Growth and Change

The past year for EurJIC has been characterized by growth and change. Both are vital for life and therefore welcomed. There is no doubt that EurJIC consequently faces many challenges − another sign of vibrant life.

The first change took effect at the beginning of 2003 when the structure of the journal changed to be anal ogous with that of other journals of the European family. Simultaneously the first indication of burgeoning submissions became evident (see Figure 1). Following the trend, early in October 2003 EurJIC had already received the same number of submissions as in 2002. The excellent support from the Editorial Board members enabled the journal to cope with this exceptional development. We thank the Board members most sincerely for their invaluable suggestions and advice that has contributed significantly to the growth in quality and not just "quantity" of EurJIC.

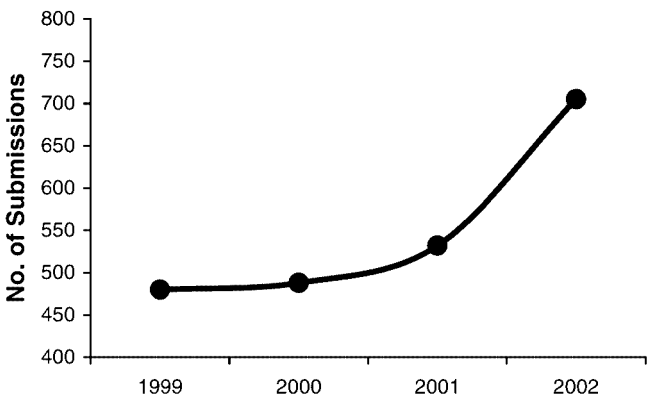

Figure 1. Number of submissions to EurJIC per year from 1999 to 2002

Invaluable support from Editorial Board

Readers will have noticed that the journal arrived twice a month, but the individual issueshardly diminished in size. We expanded the editorial office to accommodate this growth, but also introduced the publishing of articles in EarlyView to speed up the access to new publications. These EarlyView articles are fully citable by DOI, although they have not yet been assigned to an issue.

Publication times are falling as a result: even before EarlyView by DOI, the average time from submission to publication on the Web had dropped to less than five and a half months for full papers and three and a half months for the urgent Short Communications. Thus, speed of publication remains a priority, but speed is not everything. EurJIC will continue to allow peer reviewers sufficient time to comment soundly on a manuscript. Some of our referees invest a lot of time in communicating their impression of a paper in writing to the author. But the peer-review process does not stop there: many authors appreciate this new look at their work and undertake time-consuming experiments to test the ideas before submitting their revised version. All researchers profit from this process through more detailed papers, although the publication is delayed by this assiduity. Here we expressly thank each reviewer and author who exercises this dedication for the betterment of science.

The (publication) times, they are a-changin'

Peer review is a laborious process. In recognition of the load of some scientists, we attempt to keep the number of manuscripts for each reviewer down to well below one a month. With expanding submissions this is a difficult task and calls for innovative methods. We wish to thank all Editorial Board members, Advisory Board members, but also experts in fields not covered by the Boards, for their willing participation in experimentation for preselection of manuscripts. Your contribution is enormous. You keep the quality of the journal high, the work of fellow reviewers lower, and help prevent the fragmentation of our science literature into a collection of least publishable units.

Peer reviewers acknowledged

The drawbacks of modern technology also impinge on publishing. For speed, e-mail communication is preferred, but in general, partially as a result of Spam mails and stringent firewalls, about 5% of

 © 2004 Wiley-VCH Verlag GmbH & Co. KGaA, Weinheim

mail is blocked without returning a warning to the sender. A confirmation of receipt is a two-edged sword: the reviewer receives even more mail. The alternative is not knowing whether the report has arrived in the Editorial Office. Our solution to this dilemma is to send our thanks in the topic line ending with EOM (end of message). Such a mail can be clicked away without opening.

E-mail attachments are often suspect. ManuscriptXpress, the new online submission of manuscripts in conjunction with the author/referee homepage system, precludes the necessity of sending manuscripts as WORD, RTF, or PDF attachments. Directly from their computers authors can upload a document, which the system then uses to generate a PDF file. This PDF file can be easily accessed by the referees through their personal homepages, who can then submit their reports online. Authors can also conveniently gain access to their own manuscripts at any stage of publication by the same means. "No more tedious copying!" said one of our authors who preferentially submits through ManuscriptXpress. For more information, please refer to our Guidelines for Authors on page A1. There are advantages for all. Referees can refer to their reports, which are archived together with the original PDF versions of the manuscript. This system, together with the reorganization of the editorial office, has helped to reduce our publication times, in spite of an increase of 30% in the pages published.

The combined editorial office of EurJIC and EurJOC are always ready to help if anything is unclear. Early in 2003 the system was still new to authors and referees. The secretarial staff and assistants at the challenging interface between editorial office and customer did all in their power to assist, from talking an author through submission to submitting the manuscript by proxy − at a time when their learning curve with ManuscriptXpress was steep and the workload was extreme. In spite of the pressure they kept cheerful. They have deservedly earned my admiration and thanks (editor, KJH). Try them − you'll receive friendly assistance.

Unusual mention of exceptional performance

The advantages of modern technology enable scientists to keep up with the literature almost automatically! Everyone, not only subscribers, can regularly receive the Table of Contents of an issue by e-mail when it is published ("**Content Alerts**"), as well as information tailored to specific research interests about titles and authors of current articles ("**Profiled Alerts**"). More information about this service can be found at http://www.interscience.wiley.com/alerts. If you have no access to the journal but need one of the articles for your research, the Pay-per-View system will provide it in a minimum of time.

Research the literature while you sleep!

Some of these advances have been initiated by a request from an author, reviewer, or reader. EurJIC takes your suggestions seriously and encourages you to keep up the contact.

We are proud of our journal, which is developing well, as witnessed by the constant increase in the Impact Factor. EurJIC is now a well-established journal for both organometallic and material chemists, although a lot remains to be done to attract more contributions from other important areas within the inorganic chemistry community, such as bioinorganic chemistry as well as technological applications of inorganic compounds. It will be our duty to attract more submissions from these important fields and to make EurJIC a really outstanding journal for the whole community of inorganic chemists.

On behalf of the Editorial Board and the Editorial Office, the Chairman of the Board and the Editor wish you all a happy and successful 2004.

Ivano Bertini — Chairman of the Editorial Board

Karen J. Hindson — Editor

© 2004 Wiley-VCH Verlag GmbH & Co. KGaA, Weinheim

EurJIC
European Journal of Inorganic Chemistry

Issue 1/2004

Pages 1–192

Papers available ahead of print in Early View at www.interscience.wiley.com

Earliest available Table of Contents:
Automatically, free of charge by e-mail through
www.interscience.wiley.com/alerts

COVER PICTURE

The cover picture shows the synthetic pathway leading to the first polyoxometalate complex where two subunits are linked by negatively charged organic ligands via a cationic center present inside the polyoxometalate. The strategy used, together with the influence of the nature of the rare earth and the ligand concentration on the final product, are developed in the Short Communication by P. Mialane et al. on p. 33 ff.

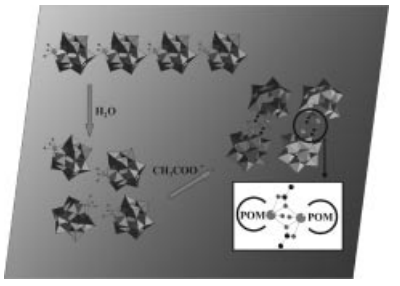

MICROREVIEW

Contents

17 **M. Jiménez-Tenorio, M. C. Puerta, P. Valerga***

Structure and Reactivity of Coordinatively Unsaturated Half-Sandwich Iron, Ruthenium and Osmium Complexes

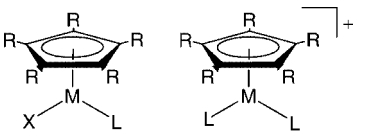

M = Fe, Ru, Os

Keywords: Transition metals / Phosphane ligands / Electron-deficient compounds / Cyclopentadienyl ligands / Agostic interactions / Sandwich complexes

 © 2004 Wiley-VCH Verlag GmbH & Co. KGaA, Weinheim

SHORT COMMUNICATION

33 **P. Mialane,* A. Dolbecq, E. Rivière, J. Marrot, F. Sécheresse**

Functionalization of Polyoxometalates by a Negatively Charged Bridging Ligand: The Dimeric $[(SiW_{11}O_{39}Ln)_2(\mu\text{-}CH_3COO)_2]^{12-}$ (Ln = Gd^{III}, Yb^{III}) Complexes

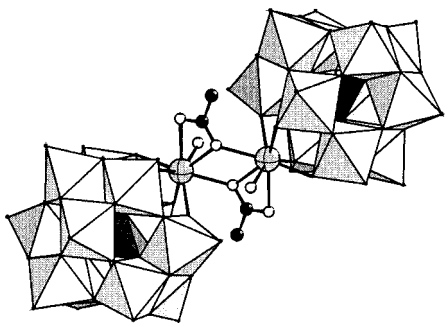

Keywords: Coordination chemistry / Lanthanides / Magnetic properties / Polyoxometalates

FULL PAPERS

37 **R. Wang, M. Hong,* D. Yuan, Y. Sun, L. Xu, J. Luo, R. Cao, A. S. C. Chan**

The Role of Spacers between Carboxylate Groups in Self-Assembly Process: Syntheses and Characterizations of Two Novel Cadmium(II) Complexes Derived from Mixed Ligands

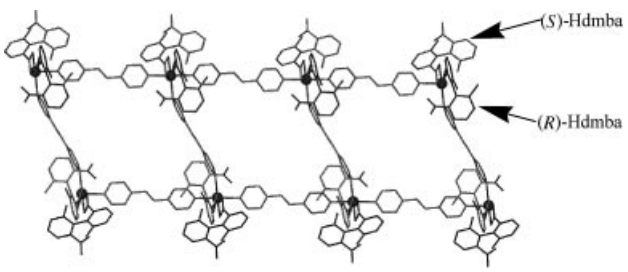

Keywords: Cadmium / Bridging ligands / X-ray diffraction / Polymers / Self assembly

44 **K. Koszinowski, D. Schröder, H. Schwarz***

Formation and Reactivity of Gaseous Iron-Sulfur Clusters

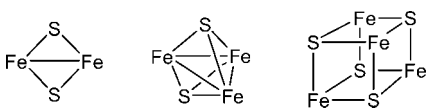

Keywords: Cluster compounds / Electron transfer / Gas-phase reactions / Iron / Sulfur

51 **M. Elhabiri, J. Hamacek, J.-C. G. Bünzli, A.-M. Albrecht-Gary***

Lanthanide Homobimetallic Triple-Stranded Helicates: Insight into the Self-Assembly Mechanism

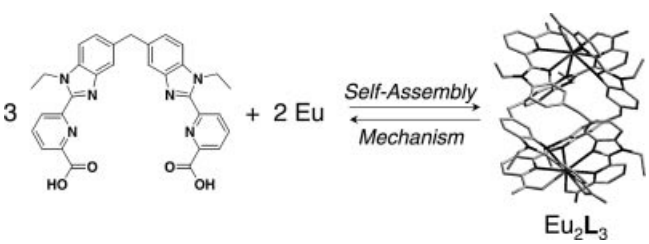

Keywords: Europium / Helicates / Mechanisms / Self-assembly / Supramolecular chemistry

63 **M. N. Sokolov,* O. A. Gerasko, D. N. Dybtsev, E. V. Chubarova, A. V. Virovets, C. Vicent, R. Llusar, D. Fenske, V. P. Fedin**

Supramolecular Chemistry Based on $[W_3S_4(H_2O)_6Cl_3]^+$ − A Versatile Building Block

Keywords: Cluster compounds / Tungsten / Antimony / Cucurbituril / Supramolecular chemistry

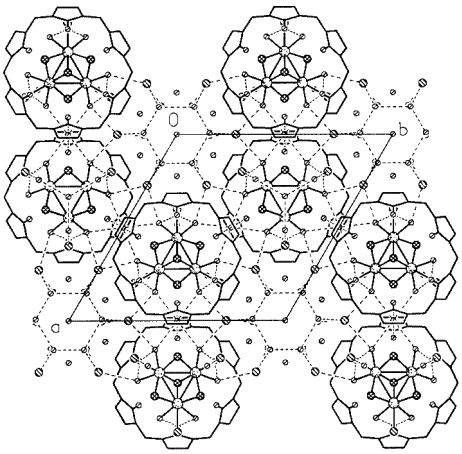

69 **F. Zhao, X. Xu, S. B. Khoo,* T. S. A. Hor***

Structure-Dependent Electrochemical Behavior of Thienylplatinum(II) Complexes of N,N-Heterocycles

Keywords: Platinum / N ligands / Cyclic voltammetry / Thin films / Heterocycles

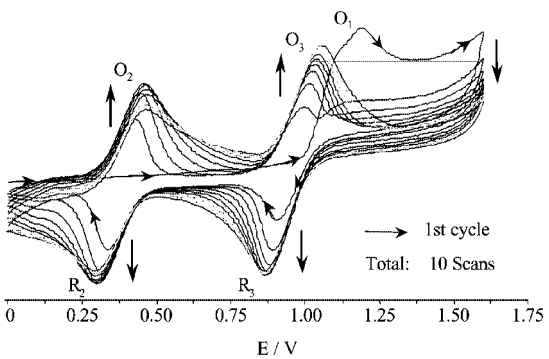

78 **K. Tang, X. Xie, L. Zhao, Y. Zhang, X. Jin***

Synthesis and Crystal Structure of $\{[HNEt_3]_{2n}[Ag_8Ag_{4/2}(SC_6H_4tBu\text{-}4)_{12}]_n \cdot nC_2H_5OH\}$ and Its Reaction Product with CS_2

Keywords: Silver / Polymers / Sulfur / Clusters

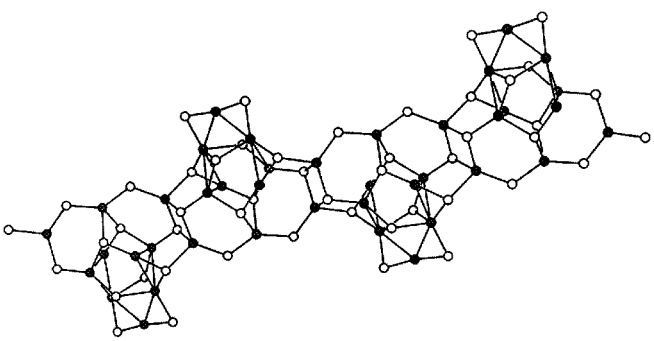

86 **J.-P. Lang,* Q.-F. Xu, W. Ji, H. I. Elim, K. Tatsumi**

Syntheses, Crystal Structures and Optical Limiting Properties of Three Novel Organometallic Tungsten-Copper-Sulfur Clusters: $[PPh_4][(\eta^5\text{-}C_5Me_5)WS_3(CuCN)_2]$, $[(\eta^5\text{-}C_5Me_5)WS_3Cu_2(PPh_3)(\mu\text{-}CN)]_2$ and $[PPh_4][\{(\eta^5\text{-}C_5Me_5)WS_3Cu_2(CN)(Py)\}_2(\mu\text{-}CN)]$

Keywords: Copper / Tungsten / Sulfur / Cluster compounds

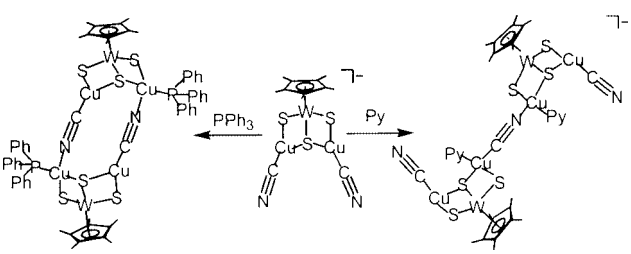

 © 2004 Wiley-VCH Verlag GmbH & Co. KGaA, Weinheim

93 **A. Eichhöfer,* D. Fenske, P. Scheer**

Investigation of the Thermal Properties of $[Cu_{20}Se_{13}(PEt_3)_{12}]$

Keywords: Cluster compounds / Mixed-valent compounds / Thermogravimetry / Copper / Selenium

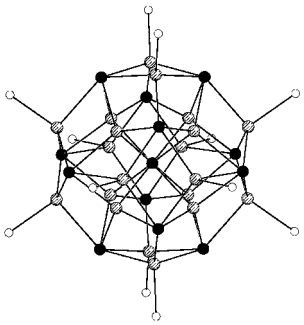

98 **H.-D. Amberger,* H. Reddmann, S. Jank, M. I. Lopes, N. Marques**

Crystal Field Strengths, Nephelauxetic Effects, and Experimentally Based Molecular Orbital Schemes (in the f Range) of Selected Cyclopentadienyl Complexes of Samarium(III)

Keywords: Lanthanides / Cyclopentadienyl ligands / Optical spectra / Crystal field analysis / Molecular orbital schemes

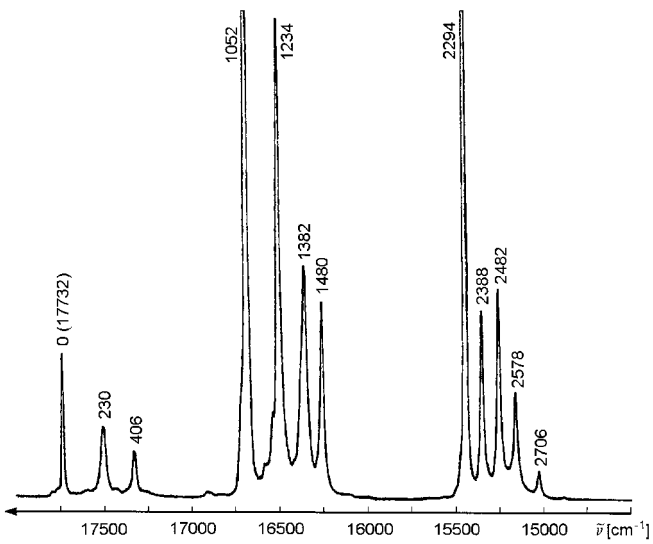

110 **D. Dobrzyńska,* M. Duczmal, L. B. Jerzykiewicz, J. Warchulska, K. Drabent**

Synthesis, Spectroscopy, and Magnetic Properties of Fe^{II} and Co^{II} Quinoline-2-carboxylates – Crystal Structure of *trans*-Bis(quinoline-2-carboxylato)bis(propanol)iron(II)

Keywords: Vibrational spectroscopy / Magnetic properties / Iron / Cobalt / Quinoline-2-carboxylates

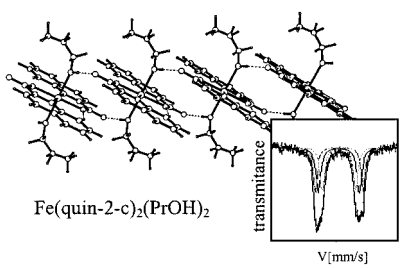

118 **V. Barba,* R. Xochipa, R. Santillan, N. Farfán**

Study of the Reaction of Tridentate Ligands with Ferrocenyl Boronic Acid

Keywords: Cyclizations / Boron / Tridentate ligands / Ferrocene

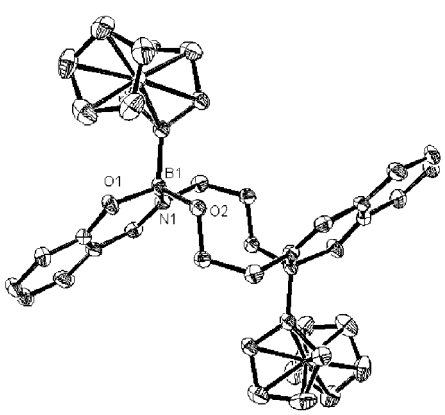

 © 2004 Wiley-VCH Verlag GmbH & Co. KGaA, Weinheim

125 **J. Tao,* X. Yin, Z.-B. Wei, R.-B. Huang, L.-S. Zheng**

Hydrothermal Syntheses, Crystal Structures and Photoluminescent Properties of Three Metal-Cluster Based Coordination Polymers Containing Mixed Organic Ligands

Keywords: Coordination polymers / Zinc / Cadmium / 5-Sulfoisophthalate / 5-Nitroisophthalate

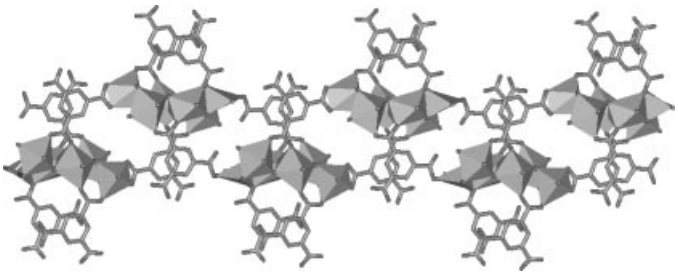

134 **Y. Yamamoto,* Y. Kosaka, Y. Tsutsumi, Y. Kaburagi, K. Kuge, Y. Sunada, K. Tatsumi**

Homo- and Heteronuclear Complexes of (Pentamethylcyclopentadienyl)rhodium(III) Bearing Bis(diphenylphosphanylmethyl)phenylphosphane

Keywords: Rhodium / Gold / Copper / Silver / Cluster compounds / P ligands

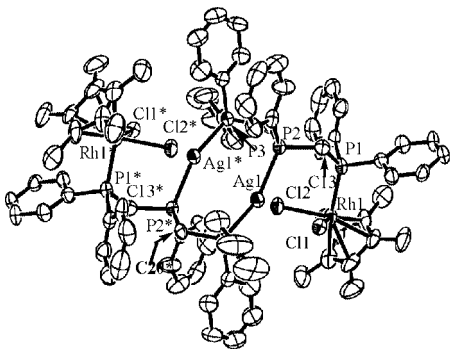

143 **A. Rodríguez-Fortea,* P. Alemany, S. Alvarez, E. Ruiz**

A Theoretical Study of the Exchange Coupling in Hydroxo- and Alkoxo-Bridged Dinuclear Oxovanadium(IV) Compounds

Keywords: Exchange coupling / Density functional calculations / Magnetic properties / Magneto-structural correlations / Vanadium

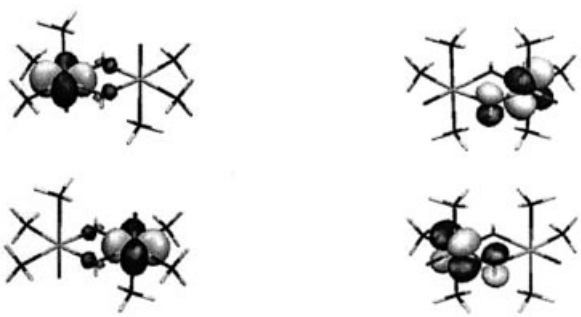

154 **G. P. M. van Klink, T. Nomoto, M. Lutz, A. L. Spek, O. S. Akkerman, F. Bickelhaupt***

In Quest of the Double Rotaxane Formation of the Bis(coronand) (1,5),(2,4)-Durenetetraylbis(18-crown-5) with Organomagnesium Compounds

Keywords: Magnesium / Mercury / Chelates / Crown compounds

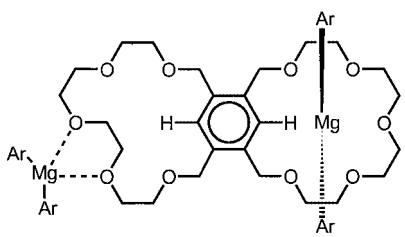

160 **J.-Y. Niu,* M.-L. Wei, J.-P. Wang,* D.-B. Dang**

1D-Polyoxometalate-Based Composite Compounds − Design, Synthesis, Crystal Structures, and Properties of $[\{Ln(NMP)_6\}(PMo_{12}O_{40})]_n$ (Ln = La, Ce, Pr; NMP = *N*-methyl-2-pyrrolidone)

Keywords: Polyoxometalates / Oxo ligands / Lanthanides / Structure elucidation / Zig-zag chain

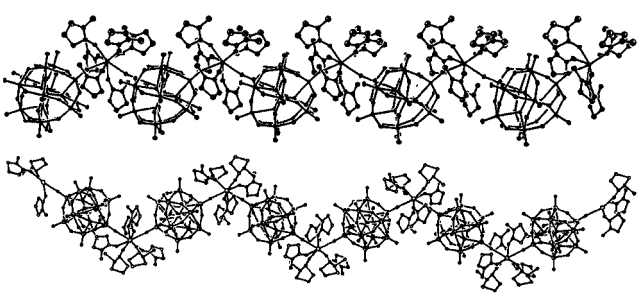

 © 2004 Wiley-VCH Verlag GmbH & Co. KGaA, Weinheim

171 **M. Afzaal, D. Crouch, M. A. Malik, M. Motevalli, P. O'Brien,* J.-H. Park, J. D. Woollins**

Deposition of II-VI Thin Films by LP-MOCVD Using Novel Single-Source Precursors

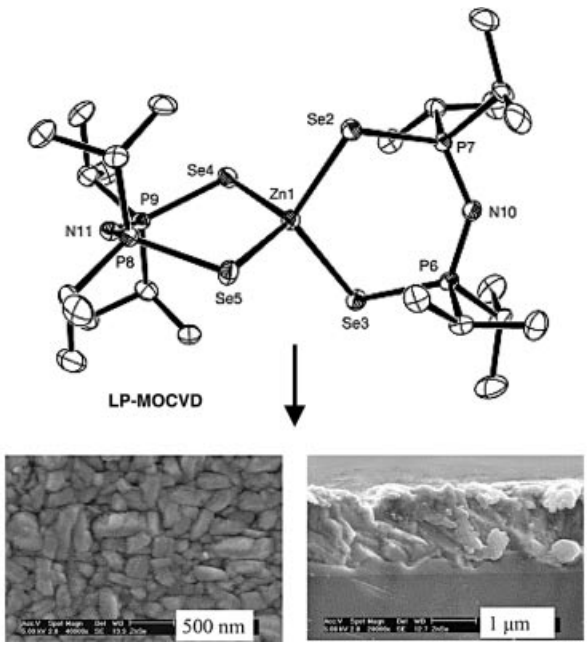

Keywords: Chemical vapour deposition / Chalcogens / Zinc / Cadmium

178 **B. K. Panda, S. Sengupta, A. Chakravorty***

Synthesis, Structure, and Properties of Biimidazole-Chelated Arylruthenium Complexes

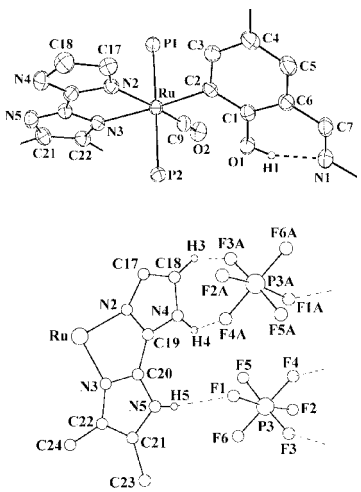

Keywords: Ruthenium / Fluorescence / Marcocyclic ligands / Hydrogen bonding

185 **X. Shi, G. Zhu,* Q. Fang, G. Wu, G. Tian, R. Wang, D. Zhang, M. Xue, S. Qiu***

Novel Supramolecular Frameworks Self-Assembled from One-Dimensional Polymeric Coordination Chains

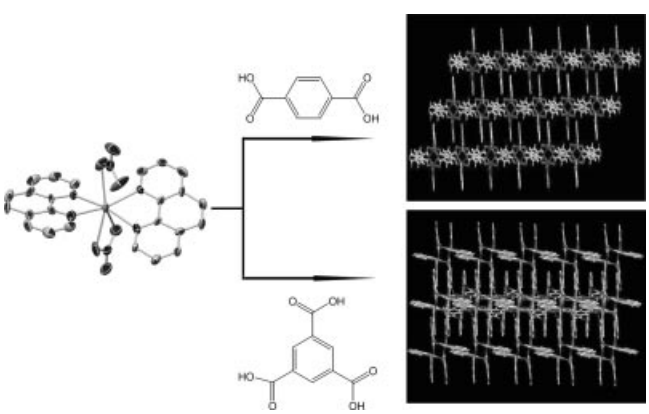

Keywords: Supramolecular chemistry / Coordination modes / Fluorescence / Polymers

 © 2004 Wiley-VCH Verlag GmbH & Co. KGaA, Weinheim

Structure and Reactivity of Coordinatively Unsaturated Half-Sandwich Iron, Ruthenium and Osmium Complexes

Manuel Jiménez-Tenorio,[a] M. Carmen Puerta,[a] and Pedro Valerga*[a]

Keywords: Transition metals / Phosphane ligands / Electron-deficient compounds / Cyclopentadienyl ligands / Agostic interactions / Sandwich complexes

This review deals with the study of coordinatively unsaturated half-sandwich iron, ruthenium and osmium complexes, in particular those bearing bulky phosphane ligands. The synthesis, properties and structure of neutral complexes of the type $[(C_5R_5)MX(L)]$ and their cationic derivatives $[(C_5R_5)M(L)_2]^+$, are described here. We will also refer to related compounds containing hydrotris(pyrazolyl)borate (Tp) ligands, given the formal relationship existing between these and those containing cyclopentadienyl groups. In addition, we discuss the reactivity of these unsaturated species towards small molecules and alkynes.

(© Wiley-VCH Verlag GmbH & Co. KGaA, 69451 Weinheim, Germany, 2004)

1. Introduction

Organometallic derivatives that do not adhere to the 18-electron rule are also known as coordinatively unsaturated organometallics, and have been referred to as the interface between Werner-type complexes and 18-electron organometallic complexes.[1] Bulky ligands are known to play an important role in the stabilization of coordinatively unsaturated metal complexes, by the steric protection provided, against the entry of additional ligands which might eventually complete the electron count at the metal centre. Since such unsaturated compounds are potential catalysts, it is

[a] Departamento de Ciencia de Materiales e Ingeniería Metalúrgica y Química Inorgánica, Facultad de Ciencias, Universidad de Cádiz,
Apartado 40, 11510 Puerto Real, Cádiz, Spain
Fax: (internat.) + 34-956/016-288
E-mail: pedro.valerga@uca.es

Manuel Jiménez-Tenorio was born in Jerez (Cádiz), Spain in 1965. He obtained his graduate degree in 1987 from the University of Cádiz and his Doctorate in 1991 with Prof. G. Jeffery Leigh at the University of Sussex, United Kingdom. In 1991 he returned to the University of Cádiz to work in collaboration with Prof. M. Carmen Puerta and Dr. Pedro Valerga. He took a permanent lectureship position in 1996 at the University of Cádiz. His current research interests are centred on the activation of dihydrogen, dinitrogen and other small molecules at coordinatively unsaturated metal centres, as well as the development of nickel and ruthenium catalysts for olefin polymerisation and alkyne coupling reactions.

Maria del Carmen Puerta, was born in Constantina (Sevilla), Spain in 1952. She obtained her graduate degree in 1974 from the University of Sevilla and her Doctorate in 1979, also at the University of Sevilla. From 1979 to 1981 she worked as a postdoc with Prof. Dieter Sellman at Friedrich-Alexander Universität Erlangen-Nürnberg. She took a permanent lectureship position at the University of Cádiz in 1983 and became a Full Professor in 2000. Her current research interests include C-H, C−C and C−X bond activation mediated by ruthenium and nickel complexes, in order to obtain high added value chemicals starting from olefins and alkynes.

Pedro Valerga, was born in Sanlúcar de Barrameda (Cádiz), Spain in 1953. He obtained his graduate degree in 1975 from the University of Sevilla and his Doctorate in 1982 with Prof. Agustín Martín-Rodríguez at the University of Cádiz. From 1985 to 1987 he worked as a postdoc with Prof. Walter L. Roth at the State University of New York at Albany. In 1987 he took a permanent lectureship position at the University of Cádiz. He has authored about 90 publications in reviewed journals. His research interests have been focused on the structural features of inorganic compounds, with special emphasis on organometallic compounds of transition metals with applications to organic synthesis and catalysis.

MICROREVIEWS: This feature introduces the readers to the author's research through a concise overview of the selected topic. Reference to important work from others in the field is included.

desirable to understand the parameters that correlate structure with stability and reactivity. Our research group has been studying the chemistry of transition metal complexes containing bulky phosphane ligands, particularly those with the strong electron-releasing phosphane 1,2-bis(diisopropylphosphano)ethane (dippe).[2−11] We have focused on the isolation of coordinatively unsaturated complexes and the study of their reactivity towards small molecules and alkynes. We initially worked with the 16-electron hydride complex $[RuH(dippe)_2][BPh_4]$.[2−4] Studies on the reactivity of this material led us to report the first example of dioxygen activation at a dihydrogen-binding site unequivocally supported by the X-ray structure analysis of the hydridodioxygen derivative *trans*-$[RuH(O_2)(dippe)_2][BPh_4]$.[2,3] Some of these results were extended later to osmium,[12,13] but we were already interested in the chemistry of half-sandwich complexes prior to that.[7−10] $[(C_5R_5)MX(L)_2]$ (R = H, Me; M = Fe, Ru, Os; X = monoanionic ligand; L = neutral ligand) derivatives constitute a very extensive class of 18-electron compounds.[14,15] Ligand dissociation from these materials gives rise to two possible types of 16-electron complexes: a) neutral complexes $[(C_5R_5)MX(L)]$ generated by dissociation of one of the neutral ligands, and b) cationic complexes $[(C_5R_5)M(L)_2]^+$ generated by dissociation of the monoanionic ligand. Both types of complexes are considered as intermediates in ligand-exchange reactions which follow a dissociative mechanism. In general, these complexes are short-lived, highly reactive transient species that are difficult to isolate. However, with a proper combination of the steric bulk and the electron-donating abilities of the ligands, the isolation of such coordinatively unsaturated species has been possible in a number of cases. These compounds are stable enough to be handled allowing their study and, in some instances, even characterisation by X-ray structure analysis. However, consistent with their coordinatively unsaturated nature, these 16-electron species remain very reactive towards a large number of substrates, including rather inert molecules such as dinitrogen. In this review we discuss the synthesis, structure and reactivity of these stable, yet reactive 16-electron half-sandwich complexes of iron, ruthenium and osmium, with emphasis on those bearing bulky phosphane ligands. We will also refer to related compounds containing hydrotris(pyrazolyl)borate (Tp) ligands, given the formal relationship existing between these and those containing cyclopentadienyl groups.[16]

2 Neutral Complexes of the Type $[(C_5R_5)M(X)(L)]$

2.1 Iron Complexes

Compared to the heavier elements in its group, iron complexes that do not follow the 18-electron rule are in general more abundant since iron is a first-row transition metal.[1] However, 16-electron complexes of formula $[(C_5R_5)Fe(X)(L)]$ are rather scarce.

Based upon the magnetic properties the complex [Cp*Fe(acac)(PMe_3)] (Cp* = C_5Me_5) is likely to have a 16-electron, spin triplet configuration with a monodentate acac ligand, or is in equilibrium with a paramagnetic product of phosphane dissociation.[17]

The reaction of $FeCl_2$ with $Li[C_5Me_4(CH_2)_2N(C_4H_8)]$ in THF/NEt_3[18] or with $Li[C_5Me_4(CH_2)_3(OCH_2CH_2)_3OMe]$ in THF[19] at low temperature yields the corresponding neutral 16-electron complexes, which appear stabilised by intramolecular coordination of the pendant amine or glycol ether moiety to iron.

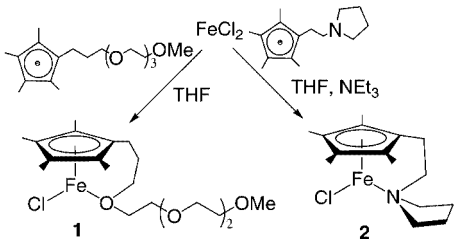

Whereas **1** appears to be stable only in solution, where it was characterised by derivatization reactions,[19] **2** has been isolated in the crystalline state.[18]

Notably, the diamagnetic 14-electron complex [Cp*Fe{$N(SiMe_3)_2$}] has been reported.[20] This compound, prepared by reaction of $FeCl_2$ with one equivalent of $K[N(SiMe_3)_2]$ in THF and subsequent addition of LiCp*, has a "pogo-stick" structure unprecedented in the chemistry of open shell organometallics (Figure 1).

In contrast with this unique compound, which contains Cp*, there is a small but growing number of 14-electron complexes of the type [Tp^RFeX] [Tp^R = hydrotris(3-*tert*-butylpyrazolyl)borate, hydrotris(3,5-diisopropylpyrazolyl)borate, hydrotris(3,4,5-trimethylpyrazolyl)borate; X = halide, alkyl, C≡CPh].[21,22] Several of these compounds have been structurally characterized by X-ray crystallography, and show a distorted tetrahedral geometry around the iron atom (Figure 2).

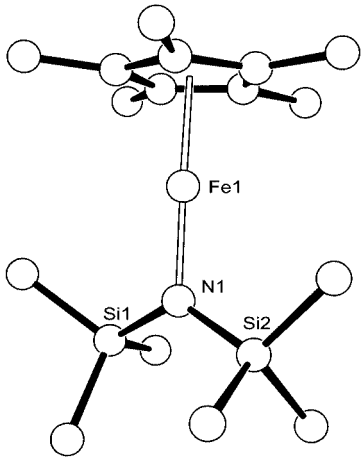

Figure 1. Molecular structure of [Cp*Fe{$N(SiMe_3)_2$}]

 © 2004 Wiley-VCH Verlag GmbH & Co. KGaA, Weinheim

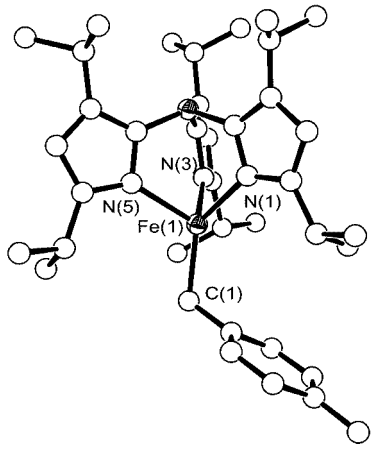

Figure 2. Molecular structure of the 14-electron complex [Tp*i*PrFeCH$_2$Tol]

[Tp^{R}FeX] derivatives, and in particular alkyl complexes such as [Tp*i*PrFeCH$_2$CH$_3$] [Tp*i*Pr = hydrotris(3,5-diisopropylpyrazolyl)borate],[22] appear to be remarkably stable despite the coordinative unsaturation, and do not undergo a β-elimination reaction. Besides, the reactions of the alkyl complexes [Tp*i*PrFeR] towards unsaturated organic substrates (olefins, acetylene) tend to be slow. This stability is attributed to the high-spin electronic configuration where four out of five frontier orbitals are singly occupied, as suggested by extended Hückel molecular orbitals (EHMO) calculations.[22]

2.2 Ruthenium Complexes

Compounds of the type [Cp*RuCl(PR$_3$)] are well-established reactive intermediates in dissociative phosphane-exchange reactions.[23] If bulky phosphane ligands are used, the isolation of the 16-electron complexes [Cp*RuCl(PR$_3$)] becomes feasible. In 1988, Tilley and co-workers prepared the compounds [Cp*RuCl(PR$_3$)] (R = *i*Pr, Cy) by reaction of tetrameric, cubane-like [(Cp*RuCl)$_4$][24] with one equivalent of the corresponding phosphane in dichloromethane.[25] Almost simultaneously, Chaudret and co-workers also reported the synthesis of these compounds by reduction of the Ru^{III} precursors [Cp*RuCl$_2$(PR$_3$)] (R = *i*Pr, Cy, *t*Bu), usually generated in situ by reaction of [Cp*RuCl$_2$]$_n$ with the appropriate amounts of phosphane and Zn in a variety of solvents.[26]

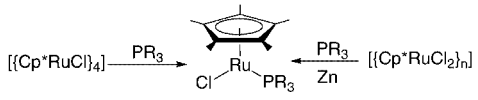

The complexes [Cp*RuCl(PMe*t*Bu$_2$)],[27] [Cp*RuCl(PPh*i*Pr$_2$)],[28] [Cp*RuCl(PMe*i*Pr$_2$)],[29] and [Cp*RuCl(η^1-(P)-PCy$_2$CH$_2$CH$_2$OMe)] (bearing a pendant ether group)[30] have also been synthesized by following any of the methods outlined above. Only bulky phosphanes with a sufficiently large cone angle allow the isolation of these 16-electron complexes. Smaller phosphanes, such as PMe$_3$ or PEt$_3$, readily form the corresponding 18-electron species [Cp*RuCl(PR$_3$)$_2$]. Furthermore, the reaction of [Cp*RuCl(PR$_3$)] (R = *i*Pr, Cy) with smaller cone angle phosphane ligands yielded complexes with filled coordination spheres. These reactions have been the subject of very detailed thermochemical investigations, which have shown that sterically demanding phosphane ligands exhibit the weakest Ru−PR$_3$ bonds.[31] There is an upper limit for the phosphane cone angle which allows the stabilization of [Cp*RuCl(PR$_3$)] species. If the cone angle is too large this results in an inefficient Ru−PR$_3$ interaction. Consistent with this, it has been noted that the reaction of [(Cp*RuCl)$_4$] with bulkier phosphanes such as PPh*t*Bu$_2$ or P(*o*-toly)$_3$ gave the unreacted starting material [(Cp*RuCl)$_4$] after 24 h at 25 °C in hexanes.[28] On the other hand, the phosphane PMe*i*Pr$_2$ defines a lower limit for the cone angle range, as both [Cp*RuCl(PMe*i*Pr$_2$)] and the 18-electron complex [Cp*RuCl(PMe*i*Pr$_2$)$_2$] are accesible depending on the phosphane to tetramer ratio.[29]

Another requirement for the stabilization of [Cp*RuX(PR$_3$)] complexes is the presence of π-electrons at the X ligand, since π-donation by lone pairs mitigates the coordinative unsaturation which would be present if the X ligand were a pure σ-donor. This is termed π-stabilized unsaturation. For this reason, these compounds have been referred to as *operationally* unsaturated, rather than *coordinatively* unsaturated.[28,32]

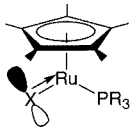

Following the initial report on the isolation of [Cp*RuCl(PR$_3$)] derivatives, the compounds of general formula [Cp*RuX(L)] (X = monoanionic ligand; L = neutral ligand) have become an important class of 16-electron complexes. Thus, alkoxo, siloxo and phenylimido complexes have been prepared. The alkoxo derivatives [Cp*Ru(OCH$_2$CF$_3$)(PR$_3$)] (PR$_3$ = PCy$_3$, PPh*i*Pr$_2$) were obtained either by reaction of the corresponding [Cp*RuCl(PR$_3$)] with Tl(OCH$_2$CF$_3$) in toluene or, alternatively, by addition of the appropriate amount of phosphane to the dimer [{Cp*Ru(μ-OCH$_2$CF$_3$)}$_2$].[28]

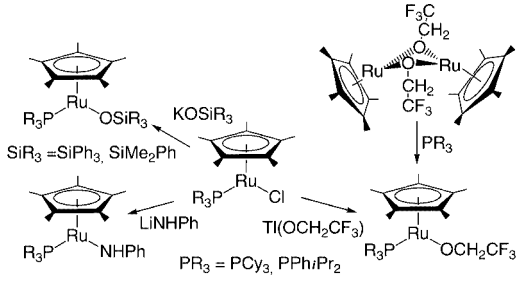

The siloxo derivatives [Cp*Ru(OSiPh$_3$)(PR$_3$)] and [Cp*Ru(OSiMe$_2$Ph)(PR$_3$)] (PR$_3$ = PCy$_3$, PPh*i*Pr$_2$) were prepared by reaction of [Cp*RuCl(PR$_3$)] with K[OSiPh$_3$] or K[OSiMe$_2$Ph] in toluene, whereas the phenylimido complexes [Cp*Ru(NHPh)(PR$_3$)] (PR$_3$ = PCy$_3$, PPh*i*Pr$_2$) were obtained in a similar fashion by reaction of [Cp*RuCl(PR$_3$)] with Li[NHPh].[28] All of these [Cp*RuX(PR$_3$)]

 © 2004 Wiley-VCH Verlag GmbH & Co. KGaA, Weinheim

derivatives contain X ligands which bear electron lone pairs at the donor atom, and hence fall into the category of π-stabilized unsaturated complexes.

The complexes [Cp*Ru(C≡CR)(PPh_3)] (R = Ph, *t*Bu) are coordinatively unsaturated species considered to be key intermediates in the catalytic coupling of alkynes.[33,34] These intermediates are generated in situ by deprotonation of the corresponding neutral vinylidene complexes [Cp*-Ru=C=CHR(Cl)(PPh_3)], but they have never been isolated as such in stable form. However, the reaction of [Cp*Ru=C=CH*t*Bu(Cl)(PPh_3)] with MeC≡CMe and NaOMe in MeOH has made possible the isolation and characterization of the β-agostic enynyl complex [Cp*Ru{C(H-CH_2)=CMeC≡C*t*Bu}(PPh_3)].[33]

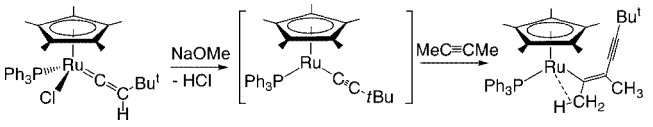

Whereas no stable compounds of the type [TpRu(X)(L)] are known, the involvement of 16-electron alkynyl species [TpRu(C≡CR)(PR_3)] in catalytic processes is well established.[35–37]

Non-phosphane ligands are also capable of stabilizing 16-electron complexes of the type [Cp*RuX(L)]. Thus, the triisopropylstibane complex [Cp*RuCl(Sb*i*Pr_3)] has been synthesized by reaction of [(Cp*RuCl)$_4$][24] with Sb*i*Pr_3 in benzene, or, alternatively, by reduction of [Cp*$RuCl_2$-(Sb*i*Pr_3)] with magnesium amalgam in THF albeit in poorer yields.[38] A series of carbene complexes of the type [Cp*RuCl(carbene)] {carbene = 1,3-R_2-imidazol-2-ylidene, R = mesityl (IMes), cyclohexyl (ICy), tolyl (ITol), 4-chlorophenyl (IpCl), adamantyl (IAd), diisopropylphenyl (IPr), (*R*)-(−)-1-cylohexylethyl [(−)ICMe], (1*S*,2*S*,3*S*,5*R*)-(+)-isopinocamphenyl [(+)I^{i}PCamp]; 1,3-dimesityl-4,5-dichloroimidazol-2-ylidene (IMesCl)} has been recently reported.[39–42] Many of these compounds have been structurally characterized, and all were prepared by reaction of the tetramer [{Cp*RuCl}$_4$][24] with the corresponding free carbene in THF.

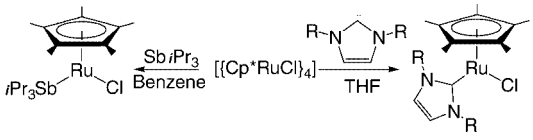

Although they do not fall specifically within the scope of this review, we should mention here a number of binuclear 16-electron complexes of the type [(Cp*Ru)$_2$(μ-$RX)_2$] {RX = OMe,[43,44] OPh,[45] OCH_2CF_3,[28] PhNH,[46] S(2,6-$Me_2C_6H_3$)[47]}, which are useful precursors for the preparation of further unsaturated complexes. These compounds display "folded" structures in the solid state and have been prepared by reaction of [(Cp*RuCl)$_4$][24] with the corresponding M^+RX^- salts or, in the case of [(Cp*Ru)$_2$(μ-$OMe)_2$], by reaction of [(Cp*$RuCl_2)_n$] with K_2CO_3 in MeOH.[43]

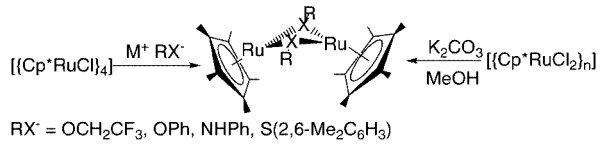

All [Cp*RuX(L)] derivatives structurally characterized display two-legged piano-stool structures, like [Cp*RuCl-(P*i*Pr_3)][25] represented in Figure 3.

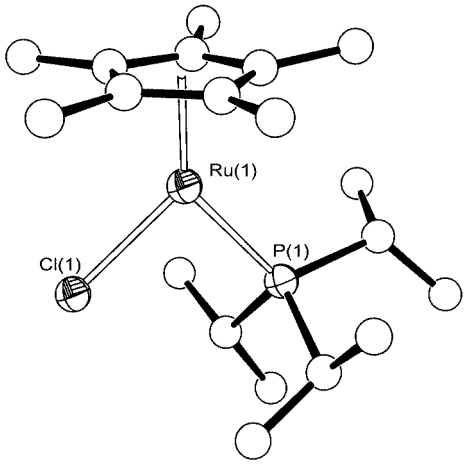

Figure 3. Molecular structure of [Cp*RuCl(P*i*Pr_3)]

Relevant bond lengths and angles for [Cp*MX(L)] (M = Ru, Os) compounds are summarized in Table 1.

The plane defined by the atoms X−Ru−L is almost perpendicular to the plane defined by the C_5 ring of Cp*. This is reflected in the pyramidalization angle α, which is the angle between the centroid of the Cp* ring, the metal atom and the centroid of the moiety X−M−L. The value of α is 170° or greater in most cases. EHMO calculations have shown the preference for a planar (non-pyramidalized, α = 180°) structure in the case of the model compounds [CpRuI-(PH_3)] and [CpRu(OH)(PH_3)], consistent with experimental data.[28] It can be said that the presence of a π-donor ligand increases the preference for a planar structure over a σ-donor ligand, whereas π-acceptor ligands favour a bent structure {α = 160° for $[CpRu(CO)_2]^+$}.[28]

In Table 1, we can see that the carbene complex [Cp*-RuCl(ICy)] has α = 143.1°. The reason for this is that this particular compound is an 18-electron chloride-bridged dimer, with a Ru−Ru separation of 3.968 Å, despite the fact that it was initially reported as a 16-electron monomer.[40] A packing diagram produced by ORTEP[48] (Figure 4) confirms the dimeric structure of [Cp*RuCl(ICy)].

A similar situation occurred for the complex [Cp*Ru-(acac)], which was initially reported as a monomer having a bent structure.[49] A packing diagram showed a 18-electron dimeric structure consisting of two independent molecules in the asymmetric unit, linked through an inversion centre, and each ruthenium bonded to the γ-carbon of the symmetry related acac group (Figure 5).[50]

Despite this, there is numerous spectral evidence in support of the coordinatively unsaturated nature of [Cp*Ru-(acac)] in solution.[51] Most likely [Cp*RuCl(ICy)] exists

 © 2004 Wiley-VCH Verlag GmbH & Co. KGaA, Weinheim

Table 1. Relevant bond lengths and angles (°) for structurally characterized neutral complexes of the type [Cp*MX(L)] (M = Ru, Os)

Compound	M−X [Å]	M−L [Å]	M−Cp*(centroid) [Å]	X−M−L [°]	α [°][a]	Ref.
[Cp*RuCl(P*i*Pr$_3$)]	2.365	2.395	1.810	91.4	175.6	[25]
[Cp*RuCl(PMe*t*Bu$_2$)]	2.395	2.392	1.770	96.32	174.5	[27]
[Cp*RuI(PPh*i*Pr$_2$)]	2.664	2.377	1.781	94.9	172.2	[28]
[Cp*Ru(OCH$_2$CF$_3$)(PCy$_3$)]	1.992	2.418	1.790	81.6	174.1	[28]
[Cp*Ru(OSiPh$_3$)(PCy$_3$)]	2.028	2.396	1.774	85.0	176.1	[28]
[Cp*RuCl(PCy$_3$)]	2.378	2.383	1.771	91.2	175.5	[39]
[Cp*RuCl(IMes)]	2.376	2.105	1.766	90.6	170.3	[39]
[Cp*RuCl(ICy)][b]	2.524	2.071	1.658	93.7	143.1	[40]
[Cp*RuCl(ITol)]	2.340	2.068	1.755	96.0	176.5	[40]
[Cp*RuCl(IAd)][c]	2.438	2.154	1.778	87.9	166.0	[40]
[Cp*RuCl(IMesCl)]	2.375	2.074	1.765	89.94	169.2	[40]
[Cp*RuCl(IPr)]	2.376	2.105	1.766	90.6	—[d]	[41]
[Cp*RuCl{(−)ICMe}]	2.377	2.097	1.763	87.1	172.4	[42]
[Cp*RuCl{(+)I^{i}PCamp}]	2.371	2.113	1.768	90.4	172.3	[42]
[Cp*Ru{PhC(N*t*Bu)$_2$}]	2.073	2.073	1.782	64.4	178.8	[53]
[Cp*OsBr(P*i*Pr$_3$)]	2.479	2.349	1.790	93.5	174.4	[63]

[a] Pyramidalization angle α = C_5 ring (centroid)−M−X(L)(centroid). [b] Reported as a 16-electron monomeric complex, it is actually a 18-electron chloride-bridged complex. [c] Displays one agostic interaction with one of the hydrogen atoms of one adamantyl group. [d] 3D-coordinates not available for calculation in the CSD.

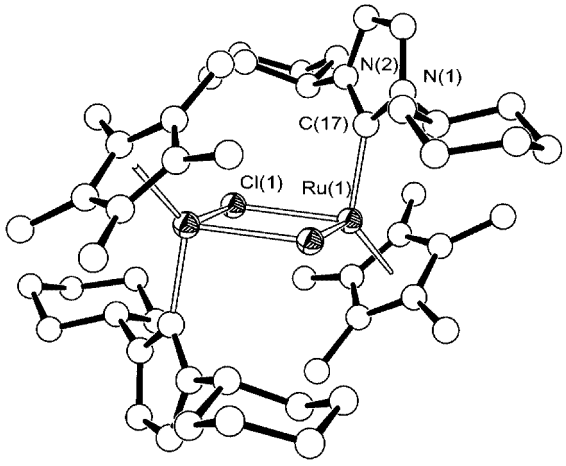

Figure 4. Molecular structure of the binuclear complex [{Cp*-Ru(ICy)}$_2$(μ-Cl)$_2$]

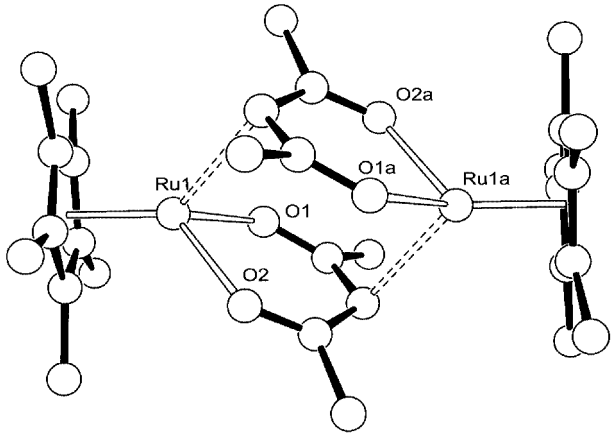

Figure 5. Molecular structure of the dimer [{Cp*Ru(acac)}$_2$]

also in solution as the monomeric species, presumably in equilibrium with its dimeric form, as has been observed for [Cp*RuCl(PMe*i*Pr$_2$)].[29]

The value of 166° found in the case of [Cp*RuCl(IAd)] is attributed to the presence of one agostic interaction with one hydrogen atom of one of the adamantyl groups (Figure 6).

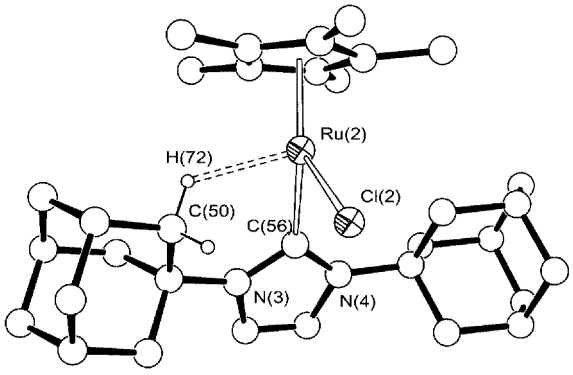

Figure 6. Molecular structure of the complex [Cp*RuCl(IAd)]; calculated average Ru···H^{agostic} 2.20 Å

The average Ru···C(H^{agostic}) distance of 2.89 Å (calculated average Ru···H^{agostic} 2.20 Å) compares well with the average value of 2.875 Å reported for the Ru···C separations in [RuPh(CO)(PMe*t*Bu$_2$)$_2$][BAr′$_4$], a complex which contains two strong agostic interactions with hydrogen atoms of the *t*Bu groups of the two phosphanes.[52]

Very recently, a series of π-stabilized complexes of the type [Cp*Ru{RC(NR′$_2$)}] (R = Me, Ph; R′ = *i*Pr, *t*Bu, Cy) has been reported.[53] In these compounds, the amidinate ligand is acting both as a σ- and π-donor to compensate coordinative unsaturation. The crystal structure of [Cp*-

 © 2004 Wiley-VCH Verlag GmbH & Co. KGaA, Weinheim

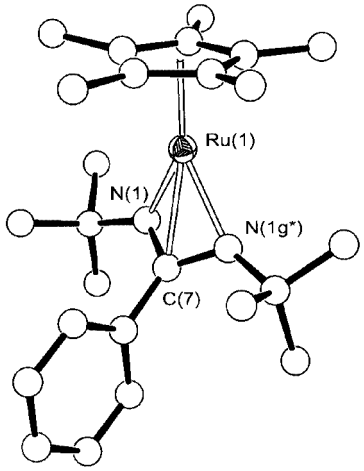

Figure 7. Molecular structure of the amidinate complex [Cp*-Ru{PhC(N*t*Bu)$_2$}]

Ru{PhC(N*t*Bu)$_2$}] (Figure 7) shows an almost perfectly planar arrangement of the Cp* centroid and the RuN_2 moiety ($\alpha = 179°$), but the NCN plane appears "folded", with an angle of 48.9° and a Ru···C separation of 2.336 Å, in a fashion which resembles that of the allyl ligands.

All coordinatively unsaturated complexes of the type [Cp*Ru(X)(L)] are extremely air sensitive materials ranging in color from dark blue to purple. The blue or purple colour is actually very characteristic of these 16-electron systems, whereas complexes having filled coordination spheres tend to be yellow, orange or red. Consistent with their coordinatively unsaturated nature, and despite any partial electronic compensation coming from π-donor ligands, [Cp*-Ru(X)(L)] derivatives are very reactive, with a strong tendency to add one ligand L (L = CO, olefins, pyridine) to attain the 18-electron configuration.[25−28] However, they are unreactive towards N_2 and are very reluctant to react with hydrogen. Thus, [Cp*RuCl(PPh*i*Pr$_2$)] shows no evidence for reaction with 2 atm of H_2 at −80 °C in [D_8]toluene. However, within 5 min of exposure of [Cp*-Ru(X)(PPh*i*Pr$_2$)] (X = Br, I) to H_2 at 25 °C in [D_8]toluene, there is evidence for the formation of the labile adducts [Cp*RuH$_2$(X)(PPh*i*Pr$_2$)] in equilibrium with [Cp*-Ru(X)(PPh*i*Pr$_2$)]. A *cisoid* square pyramidal structure has been proposed for these Ru^{IV} species. The reaction of [Cp* Ru(X)(PPh*i*Pr$_2$)] (X = CF_3CH_2O, NHPh, $OSiPh_3$) with H_2 under similar conditions involves Ru−X bond cleavage leading to [Cp*RuH$_3$(PPh*i*Pr$_2$)] plus HX.[54]

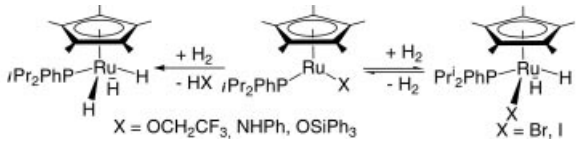

The reaction of [Cp*Ru(X)(PR$_3$)] derivatives with silicon-containing molecules has been thoroughly investigated. Intramolecular Si−H oxidative addition to ruthenium in [Cp*RuCH$_2$SiHPh$_2$(P*i*Pr$_3$)], generated by reaction of ClMgCH$_2$SiHPh$_2$ with [Cp*RuCl(P*i*Pr$_3$)], was used to produce the first isolated η^2-silene complex, [Cp*RuH(η^2-CH$_2$=SiPh$_2$)(P*i*Pr$_3$)].[55] The reaction of this compound with hydrosilanes occurs via 16-electron alkyl or silyl derivatives produced by migration of the hydride back to the silene ligand, leading to Ru^{IV} silyl hydride complexes of the types [Cp*RuH$_2$(SiR$_3$)(P*i*Pr$_3$)] and [Cp*RuH(SiR$_3$)$_2$-(P*i*Pr$_3$)].[56]

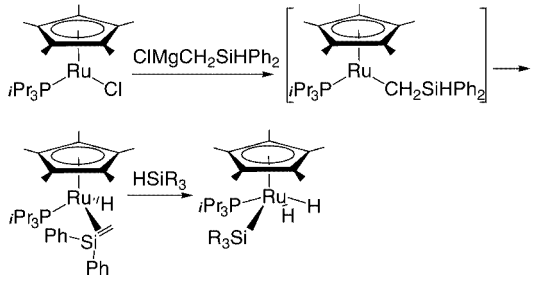

The derivatives [Cp*RuH$_2$(SiR$_3$)(PPh*i*Pr$_2$)] were generated by reaction of [Cp*Ru(OCH$_2$CF$_3$)(PPh*i*Pr$_2$)] with tertiary silanes $HSiR_3$ in pentane, whereas the reaction with the secondary silane SiH_2Ph_2 led to a mixture of [Cp*-RuH$_2$(SiHPh$_2$)(PPh*i*Pr$_2$)] and [Cp*RuH$_2${Si(OCH$_2$CF$_3$)-HPh$_2$}(PPh*i*Pr$_2$)].[54]

[Cp*RuCl(P*i*Pr$_3$)] reacts with acetylene to yield the binuclear ruthenacyclopentadiene [Cp*RuCl$_2${κ^2(*C*,*C*)-μ-C$_4$H$_4$}RuCp*],[57] whereas the reaction of the stibane homologue [Cp*RuCl(Sb*i*Pr$_3$)] with HC≡CCOOMe generates the mononuclear ruthenacyclopentadiene complex [Cp*RuCl{κ^2(*C*,*C*)-C(COOMe)=CHC(COOMe)=CH}-(Sb*i*Pr$_3$)].[38] The reaction of acetylene with [Cp*-RuCl(PPh$_3$)$_2$] also leads to the ruthenacyclopentadiene complex [Cp*RuCl{κ^2(*C*,*C*)-CH=CHCH=CH}(PPh$_3$)] by intermediacy of the 16-electron species [Cp*RuCl(PPh$_3$)] generated in situ.[58]

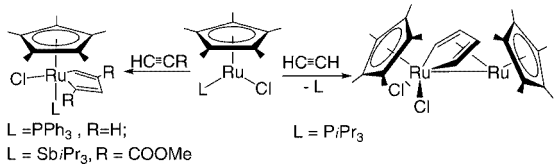

Diazo compounds add to [Cp*RuCl(PMe*i*Pr$_2$)] complexes furnishing the unstable carbene complexes [Cp*Ru=CHR(Cl)(PMe*i*Pr$_2$)] (R = COOEt, $SiMe_3$).[59] In analogous fashion, the bis(carbene) derivative [Cp*Ru=CHCOOEt-(Cl)(ICy)] is accesible by reaction of the corresponding unsaturated carbene complexes [Cp*RuCl(ICy)] with N_2CHCOOEt (EDA) in toluene at −10 °C.[60]

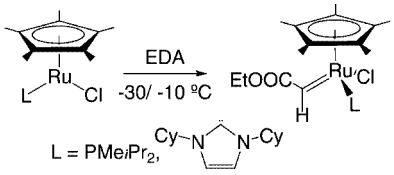

The unsaturated carbene complexes [Cp*RuCl(L)] (L = ICy, IMes) have been shown to be efficient catalysts for 1-alkyne dimerization. The conversion and selectivity of these

reactions are strongly dependent on the alkyne as well as the *N*-heterocyclic carbene substituents.[61]

[Cp*RuCl(PCy$_3$)] has recently shown to be an effective catalyst, in conjunction with Al(O*i*Pr)$_3$, for the living radical polymerization of methylmethacrylate. Although this is a versatile system which gives very narrow molecular weight distributions, the polymerizations are slow and need over 100 h for completion.[62]

2.3 Osmium Complexes

Whereas [Cp*RuCl(P*i*Pr$_3$)] was reported in 1988,[25−26] the osmium complex [Cp*OsBr(P*i*Pr$_3$)] has only been prepared very recently.[63] One possible reason for this is the unavailability of the complex [Cp*OsCl]$_4$, the homologue of [Cp*RuCl]$_4$,[24] which could serve as the starting material for the preparation of [Cp*OsCl(L)] derivatives as in the ruthenium case. Alternatively, Girolami and co-workers have described the synthesis and crystal structure of the Os^{III} dimeric complex [(Cp*OsBr)$_2$(μ-Br)$_2$],[64] providing a useful and versatile starting compound for the entry into Cp*Os chemistry. Hence, the Os^{III} phosphane complex [Cp*OsBr$_2$(P*i*Pr$_3$)] was obtained by reaction of [(Cp*-OsBr)$_2$(μ-Br)$_2$] with two equivalents of P*i*Pr$_3$ in CH_2Cl_2. Reduction of [Cp*OsBr$_2$(P*i*Pr$_3$)] with Na/Hg amalgam (0.3%, one equivalent) in THF followed by workup afforded purple-black crystals of the 16-electron complex [Cp*-OsBr(P*i*Pr$_3$)].[63] This is the only stable compound of the type [Cp*Os(X)(L)] isolated so far. X-ray crystallography showed a planar two-legged piano stool structure for this compound, just as its ruthenium congeners (Table 1).

[Cp*OsBr(P*i*Pr$_3$)] reversibly binds N_2 at low temperature to give the terminal and bridging dinitrogen complexes [Cp*OsBr(N$_2$)(P*i*Pr$_3$)] [ν(N$_2$) 2074 cm^{-1}] and [{Cp*-OsBr(P*i*Pr$_3$)}$_2$(μ-N$_2$)], which were characterized by ^{15}N NMR spectroscopy. Reaction with H_2 affords the Os^{IV} dihydrido complex [Cp*OsBrH$_2$(P*i*Pr$_3$)], whereas reaction with $PhSiH_3$ yielded the silylhydrido derivative [Cp*-OsHBr(SiH$_2$Ph)(P*i*Pr$_3$)].[63]

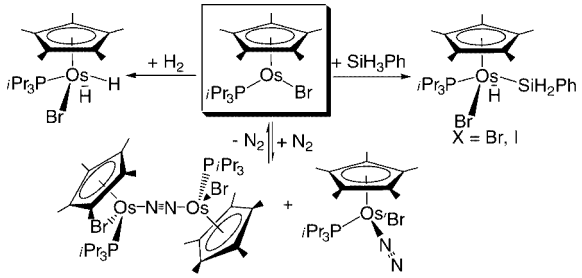

The complex [CpOsCl(P*i*Pr$_3$)$_2$] dissociates one P*i*Pr$_3$ ligand very easily in solution generating the unsaturated complex [CpOsCl(P*i*Pr$_3$)] in situ, which reacts rapidly with P(OMe)$_3$, olefins and internal alkynes furnishing 18-electron complexes of the type [CpOsCl(L)(P*i*Pr$_3$)] [L = P(OMe)$_3$, methylacrilate, bis(carboxymethyl)acetylene].[65] Besides, [CpOsCl(P*i*Pr$_3$)] is capable of H−X activation (X = H, C, Si, Ge, Sn).[66] In a similar fashion, thermolysis of the alkyl complexes [(C$_5$R$_5$)OsCH$_2$SiMe$_3$(PR$_3$)$_2$] (R = H, Me; PR$_3$ = PPh$_3$, PMe$_3$) also generates the corresponding highly reactive 16-electron complexes [(C$_5$R$_5$)OsCH$_2$SiMe$_3$(PR$_3$)] in situ, which easily undergo C−H activation processes leading to alkyl, silyl and hydridosilyl derivatives.[67]

3. Cationic Complexes of the Type [(C$_5$R$_5$)M(L)$_2$]$^+$

3.1 Iron Complexes

Although not strictly a half-sandwich complex, the 16-electron pentadienyl derivative [(η^5-pentadienyl)Fe(PEt$_3$)$_2$][PF$_6$] was reported in 1990. It was prepared by reaction of [Fe(η^5-pentadienyl)(η^3-pentadienyl)(PEt$_3$)] with Ag[PF$_6$] and PEt$_3$ in dichloromethane, or, alternatively, by addition of [HPEt$_3$][PF$_6$] to the former iron complex.[68] The first 16-electron half-sandwich complexes of iron isolated and unequivocally characterized were [(C$_5$R$_5$)Fe(dippe)][BPh$_4$] (R = H, Me).[7] These yellow-brown compounds were prepared by halide abstraction from the corresponding chloro complexes [(C$_5$R$_5$)FeCl(dippe)][6] in MeOH under argon, using NaBPh$_4$ as a chloride scavenger. The complex [Cp*Fe(dppe)][PF$_6$], prepared by oxidation of the 17-electron radical complex [Cp*Fe(dppe)] using [Cp$_2$Fe][PF$_6$], was reported shortly afterwards.[69] The related derivative [Cp*Fe(dppp)][CF$_3$SO$_3$] [dppp = 1,3-bis(diphenylphosphano)propane] has been described recently.[70] This compound was obtained by hydride abstraction from [Cp*-FeH(dppp)] using MeOSO$_2$CF$_3$ as a hydride scavenger.

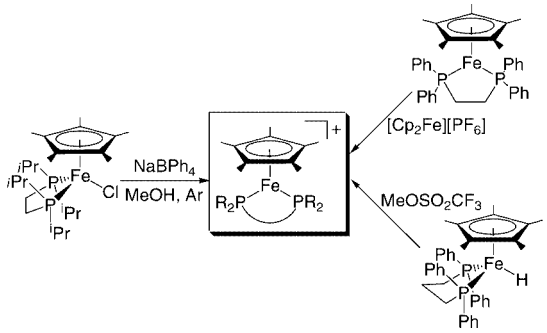

All compounds [(C$_5$R$_5$)Fe(P)$_2$]$^+$ reported to date, as well as [(η^5-pentadienyl)Fe(PEt$_3$)$_2$]$^+$, are paramagnetic species with magnetic moments ranging from 2.93 to 3.8 μ$_B$. These values for the magnetic moment are consistent with the presence of two unpaired electrons, and hence have a triplet state electron configuration. The structure of these coordinatively unsaturated two-legged piano-stool complexes has been analyzed using both extended Hückel methodology[71] and density functional theory (DFT).[71−72] Detailed DFT calculations performed on the complex [Cp*Fe(dppe)]$^+$ found a triplet ground state with a small singlet-triplet separation. Geometry optimization has shown that the structure of the compounds [(C$_5$R$_5$)Fe(PR′$_2$CH$_2$CH$_2$PR′$_2$)]$^+$ (R = H, Me; R′ = H, Ph) is planar in the triplet state (α = 177° to 180°), whereas in the singlet state it is pyramidalized, with the angle α between 145° and 162°.[72] The

 © 2004 Wiley-VCH Verlag GmbH & Co. KGaA, Weinheim

question of the spin state, geometry and structural dynamics of these systems has been explained in terms of the second-order Jahn−Teller instability of their planar (non-pyramidalized) geometry.[72] The through-space coupling (TSC) concept has also been applied to the study of the geometry of $[Cp'ML_2]$ systems (Cp′ = cyclopentadienyl or a derivative, M = Fe^{II}, Ru^{II}, L = P- or N-donor co-ligands). This concept is the molecular orbital representation of van der Waals-like repulsive-attractive forces between the ligands in addition to the interactions with the metal centre.[73] According to this, the combination of both determines whether a planar or a pyramidal structure is adopted and also whether the complex is diamagnetic or paramagnetic.[73]

The theoretical findings are supported by the experimental solid-state structures of [Cp*Fe(dippe)][BPh_4] (Figure 8),[7] [Cp*Fe(dppe)][PF_6],[69] and [Cp*Fe(dppp)]-[CF_3SO_3].[70] All of these compounds were determined by X-ray crystallography.

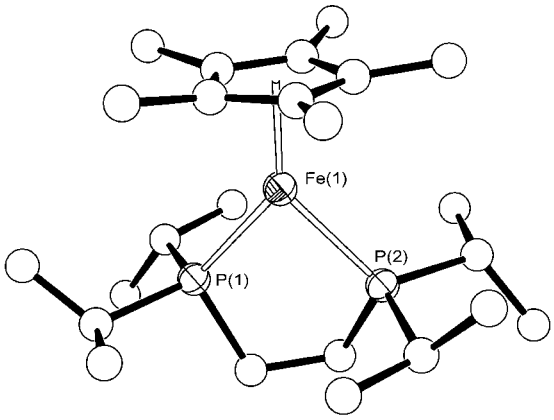

Figure 8. Molecular structure of the cation $[Cp^*Fe(dippe)]^+$

These compounds display planar two-legged piano-stool structures, and their most significant dimensions are summarized in Table 2.

There are two basic reactivity patterns for these $[(C_5R_5)Fe(P)_2]^+$ unsaturated complexes: a) addition of the ligand L to form the corresponding 18-electron complex $[(C_5R_5)Fe(L)(P)_2]^+$; and b) oxidation reactions to Fe^{III} complexes.

Complexes $[(C_5R_5)Fe(P)_2]^+$ react with a range of neutral donors such as H_2O, acetone, MeCN or CO affording the corresponding saturated complexes.[7,69,70] The resulting $[(C_5R_5)Fe(L)(P)_2]^+$ derivatives can be either diamagnetic or paramagnetic. In particular, those adducts containing oxygen-donor ligands such as acetone, H_2O or $[CF_3SO_3]^-$ in combination with Cp* as a co-ligand, all exhibit paramagnetic behaviour.[72] The complex $[Cp^*Fe(MeCN)(dippe)]^+$ is also paramagnetic at variance with its Cp counterpart, which is diamagnetic.[7] DFT has been used in an attempt to account for the unusual magnetic behaviour of these complexes.[72]

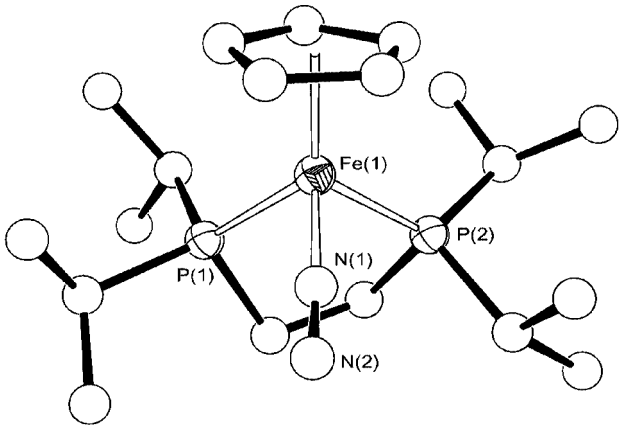

Figure 9. Molecular structure of the cationic dinitrogen complex $[CpFe(N_2)(dippe)]^+$

The complex [CpFe(dippe)][BPh_4] binds N_2 reversibly, furnishing the diamagnetic terminal dinitrogen complex [$CpFe(N_2)$(dippe)][BPh_4] [$\nu(N_2)$ 2112 cm^{-1}], which was structurally characterized (Figure 9).[7]

This dinitrogen complex exists in equilibrium with [CpFe(dippe)][BPh_4] in acetone under dinitrogen. The study of this equilibrium allowed the calculation of $\Delta H°$ and $\Delta S°$ for this process (18.2 ± 0.5 kJ·mol^{-1} and 68 ± 2 J·mol^{-1} K^{-1}, respectively).

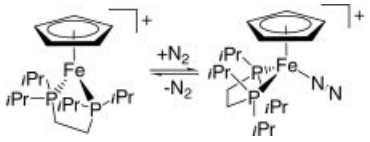

Thus, the dissociation process is entropy driven and addition of N_2 may be favoured by lowering the temperature. Poli has pointed out that the actual strength of the $Fe-N_2$ bond in this complex is greater because part of the energy spent in breaking this bond is regained as a result of the spin-state change from singlet to triplet in [CpFe-(dippe)]$^+$.[1]

3.2 Ruthenium Complexes

Cationic complexes of the type $[(C_5R_5)Ru(P)_2]^+$ are readily generated in situ by reaction of the corresponding halide

Table 2. Relevant bond lengths (Å) and angles (°) for structurally characterized cationic complexes of the type $[Cp^*Fe(P)_2]^+$

Compound	M−L [Å]	M−L [Å]	M−Cp*(centroid) [Å]	X−M−L [°]	α [°][a]	Ref.
[Cp*Fe(dippe)][BPh_4]	2.290	2.291	1.80	87.0	176	[7]
[Cp*Fe(dppe)][PF_6]	2.232	2.260	1.77	86.5	174	[69]
[Cp*Fe(dppp)][CF_3SO_3]	2.266	2.274	1.79	95.6	178	[70]

[a] Pyramidalization angle α = C_5 ring (centroid)−M−X(L)(centroid).

 © 2004 Wiley-VCH Verlag GmbH & Co. KGaA, Weinheim

complex $[(C_5R_5)RuX(P)_2]$ (X = Cl, Br, I) with a suitable halide scavenger, such as Ag^+ or Tl^+ salts. However, the resulting unsaturated cations $[(C_5R_5)Ru(P)_2]^+$ are in most cases too reactive to be isolated, and react with any suitable donor molecule in the reaction mixture to give 18-electron complexes. The donor can be a solvent molecule, particularly if it is coordinating, or, alternatively, the counterion may also act as a ligand. Hence, reports claiming the synthesis of the supposedly 16-electron complexes such as $[CpRu(dcpe)][CF_3SO_3]$ [dcpe = 1,2-bis(dicyclohexylphosphano)ethane][74] or $[Cp^*Ru(dppe)][CF_3SO_3]$[75] as orange solids which were characterized by NMR spectroscopy and microanalysis, might actually correspond to the 18-electron species $[CpRu(\eta^1\text{-}(O)\text{-}CF_3SO_3)(dcpe)]$ or $[Cp^*Ru(\eta^1\text{-}(O)\text{-}CF_3SO_3)(dppe)]$, respectively. Even counterions such as $[BPh_4]^-$ are known to bind in an η^6-fashion to ruthenium.[10] The introduction of the bulky, non-coordinating anion $[BAr'_4]^-$ {Ar′ = 3,5-$[(CF_3)_2C_6H_3]$}[76] and its use as a halide scavenger opens up new possibilities to generate and stabilize cationic, highly electrophilic 16-electron species. Thus, halide abstraction from [Cp*RuCl(TMEDA)] (TMEDA = $Me_2NCH_2CH_2NMe_2$) using $NaBAr'_4$ in Et_2O affords the blue cationic 16-electron complex [Cp*Ru(TMEDA)][BAr′4] in 92% isolated yield.[77] In a similar fashion, the reaction of $[(Cp^*RuCl)_4]$ with the diamines $Me_2NCH_2CH_2NR_2$ [R_2 = *i*Bu$_2$, $(CH_2CH_2)_2O$] and $NaBAr'_4$ in Et_2O afforded the corresponding unsaturated cationic complexes $[Cp^*Ru(Me_2NCH_2CH_2NR_2)][BAr'_4]$ in high yields. However, when the diamine $Me_2NCH_2CH_2NMePh$ was used, the 18-electron η^6-arene complex $[Cp^*Ru\{\eta^6\text{-}C_6H_5N(Me)CH_2CH_2NMe_2\}][BAr'_4]$ was obtained.[78] The complex [CpRu(TMEDA)][BAr′4] has also been synthesized following a a similar procedure, and structurally characterized (Figure 10).[79]

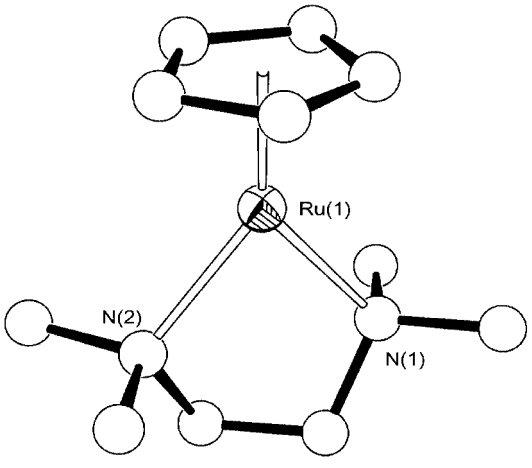

Figure 10. Molecular structure of the cation $[CpRu(TMEDA)]^+$

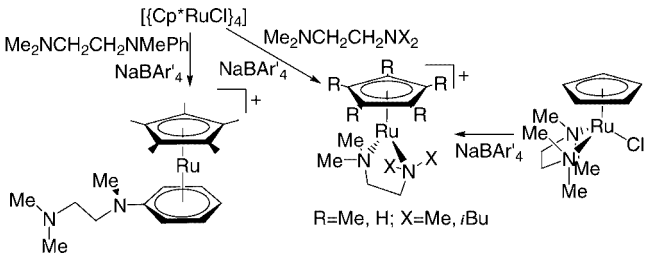

By addition of one equivalent of the dicationic carbene precursor 1,2,3,4-tetramethyl-1,2,4-triazolium bis(triflate) $[C_2HN_3Me_4][CF_3SO_3]_2$ to the dimer $[\{Cp^*Ru\}_2(\mu\text{-}OMe)_2]$,[43] the remarkably stable tricationic bis(carbene) complex $[Cp^*Ru(C_2N_3Me_4)_2][CF_3SO_3]_3$ was isolated in moderate yield.[80]

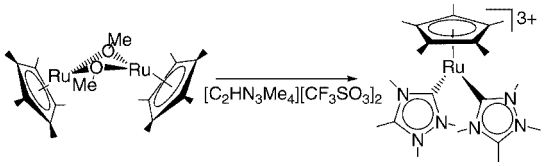

The rather long Ru−C(carbene) bond lengths in this complex (Figure 11) are in agreement with two datively bound carbenes acting as two-electron donors, and therefore the cation $[Cp^*Ru(C_2N_3Me_4)_2]^{3+}$ should be considered as a 16-electron species.

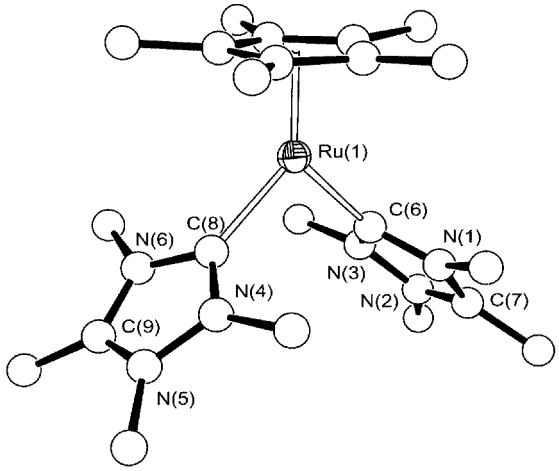

Figure 11. Molecular structure of the tricationic complex $[Cp^*Ru(C_2N_3Me_4)_2]^{3+}$

The first stable compounds of the type $[Cp^*Ru(P)_2]^+$ were unequivocally characterized and recently reported by our research group.[81,82] The complex [Cp*Ru(PMe*i*Pr$_2$)$_2$][BAr′4] (Figure 12) was prepared by reaction of [Cp*RuCl(PMe*i*Pr$_2$)][29] with $NaBAr'_4$ in fluorobenzene under argon in the presence of PMe*i*Pr$_2$, whereas the derivatives [Cp*Ru(dippe)][BAr′4] (Figure 13) and $[Cp^*Ru(PEt_3)_2]$-[BAr′4] were similarly obtained by chloride abstraction from either [Cp*RuCl(dippe)][9] or $[Cp^*RuCl(PEt_3)_2]$[83] using $NaBAr'_4$ in fluorobenzene under argon.

Although this seems to be a general reaction for the preparation of cationic 16-electron half-sandwich ruthenium complexes, the range of stable compounds of this type amenable to isolation is in fact very limited. Scheme 1 summarizes the variety of products which may result from the halide abstraction reaction of $[(C_5R_5)RuCl(P)_2]$ complexes using $NaBAr'_4$ in fluorobenzene under argon.

 © 2004 Wiley-VCH Verlag GmbH & Co. KGaA, Weinheim

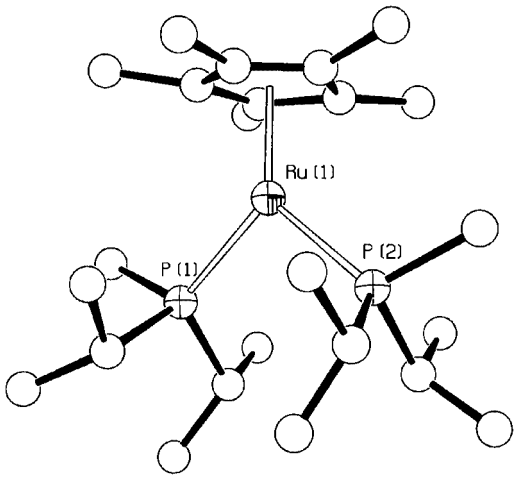

Figure 12. Molecular structure of the cation $[Cp^*Ru(PMe{\it i}Pr_2)_2]^+$

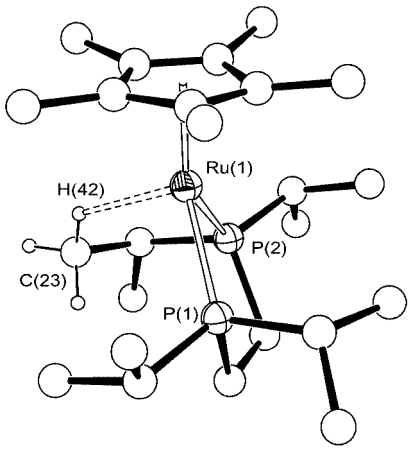

Figure 13. Molecular structure of the cation $[Cp^*Ru(dippe)]^+$; calculated $Ru\cdots H^{agostic}$ 2.262 Å

Thus, with phosphanes other than $PMe{\it i}Pr_2$, dippe or PEt_3, a variety of 18-electron compounds have been isolated. Even a non-coordinating solvent such as fluorobenzene might become a good ligand under these conditions, and hence the sandwich complex $[Cp^*Ru(\eta^6\text{-FPh})][BAr'_4]$ has been isolated from the reactions of $[Cp^*RuCl(PR_3)]$ (PR_3 = P*i*Pr$_3$, PCy_3) with $NaBAr'_4$ in fluorobenzene under argon in the presence of PR_3 in an attempt to prepare the corresponding unsaturated complexes.[82] Halide abstraction from $[Cp^*RuCl(PMe_3)_2]$ in fluorobenzene results in ligand redistribution and a mixture of $[Cp^*Ru(\eta^6\text{-FPh})][BAr'_4]$ and the tris(phosphane) complex $[Cp^*Ru(PMe_3)_3][BAr'_4]$ is obtained. If aromatic substituents are present on the phosphane ligand, the ultimate product from the halide abstraction reaction is usually the corresponding sandwich derivative $[Cp^*Ru(\eta^6\text{-}C_6H_5PR_2)][BAr'_4]$ (R = *i*Pr, Ph).[82] Another way to attain the 18-electron configuration for these systems is the formation of halide bridges. When the halide ligand is abstracted and the 16-electron fragment is generated, it can react with the remaining halo complex furnishing a cationic 18-electron halide-bridged binuclear complex. This happens in the course of the reaction of [Cp*-RuCl(dppm)] with $NaBAr'_4$ in fluorobenzene under argon, and the resulting binuclear compound undergoes phosphane rearrangement yielding $[\{Cp^*Ru\}_2(\mu\text{-Cl})(\mu\text{-dppm})_2][BAr'_4]$.[84] In a similar fashion, halide abstraction from $[Cp^*RuCl(CO)(PR_3)]$ (PR_3 = PEt_3, P*i*Pr$_2$) also leads to halide-bridged binuclear complexes $[\{Cp^*Ru(CO)(PR_3)\}_2(\mu\text{-Cl})][BAr'_4]$.[85]

The use of Cp* instead of Cp as the co-ligand is also very important for the stabilization of cationic half-sandwich 16-electron species of the type $[(C_5R_5)Ru(P)_2]^+$. Thus, when halide abstraction from $[CpRuCl(P)_2]$ [$(P)_2$ = dippe, PEt_3, P*i*Pr$_2$] using $NaBAr'_4$ in fluorobenzene under argon was

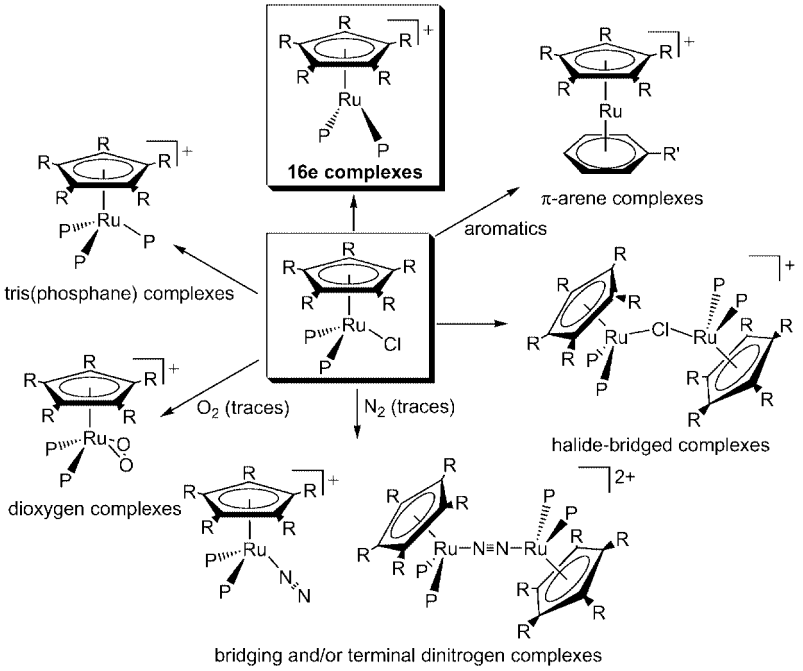

Scheme 1. Variety of products which may result from the halide abstraction reaction of $[(C_5R_5)RuCl(P)_2]$ using $NaBAr'_4$/FPh

 © 2004 Wiley-VCH Verlag GmbH & Co. KGaA, Weinheim

attempted, the resulting 16-electron species generated in this way are potentially so reactive that they scavenge trace amounts of dinitrogen present even in high-purity argon, giving dinitrogen-bridged complexes $[\{CpRu(P)_2\}_2(\mu\text{-}N_2)][BAr'_4]_2$ (Figure 14).[86]

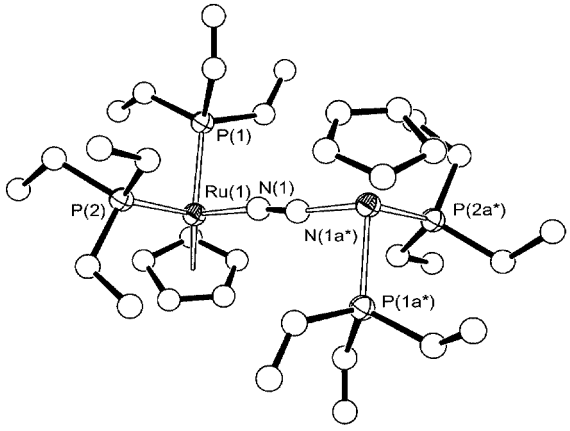

Figure 14. Molecular structure of the dicationic dinitrogen-bridged complex $[\{CpRu(PEt_3)_2\}_2(\mu\text{-}N_2)]^{2+}$

Chloride abstraction from $[CpRuCl(PMe\textit{i}Pr_2)(PPh_3)]$ under argon afforded a compound of formula $[CpRu(PMe\textit{i}Pr_2)(PPh_3)][BAr'_4]$. However, this compound is not a genuine 16-electron species, since the vacant coordination position is occupied by one of the C=C bonds of a phenyl substituent of the PPh_3 ligand (Figure 15). Hence in this case, the PPh_3 ligand adopts a very rare η^3-coordination mode[87] and the system attains the 18-electron configuration in this way.[86]

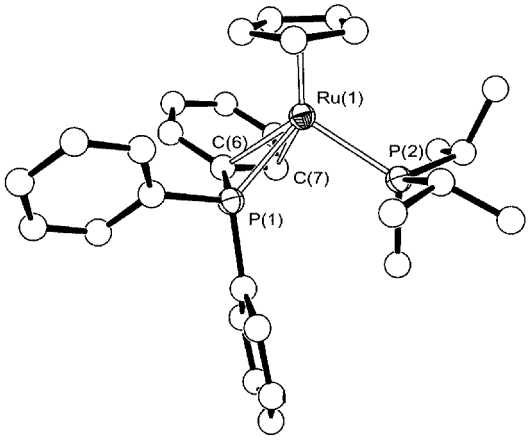

Figure 15. Molecular structure of the cation $[CpRu(\eta^3\text{-}PPh_3)(PMe\textit{i}Pr_2)]^+$

In a similar fashion, the complexes $[CpRu\{(R)\text{-}(BINAP)\}][CF_3SO_3]$[88,89] [BINAP = 2,2′-bis(diphenylphosphano)-1,1′-binaphthyl] and $[CpRu(MeO\text{-}BIPHEP)][BF_4]$[89] {MeO-BIPHEP = (6,6′-dimethoxybiphenyl-2,2′-diyl)bis[bis(3,5-di-*tert*-butylphenyl)phosphane]} contain chelating phosphane ligands acting as six-electron donors through coordination of one of the biaryl double bonds to ruthenium, also attaining the 18-electron configuration (Figure 16).

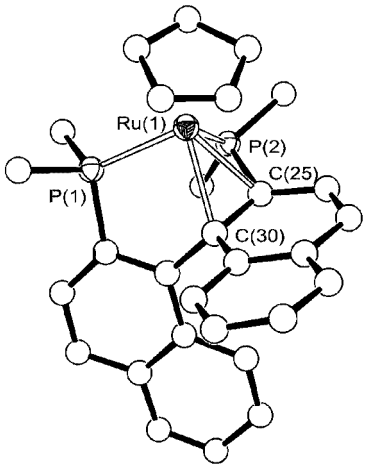

Figure 16. Molecular structure of the cation $[CpRu[(R)\text{-BINAP})]^+$; only the *ipso*-carbon atoms of the phenyl rings of the BINAP ligand are represented

All cationic compounds $[(C_5R_5)Ru(L)_2]^+$ structurally characterized display two-legged piano-stool structures (Table 3). The pyramidalization angle α falls between 170° and 180° in most cases, indicative of non-pyramidalized structures.

The angle of 160° found for $[Cp^*Ru(dippe)]^+$ is due to the presence of an agostic interaction with one of the hydrogen atoms of an isopropyl group [Figure 13; $Ru\cdots C(H^{agostic})$ distance of 2.953(4) Å, calculated $Ru\cdots H^{agostic}$ 2.262 Å].[81,82] Complexes stabilized by bonding to C=C bonds of either aryl or biarylphosphane group (Figure 15 and 16) display pyramidalization angles of 155−157°, consistent with their coordinatively saturated character. Extended Hückel[73,78,79] and DFT[73,82] calculations have been performed on several model systems $[CpRu(L)_2]^+$ $[(L)_2 = (NH_3)_2, NH_2CH_2CH_2NH_2, (PH_3)_2, PH_2CH_2CH_2PH_2]$ (Figure 17). The TSC concept has also been applied recently to the MO analysis of $[CpRu(L)_2]^+$ complexes.[73]

The calculated ground-state structure of the model phosphane complexes is strongly pyramidalized ($\alpha = 149-152°$), with an energy difference of ca. 6 kcal mol^{-1} between the ideally planar ($\alpha = 180°$) and the pyramidal geometry. In contrast, the model amine complexes adopt essentially planar structures ($\alpha = 171-179°$), with an almost flat inversion barrier.[82] It must be noted, however, that bending is hampered by bulky L_2 ligands, and the reactivity of the fragment is modified accordingly. Amine ligands participate much less than phosphane ligands in the LUMO, and this participation is further increased on bending. This is reflected in the observed agostic interaction in $[Cp^*Ru(dippe)]^+$.

Complexes $[(C_5R_5)Ru(L)_2]^+$ are highly electrophilic, as expected, although their reactivity depends strongly on the nature of both the C_5R_5 and L ligands. Thus, Cp complexes are more reactive than their Cp* homologues. For example, $[CpRu(TMEDA)]^+$ adds dihydrogen affording $[CpRu(H_2)(TMEDA)]^+$, whereas $[Cp^*Ru(TMEDA)]^+$ is unreactive

 © 2004 Wiley-VCH Verlag GmbH & Co. KGaA, Weinheim

Table 3. Relevant bond lengths (Å) and angles (°) for structurally characterized cationic complexes of the type $[(C_5R_5)Ru(L)_2]^+$

Compound	M−L [Å]	M−L [Å]	M−Cp*(centroid) [Å]	X−M−L [°]	α [°][a]	Ref.
[Cp*Ru(TMEDA)][BAr′$_4$]	2.184	2.181	1.77	80.3	179	[77]
[Cp*Ru(Me$_2$NCH$_2$CH$_2$*i*Bu$_2$)][BAr′$_4$]	2.18	2.21	1.74	78.1	168	[78]
[CpRu(TMEDA)][BAr′$_4$]	2.143	2.164	1.71	80.9	180	[79]
[Cp*Ru(C$_2$N$_3$Me$_4$)$_2$][CF$_3$SO$_3$]$_3$	2.081	2.071	1.79	93.7	180	[80]
[Cp*Ru(dippe)][BAr′$_4$][b]	2.331	2.356	1.84	83.1	160	[81,82]
[Cp*Ru(PMe*i*Pr$_2$)$_2$][BAr′$_4$]	2.393	2.395	1.83	101.4	173	[81,82]
[Cp*Ru(PEt$_3$)$_2$][BAr′$_4$]	2.28	2.36	1.85	99.3	170	[82]
[CpRu(PMe*i*Pr$_2$)(PPh$_3$)][BAr′$_4$][c]	2.295	2.372	1.84	96.8	155	[86]
[CpRu(BINAP)][BAr′$_4$][d]	2.332	2.327	1.90	90.6	155	[88]
[CpRu(MeO-BIPHEP)][BF$_4$][d]	2.273	2.317	1.86	93.5	157	[89]

[a] Pyramidalization angle α = C_5 ring (centroid)−M−X(L)(centroid). [b] Contains one agostic interaction with a hydrogen atom of an isopropyl group. [c] Attains 18-electron configuration by coordination of one C=C bond of a Ph substituent of the PPh_3 ligand. [d] Attains 18-electron configuration by coordination of one of the biaryl bonds.

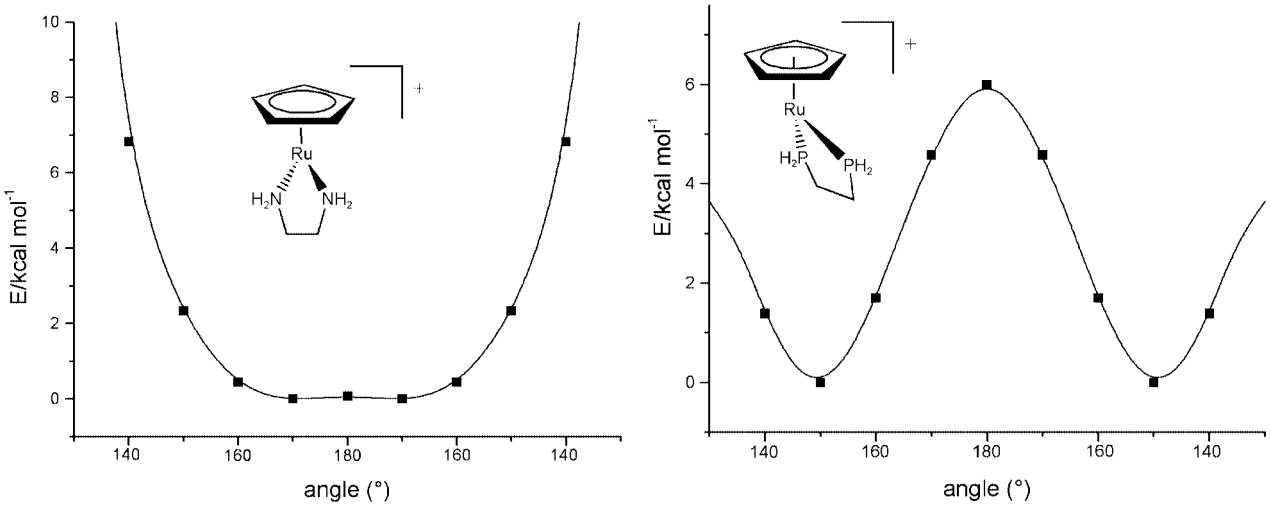

Figure 17. Energies of optimized $[CpRu(NH_2CH_2CH_2NH_2)]^+$ and $[CpRu(PH_2CH_2CH_2PH_2)]^+$ as a function of the pyramidalization angle α (°)

towards H_2.[79] In general, the transformation into the 18-electron configuration can be attained in three different ways, namely (a) direct ligand addition, (b) oxidative addition, and (c) degradation to other stable 18-electron species, such as the $[(C_5R_5)Ru(\eta^6\text{-arene})]^+$ complexes. The general reactivity patterns of $[(C_5R_5)Ru(L)_2]^+$ are summarized in Scheme 2.

All compounds $[(C_5R_5)Ru(L)_2]^+$ exhibit different degrees of affinity for an additional ligand. Whereas some compounds scavenge traces of N_2 present in argon to yield dinitrogen-bridged complexes such as $[\{CpRu(P)_2\}_2(\mu\text{-}N_2)][BAr'_4]_2$,[86] other systems {i.e. $[Cp^*Ru(TMEDA)]^+$ and $[Cp^*Ru(PMe{\it i}Pr_2)_2]^+$} are unreactive towards dinitrogen. However, most of them form terminal dinitrogen complexes $[(C_5R_5)Ru(N_2)(L)_2]^+$ {R = H, $(L)_2$ = TMEDA,[79] dippe, $(PMe{\it i}Pr_2)_2$, $(PMe{\it i}Pr_2)(PPh_3)$;[86] R = Me, $(L)_2$ = dippe,[10] dppe, dppm,[84] $(PEt_3)_2$[29]}. The reaction with oxygen often leads to the formation of stable dioxygen complexes $[(C_5R_5)Ru(O_2)(L)_2]^+$ {R = H, $(L)_2$ = TMEDA;[79] R = Me, $(L)_2$ = dppe,[75] dippe,[9] dppm,[90] $(PEt_3)_2$[29]}. All compounds of the type $[(C_5R_5)Ru(P)_2]^+$ add H_2 oxidatively furnishing the corresponding Ru^{IV} dihydride complexes $[(C_5R_5)RuH_2(P)_2]^+$. In many cases, the corresponding dihydrogen $[(C_5R_5)Ru(H_2)(P)_2]^+$ complexes have also been characterized in solution at low temperatures by NMR spectroscopy.[10,29,82]

With the exception of the reaction with HCl, the amine complexes $[(C_5R_5)Ru(TMEDA)][BAr'_4]$ (R = H, Me) are reluctant to undergo oxidative addition reactions, at variance with $[Cp^*Ru(P)_2]^+$ [$(P)_2$ = dippe, PEt_3, $PMe{\it i}Pr_2$] derivatives. One particular case is the chelate-assisted methyl C−H activation that takes place in the course of the reaction of $[Cp^*RuCl(PPh_2CH_2CH_2NMe_2)]$ with $NaBPh_4$ in CH_2Cl_2 to yield the unstable hydrido complex $[Cp^*RuH\{\kappa^3(P,N,C)\text{-}PPh_2CH_2CH_2N(=CH_2)Me\}]^+$, which is readily converted into $[Cp^*RuCl\{\kappa^3(P,N,C)\text{-}PPh_2CH_2CH_2N(=CH_2)Me\}]^+$.[91]

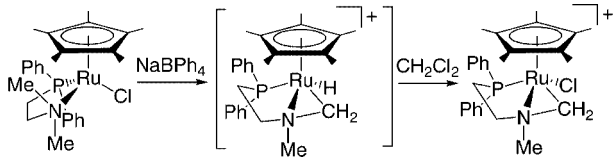

 © 2004 Wiley-VCH Verlag GmbH & Co. KGaA, Weinheim

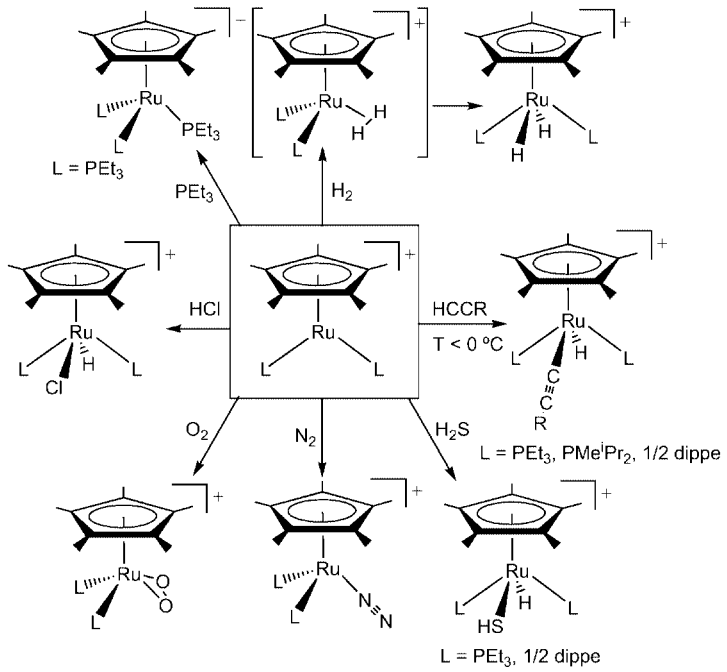

Scheme 2. General reactivity patterns of $[(C_5R_5)Ru(L)_2]^+$ complexes $[(L)_2$ = set of (NN) or (PP) ligands]

The Ru^{IV} hydridometallothiol complexes $[Cp^*RuH(SH)(P)_2]^+$ $[(P)_2$ = dippe, $PEt_3]$[83,92] result from the oxidative addition of H_2S to either $[Cp^*Ru(dippe)]^+$ or $[Cp^*Ru(PEt_3)_2]^+$. Interestingly, the addition of thiophenol yields the thiol adduct $[Cp^*Ru(HSPh)(dippe)]^+$ rather than the oxidative addition product.[92]

One of our research group contributions has been the isolation and characterization of the metastable Ru^{IV} alkynyl and hydroxyalkynyl hydrido complexes $[Cp^*RuH(C{\equiv}CR)(P)_2]^+$ $[(P)_2$ = dippe, PEt_3, $PMeiPr_2]$[8,93–97] as intermediates in the alkyne to vinylidene tautomerization process. This process takes place both in solution and in the solid state.[98]

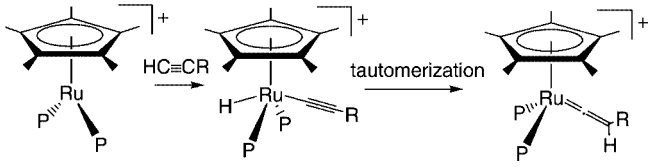

Since the initial EHMO calculations by Silvestre and Hoffmann on the alkyne to vinylidene rearrangement,[99] most theoretical studies had concluded that the intermediacy of alkynyl hydrido complexes generated by oxidative addition of the alkyne to a d^6 metal centre is too high in energy, and an alternative reaction pathway, namely a 1,2-H shift, is preferred. Recent DFT studies performed on $[CpRu(HC{\equiv}CH)(PMe_3)_2]^+$ have shown that in this particular case the energy barriers for the 1,2-H shift and the oxidative addition are almost similar, so that the latter process might become competitive.[100] Further theoretical support for the involvement of alkynyl hydrido complexes in the alkyne to vinylidene tautomerization process has been found recently, when Cp* instead of Cp is introduced in the model system for computation using a combination of DFT and quantum mechanics/molecular mechanics calculations.[97]

Whereas the solid-state structures determined by X-ray crystallography for several alkynyl hydrido complexes show a *transoid* disposition of alkynyl and hydrido ligands (Figure 18), we have spectral evidence in the case of the complexes $[Cp^*RuH(C{\equiv}CR)(PMeiPr_2)_2]^+$ [R = Ph, COOMe, *t*Bu, $CH_2(OH)$, CMeH(OH), $CMe_2(OH)$, CMePh(OH), CHPh(OH), $CPh_2(OH)$, CCy(OH)] are consistent with the occurrence of a rapid equilibrium between the *cisoid* and *transoid* isomers in solution.[96]

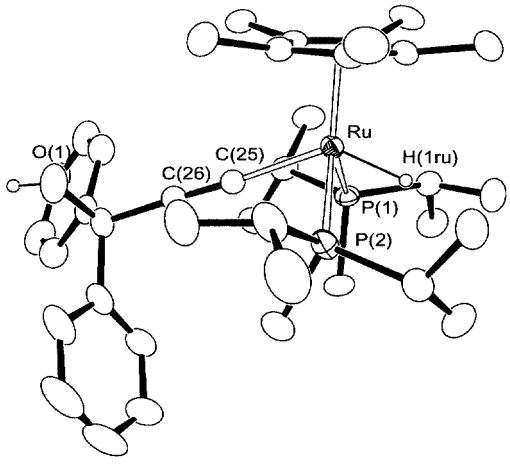

Figure 18. Molecular structure of the hydroxyalkynyl hydrido complex $[Cp^*RuH(C{\equiv}CC(OH)Ph_2(PMeiPr_2)_2]^+$

 © 2004 Wiley-VCH Verlag GmbH & Co. KGaA, Weinheim

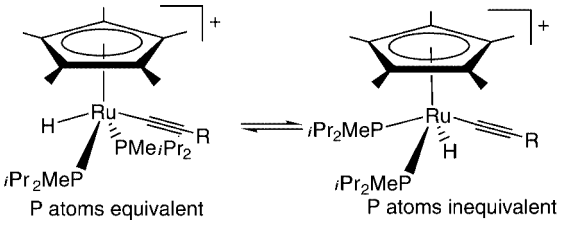

The halide abstraction reactions from hydridotris(pyrazolyl)borate $[TpRuX(L)_2]$ (L = PPh_3, dppe, dippe, PEt_3, $PMeiPr_2$, $PPh_2CH_2CH_2NMe_2$) has so far not allowed the isolation of stable 16-electron species formally analogous to their Cp*Ru counterparts.[101−105] The resulting coordinatively unsaturated fragments $[TpRu(L)_2]^+$ are extremely reactive, being trapped by any donor molecule L′ (i.e. counterion, solvent, N_2, H_2O) present in the reaction mixture to give the corresponding 18-electron complexes $[TpRu(L')(L)_2]^+$. Aquo complexes $[TpRu(H_2O)(L)_2]^+$ are often the final products isolated from halide abstraction reactions.[101,104,105] In the case of $[TpiPrRu(H_2O)(dppe)][CF_3SO_3]$, the H_2O ligand is labile and can be removed by means of molecular sieves (4 Å) affording the coordinatively unsaturated species $[TpiPrRu(dppe)][CF_3SO_3]$. This compound is stabilized by means of an agostic interaction with a hydrogen atom of one of the isopropyl groups of the Tp*i*Pr ligand, as revealed by X-ray crystallography [Figure 19; Ru···C($H^{agostic}$) 2.627(6) Å, Ru···$H^{agostic}$ 1.83(6) Å].[106] There is spectral evidence for the formation of analogous species in the cases of $[TpiPrRu(dppm)]^+$ and $[TpiPrRu(Ph_2PCH{=}CHPPh_2)]^+$, but these are too unstable to be isolated.[106]

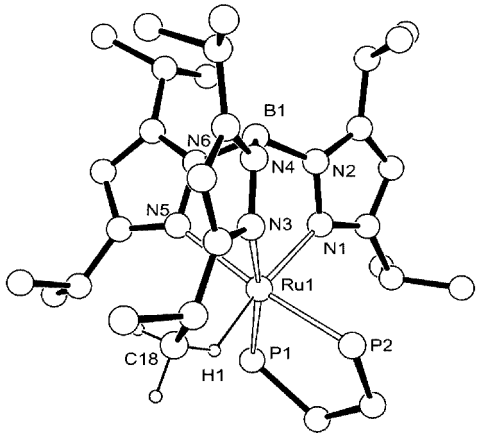

Figure 19. Molecular structure of the cationic complex $[TpiPrRu(dppe)]^+$; the phenyl rings of the dppe ligand have been omitted; the distance Ru···H^{agosti} is 1.83(6) A.

3.3 Osmium Complexes

To date, no stable compound of the type $[(C_5R_5)Os(L)_2]^+$ has been reported. Phosphane complexes $[(C_5R_5)Os(P)_2]^+$ can be generated in situ, but these are extremely reactive and easily undergo metallation reactions furnishing 18-electron organoosmium(IV) species. Thus, $[CpOsCl(PiPr_3)(PR_3)]$ (PR_3 = $PiPr_3$, PPh_3) dissociates its chloride ligand in methanol or acetone, and the resulting unsaturated metallic

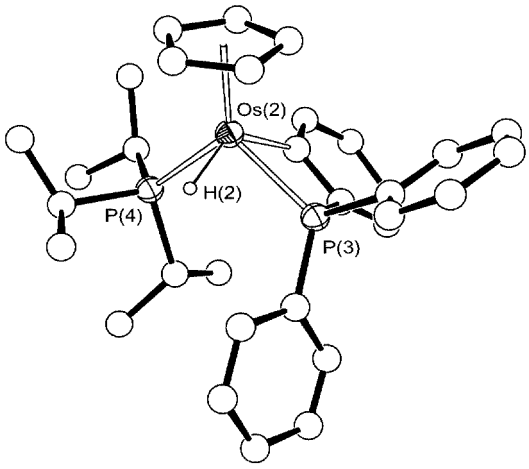

Figure 20. Molecular structure of the Os^{IV} metallated complex $[CpOsH(C_6H_4PPh_2)(PiPr_3)]^+$

fragment is capable of activating a methyl or phenyl C−H bond of a phosphane ligand to afford either $[CpOsH\{CH_2CH(CH_3)PiPr_2\}(PiPr_3)]^+$,[65] or $[CpOsH\{(C_6H_4)PPh_2\}(PiPr_3)]^+$.[107] The X-ray crystal structure of $[CpOsH\{(C_6H_4)PPh_2\}(PiPr_3)][PF_6]$ has been determined (Figure 20).[107]

In a similar fashion, the labile triflate complex $[CpOs(\eta^1\text{-}(O)\text{-}CF_3SO_3)(PPh_3)_2]$, generated by reaction of $[CpOsBr(PPh_3)_2]$ with $AgCF_3SO_3$ in toluene, undergoes spontaneous metallation both in solution and in the solid state furnishing the Os^{IV} derivative $[CpOsH\{(C_6H_4)PPh_2\}(PPh_3)][CF_3SO_3]$.[67]

Further proof of the extreme reactivity of the moieties $[(C_5R_5)Os(P)_2]^+$ comes from the fact that the fragment $\{[Cp^*Os(dmpm)]^+\}$ [dmpm = 1,2-bis(dimethylphosphano)-methane], generated in situ, has been shown to bind CH_4. The authors claimed a σ-bound methane molecule as an intermediate for hydrogen scrambling of the hydride into the methyl group in $[Cp^*OsH(CH_3)(dmpm)]^+$.[108]

Given the strong tendency displayed by the fragments $\{[(C_5R_5)Os(P)_2]^+\}$ to undergo oxidative addition reactions, the formation of Os^{IV} alkynylhydrido complexes is much easier than in ruthenium complexes. Thus, the reaction of $[CpOsCl(PiPr_3)_2]$ with $TlPF_6$ and the appropriate alkyne or alkynol in acetone/dichloromethane yields the alkynylhydrido derivatives $[CpOsH(C{\equiv}CR)(PiPr_3)_2][PF_6]$ [R = Ph, Cy, C(OH)MePh, $C(OH)Ph_2$].[109] However, at variance with their ruthenium homologues, these Os^{IV} alkynylhydrido complexes are stable species which do not rearrange into their vinylidene isomers.

4. Conclusion

Coordinatively unsaturated half-sandwich complexes of Fe, Ru and Os are very reactive species. However, with the proper combination of electron donating capabilities and steric protection of the co-ligands, the isolation of 16-electron complexes of type $[(C_5R_5)MX(L)]$ or $[(C_5R_5)M(L)_2]^+$ is possible in some cases. These species display two-legged

 © 2004 Wiley-VCH Verlag GmbH & Co. KGaA, Weinheim

piano-stool structures which exhibit different degrees of pyramidalization. These structures have been rationalised by means of several theoretical approaches, namely EHMO, TSC and DFT. The reactivity patterns of the unsaturated complexes change steadily from iron to osmium through ruthenium, with an increase in the tendency to undergo oxidative addition reactions to attain 18-electron configuration. From the knowledge of the correlations structure-reactivity of these species it should be possible in the future to develop new catalytic applications in C−C bond formation reactions such as alkyne oligomerisation or olefin polymerisation.

Acknowledgments

We thank the Ministerio de Ciencia y Tecnología of Spain (DGICYT, Project BQU2001−4046) and Junta de Andalucía (P.A.I. FQM-0188) for financial support.

[1] R. Poli, *Chem. Rev.* **1996**, *96*, 2135−2204.
[2] M. Jiménez-Tenorio, M. C. Puerta, P. Valerga, *J. Am. Chem. Soc.* **1993**, *115*, 9794−9795.
[3] M. Jiménez-Tenorio, M. C. Puerta, P. Valerga, *Inorg. Chem.* **1994**, *33*, 3515−3520.
[4] M. Jiménez-Tenorio, M. C. Puerta, P. Valerga, *J. Chem. Soc., Chem. Commun.* **1993**, 1750−1751.
[5] M. Jiménez-Tenorio, M. C. Puerta, P. Valerga, *J. Chem. Soc., Dalton Trans.* **1994**, 2431−2436.
[6] M. Jiménez-Tenorio, M. C. Puerta, P. Valerga, *Organometallics* **1994**, *13*, 3330−3337.
[7] A. de la Jara, M. Jiménez-Tenorio, M. C. Puerta, P. Valerga, *Organometallics* **1995**, *14*, 3839−3847.
[8] I. de los Ríos, M. Jiménez-Tenorio, M. C. Puerta, P. Valerga, *J. Chem. Soc., Chem. Commun.* **1995**, 1757−1758.
[9] I. de los Ríos, M. Jiménez-Tenorio, J. Padilla, M. C. Puerta, P. Valerga, *J. Chem. Soc., Dalton Trans.* **1996**, 377−381.
[10] I. de los Ríos, M. Jiménez-Tenorio, J. Padilla, M. C. Puerta, P. Valerga, *Organometallics* **1996**, *15*, 4565−4574.
[11] M. Jiménez-Tenorio, M. C. Puerta, P. Valerga, *J. Chem. Soc., Dalton Trans.* **1996**, 1305−1308.
[12] I. de los Ríos, M. Jiménez-Tenorio, M. C. Puerta, I. Salcedo, P. Valerga, *J. Chem. Soc., Dalton Trans.* **1997**, 4619−4624.
[13] M. Jiménez-Tenorio, M. C. Puerta, I. Salcedo, P. Valerga, *J. Organomet. Chem.* **1998**, *564*, 21−28.
[14] S. G. Davies, J. P. McNally, A. J. Smallridge, *Adv. Organomet. Chem.* **1990**, *30*, 1−77.
[15] G. Jia, C. P. Lau, *J. Organomet. Chem.* **1998**, *565*, 37−48.
[16] S. Trofimenko, *Chem. Rev.* **1993**, *93*, 943−980.
[17] R. A. Paciello, J. M. Manriquez, J. E. Bercaw, *Organometallics* **1990**, *9*, 260−265.
[18] K. Jonas, P. Klusmann, R. Goddard, *Z. Naturforsch., B: Chem. Sci.* **1995**, *50*, 394−404.
[19] U. Siemeling, *Chem. Rev.* **2000**, *100*, 1495−1526, and references cited therein.
[20] U. Siemeling, U. Vorfeld, B. Neumann, H. G. Stammler, *Organometallics* **1998**, *17*, 483−484.
[21] I. B. Gorrell, G. Parkin, *Inorg. Chem.* **1990**, *29*, 2452−2456.
[22] N. Shirasawa, T. T. Nguyet, S. Hikichi, Y. Moro-oka, M. Akita, *Organometallics* **2001**, *20*, 3582−3598.
[23] H. E. Bryndza, P. J. Domaille, R. A. Paciello, J. E. Bercaw, *Organometallics* **1989**, *8*, 379−385.
[24] P. J. Fagan, M. D. Ward, J. V. Caspar, J. C. Calabrese, P. J. Krusic, *J. Am. Chem. Soc.* **1988**, *110*, 2981−2983.
[25] B. K. Campion, R. H. Heyn, T. D. Tilley, *J. Chem. Soc., Chem. Commun.* **1988**, 278−280.
[26] T. Arliguie, C. Border, B. Chaudret, J. Devillers, R. Poilblanc, *Organometallics* **1989**, *8*, 1308−1314.
[27] W. E. Streib, A. A. Zlota, K. G. Caulton, *Bull. Pol. Acad. Sci., Chem.* **1994**, *42*, 197−203.
[28] T. J. Johnson, K. Folting, W. E. Streib, J. D. Martin, J. C. Huffman, S. A. Jackson, O. Eisenstein, K. G. Caulton, *Inorg. Chem.* **1995**, *34*, 488−499.
[29] M. Jiménez-Tenorio, M. C. Puerta, P. Valerga, *J. Organomet. Chem.* **2000**, *609*, 161−168.
[30] E. Lindner, M. Haustein, H. A. Mayer, K. Gierling, R. Fawzi, M. Steinmann, *Organometallics* **1995**, *14*, 2246−2252.
[31] L. Luo, S. P. Nolan, *Organometallics* **1994**, *13*, 4781−4786.
[32] K. G. Caulton, *New J. Chem.* **1994**, *18*, 25−41.
[33] C. S. Yi, N. Liu, *Organometallics* **1998**, *17*, 3158−3160.
[34] C. S. Yi, N. Liu, A. L. Rheingold, L. M. Liable-Sands, I. A. Guzei, *Organometallics* **1997**, *16*, 3729−3731.
[35] M. A. Jiménez-Tenorio, M. Jiménez-Tenorio, M. C. Puerta, P. Valerga, *Organometallics* **2000**, *19*, 1333−1342.
[36] S. Pavlik, C. Gemel, C. Slugovc, K. Mereiter, R. Schmid, K. Kirchner, *J. Organomet. Chem.* **2001**, *617−618*, 301−310.
[37] M. Jiménez-Tenorio, M. C. Puerta, P. Valerga, F. J. Moreno-Dorado, F. M. Guerra, G. M. Massanet, *Chem. Commun.* **2001**, 2324−2325.
[38] T. Braun, M. Laubender, O. Gevert, H. Werner, *Chem. Ber./Recueil* **1997**, *130*, 559−563.
[39] J. Huang, E. D. Stevens, S. P. Nolan, J. L. Petersen, *J. Am. Chem. Soc.* **1999**, *121*, 2674−2678.
[40] J. Huang, H.-J. Schanz, E. D. Stevens, S. P. Nolan, *Organometallics* **1999**, *18*, 2370−2375.
[41] L. Jafarpour, E. D. Stevens, S. P. Nolan, *J. Organomet. Chem.* **2000**, *606*, 49−54.
[42] J. Huang, L. Jafarpour, A. C. Hillier, E. D. Stevens, S. P. Nolan, *Organometallics* **2001**, *20*, 2878−2882.
[43] U. Kölle, J. Kossakowski, *J. Chem. Soc., Chem. Commun.* **1988**, 549−551.
[44] S. D. Loren, B. K. Campion, R. H. Heyn, T. D. Tilley, B. E. Bursten, K. W. Luth, *J. Am. Chem. Soc.* **1989**, *111*, 4712−4718.
[45] K. Bucken, U. Koelle, R. Pasch, B. Ganter, *Organometallics* **1996**, *15*, 3095−3098.
[46] R. E. Blake, R. H. Heyn, T. D. Tilley, *Polyhedron* **1992**, *11*, 709−710.
[47] A. Takahashi, Y. Mizobe, H. Matsuzaka, S. Dev, M. Hidai, *J. Organomet. Chem.* **1993**, *456*, 243−253.
[48] L. J. Farrugia, ORTEP-3 for Windows, Version 1.07, *J. Appl. Cryst.* **1997**, *30*, 565.
[49] U. Kölle, J. Kossakowski, G. Raabe, *Angew. Chem.* **1990**, *102*, 839−840; *Angew. Chem. Int. Ed. Engl.* **1990**, *29*, 773−774.
[50] M. E. Smith, F. J. Hollander, R. A. Andersen, *Angew. Chem.* **1993**, *105*, 1355; *Angew. Chem. Int. Ed. Engl.* **1993**, *32*, 1294.
[51] U. Koelle, C. Rietmann, G. Raabe, *Organometallics* **1997**, *16*, 3273−3281.
[52] D. Huang, W. E. Streib, J. C. Bollinger, K. G. Caulton, R. F. Winter, T. Scheirig, *J. Am. Chem. Soc.* **1999**, *121*, 8087−8097.
[53] Y. Yamaguchi, H. Nagashima, *Organometallics* **2000**, *19*, 725−727.
[54] T. J. Johnson, P. S. Coan, K. G. Caulton, *Inorg. Chem.* **1993**, *32*, 4594−4599.
[55] B. K. Campion, R. H. Heyn, T. D. Tilley, *J. Am. Chem. Soc.* **1988**, *110*, 7558−7560.
[56] B. K Campion, R. H. Heyn, T. D. Tilley, *J. Chem. Soc., Chem. Commun.* **1992**, 1201−1203.
[57] B. K. Campion, R. H. Heyn, T. D. Tilley, *Organometallics* **1990**, *9*, 1106−1112.
[58] C. S. Yi, R. Torres-Lubián, N. Liu, A. L. Rheingold, I. A. Guzei, *Organometallics* **1998**, *17*, 1257−1259.
[59] M. Jiménez-Tenorio, M. C. Puerta, P. Valerga, unpublished results.
[60] W. Baratta, E. Herdtweck, W. A. Herrmann, P. Rigo, J. Schwarz, *Organometallics* **2002**, *21*, 2101−2106.
[61] W. Baratta, W. A. Herrmann, P. Rigo, J. Schwarz, *J. Organomet. Chem.* **2000**, *593−594*, 489−493.
[62] Y. Watanabe, T. Ando, M. Kamigaito, M. Sawamoto, *Macromolecules* **2001**, *34*, 4370−4374.

 © 2004 Wiley-VCH Verlag GmbH & Co. KGaA, Weinheim

[63] P. B. Glaser, T. D. Tilley, *Eur. J. Inorg. Chem.* **2001**, 2747−2750.
[64] C. L. Gross, S. R. Wilson, G. S. Girolami, *J. Am. Chem. Soc.* **1994**, *116*, 10294−10295.
[65] M. A. Esteruelas, A. M. López, N. Ruíz, J. I. Tolosa, *Organometallics* **1997**, *16*, 4657−4667.
[66] M. Baya, P. Crochet, M. A. Esteruelas, E. Gutiérrez-Puebla, N. Ruíz, *Organometallics* **1999**, *18*, 5034−5043.
[67] P. W. Wanandi, T. D. Tilley, *Organometallics* **1997**, *16*, 4299−4313.
[68] J. R. Bleeke, R. J. Wittenbrink, T. W. Clayton, Jr., M. Y. Chiang, *J. Am. Chem. Soc.* **1990**, *112*, 6539−6545.
[69] P. Hamon, L. Toupet, J.-R. Hamon, C. Lapinte, *Organometallics* **1996**, *15*, 10−12.
[70] G. Argouarch, P. Hamon, L. Toupet, J.-R. Hamon, C. Lapinte, *Organometallics* **2002**, *21*, 1341−1348.
[71] T. R. Ward, O. Schafer, C. Daul, P. Hofmann, *Organometallics* **1997**, *16*, 3207−3215.
[72] K. Costuas, J.-Y. Saillard, *Organometallics* **1999**, *18*, 2505−2512.
[73] V. N. Sapunov, R. Schmid, K. Kirchner, H. Nagashima, *Coord. Chem. Rev.* **2003**, *238−239*, 363−382.
[74] F. L. Joslin, M. P. Johnson, J. T. Mague, D. M. Roundhill, *Organometallics* **1991**, *10*, 2781−2794.
[75] K. Kirchner, K. Mauthner, K. Mereiter, *J. Chem. Soc., Chem. Commun.* **1993**, 892−893.
[76] M. Brookhart, B. Grant, A. F. Volpe, Jr., *Organometallics* **1992**, *11*, 3920−3922.
[77] C. Gemel, K. Mereiter, R. Schmid, K. Kirchner, *Organometallics* **1997**, *16*, 5601−5603.
[78] C. Gemel, V. N. Sapunov, K. Mereiter, M. Ferencic, R. Schmid, K. Kirchner, *Inorg. Chim. Acta* **1999**, *286*, 114−120.
[79] C. Gemel, J. C. Huffman, K. G. Caulton, K. Mauthner, K. Kirchner, *J. Organomet. Chem.* **2000**, *593−594*, 342−353.
[80] A. Chaumonnot, B. Donnadieu, S. Sabo-Etienne, B. Chaudret, C. Buron, G. Bertrand, P. Metivier, *Organometallics* **2001**, *20*, 5614−5618.
[81] M. Jiménez-Tenorio, K. Mereiter, M. C. Puerta, P. Valerga, *J. Am. Chem. Soc.* **2000**, *122*, 11230−11231.
[82] H. Aneetha, M. Jiménez-Tenorio, M. C. Puerta, P. Valerga, V. N. Sapunov, R. Schmid, K. Kirchner, K. Mereiter, *Organometallics* **2002**, *21*, 5334−5346.
[83] A. Coto, M. Jiménez-Tenorio, M. C. Puerta, P. Valerga, *Organometallics* **1998**, *17*, 4392−4399.
[84] H. Aneetha, M. Jiménez-Tenorio, M. C. Puerta, P. Valerga, K. Mereiter, *Organometallics* **2003**, *22*, 1779−1782.
[85] M. Jiménez-Tenorio, M. D. Palacios, M. C. Puerta, P. Valerga, manuscript in preparation.
[86] H. Aneetha, M. Jiménez-Tenorio, M. C. Puerta, P. Valerga, K. Mereiter, *Organometallics* **2002**, *21*, 628−635.
[87] Y. Cheng, D. J. Szalda, R. M. Bullock, *Chem. Commun.* **1999**, 1629−1630.
[88] D. D. Pathak, H. Adams, N. A. Bailey, P. J. King, C. White, *J. Organomet. Chem.* **1994**, *479*, 237−245.
[89] N. Feiken, P. S. Pregosin, G. Trabesinger, A. Albinati, G. L. Evoli, *Organometallics* **1997**, *16*, 5756−5762.
[90] G. Jia, W. S. Ng, H. S. Chu, W.-T. Wong, N.-T. Yu, I. D. Williams, *Organometallics* **1999**, *18*, 3597−3602.
[91] K. Mauthner, C. Slugovc, K. Mereiter, R. Schmid, K. Kirchner, *Organometallics* **1997**, *16*, 1956−1061.
[92] A. Coto, I. de los Ríos, M. Jiménez-Tenorio, M. C. Puerta, P. Valerga, *J. Chem. Soc., Dalton Trans.* **1999**, 4309−4314.
[93] I. de los Ríos, M. Jiménez-Tenorio, M. C. Puerta, P. Valerga, *J. Am. Chem. Soc.* **1997**, *119*, 6529−6538.
[94] E. Bustelo, M. Jiménez-Tenorio, M. C. Puerta, P. Valerga, *Organometallics* **1999**, *18*, 4563−4573.
[95] E. Bustelo, M. Jiménez-Tenorio, M. C. Puerta, P. Valerga, *Eur. J. Inorg. Chem.* **2001**, 2391−2398.
[96] H. Aneetha, M. Jiménez-Tenorio, M. C. Puerta, P. Valerga, K. Mereiter, *Organometallics* **2003**, *22*, 2001−2013.
[97] E. Bustelo, J. Carbó, A. Lledós, K. Mereiter, M. C. Puerta, P. Valerga, *J. Am. Chem. Soc.* **2003**, *125*, 3311−3321.
[98] E. Bustelo, I. de los Ríos, M. Jiménez-Tenorio, M. C. Puerta, P. Valerga, *Monatsch. Chem.* **2000**, *131*, 1311−1320.
[99] J. Silvestre, R. Hoffmann, *Helv. Chim. Acta* **1985**, *68*, 1461−1506.
[100] F. De Angelis, A. Sgamellotti, N. Re, *Organometallics* **2002**, *21*, 5944−5950.
[101] G. Trimmel, C. Slugovc, P. Wiede, K. Mereiter, V. N. Sapunov, R. Schmid, K. Kirchner, *Inorg. Chem.* **1997**, *36*, 1076−1083.
[102] M. Jiménez-Tenorio, M. A. Jiménez-Tenorio, M. C. Puerta, P. Valerga, *Inorg. Chim. Acta* **1997**, *259*, 77−84.
[103] W.-C. Chan, C.-P. Lau, Y.-Z. Chen, Y.-Q. Fang, S.-M. Ng, G. Jia, *Organometallics* **1997**, *16*, 34−44.
[104] M. A. Jiménez-Tenorio, M. Jiménez-Tenorio, M. C. Puerta, P. Valerga, *J. Chem. Soc., J. Chem. Soc., Dalton Trans.* **1998**, 3601−3607.
[105] Y. Takahashi, M. Akita, S. Hikichi, Y. Moro-oka, *Inorg. Chem.* **1998**, *37*, 3186−3194.
[106] Y. Takahashi, S. Hikichi, M. Akita, Y. Moro-oka, *Organometallics* **1999**, *18*, 2571−2573.
[107] M. A. Esteruelas, E. Gutiérrez-Puebla, A. M. López, E. Oñate, J. I. Tolosa, *Organometallics* **2000**, *19*, 275−284.
[108] C. L. Gross, G. S. Girolami, *J. Am. Chem. Soc.* **1998**, *120*, 6605−6606.
[109] M. Baya, P. Crochet, M. A. Esteruelas, E. Gutiérrez-Puebla, A. M. López, J. Modrego, E. Oñate, N. Vela, *Organometallics* **2000**, *19*, 2585−2596.

Received June 3, 2003
Early View Article
Published Online October 10, 2003

 © 2004 Wiley-VCH Verlag GmbH & Co. KGaA, Weinheim

Functionalization of Polyoxometalates by a Negatively Charged Bridging Ligand: The Dimeric $[(SiW_{11}O_{39}Ln)_2(\mu\text{-}CH_3COO)_2]^{12-}$ (Ln = Gd^{III}, Yb^{III}) Complexes

Pierre Mialane,*[a] Anne Dolbecq,[a] Eric Rivière,[b] Jérôme Marrot,[a] and Francis Sécheresse[a]

Keywords: Coordination chemistry / Lanthanides / Magnetic properties / Polyoxometalates

The possibility of coupling lacunary polyoxometalates through a cationic center present in the vacancy by negatively charged organic ligands is demonstrated for the first time by single-crystal X-ray diffraction. The structure of the dimeric $K_{12}[\{Yb(\alpha\text{-}SiW_{11}O_{39})(H_2O)\}_2(\mu\text{-}CH_3COO)_2]\cdot 38H_2O$ complex, where two acetato ligands connect the ytterbium centers in a (η^2, μ-1,1) fashion, is reported. Using gadolinium instead of ytterbium, both the isostructural dimeric compound $K_{12}[\{Gd(\alpha\text{-}SiW_{11}O_{39})(H_2O)\}_2(\mu\text{-}CH_3COO)_2]\cdot 38H_2O$ and the mononuclear sandwich complex $[Gd(SiW_{11}O_{39})_2]^{13-}$ can be selectively isolated, depending on the synthetic conditions. The magnetic properties of the dimeric gadolinium complex are presented. The influence of the nature of the rare-earth metal on the final compound is further highlighted by the fact that when praseodymium is used as the rare-earth element, only the sandwich compound can be obtained.
(© Wiley-VCH Verlag GmbH & Co. KGaA, 69451 Weinheim, Germany, 2004)

Introduction

Polyoxometalates (POMs) have definite sizes and shapes and resemble discrete fragments of metal-oxide structures.[1] They are especially valuable for studies in diverse areas of current interest, which include medicine, catalysis and magnetism.[2] Among the wide variety of POMs, the Keggin series has been the most studied. These complexes have the general formula $\{XM_{12}O_{40}\}$, where X is the central atom (X = Si^{4+}, P^{5+}, As^{5+}, etc.) and M is a metal in a high oxidation state (M = $W^{5+/6+}$, $Mo^{5+/6+}$, $V^{4+/5+}$, etc.). They are usually synthesized in acidic aqueous media. The mono-, di- and trivacant species, corresponding to the formal removal of one, two or three metal centers, respectively, are successively obtained when the pH of the solution is increased. The resulting vacancies can be filled by addition of rare-earth or transition-metal cations. The vacant POM acts, for each atom incorporated in the vacancies, as a tetradentate ligand for rare-earth metals or a pentadentate ligand for transition metals. While the coupling of transition-metal or rare-earth centers coordinated to polydentate organic ligands through negatively charged bridging species (such as acetate, oxalate, squarate, phenolate, etc.) has been widely explored and has led to one of the largest family of inorganic compounds, analogous connection through either Ln^{3+} or transition-metal cations$^{2+/3+}$ present in the vacancies of POMs has not been observed. Polymeric polyoxometalate complexes have then been mainly obtained by acid-base condensation.[3] More recently, connections of the tetracapped $[\varepsilon\text{-}H_4PMo_{12}O_{40}\{La(H_2O)_4\}_4]^{5+}$ polyoxocations by carboxylates, affording multidimensional materials, have been made successfully.[4]

This lack of reactivity of polyoxoanions toward negatively charged organic ligands is mainly due to the following three characteristics of these species: (1) rare-earth- or transition-metal- substituted POMs are generally highly negatively charged, and then connection to bridging anionic ligands is not favored; (2) when a transition metal is used, as the POM acts as a pentadentate ligand, only one coordination site is available, preventing reactivity with chelating ligands; (3) due to the steric hindrance of POMs, bridging of subunits by relatively large ligands is unlikely. Nevertheless, we have developed a synthetic approach which has allowed us to overcome these difficulties. First, as the negative charge of a POM decreases with the number of vacancies, we have started our study considering a monovacant POM. Secondly, rare-earth cations have been preferred to transition-metal cations. Indeed, considering that the lanthanides have higher coordination numbers than transition metal cations, linkage to organic ligands must be facilitated. Finally, acetate has been chosen as the bridging agent, considering both its small size and its high affinity for rare-earth centers. We present here the structural characterization of compound $K_{12}[\{Yb(\alpha\text{-}SiW_{11}O_{39})(H_2O)\}_2(\mu\text{-}$

[a] Institut Lavoisier, IREM, UMR 8637, Université de Versailles Saint-Quentin,
45 Avenue des Etats-Unis, 78035 Versailles, France
E-mail: mialane@chimie.uvsq.fr
[b] Laboratoire de Chimie Inorganique, URA CNRS 420, Institut de Chimie Moléculaire d'Orsay, Université Paris-Sud,
91405 Orsay, France

$CH_3COO)_2]\cdot 38H_2O$, a unique di-μ-acetato polyoxometalate complex. The influence of the size of the rare-earth metal and of the nature of the synthetic media is discussed. Magnetic properties of the isostructural $K_{12}[\{Gd(\alpha\text{-}SiW_{11}O_{39})(H_2O)\}_2(\mu\text{-}CH_3COO)_2]\cdot 38H_2O$ complex are presented.

Results and Discussion

It has been shown recently that $[\alpha\text{-}SiW_{11}O_{39}]^{8-}$ {written below as $[SiW_{11}O_{39}]^{8-}$} reacts with rare-earth metals to afford solid-state one- or two-dimensional compounds.[5] These compounds dissociate in water leading to molecular species, of general formula $[Ln(SiW_{11}O_{39})(H_2O)_x]^{5-}$. Dissolution with heating of the precursor $K_5[Yb(SiW_{11}O_{39})(H_2O)_2]\cdot 24H_2O$ in 2 M acetate buffer has afforded crystals of the dimeric complex $K_{12}[\{Yb(SiW_{11}O_{39})(H_2O)\}_2(\mu\text{-}CH_3COO)_2]\cdot 38H_2O$ (**1**; Figure 1). In **1**, each ytterbium ion is eight-coordinate, adopting a distorted Archimedean antiprism geometry (pseudo-D_{4d}), with one $[SiW_{11}O_{39}]^{8-}$ entity acting as a tetradentate ligand and with a terminal water molecule. The remaining three coordination sites are occupied by two oxygen atoms of the bidentate-bridging acetate and one acetato-oxygen atom from the other $\{(Yb(SiW_{11}O_{39})(H_2O))(\mu\text{-}CH_3COO)_2\}$ subunits. The ytterbium ions are therefore doubly bridged by two (η^2, μ-1,1)-acetate ligands, separated by a distance of 4.085(18) Å. This connection mode has been previously encountered for two ytterbium dimers where each rare-earth center is coordinated to two cyclopentadienyl ligands, with intramolecular Yb−Yb lengths similar to that found in **1** (d_{Yb-Yb} = 3.905 and 3.930 Å).[6] The Yb−O lengths are divided into three groups, corresponding to the three different types of oxygen atoms present in the coordination sphere of the rare-earth metal [$d_{Yb-O(POM)}$ = 2.255(2)−2.289(1) Å; d_{Yb-OH_2} = 2.342(14) Å; $d_{Yb-O(Ac)}$ = 2.420(7)−2.448(4) Å]. The structure of complex **1** can be compared to the two previously reported dimeric Dawson polyoxometalates $[Ln^{III}(\alpha\text{-}n\text{-}P_2W_{17}O_{61})]^{7-}$ (Ln = Ce, n = 1; Ln = Eu, n = 2).[7] In both cases, the absence of exogenous ligands provokes the connection of each lanthanide center to the two $[P_2W_{17}O_{61}]$ subunits. Moreover, the rare-earth cations are not directly bridged with long Ln−Ln lengths [d_{Ce-Ce} = 6.0803(4) and d_{Eu-Eu} = 6.600(1) Å].

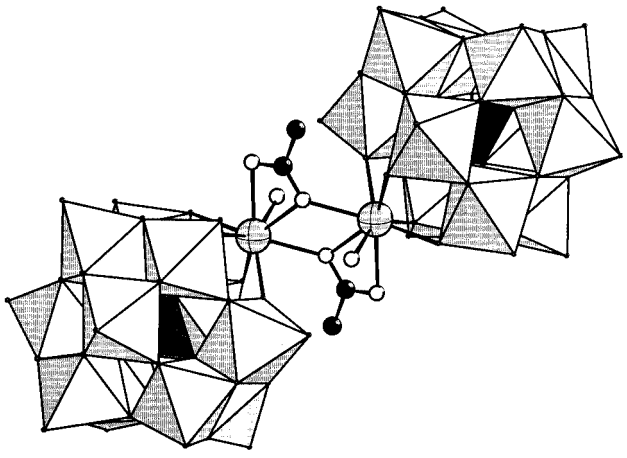

Figure 1. Polyhedral representation of complex $[\{Yb(\alpha\text{-}SiW_{11}O_{39})(H_2O)\}_2(\mu\text{-}CH_3COO)_2]^{12-}$ in **1**; grey crosshatched circles, Yb; white circles, O; light gray octahedra, $\{WO_6\}$; black tetrahedra, $\{SiO_4\}$

Syntheses in similar conditions have been performed replacing the ytterbium precursor by the related praseodymium complex **2a**. The IR spectrum of the obtained compound **2b** indicates the absence of an acetato ligand. A single-crystal X-ray diffraction study revealed that compound **2b** is the sandwich complex $K_{13}[Pr(SiW_{11}O_{39})_2]\cdot 35H_2O$, which structure has been previously postulated by Blasse et al.[8] by analogy with the known structure of $Cs_{12}[U(GeW_{11}O_{39})_2]$.[9] In **2b**, the Pr^{3+} cation is in an antiprismatic environment, coordinated to four oxygen atoms of each $[SiW_{11}O_{39}]^{8-}$ subunit [$d_{Pr-O(POM)}$ = 2.421(1)−2.518(2) Å]. Analogously, anion $[Gd(SiW_{11}O_{39})_2]^{13-}$ was obtained from heating a solution of $K_5[Gd(SiW_{11}O_{39})]\cdot 25H_2O$ in a 2 M acetate buffer. An alternative synthetic pathway was conducted to obtain the gadolinium acetato species. A concentrated acetate buffering solution was added to a solution of the gadolinium precursor dissolved in hot water and cooled to room temperature, until a 1 M acetate buffer solution was obtained. A microcrystalline compound **3** containing acetato ligands as shown by IR spectroscopy was isolated after slow evaporation. Comparison of the simulated diffraction powder pattern of **1** with the experimental X-ray diffraction powder pattern of **3** showed that **1** and **3** are isostructural. If the buffer concentration is adjusted to 2 M, the sandwich gadolinium complex $[Gd(SiW_{11}O_{39})_2]^{13-}$ is recovered. It must be noted that it has not been possible to isolate the praseodymium dimeric compound, while the ytterbium sandwich complex has never been obtained even in highly concentrated buffer solutions. It can then be concluded that as the atomic radius of the rare-earth metal decreases, the dimeric $[\{Ln(SiW_{11}O_{39})\}_2(\mu\text{-}CH_3COO)_2]^{12-}$ is preferentially formed, while an increase of the acetato buffer concentration favors the formation of the sandwich $[Ln(SiW_{11}O_{39})_2]^{13-}$ complex. It is not possible at this stage to rationalize the two observed tendencies, but clearly, this indicates that considerations on the affinity of rare-earth cations for carboxylato ligands, which increases when the size of the lanthanide decreases, are not sufficient to elucidate the reaction pathway.

The magnetic properties of $K_{12}[\{Gd(\alpha\text{-}SiW_{11}O_{39})(H_2O)\}_2(\mu\text{-}CH_3COO)_2]\cdot 38H_2O$ have been studied. The thermal dependence (χ_{MT}) of **3** is shown in Figure 2. The $\chi_M T$ curve follows a Curie law from 300 K ($\chi_M T$ = 16.2 $cm^3\cdot mol^{-1}\cdot K$) to 50 K, and then decreases from 50 K to 2 K ($\chi_M T$ = 14.6 $cm^3\cdot mol^{-1}\cdot K$). This behavior is characteristic of an antiferromagnetic coupling, in agreement with the previously reported homopolynuclear gadolinium complexes, with the exception of the dimeric Gd^{3+} salicylic complex reported by Costes et al., where the lanthanide centers were found to be ferromagnetically coupled.[10] As Gd^{3+} has an $^8S_{7/2}$ ground state, the $\chi_M T = f(T)$ curve can be fitted considering the HDVV isotropic spin Hamiltonian

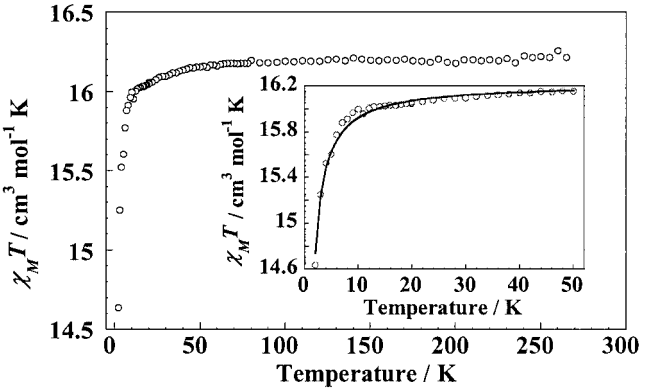

Figure 2. $\chi_M T$ per mol of compound $K_{12}[\{Gd(\alpha\text{-}SiW_{11}O_{39})(H_2O)\}_2(\mu\text{-}CH_3COO)_2]\cdot 38H_2O$ (**2**) as a function of temperature between 300 and 2 K; inset: $\chi_M T = f(T)$ between 300 and 2 K; the solid line was generated from the best fit parameters given in the text

$H = -JS_{Gd1}\cdot S_{Gd2}$, with $S_{Gd1} = S_{Gd2} = 7/2$. An excellent fit is found (Figure 2) for $J = -0.02\ cm^{-1}$ and $g = 2.02$, with an agreement factor R equal to 2.0×10^{-6} $\{R = [\Sigma(\chi_M T_{calcd.} - \chi_M T_{obsd.})^2/\Sigma(\chi_M T_{obsd.})^2]\}$. This J value is close but slightly lower than for the two previously reported dinuclear gadolinium complexes ($J = -0.05$ and $-0.21\ cm^{-1}$).[11] Nevertheless, due to the lack of structural and magnetic data, it is not possible to propose magneto-structural correlations at the moment.

Connection through Ln^{3+} or transition-metal cations$^{2+/3+}$ located in the POM vacancies has therefore been achieved. It should be noted that such dimeric lanthanide polyoxometalate compounds allow a highly accurate determination of the magnetic exchange parameters, as the Ln_2 cores are well isolated from each other due to the steric hindrance of the diamagnetic POM ligands. The magnetic study of dimeric analogous lanthanide complexes with rare-earth metals possessing a ground state with first-order orbital momentum must be performed. The reactivity of $[Ln(\alpha\text{-}SiW_{11}O_{39})(H_2O)_2]^{5-}$ ($Ln = Gd^{3+}$, Yb^{3+}) precursors with more sophisticated negatively charged organic ligands is under investigation.

Experimental Section

Synthesis: Compounds $K_5[Yb(SiW_{11}O_{39})(H_2O)_2]\cdot 24H_2O$ and $K_5[Gd(SiW_{11}O_{39})]\cdot 25H_2O$ have been prepared as described previously, for the preparation of the cesium salt[5b] but using KCl instead of CsCl. $K_5[Pr(SiW_{11}O_{39})]\cdot 26H_2O$ **2a** was prepared following the procedure described for the ytterbium compound, but using $PrCl_3\cdot 6H_2O$ instead of $YbCl_3\cdot 6H_2O$. The degree of hydration for the three precursors was determined by TGA.

$K_{12}[\{Yb(SiW_{11}O_{39})(H_2O)\}_2(\mu\text{-}CH_3COO)_2]\cdot 38H_2O$ (1): $K_5[Yb(SiW_{11}O_{39})(H_2O)_2]\cdot 24H_2O$ (350 mg, 0.1 mmol) is dissolved in potassium acetate buffer (10 mL, 2 M) and stirred at 60 °C for 1 h. After cooling to room temperature, the solution was left to evaporate. After a few days, colorless parallelopipedes of **1** were obtained. Yield: 220 mg (68 %). $C_4H_{86}K_{12}O_{122}Si_2W_{22}Yb_2$ (7002.16): calcd. Yb 4.94, W 57.76, K 6.70, C 0.68; found Yb 4.95, W 57.78, K 6.90, C 0.86. IR: $\tilde{\nu}$ = 1618 cm^{-1} (m), 1537 (m), 1453 (m), 1007 (m), 951 (s), 915 (s), 884 (s), 820 (s), 790 (s), 703 (s), 681 (s), 541 (m), 523 (m).

$K_{13}[Pr(SiW_{11}O_{39})_2]\cdot 35H_2O$ (2b): Compound **2b** was synthesized following the procedure described for **1** but with $K_5[Pr(SiW_{11}O_{39})]\cdot 26H_2O$ instead of $K_5[Yb(SiW_{11}O_{39})(H_2O)_2]\cdot 24H_2O$. After a few days, large pale green parallelepipedes of **2b** were obtained. Yield: 130 mg. $H_{70}K_{13}O_{113}PrSi_2W_{22}$ (6628.09): calcd. Pr 2.11, W 60.69, K 7.63; found Pr 1.90, W 60.77, K 7.53. IR: $\tilde{\nu}$ = 1619 cm^{-1} (m), 1005 (m), 948 (s), 906 (s), 891 (s), 827 (s), 765 (s), 720 (s), 545 (m), 526 (m), 482 (m).

$K_{12}[\{Gd(SiW_{11}O_{39})(H_2O)\}_2(\mu\text{-}CH_3COO)_2]\cdot 38H_2O$ (3): $K_5[Gd(SiW_{11}O_{39})(H_2O)_2]\cdot 24H_2O$ (350 mg, 0.1 mmol) was dissolved in water (5 mL) and heated to 60 °C. The resulting solution was cooled to room temperature. Potassium acetate buffer (5 mL, 2 M) was added and the solution left to evaporate. After a few days, colorless parallelepipedes of **3** were obtained. Yield: 170 mg (52 %). $C_4H_{86}Gd_2K_{12}O_{83}W_{22}$ (6290.40): calcd. Gd 4.50, W 57.90, K 6.72, C 0.69; found Gd 4.48, W 57.38, K 7.23, C 0.90. IR: $\tilde{\nu}$ = 1624 cm^{-1} (m), 1530 (m), 1453 (m), 999 (m), 955 (s), 906 (s), 889 (s), 812 (s), 790 (s), 755 (m), 703 (m), 693 (m), 678 (m), 543 (m), 523 (m).

X-ray Crystallography: Crystal data for **1**: monoclinic, $P2_1/c$, a = 20.0744(3), b = 12.5270(1), c = 21.1311(4) Å; β = 111.239(1)°, V = 4952.95(13) Å^3, T = 296 K, Z = 2, μ = 27.943 mm^{-1}, 34256 reflections measured, 12968 unique (R_{int} = 0.0641) which were used in all calculations. Final R indices were R_1 = 0.0430, $wR2$ = 0.0834 [$I > 2\sigma(I)$], R_1 = 0.0830, $wR2$ = 0.0960 (all data). CCDC-213782 contain the supplementary crystallographic data for this compound. These data can be obtained free of charge at www.ccdc.cam.ac.uk/conts/retrieving.html [or from the Cambridge Crystallographic Data Centre, 12, Union Road, Cambridge CB2 1EZ, UK; Fax: (internat.) +44-1223/336-033; E-mail: deposit@ccdc.cam.ac.uk]. Crystal data for **2**: triclinic, $P\bar{1}$, a = 13.7261(3), b = 19.6025(3), c = 20.6635(1) Å; α = 111.341(1), β = 105.380(1), γ = 97.683(1)°; V = 4826.31(13) Å^3, T = 296 K, Z = 2, μ = 27.282 mm^{-1}, 22578 reflections measured, 13859 unique (R_{int} = 0.0628) which were used in all calculations. Final R indices were R_1 = 0.0497, $wR2$ = 0.1081 [$I > 2\sigma(I)$], R_1 = 0.1086, $wR2$ = 0.1271 (all data). Crystallographic data for **2** have been deposited at the Fachinformationzentrum Karlsruhe, 76344 Eggenstein-Leopoldshafen, Germany [Fax: (internat.) + 49-7247-808-666; E-mail: crystdata@fiz-karlsruhe.de] on quoting the depository number CSD-413215.

Acknowledgments

We gratefully thank Laurent Lisnard for the synthesis and characterization of compounds **2** and **2b**.

[1] M. T. Pope, *Heteropoly and Isopoly Oxometalates*; Springer-Verlag: Berlin, **1983**.
[2] See special issue on Polyoxometalates; C. Hill {Guest Ed.}, *Chem. Rev.* **1998**, January/February.
[3] See, for example, for POM/TM complexes: [3a] K. Wassermann, R. Palm, H.-J. Lunk, J. Fuchs, N. Steinfeldt, R. Stösser, *Inorg. Chem.* **1995**, *34*, 5029. [3b] J. M. Clemente-Juan Coronado, J. R. Galán-Mascarós, C. J. Gómez-Garcia, *Inorg. Chem.* **1999**, *38*, 55. [3c] P. Mialane, A. Dolbecq, J. Marrot, E. Rivière, F. Sécheresse, *Angew. Chem.* **2003**, *115*, 3647; *Angew. Chem. Int. Ed.* **2003**, *42*, 3523; POM/RE complexes: [3d] K. Wassermann, M. T. Pope, *Inorg. Chem.* **2001**, *40*, 2763. [3e] R. C. Howell, F. G. Perez, S. Jain, W. DeW. Horrocks Jr., A. L. Rheingold, L. C. Francesconi, *Angew. Chem.* **2001**, *113*, 4155; *Angew. Chem.*

 © 2004 Wiley-VCH Verlag GmbH & Co. KGaA, Weinheim

Int. Ed. **2001**, *40*, 4031. [3f] K. Fukaya, T. Yamase, *Angew. Chem.* **2003**, *115*, 678; *Angew. Chem. Int. Ed.* **2003**, *42*, 654.
[4] [4a] P. Mialane, A. Dolbecq, L. Lisnard, A. Mallard, J. Marrot, F. Sécheresse, *Angew. Chem.* **2002**, *114*, 2504; *Angew. Chem. Int. Ed.* **2002**, *41*, 2398. [4b] A. Dolbecq, P. Mialane, L. Lisnard, J. Marrot, F. Sécheresse, *Chem. Eur. J.* **2003**, *9*, 2914.
[5] [5a] M. Sadakane, M. H. Dickman, M. T. Pope, *Angew. Chem.* **2000**, *112*, 3036; *Angew. Chem. Int. Ed.* **2000**, *39*, 2914. [5b] P. Mialane, L. Lisnard, A. Mallard, J. Marrot, E. Antic-Fidancev, P. Aschehoug, D. Vivien, F. Sécheresse, *Inorg. Chem.* **2003**, *42*, 2102.
[6] G. B. Deacon, G. D. Fallon, B. M. Gatehouse, A. Rabinovitch, B. W. Skelton, A. H. White, *J. Organomet. Chem.* **1995**, *501*, 23.
[7] [7a] M. Sadakane, M. H. Dickman, M. T. Pope, *Inorg. Chem.* **2001**, *40*, 2715. [7b] Q. Luo, R. C. Howell, J. Bartis, M. Dankova, W. DeW. Horrocks Jr., A. Rheingold, L. Francesconi, *Inorg. Chem.* **2002**, *41*, 6112.
[8] G. Blasse, G. J. Dirksen, F. J. Zonnevijlle, *Inorg. Nucl. Chem.* **1981**, *43*, 2847.
[9] C. M. Tourné, G. F. Tourné, M. C. Brianso, *Acta Crystallogr., Sect. B* **1980**, 2012.
[10] J.-P. Costes, J. M. Clemente-Juan, F. Dahan, F. Nicodème, M. Verelst, *Angew. Chem.* **2002**, *114*, 333; *Angew. Chem. Int. Ed.* **2002**, *41*, 323.
[11] [11a] S. Liu, L. Gelmini, S. J. Rettig, R. C. Thompson, C. Orvig, *J. Am. Chem. Soc.* **1992**, *114*, 6081. [11b] J.-P. Costes, F. Dahan, F. Nicodème, *Inorg. Chem.* **2001**, *40*, 5285.

Received August 29, 2003

 © 2004 Wiley-VCH Verlag GmbH & Co. KGaA, Weinheim

The Role of Spacers between Carboxylate Groups in Self-Assembly Process: Syntheses and Characterizations of Two Novel Cadmium(II) Complexes Derived from Mixed Ligands

Ruihu Wang,[a] Maochun Hong,*[a] Daqiang Yuan,[a] Yanqiong Sun,[a] Lijin Xu,[b] Junhua Luo,[a] Rong Cao,[a] and Albert S. C. Chan[b]

Keywords: Cadmium / Bridging ligands / X-ray diffraction / Polymers / Self assembly

Two novel cadmium(II) coordination polymers, $[Cd_2(bpda)_2(dpe)]_n$ (**1**) and $[Cd_2\{(R)\text{-Hdmpa}\}_2\{(S)\text{-Hdmpa}\}_2(dpe)_3]_n$ (**2**), [H_2bpda = 1,1′-biphenyl-3,3′-dicarboxylic acid, H_2dmpa = 6,6′-dimethyl-1,1′-biphenyl-2,2′-dicarboxylic acid, and dpe = 1,2-di(4-pyridyl)ethylene] have been prepared by hydrothermal reactions of both $Cd(NO_3)_2{\cdot}4H_2O$ and dpe with H_2bpda and H_2dmpa, respectively. **1** is a threefold interpenetrating three-dimensional coordination network composed of paddle-wheel tetracarboxylate dicadmium(II) units bridged by dpe. **2** affords an example of ligand self-discrimination in an assembly process, in which dpe connects the [Cd{(*R*)-Hdmpa}{(*S*)-Hdmpa}] building units to generate a one-dimensional ladder structure.

(© Wiley-VCH Verlag GmbH & Co. KGaA, 69451 Weinheim, Germany, 2004)

Introduction

The prospect of generating new materials with interesting structures and technologically useful functions provides significant motivation for the recent surge of research interest in organic-inorganic supramolecular frameworks.[1,2] The construction of metal−organic polymeric networks has achieved considerable progress in supramolecular chemistry and material science due to their intriguing structural diversities and potential applications in molecular adsorption, ion exchange, molecular recognition and heterogeneous catalysis.[2−5] Molecular self-assembly based on the principle of crystal engineering has proved to be efficient for the formation of these architectures. Some structural motifs with specific topologies and functions can, to a certain extent, be predicted through dominating the assembly and orientation of individual building blocks. For example, the groups of Yaghi,[3] Zaworotko,[4] and others[5] have developed a strategy to construct extended porous structures using rigid dicarboxylate ligands with different spacers and metal clusters of known geometries. However, the mechanism of molecular self-assembly is still unclear, and predictability and tinability of the exact structures of the assembly products are difficult. Thus, understanding the factors that govern the assembly process is crucial to technological development. Such factors include: the role of spacers between coordination sites in organic bridging ligands and the coordination geometry of metal ions;[6] the formation and role of the reaction precursors;[7] the formation of interpenetration and/or interdigitation lattices vs. the inclusion of solvent or guest molecules;[8] and the formation of the convergent products and the divergent products.[9]

It is well-known that the design and synthesis of bridging ligands containing appropriate coordination sites linked by spacers with specific orientations are especially crucial to the construction of desirable frameworks. By closely controlling the properties of the spacers, such as the shape, functionality, flexibility, length, and symmetry, a remarkable class of materials containing diverse architectures and functions can be obtained.[2−6] The coordination of multipyridine and multi-carboxylate ligands to metal centers has proved to be an excellent tool in the assembly process and has been highly influenced by the structural characterizations of linker groups. Moreover, as the length of organic spacer increases, interpenetration and/or interdigitation has been commonly adopted by nature in order to avoid the formation of large open channels or cavities.[10] The combination of metal ions and mixed bridging ligands containing carboxylate and pyridyl groups can allow for the formation of coordination networks possessing different structures and functional properties.[11,12] The exo-bidentate pyridyl

[a] State Key Laboratory of Structural Chemistry Fujian Institute of the Research on the Structure of Matter Chinese Academy of Sciences,
Fuzhou, Fujian, 350002, China
Fax: (internat.) +86-591-3714946
E-mail: hmc@ms.fjirsm.ac.cn
[b] Open Laboratory of Chirotechnology Department of Applied Biology and Chemical Technology, The Hong Kong Polytechnic University,
Hong Hum, Hong Kong
Fax: (internat.) +852-23649932
E-mail: bcachan@polyu.edu.hk

derivative, *trans*-1,2-di(4-pyridyl)ethylene (dpe), possesses several peculiar characteristics when used in the construction of the extended networks: 1) the double bond in the ligand can result in conformational rigidity;[13] 2) the delocalized π-system can be applied as potential electron propagating components;[14] 3) the long spacer between coordination sites can result in interpenetration and/or interdigitation;[14,15] and 4) this ligand may be used as a reaction precursor.[7a,16] However, supramolecular architectures constructed by dpe, and ligands with di- or multi-carboxylate groups, have seldom been reported to date.[16,17] Very recently, we have reported a three-dimensional pillared compound consisting of dodecanuclear cadmium(II) macrocycles $[\{Cd_2(dpa)(pya)\}_6(pya)_6(dpe)_3]_n$ (H_2dpa = diphenic acid and Hpya = isonicotinic acid),[16] in which dpe not only serves as a μ-bridge, but also acts as the precursor of pya. To systematically investigate the effects of the steric hindrance of the spacers between the carboxylate coordination sites on dpe and the assembly products, we have designed two new ligands, 1,1′-biphenyl-3,3′-dicarboxylic acid (H_2bpda) and 6,6′-dimethyl-1,1′-biphenyl-2,2′-dicarboxylic acid (H_2dmpa). The steric hinderance between the two carboxylate groups of Bpda is smaller than for H_2dpa, and this provides a greater degree of freedom for the twisting of the two phenyl rings in Bpda relative to that in H_2dpa can be more freely twisted than H_2dpa. However, not only is the steric hinderance between the two carboxylate groups of racemic dmpa greater than for H_2dpa, but dmpa can also formproducts of ligand self-discrimination or self-recognition. Herein, we wish to report the syntheses and characterizations two novel cadmium(II) complexes, $[Cd_2(bpda)_2(dpe)]_n$ (**1**), and $[Cd_2\{(R)\text{-Hdmpa}\}_2\{(S)\text{-Hdmpa}\}_2(dpe)_3]_n$ (**2**).

Result and Discussion

Synthesis and Characterization

Diphenic acid (H_2dpa) is an excellent bridging ligand for the construction of metallomacrocyclic and helical frameworks[16,18] owing to the steric hindrance between the 2,2′-positioned carboxylate groups in the assembly process, which results in a great distortion of the two phenyl rings about the central bond in dpa. Bpda and dmpa are dicarboxylate ligands that are similar to dpa. In bpda, the two carboxylate groups in the 3,3′-positions have a smaller effect on the distortion of the diphenyl spacer about the central bond in the assembly process. Dmpa is an axially chiral ligand, in which two phenyl rings cannot freely rotate about the central bond and therefore can produce two different conformations, (*R*)-dmpa and (*S*)-dmpa. Hence, it is interesting to investigate the assembly process of H_2bpda or H_2dmpa with dpe and $Cd(NO_3)_2{\cdot}4H_2O$ under the same reaction conditions as those used in the formation of $[\{Cd_2(dpa)(pya)\}_6(pya)_6(dpe)_3]_n$.[16]

The hydrothermal reaction of H_2bpda, dpe, $Cd(NO_3)_2{\cdot}4H_2O$, and NaOH, with a molar ratio of 2:2:2:3, in H_2O at 180 °C for 3 days, produced a threefold interpenetrating three-dimensional coordination polymer consisting of the dimeric cadmium−tetracarboxylate secondary building units (SBUs) bridged by dpe. Dpe has not been hydrolyzed and only serves as the axis linkers of the SBUs so as to extend the two-dimensional $[Cd_2(bpda)_2]_n$ layer into a three-dimensional framework (Scheme 1). The hydrothermal reaction of dpe, the racemic mixture of (*R*)-H_2dmpa and (*S*)-H_2dmpa, and $Cd(NO_3)_2{\cdot}4H_2O$ under the same conditions as those used in the preparation of **1** afforded the colorless crystals of **2**, in which Hdmpa undergoes ligand self-discrimination and acts as a chelating mono-bidentate ligand in the formation of the building units of [Cd{(*R*)-Hdmpa}{(*S*)-Hdmpa}].

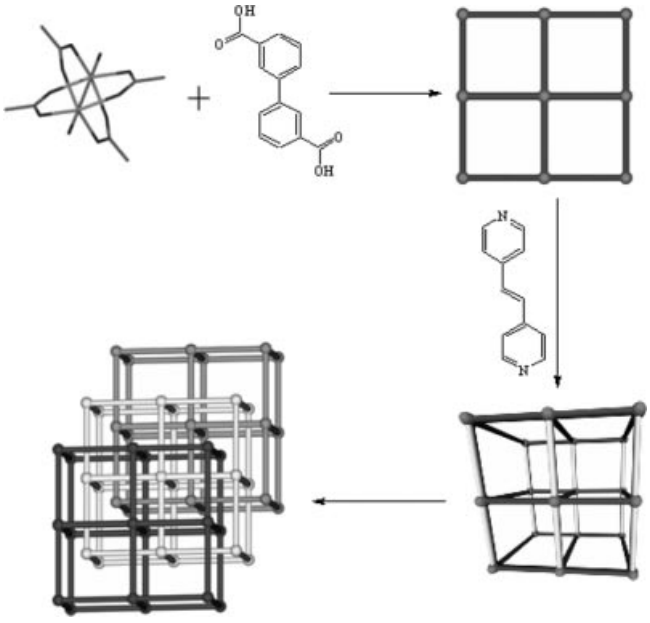

Scheme 1. Construction of the threefold interpenetrating three-dimensional framework in **1**

Thermogravimetric analysis (TGA) was performed on polycrystalline samples under a nitrogen atmosphere. No chemical decomposition was observed up to 390°C and 300 °C for **1** and **2**, respectively. The two most significant weight losses occurred between 440 and 730 °C for **1**, and between 350 and 430 °C for **2**, and are attributed to the complete decomposition of the samples to cadmium(II) oxide. Considering the formation of stoichiometric amounts of CdO, this conclusion is supported by 29.7% (above 820 °C) and 13.2% (above 540 °C) of the residues for **1** and **2**, respectively, which are in accordance with the expected values (28.9% for **1** and 13.9% for **2**).

Structural Description

$[Cd_2(bpda)_2(dpe)]_n$ (1)

Single crystal X-ray diffraction analysis reveals that compound **1** is a threefold interpenetrating three-dimensional coordination network and crystallizes in the monoclinic

 © 2004 Wiley-VCH Verlag GmbH & Co. KGaA, Weinheim

space group $P2_1/c$. As shown in Figure 1(a), the geometry around the Cd^{II} center is square-pyramidal and the metal center is coordinated by four oxygen atoms from different bpda ligands in the equatorial plane and a nitrogen atom from dpe at the axial position. Four carboxylate groups from different bpda ligands form a bridge between the two cadmium(II) centers in a *syn-syn* bidentate mode, forming a paddle-wheel secondary building unit (SBU). The Cd−Cd distance of 3.0428(14) Å suggests that there is no significant Cd^{II}−Cd^{II} interaction in the SBU (the sum of the van der Waals radii of Cd^{II} is 3.04 Å[19]); however, this distance is significantly shorter than those in discrete dimeric cadmium−tetracarboxylate complexes (3.278−3.452 Å).[20]

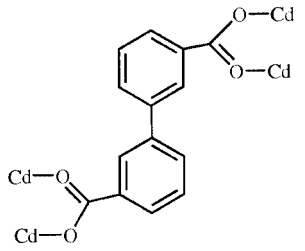

Scheme 2. Coordination mode of bpda in **1**

Bpda acts as a bis-bidentate bridging ligand by coordinating to four different Cd^{II} centers (Scheme 2). The dihedral angle between the two phenyl rings in bpda is 34.8°. The

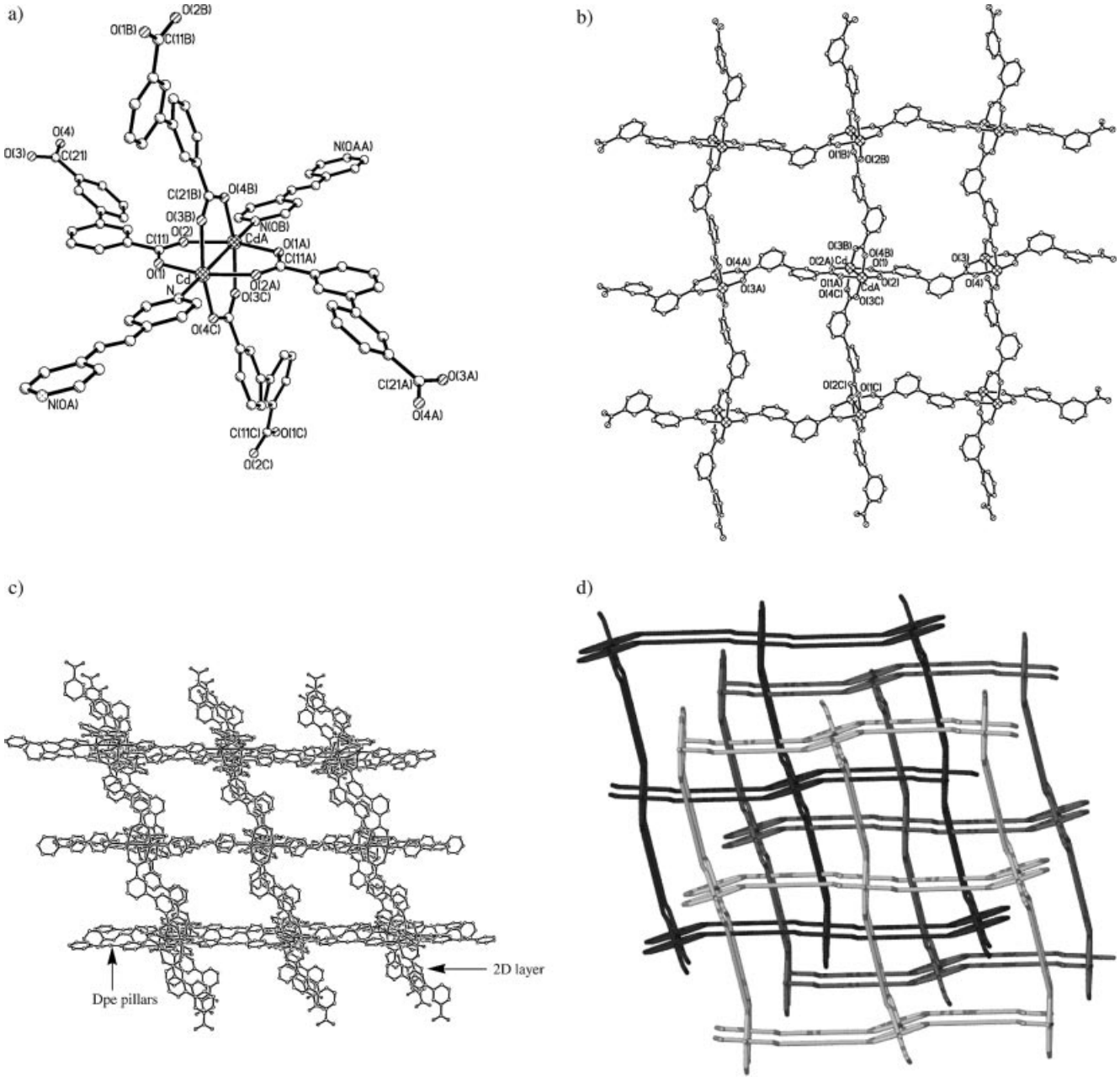

Figure 1. a) ORTEP drawing of the dinuclear cadmium(II) unit with the atom numbering scheme in **1**, b) view of the two-dimensional layer in **1** with dpe omitted, c) view of the three-dimensional layer-pillar in **1**, d) view of the threefold interpenetrating three-dimensional framework in **1**

 © 2004 Wiley-VCH Verlag GmbH & Co. KGaA, Weinheim

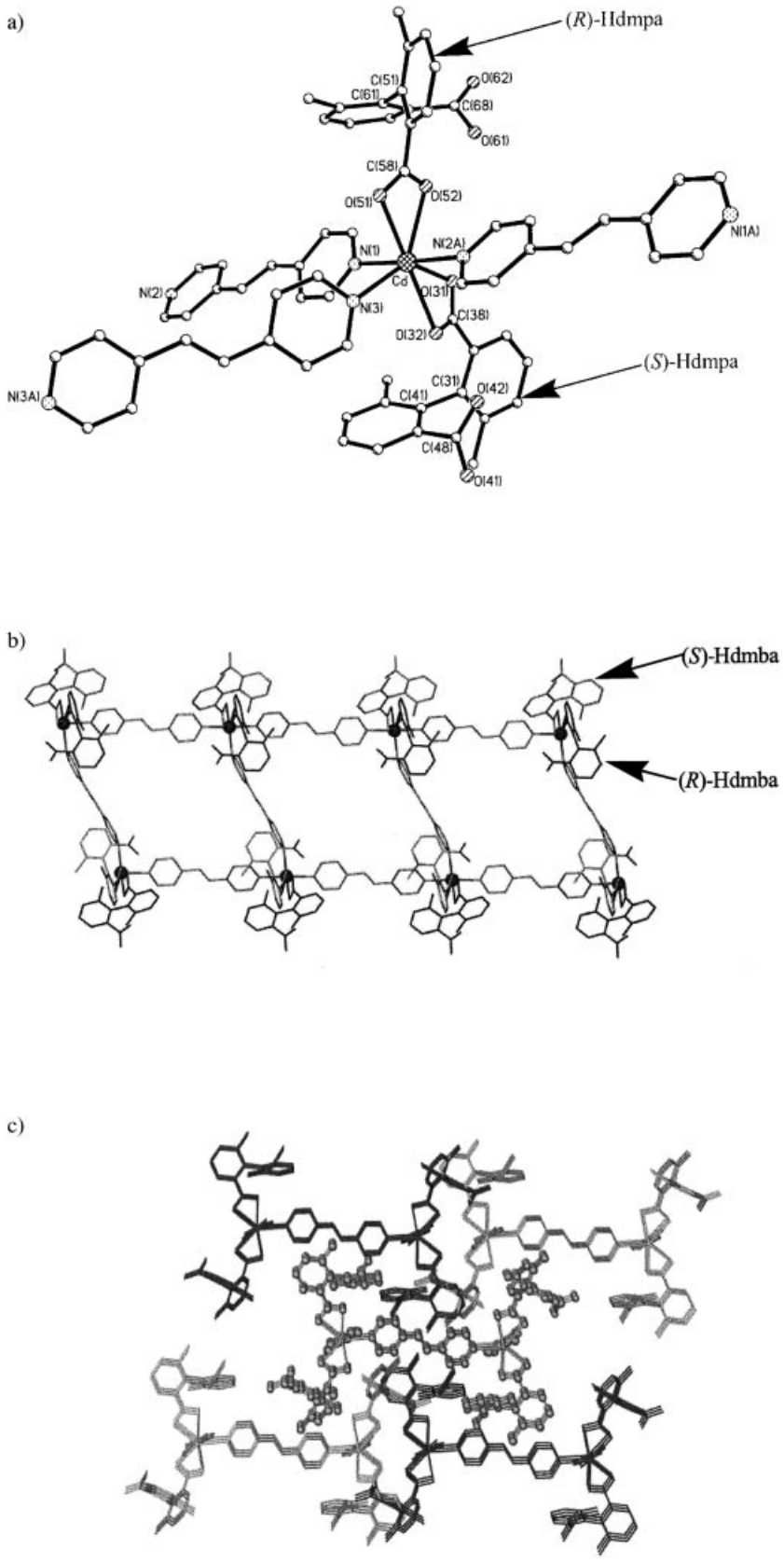

Figure 2. a) ORTEP drawing around the cadmium(II) center with atom numbering scheme in **2**, b) view of the one-dimensional ladder in **2**, c) pack diagram along the *b* axis exhibiting the interdigitation between the chains in **2**

 © 2004 Wiley-VCH Verlag GmbH & Co. KGaA, Weinheim

dihedral angles of 3.6 and 14.5° between the carboxylate groups and the linking phenyl rings allow for the formation of paddle-wheel SBUs.[21] The SBUs are inter-connected by bpda forming a two-dimensional layer with a Cd···Cd separation across bpda of 13.481 Å. To the best of our knowledge, this is the first extended structure constructed from cadmium−tetracarboxylate SBUs. The dpe ligands are *trans*-coordinated to the SBUs and form axis linkers with a Cd−N distance of 2.237(9) Å and Cd−Cd−N angle of 178.0(3)°. Thus, dpe can serve as a pillar between two adjacent two-dimensional layers thus generating a three-dimensional open framework (Figure 1,b). The Cd···Cd separation across dpe is 13.809 Å. It should be emphasized that there is a large void within the cuboidal units owing to the longer spacers between the coordination sites in dpe and bpda, but no enclathration of solvent or guest molecules is observed within the larger units. Thus, two identical frameworks fill the void in another framework, which results in the formation of a threefold interpenetrating framework (Figure 1, c).

It is worthy noting that the cuboidal units in **1** are not regular due to the fact that the coordination sites are off-axis in dpe and bpda. Klinowski et al.[11a] has recently reported a threefold interpenetrating three-dimensional modular coordination network using the more flexible biphenyl-4,4′-dicarboxylate and 1,2-bis(4-pyridyl)ethane mixed ligands, in which the cuboidal units are highly distorted owing to the high flexibility of spacers between the coordination sites. However, Chen et al.[11b] has reported a twofold interpenetrating three-dimensional structure using the mixed ligands 4,4′-bipyridine and terephthalate, in which the cuboidal units are regular due to the rigidity of the bridging ligands. This shows that the spacers between coordination sites have an important effect on the construction of the structural framework.

$[Cd_2\{(R)\text{-Hdmpa}\}_2\{(S)\text{-Hdmpa}\}_2(dpe)_3]_n$ (2)

Compound **2** is a one-dimensional ladder structure and crystallizes in the monoclinic space group $P2_1/c$. As shown in Figure 2(a), the Cd^{II} center has a distorted pentagonal bipyramidal geometry, and is coordinated by two chelating carboxylate groups from different conformational Hdmpa and three nitrogen atoms from different dpe ligands. The ligands (*R*)-Hdmpa and a (*S*)-Hdmpa are coordinated by the Cd^{II} center, which suggests an assembly process of ligand self-discrimination, therefore, no optical activity is expected in this structure. Three dpe ligands form a slightly distorted T-shaped arrangement at the seven-coordinate Cd^{II} center [N(1)−Cd−N(3) 85.0(2)°; N(2A)−Cd−N(3) 96.4(2)°; N(1)−Cd−N(2A) 177.5(2)°], in which two nitrogen atoms (N1 and N2) stand at the apical positions, the remaining nitrogen atom (N3) and four carboxylate oxygen atoms (O31, O32, O51, and O52) occupy the equatorial positions. The Cd^{II} center lies in the plane defined by the equatorial atoms, with a deviation of 0.0155 Å. Hdmpa

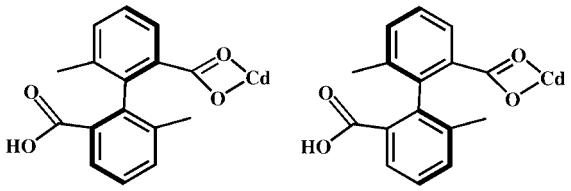

(*R*)-Hdmpa (*S*)-Hdmpa

Scheme 3. Coordination modes of (*R*)-Hdmpa and (*S*)-Hdmpa in **2**

(Scheme 3) serves as a chelating mono-bidentate ligand which is coordinated through the carboxylate group to the Cd^{II} center; carboxylic groups do not take part in coordination and do not interact with the metal centers or other ligands, therefore, this is an unusual feature of di- or multicarboxylic ligands. The dihedral angles between the two phenyl rings in (*R*)-Hdmpa and (*S*)-Hdmpa are 85.6 and 85.1°, respectively, and hence they are approximately perpendicular to each other. However, the dihedral angles between the carboxylate groups and the linking phenyl rings in (*R*)-Hdmpa and (*S*)-Hdmpa are 58.8 and 59.4°, and 29.2 and 56.1°, respectively, which are significantly larger than those in **1** and are unfavorable for the formation of the paddle-wheel SBU.[21] Dpe acts as a *trans* exo-bidentate ligand and links the [Cd{(*R*)-Hdmpa}{(*S*)-Hdmpa}] building units to form an infinite ladder structure (Figure 2, b). The methyl groups in Hdmpa prevent the formation of an extended motif. The adjacent Cd···Cd distances along the side dpe and the inner dpe are 14.069 and 13.893 Å, respectively. Owing to a longer spacer in the dpe ligand, there is a large void within the rhombohedral grids, which have been effectively filled by interdigitation of Hdmpa from the adjacent one-dimensional ladders in the *ac* plane (Figure 2, c).

Conclusions

The hydrothermal reactions of $Cd(NO_3)_2{\cdot}4H_2O$ and 1,2-di(4-pyridyl)ethylene (dpe) with dicarboxylic ligands with different steric properties, 1,1′-biphenyl-3,3′-dicarboxylic acid (H_2bpda) and 6,6′-dimethyl-1,1′-biphenyl-2,2′-dicarboxylic acid (H_2dmpa), under the same reaction conditions, produced two novel cadmium(II) coordination polymers $[Cd_2(bpda)_2(dpe)]_n$ (**1**) and $[Cd_2\{(R)\text{-Hdmpa}\}_2\{(S)\text{-Hdmpa}\}_2(dpe)_3]_n$ (**2**), respectively. In **1**, bpda and dpe link the dimeric cadmium−tetracarboxylate secondary building units (SBUs) to form a threefold interpenetrating three-dimensional coordination network. **2** is a one-dimensional ladder structure constructed from [Cd{(*R*)-Hdmpa}{(*S*)-Hdmpa}] building units and dpe bridges, and exhibits a ligand self-discrimination in an assembly process. The large void in **1** and **2** has been efficiently filled through the inter-interpenetration and inter-interdigitation of adjacent frameworks, respectively. The results show that the steric hindrance of spacers between the carboxylate coordination sites has an important effect on the coordination modes of the carboxylate groups, and different spacers between the carboxylate coordination sites can result in supramolecular architectures with different structures and functions.

 © 2004 Wiley-VCH Verlag GmbH & Co. KGaA, Weinheim

Experimental Section

1,1′-Biphenyl-3,3′-dicarboxylic acid and 6,6′-dimethyl-1,1′-biphenyl-2,2′-dicarboxylic acid were synthesized according to literature methods, using 3-aminobenzoic acid and 2-amino-3-methylbenzoic acid, respectively, as staring materials.[22] 1,2-di(4-pyridyl)ethylene and 2-amino-3-methylbenzoic acid were purchased from Aldrich and used without further purification, all the other reagents were commercially available and used as purchased. The IR spectra as KBr discs were recorded on a Magna 750 FT-IR spectrophotometer. C, H, and N elemental analyses were determined on an Elementary Vario ELIII elemental analyzer. Thermal analyzes were performed using a Thermal Analyst 2100 TA Instrument and a SDT 2960 Simultaneous TGA-DTA Instrument.

Synthesis of $[Cd_2(bpda)_2(dpe)]_n$ (1): A mixture of H_2bpda (0.12 g, 0.5 mmol), dpe (0.09 g, 0.5 mmol), $Cd(NO_3)_2{\cdot}4H_2O$ (0.15 g, 0.5 mmol) and NaOH (0.03 g, 0.75 mmol), with a molar ratio of about 2:2:2:3 in H_2O (15.0 mL), was placed in a Parr Teflon-lined stainless steel vessel and heated to 180 °C for 72 h. The reaction system was then cooled at room temperature for 24 hours. A large amount of colorless crystals were obtained and collected by filtration, washed with water and dried in air. Yield: 0.06 g (54%). Elementary analysis: calcd. for $C_{20}H_{13}CdNO_4$ (444.71): calcd. C 54.13, H 2.93, N 3.16; found C 54.07, H 2.89, N 3.18%. IR (KBr pellet): $\tilde{\nu}$ = 3469 cm^{-1} (w), 3057 (w), 1686 (w), 1622 (s), 1610 (s), 1593 (s), 1568 (s), 1433 (m), 1408 (s), 1385 (s), 1301 (vw), 1263 (w), 1169 (vw), 1024 (w), 835 (w), 758 (s), 690 (m), 623 (vw), 552 (w).

Synthesis of $\{Cd_2[(R)\text{-Hdmpa}]_2[(S)\text{-Hdmpa}]_2(dpe)_3\}_n$ (2): The procedure was similar to the synthesis of compound **1**, except that H_2dmpa (0.13 g, 0.5 mmol) was used instead of H_2bpda. Yield: 0.05 g (43% based on H_2dmpa). Elementary analysis: calcd. for $C_{50}H_{39}CdN_3O_8$ (922.24): calcd. C 65.11, H 4.23, N 4.55; found C 65.05, H 4.18, N 4.57%. IR (KBr pellet): $\tilde{\nu}$ =3051 cm^{-1} (vw), 2922 (vw), 2872 (vw), 1738 (m), 1722 (m), 1606 (s), 1560 (s), 1504 (w), 1421 (s), 1406 (s), 1389 (s), 1375 (m), 1290 (w), 1142 (vw), 1070 (vw), 1012 (w), 835 (w), 775 (w), 721 (w), 554 (w).

X-ray Crystallographic Study: Intensity data for **1** and **2** were measured on a Siemens Smart CCD diffractometer with graphite-monochromated Mo-K_α radiation (λ = 0.71073 Å) at room temperature. All empirical absorption corrections were applied using the SADABS program.[23] The structures were solved by direct methods and refined on F^2 by full-matrix least-squares using the SHELXL-97 program package.[24] The positions of the H atoms were generated geometrically (C−H bond fixed at 0.96 Å), assigned isotropic thermal parameters, and allowed to ride on their parent carbon atoms before the final cycle of refinement. The summary of the crystal data and structure determination for **1** and **2** are listed in the Table 1. The selected bond lengths and angles for **1** and **2** are listed in the Table 2.

Crystallographic data (excluding structure factors) for the two structures have been deposited with the Cambridge Crystallographic Data Centre as supplementary publication CCDC-212589 and -212590. Copies of the data can be obtained free of charge on application to CCDC, 12 Union Road, Cambridge CB2 1EZ, UK [Fax: (internat.) + 44-1223/336-033; E-mail: deposit@ccdc.cam.ac.uk].

Table 1. Summary of the crystal data and structure determination for **1** and **2**

Compound	**1**	**2**
Empirical formula	$C_{20}H_{13}CdNO_4$	$C_{50}H_{39}CdN_3O_8$
Formula mass	443.71	922.24
Crystal size [mm]	0.47 × 0.35 × 0.28	0.30 × 0.26 × 0.14
Crystal system	monoclinic	monoclinic
Space group	$P2_1/c$	$P2_1/c$
a [Å]	9.9943(8)	14.0695(3)
b [Å]	19.7593(16)	14.0633(4)
c [Å]	10.3333(8)	22.2760(4)
β [°]	111.893(2)	92.4430(10)
V [Å^3]	1893.5(3)	4403.60(18)
Z	4	4
D_c [g cm^{-3}]	1.557	1.391
μ [mm^{-1}]	1.176	0.554
T [K]	293(2)	293(2)
λ (Mo-K_α) [Å]	0.71073	0.71073
Reflections collected	6022	13408
Unique reflections	3336	7726
R_{int}	0.0585	0.0573
Parameters	235	559
S on F^2	1.111	1.187
R_1 [$I > 2\sigma(I)$][a]	0.0781	0.0767
wR_2 (all data)[b]	0.1717	0.1491
$\Delta\rho_{min}$ and $_{max}$ [e/Å^3]	1.203 and −1.525	0.706 and −0.624

[a] $R = \Sigma||F_o| - |F_c||/\Sigma|F_o|$. [b] $wR = [\Sigma w(F_o^2 - F_c^2)^2/\Sigma w(F_o^2)^2]^{1/2}$.

Table 2. Selected bond lengths [Å] and angles [°] for **1** and **2**

Compound **1**			
Cd−O(2A)[a]	2.209(8)	Cd−N	2.237(9)
Cd−O(1)	2.210(8)	Cd−O(3B)	2.240(8)
Cd−O(4C)	2.218(8)	Cd−CdA	3.043(2)
O(2A)−Cd−O(1)	158.0(4)	O(2A)−Cd−O(3B)	87.7(3)
O(2A)−Cd−O(4C)	86.7(4)	O(1)−Cd−O(3B)	86.2(3)
O(1)−Cd−O(4C)	91.5(4)	O(4)−Cd−O(3B)	159.1(4)
O(2A)−Cd−N	101.8(4)	N−Cd−O(3B)	100.1(3)
O(1)−Cd−N	100.1(4)	N−Cd−CdA	178.0(3)
O(4C)−Cd−N	100.7(3)		
Compound 2			
Cd−N(1)	2.341(5)	Cd−O(31)	2.416(5)
Cd−N(2A)	2.349(6)	Cd−O(51)	2.429(5)
Cd−O(32)	2.399(5)	Cd−O(52)	2.474(5)
Cd−N(3)	2.406(5)		
N(1)−Cd−N(2A)	177.5(2)	N(2A)−Cd−O(51)	82.3(2)
N(1)−Cd−O(32)	96.70(19)	O(32)−Cd−O(51)	163.05(17)
N(2A)−Cd−O(32)	85.4(2)	N(3)−Cd−O(51)	84.65(18)
N(1)−Cd−N(3)	85.0(2)	O(31)−Cd−O(51)	139.44(17)
N(2A)−Cd−N(3)	96.4(2)	N(1)−Cd−O(52)	91.57(19)
O(32)−Cd−N(3)	85.15(18)	N(2A)−Cd−O(52)	86.01(19)
N(1)−Cd−O(31)	82.6(2)	O(32)−Cd−O(52)	137.36(16)
N(2A)−Cd−O(31)	97.8(2)	N(3)−Cd−O(52)	137.34(18)
O(32)−Cd−O(31)	53.96(16)	O(31)−Cd−O(52)	86.12(16)
N(3)−Cd−O(31)	135.08(18)	O(51)−Cd−O(52)	53.34(16)
N(1)−Cd−O(51)	95.87(19)		

[a] Symmetry code: **1** (A) $-x+2, -y, -z$; (B) $-x+3, y+1/2, -z+1/2$; (C) $x-1, -y-1/2, z-1/2$; **2** (A) $x, y-1, z$.

Acknowledgments

This work was supported by the National Nature Science Foundation of China, Nature Science Foundation of Fujian

 © 2004 Wiley-VCH Verlag GmbH & Co. KGaA, Weinheim

Province, the Key Project of Chinese Academy of Science and Open Laboratory of Chirotechnology of the Hong Kong Polytechnic University.

[1] [1a] J.-M. Lehn, *Supramolecular Chemistry: Concepts and Perspectives*, VCH, Weinheim, **1995**. [1b] J. W. Steed, J. L. Atwood, *Supramolecular Chemistry*; John Wiley & Sons: New York, **2000**. [1c] G. R. Desiraju, *Crystal Engineering: The Design of Organic Solids*, Elsevier: New York **1989**.

[2] [2a] S. Leininger, B. Olenyuk, P. J. Stang, *Chem. Rev.* **2000**, *100*, 853−908. [2b] P. J. Hagrman, D. Hagrman, J. Zubieta, *Angew. Chem. Int. Ed.* **1999**, *38*, 2638−2684. [2c] M. Munakata, L. P. Wu, T. Kuroda-Sowa, *Adv. Inorg. Chem.* **1999**, *46*, 173−303.

[3] [3a] M. Eddauodi, J. Kim, N. Rosi, D. Vodak, J. Wachter, M. O′keeffe, O. M. Yaghi, *Science* **2002**, *295*, 469−472. [3b] M. Eddaoudi, D. B. Moler, H. Li, B. Chen, T. M. Reineke, M. O'Keeffe, O. M. Yaghi, *Acc. Chem. Res.* **2001**, *34*, 319−330.

[4] [4a] S. A. Bourne, J. Lu, A. Mondal, B. Moulton, M. J. Zaworotko, *Angew. Chem. Int. Ed.* **2001**, *40*, 2111−2113. [4b] J. Lu, A. Mondal, B. Moulton, M. J. Zaworotko, *Angew. Chem. Int. Ed.* **2001**, *40*, 2113−2116.

[5] [5a] S. I. Noro, S. Kitagawa, M. Kondo, K. Seki, *Angew. Chem. Int. Ed.* **2000**, *39*, 2081−1084. [5b] S. Dalai, P. S. Mukherjee, E. Zangrando, F. Lloret, N. R. Chaudhuri, *J. Chem. Soc., Dalton Trans.* **2002**, 822−823. [5c] A. Grirrane, A. Pastor, A. Galindo, A. Ienco, C. Mealli, P. Rosa, *Chem. Commun.* **2003**, 512−513.

[6] [6a] O. R. Evans, W. Lin, *Acc. Chem. Res.* **2002**, *35*, 511−522. [6b] H. W. Roesky, M. Andruh, *Coord. Chem. Rev.* **2003**, *236*, 91−119. [6c] D. A. McMorran, P. J. Steel, *Chem. Commun.* **2002**, 2120−2121. [6d] S. Banfi, L. Carlucci, E. Caruso, G. Ciani, D. M. Proserpio, *J. Chem. Soc., Dalton Trans.* **2002**, 2714−2721. [6e] E. Lindner, R. Zong, K. Eichele, U. Weisser, M. Ströbele, *Eur. J. Inorg. Chem.* **2003**, 705−712.

[7] [7a] A. J. Blake, N. R. Champness, S. S. M. Chung, W. S. Li, M. Schröder, *Chem. Commun.* **1997**, 1675−1676. [7b] H. K. Fun, S. S. S. Raj, R. G. Xiong, J. L. Zuo, Y. Zhi, X. Z. You, *J. Chem. Soc., Dalton Trans.* **1999**, 1915−1917.

[8] [8a] W. Lin, O. R. Evans, R. G. Xiong, Z. Wang, *J. Am. Chem. Soc.* **1998**, *120*, 13272−13273. [8b] J. S. Seo, D. Whang, H. Lee, S. I. Jun, J. Oh, Y. J. Jeon, K. Kim, *Nature* **2000**, *404*, 982−986. [8c] D. K. Chand, K. Biradha, M. Fujita, *Chem. Commun.* **2001**, 1652−1653. [8d] T. J. Prior, M. J. Rosseinsky, *Inorg. Chem.* **2003**, *42*, 1564−1575.

[9] [9a] A. J. Blake, N. R. Champness, A. N. Khlobystov, S. Parsons, M. Schröder, *Angew. Chem. Int. Ed.* **2000**, *39*, 2317−2320. [9b] S. A. Barnett, A. J. Blake, N. R. Champness, J. E. B. Nicolson, C. Wilson, *J. Chem. Soc., Dalton Trans.* **2001**, 567−573.

[10] [10a] S. R. Batten, R. Robson, *Angew. Chem. Int. Ed.* **1998**, *37*, 1460−1494. [10b] L. Carlucci, G. Ciani, D. Prosperpio, *Chem. Commun.* **1999**, 449−450. [10c] M. J. Plater, M. R. S. J. Foreman, E. Coronado, C. J. Gómez-García, A. M. Z. Slawin, *J. Chem. Soc., Dalton Trans.* **1999**, 4209−4216. [10d] Z. Y. Fu, X. T. Wu, J. C. Dai, S. M. Hu, W. X. Du, H. H. Zhang, R. Q. Sun, *Eur. J. Inorg. Chem.* **2002**, 2730−2735.

[11] [11a] F. A. A. Paz, Y. Z. Khimyak, A. D. Bond, J. Rocha, J. Klinowski, *Eur. J. Inorg. Chem.* **2002**, 2823−2828. [11b] J. Tao, M. L. Tong, X. M. Chen, *J. Chem. Soc., Dalton Trans.* **2000**, 3669−3674.

[12] [12a] S. M.-F. Lo, S. S-Y. Chui, L.-Y. Shek, Z. Lin, X. X. Zhang, G. H. Wen, I. D. Williams, *J. Am. Chem. Soc.* **2000**, *122*, 6293−6294. [12b] Z. Shi, S. H. Feng, Y. Sun, J. Hua, *Inorg. Chem.* **2001**, *40*, 5312−5313.

[13] [13a] K. D. Benkstein, J. T. Hupp, C. L. Stern, *J. Am. Chem. Soc.* **1998**, *120*, 12982−12983. [13b] D. Hagrman, R. D. Haushalter, J. Zubieta, *Chem. Mater.* **1998**, *10*, 361−365.

[14] [14a] J. A. Real, E. Andres, M. C. Munoz, M. Julve, T. Granier, A. Boussekou, F. Varret, *Science* **1995**, *268*, 265−269. [14b] G. De Munno, R. Ruiz, F. Lloret, J. Faus, R. Sessoli, M. Julve, *Inorg. Chem.* **1995**, *34*, 408−411.

[15] [15a] A. J. Blake, N. R. Champness, S. S. M. Chung, W. S. Li, M. Schröder, *Chem. Commun.* **1997**, 1005−1006. [15b] M. A. Withersby, A. J. Blake, N. R. Champness, P. A. Cooke, P. Hubberstey, A. L. Realf, S. J. Teat, M. Schröder, *J. Chem. Soc., Dalton Trans.* **2000**, 3261−3268.

[16] R. H. Wang, M. C. Hong, J. H. Luo, R. Cao, J. B. Weng, *Chem. Commun.* **2003**, 1018−1019.

[17] F. A. Cotton, C. Lin, C. A. Murillo, *Chem. Commun.* **2001**, 11−12.

[18] [18a] J.-M. Rueff, S. Pillet, N. Claiser, G. Bonaventure, M. Souhassou, P. Rabu, *Eur. J. Inorg. Chem.* **2002**, 895−900. [18b] H. Kumagai, K. Inoue, M. Kurmoo, *Bull. Chem. Soc. Jpn.* **2002**, *75*, 1283−1289. [18c] R. H. Wang, M. C. Hong, J. H. Luo, R. Cao, J. B. Weng, *Eur. J. Inorg. Chem.* **2002**, 2082−2085.

[19] A. F. Wells, *Structural Inorganic Chemistry*; Oxford University Press: London, **1962**, p. 984.

[20] [20a] T. Allman, R. Goel, N. K. Jha, A. L. Beauchamp, *Inorg. Chem.* **1984**, *23*, 914−918. [20b] S. L. Li, T. C. W. Mak, *J. Chem. Soc., Dalton Trans.* **1995**, 1519−1524.

[21] M. E. Braun, C. D. Steffek, J. Kim, P. G. Rasmussen, O. M. Yaghi, *Chem. Commun.* **2001**, 2532−2533.

[22] [22a] S. E. Denmark, H. Matsuhashi, *J. Org. Chem.* **2002**, *67*, 3479−3486. [22b] R. Curci, M. Fiorenino, M. R. Serio, *J. Chem. Soc., Chem. Commun.* **1984**, 155−156.

[23] G. M. Sheldrick, *SADABS, Program for Empirical Absorption Correction of Area Detector Data*; University of Göttingen: Göttingen, **1996**.

[24] G. M. Sheldrick, *SHELXS 97, Program for Crystal Structure Solution*; University of Göttingen: Göttingen, **1997**.

Received June 18, 2003
Early View Article
Published Online October 31, 2003

 © 2004 Wiley-VCH Verlag GmbH & Co. KGaA, Weinheim

Formation and Reactivity of Gaseous Iron-Sulfur Clusters

Konrad Koszinowski,[a] Detlef Schröder,[a] and Helmut Schwarz*[a]

Dedicated to Professor Heinz Georg Wagner on the occasion of his 75th birthday

Keywords: Cluster compounds / Electron transfer / Gas-phase reactions / Iron / Sulfur

The gas-phase reactions of Fe_n^+ clusters, n = 1–6, with COS and CS_2 have been investigated by means of Fourier-transform ion-cyclotron resonance mass spectrometry. Whereas CS_2 predominantly substitutes one Fe atom, COS exclusively affords multiple sulfur transfer and thus opens a synthetic route to gaseous $Fe_nS_x^+$ clusters. In the final products such as $Fe_2S_2^+$, $Fe_3S_2^+$, and $Fe_4S_4^+$, the sulfur atoms appear to occupy multiple coordination sites much like in the analogous biogeneous iron-sulfur clusters. Bracketing experiments find $IE(Fe_2S_2)$ = 7.2±0.3 eV besides providing upper limits for $IE(Fe_3S_2)$ and $IE(Fe_4S_4)$. In accordance with the low $IE(Fe_2S_2)$, $Fe_2S_2^+$ does not activate H_2 or small hydrocarbons and only exhibits rather limited reactivity towards more reactive substrates.
(© Wiley-VCH Verlag GmbH & Co. KGaA, 69451 Weinheim, Germany, 2004)

Introduction

Among the many functions of iron in biological systems, its involvement in redox processes is particularly important. Inter alia, electron-transfer (ET) reactions associated with photosynthesis, respiration, and nitrogen fixation rely heavily upon this transition metal. A common feature of the different enzymes mediating these processes is that their catalytically active centers are not comprised of a single iron atom but consist of several Fe atoms bound to sulfur.[1−4] The [4Fe-4S] core with its hetero-cubane structure is an especially famous example of such clusters.

Various strategies have been pursued in order to elucidate the chemical relationship between the remarkable structures of the iron-sulfur clusters and their outstanding reactivity in terms of ET. To probe the intrinsic properties of these systems, exclusion of environmental effects is warranted. This approach can be rigorously achieved by gas-phase techniques that allow a thorough investigation of the object of interest. For instance, anionic clusters of the type $Fe_nS_x^-$ have been examined by means of photoelectron spectroscopy.[5,6] In the case of their cationic counterparts, however, experiments so far have mainly centered around mononuclear systems FeS_x^+.[6−12] In a joint study with the group of Armentrout, we have recently derived thermochemical data with respect to polynuclear clusters $Fe_nS_x^+$, $n \leq 5$ and $x \leq 2$, from the kinetic energy dependences of the reactions of Fe_n^+ with COS and CS_2.[13] Although these studies provide evidence for multiple sulfur transfer, the guided-ion beam (GIB) technique applied is not the method of choice for the detailed investigation of such processes. Instead, the longer time-scale of Fourier-transform ion-cyclotron resonance mass spectrometry (FT-ICR MS) and its supreme suitability for MS^n experiments make this technique particularly adequate for the elucidation of multi-step reactions. Since it cannot compete with the GIB approach for the determination of thermochemical quantities, however, both methods are complementary. Taking advantage of this situation, the present FT-ICR study focuses on the primary and consecutive reactions between Fe_n^+ clusters, $n \leq 6$, with COS as well as CS_2. Particular attention has been paid to possible structural assignments of the evolving $Fe_nS_x^+$ ions. Moreover, the reactivity of the cluster ions $Fe_2S_2^+$, $Fe_3S_2^+$, and $Fe_4S_4^+$ has been explored briefly, with an emphasis on ET reactions and a comparison with the analogous iron-oxide clusters.

Results

Reactions with COS and CS_2

The reactions of Fe_n^+ with COS lead to stepwise sulfur transfer to the metal cluster, as shown in the reaction according to Equation (1).

$$Fe_n^+ + x\,COS \rightarrow Fe_nS^+ + CO + (x-1)\,COS \rightarrow \rightarrow Fe_nS_x^+ + x\,CO \quad (1)$$

As was established previously, mononuclear iron only accepts a single sulfur atom with an appreciable efficiency.[10] In contrast, the second sulfur transfer for Fe_2^+ is significantly faster than the first and no further reaction can be observed. Similarly, the reaction apparently stops after transfer of two S atoms in the case of Fe_3^+. For n =

[a] Institut für Chemie der Technischen Universität Berlin, Straße des 17. Juni 135, 10623 Berlin, Germany

 © 2004 Wiley-VCH Verlag GmbH & Co. KGaA, Weinheim DOI: 10.1002/ejic.200300480

4 and 6, addition of four S atoms occurs whereas even $x = 5$ is reached for Fe_5^+. Although the maximum sulfur contents observed do not necessarily correspond to the ultimate level at infinite reaction times, they nevertheless imply that any possible further reactions proceed significantly less efficiently.

A more detailed analysis required a quantitative treatment. To this end, the experimental temporal ion abundances were fitted to the kinetic model defined by reaction (1). Note that the validity of this model, postulating a stepwise sulfur transfer, can safely be assumed because no termolecular reactions are feasible at the low pressures maintained. However, a minor complication arose from side reactions with contaminants in the cases of Fe_4^+ and Fe_5^+. In order to monitor the whole series of consecutive processes, reaction times up to 30 s were necessary. Thus, continuous reactions with background oxygen and water led to the accumulation of products formed by oxidative cluster degradation and hydrolysis (for $n = 4$, species such as $Fe_2O_2^+$, $Fe_3S_2^+$, and $Fe_4S_2O^+$ are indicative of such processes). To a first approximation, similar degradation or hydrolysis probabilities may be assumed for all intermediates $Fe_nS_x^+$ within a reaction series such that the neglect of the by-products should not affect the rate constants derived for the sulfur-transfer reactions themselves. Given the relatively low amounts of the by-products resulting from contamination ($\leq 30\%$ and 15% of the total ion intensity for $n = 4$ and 5, respectively), this approach indeed appears reasonable.

The results of the kinetic modeling show uniformly high efficiencies for the reactions of the clusters with $n \geq 3$ (Table 1). In these cases, the operation of substantial enthalpic or kinetic restrictions can obviously be excluded. This finding suggests lower limits for the binding energies of the iron-sulfur clusters according to $D_{298}(Fe_nS_{x-1}^+-S) \geq D_{298}(OC-S) = 308\ kJ{\cdot}mol^{-1}$, $n = 3-6$.[14]

The reactions of Fe_n^+ with CS_2 do not afford efficient sulfur transfer but are included in the present work for comparison with the GIB data. Mononuclear Fe^+ does not react with CS_2 at thermal energies.[10,11] Similarly, the reaction of Fe_2^+ exhibits a low efficiency of $\varphi = 0.01$ with simple adduct formation as the main reaction (80% branching ratio, b.r.). Doubling of the pressure (from 1 to $2{\cdot}10^{-7}$ mbar) does not change the rate constant for this process within the relative uncertainty of 10% such that irradiative rather than termolecular stabilization seems to account for the association.[15] A second reaction channel yields $Fe_2S_2^+$ (10% b.r.). Presumably, this process involves Fe_2S^+ as an intermediate that does not build up in substantial concentrations because of a rapid second sulfur transfer. See reaction in Equation (2) with $n = 2$.

$$Fe_n^+ + 2\,CS_2 \rightarrow Fe_nS^+ + CS + CS_2 \rightarrow Fe_nS_2^+ + 2\,CS \quad (2)$$

The occurrence of CS_2^+ as a third product (10% b.r.) might point to the presence of residual amounts of electronically excited Fe_2^+ because charge transfer from ground-state Fe_2^+ to CS_2 would be strongly endothermic [$IE(Fe_2) = 6.30\pm0.01$ vs. $IE(CS_2) = 10.07\pm0.01$ eV).[16,17] Note, however, that the reaction of Fe_2^+ with CS_2 is the only case where there is a possible indication of the involvement of electronically excited states. Moreover, for the presence of large amounts of excited Fe_n^+ one would not expect the observed exponential decrease of the reactant Fe_n^+ ions as is evident from linear slopes in semi-logarithmic plots. Therefore, the formation of CS_2^+ in the reaction of Fe_2^+ is rather ascribed to the presence of small amounts of an unobserved reactive intermediate. Because of the low efficiency of this reaction channel ($\varphi = 10^{-3}$), involvement of a contaminant such as O_2 cannot be excluded either.[18]

The larger clusters react much more efficiently with CS_2 ($\varphi = 0.5-0.8$). Here, the main process corresponds to substitution of one Fe atom by CS_2 [Equation (3)]. Only for Fe_3^+, reaction (2) still takes place (25% b.r.). Obviously, CS_2 binds quite strongly to the larger Fe_n^+ clusters.

$$Fe_n^+ + CS_2 \rightarrow Fe_{n-1}CS_2^+ + Fe \quad (3)$$

The same conclusion can be drawn from the consecutive reactions that efficiently lead to the mere association of one or even two further CS_2 molecules for $n \geq 4$. Since the pressures applied for the larger cluster ions were more than an order of magnitude lower than in the case of Fe_2^+, the tendency towards termolecular stabilization should be even more reduced and, therefore, cannot account for the effective relaxation. Instead, a deep potential well of the ion-molecule complex is supposed to increase the lifetime of the collision complexes, thereby facilitating their relaxation. In comparison with Fe_2^+, the higher numbers of internal degrees of freedom in the $Fe_{n-1}CS_2^+$ clusters, $n = 4-6$, also allow a faster redistribution of the energy released upon complexation and thereby raise the lifetimes of the energetic encounter complexes as well. Such phenomena are quite

Table 1. Bimolecular rate constants k and efficiencies for the reactions of Fe_n^+ with COS derived from kinetic modeling

Reaction	$k/10^{-10}$ cm^3 s^{-1} (φ)					
$n =$	1	2	3	4	5	6
$Fe_n^+ + COS \rightarrow Fe_nS^+ + CO$	2.4[a] (0.19)	0.35 (0.032)	6.8 (0.67)	7.6 (0.77)	7.6 (0.79)	4.2 (0.44)
$Fe_nS^+ + COS \rightarrow Fe_nS_2^+ + CO$		6.8[b] (0.66)	7.9[b] (0.79)	6.4 (0.66)	7.5 (0.79)	7.4 (0.79)
$Fe_nS_2^+ + COS \rightarrow Fe_nS_3^+ + CO$				8.9 (0.93)	8.4 (0.89)	8.0 (0.86)
$Fe_nS_3^+ + COS \rightarrow Fe_nS_4^+ + CO$				6.7[b] (0.71)	7.1 (0.76)	7.1[b] (0.76)
$Fe_nS_4^+ + COS \rightarrow Fe_nS_5^+ + CO$					6.6[b] (0.71)	

[a] For the slow transfer of a second S atom and further consecutive reactions, compare: I. Kretzschmar, *Energetics and Reactivity of the Binary Transition-Metal Sulfides of the 3rd and the 4th Row*; Shaker: Aachen, **1999**. [b] Upper limits of $k < 5{\cdot}10^{-11}$ cm$^3{\cdot}$s^{-1} for a further S atom transfer can be inferred from consideration of the signal-to-noise ratios.

 © 2004 Wiley-VCH Verlag GmbH & Co. KGaA, Weinheim

common for the reactions of cluster ions in the highly diluted gas phase.[19]

Reactivity of $Fe_2S_2^+$

The reactivity of the smallest iron-sulfur cluster, i.e. $Fe_2S_2^+$, was investigated in some detail. Focusing on this cluster is advantageous for practical reasons because it can easily be generated in high abundance. Moreover, a comparison with the analogous $Fe_nO_x^+$ ions promised to be most revealing for the dinuclear systems because $Fe_2O_2^+$ has been studied extensively.[20,21]

$Fe_2S_2^+$ does not react with the inorganic substrates H_2, N_2, O_2, CO, CO_2, and H_2O ($\varphi < 10^{-3}$). Upon exposure to NH_3, $Fe_2S_2^+$ slowly binds up to three molecules of the neutral reagent. The determined rate constant $k = 3.8 \cdot 10^{-11}$ $cm^3 \cdot s^{-1}$ ($\varphi = 0.019$) does not show any dependence on the pressure [$p(NH_3)$ between 1 and $3 \cdot 10^{-7}$ mbar], thus again suggesting radiative rather than termolecular relaxation of the association complexes. Compared with H_2O, the enhanced reactivity of NH_3 reflects its higher basicity that leads to a stronger dative binding which in turn raises the lifetime of the energetic ion-molecule complexes, see above. Similarly, Nakajima et al. found association of NH_3 to be much more efficient than H_2O addition for larger $Fe_nS_x^+$ clusters. However, a comparison with these data should take into account that they refer to differently produced clusters such that the structural identities of the $Fe_nS_x^+$ species are not necessarily given.[6]

In view of the low reactivity of $Fe_2S_2^+$ towards inorganic molecules, one also does not expect it to readily activate hydrocarbons. Therefore, the reactions of $Fe_2S_2^+$ with alkanes were not investigated but its reactivity toward alkenes was addressed right away. Whereas exposure to 1-butene only afforded rather slow adduct formation ($\varphi = 0.04$), 1,4-cyclohexadiene was efficiently activated by $Fe_2S_2^+$ ($k = 6.3 \cdot 10^{-10}$ $cm^3 \cdot s^{-1}$, $\varphi = 0.61$). The reactivity of 1,4-cyclohexadiene is governed by its tendency towards H_2 elimination which meets expectation because the presumably concomitant formation of benzene provides a strong thermodynamic driving-force for this process. Consequently, loss of C_6H_6 constitutes the main reaction channel [reaction (4), 80% b.r.]. Note that this process corresponds to a formal reduction of the iron cluster-core. The second reaction channel (20%) results in hydro-desulfuration[22] [reaction (5)] and thus highlights the redox character of the reactions in an even more pronounced manner. It remains unclear whether the ionic product contains an intact benzene molecule or if further bond activation involving the remaining S atom has occurred.

$$Fe_2S_2^+ + C_6H_8 \rightarrow [Fe_2,S_2,H_2]^+ + C_6H_6 \quad (4)$$

$$Fe_2S_2^+ + C_6H_8 \rightarrow [Fe_2,S,C_6,H_6]^+ + H_2S \quad (5)$$

The primary products undergo efficient consecutive reactions. Whereas both $[Fe_2,S,C_6,H_6]^+$ and $[Fe_2,S_2,H_2]^+$ add one more 1,4-cyclohexadiene molecule under dehydrogenation [reactions (6) and (7)], the latter also loses two molecules of H_2 upon reaction with C_6H_8 [reaction (8), 70% b.r.]. Formally, this process regenerates the $Fe_2S_2^+$ cluster core with one added benzene ligand and thus corresponds to the reverse of the reduction in reaction 4. Apparently, the dinuclear cluster can easily switch from one oxidation state to another.

$$[Fe_2,S,C_6,H_6]^+ + C_6H_8 \rightarrow [Fe_2,S,C_{12},H_{12}]^+ + H_2 \quad (6)$$

$$[Fe_2,S_2,H_2]^+ + C_6H_8 \rightarrow [Fe_2,S_2,C_6,H_8]^+ + H_2 \quad (7)$$

$$[Fe_2,S_2,H_2]^+ + C_6H_8 \rightarrow [Fe_2,S_2,C_6,H_6]^+ + 2\,H_2 \quad (8)$$

ET Reactions

Given the well-known activity of biogeneous Fe_nS_x clusters in terms of ET, the respective behavior of their gaseous counterparts also deserves attention. Although the reactivity observed for $Fe_2S_2^+$ already provides some first indications with regard to its redox activity, further efforts are necessary to address this issue explicitly. Within FT-ICR mass spectrometry, a straightforward determination of *IE*s can be achieved by bracketing experiments. To this end, the ion of interest A^+ is exposed to substrates B with known *IE*s. Occurrence of ET indicates $IE(A) \geq IE(B)$, whereas in the absence of ET, the opposite relation should hold true as long as no kinetic barriers are associated with the ET process. The latter assumption is valid if the structure of the substrate B is not strongly changed upon ionization, i.e., in the case of favorable Franck−Condon factors that are usually observed for (substituted) arenes.

The bracketing method can be refined by consideration of the efficiency of the ET process instead of the only qualitative distinction between occurrence and nonoccurrence.[23] In the present case, however, major difficulties arose from the apparently rather low *IE*s of the Fe_nS_x clusters. In order to observe ET, substrates with similarly small *IE*s such as amino- or methoxy-substituted arenes were required. The low vapor pressures and the unfavorable pumping characteristics of these compounds severely complicate their handling in high-vacuum devices and prevent the determination of accurate absolute rate constants. Moreover, the appreciable basicity of aniline and its derivatives results in strong interactions between these reagents and the ionic clusters, thereby favoring mere association compared with ET. For larger clusters, adduct formation becomes even more important because of lifetime effects (see above) such that ET may no longer compete although it is still feasible thermochemically. Hence, the investigations with regard to ET had to be restricted to the smaller clusters $Fe_2S_2^+$, $Fe_3S_2^+$, and $Fe_4S_4^+$. Instead of the impractical measurement of absolute rate constants, the ratio between the rates of ET and adduct formation, as evidenced from the product distribution, was considered. For the stepwise decrease of the substrates' *IE*s, one expects the ratio k_{ET}/k_{add} to rise steeply from its low background level as soon as the *IE* of the substrate matches that of the Fe_nS_x cluster and the ET process becomes thermodynamically accessible. Indeed, this situation was found in the case of $Fe_2S_2^+$ where k_{ET}/k_{add} increases by more than one order of magnitude when changing the substrate from 1,4-dimeth-

 © 2004 Wiley-VCH Verlag GmbH & Co. KGaA, Weinheim

oxybenzene (IE = 7.56 eV)[17] to *N*-methylaniline (IE = 7.32 eV)[17] and then to *N*,*N*-dimethylaniline (IE = 7.12 eV, Figure 1).[17] This progression roughly suggests $IE(Fe_2S_2)$ = 7.2±0.3 eV. In the reaction with *N*,*N*-dimethylaniline, hydride transfer from the substrate to the $Fe_2S_2^+$ cluster occurs with approximately equal efficiency as ET [reaction (9)]. Like reaction (4) with 1,4-cyclohexadiene, this process demonstrates the ready uptake of two reduction equivalents by $Fe_2S_2^+$. Similarly, the hydro-desulfuration observed with *N*-methylaniline [reaction (10)] has its counterpart in reaction (5) for $Fe_2S_2^+$ with 1,4-cyclohexadiene.

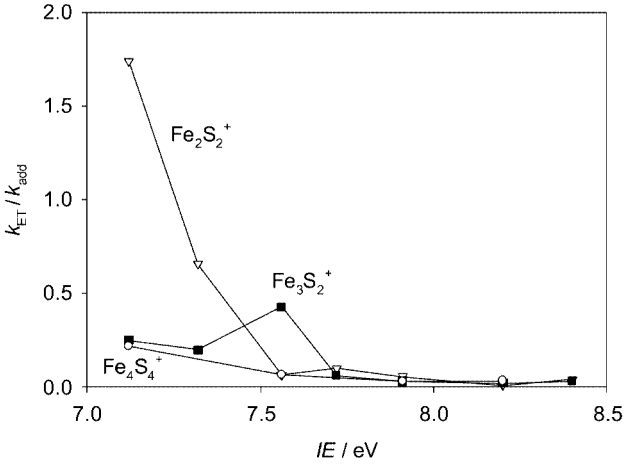

Figure 1. Ratio of ET versus addition processes for the reactions of $Fe_nS_x^+$ clusters with several substrates, B, as a function of IE(B). Specifically, the substrates applied were (in the order of increasing IE): *N*,*N*-dimethylaniline, *N*-methylaniline, 1,4-dimethoxybenzene, aniline, 2-methylnaphthalene, anisole, and mesitylene.

$$Fe_2S_2^+ + C_6H_5N(CH_3)_2 \rightarrow C_6H_5N(CH_3)CH_2^+ + [Fe_2,S_2,H] \quad (9)$$

$$Fe_2S_2^+ + C_6H_5NHCH_3 \rightarrow [Fe_2,S,C_7,H_7,N]^+ + H_2S \quad (10)$$

In the case of $Fe_3S_2^+$, the situation is more complex. The ratio k_{ET}/k_{add} substantially increases for the change from aniline (IE = 7.72 eV)[17] to 1,4-dimethoxybenzene (IE = 7.56 eV),[17] but drops again for *N*-methylaniline (IE = 7.32 eV).[17] This non-monotonic behavior might possibly result from differences between the substrates' tendencies towards adduct formation. Considering the ratio k_{ET}/k_{add} rather than the absolute rate constant k_{ET} as a criterion for ET relies on the assumption that k_{add} does not strongly change for the differently substituted arenes. However, it cannot be excluded that the small differences between the various substrates already give rise to significantly distinct lifetime effects that might account for the non-monotonic progression of k_{ET}/k_{add}. Nonetheless, it is not clear why the reaction between 1,4-dimethoxybenzene and $Fe_2S_2^+$ does not exhibit a similar anomaly.

For $Fe_4S_4^+$, low k_{ET}/k_{add} ratios were observed without exception. From the present experiments, one cannot judge whether this finding merely reflects a higher tendency towards association for the larger cluster or if a further decrease of the substrates' IEs were necessary to induce efficient ET. Note that probing the latter is far from trivial because of the low vapor pressures of the respective compounds. Hence, only upper limits for the IEs of Fe_3S_2 and Fe_4S_4 can be derived for the time being: $IE(Fe_3S_2) \leq 7.6$ and $IE(Fe_4S_4) \leq 7.6$ eV.

Discussion

Comparison between FT-ICR and GIB Data

First, the present results regarding the reactivity of Fe_n^+ clusters toward COS and CS_2 are compared with the previous GIB data.[13] With regard to the reactions with COS, both methods find sulfur transfer according to reaction (1) as the exclusive process taking place at thermal energies. Whereas the primary reactions are quite efficient for clusters sizes $n \geq 3$, a significantly decreased reactivity is consistently observed in the case of Fe_2^+ (Table 1). Since this reaction is strongly exothermic (Δ_rH° = −104±5 kJ·mol^{-1}),[13] kinetic rather than energetic restrictions must account for its low efficiency. A possible explanation suggested previously centers on the formally forbidden spin-inversion associated with the dissociation of COS ($^1\Sigma$ ground state) into CO ($^1\Sigma$) and S (^{3}P).[11,13,24] For the larger metal clusters, the presence of numerous energetically accessible electronic states mixing with the wave functions of COS is likely to weaken this restriction. In the case of the dinuclear system, however, the smaller number of electronic states appears to be insufficient for suspending spin selection-rules. This line of argument is supported by the high efficiency (φ = 0.66) observed for the consecutive reaction of Fe_2S^+ with a further COS molecule. Apparently, symmetry breaking by the sulfide ligand effectively releases spin restrictions. In addition, occurrence of the consecutive reactions for $n \geq 2$ implies negative reaction enthalpies associated with these processes. These conclusions are in full agreement with the thermochemical data derived for $Fe_2S_2^+$ and $Fe_3S_2^+$ from the GIB experiments.[13]

The agreement between the FT-ICR and GIB data also continues for the reactions of Fe_n^+ with CS_2. Here, substitution of one iron atom by CS_2 is the predominant process for $n \geq 3$ [reaction (2)] and largely suppresses sulfur transfer despite its thermochemical feasibility. In comparison with COS, the stronger binding of CS_2 presumably results from both its enhanced π-donor and π-acceptor properties. Similarly, CS is commonly known to bind to transition metals more strongly than CO.[25] Again, Fe_2^+ behaves differently from the larger clusters and does not undergo reaction 2 as both the FT-ICR and GIB approach demonstrate.[13] The CS_2 ligand probably interacts with more than one iron center such that expulsion of the second Fe atom is disfavored and instead the adduct $Fe_2CS_2^+$ is formed for n = 2. A further comment is also warranted with respect to reaction (2). Whereas the first sulfur transfer from CS_2 to Fe_2^+ is slightly endothermic (Δ_rH° = 27±6 kJ·mol^{-1}) according to the GIB method,[13] the observation of the consecutive

 © 2004 Wiley-VCH Verlag GmbH & Co. KGaA, Weinheim

$Fe_2S_2^+$ product in the present work implies feasibility of the primary reaction under FT-ICR conditions. However, its low efficiency $\varphi = 10^{-3}$ also points to the operation of energetic or kinetic restrictions. On the basis of a simple Arrhenius approach, one finds an activation energy $E_A = -RT \ln\varphi = 17$ kJ·mol^{-1} which is in reasonable agreement with the $\Delta_r H°$ value determined by the GIB method.

Structural Assignments

A principal problem of mass-spectrometric studies results from the difficulty of structural assignments because these have to rely on indirect evidence only. In the case of the $Fe_nS_x^+$ clusters, previous studies primarily focused on the mononuclear FeS_x^+ ions.[8,10,12] Upon reaction with ethylene sulfide, Fe^+ adds to up to six sulfur atoms. Ligand-exchange, photodissociation, and collision-induced dissociation experiments point to the formation of S_2 or larger S_y units in these systems.[8] Similarly, FeS_2^+ generated from the reaction of Fe^+ with COS contains an S_2 ligand as well.[10] In contrast, the GIB study provided indications for separated S atoms in $Fe_2S_2^+$ and $Fe_3S_2^+$. In particular, the high bond-dissociation energies $D_0(SFe_n^+-S)$ and $D_0(Fe_n^+-S) > 400$ kJ·mol^{-1} derived for $n \geq 2$ suggest the occupation of multiple coordination sites by sulfur.[13] The interaction with more than a single metal center should saturate the open valencies of sulfur and thus diminish its tendency towards oligomerization.

The present findings further support the presence of separate S atoms in $Fe_2S_2^+$ and $Fe_3S_2^+$. Unlike FeS_2^+, they do not undergo ligand exchange with arenes as one would expect for $Fe_n(S_2)^+$ structures. The observed saturation at $x = 2$ in the reaction of Fe_2^+ with COS is consistent with rhombic $Fe_2S_2^+$ (Scheme 1). This geometry is also known for biogeneous [2Fe-2S] clusters.[1−4] In the case of $n = 3$, saturation after the addition of two S atoms is compatible with coordination to both faces of a triangle. Such a structure would correspond to the maximum number of binding interactions between each sulfur atom and the iron centers. For Fe_4^+, the metal cluster takes up four sulfur atoms that do not undergo exchange with arenes and therefore are not assumed to combine to form S_2 or even larger units. Given that the iron core in $Fe_4S_4^+$ adopts a tetrahedral structure as in the unperturbed Fe_4^+ system,[26] the maximum coordination possible would position each of the four S atoms above one triangular face. This geometry corresponds to the hetero-cubane structure known from biological systems.[1−4] In the cases of $n = 5$ and 6, the $Fe_5S_5^+$ and $Fe_6S_4^+$ clusters resulting from sulfur transfer were not exposed to further substrates such that the questions of ligand exchange and eventual sulfur oligomerization cannot be answered. However, in analogy to their smaller homologues, multifold coordination by separate sulfur atoms appears probable for these species. Similar conclusions have been drawn by Nakajima et al. for neutral Fe_nS_x clusters produced by laser vaporization of a solid iron-sulfur mixture.[6]

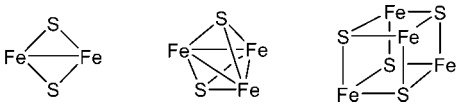

Scheme 1

Reactivity of $Fe_nS_x^+$ Clusters

The overall rather low reactivity found for $Fe_2S_2^+$ reflects the high thermochemical stability of this cluster as already inferred from the previous GIB experiments.[13] Presumably, the absence of hydrolysis and ammonolysis reactions results not only from the strength of the iron−sulfur bonds but also from the lower stability (in comparison with H_2O or NH_3) of H_2S which is the neutral by-product formed in hydrolysis or ammonolysis of $Fe_2S_2^+$. With regard to the reverse process, $Fe_2O_2^+$ indeed is known to react with two equivalents of H_2S to yield $Fe_2S_2^+$.[21] This observation indicates that hydrolysis of $Fe_2S_2^+$ is prohibited for thermochemical reasons. Compared with $Fe_2S_2^+$, the higher reactivity of $Fe_2O_2^+$ is also evident from its ability to attack non-activated hydrocarbons such as *n*-butane.[20,21] Obviously, the metal core cannot fully compensate for the electron deficiency of the O atoms such that the latter exhibit a high affinity for oxidation reactions. For $Fe_2S_2^+$, the lower electronegativity of sulfur leads to a better balanced electronic structure in this cluster and a significantly reduced oxidative power. The role of $Fe_2S_2^+$ as a mild oxidant becomes clearly visible in its reaction with 1,4-cyclohexadiene which apparently affords a reversible H_2 transfer. Moreover, this process points to the possibility of catalytic redox reactions of $Fe_2S_2^+$ which could be considered as gas-phase models for the active sites of the corresponding enyzmes.

The distinct behavior of $Fe_2S_2^+$ and $Fe_2O_2^+$ in terms of redox chemistry should also be reflected in the quantitative data derived for these systems. In comparison with $IE(Fe_2O_2) = 8.4\pm0.3$ eV,[21] $IE(Fe_2S_2) = 7.2\pm0.3$ eV is substantially lower, consistent with the arguments raised above. The present value obtained for $IE(Fe_2S_2)$ is somewhat larger than that inferred from the GIB approach, $IE_{GIB}(Fe_2S_2) = 6.64\pm0.35$ eV,[13] but both agree within the combined error margins. Note that one a priori might expect the present method to yield a slightly too high *IE* because the thermal energies of the reactants are not explicitly accounted for while they should decrease the energetic threshold of the ET reactions compared with those at $T = 0$ K. Nonetheless, the newly determined value indicates that the theoretical prediction $IE_{theo}(Fe_2S_2) = 7.76$ eV[27] does not lie as far from experiment as the comparison with $IE_{GIB}(Fe_2S_2)$ alone suggests. In the cases of Fe_3S_2 and Fe_4S_4, only upper limits could be derived for their *IE*s. Apparently, the *IE*s of these clusters are also quite low.

Conclusions

FT-ICR mass spectrometry has been used to study the formation and reactivity of cationic iron-sulfur clusters.

 © 2004 Wiley-VCH Verlag GmbH & Co. KGaA, Weinheim

$Fe_nS_x^+$ clusters can be generated by the reaction of Fe_n^+ with COS whereas exposure of Fe_n^+ to CS_2 mainly leads to substitution of one Fe atom by CS_2. These findings are fully consistent with previous results obtained by means of guided-ion beam techniques.[13] For the final products of sulfur transfer such as $Fe_2S_2^+$, $Fe_3S_2^+$, and $Fe_4S_4^+$, the absence of ligand exchange provides evidence against the presence of S_2 or larger S_y units which have been proven in the case of mononuclear FeS_x^+. This difference can be rationalized by the involvement of multiple bridging bonds between the Fe core and the sulfur atoms that are only possible for the cluster ions. The interaction with more than a single metal center saturates the open valencies of the sulfur atoms thereby preventing oligomerization. Thus, the structures of the gaseous $Fe_nS_x^+$ ions appear to strongly resemble those of biogeneous iron-sulfur clusters.

Moreover, the formation of multifold bonds substantially stabilizes the $Fe_nS_x^+$ clusters and diminishes their reactivity as demonstrated for $Fe_2S_2^+$. The low reactivity of the latter becomes particularly evident in the comparison with the analogous oxide species $Fe_2O_2^+$. Thus, the lower electronegativity of sulfur results in a well-adjusted electronic balance for $Fe_2S_2^+$ such that it does not exhibit an increased tendency towards oxidation reactions. Hence, iron-sulfur clusters seem to be intrinsically well suited for the participation in reversible redox reactions and catalytic ET processes.

Experimental Section

Experiments were performed using a Spectrospin CMS 47X FT-ICR mass spectrometer[28,29] that has recently[30] been equipped with a Smalley-type[31] cluster-ion source developed by Bondybey, Niedner-Schatteburg, and co-workers.[32] Briefly, the fundamental of a pulsed Nd:YAG laser (λ = 1064 nm, Spectron Systems) is focused onto a rotating iron target to generate a hot metal plasma. Cluster formation occurs by synchronization of a helium pulse and subsequent supersonic expansion. After passing a skimmer, the ionic components of the molecular beam are transferred into the analyzer cell where they are trapped in the field of a 7.05 T superconducting magnet. The distribution of cluster ions thus produced can be somewhat controlled by varying the delays between helium pulse, laser shot, and subsequent inlet into the analyzer cell. Whereas the abundances achieved for Fe^+ and Fe_2^+ were quite high, those for the larger clusters were significantly lower, thereby complicating the experiments in such cases. After mass-selection of a specific cluster size and removal of peaks resulting from the ^{54}Fe and ^{57}Fe isotopes by means of the FERETS ion-ejection protocol,[33] the Fe_n^+ ions were thermalyzed by an argon pulse.

Ion-molecule reactions between Fe_n^+ and COS and CS_2, respectively, were then studied by leaking-in the neutral substrate at $p \approx 5 \cdot 10^{-9}$ to $2 \cdot 10^{-7}$ mbar and recording the decline of the reactant Fe_n^+ clusters and the evolution of the products. Bimolecular rate constants k ($\pm$30% uncertainty)[34] were derived on the basis of the pseudo-first-order approximation, and the corresponding reaction efficiencies $\varphi \equiv k/k_{cap}$ were calculated according to capture theory.[35] Consecutive reactions were analyzed using numerical routines.[36,37] For the reactivity studies of the $Fe_nS_x^+$ clusters, the reactant ions were prepared by pulsing-in COS to mass-selected Fe_n^+. After further mass selection, the reactions with the permanently leaked-in substrates were recorded similarly to the way described above.

Acknowledgments

Financial support from the Deutsche Forschungsgemeinschaft and the Fonds der Chemischen Industrie is gratefully acknowledged. K.K. particularly thanks the Stiftung Stipendien-Fonds des Verbandes der Chemischen Industrie for a Kekulé scholarship.

[1] W. Lovenberg (Ed.), *Iron-Sulfur Proteins*; Academic: New York, **1973**–**1977**.
[2] T. G. Spiro (Ed.), *Iron-Sulfur Proteins*; John Wiley & Sons: New York, **1982**.
[3] H. Beinert, *FASEB J.* **1990**, *4*, 2483–2491.
[4] R. Cammack, *Advances in Inorganic Chemistry*; Academic: New York, **1992**.
[5] N. Zhang, T. Hayase, H. Kawamata, K. Nakao, A. Nakajima, K. Kaya, *J. Chem. Phys.* **1996**, *104*, 3413–3419.
[6] A. Nakajima, T. Hayase, H. Kawamata, F. Hayakawa, K. Kaya, *Chem. Phys. Lett.* **1997**, *280*, 381–389.
[7] T. C. Jackson, T. J. Carlin, B. S. Freiser, *Int. J. Mass Spectrom. Ion Processes* **1986**, *72*, 169–185.
[8] T. J. McMahon, T. C. Jackson, T. J. Carlin, B. S. Freiser, *J. Am. Chem. Soc.* **1989**, *111*, 421–427.
[9] J. N. Harvey, C. Heinemann, A. Fiedler, D. Schröder, H. Schwarz, *Chem. Eur. J.* **1996**, *2*, 1230–1234.
[10] D. Schröder, I. Kretzschmar, H. Schwarz, C. Rue, P. B. Armentrout, *Inorg. Chem.* **1999**, *38*, 3474–3480.
[11] C. Rue, P. B. Armentrout, I. Kretzschmar, D. Schröder, H. Schwarz, *J. Phys. Chem. A* **2001**, *105*, 8456–8464.
[12] For a photodissociation study on $Fe_nS_x^+$, see: Z. Yu, N. Zhang, X. Wu, Z. Gao, Q. Zhu, F. Kong, *J. Chem. Phys.* **1993**, *99*, 1765–1770.
[13] K. Koszinowski, D. Schröder, H. Schwarz, R. Liyanage, P. B. Armentrout, *J. Chem. Phys.* **2002**, *117*, 10039–10056.
[14] S. G. Lias, J. E. Bartmess, J. F. Liebman, J. L. Holmes, R. D. Levin, W. G. Mallard, *J. Phys. Chem. Ref. Data* **1998**, *17*, Suppl. 1.
[15] R. C. Dunbar, in: *Current Topics in Ion Chemistry and Physics* (Eds.: C. Y. Ng, T. Baer, I. Powis); John Wiley & Sons: New York, **1994**; vol. II.
[16] E. A. Rohlfing, D. M. Cox, A. Kaldor, K. H. Johnson, *J. Chem. Phys.* **1984**, *81*, 3846–3851.
[17] http://webbook.nist.gov/.
[18] J. Schwarz, D. Schröder, H. Schwarz, C. Heinemann, J. Hrušák, *Helv. Chim. Acta* **1996**, *79*, 1110–1120.
[19] K. Koszinowski, D. Schröder, H. Schwarz, *J. Phys. Chem. A* **2003**, *107*, 4999–5006.
[20] O. Gehret, M. P. Irion, *Chem. Eur. J.* **1996**, *2*, 598–603.
[21] P. Jackson, J. N. Harvey, D. Schröder, H. Schwarz, *Int. J. Mass Spectrom.* **2001**, *204*, 233–245.
[22] K. Eller, S. Akkök, H. Schwarz, *Helv. Chim. Acta* **1990**, *73*, 229–238.
[23] G. Bouchoux, D. Leblanc, M. Sablier, *Int. J. Mass Spectrom.* **2001**, *210/211*, 189–201.
[24] C. Rue, P. B. Armentrout, I. Kretzschmar, D. Schröder, J. N. Harvey, H. Schwarz, *J. Chem. Phys.* **1999**, *110*, 7858–7870.
[25] C. Elschenbroich, A. Salzer, *Organometallchemie*; 3rd ed., Teubner: Stuttgart, **1993**.
[26] M. Castro, D. R. Salahub, *Phys. Rev. B* **1994**, *49*, 11842–11852.
[27] O. Hübner, J. Sauer, *Phys. Chem. Chem. Phys.* **2002**, *4*, 5234–5243.
[28] K. Eller, H. Schwarz, *Int. J. Mass Spectrom. Ion Processes* **1989**, *93*, 243–257.

 © 2004 Wiley-VCH Verlag GmbH & Co. KGaA, Weinheim

[29] K. Eller, W. Zummack, H. Schwarz, *J. Am. Chem. Soc.* **1990**, *112*, 621−627.
[30] M. Engeser, T. Weiske, D. Schröder, H. Schwarz, *J. Phys. Chem. A* **2003**, *107*, 2855−2859.
[31] S. Maruyama, L. R. Anderson, R. E. Smalley, *Rev. Sci. Instrum.* **1990**, *61*, 3686−3693.
[32] C. Berg, T. Schindler, M. Kantlehner, G. Niedner-Schatteburg, V. E. Bondybey, *Chem. Phys.* **2000**, *262*, 143−149.
[33] R. A. Forbes, F. H. Laukien, J. Wronka, *Int. J. Mass Spectrom. Ion Processes* **1988**, *83*, 23−44.
[34] D. Schröder, H. Schwarz, D. E. Clemmer, Y.-M. Chen, P. B. Armentrout, V. I. Baranov, D. K. Böhme, *Int. J. Mass Spectrom. Ion Processes* **1997**, *161*, 175−191.
[35] T. Su, *J. Chem. Phys.* **1988**, *88*, 4102−4103; T. Su, *J. Chem. Phys.* **1988**, *89*, 5355.
[36] U. Mazurek, H. Schwarz, *ICR Kinetics, v. 3.0.1*, Technische Universität, Berlin, **1998**.
[37] U. Mazurek, Dissertation, D83, Technische Universität, Berlin, **2002**.

Received July 18, 2003
Early View Article
Published Online October 30, 2003

 © 2004 Wiley-VCH Verlag GmbH & Co. KGaA, Weinheim

Lanthanide Homobimetallic Triple-Stranded Helicates: Insight into the Self-Assembly Mechanism

Mourad Elhabiri,[a] Josef Hamacek,[a] Jean-Claude G. Bünzli,[b] and Anne-Marie Albrecht-Gary*[a]

Keywords: Europium / Helicates / Mechanisms / Self-assembly / Supramolecular chemistry

The self-assembly mechanism leading to the exclusive formation of a triple-stranded bimetallic helicate upon reaction of Eu^{III} with a ditopic hexadentate ligand L bearing two carboxylate moieties has been fully elucidated in water for a wide range of $[Eu]_{tot}/[L]_{tot}$ ratios. Using a fruitful combination of electrospray mass spectrometry, potentiometry, UV/Vis spectrophotometry, luminescence, and ^1H NMR spectroscopy, the final product Eu_2L_3 and the intermediate species EuL_2 and Eu_2L_2 have been characterised. The presence of terminal carboxylates in L significantly reduces the electrostatic repulsions of the coordination sites in Eu_2L_2 and Eu_2L_3 compared with the corresponding complexes formed with analogous neutral ligands and thus increases the stability of the L-europium(III) complexes. Kinetic investigations carried out with an excess of L and with an excess of Eu^{III}, show that the self-assembly proceeds through either EuL_2 or Eu_2L intermediates depending on the experimental conditions and leads to a pre-organized Eu_2L_2 complex by either a "braiding" or a "keystone" mechanism. In the last step, a fast and efficient wrapping of the third ligand strand leads to the target Eu_2L_3 helicate. The overall process is mainly governed by electrostatic interactions and proceeds via a key double stranded intermediate helicate Eu_2L_2. To the best of our knowledge, as a result of the fine-tuning of the coordination properties of L, we present one of the most efficient and cooperative metal/ligand systems for the spontaneous organization of a bimetallic triple-stranded structure.

(© Wiley-VCH Verlag GmbH & Co. KGaA, 69451 Weinheim, Germany, 2004)

Introduction

The self-assembly of supramolecular edifices, which was inspired from one of the basic principles in biology,[1] is an appealing approach to the design of novel nanomaterials with predetermined and specific properties.[2] In particular, combining the toolbox of non-covalent interactions with the intriguing chemical and physicochemical properties of transition metal ions allows one to build functional supramolecular architectures via metal-ion assisted self-assembly.[3] This strategy has successfully generated fascinating two and three-dimensional edifices from polytopic ligands, which include rods,[4] grids,[5] cages,[6] helices,[7] ladders,[8] and rings.[9] Initial studies of metallo-supramolecular helicates have mainly involved double- or triple-stranded structures containing cations such as Cu^I, Ag^I, Cu^{II}, Ni^{II}, Ga^{III}, or Fe^{III} and ligands derived from bipyridine, terpyridine, or catechol frameworks.[10,11] The specific magnetic and luminescent[12−14] properties of the trivalent lanthanide cations[15] are increasingly being taken advantage of in medical diagnoses[16,17] and therapy[18] as well as in the catalytic cleavage of DNA and RNA.[19] In this context, the synthesis of elaborate polymetallic lanthanide helicates, which are potentially chiral, may contribute to the development of such applications. However, the poor stereochemical preferences and the variable coordination numbers adopted by Ln^{III} ions render difficult a reliable molecular programming in solution. In spite of this difficulty, we have demonstrated that a careful ligand design based on the induced fit principle[20] leads to the strict self-assembly of lanthanide-containing triple-stranded helicates in organic media.[21,22] Ditopic pentadentate, hexadentate or nonadentate ligands derived from 2-pyridin-2-yl-1*H*-benzimidazole are indeed versatile building blocks and can be used to prepare bimetallic 3d−4f and 4f−4f assemblies,[23] as well as trimetallic 4f−4f−4f edifices.[24] Recently, we have also shown that grafting different substituents at the end of the hexadentate ligands results in ditopic hosts able to specifically recognize a pair of lanthanide ions in solution.[25] Bioanalytical and medical applications require water-soluble probes, so that the ditopic ligand L with two terminal carboxylate moieties was synthesized (Figure 1) and was found to yield highly stable bimetallic helicates

[a] Laboratoire de Physico-Chimie Bioinorganique, UMR 7509 du CNRS, ECPM, Université Louis Pasteur,
25 rue Becquerel, 67200 Strasbourg, France
Fax: (internat.) +33-3-90242639
E-mail: amalbre@chimie.u-strasbg.fr
[b] Swiss Federal Institute of Technology Lausanne, Institute of Molecular and Biological Chemistry,
BCH 1402, 1015 Lausanne, Switzerland
E-mail: jean-claude.bunzli@epfl.ch

Supporting information for this article is available on the WWW under http://www.eurjic.org or from the author.

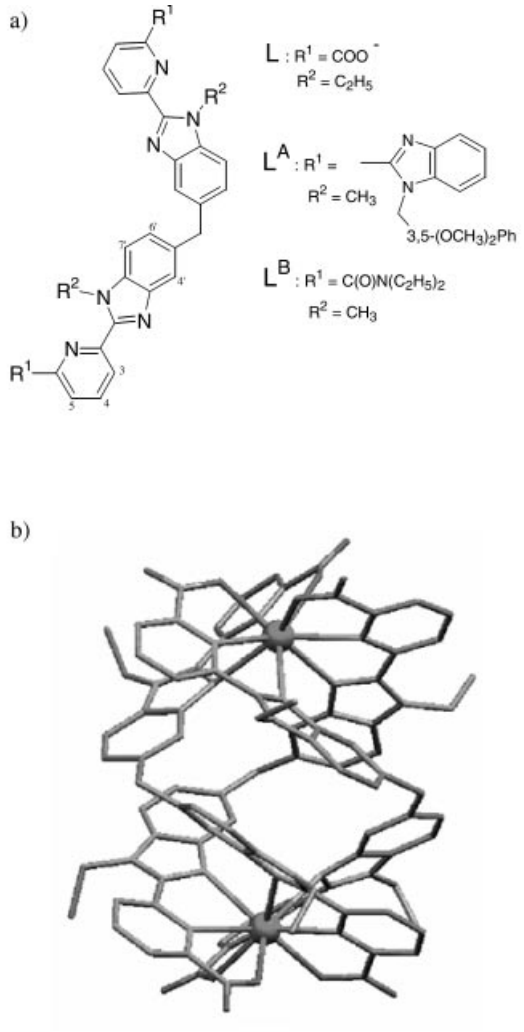

Figure 1. a) Chemical formula of deprotonated *transoid* ligand L and b) schematic view of the X-ray structure of Eu_2L_3[26]

Ln_2L_3 in water, despite the large hydration enthalpy of the metal ions.[26]

The numerous helicates reported so far[10] have been essentially characterised by their molecular structures and, sometimes, by their thermodynamic parameters. Kinetic data, which are essential for deciphering the self-assembly mechanism and, therefore for understanding the recognition process, are extremely scarce.[27–30] As part of our ongoing kinetic investigations of supramolecular edifices with polytopic ligands, dealing with either copper(I) trimetallic double-stranded[29] or lanthanide(III) bimetallic triple-stranded[30] helicates in acetonitrile, we present here a detailed physicochemical study of the Eu_2L_3 helicate in aqueous solution. The work is focused on getting a better understanding of the key steps of the self-assembly process. An original combination of potentiometry, absorption and emission spectrophotometry, ES mass spectrometry, and stopped-flow techniques, allowed us to determine both the thermodynamic and kinetic parameters characterising the formation of the bimetallic europium(III) triple-stranded helicate in water.

Results and Discussion

Ligand Properties

Detailed interpretation of thermodynamic and kinetic data requires knowledge of the ligand pK_a values, at least in the pH range in which the data are collected. Indeed, pK_a values of the carboxylic acid functions are difficult to determine in view of the extremely poor solubility of the ligand below pH 6 and its precipitation at pH 4. We have therefore investigated the acid-base properties of the ligand in the sole pH range 10.5–5.8 by various techniques. Potentiometric titrations of ca. 10^{-3} M solutions (Figure S1 in the Supporting Information; see also the footnote on the first page of this article) followed by a statistical treatment of the data[31] yielded the three protonation constants listed in Table 1. The corresponding distribution diagram is presented in Figure S2 (see Supporting Information).

Table 1. Successive protonation constants of ligand L; solvent: water; T = 25.0±0.2 °C; I = 0.1 M ($NEt_4{\cdot}ClO_4$); for the sake of simplicity charges have been omitted

Equilibrium			log K_{LH_n} ± 3σ
L + H	$\xrightarrow{K_{LH}}$ $\xleftarrow{}$	LH	10.1 ± 0.1
LH + H	$\xrightarrow{K_{LH_2}}$ $\xleftarrow{}$	LH_2	9.5 ± 0.2
LH_2 + H	$\xrightarrow{K_{LH_3}}$ $\xleftarrow{}$	LH_3	6.0 ± 0.2

In order to confirm the first pK_a, UV/Visible absorption spectra of the free ligand (see Supporting Information, Figure S3) were recorded in the range 7.38 < p[H] < 11.59 and a single cumulative protonation constant logβ_{LH_2} = 19.8±0.6 could be extracted using statistical methods[31] compared with 19.6 obtained by potentiometry.

$$L + n\,H \xrightarrow{\beta_{LH_n}} LH_n \qquad \text{with } n = 2 \tag{1}$$

We have also taken advantage of the fluorescent properties of the benzimidazole derivatives.[32,33] Decreasing the p[H] from 11.43 to 7.59 resulted in a drastic quenching of the ligand-centered fluorescence (Figure 2) and statistical treatment[31] of the data leads to the following protonation constants: logK_{LH} = 10.9±0.7 and logK_{LH_2} = 8.7±0.5. The re-calculated spectra for L, LH and LH_2 are presented in Figure S4 (see Supporting Information).

 © 2004 Wiley-VCH Verlag GmbH & Co. KGaA, Weinheim

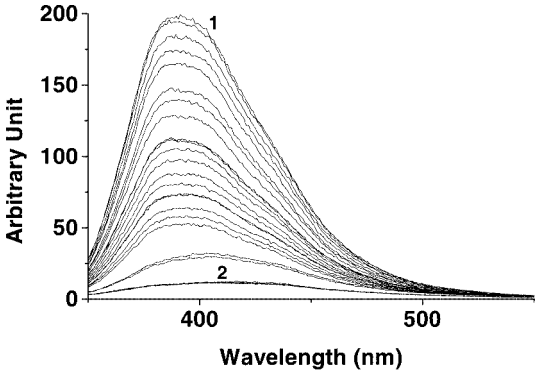

Figure 2. Corrected fluorescence spectra of L as a function of p[H]. Solvent: water; $T = 25.0 \pm 0.2$ °C; $I = 0.1$ M (NEt_4ClO_4); $l = 1$ cm; $\lambda_{exc} = 308$ nm. $[L]_{tot} = 3.56 \times 10^{-6}$ M; (**1**) p[H] 11.43; (**2**) p[H] 7.59. Spectra are not corrected for dilution

Finally, the assignment of the pK_a values was made on the basis of structural information extracted from ^{1}H and ^{13}C NMR spectra recorded at various p[D] values. These data clearly point to both monoprotonated LH and diprotonated LH_2 species retaining C_2 symmetry in the p[D] range 13.00−7.10, indicating that no intramolecular interaction occurs between the two identical subunits of the ditopic strand (Figure 1). This lack of interaction can be further confirmed by the difference between logK_{LH} and logK_{LH_2} ($\Delta \log K = 0.6$, Table 1), which is in excellent agreement with a statistical evaluation.[34] NOE effects are consistent with a *transoid* conformation for the ligand at p[D] = 13.[26] When the p[D] was decreased from 13.00 to 7.10, small but significant variations in the chemical shifts of the aromatic protons of the benzimidazole moiety ($H^{4'}$, $H^{6'}$, and $H^{7'}$) were observed whereas the ^{13}C chemical shifts related to the terminal carboxylates did not vary (Table 2). These NMR spectroscopic data strongly suggest that the first two protonation processes occur at the imidazolyl groups, an assumption confirmed by the absence of a red shift in the absorption and emission spectra in the p[H] range 11.4−7.4 (Figure 2 and Figure S3 in the Supporting Information). Such a shift would be expected if the *N*-pyridyl groups were protonated.[35,36]

In spite of the converging of the information provided by our measurements, one has to be aware that intra- and intermolecular hydrogen bonding may occur which could modify the above reasoning. For instance, in the case of 2-(2′-pyridyl)benzimidazole in hydrochloric acid, ^{15}N NMR spectroscopic measurements result in only two resonances and are consistent with the presence of fast exchanging resonance structures, one of which having a proton linked to two nitrogen atoms.[37] A similar situation is met for 1,10-phenanthroline which displays one ^{15}N signal regardless of the solvent, also pointing to the formation of bifurcated hydrogen bonds involving both nitrogen atoms.[38] In our case, formation of a hydrogen bond between the imidazolyl and the pyridine nitrogen atom is feasible and could affect the pyridyl protons, especially H^5 (Table 2 and Scheme 1).

Table 2. ^{1}H- and ^{13}C-chemical shifts δ (ppm vs. TMS) as a function of p[H]; p[H] values were determined by using p[H] = p[D] − 0.40;[88] solvent: D_2O; $[L]_{tot} = 10^{-2}$ M; $T = 25 \pm 1$ °C

	δ(^{1}H)						
	$H^{4'}$	$H^{6'}$	$H^{7'}$	H^3	H^4	H^5	
p[H] = 12.6	7.56	7.12	7.30	7.87	7.92	7.85	
p[H] = 10.0	7.54	7.08	7.26	7.86	7.91	7.82	
p[H] = 9.0	7.53	7.07	7.24	7.86	7.90	7.81	
p[H] = 6.7	7.49	7.03	7.20	7.86	7.88	7.79	
	δ (^{13}C)						
	$C^{4'}$	$C^{6'}$	$C^{7'}$	C^3	C^4	C^5	C=O
p[H] = 13.1	110.8	124.0	117.9	125.6	138.4	124.7	172.7
p[H] = 9.1	110.1	124.3	117.4	123.8	137.8	125.1	172.3
p[H] = 7.1	110.1	124.4	117.4	125.1	137.9	123.9	172.4

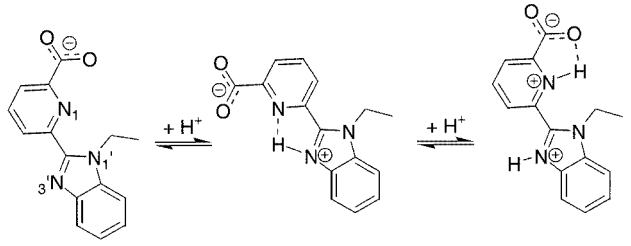

Scheme 1. Potential hydrogen bonding in two protonated subunits of L

The protonation constants logK_{LH} and logK_{LH_2} are at least 4−5 orders of magnitude larger than those reported for benzimidazole (log$K$ = 5.58)[39,40] or 2-(2′-pyridyl)benzimidazole (log$K$ = 4.41),[36] but less than two orders of magnitude smaller than the first protonation constant determined for 1,10-phenanthroline-2,9-dicarboxylic acid in water ($\log K_1 = 11.77 \pm 0.08$).[41] Carboxylic functions in positions 2 and 9 of the phenanthroline indeed induce a drastic increase in the basicity of the *N*-pyridyl atoms compared with phenanthroline ($\log K_1 = 4.77$).[42] A similar trend can be observed for the ditopic ligand L, and we note that intramolecular hydrogen bonds between N(3′) and N(1) would also contribute to increasing logK_{LH} and logK_{LH_2} (Scheme 1). If the third protonation were to take place at N(1), a large decrease in K_{LH_3} could be expected, due to both statistical effects and hydrogen bonding. The value of K_{LH_3} is about four orders of magnitude lower than K_{LH_2} and could therefore reflect these contributions and be satisfactorily compared with the constant relative to the second protonation of 1,10-phenanthroline-2,9-dicarboxylic acid ($\log K_2 = 9.04 \pm 0.14$).[41] Solubility problems below p[H] 5.89 prevented the determination of K_{LH_4}, K_{LH_5}, and K_{LH_6}. In fact, K_{LH_4} is related to K_{LH_3} in terms of symmetry (L adopting C_2 symmetry) and statistically should be smaller than the latter by approximately 0.6.[34] Much lower values of K_{LH_5} and K_{LH_6} are expected according to data available in the literature for picolinic ($\log K_2 \approx 1$)[43,44] and 1,10-phenanthroline-2,9-dicarboxylic acids ($\log K_3 = 2.37 \pm 0.21$[41]).[45] In 1.5 M $HClO_4$, slow and irreversible

 © 2004 Wiley-VCH Verlag GmbH & Co. KGaA, Weinheim

degradation of ligand L via a potential de-carboxylation reactions was observed by UV/Visible spectrophotometry (see Supporting Information, Figure S5).

Stoichiometry and Stability of Europium(III) Complexes with L

The use of electrospray mass spectrometry (ES-MS) to characterize the stoichiometry of metallic complexes in solution is well documented,[10,46] and has been employed by us for this purpose on previous occasions.[21,27−30,47−49] ES-MS measurements were carried out at two different $[Eu]_{tot}/[L]_{tot}$ ratios (Figure 3) and the corresponding spectra clearly indicate the formation of three europium(III) complexes, Eu_2L_3, Eu_2L_2, and EuL_2 (see Supporting Information, Table S1). The peaks of the triple-stranded Eu_2L_3 helicate dominate the spectra, even with an excess of Eu^{III}. The inner coordination spheres of the minor species Eu_2L_2 and EuL_2 are completed with water molecules. Since lanthanide cations possess large solvation energies,[47,48] the ES-MS responses[50] will be drastically decreased for the latter complexes compared with that of the Eu_2L_3 helicate. Loss of neutral CO_2 was also observed, as previously reported for amino acid- or peptide-metal complexes in positive[51,52] and in negative modes.[53]

To quantify the interaction between L and Eu^{III}, we titrated the ligand in water at p[H] 6.15±0.05 with europium(III) and monitored the changes occurring in solution using both absorption (Figure 4a, and Figure S6 in the Supporting Information) and gated luminescence spectroscopy (Figure 4b).

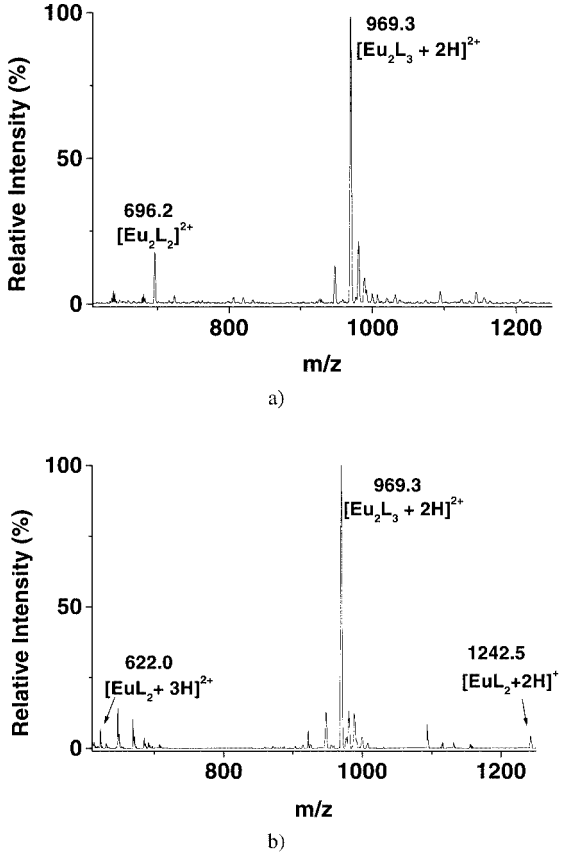

Figure 3. Electrospray mass spectra (a) $[Eu]_{tot} = 7.96 \times 10^{-4}$ M. $[L]_{tot} = 4.04 \times 10^{-4}$ M; (b) $[Eu]_{tot} = 2.05 \times 10^{-4}$ M. $[L]_{tot} = 7.96 \times 10^{-4}$ M. Solvent: CH_3OH / H_2O (80 / 20 by weight); positive mode; $V_c = 120$ V

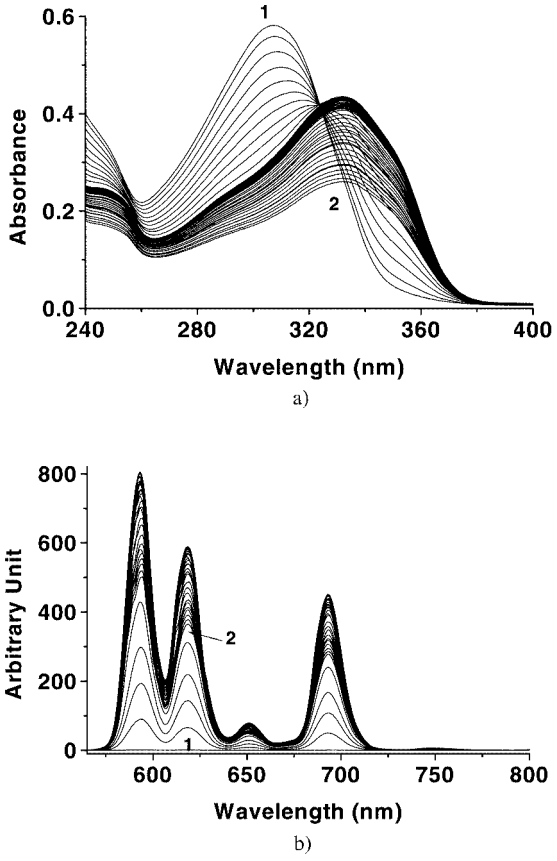

Figure 4. Spectrophotometric titrations of L versus Eu^{III} concentrations. (a) Absorption spectra: $l = 2$ cm. $[L]_{tot} = 8.22 \times 10^{-6}$ M; (1) $[Eu]_{tot}/[L]_{tot} = 0$; (2) $[Eu]_{tot}/[L]_{tot} = 23.36$. (b) Gated luminescence spectra; $\lambda_{exc} = 308$ nm; $t_d = 0.05$ ms; gate time = 1 ms; cycle time = 200 ms. $[L]_{tot} = 1.64 \times 10^{-6}$ M; (1) $[Eu]_{tot}/[L]_{tot} = 0$, (2) $[Eu]_{tot}/[L]_{tot} = 15.37$. Solvent: water; buffer MES (0.1 M); p[H] = 6.15±0.05; $T = 25.0 \pm 0.2$ °C

The formation of the helicate induces a significant red shift to 332 nm in the ligand π→π* transition band centered at 308 nm (Figure 4a). Moreover, L was reported to be a fair luminescence sensitizer for europium(III),[26] the absolute quantum yield of the metal-centered luminescence reaching 1.3% at p[H] ≈ 7.0 with a lifetime of 2.13(2) ms. Data were satisfactorily fitted to the simple model represented by Equation (2) and both experiments yielded very similar values (Table 3), in agreement with the previously

Table 3. Cumulative stability constants for the Eu_2L_3 helicate; solvent: water; $T = 25.0 \pm 0.2$ °C

Titration method	$\log\beta_{Eu_2L_3} \pm 3\sigma$[a]
UV/Vis absorption, direct	50.6 ± 2.0
Gated luminescence, direct	49.9 ± 1.3
^1H NMR, competition with DOTA	52.3 ± 2.3[26]

[a] The stability constants were calculated[89] from conditional values with the protonation constants given for L in Table 1.

 © 2004 Wiley-VCH Verlag GmbH & Co. KGaA, Weinheim

reported one obtained via ^{1}H NMR competitive titrations with various concentrations of DOTA (1,4,7,10-tetraazacyclodecane-*N*,*N*′,*N*′′,*N*′′′-tetraacetic acid) in D_2O.[26]

$$3\,L + 2\,Eu \underset{\longleftarrow}{\xrightarrow{\beta_{Eu_2L_3}}} Eu_2L_3 \quad (2)$$

Spectrophotometric (absorption and luminescence) and NMR spectroscopic data clearly demonstrate that the major species in aqueous solution at pH 6.15 and in a large range of $[Eu]_{tot}/[L]_{tot}$ ratios is the triple-stranded helicate Eu_2L_3. In addition to this main species ES-MS, which is by far a more sensitive method, indicated the presence of small amounts of Eu_2L_2 with an excess of Eu^{III}, and of EuL_2 with an excess of L. The triple stranded helicate is with no doubt a thermodynamic product and its structure in aqueous solution is the same as that determined by single-crystal X-ray diffraction.[26] Although the Eu_2L_2 species is not seen in the spectrophotometric titrations, 2:2 species have been observed with similar ligands.[21,22] In particular, $[Eu_2(L^B)_2]^{6+}$ (L^B: R^1 = C(O)NEt_2 and R^2 = CH_3, see Figure 1) adopts a box-like structure in the solid state, in which the ligand strands are arranged "side-by-side" and the two metal are ions connected via hydrogen bonds produced by four water molecules.[22] Therefore, the 2:2 species may also be considered to be a thermodynamic product. The presence of the terminal carboxylate functions of L could be expected to significantly reduce the electrostatic repulsions of the coordination sites in Eu_2L_2 and Eu_2L_3 by comparison with the corresponding complexes with L^A (R^1 = 1-(3,5-dimethoxybenzyl)-1*H*-benzimidazole and R^2 = CH_3, see Figure 1) and L^B and thus to increase the stability of the L-europium(III) complexes.[54]

Formation Kinetics in Excess of Ligand

Two series of experiments carried out with two different metal concentrations, $[Eu]_{tot} = 1.06 \times 10^{-6}$ M and 2.73×10^{-6} M, allowed us to observe two rate-limiting steps in the second and minute time spans, respectively (see Supporting Information, Figure S7). The corresponding spectrophotometric signals recorded at 350 nm undergo an increase in absorbance followed by a decrease. The variation of the two corresponding pseudo-first-order rate constants $k_{2,obs}$ and $k_{3,obs}$ (s^{-1}) versus $[L]_{tot}$ (see Supporting Information, Tables S2 and S3) is presented in Figure 5.

The variation of $k_{2,obs}$ is in good agreement with a fast pre-equilibrium for the formation of EuL, followed by a slower binding of L to EuL:

$$Eu + L \underset{\text{fast}}{\overset{K_{EuL}}{\rightleftharpoons}} EuL \quad (3)$$

$$EuL + L \underset{k_{-2}}{\overset{k_2}{\rightleftharpoons}} EuL_2 \quad (4)$$

The rate law corresponding to the equilibrium according to Equation (4) is expressed by the following Equation (5).

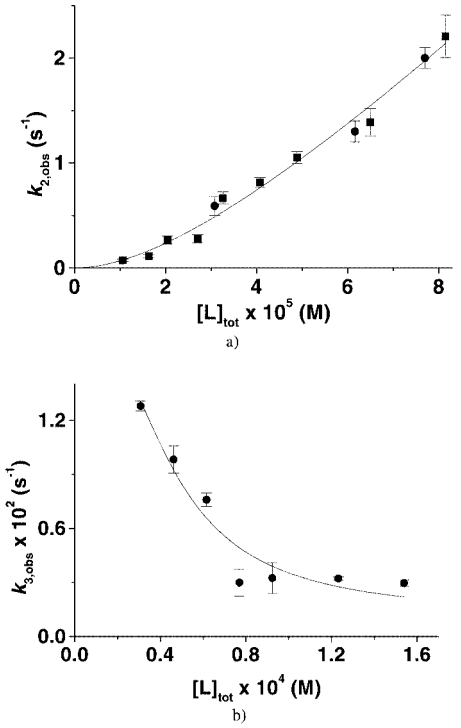

Figure 5. Variation of the pseudo-first order constants $k_{2,obs}$ (a) and $k_{3,obs}$ (b) for the formation of L-europium(III) complexes versus $[L]_{tot}$. Solvent: water; T = 25.0±0.2 °C; p[H] = 6.15±0.05 (MES buffer 0.1 M); ■ $[Eu]_{tot} = 1.06 \times 10^{-6}$ M; • $[Eu]_{tot} = 2.73 \times 10^{-6}$ M

$$d[EuL_2]/dt = k_2 \times [EuL] \times [L]_{tot} - k_{-2} \times [EuL_2] \quad (5)$$

and leads to Equation (6).[55]

$$k_{2,obs} = \frac{k_2 \times K_{EuL} \times [L]_{tot}^2}{1 + K_{EuL} \times [L]_{tot}} + k_{-2} \quad (6)$$

The rate constant k_2 and the stability constant K_{EuL} were determined by a non-linear least-squares method[56] (Table 4) but k_{-2} could not be obtained under our experimental conditions.

On the other hand, the variation of $k_{3,obs}$ versus $[L]_{tot}$ suggests the coordination of a second Eu^{III} cation to EuL_2:

$$EuL_2 + Eu \underset{k_{-3}}{\overset{k_3}{\rightleftharpoons}} Eu_2L_2 \quad (7)$$

The corresponding rate law can be written:

$$d[Eu_2L_2]/dt = k_3 \times [EuL_2] \times [Eu] - k_{-3} \times [Eu_2L_2] \quad (8)$$

Resolution of the differential Equation (8)[55] leads to the following reduced expression, under our experimental conditions:

$$k_{3,obs} = \frac{4 \times k_3 \times \beta_{EuL_2} \times [L]_{tot}^2 \times [Eu]_{tot}}{(1 + K_{EuL} \times [L]_{tot} + \beta_{EuL_2} \times [L]_{tot}^2)^2} + k_{-3} \quad (9)$$

 © 2004 Wiley-VCH Verlag GmbH & Co. KGaA, Weinheim

Table 4. Formation mechanism of Eu_2L_3 with an excess of L; solvent: water; T = 25.0 ± 0.2 °C; p[H] = 6.15±0.05 (MES buffer 0.1 M); the errors are given as standard errors[56]

Steps			Experimental values	Calculated values
Eu + L	$\overset{K_{EuL}}{\rightleftharpoons}$	EuL	$K_{EuL} = (1.9 \pm 0.8) \times 10^4$ M^{-1}	
EuL + L	$\overset{k_2}{\underset{k_{-2}}{\rightleftharpoons}}$	EuL_2	$k_2 = (4.4 \pm 0.9) \times 10^4$ M^{-1}s^{-1} $\beta_{EuL2} = (2.0 \pm 0.7) \times 10^9$ M^{-2}	$k_{-2} = \frac{k_2 \times K_{EuL}}{\beta_{EuL_2}} = 0.4 \pm 0.3$ s^{-1}
EuL_2 + Eu	$\overset{k_3}{\underset{k_{-3}}{\rightleftharpoons}}$	Eu_2L_2	$k_3 = (7.0 \pm 0.6) \times 10^3$ M^{-1}s^{-1} $k_{-3} = (1.1 \pm 0.8) \times 10^{-3}$ s^{-1}	$K_{Eu2L2} = \frac{k_3}{k_{-3}} = (6.4 \pm 4.7) \times 10^6$ M^{-1} $\beta_{Eu2L2} = \beta_{EuL2} \times K_{Eu2L2} = (1.3 \pm 1.0) \times 10^{16}$ M^{-3}
Eu_2L_2 + L	$\overset{k_4}{\underset{k_{-4}}{\rightleftharpoons}}$	Eu_2L_3	not determined	

The corresponding rate constants k_3, k_{-3} are given in Table 4.

The absorbance at 350 nm at the end of the third step (Figure S7 in the Supporting Information) is in good agreement, within experimental error, with the sum of the absorption of the excess of free ligand and of the bimetallic triple-stranded helicate ($[Eu_2L_3]_\infty$ = 1/2$[Eu]_{tot}$). This result constitutes a good indication that the last step is faster than the formation of the Eu_2L_2 precursor and that the final step in the formation of Eu_2L_3 involves the addition of a third ligand to Eu_2L_2, in a "braiding" mechanism, as opposed to a "keystone" mechanism in which the second metal ion is added to a pre-organized EuL_3 complex.[57]

Formation Kinetics with an Excess of Europium(III)

Kinetic measurements were carried out under pseudo-first order conditions. Two exponential signals were recorded at 332 nm in the second time range using a stopped-flow technique, whereas an exponential signal was measured in the hour time range on a classical spectrophotometer (Figure 6).

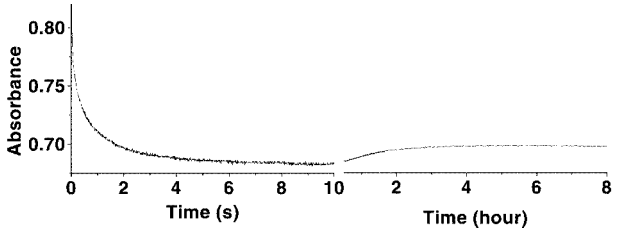

Figure 6. Variation of the absorbance at 332 nm versus time. Solvent: water; T = 25.0±0.2 °C; p[H] = 6.15±0.05 (MES buffer 0.1 M); l = 1 cm. $[L]_{tot} = 2.55 \times 10^{-5}$ M, $[Eu]_{tot} = 1.80 \times 10^{-3}$ M

Three corresponding pseudo-first-order rate constants $k'_{2,obs}$, $k'_{3,obs}$, and $k'_{4,obs}$ (s^{-1}) extracted from these data are reported in Table 5 (see also Figure S8 in the Supporting Information).

Table 5. Variation of $k'_{2,obs}$, $k'_{3,obs}$, and $k'_{4,obs}$ for the formation of L-europium(III) complexes versus $[Eu]_{tot}$; solvent: water; T = 25.0±0.2 °C; p[H] = 6.15±0.05 (MES buffer 0.1 M); $[L]_{tot} = 2.55 \times 10^{-5}$ M; reported errors are ±3σ

$[Eu]_{tot} \times 10^4$ [M]	$k'_{2,obs}$ [s^{-1}]	$k'_{3,obs}$ [s^{-1}]	$k'_{4,obs} \times 10^4$ [s^{-1}]
2.57	12.9±2.2	0.99±0.01	5.3±0.6
5.15	15.9±2.5	1.07±0.03	2.5±0.3
7.70	16.1±1.2	1.07±0.04	2.7±0.3
10.30	15.1±2.5	1.08±0.04	8.2±0.9
12.80	16.5±3.6	0.98±0.02	6.2±0.9
15.40	16.8±3.7	0.96±0.02	1.4±0.3
18.00	16.2±2.4	0.86±0.02	2.4±0.6

The pseudo-first-order rate constant $k'_{2,obs}$ increased slightly, but significantly as $[Eu]_{tot}$ was increased. A large increase of the spectrophotometric absorption occurred during the dead-time (≈ 3 ms) of the stopped-flow device and could be attributed to the initial and fast formation of EuL [Equation (3)]. The following equilibria are in satisfactory agreement with these experimental data:

$$EuL + Eu \underset{k'_{-2}}{\overset{k'_2}{\rightleftharpoons}} Eu_2L \quad (10)$$

The rate law corresponding to equilibrium (10) is expressed by:

$$d[Eu_2L]/dt = k'_2 \times [EuL] \times [Eu]_{tot} - k'_{-2} \times [Eu_2L] \quad (11)$$

and leads to Equation (12):[55]

$$k'_{2,obs} = \frac{k'_2 \times K_{EuL} \times [Eu]^2_{tot}}{1 + K_{EuL} \times [Eu]_{tot}} + k'_{-2} \quad (12)$$

 © 2004 Wiley-VCH Verlag GmbH & Co. KGaA, Weinheim

Table 6. Formation mechanism of the Eu_2L_3 helicate with an excess of Eu^{III}; solvent: water; $T = 25.0 \pm 0.2$ °C; p[H] = 6.15±0.05 (MES buffer 0.1 M); the errors are given as standard errors[56]

Steps		Experimental values	Calculated values	
$Eu + L \underset{k_{-1}}{\overset{k_1}{\rightleftharpoons}} EuL$		$K_{EuL} = (1.9 \pm 0.5) \times 10^4\ M^{-1}$		
$EuL + Eu \underset{k'_{-2}}{\overset{k'_2}{\rightleftharpoons}} Eu_2L$		$k'_2 = (1.7 \pm 0.8) \times 10^3\ M^{-1}\ s^{-1}$ $k'_{-2} = 13.8 \pm 0.9\ s^{-1}$	$K_{Eu2L} = \frac{k'_2}{k'_{-2}}$	$= (1.2 \pm 0.6) \times 10^2\ M$ $\beta_{Eu2L} = K_{Eu2L} \times K_{EuL}$ $= (2.3 \pm 1.3) \times 10^6\ M^{-2}$
$Eu_2L + L \underset{k'_{-3}}{\overset{k'_3}{\rightleftharpoons}} Eu_2L_2$		$k'_3 = (2.2 \pm 0.3) \times 10^6\ M^{-1}\ s^{-1}$	$k'_{-3} = \frac{k'_3 \times \beta_{Eu_2L}}{\beta_{Eu_2L_2}}$	$= (3.9 \pm 3.8) \times 10^{-4}\ s^{-1}$
$Eu_2L_2 + L \underset{k'_{-4}}{\overset{k'_4}{\rightleftharpoons}} Eu_2L_3$		$k'_4 = (4 \pm 1) \times 10^{-4}\ s^{-1}$	$k'_4 = \frac{k_{-4} \times \beta_{Eu_2L_3}}{\beta_{Eu_2L_2}}$	$= (6.1 \pm 4.9) \times 10^7\ M^{-1}\ s^{-1}$

If we consider that under our experimental conditions $K_{EuL} \times [Eu]_{tot} >> 1$:

$$k'_{2,obs} = k'_2 \times [Eu]_{tot} + k'_{-2} \tag{13}$$

The values of the rate constants k'_2 and k'_{-2} were calculated by a least-squares method[56] and are reported in Table 6.

When $[Eu]_{tot}$ is increased, $k'_{3,obs}$ is decreases (Table 5 and Figure S8b in the Supporting Information), which suggests that the coordination of a second ligand strand to Eu_2L takes place and leads to the bimetallic double-stranded species Eu_2L_2:

$$Eu_2L + L \underset{k'_{-3}}{\overset{k'_3}{\rightleftharpoons}} Eu_2L_2 \tag{14}$$

The rate law is then expressed by:

$$d[Eu_2L_2]/dt = k'_3 \times [Eu_2L] \times [L] - k'_{-3} \times [Eu_2L_2] \tag{15}$$

If we assume that equilibrium is reached at the end of the previous steps, we can use the corresponding stability constants to solve the mass balance equation and evaluate [L]:

$$[L] = \frac{[L]_{tot} - 2 \times [Eu_2L_2]}{1 + K_{EuL} \times [Eu]_{tot} + \beta_{Eu_2L} \times [Eu]^2_{tot}} \tag{16}$$

The new expression of the rate law becomes:

$$\frac{d[Eu_2L_2]}{dt} = \frac{k'_3 \times \beta_{Eu_2L} \times [Eu]^2_{tot} \times ([L]_{tot} - 2[Eu_2L_2])^2}{(1 + K_{EuL} \times [Eu]_{tot} + \beta_{Eu_2L} \times [Eu]^2_{tot})^2} - k'_{-3} \times [Eu_2L_2] \tag{17}$$

The resolution of this differential equation,[55] taking our experimental conditions into account, gives the reduced equation:

$$k'_{3,obs} = \frac{4 \times k'_3 \times \beta_{Eu_2L} \times [L]_{tot} \times [Eu]^2_{tot}}{(1 + K_{EuL} \times [Eu]_{tot} + \beta_{Eu_2L} \times [Eu]^2_{tot})^2} + k'_{-3} \tag{18}$$

Statistical processing[56] of the kinetic data allows estimation of k'_3, K_{EuL} and β_{Eu_2L} (Table 6), but not of k'_{-3}. It is noteworthy that the absorbance at the end of this step (Figure 6) corresponds to the absorption at 332 nm of the bimetallic triple-stranded helicate Eu_2L_3 (see Supporting Information, Figure S6). This is a sound indication that the formation of Eu_2L_2 is followed by the fast addition of a third ligand strand leading to the final thermodynamically stable helicate Eu_2L_3:

$$Eu_2L_2 + L \xrightarrow[\text{fast}]{k'_4} Eu_2L_3 \tag{19}$$

A decrease of more than four orders of magnitude was observed for $k'_{4,obs}$ compared with $k'_{3,obs}$ (Table 5), but $k'_{4,obs}$ did not vary significantly with $[Eu]_{tot}$ (see Supporting Information, Figure S8c). These data strongly suggest a slow release of L from Eu_2L_3 which was rapidly formed in the previous step:

$$Eu_2L_3 \xrightarrow{k'_{-4}} Eu_2L_2 + L \tag{20}$$

The corresponding rate law can now be expressed by the following relationship:

$$-d[Eu_2L_3]/dt = k'_{-4} \times [Eu_2L_3] \tag{21}$$

with:

$$k'_{4,obs} = k'_{-4} \tag{22}$$

We will now discuss the overall self-assembly mechanism of the bimetallic triple-stranded helicate Eu_2L_3 presented in

 © 2004 Wiley-VCH Verlag GmbH & Co. KGaA, Weinheim

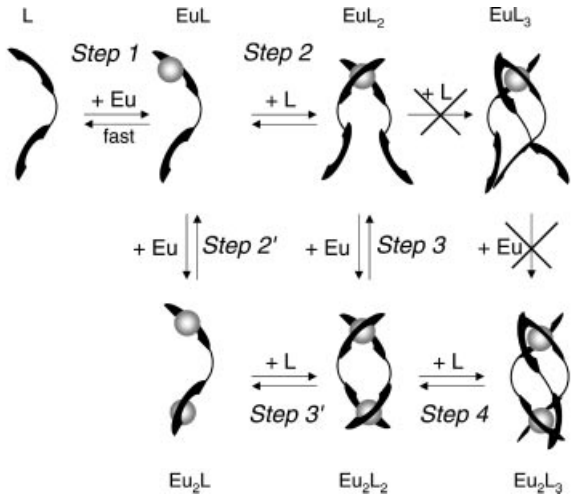

Figure 7. Schematic representation of the self-assembly mechanism of Eu_2L_3

Figure 7. The initial and final steps are independent of the stoichiometric ratio $[Eu]_{tot}/[L]_{tot}$. In contrast, the intermediate steps depend on whether the kinetics were measured in the presence of an excess of ligand or metal.

Since the water exchange rates of Ln^{III} ions are large,[58] slow complex formation is related to the ligand properties.[59–61] The ditopic molecule L was designed for the fine-tuning of the Ln^{III} coordination sphere, with a short methylenic spacer to prevent self-folding. At p[H] = 6.15, LH_2, the major species, possesses one proton on each imidazolyl group. If they are stabilized by hydrogen bonds as shown in Scheme 1, the tridentate subunits of L adopt a *cisoid* conformation (Scheme 1) which is preferable to a coordination of Eu^{III} limited by the exchange rate of the first water molecule on the lanthanide cation.[58,62] Using the water exchange rate constant k_{ex} determined by ^{17}O NMR spectroscopy for Eu^{III} (5×10^8 s^{-1}),[58,62] we calculated an outer-sphere stability constant[63,64] $K_{os} = 0.16$ M^{-1} for a triple charged cation/neutral ligand system. Under these conditions, the formation rate constant for EuL can be estimated[65] as $k_1 = K_{os} \times k_{ex} = 8 \times 10^7$ $M^{-1} \times s^{-1}$. This value is similar to the literature data reported for the formation of anthranilate-Eu^{III} (1.05×10^8 $M^{-1} \times s^{-1}$),[66,67] picolinate-La^{III} (4.9×10^8 $M^{-1} \times s^{-1}$) or picolinate-Dy^{III} (1.5×10^8 $M^{-1} \times s^{-1}$)[68,69] complexes at various temperatures and ionic strengths in water. The formation mechanism of EuL is at odds with the one determined for the EuL^A analogue, for which conformational changes lead to a slower binding rate constant and to an increased inertness.[30] The stability constant $K_{EuL} = (1.8 \pm 0.9) \times 10^4$ M^{-1}, calculated from the variation of the initial absorbance A_0 versus $[Eu]_{tot}$ in the experiments with an excess of metal (Figure 6 and Figure S9 in the Supporting Information), is in excellent agreement with the values given in Tables 4 and 6. Comparing this constant with the one obtained for the complex with the bidentate picolinate ligand ($K_1 = 1.06 \times 10^4$ M^{-1})[70] gives a good indication of a partial binding to Eu^{III} by one of the tridentate subunits in L. The dissociation rate constant $k_{-1} = k_1/K_{EuL}$ can then be estimated to be ca. 4×10^3 s^{-1}. EuL is indeed a labile species as was observed, for instance, for the anthranilate-Eu^{III} complex (3.3×10^4 s^{-1}).[66,67] Step 1 can therefore be considered as being a fast pre-equilibrium in the formation process of the target Eu_2L_3.

With an excess of L, Step 2 implies the binding of a second ligand strand to EuL, leading to the more stable complex EuL_2. The bimolecular rate constant k_2 (Table 4) is about four orders of magnitude lower than k_1. The electrostatic repulsions between the terminal carboxylate groups of the ligands probably induce conformational rearrangements which drastically slow down the coordination of L to EuL. The strong negative interactions between the ligands will prevent even more efficiently the formation of EuL_3. The addition of a second Eu^{III} cation to EuL_2 proceeds in Step 3 and leads to a very inert complex Eu_2L_2 for which either the release of a ligand ($k_{-3} \approx 10^{-3}$ s^{-1}) or of a cation ($k'_{-3} \approx 10^{-4}$ s^{-1}) is dramatically slow. Since Eu_2L_2 is a minor species, detected by ES-MS but neither by spectrophotometry nor by ^1H NMR, its stability constant could only be calculated from the rate constants (Table 4).

With an excess of Eu^{III}, the binding of a second cation (Step 2′) leads to the formation of Eu_2L. Assuming a dissociative Eigen–Wilkins[65] mechanism and using the Fuoss equation,[63] a formation rate constant equal to 5×10^3 $M^{-1} \times s^{-1}$ can be calculated, in excellent agreement with the measured rate constant k'_2 (Table 6). Therefore, the binding of a second Eu^{III} cation does not involve any structural rearrangement, but is mainly governed by the de-solvation of the entering cation and by intramolecular electrostatic repulsions. The latter induce a sizeable negative cooperative effect[27,34] as demonstrated by the ratio $K_{Eu_2L}/K_{EuL} \approx 10^{-2}-10^{-3}$. Step 3′ is related to the formation of a double-stranded bimetallic "pre-helicate" from Eu_2L. The approach of a second ligand is favored because coordination of the first ligand strand labilises the solvation sphere of the two cations and reduces the charge on the two binding sites. The estimation, via $\beta_{Eu_2L_2}$ (Tables 4 and 6), of k'_{-3} ($\approx 10^{-4}$ s^{-1}) provides information on the inertness of Eu_2L_2. A "side-by-side" arrangement, as already reported in the solid state for a closely related ligand[22] with two europium(III) cations, cannot explain an inert edifice in which the interactions between the two lanthanide ions are drastically reduced, perhaps by a "braided" structure (Figure S10, see Supporting Information).

Step 4 corresponds to the fast wrapping of the third strand around Eu_2L_2. The kinetic behavior in Step 4 is dominated by the slow solvolysis of the bimetallic triple-stranded helicate. The rate constant k_{-4} listed in Table 6 is within the range of data reported for the dissociation of various Ln^{III}-polyaminocarboxylate complexes (10^{-6} $s^{-1} < k < 10^{-3}$ s^{-1}).[71] This could also be in line with the X-ray structure of Eu_2L_3, in which two slightly different types of molecules were found, showing that an increase in the solvation of the carboxylates induces a lengthening of Eu^{III}–O distances.[26] It is noteworthy that the self-assembly mechanism of Eu_2L_3 does not exhibit any slow rearrangement from a precursor species, as previously reported by us for

 © 2004 Wiley-VCH Verlag GmbH & Co. KGaA, Weinheim

a tri-cuprous double-stranded helicate.[29] The situation is summarized in Figure 8 which displays the calculated time-dependences of the concentrations of the various Eu^{III}-containing species formed during the self-assembly process for a stoichiometric $[Eu]_{tot}/[L]_{tot}$ ratio of 0.67. The formation of the unique species Eu_2L_3 clearly occurs via the "braiding" of two ligand stands around the first Eu^{III} cation followed by the "keystone" addition of a second Eu^{III} ion and a fast wrapping of the third ligand around Eu_2L_2, the latter never being significantly accumulated.

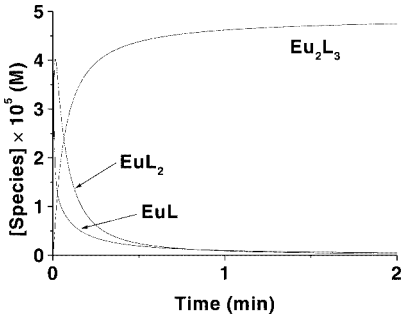

Figure 8. Calculated time dependence of the concentrations of the Eu^{III} complexes formed using the rate constants given in Tables 4 and 6.[31] Solvent: water; $T = 25.0 \pm 0.2$ °C; p[H] = 6.15±0.05 (MES buffer 0.1 M). $[L]_{tot} = 1.5 \times 10^{-4}$ M; $[Eu]_{tot}/[L]_{tot} = 0.67$

Conclusion

A fruitful combination of potentiometry, absorption and emission spectrophotometry, ^1H and ^{13}C NMR spectroscopy, and electrospray mass spectrometry allowed us to fully characterize the formation mechanism of a europium-containing triple-stranded Eu_2L_3 helicate with a hexadentate ditopic ligand. The self-assembly process implies a key bimetallic double-stranded species Eu_2L_2. This species is very inert towards the release of either a ligand or a cation, but reacts very rapidly with an additional ligand strand to yield the final triple-stranded helicate. This kinetic behavior points to the Eu_2L_2 intermediate probably adopting a structure different from the "side-by-side" arrangement observed for $Eu_2(L^B)_2$ in the solid state.[22] Indeed the formation of a 2:2 helical structure at this stage will decrease the steric hindrance and, moreover, the presence of negatively charged terminal carboxylate groups obviously contributes to prevent the formation a labile "side-by-side"[30,57] species. This is in contrast to the formation mechanism of $Eu_2(L^A)_3$ for which we propose the formation of a labile intermediate $Eu_2(L^A)_2$.[30] As far as we can tell, the increased inertness of the key intermediate is the main reason why the rate constant of the last step in the self-assembly process of Eu_2L_3 is 10^5 times larger than $Eu_2(L^A)_3$. Moreover, the addition of the successive ligand strands leads to a strong diminishing of the electrostatic interactions between the two coordination sites. These two features, which are reflected by the very low equilibrium concentrations of the intermediates, are probably of importance to "cooperatively" drive a fast and efficient self-assembly of the target triple-stranded di-europium(III) helicate.

In conclusion, the hexadentate ditopic ligand L leads to one of the most efficient cation/ligand systems for the self-assembly of a bimetallic triple-stranded helicate in water. This is mainly due to the simultaneous presence of a short spacer and of the one negative charge borne by each extremity.

Experimental Section

Starting Materials and Solvents: L was synthesized according to a previously published procedure.[26] $Eu(ClO_4)_3{\cdot}nH_2O$ was prepared from the oxide (Rhône−Poulenc, 99.99%) in the usual way.[72]

CAUTION! *Perchlorate salts combined with organic ligands are potentially explosive and should be handled in small quantities and with adequate precautions.*[73]

Distilled water was further purified by passing through a mixed bed of ion-exchanger (Bioblock Scientific R3-83002, M3-83006) and activated carbon (Bioblock Scientific ORC-83005). Spectrophotometric grade methanol (Merck, p.a.) and water were de-oxygenated using CO_2- and O_2-free argon (Sigma Oxiclear cartridge). All stock solutions were prepared using an AG 245 Mettler Toledo analytical balance (precision 0.01 mg).

Electrospray Mass Spectrometric Measurements: ES mass spectra were recorded on an HP 1100 mass spectrometer (Agilent Technologies, Palo Alto, CA, USA, formerly Hewlett−Packard Company Analytical Products Group). ES-MS was conducted in the positive ion mode. Scanning was performed from $m/z = 200$ to 1500 and the sampling cone voltage (V_c) was set at 120 V. For electrospray ionization, the drying gas was heated at 250 °C and its flow set at 3 L/min, the nebuliser pressure was 10 p.s.i. and the capillary voltage 4 kV. Solutions containing ligand L (7.96×10^{-4}, 4.04×10^{-4}, 2.02×10^{-5} M) and various equivalents of Eu^{III} were prepared in CH_3OH/H_2O (80:20 by weight). They were injected into the mass spectrometer source with a syringe pump (Harvard type PHD 2000, Harvard Apparatus Inc., South Natick, MA, USA) at a flow rate of 2 μL/min.

Potentiometric Titrations: The potentiometric titration of L ($1.036 \cdot 10^{-3}$ M) was performed using an automatic titrator system DMS 716 Titrino (Metrohm) with a combined glass electrode (Metrohm 6.0234.500, Long Life) filled with 0.1 M aqueous NaCl and connected to a microcomputer. The ionic strength was fixed at $I =$ 0.1 M with tetraethylammonium perchlorate (Fluka, puriss.). The combined glass electrode was calibrated as a hydrogen concentration probe by titrating known amounts of $HClO_4$ (9.997×10^{-2} M) with CO_2-free NMe_4OH solutions (1.040×10^{-1} M).[74] The cell was thermostatted at 25.0±0.2 °C by the flow of a Haake FJ thermostat. A stream of argon, pre-saturated with water vapour was passed over the surface of the solution. The potentiometric data (about 160 points collected over the pH range 5.9−11.0) were refined with the Hyperquad 2000[75] program which uses non-linear least-squares methods.[76] Potentiometric data points were weighted by a formula allowing greater pH errors in the region of an end-point than elsewhere. The weighting factor W_i is defined as the reciprocal of the estimated variance of measurements: $W_i = 1/\sigma_i^2 = 1/[\sigma_E^2 + (\delta E/\delta V)^2\sigma_V^2]$ where σ_E^2 and σ_V^2 are the estimated variances of the potential and volume readings, respectively. The con-

 © 2004 Wiley-VCH Verlag GmbH & Co. KGaA, Weinheim

stants were refined by minimizing the error-square sum, U, of the potentials shown below:

$$U = \sum_{i}^{N} W_i (E_{obs,i} - E_{cal,i})^2$$

Three titrations were treated either as single sets or as separated entities, for each system, without significant variation in the values of the determined constants. The quality of fit was judged by the values of the sample standard deviation, S, and the goodness of fit, χ^2, (Pearson's test). At σ_E = 0.1 mV (0.0023 σ_{pH}) and σ_V = 0.005 mL, the values of S in different sets of titrations were between 0.9 and 1.1, and χ^2 was below 12.6. The scatter of residuals versus pH was reasonably random, without any significant systematic trends, thus indicating a good fit of the experimental data. The successive protonation constants were calculated from the cumulative constants determined with the program. The uncertainties in the log K values correspond to the added standard deviations in the cumulative constants. The distribution curves of the protonated species of L as a function of pH (Figure S2, see Supporting Information) were calculated using the Haltafall program.[77]

Potentiometric and UV/Visible Titrations: A stock solution of L (8.91×10^{-5} M) was prepared by quantitative dissolution of a solid sample in deionised water and the ionic strength was adjusted to 0.1 M with NEt_4ClO_4 (Fluka, puriss). 100 mL of this solution were introduced into a jacketed cell (Metrohm) maintained at 25.0±0.2 °C (Haake FJ thermostat). The free hydrogen ion concentration was measured with a combined glass electrode (Metrohm 6.0234.500, Long Life) and a Tacussel Isis 20,000 millivoltmeter. The Ag/AgCl reference electrode was filled with NaCl (0.01 M, Fluka, p.a.) and $NaClO_4$ (0.09 M, Fluka, p.a). Standardization of the millivoltmeter and verification of the linearity (3.00 < p[H] < 9.00) of the electrode were performed using commercial buffers (Merck, Titrisol) according to classical methods.[78] The initial p[H] was adjusted to 11.59 with NMe_4OH (Merck, 10 wt.% solution in water), and the titration of the free ligand (7.38 < p[H] < 11.59) was then carried out by addition of known volumes of 1.69×10^{-2} M perchloric acid (Prolabo, normapur, 70% min) with an Eppendorf microburette. $HClO_4$ solution (Prolabo, normapur, 70% min) was titrated with NaOH (10^{-1} M, Carlo Erba, Titrisol Normex) using phenolphthalein (Prolabo, purum) as an indicator and prepared just before use. An aliquot (1 mL) was taken after each addition of acid, and simultaneous p[H] and UV/Visible spectra (230−400 nm) were recorded. Spectrophotometric measurements were made using Hellma quartz optical cells (0.2 cm) on a Kontron Uvikon 941 spectrophotometer maintained at 25.0±0.2 °C (Haake NB 22 thermostat).

UV/Visible Titrations: To probe the coordination properties of L with Eu^{III}, a solution of ligand L (8.22×10^{-6} M) at p[H] = 6.15±0.05 [0.1 M, 2-morpholinoethanesulfonic acid (MES), Fluka, microselect, 99.5%] was prepared. Europium(III) solutions were prepared immediately before use from deionised water saturated with argon. The solutions were acidified to p[H] < 4 with H_2SO_4 (Carlo Erba Reagenti, 96%) before complexometric titration to avoid hydroxide precipitation. Standardized Na_2H_2EDTA solution (Titriplex® III, Merck) in ammonium acetate (Prolabo, rectapur) buffered medium was used with xylene orange as an indicator.[79] The spectrophotometric titration of L with Eu^{III} was carried out in a Hellma quartz optical cell (2 cm). Microvolumes of a concentrated buffered (0.1 M MES, p[H] = 6.15±0.05) solution of europium(III) (4.24×10^{-4} M) were added to 4 mL of the stock ligand solution (the $[Eu]_{tot}/[L]_{tot}$ ratio varied from 0 to 23.36). Special care was taken to ensure that complete equilibration was attained. The corresponding UV/Visible spectra were recorded from 230 nm to 500 nm on a Kontron Uvikon 941 spectrophotometer maintained at 25.0±0.2 °C by the flow of a Haake NB 22 thermostat.

Potentiometric and Fluorescence Titrations: A stock solution of L (3.56×10^{-6} M, I = 0.1 M NEt_4ClO_4, Fluka, puriss) was prepared by quantitative dissolution of a solid sample and 100 mL were introduced into a jacketed cell (Metrohm) maintained at 25.0±0.2 °C by the flow of a Haake FJ thermostat. The initial p[H] was adjusted to 11.43 with NMe_4OH (Merck, 10 wt.% solution in water), and the titration of L (7.59 < p[H] < 11.43) was carried out by addition of known volumes of 1.69×10^{-2} M perchloric acid (Prolabo, normapur, 70% min) with an Eppendorf microburette. An aliquot (2 mL) was taken after each addition of acid, and simultaneous p[H] and fluorescence emission spectra were recorded (350−550 nm) with Hellma quartz optical cells (1 cm) on a Perkin−Elmer LS-50B instrument maintained at 25.0±0.2 °C by the flow of a Haake FJ thermostat. The excitation wavelength was 308±1 nm and the slit width was set at 4 nm for both excitation and emission. The source was a pulsed xenon flash lamp with a pulse width at half peak height < 10 μs and power equivalent to 20 kW.

Luminescence Titrations: Luminescence titrations were carried out on solutions with an absorbance less than 0.1 at wavelengths $\geq \lambda_{exc}$ in order to avoid any errors due to the inner filter effect. The p[H] was maintained at 6.15±0.05 by the use of 0.1 M MES (Fluka, microselect, 99.5%) and perchloric acid (Prolabo, normapur, 70% min). The titration of L (1.64×10^{-6} M) was carried out in a 1 cm Hellma quartz optical cell by addition of known microvolumes of a buffered solution of Eu^{III} (6.55×10^{-5} M) with an Eppendorf multipette® plus microburette. The $[Eu]_{tot}/[L]_{tot}$ ratio was varied from 0 to 15.37. Metal-centered luminescence spectra were recorded from 550 nm to 800 nm on a Perkin−Elmer LS-50B instrument at 25.0±0.2 °C. Gated spectra were obtained using phosphorimeter acquisition, with a delay time of 0.05 ms, a 200 ms sample window, 1 ms per flash and 1 flash per point. The slit width was 12.5 nm for both excitation and emission.

Analysis and Processing of the Spectroscopic Data: The spectrophotometric data were analyzed with both the Letagrop−Spefo[80−82] and Specfit[31] programs which adjust the absorptivities and the stability constants of the species formed at equilibrium. The Letagrop-Spefo program uses the Newton−Raphson algorithm to solve mass balance equations and a pit-mapping method to minimize the errors and determine the best parameter values. Specfit uses factor analysis to reduce the absorbance matrix and to extract the eigenvalues prior to the multiwavelength fit of the reduced data set according to the Marquardt algorithm.[83,84]

Kinetics of Formation: All kinetic measurements were performed in water at p[H] = 6.15±0.05 (0.1 M MES buffer) using a stopped-flow spectrophotometer (Applied Photophysic SX-18MV) equipped with a diode array device. The reactants were thermostatted at 25.0±0.2 °C (Lauda M12 thermostat) and mixed in a 1 cm optical cell. The data sets, averaged out of at least three replications, were recorded and analyzed with the commercial software Biokine.[85] This program fits up to three exponential functions to the experimental curves with the Simplex algorithm[86] after initialization with the Padé−Laplace method.[87]

The reaction of L with Eu^{III} in excess was followed at 332 nm. Ligand L concentration was equal to 2.55×10^{-5} M and Eu^{III} concentrations were varied from 2.57×10^{-4} M to 2.57×10^{-3} M. The reaction of Eu^{III} with ligand L in excess was followed at 350 nm.

 © 2004 Wiley-VCH Verlag GmbH & Co. KGaA, Weinheim

Two sets of experiments were carried out. Eu^{III} concentration was equal to 1.06×10^{-6} M or, 2.73×10^{-6} M and L concentrations were varied from 1.06×10^{-5} M to 8.15×10^{-5} M or from 3.08×10^{-5} M to 1.54×10^{-4} M.

Acknowledgments

This work was supported by the Centre National de la Recherche Scientifique (CNRS, UMR 7509), by the faculty of Chemistry (Université Louis Pasteur, Strasbourg, France) and the Swiss National Science Foundation. J. Hamacek thanks the European Community for granting him a Marie Curie fellowship. The authors thank Dr. S. Blanc (Université de Pau et des pays de l'Adour, Laboratoire de Chimie Structurale, Pau, France) for stimulating and helpful discussions, Dr A.-S. Chauvin for her help in acquiring the ^{13}C NMR spectroscopic data and Mr. R. Hueber for his skilful assistance in the ES-MS measurements.

[1] J. E. Vaener (Ed.), *Self-Assembly Architecture*; A. R. Liss, New York, **1988**.

[2] [2a] J. M. Lehn, *Supramolecular Chemistry: Concepts and Perspectives*, VCH, Weinheim, **1995**, chapter 9. [2b] D. Philp, J. F. Stoddart, *Angew. Chem. Int. Ed. Engl.* **1996**, *35*, 1155−1196; *Angew. Chem.* **1996**, *108*, 1242−1286. [2c] P. N. W. Baxter, *Comprehensive Supramolecular Chemistry*, Pergamon, Oxford, **1996**, chapter 6. [2d] M. Fujita, *Comprehensive Supramolecular Chemistry*, Pergamon, Oxford, **1996**, chapter 7. [2e] F. Vögtle, *Supramolecular Chemistry*, John Wiley & Sons, Chichester, **1991**. [2f]G. M. Whitesides, J. P. Mathias, C. T. Seto, *Science* **1991**, *254*, 1312−1319.

[3] [3a] V. G. Machado, P. N. W. Baxter, J. M. Lehn, *J. Braz. Chem. Soc.* **2001**, *12*, 431−462. [3b] J. M. Lehn, *Proc. Natl. Acad. Sci. USA* **2002**, *99*, 4763−4768.

[4] [4a] K. Wärnmark, P. N. W. Baxter, J. M. Lehn, *Chem. Commun.* **1998**, 993−994. [4b] F. Barigelletti, L. Flamigni, G. Calogero, L. Hammarström, J. P. Sauvage, J. P. Collin, *Chem. Commun.* **1998**, 2333−2334.

[5] [5a] I. Weissbuch, P. N. W. Baxter, S. Cohen, H. Cohen, K. Kjaer, P. B. Howes, J. Als-Nielsen, G. S. Hanan, U. S. Schubert, J. M. Lehn, L. Leiserowitz, M. Lahav, *J. Am. Chem. Soc.* **1998**, *120*, 4850−4860. [5b] A. M. Garcia, F. J. Romero-Salguero, D. M. Bassani, J. M. Lehn, G. Baum, D. Fenske, *Chem. Eur. J.* **1999**, *5*, 1803−1808. [5c] P. N. W. Baxter, J. M. Lehn, J. Fischer, M. T. Youinou, *Angew. Chem. Int. Ed. Engl.* **1994**, *33*, 2284−2287; *Angew. Chem.* **1994**, *106*, 2432−2434.

[6] [6a] K. N. Power, T. L. Hennigar, M. J. Zaworotko, *Chem. Commun.* **1998**, 595−596. [6b] M. Fujita, S. Y. Yu, T. Kusukawa, H. Funaki, K. Ogura, K. Yamaguchi, *Angew. Chem. Int. Ed.* **1998**, *37*, 2082−2085; *Angew. Chem.* **1998**, *110*, 2192−2196.

[7] [7a] A. El-ghayouy, A. Harriman, A. De Cian, J. Fischer, R. Ziessel, *J. Am. Chem. Soc.* **1998**, *120*, 9973−9974. [7b] G. Rapenne, B. T. Patterson, J. P. Sauvage, F. R. Keene, *Chem. Commun.* **1999**, 1853−1854. [7c] G. Baum, E. C. Constable, D. Fenske, C. E. Housecroft, T. Kulke, *Chem. Eur. J.* **1999**, *5*, 1862−1873. [7d] J. M. Lehn, A. Rigault, *Angew. Chem. Int. Ed. Engl.* **1988**, *27*, 1095−1097; *Angew. Chem.* **1988**, *100*, 1121−1122. [7e] M. Yamamoto, M. Takeuchi, S. Shinkai, F. Tani, Y. Naruta, *J. Chem. Soc., Perkin Trans. 2* **2000**, 9−16.

[8] [8a] P. N. W. Baxter, G. S. Hanan, J. M. Lehn, *Chem. Commun.* **1996**, 2019−2020. [8b] A. M. Garcia, D. M. Bassani, J. M. Lehn, G. Baum, D. Fenske, *Chem. Eur. J.* **1999**, *5*, 1234−1238.

[9] [9a] D. P. Funeriu, J. M. Lehn, G. Baum, D. Fenske, *Chem. Eur. J.* **1997**, *3*, 99−104. [9b] J. A. Whiteford, P. J. Stang, S. D. Huang, *Inorg. Chem.* **1998**, *37*, 5595−5601. [9c] B. Hasenknopf, J. M. Lehn, G. Baum, B. O. Kneisel, D. Fenske, *Angew. Chem. Int. Ed. Engl.* **1996**, *35*, 1838−1840; *Angew. Chem.* **1996**, *108*, 1987−1990.

[10] C. Piguet, G. Bernardinelli, G. Hopfgartner, *Chem. Rev.* **1997**, *97*, 2005−2062.

[11] M. Albrecht, *Chem. Rev.* **2001**, *101*, 3457−3497.

[12] Y. Haas, G. Stein, *J. Phys. Chem.* **1971**, *75*, 3668−3677.

[13] [13a] G. Blasse, *Phys. Stat. Sol. A* **1992**, *130*, K85−K89. [13b] J.-C. G. Bünzli, P. Froidevaux, J. M. Harrowfield, *Inorg. Chem.* **1993**, *32*, 3306−3311. [13c] S. Petoud, T. Glanzmann, J.-C. G. Bünzli, C. Piguet, Q. Xiang, R. P. Thummel, *J. Luminesc.* **1999**, *82*, 69−79.

[14] N. Sabbatini, S. Perathoner, V. Balzani, B. Alpha, J. M. Lehn, *Supramolecular Chemistry* (Ed.: V. Balzani), D. Reidel Publishing Co., Dordrecht, **1987**.

[15] J.-C. G. Bünzli, *Lanthanide Probes in Life, Chemical and Earth Sciences: Theory and Practice* (Eds.: J.-C. G. Bünzli, G. R. Choppin), Elsevier Science Publ. B. V., Amsterdam, **1989**.

[16] *The Chemistry of Contrast Agents in Medical Magnetic Resonance Imaging* (Eds.: A. E. Merbach, E. Tóth), Wiley, London, **2001**.

[17] [17a] I. Hemmilä, T. Ståhlberg, P. Mottram, *Bioanalytical Applications of Labelling Technologies*, Wallac Oy, Turku, **1995**. [17b] G. Mathis, in: *Rare Earths* (Eds.: R. Saez-Puche, P. Caro), Editorial Complutense, Madrid, **1998**.

[18] J.-C. G. Bünzli, in: *Metal Ions in Biological Systems* (Eds.: A. Sigel, H. Sigel), Marcel Dekker Inc., New York, **2003**, vol. 41, chapter 15, in press.

[19] [19a] P. Hurst, B. K. Takasaki, J. Chin, *J. Am. Chem. Soc.* **1996**, *118*, 9982−9983. [19b] T. C. Bruice, A. Tsubouchi, R. O. Dempey, L. P. Olson, *J. Am. Chem. Soc.* **1996**, *118*, 9867−9875. [19c] A. Roigk, R. Hettich, H. J. Schneider, *Inorg. Chem.* **1998**, *37*, 751−756.

[20] D. E. Koshland Jr., *Angew. Chem. Int. Ed. Engl.* **1994**, *33*, 2375−2378; *Angew. Chem.* **1994**, *106*, 2368−2371.

[21] C. Piguet, J.-C. G. Bünzli, G. Bernardinelli, G. Hopfgartner, A. F. Williams, *J. Am. Chem. Soc.* **1993**, *115*, 8197−8206.

[22] [22a] N. Martin, J.-C. G. Bünzli, V. McKee, C. Piguet, G. Hopfgartner, *Inorg. Chem.* **1998**, *37*, 577−589. [22b] C. Platas Iglesias, M. Elhabiri, M. Hollenstein, J. C. G. Bünzli, C. Piguet, *J. Chem. Soc., Dalton Trans.* **2000**, 2031−2043. [22c] R. Tripier, M. Hollenstein, M. Elhabiri, A. S. Chauvin, G. Zucchi, C. Piguet, J. C. G. Bünzli, *Helv. Chim. Acta* **2002**, *85*, 1915−1929.

[23] [23a] J.-C. G. Bünzli, C. Piguet, *Chem. Rev.* **2002**, *102*, 1897−1928. [23b] J.-C. G. Bünzli, N. André, M. Elhabiri, G. Muller, C. Piguet, *J. Alloys Compd.* **2000**, *303−304*, 66−74.

[24] [24a] B. Bocquet, G. Bernardinelli, N. Ouali, S. Floquet, F. Renaud, G. Hopfgartner, C. Piguet, *Chem. Commun.* **2002**, 930−931. [24b] S. Floquet, N. Ouali, B. Bocquet, G. Bernardinelli, D. Imbert, J. C. G. Bünzli, G. Hopfgartner, C. Piguet, *Chem. Eur. J.* **2003**, *9*, 1860−1875.

[25] N. André, R. Scopelliti, G. Hopfgartner, C. Piguet, J.-C. G. Bünzli, *Chem. Commun.* **2002**, 214−215.

[26] [26a] M. Elhabiri, R. Scopelliti, J.-C. G. Bünzli, C. Piguet, *Chem. Commun.* **1998**, 2347−2348. [26b] M. Elhabiri, R. Scopelliti, J.-C. G. Bünzli, C. Piguet, *J. Am. Chem. Soc.* **1999**, *121*, 10747−10762.

[27] S. Blanc, P. Yakirevitch, E. Leize, M. Meyer, J. Libman, A. Van Dorsselaer, A. M. Albrecht-Gary, A. Shanzer, *J. Am. Chem. Soc.* **1997**, *119*, 4934−4944.

[28] N. Fatin-Rouge, S. Blanc, E. Leize, A. Van Dorsselaer, P. Baret, J. L. Pierre, A. M. Albrecht-Gary, *Inorg. Chem.* **2000**, *39*, 5771−5778.

[29] N. Fatin-Rouge, S. Blanc, A. Pfeil, A. Rigault, A. M. Albrecht-Gary, J. M. Lehn, *Helv. Chim. Acta* **2001**, *84*, 1694−1711.

[30] J. Hamacek, S. Blanc, M. Elhabiri, E. Leize, A. Van Dorsselaer, C. Piguet, A. M. Albrecht-Gary, *J. Am. Chem. Soc.* **2003**, *125*, 1541−1550.

[31] [31a] H. Gampp, M. Maeder, C. J. Meyer, A. D. Zuberbühler, *Talanta* **1985**, *32*, 95−101. [31b] F. J. C. Rossotti, H. S. Rossotti, R. J. Whewell, *J. Inorg. Nucl. Chem.* **1971**, *33*, 2051−2065. [31c] H. Gampp, M. Maeder, C. J. Meyer, A. D. Zuberbühler, *Talanta* **1985**, *32*, 257−264. [31d] H. Gampp, M. Maeder, C. J. Meyer, A. D. Zuberbühler, *Talanta* **1986**, *33*, 943−951.

 © 2004 Wiley-VCH Verlag GmbH & Co. KGaA, Weinheim

[32] R. G. Brown, N. Entwistle, J. D. Hepworth, K. W. Hodgson, B. May, *J. Phys. Chem.* **1982**, *86*, 2418−2420.
[33] F. R. Prieto, M. Mosquera, M. Novo, *J. Phys. Chem.* **1990**, *94*, 8536−8542.
[34] B. Perlemutter-Hayman, *Acc. Chem. Res.* **1986**, *19*, 90−96.
[35] M. C. Rios Rodriguez, J. C. Penedo, R. J. Willemse, M. Mosquera, F. R. Prieto, *J. Phys. Chem. A* **1999**, *103*, 7236−7243.
[36] M. Novo, M. Mosquera, F. R. Prieto, *Can. J. Chem.* **1992**, *70*, 823−827.
[37] N. S. Rao, G. B. Rao, B. N. Murthy, M. M. Das, T. Prabhakar, M. Lalitha, *Spectrochim. Acta A* **2002**, *58*, 2737−2757.
[38] N. S. Rao, M. M. Das, G. B. Rao, D. Ziessow, *Spectrosc. Lett.* **1985**, *18*, 827−836.
[39] L. E. Kapinos, B. Song, H. Sigel, *Chem. Eur. J.* **1999**, *5*, 1794−1802.
[40] H. Xiao Feng, L. La Sheng, L. Xue Yi, C. Xiao Ming, J. Liang Nian, Z. Zhong Yuan, *Inorg. Chim. Acta* **1999**, *285*, 326−331.
[41] R. M. Dyson, G. A. Lawrance, H. Mäcke, M. Maeder, *Polyhedron* **1999**, *18*, 3243−3251.
[42] S. Yajima, Y. Hasegawa, *Bull. Chem. Soc. Jpn.* **1998**, *71*, 2825−2829.
[43] E. Kiss, K. Petrohán, D. Sanna, E. Garribba, G. Micera, T. Kiss, *Polyhedron* **2000**, *19*, 55−61.
[44] [44a] R. I. Gelb, J. S. Alper, *J. Chem. Eng. Data* **1998**, *43*, 383−385. [44b] R. W. Green, H. K. Tong, *J. Am. Chem. Soc.* **1956**, *78*, 4896−4900.
[45] In reference 26b, pK_a data are incorrect. In fact the reported figures (4.42 and 7.7) are pK_b values and not pK_a values. Recalculating these data in terms of pK_a values gives 9.6 and 6.3, two values in good agreement with those reported in Table 1, given the slightly different experimental conditions.
[46] [46a] G. Hopfgartner, C. Piguet, J. D. Henion, A. F. Williams, *Helv. Chim. Acta* **1993**, *76*, 1759−1766. [46b] G. Hopfgartner, C. Piguet, J. D. Henion, *J. Am. Soc., Mass Spectrom.* **1994**, *5*, 748−756.
[47] [47a] C. Piguet, E. Rivara-Minten, G. Hopfgartner, J.-C. G. Bünzli, *Helv. Chim. Acta* **1995**, *78*, 1541−1572. [47b] C. Piguet, G. Hopfgartner, A. F. Williams, J.-C. G. Bünzli, *J. Chem. Soc., Chem. Commun.* **1995**, 491−493.
[48] [48a] C. Piguet, J.-C. G. Bünzli, G. Bernardinelli, G. Hopfgartner, S. Petoud, O. Schaad, *J. Am. Chem. Soc.* **1996**, *118*, 6681−6697. [48b] C. Piguet, G. Bernardinelli, J.-C. G. Bünzli, S. Petoud, G. Hopfgartner, *J. Chem. Soc., Chem. Commun.* **1995**, 2575−2577.
[49] [49a] C. Piguet, E. Rivara-Minten, G. Bernardinelli, J.-C. G. Bünzli, G. Hopfgartner, *J. Chem. Soc., Dalton Trans.* **1997**, 421−433. [49b] G. Bernardinelli, C. Piguet, A. F. Williams, *Angew. Chem. Intl. Ed. Engl.* **1992**, *31*, 1622−1624; *Angew. Chem.* **1992**, *104*, 1626−1628.
[50] [50a] E. Leize, A. Jaffrezic, A. Van Dorsselaer, *J. Mass Spectrom.* **1996**, *31*, 537−544. [50b] I. I. Stewart, G. Horlick, *Anal. Chem.* **1994**, *66*, 3983−3993.
[51] J. A. Leenheer, C. E. Rostad, P. M. Gates, E. T. Furlong, I. Ferrer, *Anal. Chem.* **2001**, *73*, 1461−1471.
[52] [52a] C. L. Gatlin, R. D. Rao, F. Turecek, T. Vaisar, *Anal. Chem.* **1996**, *68*, 263−270. [52b] P. Hu, J. A. Loo, *J. Am. Chem. Soc.* **1995**, *117*, 11314−11319.
[53] [53a] A. Reiter, J. Adams, H. Zhao, *J. Am. Chem. Soc.* **1994**, *116*, 7827−7838. [53b] P. Hu, M. L. Gross, *J. Am. Soc., Mass. Spectrom.* **1994**, *5*, 137−143.
[54] S. Rigault, C. Piguet, J. C. G. Bünzli, *J. Chem. Soc., Dalton Trans.* **2000**, 2045−2053.
[55] [55a] K. A. Connors, *Chemical Kinetics. The Study of Reaction Rates in Solution*, VCH Verlagsgesellschaft, Weinheim, Germany, **1990**, chapter 3. [55b] C. Capellos, B. H. J. Bielski, *Kinetic Systems: Mathematical Description of Chemical Kinetics in Solution*, Wiley-Interscience, New York, **1972**.
[56] Microcal™ Origin™, Microcal Software, Inc., Northampton, USA.
[57] L. J. Charbonnière, A. F. Williams, A. Frey, A. E. Merbach, P. Kamalaprija, O. Schaad, *J. Am. Chem. Soc.* **1997**, *119*, 2488−2496.
[58] [58a] C. Cossy, L. Helm, A. E. Merbach, *Inorg. Chem.* **1988**, *27*, 1973−1979. [58b] C. Cossy, A. E. Merbach, *Pure Appl. Chem.* **1988**, *60*, 1785−1796. [58c] C. Cossy, L. Helm, A. E. Merbach, *Inorg. Chem.* **1989**, *28*, 2699−2703.
[59] G. U. Priimov, P. Moore, L. Helm, A. E. Merbach, *Inorg. React. Mech.* **2001**, *3*, 1−23.
[60] E. Szilágyi, É. Tóth, Z. Kovács, J. Platzek, B. Radüchel, E. Brücher, *Inorg. Chim. Acta* **2000**, *298*, 226−234.
[61] E. Brücher, D. Sherry, *Inorg. Chem.* **1990**, *29*, 1555−1559.
[62] L. Helm, A. E. Merbach, *Coord. Chem. Rev.* **1999**, *187*, 151−181.
[63] [63a] R. M. Fuoss, *J. Am. Chem. Soc.* **1958**, *80*, 5059−5061. [63b] M. Eigen, *Z. Phys. Chem.* **1954**, *1*, 176−200.
[64] [64a] J. E. Prue, *J. Chem. Soc.* **1965**, 7534−7535. [64b] D. B. Rorabacher, *Inorg. Chem.* **1966**, *5*, 1891−1899.
[65] [65a] M. Eigen, R. G. Wilkins, *Adv. Chem. Ser.* **1965**, *49*, 55−67. [65b] M. Eigen, K. Tamm, *Z. Electrochem.* **1962**, *66*, 93−107. [65c] R. G. Wilkins, *Acc. Chem. Res.* **1970**, *3*, 408−416.
[66] [66a] H. B. Silber, J. H. Swinehart, *J. Phys. Chem.* **1967**, *71*, 4344−4348. [66b] H. B. Silber, R. D. Farina, J. H. Swinehart, *Inorg. Chem.* **1969**, *8*, 819−824.
[67] Values determined at T = 12.5 °C and I = 0.2 M ($NaClO_4$) using the temperature jump relaxation method.
[68] T. E. Eriksen, I. Grenthe, I. Puigdomenech, *Inorg. Chim. Acta* **1987**, *126*, 131−135.
[69] Values determined at T = 20 °C in aqueous solutions containing 0.5 M *tert*-butyl alcohol and using the radiation induced pH-jump technique.
[70] L. C. Thompson, *Inorg. Chem.* **1964**, *3*, 1319−1321.
[71] S. Saito, H. Hoshino, T. Yotsuyanagi, *Inorg. Chem.* **2001**, *40*, 3819−3823.
[72] J. F. Desreux, *Lanthanide Probes in Life, Chemical and Earth Sciences. Theory and Practice* (Eds.: J.-C. G. Bünzli, G. R. Choppin), Elsevier Science Publ., B. V., Amsterdam, **1989**.
[73] K. N. Raymond, *Chem. Eng. News* **1983**, *61*, 4.
[74] P. Gans, B. O'Sullivan, *Talanta* **2000**, *51*, 33−37.
[75] [75a] P. Gans, A. Sabatini, A. Vacca, *HYPERQUAD2000:* Leeds, U. K., and Florence, Italy. [75b] P. Gans, A. Sabatini, A. Vacca, *Talanta* **1996**, *43*, 1739−1753.
[76] P. Gans, *Data Fitting in the Chemical Sciences*, John Wiley & Sons, Chichester, **1992**.
[77] N. Ingri, W. Kakolowicz, L. G. Sillen, B. Warnqvist, *Talanta* **1967**, *14*, 1261−1286.
[78] A. E. Martell, R. J. Motekaitis, *Determination and Use of Stability Constants*, VCH Verlagsgesellschaft, Weinheim, Germany, **1988**, chapter 1.
[79] *Méthodes d'analyses complexométriques avec les titriplex®*, 3rd edition, E. Merck Ed., Grafis: Darmstadt, **1992**.
[80] L. G. Sillen, *Acta Chem. Scand.* **1964**, *18*, 1085−1098.
[81] L. G. Sillen, B. Warnqvist, *Ark. Kemi.* **1968**, *31*, 377−390.
[82] J. Havel, *Pure Appl. Chem.* **1972**, *34*, 370−383.
[83] D. W. Marquardt, *J. Soc., Indust. Appl. Math.* **1963**, *11*, 431−441.
[84] M. Maeder, A. D. Zuberbühler, *Anal. Chem.* **1990**, *62*, 2220−2224.
[85] Bio-Logic Company, Ed. Bio-Logic Company, Echirolles, **1991**.
[86] J. A. Nelder, R. Mead, *The Computer Journal* **1965**, *7*, 308−313.
[87] E. Yeramian, P. Claverie, *Nature* **1987**, *326*, 169−174.
[88] P. K. Glasoe, F. A. Long, *J. Phys. Chem.* **1960**, *64*, 188−190.
[89] A. Ringbom, *Complexation in Analytical Chemistry*, John Wiley & Sons, Inc., New York, **1963**.

Received August 8, 2003
Early View Article
Published Online October 30, 2003

 © 2004 Wiley-VCH Verlag GmbH & Co. KGaA, Weinheim

Supramolecular Chemistry Based on $[W_3S_4(H_2O)_6Cl_3]^+$ – A Versatile Building Block

Maxim N. Sokolov,*[a] Olga A. Gerasko,[a] Danil N. Dybtsev,[a] Elena V. Chubarova,[a] Alexander V. Virovets,[a] Cristian Vicent,[b] Rosa Llusar,[b] Dieter Fenske,[c] and Vladimir P. Fedin[a]

Keywords: Cluster compounds / Tungsten / Antimony / Cucurbituril / Supramolecular chemistry

The cluster $[W_3S_4(H_2O)_6Cl_3]^+$ (which is present in solutions of $[W_3S_4(H_2O)_9]^{4+}$ in 1–4 M HCl) reacts with the macrocyclic cavitand cucurbituril ($C_{36}H_{36}N_{24}O_{12}$) to form supramolecular adducts of 2:1 cluster/cucurbituril stoichiometry, where two portals of cucurbituril (which contains a water molecule in its cavity) are closed by two cluster cations. These aggregates are bound together in the solid by complementary hydrogen bonds between coordinated Cl^- and the cations $H_9O_4^+$ to give chains. Thus, a supramolecular architecture is achieved from three different but complementary building blocks. The packing of the chains affords a honeycomb structure (hexagonal symmetry) with channels (about 5.2 Å in diameter). The overall stoichiometry is $(H_9O_4)\{[W_3S_4(H_2O)_6Cl_3]_2(C_{36}H_{36}N_{24}O_{12})\}Cl_3\cdot 16.15H_2O$ (**1**). $[W_3S_4(H_2O)_6Cl_3]^+$ reacts with $SbCl_3$ in 6 M HCl to give cuboidal $[W_3(SbCl_3)S_4(H_2O)_6Cl_3]^+$, which forms with the macrocyclic cavitand cucurbituril a 2:1 cluster/cucurbituril adduct – a discrete supramolecule consisting of five independent molecular units. In the solid it crystallizes as a salt of very rare anion $[SbCl_6]^{3-}$ with the stoichiometry $\{[W_3(SbCl_3)S_4(H_2O)_6Cl_3]_2(C_{36}H_{36}N_{24}O_{12})\}(SbCl_6)_{2/3}\cdot 12H_2O$ (**2**).

(© Wiley-VCH Verlag GmbH & Co. KGaA, 69451 Weinheim, Germany, 2004)

Introduction

Building supramolecular aggregates relies heavily upon complementary hydrogen bond formation. Much has been done in the field of pure organic supramolecular assemblies and this new branch of organic synthesis has been aptly termed "noncovalent synthesis".[1] Though the potential of hydrogen bonds for noncovalent binding in the so-called second coordination sphere was recognized about 20 years ago and a review summarizing binding of transition metal complexes (mostly ammino complexes) to crown ethers and related macrocycles (through N–H···O bonding) appeared as early as in 1983,[2] most of the spectacular success in the field of supramolecular chemistry in the last decennium was due to the skillful use of possibilities of classical coordination chemistry.[3,4] A reason for this may well be the lesser degree of liberty with which inorganic compounds containing H-bond donors (or acceptors) can be tailored to suit the requirements of complementarity. However, if we take an aqua complex in solution of an acid whose anion is only a moderate or even a weak donor, an array of mixed complexes would form, and each individual complex will have its particular geometrical arrangement of coordinated water molecules. This can be regarded as a combinatorial library and, if the interconversion between different species within the library is rapid enough, we will have a dynamic combinatorial library.[5] By introducing an organic H-bond acceptor with a purposefully chosen geometry, we could then selectively "recognize" any single desired component, making isolation of active species in equilibrium with its chemically closely congeners simple. Our previous work suggests that triangular cluster aqua ions of the general formula $[M_3Q_4Cl_x(H_2O)_{9-x}]^{4-x}$ (M = Mo, W; Q = S, Se; x = 1–5) can be regarded as components of one such library.[6–10] Specific requirements of complementarity between six-coordinated water molecules in $[M_3Q_4Cl_x(H_2O)_{9-x}]^{4-x}$ (H-bond donors) and six oxygen atoms of C=O groups of a macrocyclic cavitand cucurbituril lead to the isolation of supramolecular adducts when x = 1–3, i.e., the specific recognition of only a part of the library components, and moreover, in each case only of one of all possible isomers.[7–11]

In the present study we show, in one case – $(H_9O_4)\{[W_3S_4(H_2O)_6Cl_3]_2(C_{36}H_{36}N_{24}O_{12})\}Cl_3\cdot 16.15H_2O$ (**1**) – how the complementarity towards $[W_3S_4Cl_3(H_2O)_6]^+$ may be reinforced through introducing "guanidinium-like"

[a] A. V. Nikolaev Institute of Inorganic Chemistry of the Russian Academy of Sciences,
pr. Lavrentyeva 3, 630090 Novosibirsk, Russia
E-mail: cluster@che.nsk.su
[b] University of Jaume I, Experimental Sciences Department, P. O. Box 224, 12080 Castelló, Spain
[c] Institute of Inorganic Chemistry, University of Karlsruhe, 76128 Karlsruhe, Germany

$H_9O_4^+$ which also acts as structure-directing building block making the formation of a honeycomb-like structure possible, and, in another case – $\{[W_3(SbCl_3)S_4(H_2O)_6Cl_3]_2(C_{36}H_{36}N_{24}O_{12})\}(SbCl_6)_{2/3}\cdot 12H_2O$ (**2**) – how weak interactions other than hydrogen bonds may be exploited to build a nanosized supramolecular aggregate containing five units of three different building blocks, each of which is known as independent chemical species.

Results and Discussion

Although Cl^- coordination to $[M_3Q_4(H_2O)_9]^{4+}$ (M = Mo, W; Q = S, Se) in aqueous solutions is fairly weak {for the formation of $[Mo_3S_4(H_2O)_8Cl]^{3+}$ K is only 3.0 M^{-1}}, and no fully substituted species $[M_3Q_4Cl_9]^{5-}$ (or of other halides) have been isolated, some equilibration to the extent at least of $[M_3Q_4(H_2O)_4Cl_5]^-$ does take place in 1–6 M HCl.

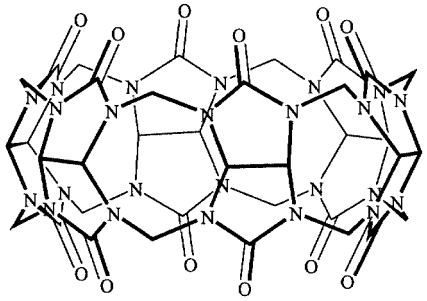

Cucurbituril

Using cucurbituril as a second coordination sphere ligand (Cuc, $C_{36}H_{36}N_{24}O_{12}$) to promote crystallization through formation of complementary associates based on hydrogen bonds between the carbonyl groups of Cuc and water molecules *cis* to the μ_3-Q ligand of the cluster it was possible to isolate the following compounds and to determine their X-ray structures: (i) monosubstituted $\{[W_3S_4(H_2O)_8Cl](pyH\subset Cuc)\}Cl_4\cdot 15.5H_2O$,[8] $\{[W_3Se_4(H_2O)_8Cl]_2(Cuc)\}Cl_6\cdot 12H_2O$[11] and $\{[Mo_3Se_4(H_2O)_8Cl]_2(Cuc)\}Cl_6\cdot 16H_2O$;[9] (ii) disubstituted $\{[W_3S_4(H_2O)_7Cl_2](Cuc)\}Cl_2\cdot 10H_2O$;[7] (iii) trisubstituted $\{[Mo_3S_4(H_2O)_6Cl_3][Mo_3S_4(H_2O)_7Cl_2](pyH\subset Cuc)\}Cl_4\cdot 17H_2O$,[7] $(H_3O)_2[Mo_3S_4(H_2O)_6Cl_3](Cuc)Cl_3\cdot 9H_2O$[10] and $\{[W_3Se_4(H_2O)_6Cl_3](pyH\subset Cuc)\}_2Cl_3\cdot 18H_2O$.[12] In all these structures the barrel-shaped cucurbituril molecule is effectively closed by one or two cluster "lids"; in some cases a small molecule (pyridinium cation) is included and retained inside the cucurbituril inner cavity.[7,8,12,13] The chloride substitution is always at the *trans* positions to the μ_3-chalcogen atom, other H_2O ligands are retained and used for complementary hydrogen bonding with Cuc. When more (5 Cl^-) enter into the cluster, as in $(H_3O)_2\{[Mo_3Se_4(H_2O)_4Cl_5]_2(Cuc)\}\cdot 15H_2O$, the complementarity is lost.[9] In all cases the $[M_3Q_4(H_2O)_6Cl_3]^+$ species are present as the most symmetrical isomers (with a threefold axis). Comparison of the geometrical parameters of $\{W_3S_4\}$ cluster cores in the aqua complexes is given in Table 1. We can see that W–W bond lengths are only slightly affected by the environment of tungsten atoms.

Formation and Structure of 1

The structure of the cluster cation $[W_3S_4(H_2O)_6Cl_3]^+$ in compounds **1** is shown in Figure 1. Main bond lengths of $\{W_3S_4\}$ cluster core are similar to that found in the tungsten aqua complexes (Table 1). Six water molecules in *cis* position to the core μ_3-S atom form hydrogen bonds with portal oxygen atoms of cucurbituril (O···O, 2.76–2.94 Å), and a complementary cationic associate $\{[W_3S_4(H_2O)_6Cl_3](Cuc)[W_3S_4(H_2O)_6Cl_3]\}^{2+}$ ("two lids on the barrel" type) is formed. It has a very high crystallo-

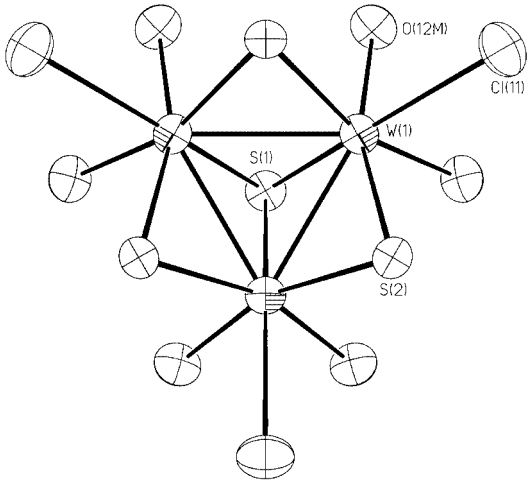

Figure 1. Cluster cation $[W_3S_4(H_2O)_6Cl_3]^+$ in the compound **1** (50% probability ellipsoids); main bond lengths [Å]: W(1)–W(1)#1 2.7360(13), W(1)–W(1)#2 2.7360(13), W(1)–S(1) 2.351(6), W(1)–S(2) 2.289(4), W(1)–S(2)#2 2.289(4), W(1)–Cl(11) 2.498(5), W(1)–O(12M) 2.175(9), W(1)–O(12M)#3 2.175(9); symmetry transformations used to generate equivalent atoms: #1: $-x+y, -x+1, z$; #2: $-y+1, x-y+1, z$; #3: $-y+1, -x+1, z$

Table 1. Average main bond lengths in the $\{W_3S_4(H_2O)_n\}$ clusters [Å]

Formula[a]	W–W	W–μ_3-S	W–μ-S	Ref.
$\{[W_3S_4(H_2O)_7Cl_2](Cuc)\}Cl_2\cdot 10H_2O$	2.714	2.340	2.285	[7]
$\{[W_3S_4(H_2O)_8Cl](pyH\subset Cuc)\}Cl_4\cdot 15.5H_2O$	2.720	2.356	2.283	[8]
$[W_3S_4(H_2O)_9](pts)_4\cdot 7H_2O$	2.724	2.345	2.282	[14]
$[W_3S_4(H_2O)_9](pts)_4\cdot 9H_2O$	2.708	2.339	2.284	[14]
$(H_9O_4)\{[W_3S_4(H_2O)_6Cl_3]_2(Cuc)\}Cl_3\cdot 16.15H_2O$	2.736	2.351	2.289	[b]

[a] pyH = pyridinium; pts = p-$CH_3C_6H_4SO_3^-$. [b] This work.

 © 2004 Wiley-VCH Verlag GmbH & Co. KGaA, Weinheim

graphic symmetry, 6bar*m*2 (D_{3h}). This associate has an ellipsoidal egg-like shape of about 19.5 Å height and 14.4 Å in diameter. The associates are arranged according to the ideal hexagonal close packing (h.c.p.) motif (Figure 2). The space group of **1** is $P6_3/mmc$ − quite common for the h.c.p. structure type (e.g. Mg metal structure). It must be stressed that the associates do not contact each other in the hexagonal layer because the distances between them (16.47 Å) are longer than the van der Waals "diameter" of the associate. It means that we have not exactly close packing, but only an h.c.p.-like motif. From this point of view, the $H_9O_4^+$ cations occupy exactly one half of the tetrahedral voids. They are planar, the central oxygen atom is surrounded by three other ones at the distance of 2.59 Å which is typical for hydroxonium cations.[15] The disordered Cl^- anions and water molecules lie in the octahedral voids playing the role of a layer between the positively charged associates. The macrocyclic cavitand cucurbituril contains a water molecule in its cavity.

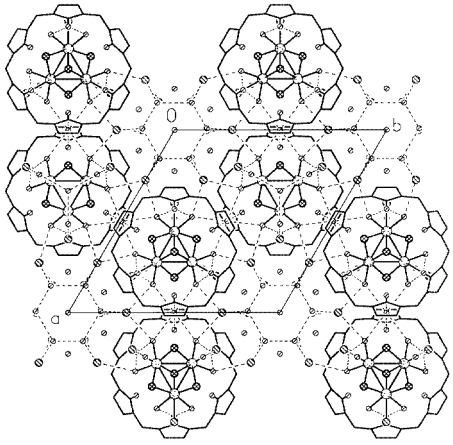

Figure 2. Crystal packing in compound **1** (projection on *a*,*b* plane); hydrogen bonds are shown as dashed lines

Once the discrete "lid-on-the-barrel" complexes between Cuc and $[M_3Q_4Cl_x(H_2O)_{9-x}]^{4-x}$ ($x = 1-3$) are formed, their further aggregation in the solid state can take place. First, through noncovalent Q···Q interactions between bridging μ_2-Q atoms (which seem to be more important when Q = Se) polymeric chains may form. This is the case for $\{[W_3Se_4(H_2O)_8Cl]_2(Cuc)\}Cl_6\cdot 12H_2O$,[11] $\{[Mo_3Se_4(H_2O)_8Cl]_2(Cuc)\}Cl_6\cdot 16H_2O$,[9] $\{[Mo_3S_4(H_2O)_6Cl_3][Mo_3S_4(H_2O)_7Cl_2](pyH\subset Cuc)\}Cl_4\cdot 17H_2O$,[7] $\{[W_3Se_4(H_2O)_6Cl_3](pyH\subset Cuc)\}_2Cl_3\cdot 18H_2O$.[12] The reluctance of the $\{W_3S_4\}$ unit to dimerise through S···S interactions is apparent here. Instead of this kind of association, in the structure of **1** the $H_9O_4^+$ cations lie between cluster−cucurbituril associates. They form hydrogen bonds with three terminal chlorine ligands of two cluster cations, Cl···O being of 3.11 Å. The guanidinium-like structure of $H_9O_4^+$ makes it suitable for complementary O−H···Cl hydrogen bonding with $[W_3S_4(H_2O)_6Cl_3]^+$. The resulting chains run along the *c* axis (Figure 3). They are shifted in such a way that each $H_9O_4^+$ cation is surrounded by four associates.

In structure **1** there are also channels along the *c* axis filled with disordered Cl^- anions and water molecules. The diameter of the channels is 5.2 Å, taking the values 1.70, 1.15, 1.40 and 1.36 Å as van der Waals radii of C, H, N and O, respectively.[16] These channels, from the h.c.p.'s point of view, are nothing else than the columns of octahedral voids. The porous frameworks built on relatively strong noncovalent interactions, like H-bonds, are of certain interest since they can be more easily disassembled than ones based on stronger covalent bonding. Kim and co-workers recently reported another cucurbituril-based honeycomb structure in $\{[Rb_2(OH)_2(CH_3OH)_2(H_2O)_2](Cuc)\}\cdot 17H_2O$ where the channels have a mean diameter of about 8.9 Å.[17]

Formation and Structure of 2

The complementarity for hydrogen bonding with cucurbituril is not lost when cuboidal chalcogen-bridged aqua complexes are dealt with since they retain the unit $\{M_3Q_4(H_2O)_6\}$. One of the most interesting properties of the triangular clusters with $\{M_3Q_4\}$ cores is their ability to incorporate a low-valent metal M′ with the formation of a cuboidal cluster $\{M_3M'Q_4\}$. In the case of $Mo_3S_4^{4+}$, some 20 transition and post-transition metals have been incorporated. It seems that all metals having $d^{10}s^2$ configuration [e.g. those of group 12 (Cd^0, Hg^0), 13 (Ga^I, In^I, Tl^I), 14 (Ge^{II}, Sn^{II}, Pb^{II}), 15 (As^{III}, Sb^{III}, Bi^{III}), and possibly group 16] can react in this way. Reactions are generally fast but in some cases (Tl^I, Pb^{II}, As^{III}, Bi^{III}) reaction does not take place in aqueous solution and/or with aqua ions, but proceed smoothly in organic solvents and with different coordination environment.[18] Antimony seems to be a border case. We observed characteristic color changes on addition of $SbCl_3$ to solutions of $[M_3Q_4(H_2O)_9]^{4+}$ in HCl, but it turned out to be difficult to characterize the reaction products.

$$[M_3Q_4(H_2O)_9]^{4+} + SbCl_3 \rightarrow [M_3(SbCl_3)Q_4(H_2O)_9]^{4+}$$

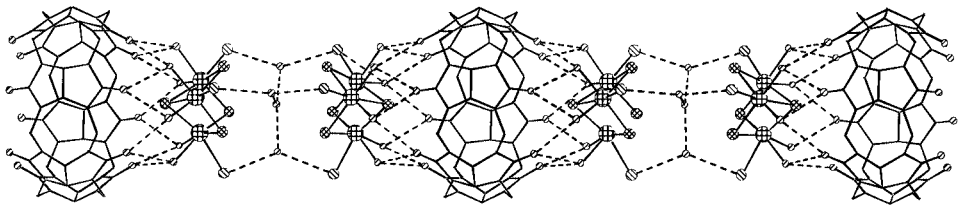

Figure 3. Fragment of the supramolecular chain in compound **1**; hydrogen bonds are shown as dashed lines

 © 2004 Wiley-VCH Verlag GmbH & Co. KGaA, Weinheim

Column purification, which is a standard procedure in this kind of chemistry, cannot be applied since (i) this equilibrium is shifted very much to the left, (ii) lowering $[H^+]$ destroys $SbCl_3$ to give oxochlorides or eventually $Sb(OH)_3$. Solutions of such cuboidal clusters in HCl are notoriously difficult to crystallize, and using Hpts (*p*-toluenesulfonic acid) for crystallization is excluded by the absence of soluble Sb^{III} cationic species in this media for the range of concentration involved (1−4 M Hpts). Therefore crystallization with cucurbituril was attempted and allowed us to isolate a cuboidal cluster $[W_3(SbCl_3)S_4(H_2O)_6Cl_3]^+$ as $\{[W_3(SbCl_3)S_4(H_2O)_6Cl_3]_2(C_{36}H_{36}N_{24}O_{12})\}(SbCl_6)_{2/3}\cdot 12H_2O$ (**2**).

The structure of the cluster cation $[W_3(SbCl_3)S_4(H_2O)_6Cl_3]^+$ in **2** is shown in Figure 4. The only other known cuboidal cluster with the $W_3SbS_4^{7+}$ core is found in $[W_3(SbI_3)S_4(OAc)(dtp)_3(DMF)]$ (dtp = diethyl dithiophosphate).[19] Also several derivatives of the $Mo_3SbS_4^{7+}$ core have been reported; they all contain dtp ligands at Mo and 3 X (X = Cl, Br, I) at Sb (Table 2).[20−22] We can see that in the case of tungsten complexes the Sb−S bond lengths are notably longer than in Mo_3SbS_4 clusters. At the same time the M−M and M−S bonds are not affected by the nature of M.

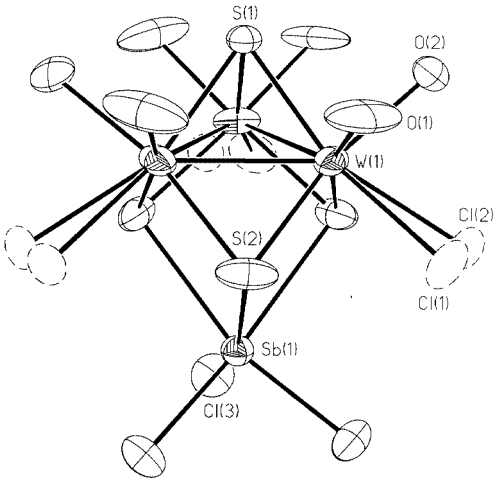

Figure 4. Cluster cation $[W_3(SbCl_3)S_4(H_2O)_6Cl_3]^+$ in the compound **2** (50% probability ellipsoids); disordered terminal chlorine ligands are shown by dashed ellipsoids, site occupancies being equal to 0.5; main bond lengths [Å]: W(1)−W(1)#1 2.7100(12), W(1)−W(1)#2 2.7100(12), W(1)−S(1) 2.349(5), W(1)−S(2) 2.300(5), W(1)···Sb(1) 3.8660(12), W(1)−Cl(1) 2.502(10), W(1)−Cl(2) 2.503(10), W(1)−O(1) 2.133(13), W(1)−O(2) 2.143(13), Sb(1)−S(2)#2 2.845(4), Sb(1)−Cl(3) 2.404(4); symmetry transformations used to generate equivalent atoms: #1: $-z+1$, $x-1/2$, $-y+1/2$; #2: $y+1/2$, $-z+1/2$, $-x+1$

In the cluster cation $[W_3(SbCl_3)S_4(H_2O)_6Cl_3]^+$ main bond lengths of $\{W_3S_4\}$ cluster core are similar to that found in the tungsten aqua complexes (Table 1). Along with the large distances W···Sb (3.87 Å) and Sb−S (2.85 Å) it makes a strong case for regarding the $[W_3(SbCl_3)S_4(H_2O)_6Cl_3]^+$ in **2** as a rather weakly bound associate of $[W_3S_4(H_2O)_6Cl_3]^+$ and $SbCl_3$. There are also a few complexes of $SbCl_3$ with thioethers [1,4,7-trithiacyclononane, 1,4,7,10,13,16-hexathiacyclooctadecane, 1,2-bis-(methylthio)ethane]. A general feature is that all of them have very long Sb−S distances, no shorter than 2.97 Å.[23,24] That in our case as well as in the other $M_3SbS_4^{7+}$ clusters the Sb−S bonds are shorter may be regarded as the result of a partial charge transfer from Sb onto M_3S_4 unit, diminishing the electron density on Sb and increasing it on S − a synergetic effect, as has been put forward to explain similar structural features of $W_3SnS_4^{6+}$.[25]

In the case of compound **2** the complementary associate cluster−cucurbituril−cluster ("two lids on the barrel" type) is also formed (Figure 5), O···O being of 2.77−2.83 Å. Thus, a nanosized supramolecular aggregate containing five units of three different building blocks, each of which is known as independent chemical species ($[W_3S_4(H_2O)_6Cl_3]^+$, $SbCl_3$ and Cuc), is formed. The largest distance between outermost chlorine atoms in this aggregate is 26.7 Å. In structure **2** associates are located on the non-intersecting

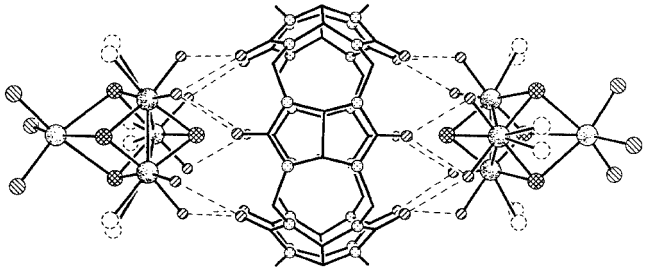

Figure 5. Complementary associate in the crystal structure of compound **2**; hydrogen bonds are shown as dashed lines

Table 2. Average main bond lengths in the $\{M_3SbS_4\}$ (M = Mo, W) clusters [Å]

Formula[a]	M−M	M···Sb	Sb−S	Ref.
$[W_3(SbI_3)S_4(\mu\text{-MeCOO})(Etdtp)_3(DMF)]\cdot H_2O$	2.719	3.902	2.846	[18]
$[Mo_3(Sb.l_3)S_4(\mu\text{-MeCOO})(Etdtp)_3(py)]\cdot MeCOOH$	2.721	3.855	2.797	[18]
$[Mo_3(SbBr_3)S_4(\mu\text{-MeCOO})(Etdtp)_3(py)]\cdot MeCOOEt$	2.703	3.850	2.793	[18]
$[Mo_3(SbI_3)S_4(\mu\text{-MeCOO})(Etdtp)_3(py)]\cdot MeCOOEt$	2.723	3.865	2.796	[18]
$[Mo_3(SbI_3)S_4(\mu\text{-}S_2CNC_4H_8)(S_2CNC_4H_8)_3(py)]\cdot 2H_2O$	2.730	3.797	2.741	[19]
$[Mo_3(Sb.l_3)S_4(\mu\text{-Etdtp})(Etdtp)_3(EtOH)]\cdot EtOH$	2.735	3.818	2.775	[20]
$[Mo_3(Sb.l_3)S_4(\mu\text{-Etdtp})(Etdtp)_3(H_2O)]\cdot 2H_2O$	2.717	3.807	2.779	[20]
$[Mo_6SbS_8(H_2O)_{18}](pts)_8\cdot 24H_2O$	2.717	3.680	2.609	[21]
$\{[W_3(SbCl_3)S_4(H_2O)_6Cl_3]_2(Cuc)\}(SbCl_6)_{2/3}\cdot 12H_2O$	2.710	3.866	2.845	[b]

[a] Etdtp = $(C_2H_5O)_2PS_2^-$; pts = $p\text{-}CH_3C_6H_4SO_3^-$; DMF = $OC(H)N(CH_3)_2$. [b] This work.

 © 2004 Wiley-VCH Verlag GmbH & Co. KGaA, Weinheim

threefold axes of $Pa\bar{3}$ space group, forming crystal packing similar to solid CO_2.

An interesting feature of this structure is the occurrence of the rare octahedron $[SbCl_6]^{3-}$ as counterion. The Sb−Cl distance is 2.678 Å, which is in agreement with the range 2.675−2.765 Å, reported for hexachloroantimonate(3−).[26,27] On the contrary, in $SbCl_6^-$ the Sb−Cl bonds are much shorter − about 2.37 Å.[28] To the best of our knowledge, there are only two other reports on $[SbCl_6]^{3-}$: in $[Co(NH_3)_6][SbCl_6]$[26] and in 2-aminoguanidinium 2-ammonioguanidinium hexachloroantimonate(III) $(CH_8N_4)(CHN_4)[SbCl_6]$.[27] In all three structures the lone pair in $[SbCl_6]^{3-}$ does not occupy a coordination site, but rather is a spherically symmetric *s* orbital.

Experimental Section

General: All reactions were carried out in air. Stock solutions of $[W_3S_4(H_2O)_9]^{4+}$ in 2 M HCl were prepared by a published procedure[29] and made up to the required $[H^+]$ concentration with 12 M HCl. Cucurbituril was synthesized by a published procedure.[30] $SbCl_3$ was of commercial quality (Aldrich). Elemental analyses were carried out in the Laboratory of Microanalysis, Institute of Organic Chemistry, Novosibirsk.

$(H_9O_4)\{[W_3S_4(H_2O)_6Cl_3]_2(C_{36}H_{36}N_{24}O_{12})\}Cl_3\cdot 16.15H_2O$ (1): A cucurbituril solution (0.3 mL, 20 mM) in 4 M HCl was added to a $[W_3S_4(H_2O)_9]^{4+}$ solution (1.5 mL, 10 mM) in 10 M HCl. The reaction mixture was stirred and left in a closed vial at room temperature for 5 d. Dark violet hexagonal crystals of **1** were collected by filtration and dried in air. Yield: 7 mg (20%). $C_{36}H_{101.3}Cl_9N_{24}O_{44.15}S_8W_6$ (3255.74): calcd. C 13.29, H 3.13, Cl 9.81, N 10.33, S 7.89; found C 13.98, H 2.59, Cl 9.00, N 10.74, S 7.94.

$\{[W_3(SbCl_3)S_4(H_2O)_6Cl_3]_2(C_{36}H_{36}N_{24}O_{12})\}(SbCl_6)_{2/3}\cdot 12H_2O$ (2): A cucurbituril solution (0.3 mL, 20 mM) in 6 M HCl was added to a mixture of a $[W_3S_4(H_2O)_9]^{4+}$ solution (1.5 mL, 10 mM) in 6 M HCl, containing 10 mg of $SbCl_3$. The reaction mixture was stirred and left in a closed vial at room temperature for 2 d. Red crystals of **2** were collected by filtration and dried in air. Yield: 8 mg (32%). $C_{36}H_{84}Cl_{16}N_{24}O_{36}S_8Sb_{2.67}W_6$ (3680.52): calcd. C 11.62, H 2.28, N 9.03; found C 11.79, H. 2.91, N 9.15.

X-ray Crystal Structure Determinations: Structures of both **1** and **2** were determined by X-ray analysis on single crystals in essentially a routine manner. **1:** $C_{36}H_{101.3}Cl_9N_{24}O_{44.15}S_8W_6$, formula mass 3255.74, hexagonal, space group $P6_3/mmc$, $Z = 2$, $a = 16.474(3)$, $c = 21.307(3)$ Å, $\gamma = 120°$, $V = 5008.0(12)$ Å^3, $D_{calcd.} = 2.159$ g·cm^{-3}, μ(Mo-K_α) = 7.362 mm^{-1}. Experimental data were measured at $T = 203$ K from a dark-violet crystal of 0.20 × 0.18 × 0.16 mm size by the standard technique with a STOE STADI4 four-cycle diffractometer using Mo-K_α radiation ($\lambda = 0.7107$ Å). A total of 6236 reflections was measured up to $2\theta_{max} = 50°$, of which 1701 are unique, $R_{int} = 0.1134$. Absorption correction was applied by measuring 3 azimuthal scans, transmission factors were from 0.7094 to 0.9965. The structure was solved by direct methods and refined by full-matrix methods for all non-hydrogen atoms using SHELX-97 program set.[31] Solvent water molecules and chlorine anions were seriously disordered. Their site occupancy factors were refined taking into account the chemical analysis data, electroneutrality and refined values of atomic thermal parameters, leading to the resulting formula that is in a good agreement with other data. $R_1 = 0.0512$ for 1089 $F \geq 4\sigma(F)$, $wR_2 = 0.1339$, $GooF = 1.142$ for all unique data. **2:** $C_{36}H_{84}Cl_{16}N_{24}O_{36}S_8Sb_{2.67}W_6$, formula mass 3680.52, cubic, space group $Pa\bar{3}$, $Z = 8$, $a = 21.788(3)$ Å, $V = 10344(2)$ Å^3, $D_{calcd.} = 2.363$ g·cm^{-3}, μ(Mo-K_α) = 7.984 mm^{-1}. Experimental data were measured at $T = 293$ K from a red crystal of 0.1 × 0.08 × 0.08 mm size by the standard technique with a Bruker SMART CCD diffractometer using Mo-K_α radiation ($\lambda = 0.7107$ Å). A total of 48756 reflections was measured up to $2\theta_{max} = 46.5°$, of which 2491 were unique, $R_{int} = 0.1968$. Absorption correction was applied empirically using the SADABS program, the ratio between minimum and maximum transmission factors was 0.8622. The structure was solved by direct methods and refined by full-matrix methods for all non-hydrogen atoms using the SHELXTL program set.[32] All non-hydrogen atoms were refined anisotropically. The Sb(1) atom was found in a special position (on a threefold axis) coordinated to three symmetry-related equivalent chlorine atoms Cl(3) and to three symmetry-related sulfur atoms S(2) (Figure 4). The hexachloroantimonate(3−) anion was found in a special position and refined as partially occupied in order to balance the overall charge of the cluster. Attempts to refine the $[SbCl_6]^{3-}$ anion with full occupancy resulted in high equivalent isotropic displacement parameters for both antimony (120 Å^2) and chlorine (240 Å^2) and a electron density hole of −3 e$^-$Å^{-3} near the antimony position. The equivalent isotropic displacement parameters in our partially occupied model were 70 Å^2 for antimony and 150 Å^2 for chlorine while the electron density hole near antimony decreased to 1.56 e$^-$Å^{-3} (highest peak is 1.30 e$^-$Å^{-3}). Based on this we decided to balance our cluster charge refining the antimony anion with partial occupancy instead of assuming the protonation of one of the crystallization water molecules. One tungsten atom per asymmetric unit was found in a general position and was coordinated to two O atoms from water molecules *cis* to μ_3-S−(W_3) [O(1) and O(2)] and to one Cl atom. The anisotropic thermal parameters of this Cl atom suggested a splitting of the electron density in two positions Cl(1) and Cl(2). The positions of all cucurbituril hydrogen atoms were generated geometrically, assigned isotropic thermal parameters and allowed to ride on the respective parent carbon atoms. Water hydrogen atoms were not refined. The five highest peaks left on the electron density map were assigned to partially occupied crystallization water molecules and refined isotropically. Convergence was reached at residuals of $R_1 = 0.0551$ and $wR_2 = 0.1348$ with a goodness-of-fit parameter of 1.041. CCDC-201934 and -201935 contain the supplementary crystallographic data for this paper. These data can be obtained free of charge at www.ccdc.cam.ac.uk/conts/retrieving.html [or from the Cambridge Crystallographic Data Centre, 12 Union Road, Cambridge CB2 1EZ, UK; Fax: (internat.) + 44-1223/336-033; E-mail: deposit@ccdc.cam.ac.uk].

Acknowledgments

The generous support by INTAS (2346, YSF 2002-432), the Russian Foundation for Basic Research (grant 02-03-32604) and Fundació Caixa Castelló-UJI (grant P1·1B2001-07) is gratefully acknowledged. One of us (A. V. V.) thanks Generalitat Valenciana (Spain) for the financial support of his visit to the University of Jaume I. Thanks are also extended to "Servei Central d'Instrumetació Científica" (SCIC) of the University Jaume I for providing us with X-ray facilities.

[1] L. J. Prins, D. N. Reinboudt, P. Timmerman, *Angew. Chem. Int. Ed.* **2001**, *40*, 2382−2426.

 © 2004 Wiley-VCH Verlag GmbH & Co. KGaA, Weinheim

[2] H. M. Colquhoun, J. F. Stoddart, D. J. Williams, *Angew. Chem. Int. Ed. Engl.* **1983**, *25*, 487−507.
[3] B. J. Holliday, C. A. Mirkin, *Angew. Chem. Int. Ed.* **2001**, *40*, 2022−2043.
[4] D. L. Caulder, K. N. Raymond, *J. Chem. Soc., Dalton Trans.* **1999**, 1185−1200.
[5] L. M. Greig, D. Philip, *Chem. Soc. Rev.* **2001**, *30*, 287−302.
[6] M. N. Sokolov, D. N. Dybtsev, V. P. Fedin, *Russ. Chem. Bull.* **2003**, *52*, 1041−1060.
[7] V. P. Fedin, A. V. Virovets, M. N. Sokolov, D. N. Dybtsev, O. A. Gerasko, W. Clegg, *Inorg. Chem.* **2000**, *9*, 2227−2230.
[8] D. N. Dybtsev, O. A. Gerasko, A. V. Virovets, M. N. Sokolov, V. P. Fedin, *Inorg. Chem. Commun.* **2000**, *3*, 345−349.
[9] V. P. Fedin, M. N. Sokolov, D. N. Dybtsev, O. A. Gerasko, A. V. Virovets, D. Fenske, *Inorg. Chim. Acta* **2002**, *331* 31−38.
[10] M. N. Sokolov, R. Hernandez-Molina, D. N. Dybtsev, E. V. Chubarova, S. F. Solodovnikov, N. V. Pervukhina, C. Vicent, R. Llusar, V. Fedin, *Z. Anorg. Allg. Chem.* **2002**, *628*, 2335−2339.
[11] M. N. Sokolov, A. V. Virovets, D. N. Dybtsev, O. A. Gerasko, V. P. Fedin, R. Hernandez-Molina, W. Clegg, A. G. Sykes, *Angew. Chem. Int. Ed.* **2000**, *112*, 1725−1727.
[12] O. A. Gerasko, A. V. Virovets, M. N. Sokolov, D. N. Dybtsev, A. V. Gerasimenko, D. Fenske, V. P. Fedin, *Russ. Chem. Bull.* **2002**, *10*, 1654−1659.
[13] A. V. Virovets, *Russ. J. Struct. Chem.* **2002**, *43*, 478−487.
[14] T. Shibahara, M. Yamasaki, G. Sakane, K. Minami, T. Yabuki, A. Ichimura, *Inorg. Chem.* **1992**, *31*, 640−647.
[15] A. F. Wells, *Structural Inorganic Chemistry*, 5th ed., Clarendon Press, Oxford, **1986**.
[16] C. C. Batsanov, *Zh. Neorg. Khim.* **1991**, *36*, 3015−3037.
[17] J. Heo, S.-Y. Kim, D. Whang, K. Kim, *Angew. Chem. Int. Ed.* **1999**, *38*, 641−643.
[18] R. Hernandez-Molina, M. N. Sokolov, A. G. Sykes, *Acc. Chem. Res.* **2001**, *34*, 223−230.
[19] J.-Q. Huang, S.-F. Lu, X.-Y. Huang, Q.-J. Wu, R.-M. Yu, *J. Cluster Sci.* **1997**, *8*, 47−50.
[20] S.-F. Lu, J.-Q. Huang, R.-M. Yu, X.-Y. Huang, Q.-Y. Wu, Y. Peng, J. Chen, Z.-X. Huang, D.-X. Wu, *Polyhedron* **2001**, *20*, 2339−2352.
[21] S.-F. Lu, J.-Q. Huang, Y.-H. Lin, J.-L. Huang, *Acta Chim. Sin.* **1987**, *3*, 191−193.
[22] G. Sakane, K. Hashimoto, M. Takahashi, M. Takeda, T. Shibahara, *Inorg. Chem.* **1998**, *37*, 4231−4234.
[23] G. R. Willey, M. T. Lakin, M. Ravindran, N. W. Alcock, *Chem. Commun.* **1991**, 271−272.
[24] A. J. Barton, N. J. Hill, W. Levason, G. Reid, *J. Chem. Soc., Dalton Trans.* **2001**, 1621−1637.
[25] A. Müller, V. P. Fedin, E. Diemann, H. Bögge, E. Krickemeyer, D. Sölter, A. M. Giuliani, R. Barbieri, P. Adler, *Inorg. Chem.* **1994**, *33*, 2243−2247.
[26] D. R. Schroeder, *Inorg. Chem.* **1973**, *12*, 210−213.
[27] M. Bujak, *Acta Crystallogr., Sect. C* **2001**, *57*, 388−390.
[28] B. Chevrier, J.-M. Le Carpentier, R. Weiss, *Acta Crystallogr., Sect. B* **1972**, *28*, 2673−2677.
[29] V. P. Fedin, M. N. Sokolov, A. V. Virovets, N. V. Podeberezskaya, V. E. Fedorov, *Inorg. Chim. Acta* **1998**, *69*, 292−296.
[30] W. A. Freeman, W. L. Mock, N.-Y. Shih, *J. Am. Chem. Soc.* **1981**, *103*, 7367−7368.
[31] G. M. Sheldrick *SHELX-97*, Release 97-2, Göttingen University, Germany **1998**.
[32] *SHELXTL Plus Structure Solution and Refinement Package*, Bruker AXS, **1998−2000**.

Received March 26, 2003
Early View Article
Published Online October 31, 2003

 © 2004 Wiley-VCH Verlag GmbH & Co. KGaA, Weinheim

Structure-Dependent Electrochemical Behavior of Thienylplatinum(II) Complexes of N,N-Heterocycles

Feng Zhao,[a] Xingling Xu,[a] Soo Beng Khoo,*[a] and T. S. Andy Hor*[a]

Keywords: Platinum / N ligands / Cyclic voltammetry / Thin films / Heterocycles

trans-[Pt(MeCN)(PPh_3)$_2$(2-thienyl)]BF_4 (**1**) serves as a convenient precursor to bifunctional mononuclear *trans*-[Pt(PPh_3)$_2$(η^1-*N*-*N*)(2-thienyl)]BF_4 [*N*-*N* = pyrazine (**2**); 2-chloropyrazine, (**3**)] and dinuclear *trans,trans*-[Pt_2(PPh_3)$_4$(μ-*N*-*N*)(2-thienyl)$_2$](BF_4)$_2$ [(*N*-*N* = 4,4′-bipyridine (**4**); 4,4′-vinylenedipyridine (**5**)] complexes. The nuclear selectivity is conveniently controlled by the choice of the heterocyclic ligands or spacers. Both structural types **3** and **5** were confirmed by single-crystal X-ray crystallographic analyses. Their solution identities were established by positive-ion Electrospray Mass Spectrometry (ESMS). The electroactivities of these complexes were studied by cyclic voltammetry (CV). Continuous CV scans of **4** and **5** revealed variations in the redox waves with the number of scans. While the initial oxidative scan exhibited only a broad, irreversible wave, further cycling showed the growth of two additional redox couples up to about the tenth cycle. The peak currents of these redox couples began to decay with prolonged potential cycling beyond the tenth cycle. These findings are consistent with the formation of electroactive oligomers/polymers, and this conclusion is supported by visible thin film formation on the electrodes. In contrast, the mononuclear complexes (**2** and **3**) do not show such behavior. The films formed were further studied by repetitive potential cycling and XPS.
(© Wiley-VCH Verlag GmbH & Co. KGaA, 69451 Weinheim, Germany, 2004)

Introduction

The preparation of macro- and supramolecular assemblies with functionalised properties is currently a major challenge in synthetic chemistry.[1] A careful selection of a transition metal and a conjugated ligand could result in not only targeted molecular sizes and shapes,[2] but also expected electrochemical, magnetic and optical properties. Incorporation of transition metals into the conjugated backbone enhances metal dπ-pπ* back-bonding, which is expected to contribute significantly to the π-electron delocalization.[3] The combination of conjugated ligands, electron-rich metal centers, and the high degree of covalence inherent in soft-soft bonding can promote low-energy electronic interactions between the metal and the ligand. Our recent interest has been focused on novel electroactive metal-organic complexes.[4] Our current interest in d^8 thienyl complexes[5] stems from their geometric directionality and conductive potential[6] upon polymerization. Recently, we have extended this study to the construction of N- and P-bridged transition metal thienyl complexes. The simplest way to achieve this is through the introduction of a bridging co-ligand, or spacer. A non-thienyl spacer would bring an extra dimension of functionality to the complex. This paper describes a combined use of thienyl and nitrogen-containing heterocyclic ligands (depicted below) in the assembly of multimeric bifunctional d^8 networks based on a readily synthesized precursor. Introduction of different N-ligands, viz. pyridine or pyrazine-based heterocycles enables us to tune the spatial and structural features that have a direct impact on the electrochemical responses.

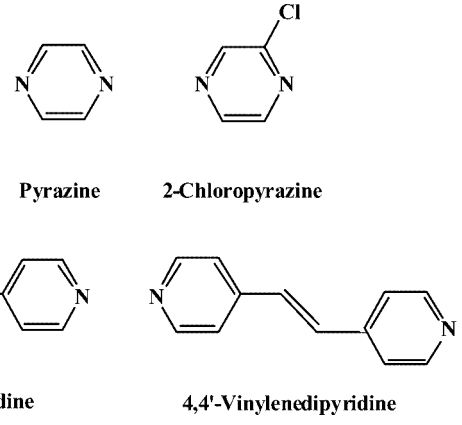

Results and Discussion

(1) Synthesis

The reaction in acetonitrile solution between equimolar *trans*-[PtBr(PPh_3)$_2$(2-thienyl)][7,8] and $AgBF_4$, gives *trans*-[Pt(MeCN)(PPh_3)$_2$(2-thienyl)]BF_4, (**1**). Its quantitative yield

[a] Department of Chemistry, Faculty of Science, National University of Singapore,
3 Science Drive 3, Singapore 117543, Singapore
Fax: (internat.) +65-6779-1691
E-mail: andyhor@nus.edu.sg

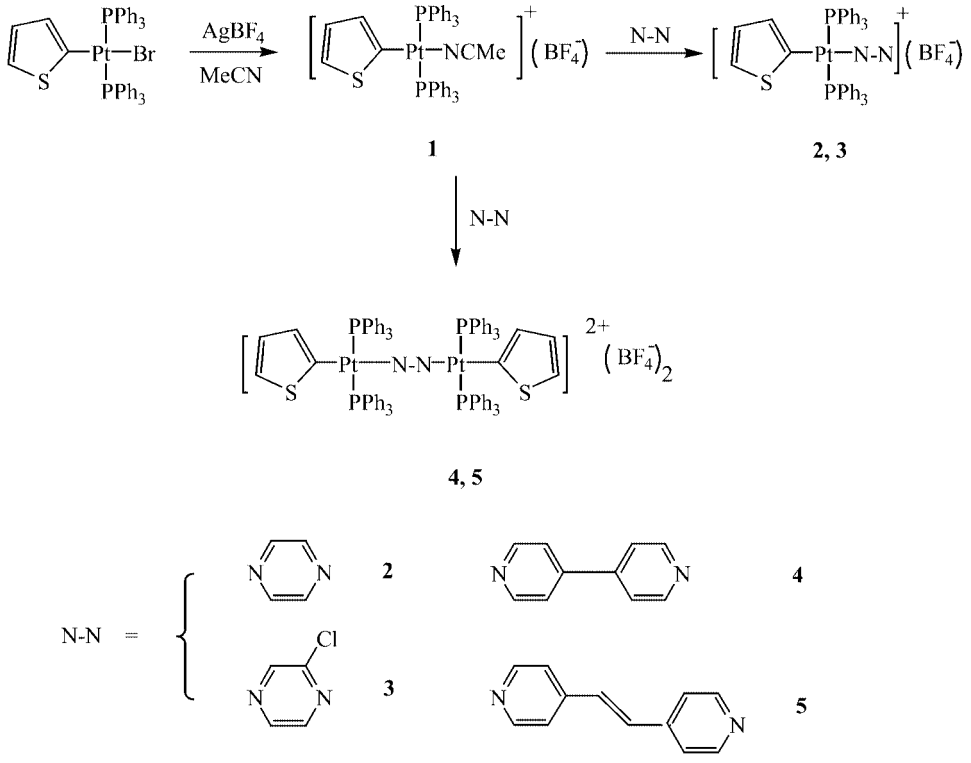

Scheme 1. Formation pathway of complexes **1**−**5**

and the presence of a labile MeCN solvent molecule make it a suitable precursor to bifunctional complexes. Although **1** can be isolated, it is more convenient to use it in situ. Upon removal of AgBr by filtration from the product mixture, addition of 4,4′-bipyridine or 4,4′-vinylenedipyridine gives dinuclear *trans,trans*-$[Pt_2(PPh_3)_4(\mu\text{-}N\text{-}N)(2\text{-thienyl})_2][BF_4]_2$ [*N*-*N* = 4,4′-bipyridine (**4**), 4,4′-vinylenedipyridine (**5**)] respectively. However, use of pyrazine and 2-chloropyrazine as substrates gives only mononuclear *trans*-$[Pt(PPh_3)_2(\eta^1\text{-}N\text{-}N)(2\text{-thienyl})][BF_4]$ [*N*-*N* = pyrazine, (**2**), 2-chloropyrazine, (**3**)] as yellow solids in high yields, despite the presence of a *trans*-disposed N-functionality (Scheme 1).

These illustrate an effective nuclear selectivity through a simple control of the N-spacer. Heterocycles in which charge delocalization is efficient, such as **2** and **3**, would have a lower nucleophilicity of the second nitrogen to an extent that it prefers to be pendant rather than bridging. The presence of the bulky PPh_3 ligand could also impede the approach of the neighboring Pt^{II} moiety towards a less protruded heterocyclic arm. Construction of cationic metal-based molecular boxes have met with a similar fate.[9,10] NMR analysis suggested that these cationic complexes are nonlabile. The ^1H coordination shifts (upfield) of the α- and β- pyrazine or pyridine hydrogen atoms (possibly due to shielding by the PPh_3 ligand) are indicative of coordinative nonlability. The α- and β-pyridine hydrogen atoms of **2** are similarly shifted upfield to δ = 8.21, 7.96 ppm, relative to free pyrazine (δ_H = 8.58), and, similarly for **5**, to δ = 7.81, 7.06 ppm, relative to free 4,4′-vinylenedipyridine (H_α δ = 8.62, H_β δ = 8.39 ppm). The ^{31}P NMR spectra of all the complexes showed the expected *trans*-phosphanes [typically $^1J_{Pt\text{-}P}$ (ca. 3480 Hz)] that are equivalent. As expected, both the shifts and couplings are fairly insensitive to subtle electronic changes in the *cis* N-ligands.

(2) Solid State Structures

Complexes **3** (Figure 1) and **5** (Figure 2) were chosen as models for X-ray crystallographic elucidation of the solid-state structures. The refinement data and bond/angle parameters are collected in Table 1 and Table 2, respectively. Complex **3** is mononuclear, comprising two *trans*-oriented phosphanes [P(2)−Pt(1)−P(2) 176.28(6)°] and a thienyl

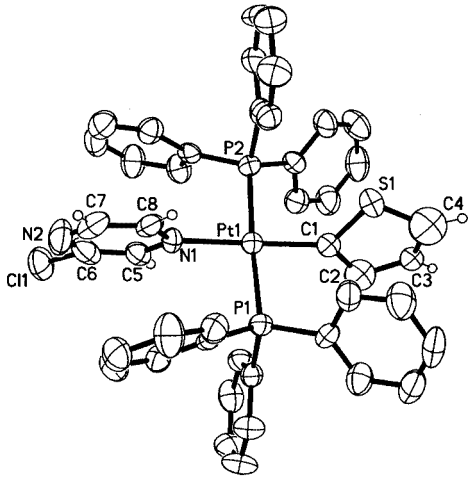

Figure 1. Thermal ellipsoids (50% probability) of **3** with the atomic numbering scheme

 © 2004 Wiley-VCH Verlag GmbH & Co. KGaA, Weinheim

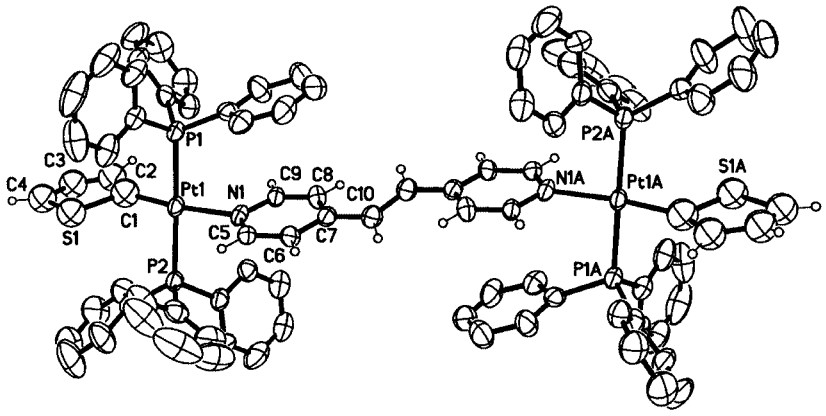

Figure 2. Thermal ellipsoids (50% probability) of **5** with the atomic numbering scheme

Table 1. Crystallographic data and structure refinement details for **3** and **5**

Complex	**3**	**5**
Empirical formula	$C_{45}H_{38}BCl_3F_4N_2P_2PtS$	$C_{92}H_{80}B_2F_8N_2O_3P_4Pt_2S_2{\cdot}CH_2Cl_2$
Formula mass	1089.02	2100.33
Color	pale yellow	yellow
Crystal size (mm)	0.26 × 0.14 × 0.10	0.28 × 0.15 × 0. 06
Crystal system	tetragonal	monoclinic
Space group	*P*4(3)	*P*2/*c*
T (K)	295(2)	223(2)
a (Å)	10.6753(5)	22.654(3)
b (Å)	10.6753(5)	11.2330(13)
c (Å)	38.654(3)	20.113(2)
α (°)	90	90
β (°)	90	111.021(2)
γ (°)	90	90
F(000)	2156	2084
V (Å^3)	4405.1(4)	4777.5(10)
Z	4	2
Absorption coefficient (mm^{-1})	3.540	3.154
Density (g·cm^{-3})	1.644	1.459
Index ranges	$-12 \le h \le 10$, $-12 \le k \le 12$, $-45 \le l \le 45$	$-26 \le h \le 26$, $-12 \le k \le 13$, $-23 \le l \le 23$
Reflections collected	25879	26547
Independent reflections	7761(R_{int} = 0.0636)	8416 (R_{int} = 0.0515)
Final *R* indices [$I > 2\sigma(I)$]	R_1 = 0.0423, wR_2 = 0.0548	R_1 = 0.0563, wR_2 = 0.1570
R indices (all data)	R_1 = 0.0546, wR_2 = 0.0565	R_1 = 0.0818, wR_2 = 0.1683
Goodness-of-fit on F^2	0.995	1.043
Largest diff. peak and hole (e·Å^{-3})	1.141 and −0.889	3.154 and −1.813

group opposite the chloropyrazine ring [N(1)−Pt(1)−C(1) 179.4(5)°]. The nitrogen atom meta to the chloro functionality is preferentially coordinated whereas the ortho counterpart is pendant. The thienyl and chloropyrazine rings are tilted at an angle of 29.5° to each other. The proximity of the phenyl rings makes the pendant nitrogen atom less susceptible to attack. Complex **5** is dinuclear with a 4,4′-vinylenedipyridine group bridging two Pt^{II} centers, opposite two thienyl terminal ligands [N(1)−Pt(1)−C(1) 168.9(2)°]. The two pyridyl rings are strictly coplanar (θ, 0°).

Complex **3** has a noncrystallographic twofold symmetry along the N(1)−Pt(1)−C(1) axis. Both substituents at the Pt(1) center, namely thienyl and 2-chloropyrazine groups are disordered along this axis. Complex **5** has a center of inversion between the methylene carbon atoms of the 4,4′-vinylenedipyridine bridging ligand, and the thienyl groups are disordered.

All Pt−N[11] [2.082(4)-2.107(4) Å] and Pt−P[10] lengths [2.3212(19)-2.323(3) Å] are normal although the Pt−N bonds of **5** are somewhat longer (in 1.2%) than in **3**. There is no evidence of perturbance to the olefinic [C(10)−C(10A) 1.352 Å] moiety at the center of the bridge.

(3) ESMS Characterization

The development of electrospray mass spectrometry (ESMS) by Fenn[12] and others[13] has provided a powerful soft technique to study multiply-charged ions, primarily large biomolecules, in solution. Recently, we have extended this development as a combinatorial-like technique to probe the chemistry of $[Pt_2(\mu\text{-}X)_2(PPh_3)_4]$ (X = S, Se).[14] In this paper we use ESMS to investigate the fragmentation of the

 © 2004 Wiley-VCH Verlag GmbH & Co. KGaA, Weinheim

Table 2. Selected bond lengths and angles for **3** and **5**

3 Bond lengths (Å)			
Pt(1)−C(1)	2.005(10)	Pt(1)−P(2)	2.323(2)
Pt(1)−N(1)	2.082(4)	Pt(1)−P(1)	2.323(2)
C(4)−S(1)	1.657(14)	C(1)−S(1)	1.705(12)
C(8)−N(1)	1.316(11)	C(5)−N(1)	1.346(10)
Bond angles (°)			
C(1′)−Pt(1)−C(1)	0.8(19)	C(1)−Pt(1)−P(2)	88.2(8)
C(1)−Pt(1)−N(1)	179.4(5)	C(1)−Pt(1)−P(1)	88.1(8)
N(1)−Pt(1)−P(2)	91.60(19)	N(1)−Pt(1)−P(1)	92.12(19)
P(2)−Pt(1)−P(1)	176.28(6)		
5 Bond lengths (Å)			
Pt(1)−C(1)	2.038(7)	Pt(1)−P(2)	2.3221(19)
Pt(1)−N(1)	2.107(4)	Pt(1)−P(1)	2.3212(19)
C(4)−S(1)	1.7997(10)	C(1)−S(1)	1.7995(10)
C(9)−N(1)	1.377(8)	C(5)−N(1)	1.348(9)
C(10)-C(10A)	1.352		
Bond angles (°)			
C(1′)−Pt(1)−C(1)	11.03(17)	C(1)−Pt(1)−P(2)	94.1(2)
C(1)−Pt(1)−N(1)	168.9(2)	C(1)−Pt(1)−P(1)	87.4(2)
N(1)−Pt(1)−P(2)	89.23(16)	N(1)−Pt(1)−P(1)	90.10(16)
P(2)−Pt(1)−P(1)	175.73(7)		

parent ions in solution. Analysis of the mononuclear complexes in CH_2Cl_2 in the positive ion mode gave a $[M(N\text{-}N)]^+$ peak for **2** (m/z = 881.7) and **3** (m/z = 915.7) [M = $Pt(PPh_3)_2$(2-thienyl); *N*-*N* = pyrazine, (**2**), 2-chloropyrazine, (**3**)]. In these complexes, there is a common peak associated with the replacement of the pyrazine ligand by MeCN viz. $[M(MeCN)]^+$ (m/z = 843.8), which was observed as the main peak for complex **1**. These data suggested that the solid-state identity of these complexes is maintained in solution.

The positive-ion ES mass spectrum of complex **5** dissolved in CH_2Cl_2 is shown in Figure 3. A possible fragmentation pathway is illustrated in Scheme 2. The presence of the intact, doubly charged molecular ion Peak A (m/z = 892.7, 100%), $[M_2(4,4'\text{-vinylenedipyridine})]^{2+}$ lends support to the suggestion that the solution and solid state structures are in agreement. Fragmentation peaks B (m/z = 802.0, 10%), D (m/z = 843.8, 4%), and C (m/z = 983.8, 32%) were also detected, corresponding to M^+, $[M(MeCN)]^+$ and $[M(4,4'\text{-vinylenedipyridine})]^+$, respectively. Similarly, in the positive-ion ES mass spectrum of complex **4**, the intact, doubly charged molecular ion peak at m/z = 880.1 was observed, together with the fragmental molecular ion peaks at m/z = 957.0 {$[M(4,4'\text{-bipyridine})]^+$}, 802.0 and 843.8.

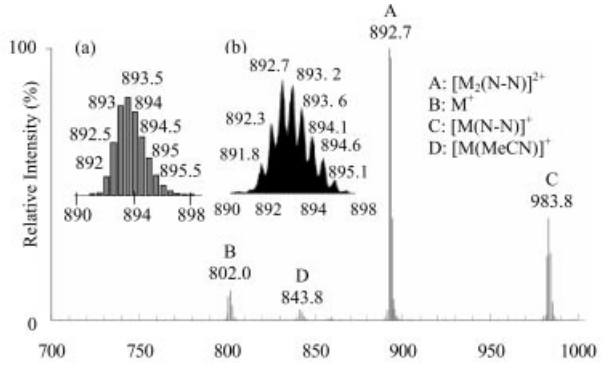

Figure 3. Positive-ion ES mass spectrum of **5** in CH_2Cl_2 solvent. The insets show the (a) calculated and (b) observed isotope distribution pattern for the intact dinuclear parent ion

Their formation can be explained by bridge cleavage by the residual MeCN molecule, thereby generating two cationic mononuclear complexes in which one bears a pendant heterocyclic ligand and the other captures the solvent ligand (Scheme 2). The ligand replacement or bridge cleavage by the strong coordination solvent MeCN has been reported before.[15] However, we should add that this takes place only when voltage is applied under spectrometric conditions. The cleavage invariably occurs at the heterocyclic junction, indicating that this is the weakest link in this series of bifunctional networks. The strong σ-donating and π-accepting character of the phosphanes as well as the anionic nature of thienyl, which electrostatically strengthens the M−C bond, make them relatively immune to such attack.

(4) Electrochemical Behavior

Cyclic voltammetric (CV) studies were performed on complexes **2**, **3**, **4** and **5** (1 mM) in CH_2Cl_2 by using Bu_4NBF_4 (0.10 M) as the supporting electrolyte. All complexes show one irreversible oxidation wave in the first scan. Complexes **4** and **5** show different electrochemical behavior from that of **2** and **3**. The repetitive cycling profiles for **5** are illustrated in Figure 4.

During the first cycle, the forward (anodic) scan gave a complex oxidation wave $\mathbf{O_1}$, which could be assigned to thiophene oxidation,[16] with at least two unresolved peaks. On reversing the scan, the reduction peaks $\mathbf{R_3}$ and $\mathbf{R_2}$ were observed. During the second cycle, new oxidation peaks $\mathbf{O_2}$ and $\mathbf{O_3}$ emerged, which were not observed on the first scan. Associated with these, the earlier oxidation wave $\mathbf{O_1}$ dropped significantly in the second anodic scan, and disappeared completely in subsequent cycles. Conversely, peaks $\mathbf{O_2/R_2}$ and $\mathbf{O_3/R_3}$ continued to increase in size to the tenth cycle, after which they began to decay with further cycles. This behavior is consistent with the formation of electroactive or conductive polymers or high oligomers.[17] Since these species are less readily soluble in the analyte solution, their formation would alter the redox pattern of the sample, and eventually render the analyte featureless in the CV scans. Polymerization is likely to take place at the thienyl site since electropolymerization of thiophene, bithiophene and substituted thiophenes is common.[18] When the electrode was removed from solution at the conclusion of the scanning experiments, rinsed with CH_2Cl_2 and dried, a greenish thin film was visible on the electrode surface. The

 © 2004 Wiley-VCH Verlag GmbH & Co. KGaA, Weinheim

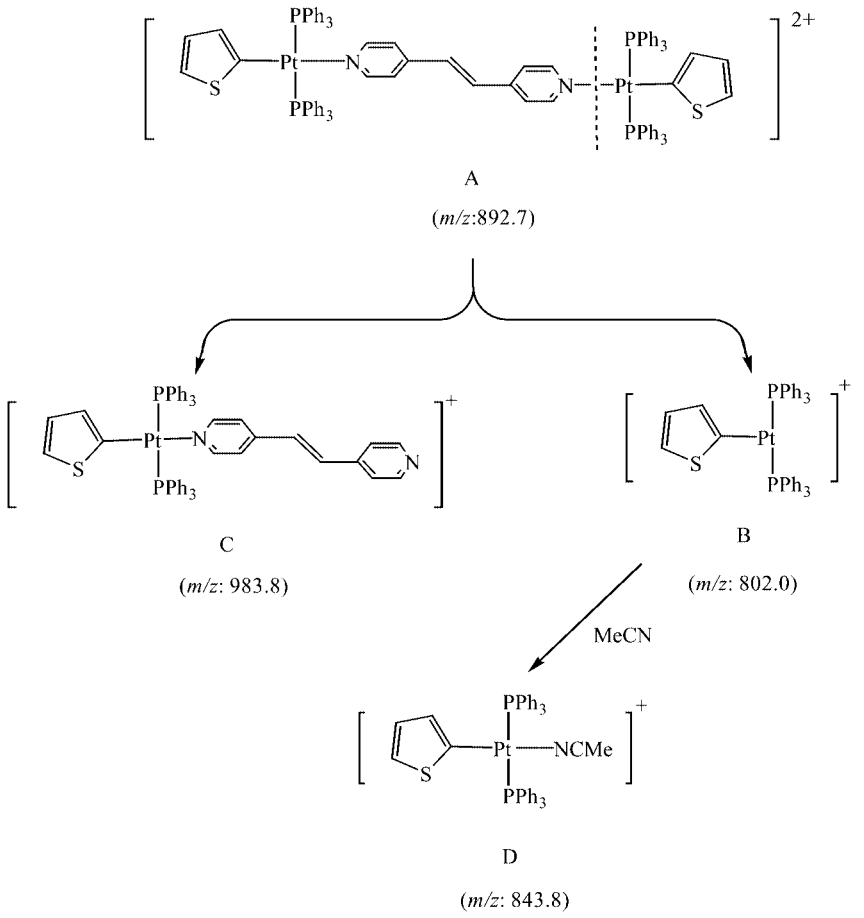

Scheme 2. Possible fragmentation pathway of **5** depicting the species observed in the positive ion ES mass spectrum

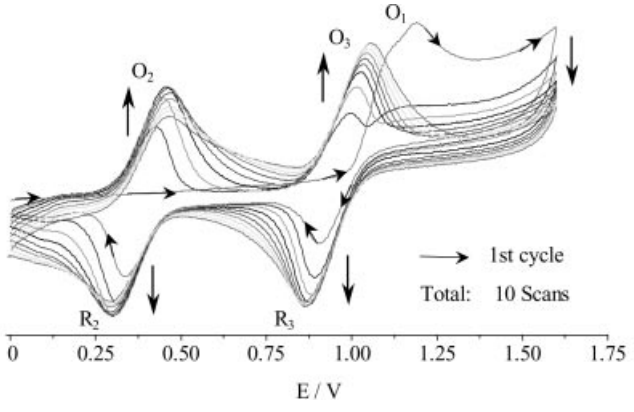

Figure 4. Continuous cyclic scanning between 0.00 to +1.60 V of **5** (0.1 mol·dm^{-3}) supported by Bu_4NBF_4 in CH_2Cl_2

material properties of this film are under investigation in our laboratory.

Cycling experiments on **4** revealed a similar decay phenomenon, with slightly different redox potentials. This suggests that the CV behavior is structurally related, and the redox potentials are sensitive to the bridging ligands. Accordingly, **2** and **3**, which are isostructural, show similar initial oxidative behavior to that of **4** and **5** (i.e. only a broad, irreversible oxidation wave) but no corresponding film formation is observed with continuous cycling. Cycling of these two analyte solutions resulted in the decrease of the oxidation wave $\mathbf{O_1}$ with no other obvious peak formation. The relevant electrochemical parameters for the complexes are summarized in Table 3. The CV profiles thus serve as supporting finger-printing diagnosis for these complexes.

In an attempt to understand this disparity, we carried out further electrochemical investigations of the films. After film formation (typically 10 scans), the potential cycling in the complex solution was terminated, and the film-coated electrode was washed with CH_2Cl_2. The electrode was then re-immersed in the blank electrolyte solution and cycled again between +0.00 V and +1.60 V. The peak heights decreased slowly with repetitive potential cycling, suggesting that the films formed from **4** and **5** are not electrochemically stable. The CV responses of these films upon treatment are also different from those seen in the $\mathbf{O_2/R_2}$ and $\mathbf{O_3/R_3}$ couples when the films were first formed. As seen in Table 3, after the tenth cycle, the anodic peak current in $\mathbf{O_2}$ is 2.79 $\times$ 10^{-5} A (i_{pc}^{R2}/i_{pa}^{O2} = 0.96 in this cycle) while that in $\mathbf{O_3}$ is 3.68 $\times$ 10^{-5} A (i_{pc}^{R3}/i_{pa}^{O3} = 1.02). This gives an $\mathbf{O_2/O_3}$ peak height ratio of 0.76. Similar analysis of the isolated film (Figure 5) shows 9.57 $\times$ 10^{-6} A for the anodic peak current in $\mathbf{O_2}$ and 1.58 $\times$ 10^{-5} A for that in $\mathbf{O_3}$, thus yielding a ratio of 0.60 (i_{pc}^{R2}/i_{pa}^{O2} = 0.86 and i_{pc}^{R3}/i_{pa}^{O3} = 0.73). The current after film formation and isolation is unusual but can be understood. Firstly, the electrogenerated cation could be a very reactive electrophilic Pt^{III}, which is

 © 2004 Wiley-VCH Verlag GmbH & Co. KGaA, Weinheim

Table 3. Electrochemical data for complexes **2**−**5** and films formed at a glassy carbon electrode

Complex[a]	E_{pa}^{O1}[b]	E_{pc}^{R3}[c]	E_{pa}^{O3}	$\Delta E_{pp(3)}$[d]	i_{pc}^{R3}/i_{pa}^{O3}[e]	E_{pc}^{R2}	E_{pc}^{O2}	$\Delta E_{pp(2)}$	i_{pc}^{R2}/i_{pa}^{O2}
2	1.26	–	–	–	–	–	–	–	–
3	1.20	–	–	–	–	–	–	–	–
4	1.16	0.91	–	–	–	0.33	–	–	–
5	1.28	0.90	–	–	–	0.31	–	–	–
Film (**4**)[f]	–	0.86	1.11	0.25	0.95	0.26	0.52	0.26	0.94
Film (**5**)[g]	–	0.82	1.12	0.30	1.02	0.25	0.51	0.26	0.96

[a] Electrochemical data for complexes **2**−**5** from cyclic voltammetry in CH_2Cl_2/0.1 M Bu_4NBF_4: potential in V vs. $Ag/AgNO_3$, scan rate 100 mV s^{-1}. [b] Anodic peak potential for irreversible oxidation. [c] Cathodic peak potential for reduction. [d] Peak-to-peak separation $\Delta E_{pp} = E_{pa} - E_{pc}$ (V). [e] The ratio of reduction current to oxidation current. [f] Film (**4**) was derived from 10 cycles of **4**. [g] Film (**5**) was derived from 10 cycles of complex **5**.

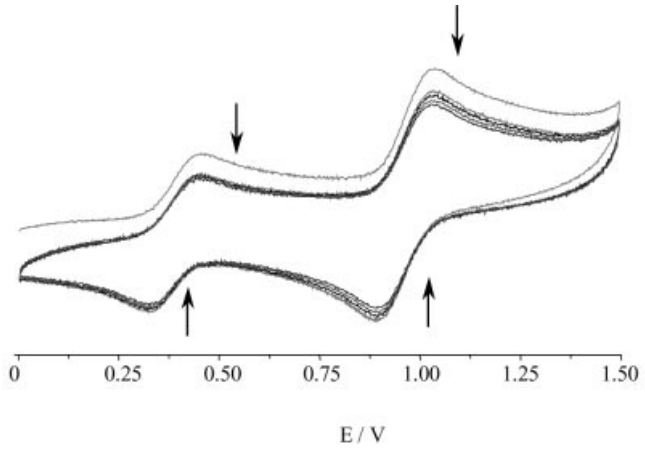

Figure 5. Continuous cyclic scanning between 0.00 to +1.60 V of the film formed from **5** in blank electrolyte solution containing 0.1 M Bu_4NBF_4 in CH_2Cl_2

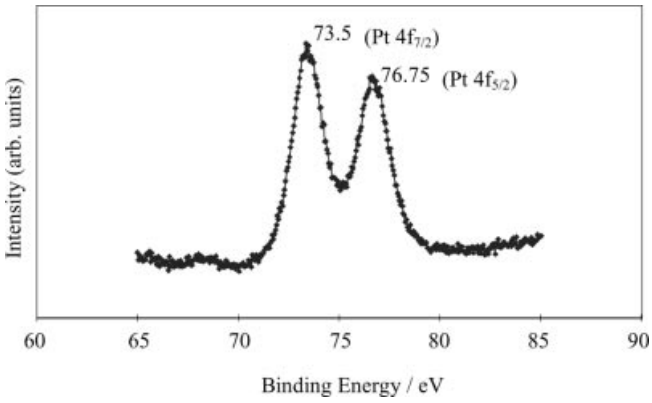

Figure 6. The XPS spectra of the film formed from **5**

bound to decay rapidly at room temperature.[19] Secondly, the stability of the film at the potentials at which it is formed could be poor, which is known as the "thiophene paradox"[20] in the synthesis of polythiophene conducting polymers via electrooxidation.

To gain some understanding of the elemental composition of the film, we carried out an XPS analysis[21] of the film formed from **5**. This film was formed typically after about 10 scans. When the potential cycling of the complex solution was terminated, the film-coated electrode was retrieved and washed with CH_2Cl_2, and the film analyzed by XPS, the Pt(4f) spectrum showed the spin-orbit components separated by 3.25 eV (Figure 6). The Pt(4f) binding energies, which compare well with those of phosphane-bearing platinum,[22] are indicative of Pt^{II}. Further S(2p), N(1s) and P(2p) spectral analyses revealed fairly typical spectra for thienyl, bipyridyl and phosphane complexes. Further studies of the film properties and characteristics, which are outside the present scope, will be a subject of our future reports.

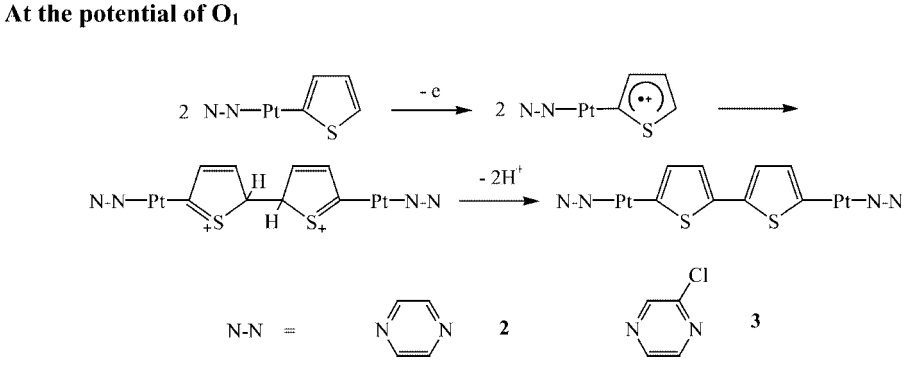

Scheme 3. Possible dimerization pathway for the mononuclear species **2** and **3** under applied potential in CV experiments

 © 2004 Wiley-VCH Verlag GmbH & Co. KGaA, Weinheim

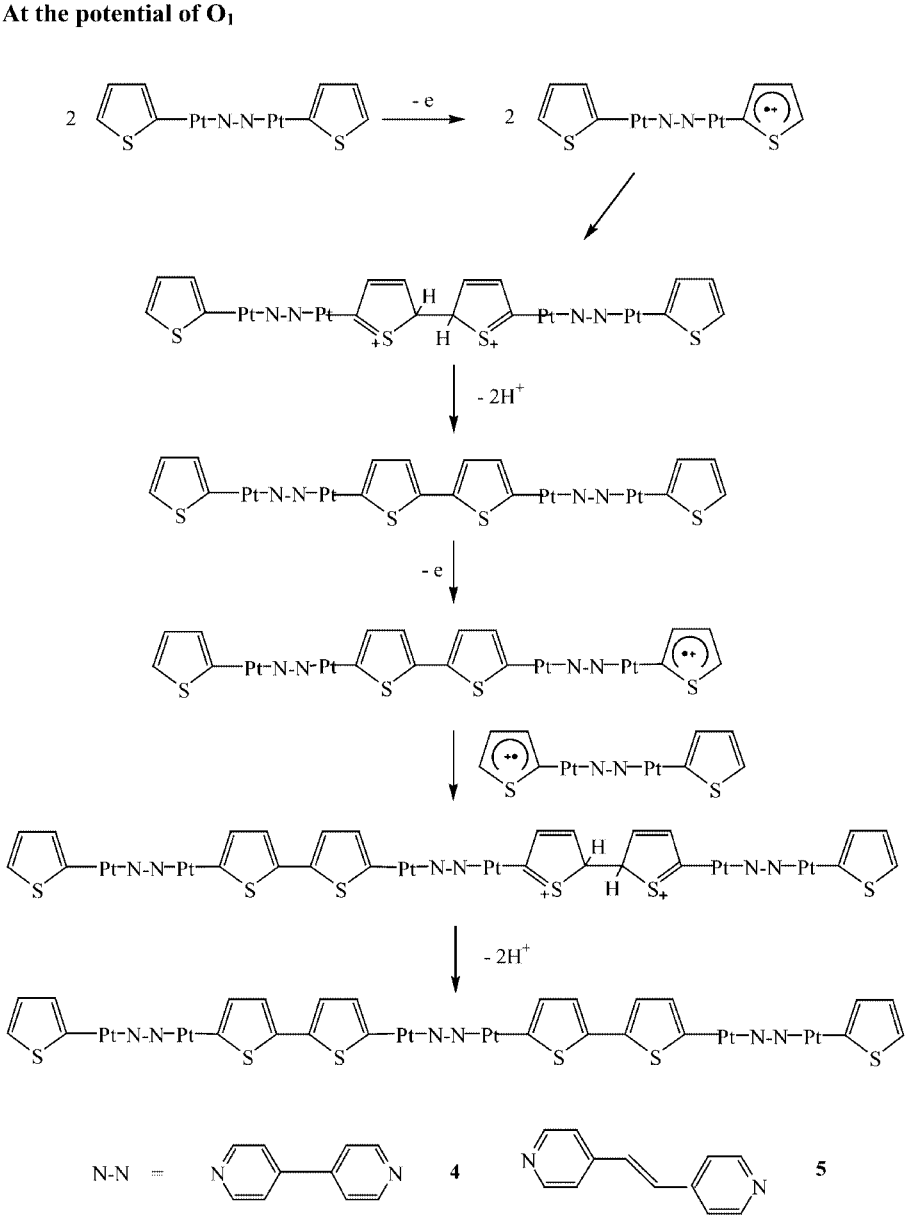

Scheme 4. Possible polymerization process for **4** and **5** that leads to film formation on the surface of the electrode from continuous scanning

It is not our primary interest to study the details of the electropolymerization mechanism, but we can propose a reasonable pathway, involving repetitive electrogeneration of a cation radical, followed by α-α coupling, that is grounded in the literature[23−25] and allows us to explain the different behavior of the mono- (Scheme 3) and dinuclear complexes (Scheme 4). At the first cycle of electropromoted coupling, the dinuclear precursors **4** and **5** yield bithiophene-bridged Pt_4 complexes that have two free ends of α-thienyl group. The latter could undergo further coupling using the free α functionality by a similar mechanism as above. This would transform a Pt_4 into a Pt_6 chain, and so on. As there is no facile chain-termination step, a film would be the obvious product on ending the electropolymerization cycles. However, for mononuclear complexes **2** and **3**, dimerization would lead to a Pt_2 complex bridged through bithiophenyl groups and with terminal N−N groups. There is no α-thienyl end and hence no further thienyl−thienyl coupling. These electrogenerated dinuclear complexes are soluble and they do not lead to further polymerization or film formation.

Conclusion

Using ESMS as a guide, we have successfully constructed novel mononuclear and dinuclear thienylplatinum complexes with different bridging coligands. The nuclear selectivity can be easily controlled by the choice of the N-spacer. The electrochemical experiments led to promising metal-

 © 2004 Wiley-VCH Verlag GmbH & Co. KGaA, Weinheim

containing thin films from electrocycling of dinuclear complexes with a thiophene function at either end. The potential for film formation from structurally characterizable materials and the possibility for adjusting the film properties through the use of different spacers would add a new dimension to our current research.

Experimental Section

All reactions were routinely performed under purified nitrogen using standard Schlenk techniques. Solvents used were of reagent grade and were freshly distilled and degassed under purified nitrogen before use. Elemental analyses were carried out in the Chemistry Department of National University of Singapore (NUS). ^{1}H and ^{31}P NMR spectra were recorded on a Bruker ACF 300 MHz spectrometer at ca. 300 K. ^{1}H and ^{31}P NMR chemical shifts are quoted in ppm downfield of Me_4Si and externally referenced to 85% H_3PO_4, respectively.

Electrospray Mass Spectrometry (ESMS): The electrospray mass spectra were recorded in positive-ion mode on a Finningan LCQ spectrometer. The spray voltage was 4.5 kV, and the capillary temperature was 40 °C. The peaks in the ESMS are identified by the most intense *m*/*z* value within the isotopic mass distribution. Isotope patterns were recorded under high-resolution conditions for all major ions and compared with theoretical patterns obtained using the Isotope program.[26] In all cases there was good agreement between the experimental and calculated isotopic mass distributions.

Cyclic Voltammetry (CV): Containers (glassware, polyethylene bottles, etc.) were soaked overnight in 10% HNO_3 prior to use. Electrochemical experiments were performed with an Autolab PGSTAT 30 electrochemical system (Eco Chemie, Netherlands). A locally made three-electrode glass cell of approximately 5 mL capacity was used for all electrochemical experiments. The reference electrode (Ag|$AgNO_3$, 0.01 M in MeCN) was placed in a compartment containing the supporting electrolyte solution separated from the working electrode compartment by a 4 mm diameter Vycor frit. Working electrodes were 3 mm diameter glassy carbon disks.

***trans*-[Pt(PPh$_3$)$_2$(pyrazine)(2-thienyl)][BF$_4$] (2):** To a stirred solution of $AgBF_4$ (19.5 mg, 0.1 mmol) in MeCN (2 mL) was added a solution of [*trans*-PtBr(PPh$_3$)$_2$(2-thienyl)] [88.3 mg, 0.1 mmol in CH_2Cl_2 (10 mL)]. The mixture was stirred, shielded from light, for 1 h and AgBr was removed by filtration. A solution of pyrazine (8.0 g, 0.1 mmol) in CH_2Cl_2 (2 mL) was then added to the colorless filtrate. The mixture was stirred at room temperature for 4 h. The clear pale yellow solution was condensed to about 2 mL under vacuum, and the pale yellow solid residue of complex **2** (92.0 mg, 95%) was collected by adding Et_2O. The product was purified by recrystallization from CH_2Cl_2/hexane to give pale yellow crystals. $C_{44}H_{37}BF_4N_2P_2PtS$ (969.69): calcd. C 54.5, H 3.85, N 2.89, S 3.30; found C 54.38, H 3.59, N 2.85, S 3.51. ^{1}H NMR ($CDCl_3$): δ = 7.2−7.5 (m, 60 H, phenyl), 8.21 (d, 1 H, pyrazine), 7.96 (d, 1 H, pyrazine), 6.93 (d, 1 H, thiophene), 6.37 (t, 1 H, thienyl), 5.94 (d, 1 H, thienyl) ppm. ^{31}P NMR ($CDCl_3$): δ = 18.34 (s) ppm.

***trans*-[Pt(2-chloropyrazine)(PPh$_3$)$_2$(2-thienyl)][BF$_4$] (3):** The synthesis follows that of **2**. 2-Chloropyrazine (11.5 mg, 0.1 mmol) and [*trans*-PtBr(2-thienyl)(PPh$_3$)$_2$] (88 mg, 0.1 mmol) gave a light yellow powder of complex **3** (98.8 mg, 94%). Recrystallization from CH_2Cl_2/Et_2O gave light yellow crystals. $C_{44}H_{36}BClF_4N_2P_2PtS$ (1004.13): calcd. C 52.63, H 3.61, N 2.79, S 3.19; found C 52.28, H 3.12, N 2.55, S 3.58. ^{1}H NMR ($CDCl_3$): δ = 7.2−7.5 (m, 60 H, phenyl), 8.69 (d, 1 H, pyrazine), 7.93 (d, 1 H, pyrazine), 7.61 (s, 1 H, pyrazine), 6.94 (d, 1 H, thiophene), 6.39 (t, 1 H, thiophene), 5.96 (d, 1 H, thiophene) ppm. ^{31}P NMR ($CDCl_3$): δ = 18.12 (s) ppm.

***trans,trans*-[Pt$_2$(μ-4,4′-bipyridine)(PPh$_3$)$_4$(2-thienyl)$_2$][BF$_4$]$_2$ (4):** The synthetic procedure is similar to that of **2**. 4,4′-Bipyridine (7.8 mg, 0.05 mmol) and complex [*trans*-PtBr(2-thienyl)(PPh$_3$)$_2$] (88 mg, 0.1 mmol) gave a pale yellow solid residue of complex **4** (78.5 mg, 80%). $C_{90}H_{74}B_2F_8N_2P_4Pt_2S_2$ (1935.38): calcd. C 55.85, H 3.85, N 1.45, S 3.31; found C 55.40, H 3.79, N 1.38, S 3.83. ^{1}H NMR (MeCN): δ = 7.2−7.5 (m, 60 H, phenyl), 8.48 (d, 4 H, pyridine), 6.89 (d, 4 H, pyridine), 7.03 (d, 2 H, thiophene), 6.35 (t, 2 H, thiophene), 5.37 (d, 2 H, thiophene) ppm. ^{31}P NMR (MeCN): δ = 18.46 (s) ppm.

***trans,trans*-[Pt$_2$(PPh$_3$)$_4$(2-thienyl)$_2$(μ-4,4′-vinylenedipyridine)][BF$_4$]$_2$ (5):** The procedure is similar to that of **2**. 4,4′-Vinylenedipyridine (9.1 mg, 0.05 mmol) and complex [*trans*-PtBr(2-thienyl)(PPh$_3$)$_2$] (88 mg, 0.1 mmol) gave a yellow solid residue of complex **5** (80.3 mg, 82%). Recrystallization from CH_2Cl_2/hexane gave pale yellow crystals. $C_{92}H_{76}B_2F_8N_2P_4Pt_2S_2$ (1961.42): calcd. C 56.34, H 3.91, N 1.43, S 3.27; found C 56.49, H 3.65, N 1.50, S 3.16. ^{1}H NMR ($CDCl_3$): δ = 7.2−7.5 (m, 60 H, phenyl), 7.81 (d, 4 H, pyridine), 7.06 (d, 4 H, pyridine), 7.07 (s, 2 H, pyridine), 6.96 (d, 2 H, thiophene), 6.41 (t, 2 H, thiophene), 5.97 (d, 2 H, thiophene) ppm. ^{31}P NMR ($CDCl_3$): δ = 18.59 (s) ppm.

Crystallography: The diffraction experiments for complexes **3** and **5** were carried out on a Bruker AXS CCD diffractometer with a Mo-K_α sealed tube. The software SMART[27] was used for collecting frames of data, indexing reflections, and determination of lattice parameters, SAINT[27] for integration of intensity of reflections and scaling, SADABS[28] for empirical absorption correction, and SHELXTL[29] for space group and structure determination, refinements, graphics, and structure reporting. In the crystal structures of **3** and **5**, the thienyl groups were disordered. Two independent models were refined in each case. The chlorine atom of the chloropyrazine ligand in **3** was also found to be disordered. The asymmetric unit in **5** has half a dichloromethane solvate molecule and 1.5 mol of disordered water molecules. The positive residual electron densities in **5** were associated with the Pt atom. A summary of crystallographic parameters for the data collections and refinements is given in Table 1. CCDC-182455 and CCDC-182456 contain the supplementary crystallographic data for this paper. These data can be obtained free of charge at www.ccdc.cam.ac.uk/conts/retrieving.html [or from the Cambridge Crystallographic Data Centre, 12, Union Road, Cambridge CB2 1EZ, UK; Fax: (internat.) + 44-1223/336-033; E-mail: deposit@ccdc.cam.ac.uk].

Acknowledgments

The authors acknowledge the National University of Singapore (NUS) for financial support and the technical staff for supporting services, in particular, J. J. Vittal and G. K. Tan for the valuable help in crystallographic analysis and interest in the project, L. J. Chen for spectroscopic assistance, and H. Xu for XPS (NUS Physics) assistance. F. Z. thanks NUS for the research scholarship. X. Xu thanks NUS for a postdoctoral fellowship. We also thank W. Henderson (Waikato) for helpful discussions and advice, and P. Teo for some experimental assistance.

[1] J.-M. Lehn, *Supramolecular Chemistry: Concepts and Perspectives*, VCH, Weinheim, **1995**, 139−160.

[2] [2a] M. Schweiger, S. R. Seidel, A. M. Arif, P. J. Stang, *Angew. Chem. Int. Ed.* **2001**, *40*, 3467−3469. [2b] S. Leininger, B. Olenyuk, P. J. Stang, *Chem. Rev.* **2000**, *100*, 853−908. [2c] M. Fujita, *Chem. Soc. Rev.* **1998**, 27, 417−425. [2d] B. Olenyuk, J. A. Whiteford, A. Fechtenkötter, P. J. Stang, *Nature* **1999**, *398*, 796−799.
[3] R. D. Markwell, I. S. Butler, A. K. Kakkar, M. S. Khan, Z. H. Al-Zakwani, J. Lewis, *Organometallics* **1996**, *15*, 2331−2337.
[4] X. Xu, S. W. A. Fong, Z. H. Li, Z. H. Loh, F. Zhao, J. J. Vittal, W. Henderson, S. B. Khoo, T. S. A. Hor, *Inorg. Chem.* **2002**, *41*, 6838−6845.
[5] Y. Xie, B. M. Wu, F. Xue, S. C. Ng, T. C. W. Mak, T. S. A. Hor, *Organometallics* **1998**, *17*, 3988−3995.
[6] A. J. Heeger, *Angew. Chem. Int. Ed.* **2001**, *40*, 2591−2611.
[7] Y. Xie, B. M. Wu, F. Xue, S. C. Ng, T. C. W. Mak, T. S. A. Hor, *J. Organomet. Chem.* **1997**, *531*, 175−181.
[8] L.-Y. Chia, W. R. McWhinnie, *J. Organomet. Chem.* **1980**, *188*, 121−128.
[9] P. J. Stang, D. H. Cao, *J. Am. Chem. Soc.* **1994**, *116*, 4981−4987.
[10] P. J. Stang, D. H. Cao, S. Saito, A. M. Arif, *J. Am. Chem. Soc.* **1995**, *117*, 6273−6283.
[11] A. Albinati, F. Isaia, W. Kaufmann, C. Sorato, L. M. Venanzi, *Inorg. Chem.* **1989**, *28*, 1112−1122.
[12] [12a] J. B. Fenn, Nobel lecture, **2002**, Stockholm University. [12b]D. L. Zhan, J. B. Fenn, *Int. J. Mass. Spectrom.* **2002**, 219, 1−10. [12c] J. B. Fenn, M. Mann, C. K. Meng, S. F. Wong, C. M. Whitehouse, *Science* **1989**, *246*, 64−71;
[13] [13a] B. F. G. Johnson, J. S. McIndoe, *Coord. Chem. Rev.* **2000**, *200*, 901−932. [13b] D. P. Gallasch, E. R. T. Tiekink, L. M. Rendina, *Organometallics* **2001**, *20*, 3373−3382. [13c] W. Henderson, B. K. Nicholson, L. J. McCaffrey, *Polyhedron* **1998**, *17*, 4291−4313.
[14] [14a] J. S. L. Yeo, J. J. Vittal, T. S. A. Hor, *Eur. J. Inorg. Chem.* **2003**, 277−280. [14b] J. S. L. Yeo, J. J. Vittal, W. Henderson, S. A. Hor, *J. Chem. Soc., Dalton Trans.* **2002**, 328−336. [14c] S. -W. A. Fong, W. T. Yap, J. J. Vittal, T. S. A. Hor, W. Henderson, A. G. Oliver, C. E. F. Rickard, *J. Chem. Soc., Dalton Trans.* **2001**, 1986−2002.
[15] M. D. Levin, J. Stang, *J. Am. Chem. Soc.* **2000**, *122*, 7428−7429.
[16] B. J. Maclean, P. G. Pickup, *J. Mater. Chem.* **2001**, *11*, 1357−1363.
[17] Y. Zhu, M. O. Wolf, *Chem. Mater.* **1999**, *11*, 2995−3001.
[18] [18a] M. Satoh, K. Imanishi, K. Yoshino, *J. Electroanal. Chem.* **1991**, *317*, 139−151. [18b] J. Heinze, H. John, M. Dietrich, P. Tschuncky, *Synth. Met.* **2001**, *119*, 49−52. [18c] J. Roncali, A. Yassar, F. Garnier, *Synth. Met.* **1989**, *28*, C275−C280.
[19] A. Klein, W. Kaim, *Organometallics* **1995**, *14*, 1176−1186.
[20] B. Krische, M. Zagorska, *Synth. Met.* **1989**, *28*, C263−C268.
[21] K. G. Neoh, E. T. Kang, K. L. Tan, *J. Phys. Chem. B* **1997**, *101*, 726−731.
[22] [22a] E. de Wolf, A. J. M. Mens, O. L. J. Gijzeman, J. H. van Lenthe, L. W. Jeneskens, B.-J. Deelman, G. van Koten, *Inorg. Chem.* **2003**, *42*, 2115−2124. [22b] B. H. Aw, K. K. Looh, H. O. Chan, K. L. Tan, T. S. Andy Hor, *J. Chem. Soc., Dalton Trans.* **1994**, 3177−3182.
[23] J. Roncali, *Chem. Rev.* **1992**, *92*, 711−738.
[24] E. Genies, G. Bidan, A. F. Diaz, *J. Electroanal., Chem.* **1983**, *149*, 113.
[25] P. Audebert, J.-M. Catel, G. Le Coustumer, V. Duchenet, P. Hapiot, *J. Phys. Chem. B* **1998**, *102*, 8661−8669.
[26] L. J. Arnold, *J. Chem. Educ.* **1992**, *69*, 811−811.
[27] *SMART & SAINT Software Reference Manuals*, Version 4.0, Siemens Energy & Automation, Inc., Analytical Instrumentation, Madison, WI, **1996**.
[28] G. M. Sheldrick, *SADABS*, a Software for Empirical Absorption Correction, University of Göttingen, **1996**.
[29] G. M. Sheldrick, *SHELXTL*, Version 5.03, Siemens Energy and Automation Inc., Analytical Instrumentation, Madison, WI, **1996**.

Received May 28, 2003
Early View Article
Published Online October 23, 2003

 © 2004 Wiley-VCH Verlag GmbH & Co. KGaA, Weinheim

Synthesis and Crystal Structure of $\{[HNEt_3]_{2n}[Ag_8Ag_{4/2}(SC_6H_4tBu\text{-}4)_{12}]_n \cdot nC_2H_5OH\}$ and Its Reaction Product with CS_2

Kaluo Tang,[a] Xiangjin Xie,[a] Liang Zhao,[a] Yaohua Zhang,[a] and Xianglin Jin*[a]

Keywords: Silver / Polymers / Sulfur / Clusters

By using an arylthiolate ligand with a substituent in the *para*-position, 4-$tBuC_6H_4S^-$, the yellow silver-thiolate complex $\{[HNEt_3]_{2n}[Ag_8Ag_{4/2}(SC_6H_4tBu\text{-}4)_{12}]_n \cdot nC_2H_5OH\}$ (**1**) has been synthesized and structurally characterized. Complex **1** is ionic composed of $[HNEt_3]^+$ cations and a polymeric $[Ag_8Ag_{4/2}(SC_6H_4tBu\text{-}4)_{12}]_n^{2n-}$ anion. Complex **1** reacts with CS_2 in acetone to give a red pentaconta-nuclear silver anionic cluster complex $\{[HNEt_3]_4[Ag_{50}S_7(SC_6H_4tBu\text{-}4)_{40}] \cdot 2CS_2 \cdot 6C_3H_6O\}$ (**2**). The core of the anionic cluster of **2** consists of fifty silver atoms and forty seven sulfur atoms, shaped like a discus with a diameter of ca. 2.0 nm. The factors influencing the structure and the formation mechanism of the large cluster are discussed.

(© Wiley-VCH Verlag GmbH & Co. KGaA, 69451 Weinheim, Germany, 2004)

Introduction

Investigations of syntheses, structures, and properties of large metal clusters, especially nano-sized cluster complexes, continues to attract increasing interest because of their potential use as new materials with unique properties.[1] Recently Müller et al.[2] reported the largest known derivative of a heteropolyacid namely $Na_{48}[H_xMo_{368}O_{1032}(H_2O)_{240}(SO_4)_{48}] \cdot nH_2O$ ($x = 16$: $n = 1000$), with a diameter of ca. 6 nm. An important part of these investigations includes the remarkably large number of reported transition metal mega-clusters with chalcogenide or chalcogenolate ligands.[3] Using the reaction of transition-metal salts with group 16 silyl derivatives $E(SiMe_3)_2$ or $RESiMe_3$ (R = alkyl or aryl; E = S, Se, Te) and tertiary phosphanes, Fenske and co-workers have successfully synthesized a series of transition metal giant clusters,[4] for instance $[Cu_{146}Se_{73}(PPh_3)_{30}]$, $[Ag_{172}Se_{40}(Se\textit{n}Bu)_{92}(dppp)_4]$, $[Ag_{38}Te_{13}(Te\textit{t}Bu)_{12}(dppe)_6]$, $[Au_{18}Se_8(dppe)_6]Cl_2$, and $[Zn_{16}Te_{13}(TePh)_6(tmeda)_5]$. In addition to these huge M−Se and M−Te clusters, two new large Ag−S cluster complexes, $[Ag_{70}S_{16}(SPh)_{34}(PhCO_2)_4$ (triphos)$_4]$ and $[Ag_{188}S_{94}(PR_3)_{30}]$ were recently synthesized by the same route.[5]

Over the last few years one of our major fields of research interest has been the synthesis of transition metal clusters with sulfur or selenium containing ligands.[6,7] We studied the insertion reaction of CS_2 into M−S bonds (M = Ag, Cu, Cd) and applied it to the synthesis of clusters.[8] It was found that the mononuclear insertion products $(PPh_3)_2M(S_2CSR)$ (M = Ag or Cu, R = alkyl or aryl) react easily with various solvents to give a series large cluster complexes, such as $[Ag_{14}(\mu_6\text{-}S)(SPh)_{12}(PPh_3)_8] \cdot 4CH_3OH \cdot 13H_2O$[9] and $[Cu_{14}(\mu_2\text{-}S)(SPh)_{12}(PPh_3)_6]$[10] etc. When cadmium thiolates were reacted with CS_2 in solvents in the absence of PPh_3, several large Cd−S cluster complexes, for example $[S_4Cd_{17}(SPh)_{24}(CH_3OCS_2)_{4/2}]_n \cdot nCH_3OH$[11] and $(Me_4N)_2[Cd_8S(SPh)_{12}Cl_4]$,[12] were obtained. In order to synthesize high-nuclearity clusters, we changed the size and the position of the substituents on the arylthiolate to affect steric control of the ligand and increase solubility. The silver complex $[AgSC_6H_2iPr_3\text{-}2,4,6]_n$ with the bulky sterically hindered arylthiolate ligand reacted with CS_2 in $CHCl_3/C_2H_5OH$ to give a deca-nuclear silver cluster complex $[Ag(SC_6H_2iPr_3\text{-}2,4,6)]_{10} \cdot 2CHCl_3 \cdot C_2H_5OH$.[13] However, the less sterically hindered 4-*tert*-butylthiophenolate containing silver anionic polymeric complex $\{[HNEt_3]_{2n}[Ag_8Ag_{4/2}(SC_6H_4tBu\text{-}4)_{12}]_n \cdot nC_2H_5OH\}$ (**1**) reacted with CS_2 in acetone to give a very large pentaconta-nuclear silver cluster complex. Here we present the syntheses and the X-ray crystal structures of the silver anionic polymeric complex **1** and its reaction product with CS_2, $[HNEt_3]_4[Ag_{50}S_7(SC_6H_4tBu\text{-}4)_{40}] \cdot 2CS_2 \cdot 6C_3H_6O$ (**2**). The latter compound has been reported as a communication.[14]

Results and Discussion

Structure of Complex 1

The X-ray crystal structure determination indicates that complex **1** is ionic and composed of $[HNEt_3]^+$ cations and a polymeric anion $[Ag_8Ag_{4/2}(SC_6H_4tBu\text{-}4)_{12}]_n^{2n-}$, the structure of which is displayed in Figure 1. Selected bond lengths and angles of **1** are presented in Table 1. One structural unit of the polymeric anion is $[Ag_8Ag_{4/2}(SC_6H_4tBu\text{-}4)_{12}]^{2-}$ (Fig-

[a] Institute of Physical Chemistry, College of Chemistry and Molecular Engineering, Peking University,
Beijing 100871, P. R. China
E-mail: jt1939@pku.edu.cn

 © 2004 Wiley-VCH Verlag GmbH & Co. KGaA, Weinheim DOI: 10.1002/ejic.200300392

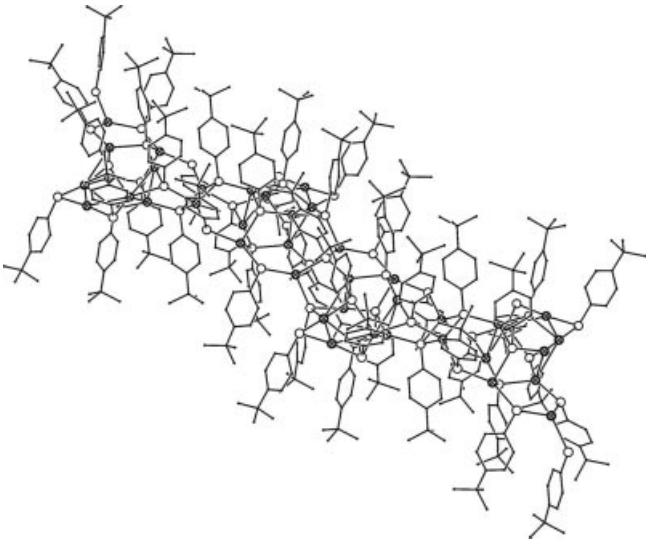

Figure 1. Structure of the polymeric anion $[Ag_8Ag_{4/2}(SC_6H_4tBu\text{-}4)_{12}]_n^{2n-}$ in **1**

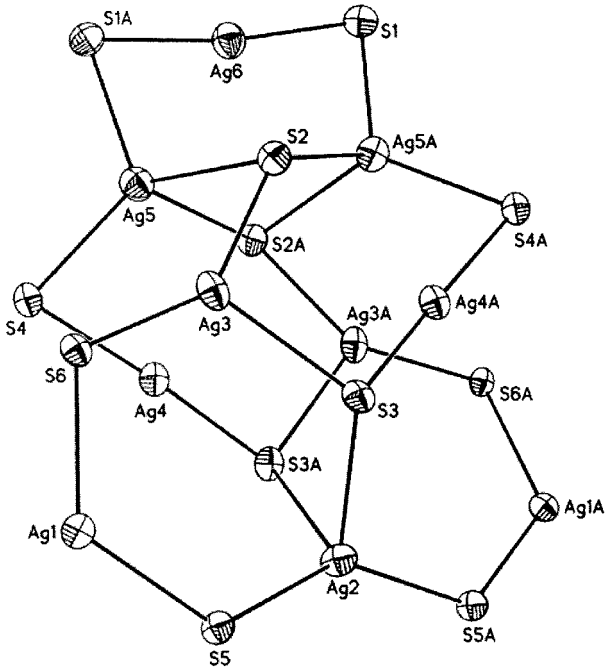

Figure 2. Structure of the $(Ag_8Ag_{4/2}S_{12})$ core of one structural unit $[Ag_8Ag_{4/2}(SC_6H_4tBu\text{-}4)_{12}]^{2-}$ in **1** with atom labeling

ure 2), in which there is a two-fold axis through the Ag2 and Ag6 atoms represented by $Ag_{4/2}$ in the formula. There are six Ag_3S_3 cycles fused into one unit. Another structural unit can be produced by the center of symmetry, which is

Table 1. Selected interatomic distances [Å] and angles [°] for complex **1**

Ag(1)−S(5)	2.5455(15)	Ag(5)−S(2)	2.6456(17)
Ag(1)−S(6)	2.5904(16)	Ag(5)−S(2)#2[a]	2.7348(17)
Ag(1)−S(4)#1[a]	2.6611(16)	Ag(5)−Ag(6)	3.0808(9)
Ag(1)−S(6)#1	2.6721(16)	Ag(6)−S(1)#2	2.3826(17)
Ag(2)−S(5)	2.5503(14)	Ag(6)−S(1)	2.3826(17)
Ag(2)−S(5)#2	2.5503(14)	Ag(6)−Ag(5)#2	3.0808(9)
Ag(2)−S(3)#2	2.6865(16)	S(1)−C(11)	1.766(6)
Ag(2)−S(3)	2.6865(16)	S(1)−Ag(5)#2	2.6058(18)
Ag(3)−S(6)	2.4442(14)	S(2)−C(21)	1.774(6)
Ag(3)−S(2)	2.4843(17)	S(2)−Ag(5)#2	2.7348(17)
Ag(3)−S(3)	2.6857(16)	S(3)−C(31)	1.775(5)
Ag(3)−Ag(4)	2.9641(9)	S(3)−Ag(4)#2	2.3686(16)
Ag(3)−Ag(5)	3.2920(9)	S(4)−C(41)	1.785(6)
Ag(4)−S(3)#2	2.3686(16)	S(4)−Ag(1)#1	2.6611(16)
Ag(4)−S(4)	2.3845(16)	S(5)−C(51)	1.778(6)
Ag(4)−Ag(5)	3.1720(9)	S(6)−C(61)	1.777(5)
Ag(5)−S(4)	2.5564(16)	S(6)−Ag(1)#1	2.6720(16)
Ag(5)−S(1)#2	2.6058(18)		
S(5)−Ag(1)−S(6)	124.67(5)	S(4)−Ag(5)−S(2)#2	107.66(5)
S(5)−Ag(1)−S(4)#1	114.08(5)	S(1)#2−Ag(5)−S(2)#2	112.07(5)
S(6)−Ag(1)−S(4)#1	112.13(5)	S(2)−Ag(5)−S(2)#2	80.44(6)
S(5)−Ag(1)−S(6)#1	122.90(5)	S(1)#2−Ag(6)−S(1)	170.44(9)
S(6)−Ag(1)−S(6)#1	88.13(5)	Ag(6)−S(1)−Ag(5)#2	76.14(5)
S(4)#1−Ag(1)−S(6)#1	86.60(5)	Ag(3)−S(2)−Ag(5)	79.77(5)
S(5)−Ag(2)−S(5)#2	139.75(7)	Ag(3)−S(2)−Ag(5)#2	128.70(6)
S(5)−Ag(2)−S(3)	99.94(5)	Ag(5)−S(2)−Ag(5)#2	94.24(5)
S(5)#2−Ag(2)−S(3)	111.19(5)	Ag(4)#2−S(3)−Ag(3)	94.32(6)
S(5)#2−Ag(2)−S(3)#2	99.94(5)	Ag(4)#2−S(3)−Ag(2)	116.53(6)
S(3)−Ag(2)−S(3)#2	78.17(7)	Ag(3)−S(3)−Ag(2)	119.19(6)
S(6)−Ag(3)−S(2)	142.86(5)	Ag(4)−S(4)−Ag(5)	79.80(5)
S(6)−Ag(3)−S(3)	115.15(5)	Ag(4)−S(4)−Ag(1)#1	108.46(6)
S(2)−Ag(3)−S(3)	101.08(5)	Ag(5)−S(4)−Ag(1)#1	130.20(6)
S(3)#2−Ag(4)−S(4)	172.33(5)	Ag(1)−S(5)−Ag(2)	122.42(6)
S(4)−Ag(5)−S(1)#2	119.01(6)	Ag(3)−S(6)−Ag(1)	112.71(6)
S(4)−Ag(5)−S(2)	125.60(5)	Ag(3)−S(6)−Ag(1)#1	118.25(6)
S(1)#2−Ag(5)−S(2)	105.38(6)	Ag(1)−S(6)−Ag(1)#1	91.87(5)

[a] Symmetry transformations used to generate equivalent atoms: #1 $-x, -y + 1, -z + 1$; #2 $-x, y, -z + 1/2$.

 © 2004 Wiley-VCH Verlag GmbH & Co. KGaA, Weinheim

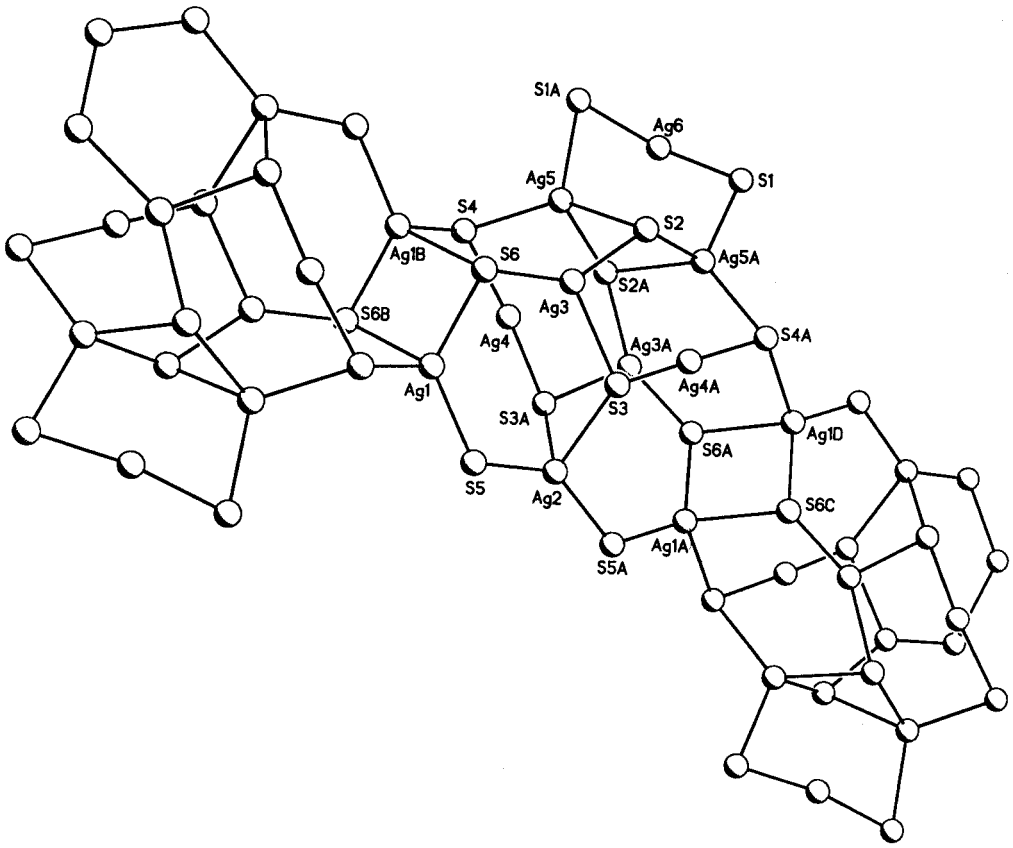

Figure 3. Structure of the $(Ag_8Ag_{4/2}S_{12})_n$ core of the polymeric anion $[Ag_8Ag_{4/2}(SC_6H_4tBu\text{-}4)_{12}]_n^{2n-}$ in **1**

at the center of the Ag_2S_2 monocycle (Ag1 S6 Ag1B S6B). Repeating the inversion symmetry operation produces a one-dimensional polymeric structure. The structure of the core of the polymeric anion of **1** is presented in Figure 3.

In the polymeric anion of **1**, all S atoms are derived from the aryl-thiolate ligands 4-tBuC$_6$H$_4$S$^-$. They are the μ_2-S (S1 and S5) and the μ_3-S (S2, S3, S4, S6) bridges to the Ag atoms. The S1 atom bridges Ag6 and Ag5A, and the angle Ag6−S1−Ag5A is 76.14 (5)°. The bond distances Ag6−S1 and Ag5A−S1 which are 2.383(2) and 2.606(2) Å, respectively are significantly different. The S5 atom bridges Ag1 and Ag2, and the angle Ag1−S5−Ag2 is 122.42(6)°. The bond distances Ag1−S5 and Ag2−S5 which are 2.546(2) and 2.550(2) Å, respectively are similar. With regards to the mean distances of the μ_3-S bridges to the Ag atoms, one is short [av. 2.449 Å (2.385−2.4845 Å)], and two are longer [av. 2.639 Å (2.556−2.735 Å)].

There are three coordination modes observed between all silver atoms and the sulfur donors: the linear, diagonally coordinated silver centers (Ag4, Ag6) exhibit an average Ag−S distance of 2.380 Å (2.383−2.369 Å), the trigonally coordinated silver centers (Ag3) exhibit an average Ag−S distance of 2.538 Å (2.444−2.686 Å) and the tetrahedrally coordinated silver centers (Ag1, Ag2, Ag5) exhibit an average Ag−S distance of 2.624 Å (2.546−2.672 Å). There are Ag−Ag interactions among the Ag atoms (Ag3, Ag4, Ag5, Ag6 Ag3A, Ag4A, Ag5A) in the unit of the polymeric anion of **1**. The Ag−Ag contacts which vary between 2.964−3.292 Å are shorter than the sum of the van der Waals radii of two Ag atoms (3.44 Å), and longer than the Ag−Ag distance in metallic Ag (2.886 Å). This may suggest they are related by so-called agentophilicity.[19] The Ag···Ag distances among those Ag atoms (Ag1, Ag2, Ag1A) are longer than 3.44 Å, which indicates that they are non-bonding and involved in very weak interactions.

Structure of Complex 2

An X-ray crystal structure determination revealed that **2** is an ionic complex composed of four $[HNEt_3]^+$ cations and an anionic cluster $[Ag_{50}S_7(SC_6H_4tBu\text{-}4)_{40}]^{4-}$. The selected bond lengths of **2** are presented in Table 2. The structure of the anionic cluster, which possesses a two-fold axis through Ag8 and Ag26, is shown in Figures 4 and . The core of the anionic cluster consists of fifty silver atoms and forty seven sulfur atoms. The shape of the core is discus-like, the inner part of which is the thickest. There is a pseudo five-fold axis at the core. The fifty Ag atoms are organized into three parts, as shown in Figure 5. In the inner part exists an Ag_{15} pentagonal prismatic unit, consisting of three overlapping Ag_5 pentagonal planar layers. The Ag−Ag distances are between 2.950 and 3.458 Å (mean 3.174 Å) in the pentagons and between 3.164 and 3.257 Å (mean 3.214 Å) between the layers. There are twenty Ag atoms in the intermediate part forming a distorted flat Ag_{20} decagonal prism, of which the

 © 2004 Wiley-VCH Verlag GmbH & Co. KGaA, Weinheim

Table 2. Selected interatomic distances [Å] for complex **2**

Ag(1)−S(1)	2.400(5)	Ag(17)−Ag(18)#1[a]	3.150(2)
Ag(1)−S(15)	2.538(5)	Ag(17)−Ag(18)	3.243(2)
Ag(1)−S(15)#1	2.614(5)	Ag(17)−Ag(2D)	4.105(4)
Ag(1)−Ag(17)	3.158(2)	Ag(18)−S(14)	2.438(5)
Ag(1)−Ag(18)	3.333(2)	Ag(18)−S(22)	2.642(4)
Ag(1)−Ag(2)	3.437(2)	Ag(18)−S(15)#1	2.698(5)
Ag(1)−Ag(1)#1	3.672(3)	Ag(18)−S(23)#1	2.710(5)
Ag(2)−S(2)	2.491(6)	Ag(18)−Ag(2B)	3.074(8)
Ag(2)−S(1)	2.493(6)	Ag(18)−Ag(17)#1	3.150(2)
Ag(2)−S(13)	2.703(5)	Ag(18)−Ag(2C)	3.270(3)
Ag(2)−S(14)	2.730(5)	Ag(18)−Ag(2A)	3.721(3)
Ag(2)−Ag(3)	3.438(3)	Ag(18)−Ag(2D)	4.224(5)
Ag(3)−S(2)	2.426(6)	Ag(19)−S(19)	2.423(5)
Ag(3)−S(12)	2.563(6)	Ag(19)−S(23)	2.463(6)
Ag(3)−S(11)	2.590(5)	Ag(19)−Ag(2A)#1	2.933(4)
Ag(3)−Ag(15)	3.154(3)	Ag(19)−Ag(2C)	3.063(3)
Ag(3)−Ag(16)	3.270(3)	Ag(19)−Ag(22)	3.094(3)
Ag(3)−Ag(4)	3.665(3)	Ag(19)−Ag(2D)	3.451(4)
Ag(4)−S(3)	2.427(7)	Ag(19)−S(31)	3.574(8)
Ag(4)−S(12)	2.475(5)	Ag(19)−Ag(2B)#1	3.596(11)
Ag(4)−S(11)	2.696(6)	Ag(2A)−Ag(2B)	1.077(9)
Ag(4)−Ag(5)	3.010(2)	Ag(2A)−S(31)#1	2.349(8)
Ag(4)−Ag(13)	3.470(3)	Ag(2A)−S(23)#1	2.539(6)
Ag(4)−Ag(14)	3.522(3)	Ag(2A)−S(21)	2.706(7)
Ag(5)−S(3)	2.456(7)	Ag(2A)−Ag(19)#1	2.933(4)
Ag(5)−S(4)	2.597(5)	Ag(2A)−Ag(2D)	3.055(4)
Ag(5)−S(10)	2.605(4)	Ag(2A)−Ag(24)	3.155(4)
Ag(5)−S(9)	2.630(5)	Ag(2A)−Ag(2C)	3.260(3)
Ag(5)−Ag(6)	3.647(2)	Ag(2B)−S(21)	2.202(11)
Ag(6)−S(4)	2.406(6)	Ag(2B)−S(23)#1	2.345(10)
Ag(6)−S(7)	2.470(6)	Ag(2B)−Ag(2C)	3.222(7)
Ag(6)−S(8)	2.811(6)	Ag(2B)−Ag(2D)	3.460(9)
Ag(6)−Ag(12)	3.102(2)	Ag(2B)−Ag(24)	3.528(9)
Ag(6)−Ag(11)	3.407(3)	Ag(2B)−Ag(19)#1	3.596(10)
Ag(6)−Ag(7)	3.747(3)	Ag(2C)−Ag(2D)	1.370(5)
Ag(7)−S(5)	2.411(6)	Ag(2C)−S(20)	2.266(6)
Ag(7)−S(7)	2.492(6)	Ag(2C)−S(22)	2.275(5)
Ag(7)−S(8)	2.752(6)	Ag(2C)−Ag(2D)#1	2.826(4)
Ag(7)−Ag(9)	3.291(2)	Ag(2C)−Ag(2F)	2.919(4)
Ag(7)−Ag(8)	3.412(2)	Ag(2D)−Ag(2D)#1	1.742(8)
Ag(7)−Ag(10)	3.425(3)	Ag(2D)−Ag(2F)	2.032(5)
Ag(8)−S(5)#1	2.483(7)	Ag(2D)−S(31)	2.609(8)
Ag(8)−S(5)	2.483(7)	Ag(2D)−S(22)	2.642(7)
Ag(8)−S(6)#1	2.715(5)	Ag(2D)−S(31)#1	2.727(7)
Ag(8)−S(6)	2.715(5)	Ag(2D)−S(20)	2.776(6)
Ag(9)−S(6)	2.404(5)	Ag(2D)−Ag(2C)#1	2.826(4)
Ag(9)−S(17)	2.454(5)	Ag(2D)−Ag(2E)	2.981(5)
Ag(9)−Ag(26)	2.946(3)	Ag(2D)−Ag(2F)#1	3.143(5)
Ag(9)−S(16)	3.055(5)	Ag(22)−S(19)	2.451(6)
Ag(9)−Ag(11)	3.091(2)	Ag(22)−S(31)	2.540(6)
Ag(9)−Ag(25)	3.100(3)	Ag(22)−S(16)	2.552(6)
Ag(9)−Ag(10)	3.109(3)	Ag(22)−Ag(2E)	3.207(4)
Ag(9)−S(7)	3.131(6)	Ag(22)−Ag(2F)	3.229(4)
Ag(10)−S(6)#1	2.410(5)	Ag(22)−Ag(25)	3.458(3)
Ag(10)−S(8)	2.668(7)	Ag(2E)−Ag(2F)	1.178(4)
Ag(10)−S(17)	2.678(5)	Ag(2E)−S(17)	2.213(6)
Ag(10)−S(18)	2.790(6)	Ag(2E)−S(20)	2.279(6)
Ag(10)−Ag(12)	3.015(3)	Ag(2E)−Ag(24)	3.117(4)
Ag(10)−Ag(25)#1	3.233(4)	Ag(2E)−Ag(26)	3.288(4)
Ag(10)−Ag(26)	3.649(3)	Ag(2E)−S(31)	3.424(8)

Table 2. *(Continued)*

Ag(11)−S(9)	2.445(5)	Ag(2F)−S(31)#1	2.559(6)
Ag(11)−S(17)	2.578(5)	Ag(2F)−S(20)	2.580(5)
Ag(11)−S(16)	2.627(6)	Ag(2F)−S(31)	2.582(7)
Ag(11)−S(7)	2.798(5)	Ag(2F)−S(17)	2.735(6)
Ag(11)−Ag(2E)	3.204(4)	Ag(2F)−Ag(26)	2.792(4)
Ag(11)−Ag(12)	3.424(3)	Ag(2F)−Ag(2D)#1	3.143(5)
Ag(11)−Ag(22)	3.475(3)	Ag(2F)−Ag(24)	3.211(4)
Ag(11)−Ag(2F)	4.081(4)	Ag(2F)−Ag(2F)#1	3.318(7)
Ag(12)−S(10)	2.419(5)	Ag(24)−S(18)	2.413(6)
Ag(12)−S(8)	2.509(6)	Ag(24)−S(21)	2.519(6)
Ag(12)−S(17)	2.657(5)	Ag(24)−S(31)#1	2.839(7)
Ag(12)−S(18)	3.119(5)	Ag(24)−Ag(25)#1	3.040(3)
Ag(12)−Ag(2E)	3.664(4)	Ag(25)−S(16)	2.394(6)
Ag(12)−Ag(24)	3.805(3)	Ag(25)−S(18)#1	2.409(6)
Ag(12)−Ag(2F)	4.609(4)	Ag(25)−Ag(24)#1	3.040(3)
Ag(13)−S(9)	2.414(5)	Ag(25)−S(31)	3.061(8)
Ag(13)−S(20)	2.520(5)	Ag(25)−Ag(26)	3.180(2)
Ag(13)−S(11)	2.686(5)	Ag(25)−Ag(10)#1	3.233(3)
Ag(13)−S(19)	2.980(6)	Ag(26)−S(17)	2.446(5)
Ag(13)−Ag(15)	3.079(2)	Ag(26)−S(17)#1	2.446(5)
Ag(13)−Ag(2E)	3.137(4)	Ag(26)−Ag(2F)#1	2.792(4)
Ag(13)−Ag(14)	3.348(3)	Ag(26)−Ag(9)#1	2.946(3)
Ag(13)−Ag(22)	3.622(3)	Ag(26)−S(31)	3.175(7)
Ag(13)−Ag(2F)	4.030(4)	Ag(26)−Ag(25)#1	3.180(2)
Ag(14)−S(10)	2.416(5)	Ag(26)−Ag(2E)#1	3.288(4)
Ag(14)−S(21)	2.606(5)	S(6)−Ag(10)#1	2.410(5)
Ag(14)−S(20)	2.612(6)	S(6)−S(6)#1	3.661(9)
Ag(14)−S(12)	2.765(6)	S(15)−Ag(1)#1	2.614(5)
Ag(14)−Ag(16)	2.994(2)	S(15)−Ag(18)#1	2.698(5)
Ag(14)−Ag(24)	3.168(4)	S(18)−Ag(25)#1	2.409(6)
Ag(14)−Ag(2E)	3.240(4)	S(22)−Ag(2C)#1	2.275(5)
Ag(14)−Ag(2F)	3.986(4)	S(22)−Ag(17)#1	2.545(4)
Ag(15)−S(13)	2.449(5)	S(22)−Ag(2D)#1	2.642(7)
Ag(15)−S(11)	2.624(6)	S(22)−Ag(18)#1	2.642(4)
Ag(15)−S(20)	2.659(5)	S(23)−Ag(2B)#1	2.345(10)
Ag(15)−S(19)	2.763(5)	S(23)−Ag(2A)#1	2.539(6)
Ag(15)−Ag(19)	3.047(3)	S(23)−Ag(18)#1	2.710(5)
Ag(15)−Ag(16)	3.270(2)	S(31)−Ag(2A)#1	2.349(8)
Ag(15)−Ag(2C)	3.331(3)	S(31)−Ag(2F)#1	2.559(6)
Ag(15)−Ag(2D)	4.382(4)	S(31)−Ag(2D)#1	2.727(7)
Ag(16)−S(14)	2.404(5)	S(31)−Ag(24)#1	2.839(7)
Ag(16)−S(20)	2.495(5)	S(22)−S(23)#1	3.631(5)
Ag(16)−S(21)	2.879(5)	S(22)−S(23)	3.631(5)
Ag(16)−S(12)	2.903(6)	S(19)−S(20)	3.690(6)
Ag(16)−Ag(2C)	3.001(3)	S(20)−S(21)	3.659(6)
Ag(16)−Ag(2B)	3.086(9)	S(16)−S(17)	3.809(7)
Ag(16)−Ag(2A)	3.882(4)	S(17)−S(18)	3.611(7)
Ag(16)−Ag(2D)	4.058(5)	S(15)−S(15)#1	3.414(10)
Ag(17)−S(13)	2.416(5)	S(13)−S(14)	3.640(6)
Ag(17)−S(22)	2.545(4)	S(11)−S(12)	3.418(7)
Ag(17)−S(15)	2.718(5)	S(9)−S(10)	3.731(6)
Ag(17)−S(23)	2.891(6)	S(7)−S(8)	3.531(7)
Ag(17)−Ag(2C)	3.083(3)	S(6)−S(6)#1	3.661(9)
Ag(17)−Ag(19)	3.094(2)		

[a] Symmetry transformations used to generate equivalent atoms: #1 $-x, -y + 1, -z + 1$; #2 $-x, y, -z + 1/2$; #3 $-x, -y, -z + 1$. Ag20, Ag21, and Ag23 (Figure 5) are disordered, corresponding to Ag2A, Ag2B, Ag2C, Ag2D, Ag2E, and Ag2F in Table 2.

five Ag_4 rectangle fragments cap the five Ag_6 side faces of the inner pentagonal prism. Each vertex of the rectangle is connected two Ag atoms on the Ag_6 face. The Ag−Ag distances are between 2.994 and 3.424 Å (mean 3.173 Å) in these rectangles and range from 2.946 to 4.137 Å (mean 3.486 Å) between the rectangles and the pentagonal prism. For the fifteen peripheral Ag centers, two out of three Ag atoms are located at the two opposite sides of a rectangle of the intermediate part. The mean Ag−Ag distance from

 © 2004 Wiley-VCH Verlag GmbH & Co. KGaA, Weinheim

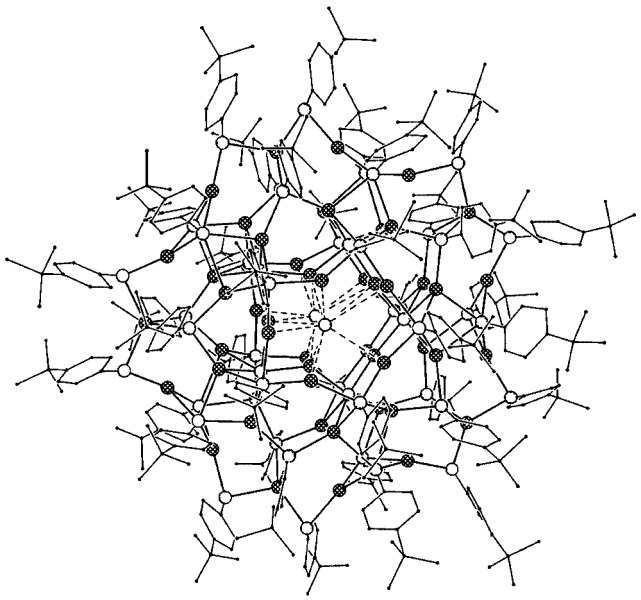

Figure 4. Structure of anionic cluster $[Ag_{50}S_7(SC_6H_4tBu\text{-}4)_{40}]^{4-}$ in **2**

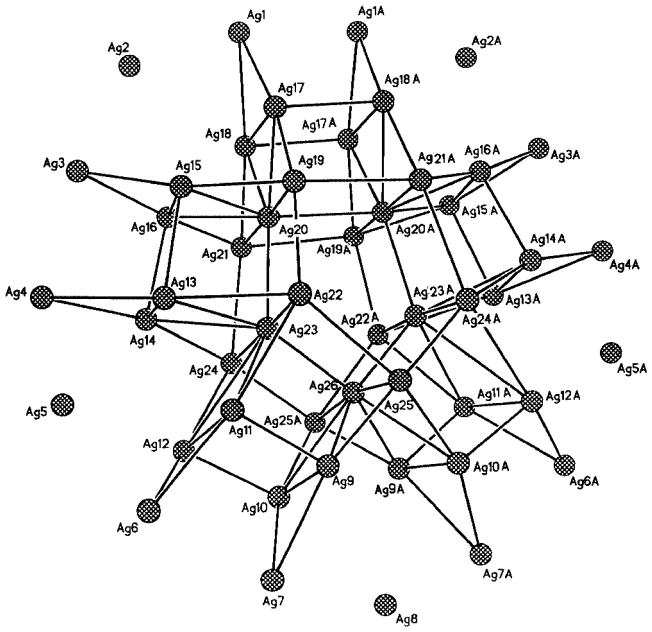

Figure 5. Skeleton structure of the Ag atoms in **2** with atom labeling

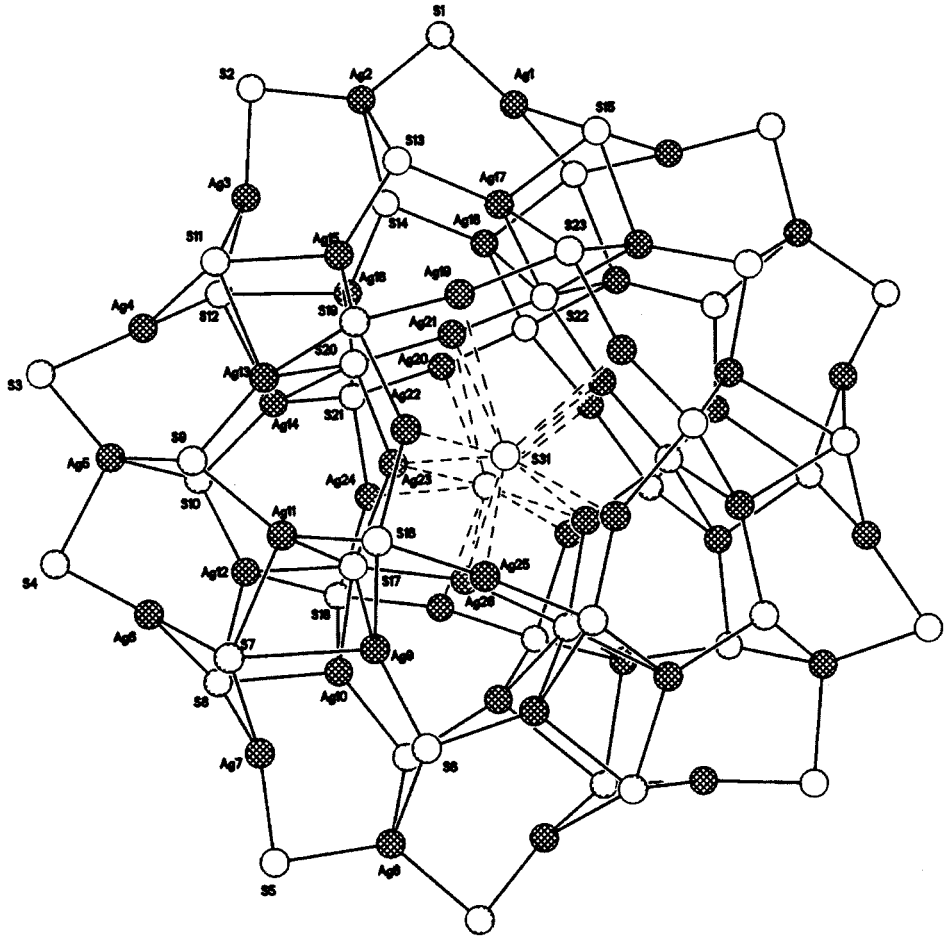

Figure 6. Structure of the $Ag_{50}S_{47}$ core of the anionic cluster in **2** with atom labeling and Ag−Ag interactions omitted; the cross-hatched circles represent the Ag atoms and the open circles represent the S atoms

 © 2004 Wiley-VCH Verlag GmbH & Co. KGaA, Weinheim

these peripheral Ag atoms to the vertices of the rectangles is 3.313 Å (3.102−3.522 Å), and the distances between two peripheral Ag atoms lie in the range of 3.010−3.747 Å.

Of the forty seven S atoms, forty of them are derived from the arylthiolate ligands 4-*t*BuC$_6$H$_4$S$^-$, and seven constitute the S^{2-} ligands. The coordination modes of these S atoms to the Ag atoms fall into several categories, as shown in Figure 6. The arrangement of the fortyfive S atoms is similar to the fifty silver atoms. In the inner region, a S_{15} pentagonal prism is located between the Ag_{15} pentagonal prism and the Ag_{20} decagonal prism, and the S_{15} pentagonal prism is staggered relative to the Ag_{15} pentagonal prism. The ten S atoms at the two outer pentagonal layers of the S_{15} unit are from the arylthiolate ligands, each of which coordinates to four silver atoms. Two of the four Ag−S distances are short (2.394−2.552Å, mean 2.452 Å) and the other two are longer (2.606−3.119Å, mean 2.842 Å). However, the five S atoms in the middle layer of the S_{15} unit exist as S^{2-} ligands, each of which bonds six Ag atoms. The mean distance of the μ_6-S bridging ligands to the silver atoms is 2.545 Å (2.430−2.678 Å). The S_{20} decagonal prism in the intermediate region is larger than the Ag_{20} decagonal prism, and also staggered relative to the Ag_{20} polyhedron. All twenty S atoms are from the arylthiolates, which coordinate to the peripheral Ag atoms and the Ag centers of the Ag_{20} unit. Ten S atoms of the S_{20} unit are μ_4-S bridges and another ten S atoms are μ_3-S bridges. With regards to the mean distance of the μ_3-S bridging ligands to the silver atoms, one is short (2.404−2.449 Å, mean 2.422 Å), and two are longer (2.605−2.730 Å, mean 2.677 Å). The μ_4-S bridging ligands exhibit two short (2.470−2.668 Å, mean 2.554 Å) and two long (2.686−3.131 Å, mean 2.796 Å) distances to the silver atoms. Finally, the peripheral ten S atoms of the arylthiolates μ_2- bridge the fifteen peripheral Ag atoms three of which have two μ_2-S bridges. The mean μ_2-S−Ag distance is 2.459 Å (2.400−2.597 Å). Additionally, there are two S^{2-} ligands in the inner Ag_{15} pentagonal prism, which are located between the pentagonal layers (Figure 6). The distances between each S^{2-} ligand and the Ag atoms are different, since the Ag20, Ag21 and Ag23 atoms are disordered. The observed Ag−S distances lie in the range of 2.449−3.781 Å. Within the S polyhedra, all the S−S distances are larger than 3.414 Å.

The core of the discus-shaped cluster, which is a nanocluster, has a diameter of ca. 2.0 nm. The core of the Ag−S cluster is surrounded by 4-*tert*-butylthiophenolate ligands leading to a diameter of ca. 2.9 nm and a maximum depth of ca. 2.2 nm. Two CS_2 solvent molecules fill in the channel-like cavities formed by the thiophenolates (Figure 7). The six acetone solvent molecules and four [HNEt$_3$]$^+$ cations are located in the bigger cavities formed by the clusters. The solvent molecules are easy to remove so that the unsolvated compound was used for elemental analysis.

It is of note that in the formation of the cluster complex **2**, the S^{2-} ligands were not added via a reagent. However, the S^{2-} ligands are essential for the formation of large clusters, since they bind the metal ions together. We have also found that in our previously reported large complexes, $[Ag_{14}(\mu_6\text{-}S)(SPh)_{12}(PPh_3)_8]\cdot 4CH_3OH\cdot 13H_2O$,[9] $[Cu_{14}(\mu_2\text{-}S)(SPh)_{12}(PPh_3)_6]$,[10] and $[S_4Cd_{17}(SPh)_{24}(CH_3OCS_2)_{4/2}]_n\cdot$

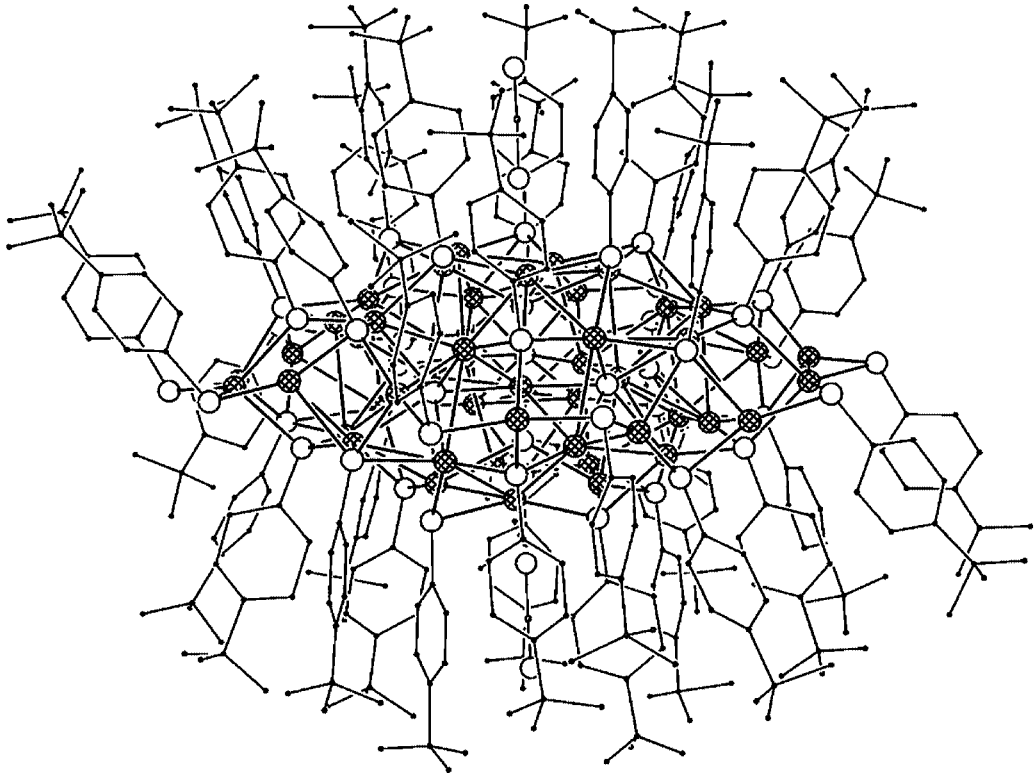

Figure 7. Structure of anionic cluster $[Ag_{50}S_7(SC_6H_4t\text{Bu-}4)_{40}]^{4-}$ in **2** with CS_2 solvent molecules in the channel-like cavities formed by the thiophenolates

 © 2004 Wiley-VCH Verlag GmbH & Co. KGaA, Weinheim

$n$$CH_3OH$[11] etc., the S^{2-} ligands are formed from the reaction of CS_2 with RS^- in solution. We suggest that when the metal thiolate compound is dissolved, the solvent causes it to dissociate into various "active fragments", including RS^-, which reacts with CS_2 resulting in the formation of S^{2-} ions, as shown in Equation (1).[8]

$$RS^- + CS_2 \longrightarrow RS\text{-}CSS \overset{RS^-}{\rightleftharpoons} RS\text{-}CS\text{-}SR + S^{2-} \quad (1)$$

The new product is formed by the optimum "self-assembly" of these active fragments and then crystallizes from the solution. This new method for the synthesis of large M-S clusters has many advantages compared with other methods. The S^{2-} anions result from the equilibrium reaction. When large clusters are formed, the S^{2-} anions are used and the position of equilibrium shifts to right and the formation of S^{2-} is slow. However, the direct addition of reagents such as Na_2S, S, NaHS, or $S(SiMe_3)_2$ may cause M_xS_y precipitation because the reaction is rapid and difficult to control. In the formation of the **2**, the reaction conditions are mild (room temperature) and easy to control and a moderate yield of 67% was observed. This result suggests that this is a promising method although further investigations are needed.

We have found that silver thiolate complexes, $(AgSR)_n$, such as $(AgS$*t*$Bu)_n$, $(AgSC_6H_5)_n$, or $(AgSC_6H_2Me_3$-2,4,6$)_n$ with less bulky substituents hardly react with CS_2 and are insoluble in inert solvents. However, by increasing the size of the substituents, the polymeric complex $(AgSC_6H_2$*i*Pr_3-2,4,6$)_n$ with sterically hindered arylthiolate ligands reacts readily with CS_2 in solution to give a decanuclear silver cluster complex $[Ag(SC_6H_2$*i*Pr_3-2,4,6$)]_{10}$.[13] The arylthiolates with bulky substituents in the *ortho*-positions are more sterically congested than those with substituents in the *para*-position and this limits the cluster size. In this study, by the use of an arylthiolate ligand, 4-*t*$BuC_6H_4S^-$, with a substituent in the *para*-position, we obtained a large pentaconta-nuclear silver cluster complex **2**. However, using the arylthiolate ligand, 4-*i*$PrC_6H_4S^-$, with a less bulky substituent in the *para*-position, a larger hexaconta-nuclear silver cluster complex $[HNEt_3]_4[Ag_{60}S_7(SC_6H_4$*i*$Pr-4)_{50}]$ (**3**) has been recently synthesized by the same method.[20] Complex **3** is also ionic composed of four $[HNEt_3]^+$ cations and an anionic cluster $[Ag_{60}S_7(SC_6H_4$*i*Pr-4$)_{50}]^{4-}$, the structure of which is very similar to that of $[Ag_{50}S_7(SC_6H_4$*t*Bu-4$)_{40}]^{4-}$, as shown in Figure 8. The core of the anionic cluster **3** consists of sixty silver atoms and fifty seven sulfur atoms. The shape of the core is discus-like, the inner part of which is the thickest. This fact once again demonstrates the rule we have observed that the less bulky the R group in $(AgSR)_n$, the more the degree of the association, n.[6] Clearly, however, the factors influencing the formation and structures of large clusters need to be further investigated.

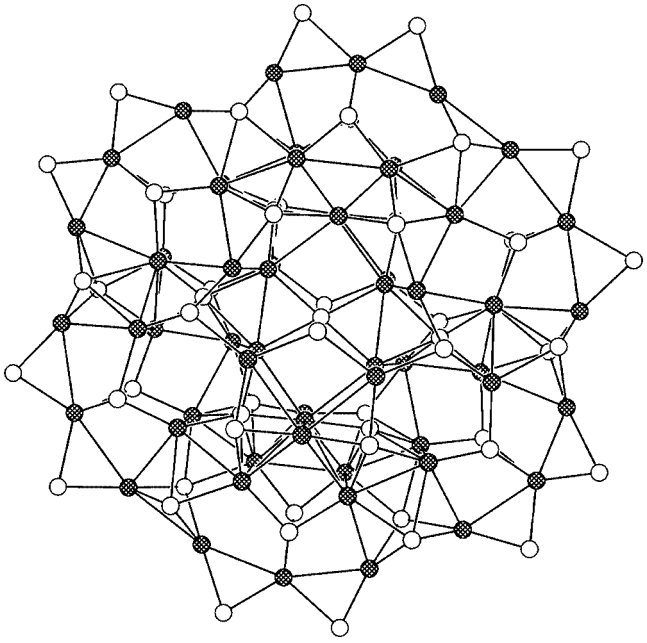

Figure 8. Structure of the $Ag_{60}S_{57}$ core of the anionic cluster $[Ag_{60}S_7(SC_6H_4$*i*Pr-4$)_{50}]^{4-}$ in **3**; the cross-hatched circles represent the Ag atoms and the open circles represent the S atoms

Experimental Section

Reactions were carried out under a nitrogen atmosphere using standard Schlenk techniques. Solvents were dried and distilled under nitrogen. Infrared spectra were recorded in KBr discs with a Nicolet-550 spectrometer. Elemental analyses were carried out using an Elemantar Vario EL analyzer. Melting points were measured with an X_6 microscopic melting point apparatus.

Complex 1: A solution of 4-*t*BuC_6H_2SH[15] (0.38 cm^3, 2.3 mmol) and Et_3N (0.32 cm^3, 2.3 mmol) in C_2H_5OH (8 cm^3) was added dropwise with stirring to a solution of $AgNO_3$ (274 mg, 1.6 mmol) in CH_3CN (5 cm^3). After stirring overnight at room temperature under a nitrogen atmosphere, the solvents were removed. The residue was dried in vacuo and then recrystallized from ethanol to afford a yellow powder (470 mg, yield 89.1%). Yellow crystals of **1** suitable for X-ray diffraction analysis were obtained by slow evaporation of the solvent from the ethanol solution of the crude product at room temperature over two days. m.p. 244.2−246.1 °C. $\{[HNEt_3]_{2n}[Ag_8Ag_{4/2}(SC_6H_4$*t*$Bu-4)_{12}]_n \cdot n C_2H_5OH\}$: calcd. C 48.64, H 6.00, N 0.833; found C 48.40, H 5.676, N 0.790%. IR: $\tilde{\nu}$ = 3057 w, 3019 vw, 2958 vs, 2915 m, 2869 m, 2789 w, 2656 w, 2468 w, 1900 w, 1629 m, 1560 vw, 1483 s, 1465 m, 1393 m, 1361 m, 1268 m, 1190 w, 1159 w, 1118 s, 1080 w, 1018 m, 821 s, 732 w, 588 w, 546 m, 465 w cm^{-1}.

Complex 2: Carbon disulfide (4 cm^3) was added to a yellow-green solution of **1** (20 mg) in acetone (4 cm^3). The solution became golden-yellow and was then filtered. The filtrate gradually became red upon standing. Red block crystals of **2** (yield 67%) suitable for X-ray diffraction analysis were obtained by evaporating the filtrate at room temperature over several days. The crystals of **2** break into pieces and desolvate in a few minutes upon removal of the mother liquor and become black very easily when exposed to light. This necessitates storage with the mother liquor and with the exclusion of light. $Ag_{50}S_{47}C_{424}H_{584}N_4$ (unsolvated): calcd. C 40.30, H 4.66, N 0.443; found C 39.89, H 4.76, N 0.399%. IR: $\tilde{\nu}$ = 3049 w, 2946 vs, 2869 s, 2789 w, 2671 w, 2472 w, 1888 w, 1621 w, 1589 w, 1485

 © 2004 Wiley-VCH Verlag GmbH & Co. KGaA, Weinheim

Table 3. Crystal data and refinement for **1** and **2**

	1	**2**
Empirical formula	$C_{68}H_{100}Ag_5NOS_6$	$C_{444}H_{620}Ag_{50}N_4O_6S_{51}$
M	1679.20	13138.00
T [K]	123(2)	123(2)
Color	yellow	red
Crystal size [mm]	0.50 × 0.20 × 0.20	0.80 × 0.60 × 0.40
Crystal system	Monoclinic	Monoclinic
Space group	*C*2/*c*	*C*2/*c*
a [Å]	38.314(8)	36.486(7)
b [Å]	18.605(4)	36.666(7)
c [Å]	20.288(4)	40.702(8)
α [°]	90.0	90.0
β [°]	103.25(3)	95.21(3)
γ [°]	90.0	90.0
V [Å^3]	14077(5)	54226(16)
Z	8	4
D_c [g·cm^{-3}]	1.585	1.609
F(000)	6832	26104
μ [mm^{-1}]	1.585	1.998
θ range [°]	2.17−27.48	0.79−25.00
No.of reflections collected/unique	56953/16058	148864/44541
R_{int}	0.0494	0.0993
Data/restraints/ parameters	16058/9/806	44541/111/1751
Goodness of fit on F^2	0.773	0.813
Final R indices	$R1$ = 0.0433	$R1$ = 0.0969
[$I > 2\sigma(I)$]	$wR2$ = 0.0916	$wR2$ = 0.2331
R indices (all data)	$R1$ = 0.1083	$R1$ = 0.2694
	$wR2$ = 0.1002	$wR2$ = 0.2907
Largest difference peak and hole [e·Å^{-3}]	1.136, −0.743	3.102, −1.596

s, 1393 m, 1363 m, 1298 w, 1267 m, 1198 w, 1156 w, 1116 s, 1084 w, 1011 m, 820 s, 736 w, 577 w, 548 m, 448 w cm^{-1}.

X-ray Crystal Structure Determination of Complexes 1 and 2: Crystallographic measurements of complexes **1** and **2** were made on a Rigaku R-AXIS RAPID Image Plate diffractometer with graphite monochromated Mo-K_α radiation (λ = 0.71073 Å) operating at 50Kv and 40 mA. Absorption corrections were applied by correction of symmetry-equivalent reflections using the ABSCOR program.[16] The structures were solved by direct methods and successive difference map (SHELXS-97)[17] and refined using full-matrix least-squares on F^2 for all unique data (SHELXL-97).[18] For complex **1**, all non-hydrogen atoms except the C and O atoms in the solvent molecule C_2H_5OH were refined anisotropically. The hydrogen atoms in the benzene groups and the three ordered *t*Bu groups were included in their calculated positions with the rigid model. Other hydrogen atoms were excluded from the refinement. The carbon atoms of the three *t*Bu groups are disordered. The occupancy of the solvent molecules C_2H_5OH were fixed at 0.7. For complex **2**, the Ag, S, and 72 C atoms are anisotropic whilst the N, O, and 150 C atoms are isotropic. Three Ag atoms and six C atoms are disordered. No hydrogen 3atoms were included in the refinement. There are 20 residual peaks (1.00−3.10 e·Å^{-3}) near the Ag atoms.

CCDC-199451 (for **1**) and -178360 (for **2**) contain the supplementary crystallographic data for this paper. These data can be obtained free of charge at www.ccdc.cam.ac.uk/conts/retrieving.html [or from the Cambridge Crystallographic Data Centre, 12, Union Road, Cambridge CB2 1EZ, UK; Fax: (internat.) + 44-1223/336-033; E-mail: deposit@ccdc.cam.ac.uk]. Crystal data and structure refinements for **1** and **2** are presented in Table 3.

Acknowledgments

The work was supported by the NNSF of China (Grant Nos. 29873080 and 29873001).

[1] *Clusters and Colloids. From Theory to Applications* (Ed.: G. Schmid), VCH, Weinheim, Germany, **1994**; *Physics and Chemistry of Metal Cluster Compounds* (Ed.: L. J. de Jongh), Kluwer, Dordrecht, **1994**.
[2] A. Müller, E. Beckmann, H. Bogge, M. Schmidtmann, A. Dress, *Angew. Chem. Int. Ed.* **2002**, *41*, 1162−1167.
[3] I. Dance, K. Fisher, *Prog. Inorg. Chem.* **1994**, *41*, 637−803; J. Arnold, *Prog. Inorg Chem.* **1995**, *43*, 353−417.
[4] H. Krautcheid, D. Fenske, G. Baum, M. Semmelmann, *Angew. Chem. Int. Ed. Engl.* **1993**, *32*, 1303−1306; D. Fenske, N. Y. Zhu, T. Langetepe, *Angew. Chem. Int. Ed.***1998**, 37, 2639−2644; T. Langetepe, D. Fenske, *Z. Anorg. Allg. Chem.* **2001**, *627*, 820−824; D. Fenske, T. Langetepe, M. M. Kappes, O. Hampe. P. Weis, *Angew. Chem. Int. Ed.* **2000**, *39*, 1857−1860; H. Pfistner, D. Fenske, *Z. Anorg. Allg. Chem.* **2001**, *627*, 575−582.
[5] X.-J. Wang, T. Langetepe, C. Persau, B.-S. Kang, G. M. Sheldrick, D. Fenske, *Angew. Chem. Int. Ed.* **2002**, *41*, 3818−3819.
[6] K. Tang, Y. Tang, *Heteroatom Chemistry* (Ed.: E. Block), VCH, New York, **1990**, pp. 345−369.
[7] K. Tang, X. Jin, H. Yan, X. Xie, C. Liu, Q. Gong, *J. Chem. Soc., Dalton Trans.* **2001**, 1374−1377.
[8] K. Tang, X. Jin, Y. Tang, *Reviews on Heteroatom Chemistry* (Ed.: S. Oae), vol. 15, MYU, Tokyo, Japan, **1996**, pp. 83−114.
[9] X. Jin, K. Tang, W. Liu, H. Zeng, H. Zhao, Y. Ouyang, Y. Tang, *Polyhedron* **1996**, *15*, 1207−1211.
[10] K. Tang, T. Xia, X. Jin, Y. Tang, *Polyhedron* **1993**, *12*, 2895−2898.
[11] X. Jin, K. Tang, S. Jia, Y. Tang, *Polyhedron* **1996**, *15*, 2617−2622.
[12] K. Tang, X. Jin, S. Jia, Y. Tang, *Chin. J. Struct. Chem.* **1995**, *14*, 399−404.
[13] X. Jin, X. Xie, H. Qian, K. Tang, C. Liu, X. Wang, Q. Gong, *Chem. Commun.* **2002**, 600−601.
[14] K. Tang, X. Xie, Y. Zhang, X. Zhao, X. Jin, *Chem. Commun.* **2002**, 1024−1025.
[15] C. Hansch, W. A. Blondon, *J. Am. Chem. Soc.* **1948**, *70*, 1561−1563; E. Bartkus, E. B. Hotelling, *J. Org. Chem.* **1960**, *25*, 232−236.
[16] T. Higashi, *ABSCOR*, Empirical Absorption Correction based on Fourier Series Approximation, Rigaku Corporation, Tokyo, **1995**.
[17] G. M. Sheldrick, *SHELXS 97*, Program for the Solution of Crystal Structures, University of Göttingen, **1997**.
[18] G. M. Sheldrick, *SHELXL 97*, Program for the Refinement of Crystal Structures, University of Göttingen, **1997**.
[19] N. Kaltsoyannis, *J. Chem. Soc., Dalton Trans.* **1997**, 1−11.
[20] K. Tang, X. Xie, L. Zhao, X. Jin, unpublished work. Crystal data for **3**: $[HNEt_3]_4[Ag_{60}S_7(SC_6H_4iPr\text{-}4)_{50}]$, monoclinic, $P2_1/n$, a = 27.891(6), b = 26.421(5), c = 39.155(8) Å, β = 93.01(3)°, V = 28813(10) Å^3, Z = 2.

Received June 24, 2003
Early View Article
Published Online November 6, 2003

 © 2004 Wiley-VCH Verlag GmbH & Co. KGaA, Weinheim

Syntheses, Crystal Structures and Optical Limiting Properties of Three Novel Organometallic Tungsten-Copper-Sulfur Clusters: $[PPh_4][(\eta^5\text{-}C_5Me_5)WS_3(CuCN)_2]$, $[(\eta^5\text{-}C_5Me_5)WS_3Cu_2(PPh_3)(\mu\text{-}CN)]_2$ and $[PPh_4][\{(\eta^5\text{-}C_5Me_5)WS_3Cu_2(CN)(Py)\}_2(\mu\text{-}CN)]$

Jian-Ping Lang,*[a,b] Qing-Feng Xu,[a] Wei Ji,[c] Hendry Izaac Elim,[c] and Kazuyuki Tatsumi[d]

Keywords: Copper / Tungsten / Sulfur / Cluster compounds

Reactions of $[PPh_4][(\eta^5\text{-}C_5Me_5)WS_3]$ with two equivalents of CuCN in MeCN produced a novel trinuclear butterfly-shaped cluster $[PPh_4][(\eta^5\text{-}C_5Me_5)WS_3(CuCN)_2]$ (**1**) in a 70% yield. Treatment of **1** with excess PPh_3 or Py gave rise to two different hexanuclear clusters $[(\eta^5\text{-}C_5Me_5)WS_3Cu_2(PPh_3)(\mu\text{-}CN)]_2$ (**2**) and $[PPh_4][\{(\eta^5\text{-}C_5Me_5)WS_3Cu_2(CN)(Py)\}_2(\mu\text{-}CN)]$ (**3**), respectively. Compounds **1**–**3** were fully characterized by spectroscopy and X-ray crystallography. The structure of the cluster anion of **1** contains a butterfly-like WS_3Cu_2 fragment in which each Cu atom is coordinated to one μ-S atom, one μ_3-S atom, and one terminal CN group. The neutral compound **2** has a double butterfly-shaped structure in which two WS_3Cu_2 fragments are interconnected by two Cu–μ-CN–Cu bridges. The anion of **3** adopts another type of double butterfly-shaped structure in which the two WS_3Cu_2 fragments are linked by a single Cu–μ-CN–Cu bridge. Compared with C_{60} in terms of the optical limiting (OL) properties measured under identical conditions, **1** and **2** exhibit a relatively good OL performance, whereas the OL effect is not observed for **3**.
(© Wiley-VCH Verlag GmbH & Co. KGaA, 69451 Weinheim, Germany, 2004)

Introduction

The reactions of thiomolybdates and thiotungstates $[MO_{4-n}S_n]^{2-}$ (M = Mo, W) with various transition metal halides has been extensively investigated as a result of their rich chemistry.[1−4] Their relation to industrial catalysis,[2] biological systems,[3] and electro/photonic materials has also been demonstrated.[4−5] However, only a few reactions have been reported that are involved in the utilization of metal cyanides such as CuCN and AgCN.[6] So far, a dozen Mo(W)/Cu(Ag)/S clusters containing either a terminal or bridging cyano group around their cluster framework have been prepared.[6−7] Among them, the polymeric clusters $\{[Et_4N]_2[MS_4Cu_4(CN)_4]\}_\infty$ (M = Mo, W) were reported to exhibit large optical limiting (OL) effects in DMF.[7b]

We have recently reported on a series of mixed-metal clusters prepared from the reactions of the organometallic trisulfido complex anions $[(\eta^5\text{-}C_5Me_5)MS_3]^-$ (M = Mo,[8a] W[8b]) with metal halides.[9] Intriguingly, when $[PPh_4][(\eta^5\text{-}C_5Me_5)WS_3]$ was treated with AgCN, a cyano-bridged helical polymer $\{[(\eta^5\text{-}C_5Me_5)WS_3]_2Ag_3(CN)\}_\infty$ was produced.[10] In order to extend the chemistry of $[PPh_4][(\eta^5\text{-}C_5Me_5)WS_3]$, we carried out the reaction of $[PPh_4][(\eta^5\text{-}C_5Me_5)WS_3]$ with CuCN. A discrete trinuclear anionic cluster $[PPh_4][(\eta^5\text{-}C_5Me_5)WS_3(CuCN)_2]$ (**1**) was the only product that was isolated. As discussed later in this paper, the anion of **1** contains two three-coordinate Cu atoms and two terminal CN groups. The coordination geometry around the Cu atoms may be completed, substitution of the CN groups may take place, and the formation of new clusters may be anticipated if suitable donor ligands are used. In this context, the reactions of **1** with excess PPh_3 or Py were performed, and two novel hexanuclear cyano-bridged clusters $[(\eta^5\text{-}C_5Me_5)WS_3Cu_2(PPh_3)(\mu\text{-}CN)]_2$ (**2**) and $[PPh_4][\{(\eta^5\text{-}C_5Me_5)WS_3Cu_2(CN)(Py)\}_2(\mu\text{-}CN)]$ (**3**) were obtained. Furthermore, in our continued efforts to search for good OL materials,[5a−5c] we have also examined the OL properties of **1**−**3** in solution with 7-ns laser pulses at 532 nm. Herein we report on the syntheses and crystal structures of **1**−**3**, along with their OL properties in solution.

[a] School of Chemistry and Chemical Engineering, Suzhou University,
Suzhou, 215006, P. R. China
Fax: (internat.) + 86-512-65224783
E-mail: jplang@suda.edu.cn
[b] State Key Laboratory of Coordination Chemistry, Nanjing University,
Nanjing, 210093, P. R. China
[c] Department of Physics, National University of Singapore,
2 Science Drive 3, 117542 Singapore
[d] Research Center for Materials Science, and Department of Chemistry, Graduate School of Science, Nagoya University,
Furo-cho, Chikusa-ku, Nagoya 464-8602, Japan

 © 2004 Wiley-VCH Verlag GmbH & Co. KGaA, Weinheim **DOI: 10.1002/ejic.200300204**

Results and Discussion

Synthesis and Spectral Characterization

As depicted in Scheme 1, addition of 2 equiv. of CuCN to a red solution of $[PPh_4][(\eta^5\text{-}C_5Me_5)WS_3]$ in MeCN generated a darkened solution, which was stirred for 1 h and filtered. The filtrate was layered with Et_2O, affording $[PPh_4][(\eta^5\text{-}C_5Me_5)WS_3(CuCN)_2]$ (**1**) as red crystals in a 70% yield. Treatment of **1** in MeCN with excess PPh_3 or Py resulted in a homogeneous solution. Subsequent standard workups produced two new clusters, $[(\eta^5\text{-}C_5Me_5)WS_3Cu_2(\mu\text{-}CN)(PPh_3)]_2$ (**2**) as red plates, and $[PPh_4][\{(\eta^5\text{-}C_5Me_5)WS_3Cu_2(CN)(Py)\}_2(\mu\text{-}CN)]$ (**3**) as orange-red needles, respectively. Compounds **1**−**3** are relatively air and moisture stable in the solid state. Compounds **1** and **3** are soluble in DMF and slightly soluble in MeCN. Both **1** and **3** are insoluble in CH_2Cl_2 and $CHCl_3$. Compound **2** dissolves in CH_2Cl_2 and $CHCl_3$, and not in MeCN and DMF.

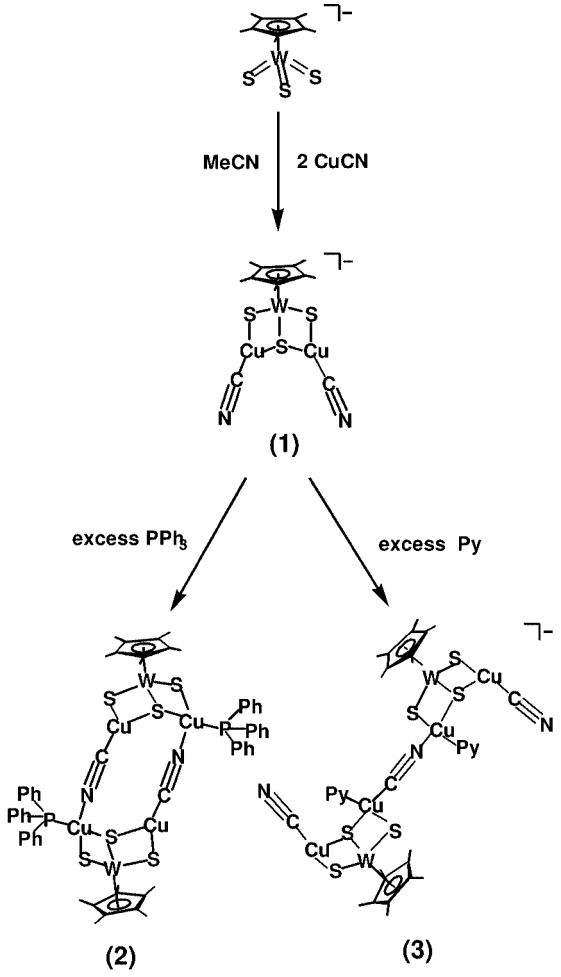

Scheme 1

The FT-IR spectra of **1**−**3** display bands assigned to the W−S_{br} stretching vibrations at 433/410 (**1**), 434/417/409 (**2**) and 445/430/413 (**3**) cm^{-1}, respectively. The IR spectrum of **1** shows a strong terminal C≡N stretching vibration at 2119 cm^{-1}, while that of **2** shows a bridging C≡N stretching vibration at 2139 cm^{-1}. Compound **3** exhibits both a terminal C≡N stretching vibration at 2053 cm^{-1} and a bridging C≡N stretching vibration at 2130 cm^{-1}. The ^1H NMR spectra of **1** and **3** in CD_3CN and of **2** in $CDCl_3$ at ambient temperature display a single resonance assigned to the $\eta^5\text{-}C_5Me_5$ group at 2.05 (**1**), 2.05 (**2**), and 2.08 (**3**) ppm, respectively. The UV/Vis spectra of **1** in MeCN and of **3** in DMF are characterized by three bands at 435, 390, and 214 nm (**1**), 452, 393, and 321 nm (**3**), while that of **2** in CH_2Cl_2 exhibits only one absorbance band at 394 nm. As the electronic spectrum of $[PPh_4][(\eta^5\text{-}C_5Me_5)WS_3]$ in MeCN shows a strong absorbance band at 381 nm,[8b] the bands at 390 (**1**), 394 (**2**), and 393 (**3**) nm observed in the UV/Vis spectra of **1**, **2**, and **3** are red-shifted (Figure 1), and they are probably dominated by the S→W^{VI} charge-transfer transitions of the $(\eta^5\text{-}C_5Me_5)WS_3$ moiety.[9c] The crystal structures of **1**−**3** were further confirmed by single crystal X-ray analysis.

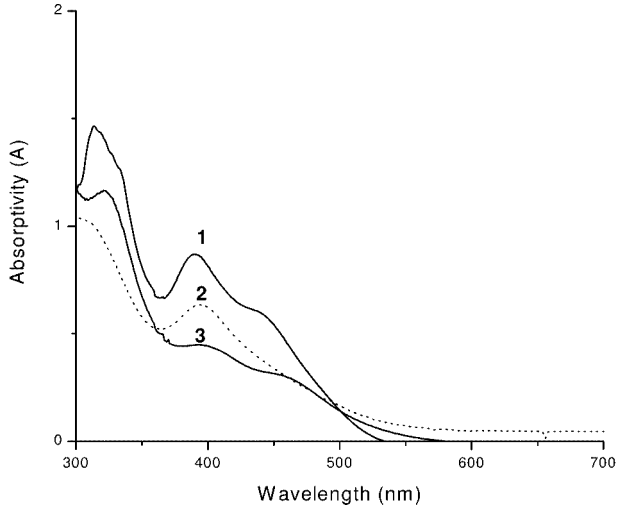

Figure 1. Absorbance spectra of **1** in MeCN, **2** in CH_2Cl_2, and **3** in DMF with a 1-mm optical length

Crystal Structure of $[PPh_4][(\eta^5\text{-}C_5Me_5)WS_3(CuCN)_2]$ (1)

Compound **1**·MeCN crystallizes in the orthorhombic space group $Pna2_1$ and the asymmetric unit contains one discrete anion $[(\eta^5\text{-}C_5Me_5)WS_3(CuCN)_2]^-$, one $[PPh_4]^+$ cation, and one MeCN solvated molecule. The $[PPh_4]^+$ cation does not interact with the cluster anion and all the bond lengths and angles related to this cation are typical. Therefore, Figure 2 only shows the structure of the cluster anion of **1**, and Table 1 lists the selected bond lengths and angles of the cluster anion of **1**. The cluster anion of **1** consists of a $(\eta^5\text{-}C_5Me_5)WS_3$ unit bound to two CuCN groups via one μ_3-S and two μ-S atoms. Alternatively, the anion of **1** may be described as containing a butterfly-shaped WS_3Cu_2 fragment, which has previously been observed in $[MoOS_3(CuSPh)_2]^{2-}$,[6a] $[(\eta^5\text{-}C_5Me_5)WS_3Cu_2(PPh_3)_2Br]$,[9d] $[MoOS_3M'_2(PPh_3)_3]$ (M = W, Mo; M′ = Cu^I, Ag^I),[11a,11b] and $[WS_4Cu_2(dppm)_3]$.[11c] The $(\eta^5\text{-}C_5Me_5)WS_3$ unit of **1** has a slightly distorted three-legged piano stool structure. The mean W−μ-S and W−μ_3-S bond lengths, 2.237 Å and 2.308 Å, are elongated by 0.05 Å and 0.12 Å, respectively,

 © 2004 Wiley-VCH Verlag GmbH & Co. KGaA, Weinheim

relative to that of $[PPh_4][(\eta^5\text{-}C_5Me_5)WS_3]$,[8b] due to the coordination of the sulfur atoms to the Cu atoms. Each Cu atom adopts a trigonal planar geometry, coordinated by one μ-S atom, one μ_3-S atom, and one terminal CN group. The mean W···Cu distance of 2.660 Å is similar to those found in the three-coordinate Cu clusters such as $[PPh_4]_2[(\eta^5\text{-}C_5Me_5)WS_3Cu_3Br_3]_2$ (2.661 Å)[9a] and $[PPh_4][\{(\eta^5\text{-}C_5Me_5)WS_3Cu_2\}_2S_2]_2$ (2.677 Å).[12] The average Cu−S length of 2.230 Å is similar to those of $[PPh_4]_2[(\eta^5\text{-}C_5Me_5)WS_3Cu_3Br_3]_2$ (2.234 Å) and $[PPh_4][\{(\eta^5\text{-}C_5Me_5)WS_3Cu_2\}_2S_2]_2$ (2.222 Å). The average terminal Cu−C length (1.892 Å) in **1** compares with those found in $[n\text{-}Pr_4N]_2[MoS_4(CuCN)]$ (1.880 Å) and $[AsPh_4]_2[MoS_4(\text{-}CuCN)_2]$ (1.886 Å).[6c]

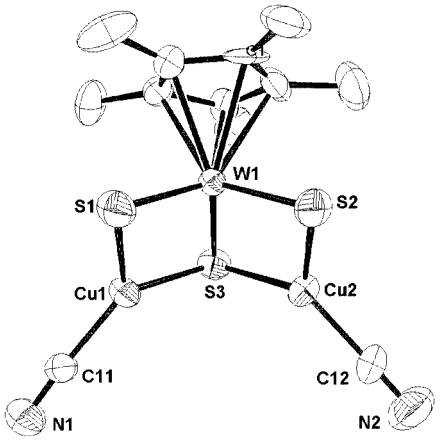

Figure 2. The perspective view of the anion of **1**. The thermal ellipsoids are drawn at the 50% probability level and the hydrogen atoms are omitted for clarity

Table 1. Selected bond lengths [Å] and angles [°] of **1**

W(1)···Cu(1)	2.6556(14)	W(1)···Cu(2)	2.6765(14)
W(1)−S(1	2.210(3)	W(1)−S(2)	2.263(3)
W(1)−S(3)	2.308(2)	Cu(1)−S(1)	2.211(3)
Cu(1)−S(3)	2.250(3)	Cu(2)−S(3)	2.226(3)
Cu(2)−S(2)	2.212(3)	Cu(1)−C(11)	1.88(1)
Cu(2)−C(12)	1.903(12)	N(1)−C(11)	1.148(13)
N(2)−C(12)	1.113(15)		
Cu(1)···W(1)···Cu(2)	78.47(4)	S(1)−W(1)−S(2)	104.29(13)
S(1)−W(1)−S(3)	106.4(1)	S(2)−W(1)−S(3)	104.8(1)
S(1)−Cu(1)−S(3)	108.4(1)	S(1)−Cu(1)−C(11)	124.9(3)
S(3)−Cu(1)−C(11)	126.7(3)	S(2)−Cu(2)−S(3)	109.31(11)
S(2)−Cu(2)−C(12)	122.4(4)	S(3)−Cu(2)−C(12)	128.2(4)
Cu(1)−N(1)−C(11)	175.0(10)	Cu(2)−C(12)−N(2)	177.5(13)
Cu(1)−S(3)−Cu(2)	97.3(1)		

Crystal Structures of $[(\eta^5\text{-}C_5Me_5)WS_3Cu_2(PPh_3)(\mu\text{-}CN)]_2$ (2) and $[PPh_4][\{(\eta^5\text{-}C_5Me_5)WS_3Cu_2(CN)(Py)\}_2(\mu\text{-}CN)]$ (3)

Compound **2** crystallizes in the monoclinic space group $P2_1/n$ and the asymmetric unit contains half a molecule of $[(\eta^5\text{-}C_5Me_5)WS_3Cu_2(PPh_3)(\mu\text{-}CN)]_2$; **3**·1.25Py crystallizes in the triclinic space group $P\bar{1}$ and the asymmetric unit consists of one discrete $[\{(\eta^5\text{-}C_5Me_5)WS_3Cu_2(CN)(Py)\}_2(\mu\text{-}CN)]^-$ anion, one $[PPh_4]^+$ cation, and 1.25 molecules of pyridine as solvated molecules. The refinements of the structures of **2** and **3** showed that the bridging cyanide groups between the Cu atoms have two orientations (i.e. the bridging cyanide groups are either coordinated through the C atoms, or through the N atoms). All the relevant C and N atoms were refined with a 50% probability of being C or N over each orientation. The derived Cu−C and Cu−N distances at the same site [e.g. Cu(1)−C(1) and Cu(1)−N(1a) in **2**, and Cu(1)−N(2) and Cu(1)−C(26a) in **3**] are identical and really express the average value. It is not known whether the distances in an ordered system would be equal. Therefore, Figure 3 shows the structure of **2** with the orientation of the bridging cyanide containing C(1) and N(1), while Figure 4 depicts the perspective view of the $[\{(\eta^5\text{-}C_5Me_5)WS_3Cu_2(CN)(Py)\}_2(\mu\text{-}CN)]^-$ anion of **3** with

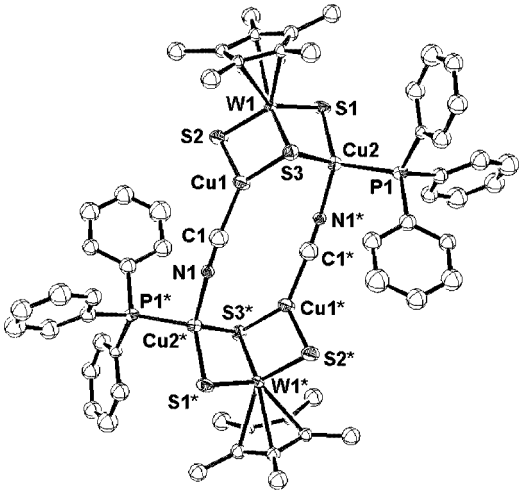

Figure 3. The perspective view of the molecular structure of **2** with 50% thermal ellipsoids. The C and N atoms of the bridging cyanide are disordered and only one orientation [C(1) and N(1)] is shown, and the hydrogen atoms are omitted for clarity.

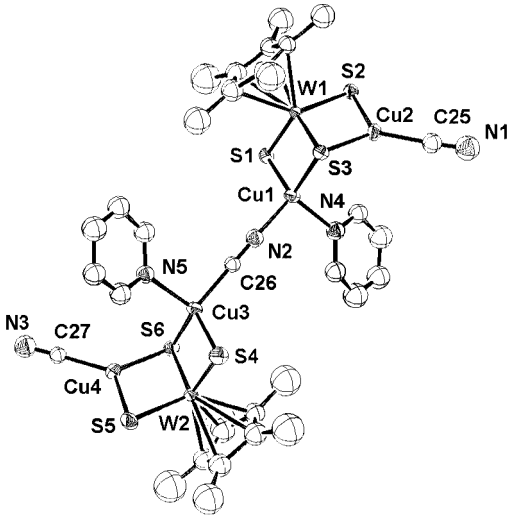

Figure 4. The perspective view of the anion of **3** with 50% thermal ellipsoids. The C and N atoms of the bridging cyanide are disordered and only one orientation [C(26) and N(2)] is shown, and the hydrogen atoms are omitted for clarity.

 © 2004 Wiley-VCH Verlag GmbH & Co. KGaA, Weinheim

Table 2. Selected bond lengths [Å] and angles [°] of **2**

W(1)···Cu(1)	2.657(2)	W(1)···Cu(2)	2.768(2)
W(1)−S(1)	2.220(4)	W(1)−S(2)	2.229(5)
W(1)−S(3)	2.291(4)	Cu(1)−S(2)	2.199(5)
Cu(1)−S(3)	2.219(5)	Cu(1)−C(1)	1.919(10)
Cu(2)−S(1)	2.272(5)	Cu(2)−S(3)	2.314(5)
Cu(2*)−N(1)	2.040(9)	Cu(2)−P(1)	2.251(5)
N(1)−C(1)	1.135(12)		
Cu(1)···W(1)···Cu(2)	70.12(6)	S(1)−W(1)−S(2)	105.3(2)
S(1)−W(1)−S(3)	104.6(2)	S(2)−W(1)−S(3)	105.1(2)
S(2)−Cu(1)−S(3)	108.6(2)	S(2)−Cu(1)−C(1)	120.5(3)
S(3)−Cu(1)−C(1)	130.9(3)	S(1)−Cu(2)−S(3)	102.2(2)
S(1)−Cu(2)−P(1)	117.8(2)	S(3)−Cu(2)−P(1)	108.4(2)
S(3)−Cu(2)−N(1*)	108.80(13)	P(1)−Cu(2)−N(1*)	103.9(2)
S(1)−Cu(2)−N(1*)	115.5(2)	Cu(1)−S(3)−Cu(2)	86.9(2)
Cu(1)−C(1)−N(1)	170.9(8)	Cu(2*)−N(1)−C(1)	160.7(7)

Table 3. Selected bond lengths [Å] and angles [°] of **3**

W(1)···Cu(1)	2.711(2)	W(1)···Cu(2)	2.657(2)
W(2)···Cu(3)	2.716(2)	W(2)···Cu(4)	2.664(2)
W(1)−S(1)	2.218(4)	W(1)−S(2)	2.231(3)
W(1)−S(3)	2.290(4)	W(2)−S(4)	2.221(4)
W(2)−S(5)	2.235(3)	W(2)−S(6)	2.295(4)
Cu(1)−S(1)	2.259(4)	Cu(1)−S(3)	2.265(4)
Cu(1)−N(2)	1.939(7)	Cu(1)−N(4)	2.11(2)
Cu(2)−S(2)	2.209(4)	Cu(2)−S(3)	2.216(4)
Cu(2)−C(25)	1.89(2)	Cu(3)−S(4)	2.265(5)
Cu(3)−S(6)	2.262(4)	Cu(3)−C(26)	1.945(8)
Cu(3)−N(5)	2.165(13)	Cu(4)−S(5)	2.202(5)
Cu(4)−S(6)	2.219(4)	Cu(4)−C(27)	1.90(2)
N(1)−C(25)	1.14(2)	N(2)−C(26)	1.154(11)
N(3)−C(27)	1.12(2)		
Cu(1)···W(1)···Cu(2)	77.89(6)	Cu(3)···W(2)···Cu(4)	76.77(6)
S(1)−W(1)−S(2)	104.3(1)	S(1)−W(1)−S(3)	106.4(1)
S(2)−W(1)−S(3)	105.35(13)	S(4)−W(2)−S(5)	104.9(2)
S(5)−W(2)−S(6)	104.9(1)	S(4)−W(2)−S(6)	106.2(2)
S(1)−Cu(1)−S(3)	105.9(2)	S(1)−Cu(1)−N(2)	115.8(2)
S(3)−Cu(1)−N(2)	115.8(2)	S(1)−Cu(1)−N(4)	102.8(4)
S(3)−Cu(1)−N(4)	113.4(4)	N(2)−Cu(1)−N(4)	102.6(4)
S(2)−Cu(2)−S(3)	108.7(2)	S(2)−Cu(2)−C(25)	122.0(5)
S(3)−Cu(2)−C(25)	129.1(5)	S(4)−Cu(3)−S(6)	105.9(2)
S(4)−Cu(3)−N(5)	101.3(4)	S(6)−Cu(3)−N(5)	115.4(3)
S(4)−Cu(3)−C(26)	117.2(3)	S(6)−Cu(3)−C(26)	114.1(2)
N(5)−Cu(3)−C(26)	102.6(5)	S(5)−Cu(4)−S(6)	108.6(2)
S(5)−Cu(4)−C(27)	123.9(5)	S(6)−Cu(4)−C(27)	127.4(5)
Cu(1)−S(3)−Cu(2)	97.7(2)	Cu(4)−S(6)−Cu(3)	96.4(2)
Cu(1)−N(2)−C(26)	179.0(6)	Cu(2)−C(25)−N(1)	177.0(17)
Cu(3)−C(26)−N(2)	179.4(7)	Cu(4)−C(27)−N(3)	178.3(15)

the orientation of the bridging cyanide containing C(26) and N(2). Tables 2 and 3 list the selected bond lengths and angles for **2** and **3** with the orientation of the bridging cyanide consisting of C(1) and N(1) in **2**, and C(26) and N(2) in **3**, respectively. The molecular structure of **2** can be viewed as a double butterfly-shaped structure in which two [(η^5-C_5Me_5)WS_3Cu_2] fragments are interconnected by a pair of Cu−μ-CN−Cu bridges. Meanwhile, the anion of **3** presents another type of double butterfly-shaped structure in which two [(η^5-C_5Me_5)WS_3Cu_2] fragments are linked by a single Cu−μ-CN−Cu bridge. To the best of our knowledge, the two structures are unprecedented in the tetrathiometallates. In both structures, each [(η^5-C_5Me_5)WS_3Cu_2] fragment shows a very similar structure to that of **1**. However, the two Cu atoms in each [(η^5-C_5Me_5)WS_3Cu_2] fragment of **2** and **3** exhibit a somewhat different coordination geometry from that of **1**. One Cu atom adopts a similar trigonal planar geometry, while the other Cu atom is coordinated by two S atoms, one CN group and one PPh_3 (**2**) or Py (**3**) group, thus exhibiting a distorted tetrahedral coordination geometry. Therefore, the different coordination geometries around the Cu atoms results in different W···Cu distances within the same [(η^5-C_5Me_5)WS_3Cu_2] fragment. The mean W···Cu distances for the three-coordinate Cu atom [2.657(2) Å in **2** and 2.661(2) Å in **3**] are similar to that of **1**. However, the mean W···Cu distance for the four-coordinate Cu atom in **2** [2.768(2) Å] is similar to those of [WS_4Cu_4(dppm)$_4$](PF_6)$_2$ (2.760 Å),[11c] but longer than those found in **3** [2.714(2) Å] and other clusters containing tetrahedral Cu atoms such as [(η^5-C_5Me_5)WS_3-Cu_2(PPh_3)$_2$Br] (2.704 Å),[9d] [Et_4N]$_2$[WS_4Cu_4(NCS)$_4$] (2.691 Å),[13a] [Et_4N]$_4$[$WS_4Cu_4I_6$] (2.692 Å),[13b] and [WS_4Cu_4(γ-MePy)$_8$][W_6O_{19}] (2.686 Å).[13c] The mean Cu−μ_3-S−Cu angle of 97.1(2)° in **3** is similar to that of **1**; however, it is about 10° smaller than that in **2**. The reason may be ascribed to the larger steric bulk of the two PPh_3 ligands coordinated at Cu(2) and Cu(2*) in **2**. The effect is also reflected in the linearity of the Cu−μ-CN−Cu bridges of **2** and **3**. The Cu−μ-CN−Cu portion in **2** is slightly bent, with Cu(1)−C(1)−N(1) and C(1)−N(1)−Cu(2*) angles of 170.9(8)° and 160.7(7)°, respectively. However, the Cu−μ-CN−Cu bridge in **3** is practically linear, with Cu(1)−N(2)−C(26) and Cu(3)−C(26)−N(2) angles of 179.0(6)° and 179.4(7)°, respectively. The Cu−C/N and Cu−N/C distances of the bridging cyanide groups in **2** and **3** range from 1.910(6) Å to 2.048(14) Å, which are similar to those found in [Cu(4-CNPy)(μ-CN)] [Cu−N/C = 1.907(2) Å and Cu−C/N = 1.999(2) Å].[13d] The mean Cu−P length of 2.251(5) Å in **2** is similar to those found in [(η^5-C_5Me_5)WS_3Cu_3(PPh_3)$_2$Br$_2$] (2.247 Å) and [PPh_4][(η^5-C_5Me_5)$WS_3Cu_3Br_3$(dppm)] (2.270 Å).[9c] The mean Cu−N(Py) length of 2.138 Å in **3** is longer than those found in [WS_4Cu_4(γ-MePy)$_8$][W_6O_{19}] (2.02 Å)[13c] and [Cu(Py)$_4$]-ClO_4 (2.046 Å).[14] The mean W−μ-S, W−μ_3-S, and Cu−S distances in both **2** and **3** compare with those found in **1**.

Optical Limiting (OL) Properties of 1−3

As shown in Figure 1, compounds **1**−**3** have a low absorbance at 532 nm. This promises low intensity loss and small temperature changes by photon absorption when the laser pulse propagates in these materials. The fluence-dependent transmission measurements of **1**−**3** are depicted in Figure 5. For **1**, the light energy transmitted begins to deviate from normal linear behavior as soon as the input light fluence reaches about 0.4 J/cm^2, and the material becomes increasingly less transparent as the light fluence rises. We define the limiting threshold as the incident fluence at which the sample transmittance falls to 50% of the corresponding linear transmittance. The limiting threshold of

 © 2004 Wiley-VCH Verlag GmbH & Co. KGaA, Weinheim

compound **1** is 7.5 J/cm^2. For **2**, when the input light fluence reaches about 2.6 J/cm^2, the light energy transmitted begins show less than linear behavior. The limiting threshold for compound **2** is larger than 10 J/cm^2. Unfortunately, no OL effects are observed for compound **3**. Although the concentration of C_{60} ($9.02\cdot10^{-4}$ M) is higher than the concentrations of **1** ($3.57\cdot10^{-4}$ M) and **2** ($1.20\cdot10^{-4}$ M), the OL performance of **1** is about 3 times better than that of C_{60} measured under identical conditions, while the OL performance of compound **2** is similar to C_{60}. The poor solubility of compounds **1** and **2** prohibits higher concentrations to be attained, and hence limits their OL performance. Better OL effects would be expected for higher concentrations of these compounds.

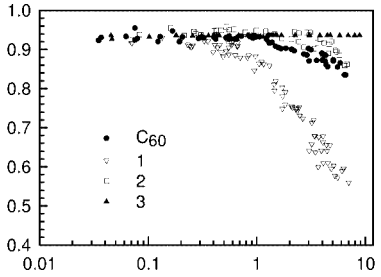

Figure 5. Optical limiting responses to 7-ns, 532 nm laser pulses, of **1** in MeCN, **2** in CH_2Cl_2, **3** in DMF, and C_{60} in toluene. Solutions with 92% transmittance at 532 nm correspond to $3.57\cdot10^{-4}$ M (**1**), $1.20\cdot10^{-4}$ M (**2**), $1.69\cdot10^{-4}$ M (**3**), and $9.02\cdot10^{-4}$ M (C_{60}), respectively

Conclusion

We demonstrated the facile synthesis of **1** and its reactivity towards PPh_3 and Py. The successful isolation of **2** and **3** shows that compound **1** can be a useful precursor for the construction of new W−Cu−S clusters in the presence of suitable donor ligands. The structures of **1**−**3** have been fully characterized by spectroscopy and X-ray analysis. Compounds **2** and **3** exhibit two types of double butterfly-shaped structures, which have not previously been observed in the chemistry of the corresponding tetrathiometallates. The OL properties of **1**−**3** in solution have been measured, and **1** and **2** exhibit relatively good OL performances when compared with C_{60}. As some preformed clusters may be assembled into supramolecular compounds via the bridging ligands such as 4,4′-bipy, and their NLO performances may be improved,[15] it is still worth screening more compounds formed from the reactions of **1** with hooking ligands such as the one mentioned above. We are currently investigating this.

Experimental Section

General: All manipulations were carried out under argon using standard Schlenk-techniques. $[PPh_4][(\eta^5\text{-}C_5Me_5)WS_3]$ was prepared as reported previously.[8b] Other chemicals were obtained from commercial sources and used as received. All solvents were predried over activated molecular sieves and refluxed over the appropriate drying agents under argon. The IR spectra were recorded on a Nicolet MagNa-IR500 FT-IR spectrometer (4000−400 cm^{-1}). ^{1}H NMR spectra were recorded at ambient temperature on a Varian UNITYplus-400 spectrometer. UV/Vis spectra were measured on a Hitachi UV-3410 spectrophotometer. The elemental analyses for C, H, and N were performed on a Carlo−Erba CHNO-S microanalyzer.

Reaction of $[PPh_4][(\eta^5\text{-}C_5Me_5)WS_3]$ with CuCN: CuCN (0.023 g, 0.26 mmol) was added to a red solution of $[PPh_4][(\eta^5\text{-}C_5Me_5)WS_3]$ (0.10 g, 0.13 mmol) in MeCN (10 mL). The solution quickly turned dark red and the mixture was stirred at room temperature for 1 h and then filtered. Diethyl ether (20 mL) was carefully layered onto the filtrate, forming red prisms of $[PPh_4][(\eta^5\text{-}C_5Me_5)WS_3(CuCN)_2]\cdot$MeCN (**1**·MeCN), which were isolated by filtration, washed with Et_2O, and dried in vacuo. Yield: 0.085 g (70%). $C_{36}H_{35}Cu_2N_2PS_3W$: calcd. C 47.02, H 4.51, N 4.49; found C 46.78, H 3.90, N 4.31%. UV/Vis (MeCN) [λ_{max}/nm (ε/M^{-1}cm^{-1})]: 435 (1700), 390 (6300), 314 (8600). IR (KBr disk): $\tilde{\nu}$ = 2119 (s), 1586 (s), 1483 (s), 1439 (vs), 1377 (m), 1318 (w), 1186 (w), 1109 (vs), 1025 (m), 995 (m), 754 (s), 724 (vs), 692 (s), 531 (s), 433 (w), 410 (m) cm^{-1}. ^{1}H NMR (CD_3CN, 400 MHz, 25 °C): δ = 7.26−7.89 (m, 20 H, PPh_4^+), 2.05 (s, 5 H, $\eta^5\text{-}C_5Me_5$) ppm.

Reaction of 1 with PPh_3: Treatment of a solution of **1** (0.042 g, 0.05 mmol) in MeCN (5 mL) with PPh_3 (0.026 g, 0.1 mmol) gave rise to a homogeneous solution, which was allowed to stir for 30 min. Diethyl ether (5 mL) was carefully layered onto the filtrate, forming red plates of $[(\eta^5\text{-}C_5Me_5)WS_3Cu_2(\mu\text{-}CN)(PPh_3)]_2$ (**2**), which were isolated by filtration, washed with Et_2O, and dried in vacuo. Yield: 0.071 g (85%). $C_{29}H_{30}Cu_2NPS_3W$: calcd. C 41.53, H 4.01, N 1.75; found C 41.89, H 3.90, N 1.68%. IR (KBr disk): $\tilde{\nu}$ = 2139 (s), 1480 (m), 1435 (s), 1376 (m), 1097 (m), 1027 (m), 747 (s), 723 (w), 695 (vs), 518 (s), 434 (m), 417 (w), 409 (w) cm^{-1}. UV/Vis (CH_2Cl_2) [λ_{max}/nm (ε/M^{-1}cm^{-1})]: 394 (5600). ^{1}H NMR ($CDCl_3$, 400 MHz, 25 °C): δ = 7.27−7.89 (m, 15 H, PPh_3), 2.05 (s, 5 H, $\eta^5\text{-}C_5Me_5$) ppm.

Reaction of 1 with Py: Compound **1** (0.042 g, 0.05 mmol) was dissolved in 1.5 mL of pyridine. The mixture was stirred at room temperature for 30 min, giving a clear solution. Diethyl ether (5 mL) was carefully layered onto the filtrate to form orange-red needles of $[PPh_4][\{(\eta^5\text{-}C_5Me_5)WS_3Cu_2(CN)(Py)\}_2(\mu\text{-}CN)]\cdot1.25$Py (**3**·1.25Py), which were isolated by filtration, washed with Et_2O, and dried in vacuo. Yield: 0.063 g (80%). $C_{29}H_{30}Cu_2NPS_3W$: calcd. C 48.42, H 4.50, N 4.12; found C 48.18, H 4.21, N 3.97%. IR (KBr disk): $\tilde{\nu}$ = 2130 (m), 2053 (m), 1483 (m), 1436 (s), 1376 (m), 1108 (vs), 996 (m), 753 (m), 724 (vs), 690 (vs), 527 (vs), 445 (w), 430 (w), 413 (w) cm^{-1}. UV/Vis (DMF) [λ_{max}/nm (ε/M^{-1}cm^{-1})]: 452 (20200), 393 (7700), 321 (5400). ^{1}H NMR ($CDCl_3$, 400 MHz, 25 °C): δ = 8.62 (br. s, 2 H, Py), 7.64−7.90 (m, 28 H, Py+PPh_4^+), 2.08 (s, 5 H, $\eta^5\text{-}C_5Me_5$) ppm.

X-ray Diffraction Crystallography: All measurements were performed on a Rigaku Mercury CCD X-ray diffractometer (3 kV, sealed tube) at −80 °C, using graphite monochromated Mo-*Kα* (λ = 0.71070 Å). A red chip of **1**·MeCN with dimensions 0.60 × 0.40 × 0.20 mm, a red prism of **2** with dimensions 0.10 × 0.05 × 0.05 mm, and a red platelet of **3**·1.25Py with dimensions 0.55 × 0.15 × 0.05 mm, were mounted at the top of a glass fiber. Diffraction data were collected at ω mode with a detector distance of 55 mm (**1**·MeCN and **2**) or 35 mm (**3**·1.25Py) to the crystal. Indexing was performed from 6 images, each of which was exposed for 15 s. A total of 1080 (**1**·MeCN) or 720 (**2** and **3**·1.25Py) oscillation images were collected in the range $1.95° < 2\theta < 54.96°$ for

 © 2004 Wiley-VCH Verlag GmbH & Co. KGaA, Weinheim

Table 4. Summary of the crystal data for the structures of **1**·MeCN, **2**, and **3**·1.25Py

	1·MeCN	**2**	**3**·1.25Py
Empirical formula	$C_{38}H_{38}Cu_2N_3PS_3W$	$C_{58}H_{60}Cu_4N_2P_2S_6W_2$	$C_{63.25}H_{66.25}Cu_4N_{6.25}PS_6W_2$
F_w	974.83	1661.32	1575.38
Crystal system	Orthorhombic	monoclinic	triclinic
Space group	$Pna2_1$	$P2_1/n$	$P\bar{1}$
a [Å]	33.919(8)	12.199(2)	9.215(1)
b [Å]	7.626(2)	15.248(3)	17.811(3)
c [Å]	15.342(3)	16.173(3)	20.900(4)
α [°]			88.383(9)
β [°]		91.879(9)	82.249(9)
γ [°]			80.901(8)
V [Å^3]	3968.6(15)	3006.9(10)	3356.0(10)
Z	4	2	2
D_c [g cm^{-3}]	1.631	1.835	1.559
μ [mm^{-1}]	4.185	5.504	3.209
Reflections [$I>3.00\sigma(I)$]	3670	2220	8875
Parameters	456	210	583
R[a]	0.032	0.043	0.058
R_w[b]	0.049	0.044	0.069
GOF[c]	1.144	0.962	1.474
Largest residual peaks and hole [e·Å^{-3}]	0.80 and −0.81	0.92 and −1.15	1.84 and −1.41

[a] $R = \Sigma F_o| - |F_c\|/\Sigma|F_o|$. [b] $R_w = \{w\Sigma(|F_o| - |F_c|)^2/\Sigma w|F_o|^2\}^{1/2}$. [c] GOF $= \{\Sigma w(|F_o| - |F_c|)^2/(M - N)\}^{1/2}$, where M is the number of reflections and N is the number of parameters.

1·MeCN, $1.97° < 2\theta < 50.04°$ for **2**, and $1.60° < 2\theta < 61.86°$ for **3**·1.25Py. The collected data were reduced by using the program CrystalClear (Rigaku and MSC, Ver. 1.3, 2001), and an empirical absorption correction was applied which resulted in transmission factors ranging from 0.266 to 0.433 for **1**·MeCN, from 0.610 to 0.759 for **2**, and from 0.623 to 0.852 for **3**·1.25Py. The reflection data were also corrected for Lorentz and polarization effects.

The structures of **1**·MeCN and **2** were solved by direct methods[16a] while that of **3**·1.25Py by heavy-atom Patterson methods,[16b] and expanded using Fourier techniques.[16c] For **1**·MeCN, all non-hydrogen atoms except those of the MeCN crystal solvent molecule were refined anisotropically. For **2**, W, Cu, S, and P atoms were refined anisotropically, while C and N atoms were refined isotropically. In both cases, all hydrogen atoms were introduced at the calculated positions and included in the structure-factor calculations. Crystal **3**·1.25Py contains 1.25 Py solvated molecules in an asymmetric unit. One Py solvent molecule is refined isotropically. The other is located on a center of symmetry and is refined with one-quarter occupancy. All non-H atoms except those of CN, Py, and η^5-C_5Me_5 were refined anisotropically. Hydrogen atoms except those of the two Py solvent molecules were placed on the idealized positions and included in the final structure-factor refinements. In the structure of **2** or **3**·1.25Py, the orientation of the bridging cyanide group was found to be disordered, and the C and N atoms were refined with a 50% probability of being C or N, i.e. C(1)/N(1a) = 0.5:0.5 and N(1)/C(1a) = 0.5:0.5 (**2**), C(26)/N(2a) = 0.5:0.5, and N(2)/C(26a) = 0.5:0.5 (**3**·1.25Py). Neutral atom scattering factors were taken from Cromer and Waber.[17a] Anomalous dispersion effects were included in $F_{calcd.}$.[17b] All calculations were performed on a Dell workstation using the CrystalStructure crystallographic software package (Rigaku and MSC, Ver. 3.0, 2002). A summary of the key crystallographic information for **1**·MeCN, **2**, and **3**·1.25Py is given in Table 4. CCDC-202420 (**1**), 202421 (**2**), and 202422 (**3**) contain the supplementary crystallographic data for this paper. These data can be obtained free of charge at http://www.ccdc.cam.ac.uk/retrieving.html [or from the Cambridge Crystallographic Data Centre, 12 Union Road, Cambridge CB2 1EZ, UK; Fax: (internat.) + 44-1223/336-033; E-mail: deposit@ccdc.cam.ac.uk].

Optical Limiting Measurements: Samples were dissolved in MeCN (**1**), CH_2Cl_2 (**2**), and DMF (**3**). The solutions with concentrations of $3.57\cdot10^{-4}$ M (**1**), $1.20\cdot10^{-4}$ M (**2**), and $1.69\cdot10^{-4}$ M (**3**) were contained in a 1-mm-thick quartz cuvette. Optical limiting experiments were performed with a Q-switched, frequency-doubled Nd:YAG laser (λ = 532 nm) with linearly polarized 7-ns pulses. The interval between the laser pulses was set at 10 s so that every pulse of light was assured to meet fresh molecules in the sample to eliminate the influence of any photo-degradation. The optical limiting phenomenon was demonstrated by measuring fluence-dependent transmissions. The laser pulses were focused on to the sample using a focusing mirror of 25-cm focal length. The spot radius of the laser pulses at the cuvette was measured to be of 35±5 μm (half width of $1/e^2$ maximum in irradiance). Both incident and transmitted laser pulses were monitored simultaneously using a calibrated beam splitter and two energy detectors (from Laser Precision, Rjp-735 energy probes). The detectors were linked to a computer by an IEEE interface. The linear (low-intensity) transmittance of all the samples was adjusted to 92%. Fullerene (C_{60}) dissolved in toluene ($9.02\cdot10^{-4}$ M) was used as a standard sample since its optical limiting performance had been well-documented.[18]

Acknowledgments

This work was supported by the National Natural Science Foundation of China (No. 20271036), the NSF of the Education Committee of Jiangsu Province (No. 02KJB150001), and the State Key Laboratory of Coordination Chemistry of Nanjing University in China.

[1] [1a] A. Müller, E. Diemann, R. Jostes, H. Bögge, *Angew. Chem. Int. Ed. Engl.* **1981**, *20*, 934−954. [1b] A. Müller, H. Bögge, U. Schimanski, M. Penk, K. Nieradzik, M. Dartmann, E. Krickemeyer, J. Schimanski, C. Römer, M. Römer, H. Dornfeld, U. Wienböker, W. Hellmann, *Monatsh. Chem.* **1989**, *120*,

 © 2004 Wiley-VCH Verlag GmbH & Co. KGaA, Weinheim

367−391. [1c] K. E. Howard, T. B. Rauchfuss, A. L. Rheingold, *J. Am. Chem. Soc.* **1986**, *108*, 297−299. [1d] M. A. Ansari, J. A. Ibers, *Coord. Chem. Rev.* **1990**, *100*, 223−266. [1e] Y. Jeannin, F. Sèheresse, S. Bernés, F. Robert, *Inorg. Chim. Acta* **1992**, *198−200*, 493−505. [1f] X.-T. Wu, P.-C. Chen, S.-W. Du, N.-Y. Zhu, J.-X. Lu, *J. Cluster Sci.* **1994**, *5*, 265−285. [1g] R. H. Holm, *Pure Appl. Chem.* **1995**, *67*, 217−224. [1h] H.-W. Hou, X.-Q. Xin, S. Shi, *Coord. Chem. Rev.* **1996**, *153*, 25−56. [1i] D.-X. Wu, M.-C. Hong, R. Cao, H.-Q. Liu, *Inorg. Chem.* **1996**, *35*, 1080−1082. [1j] D. Coucouvanis, *Adv. Inorg. Chem.* **1998**, *45*, 1−73.

[2] [2a] R. R. Chianelli, T. A. Picoraro, T. R. Halbert, W. H. Pan, E. I. Stiefel, *J. Catal.* **1984**, *86*, 226−230. [2b] M. D. Curtis, *J. Cluster Sci.* **1996**, *7*, 247−262.

[3] [3a] R. H. Holm, *Adv. Inorg. Chem.* **1992**, *38*, 1−71. [3b] E. I. Stiefel, D. Coucouvanis, W. E. Newton (Eds.), *Molybdenum Enzymes, Cofactors and Model Systems, ACS Symposium Series 535*, American Chemical Society, Washington, DC, **1993**. [3c] E. I. Stiefel, K. Matsumoto (Eds.), *Transition Metal Sulfur Chemistry, Biological and Industrial Significance, ACS Symposium Series 653*, American Chemical Society, Washington, DC, **1996**.

[4] [4a] C.-K. Chan, C.-X. Guo, R.-J. Wang, T. C. W. Mak, C.-M. Che, *J. Chem. Soc., Dalton Trans.* **1995**, 753−757. [4b] C.-M. Che, B.-H. Xia, J.-S. Huang, C.-K. Chan, Z.-Y. Zhou, K.-K. Cheung, *Chem. Eur. J.* **2001**, *7*, 3998−4006.

[5] [5a] S. Shi, W. Ji,; S.-H. Tang, J.-P. Lang, X.-Q. Xin, *J. Am. Chem. Soc.* **1994**, *116*, 3615−3616. [5b] S. Shi, W. Ji, J.-P. Lang, X.-Q. Xin, *J. Phys. Chem.* **1994**, *98*, 3570−3572. [5c] S. Shi, W. Ji, W. Xie, T.-C. Chong, H.-C. Zeng, J.-P. Lang, X.-Q. Xin, *Mater. Chem. Phys.* **1995**, *39*, 298−303. [5d] J.-P. Lang, K. Tatsumi, H. Kawaguchi, J.-M. Lu, P. Ge, W. Ji, S. Shi, *Inorg. Chem.* **1996**, *35*, 7924−7927. [5e] H.-G. Zheng, W. Ji, M. L. K. Low, G. Sakane, T. Shibahara, X.-Q. Xin, *J. Chem. Soc., Dalton Trans.* **1997**, 2375−2362. [5f] S. Shi, in: *Optoelectronic Properties of Inorganic Compounds* (Eds. D. M. Roundhill, J. P. Fackler, Jr.), Plenum Press, New York, **1998**, pp.55−105. [5g] H. Yu, Q.-F. Xu, Z.-R. Sun, Q. Liu, J.-X. Chen, S.-J. Ji, J.-P. Lang, K. Tatsumi, *Chem. Commun.* **2001**, 2614−2615.

[6] [6a] A. Müller, M. Dartmann, C. Römer, A. Clegg, G. M. Sheldrick, *Angew. Chem. Int. Ed. Engl.* **1981**, *20*, 1060−1061. [6b] S. F. Gheller, P. A. Gazzana, A. F. Masters, R. T. C. Brownlee, M. J. O'Connor, A. G. Wedd, J. R. Rodgers, M. R. Snow, *Inorg. Chim. Acta* **1981**, *54*, L131−L132. [6c] S. F. Gheller, T. W. Hambley, J. R. Rodgers, R. T. C. Brownlee, M. J. O'Connor, M. R. Snow, A. G. Wedd, *Inorg. Chem.* **1984**, *23*, 2519−2528.

[7] [7a] H.-W. Hou, H.-G. Zheng, H. G. Ang, Y.-T. Fan, M. K. M. Low, Y. Zhu, W.-L. Wang, X.-Q. Xin, W. Ji, W.-T. Wong, *J. Chem. Soc., Dalton Trans.* **1999**, 2953−2957. [7b] C. Zhang, Y.-L. Song, Y. Xu, H. K. Fun, G.-Y. Fang, Y.-X. Wang, X.-Q. Xin, *J. Chem. Soc., Dalton Trans.* **2000**, 2823−2829.

[8] [8a] H. Kawaguchi, K. Yamada, J.-P. Lang, K. Tatsumi, *J. Am. Chem. Soc.* **1997**, *119*, 10346−10358. [8b] H. Kawaguchi, K. Tatsumi, *J. Am. Chem. Soc.* **1995**, *117*, 3885−3886.

[9] [9a] J.-P. Lang, H. Kawaguchi, S. Ohnishi, K. Tatsumi, *Chem. Commun.* **1997**, 405−406. [9b] J.-P. Lang, H. Kawaguchi, K. Tatsumi, *Inorg. Chem.* **1997**, *36*, 6447−6449. [9c] J.-P. Lang, H. Kawaguchi, S. Ohnishi, K. Tatsumi, *Inorg. Chim. Acta* **1998**, *283*, 136−142. [9d] J.-P. Lang, K. Tatsumi, *J. Organomet. Chem.* **1999**, *579*, 332−337.

[10] J.-P. Lang, K. Tatsumi, *Inorg. Chem.* **1999**, *38*, 1364−1367.

[11] [11a] A. Müller, H. Bögge, J. Schimanski, *Inorg. Chim. Acta* **1983**, *76*, L245−L246. [11b] S.-W. Du, N.-Y. Zhu, X.-T. Wu, *Polyhedron* **1992**, *11*, 2489−2493. [11c] J.-P. Lang, K. Tatsumi, *Inorg. Chem.* **1998**, *37*, 6308−6316.

[12] J.-P. Lang, K. Tatsumi, *Inorg. Chem.* **1998**, *37*, 160−162.

[13] [13a] J. M. Manoli, C. Potvin, F. Sèheresse, S. Marzak, *Inorg. Chim. Acta* **1988**, *150*, 257−268. [13b] J.-P. Lang, G.-Q. Bian, J.-H. Cai, B.-S. Kang, X.-Q. Xin, *Trans. Met. Chem.* **1995**, *20*, 376−379. [13c] M. T. Pope, J.-P. Lang, X.-Q. Xin, K.-B. Yu, *Chin. J. Chem.* **1995**, *13*, 40−46. [13d] D. T. Cromer, A. C. Larson, *Acta Crystallogr., Sect. B* **1972**, *28*, 1052−1059.

[14] K. Nilsson, A. Oskarsson, *Acta Chem. Scand.* **1982**, *36*, 605−610.

[15] Q.-F. Zhang, Y.-Y. Niu, W.-H. Leung, Y. Song, I. D. Williams, X.-Q. Xin, *Chem. Commun.* **2001**, 1126−1127.

[16] [16a] G. M. Sheldrick, *SHELXS-97, Program for the Solution of Crystal Structure*, University of Göttingen, Germany, **1997**. [16b] P. T. Beurskens, G. Admiraal, G. Beurskens, W. P. Bosman, S. Garcia-Granda, R. O. Gould, J. M. M. Smits, C. Smykalla, *PATTY, The DIRDIF Program System, Technical Report of the Crystallography Laboratory*, University of Nijmegen, The Netherlands, **1992**. [16c] P. T. Beurskens, G. Admiraal, G. Beurskens, W. P. Bosman, R. de Gelder, R. Israel, J. M. M. Smits, *DIRDIF99, The DIRDIF-99 Program System, Technical Report of the Crystallography Laboratory*, University of Nijmegen, The Netherlands, **1999**.

[17] [17a] D. T. Cromer, J. T. Waber, *International Tables for X-ray Crystallography*, Vol. IV, The Kynoch Press, Birmingham, England, Table 2.2 A, **1974**. [17b] J. A. Ibers, W. C. Hamilton, *Acta Crystallogr.* **1964**, *17*, 781−782.

[18] [18a] K. M. Nashold, D. P. Walter, *J. Opt. Soc., Am. B.* **1995**, *12*, 1228−1237. [18b] R. L. McLean, M. C. Sutherland, M. C. Brant, D. M. Brandelik, P. A. Fleitz, T. Pottenger, *Opt. Lett.* **1993**, *18*, 858−860.

Received April 10, 2003
Early View Article
Published Online October 23, 2003

 © 2004 Wiley-VCH Verlag GmbH & Co. KGaA, Weinheim

Investigation of the Thermal Properties of $[Cu_{20}Se_{13}(PEt_3)_{12}]$

Andreas Eichhöfer,*[a] Dieter Fenske,[b] and Petra Scheer[a]

Keywords: Cluster compounds / Mixed-valent compounds / Thermogravimetry / Copper / Selenium

The mixed-valence cluster $[Cu_{20}Se_{13}(PEt_3)_{12}]$ has been synthesized by the reaction of CuCl and PEt_3 with $Se(SiMe_3)_2$. A powder-diffraction pattern has revealed its crystalline purity and UV/Vis reflectance spectra display an intervalence band around 1200 nm. The solid-state conversion of the cluster upon heating yields, even at moderate temperatures of around 100 °C, α-Cu_2Se and not a Cu_3Se_2 phase that should be favoured in terms of the Cu/Se ratio of 3.1:2 in the cluster complex. This thermogravimetric analysis, coupled with mass spectrometry, shows that in addition to the labile phosphane ligands selenium atoms are cleaved as $SePEt_3$ during the consolidation process.
(© Wiley-VCH Verlag GmbH & Co. KGaA, 69451 Weinheim, Germany, 2004)

Introduction

Cluster molecules of semiconductor materials, composed of tens of atoms with bonding resembling that in the solid state, are interesting molecular models for the bulk.[1] Various cluster molecules of different sizes and structures, composed of elements of either groups 11 and 16 or groups 12 and 16, have been synthesized and characterized by single-crystal XRD.[2−4] Remarkable examples include $[Cd_{32}S_{14}(SPh)_{36}(dmf)_4]$ (dmf = *N*,*N*-dimethylformamide),[5] $[Cu_{146}Se_{73}(PPh_3)_{30}]$,[6] $[Ag_{172}Se_{40}(n\text{BuSe})_{92}(dppp)_4]$ [dppp = bis(diphenylphosphanyl)propane][7] and $[Ag_{188}S_{94}(P\text{n}Pr_3)_{30}]$[8] with cluster core sizes up to 3 nm. Farneth et al. have found that the thermal properties of group 12/16 cluster molecules with the general formula $(R_4N)_4[M_{10}S_4(SPh)_{16}]$ (R = Me, Et; M = Cd, Zn) can give valuable insight into the mechanism of their solid-state conversion upon heating.[9] Investigations on $[Cu_{70}Se_{35}(PEt_2Ph)_{24}]$ reveal that the phosphane ligand shell can be cleaved at moderate temperatures (145 °C) in vacuo in a one-step process that produces nanocrystalline copper selenide.[10] Powder-diffraction measurements show that the cleavage of this ligand molecule is accompanied by an aggregation of the copper selenide cluster cores, in agreement with X-ray photoelectron spectroscopy (XPS) findings on a series of copper selenide clusters.[11] In addition, Corrigan et al. have recently investigated the mechanism of cluster condensation of the copper chalcogenolate $[Cu_6(TePh)_6(PPh_2Et)_5]$ in hexagonally ordered mesoporous MCM-41.[12]

Herein we report the thermal properties of the mixed-valence copper chalcogenide cluster $[Cu_{20}Se_{13}(PEt_3)_{12}]$ and the characterization of its thermolysis products.

Results and Discussion

The reaction of CuCl and PEt_3 with $Se(SiMe_3)_2$ in diethyl ether affords $[Cu_{70}Se_{35}(PEt_3)_{22}]$[13] while only in one experiment a small amount of $[Cu_{20}Se_{13}(PEt_3)_{12}]$ (**1**) crystals were also found. During our investigations it turned out that the use of PTFE gaskets for the stoppers, instead of grease, in combination with evacuation of the flask containing the reaction solution before refrigeration leads to the crystallization of pure **1** (Scheme 1). Obviously, the gaskets were not totally closed, allowing small amounts of oxygen and moisture to enter the flask which could affect an in situ partial oxidation of Se^{2-} to Se^{1-} or Cu^{1+} to Cu^{2+}, respectively. However, attempts to synthesize **1** by the use of an appropriate amount of $CuCl_2$ or $Cu(OOCCH_3)_2$ failed.

$$\begin{array}{l} \text{CuCl + 3 PEt}_3 \\ \text{Et}_2\text{O / −10 °C} \quad \Big| \quad \text{+ 0.5 Se(SiMe}_3)_2 \text{ / } n\text{O}_2 \\ \\ [Cu_{20}Se_{13}(PEt_3)_{12}] \quad \textbf{(1)} \end{array}$$

Scheme 1

The lattice constants of the black octahedral crystals of **1** correspond to those published[13] and the powder-diffraction pattern agrees well with the calculated values, suggesting a high crystalline purity with respect to the formation of other crystalline clusters namely $[Cu_{70}Se_{35}(PEt_3)_{22}]$

[a] Institut für Nanotechnologie, Forschungszentrum Karlsruhe, Postfach 3640, 76021 Karlsruhe, Germany
Fax: (internat.) + 49-7247-82-6368
E-mail: eichhoefer@int.fzk.de
[b] Institut für Anorganische Chemie der Universität Engesserstrasse, Geb. 30.45, 76128 Karlsruhe, Germany

Table 1. Calculated and measured powder-diffraction patterns for $[Cu_{20}Se_{13}(PEt_3)_{12}]$ (**1**) with $I(rel.) > 0.5$

Calculated			Measured		
d [Å]	2Θ [°]	I(rel.)	d [Å]	2Θ [°]	I(rel.)
13.31	6.64	100.00	13.33	6.63	100.00
11.52	7.67	39.73	11.56	7.64	40.84
8.15	10.85	1.05	8.18	10.80	0.89
6.95	12.73	0.60	6.98	12.67	0.97
5.29	16.75	2.63	5.32	16.67	3.00
5.15	17.19	4.84	5.18	17.10	7.28
4.71	18.85	0.53	4.73	18.74	0.90
			4.46	19.88	0.57
4.07	21.80	3.32	4.10	21.67	4.33
3.90	22.81	0.68	3.92	22.68	1.35
3.52	25.32	0.55	3.54	25.17	0.96
3.48	25.62	0.29	3.50	25.46	0.64
3.33	26.78	0.74	3.35	26.61	1.59
3.20	27.89	0.30	3.22	27.72	0.73
3.08	28.97	4.64	3.10	28.79	5.97
3.00	29.75	1.53	3.02	29.56	2.37
2.88	31.02	0.43	2.90	30.82	0.73
2.82	31.75	1.29	2.84	31.56	1.69
2.80	32.00	1.62	2.81	31.79	1.79
2.72	32.95	0.59	2.73	32.74	0.73
2.66	33.65	0.64	2.68	33.43	1.01
2.64	33.88	0.77	2.68	33.44	0.98
			2.66	33.66	0.98
2.58	34.79	0.60	2.59	34.57	0.82
2.53	35.45	2.71	2.55	35.22	2.71
2.42	37.18	2.54	2.43	36.94	2.04
2.32	38.85	0.58	2.33	38.59	0.64
2.26	39.86	2.83	2.28	39.59	2.08
2.23	40.45	0.44	2.23	40.37	1.92
2.22	40.65	2.41			
2.15	42.00	1.59	2.16	41.72	1.37
2.14	42.20	2.28	2.15	41.90	1.86
2.08	43.51	2.47	2.09	43.21	1.89
2.04	44.43	0.88	2.05	44.13	0.93
2.01	44.98	2.61	2.03	44.68	1.93

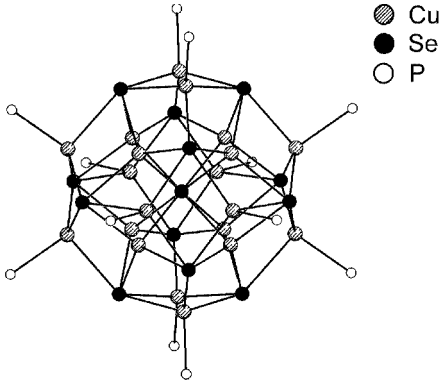

Figure 1. Molecular structure of $[Cu_{20}Se_{13}(PEt_3)_{12}]$ (**1**);[13] copper−copper contacts and carbon and hydrogen atoms omitted for clarity

(Table 1). In the molecular structure of **1** (Figure 1) 13 selenium atoms form a distorted, centered icosahedron (nonbonding Se−Se distances: 4.001−4.143 Å). Twelve of the 20 Se_3 faces are bridged by copper−phosphane units, whereas eight more copper atoms are below the remaining faces, all tetrahedrally surrounded due to an additional Cu−Se bond to the central selenium atom. Assuming a formal charge of 2− for the selenium atoms, one can assign 14 Cu^+ centers and six Cu^{2+} centers. However, the coexistence of Cu^{2+} and Se^{2-} is thermodynamically unlikely because of an electron-transfer process from the reducing Se^{2-} ligand to the oxidizing Cu^{2+} center. Additionally, the electron deficiency has to be assumed to be delocalised as there is no structural reason for it to be localised on either six of the copper atoms or on six of the selenium atoms. The compound should therefore better be described in terms of a "pure" Cu^+ substructure ligated by selenium atoms with an average charge of −1.54.

Compounds containing metal atoms in formally different oxidation states generally exhibit interesting spectroscopic behaviour. Depending on the degree of charge delocalisation in the molecular framework, one may detect additional bands in the near IR. The UV/Vis reflectance spectrum of **1** (Figure 2) shows several bands between 700 and 300 nm. The band with a maximum at 550 nm and a shoulder at 592 nm is responsible for the dark purple colour of the compound while the absorption peak at 262 nm originates most probably from charge-transfer transitions of the PEt_3 ligands. However, the broad, intense peak centered around 1200 nm can be assigned as an intervalence band, in agreement with observations made for similar copper telluride clusters.[14] According to the classification of Robin and Day,[15] which describes the different amounts of electron delocalisation between the metal atoms, **1** belongs to class IIIa (metal clusters). In this class, metal centers with different valencies cannot be distinguished, and total delocalisation of the charge is achieved.

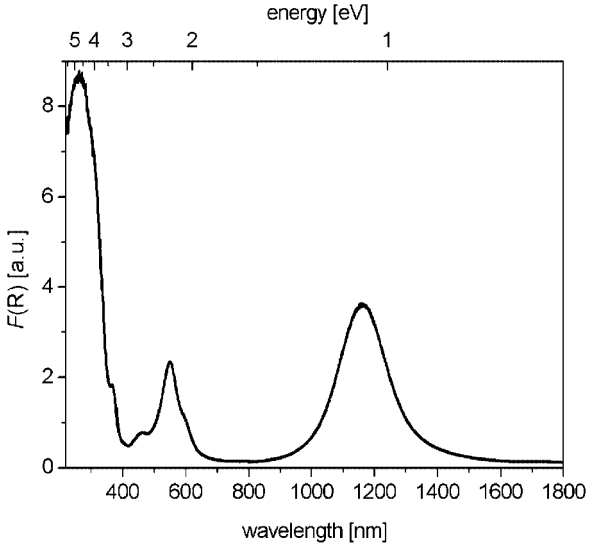

Figure 2. UV/Vis reflectance spectrum of $[Cu_{20}Se_{13}(PEt_3)_{12}]$ (**1**)

Thermogravimetric analysis of **1** in vacuo shows a one-step weight loss of 45.1% centered at 71.5 °C (Figure 3, b). As the cleavage of all the phosphane ligands leads only to

 © 2004 Wiley-VCH Verlag GmbH & Co. KGaA, Weinheim

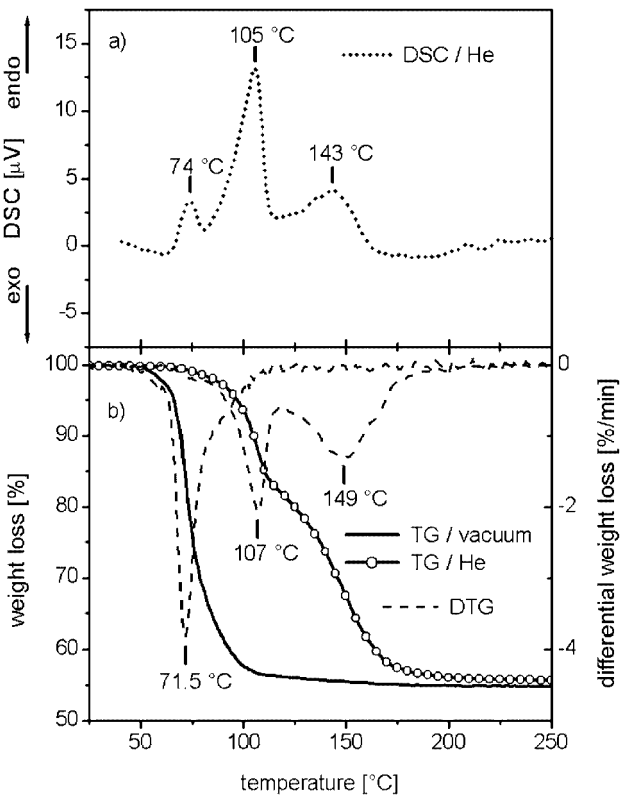

Figure 3. (a) Differential scanning calorimetry of **1**; (b) thermogravimetric analysis of $[Cu_{20}Se_{13}(PEt_3)_{12}]$ (**1**) in vacuo (straight line) and with helium flow (line with circles), the corresponding differential thermogravimetric curves are drawn as dashed lines

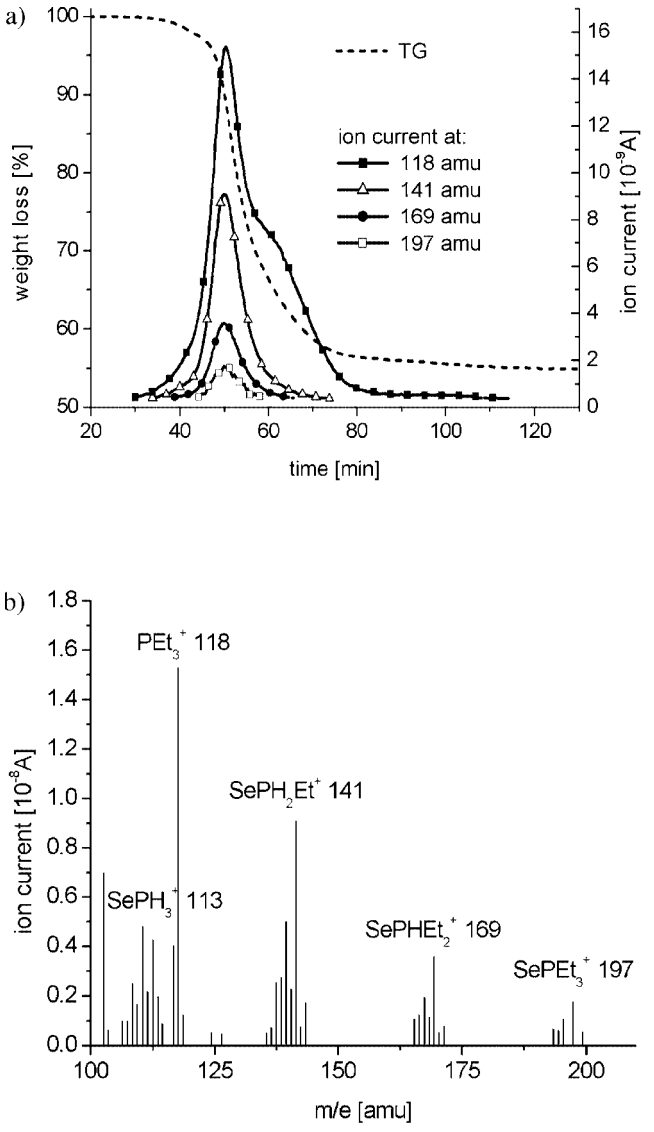

Figure 4. (a) Thermogravimetric analysis of $[Cu_{20}Se_{13}(PEt_3)_{12}]$ (**1**) in vacuo (dashed line) and ion current versus measuring time at 118, 141, 169 and 197 amu; (b) simultaneously recorded mass spectrum of the cleavage products from the thermogravimetry of **1** at cycle 131 (ca. 50 min measuring time)

a theoretical weight loss of 38.2% there appears to be additional elimination of selenium. This was confirmed by simultaneously recorded mass spectra that show peaks attributable to $SePEt_3$ and its fragmentation products (Figure 4, b). The course of the ion current caused by these species (Figure 4, a) indicates that they are formed at an early stage of the cleavage process. In contrast, the ion current for PEt_3 is spread over the whole cleavage process. Theoretical cleavage of three selenium atoms and twelve PEt_3 molecules would lead to a weight loss of 44.5%, which is close to the experimental value. Further evidence for this assumption comes from elemental analysis of the black residue obtained from the TGA, in which the Cu/Se ratio was found to be 1.97:1, in contrast to 3.1:2 in the cluster complex. The analysis further yields C 0.55%, H 0.12%, P $<$ 0.1%.

Thermogravimetric analysis of **1** in a dynamic helium gas flow showed that the thermal decomposition occurs in two successive steps, with maxima in the DTG curve at 107 and 149 °C and weight losses of approximately 17 and 27.4% (Figure 3, b). Here, the change of atmosphere increases the mean cleavage temperature, as has been observed previously for $[Cu_{70}Se_{35}(PEt_2Ph)_{24}]$.[10] The simultaneously recorded mass spectra of the volatile products show only the appropriate peaks for PEt_3 from the beginning of the first step but not for $SePEt_3$ at any stage of the cleavage process. This originates from the use of a TG-MS skimmer coupling system under normal pressure, which reduces the amount of substances reaching the detector and thus the intensity of the signal in comparison with measurements in vacuo. However, the formation of $SePEt_3$ in this case was proven by ^{31}P NMR in C_6D_6 [δ = 44.55 (m) ppm][16] and GC-MS of the collected cleavage products from a cold trap.

A more detailed investigation of the two cleavage steps suggests that in the first step only PEt_3 is cleaved and no $SePEt_3$, due to the different boiling points of the two compounds. In agreement, elemental analysis of the product at approximately 17% mass loss shows C 14.7% and H 3.1%, corresponding to the theoretical cleavage of five PEt_3 molecules (16% weight loss) which would lead to $Cu_{20}Se_{13}(PEt_3)_7$ (C 16.14%, H 3.4%) while the cleavage of three $SePEt_3$ molecules (15.6% weight loss) would give $Cu_{20}Se_{10}(PEt_3)_9$ (C 20.8%, H 4.4%). Furthermore, the cleavage of

 © 2004 Wiley-VCH Verlag GmbH & Co. KGaA, Weinheim

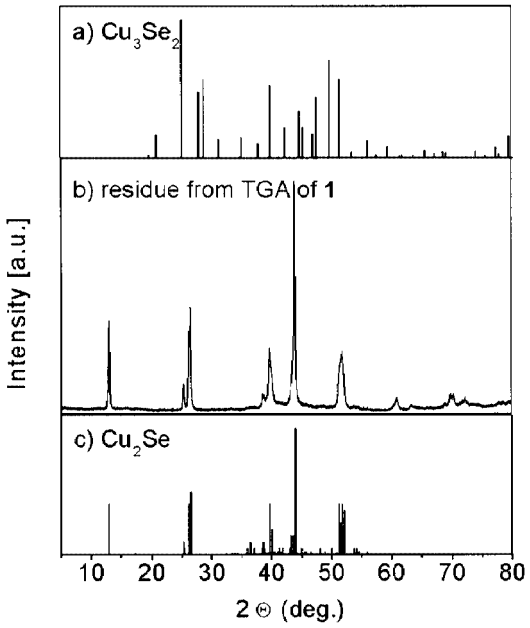

Figure 5. Room-temperature powder-diffraction patterns of (a) Cu_3Se_2;[19] (b) residue of the thermogravimetric analysis of $[Cu_{20}Se_{13}(PEt_3)_{12}]$ (**1**) in vacuo and (c) monoclinic α-Cu_2Se from ref.[18]

$SePEt_3$ in the second step can just be observed by eye upon careful stepwise heating of **1** in a glass flask and is indicated by the sudden formation of white needles on the flask walls above 100 °C. In the powder-diffraction pattern of the intermediate product (heated to 120 °C, 17% mass loss) we found no reflections due to the reported structure of Cu_3Se_2[17] but rather broad reflections pointing to the formation of Cu_2Se[18] (see discussion of powder-diffraction patterns below). Additionally, we found sharp peaks that agree with the calculated pattern of $SePEt_3$.[19] Thus, at almost below 100 °C, phosphane selenide is formed, in agreement with the vacuum TGA, but due to its higher boiling point under normal pressure it escapes from the crucible in the second step.

The differential scanning calorimetry (DSC) curve displays three separated peaks that correspond to three endothermal events in the sample under normal pressure in a dynamic helium gas flow. While the peaks at 105 and 143 °C agree with the two weight-loss steps in thermogravimetry the first endothermal reaction, centered around 74 °C, is more complicated. As the determination of the melting point of the sample gives no evidence for a related process of **1** at this temperature we suggest that the onset of the DSC signal (64 °C) depicts the limit of the thermal stability of **1**. Further heating leads to a decomposition of **1** induced by the formation of $SePEt_3$, a process that is thus clearly separated from the mass loss generated by the escape of PEt_3 and $SePEt_3$ from the crucible.

The powder-diffraction pattern of the thermogravimetric residues of **1** after heating to 250 °C are similar for measurements both in vacuo and in a helium gas flow. The peak positions (Figure 5) agree well with those reported for monoclinic α-Cu_2Se.[18] Furthermore no formation of a Cu_3Se_2 phase[19] was observed although it should be more favoured according to the Cu/Se ratio of 3.1:2 in the cluster complex. This corresponds, on the one hand, to the composition $Cu_{1.97}Se$ determined by elemental analysis and, on the other hand, to the observed mass reduction in thermogravimetry, which strongly suggests the cleavage of three selenium atoms in addition to the triethylphosphane ligands. Stevels has reported that Cu_3Se_2 disproportionates between 120 and 135 °C to form $Cu_{1.8}Se$ and CuSe.[20] In our case, vacuum conditions and the phosphanes, which allows the formation of volatile $SePEt_3$, obviously further reduces the stability of the Cu_3Se_2 phase, leading to the formation of α-Cu_2Se.

Experimental Section

General: Standard Schlenk techniques were employed throughout the syntheses using a double manifold vacuum line with high-purity dry nitrogen. Diethyl ether was dried with sodium/benzophenone and distilled under nitrogen. Anhydrous CuCl (Fluka) was purified from traces of $CuCl_2$ by subsequent washing with dilute HCl, methanol and diethyl ether followed by drying in vacuo. $Se(SiMe_3)_2$ [21] and PEt_3 [22] were prepared according to standard literature procedures. ^{31}P NMR spectra were recorded with a Bruker DPX Avance 300 with 85% H_3PO_4 as an external standard. The solid-state reflectance spectra were measured with a Varian Cary 500 spectrophotometer as micron-sized crystalline powders between quartz plates with a Labsphere integrating sphere.

$[Cu_{20}Se_{13}(PEt_3)_{12}]$ (1): PEt_3 (1.43 mL, 9.7 mmol) was added to a suspension of CuCl (0.32 g, 3.23 mmol) in diethyl ether (40 mL) and stirred for 1 h to give a clear solution. $Se(SiMe_3)_2$ (0.36 mL, 1.62 mmol) was then added at −40 °C and the flask with the PTFE gaskets as stoppers was evacuated before storage at −20 °C. A successful reaction is indicated by the formation of a violet solution. Then, after warming up to −10 °C, black octahedral crystals of **1** appeared within a few days with a final total yield of 20%. $C_{72}H_{180}Cu_{20}P_{12}Se_{13}$ (3715.3): calcd. C 23.28, H 4.88; found C 23.03, H 4.72.

X-ray Crystallography: Crystals suitable for single-crystal X-ray diffraction were obtained directly from the reaction solutions of the compound and then selected in perfluoroalkyl ether oil. Single-crystal X-ray diffraction data for determination of the cell constants of **1** were collected using graphite-monochromatized Mo-K_α radiation (λ = 0.71073 Å) with a STOE IPDS II (Imaging Plate Diffraction System). For more details concerning the crystallographic data of **1**, see ref.[13] The molecular diagram was prepared using the program SCHAKAL 97.[23] X-ray powder-diffraction (XRD) patterns were measured with a STOE STADI P diffractometer (Cu-K_α radiation, germanium monochromator, Debye−Scherrer geometry) in sealed glass capillaries. Theoretical powder-diffraction patterns for **1** were calculated on the basis of the atom coordinates obtained from single-crystal X-ray analysis by using the program package STOE WinXPOW.[24]

Thermogravimetric Analysis: Thermogravimetric analyses were run with a thermobalance STA 409 from Netzsch either in vacuo or with a dynamic helium gas flow (70 mL/min) (heating rate 2 K/min). The balance is coupled with a quadrupole mass spectrometer QMG 422 (Balzers) that includes a skimmer system for measurements under normal pressure.

 © 2004 Wiley-VCH Verlag GmbH & Co. KGaA, Weinheim

Acknowledgments

This work was supported by the Deutsche Forschungsgemeinschaft (Center of Functional Nanostructures). We thank Frau Tröster for her valuable assistance in the laboratory.

[1] *Clusters and Colloids* (Ed.: G. Schmid), VCH, Weinheim **1995**.
[2] S. Dehnen, A. Eichhöfer, D. Fenske, *Eur. J. Inorg. Chem.* **2002**, 279−317.
[3] I. Dance, K. Fisher, *Progress in Inorganic Chemistry*, vol. 41 (Ed.: Kenneth D. Karlin), John Wiley & Sons, Inc., New York, Weinheim, **1994**, p. 637−802.
[4] T. Vossmeyer, G. Reck, L. Katsikas, E. T. K. Haupt, B. Schulz, H. Weller, *Science* **1995**, *267*, 1476−1479; T. Vossmeyer, G. Reck, B. Schulz, L. Katsikas, H. Weller, *J. Am. Chem. Soc.* **1995**, *117*, 12881−12882.
[5] N. Herron, J. C. Calabrese, W. E. Farneth, Y. Wang, *Science* **1993**, *259*, 1426−1428.
[6] D. Fenske, H. Krautscheid, G. Baum, M. Semmelmann, *Angew. Chem.* **1993**, *105*, 1364−1367; *Angew. Chem. Int. Ed. Engl.* **1993**, *33*, 1303−1305.
[7] D. Fenske, T. Langetepe, N. Zhu, *Angew. Chem.* **1998**, *110*, 2783−2788; *Angew. Chem. Int. Ed.* **1998**, *37*, 2640.
[8] X.-J. Wang, T. Langetepe, C. Persau, B.-S. Kang, G. M. Sheldrick, D. Fenske, *Angew. Chem.* **2002**, *114*, 3972−3977; *Angew. Chem. Int. Ed.* **2002**, *41*, 3818−3822.
[9] W. E. Farneth, N. Herron, Y. Wang, *Chem. Mater.* **1992**, *4*, 916−922.
[10] A. Eichhöfer, E. Beckmann, D. Fenske, D. Herein, H. Krautscheid, R. Schlögl, *Isr. J. Chem.* **2001**, *41*, 31−37.
[11] D. van der Putten, D. Olevano, R. Zanoni, H. Krautscheid, D. Fenske, *J. Electron. Spectrosc. Relat. Phenom.* **1995**, *76*, 207−211.
[12] C. Kowalchuk, J. F. Corrigan, Y. Huang, *Chem. Commun.* **2000**, 1811−1812.
[13] D. Fenske, H. Krautscheid, *Angew. Chem.* **1990**, *102*, 1513−151; *Angew. Chem. Int. Ed. Engl.* **1990**, *29*, 1452−1454.
[14] A. Eichhöfer, J. F. Corrigan, D. Fenske, E. Tröster, *Z. Anorg. Allg. Chem.* **2000**, *626*, 338−348.
[15] M. B. Robin, P. Day, *Adv. Inorg. Radiochem.* **1967**, *10*, 248−422.
[16] N. Muller, P. C. Lauterbur, J. Goldenson, *J. Am. Chem. Soc.* **1956**, *78*, 3557−3561.
[17] In Powder-diffraction file PDF-2 Database Sets 1−85, **1993**, International Center for Diffraction Data, Newtown Square USA, File number 72−1421; N. Morimoto, K. Koto, *Science* **1966**, *152*, 345; R. MacLaren Murray, R. D. Heyding, *Can. J. Chem.* **1976**, *54*, 841.
[18] In Powder-diffraction file PDF-2 Database Sets 1−85, **1993**, International Center for Diffraction Data, Newtown Square USA, File number 27−1131; A. L. N. Stevels, *Philips Res. Rep. Suppl.* **1969**, *9*, 39−44.
[19] M. van Meerssche, A. Leonard, *Acta Crystallogr.* **1959**, *12*, 1053−1054.
[20] A. L. N. Stevels, *Philips Res. Rep. Suppl.* **1969**, *9*, 44−46.
[21] H. Schmidt, H. Ruf, *Z. Anorg. Allg. Chem.* **1963**, *321*, 270−273.
[22] K. Sasse in *Methoden der Organischen Chemie, Houben-Weyl*, Thieme Verlag, Stuttgart, **1963**, vol. 1, p. 32; H. D. Kaesz, F. G. Stone, *J. Org. Chem.* **1959**, *24*, 635−637.
[23] E. Keller, *SCHAKAL 97, A Computer Program for the Graphic Representation of Molecular and Crystallographic Models*, Universität Freiburg, **1997**.
[24] STOE, *WinXPOW*, STOE & Cie GmbH, Darmstadt, **2000**.

Received May 6, 2003
Early View Article
Published Online October 31, 2003

 © 2004 Wiley-VCH Verlag GmbH & Co. KGaA, Weinheim

Crystal Field Strengths, Nephelauxetic Effects, and Experimentally Based Molecular Orbital Schemes (in the f Range) of Selected Cyclopentadienyl Complexes of Samarium(III)[‡]

Hanns-Dieter Amberger,*[a] Hauke Reddmann,[a] Stefan Jank,[a] Maria Irene Lopes,[b] and Noémia Marques[b]

Keywords: Lanthanides / Cyclopentadienyl ligands / Optical spectra / Crystal field analysis / Molecular orbital schemes

The absorption and luminescence spectra of pseudo (ψ) trigonal planar [Sm(η^5-C_5H_4tBu)$_3$] (**1**), low symmetric [Sm(η^5-Cp)(η^3-Tp^{Me_2})(η^2-Tp^{Me_2})] (Cp = η^5-cyclopentadienyl; Tp^{Me_2} = hydrotris(3,5-dimethylpyrazolyl)borato) (**2**) as well as ψ trigonal pyramidal [Sm(η^5-C_5H_4tBu)$_3$(THF)] (**3**), [Sm(η^5-Cp)$_3$(THF)] (**4**) and [Sm(η^5-Cp)$_3$(CNC_6H_{11})] (**5**) have been measured at room and low temperatures. From the spectra obtained, truncated crystal field (CF) splitting patterns of these compounds could be derived, and simulated by fitting the parameters of a phenomenological Hamiltonian. On the basis of the CF parameters used, the global CF strengths experienced by the Sm^{3+} central ions of complexes **1**–**5**, as well as the individual CF strength associated with one C_5H_4tBu$^-$ ligand are estimated. The obtained Slater parameters F^2 and the spin-orbit coupling parameters ζ_{4f} allow the insertion of compounds **1**–**5** into truncated nephelauxetic and relativistic nephelauxetic series. Besides, the experimentally based non-relativistic and relativistic molecular orbital schemes (in the f range) of complexes **1** and, partly, **3** are set up and compared with the results of quantum chemical model calculations.

(© Wiley-VCH Verlag GmbH & Co. KGaA, 69451 Weinheim, Germany, 2004)

Introduction

After a successful parametric analysis of the experimentally derived crystal field (CF) splitting pattern, the global CF strength [$N_v/(4\pi)^{1/2}$] experienced by the central ion of a lanthanide [Ln(III)] compound may be calculated by the relation[2]

$$N_v / \sqrt{4\pi} = \sum_{k,q} \sqrt{\frac{(B_q^k)^2}{2k+1}}$$

where the B_q^k's represent the phenomenological CF parameters used in the fit.[3–6] The individual CF strength associated with one single ligand L^- of homoleptic neutral LnL_3 or anionic $[LnL_p]^{3-p}$ complexes is obtained by dividing $N_v/(4\pi)^{1/2}$ by three or the number of ligands (p), respectively (method A).

Alternatively, the individual CF strength of the ligand L^- of neutral $LnLL'_2$ or anionic $[LnLL'_q]^{2-q}$ complexes is nearly equal to the global CF strength if the CF strength associated with the ligands L'^- may be safely neglected (method B).

In recent years, we have parametrized the CF splitting patterns of a number of monomeric homoleptic LnL_3 [L = $C_5H_4SiMe_3^-$,[7] $N(SiMe_3)_2^-$,[8–10] $CH(SiMe_3)_2^-$,[11,12] OC_6H_3tBu$_2$-2,6$^-$[13]] complexes and — using method A — we found enormous individual CF strengths. By combining these ligands L with those producing weak CF strengths, the individual CF strength of the ligand L may also be estimated by means of method B.

Some years ago, we compared the absorption spectra of [Nd(COT)(Tp^{Me_2})] [COT = η^8-cyclooctatetraenyl; Tp^{Me_2} = hydrotris(3,5-dimethylpyrazolyl)borato] and [Nd(COT)(I)(THF)$_3$] and observed only minor differences.[14] As the CF strengths of I^- and THF are relatively small,[15] we concluded that this holds also for the Tp^{Me_2} ligand. Applying method B, the large global CF strengths found for [Ln(COT)(Tp^{Me_2})] (Ln = Pr, Nd, Sm)[16–19] were considered to be approximately equal to the individual CF strength of the COT ligand.

Up to now, the results of both methods (with the central Ln^{3+} ion as well as the ligand L^- fixed) have not been cross-checked. Because of the existence of Sm^{III} and Sm^{II} precursors, the variety of organosamarium(III) complexes is

[‡] Electronic structures of organometallic complexes of f elements, 57. Part 56: Ref.[1]

[a] Institut für Anorganische und Angewandte Chemie der Universität Hamburg,
Martin-Luther-King-Platz 6, 20146 Hamburg, Germany
Fax: (internat.) +49-(0)40-42838-2893
E-mail: fc3a501@uni-hamburg.de
[b] Departamento de Quimica, ITN,
Estrada Nacional 10, 2686, Sacavém Codex, Portugal
Fax: (internat.) +351-21-9941455
E-mail: nmarques@itn.pt

 © 2004 Wiley-VCH Verlag GmbH & Co. KGaA, Weinheim DOI: 10.1002/ejic.200300309

extremely well developed. In the framework of the present and some following estimations of the CF strengths of the strong ligands L adopting methods A and B, respectively, we will focus on the combination of the Sm^{3+} ion and (substituted) η^5-cyclopentadienyl (Cp) ligands. In this first study, we select from the series of hitherto described homoleptic $[SmCp'_3]$ [$Cp' = C_5H_4tBu^-$, $C_5H_3(1,3\text{-}SiMe_3)_2^-$, $C_5Me_5^-$, $C_5HMe_4^-$, $C_5Me_4Et^-$, $C_5H_4SiEt_3^-$, $C_5H_4CH(SiMe_3)_2^-$][20–27] and monomeric $[SmCp'L'_2]$ ($Cp' = Cp^-$, $C_5H_4tBu^-$, $C_5H_4Me^-$, $C_5Me_5^-$, $C_5H_4SiMe_3^-$, $C_5Me_4CH_2Ph^-$; $L' = Cl^-$, acac$^-$, I^-, Tp^{Me_2})[28–32] complexes the combination $[Sm(C_5H_4tBu)_3]$ (**1**)/ $[Sm(Cp)(Tp^{Me_2})_2]$ (**2**).

For the purpose of demonstrating that the CF strengths associated with the $C_5H_4tBu^-$ and Cp ligand, respectively, are comparable, it is planned to additionally analyze the absorption spectra of $[Sm(C_5H_4tBu)_3(THF)]$ (**3**) and $[Sm(Cp)_3(THF)]$ (**4**). In order to study spectroscopic and nephelauxetic effects associated with the isocyanide and nitrile ligand, respectively, we wish to compare the result of a CF analysis on $[Sm(Cp)_3(CNC_6H_{11})]$ (**5**) with that of a previous one on $[Sm(Cp)_3(NCCH_3)]$.

Organometallic π complexes of f elements usually have poor crystallizing properties, and additionally the principal rotation axes of the individual molecules in the unit cell are frequently not aligned. Even if they were aligned as in the case of low symmetric crystal systems, it is difficult to orientate these rotation axes with respect to outer homogeneous or vector fields. For this reason, the optical properties of organo-f element complexes are usually studied in solution or as pellets, thus missing the additional information obtainable from optical polarization measurements. A way out of these difficulties would be to extract a first rough set of parameters from the results of quantum chemical calculations on the compound of interest.

In order to check the predictions of previous model calculations on model pseudo (ψ) trigonal planar $[Ln(\eta^5\text{-}Cp)_3]$ (Ln = Sm, Pr, Ce)[33–35] as well as of real ψ trigonal pyramidal $[Pr(\eta^5\text{-}Cp)_3(B)]$ (B = THF, CNC_6H_{11})[35] and $[Gd(\eta^5\text{-}Cp)_3(THF)]$,[36] we wish to compare the calculated non-relativistic and relativistic molecular orbital (MO) schemes (in the f range) of these compounds with our experimentally based results.

Results and Discussion

General Symmetry Considerations, Selection Rules and the Phenomenological Hamiltonian

The crystal and molecular structure of compound **1** is unknown, however, the optical spectra of this complex exhibits the same features as those of $[Sm(C_5Me_5)_3]$ or $[Sm(C_5HMe_4)_3]$,[37] where the three Cp centroids describe a trigonal planar geometry around the Sm^{3+} ion.[23,24] Thus for **1**, we assume an effective CF of D_{3h} symmetry.

A single-crystal X-ray study of complex **2** revealed a symmetrical η^5-bonding of the Cp ring and an η^3- as well as an η^2-bonding mode of the two Tp^{Me_2} ligands[32] (Figure 1).

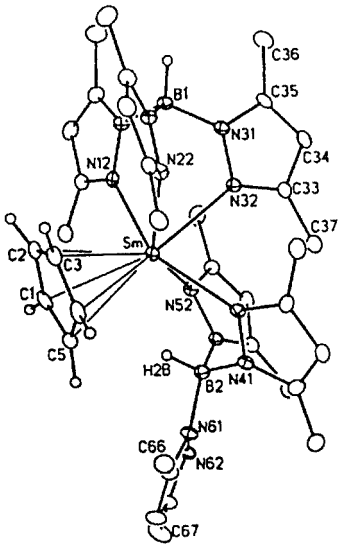

Figure 1. Molecular structure of $[Sm(\eta^5\text{-}Cp)(\eta^3\text{-}Tp^{Me_2})(\eta^2\text{-}Tp^{Me_2})]$ from a single-crystal analysis[32]

In order to simplify the parametrization of the experimentally derived energy level scheme of this low symmetric compound, we adopt the following two approaches: in analogy with our previous treatments of the CF splitting patterns of $[Ln(COT)(Tp^{Me_2})]$ (Ln = Pr, Nd, Sm)[16–19] we only consider the influence of the Cp ligand, which leads to C_{5v} symmetry. Alternatively, we approximate the real molecular geometry by a pentagonal sandwich complex (D_{5h} symmetry of the effective CF).

The electrostatic potentials of seven- and higher-membered aromatic ring ligands, experienced by f electrons, are equivalent to circles,[38] thus the effective CFs of $[Ln(COT)]^+$ fragments[16–19] are of $C_{\infty v}$ symmetry. Theoretically, in the case of lower membered aromatic ligands such as Cp, the actual C_{5v} symmetry of the $[Sm(Cp)]^{2+}$ moiety has to be considered. However, a number of previous studies of ψ trigonal pyramidal[39] and ψ trigonal bipyramidal[40] Cp complexes of rare earths showed that the five-membered Cp rings disturb the pseudo symmetry only weakly. Therefore, in the framework of this approach instead of the actual molecular C_{5v} the higher $C_{\infty v}$ symmetry is assumed. Effective CFs of D_{5h} and $C_{\infty v}$ symmetry have the same CF Hamiltonians (vide infra), thus both approaches are equivalent from the aspect of CF theory.

Single-crystal X-ray analyses of numerous mono base adducts of the type $[Ln(Cp')_3(B)]$ ($Cp' = Cp$, alkylated or silylated Cp, B = THF, CNC_6H_{11}, $NCCH_3$) revealed a ψ trigonal pyramidal structure,[20] suggesting an effective CF of C_{3v} symmetry for adducts **3–5**.

The free Sm^{3+} ion gives rise to multiplets $^{2S+1}L_J$ with $1/2 \leq J \leq 21/2$.[41] If the Sm^{3+} ion is placed into CFs of D_{3h}, $D_{5h}/C_{\infty v}$ or C_{3v} symmetry, respectively, these multiplets are split into various CF levels.[6] The wavefunctions of these levels are described to first order by $\pm M_J$ for $D_{5h}/C_{\infty v}$ symmetry, whereas different $\pm M_J$ functions with $\Delta M_J = 6$

 © 2004 Wiley-VCH Verlag GmbH & Co. KGaA, Weinheim

mix for D_{3h}, and $\Delta M_J = 3$ for C_{3v} symmetry. Table 3 of ref.[42] lists the composition of the CF eigenvectors of f^n systems (with an odd number of f electrons) exposed to a CF of D_{3h} symmetry, and correlates them with the irreducible representations (irreps) Γ_7, Γ_8 and Γ_9 of the D_{3h}' double group. In this table the convention of Koster et al.[43] is used. The convention suggested by Hüfner[44] interchanges Γ_7 and Γ_8.

In the case of $D_{5h}/C_{\infty v}$ symmetry, the CF states are sufficiently characterized by their M_J quantum numbers, and in the case of C_{3v} symmetry, the CF states transform like the irreps Γ_4 and $\Gamma_{5/6}$.

The electric dipole selection rules (odd number of f electrons) for powdered or dissolved species with an effective CF of D_{3h} symmetry are given in Table A 5.2. of ref.[6] This table shows that the only forbidden transitions for adduct **1** are of the type $\Gamma_7 \rightarrow \Gamma_7$ and $\Gamma_8 \rightarrow \Gamma_8$, respectively.

In the case of compound **2**, the ideal $D_{5h}/C_{\infty v}$ symmetry is noticeably distorted, thus we expect that each $^{2S+1}L_J$ multiplet splits into J + 1/2 levels, and all transitions are allowed. According to Table A 5.3. of ref.[6], all transitions in C_{3v} symmetry are allowed for dissolved and powdered adducts **3**−**5**.

The energy levels within f^n configuration in D_{3h}, $D_{5h}/C_{\infty v}$ and C_{3v} symmetry can be written in terms of the atomic free ion (H_{FI}) and crystal field (H_{CF}) Hamiltonians as follows:

$H = H_{FI} + H_{CF}$, where

$$H_{FI} = \sum_{k=0,2,4,6} f_k F^k(nf,nf) + a_{so}\zeta_{4f} + \alpha L(L+1) + \beta G(G_2) + \gamma G(R_7) + \sum_{i=2,3,4,6,7,8} t_i T^i + \sum_{k=0,2,4} m_k M^k + \sum_{k=2,4,6} p_k P^k \text{ [4]}, \text{ and}$$

$$H_{CF}(D_{3h}) = B_0^2 C_0^{(2)} + B_0^4 C_0^{(4)} + B_0^6 C_0^{(6)} + B_6^6 (C_{-6}^{(6)} + C_6^{(6)}) \text{ (Ref.[6], p. 242).}$$

$$H_{CF}(D_{5h}/C_{\infty v}) = B_0^2 C_0^{(2)} + B_0^4 C_0^{(4)} + B_0^6 C_0^{(6)} \text{ (Ref.[6], p. 242/245).}$$

$$H_{CF}(C_{3v}) = B_0^2 C_0^{(2)} + B_0^4 C_0^{(4)} + B_3^4 (C_{-3}^{(4)} - C_3^{(4)}) + B_0^6 C_0^{(6)} + B_3^6 (C_{-3}^{(6)} - C_3^{(6)}) + B_6^6 (C_{-6}^{(6)} + C_6^{(6)}) \text{ (Ref.[6], p. 245).}$$

The $F^k(nf,nf)$'s and ζ_{4f} terms represent, respectively, the radial parts of the electrostatic and spin-orbit interactions between f electrons, while f_k and a_{so} are the angular parts of these interactions. α, β and γ are the parameters associated with the two-body effective operators of configuration interaction, and the T^i's are the corresponding three-body effective operators. The M^k parameters represent the spin-spin, and spin-other-orbit interactions, while the P^k parameters arise from electrostatic spin-orbit interactions with higher configurations.[4] The CF interaction for the above symmetries is represented by the B_q^k parameters and the tensor operators $C_q^{(k)}$.[3]

Optical Spectra of [Sm(C$_5$H$_4$*t*Bu)$_3$]

Homoleptic base-free SmL_3 complexes with alkylated or silylated ligands are usually deeply colored[20−27] because of an energetically low-lying charge-transfer transition of the type $Sm^{III}(L^-)_3 \rightarrow Sm^{II}(L_3)^{2-}$. Thus these compounds show either no or a few luminescence transitions (on the basis of which the CF splitting patterns of Sm^{III} compounds in the low energy range < 5000 cm^{-1} are usually derived).[45] For this reason the energies of the low-lying levels of compound **1** have to be extracted mainly from "hot" transitions and IR/NIR spectra, where, however, fundamental vibrations as well as binary and ternary C−H combination vibrations and overtones are severely disturbing.

In order to partly separate stronger bands of f-f transitions from weaker vibrational signals, we also recorded the absorption spectrum of "optically empty" [La(C$_5$H$_4$*t*Bu)$_3$] in the IR/NIR range. As the NIR spectrum of this compound was poorly resolved, we also used [La(C$_5$H$_4$SiMe$_3$)$_3$] (oil at room temperature) for the above purpose.

Comparing the low-temperature IR spectra of **1** and the corresponding La compound, we could not detect any differences, thus the energies of low-lying levels have to be concluded from "hot" transitions in the UV/Vis/NIR range and the rare transitions of the luminescence spectrum. In the low temperature Vis/NIR spectrum of complex **1** some "hot" signals (with $\Delta E \approx 486$ cm^{-1} from the corresponding "cold" bands) that appear in the room temperature spectrum are missing, thus indicating an excited level at about 486 cm^{-1}.

Luminescence transitions of organometallic Sm^{III} compounds usually initiate at the lowest CF level of $^4G_{5/2}$,[45,46] which is found at 17489 cm^{-1} in the room temperature absorption spectrum of complex **1** dissolved in methylcyclohexane. In the luminescence spectrum of solid **1**, we could not detect a single luminescence transition, but a methylcyclohexane solution showed a signal at 16591 cm^{-1} (using the exciting line at 476.5 nm) which suggests the existence of a CF level at 898 cm^{-1}.

In the range 4000−4650 cm^{-1} of the IR/NIR spectrum (pellet) the expected transitions $^6H_{5/2} \rightarrow {}^6H_{11/2}$ are partially obscured by strong C−H combination vibrations and overtones, but in the remaining part of this spectrum a number of f-f transitions could be clearly identified (Figure 2, Table 1).

The UV/Vis part of the low temperature absorption spectrum is dominated by a strong broad charge-transfer band. On the low-energy side of this band one strong (17486 cm^{-1}) and three diffuse signals at approximately 18282, 19245 and 19485 cm^{-1} appeared (Table 1).

Optical Spectra of [Sm(Cp)(Tp^{Me_2})$_2$]

In order to separate bands of f-f and vibrational origin in the absorption spectrum of compound **2**, we could not make use of the corresponding "optically empty" La, Gd,

 © 2004 Wiley-VCH Verlag GmbH & Co. KGaA, Weinheim

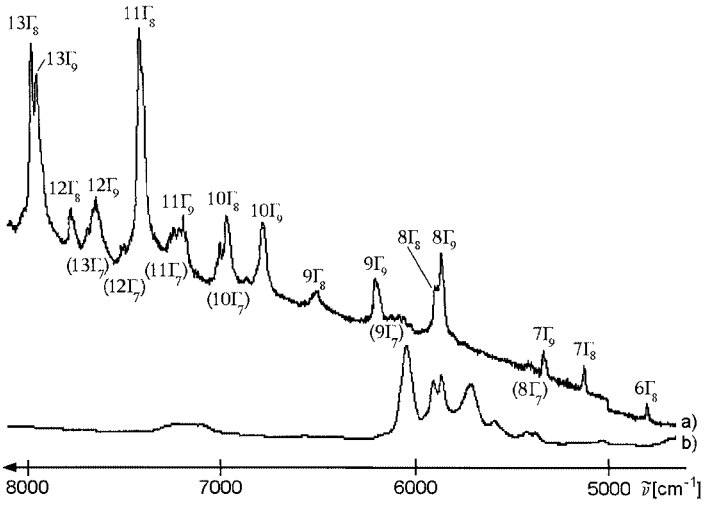

Figure 2. Absorption spectra in the range 4700−8100 cm^{-1}: a) $[Sm(C_5H_4tBu)_3]$, pellet, ca. 80 K; b) $[La(C_5H_4SiMe_3)_3]$, oil, room temperature

Table 1. Calculated and experimental energy values for $[Sm(C_5H_4tBu)_3]$; all values in cm^{-1}

Multiplet [a]	CF level		E (calcd.)	E (exp.)[b]	Multiplet	CF level		E (calcd.)	E (exp.)
$^6H_{5/2}$	$1\Gamma_7$[c]	±5/2[d]	0	0	$^6H_{15/2}$	$12\Gamma_8$	±1/2	7752	7760
$^6H_{5/2}$	$2\Gamma_9$	±3/2	493	486[e]	$^6F_{5/2}$	$13\Gamma_9$	±3/2	7930	7932
$^6H_{7/2}$	$2\Gamma_7$	±7/2	910	898[f]	$^6F_{5/2}$	$13\Gamma_8$	±1/2	7934	7960
$^6H_{5/2}$	$1\Gamma_8$	±1/2	977		$^6F_{7/2}$	$14\Gamma_7$	±7/2	8517	
$^6H_{7/2}$	$3\Gamma_7$	±5/2	1634		$^6F_{7/2}$	$14\Gamma_8$	±1/2	8607	8618
$^6H_{7/2}$	$2\Gamma_9$	±3/2	1873		$^6F_{7/2}$	$14\Gamma_9$	±3/2	8635	8618
$^6H_{7/2}$	$2\Gamma_8$	±1/2	1950		$^6F_{7/2}$	$15\Gamma_7$	±5/2	8659	(8669)
$^6H_{9/2}$	$3\Gamma_9$	±9/2	2523		$^6F_{9/2}$	$15\Gamma_8$	±1/2	9605	9616
$^6H_{9/2}$	$4\Gamma_7$	±7/2	2704		$^6F_{9/2}$	$15\Gamma_9$	±3/2	9660	
$^6H_{9/2}$	$3\Gamma_8$	±1/2	3004		$^6F_{9/2}$	$16\Gamma_7$	±5/2	9668	
$^6H_{9/2}$	$4\Gamma_9$	±3/2	3095		$^6F_{9/2}$	$16\Gamma_9$	±9/2	9835	9816
$^6H_{9/2}$	$5\Gamma_7$	±5/2	3107		$^6F_{9/2}$	$17\Gamma_7$	±7/2	9836	
$^6H_{11/2}$	$4\Gamma_8$	±11/2	3616		$^6F_{11/2}$	$16\Gamma_8$	±1/2	10874	(10772)
$^6H_{11/2}$	$5\Gamma_9$	±9/2	3853		$^6F_{11/2}$	$17\Gamma_9$	±3/2	10886	(10903)
$^6H_{11/2}$	$6\Gamma_7$	±7/2	4160		$^6F_{11/2}$	$18\Gamma_7$	±5/2	10929	
$^6H_{11/2}$	$5\Gamma_8$	±1/2	4431		$^6F_{11/2}$	$19\Gamma_7$	±7/2	11040	
$^6H_{11/2}$	$6\Gamma_9$	±3/2	4492		$^6F_{11/2}$	$18\Gamma_9$	±9/2	11212	(11216)
$^6H_{11/2}$	$7\Gamma_7$	±5/2	4570		$^6F_{11/2}$	$17\Gamma_8$	±11/2	11438	(11531)
$^6H_{13/2}$	$6\Gamma_8$	±13/2	4806	4795	$^4G_{5/2}$	$20\Gamma_7$	±5/2	17486	17486
$^6H_{13/2}$	$7\Gamma_8$	±11/2	5093	5118	$^4G_{5/2}$	$19\Gamma_9$	±3/2	18278	18282
$^6H_{13/2}$	$7\Gamma_9$	±9/2	5319	5320	$^4G_{5/2}$	$18\Gamma_8$	±1/2	18344	
$^6H_{13/2}$	$8\Gamma_7$	±7/2	5400	(5399)[g]	$^4F_{3/2}$	$20\Gamma_9$	±3/2	19210	(19245)
$^6H_{13/2}$	$8\Gamma_9$	±3/2	5872	5851	$^4F_{3/2}$	$19\Gamma_8$	±1/2	19459	(19485)
$^6H_{13/2}$	$8\Gamma_8$	±1/2	5881	5880	$^4G_{7/2}$	$21\Gamma_7$	±7/2	19855	
$^6H_{13/2}$	$9\Gamma_7$	±5/2	6097	(6104)					
$^6H_{15/2}$	$9\Gamma_9$	±15/2	6202	6190					
$^6H_{15/2}$	$9\Gamma_8$	±13/2	6507	6509					
$^6H_{15/2}$	$10\Gamma_9$	±9/2	6760	6768					
$^6H_{15/2}$	$10\Gamma_7$	±7/2	6955	6956					
$^6F_{1/2}$	$10\Gamma_8$	±1/2	6992	6993					
$^6H_{15/2}$	$11\Gamma_7$	±7/2	7196	(7210)					
$^6F_{3/2}$	$11\Gamma_9$	±3/2	7224	7176					
$^6F_{3/2}$	$11\Gamma_8$	±1/2	7388	7399					
$^6H_{15/2}$	$12\Gamma_7$	±5/2	7542	(7492)					
$^6H_{15/2}$	$12\Gamma_9$	±3/2	7631	7632					
$^6F_{5/2}$	$13\Gamma_7$	±5/2	7692	(7669)					

[a] Dominating Russell-Saunders multiplet $^{2S+1}L_J$. [b] From absorption measurements. [c] CF states (D_{3h}' double group) ordered in ascending energy. [d] Largest eigenvector component $\pm M_J$. [e] From hot transitions. [f] From luminescence measurements. [g] Values in brackets (which are presumably due to forbidden $\Gamma_7 \rightarrow \Gamma_7$ transitions) were not fitted.

 © 2004 Wiley-VCH Verlag GmbH & Co. KGaA, Weinheim

Table 2. Calculated and experimental energy values for $[Sm(Cp)(Tp^{Me_2})_2]$; all values in cm^{-1}

Multiplet [a]	CF level[b]	E (calcd.)	E (exp.)[c]	E (exp.)[d]	Multiplet [a]	CF level [b]	E (calcd.)	E (exp.) [c]	E (exp.) [d]
$^6H_{5/2}$	±5/2	0	0	0	$^6F_{5/2}$	±5/2	7244		7223
$^6H_{5/2}$	±3/2	296	230		$^6F_{5/2}$	±3/2	7263		7271
$^6H_{5/2}$	±1/2	447	406		$^6F_{5/2}$	±1/2	7274		7329
$^6H_{7/2}$	±7/2	1062	1052		$^6F_{7/2}$	±1/2	8105		8104
$^6H_{7/2}$	±5/2	1270	1234		$^6F_{7/2}$	±5/2	8113		8104
$^6H_{7/2}$	±3/2	1359	1382		$^6F_{7/2}$	±3/2	8116		8123
$^6H_{7/2}$	±1/2	1440	1480		$^6F_{7/2}$	±7/2	8139		8180
$^6H_{9/2}$	±9/2	2253	2294		$^6F_{9/2}$	±1/2	9247		9170
$^6H_{9/2}$	±7/2	2428	2388		$^6F_{9/2}$	±3/2	9249		9255
$^6H_{9/2}$	±5/2	2508	2482		$^6F_{9/2}$	±5/2	9269		9255
$^6H_{9/2}$	±3/2	2583	2578		$^6F_{9/2}$	±7/2	9314		9320
$^6H_{9/2}$	±1/2	2632	2706		$^6F_{9/2}$	±9/2	9350		9363
$^6H_{11/2}$	±11/2	3536	3574		$^6F_{11/2}$	±1/2	10585		10526
$^6H_{11/2}$	±9/2	3704	3674		$^6F_{11/2}$	±3/2	10602		10628
$^6H_{11/2}$	±7/2	3792	3800		$^6F_{11/2}$	±5/2	10633		10628
$^6H_{11/2}$	±5/2	3866	3834		$^6F_{11/2}$	±7/2	10675		10692
$^6H_{11/2}$	±3/2	3926	3892		$^6F_{11/2}$	±9/2	10725		10692
$^6H_{11/2}$	±1/2	3960	4046		$^6F_{11/2}$	±11/2	10786		10811
$^6H_{13/2}$	±13/2	4880	4910	4912	$^4G_{5/2}$	±5/2	17769	17732	
$^6H_{13/2}$	±11/2	5045	5052	5056	$^4G_{5/2}$	±3/2	18013		
$^6H_{13/2}$	±9/2	5156	5152	5149	$^4G_{5/2}$	±1/2	18177		
$^6H_{13/2}$	±7/2	5242	5228	5230	$^4F_{3/2}$	±3/2	18935		18904
$^6H_{13/2}$	±5/2	5306	5260	5263	$^4F_{3/2}$	±1/2	18956		18975
$^6H_{13/2}$	±3/2	5351	5340	5345	$^4G_{7/2}$	±7/2	19876		19927
$^6H_{13/2}$	±1/2	5373	5420	5423	$^4G_{7/2}$	±5/2	20045		20041
$^6H_{15/2}$	±15/2	6261	6212	6213	$^4G_{7/2}$	±3/2	20184		
$^6H_{15/2}$	±13/2	6403	6436	6437	$^4G_{7/2}$	±1/2	20261		
$^6F_{1/2}$	±1/2	6494	6491	6489					
$^6H_{15/2}$	±11/2	6557	6543	6553					
$^6H_{15/2}$	±9/2	6673		6660					
$^6F_{3/2}$	±3/2	6732		6743					
$^6H_{15/2}$	±7/2	6749		6750					
$^6F_{3/2}$	±1/2	6789		6791					
$^6H_{15/2}$	±5/2	6795		6791					
$^6H_{15/2}$	±3/2	6820		6826					
$^6H_{15/2}$	±1/2	6832		6826					

[a] Dominating Russell-Saunders multiplet $^{2S+1}L_J$. [b] Largest eigenvector component $\pm M_J$. [c] From luminescence measurements. [d] From absorption measurements.

Y, Lu compounds as these don't exist at this point, but as a proxy we used the combined vibrational energies of NaCp and KTp^{Me_2}. The wavenumbers of the thus separated signals of presumable f-f origin in the Vis/NIR spectrum are given in Table 2 (Figure 3).

By using all of the exciting lines of an Ar^+ laser, the best signal-to-noise ratio in the luminescence spectrum of compound **2** was observed by applying the line at 476.5 nm. Using this line, the vibrational Raman signals are well separated from the luminescence transitions.[45,46] The observed

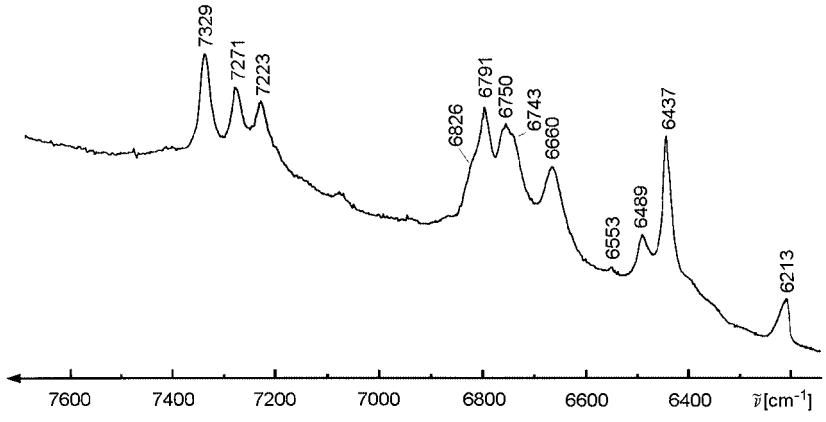

Figure 3. Absorption spectrum of $[Sm(Cp)(Tp^{Me_2})_2]$ in the range 6150−7700 cm^{-1}, pellet, ca. 80 K

 © 2004 Wiley-VCH Verlag GmbH & Co. KGaA, Weinheim

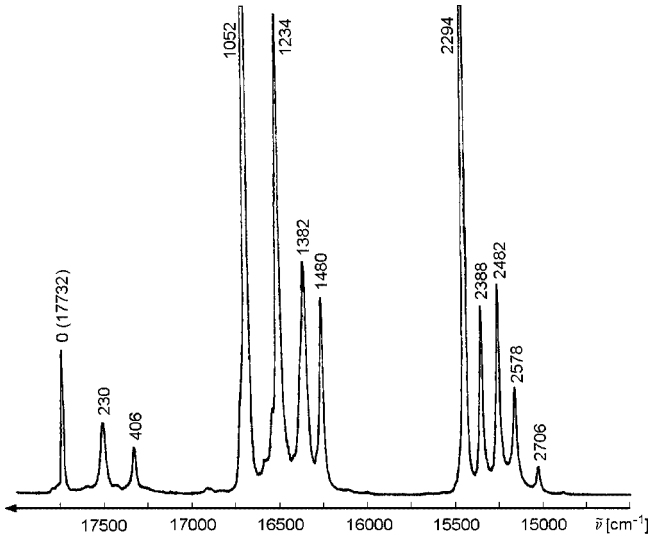

Figure 4. Luminescence spectrum of $[Sm(Cp)(Tp^{Me_2})_2]$ in the range 14500−18000 cm^{-1}, powder, ca. 90 K; the value in brackets denotes the absolute wavenumber of the fluorescing level, and those without brackets the derived CF energies.

low temperature luminescence spectrum (Figure 4) can be rationalized by identifying the fluorescing level at 17732 cm^{-1} with the lowest CF state of the multiplet $^4G_{5/2}$, and the terminal levels arising from the multiplets ^6H_J (J = 5/2, 7/2, 9/2, 11/2, 13/2, 15/2) and $^4F_{1/2}$. On this basis, the CF splitting pattern of **2** in the low-energy range could be derived (Table 2). In the overlapping region, the CF energies directly observed in the absorption spectrum and concluded from the luminescence spectrum, agree nicely (cf. Table 2).

Using the exciting line at 457.9 nm two "negative bands" with minima at 19927 cm^{-1} and 20041 cm^{-1} appeared. The existence of these signals may be explained by an absorption process from background radiation.[17] The former peak corresponds to a broad asymmetric band with the maximum at ca. 19930 cm^{-1} in the "ordinary" absorption spectrum of a pellet.

Absorption Spectra of $[Sm(C_5H_4tBu)_3(THF)]$, $[Sm(Cp)_3(THF)]$ and $[Sm(Cp)_3(CNC_6H_{11})]$

The low temperature absorption spectra of dissolved adducts **3**−**5** and previously analyzed solid $[Sm(Cp)_3(NCCH_3)]$[45] are nearly identical. The same holds for the luminescence spectra of adducts **4** and **5** and for that of $[Sm(Cp)_3(NCCH_3)]$[45] For this reason we do not present figures of the recorded spectra and refer the reader to ref.[45] Because of the deep purple color of a glassy frozen solution of compound **3**, we didn't try to record its luminescence spectrum.

CF Analyses

Because of the missing optical polarization measurements of oriented single crystals, and the principle impossi-

Table 3. Parameter values for $[Sm(C_5H_4tBu)_3]$, $[Sm(Cp)(Tp^{Me_2})_2]$, $[Sm(C_5H_4tBu)_3(THF)]$, $[Sm(Cp)_3(THF)]$, $[Sm(Cp)_3(CNC_6H_{11})]$, $[Sm(Cp)_3(NCCH_3)]$ and $[La_{0.8}Sm_{0.2}(Cp)_3(NCCH_3)_2]$; all values in cm^{-1}.

Parameter	Cpd. **1**	Cpd. **2**	Cpd. **3**	Cpd. **4**	Cpd. **5**	$[Sm(Cp)_3(NCCH_3)]$[a]	$[La_{0.8}Sm_{0.2}(Cp)_3(NCCH_3)_2]$[a]
F^2	73992	78294	75324	75773	75813	76230	77002
F^4	58470	56267	56551	56699	56445	56187	56124
F^6	37391	39760	39503	39311	39382	39636	39832
ζ_{4f}	1143	1159	1149	1149	1151	1148	1155
α	[21.6][b]	[21.6]	[21.6]	[21.6]	[21.6]	[21.6]	[21.6]
β	[-724]	[-724]	[-724]	[-724]	[-724]	[-724]	[-724]
γ	[1700]	[1700]	[1700]	[1700]	[1700]	[1700]	[1700]
T^2	[291]	[291]	[291]	[291]	[291]	[291]	[291]
T^3	[13]	[13]	[13]	[13]	[13]	[13]	[13]
T^4	[34]	[34]	[34]	[34]	[34]	[34]	[34]
T^6	[-193]	[-193]	[-193]	[-193]	[-193]	[-193]	[-193]
T^7	[288]	[288]	[288]	[288]	[288]	[288]	[288]
T^8	[354]	[354]	[354]	[354]	[354]	[354]	[354]
M^0	[2.4]	[2.4]	[2.4]	[2.4]	[2.4]	[2.4]	[2.4]
M^2	[1.34]	[1.34]	[1.34]	[1.34]	[1.34]	[1.34]	[1.34]
M^4	[0.91]	[0.91]	[0.91]	[0.91]	[0.91]	[0.91]	[0.91]
P^2	[341]	[341]	[341]	[341]	[341]	[341]	[341]
P^4	[256]	[256]	[256]	[256]	[256]	[256]	[256]
P^6	[171]	[171]	[171]	[171]	[171]	[171]	[171]
B_0^2	−2809	−1158	−1577	−1523	−1487	−1627	−953
B_0^4	1483	−81	1407	1509	1418	1291	1882
B_0^6	1278	−182	1080	1269	1243	1306	1903
B_3^4	−	−	1076	1135	1213	769	−
B_3^6	−	−	502	317	336	490	−
B_6^6	−2685	−	−2245	−2216	−2217	−2190	−2038
$N_v/(4\pi)^{1/2}$	1749	522	1371	1378	1373	1324	1222
σ	17.5 (25)[c]	35.0 (59)	30.8 (25)	30.4 (51)	25.2 (59)	31 (57)	20 (42)

[a] From ref.[45] [b] Values in square brackets were fixed at the values of $[LaCl_3:Sm^{3+}]$.[41] [c] Number of assignments in parentheses.

 © 2004 Wiley-VCH Verlag GmbH & Co. KGaA, Weinheim

bility to interpret magnetic circular dichroism measurements of dissolved systems with an odd number of f electrons,[47] the derived sequences of CF levels of compounds **1**−**5** cannot be assigned on an experimental but only on a calculational (**1**, **2**) or comparative (**3**−**5**) basis.

In order to get a first idea of the signs and magnitudes of the CF parameters of complexes **1** and **2**, we adopted the CF parameter set of ψ trigonal planar $[Pr(C_5H_4SiMe_3)_3]$[7] for **1**, and for **2**, we divided the CF parameters B_0^2, B_0^4 and B_0^6 of this compound by three. Because of the similarity of the optical spectra of $[Sm(Cp)_3(NCCH_3)]$[45] and those of adducts **3**−**5**, we used the unchanged CF parameters of $[Sm(Cp)_3(NCCH_3)]$[45] as a starting set for the latter complexes.

Together with the unchanged free-ion parameters of $LaCl_3:Sm^{3+}$ [41] for compound **2**, those of $[Sm(Cp)_3(NCCH_3)]$[45] for adducts **3**−**5** and compound **1** (however, because of presumably increased covalency the Slater parameter F^2 of the latter compound was reduced by 3%), the above mentioned sets of CF parameters were inserted into the energy matrices of the f^5 system exposed to the CFs of D_{3h}, $D_{5h}/C_{\infty v}$ and C_{3v} symmetry, respectively. Diagonalizing these matrices we calculated eigenvalues which were not too different from the experimental energies of CF states, which were thus assigned. On this basis in the framework of subsequent fitting procedures, the parameters of $H_{FI} + H_{CF}$ were fitted to the experimental CF splitting patterns. In order to reduce the number of free parameters, α, β, γ, the T^i, M^k and P^k parameters[4] were fixed at the values used in the CF analyses of $[LaCl_3:Sm^{3+}]$[41] and $[Sm(Cp)_3(NCCH_3)]$.[45] The remaining parameters were allowed to vary. For 25, 59, 25, 51 and 59 assignments, the reduced r.m.s. deviations (σ, cf. ref.[6] p.182) for compounds **1**−**5** were 17.5, 35.0, 30.8, 30.4 and 25.2 cm^{-1}, respectively.

Table 3 gives the final values of the CF and free-ion parameters for compounds **1**−**5**. For comparison purposes, the parameters of $[Sm(Cp)_3(NCCH_3)]$ and $[La_{0.8}Sm_{0.2}(Cp)_3(NCCH_3)_2]$ are also listed. In Table 1 and 2, experimental and calculated CF splitting patterns of complexes **1** and **2** are compared. Those of adducts **3**−**5** are not given because of the close similarity of the CF splitting patterns of these compounds and $[Sm(Cp)_3(NCCH_3)]$.[45]

Inserting the CF parameters of compounds **1**−**5** into the relation below[2] one ends up with $N_v/(4\pi)^{1/2}$ values of 1749, 522, 1371, 1378 and 1373 cm^{-1}, respectively.

$$N_v / \sqrt{4\pi} = \sum_{k,q} \sqrt{\frac{(B_q^k)^2}{2k+1}}$$

The above mentioned global CF strength of 1749 cm^{-1} for base-free compound **1** is the highest global CF strength ever found for a lanthanide compound. This is in agreement with the results of previous and current CF analyses of ψ trigonal planar complexes such as $[Pr(C_5H_4SiMe_3)_3]$, $[Pr(C_5H_4tBu)_3]$, $[Nd(C_5H_4SiMe_3)_3]$ and $[Nd(C_5H_4tBu)_3]$ where $N_v/(4\pi)^{1/2}$ values of 1429, 1497, 1662 and 1651 cm^{-1} were found,[7,48] which are the highest hitherto concluded for Pr^{III} and Nd^{III} compounds.

The CF strengths experienced by the Sm^{3+} central ions decrease from base-free compound **1** via mono adducts **3**−**5** to the bis adduct $[La_{0.8}Sm_{0.2}(Cp)_3(NCCH_3)_2]$ (Table 3) which is mainly due to the decreasing absolute value of B_0^2 within this series. The results[49] of basic model calculations in the framework of the angular overlap model[50−52] are consistent with the found trend for the above mentioned compounds (Table 3). The enormous decrease of CF strength going from base-free compound **1** to the mono adduct **3** is paralleled by the pair of compounds $[Sm(C_5H_4SiEt_3)_3]$/$[Sm(C_5H_4SiEt_3)_3(NCCH_3)]$ (where the former complex has a comparable CF splitting pattern as compound **1**) which have preliminary $N_v/(4\pi)^{1/2}$ values of 1721 and 1375 cm^{-1}.[53]

Applying method A on compound **1** and method B on complex **2**, $C_5H_4tBu^-$ and unsubstituted Cp produce CF strengths of 583 and 522 cm^{-1}, respectively. Comparing both values, the agreement is not too bad.

The most obvious reason for the discrepancy found would be that it is not allowed to neglect the CF strengths of the two Tp^{Me_2} ligands. Usually, nine-coordinate Ln^{3+} central ions experience low CF strengths.[54] For this reason, it was originally assumed that this also holds for homoleptic nine-coordinate $[Ln(\eta^3\text{-}Tp)_3]$ (Ln = La−Tb)[55,56] and $[Ln(COT)(\eta^3\text{-}Tp^{Me_2})]$ (Ln = Pr, Nd, Sm),[16−19] where the N atoms of the Tp^{Me_2} ligands have only somewhat shorter distances from the Ln central ions[57] as in $[Ln(Tp)_3]$.[55,56] Thus, we neglected the contribution of the Tp^{Me_2} ligand to the global CF strength and identified (adopting method B) the global CF strength of $[Ln(COT)(Tp^{Me_2})]$ (approximately 1250 cm^{-1})[16−19] with the individual CF strength of the COT ligand.

In order to examine the above assumption of a low CF strength of the Tp^{Me_2} or Tp ligand, we recently analyzed the optical spectra of homoleptic $[Ln(\eta^3\text{-}Tp)_3]$ (Ln = Eu, Pr)[56,58] and found averaged CF strengths of 149 cm^{-1} [56] and 194 cm^{-1},[58] respectively, per Tp ligand. In view of the global CF strength of approximately 1250 cm^{-1} of $[Ln(COT)(Tp^{Me_2})]$ complexes it is a somewhat rough but reasonable approximation to neglect the contribution of the Tp^{Me_2} ligand to the global CF strength.

By means of compound **1** and applying method A, the individual CF strength of the $C_5H_4tBu^-$ ligand was estimated to be 583 cm^{-1} (vide supra). This value is approximately three times greater than that of the Tp ligand and thus the contribution of the η^3- and η^2-coordinated Tp^{Me_2} ligands to the global CF strength of complex **1** cannot be neglected. In view of these facts, it is rather surprising that methods A and B, when applied to compounds **1** and **2**, lead to comparable values of the CF strength of η^5-coordinated (substituted) Cp ligands (vide supra). The most simple explanation for this finding would be that opposite effects cancel out in the case of compound **2**, thus giving almost the same individual CF strength of the Cp ligand as found for the substituted Cp ligand of compound **1**.

 © 2004 Wiley-VCH Verlag GmbH & Co. KGaA, Weinheim

If one accepts the above rough approximation for [Ln(COT)(Tp^{Me_2})], the individual CF strength of COT ligand is (with about 1250 cm^{-1}) by a factor of 2.1 greater than that which we derived for the $C_5H_4tBu^-$ ligand of compound **1** adopting method A. If one refers to the ligand field strength produced by one coordinated C atom of both ring ligands, one arrives at 156 cm^{-1} (COT) and 116 cm^{-1} (Cp).

The optical spectra of [Sm{$CH(SiMe_3)_2$}$_3$] have not been analyzed at this point, but in the case of the corresponding Nd compound we found an individual CF strength of 348 cm^{-1} for the essentially σ bonded $CH(SiMe_3)_2^-$ ligand,[12] which is considerably greater than those associated with one carbon atom of π bonded COT or Cp ligands. These findings may be partly explained by the considerably reduced average Sm−C distance of [Sm{$CH(SiMe_3)_2$}$_3$] (2.33 Å)[59] as compared to [Sm(COT)(Tp^{Me_2})] (2.622 Å)[57] and (as a proxy for compound **1**) [Sm(C_5H_3(1,3-$SiMe_3$)$_2$)$_3$] (2.76 Å).[22]

The CF parameters B_0^4 and B_0^6 of complex **2** have unusual low absolute values as compared to the remaining Cp compounds of Table 3, a fact which contributes mainly to the low global CF strength of this compound. In contrast to B_0^2, which is caused mainly by electrostatic effects the CF parameter B_0^6 is dominated by covalency effects (ref.[44] p.71). Possibly, the low covalency of complex **2** (vide infra) may be partly responsible for the low absolute values of B_0^4 and B_0^6 of this compound.

The Slater parameter F^2 and the spin-orbit coupling parameter of the gaseous Sm^{3+} ion are unknown, thus the nephelauxetic parameter beta = F^2(complex)/F^2(free ion), the relativistic nephelauxetic parameter beta′ = ζ_{4f}(complex)/ζ_{4f}(free ion), and the covalency √b [defined as √b = √(1-beta)/2 [60]] cannot be calculated. Furthermore, the Slater parameters of Sm^{III} compounds are frequently not well defined due to the limited number of $^{2S+1}$L terms (with different L or S) considered in the fits. Anyway, the insertion of compounds **1**−**5** into truncated empiric nephelauxetic and relativistic nephelauxetic series can be seen from Table 4. Evidently, the truncated nephelauxetic series for Sm^{III} compounds in Table 4 is only partly paralleled by the trend of ζ_{4f} values, and thus the relativistic nephelauxetic series.

Obviously, complex **1** has the lowest F^2 value and thus is the most covalent Sm^{III} compound hitherto analyzed, F^2 of adducts **3**−**5** moves within the typical range of mono adducts, whereas **2** has a relatively low covalency. The observed trends within compounds **1** and **3**−**5** are paralleled by the corresponding Pr and Nd complexes.[48]

Comparing the found F^2 and $N_v/(4\pi)^{1/2}$ values of adduct **5** and [Sm($Cp)_3$($NCCH_3$)] (Table 3), one has to conclude that covalency and global CF strength are more pronounced for the isocyanide than for the nitrile adduct.

The eigenvalues of an energy matrix of the spin-free f^1 system, into which the CF parameters of a parametric analysis of the compound of interest had been inserted, were defined in ref.[49] as the experimentally based non-relativistic MO scheme of this compound in the f range. Likewise, the eigenvalues of an energy matrix of the real f^1 system, into which the spin-orbit coupling as well as the CF parameters had been inserted, were defined as the experimentally based relativistic MO scheme of this compound in the f range.[66]

In Figure 5, the experimentally based non-relativistic MO schemes (in the f range) of complex **1** and [Pr(η^5-$C_5H_4SiMe_3$)$_3$][52] are compared with the non-relativistic MO scheme of fictive ψ trigonal planar [Sm(η^5-Cp)$_3$] calculated in the framework of the SW-Xα approximation.[33]

Obviously, the calculated splitting of f orbitals is considerably greater than the experimentally based ones. Moreover, the experimentally based sequences of f orbitals are roughly comparable for **1** and [Pr(η^5-$C_5H_4SiMe_3$)$_3$] (only the close-lying orbitals f_{z^3} and $f_{z(x^2-y^2)}$/f_{xyz} are interchanged) but at the first glance considerably different from the calculated one for fictive trigonal planar[Sm($Cp)_3$]. Fitting the free parameters of the phenomenological Hamiltonian of

Table 4. F^2, ζ_{4f} and $N_v/(4\pi)^{1/2}$ values of selected Sm^{III} compounds; all values in cm^{-1}.

Compound [a]	F^2	ζ_{4f}	$N_v/(4\pi)^{1/2}$	Ref.
[LaF_3:Sm^{3+}]	79805	1176	610	[61]
[Na_3[Sm($ODA)_3$]·2$NaClO_4$·6H_2O][b]	79015	1166	755	[62]
[Sm(Cp)(Tp^{Me_2})$_2$]	78293	1159	522	this work
[GdOCl:Sm^{3+}]	78196	1150	640	[63]
[$LaCl_3$:Sm^{3+}]	78125	1168	300	[41]
[$Cs_2NaSmCl_6$]	77510	1167	545	[64]
[$La_{0.8}Sm_{0.2}$($Cp)_3$($NCCH_3$)$_2$]	77002	1155	1222	[45]
[Sm[N($SiMe_3$)$_2$]$_3$(CNC_6H_{11})$_2$]	76676	1169	891	[65]
[Sm($C_5H_4CH_2CH_2OCH_3$)$_3$]	76602	1156	1198	[46]
[Sm[N($SiMe_3$)$_2$]$_3$]	76388	1164	1179	[9]
[Sm($C_5H_4SiEt_3$)$_3$($NCCH_3$)]	76305	1149	1375	[53]
[Sm($Cp)_3$($NCCH_3$)]	76230	1148	1324	[45]
[Sm($Cp)_3$(CNC_6H_{11})]	75813	1151	1373	this work
[Sm($Cp)_3$(THF)]	75773	1149	1378	this work
[Sm($C_5H_4tBu)_3$(THF)]	75324	1149	1371	this work
[Sm($C_5H_4tBu)_3$]	73992	1143	1749	this work

[a] Ordered by decreasing Slater parameter F^2. [b] ODA = oxydiacetato.

 © 2004 Wiley-VCH Verlag GmbH & Co. KGaA, Weinheim

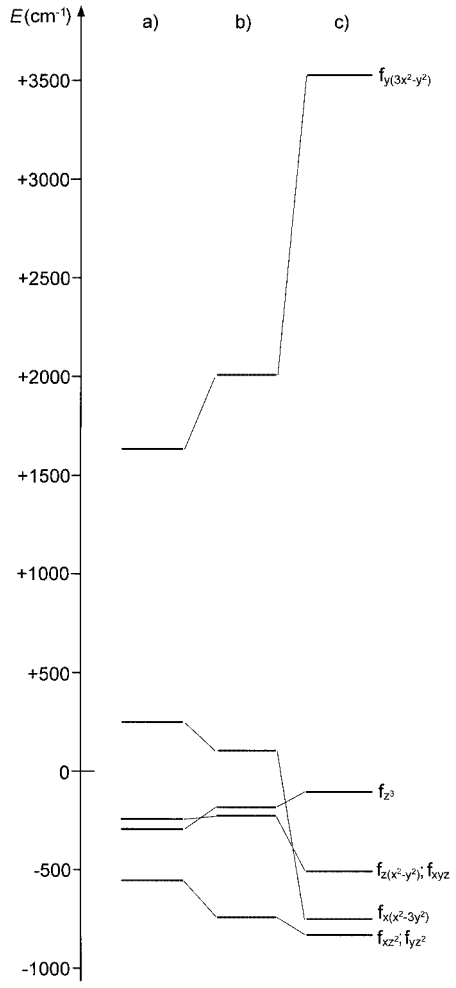

Figure 5. Experimentally based and calculated non-relativistic MO schemes of: a) $[Pr(C_5H_4SiEt_3)_3]$ (exp., from ref.[7]); b) $[Sm(C_5H_4tBu)_3]$ (exp.); c) fictive ψ trigonal planar $[Sm(Cp)_3]$ (calcd. from ref.[33])

the spin-free f^1 system to the calculated energies of f orbitals of the latter complex one arrives at $B_0^2 = -3443\ cm^{-1}$, $B_0^4 = 2817\ cm^{-1}$, $B_0^6 = 1296\ cm^{-1}$ and $B_6^6 = -6033\ cm^{-1}$. Comparing these values with those of compound **1** (Table 4), it becomes evident that first of all the CF parameters B_6^6 (which considers the interactions between the orbitals $f_{x(x^2-3y^2)}$ and $f_{y(3x^2-y^2)}$ within the framework of CF theory) but also B_0^4 are heavily overestimated by the model calculation. If one reduces B_6^6 to a quarter, not only the correct sequence of levels but also the correct total splitting of f orbitals would result. From the aspect of MO theory the required reduction of B_6^6 means that the interaction of $f_{y(3x^2-y^2)}$ with the corresponding symmetry adapted linear combination of ligand orbitals is overestimated and that of $f_{x(x^2-3y^2)}$ is underestimated by the model calculation.

The electronic structure of fictive ψ trigonal planar $[Pr(Cp)_3]$ was calculated by means of the SW-Xα[33] as well as the INDO/1[35] approximation. The SW-Xα calculation yielded a comparable MO scheme (in the f range) as for $[Sm(Cp)_3]$[33] and the more basic INDO/1 calculation led, astonishingly, to the same energetic sequence[35] as we had concluded for $[Pr(\eta^5\text{-}C_5H_4SiMe_3)_3]$ (Figure 5). However, in the case of the INDO/1 approximation the calculated total splitting of f orbitals ($1545\ cm^{-1}$ [35]) is noticeably smaller than the experimentally based one ($2189\ cm^{-1}$ [7]).

The result of a recent non-relativistic discrete variational (DV)-Xα calculation on ψ trigonal planar $[Ce(Cp)_3]$[34] is similar to that of the SW-Xα approximation.[33]

In Figure 6, the result of a previous relativistic DV-Xα calculation on fictive ψ trigonal planar $[Ce(Cp)_3]$[34] is compared with the experimentally based relativistic MO schemes of compound **1** and that of a model compound, the CF splitting pattern of which was calculated adopting the spin-orbit coupling parameter used for $[Ce(Cp)_3(NCCH_3)_2]$ ($610\ cm^{-1}$)[67] and the CF parameters of complex **1**. Obviously, the same sequences of levels exist, but the DV-Xα calculation predicts a total splitting of f levels which is a factor of 1.75 greater than that of the above characterized model compound. This is mainly due to an overestimated spin-orbit coupling parameter of the DV-Xα calculation, which is approximately twice as great ($1300\ cm^{-1}$) as those found in the framework of previous CF analyses of Ce^{III} compounds (cf. ref.[6] p. 127).

To the best of our knowledge, results of model calculations on mono adducts of the $Sm(Cp)_3$ moiety have not been published up to now. However, $[Ln(Cp)_3(THF)]$ (Ln = Pr,[35] Gd[36]) and $[Pr(Cp)_3(CNC_6H_{11})]$[35] have been the subject of INDO/1 calculations. In the case of $[Pr(Cp)_3(B)]$ ($B = CNC_6H_{11}$, THF), these calculations led to the same

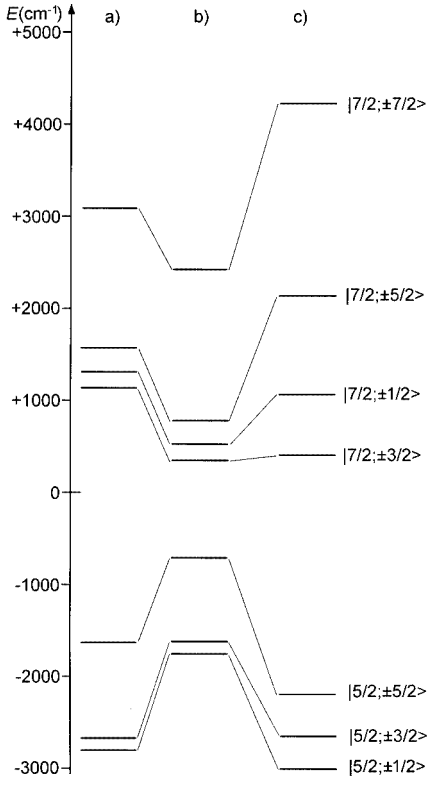

Figure 6. Experimentally based and calculated relativistic MO schemes of: a) $[Sm(C_5H_4tBu)_3]$ (exp.); b) calculated, adopting CF parameters of $[Sm(C_5H_4tBu)_3]$ and $\zeta_{4f} = 610\ cm^{-1}$; c) ψ trigonal planar $[Ce(Cp)_3]$ (calcd., from ref.[34])

 © 2004 Wiley-VCH Verlag GmbH & Co. KGaA, Weinheim

energetic sequence of f orbitals as we found on an experimental basis for these compounds[68] as well as for $[Sm(Cp)_3(NCCH_3)]$[69] and adducts **3**–**5**. However, the calculated total splitting of f orbitals of $[Pr(Cp)_3(B)]$ is with 742 cm^{-1} (B = CNC_6H_{11}) and 997 cm^{-1} (B = THF) considerably smaller than the experimentally based ones of $[Pr(Cp)_3(CNC_6H_{11})]$ (1978 cm^{-1}),[68] $[Pr(Cp)_3(THF)]$ (1722 cm^{-1} [68]), $[Sm(Cp)_3(NCCH_3)]$ (1989 cm^{-1} [69]) and compounds **3** (2043 cm^{-1}), **4** (2007 cm^{-1}) and **5** (1988 cm^{-1}).

The above-mentioned INDO calculation for $[Gd(Cp)_3(THF)]$ led to the following energetic sequence of f orbitals: $f_{z^3} < f_{xz^2}/f_{yz^2} < f_{z(x^2-3y^2)}/f_{xyz} < f_{x(x^2-3y^2)} < f_{y(3x^2-y^2)}$ (with a total splitting of f orbitals of 230 cm^{-1} [36]) which differs considerably from the experimentally based ones for mono adducts of the $[Ln(Cp)_3]$ moiety (Figure 7).

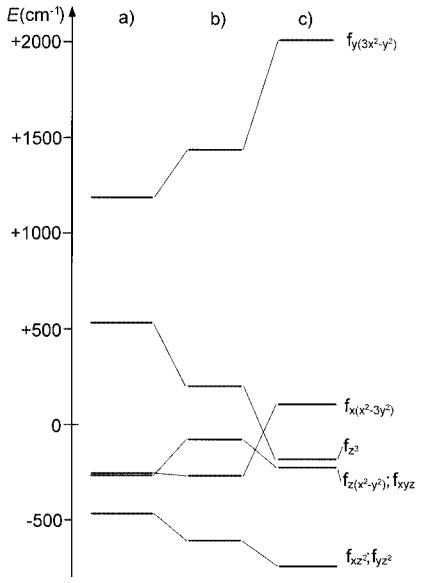

Figure 7. Experimentally based non-relativistic MO schemes of: a) $[La_{0.8}Sm_{0.2}(Cp)_3(NCCH_3)_2]$; b) $[Sm(C_5H_4tBu)_3(THF)]$; c) $[Sm(C_5H_4tBu)_3]$

To the best of our knowledge model calculations on bis adducts of the $[Ln(Cp)_3]$ moiety have not been performed, thus no calculated counterpart of the experimentally derived MO scheme of $[La_{0.8}Sm_{0.2}(Cp)_3(NCCH_3)_2]$ exists.

Going from the fictive base-free trigonal planar $[Ln(Cp)_3]$ complex via a trigonal pyramidal mono to a trigonal bipyramidal bis base adduct, the axially f_{z^3} orbital should be increasingly energetically destabilized adopting the approximation of the angular overlap model.[49] This is nicely demonstrated by the series of compounds **1**, **3** and $[La_{0.8}Sm_{0.2}(Cp)_3(NCCH_3)_2]$ (Figure 7).

Conclusion

The CF strengths of $C_5H_4tBu^-$ and Cp ligands estimated by applying method A on compound **1**, and applying method B to **2** differ by some 10%. The main reason for this discrepancy is that it is not justified to neglect the CF strength associated with the Tp^{Me_2} ligand in the case of complex **2**. This finding suggests to apply method B to other $[Sm(Cp)(L')_2]$ compounds such as $[Sm(Cp)(acac)_2]$ and $[Sm(Cp)(I)_2]$ where the CF strengths produced by the $acac^-$ and I^- ligands are probably weaker than in the case of Tp^{Me_2}.

In this work, the experimentally based MO schemes of compound **1** and the corresponding THF adduct are compared with the results of previous model calculations of different degrees of sophistication. Astonishingly, and perhaps accidentally, basic model calculations in the framework of the INDO/1 approximation on $[Pr(Cp)_3]$ and $[Pr(Cp)_3(B)]$ (B = THF, CNC_6H_{11}) would have led to correct signs but to noticeably reduced absolute values of the CF parameters as compared to those of the sets $[Pr(C_5H_4SiMe_3)_3]$/(**1**) and $[Pr(Cp)_3(B)]$/(**3**–**5**) (B = THF, CNC_6H_{11}).

Besides, applying the relativistic DV/Xα approximation to fictive ψ trigonal planar $[Ce(Cp)_3]$ a sequence of CF levels was calculated which is in agreement with the experimentally based relativistic MO scheme of complex **1**. However, this approximation seriously overestimated mainly the spin-orbit coupling parameter.

It seems that the present approximations of quantum chemistry have to be refined somewhat until they are really helpful for interpreting optical spectra of f element organyls.

Experimental Section

Compounds **1, 2**, **4** and **5** as well as the "optical empty" reference compounds $[La(C_5H_4SiMe_3)_3]$ and $[La(C_5H_4tBu)_3(THF)]$ were synthesized by adopting the procedures of Wayda,[21] Lopes et al.,[32] Birmingham et al.,[70] Fischer et al.[71] and Stults et al.[72] The absorption spectra of compounds **1** and **2** were recorded by means of KBr pellets, and those of adducts **3** and **4** (dissolved in a mixture of MeTHF/THF in the ratio 3:1) as well as those of complex **5** (dissolved in a mixture of methylcyclohexane/toluene in the ratio 3:1) as glassy frozen solutions, making use of a Cary 5e instrument. The luminescence spectra of compounds **1, 2**, **4** and **5** were run as powders (and that of **1** additionally as methylcyclohexane solution) by means of a Raman spectrometer (Jobin–Yvon, model U 1000) equipped with an Ar^+ laser (Coherent model Innova 70). In all optical low temperature measurements the samples were immersed in liquid nitrogen. Using liquid He as coolant didn't change the appearance of the spectra but worsened the signal-to-noise ratio.

The room temperature absorption spectrum of complex **1** dissolved in a mixture of glassy freezing 2-MeTHF and THF in the ratio 3:1 was identical with the data recorded by means of a KBr pellet of **1**. At 77 K, however, the absorption spectrum resembled those of $[Sm(Cp)_3(B)]$ (B = THF, $NCCH_3$, CNC_6H_{11}), thus we assume that the mono THF adduct of complex **1** (i.e. **3**) is formed quantitatively.

In order to confirm the results of the fit of compound **2**, we calculated the temperature dependence of μ^2_{eff} of this complex on the basis of calculated wavefunctions and eigenvalues, and planned to compare these data with the corresponding experimental values.

 © 2004 Wiley-VCH Verlag GmbH & Co. KGaA, Weinheim

Unfortunately, compound **2** lost weight in the framework of the susceptibility measurements,[73] thus leading to less reliable experimental μ^2_{eff} values. Nevertheless, the calculated temperature dependence of μ^2_{eff} in the range $77\ K < T < 280\ K$ was within the experimental array of curves.

Acknowledgments

H.-D. A. acknowledges D. Powietzka (ITC, Forschungszentrum Karlsruhe) for the efforts to record the temperature dependence of the paramagnetic susceptibility of $[Sm(Cp)(Tp^{Me_2})_2]$, Dr. B. Nissen-Sobocinska as well as Dr. J. Ren for communicating the results of their quantum chemical model calculations. Besides, the generous financial support of the Deutsche Forschungsgemeinschaft and the Fonds der Chemischen Industrie (H.-D. A.) as well as the NATO (N. M.) is gratefully acknowledged.

[1] H.-D. Amberger, H. Reddmann, H. H. Karsch, V. W. Graf, C. Qian, B. Wang, *J. Organomet. Chem.* **2003**, *677*, 35−45.
[2] F. Auzel, O. L. Malta, *J. Phys. (Paris)* **1983**, *44*, 201−206.
[3] B. G. Wybourne, *Spectroscopic Properties of Rare Earths*, Wiley, New York, **1965**, and references cited therein.
[4] W. T. Carnall, J. V. Beitz, H. Crosswhite, K. Rajnak, J. B. Mann, Spectroscopic Properties of the f-Elements in Compounds and Solutions, in *Systematics and Properties of the Lanthanides*, S. P. Sinha (Hrsg.), NATO ASI Series No. 109, D. Reidel, **1983**, Dordrecht, p. 389−448.
[5] D. Garcia, M. Faucher, in *Handbook on the Physics and Chemistry of Rare Earths* (Eds.: K. A. Gschneidner, Jr., L. Eyring), Vol. 21, Ch. 144, Elsevier Science B. V., Amsterdam, **1995**, pp. 263−304, and references cited therein.
[6] C. Görller-Walrand, K. Binnemans, in *Handbook on the Physics and Chemistry of Rare Earths* (Eds.: K. A. Gschneidner, Jr., L. Eyring, Vol. 22, Ch. 155, Elsevier Science B. V., Amsterdam, **1995**, p. 121−283, and references cited therein.
[7] S. Jank, H. Reddmann, H.-D. Amberger, *J. Alloys Compds.* **1997**, *250*, 387−390.
[8] H.-D. Amberger, S. Jank, H. Reddmann, N. M. Edelstein, *Mol. Phys.* **1997**, *90*, 1013−1026.
[9] H. Reddmann, S. Jank, H.-D. Amberger, *Spectrochim. Acta Part A 53* **1997**, 495−499.
[10] S. Jank, H.-D. Amberger, N. M. Edelstein, *Spectrochim. Acta Part A 54* **1998**, 1645−1650.
[11] H. Reddmann, C. Guttenberger, H.-D. Amberger, *J. Organomet. Chem.* **2000**, *602*, 65−71.
[12] C. Guttenberger, B. Unrecht, H. Reddmann, H.-D. Amberger, *Inorg. Chim. Acta* **2003**, *348*, 165−172.
[13] H.-D. Amberger, H. Reddmann, C. Guttenberger, B. Unrecht, L. Zhang, C. Apostolidis, O. Walter, B. Kanellakopulos, *Z. Anorg. Allg. Chem.* **2003**, *629*, 1522−1534.
[14] H.-D. Amberger, S. Jank, F. T. Edelmann, *J. Organomet. Chem.* **1998**, *559*, 209−213.
[15] W. Wagner, N. M. Edelstein, B. Whittaker, D. Brown, *Inorg. Chem.* **1977**, *16*, 1021−1026.
[16] H.-D. Amberger, F. T. Edelmann, *J. Organomet. Chem.* **1996**, *508*, 275−279.
[17] H.-D. Amberger, S. Jank, H. Reddmann, F. T. Edelmann, *Mol. Phys.* **1996**, *88*, 1439−1458.
[18] B. Unrecht, S. Jank, H. Reddmann, H.-D. Amberger, F. T. Edelmann, N. M. Edelstein, *J. Alloys Comp.* **1997**, *250*, 383−386.
[19] H. Reddmann, S. Jank, H.-D. Amberger, F. T. Edelmann, N. Marques, XIV. Tage der Seltenen Erden, 11.−13. Oktober **2001**, München, Poster P20.
[20] H. Schumann, J. A. Meese-Marktscheffel, L. Esser, *Chem. Rev.* **1995**, *95*, 865−986, and references cited therein.
[21] A. L. Wayda, *J. Organomet. Chem.* **1989**, *361*, 73−78.
[22] W. J. Evans, R. A. Keyer, J. W. Ziller, *J. Organomet. Chem.* **1990**, *394*, 87−97.
[23] W. J. Evans, S. L. Gonzales, J. W. Ziller, *J. Am. Chem. Soc.* **1991**, *113*, 7423−7424.
[24] H. Schumann, M. Glanz, H. Hemling, F. E. Hahn, *Z. Anorg. Allg. Chem.* **1995**, *621*, 341−345.
[25] W. J. Evans, K. J. Forrestal, J. T. Leman, J. W. Ziller, *Organometallics* **1996**, *15*, 527−531.
[26] M. Sievers, PhD Dissertation, Hamburg, **1998**.
[27] S. Al-Juaid, Y. K. Gun′ko, P. B. Hitchcock, M. F. Lappert, S. Tian, *J. Organomet. Chem.* **1999**, *582*, 143−152.
[28] R. Poli, *Chem. Rev.* **1991**, *91*, 509−551, and references cited therein.
[29] S. Manastyrskyj, R. E. Magin, M. Dubek, *Inorg. Chem.* **1963**, *2*, 904−905.
[30] Z. Ye, Y. Yu, H. Ma, *Polyhedron* **1988**, *7*, 1095−1100.
[31] V. K. Belskii, Y. K. Gunko, E. B. Lobkovskii, B. M. Bulychev, G. L. Soloveichik, *Organomet. Chem. USSR* **1991**, *4*, 202−207.
[32] I. Lopes, G. Y. Lin, A. Domingos, R. McDonald, N. Marques, J. Takats, *J. Am. Chem. Soc.* **1999**, *121*, 8110−8111.
[33] R. J. Strittmatter, B. E. Bursten, *J. Am. Chem. Soc.* **1991**, *113*, 552−559.
[34] N. Kaltsoyannis, B. E. Bursten, *J. Organomet. Chem.* **1997**, *528*, 19−33.
[35] B. Nissen-Sobocinska, private communication, April **1996**.
[36] J. Ren, private communication, February **1996**.
[37] H. Wietreich, M. Heffter, H.-D. Amberger, unpublished results.
[38] K. D. Warren, *Struct. Bonding* **1976**, *33*, 97−138, and references cited therein.
[39] H. Reddmann, S. Jank, H. Schultze, H.-D. Amberger, N. M. Edelstein, *Inorg. Chim. Acta* **2003**, *344*, 243−248, and references cited therein.
[40] H. Schulz, H. Reddmann, H.-D. Amberger, B. Kanellakopulos, C. Apostolidis, J. Rebizant, N. M. Edelstein, *J. Organomet. Chem.* **2001**, *622*, 19−32, and references cited therein.
[41] W. T. Carnall, H. Crosswhite, H. M. Crosswhite, Energy Level Structure and Transition Probabilities in the Spectra of the Trivalent Lanthanides in LaF_3, ANL Report, Appendix I, Table 1, **1977**, unpublished.
[42] S. Jank, J. Hanss, H. Reddmann, H.-D. Amberger, N. M. Edelstein, *Z. Anorg. Allg. Chem.* **2002**, *628*, 1355−1365.
[43] G. F. Koster, J. O. Dimmock, R. G. Wheeler, H. Statz, *Properties of the Thirty-Two Point Groups*; MIT Press, Cambridge, Mass., **1963**, p. 74.
[44] S. Hüfner, *Optical Spectra of Transparent Rare Earth Compounds*; Academic Press, New York, **1978**, p. 85.
[45] H. Schulz, H. Reddmann, H.-D. Amberger, *J. Organomet. Chem.* **1993**, *461*, 69−74.
[46] C. Qian, B. Wang, N. M. Edelstein, H. Reddmann, H.-D. Amberger, *J. Alloys Compds.* **1994**, *207−208*, 87−89.
[47] S. B. Piepho, P. N. Schatz, *Group Theory in Spectroscopy (With Applications To Magnetic Circular Dichroism)*, Wiley-Interscience, New York, **1983**.
[48] H.-D. Amberger, S. Jank, H. Reddmann, in preparation.
[49] S. Jank, H.-D. Amberger, *Acta Phys. Polon.* **1996**, *A90*, 21−32.
[50] C. K. Jørgensen, R. Pappalardo, H. H. Schmidtke, *J. Chem. Phys.* **1963**, *39*, 1422−1430.
[51] C. E. Schaeffer, C. K. Jørgensen, *Mol. Phys.* **1965**, *9*, 401−412.
[52] W. Urland, *Chem. Phys.* **1976**, *14*, 393−401.
[53] H. Reddmann, M. Sievers, unpublished results.
[54] K. Binnemans, C. Görller-Walrand, *J. Phys.: Condens. Matter* **1996**, *8*, 1267−1279.
[55] C. Apostolidis, J. Rebizant, B. Kanellakopulos, R. von Ammon, E. Dornberger, J. Müller, B. Powietzka, B. Nuber, *Polyhedron* **1997**, *16*, 1057−1068.
[56] C. Apostolodis, J. Rebizant, O. Walter, B. Kanellakopulos, H. Reddmann, H.-D. Amberger, *Z. Anorg. Allg. Chem.* **2002**, *628*, 2013−2025.
[57] U. Kilimann, PhD Dissertation, Göttingen, **1994**.
[58] H.-D. Amberger, H. Reddmann, C. Apostolidis, B. Kanellakopulos, *Z. Anorg. Allg. Chem.* **2003**, *629*, 147−160.

 © 2004 Wiley-VCH Verlag GmbH & Co. KGaA, Weinheim

[59] B. Hitchcock, M. F. Lappert, R. G. Smith, R. A. Bartlett, P. P. Power, *J. Chem. Soc., Chem. Commun.* **1988**, 1007−1009.
[60] S. P. Tandon, P. C. Mehta, *J. Chem. Phys.* **1970**, *52*, 5417−5420.
[61] W. T. Carnall, G. L. Goodman, K. Rajnak, R. S. Rana, *J. Chem. Phys.* **1989**, *90*, 3443−3457.
[62] S. May, M. F. Reid, F. S. Richardson, *Mol. Phys.* **1987**, *62*, 341−364.
[63] J. Hölsä, R.-J. Lamminmäki, *J. Lumin.* **1996**, *69*, 311−317.
[64] F. S. Richardson, M. F. Reid, J. J. Dallara, R. D. Smith, *J. Chem. Phys.* **1985**, *83*, 3813−3830.
[65] S. Jank, H. Reddmann, H.-D. Amberger, in preparation.
[66] S. Jank, H. Reddmann, H.-D. Amberger, *Mat. Sci. Forum* **1999**, *315−317*, 457−464.
[67] H.-D. Amberger, H. Reddmann, H. Schultze, S. Jank, B. Kanellakopulos, C. Apostolidis, *Spectrochim. Acta Part A*, in press.
[68] H. Reddmann, H.-D. Amberger, unpublished results, **1985**.
[69] H. Reddmann, H. Schulz, H.-D. Amberger, unpublished results, **1993**.
[70] J. M. Birmingham, G. Wilkinson, *J. Am. Chem. Soc.* **1956**, *78*, 42−44.
[71] E. O. Fischer, H. Fischer, *J. Organomet. Chem.* **1966**, *6*, 141−148.
[72] S. D. Stults, R. A. Andersen, A. Zalkin, *Organometallics* **1990**, *9*, 115−122.
[73] C. Apostolidis, personal communication, December **2000**.

Received May 20, 2003
Early View Article
Published Online October 23, 2003

 © 2004 Wiley-VCH Verlag GmbH & Co. KGaA, Weinheim

Synthesis, Spectroscopy, and Magnetic Properties of Fe^{II} and Co^{II} Quinoline-2-carboxylates − Crystal Structure of *trans*-Bis(quinoline-2-carboxylato)bis(propanol)iron(II)

Danuta Dobrzyńska,*[a] Marek Duczmal,[a] Lucjan B. Jerzykiewicz,[b] Jolanta Warchulska,[c] and Krzysztof Drabent[b]

Keywords: Vibrational spectroscopy / Magnetic properties / Iron / Cobalt / Quinoline-2-carboxylates

The new coordination compounds, $[Fe(quin\text{-}2\text{-}c)_2(EtOH)_2]$ (**1**), $[Co(quin\text{-}2\text{-}c)_2(EtOH)_2]$ (**2**), and $[Fe(quin\text{-}2\text{-}c)_2(PrOH)_2]$ (**3**) (where quin-2-c = quinoline-2-carboxylate) have been synthesized and investigated by ligand field, IR, Raman, and Mössbauer spectroscopy and by magnetic measurements. The X-ray analysis of the structure of **3** has been performed and refined to an *R* factor of 0.0377. The compound crystallizes in the monoclinic space group $P2_1/n$ with a = 6.104(1), b = 10.515(2), c = 19.339(4) Å, β = 92.57(3)°. The *trans* N_2O_4 environment around the Fe^{II} ion has a distorted octahedral geometry and the quin-2-c ion coordinates to iron in the equatorial plane in a chelating mode. The axial positions are occupied by propan-1-ol molecules. The spectral studies indicate the same molecular structure for all three compounds. The magnetic susceptibility and the magnetization of **2** were calculated for Co^{2+} ions in an octahedral crystal field with a rhombic zero field distortion ($|D|$ = 34 cm^{-1}, $E \approx 0$, g_{iso} = 2.35 and $N = 6.9 \cdot 10^{-4}$ emu·mol^{-1}).
(© Wiley-VCH Verlag GmbH & Co. KGaA, 69451 Weinheim, Germany, 2004)

Introduction

Carboxylate ligands are ubiquitous in biological materials and common in systems of catalytic utility. The carboxylate group offers a variety of coordination modes and many types of complexes are known.[1] Many of them, with interesting magnetic properties, have been obtained and characterized.[2]

Quinoline-2-carboxylic acid is a strong chelating agent and has been used as a reagent for the gravimetric determination of copper, cadmium, zinc and palladium.[3,4] In complexes with Rh^{I},[5−8] Rh^{III},[9] Mn^{II},[10,11] Cu^{II},[12] Ga^{III},[13] and Zn^{II}.[14] X-ray studies have revealed an N,O coordination mode of the quinoline-2-carboxylate ion. In chlorotriphenyl(quinolinium-2-carboxylato-*O*)tin(IV) monohydrate a quinoline-2-carboxylic acid binds to tin in its zwitterionic form.[15] The neutral acid molecule is demonstrated in the structure of bis(quinoline-2-carboxylic acid)tetrabromogold(III) monohydrate.[16] In the $Nd_2L_6{\cdot}3H_2O$ dimer, the coordinated quinoline-2-carboxylate ions display three modes of bonding: a bidentate carboxylate bridge, an O,O and an N,O chelating mode.[17]

It is interesting that the carboxylate group in the position *ortho* to the quinoline nitrogen, present in quin-2-c, is essential for binding Ca^{2+} and Fe^{2+} in PQQ (pyrroloquinilnequinone) which is involved as co-factor in enzymes of the quinoprotein group.[18]

In this paper, we describe the synthesis, spectroscopic and magnetic studies of low molecular weight, neutral complexes of iron(II) and cobalt(II) with the quionoline-2-carboxylate ion. The crystal structure of the ferrous compound is also presented.

Results and Discussion

Description of the Structure

The molecular geometry of $[Fe(quin\text{-}2\text{-}c)_2(PrOH)_2]$ (**3**) is shown in Figure 1, and Figure 2 (a) shows the crystal packing. Table 1 lists selected bond lengths and angles.

In the molecule of **3**, the iron(II) is six-coordinate with an O_4N_2 donor set. The coordination sphere can be described as distorted ocahedral. Two quin-2-c ligands coordinate to iron in the O,N chelating mode in the equatorial plane. The axial positions are occupied by the propanol molecules. The complex has an inversion center at the Fe^{II} ion. The Fe−O(1) bond length of 2.033(2) Å is short in comparison with the data found for iron(II) dipicolinates,[19−21] picolin-

[a] Institute of Inorganic Chemistry and Metallurgy of Rare Elements, Wrocław University of Technology,
Wybrzeże Wyspiańskiego 27, 50−370 Wrocław, Poland
Fax: (internat.) +48-(0)71-3284330
E-mail: dobrzynska@ichn.ch.pwr.wroc.pl
[b] Faculty of Chemistry, University of Wrocław,
Joliot-Curie 14, 50−383 Wrocław, Poland
[c] International Laboratory of High Magnetic Fields and Low Temperatures,
Gajowicka 95, 53−529 Wrocław, Poland

 © 2004 Wiley-VCH Verlag GmbH & Co. KGaA, Weinheim **DOI: 10.1002/ejic.200300327**

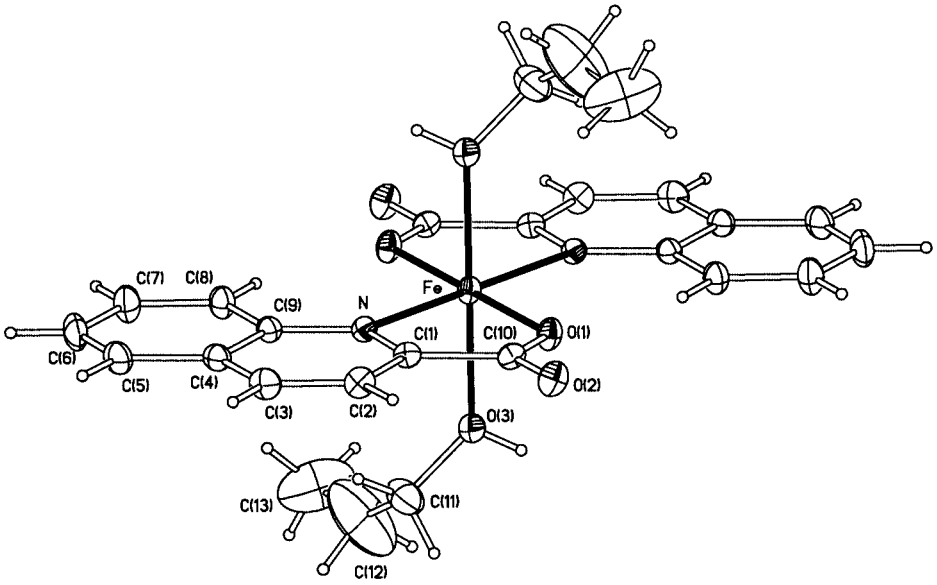

Figure 1. The molecular structure of $[Fe(quin\text{-}2\text{-}c)_2(PrOH)_2]$ with atom numbering scheme; the displacement ellipsoids are drawn at the 50% probability level

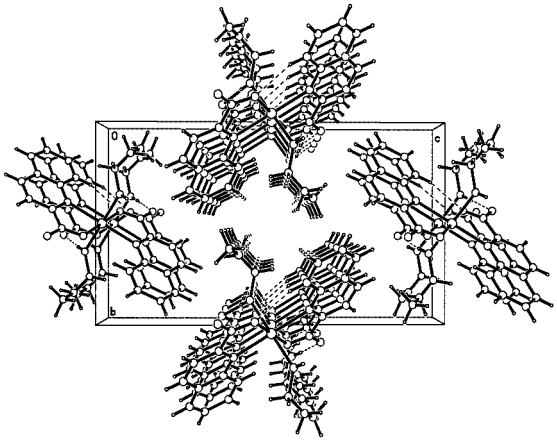

(a)

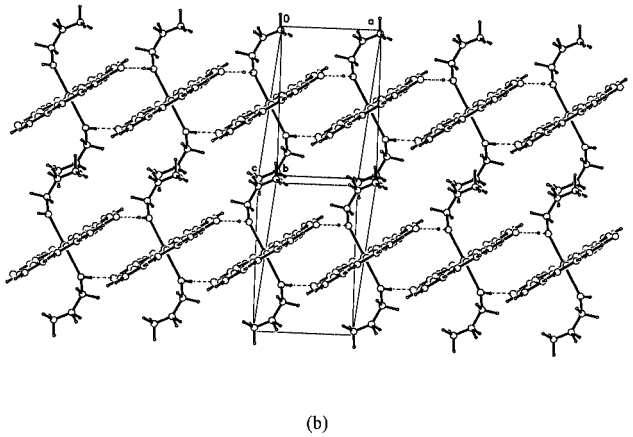

(b)

Figure 2. (a) The crystal packing of **3** viewed down the *a* axis; (b) the 1D-chains of $[Fe(quin\text{-}2\text{-}c)_2(PrOH)_2]$ molecules connected through the $O(2)^{ii}\cdots H(3O)-O(3)$ hydrogen bonds (indicated by the dashed lines)

ates,[22] and *bis*(isonicotinato)iron(II),[23] which cover the range 2.05(1)−2.37(1) Å. The Fe−N distance of 2.246(2) Å is similar to those found in ferrous dipicolinates[21] and picolinates[22] and is characteristic of high-spin Fe^{II} complexes.[24] The Fe−O(3) bond length is 2.170(3) Å. This distance is slightly shorter than the Fe^{II}−O(H)Me bond in iron(II) alkoxide cubes [2.24(2) and 2.208(2) Å][25] and in $[Fe(Pic)_2(MeOH)_2]$ [2.208(1) Å].[22]

The quinoline rings are coplanar with the equatorial chelate rings. This plane of the complex is stabilized by the weak C−H···O type intramolecular interaction [the $C(8)\cdots O(1)^{i}$ distance is 3.179(4) Å, the $C(8)-H(8)\cdots O(1)^{i}$ angle is 154(1)°, i = $-x$, $-y$, $-z$ + 1, Table 2]. Each carbonyl oxygen of the carboxylate group acts as an acceptor, resulting in a strong hydrogen bond with the hydroxyl group of the coordinated propanol molecule of an adjacent complex [the $O(2)^{ii}\cdots O(3)$ distance is 2.659(4) Å, the $O(2)^{ii}\cdots H(3O)-O(3)$ angle is 177(5)°, ii = $-x$ + 1, $-y$, $-z$ + 1]. This intermolecular interaction links the molecules into an infinite 1D-chain along the *a* axis (Figure 2, b). The Fe···Fe distance in the chain is 6.104(1) Å. In the crystal, interactions occur between the aromatic rings of the quinoline units (3.5 Å separation in stack).

Vibrational Spectra

The bands observed in the IR spectra of $[Fe(quin\text{-}2\text{-}c)_2(EtOH)_2]$ (**1**), $[Co(quin\text{-}2\text{-}c)_2(EtOH)_2]$ (**2**), and $[Fe(quin\text{-}2\text{-}c)_2(PrOH)_2]$ (**3**) and in the Raman spectrum of **2** as well as tentative assignments of these bands are given in Table 3. The IR spectra of $[Fe(quin\text{-}2\text{-}c)_2(EtOH)_2]$ and $[Co(quin\text{-}2\text{-}c)_2(EtOH)_2]$ are very similar in terms of the frequency, intensity and shape of the bands over the whole frequency region. The spectra are dominated by strong bands resulting from quinoline-2-carboxylate oscillations, but sev-

 © 2004 Wiley-VCH Verlag GmbH & Co. KGaA, Weinheim

Table 1. Bond lengths and angles for $[Fe(quin\text{-}2\text{-}c)_2(PrOH)_2]$ (**3**) (i: symmetry transformations used to generate equivalent atoms: $-x$, $-y$, $-z + 1$)

Fe−O(1)	2.033(2)
Fe−O(3)	2.170(3)
Fe−N	2.246(2)
O(1)−C(10)	1.262(3)
O(2)−C(10)	1.233(3)
O(3)−C(11)	1.385(5)
N−C(1)	1.326(4)
N−C(9)	1.370(4)
C(1)−C(2)	1.402(4)
C(1)−C(10)	1.509(4)
C(2)−C(3)	1.361(5)
C(3)−C(4)	1.397(5)
C(4)−C(5)	1.419(5)
C(4)−C(9)	1.420(4)
C(5)−C(6)	1.344(5)
C(6)−C(7)	1.397(5)
C(7)−C(8)	1.362(5)
C(8)−C(9)	1.405(4)
C(11)−C(12)	1.334(9)
C(12)−C(13)	1.200(12)
O(1)−Fe−O(3)	91.14(10)
O(1)−Fe−O(3)^{i}	88.86(10)
O(1)−Fe−N	77.12(9)
O(1)^{i}−Fe−N	102.88(9)
O(3)−Fe−N	94.04(9)
O(3)^{i}−Fe−N	85.96(9)
O(1)−Fe−N^{i}	102.88(9)
C(10)−O(1)−Fe	119.32(19)
C(11)−O(3)−Fe	129.4(3)
C(1)−N−C(9)	118.3(2)
C(1)−N−Fe	109.92(18)
C(9)−N−Fe	131.79(19)
N−C(1)−C(2)	123.1(3)
N−C(1)−C(10)	116.6(2)
C(2)−C(1)−C(10)	120.3(3)
C(3)−C(2)−C(1)	119.5(3)
C(2)−C(3)−C(4)	119.4(3)
C(3)−C(4)−C(5)	122.9(3)
C(3)−C(4)−C(9)	118.4(3)
C(5)−C(4)−C(9)	118.7(3)
C(6)−C(5)−C(4)	120.0(3)
C(5)−C(6)−C(7)	121.3(3)
C(8)−C(7)−C(6)	120.8(3)
C(7)−C(8)−C(9)	119.8(3)
N−C(9)−C(8)	119.3(3)
N−C(9)−C(4)	121.3(3)
C(8)−C(9)−C(4)	119.4(3)
O(2)−C(10)−O(1)	125.3(3)
O(2)−C(10)−C(1)	117.9(3)
O(1)−C(10)−C(1)	116.9(2)
C(12)−C(11)−O(3)	118.3(7)
C(13)−C(12)−C(11)	143.3(14)

Table 2. Hydrogen bonds for $[Fe(quin\text{-}2\text{-}c)_2(PrOH)_2]$ (**3**) (symmetry transformations used to generate equivalent atoms: i: $-x$, $-y$, $-z + 1$. ii: $-x + 1$, $-y$, $-z + 1$)

D−H···A	D−H	H···A	D···A	∠ D−H···A
O(3)−H(3O)···O(2)^{ii}	0.79(4)	1.87(4)	2.659(4)	177(5)
C(8)−H(8)···O(1)^{i}	0.930(4)	2.311(2)	3.179(4)	154(1)

eral bands characteristic of vibrations due to ethanol are also observed. Differences between these two spectra are observed in the low frequency region and are related to the bands generated by the vibrations of metal−ligand bonds.

The IR spectrum of $[Fe(quin\text{-}2\text{-}c)_2(PrOH)_2]$ is in very good agreement with the spectrum of $[Fe(quin\text{-}2\text{-}c)_2(EtOH)_2]$ in terms of the bands resulting from vibrations of the quin-2-c ion and vibrations of the coordination bonds. In particular, the bands found in the regions 1630−1150 cm^{-1} and 900−750 cm^{-1} have the same positions, intensities and shapes. The bands related to the propan-1-ol vibrations are easily found in the spectrum of **3** (Table 3).

The features which make the spectra of **1** and **2** distinct from that of **3**, apart from the previously mentioned alcohol and coordination modes, are two weak and broad bands observed near 3400 cm^{-1} and 700 cm^{-1} seen only for the ethanolic adducts. We have attributed these bands to the vibrations of trace amounts of water, $\nu(H_2O)$ and $\rho_w(H_2O)$, respectively. The positions and shapes of these bands are characteristic of coordinated water molecules.[26,27] The lower quality crystals of **1** and **2** compared with those of **3** may result from disorder in the crystals caused by the trace amounts of water. The absence of the above mentioned bands near 3400 cm^{-1} and 700 cm^{-1} in the IR spectrum of the propanol adduct **3**, the structure of which is presented here, supports our assignment.

The bands generated by the ν(OH) vibrations of alcohols are expected over a wide frequency range (3400−2500 cm^{-1}) with the frequencies considerably dependent on hydrogen bonding.[28] In the crystal of **3** the hydroxyl group of the coordinated propan-1-ol molecule forms a strong hydrogen bond with the carbonyl oxygen atom from the carboxylate group of neighbouring molecule. On this basis we have assigned the vibrations of the hydrogen bond in **3** to the medium bands observed at 2686 and 2574 cm^{-1} in its IR spectrum. The hydrogen bonding modes may also contribute to the group of strong and closely spaced bands at higher frequencies (3200−2800 cm^{-1}), but as a result of overlapping with the $\nu(C-H)_{aliph}$ and $\nu(C-H)_{arom}$ absorptions, their frequencies cannot be resolved. In the spectra of **1** and **2,** in the region 2750−2500 cm^{-1}, two doublets can be observed repeating the intensity pattern seen in the spectrum of **3** (see Table 2). These can be attributed to hydrogen bonding involving the OH group from the ethanol molecule.

The characteristic bands due to the vibrations of alcohols [with exception of the ν(OH) mode] are observed in the regions of 3100−2800 cm^{-1} [$\nu(CH_3)$ and $\nu(CH_2)$] 1100−900 cm^{-1} [ν(CO) and CH_3, CH_2 deformations] and 500−400 cm^{-1} (deformations of the C−C−O fragment) in the IR spectra of all complexes.

Inspection of the IR region 1630−1300 cm^{-1} indicates that the carboxylate group coordination mode is the same for all complexes. The values of $\Delta\nu(CO_2) = \nu_{as}(CO_2) - \nu_s(CO_2)$ are equal to 232, 225, and 234 cm^{-1} for **1**, **2**, and **3**, respectively, and indicate that the carboxylate group binds in a monodentate fashion.[29]

 © 2004 Wiley-VCH Verlag GmbH & Co. KGaA, Weinheim

Table 3. The frequencies observed in the IR spectra of $[Fe(quin\text{-}2\text{-}c)_2(EtOH)_2]$ (**1**), $[Co(quin\text{-}2\text{-}c)_2(EtOH)_2]$ (**2**), and $[Fe(quin\text{-}2\text{-}c)_2(PrOH)_2]$ (**3**) and in the Raman spectrum of **2** [cm^{-1}] and their assignment; assignment of quinoline ring vibrations was made according to Bellamy;[28] abbreviations: vs − very strong, s − strong, m − medium, w − weak, vw − very weak, b − broad, sh − shoulder, et − ethanol, prop − propanol

1 IR	2 IR	3 IR	2 R	Assignment
3386 mb	3433 mb			$\nu(H_2O)$
3064 vs	3068 m	3060 vs	3069 m	$\nu(C-H)_{quin}$
3045 s	3050 s		3054 m	$\nu(CH_3)$, $\nu(CH_2)$
3000 s,sh	3010 s,sh		3012 w	$\nu(CH_3)$, $\nu(CH_2)$
2963 vs	2964 m	2956 vs	2954 m	$\nu(CH_3)$, $\nu(CH_2)$
2916s	2920 s	2932 vs	2921 m	$\nu(CH_3)$, $\nu(CH_2)$
2905s	2907 s			$\nu(CH_3)$, $\nu(CH_2)$
2884 s	2883 s	2865 vs	2878 m	$\nu(CH_3)$, $\nu(CH_2)$
2836 vs	2813 s	2833 vs		$\nu(CH_3)$, $\nu(CH_2)$
2734 m	2735 m	2686 m		hydrogen bond vibrations
2710 m	2712 m			hydrogen bond vibrations
2584 m	2588 w	2575 m		hydrogen bond vibrations
2570 m	2561 w			hydrogen bond vibrations
1628 vs	1627 vs	1628 vs	1620 vw	$\nu(COO)_{as}$
1596 vs	1600 s	1595 s	1595 m	$\nu(C-C)$, $\nu(C-N)$ and $\delta(C-H)$ vibrations of the quinoline fragment
1564 s	1564 s	1563 s	1565 vw	$\nu(C-C)$, $\nu(C-N)$ and $\delta(C-H)$ vibrations of the quinoline fragment
1548 s	1552 m	1551 m	1547 vw	$\nu(C-C)$, $\nu(C-N)$ and $\delta(C-H)$ vibrations of the quinoline fragment
1509 m	1509 m	1509 m	1507 vw	$\nu(C-C)$, $\nu(C-N)$ and $\delta(C-H)$ vibrations of the quinoline fragment
1464 s	1466 s	1464 m	1465 m	$\nu(C-C)$, $\nu(C-N)$ and $\delta(C-H)$ vibrations of the quinoline fragment
1433 s	1432 m	1433 m	1434 w	$\nu(C-C)$, $\nu(C-N)$ and $\delta(C-H)$ vibrations of the quinoline fragment
1395 vs	1396 vs	1394 vs		$\nu(COO)_s$
1378 s	1378 s	1378 ssh	1370 vs	Ring breathing mode
1349 m	1348 m	1349 m		$\nu(C-N)$, $\nu(C-C)$ and $\delta(C-H)$ vibrations of the quinoline fragment
1301 vw	1300 vw	1300 vw		$\nu(C-N)$, $\nu(C-C)$ and $\delta(C-H)$ vibrations of the quinoline fragment
1273 w	1274 w	1274 w	1300 w	$\nu(C-N)$, $\nu(C-C)$ and $\delta(C-H)$ vibrations of the quinoline fragment
1263 vw	1265 w	1264 w	1279 vw	$\nu(C-N)$, $\nu(C-C)$ and $\delta(C-H)$ vibrations of the quinoline fragment
1218 w	1220 vw	1240 vw		$\nu(C-N)$, $\nu(C-C)$ and $\delta(C-H)$ vibrations of the quinoline fragment
1209 w	1211 vw	1215 vw		$\nu(C-N)$, $\nu(C-C)$ and $\delta(C-H)$ vibrations of the quinoline fragment
		1204 w		$\nu(C-N)$, $\nu(C-C)$ and $\delta(C-H)$ vibrations of the quinoline fragment
1181 w	1180 w	1182 w		$\delta(C-H)_{quin}$
1155 m	1154 w	1153 m		$\delta(C-H)_{quin}$
1146 w	1144 vw	1142 vw	1142 vw	
1138 vw	1135 vw	1130 vw		
1120 vw	1118 vw	1115 vw		
1098 m	1097 w	1098 vw		deformation $(CH_3)_{et,\ prop}$
		1074 m		
1056 s	1057 m	1058 m		$\nu(CO)_{et,\ prop}$
1027 w	1027 w	1020 w	1025 w	in-plane deformation modes of the quinoline ring
995 w	997 vw	995 vw		in-plane deformation modes of the quinoline ring
977 w	977 vw			in-plane deformation modes of the quinoline ring
964 w	965 w			in-plane deformation modes of the quinoline ring
902 m	903 m	902 m		in-plane deformation modes of the quinoline ring
885 m	888 w	887 w		$\nu(C-C)_{et,\ prop}$
865 m	867 m	865 m		
809 s	810 m	810 m		$\gamma(C-H)_{quin}$
781 vs	781 s	781 s	779 m	$\gamma(C-H)_{quin}$
752 vw	750 vw	751 vw		
699 vw,b	712 vw,b			$\rho_w(H_2O)$
634 m	636 m	634 w		
605 s	605w	605 m		$\delta(C=O)$
560 vw	563 vw	556 vw		out-of-plane deformations of the quinoline ring
521 w	522 w	522 w	524 w	out-of-plane deformations of the quinoline ring
502 m	503 m	503 m		out-of-plane deformations of the quinoline ring
485 vw	485 vw	485 vw		out-of-plane deformations of the quinoline ring
		472 w		$\delta(CCO)_{prop}$
		464 w		$\delta(CCC)_{prop}$
435 vw	435 w			$\delta(CCO)_{et}$
406 m	406 s	407 m	406 w	deformation mode of the quinoline rings
399 m	406 s	398 m		$\nu(M-O_{carbox})$
385 s	390 s	387 s		$\nu(M-O_{alc})$
317 m	321 s	319 m		def. mode of the quinoline rings
		264 w		
239 w	247 m	238 w		$\nu(M-N)$
204 s	205 s	205 s		deformation modes
152 m	165 m	157 w	158 m	deformation modes

 © 2004 Wiley-VCH Verlag GmbH & Co. KGaA, Weinheim

The energies of the stretching vibrations of the iron(II)-aromatic nitrogen are indicative of the spin state of the ferrous ion. The ν(Fe−N) vibrations can be observed in the range 250−220 cm^{-1} for high-spin and 530−370 cm^{-1} for low spin complexes.[30,31] In the IR spectra of **1** and **3** the ν(Fe−N) mode generates the bands located at 239 cm^{-1} and 238 cm^{-1}, respectively. The positions of the bands due to the metal-oxygen bond vibrations according to Nakamoto[27] are listed in the Table 3.

Comparison of the IR and Raman spectra of **1** and **2** with that of **3** leads to the conclusion that the molecular structures of the three complexes are very similar. Two quin-2-c ions occupy the equatorial positions and coordinate to the metal in a chelating mode via the carboxylate group and the aromatic nitrogen atom. The axial positions are occupied by two propan-1-ol molecules in **3** and by molecules of ethanol and trace amounts of water in **1** and **2**.

Electronic Spectra and Magnetic Properties

The maximum observed in the ligand field spectrum of $[Fe(quin\text{-}2\text{-}c)_2(EtOH)_2]$ at $9.5\cdot10^3$ cm^{-1} is characteristic of high spin iron(II) octahedral complexes.[32] This absorption can be attributed to the spin allowed $^5E_g \leftarrow {}^5T_{2g}(D)$ transition. A strong band, centered at $18.0\cdot10^3$ cm^{-1}, arises from an iron→ligand CT absorption. The ligand field absorption bands in the cobalt complex are found at about 8.41, 18.6, 20.9, and $22.3\cdot10^3$ cm^{-1}. These bands are commonly observed for six coordinate high-spin Co^{II} complexes.[32]

The structure of the framework of magnetic ions in $[Fe(quin\text{-}2\text{-}c)_2(PrOH)_2]$ consists of linear chains of Fe^{2+} ions along the *a* axis [Figure 2 (b)]. The M−M distance of 6.104(1) Å is rather long, precluding any direct magnetic exchange interactions. However the strong hydrogen bonds between the molecules in the chain [O(3)−H(3O)···O(2)^{ii}] make indirect interactions possible. The distance between the neighbouring chains is larger than 10 Å and the spatial arrangement of the ligands seems to rule out an effective pathway for inter-chain magnetic exchange.

The magnetic susceptibilities of $[Fe(quin-2\text{-}c)_2(EtOH)_2]$ and $[Fe(quin\text{-}2\text{-}c)_2(PrOH)_2]$ obey the Curie−Weiss law above ca. 50 K with the positive Weiss constants (+2.6 K and +7.0 K for **1** and **3**, respectively) and large magnetic moments (5.22 μ_B and 5.22 μ_B, calculated from the Curie−Weiss formula) characteristic of high-spin iron(II) complexes [Figure 3 shows the results for $[Fe(quin\text{-}2\text{-}c)_2(PrOH)_2]$. The results for $[Fe(quin\text{-}2\text{-}c)_2(EtOH)_2]$ are quite similar].

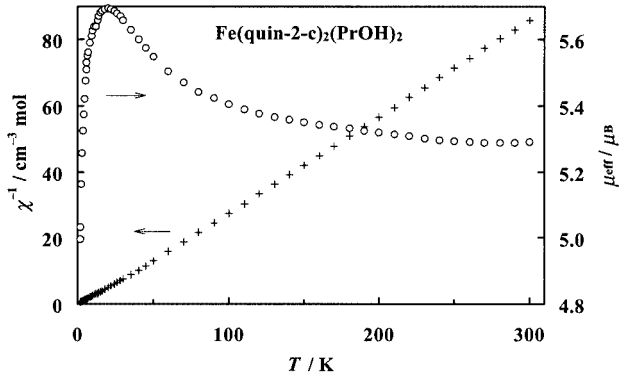

Figure 3. Temperature dependence of reciprocal susceptibility (+) and the effective magnetic moment (o) for the polycrystalline sample of $[Fe(quin\text{-}2\text{-}c)_2(PrOH)_2]$ (H = 5000 Oe)

The effective magnetic moments of the iron compounds increase with desreasing temperature, reach broad maxima at 23 K (**1**) and 20 K (**3**), then decreases quickly below T_{max}. Such behaviour is characteristic of complexes with ferro- or ferrimagnetic exchange interactions.[33] The field dependence of the magnetizations is also interesting (Figure 4). Both compounds show hysteresis at 1.9 K with the zero magnetic remanence. Similar curves have been observed for metamagnetic compounds, for example $Fe(N_2H_5)_2(SO_4)_2$.[34]

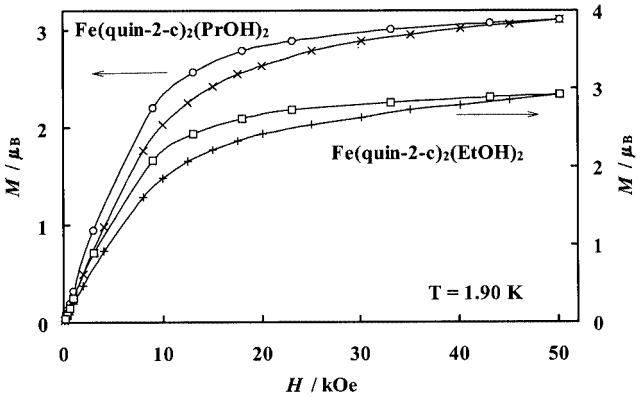

Figure 4. Field dependence of magnetization at 1.90 K for $[Fe(quin\text{-}2\text{-}c)_2(PrOH)_2]$ and $[Fe(quin\text{-}2\text{-}c)_2(EtOH)_2]$; crosses − increasing field, circles and squares − decreasing field

The magnetic properties of the iron complexes do not have a satisfactory explanation. A long-range order, which may be considered as an explanation of the behaviour of isothermal magnetization (Figure 4), is not possible in a pure one-dimensional network. However, it is not easy to see any obvious pathway for the interchain magnetic exchange. A more detailed analysis of the magnetic data is beyond the scope of this article and will be presented elsewhere.

The magnetic properties of the cobalt compound are different from those of the iron complexes. The properties of $[Co(quin\text{-}2\text{-}c)_2(EtOH)_2]$ are rather typical. The magnetic susceptibility obeys the Curie−Weiss law down to about 30 K (Figure 5). The parameters of the C−W equation depend on the Van Vleck temperature-independent paramagnetism ($N\alpha$), which is usually strong for high-spin Co^{2+} compounds.[35,36] If we assume $N\alpha = 6.9\cdot10^{-4}$ emu mol^{-1}, obtained from the fitting of the calculated and the experimental μ_{eff} (see below), the values μ = 4.57 μ_B and θ = −3.0 K are obtained (μ = 4.84 μ_B and θ = −15.6 K are found for the uncorrected susceptibility). The effective magnetic moment decreases monotonically between room temperature and 1.9 K, changing from 4.75 to 3.62 μ_B. The field dependence of magnetization shows no hysteresis and the

 © 2004 Wiley-VCH Verlag GmbH & Co. KGaA, Weinheim

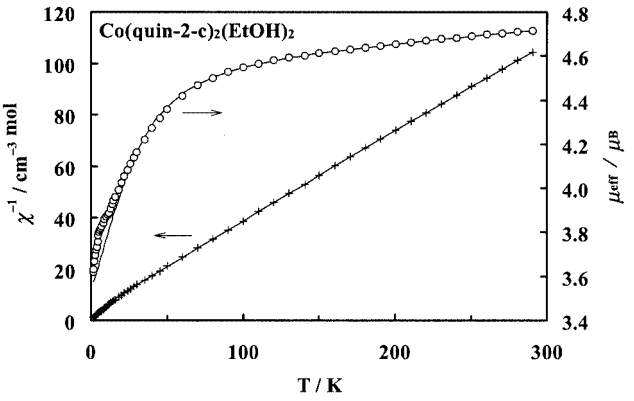

Figure 5. Temperature dependence of reciprocal susceptibility (+) and the effective magnetic moment (o) for the polycrystalline sample of $[Co(quin\text{-}2\text{-}c)_2(EtOH)_2]$ (H = 5000 Oe); the lines were calculated for S = 3/2 with the ZFS parameter $|D|$ = 34 cm^{-1}, g = 2.35 and $N\alpha = 6.9\cdot10^{-4}$ $cm^3\cdot mol^{-1}$

magnetization is almost saturated at 1.9 K in a field of 50 kOe, reaching a value of 2.2 μ_B (Figure 6).

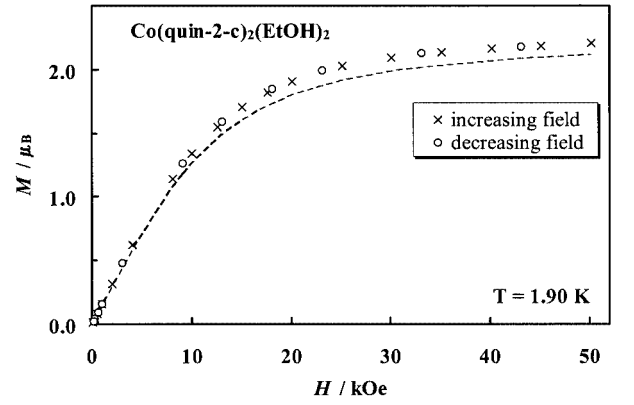

Figure 6. Field dependence of magnetization at 1.90 K for $[Co(quin\text{-}2\text{-}c)_2(EtOH)_2]$; the dashed line represents the ZFS magnetization with $|D|$ = 34 cm^{-1}, $E \approx 0$, $g_z = g_x = g_y$ = 2.35 and the Van Vleck contribution $N\alpha = 6.9\cdot10^{-4}$ $cm^3\cdot mol^{-1}$

In contrast to the iron compounds, magnetic exchange interactions are not well pronounced in the experimental results for $[Co(quin\text{-}2\text{-}c)_2(EtOH)_2]$. We therefore tried to apply the model of isolated Co^{2+} ions in the octahedral crystal field deformed by the rhombic zero field distortion. Taking into account only the second-order crystal field parameters, the spin Hamiltonian can be written as [Equation(1)], where S = 3/2.

$$H = g_z\cdot\beta\cdot H\cdot S_z + D\cdot[S_z^2 - 1/3\cdot S\cdot(S+1)] + E\cdot(S_x^2 - S_y^2) \quad (1)$$

The appropriate matrix elements and the relations between the parameters of the Hamiltonians with the different field directions were given by Abragam and Bleaney.[37] The least-squares refinement of the temperature dependence of μ_{eff} yielded $|D|$ = 34 cm^{-1}, $E \approx 0$, $g_z = g_x = g_y$ = 2.35 and the Van Vleck contribution $N\alpha = 6.9\cdot10^{-4}$ $emu\cdot mol^{-1}$. The calculated curve fits the experimental points well at higher temperatures. Below 30 K the calculated points deviate slightly from the experimental ones (Figure 5).

Moreover, the field dependence of magnetization is fairly well described by this set of parameters (Figure 6). There are at least two possible reasons of the low-temperature discrepancies: neglecting the fourth-order crystal-field parameters[38,39] and the appearance of weak magnetic exchange effects in the lowest temperature range. The large value of the axial ZFS parameter D is not unusual for Co^{2+} complexes. For example, in $Cd_2P_2S_6:Co^{2+}$ with trigonally distorted CoS_6 octahedra D = 63 cm^{-1} and it reaches a value of 84 cm^{-1} for the more covalent $Cd_2P_2Se_6:Co^{2+}$.[40,41]

The Mössbauer spectrum of $[Fe(quin\text{-}2\text{-}c)_2(EtOH)_2]$ recorded at 293 K consists of an unsymmetrical quadrupole split doublet, Figure 7.

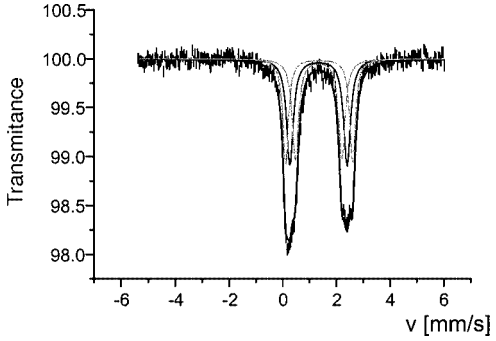

Figure 7. Room temperature Mössbauer spectrum of $[Fe(quin\text{-}2\text{-}c)_2(EtOH)_2]$

The observed asymmetry of the Mössbauer doublet cannot be attributed to the metal−metal interaction because the magnetic susceptibility data indicate that the ferrous ions are isolated. However the crystal structure of **1** is not known, although we can expect that the Fe−Fe distance in **1** is similar to that found in **3** [6.104(1) Å]. According to the least squares fitting with Lorenz curves, the Mössbauer spectrum of $[Fe(quin\text{-}2\text{-}c)_2(EtOH)_2]$ was resolved into three quadrupole doublets with *IS*, *QS*, and Γ parameters (Table 4) being very close to each other. This indicates that in the studied sample, three complexes of Fe^{II} are present having the same donor set and the same geometry. The parameters of the three components of the quadrupole split doublet are characteristic of high-spin iron(II) in an N_2O_4 octahedral environment.[18,19−21,23] The results of the Mössbauer study are consistent with the IR data and demonstrate that three compounds appear in the crystal of **1**, namely $[Fe(quin\text{-}2\text{-})_2(EtOH)_2]$, $[Fe(quin\text{-}2\text{-}c)_2(H_2O)_2]$, and $[Fe(quin\text{-}2\text{-}c)_2(EtOH)(H_2O)]$.

Table 4. Mössbauer data for $[Fe(quin\text{-}2\text{-}c)_2(EtOH)_2]$

	IS [mm/s]	*QS* [mm/s]	Γ/2 [mm/s]
I	1.378(3)	2.13(1)	0.15(3)
II	1.381(3)	1.73(1)	0.12(1)
III	1.38(1)	2.52(1)	0.14(1)

 © 2004 Wiley-VCH Verlag GmbH & Co. KGaA, Weinheim

Experimental Section

Safety Note: Perchlorates are potentially explosive. Although we have experienced no accidents so far, all compounds containing perchlorate should be handled with care and in small quantities.

***trans*-Bis(quinoline-2-carboxylato)bis(ethanol)iron(II) (1):** A solution of $Fe(ClO_4)_2 \cdot 6H_2O$ (0.100 g; 0.275 mmol) in ethanol (50 cm^3) was added to a solution of quinoline-2-carboxylic acid (0.095 g, 0.55 mmol) in ethanol (100 cm^3) at room temperature under aerobic conditions. The resultant deep red solution was allowed to stand for two days. During this period crystals of [Fe(quin-2-c)$_2$(EtOH)$_2$] appeared. The dark violet crystals were filtered, washed with ethanol and left to dry in air. Attempts to obtain X-ray quality crystals of this compound were unsuccessful. $C_{24}H_{24}FeN_2O_6$: calcd. C 58.55, H 4.89, N 5.69, Fe 11.34; found C 58.74, H 5.04, N 5.80, Fe 11.03.

***trans*-Bis(quinoline-2-carboxylato)bis(ethanol)cobalt(II) (2):** [Co(quin-2-c)$_2$(EtOH)$_2$] was obtained by a modification of the method reported for Co(quin-2-c)$_2 \cdot 1/2H_2O$.[13] A solution of $CoCl_2 \cdot 6H_2O$ (0.065 g, 0.275 mmol) in ethanol (50 cm^3) was added to a solution of quinoline-2-carboxylic acid (0.095 g, 0.55 mmol) in ethanol (100 cm^3) at room temperature. After two days pink-yellow crystals appeared. The crystals were filtered, washed with water and left to dry in air. Attempts to obtain X-ray quality crystals of this compound were unsuccessful. $C_{24}H_{24}CoN_2O_6$: calcd. C 58.19, H 4.88, N 5.65, Co 11.90; found C 58.01, H 5.20, N 5.65, Co 11.44.

***trans*-Bis(quinoline-2-carboxylato)bis(propanol)iron(II) (3):** A solution of $Fe(ClO_4)_2 \cdot 6H_2O$ (0.100 g; 0.275 mmol) in propanol (50 cm^3) was added to a solution of quinoline-2-carboxylic acid (0.095 g, 0.55 mmol) in propanol (100 cm^3) at room temperature under aerobic conditions. The resultant deep red solution was allowed to stand for two days. During this period crystals of [Fe(quin-2-c)$_2$(PrOH)$_2$] appeared. The dark violet, X-ray quality crystals were filtered, washed with propanol and left to dry in air. $C_{26}H_{28}FeN_2O_6$: calcd. C 60.01, H 5.42, N 5.38, Fe 10.73; found C 60.49, H 5.22, N 5.68, Fe 11.01.

Physical Measurements

Elemental Analyses were performed in the Analytical Laboratory, Department of Chemistry, Wrocław University of Technology.

Magnetic susceptibility down to 1.9 K and magnetization up to 50 kOe were measured with a Quantum Design SQUID magnetometer. Diamagnetic corrections were calculated using Pascal's constants[42] and were found to be $-283 \cdot 10^{-6}$ emu·mol^{-1}, $-282 \cdot 10^{-6}$ emu·mol^{-1}, and $-306 \cdot 10^{-6}$ emu·mol^{-1} for **1**, **2**, and **3**, respectively.

IR spectra were recorded in KBr pellets or nujol mulls using Perkin−Elmer FTIR-2000 and Perkin−Elmer FTIR-1600 spectrophotometers in the frequency range 50−4000 cm^{-1}. The Raman spectra of solid samples were recorded in the range 0−3600 cm^{-1} with a Bruker FIS-88 TRA-10G-Raman instrument. The excitation was provided by a diode pumped neodymium laser at 1064 nm (150 mV Nd:YAG).

Solid state UV/Vis spectra of the powdered samples were measured in the diffuse reflectance mode on a Carry 500 Scan (Varian) UV/Vis/NIR spectrophotometer.

The Mössbauer spectra of a powdered sample of [Fe(quin-2-c)$_2$(EtOH)$_2$] were recorded on a Mössbauer 2330 spectrophotometer (Polon, Poland). The isomer shift values were referenced to a sodium nitroprusside (SNP) standard. ^{57}Co in the Rh matrix of 10 mCi activity was used as the source. The spectra were processed numerically by distribution into Lorenz curves.

X-ray crystallographic Study: Crystal data collection and refinement are summarized in Table 5. Preliminary examination and intensity data collections were carried out on a KUMA KM-4 κ-axis diffractometer with graphite-monochromated Mo-K_α radiation. All data were corrected for Lorentz and polarization effects. Data reduction and analysis were carried out with the Kuma Diffraction programs.[43] The structures were solved by direct methods[44] and refined by the full-matrix least-squares method on all F^2 data using the SHELXL-97 software.[45] After refinement with isotropic displacement parameters for all atoms, an absorption correction was also applied. Carbon-bonded hydrogen atoms were included in calculated positions and refined in the riding mode using the SHELXL-97 default parameters. Other hydrogen atoms were located in a difference map and refined freely. All non-hydrogen atoms were refined with anisotropic displacement parameters.

CCDC-210965 contains the supplementary crystallographic data for this paper. These data can be obtained free of charge at www.ccdc.cam.ac.uk/conts/retrieving.html [or from the Cambridge Crystallographic Data Centre, 12 Union Road, Cambridge

Table 5. Crystal data and structure refinement for [Fe(quin-2-c)$_2$(PrOH)$_2$] (**3**)

Compound	$C_{26}H_{28}FeN_2O_6$
Empirical formula	$2\times(C_{13}H_{14}Fe_{0.50}NO_3)$
Molecular mass	520.35
λ [Å]	0.71073
T [K]	100(1)
Space group	$P2_1/n$
Crystal system	monoclinic
Unit cell dimensions:	
a [Å]	6.104(1)
b [Å]	10.515(2)
c [Å]	19.339(4)
β [°]	92.57(3)
V [Å^3]	1240.0(4)
Z	2
$D_{calcd.}$ [Mg/m^3]	1.394
F(000)	544
Habit	block
Crystal size [mm]	0.5×0.4×0.4
μ [mm^{-1}]	0.652
Absorption correction	Empirical (SHELXA)
Max. and min. transmission	0.9120 and 0.6916
Diffractometer	Kuma KM4 automatic diffractometer
Diffraction geometry	profile data from ω−2θ scans
θ range [°]	2 to 25
Number of reflections measured	2099
Number of unique reflections	1942
$R_{(int.)}$	0.0170
Number of observed reflections	1534 [$I > 2\sigma(I)$]
Refinement method	least-squares on F^2
Final R indices [$I > 2\sigma(I)$]	$R_1 = 0.0377$,[a] $wR_2 = 0.1022$[b]
Final R indices (all data)	$R_1 = 0.0552$,[a] $wR_2 = 0.1097$[b]
Goodness-of-fit (S)	1.046
Largest diff. peak and hole [e·Å^{-3}]	0.519 and −0.354

[a] $R_1 = \Sigma||F_o| - |F_c||/\Sigma|F_o|$. [b] $wR_2 = \{\Sigma[w(F_o^2 - F_c^2)^2]/\Sigma[w(F_o^2)^2]\}^{1/2}$.

 © 2004 Wiley-VCH Verlag GmbH & Co. KGaA, Weinheim

CB2 1EZ, UK; Fax: (internat.) + 44-1223-336-033; E-mail: deposit@ccdc.cam.ac.uk].

[1] C. Oldham, *Carboxylates, Squarates and Related Species*, in: *Comprehensive Coordination Chemistry* (Ed.: G. Wilkinson), Pergamon Press, Oxford, **1987**, chapter 15.6.
[2] A. Caneschi, D. Gatteschi, J. P. Renard, P. Rey, R. Sessoli, *J. Am. Chem. Soc.* **1989**, *111*, 785.
[3] A. K. Majumdar, J. G. SenGupta, *Z. Anal. Chem.* **1958**, *161*, 104.
[4] A. K. Majumdar, J. G. SenGupta, *Z. Anal. Chem.* **1958**, *161*, 181.
[5] G. J. Lamprecht, J. H. Beetge, J. G. Leipoldt, D. R. De Waal, *Inorg. Chim. Acta* **1986**, *113*, 157.
[6] M. Cano, J. V. Heras, M. A. Lobo, M. Martinez, E. Pinilla, E. Gutierrez, M. A. Monge, *Polyhedron* **1991**, *10*, 187.
[7] D. E. Graham, G. J. Lamprecht, I. M. Potegieter, A. Roodt, J. G. Leipoldt, *Trans. Met. Chem.* **1991**, *16*, 193.
[8] G. J. Lamprecht, J. G. Leipoldt, A. Roodt, *Acta Crystallogr., Sect. C* **1991**, *47*, 2209.
[9] M. Cano, J. V. Heras, M. A. Lobo, E. Pinilla, M. A. Monge, *Polyhedron* **1994**, *13*, 1563.
[10] H. M. Haendler, *Acta Crystallogr., Sect. C* **1996**, *52*, 801.
[11] M. A. S. Goher, F. A. Mautner, *Polyhedron* **1993**, *12*, 1863.
[12] H. M. Haendler, *Acta Crystallogr., Sect. C* **1986**, *42*, 147.
[13] W. Li, M. M. Olmstead, D. Miggins, R. H. Fish, *Inorg. Chem.* **1996**, *35*, 51.
[14] U. Brand, H. Varhenkamp, *Inorg. Chem.* **1995**, *34*, 3285.
[15] E. J. Gabe, F. L. Lee, L. E. Khoo, F. E. Smith, *Inorg. Chim. Acta* **1985**, *105*, 103.
[16] M. A. S. Goher, A. K. Hafez, R.-J. Wang, X. Chen, T. C. W. Mak, *Aust. J. Chem.* **1994**, *47*, 1423.
[17] P. Starynowicz, *Acta Crystallogr., Sect. C* **1990**, *46*, 2068.
[18] L. Thommasi, L. Schechter-Barloy, D. Varech, J. P. Battioni, B. Donnadieu, M. Verlest, A. Bousseksou, J-P. Tuchagues, *Inorg. Chem.* **1995**, *34*, 1514.
[19] P. Lainé, A. Gourdon, J-P. Launay, J.-P. Tuchagues, *Inorg. Chem.* **1995**, *34*, 5150.
[20] P. Lainé, A. Gourdon, J-P. Launay, *Inorg. Chem.* **1995**, *34*, 5129.
[21] P. Lainé, A. Gourdon, J-P. Launay, *Inorg. Chem.* **1995**, *34*, 5138.
[22] S. Kiani, A. Tapper, R. J. Staples, P. Stavropoulos, *J. Am. Chem. Soc.* **2000**, *122*, 7503.
[23] R. -G. Xiong, S. R. Wilson, W. Win, *J. Chem. Soc., Dalton Trans.* **1998**, 4089.
[24] Y. Zang, J. Kim, Y. Dong, E. C. Wilkinson, E. P. Appelman, L. Que Jr., *J. Am. Chem. Soc.* **1997**, *119*, 4197.
[25] K. L. Taft, A. Caneschi, L. E. Pence, Ch. D. Delfs, G. C. Papaefthymiou, S. J. Lippard, *J. Am. Chem. Soc.* **1993**, *115*, 11753.
[26] D. Michalska-Fong, P. J. McCarthy, K. Nakamoto, *Spectrochim. Acta* **1983**, *39A*, 835.
[27] K. Nakamoto, *Infrared and Raman Spectra of Inorganic and Coordination Compounds*, John Wiley & Sons, New York, **1997**.
[28] L. J. Bellamy, *The Infrared Spectra of Complex Molecules*, Chapman and Hall, London, **1975**.
[29] G. B. Deacon, R. J. Phillips, *Coord. Chem. Rev.* **1980**, *33*, 227.
[30] R. Boèa, P. Baran, L. Dlhán, H. Fuess, W. Haase, W. Linert, B. Papánková, R. Werner, *Inorg. Chim. Acta* **1998**, *278*, 190.
[31] H. A Goodwin, *Coord. Chem. Rev.* **1976**, *18*, 293.
[32] A. B. P. Lever, *Inorganic Electronic Spectroscopy*, Elsevier, Amsterdam, **1984**.
[33] O. Kahn, *Molecular Magnetism*, VCH Publishers, New York, **1993**.
[34] W. M. Reiff, H. Wong, R. B. Frankel, S. Foner, *Inorg. Chem.* **1977**, *16*, 1036.
[35] H. T. Witteveen, J. Reedijk, *J. Solid State Chem.* **1974**, *10*, 151.
[36] S. J. Gruber, C. M. Harris, E. Sinn, *J. Chem. Phys.* **1968**, *49*, 2182.
[37] A. Abragam, B. Bleaney, *Electron Paramagnetic Resonance of Transition Ions*, Clarendon Press, Oxford, **1970**.
[38] J. C. Gill, P. A. Ivey, *J. Phys. C: Solid State Phys.* **1974**, *7*, 1536.
[39] Cz. Rudowicz, *Phys. Rev.* **1980**, *B21*, 4967.
[40] G. T. Long, D. A. Cleary, *J. Phys.: Condens. Matter* **1990**, *2*, 4747.
[41] D. A. Cleary, A. H. Francis, E. Lifshitz, *Chem. Phys.* **1986**, *106*, 123.
[42] A. Weiss, H. Witte, *Magnetochemie*, Verlag Chemie, Weinheim, **1973**.
[43] *Kuma Diffraction. KM-4 User's Guide*, Version 10.1. Kuma Diffraction, Wrocław, **1998**.
[44] G. M. Sheldrick, *Acta Crystallogr., Sect. A* **1990**, *46*, 467.
[45] G. M. Sheldrick, *SHELXL-97: Program for the Refinement of Crystal Structures*, University of Göttingen, Germany, **1997**.
[46] G. M. Sheldrick, *SHELXA: Program for Post-absorption corrections*, University of Göttingen, Germany, **1997**.

Received May 30, 2003
Early View Article
Published Online October 23, 2003

 © 2004 Wiley-VCH Verlag GmbH & Co. KGaA, Weinheim

Study of the Reaction of Tridentate Ligands with Ferrocenyl Boronic Acid

Victor Barba,*[a] Rubí Xochipa,[b] Rosa Santillan,[b] and Norberto Farfán[b]

Keywords: Cyclizations / Boron / Tridentate ligands / Ferrocene

Evaluation of the reactivity of eight tridentate ligands derived from amino alcohols and salicylaldehyde, 2-hydroxyacetophenone, or 2-hydroxybenzophenone with ferrocenyl boronic acid has shown that the reaction leads to both monomeric and dimeric ferrocenyl boronates. A coordinative N–B bond is essential to give the tetrahedral boron atoms that are responsible for the formation of heterobicyclic structures containing six, seven and ten members. The purity and identity of all compounds were unequivocally established by analytical and multinuclear (^{1}H, ^{11}B, ^{13}C) magnetic resonance spectroscopic data. Furthermore, the structures of the dimeric (**2a**) and monomeric (**5b**) boron complexes were established by X-ray diffraction analyses. The dimeric compound contains a ten-membered ring in a *boat–chair–boat* conformation, while the monomeric compound has a seven-membered ring with a *chair* conformation.
(© Wiley-VCH Verlag GmbH & Co. KGaA, 69451 Weinheim, Germany, 2004)

Introduction

The synthesis and study of ferrocenyl boron derivatives has generated considerable interest due to their interesting properties and potential applications.[1−6] The boryl group attached to the Cp fragment exerts an interesting influence, attributed to $p_\pi-p_\pi$ interactions between the cyclopentadienyl system and the boron p_z orbital. Additionally, the through-space Fe−B interaction seen in (dibromoboryl)ferrocenes and (bispentafluorophenyl)boryl ferrocenes is favored because the occupied d orbitals on the iron center have the appropriate symmetry to interact with the empty p orbital of the boron center.[6b,7] Borylated ferrocenes are isoelectronic with stable ferrocenyl carbocations.[7,8] Due to possible applications of their unusual properties to electronic materials, boron compounds containing ferrocenyl units have recently been examined as charge-transfer complexes.[9−12]

Moreover, boronic acids are potentially useful for selective recognition of sugars as they can form strong boronic acid−diol interactions.[10,13,14] In addition, the complexation of boronic acids with sugars affords a fluorescence intensity that is affected by complexation.[15] Ferrocenyl boronic acid derivatives have also been used in the electrochemical detection of saccharides[13,14] and the selective recognition of fluoride, whereby the boron atom acts as a hard acid and fluoride as the hard base.[16]

Recently, ferrocenyl boron macrocycles have been prepared by the reaction of 1,1′ diborylated ferrocene [1,1′-{C_5H_4[B(R)Br]}$_2$] with tetrafunctional Lewis bases such as 2,5-di(pyrazol-1-yl)hydroquinone and quaterpyridine.[17,18] Here, formation of the dative N−B bond facilitates cyclization leading to cyclic oligomers. However, the reaction of difunctional Lewis bases such as pyrazine or 4,4′-bipyridine with 1,1-diborylated ferrocene led to polymeric materials only.[19]

Relatively few detailed studies have been performed on the coordination chemistry of ferrocenyl boronic acid. Previously, we reported the synthesis of monomeric,[20,21] dimeric,[21,22] trimeric,[23] and tetrameric[24] boron compounds by reaction of boronic acids with Schiff bases where the formation of dative N−B bonds is very important in their cyclization.[25] Here we describe the reactivity of ferrocenyl boronic acids with different tridentate ligands using simple condensation reactions.

Results and Discussion

We have investigated the reaction of boronic acids with different ligands to establish the factors involved in the formation of macrocyclic structures. To further evaluate electronic and steric factors we selected $CpFeC_5H_4B(OH)_2$, as the ferrocenyl group is bulkier and more electrophilic than a phenyl group.[22] Thus, we discuss here the reactivity of various tridentate ligands with ferrocenyl boronic acid in order to prepare new macrocyclic boron compounds.

The reaction of tridentate ligand **1a** derived from salicylaldehyde and ethanolamine with ferrocenyl boronic acid was carried out under reflux of THF to yield, after 60 min, a red solid that is stable to air (Scheme 1). The EI mass

[a] Centro de Investigaciones Químicas UAEM,
Av. Universidad 1001, C. P. 62210, Cuernavaca Morelos, México
E-mail: vbarba@ciq.uaem.mx
[b] Departamento de Química, Centro de Investigación y de Estudios Avanzados del IPN
Apdo. Postal 14-740, 07000 México, D. F., México
E-mail: jfarfan@mail.cinvestav.mx

 © 2004 Wiley-VCH Verlag GmbH & Co. KGaA, Weinheim DOI: 10.1002/ejic.200300337

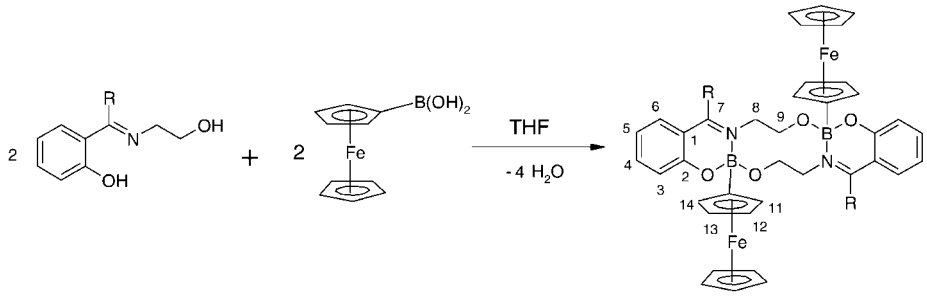

1a: R = H, **1b**: R = Me, **1c**: R = Ph

2a: R = H, **2b**: R = Me, **2c**: R = Ph

Scheme 1. Dimeric boron compounds from tridentate ligands

spectrum has a highest peak at m/z = 718, establishing the dimeric composition of compound **2a**.

To determine if a larger substituent could influence the imine bond and alter the course of the reaction, we prepared ligands derived from 2-hydroxyacetophenone (**1b**) and 2-hydroxybenzophenone (**1c**); however, these ligands react with ferrocenyl boronic acid to give dimeric boronates **2b** and **2c** in moderate yields (Scheme 1).

The dimeric composition of these compounds was established by spectroscopic analyses whereby the EI mass spectra have highest peaks at m/z = 746 and 870, which correspond to the molecular weight of **2b** and **2c**, respectively. In all cases, the base peak corresponds to the loss of one ferrocenyl moiety. NMR analyses of **2a** and **2c** could not be obtained due the compounds' insolubility in common solvents. In the NMR spectra of **2b** only a single set of signals is observed, owing to the C_2 fold axis present in the molecule. The ^{11}B NMR spectrum of **2b** shows a singlet at δ = 7.8 ppm, which is in the range expected for tetracoordinate boron atoms containing a dative N−B bond.[26]

The stretching band for the C=N group in the IR spectra is shifted to 1640, 1610, and 1606 cm^{-1} for **2a**, **2b**, and **2c**, respectively. The lower shift showed by **2b** and **2c** can be attributed to electronic and inductive effects of the methyl and phenyl groups present.

The crystal structure of **2a** confirms the dimeric nature of this compound (Figure 1). Crystallographic data and selected distances and bonds are listed in Tables 1 and 2, respectively. In analogy to the dimeric compounds previously described,[22,24,25] the structure has an inversion center at the center of the ten-membered ring. Ferrocenyl substituents on each boron atom are *trans* disposed with regard to the ten-membered macrocycle, which may be attributed to the bulkiness of the ferrocenyl moieties. A dative N−B bond, together with the required tetrahedral geometry of the boron atoms, is responsible for the dimeric form of these compounds.

Thus, B(1)−N(1) [1.632(5) Å] in **2a** is very similar to that of the boron-phenyl derivative [1.624(3) Å[24]] and accords with analogous systems.[27] The C(10)−B(1) [1.595(6) Å] is slightly shorter than in the phenyl derivative [1.601(3) Å] because the ferrocenyl group is a stronger electron donor than the phenyl group.

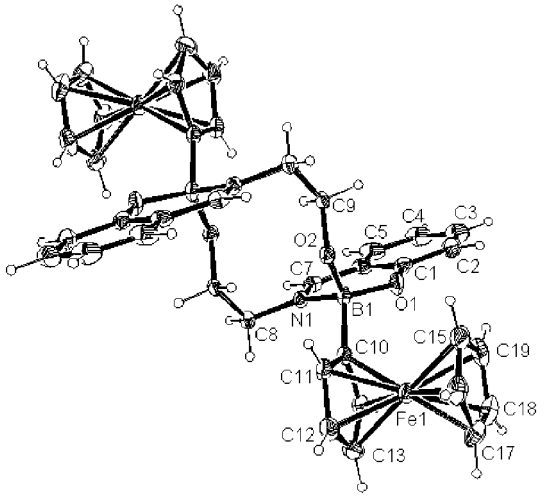

Figure 1. Molecular structure of solid-state **2a**

The tetrahedral geometry for the boron atom is evident from the bond angles, which are in the range 106.9(3)−111.5(3)°, the largest being O(1)−B(1)−C(10), which in the boron-phenyl derivative[24] is 109.4(2)°. This difference in bond angles may be attributed to the steric effect of the bulkier ferrocene unit, compared to the phenyl group. As expected, the inverse effect is observed on comparing the N(1)−(B1)−(C10) angle, which is slightly smaller [107.0(3)°] in the ferrocene derivative than in the phenyl [108.1(2)°] one.[24] The six-membered heterocycle is nearly planar, as evidenced by the O(1)−B(1)−N(1)−C(7) torsion angle (10.2°). The ten-membered heterocycle presents a *boat−chair−boat* conformation. The structure shows a relatively short transannular H···O interaction (2.47 Å) between the oxygen atom on one side of the ring with a hydrogen atom from the CH_2 group on the opposite side.

In contrast, the reaction of ligands **1d** and **1e**, obtained from salicylaldehyde and 1-aminomethylcyclohexanol, with two equivalents of ferrocenyl boronic acid provided exclusively complexes **3a** and **3b** (Scheme 2). The different reactivity, compared to **1a** and **1c** ligands, may be attributed to the cyclohexyl group at the β position relative to the nitrogen

 © 2004 Wiley-VCH Verlag GmbH & Co. KGaA, Weinheim

Table 1. Crystal data and structure refinement for **2a** and **5b**

	2a	**5b**
Empirical formula	$C_{19}H_{18}BNFeO_2$	$C_{22}H_{24}BNFeO_2$
Molecular mass	359.01	410.08
Crystal size [mm^3]	0.20 × 0.24 × 0.50	0.48 × 0.30 × 0.21
Temperature [K]	293	293
Crystal system	triclinic	monoclinic
Space group	$P\bar{1}$	$P2_1/c$
Unit cell dimensions		
a [Å]	7.7230(10)	8.5644(6)
b [Å]	10.5580(10)	11.3609(7)
c [Å]	10.7290(10)	19.1696(12)
α [°]	103.660(10)	90.00
β [°]	95.000(10)	91.5850(10)
γ [°]	109.610(10)	90.00
V [Å^3]	787.44 (15)	1864.5(2)
Z	2	4
Density (calculated) [g/cm^3]	1.51	1.429
Absorption coefficient [mm^{-1}]	0.968	0.826
Index ranges	−8/9, −12/0, −12/13	−10/10, −13/13, 0/23
Reflections collected	3117	17467
Independent reflections	2951	3283
parameters	217	246
Final R indices [$I>2\sigma(I)$]	0.049	0.0487
R indices (all data)	$wR2$ = 0.1597	$wR2$ = 0.1058
GOOF	1.005	1.219
Largest diff. peak and hole [e/Å^3]	0.437/ −0.309	0.302 / −0.297

Table 2. Selected bond lengths [Å] and angles [°] for **2a** and **5b**

	2a	**5b**
Bond lengths [Å]		
O(1)−B(1)	1.491(5)	1.481(4)
O(1)−C(1)	1.324(5)	1.333(3)
O(2)−B(1)	1.432(6)	1.426(4)
O(2)−C(9)[a]	1.413(5)	1.424(3)
B(1)−N(1)	1.632(5)	1.641(3)
B(1)−C(10)[b]	1.595(6)	1.596(4)
N(1)−C(7)	1.286(5)	1.290(4)
N(1)−C(8)[c]	1.459(5)	1.473(3)
Bond angles [°]		
B(1)−O(1)−C(1)	125.9(4)	119.6(2)
B(1)−O(2)−C(9)[a]	119.0(3)	119.0(2)
O(1)−B(1)−O(2)	111.5(4)	111.1(2)
O(1)−B(1)−N(1)	106.9(3)	105.0(2)
O(2)−B(1)−N(1)	109.1(3)	107.8(2)
O(1)−B(1)−C(10)[b]	111.5(3)	111.1(2)
O(2)−B(1)−C(10)[b]	110.6(4)	111.8(2)
N(1)−B(1)−C(10)[b]	107.0(3)	107.5(2)
B(1)−N(1)−C(7)	121.8(3)	122.7(2)
B(1)−N(1)−C(8)[c]	119.2(3)	115.0(2)
C(7)−N(1)−C(8)[c]	119.0(4)	122.3(2)

[a] For **5b** is C(12). [b] For **5b** is C(13). [c] For **5b** is C(9).

atom in ligands **1d** and **1e**, which could cause strong intramolecular interactions upon formation of either a dimeric structure or a monomeric compound containing five- and six-membered rings. Consequently, bicyclic structures are preferred. The six- and seven-membered rings contain two boron atoms, one tetrahedral and the other tricoordinate. When only one equivalent of ferrocenyl boronic acid is used, **3a** and **3b** are also formed, but in lower yields. Attempts to form the dimeric compound from this ligand by using different reaction conditions as well as other boronic acids were unsuccessful.

Bicyclic structures for **3a** and **3b** were established by MS, where the molecular peaks appear at m/z = 639 and 653, respectively. ^{11}B NMR spectra show two signals at δ = 34.8 and 8.2 ppm for **3a** and 38.3 and 7.2 ppm for **3b**, corresponding to trigonal and tetrahedral boron atoms, respectively. ^{1}H NMR shows an AB system for the NCH_2C group, due to the formation of the seven-membered heterocycle.

We then examined the ligand containing three carbon atoms between the OH and C=N groups to evaluate the effect upon ring closure. **1f** reacted with ferrocenyl boronic acid under reflux in THF (40 min) to yield a red solid that was characterized as monomeric compound **4** (Scheme 3). In accordance with previous reports,[20,28] the six-membered ring is favored (monomer) over a twelve-membered ring (dimer) in this type of ligands. The ^{11}B NMR spectrum shows a signal significantly up-field (δ = 5.0 ppm) with respect to ferrocenyl boronic acid, due to the formation of a tetrahedral boron atom. In ^{1}H NMR, an AB system appears at δ = 4.82 and 4.89 ppm, corresponding to the CH_2 group. The iminic proton is shifted to down field (9.21 ppm) in comparison with the ligand (8.57 ppm) due to formation of the dative N−B bond. All boron compounds described herein shown diastereotopic signals for the C_5H_4 moiety attached to the boron atoms, in accordance with the literature data.[2]

We also prepared ligands **1g** and **1h** from 4-aminobutanol and salicylaldehyde or 2-hydroxyacetophenone, respectively. **1g** and **1h** reacted with ferrocenyl boronic acid to give the

 © 2004 Wiley-VCH Verlag GmbH & Co. KGaA, Weinheim

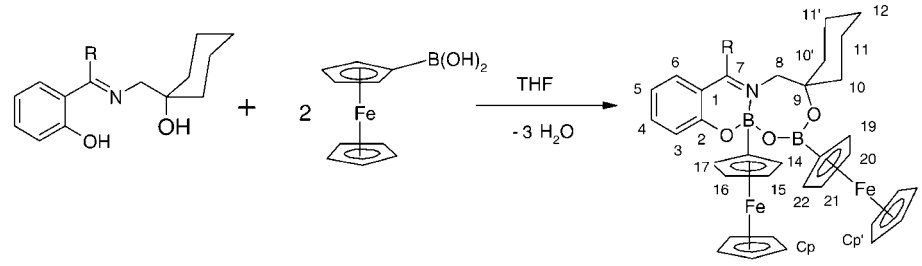

1d: R = H, **1e**: R = Me

3a: R = H, **3b**: R = Me

Scheme 2. Boron complexes having two boron atoms with different geometry

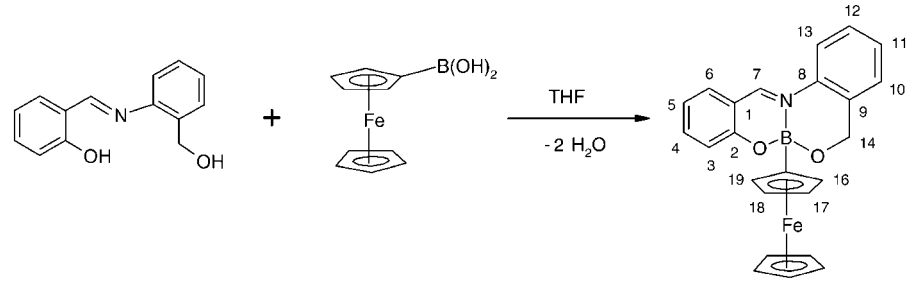

1f

4

Scheme 3. Monomeric boron compound from an aromatic tridentate ligand

monomeric compounds **5a** and **5b** with six- and seven-membered-rings (Scheme 4). Only a monomeric product was isolated, in contrast to using phenylboronic acid,[30] where both monomeric and dimeric compounds were isolated; a possible explanation is that the bulky ferrocenyl group prevents formation of the dimeric compound. Tetracoordination of the boron atom is evident in the ^{11}B NMR spectra, with signals at $\delta = 9.6$ ppm and 8.7 ppm for **5a** and **5b**, respectively, as a result of dative N−B bond formation.

Compound **5b** was characterized by X-ray crystal structure analysis (Figure 2). Selected bond lengths and angles are summarized in Table 2. The corresponding bond lengths and angles in the six-membered rings of **2a** and **5b** are indistinguishable within experimental error. Insignificant variations were found in the dative bond, for **5b** N−B bond is 1.641(3) Å and is very similar to **2a** [1.632(5) Å]. In **5b**, B−O is longer in the six-membered [1.481(4) Å] than in the seven-membered [1.426(4) Å] heterocycle, and the O−B−N bond angle is smaller in the six-membered [105.0(2)°] than in the seven-membered ring [107.8(2)°] as a result of the annular tension and planarity of the ring. The seven-membered ring has a chair conformation in the solid state (Figure 2).

Conclusions

Ferrocenyl boronic acid reacts with different tridentate ONO ligands to provide, in one step, novel dimeric and monomeric structures depending on the ligand used. Neither different groups in the imine position nor a bulky group such as ferrocenyl influence the formation of the structure. The new chemistry reported here may be useful in macrocyclic syntheses, and ferrocene derivatives could find interesting applications for molecular recognition. Current work in our laboratory involves the reactivity of analogous compounds.

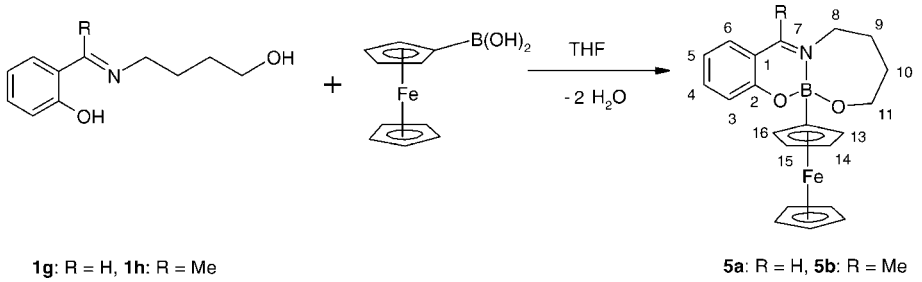

1g: R = H, **1h**: R = Me

5a: R = H, **5b**: R = Me

Scheme 4. Monomeric boron compounds from tridentate ligands derived from 4-aminobutanol

 © 2004 Wiley-VCH Verlag GmbH & Co. KGaA, Weinheim

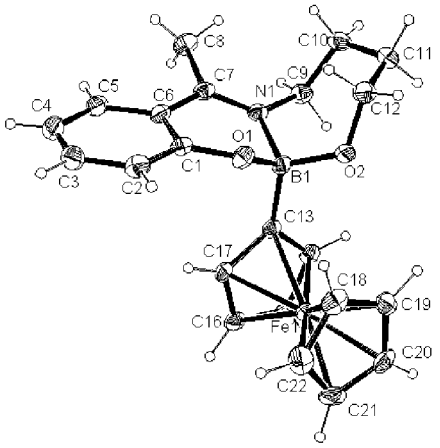

Figure 2. Molecular structure of solid-state **5b**

Experimental Section

Materials and Methods: All reagents were purchased from Aldrich and were used without further purification. NMR spectra were recorded at room temperature using the following spectrometers: Jeol GSX 270, Bruker 300, and Jeol eclipse+400. Chemical shifts are given in ppm. Infrared spectra were recorded on a Perkin−Elmer 16F-PC FT-IR spectrophotometer. Mass spectra were obtained with a HP 5989-A mass spectrometer operating in electron impact mode. Melting points were determined with a Gallenkamp MFB-595 apparatus. Elemental microanalyses were performed by Oneida Research Services (Whitesboro, NY. 13492).

Crystal Structure Determination: Single Crystals of **2a** suitable for X-ray diffraction were obtained when the reaction was performed in THF at 25 °C without stirring; crystals of **5b** suitable for X-ray structure analysis were grown by slow evaporation of a THF/CH_2Cl_2 solution of the complex. Intensity data were collected at 293 K with an Enraf−Nonius CAD4 diffractometer for compound **2a** and a Bruker-AXS APEX diffractometer with a CCD area detector for **5b**; Mo-*K*α-radiation, λ = 0.71073 Å, graphite monochromator, ω = 2θ scan. Empirical absorption corrections (DIFABS) were applied. The structures were solved by direct methods (SHELXS-86)[30] and refined using SHLXS-97.[31] All non-hydrogen atoms were refined anisotropically. Hydrogen atoms were placed in geometrically calculated positions using a riding model. Crystallographic data for the structures have been deposited at the Cambridge Crystallographic Data Center as supplementary material No. 211441 for complex **2a** and 210542 for **5b**. Copies of the data can be obtained free of charge on application to CCDC, 12 Union Road, Cambridge CB2 1EZ, UK. E-mail: deposit@ccdc.cam.ac.uk.

General Method for the Preparation of Tridentate Ligands 1a−1h: The ligands were obtained by condensation of an aldehyde or ketone with the corresponding amino alcohol under reflux in methanol for 45 min. The water formed and part of the solvent was removed using a Dean−Stark trap and the product was then dried under high vacuum. Ligands **1a**,[24] **1b**,[29] **1f**,[20] and **1g**[30] have been described previously.

General Syntheses for Boron Complexes: An equimolar solution of **1a−1h** and ferrocenyl boronic acid in THF (60 mL) was prepared and then boiled under reflux for 60 min (two equivalents of the boronic acid were used to prepare **3a** and **3b** complexes). Part of the solvent was then removed with a Dean−Stark trap so as to favor precipitation. The product was then filtered off and washed with small amounts of the same solvent.

Complex 2a: Compound **2a** was prepared from **1a** (0.50 g, 3.02 mmol) and ferrocenyl boronic acid (0.70 g, 3.02 mmol). A red solid was obtained, in 72% yield (0.78 g, 1.08 mmol), that is insoluble in all common solvents, m.p. 280−282 °C. IR ṽ = (KBr): 3412, 2930, 2850, 1640 (C=N), 1608, 1560, 1480, 1438, 1316, 1308, 1234, 1214, 1148, 1126, 1110, 1104, 1054, 1044, 1026, 1010, 970, 794, 752 cm^{-1}. EM (15 eV): *m*/*z* (%) = 718 (1) [M^+] 570 (2), 361 (25), 359 (100), 358 (35), 357 (10), 356 (3), 334 (4), 333 (2), 330 (2), 294 (6), 293 (6), 292 (4), 291 (8), 290 (3), 255 (3), 187 (7), 186 (51), 184 (4), 175 (7), 174 (50), 173 (20), 121 (2). $C_{38}H_{36}B_2Fe_2N_2O_4$: calcd. C 63.06, H 4.97, N 3.87; found C 63.38, H 5.33, N 3.84 (%).

Complex 2b: Compound **2b** was prepared from **1b** (0.50 g, 2.79 mmol) and ferrocenyl boronic acid (0.64 g, 2.79 mmol) as an orange solid, in 77% yield (0.80 g, 1.06 mmol) that is slightly soluble in chloroform, m.p. 204−206 °C. IR ṽ = (KBr): 2918, 2850, 1610 (C=N), 1550, 1456, 1444, 1332, 1276, 1214, 1144, 1134, 1118, 1106, 1004, 814, 758 cm^{-1}. MS (15 eV): *m*/*z* (%) = 746 (5) [M^+], 745 (2), 585 (3), 584 (1), 399 (3), 398 (2), 375 (3), 374 (18), 373 (74), 372 (20), 371 (5), 370 (2), 359 (2), 358 (9), 357 (2), 308 (2), 296 (2), 212 (1), 189 (11), 188 (100), 187 (43), 186 (75), 185 (5), 184 (4), 174 (5), 121 (2), 72 (4), 71 (5), 43 (3), 42 (11), 41 (4). ^{1}H NMR (300 MHz, $CDCl_3$): δ = 2.84 (s, 3 H, Me), 4.10−3.93 (m, 4 H, 8-, 9-H), 4.22 (s, 5 H, Cp-H), 4.36 (m, 2 H, 12-, 13-H), 4.44 (m, 2 H, 11-, 14-H), 6.92 (t, *J* = 7.7 Hz, 1 H, 5-H), 7.08 (d, *J* = 7.7 Hz, 1 H, 3-H), 7.54 (t, *J* = 7.7 Hz, 1 H, 4-H), 7.76 (d, *J* = 7.7 Hz, 1 H, 6-H) ppm. ^{13}C NMR (75 MHz, $CDCl_3$): δ = 16.7 (Me), 51.1 (C-8), 61.4 (C-9), 71.9 (C-Cp), 77.2 (C-11, 14), 77.6 (C-12, 13), 118.7 (C-1, 5), 120.5 (C-3), 128.5 (C-6), 136.7 (C-4), 161.4 (C-2), 175.3 (C-7) ppm. ^{11}B NMR (96 MHz, $CDCl_3$): δ = 7.8 ppm ($h_{1/2}$ = 228 Hz). $C_{40}H_{40}B_2Fe_2N_2O_4$: calcd. C 63.91, H 5.32, N 3.72; found C 63.96, H 5.78, N 3.54 (%).

Complex 2c: 2c was prepared from **1c** (0.50 g, 2.07 mmol) and ferrocenyl boronic acid (0.48 g, 2.07 mmol). A red solid was obtained, in 83% yield (0.74 g, 0.84 mmol), that is insoluble in all common solvents, m.p. 288−298 °C. IR ṽ = (KBr): 3094, 3066, 2934, 2916, 1606 (C=N), 1548, 1474, 1456, 1444, 1338, 1214, 1148, 1118, 1112, 1102, 1026, 1012, 1002, 802, 752 cm^{-1}. MS (15 eV): *m*/*z* (%) = 870 (15) [M^+], 435 (24), 311 (17), 239 (13), 368 (20), 296 (16), 250 (100), 236 (24), 186 (21), 148 (15), 98 (27), 84 (32), 44 (79). $C_{50}H_{44}B_2Fe_2N_2O_4$: calcd. C 68.56, H 5.02, N 3.20; found C 68.89, H 5.29; N 3.20 (%).

Complex 3a: 3a was prepared from **1d** (0.30 g, 1.28 mmol) and ferrocenyl boronic acid (0.30 g, 1.28 mmol) as a red solid, in 73% yield (0.60 g, 0.93 mmol), that is slightly soluble in chloroform, m.p. 228 °C. IR ṽ = (KBr): 3504, 2928, 2850, 1638 (C=N), 1552, 1474, 1458, 1446, 1406, 1390, 1382, 1270, 1260, 1214, 1176, 1148, 766 cm^{-1}. MS (15 eV): *m*/*z* (%) = 639 (100) [M^+], 595 (1), 478 (2), 427 (17), 362 (5), 320 (11), 242 (81), 212 (27), 186 (44), 148 (30), 121 (21), 95 (8), 67 (9), 56 (9). ^{1}H NMR (300 MHz, $CDCl_3$): δ = 1.81−1.17 (m, 10 H, 10-, 10′-, 11-, 11′-, 12-H), 3.24 (d, *J* = 12.9 Hz, 1 H, 8_b-H), 3.68 (m, 1 H, 16-H), 4.01 (m, 1 H, 15-H), 4.12 (m, 1 H, 17-H), 4.18 (s, 5 H, Cp-H B_{tetra}), 4.19 (d, *J* = 12.9 Hz, 1 H, 8_a-H), 4.29 (s, 5 H, Cp-H B_{tri}), 4.33 (m, 1 H, 14-H), 4.37 (m, 1 H, 21-H), 4.42 (m, 1 H, 20-H), 4.54 (m, 1 H, 22-H), 4.61 (m, 1 H, 19-H), 6.86 (t, *J* = 8.6 Hz, 1 H, 5-H), 7.13 (d, *J* = 8.6 Hz, 1 H, 3-H), 7.27 (d, *J* = 8.6 Hz, 1 H, 6-H), 7.56 (t, *J* = 8.6 Hz, 1 H, 4-H), 7.85 (s, 1 H, 7-H) ppm. ^{13}C NMR (75 MHz, $CDCl_3$): δ = 21.8 (C-11′), 21.9 (C-11), 26.0 (C-12), 34.8 (C-10′), 38.4 (C-10), 66.5 (C-8), 68.3

 © 2004 Wiley-VCH Verlag GmbH & Co. KGaA, Weinheim

(C-Cp B_{tetra}), 68.5 (C-Cp B_{tri}), 68.7 (C-16), 69.4 (C-15), 70.3 (C-21), 71.2 (C-17), 71.4 (C-14), 72.4 (C-20), 73.9 (C-9), 74.1 (C-22), 74.8 (C-19), 115.9 (C-1), 118.6 (C-5), 119.8 (C-3), 131.5 (C-6), 138.2 (C-4), 161.3 (C-2), 161.6 (C-7) ppm. ^{11}B NMR (96 MHz, $CDCl_3$): δ: B_{tri} = 34.8 ppm ($h_{1/2}$ = 260.3 Hz), B_{tetra} = 8.2 ppm ($h_{1/2}$ = 130.3 Hz). $C_{34}H_{35}B_2Fe_2NO_3$: calcd. C 63.34, H 5.43, N 2.17; found C 63.07, H 5.85, N 2.20 (%).

Complex 3b: 3b was prepared from **1e** (0.30 g, 1.21 mmol) and ferrocenyl boronic acid (28 g, 1.21 mmol) as an orange solid in 78% yield (0.62 g, 0.94 mmol), m.p. 219 °C. IR ṽ = (KBr): 2922, 1612 (C=N), 1550, 1458, 1438, 1420, 1380, 1348, 1330, 1270, 1208, 1192, 1178, 1154, 1104, 762 cm^{-1}. MS (15 eV): *m/z* (%) = 653 (97) [M$^+$], 639 (2), 467 (38), 441 (11), 426 (4), 398 (7), 376 (2), 257 (17), 256 (100), 240 (3), 212 (6), 186 (18), 162 (2). ^{1}H NMR (300 MHz, $CDCl_3$): δ = 1.80−1.10 (m, 10 H, 10-, 10′-, 11-, 11′-, 12-H), 2.50 (s, 3 H, Me), 3.52 (d, *J* = 14.9 Hz, 1 H, 8_b-H), 3.75 (s, 1 H, 16-H), 3.93 (s, 1 H, 15-H), 4.10 (s, 1 H, 17-H), 4.20 (s, 5 H, Cp-H B_{tetra}), 4.24 (s, 1 H, 14-H), 4.25 (d, *J* = 14.9 Hz, 1 H, 8_a-H), 4.29 (s, 5 H, Cp-H B_{tri}), 4.33 (s, 1 H, 21-H), 4.36 (s, 1 H, 20-H), 4.56 (s, 1 H, 22-H), 4.63 (s, 1 H, 19-H), 6.89 (td, *J* = 7.8, 1.5 Hz, 1 H, 5-H), 7.00 (dd, *J* = 7.8, 1.5 Hz, 1 H, 3-H), 7.55 (td, *J* = 7.8, 1.5 Hz, 1 H, 4-H), 7.76 (dd, *J* = 7.8, 1.5 Hz, 1 H, 6-H) ppm. ^{13}C NMR (75 MHz, $CDCl_3$): δ = 17.3 (Me), 21.8 (C-11), 22.1 (C-11′), 26.0 (C-12), 35.3 (C-10′), 36.1 (C-10), 59.3 (C-8), 68.3 (C-16), 68.4 (C-15), 68.5 (C-21), 68.6 (C-20), 68.7 (C-Cp B_{tetra}), 68.9 (C-Cp B_{tri}), 71.4 (C-17), 71.6 (C-14), 74.2 (C-22), 74.7 (C-19), 74.9 (C-9), 118.6 (C-1), 118.8 (C-5), 119.3 (C-3), 131.1 (C-6), 136.9 (C-4), 160.7 (C-2), 168.9 (C-7) ppm. ^{11}B NMR (96 MHz, $CDCl_3$): δ: B_{tri} = 38.3 ($h_{1/2}$ = 905 Hz), B_{tetra} = 7.2 ppm ($h_{1/2}$ = 148 Hz). $C_{35}H_{37}B_2Fe_2NO_3$: calcd. C 63.80, H 5.62, N 2.13; found C 64.10, H 6.08, N 2.91 (%).

Complex 4: 4 was prepared from **1f** (0.30 g, 1.32 mmol) and ferrocenyl boronic acid (0.30 g, 1.32 mmol) as a red solid in 75.5% yield (0.42 g, 1.00 mmol), m.p. 236−238 °C. IR ṽ = (KBr): 3080, 3056, 2916, 1618 (C=N), 1548, 1474, 1452, 1438, 1388, 1302, 1240, 1210, 1192, 1104, 1094, 1008, 952, 938, 816, 762 cm^{-1}. MS (15 eV): *m/z* (%) = 421 (100) [M$^+$], 420 (44), 419 (12), 418 (4), 357 (1), 356 (6), 355 (4), 354 (3), 353 (5), 352 (1), 317 (1), 312 (2), 300 (4), 299 (2), 298 (2), 297 (4), 296 (2), 290 (2), 238 (2), 237 (20), 236 (84), 235 (55), 234 (9), 225 (2), 187 (2), 186 (20), 184 (2). ^{1}H NMR (300 MHz, $CDCl_3$): δ = 3.75 (s, 5 H, Cp-H), 3.79 (m, 1 H, 18-H), 3.88 (m, 1 H, 17-H), 3.93 (m, 1 H, 19-H), 4.05 (m, 1 H, 16-H), 4.82 (d, *J* = 15.5 Hz, 1 H, 14_b-H), 4.89 (d, *J* = 15.5 Hz, 1 H, 14_a-H), 6.96 (t, *J* = 7.9 Hz, 1 H, 5-H), 7.01 (d, *J* = 7.9 Hz, 1 H, 3-H), 7.28 (d, *J* = 7.5 Hz, 1 H, 10-H), 7.40 (t, *J* = 7.5 Hz, 1 H, 11-H), 7.46 (t, *J* = 7.5 Hz, 1 H, 12-H), 7.60 (t, *J* = 7.9 Hz, 1 H, 4-H), 7.68 (d, *J* = 7.9 Hz, 1 H, 6-H), 7.97 (d, *J* = 7.5 Hz, 1 H, 13-H), 9.21 (s, 1 H, 7-H) ppm. ^{13}C NMR (75 MHz, $CDCl_3$): δ = 62.3 (C-14), 67.6 (C-Cp), 67.9 (C-18), 68.0 (C-17), 70.6 (C-19), 71.0 (C-16), 117.9 (C-1), 118.9 (C-13), 119.1 (C-3), 119.6 (C-5), 125.8 (C-11), 127.8 (C-12), 128.4 (C-10), 132.9 (C-6), 134.9 (C-9), 137.9 (C-4), 138.2 (C-8), 156.8 (C-7), 160.2 (C-2) ppm. ^{11}B NMR (96 MHz, $CDCl_3$): δ = 5.0 ppm ($h_{1/2}$ = 555 Hz). $C_{24}H_{20}B_1Fe_1N_1O_2$: calcd. C 67.99, H 4.72, N 3.30; found C 67.69, H 4.70, N 3.42 (%).

Complex 5a: 5a was prepared from **1g** (0.50 g, 2.60 mmol) and ferrocenyl boronic acid (0.60 g, 2.60 mmol) as a red solid in 88% yield (0.88 g, 2.26 mmol); it is soluble in chloroform, m.p. 223 °C. IR ṽ = (KBr): 3414, 2924, 2886, 2850, 1642 (C=N), 1608, 1560, 1476, 1460, 1228, 1212, 1114, 1106, 1000, 810, 770, 764 cm^{-1}. MS (15 eV): *m/z* (%) = 387 (100) [M$^+$], 386 (31), 385 (8), 384 (2), 322 (3), 321 (3), 203 (9), 202 (71), 201 (20), 200 (20), 187 (2), 186 (15), 148 (2), 78 (2). ^{1}H NMR (300 MHz, $CDCl_3$): δ = 1.91−1.63 (m, 4 H, 9-, 10-H), 3.69 (t, *J* = 9.0 Hz, 2 H, 8-H), 3.87 (m, 1 H, 16-H), 3.99 (t, *J* = 9.0 Hz, 2 H, 11-H), 4.10 (s, 5 H, Cp-H), 4.12 (m, 1 H, 14-H), 4.17 (m, 1 H, 15-H), 4.20 (m, 1 H, 13-H), 6.83 (td, *J* = 8.5, 1.8 Hz, 1 H, 5-H), 7.11 (d, *J* = 8.5 Hz, 1 H, 3-H), 7.26 (dd, *J* = 8.5, 1.8 Hz, 1 H, 6-H), 7.57 (td, *J* = 8.5, 1.8 Hz, 1 H, 4-H), 8.03 (s, 1 H, 7-H) ppm. ^{13}C NMR (75 MHz, $CDCl_3$): δ = 27.6 (C-10), 32.2 (C-9), 56.2 (C-11), 62.4 (C-8), 68.6 (C-Cp), 68.8 (C-15), 69.1 (C-14), 70.9 (C-16), 72.1 (C-13), 117.3 (C-1), 118.8 (C-5), 119.8 (C-3), 131.4 (C-6), 137.8 (C-4), 161.9 (C-2), 162.4 (C-7) ppm. ^{11}B NMR (96 MHz, $CDCl_3$): δ = 9.6 ppm ($h_{1/2}$ = 154.8 Hz). $C_{21}H_{22}B_1Fe_1N_1O_2$: calcd. C 64.69, H 5.64, N 3.59; found C 64.99, H 5.59, N 3.95 (%).

Complex 5b: 5b was obtained from **1h** (0.50 g, 2.41 mmol) and ferrocenyl boronic acid (0.55 g, 2.41 mmol) as a red solid, in 84.7% yield (0.82 g, 2.03 mmol), that is soluble in chloroform, m.p. 196 °C. IR ṽ = (KBr): 2914, 2894, 2364, 1624 (C=N), 1558, 1458, 1434, 1370, 1348, 1328, 1280, 1210, 1126, 1110, 996, 960, 760 cm^{-1}. MS (15 eV): *m/z* (%) = 401 (100) [M$^+$], 400 (29), 386 (5), 336 (1), 217 (11), 216 (80), 215 (22), 186 (57), 162 (4), 146 (2). ^{1}H NMR (300 MHz, $CDCl_3$): δ = 2.00−1.30 (m, 4 H, 9-, 10-H), 2.47 (s, 3 H, Me), 3.56 (m, 1 H, 15-H), 3.63 (t, *J* = 9.0 Hz, 2 H, 8-H), 3.91 (m, 1 H, 14-H), 3.93 (t, *J* = 9.0 Hz, 2 H, 11-H), 4.06 (m, 1 H, 16-H), 4.07 (s, 5 H, Cp-H), 4.19 (m, 1 H, 13-H), 6.83 (t, *J* = 7.8 Hz, 1 H, 5-H), 7.08 (d, *J* = 7.8 Hz, 1 H, 3-H), 7.45 (d, *J* = 7.8 Hz, 1 H, 6-H), 7.46 (t, *J* = 7.8 Hz, 1 H, 4-H) ppm. ^{13}C NMR (75 MHz, $CDCl_3$): δ = 15.9 (Me), 28.8 (C-10), 30.6 (C-9), 48.4 (C-11), 61.8 (C-8), 68.3 (C-Cp), 68.4 (C-15), 68.7 (C-14), 70.2 (C-16), 72.1 (C-13), 118.3 (C-5), 118.9 (C-1), 120.3 (C-3), 128.2 (C-6), 136.2 (C-4), 160.8 (C-2), 168.1 (C-7) ppm. ^{11}B NMR (96 MHz, $CDCl_3$): δ = 8.7 ppm ($h_{1/2}$ = 159 Hz). $C_{22}H_{24}B_1Fe_1N_1O_2$: calcd. C 65.42, H 5.94, N 3.47; found C 65.69, H 6.11, N 3.61 (%).

Acknowledgments

Financial support from CONACyT (Mexico) is gratefully acknowledged. The authors thank Ing. G. Cuéllar for mass spectra and Q. I. G. Uribe for NMR spectra.

[1] T. Renk, W. Ruf, W. Siebert, *J. Organomet. Chem.* **1976**, *120*, 1−25.
[2] M. Herberhold, U. Dörfler, B. Wrackmeyer, *Polyhedron* **1995**, *14*, 2683−2689.
[3] F. Jäkle, T. Priermier, M. Wagner, *Chem. Ber.* **1995**, *128*, 1163−1169.
[4] H. Braunschweig, R. Dirk, M. Müller, P. Nguyen, R. Resendes, D. P. Gates, I. Manners, *Angew. Chem. Int. Ed. Engl.* **1997**, *36*, 2338−2340. *Angew. Chem.***1997**, *109*, 2433−2435.
[5] F. Jäkle, A. Berenbaum, A. J. Lough, I. Manners, *Chem. Eur. J.* **2000**, *6*, 2762−2771.
[6] [6a] J. A. Gamboa, A. Sundararaman, L. Kakalis, A. J. Lough, F. Jäkle, *Organometallics* **2002**, *21*, 4169−4181. [6b] A. Appel, F. Jäkle, T. Priermeier, R. Schmid, M. Wagner, *Organometallics* **1996**, *15*, 1188−1194.
[7] B. E. Carpenter, W. E. Piers, M. Parvez, G. P. A. Yap, S. J. Rettig, *Can. J. Chem.* **2001**, *79*, 857−867.
[8] M. I. Rybinskaya, A. Z. Kreindlin, Y. T. Struchkov, A. I. Yanovsky, *J. Organomet. Chem.* **1989**, *359*, 233−243.
[9] K. Ma, M. Scheibitz, S. Scholz, M. Wagner, *J. Organomet. Chem.* **2002**, *652*, 11−19.
[10] A. Ori, S. Shinkai, *J. Chem. Soc., Chem. Commun.* **1995**, 1771−1772.

 © 2004 Wiley-VCH Verlag GmbH & Co. KGaA, Weinheim

[11] M. Fontani, F. Peters, W. Scherer, W. Wachter, M. Wagner, P. Zanello, *Eur. J. Inorg. Chem.* **1998**, 1453−1465.
[12] F. Fabrizi de Biani, T. Gmeinwieser, E. Herdtweck, F. Jäkle, F. Laschi, M. Wagner, P. Zanello, *Organometallics* **1997**, *16*, 4776−4787.
[13] J. C. Norrild, *J. Chem. Soc., Perkin Trans. 2* **2001**, 719−726.
[14] J. C. Norrild, I. Sotofte, *J. Chem. Soc., Perkin Trans. 2* **2001**, 727−732.
[15] T. D. James, S. Sandanayane, S. Shinkai, *Angew. Chem. Int. Ed. Engl.* **1996**, *35*, 1910−1922. *Angew. Chem.* **1996**, *108*, 2038−2050.
[16] C. Dusemund, S. Sandanayake, K. R. A. Samankurama, S. Shinkai, *J. Chem. Soc., Chem. Commun.* **1995**, 333−334.
[17] R. E. Dinnebier, L. Ding, K. Ma, M. A. Neumann, N. Tanpipat, F. J. J. Leusen, P. W. Stephens, M. Wagner, *Organometallics.* **2001**, *20*, 5642−5647.
[18] L. Ding, K. Ma, G. Dürner, M. Bolte, F. Fabrizi de Biani, P. Zanello, M. Wagner, *J. Chem. Soc., Dalton Trans.* **2002**, 1566−1573.
[19] M. Grosche, E. Herdtweck, F. Peters, M. Wagner, *Organometallics* **1999**, *18*, 4669−4672.
[20] H. Höpfl, M. Sanchez, N. Farfán, V. Barba, *Can. J. Chem.* **1998**, *76*, 1352−1360.
[21] V. Barba, D. Cuahutle, R. Santillan, N. Farfán, *Can. J. Chem.* **2001**, *79*, 1229−1237.
[22] V. Barba, R. Luna, D. Castillo, R. Santillan, N. Farfán, *J. Organomet. Chem.* **2000**, *604*, 273−282.
[23] V. Barba, E. Gallegos, R. Santillan, N. Farfán, *J. Organomet. Chem.* **2001**, *622*, 259−264.
[24] H. Höpfl, N. Farfán, *J. Organomet. Chem.* **1997**, *547*, 71−77.
[25] N. Farfán, R. Santillan, H. Höpfl, *Main. Group. Chem. News* **1999**, *7*, 3−12.
[26] H. Nöth, B. Wrackmeyer, *NMR Basic Principles and Progress*, Springer Verlag, Berlin, **1978**, *14*.
[27] H. Höpfl, *J. Organomet. Chem.* **1999**, *581*, 129−149.
[28] H. Höpfl, M. Sánchez, V. Barba, N. Farfán, S. Rojas, R. Santillan, *Inorg. Chem.* **1998**, *37*, 1679−1692.
[29] V. Barba, D. Cuahutle, M. E. Ochoa, R. Santillan, N. Farfán, *Inorg. Chim. Acta* **2000**, *303*, 7−11.
[30] G. M. Sheldrick, SHELXS-86, *Program for Crystal Structure Solution*, University of Göttingen, Germany, **1986**.
[31] G. M. Sheldrick, SHELXS-97, *A program for Crystal Structure Refinement*, University of Göttingen, Germany, **1997**.

Received June 3, 2003
Early View Article
Published Online October 22, 2003

 © 2004 Wiley-VCH Verlag GmbH & Co. KGaA, Weinheim

Hydrothermal Syntheses, Crystal Structures and Photoluminescent Properties of Three Metal-Cluster Based Coordination Polymers Containing Mixed Organic Ligands

Jun Tao,*[a] Xin Yin,[a] Zan-Bin Wei,[a] Rong-Bin Huang,[a] and Lan-Sun Zheng[a]

Keywords: Coordination polymers / Zinc / Cadmium / 5-Sulfoisophthalate / 5-Nitroisophthalate

Three novel metal-cluster based coordination polymers (MCCPs) with formulae $[Zn_4(\mu_3\text{-}OH)_2(H_2O)_2(sip)_2(4,4'\text{-}bpy)_2]\cdot 3H_2O$ (MCCP-4), $[Cd_4(\mu_3\text{-}OH)_2(H_2O)_2(sip)_2(4,4'\text{-}bpy)_4]\cdot H_2O$ (MCCP-5) and $[Cd_6(\mu_3\text{-}OH)_4(\mu_2\text{-}OH_2)_2(OH_2)_2(nip)_4(4,4'\text{-}bpy)_3]\cdot 3H_2O$ (MCCP-6) [H_2sip = 5-sulfoisophthalic acid, H_2nip = 5-nitroisophthalic acid and 4,4′-bpy = 4,4′-bipyridyl] were hydrothermally synthesized and characterized by single-crystal X-ray diffraction studies. MCCP-4 crystallizes in the triclinic space group $P\bar{1}$ with a = 10.106(2), b = 10.851(2), c = 11.125(2) Å, α = 105.66(3), β = 112.63(3), γ = 98.18(3)°, V = 1041.8(4) Å^3, and Z = 2. MCCP-5 crystallizes in the monoclinic space group $C2/c$ with a = 25.602(1), b = 16.571(1), c = 13.322(1) Å, β = 92.524(1)°, V = 5646.4(2) Å^3, and Z = 4. MCCP-4 and -5 consist of similar $[M_4(\mu_3\text{-}OH)_2]^{6+}$ tetranuclear building units that are joined through sip and 4,4′-bpy ligands to generate a two-dimensional structure (MCCP-4) and a three-dimensional structure (MCCP-5), respectively. MCCP-6 crystallizes in the triclinic space group $P\bar{1}$ with a = 14.295(2), b = 14.472(2), c = 20.204(3) Å, α = 73.362(3), β = 82.200(3), γ = 62.769(2)°, V = 3560.9(10) Å^3, and Z = 2. MCCP-6 contains unprecedented $[Cd_6(\mu_3\text{-}OH)_4(\mu_2\text{-}OH_2)_2]^{8+}$ hexanuclear building units which are linked through nip and 4,4′-bpy ligands to afford a two-dimensional structure. The infrared spectroscopy, thermal stability and photoluminescence of the three complexes were studied.

(© Wiley-VCH Verlag GmbH & Co. KGaA, 69451 Weinheim, Germany, 2004)

Introduction

Coordination polymers have attracted considerable attention in recent years due to their interesting properties and promising applications in the areas of catalysis, gas storage, magnetism and optics.[1] Concurrent with these studies has been the development of highly ordered multi-dimensional frameworks based primarily on combining organic and inorganic units through the assembly of metal centers with di- or multitopic organic ligands.[2] To date, the structures and properties of the vast majority of reported coordination polymers have been finely tuned by closely controlling the molecular properties of the organic ligands such as size, shape, functionality, flexibility and symmetry. One current challenge involves the preparation of coordination polymers in which the inorganic components display different physical properties or have different structural influences. This goal has been recently illustrated by metal-cluster based coordination polymers (MCCPs),[3] whose dimensions, geometries and properties can be controlled by the choice of metal clusters. Metal clusters can be very versatile in terms of coordination properties and rigidity as well as displaying intriguing physical properties in comparison with mono- or dinuclear species. Thus, coordination polymers constructed with metal clusters are usually more stable and promising in terms of potential applications. At present, in addition to utilizing H_2O_2 or excess base to facilitate the formation of metal clusters,[4,5] they can also be obtained from hydrothermal reactions involving in situ hydrolysis of metal ions with or without template ligands. In our group, we have focused our attention on metal-cluster based coordination polymers (particularly of Zn^{II} and Cd^{II}) with respect to their optical properties and we have found that in the presence of mixed organic ligands, metal clusters can form under hydrothermal conditions[6] e.g., $[Zn_4O(ip)_3(4,4'\text{-}bpy)]$ (MCCP-1, where ip = isophthalate), $[Zn_4(OH)_2(fa)_3(4,4'\text{-}bpy)_2]$ (MCCP-2, where fa = fumarate), $[Zn_3(OH)_2(4,4'\text{-}bpy)_{0.5}(4,4'\text{-}oba)_2]\cdot 0.5H_2O$ [MCCP-3, where 4,4′-oba = 4,4′-oxybis(benzoate)]. Based on our experience in this area and with the long-term goal of classifying the factors affecting the formation of metal clusters and metal-cluster based coordination polymers, we have started to synthesize new coordination polymers with metal clusters.

Our previous work on $[Zn_4O(ip)_3(4,4'\text{-}bpy)]$ (MCCP-1)[6a] has led us to consider whether ligands derived from isophthalate can produce similar structures, especially the 5-substituted forms of isophthalate. We selected 5-sul-

[a] Department of Chemistry and State Key Laboratory of Physical Chemistry of Solid Surfaces, Xiamen University, Xiamen 361005, China
Fax: (internat.) + 86-592-2183047
E-mail: taojun@jingxian.xmu.edu.cn

Supporting information for this article is available on the WWW under http://www.eurjic.org or from the author.

foisophthalate (sip) and 5-nitroisophthalate (nip) as ligands in which the sulfonate group shows weak coordination strength towards transition metals[7] and both sulfonate and nitro groups are suitable H-bonding acceptors.[8] As such they may be helpful for stabilizing these complexes. Herein we report three novel coordination polymers constructed from zinc and cadmium clusters and mixed organic ligands: $[Zn_4(\mu_3\text{-}OH)_2(H_2O)_2(sip)_2(4,4'\text{-}bpy)_2]\cdot 3H_2O$ (MCCP-4), $[Cd_4(\mu_3\text{-}OH)_2(H_2O)_2(sip)_2(4,4'\text{-}bpy)_4]\cdot H_2O$ (MCCP-5) and $[Cd_6(\mu_3\text{-}OH)_4(\mu_2\text{-}OH_2)_2(OH_2)_2(nip)_4(4,4'\text{-}bpy)_3]\cdot 3H_2O$ (MCCP-6).

The sip ligand was studied recently as a building block for extended frameworks. Shimizu[9] has reported a pseudo-honeycomb coordination polymer $\{[Cu_{1.5}(sip)(py)_5]\cdot(py)\cdot(H_2O)_{6.76}\}_n$, and Cao[10] reported two zeolite-like supramolecular complexes $\{[Cu(H_2O)_2(Hsip)]\cdot(H_2O)_2\cdot(pip)_{0.5}\}_n$ and $\{[Cu(H_2O)_3(Hsip)]\cdot(H_2O)_6\cdot(hmt)_{0.5}\}_n$ (pip = piperazine, hmt = hexamethylenetetramine). To date the above three Cu(sip) coordination complexes are the only transition metal sip complexes reported. In these three complexes, the sip ligands exhibit three different coordination modes, henceforth denoted as *a*-sip, *b*-sip and *c*-sip and depicted in Scheme 1. The sip ligands reported here (MCCP-4 and -5) coordinate to metal atoms in different coordination modes, namely as *d*-sip in MCCP-4 and *e*-sip in MCCP-5, respectively. With regards to the nip ligand, the only other metal-(nip) complexes which have been prepared are two Cu(nip) supramolecular isomers[11] and two Zn(nip) supramolecular structures, namely $\{[Zn(nip)(py)(H_2O)]\cdot(H_2O)\}_n$ and $\{[Zn(nip)(4,4'\text{-}bpy)_{0.5}(H_2O)_2]\cdot(H_2O)\}_n$. In the two zinc complexes that have been reported by our group,[8c,8d] the nip ligand displays two slightly different coordination modes, namely *a*-nip and *b*-nip as illustrated in Scheme 2. Interestingly, the nip ligand in MCCP-6 exhibits four different coordination modes, viz. *c*-nip, *d*-nip, *e*-nip, and *f*-nip as shown in Scheme 2.

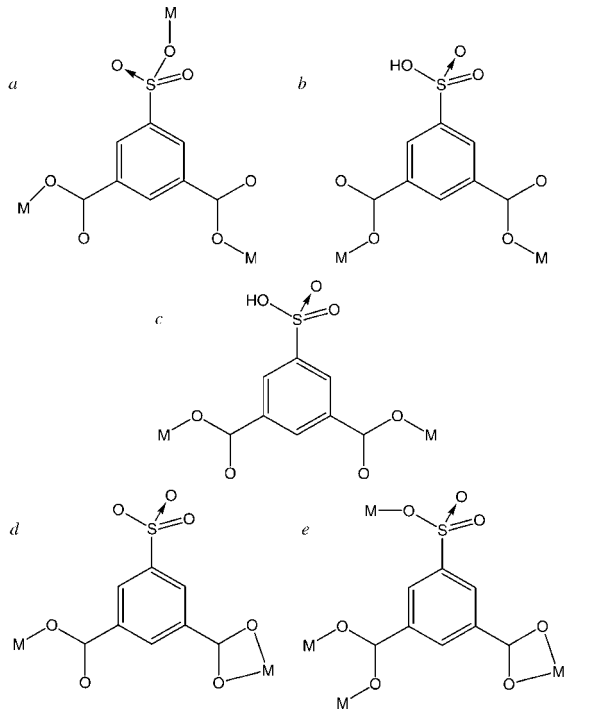

Scheme 1. The five different coordination modes of the sip ligand in refs.[9,10] (*a*, *b*, *c*), MCCP-4 (*d*) and MCCP-5 (*e*)

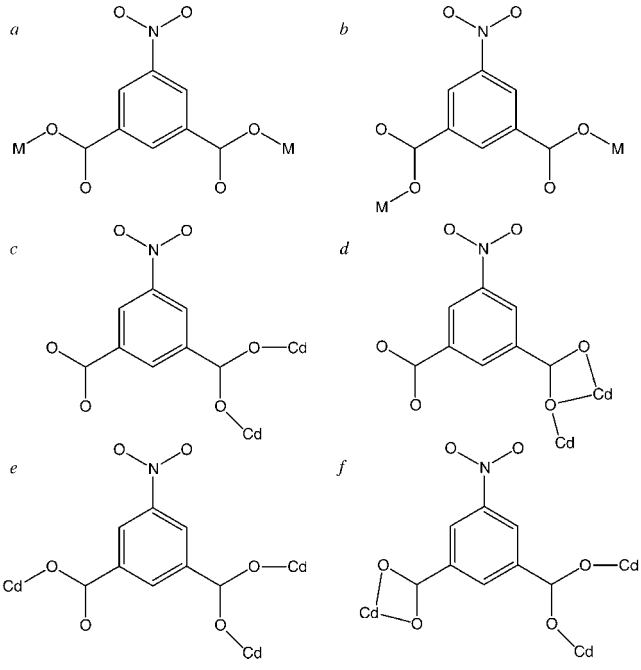

Scheme 2. The six different coordination modes of the nip ligand in refs.[8c,8d,11a] (*a*, *b*) and MCCP-6 (*c*−*f*)

Results and Discussion

Syntheses and Characterization

The hydrothermal method has been proven to be very effective for the synthesis of zeolites, nanomaterials and more recently coordination polymers. It is well known that small changes in one or more of the hydrothermal parameters, such as temperature, reaction time, pH value, and molar ratios of reactants may exert a profound influence on the final reaction products. During the past few years, we have explored the synthesis of MCCPs containing mixed organic ligands under typical hydrothermal conditions (i.e., 120−180 °C for 2−7 d), and found that a pH of 7−8 and the existence of 4,4′-bpy are most suitable in forming metal clusters as well as MCCPs. These conditions have been used directly to prepare MCCP-4, -5 and -6, where it is believed that the formation of metal clusters can be attributed to the hydrolysis of metal ions in neutral systems under hydrothermal conditions.

The FT-IR spectra of MCCP-4, -5 and -6 show no bands in the region 1690−1730 cm^{-1}, indicating complete deprotonation of the carboxyl groups. The spectra exhibit broad absorption bands in the range of 3260−3570 cm^{-1} due to the ν(OH) vibrations of coordinated water molecules. The absorptions in the region 1000−1230 cm^{-1} for MCCP-4 and -5 are typical for a sulfonate group,[12] and those at

 © 2004 Wiley-VCH Verlag GmbH & Co. KGaA, Weinheim

1360−1460 cm^{-1} for MCCP-6 characterize the asymmetric and symmetric vibrations of the nitro group.[13] The strong bands at 1360−1610 cm^{-1} for all MCCPs are characteristic of a carboxylate group. In MCCP-6 these bands probably overlap partially with those of the nitro group.

The thermogravimetric analyses (TGA) of MCCP-4 and -6 showed the occurrence of three consecutive processes, namely dehydration, ligand pyrolysis (or volatilization) and inorganic residue formation. The TGA for MCCP-4 showed the complete loss of five water molecules at ca. 135 °C (found 7.61%; calcd. 8.68%). The dehydrated compound remained stable up to ca. 360 °C without any weight loss, however, MCCP-4 decomposed when heated to 140 °C at 0.05 Torr for 12 h as evidenced by the diffraction lines observed in its X-ray powder diffraction pattern (see Supporting Information) and at a temperature range of 360−580 °C the pyrolysis (or volatilization) of both sip and 4,4′-bpy ligands occurred leaving residual ZnO (remaining weight: found 26.60%; calcd. 4ZnO: $[Zn_4(\mu_3\text{-}OH)_2(H_2O)_2(sip)_2(4,4'\text{-}bpy)_2]\cdot 3H_2O$ 27.48%). The TGA for MCCP-6 showed an initial weight loss of 3.06% from 180 to 215 °C corresponding to the removal of three lattice water molecules per formula unit (calcd. 2.49%), followed by another weight loss of 60.98% from 307 °C for elimination of the nip ligands and 4,4′-bpy pillars from the framework, the remaining residue was probably $Cd(OH)_2$. (as calcd. 6$Cd(OH)_2$: $[Cd_6(\mu_3\text{-}OH)_4(\mu_2\text{-}OH_2)_2(OH_2)_2(nip)_4(4,4'\text{-}bpy)_3]\cdot 3H_2O$ 40.42%). The TGA curve of MCCP-5 was somewhat different from those of MCCP-4 and -6. MCCP-5 remained stable under nitrogen up to 186 °C before it suffered a weight loss of 22.24% of the total weight between 186 and 335 °C. This can be assigned to the evaporation of one lattice water molecule, two-coordinated water molecules and two one-end-bound 4,4′-bpy ligands per formula (calcd. 22.22%). The second distinct weight loss appeared in the temperature range 335−550 °C and was caused by the pyrolysis (or volatilization) of the sip and μ_2-4,4′-bpy ligands resulting in a residue of $Cd(OH)_2$ (found 35.81%; calcd. 35.52%).

Description of Crystal Structures

Single-crystal X-ray diffraction analysis has revealed that MCCP-4 is a 2D-framework constructed from $[Zn_4(\mu_3\text{-}OH)_2]^{6+}$ clusters and two organic ligands. The structure contains a crystallographic inversion center located at the center of the $[Zn_4(\mu_3\text{-}OH)_2]^{6+}$ cluster with the two crystallographically nonequivalent zinc atoms assuming two different coordination geometries. Zn1 is in a distorted trigonal-bipyramidal environment and is coordinated in the equatorial plane to one μ_3-OH group, one 4,4′-bpy nitrogen atom and one oxygen atom from the monodentate carboxylate group of a *d*-sip ligand (Scheme 1). In the axial positions it is also coordinated to one μ_3-OH group and one oxygen atom from the bidentate carboxylate group of another *d*-sip ligand, as shown in Figure 1. However, the Zn1···O4B distance of 2.826(2) Å suggests a nonnegligible interaction with the uncoordinated oxygen atom of the monodentate carboxylate group of a *d*-sip ligand, which may be described as a semichelating coordination mode.[14] Hence, Zn1 may also be regarded as being in a pseudooctahedral environment. Selected bond lengths and angles are given in Table 1. Zn2 is tetrahedrally surrounded by one μ_3-OH group, one bpy nitrogen atom, one water molecule and one oxygen atom from the bidentate carboxylate group of a *d*-sip ligand. The average bond lengths around Zn2 (1.976 Å) are somewhat shorter than those of Zn1 (2.077 Å) and this is consistent with the fact that bond lengths in a tetrahedral geometry are generally shorter than those in other geometries. Two pairs of symmetry-related zinc atoms are then joined by two triply bridging μ_3-OH groups to generate the basic structural building unit $[Zn_4(\mu_3\text{-}OH)_2]^{6+}$ and the Zn−O(hydroxo) distances [1.962(2)−2.172(2) Å] are in the range of those previously reported in the literature.[4,6,15]

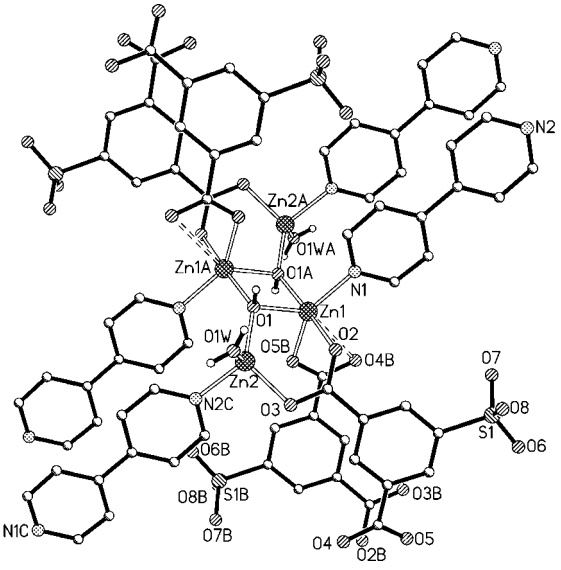

Figure 1. Perspective view of the coordination environments of zinc atoms in MCCP-4; lattice water molecules have been omitted for clarity

Table 1. Selected bond lengths [Å] and angles [°] for MCCP-4; symmetry codes A: $-x+1, -y+1, -z+1$; B: $-x+2, -y+1, -z+2$, C: $x, y+1, z+1$

Zn1−O1	2.029(2)	Zn1−O2	2.220(2)
Zn1−O1A	2.172(2)	Zn1−O5B	1.959(2)
Zn1−N1	2.005(2)	Zn1···O4B	2.826(2)
Zn2−O1	1.962(2)	Zn2−O3	1.963(2)
Zn2−O1W	1.955(2)	Zn2−N2	2.025(2)
O1−Zn1−N1	119.5(1)	O1−Zn1−O2	88.9(1)
O1−Zn1−O5B	95.6(1)	O1−Zn1−O1A	85.2(1)
N1−Zn1−O5B	144.6(1)	O1A−Zn1−O2	173.8(1)
O1−Zn2−O3	119.2(1)	O1−Zn2−O1W	109.1(1)
O3−Zn2−O1W	106.6(1)	O3−Zn2−N2C	97.8(1)

It is interesting that the $[Zn_4(\mu_3\text{-}OH)_2]^{6+}$ clusters are interlinked by the carboxylate groups of *d*-sip in mono- and bidentate fashions, resulting in one-dimensional $[Zn_4(\mu_3\text{-}OH)_2(H_2O)_2(sip)_2]_n$ chains, which are further bridged

 © 2004 Wiley-VCH Verlag GmbH & Co. KGaA, Weinheim

through μ-4,4′-bpy ligands to generate an infinite two-dimensional sheet, with uncoordinated sulfonate groups deviating from the plane and orientated on both sides (Figure 2). The distances S1−O6, S1−O7 and S1−O8 are 1.429(2), 1.462(2) and 1.442(2) Å, respectively, and all fall within the typical range of S−O bond lengths in a sulfonate anion (1.40−1.49 Å).[16] Two oxygen atoms of the sulfonate group are involved in hydrogen bonding with the μ_3-OH group and zinc-bound water molecule [O8···O1 2.703(3) Å and O7···O1 W 2.713(3) Å] on the adjacent sheets, and these hydrogen bonds serve to increase the order of the structure of MCCP-4 from two to three-dimensional.

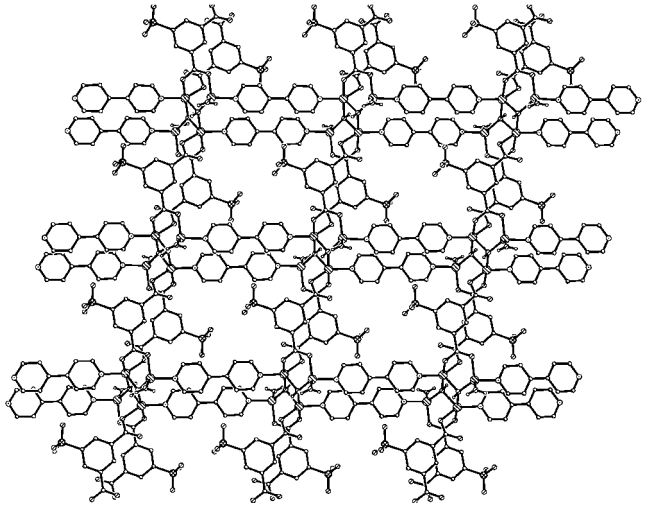

Figure 2. Perspective view of the two-dimensional sheet of MCCP-4; lattice water molecules and hydrogen bonds have been omitted for clarity

The structure of MCCP-5 is constructed from $[Cd_4(\mu_3\text{-}OH)_2]^{6+}$ clusters similar to that of MCCP-4, and also contains a crystallographic inversion center located at the center of the $[Cd_4(\mu_3\text{-}OH)_2]^{6+}$ cluster but its coordination environment around the Cd atoms is somewhat different from that of the Zn centers in MCCP-4. Selected bond lengths and angles are given in Table 2. The octahedral Cd1 atom is bound to one 4,4′-bpy nitrogen atom, three oxygen atoms from the bidentate and chelating carboxylate groups of two different *e*-sip ligands, respectively (Scheme 1). The remaining two coordination sites of the octahedron are filled by one μ_3-OH group and a sulfonate oxygen of an *e*-sip ligand (Figure 3). Cd2 adopts a slightly distorted octahedral geometry and is coordinated to two μ_3-OH groups, one 4,4′-bpy nitrogen atom and one carboxylate oxygen atom of an *e*-sip ligand in the equatorial plane, and to one water molecule and one 4,4′-bpy nitrogen atom in the axial positions. It is noteworthy that the latter 4,4′-bpy ligand uses only one nitrogen atom (N3) to coordinate to Cd2 leaving the other nitrogen (N4) free, as found in $[Zn(C_4H_4O_4)(4,4'\text{-bpy})]$ and the Co-4,4′-bpy molecular railroad.[17]

Table 2. Selected bond lengths [Å] and angles [°] for MCCP-5; symmetry codes A: $-x + 1/2, -y + 1/2, -z + 1$; B: $x, -y, -z + 1$, C $-x + 1/2, -y + 1/2, -z + 3/2$; D: $-x + 2, y + 1/2, -z + 1/2$; E: $-x, -y, -z + 1$

Cd1−O1	2.221(3)	Cd1−O2	2.451(3)
Cd1−O3	2.365(3)	Cd1−N1	2.323(3)
Cd1−O4B	2.252(3)	Cd1−O7C	2.436(4)
Cd2−O1	2.330(3)	Cd2−O1A	2.312(3)
Cd2−O1W	2.362(3)	Cd2−O5D	2.305(3)
Cd2−N3	2.417(3)	Cd2−N2E	2.385(3)
O1−Cd1−N1	113.0(1)	O1−Cd1−O4B	85.2(1)
O2−Cd1−O3	54.1(1)	O1−Cd1−O2	136.1(1)
O4B−Cd1−N1	158.2(1)	O1−Cd2−O1A	78.9(1)
O1−Cd2−O1W	81.8(1)	O1−Cd2−N3	100.3(1)
O1−Cd2−O5D	174.4(1)		

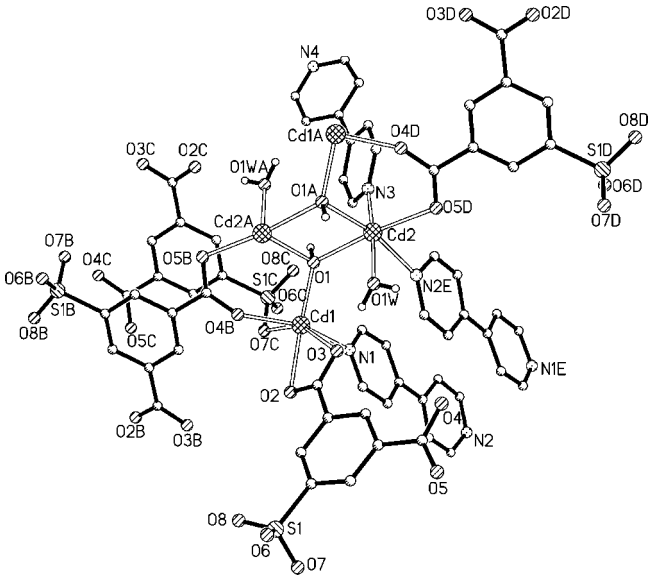

Figure 3. Perspective view of the coordination environments of cadmium atoms in MCCP-5; the coordination spheres around Cd1A and Cd2A have been drawn incompletely for clarity

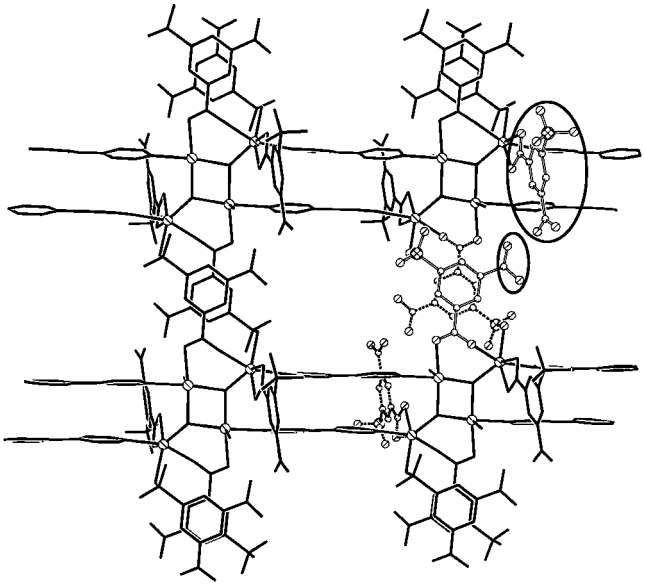

Figure 4. A section of MCCP-5 showing how the two-dimensional sheets are intersected with each other through the *e*-sip ligands

 © 2004 Wiley-VCH Verlag GmbH & Co. KGaA, Weinheim

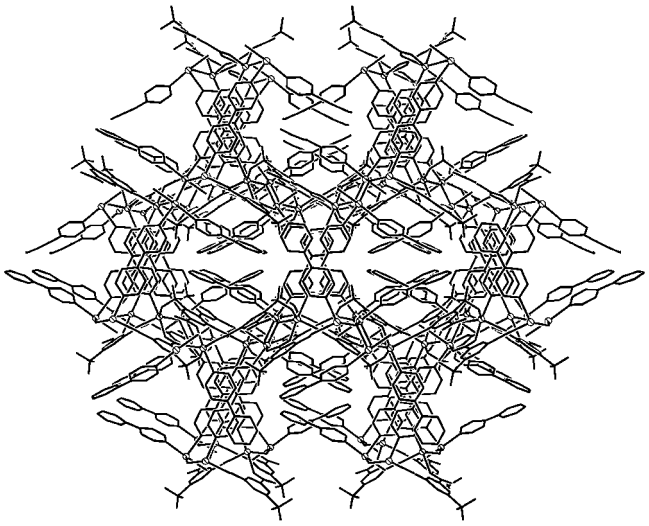

Figure 5. Perspective view of the three-dimensional structure of MCCP-5; lattice water molecules have been omitted for clarity

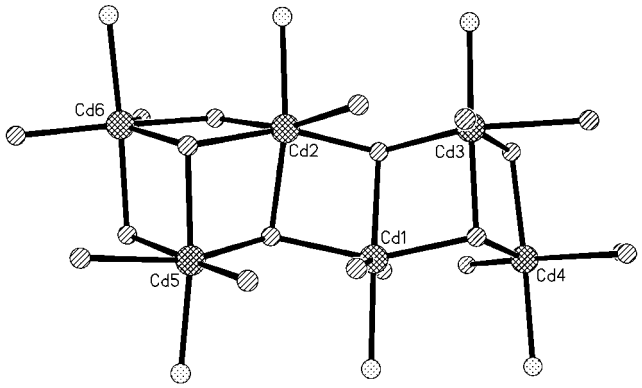

Figure 6. Perspective view of the hexanuclear cadmium cluster in MCCP-6

The most striking feature in MCCP-5 is the connection of all $[Cd_4(\mu_3\text{-}OH)_2]^{6+}$ clusters through *e*-sip ligands using their bridging bidentate carboxylate and sulfonate groups and 4,4′-bpy ligands to form an infinite two-dimensional sheet. The remaining chelating carboxylate groups orientate themselves up and down, as shown in the small circle in Figure 4. The two *e*-sip ligands drawn in open line are indeed symmetrically related (x, $-y$ +2, z − 1/2), and the chelating carboxylate group (small circle) and the *e*-sip ligand (large circle) are further coordinated to the nearest $[Cd_4(\mu_3\text{-}OH)_2]^{6+}$ cluster in the adjacent sheet which is intersected with the first one. Similarly, the two *e*-sip ligands drawn with a dashed line also are coordinated likewise. Thus, the intersected two-dimensional sheet is inter-linked through the chelating carboxylate groups of *e*-sip ligands to form an actual three-dimensional structure containing nearly hexagonal channels that are occupied by pendant 4,4′-bpy ligands and lattice water molecules, as illustrated in Figure 5. To the best of our knowledge, whereas three basic cadmium clusters have been found,[18] this is the first example of a coordination polymer constructed from $Cd_4(\mu_3\text{-}OH)_2$ clusters.

The basic building unit in MCCP-6 is the $[Cd_6(OH)_4(OH_2)_4]^{8+}$ cluster (Figure 6), which is constructed from hexameric units composed of six octahedral Cd^{II} centers in which four nip ligands doubly bridge the six cadmium clusters in *e* and *f* modes, and two nip ligands are doubly bound to four cadmium atoms in terminal *c* and *d* modes (Figure 7 and Scheme 2). Selected bond lengths and angles are listed in Table 3. Cd1 is coordinated to three μ_3-OH groups (O1, O2 and O3) and one 4,4′-bpy nitrogen

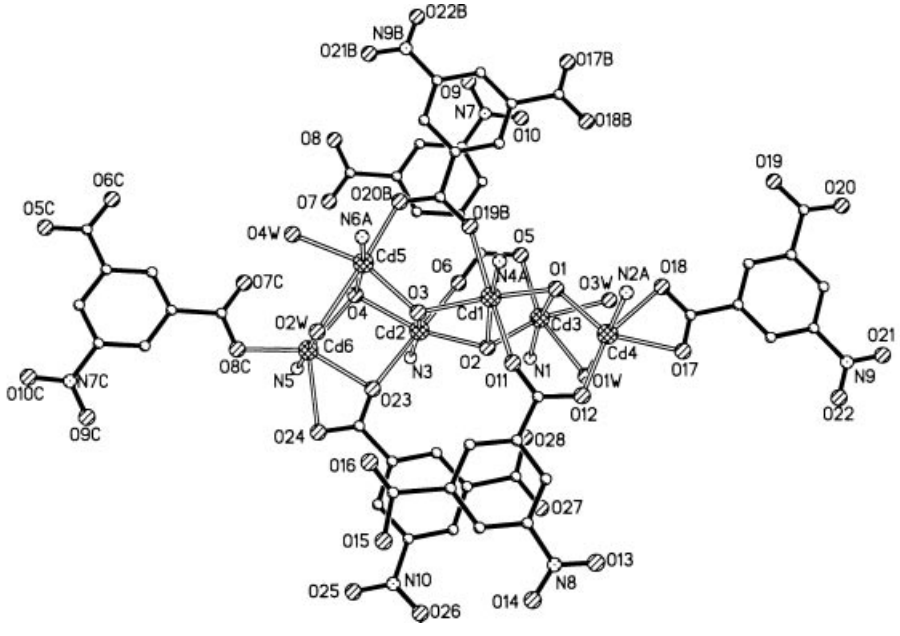

Figure 7. Perspective view of the coordination environments of cadmium atoms in MCCP-6; the carbon atoms of 4,4′-bpy ligands and lattice water molecules have been omitted for clarity

 © 2004 Wiley-VCH Verlag GmbH & Co. KGaA, Weinheim

Table 3. Selected bond lengths [Å] and angles [°] for MCCP-6; symmetry codes A: x, $y + 1$, z; B: $-x$, $-y + 1$, $-z$, C: $-x$, $-y$, $-z + 1$

Cd1−O1	2.206(6)	Cd1−O2	2.360(6)	Cd1−O3	2.219(6)	Cd1−N4A	2.284(4)
Cd1−O11	2.333(9)	Cd1−O19B	2.378(8)	Cd2−O2	2.222(6)	Cd2−O3	2.304(6)
Cd2−O4	2.282(7)	Cd2−N3	2.301(4)	Cd2−O6	2.306(8)	Cd2−O23	2.373(7)
Cd3−O1	2.259(6)	Cd3−O2	2.222(6)	Cd3−N1	2.295(5)	Cd3−O3W	2.408(8)
Cd3−O5	2.279(8)	Cd3−O1W	2.517(7)	Cd4−O1	2.247(7)	Cd4−O12	2.268(7)
Cd4−O17	2.338(7)	Cd4−O18	2.495(7)	Cd4−O1W	2.389(6)	Cd4−N2A	2.329(5)
Cd5−O3	2.217(7)	Cd5−O4	2.293(6)	Cd5−O4W	2.325(8)	Cd5−N6A	2.339(4)
Cd5−O2W	2.523(7)	Cd5−O20B	2.244(7)	Cd6−O4	2.260(6)	Cd6−O8C	2.200(8)
Cd6−O23	2.325(7)	Cd6−O24	2.610(8)	Cd6−O2W	2.369(6)	Cd6−N5	2.316(4)
O1−Cd1−O2	77.8(2)	O2−Cd1−O3	80.3(2)	O1−Cd1−N4A	103.5(2)	O3−Cd1−N4A	100.8(2)
O11−Cd1−O19B	169.5(3)	O1−Cd1−O11	93.3(4)	O2−Cd2−O3	81.5(2)	O3−Cd2−O4	78.0(2)
O2−Cd2−N3	103.5(2)	O4−Cd2−N3	98.7(2)	O3−Cd2−N3	167.9(2)	O6−Cd2−O23	162.8(3)
O1−Cd3−O2	79.7(2)	O1−Cd3−O3W	90.3(3)	O2−Cd3−N1	96.7(2)	N1−Cd3−O3W	89.5(3)
O1−Cd3−N1	167.8(3)	O5−Cd3−O1W	160.2(3)	O1−Cd4−O12	117.9(3)	O12−Cd4−O17	103.2(3)
O17−Cd4−O18	53.8(3)	O1−Cd4−O18	84.9(3)	N2A−Cd4−O1W	176.9(2)	O1−Cd4−N2A	99.3(2)
O3−Cd5−O4	79.6(2)	O4−Cd5−O4W	86.3(3)	O4 W−Cd5−N6A	90.1(3)	O3−Cd5−N6A	101.0(2)
O20B−Cd5−O2W	175.3(3)	N6A−Cd5−O2W	91.5(2)	O4−Cd6−O23	81.1(2)	O23−Cd6−O24	52.3(2)
O8C−Cd6−O24	94.9(3)	O4−Cd6−O8C	130.1(3)	N5−Cd6−O2W	177.0(2)	O4−Cd6−N5	100.4(2)

atom in the equatorial plane, and to two oxygen atoms from the bridging bidentate carboxylate group of a *c*-nip ligand (O11) and the bridging bidentate carboxylate group of an *f*-nip ligand (O19B) in the axial positions. Cd2 has a similar coordination environment and is bound to three μ_3-OH groups (O2, O3 and O4) and one nitrogen atom from the 4,4′-bpy ligand. The remaining two coordination sites of the octahedron are filled by two oxygen atoms from the bidentate carboxylate group (O6) of an *e*-nip ligand and the chelating/bridging carboxylate group (O23) of a *d*-nip ligand. Cd3 lies in the center of a distorted octahedron and is coordinated to one μ_3-OH group (O2), one μ_2-bridging water molecule (O1W), one terminal water molecule (O3W) and one oxygen atom from the bidentate carboxylate group (O5) of an *e*-nip ligand in the equatorial plane. The coordination sphere is completed by one μ_3-OH group (O1) and one nitrogen atom from the 4,4′-bpy ligand in the axial positions. Cd4 is octahedrally coordinated by one μ_3-OH group (O1), one oxygen atom from the bridging bidentate carboxylate group (O12) of a *c*-nip ligand, two oxygen atoms from the chelating carboxylate group (O17, O18) of an *f*-nip ligand, one μ_2-bridging water molecule (O1W) and one 4,4′-bpy nitrogen atom. The coordination environments around Cd5 and Cd6 are somewhat similar to those of Cd3 and Cd4, respectively, except for the different coordination modes of the nip ligands. It is noteworthy that the six cadmium atoms are interlinked through four triply bridging μ_3-OH groups to form four basic $Cd_3(OH)$ subunits, in which the Cd−O distances of between 2.211 and 2.368 Å are consistent with those of other μ_3-OH-bridged cadmium motifs.[18,19] The assignment of μ_3-OH groups was based on the near tetrahedral angles around the central O atoms with average angles between 101.1 and 106.9°, which are a little larger than those found in the $(F_5C_5CdOH)_4$ cubane.[19]

The most striking feature of MCCP-6, however, is the connection of all $[Cd_6(\mu_3\text{-}OH)_4(\mu_2\text{-}OH_2)_2(OH_2)_2]^{8+}$ building blocks through linking *e*- and *f*-nip ligands to form a slightly corrugated, infinite 1D-chain with the formula $[Cd_6(\mu_3\text{-}OH)_4(\mu_2\text{-}OH_2)_2(OH_2)_2(nip)_4]_n$ (Figure 8), in which pairs of *c*- and *d*-nip ligands are located on both sides. Obviously, the large bulk combined with short nip links does not allow for high coordination of the hexanuclear cluster because of the steric hindrance. Their links by *e*- and *f*-nip ligands are made to bind in a pairwise manner to two hexanuclear cluster as observed for ip in MOF-49.[20] As shown in Figure 7, each hexanuclear cluster is coordinated to six nitrogen atoms from six μ_2-4,4′-bpy ligands up and down, thus the adjacent 1D-chains are further interlinked through these μ_2-4,4′-bpy ligands to generate an infinite undulating 2D-sheet (Figure 9).

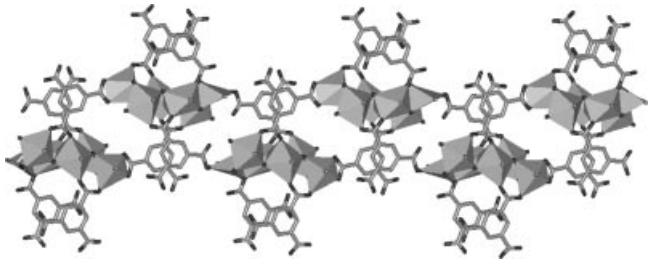

Figure 8. Perspective view of the one-dimensional chain constructed with hexanuclear cadmium clusters and nip ligands; coordinated 4,4′-bpy ligands have been omitted for clarity

Photoluminescent Properties

As we and others previously reported, coordination polymers containing zinc or cadmium oxide or hydroxide motifs exhibit photoluminescent properties[6,18b] and in this study we also investigated the photoluminescent properties of MCCP-4, -5 and -6 (Figure 10). In the solid state, the maximum of the emission bands of MCCP-4 is located at

 © 2004 Wiley-VCH Verlag GmbH & Co. KGaA, Weinheim

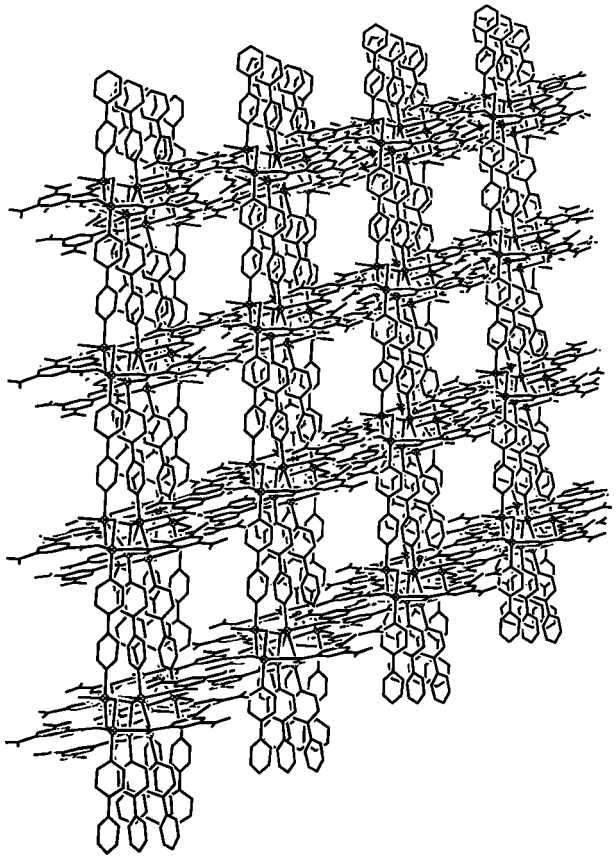

Figure 9. Perspective view of the two-dimensional structure of MCCP-6

562 nm (λ_{ex} = 505 nm), while MCCP-5 shows two emission bands at 370 nm and 468 nm (λ_{ex} = 340 nm), respectively. Since free H_2sip exhibits photoluminescence emission at 355 nm, the emission band at 370 nm of MCCP-5 may be due to the ligand donation, while the emission bands at 562 nm and 468 nm of MCCP-4 and -5 might be attributable to the formation of $[M_4(\mu_3\text{-}OH)_2]^{6+}$ (M = Zn^{II}, Cd^{II}) clusters and/or to ligand-to-metal charge transfer (LMCT).[6,21] MCCP-6 also exhibits intense photoluminescence with the maximum at 470 nm. Because the free H_2nip ligand does not emit any luminescence in the range 400−800 nm, the emission of MCCP-6 might also be assigned to the formation of $[Cd_6(\mu_3\text{-}OH)_4]^{8+}$ clusters and/or to ligand-to-metal charge transfer (LMCT).[6,21]

In conclusion, we have synthesized three novel metal-cluster-based coordination polymers, in which the sip and nip ligands show versatile coordination modes. The sulfonate groups in MCCP-4 and -5 are uncoordinated and monodentate, respectively. Furthermore, the sulfonate and nitro groups are involved in extensive inter-framework hydrogen bonding, which thus leads to extended structures with a higher order of dimensions.

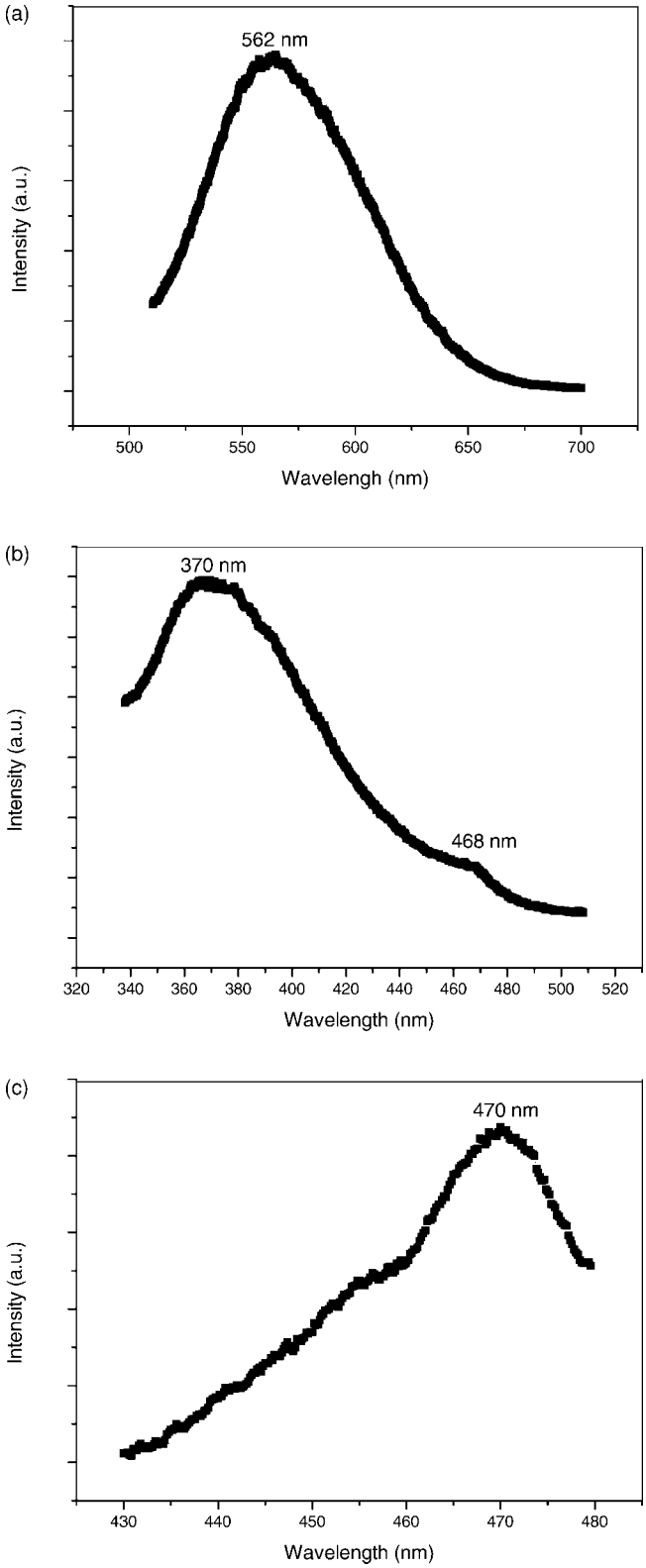

Figure 10. The solid-state photoluminescent spectra of MCCP-4 (a), -5 (b) and -6 (c) at room temperature

Experimental Section

General Remarks: All reagents were purchased from commercial sources and used without further purification. Elemental analyses

 © 2004 Wiley-VCH Verlag GmbH & Co. KGaA, Weinheim

Table 4. Crystallographic data for MCCP-4, -5 and -6

	MCCP-4	MCCP-5	MCCP-6
Empirical formula	$C_{18}H_{17}N_2O_{10.5}SZn_2$	$C_{56}H_{46}Cd_4N_8O_{19}S_2$	$C_{62}H_{54}Cd_6N_{10}O_{35}$
Formula mass	592.14	1648.73	2173.55
Crystal system	triclinic	monoclinic	triclinic
Space group	$P\bar{1}$	$C2/c$	$P\bar{1}$
a [Å]	10.106(2)	25.602(1)	14.295(1)
b [Å]	10.851(2)	16.571(1)	14.472(1)
c [Å]	11.125(2)	13.322(1)	20.204(1)
α [°]	105.66(3)	90	73.362(1)
β [°]	112.63(3)	92.524(1)	82.200(1)
γ [°]	98.18(3)	90	62.769(1)
V [Å^3]	1041.8(4)	5646.4(2)	3560.9(3)
Z	2	4	2
D_c [g·cm^{-3}]	1.888	1.940	2.027
μ [mm^{-1}]	2.467	1.646	1.862
R_1, wR_2 (obsd.)[a]	0.0273, 0.0657	0.0367, 0.0805	0.0674, 0.1234

[a] $R_1 = \Sigma||F_o| - |F_c||/\Sigma|F_o|$, $wR_2 = \{\Sigma[w(F_o^2 - F_c^2)^2]/\Sigma[w(F_o^2)^2]\}^{1/2}$.

were performed with a CE EA 1110 elemental analyzer. IR spectra were recorded from 4000 to 400 cm^{-1} with a Nicolet AVATAR FT-IR360 instrument. The thermal gravimetric analyses (TGA) were carried out under nitrogen with a NETZSCH STA 449C differential thermal analyzer with a rate of 10 °C/min.

Synthesis of MCCP-4: An aqueous solution (5 mL) of H_2sip (0.134 g, 0.50 mmol) was adjusted to pH = 7 with 1 M NaOH, and transferred into a Parr Teflon-lined stainless steel vessel (23 mL) containing $Zn(NO_3)_2{\cdot}6H_2O$ (0.158 g, 0.50 mmol) and 4,4′-bpy (0.078 g, 0.50 mmol). To the resultant mixture was added an additional 3 mL of water. The vessel was then sealed and heated to 180 °C for 3 d, followed by cooling at 2.5 °C/h to room temperature. Colorless block-like crystals were collected by hand, washed with distilled water and dried in air at ambient temperature [yield: ca. 75% based on $Zn(NO_3)_2$]. $C_{18}H_{17}N_2O_{10.5}SZn_2$ (592.14): calcd. C 36.51, H 2.89, N 4.73; found C 36.30, H 2.75, N 4.80. IR (KBr): $\tilde{\nu}$ = 3416 m, 3269 m, 3019 m, 3022 m, 1610 vs, 1560 vs, 1498 m, 1441 s, 1372 s, 1255 s, 1228 m, 1205 m, 1171 m, 1104 m, 1077 m, 1038 s, 1016 w, 912 w, 876 w, 822 m, 772 m, 731 m, 678 w, 643 m, 625 m, 593 w, 548 w, 453 w cm^{-1}.

Synthesis of MCCP-5: The synthesis of MCCP-5 was similar to the above description for MCCP-4 except that zinc nitrate hexahydrate was replaced by cadmium nitrate tetrahydrate. Yield: ca. 60% based on $Cd(NO_3)_2$. $C_{56}H_{46}Cd_4N_8O_{19}S_2$ (1648.73): calcd. C 40.79, H 2.81, N 6.80; found C 40.40, H 2.90, N 6.66. IR (KBr): $\tilde{\nu}$ = 3569 w, 3367 w, 3104 w, 3073 w, 3042 w, 3017 w, 1600 s, 1560 s, 1534 s, 1492 m, 1430 m, 1415 m, 1367 s, 1223 m, 1202 m, 1166 m, 1101 m, 1067 m, 1035 s, 996 m, 934 w, 877 w, 859 w, 821 m, 775 s, 728 s, 676 m, 619 vs, 576 m, 516 w, 464 m, 441 m cm^{-1}.

Synthesis of MCCP-6: An aqueous solution (5 mL) of H_2nip (0.106 g, 0.50 mmol) was adjusted to pH = 7 with 1 M NaOH, and transferred into a Parr Teflon-lined stainless steel vessel (23 mL) containing $Cd(NO_3)_2{\cdot}4H_2O$ (0.154 g, 0.50 mmol) and 4,4′-bpy (0.078 g, 0.50 mmol). To the resultant mixture was added an additional 3 mL of water and the vessel was then sealed and heated to 140 °C for 3 d, followed by cooling at 5 °C/h to room temperature. Colorless block-like crystals were collected by hand, washed with distilled water, and dried in air at ambient temperature [yield: ca. 40% based on $Cd(NO_3)_2$]. $C_{62}H_{54}Cd_6N_{10}O_{35}$ (2173.55): calcd. C 34.26, H 2.50, N 6.44; found C 34.10, H 2.55, N 6.15. IR (KBr): $\tilde{\nu}$ = 3410 m, 3094 m, 2914 m, 1610 vs, 1566 s, 1529 m, 1455 m, 1418 m, 1365 vs, 1219 w, 1076 w, 1009 w, 927 w, 809 m, 731 s, 630 m cm^{-1}.

Crystallographic Analyses: Diffraction data were collected with an Enraf Nonius CAD-4 diffractometer for MCCP-4 and with a Bruker APEX CCD diffractometer for MCCP-5 and MCCP-6 with graphite-monochromated Mo-K_α radiation (λ = 0.71073 Å). The three structures were solved by direct methods and refined anisotropically by full-matrix least squares based on F^2 using the SHELXTL crystallographic software package.[22] Non-hydrogen atoms in all structures were refined with anisotropic displacement parameters. Hydrogen atoms attached to carbon atoms were calculated and included as riding atoms. In the final difference Fourier map of MCCP-6 was a peak larger than 1 e·Å^{-3}. The unit cell, however, contains no residual Solvent Accessible Area as calculated by PLATON.[23] Crystal parameters and details of the data collection and refinement for the structures of MCCP-4, -5 and -6 are listed in Table 4. CCDC-201032 (MCCP-4), -201033 (MCCP-5) and -202206 (MCCP-6) contain the supplementary crystallographic data for this paper. These data can be obtained free of charge at www.ccdc.cam.ac.uk/conts/retrieving.html [or from the Cambridge Crystallographic Data Center, 12 Union Road, Cambridge CB2 1EZ, UK; Fax: (internat.) + 44-1223/336-033; E-mail: deposit@ccdc.cam.ac.uk].

Acknowledgments

This work was granted financial support from the Innovation Foundation for Young Scientific Talents of Fujian Province (No. 2002J004), the NNSF of China (No. 20023001), the Department of Science and Technology of China (No. 2002CCA01600) and the Research Program of Xiamen University (No. Y07015).

[1] [1a] J. S. Seo, D. Whang, H. Lee, S. I. Jun, J. Oh, Y. J. Jeon, K. Kim, *Nature* **2000**, *404*, 982. [1b] R. Kitaura, S. Kitagawa, Y. Kubota, T. C. Kobayashi, K. Kindo, Y. Mita, A. Matsuo, M. Kobayashi, H.-C. Chang, T. C. Ozawa, M. Suzuki, M. Sakata, M. Takata, *Science* **2002**, *298*, 2358. [1c] M. Eddaoudi, J. Kim, N. Rosi, D. Vodak, J. Wachter, M. O'Keeffe, O. M. Yaghi, *Science* **2002**, *295*, 469. [1d] G. J. Halder, C. J. Kepert, B. Mouba-

raki, K. S. Murray, J. D. Cashion, *Science* **2002**, *298*, 1762. [1e] P. Ayyappan, O. R. Evans, Y. Cui, K. A. Wheeler, W. B. Lin, *Inorg. Chem.* **2002**, *41*, 4978.

[2] [2a] S. R. Batten, R. Robson, *Angew. Chem. Int. Ed.* **1998**, *37*, 1460. [2b] O. M. Yaghi, H. Li, C. Davis, D. Richardson, T. L. Groy, *Acc. Chem. Res.* **1998**, *31*, 474. [2c] O. R. Evans, W. B. Lin, *Acc. Chem. Res.* **2002**, *35*, 511. [2d] G. K. M. Shimizu, G. D. Enright, C. I. Ratcliffe, J. A. Ripmeester, *Chem. Commun.* **1999**, 461. [2e] M. Kondo, T. Toshitomi, K. Seki, H. Matsuzaka, S. Kitagawa, *Angew. Chem. Int. Ed. Engl.* **1997**, *36*, 1725.

[3] [3a] L. A. Gerrard, P. T. Wood, *Chem. Commun.* **2000**, 2107. [3b] M. Eddaoudi, D. B. Moler, H. Li, B. Chen, T. M. Reineke, M. O'Keeffe, O. M. Yaghi, *Acc. Chem. Res.* **2001**, *34*, 319. [3c] M. Kondo, M. Miyazawa, Y. Irie, R. Shinagawa, T. Horiba, A. Nakamura, T. Naito, K. Maeda, S. Utsuno, F. Uchida, *Chem. Commun.* **2002**, 2156.

[4] [4a] D. T. Vodak, M. E. Braun, J. Kim, M. Eddaoudi, O. M. Yaghi, *Chem. Commun.* **2001**, 2534. [4b] N. L. Rosi, M. Eddaoudi, J. Kim, M. O'Keeffe, O. M. Yaghi, *Angew. Chem. Int. Ed.* **2002**, *41*, 284.

[5] [5a] S. O. H. Gutschke, D. J. Price, A. K. Powell, P. T. Wood, *Eur. J. Inorg. Chem.* **2001**, 2739. [5b] S. O. H. Gutschke, M. Molinier, A. K. Powell, P. T. Wood, *Angew. Chem. Int. Ed. Engl.* **1997**, *36*, 991.

[6] [6a] J. Tao, M.-L. Tong, J.-X. Shi, X.-M. Chen, S. W. Ng, *Chem. Commun.* **2000**, 2043. [6b] J. Tao, J.-X. Shi, M.-L. Tong, X.-X. Zhang, X.-M. Chen, *Inorg. Chem.* **2001**, *40*, 6328.

[7] [7a] S. A. Dalrymple, M. Parvez, G. K. H. Shimizu, *Inorg. Chem.* **2002**, *41*, 6986. [7b] S. A. Dalrymple, G. K. H. Shimizu, *Chem. Commun.* **2002**, 2224. [7c] C.-H. Chen, J.-W. Cai, C.-Z. Liao, X.-L. Feng, X.-M. Chen, S. W. Ng, *Inorg. Chem.* **2002**, *41*, 4967, and references cited therein.

[8] [8a] B. Szczęsna, Z. Urbańczyk-Lipkowska, *New J. Chem.* **2002**, *26*, 243. [8b] J. M. A. Robinson, D. Philp, K. D. M. Harris, B. M. Kariuki, *New J. Chem.* **2000**, *24*, 799. [8c] J. Tao, X. Yin, S.-Y. Yang, R.-B. Huang, L.-S. Zheng, *Main Group Metal Chem.* **2002**, *25*, 707. [8d] X. Yin, J. Tao, R.-B. Huang, L.-S. Zheng, *Main Group Metal Chem.* **2002**, *25*, 691. [8e] J. Tao, X. Yin, R.-B. Huang, L.-S. Zheng, S. W. Ng, *Acta Crystallogr., Sect. E* **2003**, *59*, 473.

[9] A. D. Kulynych, G. K. H. Shimizu, *Cryst. Eng. Comm.* **2002**, *4*, 102.

[10] D.-F. Sun, R. Cao, Y.-Q. Sun, X. Li, W.-H. Bi, M.-C. Hong, Y.-J. Zhao, *Eur. J. Inorg. Chem.* **2002**, 94.

[11] [11a] H. Abourahma, B. Moulton, V. Kravtsov, M. J. Zaworotko, *J. Am. Chem. Soc.* **2002**, *124*, 9990. As this manuscript was being revised, two Zn-nip and two Cd-nip coordination polymers were reported: [11b] J. Tao, X. Yin, Y.-B. Jiang, L.-F. Yang, R.-B. Huang, L.-S. Zheng, *Eur. J. Inorg. Chem.* **2003**, 2678. [11c] J. Luo, M. Hong, R. Wang, R. Cao, L. Han, Z. Lin, *Eur. J. Inorg. Chem.* **2003**, 2705.

[12] [12a] G. Socrates, *Infrared Characteristic Group Frequencies*, John Wiley & Sons, Stonebridge Press, Bristol, **1980**. [12b] Z. Wang, M. Ströbele, K.-L. Zhang, H. J. Meyer, X.-Z. You, Z. Yu, *Inorg. Chem. Commun.* **2002**, *5*, 230. [12c] J.-W. Cai, C.-H. Chen, C.-Z. Liao, J.-H. Yao, Y.-P. Hu, X. M. Chen, *J. Chem. Soc., Dalton Trans.* **2001**, 1137.

[13] [13a] D. H. Williams, I. Fleming, *Spectroscopic Methods in Organic Chemistry*, 4th ed., John Wiley & Sons, New York, **1989**. [13b] V. T. Yilmez, T. K. Yazicilar, O. Andac, H. Kutuk, Y. Bekdemir, W. T. A. Harrison, *Z. Anorg. Allg. Chem.* **2002**, *628*, 1908.

[14] [14a] J. Tao, M.-L. Tong, X. M. Chen, *J. Chem. Soc., Dalton Trans.* **2000**, 3669. [14b] G. Guilera, J. W. Steed, *Chem. Commun.* **1999**, 1563.

[15] M. Alexiou, C. Dendrinou-Samara, C. P. Raptopoulou, A. Terzis, D. P. Kessissoglou, *Inorg. Chem.* **2002**, *41*, 4732.

[16] A. Onoda, Y. Yamada, M. Doi, T. Okamura, N. Ueyama, *Inorg. Chem.* **2001**, *40*, 516.

[17] [17a] J. Tao, Y.-L. Fu, S.-L. Zheng, X.-M. Chen, S. W. Ng, *Main Group Metal Chem.* **2001**, *24*, 289. [17b] K. V. Domasevitch, G. D. Enright, B. Moulton, M. J. Zaworotko, *J. Solid State Chem.* **2000**, *152*, 280.

[18] [18a] W. Lin, Z. Wang, L. Ma, *J. Am. Chem. Soc.* **1999**, *121*, 11249. [18b] X. Xue, X.-S. Wang, L.-Z. Wang, R.-G. Xiong, B. F. Abrahams, X.-Z. You, Z.-L. Xue, C.-C. Che, *Inorg. Chem.* **2002**, *41*, 6544. [18c] T. Konno, Y. Kageyama, K. I. Okamoto, *Bull. Chem. Soc. Jpn.* **1994**, *67*, 1957.

[19] M. Weidenbruch, M. Herrndorf, A. Schafer, S. Pohl, W. Saak, *J. Organomet. Chem.* **1989**, *361*, 139.

[20] D. T. Vodak, M. E. Braun, J. Kim, M. Eddaoudi, O. M. Yaghi, *Chem. Commun.* **2001**, 2534.

[21] [21a] A. Meijerink, G. Blasse, M. Glasbeek, *J. Phys., Condens. Matter* **1990**, *2*, 6303. [21b] R. Bertoncello, M. Bettinelli, M. Cassrin, A. Gulino, E. Tondello, A. Vittadini, *Inorg. Chem.* **1992**, *31*, 1558.

[22] G. M. Sheldrick, *SHELX97*, University of Göttingen, Göttingen, Germany, **1997**.

[23] A. L. Spek, *PLATON*, University of Glasgow, Glasgow, UK, **1998**.

Received June 9, 2003
Early View Article
Published Online October 23, 2003

 © 2004 Wiley-VCH Verlag GmbH & Co. KGaA, Weinheim

Homo- and Heteronuclear Complexes of (Pentamethylcyclopentadienyl)-rhodium(III) Bearing Bis(diphenylphosphanylmethyl)phenylphosphane

Yasuhiro Yamamoto,*[a] Yosuke Kosaka,[a] Yoshihiro Tsutsumi,[a] Yoshihiro Kaburagi,[a] Katsuaki Kuge,[b] Yusuke Sunada,[b] and Kazuyuki Tatsumi[b]

Keywords: Rhodium / Gold / Copper / Silver / Cluster compounds / P ligands

Reaction of $[Cp^*RhCl_2]_2$ (**1**) with bis(diphenylphosphanylmethyl)phenylphosphane (dpmp) in the presence of KPF_6 generated the mono- or bi-nuclear complexes $[(Cp^*RhCl)(dpmp\text{-}P,P,P)(RhCl_2Cp^*)](PF_6)$ (**2**) or $[Cp^*RhCl(dpmp\text{-}P,P)](PF_6)$ (**3**), depending on the reaction conditions. These complexes have two chiral centers at Rh and the central P atoms, and the diastereomers were separated by successive recrystallization. The structures of **2(B)** with an $R_{Rh}S_P/S_{Rh}R_P$ pair and **3(A)** with an $R_{Rh}S_P/S_{Rh}R_P$ pair were elucidated by X-ray analyses. Reaction of **1** with an excess of dpmp in the presence of Ag(OTf) generated a hetero-tetranuclear complex $[\{Cp^*RhCl_2(dpmp\text{-}P,P,P)Ag\}_2](OTf)_2$ (**4**). An X-ray analysis revealed that each Cp^*RhCl_2 moiety is connected by a terminal P^1 atom of the dpmp ligand and each Ag atom is two-coordinate and is surrounded by another terminal P^3 atom, and a central P^{*2} atom of the other dpmp ligand. A mixture of **1** and dpmp was treated with $Au(SC_4H_8)$ or CuCl in the presence of KPF_6, generating the hetero-tetranuclear complexes $[\{Cp^*RhCl_2(dpmp\text{-}P,P,P)M\}_2](PF_6)_2$ (**7**: M = Au; **8**: M = Cu), in which the structures, except for the Cl-bridged structure of **8**, are fundamentally similar to that of **4**. These complexes were also prepared by the reactions of **3** with $Au(SC_4H_8)$ or CuCl. Complex **3** reacted with AgOTf to afford $[Cp^*Rh(dpmp\text{-}P,P,P)](OTf)_2$ (**5**). Treatment of **3(A)** (a diastereomer with an $R_{Rh}S_{P2}/S_{Rh}R_{P2}$ pair) with **1**, $[(p\text{-cymene})RuCl_2]_2$ or $PdCl_2(cod)$ gave $[Cp^*RhCl(dpmp\text{-}P,P,P)RhCl_2Cp^*](PF_6)$ (**2**) or $[Cp^*RhCl(dpmp\text{-}P,P,P)RuCl_2(p\text{-cymene})](PF_6)$ (**6**), respectively. These addition reactions proceeded stereoselectively.
(© Wiley-VCH Verlag GmbH & Co. KGaA, 69451 Weinheim, Germany, 2004)

Introduction

Triphosphanes, especially bis(diphenylphosphanylmethyl)-phenylphosphane (dpmp), play an important role as the backbone in the construction of polynuclear clusters. The chemistry of rhodium, iridium, and gold has been sited by Balch.[1] We have developed systematic syntheses of homo- and hetero-bimetallic and -trimetallic platinum and palladium clusters with tridentate phosphane and isocyanide ligands.[2] These complexes are constructed fundamentally of a square planar framework and contain dpmp, carbon monoxide, halogens and isocyanides as ligands. Octahedral complexes can lead to compounds with diverse dimensionality, in comparison with square-planar complexes.

Recently, we reported the preparation of supramolecular complexes based on quasi-octahedral geometries of rhodium(III) and iridium(III) bearing a pentamethylcyclopentadienyl or arene ruthenium(II) moiety. Thus, the reactions of $[Cp^*MCl_2(\mu\text{-}1,4\text{-}(CN)_2\text{-}2,3,5,6\text{-}Me_4C_6)MCl_2Cp^*]$ (M = Rh, Ir; $Cp^* = C_5Me_5$) with bidentate ligands such as pyrazine, bipyridine and di-isocyanide in the presence of AgOTf ($OTf = CF_3SO_3$) generated tetranuclear complexes with a square core.[3–5] Recently, self-assembled supramolecules with the pentamethylcyclopentadienyl or cyclopentadienyl groups in which the CN group has been generally used as a binary ligand have been reported by several researchers.[6–9]

We are interested in the chemistry of the interaction between quasi-octahedral complexes and dpmp containing three potential coordination sites because of expectation of various coordination modes and polynuclear complexes. We adopted binuclear complexes of rhodium(III), iridium(III) or ruthenium(II) containing pentamethylcyclopentadienyl or arene groups as quasi-octahedral complexes, for which the chemistry has not yet been developed. Here we report the preparation and stereochemistry of mononuclear, binuclear and polynuclear complexes of rhodium(III) bearing dpmp and pentamethylcyclopentadienyl ligands. Part of this work has already been briefly reported.[10]

[‡] Present adress: The Institute of Scientific and Industrial Research, Osaka University, Mihogaoka, Ibaraki, Osaka 567-0047, Japan. E-mail: yamamo24@sanken.osaka-u.ac
[a] Department of Chemistry, Faculty of Science, Toho University, Miyama 2-2-1, Funabashi, Chiba 274-8510, Japan
[b] Research Center for Materials Science and Department of Chemistry, Graduate School of Science, Nagoya University, Furo-cho, Chikusa-ku, Nagoya 454-8602, Japan
E-mail: i45100a@nucc.cc.nagoya-u.ac.jp
Supporting information for this article is available on the WWW under http://www.eurjic.org or from the author.

 © 2004 Wiley-VCH Verlag GmbH & Co. KGaA, Weinheim **DOI: 10.1002/ejic.200300402**

Results and Discussion

Reactions of $[Cp^*RhCl_2]_2$ (1) with dpmp in the Presence of KPF_6 or AgOTf

When $[Cp^*RhCl_2]_2$ (**1**) ($Cp^* = C_5Me_5$) was treated with an equivalent of dpmp in the presence of KPF_6 at room temperature, two kinds of complexes [**2(A)** and **2(B)**] with the empirical formula of $[Cp^*_2Rh_2Cl_3(dpmp\text{-}P,P,P)](PF_6)$ were isolated by successive recrystallization (Scheme 1). The IR spectrum of **2** showed a peak at ca. 845 cm^{-1} consistent with the presence of a PF_6 anion. The ^1H NMR spectrum of the reaction mixture indicated a ratio of 1.1:1.0 for **2(A):2(B)**. The Cp* protons appeared at δ = 1.28 (d) and 1.55 (t) for **2(A)** and at δ = 1.27 (d) and 1.73 (t) for **2(B)**, respectively. The chemical shift of the Cp* protons in the chelate ring moiety appeared at a lower magnetic field than those of the other Cp* protons since the Rh atom in a chelate ring is sufficiently electron-deficient for the transfer electron density from the Cp* ligand to the rhodium center. The X-ray analysis of **2(B)** revealed that a Rh atom is connected by the terminal and the central P atoms, and another Rh atom is coordinated to another terminal P atom.[10]

The molecule has two chiral centers namely the Rh and the central P^2 atom. Based on the priority order of the ligands around the two chiral centers,[10] compound **2(B)** was identified as the diastereomer with an $R_{Rh}S_P/S_{Rh}R_P$ pair. Thus **2(A)** is the diastereomer with an $R_{Rh}R_P/S_{Rh}S_P$ pair. The stereochemical difference is that the Cl atom and the P-substituted Ph group occupy the opposite side in **2(A)** and the same side in **2(B)**, where the structure of a **2(A)** type is designated as an *anti*-form and that of a **2(B)** type as a *syn*-form.

The reaction of **1** with an excess of dpmp in the presence of KPF_6 afforded yellow crystals of $[Cp^*RhCl(dpmp)](PF_6)$ (**3**). The ^1H NMR spectrum of the reaction mixture consists of two sets of isomers, **3(A)** and **3(B)**, with an intensity ratio of 2:1, which were separated by successive recrystallization. The X-ray study of **3(A)** revealed its stereochemistry to be that of the diastereomer with an $R_{Rh}S_P/S_{Rh}R_P$ pair (*anti*-form), based on the priority order of the ligands.[10] Thus **3(B)** is assumed to be the $R_{Rh}R_P/S_{Rh}S_P$ pair (*syn*-form). The geometries around the Rh and P^2 centers were found to be similar for **2(A)** and **3(A)**, and for **2(B)** and **3(B)**. In the ^1H NMR spectra, the Cp* protons appeared at δ = 1.74(t) for **3(A)** and at δ = 1.78 for **3(B)**. In the $^{31}P\{^1H\}$ NMR spectrum of **3**, the chemical shifts (δ = −24 ≈ −30) of the free P nuclei appeared at the higher magnetic fields by ca. 10 ≈ 20 ppm than those found for the coordinated P nuclei.[11]

Complex **3(A)** or **3(B)** was treated with **1** at room temperature, exclusively generating **2(A)** or **2(B)**, respectively. The reactions proceeded stereospecifically. Complex **2(A)** was treated with dpmp at room temperature, affording a mixture of **3(A)** and **3(B)** consisting of an approximately 5:1 molar ratio. A similar reaction of **2(B)** gave a mixture of **3(A)** and **3(B)** consisting of an approximately 1:2 molar ratio (Scheme 2). The ratios are reasonable on the basis of the formation ratio in the original reaction of **1** with dpmp. In these reactions the conversion from **2(B)** to **3** and its reverse reaction are slower than inter-conversion between **2(A)** and **3**.

Isomerization from **2(A)** [or, **3(A)**] to **2(B)** [or, **3(B)**] and its reverse reaction did not occur on standing for a long period of time (>100 h) at room temperature. When compound **2(A)** was treated with xylyl isocyanide in acetone at reflux, cleavage of the $Rh-P^3$ bond occurred, generating **3(A)** and $Cp^*RhCl_2(XylNC)$ (Scheme 2). This reaction suggests a greater bond strength in the chelate ring.

A similar reaction of **1** with dpmp was carried out in the presence of two equivalents of Ag(OTf) which afforded an orange-yellow complex **4**, formulated as $[\{Cp^*RhCl_2\text{-}(dpmp\text{-}P,P,P)Ag\}_2](OTf)_2$ (Scheme 1). The structure was

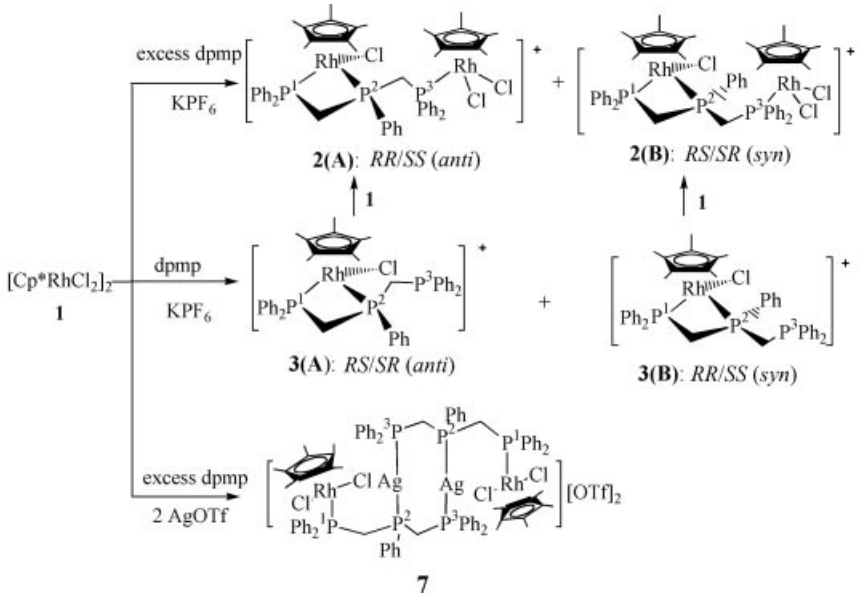

Scheme 1. Reactions of $[Cp^*RhCl_2]_2$ **1** with dpmp in the presence of KPF_6 or Ag(OTf)

 © 2004 Wiley-VCH Verlag GmbH & Co. KGaA, Weinheim

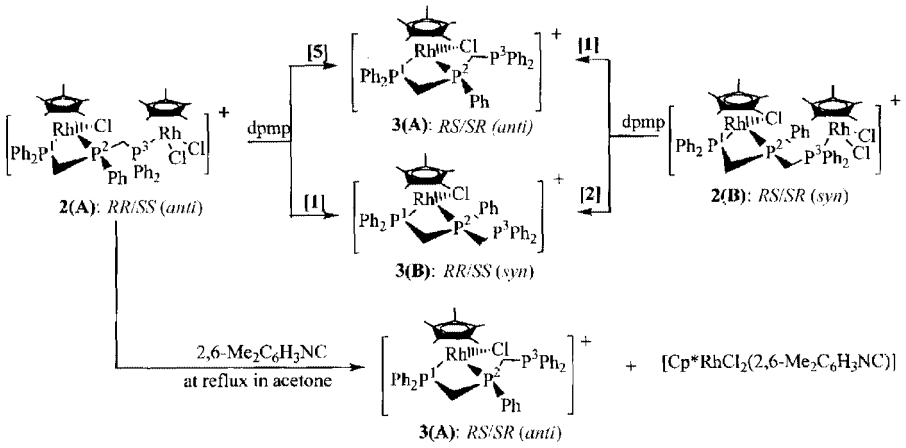

Scheme 2. Reactions of **2** with dpmp or xylyl isocyanide, where the PF_6 anion has been omitted for clarity. The formation ratio of **3(A)** and **3(B)** is designated in the bracket [].

subsequently confirmed by X-ray analysis (Figure 1). Each Cp^*RhCl_2 moiety is connected by a terminal P^1 atom of the dpmp ligand. Each Ag atom is two-coordinate and is surrounded by another terminal P^3 atom and a central P^{*2} atom of the other dpmp ligand. It is interesting to note that **4** was isolated as an addition product without the abstraction of Cl anions by Ag(OTf).

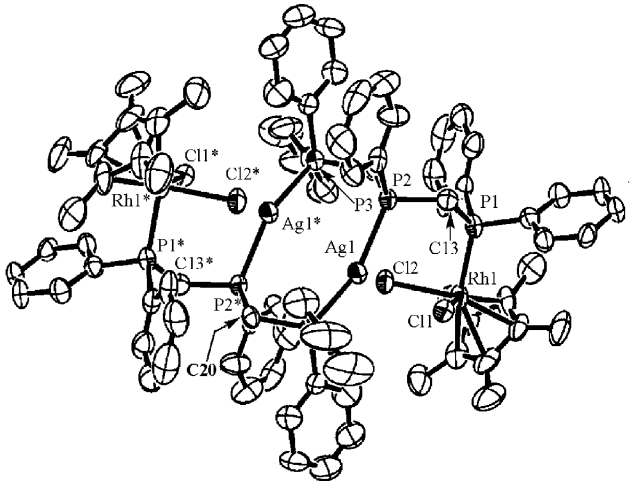

Figure 1. Molecular structure of $4{\cdot}H_2O$; the OTf anion and H_2O have been omitted for clarity and thermal ellipsoids have been drawn at the 50% probability level.

In the ^1H NMR spectrum, the Cp* protons appeared at $\delta = 1.25$ as a doublet, suggesting a symmetric structure. The $^{31}P\{^1H\}$ NMR spectrum showed a double doublet at $\delta = 28.6$ ($J_{PRh} = 146$, $J_{P,P} = 12.9$ Hz) due to the P^1 nucleus coordinated to the rhodium atom and the unresolved signals around $\delta = 2.6$ are due to the other P nuclei.

Reactions of [Cp*RhCl(dpmp-*P,P*)](PF$_6$) and [Cp*$_2$Rh$_2$Cl$_3$-(dpmp-*P,P,P*)](PF$_6$)

The mononuclear complex **3** was anticipated as being a potential precursor to hetero- or homo-multiple nuclear complexes. The reactions of **3** are depicted in Scheme 3.

In order to try to extract a Cl anion, **3** was treated with an excess of KPF_6, but only the starting material could be recovered. A similar reaction with AgOTf, however, gave the yellow η^3-complex [Cp*Rh(dpmp-*P,P,P*)](OTf)$_2$ (**5**) bearing a tridentate ligand as evidenced by the presence of a quadruplet for the Cp* protons in the ^1H NMR spectrum. The X-ray analysis was in agreement with the proposed structure (Figure 2).

When **3(A)** was treated with [(*p*-cymene)$RuCl_2]_2$ at room temperature, a reaction readily occurred, generating a brown complex **6(A)** established from elemental analysis and FAB mass spectrometry as [Cp*RhCl(dpmp-*P,P,P*)$RuCl_2$(*p*-cymene)](PF$_6$). In the ^1H NMR spectrum, the Cp* protons appeared at δ 1.52 as a triplet and the methyl protons of the isopropyl group showed two doublets at $\delta = 0.52$ and 1.00, due to nonequivalence arising from the chiral centers. The $^{31}P\{^1H\}$ NMR spectrum showed three resonances at $\delta = -12.0$ (dt, $^1J_{RhP2} = {}^2J_{P2P1} = 97.0$, $^2J_{P2P3} = 55.5$ Hz, P^2), -1.41 (t, $^1J_{P1Rh} = {}^2J_{P1P2} = 97.0$ Hz, P^1) and 23.7 (d, $^2J_{P3P2} = 55.5$ Hz, P^3) for the dpmp ligand. The stereochemistry with the *anti*-form ($R_{Rh}R_{P2}/S_{Rh}S_{P2}$) of the starting complex is assumed to be retained. Complex **6** was also prepared from the reaction of **1** with [(*p*-cymene)$RuCl_2]_2$ in a 1:1 molar ratio in the presence of KPF_6. Crystallization of the reaction mixture gave two diastereomers in a 52% yield, consisting of a 1:2 molar ratio of **6(A)** and **6(B)**, suggesting that a chelating formation including a Rh atom is preferable to one with a Ru atom. In the ^1H NMR spectrum of **6(B)**, the Cp* protons appeared at $\delta = 1.73$ and two doublets for the isopropyl protons resulted in magnetic non-equivalence. The $^{31}P\{^1H\}$ NMR

 © 2004 Wiley-VCH Verlag GmbH & Co. KGaA, Weinheim

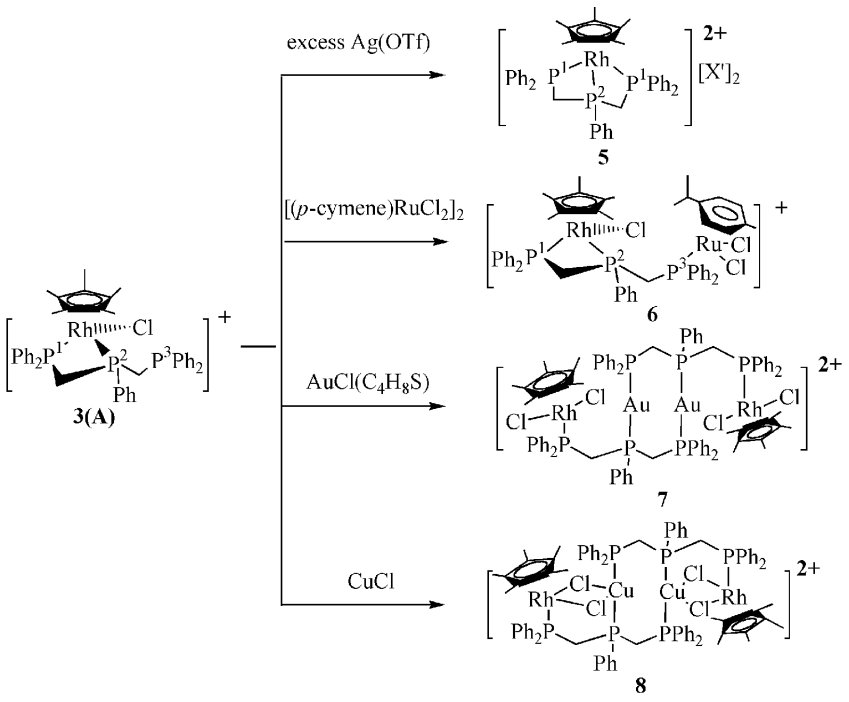

Scheme 3. Reactions of **3(A)**, where the PF_6 anions have been omitted for clarity.

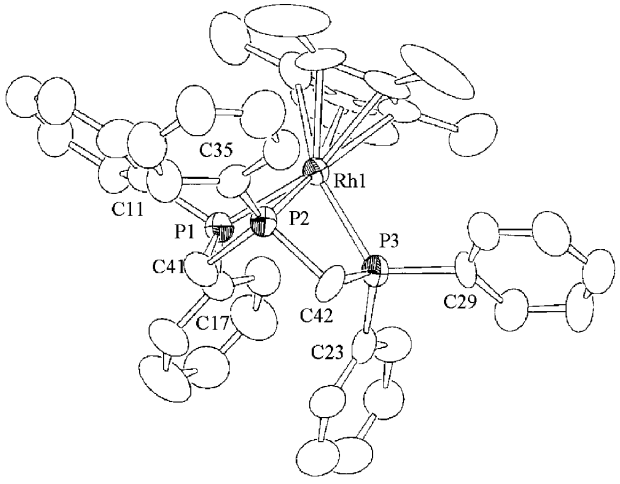

Figure 2. Molecular structure of the cation of **5**; the OTf anions have been omitted for clarity and thermal ellipsoids have been drawn at the 50% probability level.

spectrum showed three resonances at δ = −13.8 (dt, $^1J_{RhP2}$ = $^2J_{P2P1}$ = 105, $^2J_{P2P3}$ = 55.0 Hz, P^2), −10.2 (t, $^1J_{P1Rh}$ = $^2J_{P1P2}$ = 109.0 Hz, P^1) and 26.6 (d, $^2J_{P3P2}$ = 55.0 Hz, P^3) for the dpmp ligand.

Complex **3(A)** reacted readily with $AuCl(SC_4H_8)$ at room temperature, giving the reddish brown complex **7** [{Cp*$RhCl_2$(dpmp-*P,P,P*)Au}$_2$]$(OTf)_2$. X-ray analysis confirmed that the molecular structure is fundamentally similar to that of **4**.[10] Complex **7** was directly generated from **1**, $AuCl(SC_4H_8)$ and dpmp in the presence of KPF_6.

Copper(I) chloride reacted with **3(A)** at room temperature, generating the orange complex [{Cp*$RhCl_2$(dpmp-*P,P,P*)Cu}$_2$]$(PF_6)_2$ (**8**). The ^{1}H NMR spectrum showed two doublets at δ = 1.08 and 1.20 ppm with an intensity ratio of 1:2 due to the Cp* protons, suggesting the presence of diastereomers arising from two chiral centers (the central P atom of dpmp). Crystals of **8(A)** were suitable for X-ray analysis. The structure, except for the presence of two Cl bridges, is essentially similar to those of **4** and **7**. The stereochemistry was confirmed as an $R_{P2}S_{P2*}/S_{P2}R_{P2*}$ pair (Figure 3). Thus complex **8(B)**, with the chemical shift of δ = 1.08, is assumed to be a diastereomer with an $R_{P2}R_{P2*}/S_{P2}S_{P2*}$ pair.

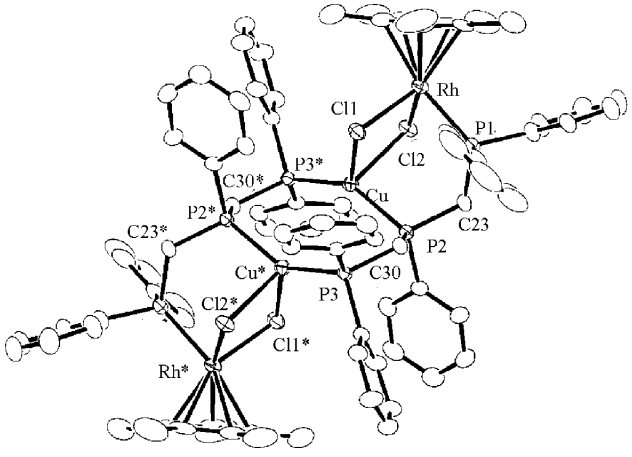

Figure 3. Molecular structure of **8**·$2CH_2Cl_2$; the OTf anions and CH_2Cl_2 molecules have been omitted for clarity and thermal ellipsoids have been drawn at the 50% probability level.

A one-pot synthesis from **1**, an excess of dpmp and CuCl in the presence of KPF_6 can also be used to prepare a mixture of the diastereomers of **8**. The BF_4 anion complex was obtained from the reaction of **1** with dpmp in the presence of $[Cu(MeCN)_4](BF_4)$.

 © 2004 Wiley-VCH Verlag GmbH & Co. KGaA, Weinheim

Complex **3(A)** was treated with S_8 at room temperature, affording an orange compound formulated from elemental analysis and FAB mass spectrometry as [Cp*RhCl(dpmp-*P,P,P*)S](PF_6) **9** (Scheme 4). The molecular structure is assumed to be consistent with addition of a S atom to the free terminal P^3 atom. This reaction is similar to the usual reaction of tertiary phosphanes with sulfur.

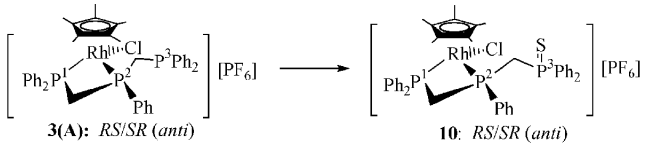

3(A): *RS/SR* (*anti*) **10**: *RS/SR* (*anti*)

Scheme 4. Reactions of **3(A)** with sulfur

The substitution reaction of **2(A)** with xylyl isocyanide (XylNC) in the presence of KPF_6 was unsuccessful, leading only to recovery of the starting materials. The reaction in the presence of Ag(OTf), however, gave [(Cp*RhCl)$_2$(dpmp-*P,P,P*)(XylNC)](OTf)$_2$ (**10**) (Scheme 5). The presence of a terminal isocyanide ligand was confirmed by appearance of a ν(N≡C) band at 2168 cm^{-1} and disappearance of a PF_6 band at ca. 850 cm^{-1}. The ^1H NMR spectrum exhibited two resonances at δ = 1.48(t) and 2.00(d) for the Cp* protons. The $^{31}P\{^1H\}$ NMR spectrum showed three resonances at δ = −15.5(ddd), −2.76(dd) and 28.6(dd) due to the P^2, P^1 and P^3 nuclei, respectively. These spectroscopic data suggest the structure depicted in Scheme 5. Since this complex has three chiral centers namely the two Rh centers and a P^2 atom, formation of two diastereomers was expected. However, no isomers were detected in the ^1H NMR spectrum. The stereochemistry for the chelating group in **10** was maintained, but the geometry around the other Rh center remains unknown.

Possible Pathway

A possible route to a hetero-nuclear complex from **1** consists of the initial formation of [Cp*RhCl(dpmp-*P,P*)]Cl **A**, followed by substitution of a Cl anion with the PF_6 or OTf anions to form **B** and AgCl (or KPF_6) (Scheme 6). This proposal was confirmed by the fact that in separate experiments, complex **A** was prepared by the reaction of **1** with an excess of dpmp, and subsequently treated with KPF_6, generating **3**. The next process is the coordination of the resultant AgCl to the free P atom of **3**, generating an intermediate **C**.

This type of species has been isolated as [Cp*IrCl(dpmp-*P,P,P*)AuCl](PF$_6$)[12] or [(C$_6$Me$_6$)Ru(dpmp-*P,P,P*)AuCl](PF$_6$)[10] by the reactions of [Cp*IrCl(dpmp-*P,P*)](PF$_6$) or [(C$_6$Me$_6$)Ru(dpmp-*P,P*](PF$_6$) with AuCl(SC$_4$H$_8$). Finally, dimerization of **D** resulting in a nucleophilic attack of the Cl anion to the Rh atom led to formation of tetranuclear complexes.

Molecular Structures

Crystal Structure of 5: A perspective drawing of **5** with the atomic numbering scheme is given in Figure 2, and selected bond lengths and angles are listed in Table 1. The dpmp ligand acts as a tridentate ligand. The average

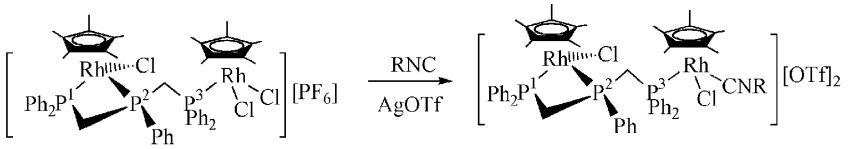

2(A): *RR/SS* (*anti*) **11** (*anti*)

Scheme 5. Reactions of **2(A)** with xylyl isocyanide in the presence of AgOTf

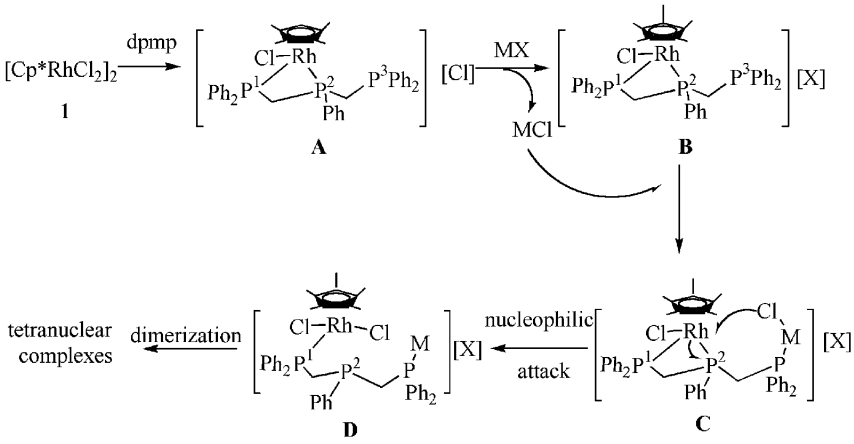

Scheme 6. Possible pathway for the formation of the hetero-tetranuclear complexes, where MX = AgOTf, [Cu(MeCN)$_4$](PF$_6$) or AuCl(SC$_4$H$_8$) and MCl = AgCl, CuCl or AuCl.

 © 2004 Wiley-VCH Verlag GmbH & Co. KGaA, Weinheim

P−Rh−P bite angle has a typical value of 70.9°, except for the P(1)−Rh−P(3) bite angle of 95.2°. The latter wide angle is a result of an unrestrained angle by a methylene chain. The Rh(1)−P(3) length of 2.369(4) Å is longer by ca. 0.05 Å than the average value of other Rh−P bonds.

Structures of 4·H_2O and 8·2CH_2Cl_2: Perspective drawings of **4** and **8** with the atomic numbering scheme are given in Figure 1 and Figure 3, and selected bond lengths and angles are listed in Table 2 and Table 3. Complexes **4** and **8** contain one H_2O and two CH_2Cl_2 solvate molecules, respectively.

Complexes **4** and **8** both have a crystallographically imposed inversion center in the middle of the Ag···Ag* and Cu···Cu vectors like that in the Au···Au vector in **7**.[10] The eight $M_2P_4C_2$ rings (M = Ag, Au, Cu) adopt a chair form to relieve the steric repulsion of the phenyl groups. Each Cp*$RhCl_2$ moiety is connected by a terminal P^1 atom of the dpmp ligand. These compounds have two chiral centers (P^2 and P^{2*}). The priority order of the ligands is M > Ph > C^2 > C^1 for the central P^2 and P^{2*}atoms, where C^1 represents the methylene carbons between the P^1 and P^2 atoms and C^2 is another methylene carbon atom. Complexes **4** and **8** have been identified as the $R_{P2}S_{P2*}/S_{P2}R_{P2*}$ pairs, similarly to **7**.[10]

An Au···Au separation of 3.203(2) Å in **7** suggests the presence of a weak interaction between the two Au centers.[10] However, the measured Ag···Ag separation of 3.385 Å in **4** suggests the absence of a metal−metal bond, since the Ag^I−Ag^I separations of 3.162−3.223 Å in [Ag_3{HC(PPh_2)$_3$}] have also suggested the absence of metal-metal bonds.[14] In comparison, [Ag_2(dpmp)$_2$](NO_3)$_2$, which is considered to have an Ag−Ag bond has an Ag−Ag separation of 3.085(1) Å.[15] A Cu···Cu separation of 3.566 Å in **8** is indicative of the absence of a metal-metal bond.

Since the M···Cl separations of 2.709 and 2.911 Å in **4** [M = Ag], and of 3.05 and 3.15 Å in **7** [M = Au] are longer than those found in each of the M−Cl-bridged bonds,[16] the Ag atoms are two-coordinate and are surrounded by two P atoms (a terminal P^{3*} atom from a dpmp ligand and a central P^2 atom from another dpmp). The P(2)−M−P(3)* angles are 150.3(1)° for **4** and 164.6(1)° for **7**, bent from the linear array to the reverse side against another Ag atom. The Cu···Cl(1) separation of 2.443 Å can be compared with the bridged Cu−Cl bond lengths of 2.448(3) Å in [$Ir_2(H)_4Cu(CO)_2$(μ-Cl)Cl(μ-dpma)$_2$]$^+$ [17] and another Cu···Cl(2) separation of 2.568 Å can be assumed to be a weak interaction, although it is somewhat longer. These Cu···Cl interaction cause the P(2)−Cu−P(3)* angle [145.77(7)°] to be more acute than those found in other complexes.

Table 1. Selected bond lengths and angles for [Cp*Rh(dpmp-*P,P,P*)]($OTf)_2$ (**5**)

Rh(1)−P(1)	2.324(3)	Rh(1)−P(2)	2.310(3)	Rh(1)−P(3)	2.369(4)
P(1)−C(41)	1.83(1)	P(2)−C(41)	1.81(1)	P(2)−C(42)	1.82(1)
P(3)−C(42)	1.83(1)				
P(1)−Rh(1)−P(2)	71.0(1)	P(1)−Rh(1)−P(3)	95.2(1)	P(2)−Rh(1)−P(3)	70.7(1)
Rh(1)−P(1)−C(41)	95.8(4)	P(1)−C(41)−P(2)	95.2(5)	Rh(1)−P(2)−C(42)	96.7(4)
P(2)−C(42)−P(3)	95.9(5)	C(41)−P(2)−C(42)	104.7(5)		

Table 2. Selected bond lengths and angles for [{Cp*RhCl(dpmp-*P,P,P*)Ag}$_2$]($PF_6)_2$·H_2O (**4**·H_2O)

Ag(1)−Cl(2)	2.706(3)	Ag(1)−P(2)	2.433(3)	Ag(1)−P(3)*	2.392(3)
Rh(1)−Cl(1)	2.425(3)	Rh(1)−Cl(2)	2.441(3)	Rh(1)−P(1)	2.327(3)
P(1)−C(13)	1.85(1)	P(2)−C(13)	1.85(1)	P(2)−C(20)	1.84(1)
P(3)−C(20)	1.84(1)				
Cl(2)−Ag(1)−P(2)	88.32(9)	Cl(2)−Ag(1)−P(3)*	120.2(1)	P(2)−Ag(1)−P(3)*	150.3(1)
Cl(1)−Rh(1)−Cl(2)	89.5(1)	Cl(1)−Rh(1)−P(1)	87.7(1)	Cl(2)−Rh(1)−P(1)	92.7(1)
Ag(1)−Cl(2)−Rh(1)	98.8(1)	Rh(1)−P(1)−C(13)	119.9(4)	P(1)−C(13)−P(2)	120.5(6)
Ag(1)−P(2)−C(13)	112.1(4)	Ag(1)−P(2)−C(20)	112.5(4)	P(2)−C(20)−P(3)	112.3(5)
Ag(1)−P(3)−C(20)	116.6(4)				
Ag(1)···Ag(1)	3.385(2)				

Table 3. Selected bond lengths and angles for [{Cp*$RhCl_2$(dpmp-*P,P,P*)Cu}$_2$]($PF_6)_2$·2CH_2Cl_2 (**8**·2CH_2Cl_2)

Cu−Cl(1)	3.443(2)	Cu−Cl(2)	2.568(2)	Cu−P(2)	2.249(2)
Cu−P(3)*	2.235(2)	Rh−Cl(1)	2.421(2)	Rh−Cl(2)	2.440(2)
Rh−P(1)	2.329(2)	P(1)−C(23)	1.836(7)	P(2)−C(23)	1.851(7)
P(2)−C(30)	1.839(7)	P(3)−C(30)	1.840(7)		
Cl(1)−Cu−Cl(2)	85.61(6)	Cl(1)−Cu−P(2)	92.02(6)	Cl(1)−Cu−P(3)*	118.80(7)
Cl(2)−Cu−P(2)	95.28(6)	Cl(2)−Cu−P(3)*	101.20(6)	P(2)−Cu−P(3)*	145.77(7)
Cl(1)−Rh−Cl(2)	88.99(6)	Cl(1)−Rh−P(1)	89.63(6)	Rh−Cl(1)−Cu	93.77(7)
Rh−Cl(2)−Cu	90.29(6)	Rh−P(1)−C(23)	101.0(3)	P(1)−C(23)−P(2)	120.0(4)
Cl(2)−Rh(1)−P(1)	88.1(2)				

 © 2004 Wiley-VCH Verlag GmbH & Co. KGaA, Weinheim

The M−P lengths increase with M in the order Cu, Au and Ag in accordance with the atomic radii of the metals. The Cl(1)−Rh−Cl(2) and Cl−Rh−P(1) angles which are in the range 87.3−92.7°are nearly perpendicular as a result of the octahedral core. The Rh−Cl bond lengths in the range 2.417−2.440 Å are typical.

Conclusion

The chemistry of dpmp has been limited to square-planar complexes of palladium, platinum and rhodium as well as two coordinate complexes of silver and gold. In this paper the chemistry of dpmp has been extended to the octahedral geometry. Pentamethylcyclopentadienyl rhodium(III) complexes bearing a dpmp ligand may be useful in the strategic synthesis of hetero-polynuclear compounds, where the cluster core could be tuned by the choice of the additional metal complex.

Experimental Section

All procedures were carried out under a nitrogen atmosphere. Dichloromethane was distilled from CaH_2 and diethyl ether was distilled from $LiAlH_4$. Isocyanides,[18] $(Ph_2PCH_2)_2PPh$,[19] $[Cp^*RhCl_2]_2$,[20] and $[Cu(MeCN)_4](BF_4)$[21] were prepared according to the literature. Infrared and electronic absorption spectra were recorded on FT/IR-5300 and U-best30 instruments, respectively. NMR spectra were recorded on a JEOL JNM-ECL-400 spectrometer. ^1H NMR spectra were measured at 400 MHz and $^{31}P\{^1H\}$ NMR spectra were measured at 161 MHz using 85% H_3PO_4 as an external reference.

Supporting Information: See also the footnote on the first page of this article. (a) Preparation of [(Cp*RhCl)(dpmp-*P,P,P*)(RhCl$_2$-Cp*)](PF$_6$) (**2**). (b) Preparation of [Cp*RhCl(dpmp-*P,P*)](PF$_6$) (**3**). (c) Preparation of [{Cp*RhCl$_2$(dpmp-*P,P,P*)Au}$_2$](PF$_6$)$_2$ (**7**). (c) Crystal structures of **2(B)**·CH_2Cl_2 and **3(A)**. (d) Table S1. Crystal data for [{Cp*$_2$Rh$_2$Cl$_3$(dpmp-*P,P,P*)}(OTf)$_2$·CH_2Cl_2 **2(B)**·CH_2Cl_2, [Cp*Rh(dpmp-*P,P*)](PF$_6$) **3(A)**, and [{Cp*RhCl$_2$(dpmp-*P,P,P*)Au}$_2$](PF$_6$)$_2$ (**7**). (e) Table S2. Selected bond lengths and angles for [Cp*$_2$Rh$_2$Cl$_3$(dpmp-*P,P,P*)](PF$_6$)·CH_2Cl_2 **2(B)**. (f) Table S3. Selected bond lengths and angles for [Cp*RhCl(dpmp-*P,P*)](PF$_6$) **3(A)**. (g) Table S4. Selected bond lengths and angles for [{Cp*RhCl$_2$(dpmp-*P,P,P*)Au}$_2$](PF$_6$)$_2$ (**7**). (h) Figure S1. ORTEP for **2(B)**. (i) Figure S2. ORTEP for 3(A). (j) Figure S3. ORTEP for **7**.

Preparation of [{Cp*RhCl$_2$(dpmp-*P,P,P*)Ag}$_2$](OTf) (4): A mixture of **1** (52.8 mg, 0.085 mmol), dpmp (107.5 mg, 0.212 mmol) and Ag(OTf) (61.4 mg, 0.239 mmol) was stirred in CH_2Cl_2 (15 mL) and acetone (10 mL) at room temperature. After 4 h the solvent was removed and the solids were washed with diethyl ether and the residue was extracted with CH_2Cl_2. The CH_2Cl_2 solution was concentrated, and diethyl ether was added to give reddish orange crystals (124.0 mg, 67.5%). UV/Vis (CH_2Cl_2): λ_{max} = 392 nm. ^1H NMR ($CDCl_3$): δ = 1.25 (d, $J_{H,P}$ = 3.5 Hz, Cp*), 1.90, 2.82, 3.13, 3.48 (m, CH_2), 5.32 (s, CH_2Cl_2), 6.8−8.2 (m, Ph). The $^{31}P\{^1H\}$ NMR ($CDCl_3$): δ = 28.6 (J_{PRh} = 146, $J_{P,P}$ = 12.9 Hz, P1), 2.6 (m, the other P nuclei), −143.6 (sept, J_{PF} = 707.5 Hz, PF_6).

Preparation of [Cp*Rh(dpmp-*P,P,P*)](OTf)$_2$ (5): A mixture of **3** (50 mg, 0.054 mmol) and AgOTf (75.4 mg, 0.293 mmol) in CH_2Cl_2 (15 mL) and acetone (5 mL) was stirred at room temperature. After 3 h, the solvent was removed and the residue was extracted with CH_2Cl_2. The solution was concentrated and diethyl ether was added to form orange crystals (41.8 mg, 72.4%). IR (nujol): $\tilde{\nu}$ = 1255, 1153, 1028 cm^{-1} (OTf). UV/Vis (CH_2Cl_2): λ_{max} = 335, 270 nm. ^1H NMR [$(CD_3)_2CO$]: δ = 1.66 (q, J_{PH} = 4.5 Hz, Cp*, 15 H), 5.49 (c, CH_2, 4 H), 7.3−8.4 (c, Ph, 25 H). $^{31}P\{^1H\}$ NMR [$(CD_3)_2CO$]: δ = −18.2 (dt, J_{P1P2} = J_{P1Rh} = 97.2 Hz, P^1), −47.4 (q, J_{P2P1} = J_{P2Rh} = 97.2 Hz, P^2), −143.6 (sept, J_{PF} = 707.5 Hz, PF_6). $C_{44}H_{44}F_6O_6P_3RhS_2$ (1042.8): calcd. C 50.68, H 4.25; found C 50.99, H 4.38.

Preparation of [Cp*RhCl(dpmp-*P,P,P*)RuCl$_2$(*p*-cymene)](PF$_6$) (6)

(1) From 3(A) and [(*p*-Cymene)RuCl$_2$]$_2$: A mixture of **3(A)** (50.4 mg, 0.054 mmol) and [(*p*-cymene)$RuCl_2$]$_2$ (19.3 mg, 0.032 mmol) was stirred in CH_2Cl_2 (10 mL) at room temperature for 5 h. The solution was concentrated to ca. 3 mL and diethyl ether was added, affording the yellow complex **6(A)** (43.6 mg, 65.6%). UV/Vis (CH_2Cl_2): λ_{max} = 361 nm. IR (nujol): $\tilde{\nu}$ = 837 cm^{-1}. FAB MS: *m*/*z* = 1085 ($[M]^+$). ^1H NMR ($CDCl_3$): δ = 0.53 (d, $J_{H,H}$ = 7.0 Hz, *i*Pr, 3 H), 1.00 (d, $J_{H,H}$ = 7.0 Hz, *i*Pr, 3 H), 1.52 (t, $J_{H,H}$ = 3.5 Hz, Cp*, 15 H), 1.75 (s, *p*-Me, 3 H), 2.41 (sept, $J_{H,H}$ = 7.0 Hz, *i*Pr, 1 H), 4.06 (c, CH_2, 2 H), 3.72 (c, CH_2, 1 H), 4.92 (c, CH_2, 1 H), 5.33, 5.44 (AB system, $J_{H,H}$ = 6.0 Hz, *p*-cymene), 6.8−8.4 (m, ph, 25 H). $^{31}P\{^1H\}$ NMR ($CDCl_3$): δ = −12.0 (dt, $^1J_{RhP2}$ = $^2J_{P2P1}$ = 97.0, $^2J_{P2P3}$ = 55.5 Hz, P^2), −1.41 (t, $^1J_{P1Rh}$ = $^2J_{P1P2}$ = 97.0 Hz, P^1) and 23.7 (d, $^2J_{P3P2}$ = 55.5 Hz, P^3), −143.5 (sept, J_{PF} = 707.5 Hz, PF_6).

(2) Direct Reaction: A mixture of $[Cp^*RhCl_2]_2$ (50.0 mg, 0.081 mmol), [(*p*-cymene)$RuCl_2$]$_2$ (50.9 mg, 0.083 mmol), dpmp (94.4 mg, 0.186 mmol) and KPF_6 (43.1 mg, 0.234 mmol) was stirred in CH_2Cl_2 (10 mL) and acetone (10 mL) at room temperature. After 20 h, the solution was evaporated to dryness and the residue extracted with CH_2Cl_2. The CH_2Cl_2 solution was concentrated to ca. 2 mL and diethyl ether was added, affording orange crystals (45.8 mg, 52.1%). The crystals were mainly isolated as the diastereomer **6(B)** based on the NMR spectrum. The ratio of **6(A)** to **6(B)** was 1:2.

6(B): ^1H NMR ($CDCl_3$): δ = 0.52 (d, $J_{H,H}$ = 7.0 Hz, *i*Pr, 3 H), 1.05 (d, $J_{H,H}$ = 7.0 Hz, *i*Pr, 3 H), 1.73 (t, $J_{H,H}$ = 4.0 Hz, Cp*, 15 H), 1.80 (s, *p*-Me, 3 H), 2.33(sept, $J_{H,H}$ = 7.0 Hz, *i*Pr, 1 H), 2.69 (dt, $J_{H,H}$ = 16.0, J_{PH} = J_{PH} = 12.0 Hz, CH_2, 1 H), 3.67 (dt, $J_{H,H}$ = 16.0, J_{PH} = J_{PH} = 12.0 Hz, CH_2, 1 H), 4.01 (ddd, $J_{H,H}$ = 16.0, J_{PH} = 7.0, $J_{P'H}$ = 4.0 Hz, CH_2, 1 H), 4.30 (ddd, $J_{H,H}$ = 16.0, J_{PH} = 7.0, J_{PH} = 4.0 Hz, CH_2, 1 H), 4.68, 5.20 (AB system, $J_{H,H}$ = 5.5 Hz, *p*-cymene), 7.0−8.5 (m, ph, 25 H). $^{31}P\{^1H\}$ NMR ($CDCl_3$): δ = −13.8 (dt, $^1J_{RhP2}$ = $^2J_{P2P1}$ = 105, $^2J_{P2P3}$ = 55.0 Hz, P^2), −10.2 (t, $^1J_{P1Rh}$ = $^2J_{P1P2}$ = 109.0 Hz, P^1) and 26.6 (d, $^2J_{P3P2}$ = 55.0 Hz, P^3), −143.5 (sept, J_{PF} = 707.5 Hz, PF_6).

Preparation of [{Cp*Rh(μ-Cl)$_2$(dpmp-*P,P,P*)Cu}$_2$](PF$_6$)$_2$ (8)

(1) One-Pot Synthesis: A mixture of **1** (32.9 mg, 0.053 mmol), dpmp (60.8 mg, 0.12 mmol) and CuCl (56.1 mg, 0.175 mmol) was stirred in CH_2Cl_2 (5 mL) and acetone (5 mL) for 24 h. The solvent was then removed and the residue extracted with CH_2Cl_2. The solution was concentrated to ca. 3 mL and diethyl ether was added, affording red crystals (47.6 mg, 43.7%).

(2) From 3: Complex **8** (16.9%) was prepared from **3(A)** and CuCl. UV/Vis (CH_2Cl_2): λ_{max} = 387, 235 nm. IR (nujol): $\tilde{\nu}$ = 835 cm^{-1}.

 © 2004 Wiley-VCH Verlag GmbH & Co. KGaA, Weinheim

^{1}H NMR (CD_2Cl_2): δ = 1.10 (d, $J_{H,P}$ = 3.5 Hz), 1.26 (d, J_{PH} = 3.5 Hz, Cp*), 2.1−3.3 (m, CH_2), 6.9−8.05 (c, Ph). $C_{84}H_{88}Cl_4Cu_2F_{12}P_8Rh_2$·1/2$CH_2Cl_2$ (2090.6): calcd. C 48.55, H 4.29; found C 48.52, H 4.25.

Preparation of [{Cp*Rh(μ-Cl)$_2$(dpmp-*P,P,P*)Cu}$_2$](BF$_4$)$_2$: The BF_4 anion complex (11.1%) was prepared from **1** (0.051 mmol), dpmp (0.011 mmol) and [Cu(MeCN)$_4$](BF_4) (0.13 mmol). The complex was established as a BF_4 anion analog of **8** by comparison with the ^{1}H NMR spectrum of **8**.

Preparation of [Cp*RhCl(dpmp=S)](PF$_6$) (9): A mixture of **3(A)** (50.9 mg, 0.055 mmol) and S_8 (7.8 mg, 0.030 mmol) was stirred in CH_2Cl_2 (5 mL) at room temperature. After 51 h, the solvent was removed under reduced pressure. After the residue was extracted with CH_2Cl_2, the solution was concentrated to ca. 2 mL, and diethyl ether was added, affording a yellow powder (16.7 mg, 31.7%). UV/Vis (CH_2Cl_2): λ_{max} = 359, 260 (sh) nm. IR (nujol): $\tilde{\nu}$ = 837 cm^{-1} (PF_6). FAB MS: *m*/*z* = 811 ([M]$^+$). ^{1}H NMR ($CDCl_3$): δ = 1.64 (t, $J_{H,P1}$ = J_{HP2} = 4.0 Hz, Cp*, 15 H), 4.3−4.9 (m, CH_2, 2 H), 6.8−8.1 (c, Ph, 25 H). ^{31}P{^{1}H} NMR ($CDCl_3$): δ = 35.6 (d, J_{P3P2} = 31.5 Hz, P^3), 0.92 (dd, J_{P1Rh} = 114.0, J_{P1P2} = 94.0 Hz, P1), −15.5 (ddd, J_{RhP2} = 114.0, J_{P2P3} = 31.5, J_{P2P1} = 94.0 Hz, P2), −143.6 (sept, J_{PF} = 707.5 Hz, PF_6). $C_{42}H_{44}ClF_6P_4RhS$ (957.1): calcd. C 49.56, H 4.45; found C 49.71, H 4.53.

Preparation of [{Cp*RhCl}(dpmp-*P,P,P*){RhCl(XylNC)Cp*}](OTf)$_2$ (10): To a mixture of **3(A)** (50.6 mg, 0.045 mmol) and Ag(OTf) (27.4 mg, 0.167 mmol) in CH_2Cl_2 (10 mL) and acetone (5 mL) was added XylNC (13.9 mg, 0.107 mmol) at room temperature. After the reaction mixture was stirred for 24 h usual workup of the mixture gave orange crystals of **10** (35.2 mg, 52.3%). IR (nujol): $\tilde{\nu}$ = 2168 cm^{-1} (N≡C). UV/Vis (CH_2Cl_2): λ_{max} = 342 nm. ^{1}H NMR ($CDCl_3$): δ = 1.48 (t, J_{PH} = 4.0 Hz, Cp*, 15 H), 1.56 (d, $^2J_{PH}$ = 3.8 Hz, Cp*, 15 H), 2.00 (s, *o*-Me, 6 H), 4.10 (m, CH_2, 1 H), 4.51 (m, CH_2, 1 H), 4.90 (m, CH_2, 2 H), 6.8−8.0 (c, 25 H). ^{31}P{^{1}H} NMR ($CDCl_3$): δ = 28.6 (dd, $^1J_{RhP3}$ = 122.2, $^2J_{P3P2}$ = 50.1 Hz, Rh(CNR)−P, P^3), −2.76 (dd, $^1J_{RhP1}$ = 113.1, $^2J_{P2P1}$ = 98.0 Hz, RhCl−P, P^1), −15.3 (ddd, $^1J_{RhP2}$ = 111.1, $^2J_{P2P1}$ = 98.0, $^2J_{P2P3}$ = 50.1 Hz, RhCl−P, P^2). $C_{63}H_{68}Cl_2F_6NO_6P_3Rh_2S_2$ (1483.0): calcd. C 50.02, H 4.62, N 0.94; found C 50.11, H 4.71, N 1.13.

Preparation of [(Cp*RhCl)(dpmp-*P,P*)]Cl (A): A mixture of [Cp*$RhCl_2$]$_2$ (30.5 mg, 0.049 mmol) and dpmp (55.2 mg, 0.109 mmol) in CH_2Cl_2 (10 mL) was stirred at room temperature for 24 h. After the removal of the solvent, the residue was washed with diethyl ether and crystallized from CH_2Cl_2 and diethyl ether to give orange crystals (28.8 mg, 36.0%). FAB MS: *m*/*z* = 780 [M$^+$]. UV/Vis (CH_2Cl_2): λ_{max} = 356, ca. 270 (sh) nm. ^{1}H NMR ($CDCl_3$): δ = 1.81 (t, *J* = 3.8 Hz, Cp*, 15 H), 3.47 (m, CH_2, 2 H), 4.24 (m, CH_2, 1 H), 5.30 (s, CH_2Cl_2), 5.49 (m, CH_2, 1 H), 7.0−7.7 (c, 25 H). ^{31}P{^{1}H} NMR ($CDCl_3$): δ = −5.10 ppm (dd, J_{P3Rh} = 115.6, J_{P2P3} = 99.0 Hz, RhCl−P, P^3), −11.0 (ddd, J_{P2Rh} = 114.1, J_{P2P3} = 99.0, J_{P2P1} = 46.5 Hz, RhCl−P, P^2), −29.4 (d, J_{P1P2} = 46.5 Hz, CH_2P, P^1). $C_{42}H_{44}Cl_2P_3Rh$·3/4CH_2Cl_2 (879.2): calcd. C 58.40, H 5.22; found C 58.03, H 5.47. The structure is assumed to be similar to that of **3(B)**, based on the ^{1}H NMR spectrum.

Reaction of 2(A) with Xylyl Isocyanide: A mixture of **2(A)** (50 mg, 0.041 mmol) and xylyl isocyanide (26.9 mg, 0.205 mmol) was heated to reflux in acetone (15 mL). After 5 h, the solvent was removed and the residue was extracted with CH_2Cl_2. The solution was concentrated and diethyl ether was added, affording a dark brown solid of [Cp*$RhCl_2$(XylNC)] (30 mg, 78%). Workup of the mother liquor gave **3(A)** (10.3 mg, 57.2%).

X-ray Data Collection: All complexes were recrystallized from CH_2Cl_2/diethyl ether. The cell constants for **5** were determined from 20 reflections on a Rigaku four-circle automated diffractometer AFC5S. Data collection was carried out using a Rigaku AFC5S diffractometer. Intensities were measured by the 2θ−ω scan method using Mo-K_α radiation (λ = 0.71069).

Table 4. [{Cp*$RhCl_2$(dpmp-*P,P,P*)Ag}$_2$](OTf)$_2$·H_2O (**4**·H_2O), [Cp*Rh(dpmp-*P,P,P*)](OTf)$_2$ (**5**), and [{Cp*$RhCl_2$(dpmp-*P,P,P*)-Cu}$_2$](OTf)$_2$·2CH_2Cl_2 (**8**)

Complex	**4**·H_2O[a]	**5**[b]	**8**·2CH_2Cl_2[a]
Empirical formula	$C_{86}H_{88}Ag_2Cl_4F_6O_7P_6Rh_2S_2$	$C_{44}H_{44}F_6O_6P_3RhS_2$	$C_{86}H_{92}Cl_8Cu_2F_{12}P_8Rh_2$
Formula mass	2160.95	1042.77	2217.97
Crystal system	orthorhombic	triclinic	monoclinic
Space group	*Pccn* (no. 46)	*P*1 (no. 2)	$P2_1/c$ (no. 14)
a /Å	31.7839(7)	12.725(10)	13.573(1)
b /Å	14.632(3)	18.23(2)	13.1107(5)
c /Å	19.9580(7)	10.90(1)	25.2635(6)
α /°	90	99.54(10)	90
β /°	90	101.70(9)	103.74(2)
γ /°	90	107.63(6)	90
V	5648(1)	2289(3)	4227(2)
Z	4	2	2
$D_{calcd.}$ /gcm^{-3}	1.546	1.513	1.643
μ(Mo-K_α) /cm^{-1}	10.89	6.39	12.79
$2\theta_{max}$	55.0	50.0	55.0
No. measured (unique)	10851	8036	10231
No. observed	5923 [$I > 3.0\sigma(I)$]	2864 [$I > 2.0\sigma(I)$]	6807 [$I > 3.0\sigma(I)$]
No. variable	523	559	532
R; *Rw*	0.090; 0.114[c]	0.062; 0.075[c]	0.155; 0.207[d]
*R*1	0.090(5923 ref)	0.062	0.074(4155 ref)
GOF	3.22	1.09	2.13

[a] Measured on a Quantum CCD Rigaku AFC7 instrument. [b] Measured on a Rigaku AFC5S instrument. [c] $R = \Sigma||F_o| - |F_c||/\Sigma|F_o|$, $R_w = (\Sigma\omega(|F_o| - |F_c|)^2/\Sigma\omega F_o^2)^{1/2}$ and $R1 = \Sigma||F_o| - |F_c||/\Sigma|F_o|$ for $I > 3.0\sigma(I)$. [d] $R = \Sigma(F_o^2 - F_c^2)/\Sigma F_o^2$, $R_w = (\Sigma\omega F_o^2 - F_c^2)^2/\Sigma\omega(F_o^2)]^{1/2}$ and $R1 = \Sigma||F_o| - |F_c|| /\Sigma|F_o|$ for $I > 2.0\sigma(I)$.

 © 2004 Wiley-VCH Verlag GmbH & Co. KGaA, Weinheim

Throughout the data collection the intensities of the three standard reflections were measured after every 200 reflections as a check of the stability of the crystals and no decay was observed. Absorption corrections were made using the ψ scan methods.

The measurements for **4**·H_2O and **8**·$2CH_2Cl_2$ were made on an MSC/ADSC Quantum CCD/Rigaku AFC7 diffractometer, using Mo-K_α radiation at 0 °C under a cold nitrogen stream. Four preliminary data frames were measured at 0.5° increments of ω in order to assess the crystal quality and preliminary unit cell parameters were calculated. The cell parameters were refined using all reflections measured in the range $2.8° < 2\theta < 40°$. The intensity images were measured at 0.5° intervals of ω for a duration of 20 s. The frame data were integrated using the d*TREK program package, and the data sets were corrected for absorption using the REQAB program.

The crystal parameters along with the details of the data collections are summarized in Table 4. Intensities were corrected for Lorentz and polarization effects. Atomic scattering factors were taken from the usual tabulation of Cromer and Waber.[22] Anomalous dispersion effects were included in F_{calcd};[23] the values of $\Delta f'$ and $\Delta f''$ were those of Creagh and McAuley.[24] All calculations were performed using the teXsan crystallographic software package.[25]

Determination of the Structures: All complexes were solved by direct methods (SIR92) except **7** which was solved by Patterson methods (DIRDIF94 PATTY) . The non-hydrogen atoms of all complexes were refined anisotropically using full-matrix least-squares based on F^2 or F values. All hydrogen atoms were calculated in ideal positions with a C−H distance of 0.95 Å. The crystal data are listed in Table 4.

CCDC-190355 for **4**·H_2O, -213525 for **5** and -190357 for **8**·$2CH_2Cl_2$ contain the supplementary crystallographic data for this paper. These data can be obtained free of charge at www.ccdc.cam.ac.uk/conts/retrieving.html [or from the Cambridge Crystallographic Data Centre, 12 Union Road, Cambridge CB2 1EZ, UK; Fax: (internat.) + 44-1223-336-033; E-mail: deposit@ccdc.cam.ac.uk].

Acknowledgments

The authors would like to thank Professor Shigetoshi Takahashi and Dr Fumie Takei of The Institute of Scientific and Industrial Research, Osaka University for performing the FAB mass spectrometry measurements. This work was partially supported by a Grant-in Aid for Scientific Research from the Ministry of Education, Science, Culture and Sports, Japan.

[1] A. P. Balch, *Homogeneous Catalysis with Metal Phosphane Complexes* (Ed.: L. H. Pignolet). Plenum Press: New York, **1983**, p. 167 and references cited therein.
[2] T. Tanase, Y. Yamamoto, *Trends Organomet. Chem.* **1999**, 35 and references cited therein.
[3] H. Suzuki, N. Tajima, K. Tatsumi, Y. Yamamoto, *Chem. Commun.* **2000**, 1801−1802.
[4] Y. Yamamoto, H. Suzuki, N. Tajima, K. Tatsumi, *Chem. Eur. J.* **2002**, *8*, 372.
[5] Y. Yamamoto, H. Nakamura, J.-F. Ma, *J. Organomet. Chem.* **2001**, *640*, 10.
[6] K. K. Klausmeyer, T. B. Rauchfuss, S. R. Wilson, *Angew. Chem.* **1998**, *110*, 1808; *Angew. Chem. Int. Ed.* **1998**, *37*, 1694.
[7] S. M. Contakes, K. K. Klausmeyer, R. M. Milberg, S. R. Wilson, T. B. Rauchfuss, *Organometallics* **1998**, *17*, 3633.
[8] D. J. Darensbourg, W.-Z. Lee, M. J. Adams, D. L. Larkins, J. H. Reibenspies, *Inorg. Chem.* **1999**, *38*, 1378.
[9] S. M. Contakes, K. K. Klausmeyer, T. B. Rauchfuss, *Inorg. Chem.* **2000**, *39*, 2069.
[10] Y. Kosaka, Y. Shinozaki, Y. Tsutsumi, Y. Kaburagi, Y. Yamamoto, Y. Sunada, K. Tatsumi, *J. Organomet. Chem.* **2003**, *671*, 8.
[11] In the $^{31}P\{^1H\}$ NMR spectra of the binuclear complexes in ref.[10] the chemical shifts of the P^3 nuclei have been erroneously assigned as $\delta = -28.1$ for an *anti*-form and at $\delta = -30.1$ for a *syn*-form. The correct values are $\delta = 28.1$ and 30.1 ppm, respectively.
[12] Y. Kosaka, Y. Yamamoto, unpublished result.
[13] P. Dierkes, P. W. N. van Leeuwen, *J. Chem. Soc., Dalton Trans.* **1999**, 1519.
[14] C.-M. Che, H.-K. Yip, V. W.-W. Yam, P.-Y. Cheung, T.-F. Lai, S.-J. Shieh, S.-M. Peng, *J. Chem. Soc., Dalton Trans.* **1992**, 427.
[15] D. M. Ho, R. Bau, *Inorg. Chem.* **1983**, *22*, 4073.
[16] A. L. Balch, M. Ghedini, D. E. Oram, P. R. Reedy, Jr., *Inorg. Chem.* **1987**, *26*, 1223.
[17] A. L. Balch, B. J. Davis, F. Neve, M. M. Olmstead, *Organometallics* **1989**, *8*, 1000.
[18] H. M. Walborsky, G. E. Niznik, *J. Org. Chem.* **1972**, *37*, 187.
[19] R. Appel, K. Geisler, H. F. Schöler, *Chem. Ber.* **1979**, *112*, 648.
[20] C. White, A. Yates, P. M. Maitlis, *Inorg. Synth.* **1992**, *29*, 228.
[21] G. J. Kubas, *Inorg. Synth.* **1979**, *19*, 90.
[22] D. T. Cromer, J. T. Waber, *International Tables for X-ray Crystallography*, Kynoch, Birmingham (England), **1974**, Table 2.2A.
[23] J. A. Ibers, W. C. Hamilton, *Acta Crystallogr.* **1964**, *17*, 718.
[24] D. C. Creagh, W. J. McAulley, *International Tables for Crystallography*, Vol. C, Kluwer, Boston, **1992**, Table 4.2.6.8, pp. 219−222.
[25] *TEXSAN*: Crystal Structure Analysis Package, Molecular Structure Corporation Houston, TX, **1985** and **1992**.

Received June 26, 2003
Early View Article
Published Online October 23, 2003

 © 2004 Wiley-VCH Verlag GmbH & Co. KGaA, Weinheim

A Theoretical Study of the Exchange Coupling in Hydroxo- and Alkoxo-Bridged Dinuclear Oxovanadium(IV) Compounds

Antonio Rodríguez-Fortea,*[a,c] Pere Alemany,[b,c] Santiago Alvarez,[a,c] and Eliseo Ruiz[a,c]

Keywords: Exchange coupling / Density functional calculations / Magnetic properties / Magneto-structural correlations / Vanadium

A density functional study of exchange coupling in hydroxo- and alkoxo-bridged dinuclear oxovanadium(IV) compounds is presented. Coupling constants calculated for full unmodeled structures are in good agreement with experimentally reported values, confirming the ability of the computational strategy used in this work to predict the exchange coupling in dinuclear V^{IV} compounds. The influence of the configuration of the $[VO(\mu\text{-}OR)_2VO]^{2+}$ core in compounds with two edge-sharing octahedrally coordinated oxovanadium(IV) centers, of the nature of the terminal ligands and of structural distortions on the coupling constant have been analyzed through model calculations. The results indicate that the coupling constant is less affected by these factors than for hydroxo- and alkoxo-bridged Cu^{II} compounds. The calculations support the orbital models usually employed in qualitative interpretations of magneto-structural correlations, showing good correlations between the calculated coupling constants and the overlap between the two magnetic orbitals or the square of the orbital gap.

(© Wiley-VCH Verlag GmbH & Co. KGaA, 69451 Weinheim, Germany, 2004)

Introduction

The phenomenon of exchange coupling between the spins of unpaired electrons located at different metal atoms in polynuclear complexes leads to magnetic behaviors that differ completely from the one predicted for independent paramagnetic entities. Antiferromagnetic coupling results when the ground state presents an antiparallel alignment of the spins, whereas ferromagnetic coupling is a consequence of the alignment of the electron spins in a parallel manner. Since the discovery of intramolecular antiferromagnetic coupling in copper(II) acetate monohydrate in 1951,[1] much experimental and theoretical work has been carried out to elucidate the mechanism of exchange coupling in polynuclear complexes. This work has led to the now well-established field of molecular magnetism, that is, the synthesis and the study of the magnetic properties of materials based on molecular entities.[2−7]

Dinuclear systems have been the most studied compounds because of their relative simplicity, especially the family of Cu^{II} compounds. This ion, with a d^9 electronic configuration, presents only one unpaired electron per metal atom, and is therefore the simplest case for the analysis of magnetic properties. A large number of compounds with different bridges have been studied and interesting relationships between the magnetic properties and the structural parameters of the bridge have been established, especially for dihydroxo-bridged compounds.[8−12] Such magneto-structural correlations are very useful for predicting magnetic properties of new compounds.

Vanadium(IV) dinuclear complexes constitute another interesting family of compounds for the study of intramolecular exchange coupling since the electronic configuration of V^{IV} is d^1, thus having one unpaired electron per metal center as in Cu^{II} compounds. A considerable number of oxovanadium(IV) dimers have been characterized, since they play an important role in biological processes[13−21] and are also relevant in solid-state chemistry,[22−28] but the established magneto-structural correlations are much fewer than for dinuclear Cu^{II} complexes.

The main difference between the Cu^{II} and V^{IV} cations is in the orbitals in which the unpaired electron is placed. In octahedral or square-planar Cu^{II} systems the unpaired electron is occupying an orbital of the e_g set, with a large contribution of the $d_{x^2-y^2}$ metal orbital, whereas for V^{IV} the only occupied orbital is of t_{2g} symmetry, mainly a d_{xy} metal orbital, if the ligands are placed along the x and y axis and the oxygen atom of the vanadyl group along the z axis. As a consequence, the exchange mechanism in dinuclear Cu^{II} and in dinuclear V^{IV} compounds is expected to be different,

[a] Departament de Química Inorgànica, Universitat de Barcelona
Diagonal 647, 08028 Barcelona, Spain
Fax: (internat.) +34-93-490-7725
E-mail: antonio.rodriguez@qi.ub.es
[b] Departament de Química Física, Universitat de Barcelona
Diagonal 647, 08028 Barcelona, Spain
[c] Centre de Recerca en Química Teòrica (CeRQT), Parc Científic de Barcelona
Baldiri i Reixach 4−6, 08028 Barcelona, Spain

since the $d_{x^2-y^2}$ metal orbital is pointing directly towards the orbitals of the bridging ligands, thus favoring a superexchange mechanism, whereas the d_{xy} metal orbital does not point to orbital ligands, but to the other d_{xy} metal orbital, leading to direct σ overlap between them and resulting in a direct through-space exchange mechanism, as suggested by Ginsberg[29] and other authors.[16,30−33]

The aforementioned direct exchange mechanism is, however, not effective in all dinuclear V^{IV} compounds, since specific geometric arrangements exist in which a direct overlap between the orbitals that bear the unpaired electron (the so called magnetic orbitals) is not possible. A useful classification of the geometries of the $[VO(\mu\text{-}OR)_2VO]^{2+}$ cores in compounds built from two edge-sharing octahedrally coordinated oxovanadium(IV) centers has been given by Plass.[34] The arrangements are classified (i) according to the orientation of the V=O groups with respect to the bridging plane, that is the plane formed by the two vanadium centers and the two oxo bridging atoms (orthogonal, coplanar or twisted), and (ii) the relative orientation of the two V=O groups (*syn* or *anti*), as shown in **1**−**5**.

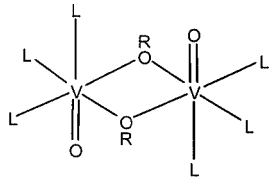

anti-orthogonal (**1**)

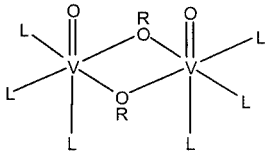

syn-orthogonal (**2**)

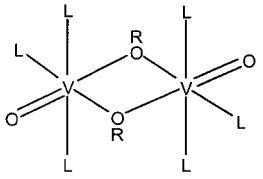

anti-coplanar (**3**)

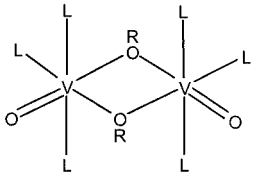

syn-coplanar (**4**)

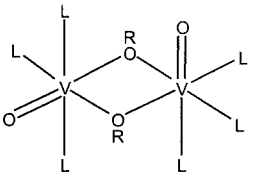

twisted (**5**)

Many dinuclear V^{IV} complexes have been reported in the two orthogonal[17,32,33,35−38] and the *anti*-coplanar configurations,[34,39−44] but the *syn*-coplanar[44,45] and the twisted arrangements[34,44] are not so frequent. There are also dinuclear V^{IV} complexes in which the metallic centers are five-coordinate in a square-pyramidal environment with the apical position occupied by the oxo group. In such a family of compounds, the classification of Plass can also be applied, the orthogonal geometries being the only possible ones.[16,20,36]

As far as the nature of the exchange coupling is concerned, it has been found that compounds with *anti*-orthogonal, *syn*-orthogonal or *syn*-coplanar configurations (**1**, **2** and **4**) present strong to moderate antiferromagnetic coupling, whereas compounds with *anti*-coplanar and twisted arrangements (**3** and **5**) show weak ferromagnetic coupling (Table 1). These experimental results have been interpreted in a qualitative way regarding the interaction between the magnetic orbitals of each center:[34] for the orthogonal configurations the direct (through-space) exchange mechanism is more effective than the superexchange pathway, and is the predominant mechanism of the exchange interaction. For *syn*-coplanar compounds, the direct exchange mechanism is not as effective as in orthogonal configurations and antiferromagnetic coupling can be qualitatively justified by considering the superexchange mechanism to be operative. For *anti*-coplanar and twisted configurations the situation is, however, different since neither mechanism seems to be effective in mediating the exchange interaction, resulting in a weak ferromagnetic coupling.[34]

Despite the large amount of experimental data for hydroxo- and alkoxo-bridged oxovanadium(IV) dinuclear complexes reported so far, theoretical studies of their magnetic properties are still rare.[34,46−49] Computation of exchange coupling constants for some structures within the density functional theory (DFT) framework has been reported by Plass, reproducing the nature of the coupling for *anti*-orthogonal (antiferromagnetic), *anti*-coplanar and twisted configurations (both ferromagnetic). Other DFT studies of the exchange interaction for hydroxo- and alkoxo-bridged oxovanadium(IV) dinuclear systems exist: (i) an analysis of the effects of the bridging V−O distance, the bridging V−O−V angle and the protonation of the bridging ligands on the coupling constant for a *syn*-coplanar core configuration,[47] and (ii) a study of the exchange interaction in the three phases of vanadyl pyrophosphate, by means of modelization with dinuclear molecular fragments.[48,49]

The aim of this contribution is to examine the exchange coupling phenomenon for hydroxo- and alkoxo-bridged oxovanadium(IV) dinuclear systems by applying a recently developed computational strategy that is able to quantitatively reproduce the coupling constants for a large variety of compounds with different bridging ligands and/or paramagnetic centers.[50−60] We will report first calculations of the exchange coupling constant for a variety of full nonmodeled structures to compare them directly with the experimental data. We will then extensively study the exchange coupling in hydroxo-bridged compounds by analyzing the influence of the $[VO(\mu\text{-}OH)_2VO]^{2+}$ core geometry on the coupling constant and studying magneto-structural correlations for distortions found in these systems. We will also study the effect of the nature of the terminal ligands on the coupling constant. Finally, we will analyze the effect that some of the aforementioned factors have on the coupling constant in the related alkoxo-bridged compounds.

 © 2004 Wiley-VCH Verlag GmbH & Co. KGaA, Weinheim

Table 1. Experimental exchange coupling constants for hydroxo- and alkoxo-bridged dinuclear V^{IV} complexes along with some of their most characteristic structural parameters: the bridging angle, V−O−V; the distance between the V atoms, V···V; the angle that measures the out-of-plane displacement of the H (or R) group from the bridging plane, τ (**7**); and the angle between the bridging plane and the plane formed by the V atom and the other two equatorially coordinated atoms, σ, defined in **6**

Compound	Bridge	Conf.	V−O−V (°)	V···V (Å)	τ (°)	σ (°)	J (cm^{-1})	Refcode	Ref.
A	OH	**1**	101.2	3.03	7.5	25.6	−354	CINKUF	[32]
B	OR	**1**	98.6	3.12	30.0	19.2	−336	DOTQAE	[37]
C	OR	**1**[a]	103.9	3.08	5.0	49.0	−214	PUTBAH	[20]
D	OH	**1**	103.2	3.12	39.2	19.4	−78	RELMAW	[35]
E	OR	**2**[b]	96.0[c]	2.95	37.7[c]	37.6[c]	−424	REPPOR	[36]
F	OH	**2**	98.1[c]	2.97	[d]	25.7[c]	−300	VAFZAD	[33]
G	OR	**2**	99.4[c]	3.08	5.1[c]	20.8[c]	−256	WARBIA	[38]
H	OH	**4**[e]	122.8	3.45	1.3	[f]	−334	YEYGAK	[45]
I	OR	**1**[b]	104.8[c]	3.11	3.1[c]	49.9[c]	−60	YIKZAT	[17]
J	OR	**3**	107.0	3.31	36.6	[f]	+3	ZUFXIH	[34]
K	OR	**5**	104.1[g]	3.22	29.0[g]	29.5	+10.6	ZUFXUT	[34]

[a] One metal ion is six-coordinate and the other one is five-coordinate. [b] The metal ions are five-coordinate. [c] The V−O−V, τ and σ angles are averages of the two different values found in each of these compounds. [d] The position of the H atoms has not been determined in the crystal structure. [e] The values for the structural parameters correspond to the bridge that is not in *trans* position with respect to the oxo ligand. [f] The σ angle is not defined for coplanar configurations. [g] Average of the two significantly different V−O−V (100.1 and 108.0°) and τ (44.1 and 13.8°) angles.

Computational Methodology

Since a detailed description of the computational strategy adopted in this work can be found elsewhere,[51,53,55,59] we will only briefly sketch its most relevant aspects here. Using a phenomenological Heisenberg Hamiltonian $\hat{H} = -J\hat{S}_1 \bullet \hat{S}_2$ to describe the exchange coupling in a dinuclear compound, where J is the coupling constant, and S_1 and S_2 the local spins on centers 1 and 2, respectively, the coupling constant J can be related to the energy difference between states with different spin multiplicity. For the case in which $S_1 = S_2$, the coupling constant may be obtained by using Equation (1), where E_{HS} is the energy of the state with the highest total spin, E_{LS} that of the lowest total spin state ($S = 0$ when $S_1 = S_2$), and S_i are the local spins on each metal atom.

$$E_{HS} - E_{LS} = -2JS_i(S_i + 1/2) \quad (1)$$

It has been found that, when using DFT-based wavefunctions, a reasonable estimate of the energy corresponding to the low spin state, E_{LS}, can be obtained directly from the energy of a broken-symmetry solution, E_{BS}.[53,61] In this case, introducing $S_i = 1/2$ in Equation (1), we arrive at the following expression for J:

$$J \approx E_{BS} - E_{HS} \quad (2)$$

Experience has shown that the use of this equation leads to a good agreement with experimental data for a large variety of compounds with exchange-coupled electrons.[50−60] The inclusion of an unspecified amount of non-dynamic correlation energy in the broken symmetry solution by means of the commonly used functionals is probably responsible for such a good agreement, as pointed out recently by Polo et al.[62]

The hybrid, DFT-based B3LYP method[63] has been used in all calculations as implemented in Gaussian-98,[64] mixing the exact Hartree−Fock exchange with Becke's expression for the exchange functional[65] and using the Lee−Yang−Parr correlation functional.[66] Double-ζ quality basis sets[67] have been employed for all atoms except for the metal ones, for which a triple-ζ basis set[68] with two extra *p* orbitals (polarization functions) has been used. Due to the small magnitude of the exchange coupling constants all energy calculations must be performed including the *SCF=Tight* option of Gaussian to ensure sufficiently well converged values for the state energies.

Results and Discussion

1. Calculations for Full Structures: In order to check the accuracy of the computational procedure employed in this work for the family of hydroxo- and alkoxo-bridged dinuclear V^{IV} complexes, we have performed calculations for several full non-modeled structures with hydroxo and alkoxo bridging ligands in which the metal atom presents distorted square-pyramidal or octahedral coordination environments (Figure 1). We note that the experimental magnetic susceptibility used to obtain the coupling constant is measured from solid samples in which packing forces can induce small deviations from the minimum energy geometry of the individual molecules. In order to be able to compare our computed coupling constants for full structures, we have used in our calculations the molecular structure as determined experimentally by X-ray diffraction rather than an optimized one, in which small changes with respect to the experimental structure could result in significant deviations of the calculated coupling constant.

The results (Table 2) show that there is a fair agreement between calculated and experimental coupling constants, reproducing the sign of the coupling constant in all cases, but obtaining rougher estimations than for other systems studied previously.[55] However, considering that the coupling constants are obtained as energy differences that are

 © 2004 Wiley-VCH Verlag GmbH & Co. KGaA, Weinheim

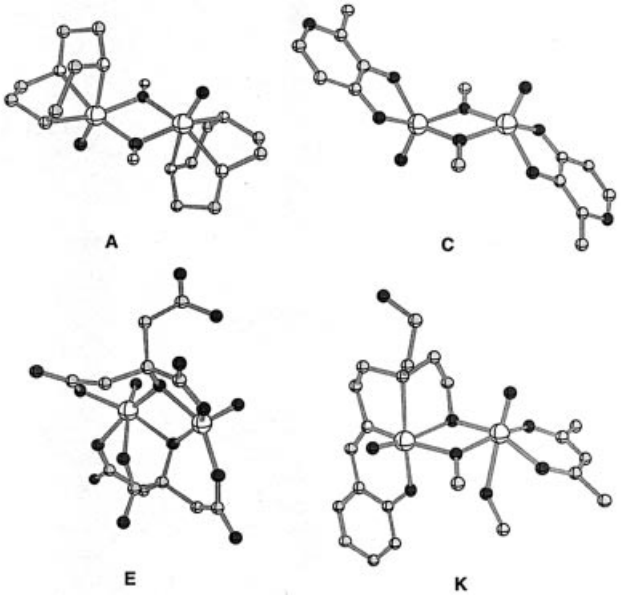

Figure 1. Crystal structures of hydroxo- and alkoxo-bridged dinuclear V^{IV} compounds whose coupling constants have been computed; large white spheres represent V atoms, medium white spheres N atoms, small white spheres H atoms, grey spheres C atoms, and dark spheres O atoms; H atoms of terminal ligands have been omitted for clarity; the labels **A**, **C**, **E** and **K** refer to Entries in Tables 1 and 2

calculated from total energy values eight or nine orders of magnitude larger, these deviations can be considered as acceptable.

2. Exchange Coupling in μ-Hydroxo Compounds: After verifying the agreement between calculated and experimental values of *J* for full non-modeled structures, we study now the effects of different factors on the coupling constant by performing calculations on a model system. In this model system, the terminal ligands present in experimental structures have been replaced by ammonia molecules (L = NH_3) and idealized structures have been considered. The bond lengths and angles used in the model system are averages of experimental values (see the Appendix). First of all, we analyze the dependence of the exchange coupling on the configuration of the $[VO(\mu\text{-}OH)_2VO]^{2+}$ core (**1**−**5**), studying then some magneto-structural correlations for distortions found in this family of compounds. Finally, we have looked at the influence of the terminal ligands on the coupling constant as well.

(a) Influence of the Configurations of the $[VO(\mu\text{-}OH)_2VO]^{2+}$ Core on the Exchange Coupling: Five different configurations of the $[VO(\mu\text{-}OH)_2VO]^{2+}$ core in complexes consisting of two edge-sharing octahedrally coordinated V^{IV} centers have been experimentally characterized (**1**−**5**). All the structural parameters are kept the same in the five models in order to study which is the effect of the core

Table 2. Experimental and calculated coupling constants for complete structures of some hydroxo- and alkoxo-bridged dinuclear V^{IV} complexes

Compound	Formula[a]	Conf.	$J_{calcd.}$ (cm^{-1})	$J_{exp.}$ (cm^{-1})	Ref.
A	$[(VO)_2(OH)_2([9]aneN_3)_2]^{2+}$	**1**	−259	−354	[32]
C	$[VO(OCH_3)(ma)]_2$	**1**[b]	−84	−214	[20]
E	$[(VO)_2(cit)(Hcit)]^{3-}$	**2**[c]	−293	−424	[36]
K	$[(VO)_2(Hsabhea)(OCH_3)(HOCH_3)(acac)]$	**5**	+15.4	+10.6	[34]

[a] Abbreviations: [9]aneN$_3$ = 1,4,7-triazacyclononane; H_4cit = citric acid; H_3sabhea = *N*-salicyclidene-2-[bis(2-hydroxyethyl)amino]ethylamine; Hacac = 2,4-pentanedione; ma = maltolato anion. [b] The metal ions are five-coordinate. [c] One metal ion is six-coordinate and the other one is five-coordinate.

Table 3. Computed coupling constants, together with the overlap integrals between BS-OMSOs for hydroxo-bridged model structures **1**−**5** (R = H) presenting different V−O−V angles (and the related V···V distances); the energy of the antiferromagnetic state relative to the minimum of each configuration is also included

Configuration	V−O−V (°)	V···V (Å)	*J* (cm^{-1})	S_{ab} x 100	$E_{rel.}$ (kcal/mol)
anti-Orthogonal (**1**)	100	3.03	−204	9.86	0.0
	104	3.12	−23.8	4.73	0.5
	108	3.20	+31.0	0.51	3.0
syn-Orthogonal (**2**)	100	3.03	−215	10.7	0.9
	104	3.12	−27.2	5.50	0.0
	108	3.20	+30.9	1.21	1.3
anti-Coplanar (**3**)	100	3.24	+3.7	1.92	6.3
	104	3.33	+7.4	1.18	1.9
	108	3.42	+8.8	0.48	0.0
syn-Coplanar (**4**)	100	3.03	−43.4	2.83	12.1
	104	3.12	−71.0	3.92	5.1
	108	3.20	−93.8	4.64	0.0
Twisted (**5**)	100	3.03	−26.7	0.52	5.9
	104	3.12	−11.7	0.37	2.1
	108	3.20	−3.3	0.25	0.0

 © 2004 Wiley-VCH Verlag GmbH & Co. KGaA, Weinheim

configuration on the coupling constant. For each core configuration the V−O−V bridging angle has been varied between 100 and 108°. The calculated coupling constant *J*, together with the overlap between the broken-symmetry occupied magnetic spin orbitals (BS-OMSOs)[69] S_{ab} and the relative energy of each configuration, are shown in Table 3.

In the orthogonal configurations (**1** and **2**), the calculated coupling constant experiences a significant variation with the V−O−V angle (more than 200 cm^{-1}), becoming more negative — enhanced antiferromagnetic coupling — for smaller values of the V−O−V bridging angle and correspondingly shorter V···V distances. The calculated values for configurations **1** and **2** are very similar, showing the small influence on the coupling constant of the orientation of the V=O groups in orthogonal configurations. These effects can be understood considering that the orbital that bears the unpaired electron is on the basal plane of the axially distorted octahedron, and its mixing with the orbitals of the ligands in the apical positions is very small for symmetry reasons. It is worth noting that the coupling constant for a model compound consisting of two edge-sharing square-pyramidally coordinated V^{IV} centers in an *anti*-orthogonal configuration with a V−O−V angle of 104° is −19.7 cm^{-1}, a value that is also in agreement with such an orbital explanation.

On the other hand, there is a much smaller variation of the coupling constant (about 50 cm^{-1}) in the model with *syn*-coplanar configuration (**4**) when the V−O−V angle is varied. Moreover, the angular dependence is opposite to that presented by orthogonal configurations, **1** and **2**, since in **4** the antiferromagnetic coupling decreases when the V−O−V angle becomes smaller. These results are consistent with the existence of different exchange mechanisms between the unpaired electrons located at the metal centers in the orthogonal and the *syn*-coplanar configurations, as suggested previously by other authors.[16,29,31−34,46] The predominant mechanism in orthogonal configurations (**1** and **2**) is direct through-space exchange, because of the important σ overlap between the d_{xy} metal orbitals (Figure 2, a) that becomes larger when the V−O−V angle and the V···V distance decrease. On the other hand, in the *syn*-coplanar configuration (**4**), the direct exchange is not so effective because the overlap between the metal orbitals that bear the unpaired electron is poor due to their relative orientation. In this case, the superexchange mechanism becomes more important since the orbitals of the bridging ligand overlap with the metal orbitals (Figure 2, b). Finally, in the *anti*-coplanar (**3**) and twisted configurations (**5**) the coupling constant is relatively small regardless of the V−O−V angle considered, showing that neither a direct exchange nor a superexchange pathway are important. It is interesting to note, though, that a weak ferromagnetic coupling is predicted for the *anti*-coplanar configuration **3**, whereas for the twisted configuration **5** weak antiferromagnetic coupling is calculated. The expectation of antiferromagnetic coupling contrasts with the experimental finding of ferromagnetic behavior for the twisted configuration **5**.[34,46] In our results we see that although the overlap between BS-OMSOs is small in the twisted configuration, it is non-zero (i.e. the orbitals are not strictly orthogonal), and the antiferromagnetic contribution to the coupling constant is larger than the ferromagnetic one, obtaining as a result a weak antiferromagnetic coupling. This result is, however, consistent with the experimental data because we use an undistorted model structure in our calculations. Distortions of the structure or the effect of terminal ligands can be at the origin of the ferromagnetic behavior shown by compound **K**,[34] whose experimental coupling constant is also well reproduced by our computational method, as shown above (Table 2).

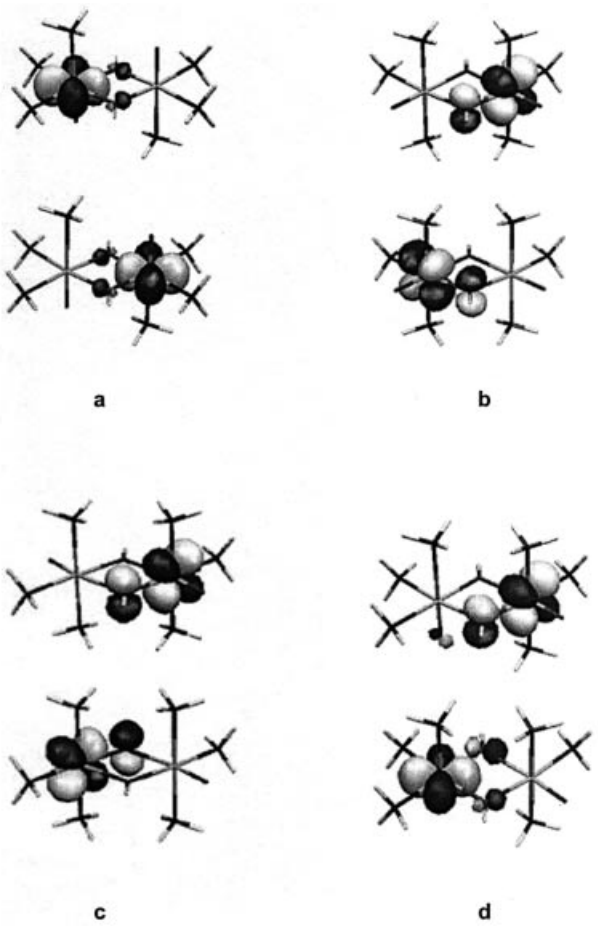

Figure 2. Computed magnetic orbitals (BS-OMSOs) for the *anti*-orthogonal (a), *syn*-coplanar (b), *anti*-coplanar (c) and twisted (d) $[VO(\mu\text{-}OH)_2VO]^{2+}$ core configurations

Together with the topology of the BS-OMSOs, two additional results support the prevalence of a direct exchange mechanism in orthogonal configurations and of a superexchange mechanism in the coplanar ones. First, a correlation between the type of core arrangement and the V···V distance exists in experimental hydroxo- and alkoxo-bridged oxovanadium(IV) dinuclear compounds: orthogonal configurations present V···V distances up to 3.20 Å, whereas in coplanar and twisted configurations the distance is larger (up to 3.45 Å), hinting to the existence of a through-space interaction in orthogonal configurations that keeps the two

 © 2004 Wiley-VCH Verlag GmbH & Co. KGaA, Weinheim

metal atoms closer than in the coplanar ones. The other result is related to the sign of the spin population in the high-spin state: in the *syn*-coplanar configuration the spin density at the oxygen atom of the only effective bridge presents the same sign as in the vanadium atoms, showing that the delocalization of the spin density is more important than the spin polarization mechanism and confirming the primacy of superexchange over the direct exchange mechanism in that core configuration. On the other hand, spin polarization predominates at the oxygen atoms of the bridge in orthogonal configurations showing that delocalization through the bridging atoms (i.e. superexchange) is not so effective in this case.

From Table 3 (last column, $E_{rel.}$), it can also be seen that the type of distortion considered here is possible from the energetic point of view for each of the five configurations studied, since only a few kcal/mol are needed to produce such a distortion. This result is in good agreement with the fact that the experimental structures of hydroxo- and alkoxo-bridged six-coordinate oxovanadium(IV) dinuclear compounds present values for the V−O−V angle over a wide range (Table 1). It is also important to note that the minimum energy for each of the configurations corresponds to a V−O−V angle of 108°, except for the orthogonal configurations in which the minimum energy corresponds to smaller angles.

The dependence of the coupling constant on the core configuration can be rationalized within the framework of the qualitative model proposed by Kahn and coworkers[3,70−76] that results in an expression for the coupling constant dependent on the overlap between non-orthogonal localized magnetic orbitals [Equation (3)].

$$J \approx 2K_{ab} + 4\beta S_{ab} \quad (3)$$

Here K_{ab} is the exchange integral involving non-orthogonal magnetic orbitals *a* and *b*, β the transfer integral and S_{ab} the overlap between the magnetic orbitals as well. The first term in Equation (3) ($2K_{ab}$) is positive and can be interpreted as a ferromagnetic contribution (J_F) to the exchange coupling constant, responsible for the stability of the triplet state, whereas the second one ($4\beta S_{ab}$) is negative and represents an antiferromagnetic term (J_{AF}) favoring the singlet state. Since within the Wolfsberg−Helmholtz approximation the transfer integral is proportional to the overlap, $\beta \propto S_{ab}$, then the antiferromagnetic contribution to the coupling constant should be proportional to the square of the overlap between magnetic orbitals, $J_{AF} \propto S_{ab}^2$.

Although Equation (3) has been obtained within the framework of the wave function based theory, it has been shown that Kohn−Shan orbitals obtained from density functional calculations are physically sound and suitable for qualitative molecular orbital theory.[77,78] In Figure 3, the values of the coupling constant corresponding to the five core configurations and three different V···V distances (Table 2) are plotted as a function of the square of the overlap between the broken-symmetry occupied magnetic spin-orbitals (BS-OMSOs).[69] We have used BS-OMSOs because they are the most suitable orbitals to represent the so-called *magnetic orbitals* for d^1 centers, since they form a non-orthogonal basis set (a must in Kahn and Briat's model) and are very similar to the localized natural orbitals as well.[79,80] From the linear fittings in Figure 3 we can find estimates for the value of the exchange integral K_{ab} by comparison with Equation (3). The estimated K_{ab} values for the five core configurations are +18.1, +15.1, +4.7, −6.9 and +1.8 cm^{-1} for the *anti*-orthogonal, *syn*-orthogonal, *anti*-coplanar, *syn*-coplanar and twisted configurations (**1**−**5**), respectively. These values are rather small compared to that found for hydroxo-bridged dinuclear Cu^{II} compounds (+412 cm^{-1}),[51] showing the low ability of hydroxo-bridged dinuclear oxovanadium(IV) compounds to propagate ferromagnetic interactions. It should be noted that although the predicted K_{ab} sign for the *syn*-coplanar configuration is wrong (−6.9 cm^{-1}, whereas K_{ab} must be positive), its value is very small, thus indicating that it must also be a small positive value as has been found for the other configurations.

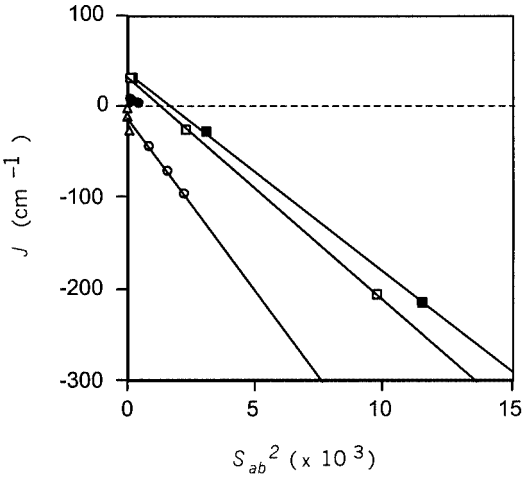

Figure 3. Dependence of the coupling constant *J* on the square of the overlap integral S_{ab}^2 (×1000) between BS-OMSOs for the different $[VO(\mu\text{-}OH)_2VO]^{2+}$ core configurations (three different V···V distances have been considered for each configuration): *anti*-orthogonal (**1**, solid squares), *syn*-orthogonal (**2**, squares), *anti*-coplanar (**3**, solid circles), *syn*-coplanar (**4**, circles) and twisted (**5**, triangles); linear fittings for the *anti*-coplanar and twisted configurations have been omitted for clarity

(b) Magnetostructural Correlations: The experimental structures for hydroxo- and alkoxo-bridged dinuclear oxovanadium(IV) compounds often deviate from the idealized geometries adopted in our model compounds. In this section we analyze the effect of the most common distortions on the coupling constant.

Effect of the V−O−V Bridging Angle (or the V···V Distance): We have studied exhaustively the dependence of the coupling constant on the V−O−V angle (or what is the same, on the V···V distance, since the V−O distance has been kept frozen), but in this section we consider only the orthogonal configurations **1** and **2**. We have checked that the variation of *J* with the V−O−V angle for each of the orthogonal configurations is almost identical, in good

 © 2004 Wiley-VCH Verlag GmbH & Co. KGaA, Weinheim

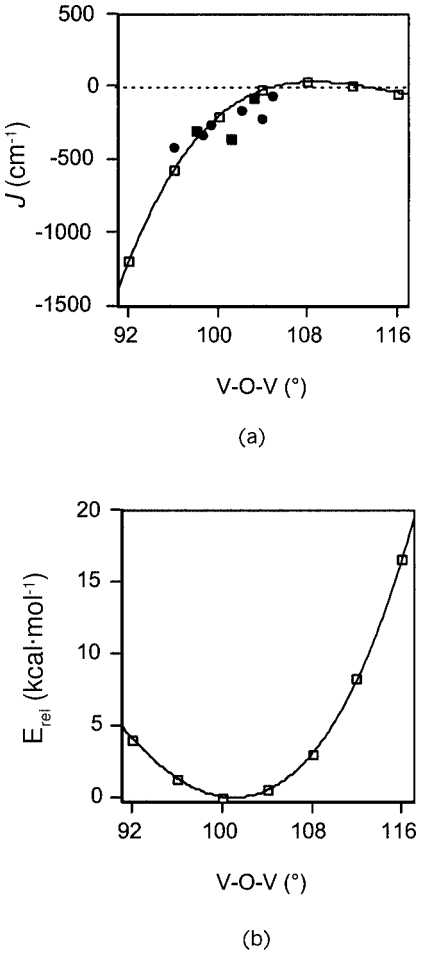

Figure 4. (a) Dependence of the calculated coupling constant J (solid line) on the bridging V−O−V angle for the model compound with an *anti*-orthogonal core configuration (**1**); black squares and circles correspond to experimental values for hydroxo- and alkoxo-bridged compounds, respectively; (b) relative energy of the ground state as a function of the V−O−V bridging angle

agreement with the simple two electrons—two orbitals approximation. In Figure 4 the results corresponding to the *anti*-orthogonal configuration are presented. From Figure 4 (a) it can be seen that strong antiferromagnetic coupling appears at small V−O−V angles (i.e. short V···V distances), as a consequence of the increased through-space overlap between the metal orbitals. This strong antiferromagnetic coupling drops sharply and becomes weakly ferromagnetic at V−O−V angles between 104° and 110° (i.e. V···V distances between 3.12 and 3.20 Å) reaching a maximum at about 108° (3.20 Å). The ferromagnetic coupling appears at much larger V−O−V angles than in the case of hydroxo-bridged dinuclear copper(II) compounds (at about 98°).[9,51] The experimental values of the coupling constant for hydroxo- and alkoxo-bridged compounds fit very well with our theoretical prediction (Figure 4a). As can be seen in Figure 4 (b), the minimum energy corresponds to the structure with a V−O−V angle of 100°. Structures with V−O−V angles ranging from 92° to 110° (V···V distances from 2.85 to 3.24 Å) are however possible (less than 5 kcal/mol), in good agreement with the fact that experimental structures present V···V distances within this range of values, as can be seen in Table 1 (configuration **1** and **2**).

The dependence of the coupling constant on the V−O−V angle for orthogonal configurations has also been analyzed by means of the qualitative model proposed by Hay, Thibeault and Hoffmann (HTH).[81] These authors obtained an approximate expression for the coupling constant of a homodinuclear complex with two unpaired electrons that predicts that the antiferromagnetic contribution to the coupling constant depends on the square of the orbital gap according to Equation (4), where K_{ab}, J_{aa}, and J_{ab} are the exchange and Coulomb integrals involving orthogonal localized orbitals a and b, and ε_1 and ε_2 are the energies of the two SOMOs of the complex.

$$E_S - E_T = J = 2K_{ab} - \frac{(\varepsilon_1 - \varepsilon_2)^2}{J_{aa} - J_{ab}} \quad (4)$$

A plot of J versus the square of the orbital gap for the *anti*-orthogonal configuration **1** is shown in Figure 5. It can be seen that the linear relation predicted by HTH holds for the hydroxo-bridged oxovanadium(IV) models studied here if the occupied magnetic spin orbitals (OMSOs)[69] are considered. An almost identical behavior is found when the *syn*-orthogonal configuration **2** is considered (not shown in Figure 5). The estimated values for K_{ab} are +13.9 and +14.7 cm^{-1} for **1** and **2**, respectively. These values are very similar to the ones predicted in Kahn and Briat's model for these core configurations (+18.1 and +15.1 cm^{-1} for **1** and **2**, respectively). Within the HTH model, it is also possible to estimate the value of $(J_{aa} - J_{ab})$ — 6.5×10^4 and 6.3×10^4 cm^{-1} for **1** and **2**, respectively — which are similar to that found for hydroxo-bridged dinuclear Cu^{II} compounds (7.2×10^4 cm^{-1}).[51,58]

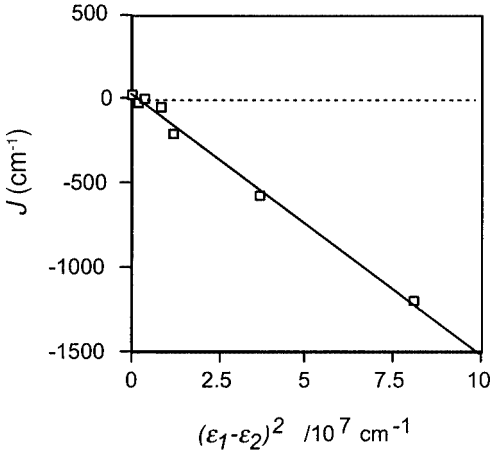

Figure 5. Dependence of the coupling constant J on the square of the energy gap between the two OMSOs for model compounds with an *anti*-orthogonal core configuration (**1**) at different values of the V−O−V bridging angle

 © 2004 Wiley-VCH Verlag GmbH & Co. KGaA, Weinheim

Effect of Bending of the Terminal Ligands: The experimental structures of some compounds with orthogonal core configurations are distorted with respect to the idealized model in the way shown in **6**.

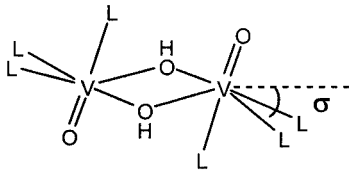

6

To study the effect of the angle σ on the coupling constant, we have performed calculations using model compounds that present an *anti*-orthogonal core configuration (**1**), keeping other structural parameters constant (a value of 104° has been taken for the V−O−V bridging angle). An increase of the antiferromagnetic coupling constant is found when σ changes from 0° (−23.8 cm^{-1}) to 30° (−86.4 cm^{-1}). This result can be rationalized by means of the HTH model since an increase in the orbital gap between OMSOs appears when the structure is distorted in this way. It is also seen that the most stable structure corresponds to that with a σ angle between 10° and 20°, in good agreement with most of the experimental structures, which present values for the σ angle of approximately 20° (Table 1). It is, however, very difficult to check the accuracy of the theoretically predicted dependence of the coupling constant on σ because *J* also depends on other structural parameters (especially on the V−O−V angle or the equivalent V···V distance) that change significantly from one structure to another.

Effect of the Orientation of the Bridge: We have also studied the dependence of the coupling constant on the displacement of hydrogen atoms out of the V_2O_2 plane for structures with an *anti*-orthogonal configuration (**1**). This type of distortion, commonly found for this family of compounds, can be represented by the structural parameter τ (**7**). The other structural parameters have been kept constant (V−O−V = 104°). A change in the nature of the magnetic coupling is found at an angle of about 20° (Figure 6), reaching a maximum of $J \approx +60$ cm^{-1}, a small value in good agreement with the predictions of qualitative models. This type of distortion is energetically possible since less than 5 kcal/mol are required to reach a τ angle of 50°, in good agreement with experimental data, where it is possible to find τ angles ranging from about 0° to 40° (Table 1).

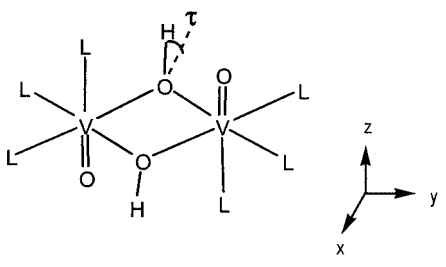

7

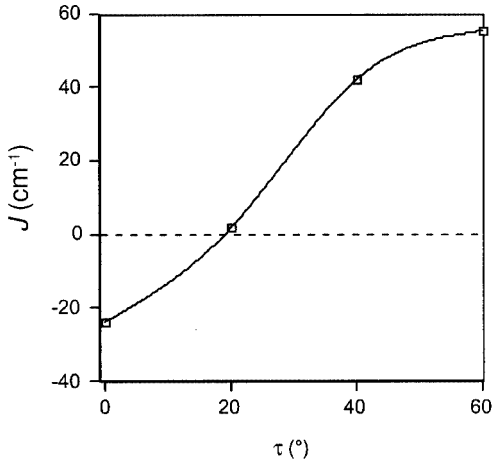

Figure 6. Dependence of the coupling constant *J* on the τ angle for the model compound with an *anti*-orthogonal core configuration (**7**)

(c) Influence of the Terminal Ligands on the Exchange Coupling Constant: The effect of changing the terminal ligands has been previously studied for several families of dinuclear Cu^{II} compounds.[50,57,59] To explain the observed shifts in the coupling constant, a detailed analysis of the magnetic orbitals for each particular case is needed and no general rules can be established.

We have studied this effect on the coupling constant of dinuclear oxovanadium(IV) compounds for two different core configurations, *anti*-orthogonal (**1**) and *syn*-coplanar (**4**). Ammonia (NH_3) and aqua (H_2O) terminal ligands have been used for the present analysis since most of the known experimental structures present N-donor and/or O-donor ligands. A value of 104° for the V−O−V angle has been employed in the model compounds. A rather small influence on the coupling constant is observed, the antiferromagnetic coupling decreasing in the *anti*-orthogonal configuration (from −23.8 to −10.0 cm^{-1}) and increasing in the *syn*-coplanar one (from −71.0 to −80.1 cm^{-1}) when ammonia is replaced by aqua ligands. This minute effect of the terminal ligands can be rationalized by the small contribution of the donor (N or O) atomic orbitals to the OMSOs: both ammonia and aqua ligands are σ-donor ligands whereas the metal orbitals that contribute to the OMSOs are of a π nature.

3. Exchange Coupling in μ-Alkoxo Compounds: Finally, we have also studied how the exchange coupling is affected by the replacement of the hydroxo bridges by alkoxo groups. We have modeled the alkoxo bridging ligands by methoxy groups (see Appendix), maintaining for the rest of the structural parameters the same values as those used in hydroxo-bridged models.

The results (Table 4) show that no significant differences appear when the hydroxo bridging ligands are replaced by methoxy groups, in contrast to the behavior found for dinuclear Cu^{II} compounds, in which an important enhancement of the antiferromagnetic coupling occurs.[51] The most

 © 2004 Wiley-VCH Verlag GmbH & Co. KGaA, Weinheim

Table 4. Computed coupling constants, together with the relative energy of the antiferromagnetic state for methoxo-bridged model structures **1**−**5** (R = Me) presenting different V−O−V angles (and the related V···V distances)

Configuration	V−O−V (°)	V···V (Å)	J (cm^{-1})	$E_{rel.}$ (kcal/mol)
anti-Orthogonal (**1**)	100	3.03	−196	0.0
	104	3.12	−13.9	0.7
	108	3.20	+34.4	3.3
syn-Orthogonal (**2**)	100	3.03	−208	0.8
	104	3.12	−17.6	0.0
	108	3.20	+34.9	1.4
anti-Coplanar (**3**)	100	3.24	+8.8	4.9
	104	3.33	+11.4	1.2
	108	3.42	+12.0	0.0
syn-Coplanar (**4**)	100	3.03	−72.9	10.7
	104	3.12	−109	4.2
	108	3.20	−137	0.0
Twisted (**5**)	100	3.03	−24.0	5.1
	104	3.12	−11.3	1.6
	108	3.20	−4.1	0.0

notable changes, even though not very significant, correspond to structures with *syn*-coplanar configurations, which show a moderate increase in the antiferromagnetic coupling constant, and the *anti*-coplanar ones, in which a slight increase of the ferromagnetic coupling is found. In orthogonal configurations, the results are almost identical to those found for hydroxo-bridged systems (the experimental alkoxo-bridged compounds fit well in the predicted dependence of J on the V−O−V angle for hydroxo-bridged model compounds, Figure 4a). The coupling constant for a model compound consisting of two edge-sharing square-pyramidally coordinated V^{IV} centers in an *anti*-orthogonal configuration, with a V−O−V angle of 104°, has been predicted to be -7.5 cm^{-1}, a value that is also similar to that in hydroxo-bridged compounds (-19.7 cm^{-1}), if somewhat smaller. Consistently, no significant differences in the experimental coupling constants are found when replacing the bridging hydroxo by alkoxo groups, and the structural parameters that play an important role in the magnetic coupling of the complexes are not very different (Table 1).

The different behavior of dinuclear V^{IV} complexes compared to that of the Cu^{II} ones is related to the predominant mechanism of exchange interaction for each family of compounds. In Cu^{II} complexes superexchange is the main mechanism and, as a consequence, the larger the orbital delocalization through the bridging ligands, the stronger the antiferromagnetic coupling. This explains the considerable enhancement of antiferromagnetic coupling when hydroxo bridging ligands are replaced by methoxo ones.[51] For V^{IV} complexes with orthogonal core configurations, the direct through-space interaction between metal orbitals is the prevalent mechanism, thus making the nature of the bridging ligands much less important. For V^{IV} complexes with *syn*-coplanar configurations, superexchange is more important than in orthogonal configurations, but still much less than in Cu^{II} complexes, thus having an intermediate behavior: a moderate enhancement of the antiferromagnetic coupling when the hydroxo bridging ligands are replaced by alkoxo ligands.

As far as the energetic cost of the V−O−V angle distortion is concerned, we obtain similar results to those found for hydroxo-bridged compounds (Table 4): (i) a few kcal/mol are needed to perform such a distortion, and (ii) the minimum energy structures present smaller V−O−V angles for orthogonal configurations **1** and **2**.

The magneto-structural correlation for the distortion corresponding to a displacement of the R group of the alkoxo bridges out of the bridging plane (**7**) has also been studied for a model structure with an *anti*-orthogonal core configuration (with an V−O−V angle of 104°). An almost identical behavior as for hydroxo-bridged compounds has been found: a change in the nature of the coupling, becoming ferromagnetic at a τ angle of about 10° and reaching a maximum of $+56$ cm^{-1} at $\tau = 40°$. It has been seen that this type of distortion is energetically possible as well: the most stable structures are the ones with τ angles about 20°, and less than 7 kcal/mol are needed to reach τ values of 40°.

Conclusions

The present contribution confirms that the computational strategy — based on density functional theory — employed to investigate the exchange coupling in hydroxo- and alkoxo-bridged dinuclear oxovanadium(IV) compounds provides fair estimates of their experimental coupling constants. With its moderate demand for computer time, it also permits us to investigate separately the effect on the coupling constant of the different types of core arrangements that exist in $[VO(\mu\text{-}OH)_2VO]^{2+}$ compounds, as well as the influence of the nature of terminal and bridging ligands and the magneto-structural correlations corresponding to the most common distortions for this family of compounds. The results confirm that different exchange mechanisms predominate in orthogonal (through-space mechanism) and coplanar configurations (superexchange mechanism). This is a consequence of the dissimilar topology of the OMSOs in each geometrical configuration. Qualitative orbital models (Kahn−Briat and Hay−Thibeault−Hoffmann) are seen to be useful in analyzing the results, giving estimates for the ferromagnetic contribution to the exchange coupling in this family of compounds. A minute influence of the nature of the terminal ligand on the coupling constant has been found, a consequence of the σ-donor character of N- and O-donor ligands considered, opposed to the π nature of the interacting electrons.

Regarding the magneto-structural correlations, a very strong antiferromagnetic coupling is found for structures that present short V···V distances when orthogonal configurations are considered, a result related to the important overlap between BS-OMSOs in such configurations. Another interesting finding is the small effect of the displacement of the hydrogen atom of the bridge out of the plane on the coupling constant, that induces a change in the nat-

 © 2004 Wiley-VCH Verlag GmbH & Co. KGaA, Weinheim

ure of the coupling (from antiferromagnetic to ferromagnetic), but that is not as important as in the case of hydroxo-bridged dinuclear Cu^{II} compounds. Finally, it is worth mentioning that important changes in the coupling are not found when the hydroxo bridging ligands are replaced by alkoxo groups, a result that differs from the behavior shown by dinuclear Cu^{II} compounds, in which an important increase in the antiferromagnetic coupling occurs.

Appendix

The bond lengths and angles used for model compounds are: 1.59 Å for the V=O bond; 1.98 Å for V−O (2.24 Å when the O bridging atom is in the *trans* position with respect to the oxo O-atom); 2.11 Å for V−N (2.34 Å when the N atom is *trans* with respect to the oxo O-atom); 0.85 Å for O−H; a value of 104° for the V−O−V bridging angle; and 91.5° for N−V−N. The N−H distance within the ammonia ligands is 1.02 Å and the H−N−H angle is 109°. For alkoxo-bridged compounds: 1.43 and 0.98 Å for O−C and C−H distances, respectively and 109° for the H−C−O angle.

Acknowledgments

Financial support to this work was provided by Dirección General de Investigación (DGI) through projects number BQU2002-04033-C02-02 and -01. Additional support came from Comissió Interdepartamental de Recerca i Innovació Tecnològica (CIRIT) through grant SGR2001-0044. The computing resources at CESCA/CEPBA were supported in part through grants from CIRIT and Universitat de Barcelona.

[1] B. Guha, *Proc. Roy. Soc.* **1951**, *206*, 353.
[2] O. Kahn, Y. Pei, Y. Journaux, *Inorganic Materials*, John Wiley & Sons, Chichester, **1992**.
[3] O. Kahn, *Molecular Magnetism*, VCH Publishers, New York, **1993**.
[4] O. Kahn, *Magnetism: A Supramolecular Function NATO ASI Series, Vol. 484*, Kluwer, Dordrecht, **1996**.
[5] D. Gatteschi, O. Kahn, J. S. Miller, F. Palacio, *Magnetic Molecular Materials*, Kluwer Academic, Dordrecht, **1991**.
[6] J. S. Miller, M. Drillon, *Magnetism: Molecules to Materials, Vol. 1 and 2*, Wiley-VCH, Weinheim, **2001**.
[7] E. Coronado, P. Delhaes, D. Gatteschi, J. S. Miller, *Magnetic Molecular Materials: From Molecular Assemblies to the Devices NATO ASI Series, Vol. 321*, Kluwer, Dordrecht, **1996**.
[8] V. H. Crawford, H. W. Richardson, J. R. Wasson, D. J. Hodgson, W. E. Hatfield, *Inorg. Chem.* **1976**, *15*, 2107.
[9] D. J. Hodgson, *Prog. Inorg. Chem.* **1975**, *19*, 173.
[10] E. D. Estes, W. E. Hatfield, D. J. Hodgson, *Inorg. Chem.* **1974**, *13*, 1654.
[11] D. L. Lewis, W. E. Hatfield, D. J. Hodgson, *Inorg. Chem.* **1972**, *11*, 2216.
[12] T. P. Mitchell, W. H. Bernard, J. R. Wasson, *Acta Crystallogr., Sect. B* **1970**, *26*, 2096.
[13] A. Butler, C. J. Carrano, *Coord. Chem. Rev.* **1991**, *109*, 61.
[14] N. D. Chasteen, *Vanadium in Biological Systems*, Kluwer Academic Publishers, Dordrecht, **1990**.
[15] D. Rehder, *Angew. Chem. Int. Ed. Engl.* **1991**, *30*, 148.
[16] C. J. Carrano, C. M. Nunn, R. Quan, J. A. Bonadies, V. L. Pecoraro, *Inorg. Chem.* **1990**, *29*, 944.
[17] S. L. Castro, M. E. Cass, F. J. Hollander, S. L. Bartley, *Inorg. Chem.* **1995**, *34*, 466.
[18] W. R. Harris, C. J. Carrano, *J. Inorg. Biochem.* **1984**, *22*, 201.
[19] Y. Sun, B. R. James, S. J. Rettig, C. Orvig, *Inorg. Chem.* **1996**, *35*, 1667.
[20] Y. Sun, M. Melchior, D. A. Summers, R. C. Thompson, S. J. Rettig, C. Orvig, *Inorg. Chem.* **1998**, *37*, 3119.
[21] M. R. Bond, L. M. Mokry, T. Otieno, J. Thompson, C. J. Carrano, *Inorg. Chem.* **1995**, *34*, 1894.
[22] G. Villeneuve, P. Amorós, D. Beltrán, M. Drillon, *Organic and Inorganic Low-Dimensional Crystalline Materials*, Plenum, New York, **1987**, Vol. B168.
[23] G. Villeneuve, K. H. Suh, P. Amorós, N. Casañ-Pastor, D. Beltrán-Porter, *Chem. Mater.* **1992**, *4*, 108.
[24] O. Centi, F. Trifiro, J. R. Ebner, V. M. Franchetti, *Chem. Rev.* **1988**, *88*, 55.
[25] D. Beltrán, P. Amorós, R. Ibañez, E. Martinez, A. Beltrán, A. LeBail, G. Ferey, G. Villeneuve, *Solid State Ionics* **1989**, *32−33*, 57.
[26] D. Beltrán-Porter, A. Beltrán-Porter, P. Amorós, R. Ibañez, E. Martinez, A. LeBail, G. Ferey, G. Villeneuve, *Eur. J. Solid State Inorg. Chem.* **1991**, *28*, 131.
[27] M. T. Pope, *Heteropoly and Isopoly Oxometalates*, Springer, New York, **1983**.
[28] V. M. Day, W. G. Klemperer, *Science* **1985**, *228*, 533.
[29] A. P. Ginsberg, E. Koubek, H. J. Williams, *Inorg. Chem.* **1966**, *5*, 1657.
[30] E. F. Hasty, T. J. Colburn, D. N. Hendrickson, *Inorg. Chem.* **1973**, *12*, 2414.
[31] A. Syamal, *Coord. Chem. Rev.* **1975**, *16*, 309.
[32] K. Wieghardt, U. Bossek, K. Volckmar, W. Swiridoff, J. Weiss, *Inorg. Chem.* **1984**, *23*, 1387.
[33] A. Neves, K. Wieghardt, B. Nuber, J. Weiss, *Inorg. Chim. Acta* **1988**, *150*, 183.
[34] W. Plass, *Angew. Chem. Int. Ed. Engl.* **1996**, *35*, 627.
[35] N. S. Dean, M. R. Bond, C. J. O′Connor, C. J. Carrano, *Inorg. Chem.* **1996**, *35*, 7643.
[36] S. Burojevic, I. Shweky, A. Bino, D. A. Summers, R. C. Thompson, *Inorg. Chim. Acta* **1996**, *251*, 75.
[37] A. S. Ceccato, A. Neves, M. A. de Brito, S. M. Drechsel, A. S. Mangrich, R. Werner, W. Haase, A. Bortoluzzi, *J. Chem. Soc., Dalton Trans.* **2000**, 1567.
[38] R. Das, K. K. Nanda, A. K. Mukherjee, M. Mukherjee, M. Helliwell, K. Nag, *J. Chem. Soc., Dalton Trans.* **1993**, 2241.
[39] F. Jiang, O. P. Anderson, S. M. Miller, J. Chen, M. Mahroof-Tahir, D. C. Crans, *Inorg. Chem.* **1998**, *37*, 5439.
[40] X. Li, M. S. Lah, V. Pecoraro, *Inorg. Chem.* **1988**, *27*, 4657.
[41] M. E. Cass, D. L. Greene, R. M. Buchanan, C. G. Pierpont, *J. Am. Chem. Soc.* **1983**, *105*, 2680.
[42] M. Velayutham, B. Varghese, S. Subramanian, *Inorg. Chem.* **1998**, *37*, 1336.
[43] Z.-H. Zhou, H.-L. Wan, S.-Z. Hu, K.-R. Tsai, *Inorg. Chim. Acta* **1995**, *237*, 193.
[44] W. Plass, *Inorg. Chem.* **1997**, *36*, 2200.
[45] M. I. Khan, Y.-D. Chang, Q. Chen, J. Salta, Y.-S. Lee, C. J. O′Connor, J. Zubieta, *Inorg. Chem.* **1994**, *33*, 6340.
[46] W. Plass, *Z. Anorg. Allg. Chem.* **1997**, *623*, 1290.
[47] L. Zhang, Z. Chen, *Chem. Phys. Lett.* **2001**, *345*, 353.
[48] L. M. Lawson Daku, S. Borshch, V. Robert, B. Bigot, *Phys. Rev. B* **2001**, *63*, 174439.
[49] S. Petit, S. A. Borshch, V. Robert, *J. Am. Chem. Soc.* **2002**, *124*, 1744.
[50] E. Ruiz, P. Alemany, S. Alvarez, J. Cano, *Inorg. Chem.* **1997**, *36*, 3683.
[51] E. Ruiz, P. Alemany, S. Alvarez, J. Cano, *J. Am. Chem. Soc.* **1997**, *119*, 1297.
[52] E. Ruiz, J. Cano, S. Alvarez, P. Alemany, *J. Am. Chem. Soc.* **1998**, *120*, 11122.
[53] E. Ruiz, J. Cano, S. Alvarez, P. Alemany, *J. Comput. Chem.* **1999**, *20*, 1391.

 © 2004 Wiley-VCH Verlag GmbH & Co. KGaA, Weinheim

[54] E. Ruiz, S. Alvarez, P. Alemany, *Chem. Commun.* **1998**, 2767.
[55] E. Ruiz, S. Alvarez, A. Rodríguez-Fortea, P. Alemany, Y. Pouillon, C. Massobrio, in *Magnetism: Molecules to Materials, Vol. 2* (Eds.: J. S. Miller, M. Drillon), Wiley-VCH, Weinheim, **2001**, p. 227−279.
[56] A. Rodríguez-Fortea, P. Alemany, S. Alvarez, E. Ruiz, *Chem. Eur. J.* **2001**, *7*, 627.
[57] J. Cano, P. Alemany, S. Alvarez, M. Verdaguer, E. Ruiz, *Chem. Eur. J.* **1998**, *4*, 476.
[58] J. Cano, E. Ruiz, P. Alemany, F. Lloret, S. Alvarez, *J. Chem. Soc., Dalton Trans.* **1999**, 1669.
[59] J. Cano, A. Rodríguez-Fortea, P. Alemany, S. Alvarez, E. Ruiz, *Chem. Eur. J.* **2000**, *6*, 327.
[60] A. Rodríguez-Fortea, P. Alemany, S. Alvarez, E. Ruiz, A. Scuiller, C. Decroix, V. Marvaud, J. Vaissermann, M. Verdaguer, I. Rosenman, M. Julve, *Inorg. Chem.* **2001**, *40*, 5868.
[61] W. Koch, M. C. Holthausen, *A Chemist's Guide to Density Functional Theory*, Wiley-VCH, Weinheim, **2000**.
[62] V. Polo, E. Kraka, D. Cremer, *Theor. Chem. Acc.* **2002**, *107*, 291.
[63] A. D. Becke, *J. Chem. Phys.* **1993**, *98*, 5648.
[64] M. J. Frisch, G. W. Trucks, H. B. Schlegel, G. E. Scuseria, M. A. Robb, J. R. Cheeseman, V. G. Zakrzewski, J. A. Montgomery, R. E. Stratmann, J. C. Burant, S. Dapprich, J. M. Millam, A. D. Daniels, K. N. Kudin, M. C. Strain, O. Farkas, J. Tomasi, V. Barone, M. Cossi, R. Cammi, B. Menucci, C. Pomelli, C. Adamo, S. Clifford, J. Ochterski, G. A. Petersson, P. Y. Ayala, Q. Cui, K. Morokuma, D. K. Malick, A. D. Rabuck, K. Raghavachari, J. B. Foresman, J. Ciolowski, J. V. Ortiz, B. B. Stefanov, G. Liu, A. Liashenko, P. Piskorz, I. Komaromi, R. Gomperts, R. L. Martin, D. J. Fox, T. A. Keith, M. A. Al-Laham, C. Y. Peng, A. Nanayakkara, C. Gonzalez, M. Challacombe, P. M. W. Gill, B. G. Johnson, W. Chen, M. W. Wong, J. L. Andres, M. Head-Gordon, E. S. Replogle, J. A. Pople, *Gaussian 98*, Gaussian, Inc., Pittsburgh, PA, **1998**.
[65] A. D. Becke, *Phys. Rev. A* **1988**, *38*, 3098.
[66] C. Lee, W. Yang, R. G. Parr, *Phys. Rev. B* **1988**, *37*, 785.
[67] A. Schaefer, H. Horn, R. Ahlrichs, *J. Chem. Phys.* **1992**, *97*, 2571.
[68] A. Schaefer, C. Huber, R. Ahlrichs, *J. Chem. Phys.* **1994**, *100*, 5829.
[69] C. Desplanches, E. Ruiz, A. Rodríguez-Fortea, S. Alvarez, *J. Am. Chem. Soc.* **2002**, *124*, 5197.
[70] O. Kahn, B. Briat, *J. Chem. Soc., Faraday Trans. 2* 1976, *72*, 1441.
[71] O. Kahn, B. Briat, *J. Chem. Soc., Faraday Trans. 2* 1976, *72*, 268.
[72] O. Kahn, B. Briat, J. Galy, *J. Chem. Soc., Dalton Trans.* **1977**, 1453.
[73] O. Kahn, M. F. Charlot, *Nouv. J. Chim.* **1980**, *4*, 567.
[74] O. Kahn, *Angew. Chem. Int. Ed. Engl.* **1985**, *24*, 834.
[75] C. Kollman, O. Kahn, *Acc. Chem. Res.* **1993**, *26*, 259.
[76] J. J. Girerd, Y. Journaux, O. Kahn, *Chem. Phys. Lett.* **1981**, *82*, 534.
[77] E. J. Baerends, O. V. Gritsenko, *J. Phys. Chem. A* **1997**, *101*, 5383.
[78] R. Stowasser, R. Hoffmann, *J. Am. Chem. Soc.* **1999**, *121*, 3414.
[79] A. Rodríguez-Fortea, E. Ruiz, P. Alemany, S. Alvarez, manuscript to be submitted.
[80] J. Cabrero, C. J. Calzado, D. Maynau, R. Caballol, J. P. Malrieu, *J. Phys. Chem. A* **2002**, *106*, 8146.
[81] P. J. Hay, J. C. Thibeault, R. Hoffmann, *J. Am. Chem. Soc.* **1975**, *97*, 4884.

Received July 18, 2003
Early View Article
Published Online October 31, 2003

 © 2004 Wiley-VCH Verlag GmbH & Co. KGaA, Weinheim

In Quest of the Double Rotaxane Formation of the Bis(coronand) (1,5),(2,4)-Durenetetrayl-bis(18-crown-5) with Organomagnesium Compounds

Gerard P. M. van Klink,[a] Tateo Nomoto,[b] Martin Lutz,[c] Anthony L. Spek,[c] Otto S. Akkerman,[d] and Friedrich Bickelhaupt*[d]

Keywords: Magnesium / Mercury / Chelates / Crown compounds

The interaction between the title compound, bis(coronand) **8**, and the diarylmagnesium compounds Ph_2Mg and $(p\text{-}tBuC_6H_4)_2Mg$ in diethyl ether leads to the formation of 1:2 complexes (**9** and **10**, respectively), irrespective of the initial ratio of the components. In [D_8]toluene, the three complex types can be discerned by ^1H NMR spectroscopy: double side-on (**9a**, **10a)**, side-on/rotaxane (**9b**, **10b)**, and, to a very minor extent, double rotaxane (**9c**, **10c**). In the case of **10a** and **10b**, the temperature dependence showed that rotaxane formation is enthalpically favored at the expense of a more negative entropy. As crystals suitable for structure determination could not be obtained from **9** and **10**, the interaction of **8** with the sterically less demanding $Hg(SCN)_2$ was studied. In this case, analogous pseudorotaxanes are formed exclusively, and both the 1:2 complex [**8**·{$Hg(SCN)_2$}$_2$] (**11**) and its 1:1 analogue **12** were observed. The double rotaxane structure of **11** was confirmed by X-ray crystal structure determination.
(© Wiley-VCH Verlag GmbH & Co. KGaA, 69451 Weinheim, Germany, 2004)

Introduction

In most respects, crown ethers derived from *m*-xylene behave as normal ligands toward organomagnesium compounds. For instance, side-on complexes involving two crown ether oxygen atoms are formed, allowing magnesium to achieve its usual coordination number of four.[1] However, a number of aspects unusual in the chemistry of organomagnesium compounds have also been encountered.[1,2] An illustration is the high organolithium-like reactivity demonstrated by intra-annular metalation of **1** to **2** (Scheme 1),[3] by metal−halogen exchange as in **3** to furnish **4**,[3,4] and by several ether cleavage reactions of substrates which are normally inert toward organomagnesium reagents.[2,5,6]

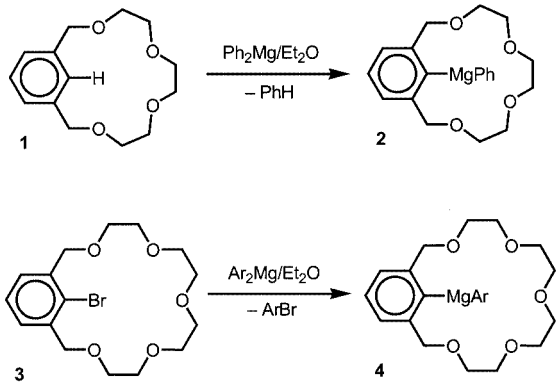

Scheme 1. Ar = Ph, *p*-$tBuC_6H_4$

Another challenging aspect is the formation of organometallic rotaxanes[7,8] such as **6**,[1,2,9,10] and even catenanes **7**[11] from **5** (Scheme 2). They are of interest not only in view of their remarkable structures, but also because of their mode of formation. The problem is that the crown ether cavity is too small to permit direct penetration by a benzene ring, so multistep processes that involve reversible ionic cleavage of a carbon-magnesium bond have to be postulated.[9−11]

In spite of the extensive literature on rotaxanes and catenanes in general,[12,13] derivatives of organometallic compounds with multiple threading have not been reported yet. On the basis of the results briefly indicated above, it seemed of interest to extend our investigations to double rotaxanes or catenanes of organomagnesium compounds for two re-

[a] Department of Metal-Mediated Synthesis, Utrecht University, Padualaan 8,
3584 CH Utrecht, The Netherlands
[b] Faculty of Education, Mie University, Tsu,
Mie 514−8507, Japan
[c] Department of Crystal and Structural Chemistry, Utrecht University, Padualaan 8,
3584 CH Utrecht, The Netherlands
[d] Scheikundig Laboratorium, Vrije Universiteit,
De Boelelaan 1083, 1081 HV Amsterdam, The Netherlands
Fax: (internat.) +31-20-4447488
E-mail: bicklhpt@few.vu.nl

 © 2004 Wiley-VCH Verlag GmbH & Co. KGaA, Weinheim DOI: 10.1002/ejic.200300427

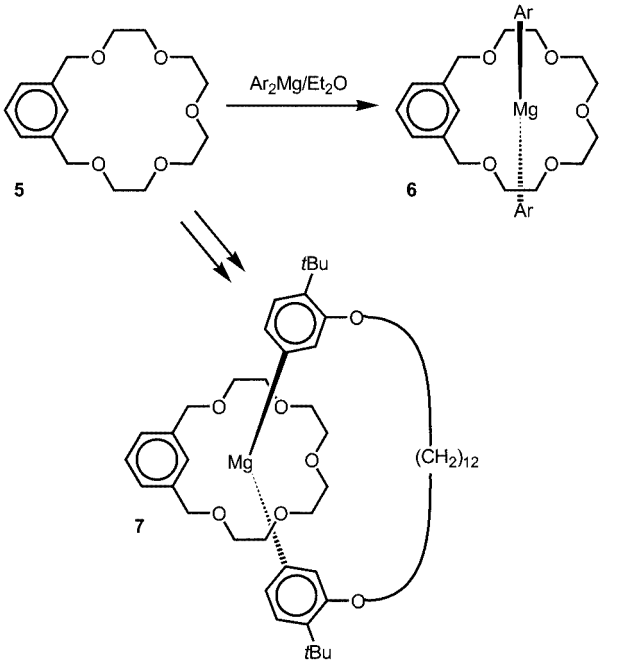

Scheme 2. Ar = Ph, *p*-*t*BuC$_6$H$_4$

asons: firstly, it was attractive to explore the transmission of conformational information between the different complexation sites, the so-called allosteric effect;[14−17] and secondly, it was conceivable that one could construct higher-order assemblies of these complex types. A good starting point for such investigations appeared to be the title compound, the bis(coronand) **8** (Scheme 3), the synthesis of which has been described.[18]

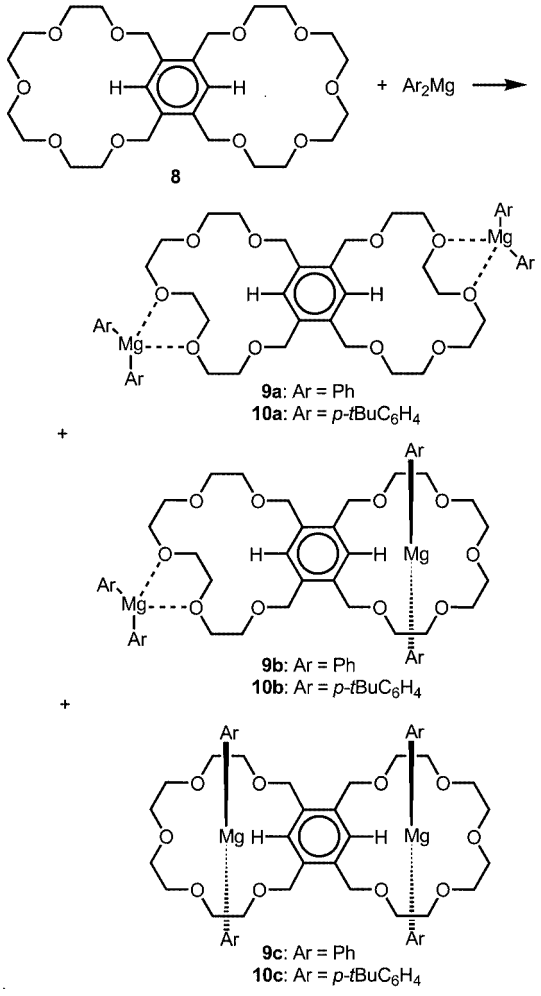

Scheme 3

Results and Discussion

Complexation of 8 with Diarylmagnesium Compounds

To study the interaction between **8** and diphenylmagnesium, diethyl ether solutions of the two compounds were mixed at room temperature in a molar ratio of 1:2. A homogeneous yellow solution resulted, but after a few minutes, a white precipitate formed. The supernatant solution was removed and hydrolyzed; it contained 10% diphenylmagnesium [according to the titration for Mg^{2+} and OH^- (acid/base and EDTA)][19] and no **8** (^{1}H NMR spectroscopy). From the precipitate, residual diethyl ether was removed by pumping under high vacuum; the resulting pale brown residue dissolved almost completely in [D$_8$]toluene. Hydrolysis of a sample followed by titration as mentioned above revealed the presence of **8** and of diphenylmagnesium in a ratio of 1:2. The ^{1}H NMR spectrum (400 MHz) in [D$_8$]toluene was rather complex. It showed, amongst others, crown

Table 1. Chemical shifts of benzylic (Ar′C*H*$_2$) and arylic (Ar′H) protons in **8** and its complexes

Compound	Ar′C*H*$_2$ free	Ar′C*H*$_2$ side-on	Ar′C*H*$_2$ rotaxane	Ar′*H* free	Ar′*H* side-on	Ar′*H* rotaxane
8[a]	4.57	–	–	7.93	–	–
8[b]	4.67	–	–	7.69	–	–
9a[a]	–	4.50	–	–	7.83	–
9b[a]	–	4.47	4.20	–	7.74	8.60
9c[a]	–	–	4.09	–	–	8.56
10a[a]	–	4.52	–	–	7.89	–
10b[a]	–	4.49	4.23	–	7.89	8.67
10c[a]	–	–	4.08?	–	–	?
11[b]	–	–	4.78	–	–	8.05
12[b]	4.59	–	4.79	7.77	–	7.79

[a] In [D$_8$]toluene. [b] In CDCl$_3$.

 © 2004 Wiley-VCH Verlag GmbH & Co. KGaA, Weinheim

ether signals at about δ = 4.2 and 4.09 ppm (Ar′CH_2) and at δ = 8.6 ppm (Ar′H; Table 1).

These Ar′CH_2 protons are shielded by about 0.4 ppm and the corresponding crown ether methylene protons (see Exp. Sect.) by 0.4−0.5 ppm are similar to those within **8**. Interestingly, the intra-annular aromatic xylylene protons Ar′H are deshielded by 0.4 ppm. This is reminiscent of analogous behavior of aryl protons inside the cavity of small metacyclophanes;[20,21] it has been ascribed to the van der Waals effect caused by steric congestion.[22] As similar changes have also been observed for **6**[9] and **7**,[11] these phenomena are indicative of the rotaxane-type threading of a diarylmagnesium into a *m*-xylylene crown ether cavity. In view of the 1:2 ratio of the two components, three structures are conceivable: the double side-on complex **9a**, the side-on/rotaxane complex **9b**, and the double rotaxane complex **9c** (Scheme 3).

Due to the complicated pattern and to partial overlap, it was difficult to assign all of the signals for the three complexes. However, based on the Ar′CH_2 signals at δ = 4.50, 4.47, 4.20, and 4.09 ppm with a relative intensity of 56:21:22:1, a tentative assignment was possible, which was supported by the intensities of the Ar′H signals at δ = 7.83, 7.74, 8.60, and 8.56 ppm, the ratio of which is Ar′CH_2/Ar′H = 4:1. As the values of δ = 4.50 and 7.83 ppm are very close to those of free **8** (δ = 4.57 and 7.93 ppm), they must be assigned to **9a**. Two other pairs of shifts at δ = 4.47 and 7.74 ppm and δ = 4.20 and 8.60 ppm have equal intensities which is in line with **9b**; this is further supported by the observation that the shifts of the first pair correspond to those of **9a** indicating side-on coordination, while those for the second pair are typical for a rotaxane structure.[9,11] The least certain assignment is that of the pair at δ = 4.09 and 8.56 ppm due to the low intensity; it cannot be excluded that these signals are caused by impurities, but on the other hand, the 4:1 ratio and the typical "rotaxane shift range" support the tentative assignment to **9c**.

An attempt to change the ratios of the three isomers by mixing **8** and diphenylmagnesium in diethyl ether in a 1:1 ratio was not successful. Again, a precipitate was formed. Analysis of the supernatant by titration and ^{1}H NMR spectroscopy (vide supra) showed it to contain only **8**. The precipitate was dissolved in [D_8]toluene; the ^{1}H NMR spectrum was practically identical to that described above, i.e. a 1:2 ratio for the components **8** and diphenylmagnesium, and the same isomer pattern as for **9**. This is remarkable insofar as the 1:2 complexes are apparently preferred even in the presence of an excess of the bis(coronand) **8**. It is unlikely that this is due to an allosteric effect; more likely, the low solubility of **9** shifts the equilibrium in its favor.

This low solubility also hampered the spectral analysis of **9**. In an attempt to obtain more soluble complexes, we performed analogous experiments by mixing **8** with di(*p*-*tert*-butylphenyl)magnesium in diethyl ether, but in this case, too, precipitation occurred. After evaporation of the diethyl ether and dissolution in [D_8]toluene, ^{1}H NMR analysis (Table 1) revealed the presence of the double side-on complex **10a** and of the side-on/rotaxane complex **10b**; the double rotaxane **10c** could not be reliably identified, but a faint signal at δ = 4.08 ppm might be due to its ArCH_2 protons. It is not surprising to find that the equilibrium between the two types of complexes is not strongly influenced by the remote *tert*-butyl group in **10**; at 298 K, the **a**/**b** ratios are 56:43 for **9** and 64.5:35.5 for **10**. According to the X-ray crystal structure of **6**,[9] one of the aryl rings is probably located partly above the aromatic ring of the crown ether; this could lead to increased steric hindrance in **10b** as compared to **9b** which explains the slightly higher preference for **10a**.

As the solubility of **10** was somewhat higher than that of **9**, we were able to check the temperature dependence of the ^{1}H NMR spectrum and its influence on the equilibrium between **10a** and **10b**. The results (Table 2) are not very reliable because a precipitate formed slowly in the NMR tube, especially at higher temperatures.

Table 2. Temperature dependence of isomer ratios **10a**:**10b**

T [K]	298	328	344	355	365
10a[a][b]	64.5	70.7	73.5	82.1	88.9
10b[a][b]	35.5	29.3	26.5	17.9	11.1

[a] In [D_8]toluene. [b] In %.

Raising the temperature shifts the equilibrium in favor of the major component **10a**. On cooling down, this process is (slowly!) reversible. In view of the precipitate formation and the few data points, it is problematic to derive quantitative values for ΔH and ΔS. However, at least a qualitative indication can be obtained if one neglects two dubious points (with more precipitate) at higher temperature. For the transformation **10a** → **10b**, the three lower points give a very good linear correlation [Equation (1)], from which ΔH = −7.8 kJ·mol^{-1} and ΔS = −31 J·mol^{-1}·K^{-1} are obtained; inclusion of all 5 temperatures would lead to ΔH = −19 kJ·mol^{-1} and ΔS = −66 J·mol^{-1}·K^{-1} (R = 0.820).

$$\Delta G = -7791 + 31.1 \cdot T \; (R = 1.000) \qquad (1)$$

With appropriate caution, one may conclude that the transformation of a side-on complex to a rotaxane in the reaction **10a** → **10b** is slightly exothermic. This is reasonable if one considers that in **10a**, the magnesium atom is coordinated to two oxygen atoms only, whereas the magnesium atom in the rotaxane cavity of **10b** weakly interacts with additional oxygens as indicated by the X-ray structures of **6** and analogous rotaxanes.[1,7−11] As expected, the reaction entropy ΔS is negative because the rotaxane is conformationally more rigid than the side-on complex. Apparently, this additional rigidity overcompensates the gain in enthalpy in the transformation of the mono rotaxanes **b** to the double rotaxanes **c**; consequently, **9c** and **10c** are minor components only.

 © 2004 Wiley-VCH Verlag GmbH & Co. KGaA, Weinheim

Complexation of 8 with $Hg(SCN)_2$

As the double rotaxane formation between **8** and diarylmagnesium compounds turned out to be unfavorable, we investigated the interaction of **8** with $Hg(SCN)_2$; the latter has served to study pseudorotaxane formation and allosteric effects in several crown ether systems.[17,23,24] When solutions of **8** and of $Hg(SCN)_2$ in acetone were mixed, a colorless precipitate was obtained. It was filtered off, dissolved in $CDCl_3$, and analyzed by ^1H NMR spectroscopy (Table 1), which revealed the formation of a single symmetrical complex. The most conspicuous signal was at δ = 8.05 ppm; the deshielding of this proton relative to its counterpart in **8** (δ = 7.69 ppm; $\Delta\delta$ = −0.36 ppm) is indicative of the intra-annular Ar*H* of a rotaxane structure (vide supra). The structural assignment of **11** (Scheme 4) is further supported by the equivalence of the two Ar*H* protons and the eight $ArCH_2$ protons. Finally, the identity of **11** was proven by an X-ray crystal structure determination (Figure 1). As the crystals were obtained directly from the reaction mixture and could not be recrystallized due to decomposition, the quality of this determination was not high ($R1$ = 0.0740); nevertheless, it unambiguously established the double pseudorotaxane threading of $Hg(SCN)_2$ through **8**.

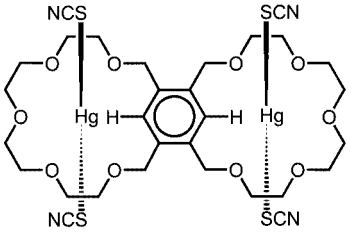

11

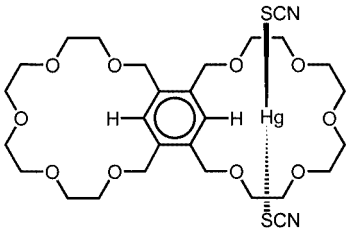

12

Scheme 4

Solutions of **11** in $CDCl_3$ deteriorated on standing as evidenced by the appearance of several new signals in the ^1H NMR spectra. When **8** and $Hg(SCN)_2$ were mixed in a 1:1 ratio, four Ar*H* signals were observed at δ = 7.69, 7.77, 7.79, and 8.05 ppm. Those at 7.69 and 8.05 ppm stem from free **8** and **11**, respectively. The two remaining signals are assigned to the mono pseudorotaxane **12**. From the signal intensities, the following ratios were derived: **8**:**12**:**11** = 20:72:8, again showing a small bias against formation of the double pseudorotaxane (**11**) which, however, is less dramatic than in the case of **9c** and **10c**. This may be ascribed to the fact that the linear $Hg(SCN)_2$ causes fewer steric interactions inside the crown ether than the aryl groups of Ar_2Mg.

Conclusion

The interaction between the title bis(coronand) **8** and the diarylmagnesium compounds Ph_2Mg and $(p\text{-}t\text{Bu}C_6H_4)_2Mg$ in diethyl ether results in the formation of 1:2 complexes (**9** and **10**, respectively), irrespective of the initial ratio of the components; presumably, this is caused by the low solubility of **9** and **10**. In [D_8]toluene, three types of complexes can be discerned by ^1H NMR spectroscopy: double side-on (**9a**, **10a**), side-on/rotaxane (**9b**, **10b**), and, to a very minor extent, double rotaxane (**9c**, **10c**); the latter two occur in approximately 1% yield only and are the first examples of organometallic double rotaxanes. In the case of **10a** and **10b**, the temperature dependence showed that rotaxane formation is enthalpically favored at the expense of a more negative entropy. Presumably, the formation of the double rotaxanes **9c** and **10c** is counteracted by interaction of the magnesium bound aryl groups across the central aromatic ring.

Due to the low solubility of **9** and **10**, crystals suitable for structure determination could not be obtained. For this reason, the interaction of **8** with the sterically less demanding $Hg(SCN)_2$ was studied. In this case, pseudorotaxanes are formed exclusively, and both the 1:2 complex [**8**·{$Hg(SCN)_2$}$_2$] (**11**) and its 1:1 analogue **12** were observed by ^1H NMR spectroscopy. The double pseudorotaxane structure of **11** was confirmed by an X-ray crystal structure determination.

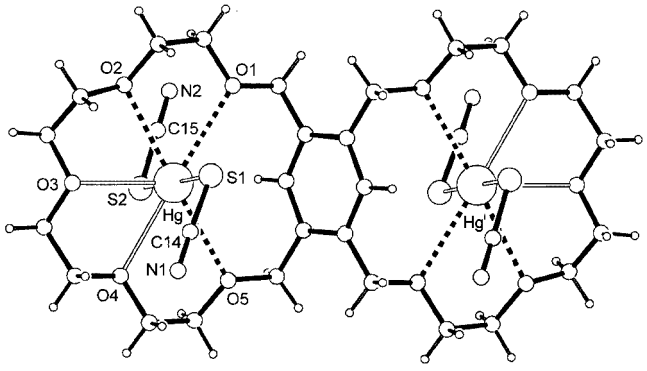

Figure 1. PLUTON[25] projection of compound **11**; symmetry operation *i*: 1 − *x*, 1 − *y*, 1 − *z*; selected bond lengths [A]: Hg−S1 2.358(4), Hg−S2 2.384(4), Hg−O3 2.737(13), Hg−O4 2.742(13), Hg−O1 2.925(12), Hg−O2 2.824(12), Hg−O5 2.898(13)

Experimental Section

General: All manipulations involving organomagnesium compounds were carried out in completely sealed glassware using standard high vacuum techniques.[19] Amounts of ′total base′ and magnesium in organomagnesium samples were determined, after hydrolysis of a sample, by titration with HCl (OH^-) and EDTA (Mg^{2+}), respectively.[19] Solvents were dried by distillation from $LiAlH_4$ after pre-drying over NaOH. NMR spectra were recorded on

 © 2004 Wiley-VCH Verlag GmbH & Co. KGaA, Weinheim

a Bruker AC 200 spectrometer (^{1}H NMR: δ = 200.1 MHz; ^{13}C NMR: δ = 50.32 MHz) or on a Bruker MSL 400 spectrometer (^{1}H NMR: δ = 400.1 MHz; ^{13}C NMR: δ = 100.6 MHz). HRMS measurements were performed on a Finnigan MAT 90 spectrometer (direct inlet). **Caution:** Organomercury compounds are poisonous!

Diphenylmagnesium: Diphenylmercury (6.39 g, 18 mmol) was stirred with doubly sublimed magnesium (4.37 g, 180 mmol) in diethyl ether (180 mL) in a fully sealed glass system for three weeks. After the magnesium amalgam had settled, the clear solution was decanted into a second vessel, and an aliquot of known volume was hydrolyzed and titrated (OH^- and Mg^{2+})[19] to establish the concentration of diphenylmagnesium.

Bis(*p*-*tert*-butylphenyl)magnesium: In a fully sealed glass system, bis(*p*-*tert*-butylphenyl)mercury (9.34 g, 20 mmol) was stirred with doubly sublimed magnesium (4.86 g, 200 mmol) in diethyl ether (200 mL) for three weeks. After settling of the magnesium amalgam, the clear solution was decanted into a second vessel, and an aliquot of known volume was hydrolyzed and titrated (OH^- and Mg^{2+})[19] to establish the concentration of bis(*p*-*tert*-butylphenyl)magnesium.

Reaction of 8 with Two Molar Equivalents of Diphenylmagnesium: Solutions of **8**[18] [7.55 mg, 0.0147 mmol in diethyl ether (2 mL)] and of diphenylmagnesium [0.03 mmol in diethyl ether (8 mL)] were combined in a fully sealed glass system. Within 15 min, the clear yellow solution decolorized, and a white precipitate was formed. After heating at 40 °C for 2 h, the clear supernatant was carefully decanted. The diethyl ether mother liquor was hydrolyzed, and the aqueous phase was titrated (OH^- and Mg^{2+}).[19] This indicated that more than 90% of the Ph_2Mg was contained in the precipitate. This titration sample was carefully extracted with benzene. The organic layers were combined, dried ($MgSO_4$), filtered, and the solvents evaporated to dryness. ^{1}H NMR spectroscopy revealed no signals that could be ascribed to starting material **8**. The solid reaction product obtained by decantation was dried by pumping under high vacuum, and toluene (10 mL) was then added, upon which most of the solid dissolved. From the supernatant, a sample was taken for characterization by ^{1}H NMR spectroscopy in [D_8]toluene. To quantify the effects of complexation on the chemical shifts of the crown ether, a reference spectrum of pure **8** was measured under identical conditions. ^{1}H NMR spectroscopy revealed that signals of the free crown ether **8** were absent. Assignment of all signals was not possible due to overlap and the complexity of the spectrum. Integration of the benzylic proton signals was used to determine the following relative yields: **9a** (55.9%), **9b** (43.2%), and **9c** (0.9%).
8: ^{1}H NMR {[D_8]toluene, 200.1 MHz, ref. $C_6D_5CD_2H$: δ = 2.03 ppm}: δ = 3.43−3.51 (br. s, 32 H, CH_2), 4.57 (s, 8 H, $ArCH_2$), 7.93 (s, 2 H, ArH) ppm. ^{13}C NMR {[D_8]toluene, 50.32 MHz, ref. $C_6D_5CD_3$: δ = 20.40 ppm}: δ = 69.61 (tt, ^1J = 139.9, ^2J = 4.2 Hz, 4C, CH_2O), 71.00 (t, ^1J = 141.9 Hz, 4C, CH_2O), 71.05 (t, ^1J = 139.9 Hz, 4C, CH_2O), 71.18 (td, ^1J = 140.4, ^3J = 3.8 Hz, 4C, $ArCH_2$), 71.46 (tt, ^1J = 140.0, ^2J = 2.5 Hz, 4C, CH_2O), 128.22 (d, ^1J = 163.8 Hz, 2C, aryl-CH), 135.50 (d, ^2J = 3.5 Hz, 2C, aryl-C) ppm.
9a: ^{1}H NMR {[D_8]toluene, 200.1 MHz, ref. $C_6D_5CD_2H$: δ = 2.03 ppm}: δ = 3.38 (s br., 16 H, CH_2), 3.41 (m, 16 H, CH_2), 4.50 (s, 8 H, $ArCH_2$), 7.24−7.26 [m, ArH(4)], 7.34 [t br., J = 6.9 Hz, ArH(3.5)], 7.83 (s, 2 H, xylyl-H), 8.11 [d br., ^3J = 6.2 Hz, ArH(2.6)] ppm.
9b: ^{1}H NMR {[D_8]toluene, 200.1 MHz, ref. $C_6D_5CD_2H$: δ = 2.03 ppm}: δ = 2.94−3.01 (m, 4 H, CH_2), 3.12−3.16 (m, 4 H, CH_2), 3.30−3.34 (m, 4 H, CH_2), 4.20 [s, 4 H, $ArCH_2$ (rotaxane)], 4.47 [s, 4 H, $ArCH_2$ (side-on)], 7.10−7.14 [m, ArH(4) (rotaxane)], 7.22 [t, J = 7.1 Hz, ArH(3.5)], 7.80 [d, ^3J = 6.4 Hz, ArH(2.6)], 7.74 [s, 1 H, xylyl-H (side-on)], 8.60 [s, 1 H, xylyl-H (rotaxane)] ppm. The other signals coincide with those of **9a**.
9c: ^{1}H NMR {[D_8]toluene, 200.1 MHz, ref. $C_6D_5CD_2H$: δ = 2.03 ppm}: δ = 4.09 (s, 8 H, $ArCH_2$), 8.56 (s, 2 H, xylyl-H) ppm. The other signals coincide with those of **9a** and **9b**.

Reaction of 8 with One Molar Equivalent of Diphenylmagnesium: Solutions of **8** (7.55 mg, 0.0147 mmol) in diethyl ether (2 mL) and of diphenylmagnesium [0.015 mmol in diethyl ether (4 mL)] were combined in a fully sealed glass system. After formation of a white suspension, the diethyl ether was distilled off and replaced by toluene (10 mL). The clear supernatant was decanted and analyzed by titration and by ^{1}H NMR spectroscopy in [D_8]toluene, which showed that only the starting material **8** was present. The pale brown precipitate was dissolved in [D_8]toluene and showed essentially the same ^{1}H NMR spectrum as that obtained in the reaction of **8** with two equivalents of Ph_2Mg, but with the products **9a** and **9b** in a ratio of 55:45. ^{1}H NMR signals of **9c** were not detected.

Reaction of 8 with Two Molar Equivalents of (p-tBuC_6H_4)$_2$Mg: A solution of (p-tBuC_6H_4)$_2$Mg (0.085 mmol) in diethyl ether (1 mL) was added to **8** (0.02167 g, 0.0421 mmol) in a fully sealed glass system, to give a clear yellow solution. After 10 min, a finely divided powder started to precipitate. After 2.5 h, the diethyl ether was distilled off, and toluene (10 mL) was added to the residue. The mixture was heated, but a clear solution was not obtained. Several attempts to crystallize the white residue in order to obtain suitable crystals for an X-ray crystal structure determination were unsuccessful. A sample was analyzed by ^{1}H NMR spectroscopy in [D_8]toluene. Assignment of all signals was not possible due to the complex nature of the spectrum. The two complexes in a mixture of **10a** and **10b** were present in a ratio of 64.5:35.5. In this case, only a faint signal of the double rotaxane complex **10c** was discernible at δ = 4.08 ppm.
10a: ^{1}H NMR {[D_8]toluene, 400.1 MHz, ref. $C_6D_5CD_2H$: δ = 2.03 ppm}: δ = 1.36 (s, 36 H, tBu), 3.37−3.45 (m, 32 H, CH_2), 4.52 (s, 8 H, $ArCH_2$), 7.45 [d, AB, ^3J = 8 Hz, 8 H, ArH(3.5)], 7.89 (s, 2 H, xylyl-H), 8.11 [d, BA, ^3J = 8 Hz, 8 H, ArH(2.6)].
10b: ^{1}H NMR {[D_8]toluene, 400.1 MHz, ref. $C_6D_5CD_2H$: δ = 2.03 ppm}: δ = 1.39 (s, 18 H, tBu) 2.93−2.99 (m, 4 H, CH_2), 3.11−3.12 (m, 4 H, CH_2), 3.17−3.23 (m, 4 H, CH_2), 3.32−3.36 (m, 4 H, CH_2), 4.23 [s, 4 H, $ArCH_2$ (rotaxane)], 4.49 [s, 4 H, $ArCH_2$ (side-on)], 7.27 [d, AB, ^3J = 7.9 Hz, 4 H, ArH(3.5)], 7.77 [d, BA, ^3J = 7.9 Hz, 4 H, ArH(2.6)], 7.89 [s, 1 H, xylyl-H (side-on)], 8.67 [s, 1 H, xylyl-H (rotaxane)] ppm. The other signals overlap with those of **10a**.

Reaction of 8 with Two Molar Equivalents of Hg(SCN)$_2$: A solution of $Hg(SCN)_2$ (0.06335 g, 0.200 mmol) in acetone (2 mL) was added to a solution of **8** (0.05143 g, 0.100 mmol) in acetone (2 mL). Within a few minutes, a white precipitate formed, which was separated by filtration and characterized by ^{1}H NMR spectroscopy as [**8**·{$Hg(SCN)_2$}$_2$] (**11**); this assignment was confirmed by the X-ray crystal structure determination.
11: ^{1}H NMR ($CDCl_3$, 200.1 MHz, ref. $CHCl_3$: δ = 7.27 ppm): δ = 3.67 (s br., 24 H, CH_2), 3.82 (m, 8 H, CH_2), 4.78 (s, 8 H, $ArCH_2$), 8.05 (s, 2 H, ArH) ppm. ^{13}C NMR ($CDCl_3$, 100.6 MHz, ref. $CDCl_3$: δ = 77.00 ppm): δ = 69.20 (t, ^1J = 145.6 Hz, 4C, CH_2), 69.42 (t, ^1J = 139.7 Hz, 4C, CH_2), 69.74 (t, ^1J = 142.7 Hz, 4C, CH_2), 69.84 (t, ^1J = 141.9 Hz, 4C, CH_2), 71.06 (t, ^1J = 140.3 Hz, 4C, $ArCH_2$), 135.72 (d, ^2J = 44.8 Hz, 2C, aryl-CH), 137.69 (br. s, 4C, aryl-C) ppm. Contrary to **12** (vide infra), **11** was not volatile under DCI conditions.

 © 2004 Wiley-VCH Verlag GmbH & Co. KGaA, Weinheim

Reaction of 8 with One Molar Equivalent of $Hg(SCN)_2$: A solution of $Hg(SCN)_2$ (0.03168 g, 0.100 mmol) in acetone (2 mL) was added to a solution of **8** (0.05143 g, 0.100 mmol) in acetone (2 mL). The mixture slowly became turbid and after one hour, the organic solvent was evaporated to dryness. The residue was dissolved in $CDCl_3$ and analyzed by ^1H NMR spectroscopy: **8** (21%), **11** (8%), and **12** (72%).

12: ^1H NMR ($CDCl_3$, 200.1 MHz, ref. $CHCl_3$: δ = 7.27 ppm): δ = 3.65 (s br., 12 H, CH_2), 3.72−3.77 (m, 20 H, CH_2), 4.59 [s, 4 H, $ArCH_2$ (rotaxane)], 4.79 [s, 4 H, $ArCH_2$ (free)], 7.77 (s, 1 H, ArH), 7.79 (s, 1 H, ArH) ppm. MS (DCI, NH_3): *m/z* (%) = 850 (10) [M + NH_4]$^+$, 791 (7) [M + NH_4-HSCN]$^+$, 632 (14), 591 (100).

X-ray Crystallographic Study: $C_{30}H_{42}Hg_2N_4O_{10}S_4$, (1148.10), colorless needles, 0.38 × 0.15 × 0.05 mm^3, triclinic, $P\bar{1}$ (no. 2), a = 7.3747(4), b = 10.0516(16), c = 14.593(3) Å, α = 89.817(15), β = 78.769(10), γ = 77.999(9)°, V = 1037.0(3) Å^3, Z = 1, ρ_x = 1.838 gcm^{-3}, 4716 measured reflections, 3633 unique reflections (R_{int} = 0.044). 161 refined parameters, R (obsd. refl.): $R1$ = 0.0740, $wR2$ = 0.2058. R (all data): $R1$ = 0.0868, $wR2$ = 0.2188, GooF = 1.055. Intensities were measured on a Enraf−Nonius CAD4T diffractometer with a rotating anode (Mo-K_α, λ = 0.71073 Å) at a temperature of 150 K. Reflection profiles for the best available crystal were structured, indicating a low quality crystal. An absorption correction was applied (program PLATON,[25] routine DELABS, μ = 7.647 mm^{-1}, 0.27−0.69 transmission). The structure was solved with Patterson methods using the program DIRDIF97,[26] and refined with the program SHELXL-97[27] against F^2 of all reflections up to a resolution of $(\sin/\lambda)_{max}$ = 0.59 Å^{-1}. Hg and O atoms and the SCN ligand were refined freely with anisotropic displacement parameters; all other carbon atoms were refined with isotropic displacement parameters. Hydrogen atoms were refined as rigid groups. The drawings, structure calculations, and checking for higher symmetry were performed with the program PLATON.[25]

CCDC-213566 contains the supplementary crystallographic data for this paper. These data can be obtained free of charge at www.ccdc.cam.ac.uk/conts/retrieving.html [or from the Cambridge Crystallographic Data Centre, 12, Union Road, Cambridge CB2 1EZ, UK; Fax: (internat.) +44-1223-336-033; E-mail: deposit@ccdc.cam.ac.uk].

Acknowledgments

Dr. B. L. M. van Baar is gratefully acknowledged for performing the HRMS and DCI measurements and Dr. F. J. J. de Kanter for the NMR experiments. This work was supported in part (M. L., A. L. S.) by The Netherlands Foundation for Chemical Sciences (CW) with financial aid from the Netherlands Organization for Scientific Research (NWO).

[1] F. Bickelhaupt in *Grignard Reagents, New Developments* (Ed.: H. G. Richey, Jr.), Wiley, Chichester, **2000**, chapter 9.
[2] F. Bickelhaupt, *Acta Chem. Scand.* **1992**, *46*, 409−417.
[3] P. R. Markies, T. Nomoto, O. S. Akkerman, F. Bickelhaupt, W. J. J. Smeets, A. L. Spek, *Angew. Chem.* **1988**, *100*, 1143−1144; *Angew. Chem. Int. Ed. Engl.* **1988**, *27*, 1084.
[4] P. R. Markies, T. Nomoto, G. Schat, O. S. Akkerman, F. Bickelhaupt, W. J. J. Smeets, A. L. Spek, *Organometallics* **1991**, *10*, 3826−3837.
[5] P. R. Markies, O. S. Akkerman, F. Bickelhaupt, W. J. J. Smeets, A. L. Spek, *J. Am. Chem. Soc.* **1988**, *110*, 4284−4292.
[6] G. J. M. Gruter, G. P. M. van Klink, O. S. Akkerman, F. Bickelhaupt, *Organometallics* **1993**, *12*, 1180−1188.
[7] H. G. Richey, Jr., D. M. Kushlan, *J. Am. Chem. Soc.* **1987**, *109*, 2510−2512.
[8] A. D. Pajerski, G. L. Bergstresser, M. Parvez, H. G. Richey, Jr., *J. Am. Chem. Soc.* **1988**, *110*, 4844−4845.
[9] P. R. Markies, T. Nomoto, O. S. Akkerman, F. Bickelhaupt, W. J. J. Smeets, A. L. Spek, *J. Am. Chem. Soc.* **1988**, *110*, 4845−4846.
[10] P. R. Markies, O. S. Akkerman, F. Bickelhaupt, W. J. J. Smeets, A. L. Spek, *Organometallics* **1994**, *13*, 2616−2627.
[11] G. J. M. Gruter, F. J. J. de Kanter, P. R. Markies, T. Nomoto, O. S. Akkerman, F. Bickelhaupt, *J. Am. Chem. Soc.* **1993**, *115*, 12179−12180.
[12] F. M. Raymo, J. F. Stoddart, *Chem. Rev.* **1999**, *99*, 1643−1663.
[13] J. W. Steed, J. L. Atwood, *Supramolecular Chemistry*, Wiley, Chichester, **2000**, chapter 7.6.
[14] J. Rebek, Jr., *Acc. Chem. Res.* **1984**, *17*, 258−264.
[15] J. Rebek, Jr., T. Costello, L. Marshal, R. Wattley, R. C. Gadwood, K. Onan, *J. Am. Chem. Soc.* **1985**, *107*, 7481−7487.
[16] Y. Rubin, K. Dick, F. Diederich, T. M. Georgiedis, *J. Org. Chem.* **1986**, *51*, 3270−3278.
[17] A. M. Costero, M. Pitarch, C. Andreu, L. E. Orchando, J. M. Amigó, T. Debaerdemaeker, *Tetrahedron* **1996**, *52*, 669−676.
[18] G. P. M. van Klink, T. Nomoto, E. van Wees, A. G. L. Ostheimer, O. S. Akkerman, F. Bickelhaupt, *SYNLETT* **1996**, 430−432.
[19] A. D. Vreugdenhil, C. Blomberg, *Recl. Trav. Chim. Pays-Bas* **1963**, *82*, 453−460.
[20] S. Hirano, H. Hara, T. Hiyama, S. Fujita, H. Nozaki, *Tetrahedron* **1975**, *31*, 2219−2227.
[21] J. W. van Straten, W. H. de Wolf, F. Bickelhaupt, *Tetrahedron Lett.* **1977**, *18*, 4667−4670.
[22] L. M. Jackman, S. Sternhell, *Applications of Nuclear Magnetic Resonance Spectroscopy in Organic Chemistry*, 2nd ed., Pergamon Press, Oxford, **1969**, p. 71−72.
[23] J. D. Owen, *J. Chem. Soc., Dalton Trans.* **1978**, 1418−1423.
[24] L. E. Ochando, J. M. Amigó, A. M. Costero, M. Pitarch, T. Debaerdemaeker, *Cryst. Res. Technol.* **1996**, *31*, 37−42.
[25] A. L. Spek, *J. Appl. Cryst.* **2003**, *36*, 7−13.
[26] P. T. Beurskens, G. Admiraal, G. Beurskens, W. P. Bosman, S. Garcia-Granda, R. O. Gould, J. M. M. Smits, C. Smykalla, The DIRDIF97 program system, Technical Report of the Crystallography Laboratory, University of Nijmegen, The Netherlands, **1997**.
[27] G. M. Sheldrick, SHELXL-97, *Program for crystal structure refinement*, University of Göttingen, Germany, **1997**.

Received July 3, 2003
Early View Article
Published Online October 23, 2003

 © 2004 Wiley-VCH Verlag GmbH & Co. KGaA, Weinheim

1D-Polyoxometalate-Based Composite Compounds − Design, Synthesis, Crystal Structures, and Properties of $[\{Ln(NMP)_6\}(PMo_{12}O_{40})]_n$ (Ln = La, Ce, Pr; NMP = *N*-methyl-2-pyrrolidone)

Jing-Yang Niu,*[a] Mei-Lin Wei,[a] Jing-Ping Wang,*[a] and Dong-Bin Dang[b]

Keywords: Polyoxometalates / Oxo ligands / Lanthanides / Structure elucidation / Zig-zag chain

The structures of three 1:1 composite compounds prepared with the polyoxometalate (POM) $[PMo_{12}O_{40}]^{3-}$ and the cations $[Ln(NMP)_6]^{3+}$ [Ln = La (**1**), Ce (**3**), Pr (**2**); NMP = *N*-methyl-2-pyrrolidone] exhibit two types of zig-zag chains with alternating cations and anions through Mo–O_t–Ln–O_t–Mo links in the crystal. The compounds were characterized by IR, UV, and ESR spectroscopy, single-crystal X-ray structural analysis, and by a study of their thermal properties. In all the compounds, the La^{3+}, Pr^{3+}, and Ce^{3+} centers are eight-coordinate with the oxygen atoms in bicapped trigonal-prismatic geometries. The variation of the average Ln–O separations along the La, Ce, and Pr series is consistent with the effects of the lanthanide contraction. The results of the single-crystal X-ray diffraction analyses and the IR spectroscopic studies are in agreement and both show the metal cation units are coordinatively bonded to the Keggin clusters. The UV spectra of the title compounds suggest that their structures are entirely disrupted in dilute solution. Low-temperature ESR spectra indicate that thermal electron delocalization occurs among the Mo atoms in the three compounds. The results of cyclic voltammetry (CV) show that compounds **1**, **2**, and **3** all undergo five two-electron reversible reductions and that the $[PMo_{12}O_{40}]^{3-}$ anions are the active centers for electrochemical redox reactions in solution, while the corresponding cations have only a small effect on the electrochemical properties. Studies of magnetic properties show that **1** is diamagnetic, while **2**and **3** exhibit antiferromagnetic Pr–Pr or Ce–Ce exchange interactions. In addition to the results of CV, the average bond lengths and the magnetic properties of compound **3** indicate that the oxidation state of cerium is iii in the compound of formula $[\{Ce(NMP)_6\}(PMo_{12}O_{40})]_n$.
(© Wiley-VCH Verlag GmbH & Co. KGaA, 69451 Weinheim, Germany, 2004)

Introduction

As a rich and diverse class of inorganic cluster systems, the polyoxometalate ions formed by the early transition metals are noted for their fascinating structural, electrochemical, catalytic, magnetic, medicinal, and photophysical properties.[1] In the field of designing and assembling molecular-based materials[2−10] with structures based on the so-called anion-cation salts or host-guest solids, polyoxometalates have been found to be extremely versatile inorganic building blocks due to their ability to accept electrons.[11] So far, many intermolecular complexes based on polyoxometalates have been synthesized and reported.[11−23] Through electron transfer between organic units and polyanions, some are able to enhance the SHG (second harmonic generation) nonlinear optical response[12] while others enhance electric or magnetic properties.[13−18] The interactions existing in the structures of organic substrates and heteropoly acids or salts are mainly facilitated by hydrogen bonds, van der Waals forces, and electrostatic forces. However, infinitely extended chains based on Keggin- or Dawson-type anions and joined together by W(Mo)−O_t−M[19] links are relatively rare. Structurally characterized notable examples include $[ET]_8[PMnW_{11}O_{39}]\cdot 2H_2O$ [ET = bis(ethylenedithio)tetrathiafulvalene],[20] $[NEt_3H]_5[XCoW_{11}O_{39}]\times 3H_2O$ (X = P or As),[21] $[Cu(en)_2(OH_2)]_2[H_2en][\{Cu(en)_2\}\text{-}P_2CuW_{17}O_{61}]\times 5H_2O$ (en = ethylenediamine), $[Cu(en)_2(OH_2)]_2[Cu(en)]_{0.5}\text{-}[H_2en]_{0.5}[\{Cu(en)_2\}P_2CuW_{17}O_{61}]\times 5H_2O$,[22] $[\{Ba(DMSO)_5\text{-}(H_2O)\}_2(SiMo_{12}O_{40})]$, $[\{Ba(DMSO)_3(H_2O)_3\}\{Ba(DMSO)_5\text{-}(H_2O)GeMo_{12}O_{40}\}]$,[11] and $[\{Ca(DMF)_5\}_2SiMo_{12}O_{40}]_n$.[23]

In polyoxometalate chemistry, one of the major challenges is the "rational" synthesis of new compounds. The development of rational methods for the modification and functionalization of polyoxometalate systems may provide the means to fully exploit the desirable attributes mentioned above. From the standpoint of molecular design, we attempted to use traditional synthesis to realize such molecular assemblies. Firstly, we introduced metal ions into the framework formed by polyanions and organic units, so that

[a] School of Chemistry and Chemical Engineering, Henan University, Kaifeng 475001, P. R. China
E-mail: jyniu@henu.edu.cn.
[b] State Key Laboratory of Coordination Chemistry, Nanjing University, Nanjing 210093, P. R. China
Supporting information for this article is available on the WWW under http://www.eurjic.org or from the author.

 © 2004 Wiley-VCH Verlag GmbH & Co. KGaA, Weinheim DOI: 10.1002/ejic.200300048

the combination of polyanions and organic units through metal ions could be achieved. Here, we chose lanthanide(III) metal ions, which have potential uses in bioinorganic chemistry and materials science.[24−26] Secondly, we chose NMP molecules as electron donors, since polyoxometalate anions are good electron acceptors, thus, they can interact leading to electron transfer. In this paper, we report the synthesis and single-crystal X-ray structural analyses of three infinitely extended polyoxometalate-based composites: $[\{Ln(NMP)_6\}(PMo_{12}O_{40})]_n$ (Ln = La, Ce, Pr; NMP = *N*-methyl-2-pyrrolidone). In the structures of these composites, the rare-earth ions are firstly coordinated by six NMP and polyanionic ligands to form a structural unit. These structural units are then connected through $Mo-O_t-Ln-O_t-Mo$[19] links to form one-dimensional chain-like structures. To the best of our knowledge, the types of structure exhibited by these compounds have not been previously reported. This paper reports studies of the magnetic and electrochemical properties as well as solid-state structural aspects of three organic-inorganic complexes with novel structures, in which infinite stacking assemblies between polyanions and cationic units have been achieved.

Results and Discussion

Experiments demonstrated that selection of a suitable solvent was crucial for growing crystals of the title compounds. Stable crystals of compounds **1**, **2**, and **3** were obtained from acetonitrile/water mixtures at room temperature. Compounds **1**, **2**, and **3** are all soluble in CH_3CN and its mixtures with water. When **1**, **2**, and **3** were dissolved in pure CH_3CN, irregular crystals were obtained because of rapid loss of solvent, therefore necessitating control of the concentration rate of the solution. This problem was overcome by simply adding water to the acetonitrile solutions. Using this method, crystals suitable for X-ray diffraction were eventually obtained. In addition, exposure of the solutions to sunlight was avoided as a result of the photosensitivity of the crystals, the reasons for which have been mentioned above.

The structures of the three composite compounds constructed from $[PMo_{12}O_{40}]^{3-}$ and the cations $[Ln(NMP)_6]^{3+}$ (Ln = La, Ce, Pr) exhibit two types of zig-zag chains with alternating cations and anions through $Mo-O_t-Ln-O_t-Mo$ links in the crystal. The novelty of these composite compounds is based on the fact that the alternating chains now contain only one cation per anion instead of two[11,23] (which is the usual case observed in other POM-cation chains). $[\{La(NMP)_6\}(PMo_{12}O_{40})]_n$ and $[\{Pr(NMP)_6\}(PMo_{12}O_{40})]_n$ show the same zig-zag chains (Figure 1). Representative molecular structural units and the coordination environment of compound **1** are shown in Figures 2 and 3(a). However, $[\{Ce(NMP)_6\}(PMo_{12}O_{40})]_n$ forms different zig-zag chains (Figure 4) from **1** and **2**, with molecular structural units and the coordination environments shown

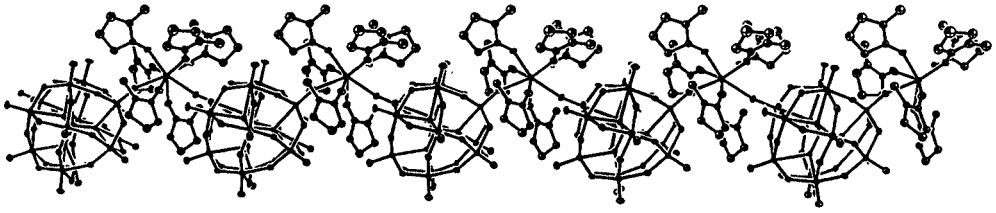

Figure 1. View of the one-dimensional chains in **1** and **2**; hydrogen atoms are omitted for clarity

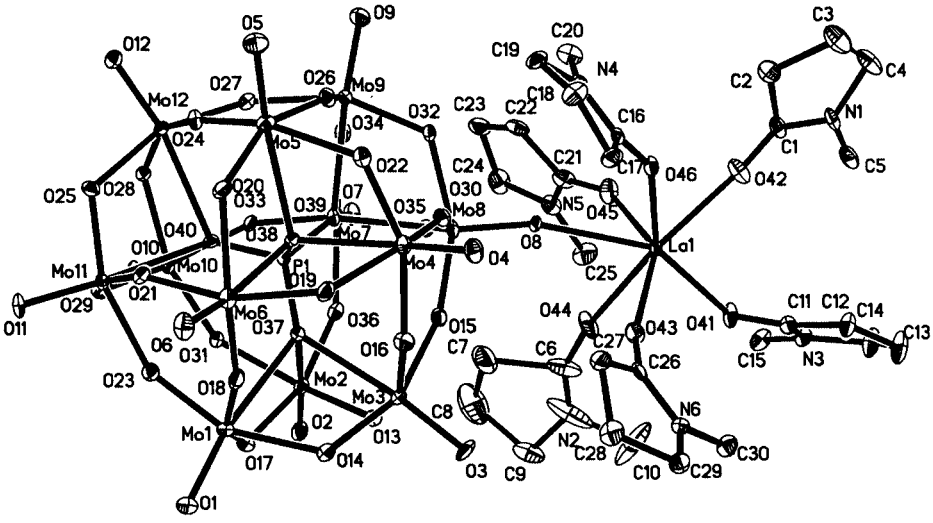

Figure 2. Molecular structural unit with atomic labeling for compound **1**; ellipsoids are shown at the 30% probability level; hydrogen atoms are omitted for clarity

 © 2004 Wiley-VCH Verlag GmbH & Co. KGaA, Weinheim

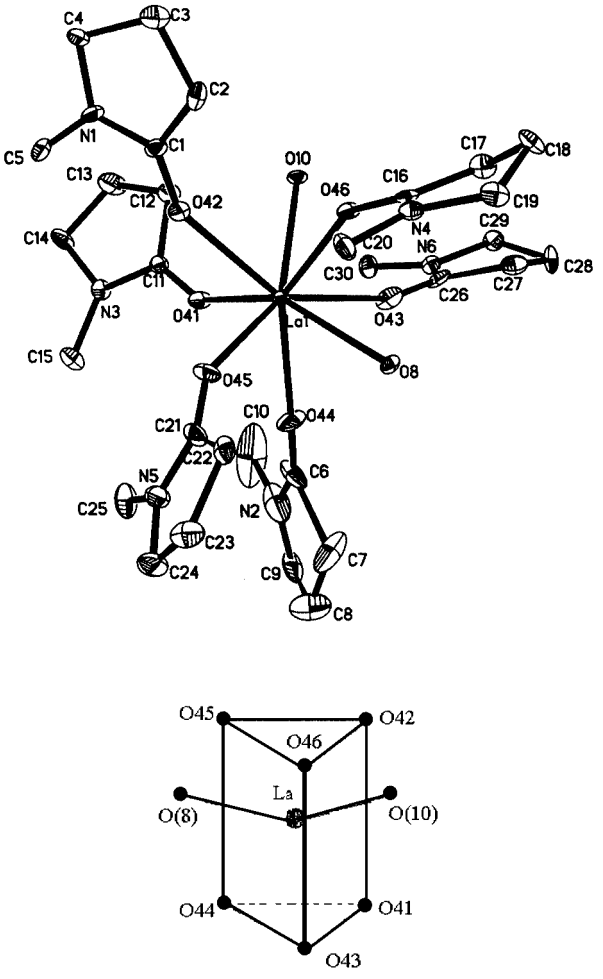

Figure 3. (a; top) Coordination environment of La^{3+} in **1**, hydrogen atoms are omitted for clarity; (b; bottom) coordination polyhedron around La^{3+} in **1**

in Figures 5 and 6. The coordination numbers of the La^{3+}, Pr^{3+} and Ce^{3+} ions are all 8 (six O atoms from the NMP ligands, and the remaining two O atoms from two adjacent heteropolyanions). The coordination environments of the La^{3+}, Pr^{3+}, and Ce^{3+} ions can be described as bicapped trigonal-prismatic, an example being that of La^{3+} shown in Figure 3(b). This is one of the common coordination geometries for complexes with a coordination number of 8.[27] In the three compounds each La^{3+}, Pr^{3+}, and Ce^{3+} ion has six O atoms from six NMP molecules forming two trigonal planes, and two terminal oxygen atoms from the polyanions occupying the caps due to the steric hindrance of the polyanions. These factors all contribute towards the stability of the title compounds. In addition, the O(10)#1−La(1)−O(8) bond angle is 124.27(15)°, the O(10)#1−Pr(1)−O(8) bond angle is 124.8 (3)°, and the O(6)#1−Ce(1)−O(6) bond angle is 122.4(3)° resulting in the formation of zig-zag chains. Comparing **3** with **1** and **2**, the striking difference lies in the type of zig-zag chains observed. In **1** and **2**, for each $[PMo_{12}O_{40}]^{3-}$ unit, there are two terminal coordinating oxygen atoms, O(10) and O(8) are almost at 90° in the Keggin-type cage while in **3**, O(6) and O(6)#1 are almost in a *para* position.

The La−O, Pr−O, and Ce−O bond lengths range from 2.397 to 2.660 Å, from 2.347 to 2.592 Å, and from 2.388 to 2.649 Å, respectively. The average bond length for all La−O bonds is 2.474 Å, which is 0.028 Å longer than the La−O1A bond length (2.446 Å) in $[La^{III}(NITBzImH)_4](ClO_4)_3\times2THF\times2H_2O$ (NITBzImH = nitronyl nitroxide radicals),[27] in which the coordination number is 8 and the coordination polyhedron around the La^{3+} ion is distorted from dodecahedral toward a square-antiprismatic geometry. This bond is 0.006 Å shorter than the La−O1A bond (2.48 Å) in $[La^{III}(NITMeBzImH)_4](ClO_4)_3\times2THF\times1H_2O$ (NITMeBzImH = nitronyl nitroxide radicals),[27] in which the coordination number of the La^{3+} ion is 8 and the coordination polyhedron around the La^{3+} ion is a distorted cube. The average bond length for all Pr−O bonds is 2.429 Å, which is 0.099 Å longer than the mean Pr(1)−O bond length (2.393 Å) of $[Pr_2(bbpen)_2(NO_3)(H_2O)]NO_3\times CH_3OH$,[28] in which the coordination number of the Pr^{3+} ion is 8 and the coordination polyhedron around the Pr^{3+} ion is a distorted cube. The average bond length for all Ce−O bonds is 2.47 Å, which is 0.064 Å shorter than the mean Ce(1)−O bond length of 2.53 Å in $[(THF)_3Ce(SC_6F_5)_3]_2$,[29] in which the coordination number of the $Ce^{3+}(1)$ ion is 8. The variation of the Ln−O average bond separations along the La, Ce, and Pr series (La−O > Ce−O > Pr−O) is consistent with the effects of the lanthanide contraction (ionic radius: $La^{3+} > Ce^{3+} > Pr^{3+}$). The fact that the mean La−O(NMOP), Pr−O(NMP), and Ce−O(NMP) bond lengths of 2.361, 2.387, and 2.405 Å, respectively, are 0.257, 0.169, and 0.244 Å shorter than the corresponding La−O_t, Pr−O_t, and Ce−O_t distances of 2.618, 2.556, and 2.649 Å indicates that the Ln−O(NMP) bonds are more stable than the Ln−O_t bonds. This is probably because the charge density at the oxygen atom of C=O is larger than that of O_t, resulting from the electron-donating effect of the methyl groups through the N atoms in the NMP molecules and the electron-withdrawing effect of the polyanions.

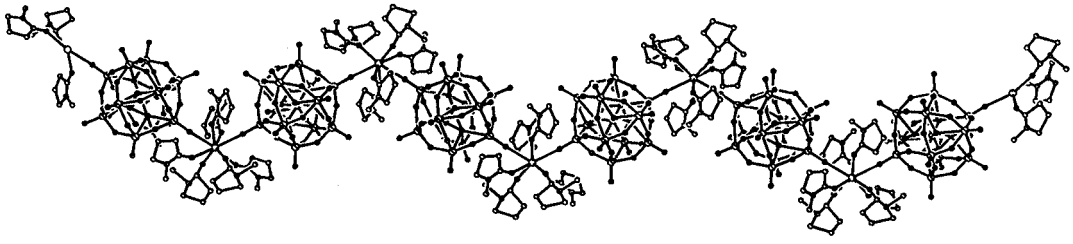

Figure 4. View of the one-dimensional chain in **3**; hydrogen atoms are omitted for clarity

 © 2004 Wiley-VCH Verlag GmbH & Co. KGaA, Weinheim

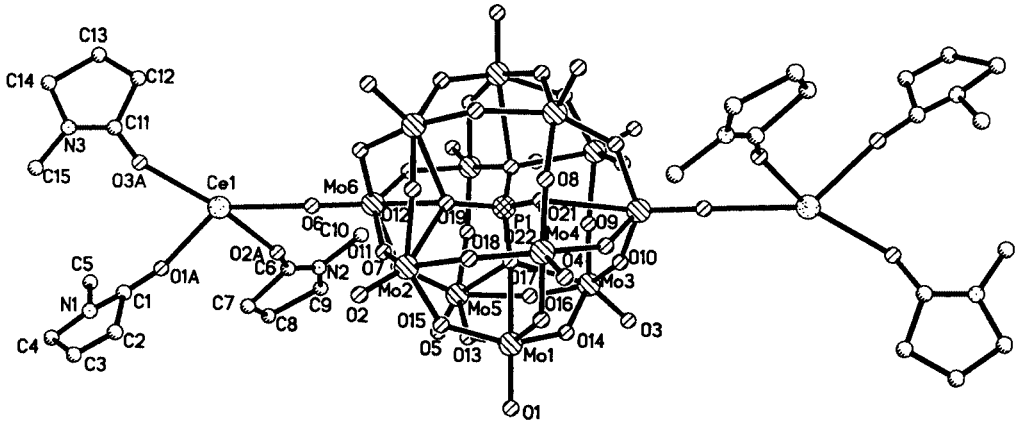

Figure 5. Molecular structural unit with atomic labeling of **3**; ellipsoids are shown at the 30% probability level; hydrogen atoms are omitted for clarity

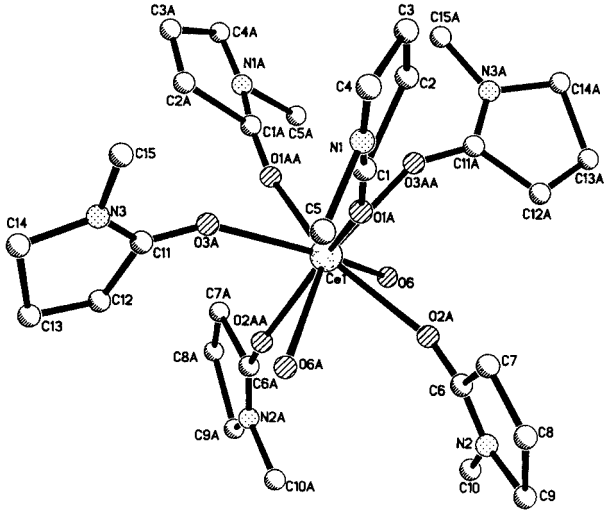

Figure 6. Coordination environment of Ce^{3+} in **3**; hydrogen atoms are omitted for clarity

The P−O bond lengths range from 1.521 to 1.546 Å for **1**, from 1.523 to 1.550 Å for **2**, and from 1.438 to 1.604 Å for **3**, respectively, with the O−P−O bond angles ranging from 108.4 to 109.9° for **1**, from 108.3 to 110.5° for **2**, and from 103.7 to 116.5° for **3**, respectively, indicating that the PO_4 tetrahedrons are distorted to a different extent in each case. The $Mo-O_t$ bond lengths range from 1.663 to 1.689 Å (av. 1.676 Å) for **1**, from 1.651 to 1.697 Å (av. 1.674 Å) for **2**, and from 1.633 to 1.664 Å (av. 1.650 Å) for **3** while the $Mo-O_a$[19] bond lengths range from 2.380 to 2.452 Å (av. 2.416 Å) for **1**, from 2.394 to 2.462 Å (av. 2.428 Å) for **2**, and from 2.384 to 2.483 Å (av. 2.427Å) for **3**. Finally, the $Mo-O_{b,c}$[19] bond lengths range from 1.804 to 2.023 Å for **1**, from 1.776 to 2.041 Å for **2**, and from 1.688 to 2.178 Å for **3**. These observations show that the MoO_6 octahedra of the polyanions in the title compounds are severely distorted because of the influence of the outer coordinating cations. Clearly, although the La^{3+}, Pr^{3+}, and Ce^{3+} ions in the title compounds have the same coordination number and coordination polyhedra, the Ce^{3+} ions distort the $[PMo_{12}O_{40}]^{3-}$ units to a larger extent than do the La^{3+} and Pr^{3+} ions. Moreover, the $Mo-O_t-Ln-O_t-Mo$ (Ln = La, Ce, Pr) links are important, firstly because polyoxometalates as ligands are electron acceptors which, in some cases, can be reduced by one or more electrons, giving rise to mixed-valence clusters. Secondly, because rare-earth atoms with magnetic properties have been introduced into the structures of compounds **1**, **2**, and **3**, they may have the potential to become novel solid-state materials in which delocalized electrons coexist with localized magnetic moments, thus affording the opportunity for the investigation of molecular systems combining magnetic and conducting properties.

There are four characteristic asymmetric vibrations resulting from heteropolyanions with the Keggin structure, namely $\nu_{as}(Mo=O_t)$, $\nu_{as}(Mo-O_b)$, $\nu_{as}(Mo-O_c)$, and $\nu_{as}(P-O_a)$. Upon comparison of the IR spectra of the title compounds with those of α-$H_3PMo_{12}O_{40}\times nH_2O$[30] the vibrational bands of the $Mo=O_t$ bonds exhibit red shifts from 975 to 961 cm^{-1} in **1**, from 975 to 959 cm^{-1} in **2** and from 975 to 961 cm^{-1} in **3**. The peaks due to the $Mo-O_c$ bonds show red shifts from 810 to 804 cm^{-1} in **1**, from 810 to 801 cm^{-1} in **2** and from 810 to 803 cm^{-1} in **3**. Lastly, the $P-O_a$ bond vibrations show red shifts from 1067 to 1063 cm^{-1} for **1**, **2**, and **3**, while the vibrational bands of the $Mo-O_b$ bonds exhibit blue shifts from 870 to 881 cm^{-1}in **1** and **3**, and from 870 to 878 cm^{-1} in **2**. These results indicate that the polyanions in the title compounds still retain the basic Keggin structure, but are distorted due to the effects of coordination. This is in agreement with the results of the single-crystal X-ray diffraction studies. In addition, there are three characteristic asymmetric vibrations resulting from NMP molecules, namely $\nu_{as}(C=O)$ (1666.1 cm^{-1}), $\nu_{as}(C-N)$ (1506 cm^{-1}), and $\nu_{as}(N-CH_3)$ (1114 cm^{-1}).[31] Upon comparison of the IR spectra of the title compounds with those of NMP molecules,[31] $\nu_{as}(C=O)$ is lower by 25.3 cm^{-1} (from 1666.1 to 1640.8 cm^{-1}) in **1**, 28.2 cm^{-1} (from 1666.1 to 1637.9 cm^{-1}) in **2**, and 27.1 cm^{-1} (from 1666.1 to 1639 cm^{-1}) in **3**, confirming that the NMP ligands are coordinated to the rare-earth ions by means of their oxygen atoms. The $\nu_{as}(C-N)$ and $\nu_{as}(N-CH_3)$ frequencies in the

 © 2004 Wiley-VCH Verlag GmbH & Co. KGaA, Weinheim

three compounds rise slightly by 8 cm^{-1} and 2−6 cm^{-1}, respectively. This can be explained by the fact that the charge density at the oxygen and carbon centers is decreased due to the O atoms of the C=O bonds being coordinated to the rare-earth ions, leading to an increase in the electron-donating effect of the methyl groups through the N atoms. The IR spectroscopic studies show that there are strong interactions between the polyanions and the organic groups in the solid state.

The UV spectra of compounds **1**, **2**, and **3** measured in aqueous solution are similar to that of α-$H_3PMo_{12}O_{40}\times nH_2O$ in the same solution. There are absorption peaks at approximately 205 nm, which can be assigned to the $O_t\rightarrow Mo$ charge-transfer bands which are also strong due to the absorption of NMP molecules at the same wavelength.[31] This suggests that although the compounds exist in polymeric form in the solid state, the polymeric chains are entirely disrupted in dilute solution. This has been observed in a previous study.[12]

The three complexes are strongly photosensitive towards irradiation with sunlight, resulting in charge-transfer by oxidation of the NMP moieties and reduction of the $[PMo_{12}O_{40}]^{3-}$ groups. ESR spectra of powders of the title compounds after exposure to sunshine are typical of molybdenum(v).[32−33] At 110 K, $g = 1.949$ for **1**, $g = 1.947$ for **2**, and $g = 1.948$ for **3**. Observation of an intense, relatively narrow ESR signal from about 3460 to 3500 G (40 G peak to peak) for **1**, **2**, and **3** at 110 K indicates that intramolecular electron transfer is relatively slow on the ESR timescale, and that the electron is delocalized.

Table 1. Cathodic peak potentials (E_{cp}) and anodic (E_{ap}) and potential differences for α-$H_3PMo_{12}O_{40}\times nH_2O$ and compounds **1** and **2** (in a mixture of 50% 1,4-dioxane and 50% H_2O containing 0.5 mol/L H_2SO_4 as the supporting electrolyte, sensitivity 10 μA, $v = 50$ mV·s^{-1}, SCE as the reference electrode)

Compound	E_{cp} [V]	E_{ap} [V]	ΔE_p [mV]	$E_{1/2}$ [V]
α-$H_3PMo_{12}O_{40}\times nH_2O$	0.308	0.339	31	0.324
	0.179	0.208	29	0.194
	−0.052	−0.022	30	−0.037
	−0.201	−0.17	31	−0.186
	−0.282	−0.244	38	−0.263
1	0.311	0.341	30	0.326
	0.181	0.212	31	0.197
	−0.050	−0.019	31	−0.035
	−0.208	−0.176	32	−0.192
	−0.286	−0.247	39	−0.267
2	0.308	0.340	32	0.324
	0.181	0.212	31	0.197
	−0.053	−0.022	31	−0.038
	−0.208	−0.179	29	−0.194
	−0.288	−0.249	39	−0.269
3	0.304	0.338	34	0.321
	0.177	0.209	32	0.193
	−0.058	−0.021	37	−0.040
	−0.210	−0.174	36	−0.192
	−0.303	−0.262	41	−0.283

Table 1 summarizes the cathodic and anionic peak potentials [V], the half-wave potentials $E_{1/2}$ [V], as well as the difference potentials for α-$H_3PMo_{12}O_{40}\times nH_2O$ and compounds **1**, **2**, and **3** (in a mixture of 50% 1,4-dioxane and 50% H_2O containing 0.5 mol/L H_2SO_4 as the supporting electrolyte, sensitivity 10 μA, $v = 50$ mV·s^{-1}, SCE as the reference electrode). Figure 7 shows the CVs for α-$H_3PMo_{12}O_{40}\times nH_2O$ and compounds **1**, **2**, and **3** carried out at a sensitivity of 10 μA. For phospho-polyoxomolybdate it is difficult to obtain well-defined redox waves in cyclic voltammetry in aqueous electrolytes due to the ease of hydrolysis of $[PMo_{12}O_{40}]^{3-}$. However, it can be stabilized by addition of comparatively large amounts of organic solvents. Thus, cyclic voltammetry was measured in organic/aqueous solvent mixtures (50% 1,4-dioxane and 50% redistilled H_2O) containing 0.5 mol/L H_2SO_4 as the supporting electrolyte. α-$H_3PMo_{12}O_{40}\times nH_2O$ as well as compounds **1**, **2**, and **3** all undergo five two-electron reversible reductions. The reversibility criterion used was $\Delta E_p = E_{ap} - E_{cp} = 59/n$ mV (n = number of electrons). The small difference in $E_{1/2}$ [V] of the three compounds shows that the $[PMo_{12}O_{40}]^{3-}$ anions are the active centers for electrochemical redox activity in the solutions, while the corresponding cations have only a small effect on the electrochemical redox behavior. Upon comparison of the results of the CVs of the three compounds, it was found that the effect of $[Ce(NMP)_6]^{3+}$ on the electrochemical redox behavior of $[PMo_{12}O_{40}]^{3-}$ is stronger than that of $[La(NMP)_6]^{3+}$ or $[Pr(NMP)_6]^{3+}$.

In aqueous solution, cerium has two accessible oxidation states namely III and IV. Only strong oxidants such as permanganate and peroxodisulfate can oxidize Ce^{III}. In general, the determination of the oxidation state of cerium is frequently a difficult problem. Previous work has shown that selected heteropolyoxotungstates can significantly influence the behavior of complex f-ions. In 1971, Peacock and Weakley reported that heteropolyoxotungstates could stabilize tetravalent cerium.[34] This stabilization was apparent from the ease of oxidation of Ce^{IV} in $[Ce(PW_{11}O_{39})_2]$, $[Ce(SiW_{11}O_{39})_2]$ and $[Ce(P_2W_{17}O_{61})_2]$. In aqueous solution, these oxidations were found to occur at +0.6 to +0.9 V vs. Ag/AgCl, which is less than the standard reduction potential of Ce^{IV}. More recently, Haraguchi et al.[35] have confirmed the shifts of the Ce^{III}/Ce^{IV} redox potentials in these heteropolyoxotungstates. The implication of their work is that the oxidation of Ce^{III} is possible with the use of only mild oxidants.[36] In contrast, the shifts of the Ce^{III}/Ce^{IV} redox potentials in heteropolymolybdates have not been reported and consequently we have examined the shift of the Ce^{III}/Ce^{IV} redox potential in $[\{Ce(NMP)_6\}(PMo_{12}O_{40})]_n$.

Figure 8 (A and B) shows the CVs of α-$H_3PMo_{12}O_{40}\times nH_2O$ (1 mmol/L) and compound **3** (1 mmol/L) in a mixture of 50% 1,4-dioxane and 50% H_2O containing 0.5 mol/L H_2SO_4 as the supporting electrolyte with Ag/AgCl as the reference electrode. Figure 8 (C) depicts the CV of compound **3** (1 mmol/L) in a mixture of 50% 1,4-dioxane and 50% H_2O containing 1.0 mol/L $HClO_4$ as the supporting electrolyte with Ag/AgCl as the reference electrode. In contrast, it was found that Ce^{III} in $[\{Ce(NMP)_6\}(PMo_{12}O_{40})]_n$ cannot be oxidized to Ce^{IV} even

 © 2004 Wiley-VCH Verlag GmbH & Co. KGaA, Weinheim

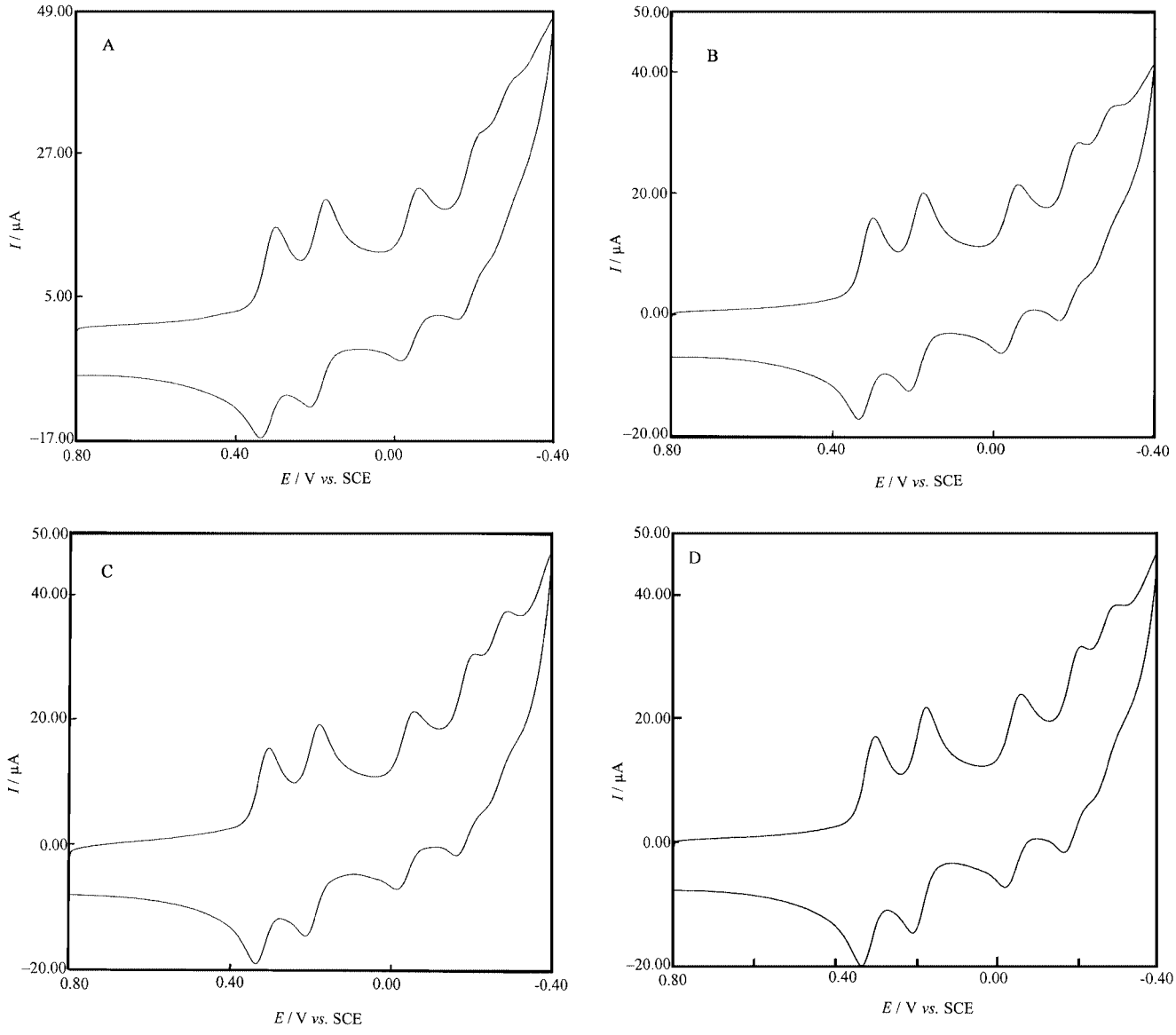

Figure 7. (A) CV of α-$H_3PMo_{12}O_{40}\times nH_2O$(1 mmol/L) in a mixture of 50% 1,4-dioxane and 50% H_2O containing 0.5 mol/L H_2SO_4 as the supporting electrolyte, sensitivity 10 μA, v = 50 mV·s^{-1}, SCE as the reference electrode; (B) CV of compound **1** (1 mmol/L) in a mixture of 50% 1,4-dioxane and 50% H_2O containing 0.5 mol/L H_2SO_4 as the supporting electrolyte, sensitivity 10 μA, v = 50 mV·s^{-1}, SCE as the reference electrode; (C) CV of compound **2** (1 mmol/L) in a mixture of 50% 1,4-dioxane and 50% H_2O containing 0.5 mol/L H_2SO_4 as the supporting electrolyte, sensitivity 10 μA, v = 50 mV s^{-1}, SCE as the reference electrode; (D) CV of compound **3** (1 mmol/L) in a mixture of 50% 1,4-dioxane and 50% H_2O containing 0.5 mol/L H_2SO_4 as the supporting electrolyte, sensitivity 10 μA, v = 50 mV s^{-1}, SCE as the reference electrode

under rigorous conditions (+1.5 V vs. Ag/AgCl; electrolyte 1 mol/L $HClO_4$ purged with O_2). These conditions are sufficient to oxidize the noncomplexed Ce^{III} aqua ion. The Ce^{III} ion in compound **3** is not oxidized at potentials higher than would be required for its oxidation in noncomplexing media, indicating a stabilization of Ce^{III} in this case. In addition, the solution chemistry of cerium(III) is similar to that of Zr, Hf and, particularly, tetravalent actinides. Thus, Ce^{III} gives phosphates insoluble in 4 mol/L HNO_3 and iodates insoluble in 6 mol/L HNO_3, as well as an insoluble oxalate. Upon addition of 5 mL of 4 mol/L NaOH to 20 mL of an aqueous solution of 1 mmol of $[\{Ce(NMP)_6\}(PMo_{12}O_{40})]_n$, which dissociates into small molecules, white deposited material can be observed. Filtration of the mixture to recover the solid, which is soluble in 5 mL of dilute HCl (0.5 mol/L), followed by the addition of two drops of concentrated phosphoric acid to the resultant solution produces a white precipitate which is soluble in 4 mol/L HNO_3.

Finally, the average $Ce^{III}-O$ distance in compound **3** is 2.47 Å, which is essentially the same as the sum of the Ce and O ionic radii of 2.49 Å for eight-coordinate Ce and two-coordinate O centers.[36]

Thus, based on the results of CV, the solution chemistry, the average bond lengths and the following magnetic susceptibilities, we can conclude that $[\{Ce(NMP)_6\}(PMo_{12}O_{40})]_n$ contains a tervalent cerium center.

 © 2004 Wiley-VCH Verlag GmbH & Co. KGaA, Weinheim

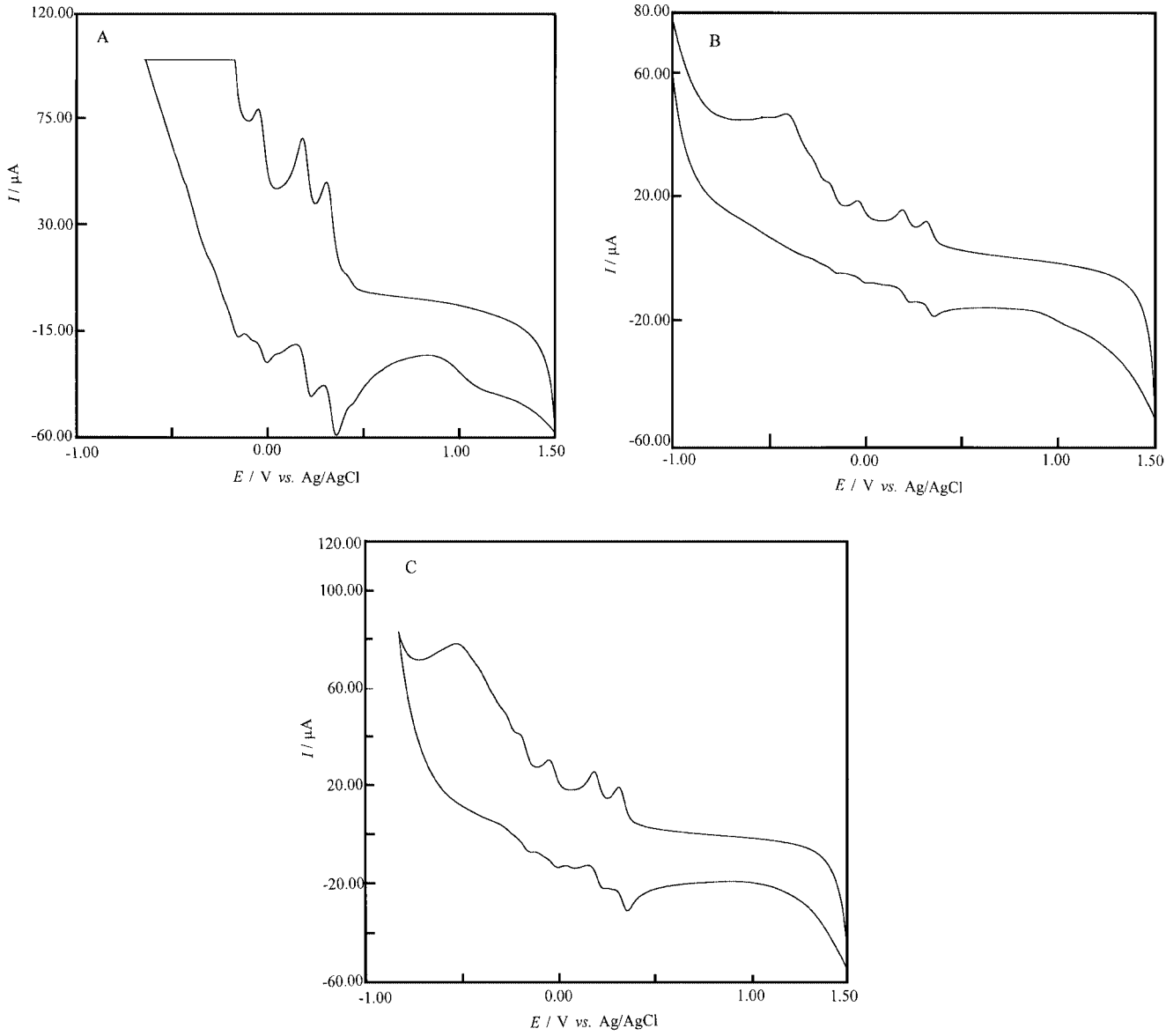

Figure 8. (A) CV of α-$H_3PMo_{12}O_{40}\times nH_2O$ (1 mmol/L) in a mixture of 50% 1,4-dioxane and 50% H_2O containing 0.5 mol/L H_2SO_4 as the supporting electrolyte, sensitivity 10 μA, v = 50 mV·s^{-1}, Ag/AgCl as the reference electrode; (B) CV of compound **3** (1 mmol/L) in a mixture of 50% 1,4-dioxane and 50% H_2O containing 0.5 mol/L H_2SO_4 as the supporting electrolyte, sensitivity 10 μA, v = 50 mV·s^{-1}, Ag/AgCl as the reference electrode; (C) CV of compound **3** (1 mmol/L) in a mixture of 50% 1,4-dioxane and 50% H_2O containing 1.0 mol/L $HClO_4$ as the supporting electrolyte, sensitivity 10 μA, v = 50 mV s^{-1}, Ag/AgCl as the reference electrode

The variable-temperature magnetic susceptibilities of polycrystalline powders of the three compounds were measured with a Cahn-2000 magnetometer between 75 and 300 K. The studies of magnetic properties show that compound **1** is diamagnetic, while compounds **2**and **3** exhibit antiferromagnetic Pr−Pr or Ce−Ce exchange interactions. The results are displayed in the form of $1/\chi_M$ (the molar magnetic susceptibility per formula unit) vs. absolute temperature in Figures 9 and 10 for compounds **2** and **3**. The mean molar magnetic susceptibility of $[\{La(NMP)_6\}(PMo_{12}O_{40})]_n$ (**1**) (−0.00018 cm^3·mol^{-1}) was used as a diamagnetic correction for the molar magnetic susceptibilities of **2** and **3**. The magnetic data for compounds **2** and **3** have been fitted to the Curie−Weiss law $\chi_M = C/(T - \theta)$ and $\chi_M = Ng^2\beta s\ (s + 1)/3k(T - \theta)$ (s_{Ce} = 1/2; s_{Pr} = 1). The Weiss constants $\theta_{Pr} = -58.88$ and $\theta_{Ce} = -108.78$ show that there are strong antiferromagnetic Pr−Pr or Ce−Ce exchange interactions in **2** and **3**.

Conclusions

Three one-dimensional composite compounds have been prepared based on the polyoxometalate anion $[PMo_{12}O_{40}]^{3-}$ and the cations $[LnNMP]_6]^{3+}$ (Ln = La, Ce, Pr). Single-crystal X-ray diffraction studies showed that the three compounds exhibit two types of zig-zag chains with alternating cations and anions through Mo−O_t−Ln−

 © 2004 Wiley-VCH Verlag GmbH & Co. KGaA, Weinheim

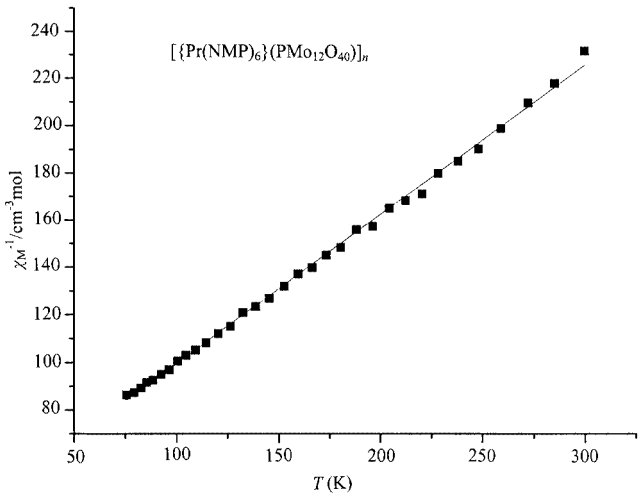

Figure 9. Plot of inverse molar susceptibility vs. absolute temperature for compound **2** (black squares); the solid line represents the best fit of the data with value in the text

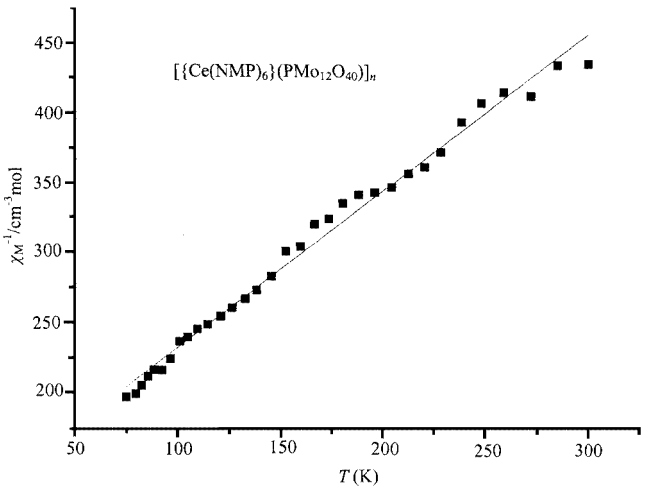

Figure 10. Plot of molar susceptibility vs. absolute temperature for compound **3** (black squares); the solid line represents the best fit of the data with value in the text

O_t−Mo links in the crystal. The variation of the Ln−O average bond separations along the La, Ce, and Pr series is consistent with the effects of the lanthanide contraction (ionic radius: $La^{3+} > Ce^{3+} > Pr^{3+}$) and the polyanions in the title compounds are severely distorted as a result of the influence of the outer coordinating cations. The polymeric structures of the compounds are entirely disrupted in dilute solution, and the cyclic voltammograms measured show that the three compounds all undergo five two-electron reversible reductions. The studies of magnetic properties indicate that **1** is diamagnetic while **2** and **3** exhibit antiferromagnetic Pr−Pr or Ce−Ce exchange interactions.

Experimental Section

Materials: All organic solvents and materials used for synthesis were of reagent grade and used without further purification. α-$H_3PMo_{12}O_{40}\times nH_2O$ was prepared according to a literature method.[30] The metal chlorides $LnCl_3$ (Ln = La, Ce, Pr) were prepared by addition of concentrated HCl to Ln_2O_3 (99.9%).

Syntheses

$[\{La(NMP)_6\}(PMo_{12}O_{40})]_n$ (1), $[\{Pr(NMP)_6\}(PMo_{12}O_{40})]_n$ (2), and $[\{Ce(NMP)_6\}(PMo_{12}O_{40})]_n$ (3): The formation of heteropolyacid lanthanide salts was accomplished by neutralization of the acids. α-$H_3PMo_{12}O_{40} \times nH_2O$ (3.8 g, 2 mmol) and $LnCl_3$ (2 mmol) were dissolved in water (15 mL) and the solution was heated to dryness at 80 °C in a water bath. NMP (2 mL) was then added to the resultant dry solid (2 g) with stirring until the mixture became a paste. After standing for ca. 15 min, the paste was dissolved in a minimum of an acetonitrile/water mixture (3:2, v/v). Finally, the solution was filtered and left standing to concentrated at room temperature. After 1−2 d, yellow crystals suitable for X-ray diffraction were obtained; yield based on α-$H_3PMo_{12}O_{40} \times nH_2O$ ca. 80%. $C_{30}H_{54}LaMo_{12}N_6O_{46}P$ (**1**) (2555.95): calcd. C 14.08, H 2.11, N 3.29; found C 13.97, H 2.01, N 3.39. $C_{30}H_{54}Mo_{12}N_6O_{46}PPr$ (**2**) (2557.95): calcd. C 14.07, H 2.11, N 3.28; found C 14.07, H 2.06, N 3.39. $C_{30}H_{54}CeMo_{12}N_6O_{46}P$ (**3**) (2557.16): calcd. C 4.08, H 2.11, N 3.28; found C 14.15, H 2.13, N 3.35. TG/DTA data: **1:** Weight loss of 23.5% below 506.3 °C without an obvious endothermic peak and with two exothermic peaks at 285 °C (where the La−O bonds

Table 2. Crystal data for **1**, **2**, and **3**

	1	**2**	**3**
Empirical formula	$C_{30}H_{54}Mo_{12}N_6O_{46}PLa$	$C_{30}H_{54}Mo_{12}N_6O_{46}PPr$	$C_{30}H_{54}Mo_{12}N_6O_{46}PCe$
Formula mass	2555.95	2557.95	2557.16
Crystal size [mm]	0.39×0.33×0.29	0.61×0.48×0.46	0.30×0.26×0.18
Crystal system	monoclinic	monoclinic	monoclinic
Space group	*Pn*	*Pn*	*C*2/*c*
Z	2	2	4
a [Å]	12.954(3)	12.947(3)	25.524(5)
b [Å]	13.417(3)	13.294(3)	12.678(3)
c [Å]	18.810(4)	18.977(4)	22.723(5)
β [°]	99.67(3)	100.77(3)	112.10(3)
V [$Å^3$]	3222.6(11)	3208.7(11)	6813(2)
μ [mm^{-1}]	3.029	3.135	3.407
Total no.of reflections	10938	10472	10788
Independent reflections; R_{int}	10929; 0.0145	10472; 0.0000	5877; 0.0164
*R*1, *wR*2 [$I > 2\sigma(I)$]	0.0278, 0.0686	0.0591, 0.1531	0.0488, 0.1365

 © 2004 Wiley-VCH Verlag GmbH & Co. KGaA, Weinheim

Table 3. Selected bond lengths [Å] and angles [°] for **1**

Mo(1)−O(14)	2.016(5)	Mo(4)−O(16)	1.989(5)
Mo(1)−O(37)	2.461(5)	Mo(4)−O(19)	1.994(5)
Mo(2)−O(2)	1.669(5)	Mo(4)−O(38)	2.434(4)
Mo(21)−O(36)	1.820(5)	Mo(5)−O(5)	1.682(5)
Mo(2)−O(13)	1.846(5)	Mo(5)−O(24)	1.821(5)
Mo(2)−O(17)	2.001(5)	Mo(5)−O(20)	1.841(5)
Mo(2)−O(31)	2.006(5)	Mo(5)−O(38)	2.438(5)
Mo(2)−O(37)	2.425(5)	Mo(6)−O(6)	1.678(5)
Mo(3)−O(3)	1.663(5)	Mo(6)−O(18)	1.816(5)
Mo(3)−O(16)	1.820(5)	Mo(6)−O(19)	1.846(5)
Mo(3)−O(14)	1.840(5)	Mo(6)−O(20)	1.997(5)
Mo(3)−O(13)	2.005(5)	Mo(6)−O(21)	2.018(5)
Mo(3)−O(15)	2.013(5)	Mo(6)−O(38)	2.452(5)
Mo(3)−O(37)	2.420(4)	Mo(8)−O(8)	1.687(4)
Mo(4)−O(4)	1.665(5)	Mo(10)−O(10)	1.689(5)
Mo(4)−O(30)	1.826(5)	O(10)−La(1)#2[a]	2.576(5)
O(41)−La(1)−O(10)#1[a]	73.27(16)	O(45)−La(1)−O(10)#1	148.16(18)
O(45)−La(1)−O(8)	77.15(18)	O(46)−La(1)−O(10)#1	72.47(16)
O(41)−La(1)−O(8)	150.11(16)	O(44)−La(1)−O(10)#1	129.8(2)
O(10)#1−La(1)−O(8)	124.27(15)	O(43)−La(1)−O(10)#1	68.62(17)

[a] Symmetry transformation used to generate equivalent atoms: #1: x, $y + 1$, z; #2: x, $y - 1$, z.

break with the oxidation of NMP molecules) and 474 °C (where the heteropolyanionic cages decompose to the lower oxides of the metals like MoO_3); calcd. 23.27% for six NMP units. **2:** Weight loss of 22.8% below 525 °C without an obvious endothermic peak and with two exothermic peaks at 287 °C (where the Pr−O bonds break with the oxidation of NMP molecules) and 493 °C (where the heteropolyanionic cages decompose to the lower oxides of the metals like MoO_3); calcd. 23.27% for six NMP units. **3:** Weight loss of 23.6% below 530 °C without an obvious endothermic peak and with two exothermic peaks at 282 °C (where the Ce−O bonds break with the oxidation of NMP molecules) and 465 °C (where the heteropoly anionic cages decompose to the lower oxides of the metals like MoO_3); calcd. 23.26% for six NMP units.

Methods: C, H, and N elemental analyses were performed with a Perkin−Elmer 240C elemental analyzer. IR spectra of samples were recorded in KBr pellets with a Nicolet 170 SXFT-IR spectrometer in the range of 4000−500cm^{-1}. UV spectra were recorded

Table 4. Selected bond lengths [Å] and angles [°] for **2**

Pr(1)−O(3A)	2.401(12)	Mo(4)−O(16)	1.998(9)
Pr(1)−O(1A)	2.404(9)	Mo(4)−O(38)	2.416(9)
Pr(1)−O(4A)	2.409(10)	Mo(5)−O(5)	1.670(9)
Pr(1)−O(2A)	2.416(10)	Mo(5)−O(24)	1.810(9)
Pr(1)−O(10)#1[a]	2.519(10)	Mo(5)−O(20)	1.844(10)
Pr(1)−O(8)	2.592(11)	Mo(5)−O(26)	1.999(9)
Mo(1)−O(1)	1.667(10)	Mo(5)−O(22)	1.999(10)
Mo(1)−O(23)	1.802(10)	Mo(5)−O(38)	2.423(8)
Mo(1)−O(17)	1.834(9)	Mo(6)−O(6)	1.658(11)
Mo(1)−O(18)	2.012(11)	Mo(6)−O(18)	1.802(10)
Mo(1)−O(14)	2.023(10)	Mo(6)−O(19)	1.857(9)
Mo(1)−O(37)	2.441(9)	Mo(6)−O(21)	1.990(10)
Mo(2)−O(2)	1.651(10)	Mo(6)−O(20)	2.000(11)
Mo(2)−O(36)	1.814(10)	Mo(6)−O(38)	2.462(9)
Mo(2)−O(13)	1.853(11)	Mo(8)−O(8)	1.697(11)
Mo(2)−O(31)	1.989(9)	Mo(10)−O(10)	1.695(10)
Mo(2)−O(17)	2.006(9)	O(10)−Pr(1)#2[a]	2.519(10)
Mo(2)−O(37)	2.409(9)	O(5A)−Pr(1)−O(10)#1	145.3(4)
Mo(3)−O(3)	1.666(11)	O(6A)−Pr(1)−O(10)#1	72.0(3)
Mo(3)−O(14)	1.819(10)	O(3A)−Pr(1)−O(10)#1	69.2(3)
Mo(3)−O(16)	1.822(10)	O(1A)−Pr(1)−O(10)#1	74.7(3)
Mo(3)−O(13)	1.997(11)	O(4A)−Pr(1)−O(10)#1	136.9(4)
Mo(3)−O(15)	2.041(10)	O(2A)−Pr(1)−O(10)#1	71.4(4)
Mo(3)−O(37)	2.432(9)	O(5A)−Pr(1)−O(8)	76.9(4)
Mo(4)−O(4)	1.696(11)	O(6A)−Pr(1)−O(8)	66.8(3)
Mo(4)−O(30)	1.829(10)	O(3A)−Pr(1)−O(8)	75.8(4)
Mo(4)−O(22)	1.830(9)	O(1A)−Pr(1)−O(8)	148.1(3)
Mo(4)−O(19)	1.986(9)	O(4A)−Pr(1)−O(8)	71.0(3)
O(10)#1−Pr(1)−O(8)	124.8(3)	O(2A)−Pr(1)−O(8)	130.8(4)

[a] Symmetry transformation used to generate equivalent atoms: #1: x, $y + 1$, z; #2: x, $y - 1$, z.

 © 2004 Wiley-VCH Verlag GmbH & Co. KGaA, Weinheim

Table 5. Selected bond lengths [Å] and angles [°] for **3**

Ce(1)−O(1A)	2.388(7)	Mo(5)−O(7)	1.824(7)
Ce(1)−O(1A)#1[a]	2.388(7)	Mo(5)−O(17)	1.985(7)
Ce(1)−O(2A)#1	2.409(7)	Mo(5)−O(8)#2[a]	1.995(9)
Ce(1)−O(2A)	2.409(7)	Mo(5)−O(21)#2	2.483(11)
Ce(1)−O(3A)	2.418(6)	Mo(5)−O(22)	2.516(10)
Ce(1)−O(3A)#1	2.418(6)	Mo(6)−O(9)#2	1.657(12)
Ce(1)−O(6)	2.649(6)	Mo(6)−O(6)	1.664(6)
Ce(1)−O(6)#1	2.649(6)	Mo(6)−O(10)#2	1.705(12)
Mo(1)−O(1)	1.633(8)	Mo(6)−O(11)	1.866(13)
Mo(1)−O(16)	1.809(7)	O(1A)−Ce(1)−O(1A)#1	119.4(4)
Mo(1)−O(14)	1.830(7)	O(1A)−Ce(1)−O(2A)#1	144.8(3)
Mo(1)−O(15)	1.990(7)	O(1A)#1−Ce(1)−O(2A)#1	83.3(3)
Mo(1)−O(13)	2.000(7)	O(1A)−Ce(1)−O(2A)	83.3(3)
Mo(1)−O(22)	2.408(11)	O(1A)#1−Ce(1)−O(2A)	144.8(3)
Mo(1)−O(20)	2.464(11)	O(2A)#1−Ce(1)−O(2A)	92.1(4)
Mo(2)−O(2)	1.662(7)	O(1A)−Ce(1)−O(3A)	76.0(3)
Mo(2)−O(15)	1.807(8)	O(1A)#1−Ce(1)−O(3A)	74.8(3)
Mo(2)−O(11)	1.818(12)	O(2A)#1−Ce(1)−O(3A)	85.9(3)
Mo(2)−O(11′)	1.888(13)	O(2A)−Ce(1)−O(3A)	139.9(3)
Mo(2)−O(12)	1.967(13)	O(1A)−Ce(1)−O(3A)#1	74.8(3)
Mo(2)−O(18)	1.990(6)	O(1A)#1−Ce(1)−O(3A)#1	76.0(3)
Mo(2)−O(12′)	2.113(13)	O(2A)#1−Ce(1)−O(3A)#1	139.9(3)
Mo(2)−O(19)	2.396(10)	O(2A)−Ce(1)−O(3A)#1	85.9(3)
Mo(3)−O(3)	1.642(7)	O(3A)−Ce(1)−O(3A)#1	120.1(4)
Mo(3)−O(12)#2	1.688(13)	O(1A)−Ce(1)−O(6)	137.1(3)
Mo(3)−O(17)	1.807(7)	O(1A)#1−Ce(1)−O(6)	75.7(2)
Mo(3)−O(14)	1.975(9)	O(2A)#1−Ce(1)−O(6)	71.1(2)
Mo(3)−O(10)	2.034(13)	O(2A)−Ce(1)−O(6)	69.8(2)
Mo(3)−O(10′)	2.066(12)	O(3A)−Ce(1)−O(6)	144.3(3)
Mo(3)−O(19)#2	2.428(10)	O(3A)#1−Ce(1)−O(6)	70.7(2)
Mo(4)−O(4)	1.639(7)	O(1A)−Ce(1)−O(6)#1	75.7(2)
Mo(4)−O(8)	1.803(9)	O(1A)#1−Ce(1)−O(6)#1	137.1(3)
Mo(4)−O(18)	1.808(7)	O(2A)#1−Ce(1)−O(6)#1	69.8(2)
Mo(4)−O(16)	2.001(8)	O(2A)−Ce(1)−O(6)#1	71.1(2)
Mo(4)−O(9)	2.041(12)	O(3A)−Ce(1)−O(6)#1	70.7(2)
Mo(4)−O(21)	2.384(11)	O(3A)#1−Ce(1)−O(6)#1	144.3(3)
Mo(5)−O(5)	1.657(7)	O(6)−Ce(1)−O(6)#1	122.4(3)
Mo(5)−O(13)	1.795(9)	Mo(6)−O(6)−Ce(1)	176.3(4)

[a] Symmetry transformation used to generate equivalent atoms: #1: $-x$, y, $-z + 1/2$; #2: $-x - 1/2$, $-y - 1/2$, $-z$.

in aqueous solution with a UV-250 spectrometer in the range of 190−400 nm. Thermogravimetric analyses (TG/DTA) were performed in air with a Perkin−Elmer-7 instrument with a heating rate of 10 °C/min from room temperature to 600 °C. ESR spectra of powdered samples of the title compounds after exposure to sunshine were recorded with a Bruker ER-200-D-SRC spectrometer in the X-band frequency at 110 K. Cyclic voltammograms were obtained with an LK98BII electrochemical analyzer at 25 °C. A glass-carbon (diameter = 3 mm) electrode was employed as the working electrode. The electrode was subjected to ultrasonic washing for 5 min followed by washing with water and acetone prior to every measurement. A platinum rod (diameter = 2 mm) was used as the counter electrode. The reference electrode was an SCE or an Ag/AgCl electrode. A Cahn-2000 magnetometer was used to measure the temperature dependence of the magnetic susceptibilities of three compounds in the 75−300 K temperature range. The crystal structures of **1**, **2**, and **3** were determined from single-crystal X-ray diffraction data. Intensity data were collected with a Rigaku RAXIS-IV image plate area detector with Mo-K_α (λ = 0.71073 Å) radiation at 293(2) K. The structures were solved by direct methods and refined using full-matrix least-squares calculations with anisotropic displacement parameters for all non-hydrogen atoms. All hydrogen atoms were geometrically fixed to allow riding on the parent atoms to which they are attached and refined with individual isotropic displacement parameters. All calculations were performed using the SHELXTL-97 program.[37] A summary of the X-ray crystal data for the three compounds is shown in Table 2. Selected bond lengths and bond angles are listed in Tables 3, 4, and 5. CCDC-201822 (**1**), -201823 (**2**), and -201821 (**3**) contain the supplementary crystallographic data for this paper. These data can be obtained free of charge at www.ccdc.cam.ac.uk/conts/retrieving.html [or from the Cambridge Crystallographic Data Centre, 12 Union Road, Cambridge CB2 1EZ, UK; Fax: (internat.) + 44-1223/336-033; E-mail: deposit@ccdc.cam.ac.uk].

Acknowledgments

This work was supported by the Natural Science Foundation of Henan Province and the Outstanding Youth Foundation of Henan Province.

[1] [1a] M. T. Pope, *Heteropoly- and Isopoly-Oxometalates*, Springer-Verlag, New York, **1983**. [1b] M. T. Pope, A. Müller, *Angew. Chem. Int. Ed. Engl.* **1991**, *30*, 34. [1c] *Polyoxometalates: From Platonic Solids to Anti-Retroviral Activity* (Eds.: M. T. Pope, A. Müller), Kluwer Academic Publishers, Dordrecht, The Netherlands, **1994**. [1d] *Chem. Rev.* **1998**, *98*, 8 (Guest Ed.: C. L. Hill).

 © 2004 Wiley-VCH Verlag GmbH & Co. KGaA, Weinheim

[2] E. Coronado, C. Gomez-Garcia, *Chem. Rev.* **1998**, *98*, 273.
[3] [3a] M. I. Khan, E. Yohannes, D. Powell, *Inorg. Chem.* **1999**, *38*, 212−213. [3b] M. I. Khan, E. Yohannes, D. Powell, *Chem. Commun.* **1999**, 23−24.
[4] M. I. Khan, *J. Solid State Chem.* **2000**, *152*, 105−112.
[5] M. Sadakane, M. H. Dickman, M. T. Pope, *Angew. Chem. Int. Ed.* **2000**, *39*, 2914−2916.
[6] H. Choi, Y.-U. Kwon, O. H. Han, *Chem. Mater.* **1999**, *11*, 1641−1643.
[7] L. G. Beauvais, M. P. Shores, J. R. Long, *Chem. Mater.* **1998**, *10*, 3783−3786.
[8] M. P. Shores, L. G. Beauvais, J. R. Long, *Inorg. Chem.* **1999**, *38*, 1648−1649.
[9] M. P. Shores, L. G. Beauvais, J. R. Long, *J. Am. Chem. Soc.* **1999**, *121*, 775−779.
[10] J.-H. Son, H. Choi, Y.-U. Kwon, *J. Am. Chem. Soc.* **2000**, *122*, 7432−7433.
[11] J.-Y. Niu, Q. Wu, J.-P. Wang, *J. Chem. Soc., Dalton Trans.* **2002**, 2512−2516.
[12] [12a] J.-Y. Niu, X.-Z. You, C.-Y. Duan, H.-K. Fun, Z.-Y. Zhou, *Inorg. Chem.* **1996**, *35*, 4211−4216. [12b] J.-Y. Niu, J.-P. Wang, W. Chen, C.-H.-L. Kennard, K.-A. Byriel, *J. Coord. Chem.* **2001**, *53*, 153−162. [12c] J.-Y. Niu, X.-Z. You, H.-K. Fun, Z.-Y. Zhou, B.-C. Yip, *Polyhedron* **1996**, *5−6*, 1003. [12d] J.-Y. Niu, B.-Z. Shan, X.-Z. You, H.-K. Fan, B.-C. Yip, *Transition Met. Chem.* **1999**, *24*, 108. [12e] J.-Y. Niu, J.-P. Wang, Y. Bo, D.-B. Dang, Z.-Z. Yuan, *J. Chem. Crystallogr.* **2000**, *30*, 43−48. [12f] H.-F. Fun, K. Chinnakali, B.-C. Yip, J.-Y. Niu, J.-P. Wang, X.-Z. You, *Acta Crystallogr., Sect. C* **1998**, *54*, 327.
[13] [13a] A. Mhanni, L. Ouahab, O. Pena, D. Grandjean, C. Garrigou-Lagrange, P. Delhaes, *Synth. Met.* **1991**, *41−43*, 1703. [13b] D. Attanasio, C. Bellitto, M. Bonamico, V. Fares, S. Patrizo, *Synth. Met.* **1991**, *41−43*, 2289. [13c] M. Clemente-León, E. Coronado, J.-M. Galán-Mascarós, C. Gimnéz-Saiz, C.-J. Gómez-García, T. Fernández-Otero, *J. Mater. Chem.* **1998**, *8*, 309.
[14] L. Ouahab, M. Bencharif, A. Mhanni, D. Pelloquin, J. F. Halet, O. Pena, J. Padiou, D. Grandjean, C. Garrigou-Lagrange, J. Amiell, P. Delhaes, *Chem. Mater.* **1992**, *4*, 666.
[15] A. Davidson, K. Boubekeur, A. Penicaud, P. Auban, C. Lenoir, P. Batail, G. Herve, *J. Chem. Soc., Chem. Commun.* **1989**, 1373.
[16] C. J. Gomez-Garcia, L. Ouahab, C. Gimenez-Saiz, S. Triki, E. Coronado, P. Delhaes, *Angew. Chem. Int. Ed. Engl.* **1994**, *33*, 223.
[17] C. J. Gomez-Garcia, C. Gimenez-Saiz, S. Triki, E. Coronado, P. Le Magueres, L. Ouahab, L. Ducasse, C. Sourisseau, P. Delhaes, *Inorg. Chem.* **1995**, *34*, 4139−4151.
[18] C. J. Gomez-Garcia, C. Gimenez-Saiz, S. Triki, E. Coronado, L. Ducasse, P. Le Magueres, L. Ouahab, P. Delhaes, *Synth. Met.* **1995**, *70*, 783.
[19] O_a refers to oxygen atoms connecting the P and Mo atoms; O_b refers to oxygen atoms located in the shared corners between two Mo_3O_{13} units; O_c refers to oxygen atoms connecting edge-sharing MoO_6 octahedra in the Mo_3O_{13} units; O_t are the terminal oxygen atoms.
[20] J. R. Galan-Mascaros, C. Gimenez-Saiz, S. Triki, C. J. Gomez-Garcia, E. Coronado, L. Ouahab, *Angew. Chem. Int. Ed. Engl.* **1995**, *24*, 1460.
[21] H. T. Evans, T. J. R. Weakey, G. B. Jameson, *J. Chem. Soc., Dalton Trans.* **1996**, 2573.
[22] B. B. Yan, Y. Xu, X. H. Bu, N. K. Goh, L. S. Chia, G. D. Stucky, *J. Chem. Soc., Dalton Trans.* **2001**, 2009−2014.
[23] J.-P. Wang, Q. Wu, J.-Y. Niu, *Sci. China, Ser. B* **2002**, *3*, 210−217.
[24] C. H. Evans, *Biochemistry of Lanthanides*, Plenum, New York, **1990**, p 47.
[25] F. H. Spedding, in *Kirk-Othmer Encyclopedia of Chemical Technology*, 3rd ed. (Eds.: M. Grayson, D. Eckroth), Wiley, New York, **1982**, vol. 19, p. 883.
[26] *Lanthanide Probes in Life, Chemical and Earth Sciences* (Eds.: J. C. G. Bünzli, G. R. Choppin), Elsevier, Amsterdam, **1989**.
[27] C. Lescop, E. Belorizky, D. Luneau, P. Rey, *Inorg. Chem.* **2002**, *41*, 3375−3384.
[28] I. A. Setyawati, S. Liu, S. J. Rettig, C. Orvig, *Inorg. Chem.* **2000**, *39*, 496−507.
[29] J. H. Melman, C. Rohde, T. J. Emge, J. G. Brennan, *Inorg. Chem.* **2002**, *41*, 28−33.
[30] R. D. Claude, F. Michael, F. Raymonde, T. Rene, *Inorg. Chem.* **1983**, *22*, 207−216.
[31] J.-Y. Niu, J.-P. Wang, L.-Q. Ma, *Chin. Sci. Bull.* **1996**, *41*, 328 (in Chinese).
[32] C. Sanchez, J. Livage, J. P. Launay, M. Fournier, Y. Jeannin, *J. Am. Chem. Soc.* **1982**, *104*, 3194−3202.
[33] J. N. Barrows, M. T. Pope, *Adv. Chem. Ser.* **1990**, *226*, 403.
[34] R. D. Peacock, T. J. R. Weakley, *J. Chem. Soc., A* **1971**, 1836−1839.
[35] N. Haraguchi, Y. Okaue, T. Isobe, Y. Matsuda, *Inorg. Chem.* **1994**, *33*, 1015−1020.
[36] M. R. Antonio, L. Soderholm, C. W. Williams, N. Ullah, L. C. Francesconi, *J. Chem. Soc., Dalton Trans.* **1999**, 3825−3830.
[37] G. M. Sheldrick, *SHELXTL-97, Program for the Refinement of Crystal Structures*, University of Göttingen, Germany, **1997**.

Received January 24, 2003
Early View Article
Published Online October 23, 2003

 © 2004 Wiley-VCH Verlag GmbH & Co. KGaA, Weinheim

Deposition of II-VI Thin Films by LP-MOCVD Using Novel Single-Source Precursors

Mohammad Afzaal,[a] David Crouch,[a] Mohmmad A. Malik,[a] Majid Motevalli,[b] Paul O'Brien,*[a] Jin-Ho Park,[a] and J. Derek Woollins[c]

Keywords: Chemical vapour deposition / Chalcogens / Zinc / Cadmium

Thin films of several zinc or cadmium chalcogenides have been deposited on glass substrates by low pressure metal-organic chemical vapour deposition (LP-MOCVD) using single-source precursors, $[M\{(EP\textit{i}Pr_2)_2N\}_2]$ (M = Cd^{II}, Zn^{II} and E = S, Se). X-ray single crystal structures show that $[Zn\{(EP\textit{i}Pr_2)_2N\}_2]$ (E = S or Se) and $[Zn\{(SePPh_2)_2N\}_2]$ are tetrahedrally distorted. TGA analyses showed that the precursors are volatile, making them suitable for MOCVD studies. As-deposited films were polycrystalline as confirmed by X-ray powder diffraction (XRPD) and their morphologies were studied by scanning electron microscope (SEM).

(© Wiley-VCH Verlag GmbH & Co. KGaA, 69451 Weinheim, Germany, 2004)

Introduction

The direct nature of band gaps in II-VI materials makes them suitable for use in devices, such as blue/blue-green laser diodes,[1−3] which could lead to high-density optical storage systems.[4−6] Cadmium chalcogenides are also useful materials in solid-state solar cells, photoconductors, field effect transistors, sensors and tranducers.[7,8]

Single-source precursors have several potential advantages over conventional MOCVD which uses dual-sources. These include limited premature reactions and good quality homogeneous films.[1] The solid-state chemistry of cadmium and zinc with the chalcogens is typified by the formation of polymeric structures with tetrahedral metal ions,[1] the admantyl structures of many thiolates with zinc and cadmium provide well-characterised examples of such behaviour,[2−4] as do the polymeric chain complexes formed by pyridinethione and 2,3-mercaptobenzothiazole with cadmium and zinc.[5,6] Bochmann et al. have extended such chemistry by producing a range of precursors based on 2,4,6-tri-*tert*-butylphenylchalcogenolate, which have been used to deposit thin films of the metal sulfides and selenides in low-pressure growth experiments.[7−9] In related work, Arnold and co-workers have also deposited a range of chalcogenides using silicon-based ligands, i.e. $[\{MESi(SiCH_3)_3\}_2]$ (M = Zn^{II}, Cd^{II}, Hg^{II} and E = S, Se or Te).[10,11]

Other classes of molecules, which have proved useful for the deposition of thin films include coordination complexes such as dialkyl dichalcogenocarbamates or dithiophosphinates.[12−16] Various groups have studied simple $[M(S_2CNEt_2)_2]$ (M = Cd^{II}, Zn^{II}) complexes and deposited CdS or ZnS films by different deposition techniques.[13−15] However, the use of metal diethyldiselenocarbamates to deposit ZnSe and CdSe on glass substrates resulted in the deposition of elemental selenium.[16] Asymmetrical alkyl substituents as in $[M(E_2CNMeHex)_2]$ (M = Cd^{II}, Zn^{II} and E = S, Se) which were originally introduced in order to increase volatility and have been successfully used to deposit II−VI films (including ZnSe and CdSe) by low pressure metal-organic chemical vapour deposition (LP-MOCVD). An investigation into decomposition mechanisms by gas chromatography mass spectroscopy (GC-MS) and electron impact mass spectroscopy (EI-MS) showed that the deposition of selenium during growth is inhibited in such compounds.[16]

We have recently identified a new class of metal-organic single-source precursors based on bis(diphenylphosphanyl-amine) e.g., $[NH(SePPh_2)_2]$ ligands (an analogue of the β-diketonates) a system pioneered by Woollins, $[M\{(SePPh_2)_2N\}_2]$ (M = Cd^{II}, Zn^{II}) complexes which have been used as precursors for zinc/cadmium selenide films by LP-MOCVD.[17] In this paper, we report crystal structures of $[Zn\{(EP\textit{i}Pr_2)_2N\}_2]$ (E = S or Se) and $[Zn\{(SePPh_2)_2N\}_2]$. We also report the deposition and characterisation of metal chalcogenide films on glass substrates from

[a] The Manchester Materials Science Centre and Department of Chemistry, The University of Manchester,
Oxford Road, Manchester, M13 9PL, UK
Fax: (internat.) +44-(0)161-2754616
E-mail: paul.obrien@man.ac.uk
[b] Department of Chemistry, Queen Mary and Westfield College, Mile End Road, London, E1 4NS, UK
[c] School of Chemistry, University of St. Andrews, Purdie Building,
St. Andrews, Fife, KY16 9ST, UK

$[M\{(EP{i}Pr_2)_2N\}_2]$ (M = Cd^{II}, Zn^{II} and E = S, Se) complexes **1**−**4**) by low-pressure MOCVD.

Results and Discussion

The syntheses of ligands $[NH(EP{i}Pr_2)_2]$ (E = S or Se) were carried out according to previously reported methods.[18,19] The synthesis of the precursor involves deprotonation of the N−H moiety, using sodium methoxide, to form anionic chelate complexes which is subsequently reacted with the metal chloride (Scheme 1). These reactions have some advantages over the routes via metal carbonates and higher yields are obtained particularly for the selenium complexes. The reactions occur efficiently and cleanly at room temperature in anhydrous methanol. All the compounds are soluble in organic solvents and are air-stable.

$$NH(SiMe_3)_2 + 2\ {}^{i}Pr_2PCl \xrightarrow[\text{stirring (3 hours)}]{50\text{–}70\ ^{\circ}C} NH(P{}^{i}Pr_2)_2 + 2\ ClSiMe_3 \quad \text{(Eq. 1)}$$

$$NH(SiMe_3)_2 \xrightarrow[\text{reflux}]{E = S,\ Se} NH(EP{}^{i}Pr_2)_2 \quad \text{(Eq. 2)}$$

$$2\ NH(EP{}^{i}Pr_2)_2 + MCl_2 \xrightarrow[MeOH]{NaOMe} M[(EP{}^{i}Pr_2)_2N]_2 + 2\ NaCl \quad \text{(Eq. 3)}$$

Scheme 1

X-ray Structures

Crystals of $[Zn\{(SePPh_2)_2N\}_2]$ suitable for X-ray diffraction studies were obtained by slow diffusion of hexane into a chloroform solution of the complex. During attempts to synthesise the mixed-alkylzinc complexes by comproportionation reactions between dimetylzinc and $[Zn\{(EP{i}Pr_2)_2N\}_2]$ (E = S or Se), the serendipitous formation of $[Zn\{(EP{i}Pr_2)_2N\}_2]$ (E = S or Se) crystals from toluene solutions occurred. The molecular structures of the compounds are shown in Figures 1−3.

X-ray single crystallographic studies carried out on $[Zn\{(EP{i}Pr_2)_2N\}_2]$ (E = S or Se) and $[Zn\{(SePPh_2)_2N\}_2]$ reveal that the complexes are tetrahedrally coordinated by two ligands. The structure of $[Zn\{(SeP{i}Pr_2)_2N\}_2]$ illustrated in Figure 1 is isostructural with its sulfur analogue (Figure 2). The Zn−Se bond lengths are in the range of 2.458(9) to 2.467(9) Å which are slightly larger than Zn−S bond lengths [2.350(11) to 2.359(11) Å]. Similarly, the Se−Zn−Se bite angles are also increased from the bite angles of S−Zn−S [111.84(4)−112.81(4)°] (Tables 2 and 3). Shortening of the P−N bonds to 1.583(3)−1.592(4) Å and

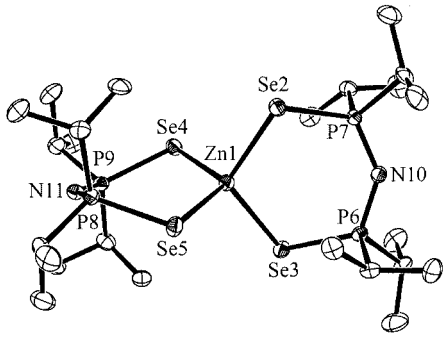

Figure 1. X-ray single crystal structure of $[Zn\{(SeP{i}Pr_2)_2N\}_2]$

Table 1. Crystallographic data collection and refinement parameters

Compound	$C_{24}H_{56}N_2P_4Se_4Zn$	$C_{24}H_{56}N_2P_4S_4Zn$	$C_{48}H_{40}N_2P_4Se_4Zn$
Formula mass	877.70	690.20	1149.91
Temperature (K)	160(2)	160(2)	433(2)
Crystal size (mm)	0.45 × 0.13 × 0.10	0.4 × 0.3 × 0.2	0.57 × 0.45 × 0.35
Crystal system	triclinic	triclinic	triclinic
Space group	$P\bar{1}$	$P\bar{1}$	$P\bar{1}$
a (Å)	9.348(2)	9.232(3)	13.727(7)
b (Å)	12.880(3)	12.678(4)	13.809(5)
c (Å)	16.389(4)	16.401(5)	14.3120(16)
α (°)	100.95(2)	92.24(2)	82.74(9)
β (°)	102.02(2)	101.77(2)	66.36(6)
γ (°)	69.64(2)	110.77(2)	70.13(4)
V (Å^3)	1794.5(7)	1744.1(10)	2337.2(15)
Z	2	2	2
$d_{calcd.}$ (mg/m^3)	1.625	1.314	1.634
Abs. coeff. (mm^{-1})	4.936	1.144	3.813
F(000)	880	736	1136
Index ranges	$0 \le h \le 11$	$-1 \le h \le 5$	$-14 \le h \le 16$
	$-14 \le k \le 15$	$-15 \le k \le 14$	$-16 \le k \le 16$
	$-19 \le l \le 19$	$-19 \le l \le 19$	$-16 \le l \le 16$
Collected/unique	6877/6313	4697/4101	8661/8661
Data/restraints/pars.	6313/0/332	4191/0/332	8661/0/4392
Goodness-of-fit on F^2	0.873	0.895	0.982
$R1$, $wR2$ [$I > 2\sigma(I)$]	0.0297, 0.0745	0.0270, 0.0662	0.0596, 0.1763
$R1$, $wR2$ (all data)	0.0592, 0.0866	0.0365, 0.0706	0.0787, 0.1963
Diff. peak, hole (e·Å^{-3})	0.545, −0.482	0.340, −0.503	1.939, −3.706

 © 2004 Wiley-VCH Verlag GmbH & Co. KGaA, Weinheim

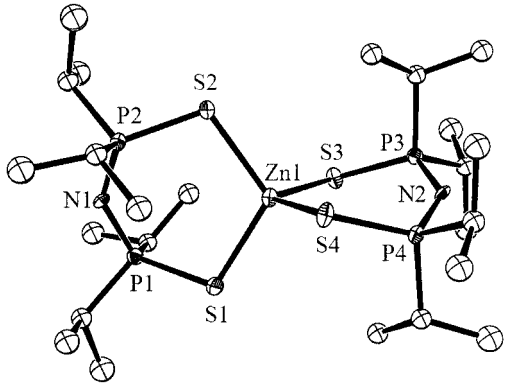

Figure 2. X-ray single crystal structure of $[Zn\{(SPiPr_2)_2N\}_2]$

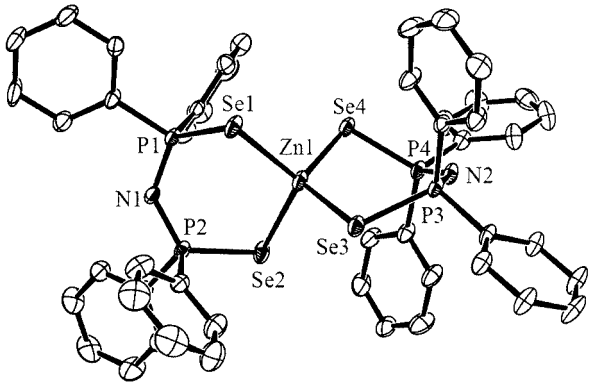

Figure 3. X-ray single crystal structure of $[Zn\{(SePPh_2)_2N\}_2]$

Table 2. Selected interatomic distances (Å) and angles (°) for $[Zn\{(SePiPr_2)_2N\}_2]$

Zn(1)−Se(2)	2.458(9)	Se(2)−Zn(1)−Se(5)	107.31(3)
Zn(1)−Se(5)	2.458(9)	Se(2)−Zn(1)−Se(4)	106.55(3)
Zn(1)−Se(4)	2.459(8)	Se(5)−Zn(1)−Se(4)	114.07(3)
Zn(1)−Se(3)	2.467(9)	Se(2)−Zn(1)−Se(3)	114.07(3)
Se(2)−P(7)	2.177(13)	Se(5)−Zn(1)−Se(3)	106.36(3)
Se(3)−P(6)	2.179(13)	Se(4)−Zn(1)−Se(3)	109.29(3)
Se(4)−P(9)	2.183(13)	P(7)−Se(2)−Zn(1)	103.30(4)
Se(5)−P(8)	2.183(13)	P(6)−Se(3)−Zn(1)	103.01(4)
P(6)−N(10)	1.592(4)	P(9)−Se(4)−Zn(1)	102.83(4)
P(8)−N(11)	1.583(3)	P(8)−Se(5)−Zn(1)	103.67(4)

Table 3. Selected interatomic distances (Å) and angles (°) for $[Zn\{(SPiPr_2)_2N\}_2]$

Zn(1)−S(4)	2.350(11)	S(4)−Zn(1)−S(2)	108.78(4)
Zn(1)−S(2)	2.347(11)	S(4)−Zn(1)−S(1)	106.98(4)
Zn(1)−S(1)	2.351(10)	S(2)−Zn(1)−S(1)	112.81(4)
Zn(1)−S(3)	2.359(11)	S(4)−Zn(1)−S(3)	111.84 (4)
S(1)−P(1)	2.027(13)	S(2)−Zn(1)−S(3)	106.59(4)
S(2)−P(2)	2.032(11)	S(1)−Zn(1)−S(3)	109.92(4)
S(3)−P(3)	2.025(11)	P(1)−S(1)−Zn(1)	105.35(5)
S(4)−P(4)	2.027(12)	P(2)−S(2)−Zn(1)	105.90 (5)
		P(3)−S(3)−Zn(1)	105.81(4)
		P(4)−S(4)−Zn(1)	105.87(4)

the subsequent extension of the P−Se bonds 2.177(13)−2.183(13) Å relative to the free ligand, indicates an increase in delocalization within the architecture due to deprotonation.[19] Crystalline $[Zn\{(SPiPr_2)_2N\}_2]$ as reported by Woollins et al. exhibits completely different unit cell parameters.[18] The unit cell described here contains two independent monomeric molecules versus four reported in the earlier paper.[18]

The zinc atom in $[Zn\{(SePPh_2)_2N\}_2]$ is also coordinated to the selenium atoms through two bidentate ligands forming six-membered chelate rings. The tetrahedral geometry around the zinc atom is distorted which is reflected in the Se−Zn−Se angles which range from 103.85(9) to 115.93(6)° (Table 4). There is no significant difference in the Zn−Se bond lengths of $[Zn\{(SePR_2)_2N\}_2]$ (R = Ph or *i*Pr). The ZnE_2P_2N (E = S or Se) rings have puckered geometries with a distorted boat conformation. This conformation appears to be the most commonly adopted for complexes containing $[R_2P(E)NP(E)R_2]^-$ (E = S or Se) ligands, although other conformations also have been reported with selenium or sulfur and phosphorous atoms at the apices.[29,30]

Table 4. Selected interatomic distances (Å) and angles (°) for $[Zn\{(SePPh_2)_2N\}_2]$

Zn(1)−Se(3)	2.459(3)	Se(3)−Zn(1)−Se(4)	115.93(6)
Zn(1)−Se(4)	2.475(15)	Se(3)−Zn(1)−Se(1)	103.85(9)
Zn(1)−Se(1)	2.482(14)	Se(4)−Zn(1)−Se(1)	111.35(8)
Zn(1)−Se(2)	2.484(19)	Se(3)−Zn(1)−Se(2)	115.03(9)
Se(1)−P(1)	2.171(3)	Se(4)−Zn(1)−Se(2)	106.10(9)
Se(2)−P(2)	2.179(2)	Se(1)−Zn(1)−Se(2)	114.71(5)
Se(3)−P(3)	2.186 (2)	P(1)−Se(1)−Zn(1)	94.11(7)
Se(4)−P(4)	2.187(2)	P(2)−Se(2)−Zn(1)	97.46(7)
		P(3)−Se(3)−Zn(1)	102.22(7)
		P(4)−Se(4)−Zn(1)	94.80(8)

Deposition Studies: In this study, metal chalcogenide thin films have been deposited using air-stable single-source precursors, $[M[(EPiPr_2)_2N\}_2]$ (M = Cd^{II}, Zn^{II} and E = S, Se). The suitability of the precursors were determined by thermogravimetric analysis (TGA) at atmospheric pressure, and all show clean sublimation without any residues, as desirable in precursors for MOCVD studies (Table 5). Deposition of thin films was attempted over a range of substrate temperatures (400 to 500 °C) on glass substrates for one hour with ca. 200 mg of precursor used for each growth experiment.

Table 5. TGA data for compounds **1**−**4**

Compound	T_s (°C)[a]	T_f (°C)[b]
$[Cd\{(SPiPr_2)_2N\}_2]$	237	355
$[Cd\{(SePiPr_2)_2N\}_2]$	310	419
$[Zn\{(SPiPr_2)_2N\}_2]$	222	366
$[Zn\{(SePiPr_2)_2N\}_2]$	240	366

[a] T_s = sublimation temp. [b] T_f = decomposition temp.

Cadmium Sulfide: CdS films were grown from $[Cd\{(SPiPr_2)_2N\}_2]$ at growth temperatures of 425 and 450 °C with a precursor temperature of 250 °C. Deposited films were yellow, transparent and well-adherent to the glass sur-

 © 2004 Wiley-VCH Verlag GmbH & Co. KGaA, Weinheim

face. At higher growth temperature (475 °C), slightly dark yellow-brown film was observed after one hour of growth. As-deposited cadmium sulfide films were analysed by XRPD, which indicated that the hexagonal CdS films (Table 6) have been deposited with a preferred orientation along the (002) plane (Figure 4). SEM studies indicate that the morphology of film deposited at 450 °C consists of randomly oriented domains of compacted thin acicular crystallites with ca. 1.75 μm in thickness (Figure 5). Similar morphology was also observed for the film deposited at 425 °C. On the basis of EDAX analyses, the films were found to be slightly cadmium rich with 52%, sulfur (46%) and phosphorous (2%).

Table 6. XRPD data for CdS grown at 425 and 450 °C from $[Cd\{(SPiPr_2)_2N\}_2]$

hkl	JCPDS (06-0314) *d* [Å] (rel. int.)	CdS (425 °C) *d* [Å] (rel. int.)	CdS (450 °C) *d* [Å] (rel. int.)
100	3.58 (75)	3.57 (2)	3.57 (2)
002	3.36 (60)	3.35 (100)	3.36 (100)
101	3.16 (100)	3.14 (5)	3.16 (14)
102	2.45 (25)	2.43 (3)	2.45 (6)
110	2.07 (55)	2.05 (3)	2.06 (2)
103	1.90 (40)	1.89 (17)	1.90 (2)
200	1.79 (18)	N/A	N/A
112	1.76 (45)	1.76 (3)	1.77 (6)

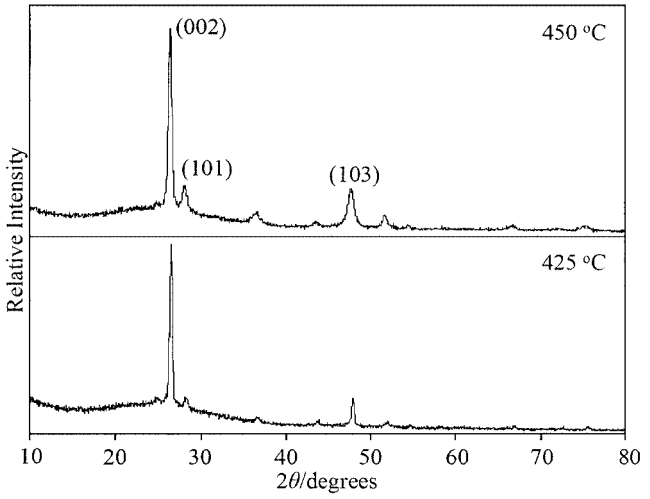

Figure 4. XRPD patterns of CdS films deposited on glass from $[Cd\{(SPiPr_2)_2N\}_2]$ by LP-MOCVD

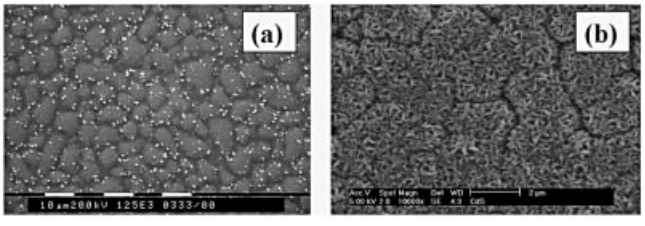

Figure 5. SEM images of CdS films from $[Cd\{(SPiPr_2)_2N\}_2]$ deposited at (a) 425 °C and 450 °C

Cadmium Selenide: Deposition of CdSe films was attempted at substrate temperatures of 425−500 °C, with the precursor temperature set at 325 °C using $[Cd\{(SePiPr_2)_2N\}_2]$. Little or no deposition was observed below 450 °C. At higher growth temperatures, 475 and 500 °C, deposited films were black and adherent to the surface. XRPD studies of the deposited films indicate that polycrystalline hexagonal CdSe films (Table 7) have been deposited with a preferred orientation along the (100) plane (Figure 6). Film deposited at 500 °C was slightly more ordered than the film grown at 475 °C indicated by the absence of (002) plane at 25.5Θ 2θ. Films grown from $[Cd\{(SePPh_2)_2N\}_2]$ also resulted in hexagonal CdSe at 500 and 525 °C but show different preferred orientations (002) and (101) respectively.[17]

Table 7. XRPD data for CdSe grown at 475 and 500 °C from $[Cd\{(SePiPr_2)_2N\}_2]$

hkl	JCPDS (08-0459) *d* [Å] (rel. int.)	CdSe (475 °C) *d* [Å] (rel. int.)	CdSe (500 °C) *d* [Å] (rel. int.)
100	3.72 (100)	3.73 (100)	3.75 (100)
002	3.51 (70)	3.51 (9)	N/A
101	3.29 (75)	3.29 (13)	3.27 (21)
102	2.55 (35)	2.55 (2)	2.54 (1)
110	2.15 (85)	2.15 (36)	2.15 (78)
103	1.98 (70)	1.98 (5)	1.97 (1)
200	1.86 (12)	1.86 (3)	1.86 (8)
112	1.83 (50)	1.83 (7)	1.83 (20)
201	1.80 (12)	1.80 (5)	1.80 (6)
202	1.65 (8)	1.64 (3)	1.64 (3)
203	1.46 (20)	1.45 (6)	1.46 (7)

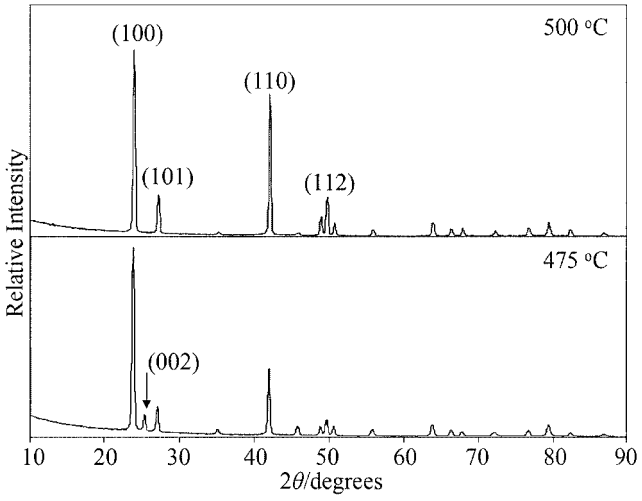

Figure 6. XRPD patterns of CdSe films deposited from $[Cd\{(SePiPr_2)_2N\}_2]$ by LP-MOCVD

SEM studies indicate that the morphology of the film grown at 500 °C consists of randomly orientated platelets (ca. 1 μm in size) (Figure 7b) with a growth rate of ca. 3 μm h^{-1}. At lower growth temperature (475 °C), film morphology consists of clusters of thin particles (Figure 7a). The surface morphology can also be compared with pre-

 © 2004 Wiley-VCH Verlag GmbH & Co. KGaA, Weinheim

vious attempts to deposit CdSe films from $[Cd\{(SePPh_2)_2N\}_2]$, which exhibited low degree of crystallinity and growth rate was also significantly lower (1 μm h^{-1}).[17] The EDAX spectrum of the film deposited at 500 °C from $[Cd\{(SeP\textit{i}Pr_2)_2N\}_2]$ shows the presence of cadmium (54%) and selenium (46%). No phosphorous contamination was detected in the films.

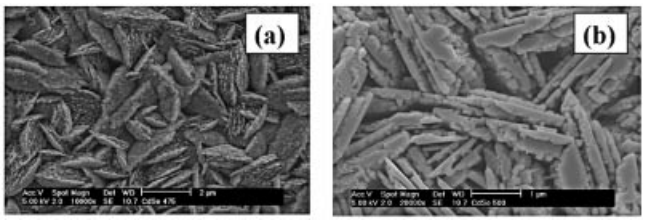

Figure 7. SEM images of CdSe films from $[Cd\{(SeP\textit{i}Pr_2)_2N\}_2]$ deposited at (a) 475 °C and 500 °C

Zinc Sulfide: Non-adherent, brown films were deposited at 450 and 475 °C maintaining precursor temperature at 250 °C using $[Zn\{(SP\textit{i}Pr_2)_2N\}_2]$. Zinc sulfide is known to exist in two phases, at low-temperature cubic polymorph (zinc blende) and at high temperature hexagonal phase (wurtzite).[31] XRPD pattern for the film deposited at 475 °C is shown in (Figure 8) and is consistent with the formation of hexagonal ZnS (JCPDS 36−1450) with a preferred orientation along the (100) plane. At higher growth temperatures (500 °C), deposited film was found to be amorphous indicated by XRPD.

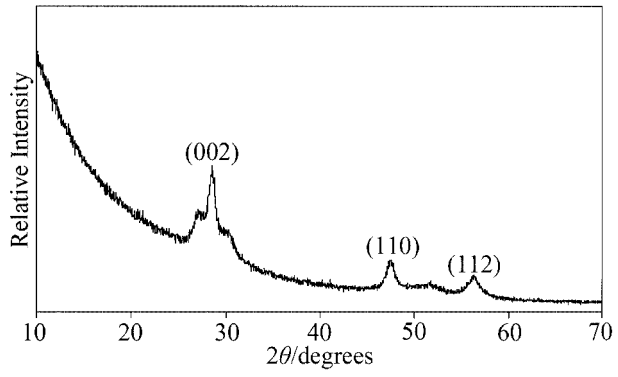

Figure 8. XRPD pattern of ZnS film deposited on glass from $[Zn\{(SP\textit{i}Pr_2)_2N\}_2]$ by LP-MOCVD

SEM micrographs for the film deposited at 475 °C shows that the film surface consists of globules ranging in size 0.25−1.25 μm. Cross-sectional SEM image of the film indicates columnar growth for ZnS and the growth rate is found to be ca. 1 μm h^{-1} (Figure 9). Similar surface morphology also has been observed for the growth of ZnS from previously studied single-source precursors by MOCVD e.g. zinc bis(diisobutyldithiophosphinate)[32] and zinc diethyldithiocarbamate.[33] EDAX indicates the presence of zinc and sulfur, however, 3% of phosphorous was also detected which is incorporated during the decomposition of precursor.

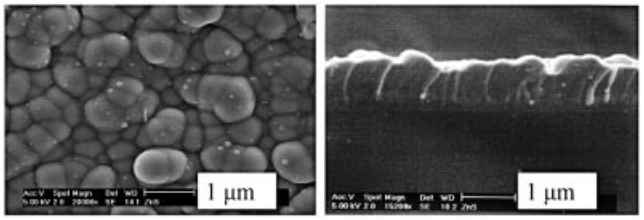

Figure 9. SEM images of ZnS films deposited at 475 °C from $[Zn\{[SP\textit{i}Pr_2)_2N\}_2]$ by LP-MOCVD

Zinc Selenide: ZnSe films were grown over a range of substrate temperatures (400−500 °C) using $[Zn\{(SeP\textit{i}Pr_2)_2N\}_2]$ but the optimum growth temperature appears to be between 425−450 °C with the precursor temperature at 275 °C. As-deposited films were orange-yellow, adherent and specular on the glass substrates. XRPD patterns indicate that the films grown at 425 and 450 °C on glass substrates showed only single-phase hexagonal ZnSe (Table 8, Figure 10). $[Zn\{(SePPh_2)_2N\}_2]$ also deposited hexagonal films at comparatively higher deposition temperatures (500 and 525 °C).[17] At higher growth temperatures

Table 8. XRPD data for ZnSe grown at 425 and 450 °C from $[Zn\{(SeP\textit{i}Pr_2)_2N\}_2]$

hkl	JCPDS (15-0105) *d* [Å] (rel. int.)	ZnSe (450 °C) *d* [Å] (rel. int.)	ZnSe (425 °C) *d* [Å] (rel. int.)
100	3.43 (100)	3.45 (95)	3.45 (100)
002	3.25 (90)	3.28 (69)	3.28 (56)
101	3.05 (70)	3.07 (28)	N/A
102	2.37 (60)	2.38 (5)	N/A
110	2.00 (100)	2.00 (100)	2.00 (70)
103	1.84 (80)	1.85 (7)	N/A
112	1.70 (70)	1.71 (41)	1.71 (25)
202	1.53 (10)	N/A	N/A
203	1.35 (60)	1.36 (2)	N/A

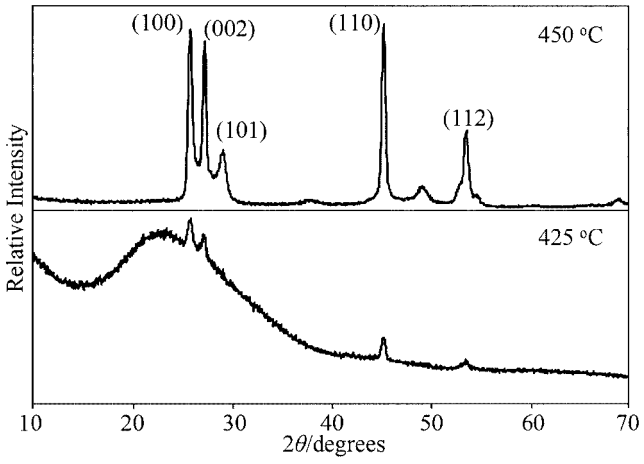

Figure 10. XRPD patterns of ZnSe films deposited from $[Zn\{(SeP\textit{i}Pr_2)_2N\}_2]$ by LP-MOCVD

 © 2004 Wiley-VCH Verlag GmbH & Co. KGaA, Weinheim

(450 °C), the crystallinity of deposited film is significantly improved. However, at lower growth temperatures (425 °C), the XRPD pattern was weak indicating a less crystalline film.

SEM micrographs for the film deposited at 450 °C on glass consists of well-defined, randomly orientated particles, with an average size of ca. 0.5 μm (Figure 11). In 1 hour growth, film with ca. 2 μm thickness has been deposited. In contrast, films deposited at 425 °C had platelike morphologies with the plates laid down horizontally with respect to the glass surface. EDAX confirms that the film is close to stoichiometric ZnSe with a small amount of phosphorous (ca. 2%).

The optical properties of the films were measured by UV/Vis spectroscopy. The bandgap values extrapolated for CdS, CdSe, ZnS and ZnSe thin films are 2.30, 1.71, 3.64 and 2.63 eV, respectively. The bandgap values are all close to the literature values of 2.53 (CdS), 1.74 (CdSe), 3.8 (ZnS) and 2.58 eV (ZnSe).[34]

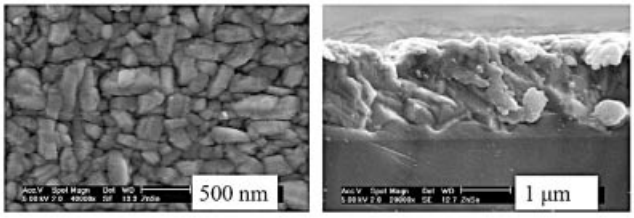

Figure 11. SEM images of ZnSe films deposited at 450 °C from $[Zn\{(SeP\textit{i}Pr_2)_2N\}_2]$ by LP-MOCVD

Conclusion

The air-stable single-source precursors $[M\{(EP\textit{i}Pr_2)_2N\}_2]$ (M = Cd^{II}, Zn^{II} and E = S, Se) have been prepared and characterised by various analytical techniques and utilised as single-source precursors for the deposition of metal chalcogenide thin films by LP-MOCVD. X-ray single crystal structures of zinc compounds indicate distorted tetrahedral geometry at the metal centres. Clean volatilisation of precursors studied by TGA makes them useful for MOCVD studies. XRPD patterns of as-deposited films show that only hexagonal phase of metal sulfide/selenide have been prepared at different growth temperatures.

Experimental Section

Precursor Synthesis: All compounds were prepared by a modified method to that reported in the literature.[18,19] The ligands $[NH(EP\textit{i}Pr_2)_2N]$ (E = S, Se) were sythesised by the reported method.[18,19]

$[Cd\{(SP\textit{i}Pr_2)_2N\}_2]$ (1):[18] In a typical preparation sodium methoxide (1.09 g, 19.7 mmol) was added to a stirred solution of $[NH(SP\textit{i}Pr_2)_2N]$ (6.00 g, 19.2 mmol) in anhydrous methanol (100 cm^3) and stirred for 10 minutes at room temperature. On addition of cadmium chloride (1.76 g, 9.5 mmol) to the resulting solution a white precipitate was formed which was furthur stirred for 2−3 hours, filtered and dried under vacuum. Recrystallisation from dichloromethane/petroleum ether (40−65 °C) yielded 6.2 g (89%) product as white solid. FT-IR: $\tilde{\nu}$ = 1224, 767 (ν P-*N*−P) cm^{-1}. ^1H NMR ($CDCl_3$): δ = 1.3 (m, 48 H, 16 CH_3-R), 2.1 (m, 8 H, 8 R-CH) ppm. ^{31}P NMR ($CDCl_3$): δ = 62.59 ppm. MS (FAB): *m*/*z* = 737 $[M + H^+]$. $C_{24}H_{56}CdN_2P_4S_4$: calcd. C 39.12, H 7.60, N 3.80, P, 16.81; found C 39.30, H 7.80, N 3.74, P 17.11.

$[Cd\{(SeP\textit{i}Pr_2)_2N\}_2]$ (2):[19] Recrystallisation of the white solid product from chloroform/methanol gave white crystals, yield 4.51 g (99%). FT-IR: $\tilde{\nu}$ = 1226, 763 (ν P-*N*−P), 425 (ν P-Se) cm^{-1}. ^1H NMR ($CDCl_3$): δ = 1.15 (m, 48 H, 16 CH_3-R), 2.1 (m, 8 H, 8 R-CH) ppm. ^{31}P NMR ($CDCl_3$): δ = 57.101 ppm. MS (FAB): *m*/*z* = 926 $[M + H^+]$. $C_{24}H_{56}CdN_2P_4Se_4$: calcd. C 31.16, H 6.10, N 3.03, P 13.39; found C 31.33, H 6.15, N 2.98, P 13.53.

$[Zn\{(SP\textit{i}Pr_2)_2N\}_2]$ (3):[18] Recrystallisation from dichloromethane/petroleum ether (40−65 °C) gave a white powder, yield 69%. FT-IR: $\tilde{\nu}$ = 1226, 773 (ν P-*N*−P) cm^{-1}. ^1H NMR ($CDCl_3$): δ = 1.3 (m, 48 H, 16 CH_3-R), 2.1 (m, 8 H, 8 R-CH) ppm. ^{31}P NMR ($CDCl_3$): δ = 63.99 ppm. MS (FAB): *m*/*z* = 689 $[M + H^+]$. $C_{24}H_{56}N_2P_4S_4Zn$: calcd. C 41.79, H 8.55, N 4.06, P 17.96; found C 41.83, H 8.56, N 4.03, P 18.64.

$[Zn\{(SeP\textit{i}Pr_2)_2N\}_2]$ (4):[19] Recrystallisation from chloroform/methanol gave white crystals, yield 4.21 g (98%) white crystals. FT-IR: $\tilde{\nu}$ = 1228, 762 (ν P-*N*−P), 427 (ν P-Se) cm^{-1}. ^1H NMR ($CDCl_3$): δ = 1.2 (m, 48 H, 16 CH_3-R), 2.0 (m, 8 H, 8 R-CH) ppm. ^{31}P NMR ($CDCl_3$): δ = 57.101 ppm. MS (FAB): *m*/*z* = 878 $[M + H^+]$. $C_{24}H_{56}N_2P_4Se_4Zn$: calcd. C 32.83, H 6.43, N 3.19, P 14.11; found C 33.02, H 6.61, N 3.12, P 14.18.

Characterisation Techniques: Unless otherwise stated, all reactions were performed under dry nitrogen using standard Schlenk techniques. All solvents and reagents were purchased from Sigma−Aldrich chemical company and used as received. In addition, toluene was distilled from over sodium under nitrogen. ^1H and ^{31}P NMR studies were carried out with a Bruker AC300 FT NMR Spectrometer. Mass spectra were recorded with a Kratos concept 1S instrument. Infrared spectra were recorded with a Specac single reflectance ATR instrument.

Growth Experiments: Low Pressure Metal-Organic Chemical Vapour Deposition (LP-MOCVD): Thin films of metal chalcogenides were grown on borosilicate glass in a low pressure (≈ 10^{-2} Torr) MOCVD reactor tube which has been described elsewhere.[21] A graphite susceptor holds the substrate dimensions (10 mm × 15 mm) which was heated by a tungsten halogen lamp.

Film Characterisations: X-ray powder diffraction studies were carried out using Philips X'Pert MPD diffractometer by using monochromated Cu-K_α radiation. The samples were mounted flat and scanned from 10° to 90° in a step size of 0.04° with a count rate of 2.5 s. Samples were carbon-coated using Edward's coating system E306A before SEM and EDAX analyses. SEM was carried out by using Philip XL30 FEG and EDAX was preformed with DX4. TGA measurements were carried out by a Seiko SSC/S200 model with a heating rate of 10 °C min^{-1} under nitrogen. Electronic absorption spectra were recorded with Helios-Beta Thermospectronic spectrophotometer.

X-ray Crystallographic Study: Single-crystal X-ray diffraction data for the compounds were collected with a CAD-4 diffractometer and Mo-K_α radiation (λ = 0.71069 Å) using ω-2θ scan. The unit cell parameters were determined by least-squares refinement on diffractometer angles (9.99° ≤ θ ≤ 12.51°) for 25 automatically centred reflections.[22] All data were corrected for absorption by empirical methods (ψ scan)[23] and for Lorentz-polarization effects

 © 2004 Wiley-VCH Verlag GmbH & Co. KGaA, Weinheim

by XCAD4.[24] The structures were solved by heavy-atom method using DIRDIF-99[25] programs, refined anisotropically(non-hydrogen atoms) by full-matrix least-squares on F^2 using SHELXL-97[26] program. The H atoms were calculated geometrically and refined with a riding model. In the final stage of refinement data were correct for absorption by DIFABS.[27] The program ORTEP-3[28] was used for drawing the molecules. Crystallographic details and selected interatomic distances and angles are given in Tables 1−4.

CCDC-204283−204285 contain the supplementary crystallographic data for this paper. These data can be obtained free of charge at www.ccdc.cam.ac.uk/conts/retrieving.html [or from the Cambridge Crystallographic Data Centre, 12, Union Road, Cambridge CB2 1EZ, UK; Fax: (internat.) +44-1223/336-033; E-mail: deposit@ccdc.cam.ac.uk].

Acknowledgments

The authors thank the EPSRC, UK for the grants to POB that have made this research possible.

[1] P. O'Brien, in *Inorganic Materials* (Eds.: D. Bruce, D. O'Hare), Wiley, Chichester, **1997**, p. 523.
[2] I. G. Dance, R. G. Garbutt, D. C. Craig, M. L. Scudder, *Inorg. Chem.* **1987**, *26*, 3732−3740.
[3] I. G. Dance, R. G. Garbutt, D. C. Craig, M. L. Scudder, *Inorg. Chem.* **1987**, *26*, 4057−4064.
[4] I. G. Dance, R. G. Garbutt, M. L. Scudder, *Inorg. Chem.* **1990**, *29*, 1571−1577.
[5] M. B. Hursthouse, O. F. Z. Khan, M. Mazid, M. Motevalli, P. O'Brien, *Polyhedron* **1990**, *9*, 541−544.
[6] O. F. Z. Khan, P. O'Brien, *Polyhedron* **1991**, *10*, 325−332.
[7] M. Bochmann, K. J. Webb, M. Harman, M. B. Hursthouse, *Angew. Chem. Int. Ed. Engl.* **1990**, *29*, 638−639.
[8] M. Bochmann, K. J. Webb, M. B. Hursthouse, M. Mazid, *J. Chem. Soc., Dalton Trans.* **1991**, 2317−2323.
[9] M. Bochmann, K. J. Webb, *J. Chem. Soc., Dalton Trans.* **1991**, 2325−2329.
[10] B. O. Dabbousi, P. J. Bonasia, J. Arnold, *J. Am. Chem. Soc.* **1991**, *113*, 3186−3188.
[11] P. J. Bonasia, J. Arnold, *Inorg. Chem.* **1992**, *31*, 2508−2514.
[12] C. Byrom, M. A. Malik, P. O'Brien, A. J. P. White, D. J. Williams, *Polyhedron* **2000**, *19*, 211−215.
[13] R. Nomura, T. Murai, T. Toyosaki, H. Matsuda, *Thin Solid Films* **1995**, *271*, 4−7.
[14] M. B. Hurthouse, M. A. Malik, M. Motevalli, P. O'Brien, *Polyhedron* **1992**, *11*, 45−48.
[15] M. Motevalli, P. O'Brien, J. R. Walsh, I. M. Watson, *Polyhedron* **1996**, *15*, 2801−2808.
[16] M. Chunggaze, M. A. Malik, P. O'Brien, *J. Mater. Chem.* **1999**, *10*, 2433−2437.
[17] M. Afzaal, S. M. Aucott, D. Crouch, P. O'Brien, J.-H. Park, J. D. Woollins, *Adv. Mater. Chem. Vap. Dep.* **2002**, *5*, 187−189.
[18] D. Cupertino, R. Keyte, A. M. Z. Slawin, D. J. Williams, J. D. Woollins, *Inorg. Chem.* **1996**, *35*, 2695−2697.
[19] D. Cupertino, D. J. Birdsall, A. M. Z. Slawin, J. D. Woollins, *Inorg. Chim. Acta* **1999**, *290*, 1−7.
[20] V. Garcia-Montalvo, J. Novosad, P. Kilian, J. D. Woollins, A. M. Z. Slawin, P. G. Y. Garcia, M. Lopez-Cardoso, G. Espinosa-Perez, R. Cea-Olivares, *J. Chem. Soc., Dalton Trans.* **1997**, 1025−1029.
[21] M. A. Malik, P. O'Brien, *Adv. Mater. Opt. Electron* **1994**, *7*, 117−121.
[22] Enraf−Nonius CAD-4/PC Software. Version 1.5c, Enraf−Nonius, Delft, The Netherlands, **1994**.
[23] A. C. T. North, D. C. Phillips, F. S. Mathews, *Acta Crystallogr., Sect. A* **1968**, A24, 351−359.
[24] Harms, S. Wocadlo, *XCAD4 − CAD4 Data Reduction*, University of Marburg, Marburg. Germany, **1995**.
[25] P. T. Beurskens, G. Beursken, W. Bosman, R. De Gelder, S. Garci-Granda, R. O. Gould, R. Israel, J. M. M. Smiths, *The DIRDIF-96 Programme system*, Crystallography Laboratory, University of Nijmegen, The Netherlands, **1996**.
[26] G. Sheldrick, M. SHELXL-97, University of Göttingen, **1997**.
[27] L. J. Farrugia, ORTEP-3 for Windows, *J. Appl. Crystallogr.* **1997**, *30*, 565.
[28] L. J. Farrugia, *WinGX − A Windows Program for Crystal Structure Analysis*, University of Glasgow, Glasgow, **1998**.
[29] J. R. Philips, A. M. Z. Slawin, A. J. P. White, D. J. Williams, J. D. Woollins, *J. Chem. Soc., Dalton Trans.* **1995**, 2467−2468.
[30] N. Zuniga-Villarreal, C. Silvestru, R. R. Lezama, S. H. Ortega, C. A. Toledano, *J. Organomet. Chem.* **1995**, *496*, 169−174.
[31] P. O'Brien, R. Nomura, *J. Mater. Chem.* **1995**, *5*, 1761−1773.
[32] Y. Takahashi, R. Yuki, M. Sugiura, S. Motijima, K. Sugiiyama, *J. Cryst. Growth* **1980**, *50*, 491−497.
[33] N. H. Tran, R. N. Lamb, G. L. Mar, *Colloids Surfaces A., Physicochem. Eng. Aspects* **1999**, *155*, 93−100.
[34] J. I. Pankove, *Optical processes in semiconductors*, Dover Publications Inc., New York, **1970**, 1327.

Received February 19, 2003
Early View Article
Published Online October 23, 2003

 © 2004 Wiley-VCH Verlag GmbH & Co. KGaA, Weinheim

Synthesis, Structure, and Properties of Biimidazole-Chelated Arylruthenium Complexes

Bikash Kumar Panda,[a] Suman Sengupta,[a] and Animesh Chakravorty*[a,b]

Keywords: Ruthenium / Fluorescence / Marcocyclic ligands / Hydrogen bonding

By reacting Ru(η^2-RL)(PPh_3)$_2$(CO)Cl (**1**) with excess 4,5-dimethyl-2,2′-biimidazole (dmbi), organometallics of the type [Ru(η^1-RL)(PPh_3)$_2$(CO)(dmbi)](PF_6) (**2**) have been isolated in excellent yield (η^2-RL is C_6H_2O-2-CHNHC_6H_4R(*p*)-3-Me-5, η^1-RL is C_6H_2OH-2-CHNC_6H_4R(*p*)-3-Me-5 and R is Me, OMe and Cl). In this process the dmbi ligand undergoes five-membered chelation, the iminium-phenolato function tautomerizes to the imine-phenol function and the Schiff base performs a large rotation around the Ru–C bond. The crystal and molecular structure of [Ru(η^1-MeL)(PPh_3)$_2$(CO)(dmbi)](PF_6)·CH_2Cl_2 is reported. For steric reasons the carbon monoxide ligand is located *syn* to the phenolic oxygen atom as opposed to *anti* in the precursor **1**. In the hydrogen bonded imine-phenol function the O–H, H···N, and N···O distances are 0.83(8), 1.77(8), and 2.552(6) Å, respectively, the O–H···N angle being 156(2)°. The Ru(dmbi) chelate along with the metallated carbon atom and the CO ligand define an equatorial plane from which the metallated aldimine fragment is rotated by 34.5° due to interligand repulsion. This results in two unequal [2.348(2) and 2.411(2) Å] Ru–P bonds and an apparent suppression of the *trans* influence of the metallated carbanionic site. The cation and anion in the complex are engaged in N–H···F and C–H···F hydrogen bonding, generating a centrosymmetric dimer in the lattice. One of the hydrogen bonds, characterized by H···F, 2.03(8) Å and N–H···F, 166(2)°, is particularly strong. Solutions of **2** absorb near 400 nm and emit near 460 nm with quantum yields and lifetimes of ca. 10^{-3} and ≤ 20 ns, respectively. The emission, which probably involves the ^{3}MLCT state incorporating a π^*(dmbi) contribution, is peculiar to the coligation of η^1-RL and dmbi to bivalent ruthenium. In dichloromethane solution **2** displays a quasireversible $\mathbf{2}^+/\mathbf{2}$ couple near 0.70 V vs. SCE [$\mathbf{2}^+$ is the ruthenium(III) analogue of **2**]. Coulometrically generated solutions of $\mathbf{2}^+$ display a strong absorption near 400 nm and rhombic EPR spectra with *g* values near 2.55, 2.15, and 1.83.

(© Wiley-VCH Verlag GmbH & Co. KGaA, 69451 Weinheim, Germany, 2004)

Introduction

New orthometallated ruthenium compounds are of current interest in terms of synthesis[1−3] reactivity[1,4−9] and photophysical properties.[10,11]

The decarbonylative metallation of 4-methyl-2,6-diformylphenol by $Ru(PPh_3)_3Cl_2$ in the presence of primary aromatic amines ($RC_6H_4NH_2$) furnishes organoruthenium species of the type Ru(η^2-RL)(PPh_3)$_2$(CO)Cl, (**1**), incorporating a four-membered chelate ring adjacent to a hydrogen-bonded iminium-phenolato ring.[12−14] The reactivity of **1** is under our scrutiny. Alkynes and isocyanides promote metallacycle expansion[5,6,8,15,16] but bidentate monoanionic σ-donor reagents such as carboxylates, nitrate, nitrite, xanthate, and pyridine-2-thiolate invariably form a four-membered chelate ring.[17−20]

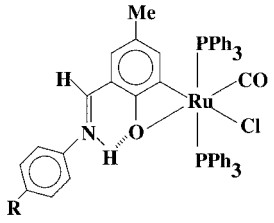

1

The richness of this reaction chemistry prompted us to explore the treatment of **1** with an electroneutral heterocyclic ligand suited for five-membered *N*,*N*-chelation − with the result that 4,5-dimethyl-2,2′-biimidazole (dmbi) has been used to afford a crystalline organoruthenium system, characterized by hydrogen bonding interactions within itself and with anions in the lattice. This is accompanied by changes in the rotameric and tautomeric states of the Schiff base ligand. The structure and properties of the new organometallics, which are also luminescent in the visible region, are scrutinized here.

Results and Discussion

Reaction of 1 with dmbi: Chelation and Tautomerization

Addition of excess dmbi to a violet solution of Ru(η^2-RL)(PPh_3)$_2$(CO)Cl (**1**) in boiling $MeOH/CH_2Cl_2$ solution

[a] Department of Inorganic Chemistry, Indian Association for the Cultivation of Science,
Kolkata 700032, India
Fax: (internat.) +91-(0)33-2473-2805
E-mail: icac@mahendra.iacs.res.in
[b] Jawaharlal Nehru Centre for Advanced Scientific Research, Bangalore 560 064, India

 © 2004 Wiley-VCH Verlag GmbH & Co. KGaA, Weinheim DOI: 10.1002/ejic.200300293

in the presence of NH_4PF_6 afforded the yellow salt [Ru(η^1-RL)(PPh_3)$_2$(CO)(dmbi)](PF_6) (**2**) according to Equation (1).

$$\mathbf{1} + \text{dmbi} + PF_6^- \rightarrow \mathbf{2} + Cl^- \quad (1)$$

In this work R = Me, OMe, and Cl, and specific compounds are identified with R in parenthesis, e.g. for **2** (Me) R = Me. Ruthenium complexes of biimidazoles have received some attention[21−25] but organoruthenium species incorporating chelation by such ligands as in **2** appear to be unprecedented. The salt **2** has been uniformly isolated in pure form in >80% yield. An isomer (the coordinating nitrogen atoms interchanged) of **2** is possible in principle but it has never been observed. Careful examination of ^{1}H NMR spectra of crude samples (before recrystallization) did not reveal any extra methyl or other signals apart from those characterizing **2** (see Exp. Sect.).

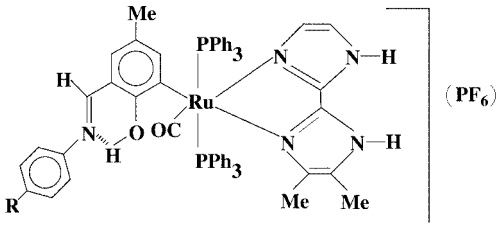

2

In Equation (1) the Ru−Cl and Ru−O (phenolato) bonds are displaced by the chelating dmbi ligand. With the liberation of the phenolato oxygen, the Schiff base fragment assumes the imine-phenol tautomeric form **3**, as opposed to the zwitterionic iminium-phenolato form **4** present in **1**.[12] This has been proven by structure determination (vide infra) and is fully consistent with spectroscopic data.

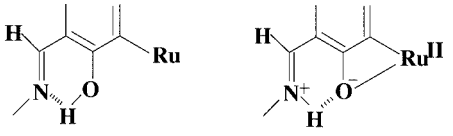

3 **4**

Thus the C=N stretching frequency in **2** is significantly lower at ca. 1600 cm^{-1} than that in **1** (ca. 1620 cm^{-1}), as expected.[26,27] Also, the aldimine CH signal in ^{1}H NMR in **2** is at a lower field, ca. 8.0 ppm as compared to ca. 7.5 ppm in **1**. The O−H resonance in **2** is a relatively sharp signal near 13 ppm, having a half-height width of ca. 30 Hz. In contrast the iminium N−H resonance in **1** is broad (width, ca. 150 Hz) due to the quadrupole moment of the nitrogen atom.[12] The prototropic transformation between **1** and **2** has certain similarities with the imine−iminium tautomerization in rhodopsins.[26]

Equation (1) is believed to proceed[17,28] via *cis* attack of chloride/O(phenolato) by dmbi as stylized in **5**. The anchored ligand can then displace both chloride and phenolato oxygen atom to achieve chelation as in **6** with concomitant prototropic and rotameric (vide infra) changes.

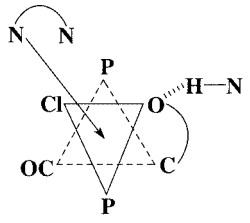

5

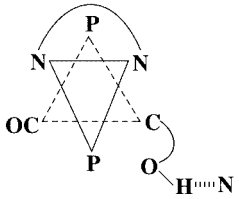

6

Characterization

Type **2** organometallics are diamagnetic (Ru^{II}, idealized t_{2g}^6) and behave as 1:1 electrolytes in acetone solution (Λ, 133−138 Ω^{-1} cm^2 mol^{-1}). The C≡O stretching frequency (ca. 1940 cm^{-1}) in **2** is indicative of dπ(Ru)−pπ(dmbi) back-bonding. In **1** as well as in the acetate and other derivatives this stretch lies systematically at lower frequencies, near 1920 cm^{-1}.[12,17−20]

In the ^{1}H NMR spectra the 3-H and 5-H proton signals of the metallated ring are sharp singlets near 6.5 ppm. The C(4)-Me signals near δ = 1.8 ppm are subject to shielding by phosphane phenyl rings.[12,17,29] The same applies to the C(22)-Me signal near 1.7 ppm; the C(21)-Me resonance is near 2.0 ppm. The PPh_3, Schiff base (C_6H_4R), and the biimidazole aromatic proton signals form a complex multiplet in the region 6.8−7.4 ppm. The dmbi N−H protons resonate near 10.2 ppm. The chemical shifts of the imine-phenol protons are considered above. The photophysical and redox properties of the complexes are examined below.

Structure: Nonbonded Interactions, Rotameric Change, and Hydrogen Bonding

The dichloromethane solvate [Ru(η^1-MeL)(PPh_3)$_2$(CO)-(dmbi)](PF_6)·CH_2Cl_2, afforded crystals suitable for structure determination. A view of the cation (Figure 1) and

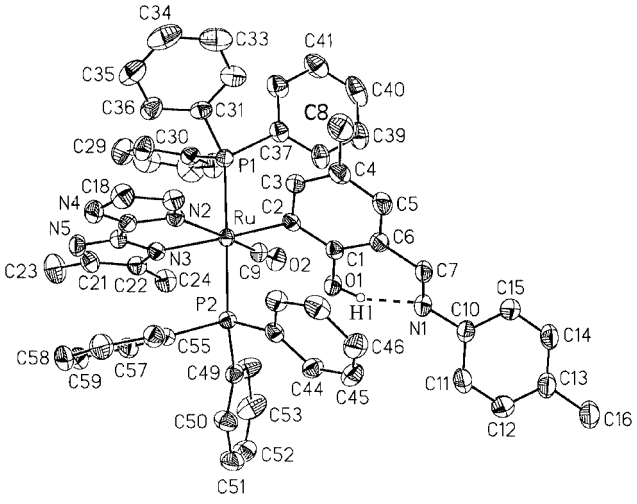

Figure 1. Perspective view and atom labeling scheme for the cation of **2**(Me)·CH_2Cl_2. All non-hydrogen atoms are represented by 30% thermal probability ellipsoids.

 © 2004 Wiley-VCH Verlag GmbH & Co. KGaA, Weinheim

Table 1. Selected bond lengths (Å) and angles (°) for complex **2**(Me)·CH_2Cl_2

Bond lengths			
Ru−P(1)	2.348(2)	Ru−N(3)	2.157(4)
Ru−P(2)	2.411(2)	C(9)−O(2)	1.152(6)
Ru−C(2)	2.068(5)	C(7)−N(1)	1.259(7)
Ru−C(9)	1.791(5)	C(1)−O(1)	1.347(6)
Ru−N(2)	2.166(4)	N(1)···O(1)	2.552(6)
Angles			
P(1)−Ru−P(2)	175.7(1)	P(2)−Ru−C(2)	87.9(1)
P(1)−Ru−N(2)	91.0(1)	Ru−C(9)−O(2)	174.8(5)
P(1)−Ru−N(3)	90.8(1)	C(2)−Ru−N(2)	95.4(2)
P(1)−Ru−C(9)	87.0(2)	C(9)−Ru−N(3)	96.5(2)
P(1)−Ru−C(2)	90.5(1)	C(9)−Ru−N(2)	172.4(2)
P(2)−Ru−N(2)	85.2(1)	N(2)−Ru−N(3)	76.3(2)
P(2)−Ru−N(3)	90.3(1)	C(9)−Ru−C(2)	91.9(2)
P(2)−Ru−C(9)	97.1(2)		

selected bond parameters (Table 1) are given here. All the hydrogen atoms in the structure, except those of CH_2Cl_2, were directly observable in difference Fourier maps, which helped in characterizing the hydrogen bonds, vide infra. In Figure 1 only the phenolic hydrogen is explicitly shown. The solvent of crystallization CH_2Cl_2 displays a nonbonded Cl···Cl interaction [3.576(4) Å] with another symmetry related CH_2Cl_2 molecule, the two forming a centrosymmetric pair in the lattice.

The $RuC_2P_2N_2$ coordination sphere has a severely distorted octahedral geometry. The angles subtended by *cis* and *trans* pairs of ligands span the ranges 76−98° and 171−176°, respectively. On the basis of covalent radii, the idealized Ru^{II}−C(sp^2) bond length is estimated to be 2.06 Å.[17,30] The observed Ru−C(2) is 2.068(5) Å. The Ru−N(3) bond is not lengthened by the *trans* influence of the carbanionic C(2) site due to certain repulsive interactions in the structure, see below.

The Ru(dmbi) chelate fragment (excluding the methyl groups) along with the metallated carbon atom C(2) and the carbon monoxide ligand constitute a satisfactory plane of mean deviation 0.03 Å (plane A). Another relevant plane (plane B) is the metallated aldimine ring defined by Ru, C(1) to C(8), N(1), O(1) (mean deviation 0.03 Å). The two planes are noncoplanar as highlighted in **7**, the dihedral angle between them is 34.5°. As a result the environment is more crowded around P(2), and Ru−P(2) [2.411(2) Å] is significantly longer than Ru−P(1) [2.348(2) Å]. In the precursor complex **1** the Schiff base lies on the equatorial plane and the two Ru−P lengths are both 2.387(2) Å.[12]

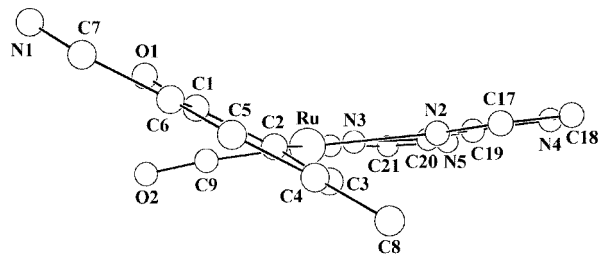

7

The noncoplanarity of A and B planes arise from the repulsive nonbonded interactions between the dmbi and Schiff base ligands. Thus C(17)···C(3) [3.298(7) Å] is less than the sum (3.40 Å) of the van der Waals (vdW) radii of the two carbon atoms.[31] The distance would have been even lower, further augmenting the repulsion, if the A and B planes were coplanar. The repulsive interaction is also expressed in an effective lengthening of the Ru−N(2) bond. The *trans* influence of the carbanionic C(2) site should normally make the Ru−N(3) bond longer than the Ru−N(2) bond although the electron-donating methyl group adjacent to N(3) may marginally counter this effect. In practice the two bond lengths − 2.157(4) and 2.166(4) Å, respectively − are equal within experimental error, primarily due to the nonbonded repulsion noted above.

The conversion of **1** into **2** is attended by a large rotation of the Schiff base fragment around the Ru−C(2) bond. The carbon monoxide ligand lies *syn* to the metallated carbon atom in both **1** and **2** but it is respectively *syn* and *anti* to the phenolic C−O function in **2** and **1**.[12] The O(1)−C(1)···C(9)−O(2) torsion angle in **2**(Me)·CH_2Cl_2 is 46.7°. The computer-generated hypothetical *anti* configuration of dmbi fragment is shown in **8** where the estimated C(17)···O(1) and N(2)···O(1) are 2.416(5) Å and 2.621(6) Å, respectively, are far below the respective sums of the vdW radii (3.20 and 3.05 Å).[31] The *anti* configuration is thus unstable and the above-noted conformational change occurs to relieve the strain. The observed C(17)···O(1) and N(2)···O(1) distances in the *syn*-configured complex are 5.660(5) and 4.930(6) Å, respectively.

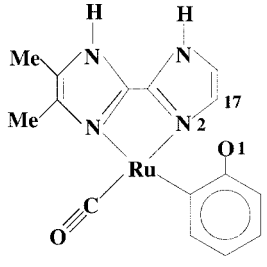

8

Within the imine-phenol fragment of **8**, O−H, H···N, and N···O are 0.83(8), 1.77(8), and 2.552(6) Å respectively, the O−H···N is 156(2)°. The hydrogen bonding is thus very unsymmetrical. In the iminium-phenolato fragment **4** of the precursor **1** the relevant bond lengths and angle are: N−H, 0.99(6) Å, H···O, 1.75(5) Å, N···O, 2.665(12) Å, and N−H···O, 144(1)°.[12] In effect, the hydrogen bonding is stronger (shorter N···O distance) in the imine-phenol species.

The dmbi ligand in the cation and the PF_6^- anion are engaged in N−H···F and C−H···F hydrogen bonding. The

 © 2004 Wiley-VCH Verlag GmbH & Co. KGaA, Weinheim

centrosymmetric dimer thus generated is shown in Figure 2 along with approximate bond parameters. In organometallic hexafluorophosphate salts, H···F distances <2.6 Å, along with X−H···F (X = C, N, O) angles >90°, generally indicate significant hydrogen bonding.[32] Of the three hydrogen bond types in Figure 3 the, N(5)−H···F(1) bond is particularly strong [H···F, 2.03(8) Å; N−H···F, 166(2)°].

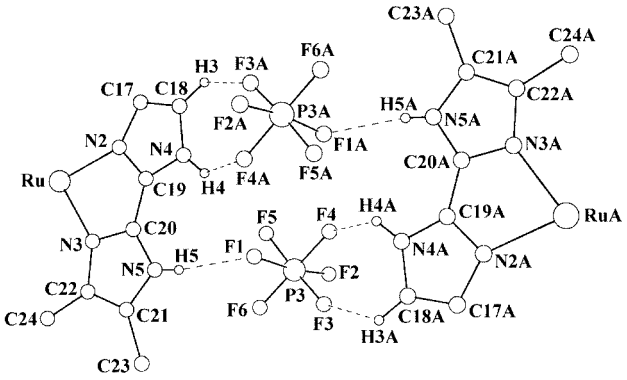

Figure 2. Hydrogen bonding in crystals of **2**(Me)·CH_2Cl_2. Relevant bond lengths (Å) and angles (°) are N(5)···F(1), 2.775(5); H(5)···F(1), 2.03(8); N(4)···F(4), 2.945(5); H(4)···F(4), 2.31(9); C(18)···F(3), 3.144(6); H(18)···F(3), 2.54(7). N(5)−H(5)···F(1), 166(2); N(4)−H(4)···F(4), 131(3); C(18)−H(18)···F(3), 123(1)

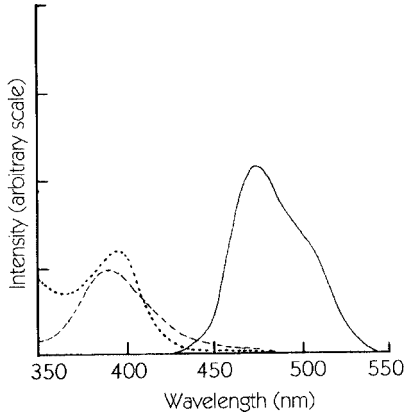

Figure 3. Absorption (···) fluorescence (——) and excitation (− − −) spectra of **2**(Cl) in dichloromethane solution.

Photophysical Properties

Type **2** complexes display two allowed transitions near 320 and 400 nm (Table 2). The later band is weaker in intensity and is believed to have significant dπ(Ru)−π*(dmbi) MLCT character. Dichloromethane solutions of **2** are fluorescent at room temperature, the emission peak lying near 460 nm. The quantum yields (φ_r) are nearly one order of magnitude lower than that of the $[Ru(bpy)_3]^{2+}$ standard[33] (Table 2).

Excitation spectral studies have revealed that the emission is associated with the absorption band near 400 nm. A representative case is shown in Figure 3. Assuming that the band has MLCT character, as suggested above, the possible involvement of the ^{3}MLCT state incorporating a π*(dmbi) contribution is implicated in the emission process. However, tris-biimidazole complexes of bivalent ruthenium are nonemitters at room temperature.[21,34] Further the parent type **1** organometallics also do not emit in the visible region. Thus the observed emission in **2** is a property peculiar to the coligation of η^1-RL and dmbi to bivalent ruthenium. Lifetime studies revealed single-exponential decay with $\tau_0 \leq 20$ ns, which is shorter than the usual (10^2-10^3 ns) lifetimes of fluorescent ruthenium(II) complexes of conjugated nitrogenous ligands.[21,23]

Electrochemistry: Metal Oxidation

In dichloromethane solution **2** displays a quasireversible (peak-to-peak separation, ca. 100 mV) cyclic voltammetric response assigned to the couple of Equation (2) where $\mathbf{2}^+$ represents the ruthenium(III) analogue of **2**.

$$\mathbf{2}^+ + e \rightarrow \mathbf{2} \quad (2)$$

The reduction potentials ($E_{1/2}$) lie near 0.70 V vs. SCE and become more positive as the electron-withdrawing power of the R group increases (OMe < Me < Cl), see Table 2. The one-electron nature of the couple is consistent with current height data, as compared to those of the one-electron standard $[Ru(bpy)_3]^{2+}$. More importantly exhaustive coulometric oxidation at 0.9 V afforded a coulomb count corresponding to a one-electron transfer (Table 2).

The trivalent organometallics $\mathbf{2}^+$, generated coulometrically, have been examined in solution. Their cyclic voltammograms (initial scan cathodic) are virtually superimposable on those of **2** (initial scan anodic), showing that $\mathbf{2}^+$ retains the gross structure of **2**. Orange-red solutions of $\mathbf{2}^+$ are characterized by an intense band near 400 nm, associ-

Table 2. Spectral and electrochemical data of **2**

Complexes	UV/Vis data[a] λ_{max}, nm (ε,[b] $M^{-1}cm^{-1}$)	Emission data λ_{max}, nm (φ_r)[a] [c]	Electrochemical data $E_{1/2}$, V (ΔE_p, mV)[d]	n[e]
2(Me)	320 (20970), 390 (4680)	464 (5.6×10^{-3})	0.69 (130)	1.07
2(OMe)	322 (23700), 394 (5210)	461 (3.0×10^{-3})	0.65 (85)	1.03
2(Cl)	321 (22760), 397 (4470)	467 (5.3×10^{-3})	0.71 (95)	0.98

[a] Solvent is dichloromethane. [b] Molar absorption coefficient. [c] Excitation at the higher wavelength absorption peak. [d] Solvent is dichloromethane; ΔE_p is peak-to-peak separation. [e] $n = Q/Q'$ where Q is the observed coulomb count and Q' is the calculated coulomb count for one-electron transfer.

 © 2004 Wiley-VCH Verlag GmbH & Co. KGaA, Weinheim

Table 3. Electronic and EPR spectroscopic data of $\mathbf{2}^+$

Complexes	UV/Vis data[a] λ_{max}, nm (ε,[b] $M^{-1}cm^{-1}$)	EPR g values[c] g_1	g_2	g_3
$\mathbf{2}(Me)^+$	324 (356560), 397(26710), 518 (4830)	2.528	2.141	1.818
$\mathbf{2}(OMe)^+$	319 (34960), 401 (24410), 512 (2530)	2.553	2.158	1.818
$\mathbf{2}(Cl)^+$	321 (37950), 403 (27710), 515 (3500)	2.578	2.159	1.856

[a] Solvent is dichloromethane. [b] Molar absorption coefficient. [c] In 1:1 dichloromethane/toluene frozen glass (77 K).

ated with a shoulder near 520 nm (Table 3). The solutions are EPR-active when frozen into the glassy state (dichloromethane/toluene, 77 K), giving rise to well-resolved rhombic spectra that are consistent with a low-spin $4d^5$ configuration in a nonaxial geometry.[35,36] A representative spectrum (Figure 4) and the g values (Table 3) are given here.

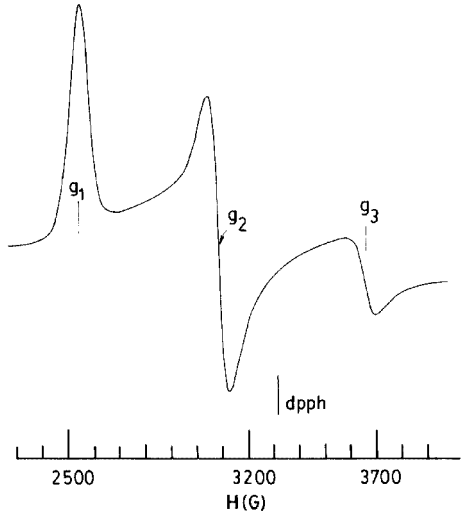

Figure 4. X-band EPR spectrum of electrogenerated $\mathbf{2}(OMe)^+$ in dichloromethane/toluene glass at 77 K. Instrument settings: power, 30 dB; modulation, 100 kHz; sweep centre, 3200 G.

Conclusions

Organometallics of type **1** are transformed into salts of type **2** upon reacting with dmbi. The conversion is attended by five-membered dmbi chelation, iminium-phenolato → imine-phenol prototropic shift and rotameric isomerization (*anti*→ *syn*) of the phenolic function with respect to the carbon monoxide ligand. The metallated aromatic ring is turned away from the dmbi chelate plane due to steric repulsion, resulting in significant inequality of the two Ru−P bonds. Also, the carbanionic *trans* influence is apparently suppressed. In solution **2** is emissive in the visible region and is electrooxidizable to its ruthenium(III) analogue $\mathbf{2}^+$, which is characterized by rhombic EPR spectra.

Experimental Section

Materials: $Ru(PPh_3)_3Cl_2$ [37] and $Ru(\eta^2\text{-RL})(PPh_3)_2(CO)Cl$[12] were prepared by reported methods, and 4,5-dimethyl-2,2′-biimidazole was obtained from Aldrich. Dichloromethane was purified for electrochemical work as described before.[35,38] All other chemicals and solvents were of analytical grade and were used as received.

Physical Measurements: Electronic and IR spectra were recorded with a Shimadzu UV-1601 PC spectrophotometer and a Nicolet Magna IR series II spectrometer respectively. ^1H NMR spectra were obtained using a Bruker 300 MHz FT NMR spectrometer. The numbering scheme used for ^1H NMR is the same as in the crystallography. Spin−spin structures are abbreviated as: s, singlet; d, doublet; t, triplet; m, multiplet. EPR spectra were recorded on a Varian E-109C X-band spectrometer fitted with a quartz dewar. Microanalyses (C, H, N) were performed using a Perkin−Elmer 240C elemental analyzer. Solution electrical conductivity was measured in acetone with a Phillips PR 9500 bridge by using a platinized electrode (cell constant of 1.05). The electrochemical measurements were performed at a platinum electrode under a nitrogen atmosphere in dichloromethane solution by using a model 620A electrochemical analyzer of CH Instruments. The supporting electrolyte was tetraethylammonium perchlorate and potentials are referenced to the saturated calomel electrode (SCE). For EPR studies $\mathbf{2}^+$ was generated coulometrically in dichloromethane solution to which dry toluene was added before freezing into the glassy state.

Fluorescence and quantum yields (using $[Ru(bpy)_3]^{2+}$ as standard,[33] $\varphi = 0.042$) were recorded with a Perkin−Elmer model LS 55 luminescence spectrometer. Luminescence lifetimes were measured in an Applied Photophysics SP-70 nanosecond fluorescence spectrometer based on a time-correlated single-photon counting technique. The decay curves were deconvoluted using the Global Fluorescence Analysis version 1.2 software of Photon Technology International.

Synthesis of Complexes: The $[Ru(\eta^1\text{-RL})(PPh_3)_2(CO)(dmbi)](PF_6)$ (**2**) complexes were synthesized in excellent yield (ca. 85%) by reacting $Ru(\eta^2\text{-RL})(PPh_3)_2(CO)Cl$ (**1**) with excess 4,5-dimethyl-2,2′-biimidazole. Details of a representative case are given below. The other compounds were prepared analogously.

2(Me): dmbi (89 mg, 0.549 mmol) was added to a hot solution of **1**(Me) (100 mg, 0.109 mmol) in a mixture of methanol (20 mL) and dichloromethane (10 mL). On subsequent heating to reflux for 3 h, the mixture changed from violet to yellow. NH_4PF_6 (30 mg, 0.184 mmol) was then added and the resultant solution was further boiled under reflux for 20 min. The solvent was then evaporated under reduced pressure and the yellow solid thus obtained was washed thoroughly with water (for removal of excess NH_4PF_6), dried, and then dissolved in dichloromethane (excess dmbi remains insoluble). The filtered solution was then stripped of solvent under reduced pressure and the residue was recrystallized from a dichloromethane/hexane (1:3) mixture followed by drying in vacuo to furnish the complex in nonsolvated form. Yield: 110 mg (85%). $C_{60}H_{54}F_6N_5O_2P_3Ru$ (1185.10): calcd. C 60.81, H 4.59, N 5.91; found C 60.75, H 4.63, N 5.85. IR (KBr): $\tilde{\nu}$ = 1939 cm^{-1}(ν_{CO}), 1591 ($\nu_{C=N}$), 847 (ν_{PF6}). ^1H NMR (300 MHz, $CDCl_3$, 298 K): δ = 12.96 (s, 1 H, O−H), 10.30 (s, 1 H, N−H), 10.20 (s, 1 H, N−H), 7.96 (s, 1 H, H7), 6.59 (s, 1 H, H5), 6.52 (s, 1 H, H3), 2.37 (s, 3 H, 13-Me), 2.02 (s, 3 H, 21-Me), 1.84 (s, 3 H, 4-Me), 1.72 (s, 3 H, 22-Me), 6.90−7.25 (m, 36 H, $2PPh_3$, H11, H12, H14, H15, H17, H18). Λ_M = 133 $\Omega^{-1}cm^2mol^{-1}$.

2(OMe): **1**(OMe) (100 mg, 0.107 mmol) and dmbi (87 mg, 0.536 mmol) were employed. Yield: 106 mg (82%). $C_{60}H_{54}F_6N_5O_3P_3Ru$ (1201.10): calcd. C 60.00, H 4.53, N 5.83; found C 60.05, H 4.58, N 5.77. IR (KBr): $\tilde{\nu}$ = 1938 cm^{-1} (ν_{CO}), 1611 ($\nu_{C=N}$), 846 (ν_{PF6}). ^1H NMR (300 MHz, $CDCl_3$, 298 K): δ = 12.99 (s, 1 H,

 © 2004 Wiley-VCH Verlag GmbH & Co. KGaA, Weinheim

Table 4. Crystallographic data for **2** (Me)·CH_2Cl_2

Empirical formula	$C_{61}H_{56}Cl_2F_6N_5O_2P_3Ru$
Molecular mass	1269.99
T/K	293(2)
Crystal system	triclinic
Space group	$P\bar{1}$
a (Å)	13.437(7)
b (Å)	13.662(8)
c (Å)	16.150(9)
α (°)	77.67(5)
β (°)	86.76(4)
γ (°)	89.46(4)
V (Å^3)	2892(3)
Z	2
Calcd. density/gm^{-3}	1.459
μ (mm^{-1})	0.514
Total reflections	8598
Independent reflections	8460
R, $\omega R2[I > 2\sigma(I)]$[a][b]	0.0574, 0.1477
Goodness-of-fit on F^2 [a][b]	1.057

[a] $R_1 = \Sigma||F_o| - |F_c||/\Sigma|F_o|$. [b] $wR2 = [\Sigma w(F_o^2 - F_c^2)^2/\Sigma(F_o^2)^2$.

O−H), 10.32 (s, 1 H, 2N−H), 10.23 (s,1 H, N−H) 7.96 (s, 1 H, H7), 6.57 (s, 1 H, H5), 6.52 (s, 1 H, H3), 2.02 (s, 3 H, 21-Me), 1.84 (s, 3 H, 4-Me), 1.75 (s, 3 H, 22-Me), 3.83 (s, 3 H, OMe), 6.98−7.25 (m, 36 H, 2 PPh_3, H11, H12, H14, H15, H17, H18). Λ_M = 137 Ω^{-1} cm^{2}mol^{-1}.

2(Cl): **1**(Cl) (100 mg, 0.107 mmol) and dmbi (87 mg, 0.536 mmol) were used. Yield: 107 mg (83%). $C_{59}H_{51}ClF_6N_5O_2P_3Ru$ (1205.52): calcd. C 58.78, H 4.26, N 5.81; found C 58.82, H 4.29, N 5.76. IR (KBr): $\tilde{\nu}$ = 1940 cm^{-1} (ν_{CO}), 1605 ($\nu_{C=N}$), 848 (ν_{PF6}). ^{1}H NMR (300 MHz, $CDCl_3$, 298 K): δ = 12.69 (s, 1 H, O-H), 10.19 (s, 1 H, N−H), 10.09 (s, 1 H, N−H), 7.95 (s, 1 H, H7), 6.62 (s, 1 H, H5), 6.54 (s, 1 H, H3), 2.02 (s, 3 H, 21-Me), 1.83 (s, 3 H, 4-Me), 1.75 (s, 3 H, 22-Me), 6.90−7.34 (m, 36 H, 2 PPh_3, H11, H12, H14, H15, H17, H18). Λ_M = 138 Ω^{-1} cm^2 mol^{-1}.

X-ray Crystallography: Bright yellow single crystals of [Ru(η^1-MeL)$(PPh_3)_2$(CO)(dmbi)](PF_6)·CH_2Cl_2 (2(Me)·CH_2Cl_2) (0.40 × 0.30 × 0.25 mm^3) were grown by slow diffusion of hexane into dichloromethane solutions at room temperature. Cell parameters were determined by a least-squares fit of 30 machine-centered reflections (2θ range 14−28°) on a Siemens R3m/V four-circle diffractometer with graphite-monochromated Mo-K_α radiation (λ = 0.71073). Two check reflections measured after every 198 reflections showed no significant intensity reduction. All data were corrected for Lorentz polarization effects and an empirical absorption correction[39] was performed on the basis of an azimuthal scan of six reflections for the crystals. The metal atom was located from Patterson maps and the rest of the non-hydrogen atoms and all the hydrogen atoms except those of CH_2Cl_2 emerged from successive Fourier syntheses. The structure was refined by a full-matrix least-squares procedure. All non-hydrogen atoms were refined anisotropically. The hydrogen atoms were refined isotropically with a fixed *U* = 0.08 Å^2. Calculations were performed using the SHELXTL, version 5.03[40] package. Crystal data are listed in Table 4. CCDC-210733 contains the supplementary crystallographic data for **2** (Me)·CH_2Cl_2. These data can be obtained free of charge at www.ccdc.cam.ac.uk/conts/retrieving.html [or from the Cambridge Crystallographic Data Centre, 12, Union Road, Cambridge CB2 1EZ, UK; Fax: (internat.) +44-1223-336-033; E-mail: deposit@ccdc.cam.ac.uk].

Computer Generation of Motif 5: The relative positions of CO and the dmbi chelate were retained as in the structure of [Ru(η^1-MeL)$(PPh_3)_2$(CO)(dmbi)](PF_6)·CH_2Cl_2 but the phenolic oxygen O(1) was shifted so as to correspond to the relative position in **1** (Me), the C−O length being set at 1.347(6) Å. The same software as noted above was used.

Acknowledgments

We are thankful to the Department of Science and Technology, the Council of Scientific and Industrial Research, New Delhi, India, for financial support. The help received from Professor M. Choudhury, Dr. S. Goswami, and Dr. D. Nath is acknowledged.

[1] M. Poyatos, J. A. Mata, E. Falomir, R. H. Crabtree, E. Peris, *Organometallics* **2003**, *22*, 1110−1114.
[2] J. Perez, V. Riera, A. Rodriguez, D. Miguel, *Organometallics* **2002**, *21*, 5437−5438.
[3] J. A. Cabeza, I. D. Rio, S. G. Granda, V. Riera, M. Suarez, *Organometallics* **2002**, *21*, 2540−2543.
[4] W. Ferstl, I. K. Sakodinskaya, N. B. Sutter, G. L. Borgne, M. Pfeffer, A. D. Ryabov, *Organometallics* **1997**, *16*, 411−418.
[5] K. Ghosh, S. Pattanayak, A. Chakravorty, *Organometallics* **1998**, *17*, 1956−1960.
[6] K. Ghosh, S. Chattopadhyay, S. Pattanayak, A. Chakravorty, *Organometallics* **2001**, *20*, 1419−1423.
[7] P. Steenwinkel, S. L. James, R. A. Gossage, D. M. Grove, H. Kooijman, W. J. J. Smeets, A. L. Spek, G. V. Koten, *Organometallics* **1998**, *17*, 4680−4693.
[8] B. K. Panda, S. Chattopadhyay, K. Ghosh, A. Chakravorty, *Organometallics* **2002**, *21*, 2773−2780.
[9] V. Ritleng, M. Pfeffer, C. Sirlin, *Organometallics* **2003**, *22*, 347−354.
[10] V. W. W. Yam, B. W. K. Chu, K. K. Cheung, *Chem. Commun.* **1998**, 2261−2262.
[11] V. W. W. Yam, B. W. K. Chu, C. C. Ko, K. K. Cheung, *J. Chem. Soc., Dalton Trans.* **2001**, 1911−1919.
[12] P. Ghosh, N. Bag, A. Chakravorty, *Organometallics* **1996**, *15*, 3042−3047.
[13] N. Bag, S. B. Choudhury, A. Pramanik, G. K. Lahiri, A. Chakravorty, *Inorg. Chem.* **1990**, *29*, 5013−5014.
[14] N. Bag, S. B. Choudhury, G. K. Lahiri, A. Chakravorty, *J. Chem. Soc., Chem. Commun.* **1990**, 1626−1627.
[15] S. Chattopadhyay, K. Ghosh, S. Pattanayak, A. Chakravorty, *J. Chem. Soc., Dalton Trans.* **2001**, 1259−1265.
[16] S. Chattopadhyay, K. Ghosh, S. Pattanayak, A. Chakravorty, *Indian J. Chem.* **2001**, 40A, 1−3.
[17] P. Ghosh, A. Pramanik, A. Chakravorty, *Organometallics* **1996**, *15*, 4147−4152.
[18] P. Ghosh, A. Chakravorty, *Inorg. Chem.* **1997**, *36*, 64−69.
[19] S. Chattopadhyay, B. K. Panda, K. Ghosh, A. Chakravorty, *Israel J. Chem.* **2001**, *41*, 139−144.
[20] B. K. Panda, S. Chattopadhyay, K. Ghosh, A. Chakravorty, *Polyhedron* **2002**, *21*, 899−904.
[21] D. P. Rillema, R. Sahai, P. Matthews, A. K. Edwards, R. J. Shaver, L. Morgan, *Inorg. Chem.* **1990**, *29*, 167−175.
[22] M. Haga, M. M. Ali, H. Maegawa, K. Nozaki, A. Yoshimura, T. Ohno, *Coord. Chem. Rev.* **1994**, *132*, 99−104.
[23] M. Haga, M. M. Ali, S. Koseki, K. Fujimoto, A. Yoshimura, K. Nozaki, T. Ohno, K. Nakajima, D. J. Stufkens, *Inorg. Chem.* **1996**, *35*, 3335−3347.
[24] M. Haga, T. Inoue, S. Yamabe, *Inorg. Chem.* **1987**, *26*, 4148−4154.
[25] P. Majumdar, S. M. Peng, S. Goswami, *J. Chem. Soc., Dalton Trans.* **1998**, 1569−1574.
[26] C. Sandorfy, D. Vocelle, *Mol. Phys. Chem. Biol.* **1989**, 4, 195−211.
[27] H. Bohme, M. Hakke, in *Advances in Organic Chemistry* (H. Bohme, H. G. Viehe, Eds.), Part 1, Vol. 9, Interscience Publication, New York, **1976**, p.1.

 © 2004 Wiley-VCH Verlag GmbH & Co. KGaA, Weinheim

[28] N. Serpone, D. G. Bickley, *Inorg. Chem.* **1972**, *17*, 391−397.
[29] P. Ghosh, *Polyhedron* **1997**, *16*, 1343−1349.
[30] A. K. Rappe, C. J. Caswit, K. Colwell, W. A. Goddard, W. M. Skiff, *J. Am. Chem. Soc.* **1992**, *114*, 10024−10035.
[31] J. E. Huheey, E. A. Keiter, R. L. Keiter, *Inorganic Chemistry: Principles of Structure and Reactivity*, Hampen Collins College Publishers, New York, **1993**, p. 292.
[32] F. Grepioni, G. Cojazzi, S. M. Drapen, N. Scully, D. Braga, *Organometallics* **1998**, *17*, 296−307.
[33] D. P. Rillema, D. G. Taghdiri, D. S. Jones, L. A. Worl, T. J. Meyer, H. A. Levy, C. D. Keller, *Inorg. Chem.* **1987**, *26*, 578−585.
[34] M. Haga, *Inorg. Chim. Acta* **1983**, *77*, L39−L41.
[35] G. K. Lahiri, S. Bhattacharya, B. K. Ghosh, A. Chakravorty, *Inorg. Chem.* **1987**, *26*, 4324−4331.
[36] P. Ghosh, A. Pramanik, N. Bag, G. K. Lahiri, A. Chakravorty, *J. Organomet. Chem.* **1993**, *454*, 237−241.
[37] T. A. Stephenson, G. Wilkinson, *J. Inorg. Nucl. Chem.* **1966**, *28*, 945−956.
[38] A. Pramanik, N. Bag, D. Ray, G. K. Lahiri, A. Chakravorty, *Inorg. Chem.* **1991**, *30*, 410−417.
[39] A. C. T. North, D. C. Phillips, F. A. Mathews, *Acta Crystallogr., Sect. A* **1968**, 24, 351−359.
[40] G. M. Sheldrick, SHELXTL, Version 5.03; *Siemens Analytical X-ray system:* Madison, WI, **1994**.

Received May 17, 2003
Early View Article
Published Online October 31, 2003

 © 2004 Wiley-VCH Verlag GmbH & Co. KGaA, Weinheim

Novel Supramolecular Frameworks Self-Assembled from One-Dimensional Polymeric Coordination Chains

Xin Shi,[a] Guangshan Zhu,*[a] Qianrong Fang,[a] Gang Wu,[a] Ge Tian,[a] Renwei Wang,[a] Daliang Zhang,[a] Ming Xue,[a] and Shilun Qiu*[a]

Keywords: Supramolecular chemistry / Coordination modes / Fluorescence / Polymers

The novel supramolecular frameworks $[Cd(BDC)(phen)(H_2O)]_n$ (**2**) and $[Cd_2(HBTC)_2(phen)_2]_{2n}\cdot nCd(HBTC)(phen)_2$ (**3**) have been synthesized by reaction of the metal source $Cd(phen)_2(NO_3)_2$ (**1**) with benzene-1,4-dicarboxylic acid (H_2BDC) and benzene-1,3,5-tricarboxylic acid (H_3BTC), respectively in a mixed solution of $DMF/C_2H_5OH/H_2O$. The three-dimensional supramolecular structure of **2** is constructed through hydrogen-bond and aromatic π–π interactions between adjacent metal-organic polymeric coordination chains. Conversely, interestingly, the supramolecular architecture **3** is formed by extending 1-D metal-organic polymeric coordination chains into a 3-D framework by hydrogen-bond interactions between polymeric coordination chains and metal-organic coordination complexes instead of by interchain hydrogen-bond interactions. Additionally, these three compounds exhibit strong fluorescence at room temperature in the solid state.

(© Wiley-VCH Verlag GmbH & Co. KGaA, 69451 Weinheim, Germany, 2004)

Introduction

Metal-organic coordination frameworks with various intriguing topologies have been extensively studied for their versatile chemical and physical properties and potential applications in functional materials.[1−8] With the development of supramolecular chemistry, self-assembly based on molecules has become an effective approach to construct functional coordination frameworks. Hydrogen bonds provide an ideal synthetic example for the rational design of an organic crystalline framework.[9] Recently, attempts have been made to combine metal−ligand coordination and hydrogen bond interactions to self-assemble multidimensional metal-organic supramolecular frameworks.[10−12] Some 3-D supramolecular frameworks have been self-assembled from one-dimensional polymeric coordination chains, which are generated by transition metal ions and multidentate units, through hydrogen bonding and π−π interactions.[11,12]

Metal-organic coordination compounds as reactants provide not only transition metal ions but also segmental organic ligands in synthesis systems. Hence novel topologies and, particularly, chemical and physical properties may be obtained if metal-organic coordination compounds are used as the metal source to prepare supramolecular frameworks; however, we could not find any reported examples.

We report here the two novel fluorescent supramolecular frameworks $[Cd(BDC)(phen)(H_2O)]_n$ (**2**) and $[Cd_2(HBTC)_2(phen)_2]_{2n}\cdot nCd(HBTC)(phen)_2$ (**3**), which are self-assembled from metal-organic coordination compound $Cd(phen)_2(NO_3)_2$ (**1**) with benzene-1,4-dicarboxylic acid (H_2BDC) and benzene-1,3,5-tricarboxylic acid (H_3BTC), respectively.

[a] Key Laboratory of Inorganic Synthesis & Preparative Chemistry Jilin University,
Changchun 130023, P. R. China
Fax: (internat.) + 86-431-5671974
E-mail: sqiu@mail.jlu.edu.cn

Results and Discussion

Description of Crystal Structure

Cd(phen)$_2$(NO$_3$)$_2$ (1)

In the asymmetric unit of coordination compound **1** (Figure 1) the seven-coordinate cadmium center is chelated by four nitrogen atoms (N1, N2; N3, N4) of two chelating

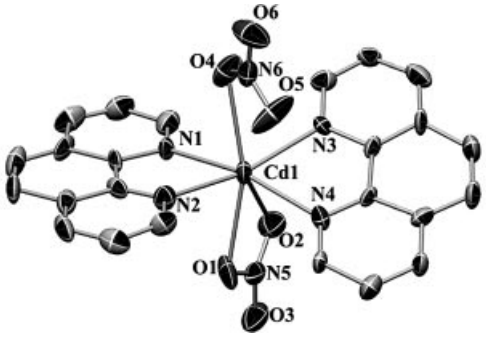

Figure 1. Asymmetry unit of **1**; thermal ellipsoids are drawn at the 50% probability level; all hydrogen atoms are omitted for clarity

 DOI: 10.1002/ejic.200300390 © 2004 Wiley-VCH Verlag GmbH & Co. KGaA, Weinheim

phen ligands and three oxygen atoms (O1, O2; O4) of two NO_3^- anions in different ways.

[Cd(BDC)(phen)(H$_2$O)]$_n$ (2)

A single-crystal X-ray analysis revealed that **2** is self-assembled from 1-D zig-zag polymeric coordination chains. In the asymmetric unit of **2**, there are one Cd atom, one BDC ligand, one phen ligand and one coordinated H_2O molecule. [Figure 2 (a)] The cadmium atom is seven-coordinate through coordination to five oxygen atoms (O1, O2; O3, O4; O5) of two chelating carboxylate groups of two BDC ligands, one water molecule and two nitrogen atoms (N1, N2) of one chelating phen ligand. The bond lengths of Cd1−O2 and Cd1−O3 are 2.567 and 2.401 Å, which are longer than those in other cadmium carboxylate coordination polymers.[13a] The distortion of the Cd−O bond may be due to the severe steric hindrance caused by the bulky phen group.

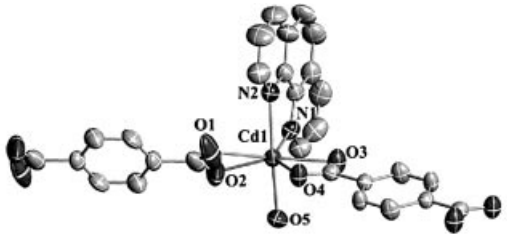

(a)

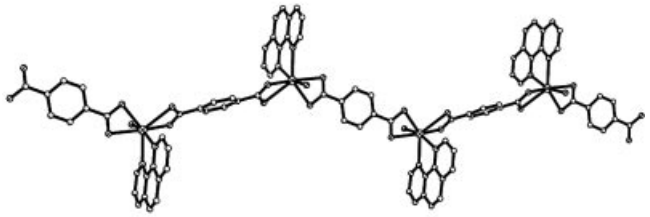

(b)

Figure 2. (a) Perspective view of the coordination environment of the cadmium atom in **2**; thermal ellipsoids are drawn at the 50% probability level; all hydrogen atoms are omitted for clarity; (b) 1-D zig-zag polymeric chain

Each BDC ligand bridges two cadmium atoms in bis(bidentate) fashion to form a 1-D infinite zig-zag chain [Figure 2(b)]. The coordinated H_2O molecules of the polymeric chains are well positioned to form interchain hydrogen bonds with the carboxylate oxygen atoms. The oxygen atoms of coordinated H_2O molecules and carboxylate oxygen atoms of BDC ligands from adjacent chains form strong hydrogen bonds (O2···O5 2.704 Å), which combine the 1-D zig-zag chains into 2-D undulating layers. Between neighboring 2-D undulating layers, C atoms with hydrogen atoms of phen ligands and carboxylate oxygen atoms of BDC ligands from neighboring layers form interlayer C−H···O hydrogen bonds (C9−H9···O4). The C9···O4 in C9−H9···O4 hydrogen bond is 3.219 Å long and the C9−H9···O4 angle is 147.20°, which are acceptable according to recent studies.[12b,14] There are also aromatic π−π stacking interactions between neighboring undulating layers. The plane−plane distance between adjacent two phen ligands of two neighboring layers is 3.517 Å, which is reasonable.[12b,15] All lateral phen ligands from neighboring undulating layers are intercalated in a zipper-like manner, which is similar to some previous examples.[12b,12c] Thus, the C−H···O hydrogen bonds along with aromatic π−π interactions further extend the 2-D undulating layers into a 3-D supramolecular framework (Figure 3).

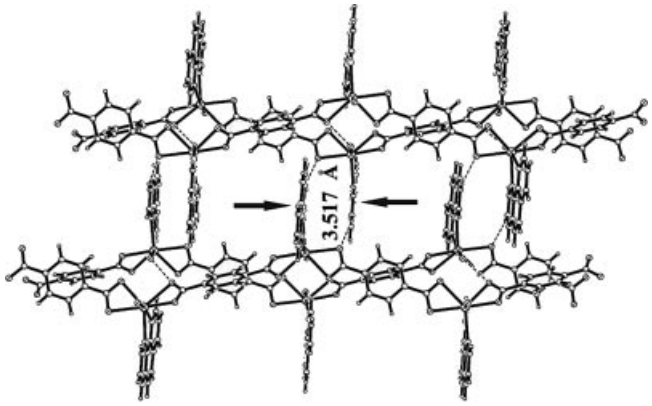

Figure 3. 3-D supramolecular framework along the [010] direction; neighboring undulating 2-D layers are intercalated in a zipper-like manner through C−H···O hydrogen bonds and π−π interactions

[Cd$_2$(HBTC)$_2$(phen)$_2$]$_{2n}$·nCd(HBTC)(phen)$_2$ (3)

X-ray crystallography reveals that **3** consists of 1-D polymeric coordination chains $[Cd_2(HBTC)_2(phen)_2]_n$ and metal-organic coordination complexes nCd(HBTC)(phen)$_2$. There are three six-coordinate cadmium centers in each asymmetric unit of **3**. Cd1 adopts a distorted octahedral geometry by coordinating to four nitrogen atoms (N1, N2; N3, N4) of two chelating phen ligands and two oxygen atoms (O14; O17) of two monodentate carboxylate groups from two H_3BTC ligands.

Two carboxylate groups from each of two crystallographically equivalent H_3BTC ligands bridge two cadmium atoms (Cd1 and Cd1A) to form a metal-organic coordination complex but the third carboxy group is uncoordinated. From the difference in bond lengths between C57−O15 [1.209(9) Å] and C57−O16 [1.326(9) Å] in the uncoordinated carboxy group, C57−O15 can be assigned to a double bond and C57−O16 to a single bond, and the hydrogen atom H16 should be linked to O16 [Figure 4 (a)].

Cd2 also adopts a distorted octahedral geometry by coordinating to four oxygen atoms (O1, O2; O5, O8) of one chelating carboxylate group of one H_3BTC ligand, two bis(monodentate) carboxylate groups of two different H_3BTC ligands and two nitrogen atoms (N5, N6) of one chelating phen ligand. The coordination environment of Cd3 is same

 © 2004 Wiley-VCH Verlag GmbH & Co. KGaA, Weinheim

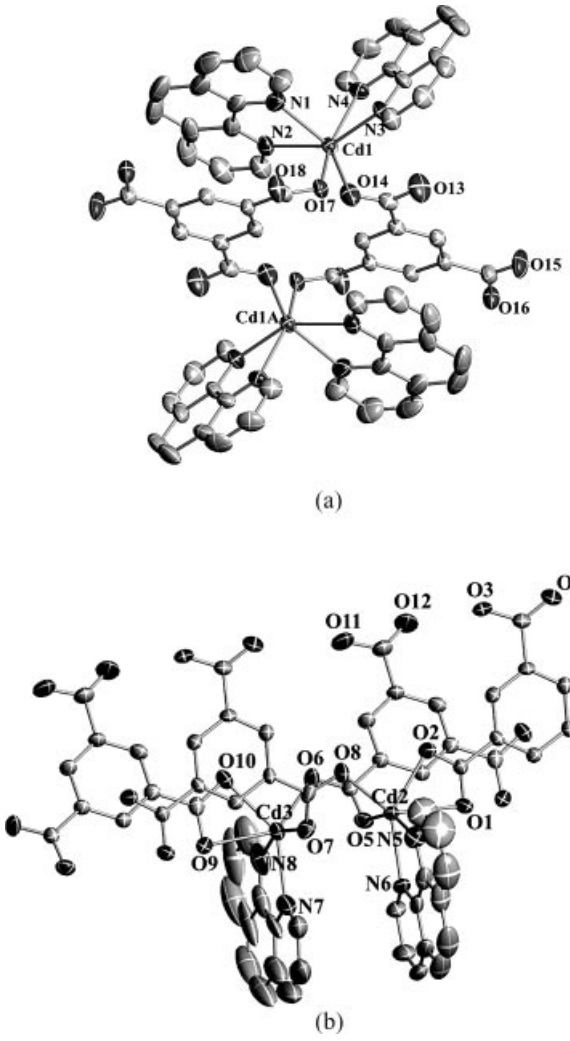

Figure 4. Perspective view of (a) the coordination environment of Cd1 in **3** and (b) the coordination environment of Cd2 and Cd3 in **3**; thermal ellipsoids are drawn at the 50% probability level; all hydrogen atoms are omitted for clarity

as that of Cd2 [Figure 4 (b)]. The bond lengths and angles of Cd−O are similar to those of cadmium trimesate polymers.[13b]

The coordinated H_3BTC ligands have two unchelated carboxy groups. The C−O bonds [C5−O3 1.298(9) Å, C40−O11 1.303(10) Å] are much longer than C=O [C5−O4 1.203(9) Å, C40−O12 1.195(10) Å] in the carboxy groups, so C5−O4 and C40−O12 can be assigned as double bonds and C5−O3 and C40−O11 as single bonds, with H3 and H11 linked to O3 and O11. The IR spectrum of **3** exhibits a broad band at ca. 3200 cm^{-1}, which is typical of the O−H vibration of a carboxy group. This shows that deprotonation of the H_3BTC ligands is incomplete, which is in good agreement with the uncoordinated carboxy groups in the structure of **3**.

Incompletely deprotonated H_3BTC ligands using the carboxylate functionality link Cd2 and Cd3 to form 1-D infinite polymeric chains $[Cd_2(HBTC)_2(phen)_2]_n$. Two adjacent 1-D chains are intercalated in a zipper-like manner[12b,12c] to form a double polymeric chain $[Cd_2(HBTC)_2(phen)_2]_{2n}$

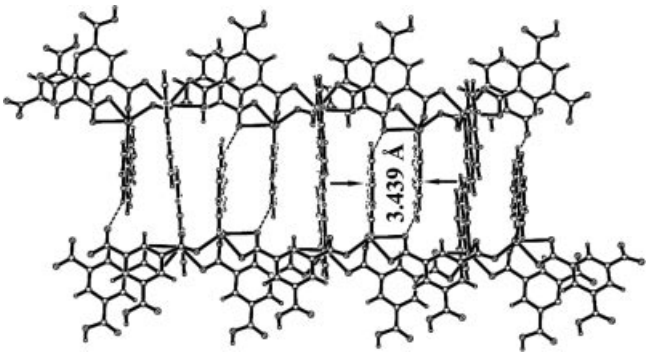

Figure 5. Double chain formed by intercalating two adjacent 1-D chains in a zipper-like manner through hydrogen bonds and π−π interactions

through C−H···O hydrogen bonds (C17···O1 2.217 Å, C17−H17···O1 154.77°)[14] and aromatic π−π stacking interactions (plane−plane distance 3.439 Å)[15] (Figure 5).

Each double polymeric chain is surrounded by metal-organic coordination complexes (Figure 6). Uncoordinated

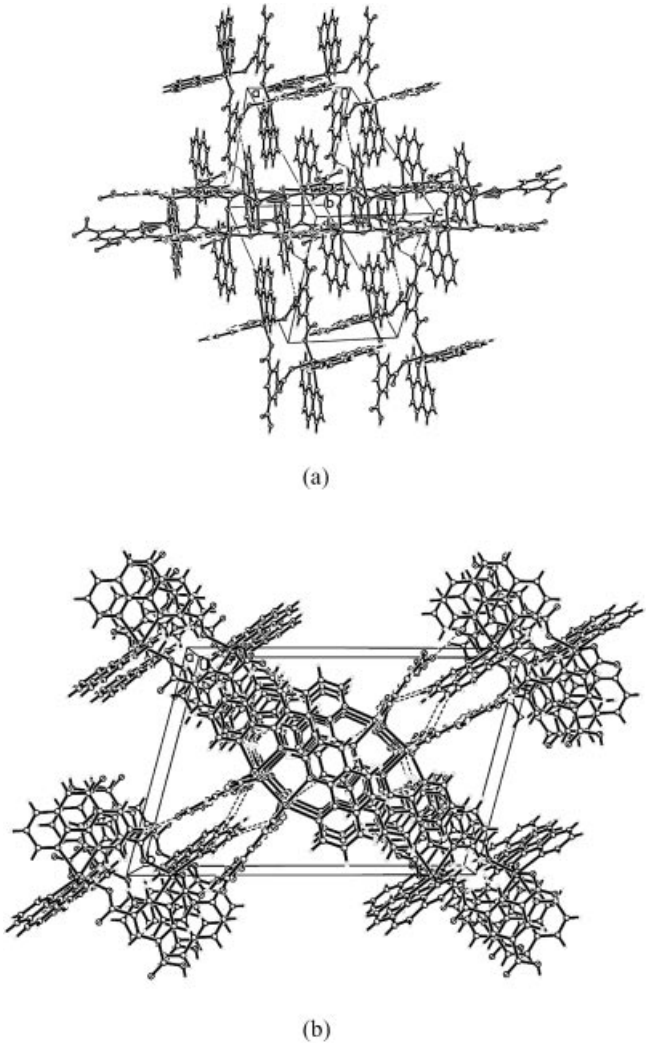

Figure 6. Perspective view of hydrogen bonds between 1-D double polymeric chains and metal-organic coordination complexes from different directions

 © 2004 Wiley-VCH Verlag GmbH & Co. KGaA, Weinheim

carboxy oxygen atoms (O3−H3 and O11−H11) of H_3BTC ligands from the double polymeric chains point outward to form hydrogen bonds (O3−H3···O18, O11−H11···O13) with the carboxylate oxygen atoms (O18 and O13) from surrounding metal-organic coordination complexes. At the same time, uncoordinated carboxy oxygen atoms (O16−H16) from the metal-organic coordination complexes are well positioned to form hydrogen bonds (O16−H16···O9) with carboxylate oxygen atoms (O9) from the double polymeric chains. The O···O distances and O−H···O angles are listed in Table 1.

Table 1. O−O distances [Å] and O−H···O angles [°] of O···O hydrogen bonds in **3** (symmetry transformations used to generate equivalent atoms: #1: $x - 1, y, z$; #2: $-x + 1, -y + 1, -z$)

D−H···A	*d*(D−H)	*d*(H···A)	*d*(D···A)	<(DHA)
O(3)−H(3)···O(18)	0.82	1.73	2.532(7)	166.6
O(11)−H(11)···O(13)#1	0.82	1.77	2.551(8)	158.9
O(16)−H(16)···O(9)#2	0.82	1.82	2.617(7)	163.4

In addition to O···O hydrogen bonds, C−H···O hydrogen bonds exist between double polymeric chains and metal-organic coordination complexes. Double polymeric chains and their surrounding metal-organic coordination complexes intercalate so as to form hydrogen bonds between them. C atoms with hydrogen atoms (C10−H10 and C16−H16a) of a phen ligand from double polymeric chains form C−H···O hydrogen bonds (C10−H10···O18 and C16−H16a···O16) with carboxylate oxygen atoms (O18 and O16) from coordination complexes. Simultaneously, C atoms with hydrogen atoms (C42−H42, C49−H49 and C72−H72) of a phen ligands from coordination complexes also form C−H···O hydrogen bonds (C42−H42···O2, C49−H49···O10 and C72−H72···O12) with carboxylate oxygen atoms (O2, O10 and O12) from double polymeric chains. The C···O distances (2.438−2.546 Å) of C−H···O hydrogen bonds (C10−H10···O18, C16−H16a···O16, C42−H42···O2, C49−H49···O10, C72−H72···O12) and the C−H···O angles (148.22−159.34°) are both within acceptable ranges.[14] Thus, two kinds of complementary hydrogen bonds form multi-linked hydrogen-bond interactions between double polymeric chains and metal-organic coordination complexes, which ultimately extend one-dimensional double polymeric chains into a three-dimensional supramolecular framework along [011] and [0−11] (Figure 7).

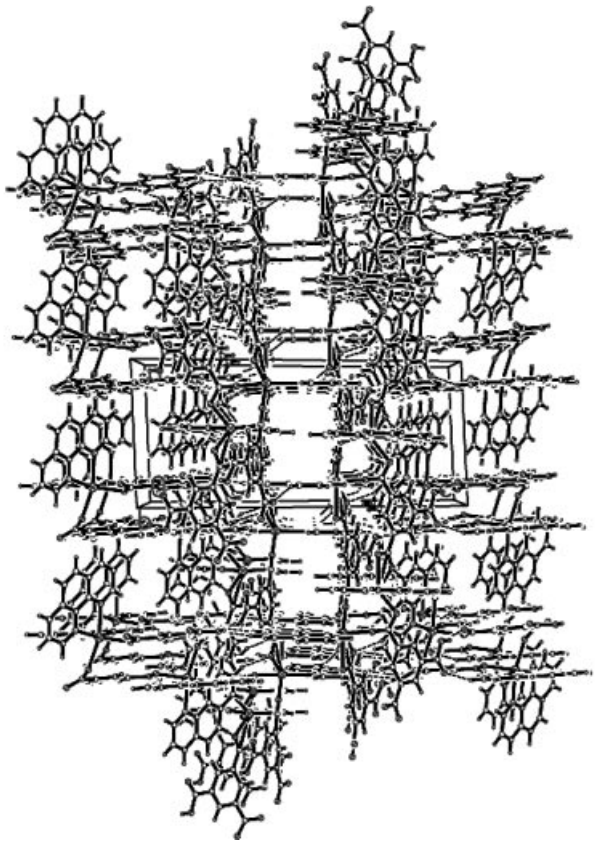

Figure 7. 3-D supramolecular architecture of **3** along [010] direction

Fluorescent Properties

Solid-state **1**, **2** and **3** exhibit strong fluorescence at room temperature. The free phen·H_2O also fluoresces in the solid state. The emission bands for free phen·H_2O are at 365 and 388 nm ($\lambda_{exc.}$ = 310 nm), which may be attributed to the $\pi^* \rightarrow \pi$ transition [Figure 8 (a)]. Of the emission bands for **1** at 366, 389 and 410 nm ($\lambda_{exc.}$ = 384 nm) [Figure 8 (b)] the first two are obviously due to intraligand charge transfer of coordinated phen ligands, similarly to the emission of free phen·H_2O. The band at 410 nm for **1** is neither LMCT (ligand-to-metal charge transfer) nor MLCT (metal-to-ligand charge transfer) in nature, and tentatively can be assigned to the intraligand fluorescent emission of coordinated phen ligands due to the planar configuration of excimeric phen molecules maintained by the cadmium ion.[16] The emission bands for **2**, at 367, 385 and 404 nm ($\lambda_{exc.}$ = 332 nm), can be assigned like those of **1** [Figure 8 (c)].[16] It is reported that free H_2BDC and free H_3BTC show fluorescence emission in the solid state. Their emission bands are mainly located at about 390 nm, with a shoulder at 370 nm for free H_3BTC (H_2BDC: $\lambda_{exc.}$ = 350 nm; H_3BTC: $\lambda_{exc.}$ = 334 nm) and are attributed to a $\pi^* \rightarrow$ n transition.[17] For **2**, the H_2BDC ligands show almost no contribution to the fluorescent emission, due to very weak fluorescent emission, resulting from a $\pi^* \rightarrow$ n transition of H_2BDC, compared with the $\pi^* \rightarrow \pi$ transition of phen and/or fluorescence quenching of carboxy groups of H_2BDC (which are strong electron-withdrawing groups). Interestingly, **3** has a single broad emission band at 380 nm ($\lambda_{exc.}$ = 330 nm), which is obviously different from the multi-bands of **2**, and may tentatively be assigned to intraligand charge transfer of coordinated phen ligands [Figure 8 (d)]. Here H_3BTC ligands also show almost no contribution to the fluorescent emission of **3**, as with **2**. The large difference between the emission bands of **2** and **3**, although they are both mixed-ligand systems, may be due to the uniquely complicated structure of **3**, with attachment of the dicadmium complex to the 1-D polymeric chain through hydrogen bonds. This complicated structure

 © 2004 Wiley-VCH Verlag GmbH & Co. KGaA, Weinheim

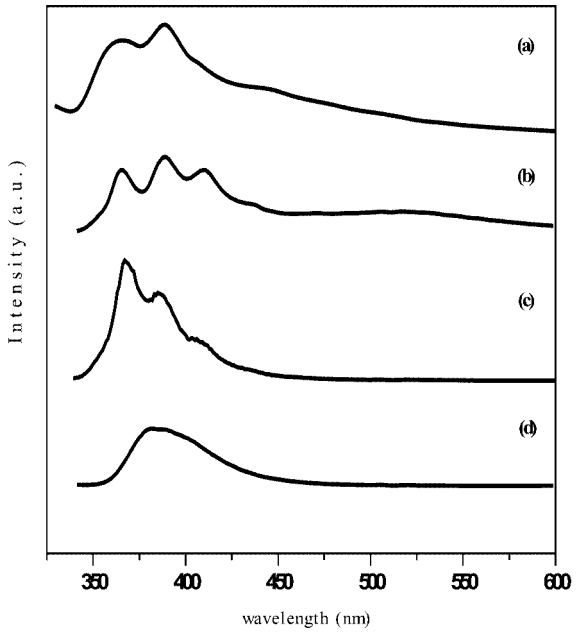

Figure 8. Solid-state fluorescent emission spectra of (a) free phen·H_2O, (b) $Cd(phen)_2(NO_3)_2$, (c) $[Cd(BDC)(phen)(H_2O)]_n$ and (d) $[Cd_2(HBTC)_2(phen)_2]_{2n}$·$n$Cd(HBTC)$(phen)_2$ at room temperature

causes multiple charge-transfer with close transition energies, which might ultimately result in a single broad emission band.

Conclusions

Two 3-D supramolecular frameworks have been synthesized by using a metal-organic coordination compound as the metal source under mild conditions. Notably for **3**, it is the hydrogen-bonding interactions between polymeric coordination chains and coordination complexes that extend the 1-D double chains into a 3-D supramolecular framework – in contrast to previously reported supramolecular structures constructed through interchain hydrogen bonds. Moreover, these compounds exhibit strong fluorescence at room temperature in the solid state.

Experimental Section

General Remarks: Elemental analyes were performed with a Perkin–Elmer 2400 element analyzer, and inductively couple plasma (ICP) analysis with a Perkin–Elmer Optima 3300DV ICP spectrometer. IR spectra were obtained with a Nicolet Impact 410 FTIR spectrometer. Fluorescence spectra were obtained with a LS 55 fluorescence/phosphorescence spectrophotometer at room temperature.

Preparation

Metal Source $Cd(phen)_2(NO_3)_2$ (1): Synthesis under hydrothermal conditions. The reaction of $Cd(NO_3)_2$·$6H_2O$ (0.308 g, 1.0 mmol) with 1,10-phenanthroline monohydrate (0.257 g, 1.3 mmol) in a solution of NaOH (10^{-3} mol/L, 10 mL) at 160 °C for 6 d produced large yellow block crystals in 86% yield (0.513 g). $C_{24}H_{16}CdN_6O_6$ (596.83): calcd. C 48.30, H 2.680, Cd 18.83, N 14.08; found C 48.36, H 2.675, Cd 18.73, N 14.12. IR (KBr): $\tilde{\nu}$ = 3066, 1600, 1588, 1495, 980, 880 cm^{-1}.

Compound 2: Preparation under mild conditions by allowing $Cd(phen)_2(NO_3)_2$ (0.158 g, 0.25 mmol) and H_2BDC (0.041 g, 0.25 mmol) to react in a solution of *N*,*N*′-dimethylformamide (DMF) (10.0 mL), absolute ethanol (2.0 mL), and distilled water (3.0 mL) at 55 °C for 4 d to produce large yellow block crystals in 59% yield (0.070 g). $C_{20}H_{14}CdN_2O_5$ (474.73): calcd. C 50.60, H 2.949, Cd 23.67, N 5.900; found C 50.52, H 2.941, Cd 23.72, N 5.884. IR (KBr): $\tilde{\nu}$ = 3325, 3079, 1625, 1606, 1541, 1418, 1012, 780 cm^{-1}.

Compound 3: Synthesis by allowing $Cd(phen)_2(NO_3)_2$ (0.158 g, 0.25 mmol) and H_3BTC (0.053 g, 0.25 mmol) to react in a solution of *N*,*N*′-dimethylformamide (DMF) (10.0 mL), absolute ethanol (2.0 mL), and distilled water (3.0 mL) at 55 °C for 6 d. The result-

Table 2. Crystal data and structure refinement for complexes **1**–**3**

	1	**2**	**3**
Empirical formula	$C_{24}H_{16}CdN_6O_6$	$C_{20}H_{14}CdN_2O_5$	$C_{75}H_{44}Cd_3N_8O_{18}$
Formula mass	596.83	474.73	1682.38
Temperature [K]	293(2)	293(2)	293(2)
Crystal system	monoclinic	monoclinic	triclinic
Space group	Cc	*C*2/*c*	$P\bar{1}$
a [Å]	11.532(2)	25.502(9)	10.192(2)
b [Å]	15.326(3)	9.866(2)	16.074(3)
c [Å]	13.330(3)	21.239(5)	23.747(5)
α [°]	90	90	104.84(3)
β [°]	104.36(3)	125.75(2)	92.26(3)
γ [°]	90	90	90.80(3)
V [Å^3]	2282.4(8)	4337(2)	3756.6(13)
Z	2	4	2
$\rho_{calcd.}$ [gcm^{-3}]	0.8680.7271.487		
μ [mm^{-1}]	0.506	0.518	0.914
Reflections collected	2617	3034	15085
Independent reflections (R_{int})	2482 (0.019)	2698 (0.041)	11446 (0.050)
R_1,wR_2 [$I > 2\sigma(I)$]	0.0196, 0.0524	0.0617, 0.1862	0.0607, 0.2104

 © 2004 Wiley-VCH Verlag GmbH & Co. KGaA, Weinheim

ant colorless block crystals were filtered off, washed with absolute ethanol and dried at room temperature. The yield was about 46% (0.064 g). $C_{75}H_{44}Cd_3N_8O_{18}$ (1682.38): calcd. C 53.54, H 2.615, Cd 20.04, N 6.660; found C 53.58, H 2.620, Cd 20.07, N 6.652. IR (KBr): $\tilde{\nu}$ = 3200, 3058, 1598, 1568, 1409, 998, 860, 676 cm^{-1}.

Single-Crystal Structure Determination: Crystallographic data for **1** and **3** were collected at 293(2) K with a Rigaku R-AXIS RAPIC IP diffractometer with Mo-K_α (λ = 0.71073 Å). Crystallographic data for **2** were collected at 293(2) K with a Bruker-AXS Smart CCD diffractometer with Mo-K_α radiation (λ = 0.71073 Å). The structures were solved by direct methods[18] and refined by full-matrix least-squares method against F^2 (SHELXL-97).[19] All non-hydrogen atoms were refined anisotropically. Hydrogen atoms of organic ligands were located geometrically. The crystallographic data for **1**−**3** are listed in Table 2, and selected bond lengths and angles for **2** and **3** are presented in Tables 3 and 4, respectively. CCDC-216289 for $[Cd(phen)_2(NO_3)_2]$, -216290 for [Cd(BDC)(phen)(H_2O)] and -216291 for $[Cd_2(HBTC)_2(phen)_2{\cdot}Cd(HBTC)(phen)_2]$ contain the supplementary crystallographic data for this paper. These data can be obtained free of charge at www.ccdc.cam.ac.uk/conts/retrieving.html [or from the Cambridge Crystallographic Data Centre, 12 Union Road, Cambridge CB2 1EZ, UK; Fax: (internat.) + 44-1223-336-033; E-mail: deposit@ccdc.cam.ac.uk].

Table 3. Selected bond lengths [Å] and angles [°] for [Cd(BDC)(phen)(H_2O)]$_n$

Cd(1)−O(1)	2.242(7)	Cd(1)−O(3)	2.401(5)
Cd(1)−N(2)	2.342(5)	Cd(1)−O(5)	2.408(5)
Cd(1)−O(4)	2.348(5)	Cd(1)−O(2)	2.567(8)
Cd(1)−N(1)	2.363(5)		
O(1)−Cd(1)−N(2)	93.6(3)	N(2)−Cd(1)−O(5)	91.02(19)
O(1)−Cd(1)−O(4)	161.3(2)	O(4)−Cd(1)−O(5)	87.53(17)
N(2)−Cd(1)−O(4)	86.26(18)	N(1)−Cd(1)−O(5)	161.41(17)
O(1)−Cd(1)−N(1)	103.3(2)	O(3)−Cd(1)−O(5)	95.38(18)
N(2)−Cd(1)−N(1)	70.68(18)	O(1)−Cd(1)−O(2)	52.5(3)
O(4)−Cd(1)−N(1)	94.32(18)	N(2)−Cd(1)−O(2)	128.8(2)
O(1)−Cd(1)−O(3)	126.1(3)	O(4)−Cd(1)−O(2)	138.6(2)
N(2)−Cd(1)−O(3)	140.09(17)	N(1)−Cd(1)−O(2)	80.8(2)
O(4)−Cd(1)−O(3)	54.86(17)	O(3)−Cd(1)−O(2)	85.54(19)
N(1)−Cd(1)−O(3)	100.81(18)	O(5)−Cd(1)−O(2)	109.8(2)
O(1)−Cd(1)−O(5)	73.8(2)		

Table 4. Selected bond lengths [Å] and angles [°] for $[Cd_2(HBTC)_2(phen)_2]_{2n}{\cdot}nCd(HBTC)(phen)_2$

Cd(1)−O(14)	2.227(5)	Cd(2)−O(5)	2.328(5)
Cd(1)−O(17)	2.288(5)	Cd(2)−N(5)	2.347(7)
Cd(1)−N(3)	2.343(5)	Cd(2)−O(1)	2.459(5)
Cd(1)−N(4)	2.359(6)	Cd(3)−O(6)	2.264(5)
Cd(1)−N(1)	2.424(6)	Cd(3)−O(7)	2.318(5)
Cd(1)−N(2)	2.407(6)	Cd(3)−N(8)	2.337(8)
Cd(2)−O(2)	2.299(5)	Cd(3)−N(7)	2.346(8)
Cd(2)−O(8)	2.294(5)	Cd(3)−O(10)	2.356(6)
Cd(2)−N(6)	2.329(5)	Cd(3)−O(9)	2.433(5)
O(14)−Cd(1)−O(17)	99.1(2)	N(6)−Cd(2)−N(5)	71.2(2)
O(14)−Cd(1)−N(3)	119.1(2)	O(5)−Cd(2)−N(5)	155.6(2)
O(17)−Cd(1)−N(3)	86.04(19)	O(2)−Cd(2)−O(1)	54.24(17)
O(14)−Cd(1)−N(4)	92.0(2)	O(8)−Cd(2)−O(1)	138.50(18)
O(17)−Cd(1)−N(4)	157.12(19)	N(6)−Cd(2)−O(1)	86.67(19)
N(3)−Cd(1)−N(4)	71.1(2)	O(5)−Cd(2)−O(1)	92.3(2)
O(14)−Cd(1)−N(1)	151.4(2)	N(5)−Cd(2)−O(1)	91.6(2)
O(17)−Cd(1)−N(1)	85.0(2)	O(6)−Cd(3)−O(7)	102.9(2)
N(3)−Cd(1)−N(1)	89.3(2)	O(6)−Cd(3)−N(8)	87.3(3)
N(4)−Cd(1)−N(1)	94.8(2)	O(7)−Cd(3)−N(8)	157.9(3)
O(14)−Cd(1)−N(2)	83.2(2)	O(6)−Cd(3)−N(7)	132.7(2)
O(17)−Cd(1)−N(2)	109.30(18)	O(7)−Cd(3)−N(7)	87.9(3)
N(3)−Cd(1)−N(2)	151.3(2)	N(8)−Cd(3)−N(7)	71.1(3)
N(4)−Cd(1)−N(2)	91.8(2)	O(6)−Cd(3)−O(10)	84.57(19)
N(1)−Cd(1)−N(2)	68.9(2)	O(7)−Cd(3)−O(10)	96.28(19)
O(2)−Cd(2)−O(8)	85.31(18)	N(8)−Cd(3)−O(10)	104.3(3)
O(2)−Cd(2)−N(6)	140.71(19)	N(7)−Cd(3)−O(10)	140.6(2)
O(8)−Cd(2)−N(6)	131.9(2)	O(6)−Cd(3)−O(9)	136.61(18)
O(2)−Cd(2)−O(5)	98.95(19)	O(7)−Cd(3)−O(9)	96.73(18)
O(8)−Cd(2)−O(5)	104.1(2)	N(8)−Cd(3)−O(9)	88.7(2)
N(6)−Cd(2)−O(5)	85.0(2)	N(7)−Cd(3)−O(9)	85.8(2)
O(2)−Cd(2)−N(5)	102.8(2)	O(10)−Cd(3)−O(9)	54.81(16)
O(8)−Cd(2)−N(5)	88.5(2)		

Acknowledgments

We are grateful for the financial support of both the State Basic Research Project (G2000077507) and the National Nature Science Foundation of China (Grant no. 29873017 and 20101004).

[1] [1a] O. M. Yaghi, H. L. Li, C. Davis, D. Richardson, T. L. Groy, *Acc. Chem. Res.* **1998**, *31*, 474−484. [1b] M. Eddaoudi, D. B. Moler, H. L. Li, B. L. Chen, T. Reineke, M. O'Keeffe, O. M. Yaghi, *Acc. Chem. Res.* **2001**, *34*, 319−330.

[2] [2a] R. Kitaura, S. Kitagawa, Y. Kubota, T. C. Kobayashi, K. Kindo, Y. Mita, *Science* **2002**, *298*, 2358−2361. [2b] J. S. Seo, D. Whang, H. Lee, S. I. Jun, J. Oh, Y. J. Jeon, K. Kim, *Nature* **2000**, *404*, 982−986.

[3] [3a] H. L. Li, A. Laine, M. O'Keeffe, O. M. Yaghi, *Science* **1999**, *283*, 1145−1147. [3b] S. S.-Y. Chui, S. M.-F. Lo, J. P. H. Charmant, A. G. Orpen, I. D. Williams, *Science* **1999**, *283*, 1148−1150. [3c] O. R. Evans, R. Xiong, Z. Wang, G. K. Wong, W. Lin, *Angew. Chem. Int. Ed.* **1999**, *38*, 536−538. [3d] M. Eddaoudi, J. Kim, M. Rosi, D. Vodak, J. Wachter, M. O'Keeffe, O. M. Yaghi, *Science* **2002**, *295*, 469−472.

[4] [4a] D. T. Vodak, M. E. Braun, J. Kim, M. Eddaoudi, O. M. Yaghi, *Chem. Commun.* **2001**, 2534−2535. [4b] M. Eddaoudi, J. Kim, M. O'Keeffe, O. M. Yaghi, *J. Am. Chem. Soc.* **2002**, *124*, 376−377. [4c] C. Z-J. Lin, S. S-Y. Chui, S. M-F. Lo, F. l-Y. Shek, M. Wu, K. Suwinska, J. Lipkowski, I. D. Williams, *Chem. Commun.* **2002**, 1642−1643. [4d] C. Livage, N. Guillou, J. Marrot, G. Ferey, *Chem. Mater.* **2001**, *13*, 4387−4392. [4e] C. Serre, G. Ferey, *J. Mater. Chem.* **2002**, *12*, 3053−3057.

[5] [5a] D. P. Cheng, M. A. Khan, R. P. Houser, *Inorg. Chem.* **2001**, *40*, 6858−6859. [5b] X. M. Zhang, M. L. Tong, X. M. Chen, *Angew. Chem. Int. Ed.* **2002**, *41*, 1029−1031. [5c] G. F. Liu, B. H. Ye, Y. H. Ling, X. M. Chen, *Chem. Commun.* **2002**, 1442−1443.

[6] [6a] S. O. H. Gutschke, D. J. Price, A. K. Powell, P. T. Wood, *Angew. Chem. Int. Ed.* **2001**, *40*, 1920−1923. [6b] S. A. Bourne, J. J. Lu, A. Mondal, B. Moulton, M. J. Zaworotko, *Angew. Chem. Int. Ed.* **2001**, *40*, 2111−2113.

[7] [7a] P. M. Forster, A. K. Cheetham, *Angew. Chem. Int. Ed.* **2002**, *41*, 457−459. [7b] B. Moulton, J. J. Lu, R. Hajndl, S. Hariharan, M. J. Zaworotko, *Angew. Chem. Int. Ed.* **2002**, *41*, 2821−2824.

[8] [8a] S. R. Seidel, P. J. Stang, *Acc. Chem. Res.* **2002**, *35*, 972. [8b] S. R. Batten, R. Robson, *Angew. Chem. Int. Ed.* **1998**, *37*, 1460−1494.

[9] [9a] K. T. Holman, A. M. Pivovar, M. D. Ward, *Science* **2001**, *294*, 1907−1911. [9b] O. Félix, M. W. Hosseini, A. De Cian, J. Fischer, *Chem. Commun.* **2000**, 281−282. [9c] R. Custelcean, M. D. Ward, *Angew. Chem. Int. Ed.* **2002**, *41*, 1724−1728.

[10] [10a] J. C. MacDonald, P. C. Dorrestein, M. M. Pilley, M. M. Foote, J. L. Lundburg, R. W. Henning, A. J. Shultz, J. L. Manson, *J. Am. Chem. Soc.* **2000**, *122*, 11692−11702. [10b] J. C. Nov-

eron, M. S. Lah, R. E. Del Sesto, A. M. Miller, J. S. Miller, P. J. Stang, *J. Am. Chem. Soc.* **2002**, *124*, 6613−6625.

[11] [11a] Yong Cui, Helen L. Ngo, Peter S. White, Wenbin Lin, *Inorg. Chem.* **2003**, *42*, 652−654. [11b] Jun-Hua Luo, Mao-Chun Hong, Rui-Hu Wang, Rong Cao, Qian Shi, Jia-Bao Weng, *Eur. J. Inorg. Chem.* **2003**, 1778−1784.

[12] [12a] Yong Cui, Helen L. Ngo, Peter S. White, Wen-bin Lin, *Chem. Commun.* **2003**, 994−995. [12b] Xiao-Ming Zhang, Ming-Liang Tong, Meng-Linan Gong, Xiao-Ming Chen, *Eur. J. Inorg. Chem.* **2003**, 138−142. [12c] S.-L. Zheng, M.-L. Tong, R.-W. Fu, X.-M. Chen, S. W. Ng, *Inorg. Chem.* **2001**, *40*, 3562−3569.

[13] [13a] Z.-F. Chen, P. Zhang, R.-G. Xiong, D.-J. Liu, X.-Z. You, *Inorg. Chem. Commun.* **2002**, 35−37. [13b] J.-C Dai, X-T. Wu, Z.-Y. Fu, C.-P. Cui, S.-M. Hu, W.-X. Du, L.-M. Wu, H.-H. Zhang, R.-Q. Sun, *Inorg. Chem.* **2002**, *41*, 1391−1396.

[14] C. R. Desiraju, *Acc. Chem. Res.* **1996**, *29*, 441−449.

[15] C. Janiak, *J. Chem. Soc., Dalton Trans.* **2000**, 3885−3896.

[16] [16a] J. Zhang, Y.-R. Xie, Q. Ye, R.-G. Xiong, Z.-L. Xue, X.-Z. You, *Eur. J. Inorg. Chem.* **2003**, 2572−2577. [16b] X.-M. Ouyang, D.-J. Liu, T. Okamura, H.-W. Bu, W.-Y. Sun, W.-X. Tang, N. Ueyama, *Dalton Trans.* **2003**, 1836−1845. [16c] Y.-P. Tian, X.-J. Zhang, J.-Y. Wu, H.-K. Fun, M.-H. Jiang, Z.-Q. Xu, A. Usman, S. Chantrapromma, L. K. Thompson, *New. J. Chem.* **2002**, *26*, 1468−1473.

[17] [17a] W. Chen, J.-Y. Wang, C. Chen, Q. Yue, H. -M. Yuan, J.-S. Chen, S.-N. Wang, *Inorg. Chem.* **2002**, *42*, 944−946.

[18] G. M. Sheldrick, *SHELXS-97, Program for Crystal Structure Solution*, Göttingen University, Germany, **1997**.

[19] G. M. Sheldrick, *SHELXL-97, Program for Crystal Structure Refinement*, Göttingen University, Germany, **1997**.

Received June 23, 2003
Early View Article
Published Online October 31, 2003

 © 2004 Wiley-VCH Verlag GmbH & Co. KGaA, Weinheim

EurJIC
European Journal of Inorganic Chemistry

Issue 2/2004

Pages 193–430

Papers available ahead of print in Early View at www.interscience.wiley.com

Earliest available Table of Contents:
Automatically, free of charge by e-mail through
www.interscience.wiley.com/alerts

COVER PICTURE

The cover picture shows the structure of the cation $[ReO(cyclen\text{-}H)I]^+$. This complex and the analogous $[ReO(cyclen\text{-}H)Cl]^+$ are the first examples of d transition metal oxo complexes anchored by a monoanionic cyclen ligand. The deprotonation of cyclen can be accounted by the enhanced Lewis acidity of the d^2 rhenium center. Although the geometric contraints of *cis*-octahedral cyclen could impose the *cis*-ReO_2 unit, the resulting *cis*-dioxo complex, *cis*-$[ReO_2(cyclen)]^+$, is very reactive, being readily converted into $[ReO(cyclen\text{-}H)X]^+$. Details are discussed in the article by I. Santos et al. on p. 243 ff.

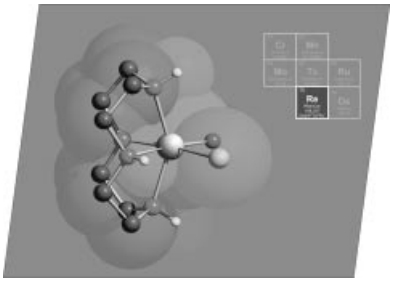

MICROREVIEW

Contents

207 **S. Shaik,* S. Cohen, S. P. de Visser, P. K. Sharma, D. Kumar, S. Kozuch, F. Ogliaro, D. Danovich**

The "Rebound Controversy": An Overview and Theoretical Modeling of the Rebound Step in C–H Hydroxylation by Cytochrome P450

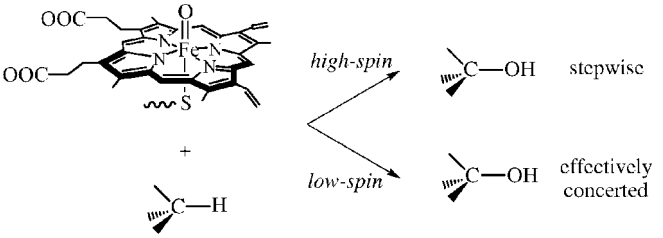

Two-state reactivity in C–H hydroxylation

Keywords: Alkanes / Cytochrome P450 / Density functional calculations / Enzyme catalysis / Free radicals / C–H hydroxylation

 © 2004 Wiley-VCH Verlag GmbH & Co. KGaA, Weinheim

SHORT COMMUNICATIONS

227 **J. M. Harrowfield, W. R. Richmond, B. W. Skelton, A. H. White***

Solid-State Models of Ion Solvation: Crystal Structures of Dimethyl Sulfoxide Solvates of Alkaline Earth Cations

Keywords: Alkaline earth metals / Dimethyl sulfoxide solvates / Solid state structures / Solvent effects

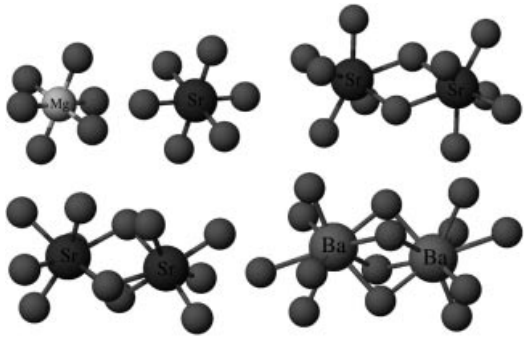

231 **M. L. Golden, S. P. Jeffery, M. L. Miller, J. H. Reibenspies, M. Y. Darensbourg***

The Construction of $(N_2S_2)Ni-Pd$ Clusters: A Slant-Chair, a Basket and a C_4-Paddlewheel Structure

Keywords: Metallothiolate ligands / Phosphane mimics / Nickel / Palladium / Cluster compounds

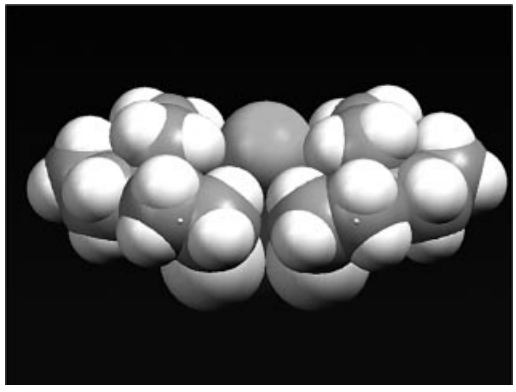

237 **L. Dai, S. Yu, Y. Shan,* M. He**

Novel Room Temperature Inorganic Ionic Liquids

Keywords: Inorganic ionic liquids / Ionic liquids / Polyoxometalates / Transition metals / Green chemistry

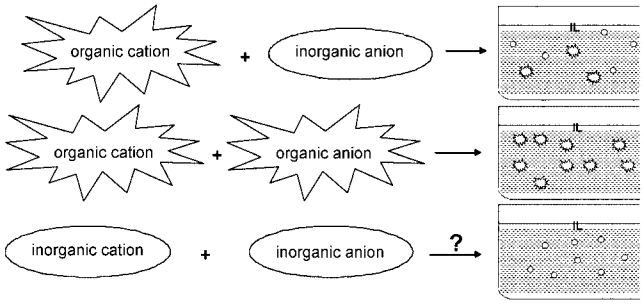

FULL PAPERS

243 **C. Xavier, A. Paulo, A. Domingos, I. Santos***

Synthesis and Structural Studies of Rhenium(V) Complexes Stabilized by a Monoanionic Cyclen Ligand

Keywords: Rhenium / Oxo ligands / Macrocycles / N ligands

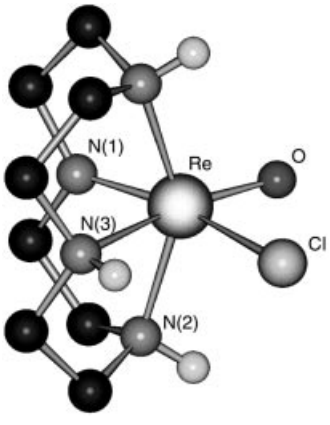

 © 2004 Wiley-VCH Verlag GmbH & Co. KGaA, Weinheim

250 **U. Ray, S. Jasimuddin, B. K. Ghosh, M. Monfort, J. Ribas,* G. Mostafa, T.-H. Lu, C. Sinha***

A New Alternating Ferro-Antiferromagnetic One-Dimensional Azido-Bridged (Arylazoimidazole)manganese(II), $[Mn(TaiEt)(N_3)_2]_n$ [TaiEt = 1-Ethyl-2-(*p*-tolylazo)imidazole], Exhibiting Bulk Weak Ferromagnetic Long-Range Ordering

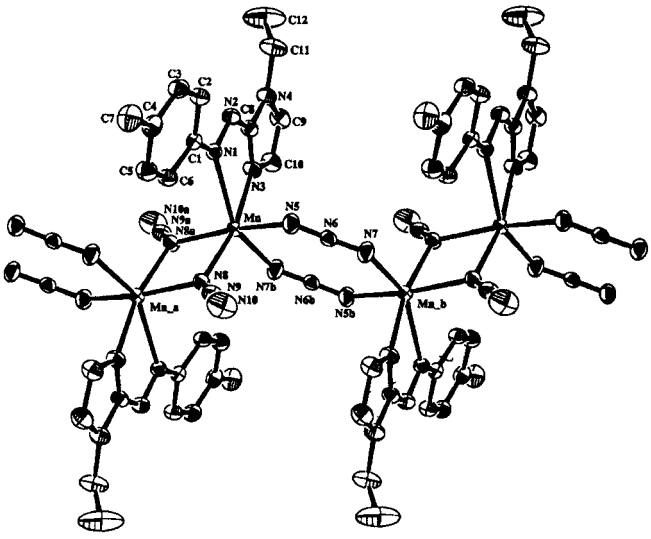

Keywords: Magnetic properties / Manganese / N ligands / Polymers

260 **A. Otero,* J. Fernández-Baeza, A. Antiñolo, J. Tejeda, A. Lara-Sánchez, L. Sánchez-Barba, A. M. Rodríguez**

New Complexes of Niobium(V) and Tantalum(V) with Monoanionic NNO Heteroscorpionate Ligands

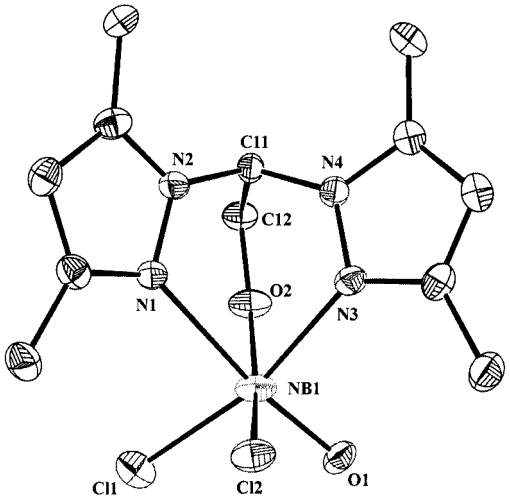

Keywords: Niobium / Tantalum / Tripodal ligands / Oxo ligands / Alkoxide ligands

267 **J. Guo, W.-K. Wong,* W.-Y. Wong**

Syntheses and Crystal Structures of Tetrakis(arylamidine)nickel(II) Chloride and Bis[2,4-dipyridyl-1,3,5-triazapentadienato]nickel(II)

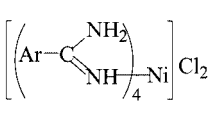

Ar = Ph, *p*-MeC_6H_4

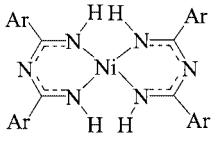

Ar = 3-pyridyl, 4-pyridyl

Keywords: Hydrogen bonds / Nickel / N ligands / Magnetic properties / Macrocyclic ligands

276 **I.-M. Mbomekalle, B. Keita, Y. W. Lu, L. Nadjo,* R. Contant, N. Belai, M. T. Pope**

Synthesis, Characterization and Electrochemistry of the Novel Dawson-Type Tungstophosphate $[H_4PW_{18}O_{62}]^{7-}$ and First Transition Metal Ions Derivatives

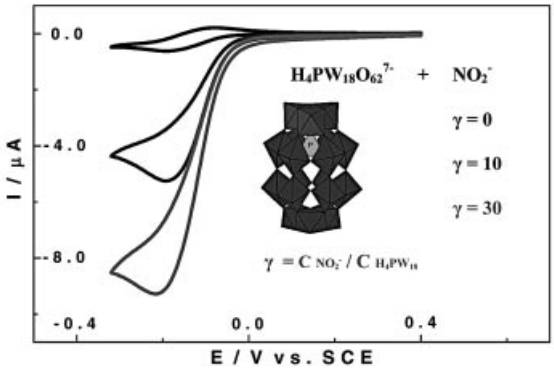

Keywords: Polyoxometalates / Tungsten / Heteropolyanions / Electrochemistry / Electrocatalysis

 © 2004 Wiley-VCH Verlag GmbH & Co. KGaA, Weinheim

286 **W. Liu, C.-H. Lee, H.-S. Chan, T. C. W. Mak, D. K. P. Ng***

Synthesis, Spectroscopic Properties, and Structure of [Tetrakis(2,4-dimethyl-3-pentyloxy)-phthalocyaninato]metal Complexes

Keywords: Macrocyclic compounds / Inclusion compounds / N ligands

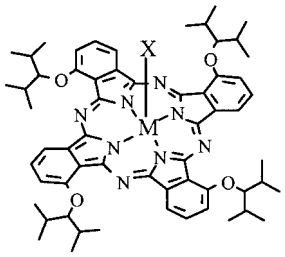

293 **M. Di Vaira, I. de los Rios, F. Mani, M. Peruzzini, P. Stoppioni***

η^1-P_{basal} Coordination of P_4X_3 (X = S, Se) Molecules toward 16e Ruthenium Fragments

Keywords: Ruthenium / Cyclopentadienyl ligands / Bidentate ligands / Density functional calculations

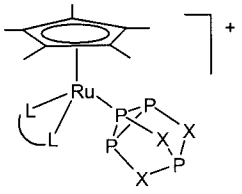

301 **V. Balland, M.-F. Charlot, F. Banse,* J.-J. Girerd,* T. A. Mattioli, E. Bill, J.-F. Bartoli, P. Battioni, D. Mansuy**

Spectroscopic Characterization of an Fe^{IV} Intermediate Generated by Reaction of XO^- (X = Cl, Br) with an Fe^{II} Complex Bearing a Pentadentate Non-Porphyrinic Ligand − Hydroxylation and Epoxidation Activity

Keywords: Iron / Oxo ligands / Bioinorganic chemistry / Epoxidation / Hydroxylation

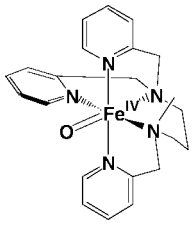

309 **A. Escuer, N. Sanz, F. A. Mautner, R. Vicente***

Phenylcyanamido Ligand Building Molecular, 1-D, and 2-D Systems − Syntheses, Crystal Structures and Magnetic Properties

Keywords: Manganese / Magnetic properties / Phenylcyanamido ligands / Bridging ligands

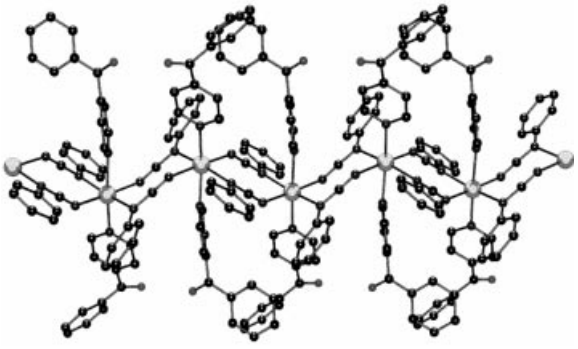

317 **R. Choukroun,* C. Lorber, L. Vendier**

Reactivity of $[Cp_2Ti(CO)_2]$ towards Nitrile and Water Adducts of $B(C_6F_5)_3$: Formation of $[Cp_2Ti(\eta^2\text{-}F_3CC_6H_4CN)\cdot B(C_6F_5)_3]$ and $[Cp_2Ti][HOB(C_6F_5)_3]$ with a Ti···F Interaction

Keywords: Titanium / Boranes / N ligands / Structure elucidation / Hydrolysis

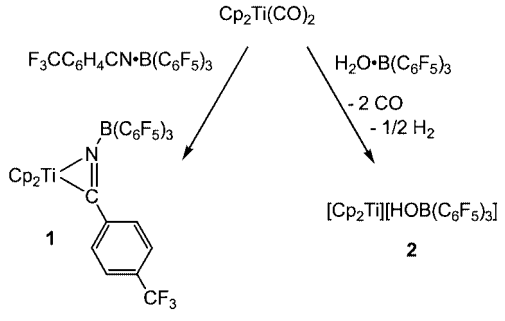

 © 2004 Wiley-VCH Verlag GmbH & Co. KGaA, Weinheim

322 **P. Noblía, E. J. Baran, L. Otero, P. Draper, H. Cerecetto, M. González, O. E. Piro, E. E. Castellano, T. Inohara, Y. Adachi, H. Sakurai, D. Gambino***

New Vanadium(V) Complexes with Salicylaldehyde Semicarbazone Derivatives: Synthesis, Characterization, and in vitro Insulin-Mimetic Activity − Crystal Structure of [$V^{V}O_2$(salicylaldehyde semicarbazone)]

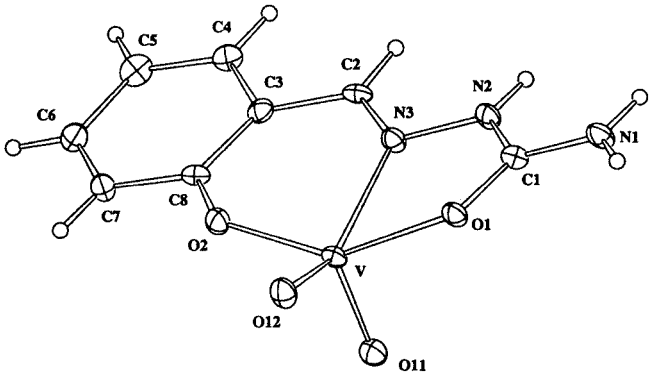

Keywords: Vanadium / Tridentate ligands / N,O,O ligands / Insulin-mimetic agents

329 **M. R. A. Al-Mandhary, P. J. Steel***

X-ray Crystallographic Study of Copper(II), Cobalt(II) and Silver(I) Complexes of Ligands Containing Two Oxine Subunits Linked by Xylylene Spacer Groups

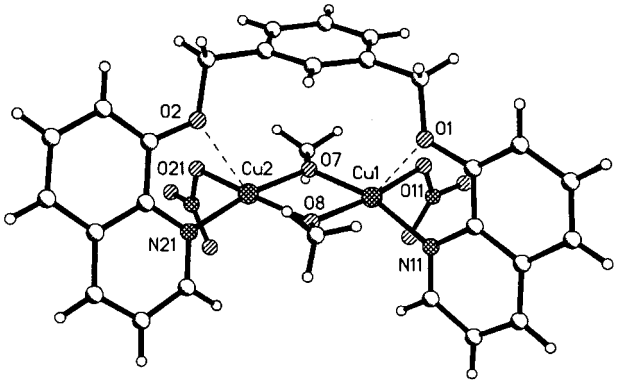

Keywords: N,O ligands / Copper / Cobalt / Silver / Bridging ligands

335 **S. P. Foxon, G. R. Torres, O. Walter, J. Z. Pedersen, H. Toftlund, M. Hüber, K. Falk, W. Haase, J. Cano, F. Lloret, M. Julve,* S. Schindler***

Syntheses, Structures, and Magnetic Properties of Copper(II) Complexes with 1,3-[Bis(2-pyridylmethyl)amino]benzene (1,3-tpbd) as Ligand

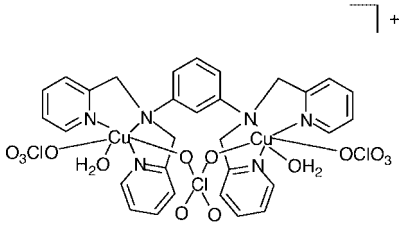

Keywords: Copper / Magnetic properties / EPR spectroscopy / Spin polarisation / Dinuclear complexes

344 **S. P. Foxon, O. Walter, R. Koch, H. Rupp, P. Müller, S. Schindler***

Tuning the Magnetic Properties of a Dinuclear Copper Complex: From Ferromagnetic to Antiferromagnetic Coupling

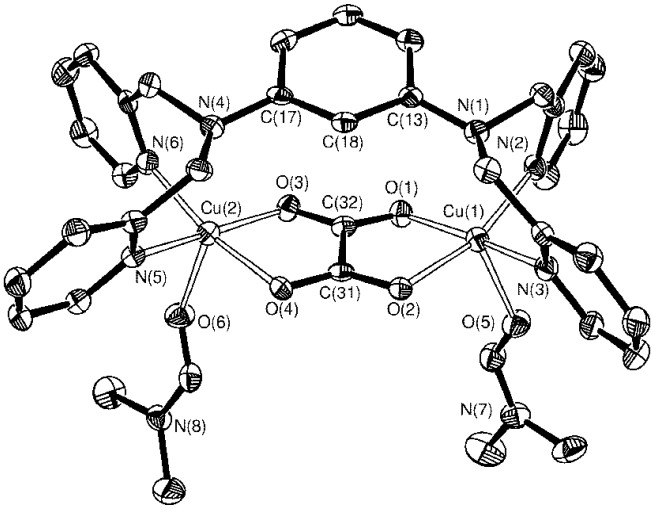

Keywords: Magnetism / Copper / Azides / Dinuclear complexes

 © 2004 Wiley-VCH Verlag GmbH & Co. KGaA, Weinheim

349 **A. Eichhöfer,* P. Deglmann**

Mercury−Chalcogenide Clusters: Synthesis and Structure of $[Hg_{10}Te_4(SePh)_{12}(PPhnPr_2)_4]$, $[Hg_{10}Te_4(TePh)_{12}(PPhnPr_2)_4]$ and $[Hg_{34}Te_{16}(SePh)_{36}(PPhnPr_2)_4]$

Keywords: Cluster compounds / Mercury / Tellurium / Selenium / DFT calculations

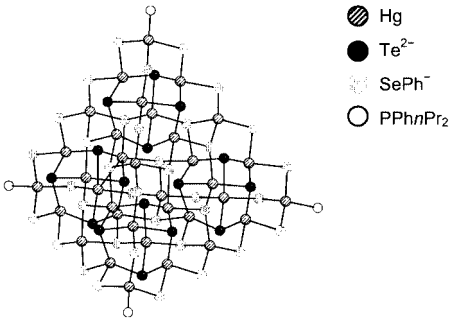

356 **T. S. Lobana,* I. Kinoshita,* K. Kimura, T. Nishioka, D. Shiomi, K. Isobe**

Pyridine-2-sulfonates as Versatile Ligands for the Synthesis of Novel Coordinative and Hydrogen-Bonded Supramolecules

Keywords: Coordination polymers / Hydrogen bonds / Supramolecular chemistry / Magnetic properties / Stacking interactions

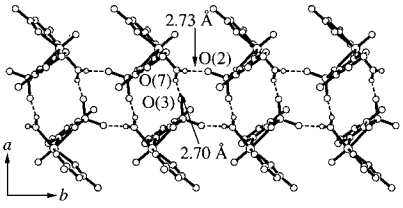

Hydrogen-bonded network of $[VO(3\text{-}mpSO_3)(acac)(H_2O)]$

368 **J. K. Bera, J. Bacsa, B. W. Smucker, K. R. Dunbar***

Heterometallic Molecular Squares and Polymers Based On Self-Assembly Reactions of Multiply Bonded Dirhenium Complexes

Keywords: Self-assembly / Polymers / Supramolecular chemistry / Rhenium / Multiple bonds

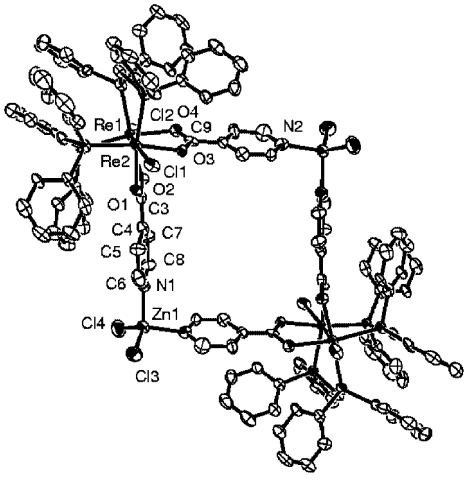

376 **P. Børsting, P. J. Steel***

Synthesis and X-ray Crystal Structures of Cobalt and Copper Complexes of 1,3-Bis(benzotriazolyl)propanes

Keywords: Copper / Cobalt / Cluster compounds / Bridging ligands / N ligands

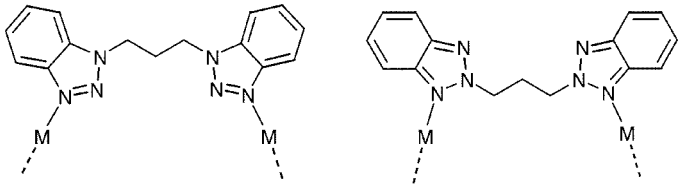

381 **K. Miqueu, J.-M. Sotiropoulos, G. Pfister-Guillouzo,* V. Rudzevich, V. Romanenko, G. Bertrand**

Role of the 2,6-Bis(trifluoromethyl)phenyl Group on the Acidity of the Corresponding Phosphane

Keywords: Photoelectron spectroscopy / DFT calculations / Phosphanide anions / Phosphanes

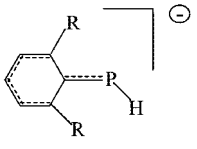

R : H, CF_3

 © 2004 Wiley-VCH Verlag GmbH & Co. KGaA, Weinheim

388 **I. L. Fedushkin,* A. A. Skatova, V. A. Chudakova, V. K. Cherkasov, G. K. Fukin, M. A. Lopatin**

Reduction of 1,2-Bis[(2,6-diisopropylphenyl)-imino]acenaphthene (dpp-bian) with Alkali Metals − A Study of the Solution Behaviour of $(dpp\text{-}bian)^{n-}[M^+]_n$ (M = Li, Na; n = 1−4) with UV/Vis, ESR and ^1H NMR Spectroscopy

Keywords: Lithium / Sodium / Bis(imino)acenaphthene / Polyanions

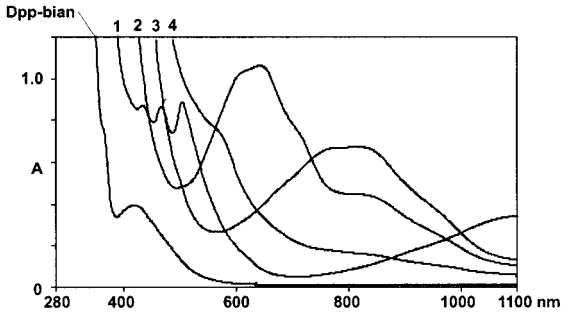

UV-VIS spectra of mono- (1), di- (2), tri- (3) and tetranion (4) of dpp-bian with lithium as counterion in TMEDA at 293 K

394 **T. Glaser,* T. Lügger, R. Fröhlich**

Synthesis, Crystal Structures, and Magnetic Properties of a Mono- and a Dinuclear Copper(II) Complex of the 2,4,6-Tris(2-pyridyl)-1,3,5-triazine Ligand

Keywords: Magnetic properties / Copper / N ligands / Coordination chemistry

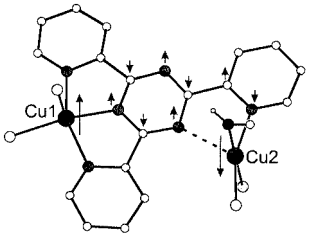

401 **H.-Z. Kou,* B. C. Zhou, S.-F. Si, R.-J. Wang**

Cyano-Bridged Dimetallic Polynuclear Cu_6Cr, Cu_6Cr_6, Cu_2W, and CuW Arrays: Synthesis, Crystal Structure, and Magnetism

Keywords: Cyano bridges / Magnetic properties / Tungsten / Copper / Chromium

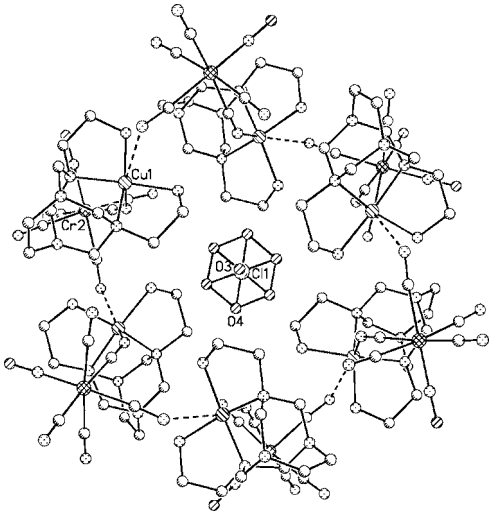

409 **J. Seebacher, M. Ji, H. Vahrenkamp***

(Neocuproin)zinc Thiolates: Attempts at Modeling Cobalamin-Independent Methionine Synthase

Keywords: Zinc / Metal complexes / Thiolates / Bioinorganic chemistry

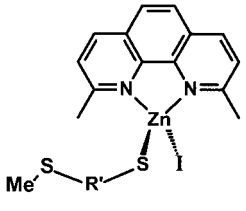

 © 2004 Wiley-VCH Verlag GmbH & Co. KGaA, Weinheim

418 **I. Özdemir, E. Çetinkaya, B. Çetinkaya,* M. Çiçek, D. Sémeril, C. Bruneau,* P. H. Dixneuf**

Access to 3-Methyl-4-methylene-*N*-tosylpyrrolidine and 3,4-Dimethyl-*N*-tosylpyrroline by Ruthenium-Catalyzed Cascade Cycloisomerization/Isomerization Reactions

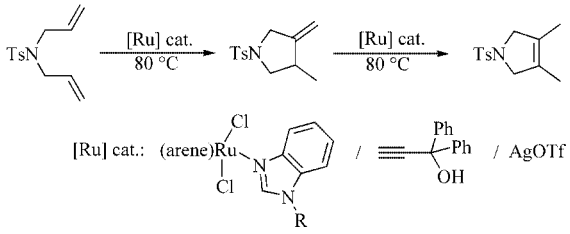

Keywords: Ruthenium / Benzimidazole / Homogeneous catalysis / Olefination

423 **O. Crespo, V. V. Brusko, M. C. Gimeno, M. L. Tornil, A. Laguna,* N. G. Zabirov**

Gold and Silver Complexes with the Ligands *N*-[Bis(isopropoxy)thiophosphoryl]thiobenzamide and *N*-[Bis(isopropoxy)thiophosphoryl]-*N*′-phenylthiourea

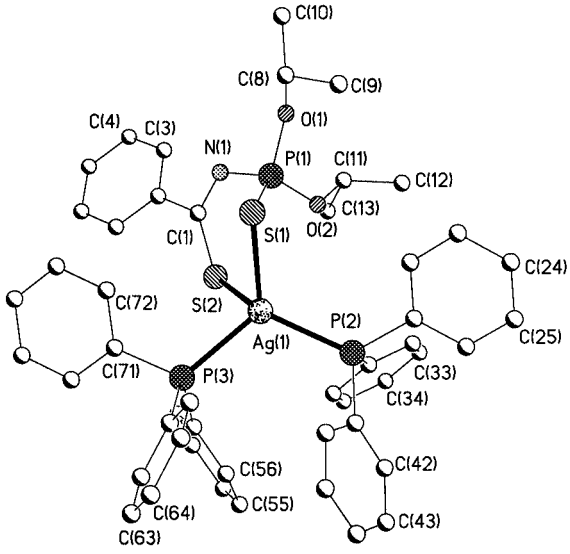

Keywords: Gold / Silver / Sulfur / Thiourea / Thioamide

 © 2004 Wiley-VCH Verlag GmbH & Co. KGaA, Weinheim

The "Rebound Controversy": An Overview and Theoretical Modeling of the Rebound Step in C−H Hydroxylation by Cytochrome P450

Sason Shaik,*[a] Shimrit Cohen,[a] Samuël P. de Visser,[a] Pankaz K. Sharma,[a] Devesh Kumar,[a] Sebastian Kozuch,[a] François Ogliaro,[a] and David Danovich[a]

Dedicated to H. F. (Fritz) Schaefer, a friend and a great scientist, on the occasion of his 60th birthday

Keywords: Alkanes / Cytochrome P450 / Density functional calculations / Enzyme catalysis / Free radicals / C−H hydroxylation

C–H hydroxylation by the enzyme cytochrome P450 is one of Nature's important and most ubiquitous processes. There is strong evidence that the mechanism proceeds by initial hydrogen abstraction, from the alkane, by the high-valent iron–oxo species of the enzyme, followed by a rebound of the alkyl radical to form the ferric–alcohol product complex (the Groves "rebound" mechanism). Nevertheless, the "rebound" mechanism is still controversial due to the ultrashort radical lifetimes deduced from radical-clock experiments. This review describes the main elements of the controversy and its updated resolution by theory, with an emphasis on the controversial rebound step. The theoretically derived model for alkane hydroxylation is found to involve two-state reactivity (TSR). In TSR, radicals are produced on two different spin-state surfaces, and thereafter they react differently; on the low-spin surface, the rebound proceeds with no product rearrangement and the lifetime of the radicals is ultrashort (or zero), while on the high-spin surface the barrier for rebound is substantial and the lifetime of the radical is sufficiently long that rearrangement may compete with product formation by rebound. A new valence-bond model is developed to model the rebound barrier on the high-spin surface and conceptualize its dependence on the nature of the alkyl radical. The possible intermediacy of carbocationic intermediates alongside radicals is discussed. It is shown that the TSR scenario provides a satisfactory rationale for the controversial findings in the field, and makes verifiable predictions. One of the predictions of TSR is that the ratio of unrearranged to rearranged products, [*U*/*R*], will be subject to an intrinsic isotope effect that is substrate-dependent. This prediction and its possible verification by experiment are discussed.
(© Wiley-VCH Verlag GmbH & Co. KGaA, 69451 Weinheim, Germany, 2004)

Introduction

Cytochrome P450, one of Nature's most potent monooxygenating enzymes in aerobic organisms,[1] has an oxidizing domain that consists of an iron−protoporphyrin complex, Figure 1, held by the protein through salt bridges to the propionate substituents and via a cysteinate (CysS) axial ligand — the "proximal ligand" — which is part of the encapsulating protein. Entrance of a substrate, RH, triggers a succession of events, which include dioxygen uptake, reduction and protonation, all of which activate the oxidase domain and convert the iron−porphyrin complex into the active species of the enzyme, the high-valent iron−oxo species called Compound I (Cpd I; Figure 1). Some of the most important functions of the enzyme involve the hydroxylation of alkanes to alcohols. As stated in the title, this paper focuses on the recent controversy that surrounds the rebound mechanism of alkane hydroxylation, and in particular on the key step of this mechanism, the rebound step itself.

In 1976 Groves and McClusky[2] suggested that alkane (Alk−H) hydroxylation by P450 proceeds by a rebound mechanism (Scheme 1). The first step in this mechanism involves hydrogen abstraction from the alkane by Cpd I. Subsequently, the alkyl radical is partitioned between two competing processes. It can either instantly rebound to form an alcohol complex, where the alcohol is unrearranged (*U*),

[a] Department of Organic Chemistry and the Lise Meitner-Minerva Center for Computational Quantum Chemistry, The Hebrew University of Jerusalem,
Givat Ram Campus, 91904 Jerusalem, Israel
Fax: (internat.) + 972-2-658-4680
E-mail: sason@yfaat.ch.huji.ac.il
Supporting information for this article is available on the WWW under http://www.eurjic.org or from the author.

MICROREVIEWS: This feature introduces the readers to the author's research through a concise overview of the selected topic. Reference to important work from others in the field is included.

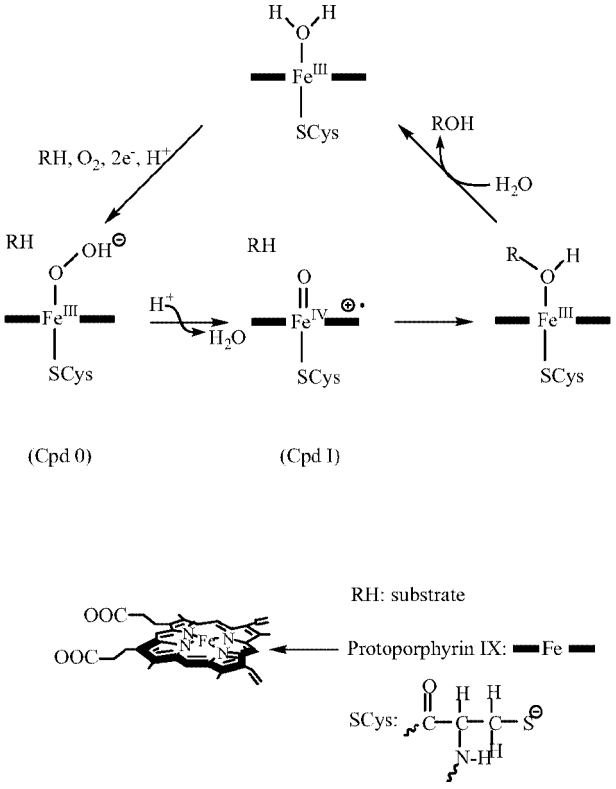

Figure 1. A truncated catalytic cycle of the enzyme cytochrome P450, showing the resting state, the active species Cpd I, its precursor, Cpd 0, and the initial product of alkane hydroxylation, the alcohol complex

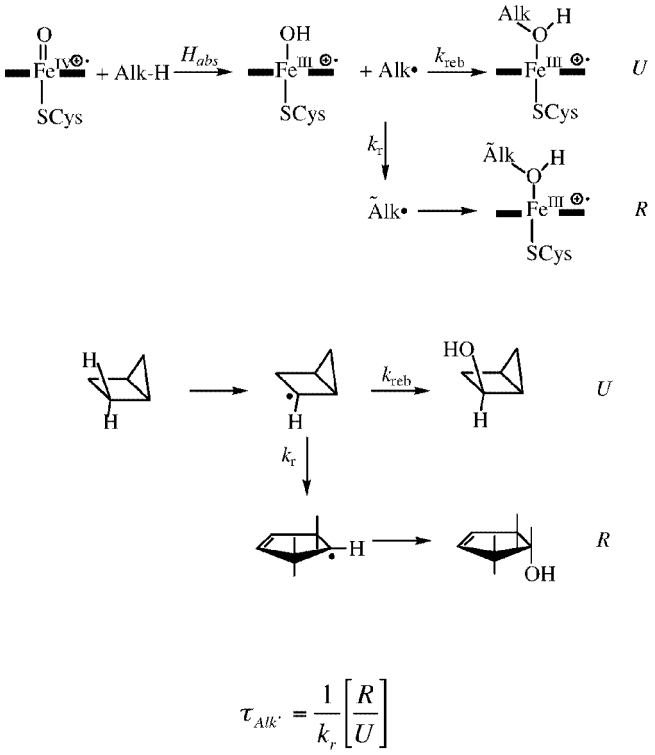

Scheme 1. The rebound mechanism, and the results of hydroxylation of bicyclo[2.1.0]pentane (ref.[12])

keeping the original stereochemical information possessed by the alkane, or it can first undergo skeletal rearrangement and then rebound to give a rearranged (*R*) alcohol product. The rebound mechanism accounts for the partial loss of stereochemistry and geometrical rearrangement data,[3] as well as for the large kinetic isotope effect (KIE) observed[4−10] when the hydrogen atom of the scissible C−H bond is replaced by a deuterium atom. However, the large degree of stereoselectivity (> 90%) and the sometimes completely stereospecific[8,11] hydroxylation suggested that the radicals are rather short-lived.

The Research Group in The Hebrew University: This Microreview summarizes the story of six years of intensive scientific discourse in the attempt to resolve the "rebound controversy" in the C−H hydroxylation chemistry by cytochrome P450. Our group entered the research on heme enzymes through the crack provided by the tiny FeO^+ diatomic that mimics the ability of cytochrome P450 to hydroxylate C−H bonds. This small diatomic posed some very enticing puzzles: the reaction with hydrocarbons was highly exothermic, apparently spin-allowed, and certainly orbitally allowed. Despite these rosy prospects, the efficiency of the reaction was extremely poor! The solution of this puzzle, together with Helmut Schwarz and Detlef Schröder, led to the development of the idea of two-state reactivity, TSR (ref.[26]), which is gaining increasing popularity in the community. Already then there was something in the air of P450 literature that spelled TSR. The "rebound controversy" was reminiscent of some TSR features, the intellectual dilemma it posed was challenging, and the chance for a scientific discourse was appealing. Our foray into the field was rather modest (ref.[33]). The three postdocs who started us off, Michael Filatov (now in Goteborg), Nathan Harris (now with Chemical Abstracts), and François Ogliaro (now in Kings College, London) were soon joined by other coworkers who are still in the group in Jerusalem, Sam de Visser (a Dutch postdoc from Amsterdam), Pankaz K. Sharma (an Indian postdoc from Hyderabad), Devesh Kumar (an Indian postdoc from Gorakhpur), Shimrit Cohen (a Ph.D. student from Jerusalem), Sebastian Kozuch (a Ph.D. student, a new immigrant from Argentina, now an M.Sc. student in Jerusalem), and David Danovich (a senior research associate, in the group since 1992). At present, the group has grown by three more postdocs and one graduate student.

The field of P450 is a vast ocean of many waters. Besides its being an intellectual arena full with enticing puzzles waiting to be solved, it is also an interdisciplinary field that is nestled in the crossroads between chemistry, biology, physics and medicine. Being active in such a field requires maintenance of many dialogues, and our group has been fortunate to enjoy and benefit from useful discussions with chemists and biologists of variegated expertise; Bernard Meunier, John Dawson, Joe Dinnocenzo, Sunichi Fukuzumi, Mike Green, Zeev Gross, Jay Groves, Fred Guengrich, Danni Harris, Jeff Jones, Isao Morishima, Marty Newcomb, Paul Ortiz de Montellano, Tom Poulos, Steve Sligar, Yoshi Watanabe, Wolf-D. Woggon, Kazunari Yoshizawa, Hendrik Zipse, and others in the heme enzyme community. As a group of theoretical chemistry, we have initially used only quantum mechanics (QM). Some controversies in the description of the active species of the enzyme by different QM modeling methods led us to the development of the concept of chameleon oxidants (ref.[27]), and very quickly it was evident that we must master also hybrid quantum mechanics/molecular mechanics (QM/MM) calculation since they enable to account for the effect of the protein environment. This is done in a fruitful and ongoing collaboration (ref.[46]) with Walter Thiel and his group members, Jan Schöneboom and Natalie Reuter (from the Max Planck Institute in Mülheim). We are even beginning to enjoy some docking calculations, and appreciate the importance of the protein motions that Judith Klinman talks about. Indeed, the field of heme enzymes has offered much more than initially expected in the fall of 1997, when I (S. S.) drew the active species of P450 for the first time and attempted to figure it out.

The first experiment to determine the lifetime of the radical was done by Ortiz de Montellano and Stearns,[3,12] using bicyclo[2.1.0]pentane (Scheme 1). Using the percentage of rearrangement [*U*/*R*] and the free-radical rearrangement rate constant, k_r, enabled them to quantitate the lifetime of the radical as 50 ps. However, since the products were exclusively the *endo* isomers, it was further concluded that the radical can rearrange but its reorientation, from the *endo* to the *exo* face, is restricted within the pocket of the protein. A similar conclusion was reached by Sligar et al.[6] for the C−H hydroxylation of camphor by P450cam, by Jones et al.[13] for C−H hydroxylation of *para*-xylene, and so on.[3] By contrast, an NMR study by Ortiz de Montellano[14] showed that a substrate like adamantane is mobile within the timescale of the enzymatic turnover within the pocket. It appears, therefore, that the restricted mobility of the radical is anisotropic. Other studies of radical clocks followed, and generated a variety of lifetime data, which indicated that the radicals are short-lived and somewhat restricted in their motions.[3]

The support for the rebound mechanism looked solid until Newcomb et al.[15−18] began their investigation of ultrafast radical clocks and carbocationic clocks. Thus, Newcomb has shown that the quantity [*U*/*R*] for a series of radical clocks does not correlate with the known lifetimes of the putative free-radical clocks.[15] Some rearrangement patterns of clocks like **1**, depicted in Scheme 2, were shown to correspond to carbocationic species.[16,18−20] Subtraction of these carbocationic rearrangements from the overall product mixture resulted in lifetimes as short as 70 fs;[16,18] durations much too short to qualify as lifetimes of a real intermediate species. These unrealistic lifetimes and the rearranged products derived from carbocations have led Newcomb and co-workers[15] to suggest that radical intermediates are not present during the reaction, and that alkane hydroxylation proceeds by two competing mechanisms nascent from two oxidant species of the enzyme, Cpd I and its precursor ferric peroxide species, so called Cpd 0 (Figure 1). As shown in Scheme 2, one mechanism involves a concerted [O] insertion from Cpd I into the C−H bond, while the second one involves hydroxonium ion (OH^+) insertion from Cpd 0 into the C−H bond. This latter process generates a protonated alcohol, which subsequently rearranges in a manner typical of a carbocation, with no intermediary of free carbocations. Newcomb's work has cast the rebound mechanism into doubt and started what is dubbed in the title of this work, as "*the rebound controversy*", which is still ongoing.[20−22]

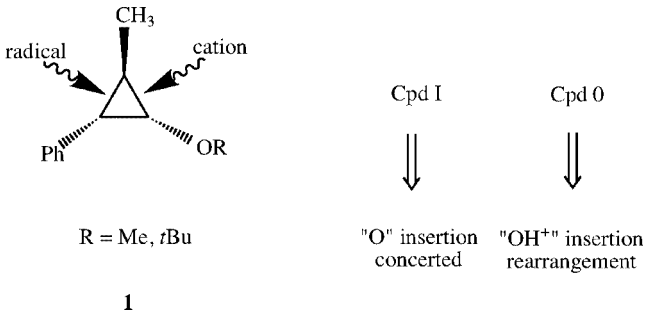

1

Scheme 2. The two-oxidant hypothesis using Cpd I and Cpd 0, and a probe substrate (**1**) that can open differently depending on whether it leads to a radical or a cationic intermediate (ref.[15])

The "rebound controversy" touches the limits of chemistry's capabilities to pinpoint complex reaction mechanisms. Its importance derives from these limits, because it forces us to grapple with the state-of-the art of our understanding of molecular processes. An eventual resolution of this controversy will no doubt come from the interplay of theory and experiment. Theory has already offered a resolution of the main elements in the controversy.[23−26] Since then, a few more theoretical studies were performed by the Jerusalem group,[27,28] and by Yoshizawa et al.[29−31] Also relevant is the molecular dynamics simulations by Gualar et al.[32] which described the rebound step in the enzyme methyl monooxygenase (MMO), and which is interesting to compare to the rebound in P450. These studies cover a range of systems and pose an opportunity to give an overview intended to refine our current understanding of the controversy, with a focus on the rebound step that appears to be the origin of the intriguing controversy.

Results and Discussion

Background: Theoretical Calculations of Alkane Hydroxylation and Key Points of Contention and Focus

In 1998, Shaik et al.[23,33] offered a possible reconciliation of the controversy based on the two-state reactivity (TSR) paradigm. Subsequently, the Jerusalem group[23,24,26,27] used density functional theory (DFT) to compute model alkane hydroxylation reactions between Cpd I (HS^- as a proximal ligand) with methane and propene. As shown in the energy profiles in Figure 2, the computations reveal that alkane hydroxylation proceeds via two states, one is a high-spin (**HS**) quartet state and the other is a low-spin (**LS**) doublet state. These two states originate in the ground state of Cpd I that possesses three unpaired electrons, which give rise to two closely lying **HS** and **LS** states, separated in energy by a few wavenumbers.[34−36] The reaction path involves a C−H activation phase, which looks like a hydrogen-abstraction process, leading to a radical, loosely coordinated to the iron−hydroxo intermediate by a C···HO hydrogen bond, followed by a reorientation phase in which the radical rotates away from the OH bond to form a direct C···O contact, and finally a rebound phase in which the radical attacks the oxygen atom to form the C−O bond of the alcohol.

The **HS** and **LS** profiles are close in energy, all the way to the PorFeOH/Alk˙ cluster, and subsequently they bifurcate. In the **LS** manifold, once the radical snaps out of the C···HO hydrogen interaction with the iron−hydroxo species, the ensuing **LS** rebound phase is barrierless.[23,24,27] By contrast, the **HS** rebound has a significant barrier to rebound, with a real transition state that has clear structural and spin density features, indicative of the source of activation. As such, the radical intermediate will have a suffic-

 © 2004 Wiley-VCH Verlag GmbH & Co. KGaA, Weinheim

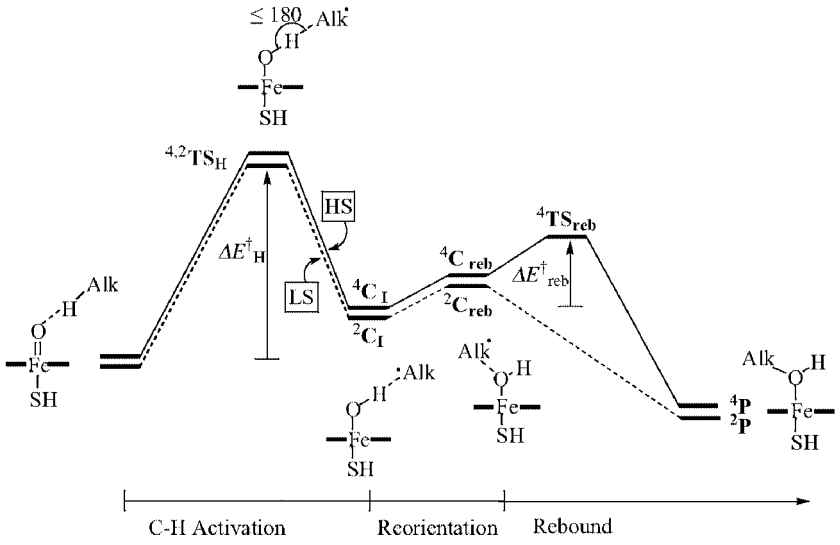

Figure 2. Reaction profile of alkane hydroxylation by Compound I, as calculated by density functional theory using porphine and L = SH^-; note the doubling of the profile to high-spin (**HS**) and low-spin (**LS**) components

iently long lifetime on the **HS** manifold. By contrast, the lifetime of the **LS** intermediate will be shorter than the **HS** and its upper limit will be set by the frequency of rotational modes, which establish a rebound position. Thus, the "lifetime of the radical" in this scenario is a two-state information content with an ultrashort component and a "normal" longer component.

Extending this picture to a clock experiment (Scheme 1) means that the amount of rearranged product *R* originates mainly in the **HS** state, while the unrearranged product *U* is contributed by both **HS** and **LS** states, although mostly by the **LS** state. Thus, the apparent radical lifetime, which is quantified from the ratio [*U*/*R*], is not a true lifetime, since it reflects the relative yields of the **HS** and **LS** processes. At the limiting case when rearrangement occurs only on the **HS** manifold, the [*U*/*R*] quantity will be equal to the percentage of the **LS** and **HS** processes in the total product yield. As a rule, within the two-state picture, the quantity [*U*/*R*] will yield apparent lifetimes that are shorter than the real ones. Ultrashort apparent lifetimes will result whenever the contribution of **HS** processes to the total hydroxylation reaction is very small. This TSR explanation[23,26] provided a reasonable solution of the controversy and revealed a scenario that, on the one hand, accommodated the KIE evidence, indicating a hydrogen-abstraction-like transition in the bond activation, and, on the other hand, demonstrated the reason for the controversial apparent lifetimes, which are determined assuming that the [*U*/*R*] quantity is a result of a single radical intermediate that is partitioned between instant rebound and rearrangement followed by rebound, as in Scheme 1.

Recent results of Newcomb et al.[37,38] indicate that the ratio [*U*/*R*] is subject to an isotope effect when the hydrogen atom is replaced by a deuterium atom in the scissile C−H bond. This finding of a product isotope effect rules out a single pathway or a single intermediate that is partitioned between rebound and rearrangement pathways. The observed product isotope effect can therefore indicate the operation of either TSR or two-oxidant (Scheme 2) scenarios. However, recent calculations by the Jerusalem group showed that Cpd 0 has a very high barrier for olefin epoxidation (its marker reaction), much higher than that which is calculated with Cpd I as an oxidant.[39] More recent DFT calculations[40] show the same trend for sulfoxidations, for which the barrier is much higher than with Cpd I, even when Cpd 0 is assisted by a powerful proton source. Thus, *DFT calculations rule out the possibility that Cpd 0 can compete with Cpd I as an oxidant*. Furthermore, the cryogenic EPR and ENDOR experiments of Davydov et al.[41] for camphor hydroxylation support oxidation by Cpd I, but not by Cpd 0. Even the most recent experimental evidence, which implies that Cpd 0 can indeed epoxidize olefins, shows that the putative reaction is sluggish compared with that of Cpd I and occurs only in the absence of Cpd I.[42] Similarly, radical-derived rearrangements were produced from model systems which involve only Cpd I as an electrophilic oxidant.[43,44] Thus, while one cannot rule out the presence of another oxidant, in the absence of Cpd I, at this stage of the research, the balance seems to favor the TSR scenario with only Cpd I as a plausible mechanism of hydroxylation by P450.[3]

Two DFT studies of ethane hydroxylation were performed by Yoshizawa et al.[29,30] using a model Cpd I with MeS^- as a proximal ligand. Their two studies indeed revealed TSR with bond-activation transition states that look like hydrogen-abstraction species. However, there were conflicting results and differences with the results of Ogliaro et al.[23,45] Thus, the study with the better basis set[29] reveals an **HS** profile that is ca. 6 kcal·mol^{-1} lower than the **LS** profile, while with a smaller basis set,[30] the **HS**−**LS** energy differences are small (0.6−3.2 kcal·mol^{-1}), but the **HS** profile is higher than the **LS**, in agreement with the results of Ogliaro et al.[23] The most recent study of camphor hydroxylation, by Kamachi and Yoshizawa,[31] which used a large

 © 2004 Wiley-VCH Verlag GmbH & Co. KGaA, Weinheim

basis set, gave a difference of 2.2 kcal·mol^{-1} between **HS** and **LS** barriers, in somewhat better agreement with Ogliaro et al.[23,45] but still the lower profile is that of the **HS** process. We think that these switches in the results originate in the choice of the thiolate ligand to model the cysteinate ligand within the protein pocket. In a recent quantum mechanical/molecular mechanical (QM/MM) study, Schöneboom et al.[46] showed that Cpd I, with MeS^- as a proximal ligand, exhibits a greater sensitivity to basis set and environmental effects, than with the model HS^- as a proximal ligand. Furthermore, it was shown that with HS^-, the gas-phase calculation of Cpd I is closer to its final state in the protein pocket.

As far as the rebound step is concerned, the earlier results of the Yoshizawa group[29,30] were in conflict with those of Ogliaro et al.,[23] although the most recent ones appear to be in good agreement. Thus, the DFT calculations of camphor hydroxylation by Kamachi and Yoshizawa,[31] with a good-quality basis set, led to a picture similar to that which was obtained by Ogliaro et al.,[23] with an **LS** rebound that has a very tiny barrier, 0.7 kcal·mol^{-1}, and an **HS** rebound that has a substantial barrier of more than 3 kcal·mol^{-1}. Even though the remaining disagreements are minimal, nevertheless these apparently conflicting results highlight both the complexity of the rebound process as well as *the need for a fundamental theoretical understanding of the rebound problem*, rather than over-reliance on computations alone. Thus, since there is an experimental and theoretical consensus about the nature of the bond-activation step, the remaining doubts concern the rebound step. As such, the major questions, which are addressed in this Microreview are the following: *What is the origin of the **HS** rebound barrier? Why does the **LS** process have a tiny rebound barrier, if at all? Will the **LS** rebound barrier always be tiny*?

There are several issues within these questions. One issue concerns the electromeric identity of the iron−hydroxo intermediate, which can either be a ferric, $Por^{\cdot+}Fe^{III}OH$, species or a ferryl, $PorFe^{IV}OH$, one. In an early paper[47] the Jerusalem group argued that in the protein pocket the ground states of the iron−hydroxo complex will be the $Por^{\cdot+}Fe^{III}OH$ species. Accordingly, the studies of Harris et al.[24] and Ogliaro et al.[23] described the rebound processes for $Por^{\cdot+}Fe^{III}OH/Alk^{\cdot}$, but pointed out that smaller barriers are expected for $PorFe^{IV}OH/Alk^{\cdot}$ ($Alk^{\cdot}$ = methyl, allyl). Recent EXAFS studies of the iron−hydroxo species of the enzyme chloroperoxidase indicate that the ground state is $PorFe^{IV}OH$,[48] and similar results were obtained computationally.[27,47,49] However, the results of Groves et al.[50] and Gross et al.[51] show that in model systems in solution, both electromers may coexist. Therefore, in the following sections, we address the question of the ground state of the iron−hydroxo species, and the respective rebound barriers of the ferric and ferryl states.

The second issue is the behavior of the **HS** vis-à-vis the **LS** rebound step. We now have data on rebound processes in methane,[23] camphor[31,52] and propene[27,49] hydroxylations, and in epoxidations of ethene[25] and propene,[27,49] as well as in methane hydroxylation by a ruthenium analog of Cpd I.[28] Based on this insight, we shall present a valence-bond model for the rebound process on the **HS** and **LS** states. Using this model we shall attempt to pattern the existing experimental data of radical scrambling during alkane hydroxylation. Finally, we shall assess the possible sources of carbocations, which are implicated by the studies of Newcomb and co-workers[15,20] and the recent studies of Ortiz de Montellano and Groves et al.[21]

Electromeric States of the Iron−Hydroxo Species and the Iron−Hydroxo/Alk$^{\cdot}$ Cluster Intermediate

The iron−hydroxo intermediate formed in the hydrogen abstraction step of Figure 2 possesses three low-lying states, shown in Scheme 3, using the d-block and other key orbitals. These are the π*-orbitals [antibonding $d_{xz,yz}$(Fe)-$p_{x,y}$(O) combinations], and the a_{2u} orbital [an antibonding a_{2u}(Por)-p_z(S) combination]. Other orbitals are the δ-orbital on the iron atom, which is always doubly occupied, and the $d_{z^2}(\sigma^*_{z^2})$ orbital, which becomes populated during the HS rebound process. The ferryl state involves two singly occupied π*-orbitals, which, together with the doubly occupied δ-orbital, correspond to a d^4 metal configuration, and hence to the $^3PorFe^{IV}OH$ electromer. The other two states involve singly occupied π^*_{yz} and a_{2u}, which, together with

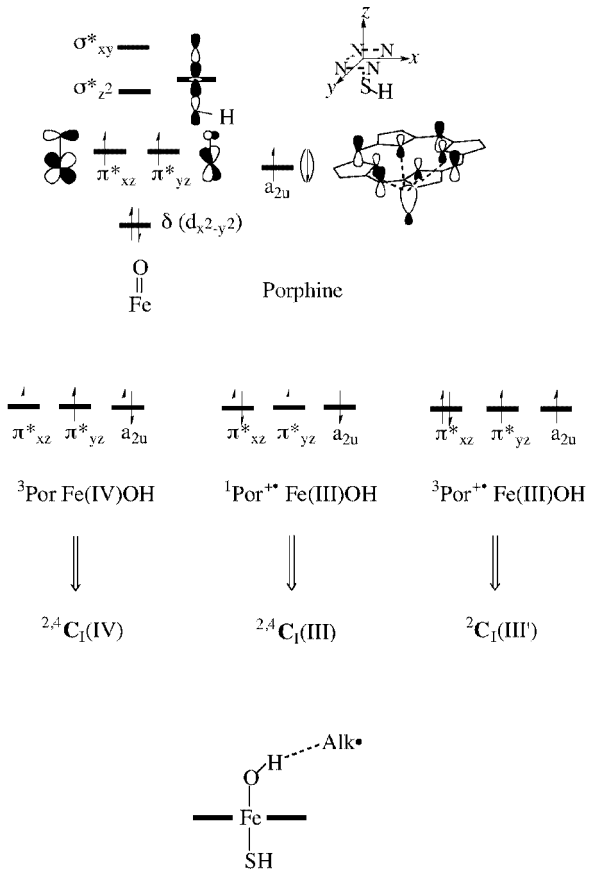

Scheme 3. An orbital diagram showing the occupancy in the ferryl(IV) electromer of the iron−hydroxo complex; below are the occupancies of the lowest electromeric species, Fe^{IV} and Fe^{III}, of this complex, along with their corresponding occupancies; the spin-state assignments are indicated by the superscripts

 © 2004 Wiley-VCH Verlag GmbH & Co. KGaA, Weinheim

the double occupancy of δ and π^*_{xz} correspond to a d^5 metal configuration and a radical cation situation formally on the porphyrin, hence the $^{1,3}Por^{\cdot+}Fe^{III}OH$ electromer states. Addition now of the alkyl radical gives rise to five different states of the iron−hydroxo/Alk$^{\cdot}$ cluster, labeled as $^{2,4}C_I(IV)$, $^{2,4}C_I(III)$ and $^{2}C_I(III')$.

The geometries and spin densities of the ferryl and ferric varieties are depicted in Figure 3a for the simple model with porphine and HS^- as proximal ligand. All values in parentheses refer to a polarizing environment, characterized by a dielectric constant, ε, of 5.7. The ferric species exhibits greater sensitivity to the polarizing environment. Thus, reminiscent of our findings for Cpd I,[46,52,53] the $Por^{\cdot+}Fe^{III}OH$ species undergoes Fe−S bond shortening and charge transfer from the porphyrin to the sulfur atom. By contrast, the ferryl species, $PorFe^{IV}OH$, is less sensitive to the environmental effect. The relative ordering of the ferric and ferryl species depends on a few variables (see detailed data in the Supporting Information) and can be described as follows. With the double-zeta LACVP(6-31G) basis set, the ground state of the bare system is the ferryl species. A larger basis set, LACV3P+*(6-311+G*), increases this preference to 5.2 kcal·mol^{-1}. Medium polarization and geometry optimization, however, stabilize the ferric states relative to the ferryl ones and decrease the difference to 3.14 kcal·mol^{-1}, as indicated in Figure 3a.

A more extensive model is the species with octamethylporphyrin and the full cysteinato ligand, shown in Figure 3b, with LACVP(6-31G) geometric values, alongside the energy differences obtained by single-point calculations with the triple-zeta LACV3P basis set and with inclusion of medium polarization. The energy difference of 1.72 kcal·mol^{-1} in favor of the ferryl situation is the highest limit of this difference. An estimate of the energy difference due to the effect of geometry optimization leads to a smaller difference of less than 0.7 kcal·mol^{-1} (values in parentheses). One can further expect that the real protoporphyrin substituents, two vinyl groups and two propionate anions, may tip the balance.[47]

Bringing in the alkyl radicals will give rise to the five states of the PorFeOH/Alk$^{\cdot}$ intermediate en route to the rebound step (see Scheme 3). The interaction of the alkyl group with the iron−hydroxo is by means of an H···C hydrogen-bonding interaction of the FeOH···C(Alk$^{\cdot}$) type, which leads to the intermediates $^{2,4}C_I$ in Scheme 3. Since the carbon atom of the alkyl group is slightly negative and the hydrogen atom of the hydroxo group is slightly positive, this hydrogen-bonding interaction will further modulate the energy differences between the ferric and ferryl states. The calculations show that the ferryl complex has a slightly larger positive charge on the hydrogen atom than in the ferric state, and therefore one might expect that the preference for the ferryl intermediate will be slightly larger in the presence of the radical, as is indeed borne out by all the calculations. However, this interaction is expected to be undermined in the presence of the screening effect of the

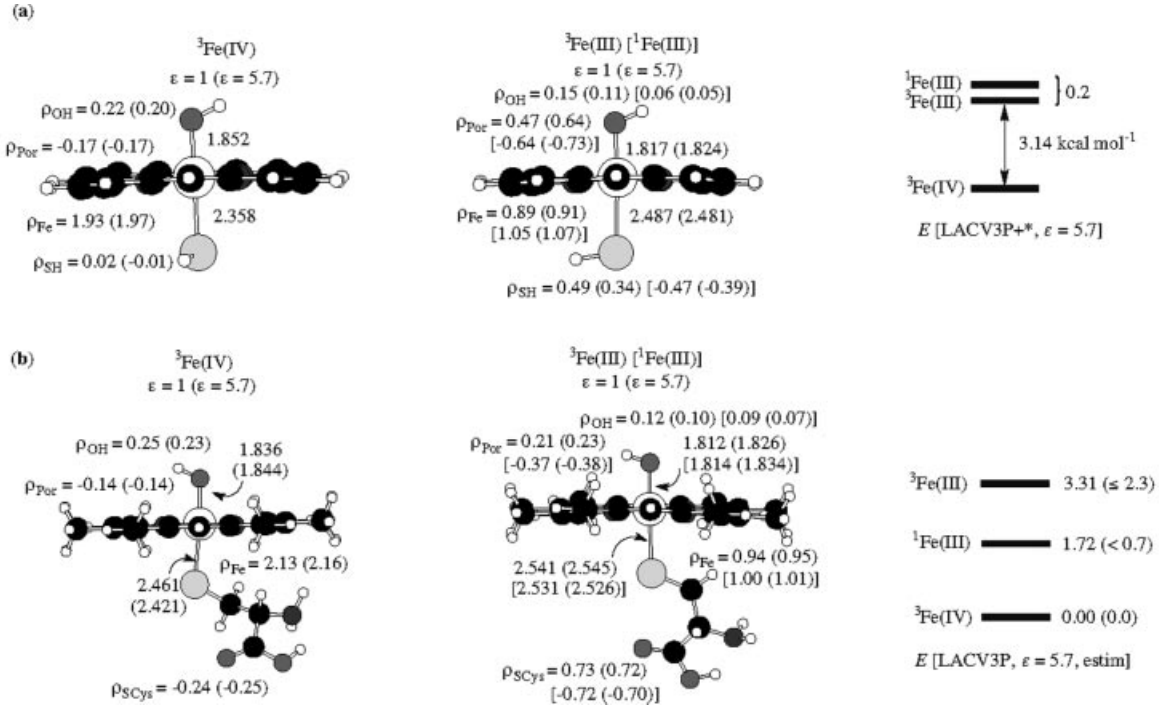

Figure 3. (a) B3LYP/LACVP geometries of the iron−hydroxo complex, using porphine and L = SH^-; the spin densities (ρ) are taken from a single point calculation with the LACV3P+* basis set in vacuo and in a dielectric medium with ε = 5.7; the diagram on the right shows relative energies calculated with the LACV3P+* basis set and in a dielectric medium with ε = 5.7; (b) B3LYP/LACVP geometries for the electromeric species of the iron−hydroxo complex, using octamethylporphyrin and L = cysteinate; structures were fully optimized in vacuo and in a solvent with a dielectric constant of ε = 5.7; the spin-density values are taken from single-point calculations with the LACV3P basis set; the diagram on the right shows relative energies calculated using the single point energies with LACV3P and in a dielectric medium with ε = 5.7; the values in parentheses are estimated relative energies corrected for the effect of geometry optimization

 © 2004 Wiley-VCH Verlag GmbH & Co. KGaA, Weinheim

protein pocket. The resulting clusters from our most recent QM/MM study of camphor hydroxylation by P450cam are depicted in Figure 4. The group spin densities clearly illustrate that, under a realistic representation of the protein environment, the ferric electromers are the ground states, but the ferryl states lie very close in energy,[52] as is indeed shown by experiment for model systems in chlorinated solvents.[50,51] Since, for realistic alkanes, all the five intermediate states will lie below the hydrogen abstraction transition states, $^{2,4}TS_H$ (Figure 2), in principle, they will all be accessible for rebound, and may further complicate the TSR picture into a multi-state scenario, where both spin and oxidation states are variable.

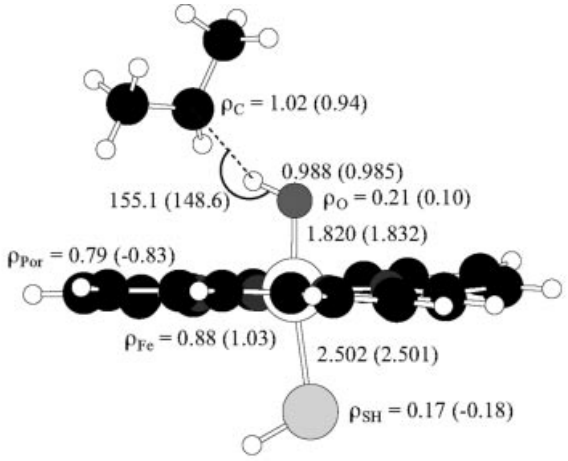

^4C_I (^2C_I)

Figure 4. A QM/MM snapshot showing only the QM subsystem of the $^{2,4}C_I$(III) clusters for camphor (truncated in the figure) hydroxylation by P450cam (ref.[52]); key geometric features and group spin densities (ρ) are indicated near the corresponding moieties; the **LS** cluster is 1.08 kcal/mol lower than the **HS** cluster

Is the Radical Free, Bound or a "Guided Radical"?

The computational data in Scheme 4 show that the strength of the FeOH···C(Alk˙) hydrogen bond in C_I is of the order of 1.9−2.7 kcal·mol^{-1}, and is marginally dependent on the radical, methyl vis-à-vis allyl. The weakness of this interaction is manifested in the presence of six-to-nine modes of very low frequencies, less than 100 cm^{-1}, and a few others with less than 200 cm^{-1}, which describe the relative movement of the alkyl radical with respect to the iron−hydroxo species, for example, ω = 81.9 cm^{-1} for the stretching mode of the hydrogen bond, H···CH_3. These frequencies are collected in the Supporting Information for the cases of methyl and allyl radicals in the ferryl states. Some of these modes are internal rotations of the radical, while others involve what may look like a stretching mode of the H···C hydrogen bond, and still others look like reorientation modes, which converts the C_I cluster to a C_H cluster held by a C−H···OFe hydrogen bond, as well as swing and flip modes. For example, a swing motion that changes the terminal of the allyl radical that is coordinated by the FeOH···C hydrogen bond, will be responsible for allylic scrambling. Likewise, a flip of the radical (self rotation), which changes the face that is coordinated to the iron−hydroxo species, will be responsible for inversion of configuration of the radical. Clearly, therefore, the radical is loosely coordinated and has a great deal of freedom at a small energy expense.

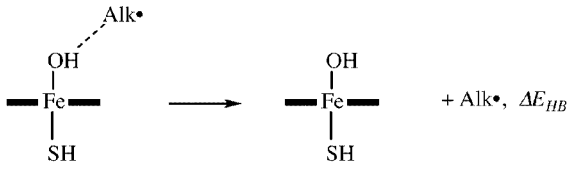

Alk	Fe	ΔE_{HB} (kcal mol^{-1})
CH_3	Fe(III)	1.9 (HS); 2.1 (LS)
CH_3	Fe(IV)	2.6 (HS); 2.7 (LS)
C_3H_5	Fe(III)	not available
C_3H_5	Fe(IV)	2.3 (HS); 2.7 (LS)

Scheme 4. OH···C hydrogen bonding energies (ΔE_{HB}) calculated at the B3LYP/LACVP level

Is the radical "bound" or is it a free radical? Since the interaction is rather small and since coordination causes the fragments to lose their individual rotational entropies ($T\Delta S \approx -6$ kcal·mol^{-1}), on the free-energy scale the separated fragments are more abundant than the FeOH···C(Alk˙) cluster, i.e., *there are more radicals that are not bound to the iron−hydroxo complex than radicals that are*. The portion of the bound species[32,54,55] will perform a periodic motion along the C···H hydrogen-bonding coordinate, as recently described in the semi-classical trajectory study of the rebound step in the enzyme MMO.[32] However, all this may be less relevant since a major consideration should be given to the situation in the protein pocket. Substrate binding by the protein is different for different P450 isozymes.[21] For example, in the enzyme $P450_{cam}$, the side chain Tyr96 holds the camphor by a hydrogen bond, C=O···HO−Tyr, to its carbonyl group.[56] This hydrogen-bonding interaction is quite exergonic, in part because it is *entropically driven* by the release of a few water molecules. Thus, this interaction appears to be more important than the weak FeOH···C(Alk˙) hydrogen bond between the alkyl group and the iron−hydroxo species. This hydrogen bonding to Tyr96 continues to hold the camphoryl radical and may even serve to reorient it towards a favorable rebound position. Thus, *we might be dealing with a "guided radical" that is conveniently oriented to the rebound position by the protein*. These protein-binding modes must be taken into account in a molecular dynamics study, and these may over-

 © 2004 Wiley-VCH Verlag GmbH & Co. KGaA, Weinheim

shadow the weak interaction found in the gas-phase calculations. Until such time when a molecular dynamics study within the protein can be conducted, we limit the analysis of the rebound step to a few essential features, which depend on clear electronic factors.

The Reorientation and Rebound Phases

Among the low-frequency vibrations of $^{2,4}C_I$, a unique mode is the one that involves either rotation of the alkyl group around the O···C axis, or the one in which the rotation of the radical is coupled to the O−H rotation around the Fe−O axis. Both movements bring the radical to the backside of the H−O bond to the rebound position (see Figure 2). This motion, which leads to the release of the radical from the FeOH···C(Alk˙) hydrogen bond, involves an energy rise of the order of 1−1.5 kcal·mol^{-1}. Both the **HS** and **LS** FeOH···C(Alk˙) species possess this feature.[23] However, once the radical snaps out of this interaction and maintains a "rebound position" with a direct O···C orientation, the **LS** and **HS** rebound processes differ in a fundamental manner. The **HS** rebound has an additional "chemical" barrier to surmount with a distinct transition state,[23,24,27] whereas the **LS** rebound is barrier-free. This, at least, is the situation in the alkyl radicals tested so far.

Table 1 collects the **HS** rebound barriers, $\Delta E^{\ddagger}_{reb}$, for the various systems studied in our group and others, including for epoxidation. These barriers are seen to be significant and to depend on the oxidation state of the iron atom in the iron−hydroxo complex [$\Delta E^{\ddagger}_{reb}$(III) > $\Delta E^{\ddagger}_{reb}$(IV)], on the identity of the transition metal [$\Delta E^{\ddagger}_{reb}$(Fe) << $\Delta E^{\ddagger}_{reb}$(Ru)], as well as on the proximal ligand [$\Delta E^{\ddagger}_{reb}$($SH^-$) > $\Delta E^{\ddagger}_{reb}$($MeSO_3^-$) ≥ $\Delta E^{\ddagger}_{reb}$(ImH)]. A polarizing field (mimicked by a dielectric constant, ε, of 5.7) raises the barrier for the Fe^{III} electromer by a significant amount, ca. 4−5 kcal·mol^{-1}, but the effect on the Fe^{IV} electromer is small and is counteracted by the effect of NH···S hydrogen bonding and further lowered by inclusion of zero-point energy effect (ZPE). As such, for the Fe^{IV} electromer, the calculated gas-phase barrier is a good approximation for the barrier that includes all these effects, while for the Fe^{III} electromer the barrier is significantly raised by the polarity of the medium.

A few rebound transition states, $^4TS_{reb}$, are depicted in Figure 5, along with a typical example of the reaction vector (the mode with imaginary frequency), which shows a clear rebound mode. The geometries of the $^4TS_{reb}$ species exhibit Fe−S and Fe−O bond elongation vis-à-vis their corresponding ^4C_I clusters. Finally, all the $^4TS_{reb}$ species exhibit reduction of the spin density on the radical and increase of the spin densities on iron, while the $^4TS_{reb}$-III species exhibit, in addition, depletion of the spin density on the porphine. Thus, both geometric as well as electronic changes accompany the **HS** rebound process.

In contrast to the **HS** rebound, once the radical in the **LS** intermediate assumes a rebound position, the ensuing rebound proceeds in a barrierless fashion for both ferryl and ferric states (Figure 2).[24,27] An illustrative example of the **LS** rebound is the behavior of $^2PorFe^{IV}OH$/allyl˙ shown in Figure 6. During the C···O shortening, the allyl radical swings around the Fe−O bond to a rebound position, the energy rises by about 1.5 kcal·mol^{-1} and then falls abruptly to the product complex, ^2P. The top structure of the potential energy profile always falls back into ^2C_I(IV) upon transition-state-optimization procedures. A frequency calcu-

Table 1. High-spin (HS) rebound barriers from the ^4C_I clusters

Entry[a]	^4C_I species	Radical	$^4\Delta E^{\ddagger}_{reb}$ [b]	$^4\Delta E^{\ddagger}_{reb}$(ZPE)[b]	$^4\Delta E^{\ddagger}_{reb}$(ε = 5.7)	$^4\Delta E^{\ddagger}_{reb}$(2NH···S)
a) Hydroxylation						
1	C_I(III)	CH_3	4.9 (5.5)	–	9.8	–
2	C_I(IV)	CH_3	3.3 (3.4)	2.9 (3.0)	4.9	–
3	C_I(IV), Ru	CH_3	12.6	–	–	–
4	C_I(IV)	C_3H_5	3.9 (3.7)	(3.4)	5.2	2.5
5	C_I(III)	C_3H_5	> 3.9	–	–	–
6	C_I(IV)	$C_{10}H_{15}O$	3.3[c]	–	–	–
7	C_I(III)	$C_{10}H_{15}O$	> 9.7[d]	–	–	–
8	C_I(IV), L = ImH	C_3H_5	(1.3)[e]	(0.7)	–	–
9	C_I(IV), L = $MeSO_3^-$	C_3H_5	1.9[f]	(1.5)	–	–
b) Epoxidation						
10	C_I(IV)	Fe−O−CH_2CH_2˙	2.3	–	–	–
11	C_I(III)	Fe−O−CH_2CH_2˙	7.2	–	–	–
12	C_I(IV)	Fe−O−CH_2CH˙(CH_3)	0.7 (0.9)	(0.3)	(0.6)	2.6
13	C_I(III)	Fe−O−CH_2CH˙(CH_3)	> 9	–	–	–

[a] In kcal/mol. Unless indicated otherwise, the proximal ligand L is thiolate, SH^-, and the transition metal is iron, Fe. All calculations refer to B3LYP/LACVP. [b] Energy values calculated with Jaguar. Energy values in parentheses calculated with Gaussian 98. [c] Camphor rebound barrier in the gas phase from ref.[31] [d] Estimated energy barrier of camphoryl rebound in the enzyme P450cam as calculated by QM/MM (value taken from the highest point in the scan, from ref.[52]). [e] Unpublished results using Cpd I model of HRP. [f] Unpublished results using Cpd I model of Woggon's reagent.

 © 2004 Wiley-VCH Verlag GmbH & Co. KGaA, Weinheim

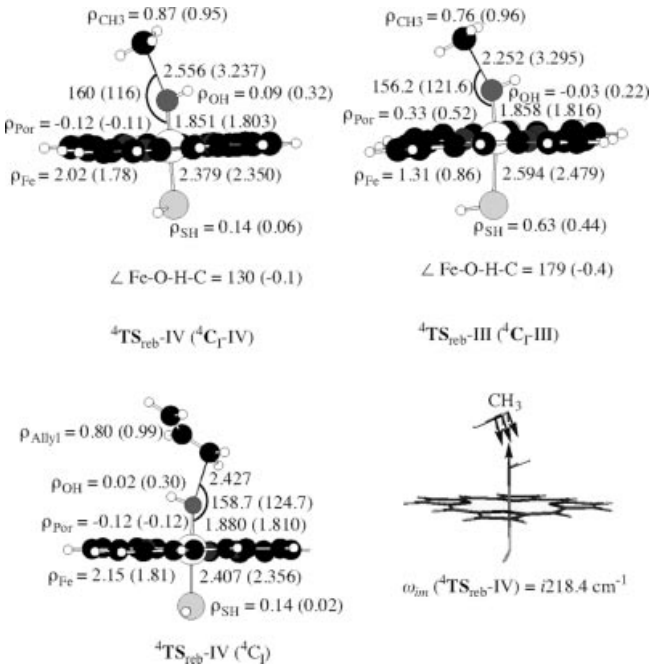

Figure 5. Rebound transition states for the **HS** process, $^4TS_{reb}$, with key geometric values and spin densities (ρ); the right-hand bottom drawing exemplifies the reaction vector (imaginary mode) for the methyl rebound $^4TS_{reb}$ species of the Fe^{IV} electromer

lation on this top structure revealed the imaginary mode displayed in the figure. It can be seen that this mode has no rebound component and is a pure rotational motion that connects the OH···C-coordinated ^2C_I(IV) conformer to the rebound conformer by a direct C···O contact. Since the latter conformer is not a real minimum, nor a saddle point, it falls abruptly to the alcohol complex product. Such rotational structures were found also for the ^2C_I(IV) intermediate of methyl radical where the imaginary rotational mode ($\omega = i92.4$ cm^{-1}) involved coupled rotation of the OH group and the methyl radical (see Supporting Information). Similar results were reported by Kamachi and Yoshizawa,[31] who located an **LS** rebound transition state with a purely rotational reaction vector ($\omega = i29.4$ cm^{-1}). The orientational nature of these structures is further evident by noting that they involve very little, if any, change in structure and spin-density distribution compared to the ^2C_I(IV) intermediate (see ρ and bond lengths in Figure 6). All the ^2C_I(III) intermediates for both allyl and methyl radicals either fell down to the corresponding alcohol products, or exhibited featureless rotational profiles en route to the products, ^2P, with structures having two or three imaginary modes corresponding to internal rotations within the cluster. Qualitatively identical results were found in our QM/MM study of the rebound process.[52]

It follows that the weak FeOH···C(Alk˙) hydrogen bond forms a flat rotational ridge that separates the **LS** iron−hydroxo/(Alk˙) intermediate and the product alcohol complex. Once the alkyl radical snaps out of this interaction, the rebound itself is a continuous downhill process. These orientational barriers amount to 0.3−1.5 kcal·mol^{-1}

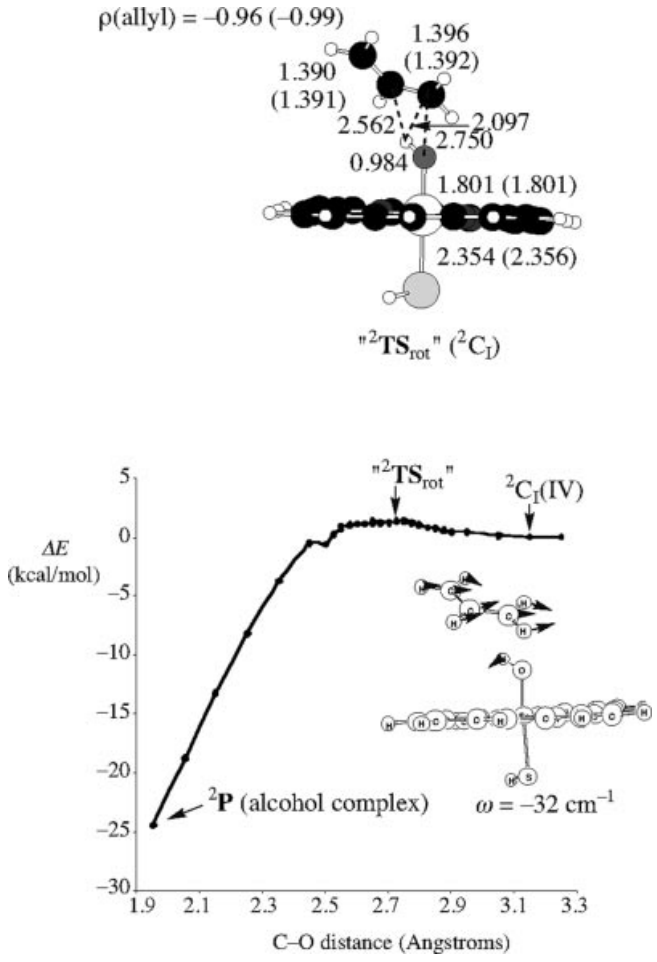

Figure 6. Illustration of the energy profile for an **LS** rebound process of the allyl radical; the topmost structure, "$^2TS_{rot}$", corresponds to a coupled rotation of the allyl radical and the OH group to assume a rebound position with a direct C···O contact; the arrows indicating the imaginary mode of "$^2TS_{rot}$" illustrate this coupled rotation; the structures on top correspond to the "$^2TS_{rot}$" species and to its precursor cluster, ^2C_I; note the virtual identity in the geometric features, and in the spin densities (ρ) of "$^2TS_{rot}$" and ^2C_I

for the various systems studied in our group. This analysis of the **LS** rebound is supported nicely by the results of the **LS** rebound in olefin epoxidation, where *the radicals are not coordinated by hydrogen bonding* to the iron−oxo complex and have barrierless rebound processes.[25,27] In conclusion, therefore, the barriers for **HS** rebound will be significantly higher than those for the **LS** rebound. Accordingly, we may expect that the lifetime of the radical on the **LS** surface will be much shorter than on the **HS** surface, and be limited by the rotational mode that the alkyl group (or OH) has to perform to establish rebound position.

The question is: Will the radical on the **LS** surface have sufficient lifetime to rearrange, or will the entire **LS** hydroxylation process be effectively concerted, while all the rearranged products will be originating in the **HS** process? In P450 hydroxylation, the rebound barriers on the **HS** surface are of the order of ≥ 4 kcal·mol^{-1} (Table 1), and are larger for the ferric states, ^4C_I(III), and within a polarizing en-

 © 2004 Wiley-VCH Verlag GmbH & Co. KGaA, Weinheim

vironment. These **HS** rebound barriers are larger than, or of the order of, the barriers for skeletal rearrangements of radicals,[57] for face-flip modes leading to inversion of chirality in the product, and for a heme alkylation process.[58] By contrast, these barriers are much larger than the ones for positional swing modes, such as migration of allylic groups that leads to allylic scrambling.[27,59] *As such, we may anticipate that the **HS** pathway will give rise to anisotropical scrambling of the stereochemical information*, in a manner that depends on the barriers for the various rearrangement modes vis-à-vis the rebound barrier, as well as on the protein environment, which restricts some modes more than others. By contrast, the reorientational barriers on the **LS** surface, about 0.3−1.5 kcal·mol^{-1}, are smaller than the barriers for skeletal rearrangement in typical clocks. In this sense, the **LS** rebound will be effectively concerted. The only rearrangement modes that may compete with the **LS** rebound are softer ones (e.g., swing), which radical clocks may be able to perform, provided no restrictions exist in the protein pocket (see ref.[21] for a similar discussion).

Finally, any quantitation of the rearrangement problem is based on the assumption that the rate of radical rearrangement in the clusters, ^4C_I, is roughly the same as that of the free radicals. Recent B3LYP/LANL2DZ(6-31G*) results by Clark[60] show that the barrier for rearrangement of the cyclopropylcarbinyl radical complexed to metal ions is about 1 kcal·mol^{-1} higher than the barrier for the free-radical rearrangement. Our own results for *trans*-phenylcyclopropylcarbinyl radical show that the rearrangements for the free radical have slightly (0.6 kcal·mol^{-1}) higher barriers than the coordinated ones.[61] These results indicate that the coordination of the radical does not dramatically change its rearrangement rate. What may change it, however, are the constraints within the protein pocket. But as yet there is no such hard evidence that can contest the assumption behind the clock experiments, namely, that the rate of rearrangement of the clock can be approximated by those of the free-radical rearrangement data.[15−19]

Origins of the Differences between LS and HS Rebounds

The difference between the **HS** and **LS** rebound processes has a fundamental origin. This can be appreciated by appeal to Figure 7, which depicts in part (a) the electronic structural changes attending the rebound processes of the ferryl $^{4,2}C_{reb}$(IV) species to the respective alcohol complexes, ^{4,2}P. During these transformations, the iron center is enriched by one electron, $Fe^{IV} \rightarrow Fe^{III}$. At the same time the Alk(C)···O linkage loses one electron and becomes a standard two-electron C−O bond. Starting from $^{4,2}C_{reb}$(III) in part (b), the porphyrin radical cation gains the electron that is lost from the C···O linkage. Thus, during rebound, *the C−O bond formation is attended by a single electron shift formally from the alkyl radical to the heme moiety.* This is common to both **LS** and **HS**. However, while in the **LS** process the electron is shifted to the low-lying orbitals (π^*_{xz} and a_{2u}), in the **HS** rebound the electron is shifted to the high-lying $\sigma^*(d_z^2)$ orbital in order to conserve the quartet spin.

As illustrative examples, we show in Figure 8 the spin-density variation along the methyl rebound path of the ferric cluster for the **HS** and **LS** states. In both states, the free spins on the methyl and porphyrin moiety diminish; however, while in the **LS** state the spin on the iron atom does not vary much, in the **HS** state the spin on the iron atom increases from an initial value of unity to about 2.5 at the end of the rebound. Therefore, relative to the **LS** rebound, the **HS** process involves an additional electronic

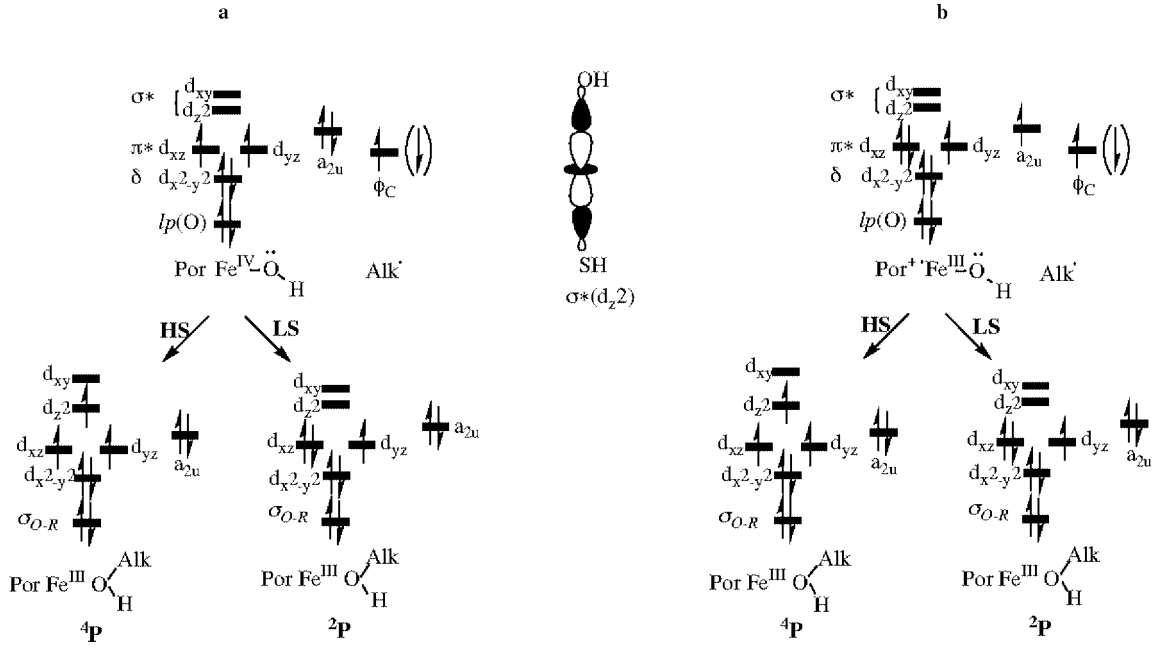

Figure 7. Orbital diagrams showing the electronic changes during rebound: (a) for the ferryl species, $^{4,2}C_I$(IV), and (b) for the ferric species, $^{4,2}C_I$(III); the $\sigma^*(d_z^2)$ orbital is drawn in between the diagrams

 © 2004 Wiley-VCH Verlag GmbH & Co. KGaA, Weinheim

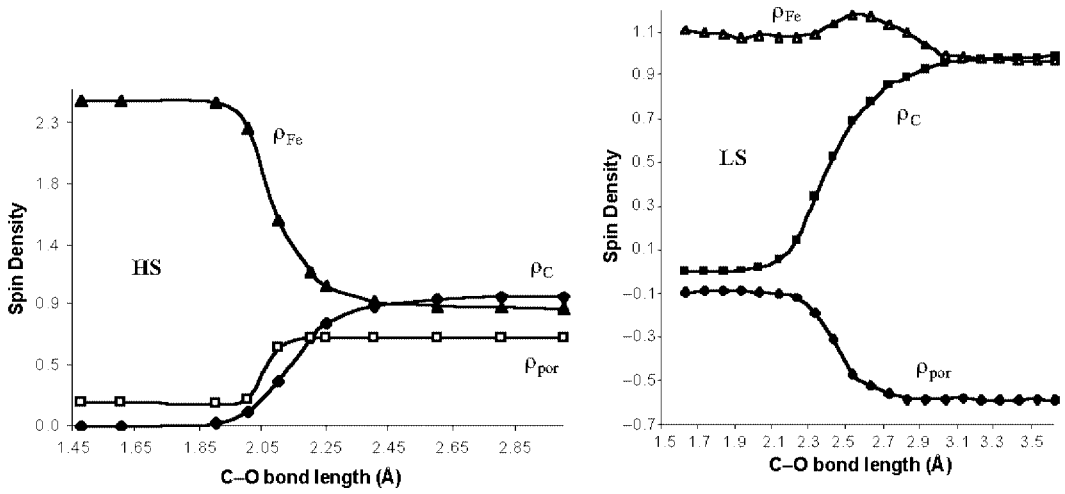

Figure 8. Spin-density (ρ) variation along the **HS** and **LS** rebound steps in methane hydroxylation; ρ_C corresponds to the spin on the methyl group, ρ_{Por} on the porphyrin and ρ_{Fe} on the iron atom

excitation within the d-block orbital.[23−25] This additional promotion to the σ*(d_z^2) orbital, which is antibonding in the S−Fe−O axis (Figure 7), is responsible for the lengthening of both Fe−S and Fe−O bonds in the $^4TS_{reb}$ species in Figure 5, and for the increase of the spin density on the iron atom and its decrease on the porphyrin in Figure 8. In turn, the lengthening of the Fe−O and Fe−S bonds is responsible for the **HS** rebound barrier. The role of the d_z^2(σ*) orbital is apparent by looking at the angle ∠FeO-C(Alk) in the $^4TS_{reb}$ species (Figure 5). This angle is very wide, ca. 156−160°, compared with the much smaller angle in the corresponding clusters, and it thereby indicates that the accepting orbital is σ*(d_z^2) that lies along the Fe−O axis (see orbital depiction in Figure 7).

In contrast with the **HS** process, the **LS** rebound does not require this electronic promotion. As such, during the **LS** rebound the Fe−S undergoes shortening and becomes strengthened; for example, in the case of allyl radical **LS** rebound, the Fe−S bond is shortened by about 0.2 Å for the various ^2C_I(III,IV) situations.[23,27] Part of this bond shortening is no doubt responsible for the fact that the **LS** rebound is considerably more exothermic (Figure 2) than the **HS** rebound, by ca. 7 kcal·mol^{-1} (for methyl) and 13 kcal·mol^{-1} (for allyl). Thus, the Fe−S bond shortening mitigates the energy rise due to the Fe−O bond lengthening and evidently eliminates altogether the rebound barrier in the **LS** manifold.

A Valence Bond (VB) Modeling of the Barrier for the Rebound Process

To outline a systematic structure-reactivity relationship for the rebound process, we present here a valence bond (VB) analysis of the origins of the barrier in the rebound step.[62] The oxidation-state changes, discussed above, which attend the rebound process correspond to an avoided crossing of the characteristic VB structures that possess these oxidation states. A typical VB diagram is shown in Figure 9, along a ''reaction coordinate'' that converts the ferryl rebound cluster (at the left hand extreme) to a ferric−alcohol complex (at the right hand extreme). A similar diagram will correspond to the conversion of the ferric intermediate, C_I(III), to the ferric−alcohol product. These valence-bond crossing patterns were recently verified computationally by creating the vertical states of the diagram and subsequently monitoring their crossover through the changes in charge and spin density on the alkyl group during the **HS** and **LS** rebound pathways for the substrate *trans*-1-isopropyl-2-phenylcyclopropane.[63]

The ground state, on the left-hand side, corresponds to a ferryl, C(IV), cluster. The excited state involves *an ion-pair* that corresponds to the vertical state in which the electron from the alkyl radical has been shifted to the iron−hydroxo moiety, to an orbital that depends on the spin state and oxidation state of the iron−hydroxo species, as discussed above in Figure 7. The vertical excited state correlates directly to the ground state of the alcohol complex product, on the left-hand side, since they possess essentially the same electronic structure. On the other hand, the ground state on the left-hand side correlates to an excited state of the alcohol product complex, in which one electron is excited from the π*(d_{xz}) orbital into the σ*(C−O) orbital. Since the two VB states have the same symmetry properties, they can mix with each other and avoid the crossing leading to an adiabatic state, which is lower by an amount *B* than the crossing point, and which corresponds to the transition state for rebound.

The rebound barrier is given by the following equation:[62]

$$\Delta E^{\ddagger}_{reb} = fG - B; f < 1 \quad (1)$$

Here, *G* is the vertical gap between the VB structures at the onset of the diagram, and *f* is the fraction of this excitation gap that enters under the crossing point of the VB

 © 2004 Wiley-VCH Verlag GmbH & Co. KGaA, Weinheim

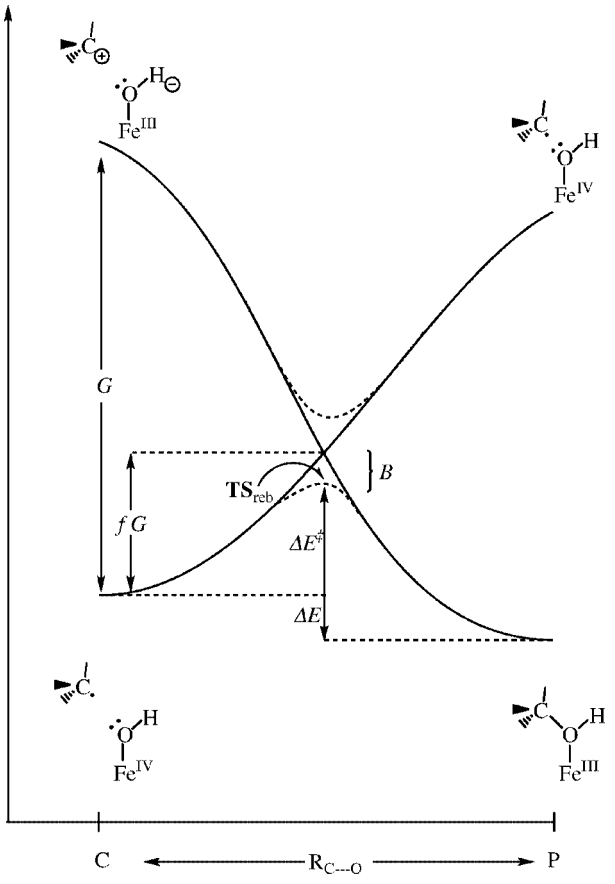

Figure 9. A valence-bond diagram (see ref.[62]) showing the origin of the rebound barrier; *G* is the vertical energy gap between the ground state of the rebound cluster, exemplified by C(IV) and the excited state where an electron was shifted to the iron d orbital; in the **LS** process the electron is shifted to the low-lying π* orbital (on the FeO moiety), while in the **HS** rebound the electron is shifted to the high-lying σ*(d_z^2) orbital; the quantity *fG* corresponds to the height of the crossing point, *B* to the quantum mechanical resonance energy due to the mixing of the valence bond forms, and Δ*E* to the energy difference between the cluster and the alcohol complex product

state curves. Finally, *B* is the VB mixing energy at the crossing point.

The vertical gap, *G*, depends on the spin state and is given by the following expression:

$$G_{\mathbf{HS}} = IP_{\mathrm{Alk.}} - EA_{\mathrm{FeOH}} + E_{\mathrm{el}} + \Delta E_{\pi^*\rightarrow\sigma^*} \quad (2a)$$

$$G_{\mathbf{LS}} = IP_{\mathrm{Alk.}} - EA_{\mathrm{FeOH}} + E_{\mathrm{el}} \quad (2b)$$

where *IP* is the ionization potential, *EA* the electron affinity, and E_{el} the electrostatic energy in the ion pair. The **HS** gap is seen to involve the additional excitation energy term, $\Delta E_{\pi^*\rightarrow\sigma^*}$, to the $d_z^2(\sigma^*)$ orbital. Calculated at the LACVP(6-31G) level, this quantity is ca. 24 kcal·mol^{-1}. The second factor, *f*, depends, inter alia, on the thermodynamic driving force of the rebound step, Δ*E*, and becomes smaller the more exothermic the rebound is.[62] Since the **LS** rebound is considerably more exothermic (Figure 2) than the **HS** rebound (e.g. by 13 kcal·mol^{-1} for allyl rebound), the *f* factor will depend on the spin state such that:

$$f_{\mathbf{LS}} < f_{\mathbf{HS}} \quad (3)$$

Therefore the height of the crossing point for the **LS** rebound will be considerably smaller than that for the **HS** rebound:

$$f_{\mathbf{LS}}G_{\mathbf{LS}} << f_{\mathbf{HS}}G_{\mathbf{HS}} \quad (4)$$

The calculated gas-phase electron affinity of the iron−hydroxo species is quite large, 63 kcal·mol^{-1} at the LACVP(6-31G) level, and in a polarizing medium (ε = 5.7) it goes up to about 100 kcal·mol^{-1}. The *IP* of radicals like allyl or cyclopropylcarbinyl is 180 kcal·mol^{-1}, and it goes down further in a polarizing medium [for allyl radical *IP*(ε = 5.7) = 131 kcal·mol^{-1}]. Thus, after inclusion of the electrostatic interaction, E_{el}, between the cation and the anion, the gap factor for the **LS** process of typical radicals (allyl, cyclopropylcarbinyl, etc.) would be rather small — $G \approx 60$ kcal·mol^{-1}. Using a typical value of $f = 0.25$, the *fG* term will be rather small, approximately 15 kcal·mol^{-1}. Since VB mixing further lowers the state by an amount *B*, which itself is of the order of 15 kcal·mol^{-1},[62] the **LS** rebound barrier will have an exceedingly small value or be virtually eliminated, as indicated by the DFT calculations. By contrast, the barrier for the **HS** rebound will persist and be significant, due to the additional excitation to the $d_z^2(\sigma^*)$ orbital and the poorer exothermicity factors. Using the computed values of the **HS** excitation energy, $\Delta E_{\pi^*\rightarrow\sigma^*}$, and a typical value for *f* ($f = 0.25$)[62] predicts that the **HS** barrier will be 6 kcal·mol^{-1} higher than the **LS** process. This is not too far from the DFT-computed difference.

The role of the excitation term to the $d_z^2(\sigma^*)$ orbital is further illustrated by the dependence of the barrier on the identity of the proximal ligand (Table 1). Thus, for thiolate, which interacts strongly with the iron atom, the $d_z^2(\sigma^*)$ orbital is high and the rebound barrier is significant. By contrast, imidazole (ImH) and methyl sulfonate ($MeSO_3^-$) proximal ligands, which are much poorer σ-binders, have much lower $d_z^2(\sigma^*)$ orbitals,[64] and consequently their rebound barriers decrease and virtually disappear, as seen in Table 1 (Entries 8 and 9).

A more striking effect is caused by changing the transition metal, i.e., when iron is replaced by ruthenium (Table 1). The 4d orbitals of ruthenium overlap much better with the 2p orbitals of the oxygen atom than the 3d orbitals of the iron atom.[28,65] Consequently, the $\sigma^*(d_z^2)$ orbital of the ruthenium−hydroxo species is much higher than the corresponding orbital of the iron−hydroxo one. This is the reason why the rebound barrier for ruthenium is almost four times larger than the corresponding barrier for iron.

The dependence of the **HS** rebound barrier on the oxidation state of the iron atom in the iron−hydroxo species can be understood by consideration of the term *B* in Equa-

 © 2004 Wiley-VCH Verlag GmbH & Co. KGaA, Weinheim

tion (1), by appeal to Figure 7. This term can be viewed as the C···O bonding energy in the transition state and along the rebound path. In the ferryl(IV) situation, the electron is shifted from the radical center directly to the $d_z^2(\sigma^*)$ orbital, and hence *B*(IV) is simply proportional to the overlap of these two orbitals, namely, $<\varphi_C|d_z^2(\sigma^*)>$. By contrast, in the ferric(III) situation, the electron cannot be shifted directly to $d_z^2(\sigma^*)$ due to spin frustration. Instead, while the spin-up electron in the φ_C orbital shifts into $d_z^2(\sigma^*)$, the spin-down electron in π^*_{xz} has to shift to a_{2u} to fill this orbital. Due to this higher order reorganization of the electronic structure, the factor *B*(III) is proportional to a product of orbital overlaps of the orbitals which participate in this electronic reshuffle, $<\varphi_C|d_z^2(\sigma^*)><\pi^*_{xz}|a_{2u}>$, and is hence smaller, namely:

$$B(\mathrm{IV}) > B(\mathrm{III}) \quad (5)$$

Since the two **HS** rebounds have approximately the same *G* and *f* factors, the stronger VB mixing for the ferryl situation will give rise to a smaller rebound barrier, as is indeed reflected by the data in Table 1.

Finally, further consideration of the term *B* shows that the rebound trajectory of the **LS** and **HS** processes must be quite different. In the **HS** rebound the electron shifts from the radical center to the $d_z^2(\sigma^*)$ orbital. Hence, to maximize the bonding term, *B*, the $^4TS_{reb}$ species must assume a structure with a large ∠FeOC angle, as is indeed shown in Figure 5 (∠FeOC ≈ 160°). By contrast, since the **LS** rebound [in the C(IV) electromer] involves a shift of the electron from the alkyl radical to the π^*_{xz} orbital, maximization of the O···C bonding along the rebound pathway requires an ∠FeOC angle of ≥ 90°. When one of these angular requirements cannot be met due to steric constraints, the corresponding barrier will increase. Such a case was recently encountered[63] in the rebound of aryl radicals, which resulted in rebound barriers in both **HS** and **LS** manifolds, since the required ∠FeOC angle of ≥ 90° for the **LS** path was barred by steric effects. These cases will not be discussed any further in the present Microreview.

Rearrangement Patterns of Radical Clocks

Clearly, the VB model in Figure 9 provides a consistent framework for analyzing and predicting trends in the rebound process. Let us now consider a series of probe substrates, which can form radicals that can undergo skeletal rearrangement, so that the unrearranged (*U*) and rearranged (*R*) forms of the radical can rebound and give rise to corresponding alcohol products, *U* and *R*, like the clock probes used by Newcomb et al.[15] The negative results of the slow clocks cannot be analyzed, but they enable us at least to bracket the barrier of the **HS** rebound to be smaller than the barrier for a slow probe like cyclopropyl carbinyl radical, which has a rearrangement barrier of approximately 6.9 kcal·mol^{-1}.[57] There are, however, [*U*/*R*] data that can be analyzed, and the question is: What can we predict for the measurable quantity [*U*/*R*], in a clock experiment?

For simplicity, we must consider a case where the only competing processes are the radical rearrangement and the **HS** and **LS** rebounds. Assuming that the **LS** rebound is effectively concerted, giving rise to only *U* products, and that the radicals on the **HS** manifold can give rise to both *U* and *R*, we can then make some predictions about the behavior of the quantity, $[U/R]_{HS}$, that arises from the **HS** rebound. A clear prediction can be made when the series meets the following conditions: (i) the rearrangement rate of the radicals is constant or quasi constant, (ii) the thermodynamics of the **HS** rebound does not vary in an adverse manner to the gap, and (iii) the rearrangement of the radical is irreversible, such that all rearranged radicals end up as rearranged alcohols.

The VB model (Figure 9) and the equation for the barrier [Equations (1) and (2)] tell us that when the above conditions hold true, the rebound barrier, $\Delta E^{\ddagger}_{reb}$, will depend on a single factor, the IP_{Alk} of the radical (within the protein pocket). The smaller the IP_{Alk} quantity, the lower the rebound barrier will be, and the shorter will be the radical lifetime on the **HS** manifold. Thus, for the above conditions, we expect that the $[U/R]_{HS}$ quantity, as well as the total [*U*/*R*], will increase as the IP_{Alk} decreases, i.e., as the radical becomes a better electron donor. Such a series was investigated by Newcomb et al.[15,17] who used clocks that are structurally related and have virtually identical rearrangement rate constants of ca. 10^{11} s^{-1}. These clocks are arranged in Scheme 5, in order of donor ability of the corresponding radical, and along with the measured [*U*/*R*] quantities. It can be seen that, in this series, which meets

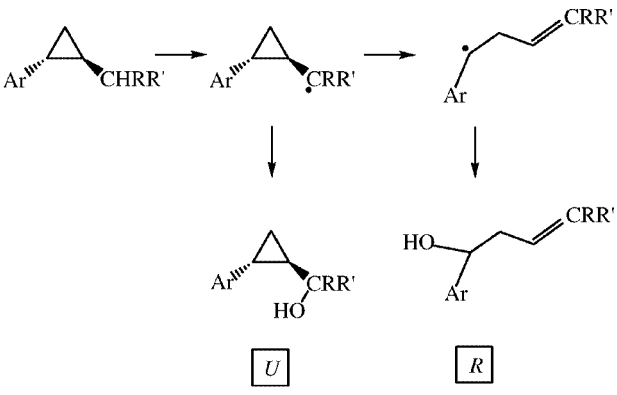

probe	Ar	R,R'	IP_{Alk}	[*U*/*R*]
2	*p*CF_3	H, H	highest	4
3	*p*H	H, H	⇑	4.3
4	*p*CF_3	H, CH_3		12
5	*p*H	H, CH_3		25
6	*p*H	CH_3, CH_3	lowest	> 100

Scheme 5. A rebound/rearrangement scheme for probe substrates (ref.[15]) and the variation of their [*U*/*R*] quantities with the ionization potentials of the corresponding alkyl radicals

 © 2004 Wiley-VCH Verlag GmbH & Co. KGaA, Weinheim

approximately the requirements stated above, the [*U*/*R*] quantity increases rapidly, with decrease of IP_{Alk}, from 4 to more than 100, as predicted by the above simple consideration. Our most recent calculations of the best donor substrate, **6**, in this series shows that, indeed, the **HS** rebound barrier vanishes, and as such both the **LS** and **HS** processes become effectively concerted.[63]

Interestingly, Newcomb, Lippard et al,[20,57] found that for MMO hydroxylation the probe substrate **3** gave no rearrangement at all, as opposed to the approximately 25% of rearranged alcohol observed during P450 hydroxylation of the same probe. This can be understood by recognizing that the electron affinity of the iron−hydroxo form of the enzyme MMO is significantly larger than that of the iron−hydroxo species of P450. As such, the energy gap factor, *G* [Equation (2)], for MMO rebound processes will generally be smaller than the same gap in P450 rebounds, leading to less rearranged products.

An interesting trend that can be predicted from the VB model refers to the effect of the strength of Fe−S binding on the **HS** rebound barrier. Weak binding will lower the energy of the $d_z^2(\sigma^*)$ orbital, and will therefore decrease the **HS** rebound barrier. Since rebound and rearrangement compete with one another, enhancement of the rebound rate will, in turn, decrease the amount of observed rearranged product. The polarity and acidity of the protein pocket affect the strength of the Fe−S bonding,[46,64,66,67] and one might therefore expect to find that the [*U*/*R*] quantity is different for different P450 isozymes. This conclusion means that [*U*/*R*] is not a pure property of the clock probe. Furthermore, studies by Newcomb et al.[38,68] and by Ortiz de Montellano and Groves et al.[21] show dependencies of the [*U*/*R*] quantity on the P450 isozyme. While we cannot rationalize the precise trends we can at least point out that the VB model predicts such behavior as the result of the variation of the Fe−S bonding with the identity of the isozyme. Presumably, this kind of information on the Fe−S bonding can ultimately be obtained by crystallography and spectroscopy.[66,69] Such a dependence of the [*U*/*R*] quantity on the identity of the isozyme is a clear demonstration that [*U*/*R*] does not measure intrinsic lifetimes of the radicals. Therefore one does not expect to find a correlation between this quantity and the rate of free-radical rearrangement, as indeed demonstrated in the study of Newcomb et al.[15]

What Does the [*U*/*R*] Quantity Actually Measure?

The above discussion considers the $[U/R]_{\mathbf{HS}}$ quantity that arises from the **HS** rebounds. However, the rebound also involves an **LS** component, and hence the total [*U*/*R*] quantity is a two-state information that must also be associated with the relative **LS/HS** yields, and not only with lifetimes as such. The question we wish to address here is: What mechanistic information is provided by the measured [*U*/*R*] quantity? One apparent aspect of the "rebound controversy" is that while the slow clocks do not lead to rearranged products, with the notable exceptions of norcarane and bicyclo[2.1.0]pentane,[20,21] the fast clocks undergo rearrangement, but lead to apparent lifetimes that are too short, sometimes as short as 70 fs.[15] Using the two-state approach enables us to understand this aspect, by appeal to Figure 2, and assuming that the **LS** pathway is effectively concerted (or leading to a negligible amount of rearranged products).

At the limit of independent **LS** and **HS** pathways with initial fractions *n* and (1 − *n*), respectively, the actual rate of rebound on the **HS** manifold is given by:[23,26]

$$k_{reb}^{(\mathbf{HS})} = k_r\{[U/R]_{tot} - F_{\mathbf{LS/HS}}\}/\{1 + F_{\mathbf{LS/HS}}\};\quad F_{\mathbf{LS/HS}} = [n/(1-n)]k_{\mathbf{LS}}/k_{\mathbf{HS}} \tag{6}$$

Here, $k_{\mathbf{LS}}$ and $k_{\mathbf{HS}}$ correspond to the rate constants for C−H bond activation for the **LS** and **HS** states, respectively, while $[U/R]_{tot}$ is the total ratio of unrearranged to rearranged products obtained from the two states:

$$[U/R]_{tot} = [(U_{\mathbf{HS}} + U_{\mathbf{LS}})/R_{\mathbf{HS}}] \tag{7}$$

The apparent rebound rate, which is quantified simply from the measured $[U/R]_{tot}$ quantity, is given on the other hand by:

$$k_{reb}^{(app)} = k_r[U/R]_{tot} \tag{8}$$

The lifetimes are inversely related to the rate constant of the rebound, and hence the ratio of the actual lifetime of the radical, on the **HS** manifold, to the apparent lifetime will be given by:

$$\tau^{(\mathbf{HS})}/\tau^{(app)} = \{[U/R]_{tot}(1 + F_{\mathbf{LS/HS}})\}/\{[U/R]_{tot} - F_{\mathbf{LS/HS}})\} > 1 \tag{9}$$

Clearly, the apparent lifetime is shorter than the actual one. The difference may be small if the relative yield quantity, $F_{\mathbf{LS/HS}}$, is close to unity. In such a case, the apparent lifetime is a reasonable approximation to the actual lifetime of the radical in the **HS** manifold. If, however, $k_{\mathbf{LS}}$ is significantly larger than $k_{\mathbf{HS}}$ and/or $n >> (1 - n)$, the result is that $F_{\mathbf{LS/HS}} >> 1$. In such a situation, the apparent lifetime will be much shorter than the actual one, leading to absurdly short lifetimes. Our recent computations of allylic hydroxylation show that under conditions that mimic the polarity and hydrogen bonding in the protein pocket, $k_{\mathbf{LS}}/k_{\mathbf{HS}}$ is approximately 10.[27,49] With such values of $F_{\mathbf{LS/HS}} \approx 10$, the apparent lifetime [Equation (8)] will be absurdly short.

In the general situation, $F_{\mathbf{LS/HS}}$ is predicted to increase[23] with the improved donor ability of the alkane, and hence to vary as the measured $[U/R]_{tot}$ quantity itself. Thus, in a series such as the Newcomb clocks in Scheme 5, the value of $F_{\mathbf{LS/HS}}$ will vary; its meaningful variation is limited by the requirement to produce only positive lifetimes. For example, with the probe **3** (Scheme 5), for which $[U/R]_{tot} \approx 4$, $F_{\mathbf{LS/HS}}$ should be < 4 (to yield a positive lifetime), while with the best donor probe, **6**, where $[U/R]_{tot} > 100$, $F_{\mathbf{LS/HS}}$

 © 2004 Wiley-VCH Verlag GmbH & Co. KGaA, Weinheim

is much larger since in this case both **HS** and **LS** processes rebound in a barrierless fashion,[63] such that, in fact, $[U/R]_{tot} \rightarrow \infty$. In any event, the actual lifetime will be longer than the apparent one by a factor N:

$$\tau^{(HS)} = N \cdot \tau^{(app)};\ N > 1 \quad (10)$$

For example, taking N to be equal to 10, the values of $F_{LS/HS}$ that will yield positive lifetimes must vary from < 3 to 9 in the Newcomb series in Scheme 5, while for $N = 5$, $F_{LS/HS}$ varies between < 2 and 4. This range of $F_{LS/HS}$ variation is reasonable, as can be judged from the DFT calculations that indicate preponderance of the **LS** process. Thus, we may bracket the value of N in Equation (10) between 5 and 10. With such N values in Equation (10), the radicals in the Newcomb series will possess real lifetimes of the order of picoseconds, which are reasonable lifetimes. Clearly, since the $[U/R]_{tot}$ quantity is a two-state information content, it does not measure the actual lifetime of the intermediate *but depends strongly on the relative yields of **HS** and **LS** reaction fluxes for a given total yield of products.*

There exist alternative scenarios, which can potentially reconcile the ''rebound controversy''. The common element to all the alternative models is that the apparent lifetime reflects the interplay of effects not present in a single state rearrangement of the ''free radical''. Let us mention three such alternative scenarios.

One possibility that has been proposed[3,10,60] is that, inside the protein, radical clocks rearrange much slower than the corresponding ''free radicals'', due to stereoelectronic constraints. This alternative has never been tested seriously, and merits evaluation. It will not, however, rule out the concomitant validity of the two-state picture.

The second scenario is the two-oxidant hypothesis[15] (Scheme 2), in which the second oxidant inserts hydroxonium ion and leads to rearrangements by anchimeric assistance typical to carbocations without having free carbocation intermediates. The problem with this otherwise perfectly legitimate hypothesis is the unknown nature of the second electrophilic oxidant. Ferric hydroperoxide, Cpd 0 (Figure 1), was tested and found to possess huge barriers for epoxidation[39,70] and sulfoxidation[40] compared with the same processes with Cpd I. This at least rules out the reactivity of Cpd 0 in the presence of Cpd I. Moreover, the sulfoxidation study[40] shows that the barrier would still be high even if the reaction of Cpd 0 were to be catalyzed by a potent proton source like H_3O^+ coordinated by a single water molecule. Thus, Cpd 0 appears to be a poor electrophile, which is expected to react only in the absence of Cpd I. Recent evidence shows that in mutants of P450, where the primary machinery of proton delivery that converts Cpd 0 to Cpd I is disrupted, the enzyme can still perform epoxidation but very sluggishly, and *it loses completely its hydroxylation capability.*[42] Thus, even if Cpd 0 functions as an oxidant, it is still doubtful, at least at the present state of experimental and theoretical understanding, that Cpd 0 can play a role in the hydroxylation mechanism.

The third alternative emerges from a recent study of a semiclassical molecular dynamics simulation of ethane hydroxylation by the enzyme MMO.[32] Applying this scenario to P450 requires a single intermediate species, which is the ^4C_I intermediate, FeOH···C(Alk), generated by a hydrogen-abstraction step. Since the hydrogen-abstraction transition state lies above the rebound transition state, part of the total reaction flux can bypass the intermediate and proceed in an effectively concerted process. In this process, the fast energy transfer of the excess energy to the OH rotational mode that is active in the rebound can carry the hydrogen-abstraction transition state directly to the final hydroxylation product, without residing in the well of the OH···C(Alk) intermediate. This concerted process results in alcohol products that conserve the stereochemical identity of the alkane. The other part of the reaction flux will pass through the well of the OH···C(Alk) intermediate, and be partitioned between rebound and rearrangement modes giving rise to a mixture of unrearranged and rearranged products. Thus, here too the $[U/R]_{tot}$ quantity reflects the interplay of two processes, one effectively concerted and the other stepwise, precisely as described above for the two-state scenario. Moreover, using the VB model (Figure 9) coupled to the dynamic scenario for analyzing the trends in the barrier of the stepwise component can, in principle, rationalize the behavior of the Newcomb probe series (Scheme 5). However, to be considered equally valid for the P450 enzyme, the dynamic scenario must fulfil the following two requirements. Firstly, the dynamics[32] have to be done within the protein environment, where fast dissipation of the excess energy to the protein modes may minimize the concerted component. Secondly, a proper dynamic study should prove or disprove the two-state scenario by including this aspect of the problem. Should such a study be carried out, and *should it indeed rule out the participation of two states*, this would then favor an original Groves mechanism,[59] within the formulation of a ''bound radical''.[32,54,55] Still, however, any mechanistic model of alkane hydroxylation must meet the challenge described in the following section.

The Product Isotope Effect and Its Mechanistic Significance in TSR

A product isotope effect (PIE) in the context of alkane hydroxylation means that when the hydrogen atom that is transferred from the alkane to the iron−oxo moiety is replaced by a deuterium atom, the product ratio $[U/R]$ will exhibit an isotope effect. *The observation of such an isotope effect means necessarily that the products U and R cannot be generated from a single intermediate or pathway and must be mediated by two pathways or from two sources.* The two-state scenario predicts that there should, in principle, be a product isotope effect (PIE) on the $[U/R]$ quantity, since U and R are produced from two pathways.[45]

To derive a simplified expression for the PIE, we assume that the rearranged alcohol is generated only on the **HS** process, and this leads to the following equation for the isotope effect on the $[U/R]$ quantity:

 © 2004 Wiley-VCH Verlag GmbH & Co. KGaA, Weinheim

$$[U/R]_H/[U/R]_D = \mathrm{PIE}[U/R] = [(k^H_{LS}/k^D_{LS})/(k^H_{HS}/k^D_{HS})]\{(k^D_r/k^H_r)[(k^H_r/k^D_{reb} + k^H_{reb}/k^D_{reb})/(1 + k^D_r/k^D_{reb})]\} = (IE_{LS}/IE_{HS})\{(1/IE_r)[(k^H_r/k^D_{reb} + IE_{reb})/(1 + k^D_r/k^D_{reb})]\} \quad (11)$$

Thus, the PIE[*U*/*R*] should depend on the ratio of intrinsic isotope effects (IEs) of the **HS** and **LS** hydrogen-abstraction steps (i.e. IE_{LS}/IE_{HS}), the isotope effect of rearrangement process (i.e. IE_r), and that of the rebound process (i.e. IE_{reb}). In the events that the rearrangement and rebound processes do not exhibit isotope effect, the expression becomes very simple, and depends only on the intrinsic IE ratio of the **LS** and **HS** hydrogen-abstraction steps, namely:

$$\mathrm{PIE}[U/R]_{TSR} \approx IE_{LS}/IE_{HS} \quad (12)$$

As such, for those systems where rearrangement and rebound processes are not subject to an isotope effect, the PIE[*U*/*R*] quantity can be predicted by straightforward DFT calculations of IE_{LS} and IE_{HS}. Using this equation, it is easily apparent that the two-state scenario would predict a product isotope effect, namely PIE[*U*/*R*] $\neq$ 1 unless the **HS** and **LS** transition states (TSs) happen to have accidentally identical structures, which they usually do not. Furthermore, the two-state mechanism predicts a substrate-dependent PIE[*U*/*R*], and this dependency can be understood by recalling,[5] that the maximal IE value is expected when the hydrogen-abstraction TS is "central" (i.e., having identical C···H and H···O bond orders/lengths), while smaller values are expected for TSs that are either "early" or "late". Thus, *the direction of the intrinsic PIE[U/R] (< 1 or > 1) quantity will generally reflect the relative positions of the hydrogen-abstraction transition states along the reaction coordinate, for the **HS** and **LS** processes.*

The ratios IE_{LS}/IE_{HS} were computed for the hydroxylation of methane,[45] propene,[27] ethane,[29,30] camphor,[31] and *trans*-1-methyl-2-phenylcyclopropane.[61] In the cases of methane, ethane and propene, the ratios are < 1, of the order of 0.7−0.8, while for camphor,[31] these ratios are either > 1 or close to 1, depending on the pattern of isotopic substitution, and on whether the IEs are inter- or intramolecular. Finally, for *trans*-[D_2]-1-methyl-2-phenylcyclopropane, the computed[61] intramolecular PIE[*U*/*R*] is 1.083−1.223, where the larger values include the effect of tunneling. Similarly, calculation of this quantity[61] for the intermolecular isotope effect (i.e., *trans*-1-methyl-2-phenylcyclopropane vs. *trans*-[D_3]-1-methyl-2-phenylcyclopropane) led to PIE[*U*/*R*] values of 0.943−1.123 where, again, the larger values involve strong tunneling correction. Other cases we studied,[63] show that the ratio of IE_{LS}/IE_{HS} can deviate from unity by as much as 40%, depending on the substrate.

Earlier experimental data by Newcomb and Ingold[37] for the two enantiomers of *trans*-1-methyl-2-phenylcyclopropane revealed ambiguous results, with values both smaller and larger than unity, PIE[*U*/*R*] $\approx$ 0.6−1.09, for the intermolecular isotope effect (i.e., *trans*-1-methyl-2-phenylcyclopropane vs. *trans*-[D_3]-1-methyl-2-phenylcyclopropane). By contrast, more recent data of Newcomb et al.[38] led to values larger than unity (e.g., the average PIE[*U*/*R*] $\approx$ 1.143) for the intramolecular isotope effect (using *trans*-[D_2]-1-methyl-2-phenylcyclopropane); the corresponding computed values using the TSR scenario[61] are 1.083−1.223. Despite this good agreement between theory[61] and the latter experimental results,[38] some qualification is in order. The experimental results are sensitive to very small changes in the percentages of the products, and gas chromatographic analysis of product distribution is subject to errors of 1−2%.[5] As such, without a proper error analysis, the recent experimental study[38] only shows that the [*U*/*R*] product ratio is likely to exhibit an isotope effect. Such an isotope effect means that the products *U* and *R* are generated by two pathways or from two sources. In this sense, the experimental results suggest the operation of TSR in alkane hydroxylation. However, should the experimental values[38] prove to be accurate, then the match between experiment and TSR theory will be a proof of principle for the operation of TSR in alkane hydroxylation.

Are There Carbocation Intermediates in P450 Hydroxylation?

Newcomb et al. have devised probes that can distinguish between cationic and radical rearrangements. One of these probes, **1** in Scheme 2, opens at the C−C bond that has an alkoxy substituent, which is the rearrangement mode expected for a carbocation intermediate. Similarly, Ortiz de Montellano, Groves et al.[21] and Newcomb et al.[20] have observed rearrangement products of norcarane that can be associated with a carbocationic rearrangement. However, Newcomb et al.[15] do not actually invoke free carbocations, but rather describe this typical rearrangement mode as being due to the presence of a protonated alcohol (nascent from OH^+ insertion, Scheme 2). By contrast, Ortiz de Montellano, Groves et al.[21] ascribe the small yield of these products to the presence of free carbocations generated by electron transfer (ET):

$$Alk^{\cdot} + \mathrm{PorFeOH} \rightarrow Alk^+ + \mathrm{PorFeOH}^-; \quad \Delta E_{ET} = IP_{Alk\cdot} - EA_{FeOH} \quad (13)$$

Right from the outset, it should be apparent that the ET process bears a resemblance to the rebound step, in the sense that in both cases the same two VB structures intersect (Figure 9). However, while during the rebound process this intersection occurs along a bond-making trajectory with a large VB mixing term *B*, and favorable exothermicity, in the ET process this will have to occur in an outer-sphere manner, with $B \rightarrow 0$, along a trajectory that avoids bond making and is thermodynamically less favorable. This typical competition between related bond-making and ET processes is well known,[62] and the bond-making process prevails unless bonding is blocked.

To assess the feasibility of ET, we calculated the energy change, ΔE_{ET}, of the reaction for a variety of alkyl radicals, using the ionization potential data in Table 2. The electron

 © 2004 Wiley-VCH Verlag GmbH & Co. KGaA, Weinheim

Table 2. Ionization potentials (in eV units) of a few radicals[a]

Entry	Radical	IP^{v}	IP^{ad}
1		8.05 (8.06)	~8.05
2		7.40	7.38
3	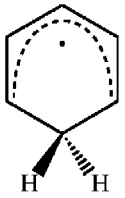	7.19	7.14
	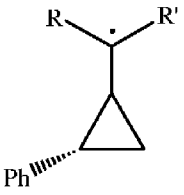 (closed) 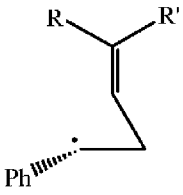 (open)		
4, R = R' = H			
4a	(closed)	7.97	
4b	(opened)	7.07	
5, R = H; R' = CH_3			
5a	(closed)	7.65	
5b	(opened)	7.03	
6, R = R' = CH_3			
6a	(closed)	7.40	
6b	(opened)	7.00	

[a] Calculated with the Green's function technique as described in refs.[74,75]

affinity of the iron−hydroxo species is 63 kcal·mol^{-1} in the gas phase, and 100 kcal·mol^{-1} in a polarizing medium with $\varepsilon = 5.7$. As we showed recently,[64] the thiolate ligand hampers the electron-acceptor properties of iron−porphyrin species, relative to non-thiolated alternatives, by as much as 30 kcal·mol^{-1} in a polarizing medium (and much more, 50−100 kcal·mol^{-1}, in the gas phase). Thus, with MMO, where the electron affinity of the diiron−hydroxo species is expected to be larger than the P450-derived iron−hydroxo one, the incursion of a carbocation species would be very much more feasible than in P450. Therefore, evidence of the presence of carbocations in MMO hydroxylations cannot constitute a proof for their existence also in the P450 reaction, unless the radical is a very good electron donor. For a radical like allyl, with calculated $IP_{allyl} = 186$ kcal·mol^{-1} (131 kcal·mol^{-1} in $\varepsilon = 5.7$) the electron-transfer reaction in Equation (13) is endothermic by 31 kcal·mol^{-1}. Even after inclusion of electrostatic interactions of ca. 14 kcal·mol^{-1} (for an ion-pair at 3 Å in an effective dielectric constant of a protein), the ET reaction is still endothermic. This should be the case for all the radicals in Table 2. However, for probes with $IP_{Alk\cdot} < 160$ kcal·mol^{-1} (< 106 kcal·mol^{-1} in $\varepsilon = 5.7$), one might anticipate an exothermic ET reaction with diffusive cationic species.

A bound carbocation that is coordinated to an iron−hydroxo anion is more likely to exist than a diffusive one. For example, in our recent study of benzene hydroxylation, we located an oxopentadienyl carbocation intermediate coordinated to the heme anion.[71] This carbocationic intermediate becomes more stable (by 4.9 kcal·mol^{-1}) than the corresponding radical in a polarizing medium ($\varepsilon = 5.7$). However, as shown in Figure 10a, the charge on the phenyl group (Q_{Ph}) is significantly less than unity. The species is therefore an intimate ion-pair with a significant degree of electronic conjugation between the radical and the iron−hydroxo moieties. To test the situation with a typical Newcomb probe system, we calculated[61] the putative cationic intermediate that can derive from *trans*-1-methyl-2-phenylcyclopropane, shown in Figure 10b. This is done by shifting the electron from the radical center on the organic moiety to the heme singly occupied orbital (π^* or a_{2u} orbital), and then letting the resulting species optimize its

 © 2004 Wiley-VCH Verlag GmbH & Co. KGaA, Weinheim

electronic structure. From the charges on the alkyl moiety (0.18−0.27), it is apparent that this species is not an ion-pair; the charge on the organic moiety is simply too small, as might be expected from its relatively high *IP* (Entry 4a in Table 2). A natural orbital analysis indicates that the species behaves as a mixed-valent state, where the electron resides partly on the radical and partly on the porphyrin in the a_{2u} orbital. This feature is depicted in Scheme 6, alongside the drawing of the natural orbitals that contain the population of 1.5 and 0.5 e^-. These orbitals are the bonding and anti-bonding combinations of the radical orbital, φ_C, and the a_{2u} orbital (the mixing is mediated by the π* orbitals of the FeO moiety). As such, this species is mostly the $Fe^{III}Por^{\cdot+}(R^{\cdot})$ species with a minor contribution from an intimate ion-pair form, $Fe^{III}Por(R^+)$. Even the best electron-donor radical in the Newcomb series (Table 2, Entry 6a) has an *IP* value close to benzene-derived pentadienyl radical (Entry 3). As such, this radical, too, generates a mixed species with a charge of +0.6 on the alkyl moiety.[63] It is doubtful that these species, even in the cases where they possess a large carbocationic character, will behave like free carbocations.

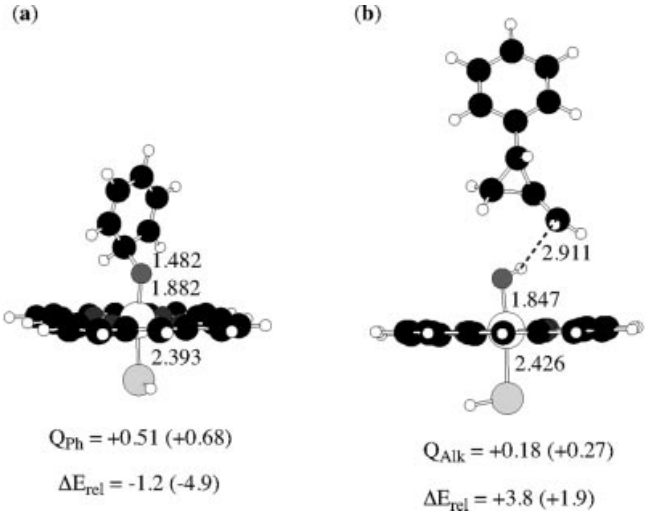

Figure 10. The geometric structures of (a) the ion-pair intermediate in benzene hydroxylation and (b) an analogous species in *trans*-1-methyl-2-phenylcyclopropane hydroxylation; below each structure we indicate the group charge of the organic moiety (*Q*) and the relative energy (ΔE_{rel}) to the radical intermediate (C_I) in vacuo (out of parentheses) and in a dielectric constant, ε = 5.7 (in parentheses)

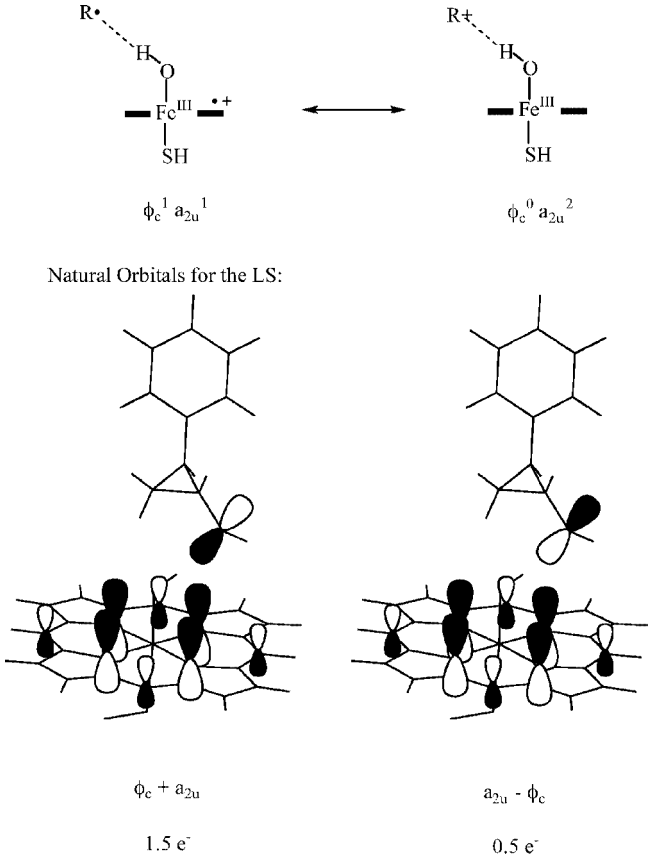

Scheme 6. The resonance structures that describe the "intimate ion-pair" species; the drawing below corresponds to the natural orbitals, which are mixtures of the radical orbital, φ_C, and the a_{2u} orbital, for the "intimate ion-pair" species derived from *trans*-1-methyl-2-phenylcyclopropane depicted in Figure 10b

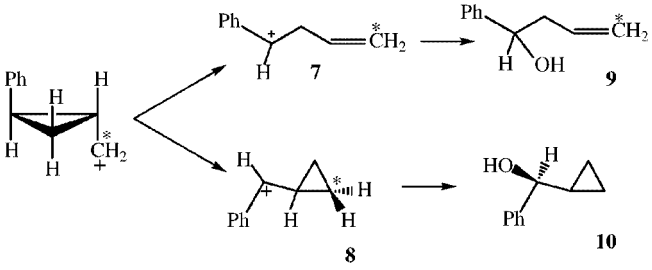

Scheme 7. The rearrangement patterns of "free" *trans*-2-phenylcyclopropylcarbinyl cation and the expected hydroxylation products

Our calculations of the rearrangement patterns of the free cation derived from *trans*-1-methyl-2-phenylcyclopropane reveals that the free cation would rearrange in a completely different manner than the corresponding radical, as summarized in Scheme 7. Alongside the "normal" rearrangement process to give **7**, the carbocation rearranges also to species **8**, in which the carbocation center is stabilized by both phenyl and cyclopropyl groups. The presence of **8** would have led to the hydroxylation product **10**, which, to the best of our knowledge, has never been reported.[15] We may therefore conclude that free carbocations are not present in the chemistry of these particular probes.

We cannot, however, rule out the presence of cations in other probes. Such cations can escape the intimate ion-pairing and be stabilized by the protein environment, subsequently undergoing typical rearrangements. How much of the carbocationic products does one expect? A direct ET to produce diffusive carbocations will always be less efficient than rebound or radical rearrangement (recall that the radical clocks rearrange very fast, e.g., $k_r \approx 10^{11}$ s^{-1}). This, in turn, would require that the amount of carbocation-derived products be smaller than the amount of radical-derived rearrangement. While some P450 hydroxylation data[16,21] indeed show that the amount of cation-derived rearranged

 © 2004 Wiley-VCH Verlag GmbH & Co. KGaA, Weinheim

product is marginally smaller than the amount of radical-derived products, other data[18,20] show the opposite trend. Alternatively, a carbocation intermediate of the intimate ion-pair type can arise directly from the C−H bond-activation phase by a hydride-abstraction process that competes with the radical-type hydrogen-abstraction process. This mechanism has not been observed yet and needs to be proven. Clearly the appearance of carbocation-derived products remains enigmatic and there is place for future experimental and theoretical studies of this issue.

Conclusion

The rebound controversy touches the limits of experimental capabilities to pinpoint complex reaction mechanisms. In such cases, theory can complement experiment by suggesting new alternatives. The two-state reactivity (TSR) scenario, which is supported by theory, provides such a paradigm. In TSR, radicals are produced on two different spin-state surfaces, and thereafter they react differently; on the low-spin surface rebound is barrierless, and hence the lifetime of the radicals is far too short to produce any rearranged products, while on the high-spin surface there is a substantial barrier for rebound, and hence the lifetime of the radical is sufficiently long so that rearrangement may compete with product formation by rebound. This paradigm provides a satisfactory rationale for the controversial findings in the field, and makes some verifiable predictions. Is this success merely accidental? This will have to be answered by future articulations of the concept.

One of the predictions of TSR is that the ratio of unrearranged to rearranged products, [*U*/*R*], is subject to an isotope effect that is substrate-dependent. Further complications in the TSR picture are caused by the presence of different electromeric states of the iron−hydroxo intermediates (Figure 2), and possibly of an intimate ion-pair carbocation, which has a mixed valent character, $PorFeOH^{-}\cdots Alk^{+} \rightleftarrows PorFeOH\cdots Alk^{\cdot}$. Finally, for sterically demanding rebound processes, as in the case of benzyl radicals for example, one may expect TSR with rebound barriers on both **HS** and **LS** manifolds. These aspects, as well as the spin crossover between the two spin states, still await a future treatment.

Theoretical Section

General Remarks: DFT calculations with the hybrid functional B3LYP were routinely used and are described in great detail in our work.[23,25,27,39,67] The calculations were carried out with JAGUAR 4.1[72] and GAUSSIAN 98 packages.[73] The standard basis involves a double zeta basis set which is called LACVP(6-31G), involving, on the iron atom, a Friesner basis set matched to an effective core potential, and a Pople 6-31G basis set on all other atoms. For some specified species, we also used more extended basis sets: one with polarization and diffuse functions on all heavy atoms, LACVP+*(6-31+G*), a fully polarized basis, LACVP**/6-31G**, and two triple zeta basis sets without and with polarization functions, LACV3P(6-311G) and LACV3P*(6-311G*). All species were characterized by geometry optimization and subsequent frequency calculations. Calculations of the species with a polarizing electric field were done with the solvent model in JAGUAR 4.1 (based on the Poisson−Boltzmann model) using a dielectric constant of $\varepsilon = 5.7$ and a probe radius, for the solvent, of 2.72 Å. Vertical ionization potentials were calculated using the outer valence Green's function (OVGF) technique, written by one of us (D. D.) and implemented in AMPAC.[74,75]

Acknowledgments

The research was supported in parts by grants (to S. S.) from the Israeli Science Foundation (ISF) and the German−Israeli Foundation (GIF).

[1] *Cytochrome P450: Structure, Mechanisms and Biochemistry* (Ed.: P. R. Ortiz de Montellano), 2nd ed., Plenum Press, New York, **1995**.
[2] J. T. Groves, G. A. McClusky, *J. Am. Chem. Soc.* **1976**, *98*, 859−861.
[3] P. R. Ortiz de Montellano, J. J. De Voss, *Natl. Prod. Rep.* **2002**, *19*, 1−18.
[4] J. T. Groves, G. A. McClusky, R. E. White, M. J. Coon, *Biochem. Biophys. Res. Commun.* **1978**, *81*, 154−160.
[5] A. Sorokin, A. Robert, B. Meunier, *J. Am. Chem. Soc.* **1993**, *115*, 7293−7299.
[6] M. H. Gelb, D. C. Heimbrook, P. Mälkönen, S. G. Sligar, *Biochemistry* **1982**, *21*, 370−377.
[7] M. Sono, M. P. Roach, E. D. Coulter, J. H. Dawson, *Chem. Rev.* **1996**, *96*, 2841−2888.
[8] W.-D. Woggon, *Top. Curr. Chem.* **1996**, *184*, 39−95.
[9] J. T. Groves, Y.-Z. Han, in *Cytochrome P450: Structure, Mechanism and Biochemistry* (Ed.: P. R. Ortiz de Montellano) 2nd ed., Plenum Press, New York, **1995**, pp. 3−48.
[10] B. Meunier, J. Bernadou, *Top. Catal.* **2002**, *21*, 47−55.
[11] H. Fretz, W.-D. Woggon, R. Voges, *Helv. Chim. Acta* **1989**, *72*, 391−400.
[12] P. R. Ortiz de Montellano, R. A. Stearns, *J. Am. Chem. Soc.* **1987**, *109*, 3415−3420.
[13] C. Audergon, K. R. Iyer, J. P. Jones, J. F. Darbyshire, W. F. Trager, *J. Am. Chem. Soc.* **1999**, *121*, 41−47.
[14] H. Lee, P. R. Ortiz de Montellano, A. E. McDermott, *Biochemistry* **1999**, *38*, 10808−10813.
[15] M. Newcomb, P. H. Toy, *Acc. Chem. Res.* **2000**, *33*, 449−455.
[16] M. Newcomb, R. Shen, S.-Y. Choi, P. H. Toy, P. F. Hollenberg, A. D. N. Vaz, M. J. Coon, *J. Am. Chem. Soc.* **2000**, *122*, 2677−2686.
[17] P. H. Toy, M. Newcomb, P. F. Hollenberg, *J. Am. Chem. Soc.* **1998**, *120*, 7719−7729.
[18] M. Newcomb, M.-H. Le Tadic-Biadatti, D. L. Chestney, E. S. Roberts, P. F. Hollenberg, *J. Am. Chem. Soc.* **1995**, *117*, 12085−12091.
[19] M. Newcomb, M.-H. Le Tadic, D. A. Putt, P. F. Hollenberg, *J. Am. Chem. Soc.* **1995**, *117*, 3312−3313.
[20] M. Newcomb, R. Shen, Y. Lu, M. J. Coon, P. F. Hollenberg, D. A. Kopp, S. J. Lippard, *J. Am. Chem. Soc.* **2002**, *124*, 6879−6886.
[21] K. Auclaire, Z. Hu, D. M. Little, P. R. Ortiz de Montellano, J. T. Groves, *J. Am. Chem. Soc.* **2002**, *124*, 6020−6027.
[22] N. Suzuki, T. Higuchi, T. Nagano, *J. Am. Chem. Soc.* **2002**, *124*, 9622−9628.
[23] F. Ogliaro, N. Harris, S. Cohen, M. Filatov, S. P. de Visser, S. Shaik, *J. Am. Chem. Soc.* **2000**, *122*, 8977−8989.

 © 2004 Wiley-VCH Verlag GmbH & Co. KGaA, Weinheim

[24] N. Harris, S. Cohen, M. Filatov, F. Ogliaro, S. Shaik, *Angew. Chem. Int. Ed.* **2000**, *39*, 2003−2007.
[25] S. P. de Visser, F. Ogliaro, N. Harris, S. Shaik, *J. Am. Chem. Soc.* **2001**, *123*, 3037−3047.
[26] S. Shaik, S. P. de Visser, F. Ogliaro, H. Schwarz, D. Schröder, *Curr. Opin. Chem. Biol.* **2002**, *6*, 556−567.
[27] S. P. de Visser, F. Ogliaro, P. K. Sharma, S. Shaik, *J. Am. Chem. Soc.* **2002**, *124*, 11809−11826.
[28] P. K. Sharma, S. P. de Visser, F. Ogliaro, S. Shaik, *J. Am. Chem. Soc.* **2003**, *125*, 2291−2300.
[29] K. Yoshizawa, Y. Kagawa, Y. Shiota, *J. Phys. Chem. B* **2000**, *104*, 12365−12370.
[30] K. Yoshizawa, T. Kamachi, Y. Shiota, *J. Am. Chem. Soc.* **2001**, *123*, 9806−9816.
[31] T. Kamachi, K. Yoshizawa, *J. Am. Chem. Soc.* **2003**, *125*, 4652−4661.
[32] V. Guallar, B. F. Gherman, W. H. Miller, S. J. Lippard, R. A. Friesner, *J. Am. Chem. Soc.* **2002**, *124*, 3377−3384.
[33] S. Shaik, M. Filatov, D. Schröder, H. Schwarz, *Chem. Eur. J.* **1998**, *4*, 193−199.
[34] F. Ogliaro, S. Cohen, M. Filatov, N. Harris, S. Shaik, *Angew. Chem.* **2000**, *112*, 4009−4013; *Angew. Chem. Int. Ed.* **2000**, *39*, 3851−3855. Erratum: *Angew. Chem. Int. Ed.* **2001**, *40*, 647.
[35] D. L. Harris, *Curr. Opin. Chem. Biol.* **2001**, *5*, 724−735.
[36] M. T. Green, *J. Am. Chem. Soc.* **1999**, *121*, 7939−7940.
[37] J. K. Atkinson, P. F. Hollenberg, K. U. Ingold, C. C. Johnson, M.-H. Le Tadic, M. Newcomb, D. A. Putt, *Biochemistry* **1994**, *33*, 10630−10637.
[38] M. Newcomb, D. Aebisher, R. Shen, R. Esala, P. Chandrasena, P. F. Hollenberg, M. J. Coon, *J. Am. Chem. Soc.* **2003**, *125*, 6064−6065.
[39] F. Ogliaro, S. P. de Visser, S. Cohen, P. K. Sharma, S. Shaik, *J. Am. Chem. Soc.* **2002**, *124*, 2806−2817.
[40] P. K. Sharma, S. P. de Visser, S. Shaik, *J. Am. Chem. Soc.* **2003**, *125*, 8698−8699.
[41] R. Davydov, T. M. Makris, V. Kofman, D. E. Werst, S. G. Sligar, B. M. Hoffman, *J. Am. Chem. Soc.* **2001**, *123*, 1403−1415.
[42] S. Jin, T. M. Markis, T. A. Bryson, S. G. Sligar, J. H. Dawson, *J. Am. Chem. Soc.* **2003**, *125*, 3406−3407.
[43] F. Hino, D. Dolphin, *Chem. Commun.* **1999**, 629−630.
[44] T. G. Traylor, K. W. Hill, W.-P. Fann, S. Tsuchiya, B. E. Dunlap, *J. Am. Chem. Soc.* **1992**, *114*, 1308−1312.
[45] F. Ogliaro, M. Filatov, S. Shaik, *Eur. J. Inorg. Chem.* **2000**, 2455−2458.
[46] J. C. Schöneboom, H. Lin, N. Reuter, W. Thiel, S. Cohen, F. Ogliaro, S. Shaik, *J. Am. Chem. Soc.* **2002**, *124*, 8142−8151.
[47] M. Filatov, N. Harris, S. Shaik, *Angew. Chem.* **1999**, *111*, 3730−3733; *Angew. Chem. Int. Ed.* **1999**, *38*, 3510−3512.
[48] M. T. Green, EXAFS data presented at the *12th International Conference on Cytochrome P450*, La Grande Motte, France, September 11−15, **2001**.
[49] S. P. de Visser, F. Ogliaro, P. K. Sharma, S. Shaik, *Angew. Chem. Int. Ed.* **2002**, *41*, 1947−1951.
[50] J. T. Groves, Z. Gross, M. K. Stern, *Inorg. Chem.* **1994**, *33*, 5065−5072.
[51] Z. Gross, S. Nimri, C. M. Barzilay, L. Simkhovich, *J. Biol. Inorg. Chem.* **1997**, *2*, 492−506.
[52] J. C. Schöneboom, S. Cohen, H. Lin, S. Shaik, W. Thiel, manuscript in preparation.
[53] F. Ogliaro, S. P. de Visser, S. Cohen, J. Kaneti, S. Shaik, *ChemBioChem* **2001**, *2*, 848−851.
[54] P. E. M. Siegbahn, R. H. Crabtree, *J. Am. Chem. Soc.* **1997**, *119*, 3103−3113.
[55] M. Torrent, D. G. Musaev, H. Basch, K. Morokuma, *J. Comp. Chem.* **2002**, *23*, 59−76.
[56] E. J. Mueller, P. J. Loida, S. G. Sligar, in *Cytochrome P450: Structure, Mechanism and Biochemistry* (Ed.: P. R. Ortiz de Montellano) 2nd ed., Plenum Press, New York, **1995**, pp. 83−124.
[57] K. E. Liu, C. C. Johnson, M. Newcomb, S. J. Lippard, *J. Am. Chem. Soc.* **1993**, *115*, 939−947.
[58] S. P. de Visser, F. Ogliaro, S. Shaik, *Angew. Chem. Int. Ed.* **2001**, *40*, 2871−2874.
[59] J. T. Groves, *J. Chem. Educ.* **1985**, *62*, 928−931.
[60] A. H. C. Horn, T. Clark, *J. Am. Chem. Soc.* **2003**, *125*, 2809−2816.
[61] D. Kumar, S. P. de Visser, S. Shaik, *J. Am. Chem. Soc.* **2003**, *125*, 13024−13025.
[62] S. Shaik, A. Shurki, *Angew. Chem. Int. Ed.* **1999**, *38*, 586−625; *Angew. Chem.* **1999**, *11*, 616−657.
[63] D. Kumar, S. P. de Visser, P. K. Sharma, S. Cohen, S. Shaik, *J. Am. Chem. Soc.*, in press.
[64] F. Ogliaro, S. P. de Visser, S. Shaik, *J. Inorg. Biochem.* **2002**, *91*, 554−567.
[65] F. Ogliaro, S. P. de Visser, J. T. Groves, S. Shaik, *Angew. Chem. Int. Ed.* **2001**, *40*, 2874−2878.
[66] T. L. Poulos, *J. Biol. Inorg. Chem.* **1996**, *1*, 356−359.
[67] F. Ogliaro, S. Cohen, S. P. de Visser, S. Shaik, *J. Am. Chem. Soc.* **2000**, *122*, 12892−12893.
[68] P. H. Toy, M. Newcomb, M. J. Coon, A. D. N. Vaz, *J. Am. Chem. Soc.* **1998**, *120*, 9718−9719.
[69] H. I. Liu, M. Sono, S. Kadkhodayan, L. P. Hager, B. Hedman, K. O. Hodgson, J. H. Dawson, *J. Biol. Chem.* **1995**, *270*, 10544−10550.
[70] T. Kamachi, Y. Shiota, T. Ohta, K. Yoshizawa, *Bull. Chem. Soc. Jpn.* **2003**, *76*, 721−732.
[71] S. P. de Visser, S. Shaik, *J. Am. Chem. Soc.* **2003**, *125*, 7413−7424.
[72] Jaguar 4.1, Schrödinger, Inc., Portland, OR, **1991−2000**.
[73] M. J. Frisch, G. W. Trucks, H. B. Schlegel, G. E. Scuseria, M. A. Robb, J. R. Cheeseman, V. G. Zakrzewski, J. A. Montgomery, Jr., R. E. Stratmann, J. C. Burant, S. Dapprich, J. M. Millam, A. D. Daniels, K. N. Kudin, M. C. Strain, O. Farkas, J. Tomasi,V. Barone, M. Cossi, R. Cammi, B. Mennucci, C. Pomelli, C. Adamo, S. Clifford, J. Ochterski, G. A. Petersson, P. Y. Ayala, Q. Cui, K. Morokuma, D. K. Malick, A. D. Rabuck, K. Raghavachari, J. B. Foresman, J. Cioslowski, J. V. Ortiz, A. G. Baboul, B. B. Stefanov, G. Liu, A. Liashenko, P. Piskorz, I. Komaromi, R. Gomperts, R. L. Martin, D. J. Fox, T. Keith, M. A. Al-Laham, C. Y. Peng, A. Nanayakkara, C. Gonzalez, M. Challacombe,P. M. W. Gill, B. Johnson, W. Chen, M. W. Wong, J. L. Andres, C. Gonzalez, M. Head-Gordon, E. S. Replogle, J. A. Pople, *Gaussian 98*, Gaussian, Inc., Pittsburgh PA, **1998**.
[74] D. Danovich, "Green's Function Method in Semiempirical Molecular Orbital Theory: Calculations of Ionization Potentials and Electron Affinities", in *Encyclopedia of Computational Chemistry* (Eds.: P. v. R. Schleyer, N. L. Allinger, T. Clark, J. Gasteiger, P. A. Kollman, H. F. Schaefer III), John Wiley & Sons, **1998**, vol. 2, p. 1190−1202.
[75] D. Danovich, Y. Apeloig, S. Shaik, *J. Chem. Soc., Perkin Trans. 2* **1993**, 321−329.

Received July 8, 2003

 © 2004 Wiley-VCH Verlag GmbH & Co. KGaA, Weinheim

Solid-State Models of Ion Solvation: Crystal Structures of Dimethyl Sulfoxide Solvates of Alkaline Earth Cations

Jack M. Harrowfield,[a] William R. Richmond,[b] Brian W. Skelton,[a] and Allan H. White*[a]

Keywords: Alkaline earth metals / Dimethyl sulfoxide solvates / Solid state structures / Solvent effects

Structural studies of the dimethyl sulfoxide solvates of the perchlorates of Mg, Sr and Ba show the presence of a variety of complex ion species indicative of the forms possible in solution. While $Mg(ClO_4)_2$·6dmso contains the expected $[Mg(dmso)_6]^{2+}$ cation, the crystallised strontium species contains a mononuclear $[Sr(dmso)_6]^{2+}$ cation and two dinuclear species, the complex $[(dmso\text{-}O)_5Sr(\mu\text{-}dmso\text{-}O)_3Sr(OH_2)(dmso\text{-}O)_3]^{4+}$ containing both seven- and eight-coordinate Sr metal centres, and $[\{(dmso\text{-}O)_5Sr(\mu\text{-}dmso\text{-}O)\}_2]^{4+}$ containing seven-coordinate Sr metal centres. The barium complex, of empirical formula $Ba(ClO_4)_2$·5dmso, contains a centrosymmetric dimer, $[Ba_2(dmso\text{-}O)_6(\mu\text{-}dmso\text{-}O)_4(O_2ClO_2)_2]^{2+}$, involving an unsymmetrically chelating perchlorate and a nine-coordinate Ba metal centre.
(© Wiley-VCH Verlag GmbH & Co. KGaA, 69451 Weinheim, Germany, 2004)

Introduction

In the sense that they are the end products of solvent removal from solutions, crystals and the species they contain may provide an indication of the species dominant in the most concentrated of solutions. In many instances, there is good evidence that the species characterised in crystalline solids are those predominant in relatively dilute solutions, though there is also evidence to the contrary.[1] At the very least nonetheless, species found in the solid state illustrate possible forms for solution species and, especially for elements which are either spectroscopically silent or inconveniently studied by spectroscopic methods, single-crystal X-ray diffraction measurements can provide by far the most efficient means of precisely defining the nature of the forms that dissolved solutes may take. This is particularly true for many metal derivatives, Sc^{III} providing an intriguing example,[2] and the case of $Pb(ClO_4)_2$ solvation by dimethyl sulfoxide (dmso) providing an example[3] of how seemingly simple stoichiometry may disguise some quite surprising coordination chemistry. In conducting an extensive structural study of solvated metal salts, we have found that dmso solvates of the alkaline earth cations provide remarkable examples of how complicated the nature of such solvates may prove to be.

Results and Discussion

Analytical characterisation of the recrystallised dmso solvates of the perchlorates of the alkaline earth metals is close to consistent with their formulations as $Be(ClO_4)_2$·4dmso[4] $Mg(ClO_4)_2$·6dmso, $Ca(ClO_4)_2$·6dmso, $Sr(ClO_4)_2$·6dmso and $Ba(ClO_4)_2$·5dmso. Given the knowledge that in numerous complexes of quite diverse ligands, the coordination number of Ba^{II} invariably equals or exceeds that of Sr^{II} in its direct analogue,[5] this fact alone indicates that some of these formulae may be oversimplified representations. In fact, this is not so for the Mg complex, for which the structure determination (Figure 1) provides a justification for its description as $[Mg(dmso\text{-}O)_6][ClO_4]_2$.

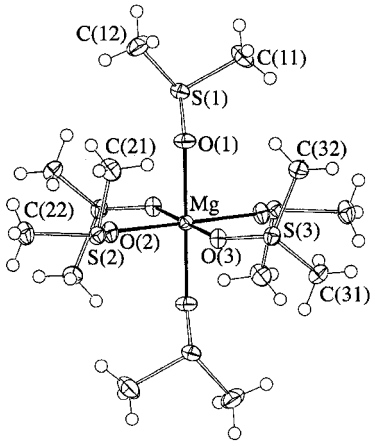

Figure 1. Projection of the centrosymmetric $[Mg(dmso\text{-}O)_6]^{2+}$ cation present in solid $Mg(ClO_4)_2$·6dmso; Mg−O(1,2,3) are 2.063(1), 2.084(1), 2.0512(9) Å, the maximum angular excursion from orthogonality being 88.60(4)°; Mg−O−S angles are 130.18(5), 127.51(7), 139.80(7)°

[a] Chemistry, School of Biomedical and Chemical Sciences, University of Western Australia,
35 Stirling Highway, Crawley WA 6009, Australia
[b] Nanochemistry Research Institute, Department of Applied Chemistry, Curtin University of Technology,
GPO Box 1987, Perth WA 6845, Australia

Although our numerous efforts to obtain crystals of both the Be and Ca complexes suitable for a structure determination have proved fruitless, so that strictly speaking the nature of the solid perchlorate species must be considered unknown, there would appear to be little doubt that the Be compound should contain tetrahedral $[Be(dmso\text{-}O)_4]^{2+}$ [4,6] while the octahedral $[Ca(dmso\text{-}O)_6]^{2+}$ species has been structurally characterised in association with two different anions.[7] The remaining two members of the alkaline earth series, however, provide some surprises. The Ba compound, which proves to have the "simpler" solid-state structure, is best formulated as the dimer $[Ba_2(dmso\text{-}O)_6(\mu\text{-}dmso\text{-}O)_4(O_2ClO_2)_2][ClO_4]_2$ and is related in structure to mixed-neutral-ligand species involving dmso[8] and dma (dimethylacetamide).[9] The dimer in the simple perchlorate (Figure 2) is centrosymmetric, with the (nine-) coordination geometry of the Ba atoms rendered somewhat irregular by the fact that four of the dmso-*O* donor atoms are bridging and one of the terminal sites on each Ba atom is occupied by unsymmetrically bidentate perchlorate [Ba−O 2.917(3), 3.056(3) Å]. If the perchlorate ligand is regarded as occupying a single coordination site, however, the geometry around the Ba metal centre is close to square antiprismatic. The perchlorate entities not found in the metal ion's primary coordination sphere appear to be involved in CH···O interactions with the dmso methyl groups (C···O approx. 3.3 Å), a mode of association which could presumably persist in solution. All the dmso molecules are coordinated and all by way of oxygen.

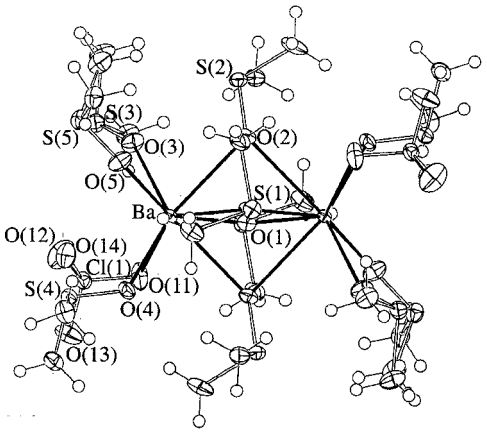

Figure 2. Projection of the centrosymmetric dinuclear cation $[(dmso\text{-}O)_3(O_2ClO_2)Ba(\mu\text{-}dmso\text{-}O)_2]_2^{4+}$; Ba−O($ClO_4$) are 2.917(3), 3.055(3); Ba−O(dmso) 2.663(3)−2.710(2), Ba-(μ-dmso-*O*) 2.797(3), 2.827(2) Å; Ba···Ba is 3.9406(4) Å; only partial atom labelling is shown for clarity

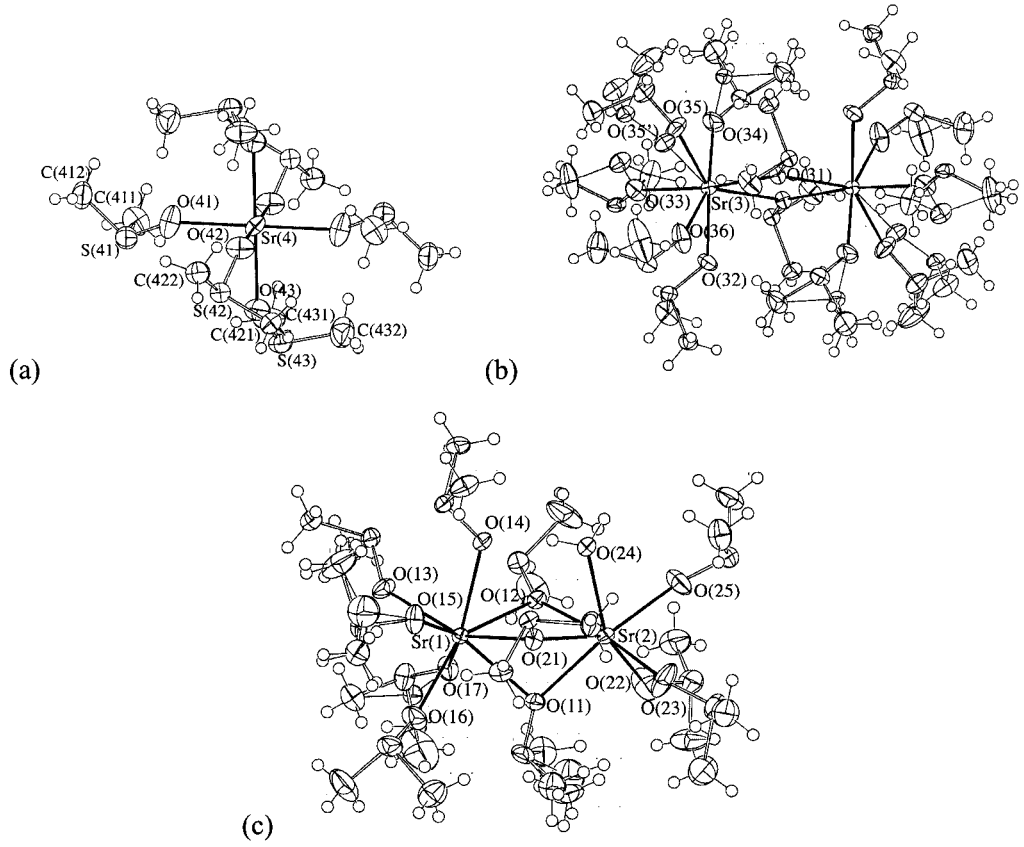

Figure 3. Projections of the cationic species in $Sr_7(ClO_4)_{14}\cdot 40dmso\cdot 2H_2O$; (a) the centrosymmetric $[Sr(dmso\text{-}O)_6]^{2+}$ cation, the maximum angular excursion from orthogonality being 91.6(2)°; Sr(4)−O(41,42,43) are 2.418(4), 2.452(5), 2.463(4) Å, corresponding Sr−O−S angles being 150.9(3), 133.0(2), 142.7(3)°; (b) the centrosymmetric $[(dmso\text{-}O)_5Sr(\mu\text{-}dmso\text{-}O)_2Sr(dmso\text{-}O)_5]_2^{4+}$ cation; Sr(3)−O(31,31′) are 2.548(3), 2.692(4), while Sr−O(unidentate dmso) range between 2.473(10) and 2.524(3) Å; (c) the $[(dmso\text{-}O)_5Sr(\mu\text{-}dmso\text{-}O)_3Sr(OH_2)(dmso\text{-}O)_3]_2^{4+}$ cation; Sr(2)−O(11,12,21) are 2.582(4), 2.490(3), 2.584(3) Å; Sr(1)−O(11,12,21) 2.659(3), 2.634(4), 2.623(3) Å, with Sr−O−Sr 94.2(1), 97.04(9), 95.01(9)°, and O(11)···O(12, 21), O(12)···O(21) 2.864(5), 2.724(5), 3.326(4) Å; Sr−O(unidentate) about Sr(2) are 2.451(4)−2.491(5) (dmso), 2.636(4) (OH_2) and about Sr(1) 2.507(5)−2.641(4) Å

 © 2004 Wiley-VCH Verlag GmbH & Co. KGaA, Weinheim

The complete coordination of dmso as an *O*-bound species is perhaps the only obvious common characteristic of both the Ba and Sr compounds. The structure determined for the Sr compound (Figure 3) shows that dmso is not the only solvent present and that the formula $Sr(ClO_4)_2$·6dmso is imprecise, a better representation being $[Sr_7(dmso)_{40}(OH_2)_2][ClO_4]_{14}$ or, better still, $[(dmso\text{-}O)_5Sr(\mu\text{-}dmso\text{-}O)_3Sr(OH_2)(dmso\text{-}O)_3]_2[\{(dmso\text{-}O)_5Sr(\mu\text{-}dmso\text{-}O)\}_2][Sr(dmso\text{-}O)_6][ClO_4]_{14}$. The presence of a water ligand may simply reflect the use of solvents which were not completely dried and may mean that different species could be obtained under different crystallisation conditions, but the particular phase presently obtained is nonetheless of interest, even if it only exemplifies possible structures. (It may also be noted that in some related systems,[8] only certain mixed solvent species are readily crystallised.) Extraordinarily, the lattice contains three distinct strontium-containing species, two of them dinuclear, in which none of them is perchlorate coordinated. Sr^{II} is found in five different coordination environments: close to regular octahedral six-coordination in the mononuclear $[Sr(dmso\text{-}O)_6]^{2+}$; irregular seven-coordination, as $[(O\text{-dmso})_5Sr(\mu\text{-}O\text{-dmso})_{(2/2)}]$, in the centrosymmetric dinuclear species, as well as in the partially aquated moiety of the unsymmetrical dinuclear species $[(dmso\text{-}O)_3(H_2O)Sr(\mu\text{-dmso-}O)_3]$; and irregular eight-coordination in the "homoleptic" component of the latter, $[(dmso\text{-}O)_5Sr(\mu\text{-dmso-}O)_3]$. The bridging units of the dinuclear arrays contain fewer (three and two) μ-dmso-*O* units than that of the above dinuclear barium species, where there are four. The mononuclear species [Figure 3(a)] is a very rare example of a homoleptic, six-coordinate Sr^{II} complex with neutral ligands, the homoleptic aqua complex, for example, being a $[Sr(OH_2)_8]^{2+}$ species.[10] There is considerable divergence in the Sr−O−S angles, but only a loose correlation between those values and their associated Sr−O distances. In the centrosymmetric dinuclear cation, [Figure 3(b)], the two Sr−O distances of the obligate planar central four-membered ring are similar and longer than the closely ranged unidentate donor distances. The stereochemistry is irregular; there is one outstandingly large angle [O(31)−Sr(3)−O(33) 171.3(1)°], but the remaining five donor atoms do not constitute an acceptable equatorial plane. All Sr−O distances are longer than those found in the six-coordinate array. Three of the unidentate dmso moieties in this array are affected by disorder; in two, this is resolvable only in the sulfur atom, distributed over positions corresponding to inversion, but in dmso (35) it is more widespread, affecting the coordinating oxygen. In the unsymmetrical aquated dinuclear cation, there are now three μ-dmso-*O* moieties, of an irregular disposition most obvious in the variation of their O···O distances, Sr−O for the eight-coordinate Sr^{I} being longer than those to the seven-coordinate Sr^{II} metal centre; the unidentate dmso-O−Sr distances follow a similar pattern, with Sr(2)−O(24) (OH_2) longer than Sr(2)−O(22,23,25).

Within the group of alkaline earth elements, the coordination chemistry of Sr^{II} generally shows closer similarities to that of Ca^{II} than Ba^{II}.[5,11] Thus, the detection of several species within crystalline solvated $Sr(ClO_4)_2$ salt can be seen as being consistent with the extensive evidence for the co-existence of various solvated forms of Ca^{II},[12] though a comparison in the particular case of dmso solvates cannot yet be made [except that the elemental analysis indicates the Ca^{II} solvate to have the composition $Ca(ClO_4)_2$·6dmso]. The higher coordination number (9) presently observed for Ba^{II} than the mean for Sr^{II} is associated with bidentate coordination of perchlorate, consistent with a rather general tendency for oxyanion coordination, especially through unsymmetrical chelation, to be prominent with very heavy metals.[13] Possibly significantly, however, is the eight-coordination for Sr^{II}, accompanied by anion coordination, is seen in solid $[Sr(dmso\text{-}O)_2(CF_3SO_3)_2]$.[14] The exploration of such subtleties by structural work can therefore be seen as providing an important contribution to the development of more sophisticated molecular models for electrolyte solutions. Following the suggestion of a referee, we note that one particular use of single-crystal data is to provide a coordination number associated with a given mean metal−donor atom distance, since solution X-ray measurements (LAXS, XAFS, EXAFS) frequently provide precise values for the latter but imprecise values for the former.[10b,12,14] Mean values for Sr−O (unidentate dmso) obtained from the present structures for six-, seven- and eight-coordination are 2.45(2), 2.50(2) and 2.56(3) Å, respectively, the value for seven-coordination being slightly less than that determined for $[Sr(dmso)_7]^{2+}$ in solution, although neither of the presently observed species containing seven-coordinate Sr is mononuclear.

Experimental Section

Synthesis and Crystal Growth

$Be(ClO_4)_2$·4dmso: Attempts to grow diffraction quality crystals of this known compound were unsuccessful.

$Mg(ClO_4)_2$·6dmso: Anhydrous $Mg(ClO_4)_2$ (1.0 g) was dissolved in ethanol (25 mL), dimethyl sulfoxide (5 mL) was added, followed by diethyl ether (25 mL) and the mixture was allowed to stand for 10 min as colourless crystals (1.90 g, 60 %) were deposited on the sides of the flask. These were recrystallised using the mixture of solvents, dmso/ethanol/diethyl ether, before crystals suitable for structural work were obtained by vapour diffusion of diethyl ether into a solution in dmso/ethanol (1:2). $C_{12}H_{36}Cl_2MgO_{14}S_6$ (692.0): calcd. C 20.83, H 5.24, S 27.80; found C 20.4, H 5.0, S (28.2).

"$Sr(ClO_4)_2$·6dmso": Concentrated perchloric acid (72 %) was added drop by drop to $SrCO_3$ (0.50 g) until most of the solid had dissolved. The mixture was transferred to a steam bath and heated. Acid addition was continued until a clear viscous solution had formed. This was heated for a further 2 min to ensure complete evolution of CO_2, then cooled to room temperature and dissolved in ethanol (40 mL). Dimethyl sulfoxide (10 mL) was added to this solution, followed by diethyl ether (50 mL). The mixture was cooled on ice to give a white, crystalline deposit (1.9 g, 75 %), which was then recrystallised twice from dmso/ethanol/diethyl ether. For elemental analysis, portion was dried by vacuum desiccation over silica gel. $C_{12}H_{36}Cl_2O_{14}S_6Sr$ (757.9): calcd. C 19.08, H 4.80, S 25.47; found C 18.9, H 4.4, S 25.1. $[Sr_7(ClO_4)_{14}$·40dmso·H_2O;

 © 2004 Wiley-VCH Verlag GmbH & Co. KGaA, Weinheim

calcd. C 18.66, H 4.74, S 24.91.] Crystals suitable for structure determination were obtained by vapour diffusion of diethyl ether into a solution of the recrystallised material in dmso/ethanol (1:2).

(The Ca analogue was prepared in the same way from $CaCO_3$. $Ca(ClO_4)_2{\cdot}6dmso = C_{12}H_{36}CaCl_2O_{14}S_6$ (708.1): calcd. C 20.4, H 5.15, Cl 10.0, S 27.2; found C 20.1, H 4.95, Cl 10.2, S 27.0. Large crystals of the complex could be obtained as for the Sr complex but they proved too fragile and too unstable for diffraction measurements to be possible.)

$Ba(ClO_4)_2{\cdot}5dmso$: $Ba(ClO_4)_2{\cdot}3H_2O$ was dissolved in dmso, ethanol and diethyl ether were added to give a white precipitate in quantitative yield. This was then twice recrystallised from dmso by addition of ethanol and diethyl ether. For analysis, the compound was dried by vacuum desiccation over silica gel. $C_{10}H_{30}BaCl_2O_{13}S_5$ (726.99): C 16.5, H 4.16, Cl 9.75; found C 16.9, H 4.22, Cl 10.0.

Structure Determinations (T ca. 153 K; monochromatic Mo-K_α radiation, $\lambda = 0.71073$ Å; Bruker AXS CCD instrument).

$Mg(ClO_4)_2{\cdot}6dmso$, $[Mg(dmso\text{-}O)_6][ClO_4]_2$: $C_{12}H_{36}Cl_2MgO_{14}S_6$ (692.0). Triclinic, $P\bar{1}$, $Z = 1$, $a = 7.6918(5)$, $b = 10.6220(7)$, $c = 10.6308(7)$ Å, $\alpha = 61.082(1)$, $\beta = 83.724(2)$, $\gamma = 84.696(2)°$, $V = 754.9$ Å^3. $D_c = 1.522$ g·cm^{-3}. $R = 0.037$, $R_w = 0.042$ for $N_o = 7706$ reflections [$F > 4\sigma(F)$] ($\theta_{max} = 60°$).

"$Ba(ClO_4)_2{\cdot}5dmso$", $[(dmso\text{-}O)_3(O_2ClO_2)Ba(\mu\text{-}dmso\text{-}O)_2]_2[ClO_4]_2$: $C_{20}H_{60}Ba_2Cl_4O_{26}S_{10}$ (1453.8). Monoclinic, $P2_1/c$, $Z = 2$ dinuclear f.u., $a = 12.046(1)$, $b = 20.560(2)$, $c = 11.5985(9)$ Å, $\beta = 110.140(2)°$, $V = 2697$ Å^3. $D_c = 1.790$ g·cm^{-3}. $R = 0.031$, $R_w = 0.040$ for $N_o = 6020$ ($\theta_{max} = 60°$). All anion and solvent species were fully ordered in the refinement, as was also true of the Mg adduct.

$Sr_7(ClO_4)_{14}{\cdot}40dmso{\cdot}2H_2O \equiv [(dmso\text{-}O)_5Sr(\mu\text{-}dmso\text{-}O)_3Sr(OH_2)(dmso\text{-}O)_3]_2[\{(dmso\text{-}O)_5Sr(\mu\text{-}dmso\text{-}O)\}_2][Sr(dmso\text{-}O)_6][ClO_4]_{14}$: $C_{80}H_{242}Cl_{14}O_{97}S_{40}Sr_7$ (5167). Triclinic, $P\bar{1}$, $Z = 1$ f.u., $a = 13.1158(6)$, $b = 19.651(1)$, $c = 23.224(1)$ Å, $\alpha = 67.478(1)$, $\beta = 75.279(1)$, $\gamma = 89.144(1)°$, $V = 5339$ Å^3. $D_c = 1.607$ g·cm^{-3}. $R_1 = 0.057$, $wR_2 = 0.072$ for No = 20926 (2θmax = 60°). Various anion and solvent components were modelled as disordered over pairs of sites, disordered fragment site occupancies refining to x, $1-x$ (minor components with isotropic displacement parameter forms), much seemingly concerted; thus for C(111, 112); S(15); S(172), C(172); S(34); O(60n); O(702−4), $x = 0.727(1)$, while for S(dmso 35); O(50n); $x = 0.5$. This affects the coordination sphere of Sr(3) where O(35)···O(35′) is 0.62(1) Å.

In the figures, non-hydrogen atoms are shown with 50 % probability amplitude displacement ellipsoids, hydrogen atoms having arbitrary radii of 0.1 Å. CCDC-14741, -214742 and -214743 contain the supplementary crystallographic data for this paper. These data can be obtained free of charge at www.ccdc.cam.ac.uk/conts/retrieving.html [or from the Cambridge Crystallographic Data Centre, 12 Union Road, Cambridge CB2 1EZ, UK; Fax: (internat.) + 44-1223/336-033; E-mail: deposit@ccdc.cam.ac.uk].

[1] [1a] I. Persson, F. Jalilehvand, M. Sandström, *Inorg. Chem.* **2002**, *41*, 192. [1b] G. Ma, A. Molla-Abbassi, M. Kritikos, A. Ilyukhin, F. Jalilehvand, V. Kessler, M. Skripkin, M. Sandström, J. Glaser, J. Näslund, I. Persson, *Inorg. Chem.* **2001**, *40*, 6432. [1c] J. Näslund, P. Lindqvist-Reis, I. Persson, M. Sandström, *Inorg. Chem.* **2000**, *39*, 4006. [1d] J. Näslund, I. Persson, M. Sandström, *Inorg. Chem.* **2000**, *39*, 4012 and references cited therein.

[2] S. A. Cotton, *Comments Inorg. Chem.* **1999**, *21*, 165.

[3] J. M. Harrowfield, B. W. Skelton, A. H. White, *J. Chem. Soc., Dalton Trans.* **1993**, 2011.

[4] P. A. Pittet, G. Elbaze, L. Helm, A. E. Merbach, *Inorg. Chem.* **1990**, *29*, 1936.

[5] See, for example: [5a] A. F. Waters, A. H. White, *Aust. J. Chem.* **1996**, *49*, 27 (see also pages 35, 61, 73, 87). [5b] D. L. Kepert, B. W. Skelton, A. F. Waters, A. H. White, *Aust. J. Chem.* **1996**, *49*, 47. [5c] B. W. Skelton, A. F. Waters, A. H. White, *Aust. J. Chem.* **1996**, *49*, 99, 137.

[6] L. Alderighi, P. Gans, S. Midollini, A. Vacca, *Adv. Inorg. Chem.* **2000**, *50*, 109.

[7] [7a] Q. Huang, X. Wu, J. Lu, *Inorg. Chem.* **1996**, *35*, 7445. [7b] S. Perruchas, F. Simon, S. Uriel, N. Avarvari, K. Boubekeur, P. Batail, *J. Organomet. Chem.* **2002**, *643*, 301.

[8] J-Y. Niu, Q. Wu, J-P. Wang, *J. Chem. Soc., Dalton Trans.* **2002**, 2512.

[9] P. Lemoine, P. Herpin, *Acta Crystallogr., Sect. B* **1980**, 2608.

[10] [10a] G. Thiele, D. Putzar, *Z. Naturforschung, Teil B* **1988**, *43*, 1224. [10b] I Persson, M. Sandström, H. Yokoyama, M. Chaudury, *Z. Naturforschung, Sect A* **1995**, *50*, 21. [10c] M. J. Hardie, A. Salinas, C. L. Raston, *Chem. Commun.* **2001**, 1850.

[11] D. E. Fenton in G. Wilkinson, J. A. McCleverty, R. D. Gillard (Eds.) *Comprehensive Coordination Chemistry*, Pergamon Press, Oxford, **1987**, vol. 3, ch. 23, p. 1.

[12] F. Jalilehvand, D. Spångberg, P. Lindqvist-Reis, K. Hermansson, I. Persson, M. Sandström, *J. Am. Chem. Soc.* **2001**, *123*, 431 and references cited therein.

[13] See, for example: [13a] J. M. Harrowfield, H. Miyamae, B. W. Skelton, A. A. Soudi, A. H. White, *Aust. J. Chem.* **2002**, *55*, 661 and references cited therein. A summary of literature concerning this issue for the lanthanides is contained in ref.[13b] [13b] J. M. Harrowfield in *Metal Ions in Biological Systems*, A. Sigel, H. Sigel (Eds.), vol. 40, ch. 4, p. 106, Marcel Dekker, New York, **2003**.

[14] G. Moreau, R. Scopelliti, L. Helm, J. Purans, A. E. Merbach, *J. Phys. Chem. A* **2002**, *106*, 9612.

Received August 21, 2003

 © 2004 Wiley-VCH Verlag GmbH & Co. KGaA, Weinheim

The Construction of $(N_2S_2)Ni-Pd$ Clusters: A Slant-Chair, a Basket and a C_4-Paddlewheel Structure

Melissa L. Golden,[a] Stephen P. Jeffery,[a] Matthew L. Miller,[a] Joseph H. Reibenspies,[a] and Marcetta Y. Darensbourg*[a]

Keywords: Metallothiolate ligands / Phosphane mimics / Nickel / Palladium / Cluster compounds

In pursuit of an analogy between bidentate diphosphane ligands and *cis*-dithiolato nickel complexes, the easily prepared [bis(mercaptoethane)diazacycloheptane]nickel complex, **Ni-1′**, has been treated with Pd^{II} and Ni^{II} sources. With the latter, trinickel species are observed with typical slant-chair structures; for palladium(ii) chloride, a basket-type structure is realized in which the floor of the basket is a PdS_4 unit and the sides are N_2S_2 units. One chloride atom is held within the basket at a Pd···Cl distance of 3.26 Å. With $Pd(NO_3)_2$ as a palladium source, a hexanuclear aggregate in the form of a C_4-paddlewheel structure is obtained. In this structure, the N_2S_2Ni complex serves as a bidentate ligand which bridges two Pd^{2+} cations at a distance of 3.132 Å.

(© Wiley-VCH Verlag GmbH & Co. KGaA, 69451 Weinheim, Germany, 2004)

Introduction

The scope of polyheterometallic cluster complexes with thiolates as bridging ligands traverses the periodic table,[1,2] and there is extensive literature of N_2S_2Ni complexes as metallothiolate ligands to nickel and palladium.[2−7] The most common composition is a trimetallic cluster complex with a slant-chair structure made of two square-planar N_2S_2Ni complexes, which flank a central planar S_4Ni unit. This form (**A**, Scheme 1) is highlighted by [bis(mercaptoethane)-diazacyclooctane]nickel, [(bme-daco)Ni^{II}], or **Ni-1**, and is known to readily capture excess Ni^{II} or Pd^{II} metal ions.[8,9] A 2:3 ratio of $ZnCl_2$ or CuBr to **Ni-1** results in a C_3-paddlewheel cluster with three **Ni-1** units performing as bidentate-bridging ligands, placing either Zn^{II} or Cu^{I} atoms in tetrahedral S_3X coordination geometry (**B**, Scheme 1).[10,11] With an excess of $Cu^{I}Cl$, an adamantane-like Ni_2Cu_4 cluster **C** results; four CuCl units bridge two (bme*-daco)Ni^{II} moieties [**Ni-1***, bme*-daco = *N*,*N*′-bis(2-mercapto-2-methylpropyl)-1,5-diazacyclooctane], engaging all available lone pairs on all sulfurs for coordinating to the soft Cu^{I} metal centers.[12] At the other extreme, the **Ni-1** moiety uses a single lone pair and binds as a monodentate ligand to iron(0) in [(**Ni-1**)$Fe(CO)_4$], D.[13]

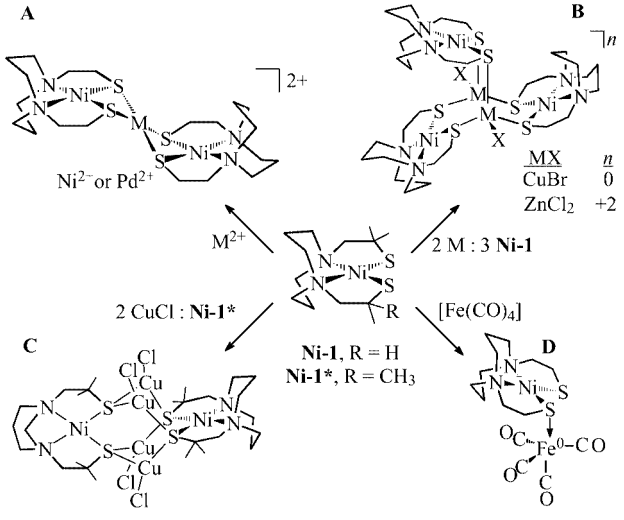

Scheme 1

The success of **Ni-1** and **Ni-1*** as metallothiolate ligands to other metals may be ascribed to the strong chelate effect of bme- and bme*-daco to Ni^{II}, as well as the generally excellent crystallinity and typical air stability of its derivatives. These features are attributed to the optimal 90° bite angles of the N−Ni−N and S−Ni−S moieties within the square-planar **Ni-1** and **Ni-1*** complexes, as well as the fused six-membered nickel-diazacyclohexane rings which adopt classic and stable chair-boat configurations.[14] Points of modification have thus far been limited to the attachment of different pendant arms to the diazacycle framework.[15−17] The readily procured seven-membered ring diazacycloheptane may be substituted for the daco ligand, generating [(bme-dach)Ni] or **Ni-1′**, whose S-based reactivity towards electrophiles such as O_2 and RX differs subtly as compared to **Ni-1**.[18] Electronic effects arising from disparities in Ni−S orbital overlap account for the differences observed. The use of **Ni-1′** as a metallothiolate ligand has not yet been explored.

[a] Texas A&M University, Department of Chemistry, College Station, TX 77843, USA
Fax: (internat.) + 1-979-845-0158
E-mail: marcetta@mail.chem.tamu.edu

It is increasingly apparent that N_2S_2Ni complexes behave toward other metals as ligands with donor abilities which are similar to phosphane ligands.[11,13,19,20] Steric and electronic modifications should lead to a class of ligands whose properties might be controlled similarly to the exceedingly versatile and technically important phosphane ligands. We report on the preparation of Ni−Pd polymetallic complexes based on **Ni-1′** as a metallothiolate ligand.

Results and Discussion

Consistent with reactions of **Ni-1** that led to structural type **A** (Scheme 1), metallation of **Ni-1′** with palladium(II) chloride produced a trimetallic species, which was discovered to be (**Ni-1′**)$_2$PdCl$_2$. X-ray diffraction studies revealed a molecular structure which is unlike any so far reported for such formulations. Rather than the slant-chair arrangement of the three d^8 square-planar conformations, the N_2S_2Ni planes emanate from the same side of the S_4Pd plane with dihedral angles of 132−134°, and Pd−Ni and Ni−Ni distances of 3.13 and 5.97 Å, respectively. As shown in Figure 1, the basket-like structure shows the 2-carbon N−N linker in both **Ni-1′** units facing inward towards an entrained chloride ion, which is located 3.26 Å above the Pd^{II} metal center. Although this distance is about 0.4 Å longer than expected for a Pd−Cl bond in square-pyramidal coordination,[21] conductivity measurements (vide infra) indicate that ion association is maintained in solution. The extended crystal packing diagram shows the second chloride ion to be located at interstitial positions throughout the crystal lattice.

While the N- and S-atom mean deviations from the best N_2S_2 and S_4 planes of [(**Ni-1′**)$_2$PdCl][Cl] are no more than 0.014 Å, the palladium atom is displaced by 0.157 Å from the S_4 plane towards the chloride ion (Table 1). The Ni^{II} cations are displaced, by 0.224 and 0.167 Å out of the S(1)−S(2)−N(1)−N(2) and N(3)−N(4)−S(3)−S(4) planes, respectively. This moves the nickel ions away from the chloride ion and into a less sterically encumbered position with respect to the hydrocarbon N to S and N to N linkages (Figure 1). The S−Ni−S angles are approximately 90°, and the bite angle imposed by the S−Ni−S metallothiolate ligand on the Pd metal center, i.e. the S−Pd−S angle, is considerably less, mean 81.4°.

Although the Ni:Pd ratio in the complex, which is derived from treating **Ni-1′** and Pd(NO$_3$)$_2$ in a 2:1 ratio, is the same as that of the chloride analogue, the composition of the isolated complex is a discrete hexanuclear cluster cation [(**Ni-1′**)$_4$Pd$_2$]$^{4+}$ with four nitrate counterions within the crystal lattice. The form of the Ni_4Pd_2 cluster (Figure 2) is that of a C_4-paddlewheel structure, which contains a Pd−Pd axis and four **Ni-1′** paddles in which S−Ni−S units

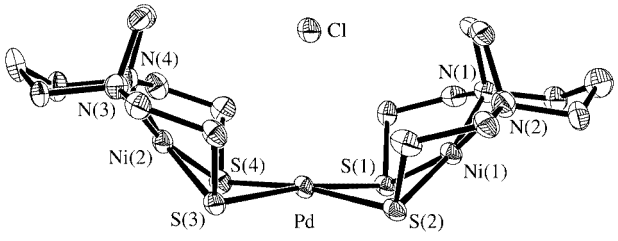

Figure 1. Molecular structure of cationic portion of [(**Ni-1′**)$_2$PdCl]$^+$[Cl]$^-$, thermal ellipsoids at 50 % probability; selected averaged distances (Å) and angles (°): Pd−S 2.369(3), Pd−Ni 3.100(2), Pd···Cl 3.262(3), Ni−N 1.957(8), Ni−S 2.190(3); S(2)−Pd−S(1) 81.02(8), S(2)−Pd−S(3) 97.43(8), S(1)−Pd−S(4) 98.80(8), S(3)−Pd−S(4) 81.74(8), N−Ni−S 92.6(2), S−Ni−S 89.7(1), N−Ni−N 83.1(3)

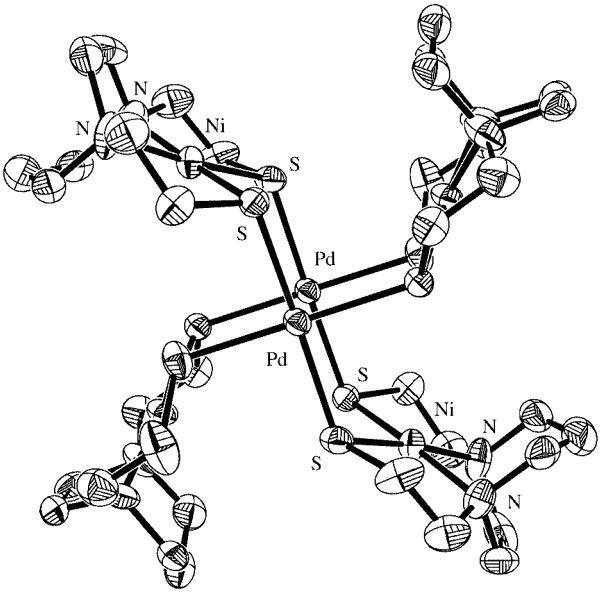

Figure 2. Molecular structure of cationic portion of [(**Ni-1′**)$_4$Pd$_2$][NO$_3$]$_4$, thermal ellipsoids at 50 % probability; selected averaged distances (Å) and angles (°): Pd−S 2.334(2), Pd···Pd 3.132(1), Ni···Ni 4.872, Ni−N 1.940(6), Ni−S 2.157(2); S−Pd−S 89.99(6), N−Ni−S 90.8(2), S−Ni−S 95.68(7), N−Ni−N 82.6(3), Pd−S−Ni 114.42(7)

Table 1. Folding angles of N_2S_2 and the S_4 planes, metal displacement from both of the planes, and M−Ni distances

Complex	Folding angles of N_2S_2 and S_4 planes (°)	Ni displacement out of N_2S_2 plane (Å)	Metal displacement out of S_4 plane (Å)	M···Ni (Å)
[(**Ni-1**)$_2$Ni][Br]$_2$	103.1	0.17	0.0	2.685
[(**Ni-1′**)$_2$NiCl][Cl]	95.2, 138.9	0.194, 0.053	0.520	2.679, 3.053
[(**Ni-1′**)$_2$Ni][Br]$_2$	121.7	0.186	0.0	2.847
[(**Ni-1′**)$_2$PdCl][Cl]	132.3, 134.0	0.167, 0.224	0.1568	3.071, 3.129
[(**Ni-1′**)$_4$Pd$_2$][NO$_3$]$_4$	−	0.066, 0.073	0.033	−

 © 2004 Wiley-VCH Verlag GmbH & Co. KGaA, Weinheim

span the palladium atoms that are 3.13 Å apart. In addition to the two rather perfect S_4Pd and four N_2S_2Ni square planes, two other planes are comprised of S_4Pd_2 units. The nitrate counterions appear to have directional long-range interactions with O−Ni and O−Pd average distances of 3.42 and 3.55 Å, respectively. This is not the first structure of its kind.[6,22] A similar C_4-paddlewheel structure, which comprise bis(aminoethanethiolate)nickel [$(H_2NCH_2CH_2S)_2$-Ni or aet_2Ni] as a metallothiolate ligand to palladium, has been reported with parallel S_4Pd planes separated by 3.02 Å.[6] The isostructural compound $[(aet_2Pd)_4Pd_2]^{4+}[Br_4]^{4-}$ has a Pd···Pd distance of 3.19 Å.[6]

A recently reported hexanickel complex was derived from the aggregation of two $Ni(BF_4)_2$ moieties with four N_2S_2Ni complexes based on the $[^-S(CH_2)_2N(Me)(CH_2)_3N$-$(Me)(CH_2)_2S^-]$ ligand.[22] The flexibility of this open-chain ligand generated torsionally distorted or twisted NiS_4 units, in contrast to the highly regular structural features of the cationic complex $[(\mathbf{Ni\text{-}1'})_4Pd_2]^{4+}$.

In order to determine the interplay of the mesocycle and counterion effects on the basket, the paddlewheel, and the slant-chair structural forms of the Ni−Pd polymetallic complexes, **Ni-1** was exposed to $Pd(NO_3)_2$ under the reaction conditions which produced the C_4-paddlewheel structure. However, the slant-chair trimetallic molecular structure was evident in the isolated crystalline material; it had no significant differences in metric parameters from those found for the chloride salt of $[(\mathbf{Ni\text{-}1})_2Pd]^{2+}$ (Scheme 1).[9]

Likewise, the **Ni-1′** moiety was treated with $NiCl_2$, which resulted in a trimetallic complex of composition [(**Ni-1′**)$_2$NiCl][Cl]. As shown in Figure 3, this trimetallic complex does not adopt the basket form of the palladium analogue $[(\mathbf{Ni\text{-}1'})_2PdCl][Cl]$, but is rather a modified slant-chair structure with a chloride ion strongly bound to a the pentacoordinate square-pyramidal nickel central atom of the S_4NiCl unit. The Ni−Cl distance is 2.304 Å, and Ni is displaced by 0.52 Å from the S_4 plane towards the apical chloride ligand. The Ni−S distances in the pentacoordinate $ClNiS_4$ unit are on average 0.27 Å longer than the Ni−S distances in the four-coordinate nickel atom within the N_2S_2Ni plane. The orientation of the chloride ligand generates distinctly different environments for Ni(3) and Ni(1). Ni(3) is displaced from its N_2S_2 ligand plane by 0.194 Å and shifts away from the chloride ligand; Ni(1) lies within the N_2S_2 plane (displacement of 0.053 Å). The closest Cl···Ni(1) and Cl···Ni(3) distances are 4.712 Å and 3.539 Å, respectively. Another consequence of this asymmetric structure is the difference in S−Ni−S angles of the N_2S_2Ni sites: the terminal S−Ni−S angles are 5° smaller than the parent N_2S_2Ni complex [90.5° and 90.46° for S(2)−Ni(3)−S(2a) and S(1)−Ni(1)−S(1a), respectively]. The central nickel atom (NiS_4) has bite angles to the N_2S_2Ni ligands of 79.2° and 77.7°.

Two other structures were determined as references for counterion interactions. The trimetallic complex prepared from the reaction of **Ni-1′** with $NiBr_2$ showed the common slant-chair arrangement, with no anion interaction with the central S_4Ni unit (Figure 4). However, the product of combining $PdBr_2$ and **Ni-1′** produced another hexanuclear, Ni_4Pd_2 C_4-paddlewheel complex with four bromide anions, as in the nitrate salt.

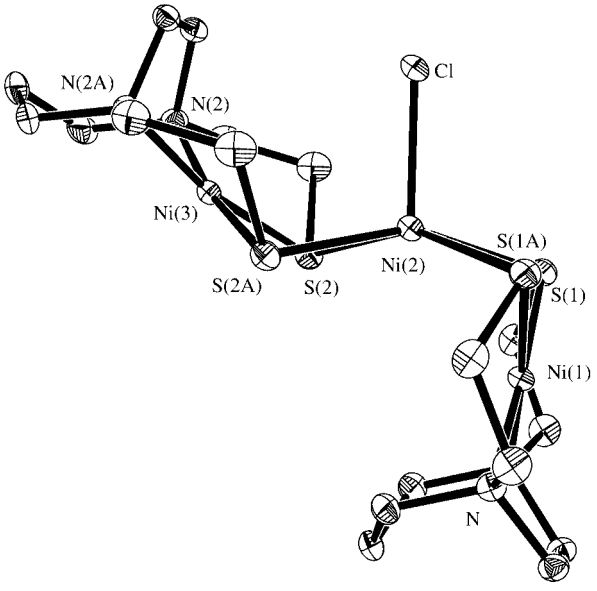

Figure 3. Molecular structure of the cationic portion of [(**Ni-1′**)$_2$NiCl]$^+$Cl$^-$, thermal ellipsoids at 50% probability; selected averaged distances (Å) and angles (°): Ni−N 1.930(4), (N_2S_2)Ni−S 2.155(1), (S_4)Ni−S 2.420(1), Ni(2)−Cl 2.304(2), Ni(1)···Ni(2) 2.679, Ni(2)···Ni(3) 3.053; N−Ni−N 83.2(3), N−Ni−S 92.63(1), S(1)−Ni(1)−S(1A) 90.46(8), S(2)−Ni(2)−S(2A) 79.20(7), S(2)−Ni(2)−S(1) 96.21(5), Cl(1)−Ni(2)−S(2) 100.59(5), Cl(1)−Ni(2)−S(1) 104.23(5)

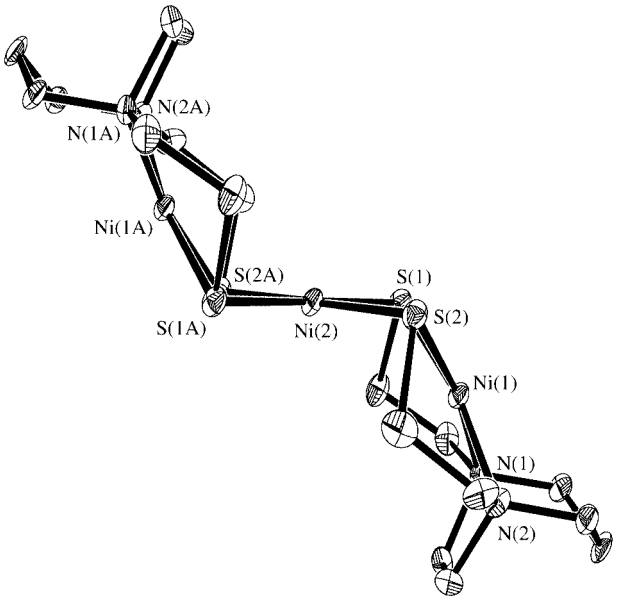

Figure 4. Molecular structure of the cationic portion of [(**Ni-1′**)$_2$Ni](Br$_2$), thermal ellipsoids at 50 % probability; selected averaged distances (Å) and angles (°): Ni−N 1.924(6), Ni(1)−S 2.149(2), Ni(2)−S 2.211(2), Ni(1)···Ni(2) 2.847(1); N−Ni−N 83.6(2), N−Ni−S 92.9(2), S(2)−Ni(1)−S(1) 88.72(7), S(2)−Ni(2)−S(1) 85.63(6), S(2)−Ni(2)−S(1A) 94.37(6)

 © 2004 Wiley-VCH Verlag GmbH & Co. KGaA, Weinheim

Solution Characterization

The colors, electronic spectral, and electrochemical features of the heterometallic complexes are ascribed to a combination of the central NiS_4 or PdS_4 units and the S-modified (bme-dach)Ni moieties. The basket and the C_4-paddlewheel palladium structures are paprika-red in color and have similar electronic spectral features. The intense L→M charge-transfer band of tan-colored **Ni-1′** at 280 nm is red-shifted on formation of the Pd derivatives to approximately 320 nm, and a broad band of lower intensity covers the 370−480 nm range. The latter has been assigned to PdS_4 coordination.[7] In contrast the trinickel slant-chair species are an intense red-black. The absorptions of the CT bands that tail off into the range of 400−500 nm have ε values of approximately 2000 $Lmol^{-1}cm^{-1}$. These values are again consistent with previous assignments to a NiS_4 chromophore.[7]

The results of molar conductivity measurements determined on CH_3OH solutions at 25 °C are listed in Table 2. The molar conductance values for the trinickel species are well within the range of three ions in CH_3OH (reported as 160−220 $cm^{-1}mol^{-1}\Omega^{-1}$),[23] indicating ion dissociation and a di-uni-uni electrolyte system. In contrast, for the [(**Ni-1′**)$_2$PdCl]Cl "basket" compound, a lower value of Λ_M = 83 $cm^{-1}mol^{-1}\Omega^{-1}$ is indicative of a uni-uni electrolyte which has a range in CH_3OH of 80−115 $cm^{-1}mol^{-1}\Omega^{-1}$.[23] From this, we conclude that the Pd−Cl interaction implied for the entrained chloride in the solid-state molecular structure remains intact in CH_3OH. The C_4-paddlewheel structure has a value of Λ_M = 136 $cm^{-1}mol^{-1}\Omega^{-1}$, which is between the two- and three-ion range in CH_3OH, and indicates that at least some of the long-range nitrate associations with the 4+ cation that was observed in the solid-state structure are maintained in solution, generating $[\{(\textbf{Ni-1}')_4Pd_2\}(NO_3)_2]^{2+}$ and two free nitrate ions.

Table 2. Molar conductivities in MeOH at 25 °C

Compound	Λ_M at 10^{-3} M ($cm^{-1}mol^{-1}\Omega^{-1}$)
[(**Ni-1**)$_2$Ni][Br]$_2$	191
[(**Ni-1′**)$_2$NiCl][Cl]	168
[(**Ni-1′**)$_2$Ni][Br]$_2$	166
[(**Ni-1′**)$_2$PdCl][Cl]	83
[(**Ni-1′**)$_4$Pd$_2$][NO$_3$]$_4$	136

Electron-spray ionization mass spectral results for the new cluster compounds were consistent with the solid-state formulations, including observation of a group of signals centered at 1508 m/z with correct isotopomer ratios computed for the intact hexanuclear cluster complex with three nitrates attached, $[\{(\textbf{Ni-1}')_4Pd_2\}^{4+}(NO_3)_3]^+$. The dicationic complex $[(\textbf{Ni-1}')_2M]^{2+}$ is a prominent species in this and all other compounds studied.

Conclusion

The graphical summary of the polymetallics based on **Ni-1′** (Scheme 2) shows the N_2S_2Ni metallothiolate ligand maintains its structural integrity whether it serves as a bidentate bridging ligand spanning two metal centers or as a that bidentate ligand to a single metal center. As can be seen in Figure 5, when **Ni-1′** is a bidentate ligand to a single metal center, the S−Ni−S angle is smaller then in its parent complex, but as a bridging bidentate ligand there is no change. Both binding modes generate stable complexes which are related to diphosphane derivatives. Analogy of **Ni-1′** in its bidentate bridging capability is towards the diphenylphosphinomethane (dppm) ligand, whose small bite angle is well-known to facilitate the formation of "A-frame" bimetallic clusters. The structure of a heptanuclear Ni_3Cu_4

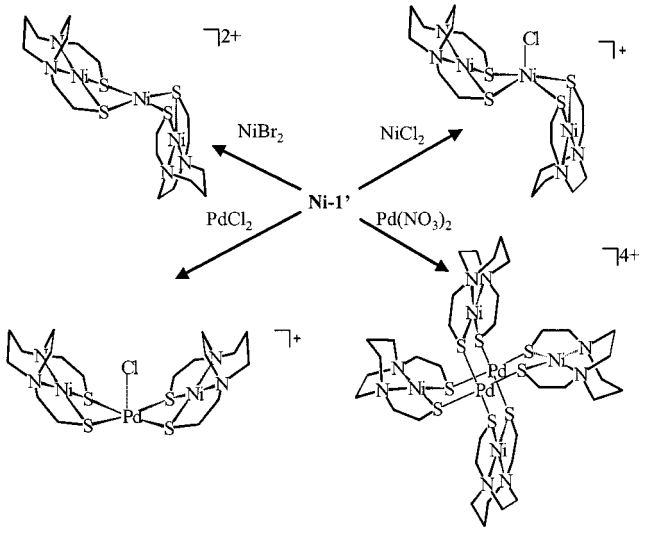

Scheme 2

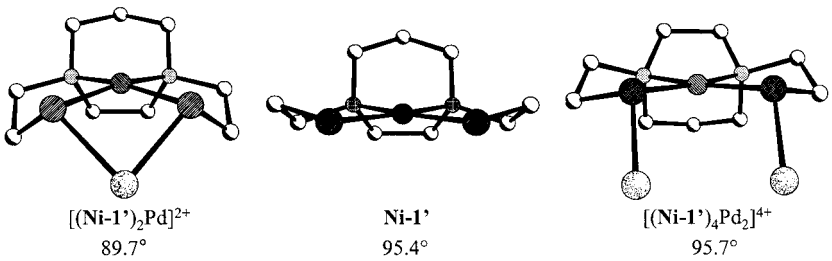

Figure 5. Comparison of the N_2S_2Ni unit as a bidentate ligand, its parent complex, and as a bidentate bridging ligand; values given are S−Ni−S angles

 © 2004 Wiley-VCH Verlag GmbH & Co. KGaA, Weinheim

cluster with a mixed set of dppm and aet_2Ni ligands support this analogy.[24] Nevertheless, dppm has also been used in the preparation of mononuclear $[M(dppm)][BF_4]_2$ salts, M = Pd, Ni;[25] these cations are analogous to our trimetallic cations.

The minor structural change from the eight-membered daco ring to the seven-membered dach framework for N_2S_2 ligand complexes resulted in structural diversity heretofore not observed in the polymetallic species. Notably, in contrast to the daco analogue, the loss of one methylene unit in the dach framework resulted in a different folding pattern as evidenced by the basket case, a different nuclearity as seen in the paddlewheel structure, and an enhanced capability to bind counterions as noted in the chloride-bound slant-chair structure. These differences appear to derive from a lesser steric requirement of the dach mesocyclic framework.

Experimental Section

General Remarks: Where anaerobic conditions were required, standard Schlenk techniques with argon and an argon glovebox were used. Solvents were dried and distilled using standard methods.[26] (bme-daco)Ni,[27] (bme-dach)Ni,[18] and [(bme-daco)$_2$Ni$_3$][Cl$_2$] [8] were synthesized according to published procedures. Anhydrous nickel(II) bromide (Strem), nickel(II) chloride hexahydrate (J.T. Baker), palladium(II) nitrate hydrate (Strem), and palladium(II) chloride (Johnson Matthey) were used as received. UV/Vis spectra were recorded on a Hewlett−Packard 8453 diode array spectrometer using quartz cells (1.00 cm path length). Elemental analyses were performed by Canadian Microanalytical Services Ltd., Delta, British Columbia, Canada. Electrospray Ionization mass spectra were recorded using a MDS-Series QStar Pulsar with a spray voltage of 5 KeV at the Laboratory for Biological Mass Spectroscopy at Texas A&M University. Conductance measurements were made using an Orion 160 conductivity meter.

[{(bme-dach)Ni}$_2$PdCl]$^+$[Cl]$^-$: Palladium chloride (0.087 g, 0.49 mmol) was refluxed under argon in CH_3CN (25 mL) until dissolved and then added to (bme-dach)Ni (0.272 g, 0.982 mmol) in CH_3CN (15 mL) to produce an orange-red precipitate. The solid was collected, redissolved in a minimum of CH_3OH, filtered and dried in vacuo. Yield: 0.336 g, 94 %. Single crystals of X-ray quality were grown from slow diffusion of diethyl ether into an CH_3CN solution. UV/Vis (CH_3OH) λ_{max} in nm (ε): 230 (22 500), 266 (19 000), 308 (20 000), 386 (6600), 420 (5700). $C_{18}H_{36}Cl_2N_4Ni_2PdS_4$ (731.5): calcd. C 29.56, N 7.66, H 4.96; found C 27.7, N 7.05, H 5.32. Mass spectrum (*m*/*z*): 330 [{(bme-dach)Ni}$_2$Pd]$^{2+}$; 696 [{(bme-dach)Ni}$_2$PdCl]$^+$.

[{(bme-dach)Ni}$_4$Pd$_2$][NO$_3$]$_4$: (bme-dach)Ni (0.116 g, 0.419 mmol) was made into a slurry with CH_3CN (25 mL). Palladium nitrate hydrate (0.049 g, 0.212 mmol) was dissolved in CH_3CN (25 mL) and transferred by cannula to the (bme-dach)Ni solution which immediately began to turn orange red. After about 10 minutes, the reaction mixture was filtered in air leaving some unchanged (bme-dach)Ni, which was washed with CH_3CN. The solution was layered with *n*-hexane and put in the refrigerator to give dark red blocks of product. Yield: 0.105 g, 64 %. UV-Vis (CH_3OH), λ_{max} in nm (ε): 230 (53 000), 266 (39 000), 308 (43 000), 386 (15 000), 420 (12 000). $C_{36}H_{72}N_{12}Ni_4O_{12}Pd_2S_8$ (1569.2): calcd. C 27.55, N 10.71, H 4.62; found C 27.36, N 10.77, H 4.73. Mass spectrum (*m*/*z*): 330 [{(bme-dach)Ni}$_2$Pd]$^{2+}$; 722 [{(bme-dach)Ni}$_2$(PdNO$_3$)]$^+$, 1507 [{(bme-dach)Ni}$_4${Pd$_2$(NO$_3$)$_3$}]$^+$, 461 [{(bme-dach)Ni}$_4$(Pd$_2$NO$_3$)]$^{3+}$.

[{(bme-daco)Ni}$_2$Pd][NO$_3$]$_2$: (bme-daco)Ni (0.230 g, 0.791 mmol) was dissolved in CH_3CN (15 mL). The yellow-brown sample of palladium nitrate hydrate (0.091 g, 0.394 mmol) was dissolved in CH_3CN (15 mL) and transferred by cannula to the purple (bme-daco)Ni solution which immediately began to turn dark red, forming a precipitate. The reaction mixture was stirred overnight and then placed in an ice-water bath. The precipitate was collected on a Büchner funnel and washed with ice cold CH_3CN. Yield: 0.178 g, 58 %. Single crystals of X-ray quality were grown from slow diffusion of diethyl ether vapor into a CH_3OH solution in the refrigerator. UV-Vis (CH_3OH), λ_{max} in nm (ε): 286 (17 700), 250 (16 000), 328 (13 000), 408 (4000), 524 (3000). $C_{20}H_{40}N_6Ni_2PdO_6S_4$ (812.6): calcd. C 29.56, N 10.34, H 4.96; found C 29.18, N 10.10, H 4.98. Mass spectrum (*m*/*z*): 343 [{(bme-daco)Ni}$_2$Pd]$^{2+}$.

[(bme-dach)$_2$Ni$_3$][Br]$_2$: A slurry containing $NiBr_2$ (0.374 g, 1.71 mmol) in 50 mL of distilled CH_3OH was added to a slurry of (bme-dach)Ni (0.535 g, 1.93 mmol) in CH_3OH (20 mL). The development of a dark red color was immediate. The solution was stirred overnight. The solvent was removed, the residue dissolved in CH_3CN, and filtered through a medium porosity frit under air. The solvent was removed in vacuo yielding a dark red solid. Yield: 0.084 g, 11%. Single crystals of X-ray quality were grown from slow evaporation of a CH_3OH solution. UV-Vis (CH_3OH), λ_{max} in nm (ε): 482 (1880), 406 (2520), 278 (16 600), 227 (19 700). $C_{18}H_{36}Br_2N_4Ni_3S_4$ (772.7): calcd. C 27.98, N 7.25, H 4.70; found C 26.83, N 7.00, H 4.73. Mass spectrum (*m*/*z*): 306 [(bme-dach)$_2$Ni$_3$]$^{2+}$; 693 [(bme-dach)$_2$Ni$_3$]$^{2+}$Br$^-$.

[(bme-dach)$_2$Ni$_3$Cl]$^+$[Cl]$^-$: [(bme-dach)$_2$Ni$_3$Cl]$^+$Cl$^-$ was synthesized in a similar fashion to [(bme-dach)$_2$Ni$_3$][Br]$_2$, using $NiCl_2{\cdot}6H_2O$ as an exogenous nickel source. Yield: 0.150 g, 60 %. $C_{18}H_{36}Cl_2N_4Ni_3S_4$ (683.8): calcd. C 29.67, N 8.19, H 5.31; found C 31.62, N 7.65, H 5.29. Mass spectrum (*m*/*z*): 306 [(bme-dach)$_2$Ni$_3$]$^{2+}$; 647 [(bme-dach)$_2$Ni$_3$Cl]$^+$.

X-ray Crystallographic Study: Low temperature X-ray diffraction data were collected on a Bruker SMART CCD-based diffractometer (Mo-K_α radiation, λ = 0.71073 Å) and covered a hemisphere of space upon combining three sets of exposures. The space groups were determined based on systematic absences and intensity statistics using the SMART[28] program for data collection and cell refinement. Raw data frame integration was performed with SAINT+.[29] Other programs used include SHELXS-86 (Sheldrick)[30] for structure solution, SHELXL-97 (Sheldrick)[31] for structure refinement and SHELXTL-Plus, version 5.1 or later (Bruker),[32] for molecular graphics and preparation of material for publication. The structures were solved by direct methods. Anisotropic displacement parameters were determined for all non-hydrogen atoms. Hydrogen atoms were added at idealized positions and refined with fixed isotropic displacement parameters equal to 1.2 (1.5 for methyl protons) times the isotropic displacement parameters of the atoms to which they were attached. Collection and refinement summaries are shown in Table 3. SADABS[31] and Wingx[33] were used on the palladium clusters. CCDC-215014 [{(**Ni-1′**)$_2$Ni}Br$_2$], CCDC-215016 [{(**Ni-1′**)$_2$NiCl}Cl], CCDC-215015 [{(**Ni-1′**)$_4$Pd$_2$}(NO$_3$)$_4$], and CCDC-215013 [{(**Ni-1′**)$_2$PdCl}Cl] contain the supplementary crystallographic data for this paper. These data can be obtained free of charge at www.ccdc.cam.ac.uk/conts/retrieving.html [or from the Cambridge Crystallographic Data Centre, 12, Union Road, Cambridge

 © 2004 Wiley-VCH Verlag GmbH & Co. KGaA, Weinheim

Table 3. Crystal data

	[(**Ni-1′**)$_2$Ni][Br$_2$]	[(**Ni-1′**)$_2$NiCl][Cl]	[(**Ni-1′**)$_4$Pd$_2$][NO$_3$]$_4$	[(**Ni-1′**)$_2$PdCl][Cl]
Formula	$C_{18}H_{36}Br_2N_4Ni_3S_4$·2$CH_3OH$	$C_{18}H_{36}Cl_2N_4Ni_3S_4$·$CH_3OH$	$C_{36}H_{72}N_{12}Ni_4O_{12}Pd_2S_8$·2$CH_3CN$	$C_{18}H_{36}Cl_2N_4Ni_2PdS_4$·$CH_3CN$
M_r (g/mol)	418.38	486.11	1651.28	772.52
T (K)	110(2)	110(2)	110(2)	110(2)
Crystal system	monoclinic	monoclinic	monoclinic	triclinic
Space group	$P2_1/n$	$P2_1/m$	$P2_1/c$	$P\bar{1}$
Unit cell				
a (Å)	7.5116(17)	9.5873(17)	12.373(3)	10.545(5)
b (Å)	15.047(3)	13.537(2)	14.585(4)	12.032(6)
c (Å)	13.664(3)	10.8074(19)	16.331(4)	12.630(6)
α (°)	90	90	90	108.548(7)
β (°)	105.643(3)	90.670(3)	91.314(5)	94.331(8)
γ (°)	90	90	90	91.978(7)
V (Å^3)	1487.2(6)	1402.5(4)	2946.3(14)	1512.1(12)
Z	2	2	4	2
GooF	0.904	1.054	1.019	1.066
Reflections collected	9483	6260	21585	8104
Reflections observed	3518	2111	5136	5037
$R1$, $wR2$ [$I > 2\sigma(I)$]	0.0593, 0.1280	0.0407, 0.1155	0.0652, 0.1656	0.0677, 0.1643
$R1$, $wR2$ (all data)	0.1096, 0.1460	0.0441, 0.1177	0.0739, 0.1800	0.0994, 0.1889

CB2 1EZ, UK; Fax: (internat.) +44-1223/336-033; E-mail: deposit@ccdc.cam.ac.uk].

Acknowledgments

Financial support from the National Science Foundation (CHE, 01−11629 for this work and CHE 98−07975 for the X-ray diffractometer and crystallographic computing system) and contributions from the R.A. Welch Foundation are gratefully acknowledged.

[1] D. W. Stephan, T. T. Nadasdi, *Coord. Chem. Rev.* **1996**, *147*, 147−208.
[2] A. R. Dias, M. H. Garcia, M. J. Villa de Brito, A. Galvão, *J. Organomet. Chem.* **2001**, *632*, 75−84.
[3] K. A. Jensen, *Z. Anorg. Chem.* **1936**, *227*, 25−31.
[4] D. C. Jicha, D. H. Busch, *Inorg. Chem.* **1962**, *1*, 872−877.
[5] D. Gibson, S. J. Lippard, *Inorg. Chem.* **1986**, *25*, 219−222.
[6] T. Konno, K. Yonenobu, J. Hidaka, K. Okamoto, *Inorg. Chem.* **1994**, *33*, 861−864.
[7] M. A. Turner, W. L. Driessen, J. Reedijk, *Inorg. Chem.* **1990**, *29*, 3331−3335.
[8] P. J. Farmer, T. Solouki, D. K. Mills, T. Soma, D. H. Russell, J. H. Reibenspies, M. Y. Darensbourg, *J. Am. Chem. Soc.* **1992**, *114*, 4601−4605.
[9] G. Musie, P. J. Farmer, T. Tuntulani, J. H. Reibenspies, M. Y. Darensbourg, *Inorg. Chem.* **1996**, *35*, 2176−2183.
[10] T. Tuntulani, J. H. Reibenspies, P. J. Farmer, M. Y. Darensbourg, *Inorg. Chem.* **1992**, *31*, 3497−3499.
[11] M. L. Golden, M. V. Rampersad, J. H. Reibenspies, M. Y. Darensbourg, *Chem. Commun.* **2003**, 1824−1825.
[12] M. L. Miller, S. A. Ibrahim, M. L. Golden, M. Y. Darensbourg, *Inorg. Chem.* **2003**, *42*, 2999−3007.
[13] C-H. Lai, J. H. Reibenspies, M. Y. Darensbourg, *Angew. Chem. Int. Ed. Engl.* **1996**, *35*, 2390−2393.
[14] A. E. Martell, R. D. Hancock, *Metal Complexes in Aqueous Solutions*; Plenum Press: New York, **1996**, ch. 3.
[15] X-H. Bu, M. Du, L. Zhang, Z-L. Shang, R-H. Zhang, M. Shionoya, *J. Chem. Soc., Dalton Trans.* **2001**, 729−735.
[16] X-H. Bu, M. Du, L. Zhang, Z-L. Shang, R-H. Zhang, D.-Z. Liao, M. Shionoya, T. Clifford, *Inorg. Chem.* **2000**, *39*, 4190−4199.
[17] X-H. Bu, M. Du, L. Zhang, D-Z. Liao, J-K. Tang, R-H. Zhang, M. Shionoya, *J. Chem. Soc., Dalton Trans.* **2001**, 593−598.
[18] J. J. Smee, M. L. Miller, C. A. Grapperhaus, J. H. Reibenspies, M. Y. Darensbourg, *Inorg. Chem.* **2001**, *40*, 3601−3605.
[19] M. A. Reynolds, T. B. Rauchfuss, S. R. Wilson, *Organometallics* **2003**, *22*, 1619−1625.
[20] R. C. Linck, C. W. Spahn, T. B. Rauchfuss, S. R. Wilson, *J. Am. Chem. Soc.* **2003**, *125*, 8700−8701.
[21] R. Bartsch, S. Hietkamp, S. Morton, H. Peters, O. Stelzer, *Inorg. Chem.* **1983**, *22*, 3624−3632.
[22] A. J. Amoroso, S. S. M. Chung, D. J. E. Spencer, J. P. Danks, M. W. Glenny, A. J. Blake, P. A. Cooke, C. Wilson, M. Schroder, *Chem. Commun.* **2003**, 2020−2021.
[23] W. J. Geary, *Coord. Chem. Rev.* **1971**, *7*, 81−122.
[24] H-W. Xu, Z-N. Chen, S. Ishizaka, N. Kitamura, J-G. Wu, *Chem. Commun.* **2002**, 1934−1935.
[25] A. Miedaner, R. C. Haltiwanger, D. L. DuBois, *Inorg. Chem.* **1991**, *30*, 417−427.
[26] A. J. Gordon, R. A. Ford, *The Chemist's Companion*; J. Wiley and Sons: New York **1972**.
[27] D. K. Mills, I. Font, P. J. Farmer, Y.-M. Hsiao, T. Tuntulani, R. M. Buonomo, D. C. Goodman, G. Musie, C. A. Grapperhaus, M. J. Maguire, C.-H. Lai, M. L. Hatley, J. J. Smee, J. A. Bellefeuille, M. Y. Darensbourg, *Inorganic Syntheses.* **1998**, *32*, 89−98.
[28] SMART 1000 CCD, Bruker Analytical X-ray Systems: Madison, WI, **1999**.
[29] SAINT-Plus, version 6.02 or later: Bruker, Madison, WI, **1999**.
[30] G. Sheldrick. SHELXS-86: *Program for Crystal Structure Solution*; Institüt für Anorganische Chemie der Universität: Göttingen, Germany, **1986**.
[31] G. Sheldrick. SHELXL-97: *Program for Crystal Structure Refinement*; Institüt für Anorganische Chemie der Universität: Göttingen, Germany, **1997**.
[32] SHELXTL, version 5.1 or later: Bruker, Madison, WI, **1998**.
[33] L. J. Farrugia, *J. Appl. Cryst.* **1999**, *32*, 837−838.

Received September 26, 2003

 © 2004 Wiley-VCH Verlag GmbH & Co. KGaA, Weinheim

Novel Room Temperature Inorganic Ionic Liquids

Liyi Dai,[a] Shuyuan Yu,[a] Yongkui Shan,*[a] and Mingyuan He[a]

Keywords: Inorganic ionic liquids / Ionic liquids / Polyoxometalates / Transition metals / Green chemistry

New inorganic ionic liquids (IIL) consisting of an inorganic polyoxometalate anion with the Keggin structure and a sodium cation, that is $Na_{13}[Ln(TiW_{11}O_{39})_2]\cdot xH_2O$ [where Ln = lanthanide (type 1)], $Na_5[MTiW_{11}O_{39}]\cdot xH_2O$ and $Na_6[MTiW_{11}O_{39}]\cdot xH_2O$ [where M = transition metal (type 2)], were prepared and their physicochemical properties were investigated. These ionic liquids were characterized by NMR and IR spectroscopy and by elemental analysis. Their melting point, viscosity, conductivity, thermal stability, and miscibility with water and organic solvents were determined. When the temperature is below ambient temperature (about 298 K) these ionic liquids are almost immiscible with water. When the temperature is raised, the solubility of the new ionic liquids increases sharply. The influence of the size and of the charge density of both the cations and anions on these properties was examined. The most remarkable feature of IILs is that water is their indispensable component. The role of the water molecule in ionic liquids is similar to that of crystalline water in hydrated compounds.

(© Wiley-VCH Verlag GmbH & Co. KGaA, 69451 Weinheim, Germany, 2004)

Introduction

Ionic liquids constitute a large, fundamental class of fluid materials that in recent years have aroused increasing interest because of their relevance to separation technologies, manufacturing processes and catalysis in green chemistry. Their properties, in fact, are low melting point, a wide liquid range, negligible vapor pressure, good solubility characteristics, relatively low viscosity, nonflammability, a wide electrochemical window, tolerance to strong acids, and excellent thermal and chemical stability.[1−10] Since the discovery of the first ionic liquid (ethylammonium nitrate) in 1914,[11] many classes of ionic liquids have been investigated. According to the current definition, ionic liquids should become liquid at or below 373 K[1] or 423 K[4]. They are typically composed of organic cations with a variety of substituents such as quaternary ammonium cations,[12,13] heterocyclic aromatic compounds,[14] pyrrolidinium cations,[15] derivatives of natural products,[16] phosphonium,[17−18] sulfonium,[19] guanidinium[20] and some more exotic cations,[21,22] and a variety of anions such as Cl^-, Br^-, NO_3^-, I^-, BF_4^-, $AlCl_4^-$, PF_6^- and others. Such ionic liquids are commonly referred to as organic−inorganic ionic liquids.[4] Only few ionic liquids comprising organic cations and organic anions (organic ionic liquids) have been investigated.[4,23−25] However, with the exception of the supercooled ionic liquid, $[Ca(NO_3)_2]_{0.4}$-$(KNO_3)_{0.6}$, reported by Moom and Jeong,[26] ionic liquids consisting of inorganic cations and inorganic anions (inorganic ionic liquids) have not yet appeared in the literature. Although their rapid emergence as environmentally benign solvents and catalysts has lead to a growing number of applications, the basic understanding and study of their physical and chemical properties has lagged behind. A significant barrier to the widespread use of ionic liquids is the lack of understanding of such properties and of the suitable manufacturing processes. It is very important to accumulate a substantial body of scientific and technological data for these fascinating fluid materials, so that their true potential as solvents and catalysts in chemical synthesis and separation processes can be realized. Here, we report the synthesis and characterization of several new inorganic ionic liquids consisting of an inorganic polyoxometalate anion with the Keggin structure and a sodium cation, that is $Na_{13}[Ln(TiW_{11}O_{39})_2]\cdot xH_2O$ [where Ln = lanthanide(type 1)], $Na_5[MTiW_{11}O_{39}]\cdot xH_2O$ and $Na_6[MTiW_{11}O_{39}]\cdot xH_2O$ [where M = transition metal (type 2)]. These materials have allowed us to further explore the formation mechanism of ionic liquids with lower melting points and to reveal the relationship between the structural features of an ionic liquid and its useful properties. Their incorporation into ionic liquids may expand the utility of ionic liquids and open up a new field of ionic liquid chemistry.

Results and Discussion

The syntheses of the novel inorganic ionic liquids were carried out in a mixture comprising an aqueous solution of sodium tungstate, tetrachlorotitanium and the related transition-metal salts (or lanthanide nitrate) at 333 K.[27] The

[a] Center for the Chemistry of Ionic Liquids, East China Normal University,
Shanghai, 200062, P. R. China
Fax: (internat.) + 86-2152510411
E-mail: ykshan@chem.ecnu.edu.cn

ionic liquids synthesized have high solubility in water at high temperatures but they are almost immiscible below ambient temperature; we were therefore able to separate the water from the synthetic mixture at low temperatures. These ionic liquids can change into amorphous powders when they are mixed with anhydrous acetone or ethanol, due to the loss of constituent water from the ionic liquids to the organic solvent. The molar ratios of the constituent elements in the investigated ionic liquids, Na:Ti:Ln:W = 13:2:1:22 (type 1), Na:Ti:M:W = 5:1:1:11 (when M = Fe, or Cr), Na:Ti:M:W = 6:1:1:11 [when M = Mn, Zn(type 2)], were determined by inductively coupled plasma-emission spectrometry. The Keggin structure characteristic of the anions was evidenced by IR spectroscopy. These results illustrate that the anion of type 1 is twice as large as that of type 2, but the charge density on the surface of the anion has no significant difference.

The most remarkable trait of IILs is that water is their indispensable component. The water content of the new ionic liquids was estimated by Karl Fischer analysis and is showed in Table 1. Although various amounts of water were also present in previously known ionic liquid systems,[4] in our IILs system water is a necessary component. Upon heating in air and in the absence of organic solvents, such ionic liquids could change into mudlike solids after loss of constituent water. This phenomenon is reminiscent of the dehydration process in crystalline solids containing crystallization water. The difference between the two phenomenona is that ionic liquids change into mudlike solids while crystals change into amorphous powders.

Table 1. Water content of the inorganic ionic liquids

Compound	H_2O (wt.-%)	x
$Na_{13}[La(TiW_{11}O_{39})_2]\cdot xH_2O$	11.18	40.0
$Na_{13}[Ce(TiW_{11}O_{39})_2]\cdot xH_2O$	9.16	32.6
$Na_{13}[Pr(TiW_{11}O_{39})_2]\cdot xH_2O$	10.08	36.3
$Na_{13}[Sm(TiW_{11}O_{39})_2]\cdot xH_2O$	10.92	39.8
$Na_{13}[Gd(TiW_{11}O_{39})_2]\cdot xH_2O$	7.72	27.1
$Na_{13}[Dy(TiW_{11}O_{39})_2]\cdot xH_2O$	8.22	29.1
$Na_{13}[Er(TiW_{11}O_{39})_2]\cdot xH_2O$	10.76	39.2
$Na_{13}[Tm(TiW_{11}O_{39})_2]\cdot xH_2O$	9.26	33.2
$Na_{13}[Yb(TiW_{11}O_{39})_2]\cdot xH_2O$	11.83	43.7
$Na_5[CrTiW_{11}O_{39}]\cdot xH_2O$	15.95	30.2
$Na_6[MnTiW_{11}O_{39}]\cdot xH_2O$	15.75	30.0
$Na_5[FeTiW_{11}O_{39}]\cdot xH_2O$	17.62	34.0
$Na_6[ZnTiW_{11}O_{39}]\cdot xH_2O$	14.70	27.2

One of the most important criteria for the evaluation of an ionic liquid is its melting point. The solid−liquid phase transition of the new inorganic ionic liquids was examined with a PerkinElmer DSC and a YAN-1 melting point apparatus and the results are summarized in Table 2. The DSC curve for $Na_{13}[Ce(TiW_{11}O_{39})_2]\cdot 33H_2O$, at a heating rate of 10 K/min, is shown in Figure 1. The DSC measurements show two distinct peaks, which demonstrate that two liquid phases, an aqueous phase and an ionic liquid phase, can be formed when the solid melts.[28] The presence of little free-water in the sample is indeed confirmed by a small

Table 2. Melting point (T_m) of the inorganic ionic liquids

Compound	T_m (K)	Compound	T_m (K)
$Na_{13}[La(TiW_{11}O_{39})_2]$	253.0	$Na_{13}[Tm(TiW_{11}O_{39})_2]$	260.2
$Na_{13}[Ce(TiW_{11}O_{39})_2]$	263.0	$Na_{13}[Yb(TiW_{11}O_{39})_2]$	267.2
$Na_{13}[Pr(TiW_{11}O_{39})_2]$	253.0	$Na_5[CrTiW_{11}O_{39}]$	261.5
$Na_{13}[Sm(TiW_{11}O_{39})_2]$	256.0	$Na_5[MnTiW_{11}O_{39}]$	253.0
$Na_{13}[Gd(TiW_{11}O_{39})_2]$	265.1	$Na_5[FeTiW_{11}O_{39}]$	257.6
$Na_{13}[Dy(TiW_{11}O_{39})_2]$	265.2	$Na_6[ZnTiW_{11}O_{39}]$	257.4
$Na_{13}[Er(TiW_{11}O_{39})_2]$	261.0		

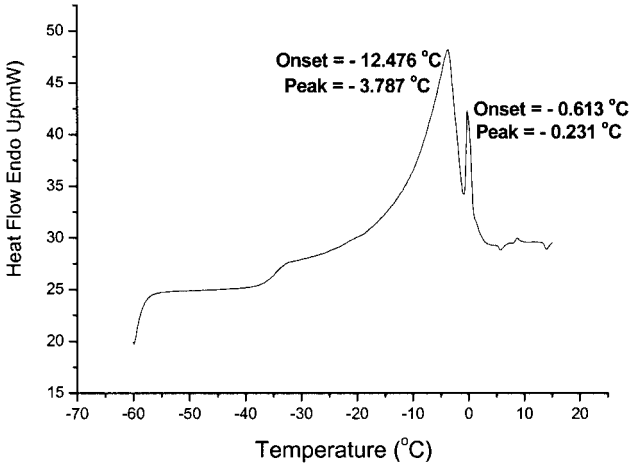

Figure 1. DSC analysis curve of $Na_{13}[Ce(TiW_{11}O_{39})_2]\cdot 33H_2O$

shoulder peak at 272.4 K. However, the main peak at 260.5 K shows that the highly hydrated inorganic ionic liquid of $Na_{13}[Ce(TiW_{11}O_{39})_2]\cdot 33H_2O$ exists in a pure phase. The results in Table 2 illustrate that all the ionic liquids possess a very low melting point and are liquid below room temperature. In general, the melting point of an ionic liquid is correlated with the symmetry, size and charge density of the component ion.[4] Hydrogen bonding and Van Der Waals interactions have also a slight influence on the melting point.[2] The low melting point of the new ionic liquids (shown in Table 2) is ascribed to the absence of hydrogen bonding between the anions and the cations and to the lower charge density on the surface of the anions.

The viscosity measurement of the new inorganic ionic liquids was carried out with an NEX-11 rotational viscosimeter. The lower viscosity (42.5−82.5 cps at 298 K) found in these ionic liquids is similar to that of [emim][BF_4](43 cps at 293 K)[29] and [bmim][CF_3SO_3](90 cps at 293 K).[30] It appears from the examination of a number of organic ionic liquids that the viscosity of the corresponding ionic liquids is related to the structure and the size of the component ions, to their tendency to form hydrogen bonding and to the strength of their van der Waals interactions.[1,31] In the inorganic ionic liquids the structures of all the component ions are very simple. For example, the cation is sodium Na^+ or hydrated sodium $Na^+(H_2O)_x$, the anion is the spherical ion with the Keggin structure $[MTiW_{11}O_{39}]^{5-}$ or $[MTiW_{11}O_{39}]^{6-}$ (where M = Cr, Mn, Fe, Zn) or the dumbbell complex ion with a double lacunary Keggin structure

 © 2004 Wiley-VCH Verlag GmbH & Co. KGaA, Weinheim

Table 3. Specific conductivity of measurable samples at 298 K

Compound	σ (×10⁴μS/cm)	Compound	σ (×10⁴μS/cm)
$Na_{13}[La(TiW_{11}O_{39})_2]$	1.10	$Na_5[CrTiW_{11}O_{39}]$	1.62
$Na_{13}[Ce(TiW_{11}O_{39})_2]$	2.02	$Na_6[MnTiW_{11}O_{39}]$	1.80
$Na_{13}[Pr(TiW_{11}O_{39})_2]$	1.85	$Na_5[FeTiW_{11}O_{39}]$	2.66
$Na_{13}[Sm(TiW_{11}O_{39})_2]$	2.24	$Na_{13}[Tm(TiW_{11}O_{39})_2]$	1.59
$Na_{13}[Er(TiW_{11}O_{39})_2]$	1.68	$Na_{13}[Yb(TiW_{11}O_{39})_2]$	1.77
$Na_{13}[Gd(TiW_{11}O_{39})_2]$	2.30	$Na_6[ZnTiW_{11}O_{39}]$	2.01
$Na_{13}[Dy(TiW_{11}O_{39})_2]$	1.92		

$[Ln(TiW_{11}O_{39})_2]^{13-}$, which has the largest ionic radius and the lowest charge density on it. The tendency to form hydrogen bonds between the cations and the anions of ionic liquids may be completely suppressed. Therefore, the viscosity in these inorganic ionic liquids is simply governed by a weak electrostatic interaction force.

The conductivity of an ionic liquid can been described by the equation below:[31]

$$\sigma = yF^2d(6\pi N_A FW\eta)[(\zeta_a r_a)^{-1} + (\zeta_{ac} r_c)^{-1}] \quad (1)$$

and can be related to its viscosity (η), formula weight (FW), density (*d*), ion radii (r_a and r_c) and to the specific interactions between the mobile ions (ζ_a and ζ_c) in an ionic liquid. The conductivity of the new inorganic ionic liquids was measured with a DDS-11 conductivitimeter and the results are shown in Table 3. Following on from the equation above, the ionic liquid containing the smallest ion should provide the highest conductivity but in our results (see Table 3) both type 1 and type 2 have some conductivity around 2×10^4 μS/cm. This phenomenon can be attributed to the similar charge density on the anionic surface of the type 1 and type 2 ionic liquids and it illustrates that one must not only focus on viscosity, molecular weight, or density, but also keep in mind the importance of the charge density on the iron when searching for highly conducting ionic liquids.

The thermal stability of the new ionic liquids in air or nitrogen was examined by Mettler Toledo thermogravimetric analysis at a heating rate of 2 K/min. Figure 2 shows the TG and SDTA data for $Na_{13}[Ce(TiW_{11}O_{39})_2]\cdot 32.6H_2O$. It is important to note that this ionic liquid is only stable up to 308 K in N_2. The two steps of water-loss and the accompanying endothermal process were observed in the TG and SDTA curves in the temperature range 291−673 K. In order to clarify the thermal behavior, the conductivity of $Na_{13}[Ce(TiW_{11}O_{39})_2]\cdot 32.6H_2O$ was measured at various temperatures after heating for 1 h in air. The experimental results are shown in Figure 3. The conductivity of this ionic liquid is almost constant in the temperature range 308−328 K and it decreases rapidly as the temperature increases, which leads to loss of constituent water. This result shows that the new ionic liquid is much less stable and possesses a liquid range of about 65 K with a melting point of around 263 K (see Table 2).

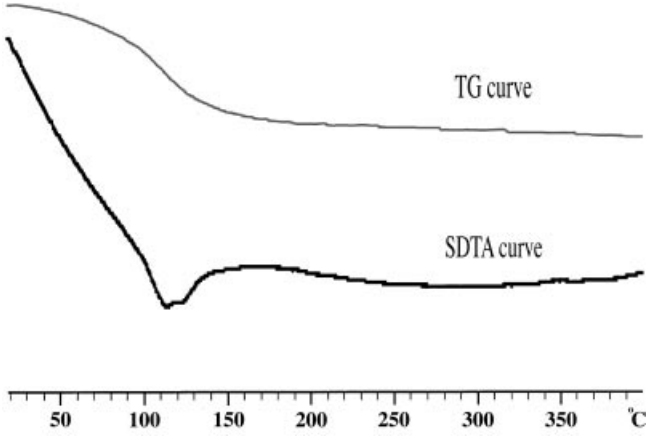

Figure 2. Thermal gravimetric curve and scanning differential thermal analysis curve of $Na_{13}[Ce(TiW_{11}O_{39})_2]\cdot 32.6H_2O$

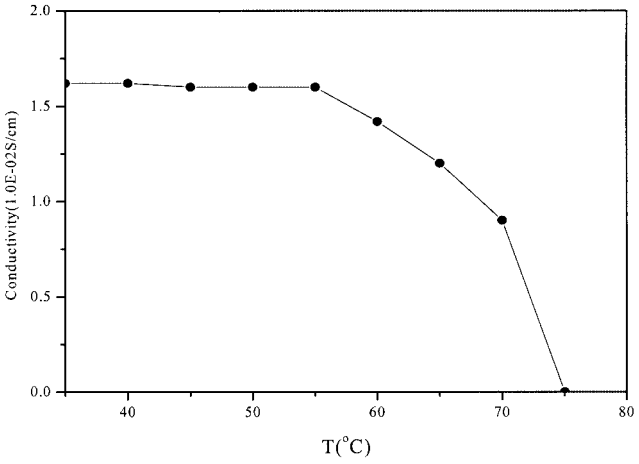

Figure 3. Specific conductivity of $Na_{13}[Ce(TiW_{11}O_{39})_2]\cdot 32.6H_2O$ at different temperatures after heating for 1h

All the investigated ionic liquids are immiscible with organic solvents having low, medium and high dielectric constants (ε): cyclohexane (ε = 2.02), benzene (ε = 2.284), carbon tetrachloride (ε = 2.238), toluene (ε = 2.379), diethyl ether (ε = 4.22), chloroform (ε = 4.724), ethyl acetate (ε = 6.02), ethanol (ε = 25.2), methanol (ε = 32.63)and acetonitrile (ε = 37.4), and so forth. They are only miscible with water but their solubility in water varies drastically depending on the temperature. When the temperature is below ambient temperature (about 293 K) these ionic liquids are almost immiscible with water. However, if the tempera-

 © 2004 Wiley-VCH Verlag GmbH & Co. KGaA, Weinheim

ture is raised , the solubility of the new ionic liquids in water increases. Most of the known ionic liquids are miscible with common organic solvents and with water, which leads us to believe that these ionic liquids may play an unexpected role in some fields such as separation and biphasic catalysis.

In order to determine the structure of the anion, the ^{183}W NMR and IR spectra of the new ionic liquids were recorded on a Bruker DRX400 nuclear magnetic resonance spectrometer, and on a Nicolet NEXUS 670 FT-IR spectrometer. The ^{183}W NMR and IR spectra of $Na_{13}[Ce(TiW_{11}O_{39})_2]\cdot 32.6H_2O$ and $Na_6(ZnTiW_{11}O_{39})\cdot 27.2H_2O$ are shown in Figures 4 and 5. The ^{183}W NMR (Figure 4) and IR (Figure 5) spectra of $Na_6(ZnTiW_{11}O_{39})\cdot 27.2H_2O$ reveal six very strong, well-resolved resonance lines and four infrared bands in the $400-1200cm^{-1}$ range, in accordance with eleven tungsten atoms involved in the expected Keggin structure (C_s symmetry) with a lacunary site.[32] The infrared spectra of $Na_{13}[Ce(TiW_{11}O_{39})_2]\cdot 32.6H_2O$ is virtually identical to that of $Na_6(ZnTiW_{11}O_{39})\cdot 27.2H_2O$, which proves that the ligand with a mono-vacant Keggin structure $(TiW_{11}O_{39})^{8-}$ consists of the new ionic liquid $Na_6(ZnTiW_{11}O_{39})\cdot 27.2H_2O$ and $Na_{13}[Ce(TiW_{11}O_{39})_2]\cdot 32.6H_2O$. However, there is a marked difference between the ^{183}W NMR spectra of $Na_6(ZnTiW_{11}O_{39})\cdot 27.2H_2O$ and that of $Na_{13}[Ce(TiW_{11}O_{39})_2]\cdot 32.6H_2O$ (see Figure 4). Ten stronger well-resolved resonance lines and some weaker resonance lines were observed in the ^{183}W NMR spectra of $Na_{13}[Ce(TiW_{11}O_{39})_2]\cdot 32.6H_2O$. This phenomenon may be due to the presence of the paramagnetic center Ce^{III} and of the isomer with a different configuration[33] or to the small magnitude of the other anionic component in the ionic liquid $Na_{13}[Ce(TiW_{11}O_{39})_2]\cdot 32.6H_2O$, as was observed in [emim]Cl-$AlCl_3$[34–36] ionic liquids.

In summary, a new series of inorganic ionic liquids consisting of an inorganic polyoxometalate anion with the Keggin structure and a sodium cation were prepared and investigated. They are the first examples of inorganic ionic liquids containing only one kind of inorganic compound and possessing different physicochemical properties from those of the known organic-inorganic ionic liquids or organic ionic liquids. Some of the characteristics of these new ionic liquids are not so desirable but they can enrich the

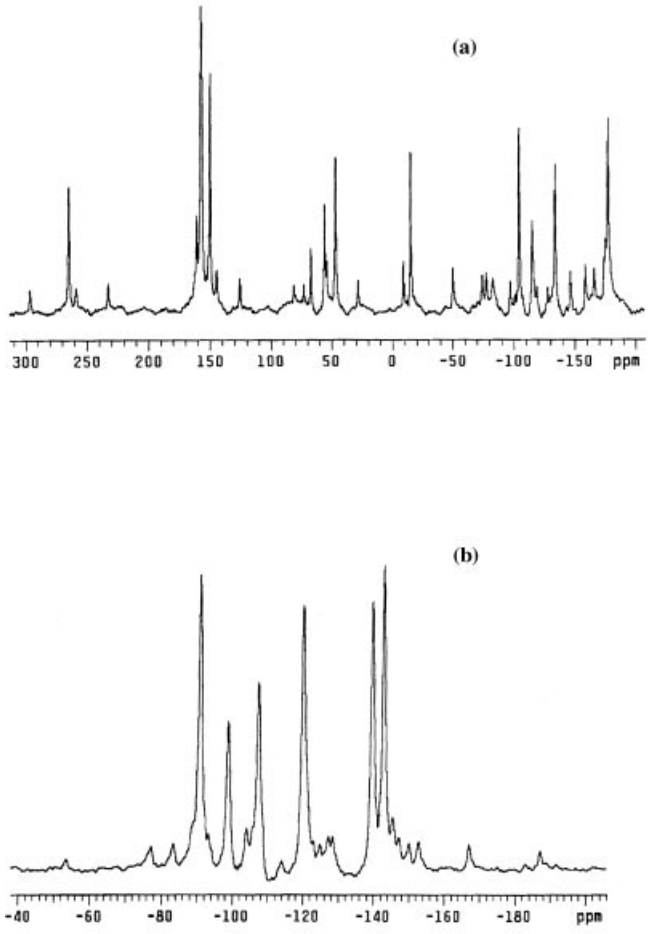

Figure 4. ^{183}W NMR spectra of $Na_{13}[Ce(TiW_{11}O_{39})_2]\cdot 32.6H_2O$ (a) and $Na_6(ZnTiW_{11}O_{39})\cdot 27.2H_2O$ (b)

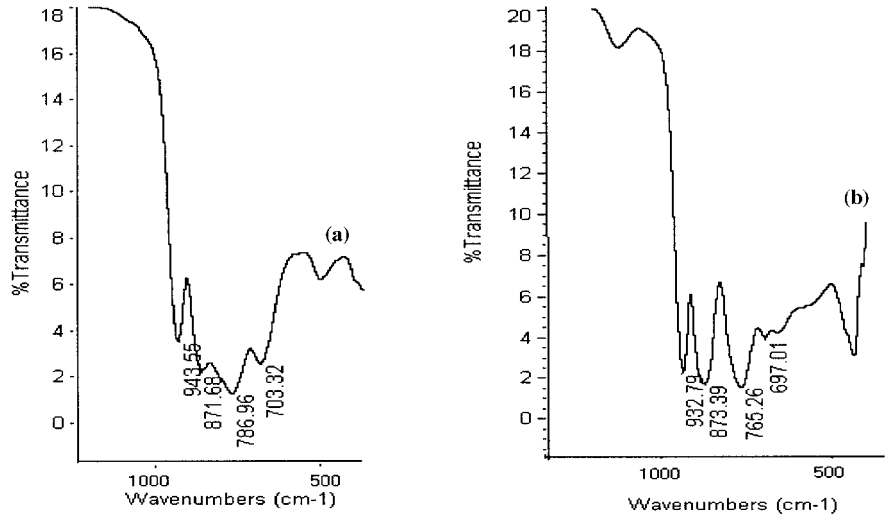

Figure 5. IR spectra of $Na_{13}[Ce(TiW_{11}O_{39})_2]\cdot 32.6H_2O$(a) and $Na_6(ZnTiW_{11}O_{39})\cdot 27.2H_2O$(b)

 © 2004 Wiley-VCH Verlag GmbH & Co. KGaA, Weinheim

chemistry of ionic liquids and open up new opportunities for further research in this field. It is extremely important to be able to access tailor-made ionic liquids for biphasic catalysis and novel separation techniques.

Experimental Section

Preparation of the Inorganic Ionic Liquids: $Na_{13}[Ln(TiW_{11}O_{39})_2]\cdot xH_2O$ (Ln = lanthanide) were prepared by dissolving sodium tungstate (36.3 g, 0.11 mol) in water (200 mL). $TiCl_4$ (1.099 mL, 0.01 mol) was added to the solution with stirring violently. The pH was adjusted to 6 with glacial acetic acid. The mixture was refluxed at 333 K for half an hour, then about 5 mL of a solution containing 0.005 mol of $Ln(NO_3)_3$ was added to the hot mixture. After stirring for 2.5 h at 333 K, the mixture was filtered and the filtrate was cooled to room temperature in a beaker. Anhydrous ethanol (50 mL) was added to the cool filtrate. The product, a colored oil, was collected at the bottom of the beaker.

The method of preparation of $Na_5[MTiW_{11}O_{39}]\cdot xH_2O$ and $Na_6[MTiW_{11}O_{39}]\cdot xH_2O$, (M = transition metal; type 2) is similar to that of type 1. The difference between the two is only the amount of metal salt used as a starting material. In the case of a transition metal, the amount of salt added is 0.01 mol, rather than 0.005 mol of the lanthanide salt.

Acknowledgments

This work was financially supported by the State Key Basic Program (No. G2000048), National Natural Science Foundation (No. 20173017 and No. 20273021) of China and the Foundation of Shanghai Science and Technology Development (No. 023012007).

[1] P. Wasserscheid, W. Keim, *Angew. Chem. Int. Ed.* **2000**, *39*, 3772−3789.
[2] T. Welton, *Chem. Rev.* **1999**, *99*, 2071−2083.
[3] J. D. Holbrey, K. R. Seddon, *Clean Products and Processes* **1999**, *1*, 223−236.
[4] J. G. Huddleston, A. E. Visser, W. M. Reichert, H. D. Willauer, G. A. Broker, R. D. Rogers, *Green Chem.* **2001**, *3*, 156−164.
[5] K. R. Seddon, *Nature Material* **2003**, *2*, 363−365.
[6] J. H. Davis Jr., P. A. Fox, *Chem. Commun.* **2003**, 1209−1212.
[7] H. Zhao, S. V. Malhotra, *Aldrichimica Acta* **2002**, *35*, 75−83.
[8] J. Dupont, R. F. de Souza, P. A. Z. Suarez, *Chem. Rev.* **2002**, 102, 3667−3692.
[9] R. Sheldon, *Chem. Commun.* **2001**, 2399−2407.
[10] C. M. Gordon, *Applied Catal., A* **2001**, *222*, 101−117.
[11] S. Sugden, H. Wilkin *J. Chem. Soc.,* 1919, 1291−1298, and references cited therein.
[12] C. F. Poole, B. R. Kersten, S. S. J. Ho, M. E. Coddens, K. C. Furton, *J. Chromatogr.* **1986**, 352, 407.
[13] P. H. Shetty, P. J. Youngberg, B. R. Kersten, C. F. Pooles, *J. Chromatogr.* **1987**, *411*, 61.
[14] V. R. Roch, C. Nanjundiah, R. T. Carlin, *World Pat. Inf.* **1997**, 9702252.
[15] D. R. Macfarlane, P. Meakin, J. Sun, N. Amini, M. Forsytl, *J. Phys. Chem. B* **1999**, *103*, 4164−4170.
[16] J. H. Davis, K. J. Forrester, T. Merrigan, *Tetrahedron Lett.* **1998**, 39, 8955−8958.
[17] P. Ludley, N. Karodia, *Tetrahedron Lett.* **2001**, *42*, 2011−2014.
[18] C. J. Bradaric, A. Downard, C. Kennedy, A. J. Robertson, Y. Zhou, *Green Chem.* **2003**, 143−152.
[19] H. Matsumoto, T. Matsuda, Y. Miyazaki, *Chem. Lett.* **2000**, 1430.
[20] N. M. M. Mateus, L. C. Branco, N. M. T. Louren, C. A. M. Afonso, *Green Chem.* **2003**, 3 347−352.
[21] K. Ito, N. Nishina, H. Ohno, *Electrochim. Acta* **2000**, 45,1295−1298.
[22] J. L. Thomas, J. Howarth, K. Hanton, D. McGuirck, *Tetrahedron Lett.* **2000**, 41,413.
[23] J. S. Wilkes, M. J. Zaworotko, *Chem. Commun.* **1992**, 965−967.
[24] J. Fuller, R. T. Carlin, H. C. Delong, D. Howorth, *Chem. Commun.* **1994**, 299−300.
[25] C. G. Swain, A. Ohno, D. K. Roe, R. Brown, T. Mangh, *J. Am. Chem. Soc.* **1967**, 89,2648−2649.
[26] I. K. Moom, Y. H. Jeong, *Thermochimica Acta* **2001**, *377*, 51−61.
[27] J. F. Liu, E-B. Wang, *Inorg. Chem.* **1991**, 7,2,160−164; J. F. Liu, W. Wang, E.-B. Wang, *Inorg. Chem.* **1992**, *8*, 1, 85−87.
[28] D. S. H. Wong, P. C Jia, M. C Jyh, H. C Cheng, *Fluid Phase Equilib.* **2002**, 194−197, 1089−1095.
[29] J. Fuller, A C. Breda, R T. Carlin, *J. Electrochem. Soc.* **1997**, 144, 67−71.
[30] K. A. Fletcher, I. A. Stoery, A. E. Hendricks, *Green Chem.* **2001**, *3*, 210−215.
[31] P. Bonhôte, A.-P. Dias, N. Papageorgiou, K. Kalyanasundaram, M. Grätzal, *Inorg. Chem.* **1996**, *35*, 1168−1178.
[32] J. D. Peter, *J. Am. Chem. Soc.* **1984**, 106, 7677.
[33] M. C Yang, D. G. Yu, *J. Appl. Polym. Sci.* **1998**, 168, 1331−1336.
[34] R. J. Gale, B. P. Gilbert, R. A. Osteryoung, *Inorg. Chem.* **1978**, 17, 2728−2736.
[35] G. Franzen, B. P. Gilbert, G. Pelzer, E. Pepauw, *Org. Mass. Spectrom.* **1986**, 21, 443−451.
[36] A. K. Abdul-Sada, A. M. Greenway, K. R. Seddon, T. Welton, *Org. Mass. Spectrom.* **1989**, 214, 917..

Received August 20, 2003

 © 2004 Wiley-VCH Verlag GmbH & Co. KGaA, Weinheim

Synthesis and Structural Studies of Rhenium(v) Complexes Stabilized by a Monoanionic Cyclen Ligand

Catarina Xavier,[a] António Paulo,[a] Angela Domingos,[a] and Isabel Santos*[a]

Keywords: Rhenium / Oxo ligands / Macrocycles / N ligands

The novel cationic (oxo)Re^{V} complexes [ReO(cyclen-H)Cl]X [X = Cl (**3a**), BPh_4 (**3b**)] and [ReO(cyclen-H)I]I (**4**) have been prepared by treating cyclen (1,4,7,10-tetrazacyclododecane) with $(Bu_4N)[ReOCl_4]$ (**1**) and *cis*-$[ReO_2I(PPh_3)_2]$ (**2**), respectively. The X-ray structural analyses of **3a** and **4**, as well as ^1H NMR spectroscopy, showed that the macrocyclic ligand is coordinated in the unprecedented monoanionic form. ^1H and ^{13}C NMR spectroscopy also demonstrated that **3a**,**b** and **4** exist in solution as single isomers. To the best of our knowledge, **3a** and **4** are the first examples of structurally characterized oxo complexes of d transition elements with cyclen bound to the metal atom through one amido and three amine groups. In both complexes, the geometry around the Re^{V} center is best described as distorted octahedral. The terminal oxo and halo ligands are coordinated in relative *cis* positions, and the amido and three amino nitrogen atoms from cyclen occupy the four remaining coordination positions. The Re–N(amido) bonds [1.894(9) Å in **3a** and 1.888(12) Å in **4**] are *trans* to the halo ligands and, as expected, are considerably shorter than the Re–N(amine) bonds, which span from 2.110(6) to 2.246(8) Å and from 2.124(8) to 2.268(10) Å for cations the cations of **3a** and **4**, respectively.
(© Wiley-VCH Verlag GmbH & Co. KGaA, 69451 Weinheim, Germany, 2004)

Introduction

Macrocyclic polyamines, especially those based on cyclen (1,4,7,10-tetrazacyclododecane) or cyclam (1,4,8,11-tetrazacyclotetradecane) frameworks are widely used in the coordination chemistry of the d and f elements in search of applications in a wide variety of areas such as catalysis, biomimicry and medicine.[1] The coordination chemistry explored with macrocyclic polyamines for rhenium has involved only cyclam[2−4] and tacn (1,4,7-triazacyclononane)[5−11] type ligands. In the case of cyclam, part of this research work has been pursued due to the relevance of rhenium complexes in the development of diagnostic or therapeutic radiopharmaceuticals.[3,4] In fact, the β-emitters ^{186}Re and ^{188}Re are potentially useful as therapeutic radionuclides, and rhenium complexes are adequate surrogates of complexes of radioactive ^{99m}Tc, which is the most widely used radionuclide in diagnostic nuclear medicine.[12−14]

The (cyclam)rhenium chemistry so far reported is restricted almost to the cationic *trans*-$[ReO_2(cyclam)]^+$ species, which contains the macrocycle coordinated in a neutral, tetradentate and equatorial fashion.[2−4] The strong tendency of cyclam to form complexes with the *trans*-$[ReO_2]^+$ core is well illustrated by the fact that *trans*-$[ReO_2(cyclam)]^+$ can be prepared using rhenium starting materials as diverse as $[ReOCl_3(PPh_3)_2]$, $[ReNCl_2(PPh_3)_2]$, or even $[ReCl_3(CH_3CN)(PPh_3)_2]$.[3] In contrast, for tacn type ligands a much more diverse rhenium chemistry has been developed. These neutral, facial and tridentate ligands allowed the stabilization of a plethora of rhenium complexes, with the metal atom in oxidation states spanning from I to VII.[5−11]

Until now, research on rhenium chemistry with cyclen, also a potentially tetradentate macrocycle like cyclam but displaying a smaller cavity size, has remained completely unexplored. Aiming to widen the scope of the chemistry of Re^{V} oxides with cyclic tetradentate polyamines, and taking into account that cyclen tends to form mainly *cis*-octahedral complexes,[15] we decided to evaluate the possibility of using cyclen as an anchor to stabilize complexes with $[Re{=}O]^{3+}$ or *cis*-$[ReO_2]^+$ cores. In this contribution we describe reactions of cyclen with the Re^{V} starting materials $(Bu_4N)[ReOCl_4]$ (**1**) and *cis*-$[ReO_2I(PPh_3)_2]$ (**2**), which led to the formation of [ReO(cyclen-H)Cl]Cl (**3a**) and [ReO(cyclen-H)I]I (**4**), respectively. Herein, we also discuss the mechanism involved in the formation of complex **4**, which most probably proceeds through the intermediate *cis*-$[ReO_2(cyclen)]^+$, as indicated by ^1H and ^{13}C NMR spectroscopic studies.

Results and Discussion

While there is an extensive literature[16] on mono(oxo)Re^{V} complexes, namely with chelating N-donor ligands, complexes with the *cis*-$[ReO_2]^+$ core are scarce. To the best of our knowledge, the latter class of compounds

[a] Departamento de Quimica, ITN
Estrada Nacional 10, 2686-953 Sacavem Codex, Portugal
Fax: (internat.) + 351-219941455
E-mail: isantos@itn.mces.pt

is comprised of only the five-coordinate *cis*-[$ReO_2I(PPh_3)_2$] (**2**)[17] and the six-coordinate *cis*-[$ReO_2(bipy)(py)_2$] (bipy = 2,2′-bipyridine)[18] and *cis*-[$ReO_2(OH_2)(Me_3tacn)]^+$ (Me_3-tacn = 1,4,7-trimethyl-1,4,7-triazacyclononane)[11]. For the synthesis of mono(oxo)Re^V complexes, several methodologies are available, namely oxygen abstraction reactions of Re^{VII} compounds already containing the ancillary ligands, reduction of perrhenate in the presence of the incoming ligands or metathesis reactions of (halo)(oxo)Re^V complexes, such as (Bu_4N)[$ReOCl_4$] (**1**) or [$ReOCl_3(PPh_3)_2$].[16,19–21] In contrast, there are no well-established synthetic methods for preparing *cis*-dioxorhenium(V) complexes.

To enter into the chemistry of mono(oxo)Re^V complexes with cyclen we decided to start from (Bu_4N)[$ReOCl_4$] (**1**),[22] while for preparing cyclen complexes with the *cis*-$[ReO_2]^+$ core we selected *cis*-[$ReOI_2(PPh_3)_2$] (**2**)[17] as the more convenient starting material. As depicted in Scheme 1, compound **1** reacts smoothly with cyclen in dichloromethane giving [ReO(cyclen-H)Cl]Cl (**3a**) in moderate yield (57%). Compound **3a** slowly precipitates from the reaction mixture as a grey-green microcrystalline solid. ^1H NMR analysis of the precipitate showed the presence of **3a** contaminated with a small amount of protonated cyclen, due to release of HCl which is scavenged by the cyclen still present in solution. To suppress the formation of protonated cyclen, we have studied the reaction of **1** with cyclen in the presence of Et_3N. However, even under these conditions **3a** co-precipitates with protonated cyclen, which was removed by successive washings with methanol. An alternative for purification of $[ReO(cyclen\text{-}H)Cl]^+$ is the replacement of the counterion in **3a** by the larger anion BPh_4^- (Scheme 1). Treatment of an aqueous solution of crude **3a** with $NaBPh_4$ was accompanied by the precipitation of [ReO(cyclen-H)Cl](BPh_4) (**3b**), which was recovered analytically pure in 65% yield, after washing with water and methanol.

The reaction of *cis*-[$ReO_2I(PPh_3)_2$] (**2**) with cyclen in dichloromethane is quite fast, resulting in a brown solution from which a red solid precipitates almost immediately. During the course of the reaction, this insoluble red solid slowly vanishes and, meanwhile, a green microcrystalline solid starts to precipitate. This green material, recovered after a reaction time of 3 h, was identified as [ReO(cyclen-H)I]I (**4**), the iodo analogue of **3** (Scheme 1). Compound **4** was obtained in approximately 40% yield after purification by successive washings with warm water to remove some protonated cyclen and perrhenate, which were formed during the reaction.

Compounds [ReO(cyclen-H)Cl]X [X = Cl (**3a**), BPh_4 (**3b**)] and [ReO(cyclen-H)I]I (**4**) were unambiguously identified by the common analytical techniques which included X-ray crystallographic analysis in the case of **3a** and **4**.

The analysis of compounds **3a**, **3b** and **4** by ^1H and ^{13}C NMR spectroscopy demonstrated that the respective complex cations exist in solution as single isomers. In fact, the ^{13}C NMR spectra of these compounds in [D_6]DMSO showed four resonances for the methylene carbon atoms of cyclen in the range δ = 49.8−71.9 ppm, and three additional resonances for the aromatic carbon atoms of the counterion in the case of **3b**. These ^{13}C NMR spectra are consistent with the solid-state structures found for **3a** and **4**, and can be accounted for by the presence of a horizontal mirror plane which bisects the macrocycle and makes each pair of chelate rings magnetically equivalent.

The ^1H NMR spectra of **3a**,**b** and **4** should display eight resonances for the 16 diastereotopic methylene protons of the monodeprotonated cyclen, one resonance for the two equivalent apical N*H* protons and one resonance for the equatorial N*H* proton. Using [D_6]DMSO as the solvent, all the expected NH resonances were observed but some signals of the methylene protons of cyclen overlapped with the signal from residual water. In **3a**,**b** and **4**, the two apical N*H* resonances appear between δ = 9.64 and 9.84 ppm, and are considerably deshielded in comparison with the equatorial NH proton which resonates between δ = 4.25 and 4.52 ppm. All spectra display four poorly resolved multiplets in the range δ = 3.50−4.00 ppm, integrating for 8 CH_2 protons, and two high-field-shifted multiplets between δ = 2.4 and 2.8 ppm, integrating each for 2 CH_2 protons. For complex **3a** there is one CH_2 resonance very close to the residual water signal, appearing at δ = 3.52 ppm, and another under the water signal as demonstrated by 2D COSY and 2D HETCOR experiments. In fact, in the COSY spectrum of **3a** three correlations were found between the water signal and three of the CH_2 resonances, while in the HETCOR spectrum one correlation was observed between the water signal and the carbon atom reson-

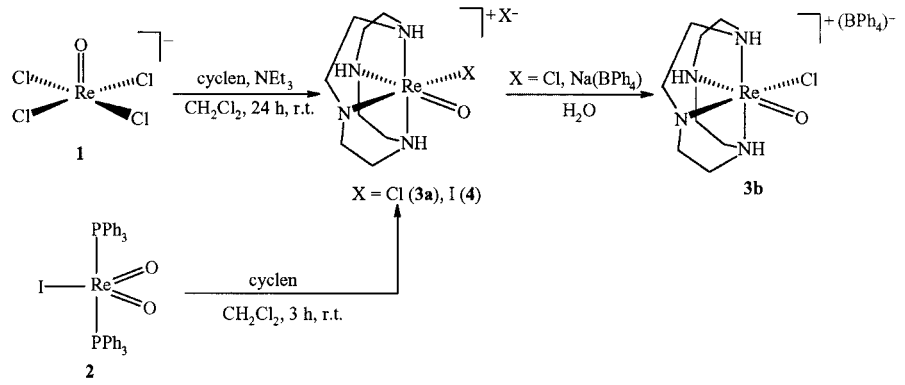

Scheme 1

 © 2004 Wiley-VCH Verlag GmbH & Co. KGaA, Weinheim

ating at δ = 64.1 ppm. In the spectra of compounds **3b** and **4**, two resonances are missing for the cyclen methylene protons. By analogy with the spectrum of 3**a**, these resonances must be under the signal of residual water, which appears at δ ≈ 3 ppm.

X-ray quality crystals of **3a** and **4** were obtained from methanol or water solutions, respectively, in the presence of air. Compound **3a** crystallized as $[ReO(cyclen\text{-}H)Cl]Cl_{0.67}(ReO_4)_{0.33}$, most probably due to partial oxidation of **3a** during the recrystallization process. Noticeably, for compound **4** no partial oxidation or hydrolysis of the rhenium−iodo bond was observed during its recrystallization from water, as evidenced by the crystal structure being consistent with intact [ReO(cyclen-H)I]I (**4**).

The crystallographic analyses showed that the complex cations **3a** and **4** are monomeric with approximately octahedral coordination geometries. ORTEP views of the structures are shown in Figures 1 and 2, and selected bond lengths and angles are listed in Tables 1 and 2, respectively.

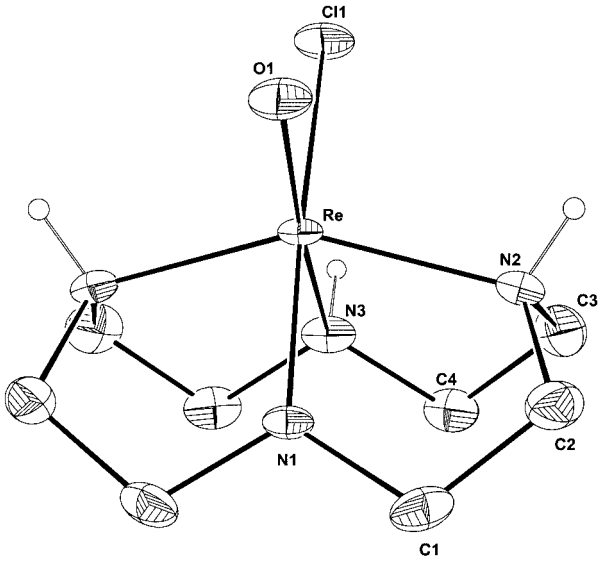

Figure 1. ORTEP view of the cationic complex **3a**; thermal ellipsoids are drawn at the 30% probability level

To the best of our knowledge, **3a** and **4** are the first reported structurally characterized examples of oxo complexes of d transition metals stabilized by a cyclen ligand. The presence of a monodeprotonated cyclen ligand is another unique feature of the structures of **3a** and **4**. In all reported structures of cyclen complexes the macrocycle is coordinated as a neutral ligand.[23−25] In both complexes, the rhenium center is coordinated by the one amido and three amine groups from cyclen, an oxo ligand and a halo ligand. The oxo and halo ligands are in *cis*-positions, as imposed by the *cis*-octahedral coordination of the tetradentate cyclen which occupies the remaining four coordination sites.

The presence of the rhenium−amido bonds is confirmed by their short lengths [Re−N(1) 1.894(9) Å in **3a**; Re−N(1) 1.888(12) Å in **4**], and by the almost planar sp^2-hybridized

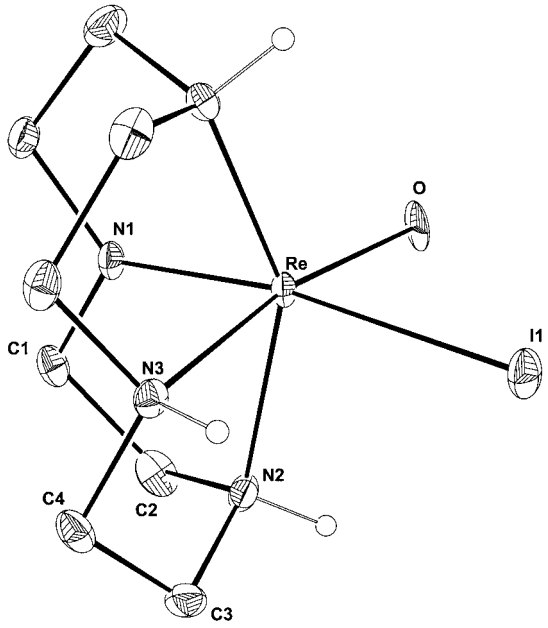

Figure 2. ORTEP view of the cationic complex **4**; thermal ellipsoids are drawn at the 30% probability level

Table 1. Selected bond lengths [Å] and angles [°] for cation **3a**

Re−O(1)	1.704(8)	Re−N(1)	1.894(9)
Re−N(2)	2.110(6)	Re−N(3)	2.246(8)
Re−Cl(1)	2.525(3)		
O(1)−Re−N(1)	108.8(3)	O(1)−Re−N(2)	105.2(2)
O(1)−Re−N(3)	164.3(4)	O(1)−Re−Cl(1)	87.8(3)
N(1)−Re−N(2)	79.8(2)	N(1)−Re−N(3)	86.9(4)
N(1)−Re−Cl(1)	163.4(3)	N(2)−Re−N(2)*[a]	147.5(3)
N(2)−Re−N(3)	76.9(2)	N(2)−Re−Cl(1)	96.1(2)
N(3)−Re−Cl(1)	76.5(3)		

[a] Equivalent atoms generated by the symmetry operation $-x$, $-x + y$, z.

Table 2. Selected bond lengths [Å] and angles [°] for cation **4**

Re−O	1.715(9)	Re−N(1)	1.888(12)
Re−N(2)	2.124(8)	Re−N(3)	2.268(10)
Re−I(1)	2.8791(10)		
O(1)−Re−N(1)	110.1(5)	O(1)−Re−N(2)	105.2(2)
O(1)−Re−N(3)	162.7(5)	O(1)−Re−I(1)	85.0(4)
N(1)−Re−N(2)	79.5(2)	N(1)−Re−N(3)	87.2(5)
N(1)−Re−I(1)	164.9(4)	N(2)−Re−N(2)*[a]	147.4(4)
N(2)−Re−N(3)	77.2(2)	N(2)−Re−I(1)	96.9(2)
N(3)−Re−I(1)	77.7(3)		

[a] Equivalent atoms generated by the symmetry operation $-x$, y, z.

N(1) atom. The Re−N(1) bond lengths in **3a** and **4** are similar to the Re−amido bond lengths recently reported for cationic (oxo)Re^V complexes with an acyclic tetradentate N-donor ligand.[16] As expected, these Re−N(1) bonds are considerably shorter than the three Re−N(amine) bonds, which span from 2.110(6) to 2.246(8) Å and from 2.124(8) to 2.268(10) Å for **3a** and **4**, respectively. Among the Re−N(amine) bonds, the longest are those corresponding to the nitrogen atom coordinated *trans* to the oxo ligand

 © 2004 Wiley-VCH Verlag GmbH & Co. KGaA, Weinheim

[Re−N(3) 2.246(8) Å in **3a**; Re−N(3) 2.268(10) Å in **4**], reflecting the *trans* effect of this multiply bound ligand. The Re=O bond lengths [1.704(8) Å in **3a**; 1.715(9) Å in **4**] are within the expected range for octahedral mono(oxo)Re^{V} complexes but the Re−Cl [2.525(3) Å in **3a**] and the Re−I [2.8791(10) Å in **4**] bonds are longer than the values usually observed in (halo)(oxo)Re^{V} complexes.[16,17]. The lengthening of the Re−X (X = Cl, I) bonds can probably be accounted for by the presence of intramolecular hydrogen bonds involving the halo ligands and the equatorial N−H hydrogen atoms [Cl···N(3) 2.968 Å in **3a**; I···N(3) 3.262 Å in **4**].

In the structures of cations **3a** and **4**, the cyclen ligands adopt a folded and butterfly-like configuration, defining four chelate rings. There is a crystallographic mirror plane which contains the Re, O, N(1), N(3) and halide atoms, bisecting the coordinated macrocycle and resulting in two pairs of crystallographically equivalent five-membered chelate rings. The crystallographically equivalent chelate rings containing the deprotonated N(1) atom {[Re, N(1), C(1), C(2), N(2)] and [Re, N(1), C(1*), C(2*), N(2*)]} adopt an envelope conformation, while the other two equivalent five-membered chelate rings {[Re, N(2), C(3), C(4), N(3)] and ([Re, N(2*), C(3*), C(4*), N(3)]} assume a twisted conformation. The small cavity size of cyclen imparts a significant angular strain on the folded ring, as clearly indicated by the axial N(2)−Re−N(2*) bond angles of 147.5(3)° in **3a** and 147.4(4)° in **4**, which bend away the macrocycle from the oxo and halo ligands coordinated in the equatorial positions. This bending is more pronounced than that usually observed in *cis*-octahedral complexes containing neutral and tetradentate cyclen, where the axial angles usually lie between 160 and 170°.[23−25] The increased bending of the macrocycle in **3a** and **4** most probably reflects the presence of the Re−N(amido) bonds, which introduce additional steric constraints in the *cis*-octahedral coordination of the small sized cyclen.

For complexes **3a** and **4**, two isomeric forms could exist, depending on the *syn* or *anti* orientation of the equatorial N−H hydrogen atoms (see Figure 3), but only one isomeric form was detected, both in solid state and in solution. In the solid-state structures found for **3a** and **4**, the two apical NH hydrogen atoms and the equatorial NH hydrogen atom are directed towards the oxo and halo ligands, corresponding to the *syn*(X) (X = Cl, I) form. The establishment of the above-mentioned intramolecular hydrogen bonds X···H

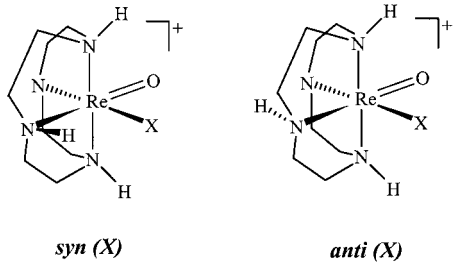

Figure 3. Schematic representation of the two possible isomers for cations $[ReO(cyclen\text{-}H)X]^{+}$ [X = Cl (**3**), I (**4**)]

[X = Cl (**3a**), I (**4**)], involving the equatorial N−H hydrogen atoms, certainly contribute to the formation of the single *syn* isomers.

Interestingly, the solid-state structures of **3a** and **4** give some support to the conjugate base catalyzed dissociative mechanism (D_{cb}), generally accepted for substitution reactions of (cyclen)Co^{III} complexes. Such mechanism involves intermediate Co^{III} complexes containing a monodeprotonated cyclen, but these intermediates were never isolated.[25]

In order to have a better insight into the nature of the intermediates involved in the formation of green [ReO(cyclen-H)I]I (**4**), we tried to identify the red solid which was formed almost immediately when *cis*-$[ReO_2I(PPh_3)_2]$ (**2**) was treated with cyclen. After a short reaction time of 30 min, the red insoluble solid was separated and washed with dichloromethane. After drying under vacuum, the recovered red and microcrystalline material was analyzed by ^{1}H and ^{13}C NMR spectroscopy. As will be discussed below, the collected NMR spectroscopic data indicated that we must have isolated the cationic complex "*cis*-$[ReO_2(cyclen)]^{+}$" (**I_1**). However, complex **I_1** was never obtained analytically pure, being always contaminated with $cyclenH^{+}$ and perrhenate. All attempts to purify **I_1** were unsuccessful because of its tendency to be transformed into [ReO(cyclen-H)I]I (**4**), even under strictly anhydrous and anaerobic conditions.

The ^{13}C NMR spectrum in [D_6]DMSO of the intermediate *cis*-$[ReO_2(cyclen)]^{+}$ (**I_1**) is even simpler than those of **3** and **4**, displaying only two methylene resonances at δ = 63.6 and 58.1 ppm for the coordinated cyclen. This pattern is consistent with the formulation proposed for **I_1**, since all the chelate rings are expected to be magnetically equivalent, due to the higher symmetry of this complex, which displays one horizontal mirror plane containing the metal atom, the oxo ligands and the equatorial nitrogen atoms, and one vertical mirror plane passing through the apical nitrogen atoms and the metal atom. Consistent with this, the ^{1}H NMR spectrum of **I_1** shows two broad resonances, centered at δ = 9.38 and 6.18 ppm and integrating for 2 protons each, which we have attributed to the two equivalent apical N*H* protons and to the two equivalent equatorial N*H* protons, by comparison with the ^{1}H NMR spectroscopic data of compounds **3a**,**b** and **4**, which have been unambiguously identified. Based on the formulation proposed for complex **I_1**, four resonances were expected for the CH_2 protons of cyclen with relative intensities of 4:4:4:4. In [D_6]DMSO, the ^{1}H NMR spectrum of **I_1** displays three resonances at δ = 3.01, 3.19 and 3.74 ppm, integrating each for 4 protons. The missing resonance also probably overlapped with the signal of residual water, as discussed above for complexes **3a**,**b** and **4**. Hence, the NMR spectroscopic properties of **I_1** seem to be in accord with its formulation as a *cis*-dioxo complex containing a tetradentate and neutral cyclen ligand.

In spite of the occurrence of parallel oxidation processes, we believe that formation of compound **4** involves **I_1** as an intermediate, as proposed in Scheme 2. The observed *cis*-dioxo intermediate **I_1** most probably rearranges into the (hydroxo)(oxo)Re^{V} derivative **I_2**, following an intramolecu-

 © 2004 Wiley-VCH Verlag GmbH & Co. KGaA, Weinheim

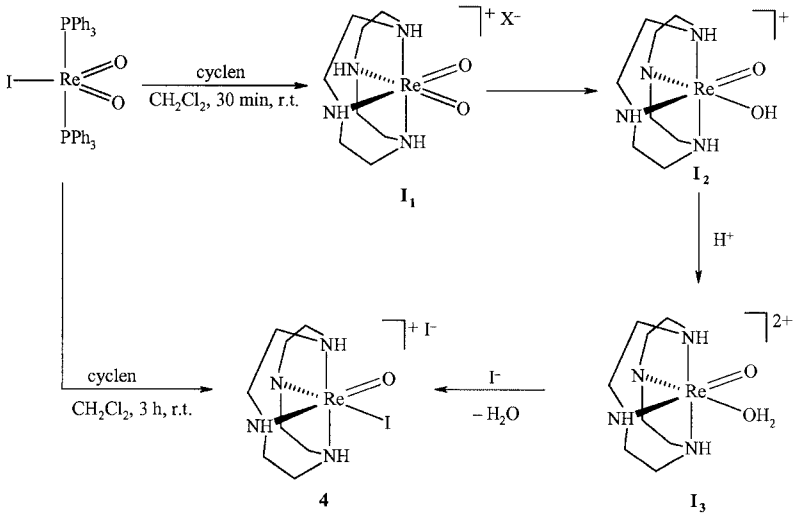

Scheme 2

lar proton transfer from cyclen to one of the oxo ligands. Further protonation of the hydroxo ligand, eventually by adventitious water, gives the intermediate aqua complex $\mathbf{I_3}$, which is finally transformed into the (iodo)(oxo) complex **4** upon replacement of the water molecule by the halide anion. The driving force for the transformation of $\mathbf{I_1}$ into **4** is certainly the basicity of the oxo ligands associated with the unstable *cis* configuration of the $[ReO_2]^+$ unit, due to the antibonding interactions between the metal d orbitals and the oxygen lone pairs.[26] In fact, the scarcity of *cis*-dioxorhenium(v) complexes has been attributed to electronic factors, the *trans* arrangement of the MO_2 unit being the most stable in octahedral dioxo transition metal complexes with a d^2 configuration.[26]

Conclusions

The novel cationic [ReO(cyclen-H)Cl]X [X = Cl (**3a**), BPh_4 (**3b**)] and [ReO(cyclen-H)I]I (**4**) were prepared in moderate yields using $(Bu_4N)[ReOCl_4]$ (**1**) or *cis*-$[ReO_2I(PPh_3)_2]$ (**2**), respectively, as the starting materials. The cations of compounds **3** and **4** are the first examples of d transition metal oxo complexes anchored to a monoanionic cyclen ligand. In the case of **3a** and **4**, the unprecedented coordination mode of the macrocycle was confirmed by X-ray crystallography, and the deprotonation of cyclen is certainly justified due to the enhanced Lewis acidity of the d^2 rhenium center. Apparently, the geometrical constraints of *cis*-octahedral cyclen could impose the *cis* geometry on the ReO_2 unit, but the resultant reactive *cis*-dioxo complex, *cis*-$[ReO_2(cyclen)]^+$, is readily converted into compound **4**. This transformation more than likely involves deprotonation of one amine group from cyclen, protonation of one of the oxo ligands from the *cis*-ReO_2 unit, and coordination of the incoming halide ion. A possible strategy for the efficient trapping of cyclen *cis*-dioxorhenium(v) derivatives could be the use of tetrasubstituted *N*-alkylated cyclen ligands, which are unable to undergo deprotonation.

Remarkably, in complexes **3** and **4** the cyclen ligand remains deprotonated even under aqueous conditions, indicating that cations **3** and **4** exhibit considerable stability in water and under aerobic conditions. These features may offer the possibility of applying such systems in the development of ^{99m}Tc or $^{186/188}Re$ radiopharmaceuticals, which is nowadays one of the most relevant areas for the application of rhenium coordination compounds.

Although not yet explored, a diverse derivative chemistry can be anticipated for complexes **3** and **4**, based on oxygen transfer or metathesis reactions, allowing an interesting comparison with the chemistry reported so far for the related macrocyclic cations $[ReO(tacn)Cl_2]^+$ and $[ReO(Me_3tacn)Cl_2]^+$.[7]

Experimental Section

General: The syntheses of the complexes were carried under nitrogen, using standard Schlenk techniques and dry CH_2Cl_2, while the workup procedures were performed under air. The starting materials $[Bu_4N][ReOCl_4]$ (**1**) and *cis*-$[ReO_2I(PPh_3)_2]$ (**2**) were prepared according to literature methods.[17,22] Other chemicals were used as purchased. ^1H and ^{13}C NMR spectra were recorded with a Varian Unity 300 MHz spectrometer. ^1H and ^{13}C chemical shifts are given in ppm and were referenced to the residual solvent resonances relative to Me_4Si. IR spectra were recorded as KBr pellets with a Perkin−Elmer 577 spectrometer. C, H and N analyses were performed with an EA 110 CE Instruments automatic analyzer.

[ReOCl(cyclen)]Cl (3a): To a solution of $[Bu_4N][ReOCl_4]$ (**1**) (200 mg, 0.34 mmol) in CH_2Cl_2 (15 mL) was added a solution of cyclen (58 mg, 0.34 mmol) and triethylamine (0.36 mmol, 50 mL) in CH_2Cl_2 (5 mL) at room temperature. The initially yellow solution became dark brown after complete addition of the ligand. The reaction mixture was stirred for 24 h and, after this time, a red

 © 2004 Wiley-VCH Verlag GmbH & Co. KGaA, Weinheim

supernatant and an insoluble gray-green solid were obtained. This solid, which was recovered using a centrifuge, was washed with methanol and formulated as **3a**. Yield: 86 mg (0.19 mmol, 57%). $C_8H_{19}Cl_2N_4ORe$ (444.38): calcd. C 21.61, H 4.27, N 12.60; found C 21.36, H 4.15, N 12.33. IR: $\tilde{\nu}$ = 940 [ν(Re=O)] cm^{-1}. ^1H NMR (300 MHz, [D$_6$]DMSO): δ = 2.49 (br., 2 H, CH_2), 2.70−2.82 (m, 2 H, CH_2), 3.40−3.52 (m, 2 H, CH_2), 3.75−4.15 (m, 8 H, CH_2), 4.24 (br., 1 H, NH), 9.84 (br., 2 H, NH) ppm. ^{13}C NMR (300 MHz, [D$_6$]DMSO): δ = 50.5, 60.9, 64.6, 71.1 ppm.

[ReOCl(cyclen)]BPh$_4$: A solution of $NaBPh_4$ (77 mg, 0.23 mmol) in distilled water (10 mL) was added to a solution of **3a** (50 mg, 0.13 mmol) in water (10 mL), causing the immediate formation of **3b** as a yellow-green microcrystalline solid. Compound **3b** was recovered using a centrifuge, followed by successive washings with methanol. Yield: 60 mg (0.085 mmol, 65%). $C_{32}H_{39}BClN_4ORe$ (728.16): calcd. C 52.78, H 5.40, N 7.69; found C 53.18, H 5.73, N 7.72. IR : $\tilde{\nu}$ = 940 [ν(Re=O)] cm^{-1}. ^1H NMR (300 MHz, [D$_6$]DMSO): δ = 2.49 (br., 2 H, CH_2), 2.72 (m, 2 H, CH_2), 3.72−4.15 (m, 8 H, CH_2), 4.24 (br.,1 H, NH), 6.78 (m, 4 H, Ar), 6.91(m, 8 H, Ar), 7.16 (m, 8 H, Ar), 9.84 (br., 2 H, NH) ppm. ^{13}C NMR (300 MHz, [D$_6$]DMSO): δ = 50.5, 60.9, 64.6, 71.1, 121.5, 125.3, 135.5 ppm.

[ReOI(cyclen)]I (4): To a solution of *cis*-[$ReO_2I(PPh_3)_2$] (130 mg, 0.15 mmol) in CH_2Cl_2 (15 mL) was added a solution of cyclen (28 mg, 0.16 mmol) in CH_2Cl_2 (5 mL). The initially purple solution became brown, and a red solid started to precipitate almost immediately. During the course of the reaction, the red solid vanished and, meanwhile, a green microcrystalline solid started to precipitate. After 3 h, the green solid, which was formulated as **4**, was recovered using a centrifuge, washed with CH_2Cl_2 and warm water, and dried under vacuum. Further purification of **4** was achieved by recrystallization from distilled water. Yield: 38 mg (0.06 mmol, 40%). $C_8H_{19}I_2N_4ORe$ (627.28): calcd. C 15.30, H 3.03, N 8.93; found C 15.65, H 2.96, N 8.79. IR: $\tilde{\nu}$ = 940 [ν(Re=O)] cm^{-1}. ^1H NMR (300 MHz, [D$_6$]DMSO): δ = 2.49−2.60 (m, 2 H,CH_2), 2.78−2.83 (m, 2 H, CH_2), 3.83−3.98 (m, 6 H, CH_2), 4.07−4.15 (m, 2 H, CH_2), 4.52 (br.,1 H, NH), 9.64 (br., 2 H, NH) ppm. ^{13}C NMR (300 MHz, [D$_6$]DMSO): δ = 51.2, 61.1, 63.4, 71.9 ppm.

X-ray Crystallographic Analysis: Crystals were obtained by recrystallization from a saturated methanol solution (**3a**) or from a saturated aqueous solution (**4**) and mounted in thin-walled glass capillaries. Data were collected at room temperature with an Enraf−Nonius CAD-4 diffractometer with graphite-monochromated Mo-K_α radiation, using an ω-2θ scan mode. The crystal data are summarized in Table 3. The data were corrected[27] for Lorentz and polarization effects, and empirically for absorption by Ψ-scans. The heavy-atom positions were located by Patterson methods using SHELXS-97.[28] The remaining atoms were located in successive Fourier difference maps and refined by least-squares refinements on F^2 using SHELXL-97.[29] All non-hydrogen atoms were refined anisotropically; the contributions of the hydrogen atoms were included in calculated positions, constrained to ride on their carbon atoms with group U_{iso} values assigned. Atomic scattering factors and anomalous dispersion terms were as in SHELXL-97.[29] The drawings were made with ORTEP-3.[30] Crystallographic data for the structure reported in this paper have been deposited with the Cambridge Crystallographic Data Centre as supplementary publication no. CCDC-215009 (**3a**) and -215010 (**4**). Copies of the data can be obtained free of charge on applicaton to CCDC, 12 Union Road, Cambridge CB2 1EZ, UK [Fax: (internat.) + 44-1223-336-033; E-mail: deposit@ccdc.cam.ac.uk].

Table 3. Crystallographic data for cations **3a** and **4**

	3a	**4**
Empirical formula	$C_8H_{19}Cl_{1.67}N_4O_{2.33}Re_{1.23}$	$C_8H_{19}I_2N_4ORe$
Formula mass	515.96	627.27
Crystal size [mm]	0.40 × 0.12 × 0.09	0.28 × 0.20 × 0.12
Crystal system	hexagonal	orthorhombic
Space group	$P6_3cm$	$Cmc2_1$
a [Å]	14.156(3) Å	8.9853(10)
b [Å]	14.156(3) Å	12.9086(14)
c [Å]	11.952(3) Å	12.3257(17)
V [Å]	2074.2(8) Å^3	1429.6(3)
Z	6	4
T [K]	293(2)	293(2)
$D_{calcd.}$ [g cm^{-3}]	2.478	2.914
μ (Mo-K_α) [mm^{-1}]	12.011	12.807
F(000)	1452	1136
No. reflections Measured	3294	1359
No. unique Reflections	1761 (0.0352)[a]	1122 (0.0202)[a]
$R1$[b]	0.0314	0.0261
wR_2	0.0451	0.0628

[a] Value of R(int). [b] The values were calculated for data with $I > 2\sigma(I)$.

Acknowledgments

C. X. would like to thank the Fundação para a Ciência e Tecnologia (National Foundation for Science and Technology) for a BIC research grant.

[1] J. Costamagna, G. Ferraudi, B. Matsuhiro, M. Campos-Vallete, J. Canales, M. Villagrán, J. Vargas, M. J. Aguirre, *Coord. Chem. Rev.* **2000**, *196*, 125.
[2] A. J. Blake, J. A. Greig, M. Schröder, *J. Chem. Soc., Dalton Trans.* **1988**, 2645.
[3] S. A. Luna, C. Bolzati, A. Duatti, G. L. Zuchini, R. F. Bandoli, *Inorg. Chem.* **1992**, *31*, 2595.
[4] B. W. Tsang, J. Reibenspies, A. E. Martell, *Inorg. Chem.* **1993**, *32*, 988.
[5] K. Wieghardt, C. Pomp, B. Nuber, J. Weiss, *Inorg. Chem.* **1986**, *25*, 1659.
[6] C. Pomp, K. Wieghardt, *Polyhedron* **1988**, *7*, 2537.
[7] R. R. Conry, J. M. Mayer, *Inorg. Chem.* **1990**, *29*, 4862.
[8] G. Böhm, K. Wieghardt, B. Nuber, J. Weiss, *Inorg. Chem.* **1991**, *30*, 3464.
[9] G. Böhm, K. Wieghardt, B. Nuber, J. Weiss, *Angew. Chem. Int. Ed. Engl.* **1990**, *29*, 787.
[10] C-M. Che, J. Y. K. Cheng, K-K. Cheung, K-Y. Wong, *J. Chem. Soc., Dalton Trans.* **1997**, 2347.
[11] J. Y. K. Cheng, K-K. Cheung, M. C. W. Chan, K-Y. Wong, C.-M. Che, *J. Chem. Soc., Dalton Trans.* **1997**, 2347.
[12] J. R. Dilworth, S. J. Parrot, *Chem. Soc. Rev.* **1998**, *27*, 43.
[13] B. Johanssen, H. Spies, *Top. Curr. Chem.* **1996**, *176*, 79.
[14] S. S. Jurisson, J. D. Lydon, *Chem. Rev.* **1999**, *99*, 2205.
[15] D. A. Buckingham, C. R. Clark, A. J. Rogers, J. Simpson, *Inorg. Chem.* **1998**, *37*, 3497, and references cited therein.
[16] L. Xu, J. Pierreroy, B. O. Patrick, C. Orvig, *Inorg. Chem.* **2001**, *40*, 2005, and references cited therein.
[17] G. F. Ciani, G. D'Alfonso, P. F. Romiti, A. Sironi, M. Freni, *Inorg. Chim. Acta* **1983**, *72*, 29.

 © 2004 Wiley-VCH Verlag GmbH & Co. KGaA, Weinheim

[18] M. S. Ram, C. S. Johnson, R. L. Blackbourn, J. T. Hupp, *Inorg. Chem.* **1990**, *29*, 238.
[19] J. D. G. Correia, A. Domingos, I. Santos, *Eur. J. Inorg. Chem.* **2000**, 1523.
[20] I. A. Degnan, J. Behm, M. R. Cook, W. A. Herrmann, *Inorg. Chem.* **1991**, *30*, 2165.
[21] [21a] A. Domingos, J. Marçalo, A. Paulo, A. Pires de Matos, I. Santos, *Inorg. Chem.* **1993**, *32*, 5114. [21b] R. Garcia, Y. H. Xing, A. Domingos, A. Paulo, I. Santos, *Inorg. Chim. Acta* **2003**, *343*, 27.
[22] R. Alberto, R. Schibili, A. Egli, P. A. Schubiger, W. A. Herrmann, G. Artus, U. Abram, T. A. Kaden, *J. Organomet. Chem.* **1995**, *493*, 119.
[23] M. Kojima, K. Nakabayashi, S. Ohba, S. Okumoto, Y. Saito, J. Fujita, *Bull. Chem. Soc. Jpn.* **1986**, *59*, 277.
[24] D. A. Buckingham, C. R. Clark, A. J. Rogers, J. Simpson, *Aust. J. Chem.* **1998**, *51*, 461.
[25] A. J. Clarkson, D. A Buckingham, A. J. Rogers, A. G. Blackman, C. R. Clark, *Inorg. Chem.* **2000**, *39*, 4769.
[26] [26a] I. Demachy, Y. Jean, *Inorg. Chem.* **1996**, *35*, 5027. [26b] I. Demachy, Y. Jean, *New J. Chem.* **1995**, *19*, 763. [26c] I. Demachy, Y. Jean, *Inorg. Chem.* **1997**, *36*, 5956.
[27] C. K. Fair, *MOLEN*, Enraf−Nonius, Delft, The Netherlands, **1990**.
[28] G. M. Sheldrick, *SHELXS-97: Program for the Solution of Crystal Structures*, University of Göttingen, Germany, **1997**.
[29] G. M. Sheldrick, *SHELXL-97, Program for the Refinement of Crystal Structures*, University of Göttingen, Germany, **1997**.
[30] L. Farrugia, *J. Appl. Crystallogr.* **1997**, *30*, 565.

Received July 21, 2003
Early View Article
Published Online November 19, 2003

 © 2004 Wiley-VCH Verlag GmbH & Co. KGaA, Weinheim

A New Alternating Ferro-Antiferromagnetic One-Dimensional Azido-Bridged (Arylazoimidazole)manganese(II), $[Mn(TaiEt)(N_3)_2]_n$ [TaiEt = 1-Ethyl-2-(*p*-tolylazo)imidazole], Exhibiting Bulk Weak Ferromagnetic Long-Range Ordering

Umasankar Ray,[a] Sk. Jasimuddin,[a] Barindra Kumar Ghosh,[a] Montserrat Monfort,[b] Joan Ribas,*[b] Golam Mostafa,[c] Tian -Huey Lu,[c] and Chittaranjan Sinha*[a]

Keywords: Magnetic properties / Manganese / N ligands / Polymers

1-Ethyl-2-(*p*-tolylazo)imidazole [*p*-Me–C_6H_4–N=N–$C_3H_2N_2$–Et-1; TaiEt], an unsymmetrical N,N′-blocker, and azide (N_3^-), a versatile intermediary, coordinate to manganese(II) forming an alternating chain with the formula $[Mn(TaiEt)(N_3)_2]_n$ (**1**). The compound crystallizes in the triclinic $P\bar{1}$ space group with a = 7.9297(7) Å, b = 9.5883(9) Å, c = 11.8366(11) Å, α = 103.555(2)°, β = 105.811(2)°, γ = 104.280(2)°, and Z = 2. The structure consists of neutral chains in which each manganese(II) center is alternately bridged by two end-on and two end-to-end azide ligands. The unsymmetrical arylazo heterocycle chelator creates a strong distortion around the metal center [N–Mn–N′ bite 67.7°; Mn–N′(azo) distance 2.562 Å]. The magnetic properties of **1** have been investigated over the temperature range 2–300 K. Magnetic data are analyzed on the basis of an alternating ferro- and antiferromagnetic Heisenberg chain of the manganese(II) ions, described by the spin Hamiltonian $H = -J_1\Sigma S_{2i}S_{2i+1} - J_2\Sigma S_{2i+1}S_{2i+2}$. The J exchange parameters are 2.65 ± 0.12 cm^{-1} and −14.5 ± 0.15 cm^{-1}, respectively. Magnetic studies at low temperatures indicate long-range ordering (canting) with a remnant magnetism that vanishes above 40 K. The canting phenomenon has been studied by various techniques including an EPR spectroscopic investigation at different temperatures and appears to be due to the local distortion around each metal center and the π-π stacking in the 3-D network.

(© Wiley-VCH Verlag GmbH & Co. KGaA, 69451 Weinheim, Germany, 2004)

Introduction

The preparation of inorganic-organic hybrid functional materials based on covalent bonds with malleable coordination spheres and non-covalent forces involving hydrogen-bonding X−H···π and π···π interactions is a field of current interest in coordination chemistry.[1−6] Self-assembly[7] is the most efficient approach in this regard. Covalent systems are particularly useful in magnetochemistry as they can provide high magnetic ordering and afford different varieties of magnetic materials.[1,2] A judicious choice of a suitable transition metal template, appropriate organic blocker and efficient magnetic coupler can lead to different molecular architectures with tunable magnetic properties. The pseudohalides, especially azide,[8] are versatile bridging ligands and allow μ-1,1 (end-on, EO), μ-1,3 (end-to-end, EE),[9] μ-1,1,3[10] and other[11,12] modes of interactions. It is established that the μ-1,1 (EO) mode gives ferromagnetic (F) and μ-1,3 (EE) gives antiferromagnetic (AF) interactions[9−12] with few exceptions.[13−16] Different combinations of azide-bridging modes have resulted in some unusual structures which consequently changes the magnetism.[9−30]

To date the maximum number of reports on azide-bridging coordination polymers with various organic blockers and investigations of their structure and magnetism have appeared for copper(II) and nickel(II).[9−21] In this regard, analogues studies of other 3d ions like manganese, iron, cobalt are less familiar. The manganese−azido system is currently attracting the attention of magnetochemists, since it enables work to be done with a greater local spin value.[9] The use of different heterocyclic N-donor ligands such as pyridine, polypyridine and their substituted derivatives, pyridine Schiff bases, are well documented.[9,22−30] But no such work has been initiated with unsymmetrical ligands having azo-N and heterocyclic-N donor centers. Arylazo heterocycles with the azoimine (−N=N−C=N−) function are unsymmetrical *N*,*N*′-end-capping chelators. For the last few years our group has been engaged[31−34] in exploring

[a] Department of Chemistry, The University of Burdwan, Burdwan 713104, India
E-mail: c_r_sinha@yahoo.com
[b] Departament de Quimica Inorganica, Universitat de Barcelona, Diagonal 647, 08028 Barcelona, Spain
E-mail: joan.ribas@qi.ub.es
[c] Department of Physics, National Tsing Hua University, Hsinchu 30043, Taiwan, ROC

 © 2004 Wiley-VCH Verlag GmbH & Co. KGaA, Weinheim DOI: 10.1002/ejic.200300415

the chemistry of such ligand systems with transition and non-transition metal ions. Ligands have been anchored on a surface to synthesize a solid-phase extractant[34] that has been used in the separation of different d^n ions from ores, alloys, medicinal samples, etc.

With this background we are interested in preparing and characterizing new polynuclear azidomanganese(II) complexes with a bidentate azoimidazole ligand, 1-ethyl-2-(*p*-tolylazo)imidazole (TaiEt). The ligand system plays a substantial role in chemistry[31−33] involving stabilizing low oxidation states of transition metal ions. We have used metal/bidentate ligands in 1:1 ratios in such a way that the four coordination vacancies around the six-coordinate manganese(II) ion should be completed by the excess azide ligands. According to this principle, we are able to prepare a new alternating double-bridged μ-1,1 (EO) and μ-1,3 (EE) azidomanganese(II) complex of TaiEt with a one-dimensional (1-D) chain along with noncovalent C−H···π and *p*···π inter-chain interactions leading to a 3-D geometry, which has been characterized by X-ray diffraction and spectroscopic studies. Magnetic measurements indicate global AF behavior with the presence of a weak F component intrinsic to the sample. The most interesting feature is the weak long-range ferromagnetic ordering likely to occur due to a canting phenomenon originating from the local distortion around the manganese(II) centers and the π-π stacking in the 3-D network.

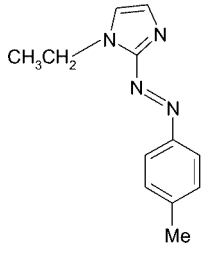

Results and Discussion

Synthesis and Formulation

The preparation of **1** can be achieved in high yield by the reaction of $Mn(OAc)_2{\cdot}4H_2O$ with TaiEt and NaN_3 in dry MeOH at room temperature. The procedure is summarized in Equation (1).

The organic blocker belongs to the unsymmetrical *N*,*N*′-chelating ligand, where N and N′ are the N(imidazole) and N(azo) donor centers, respectively. The air-stable moisture-insensitive red-brown compound is insoluble in common organic solvents. In the IR spectrum the asymmetrical azido stretch, $\nu_{assym}(N_3)$ appears as strong bands between 2095 and 2050 cm^{-1} which suggests the simultaneous existence of EE and EO bridging modes in the complex.[9,35] The azide symmetric stretch $\nu_{sym}(N_3)$ corresponding to the EO bridging mode can be observed as a band of medium intensity at 1330 cm^{-1}. This mode is not active for the symmetrical EE coordination. Finally, the band assignable to the deformation mode of the azido group, $\delta(N_3)$, found at 610, 600 cm^{-1}, is in good agreement with that observed for all polynuclear azido compounds.[9,35] Furthermore, the pertinent bands characteristic of the bound TaiEt ligand appear at 1590 [ν(C=N)] and 1395 [ν(N=N)] cm^{-1}. The diffused reflectance spectrum of $[Mn(TaiEt)(N_3)_2]_n$ exhibits an intraligand charge transfer transition at 380 nm and weak spin-forbidden *d*-*d* bands at 525 (sh) and 455 nm corresponding to an octahedral symmetry.[36]

Description of the Structure

The structure of $[Mn(TaiEt)(N_3)_2]_n$ was revealed by a single-crystal X-ray diffraction study [Figure 1, (a) and (b)]. Selected bond lengths and angles are given in Table 1. Each manganese center exhibits a distorted octahedral MnN_6 coordination sphere linked by two EO and two EE azide groups as well as two N-centers from *N*,*N*′-chelator (TaiEt), respectively, forming four-membered, eight-membered and five-membered loops around each metal center. The chelate angle =N−Mn−N′ is 67.7(1)° which is smaller than those reported values for other transition metal arylazo complexes[31−33,37,38] [76.5° for a ruthenium(II) complex[37] and 77.8° for an osmium(II) compound].[38] This may have a major influence on distortion from idealized O_h symmetry. The Mn−N(azo) bond [Mn−N(1), 2.562(2) Å] is elongated by 0.34 Å compared to the Mn−N(imidazole) distance [Mn−N(3), 2.221(2) Å]; however, it is well below the sum of the van der Waals radii of Mn^{II} and N(azo).[39] The N=N bond [N(1)−N(2), 1.267(3) Å] is longer than that of the free ligand [1.252(1) Å].[40] This increment may refer to a dπ(Mn)→π*(azo) charge transition.[32]

The atomic arrangements Mn, N1, N2, C8, N3 constitute a plane (mean deviation < 0.07 Å) and the pendant phenyl ring makes a dihedral 16.83(2)° with the plane. The manganese(II) ions are alternately linked by two EO [Mn−N(8) 2.217(2) Å, Mn−N(8a) 2.214(3) Å] and two EE [Mn−N(5) 2.204(3) Å, Mn−N(7b) 2.215(3) Å] azido bridges. The Mn−N(8)−Mn(a) angle in the EO mode is 103.53(9)° and lies within the range (100−105°)[9] for this kind of bridge. The bridging arrangement Mn−N(8)−Mn(a)−N(8a) is planar but the azide ligands do not reside within the plane. The Mn−N(5)−N(6) and Mn−N(7b)−N(6b) angles are 135.3(2)° and 130.1(2)°, respectively. The dihedral angle between the mean plane of Mn−N(5)−N(6)−N(7) and Mn−N(7b)−N(6b)−N(5b) with a chair configuration is 3.5°. The dihedral angle between the least-squares plane formed by the six N atoms of the EE double-bridging azide ligands and the N(5)−Mn−N(7b) system is 1.82(13)°. The

$$n\ Mn(OAc)_2{\cdot}4H_2O + n\ TaiEt + 2n\ NaN_3 \xrightarrow[25°C]{MeOH} [Mn(TaiEt)(N_3)_2]_n + 2n\ NaOAc + 4n\ H_2O \quad (1)$$

 © 2004 Wiley-VCH Verlag GmbH & Co. KGaA, Weinheim

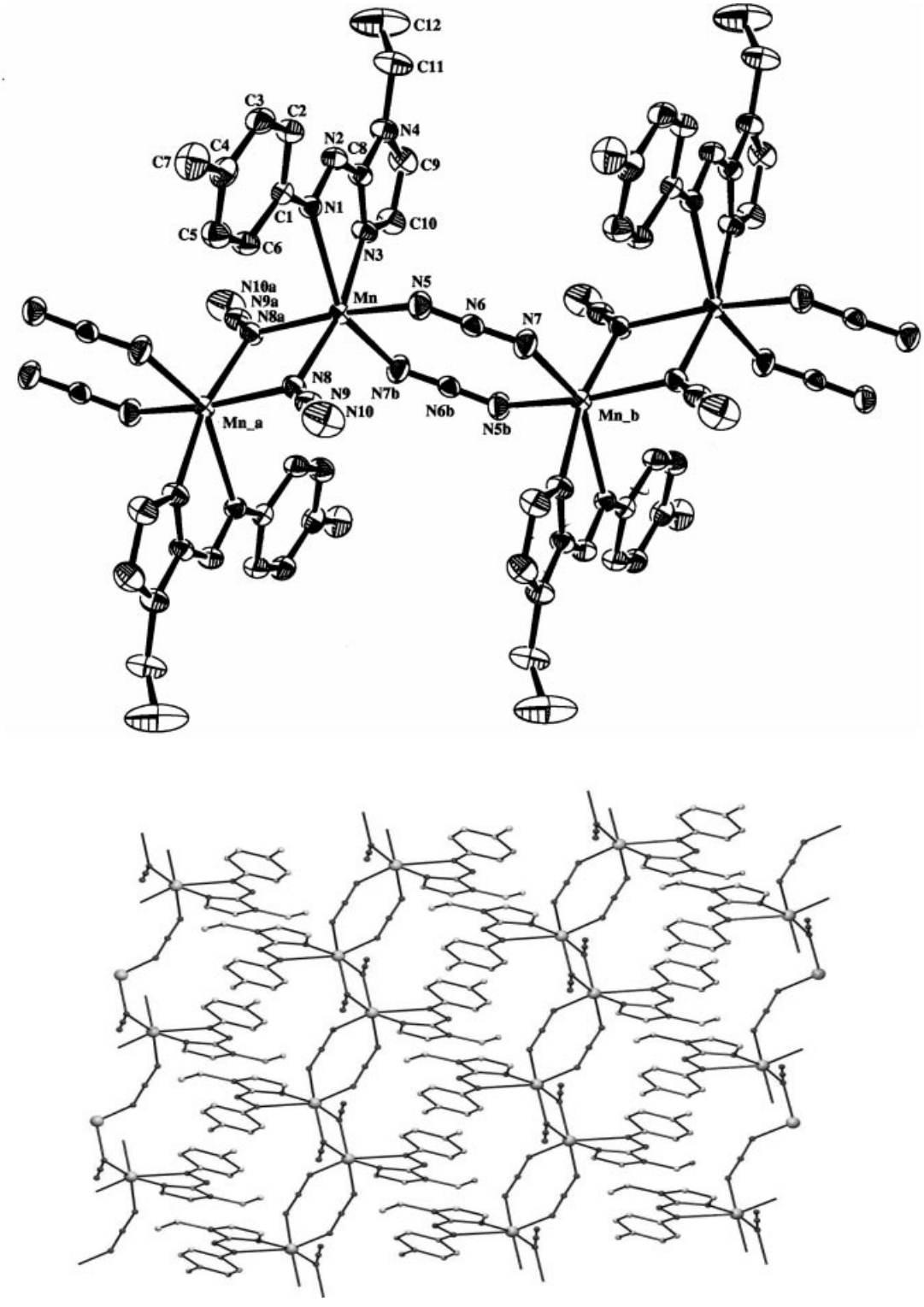

Figure1. (a; top) ORTEP view of the enchainment in $[Mn(TaiEt)(N_3)_2]_n$ with atom numbering scheme; (b; bottom) section of the packing arrangement due to noncovalent interactions of $[Mn(TaiEt)(N_3)_2]_n$ (**1**)

N−N distances of the azide ligand ranges from 1.144(4) to 1.194(3) Å and reflects typical double-bond character. In the EO mode, the N−N distance of terminal and bridging types exhibit usual distortion (ca. 0.05 Å) compared to the symmetrical bond lengths in the EE motif; but the results show that in the EE motif the azide ligand is slightly distorted from linearity [N(5)−N(6)−N(7) 177.1(3)°] compared to the EO azide form [N(8)−N(9)−N(10) 179.4(4)°]. One [N(5)] of the EE azide N atom is *trans* with that of the EO azide N atom [N(8a)] and the mutual inclination is

 © 2004 Wiley-VCH Verlag GmbH & Co. KGaA, Weinheim

Table 1. Selected bond lengths [Å] and angles [°] for **1**

Mn−N(1)	2.562(2)	Mn−N(3)	2.221(2)
Mn−N(5)	2.204(3)	Mn−N(8)	2.217(2)
Mn−N(8a)	2.214(3)	Mn−N(7b)	2.215(3)
N(1)−N(2)	1.267(3)	N(2)−C(8)	1.386(3)
N(5)−N(6)	1.162(4)	N(6)−N(7)	1.164(4)
N(8)−N(9)	1.194(3)	N(9)−N(10)	1.144(4)
Mn−Mn a	3.461	Mn−Mn b	5.400
N(3)−Mn−N(5)	97.59(9	N(3)−Mn−N(8)	167.22(10)
N(3)−Mn−N(7b)	87.46(10)	N(3)−Mn−N(8a)	95.86(9)
N(3)−Mn−N(1)	67.75(7)	N(5)−Mn−N(8a)	165.16(9)
N(5)−Mn−N(7b)	91.72(11)	N(5)−Mn−N(1)	79.61(9)
N(5)−Mn−N8	89.15(9)	N(8)−Mn−N(8a)	76.47(9)
N(8)−Mn−N(7b)	103.25(11)	N(8a)−Mn−N(7b)	95.11(11)
Mn−N(3)−C(8)	116.29(16)	N(1)−N(2)−C(8)	112.3(2)
Mn−N(5)−N(6)	135.3(2)	N(5)−N(6)−N(7)	177.1(3)
Mn(b)−N(7)−N(6)	130.1(2)	Mn−N(8)−N(9)	127.0(2)
Mn−N(8)−Mn(a)	103.53(9)	Mn(a)−N(8)−N(9)	128.0(2)
N(8)−N(9)−N(10)	179.4(4)		

Non-covalent interactions: C−H···π/π···π (coordinates)	H···C_g/C_g···C_g [Å]	Dihedral angle [°]
C(7)−H(7C)···C_g(1) (−x, 1 − y, 1 − z)	2.758(4)	146.20
C(11)−H(11b)···C_g(2) (1 − x, 1 − y, 1 − z)	2.707(3)	143.90
C_g(1)···C_g(1) (−x, −y, 1 − z)	3.416(2)	0.03
C_g(1)···C_g(2) (−x, 1 − y, 1 − z)	3.525(2)	12.60
C_g(2)···C_g(1) (1 − x, 1 − y, 1 − z)	3.136(2)	12.60
C_g(2)···C_g(2) (−x, 1 − y, 1 − z)	3.545(2)	0.00
C_g(1): N(3)−C(8)−N(4)−C(9)−C(10)		
C_g(2): C(1)−C(2)−C(3)−C(4)−C(5)−C(6)		

165.16(9)°. The imidazole N center [N(3)] of TaiEt is *trans* to the EO azide N atom [N(8)] while the azo N atom [N(1)] is *trans* to the EE azide N atom [N(7b)]. This reveals a 1-D chain structure of the molecule, which is being supported by EO and EE Mn−N_3 motifs.

The C−H···π and π···π interactions are two noncovalent forces operating among the molecules to generate a three-dimensional network.[41−43] Each molecular unit shows two C−H···π bonding interactions [C(7)−H(7C)···C_g(1) and C(11)−H(11b)···C_g(2)] with imidazole [C_g(1)] (−x, 1 − y, 1 − z) and *p*-tolyl [C_g(2)] (1 − x, 1 − y, 1 − z) rings of neighboring molecules [Table 1, Figure 1 (b)]. The C(7)−H(7c) bond is from the methyl group of (C_6H_4)−CH_3 (*p*), and C(11)−H(11b) is part of the methylene moiety of the N(4)−CH_2−(CH_3) group. Their interactions with C_g(1) and C_g(2), respectively, may provide inter-chain rigidity and is the operating force of a 3-D network. The *p*···π interactions C_g(1)···C_g(1) [3.416(2) Å], C_g(1)···C_g (2) [3.525(2) Å], C_g(1)···C_g(2) [3.136(2) Å] and C_g(2)···C_g(2) [3.545(2) Å] enhance the inter-chain networking strength. These noncovalent interactions among 1-D parallel units are ideal in forming a 3-D supramolecular continuum.

Magnetic Properties

The temperature dependence of the magnetic susceptibility is shown in Figure 2. The χ_M value is 0.0123 $cm^3 \cdot mol^{-1}$ at 300 K and increases smoothly with decreasing

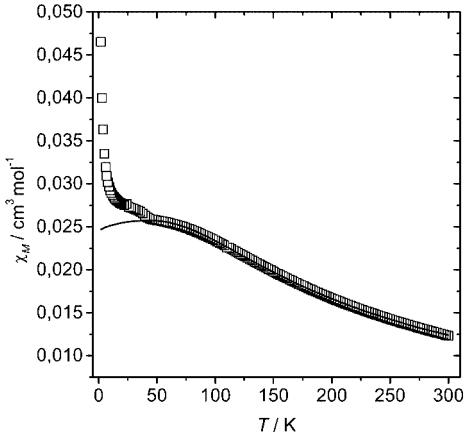

Figure 2. Plots of χ_M vs. T for **1**; the solid line represents the best fit (see text for the parameters calculated)

temperature (0.025 $cm^3 \cdot mol^{-1}$ at 50 K), and finally increases abruptly to a maximum value of 0.0465 $cm^3 \cdot mol^{-1}$ at 1.95 K. This reflects global antiferromagnetic coupling with the presence of a weak ferromagnetic long-range ordering down to 40 K presumably due to a canting phenomenon.[44] Thus, unusual χ_M values at low temperatures restrict us in fitting all of the magnetic data: it is only possible to fit the data to the temperature where the canting arises (40 K) (see below). To avoid any misleading interpretation we have carried out the fitting from 300−50 K.

 © 2004 Wiley-VCH Verlag GmbH & Co. KGaA, Weinheim

(a) High-Temperature Zone (300−50 K) − Calculation of the Coupling Parameters

The structural findings demand an alternating chain of exchange interactions with nearest neighbors that have been described by the spin Hamiltonian where J_1 and J_2 stand for the alternating exchange constants, and "classical" spin operators are expressed by S are.

$$H = -J_1\Sigma S_{2i}S_{2i+1} - J_2\Sigma S_{2i+1}S_{2i+2}$$

This approximation is justified for manganese(II) ion, which exhibits a large spin ($S = 5/2$). The fit of experimental data for such a manganese(II) 1-D system has been carried out using the reported relation[26] derived from the above Hamiltonian, in Equation (2), in which $u_1 = \coth(J_1/kT) - kT/J_1$, $u_2 = \coth(J_2/kT) - kT/J_2$ with the scaling factors $J_i = J_{i'}S(S + 1)$ and $g_i = g_{i'}[S(S + 1)]^{1/2}$.[26]

$$\chi = \frac{Ng^2\beta^2}{3kT}\left(\frac{1+u_1+u_2+u_1u_2}{1-u_1u_2}\right) \quad (2)$$

The best J parameters obtained are: 2.7 ± 0.10 cm^{-1} and -14.6 ± 0.15 cm^{-1}, $g = 2.01$ and $R = 2.56 \times 10^{-9}$. If g is kept at 2.00, which is the expected value for Mn^{II}, J_1 and J_2 do not differ significantly: 2.65 ± 0.12 cm^{-1} and -14.5 ± 0.15 cm^{-1} and $R = 1.75 \times 10^{-8}$. A negative J value (AF) can be attributed to the EE azido bridge whereas the positive J value (F) corresponds to the EO mode.[9] The main structural and magnetic parameters of the reported alternating manganese(II) 1-D azido systems along with **1** are collected in Table 2 for a comparison of the magnetic behavior. Assuming that the Mn−N distances do not vary considerably, the main factor controlling the intensity of the ferromagnetic interactions in the EO bridge appears to be the bridging Mn−N(azido)−Mn angle (θ). Density functional calculations[45,46] on some model compounds of manganese(II) show a parabolic dependence of J on this bridging angle (θ): for θ lower than 98°, AF coupling is expected; for θ greater than 98°, F coupling should result.[45] A crossover from F to AF is predicted at θ = 98°. The angles (see Table 2) are close to 100° and J values vary from 9.6 to 1.8 cm^{-1}. **1** has a very large angle (θ = 103.5°); thus, its J value should be one of the largest. However, it is one of the lowest J values (2.65 cm^{-1}) indicating that the correlation of J with θ may be complicated and a more accurate pragmatic theory is needed to systematize this behavior.

Now assuming that the Mn−N distances do not vary considerably, the most useful structural parameter for examining the magnitude of the AF coupling via EE bridges

Table 2. Main magnetostructural parameters for alternating EE−EO one-dimensional Mn−azido systems [3-bzpy = 3-benzoylpyridine; 3-Et,4-Mepy = 3-ethyl-4-methylpyridine; bpy = 2,2′-bipyridine; bpm = bis(pyrazol-1-yl)methane; dpa = 2,2′-dipyridylamine; 3-ampy = 3-aminopyridine; L^1 = *N*-phenyl-2-carbaldimine; L^2 = *N*-(*p*-tolyl)-2-carbaldimine; L^3 = *N*-(*m*-tolyl)-2-carbaldimine; L^4 = *N*-(*p*-chlorophenyl)-2-carbaldimine; L^5 = *N*-(*m*-chlorophenyl)-2-carbaldimine; TaiEt = 1-ethyl-2-(*p*-tolylazo)imidazole)]

Complex	θ[a] [°]	δ[b] [°]	*J* (*ferro*) [cm^{-1}]	*J* (*antiferro*) [cm^{-1}]	Ref.
Double EE/double EO *trans* geometry of non-azido ligands					
$[Mn(3\text{-bzpy})_2(N_3)_2]_n$	100.4	26.6	3.5	−12.3	[22]
$[Mn(3\text{-Et,4-Mepy})_2(N_3)_2]_n$	99.7	31.7	2.4	−13.7	[23]
Double EE/double EO *cis* geometry of non-azido ligands					
$[Mn(bpy)(N_3)_2]_n$	101.0	22.7	9.6	−11.9	[26]
$[Mn(bpm)(N_3)_2]_n$	102.9	20.5	15.7 (**1.80**)[c]	−63.7(−**7.28**)[c]	[27]
$[Mn(dpa)(N_3)_2]_n$	102.9	35.1	45 (**5.14**)[c]	−53 (−**6.05**)[c]	[24]
$[Mn(L^1)(N_3)_2]_n$	99.6	9.8	3.8	−15.4	[25]
$[Mn(L^2)(N_3)_2]_n$	101.6	–	5.2	−11.8	[25]
$[Mn(L^3)(N_3)_2]_n$	103.9	19.5	7.2	−13.7	[25]
$[Mn(L^4)(N_3)_2]_n$	100.6	9.8	4.1	−13.3	[25]
$[Mn(L^5)(N_3)_2]_n$	104.0	12.0	8.0	−14.4	[25]
$[Mn(TaiEt)(N_3)_2]_n$	103.5	1.82	2.65 (12)	−14.5 (15)	this work
Single EE/double EO					
$[Mn(3\text{-Et,4-Mepy})_3(N_3)_{1/2}](PF_6)$	101.4	–	3.3	−5.2	[28]
$[Mn(3\text{-ampy})_2(N_3)(H_2O)]_n$	99.6	–	2.3	−6.0	[28]

[a] θ corresponds to the Mn−N(azido)−Mn angle. [b] δ is defined in Scheme 1. [c] The J values reported in refs.[24,27] have been simulated by us because they seemed to be too large. Effectively, the simulation using the same formula indicated in the text (ref.[26]) does not agree at all with the figures of χ_M vs. T. On the contrary, dividing by $S(S + 1) = 5/2 \times 7/2 = 8.75$ the recalculated J values (indicated in parentheses in bold) perfectly agree with the figures given in refs.[24,27] This error may be due to the meaning of J given in ref.[24]; the scaling factor is $J_i = J_{i'}S(S + 1)$ used by us, which has not been used in these two papers.

 © 2004 Wiley-VCH Verlag GmbH & Co. KGaA, Weinheim

is the dihedral angle (δ) (Scheme 1). EHMO calculations[24,26] show that the AF coupling should decrease for larger values indicating that the loss of overlap due to the increase in the torsion angle becomes the driving parameter controlling the magnitude of the exchange interaction. For **1**, the δ value is the lowest reported so far (1.82°) (Table 2). Thus, the AF coupling should be greater. In fact, it is the highest $|J|$ value (14.5 cm^{-1}) reported to date. At this stage it is very difficult to draw a general conclusion. Other complexes with high δ values (close to 30°, for example, in the two complexes[22,23] with a *trans* blocker) have similar J values (Table 2) when, theoretically, this should be very small. So new compounds and more accurate calculations are necessary to systematize these kinds of magnetostructural correlations in the manganese(II) systems.

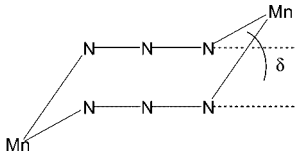

Scheme 1

(b) Low-Temperature Zone (50−2 K) − Origin of the Weak Ferromagnetism

The increase in susceptibility down to ca. 45−50 K indicates the presence of a weak intrinsic ferromagnetic contribution, possibly due to a spin canting effect.[44] A cursory report of a similar feature is found in only one of the alternating EE and EO azido-bridged 1-D manganese complexes (Table 2).[24] In the present case, extensive experiments have been performed to substantiate the long-range ordering as pointed below.

(1) An abrupt break in χ_M and $\chi_M T$ occurs at 40 K when lower fields are employed (Figure 3). This transition at 40 K, when the magnetic field changes, is indicative of the onset of long-range magnetic ordering.[47]

(2) The field-cooled magnetization (FCM) obtained on cooling within the field (50 Oe) shows the typical feature [Figure 4 (a)] of a ferromagnetic transition, i.e. a rapid increase in χ_M occurs when T decreases below 40 K and, then, appears at the beginning of saturation. If the field is switched off below 40 K, a remnant magnetization is observed. The zero-field-cooled magnetization (ZFCM) is obtained by cooling in zero-field and then applying the field and heating. At any temperature below T_c the ZFCM is smaller than the FCM, due to the fact that in this temperature range the applied field is too weak to move the domain walls. The remnant magnetization (RM) [Figure 4 (b)] indicates the presence of magnetization from 2 to 40 K. Thus, the critical temperature for the long-range magnetic ordering is 40 K.

(3) The magnetization study (from −5 T to +5 T at 2 K) shows (Figure 5) the $M/N\beta$ value to be 0.3 e^-, which is clearly indicative of the global antiferromagnetic interaction. An isolated manganese(II) ion would give 5 e^-. At the

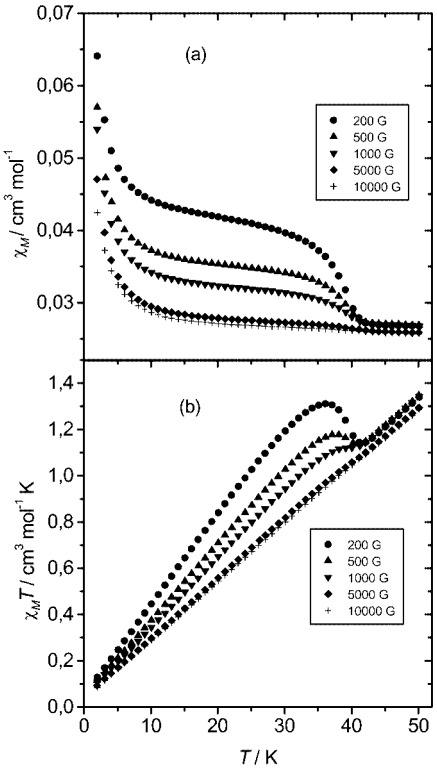

Figure 3. Plots of (a) χ_M vs. T and (b) $\chi_M T$ vs. T at different fields in the temperature range (2−50 K); at lower fields abrupt breaks are seen (see text)

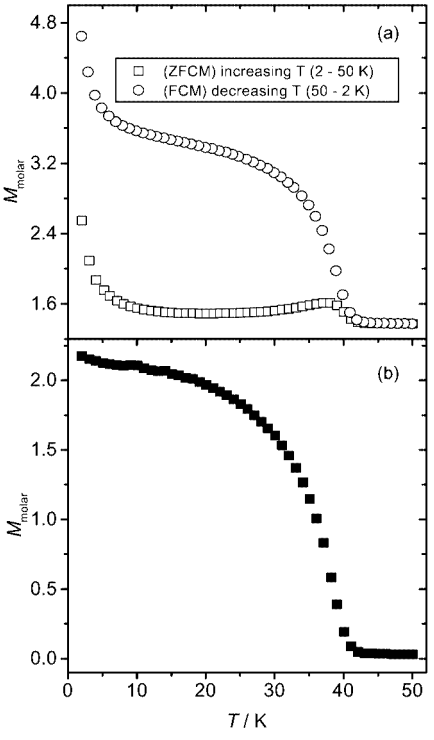

Figure 4. (a) Field-cooled magnetization (FCM) and zero-field-cooled magnetization (ZFCM) for **1**; (b) remnant magnetization as a difference of FCM and ZFCM, from 50−2 K

 © 2004 Wiley-VCH Verlag GmbH & Co. KGaA, Weinheim

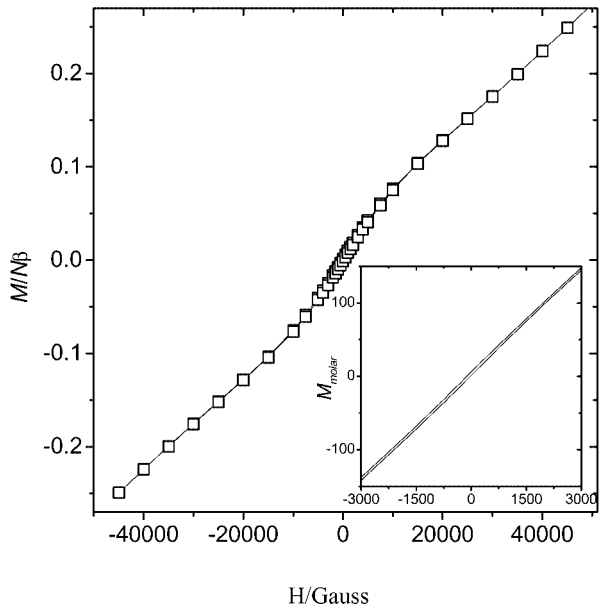

Figure 5. Reduced magnetization curve for **1**, at 2 K; (inset) central part of the magnetization curve for **1**, showing a very small hysteresis loop

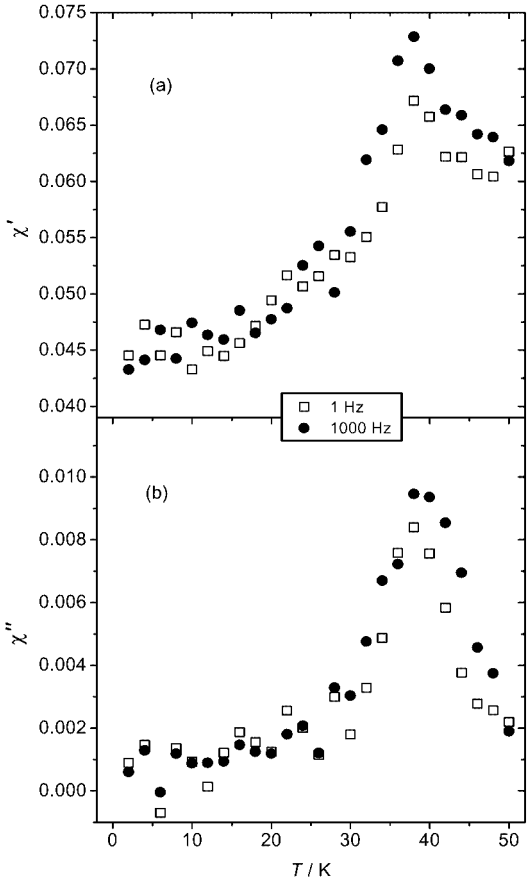

Figure 6. *In-phase* (a) and *out-of-phase* (imaginary) (b) parts of the *ac* susceptibility curves for **1** at two different frequencies (1 and 1000 Hertz)

bottom of the figure (from −0.5 T to +0.5 T) a weak hysteresis loop is seen. The coercive field is difficult to calculate, as it is too large, but the remnant magnetization at 0 K is 6.7 cm^3 Gauss·mol^{-1}, which is typical of a soft ferromagnet.

(4) The *ac* susceptibility measurements are definitely the best proof of the long-range order. The real part of the *ac* magnetic susceptibility (χ_{ac}') has a maximum at ca. 40 K, accompanied by the occurrence of non-zero field-independent χ_{ac}'' (Figure 6) suggesting that the T_c of **1** is close to 40 K. The small χ values indicate weak ferromagnetic character (in accordance with the hysteresis loop values).

(5) EPR spectroscopic measurements at room temperature (298 K) show a very intense isotropic signal centered at $g = 2.00$ (without hyperfine splitting) which is typical for the manganese(II) ion. The peak-to-peak band-width increases on lowering the temperature (at 298 K and 77 K it is ca. 150 Gauss; at 40 K it is ca. 400 Gauss) (Figure 7) and its intensity strongly diminishes. Finally, at 4 K the peak-to-peak band-width is > 2000 Gauss and 1600 times less intense than that at room temperature, which is in accordance with the behavior of long-range ordered compounds at low temperature.[48] It is worth mentioning that this feature in the EPR spectra indicates that the magnetic ordering cannot be attributed to ferromagnetic impurities and the canting phenomenon must be inherent to the sample. Canted one-dimensional (1-D)[49−51] and/or discrete[52] systems are reported in the literature though very scarce. Instead, canting is more frequent in two-dimensional (2-D) and three-dimensional (3-D) systems[53] because the canting, per se, is a three-dimensional long-range ordering. To interpret this behavior in 1-D, it is necessary to have some linkages in **1**, though weak, resulting in a 3-D network. This may be attributed to the π···π stacking (Figure 1, b) and other weak interactions. The spin canted structure is *not compatible* with the crystal structure of **1** because of the presence of an inversion center (space group $P\bar{1}$). Thus, the existence of the possible canting effect must be due to a distortion in the crystal net at low temperatures, that suppresses the inversion center. It is well known that two mechanisms lead to spin canting: (i) magnetic anisotropy (D and E) and (ii) antisymmetric exchange, $\boldsymbol{d}_{ij}[S_i \times S_j]$.[44,54] In both cases, the total energy is minimized through a compromise in which the spins are tilted away from the antiparallel towards a position in which they are perpendicular (Scheme 2). The D parameter is, in principle, non-zero because the ground state is $S = 5/2$ and there is a great distortion in the manganese(II) ion as is evident from the N−Mn−N′ angle of 67.7° created by the chelator and from lengthening of the Mn−N(azo) bond (2.56 Å) over the other five Mn−N bonds (ca. 2.2 Å). The Mn−N(azo) distance is anomalously long creating greater distortion and anisotropy. Such a coordination environment plays a major role for the canting behavior in this case and as also found in some manganese(III)[55,56] ($S = 2$) and nickel(II)[50,57] ($S = 1$) systems. The other possible origin of the canting, the antisymmetric part of the spin Hamiltonian, is proportional to $[(g - 2)/g]J$, where the intermolecular coupling, J is an average between −14.5 and 2.65 cm^{-1}. The average g value

 © 2004 Wiley-VCH Verlag GmbH & Co. KGaA, Weinheim

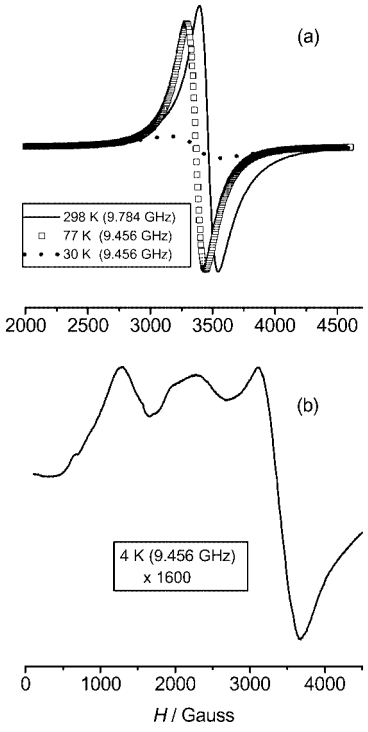

Figure 7. EPR spectra of powder sample of **1** (a) at 298 K, 77 K and 30 K with the same scale; (b) the spectrum a 4 K with a very large scale (see text)

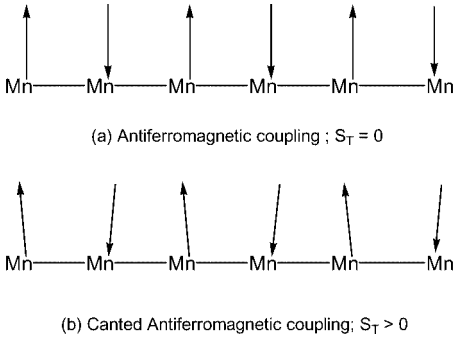

Scheme 2

is close to 2.00. Thus, although very small, this term could not be nullified. Such an explanation is found in the literature for several non-distorted iron(III),[58] manganese(II)[59,60] and copper(II) canted complexes.[61,62] In the present case, the magnetization curve allows us to calculate the (possible) canting angle. According to the literature, there are several approaches to calculate the canting angle.[22,44] The most useful is $\sin^{-1}(\mu_{RM}/\mu_{satd.})$ or $\sin^{-1}(M_{RM}/M_{satd.})$ being $\mu_{sat} = 5$ for manganese(II) ions. In complex **1**, M_{RM} is 0.3, thus the angle is very small (0.34°) and results in a very small ferromagnetic ordering.

Conclusion

We have presented here the synthesis, single-crystal X-ray structure, and magneto-structural correlation of a new 1-D azido-bridged manganese(II) coordination polymer. The structural characterization shows an alternating bis(-bridged) EE and EO azido network with a very unsymmetrical organic blocker as a *cis* chelate. The presence of C−H···π and π···π interactions leads to the generation of a three-dimensional network. From the magnetic point of view the complex shows a long-range magnetic order arising due to a canting phenomenon originated most likely from the distortion created by the low bite of the chelator resulting a very strong distortion in the Mn−N(azo) distance (2.56 Å) and 3-D structural evolution. The use of an arylazo heterocycle ligand system over pyridine or polypyridine systems[22−30] provides ample scope for such long-range magnetic ordering. We are currently working with this azo heterocycle having varied substituents on its network to prepare different molecular architectures with other 3d transition metal ions using pseudohalide intermediaries and to study their magnetic behavior towards the preparation of molecule-based magnets.

Experimental Section

Materials: Manganese(II) acetate tetrahydrate (SRL, India) and sodium azide (SRL, India) were purchased and used without further purification. 1-Ethyl-2-(*p*-tolylazo)imidazole (TaiEt) was prepared according to a reported procedure.[31] All other chemicals and solvents for preparative and spectroscopic work were of reagent grade and were used as received.

CAUTION! Azido complexes of transition metal ions containing organic ligands are potentially explosive. Only a small amount of material should be prepared, and it should be handled with care.

Physical Measurements: IR spectra (KBr discs, 4000−300 cm^{-1}) were recorded with a JASCO FTIR model 420 spectrophotometer. Microanalyses (C, H and N) were done with a Perkin−Elmer 2400 CHNS/O elemental analyzer. The diffuse reflectance spectrum was run at room temperature with a JASCO UV/Vis/NIR V-570 spectrophotometer in the 200−1000 nm range. A Bruker ES 200 spectrometer (X-band frequency) was used to record the EPR of polycrystalline samples at room (298 K) and low temperatures (77 K, 30 K, 4 K). Magnetic measurements on powdered samples were performed over the temperature range 2−300 K using a Quantum Design MPMS-7 SQUID magnetometer in a magnetic field of 0.1 T. The experimental susceptibilities were corrected for the diamagnetism of the constituent atoms (Pascal tables).

Synthesis of the Complex $[Mn(TaiEt)(N_3)_2]_n$ (1): 1 was synthesized from $Mn(OAc)_2{\cdot}4H_2O$ (0.100 g, 0.408 mmol), TaiEt (0.087 g, 0.408 mmol) and NaN_3 (0.053 g, 0.816 mmol) in dry methanol solution (25 mL). The resulting intense red solution was filtered and left to stand at room temperature. After several days, prismatic dark-red single crystals were obtained. They were separated by filtration, washed with Et_2O and dried in vacuo over indicator silica gel. Yield: 0.124 g (75%). $C_{12}H_{14}MnN_{10}$ (353.27): calcd. C 40.8, H 4.0, N 39.7; found C 40.6, H 3.9, N 39.5.

 © 2004 Wiley-VCH Verlag GmbH & Co. KGaA, Weinheim

X-ray Structure Determination: A suitable single crystal of the title complex for X-ray analysis was mounted on a Siemens SMART CCD diffractometer equipped with a graphite monochromator and Mo-K_α (λ = 0.71073 Å) radiation. Data were collected at 295 K. The crystal size was 0.08 × 0.10 × 0.18 mm. The intensity data were corrected for Lorentz and polarization effects and an empirical absorption correction was also employed using the SAINT[63] program. A summary of the crystallographic data and structure refinement parameters is given in Table 3. A total of 7947 reflections (unique reflections, 3546, R_{int} = 0.029) were collected in the range 1.9° < θ < 28.1° and 2683 were assumed applying the condition $I > 2\sigma(I)$. The structure was solved by the Patterson method using SHELXS-97[64] followed by Fourier and difference Fourier synthesis. Full-matrix least-squares refinements on F^2 were carried out using SHELXL-97 with anisotropic displacement parameters for all non-hydrogen atoms. The hydrogen atoms were fixed geometrically and refined using a riding model. In the final difference Fourier map the residual maxima and minima were 0.52 and −0.38 e·Å^{-3}. All calculations were carried out using the SHELXL-97, ORTEP-32[65], PLATON[66] programs. CCDC-193975 contains the supplementary crystallographic data for this paper. These data can be obtained free of charge at www.ccdc.cam.ac.uk/conts/retrieving.html [or from the Cambridge Crystallographic Data Centre, 12 Union Road, Cambridge CB2 1EZ, UK; Fax: (internat.) + 44-1223/336-033; E-mail: deposit@ccdc.cam.ac.uk].

Table 3. Crystal data and details of the structure determination for **1**

Empirical formula	$C_{12}H_{14}MnN_{10}$
Formula mass	353.27
Temperature [K]	295
Radiation λ [Å]	0.71073
Crystal system	triclinic
Space group	$P\bar{1}$
a [Å]	7.9297(7)
b [Å]	9.5883(9)
c [Å]	11.8366(11)
α [°]	103.555(2)
β [°]	105.811(2)
γ [°]	104.280(2)
V [Å^3]	794.05(13)
Z	2
$d_{calcd.}$ [g·cm^{-3}]	1.478
μ [mm^{-1}]	0.847
F(000)	362
Crystal size [mm]	0.08 × 0.10 × 0.18
No. of reflections collected	7947
Θ(min., max.) [°]	1.9, 28.1
Observed data [$I > 2.0\ \sigma(I)$]	2683
Refinement	
*N*ref, *N*par	3546, 208
R, *wR*2[a], *S*	0.0406, 0.1197, 1.10
Residual densitiy (min., max.) [e/Å^3]	−0.38, 0.52

[a] $w = 1/[s^2(F_o^2) + (0.0640P)^2 + 0.0109P]$ where $P = (F_o^2 + 2F_c^2)/3$.

Acknowledgments

The authors are grateful to the Council of Scientific and Industrial Research (Grant No. 01(1789)/02/EMR-II), New Delhi, India and the Spanish Government (Grant No. BQU2000/0791) for financial assistance. G. M. and T. H. L. thank the National Science Council, ROC for financial support (Grant Nos. NSC 90-2112-M-007-063 and NSC 91-2811-M-007-033). One of us (U. S. R.) thanks the UGC, for a fellowship.

[1] O. Kahn, *Molecular Magnetism*; John Wiley Sons, New York, **1993**.
[2] J. S. Miller, M. Drillon (Eds.), *Magnetism: Molecules to Materials IV*, Wiley-VCH, Weinheim, **2003**.
[3] S. R. Marder, J. E. Sohn, G. D. Stucky (Eds.), *Materials for Non-linear Optics: Chemical Perspectives*, ACS Symposium Ser., ACS, Washington, **1991**, p. 455.
[4] C. L. Bowes, G. A. Ogin, *Adv. Mater.* **1996**, *8*, 13.
[5] A. Hagfelot, M. Gratzel, *Acc. Chem. Res.* **2000**, *33*, 269.
[6] S. Chandrasekhar, *Liquid Crystals*, 2nd ed., Cambridge University Press, Cambridge, **1992**.
[7] Special issue on Focus on Self-assembly, *Acc. Chem. Res.* **1999**, *32*, no. 4.
[8] D. A. Buckingham, *Coord. Chem. Rev.* **1994**, *587*, 135.
[9] J. Ribas, A. Escuer, M. Monfort, R. Vicente, R. Cortés, L. Lezama, T. Rojo, *Coord. Chem. Rev.* **1999**, *193−195*, 1027.
[10] Z. E. Serna, L. Lezama, M. K. Urtiaga, M. Arriortua, M. G. B. Barandika, R. Cortes, T. Rojo, *Angew. Chem. Int. Ed.* **2000**, *39*, 344.
[11] G. S. Papaefstathiou, A. Escuer, C. P. Raptopoulou, A. Terzis, S. P. Perlepes, R. Vicente, *Eur. J. Inorg. Chem.* **2001**, 1567.
[12] M. A. S. Goher, J. Cano, Y. Journaux, M. A. M. Abu-Youssef, F. A. Mautner, A. Escuer, R. Vicente, *Chem. Eur. J.* **2000**, *6*, 778.
[13] C. S. Hong, S.-K. Son, Y. S. Lee, Y.-S. Kim, Y. Do, *Chem. Eur. J.* **2001**, *8*, 2239.
[14] S. Dalai, P. S. Mukherjee, T. Mallah, M. G. B. Drew, N. R. Chaudhuri, *Inorg. Chem. Commun.* **2002**, *5*, 472.
[15] Y. Xie, Q. Liu, H. Jiang, C. Du, X. Xu, M. Yu, Y. Zhu, *New J. Chem.* **2002**, *26*, 176.
[16] P. S. Mukherjee, T. Maji, A. Escuer, R. Vicente, J. Ribas, G. Rosair, F. A. Mautner, N. R. Chaudhuri, *Eur. J. Inorg. Chem.* **2002**, 943.
[17] H.-Y. Shen, W.-M. Bu, E. Q. Gao, D.-Z. Liao, Z.-H. Jiang, S. P. Yan, G.-L. Wang, *Inorg. Chem.* **2000**, *39*, 396.
[18] A. Escuer, R. Vicente, M. A. S. Goher, F. Mautner, *Inorg. Chem.* **1998**, *37*, 782.
[19] A. K. Sra, J. -P. Sutter, P. Guionneau, D. Chasseau, J. V. Yakhmi, O. Kahn, *Inorg. Chim. Acta* **2000**, 300−302, 778.
[20] P. Manikandan, R. Muthukumaran, K. R. Justin-Thomas, B. Varghese, G. V. R. Chandramouli, P. T. Manoharan, *Inorg. Chem.* **2001**, *40*, 2378 and refs. therein.
[21] L. Li, D. Liao, Z. Jiang, S. Yan, *Inorg. Chem.* **2002**, *41*, 1019.
[22] M. A. M. Abu-Youssef, A. Escuer, D. Gatteschi, M. A. S. Goher, F. A. Mautner, R. Vicente, *Inorg. Chem.* **1999**, *38*, 5716.
[23] M. A. M. Abu-Youssef, A. Escuer, M. A. S. Goher, F. A. Mautner, R. Vicente, *Eur. J. Inorg. Chem.* **1999**, 687.
[24] M. Villanueva, J. L. Mesa, M. K. Urtiaga, R. Cortes, L. Lezama, M. I. Arriortua, T. Rojo, *Eur. J. Inorg. Chem.* **2001**, 1581.
[25] E.-Q. Gao, S.-Q. Bai, Y.-F. Yue, Z.-M. Wang, C.-H. Yan, *Inorg. Chem.* **2003**, *42*, 3642.
[26] R. Cortes, M. Drillon, X. Solans, L. Lezama, T. Rojo, *Inorg. Chem.* **1997**, *36*, 677.
[27] L.-F. Tang, L. Zhang, L.-C. Li, P. Cheng, Z.-H. Wang, J.-T. Wang, *Inorg. Chem.* **1999**, *38*, 6326.
[28] M. Abu-Youssef, A. Escuer, M. A. S. Goher, F. A. Mautner, R. Vicente, *J. Chem. Soc., Dalton Trans.* **2000**, 413.
[29] H. Hou, Y. Wei, Y. Song, Z. Yinglin, Y. Zhu, L. Li, Y. Fan, *J. Mater. Chem.* **2002**, *12*, 838.
[30] J. L. Manson, A. M. Arif, J. S. Miller, *Chem. Commun.* **1999**, 1479.
[31] T. K. Misra, D. Das, C. Sinha, P. K. Ghosh, C. K. Pal, *Inorg. Chem.* **1998**, *37*, 1672.
[32] P. Byabartta, J. Dinda, P. K. Santra, C. Sinha, K. Panneerselvam, F.-L. Liao, T.-H. Lu, *J. Chem. Soc., Dalton Trans.* **2001**, 2825.
[33] P. Byabartta, Sk. Jasimuddin, B. K. Ghosh, C. Sinha, A. M. Z. Slawin, J. D. Woollins, *New J. Chem.* **2002**, *26*, 1415.
[34] D. Das, A. K. Das, C. Sinha, *Talanta* **1999**, *48*, 1013.

 © 2004 Wiley-VCH Verlag GmbH & Co. KGaA, Weinheim

[35] Nakamoto, *Infrared and Raman Spectra of Inorganic and Coordination Compounds*, 5th ed., part B, John Wiley & Sons, Inc., New York, **1997**, pp. 124.
[36] A. B. P. Lever, *Inorganic Electronic Spectroscopy*, Elsevier Science Publishers B. V., Amsterdam, **1984**.
[37] A. Seal, S. Ray, *Acta Crystallogr. Sec C, Struct. Commun.* **1984**, *40*, 929.
[38] B. K. Ghosh, A. Mukhopadhyay, S. Goswami, S. Ray, A. Chakravorty, *Inorg. Chem.* **1984**, *23*, 4633.
[39] A. G. Orpen, L. Brammer, F. H. Allen, O. Kennard, D. G. Waston, R. Taylor, *J. Chem. Soc., Dalton Trans.* **1989**, SI.
[40] D. Das, PhD Thesis, Burdwan University, **1998**.
[41] G. R. Desiraju, in *The Crystals as a Supramolecular Entity* (Ed.: J. M. Lehn), John Wiley & Sons, Chichester, U. K., **1996**, vol 2.
[42] D. Braga, L. Maini, M. Polito, L. Scaccianoc, G. Cojazzi, F. Grepioni, *Coord. Chem. Rev.* **2001**, *216−217*, 225.
[43] U. S. Ray, G. Mostafa, T.-H. Lu, C. Sinha, *Cryst. Eng.* **2002**, *5*, 95.
[44] R. C. Carlin, *Magnetochemistry*, Springer Verlag, Berlin, **1986**, pp.148;.
[45] E. Ruiz, J. Cano, S. Alvarez, P. Alemany, *J. Am. Chem. Soc.* **1998**, *120*, 11122.
[46] M. Springbong (Ed.), *Density Functional Methods: Application in Chemistry and Material Science*, John Wiley & Sons, New-York, **1997**.
[47] S. R. Batten, P. Jensen, C. J. Kepert, M. Kurmoo, B. Moubaraki, K. S. Murray, D. J. Price, *J. Chem. Soc., Dalton Trans.* **1999**, 2987.
[48] A. Bencini, D. Gatteschi, *EPR of Exchange Coupled Systems*, Springer Verlag, Berlin, **1990**.
[49] B. J. Kennedy, K. S. Murray, *Inorg. Chem.* **1985**, *24*, 1552 and references cited therein.
[50] M. L. Kirk, M. S. Lah, C. Rattopoulou, D. P. Kessissoglou, W. E. Hatfield, V. L. Pecoraro, *Inorg. Chem.* **1991**, *30*, 3900.
[51] M. A. Martínez-Lorente, J. P. Tuchagues, V. Petroulas, J. M. Savariault, R. Poinsot, M. Drillon, *Inorg. Chem.* **1991**, *30*, 3589 and references cited therein.
[52] S. O. H. Gutschke, D. J. Price, A. K. Powell, P. T. Wood, *Angew. Chem. Int. Ed.* **1999**, *38*, 1088 and references cited therein.
[53] C.-M. Liu, Z. Yu, R.-G. Xiong, K. Liu, X.-Z. You, *Inorg. Chem. Commun.* **1999**, *2*, 31.
[54] A. Escuer, R. Vicente, M. A. S. Goher, F. Mautner, *Inorg. Chem.* **1997**, *36*, 3440.
[55] T. Moriya, *in Magnetism*, vol. 1 (Eds.: G. T. Rado, H. Suhl), Academic Press, London, **1963**, pp. 85.
[56] T. Moriya, *Phys. Rev.* **1960**, *117*, 635.
[57] A. K. Gregson, N. T. Moxon, *Inorg. Chem.* **1982**, *21*, 586.
[58] D. Armentano, G. De Munno, F. Lloret, A. V. Palii, M. Julve, *Inorg. Chem.* **2002**, *41*, 2007 and references cited therein.
[59] C. S. Hong, J.-E. Koo, S.-K. Son, Y. S. Lee, Y.-S. Kim, Y. Do, *Chem. Eur. J.* **2001**, *7*, 4243.
[60] C. S. Hong, Y. Do, *Angew. Chem. Int. Ed.* **1999**, *38*, 193.
[61] S. Han, J. L. Manson, J. Kim, J. S. Miller, *Inorg. Chem.* **2000**, *39*, 4184.
[62] S. R. Batten, P. Jensen, C. J. Kepert, M. Kurmoo, B. Moubaraki, K. S. Murray, D. J. Price, *J. Chem. Soc., Dalton Trans.* **1999**, 2987.
[63] G. M. Sheldrick, *SAINT*, version 5, Siemens Analytical X-ray Instrument Inc. Madison, WI, USA, **1995**.
[64] G. M. Sheldrick, *SHELXL-PLUS*, Siemens Analytical X-ray Instruments, Inc., Madison, Wisconsin, USA, **1990**; G. M. Sheldrick, *Acta Crystallogr., Sect. A* **1990**, *46*, 467.
[65] ORTEP-3, L. J. Farrugia, *J. Appl. Crystallogr.* **1997**, *30*, 565.
[66] A. L. Spek, *PLATON99, Molecular Geometry Program*, University of Utrecht, The Netherlands, **1999**.

Received June 26, 2003
Early View Article
Published Online November 6, 2003

 © 2004 Wiley-VCH Verlag GmbH & Co. KGaA, Weinheim

New Complexes of Niobium(V) and Tantalum(V) with Monoanionic NNO Heteroscorpionate Ligands

Antonio Otero,*[a] Juan Fernández-Baeza,[a] Antonio Antiñolo,[a] Juan Tejeda,[a] Agustín Lara-Sánchez,[a] Luis Sánchez-Barba,[a] and Ana M. Rodríguez[a]

Keywords: Niobium / Tantalum / Tripodal ligands / Oxo ligands / Alkoxide ligands

A new synthetic route based on bis(3,5-dimethylpyrazol-1-yl)acetic acid (Hbdmpza) (**1**) has afforded the alcohol 2,2-bis(3,5-dimethylpyrazol-1-yl)ethanol (Hbdmpze) in good yield. This alcohol and the related lithium compound $[\{Li(bdmpza)(H_2O)\}_4]$ are excellent precursors for introducing these scorpionate ligands into transition metal complexes. For example, the lithium compound and Hbdmpze (the latter after prior addition of *n*BuLi) react with a solution of MCl_5 (M = Nb, Ta) in THF to give, after stirring for 12 h at –70 °C, a solution from which the complexes $[MCl_4(\kappa^3\text{-bdmpzx})]$ (*x* = *a*, M = Nb **2**, Ta **3**; *x* = *e*, M = Nb **4**, Ta **5**) have been isolated. When solutions of **2**–**5** in THF were stirred at ca. 20 °C for 48 h, the oxo complexes $[MCl_2(O)(\kappa^3\text{-bdmpzx})]$ (*x* = *a*, M = Nb **6**, Ta **7**; *x* = *e*, M = Nb **8**, Ta **9**) were isolated. The structures of these complexes have been determined by spectroscopic methods and the X-ray crystal structure of **8** has been established. Finally, a new class of heteroscorpionate-metal complexes containing an alkoxide ligand has been prepared. Direct reaction of the complexes $[MCl_4(\kappa^3\text{-bdmpza})]$ (M = Nb **2**, Ta **3**) with several alcohols gave the complexes $[MCl_3(\kappa^3\text{-bdmpza})(OR)]$ (M = Nb, R = Me **10**, Et **11**, *i*Pr **12**, *t*Bu **13**; M = Ta, R = Me **14**, Et **15**, *i*Pr **16**, *t*Bu **17**) after the appropriate workup.

(© Wiley-VCH Verlag GmbH & Co. KGaA, 69451 Weinheim, Germany, 2004)

Introduction

Several classes of poly(pyrazol-1-yl)borato niobium complexes containing halide, alkoxide, alkyl, imido, oxo, or alkyne ancillary ligands have been prepared.[1] We have reported the preparation of several complexes of the type $TpNb(Cl)_2(RC{\equiv}CR')$ or Tp*Nb(O)(Cl)(OR) [Tp = hydridotris(pyrazol-1-yl)borate and Tp* = hydridotris(3,5-dimethylpyrazol-1-yl)borate],[2] and have recently examined the synthesis of new "heteroscorpionate" ligands[3] that incorporate pyrazole rings. The target compounds are related to the tris(pyrazol-1-yl)methane system,[4] where one pyrazole group is replaced by a carboxylate, dithiocarboxylate or ethoxide group; i.e. bis(3,5-dimethylpyrazol-1-yl)acetate (bdmpza), bis(3,5-dimethylpyrazol-1-yl)dithioacetate (bdmpzdta) and 2,2-bis(3,5-dimethylpyrazol-1-yl)ethoxide (bdmpze). The aim is to provide a small degree of steric hindrance and considerable coordinative flexibility in the ligand. These compounds are excellent reagents for the introduction of scorpionate ligands into niobium complexes and a series of alkyne-containing niobium(III) complexes has been isolated and characterized.[5] More recently, we extended the range of complexes to include group 4 metals.[6]

In continuing such research we have further studied the synthesis of heteroscorpionate-containing niobium(V) and tantalum(V) species, where any compounds have been reported in the literature. We describe here the synthesis and characterization of new classes of heteroscorpionate-niobium and -tantalum complexes containing halide, oxo and alkoxide ancillary ligands.

Results and Discussion

The alcohol 2,2-bis(3,5-dimethylpyrazol-1-yl)ethanol (Hbdmpze) was obtained by reduction of the lithium compound $[\{Li(bdmpza)(H_2O)\}_4]$ with a 2.0 M solution of $(CH_3)_2S{\cdot}BH_3$ (borane-methyl sulfide complex) in THF at reflux in a 1:1 molar ratio (Scheme 1).[5] However, to increase the low yield (46%) of this method we proposed a new route based on the use of bis(3,5-dimethylpyrazol-1-yl)acetic acid (Hbdmpza) (**1**), which was also synthesized and characterized in this work. The lithium compound $[\{Li(bdmpza)(H_2O)\}_4]$ reacted at room temperature in a 1:1 molar ratio (Scheme 1) with hydrochloric acid to give, after appropriate workup, the acid **1** (97% yield). Reduction of this acid with a 2.0 M solution of $(CH_3)_2S{\cdot}BH_3$ gave the alcohol 2,2-bis(3,5-dimethylpyrazol-1-yl)ethanol (Hbdmpze) in 84% yield (Scheme 1). The mass spectrum (FAB) of **1** indicates a mononuclear formulation (Exp. Sect.). The IR spectrum shows two strong bands at 1578 and 1414 cm^{-1}, which are assigned to $\nu_{as}(CO_2^-)$ and

[a] Departamento de Química Inorgánica, Orgánica y Bioquímica, Universidad de Castilla-La Mancha, 13071 Ciudad Real, Spain
Fax: (internat.) + 34-926-295318
E-mail: antonio.otero@uclm.es

 © 2004 Wiley-VCH Verlag GmbH & Co. KGaA, Weinheim **DOI: 10.1002/ejic.200300451**

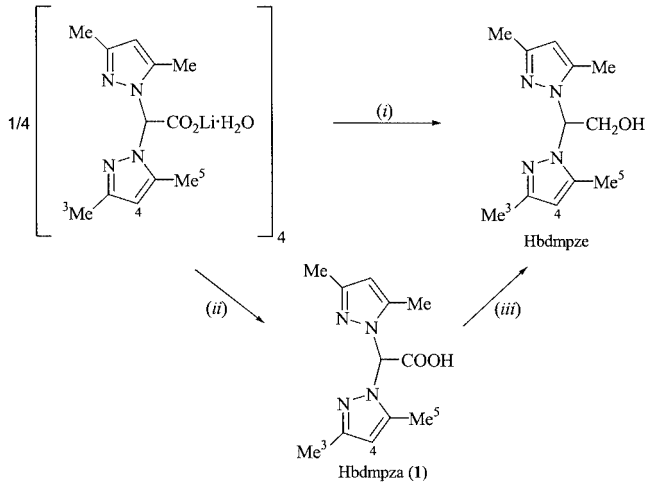

Scheme 1. Summary of reactions leading to compound **1**. Reagents and conditions: (i) $(CH_3)_2S{\cdot}BH_3$, THF, reflux, 12 h under an atmosphere of dry nitrogen, yield 46%; (ii) HCl, THF, 1 h, 20 °C, yield 97%; (iii) $(CH_3)_2S{\cdot}BH_3$, THF, reflux, 12 h under an atmosphere of dry nitrogen, yield 84%.

$\nu_s(CO_2^-)$, respectively. The ^1H NMR spectrum shows a set of resonances for H^4, Me^3 and Me^5, indicating that both pyrazole rings are equivalent in solution. In addition, all the resonances are shifted to lower fields than those for the lithium compound [{Li(bdmpza)(H_2O)}$_4$]. The $^{13}C\{^1H\}$ NMR spectra exhibit the corresponding signals for CH, C^3, C^4, C^5, Me^3, Me^5 and CO_2^- (Exp. Sect.).

[{Li(bdmpza)(H_2O)}$_4$] and (Hbdmpze) were used in the complexation of some niobium and tantalum fragments, initially with MCl_5 (M = Nb, Ta). Thus, [{Li(bdmpza)(H_2O)}$_4$] and (Hbdmpze) (the latter with prior addition of *n*BuLi) reacted with a solution of MCl_5 (Scheme 2) in THF to give, after stirring for 12 h at −70 °C, a solution from which the complexes [$MCl_4(\kappa^3$-bdmpzx)] (x = *a*, M = Nb **2**, Ta **3**; x = *e*, M = Nb **4**, Ta **5**) were isolated as red, (**2**) yellow (**3, 4**) and white (**5**) solids after the appropriate workup. When solutions of **2**−**5** in THF were stirred at ca. 20 °C for 48 h, the oxo complexes [$MCl_2(O)(\kappa^3$-bdmpzx)] (x = *a*, M = Nb **6**, Ta **7**; x = *e*, M = Nb **8**, Ta **9**) were isolated as white solids after the appropriate workup (Scheme 2). Although rigorously anhydrous experimental conditions were used, hydrolysis still occurred.

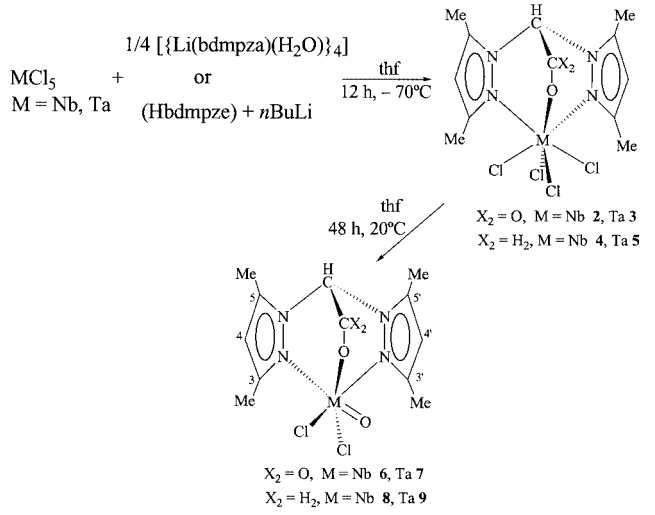

Scheme 2. Syntheses of complexes [$MCl_4(\kappa^3$-bdmpzx)] (**2**−**5**) and [$MCl_2(O)(\kappa^3$-bdmpzx)] (**6**−**9**)

The complexes were characterised spectroscopically. The mass spectra of **2**−**9** indicate a mononuclear formulation (Exp. Sect.). The ir spectra of **2**−**3** and **6**−**7** show two strong bands at ca. 1750 and 1500 cm^{-1}, which are assigned to $\nu_{as}(CO_2^-)$ and $\nu_s(CO_2^-)$, respectively. In the lithium compound [{Li(bdmpza)(H_2O)}$_4$], $\Delta\nu_{as\text{-}s}$ [$\nu_{as}(CO_2^-) - \nu_s(CO_2^-)$] is 180 cm^{-1}, and the carboxylate forms a coordinating bridge between two lithium atoms. IR spectroscopy is a good indicator of the bonding mode of carboxylate ligands:[7] bonding through the two oxygen atoms (chelate mode) leads to a decrease in $\Delta\nu_{as\text{-}s}$ in comparison to the absorptions of a bridge mode, and bonding through the single oxygen atom leads to an increase in $\Delta\nu_{as\text{-}s}$, again in comparison to a bridging mode. The $\Delta\tilde{\nu}_{as\text{-}s}$ (ca. 235 cm^{-1}) for these compounds accords with an *O*-coordination (monodentate) mode. The IR spectra of **4**, **5**, **8** and **9** contain a strong band at ca. 570 cm^{-1} that is assigned to ν(M−O). Complexes **2**−**9** show other bands of interest at ca. 420 and 315 cm^{-1}, which are assigned to ν(M−Cl) of the terminal group for a mononuclear disposition, with a seven-coordinate model or octahedral environment for each niobium atom. The ^1H and $^{13}C\{^1H\}$ NMR spectra of **2**−**5** show a single set of resonances for the pyrazole rings, indicating that the pyrazoles are equivalent. These data confirm a seven-coordinate model (Scheme 2), with κ^3-NNO coordination for the bdmpza or bdmpze.

The ^1H NMR spectra of **6**−**9** exhibit two resonances for each H^4, Me^3 and Me^5 pyrazole protons, indicating that the two pyrazole rings are non-equivalent (Exp. Sect.). These results are consistent with a proposed octahedral disposition in which the two pyrazole rings are located in *cis* and *trans* positions with respect to the oxo ligand (Scheme 2). Homonuclear NOE (nuclear Overhauser enhancement) difference spectroscopy confirmed these assignments for each pyrazole ring. In addition, the $^{13}C\{^1H\}$ NMR spectra of complexes **6**−**9** exhibit two resonances for the different pyrazole carbon atoms C^3, C^4, C^5, Me^3, Me^5 which have been assigned on the basis of $^1H-^{13}C$ HETCOR correlation experiments (Exp. Sect.). The chiral centre of the metal atom in these complexes was confirmed by the presence in solution of the two enantiomers upon addition of the chiral shift reagent (*R*)-(−)-(9-anthryl)-2,2,2-trifluoroethanol. This process gave rise to two signals for each proton in the ^1H NMR spectra, resulting from the two diastereoisomers of the corresponding two enantiomers (Figure 1).

The molecular structure of complex **8** was determined by X-ray diffraction. It crystallizes in the orthorhombic space group *Pbca* with eight molecules per unit cell, and consists of a monomeric unit with a heteroscorpionate ligand bonded to the niobium atom through the two nitrogen atoms and the oxygen from the alkoxide group (Figure 2).

 © 2004 Wiley-VCH Verlag GmbH & Co. KGaA, Weinheim

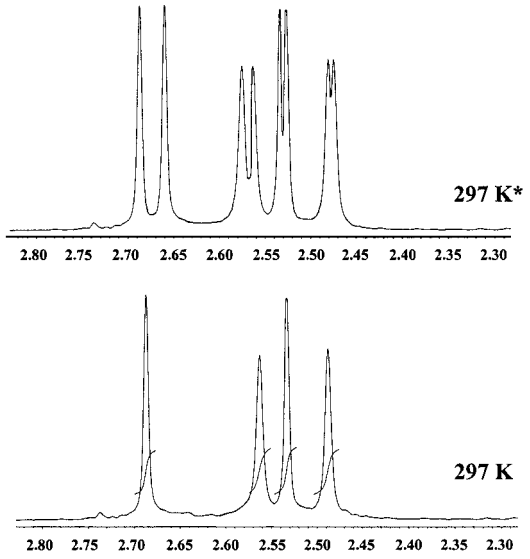

Figure 1. ^{1}H. NMR spectra in the region of the Me group of the complex [$NbCl_2(O)(\kappa^3$-bdmpza)] (**6**); *with chiral shift reagent

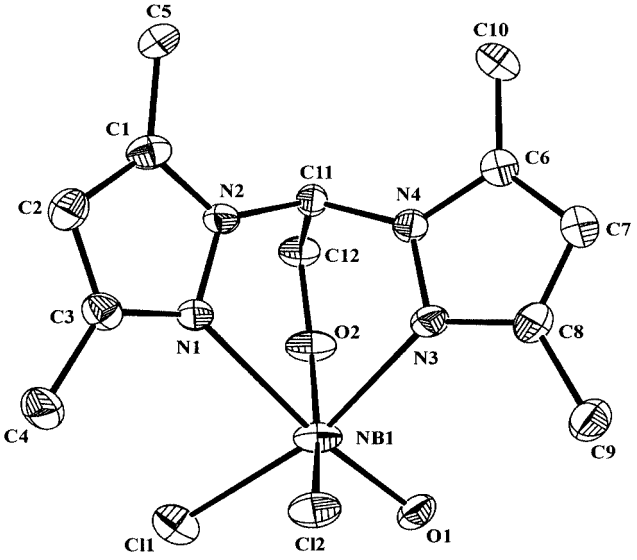

Figure 2. ORTEP drawing of the complex [$NbCl_2(O)(\kappa^3$-bdmpze)] (**8**)

In addition, the niobium centre is coordinated to two chloride atoms and one oxygen, rendering the niobium atom a chiral centre. In the solid state, due to the centrosymmetric space group, both enantiomers are present and one, *OC*−6−43(C), is depicted in Figure 2.

This complex has a pseudooctahedral geometry with an equatorial plane defined by the N1, N3, O1 and Cl1 atoms and two apical positions defined by O2 and Cl2. The major distortion appears in the O2−Nb1−Cl2 angle [157.7(2)°, Table 1]. The Nb1−N3 bond length [2.263(6) Å] is as expect for an Nb pyrazolyl complex[2] but the elongated Nb1−N1 [2.456(5) Å] indicates that O1 exerts a strong *trans* influence. The Nb1−O1 [1.796(5) Å] is as expected for a double bond.[8]

Table 1. Bond lengths (Å) and angles (°) for **8**

Nb(1)−O(1)	1.796(5)	O(1)−Nb(1)−O(2)	99.9(2)
Nb(1)−O(2)	1.903(5)	O(1)−Nb(1)−N(3)	96.7(2)
Nb(1)−N(3)	2.263(6)	O(2)−Nb(1)−N(3)	79.2(2)
Nb(1)−Cl(1)	2.337(2)	O(1)−Nb(1)−Cl(1)	97.4(2)
Nb(1)−Cl(2)	2.412(2)	O(2)−Nb(1)−Cl(1)	96.2(2)
Nb(1)−N(1)	2.456(5)	N(3)−Nb(1)−Cl(1)	165.7(1)
O(2)−C(12)	1.402(8)	O(1)−Nb(1)−Cl(2)	98.1(2)
		O(2)−Nb(1)−Cl(2)	157.7(2)
		N(3)−Nb(1)−Cl(2)	85.7(1)
		Cl(1)−Nb(1)−Cl(2)	94.49(8)
		O(1)−Nb(1)−N(1)	172.2(2)
		O(2)−Nb(1)−N(1)	78.7(2)
		N(3)−Nb(1)−N(1)	75.5(2)
		Cl(1)−Nb(1)−N(1)	90.3(1)
		Cl(2)−Nb(1)−N(1)	81.8(1)
		C(12)−O(2)−Nb(1)	136.0(4)

To extend the range of alkoxide-containing niobium and tantalum species we prepared a new class of heteroscorpionate-metal complex, which contains an alkoxide ancillary ligand. Direct reaction of complexes [$MCl_4(\kappa^3$-bdmpza)] (M = Nb **2**, Ta **3**) with several alcohols (Scheme 3) gave, after appropriate workup, the complexes [$MCl_3(\kappa^3$-bdmpza)(OR)] (M = Nb, R = Me **10**, Et **11**, *iPr* **12**, *t*Bu **13**; M = Ta, R = Me **14**, Et **15**, *iPr* **16**, *t*Bu **17**), which were isolated as yellow solids. The mass spectra of complexes **10**−**17** indicate a mononuclear formulation (Exp. Sect.). In the IR spectra $\Delta\tilde{\nu}_{as\text{-}s}$ is ca. 225 cm^{-1}, which accords with coordination by a single oxygen. Three strong bands are also observed at ca. 550, 370 and 300 cm^{-1}, and the first of these was assigned to ν(M−OR) and the latter two to ν(M−Cl). The ^{1}H NMR spectra of these complexes exhibit a single set of resonances for H^4, Me^3 and Me^5, indicating that the pyrazole rings are equivalent. These results are consistent with the proposed seven-coordinate disposition in which the alkoxide and chloride ligands bisect the plane of the scorpionate ligand (Figure 3). In addition, the $^{13}C\{^1H\}$ NMR spectra show the corresponding signals for C^3, C^4, C^5, Me^3 and Me^5 and the different carbon atoms of the corresponding alkoxide ligand (Exp. Sect.).

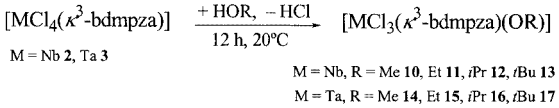

Scheme 3. Synthesis of complexes [$MCl_3(\kappa^3$-bdmpza)(OR)] **10**−**17**

Conclusion

A new synthetic route has provided the alcohol 2,2-bis(3,5-dimethylpyrazol-1-yl)ethanol (Hbdmpze) in good yield. Both this alcohol and the related lithium compound

 © 2004 Wiley-VCH Verlag GmbH & Co. KGaA, Weinheim

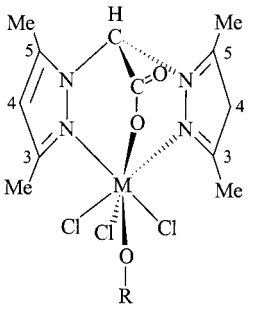

Figure 3. Proposed structure for complexes **10−17**

[{Li(bdmpza)(H_2O)}$_4$] are excellent precursors for introducing these scorpionate ligands into transition metal complexes, as confirmed by the preparation of different niobium and tantalum complexes. New classes of heteroscorpionte-niobium(v) and tantalum(v) complexes, containing halide, oxo and alkoxide ancillary ligands have also been isolated.

Experimental Section

All reactions were performed using standard Schlenk-tube techniques under an atmosphere of dry nitrogen. Solvents were distilled from appropriate drying agents and degassed before use. Microanalyses were carried out with a Perkin−Elmer 2400 CHN analyser. Mass spectra were recorded on a VG Autospec instrument using the FAB technique and 3-nitrobenzyl alcohol as matrix. Infrared spectra were recorded in the region 4000−200 cm^{-1} using a Perkin−Elmer 883 spectrophotometer. ^1H and ^{13}C NMR spectra were registered on a Varian Unity FT-300 and 200 spectrometers referenced to the residual deuterated solvent. The NOE difference spectra were recorded with the acquisition parameters: spectrum width 5000 Hz, acquisition time 3.27 s, pulse width 90°, relaxation delay 4 s, irradiation power 5−10 dB, number of scans 120. Two-dimensional NMR spectra were acquired using standard VARIANT-FT software and processed using an IPC-Sun computer.

The complexes $NbCl_5$ and $TaCl_5$ were purchased from Aldrich. The compounds [{Li(bdmpza)(H_2O)}$_4$] and Hbdmpze were prepared as reported previously.[3,5]

Preparations

Hbdmpza (1): A 10% solution of HCl (4.50 mL, 11.02 mmol) in water was added to [Li(bdmpza)(H_2O)}$_4$] (3.00 g, 11.02 mmol) dissolved in dry THF (30 mL) in a Schlenk tube (250 mL), and the resultant reaction mixture was stirred for 1 h at room temperature. The mixture was then separated and the organic layer dried with $MgSO_4$ and subsequently concentrated to afford the white solid **1**, which was washed with hexane and crystallized from a mixture of THF/hexane. Yield 97%. $C_{12}H_{16}N_4O_2$ (248.3): calcd. C 58.05, H 6.49, N 22.56; found C 58.12, H 6.65, N 22.31. ^1H NMR ($CDCl_3$, 297 K): δ = 6.89 (s, 1 H, CH), 5.91 (s, 2 H, H^4), 2.15 (s, 6 H, Me^3), 2.30 (s, 6 H, Me^5) ppm. $^{13}C\{^1H\}$ NMR ($CDCl_3$): δ = 69.3 (CH), 149.6, 142.6 (C^3 or C^5), 106.9 (C^4), 13.5 (Me^3), 11.1 (Me^5), 168.2 (CO_2^-) ppm. IR (Nujol): $\tilde{\nu}$ = 1562 ν(C=N), 1578 $\nu_{as}(CO_2^-)$, 1414 $\nu_s(CO_2^-)$ cm^{-1}. Mass spectrum (*m*/*z* assignment, % intensity): 248 $[Hbdmpza]^+$, 100.

[$NbCl_4$(κ^3-bdmpza)] (2): An equimolar quantity of [{Li(bdmpza)(H_2O)}$_4$] (1.01 g, 0.92 mmol) was added dropwise to a THF (100 mL) solution of $NbCl_5$ (1.00 g, 3.70 mmol). The resultant solution was then stirred for 12 h at −70 °C, and the solvent then removed under vacuum to give a solid that was extracted with CH_2Cl_2. The solvent was then removed to give a red solid. Yield 92%. $C_{12}H_{15}Cl_4N_4NbO_2$ (482.0): calcd. C 29.90, H 3.13, N 11.66; found C 30.02, H 3.13, N 11.72. ^1H NMR ($CDCl_3$, 297 K), δ = 6.85 (s, 1 H, CH), 6.18 (s, 2 H, H^4), 2.55 (s, 6 H, Me^3), 2.70 (s, 6 H, Me^5) ppm. $^{13}C\{^1H\}$ NMR ($CDCl_3$): δ = 72.1 (CH), 149.2, 142.3 (C^3 or C^5), 106.5 (C^4), 12.1 (Me^3), 11.6 (Me^5), 168.3 (CO_2^-) ppm. IR (Nujol): $\tilde{\nu}$ = 1575 ν(C=N), 1760 $\nu_{as}(CO_2^-)$, 1525 $\nu_s(CO_2^-)$, 429, 304 ν(Nb−Cl) cm^{-1}. Mass spectrum (*m*/*z* assignment, % intensity): 446 [M − Cl], 100.

[$TaCl_4$(κ^3-bdmpza)] (3): The synthetic procedure was the same as for complex **2**, using $TaCl_5$ (1.00 g, 2.79 mmol) and [{Li(bdmpza)(H_2O)}$_4$] (0.76 g, 0.70 mmol). The solution was stirred for 12 h at −70 °C, and the solvent was then removed under vacuum and the solid extracted with CH_2Cl_2. The latter solvent was then removed to give a yellow solid. Yield 91%. $C_{12}H_{15}Cl_4N_4O_2Ta$ (570.0): calcd. C 25.31, H 2.61, N 9.82; found C 25.34, H 2.65, N 9.86. ^1H NMR ($CDCl_3$, 297 K): δ = 7.83 (s, 1 H, CH), 6.01 (s, 2 H, H^4), 2.33 (s, 6 H, Me^3), 2.42 (s, 6 H, Me^5) ppm. $^{13}C\{^1H\}$ NMR ($CDCl_3$): δ = 73.4 (CH), 148.7, 141.2 (C^3 or C^5), 105.8 (C^4), 12.3 (Me^3), 11.1 (Me^5), 168.7 (CO_2^-) ppm. IR (Nujol): $\tilde{\nu}$ = 1572 ν(C=N), 1712 $\nu_{as}(CO_2^-)$, 1498 $\nu_s(CO_2^-)$, 405, 315 ν(Ta−Cl) cm^{-1}. Mass spectrum (*m*/*z* assignment, % intensity): 534 [M − Cl], 100.

[$NbCl_4$(κ^3-bdmpze)] (4): A 1.6 M solution of *n*BuLi in hexane (2.3 mL, 3.70 mmol) was added to a cooled (−70 °C) solution of Hbdmpze (0.87 g, 3.70 mmol) in dry THF (100 mL). After 30 min a solution of $NbCl_5$ (1.00 g, 3.70 mmol) in THF (50 mL) was added and the reaction mixture was stirred for 12 h at −70 °C. The so obtained product was then extracted into CH_2Cl_2 (50 mL) and the solvent removed under vacuum to give a yellow solid. This solid was then crystallised from a mixture of THF/hexane. Yield 90%. $C_{12}H_{17}Cl_4N_4NbO$ (468.0): calcd. C 30.73, H 3.63, N 11.91; found C 30.83, H 3.92, N 12.12. ^1H NMR ($CDCl_3$, 297 K): δ = 7.29 (t, $^3J_{H,H}$ = 5.4 Hz, 1 H, CH), 4.50 (d, $^3J_{H,H}$ = 5.4 Hz, 2 H, CH_2O), 6.04 (s, 2 H, H^4), 2.17 (s, 6 H, Me^3), 2.36 (s, 6 H, Me^5) ppm. $^{13}C\{^1H\}$ NMR ($CDCl_3$): δ = 71.7 (CH), 62.8 (CH_2O), 149.1, 141.1 (C^3 or C^5), 108.4 (C^4), 12.4 (Me^3), 11.2 (Me^5) ppm. IR (Nujol): $\tilde{\nu}$ = 1574 ν(C=N), 585 ν(Nb−O), 425, 325 ν(Nb−Cl) cm^{-1}. Mass spectrum (*m*/*z* assignment, % intensity): 432 [M − Cl], 100.

[$TaCl_4$(κ^3-bdmpze)] (5): The synthetic procedure was the same as for complex **4**, using $TaCl_5$ (1.00 g, 2.79 mmol), Hbdmpze (0.65 g, 2.79 mmol) and *n*BuLi (1.7 mL, 2.79 mmol), to give **5** as a white solid (85% yield). $C_{12}H_{17}Cl_4N_4OTa$ (556.1): calcd. C 25.92, H 3.18, N 10.08; found C 25.92, H 3.22, N 10.12. ^1H NMR ($CDCl_3$, 297 K): δ = 7.59 (t, $^3J_{H,H}$ = 4.4 Hz, 1 H, CH), 4.55 (d, $^3J_{H,H}$ = 4.4 Hz, 2 H, CH_2O), 6.06 (s, 2 H, H^4), 2.14 (s, 6 H, Me^3), 2.38 (s, 6 H, Me^5) ppm. $^{13}C\{^1H\}$ NMR ($CDCl_3$): δ = 71.3 (CH), 63.1 (CH_2O), 149.3, 141.8 (C^3 or C^5), 106.1 (C^4), 12.3 (Me^3), 11.2 (Me^5) ppm. IR (Nujol): $\tilde{\nu}$ = 1570 ν(C=N), 564 ν(Ta−O), 409, 312 ν(Ta−Cl) cm^{-1}. Mass spectrum (*m*/*z* assignment, % intensity): 520 [M − Cl], 100.

[$NbCl_2$(O)(κ^3-bdmpza)] (6): A THF (100 mL) solution of [$NbCl_4$(κ^3-bdmpza)] (**2**) (0.50 g, 1.03 mmol) was stirred for 48 h at 20 °C. The solvent was then removed under vacuum to give a white solid, which was crystallised from a mixture of THF/hexane. Yield 92%. $C_{12}H_{15}Cl_2N_4NbO_3$ (427.1): calcd. C 33.72, H 3.51, N 13.13; found C 33.72, H 3.51, N 13.13. ^1H NMR ($CDCl_3$, 297 K): δ = 6.74 (s, 1 H, CH), 6.18, 6.04 (s, 2 H, H^4 or $H^{4'}$), 2.70, 2.55 (s, 6 H, Me^3 or $Me^{3'}$), 2.54, 2.49 (s, 6 H, Me^5 or $Me^{5'}$) ppm. $^{13}C\{^1H\}$ NMR

 © 2004 Wiley-VCH Verlag GmbH & Co. KGaA, Weinheim

($CDCl_3$): δ = 66.3 (CH), 156.1, 154.9, 143.0, 141.3 (C^3 or $C^{3'}$, C^5 or $C^{5'}$), 108.9, 108.7 (C^4 or $C^{4'}$), 11.3, 10.8 (Me^3 or $Me^{3'}$), 15.3, 14.4 (Me^5 or $Me^{5'}$), 162.3 (CO_2^-) ppm. IR (Nujol): $\tilde{\nu}$ = 1579 ν(C=N), 1761 $\nu_{as}(CO_2^-)$, 1525 $\nu_s(CO_2^-)$, 926 ν(Nb=O), 429, 324 ν(Nb−Cl) cm^{-1}. Mass spectrum (*m*/*z* assignment, % intensity): 426 [M], 100.

[$TaCl_2(O)(\kappa^3$-bdmpza)] (7): The synthetic procedure was the same as for complex **6**, using [$TaCl_4(\kappa^3$-bdmpza)] **3** (0.50 g, 0.88 mmol). The solvent was removed under vacuum to give a white solid, which was crystallised from a mixture of THF/hexane. Yield 85%. $C_{12}H_{15}Cl_2N_4O_3Ta$ (515.1): calcd. C 27.92, H 2.92, N 10.81; found C 27.93, H 2.97, N 10.83. ^{1}H NMR ($CDCl_3$, 297 K): δ = 6.61 (s, 1 H, CH), 6.23, 6.08 (s, 2 H, H^4 or $H^{4'}$), 2.76, 2.57 (s, 6 H, Me^3 or $Me^{3'}$), 2.54, 2.49 (s, 6 H, Me^5 or $Me^{5'}$) ppm. $^{13}C\{^1H\}$ NMR ($CDCl_3$): δ = 66.5 (CH), 157.0, 155.5, 143.3, 141.3 (C^3 or $C^{3'}$, C^5 or $C^{5'}$), 109.4, 109.2 (C^4 or $C^{4'}$), 11.4, 10.9 (Me^3 or $Me^{3'}$), 15.7, 14.6 (Me^5 or $Me^{5'}$), 161.1 (CO_2^-) ppm. IR (Nujol): $\tilde{\nu}$ = 1569 ν(C=N), 1712 $\nu_{as}(CO_2^-)$, 1488 $\nu_s(CO_2^-)$, 897 ν(Ta=O), 405, 315 ν(Ta−Cl) cm^{-1}. Mass spectrum (*m*/*z* assignment, % intensity): 514 [M], 100.

[$NbCl_2(O)(\kappa^3$-bdmpze)] (8): The synthetic procedure was the same as for complex **6**, using [$NbCl_4(\kappa^3$-bdmpze)] (**4**) (0.50 g, 1.07 mmol). The product was extracted into CH_2Cl_2 and the solvent was then removed under vacuum to give a white solid that was crystallised from a mixture of THF/hexane. Yield 87%. $C_{12}H_{17}Cl_2N_4NbO_2$ (413.1): calcd. C 34.82, H 4.11, N 13.51; found C 34.84, H 4.14, N 13.53. ^{1}H NMR ($CDCl_3$, 297 K): δ = X 6.42, A 4.91, B 4.72 (ABX, J_{AB} = 12.2, $^3J_{AX}$ = 1.2, $^3J_{BX}$ = 2.4 Hz, 3 H, $CHCH_2O$), 6.09, 5.97 (s, 2 H, H^4 or $H^{4'}$), 2.65, 2.55 (s, 6 H, Me^3 or $Me^{3'}$), 2.48, 2.44 (s, 6 H, Me^5 or $Me^{5'}$) ppm. $^{13}C\{^1H\}$ NMR ($CDCl_3$): δ = 72.6 (CH), 65.8 (CH_2O), 153.8, 153.1, 142.8, 141.8 (C^3 or $C^{3'}$, C^5 or $C^{5'}$), 108.1, 108.0 (C^4 or $C^{4'}$), 11.5, 11.0 (Me^3 or $Me^{3'}$), 15.2, 14.5 (Me^5 or $Me^{5'}$) ppm. IR (Nujol): $\tilde{\nu}$ = 1574 ν(C=N), 570 ν(Nb−O), 930 ν(Nb=O), 421, 325 ν(Nb−Cl) cm^{-1}. Mass spectrum (*m*/*z* assignment, % intensity): 412 [M], 100.

[$TaCl_2(O)(\kappa^3$-bdmpze)] (9): The synthetic procedure was the same as for complex **6**, using [$TaCl_4(\kappa^3$-bdmpze)] (**5**) (0.50 g, 0.89 mmol). The product was extracted into CH_2Cl_2 and the solvent was then removed under vacuum to give a white solid, which was crystallised from a mixture of THF/hexane. Yield 83%. $C_{12}H_{17}Cl_2N_4O_2Ta$ (501.1): calcd. C 28.72, H 3.41, N 11.11; found C 28.77, H 3.42, N 11.13. ^{1}H NMR ($CDCl_3$, 297 K): δ = X 7.19, A 4.57, B 4.50 (ABX, J_{AB} = 22.4, $^3J_{AX}$ = $^3J_{BX}$ = 4.3 Hz, 3 H, $CHCH_2O$), 6.06, 5.97 (s, 2 H, H^4 or $H^{4'}$), 2.49, 2.34 (s, 6 H, Me^3 or $Me^{3'}$), 2.49, 2.13 (s, 6 H, Me^5 or $Me^{5'}$) ppm. $^{13}C\{^1H\}$ NMR ($CDCl_3$): δ = 72.1 (CH), 63.1 (CH_2O), 147.9, 144.8, 144.7, 143.5 (C^3 or $C^{3'}$, C^5 or $C^{5'}$), 107.9, 106.0 (C^4 or $C^{4'}$), 11.0, 10.9 (Me^3 or $Me^{3'}$), 12.6, 10.9 (Me^5 or $Me^{5'}$) ppm. IR (Nujol): $\tilde{\nu}$ = 1570 ν(C=N), 550 ν(Ta−O), 899 ν(Ta=O), 399, 316 ν(Ta−Cl) cm^{-1}. Mass spectrum (*m*/*z* assignment, % intensity): 465 [M], 100.

[$NbCl_3(\kappa^3$-bdmpza)(OMe)] (10): A MeOH (100 mL) solution of [$NbCl_4(\kappa^3$-bdmpza)] (**2**) (0.5 g, 1.03 mmol) was stirred for 12 h at 20 °C. The solvent was then removed under vacuum and the solid extracted into toluene. The toluene was then removed to give a yellow solid. Yield 81%. $C_{13}H_{18}Cl_3N_4NbO_3$ (477.6): calcd. C 32.78, H 3.64, N 11.77; found C 32.94, H 3.81, N 11.92. ^{1}H NMR ($CDCl_3$, 297 K): δ = 8.08 (s, 1 H, CH), 6.02 (s, 2 H, H^4), 2.34 (s, 6 H, Me^3), 2.46 (s, 6 H, Me^5), 3.91 (s, 3 H, OMe) ppm. $^{13}C\{^1H\}$ NMR ($CDCl_3$): δ = 69.9 (CH), 148.0, 145.4 (C^3 or C^5), 108.4 (C^4), 12.3 (Me^3), 12.0 (Me^5), 162.8 (CO_2^-), 54.2 (OMe) ppm. IR (Nujol): $\tilde{\nu}$ = 1574 ν(C=N), 1751 $\nu_{as}(CO_2^-)$, 1515 $\nu_s(CO_2^-)$, 579 ν(Nb−OMe), 385, 305 ν(Nb−Cl) cm^{-1}. Mass spectrum (*m*/*z* assignment, % intensity): 442 [M − Cl], 100.

[$NbCl_3(\kappa^3$-bdmpza)(OEt)] (11): A solution of [$NbCl_4(\kappa^3$-bdmpza)] (**2**) (0.5 g, 1.03 mmol) in EtOH (100 mL) was stirred for 12 h at 20 °C, and the solvent was then removed under vacuum and the solid extracted with toluene. The toluene was then removed to give a yellow solid. Yield 80%. $C_{14}H_{20}Cl_3N_4NbO_3$ (491.6): calcd. C 34.32, H 3.81, N 11.44; found C 34.35, H 3.82, N 11.46. ^{1}H NMR ($CDCl_3$, 297 K): δ = 7.89 (s, 1 H, CH), 5.99 (s, 2 H, H^4), 2.31 (s, 6 H, Me^3), 2.41 (s, 6 H, Me^5), 4.36 (q, $^3J_{H,H}$ = 7.0 Hz, 2 H, OCH_2CH_3), 1.30, (t, $^3J_{H,H}$ = 7.0 Hz, 3 H, OCH_2CH_3) ppm. $^{13}C\{^1H\}$ NMR ($CDCl_3$): δ = 70.4 (CH), 147.9, 144.9 (C^3 or C^5), 108.2 (C^4), 12.5 (Me^3), 11.9 (Me^5), 162.7 (CO_2^-), 63.8 (OCH_2CH_3), 13.8 (OCH_2CH_3) ppm. IR (Nujol): $\tilde{\nu}$ = 1573 ν(C=N), 1710 $\nu_{as}(CO_2^-)$, 1480 $\nu_s(CO_2^-)$, 561 ν(Nb−OEt), 374, 306 ν(Nb−Cl) cm^{-1}. Mass spectrum (*m*/*z* assignment, % intensity): 456 [M − Cl], 100.

[$NbCl_3(\kappa^3$-bdmpza)(O*i*Pr)] (12): A solution of [$NbCl_4(\kappa^3$-bdmpza)] (**2**) (0.5 g, 1.03 mmol) in *i*PrOH (100 mL) was stirred for 12 h at 20 °C. The solvent was then removed under vacuum and the solid extracted with toluene; the toluene was then removed to give a yellow solid. Yield 75%. $C_{15}H_{22}Cl_3N_4NbO_3$ (505.6): calcd. C 35.77, H 4.25, N 11.17; found C 35.63, H 4.35, N 11.23. ^{1}H NMR ($CDCl_3$, 297 K): δ = 7.56 (s, 1 H, CH), 5.94 (s, 2 H, H^4), 2.27 (s, 6 H, Me^3), 2.33 (s, 6 H, Me^5), 5.19 [m, $^3J_{H,H}$ = 7.0 Hz, 1 H, $OCH(CH_3)_2$], 1.28 [d, $^3J_{H,H}$ = 7.0 Hz, 6 H, $OCH(CH_3)_2$] ppm. $^{13}C\{^1H\}$ NMR ($CDCl_3$): δ = 71.0 (CH), 147.9, 144.2 (C^3 or C^5), 108.2 (C^4), 12.6 (Me^3), 11.7 (Me^5), 162.6 (CO_2^-), 72.1 [$OCH(CH_3)_2$], 21.4 [$OCH(CH_3)_2$] ppm. IR (Nujol): $\tilde{\nu}$ = 1569 ν(C=N), 1680 $\nu_{as}(CO_2^-)$, 1464 $\nu_s(CO_2^-)$, 552 ν(Nb−O*i*Pr), 368, 298 ν(Nb−Cl) cm^{-1}. Mass spectrum (*m*/*z* assignment, % intensity): 470 [M − Cl], 100.

[$NbCl_3(\kappa^3$-bdmpza)(O*t*Bu)] (13): A solution of [$NbCl_4(\kappa^3$-bdmpza)] (**2**) (0.5 g, 1.03 mmol) in *t*BuOH (100 mL) was stirred for 12 h at 20 °C. The solvent was then removed under vacuum and the solid extracted with toluene; the toluene was then removed to give a yellow solid. Yield 90%. $C_{16}H_{24}Cl_3N_4NbO_3$ (519.7): calcd. C 37.04, H 4.42, N 10.82; found C 37.17, H 4.54, N 10.94. ^{1}H NMR ($CDCl_3$, 297 K): δ = 7.63 (s, 1 H, CH), 6.01 (s, 2 H, H^4), 2.30 (s, 6 H, Me^3), 2.42 (s, 6 H, Me^5), 1.57 [s, 9 H, $OC(Me)_3$] ppm. $^{13}C\{^1H\}$ NMR ($CDCl_3$): δ = 70.3 (CH), 147.8, 144.9 (C^3 or C^5), 108.3 (C^4), 12.4 (Me^3), 11.8 (Me^5), 162.4 (CO_2^-), 29.3 [$OC(CH_3)_3$], 24.9 [$OC(CH_3)_3$] ppm. IR (Nujol): $\tilde{\nu}$ = 1564 ν(C=N), 1652 $\nu_{as}(CO_2^-)$, 1442 $\nu_s(CO_2^-)$, 543 ν(Nb−O*t*Bu), 358, 295 ν(Nb−Cl) cm^{-1}. Mass spectrum (*m*/*z* assignment, % intensity): 484 [M − Cl], 100.

[$TaCl_3(\kappa^3$-bdmpza)(OMe)] (14): A solution of [$TaCl_4(\kappa^3$-bdmpza)] (**3**) (0.5 g, 0.88 mmol) in MeOH (100 mL) was stirred for 12 h at 20 °C. The solvent was then removed under vacuum and the solid extracted with toluene that was then removed to give a yellow solid. Yield 82%. $C_{13}H_{18}Cl_3N_4O_3Ta$ (565.6): calcd. C 27.62, H 3.03, N 9.92; found C 27.74, H 3.06, N 9.85. ^{1}H NMR ($CDCl_3$, 297 K): δ = 7.86 (s, 1 H, CH), 6.01 (s, 2 H, H^4), 2.31 (s, 6 H, Me^3), 2.42 (s, 6 H, Me^5), 3.90 (s, 3 H, OMe) ppm. $^{13}C\{^1H\}$ NMR ($CDCl_3$): δ = 70.5 (CH), 148.3, 145.1 (C^3 or C^5), 108.4 (C^4), 12.5 (Me^3), 11.9 (Me^5), 163.2 (CO_2^-), 54.2 (OMe) ppm. IR (Nujol): $\tilde{\nu}$ = 1570 ν(C=N), 1710 $\nu_{as}(CO_2^-)$, 1503 $\nu_s(CO_2^-)$, 554 ν(Ta−OMe), 365, 301 ν(Ta−Cl) cm^{-1}. Mass spectrum (*m*/*z* assignment, % intensity): 530 [M − Cl], 100.

[$TaCl_3(\kappa^3$-bdmpza)(OEt)] (15): A solution of [$TaCl_4(\kappa^3$-bdmpza)] (**3**) (0.5 g, 0.88 mmol) in EtOH (100 mL) was stirred for 12 h at 20 °C. The solvent was then removed under vacuum and the solid

 © 2004 Wiley-VCH Verlag GmbH & Co. KGaA, Weinheim

extracted with toluene that was then removed to give a yellow solid. Yield 87%. $C_{14}H_{20}Cl_3N_4O_3Ta$ (579.6): calcd. C 29.03, H 3.21, N 9.70; found C 29.05, H 3.22, N 9.73. ^1H NMR ($CDCl_3$, 297 K): δ = 7.82 (s, 1 H, CH), 6.00 (s, 2 H, H^4), 2.30 (s, 6 H, Me^3), 2.42 (s, 6 H, Me^5), 4.35 (q, $^3J_{H,H}$ = 7.0 Hz, 2 H, OCH_2CH_3), 1.30 (t, $^3J_{H,H}$ = 7.0 Hz, 3 H, OCH_2CH_3) ppm. $^{13}C\{^1H\}$ NMR ($CDCl_3$): δ = 71.0 (CH), 148.0, 144.9 (C^3 or C^5), 108.2 (C^4), 12.5 (Me^3), 11.9 (Me^5), 162.7 (CO_2^-), 63.8 (OCH_2CH_3), 13.8 (OCH_2CH_3) ppm. IR (Nujol): $\tilde{\nu}$ = 1563 ν(C=N), 1680 $\nu_{as}(CO_2^-)$, 1468 $\nu_s(CO_2^-)$, 541 ν(Ta−OEt), 354, 298 ν(Ta−Cl) cm^{-1}. Mass spectrum (*m*/*z* assignment, % intensity): 544 [M − Cl], 100.

[$TaCl_3$(κ³-bdmpza)(O*i*Pr)] (16): A solution of [$TaCl_4$(κ³-bdmpza)] (**3**) (0.5 g, 0.88 mol) in *i*PrOH (100 mL) was stirred for 12 h at 20 °C. The solvent was then removed under vacuum and the solid extracted with toluene that was subsequently removed to give a yellow solid. Yield 68%. $C_{15}H_{22}Cl_3N_4O_3Ta$ (593.7): calcd. C 30.46, H 3.53, N 9.42; found C 30.62, H 3.66, N 9.65. ^1H NMR ($CDCl_3$, 297 K): δ = 7.77 (s, 1 H, CH), 5.98 (s, 2 H, H^4), 2.30 (s, 6 H, Me^3), 2.40 (s, 6 H, Me^5), 5.18 [m, $^3J_{H,H}$ = 7.0 Hz, 1 H, $OCH(CH_3)_2$], 1.28 [d, $^3J_{H,H}$ = 7.0 Hz, 6 H, $OCH(CH_3)_2$] ppm. $^{13}C\{^1H\}$ NMR ($CDCl_3$): δ = 70.6 (CH), 147.8, 144.7 (C^3 or C^5), 108.1 (C^4), 12.5 (Me^3), 11.8 (Me^5), 162.3 (CO_2^-), 72.3 [$OCH(CH_3)_2$], 21.4 [$OCH(CH_3)_2$] ppm. IR (Nujol): $\tilde{\nu}$ = 1568 ν(C=N), 1658 $\nu_{as}(CO_2^-)$, 1455 $\nu_s(CO_2^-)$, 539 ν(Ta−O*i*Pr), 345, 294 ν(Ta−Cl) cm^{-1}. Mass spectrum (*m*/*z* assignment, % intensity): 558 [M − Cl], 100.

[$TaCl_3$(κ³-bdmpza)(O*t*Bu)] (17): A solution of [$TaCl_4$(κ³-bdmpza)] (**3**) (0.5 g, 0.88 mmol) in *t*BuOH (100 mL) was stirred for 12 h at 20 °C. The solvent was then removed under vacuum and the solid extracted with toluene that was subsequently removed to give a yellow solid. Yield 91%. $C_{16}H_{24}Cl_3N_4O_3Ta$ (607.7): calcd. C 31.61, H 3.82, N 9.22; found C 31.63, H 3.86, N 9.26. ^1H NMR ($CDCl_3$, 297 K): δ = 7.80 (s, 1 H, CH), 6.00 (s, 2 H, H^4), 2.31 (s, 6 H, Me^3), 2.41 (s, 6 H, Me^5), 1.55 [s, 9 H, $OC(Me)_3$] ppm. $^{13}C\{^1H\}$ NMR ($CDCl_3$): δ = 70.3 (CH), 147.5, 144.3 (C^3 or C^5), 108.2 (C^4), 12.5 (Me^3), 11.7 (Me^5), 163.1 (CO_2^-), 30.1 [$OC(CH_3)_3$], 26.3 [$OC(CH_3)_3$] ppm. IR (Nujol): $\tilde{\nu}$ = 1573 ν(C=N), 1643 $\nu_{as}(CO_2^-)$, 1438 $\nu_s(CO_2^-)$, 529 ν(Ta−O*t*Bu), 334, 289 ν(Ta−Cl) cm^{-1}. Mass spectrum (*m*/*z* assignment, % intensity): 572 [M − Cl], 100.

Crystal Data for 8: Single crystals suitable for X-ray diffraction were obtained by slow evaporation of the solvent from a solution of **8** in dichloromethane. The crystals were mounted on fine glass fibres with epoxy cement. The diffractions were measured on a four-circle diffractometer (Nonius-MACH3) at 200 K using graphite-monochromated Mo-K_α radiation (λ = 0.71073 Å) and a ω/2θ scan. Two standard diffractions were monitored every hour and showed no significant intensity variation. The lattice parameters were refined by least-squares fitting from 25 automatically centred diffractions. An empirical absorption correction was made. The structure was solved by direct methods[9] yielding the positions of all non-hydrogen atoms. Refinement on F^2 was carried out by full-matrix least-squares techniques.[10] All non-hydrogen atoms were refined with anisotropic thermal parameters. The hydrogen atoms were included in calculated positions and were refined isotropically (Table 2). CCDC-208238 contains the supplementary crystallographic data for this paper. These data can be obtained free of charge at www.ccdc.cam.ac.uk/conts/retrieving.html [or from the Cambridge Crystallographic Data Centre, 12 Union Road, Cambridge CB2 1EZ, UK; Fax: (internat.) + 44-1223/336-033; E-mail: deposit@ccdc.cam.ac.uk].

Table 2. Crystal data and structure refinement for **8**

Empirical formula	$C_{12}H_{17}Cl_2N_4NbO_2$
Molecular weight	413.11
Temperature	200(2) K
Wavelength	0.71073 Å
Crystal system	orthorhombic
Space group	*Pbca*
Unit cell dimensions	
	a = 13.106(1) Å
	b = 16.463(3) Å
	c = 14.650(2) Å
Volume	3160.8(8) $Å^3$
Z	8
Density (calculated)	1.736 g/cm^3
Absorption coefficient	11.08 cm^{-1}
F(000)	1664
Crystal size	0.3 × 0.2 × 0.2 mm^3
Index ranges	$0 \le h \le 17$, $0 \le k \le 21$, $0 \le l \le 19$
Reflections collected	3787
Independent reflections	3787 [R(int) = 0.0000]
Data/restraints/parameters	3787/0/191
Goodness-of-fit on F^2	1.045
Final R indices [$I > 2\sigma(I)$]	$R1$ = 0.0758, $wR2$ = 0.1973
R indices (all data)	$R1$ = 0.0931, $wR2$ = 0.2062
Extinction coefficient	0.0001(2)
Largest diff. peak and hole	3.711 and −2.442 e·$Å^{-3}$

Acknowledgments

We gratefully acknowledge financial support from the Dirección General de Enseñanza Superior e Investigación, Spain (Grant No. PB98-0159-C02-01).

[1] [1a] L. G. Hubert-Pfalzgraf, M. Tsunoda, *Polyhedron* **1983**, *2*, 203. [1b] D. C. Bradley, M. B. Hursthouse, J. Newton, N. P. C. Walker, *J. Chem. Soc., Chem. Commun.* **1984**, 188. [1c] J. Sundermeyer, J. Putterlik, M. Foth, J. S. Field, N. Ramesar, *Chem. Ber.* **1994**, *127*, 1201. [1d] M. Etienne, P. S. White, J. L Templeton,, *Organometallics* **1991**, *10*, 3801. [1e] M. Etienne, P. S. White, J. L. Templeton, *Organometallics* **1993**, *12*, 4010. [1f] M. Etienne, P. Zeline, J. L. Templeton, P. S. White, *New. J. Chem.* **1993**, *17*, 515. [1g] M. Etienne, *Organometallics* **1994**, *13*, 410. [1h] M. Etienne, F. Biasotto, R. Mathieu, *J. Chem. Soc., Chem. Commun.* **1994**, 1661. [1i] F. Biasotto, M. Etienne, F. Dahan, *Organometallics* **1995**, *14*, 1870. [1j] M. Etienne, F. Biasotto, R. Mathieu, J. L. Templeton, *Organometallics* **1996**, *15*, 1106. [1k] P. Lorente, C. Carfagna, M. Etienne, B. Donnadieu, *Organometallics* **1996**, *15*, 1090. [1l] M. Etienne, R. Mathieu, B. Donnadieu, *J. Am. Chem. Soc.* **1997**, *119*, 3218. [1m] K. Mashima, T. Oshiki, K. Tani, *Organometallics* **1997**, *16*, 2760.

[2] [2a] M. Etienne, B. Donnadieu, R. Mathieu, J. Fernández-Baeza, F. A. Jalón, A. Otero, M. E. Rodrigo-Blanco, *Organometallics* **1996**, *15*, 4597. [2b] A. Antiñolo, F. Carrillo-Hermosilla, J. Fernández-Baeza, M. Lanfranchi, A. Lara-Sánchez, A. Otero, E. Palomares, M. A. Pellinghelli, A. M. Rodríguez, *Organometallics* **1998**, *17*, 3015.

[3] [3a] A. Otero, J. Fernández-Baeza, J. Tejeda, A. Antiñolo, F. Carrillo-Hermosilla, E. Diez-Barra, A. Lara-Sánchez, M. Fernández-López, M. Lanfranchi, M. A. Pellinghelli, *J. Chem. Soc., Dalton Trans.* **1999**, 3537. [3b] T. C. Higgs, C. J. Carrano, *Inorg. Chem.* **1997**, *36*, 291. [3c] T. C. Higgs, C. J. Carrano, *Inorg. Chem.* **1997**, *36*, 298. [3d] T. C. Higgs, K. Spartalian, C. J. O'Connor, B. F. Matzanke, C. J. Carrano, *Inorg. Chem.* **1998**, *37*, 2263. [3e] T. C. Higgs, D. Ji, R. S. Czernuszewicz, B. F. Matzanke, V. Schunemann, A. X. Trautwein, M. Helliwell, W. Ramirez, C. J. Carrano, *Inorg. Chem.* **1998**, *37*, 2383. [3f] B. S. Hammes, C. J. Carrano, *Inorg. Chem.* **1999**, *38*, 3562. [3g] B. S.

 © 2004 Wiley-VCH Verlag GmbH & Co. KGaA, Weinheim

Hammes, C. J. Carrano, *J. Chem. Soc., Dalton Trans.* **2000**, 3304. [3h] P. Ghosh, G. J. Parkin, *Chem. Commun.* **1998**, 413. [3i] C. Kimblin, T. Hascall, E. Parkin, *Inorg. Chem.* **1997**, *36*, 5680. [3j] C. Dowling, G. Perkin, *Polyhedron* **1996**, *15*, 2463. [3k] P. Ge, B. S. Haggerty, A. L. Rheingold, C. G. Riordan, *J. Am. Chem. Soc.* **1994**, *116*, 8406. [3l] R. T. Stibrany, S. Knapp, J. A. Potenza, H. J. Schugar, *Inorg. Chem.* **1999**, *38*, 132. [3m] N. Burzlaff, I. Hegelmann, B. Weibert, *J. Organomet. Chem.* **2001**, *626*, 16. [3n] A. Beck, B. Weibert, N. Burzlaff, *Eur. J. Inorg. Chem.* **2001**, 521. [3o] I. Hegelmann, A. Beck, C. Eichhorn, B. Weibert, N. Burzlaff, *Eur. J. Inorg. Chem.* **2003**, 339.

[4] [4a] J. Fernández-Baeza, F. A. Jalón, A. Otero, M. E. Rodrigo, *J. Chem. Soc., Dalton Trans.* **1995**, 1015. [4b] A. Antiñolo, F. Carrillo-Hermosilla, E. Diez-Barra, J. Fernández-Baeza, M. Fernández-Lopez, A. Lara-Sánchez, A. Moreno, A. Otero, A. M. Rodríguez, J. Tejeda, *J. Chem. Soc., Dalton Trans.* **1998**, 3737.

[5] A. Otero, J. Fernández-Baeza, J. Tejeda, A. Antiñolo, F. Carrillo-Hermosilla, E. Diez-Barra, A. Lara-Sánchez, M. Fernández-López, *J. Chem. Soc., Dalton Trans.* **2000**, 2367.

[6] [6a] A. Otero, J. Fernández-Baeza, A. Antiñolo, F. Carrillo-Hermosilla, J. Tejeda, E. Díez-Barra, A. Lara-Sánchez, L. Sánchez-Barba, I. López-Solera, M. R. Ribeiro, J. M Campos, *Organometallics* **2001**, *20*, 2428. [6b] A. Otero, J. Fernández-Baeza, A. Antiñolo, F. Carrillo-Hermosilla, J. Tejeda, A. Lara-Sánchez, L. Sánchez-Barba, M. Fernández-López, A. M. Rodríguez, I. López-Solera, *Inorg. Chem.* **2002**, *41*, 5193.

[7] K. Nakamoto, *''Infrared and Raman Spectra of Inorganic and Coordination Compounds''*, Wiley-VCH, New York, **1997**.

[8] S. Minhas, A. Devlin, D. T. Richens, A. C. Benyei, P. Lightfoot, *J. Chem. Soc., Dalton Trans.* **1998**, 953.

[9] A. Altomare, G. Cascarano, C. Giacovazzo, A. Guagliardi, M. C. Burla, G. Polidori, M. Camalli, *J. Appl. Cryst.* **1994**, 435.

[10] G. M. Sheldrick, *Program for the Refinement of Crystal Structures from Diffraction data*, University of Göttingen, Göttingen, Germany, **1997**.

Received July 9, 2003
Early View Article
Published Online November 19, 2003

 © 2004 Wiley-VCH Verlag GmbH & Co. KGaA, Weinheim

Syntheses and Crystal Structures of Tetrakis(arylamidine)nickel(II) Chloride and Bis[2,4-dipyridyl-1,3,5-triazapentadienato]nickel(II)

Jianping Guo,[a] Wai-Kwok Wong,*[a] and Wai-Yeung Wong[a]

Keywords: Hydrogen bonds / Nickel / N ligands / Magnetic properties / Macrocyclic ligands

The reaction of $LiN(SiMe_3)_2$ with arylnitrile, followed by the addition of anhydrous $NiCl_2$ gives ionic complexes of the general formula $[Ni\{H_2NC(Ar)=NH\}_4]Cl_2$ (Ar = Ph **1**, *p*-tolyl **2**). When the above reaction is carried out with cyanopyridine instead of arylnitrile under the same reaction conditions, neutral complexes of the general formula [{HN=C(Py)N=C(Py)NH}$_2$Ni] (Py = 4-pyridyl, **3**; 3-pyridyl, **4**] are obtained. Compound **1** undergoes a metathesis reaction with sodium benzoate to give the neutral complex $[(PhCO_2)_2Ni\{H_2NC(Ph)=NH\}_4]$ (**5**). Magnetic susceptibility measurements show that **1**–**4** are diamagnetic and that **5** is paramagnetic with two unpaired electrons. These results suggest that **1**–**4** are d^8 square-planar complexes and **5** is an octahedral complex. The solid state structures of compounds **1**–**5** were determined by X-ray crystallography. Structural analyses reveal that **1** and **2** form a one-dimensional network through charge-assisted hydrogen bonds; whereas **5** forms a one-dimensional network through hydrogen bonds only. In complexes **3** and **4**, the 2,4-dipyridyl-1,3,5-triazapentadienyl ligand behaves as a bidentate ligand forming a six-membered ring with the metal ion.

(© Wiley-VCH Verlag GmbH & Co. KGaA, 69451 Weinheim, Germany, 2004)

Introduction

Lithium amidinates, which can be readily generated in situ through the reaction of lithium amide with α-hydrogen-free nitriles RCN,[1] are very versatile reagents for organic and organometallic syntheses. They are the preferred bases for the formation of ketone enolates,[2] generating low steady-state concentrations of some relatively unstable carbanions,[3] and for the preparation of dithiadiazole heterocycles[4] and π-electron rich phosphorus-nitrogen hetero-donor ligands.[5] Amidinates possess a very diverse and rich coordination chemistry. As anionic ligands, they can behave as mono- and bidentate ligands when coordinated by a single metal atom, and as bridging bidentate ligands when coordinated by two metal atoms. Amidinates form coordination compounds with virtually every metal in the periodic table, ranging across the main group and transition metal series, and into the lanthanides.[6] There is a growing interest in the coordination of amidinate ligands by first-row transition metals, with the goal of creating new catalysts that have industrial use.[7] Usually these compounds were prepared by the reaction of the corresponding lithium amidinates, generated in situ, with metal halides. Metal complexes with bulky,[8] asymmetrical[9] or pendant substituents[10] on amidinato ligands, bridged amidinato ligands[11] or oxalic amidinato ligands[12] have also been synthesized. Recently, the coordination chemistry of related β-diketiminato ligands has also received increasing attention;[13] however, there are very few reports on the isoelectronic 1,3,5-triazapentadienato ligands. Herein we report on the reaction of anhydrous nickel(II) chloride with lithium *N*,*N*′-bis(trimethylsilyl)arylamidinate, $[(Me_3Si)N(Li)C(Ar)-N(SiMe_3)]$ (Ar = phenyl, tolyl, 4-pyridyl, 3-pyridyl), generated in situ from the reaction of $LiN(SiMe_3)_2$ with either benzonitrile, *p*-tolunitrile, 4-cyanopyridine or 3-cyanopyridine. Depending on the nature of the aryl group, the reactions gave either tetrakis(arylamidine)nickel(II) chloride $[Ni\{H_2NC(Ar)=NH\}_4]Cl_2$ (Ar = Ph 1, *p*-tolyl 2) or bis[2,4-dipyridyl-1,3,5-triazapentadienato]nickel(II) [{HN=C(Py)-N=C−(Py)NH}$_2$Ni] (Py = 4-pyridyl, **3**; 3-pyridyl, **4**) complexes (Scheme 1). This is in contrast to the reaction of $NiCl_2{\cdot}0.3C_4H_{10}O_2$ and $[MCl_2(PhCN)_2]$ (M = Pd or Pt) with lithium *N*,*N*′-diphenylbenzamidinate, [PhN(Li)-C(Ph)NPh], which gave the dimeric and monomeric bis(amidinato) complexes, $[Ni_2\{PhNC(Ph)NPh\}_4]$[14a] and $[M\{PhNC(Ph)NPh\}_2]$ (M = Pd, Pt),[14a,14b] respectively, in the solid state.

Results and Discussion

Synthesis and Structural Characterization

Yellow crystals of tetrakis(arylamidine)nickel(II) chloride $[Ni\{H_2NC(Ar)=NH\}_4]Cl_2$ (Ar = Ph, **1**; *p*-tolyl, **2**) were obtained in good yields (67 and 76%, respectively) when $LiN(SiMe_3)_2$ was reacted with one equivalent of benzonitrile or tolunitrile in THF, followed by the addition of half an

[a] Department of Chemistry, Hong Kong Baptist University, Waterloo Road, Kowloon Tong, Hong Kong, P. R. China
Fax: (internat.) + 852-3411-5862
E-mail: wkwong@hkbu.edu.hk

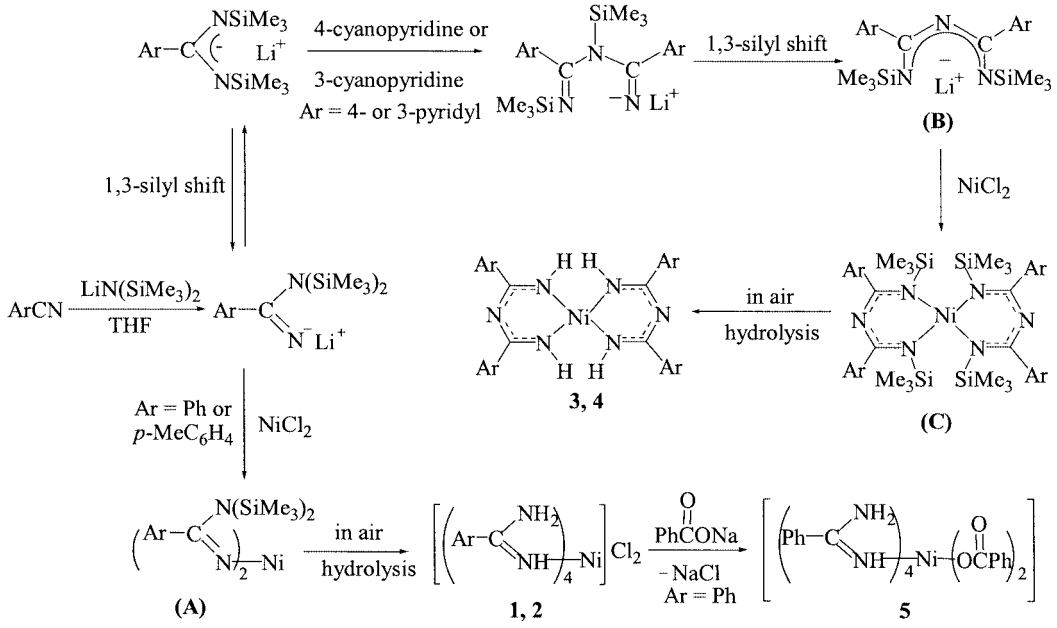

Scheme 1

equivalent of anhydrous nickel chloride and workup in air. However, when two equivalents of 4-cyanopyridine or 3-cyanopyridine were used instead of benzonitrile in the above reaction, yellow crystals of bis[2,4-dipyridyl-1,3,5-triazapentadienato]nickel(II) [{HN=C(Py)N=C(Py)NH}$_2$Ni] (Py = 4-pyridyl, **3**; 3-pyridyl, **4**), with 30 and 28% yields, respectively were obtained. Magnetic susceptibility measurements show that compounds **1**−**4** are all diamagnetic. This suggests that compounds **1**−**4** are d^8 square-planar Ni^{II} complexes. The solid state structures of these four compounds were determined by X-ray crystallography. Perspective drawings of compounds **1**−**4** are shown in Figure 1, 3, 5 and 6, respectively. Selected bond lengths and angles are given in Table 1.2

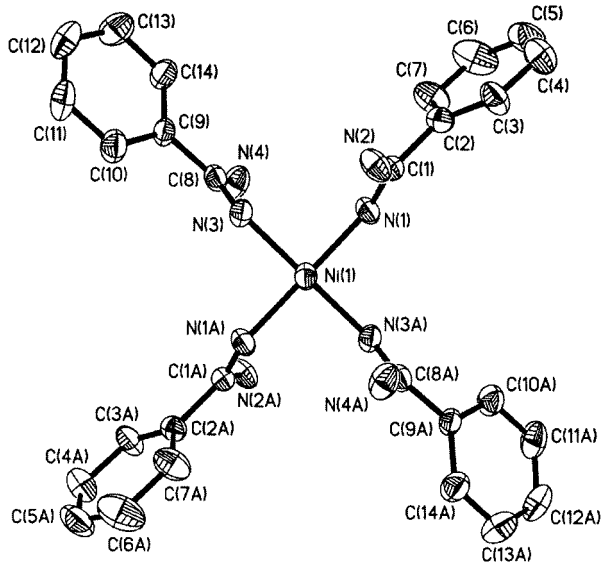

Figure 1. A perspective view of the cation of compound **1**; hydrogen atoms are omitted for clarity

The crystal structure of **1**, shown in Figure 1, reveals that the dication is centrosymmetric and that the nickel center has a square-planar geometry, the N(1)−Ni(1)−N(3) angle is 90.49(18)° and the Ni−N(coordinated) distances are 1.895(4) [Ni(1)−N(1)] and 1.885(4) Å [Ni(1)−N(3)]. The C(1)−N(1) [1.276(6) Å] and C(1)−N(2) [1.337(6) Å] distances of the N−C−N framework indicate that N(1) and N(2) are imino and amino nitrogens, respectively. The C(1)−N(2) distance, which is intermediate between a C−N single (1.47 Å) and double (1.30 Å) bond length, reflects some degree of delocalization within the N−C−N framework. The N(1)C(1)N(2) and N(3)C(8)N(4) planes form dihedral angles of 36.9 and 40.2° with the C(2)- and C(9)-phenyl planes, respectively. The distance between Ni(1B) and Cl(1A) is 3.271 Å, which is longer than the sum of the ionic radii of the Ni^{II} cation and chloride anion. This indicates that the Ni(1B) and Cl(1A) ions are held together by electrostatic attractive forces and that complex **1** is a d^8 square-planar complex. The fact that **1** is diamagnetic further supports this. The distance between Cl(1A) and N(2A) is 3.225 Å and is similar to that of the N···Cl distance of 3.332(5) Å between a NH group and a Cl^- anion involved in H-bonding.[15] The distance between Cl(1A) and the hydrogen atom bonded to N(2A) is 2.416 Å, which is the same as that between Cl(1D) and the hydrogen atom bonded to N(2AB), and is within the range (2.2−2.6 Å) observed for M−Cl···H−N distances.[16] This indicates that there is a hydrogen-bonding interaction between the chloride ion and the amino group of the benzamidine ligand. It is evident that each chloride ion interacts with one cation through electrostatic forces and with another through hydrogen−bonding. Through these interactions, the com-

 © 2004 Wiley-VCH Verlag GmbH & Co. KGaA, Weinheim

Table 1. Selected bond lengths (Å) and bond angles (°) for compounds **1**−**4**

1		**2**		**3**		**4**	
Ni(1)−N(1)	1.895(4)	Ni(1)−N(1)	1.861(4)	Ni(1)−N(1)	1.876(3)	Ni(1)−N(1)	1.847(2)
Ni(1)−N(3)	1.885(4)	Ni(1)−N(3)	1.867(4)	Ni(1)−N(2)	1.856(3)	Ni(1)−N(2)	1.855(2)
C(1)−N(1)	1.276(6)	C(1)−N(1)	1.307(6)	C(1)−N(1)	1.309(4)	C(1)−N(1)	1.307(3)
C(1)−N(2)	1.337(6)	C(1)−N(2)	1.337(6)	C(1)−N(3)	1.348(4)	C(1)−N(3)	1.341(3)
C(8)−N(3)	1.286(6)	C(9)−N(3)	1.297(6)	C(7)−N(3)	1.338(4)	C(7)−N(3)	1.354(3)
C(8)−N(4)	1.328(6)	C(9)−N(4)	1.335(6)	C(7)−N(2)	1.322(5)	C(7)−N(2)	1.307(3)
C(1)−C(2)	1.498(7)	C(1)−C(2)	1.467(7)	C(1)−C(2)	1.505(5)	C(1)−C(2)	1.496(3)
C(8)−C(9)	1.466(7)	C(9)−C(10)	1.472(7)	C(7)−C(8)	1.505(4)	C(7)−C(8)	1.493(3)
N(1)−Ni(1)−N(3)	90.49(18)	N(1)−Ni(1)−N(3)	90.18(17)	N(1)−Ni(1)−N(2)	89.12(13)	N(1)−Ni(1)−N(2)	89.14(9)
C(1)−N(1)−Ni(1)	130.6(4)	C(1)−N(1)−Ni(1)	131.6(4)	Ni(1)−N(1)−C(1)	129.5(2)	Ni(1)−N(1)−C(1)	128.01(17)
C(8)−N(3)−Ni(1)	132.3(4)	C(9)−N(3)−Ni(1)	131.3(4)	Ni(1)−N(2)−C(7)	128.6(2)	Ni(1)−N(2)−C(7)	129.85(18)
N(1)−C(1)−N(2)	121.5(5)	N(1)−C(1)−N(2)	120.1(5)	N(1)−C(1)−N(3)	125.7(3)	N(1)−C(1)−N(3)	126.7(2)
N(1)−C(1)−C(2)	120.7(5)	N(1)−C(1)−C(2)	122.2(5)	C(1)−N(3)−C(7)	120.1(3)	C(1)−N(3)−C(7)	119.96(19)
N(3)−C(8)−N(4)	119.7(5)	N(3)−C(9)−N(4)	119.9(5)	N(3)−C(7)−N(2)	127.0(3)	N(3)−C(7)−N(2)	124.4(2)
N(3)−C(8)−C(9)	122.3(5)	N(3)−C(9)−C(10)	122.1(5)	N(1)−C(1)−C(2)	121.0(3)	N(1)−C(1)−C(2)	119.2(2)
				N(2)−C(7)−C(8)	119.3(3)	N(2)−C(7)−C(8)	121.2(2)

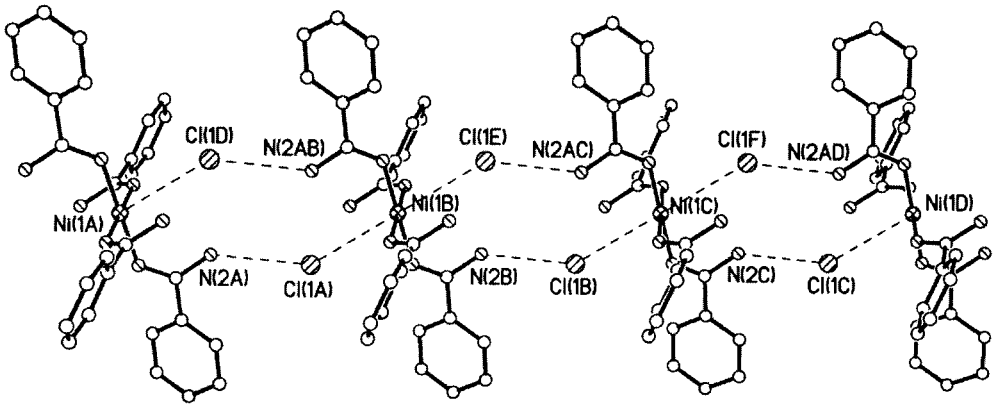

Figure 2. Crystal packing diagram for **1** showing the electrostatic and hydrogen-bonding interactions in a one-dimensional network

plex cations and chloride anions are arranged in a regular manner to form a one-dimensional network structure (Figure 2).

The solid state structure of **2** is very similar to that of **1** (Figure 3). There is centrosymmetry about the Ni center and the dication adopts a square-planar geometry with a N(1)−Ni(1)−N(3) angle of 90.18(17)°. The bond lengths between the nickel center and the coordinated nitrogen atoms are 1.861(4) [Ni(1)−N(1)] and 1.867(4) Å [Ni(1)−N(3)]. The C−N distances for the N(1)−C(1)−N(2) framework are 1.307(6) [C(1)−N(1)] and 1.337(6) Å [C(1)−N(2)], and for the N(3)−C(9)−N(4) framework are 1.297(6) [C(9)−N(3)] and 1.335(6) Å [C(9)−N(4)]. These distances again indicate some degree of delocalization within the N−C−N framework. The N(1)C(1)N(2) and N(3)C(9)N(4) planes form dihedral angles of 38.2 and 34.4° with the C(2)- and C(10)-phenyl planes, respectively. As is the case for **1**, the distance between the nickel center and the chloride atom is 3.287 Å, implying that there is an electrostatic interaction between the two ions. The N···Cl distance between Cl(1A) and N(2AB) is 3.225 Å, and the Cl···H−N distance between Cl(1A) and the hydrogen atom bonded to N(2AB), which is the same as that between

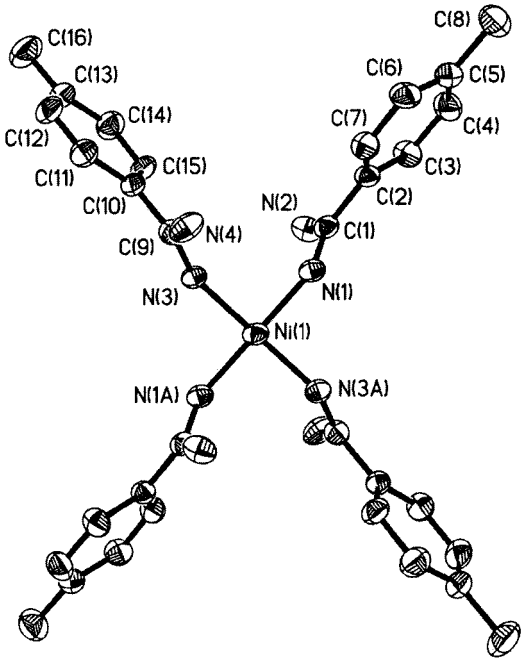

Figure 3. A perspective view of the cation of compound **2**; hydrogen atoms are omitted for clarity

 © 2004 Wiley-VCH Verlag GmbH & Co. KGaA, Weinheim

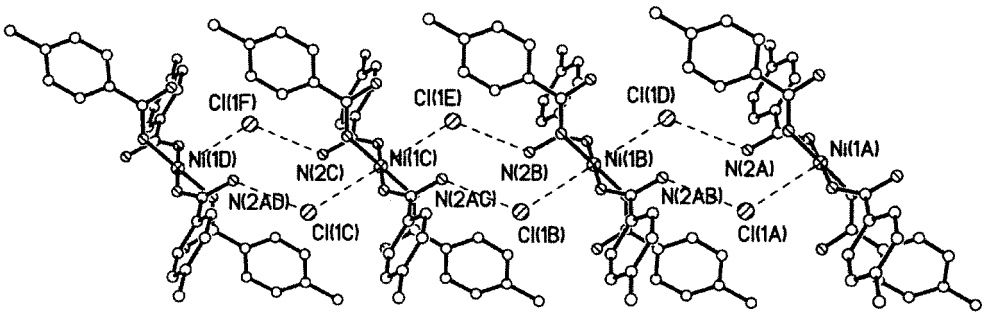

Figure 4. Crystal packing diagram for **2** showing the electrostatic and hydrogen-bonding interactions in a one-dimensional network

Cl(1D) and N(2A), is 2.505 Å. These distances indicate that there is a hydrogen-bonding interaction between the chloride ion and the nitrogen atom of the amino group. Likewise, the complex cations and chloride anions in **2** are arranged in a regular manner through charge-assisted hydrogen bonds to form a one-dimensional network structure (Figure 4).

What is perhaps remarkable in the solid state structures of **1** and **2** is the presence of both electrostatic interactions and hydrogen bonds, which link the cations and anions together to form a loose one-dimensional polymeric structure. Schröder and co-workers have also reported similar weak electrostatic forces and hydrogen-bonding interactions in a palladium complex ligated by a urea-functionalized thioether macrocycle.[15] These types of hydrogen bonds are regarded as medium-strong in strength.[17] Recently, there has been a growing interest in the use of charge-assisted hydrogen bonds for the generation of H-bonded molecular networks.[18]

The solid state structures of **3** and **4** are very similar. Structural analyses reveal that both **3** and **4** are centrosymmetric with the nickel(II) ion adopting a square-planar geometry. In complex **3**, shown in Figure 5, the nickel(II) ion is located at the center of the plane defined by the four nitrogen atoms of the two bidentate 1,3,5-triazapentadienyl ligands, $[HN{=}C(4\text{-}Py){-}N{=}C(4\text{-}Py){-}NH]^-$, with Ni−N distances of 1.876(3) [Ni−N(1)] and 1.856(3) Å [Ni−N(2)], and a N(1)−Ni(1)−N(2) angle of 89.12(13)°. Each bidentate 1,3,5-triazapentadienyl ligand forms a six-membered ring with the metal ion. The six-membered ring is almost planar, with a mean deviation of 0.0035 Å from the plane. Within the 1,3,5-triazapentadienyl ligand, the C(1)−N(1) (1.309(4) Å), C(1)−N(3) (1.348(4) Å), C(7)−N(3) (1.338(4) Å) and C(7)−N(2) (1.322(5) Å) distances are very similar, indicating complete delocalization within the N−C−N−C−N framework. The plane of the six-membered ring forms dihedral angles of 3.0 and 44.7° with the N(4)- and N(5)-pyridyl planes, respectively. Solid state packing effects presumably account for such a large difference in the above-mentioned angles.

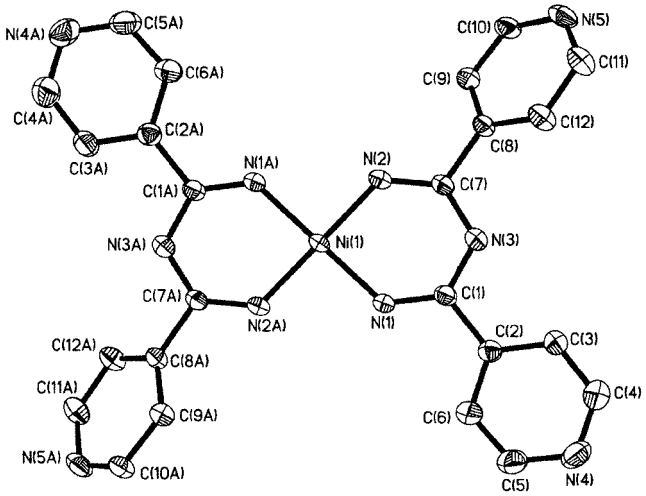

Figure 5. A perspective view of compound **3**. Hydrogen atoms are omitted for clarity

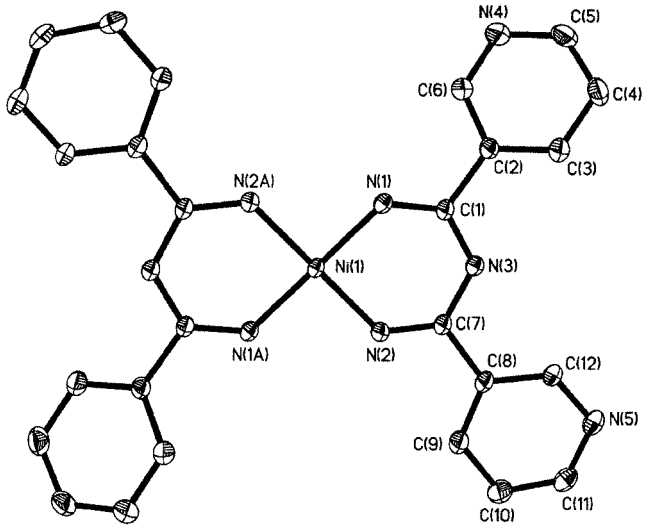

Figure 6. A perspective view of compound **4**; hydrogen atoms are omitted for clarity

Figure 6 shows the nickel(II) ion of **4** positioned at the center of the N(1)N(2)N(1A)N(2A) plane, with Ni−N distances of 1.847(2) [Ni(1)−N(1)] and 1.855(2) Å [Ni(1)−N(2)], and a N(1)−Ni(1)−N(2) angle of 89.14(9)°. Each bidentate 1,3,5-triazapentadienyl ligand forms a six-membered ring with the metal ion. The six-membered ring is almost planar, with a mean deviation of 0.0583 Å from the plane. Within the 1,3,5-triazapentadienyl ligand, the similarity between the C(1)−N(1) [1.307(3) Å], C(1)−N(3) [1.341(3) Å], C(7)−N(3) [1.354(3) Å] and C(7)−N(2)

 © 2004 Wiley-VCH Verlag GmbH & Co. KGaA, Weinheim

[1.307(3) Å] distances shows complete delocalization within the N−C−N−C−N framework. The plane of the six-membered ring forms dihedral angles of 33.8 and 9.9° with the N(4)- and N(5)-pyridyl planes, respectively.

In the literature, Lappert and co-workers reported on the formation of metal β-diketiminate complexes by the nucleophilic addition reaction of PhCN with $LiCHR_2$ or LiCHRR′.[19] The typical character of these complexes is that the ligands $[N(R^1)=C(R^2)-C(R^3)=C(R^4)-N(R^5)]^-$ form six-membered chelate rings with the metal cations. Many similar diimine ligands and complexes are also known.[20] However, there are only a few examples of transition metal complexes with the anionic 1,3,5-triazapentadienyl ligand $[HN=C(R)-N=C(R)-NH]^-$. One complex is formed by the evaporation of a methanol solution of nickel chloride hexahydrate and acetamidine,[21] the second from reacting acetonitrile with a dinuclear nickel complex $[Ni_2(\mu\text{-}OH)_2(tpa)_2](ClO_4)_2$ [tpa = tris(2-pyridylmethyl)amine],[22] and the third from reacting triazine with copper acetate.[23] The synthetic route in this paper provides a new and convenient method for the preparation of complexes with 1,3,5-triazapentadienyl ligands.

A plausible mechanism for the formation of the compounds **1**−**4** is depicted in Scheme 1. The nitrile is first attacked by $LiN(SiMe_3)_2$, giving a lithium ketimide. Reaction with benzonitrile or tolunitrile and $NiCl_2$ gives a nickel ketimide intermediate, **A**, which hydrolyzes during workup in air to give **1** or **2**, respectively. However, if 4-cyanopyridine or 3-cyanopyridine is used instead of benzonitrile or tolunitrile, the resulting lithium ketimide undergoes a rapid 1,3-silyl shift, giving a lithium *N*-silylated amidinate, which then attacks another 4-cyanopyridine. This is followed by a 1,3-silyl shift to produce the 1,3,5-triazapentadienyllithium intermediate, **B**, which then reacts with $NiCl_2$ to give the intermediate **C**, which hydrolyzes during workup in air to give **3** or **4**. We also found that varying the ratio of $LiN(SiMe_3)_2$ to the organic nitrile did not alter the results. For example, when the ratio of $LiN(SiMe_3)_2$ to benzonitrile was changed to 1:2 and that of $LiN(SiMe_3)_2$ to 4-cyanopyridine to 1:1, **1** and **3** were the only isolable products from the respective reactions. No other nickel complexes were isolated. This suggests that the resultant ketimide-amidinate $[(4\text{-}Py)C(NSiMe_3)_2]^-$ from 4-cyanopyridine reacts rapidly with another molecule of 4-cyanopyridine, thus producing the 1,3,5-triazapentadienyl anion $[(SiMe_3)NC(4\text{-}Py)NC(4\text{-}Py)N(SiMe_3)]^-$; whereas the resultant ketimide-amidinate $[PhC(NSiMe_3)_2]^-$ from benzonitrile does not react further with benzonitrile. To further support this, we also examined the hydrolysis reaction of the intermediate formed between $LiN(SiMe_3)_2$ and the organic nitriles. The $[M + 1]^+$ peak corresponding to the phenyl amidine $[PhC(=NH)NH_2]$ and the 2,4-dipyridyl-1,3,5-triazapentadiene $[HN=C(4\text{-}Py)-N=C(4\text{-}Py)-NH_2]$ was observed in the positive ESI mass spectra of the hydrolysis products obtained from the hydrolysis reaction of the intermediate derived from benzonitrile and 4-cyanopyridine, respectively. This is in agreement with the fact that the pyridyl group is a stronger electron-withdrawing substituent than the phenyl group. Therefore, the nitrile carbon atom is activated to a greater degree by the pyridyl group than the corresponding phenyl group, thus rendering it more susceptible to nucleophilic attack.

Compound **1** undergoes a metathesis reaction with sodium benzoate to give bis(benzoato)tetrakis(benzamidine)nickel(II) $[(PhCO_2)_2Ni\{H_2NC(Ph)=NH\}_4]$ (**5**) in a moderate yield (Scheme 1). Unlike **1**, which is diamagnetic, **5** is paramagnetic and has an effective magnetic moment (μ_{eff}) of 2.64 μ_B, which corresponds to two unpaired electrons. This suggests that **5** is a d^8 octahedral Ni^{II} complex. This is confirmed by the solid state X-ray structure of **5**. A perspective drawing of **5** is shown in Figure 7. Selected bond lengths and angles are given in Table 2. **5** has a distorted octahedral geometry, the two benzoato ligands are in a *trans* disposition, with N−Ni−N angles of 91.73(12) [N(1)−Ni(1)−N(3)], 176.10(12) [N(1)−Ni(1)−N(5)] and 89.39(12)° [N(1)−Ni(1)−N(7)], and a O(1)−Ni−O(3) angle of 177.51(10)°. The bond lengths between the nickel center and the coordinated nitrogen atoms are 2.075(3) [Ni(1)−N(1)], 2.073(3) [Ni(1)−N(3)], 2.096(3) [Ni(1)−N(5)] and 2.077(3) Å [Ni(1)−N(7)], and those between the nickel center and the coordinated oxygen atoms are 2.153(3) [Ni(1)−O(1)] and 2.195(3) Å [Ni(1)−O(3)]. Similar to **1** and **2**, the C(1)−N(1) (1.277(5) Å) and C(1)−N(2) (1.338(5) Å) bond lengths of the benzamidine ligand are indicative of a carbon−nitrogen double bond and single bond, respectively. The C(8)−N(3) (1.286(4) Å) and C(8)−N(4) (1.332(4) Å), C(15)−N(5) (1.270(5) Å) and C(15)−N(6) (1.338(5) Å), and C(22)−N(7) (1.284(4) Å) and C(22)−N(8) (1.338(4) Å) bond lengths also indicate that they are double and single bonds, respectively. The N(1)C(1)N(2), N(3)C(8)N(4), N(5)C(15)N(6) and N(7)C(22)N(8) planes form dihedral angles of 27.2, 36.0, 26.7 and 38.1° with the C(2)-, C(9)-, C(16)- and C(23)-phenyl planes, respectively. The benzoato ligands are almost

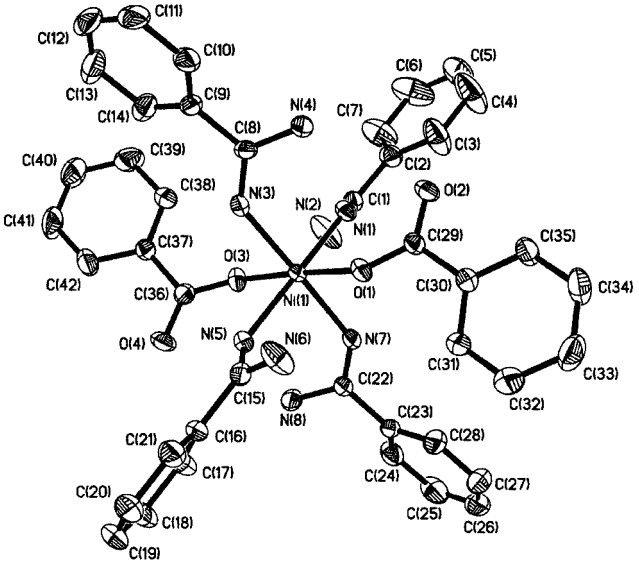

Figure 7. A perspective view of compound **5**; hydrogen atoms are omitted for clarity

 © 2004 Wiley-VCH Verlag GmbH & Co. KGaA, Weinheim

Table 2. Selected bond lengths (Å) and bond angles (°) for compound **5**

Ni(1)−N(1)	2.075(3)	Ni(1)−N(3)	2.073(3)
Ni(1)−N(5)	2.096(3)	Ni(1)−N(7)	2.077(3)
Ni(1)−O(1)	2.153(3)	Ni(1)−O(3)	2.195(3)
C(1)−N(1)	1.277(5)	C(1)−N(2)	1.338(5)
C(1)−C(2)	1.497(5)	C(8)−N(3)	1.286(4)
C(8)−N(4)	1.332(4)	C(8)−C(9)	1.495(5)
C(15)−N(5)	1.270(5)	C(15)−N(6)	1.338(5)
C(15)−C(16)	1.497(5)	C(22)−N(7)	1.284(4)
C(22)−N(8)	1.338(4)	C(22)−C(23)	1.490(5)
C(29)−O(1)	1.260(4)	C(29)−O(2)	1.252(4)
C(29)−C(30)	1.499(5)	C(36)−O(3)	1.268(4)
C(36)−O(4)	1.243(5)	C(36)−C(37)	1.505(5)
N(1)−Ni(1)−N(3)	91.73(12)	N(1)−Ni(1)−N(5)	176.10(12)
N(1)−Ni(1)−N(7)	89.39(12)	N(1)−Ni(1)−O(1)	91.63(11)
N(1)−Ni(1)−O(3)	90.18(11)	N(3)−Ni(1)−N(5)	90.00(11)
N(3)−Ni(1)−N(7)	178.81(13)	N(3)−Ni(1)−O(1)	94.39(11)
N(3)−Ni(1)−O(3)	87.27(11)	N(5)−Ni(1)−N(7)	88.90(12)
N(5)−Ni(1)−O(1)	91.72(11)	N(5)−Ni(1)−O(3)	86.41(11)
N(7)−Ni(1)−O(1)	85.18(11)	N(7)−Ni(1)−O(3)	93.13(11)
O(1)−Ni(1)−O(3)	177.51(10)	C(1)−N(1)−Ni(1)	135.5(3)
C(8)−N(3)−Ni(1)	136.3(3)	C(15)−N(5)−Ni(1)	138.4(3)
C(22)−N(7)−Ni(1)	135.5(3)	C(29)−O(1)−Ni(1)	133.4(3)
C(36)−O(3)−Ni(1)	131.2(3)	N(1)−C(1)−N(2)	120.3(4)
N(1)−C(1)−C(2)	123.7(4)	N(3)−C(8)−N(4)	121.1(3)
N(3)−C(8)−C(9)	122.9(3)	N(5)−C(15)−N(6)	120.0(4)
N(5)−C(15)−C(16)	122.8(4)	N(7)−C(22)−N(8)	121.4(3)
N(7)−C(22)−C(23)	122.8(3)	O(1)−C(29)−O(2)	124.0(4)
O(1)−C(29)−C(30)	117.1(4)	O(3)−C(36)−O(4)	124.8(4)
O(1)−C(36)−C(37)	118.8(3)		

planar. The dihedral angle between the O(1)C(29)O(2) plane and the C(30)-phenyl plane is 7.7°, and that between the O(3)C(36)O(4) plane and the C(37)-phenyl plane is 2.5°. Figure 8 shows one entity selected from its packing diagram. It is evident that the non-coordinating oxygen atoms of the two carbonyl groups of the benzoato ligands of one molecule interact with the non-coordinating nitrogen atoms of the amino group of two neighboring molecules through hydrogen bonds to form a one-dimensional infinite network. The distance between O(2A) and N(8B) is 2.891 Å, and that between O(2A) and the hydrogen atom bonded to N(8B) is 2.156 Å. The distance between O(4B) and N(4A) is 2.886 Å, and that between O(4B) and the hydrogen atom bonded to N(4A) is 2.070 Å.

Spectroscopic Properties of Compounds 1−5

The peaks in the ^{1}H NMR spectra of compounds **1** and **2** are very broad, although they are diamagnetic. This is probably due to the presence of free amidine ligands, which arise as a result of the dissociation of the complexes.[24] We were unable to locate the resonances for the NH protons of the amino and imino groups in the ^{1}H NMR spectra. However, the IR spectra of **1** and **2** exhibit strong multiple absorptions in the region between 3100−3500 cm^{-1} which are assigned to antisymmetric and symmetric NH and NH_2 stretching, and a strong absorption at 1645 cm^{-1} assigned to C=N stretching of the amidine ligands.[25] The medium strong bands around 1460 cm^{-1} can be assigned to the C−N single bond stretching. Both compounds do not show the molecular ion in their mass spectra. The LRMS (positive FAB) spectrum of **1** exhibits a peak at *m*/*z* = 453 corresponding to the $[NiL_3Cl]^+$ [L = PhC(=NH)NH_2] fragment for ^{35}Cl, and that of **2** shows a peak at *m*/*z* = 325 corresponding to the $[NiL^1(L^1-H)]^+$ [L^1 = *p*-$CH_3C_6H_4C$(=NH)NH_2; (L^1 − H) = *p*-$CH_3C_6H_4C(NH)_2^-$] fragment.

The protons at the terminal nitrogen atoms in compounds **3** and **4** are chemically equivalent, thus they have similar chemical shifts in the ^{1}H NMR spectra of **3** and **4** and appear as a singlet at δ = 7.56 for **3** and δ = 7.37 ppm for **4**. The pyridyl groups are each attached to the 1,3,5-triazapentadiento unit via a single bond, therefore, the four pyridyl rings, which are free to rotate in solution, are chemically equivalent and have similar chemical shifts. In the spectrum of **3**, the resonances for the 4-pyridyl protons appear as two doublets at δ = 8.73 (d, *J* = 4.4 Hz, 8 H) and 7.94 (d, *J* = 4.4 Hz, 8 H) ppm; whereas in the spectrum of **4**, the resonances for the 3-pyridyl protons appear as a singlet, two doublets and a doublet of doublets at δ = 9.17 (s, 4 H), 8.69 (d, *J* = 4.4 Hz, 4 H), 8.34 (d, *J* = 8.0 Hz, 4 H) and 7.51 (dd, *J* = 8.0, 4.4 Hz, 4 H) ppm, respectively. In their IR spectra, both compounds exhibit strong multiple absorptions, assigned to NH stretchings, in the region 3100−3500 cm^{-1}. Furthermore, there are other two strong absorption bands in their IR spectra. A strong broad multiple absorption band is seen between 1400−1500 cm^{-1}, and a strong single peak is seen around 1300 cm^{-1}. These can be assigned to the skeleton vibrations of the 1,3,5-triazapentadienyl ligand. The molecular ion peaks $[M + H]^+$ of

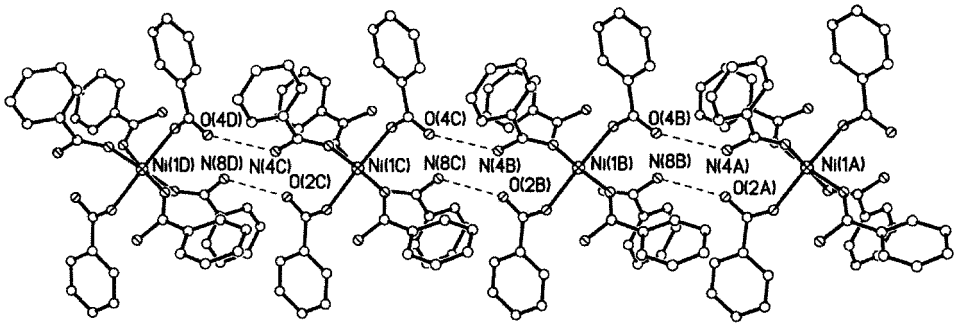

Figure 8. Crystal packing diagram for **5** showing the hydrogen-bonding in a one-dimensional network

 © 2004 Wiley-VCH Verlag GmbH & Co. KGaA, Weinheim

both **3** and **4** are exhibited at m/z = 507 in their LRMS (positive FAB) spectra.

Due to the paramagnetic nature of compound **5**, we were unable to obtain an interpretable ^{1}H NMR spectrum. In the IR spectrum, in addition to the characteristic absorption bands of the benzamidine ligands, **5** also exhibits strong absorptions at 1680 and 1136 cm^{-1}, corresponding to the C=O and C−O stretches of the benzoato ligands, respectively. No molecular ion was observed in the mass spectrum of **5**. The highest mass peak observed in the LRMS (FAB+) of **5** was at m/z = 339, which corresponds to the $[(PhCOO)_2Ni + K]^+$ fragment.

Concluding Remarks

We have developed a convenient synthetic method for some new nickel(II) complexes containing the arylamidinato and 1,3,5-triazapentadienyl ligands. The formation of one-dimensional network structures in the solid state through charge-assisted hydrogen bonds is observed for **1** and **2**; while only hydrogen-bonding interactions are apparent in the crystal lattice of **5**. We have also investigated in detail the factors that control the type of product formed, and we observed that the products obtained depend on the nature of the aryl groups used in the starting arylnitrile.

Experimental Section

General Procedures: All reactions were carried out under nitrogen in flamed Schlenk-type glassware on a dual manifold Schlenk line, unless otherwise stated. Solvents were pre-dried by standard procedures. All chemicals used were of reagent grade, obtained from Aldrich or Fisher Scientific Chemical Company. The IR spectra (KBr pellets) were recorded with a Perkin−Elmer Paragon 1000PC or Nicolet Nagan-IR 550 Series II FTIR spectrometer, and NMR spectra with a Varian INOVA 400 spectrometer. Chemical shifts for the ^{1}H NMR spectra were referenced to internal deuterated solvents and then recalculated to TMS (δ = 0.00 ppm). Fast atom bombardment (FAB) low-resolution mass spectra were obtained with a Finnigan MAT SSQ-710 spectrometer in positive mode and reported as m/z. Magnetic susceptibilities were measured with a MSB-AUTO magnetic susceptibility balance. Elemental analyses were performed by the Shanghai Institute of Organic Chemistry, Chinese Academy of Sciences.

Tetrakis(benzamidine)nickel(II) Chloride (1): Benzonitrile (0.515 mL, 5.0 mmol) and $LiN(SiMe_3)_2$ (0.837 g, 5.0 mmol) were placed in THF (20 mL) at 0 °C. The resultant yellow solution was warmed to room temperature and stirred for an additional 2 h before cooling down to −78 °C. Anhydrous $NiCl_2$ (0.324 g, 2.5 mmol) was then added to the reaction mixture, after which it was stirred at −78 °C for 1 h before warming up to room temperature. The mixture was reacted overnight. The solvent was removed in vacuo and the residue was extracted with CH_2Cl_2 (2 × 10 mL) and the solution was filtered. Removal of the solvent in vacuo gave a dark red oily product. The product was dissolved in THF (20 mL) and the solvent was evaporated slowly to give yellow crystals of **1**. Yield: 0.512 g, 67%; m.p. 174−176 °C. IR (KBr): ṽ = 3335 s, 3179 s, 1645 vs, 1606 m, 1571 s, 1457 m, 1245 w, 1127 w, 781 w and 701 s cm^{-1}. ^{1}H NMR ($CDCl_3$): δ = 7.14 (br. s, 4 H, Ph), 8.02 (br. s, 8 H, Ph) and 8.41 (br. s, 8 H, Ph) ppm; we were unable to locate the resonance due to imino NH and amino NH_2 protons. LRMS (+FAB): m/z = 453 $[(NiL_3Cl)^+$, L = PhC(=NH)NH_2] for ^{35}Cl. $C_{28}H_{32}Cl_2N_8Ni{\cdot}C_4H_8O{\cdot}0.5H_2O$ (691.33): calcd. C 55.60, H 5.98, N 16.21; found C 55.92, H 6.13, N 15.88.

Tetrakis(tolueneamidine)nickel(II) Chloride (2): Compound **2** was produced under the same reaction conditions and using the same procedures as for **1**; however, *p*-tolunitrile (0.586 g, 5.0 mmol) was used instead of benzonitrile. Yield: 0.635 g, 76%; m.p. 181−182 °C. IR (KBr): ṽ = 3326 s, 3188 s, 1645 s, 1612 s, 1565 m, 1519 w, 1460 m, 1262 w, 1133 w, 831 m, 734 m, 684 w cm^{-1}. ^{1}H NMR ($CDCl_3$): δ = 2.67 (br. m, 12 H, Me), 7.73 and 7.83 (br. m, 16 H, C_6H_4) ppm. LRMS (+FAB): m/z = 325 $\{[NiL^1(L^1-H)]^+$; L^1 = [*p*-$CH_3C_6H_4C(=NH)NH_2$], (L^1-H) = [*p*-$CH_3C_6H_4C(NH)_2^-$]. $C_{32}H_{40}Cl_2N_8Ni{\cdot}1.5H_2O{\cdot}0.4C_4H_8O$ (722.19): calcd. C 55.88, H 6.45, N 15.51; found C 55.86, H 6.37, N 15.26.

Bis[2,4-di(4-pyridyl)-1,3,5-triazapentadienato]nickel(II) (3): The procedure was similar to that of **1**. 4-Cyanopyridine (0.520 g, 5.0 mmol), $LiN(SiMe_3)_2$ (0.418 g, 2.5 mmol) and anhydrous $NiCl_2$ (0.162 g, 1.3 mmol) were used. The residue was extracted with methanol (2 × 10 mL) and the solution was filtered. Slow evaporation of the methanol solution gave yellow crystals of **3**. Yield: 0.201 g, 30%; m.p. > 300 °C. IR (KBr): ṽ = 3658 m, 3291 s, 3270 s, 3184 bw, 1601 m, 1577 m, 1533 vs, 1446 vs, 1411 s, 1315 s, 1063 m, 1003 w, 848 m, 759 s, 718 w and 595 w cm^{-1}. ^{1}H NMR ([D$_6$]DMSO): δ = 7.56 (s, 4 H, NH), 7.94 (d, J = 4.4 Hz, 8 H, pyridyl) and 8.73 (d, J = 4.4 Hz, 8 H, pyridyl) ppm. MS (+FAB): m/z = 507 [M + 1]$^+$. $C_{24}H_{20}N_{10}Ni{\cdot}0.25CH_3OH{\cdot}H_2O$ (533.21): calcd. C 54.63, H 4.35, N 26.27; found C 54.59, H 4.24, N 26.29.

Bis[2,4-di(3-pyridyl)-1,3,5-triazapentadienato]nickel(II) (4): Compound **4** was produced under the same reaction conditions and using the same procedures as for **1**. 3-Cyanopyridine (0.312 g, 3.0 mmol), $LiN(SiMe_3)_2$ (0.250 g, 1.5 mmol) and anhydrous $NiCl_2$ (0.973 g, 0.75 mmol) were used. Yield: 0.112 g, 28%; m.p. > 300 °C. IR (KBr): ṽ = 3449 m, 3305 m, 3170 m, 1643 s, 1594 s, 1548 s, 1536 s, 1480 m, 1426 m, 1303 s, 1203 m, 1023 m, 815 m, 726 s, 704 m cm^{-1}. ^{1}H NMR ([D$_6$]DMSO): δ = 7.37 (s, 4 H, NH), 7.51 (dd, J = 8.0, 4.4 Hz, 4 H, pyridyl), 8.34 (d, J = 8.0 Hz, 4 H, pyridyl), 8.69 (d, J = 4.4 Hz, 4 H, pyridyl) and 9.17 (s, 4 H, pyridyl) ppm. LRMS (+FAB): m/z = 507 [M + 1]$^+$. $C_{24}H_{20}N_{10}Ni{\cdot}CH_3OH{\cdot}1.5H_2O$ (566.25): calcd. C 53.03, H 4.81, N 24.74; found C 53.06, H 4.72, N 24.65.

Bis(benzoato)tetrakis(benzamidine)nickel(II) (5): After the preparation of **1** from benzonitrile (0.25 mL, 2.40 mmol), sodium benzoate (0.173 g, 1.20 mmol) was added to the THF mixture, and stirring was continued at room temperature for 48 h. The solvent was then removed in vacuo and dichloromethane (20 mL) was added to the residue and the solution was filtered. The solvent of the filtrate was removed in vacuo, a red oily product was obtained. The product was dissolved in THF (20 mL) and the solvent was evaporated slowly, giving pale yellow crystals of **5**. Yield: 0.261 g, 56%; m.p. > 300 °C. IR (KBr): ṽ = 3184 s, 3061 s, 1680 m, 1645 m, 1605 m, 1563 m, 1518 w, 1484 w, 1391 vs, 1136 vs, 721 w, 696 m cm^{-1}. LRMS (+FAB): m/z = 339 $[(C_6H_5COO)_2Ni + K]^+$. $C_{42}H_{42}N_8NiO_4$ (781.55): calcd. C 64.55, H 5.42, N 14.33; found C 64.38, H 5.50, N 14.25.

X-ray Crystallography: Crystals of **1**·C_4H_8O, **2**·2C_4H_8O, **3**·2CH_3OH, **4**·2CH_3OH and **5** suitable for X-ray diffraction were grown by slow evaporation of a solution of **1**, **2**, **5** in THF and **3**, **4** in CH_3OH, in air. The intensity data were collected with a Bruker

 © 2004 Wiley-VCH Verlag GmbH & Co. KGaA, Weinheim

Table 3. Crystal data and refinements for compounds **1**−**5**

Compound	**1**·C_4H_8O	**2**·2C_4H_8O	**3**·2CH_3OH	**4**·2CH_3OH	**5**
Empirical formula	$C_{32}H_{40}Cl_2N_8NiO$	$C_{40}H_{56}Cl_2N_8NiO_2$	$C_{26}H_{28}N_{10}NiO_2$	$C_{26}H_{28}N_{10}NiO_2$	$C_{42}H_{42}N_8NiO_4$
Molecular mass	682.33	810.54	571.29	571.29	781.55
Crystal system	monoclinic	triclinic	monoclinic	triclinic	triclinic
Space group	$P2_1/c$	$P\bar{1}$	$P2_1/n$	$P\bar{1}$	$P\bar{1}$
a (Å)	8.771(3)	8.404(2)	11.638(6)	7.1659(8)	9.1260(16)
b (Å)	18.813(7)	11.635(3)	6.954(4)	8.6303(10)	14.285(3)
c (Å)	10.560(4)	12.045(3)	16.500(8)	10.6513(12)	15.834(3)
α [°]	90	85.317(5)	90	76.819(2)	94.294(3)
β [°]	94.808(8)	80.593(5)	94.410(10)	87.711(2)	106.730(4)
γ [°]	90	69.049(4)	90	88.352(2)	90.162(3)
V (Å^3)	1736.4(11)	1084.8(5)	1331.3(12)	640.72(13)	1970.6(6)
Z	2	1	2	1	2
F(000)	716	430	580	298	820
$D_{calcd.}$ [g cm^{-3}]	1.305	1.241	1.405	1.481	1.317
μ(Mo-K_α) [mm^{-1}]	0.750	0.612	0.773	0.803	0.545
Reflections collected	8569	5438	6128	3805	10743
Unique reflections	3068	3750	2322	2761	7563
$R_{int.}$	0.1093	0.0466	0.0897	0.0455	0.0391
Observed reflections	1259	1818	1957	2409	4043
GOF on F^2	0.833	0.885	1.062	1.065	0.906
$R1$, $wR2$ [$I > 2\sigma(I)$][a]	0.0558, 0.1211	0.0707, 0.1631	0.0691, 0.1858	0.0484, 0.1369	0.0513, 0.1126
$R1$, $wR2$ (all data)	0.1542, 0.1484	0.1442, 0.1956	0.0771, 0.1972	0.0542, 0.1411	0.1061, 0.1447

[a] $R1 = \Sigma||F_o| - |F_c||/\Sigma|F_o|$. $wR2 = [\Sigma w(|F_o^2| - |F_c^2|)^2/\Sigma w|F_o^2|^2]^{1/2}$.

AXS SMART 1000 CCD area-detector diffractometer with graphite-monochromated Mo-K_α radiation (λ = 0.71073 Å) at 293 K. The collected frames were processed with proprietary software SAINT[26] and an absorption correction was applied (SADABS[27]) to the collected reflections. The structures of these molecules were solved by direct methods and expanded by standard difference Fourier syntheses using the software SHELXTL.[28] Structure refinements were made on F^2 using the full-matrix least-squares technique. All non-hydrogen atoms were refined with anisotropic displacement parameters. Hydrogen atoms were placed in their idealized positions and allowed to ride on the respective carbon atoms. Pertinent crystallographic data and other experimental details are summarized in Table 3. CCDC-200431 (**1**), -215047 (**2**), -200430 (**3**), -215048 (**4**) and -215049 (**5**) contain the supplementary crystallographic data for this paper. These data can be obtained free of charge at www.ccdc.cam.ac.uk/conts/retrieving.html or from the Cambridge Crystallographic Data Centre, 12 Union Road, Cambridge CB2 1EW, UK [Fax: (internat.) +44-1223-336-033; E-mail: deposit@ccdc.cam.ac.uk].

Acknowledgments

We thank the Hong Kong Baptist University and the Hong Kong Research Grants Council (HKBU 2021/99P) for financial support.

[1] [1a] R. T. Boeré, R. T. Oakley, R. W. Reed, *J. Organomet. Chem.* **1987**, *331*, 161−167. [1b] G. R. Giesbrecht, A. Shafir, J. Arnold, *J. Chem. Soc., Dalton Trans.* **1999**, 3601−3604. [1c] A. Lisovskii, M. Botoshansky, M. S. Eisen, *J. Chem. Soc., Dalton Trans.* **2001**, 1692−1698.

[2] G. L. J. van Vliet, H. Luitjes, M. Schakel, G. W. Klumpp, *Angew. Chem.* **2000**, *112*, 1707−1709; *Angew. Chem. Int. Ed.* **2000**, *39*, 1643−1645, and references cited therein.

[3] V. Snieckus, *Chem. Rev.* **1990**, *90*, 879−933, and references cited therein.

[4] [4a] M. Amin, C. W. Rees, *J. Chem. Soc., Chem. Commun.* **1989**, 1137−1138. [4b] A. W. Cordes, R. C. Haddon, R. G. Hicks, R. T. Oakley, T. T. M. Palstra, *Inorg. Chem.* **1992**, *31*, 1802−1808. [4c] A. W. Cordes, R. C. Haddon, *Can. J. Chem.* **1992**, *70*, 919−925. [4d] W. K. Wong, C. Sun, W. Y. Wong, D. W. J. Kwong, W. T. Wong, *Eur. J. Inorg. Chem.* **2000**, 1045−1054.

[5] [5a] K. Bestari, G. Ferguson, J. F. Gallagher, R. T. Oakley, *Inorg. Chem.* **1992**, *31*, 442−447. [5b] T. Chivers, K. McGregor, M. Parvez, *Inorg. Chem.* **1993**, *32*, 5119−5125. [5c] W. K. Wong, J. Jiang, D. W. J. Kwong, W. T. Wong, *Polyhedron* **1995**, *14*, 1109−1111. [5d] W. K. Wong, C. Sun, W. T. Wong, *J. Chem. Soc., Dalton Trans.* **1997**, 3387−3396.

[6] [6a] J. Barker, M. Kilner, *Coord. Chem. Rev.* **1994**, *133*, 219−300. [6b] F. T. Edelmann, *Coord. Chem. Rev.* **1994**, *137*, 403−481.

[7] J. A. R. Schmidt, J. Arnold, *J. Chem. Soc., Dalton Trans.* **2002**, 3454−3463, and references cited therein.

[8] [8a] R. T. Boeré, V. Klassen, G. Wolmershäuser, *J. Chem. Soc., Dalton Trans.* **1998**, 4147−4150. [8b] M. P. Coles, D. C. Swenson, R. F. Jordan, V. G. Young, *Organometallics* **1998**, *17*, 4042−4048. [8c] J. A. R. Schmidt, J. Arnold, *Chem. Commun.* **1999**, 2149−2150.

[9] [9a] C. Averbuj, E. Tish, M. S. Eisen, *J. Am. Chem. Soc.* **1998**, *120*, 8640−8646. [9b] L. A. Koterwas, J. C. Fettinger, L. R. Sita, *Organometallics* **1999**, *18*, 4183−4190. [9c] L. R. Sita, J. R. Babcock, *Organometallics* **1998**, *17*, 5228−5230.

[10] [10a] M. J. R. Brandsma, E. A. C. Brussee, A. Meetsma, B. Hessen, J. H. Teuben, *Eur. J. Inorg. Chem.* **1998**, 1867−1870. [10b] K. Kincaid, C. P. Gerlach, G. R. Giesbrecht, J. R. Hagadorn, G. D. Whitener, A. Shafir, J. Arnold, *Organometallics* **1999**, *18*, 5360−5366.

[11] [11a] J. R. Babcock, C. Incarvito, A. L. Rheingold, J. C. Fettinger, L. R. Siat, *Organometallics* **1999**, *18*, 5729−5732. [11b] J. R. Hagadorn, J. Arnold, *Angew. Chem.* **1998**, *110*, 1813−1815; *Angew. Chem. Int. Ed.* **1998**, *37*, 1729−1731. [11c] G. D. Whitener, J. R. Hagadorn, J. Arnold, *J. Chem. Soc., Dalton Trans.* **1999**, 1249−1256.

[12] C.-T. Chen, L. H. Rees, A. R. Cowley, M. L. H. Green, *J. Chem. Soc., Dalton Trans.* **2001**, 1761−1767.

[13] L. Bourget-Merie, M. F. Lappert, J. R. Severn, *Chem. Rev.* **2002**, *102*, 3031−3066, and references cited therein.

[14] [14a] J. Barker, M. Kilner, R. O. Gould, *J. Chem. Soc., Dalton Trans.* **1987**, 2687−2693. [14b] J. Barker, N. Cameron, M. Kilner,

M. M. Mahoud, S. C. Wallwork, *J. Chem. Soc., Dalton Trans.* **1986**, 1359−1365.

[15] J. B. Love, J. M. Vere, M. W. Glenny, A. J. Blake, M. Schröder, *Chem. Commun.* **2001**, 2678−2679.

[16] A. L. Gillon, G. R. Lewis, A. G. Orpen, S. Rotter, J. Starbuck, X.-M. Wang, Y. Rodriguez-Martin, C. Ruiz-Pérez, *J. Chem. Soc., Dalton Trans.* **2000**, 3897−3905.

[17] J. E. Delbene, *J. Phys. Chem.* **1988**, *92*, 2874−2880.

[18] [18a] B. Schmaltz, A. Jouaiti, M. W. Hosseini, A. D. Cian, *Chem. Commun.* **2001**, 1242−1243. [18b] S. Ferlay, O. Félix, M. W. Hosseine, J.-M. Planeix, N. Kyritsakas, *Chem. Commun.* **2002**, 702−703. [18c] S. Ferlay, R. Holakovsky, M. W. Hosseine, J.-M. Planeix, N. Kyritsakas, *Chem. Commun.* **2003**, 1224−1225, and references cited therein. [18d] A. Angleoni, A. G. Orpen, *Chem. Commun.* **2001**, 343−344.

[19] [19a] P. B. Hitchcock, M. F. Lappert, D.-S. Liu, *J. Chem. Soc., Chem. Commun.* **1994**, 1699−1700. [19b] P. B. Hitchcock, M. F. Lappert, M. Layh, D.-S. Liu, R. Sablong, T. Shun, *J. Chem. Soc., Dalton Trans.* **2000**, 2301−2312. [19c] P. B. Hitchcock, M. F. Lappert, M. Layh, *J. Chem. Soc., Dalton Trans.* **2001**, 2409−2416.

[20] [20a] A. Maraval, D. Arquier, A. Igau, Y. Coppel, B. Donnadieu, J.-P. Majoral, *Organometallics* **2001**, *20*, 1716−1718. [20b] S. Nückel, P. Burger, *Organometallics* **2000**, *19*, 3305−3311. [20c] V. C. Gibson, J. A. Segal, A. J. P. White, D. J. Williams, *J. Am. Chem. Soc.* **2000**, *122*, 7120−7121. [20d] C. E. Radzewich, I. A. Guzei, R. F. Jordan, *J. Am. Chem. Soc.* **1999**, *121*, 8673−8674. [20e] J. Feldman, S. J. McLain, A. Parthasarathy, W. J. Marshall, J. C. Calabrese, S. D. Arthur, *Organometallics* **1997**, *16*, 1514−1516. [20f] B. Qian, W. J. Scanlon, M. R. Smith, *Organometallics* **1999**, *18*, 1693−1698. [20g] P. H. M. Brdzelaar, R. Gelder, A. W. Gal, *Organometallics* **1998**, *17*, 4121−4123. [20h] N. J. Hardman, B. E. Eichler, P. P. Power, *Chem. Commun.* **2000**, 1991−1992. [20i] L. W. M. Lee, W. E. Piers, M. R. J. Elsegood, W. Clegg, M. Parvez, *Organometallics* **1999**, *18*, 2947−2949.

[21] R. Norrestam, *Acta Crystallogr., Sect. C* **1984**, *40*, 955−956.

[22] S. V. Kryatov, A. Y. Nazarenko, M. B. Smith, E. V. Rybak-Akimova, *Chem. Commun.* **2001**, 1174−1175.

[23] T. Kajiwara, A. Kamiyama, T. Ito, *Chem. Commun.* **2002**, 1256−1257.

[24] *Reagents for Transition Metal Complex and Organometallic Syntheses* (Ed.: R. J. Angelici), *Inorganic Syntheses*, vol. 28, John Wiley & Sons, Inc., New York, **1990**.

[25] D. Lin-Vien, N. B. Colthup, W. G. Fateley, J. G. Grasselli, *The Handbook of Infrared and Raman Characteristic Frequencies of Organic Molecules*, Academic Press Inc., San Diego, USA, **1991**, p. 61−62.

[26] *SAINT, Reference manual*, Siemens Energy and Automation, Madison, WI, **1994**−**1996**.

[27] G. M. Sheldrick, *SADABS, Empirical Absorption Correction Program*, University of Göttingen, Germany, **1997**.

[28] G. M. Sheldrick, *SHELXTL*™, Reference manual, version 5.1, Siemens, Madison, WI, **1997**.

Received July 11, 2003
Early View Article
Published Online November 19, 2003

 © 2004 Wiley-VCH Verlag GmbH & Co. KGaA, Weinheim

Synthesis, Characterization and Electrochemistry of the Novel Dawson-Type Tungstophosphate $[H_4PW_{18}O_{62}]^{7-}$ and First Transition Metal Ions Derivatives

Israel-Martyr Mbomekalle,[a] Bineta Keita,[a] Yu Wei Lu,[a] Louis Nadjo,*[a] Roland Contant,[b] Nebebech Belai,[c] and Michael T. Pope[c]

Keywords: Polyoxometalates / Tungsten / Heteropolyanions / Electrochemistry / Electrocatalysis

Following the synthesis of pure $[H_4PW_{18}O_{62}]^{7-}$ (PW_{18}), its derivatives monosubstituted with M (M = Mo^{VI}, V^{IV}, V^{V}, Mn^{II}, Fe^{III}, Co^{II}, Ni^{II} Cu^{II} and Zn^{II}) were obtained. All compounds were characterized by elemental analysis, IR, UV/visible and ^{31}P NMR spectroscopy. Their cyclic voltammetry properties were studied as a function of pH and systematically compared with those of their analogs derived from the symmetrical species, $[P_2W_{18}O_{62}]^{6-}$(P_2W_{18}). Comparison of the two unsubstituted precursors revealed that the merging of the first two waves of the monophosphate occurred in a less acidic medium than for the diphosphate. The observations point to the higher basicity of the reduced forms of PW_{18} compared with those of P_2W_{18}. The fingerprint pattern observed for α_2-$P_2W_{17}M$ derivatives in media of pH = 3 consisted of the splitting of the third W redox system into two one-electron closely spaced waves which is in contrast to the same system in α_1-$P_2W_{17}M$. This peculiarity was also obtained for several of the present α_2-$PW_{17}M$ systems in media of pH = 3 and confirmed that α_2-substituted derivatives were indeed formed. The absence of this peculiar behavior in some other derivatives is consistent with smooth variations of acid-base properties from one derivative to the next. The electrocatalytic properties of all the compounds are illustrated by the reduction of nitrite by reduced PW_{18} and of nitrate by reduced α_2-$PW_{17}Cu$.

(© Wiley-VCH Verlag GmbH & Co. KGaA, 69451 Weinheim, Germany, 2004)

Introduction

Heteropolyanions constitute a unique class of molecular metal-oxygen clusters which are remarkable in several respects: the variety of their properties based on their sizes, shapes, charge densities and reversible redox potentials and the enormous diversity of their structures.[1,2] Therefore, they appear as good candidates for applications in a wide range of areas, including catalysis, electrocatalysis, medicine, materials science, photochemistry, analytical chemistry and magnetochemistry.[3−6] Even though complete rationalization of the build-up of these structures is not available at present, very many of them might be recognized as being derived, at least partly, from lacunary Keggin and Dawson-type fragments. Keeping with the basic structures themselves, a formal direct relationship can be found between the Dawson structure and a tri-vacant Keggin structure. The appropriate Keggin fragment, A-$X^{V}W_9O_{34}$, is derived from the saturated $[XW_{12}O_{40}]^{n-}$ species by the removal of three MO_6 octahedra belonging to three different M_3O_{13} moieties. The Dawson structure is constructed from two half anions A-$X^{V}W_9O_{34}$, (with X = P^{V} or As^{V}).[7,8] Such "dimerization" mostly gives species in which the same heteroatom is present in the two halves. We were interested in the possibility of obtaining such "dimers" with two different central heteroatoms, with the complementary aim of studying the consequences of such asymmetry on the electrochemical and electrocatalytic properties of these heteropolyanions. To the best of our knowledge, the only example with two different heteroatoms in the +v oxidation state is an 18-tungsto monoarsenic monophosphoric acid, which was not fully characterized however.[9] In contrast, even though scarce, several examples of well-characterized heteropolyanions with two different heteroatoms and X atoms in the +III oxidation state have been reported namely $[H_nX^{III}W_{18}O_{60}]^{(9-n)-}$ (X = As or Sb, n = 2; X = Bi, n = 2).[10−12] Their X-ray crystal structures revealed them to be composed of two half-anions, B-XW_9O_{33}, connected by six oxygen atoms. For example, the two halves of $[H_2AsW_{18}O_{60}]^{7-}$ contain a trivalent As atom in one half and two hydrogen atoms in the other.[10] The two compounds $[H_2AsW_{18}O_{60}]^{7-}$ and $[H_2SbW_{18}O_{60}]^{7-}$ were found to differ only by the connectivity of their two halves.[11] In contrast, only recently has the description of $Na_7[H_2BiW_{18}O_{60}]$ confirmed the possibility that the Bi^{III} analog

[a] Laboratoire de Chimie Physique, UMR 8000, CNRS, Electrochimie et Photoélectrochimie, Université Paris-Sud, Bâtiment 420, 91405 Orsay Cedex, France
Fax: (internat.) +33-1-69154328
E-mail: nadjo@lcp.u-psud.fr
[b] Laboratoire de Chimie Inorganique et des Matériaux Moléculaires, UMR 7071, CNRS, Université Paris VI, 4, place Jussieu, 75252 Paris Cedex 05, France
[c] Department of Chemistry, Georgetown University, Box 571227, Washington DC 20057, USA

 © 2004 Wiley-VCH Verlag GmbH & Co. KGaA, Weinheim DOI: 10.1002/ejic.200300455

might contain two hydrogen atoms[12] instead of the three previously invoked in $(Me_4N)_6[H_3BiW_{18}O_{60}]$.[13] Finally, the present status of these asymmetric derivatives is that they are constructed from a B-XW_9O_{33} anion and a B-$H_2W_9O_{33}$ anion. To this family of asymmetric derivatives belongs the series of novel Sn^{II} substituted compounds reported recently by Krebs and co-workers.[14]

In contrast to this general situation, one of the present authors recently reported the synthesis of the novel Dawson-type tungstophosphate $[H_4PW_{18}O_{62}]^{7-}$ and its lacunary and zinc-substituted derivatives, $[H_4PW_{17}O_{62}]^{11-}$ and $[Zn(H_2O)(H_4PW_{18}O_{61})]^{9-}$, in which the two anionic halves are of the A-type with only one of them containing a central heteroatom in the +v oxidation state.[15] This pioneering report stimulated further work and, soon afterwards, our group confirmed the feasibility of this synthesis for the As^V -containing analog of the corresponding trivacant lacunary species and the synthesis of two sandwich-type derivatives, $[Zn_4(H_2O)_2(H_4AsW_{15}O_{56})_2]^{18-}$ and $[Cu_4(H_2O)_2(H_4AsW_{15}O_{56})_2]^{18-}$.[16] Finally, we have established the best experimental conditions for the synthesis of $[H_4AsW_{18}O_{62}]^{7-}$ and demonstrated that these conditions differ substantially from those necessary to obtain the well-known symmetric species $[As_2W_{18}O_{62}]^{6-}$.[17]

All of these exploratory results support the following conclusions: the putative or realized possibility of manipulating the compositions and, presumably, the acid−base and redox properties of heteropolyanions has been illustrated once more; a new family of Dawson-type heteropolyanions has been unambiguously established.

Herein we report the synthesis, characterization and electrochemistry of the hitherto unknown first-row transition metal cation-substituted heteropolyanions derived from $[H_4PW_{18}O_{62}]^{7-}$. Their electrochemistry reveals differences with the corresponding symmetric heteropolyanions. This study is completed by an evaluation of their electrocatalytic properties for the reduction of nitrate and nitrite.

Results and Discussion

All the polyanions in the present study are primarily derived from α-$[H_4PW_{18}O_{62}]^{7-}$ (abbreviated hereafter as PW_{18}) and their formulae will be written as $PW_{17}M$, with omission of oxygen atoms and overall charges when no confusion is likely to arise. M represents the substituent metal cation. The main PW_{18} isomer of interest in the following is that obtained after prolonged heating of the reaction mixture. Scheme 1 illustrates the α-structure proposed for this isomer in analogy with that of α-$[P_2W_{18}O_{62}]^{6-}$ (P_2W_{18}), an assumption based on the close resemblance of the ^{183}W NMRspectra of the two compounds.[15] In line with the numbering of tungsten atoms in α-P_2W_{18}, the IUPAC recommendations have also been followed for α-PW18. A detailed discussion[15] then shows how the results of electrochemistry, ^{31}P NMR and IR spectroscopy were combined, in this preliminary work on PW_{18}, PW_{17} and $PW_{17}Zn$, to demonstrate that the mild alkaline degradation of PW_{18} resulted in the removal of a W atom from the "cap" in the half of this molecule containing the single P atom, thus creating the first vacancy in one of the so-called α_2 positions.

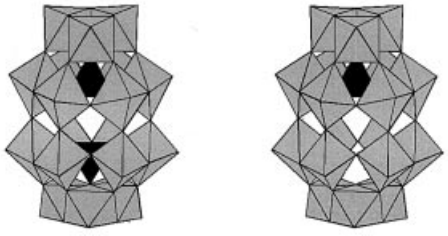

Scheme 1. Schematic representations of the Dawson-type tungstodiphosohate and tungstomonophosphate

Syntheses

A number of slight modifications were introduced into the pioneering synthesis of $K_7[H_4PW_{18}O_{62}]\cdot 18H_2O$.[15] The heating duration was prolonged to at least 96 h because we found that after the formerly proposed 60 h, the reaction mixture still contained α-$K_7[H_4PW_{18}O_{62}]\cdot 18H_2O$ as the major but not the exclusive species. Even so heating at 80 °C was ultimately necessary to obtain pure α-$K_7[H_4PW_{18}O_{62}]\cdot 18H_2O$. It is worth noting that the present procedure was essential to obtain the desired product pure and in good yield (> 65% in all preparations). Also, it must be pointed out that the optimal reagent ratios were the same as those determined previously in our synthesis of α-$K_7[H_4AsW_{18}O_{62}]\cdot 18H_2O$.[17]

The mono-lacunary derivative was obtained under mild conditions and resulted, as indicated previously, in the creation of a vacancy in a α_2-position in the half of the molecule containing the P atom. All the metal cation-substituted species were elaborated under the same conditions as the Zn^{II}-substituted compound, sometimes with slight modifications as described in the Exp. Sect. The mild conditions of the procedure leads to isomerically pure products.

UV/Visible and IR Spectroscopic Characterization

As usual, UV/Vis spectra of these compounds cannot be considered as specific fingerprints for the polyoxoanions in this series. However, the stability of the complexes in the series as a function of pH and time was studied by monitoring the UV/Vis spectra over periods of at least 24 h. The spectra were recorded between 1300 nm and 210 nm, with the maximum absorptions being located between 240 nm and 300 nm, depending on the heteropolyanion in question. The duration of observation is larger than necessary for electrochemical characterization of the complexes but was retained in order to eventually open the way for long-lasting or preparative scale catalytic or electrocatalytic processes. For this study, in addition to the mono-vacant species itself, two groups of substituted derivatives were considered. The substituted compounds are represented by α_2-$ML(PW_{17}O_{61})$, with M representing the substituent metal cation, the ligand L = O^{2-} for M = Mo^{6+}, V^{5+} and V^{4+}, while L = H_2O for all other metal cations in this work.[1,18−20] The difference between these two groups is important in that the behavior of several of these derivatives suggests only the Mo- and V-substituted compounds fea-

 © 2004 Wiley-VCH Verlag GmbH & Co. KGaA, Weinheim

ture really "saturated" substituted species while the others are close to the lacunary precursor complex. Following this classification, PW_{17} was found to be unstable regardless of the pH and to undergo fast transformation. For pH < 4, such a transformation was observed in less than one hour and the lower the pH, the faster the transformation gradually giving the saturated species PW_{18}. This behavior parallels that observed for P_2W_{17}.[1] The so-called saturated substituted compounds show stabilities close to those of unsubstituted ones: all of them were found to be stable between pH 0.3 and pH 4, with decomposition occurring to an extent of less than 20% at pH 5 and comprising between 20% and 70% at pH 6. In contrast to these results, $PW_{17}V$ remains stable up to at least pH 8. The stability domains for the other substituted complexes are shown in Table 1. Dark grey indicates the domain in which a particular derivative is stable; plain grey corresponds to a decomposition less than or equal to 20%; finally, clear grey indicates a decomposition of between 20% and 70%. Obviously, the Mn and Ni derivatives are the less stable species in the series, even though their decomposition does not reach 20% for a pH between 0.3 and 5. In contrast, Fe-, Co- and Zn-substituted complexes are stable from pH 0.3 to 5. Their transformation does not reach 20% at pH 6 and is even in the range of 6% for $PW_{17}Zn$. The case of $PW_{17}Cu$ deserves emphasis since it was observed to be stable between pH 2 and 5.

Table 1. Stability, monitored by UV/visible spectroscopy over 24 h, of α-P_2W_{18}, α-PW_{18} and the α_2-$PW_{17}M$ derivatives of the latter complex, as a function of pH. For further details, see text

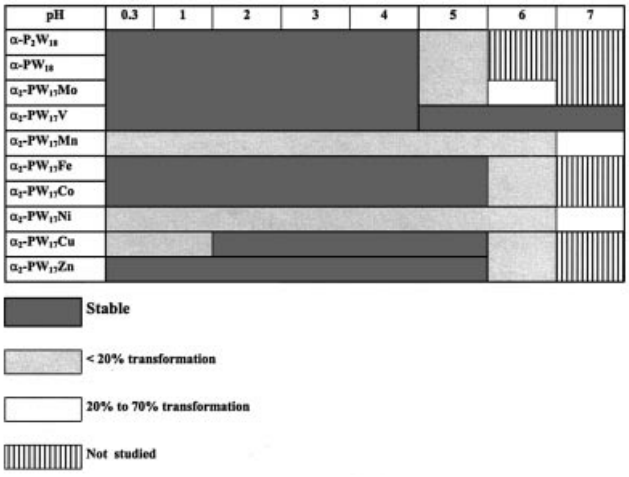

The most characteristic IR band shifts in tungstophosphates are observed between 1200 and 1000 cm^{-1} and correspond to P−O vibrations. They allow a characterization of lacunary species relative to the saturated precursor. When a substituent metal cation is introduced into the vacancy, the whole symmetry of the saturated complex tends to be restored, at least as far as the IR spectra are concerned. Table 2 lists the main IR band energies for the complexes in the present study. The complex PW_{18} is characterized by two bands observed at 1066 and 1032 cm^{-1} respectively. In contrast, they are replaced mainly by a single band located at 1033 cm^{-1} in PW_{17}. Provisionally, this modification supports the location of the vacancy in the α_2 position in the half of the molecule containing the P atom. Examination of Table 2 indicates that two kinds of spectra were obtained through the series of substituted derivatives. Complexes substituted with Mo^{VI}, V^{V}, Fe^{III}, Co^{II}, Ni^{II} and Cu^{II} behave like PW_{18} itself and show two IR bands between 1200 and 1000 cm^{-1}.Complexes containing V^{IV}, Mn^{II} or Zn^{II} have only one IR band in the same energy region. These observations reflect the alteration of symmetry around the central PO_4 moiety.[21−23] This alteration clearly appears to be a function of the substituent cation. It has also been claimed that the nature of the counter-cation seems to influence the degree of restoration of symmetry in the polyanion[24] but a study and discussion of these phenomena are beyond the scope of this work. It should be noted that, in each group, the IR spectra are very similar to one another thus preventing any reliable identification of a given anion by this spectroscopic method.

^{31}P NMR Spectroscopy

Table 3 shows the ^{31}P NMR shifts and line widths for the novel Dawson-type tungsto-monophosphates and their first row transition metal ion derivatives. At least two remarks can be made regarding these results: i) as expected, the spectrum of each of these molecules displays a unique signal ii) the shifts and line widths comply with expectations from the knowledge of shifts observed for the phosphorus atom nearer to the substituent in α_2-$P_2W_{17}M$ derivatives. Further comparison of the actual shifts among the two series and also with the corresponding α_1-$P_2W_{17}M$ derivatives[25] confirms that substitution occurs in the PW_9 moiety of PW_{18} and in the α_2-position. In several instances, larger shifts were observed in the α_2-$PW_{17}M$ compounds than in the α_2-$P_2W_{17}M$ series. Further comments on this trend are, however, beyond the scope of this paper. To the best of our knowledge, Jorris et al.[26] were the first to study the NMR of paramagnetic element-containing HPA's on P_2W_{17} derivatives. Even though their syntheses resulted in mixtures of α_1 and α_2 isomers, their pioneering work constitutes a valuable basis for the interpretation of the present observations. In these complexes, it is convenient to designate the phosphorus atom nearer to the eventually paramagnetic substituent ion as P(1) and the phosphorus atom far from this element as P(2). Observations of the ^{31}P NMR spectra of several Dawson structures substituted in the α_2 position have established that the chemical shift of P(2) is practically unaffected by the nature of the substituent element. As expected, the resonance assigned to the P atom nearest to the substitution site is considerably shifted downfield in the presence of paramagnetic cations and the shift is larger for α_1 derivatives. The ^{31}P NMR line widths depend on the particular nature of the substituent atom and especially on its electronic ground state configuration. As expected[25,26] and shown in Table 3, contrasting situations are encountered for the P(1) line with respect to its line width. The signal might be narrow or relatively narrow, or become ex-

 © 2004 Wiley-VCH Verlag GmbH & Co. KGaA, Weinheim

Table 2. Characteristic IR absorption bands of α-P_2W_{18}, α-PW_{18} and the α_2-$PW_{17}M$ derivatives of the latter complex. For further details, see text

Compound	Main IR absorption bands
α-P_2W_{18} [a]	1092(s); 1020(w); 960(s); 917(s); 780(vs); 600(vw); 568(w); 531(w); 476(vw); 374(ms); 328(m)
α-PW_{18}	1066(vs); 1032(s); 979(w); 949(w); 891(s); 763(w); 587(w); 522(s); 423(w)
$\alpha_2PW_{17}Mo$	1064(s); 1031(m); 978(sh); 948(m); 892(w); 795(w); 771(w); 587(w); 522(w)
$\alpha_2PW_{17}V^{5+}$	1057(s); 1039(sh); 947(m); 888(w); 767(w); 587(w); 521(m)
$\alpha_2PW_{17}V^{4+}$	1048(s); 939(m); 871(w); 768(w); 691(w); 588(w); 517(w)
$\alpha_2PW_{17}Mn$	1043(s); 932(m); 815(w); 767(w); 712(w); 590(w); 511(w); 415(m)
$\alpha_2PW_{17}Fe$	1057(s); 1025(s); 939(m); 875(w); 763(w); 587(w); 516(m); 467(w); 419(m)
$\alpha_2PW_{17}Co$	1047(s); 1025(w); 934(m); 860(w); 811(w); 755(w); 588(w); 512(m); 467(w); 415(w)
$\alpha_2PW_{17}Ni$	1050(s); 1022(s); 934(m); 871(w); 811(w); 767(w); 715(w); 587(w); 515(m); 467(w); 416(m)
$\alpha_2PW_{17}Cu$	1090(sh); 1047(s); 935(m); 871(w); 807(w); 751(w); 700(w); 590(w); 523(w); 467(w); 418(m)
$\alpha_2PW_{17}Zn$	1042(s); 934(m); 868(w); 815(w); 760(w); 711(w); 590(w); 511(m); 464(w); 419(m)

[a] NH_4^+ salt: R.Contant, R. Thouvenot; *Inorg. Chim. Acta* **1993**, *212*, 41−50

Table 3. ^{31}P NMR shifts (relative to 85% H_3PO_4) and line widths of α_2-monometalloheptadecatungstomonophosphate at 298 K

Compound	Δ(ppm)	Δν(Hz)	Medium in D_2O
H_4PW_{18}	−6.54 (−6.7)[a]	7	0.5 M Li_2SO_4
$\alpha_2PW_{17}V^{4+}$	6.77	2454	0.5 M HCl
$\alpha_2PW_{17}V^{5+}$	−5.13	7	0.5 M HCl
$\alpha_2PW_{17}Mn$	990	≈ 46000	0.05 M HCl
$\alpha_2PW_{17}Fe$	920	≈ 40000	0.05 M HCl
$\alpha_2PW_{17}Co$	424.5	368	0.5 M CH_3COOLi +0.5 M LiCl,
$\alpha_2PW_{17}Ni$	423	1864	0.5 M CH_3COOLi +0.5 M LiCl,
$\alpha_2PW_{17}Cu$	−34.87	3068	0.5 M CH_3COOLi +0.5 M LiCl,
$\alpha_2PW_{17}Zn$	−2.93 (−2.95)[a]	8	0.5 M CH_3COOLi +0.5 M LiCl,
$\alpha_2PW_{17}Mo$	−5.95	8	0.05 M HCl

[a] Ref.[15]

ceedingly broadened as exemplified by the case of the Mn^{II} derivative, the ground state of which is orbitally non-degenerate. Finally, it can be considered that a satisfactory agreement with the qualitative results from the observations of Jorris et al.[26] and other literature results[25] has been obtained in the present work. The same line of reasoning can also be applied to the interpretation of the spectra of the Zn^{II} and Cu^{II}-substituted derivatives. From the electronic configuration of Zn^{II}, no dramatic chemical shift is expected for the P atom compared with those observed with other diamagnetic substituents. The results in Table 3 validate this reasoning. In contrast, Cu^{II} is a paramagnetic d^9 ion that has a dramatic effect on the observed chemical shift, as expected.

Electrochemistry

Evidence for the Influence of the Asymmetry on the Voltammetric Behavior of PW_{18}: Comparison with P_2W_{18}

A comparison of the voltammetric characteristics of PW_{18} and P_2W_{18} is probably useful in highlighting the peculiarities of the former complex. Figure 1 shows the cyclic voltammograms (CV's) of the two complexes in a pH 0.3 sulfate medium superimposed on each other. The potential region was selected to avoid any deleterious derivatization of the electrode surface.[27] Furthermore, such an area is the most useful for the elucidation of electrocatalytic processes. Here, the voltammetric pattern is restricted to the first three waves observed for PW_{18} in this medium. Under the same conditions, the voltammetry of P_2W_{18} is known[28] and consists of two one-electron waves followed by two two-electron waves. These waves feature reversible diffusion-controlled processes. The comparison of the CV's of the two heteropolyanions (HPA's) is shown in Figure 1 (A) and is enlightening. The first wave of PW_{18} represents unambiguously a two-electron chemically reversible process. This point was checked by controlled potential coulometry. The two subsequent waves also feature two-electron processes. In short, the pattern for PW_{18} is composed of a set of three reversible diffusion-controlled waves. This observation was expanded by a brief study of the pattern as a function of pH. Figure 1 (B) illustrates this point and shows, in superimposition, the CV's of PW_{18} at pH 0.3 and 4. With the increase in pH, the formerly two-electron wave splits into

 © 2004 Wiley-VCH Verlag GmbH & Co. KGaA, Weinheim

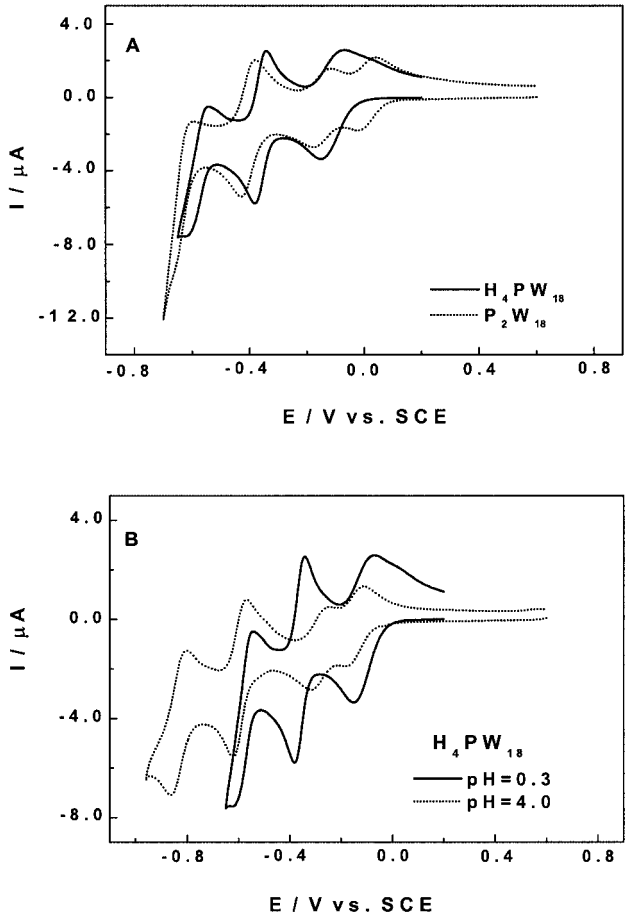

Figure 1. Cyclic voltammograms (CV's) recorded on 5×10^{-4} M solutions of the relevant polyoxometalates; scan rate: 10 $mV \cdot s^{-1}$; working electrode: glassy carbon; reference electrode: SCE; A: Comparison of the CV's observed in a pH 3 medium (0.2 M Na_2SO_4 + H_2SO_4) for the two unsubstituted tungstophosphates: PW_{18} and P_2W_{18}; B: pH Effect on the CV of PW_{18}. For further details, see text

two apparently one-electron processes. No attempt was made to ascertain quantitatively that the splitting was complete at pH 4. Turning more specifically to the comparison of the voltammetric behavior of the two HPA's, all the observations point to the higher basicity of the reduced forms of PW_{18} compared with those of P_2W_{18}. The results are consistent with the deductions which could have been forecast from their structures. Formally, PW_{18} is composed of two A-type half-anions which can be formulated as H_4W_9 and PW_9 respectively. A loose analogy might prompt us to point out the similarity between the hydrogenated fragment of PW_{18} and $[H_2W_{12}O_{40}]^{6-}$ (H_2W_{12}). This analogy should be expressed in terms of the comparable basicity between PW_{18} and P_2W_{18}, with reference to the known basicity influence in the reduction of H_2W_{12} compared with those of the corresponding species of classical Keggin-type HPA's.[28−30] In fact, polarograms (and voltammograms) of H_2W_{12} at pH < 3.5, show three waves of 2, 2 and ca. 10 electrons each,[29,30] under conditions in which the first two reductions of its analogs $[PW_{12}O_{40}]^{3-}$ and $[SiW_{12}O_{40}]^{4-}$ and even the Dawson-type P_2W_{18}, are one electron pH-independent processes. Therefore, the pH-dependent voltammetric behavior observed for PW_{18} in comparison with that of P_2W_{18} can be compared with that of H_2W_{12} vis à vis $[PW_{12}O_{40}]^{3-}$ and $[SiW_{12}O_{40}]^{4-}$. It must be concluded that PW_{18} and its first several reduced species show greater basicity compared with the corresponding P_2W_{18} species. Provisionally it is worth mentioning, in contrast, that a roughly 6 M HCl solution was necessary to make the first two waves of P_2W_{18} merge[28] and the concentration of acid reaches 7−8 M HCl in the case of $[SiW_{12}O_{40}]^{4-}$. Such merging could not be achieved for $[PW_{12}O_{40}]^{3-}$ in solution[28] and was only achieved inside polymer matrices.[31] This observation is rewarding and represents a good step in our continuous search for ways to accumulate electrons on the first or the first several waves of HPA's under mild conditions. To the best of our knowledge, this series of compounds represents the first examples in which a two-electron W-wave in a saturated species is found to appear at a relatively less negative potential and milder acidity than generally obtained in classical Dawson HPAs. This constitutes one of the favorable conditions for eventual electrocatalytic processes.

Electrochemistry of Substituted Derivatives

The lacunary precursor species PW_{17} is unstable whatever the pH of the medium which precludes a comparison of its electrochemical behavior with that of its substituted derivatives and with that of P_2W_{17}. In the study of a related series of derivatives, experimental evidence had enabled separation of the compounds into two main groups, in agreement with the discussion set down earlier in this paper.[1,18−20] Such a separation and its formerly studied electrochemical consequences should also be valid here. Following this line, the first group is composed of those derivatives that can be considered as truly saturated and include the Mo and V^V (or V^{IV})-substituted compounds; their voltammetric behavior is expected to parallel that of PW_{18} itself, in addition to the redox activity of the substituents. The second group consists of all the other derivatives and they should behave more or less like the electrochemically unknown lacunary precursor PW_{17}. Actually, we suggest that the overall electrochemical trends should be similar to those observed previously in a systematic study of α_2-$P_2W_{17}M$ derivatives[32] and should guide us toward a direct comparison of the corresponding results. The pH = 3 experiments were selected for this comparison. Figure 2 (A through C) shows representative examples of superimposed CV's. For this comparison, it is worth recalling the presence of a distinctive fingerprint for α_2-$P_2W_{17}M$ compared with α_1-$P_2W_{17}M$ at pH = 3: this peculiarity appeared in the third W-waves where a single two-electron reversible wave for the α_1 complex was replaced by two, closely spaced, presumably one-electron waves for the α_2 isomer.[32] The case of the Fe-substituted derivatives is represented in Figure 2 (A). The substituent cation is reduced within the complex more positively than the W-centers. The gross feature is that the fingerprint is present with the two one-electron waves which are more closely spaced in α_2-$PW_{17}Fe$ than in α_2-$P_2W_{17}Fe$. The presence of the fingerprint was also observed

 © 2004 Wiley-VCH Verlag GmbH & Co. KGaA, Weinheim

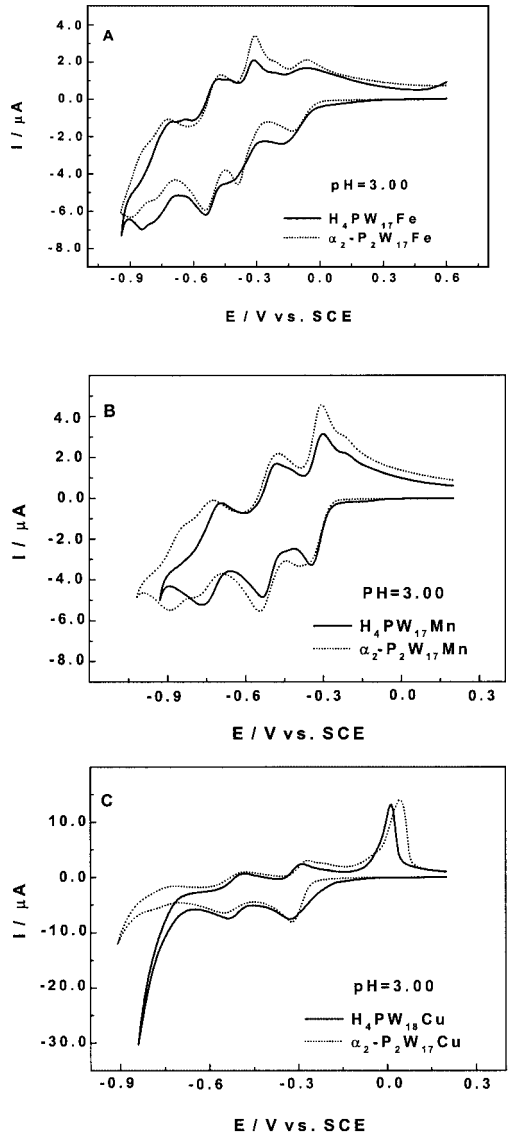

Figure 2. Comparison of the CV's observed in a pH 3 medium (0.2 M Na_2SO_4 + H_2SO_4) for representative examples of 5×10^{-4} M substituted tungstophosphates: α_2-$PW_{17}M$ and α_2-$P_2W_{17}M$; scan rate: 10 $mV.s^{-1}$; working electrode: glassy carbon; reference electrode: SCE. A: α_2-$PW_{17}Fe$ and α_2-$P_2W_{17}Fe$; B: α_2-$PW_{17}Mn$ and α_2-$P_2W_{17}Mn$; C: α_2-$PW_{17}Cu$ and α_2-$P_2W_{17}Cu$

with the V^{IV}- and Co-substituted complexes, with an almost complete merging of the waves in the latter case. In the potential region explored in Figure 2 (B), the Mn wave is not shown. The first two W-waves were observed roughly at the same potentials as the corresponding waves in α_2-$P_2W_{17}Mn$. However, the third redox system of α_2-$PW_{17}Mn$ features a single, slightly broad wave. In short, the presence of this substituent drives the third redox system in the positive potential direction and makes the fingerprint disappear. It must be pointed out that α_2-$PW_{17}Mn$ could be considered as fairly stable in the timescale of CV and the same phenomenon was seen for α_2-$PW_{17}Ni$ and α_2-$PW_{17}Zn$. Finally, the deposition of copper in Figure 2 (C) and the initiation of a probably catalytic hydrogen evolution reaction after the second W-wave precludes the observation of any possible fingerprint. In short, whatever the case, the third redox system is located at a more positive potential for α_2-$PW_{17}M$ than for α_2-$P_2W_{17}M$. Furthermore, when the fingerprint is present, the corresponding waves are more closely spaced in the former complex than in the latter. Thus, the formation of a single third W-wave is obtained through a positive move and a merging of the fingerprint waves. Such a smooth variation has not been previously observed.[32] On increasing the pH from 3 to 5, the fingerprint in the CV of α_2-$PW_{17}Fe$ becomes hardly visible. A consideration of these observations suggests that the difference in basicity between the α_2-$PW_{17}M$ and α_2-$P_2W_{17}M$ reduced forms is the basis for the splitting or otherwise of the third W-redox systems in the CV's. Such a difference in basicity is expected as a parallel to that observed between α-PW_{18} and α-P_2W_{18}. However, its intensity seems to depend critically on the substituent cations. Another outcome of this comparison is the confirmation that α_2-substituted derivatives were indeed formed.

The main other voltammetric characteristics of α_2-$PW_{17}M$ are gathered for pH 3 and pH 5 values in Table 4 for the potential locations of the first two W-waves and in Table 5 for those of the electroactive substituent cations. The values in Table 5 speak for themselves and do not call for particular comments. Even though subtle differences exist from one substituent cation to the next, a rough conclusion can be drawn from Table 4. The nature of the cation seems to induce a uniform influence on the potential locations of the two W-waves, except for the remarkable examples of Mo and Cu. The small differences are more pronounced at pH 3 than at pH 5 and more on the first wave than on the second. A combined Cu and W-wave is observed for α_2-$PW_{17}Cu$. No net separation of these two processes was obtained on going from pH 3 to 5. Controlled potential coulometry just past the peak location of this composite wave consumes four electrons per molecule for complete reduction at pH 3. Electrolysis conducted at half wave potential indicates, by spectroelectrochemistry or even by simple inspection of the solution color, that the two-electron reduction of the Cu^{2+} centre is completed before that of the W^{6+}-centres begins.

Electrocatalytic Reductions of Nitrite and Nitrate

Complexes were selected on the basis of their stability as a function of pH. Their behavior towards the electrocatalytic reductions of nitrite and nitrate in cyclic voltammetry was examined. In the potential regions explored, no direct reduction of nitrite or nitrate on the glassy carbon electrode surface could be observed.[33,34] The catalytic current intensity enhancement on the first wave or the first several waves of each HPA is preferable, with the aim of saving energy and to avoid derivatization of the electrode surface.[27] Conclusions from our previous work[16,34] are confirmed here which indicate only Cu and Ni-substituted species catalyze the reduction of nitrate, while most derivatives catalyze the reduction of nitrite. Therefore, two representative examples were selected. Figure 3 (A) illustrates the voltammetric behavior of PW_{18} towards the reduction of nitrite. For this

 © 2004 Wiley-VCH Verlag GmbH & Co. KGaA, Weinheim

Table 4. Potential locations in pH = 3.00 and pH = 5.00 media of the first two W-waves of α-H_4PW_{18} and α_2-$H_4PW_{17}M$. Cyclic voltammetry: scan rate: 10mV·s^{-1}; working electrode: glassy carbon; reference electrode: SCE; E_{pc} = cathodic peak potential, $E^\circ = (E_{pc} + E_{pa})/2$. pH = 3.00 (0.2 M Na_2SO_4 + H_2SO_4); pH = 5.00 (0.4 M CH_3COONa + CH_3COOH)

HPA	pH = 3.00				pH = 5.00			
	$-E^1_{pc}$	$-E^\circ_1$/V	$-E^2_{pc}$	$-E^\circ_2$/V	$-E^1_{pc}$	$-E^\circ_1$/V	$-E^2_{pc}$	$-E^\circ_2$/V
H_4PW_{18}	0.174	0.144	0.294	0.266	–	–	–	–
$H_4PW_{17}Mo$	0.316	0.264	0.492 0.544	0.458 0.584	–	–	–	–
$H_4PW_{17}V^{4+}$	0.418	0.390	0.588 broad	0.563	0.546	0.509	0.720	0.695
$H_4PW_{17}V^{5+}$	0.430	0.400	0.594	0.574	0.558	0.522	0.722	0.700
$H_4PW_{17}Mn$	0.346	0.324	0.536	0.507	0.568	0.513	0.656	0.628
$H_4PW_{17}Fe$	0.438	0.375	0.546	0.515	0.566	0.537	0.660	0.631
$H_4PW_{17}Co$	0.400	0.357	0.548	0.517	0.559	0.526	0.650	0.627
$H_4PW_{17}Ni$	0.420	0.357	0.552	0.521	0.548	0.517	0.664	0.639
$H_4PW_{17}Cu$	0.330 (merged with Cu wave)	0.309 (with Cu oxidation at −0.014)	0.536	0.512	0.468 (merged with Cu wave)	0.442	0.656	0.629
$H_4PW_{17}Zn$	0.396	0.365	0.540	0.515	0.554	0.527	0.664	0.641

Table 5. Potential locations in pH = 3.00 and pH = 5.00 media of the cations which may be reduced or oxidized within α_2-$H_4PW_{17}M$

Reducible cations	pH = 3.00		pH = 5.00	
	$-E_p$/V	$-E^\circ$/V	$-E_p$/V	$-E^\circ$/V
Fe^{3+}	0.188	0.123	0.250	0.166
Cu^{2+}	merged with the first W-wave	desorptive wave at +0.014	merged with the first W-wave	desorptive wave at 0.00 (single)
V^{4+}	−0.252	−0.296	−0.218	−0.276
Mo^{6+}	−0.060	−0.094	−0.060	−0.094
Oxidizable cations	E_{pa}/V	E_{pc}/V	E_{pa}/V	E_{pc}/V
V^{4+}	broad 0.394 to 0.418	0.238	0.314	broad cathodic 0.230 to 0.252
Mn^{2+}	1.106	one reduction clearly visible at 0.818	0.974	two reduction peaks observed at +0.604 and −0.082 on potential reversal
Co^{2+}	–	–	1.406	–

experiment, a medium of pH 1 was selected to obtain a complete merging of the first two waves of PW_{18}. Addition of NO_2^- [35] induced a large current intensity enhancement. No anodic trace was observed on potential reversal, even for small values of the excess parameter γ ($\gamma = C_{NO2}^-/C_{HPA}$). Increasing the concentration of nitrite still enhanced the cathodic current. It must be concluded that an efficient catalysis of the reduction of nitrite[35] can be achieved during the reduction of PW_{18}. It is worth pointing out that the catalytic process is carried out on a two-electron first wave obtained under mild conditions in the tungsten series. Provisionally, similar observations were made with the first wave of P_2W_{18}, except that this wave features a one-electron process in the medium of pH 1.

While electrocatalysis by PW_{18} is triggered by reduced W centers within the HPA, a multi-step process must be considered in the case of $PW_{17}Cu$. The phenomena will be described in terms of the example of electrocatalytic reduction of nitrate which is not common among substituted HPA's.[16,34] For example, electrocatalytic reduction of nitrate was not expected and was not observed with PW_{18}. In contrast, Figure 3 (B) shows the electrocatalytic reduction of nitrate by $PW_{17}Cu$ at pH 3. The composite nature of the first wave of $PW_{17}Cu$, described above, combines the reduction of Cu^{2+} within the complex and the first reduction of the W centers. Upon addition of increasing amounts of nitrate, a high intensity catalytic wave was observed starting just negative of the peak potential of the combined first wave. For a selected potential in the catalytic wave domain, increasing the concentration of nitrate still enhanced the cathodic wave. In the present case, electrocatalysis of nitrate was triggered by the electrodeposited copper as well as the reduced W centers. The electrocatalysis remains efficient at pH 5. Whatever the pH, the electrocatalysis of nitrate was observed at more negative potentials than for nitrite. Furthermore, in order to observe catalytic activity, larger values of the excess parameter were necessary for the former substrate than for the latter.

Conclusions

First-row transition metal cations were introduced as mono-substituents in the framework of the novel Dawson-

 © 2004 Wiley-VCH Verlag GmbH & Co. KGaA, Weinheim

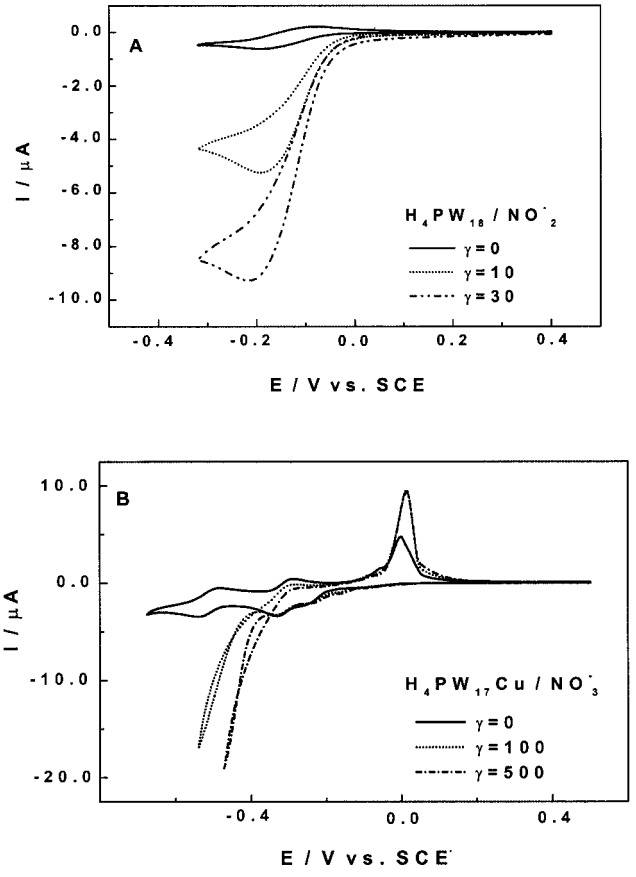

Figure 3. Cyclic voltammograms showing the catalytic activity of PW_{18} towards nitrite and α_2-$PW_{17}Cu$ towards nitrate respectively. Scan rate: 2 $mV \cdot s^{-1}$; working electrode: glassy carbon; reference electrode: SCE; A: Cyclic voltammograms at pH 1 (0.2 M Na_2SO_4 + H_2SO_4) of 2×10^{-4} M PW_{18} in the presence of increasing amounts of nitrite; the excess parameter $\gamma = C_{NO2}^{-}/C_{HPA}$ is indicated in the figure; B: Cyclic voltammograms at pH 3 (0.2 M Na_2SO_4 + H_2SO_4) of 5×10^{-4} M α_2-$PW_{17}Cu$ in the presence of increasing amounts of nitrate; the excess parameter $\gamma = C_{NO3}^{-}/C_{HPA}$ is indicated in the figure

type tungstomonophosphate PW_{18}. During this work, more prolonged heating times than used previously proved helpful in obtaining pure PW_{18} as a starting material. Comparison of the CV properties of PW_{18} and P_2W_{18} as a function of pH shows that the first two W-waves merge in less acidic solution in the former than in the latter complex. This observation leads to the conclusion that the first reduced forms of PW_{18} are more basic than the corresponding forms of P_2W_{18}. The result is interesting in at least two respects: the merging of the W-waves was obtained here through the manipulation of the acid base properties of the molecule by assembling two different building blocks; the association of such "putative" building blocks might constitute an important step in designing polyoxometalates with pre-selected properties. Another aspect of the observed basicity of PW_{18} deserves emphasis i.e. the facile formation of a two-electron first W-wave in mildly acidic media is uncommon in the classical saturated Dawson HPAs and might constitute a favorable first step in electrocatalytic processes that require several electrons in order to be effective. Concerning monosubstituted derivatives, several lines of experimental evidence converge to indicate that the substitution occurs in the α_2 position. Among them, the splitting of the third W redox system in pH 3 media was observed in several substituted derivatives. It deserves particular attention because it confirms that α_2-substituted derivatives were formed. Indeed the extent of splitting also varies smoothly from one derivative to the next, thus suggesting a simple explanation based on small basicity variations for this phenomenon.

Experimental Section

Preparations: All chemicals were of reagent grade and were used as received. The yields of finally isolated pure products ranged constantly from 60 to 95% in all the preparations.

$K_7[H_4PW_{18}O_{62}]\cdot 18H_2O$: The literature method was followed[15] with slight modifications. A sample of $Na_2WO_4\cdot 2H_2O$ (240 g, 0.73 mol) was dissolved in Millipore water (300 mL). The solution was acidified under vigorous stirring by 4 M HCl (160 mL). A mixture of 1 M H_3PO_4 (38 mL) and 4 M HCl (100 mL) was then added. The pH was adjusted to a value slightly less than 2, and the solution was heated to reflux for at least 96 h. After cooling, the solution was treated with solid KCl (100 g). The precipitate was redissolved in H_2O (150 mL) and heated at 80 °C for at least 48 h. After cooling, the clear solution was treated with solid KCl (30 g) to give a fine yellow crystalline powder. $K_7[H_4PW_{18}O_{62}]\cdot 18H_2O$ (4934.2): calcd. K 5.55, P 0.63, W 67.07; found K 5.96, P 0.63, W 66.62.

$K_{11}[H_4PW_{17}O_{61}]\cdot 18H_2O$: A sample of $K_7[H_4PW_{18}O_{62}]\cdot 18H_2O$ (8 g, 1.62 mmol) was dissolved in Millipore water (20 mL) with stirring. To the clear solution, was added a 1 M $KHCO_3$ solution (17 mL) and a white precipitate formed. Stirring was continued for roughly one more hour. The solid was then left to settle and was filtered, washed twice with ethyl alcohol, twice with diethyl ether and was air-dried by suction through a flask with a water pump. $K_{11}[H_4PW_{17}O_{61}]\cdot 18H_2O$ (4890.6): calcd. K 8.76, P 0.63, W 63.67; found K 9.66, P 0.63, W 62.80.

$K_9[H_4Zn(H_2O)PW_{17}O_{61}]\cdot 19H_2O$ (abbreviated as $PW_{17}Zn$): A sample of $Zn(NO_3)_2\cdot 6H_2O$ (0.30 g, ≈ 1 mmol) was dissolved in Millipore water (45 mL) and $K_{11}[H_4PW_{17}O_{61}]\cdot 18H_2O$ (4 g, 0.82 mmol) was added. The mixture was filtered while hot and the clear filtrate left in a beaker. A white crystalline material appeared during cooling. This material was filtered and left to dry in the open air. $K_9[H_4Zn(H_2O)PW_{17}O_{61}]\cdot 19H_2O$ (4913.8): calcd. K 7.16, P 0.63, W 63.61, Zn 1.33; found K 8.88, P 0.62, W 63.54, Zn (1.52). ^{183}W NMR: δ = −98 (2 W), −135 (2 W), −147 (2 W), −176 (2 W), −195 (2 W), −200 (2 W), −205 (2 W), −208 (2 W), −222 (1 W) ppm.

$K_9[H_4Cu(H_2O)PW_{17}O_{61}]\cdot 17H_2O$ (abbreviated as $PW_{17}Cu$): A sample of $Cu(NO_3)_2\cdot 3H_2O$ (0.25 g, ≈ 1 mmol) was dissolved in Millipore water (45 mL) and $K_{11}[H_4PW_{17}O_{61}]\cdot 18H_2O$ (4 g, 0.82 mmol) was added in small portions while heating the mixture on a water bath (≈ 60 °C). After half an hour, the mixture was filtered hot and the green clear filtrate left in a beaker. A pale green crystalline material appeared during cooling. This material was filtered and left to dry in the open air. $K_9[H_4Cu(H_2O)PW_{17}O_{61}]\cdot 17H_2O$ (4875.9): calcd. K 7.22, P 0.64, W 64.10, Cu 1.30; found K 7.11, P 0.62, W 63.42, Cu 1.44.

 © 2004 Wiley-VCH Verlag GmbH & Co. KGaA, Weinheim

$K_9[H_4Ni(H_2O)PW_{17}O_{61}]\cdot 20H_2O$ (abbreviated as $PW_{17}Ni$): A sample of $Ni(NO_3)_2\cdot 6H_2O$ (0.30 g, ≈ 1 mmol) was dissolved in Millipore water (45 mL) and $K_{11}[H_4PW_{17}O_{61}]\cdot 18H_2O$ (4 g, 0.82 mmol) was added in small portions while heating the mixture on a water bath (≈ 60 °C). After half an hour, the mixture was filtered hot and the green clear filtrate left in a beaker. A pale green yellow crystalline material appeared during cooling. This material was filtered and left to dry in the open air. $K_9[H_4Ni(H_2O)PW_{17}O_{61}]\cdot 20H_2O$ (4925): calcd. K 7.15, P 0.63, W 63.46, Ni 1.19; found K 7.40, P 0.63, W 64.11, Ni 1.29. W NMR: δ = +468 (2 W), +386 (2 W), −140 (2 W), −164 (2 W), −167 (2 W), −187 (2 W), −245 (1 W) ppm.

$K_9[H_4Co(H_2O)PW_{17}O_{61}]\cdot 20H_2O$ (abbreviated as $PW_{17}Co$): A sample of $Co(NO_3)_2\cdot 6H_2O$ (0.30 g, ≈ 1 mmol) was dissolved in Millipore water (45 mL) and $K_{11}[H_4PW_{17}O_{61}]\cdot 18H_2O$ (4 g, 0.82 mmol) was added in small portions while heating the mixture on a water bath (≈ 60 °C). After half an hour, the mixture was filtered hot and the clear dark red filtrate left in a beaker. A "terre claire'' crystalline material appeared during cooling. This material was filtered and left to dry in the open air. $K_9[H_4Co(H_2O)PW_{17}O_{61}]\cdot 20H_2O$ (4925.3): calcd. K 7.14, P 0.63, W 63.46, Co 1.20; found K 7.39, P 0.65, W 63.94, Co 1.34.

$K_8[H_4Fe(H_2O)PW_{17}O_{61}]\cdot 19H_2O$ (abbreviated as $PW_{17}Fe$): A sample of $Fe(NO_3)_3\cdot 9H_2O$ (0.40 g, ≈ 1 mmol) was dissolved in Millipore water (45 mL) and $K_{11}[H_4PW_{17}O_{61}]\cdot 18H_2O$ (4 gm, 0.82 mmol) was added in small portions while heating the mixture on a water bath (≈ 60 °C). After half an hour, the mixture was filtered hot and the yellow clear filtrate transferred to a beaker. Upon treatment of this filtrate with KCl (10 g), a pale yellow crystalline material appeared. This material was filtered and left to dry in the open air. $K_8[H_4Fe(H_2O)PW_{17}O_{61}]\cdot 19H_2O$ (4865): calcd. K 6.43, P 0.64, W 64.24, Fe 1.15; found K 6.79, P 0.64, W 63.96, Fe 1.34.

$K_9[H_4Mn(H_2O)PW_{17}O_{61}]\cdot 20H_2O$ (abbreviated as $PW_{17}Mn$): A sample of $Mn(NO_3)_2\cdot 4H_2O$ (0.25 g, ≈ 1 mmol) was dissolved in Millipore water (45 mL) and $K_{11}[H_4PW_{17}O_{61}]\cdot 18H_2O$ (4 g, 0.82 mmol) was added in small portions while heating the mixture on a water bath (≈ 60 °C). After half an hour, the mixture was filtered hot and the dark beige clear filtrate left in a beaker. A chestnut colored crystalline material appeared during cooling. This material was filtered and left to dry in the open air. $K_9[H_4Mn(H_2O)PW_{17}O_{61}]\cdot 20H_2O$ (4921.3): calcd. K 7.15, P 0.63, W 63.51, Mn 1.12; found K 7.22, P 0.62, W 65.90, Mn 1.08.

$K_9[H_4PV^{(4+)}W_{17}O_{62}]\cdot 18H_2O$ [abbreviated as $PW_{17}V^{(4+)}$]: A sample of $VOSO_4\cdot 5H_2O$ (0.42 g, 1.7 mmol) was dissolved in Millipore water (90 mL) and acidified with 4 M HCl (8.5 mL). $K_{11}[H_4PW_{17}O_{61}].18H_2O$ (8 g, 1.64 mmol) was then added in small portions with stirring. The black solution was stirred for roughly half an hour and then, treated with KCl (10 g). The grey black precipitate that resulted was recrystallized from a minimum of acidified water (HCl solution pH < 1). $K_9[H_4PV^{(4+)}W_{17}O_{62}]\cdot 18H_2O$ (4879.3): calcd. K 7.21, P 0.64, W 64.06, V 1.04; found K 7.13, P 0.62, W 64.7, V 1.05.

$K_8[H_4PV^{(5+)}W_{17}O_{62}]\cdot 18H_2O$ [abbreviated as $PW_{17}V^{(5+)}$]: To Millipore water (90 mL) was added a solution of 0.5 M HVO_4^{2-} (3.5 mL) with 4 M HCl (8.5 mL). $K_{11}[H_4PW_{17}O_{61}]\cdot 18H_2O$ (8 g, 1.64 mmol) was then added in small portions whilst stirring. The yellow solution was stirred for roughly half an hour, filtered and then treated with KCl (10 g). The yellow precipitate that resulted was recrystallized from a minimum of acidified water (HCl solution pH < 1). $K_8[H_4PV^{(5+)}W_{17}O_{62}]\cdot 18H_2O$ (4840.2): calcd. K 6.46, P 0.64, W 64.57, V 1.05; found K 5.95, P 0.63, W 65.10, V 0.95.

$K_7[H_4PMoW_{17}O_{62}]\cdot 18H_2O$ (abbreviated as $PW_{17}Mo$): A sample of $Na_2MoO_4\cdot 2H_2O$ (0.40 g, 1.7 mmol) was dissolved in Millipore water (90 mL) and acidified with 4 M HCl (8.5 mL). $K_{11}[H_4PW_{17}O_{61}]\cdot 18H_2O$ (8 g, 1.64 mmol) was then added in small portions with stirring. The clear yellow solution was stirred for roughly half an hour and then filtered and treated with KCl (10 g). The fine yellow precipitate that resulted was recrystallized from a minimum of acidified water (HCl solution pH < 1). $K_7[H_4PMoW_{17}O_{62}]\cdot 18H_2O$ (4846.1): calcd. K 5.65, P 0.64, W 64.49, Mo 1.98; found K 5.76, P 0.66, W 64.51, Mo 2.01.

General Methods and Materials: Pure water was used throughout and was obtained by passing through an RiOs 8 unit followed by a Millipore-Q Academic purification set. All reagents were of high-purity grade and were used as purchased. Elemental analyses were performed by Kanti Labs Ltd. in Mississauga, Canada. The IR spectra were recorded in KBr pellets with a Perkin−Elmer Spectrum One FT-IR spectrophotometer. The UV/Vis spectra were recorded with a Perkin−Elmer Lambda 19 spectrophotometer on 2.5 × 10^{-5} M solutions of the relevant polyanion. Matched 1.000-cm optical path quartz cuvettes were used. The compositions of the various media were as follows: for pH 0.33: 0.5 M H_2SO_4; for pH 1 to 3: 0.2 M Na_2SO_4 + H_2SO_4; for pH 4 and 5: 0.4 M CH_3COONa + CH_3COOH; for pH 6 and 7: 0.4 M NaH_2PO_4 + NaOH.

Electrochemical Experiments: The same media used for UV/visible spectroscopy were also used for electrochemistry except that the polyanion concentration was 5 × 10^{-4} M. All cyclic voltammograms were recorded at a scan rate of 10 mV·s^{-1} unless otherwise stated.

The solutions were de-oxygenated thoroughly for at least 30 min with pure argon and kept under a positive pressure of this gas during the experiments. The source, mounting and polishing of the glassy carbon electrodes (GC, Tokai, Japan) has been described.[36] The glassy carbon samples had a diameter of 3 mm. The electrochemical set-up was an EG & G 273 A system controlled by a PC with M270 software. Potentials are quoted relative to the saturated calomel electrode (SCE). The counter electrode was a platinum gauze of large surface area. All experiments were performed at room temperature.

Acknowledgments

This work was supported by the CNRS (UMR, 8000 and UMR 7071), the Universities Paris XI, Paris VI and Goergetown University. We also thank Benoît Faure for assistance with several electrochemistry experiments.

[1] M. T. Pope, *Heteropoly and Isopoly Oxometalates*, Springer-Verlag, Berlin, **1983**.
[2] M. T. Pope, A. Müller, *Angew. Chem. Int. Ed. Engl.* **1991**, *30*, 34−48.
[3] *Polyoxometalates: from Platonic Solids to Anti-Retroviral Activity* (Eds.: M. T. Pope, A. Müller); Kluwer: Dordrecht, The Netherlands, **1994**.
[4] Chemical Reviews, *Polyoxometalates* (Ed.: C. Hill), **1998**.
[5] *Polyoxometalate Chemistry: From Topology via Self-Assembly to Applications* (Eds.: M. T. Pope, A. Müller); Kluwer: Dordrecht, The Netherlands, **2001**.
[6] *Polyoxometalate Chemistry for Nano-Composite Design* (Eds.: T. Yamase, M. T. Pope); Kluwer: Dordrecht, The Netherlands, **2002**.

 © 2004 Wiley-VCH Verlag GmbH & Co. KGaA, Weinheim

[7] B. Dawson, *Acta Crystallogr.* **1953**, *3*, 113−126.
[8] H. Neubert, J. Fuchs, *Z. Naturforsch., Teil B* **1987**, *42*, 951−958.
[9] E. Van Dalen, M. G. Mellon, *Anal. Chem.* **1964**, *36*, 1068−1071.
[10] Y. Jeannin, J. Martin-Frère, *Inorg. Chem.* **1979**, *18*, 3010−3014.
[11] B. Krebs, R. Klein, in *Polyoxometalates: From Platonic Solids to Anti-Retroviral Activity* (Eds.: M. T. Pope, A. Müller), Kluwer Academic Publishers, Dordrecht, **1994**, pp. 41−57.
[12] D. Rodewald, Y. Jeannin, *C. R. Acad. Sci. Paris, Sér. IIc* **1999**, *2*, 63−67.
[13] Y. Ozawa, Y. Sasaki, *Chem. Lett.* **1987**, 923−926.
[14] B. Krebs, E. Droste, M. Piepenbrink, G. Vollmer, *C. R. Acad. Sci. Paris, Série IIc, Chim.* **2000**, *3*, 205−210.
[15] R. Contant, S. Piro-Sellem, J. Canny, R. Thouvenot, *C. R. Acad. Sci. Paris, Sér. IIc* **2000**, *3*, 157−161.
[16] B. Keita, I. M. Mbomekalle, L. Nadjo, R. Contant, *Electrochemistry Comunications* **2001**, *3*, 267−273.
[17] I. M. Mbomekalle, B. Keita, L. Nadjo, R. Contant, N. Belai, M. T. Pope, *Inorganica Chimica Acta* **2003**, *342*, 219−228.
[18] J. E. Toth, F. C. Anson, *J. Electroanal. Chem.* **1989**, *256*, 361−370.
[19] R. Contant, M. Abbessi, J. Canny, A. Belhouari, B. Keita, L. Nadjo, *Inorg. Chem.* **1997**, *36*, 4961−4967.
[20] B. Keita, A. Belhouari, L. Nadjo, R. Contant, *J. Electroanal. Chem.* **1998**, *442*, 49−57.
[21] C. Rocchiccioli-Deltcheff, R. Thouvenot, *Spectroscopy Letters* **1979**, *12*, 127−138.
[22] C. Rocchiccioli-Deltcheff, M. Fournier, R. Franck, R. Thouvenot, *Inorg. Chem.* **1983**, *22*, 207−216.
[23] R. Thouvenot, M. Fournier, R. Franck, C. Rocchiccioli-Deltcheff, *Inorg. Chem.* **1984**, *23*, 598−605.
[24] J. Gamelas, F. A. S. Couto, M. C. N. Trovao, A. M. V. Cavaleiro, J. A. S. Cavaleiro, J. D. Pedro de Jesus, *Thermochimica Acta* **1999**, *326*, 165−173.
[25] R. Contant, M. Richet, Yu Wei Lu, B. Keita, L. Nadjo, *Eur. J. Inorg. Chem.* **2002**, 2587−2593.
[26] T. L. Jorris, M. Kozik, N. Casan-Pastor, P. J. Domaille, R. G. Finke, W. K. Miller, L. C. Baker, *J. Am. Chem. Soc.* **1987**, *109*, 7402.
[27] B. Keita, L. Nadjo, *Mater. Chem. Phys.* **1989**, *22*, 77−103.
[28] B. Keita, L. Nadjo, *J. Electroanal. Chem.* **1987**, *227*, 77−98.
[29] B. Keita, A. Belhouari, L. Nadjo, *J. Electroanal. Chem.* **1993**, *355*, 235−251.
[30] J. P. Launay, PhD thesis, **1974**, Université Pierre et Marie Curie, Paris, France.
[31] A. Mahmoud, B. Keita, L. Nadjo, O. Oung, R. Contant, S. Brown, Y. de Kouchkovsky, *J. Electroanal. Chem.* **1999**, *463*, 129−145.
[32] B. Keita, F. Girard, L. Nadjo, R. Contant, J. Canny, M. Richet, *J. Electroanal. Chem.* **1999**, *478*, 76−82.
[33] A. Belhouari, B. Keita, L. Nadjo, R. Contant, *New J. Chem.* **1998**, 83−86.
[34] B. Keita, E. Abdeljalil, L. Nadjo, R. Contant, R. Belghiche, *Electrochem. Commun.* **2001**, *3*, 56−62.
[35] At pH = 1, the actual active species should be HNO_2 and/or NO. As a matter of fact, the following sequence is known: $HNO_2 \rightarrow H^+ + NO_2^-$ $pK_a = 3.3$ at 18 °C and HNO_2 disproportionates in fairly acidic solution: $3\ HNO_2 \rightarrow HNO_3 + 2\ NO + H_2O$. The rate of this reaction is known to be low.
[36] B. Keita, F. Girard, L. Nadjo, R. Contant, R. Belghiche, M. Abbessi, *J. Electroanal. Chem.* **2001**, *508*, 70−80.

Received July 11, 2003
Early View Article
Published Online November 19, 2003

 © 2004 Wiley-VCH Verlag GmbH & Co. KGaA, Weinheim

Synthesis, Spectroscopic Properties, and Structure of [Tetrakis(2,4-dimethyl-3-pentyloxy)phthalocyaninato]metal Complexes

Wei Liu,[a] Chi-Hang Lee,[a] Hoi-Shan Chan,[a] Thomas C. W. Mak,[a] and Dennis K. P. Ng*[a]

Keywords: Macrocyclic compounds / Inclusion compounds / N ligands

A series of highly soluble [tetrakis(2,4-dimethyl-3-pentyloxy)phthalocyaninato]metal complexes [$MPc(OC_7H_{15})_4$] (M = Zn, Pd, Co) were prepared by cyclic tetramerization of 3-(2,4-dimethyl-3-pentyloxy)phthalonitrile (**2**) in the presence of the corresponding metal salts and 1,8-diazabicyclo[5.4.0]undec-7-ene (DBU) in *n*-pentanol. For M = Zn and Pd, two major isomers with a C_{4h} and C_{2v} symmetry were isolated by column chromatography and characterized with various spectroscopic methods, while the cobalt analogue showed only the C_{4h} isomer. The (phthalocyaninato)manganese complex [$MnClPc(OC_7H_{15})_4$] was also synthesized by metallation of the metal-free phthalocyanine $H_2Pc(OC_7H_{15})_4$ formed by treating **2** with $CeCl_3$ and DBU in *n*-pentanol. The structures of the C_{4h} isomers of the (phthalocyaninato)zinc and -cobalt complexes and the C_4 isomer of the manganese analogue were also established by X-ray diffraction analyses. The palladium counterpart formed a novel 1:1 inclusion complex with oxalic acid, the crystal structure of which was also determined.

(© Wiley-VCH Verlag GmbH & Co. KGaA, 69451 Weinheim, Germany, 2004)

Introduction

Phthalocyanines are traditional pigments that were discovered almost a century ago. They are a unique class of macrocyclic compounds, with intriguing physical and chemical properties that allow their use in many disciplines.[1] Their well-documented functions as molecular opto-electronic materials,[2] photosensitizers for photodynamic therapy,[3] and catalysts for oxidative degradation of pollutants[4] are still being actively exploited. For some of these applications, highly soluble and non-aggregated phthalocyanines are desirable. The former property facilitates the purification and the fabrication processes, while the latter assists in characterization and allows these materials to function properly; many properties of phthalocyanines change upon aggregation.[5] As a result, a substantial number of phthalocyanines with sterically demanding substituents have been reported.[6] We describe herein a series of (phthalocyaninato)metal complexes substituted with four 2,4-dimethyl-3-pentyloxy groups. These bulky and hydrophobic substituents not only enhance the solubility of phthalocyanines in organic solvents and reduce their tendency to aggregate, but also facilitate the separation of the isomers of tetra-α-substituted phthalocyanines. Phthalocyanines containing these substituents have been briefly reported for use as optical recording materials.[7]

Results and Discussion

Synthetic Studies

In the synthesis of these (phthalocyaninato)metal complexes (Scheme 1) 3-nitrophthalonitrile (**1**) is treated with

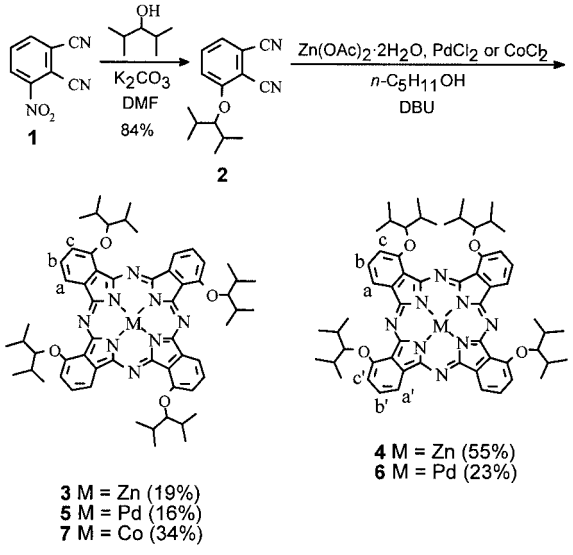

Scheme 1. Preparation of [tetrakis(2,4-dimethyl-3-pentyloxy)-phthalocyaninato]zinc, -palladium, and -cobalt complexes

[a] Department of Chemistry, The Chinese University of Hong Kong,
Shatin, N. T., Hong Kong, China
Fax: (internat.) + 852-2603-5057
E-mail: dkpn@cuhk.edu.hk

 © 2004 Wiley-VCH Verlag GmbH & Co. KGaA, Weinheim DOI: 10.1002/ejic.200300470

2,4-dimethyl-3-pentanol in the presence of K_2CO_3 in DMF to afford 3-(2,4-dimethyl-3-pentyloxy)phthalonitrile (**2**). Cyclization of **2** with zinc(II) acetate or palladium(II) chloride in the presence of DBU in *n*-pentanol then furnishes the corresponding (phthalocyaninato)metal complexes. Only the C_{4h} and C_{2v} isomers could be isolated by column chromatography, while the D_{2h} and C_s isomers were not detected. For the (phthalocyaninato)zinc complexes, the C_{4h} isomer **3** was eluted first followed by the C_{2v} isomer **4**. Interestingly, this order was reversed for the palladium analogues **5** and **6**. These isomers are usually separated by medium- or high-pressure liquid chromatography,[8] but their facile separation here may be attributed to the bulky 2,4-dimethyl-3-pentyloxy substituents at the α-positions. It is also noteworthy that for both the zinc and palladium analogues the C_{2v} isomer is produced in higher yield than the C_{4h} counterpart, which is supposed to be thermodynamically more stable. This cannot be explained by the alkoxide-induced sequential nucleophilic attack of phthalonitriles[9] and the "template" mechanism proposed by Hanack et al.,[8b] which will give predominantly the C_{4h} and C_s isomers, respectively. The reaction mechanism remains elusive but, as reported earlier,[8b] the isomer distribution of tetra-α-substituted (phthalocyaninato)metal complexes depends on many factors, including the nature of the substituent, reaction conditions, and metal center. Further investigation is clearly required.

The cobalt counterpart **7**, prepared similarly using $CoCl_2$ as the metal salt, was unstable on silica gel: the blue color faded gradually during chromatography. Preliminary purification could, however, be achieved by flash chromatography through a short column packed with neutral alumina. Further purification by recrystallization led to the pure C_{4h} isomer **7**, which was confirmed by single-crystal X-ray analysis. Other constitutional isomers, which were probably also formed during the reaction, could neither be isolated nor detected by ^{1}H NMR spectroscopy due to the paramagnetic cobalt(II) center.

Our recently reported cerium-promoted method to prepare metal-free phthalocyanines afforded high yields of 1,8,15,22-tetrakis(2,4-dimethyl-3-pentyloxy)phthalocyanine (**8**),[10] which can be used to prepare (phthalocyaninato)metal complexes. Thus, while treatment of the dinitrile **2** with $Mn(OAc)_2{\cdot}2H_2O$ and DBU in *n*-pentanol yielded a dark brown solution which did not show the typical phthalocyanines' Q-band absorption, compound **8** could be metallated with $Mn(OAc)_2{\cdot}2H_2O$ in DMF to give the (phthalocyaninato)manganese(III) complex **9** in 88% yield (Scheme 2). The manganese(II) ion was oxidized during the reaction and the axial chloro ligand came from the brine used during the workup procedure. Similar results were also observed during the preparation of (chloro)(porphyrazinato)manganese(III) complexes.[11]

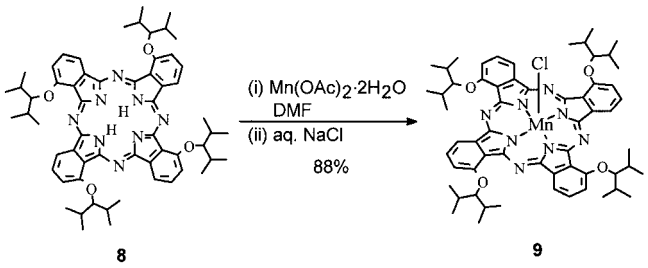

8 **9**

Scheme 2. Preparation of (phthalocyaninato)manganese complex **9**

Spectroscopic Properties

The C_{4h} and C_{2v} isomers of the (phthalocyaninato)zinc and -palladium complexes could be distinguished readily by ^{1}H NMR spectroscopy. The rather broad signals for the zinc analogues **3** and **4** in $CDCl_3$ were sharpened upon addition of a drop of [D_5]pyridine to give well-resolved spectra, due to the relief of aggregation by the axial coordination of the zinc(II) center by pyridine.[12] The spectra for the palladium analogues **5** and **6** were well resolved even in the absence of [D_5]pyridine. Figure 1 (b) shows the ^{1}H NMR spectrum of **5** in $CDCl_3$, in which all the signals can be assigned unambiguously. The spectrum shows a doublet at δ = 9.05 ppm, an overlapping doublet of doublets (or virtual triplet) at δ = 8.03 ppm, and a doublet at δ = 7.68 ppm for the three sets of ring protons. The four equivalent 2,4-dimethyl-3-pentyloxy groups resonate at δ = 4.67 (t, OCH), 2.54−2.64 (m, CH), 1.48 (d, Me), and 1.19 ppm (d, Me). All these signals are split for compound **6** [Figure 1 (a)], which clearly confirms its C_{2v} symmetry.

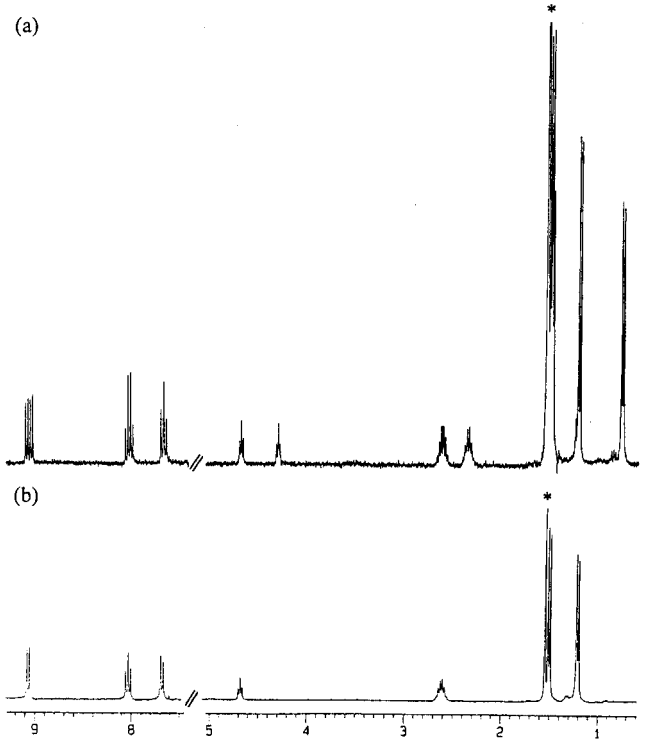

Figure 1. ^{1}H NMR spectra of **6** (a) and **5** (b) in $CDCl_3$; * water signal

The (phthalocyaninato)metal complexes **3**−**7** and **9** gave typical UV/Vis absorptions of phthalocyanines (Table 1). The absorption data of the C_{4h} and C_{2v} isomers of the (phthalocyaninato)zinc and -palladium complexes do not

 © 2004 Wiley-VCH Verlag GmbH & Co. KGaA, Weinheim

Table 1. UV/Vis data for (phthalocyaninato)metal complexes **3**−**7** and **9** in $CHCl_3$

Compound	λ_{max} [nm] (log ε)				
	B-band	LMCT	Vibronic band(s)		Q-band
$Zn[Pc(OC_7H_{15})_4]$ (**3**)	322 (4.54)	−	638 (4.37)	−	711 (5.13)
$Zn[Pc(OC_7H_{15})_4]$ (**4**)	323 (4.59)	−	638 (4.41)	−	709 (5.14)
$Pd[Pc(OC_7H_{15})_4]$ (**5**)	314 (4.31)	−	623 (4.36)	664 (4.08)	694 (5.10)
$Pd[Pc(OC_7H_{15})_4]$ (**6**)	314 (4.44)	−	625 (4.46)	671 (4.44)	696 (5.19)
$Co[Pc(OC_7H_{15})_4]$ (**7**)	313 (3.86)	−	631 (3.66)	−	702 (4.31)
$MnCl[Pc(OC_7H_{15})_4]$ (**9**)	337 (4.18)	550 (3.85)	693 (3.93)	−	775 (4.67)

show significant differences. The Q-band position, however, is highly dependent on the metal center in the order $Pd^{II} < Co^{II} < Zn^{II} << Mn^{III}$. The (phthalocyaninato)manganese complex **9** is brown instead of the characteristic blue-green as a result of the very long Q-band absorption (775 nm), which appears to be the longest wavelength recorded for (phthalocyaninato)metal complexes. This remarkably large red-shift may be attributed to the effects of metal center and the electron-donating alkoxy substituents introduced at the α-positions. A characteristic ligand-to-metal charge-transfer (LMCT) band at 550 nm was also seen for **9**.[13]

Having four bulky 2,4-dimethyl-3-pentyloxy substituents, these phthalocyanines are expected to be relatively non-aggregated in solutions. This was confirmed by variable-concentration UV/Vis studies of compounds **3**, **5**, and **9** in $CHCl_3$. For these three compounds, plots of the Q-band absorbance versus concentration (from 2×10^{-7} to 3×10^{-5} mol·dm^{-3}) gave perfect straight lines, showing that the compounds strictly follow the Lambert−Beer law. This indicates that the compounds exist mainly in monomeric form under the conditions employed. The zinc complexes **3** and **4**, however, are slightly aggregated at higher concentrations (ca. 10^{-3} mol·dm^{-3}) as shown by NMR studies (see above).

Structural Studies

Both the zinc and cobalt phthalocyanines **3** and **7** co-crystallize with a water molecule, which may come from the solvents used for recrystallization. In the molecular structure of **3** the zinc atom is disordered about the inversion center relating the two halves of the molecule (Figure 2). The oxygen atom of water occupies a site with half occupancy, giving the shortest Zn−O distance at 2.034 Å, which may be regarded as axial ligation.[14] The corresponding Co−O distance in **7** (2.494 Å), however, is significantly longer than typical $Co-OH_2$ bonds in (aquo)cobalt(II) complexes (ca. 2.1−2.2 Å).[15]

Both **3** and **7** crystallize in the monoclinic system with two molecules per unit cell. The phthalocyanine rings are arranged in a herringbone manner[16] along the crystallographic *b* axis with a stacking angle of 54.1 (**3**) or 59.7° (**7**) and an interplanar distance of 6.98 (**3**) or 7.40 Å (**7**) (Figure 3). This arrangement is similar to that of the metal-free analogue **8**[10a] and the unsubstituted phthalocyanine.[17] Due to the bulky 2,4-dimethyl-3-pentyloxy substituents, which act as spacers, the interplanar distances for these substituted phthalocyanines are much larger than that of the unsubstituted counterpart (3.31 Å).

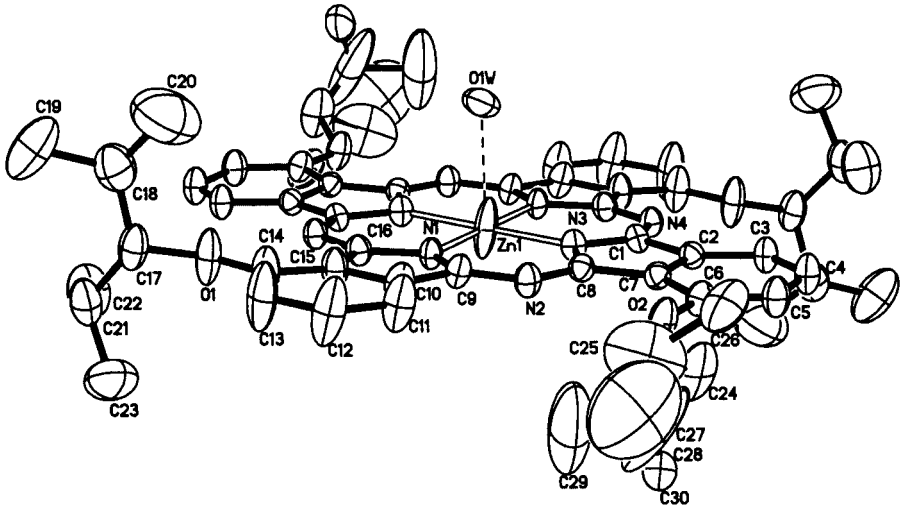

Figure 2. Molecular structure of **3** showing the 30% probability thermal ellipsoids for all non-hydrogen atoms; the zinc atom is disordered with the shortest $Zn-OH_2$ distance at 2.034 Å

 © 2004 Wiley-VCH Verlag GmbH & Co. KGaA, Weinheim

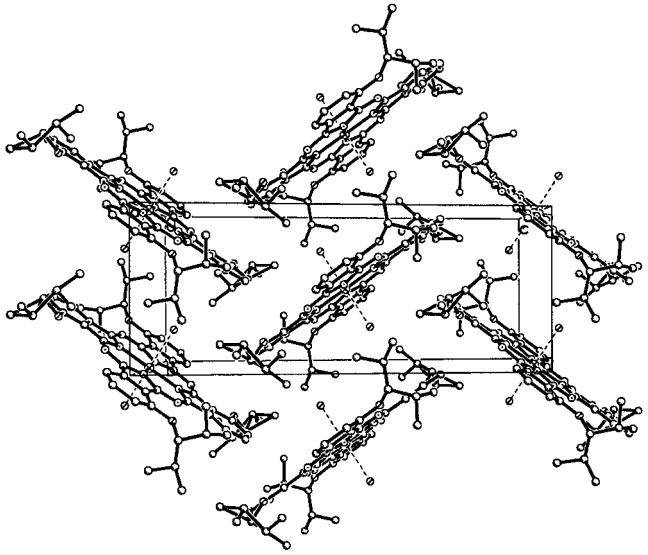

Figure 3. Packing of **3**·H_2O viewed along the *a* axis; all hydrogen atoms omitted for clarity

In the (phthalocyaninato)manganese complex **9** the manganese center is coordinated by four isoindole nitrogen atoms of the phthalocyanine ring and one terminal chloro ligand, forming a slightly distorted square pyramid (Figure 4). In contrast to the zinc and cobalt analogues, in which the metal center lies in the isoindole N_4 plane, the manganese atom is displaced 0.291 Å above the N_4 plane towards the apical chloro ligand. The displacement is similar to that in [Mn(OESTAP)Cl] [0.291 Å; OESTAP = 2,3,7,8,12,13,17,18-octakis(ethylsulfanyl)-*meso*-tetraazaporphyrinate],[18] but is 0.03 Å longer than that in [Mn(TPP)Cl] (TPP = *meso*-tetraphenylporphyrinate).[19] The average Mn−N(isoindole) distance (1.960 Å) is also similar to the average Mn−N(pyrrole) distance of [Mn(OESTAP)Cl] (1.951 Å), but shorter than that in [Mn(TPP)Cl] (2.02 Å). This is in agreement with the larger central cavity of the TPP ring. The Mn−Cl distance in **9** (2.343 A) is significantly shorter than that in [Mn(OESTAP)Cl] (2.394 Å) and [Mn(TPP)Cl] (2.37 Å). Due to the square-pyramidal structure and the C_4 disposition of the substituents, compound **9** can exhibit chirality. That the compound crystallizes in the orthorhombic system with a $P2_12_12_1$ space group shows that the crystal contains only one of the enantiomers, although a racemic mixture is expected to form during the reaction. This compound is thus a rare example of a structurally characterized manganese complex[20] and phthalocyanine with a planar asymmetry.[21]

We have recently reported a novel 1:1 inclusion complex of the metal-free phthalocyanine **8** and oxalic acid generated unexpectedly in a cerium-promoted cyclization reaction.[10a] The crystal structure shows that the oxalic acid molecules are intercalated between the phthalocyanine rings and not be hydrogen-bonded in any conventional or unconventional manner. This is very unusual for molecules, such as oxalic acid, which have good hydrogen-bonding functionalities.[22] To further explore this novel class of inclusion complexes, the (phthalocyaninato)palladium complex **5** was recrystallized in the presence of 1 equiv. of oxalic acid, giving the 1:1 inclusion complex **5**·$C_2H_2O_4$. The IR spectrum of **5**·$C_2H_2O_4$ (KBr) showed a strong band at 1671 cm^{-1} and a medium band at ca. 3400 cm^{-1}, which can be ascribed to the C=O and O−H stretches, respectively, of the oxalic acid. Figure 5 depicts the packing of molecules in the lattice viewed along the crystallographic *a* and *b* axes, which shows that the guest species are not hydrogen-bonded and simply hang between the phthalocyanine rings. The polar oxalic acid preferentially resides in the more polar cavity between the phthalocyanine rings rather than in bulk $CHCl_3$. The stacking angle is 54.3° and the interplanar distance is 7.13 Å, which are similar to those of **3** and **7**. The oxalic acid

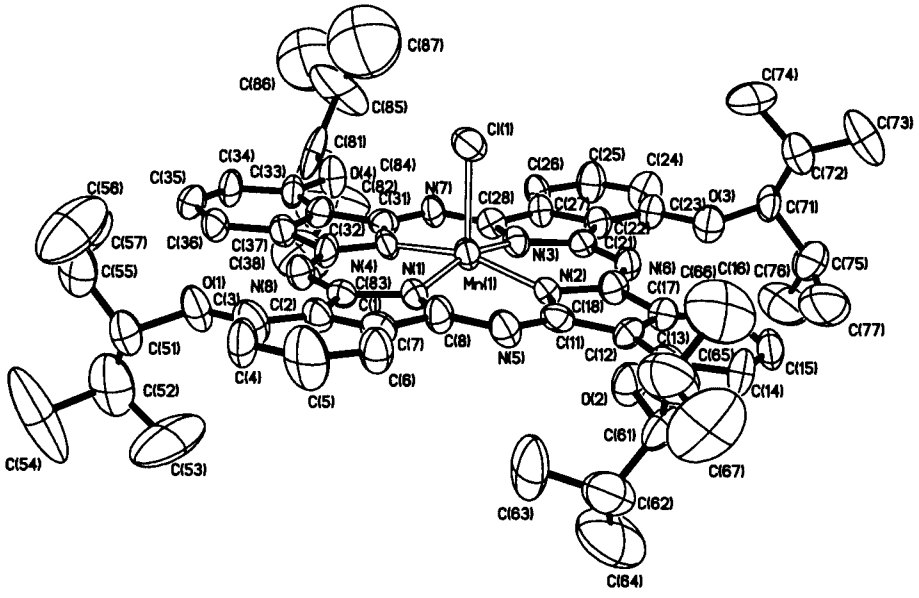

Figure 4. Molecular structure of **9** showing the 30% probability thermal ellipsoids for all non-hydrogen atoms

 © 2004 Wiley-VCH Verlag GmbH & Co. KGaA, Weinheim

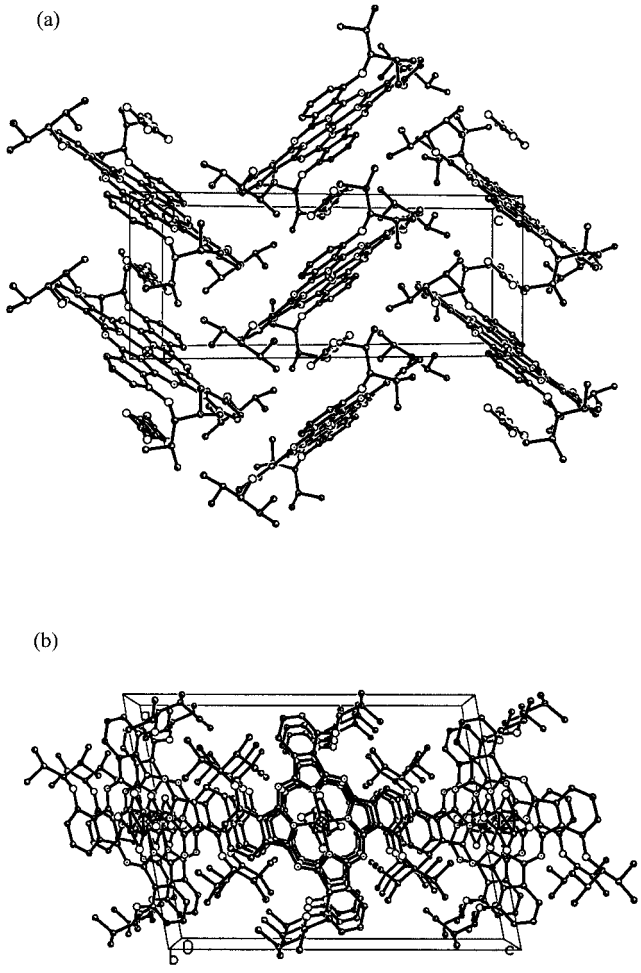

Figure 5. Crystal structure of $5 \cdot C_2H_2O_4$: views along the *a* (a) and *b* axis (b); all hydrogen atoms omitted for clarity

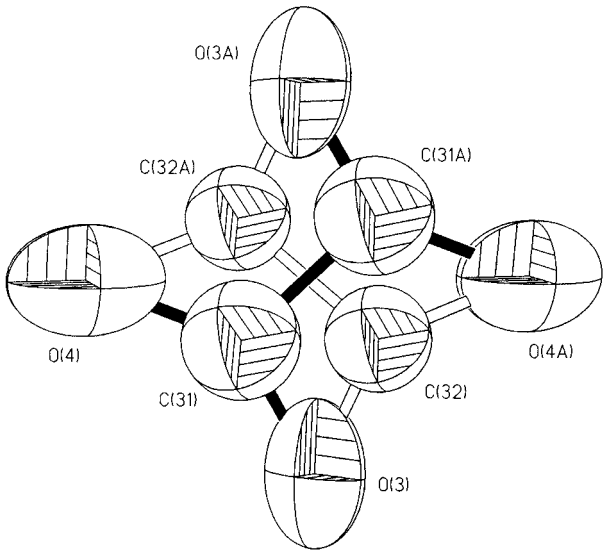

Figure 6. Molecular structure of the disordered oxalic acid in $5 \cdot C_2H_2O_4$; selected bond lengths [Å] and angles [°]: C(31)−C(31A) 1.566(10), C(31)−O(4) 1.142(16), C(31)−O(3) 1.204(18), C(32)−C(32A) 1.572(10), C(32)−O(4A) 1.176(16), C(32)−O(3) 1.229(18); O(4)−C(31)−O(3) 140.7(13), O(4)−C(31)−C(31A) 129(2), O(3)−C(31)−C(31A) 89.7(17), O(4A)−C(32)−O(3) 147.5(13), O(4A)−C(32)−C(32A) 125(2), O(3)−C(32)−C(32A) 87.7(16)

molecule is disordered (Figure 6). The average C−C, C=O, and C−O bond lengths are 1.569, 1.159, and 1.217 Å, respectively. The latter two are significantly shorter than the corresponding values for hydrogen-bonded oxalic acid (ca. 1.20 and 1.31 Å).[23]

Conclusion

We have prepared and characterized a series of (phthalocyaninato)metal complexes substituted with four bulky 2,4-dimethyl-3-pentyloxy groups. The C_{4h} isomers of the (phthalocyaninato)zinc and -cobalt complexes and the C_4 isomer of the manganese analogue have been structurally characterized. The palladium counterpart forms a rare 1:1 inclusion complex, with oxalic acid, the structure of which has also been determined.

Experimental Section

General Remarks: Reactions were performed under nitrogen. *n*-Pentanol and THF were distilled from sodium and sodium/benzophenone ketyl, respectively. DMF was predried with barium oxide and distilled under reduced pressure. Chromatographic purifications were performed on silica gel columns (Macherey−Nagel, 70−230 mesh) with the indicated eluents unless otherwise stated. Hexane used in chromatography was distilled from anhydrous $CaCl_2$. All other reagents and solvents were of reagent grade and used as received. The preparation of the metal-free phthalocyanine **8** has been reported previously.[10] ^{1}H and ^{13}C NMR spectra were recorded with a Bruker DPX 300 spectrometer (^{1}H: 300 MHz; ^{13}C: 75.4 MHz) in $CDCl_3$ solutions unless otherwise stated. Chemical shifts are relative to internal $SiMe_4$ (δ = 0 ppm). IR spectra were measured with a Nicolet Magna 550 FT-IR spectrometer as KBr pellets. UV/Vis spectra were taken with a Cary 5G UV/Vis/NIR spectrophotometer. Liquid secondary-ion (LSI) mass spectra were recorded with a Bruker APEX 47e Fourier transform ion cyclotron resonance (FTICR) mass spectrometer with a 3-nitrobenzyl alcohol matrix. Elemental analyses were performed by Medac Ltd., Brunel Science Centre, UK.

3-(2,4-Dimethyl-3-pentyloxy)phthalonitrile (2):[24] A mixture of 3-nitrophthalonitrile (**1**) (2.0 g, 12 mmol), 2,4-dimethyl-3-pentanol (4.8 g, 41 mmol), and K_2CO_3 (12.6 g, 91 mmol) in DMF (20 mL) was heated at 65 °C for 2 d. The mixture was then poured into ice-cold water (200 mL) to give a light brown solid, which was filtered off and dissolved in $CHCl_3$ (20 mL). The resultant solution was dried with anhydrous $MgSO_4$ and then concentrated in vacuo. The residue was chromatographed with $CHCl_3$ as eluent to give the product as a white solid. Further purification was achieved by recrystallization with hexane to afford white shiny needles (2.4 g, 84%), m.p. 82−83 °C. $C_{15}H_{18}N_2O$ (242.3): calcd. C 74.34, H 7.49, N 11.57; found C 74.43, H 7.28, N 11.62. ^{1}H NMR: δ = 7.50−7.55 (m, 1 H, ArH), 7.21−7.24 (m, 2 H, ArH), 4.00 (t, *J* = 6.0 Hz, 1 H, OCH), 2.02−2.11 (m, 2 H, CH), 0.94 (d, *J* = 6.9 Hz, 6 H, Me), 0.88 (d, *J* = 6.9 Hz, 6 H, Me) ppm. ^{13}C{^{1}H} NMR: δ = 163.3, 134.3, 124.5, 117.8, 117.1, 115.4, 113.3, 105.0, 90.9, 30.5, 19.8, 17.4 ppm. IR (KBr): $\tilde{\nu}$ = 2225 m cm^{-1} (C≡N). HRMS (EI): *m*/*z* calcd. for $C_{15}H_{18}N_2O$ [M$^+$] 242.1419, found 242.1435.

 © 2004 Wiley-VCH Verlag GmbH & Co. KGaA, Weinheim

[Tetrakis(2,4-dimethyl-3-pentyloxy)phthalocyaninato]zinc(II) (3 and 4): A mixture of the dinitrile **2** (100 mg, 0.41 mmol), $Zn(OAc)_2{\cdot}2H_2O$ (32 mg, 0.15 mmol), and DBU (0.2 mL) in *n*-pentanol (3 mL) was heated at 160 °C for 8 h. The volatiles were then removed in vacuo and the residue was chromatographed with hexane/ethyl acetate (2:1) as eluent. A green band was collected and the solvents were evaporated to give a crude isomeric mixture of $[ZnPc(OC_7H_{15})_4]$, which was further purified by chromatography using $CHCl_3$/ethyl acetate (10:1) as eluent. Two green bands were then developed which were collected separately to give the C_{4h} isomer **3** (20 mg, 19%) and the C_{2v} isomer **4** (59 mg, 55%), respectively. **3:** ^{1}H NMR ($CDCl_3$ with a drop of $[D_5]$pyridine): δ = 9.06 (d, *J* = 7.5 Hz, 4 H, Pc-H_a), 7.95 (t, *J* = 7.5 Hz, 4 H, Pc-H_b), 7.61 (d, *J* = 7.5 Hz, 4 H, Pc-H_c), 4.61 (t, *J* = 5.7 Hz, 4 H, OCH), 2.50−2.60 (m, 8 H, CH), 1.47 (d, *J* = 6.6 Hz, 24 H, Me), 1.14 (d, *J* = 6.6 Hz, 24 H, Me) ppm. $^{13}C\{^1H\}$ NMR ($CDCl_3$ with a drop of $[D_5]$pyridine): δ = 158.7, 153.8, 143.9, 142.0, 129.8, 125.8, 114.7, 113.6, 89.7, 31.2, 20.2, 18.4 ppm. HRMS (LSI): *m*/*z* calcd. for $C_{60}H_{73}N_8O_4Zn$ $[MH^+]$ 1033.5046, found 1033.5182. **4:** ^{1}H NMR ($CDCl_3$ with a drop of $[D_5]$pyridine): δ = 9.03−9.11 (m, 4 H, Pc-H_a and Pc-$H_{a'}$), 7.93−8.04 (m, 4 H, Pc-H_b and Pc-$H_{b'}$), 7.59−7.68 (m, 4 H, Pc-H_c and Pc-$H_{c'}$), 4.66 (t, *J* = 6.0 Hz, 2 H, OCH), 4.27 (t, *J* = 6.0 Hz, 2 H, OCH), 2.52−2.64 (m, 4 H, CH), 2.28−2.39 (m, 4 H, CH), 1.49−1.53 (m, 24 H, Me), 1.17 (d, *J* = 6.6 Hz, 12 H, Me), 0.73 (d, *J* = 6.6 Hz, 12 H, Me) ppm. HRMS (LSI): *m*/*z* calcd. for $C_{60}H_{73}N_8O_4Zn$ $[MH^+]$ 1033.5046, found 1033.5181.

[Tetrakis(2,4-dimethyl-3-pentyloxy)phthalocyaninato]palladium(II) (5 and 6): A mixture of the dinitrile **2** (100 mg, 0.41 mmol), $PdCl_2$ (21 mg, 0.12 mmol), and DBU (0.2 mL) in *n*-pentanol (3 mL) was heated at 140 °C for 18 h. The volatiles were then removed in vacuo and the residue was subjected to chromatography using $CHCl_3$ as eluent. The crude product was chromatographed again with hexane/$CHCl_3$ (2:1) as eluent to develop two green bands, which were collected and the solvents evaporated. The first band was found to be the C_{2v} isomer **6** (26 mg, 23%), while the second band was the C_{4h} isomer **5** (18 mg, 16%), which could be further purified by recrystallization from $CHCl_3$/MeOH. **5:** $C_{61}H_{73}Cl_3N_8O_4Pd$ (**5**·$CHCl_3$): calcd. C 61.39, H 6.17, N 9.40; found C 60.34, H 6.32, N 9.24. ^{1}H NMR: δ = 9.05 (d, *J* = 7.5 Hz, 4 H, Pc-H_a), 8.03 (dd, *J* = 7.5, 8.1 Hz, 4 H, Pc-H_b), 7.68 (d, *J* = 8.1 Hz, 4 H, Pc-H_c), 4.67 (t, *J* = 5.7 Hz, 4 H, OCH), 2.54−2.64 (m, 8 H, CH), 1.48 (d, *J* = 6.6 Hz, 24 H, Me), 1.19 (d, *J* = 6.6 Hz, 24 H, Me) ppm. $^{13}C\{^1H\}$ NMR: δ = 158.6, 154.7, 143.1, 141.4, 130.6, 124.2, 114.7, 113.7, 89.5, 31.4, 20.4, 18.5. HRMS (LSI): *m*/*z* calcd. for $C_{60}H_{73}N_8O_4Pd$ $[MH^+]$ 1075.4783, found 1075.4870. **6:** ^{1}H NMR: δ = 9.09 (d, *J* = 7.5 Hz, 2 H, Pc-H_a or Pc-$H_{a'}$), 9.03 (d, *J* = 7.5 Hz, 2 H, Pc-H_a or Pc-$H_{a'}$), 7.98−8.06 (m, 4 H, Pc-H_b and Pc-$H_{b'}$), 7.64−7.69 (m, 4 H, Pc-H_c and Pc-$H_{c'}$), 4.69 (t, *J* = 5.7 Hz, 2 H, OCH), 4.31 (t, *J* = 5.7 Hz, 2 H, OCH), 2.57−2.68 (m, 4 H, CH), 2.30−2.41 (m, 4 H, CH), 1.49−1.52 (m, 24 H, Me), 1.22 (d, *J* = 6.6 Hz, 12 H, Me), 0.77 (d, *J* = 6.6 Hz, 12 H, Me). $^{13}C\{^1H\}$ NMR: δ = 160.0, 158.6, 154.0, 152.0, 143.2, 143.0, 140.0 (2 overlapping signals), 130.6, 130.4, 124.2 (2 overlapping signals), 117.0, 115.0, 114.4, 113.9, 94.2, 89.4, 31.4, 29.7, 20.4, 19.9, 18.4, 18.3 ppm. HRMS (LSI): *m*/*z* calcd. for $C_{60}H_{73}N_8O_4Pd$ $[MH^+]$ 1075.4783, found 1075.5037.

[1,8,15,22-Tetrakis(2,4-dimethyl-3-pentyloxy)phthalocyaninato]-cobalt(II) (7): A mixture of the dinitrile **2** (100 mg, 0.41 mmol), anhydrous $CoCl_2$ (13 mg, 0.10 mmol), and DBU (0.2 mL) in *n*-pentanol (3 mL) was heated under reflux overnight. The volatiles were then removed in vacuo and the residue was subjected to flash chromatography on neutral alumina using hexane/ethyl acetate (1:4) as eluent. The crude product obtained was further purified by chromatography again using the same eluent to develop two blue bands. The first band was collected and the solvents were evaporated to give the C_{4h} isomer **7** as a green solid (35 mg, 34%), which could be recrystallized by layering MeOH onto a $CHCl_3$ solution. The second band contained about 5 mg of material, which could not be further purified by recrystallization because of its instability in solutions. HRMS (LSI): *m*/*z* calcd. for $C_{60}H_{72}CoN_8O_4$ $[M^+]$ 1027.5008, found 1027.4739.

Chloro[1,8,15,22-tetrakis(2,4-dimethyl-3-pentyloxy)phthalocyaninato]manganese(III) (9): A mixture of the metal-free phthalocyanine **8** (50 mg, 0.05 mmol) and $Mn(OAc)_2{\cdot}2H_2O$ (10 mg, 0.05 mmol) in DMF (3 mL) was heated at 60 °C for 4 h. Water (10 mL) was then added and the resulting mixture was washed with hexane (3 × 15 mL) to remove unchanged **8**. The obtained brown aqueous layer was mixed with saturated brine (5 mL), and the mixture was then extracted with $CHCl_3$ (3 × 15 mL). The combined reddish-brown extracts were dried with anhydrous $MgSO_4$ and the solvents evaporated in vacuo to give a brown residue, which was purified by column chromatography on neutral alumina using hexane/ethyl acetate (4:1) as eluent. The crude product was further purified by recrystallization from hexane/THF to give brown needles (48 mg, 88%). $C_{64}H_{80}ClMnN_8O_5$ (**9**·THF): calcd. C 67.93, H 7.13, N 9.91; found C 67.84, H 7.03, N 9.77. HRMS (LSI): *m*/*z* calcd. for $C_{60}H_{72}MnN_8O_4$ $[M^+ - Cl]$ 1023.5057, found 1023.4670.

X-ray Crystallographic Analyses of 3·H_2O, 5·$C_2H_2O_4$, 7·H_2O and 9·H_2O·THF: Single crystals of **3**·H_2O and **7**·H_2O were obtained by layering MeOH onto a $CHCl_3$ solution of **3** or **7**. By adding oxalic acid in the MeOH layer, single crystals of **5**·$C_2H_2O_4$ were obtained similarly. Single crystals of **9**·H_2O·THF were obtained by layering hexane onto a THF solution of **9**. Crystal data and details of data collection and structure refinement are given in Table 2. Data collection for all these compounds was performed with a Bruker SMART CCD diffractometer with Mo-K_α radiation (λ = 0.71073 Å) in a sealed tube at 293 K, using an ω-scan mode with an increment of 0.3°. Preliminary unit cell parameters were obtained from 45 frames. Final unit cell parameters were derived by global refinements of reflections obtained from integration of all of the frame data. The collected frames were integrated by using the preliminary cell-orientation matrix. The following software was employed: SMART to collect frames of data, index reflections, and determine the lattice constants; SAINT-PLUS to integrate the intensity of reflections and for scaling;[25] SADABS for absorption correction;[26] and SHELXL for space group and structure determination, refinements, graphics, and structure reporting.[27] CCDC-212501 to -212504 contain the supplementary crystallographic data for **3**·H_2O, **5**·$C_2H_2O_4$, **7**·H_2O and **9**·H_2O·THF, respectively. These data can be obtained free of charge at www.ccdc.cam.ac.uk/conts/retrieving.html [or from the Cambridge Crystallographic Data Centre, 12 Union Road, Cambridge CB2 1EZ, UK; Fax: (internat.) + 44-1223/336-033; E-mail: deposit@ccdc.cam.ac.uk].

Acknowledgments

We thank Ms. Hung-Wing Li for technical assistance in the diffraction analyses. This work was supported by The Chinese University of Hong Kong and the Hong Kong Research Grants Council.

[1] [1a] *Phthalocyanines − Properties and Applications*, vols. 1−4 (Eds: C. C. Leznoff, A. B. P. Lever), VCH, New York, **1989−1996**. [1b] N. B. McKeown, *Phthalocyanine Materials: Synthesis, Structure and Function*, Cambridge University Press, Cambridge, **1998**.

 © 2004 Wiley-VCH Verlag GmbH & Co. KGaA, Weinheim

Table 2. Crystallographic data for (phthalocyaninato)metal complexes **3**, **5**, **7**, and **9**

	3·H_2O	**5**·$C_2H_2O_4$	**7**·H_2O	**9**·H_2O·THF
Empirical formula	$C_{60}H_{74}N_8O_5Zn$	$C_{62}H_{74}N_8O_8Pd$	$C_{60}H_{74}CoN_8O_5$	$C_{64}H_{82}ClMnN_8O_6$
Formula mass	1052.64	1165.69	1046.20	1149.77
Crystal size [mm]	0.22 × 0.18 × 0.14	0.34 × 0.32 × 0.20	0.42 × 0.23 × 0.20	0.35 × 0.19 × 0.17
Crystal system	monoclinic	monoclinic	monoclinic	orthorhombic
Space group	$P2_1/c$	$P2_1/c$	$P2_1/c$	$P2_12_12_1$
a [Å]	16.024(4)	15.8995(8)	16.015(3)	13.470(3)
b [Å]	8.619(2)	8.7861(4)	8.5760(10)	31.079(6)
c [Å]	21.726(5)	21.5407(10)	21.708(3)	16.002(3)
β [°]	99.661(5)	100.3590(10)	99.493(4)	90
V [Å^3]	2958.0(12)	2960.1(2)	2940.6(8)	6699(2)
Z	2	2	2	4
F(000)	1120	1224	1114	2448
$D_{calcd.}$ [mg m^{-3}]	1.182	1.308	1.182	1.140
μ [mm^{-1}]	0.468	0.374	0.345	0.289
θ range [°]	2.11−25.00	1.92−25.00	2.11−25.00	1.31−25.00
Reflections	15498	16002	15482	36485
Unique reflections	5200 (R_{int} = 0.0915)	5213 (R_{int} = 0.0306)	5167 (R_{int} = 0.0857)	11769 (R_{int} = 0.2925)
Parameters	377	367	326	715
$R1$ [$I > 2\sigma(I)$]	0.0917	0.0382	0.1096	0.1087
$wR2$ [$I > 2\sigma(I)$]	0.2460	0.1050	0.2991	0.2473
Goodness of fit	0.918	1.005	1.049	0.913

[2] [2a] Z. Bao, A. J. Lovinger, A. Dodabalapur, *Adv. Mater.* **1997**, *9*, 42−44. [2b] G. de la Torre, P. Vázquez, F. Agulló-López, T. Torres, *J. Mater. Chem.* **1998**, *8*, 1671−1683. [2c] J. H. Schön, C. Kloc, Z. Bao, B. Batlogg, *Adv. Mater.* **2000**, *12*, 1539−1542. [2d] D. Dini, M. Barthel, M. Hanack, *Eur. J. Inorg. Chem.* **2001**, 3759−3769.

[3] [3a] H. Ali, J. E. van Lier, *Chem. Rev.* **1999**, *99*, 2379−2450. [3b] C. M. Allen, W. M. Sharman, J. E. van Lier, *J. Porphyrins Phthalocyanines* **2001**, *5*, 161−169.

[4] [4a] B. Meunier, A. Sorokin, *Acc. Chem. Res.* **1997**, *30*, 470−476. [4b] X. Tao, W. Ma, T. Zhang, J. Zhao, *Chem. Eur. J.* **2002**, *8*, 1321−1326.

[5] M. T. M. Choi, P. P. S. Li, D. K. P. Ng, *Tetrahedron* **2000**, *56*, 3881−3887 and references cited therein.

[6] See, for example: [6a] B. D. Rihter, M. D. Bohorquez, M. A. J. Rodgers, M. E. Kenney, *Photochem. Photobiol.* **1992**, *55*, 677−680. [6b] G. Gümüs, A. Gül, V. Ahsen, *New J. Chem.* **1997**, *21*, 589−594. [6c] A. C. H. Ng, X.-y. Li, D. K. P. Ng, *Macromolecules* **1999**, *32*, 5292−5298. [6d] C. J. Walsh, B. K. Mandal, *Chem. Mater.* **2000**, *12*, 287−289. [6e] A. Bilgin, Y. Gök, *Tetrahedron Lett.* **2002**, *43*, 5343−5347.

[7] [7a] T. Misawa, K. Sugimoto, T. Nishimoto, T. Tsuda, K. Takuma, *Eur. Pat. Appl.* EP 719 839, **1996** (*Chem. Abstr.* **1996**, *125*, 170866d). [7b] H. Wolleb, *PCT Int. Appl.* WO 98 14520, **1998** (*Chem. Abstr.* **1998**, *128*, 302176c).

[8] [8a] M. Hanack, G. Schmid, M. Sommerauer, *Angew. Chem. Int. Ed. Engl.* **1993**, *32*, 1422−1424. [8b] C. Rager, G. Schmid, M. Hanack, *Chem. Eur. J.* **1999**, *5*, 280−288.

[9] S. W. Oliver, T. D. Smith, *J. Chem. Soc., Perkin Trans. 2* **1987**, 1579−1582.

[10] [10a] W. Liu, C.-H. Lee, H.-W. Li, C.-K. Lam, J. Wang, T. C. W. Mak, D. K. P. Ng, *Chem. Commun.* **2002**, 628−629. [10b] C.-H. Lee, D. K. P. Ng, *Tetrahedron Lett.* **2002**, *43*, 4211−4214.

[11] L. S. Beall, N. S. Mani, A. J. P. White, D. J. Williams, A. G. M. Barrett, B. M. Hoffman, *J. Org. Chem.* **1998**, *63*, 5806−5817.

[12] X.-y. Li, D. K. P. Ng, *Eur. J. Inorg. Chem.* **2000**, 1845−1848.

[13] S. Knecht, K. Dürr, G. Schmid, L. R. Subramanian, M. Hanack, *J. Porphyrins Phthalocyanines* **1999**, *3*, 292−298.

[14] For the aquo(porphyrinato)zinc(II) complexes $Zn(OH_2)$(TPP) (TPP = *meso*-tetraphenylporphyrinate) and $Zn(OH_2)$(TMP) (TMP = *meso*-tetramesitylporphyrinate), the Zn−OH_2 distance is 2.20 and 2.22 Å, respectively; see: [14a] M. D. Glick, G. H. Cohen, J. L. Hoard, *J. Am. Chem. Soc.* **1967**, *89*, 1996−1998. [14b] H. Song, W. R. Scheidt, *Inorg. Chim. Acta* **1990**, *173*, 37−41.

[15] See, for example: [15a] E. C. Constable, M. A. M. Daniels, M. G. B. Drew, D. A. Tocher, J. V. Walker, P. D. Wood, *J. Chem. Soc., Dalton Trans.* **1993**, 1947−1958. [15b] J. D. Zubkowski, D. L. Perry, E. J. Valente, S. Lott, *Inorg. Chem.* **1995**, *34*, 6409−6411.

[16] M. K. Engel, in *The Porphyrin Handbook*, vol. 20 (Eds.: K. M. Kadish, K. M. Smith, R. Guilard), Academic Press, San Diego, **2003**, chapter 122.

[17] S. Matsumoto, K. Matsuhama, J. Mizuguchi, *Acta Crystallogr., Sect. C* **1999**, *55*, 131−133.

[18] G. Ricciardi, A. Bavoso, A. Bencini, A. Rosa, F. Lelj, F. Bonosi, *J. Chem. Soc., Dalton Trans.* **1996**, 2799−2807.

[19] L. J. Boucher, in *Coordination Chemistry of Macrocyclic Compounds* (Ed.: G. A. Melson), Plenum, New York, **1979**, p. 527.

[20] [20a] L. H. Vogt, A. Zalkin, D. H. Templeton, *Inorg. Chem.* **1967**, *6*, 1725−1730. [20b] A. Geiß, M. Keller, H. Vahrenkamp, *J. Organomet. Chem.* **1997**, *541*, 441−443.

[21] N. Kobayashi, *Coord. Chem. Rev.* **2001**, *219−221*, 99−123.

[22] G. R. Desiraju, *CrystEngComm* **2002**, *4*, 499.

[23] [23a] U. Geiser, B. L. Ramakrishna, R. D. Willett, F. B. Hulsbergen, J. Reedijk, *Inorg. Chem.* **1987**, *26*, 3750−3756. [23b] R. Baggio, M. T. Garland, M. Perec, *Inorg. Chem.* **1997**, *36*, 737−739.

[24] H. Wolleb, *Eur. Pat. Appl.* EP 703 280, **1996** (*Chem. Abstr.* **1996**, *124*, 292301r).

[25] *SMART and SAINT for Windows NT Software Reference Manuals*, Version 5.0, Bruker Analytical X-ray Systems, Madison, WI, **1997**.

[26] G. M. Sheldrick, *SADABS − A Software for Empirical Absorption Correction*, University of Göttingen, Germany, **1997**.

[27] *SHELXL Reference Manual*, Version 5.1, Bruker Analytical X-ray Systems, Madison, WI, **1997**.

Received July 16, 2003
Early View Article
Published Online November 19, 2003

 © 2004 Wiley-VCH Verlag GmbH & Co. KGaA, Weinheim

η^1-P_{basal} Coordination of P_4X_3 (X = S, Se) Molecules toward 16e Ruthenium Fragments

Massimo Di Vaira,[a] Isaac de los Rios,[a] Fabrizio Mani,[a] Maurizio Peruzzini,[b] and Piero Stoppioni*[a]

Keywords: Ruthenium / Cyclopentadienyl ligands / Bidentate ligands / Density functional calculations

Ruthenium(II) pentamethylcyclopentadienyl complexes [Ru(η^5-C_5Me_5)Cl(L–L)] [L–L = 1,2-bis(diphenylphosphanyl)-ethane, dppe (**1**), bis(diphenylphosphanyl)methane, dppm, *cis*-1,2-bis(diphenylphosphanyl)ethylene, dppet, and (1-diphenylarsanyl-2-diphenylphosphanyl)ethane, dpadppe] treated with a stoichiometric amount of P_4X_3 (X = S, Se) in THF have yielded the compounds [Ru(η^5-C_5Me_5)(L–L)-(P_4X_3)]BPh_4 (X = S, Se). In the P_4Se_3 derivatives the heptatomic cage is bound to the metal through a basal phosphorus atom. The P_4S_3 derivatives have been obtained as pairs of coordination isomers, with the cage linked either through the apical or through one of the basal P atoms, the latter form predominating (95% abundance), irrespective of the L–L ligand. The monometal complex [Ru(η^5-C_5Me_5)(dppe)(η^1-P_{basal}-P_4Se_3)]BPh_4 reacts with **1** to afford the dimetal compound [{Ru(η^5-C_5Me_5)(dppe)}$_2$(μ,$\eta^{1:1}$-P_{basal}-P_{apical}-P_4Se_3)]-(BPh_4)$_2$, where the cage exhibits both modes of bonding. The compounds have been characterized by NMR spectra (^{1}H, ^{13}C and ^{31}P) and elemental analyses. A theoretical analysis of the bonding properties of the two coordination isomer types is also presented.

(© Wiley-VCH Verlag GmbH & Co. KGaA, 69451 Weinheim, Germany, 2004)

Introduction

The mixed cage molecules E_4X_3 (E = P, As; X = S, Se) (Scheme 1, **I**) possess a unique structure exhibiting a pseudo-tetrahedral array of pnicogen atoms, where a homocyclic E_3 unit is connected via three bridging chalcogen atoms to a single pnicogen in the apical position.[1] Their behaviour towards transition metal fragments has been widely studied and various compounds containing E_mX_n units, which originate from the disruptive fragmentation of the heptatomic cages, particularly P_4S_3 and As_4S_3, have been described.[2−6] Although such units, stabilized by the metal moieties, are considered to form through stepwise disruption and/or formation of E−E bonds following the initial interaction of the intact E_4X_3 cage with the metal fragment, primary complexation of the cages has been accomplished only in few instances, e.g. with Lewis acidic metal fragments which, upon coordination, yield electronically saturated compounds having either octahedral, e.g. [$M(CO)_{5-x}(\eta^1$-$P_4S_3)_{1+x}$] [Scheme 1: M = Mo, W; x = 0

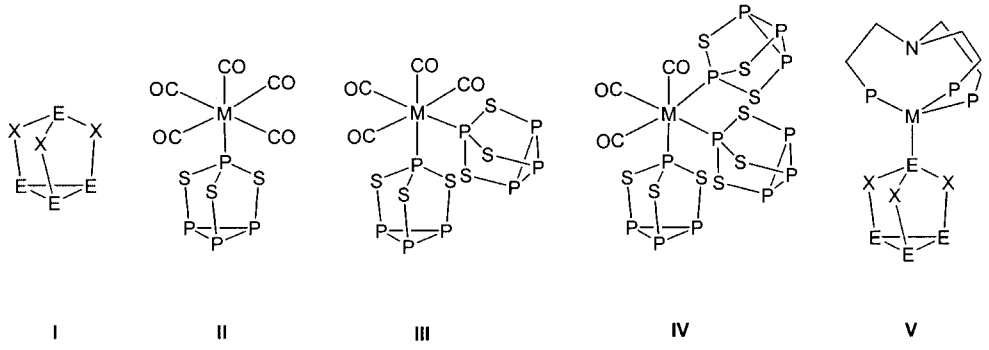

Scheme 1

[a] Dipartimento di Chimica, Università di Firenze,
via della Lastruccia n. 3, 50019 Sesto Fiorentino, Firenze, Italy
[b] ICCOM-CNR,
via Madonna del Piano, 50019 Sesto Fiorentino, Firenze, Italy
E-mail: piero.stoppioni@unifi.it

Supporting information for this article is available on the WWW under http://www.eurjic.org or from the author.

(**II**);[7] M = Cr, Mo, W; $x = 1$, (**III**);[8] M = Cr, Mo; $x = 2$ (**IV**)[8]], or tetrahedral geometry in the presence of sterically protecting groups on the coligand, e.g. $[(NP_3)M(\eta^1\text{-}P_4X_3)]$, **V** [$NP_3$ = tris(diphenylphosphanylethyl)amine; M = Ni,[9] Pd;[10] X = S, Se].

All of the above compounds, characterized by either X-ray diffraction analysis or ^{31}P NMR spectroscopy, contain the cage bound to the metal through the apical phosphorus atom, which, accordingly, has been considered a better donor than a basal phosphorus atom. Recently the 16e $[(triphos)Re(CO)_2]^+$ fragment[11] [triphos = 1,1,1-tris(diphenylphosphanylmethyl)ethane] has yielded, in the presence of P_4X_3 (X = S, Se), a mixture of Re-η^1-P_{apical} and Re-η^1-P_{basal} complexes, the latter being predominant (ca. 87%). Both, apical and basal P_4X_3 complexes with the Lewis acids BBr_3, BI_3 and $NbCl_5$ have been reported.[12] Conversely, P_4X_3 weak complexes with the silver ion have been reported in which the intact cage interacts with the metal through one sulfur and both the apical and one basal P atoms.[13]

We report here on the synthesis and characterization of the family of novel η^1-tetraphosphorus trichalcogenide complexes $[Ru(\eta^5\text{-}C_5Me_5)(L{-}L)(\eta^1\text{-}P_4X_3)]BPh_4$ [L−L = 1,2-bis(diphenylphosphanyl)ethane, dppe, bis(diphenylphosphanyl)methane, dppm, *cis*-1,2-bis(diphenylphosphanyl)ethylene, dppet, and (1-diphenylarsanyl-2-diphenylphosphanyl)ethane, dpadppe; X = S, Se]. In the P_4Se_3 derivatives the intact cage is bound to the metal fragment through a basal P atom. The P_4S_3 compounds present a mixture of Ru-η^1-P_{apical} and Ru-η^1-P_{basal} coordination isomers. All compounds have been characterized by NMR measurements. L−L ligands with different electronic and geometric requirements do not affect the binding properties of the metal fragments, which are highly specific for a basal phosphorus atom of the cage. The monometal complex $[Ru(\eta^5\text{-}C_5Me_5)(dppe)(\eta^1\text{-}P_{basal}\text{-}P_4Se_3)]BPh_4$ yields, in the presence of $[Ru(\eta^5\text{-}C_5Me_5)Cl(dppe)]$, the dinuclear compound $[\{Ru(\eta^5\text{-}C_5Me_5)(dppe)\}_2(P_4Se_3)](BPh_4)_2$ which combines the Ru-η^1-P_{apical} and Ru-η^1-P_{basal} coordination modes. Repeated attempts to obtain the compounds in crystalline form, suitable for X-ray investigations, failed. Their structures and bonding were then investigated by computational methods.

Results and Discussion

The pseudo-octahedral complexes $[Ru(\eta^5\text{-}C_5Me_5)Cl(L{-}L)]$ [L−L = ddpe (**1**), dppm (**2**), dppet (**3**), dpadppe (**4**)], which easily dissociate the chloride in solution,[14−16] react in THF with one equivalent of P_4X_3 (X = S, Se) to form a brick-red solution. Upon addition of $NaBPh_4$ and after workup the compounds $[Ru(\eta^5\text{-}C_5Me_5)(L{-}L)(\eta^1\text{-}P_4X_3)]BPh_4$ are isolated as microcrystalline solids in fairly good yield. The solids are soluble in CH_2Cl_2, THF and $(CH_3)_2CO$; they are stable under an inert atmosphere and may be handled in air for a limited time. Elemental analysis of the products confirms the formation of 1:1 adducts between the $[Ru(\eta^5\text{-}C_5Me_5)(L{-}L)]^+$ synthon and the P_4X_3 molecule. The formation of the P_4X_3 derivatives is sketched in Scheme 2.

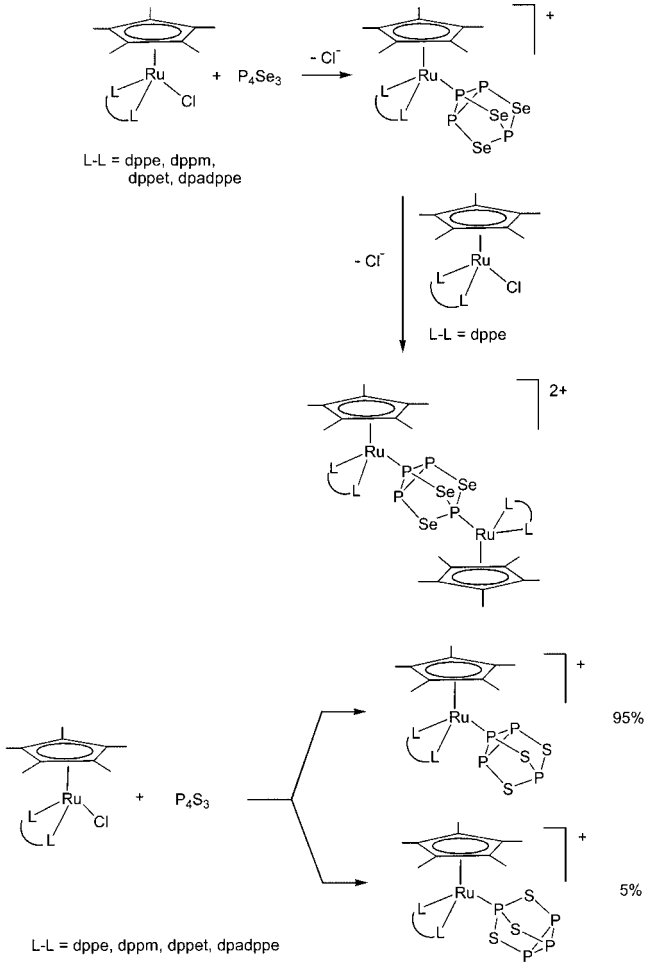

Scheme 2

The compounds have been characterized by ^1H, $^{13}C\{^1H\}$ and $^{31}P\{^1H\}$ NMR measurements. The intensity ratios of the $^{31}P\{^1H\}$ signals accord with the proposed formulae; the NMR spectroscopic data of the uncoordinated and the coordinated P_4X_3 cages, and the labelling scheme used for the different phosphorus nuclei, are shown in Table 1.

Characterization of the P_4Se_3 Coordination Compounds

The P_4Se_3 derivatives $[Ru(\eta^5\text{-}C_5Me_5)(L{-}L)(P_4Se_3)]BPh_4$ [L−L = dppe (**5**), dppm (**6**) and dppet (**7**)] exhibit in their $^{31}P\{^1H\}$ NMR spectra an A_2FM_2Q spin system which is consistent with the P_4Se_3 cage molecule being bound to the metal through one basal phosphorus atom. The diphosphane ligand P atoms (P_A) of each compound yield a doublet due to coupling with the P_Q atom of the cage bound to the metal; both the chemical shifts and coupling constants have values expected for ruthenium(II) half-sandwich compounds.[10,14,17] The heptatomic cage yields the FM_2Q part of the spin system (Table 1). The two equivalent uncoordinated basal P_M atoms yield a doublet of doublets in the

 © 2004 Wiley-VCH Verlag GmbH & Co. KGaA, Weinheim

Table 1. $^{31}P\{^1H\}$ NMR spectroscopic data of the free and coordinated P_4Se_3 and P_4S_3 ligands

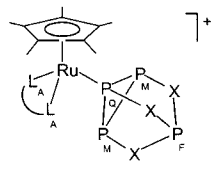

5–8 (X = Se)
10–13 (X = S), major isomer

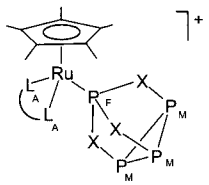

10–13 (X = S), minor isomer

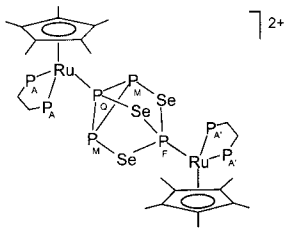

9

Compound	Chemical shift, δ(ppm)[a]			Coupling constant, J(Hz)			
	P_F	$P_M/P_{M'}$[b]	P_Q	$^2J(P_F-P_M)$	$^2J(P_F-P_Q)$	$^1J(P_M-P_Q)$/ $^1J(P_{M'}-P_Q)$[b]	$^1J(P_M-P_{M'})$[b]
P_4Se_3	30.7 (q)	−114.1 (d)		72.0			
5[c]	68.4 (dt)	−125.4 (dd)	41.2 (dtt)	59.5	51.0	244.0	
6[d]	67.7 (dt)	−131.2 (dd)	41.1 (dtt)	60.5	52.0	243.8	
7[c]	59.3 (dt)	−125.3 (dd)	40.9 (dtt)	64.1	49.8	244.1	
8[d],[e]	65.8 (dt)	−149.8 (dddd)	34.7 (dddd)	59.2	53.3	249.4	103.7
		−133.7 (ddd)				238.7	
9[c]	125.7 (dtt)	−116.8 (dd)	20.6 (dtt)	46.1	19.4	211.4	
P_4S_3	65.1 (q)	−127.3 (d)		70.0			
10 major isomer[c]	93.9 (dt)	−141.9 (dd)	35.5 (dtt)	60.2	44.9	243.2	
10 minor isomer	150.6 (m)	−120.5 (d)		22.8			
11 major isomer[c]	91.3 (dt)	−148.8 (dd)	29.7 (dtt)	60.7	46.0	243.3	
11 minor isomer	142.7 (m)	−114.9 (d)		15.0			
12 major isomer[c]	90.0 (dt)	−143.6 (dd)	31.9 (dtt)	64.1	44.8	242.3	
12 minor isomer	155.5 (m)	−119.4 (d)		20.4			
13 major isomer[c] [e]	90.4 (dt)	−149.8 (dddd)	34.7 (dddd)	61.5	47.0	244.8	101.8
		−143.4 (ddd)				236.4	
13 minor isomer	147.2 (m)	−121.9 (d)		24.4			

[a] NMR spectra were recorded at room temperature with a Varian Gemini g300bb spectrometer. Key: d = doublet, t = triplet, q = quadruplet, m = multiplet. [b] P_M atoms of compounds with the phosphars ligands **8** and **13** (major isomer) are diastereotopic. [c] Spectrum recorded in CD_2Cl_2. [d] Spectrum recorded in $(CD_3)_2CO$. [e] Only one P_A atom present.

spectra of **5, 6** and **7**, characterized by a small coupling with P_F and a large one to P_Q (ca. 240 Hz). The dpadppe compound **8** exhibits an AFMM′Q spin system in which the two basal uncoordinated phosphorus atoms of the cage are diastereotopic for L−L ligands of different donors (one P and one As) which make the ruthenium atom chiral. The resonance of P_M atoms is moderately shielded with respect to the three equivalent basal P atoms of the free cage (Table 1), whereas the P_Q resonance is shifted notably downfield. The uncoordinated P_F apical atom of the cage in **5−8** yields a doublet of triplets which is slightly downfield shifted with respect to the free ligand. The spectra of compounds **5**, **6** and **7** do not change from −60 to +50 °C (^{31}P NMR experiment in a sealed tube). Due to the limited solubility of the compounds ^{77}Se NMR spectra were not recorded.

The monometal compound [Ru(η^5-C_5Me_5)(dppe)(P_4Se_3)]BPh_4 (**5**) dissolved in THF reacts with the chloride labile **1** to form, after workup, the dimetal species [{Ru(η^5-C_5Me_5)(dppe)}$_2$(P_4Se_3)]$(BPh_4)_2$ (**9**). The ^{31}P NMR spectrum of the compound (Table 1) yields an $A_2A'_2FM_2Q$ spin system, consistent with double metallation of the P_4Se_3 molecule, which holds the two non-equivalent [{Ru(η^5-C_5Me_5)(dppe)] metal units together and is responsible for the FM_2Q part of the spin system. The coupling constants of the two resolved multiplets due to the cage phosphorus atoms (the apical and a basal one) bound to the metal fragments are particularly useful to assign the signals of the dppe ligands in the two ruthenium fragments, occurring in a narrow region (71.1 and 72.0 ppm). The apical phosphorus atom of P_4Se_3 bound to the metal undergoes a significant downfield shift upon coordination; the same trend, although less pronounced, occurs for the [(triphos)Re(CO)$_2$(P_4Se_3)]$^+$ cation.[11] Although polymetallic cluster compounds containing two[18] or three[19] bridging P_4S_3 units, formed through activation of a P−P bond, and tetrametallic compounds containing the P_4Se_3 unit, resulting from the cleavage of P−P and P−Se bonds,[6] have been described, the present dimetal species exhibits the intact P_4Se_3 molecule in a bridging position between two transition metal fragments, in analogy with the very recently reported P_4S_3 silver adducts.[13]

Characterization of the P_4S_3 Coordination Compounds

The $^{31}P\{^1H\}$ NMR spectra of the [Ru(η^5-C_5Me_5)(L-L)(P_4S_3)]BPh_4 compounds [L−L = dppe (**10**), dppm (**11**), dppet (**12**) and dpadppe (**13**)] indicate a pair of coordination isomers, present in a ratio of ca. 19:1, that differ in the bonding mode of the P_4S_3 molecule to the metal fragment: either through the apical P or through one of the

 © 2004 Wiley-VCH Verlag GmbH & Co. KGaA, Weinheim

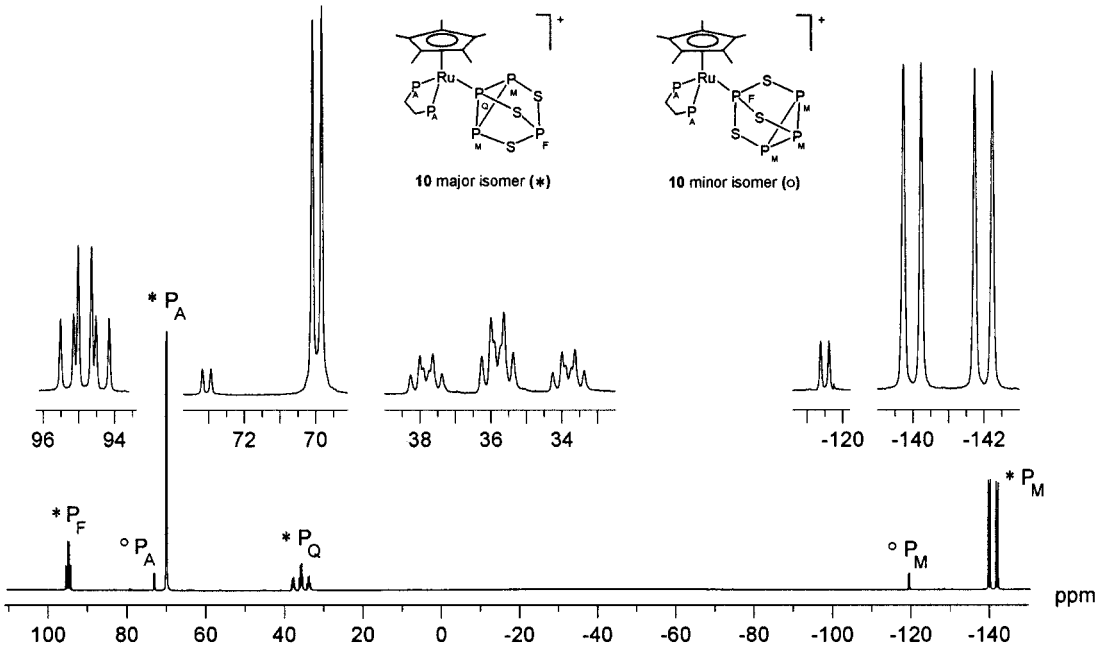

Figure 1. $^{31}P\{^{1}H\}$ NMR spectrum of $[Ru(\eta^5\text{-}C_5Me_5)(dppe)(P_4S_3)]BPh_4$ in CD_2Cl_2. The multiplet due to P_F of the minor isomer, a weak, broad signal at $\delta = 150.6$ ppm, is not reported.

basal P atoms (Scheme 2). This is supported by the $^{31}P,^{31}P$-2D COSY NMR spectra of **10** and **11**, which show two sets of correlated peaks. The $^{31}P\{^{1}H\}$ spectrum of $[Ru(\eta^5\text{-}C_5Me_5)(dppe)(P_4S_3)]BPh_4$ (**10**) is shown in Figure 1.

The major isomers of **10**, **11** and **12** exhibit an A_2FM_2Q spin system (Table 1), indicative of coordination by the cage through a basal P atom. The spectral features parallel those of the P_4Se_3 derivatives, with the cage accounting for the FM_2Q part of the spin system. The P_M signal is split, with unequal P_M-P_Q and P_M-P_F coupling constants, as found for **5**−**7** and the related rhenium compound $[(triphos)Re(CO)_2(P_4S_3)]^+$.[11] The downfield shift of the P_Q signal is larger than that of the rhenium analog.[11] As discussed above for **8**, the major isomer of the dpadppe derivative **13** exhibits an AFMM′Q spin system due to the chirality of the metal atom. The chemical shifts and coupling constants are similar to those of the major isomers of **10**−**12**.

The minor isomers of **10**, **11** and **12** exhibit an A_2FM_3 spin system (Table 1), consistent with coordination of the intact cage to the metal via the apical P_F atom. The L−L ligand P_A atoms yield a doublet at the expected field. The FM_3 part of the splitting pattern, due to the cage, exhibits chemical shifts and coupling constants in agreement with those of the corresponding coordination isomer of the rhenium compound previously described.[11] The signals of the P_4S_3 phosphorus atoms do not significantly depend on the ancillary L−L ligand (Table 1). Notably, the ruthenium-bonded P_F atom resonance occurs at low field (142−155 ppm) as a complex multiplet due to coupling with P_A and P_M; the P_F-P_M coupling constant is smaller than for the free cage (Table 1) and approaches that with the phosphane P_A. In keeping with the proposed structure, the three basal P_M atoms afford a doublet due to coupling with P_F. The minor isomer of the dpadppe derivative, **13**, yields an AFM_3 spin system, as expected, due to the presence of only one magnetically active P atom in the dpadppe ligand. The $^{31}P\{^{1}H\}$ NMR spectra of **10**, **11** and **13**, obtained in the temperatures range −60 to +50 °C (experiment in a sealed tube), do not show any dynamic process and the relative amounts of the two isomers do not change. This rules out an equilibrium between the two species which, therefore, should form through independent interactions of the basal and the apical phosphorus atoms of the cage.

Quantum-Mechanical Calculations

In the absence of crystallographic structural data on the compounds quantum-mechanical calculations were undertaken to gain information on the geometries, the relative energies of isomers and to possibly rationalize structural preferences. As described in the Exp. Sect., building on results from preliminary calculations performed on models at various levels of accuracy, the geometry of the lowest-energy conformer found for each of the coordination modes of the cage molecule in the $[Ru(\eta^5\text{-}C_5Me_5)(dppe)(P_4S_3)]^+$ cation (i.e., coordination through the apical phosphorus atom, P_{apc} hereafter, or through a basal one, P_{bas}), was optimized at the B3LYP/6−31G(d) level, with metal atom ECP functions.[20] These two models will be referred to as **10**apc and **10**bas, respectively. After Se for S substitution in the former models and subsequent optimizations, models **5**apc and **5**bas for the $[Ru(\eta^5\text{-}C_5Me_5)(dppe)(P_4Se_3)]^+$ cation were obtained. Representations of the **10**apc and **10**bas isomers are shown in Figure 2; those of the **5**apc and **5**bas models are similar and are given, with more details, with the Sup-

 © 2004 Wiley-VCH Verlag GmbH & Co. KGaA, Weinheim

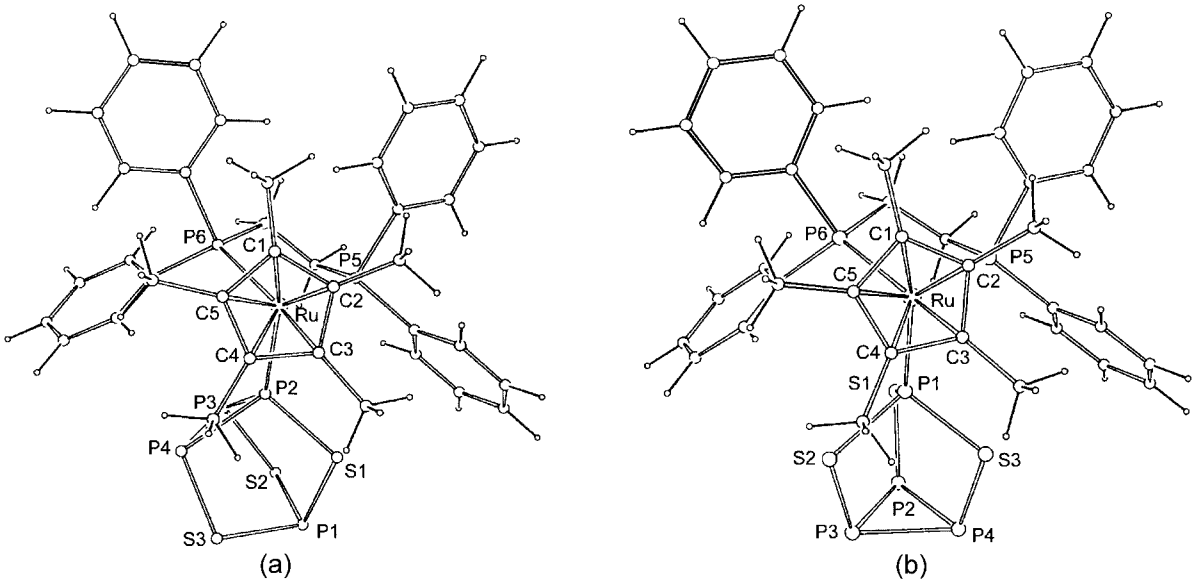

Figure 2. Optimized geometries for the $[Ru(\eta^5\text{-}C_5Me_5)(dppe)(P_4S_3)]^+$ cation with the cage molecule coordinated (a) through a basal phosphorus atom, model **10**bas, and (b) through the apical phosphorus atom, model **10**apc.

Table 2. Relative energies (kJ·mol^{-1}) and selected bond lengths (Å) for the **10**bas and **10**apc models of $[Ru(\eta^5\text{-}C_5Me_5)(dppe)(P_4S_3)]^+$ isomers and for the **5**bas and **5**apc models of $[Ru(\eta^5\text{-}C_5Me_5)(dppe)(P_4Se_3)]^+$ isomers

	10bas[a]	**10**apc[a]	**5**bas[a]	**5**apc[a]
ΔE	0	9.11	0	13.39
Ru−P(5)	2.404	2.413	2.398	2.406
Ru−P(6)	2.425	2.448	2.428	2.445
Ru−C(1)	2.318	2.317	2.316	2.316
Ru−C(2)	2.342	2.345	2.339	2.343
Ru−C(3)	2.316	2.328	2.315	2.330
Ru−C(4)	2.324	2.358	2.329	2.367
Ru−C(5)	2.320	2.323	2.323	2.329
Ru−P(n)[b]	2.346	2.339	2.360	2.364
P(1)−S(1)[c]	2.129	2.173	2.266	2.323
P(1)−S(2)	2.165	2.175	2.305	2.326
P(1)−S(3)	2.164	2.163	2.303	2.309
S(1)−P(2)	2.151	2.122	2.300	2.262
S(2)−P(3)	2.126	2.118	2.266	2.257
S(3)−P(4)	2.124	2.120	2.264	2.260
P(2)−P(3)	2.285	2.287	2.282	2.280
P(2)−P(4)	2.284	2.289	2.278	2.281
P(3)−P(4)	2.293	2.289	2.283	2.280

[a] Atomic labels as in Figure 2. [b] n = 1: **10**apc and **5**apc, n = 2: **10**bas and **5**bas. [c] Bond lengths (Å) within the free cage molecules (possessing threefold symmetry), from calculations at the B3LYP/6−31G(d) level, are [averages of experimental values from ref.[21] (P_4S_3) and refs.[10,19,22] (P_4Se_3) in parentheses]: P_4S_3, P_{apc}−S = 2.150 (2.06), P_{bas}−S = 2.139 (2.09), P_{bas}−P_{bas} = 2.276 (2.23); P_4Se_3, P_{apc}−Se = 2.276 (2.25), P_{bas}−Se = 2.264 (2.23), P_{bas}−P_{bas} = 2.270 (2.24).

porting Information (S.I.). Relative energy values within isomer pairs and essential data on geometries are presented in Table 2.

For both pairs of isomers the calculations yielded the species with the cage bound through the base as being slightly more stable than the "apical" isomer, with increasing energy separation between the isomers on going from the models of the P_4S_3 derivative to those of P_4Se_3. Although this trend qualitatively agrees with the NMR spectroscopic data, it is difficult to rationalize in terms of a restricted number of factors, due to the complexity of the systems and to the fine balance in energies. However, the following considerations may shed some light on the preferences for the two coordination modes of these cage molecules with respect to the $Ru(\eta^5\text{-}C_5Me_5)(dppe)$ metal−ligand system.

From calculations at the consistent B3LYP/6−31G(d) level on the isolated P_4S_3 and P_4Se_3 molecules, the (twofold degenerate) HOMO for both systems has important contributions from the P_{bas} atoms. An MO with dominant P_{apc} contribution lies 69.0 kJ·mol^{-1} (P_4S_3) and 89.9 kJ·mol^{-1} (P_4Se_3) below the HOMO; the situation is not substantially altered if calculations on the cages are performed at a better level, such as the B3LYP/6−31++G(2d). This suggests that, based only on these energy differences, a P_{bas} atom should be a better donor than P_{apc}, particularly for the P_4Se_3 cage, towards empty metal orbitals. Conversely, according to the localized orbital picture of the NBO approach, the lone pair (lp) of a P_{bas} atom lies at lower energy than the P_{apc} lp; however, the gap between the two decreases (from 66.9 to 26.3 kJ·mol^{-1}) on going from P_4S_3 to P_4Se_3.

The NBO analysis generally describes, at second-order perturbation theory level, the interaction between the cage and the metal as mostly consisting of donation from the P_{bas} (or P_{apc}) lp into a lobe of an antibonding orbital of the metal−ligand moiety. The **5**bas model, however, is peculiar since (a) the P_{bas} lp is involved in more than one fractional interaction of the above type, (b) Ru empty orbitals, rather than Ru-based antibonding acceptor MOs, are involved in

 © 2004 Wiley-VCH Verlag GmbH & Co. KGaA, Weinheim

such interactions and (c) no significant repulsive interactions of the P_{bas} lp with bonding (filled) orbitals of the metal moiety are detected, contrary to the other three models. These features, pointing to a comparatively higher strength of the P_{bas}−Ru interaction in the **5**bas system, result from several small changes in MO compositions and energies, and are difficult to analyse in deeper detail. Overall, the cage molecules transfer electron density to the metal moiety, with apparently negligible back-donation, according to the NBO perturbation treatment (but see below: changes in antibonding orbital populations). The amount of transferred charge (q, a.u.) increases from apical to basal coordination and, for a given coordination mode, increases on going from P_4S_3 to P_4Se_3. The, perhaps slightly overestimated, $|q|$ are: 0.196 **10**apc, 0.214 **10**bas, 0.199 **5**apc and 0.228 **5**bas.

The cage molecules undergo only small changes in geometry upon coordination, although some trends are evident. The most significant of these may be rationalized by considering the variations in the populations of the bonding and (to a greater extent) antibonding localized orbitals, according to the NBO picture. In particular, the 0.02 Å (P_4S_3) or 0.04 Å (P_4Se_3) elongation of the P_{apc}−S/Se bonds upon coordination in the apical mode (Table 2, including footnote c for the free cage molecules) can be accounted for by the modest decrease (1%) in the P_{apc}−S/Se bonding populations and considerable increase in the antibonding ones (e.g., from 0.137 to an average 0.205 a.u. for **10**apc) for both cages. Similarly, for basal coordination by P_4S_3 (**10**bas; trends are strictly similar for the Se analog **5**bas) where the P(2)−S(1) bond elongates by 0.012 Å and the S(1)−P(1) bond shortens by 0.021 Å with respect to the computed free cage values, the corresponding antibonding orbital NBO populations increase (from 0.080 to 0.153 a.u.) and, respectively, decrease (from 0.137 to 0.103 a.u.). Such trends, predominantly indicative of back donation, may be reconciled with the overall flow of negative charge *towards* the metal moiety considering that complex charge redistributions are allowed by the topology of the cage molecules.

As noted for the P_4S_3 molecule in a related study,[11] calculated bond lengths for both cage molecules here, whether coordinated or uncoordinated (Table 2), are slightly larger than the experimental values;[10,21−23] this could be due in part to effects of thermal motion causing an apparent shortening of the bonds in the diffraction experiments on the free cage molecules. The calculated Ru-P(dppe) distances (Table 2) are longer than generally found for dppe ruthenium complexes with a similar environment, although the experimental values span a large range, e.g., from 2.28 [24] to 2.41 Å.[25] Also, the calculated Ru−C are longer than the experimental ranges for η^5-C_5Me_5 (2.20−2.26 Å,[26] 2.25−2.34 Å[25]). These results may reflect the limitations of the present approach (nature of the particular DFT potential[27−29] and of the metal ECP[20] used), but may be caused by overcrowding around the metal atom in the present systems. A theoretical study on the adducts of the present cage molecules with BX_3 (X = Br, I) and $NbCl_5$ Lewis acids[12] has reached quite similar conclusions for the energetics, although more detailed comparisons are prevented by differences between the systems.

Conclusions

$[Ru(\eta^5\text{-}C_5Me_5)(L\text{-}L)]^+$ metal fragments are rather specific for basal coordination by the P_4X_3 cage molecules, independently of moderate changes in the L−L ligand. Combined with previous results for $[(triphos)Re(CO)_2(P_4X_3)]CF_3SO_3$ compounds,[11] the present ones suggest that the coordination mode of the P_4X_3 molecules through one of the basal phosphorus atoms is competitive with the apical mode and the balance between the two coordination isomers may be set by subtle properties of the metal fragments and by minor features of their interactions with the cage molecules.

Experimental Section

All reactions and manipulations were performed under an atmosphere of dry oxygen-free argon. THF was freshly distilled from sodium; dichloromethane, *n*-hexane, methanol and ethanol were degassed and flushed with argon prior to use. The ^1H, $^{31}P\{^1H\}$ and $^{13}C\{^1H\}$ NMR spectra were measured on a Varian Gemini g300bb spectrometer, equipped with a variable-temperature unit, operating at 300 MHz (^1H), 121.46 MHz (^{31}P) and 75.46 MHz (^{13}C). Chemical shifts are relative to tetramethylsilane and to H_3PO_4 85% as external standards at δ = 0.00 ppm; coupling constants are given in Hertz. Analytical data for carbon, hydrogen and sulfur were obtained from the Microanalytical Laboratory of the Department of Chemistry of the University of Firenze. The ligands 1,2-bis(diphenylphosphanyl)ethane (Aldrich), dppe, bis(diphenylphosphanyl)methane (Aldrich), dppm, *cis*-1,2-bis(diphenylphosphanyl)ethylene (Aldrich), dppet, and (1-diphenylarsanyl-2-diphenylphosphanyl)ethane (Pressure Chemical Company), dpadppe, were used as purchased. P_4S_3 was purchased from Fluka AG. and recrystallized from toluene before use. P_4Se_3 was synthesized from red phosphorus and grey selenium as described previously.[30] The complexes $[Ru(\eta^5\text{-}C_5Me_5)Cl(L\text{-}L)]$ [L−L = dppe (**1**) and dppm (**2**)] were synthesized according to the literature method.[14] The complexes $[Ru(\eta^5\text{-}C_5Me_5)Cl(L\text{-}L)]$ [L−L = dppet (**3**) and dpadppe (**4**)] are new and were synthesized by the same procedure reported for **1** and **2**.[14] The ^1H, and $^{13}C\{^1H\}$ NMR spectroscopic data of the compounds, together with the $^{31}P\{^1H\}$ NMR data of the phosphane ligands are reported here. For the minor isomers of **10**−**13** the weak ^1H resonances of the L−L ligand aliphatic protons and the ^{13}C signals were not observed. The uninformative ^1H and $^{13}C\{^1H\}$ signals of phenyl groups of the L−L ligands and of the tetraphenylborate anion, occurring in the expected regions of 6.8−7.5 and 133.5−130.0 ppm, respectively, are not reported.

Syntheses

$[Ru(\eta^5\text{-}C_5Me_5)Cl(dppet)]$ (3): Yellowish orange microcrystals, yield 85%. $C_{36}H_{37}ClP_2Ru$ (668.2): calcd. C 64.7, H 5.6; found C 64.5, H 5.8. ^1H NMR ($CDCl_3$, 298 K): δ = 2.01 [s, 15 H, br, $C_5(CH_3)_5$] and 7.85 (s, 2 H, br, PC*H*). $^{13}C\{^1H\}$ NMR ($CDCl_3$, 298 K): δ = 6.2 [br. s, $C_5(CH_3)_5$], 94.5 [br. s, $C_5(CH_3)_5$] and 137.5 (br. s, P*C*H). $^{31}P\{^1H\}$ NMR ($CDCl_3$, 298 K): δ = 94.5 (s).

$[Ru(\eta^5\text{-}C_5Me_5)Cl(dpadppe)]$ (4): Yellowish orange microcrystals, yield 82%. $C_{36}H_{39}AsClPRu$ (714.1): calcd. C 60.6, H 5.5; found C

60.4, H 5.6. ^{1}H NMR (C_6D_6, 298 K): δ = 1.67 [s, 15 H, br, $C_5(CH_3)_5$], 2.40 (s, 2 H, br, $AsCH_2$) and 2.76 (s, 2 H, br, PCH_2). $^{13}C\{^1H\}$ NMR (C_6D_6, 298 K): δ = 10.1 [br. s, $C_5(CH_3)_5$], 24.1 (br. s, $AsCH_2$), 28.7 (br. s, PCH_2) and 87.6 [br. s, $C_5(CH_3)_5$]. $^{31}P\{^1H\}$ NMR (C_6D_6, 298 K): δ = 76.4 (s).

[Ru(η^5-C_5Me_5)(dppe)(P_4Se_3)]BPh_4 (5): P_4Se_3 (175 mg, 0.5 mmol) dissolved in THF (30 mL) at 40 °C was added to a THF solution (15 mL) of (**1**) (335 mg, 0.5 mmol); neat $NaBPh_4$ (250 mg, 0.7 mmol) was then added. The resulting solution was stirred at room temperature for 2 h. An ethanol/light petroleum (1:1) solution (15 mL) was then slowly added, and orange microcrystals were obtained by slowly evaporating the resulting solution. Yield 60%. $C_{60}H_{59}BP_6RuSe_3$ (1314.7): calcd. C 54.8, H 4.5; found C 54.5, H 4.7. ^{1}H NMR (CD_2Cl_2, 298 K): δ = 1.56 [dt, 15 H, $^4J(H-P_Q)$ = 3.0, $^4J(H-P_A)$ = 1.8 Hz, $C_5(CH_3)_5$], 2.38, 2.82 (m, 4 H, PCH_2). $^{13}C\{^1H\}$ NMR (CD_2Cl_2, 298 K): δ = 10.8 [s, $C_5(CH_3)_5$], 27.3 [t, $^1J(C-P_A)$ = 22.6 Hz, PCH_2], 98.5 [s, $C_5(CH_3)_5$]. $^{31}P\{^1H\}$ NMR (CD_2Cl_2, 298 K): δ = 72.2 [2 P, d, $^2J(P_A-P_Q)$ = 27.5 Hz].

The compounds [Ru(η^5-C_5Me_5)(L-L)(P_4Se_3)]BPh_4 [L−L = dppm (**6**), dppet (**7**) and dpadppe (**8**)] were prepared by the same procedure as for **5**.

[Ru(η^5-C_5Me_5)(dppm)(P_4Se_3)]BPh_4 (6): Yield 62%. $C_{59}H_{57}BP_6RuSe_3$ (1300.7): calcd. C 54.5, H 4.4; found C 54.8, H 4.3. ^{1}H NMR [$(CD_3)_2CO$, 298 K]: δ = 1.79 [dt, 15 H, $^4J(H-P_Q)$ = 3.0, $^4J(H-P_A)$ = 2.1 Hz, $C_5(CH_3)_5$], 3.91, 4.72 (1 H each, m, PCH). $^{13}C\{^1H\}$ NMR (CD_2Cl_2, 298 K): δ = 11.7 [s, $C_5(CH_3)_5$], 46.1 [t, $^1J(C-P_A)$ = 24.0 Hz, PCH_2], 98.6 [s, $C_5(CH_3)_5$]. $^{31}P\{^1H\}$ NMR (CD_2Cl_2, 298 K): δ = 2.4 [2P, d, $^2J(P_A-P_Q)$ = 29.7 Hz].

[Ru(η^5-C_5Me_5)(dppet)(P_4Se_3)]BPh_4 (7): Yield 60%. $C_{60}H_{57}BP_6RuSe_3$ (1312.7): calcd. C 58.9, H 4.4; found C 58.6, H 4.4. ^{1}H NMR (CD_2Cl_2, 298 K): δ = 1.59 [dt, 15 H, $^4J(H-P_Q)$ = 2.7, $^4J(H-P_A)$ = 1.8 Hz, $C_5(CH_3)_5$]; the ^{1}H and ^{13}C signals of the ligand CH group were masked by the aromatic resonances. $^{13}C\{^1H\}$ NMR [$(CD_3)_2CO$, 298 K]: δ = 11.6 [s, $C_5(CH_3)_5$], 98.6 [s, $C_5(CH_3)_5$], 130.9 [vt, $^1J(C-P_A)$ = 5.8 Hz, PCH)]. $^{31}P\{^1H\}$ NMR [$(CD_3)_2CO$, 298 K]: δ = 76.7 [2P, d, $^2J(P_A-P_Q)$ = 31.9 Hz].

[Ru(η^5-C_5Me_5)(dpadppe)(P_4Se_3)]BPh_4 (8): Yield 63%. $C_{60}H_{59}AsBP_5RuSe_3$ (1358.7): calcd. C 53.0, H 4.4; found C 53.1, H 4.3. ^{1}H NMR [$(CD_3)_2CO$, 298 K]: δ = 1.66 [dd, 15 H, $^4J(H-P_Q)$ = 2.7, $^4J(H-P_A)$ = 1.8 Hz, $C_5(CH_3)_5$], 2.38 (s, 2 H, br, $AsCH_2$), 2.78 (s, 2 H, br, PCH_2). $^{31}P\{^1H\}$ NMR [$(CD_3)_2CO$, 298 K]: δ = 74.4 [1P, dd, $^2J(P_A-P_Q)$], 33.5 [$^3J(P_A-P_M)$ = 6.0 Hz].

[{Ru(η^5-C_5Me_5)(dppe)}$_2$(P_4Se_3)]$(BPh_4)_2$ (9): [Ru(η^5-C_5Me_5)Cl(dppe)] (**1**) (170 mg, 0.25 mmol) dissolved in THF (15 mL) was added to **5** (263 mg, 0.20 mmol) in THF (20 mL). The resulting solution was stirred at room temperature for 1 h; neat $NaBPh_4$ (96 mg, 0.28 mmol) was then added. Orange microcrystals were subsequently obtained by adding an ethanol/light petroleum (1:1) mixture (15 mL) and by concentrating the solution. Yield 50%. $C_{120}H_{118}B_2P_8Ru_2Se_3$ (2268.7): calcd. C 63.5, H 5.2; found C 63.3, H 5.2. ^{1}H NMR (CD_2Cl_2, 298 K): δ = 1.48 [30 H, br, $C_5(CH_3)_5$], 2.43, 2.86 (s, 8 H, br, PCH_2). $^{13}C\{^1H\}$ NMR (CD_2Cl_2, 298 K): δ = 11.2, 11.5 [s, $C_5(CH_3)_5$], 28.5, 29.7 [d, $^1J(C-P_A)$ = 24.0 Hz, (PCH_2)], 99.1, 101.1 [s, $C_5(CH_3)_5$]. $^{31}P\{^1H\}$ NMR (CD_2Cl_2, 298 K): δ = 71.1 [2P, d, P_A, $^2J(P_A-P_Q)$ = 30.4 Hz], 72.0 [2P, d, $P_{A'}$, $^2J(P_A-P_F)$ = 25.5 Hz].

[Ru(η^5-C_5Me_5)(dppe)(P_4S_3)]BPh_4 (10): A THF solution (15 mL) of **1** (335 mg, 0.5 mmol) was added to P_4S_3 (110 mg, 0.5 mmol) dissolved in THF (15 mL); neat $NaBPh_4$ (250 mg, 0.7 mmol) was then added. The resulting solution was stirred at room temperature for 2 h. An ethanol/light petroleum ether (1:1) solution (15 mL) was then slowly added, and yellow microcrystals were obtained by slowly evaporating the resulting solution. Yield 65%. $C_{60}H_{59}BP_6RuS_3$ (1174.0): calcd. C 61.4, H 5.1, S 8.2; found C 60.9, H 5.2, S 8.0. Major isomer: ^{1}H NMR (CD_2Cl_2, 298 K): δ = 1.52 [dt, 15 H, $^4J(H-P_Q)$ = 3.3, $^4J(H-P_A)$ = 1.5 Hz, $C_5(CH_3)_5$], 2.40, 2.80 (m, 4 H, PCH_2). $^{13}C\{^1H\}$ NMR (CD_2Cl_2, 298 K): δ = 10.8 [s, $C_5(CH_3)_5$], 27.4 [t, $^1J(C-P_A)$ = 22.4, PCH_2], 98.6 [s, $C_5(CH_3)_5$]. $^{31}P\{^1H\}$ NMR (CD_2Cl_2, 298 K): δ = 69.3 [2 P, d, $^2J(P_A-P_Q)$ = 31.4]. Minor isomer: ^{1}H NMR (CD_2Cl_2, 298 K): δ = 1.62 [dt, 15 H, $^4J(H-P_F)$ = 2.7, $^4J(H-P_A)$ = 1.5 Hz, $C_5(CH_3)_5$]. $^{31}P\{^1H\}$ NMR (CD_2Cl_2, 298 K): δ = 67.0 [2 P, d, $^2J(P_A-P_F)$ = 28.7 Hz].

The compounds [Ru(η^5-C_5Me_5)(L−L)(P_4S_3)]BPh_4 [L−L = dppm (**11**), dppet (**12**) and dpadppe (**13**)] were prepared by the same procedure as for **10**.

[Ru(η^5-C_5Me_5)(dppm)(P_4S_3)]BPh_4 (11): Yield 65%. $C_{59}H_{57}BP_6RuS_3$ (1160.0): calcd. C 61.4, H 5.1; found C 60.9, H 5.2. Major isomer: ^{1}H NMR (CD_2Cl_2, 298 K): δ = 1.76 [dt, 15 H, $^4J(H-P_Q)$ = 3.3, $^4J(H-P_A)$ = 2.1 Hz, $C_5(CH_3)_5$], 3.98, 4.83 (1 H each, m, PCH_2). $^{13}C\{^1H\}$ NMR (CD_2Cl_2, 298 K): δ = 10.6 [s, $C_5(CH_3)_5$], 45.4 [t, $^1J(C-P_A)$ = 26.1 Hz, PCH_2], 97.9 [s, $C_5(CH_3)_5$]. $^{31}P\{^1H\}$ NMR (CD_2Cl_2, 298 K): δ = 1.9 [2 P, d, $^2J(P_A-P_Q)$ = 30.8 Hz]. Minor isomer: ^{1}H NMR (CD_2Cl_2, 298 K): δ = 1.70 [s, 15 H, br, $C_5(CH_3)_5$]. $^{31}P\{^1H\}$ NMR (CD_2Cl_2, 298 K): δ = 1.31 [2 P, d, $^2J(P_A-P_F)$ = 31.1 Hz].

[Ru(η^5-C_5Me_5)(dppet)(P_4S_3)]BPh_4 (12): Yield 68%. $C_{60}H_{57}BP_6RuS_3$ (1172.0): calcd. C 61.5, H 4.9; found C 61.2, H 4.9. Major isomer: ^{1}H NMR (CD_2Cl_2, 298 K): δ = 1.56 [dt, 15 H, $^4J(H-P_Q)$ = 3.0, $^4J(H-P_A)$ = 1.8 Hz, $C_5(CH_3)_5$]; the CH vinyl proton of the ligand was masked by the aromatic resonances. $^{13}C\{^1H\}$ NMR (CD_2Cl_2, 298 K): δ = 10.7 [s, $C_5(CH_3)_5$], 98.8 [s, $C_5(CH_3)_5$], 129.0 [vt, $^1J(C-P_A)$ = 5.4, PCH]. $^{31}P\{^1H\}$ NMR (CD_2Cl_2, 298 K): δ = 75.7 [2 P, d, $^2J(P_A-P_Q)$ = 32.5 Hz]. Minor isomer ^{1}H NMR (CD_2Cl_2, 298 K): δ = 1.70 [s, 15 H, br, $C_5(CH_3)_5$]. $^{31}P\{^1H\}$ NMR (CD_2Cl_2, 298 K): δ = 73.2 [2 P, d, $^2J(P_A-P_F)$ = 31.6].

[Ru(η^5-C_5Me_5)(dpadppe)(P_4S_3)]BPh_4 (13): Yield 70%. $C_{60}H_{59}AsBP_5RuS_3$ (1218.0): calcd. C 59.2, H 4.9; found C 59.1, H 4.8. Major isomer: ^{1}H NMR (CD_2Cl_2, 298 K): δ = 1.58 [dd, 15 H, $^4J(H-P_Q)$ = 3.3, $^4J(H-P_A)$ = 1.8 Hz, $C_5(CH_3)_5$], 2.44 (s, 2 H, br, $AsCH_2$), 2.78 (s, 2 H, br, PCH_2). $^{13}C\{^1H\}$ NMR (CD_2Cl_2, 298 K): δ = 10.8 [s, $C_5(CH_3)_5$], 20.9 [d, $^2J(C-P_A)$ = 11.0 Hz, $AsCH_2$], 30.1 [dd, $^1J(C-P)$ = 32.7, $^3J(C-P_Q)$ = 5.4 Hz, PCH_2], 97.3 [s, $C_5(CH_3)_5$]. $^{31}P\{^1H\}$ NMR (CD_2Cl_2, 298 K): δ = 73.1 [1 P, dd, $^2J(P_A-P_Q)$ = 36.0, $^3J(P_A-P_M)$ = 7.0]. Minor isomer: ^{1}H NMR (CD_2Cl_2, 298 K): δ = 1.58 [dd, 15 H, $^4J(H-P_Q)$ = 3.3, $^4J(H-P_A)$ = 1.8 Hz, $C_5(CH_3)_5$]. $^{31}P\{^1H\}$ NMR (CD_2Cl_2, 298 K): δ = 76.1 [1 P, d, $^2J(P_A-P_F)$ = 27.4 Hz].

Computational Procedures

Calculations were performed on models of the [Ru(η^5-C_5Me_5)(dppe)(P_4S_3)]$^+$ and [Ru(η^5-C_5Me_5)(dppe)(P_4Se_3)]$^+$ cations with the GAUSSIAN 98 suite of programs,[31] using the hybrid HF-DFT B3LYP method.[27−29] Preliminary geometry optimizations (not reported), were performed (a) on simplified models of the P_4S_3 derivative, where the methyl and phenyl groups were replaced by hydrogen atoms, using the 6−31G(d,p) basis set[32] for the non-metal atoms and the LANL2DZ valence functions and effective core potential (ECP)[20] for ruthenium and (b) on "complete" models, with no simplifying replacements of methyl and phenyl groups using, however, the lower quality 3−21G (C, H) and

 © 2004 Wiley-VCH Verlag GmbH & Co. KGaA, Weinheim

3−21G* (P, S)[33,34] basis sets for the non-metal atoms. In these preliminary calculations coordination by the P_4S_3 cage molecule through the apical phosphorus atom, and through one of its basal P atoms, was considered, no symmetry was imposed. Overall, these calculations revealed a delicate energy balance between geometrical isomers differing in the mode of coordination by the cage. Moreover, for each mode the calculations on the "complete" models revealed the existence of several energy minima, characterized by small differences in the corresponding geometries. This was probably due to the effects of numerous non-bonded interactions between the bulky groups surrounding the metal atom. Computationally demanding geometry optimizations on the "complete" models at the better B3LYP/6−31G(d) level (with LANL2DZ Ru functions as above) were then performed, starting from the lowest-energy arrangement detected in the preliminary search for each of the P_4S_3 coordination modes of the $[Ru(\eta^5\text{-}C_5Me_5)(dppe)(P_4S_3)]^+$ system. The two corresponding models for the $[Ru(\eta^5\text{-}C_5Me_5)(dppe)(P_4Se_3)]^+$ cation were obtained by substitution of Se for S in the former P_4S_3 optimized models and underwent optimization in turn. Frequency calculations were performed for the four final models [a small negative (imaginary) frequency of -11 cm^{-1} for the system with apically bound P_4Se_3, at the verge of significance for residual rotational motion of CH_3 groups, was confidently ignored] and unscaled zero-point energy corrections were applied. The interpretation of results was aided by natural bond orbital (NBO) analyses.[35,36] For graphics MOLDEN[37] and ORTEP[38,39] were employed.

Acknowledgments

We acknowledge financial support from the Italian Ministero dell'Istruzione, dell'Università e della Ricerca. Thanks are also expressed to INTAS for supporting this research (project 00-00018).

[1] J. G. Riess, in *Rings, Cluster and Polymers* (Ed. A. H. Cowley), ACS Symp. Ser., **1983**, vol. 232, p. 17.
[2] M. Di Vaira, P. Stoppioni, M. Peruzzini, *Comments, Inorg. Chem.* **1990**, *11*, 1−19.
[3] M. Di Vaira, P. Stoppioni, *Coord. Chem. Rev.* **1992**, *120*, 259−279.
[4] J. Wachter, *Angew. Chem. Int. Ed.* **1998**, *37*, 751−768.
[5] L. Y. Goh, *Coord. Chem. Rev.* **1999**, *185−186*, 257−276.
[6] L. Y. Goh, W. Chen, R. C. S. Wong, *Organometallics* **1999**, *18*, 306−314.
[7] A. W. Cordes, R. D. Joyner, R. D. Shores, E. D. Dill, *Inorg. Chem.* **1974**, *13*, 132−134.
[8] R. Jefferson, H. F. Klein, J. F. Nixon, *J. Chem. Soc., Chem. Commun.* **1969**, 536−537.
[9] M. Di Vaira, M. Peruzzini, P. Stoppioni, *Inorg. Chem.* **1983**, *22*, 2196−2198.
[10] M. Di Vaira, M. Peruzzini, P. Stoppioni, *J. Organomet. Chem.* **1983**, *258*, 373−381.
[11] E. Guidoboni, I. de Rios, A. Ienco, L. Marvelli, C. Mealli, A. Romerosa, R. Rossi, M. Peruzzini, *Inorg. Chem.* **2002**, *41*, 659−668.
[12] C. Aubauer, E. Irran, T. M. Klapoetke, W. Schnick, A. Schulz, J. Senker, *Inorg. Chem.* **2001**, *40*, 4956−4965.
[13] A. Adolf, M. Gonsior, I. Krossing, *J. Am. Chem. Soc.* **2002**, *124*, 7111−7116.
[14] I. de los Rios, M. J. Tenorio, J. Padilla, M. C. Puerta, P. Valerga, *J. Chem. Soc., Dalton Trans.* **1996**, 377−381.
[15] R. J. Haines, A. L. Du Preez, *J. Organomet. Chem.* **1975**, *84*, 357−367.
[16] P. M. Treichel, D. A. Komar, P. J. Vincenti, *Inorg. Chim. Acta* **1984**, *88*, 151−152.
[17] I. de los Rios, J.-R. Hamon, P. Hamon, C. Lapinte, L. Toupel, A. Romerosa, M. Peruzzini, *Angew. Chem. Int. Ed.* **2001**, *40*, 3910−3912.
[18] C. A. Ghilardi, S. Midollini, A. Orlandini, *Angew. Chem. Int. Ed. Engl.* **1983**, *22*, 790−791.
[19] M. Di Vaira, M. Peruzzini, P. Stoppioni, *J. Chem. Soc., Dalton Trans.* **1985**, 291−295.
[20] P. J. Hay, W. R. Wadt, *J. Chem. Phys.* **1985**, *82*, 270−283.
[21] Y.-C. Leung, J. Waser, S. van Houten, A. Vos, G. A. Wiegers, E. H. Wiebenga, *Acta Crystallogr.* **1957**, *10*, 574−582.
[22] E. Keulen, A. Vos, *Acta Crystallogr.* **1959**, *12*, 323−329.
[23] J. R. Rollo, G. R. Burns, W. T. Robinson, R. J. H. Clark, H. M. Dawes, M. B. Hursthouse, *Inorg. Chem.* **1990**, *29*, 2889−2894.
[24] M. El-Khateeb, B. Wolfsberger, W. A. Schenk, *J. Organomet. Chem.* **2000**, *612*, 14−17.
[25] K. Mauthner, K. Mereiter, R. Schmid, K. Kirchner, *Organometallics* **1994**, *13*, 5054−5061.
[26] F. Morandini, A. Dondana, I. Munari, G. Pilloni, G. Consiglio, A. Sironi, M. Moret, *Inorg. Chim. Acta* **1998**, *282*, 163−172.
[27] A. D. Becke, *J. Chem. Phys.* **1993**, *98*, 5648−5652.
[28] A. D. Becke, *J. Chem. Phys.* **1993**, *98*, 1372−1377.
[29] C. Lee, W. Yang, R. G. Parr, *Physical Review B: Condensed Matter and Materials Physics* **1988,** 37, 785−789.
[30] P. Stoppioni, M. Peruzzini, *Gazz. Chim. Ital.* **1988**, *118*, 581−582.
[31] M. J. Frisch, G. W. Trucks, H. B. Schlegel, G. E. Scuseria, M. A. Robb, J. R. Cheeseman, V. G. Zakrzewski, J. A. Montgomery, Jr., R. E. Stratmann, J. C. Burant, S. Dapprich, J. M. Millam, A. D. Daniels, K. N. Kudin, M. C. Strain, O. Farkas, J. Tomasi, V. Barone, M. Cossi, R. Cammi, B. Mennucci, C. Pomelli, C. Adamo, S. Clifford, J. Ochterski, G. A. Petersson, P. Y. Ayala, Q. Cui, K. Morokuma, D. K. Malick, A. D. Rabuck, K. Raghavachari, J. B. Foresman, J. J. V. Cioslowski, A. G. Ortiz, B. B. Baboul, G. Stefanov, G. Liu, A. Liashenko, P. Piskorz, I. Komaromi, R. Gomperts, R. L. Martin, D. J. Fox, T. Keith, M. A. Al-Laham, C. Y. Peng, A. Nanayakkara, C. Gonzalez, M. Challacombe, P. M. W. Gill, B. Johnson, W. Chen, M. W. Wong, J. L. Andres, C. Gonzalez, M. Head-Gordon, E. S. Replogle, J. A. Pople, *Gaussian 98, Revision A. 7*, Gaussian, Inc., Pittsburgh PA, **1998**.
[32] R. Ditchfield, W. J. Hehre, J. A. Pople, *J. Chem. Phys.* **1971**, *54*, 724−728.
[33] J. S. Binkley, J. A. Pople, W. J. Hehre, *J. Am. Chem. Soc.* **1980**, *102*, 939−947.
[34] W. J. Pietro, M. M. Francl, W. J. Hehre, D. J. DeFrees, J. A. Pople, J. S. Binkley, *J. Am. Chem. Soc.* **1982**, *104*, 5039−5048.
[35] E. D. Glendening, A. E. Reed, J. A. Carpenter, F. Weinhold, *NBO Version 3.1*.
[36] J. P. Foster, F. Weinhold, *J. Am. Chem. Soc.* **1980**, *102*, 7211−7218.
[37] G. Schaftenaar, J. H. Noordik, *J. Comput.-Aided Mol. Design* **2000**, *14*, 123−134.
[38] C. K. Johnson, *ORTEP*, Report ORNL-5138, Oak Ridge National Laboratory, Oak Ridge/TN, USA, **1976**.
[39] L. J. Farrugia, *J. Appl. Crystallogr.* **1997**, *30*, 565.

Received July 17, 2003
Early View Article
Published Online November 19, 2003

 © 2004 Wiley-VCH Verlag GmbH & Co. KGaA, Weinheim

Spectroscopic Characterization of an Fe^{IV} Intermediate Generated by Reaction of XO^- (X = Cl, Br) with an Fe^{II} Complex Bearing a Pentadentate Non-Porphyrinic Ligand − Hydroxylation and Epoxidation Activity

Véronique Balland,[a] Marie-France Charlot,[b] Frédéric Banse,*[b] Jean-Jacques Girerd,*[b] Tony A. Mattioli,[a] Eckhard Bill,[c] Jean-François Bartoli,[d] Pierrette Battioni,[d] and Daniel Mansuy[d]

Keywords: Iron / Oxo ligands / Bioinorganic chemistry / Epoxidation / Hydroxylation

Mononuclear Fe^{IV} intermediates have been generated in MeOH upon reaction of sodium hypochlorite or hypobromite with a ferrous complex bearing the pentadentate ligands *N*-methyl-*N*,*N*′,*N*′-tris(2-pyridylmethyl)ethane-1,2-diamine (L_5^2) or *N*-methyl-*N*,*N*′,*N*′-tris(2-pyridylmethyl)propane-1,3-diamine (L_5^3). These highly unstable green complexes are characterized by an absorption band at ca. 750 nm. Mössbauer data indicate that the iron center is low spin (S = 1) with an axial electronic structure, allowing identification of the mononuclear Fe^{IV} complexes as $[L_5Fe^{IV}O]^{2+}$ or $[L_5Fe^{IV}OCH_3]^{3+}$. In acetonitrile/dichloromethane solutions, the $L_5^3Fe^{IV}$ system exhibits very selective activities toward hydroxylation of cyclohexane or epoxidation of cyclooctene and *cis*-stilbene. Computational studies performed on $[L_5Fe^{IV}O]^{2+}$ and on the model compound $[(NH_3)_5Fe^{IV}O]^{2+}$ reveal that the ground state possesses two unpaired electrons in the two π^* orbitals, as known for O_2. Electronic spectra computed by time-dependent DFT exhibit only one band in the visible region that is essentially due to d-d transitions.

(© Wiley-VCH Verlag GmbH & Co. KGaA, 69451 Weinheim, Germany, 2004)

Introduction

Porphyrinic Fe^{IV}−oxo species have been detected by spectroscopy in several heme enzymes[1−7] and their chemical models.[8−11] With respect to non-heme enzymes, studies of Fe^{IV} species are more recent and thus less advanced. Dinuclear $Fe^{III}Fe^{IV}$ or $Fe^{IV}Fe^{IV}$ species have been identified in enzymes[12,13] as well as having been chemically modeled.[14−18] The mononuclear non-heme Fe^{IV}−oxo entity has frequently been postulated in the catalytic cycle of enzymes[19,20] but to date has not been characterized. From reactivity studies of chemical models, Que et al. have postulated mononuclear Fe^{IV}−oxo intermediates.[21] Using macrocyclic tetraamido ligands, mononuclear Fe^{IV}−Cl and Fe^{IV}−CN species have been prepared and studied by Collins et al.[22,23] To the best of our knowledge, the first spectroscopic study of a non-heme mononuclear Fe^{IV}−oxo species was reported by Grapperhauser et al.[24] This complex was obtained with the macrocyclic tetraamino ligand cyclam-acetato. With the ligand tetramethylcyclam (TMC), Rohde et al. very recently obtained the complex $[Fe^{IV}(O)(TMC)(NCCH_3)]^{2+}$ after reaction of iodosylbenzene or H_2O_2 with a ferrous precursor in CH_3CN at −40 °C.[25] Moreover, they were able to obtain its X-ray crystallographic structure, since the species is stable at −40 °C in CH_3CN for at least one month. With the tetradentate tripodal ligand TPA [tris(2-pyridylmethyl)amine)], the same authors obtained the intermediate $[Fe^{IV}(O)(TPA)]^{2+}$.[26] Owing to its relative instability, the latter complex is a more efficient oxygen-atom transfer agent than $[Fe^{IV}(O)(TMC)(NCCH_3)]^{2+}$.

In this paper, we report the preparation and spectroscopic characterization of an Fe^{IV}−oxo (or methoxo) species in methanol with a non-porphyrinic nonmacrocyclic ligand as well as the preliminary study of the reactivity of the Fe^{IV}−oxo form in acetonitrile/dichloromethane.

Our strategy was to use a pentadentate ligand leaving one vacant site on the Fe center which could potentially be occupied by an oxygen species. This allowed us, and others in the past, to obtain low-spin $Fe^{III}OOH$ species.[27−34] For

[a] Laboratoire de Biophysique du Stress Oxydant, SBE/DBJC CEA/Saclay,
91191 Gif-sur-Yvette, France
[b] Laboratoire de Chimie Inorganique, UMR CNRS 8613, Université Paris-Sud,
91405 Orsay, France
[c] Max-Planck-Institut für Strahlenchemie,
45470 Mülheim an der Ruhr, Germany
[d] Chimie et Biochimie Pharmacologiques et Toxicologiques, UMR CNRS 8601, Université René Descartes (Paris V),
45 Rue des Saints-Pères, 75270 Paris cedex 06, France
Supporting information for this article is available on the WWW under http://www.eurjic.org or from the author.

instance, the $Fe^{III}OOH$ species was obtained by addition of an excess of H_2O_2 to $[L_5{}^2Fe^{II}Cl]^+$.[27,30,31,35]

In the same manner, we prepared a low-spin $Fe^{III}OOH$ species with $L_5{}^3$.[36]

In order to generate an $Fe^{IV}O$ entity we adopted the strategy of studying the reaction of the oxygen atom donors ClO^- or BrO^- with $[L_5{}^3Fe^{II}Cl]^+$ and $[L_5{}^2Fe^{II}Cl]^+$ (Scheme 1).

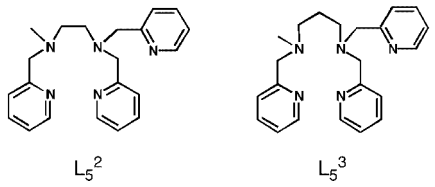

Scheme 1. Pentadentate ligands used in this study

Results and Discussion

UV/Vis Spectroscopy

The reaction of $[L_5{}^3Fe^{II}Cl]PF_6$ at −50 °C in CH_3OH with 2 equiv. of ClO^- was monitored by UV/Vis spectroscopy. Visually, a transient orange color first appeared which quickly changed to green. The green solution exhibited a band at 742 nm which persisted for about 5 min. In Mössbauer samples, this green species correspond to almost 70% of the total Fe. Taking into account the loss of this unstable species upon transfer to the Mössbauer cell, one can assume that in the solution used for UV/Vis spectroscopy, the conversion is almost quantitative. The extinction coefficient is thus $\varepsilon \approx 300\ M^{-1}cm^{-1}$.

The reaction in CH_3OH at 0 °C between $[L_5{}^3Fe^{II}Cl]PF_6$ and 100 equiv. of ClO^- was monitored by stopped-flow UV/Vis spectroscopy (Figure 1).

The maximum intensity of the band at 742 nm was obtained after 100 ms. It completely disappeared under these conditions after 2.5 s. The absorption maximum for the initial orange species was detected at 430 nm and at 0 °C it disappeared in 50 ms.

The same reaction was studied starting from $[L_5{}^2Fe^{II}Cl]PF_6$ and the series of spectra for the first 200 ms is shown in Figure 1. Even though the spectral features are very similar, some differences between the $L_5{}^2$ and $L_5{}^3$ complexes can be noted. The initial absorption band, corresponding to the orange complex, lies at 440 nm. This complex is less fleeting than its $L_5{}^3$ analog since the 440-nm band was still observable as a shoulder after 200 ms. This orange species evolved to the green complex as a clear isobestic point was observed at 503 nm. The green species was characterized by a band at 756 nm with a maximum absorbance weaker than the one observed for the $L_5{}^3$ analog, suggesting a lower conversion into the green species for the $L_5{}^2$ system. This last observation is consistent with the fact that the orange and green complexes coexist in solution in the $L_5{}^2$ system. Finally, the reactivities of $[L_5{}^3Fe^{II}Cl]PF_6$ and $[L_5{}^2Fe^{II}Cl]PF_6$ in the presence of ClO^- are similar but the stabilities of the green and orange species are different.

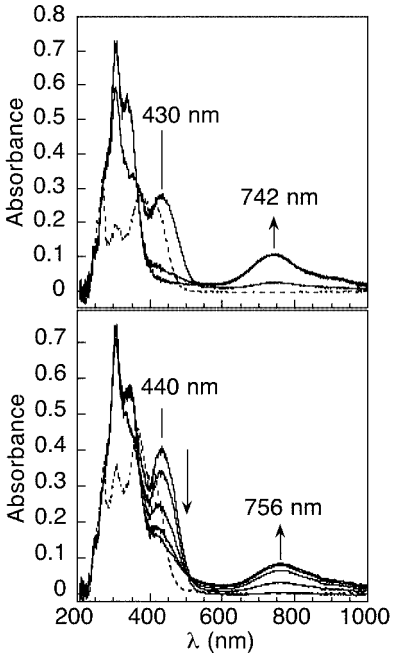

Figure 1. Evolution of the reaction between 0.5 mM $[L_5{}^3Fe^{II}Cl]PF_6$ (top) or $[L_5{}^2Fe^{II}Cl]PF_6$ (bottom) and 100 equiv. of ClO^- monitored in CH_3OH at 0 °C by stopped-flow absorption spectroscopy; the evolutions are shown between 0 and 100 ms for $L_5{}^3$ and 0 and 200 ms for $L_5{}^2$; the spectra in dashed lines are relative to the Fe^{II} starting complexes (0.5 mM)

By ozonolysis of a ferric complex with the ligand cyclamacetato, Grapperhauser obtained an $Fe^{IV}=O$ complex, characterized by a green colour (λ_{max} = 676 nm).[24] The complex $[Fe^{IV}(O)(TMC)(NCCH_3)]^{2+}$ reported by Rohde et al.[25] was also characterized by a pale green colour, with an absorption maximum at 820 nm and an extinction coefficient of 400 $M^{-1}cm^{-1}$. By using the ligand TPA, Lim and co-workers[26] were able to prepare an $Fe^{IV}=O$ complex in CH_3CN at −40 °C. This pale green intermediate exhibited a band at 724 nm with an extinction coefficient of ca. 300 $M^{-1}.cm^{-1}$. These characteristics are similar to the ones observed in the present study.

Mössbauer Spectroscopy

For Mössbauer studies a sample was prepared from $[L_5{}^3Fe^{II}Cl]PF_6$ labeled with 50% ^{57}Fe. The complex was oxidized with 2 equiv. of ClO^- at −60 °C and the green solution thus obtained was quickly frozen to 77 K.

In the absence of an applied magnetic field, the oxidation product exhibited an asymmetric quadrupole doublet at 80 K that could be deconvoluted in two symmetric subspectra. The isomer shift and quadrupole splitting of the minor species [$\delta(2) = 0.35\ mm{\cdot}s^{-1}$, $\Delta E_Q(2) = 0.88\ mm{\cdot}s^{-1}$] indicate the presence of some oxidized Fe^{III} contaminant,[37] whereas the major sub-spectrum (1) can be assigned to the green oxidation product (68% relative abundance, determined from the magnetic spectra given below). The parameters $\delta(1) = 0.02\ mm{\cdot}s^{-1}$ and $\Delta E_Q(1) = 1.20\ mm{\cdot}s^{-1}$ are indicative of low-spin Fe^{IV} species.[38]

 © 2004 Wiley-VCH Verlag GmbH & Co. KGaA, Weinheim

Applied field measurements show that the major component (1) in fact possesses integer spin. Weak fields (1 T) at 4.2 K induce only weak magnetic splittings due to the nuclear Zeeman effect resulting from the applied field (Figure 2, top), but the internal fields are vanishingly small according to dominating strong zero-field splittings (zfs) and an $M_S = 0$ ground level without significant level mixing. Sizeable internal fields were detected only at strong fields (7 T) and higher temperatures. In contrast, the contaminating species sub-spectrum (2) shows a wide magnetically split hyperfine pattern due to half-integer spin or even magnetic ordering. The large splittings attenuate the absorptions of this minor contribution to an almost vanishing baseline distortion.

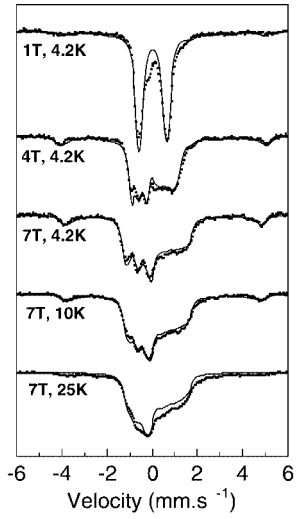

Figure 2. Mössbauer spectra of ^{57}Fe-enriched $[L_5{}^3Fe^{II}Cl]PF_6$ + 2 equiv. of ClO^- recorded at variable fields and temperatures; simulations of the spectra, made by considering a low-spin mononuclear Fe^{IV} complex, are represented by solid lines; the contamination background [sub-spectrum (2), 32% relative intensity] was taken into account by a simulation based on the equation given in the text for $S = 5/2$, $\delta = 0.4$ mm·s^{-1}, $\Delta E_Q = 0.7$ mm·s^{-1}, $D = 1$ cm^{-1}, $E/D = 0.33$, $A'_{iso}/g_N\beta_N = -19$ T

The field and temperature dependence of the magnetic Mössbauer spectra of the green oxidation product could be well simulated using the usual spin Hamiltonian

$$H = D\,[S_z{}^2 - 2/3 + E/D\,(S_x{}^2 - S_y{}^2)] + \mu_B\,\mathbf{B}\,g\,\boldsymbol{S} + H_N$$

for an electronic spin $S = 1$, where D and E/D are the zfs parameters, and H_N is the usual nuclear Hamiltonian for the ^{57}Fe nucleus.[39] The values of the spin Hamiltonian and hyperfine parameters are summarized in Table 1. We mention that alternative fits with $S = 2$ required magnetic hyperfine coupling constants with a small isotropic contribution $A'_{iso}/g_N\beta_N = -6.5$ T which is unreasonable and far below the values for known high-spin Fe^{IV}, $S = 2$, compounds.[22,40,41] This implies that the green oxidation product is an $S = 1$ species like the known oxo−ferryl compounds.

The values obtained for the green complex generated by reaction of $[L_5{}^3FeCl]^+$ with 2 equiv. of ClO^- compare well with those reported for the complexes obtained with the non-heme ligands of the cyclam family[24,25] or the amine/pyridine ligand TPA[26] (see Table 1). The Mössbauer parameters are also similar to those reported for the compound I analogue $S = 1$ Fe^{IV}=O derivative of Fe−porpholactone $[Fe^{IV}$=O**2**$]^+$.[10] For Horse Radish Peroxidase compound II, it was found that $\delta = 0.03$ mm/s and $\Delta E_Q = 1.61$ mm/s.[3] The Mössbauer analysis for the $S = 1$ porphyrinic dimethoxy complex $[Fe^{IV}(TMP)(OCH_3)_2]$ gave $\delta = -0.025$ mm/s and $\Delta E_Q = 2.1$ mm/s.[42,43] The $Fe^{IV}{}_2O_2$ diamond-core complex involving two $S = 1$ metal centers recently characterized by the group of Que yielded corresponding values for δ (0.1 mm/s) and ΔE_Q (1.75 mm/s).[18] These comparisons demonstrate that the parameters obtained from Mössbauer analysis are similar for all the Fe^{IV} species with oxygenated ligands and are independent of the nuclearity of the moieties and of the environment(s) of the metal ion(s). In contrast, low-spin $Fe^{IV}-CN$[23] and $Fe^{IV}(CN\,tBu)_2$[44] species have much larger ΔE_Q values (4.35 mm/s and 3.38 mm/s) although the δ values are similar. This strongly suggests that the $L_5{}^3Fe^{IV}$ complex has an oxygenated group as an axial ligand. The small E/D value observed here is also consistent with an axial electronic structure. This is confirmed a contrario by the larger E/D value (0.15) found by Que et al. for the dinuclear $Fe^{IV}{}_2O_2$ complex. We propose, therefore, that the green species in MeOH can be formulated as an oxo species $[L_5{}^3Fe^{IV}O]^{2+}$ or its methoxo derivative $[L_5{}^3Fe^{IV}OCH_3]^{3+}$.

We suggest that the orange species, which absorbs at 430 nm, could be the ClO^- adduct. This complex then ev-

Table 1. Mössbauer parameters obtained for several mononuclear Fe^{IV} complexes; the formulae used for the ligands are given according to the references cited

Ligand	$L_5{}^3$	TMC[25]	Cyclam-acetato[24]	**2**$^{2-}$ [10]	TPA[26]
δ [mm/s]	0.03	0.17	0.01	0.08	0.01
ΔE_Q [mm/s]	1.21	1.24	1.37	1.66	0.92
η	0.53	0.5	0.8	0.3	0.9
D [cm^{-1}]	22.5	29	23	20	28
E/D	0.01	0	0	0.1	0
g_x, g_y, g_z	2, 2, 2	2.3, 2.3, 2	2, 2, 2	2.17, 2.17, 1.99	
$A/g_N\beta_N$ [T]	−18, −20.6, −0.4	−22.5, −18, −3	−23, −23, −10	−17.5, −17.5, −10	−23.5, −23.5, −5

 © 2004 Wiley-VCH Verlag GmbH & Co. KGaA, Weinheim

olves to the high-valent iron complex characterized by an absorption band at 742 nm. The observed events can thus be summarized as shown in Scheme 2.

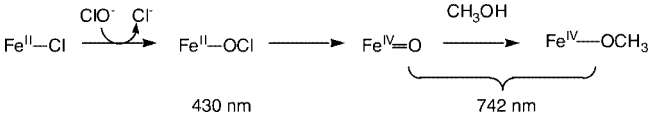

Scheme 2. Mechanism proposed for the formation of mononuclear Fe^{IV} complexes from ClO^- and $[L_5{}^3Fe^{II}Cl]^+$ or $[L_5{}^2Fe^{II}Cl]^+$

Resonance Raman Spectroscopy

We recorded resonance Raman spectra of the green species (prepared with either $Br^{16}O^-$ or $Br^{18}O^-$ in a 25 mM solution of the complex in MeOH/acetone, 2:1) using excitation at 752.5 nm and acetone was used in order to increase the solubility of the complex. In both cases, the green species was characterized by the same UV/Vis spectrum as the one observed using ClO^-. The Raman spectrum is shown in Figure 3 and the band at 752 cm^{-1} is a good candidate for the $Fe^{IV}-$oxygen vibration. Indeed, its frequency is similar to the ones reported for several ferryl−oxo heme proteins.[45] Moreover, this is the only band of the spectrum that vanishes when the green colour disappears. However, no shift was observed upon ^{18}O labelling. It is possible that either a fast exchange between $[L_5{}^3Fe^{IV}O]^{2+}$ and unlabelled H_2O occurred as reported for the intermediate ES of cytochrome c peroxidase[46,47] or that the green intermediate in the presence of methanol is an $Fe^{IV}OCH_3$ species.[48]

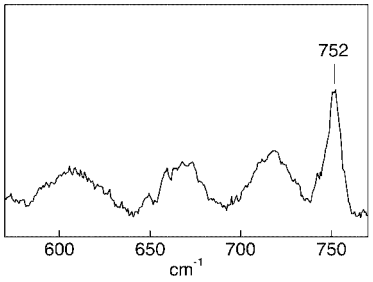

Figure 3. Resonance Raman spectrum at 10 K of the Fe^{IV} green complex prepared with a 25 mM solution of $[L_5{}^3Fe^{II}Cl]PF_6$ in presence of BrO^-; the laser wavelength used was 752.5 nm

In the case of the complex $[Fe^{IV}(O)(TMC)(NCCH_3)]^{2+}$,[25] no $Fe^{IV}=O$ vibration could be detected by Raman spectroscopy using laser excitation at 752.5 nm. However, this vibration was detected at 834 cm^{-1} by Fourier transform IR spectroscopy. With porphyrinic ligands, the $Fe^{IV}-$oxo vibration frequencies are greater than 800 cm^{-1}.[49,50] Complementary studies are therefore necessary to unambiguously assign the 752 cm^{-1} vibration observed here.

Reactivity

Reactivity studies were conducted at −20 °C with 2 equiv. of ClO^- in a mixture of acetonitrile/dichloromethane, 1:1, under aerobic conditions for cyclohexane and cyclooctene and under argon for *cis*-stilbene. The solution was stirred for 3 h and the products analyzed (Table 2).

Table 2. Yields (%/ClO^-) obtained at −20 °C for the oxidation reactions of different substrates by $[L_5{}^3FeCl]PF_6$ + 2 equiv. of ClO^- (Bzl = benzaldehyde, 800 equiv. of substrate)

Cyclohexan-		-cyclooctene		-Stilbene	
-ol	-one	Epoxy-	*cis*-	*trans*-	Bzl
10	0	15	0	10	0

The $[L_5{}^3FeCl]PF_6/ClO^-$ mixture is able to hydroxylate cyclohexane in 10% yield relative to the oxidant. Remarkably no ketone was formed. This high selectivity towards hydroxylation indicates the absence of free radical chemistry since the oxidation is performed under aerobic conditions.[51] Cyclooctene was epoxidized in a 15% yield, which is comparable to the yield of 30% reported for the intermediate $[Fe^{IV}(O)(TPA)]^{2+}$.[26] Epoxidation of *cis*-stilbene occurred with a 10% conversion but with a complete isomerization to the *trans*-epoxide. Such an isomerization has been attributed to a long-lived radical as observed with heme $Fe^{IV}=O$ species.[52] This is illustrated in Scheme 3.

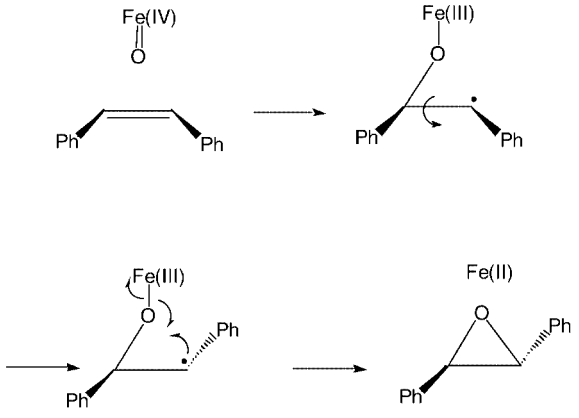

Scheme 3

With the different substrates, the same experiments performed at 20 °C did not lead to any oxidation products even in the presence of a higher ClO^- concentration. This indicates that ClO^- is not directly responsible for these oxidations. This remark is important since hypochlorite may exhibit an oxidation activity in the presence of Lewis-acidic species.[53] Moreover, at room temperature, the solution became rapidly colorless and a reddish solid precipitated which is very likely to be iron oxide as suggested by Mössbauer spectroscopy (see above). On the contrary, after 2 h at −20 °C, the solution was still yellow and only a small amount of solid was observed.

This reactivity in acetonitrile/dichloromethane strongly supports the presence of a $[L_5{}^3Fe^{IV}O]^{2+}$ species.

As pointed out by Lim et al.,[26] the reactivity of $Fe^{IV}=O$ species appears to correlate strongly with their stability:

 © 2004 Wiley-VCH Verlag GmbH & Co. KGaA, Weinheim

the less stable the species, the stronger the oxidant. The complex $[Fe^{IV}(O)(TMC)(NCCH_3)]^{2+}$, which is stable for at least one month at −40 °C, is capable of oxidizing PPh_3 but not olefins.[25] The TPA complex[26] and the porphyrin analog $[Fe^{IV}(O)(TMP)]$,[52] which are less stable than the former, are able to epoxidize olefins. The $L_5{}^3$ complex, which is much more unstable than the above complexes, is also much more reactive since it is even able to hydroxylate unactivated C−H bonds.

Quantum Calculations

The value of the molar extinction coefficient (300 $M^{-1}\cdot cm^{-1}$) of the band observed at 742 nm in methanol seems low when compared with the intense bands which have been recently detected in the 500−900-nm region for the low-spin $Fe^{IV}{}_2O_2$ model system described by Costas et al.[18] On the contrary it agrees well with the value of 400 $M^{-1}\cdot cm^{-1}$ observed at 820 nm for the X-ray characterized non-heme complex $[Fe^{IV}(O)(TMC)(NCCH_3)]^{2+}$.[25]

Spin-unrestricted DFT calculations were performed on the model compounds $[(NH_3)_5Fe^{IV}O]^{2+}$ and $[(NH_3)_5Fe^{IV}OCH_3]^{3+}$ as well as on the real complex $[L_5{}^3Fe^{IV}O]^{2+}$ using the Gaussian98 program package[54] with Becke's three parameter hybrid functional[55] and the correlation functional of Lee, Yang and Parr (B3LYP).[56] For both models, atomic distances were optimized in the two $S = 1$ and $S = 2$ spin states leading to the conclusion that the low-spin state is the more stable. The geometry of the real complex was fully optimized only in the $S = 1$ spin state. For the oxo model, the Fe−O bond length was found to be 1.635 Å, consistent with the value reported by Lehnert et al.[57,58]

The electronic absorption spectrum of the model compound $[(NH_3)_5Fe^{IV}O]^{2+}$ in the low-spin state ($S = 1$) was computed by time-dependent DFT (TDDFT) (see Exp. Sect.). It shows in the visible region only one weak band at 600 nm (oscillator strength $f = 0.0015$) (see Supporting Information). In C_{4v} symmetry (z being the Fe−O axis) this band corresponds to two degenerate transitions. The first one, with y polarization, consists of approximately equal amounts of an α excitation from the antibonding $d_{yz} - p_y$ orbital to a $d_{x^2-y^2}$-type orbital and of a β excitation from a d_{xy}-type orbital to the antibonding $d_{xz} - p_x$ orbital. The second one is the corresponding x-polarized transition involving excitation from the α-antibonding $d_{xz} - p_x$ orbitals to $d_{x^2-y^2}$ and β excitation from d_{xy} to the antibonding $d_{yz} - p_y$ orbital. These two transitions have therefore both MLCT and LMCT character. As a consequence, no appreciable charge transfer occurs and the observed band is essentially a weak-intensity d−d transition. This calculation then confirms the explanation proposed by Rohde et al. to interpret the observed low intensity.[25] The expected oxo-to-Fe^{IV} LMCT band was found at 360 nm with z polarization and involves β transitions from bonding $d_{xz} + p_x$ to antibonding $d_{xz} - p_x$ orbitals and from bonding $d_{yz} + p_y$ to antibonding $d_{yz} - p_y$ orbitals (see Supporting Information).

These conclusions can be compared with those we obtained for the Fe^{IV}−methoxo system $[(NH_3)_5Fe^{IV}OCH_3]^{3+}$. The geometry optimization led to a linear Fe−O−CH_3 motif with a short Fe−O distance of 1.709 Å, only slightly larger than the value of 1.635 Å found for the oxo model. In this case, however, the MOs containing the p_x and p_y contributions of oxygen delocalized on the CH_3 group and two essentially d−d transitions were calculated at 550 (d_{xz} or d_{yz} to d_{z^2}) and 450 nm (d_{xz} or d_{yz} to $d_{x^2-y^2}$) ($f \approx 0.0015$). The former had a zero intensity in the oxo model (see Supporting Information). The full geometry optimization of the real complex $[L_5{}^3Fe^{IV}O]^{2+}$ in the $S = 1$ state gave an Fe−O distance of 1.646 Å. In the visible region (see Supporting Information), the computed spectrum exhibits a band at 530 nm ($\varepsilon = 500\ M^{-1}.cm^{-1}$) which results from nondegenerate transitions essentially from d_{xz}- or d_{yz}-type orbitals to a $d_{x^2-y^2}$-type orbital. The LMCT transition from bonding $d + p_O$ to antibonding $d - p_O$ orbitals was calculated at 382 nm. We stress the fact that most of the informations relative to the calculated spectrum of the real complex were present in the simple model and that all orbitals of concern are strikingly similar, except for a small delocalization on the ligand $L_5{}^3$.

Finally, these calculations indicate that the weak band observed at 742 nm in MeOH for this low-spin Fe^{IV} mononuclear species has predominantly d−d character.

We would like to finish this part with some simple theoretical considerations. Is the Fe^{IV}=O notation the most accurate for a ferryl species? As is well known, the basic theoretical description of an $S = 1$ low-spin Fe^{IV}=O motif implies MOs combining the "t_{2g}" d orbitals with the p_x and p_y O orbitals to give occupied π-bonding orbitals and semi-occupied π*-antibonding orbitals with $\pi_x^* = \lambda\ d_{xz} + \mu\ p_x$ and $\pi_y^* = \lambda\ d_{yz} + \mu\ p_y$ as illustrated in Scheme 4.

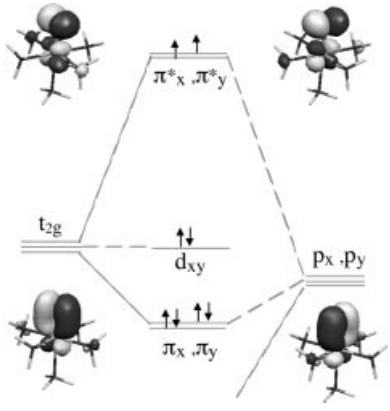

Scheme 4

This MO description enables us to understand both the delocalized spin triplet character and the double bond composed of a σ bond (not shown) and two half π bonds.

 © 2004 Wiley-VCH Verlag GmbH & Co. KGaA, Weinheim

It is instructive to examine the electronic structure of $Fe^{IV}O$ from a Valence Bond point of view. The triplet state is represented by the following Slater determinant:

$$|\pi_x^*\ \pi_y^*| = \lambda^2\,|d_{xz}\ d_{yz}| + \lambda\mu\,|d_{xz}\ p_y| + \lambda\mu\,|p_x\ d_{yz}| + \mu^2\,|p_x\ p_y|$$

The determinant $|d_{xz}\ d_{yz}|$ describes a spin triplet localized on Fe in an $Fe^{IV}{}_{LS}-O^-$ pair, the $|d_{xz}\ p_y|$ and $|p_x\ d_{yz}|$ ones describe spin triplets equally shared between Fe and O in an $Fe^{III}{}_{LS}-O^\circ$ pair and the $|p_x\ p_y|$ one describes a spin triplet localized on O in an $Fe^{II}{}_{LS}-O^{\circ\circ+}$ pair. The electron distributions related to these mesomeric forms in the ground state are represented in part a) of Scheme 5.

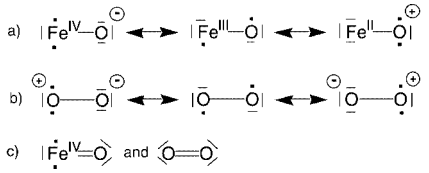

Scheme 5. In a) all forms have an actual charge of +2; the formal oxidation states are reported for Fe and the formal charges for O

Making the simplifying assumption of zero overlap between the d and p orbitals for this qualitative discussion, we deduced from the wave function $|\pi_x^*\ \pi_y^*|$ that the weight is λ^4 for the $Fe^{IV}-O^-$ form, μ^4 for the $Fe^{II}{}_{LS}-O^{\circ\circ+}$ and $2\lambda^2\mu^2$ for the $Fe^{III}{}_{LS}-O^\circ$ form, with $\lambda^2 + \mu^2 = 1$ arising from the normalization conditions of π_x^* and π_y^*. Within the same assumption of zero overlap, the spin densities are $\rho_{Fe} = 2\,\lambda^2$ and $\rho_O = 2\,\mu^2$. Scheme 6 represents the weight of each different mesomeric form as a function of μ^2.

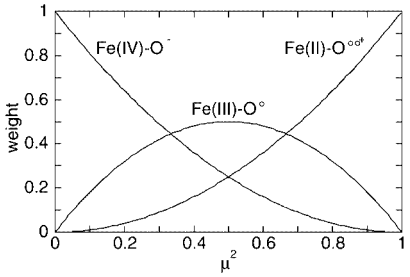

Scheme 6

The DFT calculations showed that the spin density is in fact almost equally shared between iron and oxygen, as shown in Figure 4. Within our simple hypothesis, this would imply $\lambda^2 \approx \mu^2$. When $\lambda^2 = \mu^2 = 0.5$, the $Fe^{IV}-O^-$ form amounts to 25%, the $Fe^{III}{}_{LS}-O^\circ$ form to 50% and the $Fe^{II}{}_{LS}-O^{\circ\circ+}$ form to 25%. When μ^2 decreases slightly from 0.5, the amount of $Fe^{II}{}_{LS}-O^{\circ\circ}$ evidently decreases whereas the amount of the $Fe^{IV}-O^-$ form increases. The Fe^{IV} orbitals are lowered so much in energy that they become close to the oxygen p orbitals which themselves are destabilized in O^{2-}. These AOs interact strongly and the MOs are delocalized on both Fe and O as reflected in the short Fe−O distance. The simple model of zero overlap no longer holds, but it allows us to conclude that the system has gained a significant $Fe^{III}{}_{LS}-O^\circ$ character and even $Fe^{II}{}_{LS}-O^{\circ\circ}$ character.

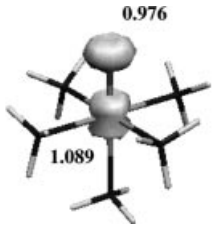

Figure 4. Spin densities calculated for the model compound $[(NH_3)_5Fe^{IV}O]^{2+}$

The description of the "$Fe^{IV}O$" species simultaneously as a diradical and a double bond system is in fact reminiscent of the electronic structure of the dioxygen molecule. It has also to be noted that, for the compound I of cytochrome P-450, the iron−oxo moiety possesses a triplet pair of electrons in π* orbitals.[59] For dioxygen the different forms are represented in part b) of Scheme 5. It is evident from symmetry that the spin is equally distributed on both oxygen atoms in triplet dioxygen. As explained by Valence Bond theory,[60] the double-bond character of O_2 arises from one σ bond, half a π_x bond and half a π_y bond and is fully compatible with a triplet state.

As represented in part c) of Scheme 5, the double-bond notation is unsatisfying both for $Fe^{IV}O$ and O_2 since this notation masks the spin density on the oxygen atom(s).

At this stage we stress that the $Fe^{III}{}_{LS}-O^\circ$ mesomeric form is dominant in the low spin ferryl system and, as for O_2, the strong radical character on O may explain the reactivity observed (see above).

We went beyond the monodeterminantal representation of the $S = 1$ ferryl ground state. We have performed a self consistent field computation (SCF) with full Configuration Interaction (CI) involving the subset of π and π* orbitals (complete active-space multi configuration SCF/CASSCF) together with localization of these orbitals into orthogonal orbitals with predominant p_x, p_y, d_{xz} and d_{yz} character. This procedure gave us the following contributions for each form: $Fe^{III}{}_{LS}-O^\circ \approx 94.5\%$, $Fe^{II}{}_{LS}-O^{\circ\circ+} \approx 5\%$ and $Fe^{IV}-O^-$ only $\approx 0.5\%$. This enrichment in $Fe^{III}{}_{LS}-O^\circ$ form is related to the removal of charge fluctuation by CI.[61] Basically, in the $Fe^{III}{}_{LS}-O^\circ$ form the monocenter electron−electron repulsion is weakened. Similarly, CI for O_2 leads to more than 80% diradical form.[62]

Conclusion

In MeOH at low temperature, we have obtained green intermediates, after reaction of XO^- (X = Cl, Br) and Fe^{II} complexes bearing the pentadentate amine/pyridine ligands $L_5{}^3$ or $L_5{}^2$. These green complexes have been assigned as Fe^{IV} entities, i.e. $[LFe^{IV}O]^{2+}$ or possibly $[LFe^{IV}OCH_3]^{3+}$ if the former reacts with MeOH. To date, $[LFe^{IV}O]^{2+}$ or $[L_5{}^3Fe^{IV}OCH_3]^{3+}$ complexes are among the first non-heme Fe^{IV} mononuclear species characterized. Spectroscopic

 © 2004 Wiley-VCH Verlag GmbH & Co. KGaA, Weinheim

studies are underway to determine which of the two possible formulations of the species is occurring in MeOH.

The reactivity, performed in acetonitrile/dichloromethane solution showed that the $ClO^-/L_5{}^3$ system is able to oxidize cyclohexane to cyclohexanol as well as cyclooctene and *cis*-stilbene to the corresponding epoxides although in the last case with a complete isomerization to the *trans* form. These very specific oxidations are consistent with the mediation of a ferryl intermediate. Moreover, we have performed DFT calculations and obtained the electronic description of the ground state for the triplet "$Fe^{IV}O$" complex. As for the triplet dioxygen molecule, the ferryl−oxo complex is actually better described as the diradical $Fe^{III}-O^{\circ}$ form. This strong radical character on the oxygen atom must be at the origin of the hydroxylation and epoxidation reactivity, in particular the isomerization observed during oxidation of the *cis*-stilbene.

Experimental Section

Materials: Starting materials were purchased from Acros. Solvents were purchased from Merck and used without further purification.

Syntheses

Ligand *N*-Methyl-*N*,*N*′,*N*′-tris(2-pyridylmethyl)ethane-1,2-diamine ($L_5{}^2$): This ligand was synthesized according to the method reported by Bernal et al.[27]

Ligand *N*-Methyl-*N*,*N*′,*N*′-tris(2-pyridylmethyl)propane-1,3-diamine ($L_5{}^3$): This ligand was obtained according to the method reported by Bernal et al.[27] using *N*-methylpropane-1,3-diamine as the starting material. The crude product obtained after evaporation of $CHCl_3$ was a dark oil purified by chromatography on Al_2O_3 (eluent $CHCl_3$/EtOH, 20:1).

Complex $[L_5{}^2Fe^{II}Cl]PF_6$: This complex was obtained as described previously.[27]

Complex $[L_5{}^3Fe^{II}Cl]PF_6$: The method described by Balland et al.[36] has been reproduced here.

^{18}O-Labelled BrO^-: ^{18}O-labelled BrO^- was prepared using $H_2{}^{18}O$ (purchased from Eurisotop, isotopic enrichment 95%) according to the method reported by Bortolini et al.[63]

Reactivity Experiments: Reactivity experiments were performed at −20 °C in CH_3CN/CH_2Cl_2, 1:1, under vigorous stirring. The amounts of reactants were: 10^{-3} mmol of Fe complex; 2 equiv. of ClO^-, and 800 equiv. of substrate. The oxidation products were analyzed by GC. The conversion of *cis*-stilbene into the *trans*-epoxide was determined by NMR spectroscopy.

Physical Measurements: UV/Vis spectra were recorded with a Varian Cary 5E spectrophotometer equipped with a Dewar fitted with quartz windows for low-temperature measurements. Stopped-flow experiments were performed with a Biologic SFM-300 instrument equipped with a Julabo F 30C cryostat. Spectra were recorded in the 200−1022-nm range with a 0.5-cm optical path and a 50-μL cuvette. The delay after mixing was 3 ms. Mössbauer data were recorded with an alternating constant-acceleration spectrometer. The minimum experimental line width was 0.24 mm·s^{-1} (full width at half-height). The sample temperature was maintained at a constant value either with an Oxford Instruments Variox or an Oxford Instruments Mössbauer-Spectromag cryostat. The latter is a split-pair superconducting magnet system for applied fields up to 8 T where the temperature of the sample can be varied in the range of 1.5−250 K. The field at the sample is perpendicular to the γ-beam. The ^{57}Co/Rh source (1.8 GBq) was positioned at room temperature inside the gap of the magnet system at a zero-field position. Isomer shifts are quoted relative to iron metal at 300 K. Samples were doped at 50% with ^{57}Fe. The solutions were prepared at −60 °C in MeOH (5.5 mM in Fe) and were studied at 77 K. Resonance Raman spectra were recorded using a Jobin Yvon spectrometer equipped with a 900 lines/mm grating and a liquid-nitrogen cooled CCD camera. The 752.5-nm line of a Kr^+ laser was used for excitation with a power of 50 mW. The samples (1.5 mM in iron) were prepared at −80 °C in CH_3OH/acetone, 2:1, then frozen and studied at 10 K.

Computational Details: Spin-unrestricted DFT calculations were performed on the model compounds $[(NH_3)_5Fe^{IV}O]^{2+}$ and $[(NH_3)_5Fe^{IV}OCH_3]^{3+}$ as well as on the real complex $[L_5{}^3Fe^{IV}O]^{2+}$ using the Gaussian98 program package[54] with Becke's three parameter hybrid functional[55] and the correlation functional of Lee, Yang and Parr (B3LYP).[56] The double zeta basis set (SV) of Ahlrichs et al.[64] was employed for all atoms. For both models the distances were optimized in the two $S = 1$ and $S = 2$ spin states leading to the conclusion that the low-spin state is the more stable and the geometry of the complex was fully optimized in the $S = 1$ spin state. The energy of the excited states and oscillator strengths, *f*, were calculated by the Time Dependent DFT (TDDFT) formalism as implemented in the Gaussian98 program.[65] The theoretical electronic spectra were then simulated using Gaussian line shapes with a bandwidth at half-height of 2000 cm^{-1}, a value which usually gives molar extinction coefficients consistent with experimental values. For the configuration interaction calculations, Slater-type orbitals (STO-3G) were used.[66]

Supporting Information: Energy diagram and contour plot of the molecular orbitals calculated by DFT for the model complex $[(NH_3)_5Fe^{IV}O]^{2+}$ in the $S = 1$ state (Figure S1). Theoretical UV/Vis spectra of the models $[(NH_3)_5Fe^{IV}O]^{2+}$ and $[(NH_3)_5Fe^{IV}OCH_3]^{+}$ and of the real complex $[L_5{}^3Fe^{IV}O]^{2+}$ (Figures S2, S3, S4, respectively).

[1] T. H. Moss, A. Ehrenberg, A. J. Bearden, *Biochemistry* **1969**, *8*, 4159.
[2] C. E. Schulz, P. W. Devaney, H. Winkler, P. G. Debrunner, N. Doan, R. Chiang, R. Rutter, L. P. Hager, *FEBS Lett.* **1979**, *103*, 102.
[3] C. E. Schulz, R. Rutter, J. T. Sage, P. G. Debrunner, L. P. Hager, *Biochemistry* **1984**, *23*, 4743.
[4] J. Terner, A. J. Sitter, C. M. Reczek, *Biochim. Biophys. Acta* **1985**, *828*.
[5] A. J. Sitter, C. M. Reczek, J. Terner, *Biochim. Biophys. Acta* **1985**, *828*, 229.
[6] S. Hashimoto, J. Teraoka, T. Inubushi, T. Yonetani, T. Kitagawa, *J. Biol. Chem.* **1986**, *261*, 11110.
[7] T. Uchida, M. Tatsushi, T. Kitagawa, *Biochemistry* **2000**, *39*, 6669.
[8] M. Schappacher, G. Chottard, R. Weiss, *J. Chem. Soc., Chem. Commun.* **1986**, 93.
[9] D. Mandon, R. Weiss, K. Jayaraj, A. Gold, J. Terner, E. Bill, A. X. Trautwein, *Inorg. Chem.* **1992**, *31*, 4404.
[10] K. Jayaraj, A. Gold, R. N. Austin, L. M. Ball, J. Terner, D. Mandon, R. Weiss, J. Fischer, A. DeCian, E. Bill, M. Müther, V. Schünemann, A. X. Trautwein, *Inorg. Chem.* **1997**, *36*, 4555.
[11] J. Terner, A. Gold, R. Weiss, D. Mandon, A. X. Trautwein, *J. Porphyrins Phthalocyanines* **2001**, *5*, 357.

 © 2004 Wiley-VCH Verlag GmbH & Co. KGaA, Weinheim

[12] L. Shu, J. Nesheim, K. Kauffmann, E. Münck, J. D. Lipscomb, L. Que, *Science* **1997**, *275*, 515.
[13] B. E. Sturgeon, D. Burdi, S. Chen, B. H. Huynh, D. E. Edmonson, J. Stubbe, B. M. Hoffman, *J. Am. Chem. Soc.* **1996**, *118*, 7551.
[14] Y. Dong, L. Que, K. Kauffmann, E. Münck, *J. Am. Chem. Soc.* **1995**, *117*, 11377.
[15] Y. Dong, Y. Zang, L. Shu, E. C. Wilkinson, L. Que, K. Kauffmann, E. Münck, *J. Am. Chem. Soc.* **1997**, *119*, 12683.
[16] D. Lee, J. L. DuBois, B. Pierce, D. Petasis, M. P. Hendrich, C. Krebs, B. H. Huynh, S. J. Lippard, *J. Am. Chem. Soc.* **1999**, *121*, 9893.
[17] H.-F. Hsu, Y. Dong, L. Shu, V. G. Young, L. Que, *J. Am. Chem. Soc.* **1999**, *121*, 5230.
[18] M. Costas, J.-U. Rohde, A. Stubna, R. Y. N. Ho, L. Quaroni, E. Münck, L. Que, *J. Am. Chem. Soc.* **2001**, *123*, 12931.
[19] N. I. Burzlaff, P. J. Rutledge, I. J. Clifton, C. M. H. Hensgens, M. Pickford, R. M. Adlington, P. L. Roach, J. E. Baldwin, *Nature* **1999**, *401*, 721.
[20] Z. H. Zhang, J. S. Ren, D. K. Stammers, J. E. Baldwin, K. Harlos, C. J. Schofield, *Nat. Struct. Biol.* **2000**, *7*, 127.
[21] H. Miyake, S. J. Lange, L. Que, *Inorg. Chem.* **2001**, *40*, 3534.
[22] K. L. Kostka, B. G. Fox, M. P. Hendrich, T. J. Collins, L. J. Rickard, L. J. Wright, E. Münck, *J. Am. Chem. Soc.* **1993**, *115*, 6746.
[23] M. J. Bartos, S. W. Gordon-Wylie, B. G. Fox, L. J. Wright, S. T. Weintraub, K. Kauffmann, E. Münck, K. L. Kostka, E. S. Uffelman, C. E. F. Rickard, K. R. Noon, T. J. Collins, *Coord. Chem. Rev.* **1998**, *174*, 361.
[24] C. A. Grapperhauser, B. Mienert, E. Bill, T. Weyhermüller, K. Wieghardt, *Inorg. Chem.* **2000**, *39*, 5306.
[25] J. U. Rohde, J. H. In, M. H. Lim, W. W. Brennessel, M. R. Bukowski, A. Stubna, E. Munck, W. Nam, L. Que, *Science* **2003**, *299*, 1037.
[26] M. H. Lim, J. U. Rohde, A. Stubna, M. R. Bukowski, M. Costas, R. Y. N. Ho, E. Munck, W. Nam, L. Que, *Proc. Natl. Acad. Sci. USA* **2003**, *100*, 3665.
[27] I. Bernal, I. M. Jensen, K. B. Jensen, C. J. McKenzie, H. Toftlund, J. P. Tuchagues, *J. Chem. Soc., Dalton Trans.* **1995**, 3667.
[28] M. Lubben, A. Meetsma, E. C. Wilkinson, B. Feringa, L. Que, *Angew. Chem. Int. Ed. Engl.* **1995**, *34*, 1512.
[29] M. E. deVries, R. M. LaCrois, G. Roelfes, H. Kooijman, A. L. Spek, R. Hage, B. L. Feringa, *Chem. Commun.* **1997**, 1549.
[30] P. Mialane, A. Novorojkine, G. Pratviel, L. Azéma, M. Slany, F. Godde, A. Simaan, F. Banse, T. Kargar-Grisel, G. Bouchoux, J. Sainton, O. Horner, J. Guilhem, L. Tchertanova, B. Meunier, J. J. Girerd, *Inorg. Chem.* **1999**, *38*, 1085.
[31] A. J. Simaan, F. Banse, P. Mialane, A. Boussac, S. Un, T. Kargar-Grisel, G. Bouchoux, J. J. Girerd, *Eur. J. Inorg. Chem.* **1999**, 993.
[32] K. B. Jensen, C. J. McKenzie, L. P. Nielsen, J. Z. Pedersen, H. M. Svendsen, *Chem. Commun.* **1999**, 1313.
[33] R. Y. N. Ho, G. Roelfes, B. L. Feringa, L. Que, *J. Am. Chem. Soc.* **1999**, *121*, 264.
[34] G. Roelfes, M. Lubben, K. Chen, R. Y. N. Ho, A. Meestma, S. Genseberger, R. M. Hermant, R. Hage, S. K. Mandal, V. G. Young, Y. Zang, H. Kooijman, A. L. Spek, L. Que, B. L. Feringa, *Inorg. Chem.* **1999**, *38*, 1929.
[35] J. J. Girerd, F. Banse, A. J. Simaan, *Struct. Bond.* **2000**, *97*, 146.
[36] V. Balland, F. Banse, E. Anxolabéhère-Mallart, M. Ghiladi, T. Mattioli, C. Philouze, G. Blondin, J.-J. Girerd, *Inorg. Chem.* **2003**, *42*, 2470.
[37] N. N. Greenwood, T. C. Gibb, *Mössbauer Spectroscopy*, Chapman and Hall Ltd., London, **1971**.
[38] E. Münck, in *Physical Methods in Bioinorganic Chemistry* (Ed.: L. Que), University Science Books, Sausalito, California, **2000**.
[39] A. X. Trautwein, E. Bill, E. Bominaar, H. Winkler, *Struct. Bond.* **1991**, *78*, 1.
[40] D. Lee, B. Pierce, C. Krebs, M. P. Hendrich, B. H. Huynh, S. J. Lippard, *J. Am. Chem. Soc.* **2002**, *124*, 3993.
[41] H. Zheng, S. J. Yoo, E. Munck, L. Que, *J. Am. Chem. Soc.* **2000**, *122*, 3789.
[42] J. T. Groves, R. Quinn, T. J. McMurry, G. Lang, B. Boso, *J. Chem. Soc., Chem. Commun.* **1984**, 1455.
[43] J. T. Groves, R. Quinn, T. J. McMurry, M. Nakamura, G. Lang, B. Boso, *J. Am. Chem. Soc.* **1985**, *107*, 354.
[44] T. J. Collins, B. G. Fox, Z. G. Hu, K. L. Kostka, E. Münck, C. E. F. Rickard, L. J. Wright, *J. Am. Chem. Soc.* **1992**, *114*, 8724.
[45] W. A. Oertling, R. T. Kean, R. Wever, G. T. Babcock, *Inorg. Chem.* **1990**, *29*, 2633.
[46] S. Hashimoto, Y. Tatsuno, T. Kitagawa, *Proc. Natl. Acad. Sci. USA* **1986**, *83*, 2417.
[47] B. Meunier, J. Bernadou, *Struct. Bond.* **2000**, *97*, 1.
[48] B. Meunier, *Chem. Rev.* **1992**, *92*, 1411.
[49] R. Weiss, A. Gold, A. X. Trautwein, J. Terner, *The Porphyrin Handbook*, Academic Press, San Diego, **2000**, vol. *4*, p. 72.
[50] Y. Watanabe, H. Fujii, *Struct. Bond.* **2000**, *97*, 59.
[51] M. Costas, K. Chen, L. Que, *Coord. Chem. Rev.* **2000**, *200−202*, 517.
[52] J. T. Groves, Z. Gross, M. K. Stern, *Inorg. Chem.* **1994**, *33*, 5065.
[53] W. Nam, J. S. Valentine, *J. Am. Chem. Soc.* **1990**, *112*, 4977.
[54] M. J. Frisch, G. W. Trucks, H. B. Schlegel, G. E. Scuseria, M. A. Robb, J. R. Cheeseman, V. G. Zakrzewski, J. A. Montgomery, Jr., R. E. Stratmann, J. C. Burant, S. Dapprich, J. M. Millam, A. D. Daniels, K. N. Kudin, M. C. Strain, O. Farkas, J. Tomasi, V. Barone, M. Cossi, R. Cammi, B. Mennucci, C. Pomelli, C. Adamo, S. Clifford, J. Ochterski, G. A. Petersson, P. Y. Ayala, Q. Cui, K. Morokuma, D. K. Malick, A. D. Rabuck, K. Raghavachari, J. B. Foresman, J. J. V. Cioslowski, A. G. Ortiz, B. B. Baboul, G. Stefanov, A. Liu, Liashenko, P. Piskorz, I. Komaromi, R. Gomperts, R. L. Martin, D. J. Fox, T. Keith, M. A. Al-Laham, C. Y. Peng, A. Nanayakkara, C. Gonzalez, M. Challacombe, P. M. W. Gill, B. Johnson, W. Chen, M. W. Wong, J. L. Andres, C. Gonzalez, M. Head-Gordon, E. S. Replogle, J. A. Pople, *Gaussian 98*, Gaussian, Inc., Pittsburgh PA, **1998**.
[55] A. D. Becke, *J. Chem. Phys.* **1993**, *98*, 5648.
[56] C. Lee, W. Yang, R. G. Parr, *Phys. Rev. B* **1988**, *37*, 785.
[57] N. Lehnert, R. Y. N. Ho, L. Que, E. I. Solomon, *J. Am. Chem. Soc.* **2001**, *123*, 8271.
[58] N. Lehnert, F. Neese, R. Y. N. Ho, L. Que, E. I. Solomon, *J. Am. Chem. Soc.* **2002**, *124*, 10810.
[59] S. Shaik, S. P. de Visser, F. Ogliaro, H. Schwarz, D. Schroder, *Curr. Opin. Chem. Biol.* **2002**, *6*, 556.
[60] P. C. Hiberty, *J. Mol. Struct.: Theochem* **1998**, *451*, 237−261.
[61] J.-P. Malrieu, in *Valence Bond Theory and Chemical Structure*, vol. 64 (Eds.: D. J. Klein, N. Trinajstic), Elsevier, Amsterdam, Oxford, New York, Tokyo, **1990**.
[62] L. Salem, *Electrons in Chemical Reactions − First Principles*, Wiley-Interscience, **1982**.
[63] O. Bortolini, M. Ricci, B. Meunier, P. Friant, I. Ascone, J. Goulon, *New. J. Chem.* **1986**, *10*, 39.
[64] A. Schaefer, H. Horn, R. Ahlrichs, *J. Chem. Phys.* **1992**, *97*, 2571.
[65] M. E. J. Casida, K. C. Casida, D. R. Salahub, *J. Chem. Phys.* **1998**, *108*, 4439.
[66] W. J. Hehre, R. F. Stewart, J. A. Pople, *J. Chem. Phys.* **1969**, *51*, 2657.

Received May 16, 2003
Early View Article
Published Online November 20, 2003

 © 2004 Wiley-VCH Verlag GmbH & Co. KGaA, Weinheim

Phenylcyanamido Ligand Building Molecular, 1-D, and 2-D Systems − Syntheses, Crystal Structures and Magnetic Properties

Albert Escuer,[a] Núria Sanz,[a] Franz A. Mautner,[b] and Ramon Vicente*[a]

Keywords: Manganese / Magnetic properties / Phenylcyanamido ligands / Bridging ligands

Several Mn^{II} compounds have been synthesised with the phenylcyanamido ligand, C_6H_5–NCN^-, and characterised by means of single crystal X-ray structure determination. The reported compounds show a wide variety of nuclearity: mononuclear, dinuclear, 1-D, and 2-D compounds are present in which the phenylcyanamido anion ($pcyd^-$) acts as a bridging ligand. The mononuclear compound $[Mn(pcyd)_2(phen)_2]$ (**1**) crystallises in the orthorhombic system, *Pbcn* space group; dinuclear compound $[\{Mn(pcyd)(phen)(MeOH)\}_2(\mu_{1,3}\text{-}pcyd)_2]$ (**2**) crystallises in the monoclinic system, *C*2/*c* space group; 1-D chain $[Mn(4\text{-}bzpy)_2(\mu_{1,3}\text{-}pcyd)_2]_n$·MeOH (**3**·MeOH) crystallises in the triclinic system, $P\bar{1}$ space group; 2-D network $[Mn(\mu_{1,3}\text{-}pcyd)_2(\mu\text{-}4,4'\text{-}bpy)]_n$·MeOH (**4**·MeOH) crystallises in the monoclinic system, C2 space group. Susceptibility measurements on compounds **2**–**4** reveal moderate AF coupling in all cases.
(© Wiley-VCH Verlag GmbH & Co. KGaA, 69451 Weinheim, Germany, 2004)

Introduction

In the last few years, a wide variety of bridging ligands have been used to promote the magnetic interaction between transition metal ions in polynuclear systems. In this sense, the anions azido[1] and dicyanamido[2] have generated a plethora of new polynuclear compounds ranging from dinuclear to 3D with different architectures. The study of the magnetic behaviour of these compounds has made for fast growth in the field molecular magnetism. However, the X-phenylcyanamido ligands (X-$pcyd^-$), Scheme 1, have practically been forgotten[3,4] as superexchange mediators in spite of the similarities with the azido or dicyanamido ligands. The $XPh-NCN^-$ group is electronically similar to the azido ligand (N_3^-), and it is reasonable to expect similar coordination modes. On the other hand, the nitrile group approaches the coordination properties of those observed for the dicyanamido ligand (mainly for M−N−C and M−N bond parameters).[2,5]

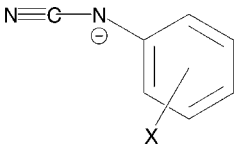

Scheme 1

With the aim of exploring the magnetic and synthetic possibilities of the R-phenylcyanamido ligands, we have recently published[5] the syntheses and structural characterisation of several representative Mn^{II} derivatives: the mononuclear compound $[Mn(3\text{-}Clpcyd)_2(H_2O)_2(4\text{-}bzpy)_2]$; the dinuclear ones $[\{Mn(3\text{-}Clpcyd)(2,2'\text{-}bpy)(S)\}_2(\mu_{1,3}\text{-}3\text{-}Clpcyd)_2]$, S = MeOH or EtOH; the 1-D $[Mn(2,2'\text{-}bpy)(\mu_{1,3}\text{-}4\text{-}Clpcyd)_2]_n$ and the 2-D $[Mn(\mu_{1,3}\text{-}3\text{-}Fpcyd)_2(\mu\text{-}4,4'\text{-}bpy)]_n$, in which 4-bzpy is 4-benzoylpyridine, 2,2′-bpy and 4,4′-bpy corresponds to the 2,2′- and 4,4′-bipyridyls. This series of compounds was obtained by using different X-phenylcyanamido derivatives: 3-$Clpcyd^-$, 4-$Clpcyd^-$ and 3-$Fpcyd^-$ are the 3-chloro-, 4-chloro-, or 3-fluorophenylcyanamido ligands, respectively. Magnetic measurements on the polynuclear $\mu_{1,3}$-X-$pcyd^-$ compounds revealed moderate AF coupling for all of them. This coupling lies in an intermediate position between the typical magnitude of the coupling induced by $\mu_{1,3}$ azido and $\mu_{1,5}$ dicyanamido bridges. MO calculations have evaluated the influence of the chair distortion of the $Mn-(NCN)_2-Mn$ unit, the effect of the halo substituent in the *para* position and the torsion effect of the phenyl rings on the superexchange interaction, and the theoretical results have been correlated with the experimental data.

In this paper, bearing in mind that the number of compounds is still low, we extend the study to the coordination compounds derived from the X-phenylcyanamido ligands by reporting the use of *only* the phenylcyanamido anion ($pcyd^-$), to synthesise a new series of $[Mn(pcyd)_2(L)_n]$ derivatives which show different nuclearities and dimensionalities. Successful syntheses and structural characterisation have been carried out for several representative complexes,

[a] Departament de Química Inorgànica, Universitat de Barcelona, c/ Martí Franquès 1−11, 08028 Barcelona, Spain
Fax: (internat.) +34-(0)93-4907725
E-mail: ramon.vicente@qi.ub.es
[b] Institut für Physikalische und Theoretische Chemie, Technische Universität Graz,
8010 Graz, Austria
E-mail: Mautner@ptc.tu-graz.ac.at

with formulae $[Mn(pcyd)_2(phen)_2]$ (**1**), $[\{Mn(pcyd)(phen)(MeOH)\}_2(\mu_{1,3}\text{-pcyd})_2]$ (**2**), $[Mn(4\text{-bzpy})_2(\mu_{1,3}\text{-pcyd})_2]\cdot MeOH$ (**3**·MeOH) and $[Mn(\mu_{1,3}\text{-pcyd})_2(\mu\text{-}4,4'\text{-bpy})]_n\cdot MeOH$ (**4**·MeOH) where 4-bzpy is 4-benzoylpyridine, 4,4′-bpy corresponds to 4,4′-bipyridyl and phen is 1,10-phenanthroline. These compounds were obtained by reaction in alcoholic media of manganese salts with the corresponding pyridinic or bipyridinic ligands and the deprotonated phenylcyanamide. The X-ray crystal structure determination reveals a wide variety of topologies and supramolecular arrangements: compound **1** is a mononuclear complex; compounds **2** a dinuclear complex bridged by double phenylcyanamido ligands, giving a supramolecular 1-D system by means of hydrogen bonds; compound **3**·MeOH is a chain of manganese atoms linked by double phenylcyanamido bridges. Finally, compound **4**·MeOH is a 2-D system formed by the crossing of phenylcyanamido and 4,4′-bpy chains. This paper gives the second structural set of data for polynuclear phenylcyanamide bridged derivatives with Mn^{II} as the central atom, together with a set of new experimental variable temperature susceptibility data for the $\mu_{1,3}$-X-pcyd$^-$ superexchange mediator.

Magnetic measurements for compounds **2**−**4** reveal a moderate AF coupling which lies in an intermediate position between the typical values of the coupling induced by $\mu_{1,3}$-azido and $\mu_{1,5}$-dicyanamido bridges. The obtained coupling constants are in accordance with the general rules for the $\mu_{1,3}$ coordination mode of pcyd$^-$ ligands discussed in the previous paper.[5]

Results and Discussion

Infrared Spectra: Neutral pcydH shows a characteristic IR ν(NCN) stretching absorption over a short wavenumber range (2225−2249 cm^{-1}), which shifts down to ca. 2120 cm^{-1} for deprotonated pcyd$^-$, suggesting a lower contribution of the resonance form containing the nitrile fragment. *N*-nitrile-coordinated X-pcyd$^-$ ligands, exhibit intermediate positions (always lower than 2200 cm^{-1}), with a dependence on the nature of the metallic centre and the number of halo groups.[3] For pcyd$^-$, the signal appears at 2108 cm^{-1} for **1** (only *N*-nitrile-coordinated pcyd$^-$ ligand), at 2168−2136 cm^{-1} for **2** (containing the two $\mu_{1,3}$-pcyd and *N*-nitrile pcyd$^-$ coordination modes) and at 2164 and 2133 cm^{-1} for **3** and **4,** respectively (containing the two $\mu_{1,3}$-X-pcyd$^-$ coordination modes). The structurally characterised $\mu_{1,3}$ copper dimer $[\{Cu(pcyd)(2,2'\text{-bpy})\}_2(\mu_{1,3}\text{-pcyd})_2]$[6] is in reasonable agreement with this assignment: it exhibits two similar absorptions at 2175 and 2103 cm^{-1}. In the mononuclear compound with the 3-Clpcyd$^-$ ligand $[Mn(3\text{-Clpcyd})_2(H_2O)_2(4\text{-bzpy})_2]$ the signal appears at 2108 cm^{-1} (only *N*-nitrile-coordinated pcyd$^-$ ligand) and at 2155−2132 cm^{-1} and 2159−2133 cm^{-1} in the dinuclear ones $[\{Mn(3\text{-Clpcyd})(2,2'\text{-bpy})(S)\}_2(\mu_{1,3}\text{-3-Clpcyd})_2]$, S = MeOH or EtOH, respectively (containing the two $\mu_{1,3}$-pcyd$^-$ and *N*-nitrile pcyd$^-$ coordination modes).[5] The wavenumber sequence for the ν(NCN) stretching absorption seems then to be pcydH > $\mu_{1,3}$-X-pcyd > *N*-nitrile coordination or anionic X-pcyd$^-$. The limited data for Mn^{II} derivatives suggest the above order, but further experimental data are required to obtain a general assignment.

Description of the Structure of $[Mn(pcyd)_2(phen)_2]$ (1): This compound consists of monomeric units in which the terminal pcyd$^-$ ligands adopt a *cis* arrangement around the central Mn^{II} ion (Figure 1). Selected bond parameters are given in Table 1.

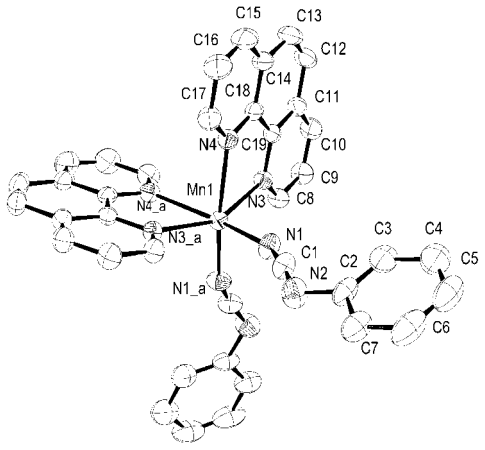

Figure 1. Labelled plot of $[Mn(pcyd)_2(phen)_2]$ (**1**)

Table 1. Selected bond lengths [Å] and angles [°] for $[Mn(pcyd)_2(phen)_2]$ (**1**)

Mn(1)−N(1)	2.131(3)	Mn(1)−N(3)	2.321(2)
Mn(1)−N(4)	2.314(2)		
N(1)−Mn(1)−N(4_a)[a]	159.5(1)	N(3)−Mn(1)−N(4)	71.3(1)
N(1)−Mn(1)−N(3)	107.2(1)	N(3)−Mn(1)−N(3_a)	155.2(1)
N(1)−Mn(1)−N(4)	90.8(1)	N(3)−Mn(1)−N(4_a)	90.1(1)
N(1)−Mn(1)−N(3_a)	88.9(1)	N(4)−Mn(1)−N(4_a)	84.1(1)
N(1)−Mn(1)−N(1_a)	100.4(1)		
N(1)−C(1)	1.154(5)	C(1)−N(2)	1.299(6)
N(2)−C(2)	1.388(6)		
Mn(1)−N(1)−C(1)	158.8(5)	N(1)−C(1)−N(2)	171.5(5)
C(1)−N(2)−C(2)	121.7(4)		

[a] Symmetry codes: _a: $-x, y, -z + 1/2$

The Mn^{2+} ion shows a strongly distorted octahedral environment imposed by the rigidity of the 1,10-phenantroline ligands. The pcyd$^-$ ligands are coordinated to the Mn atom by the nitrile N atoms. There are two kinds of bond Mn−N distances: a short distance of 2.131(3) Å between the Mn^{II} ion and the nitrile N atoms, and longer distances to the N(phen) atoms: Mn(1)−N(3) 2.312(2) Å and Mn(1)−N(4) 2.314(2) Å. The most distorted bond angles around the Mn atom are N(3)−Mn−N(4), 71.3(1)°, N(1)−Mn−N(1_a), 100.4(1)° and N(4)−Mn−N(4_a), 84.1(1)°. The coordination of the monodentate phenylcyanamido ligand to the manganese atom is not linear with a Mn(1)−N(1)−C(1) bond angle of 158.8(5)°.

The NCN unit is practically linear with a N(1)−C(1)−N(2) angle of 171.5°. NCN is asymmetric, with bond lengths of N(1)−C(1) = 1.154(5) Å and C(1)−N(2) =

 © 2004 Wiley-VCH Verlag GmbH & Co. KGaA, Weinheim

1.299(6) Å. The cyanamido unit is practically coplanar with the phenyl group of the pcyd$^-$ ligand and shows a C(1)−N(2)−C(2) bond angle of 121.7(4)°.

Description of the Structure of [{Mn(pcyd)(phen)(MeOH)}$_2$($\mu_{1,3}$-pcyd)$_2$] (2): The structure consists of centrosymmetric dinuclear Mn units linked by double end-to-end phenylcyanamido bridges (Figure 2). Selected bond parameters are given in Table 2.

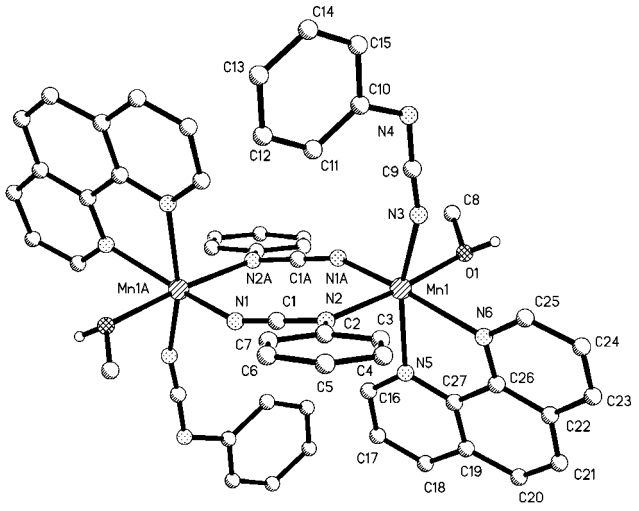

Figure 2. Labelled plot of [{Mn(pcyd)(phen)(MeOH)}$_2$($\mu_{1,3}$-pcyd)$_2$] (**2**)

Table 2. Selected bond lengths [Å] and angles [°] for [{Mn(pcyd)(phen)(MeOH)}$_2$($\mu_{1,3}$-pcyd)$_2$] (**2**)

Mn(1)−O(1)	2.235(2)	Mn(1)−N(5)	2.306(2)
Mn(1)−N(2)	2.278(2)	Mn(1)−N(6)	2.300(2)
Mn(1)−N(3)	2.140(2)	Mn(1)−N(1A)	2.166(2)
O(1)−Mn(1)−N(2)	175.1(1)	N(2)−Mn(1)−N(3)	91.2(1)
O(1)−Mn(1)−N(3)	87.4(1)	N(2)−Mn(1)−N(5)	92.8(1)
O(1)−Mn(1)−N(5)	89.8(1)	N(2)−Mn(1)−N(6)	105.5(1)
O(1)−Mn(1)−N(6)	79.2(1)	N(2)−Mn(1)−N(1A)	88.5(1)
O(1)−Mn(1)−N(1A)[a]	87.4(1)	N(5)−Mn(1)−N(6)	72.1(1)
N(3)−Mn(1)−N(5)	163.7(1)	N(5)−Mn(1)−N(1A)	91.4(1)
N(3)−Mn(1)−N(6)	91.6(1)	N(6)−Mn(1)−N(1A)	158.6(1)
N(3)−Mn(1)−N(1A)	104.6(1)		
N(1)−C(1)	1.167(3)	N(3)−C(9)	1.160(3)
C(1)−N(2)	1.296(3)	C(9)−N(4)	1.289(3)
C(2)−N(2)	1.413(3)	C(10)−N(4)	1.404(3)
Mn(1A)−N(1)−C(1)	156.2(2)	Mn(1)−N(3)−C(9)	160.3(1)
N(1)−C(1)−N(2)	176.4(2)	N(3)−C(9)−N(4)	176.5(2)
C(1)−N(2)−Mn(1)	113.2(1)	C(9)−N(4)−C(10)	117.2(2)
Mn(1)−N(2)−C(2)	129.2(1)		
C(2)−N(2)−C(1)	117.0(2)		

[a] Symmetry codes: (A) $-x$, $-y$, $-z+1$.

The six coordination sites around the Mn atoms are occupied by the two N atoms of one phen ligand, one nitrile N atom of the terminal pcyd$^-$ ligand, one nitrile and one amido nitrogen atoms of the two bridging cyanamido ligands and one O atom of the solvent molecule (methanol). The linked phen and the variety of ligands distorts the coordination polyhedron of the Mn atom: bond angles ranging between 72.1(1)° for N(5)−Mn(1)−N(6) and 105.5(1)° for N(2)−Mn(1)−N(6) are found. The different nature of the N atoms of the phenylcyanamido ligand also induces different bond parameters in the bridging region: Mn(1)−N(1) takes the value of 2.278(2) Å whereas Mn(1)−N(1A) is only 2.166(2) Å. Mn−*N*−C bond angles are also different, being Mn(1A)−N(1)−C(1) 156.2(2)° in contrast with Mn(1)−N(2)−C(1), which takes the value of 113.2(1)°. As occurs in **1**, the monodentate phenylcyanamido ligands coordinate to the manganese atom in a quasi-linear arrangement, with a Mn(1)−N(3)−C(9) bond angle of 160.3(1)°.

The C−N−C angles between the cyanamido and the phenyl groups are similar for the terminal and the bridging ligands: 117.2(2)° and 117.0(2)°, respectively. The Mn−(NCN)$_2$−Mn subunit shows a chair distortion similar to those often found in similar systems with double azido bridges.[1] This means that the two −NCN− groups are in the same plane with the manganese atoms placed 0.403(1) Å out of the main plane. The torsion angle between the plane determined by the two −NCN− groups and the N(2)−Mn(1)−N(1A) plane is 14.7(1)°. The pcyd$^-$ ligand is practically planar with a minor torsion of 4.1(2)° between the bond direction N(2)−C(2) and the (NCN)$_2$ plane. The phenylcyanamido ligand is placed out of the main (NCN)$_2$ plane, which forms an acute angle of 15.7(1)° with the N(2)−C(2) bond direction. The Mn···Mn intradimer distance is 5.479(1) Å.

The dinuclear units generate a supramolecular one-dimensional H-bonded system by means of the OH group of the coordinated methanol molecules, O(1) atom, and the N(4) atoms of the terminal pcyd$^-$ ligands. Two of these H bonds appear between each dinuclear unit, giving a structurally alternating 1-D system (Figure 3). The N(4)−O(1) distance is 2.727(2) Å and the bond angle O(1)−H(1)−N(4) has a value of 178(3)°.

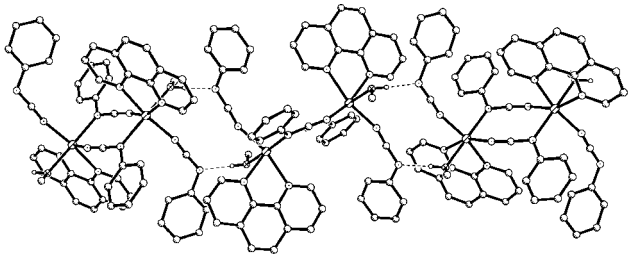

Figure 3. Hydrogen bond chain in compound **2**

Description of the Structure of [Mn(4-bzpy)$_2$($\mu_{1,3}$-pcyd)$_2$]·MeOH (3·MeOH): Selected bond parameters are given in Table 3. The structure consists of a one-dimensional Mn system where the coordination environment around the Mn atoms includes two N atoms of *trans*-4-bzpy ligands and four N atoms of bridging pcyd$^-$ ligands. The compound crystallizes with one MeOH molecule per formula unit.

 © 2004 Wiley-VCH Verlag GmbH & Co. KGaA, Weinheim

Table 3. Selected bond lengths [Å] and angles [°] for $[Mn(4\text{-bzpy})_2(\mu_{1,3}\text{-pcyd})_2]\cdot MeOH$ (**3**·MeOH)

Mn(1)−N(1)	2.168(2)	Mn(1)−N(4)	2.272(3)
Mn(1)−N(2)	2.305(3)	Mn(1)−N(5)	2.329(3)
Mn(1)−N(3)	2.195(2)	Mn(1)−N(6)	2.275(3)
N(1)−Mn(1)−N(3)	175.5(1)	N(3)−Mn(1)−N(2)	95.7(1)
N(1)−Mn(1)−N(2)	86.4(1)	N(3)−Mn(1)−N(4)	88.3(1)
N(1)−Mn(1)−N(4)	89.0(1)	N(3)−Mn(1)−N(5)	85.9(1)
N(1)−Mn(1)−N(5)	90.5(1)	N(3)−Mn(1)−N(6)	86.5(1)
N(1)−Mn(1)−N(6)	97.4(1)	N(4)−Mn(1)−N(5)	88.2(1)
N(2)−Mn(1)−N(4)	170.2(1)	N(4)−Mn(1)−N(6)	95.9(1)
N(2)−Mn(1)−N(5)	83.2(1)	N(5)−Mn(1)−N(6)	171.5(1)
N(2)−Mn(1)−N(6)	93.9(1)		
N(1)−C(1)	1.166(4)	N(3)−C(8)	1.165(4)
C(1)−N(2_a)[a]	1.300(4)	C(8)−N(4_b)	1.301(4)
N(2)−C(2)	1.413(4)	N(4)−C(9)	1.411(4)
Mn(1)−N(1)−C(1)	142.3(2)	Mn(1)−N(3)−C(8)	141.9(2)
N(1)−C(1)−N(2_a)	175.2(3)	N(3)−C(8)−N(4_b)	175.5(3)
C(1)−N(2_a)−Mn(1_a)	109.0(2)	C(8)−N(4_b)−Mn(1_b)	110.5(2)
Mn(1)−N(2)−C(2)	132.3(2)	Mn(1)−N(4)−C(9)	128.7(2)
C(2)−N(2)−C(1_a)	116.6(2)	C(9)−N(4)−C(8_b)	117.9(3)

[a] Symmetry codes: _a: $-x, -y, -z + 1$; _b: $-x + 1, -y, -z + 1$.

Double cyanamido bridges link the Mn atoms, giving a *trans* chain (Figure 4). The bond parameters in the bridging region show different bond lengths for the Mn−N(nitrile) and the Mn−N(amide) unions: Mn(1)−N(1), 2.168(2) Å and Mn(1)−N(3), 2.195(2) Å; Mn(1)−N(2), 2.305(3) Å, and Mn(1)−N(4), 2.272(3) Å. The bond angle Mn(1_a)−N(2_a)−C(1), 109.0(2)° is clearly smaller than Mn(1)−N(1)−C(1), 142.3(2)°. The Mn−$(NCN)_2$−Mn subunits show an important chair distortion: for the Mn(1)−[N(1)−C(1)−N(2)]$_2$−Mn(1_a) ring the Mn atoms are placed 0.979(1) Å out of the $(NCN)_2$ main plane and there is a dihedral angle of 37.0(1)° between the N(1)−Mn(1)−N(2) plane and the main $(NCN)_2$ plane. In this case the deviation of the phenyl groups, given by the acute angle between the bond directions N(2)−C(2) or N(4)−C(9) and the $(NCN)_2$ plane are only 9.6(2) and 7.2(2)°, respectively. The Mn atoms are placed 0.048 Å out of the $(NCN)_2$ plane in the Mn(1_b)−[N(3)−C(8)−N(4)]$_2$−Mn(1) dinuclear unit. The dihedral angle between N(3)−Mn(1)−N(4) and the main $(NCN)_2$ plane is 36.1°. The Mn···Mn intrachain distance is 5.328(1) Å, whereas the minimum interchain Mn···Mn distance is 8.520(1) Å.

Description of the Structure of $[Mn(\mu_{1,3}\text{-pcyd})_2(\mu\text{-}4,4'\text{-bpy})]_n\cdot MeOH$ (4·MeOH): The use of 4,4′-bpy determines a *trans*-octahedral arrangement around the Mn atoms (Figure 5). Selected bond parameters are given in Table 4.

The compound crystallises with a MeOH molecule per formula unit. The coordination sites around the manganese atom are occupied by two *trans* N atoms of two bridging 4,4′-bpy ligands and by four bridging $pcyd^-$ ligands. The structure may then be described as a two-dimensional sys-

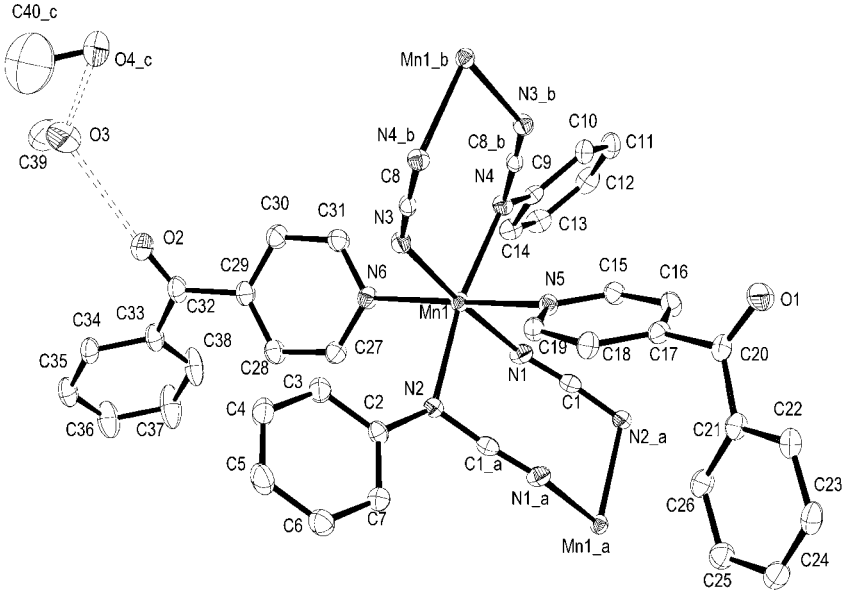

Figure 4. ORTEP plot of $[Mn(4\text{-bzpy})_2(\mu_{1,3}\text{-pcyd})_2]\cdot MeOH$ (**3**·MeOH) with thermal ellipsoids at the 40% probability level

 © 2004 Wiley-VCH Verlag GmbH & Co. KGaA, Weinheim

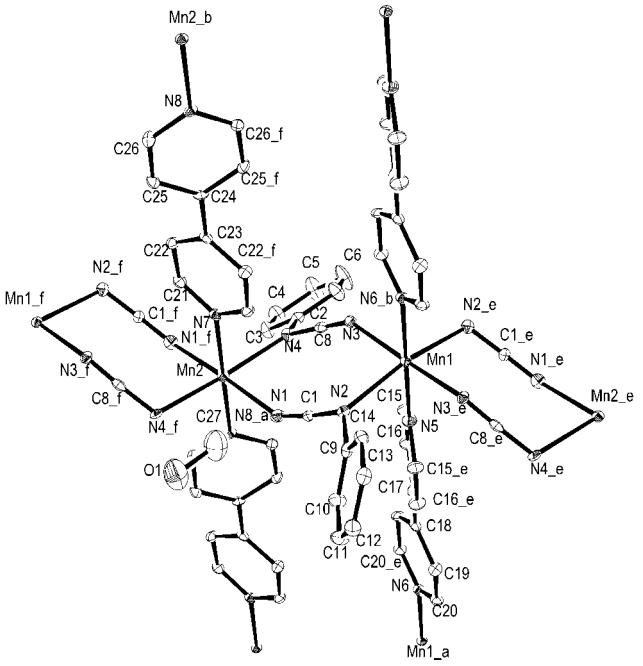

Figure 5. ORTEP plot of the basic unit of $[Mn(\mu_{1,3}\text{-pcyd})_2(\mu\text{-}4,4'\text{-bpy})]_n\cdot$MeOH (**4**·MeOH) with thermal ellipsoids at the 50% probability level

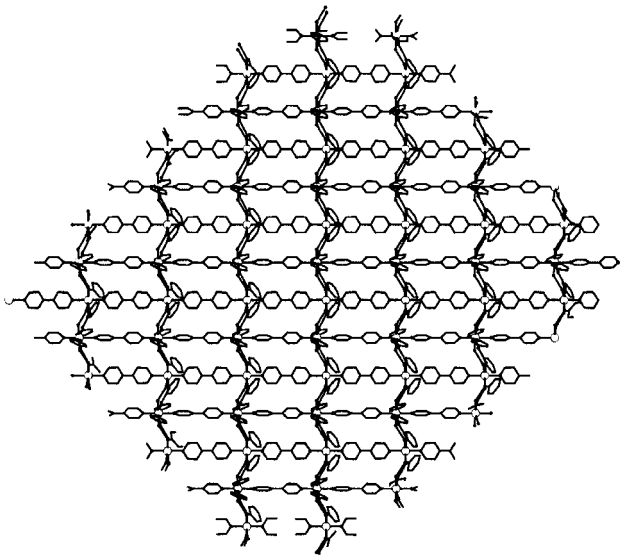

Figure 6. View of the 2-D arrangement of **4**·MeOH by means of the pcyd and 4,4′-bipy bridging ligands

tem with 4,4′-bpy-Mn chains crossed by Mn-pcyd chains (Figure 6).

The bond lengths in the bridging region again show a clear difference between nitrile and amide N atoms of the ligand: bond lengths for Mn(1)−N(3) and Mn(2)−N(1) are 2.187(4) Å and 2.173(3) Å whereas Mn(1)−N(2) and Mn(2)−N(4) are 2.315(4) Å and 2.327(4) Å, respectively. Bond angles related to the nitrile N atom Mn(1)−N(3)−C(8), 148.9(5)° and Mn(2)−N(1)−C(1), 142.3(4)° are larger than the angles related to the amide N atom Mn(1)−N(2)−C(1), 111.7(3)° and Mn(2)−N(4)−C(8), 111.2(3)°. As occurs for the above compounds, Mn−$(NCN)_2$−Mn subunits show a clear chair distortion with the Mn atoms placed 0.808(1)−0.942(1) Å out of the cyanamido plane. A dihedral angle of 30.6(2)−34.3(2)° is found between the $(NCN)_2$ planes and N(1)−Mn(2)−N(4)

Table 4. Selected bond lengths [Å] and angles [°] for $[Mn(\mu_{1,3}\text{-pcyd})_2(\mu\text{-}4.4'\text{-bpy})]_n\cdot$MeOH (**4**·MeOH)

Mn(1)−N(5)	2.350(7)	Mn(2)−N(7)	2.301(7)
Mn(1)−N(6_b)[a]	2.279(7)	Mn(2)−N(8_a)	2.312(7)
Mn(1)−N(2)	2.315(4)	Mn(2)−N(1)	2.173(3)
Mn(1)−N(3)	2.187(4)	Mn(2)−N(4)	2.327(4)
N(5)−Mn(1)−N(6_b)	180.0(6)	N(7)−Mn(2)−N(8_a)	180.0(1)
N(5)−Mn(1)−N(2)	87.6(1)	N(7)−Mn(2)−N(1)	91.7(1)
N(5)−Mn(1)−N(3)	92.4(2)	N(7)−Mn(2)−N(4)	82.8(1)
N(5)−Mn(1)−N(2_e)	87.6(1)	N(7)−Mn(2)−N(1_f)	91.7(1)
N(5)−Mn(1)−N(3_e)	92.4(2)	N(7)−Mn(2)−N(4_f)	82.8(1)
N(6_b)−Mn(1)−N(2)	92.4(1)	N(8_a)−Mn(2)−N(1)	88.3(1)
N(6_b)−Mn(1)−N(3)	87.6(2)	N(8_a)−Mn(2)−N(4)	97.2(1)
N(6_b)−Mn(1)−N(2_e)	92.4(1)	N(8_a)−Mn(2)−N(1_f)	88.3(1)
N(6_b)−Mn(1)−N(3_e)	87.6(2)	N(8_a)−Mn(2)−N(4_f)	97.2(1)
N(2)−Mn(1)−N(3)	84.8(1)	N(1)−Mn(2)−N(4)	88.8(1)
N(2)−Mn(1)−N(2_e)	175.2(2)	N(1)−Mn(2)−N(1_f)	176.7(2)
N(2)−Mn(1)−N(3_e)	95.4(1)	N(1)−Mn(2)−N(4_f)	91.6(1)
N(3)−Mn(1)−N(2_e)	95.4(1)	N(4)−Mn(2)−N(1_f)	91.6(1)
N(3)−Mn(1)−N(3_e)	175.2(1)	N(4)−Mn(2)−N(4_f)	165.3(1)
N(2_e)−Mn(1)−N(3_e)	84.8(1)	N(1_f)−Mn(2)−N(4_f)	88.8(1)
N(3)−C(8)	1.175(6)	N(1)−C(1)	1.162(6)
C(8)−N(4)	1.278(6)	C(1)−N(2)	1.299(6)
N(4)−C(2)	1.429(7)	N(2)−C(9)	1.413(7)
Mn(1)−N(3)−C(8)	148.9(5)	Mn(2)−N(1)−C(1)	142.3(4)
N(3)−C(8)−N(4)	174.4(5)	N(1)−C(1)−N(2)	177.1(6)
C(8)−N(4)−Mn(2)	111.2(3)	C(1)−N(2)−Mn(1)	111.7(3)
Mn(2)−N(4)−C(2)	128.6(3)	Mn(1)−N(2)−C(9)	132.5(3)
C(8)−N(4)−C(2)	116.0(4)	C(9)−N(2)−C(1)	115.8(4)

[a] Symmetry codes _a: $x, y-1, z$; _b: $x, y+1, z$; _e: $x, y, -z+1$; _f: $x, y, -z$.

 © 2004 Wiley-VCH Verlag GmbH & Co. KGaA, Weinheim

or N(3)−Mn(1)−N(2) planes. Bridging phenylcyanamido ligands are far from planar, showing torsion angles for N(3)−N(4)−C(2)−C(3) of 38.7(4)° and N(1)−N(2)−C(9)−C(10) of 7.7(3)°.

In this case, a small deviation of the phenyl groups is evidenced by the 26.5(3)° or 0.8(3)° acute angles between the bond directions N(2)−C(9) or N(4)−C(2) with the reference $(NCN)_2$ plane. The Mn···Mn distance through the cyanamido unit is 5.407(1) Å, through the 4,4′-bpy bridge 11.712(1) Å, and the minimum interplane Mn···Mn distance is 10.289(1) Å.

Magnetic Measurements and Coupling Constant Calculations: Magnetic measurements were performed for compounds **2**−**4** in the 300−4 K temperature range on powdered crystalline samples, (see Exp. Sect.). The overall interaction is moderately antiferromagnetic in all cases.

The susceptibility plots increase gradually on cooling for compound **2** (Figure 7), but don't reach a maximum because at low temperatures a low quantity of impurities produce a sudden increase in the susceptibility value. The experimental data were analysed with the analytical expression for an isotropic $S = 5/2$ dinuclear compound by using the analytical expression derived from the isotropic Hamiltonian $H = -JS_1 \cdot S_2$, including an impurity term. The best fit parameters were $J = -3.5(1)$ cm^{-1}, $g = 2.01(1)$, $\rho = 0.030$.

Magnetic susceptibilities for compounds **3** and **4** also increase on cooling, reaching a broad maximum at 16 K in compound **4** (Figure 7). For compound **3** a sudden increase is also observed in the susceptibility values due to paramagnetic impurities. The coupling through the 4,4′-bpy bridges is negligible, so 2-D compound **4** should be assumed to be magnetically one-dimensional through the phenylcyanamido bridges. The experimental data were analysed with the analytical expression for an isotropic $S = 5/2$ chain system[7] derived by Fisher from the Hamiltonian $H = \Sigma -JS_i \cdot S_{i+1}$, including an impurity term for **3**. The best fit parameters were $J = -2.7(1)$ cm^{-1}, $g = 2.00(1)$, $\rho = 0.027$ and $J = -2.1(1)$ cm^{-1}, $g = 2.00(1)$ for **3** and **4,** respectively.

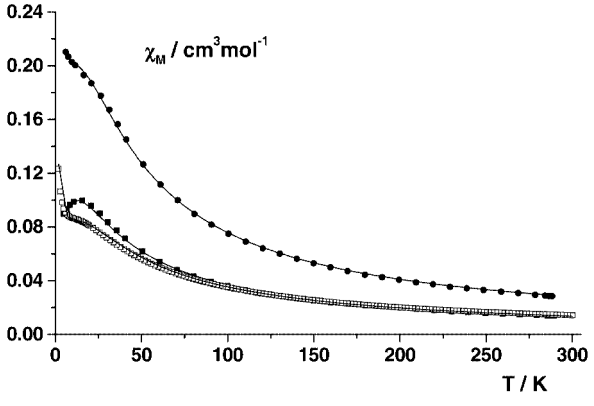

Figure 7. Plot of χ_M vs T for compounds [{Mn(pcyd)(phen)(MeOH)}$_2$($\mu_{1,3}$-pcyd)$_2$] (**2**) (solid circles) [Mn(4-bzpy)$_2$($\mu_{1,3}$-pcyd)$_2$]$_n$ (**3**) (open squares) and [Mn($\mu_{1,3}$-pcyd)$_2$(μ-4,4′-bpy)]$_n$ (**4**) (solid squares). Solid line shows the best fit of the data (see text)

EPR spectra for compound **1** show an isotropic broad band with a peak-to-peak increment (Δ_{pp}) of 674 G at room temperature, centred at $g = 2.00$. At 4 K the spectrum exhibits the main signal centred at $g = 2.00$ and a second weaker half-field band displaced at $g = 4.21$. Compound **2** shows one isotropic broad band at room temperature and 77 K, centred at room temperature at $g = 2.01$ with Δpp of 286 G. At 4 K the spectrum exhibits two main signals centred at $g = 2.01$ and 10.27 with Δpp of 438 G and 595 G, respectively, and several signals with minor intensities, which indicate some anisotropic effect at very low temperatures. Spectra of compounds **3** and **4** correspond nicely to that expected for one-dimensional systems with moderate antiferromagnetic coupling and weak dipolar interactions (Mn···Mn distances around 5.5 Å).[8] Between room temperature and 77 K the isotropic signals centered at $g = 2.01$ show a Δpp of 94 G and 92 G, respectively. Analogous Mn^{II} doubly bridged chains with end-to-end azido ligands with similar Mn···Mn intrachain distances have J values that typically lie around -10 cm^{-1}, the peak-to-peak linewidth being only 35 G due to the greater superexchange narrowing.[9] Instead, for weaker coupling, doubly dca bridged Mn^{II} chains, the peak-to-peak linewidth is much greater reaching values around 100−120 G[6] that show dipolar broadening on cooling down to 4 K.

The efficiency in transmitting the superexchange interactions is in the order $N_3^- > X\text{-pcyd}^- >> N(CN)_2^-$ [5] with typical values of the J parameter in the 1-D systems being around $-7/-15$ cm^{-1} (azido), $-1/-3$ cm^{-1} (X-pcyd$^-$) and weaker than -0.5 cm^{-1} for dicyanamide. The new series of J values reported here for the polynuclear phenylcyanamide bridged derivatives with Mn^{II} as the central atom confirms the assumption.

Conclusion

The ability of the X-phenylcyanamido ligands to act as bridging ligands has been newly confirmed by using the phenylcyanamido anion (pcyd$^-$) to synthesise a new series of formula [Mn(pcyd)$_2$(L)$_n$], L = phen, 4-bzpy and 2,2′-bpy, which show different nuclearities and dimensionalities. The coordination mode of the bridging pcyd$^-$ ligands is $\mu_{1,3}$. The magnetic measurements indicate AF coupling. The obtained coupling constant values are intermediate between the equivalent values for azido and dicianamido bridging ligands.

Experimental Section

Physical Methods: Magnetic susceptibility measurements were carried out on polycrystalline samples with a DSM8 pendulum susceptometer working in the range 4−300 K under magnetic fields of approximately 1 T. Diamagnetic corrections were estimated from Pascal tables. The infrared spectra (4000−400 cm^{-1}) were recorded from KBr pellets with a Nicolet 520 FTIR spectrophotometer. EPR spectra were recorded with a Bruker ES200 spectrometer at X-band frequency.

 © 2004 Wiley-VCH Verlag GmbH & Co. KGaA, Weinheim

Table 5. Crystal data and structure refinement for $[Mn(pcyd)_2(phen)_2]$ (**1**), $[\{Mn(pcyd)(phen)(MeOH)\}_2(\mu_{1,3}\text{-pcyd})_2]$ (**2**), $[Mn(4\text{-bzpy})_2(\mu_{1,3}\text{-pcyd})_2]_n\cdot$MeOH (**3**·MeOH) and $[Mn(\mu_{1,3}\text{-pcyd})_2(\mu\text{-}4,4'\text{-bpy})]_n\cdot$MeOH (**4**·MeOH)

	1	**2**	**3**·MeOH	**4**·MeOH
Empirical formula	$C_{38}H_{26}MnN_8$	$C_{54}H_{44}Mn_2N_{12}O_2$	$C_{39}H_{32}MnN_6O_3$	$C_{25}H_{22}MnN_6O$
M_w	649.61	1002.89	687.7	477.43
Space group	Pbcn	*C*2/*c*	$P\bar{1}$	*C*2
a, Å	13.176(5)	15.758(6)	10.043(3)	18.498(4)
b Å	10.165(4)	13.771(4)	12.840(3)	11.712(2)
c, Å	23.530(8)	22.753(7)	14.448(5)	10.472(2)
α, deg.	90	90	112.29(2)	90
β, deg.	90	93.49(2)	90.96(2)	106.43(3)
γ, deg.	90	90	101.10(2)	90
V, Å^3	3151.5(20)	4928(3)	1683(1)	2176.0(7)
Z	4	4	2	4
T, °C	25(2)	−185(2)	−173(2)	−185(2)
λ(Mo-K_α), Å	0.71069	0.71069	0.71069	0.71069
$\rho_{calcd.}$, g·cm^{-3}	1.369	1.352	1.357	1.457
μ(Mo-K_α), mm^{-1}	0.461	0.567	0.440	0.638
R[a]	0.0486	0.0376	0.0522	0.0478
ωR^2[b]	0.1431	0.0926	0.1309	0.1197

[a] $R(F_o) = \Sigma F_o - F_c/\Sigma F_o$. [b] $\omega R\,(F_o)^2 = \{\Sigma[\omega[(F_o)^2 - (F_c)^2]^2]/\Sigma[\omega[(F_o)^4]\}^{1/2}$.

Synthesis: Neutral phenylcyanamide (pcydH) was prepared by desulfurisation of the phenylthiourea with lead acetate, following the described general synthetic procedure.[11]

Compound 1: 1 was prepared by reaction of a solution of manganese nitrate hexahydrate (1 mmol) and 1,10-phenanthroline (2 mmol) in 40 mL of methanol with a solution of pcydH (2 mmol) in 10 mL of NaOH (0.2 M) to deprotonate the ligand. After the reagents were mixed, the resulting clear solution was evaporated, giving a yellow crystalline compound suitable for X-ray measurements in a few days. Yield 21%. $C_{38}H_{26}MnN_8$ (649.6): calcd. C 70.3, H 4.0, N 17.2; found C 69.8, H 4.0, N 17.5.

Compound 2: 2 was prepared by reaction of a solution of manganese nitrate hexahydrate (1 mmol) and 1,10-phenanthroline (1 mmol) in 40 mL of methanol with a solution of pcydH (2 mmol) in 5 mL of NaOH (0.2 M) to deprotonate the ligand. After the reagents were mixed, the resulting clear solution was evaporated, giving a yellow crystalline compound suitable for X-ray measurements in three days. Yield 44%. $C_{54}H_{44}Mn_2N_{12}O_2$ (1002.9): calcd. C 64.7, H 4.4, N 16.8; found C 63.7, H 4.2, N 16.7.

Compounds 3 and 4: The method was the same as that for compound **2**, using 4-benzoylpyridine (2 mmol) for **3** and 4,4′-bipyridine (1 mmol) for **4** instead of phenanthroline (1 mmol). Yield of the corresponding yellow products, was 13% and 34%, respectively. Elemental analyses were performed on **3** and **4** in powdered samples three weeks after their preparation. **Compound 3:** $C_{38}H_{28}MnN_6O_2$ (655.6): calcd. C 69.6, H 4.3, N 12.8; found C 68.5, H 4.4, N 12.8. **Compound 4:** $C_{24}H_{18}MnN_6$ (445.4): calcd. C 64.7, H 4.1, N 18.9; found C 64.4, H 4.2, N 18.9. The elemental analysis for **3** and **4** indicates the absence of crystallisation of MeOH molecules in the powdered samples. To avoid errors in the magnetic measurements, the corresponding samples of **2** were freshly extracted from the mother solutions, dried and powdered just prior to performing the measurements. Moreover, the samples of **3** and **4** were dried and powdered some days before performing the magnetic measurements.

X-ray Crystallographic Study: Crystal data and details of the structure determinations are presented in Table 5. Data were collected on a modified STOE 4-circle diffractometer with graphite-monochromated Mo-K_α radiation (λ = 0.71069 Å) and the ω-scan technique. Data of **1**−**4**·MeOH were collected at room temperature, −185(2) °C, −173(2) °C and −185(2) °C, respectively, and processed in the usual way. The structures were solved by direct methods using the SHELXS-86 computer program,[12] and refined by full-matrix least-squares methods on F^2, using the SHELXL-93 program[13] incorporated in the SHELXTL/PC V 5.03 program library[14] and the graphics program PLUTON.[15] All non-hydrogen atoms were refined anisotropically. Hydrogen atoms bonded to donor atoms were located from difference Fourier maps, and the remaining ones were located on calculated positions by using the HFIX utility of the SHELXL-93 program. Selected bond parameters are given in Table 1−4 for compounds **1**−**4**·MeOH, respectively. CCDC-201204 (**1**), -201205 (**2**), -201206 (**3**·MeOH) and -201207 (**4**·MeOH) contain the supplementary crystallographic data for this paper. These data can be obtained free of charge at www.ccdc.cam.ac.uk/conts/retrieving.html [or from the Cambridge Crystallographic Data Centre, 12, Union Road, Cambridge CB2 1EZ, UK; Fax: (internat.) + 44-1223/336-033; E-mail: deposit@ccdc.cam.ac.uk].

Acknowledgments

A.E., R.V., and N.S. wish to thank the Ministerio de Ciencia y Tecnología (Spain), project BQU2000/0791 for the financial support to carry out this research. F.A.M. wishes to thank Prof. Belaj and Prof. Kratky (University of Graz) for the use of experimental equipment and OENB (project 7967) for financial support.

[1] J. Ribas, A. Escuer, M. Monfort, R. Vicente, R. Cortés, L. Lezama, L. T. Rojo, *Coord. Chem. Rev.* **1999**, *193*−*195*, 1027.
[2] [2a] A. Escuer, N. Sanz, F. A. Mautner, R. Vicente, *Inorg. Chem.* **2000**, *39*, 1668. [2b] P. M. Van der Werff, S. R. Batten, P. Jensen, B. Moubaraki, K. S. Murray, *Inorg. Chem.* **2001**, *40*, 1718. [2c] J. W. Raebiger, J. L. Manson, R. D. Sommer, U. Geiser, A. L. Rheingold, J. S. Miller, *Inorg. Chem.* **2001**, *40*, 2578. [2d] B. Vangdal, J. Carranza, F. Lloret, M. Julve, J. Sletten, *J. Chem. Soc., Dalton Trans.* **2002**, 566. [2e] A. Escuer, F. A. Mautner, N. Sanz, R. Vicente, *Inorg. Chim. Acta* **2002**, *340*, 163. [2f] P.

 © 2004 Wiley-VCH Verlag GmbH & Co. KGaA, Weinheim

Jensen, S. R. Batten, B. Moubaraki, K. S. Murray, *J. Chem. Soc., Dalton Trans.* **2002**, 3712 and references cited therein.
[3] R. J. Crutchley, *Coord. Chem. Rev.* **2001**, *219−221*, 125.
[4] A. M. Galibert, O. Cortadellas, B. Soula, B. Donnadieu, P. L. Fabre, *J. Chem. Soc., Dalton Trans.* **2002**, 3743.
[5] A. Escuer, N. Sanz, R. Vicente, F. A. Mautner, *Inorg. Chem.* **2003**, *42*, 541.
[6] M. L. Brader, E. W. Ainscough, E. N. Baker, A. M. Brodie, *J. Chem. Soc., Dalton Trans.* **1990**, 2785.
[7] M. E. Fisher, *Am. J. Phys.* **1964**, *32*, 343.
[8] A. Bencini, D. Gatteschi, *EPR of Exchange Coupled Systems*, Springer-Verlag, Berlin, Heidelberg, **1990**, chapter 10, and references cited therein.
[9] M. A. M. Abu-Youssef, A. Escuer, D. Gatteschi, M. A. S. Goher, F. A. Mautner, R. Vicente, *Inorg. Chem.* **1999**, *38*, 5716.
[10] CACAO program (Computed Aided Composition of Atomic Orbitals), C. Mealli, D. M. Proserpio, *J. Chem. Educ.* **1990**, *67*, 399.
[11] B. R. Hollebone, R. S. Nyholm, *J. Chem. Soc., (A)* **1971**, 332.
[12] G. M. Sheldrick, SHELXS-86, Program for the Solution of Crystal Structure, University of Göttingen, Germany, **1986**.
[13] G. M. Sheldrick, SHELXL-93, Program for the Refinement of Crystal Structure, University of Göttingen, Germany, **1993**.
[14] SHELXTL 5.03 (PC-Version). Program library for the Solution and Molecular Graphics. Siemens Analytical Instruments Division, Madison WI, **1995**.
[15] A. L. Spek, PLUTON-92, University of Utrecht, 3584 CH Utrecht, The Netherlands, **1992**.

Received May 23, 2003
Early View Article
Published Online October 30, 2003

Reactivity of $[Cp_2Ti(CO)_2]$ towards Nitrile and Water Adducts of $B(C_6F_5)_3$: Formation of $[Cp_2Ti(\eta^2\text{-}F_3CC_6H_4CN)\cdot B(C_6F_5)_3]$ and $[Cp_2Ti][HOB(C_6F_5)_3]$ with a Ti···F Interaction

Robert Choukroun,*[a] Christian Lorber,[a] and Laure Vendier[a]

Keywords: Titanium / Boranes / N ligands / Structure elucidation / Hydrolysis

The reaction of $[Cp_2Ti(CO)_2]$ with borane adducts $CF_3C_6H_4CN\cdot B(C_6F_5)_3$ and $[H_2O\cdot B(C_6F_5)_3]$ has afforded the titanaazirine $[Cp_2Ti(\eta^2\text{-}C,N\text{-}F_3CC_6H_4CN)\cdot B(C_6F_5)_3]$ (**1**) and the Ti^{III} salt $[Cp_2Ti][HOB(C_6F_5)_3]$ (**2**), respectively. In both cases, a Ti···F interaction between the titanium centre and an *ortho*-fluorine atom of the tris(perfluorophenyl)borane is observed in the X-ray structure determination.

(© Wiley-VCH Verlag GmbH & Co. KGaA, 69451 Weinheim, Germany, 2004)

Introduction

The reactivity of the Lewis acid $B(C_6F_5)_3$ with organometallic complexes has been the subject of much literature, mainly concerning Ziegler−Natta catalysts in relation to the cationic group-4 complexes.[1−3] Novel aspects of the reactivity of $B(C_6F_5)_3$ recently investigated by our group on the vanadium(V) complex $[VO(OCH_2CF_3)_3]$[4] and the titanocene $[Cp_2Ti(CO)_2]$[5] led to the unexpected formation of the organometallic complex $[VO(C_6F_5)(\mu\text{-}OCH_2CF_3)(OCH_2CF_3)]_2$ and to the acylborane $[Cp_2Ti(CO)\{\eta^2\text{-}OCB(C_6F_5)_3\}]$, respectively. Addition of a Lewis acid to a nitrile allows the activation of the C−N nitrile bond; reaction with the vanadocene $[VCp_2]$ gives the vanada(IV)azirine complex $[Cp_2V\{\eta^2\text{-}RC{=}N\cdot B(C_6F_5)_3\}]$ (R = CH_3, $CF_3C_6H_4$).[6]

To prepare the titanium analogue to the vanada(IV)azirine series, we extended our findings on the reactivity of a nitrile bond activated with the Lewis acid $B(C_6F_5)_3$ toward the vanadocene[6] to the titanocene $[Cp_2Ti(CO)_2]$. In addition, a titanium(III) complex has been obtained by a controlled hydrolytic reaction with the $[H_2O\cdot B(C_6F_5)_3]$ adduct.

Results and Discussion

$[Cp_2Ti(CO)_2]$ reacts with a stoichiometric mixture of $CF_3C_6H_4CN$ and $B(C_6F_5)_3$ at 50 °C in toluene to give a red-orange crystalline complex of the titanaazirine $[Cp_2Ti(\eta^2\text{-}C,N\text{-}F_3CC_6H_4CN)\cdot B(C_6F_5)_3]$ (**1**), which has been isolated and characterized by an X-ray structure determination (Scheme 1, Figure 1).

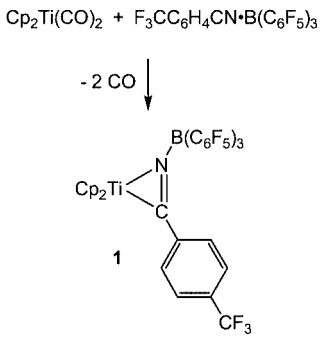

Scheme 1. Synthesis of $[Cp_2Ti(\eta^2\text{-}C,N\text{-}F_3CC_6H_4CN\cdot B(C_6F_5)_3]$ (**1**)

This is reminiscent of our recent work based on the vanadocene $[VCp_2]$ and the so-called "activated" nitrile $RCN\cdot B(C_6F_5)_3$.[6] The well-known formation of adducts between nitrile and a Lewis acid is associated with an increase in the ν(CN) frequency in the IR spectrum and an increase of the electron density on the C≡N triple bond.[3a,7]

The C−N nitrile bond is attached to the titanium atom through two σ-type Ti−C and Ti−N bonds of 2.075(2) and 2.0940(18) Å. These values are expected for such bonds, by comparison with those of the iminoacyl complex $[Ti(OAr\text{-}2,6\text{-}iPr_2)_2(\eta^2\text{-}t\text{BuNCCH}_2\text{Ph})(CH_2Ph)]$ [Ti−C 2.086(6), Ti−N 2.025(5) Å] and $[Cp_2Ti(\eta^2\text{-x,yNCPh})]$ [xy = 2,6-$(CH_3)_2C_6H_3$] [Ti−C 2.096(4), Ti−N 2.149(4) Å].[8] The carbon−nitrogen distance [1.243(3) Å] is typical of a carbon−nitrogen double bond. There are small differences between the distances and angles in the organic framework $F_3CC_6H_4CN\cdot B(C_6F_5)_3$ of **1** and those in the previously published vanadium(IV) analogue complex $[Cp_2V(\eta^2\text{-}C,N\text{-}F_3CC_6H_4CN)\cdot B(C_6F_5)_3]$.[6] The molecular geometry of **1** is

[a] Laboratoire de Chimie de Coordination, CNRS,
205 Route de Narbonne, 31077 Toulouse Cedex, France
Fax: (internat.) + 33-5-61553003
E-mail: choukrou@lcc-toulouse.fr

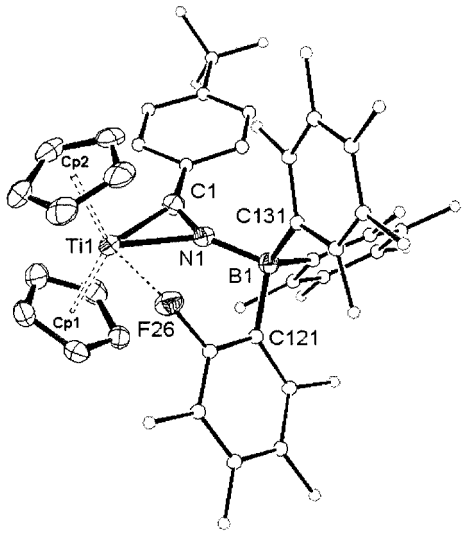

Figure 1. Molecular structure of **1**; hydrogen atoms and some labeled atoms are omitted for clarity; selected bond lengths [Å] and angles [°]: Ti(1)−C(1) 2.075(2), Ti(1)−N(1) 2.0940(18), C(1)−N(1) 1.243(3), N(1)−B(1) 1.575(3), C(1)−Ti(1)−N(1) 34.69(3), C(1)−N(1)−B(1) 147.19(9), Ti(1)−N(1)−C(1) 140.84(14)

similar to vanadium(IV) except for a C−F···Ti interaction in the solid state between an *ortho*-fluorine atom of the borane adduct and the titanium atom. The Ti···F distance (2.453 Å) is notably less than the sum of the Ti and F van der Walls radii (1.45 and 1.47 Å, respectively). This is similar to that found in $[(C_5Me_5)Ti\{C_5Me_4CH_2B(C_6F_5)_3\}]$ [Ti−*ortho*-fluorine atom = 2.406(3) Å].[9] A small but significant lengthening of the C−F(···Ti) bond [1.378(2) Å] relative to other C−F bonds (average 1.346 Å) of the perfluorophenyl groups of the borane is observed. In the ^{13}C NMR spectrum, the characteristic carbon resonance at δ = 225.6 ppm of the η²-*C,N* carbon atom is found and the corresponding ν(C=N) band appears in the IR spectrum at 1725 cm^{-1}. ^{19}F NMR obtained in $[D_8]$THF (the only solvent in which **3** is soluble) does not show a peak attributable to a Ti···F interaction at room temperature, but at 233 K the five fluorine substituents of one pentafluorophenyl group become inequivalent. This splitting exhibits a high-field ^{19}F resonance at δ = −128.1 ppm, which is characteristic for a bridging fluorine atom, in agreement with the fluorine-bridged solid-state structure. The C−F···V interaction was not observed in the vanadium analogue in the solid state but is demonstrated in solution by EPR.[6] Complex **1** can also be obtained directly by addition of a toluene solution of $CF_3C_6H_4CN$ on insoluble $[Cp_2Ti(CO)\{\eta^2\text{-}OCB(C_6F_5)_3\}]$[5] in toluene with evolution of CO.

Additionally, accidental hydrolysis during the crystallization procedure of **1** yielded a few large crystals of a blue complex. This hydrolysis was confirmed by treating the $[H_2O{\cdot}B(C_6F_5)_3]$ adduct, prepared in situ,[10] with $[Cp_2Ti(CO)_2]$ in pentane, which gave a blue complex after at least 4 d. Although an X-ray structure determination allowed us to characterize this product as the titanoxyborane $[Cp_2TiOB(C_6F_5)_3]$, careful investigation of the crystals by IR and NMR spectroscopy revealed the salt structure $[Cp_2Ti][HOB(C_6F_5)_3]$ (**2**) for the blue Ti^{III} paramagnetic crystals (vide infra) (Scheme 2). This ambiguous situation has been clarified by preparing the deuterated analogue $[Cp_2Ti][DOB(C_6F_5)_3]$ from $D_2O{\cdot}B(C_6F_5)_3$ and $[Cp_2Ti(CO)_2]$. The ν_{OH} and ν_{OD} IR frequencies (3645 and 2680 cm^{-1}, respectively) confirm chemically the formulation of the counter-anion as $[HOB(C_6F_5)_3]$; unfortunately, the hydrogen atom bound to the oxygen atom could not be located in the X-ray structure determination. Although the paramagnetic $[Cp_2Ti]^+$ fragment is NMR-silent, ^1H and ^2H NMR spectra of the diamagnetic anion show a peak at δ = 3 ppm ($\Delta\nu_{1/2}$ = 36 Hz) which could be due to a hydrogen atom in a BOH moiety. The Ti−O bond [2.1456(18) Å] is longer than a σ(Ti−O) distance,[11] which excludes the titanoxyborane formulation (Figure 2). This distance is quite similar to other Ti−O bond lengths of a coordinated alcohol on a titanium centre: $[Ti(OC_6F_5)_3(OiPr)(HOiPr)]$ 2.128(7) Å, $[Ti\{OCH(CF_3)_2\}_2(OEt)_2(HOEt)]$ 2.187(9) Å,[12] $[TiCl_2(OiPr)(HOiPr)(\mu\text{-}Cl)]_2$ 2.087(4) Å, and $[TiCl_2(O\text{-}iPr)(HOiPr)(\mu\text{-}OiPr)]_2$ 2.093(2).[13] The B−O bond [1.519(3) Å] is longer than in the anion $[(C_6F_5)_3BOH]^-$ [1.487(3) Å] [1.597(2) Å in $H_2O{\cdot}B(C_6F_5)_3$[14]]. A C−F···Ti interaction between the titanium atom and one *ortho*-fluorine atom of

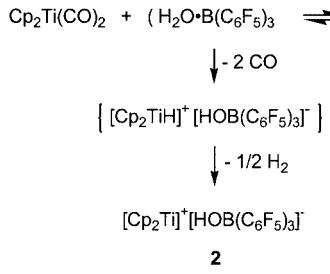

Scheme 2. Suggested hydrolytic pathway leading to $[Cp_2Ti][HOB(C_6F_5)_3]$ (**2**)

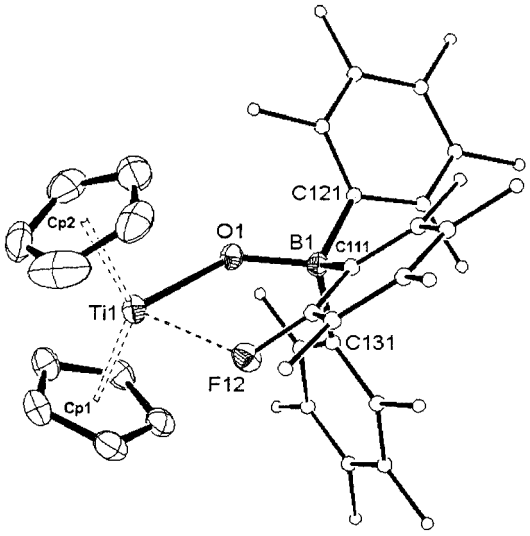

Figure 2. Molecular structure of **2**; hydrogen atoms and some labeled atoms are omitted for clarity; selected bond lengths [Å] and angles [°]: Ti(1)−O(1) 2.1456(18), O(1)−B(1) 1.519(3), Ti(1)−F(12) 2.2841(17); Ti(1)−O(1)−B(1) 137.78(14), O(1)−Ti(1)−F(12) 73.37(6)

 © 2004 Wiley-VCH Verlag GmbH & Co. KGaA, Weinheim

the $B(C_6F_5)_3$ moiety occurs in the solid-state structure. The Ti···F distance [2.2841(17) Å] is still shorter than in complex **1** and there is a lengthening of the C−F(···Ti) bond [1.375(3) Å] relative to other C−F bonds (average 1.340 Å) of the perfluorophenyl groups of the borane. A similar Ti^{III} complex as [*rac*-(ebthi)Ti][$HOB(C_6F_5)_3$] [ebthi = 1,2-ethylene-1,1′-bis(η^5-tetrahydroindenyl)], formed due to adventitious water, has been recently fully characterized by an X-ray structure analysis; the hydrogen atom attached to the oxygen atom could not be localized [*d*(Ti−O) = 2.097(3) Å; *d*(B−O) = 1.482(4) Å; *d*(Ti···F) = 2.365(2) Å].[15] Similar Ti···F distances between the titanium centre and *ortho*-fluorine atoms in zwitterionic Ti^{III} structures have also been observed {[CpTi{$C_5H_4B(C_6F_5)_3$}]: 2.248(2), 2.223(3) Å; [(*i*PrC_5H_4)Ti{*i*Pr$C_5H_3B(C_6F_5)_3$}]: 2.64(2), 2.256(2) Å}.[16,17]

Our result differs slightly from those of Green and colleagues with $[MCp_2]$ (M = Cr, Fe, Co) yielding cationic $[MCp_2]^+$ with a counter-anion such as $[(C_6F_5)_3B(\mu\text{-}OH)B(C_6F_5)_3]^-$ or $[(C_6F_5)_3BOH\cdots H_2OB(C_6F_5)_3]^-$.[14] In their case the observed difference in the anion part is due to their synthetic procedure {2 equiv. of $H_2O{\cdot}B(C_6F_5)_3$ or an equimolecular mixture of $H_2O{\cdot}B(C_6F_5)_3/B(C_6F_5)_3$ are implied in the reaction with $[MCp_2]$}. Their proposed pathway contains the suggested intermediate $[Cp_2M][HOB(C_6F_5)_3]$, which is corroborated here {Scheme 2; the first intermediate $[Cp_2TiH][HOB(C_6F_5)_3]$ is assumed only}. Complex **2** is blue, and its magnetic susceptibility (1.76 μB) and EPR spectrum in THF (g = 1.974) confirm that it is a paramagnetic Ti^{III} complex. The single line in the EPR spectrum implies that there is no interaction between the Ti atom and the *ortho*-fluorine atom (I = 1/2) in THF solution, suggesting that the solvent occupies a coordination position on the metal atom, thus releasing the Ti···F interaction. The EPR solution spectrum is unchanged at −100 °C.

In conclusion, the reactivity of the borane adducts $[RCN{\cdot}B(C_6F_5)_3]$ and $[H_2O{\cdot}B(C_6F_5)_3]$ is described with $[Cp_2Ti(CO)_2]$. As expected, the formation of the titana(IV)-azirine complex **1** confirms the role of the tris(perfluorophenyl)borane in activating a nitrile bond, as already observed in the vanadium chemistry. The formation of **2** can be controlled and derives from an hydrolytic decomposition pathway.

Experimental Section

General: All manipulations were carried out using standard Schlenk line or dry-box techniques under argon. Solvents were boiled under reflux, dried with appropriate agents under argon, collected by distillation, and then stored in a dry-box over activated molecular sieves (4 Å). Deuterated solvents were degassed and dried over activated molecular sieves (4 Å). NMR spectroscopic data were recorded using Bruker AMX-400, DPX-300, and AC-200 spectrometers, and referenced internally to residual protio solvent (^{1}H) resonances, and are reported relative to tetramethylsilane (δ = 0 ppm). ^{19}F NMR (188.298 MHz) spectra were recorded with a Bruker AC-200 spectrometer (reference CF_3CO_2H). EPR spectra were obtained by using a Bruker ESP300E spectrometer. Elemental analyses (C, H, N) were performed at the Laboratoire de Chimie de Coordination (Toulouse, France). $B(C_6F_5)_3$ was prepared according to the literature.[18]

$[Cp_2Ti(\eta^2\text{-}F_3CC_6H_4CN){\cdot}B(C_6F_5)_3]$ (1): A freshly prepared toluene (3 mL) solution of $B(C_6F_5)_3$ (51 mg, 0.01 mmol) and $CF_3C_6H_4CN$ (17 mg, 0.01 mmol) was added to $[Cp_2Ti(CO)_2]$ (23 mg, 0.01 mmol) in toluene (3 mL). The resulting red solution was heated to 50 °C for 12 h. Red crystals of **1** were formed at room temperature (15 mg). The filtrate was left for 2 d to give a further crop of microcrystalline **1** (35 mg). Yield: 58%. $C_{36}H_{14}BF_{18}NTi$ (861.19): calcd. C 50.21, H 1.64, N 1.63; found: C 50.3, H 1.58, N 1.61. IR: $\tilde{\nu}$ = 1725 [ν(C≡N)] cm^{-1}. ^{1}H NMR ([D$_8$]THF): δ = 6.18 (s, Cp), 7.85, 7.21 (d, $^1J_{C,H}$ = 8.3 Hz, C_6H_4) ppm. ^{11}B NMR ([D$_8$]THF): δ = −9.60 ppm. ^{13}C NMR ([D$_8$]THF): δ = 114.3 (d, $^1J_{C,H}$ = 174 Hz, Cp), 121 [br., $\Delta\nu_{1/2}$ = 190 Hz, *ipso*-C, $B(C_6F_5)$], 125.2 (q, $^1J_{C,F}$ = 253 Hz, *C*F$_3$), 126.8 (d, $^1J_{C,H}$ = 168 Hz, C_6H_4), 133.7, (d, $^1J_{C,H}$ = 164 Hz, C_6H_4), 134.2 (q, $^3J_{C,F}$ = 33 Hz, *C*CF$_3$), 136.1 (s, *ipso*-C, C_6H_4), 138.8 (d, $^1J_{C,F}$ = 253 Hz, C_6F_5), 141.3 (d, $^1J_{C,F}$ = 250 Hz, C_6F_5), 150.0 (d, $^1J_{C,F}$ = 237 Hz, C_6F_5), 225.6 (s, *C*=N) ppm. ^{19}F NMR (376.41 MHz, 298 K, [D$_8$]THF): δ = 13.3 (s, C*F*$_3$), −56.9 (br., 6 *o*-F, C_6F_5), −82.5 (t, 3 *p*-F, C_6F_5), −88.6 (br., 6 *m*-F, C_6F_5); (233 K): δ = 12.7 (s, C*F*$_3$), −56.8 (d, 1 *o*-F, C_6F_5), −57.2 (d, 4 *o*-F, C_6F_5), −82.2 (t, 1 *p*-F, C_6F_5), −87.5 (t, 4 *p*-F C_6F_5), −85.4 (t, 1 *m*-F, C_6F_5), −87.9 (1 *m*-F, C_6F_5), −88.5 (t, 4 *m*-F, C_6F_5), −128.1 (d, 1 *o*-F, C_6F_5) ppm.

$[Cp_2Ti][HOB(C_6F_5)_3]$ (2): $[Cp_2Ti(CO)_2]$ (23 mg, 0.01 mmol) in pentane (3 mL) was added to a pentane suspension of $B(C_6F_5)_3$ (51 mg, 0.01 mmol) in the presence of H_2O (or D_2O) (1.8 μmol). After leaving the resultant red solution for one week, blue crystalline **2** was obtained in 35% yield (25 mg). Another synthesis from a mixture of $[Cp_2Ti(CO)_2]$ (23 mg, 0.01 mmol) and $B(C_6F_5)_3$ (51 mg, 0.01 mmol) in pentane (5 mL), passed several times through undried deoxygenated Celite and left for one week, afforded large blue crystals of **2** that were suitable for X-ray analysis. $C_{28}H_{10}BF_{15}OTi$ (706.07): calcd. C 47.63, H 1.43; found: C 47.24, H 1.33. EPR: g = 1.974, a(^{49}Ti) = 11.0 G (a single line with low intensity satellites due to the interaction of d^1 electron with ^{49}Ti and ^{47}Ti isotopes (5.51% abundant, I = 7/2 and 7.75% abundant, I = 5/2, respectively), the six inner components of the ^{49}Ti octuplet exactly superimpose on the sextuplet from ^{47}Ti). μ_{eff} = 1.76 μB. ^{1}H NMR ([D$_8$]THF): δ = 3 (br., $\Delta\nu_{1/2}$ = 36 Hz, BO*H*) ppm.

Crystallographic Data for 1 and 2: For structures **1** and **2** (Table 1) data were collected using a Stoe Imaging Plate Diffraction System (IPDS). The final unit cell parameters were obtained by least-squares refinement of a set of 5000 reflections, and crystal decay was monitored by measuring 200 reflections by image. No fluctuations of the intensity were observed over the course of the data collection. A semiempirical absorption correction[19] was applied to the data. The structure was solved by direct methods using SIR92[20] and refined by least-squares procedures on F^2 with the aid of SHELXL-97[21] which is included in WinGX (version 1.63).[22] The atomic scattering factors were taken from International Tables for X-ray crystallography.[23] All hydrogen atoms were located on a difference Fourier map. All the remaining non-hydrogen atoms were anisotropically refined and in the last refinement cycles a weighting scheme was used where weights were calculated from $w = 1/[\sigma^2(F_o^2) + (aP)^2 + bP]$, where $P = (F_o^2 + 2F_c^2)/3$. The molecules were drawn using the program ORTEP32.[24] The criteria for a satisfactory complete analysis were the ratio of rms shift to standard deviation being less than 0.1 and no significant features in final difference maps. CCDC-212614 (**1**) and -212615 (**2**) contain the supplementary crystallographic data for this paper.

 © 2004 Wiley-VCH Verlag GmbH & Co. KGaA, Weinheim

Table 1. Summary of crystal data, data collection, and structure refinement parameters

	1	**2**
Empirical formula	$C_{36}H_{14}BF_{18}NTi$	$C_{28}H_{10}BF_{15}OTi$
Formula mass	861.19	706.07
Temperature [K]	160	160
Wavelength [Å]	0.71073	0.71073
Crystal system	orthorhombic	monoclinic
Space group	$P2_12_12_1$	Cc
a [Å]	9.106(5)	9.189(2)
b [Å]	18.720(5)	17.390(3)
c [Å]	19.499(5)	16.173(3)
β [°]	90.000(5)	97.63(3)
V [Å^3]	3324(2)	2561.5(9)
Z, density [g cm^{-3}]	4, 1.721	4, 1.831
F(000)	1704	1392
Absorption coefficient [mm^{-1}]	0.389	0.468
Crystal description	prismatic	prismatic
Crystal size [mm]	0.4 × 0.32 × 0.27	0.45 × 0.40 × 0.22
Collection method	rotation	rotation
2θ range for data collection [°]	3.3−52.1	3.3−52.1
No. reflections collected/unique	26272/6508 [R(int) = 0.0437]	6541/4260 [R(int) = 0.0386]
Completeness to 2θ [%]	98.4	79.8
Refinement method	Full-matrix least squares on F^2	Full-matrix least squares on F^2
Data/restraints/parameters	6508/0/514	4260/2/416
GOF on F^2	1.026	1.046
Final R indices [$I > 2\sigma(I)$]	$R1$ = 0.0314, $wR2$ = 0.0719	$R1$ = 0.0442, $wR2$ = 0.1157
R indices (total)	$R1$ = 0.0404, $wR2$ = 0.0753	$R1$ = 0.0425, $wR2$ = 0.1157
Largest difference peak and hole [e·Å^{-3}]	0.255 and −0.192 e·Å^{-3}	0.313 and −0.286 e·Å^{-3}

These data can be obtained free of charge at www.ccdc.ac.uk/conts/retrieving.html [or from the Cambridge Data Centre, 12 Union Road, Cambridge CB2 1EZ, UK; Fax: (internat.) + 44-1223/336-033; E-mail: deposit@ccdc.cam.ac.uk].

Acknowledgments

The CNRS is thanked for financial support.

[1] For leading recent reviews, see: [1a] G. W. Coates, P. D. Hustad, S. Reiinartz, *Angew. Chem. Int. Ed.* **2002**, *41*, 2236. [1b] E. You-Xian Chen, T. J. Marks, *Chem. Rev.* **2000**, *100*, 1391. [1c] G. J. P. Britovsek, V. C. Gibson, D. F. Wass, *Angew. Chem. Int. Ed.* **1999**, *38*, 428.

[2] [2a] W. E. Piers, T. Chivers, *Chem. Soc. Rev.* **1997**, *26*, 345. [2b] D. J. Parks, M. Piers, W. E. Parvez, R. Atencio, M. Zaworotko, *Organometallics* **1998**, *17*, 1369. [2c] D. J. Parks, J. M. Blackwell, W. E. Piers, *J. Org. Chem.* **2000**, 3090. [2d] D. J. Parks, R. E. von H. Spence, W. E. Piers, *Angew. Chem. Int. Ed. Engl.* **1995**, *34*, 809. [2e] J. M. Blackwell, W. E. Piers, M. Parvez, R. McDonald, *Organometallics* **2002**, *21*, 1400.

[3] [3a] H. Jacobsen, H. Berke, S. Döring, G. Kehr, G. Erker, R. Fröhlich, O. Meyer, *Organometallics* **1999**, *18*, 1724. [3b] D. Vagedes, G. Kehr, D. König, K. Wedeking, R. Frölich, G. Erker, C. Mück-Lichtenfeld, S. Grimme, *Eur. J. Inorg. Chem.* **2002**, 2015. [3c] J. Klosin, G. R. Roof, E. Y. X. Chen, *Organometallics* **2000**, *19*, 4684. [3d] D. C. Bradley, I. S. Harding, A. D. Keefe, M. Motevalli, D. H. Zheng, *J. Chem. Soc., Dalton, Trans.* **1996**, 3931. [3e] M. L. H. Green, J. Haggitt, C. P. Mehnert, *J. Chem. Soc., Chem. Commun.* **1995**, 1853. [3f] A. Antinolo, F. Carillo-Hermosilla, I. del Hierro, A. Otero, M. Fajardo, Y. Mugnier, *Organometallics* **1997**, *16*, 4161.

[4] F. Wolff, R. Choukroun, C. Lorber, B. Donnadieu, *Eur. J. Inorg. Chem.* **2003**, 628.

[5] R. Choukroun, C. Lorber, B. Donnadieu, *Organometallic.* **2003**, *22*, 1995.

[6] R. Choukroun, C. Lorber, B. Donnadieu, *Chem. Eur. J.* **2002**, *8*, 2700.

[7] R. Hoti, Z. Mihalic, H. Vancik, *Croat. Chem. Acta* **1995**, *2*, 359.

[8] [8a] L. R. Chamberlain, L. D. Durfee, P. E. Fanwick, L. Kobriger, S. L. Latesky, A. K. McMullen, I. P. Rothwell, K. Folting, J. C. Huffman, W. E. Streib, R. Wang, *J. Am. Chem. Soc.* **1987**, *109*, 390. [8b] F. van Bolhuis, E. J. M. de Boer, J. H. Teuben, *J. Organomet. Chem.* **1979**, *170*, 299.

[9] V. V. Burlakov, P. M. Pellny, P. Arndt, W. Baumann, A. Spannenberg, V. B. Shur, U. Rosenthal, *Chem. Commun.* **2000**, 241.

[10] T. Beringhelli, D. Maggioni, G. D'Alfonso, *Organometallics* **2001**, *20*, 4927.

[11] [11a] J. C. Huffman, K. G. Moloy, J. A. Marsella, K. G. Caulton, *J. Am. Chem. Soc.* **1980**, *102*, 3009. [11b] J. L. Wang, F. M. Miao, X. J. X. Fan, X. Feng, J. T. Wang, *Acta Crystallogr., Sect. C* **1990**, *46*, 1633. [11c] U. Schubert, H. Buhler, B. Hirle, *Chem. Ber.* **1992**, *125*, 999.

[12] C. Campbell, S. G. Bott, R. Larsen, W. G. Van Der Sluys, *Inorg. Chem.* **1994**, *33*, 4950.

[13] Y. T. Wu, Y. C. Ho, C. C. Lin, H. M. Gau, *Inorg. Chem.* **1996**, *35*, 5948.

[14] L. H. Doerrer, M. L. H. Green, *J. Chem. Soc., Dalton Trans.* **1999**, 4325.

[15] A. Spannenberg, V. V. Burlakov, P. Arndt, W. Baumann, V. B. Shur, U. Rosenthal, *Z. Kristallogr. NCS* **2002**, *217*, 546.

[16] V. V. Burlakov, S. I. Troyanov, A. V. Letov, L. I. Strunkina, M. Kh. Minacheva, G. G. Furin, U. Rosenthal, V. B. Shur, *J. Organomet. Chem.* **2000**, *598*, 243.

[17] V. V. Burlakov, P. Arndt, W. Baumann, A. Spannenberg, U. Rosenthal, A. V. Letov, K. A. Lyssenko, A. A. Korlyukov, L. I. Strunkina, M. Kh. Minacheva, V. B. Shur, *Organometallics* **2001**, *20*, 4072.

[18] A. G. Massey, A. J. Park, *J. Organomet. Chem.* **1966**, *5*, 218.

[19] N. Walker, D. Stuart, *Acta Crystallogr., Sect. A* **1983**, *39*, 158.

[20] A. Altomare, G. Cascarano, G. Giacovazzo, A. Guagliardi, M.

 © 2004 Wiley-VCH Verlag GmbH & Co. KGaA, Weinheim

C. Burla, G. Polidori, M. Camalli, *J. Appl. Crystallogr.* **1994**, *27*, 435.
[21] G. M. Sheldrick, *SHELX97, Programs for Crystal Structure Analysis*, University of Göttingen, Germany, **1998**.
[22] L. J. Farrugia, *J. Appl. Crystallogr.* **1999**, *32*, 837.
[23] *International Tables for X-ray Crystallography* (Eds.: J. A. Ibers, W. C. Hamilton), Kynoch Press, Birmingham, England, **1974**, vol. IV.
[24] L. J. Farrugia, *J. Appl. Crystallogr.* **1997**, *30*, 565.

Received June 12, 2003
Early View Article
Published Online November 4, 2003

 © 2004 Wiley-VCH Verlag GmbH & Co. KGaA, Weinheim

New Vanadium(V) Complexes with Salicylaldehyde Semicarbazone Derivatives: Synthesis, Characterization, and in vitro Insulin-Mimetic Activity − Crystal Structure of [$V^{V}O_2$(salicylaldehyde semicarbazone)]

Pabla Noblía,[a] Enrique J. Baran,[b] Lucía Otero,[a] Patricia Draper,[c] Hugo Cerecetto,[c] Mercedes González,[c] Oscar E. Piro,[d] Eduardo E. Castellano,[e] Toshifumi Inohara,[f] Yusuke Adachi,[f] Hiromu Sakurai,[f] and Dinorah Gambino*[a]

Keywords: Vanadium / Tridentate ligands / N,O,O ligands / Insulin-mimetic agents

The new dioxo(semicarbazone)vanadium(V) complexes *cis*-VO_2L, where L = salicylaldehyde semicarbazone (L^1), salicylaldehyde 4-*n*-butylsemicarbazone (L^2), or salicylaldehyde 4-(2-naphthyl)semicarbazone (L^3), have been synthesized, characterized by ^1H and ^{13}C NMR and FTIR spectroscopy and tested for bioactivity as potential insulin-mimetic agents. All dioxovanadium(V) complexes exhibited essentially no in vitro insulin-mimetic activity, but the VO_2L^2 complex developed activity in the presence of ascorbic acid, similar to that of vanadyl sulfate. The molecular structure of the novel complex VO_2L^1 has been solved by X-ray diffraction methods. It crystallizes in the tetragonal space group $P4_2/n$ with a = 12.7674(7), c = 11.5308(5) Å, and Z = 8. The vanadium atom is in a distorted square-pyramidal coordination, with L^1 acting as a tridentate ligand through its azomethyne nitrogen atom, carbonyl oxygen atom and deprotonated phenol oxygen atom. The coordination sphere is completed by two oxo ligands at *cis* positions.
(© Wiley-VCH Verlag GmbH & Co. KGaA, 69451 Weinheim, Germany, 2004)

Introduction

The interaction of simple vanadium species with ligand groups bearing pharmacological activity, particularly those with antitumoral and insulin-mimetic properties, is of growing interest. A more detailed physicochemical characterization of vanadium compounds with pharmacologically interesting ligands will help in furthering the inorganic pharmacology of vanadium.[1]

In particular, the discovery of the insulin-like in vitro and in vivo activity of oxovanadates(V) and oxovanadium(IV) compounds such as vanadyl sulfate has stimulated research on vanadium compounds that may have promising application in the treatment of non-insulin-dependent type-2 diabetes mellitus.[2−9] Different approaches have been attempted to develop more potent and orally active vanadium-containing insulin enhancing agents.[10] Some vanadium complexes, such as bis(alkylmaltolato)oxovanadium(IV) ones, are promising candidates as oral complements for insulin in the treatment of diabetes. Although such complexes have shown pharmacological advantages (better gastrointestinal absorption, higher potency and less toxicity) compared to the uncomplexed $VOSO_4$, further improvement in ligand design is needed, focusing on identifying new vanadium compounds with increased potency and decreased toxicity.[11]

Semicarbazones and thiosemicarbazones (Figure 1) show a wide range of biological activities.[12−15] Although some (thiosemicarbazone)vanadium complexes have been synthesized and characterized, there are very few examples of the analogous semicarbazone ligands.[12] To further discern the chelating behaviour of semicarbazones of pharmacological

[a] Cátedra de Química Inorgánica, Facultad de Química, Universidad de la República,
Gral. Flores 2124, C. C. 1157, 11800 Montevideo, Uruguay
E-mail: dgambino@fq.edu.uy
[b] Centro de Química Inorgánica (CEQUINOR/CONICET-UNLP), C. C. 962, Universidad Nacional de La Plata,
C. C. 67, 1900 La Plata, Argentina
[c] Departamento de Química Orgánica, Facultad de Química − Facultad de Ciencias, Universidad de la República,
Iguá 4225, 11400 Montevideo, Uruguay
[d] Departamento de Física and Instituto IFLP (CONICET), Facultad de Ciencias Exactas, Universidad Nacional de La Plata,
C. C. 67, 1900 La Plata, Argentina
[e] Instituto de Física de São Carlos, Universidade de São Paulo, C. P. 369, 13560 São Carlos (SP), Brazil
[f] Department of Analytical and Bioinorganic Chemistry, Kyoto Pharmaceutical University,
5 Nakauchi-cho, Misasagi, Yamashina-ku, Kyoto 607-8414, Japan
Supporting information for this article is available on the WWW under http://www.eurjic.org or from the author.

 © 2004 Wiley-VCH Verlag GmbH & Co. KGaA, Weinheim **DOI: 10.1002/ejic.200300421**

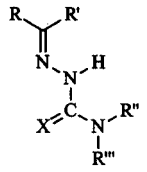

R, R', R'', R''' = H or alkyl or aryl group

Figure 1. General formula of semicarbazones (X = O) and thiosemicarbazones (X = S)

interest,[16−18] a more detailed physicochemical characterization of their vanadium complexes has been made, involving the synthesis, characterization and in vitro biological evaluation as potential insulin-mimetic agents of a series of novel (semicarbazone)VO_2^+ complexes with the general formula *cis*-V^VO_2L. Selected ligands L are salicylaldehyde semicarbazone derivatives bearing moieties with different lipophilicity − a physicochemical property that determines an adequate bioresponse of drugs, and is related to their absorption, distribution, metabolism, elimination and toxicity.[19] The ligands L (Figure 2) are salicylaldehyde semicarbazone (L^1), salicylaldehyde 4-*n*-butylsemicarbazone (L^2) and salicylaldehyde 4-(2-naphthyl)semicarbazone (L^3).

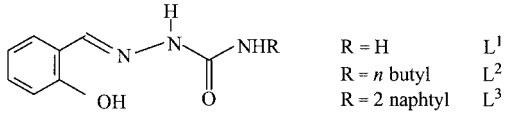

Figure 2. Selected ligands: salicylaldehyde semicarbazone (L^1), salicylaldehyde 4-*n*-butylsemicarbazone (L^2) and salicylaldehyde 4-(2-naphthyl)semicarbazone (L^3)

Although almost no $V^VO_2^+$ complex has shown good insulin-enhancing properties, V^V complexes may be reduced in vivo to form potentially bioactive $V^{IV}O^{2+}$ complexes.[20] In particular, vanadium(v) dipicolinate is an effective oral agent in live animals.[21] Thus, it seemed interesting to test the insulin-mimetic activity of the three novel complexes reported here.

Results and Discussion

Three novel V^V semicarbazone complexes have been synthesized and characterized. Complexes with the formula V^VO_2L, where L = salicylaldehyde semicarbazone (L^1), salicylaldehyde 4-*n*-butylsemicarbazone (L^2) or salicylaldehyde 4-(2-naphthyl)semicarbazone (L^3), were prepared in good yields and high purity. The analytical data agree with the proposed formulae.

In contrast to $V^{IV}O^{2+}$ complexes, those of VO_2L do not show electronic d−d transitions in the visible region due to the absence of d-electrons. Thus, the yellow color of the V^V complexes arises from intense absorption tailing-in from the UV region, originating in O→V charge transfer transitions.[22]

Selected vibration bands of the free ligands and their vanadium complexes, which are useful for determining the ligand's mode of coordination, are given in Table 1. The shifts in the ν(C=O) and the ν(C=N) bands upon coordination are consistent with bidentate coordination of the semicarbazone portion of the ligand through the carbonyl oxygen atom and azomethine nitrogen atom.[17,18] The third coordination position is the deprotonated phenol oxygen; thus the O−H stretching band is not in the spectrum of the complexes. In addition, the typical strong bands owing to asymmetric and symmetric stretching modes of the *cis*-VO_2 moiety are observed.[22]

Table 1. Selected vibration bands of the ligands L and the V^VO_2L complexes (cm^{-1}); ν: stretching; as: asymmetric, s: symmetric

Compound	ν(C=O)	ν(C=N)	ν(C−O)	ν(O−H)	$\nu_{as}(VO_2^+)$	$\nu_s(VO_2^+)$
VO_2L^1	1661	1606	1557	−	908	933
L^1	1683	1598	1522	3422	−	−
VO_2L^2	1645	1577	1473	−	933	912
L^2	1651	1573	1488	3300	−	−
VO_2L^3	1601	1560	1508	−	907	889
L^3	1647	1566	1508	3307	−	−

NMR Studies

The NMR spectra show narrow signals typical of V^V diamagnetic complexes. HETCOR experiments allowed us to assign all of signals for the studied complexes. The ^1H NMR chemical shifts along with the chemical shift differences between each complex and the corresponding ligand, expressed as Δδ, are listed in Table 2. The formula in the table shows the numbering scheme of the free ligands. The ^1H NMR integrations and signal multiplicities agree with the proposed formula. The three complexes show similar ^1H and ^{13}C chemical shifts for the salicylaldehyde semicarbazone common portion. When the ligand is coordinated, the deshielding effect of the metal atom is apparent in some protons, causing a downfield shift of the corresponding ^1H NMR peaks. Upfield shifts in the ^1H NMR spectra of the signals of 4- and 6-H of the complexes could be the result of ligand deprotonation upon coordination, due to the lack of 7-H (Table 2).[18] The upfield shift of the signal of 3-H could be due to the decreasing azomethine anisotropic effect in the coordinated form of L. When L is coordinated, the azomethine moiety is fixed by the vanadium core in an opposite spatial distribution to 3-H. Thus, after coordination, this proton is less affected by the magnetic anisotropy of the C=N double bond than in the free ligand.[23]

Structural Results

Intramolecular bond lengths and angles around the metal ion in VO_2L^1 (Table 3) and an ORTEP[24] drawing of the molecule (Figure 3) are shown here.

The X-ray diffraction study shows that the complex VO_2L^1 consists of a discrete monomeric molecule. The vanadium(v) ion is in a distorted square-pyramidal environ-

 © 2004 Wiley-VCH Verlag GmbH & Co. KGaA, Weinheim

Table 2. ^{1}H NMR chemical shifts (δ, ppm) of V^VO_2L, with L = L^1, L^2 and L^3, in [D_6]DMSO/D_2O at 303 K

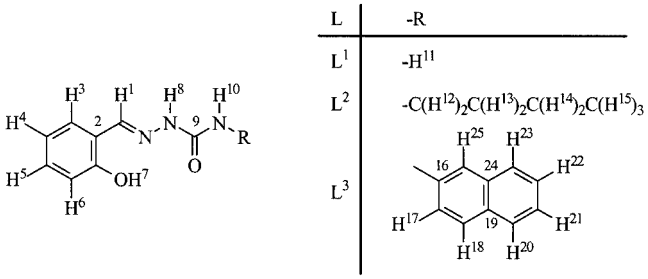

H	$V^VO_2L^1$		$V^VO_2L^2$		$V^VO_2L^3$		Δδ[a]		
	δ_{Ligand}	$\delta_{Complex}$	δ_{Ligand}	$\delta_{Complex}$	δ_{Ligand}	$\delta_{Complex}$	$\Delta\delta_{L1}$	$\Delta\delta_{L2}$	$\Delta\delta_{L3}$
1	8.14	8.58	8.12	8.63	8.21	8.69	0.44	0.51	0.48
3	7.72	7.48	7.74	7.51	7.74	[b]	−0.24	−0.23	–
4	6.81	6.79	6.85	6.85	6.87	6.85	−0.02	0	−0.02
5	7.16	7.37	7.17	7.39	7.23	[b]	0.21	0.22	–
6	6.87	6.79	6.80	6.80	6.89	6.80	−0.08	0	−0.09
7	9.85	not present	9.97	not present	10.08	not present	–	–	–
8	10.19	12.50	10.17	not observed[c]	10.70	9.93	2.31	–	−0.77
10	6.53	7.96	6.80	8.35	9.07	9.82	1.43	1.55	0.75
11			–	–	–	–		–	–
12	–	–	3.12	3.20	–	–	–	0.08	–
13	–	–	1.45	1.49	–	–	–	0.04	–
14	–	–	1.30	1.33	–	–	–	0.03	–
15	–	–	0.89	0.90	–	–	–	0.01	–
17	–	–	–	–	7.97	8.06	–	–	0.09
18	–	–	–	–	[d]	[b]	–	–	–
20	–	–	–	–	[d]	[b]	–	–	–
21	–	–	–	–	7.37	[b]	–	–	–
22	–	–	–	–	7.46	[b]	–	–	–
23	–	–	–	–	[d]	[b]	–	–	–
25	–	–	–	–	8.31	8.42	–	–	0.11

[a] $\Delta\delta = (\delta_{Complex} - \delta_{Ligand})$. [b] 7.30−7.90 ppm, as multiplet. [c] Owing to exchange with solvent protons. [d] 7.77−7.87 ppm, as multiplet.

Table 3. Bond lengths [Å] and angles [°] around the vanadium atom in [VO_2(salicylaldehyde semicarbazone)], VO_2L^1

V−O(11)	1.622(4)	O(11)−V−O(12)	108.1(2)
V−O(12)	1.641(4)	O(11)−V−O(2)	105.1(2)
V−O(2)	1.894(4)	O(12)−V−O(2)	95.9(2)
V−O(1)	1.998(4)	O(11)−V−O(1)	101.8(2)
V−N(3)	2.154(5)	O(12)−V−O(1)	92.1(2)
		O(2)−V−O(1)	147.9(2)
		O(11)−V−N(3)	102.2(2)
		O(12)−V−N(3)	148.7(2)
		O(2)−V−N(3)	83.2(2)
		O(1)−V−N(3)	74.2(2)

ment, coordinated at the pyramid basis to a salicylaldehyde semicarbazone molecule that acts as a tridentate ligand through its azomethine nitrogen atom [d(V−N) = 2.154(5) Å], and its carbonyl and deprotonated phenol oxygen atoms [V−O distances of 1.998(4) and 1.894(4) Å, respectively], and to an oxo ligand [d(V−O) = 1.641(4) Å]. The fivefold coordination is completed by another oxo ligand at the pyramid apex [d(V−O) = 1.622(4) Å]. Both oxo ligands are in *cis* positions. The average V−O bond length and O−V−O angle are quite similar to those previously reported for the *cis*-VO_2 moiety in other complexes.[25] The *trans*-ligand−V−ligand angles are O1−V−O2 147.9(2)° and N3−V−O12 148.7(2)° and the *cis*-ligand−V−ligand angles vary from 74.2(2) to 108.1(2)°.

The nitrogen atom and the three coordinated oxygen atoms at the pyramid base are nearly in a plane (rms deviation of NO_3 atoms from the least-squares plane is 0.017 Å) with the metal ion 0.401 Å apart from this plane, towards the axial oxo ligand.

The salicylaldehyde semicarbazone molecule is also nearly planar (rms deviation of ligand atoms from the least-squares plane is 0.065 Å) and subtends an angle of 5.8(1)° with the NO_3 plane. Of the possible isomeric forms for the ligand, the (*E*) isomer is preferred. The crystal is further stabilized by a net of medium-to-strong intermolecular N−H···O bonds, involving the terminal NH_2 group of a given ligand molecule and the phenol oxygen atom [d(N1···O2′) = 2.972 Å, N1−H1A···O2 = 174.9°] and the equatorial oxo ligand [d(N1···O12″) = 2.870 Å, N1−H1B···O12″ = 171.4°] of neighboring ligand molecules, and also the N−H group in an N−H···O bond with the axial oxo ligand [d(N2···O11″) = 2.723 Å, N2−H2···O11″ = 153.2°].

 © 2004 Wiley-VCH Verlag GmbH & Co. KGaA, Weinheim

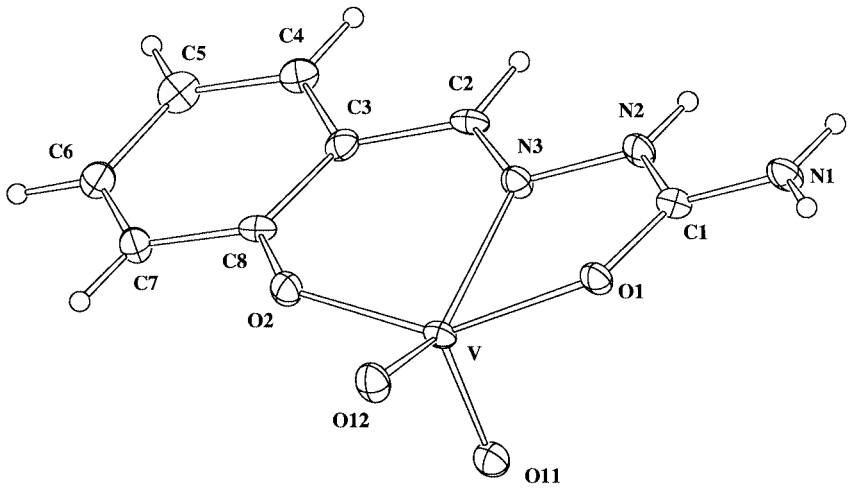

Figure 3. [VO_2(salicylaldehyde semicarbazone)] complex showing the labeling scheme of the non-H atoms and their displacement ellipsoids at the 30% probability level

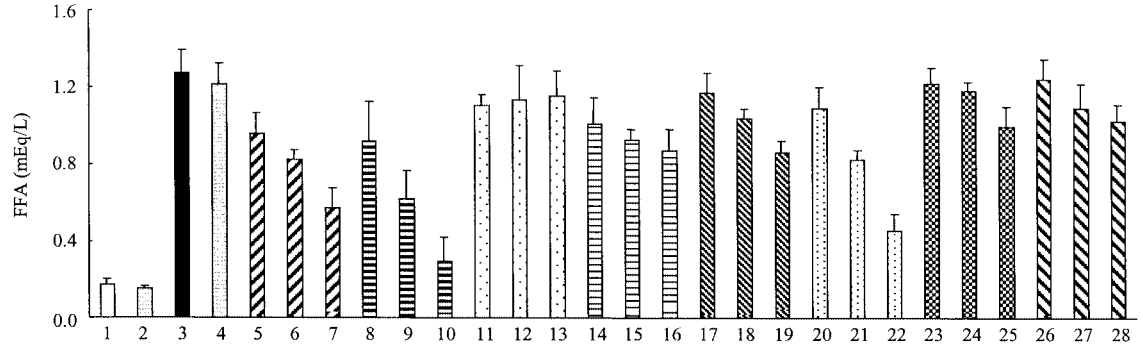

1	Blank		11	VO_2L^1	10^{-4} M	17	VO_2L^2	10^{-4} M	23	VO_2L^3	10^{-4} M
2	Blank + ascorbic acid		12		5×10^{-4} M	18		5×10^{-4} M	24		5×10^{-4} M
3	Control		13		10^{-3} M	19		10^{-3} M	25		10^{-3} M
4	Control + ascorbic acid										
5	$VOSO_4$	10^{-4} M									
6		5×10^{-4} M	14	VO_2L^1 + ascorbic acid	10^{-4} M	20	VO_2L^2 + ascorbic acid	10^{-4} M	26	VO_2L^3+ ascorbic acid	10^{-4} M
7		10^{-3} M	15		5×10^{-4} M	21		5×10^{-4} M	27		5×10^{-4} M
8	$VOSO_4$ + ascorbic acid	10^{-4} M	16		10^{-3} M	22		10^{-3} M	28		10^{-3} M
9		5×10^{-4} M									
10		10^{-3} M									

Figure 4. Inhibitory effects of $VOSO_4$ and dioxovanadium(v) complexes with or without 1 mM ascorbic acid on FFA release from isolated rat adipocytes treated with epinephrine

Biological Activity of the Complexes

In vitro insulin-mimetic activities of the three dioxovanadium(v) complexes were examined, with or without 1 mM ascorbic acid, with regard to inhibition of FFA release from isolated rat adipocytes treated with epinephrine (Figure 4). Ascorbic acid exhibited essentially no inhibitory effect on FFA release under the experimental conditions. The inhibitory effects of dioxovanadium(v) complexes were compared with those of $VOSO_4$ as a positive control (IC_{50} = 1.00 ± 0.27 mM). In the absence of ascorbic acid, all dioxovanadium(v) complexes exhibited scarcely any inhibitory effects at concentrations of 10^{-4}, 5×10^{-4} and 10^{-3} M. The in vitro insulin-mimetic activities of the three dioxovanadium(v) complexes were lower than that of $VOSO_4$. However, the addition of 1 mM ascorbic acid to $VOSO_4$ or VO_2L^2 complex ($VOSO_4$-asc and VO_2L^2-asc) significantly enhanced the inhibitory effect of FFA release (Table 4, $VOSO_4$-asc: 0.34 ± 0.15 mM, VO_2L^2-asc: 0.73 ± 0.27 mM). Thus, the in vitro insulin-mimetic activity of VO_2L^2 was improved by the addition of the reducing agent ascorbic acid, even though it remained lower than that of pure $VOSO_4$ under the same conditions.

Upon addition of $VOSO_4$ to the adipocytes under air, the vanadyl state was found to be oxidized during the 3 h of incubation (unpublished results). Therefore, the addition of ascorbic acid was thought to maintain the vanadyl state during incubation, which in turn enhances the insulin-mimetic activity of $VOSO_4$. Interestingly, of the tested dioxovanadium(v) complexes only VO_2L^2 exhibited insulin-mi-

 © 2004 Wiley-VCH Verlag GmbH & Co. KGaA, Weinheim

Table 4. Estimated IC_{50} values of the dioxovanadium(v) complexes

Compound	IC_{50} [mM]
$VOSO_4$	1.00 ± 0.27
$VOSO_4$ + ascorbic acid	0.34 ± 0.15[a]
VO_2L^1	none
VO_2L^1 + ascorbic acid	none
VO_2L^2	none
VO_2L^2 + ascorbic acid	0.73 ± 0.22[b][c]
VO_2L^3	none
VO_2L^3 + ascorbic acid	none

[a] Significance at $P < 0.05$ vs. $VOSO_4$. [b] Significance at $P < 0.05$ vs. $VOSO_4$ + ascorbic acid. [c] Significance at $P < 0.05$ vs. VO_2L^2.

metic activity in the presence of ascorbic acid, although spectroscopic experiments showed that all three complexes were reduced by the addition of ascorbic acid, as described below. These results suggest the importance of the interaction between the reduced forms of the complexes and the adipocytes, and that this interaction strongly depends on the chemical nature of the ligands.

Reaction of V^VO_2L with Ascorbic Acid

The reaction of $V^VO_2L^2$ with ascorbic acid was monitored by ^1H NMR spectroscopy at 303 K in [D_6]DMSO/D_2O. Immediately after the addition of ascorbic acid, the solution changed from yellow to dark-green and the narrow signals characteristic of the V^V diamagnetic complex were converted into broad ones. This strongly suggests that during the reaction the $V^VO_2L^2$ complex is reduced by the ascorbic acid to a paramagnetic V^{IV} species. Signals of free L^2 were not detected, indicating that the ligand remained coordinated to the central atom in the V^{IV} species.

Similar conclusions arise from the spectrophotometric study of the reduction with ascorbic acid of $V^VO_2L^2$ and $V^VO_2L^3$, as previously reported for (maltol)- and (ethylmaltol)vanadium(v) complexes.[25] In each case, after addition of the reducing agent a new band in the visible region near 670 nm was detected, which is attributable to a d−d transition of the resulting V^{IV} species.[22] After keeping the solution under air for 8 h, the new band disappeared gradually and finally the initial spectrum was obtained (Figure 5).

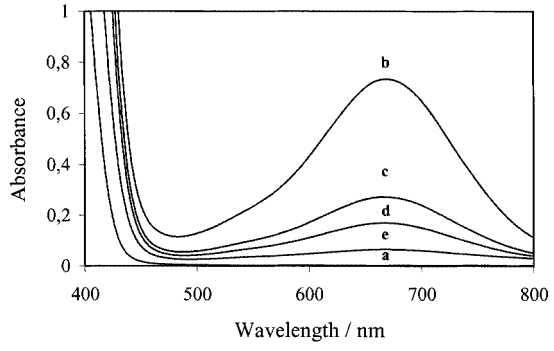

Figure 5. Electronic spectra (400−800 nm) of a 9.5×10^{-4} M DMSO solution of $V^VO_2L^2$ (a) before and (b) immediately after the addition of ascorbic acid, and (c) 20, (d) 60 and (e) 300 min after the addition

With $V^VO_2L^1$ re-oxidation of the V^{IV} species occurred almost immediately under the experimental conditions tested.

Thus, NMR and spectrophotometric experiments strongly indicate that ascorbic acid reduces V^VO_2L to a $V^{IV}O^{2+}L$ complex.

In particular, the reduction of the $V^VO_2L^2$ complex could explain the enhancement in insulin-mimetic activity of this complex in the presence of ascorbic acid.

These results, together with those of the biological tests in the presence of ascorbic acid, encouraged us to try to synthesize and isolate the $V^{IV}L^2$ complex, which could show the desirable in vitro and/or in vivo insulin-mimetic activity. We are thus extending our research to examine the structure-activity relationship of these complexes − involving redox potentials, partition coefficients, stability constants, molecular sizes and the elucidation of the chemical structure of the reduced forms. The emerging results will be the subject of a future publication.

Experimental Section

Materials: All common laboratory chemicals were purchased from commercial sources and used without further purification. 4-*n*-Butylsemicarbazide, 4-(2-naphthyl)semicarbazide and $V^{IV}O(acac)_2$, where acac = acetylacetonate, were prepared according to well-established literature procedures.[27−29] Vanadyl sulfate ($VOSO_4 \cdot 2.8H_2O$) and (+)-L-ascorbic acid were purchased from Wako Pure Chemical (Osaka, Japan). The purity of $VOSO_4 \cdot 2.8H_2O$ was determined by chelatometry using Cu-Pan [Cu-1-(2-pyridylazo-2-naphthol)]. Collagenase (Type II), bovine serum albumin (BSA; fraction V) and (±)-epinephrine hydrochloride (adrenaline) were obtained from Sigma Chemical (St. Louis, MO, USA). (+)-D-Glucose was purchased from Nacalai Tesque, Inc. (Kyoto, Japan). Other reagents were of the highest purity commercially available.

Physicochemical Characterization: C, H, N analyses were performed with a Carlo Erba Model EA1108 elemental analyzer. FTIR spectra (4000−400 cm^{-1}) were measured as KBr pellets with a Bomen M102 instrument. Electronic spectra were recorded with a Spectronic 3000 spectrophotometer. ^1H and ^{13}C NMR spectra of the free ligands and of the complexes were recorded with a Bruker DPX-400 instrument (at 400 and 100 MHz, respectively). Experiments were performed at 303 K in [D_6]DMSO/D_2O (8:2) (stability of the complexes in this medium had been tested previously). Heteronuclear correlation experiments (2D-HETCOR), HMQC (multiple quantum) and HMBC (multiple bond) were performed with the same instrument. MS experiments of the free ligands were obtained in the mass range 40−500 amu using a Shimadzu MSQP 1100 EX spectrometer with EI at 70 eV and a direct insertion probe.

Syntheses of the Ligands: All reactions were carried out under nitrogen. An equimolar mixture of 2-hydroxybenzaldehyde (salicylaldehyde) and the corresponding semicarbazide was stirred with *p*-TsOH (catalytic amounts) in dry toluene as solvent at room temperature until no more carbonyl compound was detected (SiO_2, 1% MeOH in CH_2Cl_2). For L^1 and L^2 the resulting solid was collected by filtration. For L^3 the solution was concentrated in vacuo and the solid was filtered off. The ligands were characterized by ^1H and ^{13}C NMR, IR and MS.

 © 2004 Wiley-VCH Verlag GmbH & Co. KGaA, Weinheim

Syntheses of the Complexes: The $V^{V}O_2L$ complexes were prepared by boiling under reflux $V^{IV}O(acac)_2$ (100 mg, 0.375 mmol, acac = acetylacetonate) with L (0.375 mmol) in ethanol (10 mL) for 10 h.

$V^{V}O_2L^1$: $V^{V}O_2L^1$ was filtered off from the hot solution as a yellow-greenish solid. Yield 69 mg, 70%. Single yellow-greenish crystals, suitable for X ray diffraction, were obtained by slow concentration of an ethanolic solution at room temperature. $C_8H_8N_3O_4V$ (261.1): calcd. C 36.8, H 3.09, N 16.1; found C 37.1, H 3.41, N 15.8. UV/Vis (MeOH): λ_{max} = 237, 278, 315 nm. ^{1}H NMR: δ = 6.79 (m, 2 H), 7.37 (t, 1 H), 7.48 (d, 1 H), 7.96 (br. s, 2 H), 8.58 (br. s, 1 H), 12.50 (br. s, 2 H) ppm. ^{13}C NMR: δ = 118.20, 119.30, 120.00, 133.00, 134.30, 150.0, 161.4, 164.20 ppm.

$V^{V}O_2L^2$: $V^{V}O_2L^2$ was obtained as a microcrystalline powder by slow concentration of the reaction mixture at room temperature. Yield 47 mg, 40%. $C_{12}H_{16}N_3O_4V$ (317.2): calcd. C 45.4, H 5.08, N 13.2; found C 45.1, H 5.31, N 13.1. UV/Vis (MeOH): λ_{max} = 244, 287, 359 nm. ^{1}H NMR: δ = 0.90 (t, 3 H), 1.33 (m, 2 H), 1.49 (m, 2 H), 3.20 (m, 2 H), 6.80 (d, 1 H), 6.85 (t, 1 H), 7.39 (t, 1 H), 7.51 (d, 1 H), 8.35 (br. s, 1 H), 8.63 (br. s, 1 H) ppm. ^{13}C NMR: δ = 14.40, 20.18, 31.86, 41.03, 118.66, 119.77, 120.31, 133.39, 134.65, 150.22, 160.59, 164.58 ppm.

$V^{V}O_2L^3$: $V^{V}O_2L^3$ was obtained as a yellow solid by slow concentration of the reaction mixture at room temperature, after filtering off the unreacted ligand from the hot solution. Yield 73 mg, 50%. $C_{18}H_{14}N_3O_4V$ (387.3): calcd. C 55.8, H 3.64, N 10.8; found C 55.5, H 3.90, N 10.6. UV/Vis (MeOH): λ_{max} = 242, 283, 330 nm. ^{1}H NMR: δ = 6.80 (br. t, 1 H), 6.85 (br. d, 1 H), 7.30−7.90 (m, 7 H), 8.06 (m, 1 H), 8.42 (br. s, 1 H), 8.69 (br. s, 1 H), 9.82 (br. s, 1 H), 9.93 (br. s, 1 H) ppm. ^{13}C NMR: δ = 116.90, 119.00, 120.10, 121.00, 121.75, 125.17, 127.29, 127.88, 128.34, 128.82, 129.26, 131.48, 134.28, 134.69, 137.59, 150.00, 159.66, 163.79 ppm.

X-Ray Diffraction Data and Crystal Structure Determination and Refinement: Crystal data, the data collection procedure, structure determination methods and refinement results for $V^{V}O_2L^1$ are summarized in Table 5. The hydrogen atoms were included in the molecular model at stereochemical positions and refined with the riding model. CCDC-213179 contains the supplementary crystallographic data for this paper. These data can be obtained free of charge at www.ccdc.cam.ac.uk/conts/retrieving.html [or from Cambridge Crystallographic Data Centre, 12 Union Road, Cambridge CB2 1EZ, UK; Fax: (internat.) + 44-1223/336-033; E-mail: deposit@ccdc.cam.ac.uk].

Animals: Male Wistar rats (7 weeks old) weighing 200−250 g were obtained from the Shimizu Experimental Material Co. (Kyoto, Japan). Animals were maintained on a 12 h light/dark cycle in a central animal facility. All animals were allowed free access to solid food (MF, Oriental Yeast Co. Tokyo, Japan) and tap water. All animal experiments were approved by the Experimental Animal Research Committee of Kyoto Pharmaceutical University (KPU) and were performed according to the Guidelines for Animal Experimentation of KPU.

Inhibitory Effects of $VOSO_4$ and Dioxovanadium(v) Complexes on Free Fatty Acid (FFA) Release from Isolated Rat Adipocytes Treated with Epinephrine:[4,7] Epididymal fat pads, excised from male Wistar rats (7−8 weeks) anesthetized with ether, were cut into appropriate pieces and incubated in type-II collagenase digestion in a Krebs−Ringer hydrogen carbonate (KRB) buffer (120 mM NaCl, 1.27 mM $CaCl_2$, 1.2 mM $MgSO_4$, 4.75 mM KCl, 1.2 mM KH_2PO_4 and 24 mM $NaHCO_3$; pH = 7.4) containing 2% BSA and 5 mM glucose at 37 °C with gentle shaking at 100 cycles/min for 1 h. The prepared cells were filtered through sterilized cotton gauze and were then washed with KRB buffer. Isolated rat adipocytes cells ($1.0-2.0 \times 10^6$ cells/mL) were preincubated at 37 °C for 30 min with various concentrations ($10^{-4}-10^{-3}$ M) of $VOSO_4$ or dioxovanadate complexes in KRB buffer containing 2% dimethyl sulfoxide (DMSO) with or without 1 mM (+)-L-ascorbic acid. The reaction mixtures were then incubated at 37 °C for 3 h after the addition of epinephrine (10^{-5} M, adrenaline). The reactions were stopped by soaking in ice/water and the resultant mixtures were centrifuged at 3000 rpm at 4 °C for 10 min. For the outer solution of the cells, the FFA levels were determined with an FFA kit (NEFA C-test Wako, Wako Pure Chemicals). In vitro insulin-mimetic effects of the dioxovanadate complexes were evaluated by the apparent IC_{50} value (50% inhibitory concentration of the FFA released in each system).

Reaction of $V^{V}O_2L$ with Ascorbic Acid: The reduction of $V^{V}O_2L$ by ascorbic acid was studied by electronic spectroscopy in DMSO solution. Ascorbic acid (0.047 mmol, 8.3 mg) was added to a $V^{V}O_2L$ solution (9.5×10^{-4} M, 5.0 mL) ($V^{V}O_2L$/ascorbic acid, molar ratio 1:10). The spectrum of the resultant solution was measured in the range 400−800 nm both before and after the addition and monitored with time until no bands were detected. The reaction of $V^{V}O_2L^2$ with ascorbic acid was also monitored by ^{1}H NMR at 303 K, by first dissolving $V^{V}O_2L^2$ (0.032 mmol) in [D_6]DMSO/D_2O (8:2) in an NMR tube. After purging the solution with nitrogen for 5 min, the ^{1}H NMR spectrum was measured. The ascorbic acid (0.032 mmol) was then added in one portion, and the ^{1}H NMR spectrum measured again after keeping the mixture under nitrogen for 30 min.

Acknowledgments

This work was supported by PEDECIBA, CSIC and CONICYT of Uruguay, CONICET and ANPCyT of Argentine, TWAS, FAPESP of Brazil and by the collaborative agreement between CONICET of Argentina and CNPq of Brazil.

[1] E. J. Baran, *J. Inorg. Biochem.* **2000**, *80*, 1−10.
[2] J. H. McNeill, V. G. Yuen, H. R. Hoveyda, C. Orvig, *J. Med. Chem.* **1992**, *35*, 1489−1491.
[3] K. H. Thompson, C. Orvig, *Coord. Chem. Rev.* **2001**, *219−221*, 1033−1053.
[4] H. Sakurai, Y. Kojima, Y. Yoshikawa, K. Kawabe, H. Yasui, *Coord. Chem. Rev.* **2002**, *226*, 187−198.
[5] S. Takeshita, I. Kawamura, T. Yosumo, C. Kimura, T. Yamamoto, J. Seki, A. Tamura, H. Sakurai, T. Goto, *J. Inorg. Biochem.* **2001**, *85*, 179−186.
[6] H. Sakurai, H. Sano, T. Takino, H. Yasui, *Chem. Lett.* **1999**, 913−914.
[7] H. Sakurai, H. Sano, T. Takino, H. Yasui, *J. Inorg. Biochem.* **2000**, *80*, 99−105.
[8] B. Song, N. Aebischer, C. Orvig, *Inorg. Chem.* **2002**, *41*, 1357−1364.
[9] L. C. Y. Woo, V. G. Yuen, K. H. Thompson, J. H. McNeill, C. Orvig, *J. Inorg. Biochem.* **1999**, *76*, 251−257.
[10] H. Sakurai, J. Fugono, H. Yasui, *Minirev. Med. Chem.*, accepted.
[11] K. H. Thompson, B. D. Liboiron, Y. Sun, K. D. D. Bellman, I. A. Setyawati, B. O. Patrick, V. Karunaratme, G. Rawji, J. Wheeler, K. Sutton, S. Bhanot, C. Cassidy, J. H. McNeill, V. G. Yuen, C. Orvig, *J. Biol. Inorg. Chem.* **2003**, *8*, 66−74.
[12] S. Padhye, G. B. Kauffman, *Coord. Chem. Rev.* **1985**, *63*, 127−160.
[13] H. Cerecetto, R. Di Maio, M. González, M. Risso, G. Sagrera, G. Seoane, A. Denicola, G. Peluffo, C. Quijano, M. A. Basom-

 © 2004 Wiley-VCH Verlag GmbH & Co. KGaA, Weinheim

Table 5. Crystal data and structure solution methods and refinement results for [(salicylaldehyde semicarbazone)VO_2], VO_2L[1]

Empirical formula	$C_8H_8N_3O_4V$
Formula mass	261.11
Temperature [K]	120(2)
Low-temperature device	Oxford Cryosystems
Cooling rate [K/h]	200
Crystal system	tetragonal
Space group	$P4_2/n$
Unit cell dimensions [Å][a]	$a = b = 12.7674(7)$, $c = 11.5308(5)$
Volume [Å^3]	1879.6(2)
Z, calculated density [Mg/m^3]	8, 1.845
Absorption coefficient (μ) [mm^{-1}]	1.058
F(000)	1056
Crystal size [mm]	0.190 × 0.055 × 0.037
Crystal color/shape	greenish-yellow/prism
Diffractometer/scan type	KappaCCD/φ and ω
Radiation [Å], graphite monochromator	Mo-K_α, $\lambda = 0.71073$
ϑ range for data collection [°]	2.26 to 24.99
Index ranges	$-15 \leq h \leq 13$, $-14 \leq k \leq 15$, $-12 \leq l \leq 13$
Reflections collected/unique	6324/1663 [R(int) = 0.102]
Completeness [%]	94.7 (to ϑ = 24.99°)
Reflections observed [$I > 2\sigma(I)$]	1329
Absorption correction	PLATON[29]
Max./min transm.	0.964/0.884
Data collection	COLLECT[30]
Data reduction and correction,[b] structure solution,[c] and refinement[d] programs	DENZO and SCALEPACK,[31] SHELXS-97,[32] SHELXL-97[33]
Refinement method	Full-matrix least-squares on F^2
Weights w	$[\sigma^2(F_o^2) + (0.05P)^2 + 9.68P]^{-1}$; $P = [\max(F_o^2, 0) + 2F_c^2]/3$
Data/restraints/parameters	1663/0/145
Goodness-of-fit on F^2	1.177
Final R(ind.) [$I > 2\sigma(I)$][e]	$R1 = 0.0623$, $wR2 = 0.1674$
R indices (all data)	$R1 = 0.0810$, $wR2 = 0.1766$
Largest peak/hole [e·Å^{-3}]	0.438/−0.668

[a] Least-squares refinement of the angular settings for 6324 reflections in the $2.26° < \vartheta < 24.99°$ range. [b] Corrections: Lorentz, polarization, and absorption. [c] Neutral scattering factors and anomalous dispersion corrections. [d] Structure solved by Patterson and Fourier methods. Final molecular model obtained by anisotropic full-matrix least-squares refinement of the non-hydrogen atoms. [e] R indices defined as: $R1 = \Sigma||F_o| - |F_c||/\Sigma|F_o|$, $wR_2 = [\Sigma w(F_o^2 - F_c^2)^2/\Sigma w(F_o^2)^2]^{1/2}$.

brio, M. Paulino, C. Olea-Azar, *Eur. J. Med. Chem.* **2000**, *35*, 343−350.

[14] H. Beraldo, D. Gambino, *Minirev. Med. Chem.*, accepted.

[15] J. S. Casas, M. S. García-Tesende, J. Sordo, D. X. West, A. Liberta, S. B. Padhye, R. C. Chikate, P. B. Sonawane, A. S. Kumbhar, R. G. Yerande, *Coord. Chem. Rev.* **2000**, *209*, 197−261.

[16] L. Otero, P. Noblía, D. Gambino, H. Cerecetto, M. González, A. Monge-Vega, A. López de Ceráin, O. Ezpeleta, B. Parajón-Costa, *Met. Ions Biol. Med.* **2002**, *7*, 609−613.

[17] L. Otero, P. Noblía, D. Gambino, H. Cerecetto, M. González, R. Di Maio, J. Ellena, O. E. Piro, *Inorg. Chim. Acta* **2003**, *344*, 85−94.

[18] L. Otero, P. Noblía, D. Gambino, H. Cerecetto, M. González, R. Sánchez-Delgado, E. E. Castellano, O. E. Piro, *Z. Anorg. Allg. Chem.* **2003**, *629*, 1033−1038.

[19] C. Hansch and A. Leo, *Exploring QSAR. Fundamentals and Applications in Chemistry and Biology*, ACS Professional Reference Book, Washington, **1995**.

[20] V. G. Yuen, P. Caravan, L. Gelmini, N. Glover, J. H. McNeill, L. A. Setyawati, Y. Zhon, C. Orvig, *J. Inorg. Biochem.* **1997**, *68*, 109−116.

[21] D. C. Crans, L. Yang, T. Jakusch, T. Kiss, *Inorg. Chem.* **2000**, *39*, 4409−4416.

[22] E. J. Baran, *J. Coord. Chem.* **2001**, *54*, 215−238.

[23] M. Hesse, H. Meier and B. Zeeh, *Spectroskopische Methoden in der Organischen Chemie*, Georg Thieme Verlag, Stuttgart, New York, **1995**.

[24] C. K. Johnson, *ORTEP-II, A Fortran Thermal-Ellipsoid Plot Program*, Report ORNL-5138, Oak Ridge National Laboratory, Tennessee, USA, **1976**.

[25] M. Melchior, K. H. Thompson, J. M. Jong, S. J. Rettig, E. Shuter, V. G. Yuen, Y. Zhou, J. H. McNeill, C. Orvig, *Inorg. Chem.* **1999**, *38*, 2288−2293.

[26] H. Cerecetto, R. Di Maio, G. Ibarruri, G. Seoane, A. Denicola, C. Quijano, G. Peluffo, M. Paulino, *Farmaco* **1998**, *53*, 89−94.

[27] C. P. Morley, *Inorganic Experiments* (Ed. J. Derek Woollins), VCH, Weinheim, Germany, **1994**, p. 113−114.

[28] H. Cerecetto, M. González, M. Risso, G. Seoane, A. López de Ceráin, O. Ezpeleta, A. Monge, L. Suescun, A. Mombrú, A. M. Bruno, *Arch. Pharm. (Weinheim, Ger.)* **2000**, *333*, 387−393.

[29] A. L. Spek, *Acta Crystallogr., Sect. A* **1990**, *46*, 34.

[30] Enraf−Nonius, *COLLECT*, Nonius BV, Delft, The Netherlands, **1997−2000**.

[31] Z. Otwinowski, W. Minor, *Methods Enzymol.* **1997**, *276*, 307−326.

[32] G. M. Sheldrick. *SHELXS-97, Program for Crystal Structure Resolution*, Univ. of Göttingen, Göttingen, Germany, **1997**.

[33] G. M. Sheldrick. *SHELXL-97, Program for Crystal Structures Analysis*, Univ. of Göttingen, Göttingen, Germany, **1997**.

Received July 2, 2003
Early View Article
Published Online November 19, 2003

X-ray Crystallographic Study of Copper(II), Cobalt(II) and Silver(I) Complexes of Ligands Containing Two Oxine Subunits Linked by Xylylene Spacer Groups

Muna R. A. Al-Mandhary[a] and Peter J. Steel*[b]

Keywords: N,O ligands / Copper / Cobalt / Silver / Bridging ligands

X-ray crystal structures are reported for six transition-metal complexes of the ligands 1,2-bis(8-quinolyloxymethyl)benzene (**3**) and 1,3-bis(8-quinolyloxymethyl)benzene (**4**). In three mononuclear copper(II) and cobalt(II) complexes, **3** acts as a chelating ligand with either *N*,*O*,*N*′-tridentate or *N*,*O*,*O*′,*N*′-tetradentate coordination. A novel dinuclear silver(I) complex of **3** is shown to be stabilised by a number of weak metal–ligand contacts and multiple intramolecular π–π stacking interactions. In two dinuclear copper(II) nitrate complexes of **4**, the ligand adopts very different bridging modes of coordination.

(© Wiley-VCH Verlag GmbH & Co. KGaA, 69451 Weinheim, Germany, 2004)

Introduction

Studies of combinations of organic ligands and metal-ion precursors for the controlled self-assembly of metallosupramolecular species have been the subject of a number of recent reviews.[1] Whereas rigid components are most commonly used for the rational construction of various molecular architectures, we have adopted a different approach of using flexible building blocks in order to gain access to topologies not accessible from more rigid precursors. In this context, we have recently[2] been synthesising a class of ligands represented by the general structure **1** (Scheme 1). Each of these ligands consists of a number of heterocyclic donor groups linked by flexible spacers (X) to a central arene core. This simple representation disguises the complexity of a large library of compounds that we are currently investigating. By systematically varying the number of arms, the specific heterocycle, the nature of the linking groups and the type of arene core, we can prepare ligands with a diverse range of properties.

We have found xylylene derivatives to be particularly useful components for the construction of various interesting new supramolecular architectures. For example, we have prepared new ligands consisting of *ortho*-, *meta*- and *para*-xylylene groups connected to pyrazolyl,[3] 2-pyridyloxy,[4] 2-pyridylsulfanyl[5] and benzotriazolyl[6] moieties and used them in reactions with various metals to produce metallosupramolecular species of diverse dimensionalities. In such compounds, additional stability can be imparted to the metal complexes by incorporating chelating binding domains into the ligand design. Although bridging ligands containing multiple 2,2′-bipyridine binding sites are by far the most well studied,[7] we,[8] and others,[9] have found the 3-(2-pyridyl)pyrazol-1-yl substituent to be a useful *N*,*N*′-chelating structural subunit and have attached this moiety to xylylene spacers.

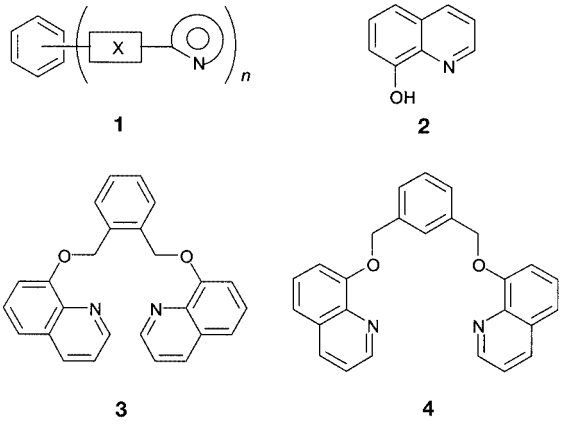

1 **2** **3** **4**

Scheme 1

Recently, we have embarked on the synthesis of a range of ligands that contain *N*,*O*-chelating moieties and have chosen 8-hydroxyquinoline (oxine; **2**) as a common starting material. Although oxine itself has a long history as a versatile bidentate ligand,[10] it has not commonly been incorporated into larger multidentate ligands. Recently, Albrecht and co-workers have reported the use of a number of ligands containing two oxine groups linked through the carbon atoms of the quinoline ring in order to prepare various complexes.[11] However, our approach has been to join the oxine subunits through the oxygen atoms.[12,13]

[a] College of Science, Sultan Qaboos University,
P. O. Box 36, Al-Khod 123, Sultanate of Oman
[b] Department of Chemistry, University of Canterbury,
Christchurch, New Zealand
Fax: (internat.) + 64-3-3642110
E-mail: p.steel@chem.canterbury.ac.nz

We herein describe the syntheses and X-ray crystal structures of a number of transition-metal complexes with ligands **3** and **4**, which consist of two oxine groups attached to the *ortho*- and *meta*-xylylene cores, respectively. Recently, we have communicated the intriguing ability of **4** to form a compact trinuclear circular helicate upon reaction with silver triflate.[14]

Results and Discussion

The ligands 1,2-bis(8-quinolyloxymethyl)benzene (**3**) and 1,3-bis(8-quinolyloxymethyl)benzene (**4**) are known compounds that were prepared by literature procedures.[15,16] We also prepared the corresponding para-isomer,[16] but were unable to form any crystalline complexes with it. Related podands, including **3**, have previously been shown to form stable complexes with alkali and alkaline earth metals.[17] Ligands **3** and **4** were treated with a variety of transition-metal salts under various reaction conditions and stoichiometric ratios. Six such reactions produced crystalline products suitable for X-ray crystal structure analysis, the structures of which we describe below. These two ligands might be expected to adopt a variety of coordination modes depending on which of the donor atoms are involved. The ligands could act as bidentate *N*,*N*′-donors in chelating or bridging modes, or as tetradentate ligands with involvement of the weaker ether oxygen donors.

Reactions of **3** with copper(II) chloride, copper(II) nitrate and cobalt(II) bromide all furnished crystalline products in good yields. Each of these complexes crystallise in the triclinic space group $P\bar{1}$ and is mononuclear with 1:1 L:MX_2 stoichiometry. Figure 1−3 show perspective views, with selected interatomic distances and angles, of the three structures in similar orientations. Although the three structures appear very similar, there are some intriguing, subtle differences. In all three structures ligand **3** adopts a very similar conformation, wherein the plane of each quinoline ring is almost orthogonal to the plane of the attached xylylene group (range of angles between planes ca. 86.3−88.8°).

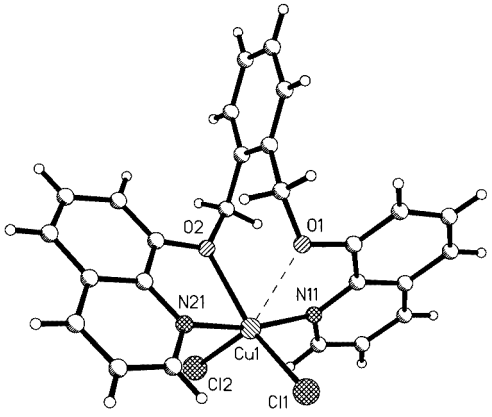

Figure 1. Perspective view of the X-ray crystal structure of **5**; selected interatomic distances (Å) and angles (°): Cu1−N11 2.025(2), Cu1−N21 2.024(2), Cu1−O1 2.466(2), Cu1−O2 2.261(2), Cu1−Cl1 2.2856(12), Cu1−Cl2 2.3688(12); N21−Cu1−N11 167.28(8), N21−Cu1−O2 74.95(8), N11−Cu1−O2 95.87(8), N21−Cu1−Cl1 95.18(7), N11−Cu1−Cl1 89.82(7), O2−Cu1−Cl1 155.85(5), N21−Cu1−Cl2 92.18(6), N11−Cu1−Cl2 96.10(6), O1−Cu1−Cl2 149.80(5), O2−Cu1−Cl2 86.59(5), Cl1−Cu1−Cl2 116.19(3)

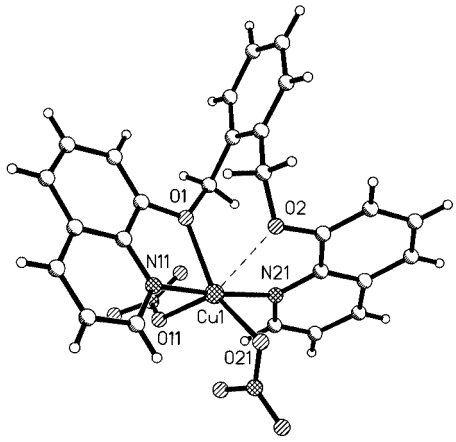

Figure 2. Perspective view of the X-ray crystal structure of **6**; the dichloromethane solvate molecule is not shown; selected interatomic distances (Å) and angles (°): Cu1−N11 1.983(3), Cu1−N21 1.998(3), Cu1−O1 2.162(3), Cu1−O2 2.457(3), Cu1−O21 2.184(4), Cu1−O11 2.217(3); N11−Cu1−N21 173.17(13), N11−Cu1−O1 77.81(11), N21−Cu1−O1 99.66(11), N11−Cu1−O21 91.58(13), N21−Cu1−O21 86.94(12), O1−Cu1−O21 144.85(11), N11−Cu1−O11 88.03(12), N21−Cu1−O11 98.08(12), O1−Cu1−O11 84.32(10), O2−Cu1−O11 150.70(10), O21−Cu1−O11 129.23(11)

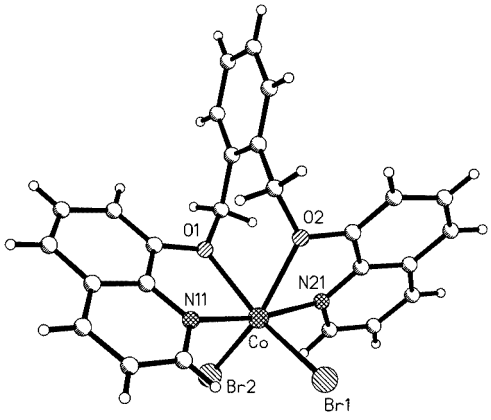

Figure 3. Perspective view of the X-ray crystal structure of **7**; selected interatomic distances (Å) and angles (????): Co−N11 2.153(2), Co−N21 2.157(2), Co−O1 2.211(2), Co−O2 2.282(2), Co−Br2 2.490(1), Co−Br1 2.496(1); N11−Co−N21 169.93(8), N11−Co−O1 73.76(7), N21−Co−O1 99.18(7), N11−Co−O2 97.68(8), N21−Co−O2 73.06(8), O1−Co−O2 72.54(7), N11−Co−Br2 92.36(6), N21−Co−Br2 94.86(6), O1−Co−Br2 90.15(5), O2−Co−Br2 156.49(5), N11−Co−Br1 94.97(6), N21−Co−Br1 89.45(6), O1−Co−Br1 159.18(5), O2−Co−Br1 92.22(5), Br2−Co−Br1 108.09(2)

However, the structures differ in the extent of interaction of the ether oxygens with the metal centre. This, in turn, is reflected in different bonding geometries at the metal centre. In the copper(II) chloride complex **5** the metal has approximately square-pyramidal five-coordinate geometry, as

 © 2004 Wiley-VCH Verlag GmbH & Co. KGaA, Weinheim

defined by a τ value of 0.19.[18] In this arrangement the atoms N11, N21, O2 and Cl1 define the basal plane and Cl2 occupies the apical position and, accordingly, has a longer bond length to the copper atom. This geometry allows for a weak interaction [2.466(2) Å] between the metal and the formally noncoordinated ether oxygen O1 (shown as a dashed line in Figure 1). However, in the copper(II) nitrate complex **6**, the geometry is intermediate between square-pyramidal and trigonal-bipyramidal with a τ value of 0.47. Once again, this geometry permits a weak interaction [2.457(3) Å] between the copper atom and O2.

In contrast, the greater requirement for six-coordination of cobalt results in the distorted octahedral geometry of complex **7** in which ligand **3** employs all of its four donor atoms. This results in two five-membered *N*,*O*-chelate rings being fused to a central seven-membered *O*,*O*′-chelate ring. The distortions from idealised octahedral geometry result from the bite angles of the chelate rings (ca. 73°) and the Br1−Co−Br2 bond angle [108.09(2)°]. Thus, in these three complexes, ligand **3** acts as a chelating ligand with either *N*,*O*,*N*′-tridentate or *N*,*O*,*O*′,*N*′-tetradentate coordination.

Previously,[14] we have described the reaction of **4** with silver triflate to produce a novel trinuclear circular helicate. The analogous reaction of **3** with silver triflate produced a very different result. The crystalline product **8** obtained from this reaction crystallises in the monoclinic space group $P2_1/c$; the asymmetric unit comprises a M_2L_3 unit, two triflate counterions and a diethyl ether solvate molecule. Figure 4 show a perspective view of the dinuclear dication, along with selected interatomic distances and angles. The nearly symmetrical structure consists of a central molecule of **3** that bridges two silver atoms, each of which is further coordinated to another molecule of **3**. The structure of **8** is interesting for a number of reasons. Each silver atom is coordinated to two quinoline nitrogen atoms with near-linear geometry. However, the bond lengths (> 2.2 Å) are somewhat long for two-coordinate silver centres.[19] The reason for this is the involvement of other donor substituents with the d^{10} silver centres.

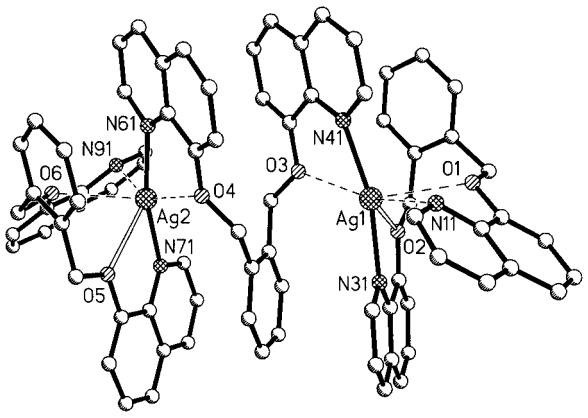

Figure 4. Perspective view of the X-ray crystal structure of **8**, hydrogen atoms, the triflate counterions and the diethyl ether solvate molecule are all omitted for clarity; selected interatomic distances (Å) and angles (°): Ag1−N41 2.213(2), Ag1−N31 2.229(2), Ag1−O2 2.595(2), Ag1−O1 2.714(2), Ag1−N11 2.714(2), Ag1−O3 2.656(2), Ag2−N61 2.230(2), Ag2−N71 2.261(2), Ag2−O5 2.575(2), Ag2−O4 2.722(2), Ag2−N91 2.722(2), Ag2−O6 2.725(2); N41−Ag1−N31 163.74(8), N41−Ag1−O2 125.39(7), N31−Ag1−O2 66.56(7), N61−Ag2−N71 167.94(8), N61−Ag2−O5 122.13(8), N71−Ag2−O5 66.53(8)

The oxygen atoms attached to the externally coordinated quinoline rings are involved in weak chelation (ca. 2.58 Å) with the silver atoms (hollow bonds in Figure 4). A notable feature of the structure is the unusual and symmetrical conformations of three molecules of **3** in this complex. We believe that each of these ligands contorts itself into the observed conformations in order to bring the remaining six potential donors into proximity with the silver atoms. Although each of these interactions (dashed bonds in Figure 4) is undoubtedly weak (ca. 2.7 Å), the combined forces of all six such interactions is likely to have a significantly stabilising influence. There is also a further stabilising factor operating in this complex, the intramolecular π−π stacking interactions between the various aromatic ring systems. Specifically, the central benzene ring of the bridging ligand is stacked between the two chelating quinolines. Additionally, the two quinoline rings of the central bridging ligand are stacked on top of one another and between the benzene rings of the outer two ligands. All of these interactions involve coplanar rings (angles between planes < 5°) separated by about 3.4 Å. Once again, although these are weak interactions, the combined influence of all five stacking interactions is likely to be significant.

Having demonstrated that ligand **3** is capable of acting as both a chelating and bridging ligand, we turned our attention to the *meta*-isomer **4**, where a chelating mode of coordination would appear less likely. Ligand **4** was treated with copper(II) nitrate in a variety of different solvents. In two cases this provided crystalline products, which were shown to be structurally very different. Reaction in methanol produced complex **9**, which crystallises in the monoclinic space group $P2_1/n$. Figure 5 shows a perspective view of **9**, with selected interatomic distances and angles.

This complex consists of a dinuclear copper pair bridged by two methoxide anions and ligand **4**. Monodentate nitrate anions complete the coordination environment of the two square-planar copper atoms. Once again the bridging ligand **4** adopts an unusual conformation, which we believe occurs in order to bring the noncoordinated ether oxygens into the coordination sphere of the copper atoms (dashed bonds in Figure 5). Relatively few dinuclear methoxide-bridged copper complexes of this type are known.[20] The Cu1−Cu2 interatomic distance [3.029(1) Å] is similar to that found in related examples.[20]

In contrast to this result, reaction of **4** with copper(II) nitrate in acetonitrile led to complex **10** which has very different architecture. It crystallises in the triclinic space group $P\bar{1}$ and has the structure shown in Figure 6. In this complex the ligand **4** acts as a more conventional bridging ligand separating two copper atoms at a distance of 10.526(1) Å. The copper atoms have square-pyramidal geometry (τ values 0.08 and 0.02 for Cu1 and Cu2, respectively) and are further coordinated to two monodentate nitrates, a water molecule and, with considerably longer bonds, to ether oxy-

 © 2004 Wiley-VCH Verlag GmbH & Co. KGaA, Weinheim

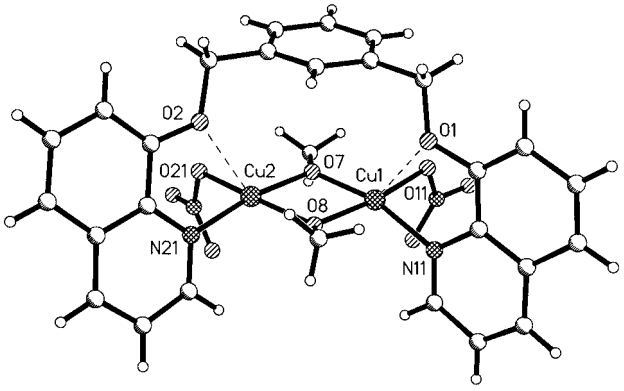

Figure 5. Perspective view of the X-ray crystal structure of **9**; selected interatomic distances (Å) and angles (°): Cu1−O7 1.928(3), Cu1−O8 1.935(3), Cu1−O11 1.996(4), Cu1−N11 2.032(4), Cu1−O1 2.451(3), Cu1−Cu2 3.029(1), Cu2−O8 1.912(3), Cu2−O7 1.946(3), Cu2−O21 1.985(3), Cu2−N21 2.043(4), Cu2−O2 2.492(3); O7−Cu1−O8 76.56(14), O7−Cu1−O11 96.85(14), O8−Cu1−O11 172.70(14), O7−Cu1−N11 165.39(17), O8−Cu1−N11 95.02(16), O11−Cu1−N11 92.08(16), O8−Cu2−O7 76.67(14), O8−Cu2−O21 168.07(14), O7−Cu2−O21 93.42(15), O8−Cu2−N21 94.69(15), O7−Cu2−N21 170.47(16), O21−Cu2−N21 94.66(16)

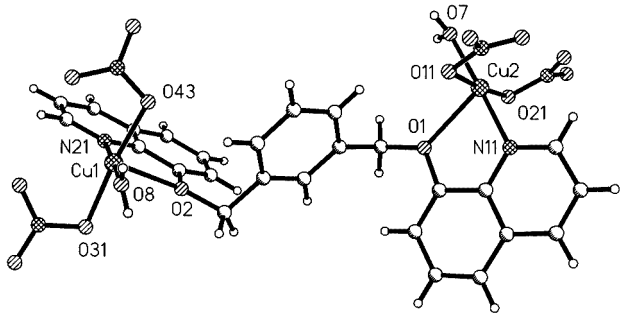

Figure 6. Perspective view of the X-ray crystal structure of **10**; diethyl ether and acetonitrile solvate molecules are not shown; selected interatomic distances (Å) and angles (°): Cu1−O8 1.935(2), Cu1−N21 1.985(2), Cu1−O43 1.987(2), Cu1−O31 1.990(2), Cu1−O2 2.391(2), Cu2−O7 1.937(2), Cu2−N11 1.975(2), Cu2−O11 1.987(2), Cu2−O21 2.010(2), Cu2−O1 2.395(2); O8−Cu1−N21 177.78(9), O8−Cu1−O43 87.87(9), N21−Cu1−O43 91.59(8), O8−Cu1−O31 86.74(9), N21−Cu1−O31 93.96(8), O43−Cu1−O31 172.91(7), O8−Cu1−O2 107.48(9), N21−Cu1−O2 74.68(7), O43−Cu1−O2 90.45(7), O31−Cu1−O2 86.78(7), O7−Cu2−N11 175.81(10), O7−Cu2−O11 88.90(9), N11−Cu2−O11 94.01(9), O7−Cu2−O21 86.22(9), N11−Cu2−O21 90.98(9), O11−Cu2−O21 174.68(8), O7−Cu2−O1 102.09(9), N11−Cu2−O1 74.76(8), O11−Cu2−O1 93.34(8), O21−Cu2−O1 89.74(8)

gens in the apical positions. Surprisingly, a search of the Cambridge Crystallographic Database revealed that this is an unprecedented geometry for a copper atom with this donor set.

Thus, ligand **4** acts as a bridging ligand in each of these two copper complexes, but in doing so, produces dinuclear complexes with very different topologies. As mentioned above, we have previously reported a novel trinuclear circular helicate resulting from reaction of **4** with silver triflate. We have since treated **4** with silver nitrate and found that this leads to a similar circular helicate, but we were unable to refine its X-ray crystal structure to a level that we consider to be acceptable (currently $R_1 = 6.5$ %). Nevertheless, this result shows that the formation of such circular helicates occurs independently of the counterion, thereby suggesting that the self-assembly process does not involve anion templation.[21]

Conclusion

In this study, we have shown that ligands comprising two oxine subunits separated by xylylene spacer groups represent useful substrates for the construction of a diverse range of interesting new complexes of varying nuclearity. These ligands have been shown to be capable of both chelating and bridging modes of coordination. Presently, we are extending this design concept to related ligands containing a greater number of oxine substructures, thereby providing access to more complex multinuclear species.

Experimental Section

Ligands **3**[15] and **4**[16] were prepared by literature procedures. Solvents were purified according to literature procedures. Other reagents were obtained from commercial sources and used as supplied. Melting points were determined using an Electrothermal melting point apparatus and are uncorrected. Elemental analyses were performed by the Campbell Microanalytical laboratory at the University of Otago.

Complex 5: $CuCl_2·2H_2O$ (8.7 mg, 0.051 mmol) dissolved in MeCN (1 mL) was layered onto a solution of ligand **3** (20 mg, 0.051 mmol) in CH_2Cl_2 (1 mL) to produce orange crystals suitable for X-ray analysis. M.p. 168 °C. Yield 21 mg (78 %). $C_{26}H_{20}Cl_2CuN_2O_2$ (526.90): C 59.27, H 3.83, N 5.32; found C 59.25, H 4.00, N 5.41.

Complex 6: $Cu(NO_3)_2·3H_2O$ (12 mg, 0.050 mmol) dissolved in MeCN (1 mL) was layered onto a solution of ligand **3** (20 mg, 0.051 mmol) in CH_2Cl_2 (1 mL) to produce yellow crystals suitable for X-ray analysis. M.p. 140−142 °C. Yield 24 mg (71 %). $C_{26}H_{20}CuN_4O_8Cu·CH_2Cl_2$ (664.94): C 48.77, H 3.33, N 8.43; found C 49.13, H 3.13, N 8.41.

Complex 7: $CoBr_2$ (22 mg, 0.10 mmol) dissolved in MeOH (1 mL) was layered onto a solution of ligand **3** (20 mg, 0.051 mmol) in CH_2Cl_2 (1 mL) to give purple crystals suitable for X-ray analysis. M.p. 240 °C (decomp.). Yield 22 mg (71 %). $C_{26}H_{20}Br_2CoN_2O_2$ (611.19) C 51.09, H 3.30, N 4.58; found C 51.17, H 3.19, N 4.67.

Complex 8: AgOTf (8.7 mg, 0.034 mmol) dissolved in MeCN (1 mL) was added to a solution of ligand **3** (20 mg, 0.051 mmol) dissolved in MeCN (1 mL). Diethyl ether (1 mL) was then added to this solution. Slow evaporation of this mixture provided colourless crystals suitable for X-ray analysis. M.p. 226−229 °C. Yield 20 mg (70 %). $C_{80}H_{60}Ag_2F_6N_6O_{12}S_2$ (1691.22): C 56.81, H 3.58, N 4.97; found C 56.63, H 3.54, N 4.91.

Complex 9: $Cu(NO_3)_2·3H_2O$ (25.6 mg, 0.102 mmol) dissolved in MeOH (1 mL) was layered onto a solution of ligand **4** (20 mg, 0.051 mmol) in CH_2Cl_2 (1 mL) to give dark green crystals suitable for X-ray analysis. M.p. 205 °C (decomp.). Yield 11 mg (31 %). $C_{28}H_{26}Cu_2N_4O_{10}$ (705.62): C 47.66, H 3.71, N 7.94; found C 47.69, H 3.85, N 7.91.

 © 2004 Wiley-VCH Verlag GmbH & Co. KGaA, Weinheim

Table 1. Crystal Data and X-ray Experimental Details for **5−10**

Complex	**5**	**6**	**7**	**8**	**9**	**10**
Empirical formula	$C_{26}H_{20}Cl_2CuN_2O_2$	$C_{27}H_{22}Cl_2CuN_4O_8$	$C_{26}H_{20}Br_2CoN_2O_2$	$C_{84}H_{70}Ag_2F_6N_6O_{13}S_2$	$C_{28}H_{26}Cu_2N_4O_{10}$	$C_{32}H_{37}Cu_2N_7O_{17}$
M_r (g.mol^{-1})	526.88	664.93	611.19	1765.32	705.61	918.77
T (K)	168(2)	168(2)	168(2)	168(2)	168(2)	168(2)
Crystal system	triclinic	triclinic	triclinic	monoclinic	monoclinic	triclinic
Space group	$P\bar{1}$	$P\bar{1}$	$P\bar{1}$	$P2_1/c$	$P2_1/n$	$P\bar{1}$
Unit cell: a (Å)	9.384(4)	9.653(2)	9.561(3)	16.648(6)	12.772(4)	9.678(4)
b (Å)	10.160(5)	11.340(3)	10.432(3)	17.329(6)	15.393(5)	13.928(6)
c (Å)	12.629(6)	13.484(3)	12.729(4)	27.222(9)	15.609(5)	16.458(7)
α (°)	106.393(5)	109.251(3)	104.861(4)	90	90	66.066(6)
β (°)	103.530(9)	91.603(4)	104.071(4)	101.753(5)	109.926(5)	87.160(6)
γ (°)	97.931(9)	104.051(3)	98.529(4)	90	90	76.302(6)
Volume (Å^3)	1095.9(9)	1342.5(6)	1159.9(6)	7689(5)	2884.9(17)	1967.4(15)
Z	2	2	2	4	4	2
Calcd. density (Mg.m^{-3})	1.597	1.610	1.750	1.52	1.625	1.551
Abs. coeff. (mm^{-1})	1.269	1.071	4.212	0.647	1.539	1.163
F(000)	538	662	606	3600	1440	944
Crystal size (mm)	0.60 × 0.51 × 0.19	0.56 × 0.56 × 0.30	0.65 × 0.38 × 0.15	0.61 × 0.35 × 0.09	0.37 × 0.16 × 0.12	0.55 × 0.35 × 0.15
Theta range (°)	2.14 to 25.00	1.97 to 25.00	1.73 to 26.37	1.93 to 26.44	2.15 to 23.50	2.17 to 26.53
Data collected	11739	9904	14208	73094	29163	25960
Unique data R_{int}	3820 [0.0327]	4727 [0.0198]	4487 [0.0178]	15297 [0.0487]	4276 [0.0622]	8025 [0.0500]
Obsd. data [$I > 2\sigma(I)$]	3427	4580	3665	10886	3268	6377
Parameters	298	379	298	1018	399	538
GooF on F^2	1.062	1.258	0.984	1.012	1.090	1.066
wR_2 (all data)	0.1061	0.1224	0.0400	0.0800	0.1358	0.1178
R_1 [$I > 2\sigma(I)$]	0.0368	0.0566	0.0297	0.0366	0.0492	0.0407

Complex 10: $Cu(NO_3)_2{\cdot}3H_2O$ (12 mg, 0.051 mmol) dissolved in MeCN (1 mL) was layered onto a solution of ligand **4** (10 mg, 0.025 mmol) in CH_2Cl_2 (1 mL) to give a green solution. Diffusion of diethyl ether into this solution gave green crystals suitable for X-ray analysis. M.p. 118 °C (decomp.). Yield 14 mg (58 %). $C_{32}H_{37}Cu_2N_7O_{17}{\cdot}Cu_2{\cdot}1/2(CH_2Cl_2)$ (961.23): C 41.61, H 3.98, N 10.21; found C 41.27, H 3.68, N 10.34.

X-ray Crystallography: The crystal data and details of the data collections and refinements for all six structures are listed in Table 1. Measurements were made with a SMART CCD area detector using graphite-monochromatized Mo-K_α (λ = 0.71073Å) radiation. The structures were solved by direct methods using SHELXS[22] and refined on F^2 using all data by full-matrix least-squares procedures with SHELXL-97.[23] All non-hydrogen atoms were refined with anisotropic displacement parameters. Hydrogen atoms were included in calculated positions with isotropic displacement parameters 1.2 times the isotropic equivalent of their carrier atoms. The functions minimised were $\Sigma w (F_o^2 - F_c^2)$, with $w = [\sigma^2(F_o^2) + aP^2 + bP]^{-1}$, where $P = [\max F_o^2 + 2F_c^2]/3$. Full tables of atom coordinates, thermal parameters, bond lengths and angles have been deposited at the Cambridge Crystallographic Data Centre. CCDC-194259−194264 contain the supplementary crystallographic data for this paper. These data can be obtained free of charge at www.ccdc.cam.ac.uk/conts/retrieving.html [or from the Cambridge Crystallographic Data Centre, 12 Union Road, Cambridge CB2 1EZ, UK; Fax: (internat.) + 44-1223/336-033; E-mail: deposit@ccdc.cam.ac.uk].

Acknowledgments

We thank the Royal Society of New Zealand Marsden Fund for financial support and Sultan Qaboos University for sabbatical leave to M. Al-Mandhary. We also thank Chris Fitchett and John Cannon for important contributions to the crystallography.

[1] For recent reviews, see: [1a] S. Leininger, B. Olenyuk, P. J. Stang, *Chem. Rev.* **2000**, *100*, 853−908. [1b] G. F. Swiegers, T. J. Malefetse, *Chem. Rev.* **2000**, *100*, 3483−3538. [1c] B. Moulton, M. J. Zaworotko, *Chem. Rev.* **2001**, *101*, 1629−1658. [1d] M. Fujita, K. Umemoto, M. Yoshizawa, N. Fujita, T. Kusukawa, K. Biradha, *Chem. Commun.* **2001**, 509−518. [1e] D. W. Johnson, K. N. Raymond, *Supramol. Chem.* **2001**, *13*, 639−659. [1f] B. J. Holliday, C. A. Mirkin, *Angew. Chem. Int. Ed.* **2001**, *40*, 2022−2043. [1g] G. F. Swiegers, T. J. Malefetse, *Coord. Chem. Rev.* **2002**, *225*, 91−121.
[2] C. M. Hartshorn, P. J. Steel, *Inorg. Chem.* **1996**, *35*, 6902−6903.
[3] [3a] C. M. Hartshorn, P. J. Steel, *Aust. J. Chem.* **1995**, *48*, 1587−1599. [3b] C. M. Hartshorn, P. J. Steel, *Organometallics* **1998**, *17*, 3487−3496.
[4] C. M. Hartshorn, P. J. Steel, *J. Chem. Soc., Dalton Trans.* **1998**, 3927−3934.
[5] C. M. Hartshorn, P. J. Steel, *J. Chem. Soc., Dalton Trans.* **1998**, 3935−3940.
[6] B. J. O'Keefe, P. J. Steel, *Inorg. Chem. Commun.* **2000**, *3*, 473−475.
[7] C. Kaes, A. Katz, M. W. Hosseini, *Chem. Rev.* **2000**, *100*, 3553−3590.
[8] C. M. Hartshorn, P. J. Steel, *Inorg. Chem. Commun.* **2000**, *3*, 476−481.
[9] M. D. Ward, J. A. McCleverty, J. C. Jeffery, *Coord. Chem. Rev.* **2001**, *222*, 251−272.
[10] J. P. Phillips, *Chem. Rev.* **1956**, *56*, 271−297.
[11] [11a] M. Albrecht, O. Blau, *Synthesis* **1997**, 213−216. [11b] M. Albrecht, O. Blau, *Chem. Commun.* **1997**, 345−346. [11c] M. Albrecht, O. Blau, R. Fröhlich, *Chem. Eur. J.* **1999**, *5*, 48−56.

 © 2004 Wiley-VCH Verlag GmbH & Co. KGaA, Weinheim

[11d] M. Albrecht, O. Blau, J. Zauner, *Eur. J. Org. Chem.* **1999**, 3165−3169. [11e] M. Albrecht, O. Blau, E. Wegelius, K. Rissanen, *New J. Chem.* **1999**, *23*, 667−668.
[12] M. R. A. Al-Mandhary, P. J. Steel, *Aust. J. Chem.* **2002**, *55*, 705−708.
[13] M. R. A. Al-Mandhary, P. J. Steel, *Inorg. Chim. Acta* **2003**, *351*, 7−11.
[14] M. R. A. Al-Mandhary, P. J. Steel, *Inorg. Chem. Commun.* **2002**, *5*, 954−957.
[15] K. Hiratani, K. Taguchi, H. Sugihara, T. Okaida, *Chem. Lett.* **1986**, 197−200.
[16] B. Tümmler, G. Maass, F. Vögtle, H. Sieger, U. Heimann, E. Weber, *J. Am. Chem. Soc.* **1979**, *101*, 2588−2598.
[17] F. Vögtle, E. Weber, *Angew. Chem. Int. Ed. Engl.* **1979**, *18*, 753−776.
[18] A. W. Addison, T. Nageswara Rao, J. Reedijk, J. van Rijn, G. C. Verschoor, *J. Chem. Soc., Dalton Trans.* **1984**, 1349−1356.
[19] M. Munakata, L. P. Wu, T. Kuroda-Sowa, *Adv. Inorg. Chem.* **1998**, *46*, 173−303.
[20] [20a] V. K. Voronkova, L. V. Mosina, Y. V. Yablokov, M. A. Yampolskaya, G. S. Matuzenko, Y. A. Simonov, B. Y. Kuyavskaya, N. V. Gerbeleu, V. K. Belskii, *Zh. Strukt. Khim.* **1986**, *27*, 69−79. [20b] S. A. Komaei, G. A. van Albada, I. Mutikainen, U. Turpeinen, J. Reedijk, *Eur. J. Inorg. Chem.* **1998**, 1577−1579. [20c] D. M. L. Goodgame, I. Hussain, A. J. P. White, D. J. Williams, *J. Chem. Soc., Dalton Trans.* **1999**, 2899−2900. [20d] A. M. Guidote, K. Ando, K. Terada, Y. Kurusu, H. Nagao, Y. Matsuyama, *Inorg. Chim. Acta* **2001**, *324*, 203−211.
[21] [21a] M. Albrecht, *Chem. Rev.* **2001**, *101*, 3457−3497. [21b] R. Vilar, *Angew. Chem. Int. Ed.* **2003**, *42*, 1460−1477.
[22] G. M. Sheldrick, *Acta Crystallogr., Sect. A* **1990**, *46*, 467−473.
[23] G. M. Sheldrick, *SHELXL-97*, University of Göttingen, **1997**.

Received July 3, 2003
Early View Article
Published Online October 31, 2003

 © 2004 Wiley-VCH Verlag GmbH & Co. KGaA, Weinheim

Syntheses, Structures, and Magnetic Properties of Copper(II) Complexes with 1,3-[Bis(2-pyridylmethyl)amino]benzene (1,3-tpbd) as Ligand

Simon P. Foxon,[a] Gemma Romualdo Torres,[a] Olaf Walter,[b] Jens Zacho Pedersen,[c] Hans Toftlund,[c] Martina Hüber,[d] Karsten Falk,[d] Wolfgang Haase,[d] Joan Cano,[e] Francesc Lloret,[e] Miguel Julve,*[e] and Siegfried Schindler*[a]

Keywords: Copper / Magnetic properties / EPR spectroscopy / Spin polarisation / Dinuclear complexes

The dinuclear copper(II) complexes $\{[Cu_2(1,3\text{-tpbd})(H_2O)(OAc)_2](ClO_4)_2\}_{0.23}\{[Cu_2(1,3\text{-tpbd})(H_2O)_2(OAc)](ClO_4)_3\}_{0.77}\cdot 0.77H_2O$ (**1**), $[Cu_2(1,3\text{-tpbd})(H_2O)_2(OAc)_2](ClO_4)_2\cdot 2H_2O$ (**2**), and the tetranuclear copper(II) complex $[Cu_4(1,3\text{-tpbd})_2(H_2O)_2(SO_4)_4]\cdot 8H_2O$ (**3**) {1,3-tpbd = 1,3-bis[bis(2-pyridylmethyl)amino]benzene} were synthesised and structurally characterised by X-ray diffraction. Variable-temperature (2.0–290 K) magnetic susceptibility measurements on these complexes as well as on the dinuclear copper(II) complex $[Cu_2(1,3\text{-tpbd})(H_2O)_2(ClO_4)_3]ClO_4$ (**4**) (whose structure was published earlier) were performed. In contrast to **2** and **3**, significant ferromagnetic coupling with $J = +9.3$ cm^{-1} was observed for **4** (the Hamiltonian being defined as $\hat{H} = -J\,\hat{S}_1\cdot\hat{S}_2$). Density functional theory (DFT) calculations were used successfully for the interpretation of the ferromagnetic coupling observed in **4**.
(© Wiley-VCH Verlag GmbH & Co. KGaA, 69451 Weinheim, Germany, 2004)

Introduction

Continuing interest in the synthesis and characterisation of polynuclear copper(II) complexes derives from the efforts to understand the factors that are responsible for the magnetic exchange interactions between coupled metal centres. Attention has been focused on the magnetostructural correlations and the exchange mechanism involving different bridging groups.[1−7]

The symmetry and energy of the SOMOs ("magnetic orbitals": the molecular orbitals which define each unpaired electron of a paramagnetic centre) and the molecular orbitals of the bridging ligands are important for the understanding of the magnetic exchange phenomena in polynuclear complexes.[3,8−10] The most common situation for magnetic coupling through extended bridges is the antiferromagnetic interaction: the larger the overlap integral between the SOMOs involved, the larger the antiferromagnetic coupling. However, ferromagnetic coupling is observed when the interacting SOMOs are orthogonal to one another: the larger the overlap density between orthogonal SOMOs, the larger the ferromagnetic coupling. Orthogonality can be achieved by either geometrical or topological symmetry; geometrical symmetry has been successfully applied to bimetallic compounds[3] and metal−radical systems.[11] Topological symmetry is being used extensively in designing high-spin organic polyradical species; the intramolecular spin alignment can be explained in terms of the spin polarisation mechanism.[12,13] This mechanism describes how an unpaired electron on one atom polarizes the electron cloud on the adjacent atom in the opposite sense.

Although the spin polarisation mechanism was shown to be valid for some oxygen or nitrogen perturbed systems[14,15] as well as for some organic radical-paramagnetic transition metal ion type systems,[16] the limits of its application are unclear, especially for coordination compounds containing transition metal ions as the only spin sources. In fact, polymeric transition metal complexes containing pyrimidine bridges have been designed as an approach to molecule-based ferromagnets.[17−22] Ward and co-workers provided examples of antiferromagnetic/ferromagnetic coupling between transition metal ions connected by conjugated bridges with an even/odd number of atoms.[19,20]

[a] Institut für Anorganische und Analytische Chemie, Justus-Liebig-Universität Gießen,
Heinrich-Buff-Ring 58, 35392 Gießen, Germany
Fax: (internat.) +49-641-9934-149
E-mail: Siegfried.Schindler@anorg.chemie.uni-giessen.de
[b] Forschungszentrum Karlsruhe, ITC-CPV,
Postfach 3640, 76021 Karlsruhe, Germany
[c] Department of Chemistry, Odense University,
Campusvej 55, 5230 Odense M, Denmark
[d] Institute for Physical Chemistry, Technical University of Darmstadt,
Petersenstraße 20, 64287 Darmstadt, Germany
[e] Department de Química Inorgànica, Facultat de Química, Universitat de València,
Dr. Moliner 50, 46100 Burjassot, València, Spain
Fax: (internat.) +34-96-3544-322
E-mail: miguel.julve@uv.es

Some of us have investigated dinuclear copper complexes with ligands derived from 1,3-phenylenediamine which can be regarded as model compounds for copper proteins.[23,24] However, only a few ligands are described in the literature that are based on a 1,3-phenylenediamine unit.[21,25−30]

We have synthesised and characterised dinuclear copper(I) and copper(II) complexes with the ligand 1,3-bis[bis(2-pyridylmethyl)amino]benzene (1,3-tpbd).[23] A schematic representation of the cation of the copper(II) complex $[Cu_2(1,3\text{-tpbd})(H_2O)_2(ClO_4)_3]ClO_4$ characterised by single-crystal X-ray diffraction is shown below in Figure 1.

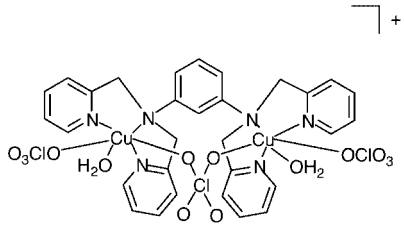

Figure 1. Schematic representation of the molecular structure of the cation of $[Cu_2(1,3\text{-tpbd})(H_2O)_2(ClO_4)_3]ClO_4$ (**4**)

To investigate the effect of substituting the perchlorate bridge in $[Cu_2(1,3\text{-tpbd})(H_2O)_2(ClO_4)_3]ClO_4$ with other anions we synthesised and structurally characterised the dinuclear copper(II) complexes $\{[Cu_2(1,3\text{-tpbd})(H_2O)(OAc)_2](ClO_4)_2\}_{0.23}\{[Cu_2(1,3\text{-tpbd})(H_2O)_2(OAc)](ClO_4)_3\}_{0.77}\cdot 0.77H_2O$ (**1**), $[Cu_2(1,3\text{-tpbd})(H_2O)_2(OAc)_2](ClO_4)_2\cdot 2H_2O$ (**2**), and the tetranuclear copper(II) complex $[Cu_4(1,3\text{-tpbd})_2(H_2O)_2(SO_4)_4]\cdot 8H_2O$ (**3**) and furthermore investigated their magnetic behaviour in comparison with $[Cu_2(1,3\text{-tpbd})(H_2O)_2(ClO_4)_3]ClO_4$ (**4**).

Results and Discussion

Synthesis and Crystal Structures

$[Cu_2(1,3\text{-tpbd})(H_2O)_2(ClO_4)_3](ClO_4)$ (**4**) was prepared and characterised as described previously.[23] Dinuclear cop-

Table 1. Selected bond lengths and bond angles with standard deviations in parentheses for **1a/1b**, **2** and **3**

1a/1b					
Cu(1)−N(1)	2.049(3)	Cu(1)−N(2)	1.951(3)	Cu(1)−N(3)	1.943(3)
Cu(1)−O(2)	1.944(2)	Cu(2)−N(4)	2.100(3)	Cu(2)−N(5)	1.973(3)
Cu(2)−N(6)	1.966(3)	Cu(2)−O(3)	2.215(3)	Cu(2)−O(4)	2.020(3)
O(1)···H(31)	1.81	O(3)−H(31)	0.91		
N(1)−Cu(1)−N(2)	84.51(11)	N(1)−Cu(1)−N(3)	85.05(11)	N(2)−Cu(1)−N(3)	158.73(12)
N(1)−Cu(1)−O(2)	166.91(11)	N(2)−Cu(1)−O(2)	98.29(11)	N(3)−Cu(1)−O(2)	96.06(11)
N(4)−Cu(2)−N(5)	82.68(12)	N(4)−Cu(2)−N(6)	83.38(12)	N(5)−Cu(2)−N(6)	163.70(13)
N(4)−Cu(2)−O(3)	106.24(13)	N(5)−Cu(2)−O(3)	99.40(12)	N(6)−Cu(2)−O(3)	92.58(13)
N(4)−Cu(2)−O(4)	161.12(13)	N(5)−Cu(2)−O(4)	96.71(13)	N(6)−Cu(2)−O(4)	93.75(13)
O(3)−Cu(2)−O(4)	92.51(15)	O(1)···H(31)−O(3)	173.3		
2					
Cu(1)−N(1)	2.067(2)	Cu(1)−N(2)	1.983(2)	Cu(1)−N(3)	1.986(2)
Cu(1)−O(1)	1.999(2)	Cu(1)−O(5)	2.330(2)	Cu(2)−N(4)	2.108(2)
Cu(2)−N(5)	1.969(2)	Cu(2)−N(6)	1.972(2)	Cu(2)−O(3)	1.983(2)
Cu(2)−O(6)	2.194(2)				
N(1)−Cu(1)−N(2)	83.12(9)	N(1)−Cu(1)−N(3)	84.15(9)	N(2)−Cu(1)−N(3)	165.07(10)
N(1)−Cu(1)−O(1)	164.87(9)	N(2)−Cu(1)−O(1)	96.14(9)	N(3)−Cu(1)−O(1)	98.18(9)
N(1)−Cu(1)−O(5)	98.10(9)	N(2)−Cu(1)−O(5)	88.18(9)	N(3)−Cu(1)−O(5)	85.92(9)
N(4)−Cu(2)−N(5)	83.35(9)	N(4)−Cu(2)−N(6)	83.20(9)	N(5)−Cu(2)−N(6)	163.18(9)
N(4)−Cu(2)−O(3)	162.13(8)	N(5)−Cu(2)−O(3)	96.62(9)	N(6)−Cu(2)−O(3)	93.11(9)
3					
Cu(1)−N(1)	2.062(3)	Cu(1)−N(2)	2.032(3)	Cu(1)−N(3)	2.003(3)
Cu(1)−O(1)	1.953(2)	Cu(1)−O(5)	2.159(3)	Cu(2)−N(4)	2.038(3)
Cu(2)−N(5)	2.001(3)	Cu(2)−N(6)	1.986(3)	Cu(2)−N(6)	1.986(3)
Cu(2)−O(6)	1.963(2)	Cu(2)−O(6)#1	2.398(2)	S(1)−O(1)	1.510(2)
S(1)−O(2)	1.469(2)	S(1)−O(3)	1.469(2)	S(1)−O(4)	1.456(2)
S(2)−O(6)	1.528(2	S(2)−O(7)	1.459(3)	S(2)−O(8)	1.462(2)
S(2)−O(9)	1.464(2)	Cu(2)···Cu(2a)	3.316		
N(1)−Cu(1)−N(2)	81.86(10)	N(1)−Cu(1)−N(3)	81.52(11)	N(2)−Cu(1)−N(3)	163.34(11)
N(1)−Cu(1)−O(1)	162.48(10)	N(1)−Cu(1)−O(5)	103.93(12)	N(2)−Cu(1)−O(1)	103.86(10)
N(2)−Cu(1)−O(5)	90.58(11)	N(3)−Cu(1)−O(1)	91.71(11)	N(3)−Cu(1)−O(5)	94.63(11)
O(1)−Cu(1)−O(5)	92.66(11)	N(4)−Cu(2)−N(5)	83.16(11)	N(4)−Cu(2)−N(6)	82.88(11)
N(5)−Cu(2)−N(6)	165.44(11)	N(4)−Cu(2)−O(6)	177.28(10)	N(4)−Cu(2)−O(6)#1	95.90(9)
N(5)−Cu(2)−O(6)	98.03(10)	N(5)−Cu(2)−O(6)#1	98.79(9)	N(6)−Cu(2)−O(6)	96.09(10)
N(6)−Cu(2)−O(6)#1	86.77(9)	O(6)−Cu(2)−O(6)#1	81.51(9)		

 © 2004 Wiley-VCH Verlag GmbH & Co. KGaA, Weinheim

Table 2. Crystal data and structure refinement parameters for **1a/1b**, **2** and **3**

Complex	$(\mathbf{1a})_{0.23}(\mathbf{1b})_{0.77}\cdot 0.77H_2O$	**2**	**3**
Empirical formula	$C_{32.44}H_{33.67}Cl_{2.78}Cu_2N_6O_{16.11}$	$C_{34}H_{42}Cl_2Cu_2N_6O_{16}$	$C_{60}H_{76}Cu_4N_{12}O_{26}S_4$
Molecular mass	990.93	988.72	1763.72
Temperature /K	293(2)	293(2)	200(2)
Crystal system	monoclinic	monoclinic	monoclinic
Space group	$P2_1/c$ (No. 14)	$P2_1/n$ (No. 14)	$P2_1/n$ (No. 14)
a (Å)	23.6166(1)	16.995(3)	11.8974(3)
b (Å)	10.0463(2)	12.594(3)	10.7422(2)
c (Å)	17.2188(3)	20.046(4)	27.9871(6)
β /°	102.0280(10)	109.702(17)	101.9850(10)
V (Å^3)	3995.63(11)	4039.5(14)	3498.90(13)
Z	4	4	2
$D_{calcd.}$ /g·cm^{-3}	1.647	1.626	1.674
μ/mm^{-1}	1.329	1.265	1.410
F(000)	2018	2032	1816
Crystal size (mm^3)	0.30 × 0.30 × 0.30	0.20 × 0.20 × 0.25	0.25 × 0.20 × 0.10
θ range for data collection	1.76 to 28.32	1.93 to 28.29	1.49 to 28.30
Index ranges	$-31 \le h \le 31$	$-22 \le h \le 22$	$-15 \le h \le 15$
	$-13 \le k \le 13$	$-16 \le k \le 16$	$-14 \le k \le 13$
	$-22 \le l \le 22$	$-26 \le l \le 26$	$-36 \le l \le 37$
Reflections measured	40879	41742	35485
Unique reflections, R_{int}	9818, 0.0552	9895, 0.0500	8516, 0.0815
Completeness to θmax	93.3%	94.4%	93.1%
Data/restraints/parameters	9818/0/620	9895/0/641	8516/0/527
Goodness of fit on F^2	1.016	0.999	0.999
Final R indices	$R1 = 0.0498$	$R1 = 0.0429$	$R1 = 0.0471$
$[I > 2\sigma(I)]$	$wR2 = 0.1258$	$wR2 = 0.0972$	$wR2 = 0.0801$
R indices (all data)	$R1 = 0.0933$	$R1 = 0.0812$	$R1 = 0.0996$
	$wR2 = 0.1454$	$wR2 = 0.1125$	$wR2 = 0.0968$
Max./min. electron density /e·Å^{-3}	+0.929/−0.939	+1.287/−0.809	+0.519/−0.489

per(II) complexes with acetate or sulfate as additional anionic ligands in place of perchlorate were obtained by mixing the appropriate copper(II) salts with 1,3-tpbd in methanol/water mixtures.

Acetate can display varying modes of coordination in its copper(II) complexes: bridging, bidentate and monodentate coordination modes of this ligand are well-known and for the sake of brevity only a few examples are given in the cited references.[31−37] Our first attempt of reacting together 1,3-tpbd, copper(II) perchlorate and copper(II) acetate resulted in a mixture of blue and green crystals. The molecular structure of both compounds was solved by single-crystal X-ray diffraction; the blue crystals showed disorder at one copper(II) ion indicating that in the unit cell there were two different complexes present, denoted **1a** and **1b**, which were found in a 23 to 77 ratio respectively. The contents of the unit cell can be represented as $\{[Cu_2(1,3\text{-tpbd})(H_2O)(OAc)_2](ClO_4)_2\}_{0.23}\{[Cu_2(1,3\text{-tpbd})(H_2O)_2(OAc)](ClO_4)_3\}_{0.77}\cdot 0.77H_2O$ ($\mathbf{1a}_{0.23}\mathbf{1b}_{0.77}\cdot 0.77H_2O$). In **1a** the copper(II) ion Cu(1) is tetra-coordinated to three N-donor atoms of the 1,3-tpbd ligand and one O atom of an acetate, the ligands forming a distorted square planar environment around the copper(II) ion (Figure 2 and Table 1 and 2). The coordination geometry around the copper(II) ion Cu(2) is square pyramidal; Cu(2) is bound to three N-donor atoms of the 1,3-tpbd ligand, one O atom of an acetate ion [O(4) in Figure 2] and one O-donor atom of a coordinated water molecule.

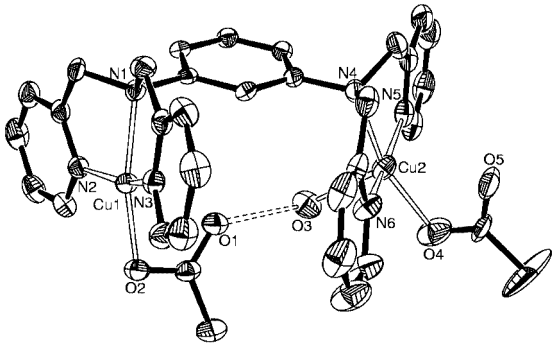

Figure 2. ORTEP representation (30% probability displacement ellipsoids) of the cation of **1a** (hydrogen atoms are omitted for clarity)

The copper(II) coordination environments in **1a** and **1b** differ; one of the coordinated acetate anions in **1a** [O(4) in Figure 2] is replaced by a water solvent molecule and an additional perchlorate anion is found in the unit cell.

An intramolecular hydrogen bond formed by the water solvent molecule O(3), which is always coordinated to Cu(2), and the non-coordinated O atom O(1) of the acetate ligand bound to the other copper ion Cu(1) leads to further stabilisation (Table 2).

The dark green crystals were characterised as $[Cu_2(1,3\text{-tpbd})(H_2O)_2(OAc)_2](ClO_4)_2\cdot 2H_2O$ (**2**) and the molecular

 © 2004 Wiley-VCH Verlag GmbH & Co. KGaA, Weinheim

structure of the cation of **2** is shown in Figure 3 (Table 1 and 2). Each copper(II) centre is five-coordinate and their coordination geometries are best described as square pyramidal.

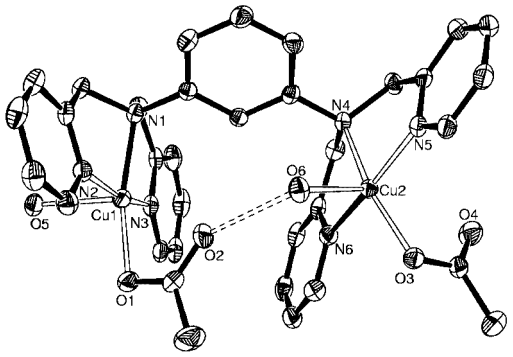

Figure 3. ORTEP representation (30% probability displacement ellipsoids) of the cation of **2** (hydrogen atoms are omitted for clarity)

2 was obtained in a pure form by mixing 1,3-tpbd and copper(II) acetate stoichiometrically (1:2) in methanol/water with an excess of sodium perchlorate. Only large green crystals of **2** were grown from that solution. An excess of acetate ions in solution is necessary to avoid substitution of the acetate ligands by water molecules.

In contrast to **4**, where a perchlorate ion bridges the two copper(II) ions in the solid state, the acetate ions in **1a**, **1b** and **2** coordinate only in a monodentate fashion. The Cu−O bond lengths in **1a**, **1b** and **2** (Table 2) are similar to those found in other monodentate acetate-containing copper(II) complexes and the $Cu-N_{pyridine}$ bonds are shorter than the $Cu-N_{amine}$ bonds.[35,37] In the cases where the copper(II) ion is coordinated by an axial ligand, the bond lengths of Cu−O are clearly longer than those in the equatorial positions. Bond lengths and angles of **1** and **2** compare well with **4**. The Cu···Cu distances in **1** (6.06 Å) and **2** (5.85 Å) are similar to **4** (5.87 Å)[23] even though the two copper(II) ions are not bridged by acetate.

Sulfate was also chosen to replace the perchlorate bridge in **4**. There are numerous examples of structurally characterised transition metal complexes with sulfate as a bridging ligand (a limited number of examples are given in the references).[38−43] Mixing stoichiometric amounts of copper(II) sulfate and 1,3-tpbd (2:1) in water lead to the formation of dark blue crystals after slow evaporation at room temperature. The molecular structure revealed that the tetranuclear complex $[Cu_4(1,3\text{-tpbd})_2(H_2O)_2(SO_4)_4]\cdot 8H_2O$ (**3**) formed (Figure 4 and Table 1 and 2) with the sulfate ion acting as both a terminal ligand and as a bridging ligand.

Each copper(II) ion in **3** is five-coordinate and their coordination geometries are best described as distorted square pyramidal. The two sulfate-bridged copper(II) ions are separated by 3.316 Å. The sulfate anions exhibit an unusual one atom bridging mode which is reflected in the different S−O bond lengths of 1.515(2) Å (coordinated oxygen) and 1.461(2) Å (mean value, uncoordinated oxygens). The Cu···Cu distances through the bridging 1,3-tpbd units (7.20 Å) in **3** are much longer than in **1**, **2** or **4**. We are aware of only one other example of a bis-sulfate bridged copper(II) complex $[Cu(HL)(SO_4)]_2$ (HL = 2-formylpyridine thiosemicarbazone) which has been structurally characterised.[39] The geometry of the coordination sphere around the copper(II) ions in $[Cu(HL)(SO_4)]_2$ is distorted square-pyramidal, with bond lengths and angles for $[Cu(HL)(SO_4)]_2$ similar to those observed in **3**.

Magnetic Properties of 2, 3 and 4

The temperature dependence of $\chi_M T$ for **4** (χ_M is the magnetic susceptibility per two copper(II) ions) is shown in Figure 5.

At room temperature, $\chi_M T$ is equal to 0.85 $cm^3\cdot K\cdot mol^{-1}$, the expected value for two magnetically isolated spin doublets. Upon cooling, the value of $\chi_M T$ increases, attaining a maximum at 3.5 K and then decreasing slightly further. This behaviour is typical of a ferromagnetically coupled dinuclear copper(II) complex, the small decrease of $\chi_M T$ in the low temperature range being due to weak intermolecular magnetic interactions.

The susceptibility data of **4** were analysed through a simple Bleaney−Bowers expression[44] for two magnetically interacting local spin doublets derived from the Hamiltonian $\hat{H} = -J\,\hat{S}_1\cdot\hat{S}_2$ ($\hat{S}_1 = \hat{S}_2 = 1/2$) with the inclusion of a θ parameter to account for the intermolecular interactions. Least-squares best-fit results are: $J = +9.3\ cm^{-1}$, $g = 2.12$, $\theta = -0.08$ K and $R = 1.8 \times 10^{-6}$ (R is the agreement factor defined as $\Sigma_i[(\chi_M T)_{obsd.}(i) - (\chi_M T)_{calcd.}(i)]^2/$

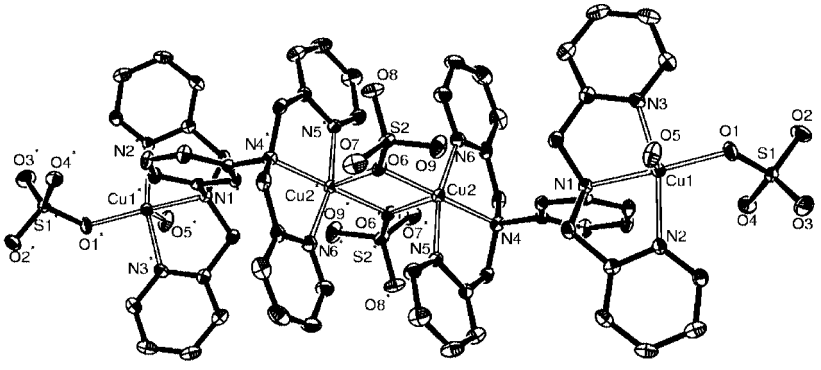

Figure 4. ORTEP representation (30% probability displacement ellipsoids) of **3** (hydrogen atoms are omitted for clarity)

 © 2004 Wiley-VCH Verlag GmbH & Co. KGaA, Weinheim

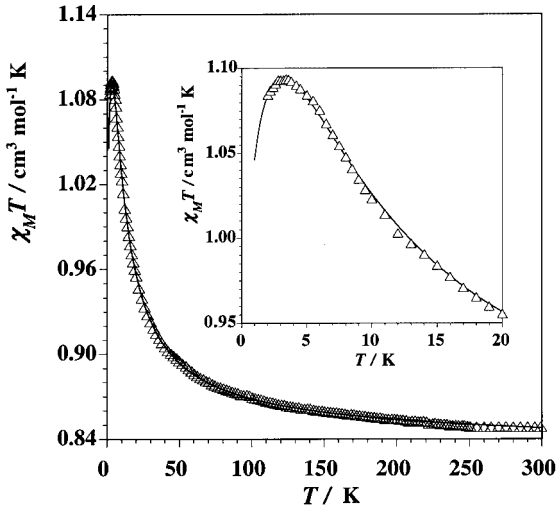

Figure 5. Thermal variation of $\chi_M T$ for **4**: (△) experimental data; (−) best fit (see text). The inset shows the maximum of $\chi_M T$ in the low-temperature region (applied magnetic field of 0.1 T)

$\Sigma_i[(\chi_M T)_{obsd.}(i)]^2$). The theoretical curve (solid line in Figure 5) fits the experimental data well as indicated by the low value of the agreement factor. The magnetisation versus H plot up to 5 T (maximum available magnetic field with our SQUID) at 2 K (Figure 6) tends to a saturation value of ca. 2.1 BM as expected for a $S = 1$ spin state with $g = 2.12$.

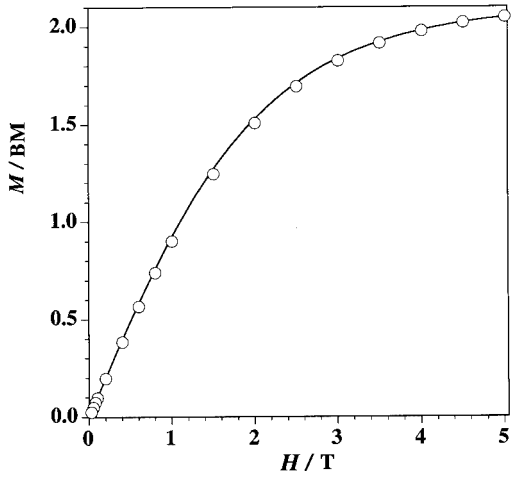

Figure 6. M versus H plot at 2 K for **4**: (o) experimental data; (–) Brillouin function for an $S = 1$ spin state with $g = 2.12$

The EPR spectrum of **4** in methanol (Figure 7) was recorded at X-band frequency at 100 K to elucidate further the nature of the magnetic coupling. The spectrum shows a seven line splitting pattern in the $g_{||}$ region, with the 1:2:3:4:3:2:1 intensity pattern characteristic of a coupled dinuclear Cu^{II} system. A similar signal, but with much lower intensity, due to the forbidden $\Delta M = \pm 2$ state was observed around 1500 G. The observed half-field signal confirms the presence of a $Cu^{II}-Cu^{II}$ triplet state. No changes in the positions of the signals were observed in this spectrum when working at 5 K.

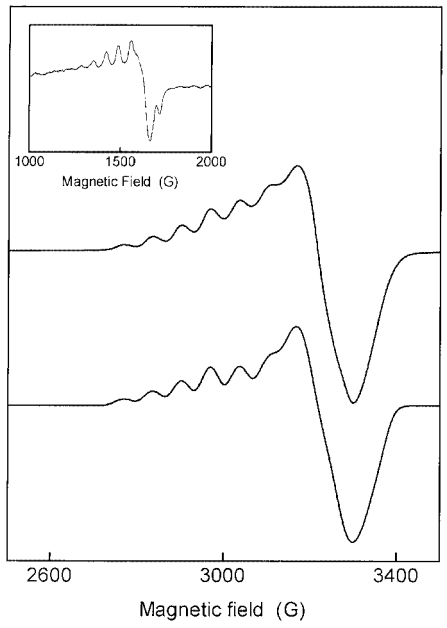

Figure 7. Top: Measured EPR spectrum of **4** in methanol/water; Bottom: Simulated spectrum. The inset shows the measured EPR spectrum at half-field

Magnetic susceptibility measurements of **2** were problematic. A large crystal, which was taken out of the mother liquor, was investigated immediately and no magnetic coupling could be detected during the magnetic measurements. This behaviour changed when the crystal became dry with a ferromagnetic coupling of ca. $J = +9.1$ cm^{-1} observed. Ferromagnetic coupling was observed when smaller crystals were used which seemed to loose water molecules when a vacuum was applied during the magnetic measurements. Most likely, carboxylate-assisted water loss occurs and the structural change associated with this process [carboxylate bridge between Cu(1) and Cu(2)] would lead to a 1,3-tbpd-bridged dicopper(II) fragment very close in nature to that observed for **4**, the magnetic coupling of the anhydrous phase of **2** being essentially identical to that of **4**.

EPR measurements of **2** were unsuccessful in providing a complete description of the magnetic behaviour. The EPR spectrum of the pure green crystals dissolved in methanol demonstrated that at least a mixture of three species exists under these conditions. This is similar to our findings during the structural characterisation of the complexes, where from one solution three different complexes were obtained. Clear changes in the EPR spectra were observed by adding sodium perchlorate or sodium acetate indicating the presence of equilibria in solution. Even though no "clean" EPR spectrum could be measured for **2**, we observed that no triplet state at half field was detected under the same conditions as for **4**, in agreement with the magnetic susceptibility measurements of the large crystal. Therefore, it is clear that none of the acetate complexes in methanolic solutions [most likely species consisting of differing amounts of acetate and water molecules coordinated to the copper(II)

 © 2004 Wiley-VCH Verlag GmbH & Co. KGaA, Weinheim

ions as shown in Figure 2 and 3] provide a magnetic exchange pathway for ferromagnetic coupling.

Magnetic susceptibility measurements of **3** failed to provide any information that magnetic coupling between the copper(II) ions in this complex takes place. **3** showed typical normal magnetic behaviour of four magnetically isolated copper(II) ions and the data followed a Curie law. This finding is the same as the findings obtained for $[Cu(HL)(SO_4)]_2$ where no magnetic exchange phenomena were detected.[39] EPR spectra of **3** could not be obtained because the complex is insoluble in methanol and those performed in water or methanol/water mixtures were not well resolved.

The number of ferromagnetically coupled dinuclear copper(II) complexes is small when compared to that of antiferromagnetically coupled ones.[1,3,32,34,45–52] Herein, different bridging groups were found to provide a magnetic exchange pathway for ferromagnetic coupling in dinuclear copper(II) complexes. However, in all these cases (with the exception of a related complex reported recently[21]) the distance between the two copper(II) ions is much less than 5.87 Å as in **4**. Moreover, magnetic exchange coupling over large distances is often weak and antiferromagnetic.[3,6,53,54]

Examining the structure of **4** (Figure 1), two possible exchange pathways could be operative, one involving the phenylenediamine unit and the other involving the perchlorate bridge. The latter pathway is ruled out taking into account that the perchlorate oxygen is axially coordinated to the copper(II) ion [2.39 Å for Cu–O(perchlorate)].[23] As the unpaired electron of the copper(II) ion is delocalised only in the four short equatorial bonds, it is clear that the spin density on the perchlorate oxygen should be very small. A similar conclusion was reached by Murray and coworkers for the perchlorate bridged complex $[Cu_2L^1(ClO_4)_2]\cdot 2H_2O$ [L^1 = *N*-(2-pyridinyl)acetoacetamide].[55] Furthermore, from the X-ray structure data of **4** the intermolecular exchange interaction can be excluded: the shortest intermolecular copper–copper distance is 8.67 Å, with no ligand present which could provide a possible exchange pathway. Consequently, the exchange pathway involved in the ferromagnetic coupling observed in **4** is operating through the *meta*-phenylenediamine bridge. In contrast to **4**, complexes with either a *para*-phenylenediamine (pd) bridge as in $[(tren)Cu(pd)Cu(tren)]^{4+}$[56,57] [tren = tris(2-aminoethyl)amine], or the dinuclear copper(II) complex of the *para* homologue of 1,3-tpbd, $[Cu_2(1,4\text{-tpbd})(H_2O)_4](S_2O_6)_2$ ($J = -15.56$ cm^{-1}),[58] show weak antiferromagnetic coupling.

The relatively weak exchange coupling of the unpaired electrons of the copper(II) ions in **4** is expected since the superexchange pathway, attributed to magnetic exchange coupling interactions, is most often described as operating via the sigma bond framework. In the case of $[Cu_2(1,4\text{-tpbd})(H_2O)_4](S_2O_6)_2$ the pathway is seven bonds long. A comparison of the magnetic coupling observed in $[Cu_2(1,4\text{-tpbd})(H_2O)_4](S_2O_6)_2$ with the magnetic coupling observed in **4** provides a demonstration of the spin-polarisation mechanism between paramagnetic ions via an aromatic organic bridging group. Ferromagnetism is predicted in cases where there is an odd number of bridging atoms and antiferromagnetic exchange coupling with an even number of bridging atoms. With five atoms between the copper(II) ions in **4**, the σ framework is one bond shorter than that in $[Cu_2(1,4\text{-tpbd})(H_2O)_4](S_2O_6)_2$. The two SOMOs involved in **4** are almost perpendicular to the phenyl ring and the unpaired electrons in the $d_{x^2-y^2}$ orbitals of both copper(II) ions can interact via this pathway. Thus the nature of the exchange coupling observed in these two complexes (ferro- in **4** and antiferromagnetic in $[Cu_2(1,4\text{-tpbd})(H_2O)_4](S_2O_6)_2$] is expected using this model.

In order to interpret the ferromagnetic interaction present in **4**, DFT calculations were performed (see paragraph of Computational Methodology in the Exp. Sect.)[23] on the model systems depicted in Figure 8 (**I**–**IV**), where the donor nitrogen atoms of 1,3-tpbd have been replaced by ammonia molecules (model **IV** corresponds to the complex **4**).

In the four models, the unpaired electron on each copper(II) ion (that is the SOMO) lies in the basal plane of the

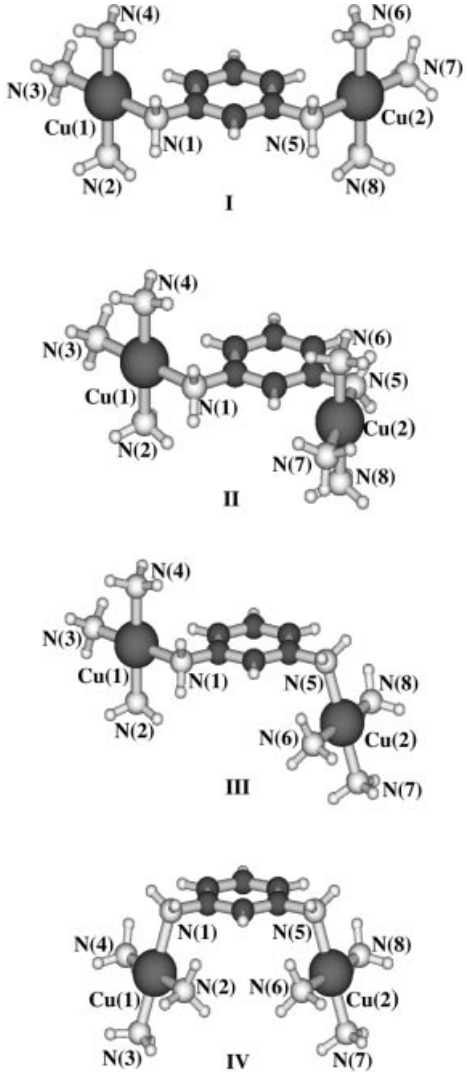

Figure 8. Model systems (**I**–**IV**) of dinuclear copper(II) complexes which were used to carry out the DFT type calculations (see text)

 © 2004 Wiley-VCH Verlag GmbH & Co. KGaA, Weinheim

metal ion [comprising of atoms N(1), N(2), N(3), and N(4) for Cu(1) and N(5), N(6), N(7), and N(8) for Cu(2)]. The orientation of the two SOMOs with respect to the phenylenediamine plane is gradually varied in **I**−**IV** in such a manner that the exchange interaction is transmitted through either pure σ (**I** and **II**) or π (**IV**) pathways, whereas **III** is a mixed σ-π type. The calculated values of *J* for models **I**−**IV** are −1.7, −0.1, +0.6 and +7 cm^{-1}, respectively.

The analysis of the trend for the observed *J* values shows that the magnetic interaction is weak and antiferromagnetic in **I** and **II**, with that of **I** being somewhat larger. The SOMOs in these models are perpendicular to the plane of the phenylenediamine plane, but they differ in their conformation: *anti-anti* in **I** versus *anti-syn* in **II**. The σ in-plane overlap between the SOMOs of Cu(1) and Cu(2), through the long pathway Cu(1)−N(1)−C−C−C−N(5)−Cu(2) in both models, is expected to be weak and poorer in the case of **II** because of its *anti-syn* configuration. Since the antiferromagnetic interaction in a dinuclear copper(II) complex is proportional to the square of the overlap integral between the SOMOs,[56,57] the value of the antiferromagnetic coupling in **I** and **II** is expected to be very small and weaker for **II**. In the case of **III** the SOMO of Cu(2) lies below the plane of the phenylenediamine plane, whereas that of Cu(1) remains unchanged. In this situation, although the set of atoms involved in the exchange pathway is the same as in **I** and **II** [Cu(1)−N(1)−C−C−C−N(5)−Cu(2)], the spin density on N(1) is of a σ type whereas that on N(5) is of a π type. Consequently, a zero overlap between the SOMOs will result (case of accidental orthogonality) and a ferromagnetic coupling interaction is expected. This coupling has to be small because of the extended bridging pathway involved.[56,57] In the case of model **IV** the two SOMOs, being perpendicular to the phenylenediamine plane, lie below this plane. The spin density on the N(1) and N(5) amine nitrogens is of the π type. The DFT calculations for this model indicate a ground triplet spin state lying below the excited singlet spin state. The calculated value of *J* for **IV** (+7 cm^{-1}) agrees well with the experimental value obtained for **4** from the fit of the susceptibility data ($J = +9.3\ cm^{-1}$). To qualitatively understand this result, a focus on the nature of the singly occupied molecular orbitals (SOMOs) depicted in Figure 9 (a) is helpful.

The SOMOs are composed of the in-phase and out-of-phase combinations of the 3d orbitals of the copper(II) ions with two π-type nonbonding molecular orbitals of appropriate symmetry of the *meta*-phenylenediamine unit. In these SOMOs there is an antibonding interaction between the $d_{x^2-y^2}$ orbital of the copper(II) ion and the p_z atomic orbital of the nitrogen atoms of the bridging ligand. This interaction involves: i) an energy gap between the two SOMOs following the rules formulated by Kanamori and Goodenough or Kahn's model.[3,8−10] Since the orbitals of the ligands involved in the building of these SOMOs are of a non-bonding character and, consequently, similar energies, and since the electronic densities on the nitrogen atoms are also similar in both orbitals, the two resultant SOMOs

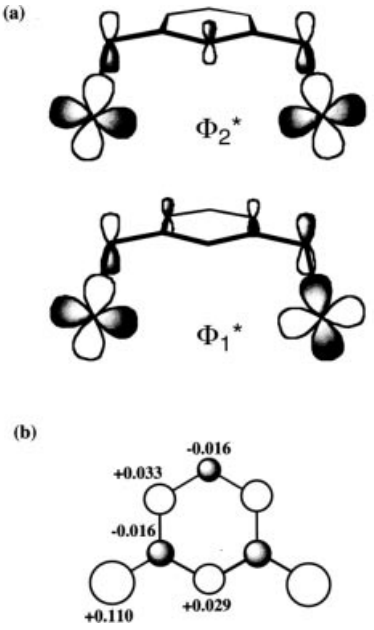

Figure 9. Schematic representation of (a) the two SOMOs and (b) the spin density distribution on the bridge region for **4** on the basis of DFT calculations. Empty and full contours represent positive and negative spin densities, respectively. Calculated average atomic spin densities are presented

(φ_1* and φ_2*) are practically degenerate, with a small energy gap of 347 cm^{-1}; ii) a spin delocalisation from the copper(II) ion to the nitrogen atom of the π system of the bridging skeleton, that accounts for the transmission of the exchange. Thus, the direct overlap between the $d_{x^2-y^2}$ orbital of the metal ion and the π system of the pyridyl ligand allows the unpaired spin of the metal to induce a polarisation of spin on the bridging skeleton (see Figure 9), as occurs in similar compounds described by Ung et al.[20] These systems constitute very interesting cases because of the strong competition between spin delocalisation and spin polarisation, prevailing the alternating spin rule in our case, as shown by experimental data and theoretical calculations.

Conclusion

Complex **4** is an example of a dinuclear copper(II) complex showing ferromagnetic exchange coupling over quite a long distance. The ferromagnetic coupling in **4** is due to the non-coplanarity of the metal coordination planes, leading to a folded structure, placing the two SOMOs in **4** practically perpendicular to the phenyl ring. The symmetry in **4** breaks down if the bridging perchlorate ion is substituted by a non-bridging acetate ion as in **2** and the magnetic interaction vanishes. The magnetic coupling in the dehydrated phase of **2** is essentially identical to that of **4**. Such a fact suggests that the carboxylate-assisted loss of the coordinated water molecule in **2** leads to a carboxylato-bridged species where the carboxylato group mimics the perchlorato group in **4**, leading to a very similar structure. The relative arrangement of the SOMOs of the copper(II) ions, with re-

 © 2004 Wiley-VCH Verlag GmbH & Co. KGaA, Weinheim

spect to the *meta*-phenylenediamine plane, and the fact that the sulfate-oxygen occupies an equatorial position of one copper(II) ion [Cu(2A)] and the axial one at the adjacent copper(II) ion [Cu(2)] account for the lack of magnetic coupling in the tetrameric complex **3**.

Experimental Section

General Remarks: Reagents and solvents used were of commercially available reagent grade quality. 1,3-tpbd and **4** were synthesised as described previously.[23] Electron spin resonance measurements at X-band frequency were obtained using a Bruker EMX-113 spectrometer. Samples in methanol or methanol water (9:1) mixtures were measured at 100 K. Simulation of all EPR spectra was made with the Bruker SimFonia program. Magnetic susceptibility data were collected: a) Over the temperature range 4.2−295 K at an applied magnetic field of 0.56−1.5 T. The measurements were performed using a Faraday-type magnetic balance, equipped with a Cahn D-200 microbalance and a Bruker B-MN 200/60 electromagnet.[59] The sample constituted of microcrystals contained in a quartz basket which was calibrated independently, using $HgCo(SCN)_4$ as calibrant. The diamagnetic correction of the magnetic susceptibility was calculated using Pascal's constants. b) Over the temperature range 2.0−290 K with a Quantum Design SQUID susceptometer and using an applied magnetic field of 0.1 T (compounds **2** and **4**). The susceptometer was calibrated with $(NH_4)_2Mn(SO_4)_2{\cdot}12H_2O$.

Computational Methods: The computational strategy used in the present work has been fully described elsewhere,[60] and it is briefly outlined here. For the evaluation of the coupling constant for each model compound (**I**−**IV**, Figure 8), two separate calculations were carried out using DFT, one for the triplet state and another one for the low-spin, broken symmetry state. The hybrid B3LYP method[61] was been used in the calculations as implemented in GAUSSIAN 98,[61] with all-electron double-ζ basis proposed by Ahlrichs and co-workers except for copper where we have used a triple-ζ basis.[62] Ammonia molecules were used as peripheral ligands in **I**−**IV** and the bond lengths and angles are those of the average values of the real structures. The complete dimeric structures were used in the calculations to estimate the values of *J*.

Caution! *Perchlorate salts are potentially explosive and should be handled with great care. Our preparations were carried out on mmol scale and heating was avoided.*

Mixture of $[Cu_2(1,3\text{-tpbd})(H_2O)(OAc)_2](ClO_4)_2$/$[Cu_2(1,3\text{-tpbd})(H_2O)_2(OAc)](ClO_4)_3$ (1a/1b) and $[Cu_2(1,3\text{-tpbd})(H_2O)_2(OAc)_2](ClO_4)_2$ (2): To a suspension of 1,3-tpbd (250 mg, 0.5 mmol) in methanol (15 mL) was added a solution of $Cu(ClO_4)_2{\cdot}6H_2O$ (195 mg, 0.525 mmol) and $Cu(OAc)_2{\cdot}H_2O$ (104 mg, 0.525 mmol) in water (20 mL). The green solution was stirred for a few minutes, filtered and crystals suitable for X-ray analysis formed after a few days.

$[Cu_2(1,3\text{-tpbd})(H_2O)_2(OAc)_2](ClO_4)_2{\cdot}2H_2O$ (2): To a suspension of 1,3-tpbd (250 mg, 0.5 mmol) in methanol (15 mL) was added a solution of $Cu(OAc)_2{\cdot}H_2O$ (208 mg, 1.05 mmol) in 20 mL of water. After an excess of solid $NaClO_4$ was added to the green solution it was stirred for a few minutes, filtered and left on the shelf. Crystals suitable for X-ray analysis formed after a few days. Yield 267 mg (54%). $C_{34}H_{42}Cl_2Cu_2N_6O_{16}$ (988.7): calcd. C 41.30, H 4.28, N 8.50; found C 40.94, H 4.06, N 8.48.

$[Cu_4(1,3\text{-tpbd})_2(H_2O)_2(SO_4)_4]{\cdot}8H_2O$ (3): To a suspension of 1,3-tpbd (300 mg, 0.63 mmol) in methanol (15 mL) was added a solution of $Cu(SO_4)_2{\cdot}6H_2O$ (315 mg, 1.26 mmol) in water (20 mL). The deep green solution was stirred for a few minutes, filtered and blue crystals suitable for X-ray analysis formed after a few days. Yield 220 mg (40%). $C_{60}H_{76}Cu_4N_{12}O_{26}S_4$ (1763.7): calcd. C 40.86, H 4.34, N 9.53; found C 40.86, H 4.58, N 9.40.

X-ray Crystallographic Study: Crystal data and experimental conditions are listed in Table 2. The molecular structures are illustrated in Figures 2−4. Selected bond lengths and bond angles with standard deviations in parentheses are presented in Table 1. Intensity data were collected on a Siemens SMART 5000 CCD-Diffractometer with graphite monochromated Mo-K_α radiation (λ = 0.71073 Å). The collected reflections were corrected for Lorentz, polarisation and absorption effects.[63] The structures were solved by direct methods and refined by full-matrix-least-squares methods on F^2.[64,65] CCDC-204112, -204113, and -204114 contain the supplementary crystallographic data for this paper. These data can be obtained free of charge at www.ccdc.cam.ac.uk/conts/retrieving.html [or from the Cambridge Crystallographic Data Centre, 12 Union Road, Cambridge CB2 1EZ, UK; Fax: (internat.) + 44-1223/336-033; E-mail: deposit@ccdc.cam.ac.uk].

Acknowledgments

S. S. and W. H. gratefully acknowledge financial support from the Volkswagen-Stiftung and the Deutsche Forschungsgemeinschaft. Furthermore, we thank Dr. Achim Elvers and Prof. Dr. Ulrich Zenneck (University of Erlangen-Nürnberg) for their assistance with the first EPR measurements and helpful discussions. S. S. furthermore thanks Prof. Dr. Rudi van Eldik (University of Erlangen-Nürnberg) for his support of this work. Financial support from the Spanish Ministry of Science and Technology through Project BQ2001−2928 is also acknowledged.

[1] O. Kahn, *Comments, Inorg. Chem.* **1984**, *3*, 105.
[2] O. Kahn, *Angew. Chem. Int. Ed. Engl.* **1985**, *24*, 834.
[3] O. Kahn, *Molecular Magnetism*, Wiley-VCH, Weinheim, **1993**.
[4] M. Kato, Y. Muto, *Coord. Chem. Rev.* **1988**, *92*, 45.
[5] W. E. Hatfield, *Comments, Inorg. Chem.* **1981**, *1*, 105.
[6] K.-S. Bürger, P. Chaudhuri, K. Wieghardt, B. Nuber, *Chem. Eur. J.* **1995**, *1*, 583.
[7] R. D. Willet, D. Gatteschi, O. Kahn, *Magneto-Structural Correlations in Exchange Systems*; Reidel, Dordrecht, **1985**.
[8] J. B. Goodenough, *Phys. Rev.* **1955**, *100*, 654.
[9] J. Kanamori, *J. Phys. Chem. Solids* **1959**, *10*, 87.
[10] P. W. Anderson, *Solid State Phys.* **1963**, *14*, 99.
[11] A. Caneschi, D. Gatteschi, R. Sessoli, *Acc. Chem. Res.* **1989**, *22*, 392.
[12] H. M. McConnell, *J. Chem. Phys.* **1963**, *39*, 1910.
[13] N. Mataga, *Theor. Chim. Acta* **1968**, *10*, 372.
[14] F. Kanno, K. Inoue, N. Koga, H. Iwamura, *J. Phys. Chem.* **1993**, *97*, 13267.
[15] M. Kitano, Y. Ishimaru, K. Inouw, N. Koga, H. Iwamura, *Inorg. Chem.* **1994**, *33*, 6012.
[16] N. Koga, H. Ishimanu, H. Iwamara, *Angew. Chem. Int. Ed. Engl.* **1996**, *108*, 815.
[17] T. Ishida, T. Nogami, *Recent Res. Dev. Pure Appl. Chem.* **1997**, *1*, 1.
[18] H. Oshio, *J. Chem. Soc., Chem. Commun.* **1991**, 240.
[19] A. M. W. C. Thompson, D. Gatteschi, J. A. McCleverty, J. A. Navas, E. Rentschler, M. D. Ward, *Inorg. Chem.* **1996**, *35*, 2701.
[20] V. A. Ung, A. M. W. C. Thompson, D. A. Bardwell, D. Gatteschi, J. C. Jeffery, J. A. McCleverty, F. Totti, M. D. Ward, *Inorg. Chem.* **1997**, *36*, 3447.

 © 2004 Wiley-VCH Verlag GmbH & Co. KGaA, Weinheim

[21] I. Fernández, R. Ruiz, J. Faus, M. Julve, F. Lloret, J. Cano, X. Ottenwaelder, Y. Journaux, M. C. Munõz, *Angew. Chem. Int. Ed.* **2001**, *113*, 3129.
[22] T. Glaser, M. Gerenkamp, R. Fröhlich, *Angew. Chem. Int. Ed.* **2002**, *114*, 3984.
[23] S. Schindler, D. J. Szalda, C. Creutz, *Inorg. Chem.* **1992**, *31*, 2255.
[24] S. Schindler, *Eur. J. Inorg. Chem.* **2000**, 2311.
[25] T. N. Sorrell, M. L. Garrity, D. J. Ellis, *Inorg. Chim. Acta* **1989**, *166*, 71.
[26] N. N. Murthy, M. Mahroof-Tahir, K. D. Karlin, *J. Am. Chem. Soc.* **1993**, *115*, 10404.
[27] M. Mahroof-Tahir, N. N. Murthy, K. D. Karlin, N. J. Blackburn, S. N. Shaikh, J. Zubieta, *Inorg. Chem.* **1992**, *31*, 3001.
[28] M. Mahroof-Tahir, K. D. Karlin, *J. Am. Chem. Soc.* **1992**, *114*, 7599.
[29] R. Hernández-Molina, A. Mederos, P. Gili, S. Domínguez, F. Lloret, J. Cano, M. Julve, C. Ruiz-Pérez, X. Solans, *J. Chem. Soc., Dalton Trans.* **1997**, 4327.
[30] S. Domínguez, A. Mederos, P. Gili, A. Rancel, A. E. Rivero, F. Brito, F. Lloret, X. Solans, C. Ruiz-Pérez, M. L. Rodríguez, I. Brito, *Inorg. Chim. Acta* **1997**, *255*, 367.
[31] T. N. Sorrell, C. O′Connor, O. P. Anderson, J. H. Reibenspies, *J. Am. Chem. Soc.* **1985**, *107*, 4199.
[32] V. McKee, M. Zvagulis, J. V. Dagdigian, M. G. Patch, C. A. Reed, *J. Am. Chem. Soc.* **1984**, *106*, 4765.
[33] P. K. Coughlin, S. J. Lippard, *J. Am. Chem. Soc.* **1984**, *106*, 2328.
[34] G. Christou, S. P. Perlepes, E. Libby, K. Folting, J. C. Huffmann, R. J. Webb, D. N. Hendrickson, *Inorg. Chem.* **1990**, *29*, 3657.
[35] M. Vaidyanathan, R. Viswanathan, M. Palaniandavar, T. Balasubramanian, P. Prabhaharan, T. P. Muthiah, *Inorg. Chem.* **1998**, *37*, 6418.
[36] Y. Nishida, M. Takeuchi, K. Takahashi, S. Kida, *Chem. Letters* **1983**, 1815.
[37] J. A. Halfen, W. B. Tolman, *J. Am. Chem. Soc.* **1994**, *116*, 5475.
[38] H. Endres, D. Nothe, E. Rossato, W. E. Hatfield, *Inorg. Chem.* **1984**, *23*, 3467.
[39] A. G. Bingham, H. Bögge, A. Müller, E. W. Ainscough, A. M. Brodie, *J. Chem. J. Chem. Soc., Dalton Trans.* **1987**, 493.
[40] D. A. Buckinham, C. R. Clark, J. Simpson, W. T. Robinson, *Inorg. Chem.* **1988**, *27*, 3544.
[41] K. Wieghardt, S. Drueke, P. Chaudhuri, U. Florke, H.-J. Haupt, B. Nuber, J. Weiss, *Z. Naturforsch., Teil B* **1989**, *44*, 1093.
[42] M. A. de Britto, A. Neves, I. Vencato, C. Zucco, V. Drago, K. Giesar, W. Haase, *J. Braz. Chem. Soc.* **1997**, *8*, 443.
[43] L. K. Thompson, X. Zhiqiang, A. E. Goeta, J. A. K. Howard, H. J. Clase, D. O. Miller, *Inorg. Chem.* **1998**, *37*, 3217.
[44] B. Bleaney, K. Bowers, *Proc. Roy. Soc., Sect. A* **1952**, *214*, 451.
[45] A. M. Greenaway, C. J. O′Connor, J. W. Overman, E. Sinn, *Inorg. Chem.* **1981**, *20*, 1508.
[46] A. K. Gregson, N. T. Moxon, *Inorg. Chem.* **1982**, *21*, 3464.
[47] A. L. van den Brenk, K. A. Byriel, D. P. Fairlie, L. R. Gahan, G. R. Hanson, C. J. Hawkins, A. Jones, C. H. L. Kennard, B. Moubaraki, K. Murray, *Inorg. Chem.* **1994**, *33*, 3549.
[48] Y. Zang, Z. Yin, G. Wang, C. Zeng, A. Dai, Z. Zhou, *Inorg. Chem.* **1990**, *29*, 560.
[49] G. Kolks, S. J. Lippard, J. V. Waszczak, *J. Am. Chem. Soc.* **1980**, *102*, 4832.
[50] J. F. Villa, W. E. Hatfield, *J. Chem. Phys.* **1971**, *55*, 4758.
[51] J. F. Villa, W. E. Hatfield, *Inorg. Chem.* **1971**, *10*, 2038.
[52] P. Illiopoulos, K. S. Murray, R. Robson, J. Wilson, G. A. Williams, *J. Chem. Soc., Dalton Trans.* **1987**, 1585.
[53] R. Veit, J. J. Girerd, O. Kahn, F. Robert, Y. Jeannin, *Inorg. Chem.* **1986**, *25*, 4175.
[54] R. Vicente, J. Ribas, S. Alvarez, A. Segui, X. Solanz, M. Verdaguer, *Inorg. Chem.* **1987**, *26*, 4004.
[55] P. Illiopoulos, G. D. Fallon, K. S. Murray, *J. Chem. Soc., Dalton Trans.* **1986**, 437.
[56] T. R. Felthouse, E. N. Duesler, D. N. Hendrickson, *J. Am. Chem. Soc.* **1978**, *100*, 618.
[57] T. R. Felthouse, D. N. Hendrickson, *J. Am. Chem. Soc.* **1978**, *17*, 2636.
[58] T. Buchen, A. Hazell, L. Jessen, C. J. McKenzie, L. Preuss Nielson, J. Z. Pedersen, D. Schollmeyer, *J. Chem. Soc., Dalton Trans.* **1997**.
[59] S. Gehring, P. Fleischhauer, H. Paulus, W. Haase, *Inorg. Chem.* **1993**, *32*, 54.
[60] E. Ruiz, P. Alemany, S. Alvarez, J. Cano, *J. Am. Chem. Soc.* **1997**, *119*, 1297.
[61] A. D. Becke, *J. Chem. Phys.* **1993**, *98*, 5648.
[62] A. Schaefer, H. Horn, R. Ahlrichs, *J. Chem. Phys.* **1992**, *97*, 2571.
[63] Siemens Area Detector Absorption Correction, Siemens.
[64] G. M. Sheldrick, *SHELX-97*, University of Göttingen, **1997**.
[65] L. Zsolnai, *XPMA*, University of Heidelberg, **1997**.

Received July 1, 2003
Early View Article
Published Online November 4, 2003

 © 2004 Wiley-VCH Verlag GmbH & Co. KGaA, Weinheim

Tuning the Magnetic Properties of a Dinuclear Copper Complex: From Ferromagnetic to Antiferromagnetic Coupling

Simon P. Foxon,[a] Olaf Walter,[b] Robert Koch,[c] Holger Rupp,[c] Paul Müller,[c] and Siegfried Schindler*[a]

Keywords: Magnetism / Copper / Azides / Dinuclear complexes

A novel structural motif in oxalate bridged copper(II) complexes has been prepared namely a metallamacrocyclic compound of the dinucleating ligand 1,3-bis[bis(2-pyridylmethyl)-amino]benzene (= 1,3-tpbd). It could be demonstrated that the magnetic properties of copper(II) complexes of the 1,3-tpbd ligand can be adjusted from weakly ferromagnetic (J = +9.3 cm^{-1}) to strongly antiferromagnetic [J = –366(9) cm^{-1}] by variation of the additional ligands (e.g. perchlorate, azide, oxalate etc.).

(© Wiley-VCH Verlag GmbH & Co. KGaA, 69451 Weinheim, Germany, 2004)

Introduction

We have previously demonstrated that the ligand 1,3-tpbd {tpbd = 1,3-bis[bis(2-pyridylmethyl)amino]benzene}, a derivative of 1,3-phenylenediamine, provides a rigid structural framework in which two copper(I) or copper(II) ions can bind in close proximity to one another.[1] A magnetic study on the structurally characterised perchlorate bridged dinuclear copper(II) complex $[Cu_2(1,3\text{-tpbd})(H_2O)_2(ClO_4)_3](ClO_4)$ (**1**, Figure 1) showed that a significant ferromagnetic coupling (J = +9.3 cm^{-1}, the Hamiltonian being defined as $\mathbf{H} = -J\mathbf{S}_1\cdot\mathbf{S}_2$) mediated by the phenylenediamine unit could be observed[2] and the intramolecular Cu···Cu distance is 5.873(1) Å.[1] Ferromagnetic coupling has also been reported recently for a related dinuclear complex.[3] The ferromagnetic coupling following the spin polarisation mechanism was successfully interpreted for both complexes using density functional theory (DFT) calculations.[2,3]

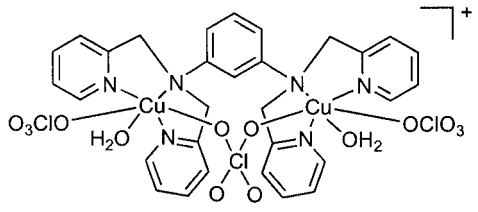

Figure 1. Schematic representation of the cation of **1**

In contrast, no magnetic exchange coupling was observed when the perchlorate group in **1** was substituted with acetate {which did not bridge the two copper(II) ions} or sulfate {the sulfate ion acting as both a terminal ligand and a one-atom bridging ligand in the tetranuclear complex $[Cu_4(1,3\text{-tpbd})_2(H_2O)_2(SO_4)_4]$}.[2]

Besides acetate, azide, and oxalate are typical multidentate ligands employed in copper(II) chemistry in order to achieve strong magnetic coupling between two metal centres.[4] Polynuclear copper(II) complexes with bridging azide ligands have received much attention due to the diverse range of their structural and magnetic properties.[4] Interest originates from the variety of coordination modes the azide anion can exhibit. It can act either as a terminal ligand or as a bridging ligand. For the latter case, three different types of structure may be observed: N_3^- can bridge through just one of the terminal nitrogen atoms (μ-1,1)[5–16] or through both terminal nitrogen atoms (μ-1,3) either symmetrically or asymmetrically.[5,17–23] The magnetic behaviour of the respective modes of coordination has been well established. The μ-1,1 mode mediates strong ferromagnetic exchange interactions and the symmetric μ-1,3 mode mediates strong antiferromagnetic exchange interactions.

During the last 20 years extensive theoretical and experimental studies by Kahn[9,24,25] and others[26,27] have been carried out in order to understand the exceptional ability of the oxalate bridge in mediating very weak to quite strong antiferromagnetic coupling between copper(II) centres separated by more than 5.5 Å. Kahn et al. elegantly demonstrated that in a series of dinuclear copper(II) μ-oxalate

[a] Institut für Anorganische und Analytische Chemie, Justus-Liebig-Universität,
Heinrich-Buff-Ring 58, 35392 Gießen, Germany
Fax: (internat.) + 49-641-9934149
E-mail: siegfried.schindler@anorg.chemie.uni-giessen.de
[b] ITC-CPV, Forschungszentrum Karlsruhe GmbH, ITC-CPV, Postfach 3640, 76021 Karlsruhe, Germany
[c] Physikalisches Institut III, Universität Erlangen-Nürnberg, Erwin-Rommel-Str. 1, 91058 Erlangen, Germany

 © 2004 Wiley-VCH Verlag GmbH & Co. KGaA, Weinheim **DOI: 10.1002/ejic.200300456**

complexes it was possible to "tune" the singlet-triplet energy gap (2J) over a wide range ($0 < 2J < 400$ cm^{-1}) by keeping the [Cu(μ-oxalate)Cu]$^{2+}$ core constant and varying only the nature of the amine ligands.[28]

We decided to exploit the fact that the ligand 1,3-tpbd is capable of binding two metal ions at a fixed distance in order to prepare a novel dinuclear copper(II) bridging oxalate complex. It was envisaged that the 1,3-tpbd backbone would "fix" the [Cu(μ-oxalate)Cu]$^{2+}$ core in a rigid planar conformation leading to a strong antiferromagnetic interaction between the two copper(II) centres mediated by the oxalate bridge. Herein, we report the synthesis, structural characterisation, and magnetic behaviour of 1,3-tpbd copper(II) complexes with azide and oxalate as co-ligands.

Results and Discussion

Crystal Structure of [Cu_2(1,3-tpbd)(N_3)$_4$] (2)

The mode of azide binding which would occur in the copper(II) complex of 1,3-tpbd [Cu_2(1,3-tpbd)(N_3)$_4$] (**2**) was not at all predictable. We assumed the azide ligands would most likely adopt an intra- or intermolecular bridging mode (the common case). A structural determination of **2** revealed, however, two terminal azide anions coordinated to each copper(II) ion (the less common case). An ORTEP[29] representation of the crystal structure of **2** is shown below in Figure 2. Crystallographic data for **2** are presented in Table 2 with selected bond lengths and angles in Table 1.

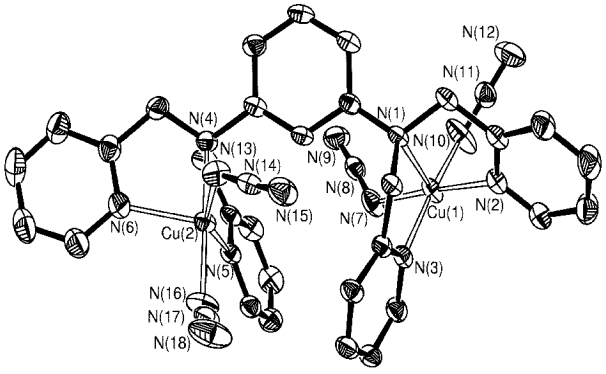

Figure 2. ORTEP[29] representation (50% probability displacement ellipsoids) of **2**. Hydrogen atoms omitted for clarity

Each copper(II) ion in **2** is five-coordinate [intramolecular separation Cu(1)···Cu(2) = 6.160(2) Å] being ligated by five nitrogen donor atoms, three nitrogen atoms from the 1,3-tpbd ligand and two azide ions. The coordination geometry around Cu(1) and Cu(2) is best described as distorted square-based pyramidal, with Cu(1) adopting a closer to ideal square-based pyramidal geometry than Cu(2). For Cu(1) the trigonality index parameter[30] $\tau = 0.06$ [where $\tau = (\beta - \alpha)/60$, with α and β being the two largest coordination angles around the metal centre. For ideal square-pyramidal geometry $\tau = 0$, while for perfect trigonal-bipyramidal geometry $\tau = 1$]. The equatorial plane around Cu(1) consists of the pyridyl donor atoms N(2) and N(3) of the ligand and the azide donor atoms N(7) and N(10) [Cu(1)−N(2) = 2.036(2) Å, Cu(1)−N(3) = 2.044(2) Å, Cu(1)−N(7) = 1.955(2) Å, Cu(1)−N(10) = 1.975(2) Å]. Occupying the apical coordination site is the tertiary amine atom N(1) of the ligand [Cu(1)−N(1) = 2.474(2) Å]. Around Cu(2) the coordination geometry is significantly distorted from square pyramidal towards trigonal bipyramidal (τ[30] = 0.36). The apical coordination site of Cu(2) however is occupied by the pyridyl donor atom N(6) of the ligand [Cu(2)−N(6) = 2.176(2) Å] and not by the tertiary amine atom N(4), which is in contrast to what is evident for Cu(1). The equatorial plane around Cu(2) consists of

Table 1. Selected bond lengths [Å] and angles [°] in **2** and **3**

2			
Cu(1)−N(1)	2.474(2)	Cu(2)−N(4)	2.138(2)
Cu(1)−N(2)	2.036(2)	Cu(2)−N(5)	2.029(2)
Cu(1)−N(3)	2.044(2)	Cu(2)−N(6)	2.176(2)
Cu(1)−N(7)	1.955(2)	Cu(2)−N(13)	1.979(2)
Cu(1)−N(10)	1.975(2)	Cu(2)−N(16)	1.959(2)
Cu(1)···Cu(2)	6.160(2)		
N(1)−Cu(1)−N(2)	75.08(6)	N(2)−Cu(1)−N(3)	90.88(6)
N(1)−Cu(1)−N(3)	77.42(5)	N(2)−Cu(1)−N(7)	176.16(6)
N(1)−Cu(1)−N(7)	105.04(7)	N(3)−Cu(1)−N(10)	172.58(8)
N(1)−Cu(1)−N(10)	110.00(8)		
3			
Cu(1)···N(1)	2.509(2)	Cu(1)−O(1)	2.013(2)
Cu(1)−N(2)	2.026(3)	Cu(1)−O(2)	1.996(2)
Cu(1)−N(3)	2.027(3)	Cu(1)−O(5)	2.242(2)
Cu(1)···Cu(2)	5.188(2)	C(31)−C(32)	1.540(4)
N(2)−Cu(1)−N(3)	99.6(1)	N(3)−Cu(1)−O(2)	87.73(9)
N(2)−Cu(1)−O(1)	88.07(9)	N(3)−Cu(1)−O(5)	91.54(9)
N(2)−Cu(1)−O(2)	163.38(9)	O(1)−Cu(1)−O(2)	83.21(9)
N(2)−Cu(1)−O(5)	92.32(9)	O(1)−Cu(1)−O(5)	94.79(8)
N(3)−Cu(1)−O(1)	169.88(9)	O(2)−Cu(1)−O(5)	102.46(8)

Table 2. Crystallographic data for **2** and **3**

	2	**3**
Formula	$C_{30}H_{28}Cu_2N_{18}$	$C_{41}H_{49}Cl_2Cu_2N_9O_{15}$
M	767.78	1105.87
Crystal system	triclinic	triclinic
Space group	$P\bar{1}$	$P\bar{1}$
a [Å]	9.0968(7)	12.6529(7)
b [Å]	12.769(1)	12.9553(8)
c [Å]	15.804(2)	15.5846(9)
α [°]	66.918(1)	78.084(1)
β [°]	81.261(1)	67.703(1)
γ [°]	74.051(1)	81.976(1)
U [Å^3]	1621.7(2)	2307.4(2)
Z	2	2
D_c [g·cm^{-3}]	1.572	1.592
μ [mm^{-1}]	1.366	1.117
Reflections measured	17240	25012
Unique reflections	7655	11012
R_{int}	0.0195	0.0476
Parameters	460	645
R (F, $F^2 > 2\sigma$)	0.0293	0.0453
R_w (F^2, all data)	0.0814	0.1055

 © 2004 Wiley-VCH Verlag GmbH & Co. KGaA, Weinheim

the tertiary amine atom N(4) and the pyridyl donor atom N(5) of the ligand and the donor atoms N(13) and N(16) of the two azide ligands [Cu(2)−N(4) = 2.138(2) Å, Cu(2)−N(5) = 2.029(2) Å, Cu(2)−N(13) = 1.979(2) Å, Cu(2)−N(16) = 1.959(2) Å]. Cu(2) deviates from the mean plane of the square pyramid towards the apical N(6) by ca. 0.22 Å.

Asymmetric azide stretching vibrations generally occur above 2000 cm^{-1}, and the appearance of more than one band is a good indication that more than one type of azide ligand is present. In the solid state the N_3^- stretching frequency in **2** appears as a sharp band at 2048 cm^{-1}, a value which is in agreement with other structurally and spectroscopically characterised dinuclear copper(II) complexes containing terminal azide ligands.[11,31]

$[Cu_2(1,3\text{-tpbd})(C_2O_4)(DMF)_2](ClO_4)_2\cdot DMF$ (3)

Reacting sodium oxalate with **1** led to the initial isolation of a turquoise coloured precipitate. Recrystallisation of the precipitate by slow diffusion of diethyl ether into a DMF containing solution led to the formation of the dinuclear complex $[Cu_2(1,3\text{-tpbd})(C_2O_4)(DMF)_2](ClO_4)_2\cdot DMF$ (**3**). An ORTEP[29] representation of the crystal structure of the cation of **3** is shown below in Figure 3. Crystallographic data for **3** are presented in Table 2 and selected bond lengths and angles are in Table 1.

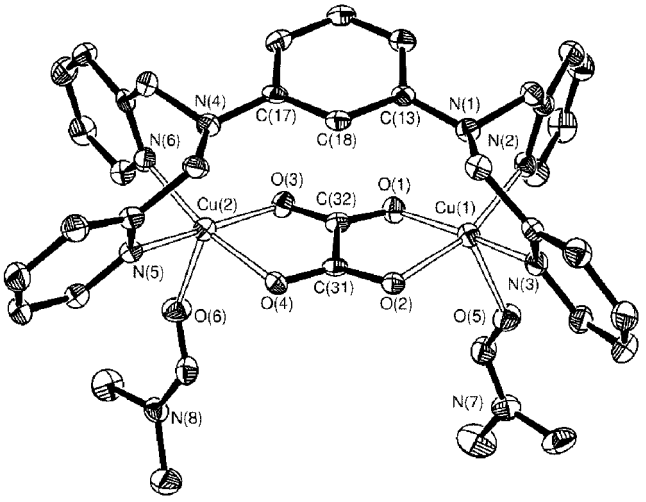

Figure 3. ORTEP[29] representation (50% probability displacement ellipsoids) of **3**. Hydrogen atoms and one DMF solvent molecule omitted for clarity

The cation of **3** consists of two copper(II) ions [intramolecular separation Cu(1)···Cu(2) = 5.188(2) Å] with the copper(II) ions being bridged by the bis-bidentate oxalate ion. Both the copper(II) centres are best described as having a "4+1" square pyramidal coordination geometry and the geometrical parameters around each copper(II) centre do not differ significantly from one another. The basal plane around Cu(1) consists of the two pyridine nitrogen atoms of the ligand [Cu(1)−N(2) = 2.026(3) Å and Cu(1)−N(3) = 2.027(3) Å] and two oxygen atoms of the oxalate anion [Cu(1)−O(1) = 2.013(2) Å and Cu(1)−O(2) = 1.996(2) Å]. A DMF solvent molecule occupying the apical site [Cu(1)−O(5) = 2.242(2) Å] completes the coordination environment around Cu(1). The tertiary amine nitrogen N(1) forms a very weak interaction with Cu(1) [Cu(1)···N(1) = 2.509(2) Å]. This is most likely the reason for the much smaller distance between the copper(II) ions in **3** compared with **1** or **2**. The dimensions of the oxalate anion show no abnormalities and are typical of those found in other structurally characterised copper(II) complexes. The basal planes around Cu(1) and Cu(2) do not lie perfectly coplanar with the plane containing the oxalate bridge: the oxalate bridge is slightly "puckered", giving rise to a "boat type" conformation.[27] The oxalate anion and the central aromatic ring of the 1,3-tpbd moiety are not coplanar with one another and, moreover, the oxalate anion does not lie directly beneath the aromatic ring. However, the central aromatic ring carbon atoms C(13), C(17), and C(18) make several close contacts with the oxalate anion: [C(13)···O(1) = 3.333 Å, C(18)···C(31) = 3.018 Å, C(18)···C(32) = 3.171 Å, and C(17)···O(3) = 3.262 Å].

Many structurally characterised oxalate bridged complexes are known: a search of the Cambridge Structural Database[32] for dinuclear copper(II) complexes of amine ligands containing a bridging bis-bidentate oxalate unit reveals there to be between 40 and 50 such structures.[28,33−37]

However, in contrast to these compounds, complex **3** presents a novel structural motif in which the two copper(II) ions are furthermore bridged by the dinucleating 1,3-tpbd ligand, thus leading to a metallamacrocyclic complex when oxalate is coordinated. There are only two other examples of structurally characterised dinuclear copper(II) complexes that use oxalate only as an additional bridging ligand.[38,39] However, these complexes contain macrocyclic ligands prior to their binding to oxalate and the magnetic properties of these complexes have not been described.

Magnetic Measurements

Measurements of the magnetic properties on powder samples of **2** and **3** were performed. A plot of $m\cdot T/B$ vs. temperature for **2** at a magnetic field of 5.5 T showed no maximum which is characteristic of antiferromagnetic coupling and is shown below in Figure 4.

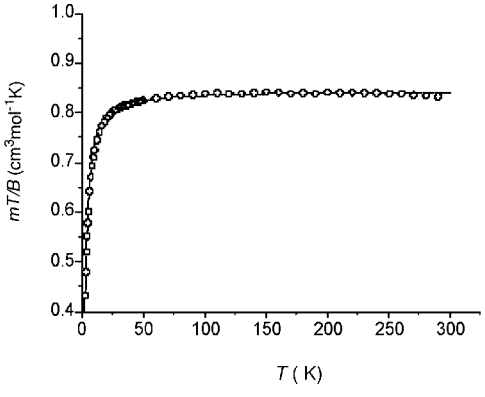

Figure 4. $m\cdot T/B$ vs. temperature of **2**. Circles represent experimental data, the solid line represents the fit

For $T > 50$ K the system behaves like an uncoupled dimer as the signal is constant at a value of 0.8 $cm^3 \cdot mol^{-1} \cdot K$. At low temperatures, the signal decreases with temperature, an indication that the value of $|J|$ is small. Quantitative analysis of the data using the Hamiltonian $H = -J\, \boldsymbol{S}_1 \cdot \boldsymbol{S}_2 + \mu_B g \boldsymbol{S} \cdot \boldsymbol{B}$, where J denotes the exchange coupling parameter, g the Zeeman factor, $\boldsymbol{S}_1$, $\boldsymbol{S}_2$, and $\mathbf{S}$ the Spin Operators for each copper(II) ion and for the coupled system] revealed as a best fit the following parameters: $J = -2.1(4)$ cm^{-1}, $g = 2.10(8)$ with $R = 1.25 \cdot 10^{-5}$ ($R = \{\Sigma[(\chi_m T)_{exp} - (\chi_m T)_{calc}]^2\}/[\Sigma(\chi_m T)^2_{exp}]\}$. As the azide anions do not act as bridging ligands, no suitable magnetic exchange pathway is available between the unpaired electrons of each copper(II) ion. Ferromagnetic coupling is no longer possible because one of the amine nitrogen donor atoms N(1) occupies the axial site of Cu(1) and is no longer in an equatorial position of the complex.

The magnetic behaviour of **3** is shown in Figure 5 as a plot of $\chi_m \cdot T$ vs. temperature, where χ_m denotes the molar susceptibility. The signal decreases with temperature down to 100 K. At lower temperatures the signal vanishes indicating an antiferromagnetic $\mathbf{S} = 0$ ground state. For theoretical analysis the same spin Hamiltonian as above was employed. At 300 K the signal is well below the value expected for two isolated copper(II) ions (0.8 $cm^3 \cdot mol^{-1} \cdot K$) indicating a huge value for $|J|$. The parameters obtained from a best fit obtained from a least-squares analysis are: $J = -366(9)$ cm^{-1}, $g = 2.18(2)$ and $R = 7.3 \cdot 10^{-6}$. The theoretical curve using the above parameters is shown in Figure 5.

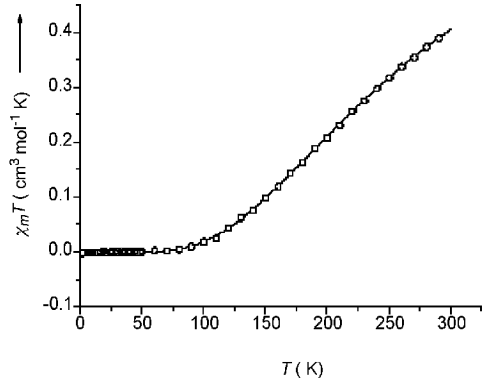

Figure 5. $\chi_m \cdot T$ vs. temperature of **3**. Circles represent experimental data, the solid line represents the fit

In contrast to **1**, ferromagnetic coupling in **3** via a spin polarisation pathway through the phenylenediamine backbone is completely excluded because the tertiary amine nitrogen atoms N(1) and N(4) of the ligand (see Figure 3 above) are not coordinated to the copper(II) ions. However, in contrast to **2**, the bridging oxalate ligand in **3** offers a pathway for strong antiferromagnetic coupling. The J value lies in the expected range for a square pyramidal copper(II) centre, albeit towards the strongest coupling observed for a Cu(ox)Cu complex containing only nitrogen donor ligands. The antiferromagnetic coupling is only slightly smaller than that found in the $[tmen(H_2O)Cu(\mu\text{-}C_2O_4)Cu(H_2O)tmen]^{2+}$ cation ($J = -384.5$ cm^{-1}).[4]

Conclusion

From the results presented herein together with an earlier report we have clearly demonstrated that the magnetic properties of copper(II) complexes of the 1,3-tpbd ligand can be adjusted from weakly ferromagnetic to strongly antiferromagnetic. However normal magnetic behaviour of magnetically isolated copper(II) ions (data following the Curie Law) as well as very weak antiferromagnetic behaviour can also be achieved. Often changes in the magnetic properties of dinuclear copper(II) complexes can be achieved by varying the nature of the ligand, and not the magnetic coupling unit e.g. azide or oxalate.

Experimental Section

General Remarks: The ligand 1,3-tpbd was synthesised as described previously.[1] Reagents and solvents were of commercially available reagent grade quality and were used without further purification. Magnetic susceptibility data for **2** and **3** were collected in the temperature range of 1.8−300 K on a Quantum Design MPMS-7 SQUID magnetometer. Two samples of each compound were investigated. The powder samples (typically 0.5 mg) were mixed with apiezon grease and fixed on a plastic straw. The signal of the grease could be subtracted from the experimental measurements, whereas the signal due to the straw was negligible.

Caution! *The syntheses and procedures described below involve compounds that contain perchlorate and azide ions, which can detonate explosively and without warning. Although we have not encountered any problems with the compounds used in this study, they should be handled with extreme caution.*

$[Cu_2(1,3\text{-tpbd})(N_3)_2]$ (2): 1,3-tpbd (0.100 g, 0.21 mmol) was suspended in acetonitrile (3 cm^3). To this suspension was added $Cu(OAc)_2 \cdot H_2O$ (0.085 g, 0.42 mmol) in water (2 cm^3). The green coloured solution was stirred for a few minutes and sodium azide (0.055 g, 0.84 mmol) in water (2 cm^3) was added dropwise. The solution became dark green. Within the period of a few hours a precipitate had formed which was removed and discarded. The remaining dark green coloured solution was allowed to evaporate slowly at room temperature. Within one week small dark green coloured needles of **2** appeared which were suitable for a single-crystal X-ray structural determination; found C 46.64, H 3.75, N 33.00. $C_{30}H_{28}Cu_2N_{18}$ (767.770) requires C, 46.93, H 3.68, N 32.84%.

$[Cu_2(1,3\text{-tpbd})(C_2O_4)(DMF)_2](ClO_4)_2 \cdot DMF$ (3): 1,3-tpbd (0.100 g, 0.21 mmol) was suspended in methanol (3 cm^3). To this suspension was added $Cu(ClO_4)_2 \cdot 6H_2O$ (0.157 g, 0.42 mmol) in water (2 cm^3). The dark green coloured solution was stirred for a few minutes and sodium oxalate (0.0284 g, 0.21 mmol) in water (2 cm^3) was added dropwise. A turquoise coloured precipitate appeared immediately. The precipitate was filtered, washed with a little water and diethyl ether, and dried (0.178 g, 0.19 mmol, 91%). The blue coloured powder was dissolved in dimethylformamide (2 cm^3). Diethyl ether was allowed to slowly diffuse into the solution and within the period of a few days small light green coloured crystals appeared which were suitable for a single-crystal X-ray structural determination; found C 44.62, H 4.74, N 11.14. $C_{41}H_{49}Cl_2Cu_2N_9O_{15}$ (1105.897) requires C 44.53, H 4.47, N 11.40%. IR (KBr disc): $\tilde{\nu}/cm^{-1}$: 1661 ($\tilde{\nu}_{asym}$OCO oxalate); 1348, 1306 ($\tilde{\nu}_{sym}$OCO oxalate); 774 (δ_{sym}OCO oxalate).

 © 2004 Wiley-VCH Verlag GmbH & Co. KGaA, Weinheim

X-ray Crystallographic Studies: The details of structure solution and refinement are given in Table 2. Cell dimensions and intensity data for **2** and **3** were measured at 200(2) K on a Siemens SMART 1000 CCD diffractometer with graphite-monochromated Mo-K_α radiation ($\lambda = 0.71073$ Å). The collected reflections were corrected for Lorentz, polarisation, and absorption effects. The structures were solved by direct methods and refined by full-matrix least-squares procedures on F^2.[40−42] Anisotropic displacement parameters were refined for all non-hydrogen atoms, and isotropic hydrogen atoms were included with riding model constraints.

CCDC-207005 for **2** and -207004 for **3** contain the supplementary crystallographic data for this paper. These data can be obtained free of charge at www.ccdc.cam.ac.uk/conts/retrieving.html [or from the Cambridge Crystallographic Data Centre, 12 Union Road, Cambridge CB2 1EZ, UK; Fax: (internat.) + 44-1223/336-033; E-mail: deposit@ccdc.cam.ac.uk].

[1] S. Schindler, D. J. Szalda, C. Creutz, *Inorg. Chem.* **1992**, *31*, 2255.
[2] S. P. Foxon, G. Romualdo Torres, O. Walter, J. Z. Pedersen, H. Toftlund, M. Hüber, K. Falk, W. Haase, J. Cano, F. Lloret, M. Julve, S. Schindler, *Eur. J. Inorg. Chem.* **2003**, 335−343.
[3] I. Fernández, R. Ruiz, J. Faus, M. Julve, F. Lloret, J. Cano, X. Ottenwaelder, Y. Journaux, M. C. Muñoz, *Angew. Chem. Int. Ed.* **2001**, *40*, 3039.
[4] O. Kahn, *Molecular Magnetism*, VCH, Weinheim, **1993**.
[5] A. Escuer, M. A. S. Goher, F. A. Mautner, R. Vicente, *Inorg. Chem.* **2000**, *39*, 2107.
[6] P. Manikandan, R. Muthukumaran, K. R. J. Thomas, B. Varghese, G. V. R. Chandramouli, P. T. Manoharan, *Inorg. Chem.* **2001**, *40*, 2378.
[7] L. K. Thompson, S. S. Tandon, F. Lloret, J. Cano, M. Julve, *Inorg. Chem.* **1997**, *36*, 3301.
[8] X. H. Bu, M. Du, Z. L. Shang, R. H. Zhang, D. Z. Liao, M. Shionoya, T. Clifford, *Inorg. Chem.* **2000**, *39*, 4190.
[9] O. Kahn, S. Sikorav, J. Gouteron, S. Jeannin, Y. Jeannin, *Inorg. Chem.* **1983**, *22*, 2877.
[10] G. A. van Albada, M. T. Lakin, N. Veldman, A. L. Spek, J. Reedijk, *Inorg. Chem.* **1985**, *34*, 4910.
[11] S. S. Tandon, L. K. Thompson, M. E. Manuel, J. N. Bridson, *Inorg. Chem.* **1994**, *33*, 5555.
[12] M. F. Charlot, O. Kahn, M. Chaillet, C. Larrieu, *J. Am. Chem. Soc.* **1986**, *108*, 2574.
[13] J. Comarmond, P. Plumeré, J.-M. Lehn, Y. Agnus, R. Louis, R. Weiss, O. Kahn, I. Morgenstern-Badarau, *J. Am. Chem. Soc.* **1982**, *104*, 6330.
[14] R. Cortés, M. K. Urtiaga, L. Lezama, J. I. R. Larramendi, M. I. Arriortua, T. Rojo, *J. Chem. Soc., Dalton Trans.* **1992**, 3685.
[15] K. D. Karlin, J. C. Hayes, J. P. Hutchinson, J. Zubieta, *J. Chem. Soc., Chem. Commun.* **1983**, 376.
[16] S. Sikorav, I. Bkouche-Waksman, O. Kahn, *Inorg. Chem.* **1984**, *23*, 490.
[17] Y. Agnus, R. Louis, R. Weiss, *J. Am. Chem. Soc.* **1979**, *101*, 3381.
[18] F. A. Mautner, M. A. S. Goher, *Polyhedron* **1992**, *11*, 2537.
[19] M. A. S. Goher, F. A. Mautner, *Polyhedron* **1998**, *17*, 1561.
[20] Z. Shen, J. L. Zuo, S. Gao, Y. Song, C. M. Che, H. K. Fun, X. Z. You, *Angew. Chem. Int. Ed.* **2000**, *39*, 3633.
[21] Z. Shen, J. L. Zuo, Z. Yu, Y. Zhang, J. F. Bai, C. M. Che, H. K. Fun, J. J. Vittal, X. Z. You, *J. Chem. Soc., Dalton Trans.* **1999**, 3393.
[22] T. R. Felthouse, D. N. Hendrickson, *Inorg. Chem.* **1978**, *17*, 444.
[23] A. Escuer, M. Font-Bardía, E. Peñalba, X. Solans, R. Vicente, *Inorg. Chim. Acta* **2000**, *298*, 195.
[24] O. Kahn, M. F. Charlot, *Nouv. J. Chim.* **1980**, *4*, 567.
[25] O. Kahn, *Inorg. Chim. Acta* **1982**, *62*, 3.
[26] P. J. Hay, J. C. Thibeault, R. Hoffmann, *J. Am. Chem. Soc.* **1975**, *97*, 4884.
[27] S. Alvarez, M. Julve, M. Verdaguer, *Inorg. Chem.* **1990**, *29*, 4500.
[28] M. Julve, M. Verdaguer, O. Kahn, A. Gleizes, M. Philoche-Levisalles, *Inorg. Chem.* **1983**, *22*, 368.
[29] L. J. Farrugia, *J. Appl. Cryst.* **1997**, *30*, 565.
[30] A. W. Addison, T. N. Rao, J. Reedijk, J. van Rijn, G. C. Verschoor, *J. Chem. Soc., Dalton Trans.* **1984**, 1349.
[31] G. De Munno, M. G. Lombardi, M. Julve, F. Lloret, J. Faus, *Inorg. Chim. Acta* **1998**, *282*, 82.
[32] F. H. Allen, *Acta Crystallogr., Sect. B* **2002**, *58*, 380.
[33] M. Julve, M. Verdaguer, A. Gleizes, M. Philoche-Levisalles, O. Kahn, *Inorg. Chem.* **1984**, *23*, 3808.
[34] R. Vicente, A. Escuer, X. Solans, M. Font-Bardía, *J. Chem. Soc., Dalton Trans.* **1996**, 1835.
[35] T. R. Felthouse, E. J. Laskowski, D. N. Hendrickson, *Inorg. Chem.* **1977**, *16*, 1077.
[36] L. J. Farrugia, S. Lopinski, P. A. Lovatt, R. D. Peacock, *Inorg. Chem.* **2001**, *49*, 558.
[37] I. Castro, J. Faus, M. Julve, A. Gleizes, *J. Chem. Soc., Dalton Trans.* **1991**, 1937.
[38] Q. Lu, J. J. Reibenspies, A. E. Martell, R. J. Motekaitis, *Inorg. Chem.* **1996**, *35*, 2630.
[39] S. Warzeska, R. Krämer, *Chem. Ber.* **1995**, *128*, 115.
[40] Siemens Area Detector Absorption Correction, Siemens.
[41] G. M. Sheldrick, *SHELX-97. Program for the Refinement of Crystal Structures*, University of Göttingen, **1997**.
[42] L. Zsolnai, *XPMA, ZORTEP*, University of Heidelberg, **1997**.

Received July 11, 2003
Early View Article
Published Online November 4, 2003

Mercury−Chalcogenide Clusters: Synthesis and Structure of $[Hg_{10}Te_4(SePh)_{12}(PPhnPr_2)_4]$, $[Hg_{10}Te_4(TePh)_{12}(PPhnPr_2)_4]$ and $[Hg_{34}Te_{16}(SePh)_{36}(PPhnPr_2)_4]$

Andreas Eichhöfer*[a] and Peter Deglmann[b]

Keywords: Cluster compounds / Mercury / Tellurium / Selenium / DFT calculations

The reaction of $HgCl_2$ with $PPhnPr_2$, $Te(SinBu_3)_2$ and $PhESiMe_3$ (E = Se, Te) in DME at –30 °C results in the formation of yellow octahedral crystals of $[Hg_{10}Te_4(SePh)_{12}(PPhnPr_2)_4]$ and $[Hg_{10}Te_4(TePh)_{12}(PPhnPr_2)_4]$ respectively. The molecular structures of the clusters are similar to those of other $[M_{10}Se_4(SePh)_{12}(PR_3)_4]$ (M = Cd, Zn; R = org. group) cluster compounds, but are the first of this type with tellurium as the group 16 metal atom. Dissolution of $[Hg_{10}Te_4(SePh)_{12}(PPhnPr_2)_4]$ in benzene/toluene at 5 °C leads to the formation of the larger cluster $[Hg_{34}Te_{16}(SePh)_{36}(PPhnPr_2)_4]$ which displays a new structure type for group 12–16 cluster molecules. The "$Hg_{34}Te_{16}Se_{36}$" cluster core can be considered as an idealized tetrahedral fragment, 15 Å in diameter, of the cubic sphalerite lattice with a vacancy in the center. Theoretical investigations on the basis of density functional theory (DFT) reproduce the structural data and the measured electronic spectra for this cluster. Additionally we found that formal occupation of the vacancy by a mercury ion would lead to an ionic cluster $[Hg_{35}Te_{16}(SeMe)_{36}(PMe_3)_4]^{2+}$ which should be stable according to the results of the calculations. This suggests that the formation of the vacancy is probably driven by the absence of an appropriate counterion in the reaction which might stabilize such an ionic cluster molecule.

(© Wiley-VCH Verlag GmbH & Co. KGaA, 69451 Weinheim, Germany, 2004)

Introduction

Systematic studies of the size dependent optical and electronic properties of CdSe cluster-molecules show that the quantum confinement effect common with larger CdSe nanocrystals also occurs in these small molecular systems.[1] Synthesis and structural characterization of group 12−16 cluster molecules has mostly focused on ZnS,[2] ZnSe,[3] ZnTe[4] and CdS.[5,6] Chalcogenide cluster compounds with mercury are still rare even though these materials possess interesting properties as bulk- or nano-materials. The alloy $Cd_{1-x}Hg_xTe$ is a well known material in long-wavelength IR detector technologies for example, and HgTe nanoparticles have been proposed as potential amplifiers operating at wavelengths of 1.3 μm and 1.55 μm in telecommunication devices.[7,8] Recent investigations on mercury selenide clusters reveal that the smaller cluster $[Hg_{10}Se_4(SePh)_{12}(PPh_2nPr)_4]$ is converted in benzene to a larger cluster $[Hg_{32}Se_{14}(SePh)_{36}]$.[9,10] In order to extend optical investigations on group 12−16 cluster molecules and to study further the mechanism of structural growth of nanoclusters in this size regime we investigated the synthesis and crystallization of mercury selenide and mercury telluride cluster molecules.

[a] Institut für Nanotechnologie (INT), Forschungszentrum Karlsruhe
Postfach 3640, 76021 Karlsruhe, Germany
Fax: (internat.) + 49-7247-82-6368
E-mail: eichhoefer@int.fzk.de
[b] Institut für Physikalische Chemie, Lehrstuhl für Theoretische Chemie Universität Karlsruhe,
Kaiserstr. 12, 76128 Karlsruhe, Germany

Results and Discussion

Synthesis and Structure

The reaction of $HgCl_2$ with $PPhnPr_2$, $Te(SinBu_3)_2$ and $PhESiMe_3$ (E = Se, Te) in DME at −30 °C results in the formation of yellow octahedral crystals of $[Hg_{10}Te_4(SePh)_{12}(PPhnPr_2)_4]$ (**1**) and $[Hg_{10}Te_4(TePh)_{12}(PPhnPr_2)_4]$ (**2**), respectively (Scheme 1).

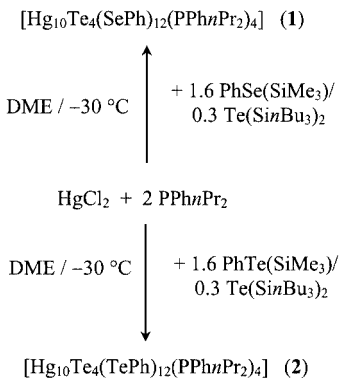

Scheme 1

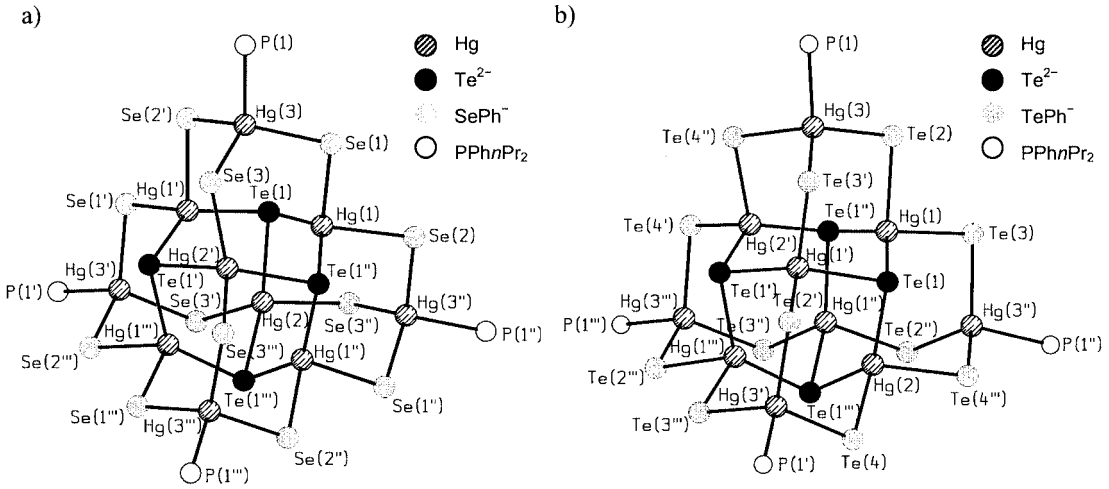

Figure 1. a) The $Hg_{10}Te_4Se_{12}P_4$ cluster core as a section of the molecular structure of $[Hg_{10}Te_4(SePh)_{12}(PPhnPr_2)_4]$ (**1**) (symmetry transformations for generating equivalent atoms: $-y + 1/4$, $x + 1/4$, $-z + 1/4$; $y - 1/4$, $-x + 1/4$, $-z + 1/4$; $-x$, $-y + 1/2$, z; $-x$, $-y + 1$, $-z + 1$). b) The $Hg_{10}Te_{16}P_4$ cluster core as a section of the molecular structure of $[Hg_{10}Te_4(TePh)_{12}(PPhnPr_2)_4]$ (**2**) (symmetry transformations for generating equivalent atoms: $y - 1/4$, $-x + 1/4$, $-z + 1/4$; $-y + 1/4$, $x + 1/4$, $-z + 1/4$; $-x$, $-y + 1/2$, z). C and H atoms are omitted for clarity.

Figure 1(a) shows the molecular structure of the $[Hg_{10}Te_4Se_{12}P_4]$ cluster core of **1** determined by single-crystal X-ray diffraction (see also Table 3). The compound crystallizes in the tetragonal space group $I4_1/a$ (4bar site symmetry). The cluster core, which is comprised of four adamantane cages each of which is formed by three tellurium, three selenium and four mercury atoms, is a macrotetrahedral fragment of the sphalerite structure, which is also found in HgSe and HgTe.[11] The resultant tetrahedron, with the four phosphane atoms in the apex positions, has edge lengths of 1240.6−1284.2 pm and has a diameter of 820 pm (from the mercury atom at the vertex of the tetrahedron to the center of the opposite tetrahedral face).

The mercury atoms Hg1−Hg3 have distorted tetrahedral environments, coordinated by the selenium atoms of the μ_2-$SePh^-$ ligands (Se1, Se2, Se3) and the μ_3-Te^{2-} ligands (Te1) as well as the phosphorus atoms of the $PPhnPr_2$ ligands (P1) (bond angles are: Se−Hg−Se 96.59−112.26(3); Se−Hg−Te 92.17−113.73(3); Te−Hg−Te 134.47−137.15(4); P−Hg−Se 104.76−108.22(11)°]. The Hg−SePh bond lengths which range from 263.44−278.09(10) pm are similar to those found in $[Hg_{10}Se_4(SePh)_{12}(PPh_2nPr)_4]$[10] while the Hg−Te bond lengths between 270.92−274.13(7) pm are shorter than those in HgTe (279 pm).[12] The Hg−P1 bond length of the four outer Hg3 atoms coordinated by the $PPhnPr_2$ ligands is 256.9(3) pm.

Figure 1(b) shows the molecular structure of the $[Hg_{10}Te_{16}P_4]$ cluster core of **2** determined by single-crystal X-ray diffraction which is isostructural with **1**. Due to the larger covalent radii of the tellurium atoms the cluster core is slightly larger in comparison with **1** as indicated by edge lengths of 1289.3−1298.7 pm of the tetrahedron formed by the four phosphane atoms and a diameter of 840 pm taken from the mercury atom at the vertex of the tetrahedron to the center of the opposite tetrahedral face. The Hg−TePh bond lengths range from 278.02−291.11(11) pm corresponding to values found in $[Hg_6(\mu\text{-}Br_2)Br_2(\mu\text{-}TePh)_8(py)_2]$[13] and the Hg−Te bond lengths from

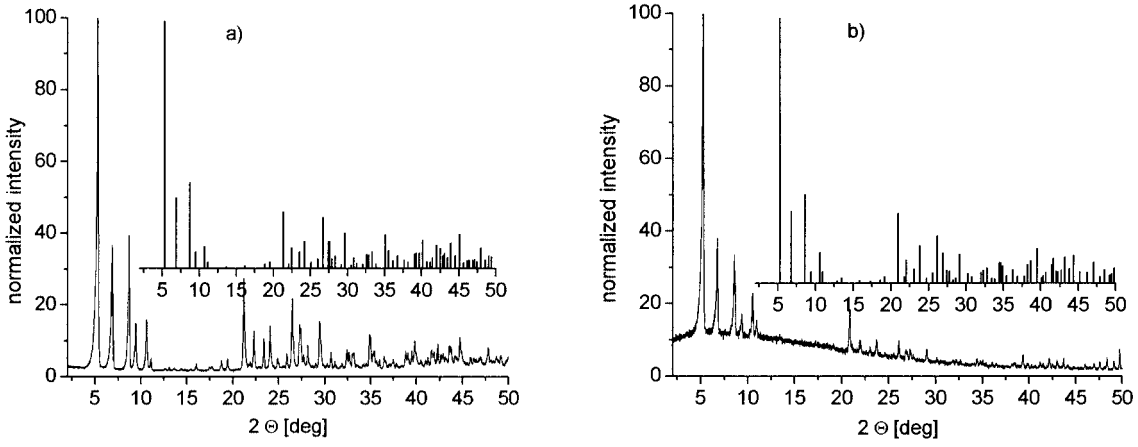

Figure 2. Measured X-ray powder pattern and calculated peak pattern for a) $[Hg_{10}Te_4(SePh)_{12}(PPhnPr_2)_4]$ (**1**) and b) $[Hg_{10}Te_4(TePh)_{12}(PPhnPr_2)_4]$ (**2**).

 © 2004 Wiley-VCH Verlag GmbH & Co. KGaA, Weinheim

272.39−275.74(10) pm are similar to those in **1**. The value of the Hg−P1 bond length for the four outer Hg3 atoms coordinated by the PPh*n*Pr$_2$ ligands is 261.1(4) pm.

Filtration of **1** and **2** at −30 °C and subsequent drying in vacuo resulted in yellow powders which are stable under nitrogen at room temperature. Powder diffraction patterns of the two compounds show their crystalline purity (Figure 2). If **2** is dissolved in benzene/toluene at 5 °C the formation of an orange solution can be observed from which **3** crystallizes within a few days (Scheme 2).

$$4\ [Hg_{10}Te_4(SePh)_{12}(PPh\mathit{n}Pr_2)_4]\ \ (\mathbf{1})$$

$$\xrightarrow[5\ ^\circ C]{C_6H_6/\text{toluene}}$$

$$[Hg_{34}Te_{16}(SePh)_{36}(PPh\mathit{n}Pr_2)_4]\ \ (\mathbf{3})$$
$$+$$
$$6\ Hg(SePh)_2\ +\ 12\ PPh\mathit{n}Pr_2$$

Scheme 2

The compound crystallizes in the triclinic space group $P\bar{1}$ (see also Table 3). The $Hg_{34}Te_{16}Se_{36}$ cluster framework is formed from four fused $Hg_{10}Te_4Se_{12}$ cluster cores and thus 16 $Hg_6Te_3Se_3$ adamantane like cages with a tetrahedral hole in the center of the molecule (Figure 3).

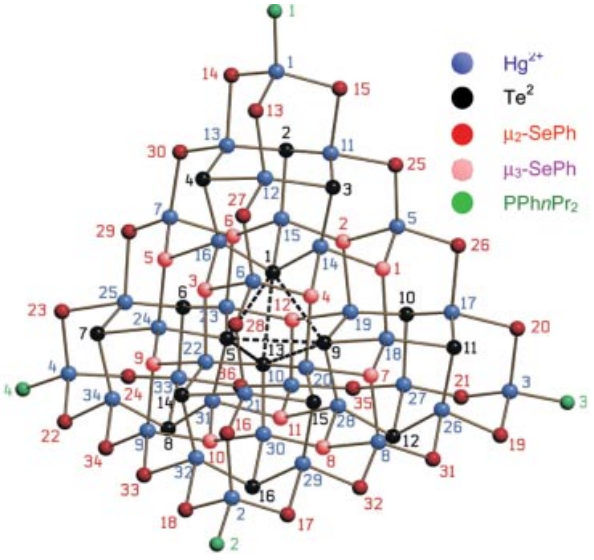

Figure 3. The $Hg_{34}Te_{16}Se_{36}P_4$ cluster core as a section of the molecular structure of $[Hg_{34}Te_{16}(SePh)_{36}(PPh\mathit{n}Pr_2)_4]$ (**3**). Atoms are labeled with numbers only. Nonbonding Te−Te distances (dashed line): Te1−Te9: 376.4 ; Te5−Te13: 385.5 pm. C and H atoms are omitted for clarity.

Thus one could formally explain the formation of **3** in terms of a direct condensation reaction of four "$Hg_{10}Te_4(SePh)_{12}$" cluster cores accompanied by the formal cleavage of six "$(PPhnPr_2)_2Hg(SePh)_2$" units (Scheme 2). In agreement with this, small amounts of $Hg(SePh)_2$ could be crystallized upon layering supernatant reaction solutions of **3** during which the formation of HgTe was not observed. Formal occupation of the tetrahedral hole by a mercury atom would lead to an ideal tetrahedral fragment of the cubic sphalerite structure. The diameter of the cluster core taken as the distance from the Hg atom at the vertex of the tetrahedron to the center of the opposite tetrahedral face is about 1500 pm.

Whereas the known cluster $[Hg_{32}Se_{14}(SePh)_{36}]$[10,11] is, according to theoretical considerations, a larger homolog of the cluster $[Hg_{17}Se_4(SePh)_{28}]^{2-}$, compound **3** is in fact a larger homolog of the cluster $[Hg_{10}Te_4(SePh)_{12}(PPhnPr_2)_4]$.[14] In contrast to the predicted formula by Dance et al. for such a group 12−16 metal chalcogenide cluster $[M_{35}E_{28}(ER)_{24}(PR_3)_4]^{10-}$ (M = Zn, Cd, Hg; E = S, Se, Te) we observed in **3**, a formal exchange of E^{2-} ions by additional ER^- ligands resulting in an overall zero charge. These 12 additional $SePh^-$ ligands are therefore each bridging three mercury atoms in contrast to the other 24 μ_2-$SePh^-$ ligands, a bonding mode which had not been observed before for $SePh^-$ ligands in group 12−16 cluster molecules. Although all mercury atoms Hg1−Hg34 have distorted tetrahedral coordination geometries, three different atomic environments coexist. The atoms Hg1−Hg4 are each coordinated by one phosphorous atom (P1−P4) of the PPh*n*Pr$_2$ ligands and three selenium atoms of the μ_2-$SePh^-$ ligands (Se13−Se24) (for selected bond length and angles see Table 1). Six of the mercury atoms namely Hg5−Hg10 are each bonded to four selenium atoms, two of them belonging to the remaining μ_2-$SePh^-$ ligands (Se25−Se36) and two of them to the μ_3-$SePh^-$ ligands (Se1−Se12). The remaining 24 mercury atoms (Hg11−Hg34) are each surrounded by two selenium atoms from either the two μ_2-$SePh^-$ ligands or the two μ_3-$SePh^-$ ligands and two tellurium atoms from the μ_3-Te^{2-} ligands (Te1−Te16). The Hg−SePh bond lengths and the Hg−Te bond lengths which range from 262.1−293.3(4) pm and 268.4−279.3(3) pm respectively correspond to those found in **1** but show a broader range due to larger distortions of the ideal tetrahedral cluster molecule.

Interestingly a similar cluster core structure was predicted by Spanhel et al. for a group 12−16 cluster of the formal composition $[Cd_{34}Se_{19}(COOCH_3)_{25}(OH)(P\mathit{n}Bu_3)_{7.5}]$ on the basis of a powder X-ray pattern, SAXS, chemical elemental analysis and FTIR spectroscopy.[15] They derived this structure from similar cage like tetrahedral pyramids (Koch pyramids) which are well known from fractal geometry.[16] According to this, the cluster structure "$Hg_{34}Te_{16}(SePh)_{36}$" corresponds to the third hierarchical level of self-similar Koch pyramids with a fractal dimension 2.

UV/Vis Spectroscopy

To investigate the electronic structure of the cluster-molecules, we measured the UV/Vis reflectance spectra of **1**−**3** as nujol mulls. The spectra are shown in Figure 4. A systematic behavior is seen for the absorption onsets reflecting the position of the first optically allowed transition. The onset shows a small shift to lower energy upon substitution of the atom in the E′ position from Se to Te in

 © 2004 Wiley-VCH Verlag GmbH & Co. KGaA, Weinheim

Table 1. Selected mean interatomic distances [pm] and angles [deg] for $[Hg_{34}Te_{16}(SePh)_{36}(PPhnPr_2)_4]$ (**3**)

Coordination environment	Atoms	Range of distances [pm]	Range of angles [deg]
PHg$(SePh)_3$	Hg1−Hg4	Hg2−P2: **254.4(10)** − Hg4−P4: **255.7(11)**	P2−Hg2−Se18: **101.6(3)** − P2−Hg2−Se16: **117.5(2)**
		Hg2−Se16: **263.0(3)** − Hg2−Se18: **268.7(4)**	Se17−Hg2−Se18: **96.8(1)** − Se16−Hg2−Se17: **116.8(1)**
Hg$(SePh)_4$	Hg5−Hg10	Hg5−Se25: **262.1(3)** − Hg8−Se8: **275.1(4)**	Se7−Hg8−Se8: **97.8(1)** − Se33−Hg9−Se9: **118.5(1)**
$(Te)_2$**Hg**$(SePh)_2$	Hg11−Hg34	Hg27−Se21: **273.1(4)** − Hg14−Se4: **293.3(4)**	Te10−Hg17−Te11: **132.2(1)** − Te15−Hg20−Te13: **140.2(9)**
		Hg16−Te4: **268.4(2)** − Hg34−Te8: **279.2(3)**	Se17−Hg29−Te16: **91.6(1)** − Te7−Hg34−Se34: **115.1(1)**
			Se18−Hg32−Se33: **97.5(2)** − Se16−Hg21−Se28: **105.1(1)**
μ_3-**Te**$(Hg)_3$	Te1, Te5, Te9, Te13	Hg16−Te1: **271.4(3)** − Hg22−Te13: **273.8(3)**	Hg30−Te13−Hg20: **90.6(1)** − Hg23−Te5−Hg24: **95.1(1)**
	Te2−Te4, Te6−Te8	Hg16−Te4: **268.4(2)** − Hg34−Te8: **279.2(3)**	Hg24−Te7−Hg25: **89.9(1)** − Hg32−Te16−Hg29: **98.1(1)**
	Te10−Te12, Te14−Te16		
μ_3-**Se**$Ph(Hg)_3$	Se1−Se12	Hg10−Se11: **266.0(4)** − Hg14−Se4: **293.3(4)**	Hg6−Se3−Hg22: **103.8(1)** − Hg18−Se7−Hg20: **123.4(1)**
μ_2-**Se**$Ph(Hg)_2$	Se13−Se24	Hg2−Se16: **262.9(3)** − Hg25−Se23: **279.6(4)**	Hg3−Se21−Hg27: **100.7(1)** − Hg2−Se17−Hg29: **110.1(1)**
	Se25−Se36	Hg5−Se25: **262.1(3)** − Hg13−Se30: **283.2(4)**	Hg9−Se33−Hg32: **106.5(1)** − Hg7−Se30−Hg13: **111.3(1)**

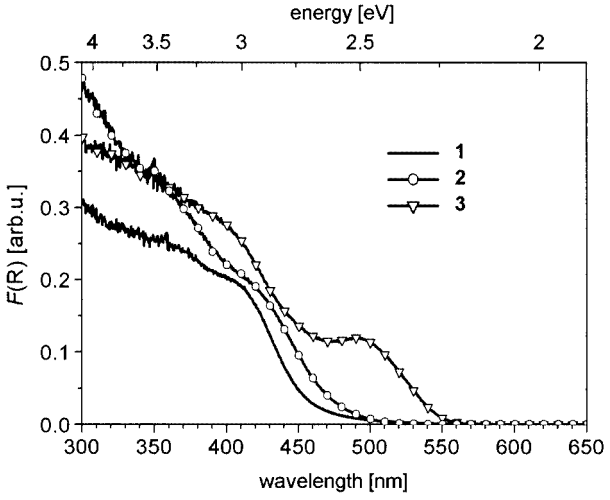

Figure 4. Reflectance spectra of $[Hg_{10}Te_4(SePh)_{12}(PPhnPr_2)_4]$ (**1**), $[Hg_{10}Te_4(TePh)_{12}(PPhnPr_2)_4]$ (**2**) and $[Hg_{34}Te_{16}(SePh)_{36}(PPhnPr_2)_4]$ (**3**) as microcrystalline powders in oil between two quartz plates.

$[Hg_{10}Te_4(E'Ph)_{12}(PPhnPr_2)_4]$ (**1**, **2**). This is consistent with the known dependence of the band gap in the corresponding bulk semiconductors HgTe and HgSe. An increase of cluster size in **3** is accompanied by a shift of the band gap to lower energies of about 0.5 eV compared with **1**. This can be interpreted in terms of the quantum confinement effect observed in larger group 12−16 nanocrystals. For **1** and **2** the spectra display two weakly resolved absorption shoulders at 400/355 nm and 410/355 nm respectively, a pattern which was also observed for $[Hg_{10}Se_4(SePh)_{12}(PPh_2nPr)_4]$ and $[Cd_{10}E_4(E'Ph)_{12}(PR_3)_4]$ (E = Se, Te; E′ = S, Se, Te).[10,17] Cluster **3** shows one well resolved absorption maximum at 493 nm followed by a further broad shoulder extending to 300 nm which shows no distinct maximum. The spectrum of **3** is therefore different from those of $[Cd_{32}Se_{14}(SePh)_{36}(PPh_3)_4]$ and $[Hg_{32}Se_{14}(SePh)_{36}]$ which both show two distinct absorption maxima in the low energy region of the spectra.[1,10] Furthermore the first electronic transition for $[Hg_{32}Se_{14}(SePh)_{36}]$ lies 50 nm lower in energy at 550 nm compared with **3** although the latter contains two additional mercury atoms and 16 tellurium atoms instead of the selenium atoms. These absorption features are therefore most probably related to the difference in the structure of the cluster core in particular the mercury vacancy in the center of **3**. The dissolution of **3** in THF at −25 °C followed by careful warming to room temperature resulted in a clear orange solution which showed an absorption spectrum similar to that of the crystalline powder as a mull in oil. This is also evidence for the stability of **3** in solution at room temperature.

Compound **2** dissolved in THF at −25 °C to yield a clear red orange solution from which a deep red microcrystalline powder precipitated upon warming to room temperature. The X-ray powder diffraction pattern shows in the low 2 theta region (2θ = 2−7 deg.) several well resolved peaks suggesting crystallization of cluster molecules. Furthermore, this red powder displays an absorption onset at 650 nm with a shoulder at about 530 nm. The elemental analysis (found C 18.69, H 1.46%) shows unusually good agreement with the calculated values for the formula $[Hg_{34}Te_{16}(TePh)_{36}](PPhnPr_2)_4]$ (calcd. C 18.64, H 1.52%).

Theory

Density functional investigations have been carried out to elucidate certain features of **3**. All calculations were performed with the RI-DFT modules[18] (RI means the "resolution of the identity", i.e. an auxiliary basis set expansion is used, to process Coulomb-energy contributions more efficiently) of the TURBOMOLE[19] program system employing the BP86-functional,[20] which is a rather reliable functional for treatment of transition metal compounds, and (if not mentioned otherwise) a "split valence plus polarization" basis set − SV(P)[21] − where the brackets indicate that the polarization functions were omitted for H.

The first point of interest concerns the hole in the center of **3**. A condensation of **1** might also be expected to lead to a "real cubic sphalerite cluster" with one further mercury atom in the vacancy (and perhaps two phosphane ligands being replaced by μ_1-$SePh^-$ to maintain the overall zero charge). Thus we performed geometry optimizations of the model clusters $[Hg_{34}Te_{16}(SeMe)_{36}(PMe_3)_4]$, $[Hg_{35}Te_{16}(SeMe)_{36}(PMe_3)_4]^{2+}$ (both *T*-symmetry) and $[Hg_{35}Te_{16}(Se-$

 © 2004 Wiley-VCH Verlag GmbH & Co. KGaA, Weinheim

$Me)_{38}(PMe_3)_2]$ (*C*2-symmetry). A drastic lowering of the HOMO−LUMO gap was observed upon introducing μ_1-SeR^- ligands (from 1.52 eV for $[Hg_{34}Te_{16}(SeMe)_{36}(PMe_3)_4]$ and 1.17 eV in $[Hg_{35}Te_{16}(SeMe)_{36}(PMe_3)_4]^{2+}$ to only 0.23 eV for $[Hg_{35}Te_{16}(SeMe)_{38}(PMe_3)_2]$), which indicates that this kind of coordination should be unfavorable. Another way of obtaining a neutral cluster with 35 Hg atoms might be substitution of two μ_3-SeR^- ligands by Te^{2-}, but in the observed condensation reaction all Te^{2-} available from **1** is already incorporated in the structure with the central hole, so if there is no other source of chalcogenide dianions, the loss of electroneutrality might be one reason for the formation of **3**. However, geometrical reasons also seem at a first glance to prevent a "filled" cluster core because the vacancy is simply not large enough to be occupied by Hg^{2+}. The computed Te−Te distances of 398.7 pm for $[Hg_{34}Te_{16}(SeMe)_{36}(PMe_3)_4]$ in the central Te_4-unit would lead to Hg−Te distances of 244.1 pm for a mercury atom in the center of this Te_4-tetrahedron while the Te−Te distances found in the X-ray structure of **3** are even shorter (376.4−385.5 pm). It seems as if the $PhSe^-$-ligands on the edges of this mixed chalcogenide cluster are responsible for this, because the predicted value for a hypothetical $[Hg_{34}Te_{16}(TeMe)_{36}(PMe_3)_4]$ cluster is 434.2 pm which is only slightly shorter than the observed Te−Te distance (456 pm) and the Hg−Te bond length (279 pm) in bulk HgTe.[13] The insertion of a central Hg^{2+} in **3**, leading to $[Hg_{35}Te_{16}(SeMe)_{36}(PMe_3)_4]^{2+}$, resulted in a significant increase of the predicted Te−Te distances with values of 470.7 pm which might cause high tension and reduced stability for the latter system. Interestingly however, the size of the tetrahedron of the outer Hg-atoms (Hg1−Hg4 in Figure 3) only increased from 1722.5 pm to 1754.7 pm when going from $[Hg_{34}Te_{16}(SeMe)_{36}(PMe_3)_4]$ to $[Hg_{35}Te_{16}(SeMe)_{36}(PMe_3)_4]^{2+}$ and all other bond lengths did not change by more than 7 pm. The tension caused by the stretching of the central Te_4 tetrahedra is rather compensated for by a deformation of the bond angles which is of course mostly significant for the four tellurium atoms in the center (Te1, Te5, Te9, Te13) changing from μ_3-bridging (Hg−Te−Hg: 92.86°) to a distorted tetrahedral coordination (Hg−Te−Hg: 104.73−113.87°) while all the other bond angles did not change by more than 4.3°. These findings suggest that from the theoretical point of view such an ionic cluster molecule could be stable but its formation is not favored in the present reaction due to the absence of an appropriate counterion.

$[Hg_{32}Se_{14}(SePh)_{36}]$ and **3** are obviously different in their coordination behavior towards phosphane ligands. Although both clusters are synthesized starting from phosphane-coordinated "Hg_{10}" cluster molecules, **3** appears with all four Hg corners saturated by $PPhnPr_2$ whereas in the cluster with 32 mercury atoms all four mercury atoms at the corners are only trigonally coordinated by three $SePh^-$ ligands. Since a comparison of the influence of the phosphane ligands on the electronic structure of $[Hg_{34}Te_{16}(SeMe)_{36}(PMe_3)_4]$ and $[Hg_{32}Se_{14}(SeMe)_{36}(PMe_3)_4]$ showed no real differences between these two model compounds, we performed further geometry optimizations of the more realistic systems $[Hg_{34}Te_{16}(SePh)_{36}(PMe_3)_4]$, $[Hg_{34}Te_{16}(SePh)_{36}(PPh_3)_4]$, $[Hg_{32}Se_{14}(SePh)_{36}(PMe_3)_4]$, and $[Hg_{32}Se_{14}(SePh)_{36}(PPh_3)_4]$. This however was only possible using two different small basis sets (single zeta quality) for the organic ligands, which are specially optimized for the description of phenyl- and methyl-substituents (available as "SZ.benzene" and "sz.methane" in TURBOMOLE). The energies for the detachment of the PMe_3 ligands from $[Hg_{34}Te_{16}(SePh)_{36}(PMe_3)_4]$ and $[Hg_{32}Se_{14}(SePh)_{36}(PMe_3)_4]$ are quite similar (+44.6 kJ/mol and +43.8 kJ/mol per ligand, respectively). In contrast to this, the corresponding Hg−P bond strengths are clearly lower in the case of PPh_3 (+23.2 kJ/mol in $[Hg_{34}Te_{16}(SePh)_{36}(PPh_3)_4]$ and only +7.8 kJ/mol in $[Hg_{32}Se_{14}(SePh)_{36}(PPh_3)_4]$), which can be explained by the higher steric demands of the phenyl substituent. Especially in the $[Hg_{32}Se_{14}(SePh)_{36}]$ cluster core the μ_2-$SePh^-$ groups near the terminal Hg-atoms protrude so much that repulsion effects prevent a stronger metal-ligand interaction. The nuclear arrangement in the clusters with 34 Hg-atoms, i.e. in a $[Hg_{34}Te_{16}(SePh)_{36}]$ cluster core, is more favorable for the uptake of bulky ligands, and additionally, the experiments leading to **3** were carried out with $PPhnPr_2$. The steric properties of the latter phosphane should be somewhere in between those of PMe_3 and PPh_3. This clearly accounts for the experimental findings.

The differences between the UV/Vis spectra of **3** and $[Hg_{32}Se_{14}(SePh)_{36}]$ are also in line with theoretical results obtained by time dependent DFT as shown in Table 2. Electronic excitations were calculated using the TURBOMOLE module "ESCF".[22,23] The experimental absorbance maximum of **3** appears at 493 nm, which means an excitation energy of 2.51 eV, whereas two distinct maxima in $[Hg_{32}Se_{14}(SePh)_{36}]$ are located at 2.27 eV and 2.47 eV. Once again, for the model compounds $[Hg_{34}Te_{16}(SeMe)_{36}(PMe_3)_4]$ and $[Hg_{32}Se_{14}(SeMe)_{36}]$, we calculated the energies of the twenty lowest singlet transitions in the dipole-allowed irreducible representation *t*. The red-shift of time dependent DFT[24] was taken into account by adding a systematic offset of 0.8 eV. As a result, there are two strong low energy

Table 2. Comparison of experimental and calculated (TDDFT) spectra of $[Hg_{32}Se_{14}(SePh)_{36}]$ and $[Hg_{34}Te_{16}(SeMe)_{36}(PMe_3)_4]$.

	Transition energy (exp.) in eV	Transition energy (TDDFT) in eV	Oscillator strength (TDDFT)
$Hg_{32}Se_{14}(SePh)_{36}$	2.27	2.221	0.30
	2.47	2.353	0.05
$Hg_{34}Te_{16}(SeMe)_{36}(PMe_3)_4$	2.51	2.411	0.25
		2.495	0.10

 © 2004 Wiley-VCH Verlag GmbH & Co. KGaA, Weinheim

transitions in the predicted spectrum of $[Hg_{34}Te_{16}(SeMe)_{36}(PMe_3)_4]$ at 2.41 eV and 2.49 eV − the experimental procedure might not be able to resolve this small energetic separation which would explain the solitary maximum at 2.51 eV in the spectrum of **3**. For $[Hg_{32}Se_{14}(SeMe)_{36}]$, apart from transitions with negligibly small oscillator strengths, one also finds two important excitations at 2.22 eV and 2.35 eV, which closely resemble the measured values in the spectrum of the corresponding phenyl cluster (it should be noted, that the calculated oscillator strength of the second transition is smaller than for the first excitation, which is also the case in the experimental spectrum, though however not to this extent).

Conclusions

We have shown that reactions of $HgCl_2$ with $PPhnPr_2$, $Te(SinBu_3)_2$ and $PhESiMe_3$ (E = Se, Te) in DME result in the formation of $[Hg_{10}Te_4(EPh)_{12}(PPhnPr_2)_4]$ (E = Se **1,** E = Te **2**). Investigations in solution reveal that the cluster $[Hg_{10}Te_4(SePh)_{12}(PPh_2nPr)_4]$ (**1**) is a metastable compound which is converted in benzene/toluene at room temperature to $[Hg_{34}Te_{16}(SePh)_{36}(PPhnPr_2)_4]$ (**3**). The "$Hg_{34}Te_{16}Se_{36}$" cluster core of **3** consists of four tetrahedral "$Hg_{10}Te_4(SePh)_{12}$" cages each sharing three "$Hg(SePh)_3$" edges, a cage structure well known in fractal geometry as a "Koch pyramid". Thus the structure can be described as an ideal tetrahedral fragment, 1500 pm in diameter, of the cubic sphalerite lattice with one mercury vacancy in the center. The molecular structure of **3** with mixed chalcogen atoms is therefore different from that of $[Hg_{32}Se_{14}(SePh)_{36}]$ which is a product of the recrystallization of the pure selenide cluster $[Hg_{10}Se_4(SePh)_{12}(PPh_2nPr)_4]$.[10] DFT calculations reveal that an ionic cluster $[Hg_{35}Te_{16}(SeMe)_{36}(PMe_3)_4]^{2+}$ in which the vacancy is filled by a mercury ion could also be stable. This suggests that the formation of the vacancy is probably mostly driven by the absence of an appropriate counterion in the reaction which would stabilize such an ionic cluster molecule. This peculiarity of the structure has also a distinct influence on the electronic structure of **3** in comparison with $[Hg_{32}Se_{14}(SePh)_{36}]$ as can be seen from the UV/Vis reflectance spectra. In future we will target the development of conditions for further controlled cluster growth of these molecules.

Experimental Section

Standard Schlenk techniques were employed throughout the syntheses using a double manifold vacuum line with high purity dry nitrogen. The solvents tetrahydrofuran (THF), dimethylethylene glycol (DME) and benzene were dried over sodium-benzophenone and toluene over $LiAlH_4$, and distilled under nitrogen. Anhydrous $HgCl_2$ was purchased from Aldrich. $PhSeSiMe_3$,[24] $Se(SiMe_3)_2$ [25] and $PhTeSiMe_3$ [26] were prepared according to standard literature procedures. $Te(SinBu_3)_2$ was prepared accordingly to the synthesis of $Se(SiMe_3)_2$ by the use of $ClSinBu_3$ instead of $ClSiMe_3$.

UV/Vis absorption spectra of cluster molecules in solution were measured on a Varian Cary 500 spectrophotometer in quartz corvettes. Solid state reflection spectra were measured as micron sized crystalline powders between quartz plates with a Labsphere integrating sphere.

1: $HgCl_2$ (0.27 g, 0.99 mmol) was dissolved in DME (40 mL) with the addition of $PPhnPr_2$ (0.42 mL, 1.99 mmol). $PhSeSiMe_3$ (0.34 mL, 1.79 mmol) was then added at 0 °C and the resultant clear yellow solution stirred for half an hour. Addition of $Te(SinBu_3)_2$ (0.14 mL, 0.3 mmol) at −40 °C led to the formation of a pale yellow solution from which $[Hg_{10}Se_4(TePh)_{12}(PPhnPr_2)_4]$ (**1**) could be crystallized at −30 °C (60% yield). $C_{120}H_{136}Hg_{10}P_4Se_{12}Te_4$ (5166.11): calcd. C 27.89, H 2.65; found C 27.79, H 2.72.

2: $HgCl_2$ (0.23 g, 0.85 mmol) was dissolved in DME (35 mL) with the addition of $PPhnPr_2$ (0.36 mL, 1.69 mmol). $PhTeSiMe_3$ (0.31 mL, 1.36 mmol) was then added at 0 °C and the resultant clear yellow solution stirred for an hour. Addition of $Te(SinBu_3)_2$ (0.12 mL, 0.25 mmol) at −40 °C led to the formation of a pale yellow solution from which $[Hg_{10}Te_4(TePh)_{12}(PPhnPr_2)_4]$ (**2**) could be crystallized at −30 °C (63% yield). $C_{120}H_{136}Hg_{10}P_4Te_{16}$ (5749.79): calcd. C 25.06, H 2.38; found C 24.95, H 2.26.

3: Compound **1** (0.11 g, 0.019 mmol) was dissolved in a mixture of benzene (4 mL) and toluene (16 mL) at 5 °C giving an orange solution. The solution was then gradually allowed to warm up in the cooling bath and over the period of one week orange crystals of $[Hg_{34}Te_{16}(SePh)_{36}(PPhnPr_2)_4]$ (**3**) were formed (yield 70% calculated for Scheme 2). $C_{264}H_{256}Hg_{34}P_4Se_{36}Te_{16}$ (15257.05): calcd. C 20.78, H 1.69; found C 20.41, H 1.60.

Crystals suitable for single-crystal X-ray diffraction were obtained directly from the reaction solutions of the compounds and then selected in perfluoroalkyl ether oil.

Single-crystal X-ray diffraction data were collected using graphite-monochromated Mo-K_α radiation (λ = 0.71073 Å) on a STOE IPDS II (Imaging Plate Diffraction System). The structures were solved with the direct methods program SHELXS[27] of the SHELXTL PC suite of programs and were refined with the use of the full-matrix least-squares program SHELXL.[28] Molecular diagrams were prepared using the program SCHAKAL 97[28] and DIAMOND.[29]

All Hg, Te, Se and P atoms were refined with anisotropic displacement parameters. In **2** the C atoms were also refined anisotropically. The C atoms in **1** were refined isotropically while the C atoms of the phenyl groups in **3** were refined isotropically as rigid groups. H atoms of the SePh groups were included in calculated positions for **2**. C_6H_6 solvent molecules in **3** were refined as rigid groups with half occupancy. Residual electron density in the difference Fourier map of **3** indicates the existence of additional disordered solvent molecules in the crystal lattice which could not be refined successfully (see Table 3).

Numerical absorption corrections were applied to the data of **2** and **3**.

CCDC-205710 (**1**), -205711 (**2**), and -205712 (**3**) contain the supplementary crystallographic data for this paper. These data can be obtained free of charge at www.ccdc.cam.ac.uk/conts/retrieving.html (or from the Cambridge Crystallographic Data Centre, 12 Union Road, Cambridge CB2 1EZ, UK; Fax: (internat.) + 44-1223-336-033; E-mail: deposit@ccdc.cam.ac.uk).

 © 2004 Wiley-VCH Verlag GmbH & Co. KGaA, Weinheim

Table 3. Crystallographic data for $[Hg_{10}Te_4(SePh)_{12}(PPhnPr_2)_4]$ (**1**), $[Hg_{10}Te_4(TePh)_{12}(PPhnPr_2)_4]$ (**2**) and $[Hg_{34}Te_{16}(SePh)_{36}(PPhnPr_2)_4]$ (**3**)

	1	**2**	**3**·2C$_6$H$_6$
Formula mass	5165.99	5749.67	15413.0
Crystal system	tetragonal	tetragonal	triclinic
Space group	$I4_1/a$	$I4_1/a$	$P\bar{1}$
a [pm]	2550.7(4)	2601.9(4)	2468.4(5)
b [pm]			3109.8(6)
c [pm]	2164.2(4)	2187.1(4)	3163.9(6)
α [°]			104.41(3)
β [°]			108.35(3)
γ [°]			103.31(3)
V [10^{6}pm^3]	14081(4)	14807(4)	21031(7)
Z	4	4	2
T [K]	180	180	210
d_c [g cm^{-3}]	2.437	2.579	2.434
μ(Mo-K_α) [mm^{-1}]	14.859	13.499	16.607
F[000]	9328	10192	13520
$2\theta_{max}$ [°]	52	52	44.5
Measured reflections	31108	18281	98038
Unique reflections	6892	6694	49871
R_{int}	0.0966	0.1103	0.0958
Reflections with $I > 2\sigma(I)$.	5111	4744	20920
Refined parameters	213	339	1463
$R1[I > 2\sigma(I)]$[a]	0.0404	0.0468	0.0581
$wR2$(all data)[b]	0.1308	0.1441	0.1974

[a] $R1 = \Sigma||F_o| - |F_c||/\Sigma|F_o|$. [b] $wR2 = \{\Sigma[w(F_o^2 - F_c^2)^2]/\Sigma[w(F_o^2)^2]\}^{1/2}$.

X-ray powder diffraction patterns (XRD) were measured on a STOE STADI P diffractometer (Cu-K_α radiation, Germanium monochromator, Debye−Scherrer geometry) in sealed glass capillaries. Theoretical powder diffraction patterns for **1** and **2** were calculated on the basis of the atom coordinates obtained from single-crystal X-ray analysis by using the program package STOE WinXPOW.[30]

Acknowledgments

This work was supported by the Deutsch-Israelisches Programm (DIP) and the Deutsche Forschungsgemeinschaft (Center for Functional Nanostructures CFN). A. E. is grateful to Prof. D. Fenske for helpful discussions and for providing excellent working conditions, E. Tröster for her invaluable assistance in the practical work and Dr. Susan Anson for careful revision of the manuscript.

[1] V. Soloviev, A. Eichhöfer, D. Fenske, U. Banin, *J. Am. Chem. Soc.* **2001**, *123*, 2354−2364.
[2] A. Eichhöfer, O. Hampe, M. Blom, *Eur. J. Inorg. Chem.* **2003**, 1307 −1314; S. Behrens, M. Bettenhausen, A. Eichhöfer, D. Fenske, *Angew. Chem.* **1997**, *109*, 2874−2876; *Angew. Chem. Int. Ed. Engl.* **1997**, *24*, 2797−2799; S. Behrens, D. Fenske, *Ber. Bunsenges. Phys. Chem.* **1997**, *101*, 1588−1592.
[3] B. Ali, I. G. Dance, D. C. Craig, M. L. Scudder, *J. Chem. Soc., Dalton Trans.* **1998**, 1661−1667; M. D. Nyman, M. J. Hampden-Smith, E. N. Duesler, *Inorg. Chem.* **1996**, *35*, 802−803.
[4] A. Eichhöfer, D. Fenske, H. Pfistner, M. Wunder, *Z. Anorg. Allg. Chem.* **1998**, *624*, 1909−1914.
[5] H. Pfistner, D. Fenske, *Z. Anorg. Allg. Chem.* **2001**, *627*, 575−582.
[6] G. S. H. Lee, K. J. Fisher, D. C. Craig, M. L. Scudder, I. G. Dance, *J. Am. Chem. Soc.* **1990**, *112*, 6435−6437; G. S. H. Lee, D. C. Craig, I. Ma, M. L. Scudder, T. D. Bailey, I. G. Dance, *J. Am. Chem. Soc.* **1988**, *110*, 4863−4864; I. G. Dance, A. Choy, M. L. Scudder, *J. Am. Chem. Soc.* **1984**, *106*, 6285−6295.
[7] T. Vossmeyer, G. Reck, L. Katsikas, E. T. K. Haupt, B. Schulz, H. Weller, *Science* **1995**, *267*, 1476−1479; T. Vossmeyer, G. Reck, B. Schulz, L. Katsikas, H. Weller, *J. Am. Chem. Soc.* **1995**, *117*, 12881−12882.
[8] A. Rogach, S. Kershaw, M. Burt, M. Harrison, A. Kornowski, A. Eychmüller, H. Weller, *Adv. Mater.* **1999**, *11*, 552−555.
[9] M. Harrison, S. Kershaw, A. Rogach, A. Kornowski, A. Eychmüller, H. Weller, *Adv. Mater.* **2000**, *12*, 123−125.
[10] A. Eichhöfer, E. Tröster, *Eur. J. Inorg. Chem.* **2002**, 2253−2256.
[11] S. Behrens, M. Bettenhausen, A. C. Deveson, A. Eichhöfer, D. Fenske, A. Lohde, U. Woggon, *Angew. Chem.* **1996**, *108*, 2360−2363; *Angew. Chem. Int. Ed. Engl.* **1996**, *35*, 2215−2218.
[12] Landolt-Börnstein, *Gruppe III: Kristall und Festkörperphysik*, vol. 17, *Halbleiter* (Ed.: O. Madelung), Springer, Berlin, **1982**, p. 236.
[13] J. Waser, L. Pauling, *J. Chem. Phys.* **1950**, *18*, 747.
[14] E. Schulz Lang, R. A. Zan, C. C. Gatto, R. A. Burrow, E. M. Vázquez-López, *Eur. J. Inorg. Chem.* **2002**, 331−333.
[15] I. Dance and G. Lee in *Perspectives in Coordination Chemistry* (Ed.: A. F. Williams) Helvetica Chimica Acta Basel; VCH, Weinheim, **1992**, p. 86−94.
[16] V. Ptatschek, T. Schmidt, M. Lerch, G. Müller, L. Spanhel, A. Emmerling, J. Fricke, A. H. Foitzik, E. Langer, *Ber. Bunsenges. Phys. Chem.* **1998**, *102*, 85−95.
[17] H. O. Peitgen, H. Jürgens and D. Saupe in *Bausteine des Chaos − Fraktale*, Springer Berlin, Klett-Cotta, Stuttgart, **1992**.
[18] A. Eichhöfer, A. Aharoni, U. Banin, *Z. Anorg. Allg. Chem.* **2002**, *628*, 2415−2421.
[19] O. Treutler, R. Ahlrichs, *J. Chem. Phys.* **1995**, *102*, 346; K. Eichkorn, O. Treutler, H. Öhm, M. Häser, R. Ahlrichs, *Chem. Phys. Lett.* **1995**, *242*, 652, K. Eichkorn, F. Weigend, O. Treutler, R. Ahlrichs, *Theo. Chem. Acc.* **1997**, *97*, 119.
[20] M. Bär, M. Häser, H. Horn, C. Kölmel, R. Ahlrichs, *Chem. Phys. Lett.* **1989**, *162*, 165.
[21] A. D. Becke, *Phys. Rev. A* **1988**, *38*, 3098; S. H. Vosko, L. Wilk, M. Nusair, *Can. J. Phys.* **1980**, *58*, 1200; J. P. Perdew, *Phys. Rev. B* **1986**, *33*, 8822.
[22] A. Schäfer, H. Horn, R. Ahlrichs, *J. Chem. Phys.* **1992**, *97*, 2571.
[23] R. Bauernschmitt, R. Ahlrichs, *Chem. Phys. Lett.* **1996**, *256*, 454.
[24] R. Bauernschmitt, R. Ahlrichs, *J. Chem. Phys.* **1996**, *104*, 9047.
[25] N. Miyoshi, H. Ishii, K. Kondo, S. Mui, N. Sonoda, *Synthesis* **1979**, 301−304.
[26] H. Schmidt, H. Ruf, *Z. Anorg. Allg. Chem.* **1963**, *321*, 270−273.
[27] K. Praefcke, C. Weichsel, *Synthesis* **1980**, 216.
[28] G. M. Sheldrick, SHELXTL PC version 5.1 An Integrated System for Solving, Refining, and Displaying Crystal Structures from Diffraction Data, Bruker Analytical X-ray Systems, Karlsruhe, **2000**.
[29] E. Keller, SCHAKAL 97, A Computer Program for the Graphic Representation of Molecular and Crystallographic Models, Universität Freiburg, **1997**.
[30] K. Brandenburg, DIAMOND version 2.1d, Visual Crystal Structure Information System, Bonn, **2000**.
[31] STOE, WinXPOW, STOE & Cie GmbH, Darmstadt, **2000**.

Received July 9, 2003
Early View Article
Published Online November 19, 2003

 © 2004 Wiley-VCH Verlag GmbH & Co. KGaA, Weinheim

Pyridine-2-sulfonates as Versatile Ligands for the Synthesis of Novel Coordinative and Hydrogen-Bonded Supramolecules

Tarlok S. Lobana,*[a,b] Isamu Kinoshita,*[a] Kentaro Kimura,[a] Takanori Nishioka,[a] Daisuke Shiomi,[a] and Kiyoshi Isobe[a]

Keywords: Coordination polymers / Hydrogen bonds / Supramolecular chemistry / Magnetic properties / Stacking interactions

The reactions of 3-methylpyridine-2-sulfonic acid (3-mpSO$_3$H) with Cu^{II} and 4-methylpyridine-2-sulfonic acid (4-mpSO$_3$H) with Zn^{II} in water formed one-dimensional infinite coordination polymers, [Cu(3-mpSO$_3$)$_2$]$_n$ (**1**) and [Zn(4-mpSO$_3$)$_2$]$_n$ (**2**). Similarly, two-dimensional hydrogen-bonded supramolecules of stoichiometries, [ML$_2$(H$_2$O)$_2$] [L = 3-methylpyridine-2-sulfonate (3-mpSO$_3$), M = Mn (**3**), Fe (**4**), Co (**5**), Zn (**6**); L = 5-methylpyridine-2-sulfonate (5-mpSO$_3$), M = Zn (**7**); L = pyridine-2-sulfonate (PySO$_3$), M = Zn (**8**); L = 4-mpSO$_3$, M = Co (**9**)], [Ni(3-mpSO$_3$)$_2$(H$_2$O)$_2$]·H$_2$O (**10**) and the one-dimensional hydrogen-bonded network [VO(acac)(3-mpSO$_3$)(H$_2$O)] (**11**) (acac = acetylacetonate) have been prepared. The ligands are tridentate [*N*,*O*-chelating-Cu-μ-*O*-bridging] in **1** and **2**, while in all the other compounds the N,O-chelating and uncoordinated O atoms are engaged in intermolecular hydrogen bonding leading to the formation of hydrogen-bonded networks. The geometry around each metal center is octahedral (**9**) or distorted octahedral (**1**–**8**, **10** and **11**). The compounds **3**–**8**, and **10** showed novel π–π stacking interactions, not shown by **9** and **11**. The magnetic behavior of **3** and **11** indicates lack of any intermolecular magnetic interactions. The position of the substituents in the pyridyl ring and Jahn–Teller effect (Cu^{II}) appear to determine the stacking interactions as well as the density of ligands with regard to the formation of coordinative and hydrogen-bonded supramolecules.
(© Wiley-VCH Verlag GmbH & Co. KGaA, 69451 Weinheim, Germany, 2004)

Introduction

The hydrogen bonding and coordinative bond are the two main principles involved in the synthesis of supramolecules.[1−4] The intrinsic magnetic, optical, catalytic and structural properties of the metal ions are the prerequisites, in the field of crystal engineering, for non-linear optic, ferromagnetic, superconducting and gas-occlusion materials. The self-assembled metal complexes having one-, two-, or three-dimensional solid state networks are expected to play vital roles in the specific functions of materials.[5−8]

Pyridine-2-thione, the simplest prototype of heterocyclic thioamides, has shown its versatility in the formation of a wide range of mononuclear through to polynuclear compounds with interesting structural novelties, magnetic, electrochemical, spectral and conduction properties.[9−14] A remarkable observation is that it can bind one to four metals giving rise to polymetallic materials.[9,12] This unusual property of pyridine-2-thiolates prompted us to investigate pyridine-2-sulfonates, which are extensions of pyridine-2-thiones involving oxidation of sulfur at the 2-position of the pyridine rings. These pyridine-2-sulfonates possess one N and three O atoms (N, 3O donor set) which could provide several possibilities for coordinative and other types of bonding interactions. It may be mentioned here that only the limited coordination chemistry of pyridine-2-sulfonates is known.[15,16]

The aerobic oxidation of sulfur in 2,2′-bis(3-methylpyridine) disulfide in the presence of copper(II) bromide in methanol generated 3-methylpyridine-2-sulfonic acid, which subsequently formed an infinite one-dimensional polymer, [Cu(3-mpSO$_3$)$_2$]$_n$. A direct reaction of 3-methylpyridine-2-sulfonic acid (3-mpSO$_3$H) with Zn^{II} bromide also formed a two-dimensional hydrogen-bonded polymer, [Zn(3-mpSO$_3$)$_2$(H$_2$O)$_2$].[17] These observations stimulated our interest to systematically investigate the coordination behavior of pyridine-2-sulfonic acids. The oxidation of sulfur by the metal ions and C−S bond cleavage reactions mimic the metabolism of organic sulfur in mammals.[17,18]

In this paper, we report on novel coordination polymers and hydrogen-bonded supramolecules prepared using pyri-

[a] Department of Material Science, Graduate School of Science, Osaka City University,
Sugimoto, Sumiyoshi-ku, Osaka 558-8585, Japan
Fax: (internat.) + 81-6-6690-2753
E-mail: isamu@sci.osaka-cu.ac.jp
[b] On leave from:
Department of Chemistry, Guru Nanak Dev University, Amritsar 143005, India
Fax: (internat.) + 91-183-2-258820
E-mail: tarlokslobana@yahoo.co.in

 © 2004 Wiley-VCH Verlag GmbH & Co. KGaA, Weinheim DOI: 10.1002/ejic.200300251

dine-2-sulfonic acid, 3-, 4- and 5-methylpyridine-2-sulfonic acids (Scheme 1) and divalent cations/oxocations, viz. VO^{2+}, Mn^{2+}, Fe^{2+}, Co^{2+}, Ni^{2+}, Cu^{2+} and Zn^{2+}. These ligands might act as multidentate ones involving *N*,*O*−chelation, *N*,*O*−chelation-Cu-μ-*O*-bridging, hydrogen bonding and π−π (pyridine ring based) interactions. All these compounds are characterized using analytical data, IR and NMR spectroscopy, X-ray crystallography and magnetic moment studies.

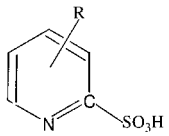

1

	Ligand
R = H	Pyridine-2-sulfonic acid ($PySO_3H$)
3-Me	3-Methylpyridine-2-sulfonic acid (3-mpSO_3H)
4-Me	4-methylpyridine-2-sulfonic acid (4-mpSO_3H)
5-Me	5-Methylpyridine-2-sulfonic acid (5-mpSO3H)

Scheme 1

Results and Discussion

Compounds **1**−**11** were prepared by the reactions of divalent cations/oxocations with neutral pyridine/substituted pyridine-2-sulfonic acids or their sodium salts. The reactions may be labeled as metathetical ones with the exchange of an anion with a metal salt by the RSO_3 anion (R = Py, x-Py, x = 3-Me, 4-Me, 5-Me) of a pyridine sulfonic acid. Allowing the reaction mixture to stand at room temperature gave crystals suitable for X-ray crystallography in many cases, while in some other cases the volume of the reaction mixture was reduced to obtain the crystals. The complexes are soluble in water as well as in alcoholic solvents such as ethanol, methanol etc. On the basis of stoichiometry, as revealed by the elemental analyses, and later confirmed by X-ray crystallography (vide infra), the complexes are grouped into four types: (a) $[ML_2]_n$ [L, M: 3-mpSO_3, Cu (**1**), 4-mpSO_3, Zn (**2**)]; (b) $[ML_2(H_2O)_2]$ [L, M: 3-mpSO_3, Mn (**3**), Fe (**4**), Co (**5**), Zn (**6**); 5-mpSO_3, Zn (**7**); $PySO_3$, Zn (**8**); 4-mpSO_3, Co (**9**)]; (c) $[Ni(3\text{-mpSO}_3)_2(H_2O)_2]\cdot H_2O$ (**10**) and (d) [VO(acac)(3-mpSO_3)(H_2O)] (**11**) (Hacac = acetylacetone). *Type a* compounds (**1**, **2**) are found to be one-dimensional covalently bonded infinite polymers, while *types b*−*d* are hydrogen-bonded (noncovalent) one- or two-dimensional (**3**−**11**) infinite polymers. Table 3 contains the crystal data and Table 1 contains bond lengths and bond angles of the compounds **1**−**11**.

The major IR spectral bands of the compounds **1**−**11** and those of the ligands are listed in the Exp. Sect. The presence of water is clearly identified by the well-defined, strong bands of the ν(O−H) and δ(O−H) stretching vibrations. The compounds **3**−**6** and **10** show three ν(O−H) peaks each, while **7**−**9** and **11** show only two such bands; however, all show one δ(O−H) stretching vibration. The splitting of the ν(O−H) peaks shows an unequivalent chemical environment in the vicinity of the O−H groups which are modulated by the hydrogen bonding; the compounds **1** and **2** show no water peaks. The peaks due to the pyridine ring are relatively strong versus those due to the methyl group. The sulfonate group RSO_3^- shows strong bands due to ν(S−O) vibrations generally found in the region 1300−1055 cm^{-1}. The ν(C−S) peak of free 3-mpSO_3H at 1035 cm^{-1} shifts to the low energy region, and were thus found in the region 1015−1031 cm^{-1}; **1** showed the largest shift.[19] Other ligands also show shifts in the ν(C−S) peaks to lower energies in their complexes. A characteristic peak due to the rocking mode of the methyl group, δ(C−CH_3) is assigned in the region 800−850 cm^{-1}. The absorption due to the vanadyl group, ν(V−O), is observed at 974 cm^{-1} as a strong peak.

Table 1−3 give a summary of important highlights of compounds **1**−**11**, bond parameters and crystal data, respectively.

Coordination Polymers

Type a compounds (**1**, **2**) belong to this category and have one-dimensional polymeric structures. The reaction of copper(II) bromide with 3-mpSO_3H in a methanol/water mixture formed monoclinic green crystals of empirical formula, Cu(3-mpSO_3)$_2$ and X-ray crystallography has shown that it exists as a one-dimensional covalently bonded polymer, $[Cu(3\text{-mpSO}_3)_2]_n$ (**1**). It is interesting to note that the aerial oxidation of 2,2′-bis(3-methylpyridine) disulfide in the presence of copper(II) bromide in methanol formed triclinic green crystals with the same crystal structure as **1**.[17] The different crystal modifications may be the consequence of the reaction conditions involved in the two cases (Table 2 and 3).

The reaction of 3-mpSO_3H with zinc(II) bromide in water did not form a polymer similar to **1**, but rather a complex with the stoichiometry, $[Zn(3\text{-mpSO}_3)_2(H_2O)_2]$ (**6**, vide infra) was formed. However, the related ligand, 4-mpSO_3H with zinc(II) bromide formed a complex of stoichiometry, Zn(4-mpSO_3)$_2$ which is also an one-dimensional coordination polymer **2**.

Figure 1 and 2 show the polymers along the *c* axis and *a* axis, respectively, with the numbering schemes (3 metal atoms shown in each case). The formation of **1** is believed to take place by initially forming the moiety, *trans*-Cu(3-mpSO_3)$_2$ (A) in which 3-mpSO_3 forms five-membered rings. This moiety (repeat unit) combines with another unit via free oxygen atoms along the axial side forming the dimer with eight-membered rings [$Cu_2O_4S_2$ core] and this process continues to finally form the one-dimensional infinite polymer. In this polymer each Cu atom is bonded to 2 N and 4 O atoms; two N and two O atoms occupy *trans* positions of the square plane of the CuN_2O_2 core and the geometry around each Cu center is elongated octahedral. The axial Cu−O [2.438(10) Å] bonds are longer than the equatorial Cu−O bonds [1.989(8) Å] by ca. 0.45 Å. Further, the equatorial Cu−O and Cu−N [1.97(10) Å] bond lengths are close to the sum of the covalent radii of Cu and O (1.93 Å) or Cu and N (1.95 Å), respectively. The longer Cu−O axial bonds lead to shorter S(1)−O(3) bonds and the free S(1)−O(2) bond length is in between the two extremes. These S−O distances are much less than the sum of the

 © 2004 Wiley-VCH Verlag GmbH & Co. KGaA, Weinheim

Table 1. Bond lengths (Å) and angles (°) for compounds **1**−**11**

$[ML_2]_n$ L = 3-mpSO$_3$	$[CuL_2]_n$ (**1**) L = 4-mpSO$_3$	$[ZnL_2]_n$(**2**) L = 3-mpSO$_3$	[VOL(acac)(H$_2$O)] (**11**)	
M(1)−O(1)	1.989(8)	2.111(1)	V(1) −O(1)	2.171(2)
M(1) − O(3**)	2.438(10)	2.182(1)	V(1)−O(4), O(5)	1.974(2), 1.975(2)
M(1)−N(1)	1.97(1)	2.069(1)	V(1)−N(1)	2.155(2)
S(1)−C(1)	1.81(1)	1.790(2)	S(1)−C(1)	1.786(2)
S(1)−O(1)	1.488(8)	1.469(1)	S(1)−O(1)	1.467(2)
S(1)−O(2)	1.449(10)	1.433(1)	V(1)−O(6)	1.588(2)
S(1)−O(3)	1.409(10)	1.462(1)	V(1)−O(7)	2.060(2)
N(1)−M(1) −N(1*)	180.0	180.0	N(1)−V(1) −O(1)	76.04(6)
O(1)−M(1) −O(1*)	180.0	180.0	O(1)−V(1) −O(6)	169.59(8)
O(1)−M(1) −N(1)	86.1(4)	82.85(5)	O(4) −V (1) −O(5)	89.75(7)
M(1)−O(1) −S(1)	118.4(5)	117.74(6)	V(1) −O(1) −S(1)	123.13(9)
O(1)−S(1) −C(1)	101.8(5)	104.46(7)	O(1) −S(1) −C(1)	103.13(10)
S(1) −C(1) −N(1)	115.3(9)	116.3(1)	S(1) −C(1) −N(1)	113.7(1)
C(1) −N(1) −M(1)	116.7(8)	117.2(1)	C(1) −N(1)−V(1)	121.8(1)
			O(7) −V(1) −O(4)	91.08(8)
Intermolecular parameters				
			O(3) ··· O(7)	2.697(3)
			O(2) ··· O(7)	2.730(3)

$[ML_2(H_2O)_2]$ L = 3-mpSO$_3$	$[MnL_2(H_2O)_2]$ (**3**)	$[FeL_2(H_2O)_2]$ (**4**)	$[CoL_2(H_2O)_2]$ (**5**)	$[ZnL_2(H_2O)_2]$ (**6**)
M(1)−O(1)	2.187(2)	2.137(2)	2.103(2)	2.155(1)
M(1)−O(4)	2.164(2)	2.109(2)	2.090(2)	2.095(1)
M(1)−N(1)	2.242(2)	2.175(2)	2.126(2)	2.109(1)
S(1)−C(1)	1.802(2)	1.796(2)	1.797(2)	1.797(2)
S(1)−O(1)	1.457(2)	1.459(2)	1.463(2)	1.458(1)
S(1)−O(2)	1.443(2)	1.444(2)	1.442(2)	1.443(2)
S(1)−O(3)	1.451(2)	1.446(2)	1.444(2)	1.447(1)
N(1)−M(1)−N(1*)	155.01(9)	157.1(1)	159.8(1)	158.12(8)
O(1)−M(1)−O(1*)	96.9(1)	96.5(1)	98.1(1)	97.76(9)
O(1)−M(1)−N(1)	76.28(6)	77.99(7)	80.0(7)	79.90(5)
O(4)−M(1)−O(4*)	82.8(2)	82.3(1)	83.7(1)	83.51(9)
M(1)−O(1)−S(1)	123.75(10)	123.0(1)	121.75(10)	120.37(7)
O(1)−S(1)−C(1)	104.8(1)	104.3(1)	104.4(1)	104.82(8)
S(1)−C(1)−N(1)	114.2(1)	114.1(1)	114.1(2)	114.6(1)
C(1)−N(1)−M(1)	120.5(1)	120.2(1)	119.4(1)	120.0(1)
Intermolecular parameters				
O(2) ··· O(4)	2.814(3)	2.812(3)	2.837(3)	2.818(2)
O(3) ··· O(4)	2.718(3)	2.718(3)	2.729(3)	2.723(2)
Stacking interaction	ca. 3.47	ca. 3.48	ca. 3.49	ca. 3.50

$[ML_2(H_2O)_2]$	$[ZnL_2(H_2O)_2]$ (**7**) L = 5-mpSO$_3$	$[ZnL_2(H_2O)_2]$ (**8**) L = PySO$_3$	$[CoL_2(H_2O)_2]$ (**9**) L = 4-mpSO$_3$	$[NiL_2(H_2O)_2]\cdot H_2O$ (**10**) L = 3-mpSO$_3$
M(1)−O(1)	2.189(2)	2.156(3)	2.118(1)	2.057(2)
M(1)−O(4)	2.073(2)	2.051(3)	2.071(2)	2.057(2)
M(1)−N(1)	2.102(2)	2.144(3)	2.120(2)	2.085(2)
S(1)−C(1)	1.787(2)	1.783(3)	1.785(2)	1.795(3)
S(1)−O(1)	1.454(2)	1.453(3)	1.466(1)	1.466(2)
S(1)−O(2)	1.448(2)	1.440(3)	1.448(2)	1.440(2)
S(1)−O(3)	1.442(2)	1.438(3)	1.447(2)	1.444(3)
N(1)−M(1)−N(1*)	161.07(9)	165.2(2)	180.0	169.6(1)
O(1)−M(1)−O(1*)	98.18(10)	93.0(2)	180.0	94.3(1)
O(1)−M(1)−N(1)	80.16(6)	80.7(1)	81.37(5)	82.27(8)
O(4)−M(1)−O(4*)	85.66(10)	86.1(2)	180.0	86.6(1)
M(1)−O(1)−S(1)	117.62(9)	118.6(1)	116.98(8)	120.1(1)
O(1)−S(1)−C(1)	104.29(9)	105.3(2)	103.85(8)	104.9(1)
S(1)−C(1)−N(1)	115.3(1)	116.0(2)	114.4(1)	114.0(2)
C(1)−N(1)−M(1)	118.8(1)	117.2(2)	116.7(1)	118.4(2)
Intermolecular parameters				
O(2) ··· O(4)	2.760(2)	2.730(4)	2.769(2)	2.715(3)
O(3) ··· O(4)	2.748(2)	2.704(4)	2.741(2)	–
O(3) ··· O(5)	–	–	–	2.784(3)
O(4) ··· O(5)	–	–	–	2.760(4)
Stacking interaction	ca. 3.96	ca. 3.70	–	ca. 3.82

covalent radii of S and O atoms (1.75 Å).[20] It shows partial double bond character of the S−O bonds. The S(1)−C(1) distance is close to that of a single covalent bond length (1.79 Å) (Table 1).

The formation of polymer **2** can be viewed in a manner similar to that of **1**; however the axial Zn−O [2.182(1) Å] and equatorial Zn−O [2.111(1) Å] bond lengths are comparable and coupled with the bond angles, the geometry around each zinc(II) center is close to an ideal octahedron. It may be noted that the variations in coordinated bond lengths are controlled by the metal-oxygen interactions. The stronger M−O bonds lead to long S−O bonds and vice

Table 2. A summary of important highlights of compounds **1**−**11**

Compound	Structure type	Crystal system	Space group	π−π (Å)
$[\{Cu(3\text{-}mpSO_3)_2\}_n]$ (**1**)	Coordination polymer	monoclinic	$P2_1/n$(no. 14)	Nil
$[\{Zn(4\text{-}mpSO_3)_2\}_n]$ (**2**)	Coordination polymer	monoclinic	$P2_1/c$(no. 14)	Nil
$Mn(3\text{-}mpSO_3)_2(H_2O)_2]$ (**3**)	H-bonded polymer	monoclinic	$C2/c$(no. 15)	3.47
$Fe(3\text{-}mpSO_3)_2(H_2O)_2]$ (**4**)	H-bonded polymer	monoclinic	$C2/c$(no. 15)	3.48
$Co(3\text{-}mpSO_3)_2(H_2O)_2]$ (**5**)	H-bonded polymer	monoclinic	$C2/c$(no. 15)	3.49
$Zn(3\text{-}mpSO_3)_2(H_2O)_2]$ (**6**)	H-bonded polymer	monoclinic	$C2/c$(no. 15)	3.50
$[Zn(5\text{-}mpSO_3)_2(H_2O)_2]$ (**7**)	H-bonded polymer	monoclinic	$C2/c$(no. 15)	3.96
$[Zn(PySO_3)_2(H_2O)_2]$ (**8**)	H-bonded polymer	monoclinic	$C2/c$(no. 15)	3.70
$[Co(4\text{-}mpSO_3)_2(H_2O)_2]$ (**9**)	H-bonded polymer	triclinic	$P\bar{1}$(no. 2)	Nil
$[Ni(3\text{-}mpSO_3)_2(H_2O)_2]H_2O$ (**10**	H-bonded polymer	monoclinic	$C2/c$(no. 15)	3.82
$[VO(3\text{-}mpSO_3)(acac)(H_2O)]$ (**11**)	H-bonded polymer	monoclinic	$P2_1/c$(no. 14)	Nil

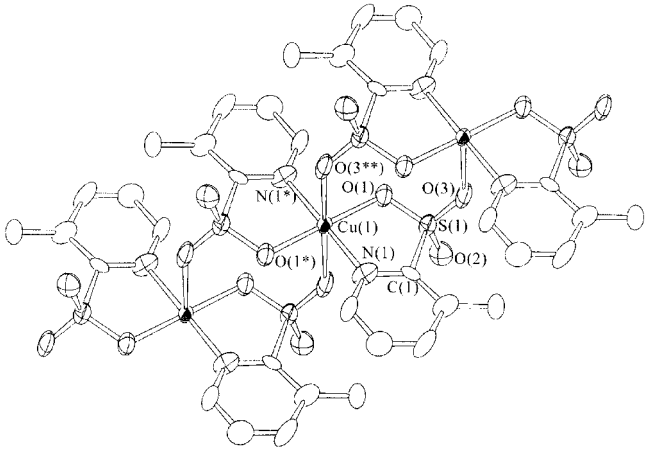

Figure 1. One-dimensional infinite structure of $[\{Cu(3\text{-}mpSO_3)_2\}_n]$ (**1**) along the *c* axis

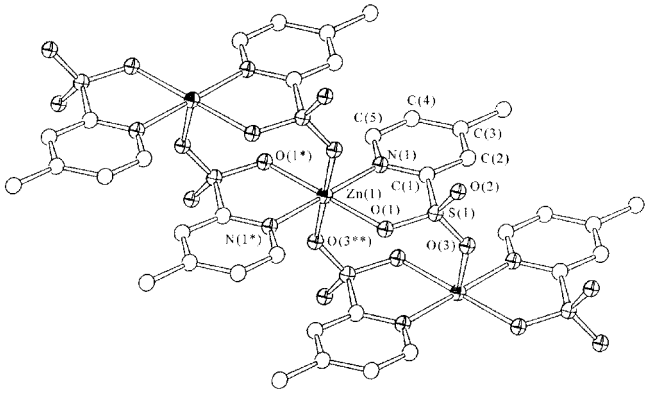

Figure 2. One-dimensional infinite structure of $[Zn(4\text{-}mpSO_3)_2]_n$ (**2**) along the *a* axis

versa. The S(1)−O(2) bonds of the RSO_3 groups, which are not involved in bonding to the metals in polymers **1** and **2** are also marginally affected by the change of the metal (Table 1). The OMN bite angle is 86.1(4)° in the Cu polymer and 82.85(5)° in the zinc polymer and this is probably linked with the size of the metal center. The angles at O(1), S(1), C(1) and N(1) are also affected by the bite angles. The large bite angle at the Cu^{I} center is accompanied by a relatively large angle at O(1) and smaller angles at S(1), C(1), and N(1), while the reverse trend is shown by the zinc polymer. Thus in compounds **1** and **2**, $3\text{-}mpSO_3^-$ and $4\text{-}mpSO_3^-$ ligands act as N,O,O donor sets with one free S−O bond in each case.

Structures of Mononuclear Units (*Types b*−*d*)

Compounds **3**−**9** (*type b*) have the same structural formula, $[ML_2(H_2O)_2]$ and the differences lie in the nature of the metal, presence of a methyl substituent in the pyridyl ring and the position of the water ligands. Thus the compounds, **3**−**6** have $3\text{-}mpSO_3^-$ while **7**−**9** have $5\text{-}mpSO_3^-$, $PySO_3^-$ and $4\text{-}mpSO_3^-$, respectively, as the anionic ligands. Further, H_2O molecules occupy *cis* positions of the octahedral compounds **3**−**8** (Figure 3) and *trans* positions in compound **9** (Figure 4).

Compounds **3**−**8** are monoclinic with space groups, $C2/c$, **9** has triclinic crystals with space group $P\bar{1}$, and **3**−**6** are isomorphic. It shows that the position of water in the octahedron and not the substituent of the pyridyl ring most probably determines the crystal system (Table 2 and 3). Figure 3 (only structure of compound **3** shown) and Figure 4 (compound **9**) show the numbering schemes of the complexes. The molecular structure of each of compounds **3**−**9** consists of two N,O-chelating RSO_3^- (R = Py, x-Py) ligands and two water molecules; the divalent metal center, Co^{II} is located on the crystallographic inversion center in compound **9**.

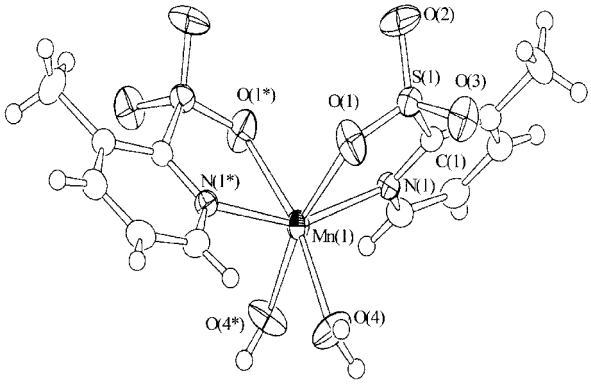

Figure 3. ORTEP drawing of $[Mn(3\text{-}mpSO_3)_2(H_2O)_2]$ (**3**) showing the numbering scheme

 © 2004 Wiley-VCH Verlag GmbH & Co. KGaA, Weinheim

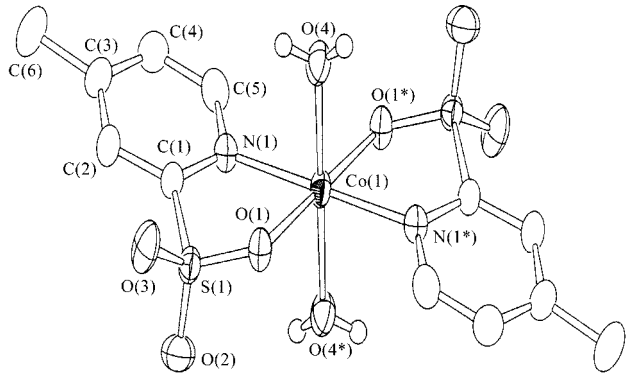

Figure 4. ORTEP view of *trans*-[Co(4-mpSO$_3$)(H$_2$O)$_2$] (**9**) showing the numbering scheme

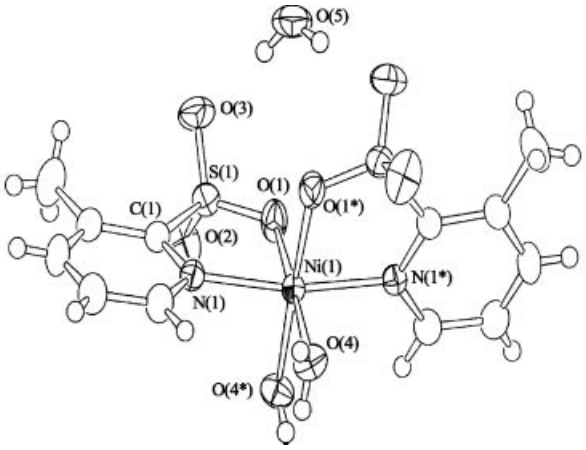

Figure 5. ORTEP view of *cis*-[Ni(3-mpSO$_3$)$_2$(H$_2$O)$_2$]·H$_2$O (**10**)

A discussion on the differences in the bond parameters of **3**−**9** now follows. In these compounds, M(1)−O(1), O(1*), N(1) and N(1*) bonds are related to the RSO$_3^-$ moiety and M−O(4), O(4*) bonds refer to the coordinated H$_2$O molecules. The oxygen atoms of S−O(2) and S−O(3) bonds are free and engage in the intermolecular hydrogen bonding (vide infra). In compound **3**, the M(1)−O(1) bond length, 2.187(2) Å, is close to the sum of the covalent radii of Mn and O (2.12 Å).[20] The Mn(1)−O(4) bond length, 2.164(2) Å, is less than the Mn(1)−O(1) bond length and it shows that water is relatively more tightly bonded to Mn(1). The Mn(1)−N(1) bond length, 2.242(2) Å, is also close to the sum of the covalent radii of Mn and N (2.14 Å).[20] The trend in M(1)−O(1), O(4), N(1) bond lengths for compounds **4**−**9** is similar. The metal−ligand bond lengths clearly vary with the size of the central metal atom: Mn > Fe > Co > Ni. The coordinated S(1)−O(1) bond is only marginally longer than the uncoordinated S(1)−O(2), O(3) bonds in all these compounds (Table 1). All these S−O bond lengths are less than the sum of the covalent radii of S and O atoms (1.75Å).[20] Finally, S(1)−C(1) distances lie in the narrow range ca.1.783−1.802 Å and close to the single covalent bond length (1.79 Å).

Each of compounds **3**−**8** have a distorted octahedral geometry and the *trans* N(1)−M−N(1*) bond angles are in the range, ca. 155−165°; however, compound **9** has a perfect octahedral geometry. The bite angle, O(1)−M(1)−N(1) of the pyridine-2-sulfonates lie in the range, ca. 76−81° in compounds **3**−**9** and these bite angles are less than those shown by **1** (ca. 86°) and **2** (ca. 83°). Thus compound **1** showed the largest bite angle among complexes **1**−**9**. The coordinated H$_2$O molecules are *trans* in compound **9** and cause the O(4)−M−O(4*) bond angles to be ca. 82−86° in complexes **3**−**8**. The trend of bond angles at O(1), S(1), C(1) and N(1) atoms is similar to that observed in compounds **1** and **2** (Table 1).

Figure 5 and 6 show molecular structures with numbering schemes of compounds **10** (*type c*) and **11** (*type d*), respectively. Compound **10** has two chelating 3-mpSO$_3^-$ ligands, two coordinated water molecules and one lattice water molecule. It also crystallizes in the *C*-centered monoclinic space group *C*2/*c* (Table 2 and 3) and it has a molecular structure similar to that of **3** (Figure 3). The bond parameters are also similar to those of compounds 3−9 except that Ni(1)−O(1) and Ni(1)−(4) (coordinated H$_2$O) have the same bond lengths. Finally compound **11** formed monoclinic crystals with space group, $P2_1/c$ and in this compound the VO^{2+} ion is coordinated by a water molecule and two different chelating ligands, acac$^-$ and 3-mpSO$_3^-$(Table 3). The geometry around the vanadium(IV) center is distorted octahedral. The equatorial plane of the vanadyl is occupied by the O atom of the water molecule, N atom of 3-mpSO$_3^-$ and two O atoms of acac. One oxygen atom of 3-mpSO$_3$ occupies a position *trans* to the V=O group. The bond angles and lengths show trends similar to those of compounds **3**−**10**; the V=O bond as expected, is the shortest bond [V(1)−O(6) = 1.588(2) Å]. The acac$^-$ ion forms bonds stronger than those formed by the oxygen atom of 3-mpSO$_3^-$ or it may be the *trans* effect of V=O bond which lengthens V(1)−O(1) bond vis-à-vis V(1)−O(4), O(5) bonds which are short.

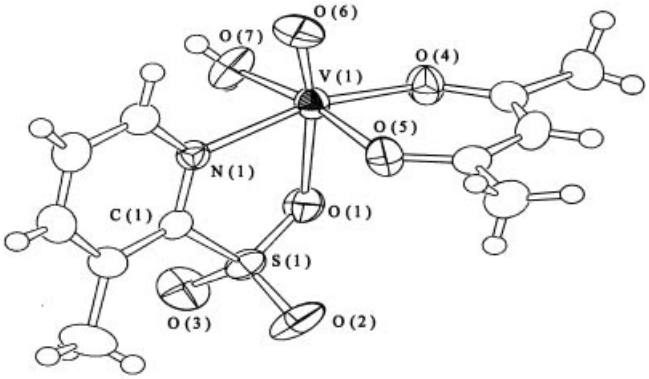

Figure 6. ORTEP drawing of [VO(acac)(3-mpSO$_3$)(H$_2$O)] (**11**)

Hydrogen-bonded Supramolecules

The coordinated water molecules of mononuclear compounds **3**−**11** as well as the lattice water molecule of **10** are engaged in the formation of intermolecular hydrogen bonds between the mononuclear units leading to the construction

 © 2004 Wiley-VCH Verlag GmbH & Co. KGaA, Weinheim

Table 3. Crystal data for compounds **1**−**11**

Compound	**1**	**2**	**3**	**4**
T/K	296	296	296	296
Empirical formula	$C_{12}H_{12}CuN_2O_6S_2$	$C_{12}H_{12}N_2O_6S_2Zn$	$C_{12}H_{16}MnN_2O_8S_2$	$C_{12}H_{16}FeN_2O_8S_2$
M_r	407.90	409.74	435.32	436.23
Crystal system	monoclinic	monoclinic	monoclinic	monoclinic
Space group	$P2_1/n$(No. 14)	$P2_1/c$(No. 14)	$C2/c$(No. 15)	$C2/c$(No. 15)
a (Å)	18.627(2)	4.993(1)	19.152(4)	19.069(2)
b (Å)	7.890(2)	14.691(1)	7.472(4)	7.427(2)
c (Å)	4.960(2)	10.194(1)	14.303(4)	14.224(2)
β [°]	89.96(2)	102.40(1)	125.709(10)	125.757(4)
V (Å^3)	729.0(4)	730.4(2)	1661.9(9)	1634.8(4)
Z	2	2	4	4
$D_{calcd.}$ [g cm^{-3}]	1.858	1.863	1.740	1.772
μ [mm^{-1}]	1.817	2.00	1.090	1.223
F(000)	414.00	416.00	892.00	896.00
Data collected	2310	2430	2677	2637
Unique data(R_{int})	2253(0.021)	2209(0.016)	2603(0.015)	2566(0.021)
Observed data [$I > 3\sigma(I)$]	1726	1920	1999	1979
Final *R* [$I > 3\sigma$(I)]	0.124	0.024	0.040	0.036
wR	0.192	0.039	0.053	0.053
Goodness of fit, *S*	5.29	1.55	1.71	1.76
$\Delta\rho_{min.}$, $\Delta\rho_{max.}$ [e·Å^{-3}]	−2.98, 3.36	−0.58, 0.30	−0.69, 0.40	−0.55, 0.36

Compound	**5**	**6**	**7**	**8**
T/K	296	296	296	296
Empirical formula	$C_{12}H_{16}CoN_2O_8S_2$	$C_{12}H_{16}N_2O_8S_2Zn$	$C_{12}H_{16}N_2O_8S_2Zn$	$C_{10}H_{12}N_2O_8S_2Zn$
M_r	439.32	445.77	445.77	417.71
Crystal system	monoclinic	monoclinic	monoclinic	monoclinic
Space group	$C2/c$(No. 15)	$C2/c$(No. 15)	$C2/c$(No. 15)	$C2/c$(No. 15)
a (Å)	19.091(2)	19.058(1)	13.884(2)	13.714(3)
b (Å)	7.367(4)	7.381(1)	7.336(1)	7.150(3)
c (Å)	14.313(2)	14.321(1)	17.932(2)	15.985(3)
β [°]	126.063(6)	126.176(4)	114.065(7)	107.16(1)
V (Å^3)	1627.4(6)	1626.2(3)	1667.7(4)	1497.6(7)
Z	4	4	4	4
$D_{calcd.}$ [g cm^{-3}]	1.793	1.821	1.775	1.852
μ [mm^{-1}]	1.357	1.813	1.768	1.962
F(000)	900.00	912.00	912.00	848.00
Data collected	2636	2630	2714	2433
Unique data(R_{int})	2564(0.021)	2556(0.021)	2612(0.015)	2341(0.016)
Observed data [$I > 3\sigma(I)$]	1776	2056	2274	1746
Final *R* [$I > 3\sigma(I)$]	0.033	0.027	0.033	0.046
wR	0.043	0.038	0.054	0.065
Goodness of fit, *S*	1.25	1.34	1.34	2.19
$\Delta\rho_{min.}$, $\Delta\rho_{max.}$ [e·Å^{-3}]	−0.48, 0.35	−0.47, 0.30	−1.13, 0.35	−1.42, 0.44

Compound	**9**	**10**	**11**
T/K	296	296	296
Empirical formula	$C_{12}H_{16}CoN_2O_8S_2$	$C_{12}H_{18}N_2NiO_9S_2$	$C_{11}H_{15}NO_7SV$
M_r	439.32	457.10	356.24
Crystal system	triclinic	monoclinic	monoclinic
Space group	$P\bar{1}$(No. 2)	$C2/c$(No. 15)	$P2_1/c$(No. 14)
a (Å)	7.430(2)	18.711(3)	13.759(2)
b (Å)	8.507(2)	8.364(2)	7.114(1)
c (Å)	7.207(1)	13.943(2)	15.503(1)
α [°]	99.01(2)		
β [°]	95.35(2)	124.851(8)	103.660(8)
γ [°]	69.45(1)		
V (Å^3)	420.9(1)	1790.7(6)	1474.6(3)
Z	1	4	4
$D_{calcd.}$ [g cm^{-3}]	1.733	1.695	1.605
μ [mm^{-1}]	1.312	1.366	0.844
F(000)	225.00	944.00	732.00
Data collected	5276	2843	4796
Unique data(R_{int})	2456(0.040)	2766(0.031)	4622(0.022)
Observed data [$I > 3\sigma(I)$]	2131	1929	2899
Final *R* [$I > 3\sigma(I)$]	0.034	0.040	0.034
wR	0.048	0.048	0.044
Goodness of fit, *S*	1.72	1.45	1.38
$\Delta\rho_{min.}$, $\Delta\rho_{max.}$ [e·Å^{-3}]	−0.48, 0.31	−1.15, 0.47	−0.35, 0.26

of the two-dimensional (**3**−**10**) and one-dimensional (**11**) supramolecules. Compounds **3**−**8** and **10** showed additional noncovalent π−π interactions, not shown by compounds **9** and **11**. The uncoordinated sulfonato oxygen atoms and coordinated water molecules of compounds **3**−**6** containing 3-mpSO_3^- ligands connect each mononuclear

 © 2004 Wiley-VCH Verlag GmbH & Co. KGaA, Weinheim

unit via the intermolecular hydrogen bonds, O(2)··· H-O(4) and O(3)··· H−O(4) (Table 1) to form two-dimensional hydrogen-bonded networks parallel to the *bc* plane. For example, Figure 7 shows the H bonded network of compound **3** parallel to the *bc* plane. In the two-dimensional network, the adjacent molecules along the *b* axis have the same orientation, while the neighboring molecules along the *c* axis have inverted structures of the original molecule and are in the opposite orientation to the original. All of the pyridine rings of the 3-mpSO$_3^-$ ligands are stacked by relatively strong π−π interactions (ca. 3.47Å) as shown for the crystal packing of **3** in Figure 8. Compounds **4**−**6** have the same hydrogen and π−π stacking patterns and their intermolecular parameters are listed in Table 1.

The hydrogen bonding in compound **8** containing the pySO$_3^-$ ligand forms a two-dimensional network parallel to the *ab* plane (Figure 9). The two dimensional hydrogen-bonded sheets are stacked over each other by π−π interactions (ca. 3.70 Å) of the pyridine rings in an offset geometry as shown in Figure 10.

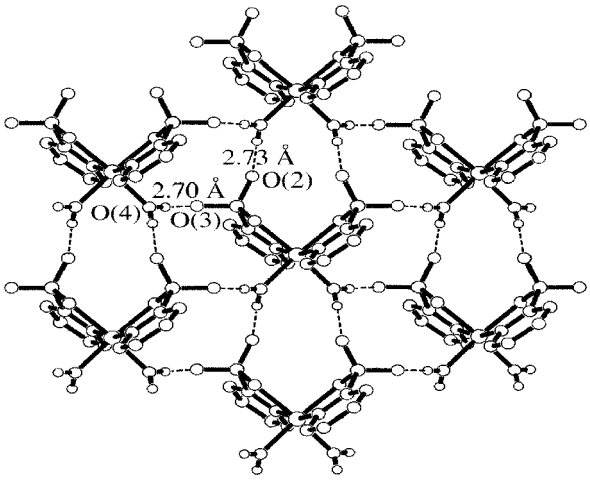

Figure 9. H bonded network of [Zn(PySO$_3$)$_2$(H$_2$O)$_2$] (**8**) parallel to the *ab* plane

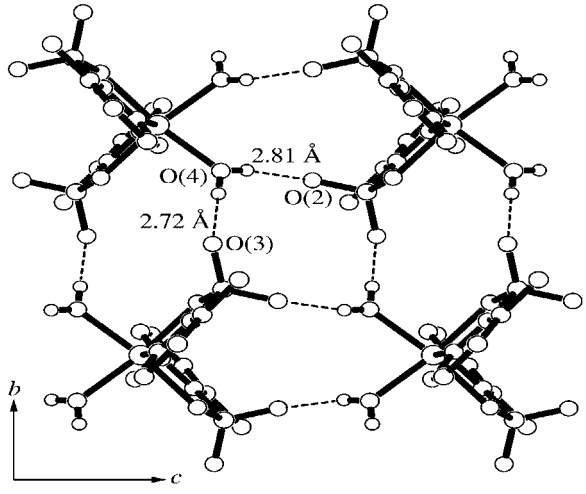

Figure 7. H bonded network of [Mn(3-mpSO$_3$)$_2$(H$_2$O)$_2$] (**3**) parallel to the *bc* plane

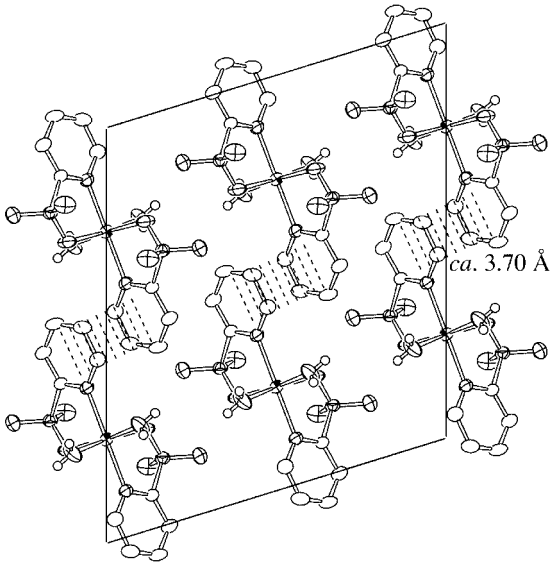

Figure 10. Crystal packing of [Zn(PySO$_3$)$_2$(H$_2$O)$_2$] (**8**) when viewed along the *b* axis

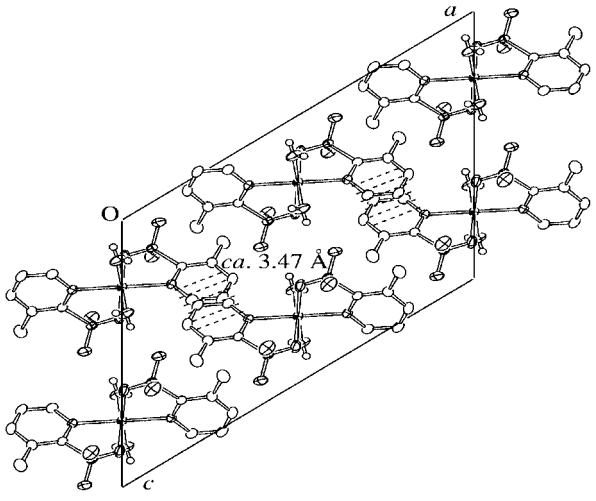

Figure 8. Crystal packing of [Mn(3-mpSO$_3$)$_2$(H$_2$O)$_2$] (**3**) when viewed along the *b* axis

The hydrogen-bonded network of compound **7** containing the 5-mpSO$_3^-$ ligand is also similar to that of **8.** Figure 11 shows that the pyridine rings of the 5-mpSO$_3^-$ ligands are most weakly stacked over each other (ca. 3.96 Å), as compared to the aromatic stacking in the crystals of **3**−**6**, **8** and **10**. Therefore, the calculated density for **7** (1.775 g·cm^{-3}) is clearly less than that for compound **6** (1.821 g·cm^{-3}) even though the two zinc complexes have a common chemical formula. It may be further noted that the

 © 2004 Wiley-VCH Verlag GmbH & Co. KGaA, Weinheim

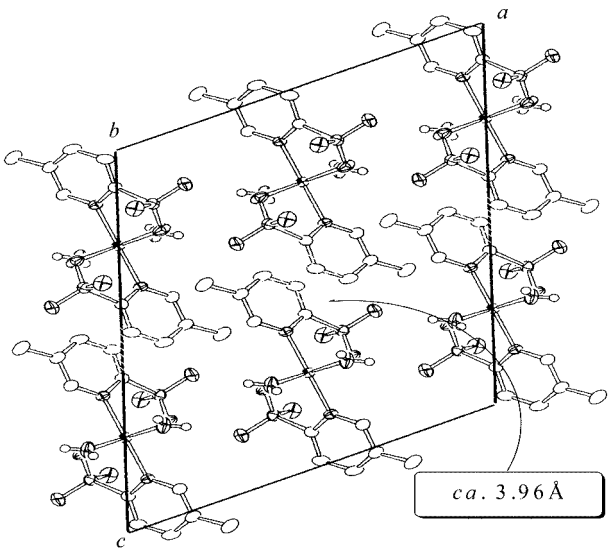

Figure 11. Crystal packing of $[Zn(5\text{-}mpSO_3)_2(H_2O)_2]$ (**7**) when viewed along the *b* axis, geometry as shown in Figure 10

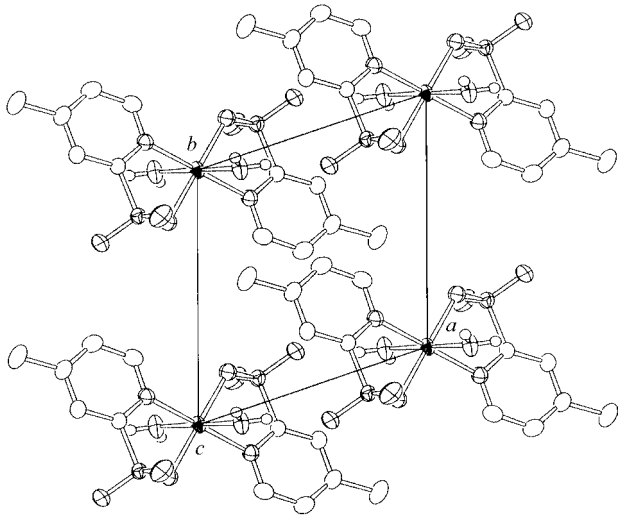

Figure 13. Crystal packing of $[Co(4\text{-}mpSO_3)_2(H_2O)_2]$ (**9**) when viewed along the *c* axis

stacking interaction in compound **6** (ca. 3.50 Å) is stronger than that in compound **8** (above).

It may be interesting to add here that the stoichiometry of zinc(II) complexes **6**−**8** is different from that of **2** which is a one-dimensional polymer as described earlier. The exceptional behavior can be ascribed to the steric effect of the methyl group at the 4-position in the pyridine ring of the 4-$mpSO_3^-$ ligand in **2**. The methyl group sticking out along the Zn(1)-N(1)···C(3) line is probably unfavorable for the formation of hydrogen-bonded networks similar to those of complexes **6**−**8**.

In compound **9**, the hydrogen-bonded network is spread out parallel to the *ac* plane (Figure 12) and it does not show any π−π interaction in the crystal structure (Figure 13) unlike that shown by compound **5**. The methyl group at the 4-position in the 4-$mpSO_3^-$ ligand elongates the structure of **9** along the Co(1)-N(1)···C(3) line and this structural elongation may be the main factor for the absence of π−π interactions in its crystal structure. In compound **10**, two uncoordinated oxygen atoms of 3-$mpSO_3^-$ [O(2), O(3)] participate in intermolecular hydrogen bonds with the coordinated and lattice water molecules leading to the formation of two-dimensional hydrogen-bonded networks (Figure 14). The H bonded sheets are stacked by the π−π interactions of the pyridyl rings in an offset geometry (Figure 15). Finally for compound **11**, the self-assembly of the mononuclear complexes results in the formation of a one-dimensional supramolecular structure along the crystallographic *b* axis (Figure 16).

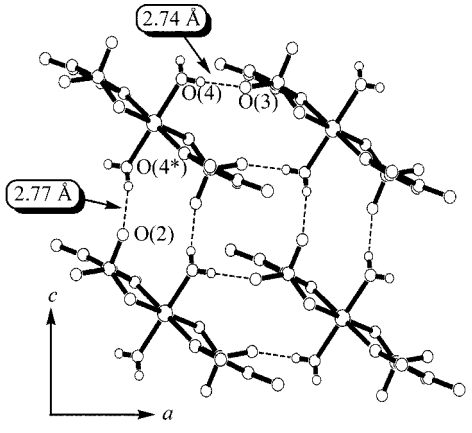

Figure 12. H bonded network of $[Co(4\text{-}mpSO_3)_2(H_2O)_2]$ (**9**) parallel to the *ac* plane

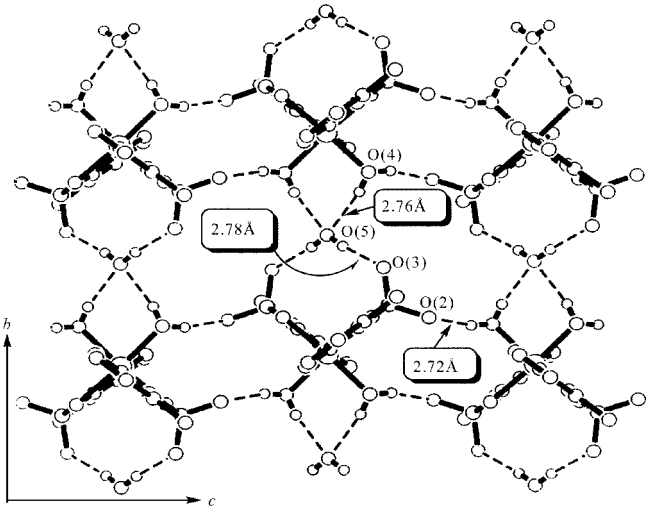

Figure 14. H-bonded network of $[Ni(3\text{-}mpSO_3)_2(H_2O)_2]\cdot H_2O$ (**10**) parallel to the *bc* plane

Magnetic Properties

The magnetic measurement studies of compounds **3** and **11** were carried out in order to check for possible magnetic exchange interactions, if any, between adjacent metal centers of the hydrogen-bonded networks. The variable temperature magnetic susceptibility studies revealed that these compounds are typical paramagnetic compounds with ground spin-states of $S = 5/2$ for **3** and $S = 1/2$ for **11**. The

 © 2004 Wiley-VCH Verlag GmbH & Co. KGaA, Weinheim

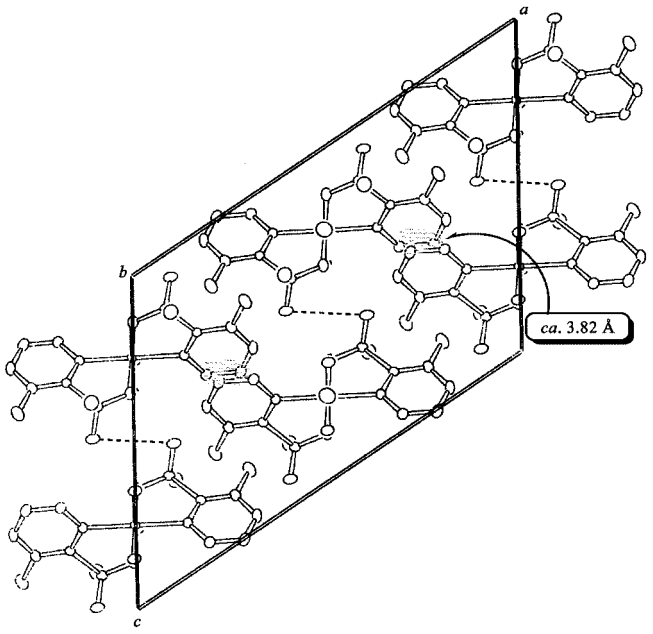

Figure 15. Crystal packing of $[Ni(3\text{-}mpSO_3)_2(H_2O)_2]\cdot H_2O$ (**10**) when viewed along the *b* axis

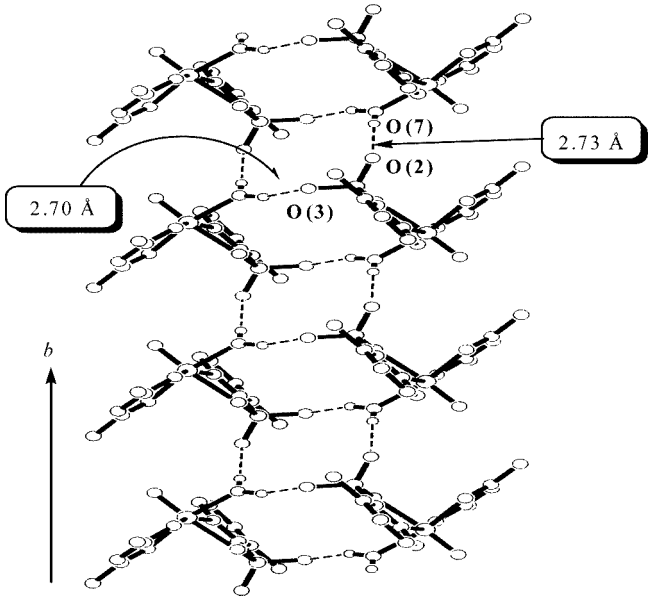

Figure 16. One-dimensional hydrogen-bonded network of complex **11**

magnetic behavior indicates that the intermetallic distances (7.11−7.47 Å) in these network structures are too long to cause any intermolecular magnetic interactions. Other complexes (**1**, **4**, **5**, **9** and **10**) also showed typical paramagnetic behavior.

Solution Phase Behavior

The NMR spectroscopic data of the ligands and zinc(II) complexes recorded in CD_3OD solvent are listed in the Exp. Sect. The ligand spectra are broad as well as partially resolved in view of the exchange of a proton between a N atom and sulfonate SO_3 groups and after the deprotonation of the complexes, the spectra generally become sharp as well as better resolved indicating metal−ligand interaction. Consider first $PySO_3$ and its compound **8**, three pyridyl ring protons show a high-field shift and the magnitude of the shift varies as follows: H(4) > H(5) > H(3). The H(6) proton close to the N coordinating center can be considered as essentially unchanged. The same trend is shown by the compounds **2**, **6** and **7**. The methyl group of $3\text{-}mpSO_3^-$ in compound **6** shows a low-field shift, but the 4-and 5-methyl groups of compounds **2** and **7** show high-field shifts. This difference is understandable in view of the deshielding influence of the sulfonate group, which exerts the largest effect on the methyl group at the 3-position. This is in line with the relatively low up-field shift of H(3) protons of compounds **2**, **7** and **8** which are close to the SO_3 group. NMR spectroscopic studies reveal one very interesting observation that electron density of pyridyl rings is highly polarized and the H(4) (or, 4-Me) and H(5) (or, 5-Me) protons experience high diamagnetic shielding. The NMR spectrum of compound **6** shows that the group $3\text{-}mpSO_3^-$ has distinctly different behavior, which was also reflected in the solid state (compounds **3**−**6**, vide supra).

Conclusions

The location of methyl substituents at the 3-position of the pyridyl ring ($3\text{-}mpSO_3$ ligand) appears to be most suited to induce close π−π stacking interactions (3.47−3.50 Å), a prerequisite for possible electrical conductivity properties. $PySO_3^-$ in compound **8** showed π−π stacking interactions of medium strength (3.70 Å) and the 5-methyl substituent in compound **7** appears to disfavor such interactions leading to a very weak interaction, ca. 3.96 Å. The stacking in $[Ni(3\text{-}mpSO_3)_2(H_2O)_2]\cdot H_2O$ (**10**) is weakened by the presence of water of hydration which increases π−π stacking distance to 3.82 Å compared to other $3\text{-}mpSO_3$ analogs (compounds **3**−**6**). Interestingly the methyl substituent at the 4-position totally disfavors the π−π stacking interactions as for example in compound, $[Co(4\text{-}mpSO_3)_2(H_2O)_2]$ (**9**), because of elongation of the structure along the Co(1)-N(1)···C(3) line. Compound **11** has a columnar one-dimensional structure, which is not suited for such stacking interactions. An analysis of metal−oxygen and metal−nitrogen bond lengths (Table 1) reveals that (i) along the axial side Cu−O bond is weakest, while the Cu−N bonds are shortest and (ii) that water forms very strong metal−oxygen bonds in all the water ligated compounds (**3**−**11**). The longer Cu−O axial bonds are due to Jahn−Teller distortion. Thus copper(II) water ligation appears to be energetically less favored over copper(II) polymer formation as in compound **1**. The factors for the formation of the coordination polymer $[\{Zn(4\text{-}mpSO_3)_2\}_n]$ (**2**), unlike hydrogen-bonded compound of type **9**, are not well understood. However, the compact polymeric structure as in **2** appears energetically more favored.

 © 2004 Wiley-VCH Verlag GmbH & Co. KGaA, Weinheim

Experimental Section

Materials and Physical Measurements: All chemicals were purchased from Aldrich, Nacharai Tesque, and Wako Pure Chemical. All reagents and solvents were used without further purification. Infrared spectra in the range 4000−400 cm^{-1} were recorded on KBr discs with a JASCO FTIR 420 spectrophotometer. The ^1H NMR spectra were measured with a JEOL Lambda 400 spectrometer. The magnetic susceptibilities were measured with a Quantum Design SQUID magnetometer MPMS. Elemental analyses were carried out by the Analytical Center of Graduate School of Science in Osaka City University.

Synthesis of Ligands: Pyridine-2-sulfonic acid and its methyl-substituted analogs were prepared by the oxidation of the corresponding pyridine-2-thiones as reported in the literature.[21] The substituted pyridine-2-thiones, namely, 1-H-*x*-methylpyridine-2-thiones (*x* = 3, 4, 5) were synthesized via sulfhydrylation of their corresponding 2-bromopyridines.[22] 1-H-*x*-methylpyridine-2-thione (2.25 g, 0.018mol) was dissolved in 40 mL of glacial acetic acid and then 6.5 mL (0.058 mol) of 30% hydrogen peroxide was added to the mixture. The reaction mixture was heated to 80 °C with stirring until the color of the thione completely disappeared. After removal of the solvent by evaporation under a reduced pressure, the resulting residue was recrystallized from water/methanol (1:1, by volume) to afford colorless crystal of *x*-methylpyridine-2-sulfonic acids.

Caution! *The mixture of acetic acid and hydrogen peroxide produces potentially explosive materials. It is preferable that only limited amounts are prepared at a time, while the temperature is maintained with care. Stirring of the reaction mixture should also be well controlled.*

Pyridine-2-sulfonic Acid ($PySO_3H$): Yield 1.77 g (55%). $C_5H_5NO_3S$ (159.17): calcd. C 37.73, H 3.17, N 8.80; found C 37.72, H 3.09, N 8.77. IR: $\tilde{\nu}$ = ν(N−H) + ν(O−H) 3445 (br. w), 3198 (m), 3132 (s) cm^{-1}; ν(C−H) 3110−2931 (w); δ(N−H) + δ(O−H) 1618 (s); ν(C−N) 1600 (s); ν(C−C) 1520 (s); δ(C−H) 1459 (s), 1417 (w), 1359 (w); ν(S−O) 1303 (s), 1269 (vs), 1247 (vs), 1206 (vs), 1166 (s), 1148 (vs), 1090 (s); ν(C−S) 1041 (vs) cm^{-1}. ^1H NMR (400 MHz, [D_4]methanol, 22 °C): δ = 8.76 (br. s, 1 H, 6-H), 8.69 (t, $J_{H,H}$ = 10.3 Hz, 1 H, 4-H), 8.36 (br. s, 1 H, 5-H), 8.10 (br. s, 1 H, 3-H) ppm.

3-Methylpyridine-2-sulfonic Acid (3-$mpSO_3H$): Yield 1.75 g (50%). $C_6H_7NO_3S$ (173.2): calcd. C 41.61, H 4.07, N 8.09; found C 41.52, H 4.04, N 8.08. IR: $\tilde{\nu}$ = ν(N−H) + ν(O−H) 3210 (m), 3165 (s) cm^{-1}; ν(PyC−H) 3106 (s), 3055 (s); δ(N−H) + δ(O−H) 1614 (m); ν(C−N) 1594 (w); ν(C−C) 1511 (s); δ(C−H) 1459 (m),1446 (m), 1388 (m); ν(S−O) 1316 (m), 1292 (m), 1269 (vs), 1251 (vs), 1237 (s), 1217 (vs), 1210 (sh), 1186 (s), 1158 (s), 1146 (m), 1112 (m); ν(C−S) 1035 (vs); δ(C−CH_3) 816 (m), 802 (m). ^1H NMR (400 MHz, [D_4]methanol, 22 °C): δ = 8.53 (d, $J_{H,H}$ = 6.7 Hz, 2 H, 4-H, 6-H), 7.99 (t, $J_{H,H}$ = 6.7 Hz, 1 H, 5-H); 3.27 (s, 3 H, CH_3) ppm.

4-Methylpyridine-2-sulfonic Acid (4-$mpSO_3H$): Yield 1.93 g (55%). $C_6H_7NO_3S$ (173.2): calcd. C 41.61, H 4.07, N 8.09; found C 41.51, H 4.22, N 8.06. IR: $\tilde{\nu}$ = ν(N−H) + ν(O−H) 3532 (br. vs), 3466 (br. vs), 3363 (m), 3238 (m) cm^{-1}; ν(PyC−H) 3091 (m), 3064 (w); ν(MeC−H) 3008−2858 (w); δ(N−H) + δ(O−H) 1626 (s); ν(C−N) 1602 (m); ν(C−C) 1516 (m); δ(C−H) 1463 (br. s), 1367 (w); ν(S−O) 1297 (m), 1271 (vs), 1245 (vs), 1225 (s), 1200 (m), 1133 (m), 1112 (m); ν(C−S) 1054 (vs); δ(C−CH_3) 836 (vs). ^1H NMR (400 MHz, [D_4]methanol, 22 °C): δ = 8.57 (d, $J_{H,H}$ = 5.9 Hz, 1 H, 6-H), 8.20 (s, 3-H, 1 H), 7.92 (d, $J_{H,H}$ = 5.9 Hz, 1 H, 5-H), 3.24 (s, 3 H, CH_3) ppm.

5-Methylpyridine-2-sulfonic Acid (5-$mpSO_3H$): Yield 1.75 g (50%). $C_6H_7NO_3S$ (173.2): calcd. C 41.61, H 4.07, N 8.09; found C 41.57, H 4.09, N 8.08. IR: $\tilde{\nu}$ = ν(N−H) + ν(O−H) 3475 (br. vs), 3417 (br. vs), 3250 (sh), 3175(sh) cm^{-1}; ν(PyC−H) 3101(m); ν(MeC−H) 3000−2800 (w); δ(N−H) + δ(O−H) 1634 (s); ν(C−N) 1620 (m); ν(C−C) 1556 (m); δ(C−H) 1458 (m), 1436 (m); ν(S−O) 1301 (m), 1267 (vs), 1218 (vs), 1153 (s), 1137 (m); ν(C−S) 1048 (vs); δ(C−CH_3) 849 (s). ^1H NMR (400 MHz, [D_4]methanol, 22 °C): δ = 8.60 (s, 1 H, 6-H), 8.52 (d, $J_{H,H}$ = 7.7 Hz, 1 H, 4-H), 8.23 (d, $J_{H,H}$ = 7.7 Hz, 1 H, 3-H); 3.60 (s, CH_3, 3 H) ppm.

Syntheses of Compounds 1−11

[{Cu(3-$mpSO_3$)$_2$}$_n$] (1): A solution of copper(II) bromide (0.20 g, 0.90 mmol) in 3 mL of water was placed at the bottom of an H-shaped cell, and a solution of 3-$mpSO_3H$ (0.31 g, 1.8 mmol) in 3 mL of water was settled at the other bottom of the cell. The bridging part of the cell was slowly immersed with a methanol/water mixture (1:1 by volume), and the cell was kept steady for 2 weeks. Pale blue crystals of **1** were formed at the bridging part of the cell. Yield 0.140 g (38%). $C_{12}H_{12}CuN_2O_6S_2$ (407.90): calcd. C 35.30, H 2.94, N 6.86; found C 35.28, H 2.92, N 6.76. IR: $\tilde{\nu}$ = ν(PyC−H) 3086 (m) cm^{-1}; ν(MeC−H) 3015−2828 (w); ν(C−N) 1589 (m); ν(C−C) 1580 (w); δ(C−H) 1451 (s), 1374 (w); ν(S−O) 1280 (vs), 1208 (m), 1170 (vs), 1147 (vs), 1075 (m); ν(C−S) 1041 (w), 1015 (s); δ(C−CH_3) 847 (m), 813 (s).

[{Zn(4-$mpSO_3$)$_2$}$_n$] (2): An aqueous solution of 4-$mpSO_3H$ (0.14 g, 0.80 mmol) was neutralized with a diluted aqueous sodium hydroxide solution, and the solvent was evaporated to dryness under reduced pressure. The residue was dissolved in 3 mL of water. The resulting solution was mixed with a solution of zinc(II) bromide (0.091 g, 0.40 mmol) in 1 mL of water. The mixture was stirred for 10 minutes. and subsequently allowed to stand for 1 month at room temperature to obtain colorless crystals of **2**. Yield 0.038 g (23%). $C_{12}H_{12}N_2O_6S_2Zn$ (409.74): calcd. C 35.14, H 2.93, N 6.83; found C 35.15, H 2.90, N 6.73. IR: $\tilde{\nu}$ = ν(PyC−H) 3087 (m) cm^{-1}; ν(MeC−H) 2900−3070 (vw); ν(C−N) 1612 (s); ν(C−C) 1551 (w); δ(C−H) 1437 (m), 1401 (m), 1376 (m); ν(S−O) 1285 (sh), 1277 (vs), 1240 (s), 1172 (vs), 1137 (s), 1114 (s); ν(C−S) 1042 (s), 1024 (s) (νC−S); δ(C−CH_3) 849(s).). ^1H NMR (400 MHz, [D_4]methanol, 22 °C)(ppm): δ = 8.52 (br. d, 1 H, 6-H), 7.90 (s, 1 H, 3-H), 7.50 (s, br., 1 H, 5-H), 2.73 (s, 3 H, CH_3) ppm. Compounds **7** and **9** were prepared similarly.

[Mn(3-$mpSO_3$)$_2$(H_2O)$_2$] (3): A solution of manganese(II) acetate (0.10 g, 0.58 mmol) in 2 mL of water was added to a solution of 3-$mpSO_3H$ (0.20 g, 1.2 mmol) in 4 mL of water and the mixture was stirred for 10 minutes. The solution was kept steady for a week to yield colorless crystals of **3**. Yield 0.096 g (38%). $C_{12}H_{16}MnN_2O_8S_2$ (435.32): calcd. C 33.08, H 3.68, N 6.43; found C 33.17, H 3.67, N 6.43. IR: $\tilde{\nu}$ = ν(O−H) 3409 (br. vs), 3352 (br. vs), 3253 (br. s) cm^{-1}; ν(PyC−H) 3090 (w); ν(MeC−H) 3050−2800 (vw); δ(O−H) 1657 (s); ν(C−N) + ν(C−C) 1583 (m); δ(C−H) 1455 (m), 1415 (w), 1392 (w); ν(S−O) 1238 (vs), 1217 (s), 1191 (vs), 1154 (s), 1123 (w), 1076 (m); ν(C−S) 1029 (vs); δ(C−CH_3) 839 (m), 804 (s). Compounds **8** and **10** were prepared similarly.

[Fe(3-$mpSO_3$)$_2$(H_2O)$_2$] (4): A vial containing iron(II) chloride tetrahydrate (0.16 g, 0.80 mmol) was placed under argon to displace the air, and then 2 mL of degassed water was added to the vial to dissolve the salt. A solution of 3-$mpSO_3H$ (0.28 g, 1.6 mmol) in

 © 2004 Wiley-VCH Verlag GmbH & Co. KGaA, Weinheim

5 mL of degassed water was added dropwise to the metal-containing solution by a syringe. The mixture was allowed to stand for 2 days, yielding yellow crystals of **4**, stable in air and moisture. Yield 0.069 g (20%). $C_{12}H_{16}FeN_2O_8S_2$ (436.23): calcd. C 33.01, H 3.67, N 6.42; found C 33.04, H 3.68, N 6.46. IR: $\tilde{\nu}$ = ν(O−H) 3417 (br. vs), 3349 (br. vs), 3253 (br. s) cm^{-1}; ν(PyC−H) 3092 (w), 3064 (w); ν(MeC−H) 3020−2881 (w); δ(O−H) 1658 (s); ν(C−N) + ν(C−C) 1581 (m); δ(C−H) 1456 (m), 1416 (w), 1391 (w); ν(S−O) 1238 (vs), 1217 (w), 1194 (s), 1154 (s), 1125 (w), 1076 (m); ν(C−S) 1027 (s); δ(C−CH_3) 840 (m), 804 (s).

[Co(3-mpSO$_3$)$_2$(H$_2$O)$_2$] (5): A solution of cobalt(II) bromide hexahydrate (0.10 g, 0.31 mmol) in 2 mL of water was added to a solution of 3-mpSO$_3$H (0.11 g, 0.62 mmol) in 5 mL of water and the mixture was stirred for 10 minutes. The solution was concentrated slowly to ca. 3 mL in a dessicator under water vapor pressure, yielding reddish purple crystals of **5**. Yield 0.049 g (36%). $C_{12}H_{16}CoN_2O_8S_2$ (439.32): calcd. C 32.78, H 3.64, N 6.37; found C 32.73, H 3.64, N 6.37. IR: $\tilde{\nu}$ = ν(O−H) 3433 (br. vs), 3358 (br. vs), 3260 (br. s) cm^{-1}; ν(PyC−H) 3092 (w), 3065 (w); ν(MeC−H) 3000−2827 (vw); δ(O−H) 1657 (s); ν(C−N) + ν(C−C) 1586 (m); δ(C−H) 1458 (s), 1391 (w); ν(S−O) 1241 (vs), 1219 (m), 1186 (vs), 1152 (s), 1127 (m), 1076 (m); ν(C−S) 1027 (vs);); δ(C−CH_3) 841 (m), 805 (s).

[Zn(3-mpSO$_3$)$_2$(H$_2$O)$_2$] (6): A solution of zinc(II) bromide (0.091 g, 0.40 mmol) in 2 mL of water was added to a solution of 3-mpSO$_3$H (0.14 g, 0.80 mmol) in 5 mL of water, and the mixture was stirred for 10 minutes. The solution was left for two weeks to yield colorless crystals of **6**. Yield 0.040 g (22%). $C_{12}H_{16}N_2O_8S_2Zn$ (445.77): calcd. C 32.30, H 3.59, N 6.28; found C 32.30, H 3.58, N 6.26. IR: $\tilde{\nu}$ = ν(O−H) 3424 (br. vs), 3356 (vs), 3255 (vs) cm^{-1}; ν(PyC−H) 3093 (m), 3066 (m); ν(MeC−H) 3025−2856 (w); δ(O−H) 1655 (s); ν(C−N) 1587 (s); ν(C−C) 1541 (w); δ(C−H) 1454 (s), 1419 (w), 1391 (m); ν(S−O) 1282 (m), 1237 (vs), 1197 (vs), 1157 (vs), 1127 (s), 1078 (s); ν(C−S) 1031 (vs); δ(C−CH_3) 842 (m), 806 (s). ^{1}H NMR (400 MHz, [D$_4$]methanol, 22 °C): δ = 8.60 (d, $J_{H,H}$ = 4.9 Hz, 1 H, 6-H), 7.99 (d, $J_{H,H}$ = 7.7 Hz, 1 H, 4-H); 7.59 (dd, $J_{H,H}$ = 4.9, 7.7 Hz, 1 H, 5-H), 3.41 (s, 3 H, CH_3) ppm.

[Zn(5-mpSO$_3$)$_2$(H$_2$O)$_2$] (7): Yield 0.068 g (34%). $C_{12}H_{16}N_2O_8S_2Zn$ (445.77): calcd. C 32.30, H 3.59, N 6.28; found C 32.43, H 3.58, N 6.20. IR: $\tilde{\nu}$ = ν(O−H) 3359 (vs), 3245 (s) cm^{-1}; ν(PyC−H) + ν(MeC−H) 3100−2900 (vw); δ(O−H) 1649 (s); ν(C−N) 1598(m); ν(C−C) 1577 (w); δ(C−H) 1473 (m), 1378 (m); ν(S−O) 1298 (m), 1233 (vs), 1207 (vs), 1157 (s), 1125 (s); ν(C−S) 1030 (vs); δ(C−CH_3) 835 (s). ^{1}H NMR (400 MHz, [D$_4$]methanol, 22 °C): δ = 8.58 (s, 1 H, 6-H), 8.02 (d, $J_{H,H}$ = 8.2 Hz, 1 H, 4-H), 7.95 (d, $J_{H,H}$ = 8.2 Hz, 1 H, 3-H); 3.05 (s, 3 H, CH_3) ppm.

[Zn(PySO$_3$)$_2$(H$_2$O)$_2$] (8): Yield 0.016 g (31%). $C_{10}H_{12}N_2O_8S_2Zn$ (417.71): calcd. C 28.73, H 2.87, N 6.70; found C 28.84, H 2.82, N 6.70. IR: $\tilde{\nu}$ = ν(O−H) 3335 (br. vs), 3240 (s) cm^{-1}; ν(PyC−H) 3107(m); δ(O−H) 1650 (s); ν(C−N) 1596 (s); ν(C−C) 1568 (w); δ(C−H) 1470 (m), 1436 (s); ν(S−O) 1300 (m), 1235 (vs), 1205 (vs), 1170 (s), 1159 (s), 1101 (m), 1056 (m); ν(C−S) 1032 (vs). ^{1}H NMR (400 MHz, [D$_4$]methanol, 22 °C): δ = 8.72 (d, $J_{H,H}$ = 5.1 Hz, 1 H, 6-H), 8.18 (t, $J_{H,H}$ = 7.8 Hz, 1 H, 4-H), 8.08 (d, $J_{H,H}$ = 7.8 Hz, 1 H, 3-H), 7.69 (t, $J_{H,H}$ = 6.2 Hz, 1 H, 5-H) ppm.

[Co(4-mpSO$_3$)$_2$(H$_2$O)$_2$] (9): Yield 0.130 g (38%). $C_{12}H_{16}CoN_2O_8S_2$ (439.32): calcd. C 32.78, H 3.64, N 6.37; found C 32.94, H 3.64, N 6.42. IR: $\tilde{\nu}$ = ν(O−H) 3375 (br. vs), 3260 (br. s) cm^{-1}; ν(PyC−H) 3081 (m); ν(MeC−H) 2964−2834 (w); δ(O−H) 1654 (s); ν(C−N) 1611 (s); ν(C−C) 1555 (w); δ(C−H) 1473 (m), 1438 (m), 1405 (m), 1376 (m); ν(S−O) 1240 (vs), 1188 (vs), 1141 (s), 1113 (s), 1036 (s); ν(C−S) 1018 (vs); δ(C−CH_3) 847 (s).

[Ni(3-mpSO$_3$)$_2$(H$_2$O)$_2$].H$_2$O (10): Yield 0.12 g (66%). $C_{12}H_{18}N_2NiO_9S_2$ (457.10): calcd. C 31.50, H 3.94, N 6.13; found C 31.78, H 3.90, N 6.23. IR: $\tilde{\nu}$ = ν(O−H) 3453 (br. vs), 3366 (br. vs), 3266 (br. s) cm^{-1}; ν(PyC−H) 3094 (m), 3066 (m); ν(MeC−H) 3000−2800 (vw); δ(O−H) 1655 (s); ν(C−N) + ν(C−C) 1588 (m); δ(C−H) 1457 (s), 1391 (m); ν(S−O) 1243 (vs), 1186 (vs), 1155 (vs), 1077 (s); ν(C−S) 1026 (vs); δ(C−CH_3) 843 (s), 807 (s).

[VO(acac)(3-mpSO$_3$)(H$_2$O)] (11): A solution of bis(acetylacetonato)vanadium(IV) oxide (0.11 g, 0.40 mmol) in 2 mL of methanol was added to a solution of 3-mpSO$_3$H (0.14 g, 0.80 mmol) in 5 mL of water. The navy blue mixture was stirred for 5 minutes and left at room temperature for 2 days to afford navy blue crystals of **11**. Yield 0.098 g (68%). $C_{11}H_{15}NO_7SV$ (356.24): calcd. C 37.05, H 4.24, N 3.93; found C 37.17, H 4.27, N 3.96. IR: $\tilde{\nu}$ = ν(O−H) 3324 (br. vs), 3222 (br. vs) cm^{-1}; ν(PyC−H) 3092 (w); ν(MeC−H) 3001−2884 (w); δ(O−H) 1648 (s); ν(C−N) + ν(C−C) + ν(C−O) 1578 (vs), 1525 (vs); δ(C−H) + ν(CH=C) 1452 (m), 1430 (m), 1366 (vs); ν(S−O) 1284 (s), 1259 (vs), 1192 (vs), 1156 (s), 1077 (m); ν(C−S) 1031 (vs); ν(V−O) 974 (vs); δ(C−CH_3) 841 (m), 811 (s).

X-ray Crystallography: For all crystals intensity data were collected on a Rigaku AFC-7S diffractometer with a graphite-monochromated Mo-K_α radiation (λ = 0.71069 Å) at 296 K using the ω−2θ scan technique to a maximum 2θ value of 60.° Three standard reflections monitored after every 150 reflections were used for the crystal decay corrections. The observed reflections [$I > 3\sigma(I)$] were extracted from the unique reflections, and the data were corrected for Lorentz and polarization effects. An absorption correction was applied using the empirical ψ-scan method. All crystallographic calculations were carried out using teXsan programs.[23] The structure was solved by the direct methods (SIR92),[24] and refined with full-matrix least-squares techniques,[25] with anisotropic displacement parameters for the non-hydrogen atoms. Some hydrogen atoms were located on difference Fourier maps and refined isotropically, the rest were located in calculated positions and included in the refinement. Table 3 contains crystal data for complexes **1**−**11**. CCDC-205227 to -205236 for complexes **1**−**5**, **7**−**11**, respectively, and -116650 for complex **6** contain the supplementary crystallographic data for this paper. These data can be obtained free of charge at www.ccdc.cam.ac.uk/conts/retrieving.html [or from the Cambridge Crystallographic Data Centre, 12 Union Road, Cambridge CB2 1EZ, UK; Fax: (internat.) + 44-1223-336-033; E-mail: deposit@ccdc.cam.ac.uk]

Acknowledgments

T. S. L. thanks the Japan Society for Promotion of Science for Invitation Fellowship. He also thanks the Guru Nanak Dev University, Amritsar, India for leave. Financial assistance from Ministry of Education, Science and Culture, Japan. Elemental analysis services rendered by the Analytical Center of Osaka City University are gratefully acknowledged. The authors are grateful to the referees for useful comments.

[1] J. M. Lehn, *Supramolecular Chemistry: Concepts and Perspectives*; Wiley-VCH, Weinheim, **1995**, p. 89 and 139.
[2] G. R. Desiraju, *Angew. Chem. Int. Ed. Engl.* **1995**, *34*, 2311−2327.
[3] V. Baron, B. Gillon, A. Cousson, C. Mathoniere, O. Kahn, A. Grand, L. Ohrstrom, B. Delley, M. Bonnet, J. X. Boucherle, *J. Am. Chem. Soc.* **1997**, *119*, 3500−3506.

 © 2004 Wiley-VCH Verlag GmbH & Co. KGaA, Weinheim

[4] M. Munakata, L. P. Wu, T. K. Sowa, *Adv. Inorg. Chem.* **1999**, *46*, 173−303.
[5] H. Zhang, X. Wang, B. K. Teo, *Coord. Chem. Rev.* **1999**, *183*, 157−195.
[6] R. Cortes, L. Lezama, J. L. Pizarro, M. I. Arriortua, T. Rojo, *Angew. Chem. Int. Ed. Engl.* **1996**, *35*, 1810−1812.
[7] H. Kobayashi, H. Tomita, T. Naito, A. Kobayashi, F. Sakai, T. Watanabe, P. Cassoux, *J. Am. Chem. Soc.* **1996**, *118*, 368−377.
[8] S. Kitagawa, M. Kondo, *Bull. Chem. Soc. Jpn.* **1998**, *71*, 1739−1753.
[9] E. S. Raper, *Coord. Chem. Rev.* **1997**, *165*, 475−567 (and refs. therein).
[10] K. Kitano, R. Tanaka, T. Kimura, T. Tsuda, S. Shimizu, H. Takagi, T. Nishioka, D. Shiomi, A. Ichimura, I. Kinoshita, K. Isobe, S. Ooi, *J. Chem. Soc., Dalton Trans.* **2000**, 995−1000 (and refs. therein).
[11] T. S. Lobana, A. Castineiras, *Polyhedron* **2002**, *21*, 1603−1611.
[12] W. Su, M. Hong, J. Weng, Y. Liang, Y. Zhao, R. Cao, Z. Zhou, A. S. C. Chan, *Inorg. Chim. Acta* **2002**, *331*, 8−15 (and refs. therein).
[13] M. Hong, Y. Zhao, W. Su, R. Cao, M. Fujita, Z. Zhou, A. S. C. Chan, *Angew. Chem. Int. Ed.* **2000**, *39*, 2468−2470.
[14] T. S. Lobana, S. Paul, A. Castineiras, *J. Chem. Soc., Dalton Trans.* **1999**, 1819−1824.
[15] F. Charbonnier, R. Faure, H. Loiseleur, *Cryst. Struct. Commun.* **1981**, *10*, 1129−1132.
[16] M. Murata, M. Kojima, A. Hioki, M. Miyagawa, M. Hirotsu, K. Nakajima, M. Kita, S. Kashino, Y. Yoshikawa, *Coord. Chem. Rev.* **1998**, *174*, 109−131.
[17] K. Kimura, T. Kimura, I. Kinoshita, N. Nakashima, K. Kitano, T. Nishioka, K. Isobe, *Chem. Commun.* **1999**, 497−498.
[18] K. Umakoshi, T. Yamasaki, A. Fukuoka, H. Kawano, M. Ichikawa, M. Onishi, *Inorg. Chem.* **2002**, *41*, 4093−4095.
[19] E. M. Barranco, O. Crespo, M. C. Giemno, P. G. Jones, A. Laguna, C. Sarroca, *J. Chem. Soc., Dalton Trans.* **2001**, 2523−2529.
[20] (Eds.: J. E. Huheey, E. A. Keiter, R. L. Keiter), *Inorganic Chemistry: Principles of Structure and Reactivity*, 4th Ed., Harper Collins College Publishers, New York, **1993**.
[21] A. M. Comrie, J. B. Stenlake, *J. Chem. Soc.* **1958**, 1853−1854.
[22] E. C. Horning, *Organic Synthesis*, John Wiley & Sons, Inc., New York, **1955**, vol. 3, p. 136−139.
[23] teXsan, *Crystal Structure Analysis Package, Molecular Structure Corporation*, **1985** and **1999**.
[24] A. Altomare, G. Cascarano, C. Giacovazzo, A. Guagliardi, M. C. Burla, G. Polidori, M. Camalli, *J. Appl. Cryst.* **1994**, *27*, 435−436.
[25] G. M. Sheldrick, *SHELXL-97. Program for the Refinement of Crystal Structures.* University of Göttingen, Germany, **1997**.

Received April 30, 2003
Early View Article
Published Online December 4, 2003

 © 2004 Wiley-VCH Verlag GmbH & Co. KGaA, Weinheim

Heterometallic Molecular Squares and Polymers Based On Self-Assembly Reactions of Multiply Bonded Dirhenium Complexes

Jitendra K. Bera,[a] John Bacsa,[a] Bradley W. Smucker,[a] and Kim R. Dunbar*[a]

Keywords: Self-assembly / Polymers / Supramolecular chemistry / Rhenium / Multiple bonds

Self-assembly reactions of the triply-bonded dirhenium complex *cis*-$[Re_2Cl_2(dppm)_2(O_2CC_5H_4N\text{-}4)_2]$ with *cis*-protected Pt^{II} and Zn^{II} precursors have produced heterometallic squares. Analogous reactions with $Ag(O_3SCF_3)$, *cis*-$[Re_2Cl_4(O_2CCH_3)_2(H_2O)_2]$ and $[Rh_2(O_2CCH_3)_4]$ have yielded mixed-metal polymeric structures. These results demonstrate that the isonicotinate ligand is useful for accessing heterometallic structures involving metal–metal bonded complexes.
(© Wiley-VCH Verlag GmbH & Co. KGaA, 69451 Weinheim, Germany, 2004)

Introduction

The assembly of metal-based units into supramolecular structures may furnish interesting conducting,[1] magnetic,[2] optical,[3] or catalytic properties.[4] Among the complexes that have been synthesized in this vein are dimetal (M_2) "lantern" complexes as building blocks for homometallic supramolecular assemblies, efforts that have largely focused on the use of dicarboxylic acids.[5] In addition, edge-sharing bi-octahedral dirhenium units can be linked by cyanide and thiocyanate to yield mixed metal Re_4Pd_2, Re_2Ag, Re_2W, Re_2Pt, and Re_2Rh complexes.[6] Recently, we reported a new type of self-assembly reaction that affords molecules with both M_2 and M′ units. The isonicotinate ligand was used as it binds to three metals (Scheme 1). Specifically, the precursor molecule *cis*-$[Re_2Cl_2(dppm)_2(O_2CC_5H_4N\text{-}4)_2]$ (**1**) was synthesized and treated with *cis*-$[Pt(dbbpy)(Otf)_2]$ (dbbpy = 4,4′-di-*tert*-butyl-2,2′-bipyridine; Otf = O_3SCF_3) to yield a molecular square composed of alternating dirhenium and platinum corners.[7] Herein we report further reactions of **1** with various metal complexes to yield a new heterometallic molecular square with alternating Re_2 and Zn corners and three open-chain polymers consisting of 1:1 Re_2/Ag, Re_2/Re_2, and Re_2/Rh_2 units.

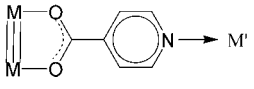

Scheme 1

[a] Department of Chemistry, Texas A&M University, College Station, Texas 77842-3012 (USA)
Fax: (internat.) + 1-979-845-7177
E-mail: dunbar@mail.chem.tamu.edu

Results and Discussion

The molecular structure of complex **1** involves orthogonally disposed isonicotinate groups with two dangling nitrogen donors available for further coordination. Reactions of **1** with *cis* and *trans* accessible transition metal precursors can, in principle, generate various cyclic and open-frame oligomers as well as polymers (Scheme 2). Self-assembly reactions typically yield one major product in a high yield as dictated by a combination of enthalpic and entropic contributions. Here, various building blocks have been employed in reactions of **1**, including $[Pt(dbbpy)(O_3SCF_3)_2]$, $ZnCl_2$, $Ag(O_3SCF_3)$, *cis*-$[Re_2Cl_4(O_2CCH_3)_2(H_2O)_2]$, and $[Rh_2(O_2CCH_3)_4]$, all of which have at least two positions available for facile substitution, but differ in the geometry and disposition of the available metal binding sites. *Hybrid* molecular squares $[\{cis\text{-}Re_2(O_3SCF_3)_2(dppm)_2(O_2CC_5H_4N\text{-}4)_2\}\{Pt(dbbpy)\}]_2(O_3SCF_3)_4$ (**2**) and $[\{cis\text{-}Re_2Cl_2(dppm)_2(O_2CC_5H_4N\text{-}4)_2\}\{ZnCl_2\}]_2$ (**3**), composed of alternating $Re_2^{II,II}$ and M^{II} (M = Pt and Zn) corners, have been isolated from the reactions of **1** with $[Pt(dbbpy)(O_3SCF_3)_2]$[7] and $ZnCl_2$, respectively. In contrast, the reactions of **1** with $Ag(O_3SCF_3)$, *cis*-$[Re_2Cl_4(O_2CCH_3)_2(H_2O)_2]$ and $[Rh_2(O_2CCH_3)_4]$ yield open-chain polymeric structures $[\{cis\text{-}Re_2(OReO_3)_2(dppm)_2(O_2CC_5H_4N\text{-}4)_2\}\{Ag{\cdot}ReO_4\}]_\infty$ (**4**), $[\{cis\text{-}Re_2Cl_2(dppm)_2(O_2CC_5H_4N\text{-}4)_2\}\{cis\text{-}Re_2Cl_4(O_2CCH_3)_2\}]_\infty$ (**5**), and $[\{cis\text{-}Re_2Cl_2(dppm)_2(O_2CC_5H_4N\text{-}4)_2\}\{Rh_2(O_2CCH_3)_4\}]_\infty$ (**6**), respectively. These reactions are essentially instantaneous as judged by the rapid formation of insoluble solids. Crystals of complexes **3**–**6** were obtained by slow diffusion. Regardless of the ratio of complex **1** and the metal precursors, the isolated products are essentially the same. The new compounds **3**–**6** are insoluble in common organic solvents, which prevents measurements of their physical properties in solution.

 © 2004 Wiley-VCH Verlag GmbH & Co. KGaA, Weinheim **DOI: 10.1002/ejic.200300268**

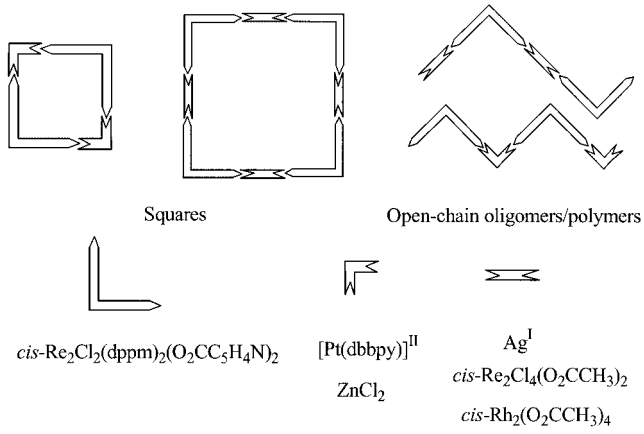

Scheme 2

Complex **3**·10($C_2H_4Cl_2$)·11(CH_3OH)·(H_2O) is a molecular square consisting of alternating $(dppm)_2Re_2^{II}$ and $Zn^{II}Cl_2$ units at the vertices and isonicotinate ligands along the edges (Figure 1). Selected bond lengths and angles are provided in Table 1. The square is considerably distorted, as evidenced by the Zn···Zn diagonal distance of 11.881(5) Å whereas the diagonal defined by the midpoints of the two Re_2 units is 13.608(3) Å. These distances are strikingly similar to the corresponding values in complex **2** (11.971(3) and 13.263(3) Å], the structure of which is identical to complex **3** except that the $ZnCl_2$ corners are replaced by Pt(dbbpy) units (Figure 2). The Re−Re [2.318(1) Å] and the Re−P [2.387(4)−2.412(3) Å], Re−O [2.133(8)−2.160(9) Å], and Re−Cl distances [2.513(3) and 2.523(3) Å] are similar to the corresponding distances in the precursor complex **1**. The vertex angle subtended by the Re_2 units is less than the ideal 90° [O1−Re2−O3 80.6(3)° and O2−Re1−O4 80.0(3)°]. The coordination environment around Zn is best described as distorted tetrahedral. The N1−Zn1−N2 vertex angle is 101.0(5)° while Cl3−Zn1−Cl4 is significantly larger [122.8(2)°], presumably due to non-bonded repulsions between the adjacent chlorine atoms.

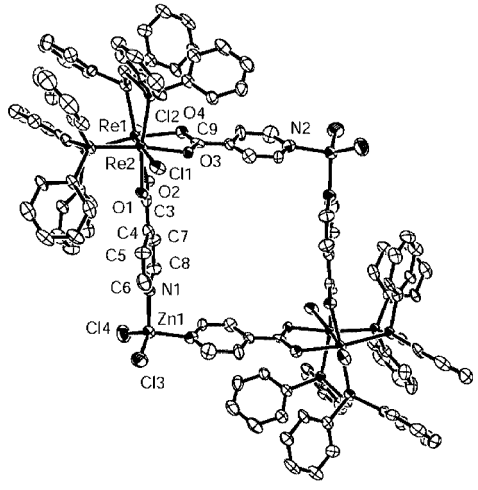

Figure 1. ORTEP representation of the neutral molecular square [{*cis*-$Re_2Cl_2(dppm)_2(O_2CC_5H_4N\text{-}4)_2$}{$ZnCl_2$}]$_2$ in **3**·10($C_2H_4Cl_2$)·11(CH_3OH)·(H_2O) with important atoms labeled. Thermal ellipsoids are at the 50% probability level; hydrogen atoms have been omitted for clarity

Table 1. Selected bond lengths [Å] and angles [deg] for **3**

Bond lengths			
Re1−Re2	2.3175(10)	Re2−O1	2.133(8)
Re1−P2	2.402(3)	Re2−P1	2.394(4)
Re1−P4	2.387(4)	Re2−P3	2.412(3)
Re1−O2	2.160(9)	Zn1−N1	2.041(12)
Re1−O4	2.149(9)	Zn1−N2	2.052(13)
Re1−Cl2	2.513(3)	Zn1−Cl3	2.232(5)
Re2−Cl1	2.523(3)	Zn1−Cl4	2.202(5)
Bond angles			
O4−Re1−O2	80.0(3)	N1−Zn1−N2	101.0(5)
O4−Re1−P4	95.3(3)	N1−Zn1−Cl4	107.8(4)
Re2−Re1−P4	98.71(8)	N2−Zn1−Cl4	110.2(4)
O2−Re1−P2	89.8(3)	N1−Zn1−Cl3	106.1(4)
Re2−Re1−P2	96.06(8)	N2−Zn1−Cl3	106.8(4)
P4−Re1−P2	94.12(12)	Cl4−Zn1−Cl3	122.8(2)

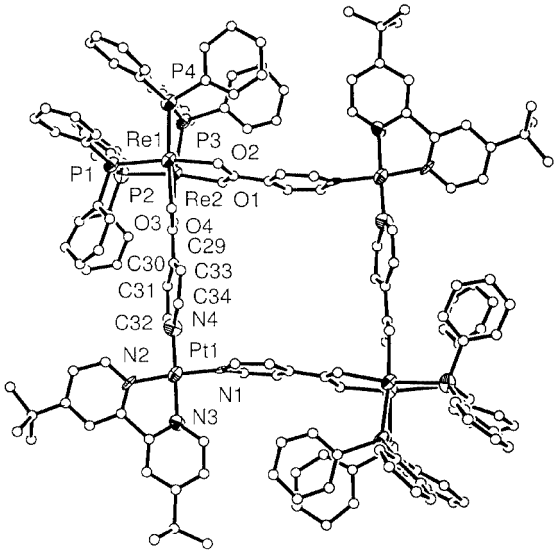

Figure 2. ORTEP representation of the molecular square [*cis*-$Re_2(dppm)_2(O_2CC_5H_4N\text{-}4)_2Pt(dbbpy)]_2$ with important atoms labeled. Thermal ellipsoids are at the 50% level except for the carbon and oxygen atoms which are represented as circles of arbitrary radius. Note that the C, O, F, and S atoms of the triflate anions are axially coordinated, and the hydrogen atoms are removed for clarity

A cyclic voltammetric study of **2** in a 0.1 M nBu_4NPF_6/CH_2Cl_2 solution reveals weak electronic coupling between the dirhenium units through the Pt centers ($\Delta E_{1/2}$ = 130 mV; K_c = 158). The extent of coupling is similar to that estimated for complexes in which dirhenium units are connected by terephthalate ligands.[5]

In complex **4**, the structure of which has been confirmed by X-ray diffraction, the axial chloride ligands have, surprisingly, been replaced by $[ReO_4]^-$ ions. Moreover, it does not contain an outer-sphere triflate anion, rather a second $[ReO_4]^-$ unit is located in the interstices. The $[ReO_4]^-$ anion is a result of oxidative decomposition of **1**, which also explains the relatively low yield of complex **4**. The intense IR

 © 2004 Wiley-VCH Verlag GmbH & Co. KGaA, Weinheim

resonances seen between 890 and 950 cm^{-1} indicate ν(Re−O) stretches.

The cationic $[\{cis\text{-}Re_2(OReO_3)_2(dppm)_2(O_2CC_5H_4N\text{-}4)_2\}\{Ag\}]^+$ repeat unit in the crystal structure of **4**·1.5($C_2H_4Cl_2$)·2(CH_3OH) (Figure 3) and selected distances and angles (Table 2) are given here. Each of the $\{Re_2(OReO_3)_2(dppm)_2(O_2CC_5H_4N\text{-}4)_2\}$ units is connected by Ag^I ions.[8] The *anti* orientation of one set of the isonicotinate ligands in adjacent dirhenium units results in a zig-zag pattern for the polymeric structure (see Figure 4, a). The axial positions of the Re_2 unit in complex **4** are occupied by the $[ReO_4]^-$ anion (instead of the original Cl^- ion in **1**) which leads to a slightly shorter Re−Re distance [2.2850(13) Å] as compared to **1** [2.3271(4) Å]. All metrical parameters involving the dirhenium units are typical of other dirhenium−diphosphane complexes.[9] The two-coordinate Ag^I ion is in a nearly linear geometry (N6−Ag1−N18 172.3(8)°] with Ag1−N6 and Ag1−N18 distances of 2.130(18) and 2.128(18) Å, respectively.

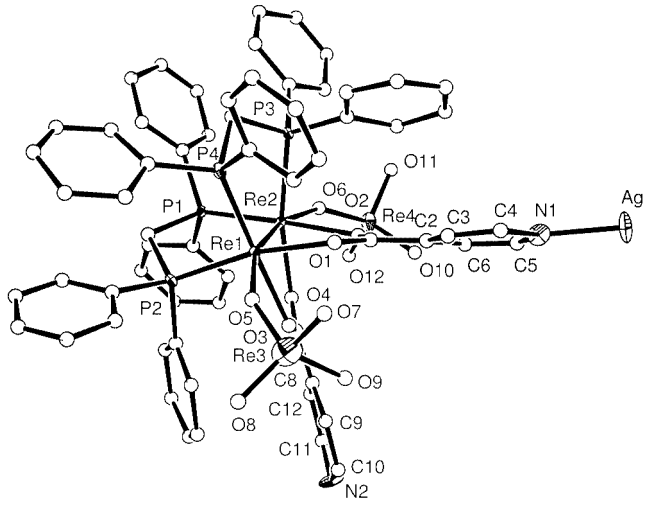

Figure 3. ORTEP representation of the repetitive cationic fragment $[\{cis\text{-}Re_2(OReO_3)_2(dppm)_2(O_2CC_5H_4N\text{-}4)_2\}\{Ag\}]^+$ in **4**·1.5($C_2H_4Cl_2$)·2(CH_3OH) with important atoms labeled. Thermal ellipsoids are at the 40% level except for the carbon and oxygen atoms which are represented as circles of arbitrary radius. Hydrogen atoms have been omitted for clarity

As the complexes *cis*-$[Re_2Cl_4(O_2CCH_3)_2(H_2O)_2]$[10] and $[Rh_2(O_2CCH_3)_4]$[11] engage in axial interactions, they were used here as linkers for complex **1**. Although structurally similar, the difference in the lengths of the quadruple bond in the dirhenium complex [2.224(5) Å] and the single bond in the dirhodium compound [2.403(2) Å] allowed us to vary the linker length. The axial water ligands in *cis*-$[Re_2Cl_4(O_2CCH_3)_2(H_2O)_2]$ are readily replaced by the nitrogen atoms of the isonicotinate ligands in complex **1**. Each of the $\{cis\text{-}Re_2Cl_2(dppm)_2(O_2CC_5H_4N\text{-}4)_2\}$ moieties is coordinated to two different $\{cis\text{-}Re_2Cl_4(O_2CCH_3)_2\}$ units. The isonicotinate ligands of neighboring $\{cis\text{-}Re_2Cl_2(dppm)_2(O_2CC_5H_4N\text{-}4)_2\}$ units are *anti*, leading to a zig-zag chain structure with alternating triply bonded $Re_2^{II,II}$ and quadruply bonded $Re_2^{III,III}$ units (Figure 4, b). A portion of the polymer, namely the $[\{cis\text{-}Re_2Cl_2(dppm)_2(O_2CC_5H_4N\text{-}4)_2\}\{cis\text{-}Re_2Cl_4(O_2CCH_3)_2\}]$ unit, is depicted in Figure 5. Selected bond lengths and angles are provided in Table 3. The Re−Re of 2.3143(9) Å, Re−P [2.371(4)−2.410(4) Å], Re−Cl [2.530(4), and 2.538(4) Å] are all typical of triply bonded dirhenium complexes with similar ligands.

Table 2. Selected bond lengths [Å] and angles [deg] for **4**

Bond lengths			
Re2−Re1	2.2850(13)	Re1−O3	2.133(14)
Ag1−N6	2.13(2)	Re1−O5	2.22(2)
Ag1−N18	2.128(18)	Re2−P1	2.401(5)
Re2−O2	2.120(13)	Re2−P3	2.419(5)
Re2−O4	2.147(13)	Re1−P2	2.405(6)
Re2−O9	2.230(14)	Re1−P4	2.408(6)
Re1−O1	2.133(13)		
Bond angles			
N6−Ag1−N18	172.3(8)	O1−Re1−O3	79.4(5)
O2−Re2−O4	79.4(5)	O1−Re1−O5	78.4(6)
O2−Re2−O9	80.9(5)	O3−Re1−O5	77.9(6)
O4−Re2−O9	80.2(5)	O1−Re1−P2	168.9(4)
O2−Re2−P1	169.5(4)	O3−Re1−P2	90.1(4)
O4−Re2−P1	94.1(4)	O5−Re1−P2	96.0(5)
O9−Re2−P1	90.0(4)	O1−Re1−P4	95.6(4)
O2−Re2−P3	89.9(4)	O3−Re1−P4	171.2(4)
O4−Re2−P3	168.7(4)	O5−Re1−P4	94.0(5)
O9−Re2−P3	94.4(4)	P2−Re1−P4	94.4(2)
P1−Re2−P3	95.83(18)		

The Re(1)−Re(2) [2.244(1) Å] in the $\{Re_2Cl_4(O_2CCH_3)_2\}$ unit is characteristic of a Re−Re quadruple bond, and is slightly longer than the Re−Re bond [2.224(5) Å] in *cis*-$[Re_2(O_2CCH_3)_2Cl_4(H_2O)_2]$. The Re−O and Re−Cl distances are typical of values reported for similar complexes,[12] and the Re−Re−O angles [89.3(3)−90.3(3)°] are close to 90°. The corresponding angles involving the equatorial Cl^- ligands [103.6(1)−104.4(1)°] are much wider. This "bending back" of the chloride ligands away from the Re−Re bond and towards the axial sites leads to a marked non-linearity of the Re−Re−N (axial) units as evidenced by the Re4−Re3−N2 and Re3−Re4−N1 angles of 163.2(3) and 163.6(4)°, respectively.

Reaction of $[Rh_2(O_2CCH_3)_4]$ with **1** also produced crystals of a zig-zag polymeric chain compound with alternating triply bonded $Re_2^{III,III}$ and singly bonded $Rh_2^{II,II}$ units (Figure 4, c). A diagram of the unit $[\{cis\text{-}Re_2Cl_2(dppm)_2(O_2CC_5H_4N\text{-}4)_2\}\{Rh_2(O_2CCH_3)_4\}]$ is shown in Figure 6. Selected bond lengths and angles are provided in Table 4. The metrical parameters involving the triply bonded dirhenium units are similar to those observed in analogous complexes. The two sets of Rh−Rh distances [2.417(6) and 2.392(5) Å] observed in the crystal structure are both typical of singly bonded Rh_2^{4+} units with axial nitrogen donor ligands.[11] The axial Rh−N distances are 2.27(4) and 2.22(2) Å. The Rh1−Rh1′−N1 and Rh2−Rh2′−N2 angles are much closer to linearity at 177.6(7) and 176.3(7)° in complex **6** while the corresponding angles in complex **5** are significantly smaller.

 © 2004 Wiley-VCH Verlag GmbH & Co. KGaA, Weinheim

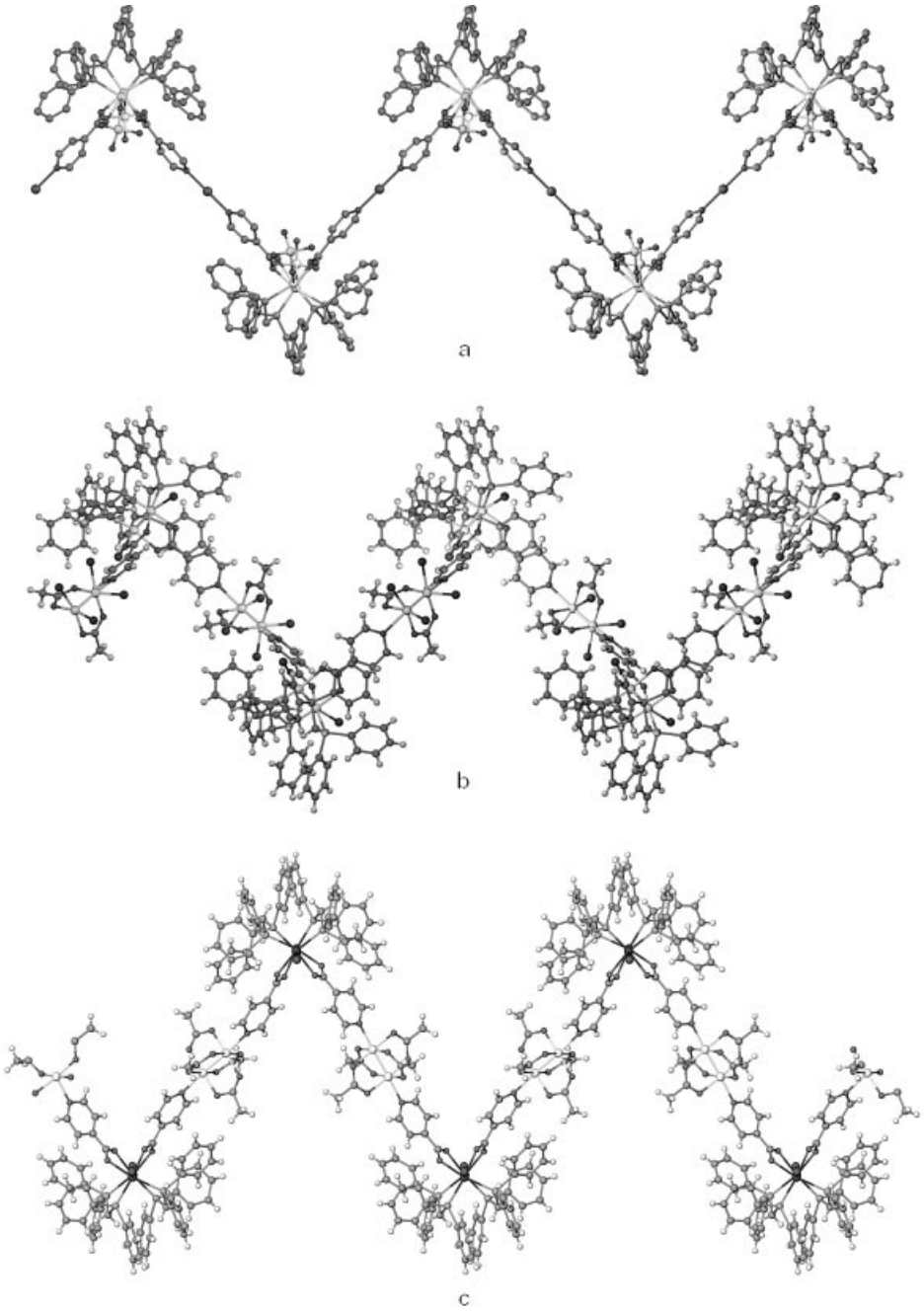

Figure 4. Graphical representation of the zig-zag patterns of the polymeric structures of complexes **4** (a), **5** (b), and **6** (c)

The crystal packing of compounds **2**−**6** share a common interesting feature, namely the phenyl groups of the dppm ligands from the neighboring molecules are engaged in close phenyl−phenyl contacts.[13] A representative example of the packing of Re_2/Zn squares in complex **3** is shown in Figure 7. Such arrangements create a cavity in the crystal lattice in which several solvent molecules are trapped during crystallization.

As documented here, self-assembly the reactions of **1** with *cis* and *trans* disposed linkers can yield discrete cyclic structures or polymers. The rationale for the formation of low-nuclearity species is based solely on the entropy factor. There is also a slight favorable enthalpic contribution for the stabilization of the cyclic structures versus the open-frame oligomers, as the former involves more metal−ligand interactions. Finally, the formation of the heterometallic squares **2** and **3** as the major products, rather than smaller or larger sized rings, is presumably a consequence of the ring-strain of the metallacyclophane. Having stated these points, why do the reactions of $Ag(O_3SCF_3)$, *cis*-$[Re_2Cl_4(O_2CCH_3)_2(H_2O)_2]$, and $[Rh_2(O_2CCH_3)_4]$ react with **1** to yield polymers instead of squares of larger dimensions? A common explanation is the role of concentration in the self-assembly reactions. Dilute solutions typically lead to cyclic

 © 2004 Wiley-VCH Verlag GmbH & Co. KGaA, Weinheim

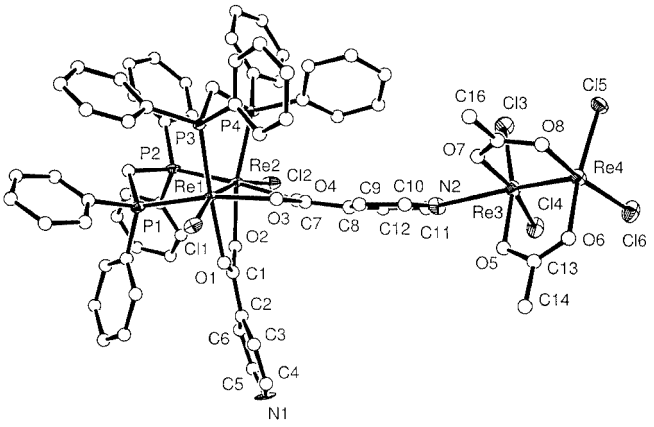

Figure 5. ORTEP representation of the repetitive neutral fragment [{*cis*-$Re_2Cl_2(dppm)_2(O_2CC_5H_4N\text{-}4)_2$}{*cis*-$Re_2Cl_4(O_2CCH_3)_2$}] in **5**·3($C_3H_6O$)·2($CH_2Cl_2$) with important atoms labeled. Thermal ellipsoids are at the 40% level except for the carbon and oxygen atoms which are represented as circles of arbitrary radius. Hydrogen atoms have been omitted for clarity

Table 3. Selected bond lengths [Å] and angles [deg] for **5**

Bond lengths			
Re1−Re2	2.3143(9)	Re2−P2	2.371(4)
Re4−Re3	2.2440(10)	Re2−P4	2.397(4)
Re3−N2	2.439(14)	Re2−Cl2	2.538(4)
Re4−N1	2.434(13)	Re3−O7	2.016(12)
Re1−O3	2.150(10)	Re3−O5	2.033(11)
Re1−O1	2.155(9)	Re3−Cl4	2.292(4)
Re1−P3	2.377(4)	Re3−Cl3	2.297(4)
Re1−P1	2.410(4)	Re4−O6	2.045(10)
Re1−Cl1	2.530(4)	Re4−O8	2.068(11)
Re2−O4	2.122(9)	Re4−Cl6	2.288(5)
Re2−O2	2.130(10)	Re4−Cl5	2.323(4)
Bond angles			
O3−Re1−O1	80.8(4)	Re4−Re3−Cl3	104.36(12)
O3−Re1−Re2	88.0(3)	Cl6−Re4−Cl5	93.42(17)
O3−Re1−Cl1	83.4(3)	O6−Re4−N1	78.0(5)
O1−Re1−Cl1	81.7(3)	O8−Re4−N1	78.6(5)
Re2−Re1−Cl1	167.90(10)	Cl6−Re4−N1	87.0(4)
O4−Re2−O2	79.8(4)	Cl5−Re4−N1	87.8(3)
O4−Re2−Cl2	83.4(3)	O7−Re3−O5	89.1(5)
O2−Re2−Cl2	80.8(3)	O7−Re3−Re4	89.3(3)
Re1−Re2−Cl2	167.01(10)	O5−Re3−Re4	89.9(3)
O6−Re4−O8	87.1(5)	O7−Re3−Cl4	166.7(3)
O6−Re4−Re3	89.6(3)	O5−Re3−Cl4	88.3(4)
O8−Re4−Re3	90.3(3)	O7−Re3−Cl3	86.8(4)
O6−Re4−Cl6	90.0(3)	O8−Re4−Cl5	86.0(3)
Cl4−Re3−Cl3	92.44(17)	O7−Re3−N2	78.7(5)
Re3−Re4−Cl6	103.81(12)	O5−Re3−N2	78.4(5)
Re3−Re4−Cl5	103.64(11)	Re3−Re4−N1	163.6(4)
Re4−Re3−Cl4	103.73(12)	Re4−Re3−N2	163.2(3)

products whereas concentrated solutions produce polymers. However, we found no evidence of lower nuclearity products, regardless of the concentrations of the precursors. Polymer formation may occur because squares of larger dimensions would require many solvent molecules to crystallize in the void space. Close-packed polymers also contain solvent molecules, but the packing of larger squares is expected to be much less efficient.

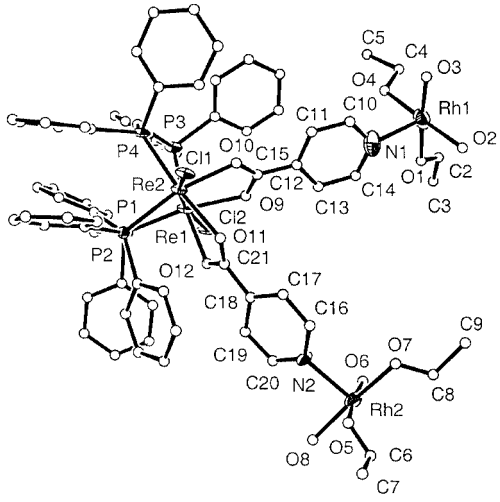

Figure 6. ORTEP representation of the repetitive neutral fragment [{*cis*-$Re_2Cl_2(dppm)_2(O_2CC_5H_4N\text{-}4)_2$}{$Rh_2(O_2CCH_3)_4$}] in **6**·1.5($C_3H_6O$)·2($CH_2Cl_2$)·$H_2O$ with important atoms labeled. Thermal ellipsoids are at the 40% level except for the carbon and oxygen atoms which are represented as circles of arbitrary radius. Hydrogen atoms have been omitted for clarity

Table 4. Selected bond lengths [Å] and angles [deg] for **6**

Bond lengths			
Re1−Re2	2.3425(15)	Re2−P2	2.438(6)
Rh1−Rh1	2.417(6)	Rh1−O2	2.02(3)
Rh2−Rh2	2.392(5)	Rh1−O4	2.02(3)
Re1−P1	2.408(7)	Rh1−O1	2.09(3)
Re1−P3	2.434(7)	Rh1−O3	2.10(3)
Re1−O12	2.165(18)	Rh1−N1	2.27(4)
Re1−O9	2.193(15)	Rh2−N2	2.22(2)
Re1−Cl2	2.529(6)	Rh2−O5	2.02(4)
Cl1−Re2	2.551(6)	Rh2−O7	2.04(3)
Re2−O10	2.179(17)	Rh2−O8	2.08(2)
Re2−O11	2.211(17)	Rh2−O6	2.09(3)
Re2−P4	2.407(7)		
Bond angles			
O12−Re1−O9	79.6(7)	P1−Re1−P3	95.7(2)
O12−Re1−Re2	88.2(5)	Re2−Re1−Cl2	166.81(19)
O9−Re1−Re2	86.1(4)	O2−Rh1−O1	88.0(12)
O12−Re1−P1	93.3(5)	O4−Rh1−O1	90.3(12)
O9−Re1−P1	169.6(5)	O2−Rh1−O3	87.7(16)
Re2−Re1−P1	101.48(15)	O4−Rh1−O3	93.9(17)
O12−Re1−P3	169.8(5)	N1−Rh1−Rh1	176.3(7)
O9−Re1−P3	90.8(5)	N2−Rh2−Rh2	177.6(7)

Concluding Remarks

The results of this study demonstrate the feasibility of preparing both discrete cyclic products and open-chain polymers based on the self-assembly of triply-bonded dirhenium units with various inorganic precursors. Dirhodium

 © 2004 Wiley-VCH Verlag GmbH & Co. KGaA, Weinheim

Figure 7. Packing diagram of the Re_2/Zn molecular squares in the crystal structure of complex **3**

complexes with isonicotinate ligands as well as 4-cyanobenzoate groups have been prepared recently and it appears that this will be a generally useful method for preparing mixed-metal clusters.[14] The title compound **1** provides access to different types of heterometallic structures, and its reactions illustrate the usefulness of such molecules for incorporating electron-rich metal−metal bonded complexes into cyclic and acyclic architectures that contain a second type of metal site.[15]

Experimental Section

Solvents were dried by conventional methods, distilled from over nitrogen and deoxygenated prior to use. The starting materials *cis*-$[Re_2Cl_2(dppm)_2(O_2CC_5H_4N\text{-}4)_2]$,[7] *cis*-$[Re_2Cl_4(O_2CCH_3)_2(H_2O)_2]$,[16] $[Rh_2(O_2CCH_3)_4]$[17] were synthesized by literature methods. Silver triflate and zinc chloride were purchased from Aldrich and used without further purification. Infrared spectra were recorded in the range 400−4000 cm^{-1} using a Nicolet 470 FT-IR spectrometer as Nujol mull samples suspended between KBr plates. Elemental microanalyses were performed by Dr. H. D. Lee of the Purdue University Microanalytical Laboratory.

Synthesis of [{*cis*-$Re_2(O_3SCF_3)_2(dppm)_2(O_2CC_5H_4N\text{-}4)_2$}{Pt(dbbpy)}]$_2(O_3SCF_3)_4$ (2): A mixture of *cis*-$[Re_2Cl_2(dppm)_2(O_2CC_5H_4N\text{-}4)_2]$ (0.095 g, 0.07 mmol) and 0.052 g (0.07 mmol) of $[Pt(dbbpy)(O_3SCF_3)_2]$ was stirred in CH_2Cl_2 for 8−10 h. The resultant red solution was then concentrated and treated with diethyl ether to yield a solid that was collected by filtration, washed with fresh diethyl ether (3 × 5 mL) and dried in vacuo. Single crystals were grown by slow diffusion of Et_2O into a solution of **2** in CH_2Cl_2. Yield: 34 mg (42%). ^1H NMR (δ in $CDCl_3$): 5.05 and 6.50 (m, 4 H, -CH_2- of dppm); 6.8−7.2, 7.42, 7.60 (m, 40 H, Ph of dppm); 8.01 and 8.80 (m, 8 H, isonicotinate), 8.19, 8.28, 9.42 (m, 6 H, aromatic, dbbpy), 1.45 (m, 18 H, CH_3 of dbbpy) ppm. $^{31}P\{^1H\}$ NMR (δ in $CDCl_3$): −9.88 ppm.

Synthesis of [{*cis*-$Re_2Cl_2(dppm)_2(O_2CC_5H_4N\text{-}4)_2$}{$ZnCl_2$}]$_2$ (3): A CH_3OH solution (10 mL) of $ZnCl_2$ (5 mg, 0.04 mmol) was carefully layered over a solution of 1,2-dichloroethane (10 mL) that contained *cis*-$Re_2Cl_2(dppm)_2(O_2CC_5H_4N\text{-}4)_2$ (50 mg, 0.03 mmol). After 7 days, a crop of bright-red crystals was collected by filtration, washed with methanol (3 × 5 mL) followed by dichloromethane (3 × 5 mL) and dried in vacuo. Yield: 48 mg (87%). $C_{67}H_{64}Cl_8N_2O_5P_4Re_2Zn$ (i.e. **2**·$2C_2H_4Cl_2$·CH_3OH): calcd. (%) C 44.15, N 1.54, H 3.54, Cl 15.56; found C 44.01; N 1.52, H 3.51, 15.07.

Synthesis of [{*cis*-$Re_2(OReO_3)_2(dppm)_2(O_2CC_5H_4N\text{-}4)_2$}{Ag·$ReO_4$}] (4): A CH_3OH solution of AgO_3SCF_3 (10 mg, 0.04 mmol) was layered over a solution of *cis*-$[Re_2Cl_2(dppm)_2(O_2CC_5H_4N\text{-}4)_2]$ (50 mg, 0.03 mmol) in 1,2-dichloroethane (10 mL). The Schlenk-tube was then wrapped with foil to avoid light and stored in a refrigerator. After 7 days, a small quantity of block-shaped crystals of **2** had formed along with a gray precipitate. The crystals were separated from the solid, washed with methanol (3 × 5 mL) followed by dichloromethane (3 × 5 mL) and dried in vacuo. Yield: 16 mg (21%). $C_{62}H_{52}AgN_2O_{16}P_4Re_5$: calcd. C 33.19, N 1.25, H 2.34; found C 32.92; N 1.28, H 2.32.

Synthesis of [{*cis*-$Re_2Cl_2(dppm)_2(O_2CC_5H_4N\text{-}4)_2$}{*cis*-$Re_2Cl_4(O_2CCH_3)_2$}] (5): An acetone solution (10 mL) of *cis*-$[Re_2Cl_4(O_2CCH_3)_2(H_2O)_2]$ (25 mg, 0.04 mmol) was carefully layered over a dichloromethane solution of *cis*-$[Re_2Cl_2(dppm)_2(O_2CC_5H_4N\text{-}4)_2]$ (50 mg, 0.03 mmol). After 2 days, the dark blue crystals that had formed were collected by filtration, washed with acetone (3 × 5 mL) followed by dichloromethane (3 × 5 mL) and dried in vacuo. Yield: 66 mg (92%). $C_{66}H_{58}Cl_6N_2O_8P_4Re_4$: calcd. (%) C 37.95, N 1.34, H 2.80; Cl 10.18; found C 37.65; N 1.31, H 2.73, Cl 10.03.

Synthesis of [{*cis*-$Re_2Cl_2(dppm)_2(O_2CC_5H_4N\text{-}4)_2$}{$Rh_2(O_2CCH_3)_4$}] (6): An acetone solution (10 mL) of $[Rh_2(O_2CCH_3)_4]$ (17 mg, 0.04 mmol) was carefully layered over a dichloromethane solution of *cis*-$[Re_2Cl_2(dppm)_2(O_2CC_5H_4N\text{-}4)_2]$ (50 mg, 0.03 mmol). After 7 days, the resultant red crystals were collected by filtration, washed with acetone (3 × 5 mL) and dichloromethane (3 × 5 mL), and dried in vacuo. Yield: 56 mg (86%). $C_{70}H_{64}Cl_2N_2O_{12}P_4Re_2Rh_2$: calcd. (%) C 44.29, N 1.48, H 3.40; found C 44.11; N 1.56, H 3.27.

X-ray Crystallography: Crystals of **3**−**6** were harvested directly from the slow diffusion reactions as described in the synthesis section. Single-crystal X-ray intensities were collected at 110(2) K on a Bruker SMART CCD based X-ray diffractometer with 1.5 kW graphite monochromated Mo-K_α radiation (λ = 0.71073 Å). Data reduction, cell-refinement, and corrections for Lorentz and polarization effects were carried out with the program SAINT.[18] Semi-empirical absorption corrections were carried out with the program SADABS.[19] The structures were solved and refined using X-SEED,[20] a graphical interface to SHELX.[21] Additional crystallographic calculations were performed by the programs PLATON[22] and PARST.[23] The hydrogen atoms were refined in a riding mode with values of U_{eq} that were 1.2 times the U_{eq} for the heavy atoms to which they are bonded. Experimental details and pertinent crystallographic data for complexes **3**−**6** are summarized in Table 5.

[{*cis*-$Re_2Cl_2(dppm)_2(O_2CC_5H_4N\text{-}4)_2$}{$ZnCl_2$}]$_2$·10($C_2H_4Cl_2$)·11($CH_3OH$)·($H_2O$) [3·10($C_2H_4Cl_2$)·11($CH_3OH$)·($H_2O$)]: The data were collected using ω-scans in the range $1.67 < \theta < 27.82°$. The detector to crystal distance was set at 60 mm. Exposure times of 20 s per frame and scan widths of 0.3° were used throughout the data collection. The fact that the beta angle is close to 90° combined with the large R-merge value indicated possible pseudo-

 © 2004 Wiley-VCH Verlag GmbH & Co. KGaA, Weinheim

Table 5. Crystallographic data for complexes **3**−**6**

	3·10$C_2H_4Cl_2$·11CH_3OH·H_2O	**4**·1.5($C_2H_4Cl_2$)·2(CH_3OH)	**5**·3(C_3H_6O) ·2(CH_2Cl_2)	**6**·1.5(C_3H_6O)·2(CH_2Cl_2)·H_2O
Formula	$C_{155}H_{190}Cl_{28}N_4O_{20}P_8Re_4Zn_2$	$C_{67}H_{66}AgCl_3N_2O_{18}P_4Re_5$	$C_{77}H_{80}Cl_{10}N_2O_{11}P_4Re_4$	$C_{76.50}H_{79}Cl_6N_2O_{14.5}P_4Re_2Rh_2$
Molecular mass	4545.01	2456.32	2432.61	2173.22
Crystal system	monoclinic	monoclinic	orthorhombic	monoclinic
Space group	$P2_1/n$ (No. 14)	$P2_1/c$ (No. 14)	*Pbcn* (No. 60)	$P2_1/n$ (No. 14)
a [Å]	16.289(3)	19.504(4)	23.150(5)	16.209(3)
b [Å]	35.117(7)	16.407(3)	24.220(5)	38.889(8)
c [Å]	17.001(3)	24.360(5)	33.300(7)	17.363(4)
β [deg]	90.08(3)	92.68(3)		90.42(3)
V [Å^3]	9725(3)	7787(3)	18671(6)	10945(4)
Z	2	4	8	4
$\rho_{calcd.}$ [g/cm^3]	1.552	2.095	1.731	1.319
μ (Mo-K_α) [mm^{-1}]	3.229	8.238	5.577	2.753
F(000)	4528	4636	9392	4280
Reflections collected	56099	51822	81011	74227
Independent	21289	14162	13495	13984
Observed [$I > 2\sigma(I)$]	12028	7692	8618	6996
No. of variables	952	508	868	585
R_1[a]	0.092	0.093	0.092	0.127
wR_2[b]	0.211	0.247	0.189	0.331
Goodness-of-fit	1.017	1.025	1.144	1.020

[a] $R1 = \Sigma||F_o| - |F_c||/\Sigma F_o$ with $F_o^2 > 2\sigma(F_o^2)$. [b] $wR_2 = [\Sigma w(|F_o^2| - |F_c^2|)^2/\Sigma|F_o^2|^2]^{1/2}$.

merohedral twinning of the crystal. A search for possible twin laws was carried out, but none of them reduced the *R*-factor appreciably. As the final discrepancy indices of both R_1 and R_{int} were small for a potentially twinned data set, we surmised that the major contribution to the integrated data was from one component of the twin and therefore a twin correction would not improve the model significantly. Disordered solvent molecules with fractional site occupancies were modeled with restraints. All non-hydrogen atoms except the carbon and oxygen atoms of the methanol and water molecules were refined anisotropically.

[{*cis*-$Re_2(OReO_3)_2(dppm)_2(O_2CC_5H_4N$-4)$_2$}{Ag·$ReO_4$}]·1.5($C_2H_4Cl_2$)·2-($CH_3OH$) [4·1.5($C_2H_4Cl_2$)·2($CH_3OH$)]: Exposure times of 25 s per frame and scan widths of 0.3° were used throughout the data collection. The data were collected using ω-scans in the θ range 1.53 to 25.35°. The numerous heavy metal atoms resulted in the crystal exhibiting a large absorption coefficient. Unfortunately, the weak nature of the diffraction prevented the use of very small crystal that would minimize the effects of absorption. The isolated $[ReO_4]^-$ ions are disordered over two positions and were modeled using two components with restraints on the Re−O and O···O distances and site occupancies. All the non-hydrogen atoms except the carbon and oxygen atoms were refined anisotropically.

[{*cis*-$Re_2Cl_2(dppm)_2(O_2CC_5H_4N$-4)$_2$}{*cis*-$Re_2Cl_4(O_2CCH_3)_2$}]·3-($C_3H_6O$)·2($CH_2Cl_2$) [5·3($C_3H_6O$)·2($CH_2Cl_2$)]: The data were collected using ω-scans in the range $1.22 < \theta < 23.34°$. The diffraction patterns were indexed using a primitive orthorhombic cell, and the structure was solved and refined in the space group *Pbcn*. A disordered dichloromethane solvent molecule was modeled using two components with restraints on the C−Cl and Cl···Cl distances and site occupancies for the two fragments set to 0.5 each. In the final cycles of refinement, all non-hydrogen atoms, except those belonging to solvent molecules, were refined anisotropically.

[{*cis*-$Re_2Cl_2(dppm)_2(O_2CC_5H_4N$-4)$_2$}{$Rh_2(O_2CCH_3)_4$}]·1.5-($C_3H_6O$)·2($CH_2Cl_2$)·$H_2O$ [6·1.5(C_3H_6O)·2(CH_2Cl_2)·H_2O]: The crystal selected for data collection was removed from the solvent and quickly placed in a cold-stream to prevent decay. The detector-to-crystal distance was set at 60 mm. Exposure times of 40 s per frame and scan widths of 0.3° were used throughout the data collection. The data were collected using ω-scans in the θ range 1.57 to 23.14°. The diffraction patterns were indexed using a primitive monoclinic cell. The space group $P2_1/n$ was chosen on the basis of the systematic absences in the diffraction pattern. In the final cycles of refinement the Re, Cl, P, and O atoms belonging to the coordination polymer were refined anisotropically. Anisotropic refinement of carbon atoms and the atoms belonging to guest molecules resulted in these atoms having non-positive definite displacement parameters.

Acknowledgments

K. R. D. gratefully acknowledges the Welch Foundation and the National Science Foundation for a PI Grant (CHE-9906583) and for equipment grants to purchase the CCD X-ray equipment (CHE-9807975). K. R. D. also thanks Johnson-Matthey for a generous loan of rhodium trichloride.

[1] [1a] O. Ermer, *Adv. Mater.* **1991**, *3*, 608, and references therein. [1b] A. Aumuller, P. Erk, G. Klebe, S. Hünig, J. U. von Schütz, H. P. Werner, *Angew. Chem. Int. Ed. Engl.* **1986**, *25*, 740.

[2] C. S. Campos-Fernández, J. R. Galán-Mascarós, B. W. Smucker, K. R. Dunbar, *Eur. J. Inorg. Chem.* **2003**, 988, and references cited therein.

[3] [3a] U. Hahn, M. Gorka, F. Vogtle, V. Vicinelli, P. Ceroni, M. Maestri, V. Balzani, *Angew. Chem. Int. Ed.* **2002**, *41*, 3595. [3b] V. Balzani, P. Ceroni, A. Juris, M. Venturi, S. Campagna, F. Puntoriero, S. Serroni, *Coord. Chem. Rev.* **2001**, *219*, 545, and references cited therein.

[4] [4a] M. Abrantes, A. Valente, M. Pillinger, I. S. Goncalves, J. Rocha, C. C. Romao, *J. Catal.* **2002**, *209*, 237. [4b] R. Tannenbaum, *J. Mol. Catal. A: Chem.* **1996**, *107*, 207. [4c] M. Fujita, Y. J. Kwon, S. Washizu, K. Ogura, *J. Am. Chem. Soc.* **1994**, *116*, 1151.

[5] [5a] F. A. Cotton, C. Lin, C. A. Murillo, *Acc. Chem. Res.* **2001**, *34*, 759 and references cited therein. [5b] J. K. Bera, R. Clérac, P. E. Fanwick, R. A. Walton, *J. Chem. Soc., Dalton Trans.* **2002**, 2168. [5c] J. K. Bera, P. Angaridis, F. A. Cotton, M. A.

Petrukhina, P. E. Fanwick, R. A. Walton, *J. Am. Chem. Soc.* **2001**, *123*, 1515. [5d] R. H. Cayton, M. H. Chisholm, J. C. Huffman, E. B. Lobkovsky, *J. Am. Chem. Soc.* **1991**, *113*, 8709.
[6] [6a] S.-M. Kuang, P. E. Fanwick, R. A. Walton, *Inorg. Chem.* **2002**, *41*, 1036; *Inorg. Chem.* **2002**, *41*, 147; *Inorg. Chem.* **2001**, *40*, 5682; *Inorg. Chem.* **2000**, *39*, 2968.
[7] J. K. Bera, B. W. Smucker, R. A. Walton, K. R. Dunbar, *Chem. Commun.* **2001**, 2562.
[8] For other references to the use of Ag^{I} as a linking cation see: [8a] D. Braga, M. Polito, M. Bracaccini, D. D'Addario, E. Tagliavini, D. M. Proserpio, F. Grepioni, *Chem. Commun.* **2002**, 1080. [8b] R. Schneider, M. W. Hosseini, J.-M. Plainex, A. De Cian, J. Fisher, *Chem. Commun.* **1998**, 1625.
[9] A. R. Cutler, D. R. Derringer, P. E. Fanwick, R. A. Walton, *J. Am. Chem. Soc.* **1988**, *110*, 5024.
[10] [10a] J. K. Bera, T.-T. Vo, R. A. Walton, K. R. Dunbar, *Polyhedron*, in press. [10b] Y. Ding, S. S. Lau, P. E. Fanwick, R. A. Walton, *Inorg. Chim. Acta* **2000**, *300–302*, 505.
[11] F. A. Cotton, E. V. Dikarev, M. A. Petrukhina, M. Schmitz, P. J. Stang, *Inorg. Chem.* **2002**, *41*, 2903, and references cited therein.
[12] F. A. Cotton, R. A. Walton, *Multiple Bonds Between Metal Atoms*, 2nd ed., Clarendon Press, Oxford, **1993**.
[13] I. Dance, M. Scudder, *Chem. Eur. J.* **1996**, *2*, 481.
[14] S. L. Schiavo, F. Nicolò, G. Tresoldi, P. Piraino, *Inorg. Chim. Acta* **2003**, *343*, 351.
[15] J. K. Bera, J. Bacsa, K. R. Dunbar, unpublished work.
[16] A. R. Chakravarty, F. A. Cotton, A. R. Cutler, R. A. Walton, *Inorg. Chem.* **1986**, *25*, 3619.
[17] G. A. Rempel, P. Legzdins, H. Smith, G. Wilkinson, *Inorg. Synth.* **1972**, *13*, 87.
[18] *SAINT*, Program for area detector absorption correction, Siemens Analytical X-ray Instruments Inc., Madison, WI 53719, USA, **1994–1996**.
[19] G. M. Sheldrick, *SADABS*, Program for Siemens area detector absorption correction, Univ. of Göttingen, Germany, **1996**.
[20] L. J. Barbour, *X-Seed*, Graphical interface to SHELX-97 and POV-Ray, **1999** (http://www.x-seed.net).
[21] G. M. Sheldrick, *SHELXS-97, A Program for Crystal Structure Solution,* Univ. of Göttingen, Germany, **1997**. G. M. Sheldrick, *SHELXL-97, A Program for Crystal Structure Refinement,* Univ. of Göttingen, Germany, **1997**.
[22] A. L. Spek, *PLATON*, University of Utrecht, The Netherlands, **2001**.
[23] *PARST:* M. Nardelli, *J. Appl. Crystallogr.* **1995**, *28*, 659.

Received May 6, 2003
Early View Article
Published Online November 6, 2003

 © 2004 Wiley-VCH Verlag GmbH & Co. KGaA, Weinheim

Synthesis and X-ray Crystal Structures of Cobalt and Copper Complexes of 1,3-Bis(benzotriazolyl)propanes

Philip Børsting[a] and Peter J. Steel*[a]

Keywords: Copper / Cobalt / Cluster compounds / Bridging ligands / N ligands

Two propylene-bridged bis-benzotriazole ligands, **1** and **2**, were used to obtain three novel coordination polymers with cobalt(II), copper(II) and copper(I). The complexes were structurally characterised by X-ray crystallography. The complex $[Co(1)Cl_2]_n$, **3**, possesses a helical zigzag chain structure in which tetrahedral $CoCl_2$ centres are bridged by molecules of **1** having an extended conformation. The complex $[Cu(1)Cl_2]_n$, **4**, exhibits a more complex supramolecular architecture, which extends in two dimensions, with bridging through Cu_2Cl_4 dimeric units in one direction and through the organic ligand in an orthogonal direction. The complex $[Cu(2)Cl]_n$, **6**, has a one-dimensional polymeric structure involving 16-membered M_2L_2 rings bridged by Cu_2Cl_2 units.

(© Wiley-VCH Verlag GmbH & Co. KGaA, 69451 Weinheim, Germany, 2004)

Introduction

The use of linear and angular components for the controlled self-assembly of two- and three-dimensional metallosupramolecular species has been the subject of considerable study in recent years.[1] The most commonly employed organic-connecting components are rigid, linear, bridging heterocyclic ligands, such as pyrazine and 4,4′-bipyridine. More recently, flexible ligands have been employed in order to gain access to topologies not available from logical combination of rigid building blocks. The simplest way to introduce flexibility into ligand design is by incorporation of alkyl chain spacer groups. For example, symmetrical ligands containing propylene spacer groups between 4-pyridyl,[2] 8-quinolyloxy,[3] 1-pyrazolyl,[4] 1-triazolyl,[5] and 2-benzimidazolyl[6] donor groups have recently been used for the construction of interesting new supramolecular architectures.

For some years now we have been involved in the synthesis and study of ligands containing less commonly studied heterocyclic ring systems.[7] One such heterocycle is benzotriazole, which is extensively used as a synthetic auxiliary in organic chemistry[8] but has been largely ignored by coordination chemists. The parent heterocycle can coordinate up to three metals in its deprotonated form.[9] Particular emphasis has been placed on copper complexes, due to the importance of benzotriazole as a corrosion inhibitor.[10] We have recently reported the incorporation of benzotriazole groups into a number of chelating ligands[11] and into a bidentate bridging ligand that forms a triple stranded helicate.[12] We now describe complexes of two symmetrical, isomeric ligands, **1** and **2**, which contain benzotriazole groups separated by flexible propylene spacer units (see Figure 1).

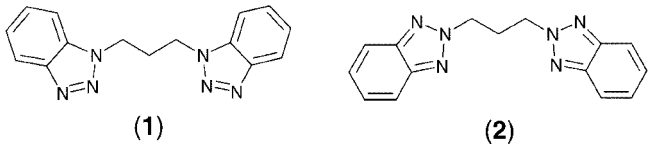

(1) (2)

Figure 1. Structural formulae of ligands **1** and **2**

Results and Discussion

The ligands **1** and **2** were prepared by reaction of benzotriazole with 1,3-dibromopropane in the presence of sodium hydroxide in DMSO solution, as described previously by Katritzky et al.[13] This reaction produces a mixture of the symmetrical 1,1′- and 2,2′-isomers **1** and **2**, along with the unsymmetrical 1,2′-isomer. The three isomers were separated by column chromatography on silica gel and recrystallized from absolute ethanol, and their properties were in agreement with those described previously.[13] However, ligand **1** has recently been described by other workers,[14] who reported a ^1H NMR spectrum that we believe to be that of isomer **2**. In order to resolve this discrepancy unambiguously, we carried out an X-ray crystal structure determination of the compound we identified as **2**.

Figure 2 shows a perspective view of the structure of this ligand, which is indeed the 2,2′-isomer, in agreement with the NMR assignment of Katritzky et al.[13] The compound crystallizes in the orthorhombic space group $P2_12_12_1$ with

[a] Department of Chemistry, University of Southern Denmark, Campusvej 55, 5230 Odense M, Denmark
[b] Department of Chemistry, University of Canterbury, Christchurch, New Zealand
Fax: (internat.) +64-(0)3-3642110
E-mail: p.steel@chem.canterbury.ac.nz

 © 2004 Wiley-VCH Verlag GmbH & Co. KGaA, Weinheim DOI: 10.1002/ejic.200300271

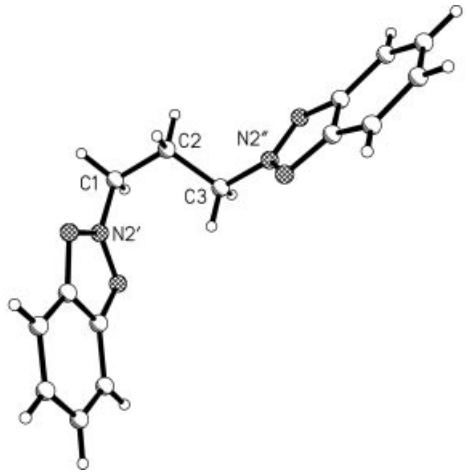

Figure 2. Perspective view of the X-ray molecular crystal structure of ligand **2**

a complete molecule in the asymmetric unit. The bonding geometry of the benzotriazole rings is similar to that in other 2-alkylbenzotriazoles.[13,15] In the solid state it adopts an unsymmetrical conformation about the central propylene spacer group. Specifically, one of the benzotriazole rings exists in a *gauche* conformation [N2′−C1−C2−C3 torsional angle = 59.0(2)°], while the other ring has the expected *anti* conformation [C1−C2−C3−N2′′ torsional angle = 172.2(1)°]. This unusual shape undoubtedly results from a complex system of intermolecular forces, comprising face-to-face and edge-to-face aromatic interactions,[16] as well as C−H···N interactions,[17] all of which are now well-known to contribute significantly to the solid-state structures of heteroaromatic compounds.

Having unambiguously established the structures of the ligands, we proceeded to study their coordination chemistry. All three ligands were treated with a variety of first row transition metal salts. Complexes of the unsymmetrical 1,2′-isomer failed to assemble into any crystalline product. However, reactions of **1** and **2** with both cobalt(II) chloride and copper(II) chloride furnished single crystals suitable for X-ray structure determination.

Reaction of cobalt(II) chloride with **1** formed $[Co(1)Cl_2]_n$, **3**, which is a one-dimensional coordination polymer. Figure 3 shows a perspective view of a section of the extended

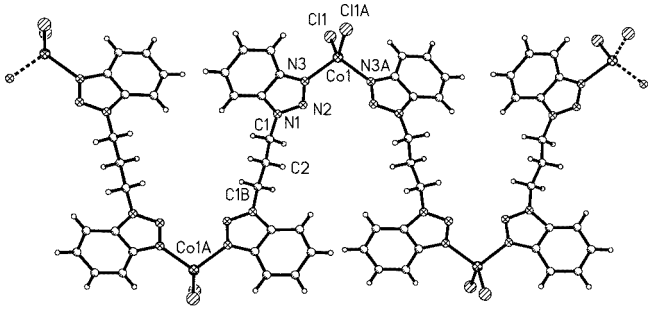

Figure 3. Perspective view, with selected atom labelling, of the one-dimensional coordination polymer $[Co(1)Cl_2]_n$, **3**; selected bond lengths (Å) and angles (°): Co1−N3 2.011(2); Co-Cl1 2.2235(6); N3−Co1−N3A 108.2(1); N3−Co1−Cl1 104.33(5); N3−Co1−Cl1A 112.02(5)

structure with selected atom labelling. The complex crystallizes in the orthorhombic space group *Pnna*, with half the ligand and half a $CoCl_2$ in the asymmetric unit. Thus, the distorted tetrahedral cobalt atom and the central carbon of the propylene group (C2) each lie on different two-fold rotation axes. The resulting polymer chains extend into a helical zigzag pattern, in which the bridging ligand adopts the most extended possible form, with *anti* conformations of the propylene spacer [N1−C1−C2−C1B torsional angle = 179.6(2)°] and coordination by the less sterically hindered N3 nitrogen atoms, as was observed for the $CuCl_2$ complex of the related ligand with a methylene spacer group.[11] As a result, the ligand bridges the cobalt atoms, which are separated by 12.462(1) Å. The polymer chains stack on each other by face-to-face interactions between the benzotriazole groups in such a way that each chain stacks with four other chains.

An analogous reaction of **1** with copper(II) chloride led to a complex, $[Cu(1)Cl_2]_n$, **4**, with a more complex supramolecular architecture. The compound crystallizes in the monoclinic space group $P2_1/n$ with a dichlorocopper(II) unit and a whole bridging ligand in the asymmetric unit. Figure 4 shows a perspective view of the contents of the asymmetric unit and the symmetry-related connecting atoms. The benzotriazole rings are both coordinated through the N3 nitrogen atoms in preference to the more sterically congested N2 nitrogen atoms. Within complex **4** the bridging ligand exists in a more compact conformation than was observed in **3**. In particular, the propylene bridge folds into a *gauche-gauche* conformation [N1"−C1−C2−C3 torsional angle = 57.2(3)° and C1−C2−C3−N1′ torsional angle = 68.0(3)°], which is similar to that observed in a zinc(II) thiocyanate complex of the same ligand.[14] As a consequence, copper atoms bridged by ligand **1** are separated by only 9.157(1) Å, much less than the metal−metal separation in **3**.

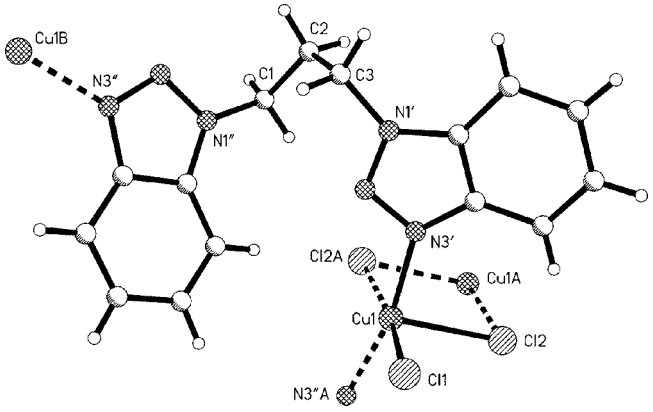

Figure 4. Perspective view showing the contents of the asymmetric unit and the connected atoms (dashed bonds), with selected atom labelling, in the crystal structure of $[Cu(1)Cl_2]_n$, **4**; selected bond lengths (Å) and angles (°): Cu1−N3′ 2.014(2); Cu1−N3′′A 2.026(2); Cu1−Cl1 2.2834(8); Cu1−Cl2 2.6442(8); Cu1−Cl2A 2.3238(8); N3′−Cu1−N3′′A 166.56(8); N3′−Cu1−Cl1 88.57(6); N3′′A−Cu1−Cl1 90.75(6); N3′−Cu1−Cl2A 87.95(6); N3′′A−Cu1−Cl2A 90.21(6); Cl1−Cu1−Cl2A 168.94(3); N3′−Cu1−Cl2 96.83(6); N3′′A−Cu1−Cl2 96.49(6); Cl1−Cu1−Cl2 100.47(3); Cl2A−Cu1−Cl2 90.36(2); Cu1−Cl2−Cu1A 89.64(2)

 © 2004 Wiley-VCH Verlag GmbH & Co. KGaA, Weinheim

The copper atom is five-coordinate, being bonded to two molecules of **1** that are related by a crystallographic glide plane, a terminal chlorine atom and two bridging chlorines that are related by a centre of inversion. The geometry of the copper is square pyramidal with a τ value[18] of 0.088; one of the bridging chlorines occupies the axial site. The terminal chlorine has a bond length of 2.283(1) Å and the two bridging chlorine atoms have bond lengths of 2.324(1) and 2.644(1) Å, giving the Cu_2Cl_2 unit a parallelogram-like shape, which, by virtue of the crystallographic centre of inversion, is strictly planar. The Cu1···Cu1A interatomic distance across the parallelogram is 3.509(1) Å. These distances are within the range of other known di-μ-chlorocopper(II) complexes.[7,10b,19]

The bridging nature of the heterocyclic ligand serves to extend the structure in one dimension. Further bridging by the chlorine atoms results in an orthogonal extension of the structure that produces a complicated two-dimensional network. Large 44-membered fused metallacyclic ring-systems exist within this network as M_6L_4 units, one of which is shown in Figure 5. A stabilising influence within this structure appears to come from π−π stacking between the benzotriazole rings separated by the Cu_2Cl_2 units. These rings lie perpendicular to the Cu_2Cl_2 plane and are separated by approximately 3.5 Å, although they are offset such that the centroids of the benzo rings are separated by ca. 4.18 Å.

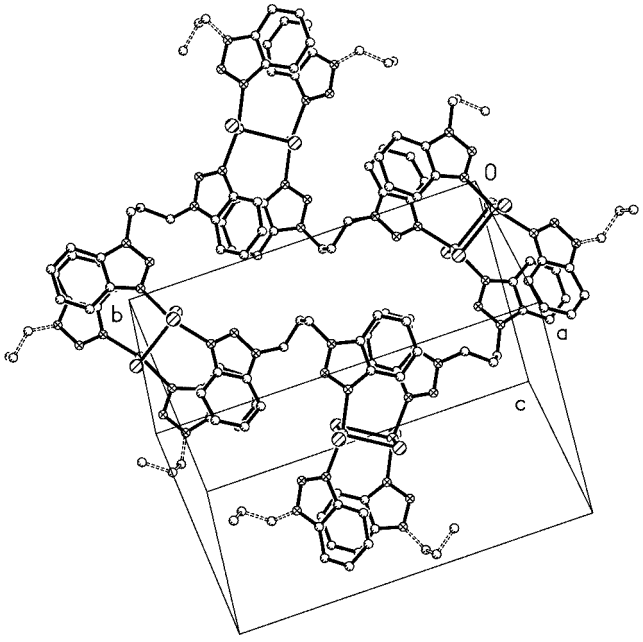

Figure 5. Perspective view of a section of the extended two-dimensional polymeric structure of **4**; the unit cell is indicated

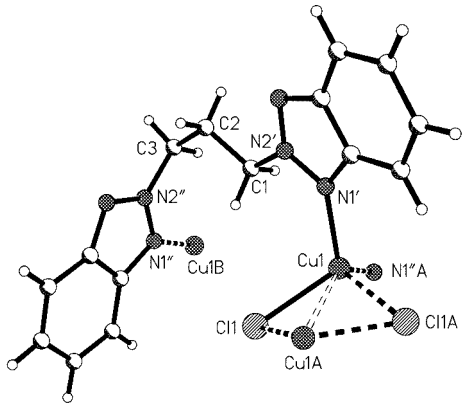

Figure 6. Perspective view showing the contents of the asymmetric unit and the connected atoms (dashed bonds), with selected atom labelling, in the crystal structure of $[Cu(2)Cl]_n$, **6**; selected bond lengths (Å) and angles (°): Cu1−N1′ 2.011(3); Cu1−N1′′A 2.015(3); Cu1−Cl1 2.3724(9); Cu1−Cl1A 2.4287(9); N1′−Cu1−N1′′A 115.3(1); N1′−Cu1−Cl1 112.29(8); N1′′A−Cu1−Cl1 111.19(8); N1′−Cu1−Cl1A 108.30(8); N1′′A−Cu1−Cl1A 107.59(8); Cl1−Cu1−Cl1A 101.01(3)

Reaction of **2** with cobalt(II) chloride gave a $[Co(2)Cl_2]_n$ complex, **5**, as a light blue solid, which failed to produce any crystals suitable for X-ray crystallography. In contrast, reaction of **2** with copper(II) chloride in methanol gave, quite unexpectedly, a copper(I) species as lemon-coloured crystals. This surprising result proved to be quite reproducible, although the identity of the metal reductant remains undetermined. The resulting polymeric $[Cu(2)Cl]_n$ complex, **6**, crystallizes in the monoclinic space group *C*2/*c*, with a copper(I) chloride unit and a whole bridging ligand in the asymmetric unit. Figure 6 shows a perspective view of the contents of the asymmetric unit and the symmetry-related connecting atoms.

Within the complex the ligand adopts a conformation quite similar to that found in the structure of the free ligand **2**, in which one benzotriazole group adopts a *gauche* conformation to the propylene linker [C1−C2−C3−N2′′ torsional angle = 64.9(4)°] and the other group an *anti* conformation [N2′−C1−C2−C3 torsional angle = 177.8(3)°].

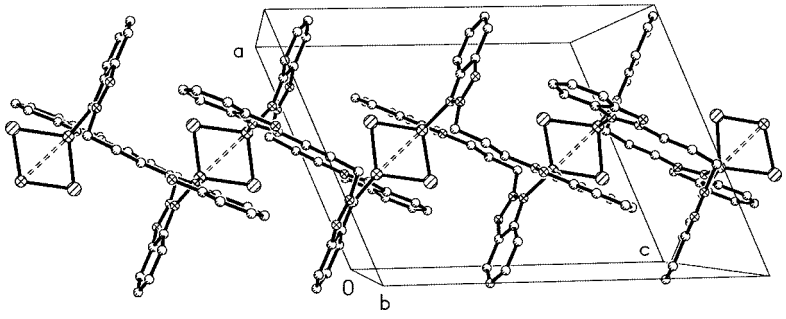

Figure 7. Perspective view of a section of the extended one-dimensional polymeric structure of **6**; the unit cell is indicated

This results in a relatively short intermetallic separation across the ligand bridge [Cu1···Cu1B = 6.010(1) Å]. The copper(I) atom has tetrahedral geometry with coordination to two bridging chlorine atoms, related by a twofold rotation axis, and two nitrogen atoms of different ligands, related by a centre of inversion. The Cu−Cl bond lengths are relatively symmetric [2.372(1) and 2.429(1) Å] and are in the range of other known binuclear Cu_2Cl_2 complexes.[20] The Cu_2Cl_2 unit is nonplanar with a rather short Cu···Cu contact [Cu1···Cu1A = 2.8093(8) Å]. The Cu−N1 distances are also within the range of similar known binuclear Cu_2Cl_2 complexes.[20] Two molecules of ligand **2** bridge two copper atoms, thereby generating a 16-membered M_2L_2 ring structure about a crystallographic centre of inversion. As shown in Figure 7, these rings further extend into a one-dimensional polymeric structure through the chloro bridges. Once again, the extended structure appears to be stabilised by π−π stacking interactions across the Cu_2Cl_2 units between adjacent benzotriazole systems, whose mean planes are separated by ca. 3.5 Å.

Conclusion

The present study has shown that benzotriazole is a useful heterocyclic ring system for incorporation into bridging ligands. The bidentate ligands **1** and **2**, having flexible propylene linkers, generate one- and two-dimensional coordination polymer networks with copper and cobalt chlorides.

Experimental Section

General Procedures and Ligand Syntheses: NMR spectra were recorded on a Varian Unity 300 spectrometer with a 3 mm probe and operating at 300 MHz and 75 MHz for ^1H and ^{13}C, respectively. Melting points were determined using an electrothermal melting point apparatus and are uncorrected. Elemental analyses were performed by the Campbell Microanalytical laboratory at the University of Otago.

The ligands were prepared according to the procedure of Katritzky et al.[13] This gave a mixture of **1** [m.p. 139−139.5 °C (ref.[13] 119−121 °C)], **2** [119−121 °C (ref.[13] 116−118 °C)] and the unsymmetrical 1,2′-disubstituted isomer [80−81 °C (ref.[13] 83−83.5 °C)], which were separated by chromatography on silica gel and recrystallized from ethanol.

Preparation of Complexes

Cobalt(II) Chloride Complex of 1, viz. 3: 1,3-Bis(benzotriazolyl)propane (10 mg, 0.036 mmol) was dissolved in boiling MeOH (1 mL) and added to a solution of $CoCl_2·6H_2O$ (8.5 mg, 0.036 mmol) in MeOH (1 mL). After 20 days blue plate crystals suitable for X-ray crystallography had formed. The crystals were removed and washed with MeOH. Yield: 8.5 mg (58%), m.p. 322 °C. $C_{15}H_{14}Cl_2CoN_6$ (408.15): calcd. C 44.14, H 3.46, N 20.59 %; found: C 44.28, H 3.27, N 20.48 %.

Copper(II) Chloride Complex of 1, viz. 4: $CuCl_2·2H_2O$ (6.0 mg, 0.035 mmol) was dissolved in MeOH (3 mL) and added to a solution of 1,3-bis(benzotriazolyl)propane (10 mg, 0.036 mmol) dissolved in hot MeOH (3 mL). The light green mixture was mixed well and left standing at room temperature. After a few minutes blue crystals began to form and after 1 hour the solution was colourless. The blue block-shaped crystals are stable in air and suitable for X-ray diffraction. Yield: 11.9 mg (82%), m.p. 274 °C. $C_{15}H_{14}Cl_2CuN_6$ (412.76): calcd. C 43.65, H 3.42, N 20.36 %; found: C 43.76, H 3.37, N 20.15 %.

Cobalt(II) Chloride Complex of 2, viz. 5: 1,3-Bis(benzotriazol-2-yl)-propane (32.4 mg, 0.116 mmol) and $CoCl_2·6H_2O$ (25.2 mg, 0.106 mmol) were stirred and refluxed in MeOH (8 mL) for 16 h, which resulted in a blue solution. The blue solution was evaporated

Table 1. X-ray crystal data and details of data collections and structure refinements

Compound	**2**	**3**	**4**	**6**
Empirical formula	$C_{15}H_{14}N_6$	$C_{15}H_{14}N_6CoCl_2$	$C_{15}H_{14}N_6CuCl_2$	$C_{15}H_{14}N_6CuCl$
Molecular mass	278.32	408.15	412.76	377.31
Crystal system	orthorhombic	orthorhombic	monoclinic	monoclinic
a (Å)	5.8393(6)	14.377(2)	9.692(2)	11.693(1)
b (Å)	5.9826(6)	13.997(2)	15.309(3)	17.876(1)
c (Å)	38.695(4)	8.037(1)	11.093(2)	15.444(1)
β (°)	90	90	91.312(2)	112.131(1)
V (Å^3)	1351.8	1617.2(3)	1645.5(5)	2990.5(4)
Space group	$P2_12_12_1$	Pnna	$P2_1/n$	$C2/c$
Z	4	4	4	8
D_c (mg·m^{-3})	1.368	1.676	1.666	1.647
F (000)	584	828	836	1536
Temperature (K)	168(2)	165(2)	295(2)	165(2)
Crystal form	colourless block	blue plate	blue block	lemon-coloured block
Crystal size (mm)	0.61 × 0.57 × 0.24	0.40 × 0.39 × 0.03	0.34 × 0.14 × 0.14	0.65 × 0.14 × 0.11
μ (mm^{-1})	0.088	1.401	1.661	1.647
$2\theta_{max}$ (°)	52.78	53.12	52.80	50.00
Unique reflections	2752	1680	3297	2638
Completeness (%)	99.5	99.0	97.6	99.8
Parameters	190	110	217	208
R[a] [$I > 2\sigma(I)$][a]	0.0351	0.0304	0.0298	0.0421
wR[b] (all data)	0.0832	0.0776	0.0846	0.1050

[a] $R = \Sigma(|F_o| - |F_c|)/\Sigma|F_o|$. [b] $wR = (\Sigma[w(F_o^2 - F_c^2)^2]/\Sigma[w(F_o^2)^2])^{1/2}$.

 © 2004 Wiley-VCH Verlag GmbH & Co. KGaA, Weinheim

in vacuo, the resulting solid was redissolved in $CHCl_3$ (2 mL) and the solution was subjected to slow evaporation, which gave a light blue solid. Yield: 39 mg (90%), m.p. 265−266 °C. $C_{15}H_{14}Cl_2CoN_6$ (408.15): calcd. C 44.14, H 3.46, N 20.59 %; found: C 43.89, H 4.07, N 20.29 %.

Copper(I) Chloride Complex of 2, viz. 6: 1,3-Bis(benzotriazol-2-yl)-propane (10 mg, 0.036 mmol) was dissolved in boiling MeOH (1 mL), and $CuCl_2{\cdot}2H_2O$ (6.0 mg, 0.036 mmol) dissolved in MeOH (1 mL) was added. The pale green solution was mixed well. After a few days, lemon-coloured crystals suitable for X-ray crystallography had formed. The crystals were filtered off and washed with MeOH. Yield: 4.9 mg (36%), m.p. 199 °C. $C_{15}H_{14}ClCuN_6$ (377.31): calcd. C 47.64, H 3.73, N 22.22 %; found: C 47.69, H 3.58, N 22.06.

X-ray Crystallography: Crystal data and experimental details of the data collections and structure refinements are listed in Table 1. Data were collected with a Siemens SMART CCD area detector, using graphite monochromatised Mo-K_α radiation (λ = 0.71073 Å). Almost complete spheres of data were collected. The structures were solved by direct methods using SHELXS,[21] and refined on F^2 using all data by full-matrix least-squares procedures with SHELXL-97.[22] Hydrogen atoms were included in calculated positions with isotropic displacement parameters 1.3 times the isotropic equivalent of their carrier atoms. The function minimised was $\Sigma w(F_o^2 - F_c^2)^2$, with $w = [\sigma^2(F_o^2) + (aP)^2 + bP]^{-1}$, where $P = [\max(F_o,0)^2 + 2F_c^2]/3$. CCDC-207061 (for **3**), -207062 (for **4**), -207063 (for **2**), -207064 (for **6**) contain the supplementary crystallographic data for this paper. These data can be obtained free of charge at www.ccdc.cam.ac.uk/conts/retrieving.html or from the Cambridge Crystallographic Data Centre, 12 Union Road, Cambridge CB2 1EZ, UK; Fax: (internat.) + 44-1223/336-033; E-mail: deposit@ccdc.cam.ac.uk.

[1] For recent reviews, see: [1a] S. Leininger, B. Olenyuk, P. J. Stang, *Chem. Rev.* **2000**, *100*, 853−908. [1b] G. F. Swiegers, T. J. Malefetse, *Chem. Rev.* **2000**, *100*, 3483−3538. [1c] B. Moulton, M. J. Zaworotko, *Chem. Rev.* **2001**, *101*, 1629−1658. [1d] M. Fujita, K. Umemoto, M. Yoshizawa, N. Fujita, T. Kusukawa, K. Biradha, *Chem. Commun.* **2001**, 509−518. [1e] D. W. Johnson, K. N. Raymond, *Supramol. Chem.* **2001**, *13*, 639−659. [1f] B. J. Holliday, C. A. Mirkin, *Angew. Chem. Int. Ed.* **2001**, *40*, 2022−2043. [1g] G. F. Swiegers, T. J. Malefetse, *Coord. Chem. Rev.* **2002**, *225*, 91−121.

[2] For recent examples, see: [2a] M. J. Plater, M. R. S. J. Foreman, T. Gelbrich, S. J. Coles, M. B. Hursthouse, *J. Chem. Soc., Dalton Trans.* **2000**, 3065−3073. [2b] F. M. Tabellion, S. R. Seidel, A. M. Arif, P. J. Stang, *Angew. Chem. Int. Ed.* **2001**, *40*, 1529−1532. [2c] F. M. Tabellion, S. R. Seidel, A. M. Arif, P. J. Stang, *J. Am. Chem. Soc.* **2001**, *123*, 11982−11990. [2d] M. J. Plater, M. R. S. J. Foreman, T. Gelbrich, M. B. Hursthouse, *Inorg. Chim. Acta* **2001**, *318*, 171−174. [2e] L. Pan, E. B. Woodlock, X. Wang, K.-C. Lam, A. L. Rheingold, *Chem. Commun.* **2001**, 1762−1763. [2f] L. Carlucci, G. Ciani, M. Moret, D. M. Proserpio, S. Rizzato, *Chem. Mater.* **2002**, *14*, 12−16. [2g] W. J. Belcher, C. A. Longstaff, M. R. Neckenig, J. W. Steed, *Chem. Commun.* **2002**, 1602−1603. [2h] E.-Q. Gao, Z.-W. Wang, C.-S. Liao, C.-H. Yan, *New J. Chem.* **2002**, *26*, 1096−1098. [2i] M. T. Bujaci, X. Wang, S. Li, C. Zheng, *Inorg. Chim. Acta* **2002**, *333*, 152−154.

[3] M. R. A. Al-Mandhary, P. J. Steel, *Aust. J. Chem.* **2002**, *55*, 705−708.

[4] [4a] A. M. Schuitema, M. Engelen, I. A. Koval, S. Gorter, W. L. Driessen, J. Reedijk, *Inorg. Chim. Acta* **2001**, *324*, 57− 64. [4b] D. A. McMorran, S. Pfadenhauer, P. J. Steel, *Aust. J. Chem.* **2002**, *55*, 519−522.

[5] [5a] G. A. Van Albada, R. C. Guijt, J. G. Haasnoot, M. Lutz, A. L. Spek, J. Reedijk, *Eur. J. Inorg. Chem.* **2000**, 121−126. [5b] Q. Zhao, H. Li, X. Wang, Z. Chen, *New J. Chem.* **2002**, *26*, 1709−1710.

[6] [6a] G. A. van Albada, M. T. Lakin, N. Veldman, A. L. Spek, J. Reedijk, *Inorg. Chem.* **1995**, *34*, 4910−4917. [6b] G. A. van Albada, W. J. J. Smeets, A. L. Spek, J. Reedijk, *Inorg. Chim. Acta* **2000**, *299*, 35−40. [6c] I. Riggio, G. A. van Albada, D. D. Ellis, I. Mutikainen, A. L. Spek, U. Turpeinen, J. Reedijk, *Polyhedron* **2001**, *20*, 2659−2666.

[7] C. Richardson, P. J. Steel, *Eur. J. Inorg. Chem.* **2003**, 405−408, and references cited therein.

[8] A. R. Katritzky, X. Lan, J. Z. Yang, O. V. Denisko, *Chem. Rev.* **1998**, *98*, 409−548.

[9] [9a] D. S. Moore, S. D. Robinson, *Adv. Inorg. Chem.* **1988**, *32*, 171−239, and references cited therein. [9b] M. Murrie, D. Collison, C. D. Garner, M. Helliwell, P. A. Tasker, S. S. Turner, *Polyhedron* **1998**, *17*, 3031−3043.

[10] [10a] R. Walker, *J. Chem. Educ.* **1980**, *57*, 789−791. [10b] I. Soetofte, K. Nielsen, *Acta Chem. Scand., Ser. A* **1981**, *35*, 733−738. [10c] H. M. J. Hendriks, J. J. M. W. L. Birker, G. C. Verschoor, J. Reedijk, *J. Chem. Soc., Dalton Trans.* **1982**, 623−631. [10d] G. F. Kokoszka, J. Baranowski, C. Goldstein, J. Orsini, A. D. Mighell, V. L. Himes, A. R. Siedle, *J. Am. Chem. Soc.* **1983**, *105*, 5627−5633. [10e] J. Reedijk, A. R. Siedle, R. A. Velapoldi, J. A. M. Van Hest, *Inorg. Chim. Acta* **1983**, *74*, 109−118.

[11] C. Richardson, P. J. Steel, *Dalton Trans.* **2003**, 992−1000.

[12] B. J. O'Keefe, P. J. Steel, *Inorg. Chem. Commun.* **2000**, *3*, 473−475.

[13] A. R. Katritzky, A. Jesorka, J. Wang, B. Yang, J. Wu, P. J. Steel, *Liebigs Ann.* **1996**, 745−755.

[14] X. Meng, Y. Song, H. Hou, Y. Fan, G. Li, Y. Zhu, *Inorg. Chem.* **2003**, *42*, 1306−1318.

[15] [15a] A. R. Katritzky, J. Wu, W. Kuzmierkiewicz, S. Rachwal, M. Balasubramanian, P. J. Steel, *Liebigs Ann. Chem.* **1994**, 7−12. [15b] A. R. Katritzky, P. J. Steel, S. N. Denisenko, *Tetrahedron* **2001**, *57*, 3309−3314.

[16] [16a] C. A. Hunter, K. R. Lawson, J. Perkins, C. J. Urch, *J. Chem. Soc., Perkin Trans. 2* **2001**, 651−669. [16b] W. B. Jennings, B. M. Farrell, J. F. Malone, *Acc. Chem. Res.* **2001**, *34*, 885−894. [16c] E. A. Meyer, R. K. Castellano, F. Diederich, *Angew. Chem. Int. Ed.* **2003**, *42*, 1210−1250.

[17] J. J. M. Amoore, L. R. Hanton, M. D. Spicer, *Dalton Trans.* **2003**, 1056−1058, and references cited therein.

[18] A. W. Addison, T. Nageswara Rao, J. Reedijk, J. van Rijn, G. C. Verschoor, *J. Chem. Soc., Dalton Trans.* **1984**, 1349−1356.

[19] [19a] P. C. Christidis, C. A. Bolos, G. S. Nikolov, *Inorg. Chim. Acta* **1995**, *237*, 123−130. [19b] M. Melnik, M. Kabesova, M. Koman, L. Macaskova, J. Garaj, C. E. Holloway, A. Valent, *J. Coord. Chem.* **1998**, *45*, 147−359.

[20] [20a] O. M. Yaghi, G. Li, *Angew. Chem. Int. Ed. Engl.* **1995**, *34*, 207−209. [20b] Y. C. M. Pennings, W. L. Driessen, J. Reedijk, *Polyhedron* **1988**, *7*, 2583−2589.

[21] G. M. Sheldrick, *Acta Crystallogr., Sect. A* **1990**, *46*, 467−473.

[22] G. M. Sheldrick, *SHELXL-97*, University of Göttingen, **1997**.

Received May 7, 2003
Early View Article
Published Online October 31, 2003

Role of the 2,6-Bis(trifluoromethyl)phenyl Group on the Acidity of the Corresponding Phosphane[‡]

Karinne Miqueu,[a] Jean-Marc Sotiropoulos,[a] Geneviève Pfister-Guillouzo,*[a] Valentyn Rudzevich,[b] Vadim Romanenko,[b] and Guy Bertrand[b]

Keywords: Photoelectron spectroscopy / DFT calculations / Phosphanide anions / Phosphanes

The proton affinities of $PhPH^-$ (**1**) and Ar_fPH^- (**2**) were calculated using the B3LYP hybrid functional and the 6-31+G(d,p) basis set. For both anions a net difference was observed. The study of the structural and electronic properties of the anionic species and the corresponding phosphanes $PhPH_2$ (**3**) and Ar_fPH_2 (**4**) allowed us to unsderstand this results and point out the specific role of the 2,6-bis(trifluoromethyl)phenyl (Ar_f) substituent.
(© Wiley-VCH Verlag GmbH & Co. KGaA, 69451 Weinheim, Germany, 2004)

Introduction

During the last two decades the 2,6-bis(trifluoromethyl)-phenyl (Ar_f) and 2,4,6-tris(trifluoromethyl)phenyl substituents have been widely used in main-group element chemistry,[2] because they feature a unique combination of steric and electronic properties. The steric effects of perfluoroalkylated aryl groups are well established and highlighted by the synthesis of a wide range of the kinetically stabilized low-coordinated main-group element derivatives, such as phosphaalkenes,[3] diphosphenes,[4] iminoarsanes[5] and their transition metal derivatives. The electronic effects of Ar_f groups are less studied and represent a more recent and developing area.[6]

In a preliminary communication[7] we reported the synthesis and molecular structure of the ion-separated salt $[P(H)Ar_f][K(benzo\text{-}15\text{-}crown\text{-}5)_2]$ representing the first structurally characterized example of a dicoordinated monoorganylphosphanide anion. The use of other bulky substituents (without fluorinated groups) does not allow for the isolation and characterization of such anionic species. Therefore, it was of interest to rationalize this experimental observation and to understand the electronic effects of the Ar_f group. Moreover, information about specific behavior of this latter can be obtained by calculation of the proton affinities of $PhPH^-$ (**1**) and Ar_fPH^- (**2**). This involves naturally the theoretical study of the anions, performed here for the first time, but also the knowledge of the neutral species. The coupling between UV photoelectron spectroscopy and calculations allows us to obtain structural and electronic properties of the phosphanes $PhPH_2$ (**3**) and Ar_fPH_2 (**4**).

For the neutral species, previous works[8] on the basic properties of arylphosphanes had shown that the orientation of the phosphorus lone pair relative to the aromatic ring was an important factor. However, reinvestigating the photoelectron spectrum of $PhPH_2$ (**3**) Veszpremi et al. concluded that the conjugative interaction between the phosphorus lone pair and the phenyl ring is of minor importance in agreement with other spectroscopic and quantum chemical results (MNDO and HF/MP2).[9] The rotational barrier of the phenyl group in **3** has been found to be rather low.

No experimental and theoretical data exist concerning the [2,6-bis(trifluoromethyl)phenyl]phosphane (**4**). Considering the importance of electron correlation for the geometry optimization of compounds having a flat potential energy surface, we investigated the rotational barriers for $PhPH_2$ (**3**) and Ar_fPH_2 (**4**) using the density functional theory. Moreover, the He-I photoelectron spectra of **3** and **4** were carried out and the data compared with the theoretical results. Such an approach would allow to determine if neutral species show notable differences.

First, we are going to present the theoretical results concerning the anionic species and then the PE spectra as well as the calculations of the corresponding phosphanes.

[‡] Application of Photoelectron Spectroscopy to Molecular Properties, 63. Part 62: Ref.[1]

[a] Laboratoire de Chimie-Théorique et Physico-Chimie Moléculaire, CNRS UMR 5624, Université de Pau et des Pays de l'Adour Avenue de l'Université,
B. P. 1155, 64013 Pau cedex, France
Fax: (internat.) + 33-5-59407588
E-mail: genevieve.pfister@univ-pau.fr
[b] UCR-CNRS Joint Research Chemistry Laboratory, UMR 2282, Department of Chemistry, University of California, Riverside, CA 92521-0403, U.S.A.
Fax: (internat.) + 1-909-787-4713
E-mail: gbertran@mail.ucr.edu

Results and Discussion

Anionic Species

The geometrical parameters for the anionic species **1** and **2** are summarized in Table 1. For the two systems $PhPH^-$ (**1**) and Ar_fPH^- (**2**), the lowest energetic form (form **1A** and **2A**, respectively) is planar. The C^1-P-H angle is 95.8° for **1** and 97.5° for **2**. Such a structure presents a lone pair in the C^1PH plane with a strong s character and a pure p orthogonal lone pair. The transition states corresponding to the rotation around the C^1-P bond (form **1B** and **2B**; PH perpendicular to the phenyl ring) are calculated to be 8.76 and 15.52 kcal/mol (ZPE correction) for $PhPH^-$ and Ar_fPH^-, respectively, higher than their minima.

Table 1. Selected bond lengths [Å] and bond angles [°] for the privileged structures and the transition states of $PhPH^-$ (**1**) and Ar_fPH^- (**2**) calculated with the B3LYP hybrid functional and the basis set 6-31+G(d,p)

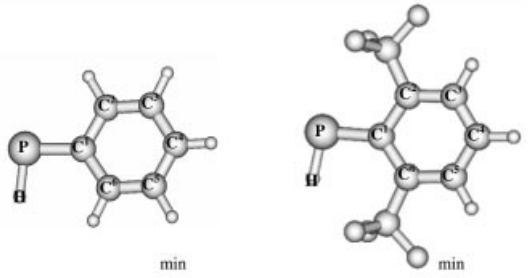

	1A min H–P^1–C^1–C^6 = 0° calcd.	**1B** T.S. H–P^1–C^1–C^6 = 90° calcd.	**2A** min H–P^1–C^1–C^6 = 0° calcd.	**2A** min exp.	**2B** T.S. H–P^1–C^1–C^6 = 89.9° calcd.
P–C^1	1.811	1.886	1.787	1.795	1.884
C^1–C^2	1.428	1.413	1.459	1.453	1.426
C^2–C^3	1.391	1.400	1.391	1.394	1.401
C^3–C^4	1.406	1.399	1.397	1.392	1.394
C^4–C^5	1.404	1.399	1.395	1.390	1.389
C^5–C^6	1.393	1.400	1.394	1.399	1.405
C^1–C^6	1.427	1.413	1.457	1.452	1.428
H–P–C^1	95.82	93.72	97.50	–	95.31
C^6–C^1–C^2	114.77	115.76	112.62	113.3	114.24

The stabilization of the planar structure can be explained by the interaction between the π phosphorus lone pair (p character) and the π^*_{b1} orbital of the ring, localized on the C^1 (and C^4) atoms (Figure 1). In fact, for the two minima **1A** and **2A** the HOMO is stabilized by about 0.27 eV for **1** and 0.53 eV for **2**, compared to the transition states **1B** and **2B** (HOMO: n_P^{π}). In contrast, for the transition states **1B** and **2B** we notice a strong destabilizing of the HOMO-1 (around 0.5 eV), compared to **1A** and **2A** due to an interaction between the s lone pair and the b_1 orbital.

For the fluorinated compound **2**, the inductive effect of the CF_3 groups stabilizes the b_1, a_2, a_2^*, and b^*_1 orbitals of the phenyl ring. In this case the destabilizing interaction between the π phosphorus lone pair and the b_1 orbital does not exist and only the stabilizing interaction occurs with the b^*_1. So, the π stabilizing interaction between n_P^{π} and π^*_{b1} is more important for **2** than for **1** as displayed Figure 1.

For the privileged forms **1A** and **2A**, we observe a shortening of the $P-C^1$ bond and a lengthening of the C^1-C^2 and C^1-C^6 bonds compared to the neutral species

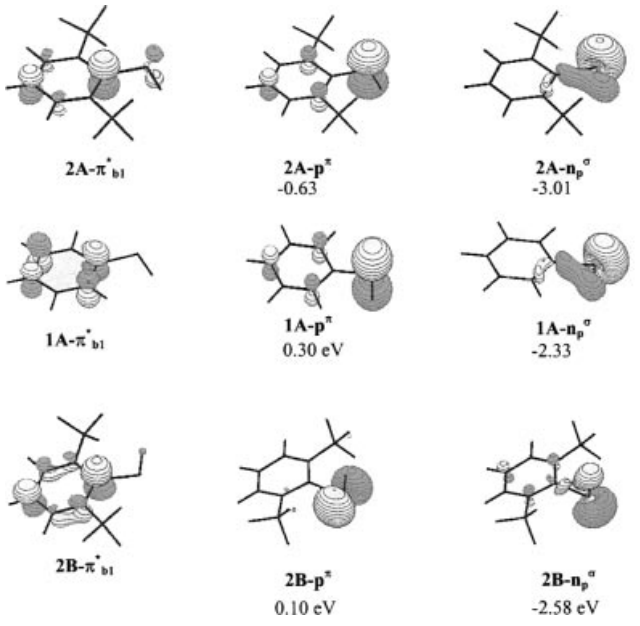

Figure 1. Plot of the molecular orbitals for the minima of $PhPH^-$ (**1A**) and Ar_fPH^- (**2A**) and the corresponding transition states **1B** and **2B**

(Table 2). This effect is more pronounced for **2** than **1** (**2**: $P-C^1$: 1.787 Å, C^1-C^2: 1.459 Å, C^1-C^6: 1.457 Å; **1**: $P-C^1$: 1.811 Å, C^1-C^2: 1.428 Å and C^1-C^6: 1.427 Å). These geometrical changes are due to the stabilizing interaction $n_P^{\pi} \rightarrow \pi^*_{b1}$. For the anion **2**, these calculated geometric parameters are in particularly good agreement with the X-ray values[7] ($P-C^1$: 1.795 Å, C^1-C^2: 1.453 Å, and C^1-C^6: 1.452 Å). The delocalization of the negative charge (NBO analysis) to the aryl group is well described by the electronic distribution (Table 3). Noteworthy is the π-electronic trans-

Table 2. Selected bond lengths [Å] and bond angles [°] for the privileged structures of $PhPH_2$ (**3A**) and Ar_fPH_2 (**4A**) and their transition states (T.S.) (**3B** and **3C** for $PhPH_2$ and **4B** for Ar_fPH_2), calculated with the B3LYP hybrid functional and the basis set 6-31+G(d,p) (θ = Lp $P-C^1-C^2$ [°]); energetic difference between T.S. and the minimum [kcal/mol]

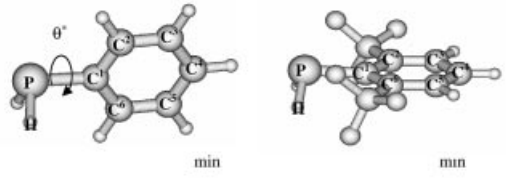

	3A min θ = 10.5°	**3B** T.S. θ = 90°	**3C** T.S. θ = 0°	**4A** min θ = 90°	**4B** T.S. θ = 0°
P–C^1	1.856	1.855	1.858	1.876	1.891
C^1–C^2	1.404	1.404	1.403	1.416	1.414
C^2–C^3	1.399	1.397	1.399	1.399	1.400
C^3–C^4	1.396	1.397	1.395	1.390	1.389
C^4–C^5	1.399	1.397	1.399	1.390	1.391
C^5–C^6	1.396	1.397	1.396	1.399	1.399
C^1–C^6	1.405	1.404	1.406	1.416	1.417
H–P–C^1	98.11	97.22	97.95	96.70	96.33
C^6–C^1–C^2	118.54	118.54	118.55	116.32	116.61
ΣP	288.94	288.26	289.04	287.13	286.22
$E_{TS} - E_{min}$	0	0.6	insignifiant	0	1.99

 © 2004 Wiley-VCH Verlag GmbH & Co. KGaA, Weinheim

fer of about 0.7 π e^- from the phosphorus lone pair to the π system of the phenyl ring (**1**: 0.62 π e^-; **2**: 0.76 π e^-).[10]

Table 3. NBO charges computed at the B3LYP/6-31G(d,p) level for $PhPH^-$ (**1**) and Ar_fPH^- (**2**)

	$PhPH^-$ (**1A**)	Ar_fPH^- (**2A**)
P	−0.26	−0.09
C^1	−0.32	−0.32
C^2	−0.27	−0.22
C^3	−0.25	−0.20
C^4	−0.33	−0.34
C^5	−0.25	−0.20
C^6	−0.28	−0.23
H^1	−0.08	−0.06

For the transition states **1B** and **2B**, the calculated P−C bonds (1.886 and 1.884 Å, respectively) are longer than those for **1A** and **2A**. The C^1-C^2 and C^1-C^6 bond lengths (ca. 1.427 Å) for **2B** also agree with a weak delocalization of the phosphorus lone pair, with an s character, in the ring as shown in Figure 1.

Thus, considering the charges and the geometric parameters it appears that the phenyl ring substituted by CF_3 groups acts as an electron acceptor by the π^*_{b1} orbital and contributes to the stability of the Ar_fPH^- anion (**2**) which features a quinoid structure.

However, the stabilization of the anion **2** is not the only factor that explains the isolation of such species from the phosphane Ar_fPH_2 precursor **4**. A second reason can be proposed: the presence of the CF_3 groups must induce destabilizing interactions into the neutral molecule. In order to check such a hypothesis, we theoretically determined the stationary points (minima and saddle points) corresponding to the rotation process of the two phosphanes **3** and **4**. In addition, the photoelectron spectra were recorded to determine the possibility of a favored orientation between the aryl group and the phosphorus lone pair. The agreement between theoretical data and PE experiments allow us to determine the importance of interactions between the π system of this aryl group and the n_p phosphorus lone pair.

Phenylphosphane (3)

For the phenylphosphane the energetically privileged rotamer **3A** presents a *gauche* orientation of the phenyl ring ($H^1-P-C^1-C^2$: −112.7°, $H^2-P-C^1-C^2$: 152.9°; Lp $P-C^1-C^2$: 10.5°). In this case, there is a very weak interaction between the π-system of the phenyl ring and the phosphorus lone pair. During the rotation process, two transition states (**3B**; Lp $P-C^1-C^2$: 90°) and (**3C**; Lp $P-C^1-C^2$: 0°) have been found on the potential energy surface. For **3B**, there is a maximal interaction between the phosphorus lone pair and the π system of the phenyl ring, whereas **3C** presents no interaction. The geometrical parameters are described in Table 2. The energy difference between the different transition states (**3B** or **3C**) and the minimum **3A** is very weak (calculated at 0.6 kcal/mol for **3B**) or negligible (for **3C**). It means that a free rotation of the phenyl group in the gas phase can occur. This result is in agreement with the one reported by Veszpremi et al. (HF/MP2 calculations).[9a]

For these different structures the electronic and nuclear repulsion energies are summarized in Table 4. We can note that the lowest energy structure corresponds to a form where the electronic and nuclear repulsion energies are intermediate between those of the two transition states. For **3B**, the electronic and the repulsion energies are strongest, this latter being predominating.

Table 4. Electronic and nuclear repulsion energies [hartrees] for the different structures of $PhPH_2$ (**3**) and Ar_fPH_2 (**4**)

	E_{elec}	E_{rep}
$PhPH_2$ (**3A**) min	−893.013421	318.800771
$PhPH_2$ (**3B**)	−893.206339	318.994787
$PhPH_2$ (**3C**)	−892.953020	318.740385
Ar_fPH_2 (**4A**) min	−2453.638501	1205.321897
Ar_fPH_2 (**4B**)	−2450.487236	1202.174381

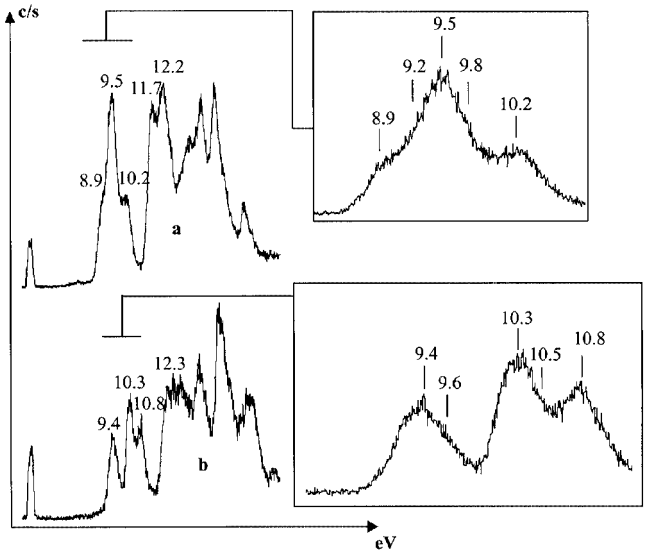

Figure 2. **a**: He-I spectrum of $PhPH_2$ (**3**); **b**: He-I spectrum of Ar_fPH_2 (**4**)

For compound **3**, the PE spectrum (Figure 2) presents, at low energies, three bands of different intensities at 8.9, 9.5 and 10.2 eV, the second one being the most intense.

For the lowest energy structure **3A**, the three first Kohn−Sham (K-S) orbitals are energetically close (Table 5: $\pi_{b1} - n_P$: −6.92; π_{a2}: −7.17; $\pi_{b1} + n_P$: −7.43 eV). Thus, the PE spectrum would present three bands with the same intensities, each separated by about 0.25 eV, or a unique broad band. The experimental spectrum cannot correspond to **3A** since, experimentally, the separation between the first and the third band is about 1.2 eV and the second band is more intense than the first and third ones. This observation suggests the presence of other rotamers. In fact, this PE

 © 2004 Wiley-VCH Verlag GmbH & Co. KGaA, Weinheim

spectrum would be a superposition of all rotamers' ionizations (Figure 3), as previously observed.[9a]

Table 5. Kohn−Sham energies and ΔSCF values for $PhPH_2$ (minimum **3A** and transition states **3B** and **3C**) and Ar_fPH_2 (minimum **4A** and transition state **4B**) calculated with the B3LYP hybrid functional and the basis set 6-31+G(d,p)

Kohn−Sham energies [eV] (Δ*SCF values*)				
$PhPH_2$ (**3A**)	$PhPH_2$ (**3B**)	$PhPH_2$ (**3C**)	Ar_fPH_2 (**4A**)	Ar_fPH_2 (**4B**)
−6.92	−6.47	−7.13	−7.22	−7.57
$\pi_{b1} - n_P$ (*8.86 eV*)	$\pi_{b1} - n_P$ (*8.41 eV*)	π_{a2} (*9.10 eV*)	$\pi_{b1} - n_P$ (*9.14 eV*)	n_P (*9.86 eV*)
−7.17	−7.14	−7.19	−8.25	−8.08
π_{a2}	π_{a2}	π_{b1}	π_{a2}	π_{a2}
−7.43	−7.94	−7.19	−8.67	−8.28
$\pi_{b1} + n_P$	$\pi_{b1} + n_P$	n_p	$\pi_{b1} + n_P$	π_{b1}

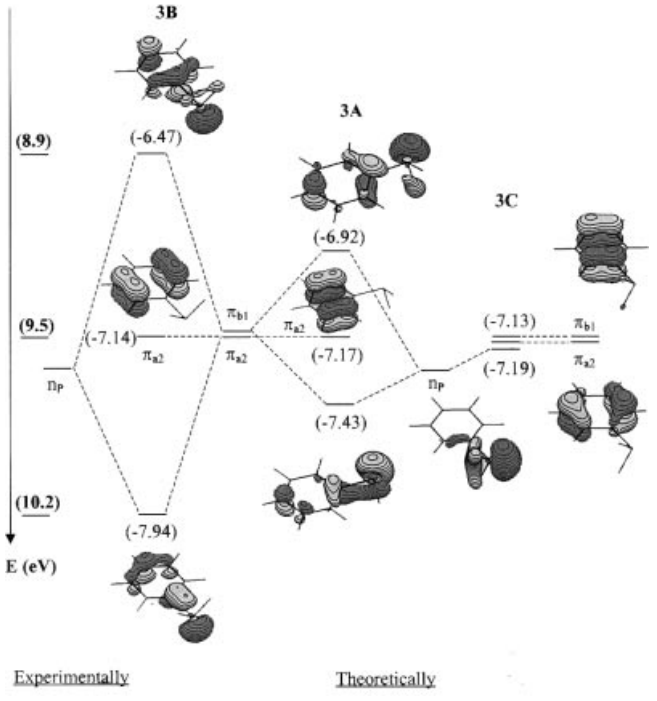

Figure 3. Experimental ionization potentials, molecular orbitals and Kohn−Sham values of $PhPH_2$ (minimum **3A** and transition states **3B** and **3C**)

For **3C** the K-S energies (−7.13: π_{a2}; −7.19 eV: π_{b1} and n_P) of the first three orbitals are almost identical (Table 5). These three ionizations would appear in a unique band, like for **3A**. Taking into account the similar K-S energies for **3A** and **3C** as well as the π_{a2} and π_{b1} ionization potentials of the phenyl ring,[11] the first three ionizations of these two rotamers will be at the same energy (9.5 eV). Thus, the second band can be assigned to the removal of an electron from the $\pi_{b1} - n_P$, π_{a1}, $\pi_{b1} + n_P$ orbitals of **3A** as well as the π_{a2}, π_{b1}, and n_P orbitals of all rotamers around **3C**. This rotamer population explains the intensity of this latter in the PE spectrum.

For **3B**, the first three Kohn−Sham energies (Table 5) are calculated at −6.47: $\pi_{b1} - n_P$; −7.14: π_{a2}; −7.94 eV: $\pi_{b1} + n_P$, respectively. Only the presence of rotamers population with a structure close to **3B** allows the assignment of the complete experimental spectrum. Like for **3A** and **3C**, the second ionization π_{a2} corresponds to the experimental band centered at 9.5 eV. Taking into account the theoretical difference between the first and second ionization (0.67 eV) the band at 8.9 eV corresponds to the removal of an electron from the $\pi_{b1} - n_P$ orbital. Moreover, the comparison between the experimental (1.3 eV) and theoretical (1.4 eV) energetic gap between the first and third band allows us to associate the third ionization to the band at 10.2 eV.

These assignments are consistent with the expanded spectra (Figure 2) where we observe an intense band centered at 9.5 eV with a shoulder between 8.6 and 9.0 eV and a broad shoulder between 9.8 and 10.3 eV.

[2,6-Bis(trifluoromethyl)phenyl]phosphane (4)

For **4**, one minimum is found on the potential energy surface (Table 2). This lowest energy structure (**4A**) corresponds to a maximal interaction between the phosphorus lone pair and the π system. A comparison between **4A** and **3B** (phenyl ring with the same orientation) shows a slight lengthening of the P−C^1 bond length (1.876 Å for **4A** and 1.855 Å for **3B**) and a phosphorus pyramidalization more pronounced for **4** (ΣP angle: 287.13° for **4A**, 288.26° for **3B**). An explanation is found considering the strong interatomic and electronic repulsions between the phosphorus lone pair and the CF_3 substituents. For **4A**, the theoretical H−F and P−F distances (2.46 and 2.92 Å, respectively) correspond to a van der Waals contact (2.55 and 3.25 Å, respectively). However, there is a compensation between these high steric repulsions, which destabilize the system and an electronic delocalization between the phosphorus lone pair and the aromatic system, which is stabilizing.

The ring system of the transition state **4B** has similar orientation than **3C** [no interaction between n_P and $\pi_{C=C}$]. It is found to be 1.99 kcal/mol higher in energy than the minimum. As for $PhPH_2$, a free rotation can also be proposed in this case. A lengthening of the P−C^1 bond is noteworthy when we compared the calculated geometric parameters of **4B** and **3C** (Table 2).

For these two structures **4A** and **4B** the electronic and nuclear repulsion energies are summarized Table 4. The lowest energy structure **4A** corresponds to the form where the electronic energy is the more important. The presence of σ-attractor CF_3 groups involves an electronic delocalization between the phosphorus lone pair and the aromatic system (π^*_{b1}) which stabilizes the system and counterbalances the high steric interactions (Figure 4). For **4** the photoelectron spectrum (Figure 2) shows three well-separated first bands which appear at 9.4, 10.3, and 10.8 eV, respectively.

 © 2004 Wiley-VCH Verlag GmbH & Co. KGaA, Weinheim

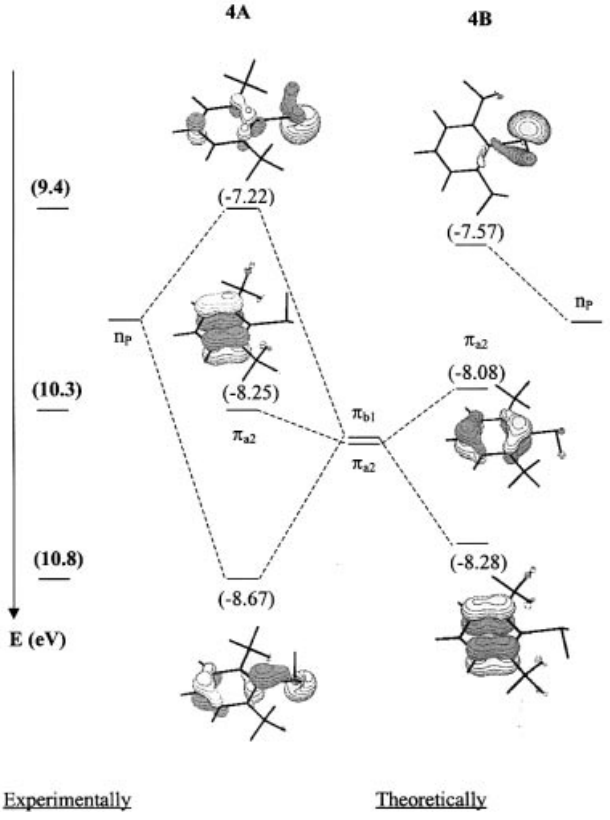

Figure 4. Experimental ionization potentials, molecular orbitals and Kohn−Shan values of Ar_fPH_2 (minimum **4A** and T.S. **4B**)

For the lowest energy structure (**4A**) the three K-S energies (Table 5) are calculated at −7.22: $\pi_{b1} - n_P$; −8.25: π_{a2}; −8.67 eV: $\pi_{b1} + n_P$, respectively. In the PE spectrum the second band, centered at 10.3 eV is associated with the ionization of the π_{a2} orbital.[12] The experimental separation between the first and the third band is about 1.4 eV. Taking into account the calculated energetic gap between the first and third ionizations (1.45 eV), we assign the first band (9.4 eV) to the ionization from the $\pi_{b1} - n_P$ orbital and the third band (10.8 eV) to the $\pi_{b1} + n_P$ orbital.

The weak energy difference between the two rotamers **4A** and **4B**, as previously observed in the case of **1**, involves the existence of a free rotation process. It means that the ionizations of **4B** are going to also appear in the experimental spectrum. For **4B** the K-S energies are the following: −7.57: n_P; −8.08: π_{a2}; −8.28 eV: π_{b1} (Table 5). Thus, for this rotamer, the ionization of the phosphorus lone pair is located in the shoulder of the first band (9.4 eV) and the π_{a2} and π_{b1}' ionizations in the second band centered at 10.3 eV, which explains its intensity. The expanded spectrum allows us to check the existence of a shoulder (9.6 eV) in the first band and the presence of several ionizations near 10.3 eV.

The photoelectron study shows that for these neutral species, the ring orientation is of minor importance.

Proton Affinity

Considering the previous results on the phosphanides and corresponding phosphanes, it was of interest to focus our attention on the proton affinity (PA) of the anion (or the acidity of the phosphane).

Taking into account the equation $A^- + H^+ \rightarrow HA$, PA is the result of the energiy difference between the neutral and the anion species. A net difference is observed between the two anions since PA is calculated at 352.93 kcal/mol for $PhPH^-$ (**1**) and 337.37 kcal/mol for Ar_fPH^- (**2**). Such results are coherent with the existence of the naked phosphanide **2**, both in the solid state and in solution. In fact the Ar_f substituent involves a stabilization of the anion species (interaction $p^{\pi} \rightarrow \pi^*_{b1}$) but also a destabilization of the corresponding phosphane (important steric repulsion between the phosphorus and fluorine lone pairs). These two factors lead to a peculiar gas-phase acidity for the Ar_fPH_2 compound. It is noteworthy that the gas-phase acidity of **4** is stronger than the one of PH_3 (expt. 370.8 kcal/mol; calcd. 364.7 kcal/mol) and close to the one of HCOOH (found 345 kcal/mol; calcd. 335.5 kcal/mol).

The calculation of the proton affinity can also be performed by the isodesmic reaction $NH_4^+ + Ar_fPH^- \rightarrow Ar_fPH_2 + NH_3$. In this case the PA can reliably be anchored on the experimental value of NH_3 (202.3 kcal/mol[13]). Noteworthy that the PA values resulting from the isodesmic reaction are calculated at 352.0 kcal/mol for **1** and 336.44 kcal/mol for **2**. These latter are very close to the previous ones which result from the energies difference between the neutral and the anion species.

Conclusion

The stabilization of the fluorinated anion Ar_fPH^- (**2**) as well as the presence of destabilizing interactions into the corresponding neutral molecule Ar_fPH_2 (**4**) allow us to explain the difference observed in the calculated proton affinities for **1** and **2**. For the anionic species we theoretically showed that favored form is planar because of stabilizing interaction between the π phosphorus lone pair (p character) and the π^*_{b1} orbital. This latter seems to be more important for the fluorinated compound **2** compared to **1** since the inductive effect of the CF_3 groups involves a stabilization of the a_2, b_1, a^*_2, and b^*_1 orbitals of the aryl group, and decreases the $p^{\pi} \rightarrow \pi^*_{b1}$ energetic gap. In this case Ar_f is an electron acceptor by its LUMO orbital and contributes to the observed stability of the corresponding anion.

With regard to neutral species, the coupling of UV Photoelectron Spectroscopy and DFT calculations, showed that a free rotation of the aryl group occurs in the gas phase. However, the phosphanes **3** and **4** exhibit different favored forms: the phosphorus lone pair is in maximal interaction with the π system of the ring for **4**, while almost no interaction exists for **3**. For the bulky compound **4**, the orientation of the phenyl ring allows a compensation between two competitive factors: high steric repulsions (between phosphorus and fluorine lone pairs) which destabilize

 © 2004 Wiley-VCH Verlag GmbH & Co. KGaA, Weinheim

the system and an electronic delocalization between the phosphorus lone pair and the aromatic system, which is stabilizing.

Computational Details

Calculations were performed with the Gaussian 98 program[14,15] using the density functional theory.[16] The various structures were fully optimized at the B3LYP level.[17] This functional is built with Becke's three-parameter exchange functional[17a] and the Lee−Yang−Parr correlation functional.[17c] Kass et al.[18] have shown, with 35 different anionic species, that the density functional theory provides reasonable results concerning acidities compared to the experimental data. Thus, calculations for the anions $PhPH^-$ (**1**) and Ar_fPH^- (**2**) have been carried out using the B3LYP hybrid functional and the 6-31+G(d,p) basis set, with polarization functions on all the atoms and diffuse functions on all non-hydrogen atoms. Moreover, the use of density functional theory (DFT) within its Kohn−Sham (K-S) presents many advantages. First, the cost of a K-S DFT calculation is at most of the same order of magnitude as a Hartree−Fock one whereas most of the description of electron correlation is taken into account. Thus, it is substantially less expensive than traditional correlated techniques. The basis set used for all calculations is the 6-31G+(d,p) set which is augmented with polarisation functions on all the atoms and diffuse functions on all non-hydrogen atoms since the inclusion of polarization is necessary for the obtention of accurate energies. The structures were optimized and the second derivatives were calculated in order to determine if a minimum or a transition state (one negative eigenvalue) existed for the resulting geometry. All total energies have been zero-point energy (ZPE) and temperature corrected using unscaled density functional frequencies. For the large molecules, association between ionization potential and Kohn−Sham (K-S) energies calculated with common functionals (Koopmans' theorem like) has been discussed in depth. Arduengo and co-workers[19] first used DFT calculations at the nonlocal level to assign their photoelectron spectra. They applied a uniform shift to the orbital energies considering the difference between the calculated and experimental molecular ionization potential. The aim was to directly compare the K-S energies to the experimental energies. Moreover, Werstiuk and Rademacher[20] have developed and successfully applied a routine for the interpretation of PE spectra based on B3LYP theory. This routine requires the calculation of the molecule's first vertical ionization potential IP_v. Calculated orbital energies $-\varepsilon$ are then shifted uniformly so that the HOMO energy equals that of the IP_v, giving the higher IPs. More recently, Hoffmann[21] underlined that the K-S orbitals are a good basis for a qualitative interpretation of molecular orbitals. He concludes that if we want to go a step beyond a qualitative interpretation and look at orbital energies as rough ionization potentials and if the DFT calculations are done with commonly used potentials, then it appears we must take the absolute constant and linear orbital energy shift into account by applying a suitable $ax + b$ scaling. In the case of large molecules, the ordering of levels found using the DFT calculations, seems to be qualitatively well translated as well by using HF methods. This fact, despite the evident limits of correlation, gives a good base to discuss the ionizations assignments which cannot be reached by a direct calculation. The "natural population analysis" (NBO calculations) at the given optimized geometries, allowing to calculate orbital populations of molecular wave functions, was carried out according to the Weinhold−Reed partitioning scheme.[22]

Photoelectron Spectra: The photoelectron spectra were recorded with a Helectros 0078 instrument equipped with 127° cylindrical analyser and monitored by a microcomputer supplemented with a digital/analog (D/A) converter. The spectra were calibrated with the known auto-ionisation of helium at 4.98 eV [He-II(He)] and nitrogen ionisation at 15.59 eV.

Acknowledgments

Financial support of this work by the CNRS (France) is gratefully acknowledged. We also thank the Institut du Developpement de Ressources en Informatique Scientifique (IDRIS, Orsay, France), administered by the CNRS, for the calculation facilities, Dr. Gijs Schaftenaar for allowing us to use his graphic program Molden,[23] and the "Societé de Secours des Amis des Sciences" for financial support of K. M.

[1] A. Chrostowska, V. Lemierre, T. Pigot, G. Pfister-Guillouzo, I. Saur, K. Miqueu, G. Rima, J. Barrau, *Main Group Met. Chem.* **2002**, *25*, 469.
[2] For a review on this topic see: F. T. Edelmann, *Comments Inorg. Chem.* **1992**, *12*, 259.
[3] K. B. Dillon, H. P. Goodwin, *J. Organomet. Chem.* **1994**, *469*, 125.
[4] [4a] K. B. Dillon, H. P. Goodwin, *J. Organomet. Chem.* **1992**, *429*, 169. [4b] K. B. Dillon, V. C. Gibson, L. I. Sequeira, *J. Chem. Soc., Chem. Commun.* **1995**, 2429. [4c] K. B. Dillon, V. C. Gibson, J. A. K. Howard, L. I. Sequeira, J. W. Yao, *Polyhedron* **1996**, *15*, 4173.
[5] J.-Th. Ahlemann, A. Künzel, H. W. Roesky, M. Noltemeyer, L. Markovskii, H. G. Schmidt, *Inorg. Chem.* **1996**, *35*, 6644.
[6] [6a] M. G. Davidson, K. B. Dillon, J. A. K. Howard, S. Lamb, M. D. Roden, *J. Organomet. Chem.* **1998**, *550*, 481. [6b] J. E. Bender IV, M. M. Banaszak Holl, J. W. Kampf, *Organometallics* **1997**, *16*, 2743. [6c] J. E. Bender IV, A. J. Shusterman, M. M. Banaszak Holl, J. W. Kampf, *Organometallics* **1999**, *18*, 1547. [6d] N. Burford, Ch. L. B. Macdonald, D. J. LeBlanc, T. S. Cameron, *Organometallics* **2000**, *19*, 152. [6e] G. M. Benedikt, B. L. Goodall, S. Iyer, L. H. McIntosh III, R. Mimna, L. F. Rhodes, C. S. Day, V. W. Day, *Organometallics* **2001**, *20*, 2565.
[7] L-V. Rudzevich, H. Gornitzka, V-D. Romanenko, G. Bertrand, K. Miqueu, J-M. Sotiropoulos, G. Pfister-Guillouzo, *Angew. Chem. Int. Ed.* **2001**, *41*, 7, 1193.
[8] [8a] S. Ikuta, P. Kebarle, *Can. J. Chem.* **1983**, *61*, 97. [8b] S. T. Howard, J. A. Platts, *J. Phys. Chem.* **1995**, *99*, 9027. [8c] S. T. Howard, J. P. Foreman, P. G. Edwards, *Inorg. Chem.* **1996**, *35*, 5812.
[9] [9a] L. Nyulaszi, D. Szieberth, G. I. Csonka, J. Reffy, J. Heinicke, T. Veszpremi, *Struct. Chem.* **1995**, *6*, 1. [9b] D. E. Cabelli, A. H. Cowley, M. J. S. Dewar, *J. Am. Chem. Soc.* **1981**, *103*, 3286. [9c] D. E. Cabelli, A. H. Cowley, M. J. S. Dewar, *J. Am. Chem. Soc.* **1981**, *103*, 3290.

 © 2004 Wiley-VCH Verlag GmbH & Co. KGaA, Weinheim

[10] These charges are computed with B3LYP/6-31G(d,p).

[11] Experimentally, the π ionizations (π_{b1}, π_{a1}) of the phenyl ring appear at 9.24 eV.[24] Theoretically the K-S energies of the π ionizations are −7.01 eV.

[12] For $Ph(CF_3)_2$ the experimental π_{a2} and π_{b1} ionization potentials are 10.41 eV.

[13] [13a] R. Yamdagni, P. Kebarle, *J. Am. Chem. Soc.* **1973**, *95*, 3504. [13b] R. Yamdagni, P. Kebarle, *J. Am. Chem. Soc.* **1976**, *98*, 1320. [13c] J. F. Wolf, R. H. Staley, I. Koppel, M. Taagepera, R. T. Mciver, J. L. Beauchamp, R. W. Taft, *J. Am. Chem. Soc.* **1977**, *99*, 5417.

[14] M. J. Frisch, G. W. Trucks, H. B. Schlegel, G. E. Scuseria, M. A. Robb, J. R. Cheeseman, V. G. Zakrzewski, J. A. Montgomery, R. E. Stratman, J. C. Burant, S. Dapprich, J. M. Millam, A. D. Daniels, K. N. Kudin, M. C. Strain, O. Farkas, J. Tomasi, V. Barone, M. Cossi, R. Cammi, B. Mennucci, C. Pomelli, C. Adamo, S. Clifford, J. Ochterski, G. A. Petersson, P. Y. Ayala, Q. Cui, K. Morokuma, D. K. Malick, A. D. Rabuck, K. Raghavachari, J. B. Foresman, J. Cioslowswi, J. V. Ortiz, A. G. Baboul, B. B. Stefanov, G. Liu, A. Liashenko, P. Piskorz, I. Komaromi, R. Gomperts, R. Martin, D. J. Fox, T. Keith, M. A. Al-Laham, C. Y. Peng, A. Nanayakkara, C. Gonzalez, M. Challacombe, P. M. W. Gill, B. Jonhson, W. Chen, M. W. Wong, J. L. Andres, M. Head-Gordon, E. S. Replogle, J. A. Pople, *Gaussian 98*, Revision A.7, Gaussian, Inc., Pittsburgh PA, **1998**.

[15] W. J. Hehre, L. Radom, P. v. R. Schleyer, J. A. Pople, *Ab Initio Molecular Orbital Theory*, John Wiley and Sons, New York, **1986**.

[16] R. G. Parr, W. Yang, *Functional Theory of Atoms and Molecules* (Eds.: R. Breslow, J. B. Goodenough), Oxford University Press, New York, **1989**.

[17] [17a] A. D. Becke, *Phys. Rev.* **1988**, *A38*, 3098. [17b] A. D. Becke, *J. Chem. Phys.* **1993**, *98*, 5648. [17c] C. Lee, W. Yang, R. G. Parr, *Phys. Rev.* **1988**, *B37*, 785.

[18] G. N. Merill, S. R. Kass, *J. Phys. Chem.* **1996**, *100*, 17465.

[19] A. J. Arduengo III, H. Bock, H. Chen, M. Denk, D. A. Dixon, J. C. Green, W. A. Hermann, N. L. Jones, M. Wagner, R. West, *J. Am. Chem. Soc.* **1994**, *116*, 6641.

[20] [20a] H. M. Muchall, P. Rademacher, *J. Mol. Struct.* **1997**, *435*, 157. [20b] H. M. Muchall, P. Rademacher, *J. Mol. Struct.* **1998**, *471*, 189. [20c] H. M. Muchall, N. H. Werstiuk, B. Choudhurry, *Can. J. Chem.* **1998**, *76*, 221. [20d] H. M. Muchall, N. H. Werstiuk, B. Choudhurry, J. Ma, J. Warkentin, J. P. Pezacki, *Can. J. Chem.* **1998**, *76*, 238.

[21] R. Stowasser, R. Hoffmann, *J. Am. Chem. Soc.* **1999**, *121*, 3414.

[22] [22a] A. E. Reed, L. A. Curtiss, F. Weinhold, *J. Chem. Rev.* **1988**, *88*, 899. [22b] J. P. Foster, F. Weinhold, *J. Am. Chem. Soc.* **1980**, *102*, 7211.

[23] G. Schaftenaar, J. H. J. Noordik, *Comput.-Aided Mol. Des.* **2000**, *14*, 123.

[24] K. Kimura, S. Katsumata, Y. Achiba, T. Yamazaki, S. Iwata, *Handbook of He I Photoelectron Spectroscopy of Fundamental Organic Molecules*, Japan Scientific Societies Press, Tokyo, Japan, **1981**.

Received May 27, 2003
Early View Article
Published Online October 30, 2003

 © 2004 Wiley-VCH Verlag GmbH & Co. KGaA, Weinheim

Reduction of 1,2-Bis[(2,6-diisopropylphenyl)imino]acenaphthene (dpp-bian) with Alkali Metals − A Study of the Solution Behaviour of (dpp-bian)$^{n-}$[M$^+$]$_n$ (M = Li, Na; n = 1−4) with UV/Vis, ESR and ^{1}H NMR Spectroscopy

Igor L. Fedushkin,*[a] Alexandra A. Skatova,[a] Valentina A. Chudakova,[a] Vladimir K. Cherkasov,[a] Georgy K. Fukin,[a] and Mikhail A. Lopatin[a]

Keywords: Lithium / Sodium / Bis(imino)acenaphthene / Polyanions

An excess of lithium or sodium in diethyl ether consistently reduces 1,2-bis[(2,6-diisopropylphenyl)imino]acenaphthene (dpp-bian) to the mono-, di-, tri- and tetraanion, (dpp-bian)$^{n-}$[M$^+$]$_n$ (M = Li, Na; n = 1–4). The process of reduction is easily observed by the change in colour of the solution, on going from the neutral ligand (yellow) to the monoanion (red), the dianion (green for Na or Li in Et_2O; dark blue, followed by green, for Li in TMEDA), the trianion (brown) and the tetraanion (red-brown). In each reduction the maximum of the absorption, caused by electron transition from the HOMO of the respective form (dpp-bian)$^{n-}$ (n = 1–4), is shifted to the long-wavelength region in comparison to the previously reduced state. The disproportionation reactions (dpp-bian)$^{1-}$ → (dpp-bian)^0 + (dpp-bian)$^{2-}$ and (dpp-bian)$^{2-}$ → (dpp-bian)$^{1-}$ + (dpp-bian)$^{3-}$ take place in solution along with the reduction process, thus causing the presence of three reduced forms of the ligand at the same time in the first and second stages of the reduction. Paramagnetic (dpp-bian)$^{1-}$ and (dpp-bian)$^{3-}$ are characterised by ESR spectroscopy. For the diamagnetic forms (dpp-bian)$^{2-}$ and (dpp-bian)$^{4-}$ ^{1}H NMR spectra were recorded. The complex [Li$^+$(dpp-bian)(TMEDA)] (**1**), which formed from the initial stage of the reduction of dpp-bian with lithium metal in TMEDA, was isolated in a crystalline form and its molecular structure was determined by single-crystal X-ray diffraction.

(© Wiley-VCH Verlag GmbH & Co. KGaA, 69451 Weinheim, Germany, 2004)

Introduction

Within the last few years 1,2-bis[(2,6-diisopropylphenyl)imino]acenaphthene (dpp-bian) began to be used widely in coordination chemistry of transition metals.[1] Several interesting chemical reactions of metal complexes based on this ligand were reported. Until recently only complexes of transition metals and only with the neutral dpp-bian ligand were studied. These complexes are active as catalysts in alkyne hydrogenation[2a], C−C[2b] and C−Sn[2c] bond formation, and especially in olefin polymerisation.[3] We have reported on the synthesis, isolation of crystals and detailed characterisation of the magnesium and calcium complexes with the dpp-bian dianion, (dpp-bian)$^{2-}$M^{2+}(L)$_n$ (M = Mg, L = THF, n = 2, 3 and L = Py, n = 3; M = Ca, L = THF, n = 3, 4).[4] These Mg and Ca complexes are easy to synthesise by direct reduction of the ligand with metallic magnesium or calcium. The use of sodium metal has allowed the reduction of dpp-bian leading to the formation of the dianion and also the tetraanion. Thus, sodium salts of mono-, di-, tri- and tetraanions of the ligand, [Na$^+$(dpp-bian)$^-$]$_2$, [Na$^+_2$(Et$_2$O)$_3$(dpp-bian)$^{2-}$], [Na$^+_3$(Et$_2$O)$_2$(dpp-bian)$^{3-}$]$_2$, [Na$^+_4$(THF)$_4$(dpp-bian)$^{4-}$]$_2$, were isolated in crystalline form and characterised by single-crystal X-ray diffraction.[5] Thus, for the first time four anionic forms of a single ligand were isolated on a preparative scale and characterised by single-crystal X-ray structure analysis. At present one of our objectives is to use these sodium salts for synthesis of other non-transition metal complexes, which in turn, can be used as reducing agents of various classes of organic substrates, working over a wide range of the redox potentials.

To find an optimal synthetic approach to other metal complexes by metathetical reactions using the sodium salts (dpp-bian)$^{n-}$(Na$^+$)$_n$ (n = 1−4), more insight into their solution behaviour is needed. Therefore, we started the UV/Vis and ESR spectroscopic study of (dpp-bian)$^{n-}$(Na$^+$)$_n$ (n = 1−4) in solution. We also report here on the solution behavior of the lithium salts (dpp-bian)$^{n-}$(Li$^+$)$_n$ (n = 1−4) prepared in situ in both diethyl ether and TMEDA as well as the solid-state molecular structure of the TMEDA adduct [Li$^+$(dpp-bian)$^-$(TMEDA)] (**1**).

[a] G. A. Razuvaev Institute of Organometallic Chemistry of Russian Academy of Sciences,
Russian Federation, Tropinina 49, 603950 Nizhny Novgorod GSP-445,
Fax: (internat.) + 7-8312-661-497
E-mail: igorfed@imoc.sinn.ru

 © 2004 Wiley-VCH Verlag GmbH & Co. KGaA, Weinheim **DOI: 10.1002/ejic.200300351**

Results and Discussion

Reduction of dpp-bian with Sodium and Lithium − The Solution UV/Vis Spectroscopy

In general, a solution of the dpp-bian ligand was added into an ampoule which contained the appropriate alkali metal and was connected to the spectroscopic cell. Then the ampoule was sealed off under vacuum. On shaking the ampoule for several hours, a colour change was observed and monitored by UV/Vis spectroscopy. Figure 1 represents the electronic absorption spectra of $[Na^+_n(dpp\text{-}bian)^{n-}]$ (n = 1−4) obtained by reduction of dpp-bian with sodium metal in diethyl ether. The curves 1−9 reflect the change of spectra in a chronological sequence. The reduction is completed within 6 h upon intense shaking at room temperature. The neutral ligand exhibits an absorption at 420 nm, which corresponds to a yellow solution. Over the course of reduction the colour of the solution becomes darker, the band of absorption of the initial ligand gradually disappears, and the absorption of the radical anion $(dpp\text{-}bian)^-$ (435, 460 and 495 nm) (Figure 1, a, spectrum 1) becomes visible. As the reduction proceeds, the absorption band of $(dpp\text{-}bian)^-$ is lowered again and the absorption of the dianion (640 nm) is enhanced (Figure 1, a, spectrum 2). Spectrum 3 (Figure 1, a) shows the absorption of the dianion (640 nm) becoming more intensive and indicates the prevalence of the dianion in solution. The compound $[Na_2(Et_2O)_3(dpp\text{-}bian)]$, isolated in crystalline form,[5] exhibits the same spectrum. Figure 1 (b) reflects changes on going from $(dpp\text{-}bian)^{2-}$ to $(dpp\text{-}bian)^{3-}$. The absorption at 840 nm indicates the formation of the trianion $[Na^+_3(dpp\text{-}bian)^{3-}]$. As seen from Figure 1 (a and b), three reduced forms of the ligand are present at the same time in solution. This may be explained by the disproportionation: $(dpp\text{-}bian)^{1-} \rightarrow (dpp\text{-}bian)^0 + (dpp\text{-}bian)^{2-}$ and $(dpp\text{-}bian)^{2-} \rightarrow (dpp\text{-}bian)^{1-} + (dpp\text{-}bian)^{3-}$. Upon further reduction of $(dpp\text{-}bian)^{3-}$ with sodium the absorption of the trianion (840 nm) disappears (Figure 1, c). Spectrum 9 in Figure 1 (c) indicates the complete reduction of the ligand to the tetraanion. The tri- and tetraanions of the ligand show similar absorbance in the wavelength region (400−600 nm), but differ in the region of 700−1100 nm. It should be noted that this difference cannot be visually observed. Therefore, it is difficult to distinguish the colour of solutions of the tri- and tetraanions. Taking into account the observation that the absorption of every next reduced form has a lower absorption compared to that of the previous form, one can suggest that the absorption of the tetraanion, which originates from the electron transfer from the HOMO, is shifted into the near IR region. Although there is no isosbestic point in spectra 7−9, one can conclude that the disproportionation process $(dpp\text{-}bian)^{3-} \rightarrow (dpp\text{-}bian)^{2-} + (dpp\text{-}bian)^{4-}$ does not take place because of the absence of the absorption of the dianion (Figure 1, c).

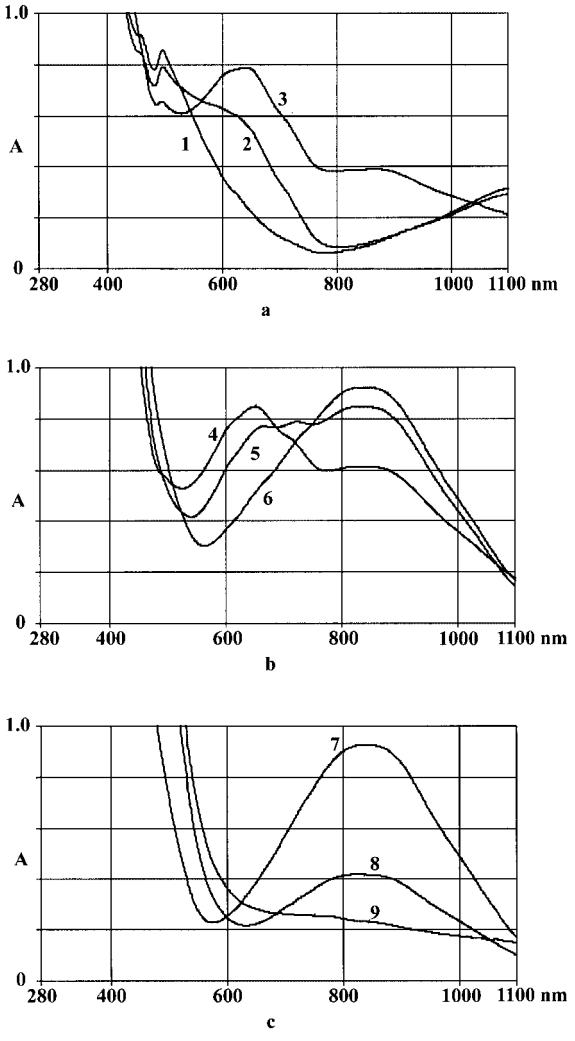

Figure 1. UV/Vis spectra of $(dpp\text{-}bian)^{n-}Na^+_n$ (n = 1−4) in Et_2O (10^{-3} mol/L) in the Pyrex cell (3.5 mm): (a) $(dpp\text{-}bian) \rightarrow (dpp\text{-}bian)^-$, (b) $(dpp\text{-}bian)^- \rightarrow (dpp\text{-}bian)^{2-} \rightarrow (dpp\text{-}bian)^{3-}$, (c) $(dpp\text{-}bian)^{3-} \rightarrow (dpp\text{-}bian)^{4-}$; the curves **1−9** reflect the change of spectra in a chronological sequence

The process of the reduction of the dpp-bian ligand with lithium metal was also investigated by electron absorption spectroscopy. The spectra, which correspond to the intermediate reduced forms of the ligand, are presented in Figure 2. Spectra 1−3 indicate the consecutive transformation of the radical anion $(dpp\text{-}bian)^-$ to the dianion $(dpp\text{-}bian)^{2-}$ (432, 468, 503 nm and 595, 650 nm, respectively). In spectrum 2 the simultaneous presence of the three forms in solution is clearly visible. The trianion $(dpp\text{-}bian)^{3-}$ has a maximum at 718 nm, which confirms the dissproportionation of the dianion to the radical anion and trianion. Figure 2 (b) reflects a gradual transition of $(dpp\text{-}bian)^{2-}$ into $(dpp\text{-}bian)^{3-}$ (718 and 780 nm). Spectrum 6 corresponds to a solution in which the $(dpp\text{-}bian)^{3-}$ form is dominant. Figure 2 (c) shows changes in solution on going from the trianion to the tetraanion. The existence of the isosbestic point in spectra 7−9 indicates that the trianion is completely converted by lithium under electron transfer into the tetranion without any side reactions (disproportionation etc.).

Upon reduction of dpp-bian with lithium in a diluted diethyl ether solution, we observed at the initial stages an appearance of an intense blue colour on cooling to about

 © 2004 Wiley-VCH Verlag GmbH & Co. KGaA, Weinheim

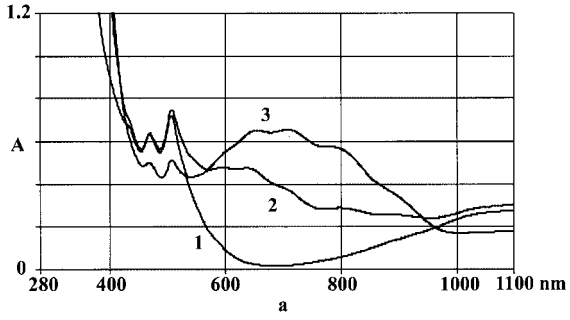

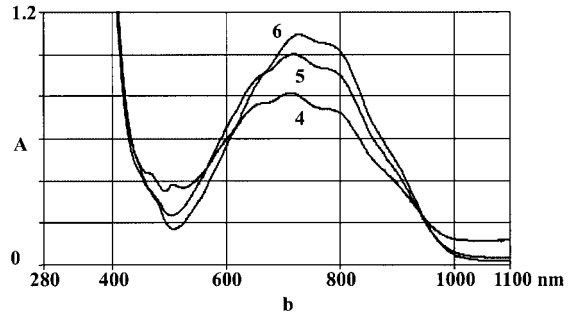

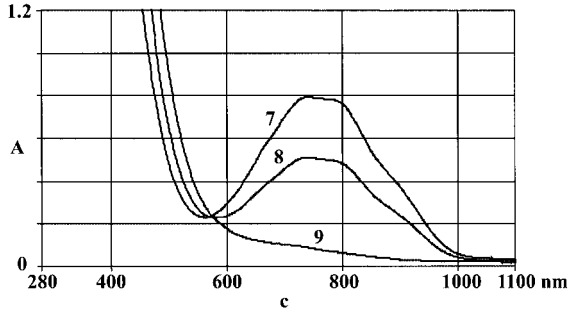

Figure 2. UV/Vis spectra of $(dpp\text{-}bian)^{n-}Li^{+}_{n}$ ($n = 1-4$) in Et_2O (10^{-3} mol/L) in the Pyrex cell (3.5 mm): (a) (dpp-bian) → (dpp-bian)$^{-}$, (b) (dpp-bian)$^{-}$ → (dpp-bian)$^{2-}$ → (dpp-bian)$^{3-}$, (c) (dpp-bian)$^{3-}$ → (dpp-bian)$^{4-}$; the curves **1**−**9** reflect the change of spectra in a chronological sequence

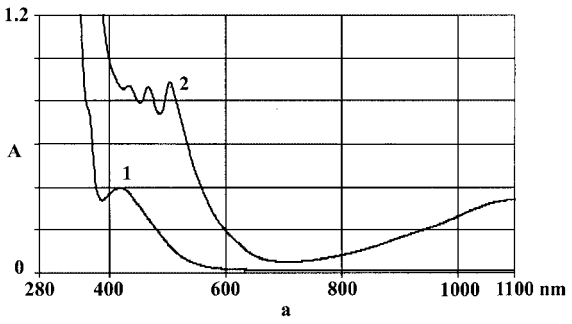

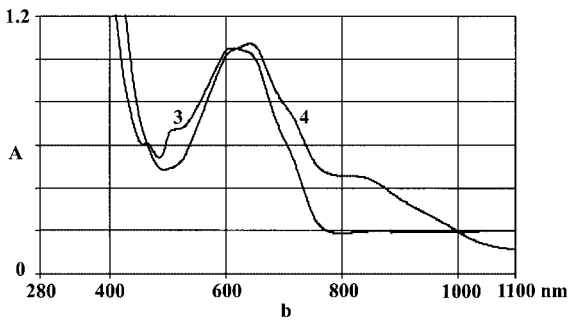

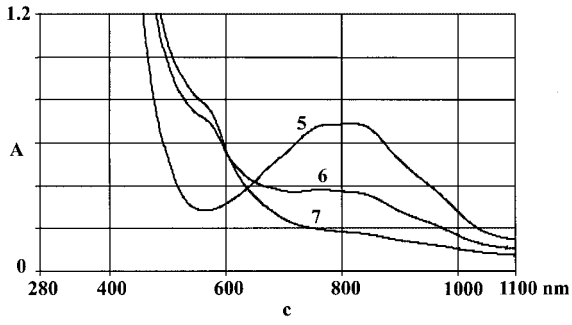

Figure 3. UV/Vis spectra of $(dpp\text{-}bian)^{n-}Li^{+}_{n}$ ($n = 1-4$) in TMEDA (10^{-3} mol/L) in a Pyrex cell (3.5 mm): (a) (dpp-bian) → (dpp-bian)$^{-}$, (b) (dpp-bian)$^{-}$ → (dpp-bian)$^{2-}$ → (dpp-bian)$^{3-}$, (c) (dpp-bian)$^{3-}$ → (dpp-bian)$^{4-}$; the curves **1**−**7** reflect the change of spectra in a chronological sequence

−50 °C. It was neither observed in the case of sodium nor at higher concentrations of the ligand in the case of lithium. Thawing of the ether solution leads to a colour change from blue to green. A similar colour has been observed earlier for THF solutions of lanthanide complexes with the naphthalene dianion {575 nm for $[EuI(THF)_4]_2(\mu\text{-}C_{10}H_8)$ and 604 nm for $[LaI_2(THF)_3]_2(\mu\text{-}C_{10}H_8)$}.[6] One can suggest that in the diluted Et_2O solution, at different temperatures, the mutual transition of two electronic isomers of the ligand takes place. In one of these forms the negative charge is, presumably, located mainly on the diimine function of the ligand (green) and in the second form on the naphthalene rings (deep blue). The latter form of the dpp-bian ligand may be considered as a dianion of the 1,8-disubstituted naphthalene. We suppose that transformation of the green dianion to the blue dianion is forced by the separation of the cation from the dianion by the solvent.

In order to find an experimental confirmation for this assumption we have tried to stabilise the dark blue form of $(dpp\text{-}bian)^{2-}$ using TMEDA as a solvent. Earlier, TMEDA was successfully used for the stabilisation of the lithium complex with the naphthalene dianion $[Li(TMEDA)]_2(\mu\text{-}C_{10}H_8)$.[7] The electronic absorption spectra of the reduction of dpp-bian with lithium in TMEDA are given in Figure 3. For the transition from $(dpp\text{-}bian)^{-}$ [432, 465 and 502 nm; Figure 3 (a), spectrum 2] to $(dpp\text{-}bian)^{2-}$ [Figure 3 (b), spectrum 3] the absorption that reflects the dianion formation, has a maximum at 612 nm and a shoulder at 645 nm. This spectrum corresponds to a dark blue colour of the solution. Further, this dark blue colour changes to a blue-green colour (spectrum 4). At that moment the absorption at 645 nm becomes most intense, and the maximum at 612 nm becomes a shoulder. We believe, that at the initial stages of the dianion formation, when its concentration is still very small, $Li^{+}_{2}(dpp\text{-}bian)^{2-}$ exists in solution as a solvent-separated ion pair. The negative charge of the dianion is located mostly on the naphthalene part of the molecule. Figure 3 (c) presents the transition from (dpp-

 © 2004 Wiley-VCH Verlag GmbH & Co. KGaA, Weinheim

bian)$^{3-}$ to (dpp-bian)$^{4-}$. The absorption of the trianion (760 and 837 nm) gradually disappears in the sequence 5 → 6 → 7. We have not had an opportunity to record the spectrum of (dpp-bian)$^{4-}$ in the region of 1100−2000 nm, but we suggest that the absorption of (dpp-bian)$^{4-}$, which corresponds to the excitation of an electron from the HOMO of the tetraanion, shifts to the long-wavelength region (> 1100 nm).

Molecular Structure of [Li$^+$(dpp-bian)$^-$(TMEDA)] (1)

Suitable crystals of **1** were obtained for X-ray structure determination by concentration of the TMEDA solution of **1**. The lithium atom in **1** has a distorted tetrahedral environment (Figure 4). The bite angles N(1)−Li(1)−N(2) and N(3)−Li(1)−N(4) are 87.03 and 83.90°, respectively. The lithium−dpp-bian bonds [Li(1)−N(1) 2.0365(18) and Li(1)−N(2) 2.0603(18) Å] are notably shorter than the lithium−TMEDA bonds [Li(1)−N(3) 2.1201(19) and Li(1)−N(4) 2.1701(19) Å]. The anionic character of the radical of the dpp-bian ligand in **1** is evident from the elongation of the C−N bond of the diimine moiety [C(1)−N(1) 1.3295(11) Å and C(11)−N(2) 1.3303(11) Å], compared with that of the neutral related ligand *p*-tol-bian [1.267(3) Å],[1b] the four-coordinate Pd^{II} complex [(dpp-bian)PdCl(CH$_3$)][1b] (1.287 Å) and the five-coordinate Cu^{II} complex [(dpp-bian)CuCl$_2$(AcOH)][8] (1.287 Å). On the other hand, the bonds C(1)−N(1) and C(11)−N(2) are very close to the respective bonds in [Na$^+$(dpp-bian)$^-$]$_2$ [1.3239(18) Å and 1.3326(19) Å][5] and substantially shorter than in the sodium complex with the dpp-bian dianion [Na$^+_2$(Et$_2$O)$_3$(dpp-bian)$^{2-}$] [1.387(4) and 1.386(4) Å].[5]

ESR Spectroscopy of (dpp-bian)$^{n-}$[M$^+$]$_n$ (M = Li, Na; *n* = 1 or 3)

The mono- and trianions of dpp-bian consist of an unpaired electron making them detectable by ESR spectroscopy. Figures 5 and 6 represent the ESR spectra of (dpp-bian)$^-$ and (dpp-bian)$^{3-}$, respectively (upper spectra − observed; lower spectra − simulated). In a toluene solution [Na$^+$(dpp-bian)$^-$] reveals an ESR signal of six lines (g = 2.0025) due to the coupling of the unpaired electron to two ^{14}N nuclei (I = 1, natural abundance 99.6%) and

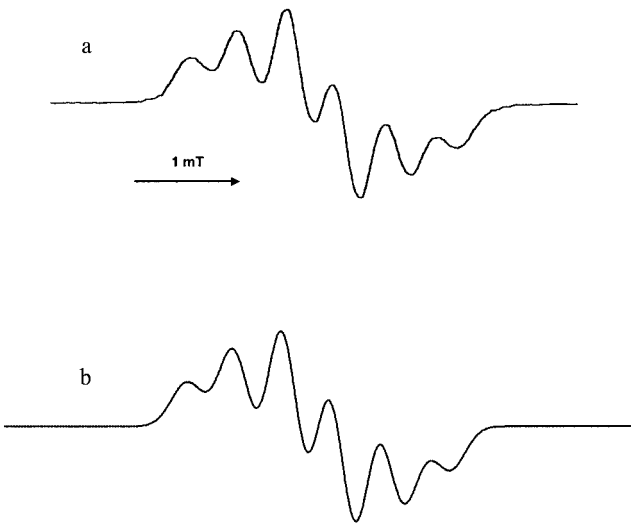

Figure 5. X-band ESR spectrum of [Na$^+$(dpp-bian)$^-$] in toluene at 285 K: (a) experimental; (b) simulated [A_N = 0.46 (2 N), A_{Na} = 017 (1 Na) mT, line width −0.31 mT)]

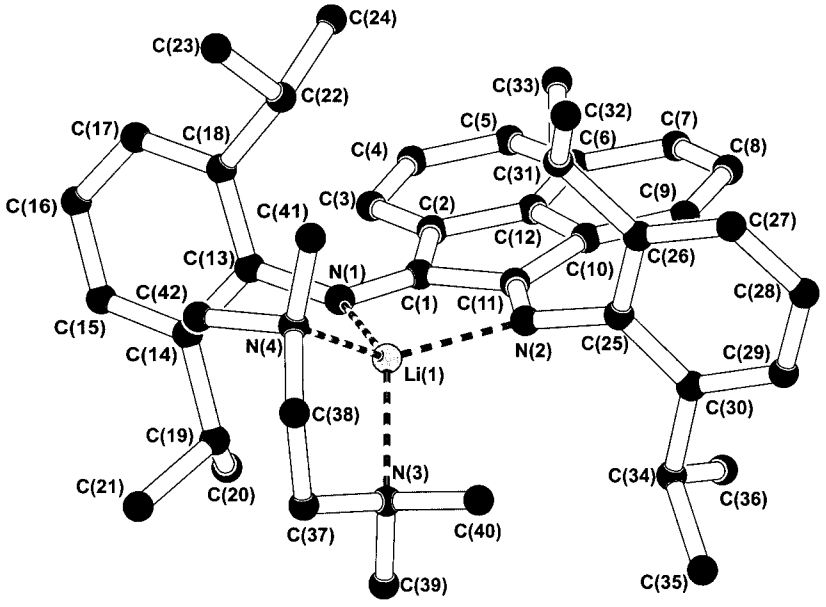

Figure 4. PLATON plot of the molecular structure of complex **1**; hydrogen atoms are omitted; selected bond lengths [Å] and angles [°]: Li(1)−N(1) 2.0365(18), Li(1)−N(2) 2.0603(18), Li(1)−N(3) 2.1201(19), Li(1)−N(4) 2.1701(19), N(1)−C(1) 1.3295(11), N(2)−C(11) 1.3303(11), N(1)−C(13) 1.4231(11), N(2)−C(25) 1.4206(11), C(1)−C(11) 1.4538(12), C(1)−C(2) 1.4768(12), C(2)−C(3) 1.3821(12), C(4)−C(5) 1.3766(15), C(2)−C(12) 1.4218(12), C(3)−C(4) 1.4216(13), C(5)−C(6) 1.4217(14), C(6)−C(7) 1.4263(14), C(6)−C(12) 1.3949(12), C(7)−C(8) 1.3747(15), C(8)−C(9) 1.4222(13), C(10)−C(12) 1.4219(12), C(9)−C(10) 1.3859(13), C(10)−C(11) 1.4793(12); N(1)−Li(1)−N(2) 87.03(7), N(3)−Li(1)−N(4) 83.90(7), N(2)−Li(1)−N(3) 110.21(9), N(1)−Li(1)−N(4) 113.44(9), N(2)−Li(1)−N(4) 135.97(9), N(1)−Li(1)−N(3) 133.90(9)

 © 2004 Wiley-VCH Verlag GmbH & Co. KGaA, Weinheim

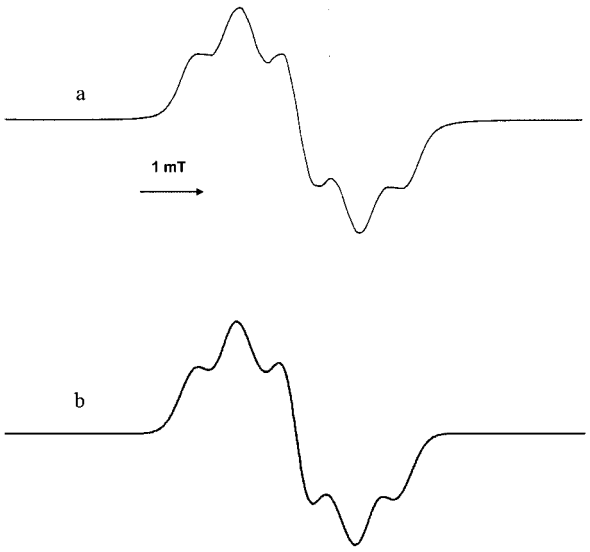

Figure 6. X-band ESR spectrum of $[Na^+{}_3(dpp\text{-}bian)^{3-}]$ in THF at 293 K: (a) experimental; (b) simulated [A_H = 0.027 (2 H), 0.39 (2 H), 0.66 (2 H) mT, line width −0.42 mT)]

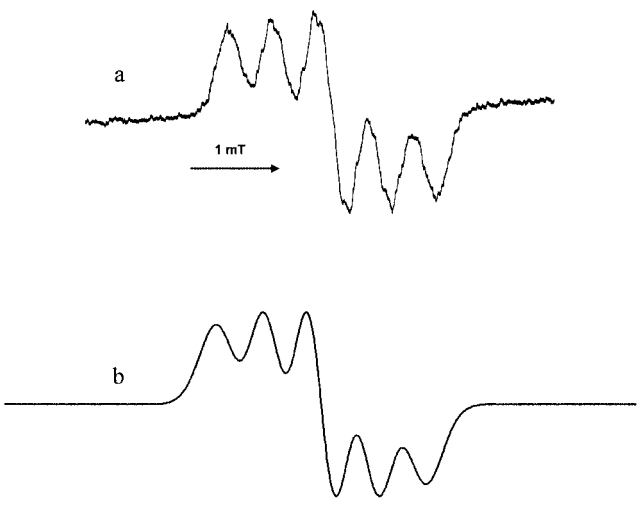

Figure 7. X-band ESR spectrum of $[Li^+(dpp\text{-}bian)^-]$ in TMEDA at 280 K: (a) experimental; (b) simulated [A_N = 0.46 (2 N) mT, line width −0.42 mT)]

the ^{23}Na nucleus (I = 3/2, natural abundance 100%). The hyperfine coupling constants [A_N = 0.46 (2 N) and A_{Na} = 0.17 (1 Na) mT)] of this signal indicate that: (i) the unpaired electron is mainly localized over the diimine part of the dpp-bian molecule and (ii) the complex exists in THF solution as a contact ion pair with the sodium atom being coordinated by two nitrogen atoms of the ligand. In contrast, the ESR signal of the trianion $[Na^+{}_3(dpp\text{-}bian)^{3-}]$ (g = 2.0023) exhibits a hyperfine structure due to the coupling of the unpaired electron to three different pairs of ^1H nuclei [A_H = 0.027 (2 H), A_H = 0.39 (2 H) and A_H = 0.66 (2 H) mT] (Figure 6). As there is no coupling to ^{14}N nuclei in the ESR signal of the trianion, we conclude that in $(dpp\text{-}bian)^{3-}$ the unpaired electron is delocalised over the naphthalene part of the dpp-bian ligand. These findings are in good agreement with the solid-state structures of $[Na^+(dpp\text{-}bian)^-]_2$ and $[Na^+{}_3(Et_2O)_2(dpp\text{-}bian)^{3-}]_2$.[5] In contrast to the sodium salt of the monoanion $(dpp\text{-}bian)^-$ the lithium derivative $[Li^+(dpp\text{-}bian)^-(TMEDA)]$ in TMEDA shows the ESR signal of five components (Figure 7). The hyperfine structure of this signal [g = 2.0021, A_N = 0.46 (2 N) mT] is caused by the coupling of the unpaired electron to only two ^{14}N nuclei, thus indicating that in TMEDA complex **1** exists as a solvent-separated ion pair. The ESR signal of $[Na^+(dpp\text{-}bian)^-]$ in THF is similar to that of complex **1** in TMEDA. However, in this spectrum there is a line of low intensity, which appears exactly in the middle of the quintuplet. The observed spectrum may be attributed to two overlapped signals of five and six lines. These signals correspond to the contact and solvent-separated ion pairs $[Na^+(dpp\text{-}bian)^-]$ (quintuplet) and $[Na(THF)_n]^+[dpp\text{-}bian]^-$ (sextuplet).

^1H NMR Spectroscopy of $(dpp\text{-}bian)^{n-}[M^+]_n$ (M = Na, n = 2 or 4)

As anticipated, complexes $[Na^+{}_2(Et_2O)_3(dpp\text{-}bian)^{2-}]$ and $[Na^+{}_4(THF)_4(dpp\text{-}bian)^{4-}]_2$ are diamagnetic and therefore are detectable by NMR spectroscopy. The signals of the paramagnetic mono- and trianionic species, which appear in the solution due to disproportionation of $[Na^+{}_2(Et_2O)_3(dpp\text{-}bian)^{2-}]$, are not visible in the ^1H NMR spectrum because of their broadening. In the ^1H NMR solution spectrum in C_6D_6 the methyl groups of the isopropyl group appear as two doublets centred at δ = 1.41 ppm and for $[Na^+{}_2(Et_2O)_3(dpp\text{-}bian)^{2-}]$, due to hindered rotation about the aryl carbon−nitrogen bond, at δ = 1.33 ppm (^3J = 8.0 Hz for both doublets). The signal for the four $H-C(CH_3)_2$ protons appears as a septuplet at δ = 3.85 ppm (^3J = 8.0 Hz). The signals of the twelve aromatic protons are found in a relatively narrow region (δ = 7.32−6.51 ppm). Despite the extreme sensitivity of complex $[Na^+{}_4(THF)_4(dpp\text{-}bian)^{4-}]_2$ towards air and moisture, attempts to obtain its ^1H NMR spectrum were undertaken. The spectrum obtained in $[D_8]$THF revealed the presence of some impurities amounting to about 10%. These narrow signals are attributable to those observed for $[Na^+{}_2(Et_2O)_3(dpp\text{-}bian)^{2-}]$ in C_6D_6. The dominant signals in the spectrum are noticeably broadened, high-field shifted, and probably belong to the aromatic protons of the tetraanion (δ = 6.56, 6.45, 5.83, 4.64, 3.93, 2.83 ppm). The signal corresponding to the $H-C(CH_3)_2$ proton appears to be partly overlapping with the THF signal at δ = 3.60 ppm. The methyl protons of the isopropyl groups are observed as a broad single signal at δ = 0.91 ppm.

Conclusion

Based on the UV/Vis spectroscopy data for $(dpp\text{-}bian)^{n-}[M^+]_n$ (M = Li, Na; n = 1−4), we have established that in solution $(dpp\text{-}bian)^-$ and $(dpp\text{-}bian)^{2-}$ undergo disproportionation to species which can be oxidised and reduced by one electron. Nevertheless, as reported recently,[5] every reduced form of $(dpp\text{-}bian)^{n-}$ (n = 1−4) may be isolated from solution in the individual state. The ESR spec-

 © 2004 Wiley-VCH Verlag GmbH & Co. KGaA, Weinheim

troscopy data for lithium and sodium salts of the monoanion $(dpp\text{-}bian)^-$ show that these salts may exist in solution either as solvent-separated or contact ion pairs.

Experimental Section

General Remarks: All manipulations were carried out under vacuum using Schlenk ampoules. Prior to use THF, toluene and diethyl ether were distilled from sodium/benzophenone. TMEDA was dried with lithium and condensed prior to use. 1,2-Bis[(2,6-diisopropylphenyl)imino]acenaphthene (dpp-bian) was prepared according to a published procedure.[8] The UV/Vis spectra were recorded with a Perkin−Elmer Lambda 25 spectrometer. Into the ampoule for UV/Vis spectroscopy, which contained sodium or lithium metal (10- to 20-fold excess calculated on the ligand), the solution of dpp-bian (20 mg, 0.04 mmol) in diethyl ether (40 mL) or in TMEDA (40 mL) was added. This ampoule was then sealed off under vacuum. The ESR spectra were recorded with a Bruker ER 200D-SRC spectrometer. The ESR signals were referenced to the signal of diphenylpicrylhydrazyl (DPPH, $g = 2.0037$).

[Li(dpp-bian)(TMEDA)] (1): A suspension of dpp-bian (0.5 g, 1.0 mmol) in TMEDA (30 mL) was added into a Schlenk ampoule, which contained lithium (1.0 g, 0.14 mmol). The mixture was stirred for 1 h. While stirring, the solution turned cherry-red. The solution was decanted from the lithium metal and then concentrated to 15 mL by evaporation of the solvent in vacuo on heating affording 0.34 g (55%) of **1** as dark red crystals. M.p. 199−201 °C. $C_{42}H_{56}LiN_4$ (623.85): calcd. C 80.72, H 9.11; found C 80.86, H 9.05.

Single-Crystal X-ray Structure Determination of 1: The data were collected with a SMART APEX diffractometer (graphite-monochromated, Mo-K_α radiation, ω- and ψ-scan technique, $\lambda = 0.71073$ Å). The structures were solved by direct methods using SHELXS-97[9] and were refined on F^2 using SHELXL-97[10]. All non-hydrogen atoms were refined anisotropically and the hydrogen atoms were placed in calculated positions and assigned to an isotropic displacement parameter of 0.08 Å^2. SADABS[11] was used to perform area-detector scaling and absorption corrections (max./min. transmission 0.9811/0.9688). The geometrical aspects of the structure were analysed using PLATON.[12] Data collection: crystal dimensions 0.50 × 0.40 × 0.30 mm, triclinic, $P\bar{1}$, $a = 10.5011(9)$ Å, $b = 13.2585(12)$ Å, $c = 14.0911(12)$ Å, $\alpha = 98.926(2)°$, $\beta = 104.293(2)°$, $\gamma = 91.076(2)°$, $V = 1874.8(3)$ Å^3, $Z = 2$, $\rho_{calcd.} = 1.105 \times 10^3$ kg m^{-3}, $\mu = 0.064$ mm^{-1}, $F(000) = 678$, $1.98° \le \theta \le 29.00°$, $-14 \le h \le 14$, $-18 \le k \le 17$, $-19 \le l \le 19$, 19549 data collected, 9690 unique data ($R_{int} = 0.0223$), 648 refined parameters, GOF(F^2) = 1.030, final R indices $\{R_1 = \Sigma F_o - F_c/\Sigma F_o$, $wR_2 = [\Sigma w(F_o^2 - F_c^2)^2/\Sigma w(F_o^2)^2]^{1/2}\}$ $R_1 = 0.0515$, $wR_2 = 0.1204$, max./min. residual electron density 0.422/−0.210 e·Å^{-3}. CCDC-210160 (**1**) contains the supplementary crystallographic data, which can be obtained free of charge at www.ccdc.cam.ac.uk/conts/retrieving.html or from the Cambridge Crystallographic Data Centre, 12 Union Road, Cambridge CB2 1EZ, UK; Fax: (internat.) + 44-1223/336-033; E-mail: deposit@ccdc.cam.ac.uk.

Acknowledgments

This work was supported by the Russian Foundation for Basic Research (Grant RFBR No. 03-03-32246a). The spectroscopic studies were carried out in the Analytical Center of the IOMC RAS (Grant RFBR No. 00-03-40116).

[1] [1a] R. van Asselt, K. Vrieze, C. J. Elsevier, *J. Organomet. Chem.* **1994**, *480*, 27−40. [1b] R. van Asselt, C. J. Elsevier, W. J. J. Smeets, A. L. Spek, R. Benedix, *Recl. Trav. Chim. Pays-Bas* **1994**, *113*, 88−98. [1c] R. van Asselt, C. J. Elsevier, *Organometallics* **1994**, *13*, 1972−1980. [1d] R. van Asselt, C. J. Elsevier, W. J. J. Smeets, A. L Spek, *Inorg. Chem.* **1994**, *33*, 1521−1531. [1e] R. van Asselt, E. Rijnberg, C. J. Elsevier, *Organometallics* **1994**, *13*, 706−720. [1f] R. van Asselt, E. E. C. G. Gielens, R. E. Rulke, K. Vrieze, C. J. Elsevier, *J. Am. Chem. Soc.* **1994**, *116*, 977−985. [1g] R. van Asselt, E. E. C. G. Gielens, R. E. Rulke, C. J. Elsevier, *J. Chem. Soc., Chem. Commun.* **1993**, 1203−1204.

[2] [2a] M. W. van Laren, C. J. Elsevier, *Angew. Chem. Int. Ed.* **1999**, *38*, 3715−3717. [2b] R. van Belzen, H. Hoffmann, C. J. Elsevier, *Angew. Chem. Int. Ed. Engl.* **1997**, *36*, 1743−1745. [2c] E. Shirakawa, T. Hiyama, *J. Organomet. Chem.* **2002**, *653*, 114−121.

[3] [3a] D. Pappalardo, M. Mazzeo, S. Antinucci, C. Pellecchia, *Macromolecules* **2000**, *33*, 9483−9487. [3b] D. J. Tempel, L. K. Johnson, R. L. Huff, P. S. White, M. Brookhart, *J. Am. Chem. Soc.* **2000**, *122*, 6686−6700. [3c] D. P. Gates, S. A. Svejda, E. Onate, Ch. M. Killian, L. K. Johnson, P. S. White, M. Brookhart, *Macromolecules* **2000**, *33*, 2320−2334. [3d] S. A. Svejda, M. Brookhart, *Organometallics* **1999**, *18*, 65−74. [3e] M. Gasperini, F. Ragaini, S. Cenini, *Organometallics* **2002**, *21*, 2950−2957.

[4] I. L. Fedushkin, A. A. Skatova, V. A. Chudakova, G. K. Fukin, S. Dechert, H. Schumann, *Eur. J. Inorg. Chem.* **2003**, 3336−3346.

[5] I. L. Fedushkin, A. A. Skatova, V. A. Chudakova, G. K. Fukin, *Angew. Chem. Int. Ed.* **2003**, *42*, 3294−3298.

[6] I. L. Fedushkin, M. N. Bochkarev, H. Schumann, L. Esser, G. Kociok-Kohn, *J. Organomet. Chem.* **1995**, *489*, 145−151.

[7] J. J. Brooks, W. Rhine, G. D. Stucky, *J. Am. Chem. Soc.* **1972**, *94*, 7346−7351.

[8] A. A. Paulovicova, U. El-Ayaan, K. Shibayama, T. Morita, Y. Fukuda, *Eur. J. Inorg. Chem.* **2001**, 2641−2646.

[9] G. M. Sheldrick, *SHELXS-97, Program for the Solution of Crystal Structures*, Universität Göttingen, **1990**.

[10] G. M. Sheldrick, *SHELXL-97, Program for the Refinement of Crystal Structures*, Universität Göttingen, **1997**.

[11] G. M. Sheldrick, *SADABS, Program for Empirical Absorption Correction of Area Detector Data*, Universität Göttingen, **1996**.

[12] A. L. Spek, *PLATON, A Multipurpose Crystallographic Tool*, Utrecht University, **2000**.

Received June 7, 2003
Early View Article
Published Online November 6, 2003

 © 2004 Wiley-VCH Verlag GmbH & Co. KGaA, Weinheim

Synthesis, Crystal Structures, and Magnetic Properties of a Mono- and a Dinuclear Copper(II) Complex of the 2,4,6-Tris(2-pyridyl)-1,3,5-triazine Ligand

Thorsten Glaser,*[a] Thomas Lügger,[a] and Roland Fröhlich[b]

Keywords: Magnetic properties / Copper / N ligands / Coordination chemistry

The reaction of 2,4,6-tris(2-pyridyl)-1,3,5-triazine (tptz) with $Cu(BF_4)_2 \cdot 3H_2O$ and *N*,*N*-bis(3-aminopropyl)methylamine (Medpt) yielded the monomeric complex $[(tptz)Cu^{II}(Medpt)](BF_4)_2 \cdot 2MeOH$ (**1**) whereas reaction of tptz with $CuCl_2 \cdot 2H_2O$ yielded the dinuclear complex $[\{Cu^{II}Cl_2\}(tptz)\{Cu^{II}Cl_2(MeOH)\}]$ (**2**). The molecular structures of **1** and **2** were established by single-crystal X-ray diffraction studies. The copper ion in complex **1** is elongated octahedral with the nitrogen atoms of Medpt and the triazine nitrogen atom of tptz in the equatorial positions, and the two pyridyl nitrogen atoms of tptz in axial positions. The two Cu^{II} ions in complex **2** are bridged by tptz, coordinating to Cu1 in a terpyridine-like fashion and to Cu2 in a bipyridine-like coordination mode. The triazine nitrogen atom bound to Cu1 is coordinated in an equatorial position whereas the triazine nitrogen atom bound to Cu2 is situated in the apical position. The equatorial plane of Cu1 is coplanar with the 1,3,5-triazine plane whereas the equatorial plane of Cu2 is perpendicular to the 1,3,5-triazine plane. Intermolecular interactions in the solid state result in both compounds in "dimeric units" due to hydrogen bonding. Both complexes were investigated by variable-temperature magnetic susceptibility measurements. Through-space dipolar couplings and/or weak through-bond interactions in complex **1** result in a small intermolecular antiferromagnetic interaction ($J = -0.09$ cm^{-1}). The intramolecular exchange coupling in the dinuclear complex **2** is antiferromagnetic ($J = -2.5$ cm^{-1}). This antiferromagnetic interaction was analyzed in view of the molecular structure considering spin-polarization, superexchange and orbital-orthogonality. A spin-polarization pathway seems to be the leading contribution which does not involve the 1,3 bridging pathway.
(© Wiley-VCH Verlag GmbH & Co. KGaA, 69451 Weinheim, Germany, 2004)

Introduction

The rational design of polynuclear complexes with ferromagnetic interactions between the paramagnetic centers is central to the development of new classes of molecule-based magnets.[1] One strategy for synthesizing materials with ferromagnetic interactions is provided by the *meta*-phenylene linkage of organic radicals and carbenes utilizing the spin-polarization mechanism.[2] This concept has been applied to binuclear transition metal complexes bridged in a *meta*-phenylene arrangement using a variety of bridging ligands.[3] Some of these compounds do indeed exhibit ferromagnetic interactions between the transition metal ions.[4−7] However, many complexes with the same kinds of bridging ligands exhibit antiferromagnetic interactions between the transition metal ions.[8] Several theoretical investigations have been performed in order to obtain an insight into the question of why the concept of spin-polarization cannot be applied in a straightforward manner to transition metal complexes. Bencini et al. showed on resorcinol- and hydrochinone-bridged dinuclear Mo^V complexes that for both bridging units not only is the spin-polarization mechanism active but also the superexchange interaction.[9] The orientation of the magnetic orbital on each metal site relative to the plane of the bridging benzene ring was found to be crucial for a ferromagnetic or an antiferromagnetic contribution of the superexchange interaction as well as of the spin-polarization mechanism. Takano et al. investigated dinuclear Cu^{II} and Mn^{II} complexes with a bridging pyrimidine ligand using DFT and post-Hartree−Fock methods.[10] They concluded that superexchange interactions leading to antiferromagnetic interactions are more important in *meta*-phenylene bridged transition metal complexes compared with *meta*-phenylene bridged organic carbenes and radicals. Finally, ferromagnetic interactions were proposed in pyrimidine-bridged dinuclear Cu^{II} complexes when the pyrimidine-nitrogen donor of one Cu^{II} center is coordinated equatorially and the pyrimidine-nitrogen donor of the other Cu^{II} center is coordinated axially. Antiferromagnetic interactions were proposed when both nitrogen atoms are coordinated equatorially.[8a,11]

Recently, we reported the use of modified 1,3,5-trihydroxybenzene (phloroglucinol) ligands to bridge three

[a] Institut für Anorganische und Analytische Chemie, Westfälische Wilhelms-Universität Münster
Wilhelm-Klemm-Str. 8, 48149 Münster, Germany
Fax: (internat.) +49-251-833-3108
E-mail: tglaser@uni-muenster.de
[b] Organisch-Chemisches Institut, Westfälische Wilhelms-Universität Münster
Corrensstr. 40, 48149 Münster, Germany

 © 2004 Wiley-VCH Verlag GmbH & Co. KGaA, Weinheim **DOI: 10.1002/ejic.200300443**

Cu^{II} ions in a *meta*-phenylene linkage.[12] These complexes exhibit ferromagnetic interactions between the three $S_i = {}^1/_2$ sites to result in a $S_t = {}^3/_2$ spin ground state due to the spin-polarization mechanism (**I** in Scheme 1). In an extended version of these ligands, we incorporated salen-like coordination environments because salen-like ligands form stable complexes with most metal ions.[13] Just as phloroglucinol is the triangularly topological extension of resorcinol, the triangularly topological extension of pyrimidine is 1,3,5-triazine. We wanted to investigate whether modified 1,3,5-triazine-ligands may be used for the synthesis of trinuclear transition metal complexes with ferromagnetic interactions between the paramagnetic centers based on the spin-polarization mechanism (**II** in Scheme 1).

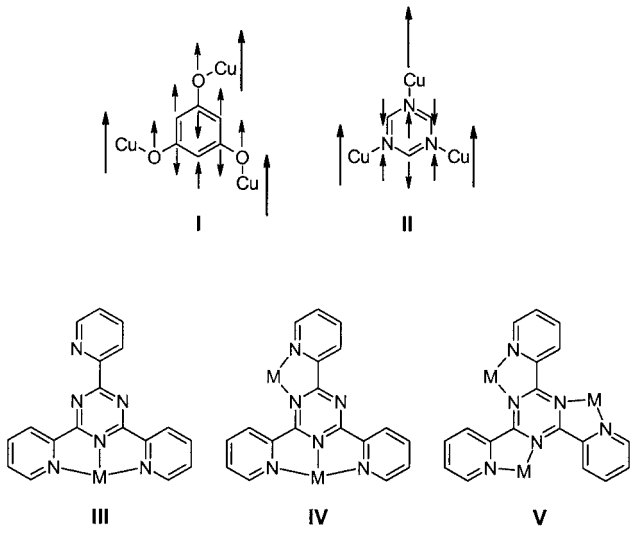

Scheme 1

Hendrickson and co-workers reported a series of trinuclear Ti^{III} complexes using the tri-anions of cyanuric acid and trithiocyanuric acid as bridging ligands.[14] While the Ti^{III} centers in the cyanuric bridged complex are antiferromagnetically coupled, a ferromagnetically coupled system was found in the trithiocyanuric system. Recently, Dunbar and co-workers used 1,3,5-triazine-2,4,6-tricarboxyclic acid for the synthesis of a one-dimensional chain compound with Fe^{II} ions. However, no exchange interactions between the Fe^{II} centers were observed and this was attributed to the large distance between the paramagnetic centers in the chain. The ferrous ions are not bridged by coordination to one 1,3,5-triazine ring. The ligand bridges the Fe^{II} ions by use of one 1,3,5-triazine nitrogen donor at one site and by a carboxylic group at the other site.[15] Gamez, Reedijk and co-workers reported an interesting copper coordination polymer using 2,4,6-tris(dipyridin-2-ylamino)-1,3,5-triazine which demonstrated the use of modified 1,3,5-triazine ligands for the construction of higher-dimensional assemblies.[16]

The modified 1,3,5-triazine ligand 2,4,6-tris(2-pyridyl)-1,3,5-triazine (tptz)[17] has been used in the spectrophotometric determination of transition metal ions[18] and as a solvent extraction reagent.[19] Several transition-metal complexes using the ligand tptz have been reported.[20−22] The predominant coordination mode of tptz is tri-dentate terpyridine-like (**III** in Scheme 1). However, tptz is also capable of bridging two metal centers in one terpyridine- and one bipyridine-like coordination mode (**IV** in Scheme 1) but no magnetic properties were reported. Several reports have described that coordination of one metal ion, especially Cu^{II}, to tptz induces the hydrolysis of tptz to form bis(2-pyridylcarbonyl)amine and its complexes.[22,23]

In order to use tptz as a ferromagnetic coupler between three transition metal ions we investigated whether complexes with tptz as a bridging ligand between three metal ions in bipyridine-like sites would be accessible (**V** in Scheme 1). Herein we report the reaction of tptz with an excess of Cu^{II} ions. In the presence of *N*,*N*-bis(3-aminopropyl)methylamine (Medpt), only the mononuclear complex $[(tptz)Cu^{II}(Medpt)](BF_4)_2{\cdot}2MeOH$ (**1**) was isolated. In contrast, reaction of tptz with an excess of $CuCl_2{\cdot}2H_2O$ resulted in the dinuclear complex $[\{Cu^{II}Cl_2\}(tptz)\{Cu^{II}Cl_2(MeOH)\}]$ (**2**). No indications of hydrolysis of tptz were observed. Both complexes were fully characterized by single-crystal X-ray diffraction studies and magnetic measurements. To the best of our knowledge complex **2** is the first dinuclear copper complex of tptz and this is the first determination of exchange interactions mediated by the tptz ligand.

Results and Discussion

Synthesis and Spectroscopy

In order to synthesize a trinuclear Cu^{II} complex of type **V** (Scheme 1) with three bipyridine-like coordination sites, additional ligands for complexation of the Cu^{II} centers have to be provided. Since the preferred coordination number of Cu^{II} ions is five, we used an additional tridendate ligand (Medpt). The reaction of tptz with three equivalents of $Cu(BF_4)_2{\cdot}3H_2O$ and three equivalents of Medpt in methanol resulted in a blue solution from which green crystals of **1** separated upon diffusion of diethyl ether into the solution. The FTIR spectrum of **1** confirmed the presence of the tptz ligand by the absorptions in the 400 to 1600 cm^{-1} region. Two intense N−H bands at 3173 and 3077 cm^{-1} and C−H bands of aliphatic groups between 2800 and 3000 cm^{-1} demonstrate the presence of the Medpt ligand. Additionally, the typical bands of BF_4^- show the cationic nature of the complex. The electrospray mass spectrum of **1** exhibits a prominent ion at a mass-to-charge ratio (*m*/*z*) of 259.9, with mass and isotopic distribution patterns corresponding to $[(tptz)Cu(Medpt)]^{2+}$ (calculated *m*/*z* of 260.1). The elemental analysis combined with these data are in accordance with the formulation of **1** as $[(tptz)Cu^{II}(Medpt)](BF_4)_2{\cdot}2CH_3OH$ which was corroborated by an X-ray diffraction study.

The reaction of tptz with 15 equivalents of $CuCl_2{\cdot}2H_2O$ in MeOH resulted in a green solid. Elemental analysis gave a tptz/Cu/Cl ratio of 1:2:4 corresponding to a dinuclear complex and not the 1:3:6 ratio expected for a trinuclear

 © 2004 Wiley-VCH Verlag GmbH & Co. KGaA, Weinheim

complex. Diffusion of methanolic solutions of tptz and an excess of $CuCl_2 \cdot 2H_2O$ yielded green needles suitable for single-crystal X-ray diffraction. The FTIR spectrum of **2** exhibits a broad absorption between 2500 and 3200 cm^{-1} indicating the presence of hydrogen bonded O−H groups. The spectrum shows the main signals of the free tptz ligand which are slightly shifted and in most cases split. Structural characterization by a single-crystal X-ray diffraction study enabled the formulation of **2** as [{$Cu^{II}Cl_2$}(tptz)-{$Cu^{II}Cl_2$(MeOH)}].

Crystal Structures

Figure 1a shows the molecular structure of the dication $[(tptz)Cu^{II}(Medpt)]^{2+}$ in **1** and the labeling scheme used. The asymmetric unit consists of the dication, two BF_4^- anions and two methanol molecules. Selected interatomic distances and angles are listed in Table 1. The copper ion is coordinated by six nitrogen donors (N1, N4, N5 of tptz; N7, N8, N9 of Medpt). The distance between Cu and the triazine nitrogen donor N1 is 2.15 Å whereas the distances with the two pyridyl nitrogen donors N4 and N5 are long at 2.41 Å and 2.50 Å, respectively. The central tertiary amine donor N9 of Medpt is coordinated trans to the triazine nitrogen donor with a bond length of 2.13 Å whereas the primary amine donors N7 and N8 form short bonds of 1.99 Å and 2.00 Å, respectively. The coordination environment of the Cu^{II} ion is best described as an axially elongated octahedron with severe distortion. The equatorial plane consists of N1, N7, N8, and N9 and is orientated perpendicular to the 1,3,5-triazine plane. The angle of 142° subtended by the two axial donors N4 and N5 and the copper center deviates strongly from the ideal N−Cu−N angle of 180°. However, this decreased angle is typical for a Cu^{II} ion in a terpyridine-like environment with the two pyridyl donors in axial positions.

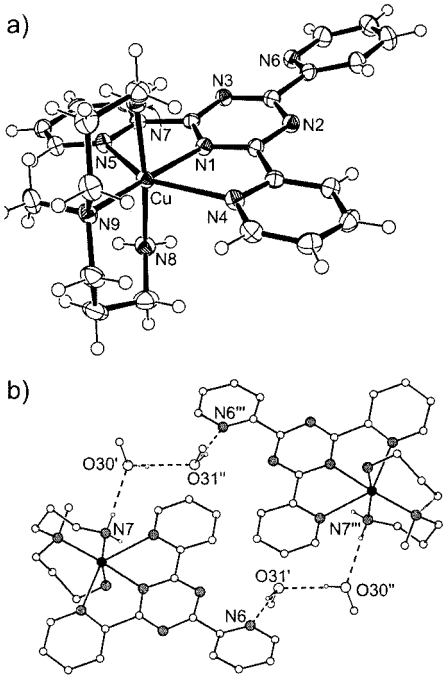

Figure 1. a) Molecular structure of the dication $[(tptz)Cu(Medpt)]^{2+}$ in crystals of **1**. Thermal ellipsoids represent the 50% probability surfaces. b) Schematic view of the "dimeric unit" in **1** formed by hydrogen bonding. [symmetry code: (′) $1-x$, $1-y$, $1-z$; (″) x, y, $1+z$; (‴) $1-x$, $1-y$, $2-z$]

Table 1. Selected bond lengths [Å] and angles [°] for **1**

Cu−N1	2.151(2)
Cu−N4	2.414(2)
Cu−N5	2.496(3)
Cu−N7	1.993(2)
Cu−N8	1.995(2)
Cu−N9	2.129(2)
N1−Cu−N4	72.37(6)
N1−Cu−N5	70.37(6)
N1−Cu−N7	86.88(7)
N1−Cu−N8	90.19(7)
N1−Cu−N9	174.20(6)
N4−Cu−N5	142.44(5)
N4−Cu−N7	97.59(7)
N4−Cu−N8	92.57(7)
N4−Cu−N9	102.37(6)
N5−Cu−N7	85.97(7)
N5−Cu−N8	83.02(7)
N5−Cu−N9	115.05(6)
N7−Cu−N8	168.03(8)
N7−Cu−N9	91.48(7)
N8−Cu−N9	92.52(7)

The two di-cations are organized in pairs as "dimers" held together by hydrogen bonds with the methanol solvate molecules (Figure 1b). One methanol forms a hydrogen bond with the uncoordinated pyridyl nitrogen atom (N6−O31′ and N6‴−O31″ 2.80 Å). This methanol forms an additional hydrogen bond to a second methanol (O31′−O30″ and O31″−O30′ 2.73 Å) while this second methanol forms a hydrogen bond with a coordinated primary amine of a second di-cation (O30″−N7‴ and O30′−N7 3.03 Å). The Cu−Cu‴ distance is 11.5 Å. However, the shortest Cu−Cu distance in **1** is 7.77 Å. The packing is governed mainly by weak interactions, *viz.* long N−H···F, C−H···F, π-π interactions (there are no strong π-π interactions in **1**) etc.

Figure 2a shows the molecular structure of the dinuclear complex [{$Cu^{II}Cl_2$}(tptz){$Cu^{II}Cl_2$(MeOH)}] (**2**) and the labeling scheme used. Selected interatomic distances and angles are listed in Table 2. Cu1 is coordinated by tptz in a terpyridine-like coordination mode (**III** in Scheme 1) with two additional chloride donors resulting in five-fold coordination. The Cu1−N1 distance of the triazine nitrogen donor is 1.94 Å and the distances with the two pyridyl donors N26 and N66 of tztp are both 2.07 Å. The chloride Cl12 is coordinated trans to the triazine nitrogen donor N1 at a distance of 2.22 Å whereas chloride Cl11 forms a long bond of 2.51 Å. The coordination geometry of Cu1 may best be described as distorted square pyramidal with N1, N26, N66, and Cl12 forming the equatorial plane and Cl11 occupying the apical position. This equatorial plane is almost coplanar with the 1,3,5-triazine plane. The N26−Cu1−N66 angle of 154° of the terpyridine-like unit is significantly larger compared with the analogous

 © 2004 Wiley-VCH Verlag GmbH & Co. KGaA, Weinheim

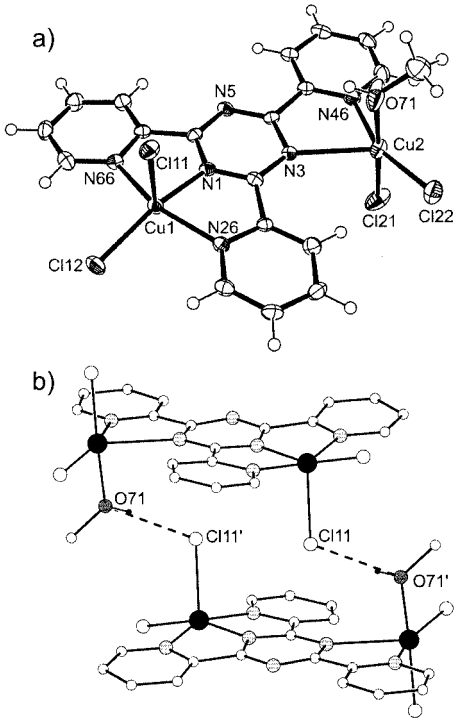

Figure 2. a) Molecular structure of the dinuclear complex [{$Cu^{II}Cl_2$}(tptz){$Cu^{II}Cl_2$(MeOH)}] in crystals of **2**. Thermal ellipsoids represent the 50% probability surfaces. b) Schematic view of the "dimeric unit" in **2** formed by hydrogen bonding. [symmetry code: (′) $2 - x, -y, 2 - z$]

Table 2. Selected bond lengths [Å] and angles [°] for **2**

Cu1−N1	1.942(3)
Cu1−N26	2.072(3)
Cu1−N66	2.073(3)
Cu1−Cl12	2.2192(9)
Cu1−Cl11	2.5093(9)
Cu2−N3	2.454(3)
Cu2−N46	2.023(3)
Cu2−O71	2.045(3)
Cu2−Cl22	2.2220(10)
Cu2−Cl21	2.2391(11)
N1−Cu1−N26	77.60(11)
N1−Cu1−N66	78.45(11)
N1−Cu1−Cl11	98.13(8)
N1−Cu1−Cl12	159.16(8)
N26−Cu1−N66	153.68(10)
N26−Cu1−Cl11	95.02(7)
N26−Cu1−Cl12	100.99(8)
N66−Cu1−Cl11	99.01(8)
N66−Cu1−Cl12	97.50(8)
Cl11−Cu1−Cl12	102.70(4)
N3−Cu2−N46	74.93(10)
N3−Cu2−Cl21	92.63(7)
N3−Cu2−Cl22	123.26(6)
N3 −Cu2−O71	85.07(11)
N46−Cu2−Cl21	90.27(8)
N46−Cu2−Cl22	160.40(9)
N46−Cu2−O71	85.54(13)
Cl21−Cu2−Cl22	95.63(4)
Cl21−Cu2−O71	175.63(10)
Cl22−Cu2−O71	88.73(10)

N4−Cu−N5 angle in **1**. This increase originates from the decreased Cu1−N1 bond length of 1.94 Å compared with 2.15 Å in **1** and the different coordination mode of the two pyridyl rings. In **2**, the pyridyl rings are in the equatorial plane (short bonds, 2.07 Å) which is in contrast to **1** where the pyridyl rings occupy axial positions (long bonds, 2.41 and 2.50 Å).

Cu2 is coordinated by tptz in a bipyridine-like coordination mode (**IV** in Scheme 1) with two additional chloride donors and one methanol ligand resulting in a five-fold coordination. The Cu2−N3 bond length of the triazine nitrogen donor at 2.45 Å is the longest found in the two complexes. Conversely, the pyridyl nitrogen donor of tztp N46 forms the shortest pyridyl nitrogen−copper bond at 2.02 Å. Chloride Cl22 is coordinated trans to the pyridyl nitrogen donor at a distance of 2.22 Å and chloride Cl21 is coordinated cis to the pyridyl nitrogen donor at a distance of 2.24 Å. The Cu2−O71 bond length of the coordinated methanol ligand is 2.05 Å. The coordination geometry of Cu2 may also best be described as distorted square pyramidal but in contrast to Cu1 the 1,3,5-triazine nitrogen donor occupies the axial position and the equatorial plane formed by N46, Cl21, Cl22, and O71 is oriented perpendicular to the 1,3,5-triazine plane. With implications for the magnetic properties it is interesting to note that the axial ligand N3 is tilted from a perfect axial position as indicated by the acute N3−Cu2−N46 angle of 75°.

Two molecules of **2** form dimers as a result of two hydrogen bonds which are symmetry related (Figure 2b). The chloride ligand coordinated in the axial position of Cu1 in one molecule forms a hydrogen bond with the coordinated methanol ligand of Cu2 of the other molecule at a distance of 3.01 Å.

Magnetic Properties

The magnetic susceptibilities of **1** and **2** were measured in the temperature range 2−300 K. The raw data were corrected for underlying diamagnetism by using tabulated Pascal's constants and for temperature-independent paramagnetism, χ_{TIP}, which was obtained as a fit parameter. The magnetic properties were analyzed by using the spin Hamiltonian in Equation (1) including the isotropic Heisenberg−Dirac−van Vleck (HDvV) exchange Hamiltonian and the single-ion Zeeman interaction by using a full-matrix diagonalization approach.

$$H = -2J\mathbf{S}_1\mathbf{S}_2 + \sum_i [\mu_B g_i \mathbf{S}_i \mathbf{B}] \quad (1)$$

The effective magnetic moment, μ_{eff}, of complex **1** has a temperature-independent value of 1.84 μ_B in the range 300−30 K and decreases below 30 K to a value of 1.53 μ_B at 2 K (not shown). These data were simulated by using the spin-Hamiltonian for an isolated $S_i = {}^1/_2$ system with $g = 2.123$ and $\chi_{TIP} = 33 \cdot 10^{-6}$ cm^3·mol^{-1}. However, the decrease below 30 K could not be well reproduced although saturation effects were already taken into account. Thus, the decrease in μ_{eff} reflects intermolecular antiferromagnetic

 © 2004 Wiley-VCH Verlag GmbH & Co. KGaA, Weinheim

interactions. We tried to simulate this decrease by introducing a Weiss temperature Θ. The simulation using Θ = −0.14 K resulted in a better agreement, but the simulation was still not satisfactory in the low temperature region. We tried to simulate the magnetic data of **1** using spin Hamiltonian in Equation (1) for a weak exchange coupled dimer. Figure 3 (top) shows the temperature dependence of μ_{eff} calculated for the "dimer $\mathbf{1}_2$". This model, using the same *g*-value and χ_{TIP} per site as for the monomeric model described above, gave a satisfactory agreement between experimental and simulated data even in the low temperature range with $J = -0.09$ cm^{-1}. It was not possible to assign the origin of this weak intermolecular antiferromagnetic interaction. Through-space dipolar couplings (closest Cu−Cu distance 7.77 Å) and/or through-bond interactions may account for this weak intermolecular interaction.

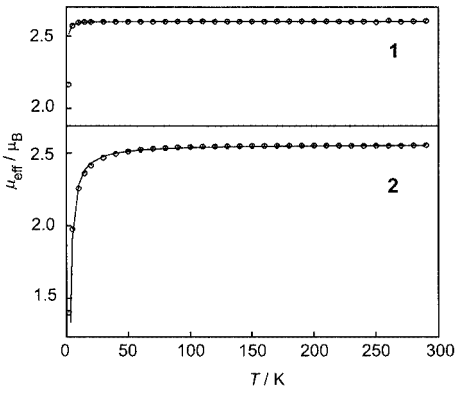

Figure 3. Top: Temperature dependence of the effective magnetic moment, μ_{eff}, calculated for the "dimeric unit" of complex **1** at 1 T. The solid line is a fit of the experimental data using the spin Hamiltonian in Equation (1) with $S_1 = S_2 = 1/2$, $g_1 = g_2 = 2.123$, $\chi_{TIP} = 66{\cdot}10^{-6}$ cm^3·mol^{-1} for the "dimer", and $J = -0.09$ cm^{-1}. Bottom: Temperature dependence of the effective magnetic moment, μ_{eff}, of complex **2** at 1 T. The solid line is a fit of the experimental data using the spin Hamiltonian (1) with $S_1 = S_2 = 1/2$, $g_1 = g_2 = 2.090$, $\chi_{TIP} = 180{\cdot}10^{-6}$ cm^3·mol^{-1}, and $J = -2.5$ cm^{-1}.

The effective magnetic moment, μ_{eff}, of the dinuclear complex **2** has a temperature-independent value of 2.55 μ_B in the range 300−110 K and decreases below 110 K to a value of 1.40 μ_B at 2 K (Figure 3 bottom). This is typical behavior for an antiferromagnetically coupled Cu^{II} dimer. The simulation using the spin Hamiltonian in Equation (1) with $g = 2.090$, $\chi_{TIP} = 180{\cdot}10^{-6}$ cm^3·mol^{-1}, and $J = -2.5$ cm^{-1} nicely reproduces the experimental data. Thus, there is a sizeable exchange coupling through the tptz ligand which is antiferromagnetic in nature.

To the best of our knowledge, the determination of the exchange coupling in **2** is the first established for the tptz ligand. The antiferromagnetic interaction is, at a first glance, counterintuitive to the spin-polarization mechanism mediated by the *meta*-phenylene arrangement of the two copper centers. The spin-polarization should result in a ferromagnetic coupling as depicted in Scheme 2a. However, a close inspection of the molecular structure of **2** results in a deeper understanding of the exchange coupling in **2**. The magnetic orbitals $d_{x^2-y^2}$ of square-pyramidal-coordinated Cu^{II} ions are located in the equatorial plane. The equatorial plane of Cu1 is orientated parallel to the 1,3,5-triazine ring consisting of N1, N26, N66, and Cl12. In contrast, the equatorial plane of Cu2 is oriented perpendicular to the 1,3,5-triazine ring and consists of N46, Cl12, Cl22, and O71. The $d_{x^2-y^2}$ orbital of Cu1 is delocalized to N1 in a σ-type pathway. There is no delocalization of the $d_{x^2-y^2}$ orbital of Cu2 to N3. First, the Cu2−N3 distance of 2.45 Å is too long for significant delocalization and secondly, the $d_{x^2-y^2}$ orbital of Cu2 is of δ-type symmetry with respect to the Cu2−N3 bond. There is however a strong delocalization of the $d_{x^2-y^2}$ of Cu2 to N46 (Cu2−N46 2.02 Å) in a σ-type pathway. Thus, the spin-polarization mechanism is not operative through the pathway depicted in Scheme 2a but it is operative through a pathway incorporating the pyridyl ring of N46. This pathway for the spin-polarization leads to an antiferromagnetic coupling between the two copper centers (Scheme 2b) and is consistent with the experimental data. The ability of polypyridyl type bridging ligands to mediate spin-polarization over long distances of a ferro- and antiferromagnetic nature depending on the relative arrangement of the pyridyl rings has been demonstrated by McCleverty, Ward, and co-workers.[3,7]

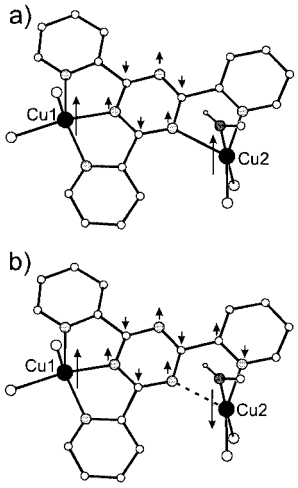

Scheme 2

As indicated in the introduction, not only the spin-polarization contribution to the exchange coupling but also the superexchange contribution seems to be effective. The orientation of the equatorial planes of the two copper centers is orthogonal. Thus, the magnetic orbitals of Cu1 and Cu2 are orthogonal to each other. This orbital orthogonality was used to understand the ferromagnetic interactions observed in pyrimidine bridged dinuclear Cu^{II} complexes with an equatorial-axial ligation of the pyrimidine bridging ligand.[8a,11] However, the deviation of the axial triazine nitrogen donor N3 of Cu2 from perfect axial ligation (vide supra) removes the strict orthogonality of the magnetic orbitals and some positive overlap of the $d_{x^2-y^2}$ orbital of Cu2 with the *p*-orbitals of N3 might occur. Due

 © 2004 Wiley-VCH Verlag GmbH & Co. KGaA, Weinheim

to the long bond length, this overlap is weak and gives a small further contribution to the observed antiferromagnetic exchange interaction.

Experimental Section

General Methods and Materials: Infrared spectra (400−4000 cm^{-1}) of solid samples were recorded on a Bruker Vector 22 spectrometer as KBr disks. ESI mass spectra were recorded on a Micromass Quattro LC mass spectrometer. All starting materials were obtained commercially and used without further purification. Temperature-dependent magnetic susceptibilities of finely ground crystals were measured using a SQUID magnetometer (Quantum Design) at 1.0 T (2.0−300 K). For calculations of the molar magnetic susceptibility, χ_M, the measured susceptibilities were corrected for the underlying diamagnetism of the sample using tabulated Pascal's constants. The JULIUS routine was used for spin Hamiltonian simulations using a full-matrix diagonalization approach of the data.[24]

[(tptz)Cu^{II}(Medpt)]$(BF_4)_2$·2MeOH (1): A solution of Medpt (84 mg, 0.57 mmol) in methanol (5 mL) was added dropwise to a green solution of tptz (60 mg, 0.19 mmol) and $Cu(BF_4)_2$·$3H_2O$ (168 mg, 0.57 mmol) in methanol (15 mL). The resultant blue solution was stirred for 3 hours. Diffusion of diethyl ether into this solution afforded green crystals. Yield: 95 mg (65%). ESI-MS (positive ion mode): m/z = 260 $[(tptz)Cu(Medpt)]^{2+}$. IR (KBr): $\tilde{\nu}$/cm^{-1} = 3315 w, 3173 m, 3077 m, 2956 w, 2883 w, 2081 w, 1660 m, 1590 w, 1562 w, 1522 m, 1523 s, 1486 w, 1470 w, 1434 w, 1401 w, 1385 s, 1377 s, 1294 w, 1264 m, 1215 w, 1181 w, 1084 s, 1032 s, 1001 w, 929 w, 862 w, 763 s, 738 w, 675 m, 667 m, 628 w, 620 w, 533 m, 522 m; elemental analysis calcd. (%) for [(tptz)Cu^{II}(Medpt)]$(BF_4)_2$·2MeOH $C_{27}H_{39}B_2CuF_8N_9O_2$ (758.83): calcd. C 42.74, H 5.18, N 16.61; found C 42.40, H 4.88, N 16.59.

[{$Cu^{II}Cl_2$}(tptz){$Cu^{II}Cl_2$(MeOH)}] (2): Solid tptz (10 mg, 0.032 mmol) and solid $CuCl_2$·$2H_2O$ (50 mg, 0.29 mmol) were each placed in one arm of an H-shaped tube. The tube was filled carefully with methanol allowing for diffusion of the two solutions between the two arms. During the course of 7 days, green needles appeared. Yield: 19 mg (97%). IR (KBr): $\tilde{\nu}$/cm^{-1} = 3417 m, 3137 m, 3093 m, 3042 m, 1608 w, 1578 s, 1563 m, 1544 s, 1494 m, 1475 m, 1445 w, 1408 m, 1396 w, 1377 s, 1308 w, 1264 m, 1154 w, 1097 w, 1039 w, 1016 m, 773 s, 687 m, 668 m, 661 m, 641 w; elemental analysis calcd. (%) for [{$Cu^{II}Cl_2$}(tptz){$Cu^{II}Cl_2$(MeOH)}] $C_{19}H_{16}Cl_4Cu_2N_6O$ (613.26): calcd. C 37.21, H 2.63, N 13.70; found C 36.88, H 2.65, N 13.50.

X-ray Crystal Structure Analysis of [(tptz)Cu^{II}(Medpt)]$(BF_4)_2$·2MeOH (1): Formula $C_{27}H_{39}B_2CuF_8N_9O_2$, M = 758.83 g·mol^{-1}, green crystal 0.45 × 0.29 × 0.12 mm, a = 11.857(2), b = 12.370(2), c = 13.033(2) Å, α = 103.01(1), β = 109.01(1), γ = 103.13(1)°, V = 1664.6(4) $Å^3$, $\rho_{calcd.}$ = 1.514 g·cm^{-3}, μ = 7.43 cm^{-1}, empirical absorption correction (0.731 ≤ T ≤ 0.916), Z = 2, triclinic, space group $P\bar{1}$ (No. 2), λ = 0.71073 Å, T = 153 K, ω and φ scans, 16469 reflections collected (±h, ±k, ±l), [(sinθ)/λ] = 0.65 $Å^{-1}$, 7635 independent (R_{int} = 0.027) and 6466 observed reflections [$I \geq 2\ \sigma(I)$], 621 refined parameters, R = 0.040, wR^2 = 0.098, max. residual electron density 0.51 (−0.47) e·$Å^{-3}$, hydrogens calculated and refined as riding atoms.

X-ray Crystal Structure Analysis of [{$Cu^{II}Cl_2$}(tptz){$Cu^{II}Cl_2$(MeOH)}] (2): formula $C_{19}H_{16}Cl_4Cu_2N_6O$, M = 613.26 g·mol^{-1}, green crystal 0.60 × 0.10 × 0.03 mm, a = 8.332(1), b = 26.006(1), c = 10.496(1) Å, β = 99.09(1)°, V = 2245.7(4) $Å^3$, $\rho_{calcd.}$ = 1.814 g·cm^{-3}, μ = 23.96 cm^{-1}, empirical absorption correction (0.327 ≤ T ≤ 0.932), Z = 4, monoclinic, space group $P2_1/c$ (No. 14), λ = 0.71073 Å, T = 198 K, ω and φ scans, 8930 reflections collected (±h, ±k, ±l), [(sinθ)/λ] = 0.66 $Å^{-1}$, 5113 independent (R_{int} = 0.040) and 3665 observed reflections [$I \geq 2\ \sigma(I)$], 293 refined parameters, R = 0.043, wR^2 = 0.094, max. residual electron density 0.89 (−0.59) e·$Å^{-3}$, hydrogens calculated and refined as riding atoms.

Data sets were collected with Bruker AXS APEX and Nonius Kappa CCD diffractometers, equipped with rotating anode generators. Programs used: data collection SMART[25] and COLLECT,[26] data reduction SAINT[25] and Denzo-SMN,[27] absorption correction SADABS[25] and SORTAV,[28] structure solution SHELXS-97,[29] structure refinement SHELXL-97.[30]

CCDC-211262 and -211263 contain the supplementary crystallographic data for this paper. These data can be obtained free of charge at www.ccdc.cam.ac.uk/conts/retrieving.html [or from the Cambridge Crystallographic Data Centre, 12 Union Road, Cambridge CB2 1EZ, UK; Fax: (internat.) + 44-1223-336-033; E-mail: deposit@ccdc.cam.ac.uk].

Acknowledgments

T. G. gratefully acknowledges Professor F. E. Hahn for his generous support. This work was supported by the Fonds der Chemischen Industrie (Liebig-Stipendium for T. G.) and the BMBF (Kooperationsbereich Neue Materialien). Dr. E. Bill (Max-Planck-Institut für Strahlenchemie, Mülheim an der Ruhr) is thanked for the magnetic measurements and for valuable discussions.

[1] O. Kahn, *Acc. Chem. Res.* **2000**, *33*, 647−657.
[2] [2a] H. C. Longuet-Higgins, *J. Chem. Phys.* **1950**, *18*, 265−274. [2b] H. M. McConnell, *J. Chem. Phys.* **1963**, *39*, 1910. [2c] H. Iwamura, *Adv. Phys. Org. Chem.* **1990**, *26*, 179−253. [2d] A. Rajca, *Chem. Eur. J.* **2002**, *8*, 4834−4841.
[3] J. A. McCleverty, M. D. Ward, *Acc. Chem. Res.* **1998**, *31*, 842−851.
[4] Pyrimidine-bridged complexes: [4a] S.-i. Mitsubori, T. Ishida, T. Nogami, H. Iwamura, *Chem. Lett.* **1994**, 285−288. [4b] F. Lloret, G. De Munno, M. Julve, J. Cano, R. Ruiz, A. Caneschi, *Angew. Chem.* **1998**, *110*, 143−145; *Angew. Chem. Int. Ed.* **1998**, *37*, 135−138. [4c] T. Ishida, K. Nakayama, M. Nakagawa, W. Sato, Y. Ishikawa, M. Yasui, F. Iwasaki, T. Nogami, *Synth. Met.* **1997**, *85*, 1655−1658. [4d] T. Ishida, S.-i. Mitsubori, T. Nogami, N. Takeda, M. Ishikawa, H. Iwamura, *Inorg. Chem.* **2001**, *40*, 7059−7064.
[5] Resorcinol-bridged complexes: [5a] V. Â. Ung, A. M. W. Cargill Thompson, D. A. Bardwell, D. Gatteschi, J. C. McCleverty, F. Totti, M. D. Ward, *Inorg. Chem.* **1997**, *36*, 3447−3454. [5b] V. Â. Ung, S. M. Couchman, J. C. Jeffery, J. A. McCleverty, M. D. Ward, F. Totti, D. Gatteschi, *Inorg. Chem.* **1999**, *38*, 365−369. [5c] H. Oshio, H. Ichida, *J. Phys. Chem.* **1995**, *99*, 3294−3302.
[6] 1,3-Diaminophenylene-bridged complex: I. Fernández, J. Faus, M. Julve, F. Lloret, J. Cano, X. Ottenwaelder, Y. Journeaux, M. C. Muñoz, *Angew. Chem.* **2001**, *113*, 3129−3132; *Angew. Chem. Int. Ed.* **2001**, *40*, 3039−3042.
[7] Extended Polypyridyl-bridged complexes: A. M. W. Cargill Thompson, D. Gatteschi, J. A. McCleverty, J. A. Navas, E. Rentschler, M. D. Ward, *Inorg. Chem.* **1996**, *35*, 2701−2703.
[8] [8a] T. Ishida, T. Kawakami, S.-i. Mitsubori, T. Nogami, K. Yamaguchi, H. Iwamura, *J. Chem. Soc., Dalton Trans.* **2002**, 3177−3186. [8b] K. Nakayama, T. Ishida, R. Takayama, D. Hashizume, M. Yasui, F. Iwasaki, T. Nogami, *Chem. Lett.*

 © 2004 Wiley-VCH Verlag GmbH & Co. KGaA, Weinheim

1998, 497−498. [8c] R. Feyderherm, S. Abens, D. Günther, T. Ishida, M. Meißner, M. Meschke, T. Nogami, M. Steiner, *J. Phys.: Condens. Matter* **2000**, *12*, 8495−8509. [8d] J. Omata, T. Ishida, D. Hashizume, F. Iwasaki, T. Nogami, *Inorg. Chem.* **2001**, *40*, 3954−3958. [8e] T. Kusaka, T. Ishida, D. Hashizume, F. Iwasaki, T. Nogami, *Chem. Lett.* **2000**, 1146−1147. [8f] D. R. Corbin, L. B. Francesconi, D. H. Hendrickson, G. D. Stucky, *Inorg. Chem.* **1981**, *20*, 2084−2089.

[9] A. Bencini, D. Gatteschi, F. Totti, D. N. Sanz, J. A. McCleverty, M. D. Ward, *J. Phys. Chem. A* **1998**, *102*, 10545−10551.

[10] Y. Takano, T. Onishi, Y. Kitagawa, T. Soda, Y. Yoshioky, K. Yamaguchi, *Int. J. Quant. Chem.* **2000**, *80*, 681−691.

[11] [11a] M. Yasui, Y. Ishikawa, N. Akiyama, T. Ishida, T. Nogami, F. Iwasaki, *Acta Crystallogr., Sect. B* **2001**, *57*, 288−295. [11b] F. Mohri, K. Yoshizawa, T. Yamabe, T. Ishida, T. Nogami, *Mol. Eng.* **1999**, *8*, 357−373.

[12] T. Glaser, M. Gerenkamp, R. Fröhlich, *Angew. Chem.* **2002**, *114*, 3984−3986; *Angew. Chem. Int. Ed.* **2002**, *41*, 3823−3825.

[13] [13a] T. Glaser, M. Heidemeier, T. Lügger, *J. Chem. Soc., Dalton Trans.* **2003**, 2381−2383. [13b] T. Glaser, M. Heidemeier, E. Bill, unpublished results.

[14] [14a] B. F. Fieselmann, D. N. Hendrickson, G. D. Stucky, *Inorg. Chem.* **1978**, *17*, 1841−1848. [14b] D. R. Corbin, L. B. Francesconi, D. H. Hendrickson, G. D. Stucky, *Inorg. Chem.* **1979**, *18*, 3069−3074. [14c] L. B. Francesconi, D. R. Corbin, D. H. Hendrickson, G. D. Stucky, *Inorg. Chem.* **1979**, *18*, 3074−3080.

[15] R.-R. Galan-Mascaros, J. M. Clemente-Juan, K. R. Dunbar, *J. Chem. Soc., Dalton Trans.* **2002**, 2710−2713.

[16] P. Gamez, P. de Hoog, O. Roubeau, M. Lutz, W. L. Driessen, A. L. Spek, J. Reedijk, *Chem. Commun.* **2002**, 1488−1489.

[17] F. H. Case, E. J. Koft, *J. Am. Chem. Soc.* **1959**, *81*, 905−906.

[18] Fe: [18a] P. Collins, H. Diehl, G. F. Smith, *Anal. Chem.* **1959**, *31*, 1862−1867. [18b] H. Diehl, E. B. Buchanan Jr, G. F. Smith, *Anal. Chem.* **1960**, *32*, 1117−1119. Ru: [18c] W. A. Embry, G. H. Ayres, *Anal. Chem.* **1968**, *40*, 1499−1501. Co: [18d] M. J. Jammohamed, G. H. Ayres, *Anal. Chem.* **1972**, *44*, 2263−2268.

[19] C. Musikas, X. Vitart, J. Y. Pasquiou, R. Hoel, in *Chemical Separations*, Vol. 1, C. J. King. J. D. Navratil (eds), Litarvan Literature, Denver **1986**.

[20] [20a] R. S. Vagg, R. N. Warrener, E. C. Watton, *Aust. J. Chem.* **1967**, *20*, 1841−1857. [20b] G. A. Barclay, R. S. Vagg, E. C. Watton, *Aust. J. Chem.* **1969**, *22*, 643−645. [20c] R. S. Vagg, R. N. Warrener, E. C. Watton, *Aust. J. Chem.* **1969**, *22*, 141−152. [20d] H. A. Goodwin, R. N. Sylva, R. S. Vagg, E. C. Watton, *Aust. J. Chem.* **1969**, *22*, 1605−1611. [20e] G. A. Barclay, R. S. Vagg, E. C. Watton, *Acta Crystallogr., Sect. B* **1977**, *33*, 3487−3491. [20f] G. A. Barclay, R. S. Vagg, E. C. Watton, *Acta Crystallogr., Sect. B* **1978**, *34*, 1833−1837. [20g] B. N. Figgis, E. S. Kucharski, S. Mitra, B. W. Skelton, A. H. White, *Aust. J. Chem.* **1990**, *43*, 1269−1276.

[21] [21a] X. Chen, F. J. Fernia, J. W. Babich, J. A. Zubieta, *Inorg. Chem.* **2001**, *40*, 2769−2777. [21b] S. A. Cotton, V. Franckevicius, J. Fawcett, *Polyhedron* **2002**, *21*, 2055−2061. [21c] E. Freire, S. Baggio, J. C. Munoz, R. Baggio, *Acta Crystallogr., Sect. C* **2002**, *58*, m221−m224. [21d] P. Byers, G. Y. S. Chan, M. G. B. Drew, M. J. Hudson, *Polyhedron* **1196**, *15,* 2845−2849. [21e] N. Gupta, N. Grover, G. A. Neyhart, P. Singh, H. H. Thorp, *Inorg. Chem.* **1993**, *32*, 310−316.

[22] [22a] A. Canarero, J. M. Amigo, J. Faus, M. Julve, T. Debaerdemaeker, *J. Chem. Soc., Dalton Trans.* **1988**, 2033−2039. [22b] J. Faus, M. Julve, J. M. Amigo, T. Debaerdemaeker, *J. Chem. Soc., Dalton Trans.* **1989**, 1681−1687.

[23] [23a] E. I. Lerner, S. J. Lippard, *J. Am. Chem. Soc.* **1976**, *98*, 5397−5398. [23b] E. I. Lerner, S. J. Lippard, *Inorg. Chem.* **1977**, *16*, 1546−1551. [23c] T. Kajiwara, A. Kamiyama, T. Ito, *Chem. Commun.* **2002**, 1256−1257. [23d] A. Kamiyama, T. Noguchi, T. Kajiwara, T. Ito, *Inorg. Chem.* **2002**, *41*, 507−512. [23e] P. Paul, B. Tyagi, M. M. Bhadbhade, E. Suresh, *J. Chem. Soc., Dalton Trans.* **1997**, 2273−2277.

[24] C. Krebs, E. Bill, F. Birkelbach, V. Stämmler, unpublished results.

[25] *SMART*, Bruker AXS, **2000**.

[26] Nonius B. V., **1998**.

[27] Z. Otwinowski, W. Minor, *Methods in Enzymology* **1997**, *276*, 307−326.

[28] [28a] R. H. Blessing, *Acta Crystallogr., Sect. A* **1995**, *51*, 33−37. [28b] R. H. Blessing, *J. Appl. Cryst.* **1997**, *30*, 421−426.

[29] G. M. Sheldrick, *Acta Crystallogr., Sect. A* **1990**, *46*, 467−473.

[30] *SHELXL-97*, G. M. Sheldrick, Universität Göttingen, **1997**.

Received July 8, 2003
Early View Article
Published Online November 19, 2003

 © 2004 Wiley-VCH Verlag GmbH & Co. KGaA, Weinheim

Cyano-Bridged Dimetallic Polynuclear Cu_6Cr, Cu_6Cr_6, Cu_2W, and CuW Arrays: Synthesis, Crystal Structure, and Magnetism

Hui-Zhong Kou,*[a] Bei Chuan Zhou,[a] Shu-Feng Si,[a] and Ru-Ji Wang[a]

Keywords: Cyano bridges / Magnetic properties / Tungsten / Copper / Chromium

The synthesis, structure, and properties of the dimetallic complexes $[CuLCr(CN)_6]_6\cdot[\{CuL(H_2O)\}_6Cr(CN)_6](ClO_4)_3\cdot 16H_2O$ (**1**), $[CuLCr(CN)_5(NO)]_6\cdot[\{CuL(H_2O)\}_6Cr(CN)_5(NO)](ClO_4)_3\cdot 16H_2O$ (**2**) and $[CuL]_3[W(CN)_8]_2\cdot 4H_2O$ (**3**) {L = 3,7-bis(2-aminoethyl)-1,3,5,7-tetraazabicyclo[3.3.2]decane} are presented. The structures of **1** and **2** are isomorphous and consist of novel cyano-bridged $[CuL(\mu\text{-}CN)_2Cr(CN)_4]_6$ dodecanuclear units and $[CuL(H_2O)(\mu\text{-}CN)]_6Cr$ heptanuclear moieties. Every cyclic dodecanuclear Cu_6Cr_6 group embeds a ClO_4^- anion. The heptanuclear and the dodecanuclear units are connected through hydrogen bonds to generate a vacant hole, in which another ClO_4^- anion is accommodated. Complex **3** contains cyano-bridged Cu_2W trimers and CuW dimers. Magnetic studies have shown that the three complexes display ferromagnetic coupling across the Cr–CN–Cu or W–CN–Cu linkages. The best fit to the magnetic data gave for complex **1** $J_{CuCr} = +2.40\ cm^{-1}$, $g_{Cr} = 1.99$, $g_{Cu} = 2.09$, and an intermolecular coupling constant $\theta = +0.23$ K while for complex **2** $J_{CuCr} = +12\ cm^{-1}$, $g = 2.13$, and $\theta = -0.49$ K. Ferromagnetic Cu^{II}-W^{V} coupling is operative in complex **3**.
(© Wiley-VCH Verlag GmbH & Co. KGaA, 69451 Weinheim, Germany, 2004)

Introduction

The magnetic properties of cyano-bridged dimetallic assemblies have been actively researched.[1−55] Exciting findings include the design and synthesis of cyano-bridged room-temperature molecule-based magnets[1] and magnetically tunable materials.[2−5] In particular, cyano-bridged polynuclear species can be used to elucidate the strength of intermetallic coupling through the bridges and to search for single-molecule magnets.[10−21] Until now, cyano-bridged star-like heptanuclear complexes $\{[ML^1]_6[M'(CN)_6]\}^{n+}$ (M = Cu^{II}, Ni^{II}, or $Mn^{II/III}$; L^1 = organic ligands; M′ = Fe^{III}, Cr^{III}) have been synthesized,[21−29] some of which have been structurally characterized. The magnetism of cyano-bridged tri-, tetra-, penta-, and pentadecanuclear complexes has also been reported.[34−50] These studies show that the coupling constants of Ni^{II}-Fe^{III}, Mn^{II}-Fe^{III}, Ni^{II}-Cr^{III}, Mn^{II}-Cr^{III}, and Cu^{II}-Cr^{III} through the cyano bridges are generally less than 20 cm^{-1} (absolute values). Very recently, a cyano-bridged Mo_6Mn complex has been found to exhibit interesting single-molecule magnet behavior.[20] Our interest in low-dimensional cyano-bridged dimetallic complexes[41,46] has suggested that treating the Cu^{II} building block $[CuL](ClO_4)_2$ {L = 3,7-bis(2-aminoethyl)-1,3,5,7-tetraazabicyclo[3.3.2]decane} with $[Cr(CN)_6]^{3-}$, $[Cr(CN)_5(NO)]^{3-}$ or $[W(CN)_8]^{3-}$ will generate cyano-bridged species since the cyano nitrogen atoms can replace the weakly coordinated ClO_4^- oxygen atoms around the Cu^{II} atom.[56] Three novel polynuclear dimetallic complexes have been obtained and investigated for their magnetic properties. We report our findings here.

[a] Department of Chemistry, Tsinghua University, Beijing 100084, P. R. China
E-mail: kouhz@mail.tsinghua.edu.cn
Supporting information for this article is available on the WWW under http://www.eurjic.org or from the author.

Results and Discussion

Synthesis and Physical Characterization

$[Cr(CN)_6]^{3-}$/$[Cr(CN)_5(NO)]^{3-}$ and $[CuL](ClO_4)_2$ react to form the new complexes **1** and **2** irrespective of the molar ratios of two precursors. Usually, di- or trinuclear and 1D chain complexes are produced by the reactions of hexacyanometallate with Cu^{II} complexes.[30,43−45,47−49] Thus, the formation of cyano-bridged dodecanuclear Cu_6Cr_6 and heptanuclear Cu_6Cr moieties is unexpected. Similarly, an attempt to synthesize Cu_6Fe complexes led to the cocrystallisation of heptanuclear and pentanuclear moieties.[23]

Similar to the reaction of $[Cu(en)_2]^{2+}$ with $[W(CN)_8]^{3-}$, $[CuL]^{2+}$ with $[W(CN)_8]^{3-}$ affords a cyano-bridged polynuclear Cu_3W_2 complex (**3**). Although a cyano-bridged 3D molecular structure is assumed for $Cu(en)_2-W(CN)_8$, it may be best regarded as polynuclear owing to its considerably weak $Cu-N_{cyano}$ coordination bonds.[52]

The three strong IR bands at 2129, 2119, and 2112 cm^{-1} for complex **1**, and 2115, 2110, 2098 cm^{-1} for complex **2** are attributed to C≡N stretching modes. The splitting of $\nu_{C\equiv N}$ indicates the presence of both bridging and nonbridging cyano ligands, which is consistent with the X-ray structural results (vide infra). The strong band centred at 1089 cm^{-1} (ν_{Cl-O}) indicates the existence of ClO_4^- anions. The

 DOI: 10.1002/ejic.200300500 © 2004 Wiley-VCH Verlag GmbH & Co. KGaA, Weinheim

very strong band at 1664 cm^{-1} ($\nu_{O=N}$) shows the presence of NO^+ groups in complex **2**.[55,57,58]

The solution electronic spectrum of complex **1** shows a weak broad band centred at 530 nm due to the d−d transition of Cu^{II}.[56] The d−d transition of Cr^{III} may be masked by that of Cu^{II}.

The powder X-band EPR spectrum of **1** at room temperature shows a broad, nearly isotropic signal that affords a g_{iso} value of 2.02. No half-field transition was observed. The broad isotropic signal differs from that of an axial $S = 1/2$ Cu^{II} complex. With the presence of nearly isolated Cu^{II} moieties in the complex, the EPR spectrum can be tentatively explained as the superimposition of the transitions for $S = 3/2$ (Cr^{III}), $S = 1/2$ (Cu^{II}) and the ferromagnetically coupled ground state $S = 2$ for $Cu^{II}Cr^{III}$ (vide infra).

Crystal Structures

The structures of complexes **1** and **2** are shown in Figures 1, 2, and 3. Figure 4 shows the Cu_6Cr_6 dodecanuclear unit of both complexes. The cell packing plots of three complexes are shown in the Supporting Information. The structure of the polynuclear units for complex **3** is shown in Figure 6. Selected bond lengths and angles are listed in Tables 1 and 2.

Complex **1** is isostructural to complex **2**. The structure of both complexes confirms the cocrystallization of heptanuclear Cu_6Cr^{9+} cations, cyclic $Cu_6Cr_6^{6-}$ anions, and ClO_4^- counter-anions. The molar ratio of the constituents is 1:1:3.

The $Cu_6Cr_6^{6-}$ anion consists of six $[CuL]^{2+}$ moieties and six $[Cr(CN)_6]^{3-}$ (**1**) or $[Cr(CN)_5(NO)]^{3-}$ (**2**), which are alternatively connected by the cyano ligands. The coordination environment of Cu^{II} is distorted octahedral (4 + 1 + 1) with the N_{cyano} atom at the axial position [Cu(1)−N(2) and Cu(1)−N(4A) bond lengths are 2.506(5) and 3.072(6) Å for **1**, and 2.378(5) and 3.082(6) Å for **2**].

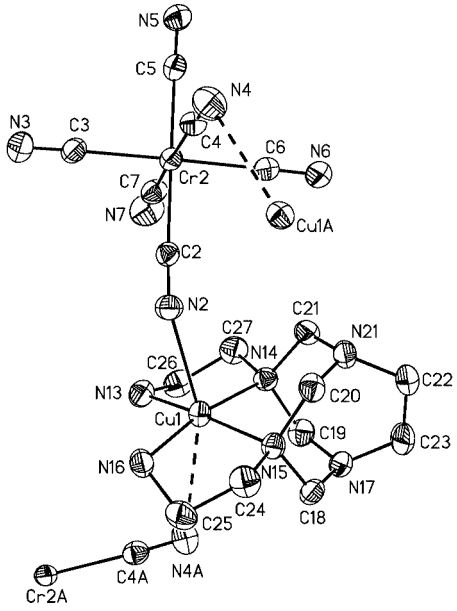

Figure 1. ORTEP diagram of the asymmetric unit of Cu_6Cr_6 for complex **1** with thermal ellipsoids at 30% probability

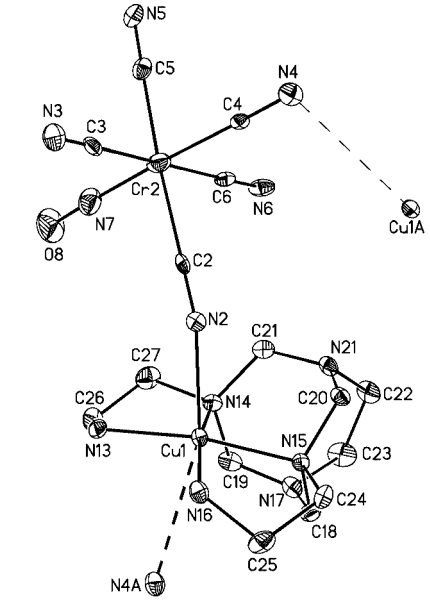

Figure 2. ORTEP diagram of the asymmetric unit of Cu_6Cr_6 for complex **2** with thermal ellipsoids at 30% probability

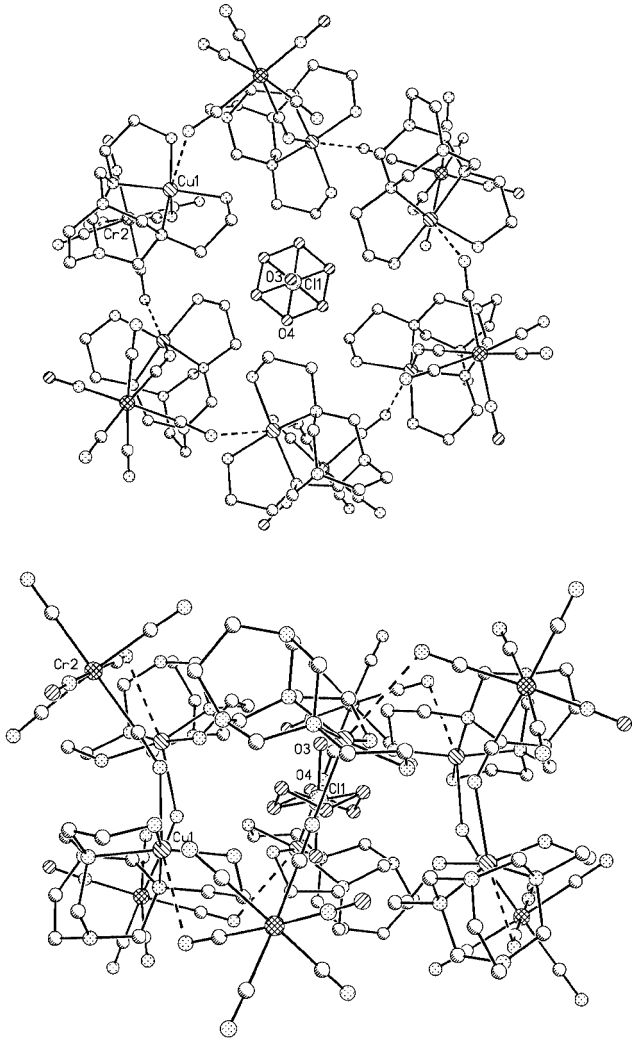

Figure 3. Cyclic Cu_6Cr_6 unit of complexes **1** and **2** showing the encapsulated ClO_4^- anion; (a) top view, (b) side view

 © 2004 Wiley-VCH Verlag GmbH & Co. KGaA, Weinheim

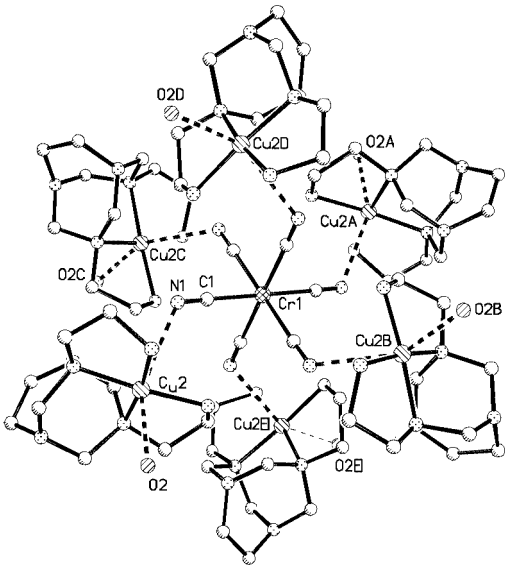

Figure 4. Star-like Cu_6Cr cation of **1**; the Cu_6Cr cation of **2** is similar to that of **1** except that one of the cyanide ligands is replaced by NO^+

Table 1. Selected bond lengths [Å] and angles [°] for **1** and **2**

1		**2**	
Cu(1)−N(16)	2.000(5)	Cu(1)−N(16)	2.001(5)
Cu(1)−N(13)	2.006(5)	Cu(1)−N(13)	2.034(5)
Cu(1)−N(14)	2.016(4)	Cu(1)−N(14)	2.023(5)
Cu(1)−N(15)	2.029(4)	Cu(1)−N(15)	2.028(5)
Cu(1)−N(2)	2.506(5)	Cu(1)−N(2)	2.378(5)
Cu(1)−N(4)#1[a]	3.072(6)	Cu(1)−N(4)#1	3.082(6)
Cu(2)−N(9)	2.023(5)	Cu(2)−N(9)	2.036(7)
Cu(2)−N(10)	1.997(5)	Cu(2)−N(10)	1.984(7)
Cu(2)−N(11)	2.001(5)	Cu(2)−N(11)	1.985(7)
Cu(2)−O(2)	2.463(5)	Cu(2)−O(2)	2.464(7)
Cu(2)−N(1)	3.021(5)	Cu(2)−N(1)	2.950(7)
Cr(2)−C(7)	2.079(7)	Cr(2)−N(7)	1.886(8)
Cr(2)−C(6)	2.080(6)	Cr(2)−C(6)	2.036(7)
Cr(2)−C(5)	2.073(6)	Cr(2)−C(5)	1.985(8)
Cr(2)−C(4)	2.079(7)	Cr(2)−C(4)	2.016(7)
Cr(2)−C(3)	2.081(6)	Cr(2)−C(3)	2.037(8)
Cr(2)−C(2)	2.101(6)	Cr(2)−C(2)	2.099(7)
Cr(1)−C(1)	2.078(6)	Cr(1)−C(1)/N(30)	1.989(6)
N(1)−C(1)−Cr(1)	174.0(6)	N(1)−C(1)−Cr(1)	173.9(7)
N(2)−C(2)−Cr(2)	176.4(5)	N(2)−C(2)−Cr(2)	176.2(5)
N(3)−C(3)−Cr(2)	178.7(6)	N(3)−C(3)−Cr(2)	178.7(6)
N(4)−C(4)−Cr(2)	176.8(6)	N(4)−C(4)−Cr(2)	175.4(6)
N(5)−C(5)−Cr(2)	179.1(5)	N(5)−C(5)−Cr(2)	179.2(6)
N(6)−C(6)−Cr(2)	177.8(6)	N(6)−C(6)−Cr(2)	177.7(7)
N(7)−C(7)−Cr(2)	177.7(6)	O(8)−N(7)−Cr(2)	177.7(6)
C(2)−N(2)−Cu(1)	142.7(6)	C(2)−N(2)−Cu(1)	144.8(5)
C(1)−N(1)−Cu(2)	129.1(5)	C(1)−N(1)−Cu(2)/ N(30)−O(9)−Cu(2)	129.8(5)

[a] Symmetry operation: #1: $2/3 + x - y$, $1/3 + x$, $1/3 - z$.

The Cu^{II} ion is equatorially coordinated by four nitrogen atoms from the L ligand. The cyano ligand coordinates to the Cu^{II} ion in a bent fashion with Cu−N−C angles of 142.7(6) and 114.1(5)° for **1**, and 144.8(5)° and 112.2(5)° for **2**. In **2**, the bridging cyano ligands are *cis* or *trans* to the NO^+ ligand (Figure 2). The Cr···Cu distances through the cyano bridge are 5.427(1), 5.248(1) Å for **1** and 5.333(1), 5.225(1) Å for **2**. Within the cyclic Cu_6Cr_6 group, a perchlorate anion [Cl(1)] is embedded, which is disordered over two sets of positions (Figure 3).

Table 2. Selected bond lengths [Å] and angles [°] for **3**

W(2)−C(1)	2.154(6)	W(1)−C(40)	2.157(6)
W(2)−C(2)	2.148(6)	W(1)−C(41)	2.171(5)
W(2)−C(3)	2.162(6)	W(1)−C(42)	2.155(6)
W(2)−C(4)	2.143(7)	W(1)−C(43)	2.157(6)
W(2)−C(5)	2.163(7)	W(1)−C(44)	2.158(6)
W(2)−C(6)	2.123(5)	W(1)−C(45)	2.179(5)
W(2)−C(7)	2.190(7)	W(1)−C(46)	2.146(6)
W(2)−C(8)	2.155(7)	W(1)−C(47)	2.160(6)
Cu(1)−N(1)	2.300(5)	Cu(2)−N(6)	2.210(5)
Cu(1)−N(9)	2.003(5)	Cu(2)−N(15)	2.016(6)
Cu(1)−N(10)	2.002(5)	Cu(2)−N(16)	2.004(6)
Cu(1)−N(11)	2.029(5)	Cu(2)−N(18)	1.994(5)
Cu(1)−N(13)	2.011(4)	Cu(2)−N(20)	2.003(6)
Cu(1)−N(9)	2.003(5)	Cu(1)−N(10)	2.002(5)
Cu(1)−N(11)	2.029(5)	Cu(1)−N(13)	2.011(4)
Cu(3)−N(47)	2.368(4)		
C(1)−N(1)−Cu(1)	161.0(5)	C(6)−N(6)−Cu(2)	169.3(8)
C(47)−N(47)−Cu(3)	147.5(4)		

The $[Cr(CN)_6]^{3-}$ anion is nearly octahedral: the *cis*- and *trans*-C−Cr−C angles are close to 90° and 180°, respectively. The Cr−C−N linkages show only a slight deviation from linearity. The $[Cr(CN)_5(NO)]^{3-}$ anion has a distorted octahedral environment (C_{4v} symmetry): the Cr−*N*−O and Cr−C−N linkages are nearly linear, and the N−Cr−C *cis* angles are > 90° due to the greater electronegativity (EN) of the nitrosyl group with respect to the cyanide groups. This agrees with the EN calculations of Huheey ($NO^+ > CN^- > H_2O$).[59] The Cr−C bonds range from 1.985(8) to 2.099(7) Å, while the Cr−N distance is 1.886(8) Å. These data are in good agreement with complexes incorporating $[Cr(CN)_5(NO)]^{3-}$.[55,58]

In the heptanuclear cation (Figure 4), $[Cr(CN)_6]^{3-}$ (**1**) or $[Cr(CN)_5(NO)]^{3-}$ (**2**) is encapsulated by six $[CuL(H_2O)]^{2+}$ units through the weak $Cu-N_{cyano}$ coordination bonds [Cu−N = 3.021(5) Å for **1** and 2.950(7) Å for **2**], forming an almost spherical cluster. The Cu(2) coordination geometry is elongated octahedral with four nitrogen atoms of L at the equatorial plane, and the oxygen atom [O(2)] of one water molecule and one nitrogen atom of the bridging CN^- ligand at the axial positions [Cu(2)−O(2) = 2.463(5) Å for **1** and 2.464(7) Å for **2**]. The disorder of NO^+ over six positions in **2** precludes an accurate determination of the Cu−O(NO^+) bond length. However, the encapsulation of the $[CuL(H_2O)]^{2+}$ group reveals an NO^+ bridge.

The Cu−N≡C angles in the heptanuclear cations [129.1(5)° for **1** and 129.8(5)° for **2**] show a greater deviation from linearity. The axial O(2)−Cu(1)−N(1) angles also deviate from linearity [154.9(2)° for **1** and 155.6(2)° for **2**]. The Cr···Cu distances through the cyano bridge are 5.591(1) Å (**1**) and 5.489(1) Å (**2**).

 © 2004 Wiley-VCH Verlag GmbH & Co. KGaA, Weinheim

Cl(1) and Cr(1) lie in special positions, viz. at the $\bar{3}$ rotation axis along the *c* axis, resulting in the disorder of the ClO_4^- anion. Also, the heptanuclear and the dodecanuclear units pack along the *c* axis (Figure 5), and are connected through hydrogen bonds [O(2)···N(3A)] (Figure 6). A ClO_4^- anion is accommodated between the two polynuclear units, and is hydrogen-bonded to the nitrogen atoms [N(8)] of L.

The structure of **3** consists of two cyano-bridged trimeric Cu_2W and dimeric CuW moieties (Figure 6). In the Cu_2W trimer, $[W(CN)_8]^{3-}$ uses two cyano ligands to connect two $[CuL]^{2+}$ groups, giving rise to a "V"-shaped structure. The Cu^{II} ions are five-coordinate with four nitrogen atoms of the L ligand occupying the equatorial plane and one cyano nitrogen atom at the apical position. The $Cu-N_{cyano}$ bond lengths are 2.300(5) Å for Cu(1)−N(1) and 2.210(5) Å for Cu(2)−N(6). The cyano bridging ligands coordinate to the copper ions with bond angles of 161.0(5)° for Cu(1)−N(1)−C(1) and 169.3(8)° for Cu(2)−N(6)−C(6). The CuW dimer differs from the trimer in that it contains only one cyano bridge linking two metal ions. The cyano bridging ligand coordinates to the copper ion [Cu(3)−N(47) = 2.368(4) Å] with a bond angle of 147.5(4)°. Based on the $Cu-N_{cyano}$ bond lengths and the corresponding Cu−N−C bond angles, the shorter the $Cu-N_{cyano}$ bond lengths the larger are the Cu−N−C bond angles. The corresponding metal−metal separations are 5.535 Å for Cu(1)−W(2), 5.458 Å for Cu(2)−W(2) and 5.436 Å for W(1)−Cu(3). In the cell, two polynuclear moieties are linked through weak intermolecular contacts ($Cu-N_{cyano} > 3.16$ Å) giving rise to a 3D network (see Supporting Information). Water molecules within the network are hydrogen-bonded to the primary amine nitrogen atoms and the nonbridging cyano nitrogen atoms.

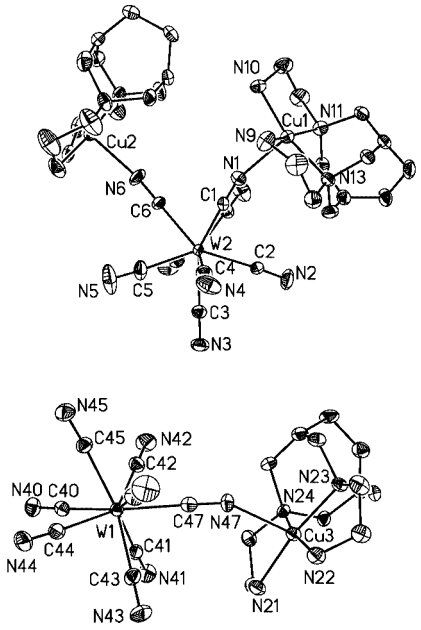

Figure 6. Structure of complex **3**, showing the discrete trimeric and dimeric units

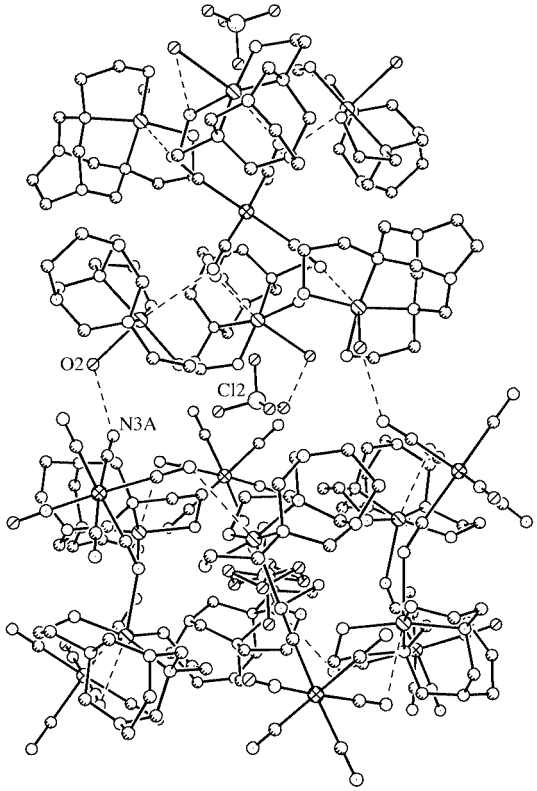

Figure 5. Hydrogen-bonded cyclic Cu_6Cr_6 and spherical Cu_6Cr units of **1** and **2** showing the encapsulation of the ClO_4^- anion (Cl2)

Magnetic Properties

The magnetic susceptibilities of the three complexes have been measured, and plots of $\chi_m T$ vs. T are shown in Figures 7, 8, and 9, where χ_m is the magnetic susceptibility per $Cu_{12}Cr_7$ unit or per Cu_3W_2 unit.

With decreasing temperature, $\chi_m T$ of **1** increases slowly until ca. 30 K and then sharply reaches a maximum of 23.0 emu·K·mol^{-1} at 4 K. The magnetic susceptibilities obey the Curie−Weiss law with a positive Weiss constant of +2.1 K and a Curie constant of 17.9 emu·K·mol^{-1} (calculated

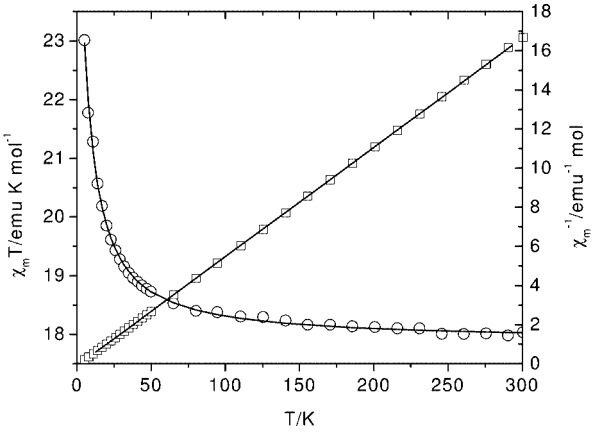

Figure 7. Temperature dependence of $\chi_m T$ and χ_m for **1**; the solid line is the best fit with the parameters in the text

 © 2004 Wiley-VCH Verlag GmbH & Co. KGaA, Weinheim

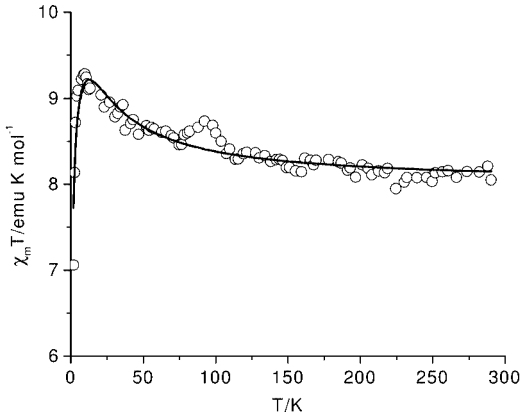

Figure 8. Temperature dependence of $\chi_m T$ for **2**; the solid line is the fit to the Curie−Weiss law

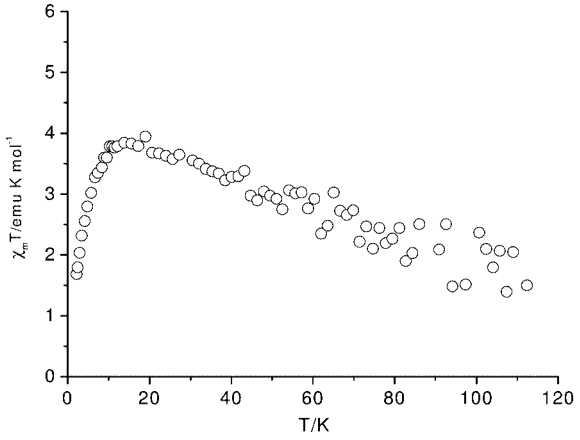

Figure 9. Temperature dependence of $\chi_m T$ for **3**

value is 17.75 emu·K·mol^{-1} assuming $g = 2$). This magnetic behaviour reveals ferromagnetic coupling between the $Cu^{II}-Cr^{III}$ ions through the cyanide bridges. The ferromagnetic interaction between the Cr^{III} and Cu^{II} ions is due to the orthogonality of the magnetic orbitals of Cr^{III} (t_{2g}^3) and Cu^{II} (e_g^3).

From the structural information of **1**, the system can be treated as six strongly interacting CuCr dimers [$Cu-N_{cyano}$ = 2.506(5) Å] between which a weak interaction is present [$Cu-N_{cyano}$ = 3.072(6) Å] and weakly interacting Cu_6Cr clusters [$Cu-N_{cyano}$ = 3.021(6) Å]. The weak interactions are negligibly small and can be included in the intermolecular field term during the fit. Hence, the magnetic susceptibilities can be simulated by Equations (1) and (2) based on the isotropic spin Hamiltonian $\hat{H} = -2J_d S_{Cr} S_{Cu}$ for the strongly interacting $Cu^{II}Cr^{III}$ dimer, where g_1 and g_2 are the g factors for the total spin states of $S_T = 1$ and 2, respectively, and θ accounts for the interdimeric coupling. The g_1 and g_2 factors are related to g_{Cu} and g_{Cr}, viz. $g_1 = 3/4g_{Cr} - 1/4g_{Cu}$ and $g_2 = 3/4g_{Cr} + 1/4g_{Cu}$ according to the literature method.[61−63]

$$\chi_d = \frac{Ng^2\beta^2}{k(T-\theta)} \cdot \frac{2g_1^2 + 10g_2^2 \exp(4J_d/kT)}{3 + 5\exp(4J_d/kT)} \quad (1)$$

$$\chi_m = 6\times\chi_d + 6\times\frac{Ng_{Cu}^2\beta^2}{3kT} S_{Cu}(S_{Cu}+1) + \frac{Ng_{Cr}^2\beta^2}{3kT} S_{Cr}(S_{Cr}+1) \quad (2)$$

The best fit to the magnetization data gives g_{Cu} = 2.09, g_{Cr} = 1.99, J_d = +2.40 cm^{-1} and θ = +0.23 K (Figure 7). To approximate the $Cu^{II}-Cr^{III}$ coupling in the Cu_6Cr moieties we used an identical θ, giving rise to a similar result with g_{Cu} = 2.09, g_{Cr} = 1.99, J_d = +2.37 cm^{-1} and θ = +0.17 K. The positive θ indicates weak intermolecular ferromagnetic interactions. Of course, this θ includes two effects: the $Cu^{II}-Cr^{III}$ magnetic coupling through the weak bridging cyano ligands and the intercluster magnetic exchange. The $Cu^{II}-Cr^{III}$ coupling constant is similar to those reported for the cyano-bridged 1D CuCr complexes $\{[Cu(L^2)][Cu(L^2)Cr(CN)_6]ClO_4\cdot 2H_2O\}_n$ (L^2 = *meso*-5,5,7,12,12,14-hexamethyl-1,4,8,11-tetraazacyclotetradecane) (J = +4.82 cm^{-1}) and $[Cu(cyclam)]_3[Cr(CN)_6]_2\cdot 4H_2O$ (J = +4.33 cm^{-1}),[64,30] and is lower than that of the cyano-bridged Cu_3Cr complex $[Cu(edma)]_3Cr(CN)_6$ ($edma^-$ = ethylenediaminemonoacetate) (J = +9.16 cm^{-1}).[44]

A Cu^{II} ion in elongated octahedral surroundings has a magnetic orbital built from a $d_{x^2-y^2}$ orbital (x and y axes are taken along the $Cu-N_{equatorial}$ directions) with little contribution from the d_z^2 orbital and localized in the equatorial plane. A weak magnetic interaction is anticipated due to the little delocalization of the magnetic orbital towards the axial position by the bridging cyano atom for complex **1** and $\{[Cu(L^2)][Cu(L^2)Cr(CN)_6]ClO_4\cdot 2H_2O\}_n$.[64] That the strongest Cu···Cr coupling is present in the Cu_3Cr complex is understandable because the bridging cyano atom is situated within the coordination plane (xy plane).

The magnetic behaviour of complex **2** is similar to that of complex **1** (Figure 8); $\chi_m T$ increases smoothly as the temperature is lowered to ca. 9.6 K, reaching a maximum of 9.3 cm^3·K·mol^{-1}, and then decreases. The anomaly at ca. 90 K is due to experimental errors. Such magnetic behaviour is characteristic of an unambiguous local ferromagnetic interaction. The magnetic susceptibility in the range 10−300 K has been fitted by the Curie−Weiss expression that is usually used to describe weakly coupled systems. The positive Weiss constant obtained (+4.0 K) suggests a ferromagnetic interaction. The Curie constant C (8.0 emu·K·mol^{-1}) is consistent with the theoretical value of 8.00 emu·K·mol^{-1} with g = 2.12.

The fit to the magnetic data of **2** with a model similar to complex **1** affords g = 2.13, J_d = +12 cm^{-1}, and θ = −0.49 K. The $Cu^{II}-Cr^{I}$ magnetic coupling constant (J_d) is positive, indicating a ferromagnetic interaction between the metal ions.

Complex **2** is the first example incorporating Cu^{II} and low-spin Cr^{I} ions. Analogously, the ferromagnetic nature of

 © 2004 Wiley-VCH Verlag GmbH & Co. KGaA, Weinheim

the $Cu^{II}-Cr^{I}$ coupling can be interpreted by the orthogonality of the magnetic orbitals of the low-spin Cr^{I} [$3d^5$, $(d_{xy})^1$] and Cu^{II} [$3d^9$, $(d_{x^2-y^2})^1$] ions.[55]

The comparatively large Weiss constant and J_d compared to that of complex **1** may be partially due to the shorter Cu(1)−N(2) bond length in complex **2**, which favours a stronger Cu···Cr coupling through the cyano bridge.

The magnetic behavior of complex **3** indicates a ferromagnetic nature (Figure 9), which is consistent with the reported analogous cyano-bridged $Cu^{II}-W^{V}$ complexes, in which ferromagnetic $Cu^{II}-W^{V}$ coupling is always observed.[50,52] The decrease of $\chi_m T$ below 18 K may be due to intermolecular antiferromagnetic interaction through the weak cyano contacts and the field saturation effect.

Conclusion

The self-assembly of the $[CuL]^{2+}$ precursor, and $K_3[Cr(CN)_6]$, $K_3[Cr(CN)_5(NO)]$, or $K_3[W(CN)_8]$ affords a series of cyano-bridged polynuclear complexes. X-ray diffraction analysis shows that they consist of novel polynuclear star-like Cu_6Cr and cyclic Cu_6Cr_6 moieties, and that the CuW complex has a cyano-bridged dinuclear and trinuclear structure. Variable-temperature magnetic susceptibility measurements show that the three complexes exhibit ferromagnetic coupling between neighbouring metal ions.

Experimental Section

General Remarks: Elemental analyses of carbon, hydrogen, and nitrogen were carried out with an Elementar Vario EL. Infrared spectroscopy was performed with a Magna-IR 750 spectrophotometer in the 4000−650 cm^{-1} region. The electronic spectrum of **1** was measured with a Perkin−Elmer Hitachi-240 spectrophotometer in water. The room-temperature EPR powder spectrum of **1** was recorded at the X-band with a Bruker ER 200B spectrometer. Variable-temperature magnetic susceptibility measurements of **1** were performed with a Quantum Design MPMS SQUID magnetometer, while those of **2** and **3** were carried out with a MagLab 2000 magnetometer. The experimental susceptibilities were corrected for the diamagnetism of the constituent atoms (Pascal's Tables) and the sample holder (gelatine capsule). All chemicals and solvents used in the synthesis were of reagent grade. $[CuL](ClO_4)_2$, $K_3[Cr(CN)_6]$, $K_3[Cr(CN)_5(NO)]$, and $K_3[W(CN)_8]$ were prepared according to literature methods.[56,57,60,65] ***Caution!*** Perchlorate salts of metal complexes are potentially explosive; only a small amount of material should be prepared, and it should be handled with care.

$[CuLCr(CN)_6]_6[\{CuL(H_2O)\}_6Cr(CN)_6](ClO_4)_3\cdot 16H_2O$ (1): Cubic red single crystals were obtained by slow concentration of an aqueous solution (15 mL) of $[CuL](ClO_4)_2$ (0.1 mmol) and $K_3[Cr(CN)_6]$ (0.1 mmol) in a molar ratio of 1:1. Yield: 23 mg, 40% (based on Cu). IR: $\tilde{\nu}$ = 2129 s, 2119 s, 2112 s ($\nu_{C\equiv N}$); 1086 br (ν_{Cl-O}) cm^{-1}. UV/Vis: λ = 530 nm.

$[CuLCr(CN)_5(NO)]_6\cdot[\{CuL(H_2O)\}_6Cr(CN)_5(NO)](ClO_4)_3\cdot 16H_2O$ (2): Red single crystals of **2** were prepared by a procedure similar to that for **1**, using $K_3[Cr(CN)_5(NO)]$ instead of $K_3[Cr(CN)_6]$. Yield: 24 mg, 50% (based on Cu). IR: 2115 s, 2110 s, 2098 sh ($\nu_{C\equiv N}$); 1664 vs ($\nu_{O=N}$); 1089 vs (ν_{Cl-O}) cm^{-1}.

$[CuL]_3[W(CN)_8]_2\cdot 4H_2O$ (3): Violet single crystals were obtained by slow concentration of an aqueous solution (10 mL) of $[CuL](ClO_4)_2$ (0.1 mmol) and $K_3[W(CN)_8]$ (0.1 mmol) in a molar ratio of 1:1. Yield: 11 mg, 20% (based on Cu). IR: 2142 s, 2105 sh ($\nu_{C\equiv N}$) cm^{-1}.

X-ray Crystallographic Study: The data collections of **1**, **3**, and **2** were made with a Bruker Siemens P4 and a Rigaku R-Axis RIPID IP diffractometer at 293 K, respectively. The structures were solved by direct methods (SHELXS-97) and refined by full-matrix least squares (SHELEXL-97) on F^2.[66] Anisotropic thermal parameters were used for the non-hydrogen atoms and isotropic parameters for the hydrogen atoms. Hydrogen atoms were added geometrically and refined by using a riding model. Weighted R factors wR and goodness of fit values (S) are based on F^2, conventional R factors are based on F, with F set to zero for negative F^2. Crystal data are summarized in Table 3. During the solution of the crystal structure of complex **2**, it was found that the atoms (five C and one N) lie from 1.886(8) to 2.099(7) Å away from Cr. Considering that the usual Cr−C bond length is approximately 2.0 Å and that the Cr−N bond length is ca. 1.8 Å,[55,58] the N atom was unambiguously assigned a Cr−N distance of 1.886(8) Å. CCDC-207494 (**1**), -207495 (**2**), -215992 (**3**) contain the supplementary crystallographic data for this paper. These data can be obtained free of charge at www.ccdc.cam.ac.uk/conts/retrieving.html [or from the Cambridge

Table 3. Crystallographic data for complexes **1**−**3**

	1	**2**	**3**
Empirical formula	$C_{162}H_{324}Cl_3Cr_7Cu_{12}N_{114}O_{34}$	$C_{155}H_{324}Cl_3Cr_7Cu_{12}N_{114}O_{41}$	$C_{46}H_{79}Cu_3N_{34}O_4W_2$
Formula mass	5646.18	5674.11	1730.75
Space group	$R\bar{3}$	$R\bar{3}$	$P2_12_12_1$
a [Å]	28.866(6)	28.402(4)	11.318(2)
b [Å]	28.866(6)	28.402(4)	15.998(3)
c [Å]	25.145(7)	24.786(5)	36.261(7)
V [Å^3]	18144(7)	17316(5)	6566(2)
Z	3	3	4
μ(Mo-K_a) [mm^{-1}]	1.449	1.521	1.751
Data/restraints/parameters	7181/0/500	12854/0/500	23770/0/802
R_{int} (on F^2)	0.0343	0.0440	0.0607
Goodness of fit on F^2	1.185	1.110	0.964
$R1$ [$I > 2\sigma(I)$]	0.0553	0.0722	0.0461
$wR2$ (all data)	0.1477	0.1556	0.0933

Crystallographic Data Centre, 12 Union Road, Cambridge CB2 1EZ, UK; Fax: (internat.) + 44-1223-336-033; E-mail: deposit@ccdc.cam.ac.uk].

Acknowledgments

This work was supported by the National Natural Science Foundation of China (project nos. 20201008 and 50272034).

[1] S. M. Holmes, G. S. Girolami, *J. Am. Chem. Soc.* **1999**, *121*, 5593.
[2] S. Ferlay, T. Mallah, R. Ouahes, P. Veillet, M. Verdaguer, *Nature* **1995**, *378*, 701.
[3] T. Mallah, S. Thiebaut, M. Verdaguer, P. Veillet, *Science* **1993**, *262*, 1554.
[4] O. Sato, T. Iyoda, A. Fujishima, K. Hashimoto, *Science* **1996**, *272*, 704.
[5] S.-I. Ohkoshi, Y. Abe, A. Fujishima, K. Hashimota, *Phys. Rev. Lett.* **1999**, *82*, 1285.
[6] M. Ohba, N. Usuki, N. Fukita, H. Okawa, *Angew. Chem. Int. Ed.* **1999**, *38*, 1795.
[7] H. Miyasaka, N. Matsumoto, H. Okawa, N. Re, E. Gallo, C. Floriani, *J. Am. Chem. Soc.* **1996**, *118*, 981.
[8] H. Miyasaka, N. Matsumoto, H. Okawa, N. Re, E. Gallo, C. Floriani, *Angew. Chem. Int. Ed. Engl.* **1995**, *34*, 1446.
[9] N. Re, E. Gallo, C. Floriani, H. Miyasaka, N. Matsumoto, *Inorg. Chem.* **1996**, *35*, 6004.
[10] H. Miyasaka, N. Matsumoto, N. Re, E. Gallo, C. Floriani, *Inorg. Chem.* **1997**, *36*, 670.
[11] H. Miyasaka, H. Ieda, N. Matsumoto, K.-i. Sugiura, M. Yamashita, *Inorg. Chem.* **2003**, *42*, 3509−3515.
[12] J. A. Smith, J.-R. Galan-Mascaros, R. Clerac, K. R. Dunbar, *Chem. Commun.* **2000**, 1077.
[13] H.-Z. Kou, S. Gao, J. Zhang, G.-H. Wen, G. Su, R. K. Zheng, X. X. Zhang, *J. Am. Chem. Soc.* **2001**, *123*, 11809.
[14] F. Thétiot, S. Triki, J. S. Pala, C. J. Gómez-García, S. Golhen, *Chem. Commun.* **2002**, 1078.
[15] M. S. El Fallah, E. Rentschler, A. Caneschi, R. Sessoli, D. Gatteschi, *Angew. Chem. Int. Ed. Engl.* **1996**, *35*, 1947.
[16] E. Coronado, C. J. Gomez-Garcia, A. Nuez, F. M. Romero, E. Rusanov, H. Stoeckli-Evans, *Inorg. Chem.* **2002**, *41*, 4615.
[17] K. Inoue, H. Imai, P. S. Ghalsasi, K. Kikuchi, M. Ohba, H. Okawa, J. V. Yakhmi, *Angew. Chem. Int. Ed.* **2001**, *40*, 4242.
[18] P. A. Berseth, J. J. Sokol, M. P. Shores, J. L. Heinrich, J. R. Long, *J. Am. Chem. Soc.* **2000**, *122*, 9655.
[19] M. P. Shores, J. J. Sokol, J. R. Long, *J. Am. Chem. Soc.* **2002**, *124*, 2279.
[20] J. J. Sokol, A. G. Hee, J. R. Long, *J. Am. Chem. Soc.* **2002**, *124*, 7656.
[21] R. J. Parker, D. C. Hockless, B. Moubaraki, K. S. Murray, L. Spiccia, *Chem. Commun.* **1996**, 2789.
[22] R. J. Parker, L. Spiccia, S. R. Batten, J. D. Cashion, G. D. Fallon, *Inorg. Chem.* **2001**, *40*, 4696.
[23] R. J. Parker, L. Spiccia, B. Moubaraki, K. S. Murray, D. C. R. Hockless, A. D. Rae, A. C. Willis, *Inorg. Chem.* **2002**, *41*, 2489.
[24] R. J. Parker, L. Spiccia, K. J. Berry, G. D. Fallon, B. Moubaraki, K. S. Murray, *Chem. Commun.* **2001**, 333.
[25] X. Shen, B. Li, J. Zou, Z. Xu, *Transition Met. Chem.* **2002**, *27*, 372.
[26] T. Mallah, C. Auberger, M. Verdaguer, P. Veillet, *J. Chem. Soc., Chem. Commun.* **1995**, 61.
[27] A. Scuiller, T. Mallah, A. Nivorozkhin, J.-L. Tholence, M. Verdaguer, P. Veillet, *New J. Chem.* **1996**, *20*, 1.
[28] G. Rogez, S. Parsons, V. Villar, T. Mallah, *Inorg. Chem.* **2001**, *40*, 3836.
[29] V. Marvaud, C. Decroix, A. Scuiller, C. Guyard-Duhayon, J. Vaissermann, F. Gonnet, M. Verdaguer, *Chem. Eur. J.* **2003**, *9*, 1678.
[30] M. S. El Fallah, J. Ribas, X. Solans, M. Font-Bardia, *New J. Chem.* **2003**, *27*, 895.
[31] Z. J. Zhong, H. Seino, Y. Mizobe, M. Hidai, A. Fujishima, S. Ohkoshi, K. Hashimoto, *J. Am. Chem. Soc.* **2000**, *122*, 2952.
[32] J. Larionova, M. Gross, M. Pilkington, H. Audres, H. Stoeckli-Evans, H. U. Gudel, S. Decurtins, *Angew. Chem. Int. Ed.* **2000**, *39*, 1605.
[33] F. Bonadio, M. Gross, H. Stoeckli-Evans, S. Decurtins, *Inorg. Chem.* **2002**, *41*, 5891.
[34] S. Tanase, M. Andruh, N. Stanica, C. Mathoniere, G. Rombaut, S. Golhen, L. Ouahab, *Polyhedron* **2003**, *22*, 1315.
[35] K. V. Langenberg, S. R. Batten, K. J. Berry, D. C. R. Hockless, B. Moubaraki, K. S. Murray, *Inorg. Chem.* **1997**, *36*, 5006.
[36] C. P. Berlinguette, D. Vaughn, C. Canada-Vilalta, J. R. Gala′n-Mascaro′s, K. R. Dunbar, *Angew. Chem. Int. Ed.* **2003**, *42*, 1523.
[37] C. P. Berlinguette, J. R. Gala′n-Mascaro′s, K. R. Dunbar, *Inorg. Chem.* **2003**, *42*, 3416.
[38] K. E. Vostrikova, D. Luneau, W. Wernsdorfer, P. Rey, M. Verdaguer, *J. Am. Chem. Soc.* **2000**, *122*, 718.
[39] A. Marvilliers, Y. Pei, J. C. Boquera, K. E. Vostrikova, C. Paulsen, E. Rivière, J.-P. Audière, T. Mallah, *Chem. Commun.* **1999**, 1951.
[40] R. Podgajny, C. Desplanches, B. Sieklucka, R. Sessoli, V. Villar, C. Paulsen, W. Wernsdorfer, Y. Dromzee, M. Verdaguer, *Inorg. Chem.* **2002**, *41*, 1323.
[41] H.-Z. Kou, B. C. Zhou, D.-Z. Liao, R.-J. Wang, Y. D. Li, *Inorg. Chem.* **2002**, *41*, 6887.
[42] J. A. Smith, J. R. Galan-Mascaros, R. Clerac, J. S. Sun, O. Y. Xiang, K. R. Dunbar, *Polyhedron* **2001**, *20*, 1727.
[43] N. Mondal, S. Mitra, G. Rosair, *Polyhedron* **2001**, *20*, 2473.
[44] D. G. Fu, J. Chen, X. S. Tan, L. J. Jiang, S. W. Zhang, W. X. Tang, *Inorg. Chem.* **1997**, *36*, 220.
[45] H. Oshio, O. Tamada, H. Onodera, T. Ito, T. Ikoma, S. Tero-Kubota, *Inorg. Chem.* **1999**, *38*, 5686.
[46] H.-Z. Kou, S. Gao, C.-H. Li, D.-Z. Liao, B.-C. Zhou, R.-J. Wang, Y. D. Li, *Inorg. Chem.* **2002**, *41*, 4756.
[47] R. J. Parker, K. D. Lu, S. R. Batten, B. Moubaraki, K. S. Murray, L. Spiccia, J. D. Cashion, A. D. Rae, A. C. Willis, *J. Chem. Soc., Dalton Trans.* **2002**, 3723.
[48] R. Lescouezec, J. Vaissermann, F. Lloret, M. Julve, M. Verdaguer, *Inorg. Chem.* **2002**, *41*, 5943.
[49] V. Marvaud, C. Decroix, A. Scuiller, F. Tuyeras, C. Guyard-Duhayon, J. Vaissermann, J. Marrot, F. Gonnet, M. Verdaguer, *Chem. Eur. J.* **2003**, *9*, 1692.
[50] D. F. Li, S. Gao, L. M. Zheng, K. B. Yu, W. X. Tang, *New J. Chem.* **2002**, *26*, 1190.
[51] D. F. Li, S. Gao, L. M. Zheng, K. B. Yu, W. X. Tang, *J. Chem. Soc., Dalton Trans.* **2002**, 2805.
[52] D. F. Li, S. Gao, L. M. Zheng, W. Y. Sun, T. Okamura, N. Ueyama, W. X. Tang, *New J. Chem.* **2002**, *26*, 485.
[53] Y. Song, S. Ohkoshi, Y. Arimoto, H. Seino, Y. Mizobe, K. Hashimoto, *Inorg. Chem.* **2003**, *42*, 1848.
[54] J. Koo, D.-h. Kim, Y.-S. Kim, Y. Do, *Inorg. Chem.* **2003**, *42*, 2983−2987.
[55] H.-Z. Kou, S. Gao, B.-Q. Ma, D.-Z. Liao, *Chem. Commun.* **2000**, 713.
[56] Y. He, H.-Z. Kou, Y. Li, B. C. Zhou, M. Xiong, Y. D. Li, *Inorg. Chem. Commun.* **2003**, *6*, 38.
[57] W. P. Griffith, J. Lewis, G. Wilkinson, *J. Chem. Soc.* **1959**, 872.
[58] J. H. Enemark, M. S. Quinby, L. L. Reed, M. J. Steuck, K. K. Walthers, *Inorg. Chem.* **1970**, *9*, 2397.
[59] J. E. Huheey, *J. Phys. Chem.* **1965**, *69*, 3284.
[60] F. V. D. Cruser, E. H. Miller, *J. Am. Chem. Soc.* **1906**, *28*, 1132.
[61] M. Ohba, H. Tamaki, N. Matsumoto, H. Okawa, *Inorg. Chem.* **1993**, *32*, 5385.
[62] C. C. Chao, *J. Magn. Reson.* **1973**, *10*, 1.

 © 2004 Wiley-VCH Verlag GmbH & Co. KGaA, Weinheim

[63] R. P. Scaringe, D. Hodgson, W. E. Hatfield, *Mol. Phys.* **1978**, *35*, 701.
[64] M. S. El Fallah, J. Ribas, X. Solans, M. Font-Bardia, *J. Chem. Soc., Dalton Trans.* **2001**, 247.
[65] H. Baadsgaard, W. D. Treadwell, *Helv. Chim. Acta* **1955**, *38*, 1669.
[66] G. M. Sheldrick, *SHELXL97* and *SHELXS97*, University of Göttingen, Germany.

Received July 23, 2003
Early View Article
Published Online November 19, 2003

 © 2004 Wiley-VCH Verlag GmbH & Co. KGaA, Weinheim

(Neocuproin)zinc Thiolates: Attempts at Modeling Cobalamin-Independent Methionine Synthase

Jan Seebacher,[a] Mian Ji,[a] and Heinrich Vahrenkamp*[a]

Keywords: Zinc / Metal complexes / Thiolates / Bioinorganic chemistry

Several new complexes [(neo)Zn(SR)$_2$] [neo = neocuproin (2,9-dimethylphenanthroline)] have been synthesized and structurally characterised. They react in a stepwise fashion with the alkylating agents CH_3I and $(CH_3)_2SO_4$ to afford the thioethers CH_3SR and first the mixed complexes [(neo)Zn(SR)X] (X = I, CH_3SO_4) and then [(neo)ZnX$_2$]. Similar alkylations occur with benzyl iodide, but not with trimethyl phosphate in nonpolar media. Under these conditions, thiolate exchange with [PPN]SR does not occur which indicates that the alkylations take place at the zinc-bound thiolates. In polar solvents (methanol, DMSO), thiolate exchange occurs readily, and at higher temperatures $(CH_3)_3PO_4$ also acts as an alkylating agent which indicates that under these conditions free thiolate is available in solution. Qualitative kinetic data support the associative alkylation mechanism in nonpolar media and the change of mechanism in polar media.

(© Wiley-VCH Verlag GmbH & Co. KGaA, 69451 Weinheim, Germany, 2004)

Introduction

In recent years the well-investigated classes of zinc enzymes, i.e. those for hydrolytic reactions and those of the alcoholdehydrogenase family, have been accompanied by a new class responsible for thiolate alkylations. Their most prominent function is the synthesis of methionine from homocysteine.[1,2] Other thiolate-alkylating enzymes include betain:homocysteine *S*-methyltransferase,[3] protein prenyltransferases[4−6] like farnesyl transferase,[7] methanol:CoM methyltransferase,[8] and the Ada repair protein.[9,10] It is believed that all these enzymes activate the thiol by attaching it to zinc as a thiolate.[5,11] We were able to show that this correlates with the ability of low-coordinate zinc to lower the pK_a of zinc-bound water to 7 or below, thereby generating Zn−OH species under physiological conditions which react with thiols to produce Zn−SR species and water.[12]

In cobalamin-independent methionine synthase[13] and several of the related enzymes,[14] zinc is attached to the protein by one histidine and two cysteinate residues and bears a labile ligand, typically water. Thereby its coordination in the resting state is $ZnNS_2O$, and after substrate attachment it is $ZnNS_3$. Several compounds modeling methionine synthase with zinc complexes have approximated this coordination. Darensbourg[15] alkylated ZnN_2S_2 species, Carrano[16−18] various ZnN_2SX and ZnN_2S_2 species, Parkin[19] a ZnS_4 complex, Riordan prepared $ZnNS_3$ and ZnS_4 complexes[20] and studied the alkylation of an NiN_4S complex,[21] and very recently Darbre[22] found that the ZnN_2S_2 complex [Zn(MEPA)$_2$] previously reported by us[23] can be methylated with trimethyl phosphate. So far the alkylation of a close model complex, i.e. one with $ZnNS_3$ coordination, has not been studied. In the cases where mechanistic investigations were undertaken, they indicated that the thiolates are alkylated in the zinc-bound state and the resultant thioethers are subsequently released. Only in the alkylation of anionic $[Zn(SR)_4]^{2-}$, which was studied as a model for the Ada repair protein, was it observed that the thiolate dissociates from zinc prior to being attacked by the alkylating agent.[24]

Our own contributions to this field have so far consisted of the investigation of (pyrazolylborato)zinc thiolate (Tp* Zn−SR) complexes, i.e. ZnN_3S systems. During the synthetic studies[25−28] it was found that such complexes are easily formed in neutral solutions from TpZn−OH and the corresponding thiol, i.e. their formation does not require a base. Detailed mechanistic studies[29,30] then revealed that the alkylation of their thiolates occurs intramolecularly and that the zinc−sulfur bond is broken after the formation of the thioether. The drawback of the model chemistry using TpZn−SR complexes is that their zinc coordination is different from that in the enzyme ($ZnNS_3$) and that they are not reactive toward the biological alkylating agents *N*-methyltetrahydrofolate or organic phosphates nor analogues thereof in the form of alkylammonium salts or trimethyl phosphate.

With the hope of increasing the reactivity of the zinc thiolates and to approximate the natural binding situation of zinc we therefore set out to investigate zinc thiolates with

[a] Institut für Anorganische und Analytische Chemie der Universität Freiburg
Albertstr. 21, 79104 Freiburg, Germany
Fax: (internat.) + 49-761/203-6001
E-mail: vahrenka@uni-freiburg.de

a more sulfur-rich ligand environment. This paper describes the chemistry of ZnN_2S_2 systems and work on $ZnNS_3$ and ZnS_4 systems is in progress. Ideally one would have taken a pyrazolylborate-derived tripodal N_2S ligand to study $(N_2S)Zn-SR$ complexes for this purpose. Since such a ligand is not available as yet, however, we resorted to an appropriate chelating N_2 ligand and the corresponding $(N_2)Zn(SR)_2$ complexes. Based on previous favourable experience with such complexes[31–34] we opted for neocuproin (neo, 2,9-dimethylphenanthroline). This paper reports the syntheses and structures of some new $[(neo)Zn(SR)_2]$ complexes and reactivity studies related to the stepwise removal of their thiolate ligands as thioethers by means of alkylation with various alkylating agents under a variety of conditions.

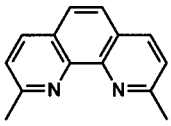

neocuproin (neo)

Results and Discussion

(Neocuproin)zinc Bis(thiolate) Complexes

The neocuproin ligand is favourable for stable and tetrahedral zinc complexes. It has already been observed that this is also true for bis(thiolate) complexes.[31–34] For the simple bis(thiolates), the benzenethiolate,[34] and the phenylethanethiolate[31] have also been structurally characterized and we now contribute the bis(thiolates) **1a**–**h**. Their preparation can be achieved with comparable yields by two alternative methods. The first of these consists of the successive treatment of sodium methoxide with the thiol, hydrated zinc perchlorate and then neocuproin. The other uses zinc bis[bis(trimethylsilyl)]amide as the base and the zinc precursor, which is added to a mixture of the thiol and neocuproin.

R	C_2H_5	$CH_2C_6H_5$	*p*-$CH_3C_6H_4$	*p*-$NO_2C_6H_4$	2,6-$(C_6H_5)_2C_6H_3$
	1a	**1b**	**1c**	**1d**	**1e**

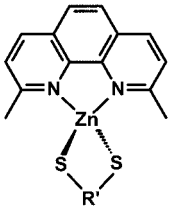

R'	C_2H_4	*o*-$CH_2C_6H_4CH_2$	*o*-$CH_2C_6H_4$
	1f	**1g**	**1h**

In complexes **1a**–**e**, the monodentate thiolates were varied so as to have aliphatic, benzylic, and aromatic substituents, and among the aromatic substituents the electron density and the steric bulk were varied. The same aliphatic/benzylic/aromatic variation was the reason for the choice of the three bidentate thiolate ligands in **1f**–**h**. Specifically in **1h** the thiolate ligand is benzylic at one sulfur atom and aromatic at the other, and it was hoped that this would be reflected in the reactivity of the two thiolate functions.

All complexes **1** are yellow crystalline solids. Their IR spectra are not diagnostic since there are hardly any band shifts for the ligands upon coordination to zinc. Similarly the ^1H NMR spectra are characteristic only for the thiolate ligands (see Exp. Sect.), while the neocuproin resonances [typical values in $CDCl_3$: δ = 3.1 (s, CH_3), 7.5 (d, J = 8.4 Hz, 4-H), 7.9 (s, 5-H), 8.3 (d, J = 8.4 Hz, 3-H) ppm] show only very small shifts upon coordination.

Four of the eight bis(thiolate) complexes were subjected to structural determinations. One typical example of each of the monodentate (**1c**) and bidentate thiolates (**1h**) are presented as Figures 1 and 2. A summary of selected bond

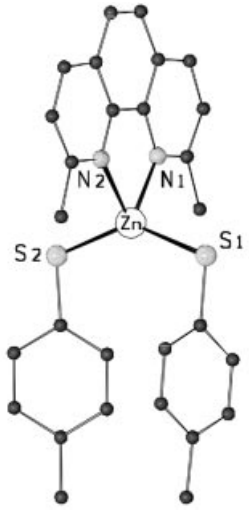

Figure 1. Molecular structure of complex **1c**

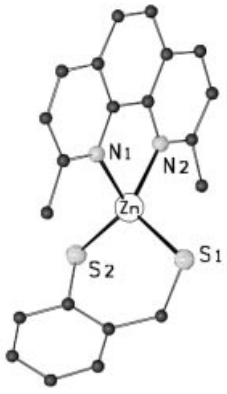

Figure 2. Molecular structure of complex **1h**

 © 2004 Wiley-VCH Verlag GmbH & Co. KGaA, Weinheim

lengths and angles for all four structures is given in Table 1. The table shows {as does the comparison with previously reported [(neo)Zn(SR)] complexes[31,33,34]} that the Zn−N and Zn−S bond lengths are rather constant, irrespective of the electronic nature of the thiolate ligands. Likewise the N−Zn−N angle is fixed to its low value due to the steric constraints of the neocuproin ligand. The only variable quantities are the S−Zn−S and N−Zn−S angles. While the chelating bis(thiolate) in **1h** fixes the S−Zn−S angle near the tetrahedral value, it can extend to almost 140° in the absence of any restraints, as in **1c**. The average size of the N−Zn−N angle which is large for **1h** and small for **1c** is a mere consequence of the size of the S−Zn−S angles.

Table 1. Bond lengths [Å] and angles [°] for complexes **1**

	1c	**1d**	**1g**	**1h**
Zn−S1	2.266(2)	2.287(1)	2.249(1)	2.271(3)
Zn−S2	2.267(2)	2.289(2)	2.260(1)	2.275(3)
Zn−N1	2.121(4)	2.104(2)	2.115(3)	2.081(8)
Zn−N2	2.121(4)	2.103(2)	2.122(3)	2.062(8)
S−Zn−S	137.62(5)	120.76(2)	123.58(5)	108.4(1)
N−Zn−N	78.85(1)	80.34(7)	79.1(1)	81.3(3)
S−Zn−N	103.0−109.7	106.6−118.4	109.6−113.6	114.8−119.2

Alkylation Reactions

As before,[30] the most convenient reagent for alkylation of the zinc-bound thiolates was methyl iodide. With the exception of **1e** all thiolates **1** were treated with 1 mol-equiv. of CH_3I in chloroform. Clean reactions occurred with the bis(thiolates) **1a−c** resulting in the liberation of the thioether CH_3SR and isolation of the iodide thiolate complexes **2a−c**. Complex **1d** reacted too slowly at room temperature, but yielded decomposition products at elevated temperatures which prevented the isolation of pure **2d**. Of the chelating bis(thiolates), **1f** and **1g** underwent clean release of one thiolate function, producing **2f** and **2g** with thioether thiolate ligands. The asymmetric chelating bis(thiolate) **1h** was found by NMR observation to be, as expected, more reactive at the benzylthiolate than at the phenylthiolate function, yet the methylation of the benzylthiolate unit did not go to completion before methylation of the phenylthiolate began. As a result the thioether thiolate complex **2h**, like **2d**, could only be identified by its NMR spectroscopic data.

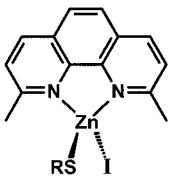

R	C_2H_5	$CH_2C_6H_5$	*p*-$CH_3C_6H_4$	*p*-$NO_2C_6H_4$
	2a	**2b**	**2c**	**2d**

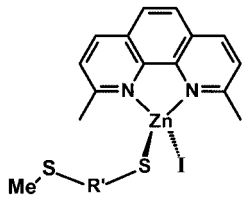

R'	C_2H_4	*o*-$CH_2C_6H_4CH_2$	*o*-$CH_2C_6H_4$
	2f	**2g**	**2h**

Alkylations with benzyl iodide were performed with the chelate complexes **1f** and **1g**. They were slightly faster than the methyl iodide reactions and yielded the thioether thiolate complexes **3f** and **3g**.

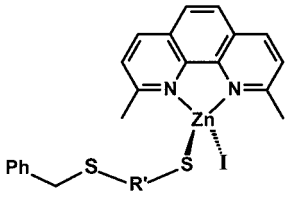

R'	C_2H_4	*o*-$CH_2C_6H_4CH_2$
	3f	**3g**

Crystals of **3g** suitable for an X-ray analysis were obtained. Figure 3 shows the molecular shape which is an indication of the intramolecular nature of the alkylation reactions. The coordination of zinc in **3g** largely resembles that in the bis(thiolate) complexes **1**. Notably the N−Zn−S angles are spread over a range of 14°, and the S−Zn−I angle is close to the tetrahedral value.

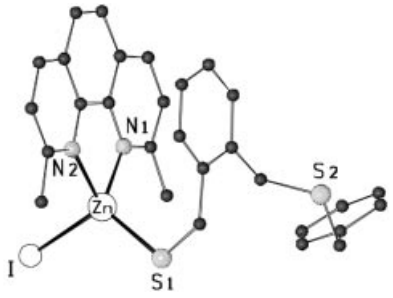

Figure 3. Molecular structure of **3g**; selected bond lengths [Å] and angles [°]: Zn−I 2.580(1), Zn−S 2.244(2), Zn−N1 2.082(5), Zn−N2 2.074(5); S−Zn−I 111.87(6), N1−Zn−N2 80.8(2), N1−Zn−S 118.2(2), N2−Zn−S 122.6(2), N1−Zn−I 110.6(1), N2−Zn−I 109.0(1)

When 2 equiv. of methyl iodide were allowed to react with **1a−c**, **1f**, and **1g**, complete removal of the thiolate ligands occurred and the resultant methyl thioethers could be identified by their ^1H NMR spectra. The remaining zinc complex (neo)ZnI_2 was isolated from the reactions of **1c** and **1f** and characterised and its crystal structure deter-

 © 2004 Wiley-VCH Verlag GmbH & Co. KGaA, Weinheim

mined (see Exp. Sect.). It was observed that the second step of the alkylations is not significantly slower than the first step. This also means that even with 1 equiv. of methyl iodide part of the starting materials **1** are converted into (neo)ZnI_2 and 2 equiv. of the thioether, which in some cases hampered the isolation of the mixed complexes **2**.

We have previously observed[30] that dimethyl sulfate is as good as methyl iodide for the alkylation of zinc-bound thiolates, but that the low stability of the resultant zinc−(methyl sulfate) complexes creates preparative problems. This was not so pronounced in the present study. Complexes **1a**, **b**, **f**, and **g** were chosen for the dimethyl sulfate reactions, representing two cases each of monodentate and chelating bidentate thiolates. Treatment with 1 equiv. of dimethyl sulfate produced the corresponding methyl thioethers, as evidenced by ^1H NMR spectroscopy. The resultant zinc complexes **4**, of which **4f** and **g** still contain the thioether as a ligand, were isolated in good yields. They are methyl sulfate complexes which are stable at room temperature. Yet both their NMR spectra and their elemental analyses showed that they were not pure, and attempts at purifying them by recrystallisation only increased their impurity content.

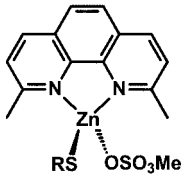

R	Et	Bn
	4a	**4b**

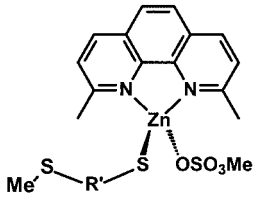

R'	C_2H_4	*o*-$CH_2C_6H_4CH_2$
	4f	**4g**

Treatment of **4a**, **b**, **f**, or **g** with an excess of dimethyl sulfate resulted in complete release of the corresponding methyl thioethers just as in the methyl iodide reactions, but the fate of the remaining zinc species is unclear. No evidence for the formation of [(neo)$Zn(OSO_3CH_3)_2$] was obtained. Only in one case could a small amount of a crystalline product be isolated from the reaction of **1f**. A structural determination, the result of which is shown in Figure 4, identified this product as complex **5**.

5: [$(neo)_2Zn-OSO_3Me$](OSO_3Me)

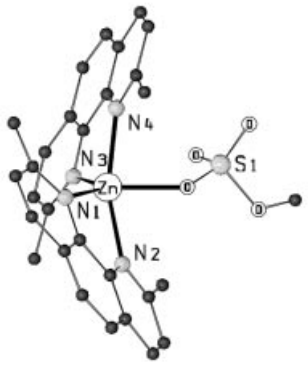

Figure 4. Molecular structure of **5**; selected distances [Å] and angles [°] in the complex cation: Zn−O 2.138(2), Zn−N1 2.093(2), Zn−N2 2.130(2), Zn−N3 2.059(2), Zn−N4 2.135(2), (Zn)O−S 1.465(2), S=O 1.435(2) and 1.437(2), S−O(C) 1.592(2); N2−Zn−N4 161.9(1), O1−Zn−N1 119.5(1), O1−Zn−N3 119.8(1), N1−Zn−N3 120.7(1); in the methyl sulfate anion: S=O 1.394(3), 1.430(5) and 1.420(7), S−O(C) 1.589(10)

The major piece of information from the structure of **5** is the demonstration of the existence of zinc−(alkyl sulfate) binding. The coordination of the zinc ion in **5** is somewhere between square-pyramidal and trigonal-bipyramidal. The suggested square-pyramidal coordination is impossible because the four methyl groups of the neocuproin ligands prevent a symmetric basal arrangement. The alternative trigonal-bipyramidal coordination is impossible because of the small intra-chelate-ligand N−Zn−N angles. The molecular shape of **5** and its bonding parameters closely resemble those in the corresponding nitrate complex.[35] The S=O bond lengths in the ligated and the free methyl sulfate groups do not differ significantly. This holds specifically for the S−O(Zn) bond which is much closer in length to the S=O bonds than to the real single bonds S−O(C). This situation resembles that in the zinc−(organyl phosphate) complexes[36,37] and, just as for the latter, indicates that there is a considerable amount of ionic character in the Zn−O bond.

A more "biological" alkylating agent is trimethyl phosphate, since the Ada repair protein dealkylates alkyl phosphates by transferring the alkyl groups from phosphate to thiolate.[9,10] As before,[30] we also found here that trimethyl phosphate does not alkylate the thiolate ligands of complexes **1** in nonpolar media. It has, however, been reported in the literature[22,24] that in strongly polar solvents and at elevated temperatures the alkylation does take place. This could be reproduced by us using complex **1c**. Heating equimolar amounts of **1c** and $PO(OMe)_3$ in DMSO to 80 °C for 2 weeks produced an almost quantitative formation (by NMR) of $MeSC_6H_4$-*p*-CH_3 and a good isolated yield of the phosphate complex **6**. Likewise with a fivefold amount of $PO(OMe)_3$ nearly quantitative formation of the bis(phosphate) complex **7** took place. The harsh reaction conditions required due to the low alkylating strength of trimethyl phosphate most probably involve a change in the mechanism of the alkylation. As suggested before,[22,24] we con-

 © 2004 Wiley-VCH Verlag GmbH & Co. KGaA, Weinheim

clude (see below) that in these cases free thiolate is liberated and alkylated without the involvement of zinc.

6: [(neo)Zn(S−*p*-Tol)OPO(OMe)$_2$]

7: [(neo)Zn{OPO(OMe)$_2$}$_2$]

The biological alkylating agent in cobalamin-independent methionine synthase is N^5-methyltetrahydrofolic acid, a methylammonium salt. Two synthetic analogues, *N*,*N*,*N*-trimethylanilinium iodide and *N*-methyltetrahydroquinoxalinium iodide, were found to be good mimics,[38] yet they showed no methylating tendency even towards **1b**, the most reactive of the thiolates investigated here even at elevated temperatures.

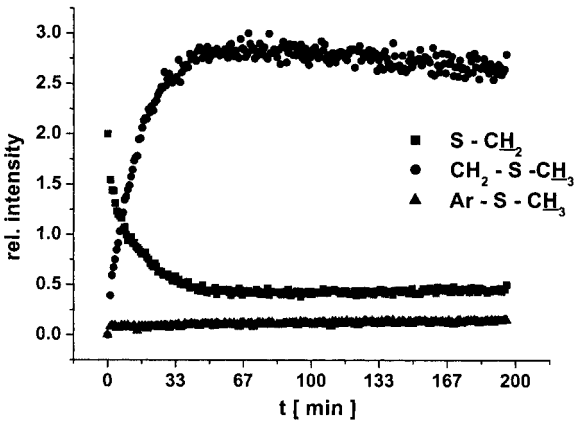

Figure 5. Kinetic traces (by ^{1}H NMR) for the reaction of **1h** (0.005 M) with a four-fold excess of CH_3I in chloroform at 300 K

Mechanistic Considerations

The question of whether the alkylation occurs at the zinc-bound or at the free anionic thiolates was addressed with the same procedures as used in our preceding work.[30] Both thiolate exchange experiments and kinetic investigations led to the conclusion that the [(neo)Zn(SR)$_2$] complexes just like the Tp*Zn−SR complexes undergo intramolecular alkylation, i.e. they do not dissociate in nonpolar media.

The thiolate exchange experiments were monitored by ^{1}H NMR spectroscopy. In no case could a replacement of SR in [(neo)Zn(SR)$_2$] by SR′ from [PPN]SR be observed in chloroform. In methanol, however, fast exchange between [(neo)Zn(SBn)$_2$] (**1b**) and NaSEt took place. Starting with a 1:1 mixture of the reagents, an equilibrium was reached in which [(neo)Zn(SBn)$_2$] and [(neo)Zn(SEt)$_2$] exist in a 10:1 ratio. When treating [(neo)Zn(SBn)$_2$] with the chelating thiolate $Na_2(SCH_2-C_6H_4-CH_2S)$, a quantitative conversion into the chelating dithiolate complex **1g** and NaSBn occurred within minutes. The driving force for this reaction is the precipitation of **1g** from the methanolic solution.

Kinetic data were accumulated for several of the alkylation reactions under pseudo-first-order conditions. Yet in no case could they be fitted cleanly by assuming first-order behaviour. The reasons for this are mainly due to the early onset of the second alkylation step and precipitation of some of the mixed iodide thiolate complexes **2**. A characteristic plot is displayed in Figure 5 which shows in the trace at the bottom the formation of the doubly alkylated bis(thiolate) and in the trace at the top the appearance and subsequent disappearance of the monoalkylated species **2h**.

A qualitative estimate of the second-order rate constant could be obtained for the reaction of **1g** with an excess of methyl iodide. By comparing initial rates at identical concentrations with those of the previously reported Tp*Zn−SR/MeI reaction[30] a value of k'' of the order of 10^{-4} $M^{-1}s^{-1}$ was obtained. This is considerably slower than for [Tp*Zn−SR] complexes, but compares favourably with the k'' value obtained by Carrano[18] for the MeI methylation of an [(N_2O)Zn−SPh] complex. There still exist too few second-order rate constants for such alkylations to allow a meaningful discussion, however.

Finally, another argument in favour of a dissociative alkylation process in polar media (i.e. a nondissociative process in chloroform) was found in the comparison of reaction speeds: in methanol the reaction between **1b** and methyl iodide is roughly one order of magnitude faster than in chloroform. As for the thiolate exchange reactions and for the alkylations with trimethyl phosphate (see above) the simplest explanation for this is the existence of free anionic thiolate in the polar medium.

Conclusions

The present work represents the second step in our investigations on modeling biological thiolate alkylations with tetrahedral zinc complexes. After the ZnN_3S situation in (pyrazolylborato)zinc thiolates the ZnN_2S_2 situation in (neocuproin)zinc thiolates was addressed. Again, the accumulated evidence indicates that the thiolates are alkylated in the zinc-bound state. Furthermore, while the coordination environment of zinc in the enzymes could be approximated, the alkylating agents had to be much stronger than the naturally occuring *N*-methyltetrahydrofolate.

It was found that both thiolate ligands in the [(neo)Zn(SR)$_2$] complexes are alkylated in a stepwise fashion. When, as in complex **1h**, both an aromatic and a benzylic thiolate are offered, the benzylic one as expected reacts first, although not significantly faster than the aromatic one. Compared with the [Tp*Zn−SR] complexes the [(neo)Zn(SR)$_2$] complexes are more reactive due to their more electron-rich ZnN_2S_2 situation.

Unlike the pyrazolylborate ligands the neocuproin ligand cannot encapsulate the zinc ion, thereby approximating its enzymatic environment. This would call for tripodal N_2S ligands, possibly derived from the pyrazolylborates. The synthesis of such ligands is still a challenge. Similar tripodal ligands of the NS_2 and S_3 type exist, however,[39,40] and we are investigating thiolate alkylations of [L·Zn−SR] complexes derived from them.

 © 2004 Wiley-VCH Verlag GmbH & Co. KGaA, Weinheim

Experimental Section

General: For general working and measuring procedures, see ref.[41] Starting materials were obtained commercially, except for $Zn[N(SiMe_3)_2]_2$,[42] *o*-(mercaptomethyl)thiophenol,[43] and *o*-bis-(mercaptomethyl)benzene.[44] The methyl thioethers resulting from the methylations have been described[45−48] and were identified by their ^1H NMR spectra. The PPN salts of the thiols were prepared by cation exchange as described.[49]

Elemental Analyses: All new compounds were characterized by elemental analyses which were satisfactory in most cases. Yet, as mentioned in the text, several of the alkylation reactions yielded product mixtures, from which the expected products could not be isolated in a fully pure form. For these products four elements were analyzed, giving an overall satisfactory picture for **1b**, **1e**, **1g**, **4a**, **4b**, and **4g**. Only for **2f**, **3f**, and **4f** was the purity obviously insufficient.

Complex 1a: A solution of $Zn[N(SiMe_3)_2]_2$ (1.71 g, 4.42 mmol) in toluene (50 mL) was added slowly with stirring to a solution of neo·H_2O (1.00 g, 4.42 mmol) and ethanethiol (0.66 mL, 550 mg, 8.8 mmol) in toluene (100 mL) over a period of 2 h. A light yellow precipitate resulted which was filtered and washed two times each with toluene (3 mL) and diethyl ether (3 mL). **1a** (1.50 g, 86%) remained as a light yellow powder, m.p. 250 °C (dec.). $C_{18}H_{22}N_2S_2Zn$ (395.91): calcd. C 54.61, H 5.60, N 7.08, Zn 16.52; found C 53.02, H 5.64, N 6.75, Zn 15.89. ^1H NMR ($CDCl_3$): δ = 1.16 [t, *J* = 7.4 Hz, 6 H, CH_3(Et)], 2.46 [q, *J* = 7.4 Hz, 4 H, CH_2(Et)] ppm.

Complex 1b: Similar procedure to that for **1a** from $Zn[N(SiMe_3)_2]_2$ (1.71 g, 4.42 mmol), neo·H_2O (1.00 g, 4.42 mmol), and benzylmercaptan (1.10 g, 8.84 mmol). Yield 2.10 g (91%) of **1b** as light yellow powder, m.p. 148 °C. $C_{28}H_{26}N_2S_2Zn$ (520.05): calcd. C 64.67, H 5.04, N 5.39, Zn 12.57; found C 65.98, H 5.27, N 4.87, Zn 11.49. ^1H NMR ($CDCl_3$): δ = 3.54 [s, 4 H, CH_2(Bn)], 6.65−6.71 (m, 6 H, Bn), 6.86−6.91 (m, 4 H, Bn) ppm.

Complex 1c: A solution of $Zn(ClO_4)_2·6H_2O$ (0.372 g, 1.00 mmol) in methanol (80 mL) was added very slowly with stirring to a solution of *p*-thiocresol (0.248 g, 2.00 mmol) and NaOMe (0.108 g, 2.00 mmol) in methanol (100 mL) over a period of 3 h; neo·H_2O (0.208 g, 1.00 mmol) in methanol (15 mL) was then added and the mixture stirred overnight. The volume was reduced to 30 mL in vacuo, the precipitate filtered, dried in vacuo, and recrystallized from hot methanol; **1c** (0.41 g, 79%) resulted as yellow crystals, m.p. 207 °C. $C_{28}H_{26}N_2S_2Zn$ (520.05): calcd. C 64.67, H 5.04, N 5.39, S 12.33; found C 64.54, H 5.53, N 5.59, S 12.25. ^1H NMR ([D_6]DMSO): δ = 1.89 [s, 6 H, CH_3(Tol)], 6.28 (d, *J* = 8.0 Hz, 4 H, Tol), 6.64 (d, *J* = 8.0 Hz, 4 H, Tol) ppm.

Complex 1d: Similar to **1a** from $Zn[N(SiMe_3)_2]_2$ (1.46 g, 3.77 mmol), neo·H_2O (0.785 g, 3.77 mmol), and *p*-nitrothiophenol (1.17 g, 7.54 mmol). Recrystallization from toluene yielded **1d** as dark yellow crystals (1.05 g, 48%), m.p. 213 °C. $C_{26}H_{20}N_4O_4S_2Zn$ (581.99): calcd. C 53.66, H 3.46, N 9.63, S 11.02; found C 53.45, H 3.53, N 9.78, S 10.76. ^1H NMR ($CDCl_3$): δ = 7.20 (d, *J* = 8.0 Hz, 4 H, Ar), 7.54 (d, *J* = 8.0 Hz, 4 H, Ar) ppm.

Complex 1e: Like **1c** from $Zn(ClO_4)_2·6H_2O$ (0.093 g, 0.25 mmol), 2,6-diphenylthiophenol (0.131 g, 0.50 mmol), NaOMe (0.027 g, 0.50 mmol), and neo·H_2O (0.052 g, 0.25 mmol). Yield 0.114 g (57%) of **1e** as yellow crystals, m.p. 260 °C (dec.). $C_{50}H_{38}N_2S_2Zn$ (796.39): calcd. C 75.41, H 4.81, N 3.52, S 8.05; found C 74.35, H 4.95, N 3.45, S 7.97. ^1H NMR ($CDCl_3$): δ = 6.74−6.92 (m, 18 H, Ar), 7.11−7.16 (m, 8 H, Ar) ppm.

Complex 1f: Like **1a** from $Zn[N(SiMe_3)_2]_2$ (1.71 g, 4.42 mmol), neo·H_2O (1.00 g, 4.42 mmol) and ethanedithiol (0.41 g, 4.4 mmol). Yield 1.12 g (69%) of **1f** as a yellow solid, m.p. 270 °C (dec.). $C_{16}H_{16}N_2S_2Zn$ (365.84): calcd. C 52.53, H 4.41, N 7.66, S 17.87; found C 52.59, H 4.44, N 7.59, S 17.10. ^1H NMR ($CDCl_3$): δ = 3.03 (s, 4 H, CH_2) ppm.

Complex 1g: Like **1c** from $Zn(ClO_4)_2·6H_2O$ (0.447 g, 1.20 mmol), *o*-bis(mercaptomethyl)benzene (0.204 g, 1.20 mmol), NaOMe (2.45 mmol of a 0.25 M solution), and neo·H_2O (0.272 g, 1.20 mmol). Yield 0.240 g of **1g** as a light yellow powder and, after reducing the volume of the filtrate and cooling, 0.030 g of **1g** as yellow crystals. Total yield 0.270 g (51%) of **1g**, m.p. 270 °C (dec.). $C_{22}H_{20}N_2S_2Zn$ (441.94): calcd. C 59.79, H 4.56, N 6.34, Zn 14.80; found C 58.14, H 4.45, N 6.01, Zn 13.70. ^1H NMR ($CDCl_3$): δ = 4.03 (s, 4 H, CH_2), 7.12−7.18 (m, 2 H, Ph), 7.35−7.39 (m, 2 H, Ph) ppm.

Complex 1h: Like **1c** from $Zn(ClO_4)_2·6H_2O$ (2.62 g, 7.04 mmol), *o*-(mercaptomethyl)thiophenol (1.10 g, 7.04 mmol), NaOMe (0.807 g, 14.9 mmol), and neo·H_2O (1.59 g, 7.04 mmol). Yield 1.56 g of **1h** as a yellow powder and, after reducing the volume of the filtrate and cooling, 0.16 g of **1h** as yellow crystals. Total yield 1.72 g (58%) of **1h**, m.p. 265 °C (dec.). $C_{21}H_{18}N_2S_2Zn$ (427.91): calcd. C 58.95, H 4.24, N 6.55, S 14.99; found C 58.49, H 3.78, N 6.02, S 14.34. ^1H NMR (CD_3OD): δ = 3.97 (s, 2 H, CH_2), 6.95−7.07 (m, 2 H, Ar), 7.27−7.32 (m, 1 H, Ar), 7.46−7.55 (m, 1 H, Ar) ppm.

Alkylations with Methyl Iodide

2a: Complex **1a** (500 mg, 1.26 mmol) and MeI (79 μL, 180 mg, 1.26 mmol) in chloroform (40 mL) were stirred for 2 d. Reduction of the volume in vacuo to 20 mL and layering with diethyl ether (10 mL) yielded **2a** (17 mg, 3%) as a colourless powder, m.p. 300 °C (dec.). $C_{16}H_{17}IN_2SZn$ (461.68): calcd. C 41.63, H 3.71, N 6.07, Zn 14.16; found C 41.00, H 3.58, N 5.86, Zn 14.63. ^1H NMR ($CDCl_3$): δ = 1.33 [t, *J* = 7.3 Hz, 3 H, CH_3(Et)], 2.73 [q, *J* = 7.3 Hz, 2 H, CH_2(Et)] ppm.

2b: Complex **1b** (100 mg, 0.19 mmol) and MeI (12 μL, 27.3 mg, 0.19 mmol) in chloroform (25 mL) were stirred for 2 d. The volume was reduced to 1 mL in vacuo. The precipitate was filtered and washed three times with cold chloroform (1 mL) leaving behind **2b** (90 mg, 89%) as a colourless solid, m.p. 270 °C (dec.) which was not analytically pure. $C_{21}H_{19}IN_2SZn$ (523.75): EI MS: *m/z* (%) = 399.2 (100) [$M^+ - C_6H_5CH_2S$], 314.2 (30) [$C_6H_5CH_2SZnI$]. ^1H NMR ($CDCl_3$): δ = 3.54 (s, 2 H, CH_2), 7.02−7.12 (m, 5 H, Ph) ppm.

2c: Like **1b** with **1c** (133 mg, 0.26 mmol) and MeI (36 mg, 0.26 mmol) for one week. Yield 56 mg (40%) of **2c** as a light yellow solid, m.p. 200 °C. $C_{21}H_{19}IN_2SZn$ (523.75): calcd. C 48.16, H 3.66, N 5.35, S 6.12; found C 48.00, H 3.99, N 5.42, S. 5.75. ^1H NMR ([D_6]DMSO): δ = 1.89 [s, 3 H, Me(Tol)], 6.29 (d, *J* = 7.8 Hz, 2 H, Tol), 6.64 (d, *J* = 7.8 Hz, 2 H, Tol) ppm.

2f: Like **1a** with **1f** (250 mg, 0.68 mmol) and MeI (97 mg, 0.68 mmol). Yield 167 mg (48%) of **2f** as light yellow crystals, m.p. 210 °C (dec.). $C_{17}H_{19}IN_2S_2Zn$ (507.78): calcd. C 40.21, H 3.77, N 5.52, Zn 12.88; found C 36.29, H 3.08, N 5.10, Zn 12.40. ^1H NMR ($CDCl_3$): δ = 2.16 (s, 3 H, SCH_3), 2.77−2.89 (m, 2 H, CH_2), 2.91−3.02 (m, 2 H, CH_2) ppm.

2g: Complex **1g** (500 mg, 1.13 mmol) and MeI (161 mg, 1.13 mmol) in chloroform (40 mL) were stirred for 1 d. The resultant precipitate was filtered, washed with diethyl ether, and dried in vacuo, leaving behind **2g** (302 mg, 47%) as a colourless powder, m.p. 220

 © 2004 Wiley-VCH Verlag GmbH & Co. KGaA, Weinheim

°C (dec.). $C_{23}H_{23}IN_2S_2Zn$ (583.87): calcd. C 47.31, H 3.97, N 4.80, Zn 11.20; found C 47.16, H 3.89, N 4.67, Zn 12.50. ^{1}H NMR ($CDCl_3$): δ = 2.02 (s, 3 H, SMe), 3.90 [s, 2 H, CH_2(Ar)], 3.96 [s, 2 H, CH_2(Ar)], 6.57−6.70 (m, 1 H, Ar), 6.72−6.84 (m, 1 H, Ar), 6.87−6.95 (m, 1 H, Ar), 6.97−7.05 (m, 1 H, Ar) ppm.

Alkylations with Benzyl Iodide

3f: Complex **1f** (250 mg, 0.68 mmol) and benzyl iodide (149 mg, 0.68 mmol) in chloroform (50 mL) were stirred for 1 d. Layering with hexane yielded **3f** (323 mg, 81%) as a colourless powder, m.p. 330 °C (dec.) which was filtered and dried in vacuo. $C_{23}H_{23}IN_2S_2Zn$ (583.87): calcd. C 47.31, H 3.97, N 4.80, S 10.98; found C 48.61, H 4.33, N 4.52, S 10.14. ^{1}H NMR ($CDCl_3$): δ = 2.79−2.85 (m, 2 H, CH_2), 2.91−2.99 (m, 2 H, CH_2), 3.79 [s, 2 H, CH_2(Bn)], 7.23−7.40 (m, 5 H, Ph) ppm.

3g: Like **1f** with **1g** (567 mg, 1.28 mmol) and benzyl iodide (279 mg, 1.28 mmol). Yield 228 mg (27%) of **3g** as colourless crystals, m.p. 220 °C (dec.). $C_{29}H_{27}IN_2S_2Zn{\cdot}0.5CHCl_3$ (659.97 + 119.38): calcd. C 49.23, H 3.85, N 3.98; found C 49.68, H 3.79, N 4.18. ^{1}H NMR ($CDCl_3$): δ = 3.64 [s, 2 H, CH_2(Ph)], 3.81 [s, 2 H, CH_2(Ph)], 3.91 [s, 2 H, CH_2(Ph)], 6.54−6.62 (m, 1 H, Ar), 6.68−6.75 (m, 1 H, Ar), 6.84 (d, *J* = 7.6 Hz, 1 H, Ar), 7.00 (d, *J* = 7.6 Hz, 1 H, Ar), 7.05−7.30 (m, 5 H, Ar) ppm.

Twofold Methylations

With 1c: Complex **1c** (103 mg, 0.20 mmol) and CH_3I (450 mg, 3.2 mmol) in chloroform (25 mL) were stirred for 2 d. All volatiles were then removed in vacuo and the residue washed with diethyl ether (2 mL) and dichloromethane (2 mL), leaving behind (neo)ZnI_2 (48 mg, 46%) as a colourless powder, m.p. 320 °C (dec.). Crystals for the structure determination were obtained by recrystallization from chloroform. $C_{14}H_{12}I_2N_2Zn$ (527.46): calcd. C 31.88, H 2.29, N 5.31; found C 31.67, H 2.41, N 5.04. ^{1}H NMR ($CDCl_3$): δ = 3.25 (s, 6 H, CH_3), 7.78 (d, *J* = 8.4 Hz, 2 H, H_B), 7.95 (s, 2 H, H_C), 8.47 (d, *J* = 8.4 Hz, 2 H, H_A).

With 1f: Complex **1f** (50 mg, 0.14 mmol) and CH_3I (2.27 g, 16.0 mmol) in chloroform (25 mL) were stirred for 1 week. Workup as above yielded (neo)ZnI_2 (12 mg, 17%).

Methylations with Dimethyl Sulfate

4a: Complex **1a** (281 mg, 0.71 mmol) and $(MeO)_2SO_2$ (67 μL, 89 mg, 0.71 mmol) in chloroform (40 mL) were stirred for 2 d. Reduction of the volume to 20 mL in vacuo and layering with diethyl ether yielded a precipitate which was filtered and washed twice with diethyl ether (5 mL), leaving behind **4a** (285 mg, 90%) as a colourless powder, m.p. 300 °C (dec.). $C_{17}H_{20}N_2O_4S_2Zn$ (445.88): calcd. C 45.79, H 4.52, N 6.28, Zn 14.67; found C 43.48, H 4.15, N 6.07, Zn 14.26. ^{1}H NMR ($CDCl_3$): δ = 1.34 [t, *J* = 7.3 Hz, 3 H, CH_3(Et)], 2.58 [q, *J* = 7.3 Hz, 2 H, CH_2(Et)], 3.68 (s, 3 H, OMe) ppm.

4b: Like **1a** with **1b** (150 mg, 0.29 mmol) and $(MeO)_2SO_2$ (27 μL, 36 mg, 0.29 mmol), yielded **4b** (146 mg, 99%) as a colourless powder, m.p. 150 °C. $C_{22}H_{22}N_2O_4S_2Zn$ (507.95): calcd. C 52.02, H 4.37, N 5.52, Zn 12.87; found C 48.70, H 4.42, N 5.25, Zn 11.57. ^{1}H NMR ($CDCl_3$): δ = 3.66 (s, 3 H, OMe), 3.72 (s, 2 H, CH_2), 6.36−6.51 (m, 3 H, Ph), 6.76−6.85 (m, 2 H, Ph) ppm.

4f: Complex **1f** (160 mg, 0.44 mmol) and $(MeO)_2SO_2$ (45 μL, 60 mg, 0.48 mmol) in chloroform (20 mL) were stirred for 2 d. Layering with hexane (30 mL) yielded, within one week, a mixture of a colourless powder and colourless crystals, which was filtered, washed with diethyl ether, and dried in vacuo. Manual removal of the crystals left behind **4f** (25 mg, 12%), m.p. 270 °C (dec.). $C_{18}H_{22}N_2O_4S_3Zn$ (491.97): calcd. C 43.95, H 4.51, N 5.69, Zn 13.29; found C 42.15, H 3.84, N 6.22, Zn 13.62. ^{1}H NMR ($CDCl_3$, ppm): δ = 2.06 (s, 3 H, SMe), 2.72−2.85 (m, 2 H, CH_2), 2.91−3.01 (m, 2 H, CH_2), 3.69 (s, 3 H, OMe) ppm. The crystals amounted to 5 mg (2%) of **5**, m.p. 254 °C, which was identified by the structural determination.

4g: Like **1f** with **1g** (500 mg, 1.13 mmol) and $(MeO)_2SO_2$ (107 μL, 143 mg, 1.13 mmol), yield **4g** (520 mg, 81%) as a colourless powder, m.p. 160 °C. $C_{24}H_{26}N_2O_4S_3Zn$ (568.07): calcd. C 50.74, H 4.61, N 4.93, Zn 11.50; found C 48.82, H 4.34, N 4.96, Zn 11.47. ^{1}H NMR ($CDCl_3$): δ = 1.89 (s, 3 H, SMe), 3.70 (s, 3 H, OMe), 3.76 (s, 2 H, CH_2), 3.83 (s, 2 H, CH_2), 6.02−6.17 (m, 1 H, C_6H_4), 6.30−6.45 (m, 1 H, C_6H_4), 6.47−6.63 (m, 2 H, C_6H_4).

Methylations of 1c with Trimethyl Phosphate

With 1 Equiv.: Complex **1c** (200 mg, 0.38 mmol) and $PO(OMe)_3$ (54 mg, 0.38 mmol) in DMSO (10 mL) were stirred at 80 °C for 2 weeks. All volatiles were then removed in vacuo at 80 °C. The residue was washed with diethyl ether and dried in vacuo, leaving behind **6** (135 mg, 67%) as a light yellow powder, m.p. 148 °C. $C_{23}H_{25}N_2O_4PSZn$ (521.89): calcd. C 52.93, H 4.83, N 5.37, S 6.14; found C 53.56, H 4.92, N 6.32, S 7.08. ^{1}H NMR ([D$_6$]DMSO): δ = 1.91 [s, 3 H, CH_3(Tol)], 3.30 (d, *J* = 5.2 Hz, 6 H, OMe), 6.34 (d, *J* = 7.0 Hz, 2 H, Tol), 6.70 (d, *J* = 7.2 Hz, 2 H, Tol) ppm.

With 2 Equiv.: As above with **1c** (100 mg, 0.19 mmol) and $PO(OMe)_3$ (133 mg, 0.95 mmol), yielded **7** (85 mg, 85%) as a light yellow powder, m.p. 142 °C. $C_{18}H_{24}N_2O_8P_2Zn{\cdot}H_2O$ (523.73 + 18.02): calcd. C 39.91, H 4.84, N 5.17; found C 39.89, H 5.02, N 4.69. ^{1}H NMR ($CDCl_3$): δ = 1.50 (s, 2 H, H_2O), 3.59 (d, *J* = 10.9 Hz, 12 H, OMe) ppm.

NMR Experiments: For all alkylation reactions described above, from which zinc complexes were isolated, the resultant alkyl thioethers which are known compounds[45−48] were identified by ^{1}H NMR spectroscopy, specifically by their characteristic *S*-methyl resonances. The NMR spectroscopic data showed that none of the reactions were clean, i.e. decomposition reactions and subsequent alkylations set in before the first alkylation step was complete. In those cases where the resultant zinc complexes could not be isolated, i.e. in the CH_3I methylations of **1d** and **1h** and the double methylations with CH_3I and $(CH_3O)_2SO_2$, the information on the reaction course rests on the NMR spectroscopic data alone. Likewise the qualitative determinations of reaction rates were done by ^{1}H NMR spectroscopy. This concerns the rates for methylations versus benzylations, for single versus double methylations and for methylations in chloroform versus methanol.

Thiolate Exchange: 1. A mixture of **1b** (9.9 mg, 19.0 μmol) and NaSEt (1.6 mg, 19.0 μmol) in CD_3OD (0.5 mL) reached equilibrium within 1 h. The intensity ratio of the benzyl CH_2 singlets for **1b** vs. NaSBn was 10:1. 2. **1b** (12.3 mg, 23.8 μmol) and $Na_2[SCH_2-C_6H_4-CH_2S]$ (5.1 mg, 23.8 μmol) in CD_3OD (0.25 mL) immediately produced a light yellow precipitate of **1g**. ^{1}H NMR of the solution showed that no more **1b** remaind and the major organic component was NaSBn.

Kinetic Measurements: The measurements were performed on 0.005−0.02 M $CDCl_3$ solutions of the zinc complex. Kinetic traces were recorded at 10-min intervals for reaction mixtures containing 4−10 mol-equiv. of CH_3I. The intensities of isolated ^{1}H NMR resonances were recorded. In all cases it was observed that the second alkylation sets in before the first half-life of the first alkylation is

 © 2004 Wiley-VCH Verlag GmbH & Co. KGaA, Weinheim

Table 2. Crystallographic details

	1c	**1d**	**1g**	**1h**	**3g**	(neo)ZnI_2	**5**
Empirical formula	$C_{28}H_{26}N_2S_2Zn$	$C_{26}H_{20}N_4O_4S_2Zn$	$C_{22}H_{20}N_2S_2Zn{\cdot}CH_2Cl_2$	$C_{21}H_{18}N_2S_2Zn$	$C_{29}H_{27}IN_2S_2Zn$	$C_{14}H_{12}I_2N_2Zn$	$C_{30}H_{30}N_4O_8S_2Zn$
Formula mass	520.00	581.95	526.82	427.86	659.97	703.23	704.10
Crystal size [mm]	0.3 × 0.2 × 0.1	0.3 × 0.3 × 0.2	0.3 × 0.2 × 0.2	0.3 × 0.2 × 0.2	0.4 × 0.2 × 0.2	0.4 × 0.2 × 0.2	0.5 × 0.5 × 0.4
Space group	*Pbca*	$P2_1/c$	$P2_1/c$	$P2_1/n$	$P2_1/c$	$P2_1/n$	$P2_1/c$
Z	8	4	4	4	4	4	4
a [Å]	15.929(1)	12.369(5)	12.794(3)	9.722(4)	8.011(2)	8.287(1)	17.739(4)
b [Å]	11.056(1)	18.502(7)	14.928(3)	16.288(6)	37.246(7)	14.221(2)	13.653(3)
c [Å]	28.218(1)	12.005(5)	13.356(3)	11.688(5)	10.485(4)	13.765(2)	12.885(3)
α [°]	90	90	90	90	90	90	90
β [°]	90	116.651(6)	115.38(3)	92.116(7)	117.09(2)	103.376(3)	105.85(3)
γ [°]	90	90	90	90	90	90	90
V [Å^3]	4969.5(5)	2455.4(16)	2304.6(8)	1849.6(13)	2785.2(13)	1578.2(3)	3002(1)
$d_{calcd.}$ [g cm^{-3}]	1.39	1.57	1.52	1.54	1.57	2.22	1.56
μ(Mo-$K_α$) [mm^{-1}]	1.18	1.21	1.49	1.56	2.16	5.46	1.02
hkl range	*h*: −21 to 21	*h*: −16 to 11	*h*: −14 to 15	*h*: −12 to 11	h:-9 to 0	*h*: −9 to 9	*h*: −20 to 19
	k: −14 to 14	*k*: −23 to 24	*k*: 0 to 18	*k*: −19 to 9	*k*: 0 to 45	*k*: −15 to 15	*k*: −16 to 15
	l: −37 to 37	*l*: −15 to 16	*l*: −16 to 0	*l*: −11 to 15	*l*: −11 to 12	*l*: −15 to 15	*l*: 0 to 14
Reflections measured	43154	15529	4725	5544	5842	10802	10671
Independent reflections	6163	5941	4521	3991	5450	2269	5507
Obsd. reflections [$I > 2σ(I)$]	3094	4627	3339	1357	3603	1735	4495
Parameters	298	334	271	235	316	172	438
Reflections refined	6163	5941	4521	3991	5450	2269	5507
*R*1 (obsd. reflections)	0.056	0.031	0.049	0.076	0.051	0.023	0.036
*wR*2 (all reflections)	0.156	0.091	0.161	0.272	0.161	0.051	0.125
Residual density [e/Å^{-3}]	+0.6/−0.6	+0.5/−0.4	+0.6/−0.8	+0.8/−1.1	+0.8/−1.0	+0.5/−0.5	+1.6/−0.5

reached. This virtually prevented the determination of rate constants. Detailed investigations were made for the CH_3I methylation of **1g** and **1h**. Taking the data for the first hour of the methylation of **1g** (ca. 40% conversion), pseudo-first-order rate constants could be obtained which were roughly 100 times smaller than those for the methylation of $Tp^{Ph,Me}Zn-SBn$ under similar conditions.[30] The methylation of **1h**, for which the kinetic traces are displayed in Figure 5, is about one order of magnitude faster.

Structural Determiantions:[50] Crystals were obtained as described in the Exp. Sect. Diffraction data were recorded at room temp. [**1g**, **1h**, **3g**, (neo)ZnI_2, **5**] and at −90 °C (**1c**, **1d**) with a Nonius CAD4 (**5**) or a Bruker Smart CCD diffractometer [**1c**, **1d**, **1g**, **1h**, **3g**, (neo)ZnI_2]. Empirical absorption corrections were applied for **1c**, **1d**, **1g**, **1h**, **3g**, and (neo)ZnI_2. The structures were solved with direct methods and refined anisotropically using the SHELX[51] program suite. Hydrogen atoms were included at fixed distances and isotropic temperature factors 1.2 times those of the atoms to which they are attached. Parameters were refined against F^2. Drawings were produced with SCHAKAL.[52] Table 2 lists the crystallographic data.

Acknowledgments

This work was supported by the Deutsche Forschungsgemeinschaft and the Fonds der Chemischen Industrie. We thank Drs. W. Deck and H. Brombacher for help with the crystal-structure determinations.

[1] R. G. Mathews, J. T. Drummond, *Chem. Rev.* **1990**, *90*, 1275−1290.
[2] J. Eichel, J. C. Gonzales, M. Hotze, R. G. Mathews, J. Schröder, *Eur. J. Biochem.* **1995**, *230*, 1053−1058.
[3] A. P. Breksa, T. A. Garrow, *Biochemistry* **1999**, *38*, 13991−13998.
[4] M. H. Gelb, *Science* **1997**, *275*, 1750−1751.
[5] K. E. Hightower, C. A. Fierke, *Curr. Opin. Chem. Biol.* **1999**, *3*, 176−181.
[6] H. Zhang, M. C. Seabra, J. Deisenhofer, *Structure* **2000**, *8*, 241−251.
[7] H. W. Park, S. R. Boduluri, J. F. Moomaw, P. J. Casey, L. Beese, *Science* **1997**, *275*, 1800−1801.
[8] K. Sauer, R. Thauer, *Eur. J. Biochem.* **1997**, *249*, 280−285.
[9] L. C. Myers, M. P. Terranova, A. E. Ferentz, G. Wagner, G. L. Verdine, *Science* **1993**, *261*, 1164−1167.
[10] L. J. Sun, C. K. Yim, G. L. Verdine, *Biochemistry* **2001**, *40*, 11596−11603.
[11] R. G. Matthews, C. W. Goulding, *Curr. Opin. Chem. Biol.* **1997**, *1*, 332−339.
[12] H. Vahrenkamp, *Acc. Chem. Res.* **1999**, *32*, 589−596.
[13] K. Peariso, Z. S. Zhou, A. E. Smith, R. G. Matthews, J. E. Penner-Hahn, *Biochemistry* **2001**, *40*, 987−993.
[14] S. A. Ensign, *Biochemistry* **2001**, *40*, 5845−5853.
[15] C. A. Grapperhaus, T. Tuntulani, J. H. Reibenspies, M. Y. Darensbourg, *Inorg. Chem.* **1998**, *37*, 4052−4058.
[16] B. S. Hammes, C. J. Carrano, *Inorg. Chem.* **1999**, *38*, 4593−4600.
[17] B. S. Hammes, C. J. Carrano, *Inorg. Chem.* **2001**, *40*, 919−927.
[18] B. S. Hammes, C. R. Warthen, D. C. Crans, C. J. Carrano, *J. Biol. Inorg. Chem.* **2001**, *6*, 82−90.
[19] B. M. Bridgewater, T. Fillebeen, R. A. Friesner, G. Parkin, *J. Chem. Soc., Dalton Trans.* **2000**, 4494−4496.
[20] S. J. Chiou, J. Innocent, C. G. Riordan, K. C. Lam, L. Liable-Sands, A. L. Rheingold, *Inorg. Chem.* **2000**, *39*, 4347−4353.
[21] M. S. Ram, C. G. Riordan, R. Ostrander, A. L. Rheingold, *Inorg. Chem.* **1995**, *34*, 5884−5892.
[22] M. Machuqueiro, T. Darbre, *J. Inorg. Biochem.* **2003**, *94*, 193−196.
[23] U. Brand, H. Vahrenkamp, *Inorg. Chem.* **1995**, *34*, 3285−3293.
[24] J. J. Wilker, S. Lippard, *Inorg. Chem.* **1997**, *36*, 969−978.
[25] R. Alsfasser, A. K. Powell, S. Trofimenko, H. Vahrenkamp, *Chem. Ber.* **1993**, *126*, 685−694.

 © 2004 Wiley-VCH Verlag GmbH & Co. KGaA, Weinheim

[26] M. Ruf, R. Burth, K. Weis, H. Vahrenkamp, *Chem. Ber.* **1996**, *129*, 1251−1257.
[27] R. Burth, H. Vahrenkamp, *Z. Anorg. Allg. Chem.* **1998**, *624*, 381−385.
[28] M. Rombach, H. Vahrenkamp, *Inorg. Chem.* **2001**, *40*, 6144−6150.
[29] U. Brand, M. Rombach, H. Vahrenkamp, *Chem. Commun.* **1998**, 2717−2718.
[30] U. Brand, M. Rombach, J. Seebacher, H. Vahrenkamp, *Inorg. Chem.* **2001**, *40*, 6151−6157.
[31] R. Burth, H. Vahrenkamp, *Inorg. Chim. Acta* **1998**, *228*, 193−199.
[32] A. Meißner, W. Haehnel, H. Vahrenkamp, *Chem. Eur. J.* **1997**, *3*, 261−267.
[33] M. Tesmer, H. Vahrenkamp, *Eur. J. Inorg. Chem.* **2001**, 1183−1188.
[34] K. J. Jordan, W. F. Wacholtz, G. A. Crosby, *Inorg. Chem.* **1991**, *30*, 4588−4593.
[35] A. J. Pallenberg, T. M. Marschner, D. M. Barnhart, *Polyhedron* **1997**, *16*, 2711−2719.
[36] K. Weis, M. Rombach, M. Ruf, H. Vahrenkamp, *Eur. J. Inorg. Chem.* **1998**, 263−270.
[37] K. Weis, H. Vahrenkamp, *Eur. J. Inorg. Chem.* **1998**, 271−274.
[38] G. P. Tuszynski, M. Frederick, R. G. Kallen, *J. Am. Chem. Soc.* **1975**, *97*, 7359−7370.
[39] M. Tesmer, M. Shu, H. Vahrenkamp, *Inorg. Chem.* **2001**, *40*, 4022−4029.
[40] M. Shu, R. Walz, B. Wu, J. Seebacher, H. Vahrenkamp, *Eur. J. Inorg. Chem.* **2003**, 2502−2511.
[41] M. Förster, R. Burth, A. K. Powell, T. Eiche, H. Vahrenkamp, *Chem. Ber.* **1993**, *126*, 2643−2648.
[42] H. Bürger, W. Sawodny, U. Wannagat, *J. Organomet. Chem.* **1965**, *3*, 113−120.
[43] A. Lüttringhaus, K. Hägele, *Angew. Chem.* **1955**, *67*, 304−305.
[44] J. J. Mayerle, S. E. Denmark, P. V. dePamphilis, J. A. Ibers, R. H. Holm, *J. Am. Chem. Soc.* **1975**, *97*, 1032−1045.
[45] P. Bonviccini, A. Levi, V. Lucchini, G. Scorrano, *J. Chem. Soc., Perkin Trans. 2* **1972**, 2267−2269.
[46] D. Villemin, M. Hachemi, *Synth. Commun.* **1996**, *26*, 2449−2460.
[47] R. C. Chambers, C. L. Hill, *J. Am. Chem. Soc.* **1990**, *112*, 8427−8433.
[48] T. Okajima, Z. H. Wang, Y. Fukazawa, *Chem. Lett.* **1991**, *1*, 37−40.
[49] W. F. Law, C. Kim, M. Y. Darensbourg, A. L. Rheingold, *J. Am. Chem. Soc.* **1989**, *111*, 3591−3597.
[50] CCDC-215926 (**1c**), -215927 (**1d**), -215928 (**1g**), -215929 (**1h**), -215930 (**3g**), -215932 [(neo)ZnI_2], and -215931 (**5**) contain the supplementary crystallographic data for this paper. These data can be obtained free of charge at www.ccdc.cam.ac.uk/conts/retrieving.html [or from the Cambridge Crystallographic Data Centre, 12 Union Road, Cambridge CB2 1EZ, UK; Fax: (internat.) + 44-1223/336-033; E-mail: deposit@ccdc.cam.ac.uk].
[51] G. M. Sheldrick, *SHELXS-86 and SHELXL-93, Programs for Crystal Structure Determination*, University of Göttingen, **1986** and **1993**.
[52] E. Keller, *SCHAKAL for Windows*, Universität Freiburg, **2001**.

Received July 24, 2003
Early View Article
Published Online November 19, 2003

 © 2004 Wiley-VCH Verlag GmbH & Co. KGaA, Weinheim

Access to 3-Methyl-4-methylene-*N*-tosylpyrrolidine and 3,4-Dimethyl-*N*-tosylpyrroline by Ruthenium-Catalyzed Cascade Cycloisomerization/Isomerization Reactions

Ismail Özdemir,[a] Engin Çetinkaya,[b] Bekir Çetinkaya,*[b] Metin Çiçek,[a] David Sémeril,[c] Christian Bruneau,*[c] and Pierre H. Dixneuf[c]

Keywords: Ruthenium / Benzimidazole / Homogeneous catalysis / Olefination

New $RuCl_2$(benzimidazole)(arene) complexes have been prepared. Upon reaction with 1,1-diphenylprop-2-ynol they generate catalyst precursors which perform the cycloisomerization of diallyltosylamide into 3-methyl-4-methylene-*N*-tosylpyrrolidine. The presence of *N*-(2,4,6-trimethylbenzyl)benzimidazole as ligand leads to a subsequent isomerization and gives the 3,4-dimethyl-*N*-tosylpyrroline.

(© Wiley-VCH Verlag GmbH & Co. KGaA, 69451 Weinheim, Germany, 2004)

Introduction

Transition metal complexes with nitrogen-containing ligands have recently shown their potential to perform selective catalytic transformations of molecules with atom economy.[1] Especially, a variety of RuX_2(arene)(L) complexes promoting catalytic reactions such as nucleophilic addition to triple bonds to form furans (L = imidazoline, tetrahydropyrimidine,[2] benzimidazole[3]), hydrogen transfer (L = amino acid,[4] amino alcohol,[5] diamine[6]), cyclopropanation (L = diamine[7]), or Diels−Alder cycloaddition and Claisen rearrangement [L = bis(oxazoline)[8,9]]. It is also well established that $RuCl_2$(arene)(L) complexes can easily be transformed by activation of propargylic alcohols into cationic ruthenium(allenylidene) complexes, which have shown catalytic properties in olefin metathesis.[10]

We now report (i) the straightforward preparation of new $RuCl_2$(η^6-arene)(L) complexes with an *N*-coordinated benzimidazole ligand and (ii) their in situ transformation into efficient catalyst precursors for cycloisomerization of diallyltosylamide into 3-methy-4-methylene-*N*-tosylpyrrolidine followed, when a suitable benzimidazole is used (R = mesityl-CH_2), by double bond isomerization to form a pyrroline derivative. This study reveals a very efficient ruthenium catalyst for isomerization of the exocyclic C=CH_2 double bond of 3-methyl-4-methylenepyrrolidine into the tetrasubstituted C=C bond of 3,4-dimethylpyrrolidine derivatives (Scheme 1).

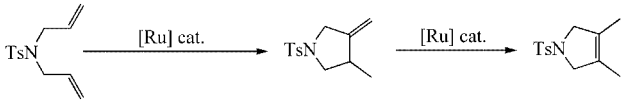

Scheme 1

Results and Discussion

The reaction of *N*-alkylbenzimidazoles **2**−**4** and the *N*-(aralkyl)benzimidazole **5** with the dinuclear [$RuCl_2$(*p*-cymene)]$_2$ (**1a**) and [$RuCl_2$(hexamethylbenzene)]$_2$ (**1b**) com-

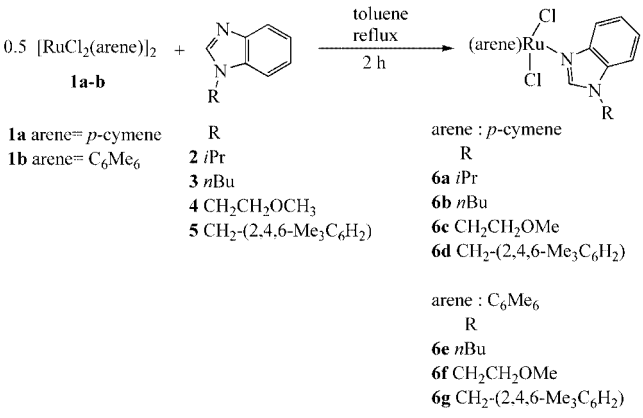

Scheme 2

[a] Inönü Üniversitesi Fen-Edebiyat Fakültesi, 44069 Malatya, Turkey
[b] Ege University, Department of Chemistry, 35100 Bornova-Izmir, Turkey
[c] Institut de Chimie, UMR 6509: CNRS − Université de Rennes, Organométalliques et Catalyse, Campus de Beaulieu, 35042 Rennes, France

 © 2004 Wiley-VCH Verlag GmbH & Co. KGaA, Weinheim DOI: 10.1002/ejic.200300224

Table 1. Selected analytical data for the new (benzimidazole)ruthenium complexes (**6**)

Complex	Yield of isolated product [%]	M.p. [°C]	$\nu_{(C-N)}$ [cm^{-1}]	^{13}C NMR, C-2 signals δ [ppm] ($^{1}J_{C,H}$ [Hz])	^{1}H NMR, 2-H signals δ [ppm]
6a	85	183.0	1506	142.96 (197.3)	8.44
6b	87	206.5	1612	144.52 (198.8)	8.34
6c	87	197.0	1616	145.54 (199.5)	8.22
6d	90	224.0	1610	144.18 (203.0)	7.92
6e	86	307.5	1612	145.08 (201.4)	8.12
6f	82	276.0	1508	146.18 (202.6)	7.97
6g	86	310.5	1612	144.81 (205.6)	7.70

plexes proceeded smoothly in refluxing toluene to give the $RuCl_2$(benzimidazole)(arene) complexes **6a**−**g** as crystalline solids in 82−90% yields (Scheme 2, Table 1).

Complexes **6a**−**g**, which are very stable in the solid state have been characterized by analytical and spectroscopic techniques (Table 1). The IR data show the presence of a C=N bond with a ν(C=N) vibration at 1506−1616 cm^{-1}, and the ^{1}H NMR spectra clearly exhibit a singlet at δ = 7.70−8.44 ppm typical of the N=CH−N fragment. In the ^{13}C NMR spectrum, the chemical shift of the corresponding C-2 atom was detected in the region δ = 142.96−146.18 ppm with a $^{1}J_{C,H}$ coupling constant close to 200 Hz. These new complexes show typical spectroscopic signatures which are in line with those recently reported for other $RuCl_2$(arene)(benzimidazole) complexes with R = Me, Et, $(CH_2)_2NEt_2$, $(CH_2)_2CO_2Et$.[3]

In contrast with the related (arene)$RuCl_2$(phosphane),[11] (arene)$RuCl_2$(diaminocarbene) complexes,[12,13a] **6** presented no metathesis catalytic activity for the transformation of *N*,*N*-diallyltosylamide (**8**). The known catalytic activities of [RuCl(=C=C=CPh_2)(arene)(L)][X] (L = PCy_3,[10] diaminocarbene[13]) to perform the ring-closing metathesis of dienes and ring-opening metathesis polymerization of cyclic olefins, provided impetus to prepare the corresponding cationic ruthenium(allenylidene)(benzimidazole) complexes according to the reaction depicted in Scheme 3. Indeed, purple complexes were prepared in dichloromethane but they were not stable enough to be cleanly isolated and characterized. Based on previous results obtained with more stable ruthenium(allenylidene) complexes from analogous precursors,[10,13] we assumed that the new organometallic species **7a**−**g** (Scheme 3) contained the $[RuCl(arene)(benzimidazole)(allenylidene)]^+$ cation. In order to circumvent this instability problem, they were generated in situ from complexes **6a**−**g** just before use, by abstraction of chloride with silver triflate followed by addition of 1,1-diphenylprop-2-ynol at room temperature in the selected solvent (Scheme 3).

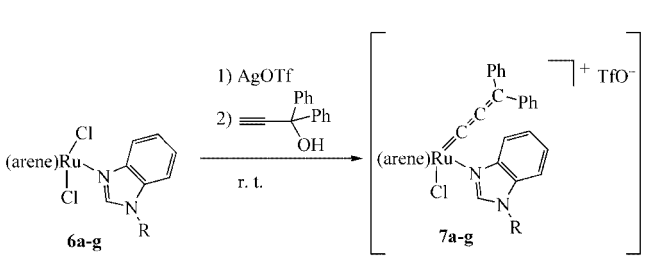

Scheme 3

The catalytic performances of these in situ generated precursors were evaluated in the transformation of *N*,*N*-diallyltosylamide (**8**) at 80 °C in various solvents (Scheme 4, Table 2).

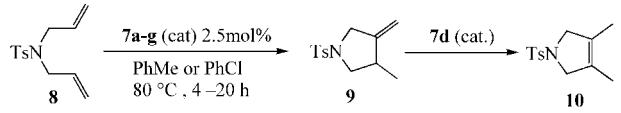

Scheme 4

Table 2. Catalytic transformation of *N*,*N*-diallyltosylamide (**8**)

Catalyst	Solvent	Time [h]	Conversion [%]	**9** [%]	**10** [%]
7a	PhCl	18	100	100	
7b	PhMe	13	76	76	
7b	PhCl	10	100	100	
7c	PhMe	12	37	37	
7c	PhCl	10	82	82	
7d	PhMe	4	100	100	
7d	PhMe	10	100		100
7d	PhCl	6	98	60	38
7d	PhCl	10	100		100
7e	PhCl	18	65	65	
7f	PhMe	10	58	58	
7f	PhCl	20	100	100	
7g	PhCl	20	79	40	39

Thus, the catalyst was first generated by successive additions of silver triflate (0.0125 mmol) and HC≡$CCPh_2OH$ (0.0125 mmol) to a solution of **6** (0.0125 mmol, 2.5 mol %) in 2.5 mL of solvent and stirred at room temperature for 20 min. The diene **8** (0.5 mmol) was then added and the solution was heated at 80 °C for 4−20 h. The catalytic precursors thus prepared in situ showed catalytic activity for the transformation of the 1,6-diene **8** into the cycloisomerization compounds **9** or **10**. According to this procedure, the presence of the diene **8** added just after the preparation of **7** might stabilize organometallic intermediates and generate catalyst precursors with long-lasting activity.

In contrast with the catalyst arising from the allenylidene complex [RuCl(=C=C=CPh_2)(PCy_3)(*p*-cymene)][OTf],[10]

 © 2004 Wiley-VCH Verlag GmbH & Co. KGaA, Weinheim

no trace of *N*-tosyl-2,5-dihydropyrrole was detected, which indicated that no metathesis reaction took place with precursors **7**.

The catalysts resulting from **6a**−**c** and **6e**−**f**, which bear an aliphatic R group as substituent of the benzimidazole ligand led to the formation of the 3-methyl-4-methylene heterocycle **9**. The reaction was faster in chlorobenzene than in toluene and the total conversion of the starting substrate could be achieved in 10 h with the precatalyst **7b** and within 18−20 h with **7a** and **7f**.

The catalytic species generated from **7d** containing the *N*-(2,4,6-trimethylbenzyl)-substituted benzimidazole ligand **5** was much more efficient and the complete conversion of **8** to **9** was carried out in toluene in less than 4 h. Under the reaction conditions, a subsequent isomerization took place which led to 3,4-dimethyl-*N*-tosylpyrroline (**10**) bearing a tetrasubstituted endocyclic double bond in quantitative yield at 80 °C after 10 h, whatever the solvent. Apparently, in toluene, as the formation of **10** starts only after complete conversion of **8**, the presence of the starting diene inhibits the isomerization of **9** to **10**. The analogous catalytic system **7g** resulting from the C_6Me_6-containing precursor was less active at 80 °C after 20 h, as the conversion reached only 79 % and a 1:1 mixture of **9** and **10** was obtained. This observation is consistent with the hypothesis of the initial displacement of the arene ligand to generate the catalytic species (Scheme 5).[13b,14,15] During the catalytic process, the formation of indenylidene complexes by rearrangement of the allenylidene ligand, cannot be ruled out.[16]

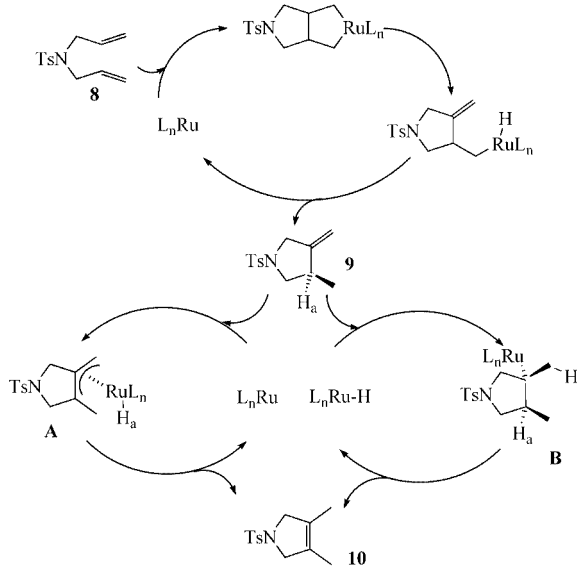

Scheme 5

From a separate experiment, it was possible to show that **10** resulted from the catalytic isomerization of **9** in the presence of **7d** as catalyst. Thus, by using the catalytic system prepared in situ from 2.5 mol % of the ruthenium precursor **6d**, AgOTf (2.5 mol %) and HC≡CCPh$_2$OH (2.5 mol %) in 2.5 mL of toluene, **9** (0.5 mmol) was completely converted into **10** at 80 °C after 4 h. Two possible mechanisms could account for this isomerization: (i) allylic C−H activation and H migration via an (allyl)(hydrido)ruthenium intermediate **A** or (ii) if a Ru−H species is formed, by insertion of the exocyclic double bond into a Ru−H bond followed by β-elimination (Scheme 5). Both processes should be stereoselective as the coordination of the Ru atom should preferentially take place on the less hindered face of **9**. Thus, β-elimination from **B** should be favored with H_a in the *syn* position, as well as the (allyl)ruthenium formation by coordination to **9** on the sterically less hindered face.

Transition-metal-catalyzed cycloisomerization reactions from α,ω-dienes is a topic of current interest.[17] The formation of 3-methyl-4-methylene cyclic derivatives of type **9** has already been observed with several metal catalysts including palladium,[18,19] nickel,[19] rhodium[20] and titanium.[21] Other efficient catalytic systems based on ruthenium precursors such as $[Ru(cod)Cl_2]_n$ or Cp*Ru(cod)Cl in protic solvents,[22] or generated in situ from $[RuCl_2(p\text{-cymene})]_2$, an imidazolinium salt and a base,[15] have been reported.

A few examples of cycloisomerization of 1,6-diene into 1,2-dimethylcyclopentene derivatives involve palladium catalysts in the presence of silane[23] or rhodium catalysts,[20] and most of the substrates which lead to these cycloisomerization products are 2,2-diallylmalonate derivatives. In the present ruthenium-catalyzed isomerization of **8** to **10**, the role of the 2,4,6-trimethylbenzyl ligand in **7d** appears to be crucial. It might result from temporary interaction of the mesityl group with the metal center as its coordination operates with closely related diaminocarbene ligands.[13b,14]

Conclusion

New ruthenium species generated in situ from $RuCl_2$(arene)(benzimidazole) complexes in the presence of 1,1-diphenylprop-2-ynol are active catalysts to perform the cycloisomerization of *N*,*N*-diallyltosylamide to the *N*-tosylpyrrolidine **9** featuring an exocyclic methylene group under neutral and mild conditions. The catalyst containing the benzimidazole **5** (R = 2,4,6-$Me_3C_6H_2CH_2$) exhibits specific catalytic properties. It leads to the fastest cycloisomerization reaction and in addition offers the first example of ruthenium-catalyzed isomerization of 3-methyl-4-methylene-*N*-tosylpyrrolidine (**9**) to 3,4-dimethyl-*N*-tosylpyrroline (**10**).

Experimental Section

General: Manipulations were carried out with standard Schlenk techniques under nitrogen with previously dried solvents. The complexes $[RuCl_2(arene)]_2$ were prepared according to known methods.[24] 1-Substituted benzimidazoles **2**−**5** were prepared by alkylation of the potassium salt of benzimidazole. Infrared spectra were recorded as KBr pellets in the range 400−4000 cm^{-1} with an ATI UNICAM 2000 spectrometer. ^{1}H NMR (300 MHz) and ^{13}C NMR (75.5 MHz) were recorded with a Bruker AM 300 WB FT spectrometer with chemical shifts referenced to residual solvent $CDCl_3$. Microanalyses were performed by the TÜBITAK analyses centre.

 © 2004 Wiley-VCH Verlag GmbH & Co. KGaA, Weinheim

Preparation of the Ruthenium(benzimidazole) Complexes 6a−g: A solution of the *N*-substituted benzimidazole **2**−**5** (1.05 mmol) and $[RuCl_2(p\text{-cymene})]_2$ or $[RuCl_2(hexamethylbenzene)]_2$ (0.5 mmol) in toluene (15 mL) were heated under reflux for 2 h. Upon cooling to room temperature, orange crystals of **6a**−**g** were obtained. The crystals were filtered, washes with diethyl ether (3 × 10 mL) and dried under vacuum.

$RuCl_2$(*p*-cymene)(*N*-isopropylbenzimidazole) (6a): ^{1}H NMR (300 MHz, $CDCl_3$): δ = 8.44 (s, 1 H, N=C*H*), 7.33 (m, 4 H, C_6H_4), 5.42 and 5.32 [2 × d, *J* = 6.00 Hz, 4 H, $(CH_3)_2CHC_6H_4CH_3$], 4.58 [sept, *J* = 6.70 Hz, 1 H, C*H*$(CH_3)_2$], 2.06 [s, 3 H, $(CH_3)_2CHC_6H_4CH_3$], 1.83 [sept, *J* = 7.00 Hz, 1 H, $(CH_3)_2CHC_6H_4CH_3$], 1.49 [d, *J* = 6.70 Hz, 6 H, CH$(CH_3)_2$], 1.18 [d, *J* = 7.00 Hz, 6 H, $(CH_3)_2CHC_6H_4CH_3$] ppm. ^{13}C NMR (75.5 MHz, $CDCl_3$): δ = 142.9 (N=*C*H), 142.2, 133.2, 123.8, 123.5, 120.7, 111.5 (m, C_6H_4), 102.4, 97.9, 82.8, 81.2 $[(CH_3)_2CHC_6H_4CH_3]$, 49.0 [*C*H$(CH_3)_2$], 30.7 $[(CH_3)_2CHC_6H_4CH_3]$, 22.5 [CH$(CH_3)_2$], 22.3 $[(CH_3)_2CHC_6H_4CH_3]$, 18.5 $[(CH_3)_2CHC_6H_4CH_3]$ ppm. Yield 0.39 g (85%). $C_{20}H_{26}Cl_2N_2Ru$ (466.42): calcd. C 51.50, H 5.62, N 6.01; found C 51.40, H 5.71, N 6.10.

$RuCl_2$(*p*-cymene)(*N*-butylbenzimidazole) (6b): ^{1}H NMR (300 MHz, $CDCl_3$): δ = 8.34 (s, 1 H, N=C*H*), 7.95−7.27 (m, 4 H, C_6H_4), 5.47 and 5.32 [2 × d, *J* = 5.96 Hz, 4 H, $(CH_3)_2CHC_6H_4CH_3$], 3.98 (t, *J* = 7.21 Hz, 2 H, CH_2CH$_2$CH$_2$CH$_3$), 2.77 [sept, *J* = 6.89 Hz, 1 H, $(CH_3)_2CHC_6H_4CH_3$], 2.05 [s, 3 H, $(CH_3)_2CHC_6H_4CH_3$], 1.72 (m, 2 H, CH$_2$CH_2CH$_2$CH$_3$), 1.26 (m, 2 H, CH$_2$CH$_2$CH_2CH$_3$), 1.21 [d, *J* = 4.82 Hz, 6 H, $(CH_3)_2CHC_6H_4CH_3$], 0.86 (t, *J* = 7.38 Hz, 3 H, CH$_2$CH$_2$CH$_2$CH_3) ppm. ^{13}C NMR (75.5 MHz, $CDCl_3$): δ = 144.5 (N=*C*H), 142.5, 133.7, 124.0, 123.4, 120.5, 110.9, (C_6H_4), 102.4, 97.8, 82.9, 81.1$[(CH_3)_2CHC_6H_4CH_3]$, 45.7 (*C*H$_2$CH$_2$CH$_2$CH$_3$), 31.6 (CH$_2$*C*H$_2$CH$_2$CH$_3$), 30.7 $[(CH_3)_2CHC_6H_4CH_3]$, 22.3 $[(CH_3)_2CHC_6H_4CH_3]$, 19.9 (CH$_2$CH$_2$*C*H$_2$CH$_3$), 20.0 $[(CH_3)_2CHC_6H_4CH_3]$, 13.6 (CH$_2$CH$_2$CH$_2$*C*H$_3$) ppm. Yield 0.42 g (87%). $C_{21}H_{28}Cl_2N_2Ru$ (480.45): calcd. C 52.50, H 5.87, N 5.83; found C 52.43, H 6.01, N 5.96.

$RuCl_2$(*p*-cymene)[*N*-(2-methoxyethyl)benzimidazole] (6c): ^{1}H NMR (300 MHz, $CDCl_3$): δ = 8.22 (s, 1 H, N=C*H*), 7.94−7.26 (m, 4 H, C_6H_4), 5.47 and 5.31 [2 × d, *J* = 6.00 Hz, 4 H, $(CH_3)_2CHC_6H_4CH_3$)], 3.92 (t, *J* = 5.00 Hz, 2 H, CH$_2$CH_2OCH$_3$), 3.47 (t, *J* = 5.10 Hz, 2 H, CH_2CH$_2$OCH$_3$), 3.16 (s, 3 H, CH$_2$CH$_2$OCH_3), 2.78 [sept, *J* = 6.90 Hz, 1 H, $(CH_3)_2CHC_6H_4CH_3$], 2.38 [d, *J* = 6.90 Hz, 6 H, $(CH_3)_2CHC_6H_4CH_3$)], 2.03 [s, 3 H, $(CH_3)_2CHC_6H_4CH_3$)] ppm. ^{13}C NMR (75.5 MHz, $CDCl_3$): δ = 145.5 (N=*C*H), 142.2, 133.4, 124.1, 123.2, 120.2, 111.3 (C_6H_4), 102.5, 97.8, 82.9, 81.2 $[(CH_3)_2CHC_6H_4CH_3)]$, 69.9 (CH$_2$*C*H$_2$OCH$_3$), 58.7 (CH$_2$CH$_2$O*C*H$_3$), 45.6 (*C*H$_2$CH$_2$OCH$_3$), 30.6 $[(CH_3)_2CHC_6H_4CH_3]$, 21.9 $[(CH_3)_2CHC_6H_4CH_3)]$, 18.4 $[(CH_3)_2CHC_6H_4CH_3)]$ ppm. Yield 0.42 (87%). $C_{20}H_{26}Cl_2N_2ORu$ (482.42): calcd. C 49.80, H 5.43, N 5.81; found C 49.97, H 5.55, N 6.03.

$RuCl_2$(*p*-cymene)[*N*-(2,4,6-trimethylbenzyl)benzimidazole] (6d): ^{1}H NMR (300 MHz, $CDCl_3$): δ = 7.92 (s, 1 H, N=C*H*), 7.99−7.20 (m, 4 H, C_6H_4), 6.85 [s, 2 H, $(CH_3)_3C_6H_2CH_2$], 5.29 and 5.20 [2 × d, *J* = 5.75 Hz, 4 H, $(CH_3)_2CHC_6H_4CH_3$], 5.14 [s, 2 H, $(CH_3)_3C_6H_2CH_2$], 2.54 [sept, *J* = 6.90 Hz, 1 H, $(CH_3)_2CHC_6H_4CH_3$], 2.26 [s, 3 H, $(CH_3)_2CHC_6H_4CH_3$), 2.13, 2.23 [s, 9 H, 2,4,6-$(CH_3)_3C_6H_2CH_2$], 1.01 [d, *J* = 6.90 Hz, 6 H, $(CH_3)_2CHC_6H_4CH_3$] ppm. ^{13}C NMR (75.5 MHz, $CDCl_3$): δ = 144.2 (N=*C*H), 142.5, 133.7, 124.0, 123.4, 120.5, 110.9 (C_6H_4), 139.1, 137.8, 129.9, 126.7 $[(CH_3)_3C_6H_2CH_2]$, 101.9, 98.1, 83.0, 80.9 $[(CH_3)_2CHC_6H_4CH_3]$, 43.9 $[(CH_3)_3C_6H_2CH_2]$, 30.6 $[(CH_3)_2CHC_6H_4CH_3]$, 24.1 $[(CH_3)_2CHC_6H_4CH_3]$, 21.1, 19.8 $[(CH_3)_3C_6H_2CH_2]$, 18.5 $[(CH_3)_2CHC_6H_4CH_3]$ ppm. Yield 0.5 g (90%). $C_{27}H_{32}Cl_2N_2Ru$ (556.54): calcd. C 58.27, H 5.80, N 5.04; found C 58.32, H 5.86, N 5.21.

$RuCl_2$(hexamethylbenzene)(*N*-butylbenzimidazole) (6e): ^{1}H NMR (300 MHz, $CDCl_3$): δ = 8.12 (s, 1 H, N=C*H*), 7.80−7.21 (m, 4 H, C_6H_4), 3.99 (t, *J* = 7.20 Hz, 2 H, CH_2CH$_2$CH$_2$CH$_3$), 1.96 [s, 18 H, $C_6(CH_3)_6$], 1.67 (m, 2 H, CH$_2$CH_2CH$_2$CH$_3$), 1.25 (m, 2 H, CH$_2$CH$_2$CH_2CH$_3$), 0.87 (t, *J* = 7.38 Hz, 3 H, CH$_2$CH$_2$CH$_2$CH_3) ppm. ^{13}C NMR (75.5 MHz, $CDCl_3$): δ = 145.1 (N=*C*H), 133.7, 128.2, 123.8, 121.2, 110.6 (C_6H_4), 90.9 $[C_6(CH_3)_6]$, 45.5 (*C*H$_2$CH$_2$CH$_2$CH$_3$), 31.7 (CH$_2$*C*H$_2$CH$_2$CH$_3$), 20.1 (CH$_2$CH$_2$*C*H$_2$CH$_3$), 15.8 $[C_6(CH_3)_6]$, 13.6 (CH$_2$CH$_2$CH$_2$*C*H$_3$) ppm. Yield 0.44 g (86%). $C_{23}H_{32}Cl_2N_2Ru$ (508.49): calcd. C 54.33, H 6.34, N 5.51; found C 54.58, H 6.19, N 5.73.

$RuCl_2$(hexamethylbenzene)[*N*-(2-methoxyethyl)benzimidazole] (6f): ^{1}H NMR (300 MHz, $CDCl_3$): δ = 7.97 (s, 1 H, N=C*H*), 7.20−7.90 (m, 4 H, C_6H_4), 3.85 (t, *J* = 5.00 Hz, 2 H, CH$_2$CH_2OCH$_3$), 3.41 (t, *J* = 5.09 Hz, 2 H, CH_2CH$_2$OCH$_3$), 3.12 (s, 3 H, CH$_2$CH$_2$OCH_3), 1.94 [s, 18 H, $C_6(CH_3)_6$] ppm. ^{13}C NMR (75.5 MHz, $CDCl_3$): δ = 146.2 (N=*C*H), 140.5, 133.2, 123.8, 122.4, 120.7, 111.2 (C_6H_4), 90.9 $[C_6(CH_3)_6]$, 69.8 (CH$_2$*C*H$_2$OCH$_3$), 58.6 (CH$_2$CH$_2$O*C*H$_3$), 45.3 (*C*H$_2$CH$_2$OCH$_3$), 15.7 $[C_6(CH_3)_6]$ ppm. Yield 0.42 g (82%). $C_{22}H_{30}Cl_2N_2ORu$ (510.47): calcd. C 51.76, H 5.92, N 5.49; found C 51.70, H 5.83, N 5.67.

$RuCl_2$(hexamethylbenzene)[*N*-(2,4,6-trimethylbenzyl)benzimidazole] (6g): ^{1}H NMR (300 MHz, $CDCl_3$): δ = 7.70 (s, 1 H, N=C*H*), 8.05−7.26 (m, 4 H, C_6H_4), 6.95 [s, 2 H, $(CH_3)_3C_6H_2CH_2$], 5.21 [s, 2 H, $(CH_3)_3C_6H_2CH_2$], 2.31, 2.23 [s, 9 H, $(CH_3)_3C_6H_2CH_2$], 1.87 [s, 18 H, $C_6(CH_3)_6$] ppm. ^{13}C NMR (75.5 MHz, $CDCl_3$): δ = 141.8 (N=*C*H), 141.2, 134.1, 123.9, 123.0, 121.0, 110.3 (C_6H_4), 139.1, 137.3, 129.7, 126.9 $[(CH_3)_3C_6H_2CH_2]$, 90.7 $[C_6(CH_3)_6]$, 43.7 $[(CH_3)_3C_6H_2CH_2]$, 21.1, 19.8 $[(CH_3)_3C_6H_2CH_2]$, 15.6 $[C_6(CH_3)_6]$ ppm. Yield 0.50 g (86%). $C_{29}H_{36}Cl_2N_2Ru$ (584.60): calcd. C 59.58, H 6.21, N 4.79; found C 59.37, H 6.26, N 4.93.

Compounds **9**[15a] and **10**[25] were separated by GCMS chromatography and identified by ^{1}H NMR and compared with data from the literature.

3-Methyl-4-methylene-*N*-tosylpyrrolidine (9): ^{1}H NMR (200 MHz, $CDCl_3$): δ = 7.68 (d, *J* = 8.1 Hz, 2 H, arom. C*H*), 7.30 (d, *J* = 8.1 Hz, 2 H, arom. C*H*), 4.93 (dm, *J* = 1.6 Hz, 1 H, C=CH*H*), 4.88 (dm, *J* = 1.6 Hz, 1 H, C=C*H*H), 3.93 (dm, *J* = 14.1 Hz, 1 H, CH_2C=), 3.71 (dm, *J* = 14.1 Hz, 1 H, CH_2C=), 3.35−3.65 (m, 1 H, C*H*Me), 2.66 (m, 2 H, NCH_2CH), 2.41 (s, 3 H, CH_3Ar), 1.01 (d, *J* = 6.3 Hz, 3 H, CHMe) ppm. ^{13}C NMR (75.5 MHz, $CDCl_3$): δ = 149.3, 143.7, 137.1, 129.7, 127.8, 106.1, 55.1, 52.2, 37.5, 21.6, 16.1 ppm.

3,4-Dimethyl-*N*-tosylpyrroline (10): ^{1}H NMR (200 MHz, $CDCl_3$): δ = 7.36 (m, 4 H, arom. C*H*), 4.04 (s, 4 H, 2 × CH_2), 2.48 (s, 3 H, CH_3Ar),1.60 (s, 6 H, 2 × CH_3C=) ppm. ^{13}C NMR (75.5 MHz, $CDCl_3$): δ = 143.7, 134.6, 130.2, 128.2, 127.3, 126.6, 66.3, 21.9, 11.6 ppm.

Acknowledgments

The authors are grateful to the EU COST Chemistry programme (D17/0003/00) and TUBITAK (MISAG-COST-D17) for support.

 © 2004 Wiley-VCH Verlag GmbH & Co. KGaA, Weinheim

[1] A. Togni, L. M. Venanzi, *Angew. Chem.* **1994**, *106*, 517−547; *Angew. Chem. ; Int. Ed. Engl.* **1994**, *33*, 497; F. Fache, E. Schulz, M. L. Tommasino, M. Lemaire, *Chem. Rev.* **2000**, *100*, 2159−2232.
[2] B. Çetinkaya, B. Alici, I. Özdemir, C. Bruneau, P. H. Dixneuf, *J. Organomet. Chem.* **1999**, *575*, 187−192.
[3] B. Çetinkaya, I. Özdemir, C. Bruneau, P. H. Dixneuf, *Eur. J. Inorg. Chem.* **2000**, 29−32.
[4] D. Carmona, M. Pilar Lamata, F. Viguri, I. Dobrinovich, F. J. Lahoz, L. A. Oro, *Adv. Synth. Catal.* **2002**, *344*, 495−498.
[5] K. Everaere, A. Mortreux, J. F. Carpentier, *Adv. Synth. Catal.* **2003**, *345*, 67−77; D. A. Alonso, P. Brandt, S. J. M. Nordin, P G. Andersson, *J. Am. Chem. Soc.* **1999**, *121*, 9580−9588.
[6] R. Noyori, S. Hashiguchi, *Acc. Chem. Res.* **1997**, *30*, 97−102.
[7] F. Simal, A. Demonceau, A. F. Noels, *Tetrahedron Lett.* **1998**, *39*, 3493−3496.
[8] J. W. Faller, A. Lavoie, *J. Organomet. Chem.* **2001**, *630*, 17−22.
[9] H. Ben Ammar, J. Le Nôtre, M. Salem, M. T. Kaddachi, P. H. Dixneuf, *J. Organomet. Chem.* **2002**, *662*, 63−69.
[10] M. Picquet, D. Touchard, C. Bruneau, P. H. Dixneuf, *New J. Chem.* **1999**, 141−143; A. Fürstner, M. Liebl, C. W. Lehmann, M. Picquet, R. Kunz, C. Bruneau, D. Touchard, P. H. Dixneuf, *Chem. Eur. J.* **2000**, *6*, 1847−1857; R. Castarlenas, D. Sémeril, A. F. Noels, A. Demonceau, P. H. Dixneuf, *J. Organomet. Chem.* **2002**, *663*, 235−238.
[11] A. Fürstner, L. Ackermann, *Chem. Commun.* **1999**, 95−96.
[12] L. Delaude, A. Demonceau, A. F. Noels, *Chem. Commun.* **2001**, 986−987.
[13] [13a] L. Jafarpour, J. Huang, E. D. Stevens, S. P. Nolan, *Organometallics* **1999**, *18*, 3760−3763. [13b] B. Çetinkaya, S. Demir, I. Özdemir, L. Toupet, D. Sémeril, C. Bruneau, P. H. Dixneuf, *New J. Chem.* **2001**, *25*, 519−521.
[14] B. Çetinkaya, S. Demir, I. Özdemir, L. Toupet, D. Sémeril, C. Bruneau, P. H. Dixneuf, *Chem. Eur. J.* **2003**, *9*, 2323−2330.
[15] [15a] D. Sémeril, C. Bruneau, P. H. Dixneuf, *Helv. Chim. Acta* **2001**, *84*, 3335−3341. [15b] D. Sémeril, C. Bruneau, P. H. Dixneuf, *Adv. Synth. Catal.* **2002**, *344*, 585−595.
[16] H.-J. Schanz, L. Jafarpour, E. D. Stevens, S. P. Nolan, *Organometallics* **1999**, *18*, 5187−5190; A. Fürstner, O. R. Thiel, L. Ackermann, H.-J. Schanz, S. P. Nolan, *J. Org. Chem.* **2000**, *65*, 2204−2207.
[17] G. C. Lloyd-Jones, *Org. Biomol. Chem.* **2003**, *1*, 215−236; B. M. Trost, M. J. Krische, *Synlett* **1998**, 1−16.
[18] A. Heumann, M. Moukhliss, *Synlett* **1998**, 1211−1212; R. Grigg, T. R. B. Mitchell, A. Ramasubbu, *J. Chem. Soc., Chem. Commun.* **1979**, 669−670.
[19] B. Radetich, T. V. Rajanbabu, *J. Am. Chem. Soc.* **1998**, *120*, 8007−8008.
[20] R. Grigg, J. F. Malone, T. R. B. Mitchell, A. Ramasubbu, R. M. Scott, *J. Chem. Soc., Perkin Trans.* **1984**, 1745−1754; A. Bright, J. F. Malone, J. K. Nicolson, J. Powell, B. L. Shaw, *J. Chem. Soc., Chem. Commun.* **1971**, 712.
[21] S. Okamoto, T. Livinghouse, *J. Am. Chem. Soc.* **2000**, *122*, 1223−1224.
[22] Y. Yamamoto, Y. Nakagai, N. Ohkoshi, K. Itoh, *J. Am. Chem. Soc.* **2001**, *123*, 6372−6380; Y. Yamamoto, N. Ohkoshi, M. Kameda, K. Itoh, *J. Org. Chem.* **1999**, *64*, 2178−2179; M. Michaut, M. Santelli, J.-L. Parrain, *Tetrahedron Lett.* **2003**, *44*, 2157−2159.
[23] P. Kisanga, R. A. Widenhoefer, *J. Am. Chem. Soc.* **2000**, *122*, 10017−10026; R. A. Widenhoefer, N. S. Perch, *Org. Lett.* **1999**, *1*, 1103−1105.
[24] M. A. Bennett, T. N. Huang, T. W Matheson, A. K. Smith, *Inorg. Synth.* **1982**, *21*, 74.
[25] A. Padwa, H. Nimmesgern, G. S. K. Wong, *J. Org. Chem.* **1985**, *50*, 5620−5627.

Received April 17, 2003
Early View Article
Published Online October 30, 2003

 © 2004 Wiley-VCH Verlag GmbH & Co. KGaA, Weinheim

Gold and Silver Complexes with the Ligands *N*-[Bis(isopropoxy)-thiophosphoryl]thiobenzamide and *N*-[Bis(isopropoxy)thiophosphoryl]-*N′*-phenylthiourea

Olga Crespo,[a,b] Vasiliy V. Brusko,[c] M. Concepción Gimeno,[a] M. Loreto Tornil,[b] Antonio Laguna,*[a] and Nail G. Zabirov[c]

Keywords: Gold / Silver / Sulfur / Thiourea / Thioamide

Gold and silver complexes with the *N*-[bis(isopropoxy)-thiophosphoryl]thiobenzamide (HL^1) and *N*-[bis(isopropoxy)-thiophosphoryl]-*N′*-phenylthiourea (HL^2) ligands are reported. The compounds $[M(HL)(PPh_3)]TfO$, $[Ag(HL)(TfO)]$ and $[Ag(HL)(PPh_3)_2]TfO$ were obtained by the reaction of both ligands with the corresponding trifluoromethanesulfonate salts. The (acetylacetonato)gold and -silver materials $[M(acac)(PPh_3)]$ or $[Au(acac)(C_6F_5)_2]$ cause deprotonation of the ligands and afford $[ML(PPh_3)]$ or $[AuL(C_6F_5)_2]$, whereas the reaction of $[Au(TfO)(PPh_3)]$ with HL^1 in a 2:1 molar ratio in KOH/MeOH affords $[Au_2(L^1)(PPh_3)_2]TfO$. The first homoleptic anionic metal compounds $[Au^IL_2]^-$ are also reported.
(© Wiley-VCH Verlag GmbH & Co. KGaA, 69451 Weinheim, Germany, 2004)

Introduction

The chemistry of chelating ligands attached to metal centers through sulfur atoms has been extensively investigated. Unusual coordination at the metal centers and interesting stereochemistries of the chelate rings have been found. Among them, the coordination chemistry of *N*-(thiophosphoryl)thioamides or *N*-(thiophosphoryl)thioureas has been studied and extraction of metals using *N*-[bis(isopropoxy)thiophosphoryl]thiobenzamide has been reported[1] as well as a liquid ion-selective electrode for Hg^{2+} determination.[2] Different $R^1C(X)NHP(Y)R^2R^3$ ligands have been reported[3−10] (R^1 = R-NH or NX_2 X = H, alkyl or aryl group; R^2, R^3 = alkyl, aryl, alkoxy or aryloxy group, X = O, S; Y = O, S, Se) and despite the tautomeric forms in which they can exist, infrared studies on some of them support the presence of structures in which two double bonds C=S and P=S are present[7] although delocalization of the C−NH−P unit has been found as more representative of the bonding in the crystal structures[11] of $PhC(S)NHP(S)(OR)_2$ (R = *i*Pr, Et). The species consisting on one 1,10-diaza-18-crown-6 with two "$(O\textit{i}Pr)_2P(S)NHC(S)$" units bonded to the nitrogen atoms has also been described.[8]

A brief overview of the chemistry with representative elements includes the potassium derivatives in which the metal atom is bonded to the sulfur atoms of "$(O\textit{i}Pr)_2P(S)NHC(S)Ph$". The potassium atom can be in the center of a diaza-18-crown-6 cycle, or as part of a more complicated structure.[12,13] Other examples of coordination to representative elements include the mononuclear hexacoordinate compounds prepared from the reactions of different ligands with $SnCl_4$ although the geometries were not confirmed by X-ray studies,[14] and the lead derivatives $[Pb\{(O\textit{i}Pr)_2P(X)NC(S)Ph\}_2]$.[15] The $[M^{2+}L_2]$ stoichiometry is the most common among the transition metal complexes described so far (M = Ni, Co, Pt, Pd, Zn, Cd)[6,7,16−22] which have been confirmed in many cases by single-crystal X-ray diffraction studies.

Among the reported complexes, those containing the coinage metals are however scarcely represented. The synthesis of $[Cu\{PhNHC(S)NP(S)(O\textit{i}Pr)_2\}]$[5] and also the reduction of Cu^{II} to Cu^I with other ligands[23] such us $PhNHC(S)NHP(S)Ph_2$, $Me_2NC(S)NHP(S)Ph_2$, or $Et_2NC(S)NHP(S)(OPh)_2$ have been described. For the latter, the crystal structure[24] consists on a trinuclear derivative of formula $[Cu\{Et_2NC(S)NP(S)(OPh)_2\}]_3$. The three-coordinate environment of the copper atom in $[Cu\{PhC(O)NP(S)Ph_2\}(PPh_3)]$[7] has also been described. To the best of our knowledge the only such silver complex reported is the tetranuclear derivative $[Ag\{PhC(S)NP(S)(O\textit{i}Pr)_2\}]_4$,[25] but no related gold complexes have been described. In this paper we report the synthesis and characterization of gold and silver complexes with the *N*-[bis(isopropoxy)thiophosphoryl]thiobenzamide

[a] Departamento de Química Inorgánica, Instituto de Ciencia de Materiales de Aragón, Universidad de Zaragoza-CSIC, 50009 Zaragoza, Spain
[b] Escuela Politécnica Superior de Huesca, Carretera de Cuarte s/n 22071 Huesca, Spain
[c] Kazan State University, Kremlevskaya, st. 18, Kazan 420008, Russia

[PhC(S)NHP(S)(O*i*Pr)$_2$, HL^1) and *N*-[bis(isopropoxy)-thiophosphoryl]-*N*′-phenylthiourea (PhNHC(S)NHP(S)-(O*i*Pr)$_2$, HL^2) ligands (see Schemes 1 and 2). The first homoleptic anionic metal compounds [Au^{I}L$_2$]$^-$ are also reported. The previously reported derivatives are neutral (the metal oxidation state is +II) and different stoichiometries were obtained when the oxidation state was +I. In many of the derivatives shown here, coordination of the ligand takes place without any previous deprotonation of the ligands.

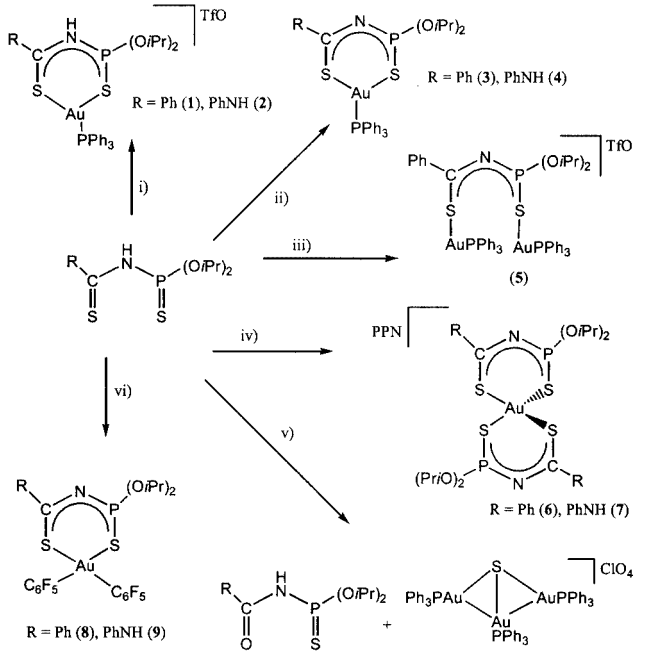

Scheme 1. i) [Au(TfO)(PPh$_3$)]/CH$_2$Cl$_2$, ii) [Au(TfO)(PPh$_3$)]/KOH, MeOH, iii) 2 [Au(TfO)(PPh$_3$)]/KOH, MeOH, iv) 1/2 PPN[Au(acac)$_2$]/CH$_2$Cl$_2$, 1/2 PPN[AuCl$_2$]/KOH, MeOH, v) [O{Au(PPh$_3$)}$_3$]ClO$_4$/CH$_2$Cl$_2$, vi) [Au(C$_6$F$_5$)$_2$(acac)]/CH$_2$Cl$_2$, NBu$_4$[Au(C$_6$F$_5$)$_2$]/KOH, MeOH

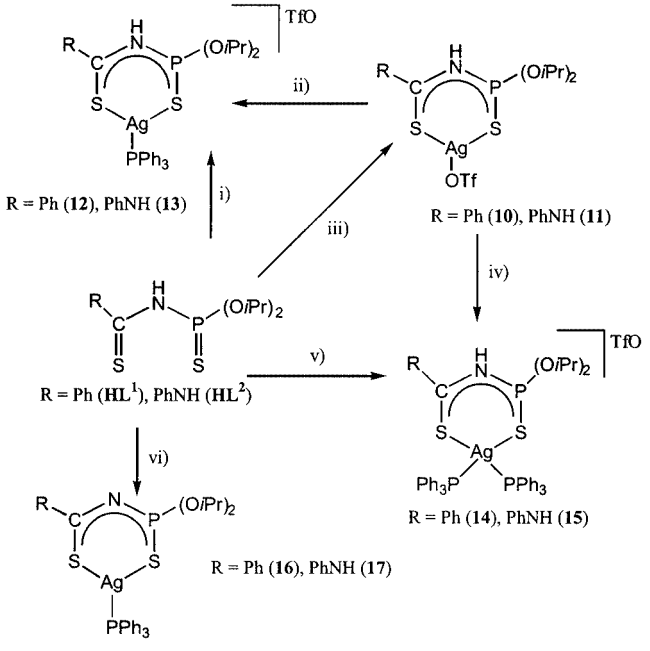

Scheme 2. i) [Ag(TfO)(PPh$_3$)]/CH$_2$Cl$_2$, ii) PPh$_3$, iii) AgTfO/CH$_2$Cl$_2$, iv) 2 PPh$_3$, v) [Ag(TfO)(PPh$_3$)$_2$]/CH$_2$Cl$_2$, vi) [Ag(TfO)(PPh$_3$)]/KOH, MeOH, [Ag(acac)(PPh$_3$)]/CH$_2$Cl$_2$

Results and Discussion

All the complexes described below are air and moisture stable. The behavior of their acetone solutions corresponds to their proposed neutral or ionic structures (Tables 1 and 2 show the conductivity values, yields, elemental analyses for C, H, N and S, NMR and mass spectral data for all the complexes presented). Characteristic absorptions are present in the IR spectra of the ligands.

Thus, in HL^1 the ν(NH) vibration appears at 3240 cm^{-1} and the ν(P=S) at 648. In HL^2 the ν(P=S) vibration appears at 640 cm^{-1}. Two ν(NH) vibrations appear at 3200 (Ph−NH) and 3063 cm^{-1} (C−NH−P), the second being observed as a shoulder of the nujol band in the spectrum of HL^2. In the discussion we will comment on the modification of the first band and the other band always appears as a shoulder on the nujol band in the complexes in which the ligand HL^2 has not been deprotonated. The shifts of the ν(P=S) IR band and the ^{31}P{^{1}H} NMR resonance due to the phosphorus atom of the ligand from those in the free ligands point to the involvement of the sulfur atom of the PS unit in the formation of the complexes. The shift of the ν(NH) vibration in the SCN(H)PS unit in the complexes which contain ligands which have not been deprotonated could point to the formation of a six-membered chelating ring. This is a reasonable proposal since tendency of the ligands to coordinate in a chelating form has already been shown in the literature and has also been confirmed by the X-ray structures of two of the compounds described herein.

Gold Complexes

The displacement of the labile trifluoromethanesulfonate ligand in [Au(TfO)(PPh$_3$)] affords the complexes [Au(HL^1)(PPh$_3$)]TfO (**1**) and [Au(HL^2)(PPh$_3$)]TfO (**2**). The vibrations corresponding to the anionic TfO groups are present in their IR spectra [$\nu_{asym}(SO_3)$ 1270, $\nu_{sym}(CF_3)$ 1225, $\nu_{asym}(CF_3)$ 1151, $\nu_{sym}(SO_3)$ 1033 cm^{-1}].[26] In **1** the ν(NH) absorption appears at 3242 cm^{-1} and the ν(P=S) at 579. In **2** they appear at 3205 and 580 cm^{-1}, respectively. In their ^{1}H NMR spectra the isopropyl hydrogen atoms appear at approximately δ = 1.3 (CH$_3$) and 5.0 (CH) ppm. The NH hydrogen atoms of the amido-thiophosphoryl groups appear at around δ = 10 (**1**) or 11 (**2**) ppm. The values in each case are at lower fields than in the corresponding ligands (δ = 8.05 ppm HL^1; 9.61 ppm HL^2). In the spectrum of **2** the shift of the other NH hydrogen atom (δ = 9.69 ppm) also appears downfield of the corresponding shift in HL^2 (δ = 7.01 ppm).

The ^{31}P{^{1}H} NMR spectra show two resonances, as expected, for the two nonequivalent phosphorous atoms. Those observed near δ = 50 ppm can be assigned to the phosphorous atoms of the HL^1 or HL^2 coordinated fragments. In **1** the signal is δ = 2.6 ppm upfield from that in

 © 2004 Wiley-VCH Verlag GmbH & Co. KGaA, Weinheim

Table 1. Data for gold complexes **1**−**9**

Compound	Elemental Analysis[a] C	H	N	S	Yield (%)	Λ_M[b]	^{1}H NMR[c][d]	^{31}P{^{1}H}[c]
[Au(L^{1}H)(PPh$_3$)]TfO (**1**)	41.65 (41.5)	3.55 (3.8)	1.75 (1.5)	10.15 (10.4)	78	160	1.36 (br. m, 12 H, *i*Pr-CH$_3$), 4.95 (br. m, 2 H, *i*Pr-CH), 7.20−7.79 (v.m., br, 20 H, Ph), 10.00 (br. s, 1 H, C-HN-P)	55.1 (s), 36.9 (s)
[Au(L^2 H)(PPh$_3$)]TfO (**2**)	40.5 (40.85)	3.45 (3.85)	2.75 (3.0)	10.35 (10.2)	84	132	1.31−1.51 (v.m., br, 12 H, *i*Pr-CH$_3$), 4.85 (br. m, 2 H, *i*Pr-CH), 7.20−7.38 (v.m., br, 20 H, Ph), 9.69 (br. s, 1 H, C-HN-P), 10.83 (br. s, Ph-HN)	54.9 (s), 36.8 (s)
[Au(L^1)(PPh$_3$)] (**3**)	47.65 (48.0)	3.95 (4.4)	1.3 (1.8)	7.95 (8.3)	58	1	1.26 (br. m, 12 H, *i*Pr-CH$_3$), 4.76 (br. m, 2 H, *i*Pr-CH), 7.20−7.47 (br. m, 20 H, Ph)	55.7 (s), 37.7 (s)
[Au(L^2)(PPh$_3$)] (**4**)	46.85 (47.1)	4.05 (4.45)	3.15 (3.55)	7.65 (8.1)	48	3	1.25 (br. m, 12 H, *i*Pr-CH$_3$), 4.73 (br. m, 2 H, *i*Pr-CH), 7.24−7.58 (m., br, 20 H, Ph + 1 Ph-HN)	54.8 (s), 37.9 (s)
[Au$_2$(L^1)(PPh$_3$)$_2$]TfO (**5**)	43.05 (43.4)	3.35 (3.55)	0.6 (1.0)	7.25 (6.95)	72	178	1.43 (br. m, 12 H, *i*Pr-CH$_3$), 4.92 (br. m, 2 H, *i*Pr-CH), 7.18 (v.m., br, 20 H, Ph)	49.4 (s), 36.2 (s)
PPN[Au(L^1)$_2$] (**6**)	54.45 (54.4)	4.6 (5.0)	2.8 (3.05)	8.95 (9.35)	69	77	1.27 (br. m, 24 H, *i*Pr-CH$_3$), 4.83 (br. m, 4 H, *i*Pr-CH), 7.01−7.85 (v.m., br, 40 H, Ph)	63.1 (s)
PPN[Au(L^2)$_2$] (**7**)	53.4 (53.85)	4.9 (5.05)	4.15 (4.05)	8.95 (9.25)	64	88	1.24 (br. m, 24 H, *i*Pr-CH$_3$), 4.80 (br. m, 4 H, *i*Pr-CH), 7.09−7.63 (v.m., br, 20 H, Ph), 8.52 (br. s, 2 H, Ph-HN-C)	63.7 (s)
[Au(L^1)(C$_6$F$_5$)$_2$] (**8**)	35.55 (35.45)	2.5 (2.25)	1.55 (1.65)	7.5 (7.55)	54	2	1.25−1.48 (v.m., br, 12 H, *i*Pr-CH$_3$), 4.95 (br. m, 2 H, *i*Pr-CH), 7.36−8.14 (v.m., br, 5 H, Ph)	41.8 (s)
[Au(L^2)(C$_6$F$_5$)$_2$] (**9**)	35.3 (34.8)	2.5 (2.35)	3.2 (3.25)	7.15 (7.45)	61	1	1.39 (br. m, 12 H, *i*Pr-CH$_3$), 4.82 (br. m, 2 H, *i*Pr-CH), 7.22−7.90 (v.m., br, 5 H, Ph + 1 Ph-HN)	43.5 (s)

[a] Calcd. values in parentheses. [b] $\Omega^{-1}cm^2mol^{-1}$. [c] δ in ppm. [d] v.m. means more than one multiplet.

the free ligand and in **2** it is shifted δ = 2.1 ppm downfield of that in free HL^2. The signal in the higher field region can be assigned to the triphenylphosphane ligand. In the Liquid Secondary Ion Mass Spectra (LSIMS +) of **2** the cation molecular peak can be observed at *m*/*z* = 792 (13 % intensity), although the most intense peak corresponds to the species [Au(PPh$_3$)]$^+$ (*m*/*z* = 459). The cationic molecular peak was not observed in the spectrum of **1** and the most intense peak corresponds to the species [Au(PPh$_3$)]$^+$ in this case also. An observation of note is the presence in both spectra of the peak corresponding to [Au$_2$L(PPh$_3$)$_2$]$^+$ which indicates the important stability of these species. This observation led us to specifically investigate the synthesis of complexes of higher nuclearity. The starting compound [O{Au(PPh$_3$)}$_3$]$^+$ is a good deprotonating agent which can also be used to introduce between one and three "Au(PPh$_3$)" fragments. The results of such reactions with both ligands in a 1:1 molar ratio are shown in Scheme 1. In both cases, the cleavage of the C=S bond and the formation of the corresponding *N*-[bis(isopropoxy)thiophosphoryl]-benzamide [^{31}P{^{1}H} NMR: δ = 58.7(s)ppm] or *N*-[bis(isopropoxy)thiophosphoryl]-*N*′-phenylurea [^{31}P{^{1}H} NMR: δ = 58.2(s) ppm] and the gold complex [S{Au(PPh$_3$)}$_3$]$^+$ (^{31}P{^{1}H} NMR: δ: s, 33.4 ppm) were observed. Deprotonation of the ligands and coordination of only one "Au(PPh$_3$)" fragment is possible by using the starting compound [Au(acac)(PPh$_3$)] (acac = acetylacetonate). This reaction afforded [AuL^1(PPh$_3$)] (**3**) and [AuL^2(PPh$_3$)] (**4**). In the IR spectra of the latter complexes, the ν(P=S) vibrations appear at 584 and 577 cm^{-1}, respectively. The ν(NH) vibrations due to the "CN(H)P" fragments were not observed and in the spectrum of **4** the ν(NH) vibration corresponding to the "PhNH" unit appears at 3293 cm^{-1}. The ^{1}H NMR spectra also corroborate the observed deprotonation of the ligands since no signal corresponding to the "CN(H)P" fragment could be observed. In the spectrum of **4** the signal corresponding to the "PhNH" hydrogen atom overlaps with the broad signal arising from the protons of the PPh$_3$ group. The ^{31}P{^{1}H} NMR spectra of **3** and **4** show similar patterns to those observed in the spectra of **1** and **2**. It is of note that the chemical shifts observed for the thiophosphoryl phosphorous atoms are less significant compared with those of the analogous nondeprotonated complexes **1** and **2**. The signals corresponding to the triphenylphosphane ligands are shifted about 1 ppm downfield in both cases. In the LSIMS + the molecular peaks

 © 2004 Wiley-VCH Verlag GmbH & Co. KGaA, Weinheim

Table 2. Data for silver complexes **10**−**17**

Compound	Analytical data[a] C	H	N	S	Yield (%)	Λ_M[b]	^{1}H NMR[c][d]	^{31}P{^{1}H}[c]
[Ag(TfO)(L^{1}H)] (**10**)	30.7 (29.3)	4.0 (3.5)	2.45 (2.45)	15.35 (16.75)	53	67	1.39 (br. m, 12 H, *i*Pr-CH$_3$), 4.89 (br. m, 2 H, *i*Pr-CH), 7.36−8.22 (v.m., br, 5 H, Ph + 1 C-HN-P)	52.2
[Ag(TfO)(L^{2}H)] (**11**)	29.0 (28.55)	4.0 (3.6)	4.5 (4.75)	15.05 (16.3)	78	72	1.40 (br. m, 12 H, *i*Pr-CH$_3$), 4.88 (br. m, 2 H, *i*Pr-CH), 7.37 (br. m, 5 H, Ph), 9.58 (br. s, 1 H, C-HN-P), 10.65 (br. s, Ph-HN)	54.0
[Ag(L^{1}H)(PPh$_3$)]TfO (**12**)	45.75 (45.95)	4.25 (4.2)	1.55 (1.65)	11.25 (11.5)	75	136	1.37 (br. m, 12 H, *i*Pr-CH$_3$), 4.99 (br. m, 2 H, *i*Pr-CH), 7.20−7.88 (m., br, 20 H, Ph), 11.57 (br. s, 1 H, C-HN-P)	53.7 (s), 15.3 (dd), 627.4, 543.9
[Ag(L^2 H)(PPh$_3$)]TfO (**13**)	45.35 (45.15)	4.05 (4.25)	3.65 (3.9)	10.95 (11.3)	94	132	1.19−1.40 (v.m., br, 12 H, *i*Pr-CH$_3$), 4.89 (br. m, 2 H, *i*Pr-CH), 7.20−7.38 (v.m., br, 20 H, Ph), 9.61 (br. s, 1 H, C-HN-P), 10.42 (br. s, Ph-HN)	54.8 (s), 14.5(dd), 617.9, 535.7
[Ag(L^{1}H)(PPh$_3$)$_2$]TfO (**14**)	54.2 (54.65)	4.35 (4.6)	1.1 (1.25)	7.3 (8.75)	85	155	1.33 (br. m, 12 H, *i*Pr-CH$_3$), 4.79 (br. m, 2 H, *i*Pr-CH), 7.21−7.62 (v.m., br, 35 H, Ph + 1 C-HN-P)	54.5 (s), 7.3 (br)
[Ag(L^{2}H)(PPh$_3$)$_2$]TfO (**15**)	53.8 (53.9)	4.45 (4.6)	2.4 (2.5)	7.44 (8.65)	84	140	1.38 (br. m, 12 H, *i*Pr-CH$_3$), 4.78 (br. m, 2 H, *i*Pr-CH), 7.12−7.31 (v.m., br, 35 H, Ph), 9.27 (br. s, 1 H, C-HN-P), 9.83 (br. s, 1 H, Ph-HN)	54.9 (s), 6.1 (dd), 409.8, 360.0
[Ag(L^1)(PPh$_3$)] (**16**)	53.65 (54.25)	4.8 (5.0)	1.95 (2.05)	9.05 (9.35)	66	1	1.27 (br. m, 12 H, *i*Pr-CH$_3$), 4.81 (br. m, 2 H, *i*Pr-CH), 7.22−7.61 (v.m., br, 20 H, Ph)	57.1 (s), 14.1 (dd), 570.3, 494.7
[Ag(L^2)(PPh$_3$)] (**17**)	52.65 (53.05)	4.45 (5.05)	3.55 (4.0)	8.75 (9.15)	54	1	1.21−1.49 (v.m., br, 12 H, *i*Pr-CH$_3$), 4.72 (br. m, 2 H, *i*Pr-CH), 6.94−7.68 (v.m., br, 20 H, Ph) + 1 Ph-HN)	58.4 (s), 14.3 (br)

[a] Theoretical values in brackets. [b] $\Omega^{-1}cm^2mol^{-1}$. [c] δ in ppm. [d] v.m. means more than one multiplet.

appear at *m*/*z* = 776 (16 %) (**3**) and 791 (8 %) (**4**). The reaction of HL^1 or HL^2 with [Au(TfO)(PPh$_3$)] in a 1:1 molar ratio in MeOH with a stoichiometric amount of KOH affords **3** or **4**. The reaction in a 1:2 molar ratio of HL^1 with [Au(TfO)(PPh$_3$)] in KOH/MeOH affords [Au$_2$L^1(PPh$_3$)$_2$]TfO (**5**). In the IR spectrum of **5** the vibrations corresponding to the anionic trifluoromethanesulfonate are observed and the ν(P=S) band appears at 579 cm^{-1}. The ligand deprotonation is confirmed by the absence of the NH vibration in the IR spectrum and an analysis of the ^{1}H NMR spectrum in which only those absorptions corresponding to the isopropyl and phenyl groups are observed. The ^{31}P{^{1}H} NMR spectrum display two signals, that at δ = 49.9 ppm can be assigned to the phosphorus atom of the thiophosphoryl group with the other (a broad signal) corresponding to the triphenylphosphane ligands. The cationic molecular peak is present in the LSIMS + (*m*/*z* = 1234, 52 %). The same reaction with HL^2 affords a solid, the ^{31}P{^{1}H} NMR spectrum of which displays five signals. The most intense resonance corresponds to the [S{Au(PPh$_3$)}$_3$]$^+$ cation and two of the signals which appear with very weak intensities at 54.9 and 37.0 ppm possibly correspond to the analog of **5** i.e. [Au$_2$L^2(PPh$_3$)$_2$]TfO. In fact, the LSIMS + shows a peak corresponding to the species [Au$_2$L^2(PPh$_3$)$_2$] (*m*/*z* = 1249, 28 %) and the proposed structure is shown in Scheme 1.

We have also investigated the reactivity of these ligands towards PPN[Au(acac)$_2$] in a molar ratio of 2:1. The resultant compounds PPN[Au(L^1)$_2$] (**6**) and PPN[Au(L^2)$_2$] (**7**) show ν(P=S) bands at 610 and 578 cm^{-1}, respectively. In **7** the ν(NH) vibration appears at 3302 cm^{-1}. The ^{1}H NMR spectra show the phenyl and isopropyl protons and in the case of compound **7** the NH hydrogen atom appears at δ = 8.52 ppm. Two signals are present in their ^{31}P{^{1}H} NMR spectra. The resonance at approximately δ = 63 ppm can be assigned to the thiophosphoryl group which shows a very significant downfield shift from the signals of the ligands. The other signal at δ = 21.2 ppm corresponds to the PPN cation. The anionic molecular peak of compound **6** is present in the LSIMS − (*m*/*z* = 829, 85 %). Although no structural confirmation has been obtained by X-ray crystallography, a homoleptic mononuclear derivative has been proposed. More complicated arrangements consisting of more that one "[AuL$_2$]$^+$" unit could give rise to the same conductivity and elemental analysis values but are considered to be much less probable. Based on the probable chelate mode

 © 2004 Wiley-VCH Verlag GmbH & Co. KGaA, Weinheim

of the ligand and the results of similar studies with other metals we are inclined to favor a tetra-coordinated arrangement as the most likely structure.

The syntheses of gold(III) complexes derived from [Au(acac)(C_6F_5)$_2$] have also been carried out. The resultant products, [Au(C_6F_5)$_2$(L^1)] (**8**) and [Au(C_6F_5)$_2$(L^2)] (**9**), show ν(P=S) vibrations at 567 and 591 cm^{-1}, respectively, and in **9** the ν(NH) vibration appears at 3403 cm^{-1}. The vibrations corresponding to the pentafluorophenyl rings are also present at around 1508, 964 and 784 cm^{-1}. In both derivatives the deprotonation of the ligands is evident from the ^{1}H NMR spectra. Very notable high field shifts from the values in the free ligands were observed in the ^{31}P{^{1}H} spectra for both complexes (see Table 1). The ^{19}F spectra show the presence of two nonequivalent pentafluorophenyl rings, five signals were observed in the ratio of 1(F_p):1(F_p):2(F_o):2(F_o):4(F_m). The signal at approximately δ = −160 ppm corresponds to the *meta* fluorine atoms. The fluorine atoms in the *para*- and *ortho*-positions give rise to two triplets at around δ = −158 ppm and two multiplets at approximately δ = −121 ppm, respectively. The molecular peaks are present in the LSIMS + at *m*/*z* = 848 (24 %) (**8**) and 863 (42 %; **9**).

Silver Complexes

The reaction of AgTfO with both ligands in a molar ratio of 1:1 afforded the complexes [Ag(TfO)(HL^1)] (**10**) and [Ag(TfO)(HL^2)] (**11**). Their conductivity values in acetone solution are between those described for the presence of no electrolyte and a 1:1 electrolytic species. This is due to the lability of the trifluoromethanesulfonate anion. In their IR spectra the vibrations corresponding to the presence of covalent TfO[26] groups are present [$\nu_{asym}(SO_3)$ 1283 and 1240, $\nu_{sym}(CF_3)$ 1220, $\nu_{asym}(CF_3)$ 1180, $\nu_{sym}(SO_3)$ 1030 cm^{-1}]. The ν(NH) and ν(P=S) vibrations appear at 3290, 575 (**10**) or 3270, 598 (**11**) cm^{-1}. In the ^{1}H NMR spectrum of **10** the NH hydrogen atom bonded to the thiophosphoryl group is coincidental with the multiplet which corresponds to the phenyl protons whereas in **11**, it appears at δ = 10.65 ppm. The other NH proton in **11** shows a resonance at δ = 9.58 ppm. Their ^{31}P{^{1}H} NMR spectra both display one singlet near δ = 50 ppm. These resonances are shifted upfield by δ = 5.5 ppm in (**10**) and downfield by δ = 1.2 ppm in (**11**) from those of the free ligands. The LSIMS + of complex **11** shows the cationic molecular peak [Ag(HL^2)]$^+$ at *m*/*z* = 441 (47 %).

Displacement of the trifluoromethanesulfonate anion and deprotonation in **10** and **11** allows the synthesis of different complexes. Thus, the reaction with triphenylphosphane in a 1:1 or 1:2 molar ratio affords the three-coordinate [Ag(HL^1)(PPh_3)]TfO (**12**), [Ag(HL^2)(PPh_3)]TfO (**13**) or four-coordinate [Ag(HL^1)(PPh_3)$_2$]TfO (**14**) and [Ag(HL^2)(PPh_3)$_2$]TfO (**15**) complexes. Compounds **12** and **13** can also be obtained by reaction of the ligands with [Ag(TfO)(PPh_3)] in a 1:1 molar ratio. In their IR spectra the vibrations corresponding to the TfO$^-$ anion are present and those due to ν(P=S) appear at 575 (**12**) and 574 cm^{-1} (**13**). The NH bands appear at 3260 (**12**) or 3220 (**13**) cm^{-1}. In the ^{1}H NMR spectra, resonances arising from the hydrogen atoms of the NH groups bonded to the thiophosphoryl groups are shifted to low field from those of the free ligands. An additional signal is present in **13** at δ = 9.61 ppm due to the hydrogen atom of the NH urea unit. In the ^{31}P{^{1}H} NMR spectra the two nonequivalent phosphorus atoms display resonances with different shapes. One of them, assigned to the thiophosphoryl group, is a narrow resonance which appears at about δ = 54 ppm while the other is broad and corresponds to the triphenylphosphane ligand. When the spectra were recorded at −55 °C the broad resonances split into two doublets as a consequence of the phosphorus atom coupling to the two silver isotopes, ^{107}Ag and ^{109}Ag. The LSIMS + show the cationic molecular peaks in both cases [*m*/*z* = 686, 28 % (**12**); 704, 31 % (**13**)].

Like **12** and **13**, complexes **14** and **15** can also be obtained by reaction of the ligands with [Ag(TfO)(PPh_3)$_2$] in a 1:1 molar ratio. In their IR spectra the ν(P=S) vibrations appear at 571 (**14**) and 573 (**15**) cm^{-1}, and those arising from the NH groups come at 3280 (**14**) and 3220 (**15**) cm^{-1}. In the ^{1}H NMR spectra of **15** both the NH resonances can be observed whereas in **14** the resonance of the hydrogen atom of the NH group is obscured by the phenyl hydrogen resonances. The ^{31}P{^{1}H} NMR spectra show the same patterns observed for **12** and **13** but only in the case of **15** the broad signal becomes split at low temperature (even at −85 °C). For these four-coordinate complexes the resonances due to the triphenylphosphane ligands appear near δ = 7 ppm which is upfield of those in the three-coordinate analogs. The structure of both complexes have been analyzed by X-ray studies which reveal the expected four-coordination (tetrahedral geometry) around the silver center (Figure 1, Figure 2). In compound **14** the ring defined by Ag(1), S(1), P(1), N(1), C(1) and S(2) adopts a boat conformation in which the angle between the planes defined by S(1), P(1), Ag(1), S(2) and P(1), N(1), C(1), S(2) is 53.7°. Compound **15** shows a twist boat conformation in which the atoms S(1), Ag(1), S(2) and C(1) lie in the same plane. Similar Ag−P bond lengths (Tables 2 and 3) can be observed in both complexes which vary from 2.4712(8) to 2.4909(7) Å. The shortest values of those found in [Ag(dppe)$_2$]NO_3 [2.488(3)−2.527(3) Å][27] are very close to those in **14** and **15** and also those found in [Ag(phen){(PPh_2)$_2$$C_2B_{10}H_{10}$}]$ClO_4$ [2.463(2), 2.479(2) Å].[28] Longer values have been found in [Ag{($SPPh_2$)$_2$$CH_2$}{($PPh_2$)$_2$$C_2B_{10}H_{10}$}]$ClO_4$ [2.526(2), 2.532(2) Å][28] and in [Ag(PPh_3)$_4$]ClO_4 (1 × 2.650(2), 3 × 2.668(5) Å].[29] Two different Ag−S bond lengths are present in each complex, the distances to the sulfur atoms of the thiophosphoryl groups are longer [2.6952(8) Å (**14**), 2.6648(8) (**15**) Å] than the other Ag-S distances [2.5892(2) Å (**14**), 2.5379(8) (**15**) Å] in both complexes (Table 4). These values can be compared with those found in other tetrahedral silver complexes such as [AgBr(18S_6)] (18S_6 = 1,4,7,10,13,16-hexathiacyclooctadecane) [2.514(1)−2.636(1) Å],[30] [Ag{($SPPh_2$)$_2$$CH_2$}{($PPh_2$)$_2$$C_2B_{10}H_{10}$}]$ClO_4$ [2.540(2), 2.588(2) Å],[28] [Ag{$S_2C_2(CN)_2$}(PPh_3)$_4$][31]

 © 2004 Wiley-VCH Verlag GmbH & Co. KGaA, Weinheim

[2.568(7), 2.653(7) Å], or in $[Ag_4(\mu_3\text{-}SC_2B_{10}H_{11})_2(\mu\text{-}O_3SCF_3)_2(PPh_3)_2]$[32] [two tetrahedral, two trigonal silver atoms, Ag(tetrahedral)−S distances 2.5467(14), 2.6508(14) Å].

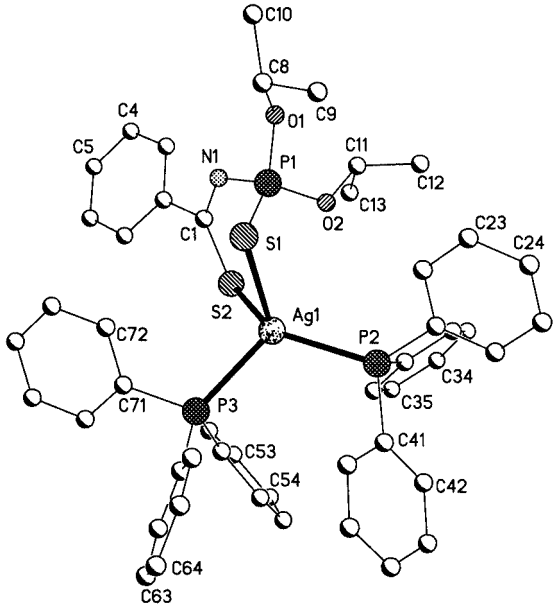

Figure 1. Molecular structure of the cation of compound **14**; hydrogen atoms have been omitted for clarity

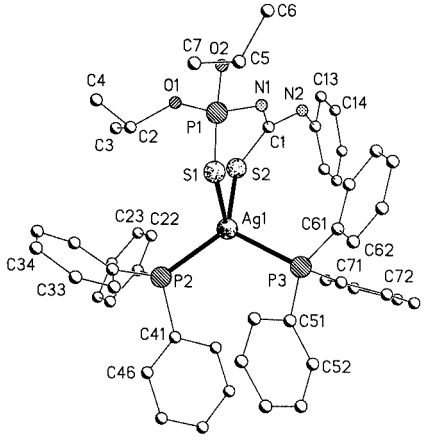

Figure 2. Molecular structure of the cation of compound **15**; hydrogen atoms have been omitted for clarity

Table 3. Selected bond lengths [Å] and angles [°] for **14**

Ag(1)−P(2)	2.4711(8)	N(1)−C(1)	1.355(3)
Ag(1)−P(3)	2.4907(7)	N(1)−P(1)	1.685(2)
Ag(1)−S(1)	2.5893(7)	P(1)−O(2)	1.550(2)
Ag(1)−S(2)	2.6954(7)	P(1)−O(1)	1.556(2)
S(1)−P(1)	1.9440(10)	S(2)−C(1)	1.666(3)
P(2)−Ag(1)−P(3)	116.11(2)	C(1)−S(2)−Ag(1)	114.36(10)
P(2)−Ag(1)−S(1)	117.50(2)	C(1)−N(1)−P(1)	128.2(2)
P(3)−Ag(1)−S(1)	115.56(2)	O(2)−P(1)−O(1)	106.61(11)
P(2)−Ag(1)−S(2)	117.29(2)	O(1)−P(1)−N(1)	99.81(11)
P(3)−Ag(1)−S(2)	90.74(2)	O(2)−P(1)−S(1)	112.25(8)
S(1)−Ag(1)−S(2)	94.48(2)	O(1)−P(1)−S(1)	115.66(9)
P(1)−S(1)−Ag(1)	92.47(3)	N(1)−P(1)−S(1)	114.52(9)

Table 4. Bond lengths [Å] and angles [°] for **15**

Ag(1)−P(2)	2.4510(8)	P(2)−C(41)	1.816(3)
Ag(1)−P(3)	2.4808(8)	P(2)−C(21)	1.820(3)
Ag(1)−S(2)	2.5379(8)	P(3)−C(51)	1.820(3)
Ag(1)−S(1)	2.6648(8)	P(3)−C(71)	1.824(3)
P(1)−O(1)	1.557(2)	P(3)−C(61)	1.827(3)
P(1)−O(2)	1.562(2)	S(2)−C(1)	1.682(3)
P(1)−N(1)	1.674(3)	N(1)−C(1)	1.368(4)
P(1)−S(1)	1.9390(10)	N(2)−C(1)	1.336(4)
P(2)−C(31)	1.814(3)	N(2)−C(11)	1.422(4)
P(2)−Ag(1)−P(3)	118.51(3)	O(1)−P(1)−O(2)	104.35(11)
P(2)−Ag(1)−S(2)	113.46(3)	O(1)−P(1)−N(1)	102.18(12)
P(3)−Ag(1)−S(2)	114.78(3)	O(2)−P(1)−N(1)	99.64(12)
P(2)−Ag(1)−S(1)	111.39(3)	O(1)−P(1)−S(1)	116.81(8)
P(3)−Ag(1)−S(1)	98.05(3)	O(2)−P(1)−S(1)	113.93(8)
S(2)−Ag(1)−S(1)	97.08(2)	N(1)−P(1)−S(1)	117.63(10)

The syntheses of deprotonated derivatives have been carried out by two synthetic routes just as for the gold complexes. The first is the use of $(acac)^-$ as a deprotonating agent, the other using methanol and KOH. The reactions afford $[AgL^1(PPh_3)]$ (**16**) or $[AgL^2(PPh_3)]$ (**17**). In the IR spectrum of **17** the ν(P=S) vibration appears at 575 cm^{-1} and the ν(NH) at 3203 cm^{-1}. Due to a poor mixture between **16** and Nujol, no satisfactory IR spectrum for **16** could be recorded. The deprotonation of the ligands is evident from the ^1H NMR spectra. Moreover, two resonances are present in the $^{31}P\{^1H\}$ NMR spectra and only in the case of compound **16**, the broad signal is split into two doublets.

Conclusions

The reactions studied indicate that a great variety of coordination types and complexes can be prepared (Schemes 1 and 2). Some notable points are a) The use of acetylacetonate as a suitable deprotonating agent. This is a new synthetic pathway that allows the use of solvents other than alcohols. The mixture MeOH/KOH, widely described in the literature, may not be the best since some metallic fragments may not be soluble in alcohol. b) The [Ag(HL)(TfO)] compounds synthesized are interesting starting materials which allow the incorporation of the "Ag(HL)" unit (also deprotonated) into more complicated structures. c) Cleavage of the C=S bond occurs upon the reaction of the oxonium salt $[O\{Au(PPh_3)\}_3]$ with the ligands.

Experimental Section

Reagents: AgTfO and PPh_3 were purchased from Aldrich and were used as received. The ligands (HL^1)[4] and (HL^2)[5] and the starting materials $[Au(acac)(PPh_3)]$,[33] $[O\{Au(PPh_3)\}_3]ClO_4$,[34] $[Au(acac)(C_6F_5)_2]$,[35] $PPN[Au(acac)_2]$,[33,36] $[Ag(TfO)(PPh_3)]$,[37] $[Ag(TfO)(PPh_3)_2]$[37] were synthesized according to literature methods. $[Au(TfO)(PPh_3)]$ was synthesized from $[AuCl(PPh_3)]$[38] and AgTfO in dichloromethane.

 © 2004 Wiley-VCH Verlag GmbH & Co. KGaA, Weinheim

General Procedures: Infrared spectra were recorded on a Perkin−Elmer FT-IR Spectrum 1000 spectrophotometer in the range 4000−400 cm^{-1} using Nujol mulls between polyethylene sheets. Conductivities were measured in (ca. 5×10^{-4}) M acetone solutions with a Jenway 4010 conductimeter. Elemental analyses of C, H, N and S were carried out with a Perkin−Elmer 240C microanalyzer. Mass spectra were recorded on a VG Autospec instrument using the LSIMS (+, −) techniques and nitrobenzyl alcohol as a matrix and on an HP59987 A ELECTROSPRAY. ^{1}H, ^{19}F and ^{31}P NMR spectra were recorded on a Bruker ARX 300 spectrometer in $CDCl_3$ or $(CD_3)_2CO$. Chemical shifts are quoted relative to external $SiMe_4$ (^{1}H), $CFCl_3$ (^{19}F) or 85 % H_3PO_4 (^{31}P).

Syntheses: [Au(HL)(PPh$_3$)]TfO [L = L^1(1), L^2(2)]: HL^1 (0.1 mmol, 0.032 g) or HL^2 (0.1 mmol, 0.033 g) was added to a dichloromethane solution (20 mL) of [Au(TfO)(PPh_3)] (0.1 mmol, 0.0610 g). After stirring for 15 min the solvent was reduced to about 5 mL. Addition of *n*-hexane (20 mL) led to precipitation of an orange (**1**) or white (**2**) solid. Recrystallization from dichloromethane/hexane afforded the pure compounds.

[Au(L)(PPh$_3$)] [L = L^1(3), L^2(4)] Method a: KOH (0.1 mmol, 0.006 g) and then HL^1 (0.1 mmol, 0.032 g) or HL^2 (0.1 mmol, 0.033 g) was added to a solution of [Au(TfO)(PPh_3)] (0.1 mmol, 0.0610 g) in methanol (20 mL). After stirring for 15 min the solvent was reduced to about 5 mL. Addition of *n*-hexane (20 mL) led to precipitation of a yellow (**3**) or white (**4**) solid.

Method b: HL^1 (0.1 mmol, 0.032 g) or HL^2 (0.1 mmol, 0.033 g) was added to a solution of [Au(acac)(PPh_3)] (0.1 mmol, 0.056 g) in dichloromethane. After stirring for 15 min the solution was filtered through celite and the filtrate concentrated to about 5 mL. Addition of *n*-hexane (20 mL) led to precipitation of a yellow (**3**) or white (**4**) solid**.** Recrystallization from dichloromethane/hexane afforded the pure compounds.

[Au$_2$(L^1)(PPh$_3$)$_2$]TfO (5): KOH (0.1 mmol, 0.006 g) and HL^1 (0.1 mmol, 0.032 g) were added to a solution of [Au(TfO)(PPh_3)] (0.2 mmol, 0.121 g) in methanol (20 mL). After stirring for 15 min the solvent was concentrated to about 5 mL. Addition of *n*-hexane (20 mL) led to precipitation of a yellow solid (**5**). Recrystallization from dichloromethane/hexane afforded the pure compound.

PPN[Au(L)$_2$] [L = L^1(6), L^2 (7)]: HL^1 (0.2 mmol, 0.064 g) or HL^2 (0.2 mmol, 0.066 g) was added to a solution of PPN[Au(acac)$_2$] (0.1 mmol, 0.093 g) in dichloromethane (20 mL). After stirring for 15 min the solution was filtered through celite and the filtrate concentrated to about 5 mL. Addition of *n*-hexane (20 mL) led to precipitation of a pale yellow (**6**) or brown (**7**) solid. Recrystallization from dichloromethane/hexane afforded the pure compounds.

[Au(C$_6$F$_5$)$_2$(L)] [L = L^1 (8), L^2 (9)]: HL^1 (0.1 mmol, 0.032 g) or HL^2 (0.1 mmol, 0.033 g) was added to a solution of [Au(C_6F_5)$_2$(acac)] (0.1 mmol, 0.063 g) in dichloromethane (20 mL). The stirred solution was filtered through celite and the filtrate concentrated to about 5 mL. Addition of *n*-hexane (20 mL) led to precipitation of a yellow solid (**8** or **9**). Recrystallization from dichloromethane/hexane afforded the pure compounds. ^{19}F NMR for **8**: δ = −160 (m, *m*-F, 4F), 156 (t, *p*-F, ^{3}J(FF) 20.0 Hz), 155.7 (t, *p*-F, ^{3}J(FF) 19.8 Hz), −121.9 (m, *o*-F, 2F), −121.7 (m, *o*-F, 2F) ppm. ^{19}F NMR for **9**: δ = −161.8 (m, *m*-F, 4F), 157.2 (t, *p*-F, ^{3}J(FF) 20.0 Hz), 156.8 (t, *p*-F, ^{3}J(FF) 19.6 Hz), −122.4 (m, *o*-F, 2F), −122.1 (m, *o*-F, 2F).

[Ag(HL)(TfO)] [L = L^1 (10), L^2 (11)]: HL^1 (0.1 mmol, 0.032 g) or HL^2 (0.1 mmol, 0.033 g) was added to a dichloromethane solution (20 mL) of Ag(TfO) (0.1 mmol, 0.026 g). After stirring for 4 hours the solvent was reduced to about 5 mL. Addition of *n*-pentane (20 mL) led to precipitation of a yellow (**10**) or white (**11**) solid. Recrystallization from dichloromethane/pentane afforded the pure compounds.

[Ag(HL)(PPh$_3$)]TfO [L = L^1 (12), L^2 (13)] Method a: PPh_3 (0.1 mmol, 0.026 g) was added to a solution of [Ag(HL)(TfO)] (0.1 mmol; L^1 0.057 g, L^2 0.058 g) in dichloromethane (20 mL). After stirring for 15 min the solvent was concentrated to about 5 mL. Addition of *n*-hexane (20 mL) led to precipitation of a yellow (**12**) or white (**13**) solid.

Method b: HL^1 (0.1 mmol, 0.032 g) or HL^2 (0.1 mmol, 0.033 g) was added to a solution of [Ag(TfO)(PPh_3)] (0.1 mmol, 0.052 g) in dichloromethane (20 mL). The stirred solution was concentrated to about 5 mL. Addition of *n*-hexane (20 mL) led to precipitation of a yellow (**12**) or white (**13**) solid. Recrystallization from dichloromethane/hexane afforded the pure compounds.

[Ag(HL)(PPh$_3$)$_2$]TfO [L = L^1 (14), L^2 (15)] Method a: PPh_3 (0.2 mmol, 0.053 g) was added to a solution of [Ag(HL)(TfO)] (0.1 mmol; L^1 0.057 g, L^2 0.058 g) in dichloromethane (20 mL). After stirring for 15 min the solvent was concentrated to about 5 mL. Addition of *n*-hexane (20 mL) led to precipitation of a yellow (**14**) or white (**15**) solid.

Table 5. Details of data collection and structure refinement for **14** and **15**

Compound	**14**	**15**
Chemical formula	$C_{50}H_{50}AgF_3NO_5P_3S_3$	$C_{50}H_{51}AgF_3N_2O_5P_3S_3$
Crystal habit	colorless prism	yellow tablet
Crystal size (mm)	0.5 × 0.2 × 0.14	0.32 × 0.28 × 0.2
Crystal system	monoclinic	triclinic
Space group	$P2_1/c$	$P\bar{1}$
a (Å)	22.0613(19)	12.9484(18)
b (Å)	12.8679(11)	13.3524(19)
c (Å)	18.8993(16)	15.831(2)
α (°)	90	71.895(2)
β (°)	113.755(1)	79.351(3)
γ (°)	90	76.764(2)
V (Å^3)	4910.6(7)	2513.3(6)
Z	4	2
D_c (g cm^{-3})	1.486	1.472
M_r	1098.87	1113.89
F(000)	2256	1144
T (°C)	−100	−100
$2\theta_{max}$ (°)	58	56
μ(Mo-K_α) (mm^{-1})	0.695	0.680
No. of reflections measured	31073	16548
No. of unique reflections	11287	11100
R_{int}	0.0769	0.0386
$R1$[a] [$F > 4\sigma(F)$]	0.0500	0.0446
$wR2$[b](F^2, all refl.)	0.1322	0.1006
No. of reflections used	11287	11100
No. of parameters	603	616
No. of restraints	0	0
S[c]	1.032	0.983
Δρ (Å^{-3})	2.026	1.222

[a] $R1\ (F) = \Sigma||F_o| - |F_c||/\Sigma|F_o|$. [b] $wR2\ (F^2) = [\Sigma\{w(F_o^2 - F_c^2)^2\}/\Sigma\{w(F_o^2)^2\}]^{0.5}$; $w^{-1} = \sigma^2(F_o^2) + (aP)^2 + bP$, where $P = [F_o^2 + 2F_c^2]/3$ and *a* and *b* are constants adjusted by the program. [c] $S = [\Sigma\{w(F_o^2 - F_c^2)^2\}/(n - p)]^{0.5}$, where *n* is the number of data and *p* the number of parameters.

 © 2004 Wiley-VCH Verlag GmbH & Co. KGaA, Weinheim

Method b: HL^1 (0.1 mmol, 0.032 g) or HL^2 (0.1 mmol, 0.033 g) was added to a solution of $[Ag(TfO)(PPh_3)_2]$ (0.1 mmol, 0.078 g) in dichloromethane (20 mL). The stirred solution was concentrated to about 5 mL. Addition of *n*-hexane (20 mL) led to precipitation of a yellow (**14**) or white (**15**) solid. Recrystallization from dichloromethane/hexane afforded the pure compounds.

$[Ag(L)(PH_3)]$ [L = L^1 (16), L^2 (17)] Method a: KOH (0.1 mmol, 0.006 g) and HL^1 (0.1 mmol, 0.032 g) or HL^2 (0.1 mmol, 0.033 g) were added to a solution of $[Ag(TfO)(PPh_3)]$ (0.1 mmol, 0.052 g) in methanol (20 mL). After stirring for 15 min the solvent was concentrated to about 5 mL. Addition of *n*-hexane (20 mL) led to precipitation of a pale yellow (**16**) or white (**17**) solid.
Method b: HL^1 (0.1 mmol, 0.032 g) or HL^2 (0.1 mmol, 0.033 g) was added to a solution of $[Ag(acac)(PPh_3)]$ (0.1 mmol, 0.047 g) in dichloromethane. The stirred solution was filtered through celite and the filtrate concentrated to about 5 mL. Addition of *n*-hexane (20 mL) led to precipitation of a pale yellow (**16**) or white (**17**) solid. Recrystallization from dichloromethane/hexane afforded the pure compounds.

X-ray Crystallographic Study: The crystals were mounted in inert oil on a glass fiber and transferred to the cold gas stream of a Bruker SMART APEX CCD system diffractometer. Data were collected using monochromated Mo-K_α radiation (λ = 0.71073 Å). Absorption corrections were based on multiple scans (program SADABS). The structures were refined on F^2 using the program SHELXL-97.[39] All non-hydrogen atoms were refined anisotropically. CCDC 203107 and 203108 contain the supplementary crystallographic data for this paper. These data can be obtained free of charge at www.ccdc.cam.ac.uk/conts/retrieving.html [or from the Cambridge Crystallographic Data Center, 12, Union Road, Cambridge CB2 1EZ, UK; fax: (internat.) +44-1223/336-033; E-mail: deposit@ccdc.cam.ac.uk].

Acknowledgments

We thank the Dirección General de Investigación no. BQU2001-2409-C02-01 for financial support. V. V. B. and N. G. Z. thank the Russian Foundation for Basic Research (no. 03-03-32372a and 03-03-96225r2003tatarstan-0).

[1] V. F. Toropova, T. A. Lazareva, F. M. Batyrshina, M. G. Zimin, *Zh. Anal. Khim.* **1982**, *37*, 1739−1743.
[2] W. Szczepaniak, J. Oleksy, *Anal. Chim. Acta* **1986**, *189*, 237−243.
[3] M. G. Zimin, G. A. Lazareva, N. I. Savel′eva, R. G. Islamov, N. G. Zabirov, V. F. Toropova, A. N. Pudovik, *J. Gen. Chem. USSR* **1982**, *52*, 1573−1581.
[4] A. N. Pudovik, R. A. Cherkasov, M. G. Zimin, N. G. Zabirov, *Izv. Akad, Nauk SSSR* **1979**, 861−866.
[5] M. G. Zimin, R. M. Kamalov, R. A. Cherkasov, A. N. Pudovik, *Phosphorus Sulfur* **1982**, *13*, 371−382.
[6] A. Ziegler, V. P. Botha, I. Haiduc, *Inorg. Chim. Acta* **1975**, *15*, 123−128.
[7] D. J. Birdsall, J. Green, T. Q. Ly, J. Novosad, M. Necas, A. M. Z. Slawin, J. D. Woollins, Z. Zak, *Eur. J. Inorg. Chem.* **1999**, 1445−1452.
[8] A. N. Chekhlov, N. G. Zabirov, R. A. Cherkasov, I. V. Martynov, *Dokl. Akad. Nauk. SSSR* **1989**, *307*, 129−135.
[9] N. G. Zabirov, F. M. Shamsevaleev, R. A. Cherkasov, *Usp. Khim.* **1991**, *60*, 2189−2192.
[10] R. M. Kamalov, M. G. Zimin, A. N. Pudovik, *Usp. Khim.* **1985**, *54*, 2044−2075.
[11] V. N. Solov′ev, A. N. Chekhlov, N. G. Zabirov, R. A. Cherkasov, I. V. Martynov, *Zh. Strukt. Khim.* **1990**, *31*, 103−104.
[12] N. G. Zabirov, F. M. Shamsevaleev, V. A. Shcherbakova, R. A. Cherkasov, V. N. Solov′ev, A. N. Cheklov, G. M. Dmitrieva, I. V. Martynov, *Zh. Obshch. Khim.* **1990**, *60*, 1997−2004.
[13] V. N. Solov′ev, A. N. Chekhlov, I. V. Martynov, *Koord. Khim.* **1991**, *17*, 618−625.
[14] N. G. Zabirov, A. A. Muratova, S. V. Kashevarov, R. A. Cherkasov, *J. Gen. Chem. USSR* **1996**, *66*, 406−408.
[15] N. G. Zabirov, V. N. Solov′ev, F. M. Shamsevaleev, R. A. Cherkasov, A. N. Chekhlov, A. G. Tsifarkin, I. V. Martynov, *J. Gen. Chem. USSR* **1991**, *61*, 597−604.
[16] S. V. Mashkina, N. Yu. Pestova, N. A. Ulakhovich, N. G. Zabirov, *J. Gen. Chem. USSR* **1996**, *66*, 515−533.
[17] N. G. Zabirov, I. A. Litvinov, O. N. Kataeva, S. V. Kashevarov, F. D. Sokolov, R. A. Cherkasov, *Russ. J. Gen. Chem.* **1998**, *68*, 1408−1410.
[18] N. G. Zabirov, V. N. Solov′ev, F. M. Shamsevaleev, R. A. Cherkasov, I. V. Martynov, *J. Gen. Chem. USSR* **1991**, *61*, 1608−1613.
[19] T. Iwamoto, F. Ebina, H. Nakazawa, C. Nakatsuka, *Bull. Chem. Soc. Jpn.* **1979**, *52*, 1857−1858.
[20] Z. Zak, T. Glowiak, N. T. T. Chau, E. Herrmann, *Z. Anorg. Allg. Chem.* **1990**, *586*, 136−140.
[21] V. P. Botha, A. Ziegler, I. Haiduc, *Inorg. Chim. Acta* **1976**, *17*, 13−16.
[22] V. V. Brus'ko, A. I. Rakhmatullin, N. G. Zabirov, *Russ. J. Gen. Chem.* **2000**, *70*, 1603−1609.
[23] I. Ojima, T. Onishi, T. Iwamoto, N. Inamoto, K. Tamaru, *Bull. Chem. Soc. Jpn.* **1971**, *44*, 2150−2154.
[24] E. Herrmann, R. Richter, N. T. T. Chau, *Z. Anorg. Allg. Chem.* **1997**, *623*, 403−408.
[25] V. N. Solov'ev, A. N. Chekhlov, N. G. Zabirov, I. V. Martynov, *Dokl. Akad. Ross. Nauk. SSSR* **1995**, *341*, 502−506.
[26] [26a] D. H. Johnson, D. F. Shriver, *Inorg. Chem.* **1993**, *32*, 1045−1047. [26b] G. A. Lawrance, *Chem. Rev.* **1986**, *86*, 17−33.
[27] C. S. W. Harker, E. R. T. Tiekink, *J. Coord. Chem.* **1990**, *21*, 287−293.
[28] E. Bembenek, O. Crespo, M. C. Gimeno, P. G. Jones, A. Laguna, *Chem. Ber.* **1994**, *127*, 835−840.
[29] L. M. Engelhard, C. Pakawatchai, A. H. White, P. C. Healy, *J. Chem. Soc., Dalton Trans.* **1985**, 125−133.
[30] P. J. Blower, J. A. Clackson, S. C. Rawle, J. R. Hartman, R. E. Wolf, R. Yagbasan, S. G. Bott, S. R. Cooper, *Inorg. Chem.* **1989**, *28*, 4040−4046.
[31] D. D. Heinrich, J. P. Fackler, P. Lahuerta, *Inorg. Chim. Acta* **1986**, *116*, 15−19.
[32] M. M. Artigas, O. Crespo, M. C. Gimeno, P. G. Jones, A. Laguna, M. D. Villacampa, *Inorg. Chem.* **1997**, *36*, 6454−6456.
[33] J. Vicente, M. T. Chicote, R. M. Dávila, M. S. Adrian, J. P. Fackler Jr., *Inorg. Synth.* **1998**, *32*, 173−177.
[34] M. I. Bruce, B. K. Nicholson, O. B. Shawkataly, *Inorg. Synth.* **1989**, *26*, 326.
[35] R. Uson, A. Laguna, M. Laguna, M. Abad, *J. Organomet. Chem.* **1983**, *249*, 437−443.
[36] E. J. Fernández, M. C. Gimeno, P. G. Jones, A. Laguna, M. Laguna, J. M. López-de-Luzuriaga, *J. Chem. Soc., Dalton Trans.* **1992**, 3365−3370.
[37] M. Bardaji, O. Crespo, A. Laguna, A. K. Fischer, *Inorg. Chim. Acta* **2000**, *304*, 7−16.
[38] R. Uson, A. Laguna, *Inorg. Synth.* **1982**, *21*, 71.
[39] G. M. Sheldrick. *Program for Crystal Structure Refinement*, University of Göttingen, Göttingen, Germany, **1997**.

Received May 30, 2003
Early View Article
Published Online November 4, 2003

EurJIC
European Journal of Inorganic Chemistry

Issue 3/2004

Pages 431–660

Papers available ahead of print in Early View at www.interscience.wiley.com

Earliest available Table of Contents:
Automatically, free of charge by e-mail through
www.interscience.wiley.com/alerts

COVER PICTURE

The cover picture shows the dissociative character of the displacement of a coordinated solvent molecule *trans* to the alkyl group in cobalt(III) complexes. Details are discussed in the article by R. van Eldik et al. on p. 653ff. The work has benefited greatly from an international collaboration.

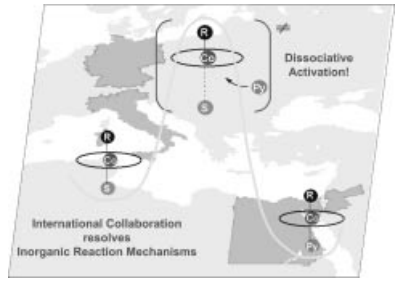

MICROREVIEW

Contents

445 **M. Gielen,* M. Biesemans, R. Willem, E. R. T. Tiekink**

Diorganotin Salicylaldoximate Clusters: Their Fascinating Chemistry and Structures

Keywords: Cluster compounds / NMR spectroscopy / Substitution reactions / Tin / X-ray diffraction

 © 2004 Wiley-VCH Verlag GmbH & Co. KGaA, Weinheim

SHORT COMMUNICATIONS

453 **P. Grosshans, A. Jouaiti, V. Bulach, J.-M. Planeix, M. W. Hosseini,* N. Kyritsakas**

Design and Structural Analysis of Metallamacrocycles Based on a Combination of Ethylene Glycol Bearing Pyridine Units with Zinc, Cobalt and Mercury

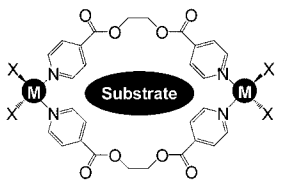

Keywords: Glycol / Pyridine / Zinc / Cobalt / Mercury / Metallamacrocycle

459 **S.-C. Hsu, Y.-C. Lin,* S.-L. Huang, Y.-H. Liu, Y. Wang, H. Liu**

Novel Thiotetraazapentalene Complexes from the Reaction of Ruthenium Azide Complex with Alkyl Isothiocyanates

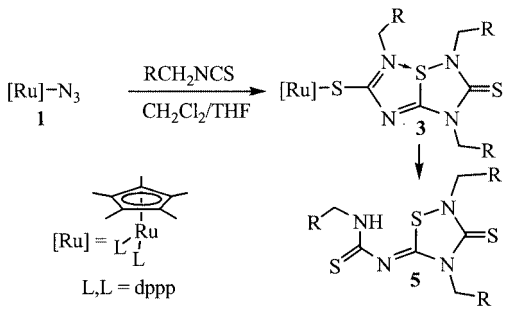

Keywords: Ruthenium / Azides / Isothiocyanates / Thiotetraazapentalene

FULL PAPERS

463 **S. Laurent, F. Botteman, L. Vander Elst, R. N. Muller***

New Bifunctional Contrast Agents: Bis-Amide Derivatives of *C*-Substituted Gd-DTPA

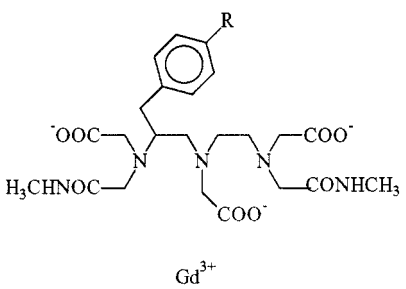

Keywords: Gadolinium / Zinc / Metallation / Amides

469 **S. Jung, K. Ilg, C. D. Brandt, J. Wolf, H. Werner***

A Series of Vinylidene-, Vinyl-, Carbene- and Carbyneruthenium(II) Complexes with $[Ru(PCy_3)_2]$ and $[Ru(PiPr_3)_2]$ as Molecular Building Blocks

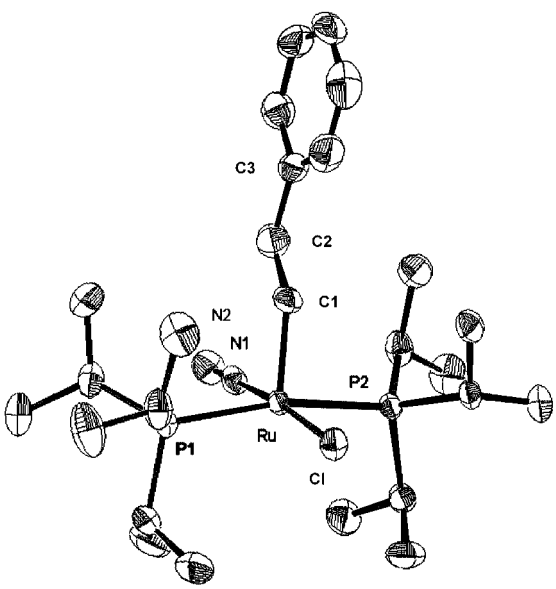

Keywords: Carbene complexes / Carbyne complexes / Ruthenium / Vinyl complexes / Vinylidene complexes

 © 2004 Wiley-VCH Verlag GmbH & Co. KGaA, Weinheim

481 **P. Krüger, H. Werner***

Mono- and Dinuclear Rhodium and Iridium Complexes with Chiral Phospholanes as Ligands

Keywords: Allyl ligands / Carbonyl ligands / Hydrido complexes / Phospholanes / Rhodium

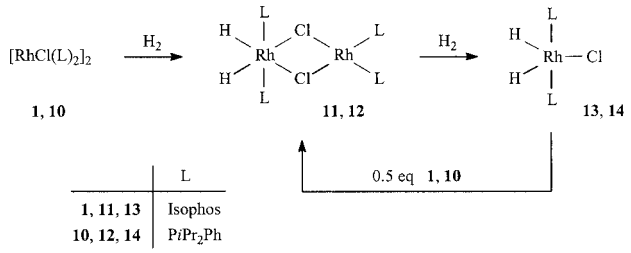

492 **J. Bley-Escrich, J.-P. Gisselbrecht,* M. Michels, L. Zander, E. Vogel, M. Gross***

Electrochemical and Spectroelectrochemical Investigations of Mono- and Binuclear Cobalt(II) Complexes of "Figure-Eight" Octapyrrolic Macrocycles

Keywords: Macrocyclic ligands / Cobalt / Cluster complexes / Electrochemistry

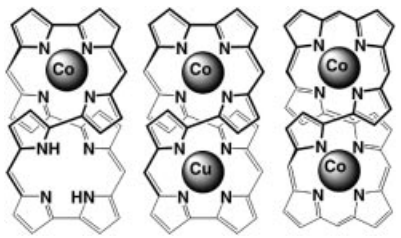

500 **G. Malandrino, R. Lo Nigro, I. L. Fragalà,* C. Benelli**

Yttrium β-Diketonate Glyme MOCVD Precursors: Effects of the Polyether Length on Stabilities, Mass Transport Properties and Coordination Spheres

Keywords: Yttrium / Thermogravimetry / Superconductors

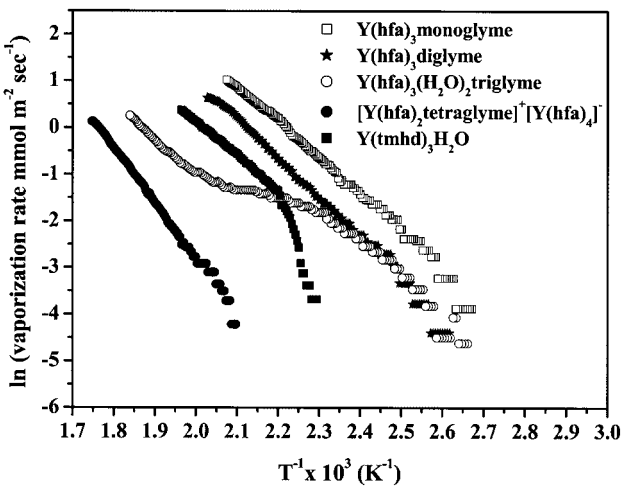

510 **P. Zhu, F. Lu, N. Pan, D. P. Arnold,* S. Zhang, J. Jiang***

Comparative Electrochemical Study of Unsubstituted and Substituted Bis(phthalocyaninato) Rare Earth(III) Complexes

Keywords: Phthalocyanines / Sandwich complexes / Rare earths / Electrochemistry

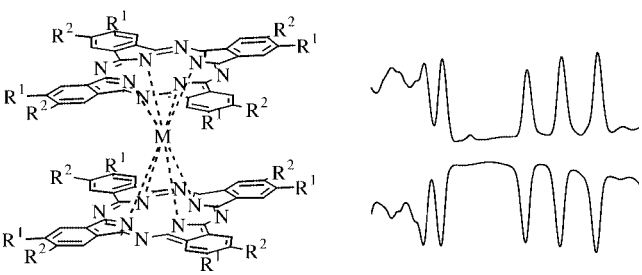

518 **P. Zhu, N. Pan, C. Ma, X. Sun, D. P. Arnold,* J. Jiang***

Electrochemistry of Heteroleptic Tris(phthalocyaninato) Rare Earth(III) Complexes

Keywords: Phthalocyanines / Sandwich complexes / Rare earths / Electrochemistry

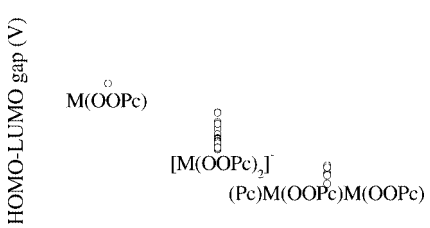

 © 2004 Wiley-VCH Verlag GmbH & Co. KGaA, Weinheim

524 **A. Del Zotto,* W. Baratta, M. Sandri, G. Verardo, P. Rigo**

Cyclopentadienyl Ru^{II} Complexes as Highly Efficient Catalysts for the *N*-Methylation of Alkylamines by Methanol

Keywords: Homogeneous catalysis / Ruthenium / Amines / *N*-methylation / Imines

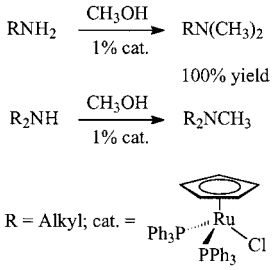

530 **Z. Fei, R. Scopelliti, P. J. Dyson***

On the Reactivity of the Iminodiphosphane $C_6H_4(o\text{-}CN)N{=}PPh_2{-}PPh_2$: Fragmentation Versus Isomerisation

Keywords: N,P ligands / Palladium / Platinum / Reaction mechanisms / Structure elucidation

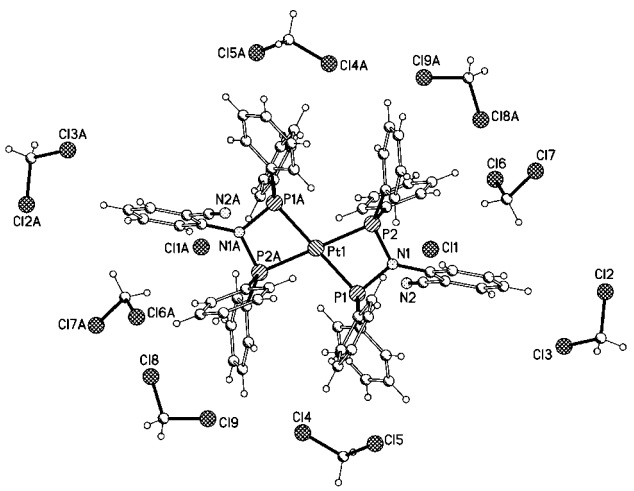

538 **J.-L. Song, J.-G. Mao,* H.-Y. Zeng, Z.-C. Dong**

Syntheses, Crystal Structures and Magnetic Properties of Four Cu^{II}-Hg^{II} Mixed-Metal Halide Oligomers

Keywords: Copper / Mercury / Magnetic properties / Cluster compounds

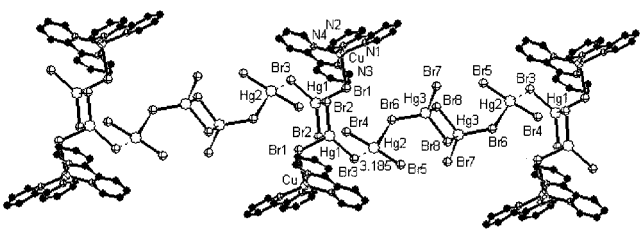

544 **X.-M. Zhang***

A Microporous Zinc Phosphonocarboxylate with a Zeolite ABW Framework via the Trialkyl Phosphonocarboxylate Route: In situ Synthesis and Characterization of $Na[Zn(O_3PC_2H_4CO_2)]\cdot H_2O$

Keywords: Microporous materials / Organic-inorganic hybrid / Zeolites / Zinc

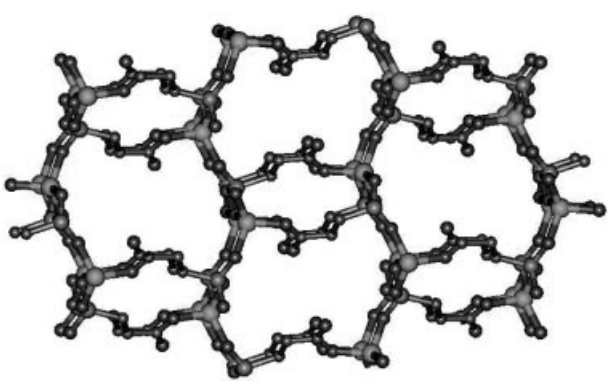

 © 2004 Wiley-VCH Verlag GmbH & Co. KGaA, Weinheim

549 **A. Guerrero, F. A. Jalón, B. R. Manzano,* A. Rodríguez, R. M. Claramunt,* P. Cornago, V. Milata, J. Elguero**

Apparent Allyl Rotation in New Allylpalladium(II) Complexes with Pyrazolyl *N*-Donor Ligands

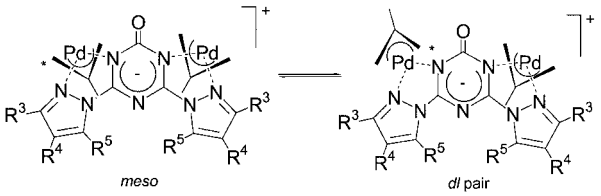

Keywords: Fluxionality / N ligands / Allyl ligands / Palladium

557 **S. Gao, L. Zhu, Y. Xie,* X. Qian**

Formation of Cubic GaN Nanocrystals: A Study of the Thermal Stability of GaP Nanocrystals under Nitrogen

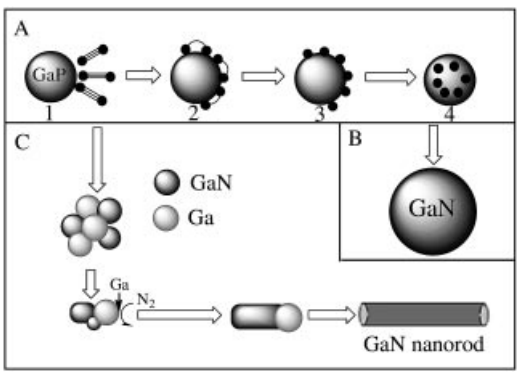

Keywords: Gallium / Phosphorus / Nitrides / Nanostructures / Thermochemistry

562 **X.-Y. Chen, B. Zhao, P. Cheng,* B. Ding, D.-Z. Liao, S.-P. Yan, Z.-H. Jiang**

Multi-Dimensional Systems Built from Dichromate Anions − Syntheses, Crystal Structures, and Magnetic Properties

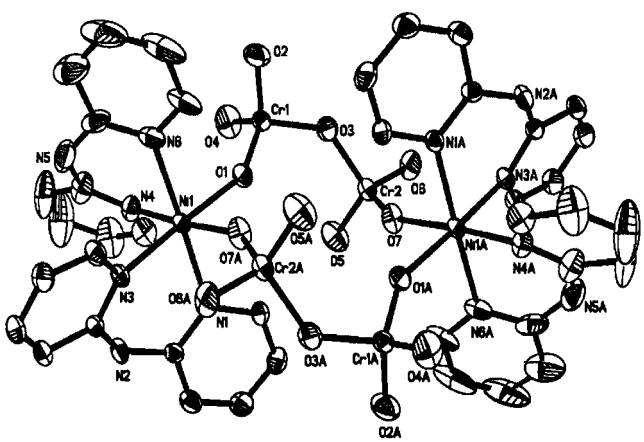

Keywords: Chromium / Magnetic properties / N ligands / Self-assembly

570 **V. Zima,* K. Melánová, L. Beneš, M. Trchová, J. Dybal**

Intercalation of γ-Butyrolactone into Vanadyl Phosphate and Niobyl Arsenate

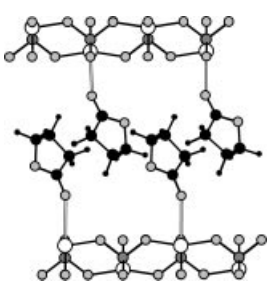

Keywords: Intercalations / Powder X-ray diffraction / Vibrational spectroscopy / ab initio calculations

 © 2004 Wiley-VCH Verlag GmbH & Co. KGaA, Weinheim

575 **E. G. Sakellariou, J.-P. Collin,* C. O. Dietrich-Bucheker, J.-P. Sauvage***

Copper(I)-Assembled Pseudorotaxanes Bearing Bis(nitrile) Ligands: Selective Formation of Large Chelate Rings

Keywords: Copper / N ligands / Macrocycles / Chelates

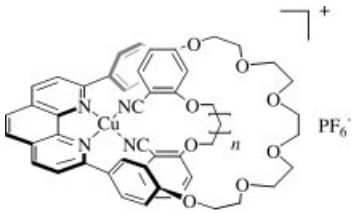

581 **D. Sellmann, K. P. Peters,* F. W. Heinemann**

New Pentadentate Carboxylate-Derivatized Sulfur Ligands Affording Water Soluble Iron Complexes with [Fe(NS_4)] Cores that Bind Small Molecules (CO, NO, PMe_3) as Co-Ligands

Keywords: Iron / Nickel / S ligands / P ligands / Water solubility

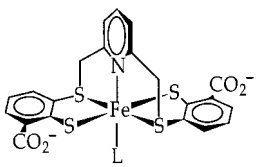

591 **I. A. Koval, M. Huisman, A. F. Stassen, P. Gamez, M. Lutz, A. L. Spek, J. Reedijk***

Unusual Cu^{II} and Mn^{II} Complexes of Phenol-Based Ligands Containing Amine, Pyridine and Formyl Functions: Unexpected Structural Features and Solution Studies

Keywords: Copper / Manganese / Magnetic properties / EPR spectroscopy / Cyclic voltammetry

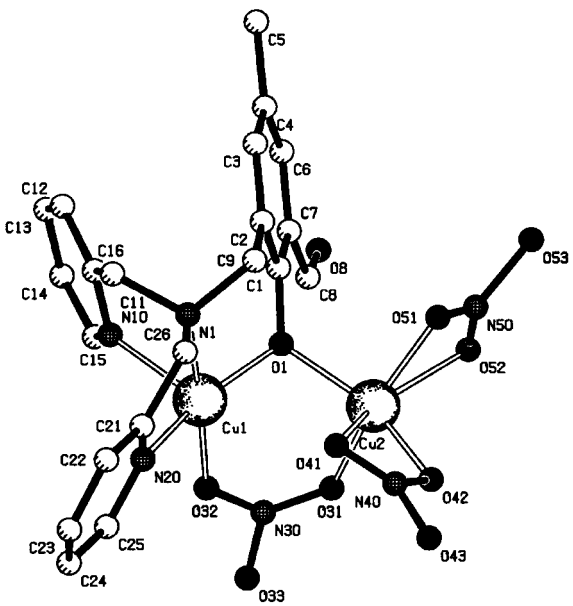

601 **J. C. Gávalez-Ruiz, C. Guadarrama-Pérez, H. Nöth, A. Flores-Parra***

Group 13 Complexes of 5-Methyl-1,3,5-dithiazinane

Keywords: Aluminum / Halides / Indium / Conformational analysis

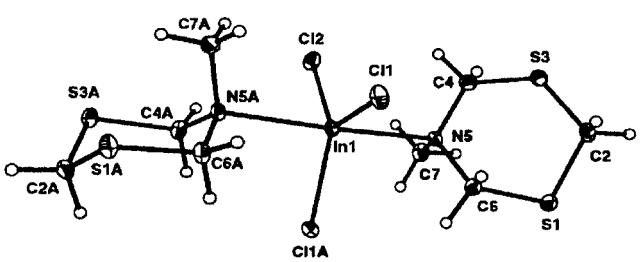

 © 2004 Wiley-VCH Verlag GmbH & Co. KGaA, Weinheim

612 **X. Sala, A. Poater, I. Romero, M. Rodríguez, A. Llobet,* X. Solans, T. Parella, T. M. Santos**

Synthesis, Structure, and Redox Properties of a New Aqua Ruthenium Complex Containing the Tridentate [9]aneS_3 and the Didentate 1,10-Phenanthroline Ligands

Keywords: Crown compounds / Catalysis / Oxidations / Redox chemistry / Ruthenium

619 **M. S. Balula, J. A. Gamelas, H. M. Carapuça, A. M. V. Cavaleiro,* W. Schlindwein**

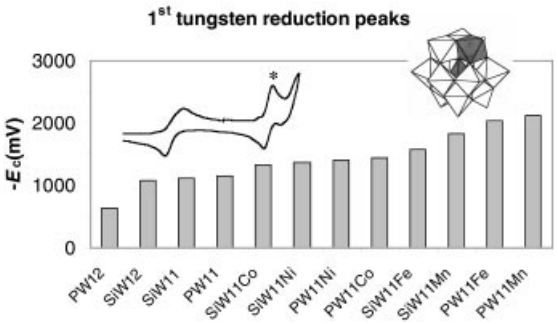

Electrochemical Behaviour of First Row Transition Metal Substituted Polyoxotungstates: A Comparative Study in Acetonitrile

Keywords: Polyoxometalates / Sandwich complexes / Transition metals / Electrochemistry

629 **K. N. Gavrilov,* V. N. Tsarev, A. A. Shiryaev, O. G. Bondarev, S. E. Lyubimov, E. B. Benetsky, A. A. Korlyukov, M. Y. Antipin, V. A. Davankov, H.-J. Gais**

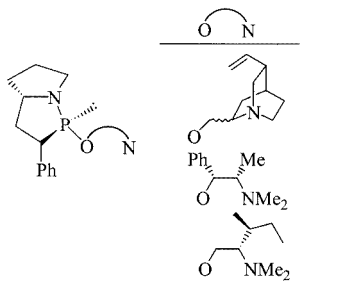

*P**,*N*-Bidentate Amino Phosphoramidites: New Highly Effective Ligands for Pd-Catalysed Asymmetric Allylic Substitution

Keywords: Asymmetric catalysis / *P*,*N*-ligands / Allylation / Palladium / Rhodium

635 **I. Beloso, J. Borrás, J. Castro,* J. A. García-Vázquez, P. Pérez-Lourido, J. Romero, A. Sousa***

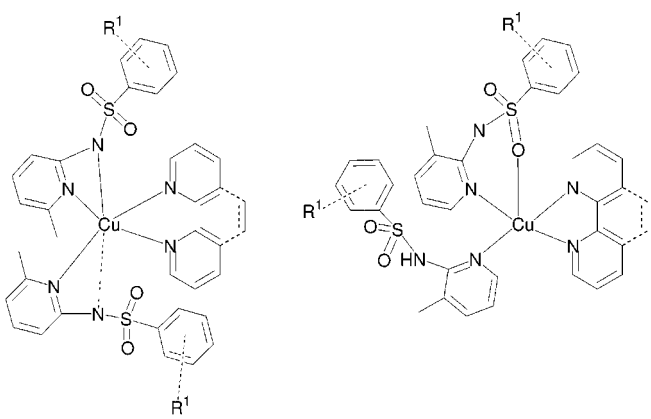

Flexidentate Behaviour of 2-Pyridylsulfonamides − Direct Electrochemical Synthesis and Spectroscopic and X-ray Characterisation of Neutral Copper(II) Complexes of *N*-(2-Pyridyl)sulfonamides

Keywords: Copper / S ligands / Electrochemical synthesis / N ligands

 © 2004 Wiley-VCH Verlag GmbH & Co. KGaA, Weinheim

646 **B. Arezzini, M. Ferrali, E. Ferrari, R. Grandi, S. Monti, M. Saladini***

Glycosyl-Curcuminoids as Potential New Chelating Agents in Iron Overload Chelation Therapy

Keywords: Chelates / Iron / Gallium / Redox chemistry / Bioinorganic chemistry

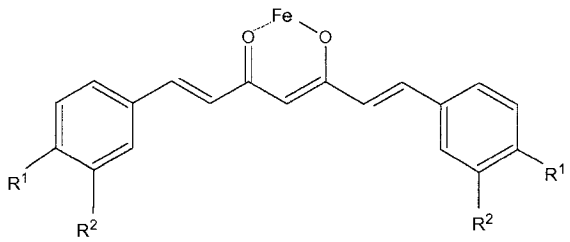

653 **B. M. Alzoubi, M. S. A. Hamza, A. Felluga, L. Randaccio, G. Tauzher, R. van Eldik***

Kinetics and Mechanism of Axial Ligand Substitution of Alkyl Cobaloximes by Substituted Pyridines in Different Solvents

Keywords: Cobaloximes / Solvent effects / *trans* effect / Ligand-substitution reactions / Nitrogen heterocycles

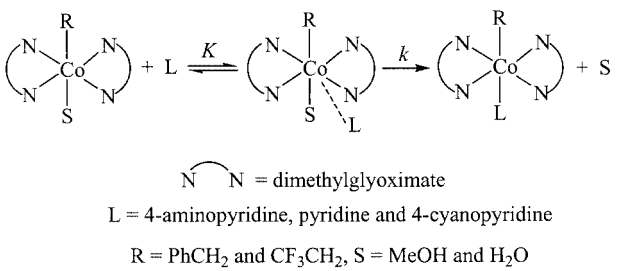

 © 2004 Wiley-VCH Verlag GmbH & Co. KGaA, Weinheim

Diorganotin Salicylaldoximate Clusters: Their Fascinating Chemistry and Structures

Marcel Gielen,*[a] Monique Biesemans,[a] Rudolph Willem,[a] and Edward R. T. Tiekink[b]

Keywords: Cluster compounds / NMR spectroscopy / Substitution reactions / Tin / X-ray diffraction

A large variety of small oxotin clusters, characterised as stable crystalline products or solution transients, has been obtained by the reaction of various diorganotin oxides and salicylaldoxime. The structures were investigated by high resolution multinuclear NMR methods and X-ray crystallography. The predominant trinuclear clusters contain one seven- and two five-coordinate tin atoms and undergo a series of reversible substitution reactions, including those leading to clusters of differing nuclearity, in solution at room temperature. Such a variety of structures is rather unusual in organotin chemistry.
(© Wiley-VCH Verlag GmbH & Co. KGaA, 69451 Weinheim, Germany, 2004)

[a] Vrije Universiteit Brussel (VUB), High Resolution NMR Centre (HNMR),
Pleinlaan, 2, 1050 Brussel, Belgium
E-mail: mgielen@vub.ac.be
mbiesema@vub.ac.be
rwillem@vub.ac.be
[b] Department of Chemistry, National University of Singapore, Singapore 117543
E-mail: chmtert@nus.edu.sg

Introduction

An interesting review paper by White, Tasker and Smith[1] gives an overview of the crystal structural chemistry of phenolic oximes and their metal complexes. This review underlines that for both the free ligand and its metal complexes, hydrogen bonds between the oximic proton and

Marcel Gielen was born in Brussels in 1938. He received his PhD at the Université Libre de Bruxelles in 1963 with Professor Jacques Nasielski, in the field of the kinetics and mechanisms of the bimolecular electrophilic aliphatic substitutions. He was a fellow of the Fonds National de la Recherche Scientifique until he received a position of lecturer at the newly created Vrije Universiteit Brussel in 1966, where he became full professor in 1972. His main research interests were, and still are, the stereochemistry at carbon of S_E2 reactions at a saturated carbon atom, the fluxionality of inorganic and organometallic complexes, the stereochemistry of S_N2 reactions at tetrahedrally substituted atoms and the development of metal-based drugs. He is the author of 300 papers devoted to organometallic chemistry, devoted for instance to the synthesis, characterization and antitumour activities of organotin compounds. He has been the editor of several books and journals and is now, with Edward Tiekink, Narayan Hosmane and Rudolph Willem, the coordinating editor of the section "Main Group Metal Compounds" of Applied Organometallic Chemistry. He is, with Rudi Willem and Bernd Wrackmeyer, the editor of the series "Physical Organometallic Chemistry" published by Wiley; the fourth volume, Fluxional Organometallic Compounds, is in press. He is also, with Edward Tiekink, the editor of another book published by Wiley entitled "Metallotherapeutic Agents" that appears in 2004.

Monique Biesemans received her PhD in Organic Chemistry in 1978 at the Vrije Universiteit Brussel (VUB), where she studied the interaction between proteins and organic substrates by NMR spectroscopy under the supervision of Prof. Georges Van Binst. She worked since 1969 as assistant, and later as Doctor-Assistant at the VUB, under the leadership of Prof. Louis Van Hove, a specialist in steroid chemistry. In 1990, she joined the group of Prof. Marcel Gielen, where she directed her research to advanced structure determinations by multinuclear NMR spectroscopy, focussing on applied organotin chemistry, and more recently on organotin interface chemistry. She is the author or co-author of over 140 peer-reviewed publications on these subjects.

Rudolph Willem was born in 1948 and received his PhD in Theoretical Chemistry at the Université Libre de Bruxelles in 1975, active in group theoretical modelling of stereochemically dynamic processes under the supervision of Prof. Jean Brocas. He became assistant, and later Doctor-Assistant at the Vrije Universiteit Brussel (VUB) from 1972, under the leadership of Prof. Marcel Gielen. He is known as an active researcher in the field of experimental NMR applications on dynamic stereochemistry and in cellular NMR during a post-doctoral stay in the Max Planck Institute for Physiology in Dortmund, Germany, under the supervision of Prof. R. Kinne in 1987. He became an Associate Professor at the Engineering Science Faculty of the VUB from 1988, and the head of the NMR Department of the VUB from 1989. He received the titles Professor of Chemistry in 1997 and Full Professor and Vice-Dean of the Faculty in 2002. He is the author or coauthor of over 240 peer-reviewed publications on structural chemistry and advanced NMR applications to structure determinations, with focus on applied organotin chemistry, and more recently on organotin interface chemistry and tin NMR spectroscopy.

Edward R. T. Tiekink is a Ph.D. (1985) graduate of The University of Melbourne. After moving to The University of Adelaide, first as a Research Associate and later as a member of the academic staff, he made the move to the National University of Singapore (2001) where he pursues research interests in crystal engineering, nanoparticles generation of main group element sulfides, and the development of metal-based drugs. His research has resulted in over 850 publications and currently he serves on the editorial boards of "Zeitschrift für Kristallographie" (Co-Editor), "Acta Crystallographica E" (founding Co-Editor), "Applied Organometallic Chemistry" (Section Co-Editor), and "Bioinorganic Chemistry & Applications".

MICROREVIEWS: This feature introduces the readers to the author's research through a concise overview of the selected topic. Reference to important work from others in the field is included.

phenolic oxygen atom play a fundamental role in the structural chemistry of these compounds. Whereas this review focuses on structures obtained from X-ray crystallography, the present review will be devoted, in the main, to the solution chemistry of tin salicylaldoximate clusters and will outline more particularly the existence of transient species generated upon dissolution (chloroform) of pure single crystals of these clusters. The use of 2D heteronuclear NMR techniques involving the ^{119}Sn nucleus is revealed as the optimal tool to investigate the structural chemistry of this system.

Many series of diorganotin carboxylates have been synthesized, either for investigating their solid state or solution structure,[2] or for assessing their performance as PVC stabilizers,[3] biocides,[4] anti-tumour agents,[5] anion-recognition agents,[6] and catalysts for polyurethane foams,[7] for room temperature vulcanisation of silicon rubbers,[8] for transesterifications,[9] for acetylations of alcohols,[10] and for dehydrations of alcohols to ethers.[11] They can be synthesized by condensing diorganotin oxides with carboxylic acids.[5] Two types of structures can be obtained, depending basically on the diorganotin oxide/carboxylic acid molar ratio. When a 1:1 ratio is used, dimeric dicarboxylatotetraorganodistannoxanes are generally generated through a diorganotin carboxylate hydroxide intermediate:

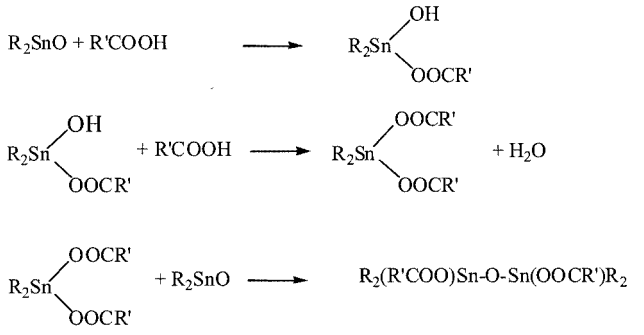

The latter compound dimerises as follows:

$$2\,[R_2(R'COO)Sn-O-Sn(OOCR')R_2] \rightarrow [R_2(R'COO)Sn-O-Sn(OOCR')R_2]_2$$

Moreover, a distannoxane unit can react with 2 equiv. of carboxylic acid to yield the diorganotin dicarboxylate:

$$R_2(R'COO)Sn-O-Sn(OOCR')R_2 + 2\,R'COOH \rightarrow H_2O + 2\,(R'COO)_2SnR_2$$

The dimeric centrosymmetric distannoxane is characterized by an Sn_2O_2 four-membered ring with two endocyclic five-coordinate tin atoms (quite common in organotin chemistry) that is linked, by the bridging oxygen atoms, to two exocyclic five-coordinate diorganotin moieties (Figure 1) so that the structure contains two μ_3-oxo functionalities.

When salicylaldoxime, represented hereafter as HOZNOH (see Scheme 1) rather than a carboxylic acid, is involved in condensation reactions with a diorganotin oxide,[12] a totally different coordination chemistry takes

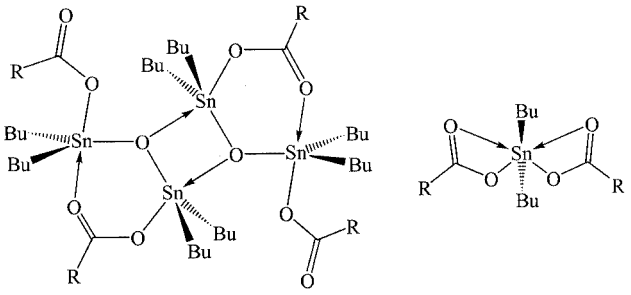

Figure 1. Structures of dimeric dicarboxylatotetraorganodistannoxanes and diorganotin dicarboxylates

place at the tin atom. This paper provides a review of the syntheses, structures and solution chemistry of tin salicylaldoximates, as investigated over the last decade or so.

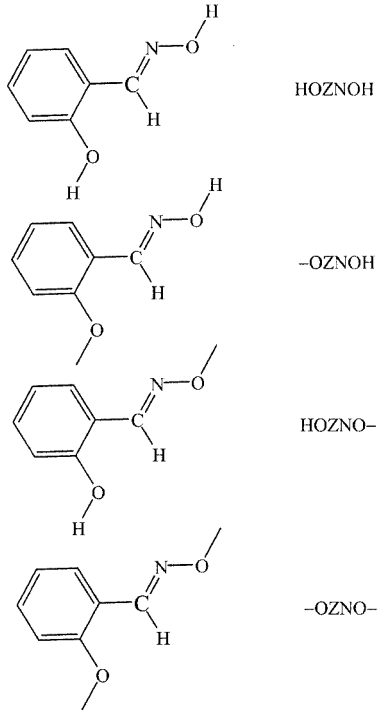

Scheme 1

Structures and Chemistry of Diorganotin Salicylaldoximates

One of the reasons for the difference in the organotin chemistry of salicylaldoxime is the presence of two constitutionally different hydroxylic protons that can potentially be substituted by a metal atom. Reaction of salicylaldoxime with di-*n*-butyltin oxide gives rise to a cluster,[13–15] the structure[16] of which was determined by X-ray crystallography (see Figure 2) and investigated in solution by 1D and 2D multinuclear (^{1}H, ^{13}C, ^{119}Sn) NMR techniques.[16]

This complex is generated irrespective of the starting ratio between nBu$_2$SnO and HOZNOH, and can be formulated as [(Bu$_2$Sn)(Bu$_2$SnO)(Bu$_2$SnOH)(OZNO)(OZNOH)] (**1**). It contains a protonated distannoxane unit with two

 © 2004 Wiley-VCH Verlag GmbH & Co. KGaA, Weinheim

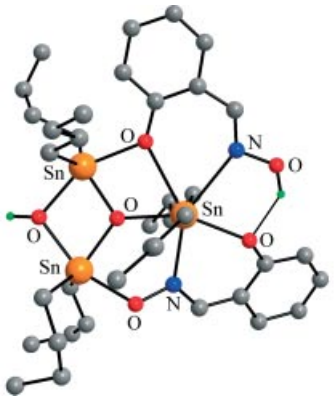

Figure 2. Structure of the crystalline organotin cluster $[(Bu_2Sn)(Bu_2SnO)(Bu_2SnOH)(OZNO)(OZNOH)]$ (**1**); in this diagram and in subsequent molecular structures, drawn with DIAMOND™, only the acidic hydrogen atoms are shown for reasons of clarity; colour code for all molecular structures in this review: orange, tin; red, oxygen; blue, nitrogen; turquoise, halide; grey, carbon; and green, hydrogen

five-coordinate tin atoms, which are in turn connected through a three-coordinate oxygen atom to a third, seven-coordinate tin atom, also coordinated by two differently bonded salicylaldoximate ligands. Another form (**1′**) related to cluster **1** arises from proton transfer from the SnOH moiety in the Sn_2O_2 group to the oxygen of the NO function of the OZNO ligand, as evidenced by ^{1}H NMR spectroscopy. The formula of **1′** is best represented as $[(Bu_2Sn)(Bu_2SnO)_2(OZNOH)_2]$ (see Figure 3).

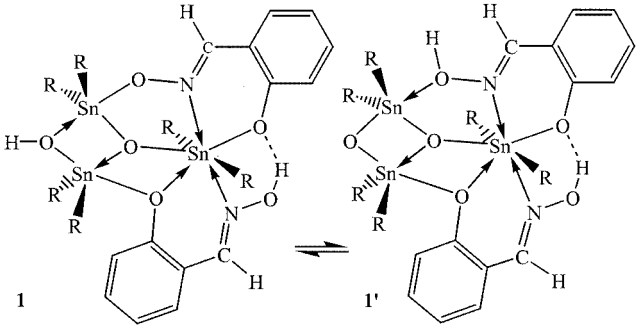

Figure 3. Structures in solution for the organotin cluster $[(Bu_2Sn)(Bu_2SnO)(Bu_2SnOH)(OZNO)(OZNOH)]$ (**1**) as found in the crystalline state, in equilibrium with a proton transfer isomer $[(Bu_2SnO)_2(Bu_2Sn)(OZNOH)_2]$ (**1′**)

In the latter formulation, a cyclodimer of diorganotin oxide is interacting with the one salicylaldoximate ligand through a PhO→Sn interaction and with the other one by a C=NO→Sn coordination, and an $(nBu_2Sn)_2O$→Sn contact from one oxygen atom of the four-membered Sn_2O_2 ring to the seven-coordinate tin atom. This suggests that the soluble cluster could act as an in situ reservoir of soluble diorganotin oxide, although this remains to be proven.[17,18]

Upon dissolution of monocrystalline **1** in $CDCl_3$, intense ^{119}Sn NMR resonances are observed for cluster **1**, together with other minor resonances that were assigned to other species as discussed below. Thus, a set of three minor, equally intense ^{119}Sn resonances were assigned to another cluster, **2**, that was subsequently synthesized independently from the reaction:

$$3\ HOZNOH + 3/n\ (R_2SnO)_n \rightarrow 2\ H_2O + [(R_2SnO)(R_2Sn)_2(HOZNO)(ZNOH)(OZNO)]\ (\mathbf{2})$$

Cluster **2** has three constitutionally different salicylaldoximate ligands. Its structural formula is shown in Figure 4, together with a crystal structure for the case when R = Me. Attempts to recrystallise **2** often failed for R = Me or provided crystals of **1** from undried solvents for R = *n*Bu. It was only under very carefully controlled crystallization conditions[19] that crystals of **2** could eventually be obtained for R = Me.

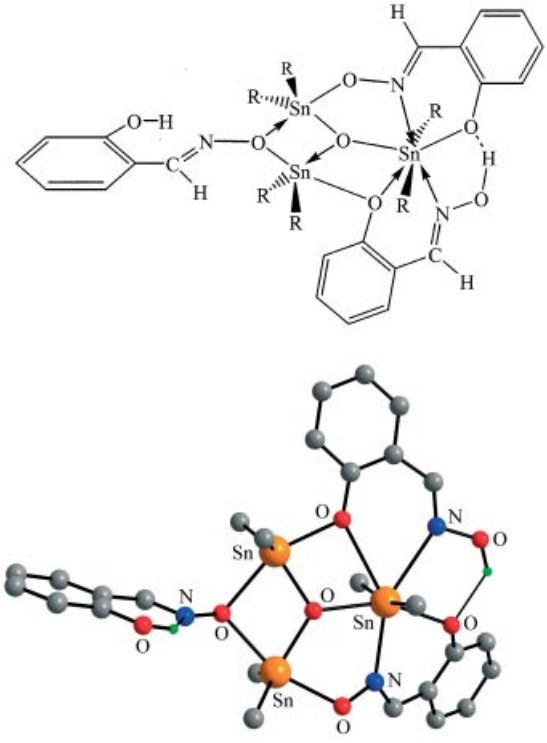

Figure 4. Lewis formula (top) and molecular structure (bottom) of the organotin cluster $[(R_2SnO)(R_2Sn)_2(HOZNO)(OZNOH)(OZNO)]$ (**2**; R = Me)

The μ_2-salicylaldoximate ligand of **2** is oriented in an approximately perpendicular position with respect to the almost planar trinuclear cluster. This yields a chiral skeleton in the solid state where the three tin atoms are inequivalent. The consequences of this chirality observed in the crystal are not observable in solution, suggesting a fast inversion of the skeletal chirality on the NMR timescale.[20]

The water generated in the synthesis of **2** is available in situ to convert **2** into **1**, which, at least for R = *n*Bu, explains the formation of the crystalline cluster **1** (Figure 2):

$$[(Bu_2SnO)(Bu_2Sn)_2(HOZNO)(OZNOH)(OZNO)] + H_2O \rightarrow [(Bu_2SnO)(Bu_2Sn)(Bu_2SnOH)(OZNOH)(OZNO)] + HOZNOH$$

 © 2004 Wiley-VCH Verlag GmbH & Co. KGaA, Weinheim

The water converts the μ^2-bridging HOZNO ligand into the good nucleophilic leaving group HOZNOH in such a way so that the substitution reaction of the HOZNO ligand by HO can occur because it is catalysed through electrophilic assistance by a hydroxylic proton available in the medium (e.g. from water generated in situ and/or present in undried solvents).

The structures of **1** and **2** are quite similar, as can be deduced from the similarity of their tin NMR spectra as well as their crystalline structures. Both are unsymmetrical networks of tin−oxygen and tin−nitrogen bonds with one seven-coordinate tin atom and two five-coordinate tin atoms.

Another series of weak ^{119}Sn resonances arising upon dissolution of crystalline **1** originate from another totally different tin cluster, **3**, the structure of which, determined by multinuclear NMR spectroscopy, is shown in Figure 5. It contains two six- and two five-coordinate tin atoms and two salicylaldoximate moieties.

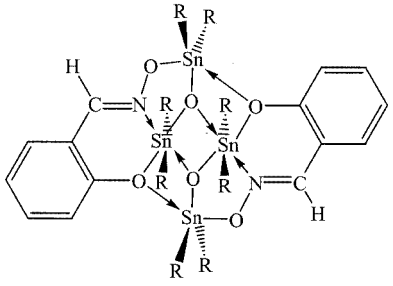

Figure 5. Structure of the organotin cluster $[(R_2Sn)_2(R_2SnO)_2(OZNO)_2]$ (**3**)

Lastly, a single ^{119}Sn resonance arises from a third very symmetrical cluster, **4** (Figure 6), containing four six-coordinate tin atoms and four salicylaldoximate ligands, as deduced from the relative intensities of $^2J(^{119}SnO\text{-}^{117}Sn)$ coupling satellites with respect to their parent signal.

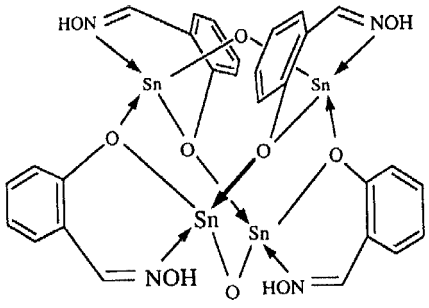

Figure 6. Structure of the organotin cluster $[(R_2Sn)_2(R_2SnO)_2(OZNOH)_4]$ (**4**); the tin-bound R groups have been omitted for clarity

An explanation for the formation of the first of the two minor species, $[(R_2Sn)_2(R_2SnO)_2(OZNO)_2]$ (**3**), observed in the solution generated from crystalline **1**, is shown in Figure 7:

$$2[(R_2SnO)(R_2Sn)(R_2SnOH)(OZNO)(OZNOH)] \rightarrow [(R_2Sn)(R_2SnO)(OZNOH)_2] + H_2O + 2[(R_2Sn)(R_2SnO)(OZNO)]$$

followed by

$$2[(R_2Sn)(R_2SnO)(OZNO)] \rightarrow [(R_2Sn)_2(R_2SnO)_2(OZNO)_2] \quad (3)$$

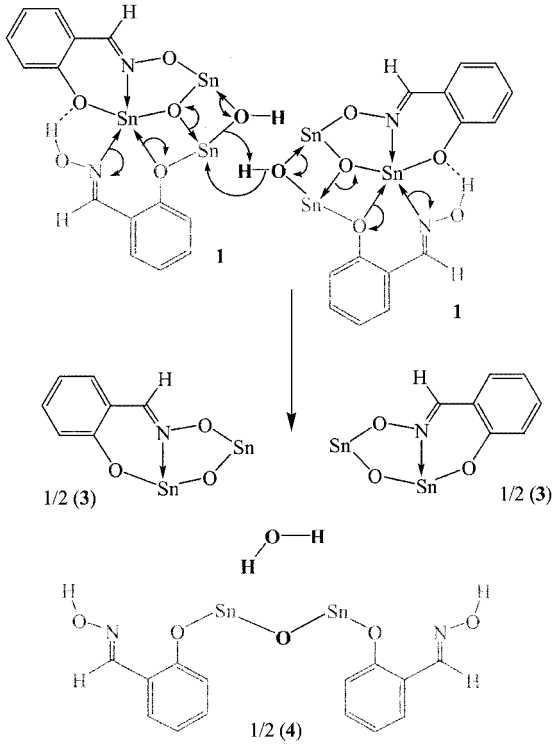

Figure 7. Reaction of two cluster units **1** yielding water, two identical molecules that, upon aggregation, provide **3**, as well as a distannoxane, the dimer of which is cluster **4**; the tin-bound R groups have been omitted for clarity

The second minor species, $[(R_2Sn)_2(R_2SnO)_2(OZNOH)_4]$ (**4**), is then formed by the dimerisation of $[(R_2Sn)(R_2SnO)(OZNOH)_2]$ generated by the reaction shown in Figure 7.

Another relatively straightforward reaction explains the presence of the latter minor compound **4**:

$$[(R_2Sn)(R_2SnO)(R_2SnOH)(OZNO)(OZNOH)] \rightarrow R_2SnO + [(R_2Sn)(R_2SnO)(OZNOH)_2]$$

which is again the monomeric precursor of **4**, R_2SnO precipitating in its usual polymeric form $(R_2SnO)_n$, in agreement with the experimental observation of precipitate formation.

Another reaction consistent with the presence of the minor species is given in Figure 8. Compound **1** can react with $[(R_2Sn)(R_2SnO)(OZNOH)_2]$ to yield $[(R_2SnO)(R_2Sn)_2(HOZNO)(OZNOH)(OZNO)]$ (**2**), H_2O

and $[(R_2Sn)(R_2SnO)(OZNO)]$, the monomeric precursor of **3**, already described above.

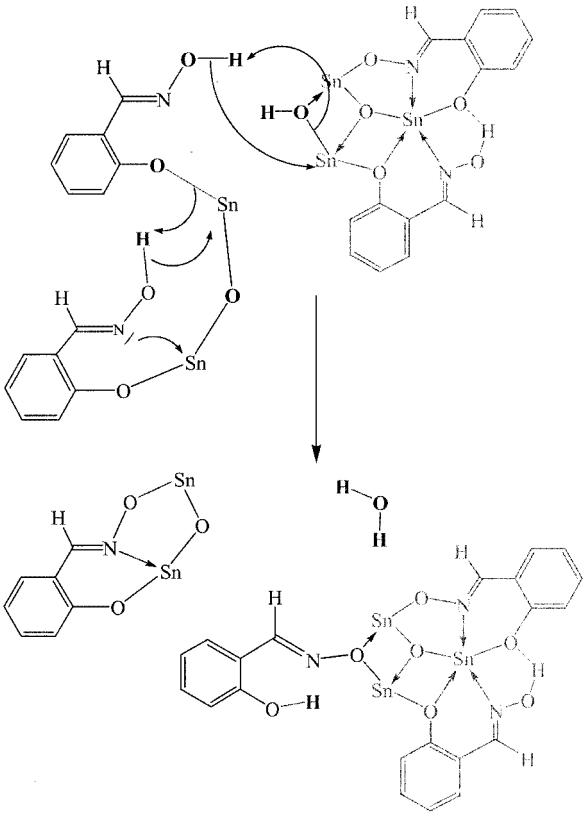

Figure 8. Reaction of cluster **1** with $[(R_2Sn)(R_2SnO)(OZNOH)_2]$, yielding water, cluster **2** and a distannoxane, the dimer of which is cluster **3**; the tin-bound R groups have been omitted for clarity

When both organic substituents on the tin atom are methyl groups, the dimethyl analogue of **1** can no longer be obtained in crystalline form. When alcohols R′OH are used for the crystallization, the crystals formed arise from novel structures containing an R′O group bridging the two five-coordinate tin atoms, instead of the OH group present in **1** (Figure 9),[21,22] i.e. $[(R_2Sn)(R_2SnO)(R_2SnOR')(OZNO)(OZNOH)]$ (see Table 1).

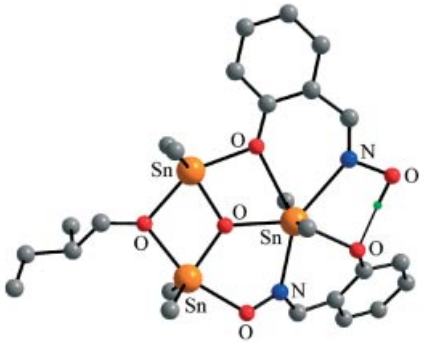

Figure 9. Structure of the organotin cluster $[(Me_2Sn)(Me_2SnO)(Me_2SnOCH_2CHMeEt)(OZNO)(OZNOH)]$ (**9**)

A mechanism similar to the one described for the transformation of **2** into **1** by the action of water remains applicable for the generation of **3** and **5**−**9** from **4**. This consists of protonation of the oximic oxygen atom of (HOZNO) in **4**, utilizing the proton from the entering R′OH to promote substitution with HOZNOH, which is the stable leaving group.

Table 1. Compounds obtained by treating di-*n*-butyl or dimethyltin oxide with salicylaldoxime; in the case when R = Me, compound **3** was observed solely as a transient, **4** was obtained as a crystalline solid, and compounds **5**−**9** were isolated from solutions in the corresponding alcohol R′OH

Compd.	R′O	R
1	HO	*n*Bu
2	*o*-HOZNO	*n*Bu
3	HO	Me
4	*o*-HOZNO	Me
5	MeO	Me
6	EtO	Me
7	PrO	Me
8	*i*PrO	Me
9	(*R*)-2-methylbutoxy	Me

More sterically hindered alcohols did not yield the corresponding alkoxy-bridged clusters. It should also be mentioned that the alkoxy-bridged compounds **5**−**9** are somewhat unstable since, upon ageing, their benzene solutions reveal the appearance of **4** and **3** as transients.

Because an electrophilic assistance by the proton of the entering R′OH appeared necessary in all these reactions to allow for the substitution of YO (YO = HOZNO or HO) by R′O, it was assessed whether other nucleophiles possessing a transferable proton are suitable for a similar substitution reaction. It appears that the MeO group of **5** can, indeed, be substituted for the PhCH=NO group (Figure 10),[22] yielding cluster **10**.

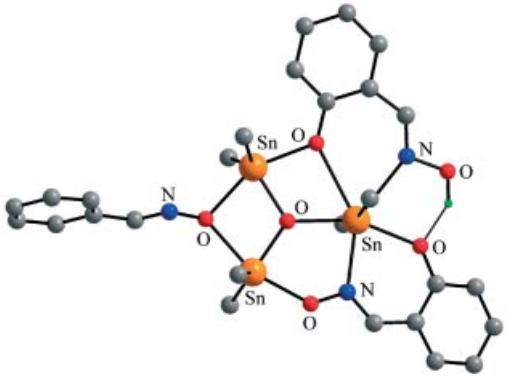

Figure 10. Structure of the organotin cluster $[(Me_2Sn)(Me_2SnO)(Me_2SnON{=}CHPh)(OZNO)(OZNOH)]$ (**10**)

Table 2 shows that phenols, ArOH, are also capable of inducing such reactions (Figure 11).[22]

Steric hindrance likewise hampers the substitution reaction in aryloxy cluster formation, as for the alkoxy cluster analogues, since 2,6-dimethylphenol, with a pK_a similar to the 3,5 analogue, is not capable of converting the methoxy

 © 2004 Wiley-VCH Verlag GmbH & Co. KGaA, Weinheim

Table 2. Dimethyltin phenolate salicylaldoximato clusters synthesized from **5** and ArOH

Compd.	Ar
11	*p*-MeC_6H_4
12	*p*-BrC_6H_4
13	*m*-ClC_6H_4
14	*m*-$O_2NC_6H_4$
15	3,5-$Me_2C_6H_3$

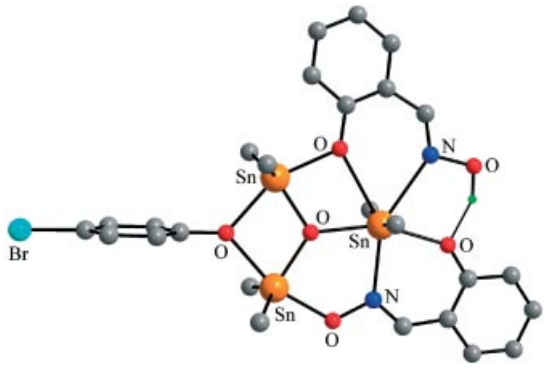

Figure 11. Structure of the organotin cluster [(Me_2Sn)(Me_2SnO)-($Me_2SnOC_6H_4$-*p*-Br)(OZNO)(OZNOH)] (**12**)

cluster into the corresponding 2,6-dimethylphenolate in pure form, as is the case with the 3,5 compound, **15**.

When treated with **5**, phenols with a pK_a slightly lower than 8.0, like *p*-cyanophenol (pK_a = 7.95) or *p*-nitrophenol (pK_a = 7.16), do not yield any substitution products that could be isolated as pure compounds, being observed solely as unstable transients. The threshold pK_a above which a substitution converts **5** into its aryloxy-substituted analogue in a way amenable to isolation and purification, lies in the range 8.0−8.4. Very acidic phenols, such as 2,4-dinitrophenol, completely destroy the cluster structure.

The acidity of carboxylic acids is also sufficient to destroy the cluster skeleton, yielding the usual carboxylatodistannoxane dimers discussed in the Introduction. However, the low acidity of the nucleophile is not sufficient to allow for a smooth substitution, since the weakly acidic acetylacetone (acacH) converts **5** into [$Me_2Sn(acac)_2$]. When **5** is treated with ethylene glycol, 2,2-dimethyl-1,3-dioxa-2-stannacyclopentane is generated.

A special case is provided by cluster **16** (Figure 12)[23] where the nucleophile bridging both five-coordinate tin atoms is simply a fluoride ion. Cluster **16** was obtained by reaction of **4** with NH_4F, showing that the necessary acidic reaction activation is ensured by a proton of the ammonium cation being transferred to the bridging HOZNO ligand to be substituted as HOZNOH. The mechanism of the substitution reaction of fluoride towards **4** or **5** was completely elucidated, taking advantage of the benefits of ^{19}F and ^{119}Sn NMR spectroscopy, in particular the associated spectral patterns arising from $^1J(^{19}F\text{-}^{119/117}Sn)$ scalar couplings. It was unambiguously established that the substitution occurs through an addition/elimination reaction mechanism, involving an intermediate where the entering and leaving nucleophiles are part of a motif where the transferred proton acts as a hydrogen bond connecting them (see Scheme 2).

Figure 12. Structure of the organotin cluster [(Me_2Sn)(Me_2SnO)-(Me_2SnF)(OZNO)(OZNOH)] (**16**)

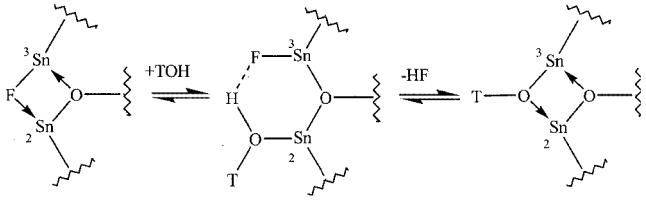

Scheme 2

Conclusion

It can be stated that a large variety of small clusters can be obtained as stable crystalline products or solution transients upon reaction between diorganotin oxides and salicylaldoxime. The basic coordination pattern consists of one seven- and two five-coordinate tin atoms. In solution, such clusters undergo readily reversible substitution reactions under very mild conditions revealing a very broad panel of novel clusters. This variety is rather unusual in organotin chemistry.

Acknowledgments

R. W. and M. B. thank the Fonds voor Wetenschappelijk Onderzoek − Vlaanderen (contract G. 0016.02) and the Research Council of the VUB for financial support. M. G. is also grateful to the Fonds voor Wetenschappelijk Onderzoek − Vlaanderen that provided funds to the laboratory (contract G.0074.00). The National University of Singapore is thanked for a grant (R-143-000-186-112) supporting research in organotin chemistry.

[1] A. G. White, P. A. Tasker, D. J. Smith, *Coord. Chem. Rev.*, in press.
[2] E. R. T. Tiekink, *Appl. Organomet. Chem.* **1991**, *1*, 1−23; *Trends Organomet. Chem.* **1994**, *1*, 71−116.
[3] R. C. Poller, *The Chemistry of Organotin Compounds*, Logos Press, London, **1970**.
[4] H. V. Smith, *Organotin Stabilizers*, The Tin Research Institute, Greenford, **1959**.

 © 2004 Wiley-VCH Verlag GmbH & Co. KGaA, Weinheim

[5] M. Gielen, *Appl. Organomet. Chem.* **2002**, *16*, 481−494.
[6] J. K. Tsagatakis, N. A. Chaniotakis, R. Altmann, K. Jurkschat, R. Willem, J. C. Martins, E. Bakker, Y. Qin, *Helv. Chim. Acta* **2001**, *84*, 1952−1961.
[7] S. Karpel, *Tin and its Uses* **1980**, *125*, 1−6.
[8] W. Knoll, *Chemistry and Technology of Silicones*, Academic Press, New York, **1968**.
[9] J. Otera, *Chem. Rev.* **1993**, *93*, 1449−1470.
[10] S. Durand, K. Sakamoto, A. Orita, J. Otera, A. Duthie, D. Dakternieks, M. Schulte, K. Jurkschat, *Organometallics* **2000**, *19*, 3220−3223.
[11] D. Marton, D. Slaviero, G. Tagliavini, *Tetrahedron* **1989**, *45*, 7099−7108.
[12] M. Bouâlam, M. Biesemans, J. Meunier-Piret, R. Willem, M. Gielen, *Appl. Organomet. Chem.* **1992**, *6*, 197−205.
[13] R. R. Holmes, *Acc. Chem. Res.* **1989**, *22*, 190−197.
[14] V. Chandrasekhar, S. Nagendran, V. Baskar, *Coord. Chem. Rev.* **2002**, *235*, 1−52.
[15] C. Ma, Q. Jiang, R. Zhang, D. Wang, *Dalton Trans.* **2003**, 2975−2978.
[16] F. Kayser, M. Biesemans, M. Bouâlam, E. R. T. Tiekink, A. El Khloufi, J. Meunier-Piret, A. Bouhdid, K. Jurkschat, M. Gielen, R. Willem, *Organometallics* **1994**, *13*, 1098−1113.
[17] D. Dakternieks, K. Jurkschat, S. van Dreumel, E. R. T. Tiekink, *Inorg. Chem.* **1997**, *36*, 2023−2029.
[18] J. Beckmann, K. Jurkschat, B. Mahieu, M. Schurmann, *Main Group Met. Chem.* **1998**, *21*, 113−122.
[19] F. A. G. Mercier, A. Meddour, M. Gielen, M. Biesemans, R. Willem, E. R. T. Tiekink, *Organometallics* **1998**, *17*, 5933−5936.
[20] A. Meddour, A. Bouhdid, M. Gielen, M. Biesemans, F. Mercier, E. R. T. Tiekink, R. Willem, *Eur. J. Inorg. Chem.* **1998**, 1467−1472.
[21] R. Willem, A. Bouhdid, F. Kayser, A. Delmotte, M. Gielen, J. C. Martins, M. Biesemans, B. Mahieu, E. R. T. Tiekink, *Organometallics* **1996**, *15*, 1920−1929.
[22] R. Willem, A. Bouhdid, A. Meddour, C. Camacho-Camacho, F. Mercier, M. Gielen, M. Biesemans, F. Ribot, C. Sanchez, E. R. T. Tiekink, *Organometallics* **1997**, *16*, 4377−4385.
[23] A. Meddour, F. Mercier, J. C. Martins, M. Gielen, M. Biesemans, R. Willem, *Inorg. Chem.* **1997**, *36*, 5712−5715.

Received October 13, 2003

 © 2004 Wiley-VCH Verlag GmbH & Co. KGaA, Weinheim

Design and Structural Analysis of Metallamacrocycles Based on a Combination of Ethylene Glycol Bearing Pyridine Units with Zinc, Cobalt and Mercury

Philippe Grosshans,[a] Abdelaziz Jouaiti,[a] Véronique Bulach,[a] Jean-Marc Planeix,[a] Mir Wais Hosseini,*[a] and Nathalie Kyritsakas[b]

Keywords: Glycol / Pyridine / Zinc / Cobalt / Mercury / Metallamacrocycle

In the presence of MX_2 salts, ligand **1** (in a M/L ratio of 2:2, M = Zn, Hg, Co, X = Cl or I), based on the ethylene glycol fragment bearing two pyridine units as monodentate coordination sites, leads to isostructural square-shaped neutral metallamacrocycles as demonstrated by X-ray diffraction on single crystals. For all dinuclear complexes generated, the dicationic metal centre adopts a distorted tetrahedral coordination geometry and its coordination sphere is composed of the X_2N_2 set of coordinating atoms. For all complexes, the parallel packing of the cyclic structures generates channels which are occupied by solvent molecules. The solvent molecules, which behave as substrates, are positioned within the cavity of the metallamacrocycles. Control of the dimension of the macrocycles, by varying the size of the connecting metal centre, has also been demonstrated.

(© Wiley-VCH Verlag GmbH & Co. KGaA, 69451 Weinheim, Germany, 2004)

Introduction

Metallamacrocycles are finite entities composed of organic fragments and endocyclic metal centres.[1−11] These species may be described as cyclic structures either resulting from the bridging of metal centres by organic ligands that possess at least two coordinating sites or from the interconnection of organic ligands by the metal centres. For the design of metallamacrocycles, one must take into account the characteristics of the organic ligand (shape, rigidity, number and disposition of the coordinating sites) as well as the stereochemical requirements of the metal centre (oxidation state, geometry, number and disposition of free coordination sites).[3]

The majority of metallamacrocycles reported to date are based on the combination of *cis*-protected cationic square-planar metal units such as diphosphane or ethylenediamine complexes of Pd^{II} and Pt^{II} and often bis(pyridine) neutral ligands.[2−4] For these cases, due to the neutral nature of the ligands used, the metallamacrocycles formed are cationic in nature and thus are associated with anions for charge neutrality purposes. In order to generate uncharged metallamacrocycles, one may consider a combination of neutral metal complexes and organic ligands. This has been previously demonstrated with metal halide complexes.[11,12] Indeed, in that case, the coordinating halide centres not only neutralise the cationic charge of the metal cation, but also, by occupying some of the coordination sites within the first coordination sphere around the metal, allow the disposition of the remaining unoccupied sites to be controlled. This aspect has been demonstrated by us both in the case of discrete metallamacrocycles[12] and for coordination networks.[13−20]

Another important issue associated with the metallamacrocycles is the control of the nuclearity (i.e. the metal to ligand ratio). Indeed, depending on the nature of the bis(monodentate) ligand (rigidity, positioning of the coordinating sites) and the metal cation used (number and disposition of coordination sites), different cyclic structures such as [1.1] I, [2.2] II, [3.3] III, [4.4] IV etc. may be expected (Figure 1).[3,21]

Here, in the continuation of our investigations on the design of metallamacrocycles,[12,21−27] we describe the formation of four new neutral metallamacrocycles based on the use of the bis(monodentate) ligand **1** and neutral metal halide complexes (MX_2: M = Zn, Hg, Co; X = Cl or I).

Results and Discussion

The design of ligand **1** (Scheme 1) is based on the ethylene glycol fragment **2** as a spacer connecting two monodentate pyridine derivatives. The connection between the two

[a] Université Louis Pasteur, Laboratoire de Chimie de Coordination Organique, Institut Le Bel,
4, rue Blaise Pascal, 67000 Strasbourg, France
Fax: (internat.) + 33-3-90241325
E-mail: hosseini@chimie.u-strasbg.fr
[b] Université Louis Pasteur, Service Commun des Rayons X, Institut Le Bel,
4, rue Blaise Pascal, 67000 Strasbourg, France

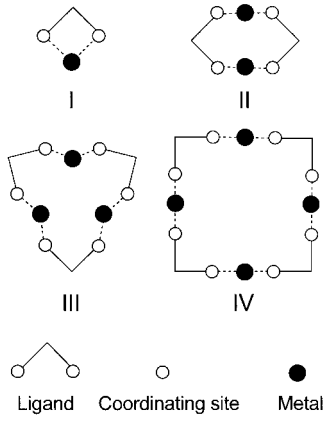

Figure 1. Schematic representations of the formation of metallamacrocycles of different nuclearity between a bis-monodentate fragment and a metal centre possessing two free coordination sites

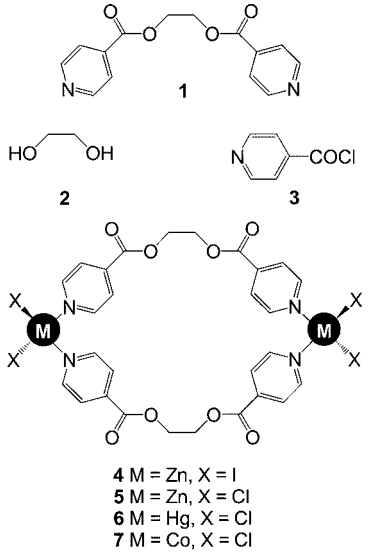

Scheme 1

units is achieved through an ester group at the 4-position of the pyridine ring. Although the straight forward synthesis of **1** has been reported,[28] we used our own methodology consisting of the condensation of ethylene glycol **2** with **3** in dry THF and in the presence of Et_3N (see Exp. Sect.).

Compound **1**, which is of the bis(monodentate) type, may either behave as a ligand and thus lead to metallamacrocyclic complexes or act as a tecton and generate coordination networks in the presence of appropriate metal centres.[29,30] We have previously demonstrated the latter case using analogous oligoethylene glycol based tectons, which lead to the formation of double-helical infinite networks when combined with silver cations.[31,32] Ligand **1** has also been used for the formation of 1D coordination networks in the presence of copper bromide.[33] The formation of coordination networks based on an analogous compound for which the ethylene glycol unit is replaced by an ethylene diamine fragment has also been reported.[34]

For the generation of metallamacrocycles under self-assembly processes, the choice of the coordinating heteroatoms and the cationic metal centre is crucial. Indeed, the self-assembly phenomena requires reversible coordination bond formation. Since ligand **1** contains two pyridine units as coordinating sites, zinc(II), mercury(II) and cobalt(II) halides have been chosen because the binding of pyridine to these metals in the oxidation state II is reversible. Thus, although many different species may be formed in solution, the selection of a metallamacrocycle with a given nuclearity may be achieved by the crystallisation process. In the present investigation, zinc(II), mercury(II) and cobalt(II) halides were combined with ligand **1** under crystallisation conditions leading exclusively to four new metallamacrocycles **4**−**7**, which were characterised by elemental analysis and X-ray diffraction on single crystals (Table 1). All four metallamacrocycles were found to be insoluble in common solvents such as CH_2Cl_2, $CHCl_3$, MeOH, EtOH, THF, CH_3CN and dioxane and for that reason they could not be characterised by NMR spectroscopy. The metallamacrocycles **4**−**7** were slightly soluble in DMF and readily soluble in DMSO. However, the ^1H NMR solution study in DMSO revealed that the chemical shifts observed for all signals were identical to those observed for the free ligand in the same solvent, probably implying that the metallamacrocycles are degraded in DMSO.

Treatment of ligand **1** with ZnI_2, produced slightly yellowish single crystals upon slow diffusion of a solution of ZnI_2 in EtOH into a solution of **1** in $CHCl_3$. The X-ray diffraction study of **4** (Table 1) revealed that the crystal (triclinic, $P\bar{1}$) is composed of one ZnI_2 dinuclear [2.2] complex **4** (Type II; Figure 1) and one disordered $CHCl_3$ solvent molecule. The solvent molecule is located within the cavity of the metallamacrocycle of the cyclophane (there are four edges, each defined by one pyridine unit), which leads to an inclusive complex in the crystalline phase (Figure 2).

The shape of the metallamacrocycle is a very slightly distorted square (8.65 Å × 8.72 Å) with the two ZnI_2 units occupying diagonal corners (Zn···Zn distance 12.25 Å). For ligand **1**, the ethylene glycol fragment adopts a gauche conformation with the O−C−C−O dihedral angles of −80.2° and +80.3°. The plane of the two ester groups (average C−O and C=O distances are approximately 1.32 Å and 1.19 Å, respectively; the O−C−O angle lies between 123.6° and 125.0°) is slightly tilted with respect to the connected pyridine unit (C−C−C−O dihedral angles of 2.3° and 6.2°). The coordination sphere around the metal is composed of two I^- anions and two N atoms belonging to two pyridine units of two different ligands (**1**) with average Zn−N and Zn−I bond lengths of approximately 2.06 Å and 2.54 Å, respectively (Figure 2). The metal centre adopts a distorted tetrahedral coordination geometry with N−Zn−N and I−Zn−I angles of 102.8° and 121.0°, respectively. The N−Zn−I angle varies between 106.4° and 107.4°. The slightly distorted square metallamacrocycles are packed in a parallel fashion thus generating channels occupied by solvent molecules. In one direction of space, the metallamacrocycles probably interact through stacking be-

 © 2004 Wiley-VCH Verlag GmbH & Co. KGaA, Weinheim

Table 1. X-ray data for metallamacrocycles **4**−**7** formed between ligand **1** and metal halides

	4:**1**-ZnI_2	**5**:**1**-$ZnCl_2$	**6**:**1**-$HgCl_2$	**7**:**1**-$CoCl_2$
Chemical Formula	$C_{29}H_{25}Cl_3I_4N_4O_8Zn_2$	$C_{29}H_{24}Cl_7N_4O_8Zn_2$	$C_{15}H_{13}Cl_4HgN_2O_4$	$C_{15}H_{13}Cl_4CoN_2O_4$
Molecular mass	1302.23	935.45	627.68	486.024
Crystal system	triclinic	monoclinic	monoclinic	monoclinic
Space group	$P\bar{1}$	$P2_1/c$	$P2_1/c$	$P2_1/c$
a (Å)	9.860(2)	9.6818(4)	10.0469(2)	10.030(2)
b (Å)	10.042(3)	18.9516(13)	19.3318(4)	18.899(5)
c (Å)	10.228(3)	10.2085(7)	10.3355(2)	10.112(2)
α (°)	81.30(2)	90.00	90.00	90.00
β (°)	81.81(2)	98.198(5)	98.814(5)	98.85(3)
γ (°)	86.97(2)	90.00	90.00	90.00
V (Å^3)	990.4(4)	1854.0(2)	1983.70(7)	1894.0(8)
$D_{calcd.}$ (gcm^{-3})	2.184	1.676	2.10	1.70
Z	1	2	4	4
Colour	colourless	colourless	colourless	blue
Crystal size (mm)	0.37 × 0.21 × 0.08	0.40 × 0.20 × 0.15	0.20 × 0.15 × 0.06	0.15 × 0.07 × 0.01
μ(Mo-K_α) (mm^{-1})	4.580	1.850	8.320	1.494
T (K)	173	173	173	173
Data collected	5760	5399	10139	34078
Obsd. data [$I > 3\sigma(I)$]	4916	3785	3570	3341
$R1$	0.039	0.050	0.029	0.043
$wR2$	0.129	0.113	0.046	0.156
GooF	1.116	1.035	1.008	1.114
CCDC No	216069	216070	216071	216073

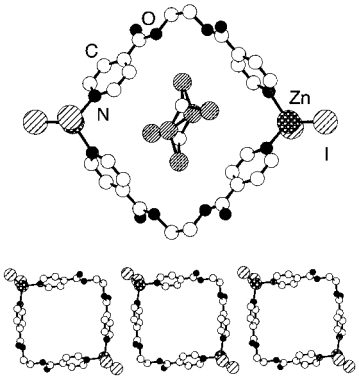

Figure 2. Solid-state structure of the dinuclear zinc metallamacrocycle **4** obtained upon reacting ligand **1** with ZnI_2; the cavity of the square macrocycle is occupied by a disordered $CHCl_3$ molecule (top) and in one direction of space; the metallamacrocycles interact through stacking between pyridine units (bottom); H atoms are not represented for clarity; for bond lengths and angles see text

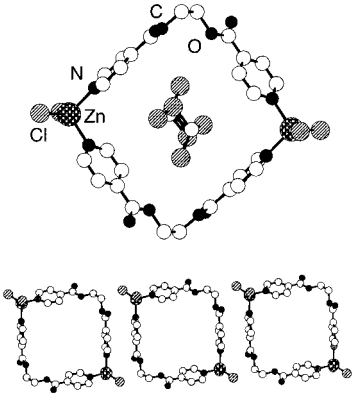

Figure 3. The solid-state structure of the dinuclear zinc metallamacrocycle **5** (top) obtained upon reacting ligand **1** with $ZnCl_2$; the square macrocycle forms an inclusive complex with a $CHCl_3$ molecule (disordered) and the packing of consecutive units (bottom); H atoms are not represented for clarity; for bond lengths and angles see text

tween pyridine units disposed in an anti-parallel manner (shortest distance between carbon atoms of two pyridines belonging to two consecutive metallamacrocycles is ca. 3.80 Å).

As expected, when ZnI_2 was replaced by $ZnCl_2$ under the same conditions, the X-ray diffraction study (Table 1) again revealed a similar metallamacrocycle **5** (Figure 3). The crystal structure (monoclinic, $P2_1/c$) is again composed of one $ZnCl_2$ dinuclear complex **5** and one disordered $CHCl_3$ solvent molecule. The latter, as mentioned above, is located within the cavity of the metallamacrocycle (Figure 3). The metallamacrocycle adopts a similarly distorted square form as above with almost identical dimensions (8.64 Å × 8.73 Å, Zn···Zn distance is 12.36 Å). Ligand **1** presents the same characteristics as those observed for the ZnI_2 complex **4**, that is, gauche conformation of the ethylene glycol fragment (O−C−C−O dihedral angles −77.2° and +77.2°). The plane of the two ester groups (average C−O and C=O distances are ca. 1.32 Å and 1.19 Å, respectively; the O−C−O angle lies between 124.6° and 125.2°) is again slightly tilted with respect to the connected pyridine unit (C−C−C−O dihedral angles of −0.8° and +10.2°). The coordination sphere around the metal centre is composed of two Cl^- anions and two N atoms belonging to two pyridine units of two different ligands (**1**) with Zn−N and Zn−Cl average bond lengths of approximately 2.05 Å and 2.21 Å, respectively (Figure 2). The metal centre adopts a distorted tetrahedral coordination geometry with N−Zn−N and Cl−Zn−Cl angles of 101.6° and 121.5°, respectively. The

 © 2004 Wiley-VCH Verlag GmbH & Co. KGaA, Weinheim

N−Zn−Cl angle varies between 105.9° and 111.4°. Again, as for the previous case mentioned above, the square metallamacrocycles are packed in a parallel fashion generating channels. Also, in one direction of space, the metallamacrocycles probably interacts through stacking between pyridine units disposed in an anti-parallel fashion (shortest distance between carbon atoms of two pyridines belonging to two consecutive metallamacrocycles is ca. 3.67 Å). Comparison of structures **4** and **5** shows that changing the steric demand of the halogen atoms coordinated to the metal centre has almost no effect on the size of the metallamacrocycle.

In order to increase the dimensions of the metallamacrocycle, that is, the size of the endocyclic cavity, it may be possible to increase the size of the metal centre. For that reason, ligand **1** was treated with $HgCl_2$. Upon slow diffusion of a solution of $HgCl_2$ in EtOH into a solution of **1** in $C_2H_2Cl_4$, colourless crystals were obtained (Table 1). The crystal structure (monoclinic, $P2_1/c$) is composed of one neutral metallamacrocycle **6** and one tetrachloroethane solvent molecule. The solvent molecule is again located within the cavity of the metallamacrocycle **6** (Figure 4). The structure again adopts a slightly distorted square form with larger dimensions, as expected (8.98 Å × 9.05 Å, the Hg···Hg distance is 13.29 Å). Ligand **1** presents the same characteristics as those observed for the dinuclear metallamacrocycles **4** and **5** obtained with zinc, that is, gauche conformation of the ethylene glycol fragment (O−C−C−O dihedral angles −81.8° and +81.8°). The plane of the two ester groups (average C−O and C=O distances are ca 1.33 Å and 1.19 Å, respectively, the O−C−O angle lies between 123.6° and 123.8°) is again slightly tilted with respect to the connected pyridine unit (C−C−C−O dihedral angles of −1.2° and −8.9°). The coordination sphere around the Hg^{2+} cation is composed of two Cl^- anions and two N atoms belonging to two pyridine units of two different ligands (**1**) with Hg−N and Hg−Cl average bond lengths of approximately 2.39 Å and 2.36 Å, respectively. The metal centre adopts a distorted tetrahedral coordination geometry with N−Hg−N and Cl−Hg−Cl angles of 97.0° and 141.7°, respectively. The N−Hg−Cl angle varies between 97.0° and 104.7°. As for the previous cases mentioned above, the square metallamacrocycles are packed in a parallel fashion with stacking interactions (shortest distance between carbon atoms of two pyridines belonging to two consecutive metallamacrocycles ca. 3.60 Å) in one direction of space between consecutive metallamacrocycles **6** (Figure 4).

Finally, ligand **1** was allowed to react with $CoCl_2$ under crystallisation conditions. The slow diffusion of a solution of $CoCl_2{\cdot}6H_2O$ in EtOH into a solution of **1** in $C_2H_2Cl_4$ afforded blue crystals (Table 1). The crystal structure (monoclinic, $P2_1/c$) is composed of one $CoCl_2$ dinuclear complex **7** and one tetrachloroethane solvent molecule. Again the solvent molecule is located within the cavity of the metallamacrocycle **7** (Figure 5), which adopts a slightly distorted square shape with similar dimensions (8.63 Å × 8.71 Å, Co···Co distance is ca. 12.22 Å) close to those observed for the Zn complexes **4** and **5**. Ligand **1** presents the same characteristics as those observed for the dinuclear metallamacrocycles **4**−**6** which were obtained with zinc and mercury, that is, gauche conformation of the ethylene glycol fragment (O−C−C−O dihedral angles −77.8° and +77.9°). The plane of the two ester groups (average C−O and C=O distances are ca. 1.33 Å and 1.19 Å, respectively; O−C−O angles lie between 124.2° and 125.0°) is again tilted with respect to the connected pyridine unit (C−C−C−O dihedral angles of −1.5° and +9.9°). Interestingly, the coordination sphere around the Co^{2+} cation is only composed of two Cl^- anions and two N atoms belonging to two pyridine units of two different ligands (**1**) with Co−N and Co−Cl average bond lengths of approximately 2.04 Å and 2.22 Å, respectively. The metal centre adopts a distorted tetrahedral coordination geometry with N−Co−N and Cl−Co−Cl angles of 105.7° and 120.4°, respectively. The N−Co−Cl angle varies between 105.4° and 110.2°. This coordination geometry around Co^{II} with the (X_2N_2) set of coordinating centres differs from the previously observed octahedral geometry with the same type of donor sites (pyridine and Cl^-).[13−18] Once again, as for

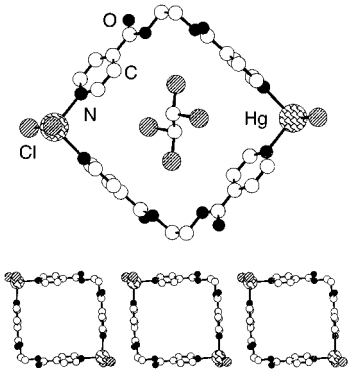

Figure 4. The solid-state structure of the dinuclear mercury metallamacrocycle **6** (top) obtained upon reacting ligand **1** with $HgCl_2$; the square macrocycle forms an inclusive complex with tetrachloroethane molecule; the packing of consecutive units generates channels (bottom); H atoms are not represented for clarity; for bond lengths and angles see text

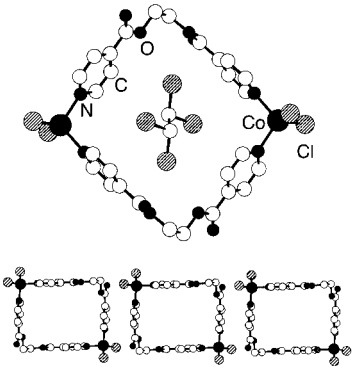

Figure 5. The solid-state structure of the dinuclear cobalt metallamacrocycle **7** (top) obtained upon reacting ligand **1** with $CoCl_2$; the Co^{II} centre adopts a distorted tetrahedral coordination geometry; the square macrocycle forms an inclusive complex with tetrachloroethane molecule; the packing of consecutive units generates channels (bottom); H atoms are not represented for clarity; for bond lengths and angles see text

 © 2004 Wiley-VCH Verlag GmbH & Co. KGaA, Weinheim

the previous cases mentioned above, the slightly distorted square metallamacrocycles are packed in a parallel fashion with stacking interactions (shortest distance between carbon atoms of two pyridines belonging to two consecutive metallamacrocycles is ca. 3.60 Å) are in one direction of space between consecutive metallamacrocycles of **7**.

In summary, the rather simple ligand **1**, composed of an ethylene glycol unit bearing two pyridines as monodentate coordination sites, leads in the presence of metal halides (MX_2: M = Zn, Hg, Co; X = Cl or I) in a M/L ratio of 2:2 to isostructural square-shape neutral metallamacrocycles. The metallamacrocyclic structures offer rather large cavities of the cyclophane type which are occupied by solvent molecules. In the crystal, the square-cyclic units are packed in a parallel fashion, thus generating channels occupied by solvent molecules. In one direction of space, the metallamacrocycles probably interact with each other through stacking of the pyridine units belonging to consecutive units and are disposed in an anti-parallel manner. Since the solvent molecules included in the cavity of the metallamacrocycles may play a template role and thus define the nuclearity of the complex, we are currently evaluating this aspect. The formation of other types of finite metallamacrocycles using ligand **1**, other metal centres and the generation of infinite coordination networks are currently under investigation. The ability of the analogous ligand for which the pyridine units are connected at the 3-position to generate metallamacrocycles and/or coordination networks with a variety of metal complexes is also currently being investigated.

Experimental Section

General: All commercially available reagents were purchased and used without further purification. ^1H and ^{13}C NMR spectra were recorded on Bruker spectrometers at 400 and 300 MHz and at 50 MHz, respectively. Microanalyses were performed by the Service de Microanalyses de la Fédération de Recherche Chimie, Université Louis Pasteur, Strasbourg.

Synthesis of Ligand 1: A solution of **3** as its hydrochloride salt (2.15 g, 12 mmol) in dry THF (30 mL) was added to ethylene glycol **2** (0.3 g, 4.8 mmol) under argon. The mixture was stirred before Et_3N (5 mL) was added and stirred at room temperature for a further 12 hours. The brownish solution was evaporated to dryness under reduced pressure. A saturated aqueous hydrogenocarbonate solution (50 mL) was added to the residue and the mixture was extracted with CH_2Cl_2 (3 × 50 mL). The organic solvent was removed and the residue purified by column chromatography (SiO_2, CH_2Cl_2-0-2 % MeOH) affording the pure compound **1** (0.66 g, 51 %) as a slightly yellowish oil. $C_{14}H_{12}N_2O_4$ (272.26): calcd. C 61.76, H 4.44, N 10.29; found C 61.59, H 4.53, N 9.96. ^1H NMR ($CDCl_3$, 300 MHz, 25 °C): δ = 4.71 (s, 4 H, CH_2O), 7.84 (dd, 4 H, J = 1.65 and 4.41 Hz), 8.79 (dd, J = 1.6, 4.4 Hz, 4 H) ppm. ^{13}C NMR ($CDCl_3$; 300 MHz; 25 °C): δ = 63.2, 122.8, 136.7, 150.7, 164.9 ppm.

Synthesis of Metallamacrocycles 4−7: Single crystals of suitable quality for X-ray diffraction investigations were obtained within 2−4 days at room temperature, upon slow diffusion of a $CHCl_3$ or $C_2H_2Cl_4$ solution (1 mL) of **1** (5 mg) into a EtOH (2 mL) solution of ZnI_2, $ZnCl_2$, $HgCl_2$ or $CoCl_2·6H_2O$ (1.5 mg); **4**: $C_{14}H_{12}O_4N_2·ZnI_2$ (591.45): calcd. C 28.43, H 2.05, N 4.74; found C 28.38, H 2.12, N 4.68; **5**: $C_{14}H_{12}N_2O_4·ZnCl_2$ (408.55): calcd. C 41.16, H 2.96, N 6.86; found C 41.33, H 3.08, N 6.90; **6**: $C_{14}H_{12}N_2O_4·HgCl_2$ (543.76): calcd. C 30.92, H 2.22, N 5.15; found C 30.89, H 2.32, N 5.46; **7**: $C_{14}H_{12}N_2O_4·CoCl_2$ (410.10): calcd. C 41.82, H 3.10, N 6.97; found C 41.88, H 3.06, N 6.99.

Crystal Structure Characterisation: X-ray diffraction data was carried out on a Kappa CCD diffractometer equipped with an Oxford Cryosystem liquid N_2 device, with graphite-monochromated Mo-K_α radiation (Table 1). In the case of **6**, diffraction data were corrected for absorption and analysed using the OpenMolen package,[35] whereas for the other three metallamacrocycles **4**, **5** and **7**, Nonius−Maxus Package 4.3 was used. All non-H atoms were refined anisotropically. CCDC-216069 to -216071 and -216073 contain the supplementary crystallographic data for this paper. These data can be obtained free of charge at www.ccdc.cam.ac.uk/conts/retrieving.html or from the Cambridge Crystallographic data Centre, 12 Union Road, Cambridge CB2 1EZ, UK; Fax: (internat.) +44-1223/336-033; E-mail: deposit@ccdc.cam.ac.uk.

Acknowledgments

Thanks to Université Louis Pasteur and the Ministry of Research and Technology for financial support and a scholarship to P. G.

[1] R. W. Saalfrank, A. Stark, K. Peters, H.-G. von Schnering, *Angew. Chem. Int. Engl.* **1988**, *27*, 851−853.
[2] [2a] M. Fujita in *Comprehensive Supramolecular Chemistry*, (Eds.) J. L. Atwood, J. E. D. Davies, D. D. MacNicol, F. Vögtle, vol. 9 (Eds.: J. P. Sauvage, M. W. Hosseini), Elsevier, Oxford, **1996**, p. 253−282. [2b]M. Fujita, *Acc. Chem. Res.* **1999**, *32*, 53−61.
[3] P. J. Stang, B. Olenyuk, *Acc. Chem. Res.* **1997**, *30*, 502−518.
[4] G. F. Swiegers, T. J. Malefetse, *Chem. Rev.* **2000**, *100*, 3483−3537.
[5] J. K. M. Sanders (Eds.: J. L. Atwood, J. E. D. Davies, D. D. MacNicol, F. Vögtle), vol. 9 (Eds.: J. P. Sauvage, M. W. Hosseini), Elsevier, **1996**, p. 131−164.
[6] C. M. Drain, J.-M. Lehn, *J. Chem. Soc., Chem. Commun.* **1994**, 2313−2314.
[7] F. M. Romero, R. Ziessel, A. Dupont-Gervais, A. van Dorsselaer, *Chem. Commun.* **1996**, 551−552.
[8] T. Habicher, J. F. Nierengarten, V. Gramlich, F. Diederich, *Angew. Chem. Int. Ed.* **1998**, *37*, 1916−1919.
[9] D. W. Johnson, J. Xu, R. W. Saalfrank, K. N. Raymond, *Angew. Chem. Int. Ed.* **1999**, *38*, 2882−2885.
[10] K. R. J. Thomas, J. T. Lin, Y.-Y. Lin, C. Tsai, S.-S. Sun, *Organomet.* **2001**, *20*, 2262−2269.
[11] D. Braga, M. Polito, M. Bracaccini, D. D'Addario, E. Tagliavini, D. M. Proserpio, F. Grepioni, *Chem. Commun.* **2002**, 1080−1081.
[12] C. Klein, E. Graf, M. W. Hosseini, A. De Cian, N. Kyritsakas-Gruber, *Eur. J. Inorg. Chem.* **2002**, 1299−1302.
[13] M. Loï, E. Graf, M. W. Hosseini, A. De Cian, J. Fischer, *Chem. Commun.* **1999**, 603−604.
[14] A. Jouaiti, M. W. Hosseini, A. De Cian, *Chem. Commun.* **2000**, 1863−1864.
[15] A. Jouaiti, V. Jullien, M. W. Hosseini, J.-M. Planeix, A. De Cian, *Chem. Commun.* **2001**, 1114−1115.
[16] A. Jouaiti, M. W. Hosseini, N. Kyritsakas, *Chem. Comm* **2002**, 1898.
[17] P. Grosshans, A. Jouaiti, M. W. Hosseini, N. Kyritsakas, *New. J. Chem.* **2003**, *27*, 793−797.

 © 2004 Wiley-VCH Verlag GmbH & Co. KGaA, Weinheim

[18] P. Grosshans, A. Jouaiti, N. Kardouh, M. W. Hosseini, N. Kyritsakas, *New. J. Chem.* **2003**, submitted.
[19] B. Zimmer, M. Hutin, V. Bulach, M. W. Hosseini, A. De Cian, N. Kyritsakas, *New. J. Chem.* **2002**, *26*, 1532−1535.
[20] B. Zimmer, V. Bulach, M. W. Hosseini, A. De Cian, N. Kyritsakas, *Eur. J. Inorg. Chem.* **2002**, 3079−3080.
[21] P. Grosshans, A. Jouaiti, M. W. Hosseini, A. De Cian, N. Kyritsakas, *Tetrahedron Lett.* **2003**, *44*, 1457−1460.
[22] G. Oddon, M. W. Hosseini, *Tetrahedron Lett.* **1993**, *34*, 713−7416.
[23] R. Schneider, M. W. Hosseini, J.-M. Planeix, A. De Cian, J. Fischer, *Chem. Commun.* **1998**, 1625−1626.
[24] M. Loï, M. W. Hosseini, A. Jouaiti, A. De Cian, J. Fischer, *Eur. J. Inorg. Chem.* **1999**, 1981−1985.
[25] A. Jouaiti, M. Loï, M. W. Hosseini, A. De Cian, *Chem. Commun.* **2000**, 2085−2086.
[26] V. Jullien, J.-M. Planeix, M. W. Hosseini, A. De Cian, *J. Org. Met. Chem.* **2002**, *643−644*, 376−380.
[27] A. Jouaiti, M. W. Hosseini, N. Kyritsakas, *Eur. J. Inorg. Chem.* **2002**, 57−61.
[28] C. O. Badgett, C. F. Woodward, *J. Am. Chem. Soc.* **1947**, 2907.
[29] S. R. Batten, R. Robson, *Angew. Chem. Int. Ed.* **1998**, *37*, 1460−1494.
[30] B. Moulton, M. J. Zaworotko, *Chem. Rev.* **2001**, *101*, 1629−1658.
[31] B. Schmaltz, A. Jouaiti, M. W. Hosseini, A. De Cian, *Chem. Commun.* **2001**, 1242−1243.
[32] A. Jouaiti, M. W. Hosseini, N. Kyritsakas, *Chem. Commun.* **2003**, 423−424.
[33] L.-C. Song, W.-X. Zhang, J.-Y. Wang, *Trans. Met. Chem.* **2002**, *27*, 526−531.
[34] S. Muthu, J. H. K. Yip, J. J. Vittal, *J. Chem. Soc., Dalton Trans.* **2001**, 3577−3584.
[35] OpenMolenN, Interactive Structure Solution, Nonius B. V., Delft, The Netherlands, **1997**.

Received August 25, 2003

 © 2004 Wiley-VCH Verlag GmbH & Co. KGaA, Weinheim

Novel Thiotetraazapentalene Complexes from the Reaction of a Ruthenium Azide Complex with Alkyl Isothiocyanates

Sheng-Chin Hsu,[a,b] Ying-Chih Lin,*[a] Shou-Ling Huang,[a] Yi-Hung Liu,[a] Yu Wang,[a] and Hwang Liu[b]

Keywords: Ruthenium / Azides / Isothiocyanates / Thiotetraazapentalene

Reactions of the ruthenium azide complex **1** with alkyl isothiocyanates give novel ruthenium thiotetraazapentalenedithione complexes **3a–c** containing a hypervalent sulfur atom. The ligand, bound through one sulfur atom, is derived from three isothiocyanate molecules and one nitrogen atom from an azide ion. The synthesis and structural determination of **3a–c**, as well as a possible mechanism for their formation is described.
(© Wiley-VCH Verlag GmbH & Co. KGaA, 69451 Weinheim, Germany, 2004)

Introduction

Isothiocyanates are known to undergo reactions with unsaturated substrates (including Diels−Alder reactions and nucleophilic additions) to provide heterocyclic derivatives.[1] The pathways for these conversions are controlled by the character of the substrates as well as by the type of reagent.[2−4] For example, addition to the C=S or C=N bond of the heteroallene moiety can occur, leading to polymerization,[5,6] whereas the reactions of acyl/thioacyl isothiocyanates often lead to the formation of 1,4-cycloadducts.[7] The organic chemistry of these isothiocyanate heteroallenes has been described in several reviews,[8,9] but reactions of isothiocyanates with metal complexes have not yet been comprehensively investigated. We reported previously the reactions of ruthenium acetylide complexes with isothiocyanate, which yielded ligands containing four- and six-membered heterocyclic rings.[10,11] Because the reaction of arylsulfonyl isothiocyanates with alkyl azides is known[12] to give 4-alkyl-5-arylsulfonylimino-1,2,3,4-thiatriazolines we were interested in studying the reactions of ruthenium azide complexes with isothiocyanates. Surprisingly, these reactions give ruthenium thiotetraazapentalene[13,14] complexes containing a hypervalent sulfur atom. It is known that thiotetraazapentalene can be prepared from the reaction of thiourea with isothiocyanate,[15,16] but metal-coordinated species are relatively rare. The synthesis and structural characterization of these novel thiotetraazapentalene ruthenium complexes **3a−c** are described below. The isolation of several minor products led to the elucidation of a possible mechanism.

Results and Discussion

The reaction of $[Ru]N_3$ (**1**, [Ru] = (η^5-C_5Me_5)(dppp)Ru, dppp = 1,3-bis(diphenylphosphanyl)propane) with a fivefold excess of $PhCH_2NCS$ in THF under nitrogen for one day gave **3a** in 40 % yield. This compound was identified as a ruthenium thiotetraazapentalene complex by single-crystal X-ray diffraction analysis. About 35 % of the unchanged azide was also isolated. Interestingly, the reaction of **1** with a tenfold excess of $PhCH_2NCS$ in THF gave $\{[Ru]NCS[Ru]\}^+NCS^-$ (**2**) as the major product in 55 % yield and complex **3a** in only 20 % yield (Scheme 1). Following removal of **2** and **3a**, two minor products, [Ru]SC(=NH)$NHCH_2Ph$ (**4**) and **5** (Scheme 2) could be separated from the reaction mixture by fractional crystallization in 5 % and 6 % yield respectively (based on **1**). The reaction of **1** with other alkyl isothiocyanates (EtNCS and MeNCS) in a fivefold excess resulted in the formation of the analogous ruthenium thiotetraazapentalene complexes **3b** and **3c** (Scheme 1) in comparable yields.

Varying the relative amounts of the reactants gave similar yields of the product, however no attempt was made to isolate the compounds analogous to **4** and **5** because of their low yields. Interestingly, the reaction of **1** with phenyl isothiocyanate yielded the monomeric complex [Ru]NCS (**6**) as the only isolable product.

The IR spectrum of **3a** displays absorption bands at 1174 and 699 cm^{-1}, assignable to the $\nu_{C=S}$ and ν_{C-S} stretches respectively.[17,18] In the ^1H NMR spectrum of **3a** at room

[a] Department of Chemistry, National Taiwan University, Taipei, Taiwan 106, Republic of China
Fax: (internat.) + 886-2-23636359
E-mail: yclin@ntu.edu.tw
[b] Scientific & Technical Research Center, Investigation Bureau, Ministry of Justice, Hsintien City, Taipei County, Taiwan 231, Republic of China
Supporting information for this article is available on the WWW under http://www.eurjic.org or from the author.

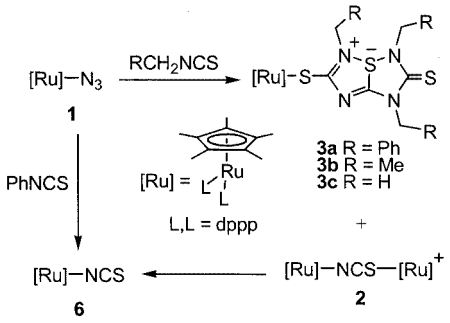

Scheme 1

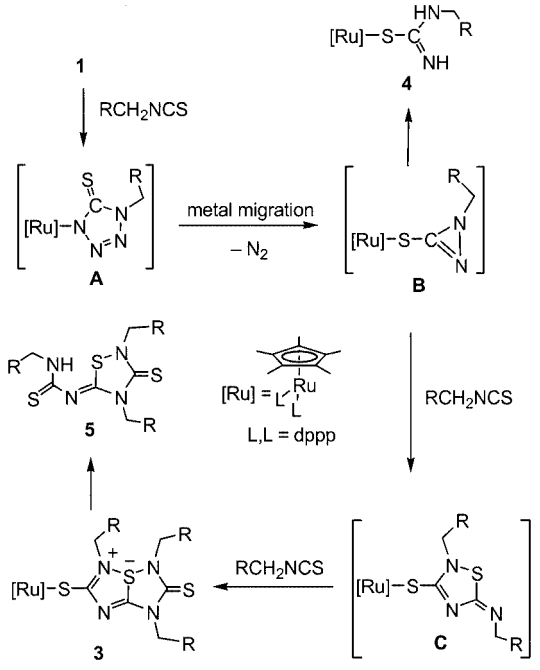

Scheme 2

temperature (in addition to the singlet at δ = 1.51 ppm due to Cp*), there is a very broad resonance at δ = 5.07 ppm and two sharp singlet resonances at δ = 4.86 and 4.72 ppm, which are assignable to the three methylene groups. At 233 K, these resonances resolve into two AX patterns at δ = 5.57 and 3.93 ppm ($J_{H,H}$ = 16.09 Hz) and δ = 5.16 and 4.67 ppm ($J_{H,H}$ = 14.39 Hz), and an AB pattern at δ = 5.13 and 5.07 ppm ($J_{H,H}$ = 17.02 Hz). The ^{31}P NMR spectrum at room temperature displays a broad singlet resonance at δ = 37.54 ppm, which splits into two doublets at δ = 40.51 and 34.81 ppm with $J_{P,P}$ = 51.7 Hz at 233 K. This is possibly because of the hindered rotation of the Ru−S bond at low temperature.[12,19,20] Consistent with this structure, the FAB mass spectrum shows a parent peak at *m*/*z* = 1110.1. Single crystals of **3a** readily formed in a mixture of hexane and THF, enabling the structure of **3a** to be unambiguously determined by single-crystal X-ray diffraction analysis (Figure 1).

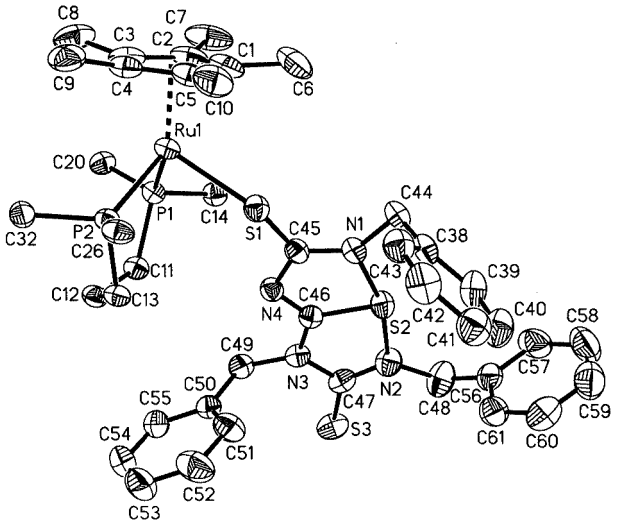

Figure 1. X-ray crystal structure of **3a** with thermal ellipsoids at the 30 % probability level; the four dppp phenyl groups and all of the hydrogen atoms have been omitted for clarity; selected bond lengths (Å): Ru(1)−S(1) 2.4427(8), S(1)−C(45) 1.739(3), C(45)−N(1) 1.305(4), C(45)−N(4) 1.370(4), C(47)−N(2) 1.296(5), C(47)−N(3) 1.406(4), C(46)−N(3) 1.370(4), C(46)−N(4) 1.314(4), S(2)−N(1) 1.884(3), S(2)−N(2) 1.969(3), C(46)−S(2) 1.722(3), C(47)−S(3) 1.683(3); selected bond angles (deg): C(45)−S(1)−Ru(1) 126.56(10), N(1)−S(2)−C(46) 81.80(14), S(2)−C(46)−N(4) 120.4(2), N(3)−C(46)−S(2) 116.6(2), C(46)−N(4)−C(45) 110.9(3), C(45)−N(1)−S(2) 113.1(2), N(2)−C(47)−N(3) 109.8(3), C(46)−N(3)−C(47) 116.1(3), C(46)−S(2)−N(2) 82.79(14), S(2)−N(2)−C(47) 114.7(2), N(1)−C(45)−S(1) 122.4(2), N(4)−C(45)−S(1) 123.7(2), N(2)−C(47)−S(3) 128.2(3), N(3)−C(47)−S(3) 122.1(3)

Thiatetraazapentalenes have been prepared from cyclic thioureas and two equivalents of RNCS.[15,16] A bis(thiatetraazapentalenedithione)copper(I) complex has also been reported, in which four sulfur atoms in the thiocarbonyl groups coordinate tetrahedrally to the copper atom, to form a one-dimensional coordination polymer.[21]

Even though complexes **2** and **6** have the same empirical formula, their spectra are quite distinctive. For example, in **2**, there are two singlets (with equal intensities) at δ = 37.93 and 35.38 ppm in the ^{31}P NMR spectrum and likewise at δ = 1.31 and 1.29 ppm in the ^{1}H NMR spectrum, attributable to the two Cp* groups. In contrast, there is a singlet at δ = 37.86 ppm in the ^{31}P NMR spectrum of **6** and a singlet at δ = 1.29 ppm in the ^{1}H NMR spectrum. The FAB mass spectrum of **2** also displays parent peaks at *m*/*z* = 1356.3, consistent with its formula. Generally, ruthenium isothiocyanate complexes form N-bound linkage isomers,[22−26] but many S-bound isothiocyanate ruthenium complexes are also known, one of which was recently characterized by single-crystal X-ray diffraction analysis.[27] Dinuclear Ru complexes bridged by isothiocyanate ligands are also known in the literature.[28,29]

Complex **4** was characterized by spectroscopic as well as elemental analysis. In the IR spectrum of **4**, two absorption bands at 1617 and 699 cm^{-1} (assignable to the $\nu_{C=N}$ and ν_{C-S} stretches respectively) were observed, with the $\nu_{C=S}$

being absent. In the ^{1}H NMR spectrum, the Cp* ligand appeared as a singlet at δ = 1.22 ppm, a broad resonance at δ = 6.01 ppm was attributed to the amine proton, and a broad resonance at δ = 4.08 ppm was identified as belonging to the methylene protons of the benzyl group. These last two resonances showed $^3J_{H,H}$ coupling in the COSY spectrum. In addition, the broad resonance at δ = 4.32 ppm was assigned to the =NH proton of the imine group. The room temperature ^{31}P NMR spectrum of **4** displays a singlet at δ = 37.09 ppm. The crystal structure of **4** indicates that the isothiourea ligand is bound to the ruthenium metal through the sulfur atom (Figure 2).

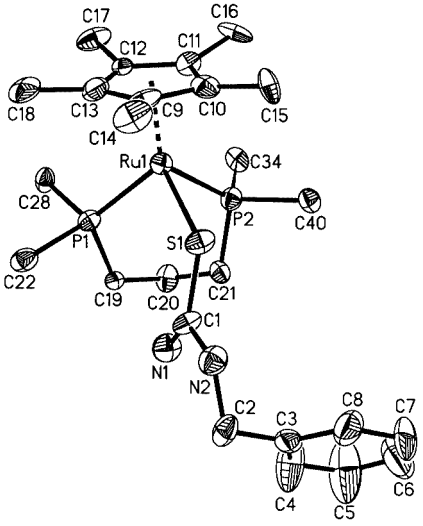

Figure 2. Structural drawing of **4** with thermal ellipsoids at the 30 % probability level; the four dppp phenyl groups and all of the hydrogen atoms have been omitted for clarity; selected bond lengths (Å): Ru(1)−S(1) 2.415(3), S(1)−C(1) 1.726(12), C(1)−N(1) 1.22(2), C(1)−N(2) 1.371(13); selected bond angles (deg): Ru(1)−S(1)−C(1) 126.0(4), S(1)−C(1)−N(1) 126.8(10), S(1)−C(1)−N(2) 112.4(9), N(1)−C(1)−N(2) 120.1(12)

The product **5** was identified by spectroscopic methods as being a five-membered 5-imino-1,2,4-thiadiazolidin-3-thione (Scheme 2).

In the IR spectrum of **5**, absorption bands at 1617, 1184 and 698 cm^{-1} were assigned to $\nu_{C=N}$, $\nu_{C=S}$ and ν_{C-S} stretches, respectively. The high resolution FAB mass spectrum of **5** has a parent peak at *m*/*z* = 463.1807, consistent with the molecular formula. Two isomers (*E* and *Z* forms) in a ratio of 3:2 were apparent from the NMR spectrum of **5**. The fact that the five-membered ring had opened was clear from the presence of a doublet at δ = 4.62 ppm, assigned to one of the methylene groups from its coupling to the NH proton. The resonances for the other two methylene groups at δ = 5.18 and 5.70 ppm remain as singlets. This indicates that the formation of **5** could result from cleavage of the dative N−S bond of **3a**, followed by cleavage of the Ru−S bond. Non metal-containing compounds with similar structures have been reported in the literature;[30] (*E*) and (*Z*) isomers arising from the imine bond are also known.

As mentioned in the literature,[12] it is common to observe the [3+2] cycloaddition of organic azides with the C=N bond of isothiocyanates. However, the thiatetraazapentalenes **3** incorporate three isothiocyanate molecules and only one nitrogen atom from the azide ligand. A possible mechanism for the formation of **3** is depicted in Scheme 2. Cycloaddition of the azide ligand of complex **1** with the C=N bond of the isothiocyanate to form **A** is followed by loss of nitrogen and migration of the ruthenium metal from nitrogen to sulfur to give **B**, which could provide the S-metalated isothiourea complex **4** as a minor product. Complex **B** could then undergo two successive [3+2] cycloadditions; the first with the C=S bond[31,32] of isothiocyanate (to give **C**), and the second with the C=N bond[33] of isothiocyanate, to afford **3**. Formation of **5** (R = Ph) might then be accounted for by loss of the metal from **3a**.

Conclusion

In summary, a novel metallated thiatetraazapentalene has been isolated from the reaction of a ruthenium azide with alkyl thioisocyanates. Formation of this product may proceed through a tandem process that involves three consecutive [3+2] cycloadditions with an alkyl thioisocyanate, a new method for the preparation of this type of compound. Isolation of the S-metalated isothiourea complex **4** and the 5-imino-[1,2,4]thiadiazolidine-3-thione **5** as minor products provides insight into a mechanism for the formation of **3**. Detailed mechanistic studies (including the use of ^{15}N-labeled azide as the starting material) are currently underway.

Experimental Section

Synthesis of 3a: A mixture of [Ru]N_3 **1** (0.45 g, 0.65 mmol) and $PhCH_2NCS$ (0.90 mL, 10.3 mmol) in THF (30 mL) was heated at reflux for one day under nitrogen. The solvent was evaporated under reduced pressure and enough *n*-hexane added to cause precipitation of a yellow solid, which was isolated by filtration and washed with *n*-hexane to give {[Ru]NCS[Ru]}$^+$NCS$^-$ **2** (0.13 g, 14 %). (Upon recrystallization, only the monomeric complex [Ru]NCS **6** was obtained.) Red crystals formed in the filtrate, which were isolated by filtration, washed with diethyl ether and *n*-hexane and dried under vacuum. This product was identified as **3a** (0.29 g, 40 %). Orange crystals formed in the remaining filtrate, which were isolated by filtration to provide **4** (0.03 g, 5 %). Finally, a white compound crystallized from the residual solution, identified as **5** (0.02 g, 6 %), in both the (*E*) and (*Z*) forms.

Data for 3a: $C_{61}H_{62}N_4P_2RuS_3$ (1110.27): calcd. C 65.98, H 5.63, N 5.05, S 8.66; found C 66.04, H 5.70, N 4.98, S 8.70. MS (FAB, ^{102}Ru): *m*/*z* = 1110.1 [M]$^+$, 649.1 [M − N($PhCH_2NCS)_3$]$^+$. IR (KBr): $\tilde{\nu}$ = 1174 (C=S), 699 (C−S) cm^{-1}. ^{1}H NMR ([D_8]THF): δ = 7.46−6.89 (m, 20 H, Ph), 5.07 (br. s, 2 H, CH_2), 4.86 (s, 2 H, CH_2), 4.72 (s, 2 H, CH_2), 2.83−1.35 (m, 6 H, CH_2), 1.51 (s, 15 H, Cp*-CH_3) ppm. ^{31}P NMR ([D_8]THF): δ = 37.54 (br. s) ppm.

X-ray Crystallographic Studies: Data was collected at room temperature from epoxy-coated crystals mounted on a glass fiber. All measurements were made on a CCD Smart diffractometer with

 © 2004 Wiley-VCH Verlag GmbH & Co. KGaA, Weinheim

graphite-monochromated Mo-K_α radiation (λ = 0.71073 Å). Empirical absorption corrections were applied in each case. The relevant crystallographic data are presented in Table 1. The structure was solved by direct methods using the program SHELXTL (Sheldrick, 1997).[34] Hydrogen atoms were placed geometrically using the riding model with thermal parameters set to 1.2 times that for the atoms to which the hydrogen is attached and 1.5 times that for the methyl hydrogens. CCDC-217188 (**3a**) and -217289 (**4**) contain the supplementary crystallographic data for this paper. These data can be obtained free of charge at www.ccdc.cam.ac.uk/conts/retrieving.html [or from the Cambridge Crystallographic Data Centre, 12 Union Road, Cambridge CB2 1EZ, UK; Fax: (internat.) + 44-1223/336-033, E-mail: deposit@ccdc.cam.ac.uk].

Table 1. Crystal data and structure refinement for **3a** and **4**

	3a	**4**
Empirical formula	$C_{61}H_{63}N_4P_2RuS_3$	$C_{48}H_{56}N_2P_2RuS$
Molecular mass	1111.34	856.02
T (K)	295(2)	295(2)
Crystal system	monoclinic	triclinic
Space group	$P2_1$	$P\bar{1}$
a (Å)	11.55600(10)	13.3770(3)
b (Å)	18.0640(2)	18.4420(4)
c (Å)	13.33100(10)	20.4070(5)
α (°)	90	110.9660(10)
β (°)	97.5110(10)	90.8920(10)
γ (°)	90	111.2670(10)
V (Å^3)	2758.94(4)	4319.4(2)
Z	2	4
ρ(calcd.) (Mg/m^3)	1.338	1.316
F(000)	1158	1792
Data/parameters	12253/641	14753/982
GOF	1.112	0.990
$R1$, $wR2$ [$I > 2\sigma(I)$][a]	0.0372, 0.0902	0.0595, 0.1314
(all data)	0.0458, 0.1032	0.1736, 0.1992

[a] $R1 = \Sigma||F_o| - |F_c||/\Sigma|F_o|$, $wR2 = [\Sigma w(F_o^2 - F_c^2)^2/ \Sigma w(F_o^2)^2]^{1/2}$.

Acknowledgments

We thank the National Science Council of Taiwan for financial support. Assistance to S. C. H. from The Bureau of Investigation, Ministry of Justice, Taiwan, R. O. C. is also gratefully acknowledged.

[1] H. Urich, B. Tucher, A. A. R. Satigh, *Tetrahedron* **1966**, *22*, 1565.
[2] G. G. Furin, E. L. Zhuzhgov, *Chem. Heterocycl. Comp.* **2002**, *38*, 129.
[3] L. Brandsma, N. A. Nedolya, O. A. Tarasova, B. A. Trofimov, *Chem. Heterocycl. Comp.* **2000**, *36*, 1241.
[4] L. Drobnica, P. Kristian, J. Augustin, in *The Chemistry of Cyanates and Their Thio Derivatives*, S. Patai (Ed.), John Wiley and Sons, New York, **1977**, Part 2, p. 1003.
[5] W. Buchmann, B. Desmazieres, J. P. Morizur, H. A. Nguyen, H. Cheradame, *Macromolecules* **2001**, *34*, 2783.
[6] W. Buchmann, B. Desmazieres, J.-P. Morizur, H. A. Nguyen, H. Cheradame, *Macromolecules* **2000**, *33*, 660.
[7] O. Tsuge, in *The Chemistry of Cyanates and Their Thio Derivatives*, S. Patai (Ed.), John Wiley & Sons, New York, **1977**, Part 1, p. 445.
[8] C. W. J. Chang, *Prog. Chem. Org. Nat. Prod.* **2000**, *80*, 1.
[9] A. Hartmann, *Methoden Org. Chem. Houben-Weyl* **1983**, *E4*, 834.
[10] C. W. Chang, Y. C. Lin, G. H. Lee, S. L. Huang, Y. Wang, *Organometallics* **1998**, *17*, 2534.
[11] C. W. Chang, Y. C. Lin, G. H. Lee, Y. Wang, *Organometallics* **1999**, *18*, 3445.
[12] G. L'abbé, G. Verhelst, S. Toppet, *J. Org. Chem.* **1977**, *42*, 1159.
[13] K. Akiba, M. Ohsugi, H. Iwasaki, K. Ohkata, *J. Am. Chem. Soc.* **1988**, *110*, 5576.
[14] N. Matsumura, J. Kawano, N. Fukunishi, H. Inoue, M. Yasui, F. Iwasaki, *J. Am. Chem. Soc.* **1995**, *117*, 3623.
[15] N. Matsumura, M. Tomura, Y. Tsuchiya, S. Yoneda, M. Nakamura, *Chem. Express* **1986**, *1*, 487.
[16] L.-L. Lai, D. H. Reid, *Heteroatom. Chem.* **1997**, *8*, 13.
[17] R. T. Jashav, M. G. Paranjpe, *J. Indian Chem. Soc.* **1982**, *59*, 71.
[18] M. Komatsu, Y. Ohshiro, K. Yasuda, S. Ichijima, T. Agawa, *J. Org. Chem.* **1974**, *7*, 957.
[19] N. Matsummura, M. Kusamiya, H. Inoue, *J. Heterocycl. Chem.* **1995**, *4*, 1269.
[20] R. J. S. Beer, H. Singh, D. Wright, L. K. Hansen, *Tetrahedron* **1981**, *14*, 2485.
[21] F. Iwasaki, M. Yasui, S. Yoshida, H. Nishiyama, S. Shimamoto, N. Matsumura, *Bull. Chem. Soc. Jpn.* **1996**, *69*, 2759.
[22] R. Parashad, S. K. S. Yadav, U. Agarwala, *J. Inorg. Nucl. Chem.* **1981**, *43*, 2359.
[23] M. Rowley, J. W. Steed, D. A. Tocher, *Polyhedron* **1995**, *14*, 1415.
[24] W. Preetz, H. H. Fricke, *Z. Anorg. Allg. Chem.* **1982**, *486*, 49.
[25] R. K. Poddar, R. Parashad, U. Agarwala, *J. Inorg. Nucl. Chem.* **1980**, *42*, 837.
[26] O. Kohle, S. Ruile, M. Grätzel, *Inorg. Chem.* **1996**, *35*, 4779.
[27] P. Homanen, M. Haukka, T. A. Pakkanen, J. Pursiainen, R. H. Laitinen, *Organometallics* **1996**, *15*, 4081.
[28] V. Palaniappan, S. K. S. Yadav, U. C. Agarwala, *Polyhedron* **1985**, *4*, 1457.
[29] J. W. Steed, D. A. Tocher, *J. Chem. Soc., Dalton Trans.* **1992**, 459.
[30] A. Martinez, M. Alonso, A. Castro, C. Perez, F. J. Moreno, *J. Med. Chem.* **2002**, *45*, 1292.
[31] J. O. Baeg, H. Alper, *J. Org. Chem.* **1995**, *60*, 3092.
[32] Y. Yamamoto, H. Takagishi, K. Itoh, *J. Am. Chem. Soc.* **2002**, *124*, 29.
[33] A. Dondoni, L. Knieio, A. Medici, *J. Org. Chem.* **1982**, *47*, 3994.
[34] G. M. Sheldrick, (1997), SHELXTL V5.1 Software Reference Manual, Bruker AXS Inc., Madison, Wisconsin, USA.

Received August 19, 2003

 © 2004 Wiley-VCH Verlag GmbH & Co. KGaA, Weinheim

New Bifunctional Contrast Agents: Bis-Amide Derivatives of *C*-Substituted Gd-DTPA

Sophie Laurent,[a] François Botteman,[a] Luce Vander Elst,[a] and Robert N. Muller*[a]

Keywords: Gadolinium / Zinc / Metallation / Amides

In order to expand upon and confirm previous observations on the positive and adverse roles played by the functionalization and substitution of the parent MRI contrast agent Gd-DTPA, two new bi-functionalized contrast agents namely Gd-(*S*)-EOB-DTPA-BMA and Gd-(*S*)-C_4Bz-DTPA-BMA have been synthesized, purified, and characterized by multinuclear NMR studies. Water ^{1}H nuclear magnetic relaxation dispersion profiles were recorded at several temperatures. τ_R was determined by ^{2}H NMR on the diamagnetic lanthanum complex. τ_M, the water residence time, was obtained by ^{17}O NMR measurements and the stability versus transmetallation by zinc was evaluated by proton relaxometry. The residence time of water molecules in the first coordination sphere of the Gd complexes has confirmed the antagonistic effects of amide functions and C-4 substitution on the reduction of the water residence time, a critical parameter of relaxivity. This C-4 position is thus particularly appropriate for the substitution required by the design of new contrast agents covalently bound to macromolecules or carrying specific vectors.

(© Wiley-VCH Verlag GmbH & Co. KGaA, 69451 Weinheim, Germany, 2004)

Introduction

The efficacy of the gadolinium complexes currently used as contrast agents in Magnetic Resonance Imaging results partly from the presence of water molecules in the first coordination sphere of the ion and from the exchange of these coordinated molecules with the bulk. An exchange rate which is too slow or too fast limits the efficacy of the contrast agent. In a previous report,[1] we have shown that Gd-DTPA derivatives carrying benzyl groups are characterized by water exchange rates which differ according to the position of the group: the complex *C*-substituted on an ethylenic carbon i.e. [Gd-(*S*)-C_4Bz-DTPA] has a faster water exchange rate and an higher relaxivity, the bis(benzylamide) (Gd-DTPA-BBzA) has a slightly higher proton relaxivity at 37 °C than the parent compound but the longer residence time of its coordinated water molecules (τ_M) clearly limits the relaxivity at low temperatures and, finally, the bis-ester derivative (Gd-DTPA-BBzE) behaves like Gd-DTPA. Another *C*-substituted derivative, Gd-(*S*)-EOB-DTPA, was also shown to be characterized by an increased water exchange rate compared with the parent compound.[2] On the contrary, amide derivatives of Gd-DTPA or Gd-DOTA are known to be characterized by slower water exchange rates than those of their parent structures.[3−5]

In this work, the influence of the *C*-substitution on the behavior of bis-amide derivatives was thus studied on two compounds, both substituted on the ethylenic C-4 carbon. Gd-(*S*)-EOB-DTPA-BMA (**1**) and Gd-(*S*)-C_4Bz-DTPA-BMA (**2**) (Figure 1) were synthesized and their gadolinium complexes were characterized by: i) proton relaxation rate measurements between 0.5 mT and 7.05 T (NMRD profiles), ii) estimation of their rotational correlation times through the analysis of the deuterium relaxation rates of their specifically labeled La-analogues, and iii) determination of the water residence times of their coordinated water molecules through the analysis of the temperature dependence of the ^{17}O transverse relaxation rates of water. Their stability versus transmetallation by Zn^{2+}, an important endogenous ion, was also studied. Finally, all these parameters, compared with those of parent and analogous compounds, are discussed in the context of the structure−relaxivity relationship.

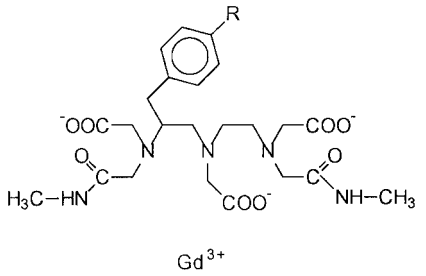

Gd-(*S*)EOB-DTPA-BMA **1** : R = -OC_2H_5

Gd-(*S*)C_4Bz-DTPA-BMA **2**: R = -H

Figure 1. Chemical structures of Gd-(*S*)-EOB-DTPA-BMA (**1**) and Gd-(*S*)-C_4Bz-DTPA-BMA (**2**)

[a] NMR Laboratory, Department of Organic Chemistry, University of Mons-Hainaut,
7000 Mons, Belgium,
Fax: (internat.) + 32-65-373520
E-mail: robert.muller@umh.ac.be

Results and Discussion

The bis-amide complexes **1** and **2** (Figure 1) were synthesized by the classical method starting from the reaction of the pentacarboxylated ligands with acetic anhydride in the presence of pyridine to produce *C*-functionalized DTPA bis-anhydrides. The subsequent amination was carried out with an excess of methylamine.

NMRD profiles recorded at 310 K show that, in general, the relaxivities (r_1) of all the *C*-substituted derivatives are higher than those of Gd-DTPA and Gd-DTPA-BMA (Figure 2). At low magnetic fields, the relaxivities of the bis-amide derivatives of the *C*-substituted complexes are slightly lower than those of their carboxylate analogues. At higher fields, however, the relaxivities of the bis-amides **1** and **2** are similar to those of their parent compounds Gd-(*S*)-EOB-DTPA (**5**) or Gd-(*S*)-C_4Bz-DTPA (**6**) but still markedly higher than those of the unsubstituted structures Gd-DTPA (**3**) or Gd-DTPA-BMA (**4**). At 0.47 T (20 MHz) and 310 K, the relaxivity values of Gd-(*S*)-EOB-DTPA (**5**), Gd-(*S*)-EOB-DTPA-BMA (**1**), Gd-(*S*)-C_4Bz-DTPA (**6**), Gd-(*S*)-C_4Bz-DTPA-BMA (**2**), Gd-DTPA (**3**), and Gd-DTPA-BMA (**4**) are 5.5, 5.0, 4.8, 4.7, 3.9, and 3.8 $s^{-1}\cdot mM^{-1}$ respectively.

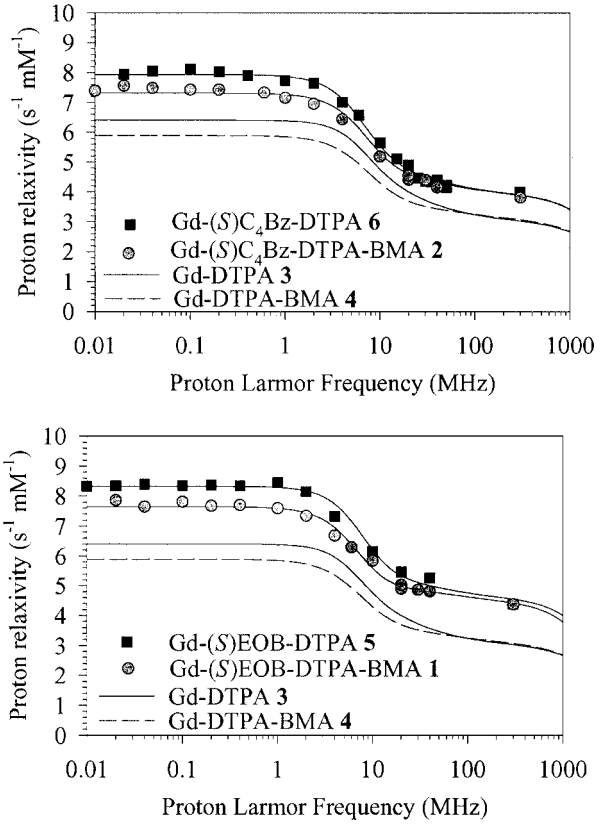

Figure 2. ^{1}H NMRD relaxivity profiles of Gd-(*S*)-C_4Bz-DTPA-BMA (**2**) and Gd-(*S*)-C_4Bz-DTPA (**6**) in water at 310 K ([Gd complex] = 1 mM) (top graph) and of Gd-(*S*)-EOB-DTPA-BMA (**1**) and Gd-(*S*)-EOB-DTPA (**5**) in water at 310 K ([Gd complex] = 1 mM) (bottom graph). The fittings of the NMRD profiles of Gd-DTPA (**3**) and Gd-DTPA-BMA (**4**) are shown for comparison. The lines correspond to the theoretical fittings of the data points.

The longitudinal relaxivity, r_1, arises from both short (inner sphere) and long (outer sphere) distance magnetic interactions. The inner sphere contribution can be described by the Solomon−Bloembergen equations,[6−7] while the outer sphere contribution can be accounted for by the Freed model[8] (see ref.[2] for the description of the models). A rather large number of structural parameters is included in those models: q the number of water molecules in the first coordination sphere, τ_M the residence time describing the exchange between coordinated and bulk water, r the distance between coordinated water protons and the unpaired electron spin, d the distance of closest approach, D the relative diffusion constant, τ_R the rotational correlation time of the hydrated complex and $\tau_{s1,2}$ the longitudinal and transverse relaxation times of the electron. These latter parameters are field dependent with τ_{SO} being the value of $\tau_{s1,2}$ at zero field and τ_v the correlation time modulating the interaction responsible of the electronic relaxation.

Therefore, the analysis of the proton NMRD curves by a multi-parametric fitting procedure takes advantage of the knowledge of some of the parameters.[2,9] In previous studies,[2,4,9−12] it has been shown that q, τ_R, and τ_M could be evaluated by specific NMR techniques and reduce the ambiguity of the analysis of the proton NMRD curves. By analogy with similar complexes [Gd-(*S*)-EOB-DTPA (**5**), Gd-DTPA-BMA (**4**) or Gd-DTPA (**3**)], q was assumed to be equal to one and d and D^{310} were set to 0.36 nm and 3.3 $\times 10^{-9}$ $m^2\cdot s^{-1}$ respectively.

The determination of τ_R was performed at five temperatures (from 278 K to 318 K) on the diamagnetic lanthanum complexes deuterated at the α positions of the carbonyl groups[13] through the analysis of the deuterium longitudinal rates.[2] At 310 K, the values of τ_R are fairly close {τ_R [La-(*S*)-[D_8]EOB-DTPA-BMA] = 63 ± 7 ps; τ_R [La-(*S*)-[D_{10}]EOB-DTPA] = 66 ± 7 ps; τ_R [La-(*S*)-[D_8]C_4Bz-DTPA-BMA] = 60 ± 6 ps; τ_R [La-(*S*)-[D_{10}]C_4Bz-DTPA] = 65 ± 7 ps; τ_R [La-[D_8]DTPA-BMA] = 67 ± 7 ps; and τ_R [La-[D_{10}]DTPA] = 60 ± 6 ps}. The activation energies for the rotations calculated from the evolutions of τ_R with temperature are comparable for all the complexes (E_R = 20 −24 kJ/mol).

Among the two relaxation mechanisms, i.e. the outer sphere and the inner sphere contributions, only the latter is influenced by the water residence time and can thus be quenched at low temperatures while the former always increases when the temperature is lowered. Therefore, as long as the water residence time is not limiting the propagation of the relaxation ($\tau_M < T_{1M}$ where T_{1M} is the relaxation time of the protons of the coordinated water molecule), the global relaxivity increases when temperature decreases. If this condition is not fulfilled, the global relaxivity may reach a plateau or even decrease at low temperatures. The possible influence of τ_M on the proton relaxivity was evaluated at 0.47 T over a range of temperatures between 278 K and 318 K (Figure 3). Like Gd-DTPA itself, its *C*-functionalized derivatives exhibit a continuous increase in r_1 when the temperature is lowered, revealing that τ_M does not limit the relaxation rate. On the contrary, the bis-amide

 © 2004 Wiley-VCH Verlag GmbH & Co. KGaA, Weinheim

complexes Gd-DTPA-BMA **4**, Gd-(*S*)-C_4Bz-DTPA-BMA **2**, and Gd-(*S*)-EOB-DTPA-BMA **1** show a clear limitation of their relaxivity by the water exchange below 310 K.

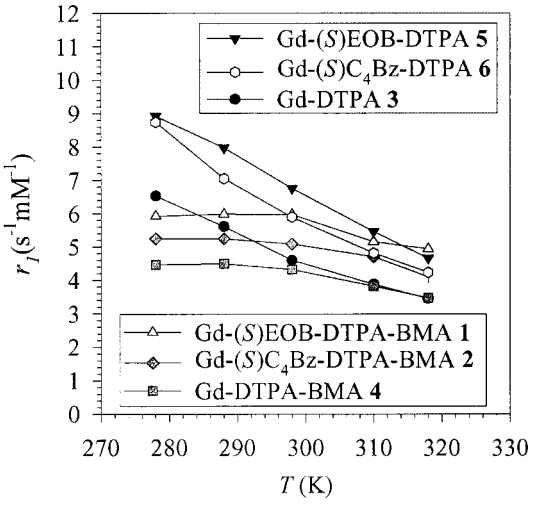

Figure 3. Temperature dependence of the proton relaxivities of the various Gd complexes at 0.47 T.

A quantitative estimation of the residence times of water molecules in the first coordination spheres of the gadolinium complexes (τ_M) was obtained from the analysis of the temperature dependence of the ^{17}O transverse relaxation rates of solutions containing 13−50 mM of the gadolinium complexes. Various parameters are involved in the theoretical fitting of the ^{17}O data: $A/\hbar$, the hyperfine coupling constant between the oxygen nucleus of bound water molecules and the Gd^{3+} ion; τ_V, the correlation time modulating the electronic relaxation of Gd^{3+}; E_v, the activation energy related to τ_V; Δ^2, the mean-square zero field splitting energy (Δ^2 is related to τ_{SO} by $\tau_{SO} = [12\ \Delta^2\tau_V]^{-1}$); and $\Delta H^{\#}$ and $\Delta S^{\#}$, the enthalpy and entropy of the water exchange process. The theoretical fitting of the transverse relaxation rates obtained over a temperature range from 280 K to 350 K gives values of τ_M^{310} for Gd-(*S*)-EOB-DTPA-BMA (**1**) and Gd-(*S*)-C_4Bz-DTPA-BMA (**2**) of 472 ± 38 ns and 429±23 ns, respectively. These values are between those reported for pentacarboxylate complexes {τ_M^{310} [Gd-DTPA (**3**)] = 143±25 ns; τ_M^{310} [Gd-(*S*)-EOB-DTPA (**5**)] = 82 ± 21 ns; τ_M^{310} [Gd-(*S*)-C_4Bz-DTPA (**6**)] = 86 ± 8 ns} and the bis-amide parent structure (τ_M^{310} [Gd-DTPA-BMA (**4**)] = 967±36 ns) (Table 1). These results are in good agreement with the temperature dependence of r_1 at 0.47 T and they confirm that the presence of amide functions on the structure of the DTPA ligand considerably decreases the exchange rate and that a conformational or steric effect, induced by substitution on the C_4 of the ligand, counteracts this unfavorable effect.

The fittings of the proton NMRD profiles were performed with the distance *r* fixed to the usual value of 0.31 nm for Gd-DTPA (**3**) and Gd-DTPA-BMA (**4**). For the *C*-functionalized complexes, such a distance results in τ_R values significantly larger than those obtained by deuterium relaxometry (τ_R^{310}= 112 ps, 91 ps, 109 ps, and 84 ps for complexes **1**, **2**, **5**, and **6** respectively). Shorter effective distances (0.291 nm and 0.3 nm) were therefore used to fit the data (Table 2). For complexes **1** and **5**, τ_R values obtained for the distance r equal to 0.291 nm are in better agreement with the values obtained by deuterium relaxometry, whereas for complexes **2** and **6**, both distances (0.291 nm and 0.3 nm) can account for the experimental results. The fitted values of τ_{SO} and τ_V (Table 2) are in the same range for all the complexes and agree with those obtained by the fitting of the ^{17}O data (Table 1). At low magnetic fields, the lower relaxivity of the bis-amide *C*-substituted complexes **1** and **2**, compared with their parent complexes **5** and **6**, can be related to their longer τ_M values which result in a more marked limitation of the relaxivity at low rather than at high fields.

The NMRD profiles of Gd-(*S*)-EOB-DTPA-BMA (**1**) and Gd-(*S*)-C_4Bz-DTPA-BMA (**2**) at 298 K and 310 K are shown in Figure 4. The data recorded at 298 K are only slightly greater than those obtained at 310 K, confirming that τ_M is indeed limiting the relaxivity. The parameters obtained from the theoretical fitting are shown in Table 2.

Table 1. Parameters obtained from the fitting of the reduced transverse relaxation rate of ^{17}O

	Gd-(*S*)-EOB-DTPA-BMA (**1**)	Gd-(*S*)-C_4Bz-DTPA-BMA (**2**)	Gd-DTPA (**3**)	Gd-DTPA-BMA (**4**)	Gd-(*S*)-EOB-DTPA (**5**)	Gd-(*S*)-C_4Bz-DTPA (**6**)
Δ^2 (10^{20} s^{-2})	0.98 ± 0.10	0.92 ± 0.03	1.08 ± 0.03	0.85 ± 0.03	1.05 ± 0.12	1.17 ± 0.03
τ_V^{310} (ps)	16 ± 2.0	16 ± 0.4	23 ± 0.3	16 ± 0.6	17 ± 2	10 ± 0.3
$\lvert A/\hbar \rvert$ (10^6 rad s^{-1})	2.99 ± 0.23	2.80 ± 0.20	3.4 ± 0.1	3.16 ± 0.04	4.1 ± 0.5	3.19± 0.06
$\Delta H^{\#}$ (kJ/mol)	43.9 ± 0.14	37.1 ± 0.07	51.5 ± 0.3	48 ± 0.05	53.5 ± 0.3	50.1 ± 0.13
$\Delta S^{\#}$ (J/mol K)	17.6 ± 0.23	−3.54 ± 0.23	52.1 ± 0.6	24.9 ± 0.2	63 ± 1.3	51.8 ± 0.4
E_V (kJ/mol)	0.95 ± 1.44	0.90 ± 12.4	4.5 ± 4.2	15.0 ± 10.9	7.1 ± 5.9	8.7 ± 3.9
τ_M^{310} (ns)	472± 38	429 ± 23	143 ± 25	967 ± 36	82 ± 21	86 ± 8
τ_{SO}^{310} (ps)[a]	54±27	58 ± 4	67 ± 11	56 ± 4	58 ± 14	69 ± 4

[a] Calculated from the values of Δ^2 and τ_V^{310}.

 © 2004 Wiley-VCH Verlag GmbH & Co. KGaA, Weinheim

Table 2. Values of τ_R, τ_{SO}, τ_V, and r obtained by fitting of the proton NMRD data at 310 K and 298 K

T = 310 K	τ_R (ps)	τ_M (ns)[a]	τ_{so} (ps)	τ_v (ps)	r (nm)
Gd-(*S*)-EOB-DTPA-BMA (**1**)	71 (63)[b]	472	72	16	0.291
	92	472	79	21	0.3
Gd-(*S*)-C_4Bz-DTPA-BMA (**2**)	61 (60)[b]	429	76	11	0.291
	70	429	86	16	0.3
Gd-DTPA (**3**)	57 (60)[b]	143	83	23	0.31
Gd-DTPA-BMA (**4**)	64 (67)[b]	967	74	12	0.31
Gd-(*S*)-EOB-DTPA (**5**)	71 (66)[b]	82	76	23	0.291
	86	82	88	28	0.3
Gd-(*S*)-C_4Bz-DTPA (**6**)	61 (65)[b]	86	77	14	0.291
	72	86	91	17	0.3
T = 298 K	τ_R (ps)	τ_M (ns)[a]	τ_{so} (ps)	τ_v (ps)	r (nm)
Gd-(*S*)-EOB-DTPA-BMA (**1**)	84 (86)[b]	976	69	17	0.291
	97	976	78	24	0.3
Gd-(*S*)-C_4Bz-DTPA-BMA (**2**)	73 (83)[b]	798	72	13	0.291
	82	798	88	15	0.3

[a] τ_M values were obtained from ^{17}O NMR. [b] The values in parentheses are those obtained by ^2H NMR spectroscopy on the lanthanum analogue.

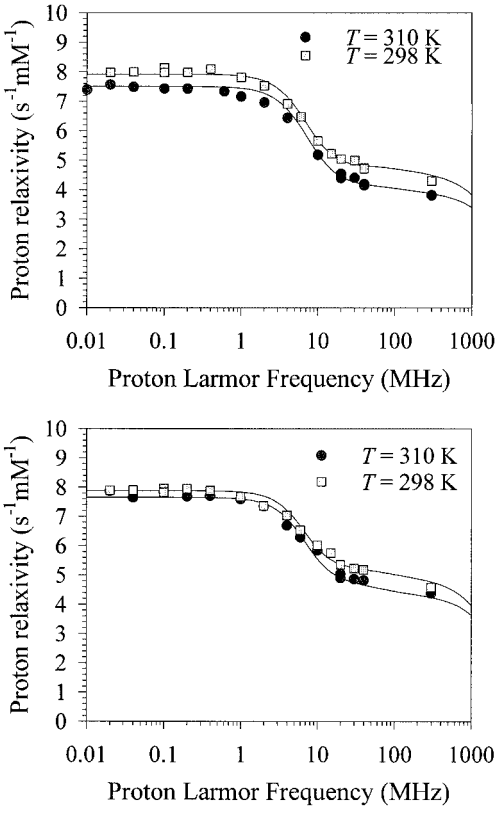

Figure 4. ^1H NMRD relaxivity profiles of Gd-(*S*)-C_4Bz-DTPA-BMA (**2**) (top graph) and Gd-(*S*)-EOB-DTPA-BMA (**1**) (bottom graph) in water at 298 K and 310 K ([Gd complex] = 1 mM). The lines correspond to the theoretical fittings of the data points

Finally, the transmetallation of the gadolinium complex by Zn^{2+} has been assessed. In a phosphate buffer (pH = 7), a precipitation of gadolinium ions expelled from the complex by Zn^{2+} occurs resulting in a decrease of the proton paramagnetic relaxation rate of the solution. The time evolution of the proton relaxation rate was monitored at 0.47 T and 310 K. Previous results showed that, on the one hand, the *C*-functionalized carboxylate complexes are kinetically and thermodynamically more stable than the parent compound Gd-DTPA and, on the other hand, that bis-amide derivatives are less stable.[14] For the bis-amide *C*-substituted compounds, the C-substitution and the bis-amide functions have opposite effects. The "kinetic index", which is the time required to reach 80 percent of the initial R_1^P value, and the "thermodynamic index", which is the R_1^P (t)/R_1^P (0) value measured after 3 days, indeed show a faster and more extensive transmetallation of Gd-(*S*)-EOB-

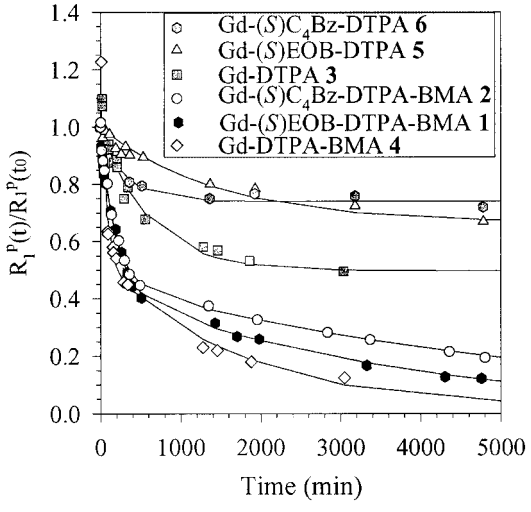

Figure 5. Evolution of the R_1^p (t)/ R_1^p (t = 0) ratio as a function of time for Gd-(*S*)-C_4Bz-DTPA (**6**), Gd-(*S*)-EOB-DTPA (**5**), Gd-DTPA (**3**), Gd-(*S*)-C_4Bz-DTPA-BMA (**2**), Gd-(*S*)-EOB-DTPA-BMA(**1**), and Gd-DTPA-BMA (**4**) (concentrations of Gd complexes and $ZnCl_2$ are 2.5 mM in a phosphate buffer of pH = 7, T = 310 K, B_0 = 0.47 T)

 © 2004 Wiley-VCH Verlag GmbH & Co. KGaA, Weinheim

Table 3. Values of the kinetic and thermodynamic indexes obtained during the transmetallation process

	Kinetic index (min)[a]	Thermodynamic index (%)[b]
Gd-(*S*)-EOB-DTPA-BMA (**1**)	70	13
Gd-(*S*)-C_4Bz-DTPA-BMA (**2**)	80	22
Gd-DTPA (**3**)[c]	260−280	49
Gd-DTPA-BMA (**4**) [c]	50−60	9
Gd-(*S*)-EOB-DTPA (**5**) [c]	1500	69
Gd-(*S*)-C_4Bz-DTPA (**6**) [c]	300	73

[a] The kinetic index is defined here as the time required to attain 80 % of the initial value of R_1^P. [b] The thermodynamic index is defined here as the ratio between R_1^P at 4320 min and the initial R_1^P. [c] From ref.[14].

DTPA-BMA (**1**) and Gd-(*S*)-C_4Bz-DTPA-BMA (**2**) than that observed for the parent compound Gd-DTPA (**3**). Only a slight stabilization was observed with respect to the unsubstituted bis-amide derivative (Figure 5 and Table 3).

Conclusion

Two new bi-functionalized compounds, Gd-(*S*)-EOB-DTPA-BMA (**1**) and Gd-(*S*)-C_4Bz-DTPA-BMA (**2**), have been successfully synthesized. The τ_M values obtained by ^{17}O NMR spectroscopy confirm the lengthening and adverse effect of the amide functions and demonstrate the beneficial effect of a C-4 substitution on the reduction of the water residence time. As assessed by the Zn^{2+} transmetallation process, the two new bis-amides are less stable than Gd-DTPA and slightly more stable than Gd-DTPA-BMA (**4**). In conclusion, although more difficult to synthesize, C-4-substituted DTPA complexes are better suited for the covalent binding to macromolecules or to specific vectors in the context of the design of new specific contrast agents for molecular imaging.

Experimental Section

General

Chemicals: Gd-DTPA (**3**), Gd-(*S*)-EOB-DTPA (**5**), and the ligand EOB-DTPA were provided by Schering AG (Berlin, Germany). The ligand (*S*)-C_4Bz-DTPA and the corresponding gadolinium complex were obtained as described earlier.[1] The organic reactants and intermediates were purchased from Aldrich (Bornem, Belgium). NMR Spectroscopy: ^1H and ^{13}C NMR spectra were recorded with a Bruker AMX-300 instrument (Bruker, Karlsruhe, Germany). Chemical shifts (in ppm) are referred to the solvent peak. For ^{13}C NMR, the methyl signal of *tert*-butanol was used as reference (δ = 31.2 ppm). Mass Spectrometry: Mass spectra (LSIMS) were obtained with a VG AUTOSPEC mass spectrometer (VG Analytical, Manchester, UK). Samples were dissolved in water and deposited in a glycerol matrix. Chromatography: High-performance liquid chromatography (HPLC) was performed with a Waters 600 multisolvent delivery system equipped with a Rheodyne injection valve (20μL loop) and controlled by the Millenium software (Waters, Milford, USA). A Novapak C18 column (4.56 mm × 150 mm) was used. Elution was performed with a linear gradient of pure 0.05 M triethylammonium acetate (pH = 6) to 100 % methanol at a flow rate of 1 mL/min for 20 min. A fluorescence detector was used to monitor the elution of the gadolinium complex. Relaxometry: Proton Nuclear Magnetic Relaxation Dispersion (NMRD) profiles were recorded with a Field Cycling Relaxometer working between 0.02 and 50 MHz. Additional points at 20 and 300 MHz respectively were obtained on a Bruker Minispec PC-20 thermostatically controlled by a tetrachloroethylene flow and with a Bruker AMX 300 spectrometer. Fitting of the ^1H NMRD curves was performed with previously described software using minimization routines (Minuit, CERN Library).[15,16] The deuterium and ^{17}O measurements were carried out with 2 mL samples contained in 10-mm o.d. tubes with a Bruker AMX-300 spectrometer equipped with a broadband probe. The field homogeneity was optimized on the proton free induction decay using the decoupling coil. The temperature was regulated by air or nitrogen flow (Bruker BVT-2000 unit). Deuterium longitudinal relaxation rates were measured using an inversion recovery Fourier transform sequence on solutions containing the labeled diamagnetic lanthanum complex dissolved in deuterium depleted water (Aldrich, Bornem, Belgium). The experimental data were fitted with a three-parameter minimization routine. Diamagnetic transverse relaxation times of ^{17}O water (pH ≈ 6.5) were measured at natural abundance using a Carr−Purcell−Meiboom−Gill sequence and a two-parameter fit of the data. ^{17}O transverse relaxation times of water (natural abundance) in solutions containing paramagnetic complexes were calculated directly from the linewidth. All ^{17}O NMR spectra were proton decoupled. The theoretical fitting of the data was performed as described previously.[1,2,9]

Synthesis of Ligands

3,6,9-Tris(carboxymethyl)-4-ethoxybenzyl-1,11-bis(methylamino)-3,6,9-triazaundeca-1,11-dione [(*S*)-EOB-DTPA-BMA (1)]: A mixture of (*S*)-EOB-DTPA (0.4 g), acetic anhydride (0.6 mL), and pyridine (0.5 mL) was heated at 70 °C for 24 h. The suspension was cooled, a 2 M methylamine (methanol solution) was added (3 mL) and the mixture was stirred for around 24 h. After addition of methanol (50 mL), the mixture was filtered. The filtrate was evaporated to dryness under reduced pressure. Water (5 mL) was then added and the pH was adjusted to 2 with 2 N HCl. The solution was passed through a DOWEX AG 50 W-X8 (H^+ form) cation-exchange resin which was first eluted with water and the product was recovered from the resin by elution with 2 N aqueous ammonia. The residue obtained after evaporation of the solution was dissolved in acetic acid and precipitated with ethyl acetate. The crude product was recovered by filtration. Yield: 0.16 g (38 %). ^1H NMR (D_2O): δ = 6.9−6.7 (4 H, AA′BB′, Ph), 3.8 (q, 2 H, CH_2), 3.6−2.8 (m, 19 H, 8 × CH_2, CH), 2.5 (s, 3 H, CH_3), 2.45 (s, 3 H, CH_3), 1.1 (t, 3 H, CH_3) ppm. ^{13}C NMR (D_2O): δ = 178.1, 171.8, 171.2, 170.6, 170.4, 166.1, 114.2, 128.9, 130.4, 65.1, 62.5, 61.1, 58.9,

 © 2004 Wiley-VCH Verlag GmbH & Co. KGaA, Weinheim

57.3, 57.2, 56.5, 55.1, 53.7, 52.3, 51.8, 26.4, 26.3, 14.3 ppm. LSIMS: $[M + 1]^+$: 554^+. HPLC: 13.3 min.

4-Benzyl-3,6,9-tris(carboxymethyl)-1,11-bis(methylamino)-3,6,9-triazaundeca-1,11-dione [(*S*)-C_4Bz-DTPA-BMA (2)]: This compound was obtained from (*S*)-C_4Bz-DTPA[1] as described for (*S*)-EOB-DTPA-BMA above. Yield: 0.142 g (32 %). ^{1}H NMR (D_2O): δ = 7.3−7.0 (m, 5 H, Ph), 3.45−2.6 (m, 19 H, 9 × CH_2, CH), 2.5 (s, 3 H, CH_3), 2.45 (s, 3 H, CH_3) ppm. ^{13}C NMR (D_2O): δ = 177.9, 171.9, 171.3, 170.6, 170.3, 138.8, 128.6, 128.3, 125.8, 62.4, 61.0, 58.8, 57.2, 57.1, 56.6, 55.2, 53.6, 52.4, 51.7, 26.4, 26.3 ppm. LSIMS: $[M + 1]^+$: 536^+. HPLC: 12.5 min.

Complexation: The La^{III} or Gd^{III} complexes were prepared by mixing aqueous solutions of equimolar amounts of hydrated $LaCl_3$ or $GdCl_3$ and the ligand. The pH was adjusted to between 6.5 and 7. The absence of free La or Gd ions was checked with xylenol orange indicator. The complexes were passed through a Sep-Pak column (Waters, Accell Plus QMA Cartridges) and the eluted solutions were freeze-dried. The purities of the chelates were verified by HPLC and their masses confirmed by LSIMS.

Deuteration: Deuteration of the ligands [(*S*)-EOB-DTPA-BMA and (*S*)-C_4Bz-DTPA-BMA] or of the lanthanum complexes at the α position of the carbonylic groups was performed by the procedure described by Wheeler and Legg.[13] The ligand or complex (4 mmol) was dissolved in D_2O (40 mL), the pD was adjusted to 10.6 by addition of K_2CO_3 and the mixture was heated to reflux for 24 h with stirring. The pD was then adjusted to 2 (ligand solution) or 6 (lanthanum complex solution) with concentrated hydrochloric acid, the solution was evaporated to a final volume of 10 mL and the solid KCl was removed by filtration. Acetone was added to induce precipitation of the deuterated compounds, which were recovered by filtration, dissolved in H_2O and isolated after lyophilization. The deuteration (> 95 %) was confirmed by ^{1}H NMR spectroscopy.

(*S*)-[D_8]EOB-DTPA-BMA: NMR (D_2O, pH = 10): δ = 6.9−6.7 (4 H, AA′BB′, Ph), 3.8 (q, 2 H, CH_2), 3.6−2.8 (m, 11 H, 5 × CH_2, CH), 2.5 (s, 3 H, CH_3), 2.45 (s, 3 H, CH_3), 1.1 (t, 3 H, CH_3) ppm.

(*S*)-[D_8]C_4Bz-DTPA-BMA: NMR (D_2O, pH = 10): δ = 7.4−7.1 (m, 5 H, Ph), 3.45−3.0 (m, 5 H, 2 × CH_2, CH), 2.9−2.6 (m, 6 H, 3 × CH_2), 2.5 (s, 3 H, CH_3), 2.45(s, 3 H, CH_3) ppm.

Kinetics of the Transmetallation: The technique is based on the evolution of the paramagnetic proton longitudinal relaxation rate (R_1^p) of a phosphate buffer solution (pH, 7, $[H_2PO_4^-]$ + $[HPO_4^{2-}]$ + $[PO_4^{3-}]$ = 67 mM) containing 2.5 mM of gadolinium complex and 2.5 mM of $ZnCl_2$.[14] The measurements were performed with a Bruker Minispec PC 120 (20 MHz) spin analyzer at 310 K.

Acknowledgments

The authors thank Mrs Patricia de Francisco for her help in preparing the manuscript. This work was supported by the ARC Program 95/00−194 of the French Community of Belgium, and the Fonds National de la Recherche Scientifique (FNRS) of Belgium. FB thanks the Fonds pour la Recherche dans l'Industrie et l'Agriculture (FRIA) of Belgium for their financial help.

[1] S. Laurent, L. Vander Elst, S. Houzé, N. Guerit, R. N. Muller, *Helv. Chim. Acta* **2000**, *83*, 394−406.
[2] L. Vander Elst, F. Maton, S. Laurent, F. Seghi, F. Chapelle, R. N. Muller, *Magn. Reson. Med.* **1997**, *38*, 604−614.
[3] S. Aime, M. Botta, M. Fasano, S. Paoletti, L. Anelli, F. Uggeri, M. Virtuani, *Inorg. Chem.* **1994**, *33*, 4707−4711.
[4] E. Toth, D. Pubanz, S. Vauthey, L. Helm, A. E. Merbach, *Chem. Eur. J.* **1996**, *2*, 1607−1615.
[5] S. Aime, A. Barge, J. I. Bruce, M. Botta, J. A. K. Howard, J. M. Moloney, D. Parker, A. S. de Sousa, M. Woods, *J. Am. Chem. Soc.* **1999**, *121*, 5762−5771.
[6] I. Solomon, *Phys. Rev.* **1955**, *99*, 559−565.
[7] N. Bloembergen, *J. Chem. Phys.* **1957**, *27*, 572−573.
[8] J. H. Freed, *J. Chem. Phys.* **1978**, *68*, 4034−4037.
[9] R. N. Muller, B. Radüchel, S. Laurent, J. Platzek, C. Piérart, P. Mareski, L. Vander Elst, *Eur. J. Inorg. Chem.* **1999**, 1949−1955.
[10] M. C. Alpoim, A. M. Urbano, C. F. G. C. Géraldes, J. A. Peters, *J. Chem. Soc., Dalton Trans.* **1992**, 463−467.
[11] K. Micskei, L. Helm, E. Brücher, A. E. Merbach, *Inorg. Chem.* **1993**, *32*, 3844−3850.
[12] F. Botteman, G. Nicolle, L. Vander Elst, S. Laurent, A. E. Merbach, R. N. Muller, *Eur. J. Inorg. Chem.* **2002**, 2686−2693.
[13] W. D. Wheeler, J. I. Legg, *Inorg. Chem.* **1985**, *24*, 1292−1297.
[14] S. Laurent, L. Vander Elst, F. Copoix, R. N. Muller, *Invest. Radiol.* **2001**, *36*, 115−122.
[15] R. N. Muller, D. Declercq, P. Vallet, F. Giberto, B. Daminet, H. W. Fischer, F. Maton, Y. Van Haverbeke, in *Implementation and operation of an integrated and comprehensive relaxometric data bank, Proc. ESMRMB*, 7th Annual Congress, Strasbourg, **1990**, p. 394.
[16] P. Vallet, in *Relaxivity of nitroxide stable free radicals. Evaluation by field cycling method and optimisation*, PhD Thesis, University of Mons-Hainaut, Belgium, **1992**.

Received July 11, 2003
Early View Article
Published Online December 12, 2003

 © 2004 Wiley-VCH Verlag GmbH & Co. KGaA, Weinheim

A Series of Vinylidene-, Vinyl-, Carbene- and Carbyneruthenium(II) Complexes with $[Ru(PCy_3)_2]$ and $[Ru(P\mathit{i}Pr_3)_2]$ as Molecular Building Blocks

Stefan Jung,[a] Kerstin Ilg,[a] Carsten D. Brandt,[a] Justin Wolf,[a] and Helmut Werner*[a]

Dedicated to Professor Michael F. Lappert on the occasion of his 75th birthday

Keywords: Carbene complexes / Carbyne complexes / Ruthenium / Vinyl complexes / Vinylidene complexes

The hydrido(vinylidene) complexes $[RuHCl(=C=CHR)(L)_2]$ (R = H, *t*Bu, Ph; L = PCy_3, $P\mathit{i}Pr_3$) undergo metathesis reactions in the presence of KX (X = I, NCO, OPh, CH_3CO_2, CF_3CO_2) to give the substitution products $[RuHX(=C=CHR)(L)_2]$ (**6**–**15**) in good to excellent yields. Treatment of $[RuHX(=C=CHR)(L)_2]$ with HBF_4 in diethyl ether affords the cationic carbyneruthenium(II) derivatives $[RuHX(\equiv CCH_2R)(OEt_2)(L)_2]BF_4$ (**17**, **18**, **20**, **21**) and $[RuH(\kappa^2\text{-}O_2CCH_3)(\equiv CCH_2R)(L)_2]BF_4$ (**19**, **22**). The reactions of $[RuHCl(=C=CHR)(L)_2]$ with MX [X = BF_4, PF_6, BPh_4, $B(Ar_f)_4$] in acetonitrile lead to the formation of cationic five- and six-coordinate vinylruthenium(II) compounds **26a**–**d** and **27a**–**d** of which $[Ru(CH=CH_2)(CH_3CN)_2(PCy_3)_2]BPh_4$ (**26c**) has been characterized by X-ray crystallography. The starting material $[RuHCl(=C=CHPh)(P\mathit{i}Pr_3)_2]$ reacts with CO to give $[RuCl(CH=CHPh)(CO)_2(P\mathit{i}Pr_3)_2]$ (**28**) and with N_2 to produce $[RuCl(CH=CHPh)(N_2)(P\mathit{i}Pr_3)_2]$ (**29**). The molecular structure of **29** has been determined. Protonation of $[Ru(CH=CH_2)(CH_3CN)_2(PCy_3)_2]X$ and $[Ru(CH=CHPh)(CH_3CN)_3(P\mathit{i}Pr_3)_2]X$ with HBF_4 and $HB(Ar_f)_4$ yields the dicationic carbeneruthenium(II) complexes $[Ru(=CHCH_3)(CH_3CN)_2(PCy_3)_2]X_2$ (**30a**,**b**) and $[Ru(=CHCH_2Ph)(CH_3CN)_3(P\mathit{i}Pr_3)_2][B(Ar_f)_4]_2$ (**31**), the latter of which eliminates styrene to give $[Ru(CH_3CN)_3(P\mathit{i}Pr_3)_2][B(Ar_f)_4]_2$ (**32**).
(© Wiley-VCH Verlag GmbH & Co. KGaA, 69451 Weinheim, Germany, 2004)

Introduction

In the context of our investigations on the preparation and reactivity of vinylideneruthenium(II) complexes,[1] we recently reported that the reaction of the five-coordinate hydrido(vinylidene) compound $[RuHCl(=C=CH_2)(PCy_3)_2]$ with acids HA, containing an anion that does *not* coordinate to the metal center, in diethyl ether affords the cationic carbyne(hydrido) complex $[RuHCl(\equiv CCH_3)(PCy_3)_2(OEt_2)]^+$ instead of the anticipated isomeric carbene derivative $[RuCl(=CHCH_3)(PCy_3)_2(OEt_2)]^+$.[2] This cation, as well as the corresponding cations with coordinated water or dimethylaniline instead of diethyl ether, turned out to be a highly efficient catalyst for olefin metathesis, including the cross-olefin metathesis of cyclopentene with methylacrylate to afford multiply unsaturated esters $CH_2(C_5H_8)_nCHCO_2Me$ (n = 1−3). The cations $[RuHCl(\equiv CCH_3)(PCy_3)_2(S)]^+$, however, in the absence of excess HA are rather labile and decompose in solution within 20 min at room temperature. For this reason, we set out to prepare more stable ruthenium carbynes by modifying the coordination sphere and using different ruthenium vinylidenes as the precursors.

In this paper we report the synthesis of a series of new hydrido(vinylidene) complexes $[RuHX(=C=CHR)(PCy_3)_2]$ and $[RuHX(=C=CHPh)(P\mathit{i}Pr_3)_2]$, their conversion into the corresponding cationic ruthenium carbynes and into neutral as well as cationic vinylruthenium compounds, and also the formation of dicationic, five-coordinate ruthenium carbenes. Some preliminary results have already been communicated.[3]

[a] Institut für Anorganische Chemie der Universität Würzburg, Am Hubland, 97074 Würzburg, Germany
E-mail: helmut.werner@mail.uni-wuerzburg.de

Results and Discussion

The hydrido(dihydrogen) complex $[RuHCl(H_2)(PCy_3)_2]$ (**1**), which can be prepared from $RuCl_3{\cdot}3H_2O$ in high yield,[2,4] is not only an appropriate starting material for $[RuHCl(=C=CH_2)(PCy_3)_2]$ (**3**) and $[RuHCl(=C=CHPh)(PCy_3)_2]$ (**4**) but also for the *tert*-butylvinylidene counterpart **2** [see Equation (1)]. Treatment of a solution of **1** in CH_2Cl_2 with two equivalents of tBuC≡CH at −78 °C leads to the formation of **2** which, after removal of the solvent, was isolated as a brown air-sensitive solid in 72% yield. In contrast to **3** and **4**, compound **2** decomposes slowly in solution even at low temperatures and thus only ^1H and ^{31}P NMR spectroscopic data could be obtained. The ^1H NMR spectrum displays the signal for the vinylidene proton as a triplet at δ = 2.87 ppm and the resonance for the hydride, also as a triplet, at δ = −13.89 ppm.

$$[RuHCl(H_2)(PCy_3)_2] \xrightarrow[-CH_2=CHtBu]{2HC\equiv CtBu} [RuHCl(=C=CHtBu)(PCy_3)_2] \quad (1)$$

1 **2**

While attempts to replace the chloro ligand in **2** by iodide or isocyanate led to a mixture of products that could not be separated by fractional crystallization, a clean reaction occurs between **2** and excess CH_3CO_2K that affords the acetato derivative **6** in virtually quantitative yield. The characteristic signals for the =CH and the RuH protons appear in the ^1H NMR spectrum at $\delta = 2.12$ and -12.48 ppm, respectively, and are split into triplets due to ^1H-^{31}P coupling. The IR spectrum of **6** shows two bands for the asymmetric and symmetric OCO stretching modes at 1635 and 1448 cm^{-1}, respectively, which, in agreement with literature data,[5] indicate a chelating coordination of the acetate unit.

The reactions of compounds **3** and **4**, being significantly more stable than **2**, with both KOCN and CH_3CO_2K in THF proceed cleanly and give the substitution products **7**−**10** in good to excellent yields. Apart from the elemental analyses, the spectroscopic data support the proposed structure shown in Scheme 1. Since the IR spectra of **7** and **9** display the symmetric ν(NCO) stretch at 1446 cm^{-1}, we assume that the NCO ligand is *N*-bonded. In case of an *O*-coordination, the corresponding absorption is expected to appear below 1200 cm^{-1}.[6]

Both the hydrido(vinylidene) complex **5**, containing two triisopropylphosphane ligands, and the compounds **11**−**15** obtained by salt metathesis with KX in THF (Scheme 1) are considerably more stable than their PCy_3 counterparts. In solution (C_6H_6 or CH_2Cl_2) they do not decompose even after 24 h. In the ^1H NMR spectra of **11**−**15**, the vinylidene =CH proton resonates at between $\delta = 4.25$ and 4.40 ppm and the RuH proton at between $\delta = -9.3$ and -13.6. In the low-field region the ^{13}C NMR spectra of **11**−**15** display two triplets, one between $\delta = 327$ and 338 ppm and the other between $\delta = 108$ and 110 ppm, which are assigned to the α- and β-carbon atoms of the vinylidene ligand. For the Ru(NCO) compound **12** and the Ru(κ^2-O_2CCR_3) de-

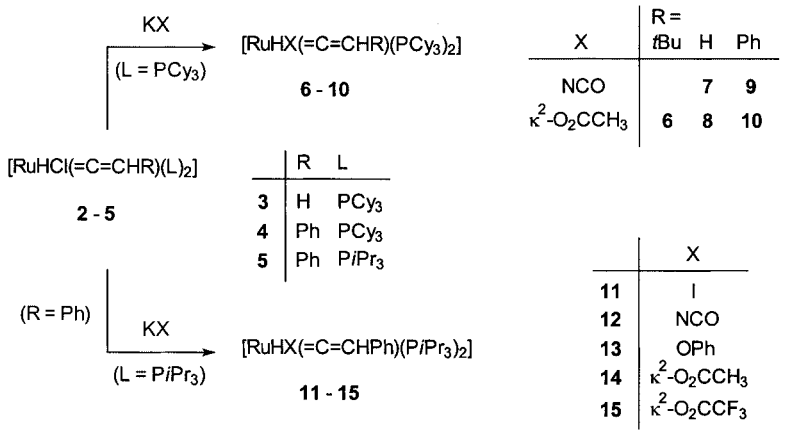

X	R = tBu	H	Ph
NCO		7	9
κ^2-O_2CCH_3	6	8	10

	R	L
3	H	PCy_3
4	Ph	PCy_3
5	Ph	$PiPr_3$

	X
11	I
12	NCO
13	OPh
14	κ^2-O_2CCH_3
15	κ^2-O_2CCF_3

Scheme 1

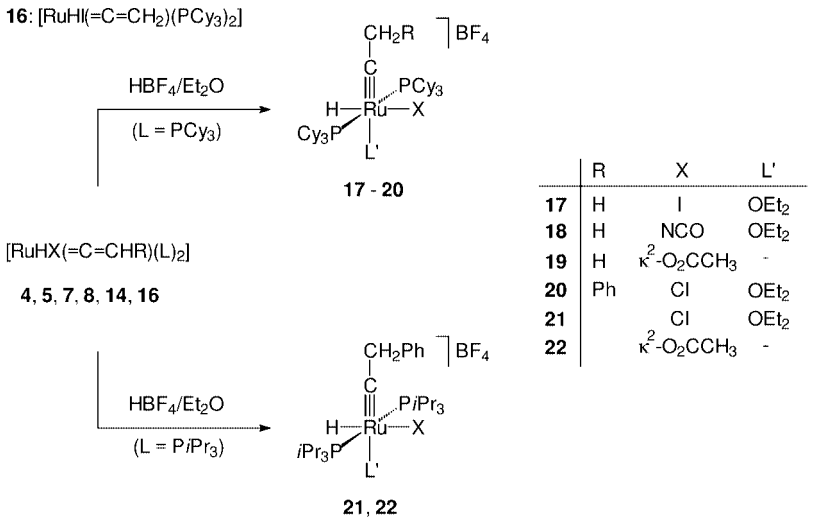

	R	X	L'
17	H	I	OEt_2
18	H	NCO	OEt_2
19	H	κ^2-O_2CCH_3	-
20	Ph	Cl	OEt_2
21		Cl	OEt_2
22		κ^2-O_2CCH_3	-

Scheme 2

 © 2004 Wiley-VCH Verlag GmbH & Co. KGaA, Weinheim

rivatives **14** and **15** the positions of the ligand vibrations in the IR spectra are quite similar to those of **7** and **9** and **8** and **10**, respectively, and thus an *N*-linkage for the NCO^- anion and a chelating coordination mode for the carboxylate unit can be assumed.

The ruthenium vinylidenes **4**, **5**, **7**, **8**, **14** and **16** are readily protonated with a solution of HBF_4 in diethyl ether at low temperatures to give the six-coordinate cationic carbyne complexes **17**−**22** in 55−73% yield. The products were isolated as light yellow, moderately air-sensitive solids by precipitation with diethyl ether. While solutions of the acetato derivatives **19** and **22** (see Scheme 2) are stable for about one hour, the related compounds **17**, **18** and **20**, **21** decompose more readily, for example in dichloromethane in ca. 30 min even at 0 °C. Conductivity measurements (in nitromethane) confirm the presence of 1:1 electrolytes. The ^1H NMR spectra of **17** and **18** show a singlet for the methyl protons of the carbyne ligand at δ = 2.51 (**17**) and 2.23 ppm (**18**), while the spectra of **20**−**22** display the resonance (also a singlet) for the CH_2Ph protons at δ = 3.66−4.03 ppm. The hydride signal appears between δ = −6.41 and −7.46 ppm and is thus shifted downfield by ca. 3−6 ppm compared with the hydrido(vinylidene) precursors. The ^1H NMR spectra of **17**, **18** and **20**, **21** also confirm the coordination of one molecule of diethyl ether which is noteworthy insofar as in the five-coordinate carbyneruthenium complexes $[RuCl_2(\equiv CCH_2R)(PR'_3)_2]^+$ (R = Ph, *t*Bu; R′ = Cy, *i*Pr) the position *trans* to the carbyne ligand is not occupied by a solvent molecule.[7]

Similarly to the chloro derivative $[RuHCl(\equiv CCH_3)(PCy_3)_2(OEt_2)]BF_4$,[2] the cationic carbyne(hydrido) compounds **17** and **18** also catalyze the ring opening metathesis polymerization (ROMP) of cyclooctene. While for **18**, the rate, the yield of the polymer and the ratio of the *trans*- and *cis*-oriented carbon-carbon double bonds of the polymer are almost identical to the data obtained with the Grubbs catalyst $[RuCl_2(=CHPh)(PCy_3)_2]$, for **17** the results are less good. Under the same conditions (CH_2Cl_2, room temperature, ratio cyclooctene to ruthenium complex = 500:1), the acetato compound **19** is nearly inert in the ROMP of cyclooctene, which is probably due to the coordination number of six at ruthenium(II). The entering olefin can thus not bind to the metal center and can also not initiate the conversion of the $RuH(\equiv CCH_3)$ to the active $Ru(=CHCH_3)$ moiety.

Taking into consideration the fact that hydrido(vinylidene)ruthenium compounds $[RuHCl(=C=CHR)(PR'_3)_2]$ react with one equivalent of HCl to give the Grubbs-type carbene complexes $[RuCl_2(=CHCH_2R)(PR'_3)_2]$,[4] we also attempted to convert the relatively stable isocyanato derivative **12** into the corresponding metal carbene. However, while the dichloro compound **23** was exclusively formed with two equivalents of HCl, the reaction of **12** with HCl in the molar ratio 1:0.9 gave a mixture of four products. Apart from the hydrido(vinylidene) complex **5** three carbene derivatives could be detected, which in the ^{31}P NMR spectrum give rise to three singlets at δ = 45.2, 47.0 and 48.3 ppm. The ^1H NMR spectrum of the mixture equally shows three resonances for the carbene Ru=CH proton at δ = 19.06, 19.50 and 19.95 ppm, which are split into triplets due to ^1H-^{31}P coupling. While the signals at δ = 45.2 (^{31}P) and 19.95 ppm (^1H) belong to the dichloro compound **23**,[1d,1e] the corresponding resonances at δ = 48.3 (^{31}P) and 19.06 ppm (^1H) are assigned to the bis(isocyanato) counterpart **25**, which was prepared from **23** and excess KOCN in THF (see Scheme 3). The mixed ligand RuCl(NCO) species **24** is thus characterized by the signals at δ = 47.0 (^{31}P) and 19.50 ppm (^1H). To explain the formation of the unexpected products **23** and **25** in the reaction of **12** with HCl, we assume that the acid attacks both the C=C bond of the vinylidene and the metal, leading to an NCO/Cl exchange and formation of both **5** and HNCO. The starting material **12** can therefore react either with HCl to give **24** or with HNCO to afford **25**. Analogously, the reaction of **5** (generated from **12** and HCl) furnishes **23** (with HCl) and **24** (with HNCO). All attempts to separate the reaction mixture consisting of **5**, **23**, **24** and **25** by fractional crystallization or low-temperature column chromatography failed.

Since the Ru−Cl bond of the hydrido(vinylidene) complexes is quite labile, we were tempted to replace the chloride not only by other anions but also by a neutral Lewis

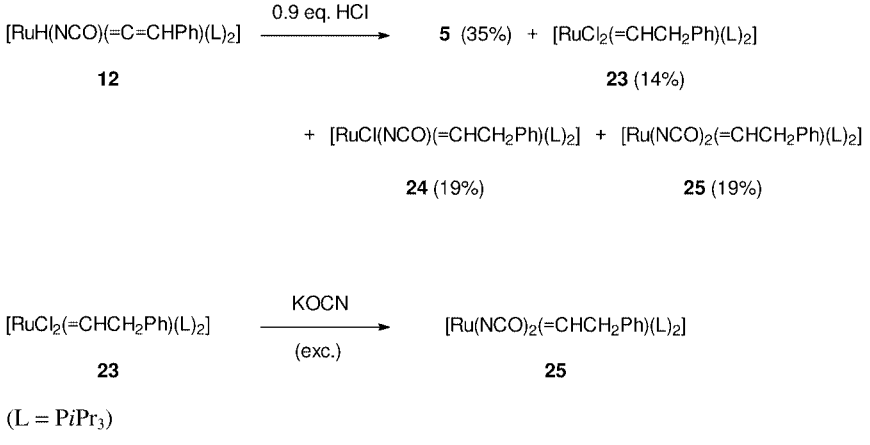

Scheme 3

 © 2004 Wiley-VCH Verlag GmbH & Co. KGaA, Weinheim

base such as acetonitrile. Treatment of a solution of **3** in CH_2Cl_2 with MeCN led, indeed, to a quick change of color from deep red to brown-yellow but afforded, after conventional workup, the cationic vinyl compound [Ru(CH=CH_2)$(NCMe)_2(PCy_3)_2$]Cl instead of a vinylidene complex. Because this compound, even as a solid, is rather unstable, the reaction was repeated in the presence of $NaBF_4$ or KPF_6 and gave the more stable complexes **26a** and **26b** in about 90% yield (Scheme 4). Salt metathesis with $NaBPh_4$ and $NaB(Ar_f)_4$ [Ar_f = 3,5-$C_6H_3(CF_3)_2$] in methanol led to the formation of **26c** and **26d**, respectively. Compounds **26a**−**d** are red-brown or orange-red, only slightly air-sensitive solids, which, in contrast to the analogous chloride, can be stored under argon at room temperature for weeks without decomposition. The composition of **26a**−**d** has been confirmed by elemental analysis and conductivity measurements. Typical spectroscopic features of **26a**−**d** are the three resonances for the vinyl protons which, taking **26a** as an example, appear at δ = 7.38, 4.84 and 4.70 ppm. The signal at lowest field is a doublet of doublets with a large *trans*-^{1}H-^{1}H and a smaller *cis*-^{1}H-^{1}H coupling and is assigned to the C*H*=CH_2 proton. The two other signals are doublets and belong to the methylene protons. The ^{31}P NMR spectra of **26a**−**d** display a single resonance confirming that the two phosphane ligands are stereochemically equivalent.

The result of the X-ray crystal structure analysis of **26c** is shown in Figure 1. The coordination geometry around the metal center of the cation corresponds to that of a square pyramid with the two phosphanes and the two acetonitriles *trans*-disposed. The atoms C(5) and C(6) of the vinyl ligand (which occupies the apical position) lie in the same plane as the nitrogen and carbon atoms of the MeCN units. In contrast to the nearly linear N(1)−Ru−N(2) axis, the P(1)−Ru−P(2) axis is slightly bent, with the phosphorus atoms pointing away from the CH=CH_2 moiety.

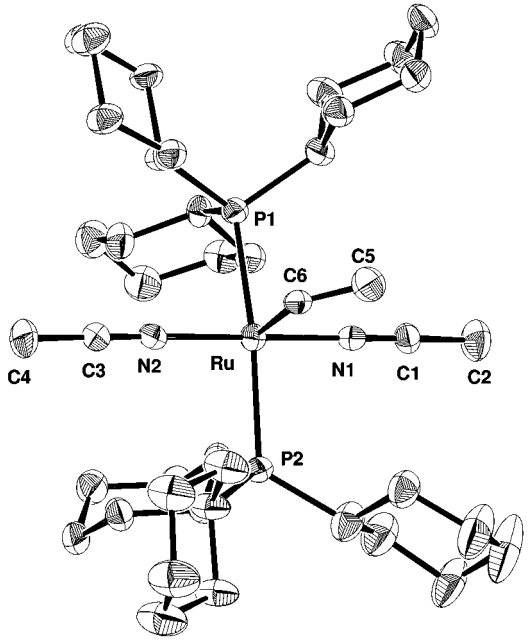

Figure 1. Molecular structure of **26c** (hydrogen atoms are omitted for clarity); selected bond lengths [Å] and angles [°]: Ru−P(1) 2.3975(13), Ru−P(2) 2.3979(12), Ru−N(1) 2.008(4), Ru−N(2) 2.006(4), Ru−C(6) 2.001(5), C(6)−C(5) 1.340(7), N(1)−C(1) 1.160(6), N(2)−C(3) 1.142(6); P(1)−Ru−P(2) 171.04(4), N(1)−Ru−N(2) 178.05(15), P(1)−Ru−C(6) 92.48(12), P(2)−Ru−C(6) 96.24(12), N(1)−Ru−C(6) 92.35(16), N(2)−Ru−C(3) 89.52(16), Ru−N(1)−C(1) 176.9(4), Ru−N(2)−C(3) 179.0(4), N(1)−C(1)−C(2) 178.7(5), N(2)−C(3)−C(4) 179.0(5), Ru−C(6)−C(5) 129.8(4)

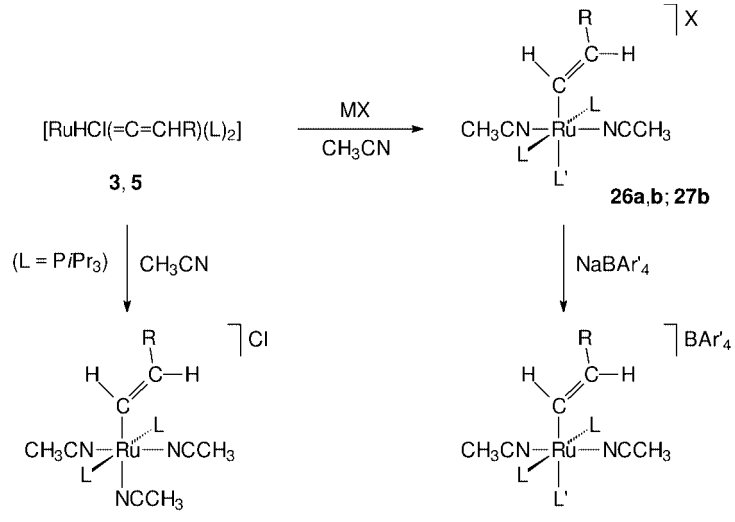

	R	L	L'	X
26a	H	PCy_3	-	PF_6
26b	H	PCy_3	-	BF_4
27b	Ph	P*i*Pr_3	CH_3CN	PF_6

	R	L	L'	Ar'
26c	H	PCy_3	-	Ph
26d	H	PCy_3	-	(Ar_f)
27c	Ph	P*i*Pr_3	CH_3CN	Ph
27d	Ph	P*i*Pr_3	CH_3CN	(Ar_f)

Scheme 4

 © 2004 Wiley-VCH Verlag GmbH & Co. KGaA, Weinheim

The distance Ru−C(6) of 2.001(5) Å is relatively short but similar to that in other ruthenium compounds with a Ru−C(sp^2) bond.[8] The Ru−P bond lengths of 2.3975(13) and 2.3979(12) Å lie in the expected range and are nearly identical to those found in five-coordinate carbeneruthenium(II) complexes containing a [Ru(PCy_3)$_2$] fragment.[9,10]

The bis(triisopropylphosphane) compound **5** behaves similarly to **3** and reacts with acetonitrile in CH_2Cl_2 to give **27a** (Scheme 4). In the presence of KPF_6, the hexafluorophosphate **27b** is formed, which, upon salt metathesis, affords **27c** and **27d**. The elemental analyses as well as the spectroscopic data of the vinyl complexes **27a**−**d** confirm that, in contrast to **26a**−**d**, *three* acetonitrile ligands are coordinated to the metal center. The smaller cone angle of P*i*Pr$_3$ (160°) compared to PCy_3 (170°)[11] probably favors the increase of the coordination number from five to six in the [Ru(P*i*Pr$_3$)$_2$] derivatives. An uncharged six-coordinate ruthenium compound of composition [$RuCl_2$(NCMe)$_2$(P*i*Pr$_3$)$_2$] has recently been prepared by Katayama and Ozawa from [(*p*-cymene)$RuCl_2$]$_2$ and P*i*Pr$_3$ in toluene/acetonitrile.[12] Moreover, Caulton et al. have found that the hydrido(iodo) complex [RuHI(=C=CHSiMe$_3$)(P*t*Bu$_2$Me)$_2$] reacts with excess methyl isocyanide to give the substituted vinylruthenium(II) derivative [Ru(CH=CHSiMe$_3$)(CNMe)$_3$(P*t*Bu$_2$Me)$_2$]I.[13]

An intramolecular migration of the hydride to the α-carbon atom of the vinylidene ligand also occurs upon treatment of compound **5** with carbon monoxide. This reaction is accompanied by a quick change of color from olive-green to red and then to pale yellow. The final product is the six-coordinate dicarbonyl complex **28** (Scheme 5), which is probably formed via the corresponding red, monocarbonyl complex [RuCl{(*E*)-CH=CHPh)}(CO)(P*i*Pr$_3$)$_2$]. This monocarbonyl compound was previously prepared in our laboratory from [RuHCl(CO)(P*i*Pr$_3$)$_2$] and phenylacetylene and shown to react readily with CO to give **28**.[14]

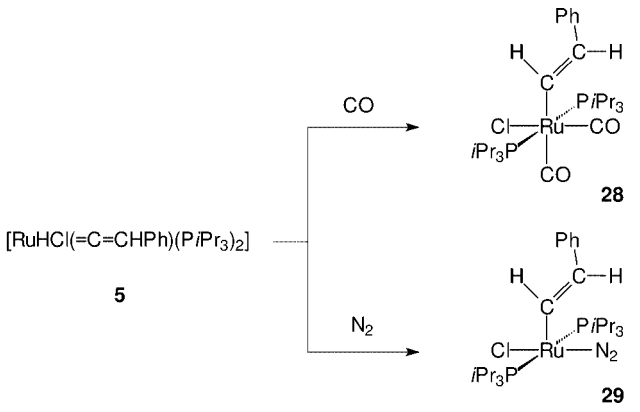

Scheme 5

Quite unexpectedly, the hydride shift to afford a RuCH=CHPh unit can also be initiated by N_2. Stirring a solution of **5** in pentane under an atmosphere of dinitrogen leads to a smooth change of color from olive-green to red-brown and gives, after low-temperature crystallization and drying the precipitate in a stream of N_2, the insertion product **29** in 92% isolated yield. In the IR spectrum of **29**, the $\nu(N_2)$ stretching mode appears at 2067 cm^{-1} and thus at a similar position as for a [Ru(N_2)(P*i*Pr$_3$)] complex with a tetradentate *N*,*S*,*S*,*N*-bonded chelate ligand.[15] The ^{1}H NMR spectrum of **29** displays the two signals for the vinyl protons at δ = 9.50 (RuCH) and 6.37 ppm (=CH) while the resonances for the corresponding carbon atoms appear at δ = 147.5 (RuC) and 130.2 ppm (C=*C*), respectively.

The formation of **29** from **5** is reversible. If a solution of **29** in benzene is stored at room temperature for ca. 2 h, the ^{1}H NMR spectrum reveals the presence of **5** and **29** in the ratio of 2:3. After evaporation of the solvent in vacuo, only the hydrido(vinylidene) complex can be detected. The elimination of N_2, accompanied by an α-shift of the RuCH proton from carbon to the metal, also takes place in the thermal reaction of **29**, which has been studied by differential thermal analysis (DTA). The ^{1}H NMR spectrum of the remaining product is identical to that of **5**. An analogous reversible formation of a vinylmetal compound has also been observed by Bercaw et al. who reacted [(η^5-C_5Me_5)$_2$TaH(=C=CH_2)] with CO to give [(η^5-C_5Me_5)$_2$Ta(CH=CH_2)(CO)] and regenerated the hydrido(vinylidene) precursor photochemically.[16]

The proposed structure of the dinitrogen complex **29** has been confirmed crystallographically (see Figure 2). As in the cationic vinyl compound **26c**, the coordination geometry around the metal center is square-pyramidal with the vinyl ligand in the apical position. The bending of the P(1)−Ru−P(2) axis [168.74(3)°] is somewhat more pronounced than in **26c** [171.04(4)°], which could be due to a slightly stronger steric repulsion between the phenyl and the

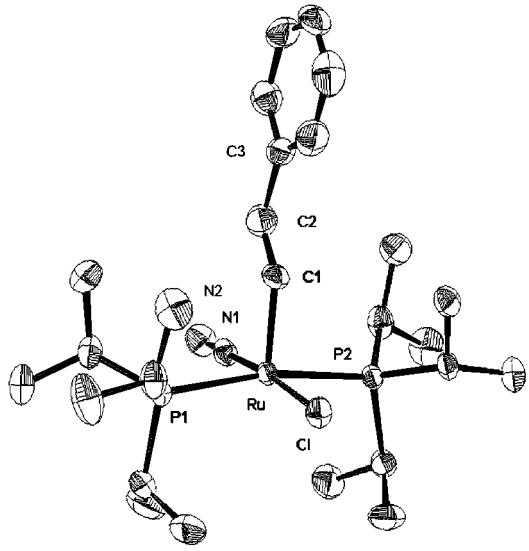

Figure 2. Molecular structure of **29** (hydrogen atoms are omitted for clarity); selected bond lengths [Å] and angles [°]: Ru−P(1) 2.4021(7), Ru−P(2) 2.4005(7), Ru−N(1) 1.869(5), Ru−Cl 2.3959(19), Ru−C(1) 1.973(3), C(1)−C(2) 1.296(5), N(1)−N(2) 1.088(8); P(1)−Ru−P(2) 168.74(3), N(1)−Ru−Cl 174.13(17), P(1)−Ru−Cl 98.15(9), P(2)−Ru−Cl 93.12(9), N(1)−Ru−P(1) 89.42(17), N(1)−Ru−P(2) 90.59(17), Cl−Ru−P(1) 89.33(4), Cl−Ru−P(2) 89.52(4), Cl−Ru−N(1) 90.63(19), Cl−Ru−C(1) 95.23(11), Ru−N(1)−N(2) 179.2(7), Ru−C(1)−C(2) 135.0(3), C(1)−C(2)−C(3) 125.1(3)

 © 2004 Wiley-VCH Verlag GmbH & Co. KGaA, Weinheim

isopropyl groups. The Ru−N(1)−N(2) axis is perfectly linear while in the related complex $[RuHCl(N_2)(P\mathit{i}Pr_3)_2]$ the bond angle Ru−*N*−N is 175(2)°.[17] The bond lengths Ru−N(1) and N(1)−N(2) are, respectively, 1.869(5) and 1.088(8) Å and thus quite similar to those in $[RuHCl(N_2)(P\mathit{i}Pr_3)_2]$.

The reactions of the vinyl complexes $[Ru(CH{=}CHR)(NCMe)_n(L)_2]X$ (L = PCy_3: *n* = 2; L = $P\mathit{i}Pr_3$: *n* = 3) with strong acids lead to a conversion of the vinyl ligand into a coordinated carbene. While the protonation of **26a** or **26c** with excess HBF_4 in diethyl ether gives a salt-like product with $[Ru(=CHCH_3)(NCMe)_2(PCy_3)_2]^{2+}$ as the cation and different ratios of, respectively, PF_6^-/BF_4^- and BPh_4^-/BF_4^- as the anion, the reaction of **26b** with HBF_4 affords the bis(tetrafluoroborate) **30a** cleanly in 75% yield (Scheme 6). In a similar way, compound **30b** was prepared on treatment of **26d** with Brookhart's acid $[H(OEt_2)_2][B(Ar_f)_4]$.[18] Both **30a** and **30b** are yellow, moderately air-stable solids, the conductivity of which (in nitromethane) corresponds to that of 1:2 electrolytes. Regarding the spectroscopic data, the most typical features are the signal for the carbene =CH proton at δ = 17.70 (**30a**) and 17.20 ppm (**30b**) in the ^1H NMR spectra and the multiplet for the carbene carbon atom at δ = 335.1 ppm (**30b**) in the ^{13}C NMR spectrum. The single resonance for the phosphorus nuclei in the ^{31}P NMR spectra of **30a** and **30b** suggests that the phosphane ligands are stereochemically equivalent and thus in a *trans* disposition. Attempts to generate the dication $[Ru(=CHCH_3)(NCMe)_2(PCy_3)_2]^{2+}$ from $[RuCl_2(=CHCH_3)(PCy_3)_2]$ by substitution of the chloro ligands for acetonitrile failed.

In contrast to **26d**, the related bis(triisopropylphosphane) compound **27d** reacts with an equimolar amount of $[H(OEt_2)_2][B(Ar_f)_4]$ in CH_2Cl_2 at 0 °C to give a 1:1 mixture of the dicationic complexes **31** and **32**. Since both compounds are readily soluble in dichloromethane but insoluble in benzene or pentane, they could not be separated by fractional crystallization. The ^1H NMR spectrum of the mixture displays a triplet at δ = 17.32 ppm, assigned to the =CH proton, and a multiplet, which becomes a doublet in off-resonance, at δ = 4.22 ppm for the CH_2Ph protons of the carbene ligand of **31**. In the ^{31}P NMR spectrum, a single resonance for the ^{31}P nuclei of **31** is observed.

Stirring the solution of **31** and **32** for 2 h at room temperature leads to a complete conversion of **31** into the carbene-free complex **32**, which was isolated as a green, moderately air-stable solid in 90% yield. As a by-product, styrene was detected both by ^1H NMR spectroscopy and GC/MS analysis. Since both the ^1H and ^{13}C NMR spectra of **32** show a single set of signals for the protons and carbon atoms of the CH_3CN ligands and since the molecule is diamagnetic, instead of a trigonal-bipyramidal structure a fluxional square-pyramidal geometry is more likely. With regard to the mechanism of the conversion of **31** to **32**, we assume, in agreement with results recently reported by Carmona[19] and Gimeno[20] and their co-workers, that the carbene ligand $CHCH_2Ph$ rearranges by an intramolecular 1,2-H shift to styrene. As the bonding of an olefin to a twofold positively charged metal center is, in general, considered to be weak, styrene is eliminated from the intermediate and the five-coordinate complex **32** is formed.

The formation of a metal carbene from a metal vinyl precursor is not without precedence. Casey[21] and Helquist[22] et al. showed already in 1982 that neutral cyclopentadienyliron compounds with $Fe-CR{=}CH_2$ as a linkage can be converted with HBF_4 into the corresponding cationic carbene derivatives. Similar transformations of neutral vinyl to monocationic carbene complexes by attack of an electrophile at the β-carbon atom of the vinyl ligand have since been carried by various research groups[23] including ours.[24] However, we note that: (1) as far we know there is no report about the preparation of a *dicationic* metal

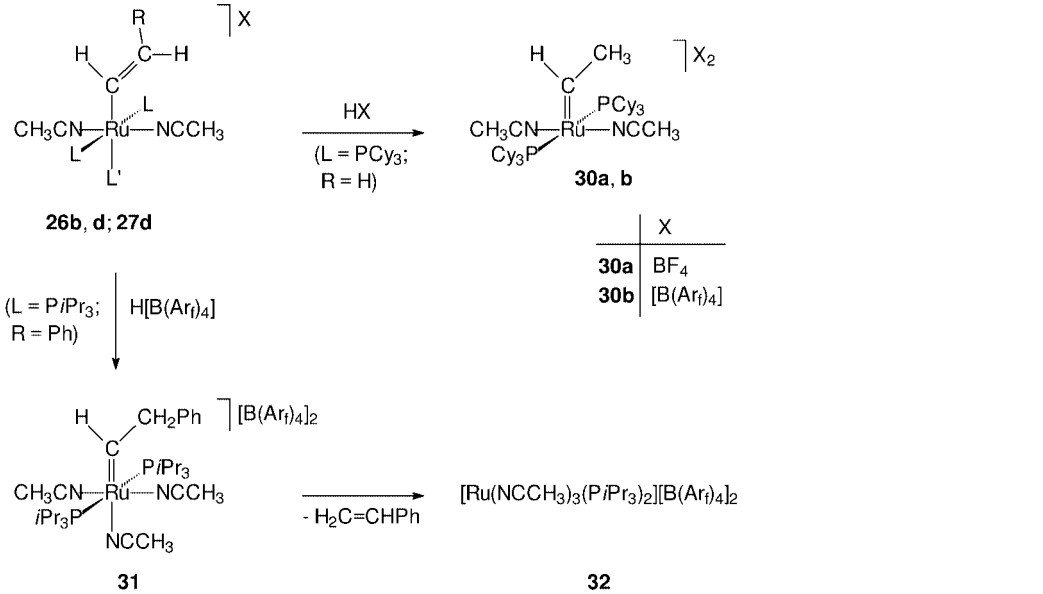

Scheme 6

carbene from a *monocationic* vinylmetal precursor by protonation, and (2) to the best of our knowledge **30a** and **30b** are the first dicationic five-coordinate carbeneruthenium complexes described as yet.

Experimental Section

All operations were carried out under argon using Schlenk techniques. The starting materials **1**,[4,25] **3**−**5**,1d][1e,25] **16**,[4,25] and **23**[1d,1e] were prepared as described in the literature. IR spectra were recorded on a Bruker IFS 25 FT-IR infrared spectrometer, and NMR spectra were recorded at room temperature on Bruker AC 200 and AMX 400 instruments, unless otherwise stated. The molar conductivity Λ_M was determined in nitromethane. Melting points were measured by differential thermal analysis (DTA) with a Thermoanalyzer Du Pont 9000. Abbreviations used: s, singlet; d, doublet; t, triplet; q, quadruplet; sept, septet; m, multiplet; vt, virtual triplet; br, broadened signal; $N = {}^3J_{P,H} + {}^5J_{P,H}$ or ${}^1J_{P,C} + {}^3J_{P,C}$.

Preparation of [RuHCl(=C=CH*t*Bu)(PCy$_3$)$_2$] (2): A solution of **1** (177 mg, 0.25 mmol) in CH_2Cl_2 (15 mL) was treated at −78 °C with *tert*-butylacetylene (0.1 mL, 0.82 mmol). After stirring the reaction mixture for 30 s, the solvent was removed in vacuo. A brown solid was obtained, which was washed at −78 °C with pentane (6 mL) and dried in vacuo; yield 143 mg (72%); m.p. 80 °C (decomp). IR (KBr): ν(RuH) = 2106, ν(C=C) = 1637 cm^{-1}. ^{1}H NMR (200 MHz, C_6D_6): δ = 2.87 (t, $J_{P,H}$ = 3.7 Hz, 1 H, Ru=C=CH), 2.61−1.20 (m, 66 H, C_6H_{11}), 1.27 (s, 9 H, CCH_3), −13.89 (t, $J_{P,H}$ = 17.8 Hz, 1 H, RuH) ppm. ^{31}P NMR (81.0 MHz, C_6D_6): δ = 39.0 (s) ppm. $C_{42}H_{77}ClP_2Ru$ (780.5): calcd. C 64.63, H 9.94; found C 63.95, H 9.72.

Preparation of [RuH(κ^2-O$_2$CCH$_3$)(=C=CH*t*Bu)(PCy$_3$)$_2$] (6): A solution of **2** (97 mg, 0.12 mmol) in THF (8 mL) was treated with finely divided potassium acetate (280 mg, 2.85 mmol) and stirred for 20 min at room temperature. The solvent was evaporated in vacuo and the residue was extracted with benzene (10 mL). The extract was dried in vacuo, and the remaining off-white solid was washed twice with pentane (3 mL each) and dried; yield 93 mg (96%); m.p. 50 °C (decomp). IR (KBr): ν(RuH) = 2053, ν($OCO_{asym.}$) = 1635, ν(C=C) = 1546, ν($OCO_{sym.}$) = 1448 cm^{-1}. ^{1}H NMR (400 MHz, CD_2Cl_2): δ = 2.12 (t, $J_{P,H}$ = 3.3 Hz, 1 H, Ru=C=CH), 1.97−0.87 (m, 66 H, C_6H_{11}), 1.43 (s, 3 H, CH_3CO_2), 0.73 (s, 9 H, CCH_3), −12.48 (t, $J_{P,H}$ = 19.6 Hz, 1 H, RuH) ppm. ^{13}C NMR (100.6 MHz, CD_2Cl_2): δ = 180.3 (s, CH_3CO_2), 114.8 (s, Ru=C=*C*H), 33.4 (vt, *N* = 17.8 Hz, C1 of C_6H_{11}), 32.4 (s, *C*CH_3), 30.1 (s, C3 or C5 of C_6H_{11}), 29.4 (s, C3 or C5 of C_6H_{11}), 28.2, 28.0 (both vt, *N* = 10.2 Hz, C2,6 of C_6H_{11}), 26.9 (s, C4 of C_6H_{11}), 24.4 (s, *C*H_3CO_2) ppm; the signal of the Ru=C carbon atom could not be located exactly. ^{31}P NMR (162.0 MHz, CD_2Cl_2): δ = 38.0 (s) ppm. $C_{44}H_{80}O_2P_2Ru$ (804.1): calcd. C 65.72, H 10.03; found C 65.62, H 10.19.

Preparation of [RuH(NCO)(=C=CH$_2$)(PCy$_3$)$_2$] (7): A solution of **3** (80 mg, 0.11 mmol) in THF (8 mL) was treated with an excess of finely divided KOCN (400 mg, 4.93 mmol) and stirred for 30 min at room temperature. A gradual change of color from red-brown to brown occurred. The solvent was evaporated in vacuo, the residue was extracted with benzene (10 mL), and the extract was again dried in vacuo. After the oily residue was layered with pentane (5 mL), a brown solid precipitated which was separated from the mother liquor and dried; yield 63 mg (78%); m.p. 42 °C (decomp). IR (KBr): ν($NCO_{asym.}$) = 2219, ν(RuH) = 2072, ν(C=C) = 1612, ν($NCO_{sym.}$) = 1446 cm^{-1}. ^{1}H NMR (200 MHz, C_6D_6): δ = 2.66 (t, $J_{P,H}$ = 3.7 Hz, 2 H, Ru=C=CH_2), 2.47−0.81 (m, 66 H, C_6H_{11}), −18.30 (t, $J_{P,H}$ = 18.3 Hz, 1 H, RuH) ppm. ^{31}P NMR (81.0 MHz, C_6D_6): δ = 43.9 (s) ppm. $C_{39}H_{69}NOP_2Ru$ (731.0): calcd. C 64.08, H 9.51, N. 1.92; found C 63.16, H 9.41, N. 2.07.

Preparation of [RuH(κ^2-O$_2$CCH$_3$)(=C=CH$_2$)(PCy$_3$)$_2$] (8): This compound was prepared as described for **6**, with **3** (74 mg, 0.10 mmol) and potassium acetate (250 mg, 2.55 mmol) as starting materials. Pale brown solid; yield 70 mg (94%); m.p. 50 °C (decomp). IR (KBr): ν(RuH) = 2064, ν($OCO_{asym.}$) = 1601, ν(C=C) = 1549, ν($OCO_{sym.}$) = 1447 cm^{-1}. ^{1}H NMR (200 MHz, C_6D_6): δ = 2.74 (t, $J_{P,H}$ = 3.3 Hz, 2 H, Ru=C=CH_2), 2.44−1.07 (m, 66 H, C_6H_{11}), 1.94 (s, 3 H, CH_3CO_2), −11.84 (t, $J_{P,H}$ = 19.1 Hz, 1 H, RuH) ppm. ^{13}C NMR (100.6 MHz, C_6D_6): δ = 330.0 (t, $J_{P,C}$ = 15.3 Hz, Ru=*C*=CH_2), 197.7 (s, CH_3CO_2), 84.6 (t, $J_{P,C}$ = 3.8 Hz, Ru=C=*C*H_2), 33.1 (vt, *N* = 17.8 Hz, C1 of C_6H_{11}), 29.5, 28.9 (both s, C3,5 of C_6H_{11}), 27.6, 27.4 (both vt, *N* = 10.2 Hz, C2,6 of C_6H_{11}), 26.2 (s, C4 of C_6H_{11}), 23.8 (s, *C*H_3CO_2) ppm. ^{31}P NMR (162.0 MHz, C_6D_6): δ = 39.4 (s) ppm. $C_{40}H_{72}O_2P_2Ru$ (748.0): calcd. C 64.23, H 9.70, Ru 13.51; found C 63.70, H 9.00, Ru 13.63.

Preparation of [RuH(NCO)(=C=CHPh)(PCy$_3$)$_2$] (9): This compound was prepared as described for **7**, with **4** (133 mg, 0.17 mmol) and KOCN (300 mg, 3.70 mmol) as starting materials. Olive-green solid; yield 92 mg (67%); m.p. 50 °C (decomp). IR (KBr): ν($NCO_{asym.}$) = 2205, ν(RuH) = 2071, ν(C=C) = 1615, ν($NCO_{sym.}$) = 1446 cm^{-1}. ^{1}H NMR (200 MHz, C_6D_6): δ = 7.15−6.76 (m, 5 H, C_6H_5), 4.34 (t, $J_{P,H}$ = 3.9 Hz, 1 H, Ru=C=CH), 2.37−1.17 (m, 66 H, C_6H_{11}), −14.42 (t, $J_{P,H}$ = 17.2 Hz, 1 H, RuH) ppm. ^{31}P NMR (C_6D_6, 81.0 MHz): δ = 43.1 (s) ppm. $C_{45}H_{73}NOP_2Ru$ (807.1): calcd. C 66.97, H 9.12, N 1.74; found C 66.80, H 8.89, N 2.07.

Preparation of [RuH(κ^2-O$_2$CCH$_3$)(=C=CHPh)(PCy$_3$)$_2$] (10): This compound was prepared as described for **6**, with **4** (81 mg, 0.10 mmol) and potassium acetate (230 mg, 2.34 mmol) as starting materials. Pale brown solid; yield 68 mg (83%); m.p. 42 °C (dec.). IR (KBr): ν(RuH) = 2099, ν(C=C) = 1610, ν($OCO_{asym.}$) = 1588, ν($OCO_{sym.}$) = 1446 cm^{-1}. ^{1}H NMR (200 MHz, C_6D_6): δ = 7.29−6.92 (m, 5 H, C_6H_5), 4.35 (t, $J_{P,H}$ = 3.3 Hz, 1 H, Ru=C=CH), 2.31−1.07 (m, 66 H, C_6H_{11}), 1.95 (s, 3 H, CH_3CO_2), −10.66 (t, $J_{P,H}$ = 19.1 Hz, 1 H, RuH) ppm. ^{31}P NMR (81.0 MHz, C_6D_6): δ = 40.1 (s) ppm. $C_{46}H_{76}O_2P_2Ru$ (824.1): calcd. C 67.04, H 9.29; found C 66.20, H 9.25.

Preparation of [RuHI(=C=CHPh)(P*i*Pr$_3$)$_2$] (11): A solution of **5** (73 mg, 0.13 mmol) in THF (7 mL) was treated with an excess of finely divided KI (250 mg, 1.51 mmol) and stirred for 20 min at room temperature. The solvent was evaporated in vacuo, the residue was extracted with benzene (8 mL), and the extract was again dried in vacuo. After the residue was layered with pentane (5 mL) and the solution stored at −78 °C, a brown solid formed which was washed with small quantities of pentane and dried; yield 71 mg (84%); m.p. 36 °C (decomp). IR (KBr): ν(RuH) = 2075, ν(C=C) = 1609 cm^{-1}. ^{1}H NMR (200 MHz, C_6D_6): δ = 7.54−6.83 (m, 5 H, C_6H_5), 4.33 (t, $J_{P,H}$ = 3.3 Hz, 1 H, Ru=C=CH), 2.56 (m, 6 H, PC*H*CH_3), 1.21 (m, 36 H, PCHC*H*$_3$), −9.32 (t, $J_{P,H}$ = 18.0 Hz, 1 H, RuH) ppm. ^{13}C NMR (50.3 MHz, C_6D_6): δ = 326.8 (t, $J_{P,C}$ = 15.3 Hz, Ru=*C*=CHPh), 132.8 (s, *ipso*-C of C_6H_5), 128.3, 127.8, 123.9 (all s, C_6H_5), 109.1 (t, $J_{P,C}$ = 4.4 Hz, Ru=C=*C*HPh), 25.7 (vt, *N* = 20.4 Hz, P*C*HCH$_3$), 20.4, 20.3 (both s, PCH*C*H$_3$) ppm. ^{31}P NMR (81.0 MHz, C_6D_6): δ = 51.6 (s) ppm. $C_{26}H_{49}IP_2Ru$ (651.6): calcd. C 47.93, H 7.58, Ru 15.51; found C 47.75, H 7.30, Ru 15.46.

 © 2004 Wiley-VCH Verlag GmbH & Co. KGaA, Weinheim

Preparation of [RuH(NCO)(=C=CHPh)(P*i*Pr$_3$)$_2$] (12): This compound was prepared as described for **11**, with **5** (78 mg, 0.14 mmol) and KOCN (250 mg, 3.08 mmol) as starting materials; reaction time 15 min. Dark green solid; yield 77 mg (97%); m.p. 56 °C (decomp). IR (KBr): ν(NCO$_{asym.}$) = 2213, ν(RuH) = 2075, ν(C=C) = 1610, ν(NCO$_{sym.}$) = 1464 cm^{-1}. ^{1}H NMR (200 MHz, C_6D_6): δ = 7.20−6.75 (m, 5 H, C_6H_5), 4.29 (t, $J_{P,H}$ = 3.3 Hz, 1 H, Ru=C=CH), 2.29 (m, 6 H, PC*H*CH$_3$), 1.12 (m, 36 H, PCHC*H*$_3$), −13.37 (t, $J_{P,H}$ = 17.4 Hz, 1 H, RuH) ppm. ^{13}C NMR (50.3 MHz, C_6D_6): δ = 333.3 (t, $J_{P,C}$ = 14.9 Hz, Ru=*C*=CHPh), 144.0 (s, NCO), 133.8 (s, *ipso*-C of C_6H_5), 128.2, 126.3, 123.8 (all s, C_6H_5), 110.3 (t, $J_{P,C}$ = 3.8 Hz, Ru=C=*C*HPh), 24.7 (vt, *N* = 20.4 Hz, P*C*HCH$_3$), 20.2, 20.0 (both s, PCH*C*H$_3$) ppm. ^{31}P NMR (81.0 MHz, C_6D_6): δ = 52.3 (s) ppm. $C_{27}H_{49}NOP_2Ru$ (566.7): calcd. C 57.22, H, 8.71, N, 2.47; found C 57.24, H 8.62, N 2.47.

Preparation of [RuH(OPh)(=C=CHPh)(P*i*Pr$_3$)$_2$] (13): This compound was prepared as described for **11**, with **5** (209 mg, 0.37 mmol) and KOPh (300 mg, 2.27 mmol) as starting materials; reaction time 10 min. Brown solid; yield 80 mg (35%); m.p. 80 °C (decomp). IR (KBr): ν(RuH) = 2058, ν(C=C) = 1606 cm^{-1}. ^{1}H NMR (400 MHz, C_6D_6): δ = 7.25−6.76 (m, 10 H, C_6H_5 and OC_6H_5), 4.40 (t, $J_{P,H}$ = 3.1 Hz, 1 H, Ru=C=CH), 2.16 (m, in ^{1}H{^{31}P} sept, $J_{H,H}$ = 7.0 Hz, 6 H, PC*H*CH$_3$), 1.15, 1.13 (both m, in ^{1}H{^{31}P} both d, $J_{H,H}$ = 7.0 Hz, 18 H each, PCHC*H*$_3$), −13.59 (t, $J_{P,H}$ = 18.3 Hz, 1 H, RuH) ppm. ^{13}C NMR (100.6 MHz, C_6D_6): δ = 329.6 (t, $J_{P,C}$ = 15.9 Hz, Ru=*C*=CHPh), 133.6, 129.4, 128.5, 128.1, 123.3, 123.2, 118.0, 116.3 (all s, C_6H_5 and OC_6H_5), 110.4 (t, $J_{P,C}$ = 3.8 Hz, Ru=C=*C*HPh), 24.5 (vt, *N* = 19.0 Hz, P*C*HCH$_3$), 20.3, 20.2 (both s, PCH*C*H$_3$) ppm. ^{31}P NMR (162.0, MHz C_6D_6): δ = 50.5 (s) ppm. $C_{32}H_{54}OP_2Ru$ (617.8): calcd. C 62.21, H 8.81; found C 61.91, H 8.33.

Preparation of [RuH(κ^2-O$_2$CCH$_3$)(=C=CHPh)(P*i*Pr$_3$)$_2$] (14): This compound was prepared as described for **11**, with **5** (67 mg, 0.12 mmol) and potassium acetate (250 mg, 2.55 mmol) as starting materials; reaction time 10 min. Orange-red solid; yield 65 mg (92%); m.p. 62 °C (decomp). IR (KBr): ν(RuH) = 2021, ν(C=C) = 1603, ν(OCO$_{asym.}$) = 1586, ν(OCO$_{sym.}$) = 1449 cm^{-1}. ^{1}H NMR (400 MHz, C_6D_6): δ = 7.25−6.84 (m, 5 H, C_6H_5), 4.31 (t, $J_{P,H}$ = 3.5 Hz, 1 H, Ru=C=CH), 2.39 (m, in ^{1}H{^{31}P} sept, $J_{H,H}$ = 7.0 Hz, 6 H, PC*H*CH$_3$), 1.82 (s, 3 H, CH_3CO_2), 1.28, 1.25 (both m, in ^{1}H{^{31}P} both d, $J_{H,H}$ = 7.0 Hz, 18 H each, PCHC*H*$_3$), −10.58 (t, $J_{P,H}$ = 18.7 Hz, 1 H, RuH) ppm. ^{13}C NMR (100.6 MHz, C_6D_6): δ = 335.2 (t, $J_{P,C}$ = 15.3 Hz, Ru=*C*=CHPh), 181.3 (s, CH_3CO_2), 134.9 (s, *ipso*-C of C_6H_5), 128.3, 123.8, 123.0 (all s, C_6H_5), 108.6 (t, $J_{P,C}$ = 3.8 Hz, Ru=C=*C*HPh), 24.6 (s, CH_3CO_2), 24.4 (vt, *N* = 19.0 Hz, P*C*HCH$_3$), 20.1, 19.5 (both s, PCH*C*H$_3$) ppm. ^{31}P NMR (162.0 MHz, C_6D_6): δ = 49.1 (s) ppm. $C_{28}H_{52}O_2P_2Ru$ (583.7): calcd. C 57.61, H 8.98, Ru 17.31; found C 57.99, H 8.73, Ru 17.84.

Preparation of [RuH(κ^2-O$_2$CCF$_3$)(=C=CHPh)(P*i*Pr$_3$)$_2$] (15): This compound was prepared as described for **11**, with **5** (153 mg, 0.27 mmol) and CF_3CO_2K (400 mg, 2.63 mmol) as starting materials. The residue was extracted with toluene (9 mL); reaction time 10 min. Red solid; yield 157 mg (91%); m.p. 54 °C (decomp). IR (KBr): ν(RuH) = 2044, ν(C=C) = 1628, ν(OCO$_{asym.}$) = 1588, ν(OCO$_{sym.}$) = 1444 cm^{-1}. ^{1}H NMR (400 MHz, C_6D_6): δ = 7.22−6.85 (m, 5 H, C_6H_5), 4.24 (t, $J_{P,H}$ = 3.5 Hz, 1 H, Ru=C=CH), 2.29 (m, in ^{1}H{^{31}P} sept, $J_{H,H}$ = 7.0 Hz, 6 H, PC*H*CH$_3$), 1.19, 1.16 (both m, in ^{1}H{^{31}P} both d, $J_{H,H}$ = 7.0 Hz, 18 H each, PCHC*H*$_3$), −11.51 (t, $J_{P,H}$ = 18.4 Hz, 1 H, RuH) ppm. ^{13}C NMR (100.6 MHz, C_6D_6): δ = 338.1 (t, $J_{P,C}$ = 15.3 Hz, Ru=*C*=CHPh), 163.4 (q, $J_{F,C}$ = 36.9 Hz, CF_3CO_2), 133.4 (s, *ipso*-C of C_6H_5), 128.5, 124.0, 123.7 (all s, C_6H_5), 115.2 (q, $J_{F,C}$ = 287.3 Hz, *C*F$_3$CO$_2$), 108.9 (t, $J_{P,C}$ = 3.8 Hz, Ru=C=*C*HPh), 24.5 (vt, *N* = 20.4 Hz, P*C*HCH$_3$), 20.0, 19.5 (both s, PCH*C*H$_3$) ppm. ^{19}F NMR (376.5 MHz, C_6D_6): δ = −75.2 (s) ppm. ^{31}P NMR (162.0 MHz, C_6D_6): δ = 48.2 (s) ppm. $C_{28}H_{49}F_3O_2P_2Ru$ (637.7): calcd. C 52.74, H 7.74, Ru 15.85; found C 52.60, H 7.50, Ru 16.80.

Preparation of [RuHI(≡CCH$_3$)(OEt$_2$)(PCy$_3$)$_2$]BF$_4$ (17): A solution of **16** (123 mg, 0.15 mmol) in a 1:1 mixture of CH_2Cl_2 (5 mL) and diethyl ether (5 mL) was treated at −78 °C with a 1.6 M solution of HBF_4 in diethyl ether (0.15 mL, 0.24 mmol). After warming the solution to 0 °C the solvent was evaporated in vacuo and the residue was layered with diethyl ether (5 mL). A light yellow solid precipitated, which was filtered, washed with pentane (5 mL) and dried; yield 86 mg (59%); m.p. 45 °C (decomp). Λ_M (Ω^{-1}cm^{2}mol^{-1}) = 54. ^{1}H NMR (200 MHz, CD_2Cl_2): δ = 3.42 (q, $J_{H,H}$ = 7.3 Hz, 4 H, OC*H*$_2$CH$_3$), 2.51 (s, 3 H, Ru≡CCH$_3$), 2.37−1.32 (m, 66 H, C_6H_{11}), 1.15 (t, $J_{H,H}$ = 7.3 Hz, 6 H, OCH$_2$C*H*$_3$), −6.87 (t, $J_{P,H}$ = 15.3 Hz, 1 H, RuH) ppm. ^{31}P NMR (81.0 MHz, CD_2Cl_2): δ = 55.7 (s) ppm. $C_{42}H_{80}BF_4IOP_2Ru$ (977.8): calcd. C 51.59, H 8.25; found C 51.45, H 7.98.

Preparation of [RuH(NCO)(≡CCH$_3$)(OEt$_2$)(PCy$_3$)$_2$]BF$_4$ (18): This compound was prepared as described for **17**, from **7** (45 mg, 0.06 mmol) and a 1.6 M solution of HBF_4 in diethyl ether (0.3 mL, 0.48 mmol). Light yellow solid; yield 39 mg (73%); m.p. 69 °C (decomp). Λ_M (Ω^{-1}cm^{2}mol^{-1}) = 95. IR (KBr): ν(NCO$_{asym.}$) = 2229, ν(RuH) = 1973, ν(NCO$_{sym.}$) = 1448 cm^{-1}. ^{1}H NMR (200 MHz, CD_2Cl_2): δ = 3.42 (q, $J_{H,H}$ = 7.3 Hz, 4 H, OC*H*$_2$CH$_3$), 2.23 (s, 3 H, Ru≡CCH$_3$), 2.30−1.31 (m, 66 H, C_6H_{11}), 1.15 (t, $J_{H,H}$ = 7.3 Hz, 6 H, OCH$_2$C*H*$_3$), −7.46 (t, $J_{P,H}$ = 16.3 Hz, 1 H, RuH) ppm. ^{31}P NMR (81.0 MHz, CD_2Cl_2): δ = 46.8 (s) ppm.

Preparation of [RuH(κ^2-O$_2$CCH$_3$)(≡CCH$_3$)(PCy$_3$)$_2$]BF$_4$ (19): A solution of **8** (81 mg, 0.11 mmol) in toluene (5 mL) was treated at 0 °C with a 1.6 M solution of HBF_4 in diethyl ether (0.3 mL, 0.48 mmol) and stirred for 15 min at 0 C. The solvent was evaporated in vacuo, the remaining light yellow resisue was washed with pentane (5 mL) and dried; yield 61 mg (66%); m.p. 60 °C (decomp). Λ_M (Ω^{-1}cm^{2}mol^{-1}) = 113. IR (KBr): ν(RuH) = 2066, ν(OCO$_{asym.}$) = 1629, ν(OCO$_{sym.}$) = 1448 cm^{-1}. ^{1}H NMR (200 MHz, CD_2Cl_2): δ = 2.50−1.30 (m, 72 H, C_6H_{11}, Ru≡CCH$_3$ and CH_3CO_2), −7.31 (t, $J_{P,H}$ = 17.0 Hz, 1 H, RuH) ppm. ^{31}P NMR (81.0 MHz, CD_2Cl_2): δ = 48.7 (s) ppm.

Preparation of [RuHCl(≡CCH$_2$Ph)(OEt$_2$)(PCy$_3$)$_2$]BF$_4$ (20): This compound was prepared as described for **17**, from **4** (93 mg, 0.12 mmol) and a 1.6 M solution of HBF_4 in diethyl ether (0.2 mL, 0.32 mmol). Light yellow solid; yield 75 mg (65%); m.p. 55 °C (decomp). Λ_M (Ω^{-1}cm^{2}mol^{-1}) = 61. ^{1}H NMR (200 MHz, CD_2Cl_2): δ = 7.42−6.69 (m, 5 H, C_6H_5), 4.03 (s, 2 H, Ru≡CC*H*$_2$Ph), 3.44 (q, $J_{H,H}$ = 7.3 Hz, 4 H, OC*H*$_2$CH$_3$), 2.83−1.26 (m, 66 H, C_6H_{11}), 1.15 (t, $J_{H,H}$ = 7.3 Hz, 6 H, OCH$_2$C*H*$_3$), −6.41 (br. s, 1 H, RuH) ppm. ^{31}P NMR (81.0 MHz, CD_2Cl_2): δ = 56.0 (s) ppm. $C_{48}H_{84}BClF_4OP_2Ru$ (962.5): calcd. C 59.90, H 8.80; found C 58.91, H 8.50.

Preparation of [RuHCl(≡CCH$_2$Ph)(OEt$_2$)(P*i*Pr$_3$)$_2$]BF$_4$ (21): A solution of **5** (56 mg, 0.10 mmol) in a 1:1 mixture of CH_2Cl_2 (3 mL) and diethyl ether (3 mL) was treated at −78 °C with a 1.6 M solution of HBF_4 in diethyl ether (0.2 mL, 0.32 mmol). After warming the solution to 0 °C, the solvent was evaporated in vacuo, and the residue was treated with diethyl ether (10 mL). The suspension was stirred for 15 min at 0 °C which led to the precipitation of a light yellow solid. This was separated from the mother liquor, washed with diethyl ether (5 mL) and dried; yield 40 mg (55%); m.p. 60 °C (decomp). Λ_M (Ω^{-1}cm^{2}mol^{-1}) = 61. ^{1}H NMR (200 MHz,

 © 2004 Wiley-VCH Verlag GmbH & Co. KGaA, Weinheim

CD_2Cl_2): δ = 7.41−7.27 (m, 5 H, C_6H_5), 3.95 (s, 2 H, Ru≡CCH_2Ph), 3.43 (q, $J_{H,H}$ = 7.3 Hz, 4 H, OCH_2CH$_3$), 2.76 (m, 6 H, PCHCH$_3$), 1.31 (m, 36 H, PCHCH_3), 1.14 (t, $J_{H,H}$ = 7.3 Hz, 6 H, OCH$_2$CH_3), −6.73 (br. s, 1 H, RuH) ppm. ^{31}P NMR (81.0 MHz, CD_2Cl_2): δ = 63.6 (s) ppm.

Preparation of [RuH(κ^2-O$_2$CCH$_3$)(≡CCH$_2$Ph)(P*i*Pr$_3$)$_2$]BF$_4$ (22): A solution of **14** (67 mg, 0.11 mmol) in toluene (7 mL) was treated at 0 °C with a 1.6 M solution of HBF_4 in diethyl ether (0.4 mL, 0.64 mmol) and stirred for 15 min at 0 °C. The solution was warmed to room temperature and then concentrated to ca. 1 mL in vacuo. A light yellow solid precipitated, which was separated from the mother liquor, washed with pentane (5 mL, 0 °C) and dried; yield 43 mg (55%); m.p. 48 °C (decomp). Λ_M (Ω^{-1}cm^{2}mol^{-1}) = 96. IR (KBr): ν(RuH) = 2072, ν(OCO$_{asym.}$) = 1587, ν(OCO$_{sym.}$) = 1465 cm^{-1}. ^{1}H NMR (200 MHz, CD_2Cl_2, 295 K): δ = 7.40−7.18 (m, 5 H, C_6H_5), 3.90 (s, 2 H, Ru≡CCH_2Ph), 2.34 (s, 3 H, CH_3CO_2), 2.33 (m, 6 H, PCHCH$_3$), 1.34 (m, 36 H, PCHCH_3), −6.90 (br. s, 1 H, RuH) ppm. ^{1}H NMR (200 MHz, CD_2Cl_2, 263 K): δ = −6.75 (t, $J_{P,H}$ = 17.4 Hz, 1 H, RuH) ppm. ^{31}P NMR (81.0 MHz, CD_2Cl_2, 295 K): δ = 59.1 (br. s) ppm. ^{31}P NMR (81.0 MHz, CD_2Cl_2, 263 K): δ = 59.0 (s) ppm. $C_{28}H_{53}BF_4O_2P_2Ru$ (671.5): calcd. C 50.08, H 7.95; found C 49.73, H 7.75.

Reaction of 12 with HCl: A solution of **12** (87 mg, 0.16 mmol) in benzene (10 mL) was treated with a 0.42 M solution of HCl in benzene (0.33 mL, 0.14 mmol) and stirred for 10 min at room temperature. The solvent was evaporated in vacuo and the red-brown residue was dissolved in C_6D_6 (0.5 mL). The NMR spectra indicated that besides the starting material **12** (13%) a mixture of four products was formed, of which **5** (35%) and [RuCl$_2$(=CHCH$_2$Ph)(P*i*Pr$_3$)$_2$] (**23**, 14%) were identified by comparison with authentic samples.[1d,1e] The other two products were assumed to be [RuCl(NCO)(=CHCH$_2$Ph)(P*i*Pr$_3$)$_2$] (**24**, 19%) and [Ru(NCO)$_2$(=CHCH$_2$Ph)(P*i*Pr$_3$)$_2$] (**25**, 19%). Characteristic data for **24**: ^{1}H NMR (200 MHz, C_6D_6): δ = 19.50 (t, $J_{H,H}$ = 5.1 Hz, Ru=CH), 4.15 (d, $J_{H,H}$ = 5.1 Hz, CH_2Ph).

Preparation of [Ru(NCO)$_2$(=CHCH$_2$Ph)(P*i*Pr$_3$)$_2$] (25): A solution of **23** (102 mg, 0.17 mmol) in a mixture of THF (10 mL) and CH_2Cl_2 (3 mL) was treated with finely divided KOCN (150 mg, 1.85 mmol) and stirred for 24 h at room temperature. After evaporation of the solvent in vacuo, the residue was extracted twice with benzene (9 mL each). The combined extracts were dried in vacuo, the remaining violet solid was washed three times with pentane (5 mL each) and dried; yield 98 mg (94%); m.p. 82 °C (decomp). IR (KBr): ν(NCO$_{asym.}$) = 2230, ν(NCO$_{sym.}$) = 1450 cm^{-1}. ^{1}H NMR (400 MHz, C_6D_6): δ = 19.06 (t, $J_{H,H}$ = 5.2 Hz, 1 H, Ru=CH), 7.24−7.04 (m, 5 H, C_6H_5), 3.99 (d, $J_{H,H}$ = 5.2 Hz, 2 H, CH_2Ph), 2.14 (m; in ^{1}H{^{31}P} sept, $J_{H,H}$ = 7.0 Hz, 6 H, PCHCH$_3$), 0.98 (dvt, N = 14.0, $J_{H,H}$ = 7.0 Hz, 36 H, PCHCH_3) ppm. ^{13}C NMR (100.6 MHz, C_6D_6): δ = 319.5 (br. s, Ru=CH), 139.9 (s, NCO), 136.6 (s, *ipso*-C of C_6H_5), 127.9, 127.3, 125.9 (all s, C_6H_5), 64.3 (s, CH$_2$Ph), 22.4 (vt, N = 20.4 Hz, PCHCH$_3$), 18.1 (s, PCHCH$_3$) ppm. ^{31}P NMR (162.0 MHz, C_6D_6): δ = 48.3 (s) ppm. $C_{28}H_{50}N_2O_2P_2Ru$ (609.7): calcd. C 55.16, H 8.26, N 4.59; found C 54.69, H 8.24, N 4.44.

Preparation of [Ru(CH=CH$_2$)(NCCH$_3$)$_2$(PCy$_3$)$_2$]PF$_6$ (26a): A solution of **3** (270 mg, 0.39 mmol) in a 1:1 mixture of CH_2Cl_2 and acetonitrile (30 mL) was treated with KPF_6 (250 mg, 1.36 mmol) and stirred for 35 min at room temperature. A gradual change of color from red-brown to light brown occurred. The solvent was evaporated in vacuo and the residue was extracted twice with CH_2Cl_2 (10 mL each). The combined extracts were dried in vacuo, the remaining brown solid was washed twice with pentane (8 mL each) and dried; yield 307 mg (87%); m.p. 55 °C (dec.). Λ_M (Ω^{-1}cm^{2}mol^{-1}) = 69. IR (KBr): ν(CN) = 2253 cm^{-1}. ^{1}H NMR (400 MHz, CD_2Cl_2): δ = 7.38 (dd, $J_{H,H}$ = 15.8, $J_{H,H}$ = 7.9 Hz, 1 H, CH=CH$_2$), 4.84 (d, $J_{H,H}$ = 7.9 Hz, 1 H, *cis*-H of CH=CH_2), 4.70 (d, $J_{H,H}$ = 15.8 Hz, 1 H, *trans*-H of CH=CH_2), 2.49 (s, 6 H, CH_3CN), 2.24−1.22 (m, 66 H, C_6H_{11}) ppm. ^{13}C NMR (100.6 MHz, CD_2Cl_2): δ = 150.2 (br. s, RuCH), 125.5 (s, CN), 117.3 (s, CH=CH$_2$), 34.3 (vt, N = 16.2 Hz, C1 of C_6H_{11}), 29.7 (s, C3,5 of C_6H_{11}), 28.1 (vt, N = 10.2 Hz, C2,6 of C_6H_{11}), 26.5 (s, C4 of C_6H_{11}), 5.0 (s, CH$_3$CN) ppm. ^{31}P NMR (162.0 MHz, CD_2Cl_2): δ = 22.4 (s, PCy$_3$), −144.0 (sept, $J_{F,P}$ = 709.4 Hz, PF_6) ppm. $C_{42}H_{75}F_6N_2P_3Ru$ (916.0): calcd. C 55.07, H 8.25, N 3.06, Ru 11.03; found C 54.89, H 7.81, N 3.06, Ru 10.76.

Preparation of [Ru(CH=CH$_2$)(NCCH$_3$)$_2$(PCy$_3$)$_2$]BF$_4$ (26b): This compound was prepared as described for **26a**, from **3** (101 mg, 0.14 mmol) and $NaBF_4$ (250 mg, 2.28 mmol) in a 2:1 mixture of CH_2Cl_2 and acetonitrile (15 mL). Orange-red solid; yield 109 mg (91%); m.p. 52 °C (decomp). Λ_M (Ω^{-1}cm^{2}mol^{-1}) = 58. IR (KBr): ν(CN) = 2254 cm^{-1}. ^{1}H NMR (400 MHz, CD_2Cl_2): δ = 7.21 (dd, $J_{H,H}$ = 15.6, $J_{H,H}$ = 7.7 Hz, 1 H, CH=CH$_2$), 4.62 (d, $J_{H,H}$ = 7.7 Hz, 1 H, *cis*-H of CH=CH_2), 4.54 (d, $J_{H,H}$ = 15.6 Hz, 1 H, *trans*-H of CH=CH_2), 2.39 (s, 6 H, CH_3CN), 2.25−1.10 (m, 66 H, C_6H_{11}) ppm. ^{13}C NMR (100.6 MHz, CD_2Cl_2): δ = 148.7 (br. s, RuCH), 125.6 (s, CN), 117.1 (s, CH=CH$_2$), 34.2 (vt, N = 16.2 Hz, C1 of C_6H_{11}), 29.7 (s, C3,5 of C_6H_{11}), 28.0 (vt, N = 9.5 Hz, C2,6 of C_6H_{11}), 26.5 (s, C4 of C_6H_{11}), 5.0 (s, CH$_3$CN) ppm. ^{31}P NMR (162.0 MHz, CD_2Cl_2): δ = 22.5 (s) ppm. $C_{42}H_{75}BF_4N_2P_2Ru$ (857.9): calcd. C 58.80, H 8.81, N 3.27; found C 58.55, H 8.54, N 3.36.

Preparation of [Ru(CH=CH$_2$)(NCCH$_3$)$_2$(PCy$_3$)$_2$]BPh$_4$ (26c): A solution of **26a** (450 mg, 0.49 mmol) in methanol (20 mL) was treated with $NaBPh_4$ (200 mg, 0.58 mmol) and stirred for 15 min at room temperature. An orange-red solid precipitated, which was separated from the mother liquor, washed three times with methanol (10 mL each) and dried in vacuo; yield 416 mg (78%); m.p. 100 °C (decomp). Λ_M (Ω^{-1}cm^{2}mol^{-1}) = 63. IR (KBr): ν(CN) = 2244 cm^{-1}. ^{1}H NMR (400 MHz, CD_2Cl_2): δ = 7.33−6.86 (m, 21 H, CH=CH$_2$ and BC$_6$H$_5$), 4.70 (d, $J_{H,H}$ = 7.3 Hz, 1 H, *cis*-H of CH=CH_2), 4.63 (d, $J_{H,H}$ = 15.2 Hz, 1 H, *trans*-H of CH=CH_2), 2.33 (s, 6 H, CH_3CN), 2.24−1.24 (m, 66 H, C_6H_{11}) ppm. ^{13}C NMR (100.6 MHz, CD_2Cl_2): δ = 164.1 (q, $J_{B,C}$ = 49.6 Hz, *ipso*-C of BC$_6$H$_5$), 147.2 (br. s, RuCH), 136.0 (s, CH of BC$_6$H$_5$), 125.7 (q, $J_{B,C}$ = 3.2 Hz, *ortho*-C of BC$_6$H$_5$), 121.7 (s, BC$_6$H$_5$), 117.2 (s, CH=CH$_2$), 34.3 (vt, N = 16.5 Hz, C1 of C_6H_{11}), 29.8 (s, C3,5 of C_6H_{11}), 28.1 (vt, N = 10.2 Hz, C2,6 of C_6H_{11}), 26.5 (s, C4 of C_6H_{11}), 4.8 (s, CH$_3$CN) ppm; the signal of the CN carbon atom could not be located exactly. ^{31}P NMR (162.0 MHz, CD_2Cl_2): δ = 23.0 (s) ppm. $C_{66}H_{95}BN_2P_2Ru$ (1090.3): calcd. C 72.71, H 8.78, N 2.57; found C 72.53, H 7.96, N 2.65.

Preparation of [Ru(CH=CH$_2$)(NCCH$_3$)$_2$(PCy$_3$)$_2$][B(Ar$_f$)$_4$] (26d): A suspension of **26a** (54 mg, 0.06 mmol) in diethyl ether (6 mL) was treated at 0 °C with a solution of Na[B(Ar$_f$)$_4$] (55 mg, 0.06 mmol) in diethyl ether (5 mL). After stirring the reaction mixture for 10 min, a white solid precipitated. The solution was filtered and the filtrate dried in vacuo. The remaining red-brown solid was washed three times with pentane (5 mL each) and dried in vacuo; yield 94 mg (96%); m.p. 70 °C (decomp). Λ_M (Ω^{-1}cm^{2}mol^{-1}) = 78. ^{1}H NMR (400 MHz, CD_2Cl_2): δ = 7.72 [br. s, 8 H, *ortho*-H of B(Ar$_f$)$_4$], 7.57 [br. s, 4 H, *para*-H of B(Ar$_f$)$_4$], 7.29 (dd, $J_{H,H}$ = 15.3, $J_{H,H}$ = 7.6 Hz, 1 H, CH=CH$_2$), 4.70 (dt, $J_{H,H}$ = 7.6, $J_{P,H}$ = 2.5 Hz,

 © 2004 Wiley-VCH Verlag GmbH & Co. KGaA, Weinheim

1 H, *cis*-H of CH=CH_2), 4.65 (dt, $J_{H,H}$ = 15.3, $J_{P,H}$ = 2.0 Hz, 1 H, *trans*-H of CH=CH_2), 2.51 (s, 6 H, CH_3CN), 2.25−1.13 (m, 66 H, C_6H_{11}) ppm. ^{13}C NMR (100.6 MHz, CD_2Cl_2): δ = 161.8 [q, $J_{B,C}$ = 49.9 Hz, *ipso*-C of $B(Ar_f)_4$], 147.2 (br. s, RuCH), 134.9 [br. s, *ortho*-C of $B(Ar_f)_4$], 129.0 [br. q, $J_{F,C}$ = 31.5 Hz, *meta*-C of $B(Ar_f)_4$], 125.4 (s, CN), 124.7 (q, $J_{F,C}$ = 272.4 Hz, CF_3), 117.5 [m, *para*-C of $B(Ar_f)_4$], 117.2 (t, $J_{P,C}$ = 3.4 Hz, CH=*C*H_2), 34.3 (vt, *N* = 15.2 Hz, C1 of C_6H_{11}), 29.8 (s, C3,5 of C_6H_{11}), 28.1 (vt, *N* = 9.5 Hz, C2,6 of C_6H_{11}), 26.4 (s, C4 of C_6H_{11}), 5.0 (s, *C*H_3CN) ppm. ^{19}F NMR (376.5 MHz, CD_2Cl_2): δ = −62.7 (s) ppm. ^{31}P NMR (162.0 MHz, CD_2Cl_2): δ = 22.9 (s) ppm. $C_{74}H_{87}BF_{24}N_2P_2Ru$ (1634.3): calcd. C 54.39, H 5.36, N 1.71; found C 53.82, H 5.12, N 1.68.

Preparation of [Ru{(*E*)-CH=CHPh}(NCCH$_3$)$_3$(P*i*Pr$_3$)$_2$]Cl (27a): A solution of **5** (81 mg, 0.14 mmol) in CH_2Cl_2 (8 mL) was treated with acetonitrile (3 mL, 0.06 mol) and stirred for 10 min at room temperature. The solvent was evaporated in vacuo, the remaining light yellow solid was washed twice with pentane (8 mL each) and dried; yield 87 mg (91%); m.p. 50 °C (decomp). Λ_M ($\Omega^{-1}cm^2mol^{-1}$) = 56. IR (KBr): ν(CN) = 2251 cm^{-1}. ^1H NMR (200 MHz, CD_3CN): δ = 8.74 (dt, $J_{H,H}$ = 17.2, $J_{P,H}$ = 1.8 Hz, 1 H, C*H*=CHPh), 7.15−6.90 (m, 5 H, C_6H_5), 6.43 (dt, $J_{H,H}$ = 17.2, $J_{P,H}$ = 1.8 Hz, 1 H, CH=C*H*Ph), 2.46 (m, 6 H, PC*H*CH_3), 2.38 (s, 9 H, CH_3CN), 1.26 (m, 36 H, PCHC*H*$_3$) ppm. ^{13}C NMR (50.3 MHz, CD_3CN): δ = 164.2 (br. s, RuCH), 142.6 (s, *ipso*-C of C_6H_5), 133.8 (s, CH=*C*HPh), 129.2, 124.3, 123.7 (all s, C_6H_5), 126.9 (s, CN), 24.8 (vt, *N* = 17.1 Hz, P*C*HCH$_3$), 19.7 (s, PCH*C*H$_3$), 5.3, 5.0 (both s, *C*H_3CN) ppm. The second signal of the CN carbon atoms is probably covered by the signals of the phenyl carbon atoms. ^{31}P NMR (81.0 MHz, CD_3CN): δ = 28.8 (s) ppm. $C_{32}H_{58}ClN_3P_2Ru$ (683.3): calcd. C 56.25, H 8.55, N 6.15; found C 55.89, H 8.05, N 5.56.

Preparation of [Ru{(*E*)-CH=CHPh}(NCCH$_3$)$_3$(P*i*Pr$_3$)$_2$]PF$_6$ (27b): This compound was prepared as described for **26a**, from **27a** (85 mg, 0.12 mmol) and KPF_6 (150 mg, 0.81 mmol) in a 5:3 mixture of CH_2Cl_2 and acetonitrile (8 mL). Orange solid; yield 73 mg (77%); m.p. 36 °C (dec.). Λ ($\Omega^{-1}cm^2mol^{-1}$) = 66. IR (KBr): ν(CN) = 2260 cm^{-1}. ^1H NMR (200 MHz, CD_2Cl_2): δ = 8.56 (d, $J_{H,H}$ = 16.8 Hz, 1 H, C*H*=CHPh), 7.20−6.89 (m, 5 H, C_6H_5), 6.34 (d, $J_{H,H}$ = 16.8 Hz, 1 H, CH=C*H*Ph), 2.46 (m; in $^1H\{^{31}P\}$ sept, $J_{H,H}$ = 7.4 Hz, 6 H, PC*H*CH_3), 2.42 (s, 6 H, CH_3CN), 2.31 (s, 3 H, CH_3CN), 1.27 (dvt, *N* = 12.3, $J_{H,H}$ = 7.4 Hz, 36 H, PCHC*H*$_3$) ppm. ^{13}C NMR (50.3 MHz, CD_2Cl_2): δ = 159.7 (br. s, RuCH), 141.2 (s, *ipso*-C of C_6H_5), 133.3 (s, CH=*C*HPh), 128.2, 123.6, 123.1 (all s, C_6H_5), 125.4, 123.3 (both s, CN), 24.1 (vt, *N* = 17.1 Hz, P*C*HCH$_3$), 19.1 (s, PCH*C*H$_3$), 5.0, 3.3 (both s, *C*H_3CN) ppm. ^{31}P NMR (81.0 MHz, CD_2Cl_2): δ = 28.3 (s, P*i*Pr$_3$), −144.0 (sept, $J_{F,P}$ = 709.4 Hz, PF_6) ppm. $C_{32}H_{58}F_6N_3P_3Ru$ (792.8): calcd. C 48.48, H 7.37, N 5.30; found C 48.07, H 6.95, N 5.44.

Preparation of [Ru{(*E*)-CH=CHPh}(NCCH$_3$)$_3$(P*i*Pr$_3$)$_2$]BPh$_4$ (27c): This compound was prepared as described for **26c**, from **27b** (230 mg, 0.23 mmol) and $NaBPh_4$ (200 mg, 0.58 mmol) in methanol (15 mL). Orange-brown solid; yield 162 mg (73%); m.p. 114 °C (decomp). Λ_M ($\Omega^{-1}cm^2mol^{-1}$) = 42. IR (KBr): ν(CN) = 2258 cm^{-1}. ^1H NMR (400 MHz, CD_2Cl_2): δ = 8.48 (d, $J_{H,H}$ = 16.6 Hz, 1 H, C*H*=CHPh), 7.35−6.88 (m, 25 H, C_6H_5 and BC_6H_5), 6.30 (d, $J_{H,H}$ = 16.6 Hz, 1 H, CH=C*H*Ph), 2.46 (m; in $^1H\{^{31}P\}$ sept, $J_{H,H}$ = 7.0 Hz, 6 H, PC*H*CH_3), 2.24 (s, 6 H, CH_3CN), 2.08 (s, 3 H, CH_3CN), 1.27 (dvt, *N* = 12.6, $J_{H,H}$ = 7.0 Hz, 36 H, PCHC*H*$_3$) ppm. ^{13}C NMR (100.6 MHz, CD_2Cl_2): δ = 164.1 [q, $J_{B,C}$ = 49.5 Hz, *ipso*-C of BC_6H_5], 140.7 (s, *ipso*-C of C_6H_5), 133.2 (s, CH=*C*HPh), 136.0, 128.3, 123.7, 123.4, 121.8 (all s, C_6H_5 and BC_6H_5), 125.7 (q, $J_{B,C}$ = 3.1 Hz, *ortho*-C of BC_6H_5), 24.1 (vt, *N* = 17.3 Hz, P*C*HCH$_3$), 19.3 (s, PCH*C*H$_3$), 4.9, 3.3 (both s, *C*H_3CN) ppm. The signals of the CN carbon atoms and of the RuCH carbon atom are probably covered by the signals of the phenyl carbon atoms. ^{31}P NMR (162.0 MHz, CD_2Cl_2): δ = 28.6 (s) ppm. $C_{56}H_{78}BN_3P_2Ru$ (967.1): calcd. C 69.55, H 8.13, N 4.35; found C 68.73, H 8.09, N 4.14.

Preparation of [Ru{(*E*)-CH=CHPh}(NCCH$_3$)$_3$(P*i*Pr$_3$)$_2$][B(Ar$_f$)$_4$] (27d): This compound was prepared as described for **26d**, from **27b** (73 mg, 0.09 mmol) and a solution of Na[$B(Ar_f)_4$] (77 mg, 0.09 mmol) in diethyl ether (6 mL). Red-brown solid; yield 83 mg (61%); m.p. 70 °C (decomp). Λ_M ($\Omega^{-1}cm^2mol^{-1}$) = 54. IR (KBr): ν(CN) = 2263 cm^{-1}. ^1H NMR (300 MHz, CD_2Cl_2): δ = 8.44 (dt, $J_{H,H}$ = 16.6, $J_{P,H}$ = 2.1 Hz, 1 H, C*H*=CHPh), 7.73 [br. s, 8 H, *ortho*-H of $B(Ar_f)_4$], 7.58 [br. s, 4 H, *para*-H of $B(Ar_f)_4$], 7.21−6.92 (m, 5 H, C_6H_5), 6.28 (d, $J_{H,H}$ = 16.6 Hz, 1 H, CH=C*H*Ph), 2.49−2.40 (m, 12 H, CH_3CN and PC*H*CH_3), 2.23 (s, 3 H, CH_3CN), 1.25 (m, 36 H, PCHC*H*$_3$) ppm. ^{13}C NMR (75.5 MHz, CD_2Cl_2): δ = 161.8 [q, $J_{B,C}$ = 49.8 Hz, *ipso*-C of $B(Ar_f)_4$], 140.6 (s, *ipso*-C of C_6H_5), 134.9 [br. s, *ortho*-C of $B(Ar_f)_4$], 133.3 (m, CH=*C*HPh), 128.9 [qq, $J_{F,C}$ = 31.5, $J_{F,C}$ = 2.9 Hz, *meta*-C of $B(Ar_f)_4$], 128.3, 123.8, 123.5 (all s, C_6H_5), 125.5 (s, CN), 124.7 (q, $J_{F,C}$ = 272.6 Hz, CF_3), 117.6 [m, *para*-C of $B(Ar_f)_4$], 24.1 (vt, *N* = 17.2 Hz, P*C*HCH$_3$), 19.2 (s, PCH*C*H$_3$), 5.6, 4.1 (both s, *C*H_3CN) ppm. The second signal of the CN carbon atoms and the signal of the RuCH carbon atom are probably covered by the signals of the phenyl carbon atoms. ^{19}F NMR (282.4 MHz, CD_2Cl_2): δ = −63.3 (s) ppm. ^{31}P NMR (CD_2Cl_2, 81.0 MHz): δ = 29.2 (s) ppm. $C_{64}H_{70}BF_{24}N_3P_2Ru$ (1511.1): calcd. C 50.87, H 4.67, N 2.78; found C 50.58, H 4.45, N 2.57.

Generation of [RuCl{(*E*)-CH=CHPh}(CO)$_2$(P*i*Pr$_3$)$_2$] (28): In an NMR tube, a solution of **5** (28 mg, 0.05 mmol) in C_6D_6 (0.5 mL) was cooled to −78 °C. The tube was evacuated in vacuo and then filled with CO. Upon warming to room temperature, a change of color from olive-green to red and finally to pale yellow occurred. The ^1H and ^{31}P NMR spectra of the solution revealed that compound **28** was formed in quantitative yield. It was identified by comparison of the NMR spectroscopic data with those of an authentic sample.[14]

Preparation of [RuCl{(*E*)-CH=CHPh}(N$_2$)(P*i*Pr$_3$)$_2$] (29): A solution of **5** (68 mg, 0.12 mmol) in pentane (8 mL) was stirred under a nitrogen atmosphere for 2 h at room temperature. A change of color from olive-green to brown occurred and a red-brown solid precipitated. After storing the solution for 12 h at −20 °C, the mother liquor was separated and the remaining red-brown solid dried in a stream of N_2; yield 65 mg (92%); m.p. 34 °C (decomp). IR (KBr): ν(N_2) = 2067 cm^{-1}. ^1H NMR (400 MHz, C_6D_6): δ = 9.50 (dt, $J_{H,H}$ = 16.6, $J_{P,H}$ = 1.5 Hz, 1 H, C*H*=CHPh), 7.39−6.86 (m, 5 H, C_6H_5), 6.37 (dt, $J_{H,H}$ = 16.6, $J_{P,H}$ = 1.9 Hz, 1 H, CH=C*H*Ph), 2.62 (m; in $^1H\{^{31}P\}$ sept, $J_{H,H}$ = 7.2 Hz, 6 H, PC*H*CH_3), 1.17, 1.15 (both m; in $^1H\{^{31}P\}$ both d, $J_{H,H}$ = 7.2 Hz, 18 H each, PCHC*H*$_3$) ppm. ^{13}C NMR (100.6 MHz, C_6D_6): δ = 147.5 (t, $J_{P,C}$ = 10.8 Hz, RuCH), 138.0 (s, *ipso*-C of C_6H_5), 130.2 (t, $J_{P,C}$ = 3.2 Hz, CH=*C*HPh), 127.9, 123.2, 123.1 (all s, C_6H_5), 22.5 (vt, *N* = 17.8 Hz, P*C*HCH$_3$), 18.8, 18.7 (both s, PCH*C*H$_3$) ppm. ^{31}P NMR (162.0 MHz, C_6D_6): δ = 33.3 (s) ppm. $C_{26}H_{49}ClN_2P_2Ru$ (588.2): calcd. C 53.10, H 8.40, N 4.76; found C 53.24, H 8.30, N 3.86.

Preparation of [Ru(=CHCH$_3$)(NCCH$_3$)$_2$(PCy$_3$)$_2$](BF$_4$)$_2$ (30a): A solution of **26b** (275 mg, 0.32 mmol) in CH_2Cl_2 (8 mL) was treated with a 1.6 M solution of HBF_4 in diethyl ether (1.0 mL, 1.60 mmol) at room temperature. A change of color from red to yellow-orange

 © 2004 Wiley-VCH Verlag GmbH & Co. KGaA, Weinheim

occurred. The solvent was evaporated in vacuo, the remaining yellow solid was washed three times with pentane (5 mL each) and dried; yield 225 mg (75%); m.p. 55 °C (decomp). Λ ($\Omega^{-1}cm^2mol^{-1}$) = 99. IR (KBr): ν(CN) = 2275 cm^{-1}. ^1H NMR (200 MHz CD_2Cl_2): δ = 17.70 (m, 1 H, =C*H*CH_3), 2.96 (br.s, 3 H, =CHC*H*$_3$), 2.79 (s, 6 H, CH_3CN), 2.53−1.31 (m, 66 H, C_6H_{11}) ppm. ^{31}P NMR (81.0 MHz, CD_2Cl_2): δ = 38.0 (s) ppm. $C_{42}H_{76}B_2F_8N_2P_2Ru$ (945.7): calcd. C 53.34, H 8.10, N. 2.96; found C 53.01, H 7.73, N 3.42.

Preparation of [Ru(=CHCH$_3$)(NCCH$_3$)$_2$(PCy$_3$)$_2$][B(Ar$_f$)$_4$]$_2$ (30b): A solution of **26d** (94 mg, 0.06 mmol) in CH_2Cl_2 (8 mL) was treated at 0 °C with a solution of $[H(OEt_2)_2][B(Ar_f)_4]$ (58 mg, 0.06 mmol) in CH_2Cl_2 (4 mL). A change of color from red to yellow occurred. After warming the solution to room temperature, the solvent was evaporated in vacuo, and the remaining yellow solid was washed three times with pentane (5 mL each) and dried; yield 130 mg (87%); m.p. 130 °C (decomp). Λ_M ($\Omega^{-1}cm^2mol^{-1}$) = 139. ^1H NMR (400 MHz, CD_2Cl_2): δ = 17.20 (q, $J_{H,H}$ = 5.9 Hz, 1 H, =C*H*CH_3), 7.72 [br. s, 16 H, *ortho*-H of $B(Ar_f)_4$], 7.57 [br. s, 8 H, *para*-H of $B(Ar_f)_4$], 2.87 (d, $J_{H,H}$ = 5.9 Hz, 3 H, =CHC*H*$_3$), 2.75 (s, 6 H, CH_3CN), 2.17−1.23 (m, 66 H, C_6H_{11}) ppm. ^{13}C NMR (100.6 MHz, [D$_6$]acetone): δ = 335.1 (m, Ru=C), 163.0 [q, $J_{B,C}$ = 49.6 Hz, *ipso*-C of $B(Ar_f)_4$], 135.9 [br. s, *ortho*-C of $B(Ar_f)_4$], 130.4 [br. q, $J_{F,C}$ = 31.8 Hz, *meta*-C of $B(Ar_f)_4$], 125.7 (q, $J_{F,C}$ = 272.1 Hz, CF_3), 118.8 [m, *para*-C of $B(Ar_f)_4$], 48.5 (s, =CH*C*H$_3$), 35.3 (vt, *N* = 19.1 Hz, C1 of C_6H_{11}), 30.8 (s, C3, 5 of C_6H_{11}), 28.5 (vt, *N* = 10.2 Hz, C2, 6 of C_6H_{11}), 26.1 (s, C4 of C_6H_{11}), 5.7 (s, *C*H$_3$CN) ppm. The signal of the CN carbon atom could not be located exactly. ^{19}F NMR (376.5 MHz, [D$_6$]acetone): δ = −62.9 (s) ppm. ^{31}P NMR (162.0 MHz, [D$_6$]acetone): δ = 41.0 (s) ppm. $C_{106}H_{100}B_2F_{48}N_2P_2Ru$ (2498.5): calcd. C 50.96, H 4.03, N 1.12; found C 50.72, H 3.77, N 1.13.

Generation of [Ru(=CHCH$_2$Ph)(NCCH$_3$)$_3$(P*i*Pr$_3$)$_2$][B(Ar$_f$)$_4$]$_2$ (31): A solution of **27d** (48 mg, 0.03 mmol) in CH_2Cl_2 (5 mL) was treated at 0 °C with a solution of $[H(OEt_2)_2][B(Ar_f)_4]$ (32 mg, 0.03 mmol) in CH_2Cl_2 (3 mL). A change of color from red to light green occurred. After stirring the solution for 2 min, it was filtered and the filtrate was dried in vacuo. The ^1H and ^{31}P NMR spectra of the light green residue revealed that it consisted of equal amounts of **31** and **32**. Data for **31**: ^1H NMR (400 MHz, CD_2Cl_2): δ = 17.32 (t, $J_{H,H}$ = 5.1 Hz, 1 H, =C*H*CH_3), 4.42 (m; in $^1H\{^{31}P\}$ d, $J_{H,H}$ = 5.1 Hz, 2 H, C*H*$_2$Ph) ppm. ^{31}P NMR (162.0 MHz, CD_2Cl_2): δ = 51.5 (s) ppm.

Preparation of [Ru(NCCH$_3$)$_3$(P*i*Pr$_3$)$_2$][B(Ar$_f$)$_4$]$_2$ (32): A solution of **27d** (80 mg, 0.05 mmol) in CH_2Cl_2 (6 mL) was treated with a solution of $[H(OEt_2)_2][B(Ar_f)_4]$ (53 mg, 0.05 mmol) in CH_2Cl_2 (4 mL) and stirred for 2 h at room temperature. The solution was filtered, and the filtrate was dried in vacuo. The remaining green solid was washed twice with pentane (5 mL each) and dried; yield 102 mg (90%); m.p. 68 °C (decomp). Λ_M ($\Omega^{-1}cm^2mol^{-1}$) = 153. IR (KBr): ν(CN) = 2288 cm^{-1}. ^1H NMR (400 MHz, CD_2Cl_2): δ = 7.72 [br. s, 16 H, *ortho*-H of $B(Ar_f)_4$], 7.57 [br. s, 8 H, *para*-H of $B(Ar_f)_4$], 2.48 (m; in $^1H\{^{31}P\}$ sept, $J_{H,H}$ = 7.2 Hz, 6 H, PC*H*CH_3), 2.40 (s, 9 H, CH_3CN), 1.32, 1.31 (both dvt, *N* = 13.5, $J_{H,H}$ = 7.2 Hz, 18 H each, PCHC*H*$_3$) ppm. ^{13}C NMR (100.6 MHz, C_6D_6): δ = 161.8 [q, $J_{B,C}$ = 49.8 Hz, *ipso*-C of $B(Ar_f)_4$], 134.9 [br. s, *ortho*-C of $B(Ar_f)_4$], 128.9 [br. q, $J_{F,C}$ = 31.8 Hz, *meta*-C of $B(Ar_f)_4$], 127.5 (s, CN), 124.7 (q, $J_{F,C}$ = 272.7 Hz, CF_3), 117.6 [m, *para*-C of $B(Ar_f)_4$], 24.0 (vt, *N* = 19.1 Hz, P*C*HCH$_3$), 19.0 (s, PCH*C*H$_3$), 4.7 (s, *C*H$_3$CN) ppm. ^{19}F NMR (376.5 MHz, CD_2Cl_2): δ = −62.8 (s) ppm. ^{31}P NMR (162.0 MHz, CD_2Cl_2): δ = 27.9 (s) ppm. $C_{88}H_{75}B_2F_{48}N_3P_2Ru$ (2271.1): calcd. C 46.54, H 3.33, N 1.85; found C 46.65, H 3.35, N 2.31.

X-ray Structure Determination of Compounds 26c and 29: Single crystals of **26c** were grown from CH_2Cl_2 at −20 °C and those of **29** from pentane at −78 °C. Crystal data collection parameters for these structures are presented in Table 1. The data were collected on a Stoe IPDS diffractometer (**26c**) and a Bruker Smart Apex diffractometer (**29**) using monochromated Mo-K_α radiation (λ = 0.71073 Å). Intensity data were corrected for Lorentz and polarization effects and an empirical absorption correction was applied (SADABS2.0). The structures were solved by direct methods (SHELXS-97).[26] Atomic coordinates and anisotropic thermal parameters of the non-hydrogen atoms were refined by the full-matrix least-squares method on F^2 using SHELXL-97.[27] The asymmetric unit of **26c** includes a molecule of dichloromethane, the chloro atoms of which are disordered (ratio of occupancy factors Cl1/Cl2:Cl1′/Cl2′ = 82:18). The hydrogen atoms of the vinyl ligand were found in a difference-Fourier synthesis and refined without restraints. The positions of all other hydrogen atoms were calculated according to the ideal geometry and refined by the riding method. The chloro and the nitrogen ligands of **29** are disordered and could be refined anisotropically without restraints (occupancy factor 80:20).

Ref. code MIKMUO (**26c**) and CCDC-215082 (**29**) contain the supplementary crystallographic data for this paper. These data can be obtained free of charge at www.ccdc.cam.ac.uk/conts/retrieving.html [or from the Cambridge Crystallographic Data Centre, 12, Union Road, Cambridge CB2 1EZ, UK; Fax: (internat.) +44-1223-336-033; E-mail: deposit@ccdc.cam.ac.uk].

Table 1. Crystal data for complexes **26c** and **29**

	26c·CH_2Cl_2	**29**
Empirical formula	$C_{67}H_{97}BCl_2N_2P_2Ru$	$C_{26}H_{49}ClN_2P_2Ru$
M	1189.35	588.13
Crystal size (mm)	0.19 × 0.16 × 0.12	0.40 × 0.24 × 0.12
Crystal system	triclinic	monoclinic
Space group	$P\bar{1}$ (no. 2)	$P2_1/c$ (no. 14)
a (Å)	12.7193(17)	16.4389(8)
b (Å)	15.482(2)	10.9929(5)
c (Å)	17.447(2)	17.0126(8)
α (°)	88.771(16)	90
β (°)	79.913(15)	105.4450(10)
γ (°)	69.452(15)	90
V (Å^3)	3164.3(7)	2963.3(2)
Z	2	4
D_c (g cm^{-3})	1.227	1.318
Temperature (K)	173(2)	173(2)
μ (mm^{-1})	0.423	0.743
2Θ(max) (°)	50.06	50.00
No. reflections measured	25291	41784
No. unique reflections (R_{int})	10533 (0.0637)	5210 (0.0291)
No. observed reflections [$I > 2\sigma(I)$]	6204	5026
Parameters refined	686	331
R_1	0.0495	0.0363
wR_2	0.1280	0.0827
Reflection/parameter ratio	15.4	15.74
Residual electron density (e·Å^{-3})	+1.064/−0.948	+1.025/−0.343

 © 2004 Wiley-VCH Verlag GmbH & Co. KGaA, Weinheim

Acknowledgments

This work was supported by the Deutsche Forschungsgemeinschaft (SFB 347), the BASF AG, and the Fonds der Chemischen Industrie. We are grateful to the latter in particular for a PhD grant (to K. I.). Moreover, we thank Mrs. M.-L. Schäfer and Dr. W. Buchner for NMR measurements, Mrs. R. Schedl and Mr. C. P. Kneis for elemental analyses and DTA measurements, and Mr. S. Stellwag for technical assistance.

[1] [1a] H. Werner, A. Stark, M. Schulz, J. Wolf, *Organometallics* **1992**, *11*, 1126−1130. [1b] H. Werner, A. Stark, P. Steinert, C. Grünwald, J. Wolf, *Chem. Ber.* **1995**, *128*, 49−62. [1c] M. Martin, O. Gevert, H. Werner, *J. Chem. Soc., Dalton Trans.* **1996**, 2275−2283. [1d] C. Grünwald, O. Gevert, J. Wolf, P. González-Herrero, H. Werner, *Organometallics* **1996**, *15*, 1960−1962. [1e] J. Wolf, W. Stüer, C. Grünwald, O. Gevert, M. Laubender, H. Werner, *Eur. J. Inorg. Chem.* **1998**, 1217−1224.

[2] W. Stüer, J. Wolf, H. Werner, P. Schwab, M. Schulz, *Angew. Chem.* **1998**, *110*, 3603−3606; *Angew. Chem. Int. Ed.* **1998**, *37*, 3421−3423.

[3] S. Jung, K. Ilg, J. Wolf, H. Werner, *Organometallics* **2001**, *20*, 2121−2123.

[4] W. Stüer, Dissertation, Universität Würzburg, **1999**.

[5] [5a] S. D. Robinson, M. F. Uttley, *J. Chem. Soc., Dalton Trans.* **1973**, 1912−1920. [5b] G. B. Deacon, R. J. Phillips, *Coord. Chem. Rev.* **1980**, *33*, 227−250. [5c] C. Oldham, in *Comprehensive Coordination Chemistry* (Eds.: G. Wilkinson, R. D. Gillard, J. A. McCleverty), Pergamon Press, Oxford, **1987**, Vol. 2, p. 435−459.

[6] [6a] J. L. Burmeister, E. A. Deardorf, A. Jensen, V. H. Christiansen, *Inorg. Chem.* **1970**, *9*, 58−63. [6b] U. Müller, *Z. Anorg. Allg. Chem.* **1973**, *396*, 187−198.

[7] P. González-Herrero, B. Weberndörfer, K. Ilg, J. Wolf, H. Werner, *Organometallics* **2001**, *20*, 3672−3685.

[8] T. Daniel, N. Mahr, T. Braun, H. Werner, *Organometallics* **1993**, *12*, 1475−1477.

[9] P. Schwab, R. H. Grubbs, J. W. Ziller, *J. Am. Chem. Soc.* **1996**, *118*, 100−110.

[10] B. Weberndörfer, Dissertation, Universität Würzburg, **2001**.

[11] C. A. Tolman, *Chem. Rev.* **1977**, *77*, 313−348.

[12] H. Katayama, F. Ozawa, *Organometallics* **1998**, *17*, 5190−5196.

[13] M. Oliván, E. Clot, O. Eisenstein, K. G. Caulton, *Organometallics* **1998**, *17*, 3091−3100.

[14] H. Werner, M. A. Esteruelas, H. Otto, *Organometallics* **1986**, *5*, 2295−2299.

[15] D. Sellmann, B. Hautsch, A. Rösler, F. W. Heinemann, *Angew. Chem.* **2001**, *113*, 1553−1555; *Angew. Chem. Int. Ed.* **2001**, *40*, 1505−1507.

[16] A. van Asselt, B. J. Burger, V. C. Gibson, J. E. Bercaw, *J. Am. Chem. Soc.* **1986**, *108*, 5347−5349.

[17] J. N. Coalter III, J. C. Bollinger, J. C. Huffman, U. Werner-Zwanziger, K. G. Caulton, E. R. Davidson, H. Gérard, E. Clot, O. Eisenstein, *New. J. Chem.* **2000**, *24*, 9−26.

[18] M. Brookhart, B. Grant, A. F. Volpe, *Organometallics* **1992**, *11*, 3920−3922.

[19] F. M. Alías, M. L. Poveda, M. Sellin, E. Carmona, *J. Am. Chem. Soc.* **1998**, *120*, 5816−5817.

[20] M. P. Gamasa, J. Gimeno, B. M. Martín-Vaca, *Organometallics* **1998**, *17*, 3707−3715.

[21] C. A. Casey, W. H. Miles, H. Tukada, J. M. O'Connor, *J. Am. Chem. Soc.* **1982**, *104*, 3761−3762.

[22] K. A. M. Kremer, G.-H. Kuo, E. J. O'Connor, P. Helquist, R. C. Kerber, *J. Am. Chem. Soc.* **1982**, *104*, 6119−6121.

[23] [23a] G. S. Bodner, D. E. Smith, W. G. Hatton, P. C. Heah, S. Georgiou, A. L. Rheingold, S. J. Geib, J. P. Hutchinson, J. A. Gladysz, *J. Am. Chem. Soc.* **1987**, *109*, 7688−7705. [23b] M. A. Esteruelas, F. J. Lahoz, E. Oñate, L. A. Oro, B. Zeier, *Organometallics* **1994**, *13*, 4258−4265. [23c] G. Jia, W. F. Wu, R. C. Y. Yeung, H. Xia, *J. Organomet. Chem.* **1997**, *538*, 31−40. [23d] F. M. Alias, M. L. Poveda, M. Sellin, E. Carmona, E. Gutiérrez-Puebla, A. Monge, *Organometallics* **1998**, *17*, 4124−4126.

[24] H. Werner, S. Jung, P. González-Herrero, K. Ilg, J. Wolf, *Eur. J. Inorg. Chem.* **2001**, 1957−1961.

[25] J. Wolf, W. Stüer, C. Grünwald, H. Werner, P. Schwab, M. Schulz, *Angew. Chem.* **1998**, *110*, 1165−1167; *Angew. Chem. Int. Ed.* **1998**, *37*, 1124−1126.

[26] G. M. Sheldrick, *Acta Crystallogr., Sect. A* **1990**, *46*, 467−473.

[27] G. M. Sheldrick, *SHELXL-97*, University of Göttingen, Göttingen, Germany, **1997**.

Received July 23, 2003
Early View Article
Published Online November 28, 2003

 © 2004 Wiley-VCH Verlag GmbH & Co. KGaA, Weinheim

Mono- and Dinuclear Rhodium and Iridium Complexes with Chiral Phospholanes as Ligands

Peter Krüger[a] and Helmut Werner*[a]

Dedicated to Professor Christoph Elschenbroich on the occasion of his 65th birthday

Keywords: Allyl ligands / Carbonyl ligands / Hydrido complexes / Phospholanes / Rhodium

The dinuclear complexes $[RhCl(L)_2]_2$ (**1**, **2**) with L = 1-isopropyl-(2*S*,5*S*)-2,5-dimethylphospholane (Isophos) and (2*S*,5*S*)-2,5-dimethyl-1-phenylphospholane (Phephos), respectively, prepared from $[RhCl(C_8H_{14})_2]_2$ and four equivalents of L, react with Lewis bases such as L, CO, ethene and diphenylacetylene by cleavage of the chloride bridges. Mononuclear compounds of the general composition $[RhCl(L)_3]$ (**3**, **4**) and *trans*-$[RhCl(L')(L)_2]$ (**5**–**9**; L′ = CO, C_2H_4, C_2Ph_2) were obtained, of which **4** (L = Phephos) and **8** (L′ = C_2H_4; L = Phephos) are in equilibrium with the precursors. Oxidative addition of H_2 to **1** (L = Isophos) and $[RhCl(PiPr_2Ph)_2]_2$ (**10**) affords the mononuclear dihydrido complexes $[RhH_2Cl(L)_2]$ (**13**) and $[RhH_2Cl(PiPr_2Ph)_2]$ (**14**), respectively, via the unsymmetrical compounds $[RhH_2(L)_2(\mu\text{-}Cl)_2Rh(L)_2]$ (**11**) and $[RhH_2(PiPr_2Ph)_2(\mu\text{-}Cl)_2Rh(PiPr_2Ph)_2]$ (**12**) as intermediates. These intermediates can be isolated by treatment of **13** and **14** with one half equivalent of **1** or **10**, respectively. The hydrogenation of the η^3-allyl and η^3-benzyl complexes $[(\eta^3\text{-}2\text{-}RC_3H_4)Rh(L)_2]$ (**16**–**18**) and $[(\eta^3\text{-}CH_2Ph)Rh(L)_2]$ (**19**, **20**), which were prepared from **1** or **2** and the corresponding Grignard reagent, leads to the dinuclear $Rh^{III}Rh^{I}$ products $[RhH_2(L)_2(\mu\text{-}H)_2Rh(L)_2]$ (**21**, **22**), which are structurally related to the dichloro(dihydrido) derivatives **11** and **12**. Compound **21** (L = Isophos) reacts with CO to give *trans*-$[RhH(CO)(L)_2]$ (**23**). While treatment of **1** with phenylacetylene yields the vinylidene complex *trans*-$[RhCl(=C=CHPh)(Isophos)_2]$ (**26**), via η^2-alkyne and alkynyl(hydrido) intermediates, the reaction of **2** with PhC≡CH affords the labile enyne compound *trans*-$[RhCl\{\eta^2\text{-}(E)\text{-}PhC{\equiv}CCH{=}CHPh\}(Phephos)_2]$ (**27**). Reaction of **27** with CO gives **6** and the free enyne. The carbene complexes *trans*-$[RhCl(=CPh_2)(L)_2]$ (**30**, **31**), obtained from *trans*-$[RhCl(=CPh_2)(SbiPr_3)_2]$ (**29**) and L, react with ethene not by olefin metathesis but by formation of the isomeric olefins $Ph_2C{=}CHCH_3$ (**32**) and $CH_2{=}CHCHPh_2$ (**33**) in different ratios. With iridium as the metal center, carbonyl, dihydrido, and dihydrido(carbonyl) compounds with $[IrCl(Isophos)_2]$ as the building block have been prepared.
(© Wiley-VCH Verlag GmbH & Co. KGaA, 69451 Weinheim, Germany, 2004)

Introduction

In the context of our investigations on low-valent organorhodium compounds containing bulky tertiary phosphanes as supporting ligands,[1] we recently observed that even an apparently minor change in the size of the phosphane upon going from $PiPr_3$ to $PiPr_2Ph$ causes a difference in the reactivity of the corresponding complexes.[2] A striking example is the behavior of the acetato derivatives $[Rh(\kappa^2\text{-}O_2CCH_3)(PiPr_3)_2]$ and $[Rh(\kappa^2\text{-}O_2CCH_3)(PiPr_2Ph)_2]$, of which the first reacts with two equivalents of phenylacetylene to give a vinylrhodium(III) compound containing a Rh(CH=CHPh) unit,[3] while under the same conditions the second affords a product with $Rh(CPh{=}CH_2)$ as a molecular fragment.[2]

Taking these results into consideration, we started a systematic study of the reactivity of rhodium (and some iridium) complexes with 1-isopropyl-(2*S*,5*S*)-2,5-dimethylphospholane (abbreviated as Isophos) and (2*S*,5*S*)-2,5-dimethyl-1-phenylphospholane (abbreviated as Phephos) as ligands. As depicted in Scheme 1, these phospholanes are similar in size to $PiPr_3$ and $PiPr_2Ph$, but in contrast to these tertiary phosphanes are chiral, which for catalytic purposes

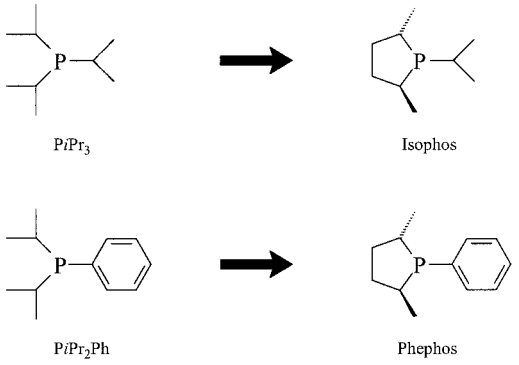

Scheme 1

[a] Institut für Anorganische Chemie der Universität Würzburg, Am Hubland, 97074 Würzburg, Germany
E-mail: helmut.werner@mail.uni-wuerzburg.de

could be an important factor. In this paper we report the preparation of the starting materials $[RhCl(Isophos)_2]_2$ (**1**) and $[RhCl(Prephos)_2]_2$ (**2**), the reactivity of these compounds toward H_2, CO, ethene, internal and terminal alkynes, and the conversion of **1** and **2** to η^3-allyl- and η^3-benzylrhodium(I) complexes, and discuss very briefly some exploratory experiments regarding the synthesis and reactivity of iridium compounds with Isophos as ligand.

Results and Discussion

The method previously used by us for the preparation of $[RhCl(P\mathit{i}Pr_3)_2]_2$ [4] could also be applied to the synthesis of **1** and **2** (Scheme 2). Treatment of a suspension of the bis(cyclooctene) derivative $[RhCl(C_8H_{14})_2]_2$ with four equivalents of Isophos[5] or Phephos[6] in acetone or benzene gives the required products in 92% (**1**) and 75% (**2**) isolated yields. Both **1** and **2** are red or orange-red solids, which, like $[RhCl(P\mathit{i}Pr_3)_2]_2$, are thermally not very stable, but in contrast to their $P\mathit{i}Pr_3$ counterpart are less air-sensitive. The ^{31}P NMR spectra of **1** and **2** display a sharp doublet with a large $^1J_{Rh,P}$ coupling constant of 196.2 Hz (**1**) and 198.0 Hz (**2**) that is characteristic for a $Rh(PR_3)_2$ moiety with the P-donors in a *cis* arrangement.[4,7] The ^1H NMR spectra of **1** and **2** show two signals for the protons of the different methyl groups of the phospholane units but are otherwise quite complicated due to the overlap of the resonances for the CH_2 and CH protons of the five-membered ring. Similar observations have also been made for the other Isophos and Phephos complexes described in this paper and thus the corresponding ^1H NMR spectroscopic data will not be discussed.

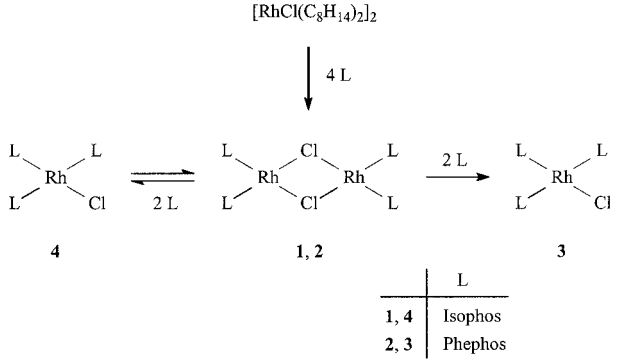

Scheme 2

Treating a suspension of $[RhCl(C_8H_{14})_2]_2$ with eight instead of four equivalents of Isophos or Phephos leads to the formation of the mononuclear compounds **3** and **4**, respectively (see Scheme 2). However, while **3** could be isolated as an analytically pure product, the analogue **4** is in equilibrium with **1** and free Isophos. The equilibrium lies completely on the side of **4** only in the presence of excess Isophos and thus all attempts to obtain **4** without Isophos as a by-product failed. The ^{31}P NMR spectrum of **3** at room temperature displays, apart from a sharp doublet of triplets for the ^{31}P nuclei *trans* to chloride, a broad signal that becomes a doublet of doublets at 330 K owing to an increase in the rate of the exchange process for the phospholanes. The $^1J_{Rh,P}$ and $^2J_{P,P}$ coupling constants for **3** are very similar to those of the Wilkinson complex $[RhCl(PPh_3)_3]$.[8]

The reactions of compounds **1** and **2** with CO, ethene and diphenylacetylene, that all lead to cleavage of the chloro bridges, are summarized in Scheme 3. The carbonyl complexes **5** and **6** are formed almost instantaneously and were isolated as yellow, moderately air-sensitive solids in ca. 90% yields. Compound **5** is also accessible from **7** and CO and compound **6** similarly from **3** and carbon monoxide by ligand exchange. In contrast to the behavior of **1** and **2** toward an excess of Isophos or Phephos, the reaction of **2** (with Phephos as ligand) with ethene approaches an equilibrium, while the corresponding reaction of **1** (with Isophos as ligand) affords the mononuclear complex **7** nearly quantitatively. Treatment of **2** with diphenylacetylene does not lead to an equilibrium but gives compound **9** as a yellow solid in 72% yield. The ^{31}P NMR spectra of **5**−**9** all display one sharp doublet, indicating that in each case the two phospholane ligands are *trans*-disposed. The wavenumbers for the ν(CO) stretching mode in the IR spectra of **5** and **6** (1947 and 1961 cm^{-1}) are nearly identical to those of their phosphane counterparts *trans*-$[RhCl(CO)(P\mathit{i}Pr_3)_2]$ (1943 cm^{-1})[9] and *trans*-$[RhCl(CO)(P\mathit{i}Pr_2Ph)_2]$ (1960 cm^{-1})[10] which suggests that the coordinative capabilities of $P\mathit{i}Pr_3$ and $P\mathit{i}Pr_2Ph$ on one hand and those of the phospholanes on the other are similar. With regard to the lability of **8** we note that the bis(triphenylphosphane) complex *trans*-$[RhCl(C_2H_4)(PPh_3)_2]$ also loses the ethene ligand in the absence of an excess of C_2H_4 and rearranges to $[RhCl(PPh_3)_2]_2$.[11]

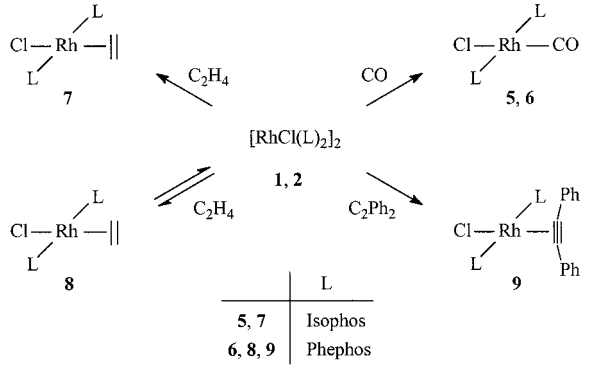

Scheme 3

The course of the oxidative addition of H_2 to the metal centers of **1**, **2** and the related compound $[RhCl(P\mathit{i}Pr_2Ph)_2]_2$ (**10**)[2] is also dependent on the type of phosphorus donor. Passing a slow stream of dry dihydrogen through a solution of **1** or **10** in toluene or pentane at low temperatures leads, after warming to 20 °C, to the formation of the dihydrido complexes **13** and **14** in 76−87% isolated yields. In contrast, the reaction of **2** with H_2 generates an equilibrium which, even after stirring the solution for 12 h under a dihydrogen

 © 2004 Wiley-VCH Verlag GmbH & Co. KGaA, Weinheim

atmosphere, could not be completely shifted to the side of product **15** (Scheme 4). In the absence of H_2, **15** is reconverted into **2**. The fact that **15** is not an analogue of **13** and **14** is confirmed by the ^{31}P NMR spectrum, which displays two resonances (both doublets) at $\delta = 69.9$ and 52.2 ppm, respectively. Since the signal at lower field shows a large $^1J_{Rh,P}$ coupling constant of 195.8 Hz, it is assigned to the *cis*-oriented phospholanes at the lower coordinated rhodium center. The chemical shift and the coupling constant (118.4 Hz) for the signal at higher field are very similar to those of **14** ($\delta = 53.7$ ppm; $^1J_{Rh,P} = 119.1$ Hz) with P*i*Pr$_2$Ph as ligand. The ^{31}P NMR spectra of **13** and **14** (which are both yellow solids that can be stored under argon for weeks) show only one resonance, confirming that the two P-donors are in the *trans* positions. In the ^1H NMR spectra of **13** and **14** there is also only one set of signals (doublet of triplets) at $\delta = -22.00$ and -21.24 ppm for the hydride ligands, which is in agreement with the proposed structure shown in Scheme 4. An X-ray crystal structure analysis of [RhH$_2$Cl(P*i*Pr$_3$)$_2$] has been carried out, and this proved that the coordination geometry is trigonal bipyramidal with the phosphanes in the apical positions.[12]

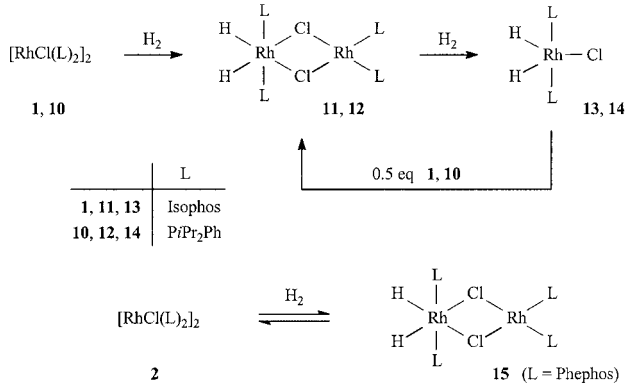

Scheme 4

The plausible assumption that compounds **13** and **14** are formed via **11** and **12** as intermediates was confirmed by the reactions of **13** and **14** with one half equivalent of **1** or **10**, respectively. The conversion is relatively slow (3 h at 20 °C in C_6D_6) and was monitored by NMR spectroscopy. The ^1H and ^{31}P NMR spectra of **11** and **12** are similar to those of **15** and also to those of [RhH$_2$(PPh$_3$)$_2$(μ-Cl)$_2$Rh(PPh$_3$)$_2$], which is the first compound of this structural type reported in the literature.[8] It should be mentioned that dimer **1**, with Isophos as ligand, reacts in C_6D_6 at 60 °C with a tenfold excess of cyclooctane to give **11** and cyclooctene. However, this dehydrogenation is a stoichiometric reaction and all attempts to convert C_8H_{16} into C_8H_{14} catalytically using **1** as the catalyst failed.

In analogy to the preparation of [Rh(η^3-C$_3$H$_5$)(PR$_3$)$_2$] (PR$_3$ = P*i*Pr$_3$,[7,13] P*i*Pr$_2$Ph[2]), the starting materials **1** and **2**, both generated in situ from [RhCl(C$_8$H$_{14}$)$_2$]$_2$ and the corresponding phospholane, react with a solution of the Grignard reagent 2-RC$_3$H$_4$MgBr in diethyl ether to give the η^3-allyl complexes **16**−**18** in 72−82% isolated yield (Scheme 5). The Phephos derivative **18** is equally accessible from **3** and C$_3$H$_5$MgBr in the molar ratio of 1:4. Similarly to the related P*i*Pr$_3$ and P*i*Pr$_2$Ph compounds, **16**−**18** are orange-yellow solids that are not only air sensitive but also thermally quite labile. In contrast to the ^{31}P NMR spectra of [Rh(η^3-C$_3$H$_5$)(PR$_3$)$_2$] (PR$_3$ = P*i*Pr$_3$, P*i*Pr$_2$Ph) and [Rh(η^3-2-MeC$_3$H$_4$)(P*i*Pr$_3$)$_2$],[2,13] which display a sharp doublet, the ^{31}P NMR spectra of **16**−**18** exhibit the AB part of an ABX system, which reflects the non-equivalence of the chiral phospholane ligands. Owing to this non-equivalence, the ^1H NMR spectra of **16**−**18** show two signals for the *anti*- and two for the *syn*-protons of the terminal allylic CH$_2$ units, with a significant difference in the chemical shifts. Since the spectrum of **16** remains unchanged in the temperature range between 278 and 330 K, there is no doubt that in solution the Rh(η^3-2-MeC$_3$H$_4$) moiety is rigid on the NMR timescale and does not undergo an η^3-η^1-η^3 rearrangement.[14]

Under similar conditions as used for the preparation of **16**−**18**, the in situ generated dimers **1** and **2** also react with the benzyl Grignard reagent PhCH$_2$MgBr to give the η^3-benzylrhodium(I) compounds **19** and **20** in about 80% yield. The red air-sensitive solids are thermally even less stable than their Rh(η^3-C$_3$H$_5$) counterparts **17** and **18** and under argon slowly decompose at room temperature. In benzene, **19** and **20** are stable for ca. 1 h, while in CHCl$_3$ and CH$_2$Cl$_2$ they decompose almost instantaneously. The ^1H NMR spectrum of **19** shows, apart from a triplet for the CH$_2$ protons of the benzylic group, five distinct resonances for the six-membered ring protons H^3 − H^7, which, as for **16**−**18**, indicates that the bonding between the C$_6$H$_5$CH$_2$ ligand and the metal is rigid on the NMR timescale. As expected, the ^{31}P NMR spectra of **19** and **20** display two doublets of doublets of which those at lower fields ($\delta = 76.0$ ppm for **19** and $\delta = 65.2$ ppm for **20**), owing to their larger $^1J_{Rh,P}$ coupling constant of ca. 260 Hz, are assigned to the ^{31}P nuclei *trans* to the ring and those at higher fields ($\delta = 64.9$ ppm for **19** and $\delta = 58.1$ ppm for **20**), with a $^1J_{Rh,P}$ coupling constant of ca. 180 Hz, to the ^{31}P nuclei *trans* to the benzylic CH$_2$ unit.

The η^3-allyl and η^3-benzyl complexes **17**, **19** and **20** react smoothly with H_2 at a pressure of 1 bar to give the Rh$_2$H$_4$ derivatives **21** and **22**, respectively (see Scheme 5). Compounds of the general composition [Rh$_2$H$_4$(L)$_4$] with L = P*i*Pr$_3$,[15] P(OR)$_3$,[16] P(NMe$_2$)$_3$,[17] and L$_2$ = *i*Pr$_2$P(CH$_2$)$_n$-P*i*Pr$_2$ (n = 2, 3)[18] are well-known, but in most cases are rather labile and can be handled only under a hydrogen atmosphere. The X-ray crystal structure analysis of the stable complex [Rh$_2$H$_4$\{P(NMe$_2$)$_3$\}$_4$] revealed that the two rhodium centers, which are bridged by two hydride ligands, have a different coordination geometry, one being octahedral and the other square planar.[17] According to the spectroscopic data, we assume that the phospholane complexes **21** and **22** are structurally related to their P(NMe$_2$)$_3$ counterpart. The ^1H NMR spectrum of **21** (which is a dark green, extremely air-sensitive solid) displays two resonances at $\delta = -10.20$ and -17.50 ppm in the high-field region, of which the first is split into a triplet of quintets due to ^{103}Rh-

 © 2004 Wiley-VCH Verlag GmbH & Co. KGaA, Weinheim

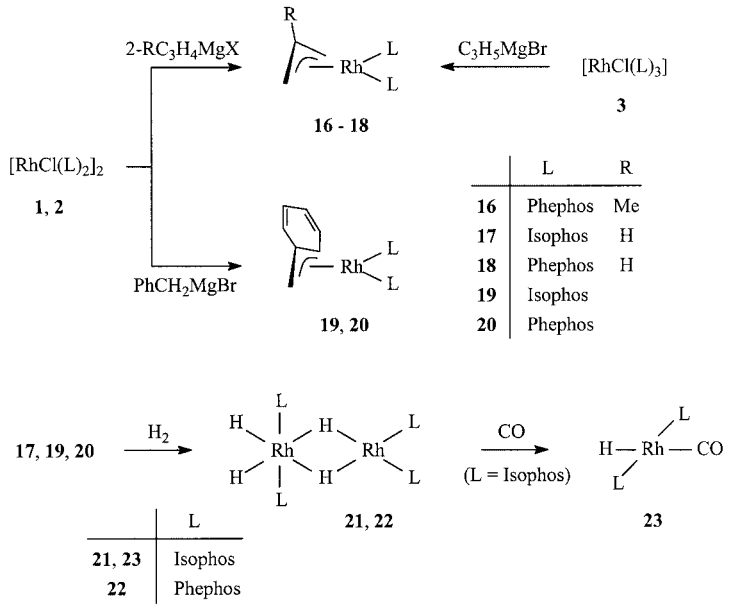

Scheme 5

^{1}H and ^{31}P-^{1}H couplings. Therefore, this signal is assigned to the bridging hydrides. The second resonance is a doublet of triplets and belongs to the terminal hydrides at the Rh^{III} center. The ^{1}H NMR spectrum of **22** also shows two hydride signals (with similar chemical shifts as for **21**), but these signals are rather broad, possibly due to a slow intramolecular rearrangement process as found for $[Rh_2H_4\{P(O\textit{i}Pr)_3\}_4]$.[19] In agreement with the proposed structure, the ^{31}P NMR spectra of **21** and **22** display two doublets at δ = 77.8 and 72.1 ppm (**21**) and δ = 73.8 and 65.4 ppm (**22**) with similar intensities, confirming that the four phospholane units are pairwise equivalent. Owing to the significant difference in the coupling constants, the signals at lower field are assigned to the *trans*-disposed P-donors at the Rh^{III} centers and the signals at higher field to the *cis*-disposed P-donors at the Rh^{I} centers of the molecules.

The Isophos complex **21** reacts quite rapidly with CO by cleavage of the hydride bridges and elimination of H_2 to afford the mononuclear carbonyl(hydrido)rhodium(I) compound **23** in nearly quantitative yield (see Scheme 5). Typical spectroscopic features of **23** (which is a yellow air-sensitive solid for which a correct elemental analysis has been obtained) are the sharp doublet at δ = 64.7 ppm in the ^{31}P NMR spectrum, confirming the equivalence of the phospholane ligands, the doublet of triplets at δ = −10.36 ppm for the hydride in the ^{1}H NMR spectrum, and the ν(CO) and ν(RhH) stretching modes at 1965 and 2065 cm^{-1} in the IR spectrum. Whereas the triisopropylphosphane derivative $[Rh_2H_4(P\textit{i}Pr_3)_4]$ reacts smoothly with CO to give $[Rh(CO)_3(P\textit{i}Pr_3)]_2$,[15b] a similar conversion of **23** to $[Rh(CO)_3(Isophos)]_2$ was not observed, even if the carbonyl(hydrido) compound is stored for 12 h under a CO atmosphere.

The reactivity of the Isophos complex **1** toward phenylacetylene is quite similar to that of the phosphane analogue $[RhCl(P\textit{i}Pr_3)_2]_2$.[20] Treatment of a solution of **1** in benzene with two equivalents of PhC≡CH at room temperature leads to a quick change of color from brick-red to yellow. If the reaction is carried out in C_6D_6 and monitored by ^{1}H NMR spectroscopy, after a few minutes a doublet is observed at δ = 4.11 ppm, which we assign to the alkyne proton of the η^2-alkyne intermediate **24** (Scheme 6). The ^{31}P NMR spectrum of **24** exhibits the AB part of an ABX spin system indicating that the rotation of the alkyne around the metal-alkyne axis is slow on the NMR timescale.

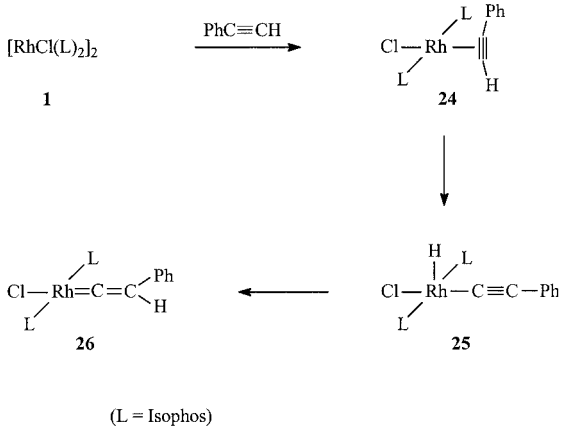

Scheme 6

Only 10 min after the signals of **24** have appeared, a subsequent rearrangement takes place which generates the alkynyl(hydrido)rhodium(III) species **25**. Noteworthy spectroscopic data of this intermediate are the hydride signal in the ^{1}H NMR spectrum at δ = −19.38 ppm, which is split by the ^{103}Rh and ^{31}P nuclei into a doublet of triplets, and the doublet at δ = 50.1 ppm in the ^{31}P NMR spectrum. The $^1J_{Rh,P}$ coupling constant of 99.2 Hz is consistent with a *trans* disposition of the two phospholanes, and thus a

 © 2004 Wiley-VCH Verlag GmbH & Co. KGaA, Weinheim

square-pyramidal structure for the five-coordinate compound can be proposed.

The final conversion of **25** to the stable isomer **26** proceeds upon warming the solution to 80 °C and affords, after chromatographic workup, the vinylidene complex in 84% isolated yield. In contrast to yellow **24** (which we failed to isolate), **26** is a violet, moderately air-stable solid, which is soluble in all common organic solvents apart from pentane and hexane. The ^{13}C NMR spectrum of **26** shows two resonances (both doublets of triplets) in the low-field region at δ = 296.3 and 112.3 ppm, which are characteristic for a Rh=C=CHR unit.[20,21] With regard to the course of the conversion of **25** to **26**, we note that owing to recent ab inito MO calculations both a mononuclear as well as a bimolecular mechanism seems possible.[22] In contrast to the related ruthenium system,[23] the alkynyl(hydrido)rhodium(III) species lies in a relative energy minimum, which is in agreement with the results presented in Scheme 6.

Compared with its Isophos counterpart **1**, the Phephos complex **2** behaves differently toward PhC≡CH. Instead of a vinylidene compound, the square-planar enynerhodium(I) complex **27** is generated which, however, is quite labile and could not be isolated in an analytically pure state. The ^1H NMR spectrum of **27** displays two signals for the olefinic protons at δ = 6.88 and 7.36 ppm, which, as indicated by the large $^3J_{H,H}$ coupling constant of 15.4 Hz, are *trans*-disposed at the C=C double bond. Other spectroscopic data are similar to those of *trans*-[RhCl{η^2-(*E*)-PhC≡CCH=CHPh}($P i Pr_3$)$_2$], which is obtained from the alkynyl(vinylidene) derivative *trans*-[Rh(C≡CPh)(=C=CHPh)($P i Pr_3$)$_2$] and protic acids.[3,24]

Upon passing a slow stream of CO through a solution containing **27**, a gradual change of color from yellow to pale yellow occurs and the formation of the carbonyl complex **6** and free (*E*)-PhC≡CCH=CHPh (**28**) can be detected (Scheme 7). It should be mentioned that the reaction of [RhCl(PMe_3)$_2$]$_2$ with excess phenylacetylene leads to PhC≡CC(Ph)=CH_2, which means that in this case the head-to-tail instead of the head-to-head dimerization is preferred.[25]

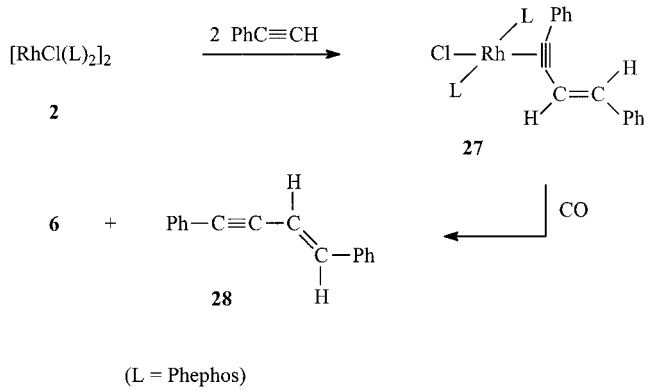

Scheme 7

Square-planar rhodium carbenes of the general composition *trans*-[RhCl(=CPh_2)(L)$_2$] could be obtained with both Isophos and Phephos as ligands L. The reaction of the starting material **29** with two equivalents of the corresponding phospholane proceeds under mild conditions and affords the required products **30** and **31** in 79−93% isolated yield (Scheme 8). The carbene complexes are green air-sensitive solids that decompose slowly in benzene and acetone but rapidly in $CHCl_3$ solution. Since the ^{31}P NMR spectra of **30** and **31** show a single resonance (doublet), there is no doubt that the two phospholane ligands are coordinated in the *trans* positions.

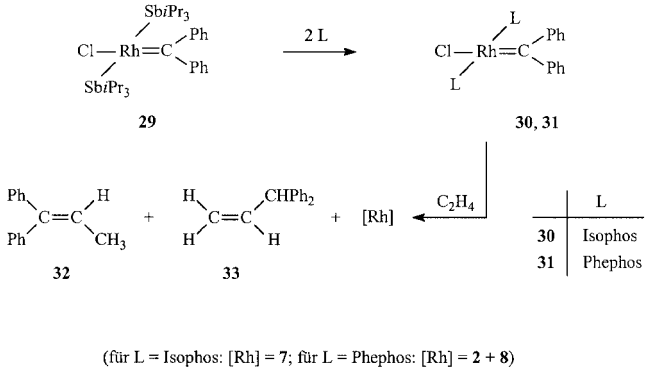

Scheme 8

Similarly to **29** and the phosphane analogues *trans*-[RhCl(=CPh_2)(PR_3)$_2$] (PR_3 = $P i Pr_3$, $P i Pr_2 Ph$, $P i PrPh_2$, PPh_3),[26] the related phospholane derivatives **30** and **31** are catalytically inactive in olefin metathesis. However, they do react with ethene relatively fast (10 min in C_6D_6 at room temperature) to give, apart from the ethene complexes **7** and **8** (and the dimer **2** in the case of Phephos as ligand), a mixture of two olefins **32** and **33** (see Scheme 8). With **30** as the precursor, the ratio of **32**:**33** is 94:6, while with **31** as precursor the ratio is 86:14. In our previous work we have already postulated that the major isomer **32** is probably generated via a rhodiacyclobutane, which, following a β-H shift, affords a RhH(η^3-CH_2CHCPh_2) intermediate. This reacts, in the presence of ethene, by reductive elimination to give the trisubstituted olefin.[3] The route to the minor isomer is not clear as yet, but possibly also proceeds via a rhodiacyclobutane as an intermediate.[27] For comparison it should be mentioned that by using *trans*-[RhCl(=CPh_2)($P i Pr_3$)$_2$] as the precursor, the ratio of **32**:**33** is 90:10 and with *trans*-[RhCl(=CPh_2)($P i Pr_2 Ph$)$_2$] it is 81:19.[27]

Some preliminary results regarding the preparation of iridium complexes with Isophos as ligand are summarized in Scheme 9. In contrast to [RhCl(C_8H_{14})$_2$]$_2$, the iridium counterpart reacts with four equivalents of Isophos to give a product which, even after storing for 12 h in vacuo, contains some cyclooctene. A similar situation results if [IrCl(C_8H_{14})$_2$]$_2$ is treated with $P i Pr_3$ in a 1:4 molar ratio.[28] Attempts to crystallize the crude product, obtained from [IrCl(C_8H_{14})$_2$]$_2$ and Isophos, from acetone led partly to the carbonyl derivative **34**. This complex is more conveniently prepared if a slow stream of CO is passed through the solution generated from [IrCl(C_8H_{14})$_2$]$_2$ and Isophos. The IR spectrum of the yellow solid displays a ν(CO) stretch at

 © 2004 Wiley-VCH Verlag GmbH & Co. KGaA, Weinheim

1937 cm^{-1} which is nearly identical to the value (1935 cm^{-1}) reported for *trans*-[IrCl(CO)(P*i*Pr$_3$)$_2$].[29]

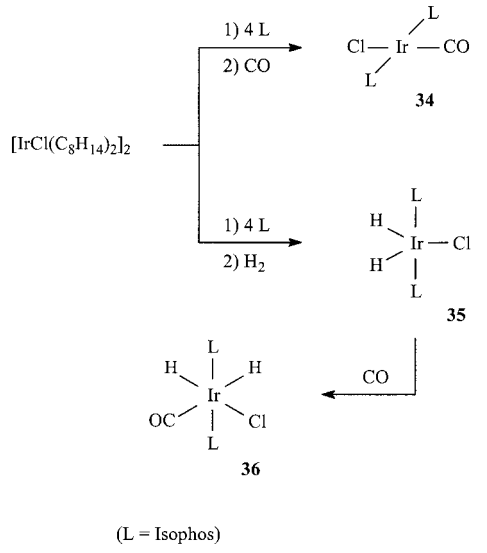

Scheme 9

If instead of CO a stream of H_2 is passed through the solution obtained from [IrCl(C_8H_{14})$_2$]$_2$ and Isophos, the dihydridoiridium(III) compound **35** is generated. Similarly to the rhodium analogue **13**, it is a yellow air-sensitive solid which is readily soluble in all common organic solvents. Since there is only one resonance (triplet) for the hydrides at $\delta = -26.98$ ppm in the ^{1}H NMR spectrum and only one singlet (triplet in off-resonance) for the ^{31}P nuclei at $\delta = 51.2$ ppm in the ^{31}P NMR spectrum, we assume that the coordination geometry around the iridium center corresponds to a trigonal bipyramid with the P-donors in the apical positions. This geometry has been confirmed crystallographically for [IrH$_2$Cl(*t*Bu$_2$PCH$_2$CMe$_3$)$_2$].[30] As expected, the five-coordinate dihydrido complex **35** adds one molecule of CO to give the octahedral compound **36**, which, in contrast to the precursor, is only slightly air sensitive. The ^{1}H NMR spectrum of **36** displays two signals in the high-field region at $\delta = -8.57$ ppm and $\delta = -19.97$ ppm, which is consistent with the assumption that one of the hydrido ligands is *trans* to CO and the other *trans* to chloride. The triisopropylphosphane counterpart [IrH$_2$Cl(CO)(P*i*Pr$_3$)$_2$] is also known and shows the hydride resonances in the ^{1}H NMR spectrum at $\delta = -8.64$ ppm and $\delta = -20.20$ ppm, respectively.[31]

In conclusion, the work described in this paper illustrates that a series of rhodium and iridium complexes with the phospholanes Isophos and Phephos is accessible following similar preparative routes to those used for the synthesis of the P*i*Pr$_3$ and P*i*Pr$_2$Ph analogues. Owing to the similar size of the phosphanes and the phospholanes (see Scheme 1) and owing to the related donor/acceptor capabilities, it is also not surprising that both the chemical properties and the spectroscopic data of the M(P*i*Pr$_3$)$_2$ and the M(Isophos)$_2$ as well as those of the Rh(P*i*Pr$_2$Ph)$_2$ and the Rh(Phephos)$_2$ complexes are similar. Some preliminary results from catalytic studies reveal that in the hydrogenation of styrene (toluene, 60 °C, ratio catalyst to substrate = 1:100) the Isophos derivative **1** is significantly less active (TOF = 46.6 h^{-1}) than the Wilkinson complex [RhCl(PPh$_3$)$_3$] (TOF = 1250 h^{-1}). Moreover, the optical yield in the hydrogenation of PhCH=C(CO$_2$R)NHC(O)Me (R = H, Me) with **1** as the catalyst under similar conditions is rather low (14% *ee*) and could only be improved slightly in the presence of excess Isophos. Therefore, the aim for the future is to modify the coordination sphere around rhodium (and possibly iridium) in such a way that the phospholanes also become attractive ligands for catalysis, not necessarily only for hydrogenation reactions.

Experimental Section

All operations were carried out under argon using standard Schlenk techniques. The starting materials [RhCl(C_8H_{14})$_2$]$_2$,[32] [RhCl(P*i*Pr$_2$Ph)$_2$]$_2$ (**10**),[2] *trans*-[RhCl(=CPh$_2$)(Sb*i*Pr$_3$)$_2$] (**29**),[26] and [IrCl(C_8H_{14})$_2$]$_2$ [33] were prepared as described in the literature. NMR spectra were recorded at room temperature (if not otherwise stated) on Bruker AC 200 and AMX 400 instruments and IR spectra on a Perkin−Elmer 1420 infrared spectrophotometer. Abbreviations used: s = singlet; d = doublet; t = triplet; q = quadruplet; quin = quintet; m = multiplet; vt = virtual triplet; br = broadened signal, $N = {}^3J_{P,H} + {}^5J_{P,H}$ or ${}^1J_{P,C} + {}^3J_{P,C}$. Melting points were measured by differential thermal analysis (DTA).

Preparation of [RhCl(Isophos)$_2$]$_2$ (1): A suspension of [RhCl(C_8H_{14})$_2$]$_2$ (176 mg, 0.25 mmol) in acetone (2 mL) was treated with Isophos (166 mg, 1.05 mmol) and stirred for 10 min at room temperature. A brick-red solid precipitated which was filtered, washed three times with 1 mL portions of pentane (0 °C) and dried; yield 209 mg (92%); m.p. 54 °C (dec.). ^{1}H NMR (200 MHz, C_6D_6): δ = 2.20 [m, 8 H, CH(ring)], 2.01 [m, 4 H, CH(*i*Pr)], 1.85 [m, 12 H, CH$_3$(*i*Pr)], 1.81 [dvt, $N = 23.3$, $J_{H,H} = 6.9$ Hz, 8 H, CH$_2$(ring)], 1.70 [dvt, $J_{P,H} = 20.8$, $J_{H,H} = 7.3$ Hz, 12 H, CH$_3$(*i*Pr)], 1.40 [m, 8 H, CH$_2$(ring)], 1.38 [dvt, $N = 19.9$, $J_{H,H} = 7.1$ Hz, 12 H, CH$_3$(ring)], 1.17 [dvt, $N = 19.0$, $J_{H,H} = 7.3$ Hz, 12 H, CH$_3$(ring)] ppm. ^{13}C NMR (50.3 MHz, C_6D_6): δ = 37.1 [dt, $J_{Rh,C} = 11.1$, $J_{P,C} = 3.7$ Hz, CH$_2$(ring)], 36.2, 35.0 [both s, CH(ring)], 34.8 [t, $J_{Rh,C} = 12.0$ Hz, CH$_2$(ring)], 28.7 [vt, $N = 18.6$ Hz, CH(*i*Pr)], 22.9 [d, $J_{Rh,C} = 29.6$ Hz, CH$_3$(ring)], 22.4, 17.3 [both s, CH$_3$(*i*Pr)], 14.9 [s, CH$_3$(ring)] ppm. ^{31}P NMR (81.0 MHz, C_6D_6): δ = 75.8 (d, $J_{Rh,P} = 196.2$ Hz) ppm. $C_{36}H_{76}Cl_2P_4Rh_2$ (909.6): calcd. C 47.54, H 8.42; found C 47.43, H 8.18.

Preparation of [RhCl(Phephos)$_2$]$_2$ (2): A suspension of [RhCl(C_8H_{14})$_2$]$_2$ (116 mg, 0.16 mmol) in benzene (2 mL) was treated with Phephos (127 mg, 0.66 mmol) and stirred for 10 min at room temperature. A clear orange-red solution was generated which, after stirring for 2 h, was dried in vacuo. The remaining orange-red solid was washed three times with 1 mL portions of pentane (−78 °C) and dried; yield 125 mg (75%); m.p. 60 °C (dec.). ^{1}H NMR (200 MHz, C_6D_6): δ = 7.74−6.84 (m, 20 H, C_6H_5), 1.62−0.75 [m, 24 H, CH(ring) and CH$_2$(ring)], 1.19, 0.67 [both m, 12 H each, CH$_3$(ring)] ppm. ^{31}P NMR (81.0 MHz, C_6D_6): δ = 71.1 (d, $J_{Rh,P} = 198.0$ Hz) ppm. $C_{48}H_{68}Cl_2P_4Rh_2$ (1045.7): calcd. C 55.13, H 6.55; found C 54.59, H 7.22.

Preparation of [RhCl(Phephos)$_3$] (3): This compound was prepared as described for **2**, with [RhCl(C_8H_{14})$_2$]$_2$ (120 mg, 0.17 mmol) and

 © 2004 Wiley-VCH Verlag GmbH & Co. KGaA, Weinheim

Prephos (257 mg, 1.34 mmol) in acetone (2 mL) as starting materials. Orange solid; yield 204 mg (84%); m.p. 59 °C (dec.). ^{1}H NMR (200 MHz, C_6D_6, 295 K): δ = 7.86−6.90 (m, 15 H, C_6H_5), 3.20−0.02 (m, 36 H, ring protons) ppm. ^{13}C NMR (50.3 MHz, C_6D_6, 295 K): δ = 137.9 (br. d, $J_{P,C}$ = 26.8 Hz, *ipso*-C of PC_6H_5), 136.8 (vt, *N* = 26.9 Hz, *ipso*-C of PC_6H_5), 134.0 (vt, *N* = 9.2 Hz, *ortho*-C of PC_6H_5), 133.5 (d, $J_{P,C}$ = 8.3 Hz, *ortho*-C of PC_6H_5), 130.4, 128.7 (both s, *para*-C of PC_6H_5), 126.9 (vt, *N* = 9.2 Hz, *meta*-C of PC_6H_5), 126.8 (d, $J_{P,C}$ = 8.3 Hz, *meta*-C of PC_6H_5), 38.0 (br. dvt, *N* = 23.1 Hz, CH), 34.6, 34.4, 34.3, 34.2 (all br. s, CH_2), 33.7 (br. s, CH), 31.9 (d, $J_{P,C}$ = 25.9 Hz, CH), 23.7 [d, $J_{P,C}$ = 12.0 Hz, CH_3(ring)], 23.3 [vt, *N* = 12.0 Hz, CH_3(ring)], 16.6, 15.9 [both s, CH_3(ring)] ppm. ^{31}P NMR (81.0 MHz, C_6D_6, 295 K): δ = 69.1 (dt, $J_{Rh,P}$ = 145.2, $J_{P,P}$ = 39.6 Hz, Phephos *trans* to Cl), 49.4 (br. s, Phephos *cis* to Cl) ppm. ^{31}P NMR (81.0 MHz, C_6D_6, 330 K): δ = 69.4 (dt, $J_{Rh,P}$ = 185.1, $J_{P,P}$ = 39.2 Hz, Phephos *trans* to Cl), 49.9 (dd, $J_{Rh,P}$ = 137.9, $J_{P,P}$ = 39.2 Hz, Phephos *cis* to Cl) ppm. $C_{36}H_{51}ClP_3Rh$ (715.1): calcd. C 60.47, H 7.19; found C 60.34, H 7.08.

Generation of [RhCl(Isophos)$_3$] (4): A solution of $[RhCl(C_8H_{14})_2]_2$ (70 mg, 0.10 mmol) in [D_8]toluene (0.5 mL) was treated with Isophos (127 mg, 0.80 mmol) and stirred for 10 min at room temperature. The ^{31}P NMR spectrum revealed that a mixture of **1** and **4** in the ratio of 1:9 was formed. Attempts to separate **4** from the by-product failed. Data for **4**: ^{31}P NMR (81.0 MHz, [D_8]toluene): δ = 84.2 (dt, $J_{Rh,P}$ = 190.7, $J_{P,P}$ = 41.2 Hz, Isophos *trans* to Cl), 59.0 (br. s, Isophos *cis* to Cl].

Preparation of *trans*-[RhCl(CO)(Isophos)$_2$] (5): A slow stream of CO was passed through a solution of either **1** (120 mg, 0.13 mmol) or **7** (24 mg, 0.05 mmol) in benzene (5 mL) for 30 s at room temperature. A change of color from brick-red to pale yellow occurred. The solvent was evaporated in vacuo and, after recrystallization of the residue from pentane at −78 °C, a pale yellow solid was isolated; yield 111 mg (88%) from **1** or 22 mg (92%) from **7**; m.p. 174 °C (dec.). IR (benzene): ν(CO) = 1947 cm^{-1}. ^{1}H NMR (200 MHz, C_6D_6): δ = 2.10−1.60 [m, 10 H, CH(ring), CH(*i*Pr), CH_2(ring)], 1.55 [dvt, *N* = 24.3, $J_{H,H}$ = 7.1 Hz, 6 H, CH_3(*i*Pr)], 1.40 [m, 4 H, CH_2(ring)], 1.31 [dvt, *N* = 23.0, $J_{H,H}$ = 7.1 Hz, 6 H, CH_3(*i*Pr)], 1.19 [dvt, *N* = 21.2, $J_{H,H}$ = 7.0 Hz, 6 H, CH_3(ring)], 1.18 [dvt, *N* = 21.6, $J_{H,H}$ = 7.1 Hz, 6 H, CH_3(ring)] ppm. ^{13}C NMR (50.3 MHz, C_6D_6): δ = 189.3 (dt, $J_{Rh,C}$ = 73.7, $J_{P,C}$ = 15.3 Hz, RhCO), 36.5 [vt, *N* = 28.1 Hz, CH(ring)], 36.0, 35.8 [both s, CH_2(ring)], 34.8 [vt, *N* = 24.1 Hz, CH(ring)], 25.0 [vt, *N* = 20.0 Hz, CH(ring)], 21.3 [s, CH_3(ring)], 20.5 [vt, *N* = 9.0 Hz, CH_3(ring)], 18.9, 15.4 [both s, CH_3(ring)] ppm. ^{31}P NMR (81.0 MHz, C_6D_6): δ = 53.1 (d, $J_{Rh,P}$ = 118.2 Hz) ppm. $C_{19}H_{38}ClOP_2Rh$ (482.82): calcd. C 47.27, H 7.93; found C 47.30, H 8.02.

Preparation of *trans*-[RhCl(CO)(Phephos)$_2$] (6): A slow stream of CO was passed through a solution of either **2** (120 mg, 0.12 mmol) or **3** (50 mg, 0.07 mmol) in benzene (5 mL) for 30 s at room temperature. The solution was then worked-up as described for **5**. Pale yellow solid; yield 111 mg (88%) from **2** or 36 mg (94%) from **3**; m.p. 131 °C (dec.). IR (benzene): ν(CO) = 1961 cm^{-1}. ^{1}H NMR (200 MHz, C_6D_6): δ = 7.96 (m, 4 H, *ortho*-H of C_6H_5), 7.10 (m, 6 H, *meta*-, *para*-H of C_6H_5), 3.39−0.75 [m, 12 H, CH(ring), CH_2(ring)], 1.72, 0.86 [both m, 6 H each, CH_3(ring)] ppm. ^{13}C NMR (50.3 MHz, C_6D_6): δ = 186.5 (dt, $J_{Rh,C}$ = 74.0, $J_{P,C}$ = 16.2 Hz, RhCO), 134.1 (vt, *N* = 12.0 Hz, *ortho*-C of C_6H_5), 132.5 (vt, *N* = 32.4 Hz, *ipso*-C of C_6H_5), 129.7 (s, *para*-C of C_6H_5), 127.6 (vt, *N* = 9.2 Hz, *meta*-C of C_6H_5), 35.1 [d, $J_{P,C}$ = 25.0 Hz, CH(ring)], 34.3 [d, $J_{P,C}$ = 13.9 Hz, CH(ring)], 33.6 [vt, *N* = 13.0 Hz, CH_2(ring)], 21.3 [vt, *N* = 12.0 Hz, CH_3(ring)], 14.9 [s, CH_3(ring)] ppm. ^{31}P NMR (81.0 MHz, C_6D_6): δ = 48.6 (d, $J_{Rh,P}$ = 123.9 Hz) ppm. $C_{25}H_{34}ClOP_2Rh$ (550.85): calcd. C 54.51, H 6.22; found C 54.37, H 6.27.

Preparation of *trans*-[RhCl(C_2H_4)(Isophos)$_2$] (7): A slow stream of ethene was passed through a solution of **1** (120 mg, 0.13 mmol) in benzene (5 mL) for 2 min at room temperature. A change of color from brick-red to pale yellow occurred. The solution was worked up as described for **5**. Pale yellow solid; yield 110 mg (88%); m.p. 72 °C. IR (hexane): ν(C=C) = 1510 cm^{-1}. ^{1}H NMR (200 MHz, C_6D_6): δ = 2.52, 2.28 (both m, 2 H each, C_2H_4), 2.12−1.80 [m, 10 H, CH(ring), CH(*i*Pr), CH_2(ring)], 1.78 [dd, $J_{P,H}$ = 16.0, $J_{H,H}$ = 8.7 Hz, 6 H, CH_3(*i*Pr)], 1.63 [dd, $J_{P,H}$ = 14.6, $J_{H,H}$ = 7.3 Hz, 6 H, CH_3(*i*Pr)], 1.33 [m, 4 H, CH_2(ring)], 1.26 [dd, $J_{P,H}$ = 14.7, $J_{H,H}$ = 7.3 Hz, 6 H, CH_3(ring)], 1.02 [dd, $J_{P,H}$ = 13.9, $J_{H,H}$ = 6.9 Hz, 6 H, CH_3(ring)] ppm. ^{31}P NMR (81.0 MHz, C_6D_6): δ = 46.7 (d, $J_{Rh,P}$ = 121.4 Hz) ppm. $C_{20}H_{42}ClP_2Rh$ (482.87): calcd. C 49.75, H 8.77; found C 49.30, H 8.72.

Generation of *trans*-[RhCl(C_2H_4)(Phephos)$_2$] (8): A slow stream of ethene was passed through a solution of **2** (50 mg, 0.05 mmol) in C_6D_6 (0.5 mL) for 5 min at room temperature. The ^{31}P NMR spectrum revealed that **2** and **8** were present in equal amounts. If the ethene atmosphere was replaced by argon, the starting material was regenerated. Attempts to separate the two compounds failed. Data for **8**: ^{31}P NMR (81.0 MHz, C_6D_6): δ = 48.8 (d, $J_{Rh,P}$ = 125.5 Hz) ppm.

Preparation of *trans*-[RhCl(PhC≡CPh)(Phephos)$_2$] (9): A solution of $[RhCl(C_8H_{14})_2]_2$ (85 mg, 0.12 mmol) in benzene (10 mL) was treated dropwise with a solution of Phephos (102 mg, 0.53 mmol) in benzene (2 mL) at room temperature. After stirring the solution for 30 min, a solution of diphenylacetylene (21 mg, 0.12 mmol) in benzene (2 mL) was added. The reaction mixture was stirred for 4 h and then the solvent was evaporated in vacuo. The residue was dissolved in acetone (1 mL), the solution was layered with pentane (5 mL) and stored for 12 h at −78 °C. Orange-yellow crystals precipitated which were filtered, washed twice with 2 mL portions of pentane (0 °C) and dried; yield 109 mg (72%); m.p. 81 °C (dec.). ^{1}H NMR (200 MHz, C_6D_6): δ = 8.25, 7.86 (both m, 4 H each, C_6H_5), 7.65 (m, 2 H, C_6H_5), 7.24 (m, 10 H, C_6H_5), 2.78−1.05 [m, 6 H, CH(ring), CH_2(ring)], 2.22 [br. vt, *N* = 24.0 Hz, 6 H, CH_3(ring)], 0.68 [br. vt, *N* = 19.3 Hz, 6 H, CH_3(ring)] ppm. ^{13}C NMR (50.3 MHz, C_6D_6): δ = 135.0 (vt, *N* = 10.8 Hz, *ortho*-C of PC_6H_5), 132.7 (vt, *N* = 28.0 Hz, *ipso*-C of PC_6H_5), 132.0, 129.2, 128.7, 128.3 (all s, C_6H_5), 127.4 (vt, *N* = 8.2 Hz, *meta*-C of PC_6H_5), 88.2 (dt, $J_{Rh,C}$ = 15.7, $J_{P,C}$ = 2.8 Hz, Ph*C*≡*C*Ph), 37.1 [vt, *N* = 24.4 Hz, CH(ring)], 35.8, 35.5 [both s, CH_2(ring)], 31.9 [vt, *N* = 23.0 Hz, CH(ring)], 21.0 [vt, *N* = 11.6 Hz, CH_3(ring)], 15.7 [s, CH_3(ring)] ppm. ^{31}P NMR (81.0 MHz, C_6D_6): δ = 41.9 (d, $J_{Rh,P}$ = 121.3 Hz) ppm. $C_{38}H_{44}ClP_2Rh$ (701.1): calcd. C 65.10, H 6.33; found C 64.85, H 6.09.

Generation of [RhH_2(Isophos)$_2$(μ-Cl)$_2$Rh(Isophos)$_2$] (11): A solution of **1** (45 mg, 0.05 mmol) and **13** (45 mg, 0.10 mmol) in C_6D_6 (0.5 mL) was stirred for 3 h at room temperature. The ^{1}H and ^{31}P NMR spectra revealed that compound **11** was generated. Attempts to isolate **11** failed. Characteristic data for **11**: ^{1}H NMR (200 MHz, C_6D_6): δ = −21.50 (dt, $J_{Rh,H}$ = 24.7, $J_{P,H}$ = 14.5 Hz) ppm. ^{31}P NMR (81.0 MHz, C_6D_6): δ = 74.5 [d, $J_{Rh,P}$ = 193.3 Hz, *cis*-Rh(Isophos)$_2$], 64.0 [d, $J_{Rh,P}$ = 114.4 Hz, *trans*-Rh(Isophos)$_2$] ppm.

Generation of [RhH_2(P*i*Pr_2Ph)$_2$(μ-Cl)$_2$Rh(P*i*Pr_2Ph)$_2$] (12): A solution of **10** (21 mg, 0.02 mmol) and **14** (21 mg, 0.04 mmol) in C_6D_6 (0.5 mL) was stirred for 3 h at room temperature. The ^{1}H and ^{31}P NMR spectra revealed that compound **12** had formed. Attempts

 © 2004 Wiley-VCH Verlag GmbH & Co. KGaA, Weinheim

to isolate **12** failed. Characteristic data for **12**: ^{1}H NMR (200 MHz, C_6D_6): δ = −21.46 (dt, $J_{Rh,H}$ = 22.8, $J_{P,H}$ = 16.0 Hz) ppm. ^{31}P NMR (81.0 MHz, C_6D_6): δ = 55.7 [d, $J_{Rh,P}$ = 196.2 Hz, *cis*-Rh(P*i*Pr$_2$Ph)$_2$], 48.5 [d, $J_{Rh,P}$ = 117.1 Hz, *trans*-Rh(P*i*Pr$_2$Ph)$_2$] ppm.

Preparation of [RhClH$_2$(Isophos)$_2$] (13): A solution of **1** (120 mg, 0.13 mmol) in toluene (5 mL) was stirred for 5 min at −78 °C under a H_2 atmosphere. Upon warming the solution slowly to room temperature, a change of color from brick-red to yellow occurred. After stirring for 15 min, the solvent was evaporated in vacuo and the residue was extracted with pentane (10 mL). The extract was dried in vacuo to give a yellow solid; yield 90 mg (76%); m.p. 64 °C (dec.). IR (KBr): ν(RhH) = 2155 cm^{-1}. ^{1}H NMR (200 MHz, C_6D_6): δ = 2.04−1.84 [m, 10 H, CH(ring), CH(*i*Pr), CH$_2$(ring)], 1.83 [dd, $J_{P,H}$ = 16.3, $J_{H,H}$ = 6.9 Hz, 6 H, CH$_3$(*i*Pr)], 1.46 [dd, $J_{P,H}$ = 13.6, $J_{H,H}$ = 7.0 Hz, 6 H, CH$_3$(*i*Pr)], 1.32 [m, 4 H, CH$_2$(ring)], 1.30 [dd, $J_{P,H}$ = 13.9, $J_{H,H}$ = 6.9 Hz, 6 H, CH$_3$(ring)], 1.10 [dd, $J_{P,H}$ = 13.6, $J_{H,H}$ = 6.8 Hz, 6 H, CH$_3$(ring)], −22.00 (dt, $J_{Rh,H}$ = 26.0, $J_{P,H}$ = 14.6 Hz, 2 H, RhH) ppm. ^{31}P NMR (81.0 MHz, C_6D_6): δ = 64.0 (d, $J_{Rh,P}$ = 113.1 Hz) ppm. $C_{18}H_{40}ClP_2Rh$ (456.8): calcd. C 47.33, H 8.83; found C 47.30, H 8.82.

Preparation of [RhClH$_2$(P*i*Pr$_2$Ph)$_2$] (14): A suspension of **10** (100 mg, 0.095 mmol) in pentane (2 mL) was stirred for 5 min at −50 °C under a H_2 atmosphere. The suspension was slowly warmed to room temperature, which led to a smooth change of color from dark violet to yellow. After stirring for 1 h at 20 °C, the yellow solution was concentrated in vacuo to ca. 1 mL and stored for 3 h at 0 °C. A yellow solid precipitated, which was separated from the mother liquor and dried; yield 88 mg (87%); m.p. 67 °C (dec.). IR (KBr): ν(RhH) = 2164 cm^{-1}. ^{1}H NMR (200 MHz, CD_2Cl_2): δ = 7.85 (m, 4 H, *ortho*-H of C_6H_5), 7.12 (m, 6 H, *meta*- and *para*-H of C_6H_5), 2.63 (m, 4 H, PC*H*CH$_3$), 1.29 (dvt, *N* = 15.0, $J_{H,H}$ = 7.1 Hz, 12 H, PCHC*H*$_3$), 1.01 (dvt, *N* = 14.3, $J_{H,H}$ = 7.0 Hz, 12 H, PCHC*H*$_3$), −21.24 (dt, $J_{Rh,H}$ = 24.8, $J_{P,H}$ = 14.4 Hz, 2 H, RhH$_2$) ppm. ^{13}C NMR (50.3 MHz, C_6D_6): δ = 134.8 (vt, *N* = 11.6 Hz, *ortho*-C of C_6H_5), 129.9 (s, *para*-C of C_6H_5), 127.9 (vt, *N* = 9.1 Hz, *meta*-C of C_6H_5), 127.7 (d, $J_{P,C}$ = 18.5 Hz, *ipso*-C of C_6H_5), 24.3 (vt, *N* = 24.6 Hz, P*C*HCH$_3$), 19.4, 18.9 (both s, PCH*C*H$_3$) ppm. ^{31}P NMR (81.0 MHz, CD_2Cl_2): δ = 53.7 (d, $J_{Rh,P}$ = 119.1 Hz) ppm. $C_{24}H_{40}ClP_2Rh$ (528.9): calcd. C 54.50, H 7.62; found C 54.24, H 7.49.

Generation of [RhH$_2$(Phephos)$_2$(μ−Cl)$_2$Rh(Phephos)$_2$] (15): A slow stream of H_2 was passed for 20 s through a solution of **2** (50 mg, 0.05 mmol) in C_6D_6 (0.5 mL) at room temperature. The ^{1}H and ^{31}P NMR spectra revealed that an equilibrium between **2** and **15** was established which, even after repeated addition of H_2, could not be completed shifted to the side of the dinuclear complex. If the hydrogen atmosphere was replaced by argon, compound **15** was reconverted into **2**. Characteristic data for **15**: ^{1}H NMR (200 MHz, C_6D_6): δ = −20.77 (dt, $J_{Rh,H}$ = 24.7, $J_{P,H}$ = 14.5 Hz) ppm. ^{31}P NMR (81.0 MHz, C_6D_6): δ = 69.9 [d, $J_{Rh,P}$ = 195.8 Hz, *cis*-Rh(Phephos)$_2$], 52.2 [d, $J_{Rh,P}$ = 118.4 Hz, *trans*-Rh(Phephos)$_2$] ppm.

Preparation of [Rh(η^3-2-MeC$_3$H$_4$)(Phephos)$_2$] (16): A suspension of [RhCl(C$_8$H$_{14}$)$_2$]$_2$ (82 mg, 0.11 mmol) in diethyl ether (2 mL) was treated at 0 °C with Phephos (88 mg, 0.46 mmol) and stirred for 30 min at 0 °C. A clear orange-red solution was formed to which a 0.8 M solution of 2-MeC$_3$H$_4$MgCl in THF (0.58 mL, 0.46 mmol) was added dropwise. A change of color from orange-red to yellow occurred. After stirring the reaction mixture for 30 min at room temperature, the solvent was removed in vacuo and the residue was extracted with pentane (20 mL). The extract was dried in vacuo, the remaining orange-yellow air-sensitive solid was washed three times with 1 mL portions of acetone (0 °C) and dried; yield 98 mg (82%); m.p. 55 °C (dec.). ^{1}H NMR (200 MHz, 278 K, C_6D_6): δ = 7.52 (m, 6 H, *meta*-, *para*-H of C_6H_5), 7.20 (m, 4 H, *ortho*-H of C_6H_5), 2.92−0.72 [m, 12 H, CH(ring), CH$_2$(ring)], 2.84 (d, $J_{P,H}$ = 3.3 Hz, 1 H, allyl-H$_{syn}$), 2.64 (d, $J_{P,H}$ = 2.9 Hz, 1 H, allyl-H$_{syn}$), 2.18 (d, $J_{P,H}$ = 6.2 Hz, 1 H, allyl-H$_{anti}$), 1.78 (d, $J_{P,H}$ = 5.8 Hz, 1 H, allyl-H$_{anti}$), 1.66 (d, $J_{Rh,H}$ = 2.2 Hz, 3 H, allyl-CH$_3$), 1.31 [dd, $J_{P,H}$ = 15.4, $J_{H,H}$ = 7.3 Hz, 3 H, CH$_3$(ring)], 1.22 [dd, $J_{P,H}$ = 15.4, $J_{H,H}$ = 6.9 Hz, 3 H, CH$_3$(ring)], 0.49 [dd, $J_{P,H}$ = 13.2, $J_{H,H}$ = 6.9 Hz, 3 H, CH$_3$(ring)], 0.35 [dd, $J_{P,H}$ = 13.5, $J_{H,H}$ = 6.9 Hz, 3 H, CH$_3$(ring)] ppm. ^{13}C NMR (50.3 MHz, C_6D_6): δ = 139.9 (d, $J_{P,C}$ = 21.3 Hz, *ipso*-C of C_6H_5), 139.4 (d, $J_{P,C}$ = 22.2 Hz, *ipso*-C of C_6H_5), 134.1 (d, $J_{P,C}$ = 2.8 Hz, *ortho*-C of C_6H_5), 133.8 (d, $J_{P,C}$ = 1.9 Hz, *ortho*-C of C_6H_5), 128.8, 128.7 (both s, *para*-C of C_6H_5), 127.5, 127.4 (both d, $J_{P,C}$ = 3.7 Hz, *meta*-C of C_6H_5), 117.0 [d, $J_{Rh,C}$ = 6.5 Hz, CH$_2$*C*(CH$_3$)CH$_2$], 51.6, 51.2 [both ddd, $J_{P,C}$ = 12.0 and 7.4, $J_{Rh,C}$ = 1.9 Hz, *C*H$_2$C(CH$_3$)CH$_2$], 40.9 [ddd, $J_{P,C}$ = 41.6 and 19.5, $J_{Rh,C}$ = 3.7 Hz, CH(ring)], 35.4 [s, CH$_2$(ring)], 33.2 [t, $J_{P,C}$ = 19.0 Hz, CH(ring)], 26.4 [s, CH$_3$(ring)], 23.5 [d, $J_{P,C}$ = 16.1 Hz, CH$_2$C(*C*H$_3$)CH$_2$], 14.7 [s, CH$_3$(ring)] ppm. ^{31}P NMR (81.0 MHz, C_6D_6): δ$_A$ = 62.1, δ$_B$= 62.9 (AB part of ABX spectrum; A, B = P, X = Rh; $J_{A,B}$ = 27.8, $J_{A,X}$ = 195.0, $J_{B,X}$ = 195.7 Hz) ppm. $C_{28}H_{41}P_2Rh$ (542.5): calcd. C 61.99, H 7.62; found C 62.06; H 7.58.

Preparation of [Rh(η^3-C$_3$H$_5$)(Isophos)$_2$] (17): This compound was prepared as described for **16**, with [RhCl(C$_8$H$_{14}$)$_2$]$_2$ (169 mg, 0.24 mmol), Isophos (168 mg, 1.06 mmol) and a 0.56 M solution of C$_3$H$_5$MgBr in diethyl ether (0.42 mL, 0.48 mmol) as starting materials. Orange-yellow air-sensitive solid; yield 159 mg (72%); m.p. 71 °C (dec.). ^{1}H NMR (200 MHz, C_6D_6): δ = 4.76 (m, 1 H, CH$_2$C*H*CH$_2$), 3.55, 3.42 (both m, 1 H each, allyl-H$_{syn}$), 2.31−1.62 [m, 12 H, CH(ring), CH(*i*Pr), CH$_2$(ring), allyl-H$_{anti}$], 1.35 [m, 4 H, CH$_2$(ring)], 1.24 [dd, $J_{H,H}$ = 7.6, $J_{P,H}$ = 3.3 Hz, 6 H, CH$_3$(*i*Pr)], 1.20 [dd, $J_{P,H}$ = 11.0, $J_{H,H}$ = 7.1 Hz, 6 H, CH$_3$(*i*Pr)], 1.15 [dd, $J_{P,H}$ = 11.0, $J_{H,H}$ = 7.1 Hz, 6 H, CH$_3$(ring)], 1.07 [dd, $J_{H,H}$ = 7.1, $J_{P,H}$ = 5.1 Hz, 6 H, CH$_3$(ring)] ppm. ^{31}P NMR (81.0 MHz, C_6D_6): δ$_A$ = 65.7, δ$_B$= 67.7 (AB part of ABX spectrum; A, B = P, X = Rh; $J_{A,B}$ = 24.7, $J_{A,X}$ = 206.4, $J_{B,X}$ = 206.0 Hz) ppm. $C_{21}H_{43}P_2Rh$ (460.4): calcd. C 54.78, H 9.41; found C 55.23, H 9.78.

Preparation of [Rh(η^3-C$_3$H$_5$)(Phephos)$_2$] (18): a) This procedure was analogous to that described for **16**, with [RhCl(C$_8$H$_{14}$)$_2$]$_2$ (67 mg, 0.09 mmol), Phephos (72 mg, 0.37 mmol) and a 0.74 M solution of C$_3$H$_5$MgBr in diethyl ether (0.5 mL, 0.37 mmol) as starting materials. Orange-yellow air-sensitive solid; yield 70 mg (74%). b) A suspension of **3** (100 mg, 0.14 mmol) in benzene (5 mL) was treated with a 0.70 M solution of C$_3$H$_5$MgBr in diethyl ether (0.8 mL, 0.56 mmol) at room temperature. A quick change of color from orange to yellow occurred. After stirring the reaction mixture for 30 min, the solvent was evaporated in vacuo, the residue was extracted with pentane (5 mL) and the extract was dried in vacuo. The residue was recrystallized from acetone (1 mL) at −78 °C to give an orange-yellow air-sensitive solid; yield 55 mg (75%), m.p. 49 °C (dec.). ^{1}H NMR (200 MHz, 278 K, C_6D_6): δ = 7.61−7.48 (m, 6 H, *meta*-, *para*-H of C_6H_5), 7.06 (m, 4 H, *ortho*-H of C_6H_5), 5.11 (m, 1 H, CH$_2$C*H*CH$_2$), 3.50, 3.29 (both m, 1 H, allyl-H$_{syn}$), 2.66−1.11 [m, 14 H, CH(ring), CH$_2$(ring), allyl-H$_{anti}$], 1.34, 1.31 [both dd, $J_{P,H}$ = 15.0, $J_{H,H}$ = 7.5 Hz, 3 H each, CH$_3$(ring)], 0.69, 0.47 [both dd, $J_{P,H}$ = 13.4, $J_{H,H}$ = 6.9 Hz, 3 H each, CH$_3$(ring)] ppm. ^{13}C NMR (50.3 MHz, C_6D_6): δ = 139.5, 139.3 (both d, $J_{P,C}$ = 19.5 Hz, *ipso*-C of C_6H_5), 133.7 (d, $J_{P,C}$ = 4.6 Hz, *ortho*-C of C_6H_5), 133.5 (d, $J_{P,C}$ = 3.7 Hz, *ortho*-C of C_6H_5), 128.3, 128.2

 © 2004 Wiley-VCH Verlag GmbH & Co. KGaA, Weinheim

(both s, *para*-C of C_6H_5), 127.1, 127.0 (both d, $J_{P,C}$ = 2.8 Hz, *meta*-C of C_6H_5), 105.9 (d, $J_{P,C}$ = 5.9 Hz, CH_2CHCH_2), 52.4 (ddd, $J_{P,C}$ = 25.0 and 7.4, $J_{Rh,C}$ = 1.9 Hz, CH_2CHCH_2), 51.2 (ddd, $J_{P,C}$ = 25.0 and 7.4, $J_{Rh,C}$ = 2.8 Hz, CH_2CHCH_2), 40.9 [ddd, $J_{P,C}$ = 41.6, $J_{P,C}$ = 19.5, $J_{Rh,C}$ = 3.7 Hz, CH(ring)], 35.4 [d, $J_{P,C}$ = 11.9 Hz, CH_2(ring)], 35.2 [s, CH_2(ring)], 34.3 [d, $J_{P,C}$ = 21.1 Hz, CH(ring)], 33.3 [d, $J_{P,C}$ = 20.5 Hz, CH(ring)], 23.0 [d, $J_{P,C}$ = 15.7 Hz, CH_3(ring)], 22.6 [d, $J_{P,C}$ = 17.6 Hz, CH_3(ring)], 14.6, 14.5 [both s, CH_3(*i*Pr)] ppm. ^{31}P NMR (81.0 MHz, C_6D_6): δ_A = 58.5, δ_B = 61.0 (AB part of ABX spectrum; A, B = P, X = Rh; $J_{A,B}$ = 27.9, $J_{A,X}$ = 116.2, $J_{B,X}$ = 116.9 Hz) ppm. $C_{27}H_{39}P_2Rh$ (528.5): calcd. C 61.37, H 7.44; found C 61.41, H 7.38.

Preparation of [Rh(η^3-$CH_2C_6H_5$)(Isophos)$_2$] (19): A suspension of **1** (90 mg, 0.10 mmol) in diethyl ether (10 mL) was treated dropwise at 0 °C with a 0.86 M solution of $C_6H_5CH_2MgBr$ in diethyl ether (0.23 mL, 0.20 mmol). A gradual change of color from brick-red to deep red occurred. After stirring the reaction mixture for 30 min, it was warmed to room temperature, and then the solvent was evaporated in vacuo. The residue was extracted with pentane (20 mL) and the extract was dried in vacuo. The remaining deep red, air-sensitive solid was washed three times with 1 mL portions of acetone (0 °C) and dried; yield 83 mg (82%). ^{1}H NMR (200 MHz, [D$_8$]toluene): δ = 7.17 (t, $J_{H,H}$ = 8.2 Hz, 1 H, H^3), 7.07 (t, $J_{H,H}$ = 6.9 Hz, 1 H, H^4), 6.72 (t, $J_{H,H}$ = 6.9 Hz, 1 H, H^2), 6.16 (d, $J_{H,H}$ = 6.2 Hz, 1 H, H^1), 5.79 (d, $J_{H,H}$ = 6.2, 1 H, H^5), 2.11 (t, $J_{P,H}$ = 2.4 Hz, 2 H, CH_2), 2.30−0.23 (m, 38 H, Isophos protons) ppm; the phenyl protons are numbered clockwise beginning at the position next to the carbon atom carrying the CH_2 group. ^{31}P NMR (81.0 MHz, [D$_8$]toluene): δ = 76.0 (dd, $J_{Rh,P}$ = 260.8, $J_{P,P}$ = 24.0 Hz), 64.9 (dd, $J_{Rh,P}$ = 177.7, $J_{P,P}$ = 24.4 Hz) ppm. $C_{25}H_{45}P_2Rh$ (510.5): calcd. Rh 20.16; found Rh 20.08.

Preparation of [Rh(η^3-$CH_2C_6H_5$)(Phephos)$_2$] (20): This compound was prepared as described for **16**, with $[RhCl(C_8H_{14})_2]_2$ (120 mg, 0.17 mmol), Phephos (135 mg, 0.70 mmol) and a 0.86 M solution of $C_6H_5CH_2MgBr$ in diethyl ether (0.39 mL, 0.34 mmol) as starting materials. Deep red, air-sensitive solid; yield 156 mg (80%). ^{1}H NMR (200 MHz, C_6D_6): δ = 7.73−6.90 (m, 10 H, C_6H_5), 6.60 (t, $J_{H,H}$ = 7.3 Hz, 1 H, H^2), 6.11 (d, $J_{H,H}$ = 7.3 Hz, 1 H, H^1), 6.04 (d, $J_{H,H}$ = 7.7 Hz, 1 H, H^5), 2.74−0.23 [m, 12 H, CH(ring), CH_2(ring)], 0.78 [dd, $J_{P,H}$ = 14.3, $J_{H,H}$ = 7.3 Hz, 6 H, CH_3(ring)], 0.66 [dd, $J_{P,H}$ = 15.7, $J_{H,H}$ = 7.3 Hz, 3 H, CH_3(ring)], 0.46 (dd, $J_{P,H}$ = 13.2, $J_{H,H}$ = 7.0 Hz, 3 H, CH_3(ring)] ppm; the phenyl protons are numbered clockwise beginning at the position next to the carbon atom carrying the CH_2 group; signal for benzylic CH_2 protons partially covered by signals of H^1 and H^2, signals of H^3 and H^4 probably covered by that of the C_6H_5 protons. ^{13}C NMR (50.3 MHz, C_6D_6): δ = 139.1 (d, $J_{P,C}$ = 23.1 Hz, *ipso*-C of C_6H_5), 137.8 (d, $J_{P,C}$ = 19.4 Hz, *ipso*-C of C_6H_5), 133.1 (d, $J_{P,C}$ = 4.6 Hz, *ortho*-C of C_6H_5), 132.9 (d, $J_{P,C}$ = 2.8 Hz, *ortho*-C of C_6H_5), 132.1 (s, C^{2,4}), 129.3, 128.8 (both s, *para*-C of C_6H_5), 126.9, 126.7 (both d, $J_{P,C}$ = 2.8 Hz, *meta*-C of C_6H_5), 120.5 (s, CCH_2), 115.8 (s, C^3), 105.8 (d, $J_{P,C}$ = 7.4 Hz, C^{1,3}), 39.0 [br. d, $J_{P,C}$ = 25.0 Hz, CH(ring)], 37.8 [d, $J_{P,C}$ = 25.6 Hz, CH(ring)], 36.1 [d, $J_{P,C}$ = 17.6 Hz, CH(ring)], 34.5, 32.5 [both m, CH_2(ring)], 31.6 [d, $J_{P,C}$ = 19.4 Hz, CH(ring)], 23.6 [d, $J_{P,C}$ = 14.8 Hz, CH_3(ring)], 22.5 [d, $J_{P,C}$ = 16.7 Hz, CH_3(ring)], 14.6, 13.1 [both d, $J_{P,C}$ = 2.8 Hz, CH_3(ring)] ppm; signal of benzylic CH_2 carbon atom not located exactly. ^{31}P NMR (81.0 MHz, C_6H_6): δ = 65.2 (dd, $J_{Rh,P}$ = 256.8, $J_{P,P}$ = 28.0 Hz), 58.10 (dd, $J_{Rh,P}$ = 180.6, $J_{P,P}$ = 30.5 Hz) ppm. $C_{31}H_{41}P_2Rh$ (578.5): calcd. Rh 17.79; found Rh 18.21.

Preparation of [Rh_2H_4(Isophos)$_4$] (21): A solution of **17** (150 mg, 0.33 mmol) in pentane (10 mL) was stirred at −78 °C for 5 min under a H_2 atmosphere. The solution was then slowly warmed to room temperature, which led to a change of color from yellow dark green. After stirring for 15 min, the solvent was evaporated in vacuo, the remaining dark green, extremely air-sensitive solid was washed three times with 2 mL portions of acetone (−78 °C) and dried; yield 128 mg (92%). IR (hexane): ν(RhH) = 2001 cm^{-1}. ^{1}H NMR (200 MHz, C_6D_6): δ = 2.76−0.18 (m, 76 H, Isophos protons), −10.20 (tquint, $J_{P,H}$ = 27.6, $J_{Rh,H}$ = 8.2 Hz, 2 H, RhH_2Rh), −17.50 (dt, $J_{P,H}$ = 16.7, $J_{Rh,H}$ = 1.5 Hz, 2 H, RhH_2) ppm. ^{31}P NMR (81.0 MHz, C_6D_6): δ = 77.8 [d, $J_{Rh,P}$ = 109.0 Hz, *trans*-Rh(Isophos)$_2$], 72.1 [d, $J_{Rh,P}$ = 161.3 Hz, *cis*-Rh(Isophos)$_2$] ppm. Alternatively, instead of **17** compound **19** could be used as starting material; the yield of **21** (determined by NMR spectroscopy) was quantitative.

Generation of [Rh_2H_4(Prephos)$_4$] (22): A slow stream of H_2 was passed through a solution of **20** (50 mg, 0.09 mmol) in C_6D_6 (0.5 mL) at room temperature. A change of color from deep red to black occurred. Removal of the solvent in vacuo led to quick decomposition. Therefore, the product was characterized by ^{1}H and ^{31}P NMR spectroscopy in the presence of hydrogen. Data for **22**: ^{1}H NMR (200 MHz, C_6D_6): δ = −11.2 (br. m), −18.1 (br. m) ppm. ^{31}P NMR (81.0 MHz, C_6D_6): δ = 73.8 [d, $J_{Rh,P}$ = 111.9 Hz, *trans*-Rh(Prephos)$_2$], 65.4 [d, $J_{Rh,P}$ = 157.7 Hz, *cis*-Rh(Prephos)$_2$].

Preparation of *trans*-[RhH(CO)(Isophos)$_2$] (23): A slow stream of CO was passed through a solution of **21** (130 mg, 0.15 mmol) in hexane (10 mL) for 30 s at room temperature. A quick change of color from dark green to yellow occurred. The solvent was evaporated in vacuo, the residue was dissolved in pentane (3 mL) and the solution was stored for 12 h at −78 °C. Yellow air-sensitive crystals precipitated which were separated from the mother liquor and dried; yield 126 mg (94%); m.p. 64 °C. IR (hexane): ν(RhH) = 2065, ν(CO) 1965 cm^{-1}. ^{1}H NMR (200 MHz, C_6D_6): δ = 2.15 [m, 2 H, CH(*i*Pr)], 2.00−1.43 [m, 12 H, CH(ring), CH_2(ring)], 1.24 [dvt, *N* = 23.6, $J_{H,H}$ = 6.9 Hz, 6 H, CH_3(*i*Pr)], 1.10 [dvt, *N* = 23.7, $J_{H,H}$ = 7.9 Hz, 6 H, CH_3(*i*Pr)], 1.09 [dvt, *N* = 21.7, $J_{H,H}$ = 6.9 Hz, 6 H, CH_3(ring)], 0.88 [dvt, *N* = 21.7, $J_{H,H}$ = 6.9 Hz, 6 H, CH_3(ring)], −10.36 (dt, $J_{P,H}$ = 6.9, $J_{Rh,H}$ = 4.9 Hz, 1 H, RhH) ppm. ^{31}P NMR (81.0 MHz, C_6D_6): δ = 35.8 (d, $J_{Rh,P}$ = 136.6 Hz) ppm. $C_{19}H_{39}OP_2Rh$ (448.4): calcd. C 50.90, H 8.77; found C 51.04, H 8.79.

Generation of *trans*-[RhCl(PhC≡CH)(Isophos)$_2$] (24) and [RhHCl-(C≡CPh)(Isophos)$_2$] (25): A solution of **1** (15 mg, 0.02 mmol) in C_6D_6 (0.5 mL) was treated dropwise with phenylacetylene (11 μL, 10 mg, 0.10 mmol) at room temperature. A quick change of color from brick-red to yellow occurred. The ^{1}H and ^{31}P NMR spectra indicated that compound **24** had formed. If the solution was stored for 10 min, new signals appeared in the NMR spectra which were assigned to intermediate **25** and the final product **26**. Attempts to isolate **24** or to separate **25** from **26** failed. Characteristic data for **24**: ^{1}H NMR (200 MHz, C_6D_6): δ = 4.11 (d, $J_{Rh,H}$ = 2.9 Hz, ≡CH), 1.88 (m, 6 H, CH_3), 1.59 (m, 6 H, CH_3), 1.30 (m, 6 H, CH_3), 0.90 (m, 3 H, CH_3), 0.60 (m, 3 H, CH_3) ppm. ^{31}P NMR (81.0 MHz, C_6D_6): δ_A = 44.8, δ_B = 44.0 (AB part of ABX spectrum; A, B = P, X = Rh; $J_{A,B}$ = 36.0, $J_{A,X}$ = 116.2, $J_{B,X}$ = 117.0 Hz) ppm. Characteristic data for **25**: ^{1}H NMR (200 MHz, C_6D_6): δ = −19.38 (dt, $J_{Rh,H}$ = 21.8, $J_{P,H}$ = 11.6 Hz) ppm. ^{31}P NMR (81.0 MHz, C_6D_6): δ = 50.1 (d, $J_{Rh,P}$ = 99.2 Hz) ppm.

Preparation of [RhCl(=C=CHPh)(Isophos)$_2$]$_2$ (26): A solution of **1** (80 mg, 0.09 mmol) in benzene (5 mL) was treated dropwise with a solution of phenylacetylene (24 μL, 22 mg, 0.22 mmol in benzene (2 mL) at room temperature. A quick change of color from brick-

 © 2004 Wiley-VCH Verlag GmbH & Co. KGaA, Weinheim

red to yellow occurred. After the solution was stirred for 3 h at 90 °C, a subsequent change of color from yellow to violet took place. The solution was cooled to room temperature, the solvent was evaporated in vacuo, the residue was dissolved in benzene (2 mL) and the solution was chromatographed on Al_2O_3 (neutral, activity grade III, length of column 5 cm). With benzene (20 mL) a colorless fraction was eluted which was discarded. With a mixture of benzene/acetone (10:1), a violet fraction was eluted which was dried in vacuo. The remaining violet solid was washed three times with 2 mL portions of pentane (0 °C) and dried; yield 47 mg (84%); m.p. 118 °C (dec.). ^{1}H NMR (200 MHz, C_6D_6): δ = 7.32−6.83 (m, 5 H, C_6H_5), 3.20−0.84 [m, 14 H, CH(ring), CH(*i*Pr), CH_2(ring)], 1.87 (dt, $J_{P,H}$ = 3.3, $J_{Rh,H}$ = 1.2 Hz, 1 H, =C*H*Ph), 1.61 (m, 6 H, CH_3), 1.34 (m, 12 H, CH_3), 1.17 (m, 6 H, CH_3) ppm. ^{13}C NMR (50.30 MHz, C_6D_6): δ = 296.3 (dt, $J_{Rh,C}$ = 58.5, $J_{P,C}$ = 17.2 Hz, Rh=*C*=C), 128.9, 128.4, 125.4, 125.1 (all s, C_6H_5), 112.3 (dt, $J_{Rh,C}$ = 15.3, $J_{P,C}$ = 7.0 Hz, Rh=C=*C*), 35.6 (s, CH_2), 34.8 [vt, *N* = 23.0 Hz, CH(ring)], 34.4, 34.3 (both vt, *N* = 23.2 Hz, P*C*HCH$_3$), 24.7 [vt, *N* = 17.6 Hz, CH(ring)], 21.5, 21.4 [both s, CH_3(ring)], 19.9, 15.0 (both s, PCH*C*H$_3$) ppm. ^{31}P NMR (81.0 MHz, C_6D_6): δ = 47.7 (d, $J_{Rh,P}$ = 134.8 Hz) ppm. $C_{26}H_{44}ClP_2Rh$ (556.9): calcd. C 56.07, H 7.96; found C 55.76, H 7.92.

Generation of *trans*-[RhCl(η^2-(*E*)-PhC≡CCH=CHPh)(Phephos)$_2$] (27): A solution of **2** (100 mg, 0.19 mmol) in C_6D_6 (0.5 mL) was treated dropwise with phenylacetylene (0.12 mL, 1.14 mmol) at room temperature. A gradual change of color from orange-red to deep red occurred. The reaction was monitored by NMR spectroscopy. After 1 h, the starting material had been consumed and the signals of a new compound were observed. Typical data for **27**: ^{1}H NMR (200 MHz, C_6D_6): δ = 7.36, 6.88 (both d, $J_{H,H}$ = 15.4 Hz, CH=CH *trans*-disposed) ppm. ^{31}P NMR (81.0 MHz, C_6D_6): δ = 43.4 (d, $J_{Rh,P}$ = 136.2 Hz) ppm.

Reaction of Compound 27 with CO: A slow stream of CO was passed through a solution of **27**, generated as described above, for 20 s at room temperature. The ^{1}H NMR spectrum revealed that besides **6** the enyne (*E*)-PhC≡CCH=CHPh (**28**) was formed which was identified by comparison of the NMR spectroscopic data with those of an authentic sample.[3]

Preparation of *trans*-[RhCl(=CPh$_2$)(Isophos)$_2$] (30): A suspension of **29** (50 mg, 0.06 mmol) in pentane (10 mL) was treated at −78 °C with a solution of Isophos (20 mg, 0.12 mmol) in pentane (5 mL) and, after warming to room temperature, stirred for 1 h. The solvent was evaporated in vacuo, the residue was dissolved in hexane (2 mL) and the solution was chromatographed on Al_2O_3 (neutral, activity grade III, length of column 3.0 cm). With diethyl ether a green fraction was eluted, which was dried in vacuo. The remaining green solid was washed twice with 2 mL portions of hexane (0 °C) and dried; yield 30 mg (79%); m.p. 65 °C (dec.). ^{1}H NMR (200 MHz, C_6D_6): δ = 7.99 (m, 2 H, *ortho*-H of C_6H_5), 7.30 (m, 1 H, *para*-H of C_6H_5), 6.98 (m, 2 H, *meta*-H of C_6H_5), 2.37−0.69 [m, 12 H, CH(ring), CH(*i*Pr), CH_2(ring)], 1.90 [dvt, *N* = 16.9, $J_{H,H}$ = 7.2 Hz, 6 H, CH_3(ring)], 1.44 [dvt, *N* = 13.5, $J_{H,H}$ = 7.0 Hz, 6 H, CH_3(*i*Pr)], 1.09 [dvt, *N* = 14.2, $J_{H,H}$ = 7.2 Hz, 6 H, CH_3(*i*Pr)], 0.74 [dvt, *N* = 12.3, $J_{H,H}$ = 7.0 Hz, 6 H, CH_3(ring)] ppm. ^{31}P NMR (81.0 MHz, C_6D_6): δ = 29.5 (d, $J_{Rh,P}$ = 166.9 Hz) ppm. $C_{31}H_{48}ClP_2Rh$ (621.0): calcd. C 59.96, H 7.79, Rh 16.57; found C 60.87, H 7.43, Rh 16.48.

Preparation of *trans*-[RhCl(=CPh$_2$)(Phephos)$_2$] (31): A solution of **29** (112 mg, 0.14 mmol) in pentane (10 mL) was treated at −78 °C with a solution of Phephos (56 mg, 0.29 mmol) in pentane (2 mL) and, after warming to room temperature, stirred for 1 h. The solution was concentrated to ca. 1 mL in vacuo and stored for 2 h. A green microcrystalline solid precipitated, which was separated from the mother liquor, washed twice with 2 mL portions of pentane (0 °C) and dried; yield 90 mg (93%); m.p. 70 °C. ^{1}H NMR (200 MHz, C_6D_6): δ = 7.38−6.64 (m, 20 H, C_6H_5), 3.31−1.10 [m, 12 H, CH(ring), CH_2(ring)], 2.09, 0.85 [both m, 6 H each, CH_3(ring)] ppm. ^{13}C NMR (50.3 MHz, C_6D_6): δ = 162.2 (vt, *N* = 7.6 Hz, *ipso*-C of C_6H_5), 134.5 (s, *ortho*-C of C_6H_5), 133.2 (vt, *N* = 11.1 Hz, *ortho*-C of C_6H_5), 128.3, 127.5 (both s, *para*-C of C_6H_5), 126.8 (vt, *N* = 7.6 Hz, *meta*-C of C_6H_5), 126.7 (s, *meta*-C of C_6H_5), 34.9, 34.0 [both s, CH_2(ring)], 33.9, 32.0 [both vt, *N* = 22.8 Hz, CH(ring)], 22.5 [vt, *N* = 10.2 Hz, CH_3(ring)], 15.21 [s, CH_3(ring)] ppm; signal of carbene carbon atom could not be exactly located. ^{31}P NMR (81.0 MHz, C_6D_6): δ = 37.3 (d, $J_{Rh,P}$ = 172.5 Hz) ppm. $C_{37}H_{44}ClP_2Rh$ (689.1): calcd. C 64.49, H 6.44, Rh 14.93; found C 64.56, H 6.43, Rh 15.12.

Preparation of *trans*-[IrCl(CO)(Isophos)$_2$] (34): A suspension of $[IrCl(C_8H_{14})_2]_2$ (140 mg, 0.16 mmol) in pentane (10 mL) was treated with Isophos (99 mg, 0.62 mmol) and stirred for 5 min at room temperature. A slow stream of CO was then passed through the solution for 10 min. A yellow solid precipitated which was filtered and recrystallized from a mixture of pentane/THF (10:1). Yellow air-stable crystals were isolated; yield 148 mg (81%); m.p. 232 °C (dec.). IR (CH_2Cl_2): ν(CO) = 1937 cm^{-1}. ^{1}H NMR (200 MHz, C_6D_6): δ = 2.00−1.54 [m, 10 H, CH(ring), CH(*i*Pr), CH_2(ring)], 1.46 [dvt, *N* = 22.8, $J_{H,H}$ = 7.0 Hz, 6 H, CH_3(*i*Pr)], 1.38 [m, 4 H, CH_2(ring)], 1.29 [dvt, *N* = 23.2, $J_{H,H}$ = 7.0 Hz, 6 H, CH_3(*i*Pr)], 1.18 [dvt, *N* = 21.5, $J_{H,H}$ = 7.1 Hz, 6 H, CH_3(ring)], 1.11 [dvt, *N* = 21.4, $J_{H,H}$ = 6.9 Hz, 6 H, CH_3(ring)] ppm. ^{31}P NMR (81.0 MHz, C_6D_6): δ = 7.3 (s) ppm. $C_{19}H_{38}ClIrOP_2$ (572.1): calcd. C 39.89, H 6.70; found C 39.47, H 6.70.

Preparation of [IrClH$_2$(Isophos)$_2$] (35): A suspension of $[IrCl(C_8H_{14})_2]_2$ (140 mg, 0.16 mmol) in hexane (10 mL) was treated with Isophos (99 mg, 0.62 mmol) and stirred for 5 min at room temperature. A slow stream of H_2 was then passed through the solution for 10 min. The solvent was evaporated in vacuo, the residue was dissolved in pentane (3 mL) and the solution was stored for 12 h at −78 °C. Pale yellow air-sensitive crystals precipitated which were filtered, washed twice with 0.5 mL portions of pentane (−20 °C) and dried; yield 133 mg (76%); m.p. 98 °C (dec.). IR (KBr): ν(IrH) = 2290 cm^{-1}. ^{1}H NMR (200 MHz, C_6D_6): δ = 2.10−1.70 [m, 10 H, CH(ring), CH(*i*Pr), CH_2(ring)], 1.78 [dvt, *N* = 22.3, $J_{H,H}$ = 6.9 Hz, 6 H, CH_3(*i*Pr)], 1.44 [dvt, *N* = 21.2, $J_{H,H}$ = 7.0 Hz, 6 H, CH_3(*i*Pr)], 1.34 [m, 4 H, CH_2(ring)], 1.28 [dvt, *N* = 20.7, $J_{H,H}$ = 6.9 Hz, 6 H, CH_3(ring)], 1.08 [dvt, *N* = 21.1, $J_{H,H}$ = 6.9 Hz, 6 H, CH_3(ring)], −26.98 [t, $J_{P,H}$ = 14.2 Hz, 2 H, IrH] ppm. ^{31}P NMR (81.0 MHz, C_6D_6): δ = 51.2 (br. s, t in off-resonance) ppm. $C_{18}H_{40}ClIrP_2$ (546.1): calcd. C 39.59, H 7.38; found C 39.43, H 7.38.

Preparation of [IrClH$_2$(CO)(Isophos)$_2$] (36): A slow stream of CO was passed through a solution of **35** (120 mg, 0.22 mmol) in pentane (5 mL) for 10 min at room temperature. A pale yellow solid precipitated which was filtered and then dissolved in methanol (10 mL). The solution was concentrated to ca. 2 mL in vacuo and stored for 6 h at −78 °C. Pale yellow, moderately air-sensitive crystals precipitated which were washed twice with 0.5 mL portions of methanol (−20 °C) and dried; yield 99 mg (78%); m.p. 185 °C (dec.). IR (KBr): ν(IrH) = 2210, 2005, ν(CO) 1975 cm^{-1}. ^{1}H NMR (200 MHz, C_6D_6): δ = 2.10−1.60 [m, 10 H, CH(ring), CH(*i*Pr), CH_2(ring)], 1.54 [dvt, *N* = 22.7, $J_{H,H}$ = 6.9 Hz, 6 H, CH_3(*i*Pr)], 1.48 [dvt, *N* = 21.2, $J_{H,H}$ = 7.0 Hz, 6 H, CH_3(*i*Pr)], 1.28 [m, 4 H,

 © 2004 Wiley-VCH Verlag GmbH & Co. KGaA, Weinheim

CH_2(ring)], 1.24 [dvt, N = 21.2, $J_{H,H}$ = 7.0 Hz, 6 H, CH_3(ring)], 0.94 [dvt, N = 19.7, $J_{H,H}$ = 6.9 Hz, 6 H, CH_3(ring)], −8.57 (dt, $J_{P,H}$ = 18.9, $J_{H,H}$ = 5.8 Hz, 1 H, IrH *trans* to CO), −19.97 (dt, $J_{P,H}$ = 11.6, $J_{H,H}$ = 5.8 Hz, 1 H, IrH *trans* to Cl) ppm. ^{31}P NMR (81.0 MHz, C_6D_6): δ = 36.1 (s, t in off-resonance) ppm. $C_{19}H_{40}ClIrOP_2$ (574.1): calcd. C 39.75, H 7.02; found C 39.70, H 7.01.

Acknowledgments

This work was supported by the Deutsche Forschungsgemeinschaft (SFB, 347) and the Fonds der Chemischen Industrie. We thank Mrs. R. Schedl and Mr. C. P. Kneis for elemental analysis and DTA measurements and Mrs. M.-L. Schäfer and Dr. W. Buchner for NMR spectra.

[1] Reviews: [1a] H. Werner, *Nachr. Chem. Tech. Lab.* **1992**, *40*, 435−444. [1b] H. Werner, *J. Organomet. Chem.* **1994**, *475*, 45−55. [1c] H. Werner, *Chem. Commun.* **1997**, 903−910.
[2] H. Werner, F. Kukla, P. Steinert, *Eur. J. Inorg. Chem.* **2002**, 1377−1389.
[3] M. Schäfer, J. Wolf, H. Werner, *J. Organomet. Chem.* **1995**, *485*, 85−100.
[4] H. Werner, J. Wolf, A. Höhn, *J. Organomet. Chem.* **1985**, *287*, 395−407.
[5] [5a] W. Oppolzer, M. Wills, C. Starkemann, G. Bernardinelli, *Tetrahedron Lett.* **1990**, 4117−4120. [5b] J. Bakos, A. Orosz, B. Heil, M. Laghmari, P. Lhoste, D. Sinou, *J. Chem. Soc., Chem. Commun.* **1991**, 1684−1685.
[6] M. J. Burk, *J. Am. Chem. Soc.* **1991**, *113*, 8518−8519.
[7] H. Werner, M. Schäfer, O. Nürnberg, J. Wolf, *Chem. Ber.* **1994**, *127*, 27−38.
[8] C. A. Tolman, P. Z. Meakin, D. L. Lindner, J. P. Jesson, *J. Am. Chem. Soc.* **1974**, *96*, 2762−2774.
[9] K. Wang, M. E. Goldman, T. J. Emge, A. S. Goldman, *J. Organomet. Chem.* **1996**, *518*, 55−68.
[10] F. Kukla, Dissertation, University of Würzburg, **1997**.
[11] [11a] J. A. Osborn, F. H. Jardine, J. F. Young, G. Wilkinson, *J. Chem. Soc., A* **1966**, 1711−1732. [11b] Y. Ohtani, A. Yamagishi, M. Fujimoto, *Chem. Lett.* **1977**, 1187−1190.
[12] R. L. Harlow, D. L. Thorn, R. T. Baker, N. L. Jones, *Inorg. Chem.* **1992**, *31*, 993−997.
[13] M. Schäfer, Dissertation, University of Würzburg, **1994**.
[14] K. Vrieze, H. C. Volger, P. W. N. M. van Leeuwen, *Inorg. Chim. Acta Rev.* **1977**, *16*, 211−239.
[15] [15a] D. L. Thorn, J. A. Ibers, *Adv. Chem. Ser.* **1982**, *196*, 117−131. [15b] J. Wolf, O. Nürnberg, M. Schäfer, H. Werner, *Z. Anorg. Allg. Chem.* **1994**, *620*, 1157−1162.
[16] R. K. Brown, J. M. Williams, A. J. Sivak, E. L. Muetterties, *Inorg. Chem.* **1980**, *19*, 370−374.
[17] E. B. Meier, R. R. Burch, E. L. Muetterties, V. W. Day, *J. Am. Chem. Soc.* **1982**, *104*, 2661−2663.
[18] M. D. Fryzuk, W. E. Piers, S. J. Rettig, F. W. B. Einstein, T. Jones, T. A. Albright, *J. Am. Chem. Soc.* **1989**, *111*, 5709−5721.
[19] [19a] A. J. Sivak, E. L. Muetterties, *J. Am. Chem. Soc.* **1979**, *101*, 4878−4887. [19b] R. R. Burch, E. L. Muetterties, V. W. Day, *Organometallics* **1982**, *1*, 188−197.
[20] H. Werner, F. J. Garcia-Alonso, H. Otto, J. Wolf, *Z. Naturforsch., Teil B* **1988**, *43*, 722−726.
[21] H. Werner, U. Brekau, *Z. Naturforsch., Teil B* **1989**, *44*, 1438−1446.
[22] Y. Wakatsuki, N. Koga, H. Werner, K. Morokuma, *J. Am. Chem. Soc.* **1997**, *119*, 360−366.
[23] Y. Wakatsuki, N. Koga, H. Yamazaki, K. Morokuma, *J. Am. Chem. Soc.* **1994**, *116*, 8105−8111.
[24] M. Schäfer, J. Wolf, H. Werner, *J. Chem. Soc., Chem. Commun.* **1991**, 1341−1343.
[25] W. T. Boese, A. S. Goldman, *Organometallics* **1991**, *10*, 782−786.
[26] H. Werner, P. Schwab, E. Bleuel, N. Mahr, P. Steinert, J. Wolf, *Chem. Eur. J.* **1997**, *3*, 1375−1384.
[27] E. Bleuel, Dissertation, University of Würzburg, **2000**.
[28] M. Schulz, Dissertation, University of Würzburg, **1993**.
[29] W. Strohmeier, W. Rheder-Stirnweiss, *Z. Naturforsch., Teil B* **1969**, *24*, 939−940.
[30] L. Dahlenburg, A. Yardimcioglu, *J. Organomet. Chem.* **1985**, *291*, 371−386.
[31] H. Werner, A. Höhn, M. Dziallas, *Angew. Chem.* **1986**, *98*, 1112−1114; *Angew. Chem. Int. Ed. Engl.* **1986**, *25*, 1090−1092.
[32] A. van der Ent, A. L. Onderdelinden, *Inorg. Synth.* **1990**, *28*, 90−92.
[33] [33a] A. van der Ent, A. L. Onderdelinden, *Inorg. Synth.* **1973**, *14*, 94−95. [33b] J. L. Herde, J. C. Lambert, C. V. Senoff, *Inorg. Synth.* **1974**, *15*, 18−20.

Received August 6, 2003
Early View Article
Published Online December 4, 2003

 © 2004 Wiley-VCH Verlag GmbH & Co. KGaA, Weinheim

Electrochemical and Spectroelectrochemical Investigations of Mono- and Binuclear Cobalt(II) Complexes of "Figure-Eight" Octapyrrolic Macrocycles

Jordi Bley-Escrich,[a] Jean-Paul Gisselbrecht,*[a] Martin Michels,[b] Lars Zander,[b] Emanuel Vogel,[b] and Maurice Gross*[a]

Keywords: Macrocyclic ligands / Cobalt / Cluster complexes / Electrochemistry

In this paper, electrochemical investigations of a set of three cyclooctaphyrin complexes containing divalent cobalt are reported. These complexes are the homodinuclear cobalt-cobalt complex Co_2L_1 with the ligand H_4L_1, the mononuclear cobalt complex CoH_2L_2 and the heterodinuclear copper(II)-cobalt complex $CoCuL_2$ with the ligand H_4L_2. All of these species undergo two reduction and three oxidation processes, all of which are reversible one-electron transfers. The two reduction and first two oxidation steps are ligand-centered, as confirmed by spectroelectrochemical investigations. In contrast, the third oxidation corresponds to a metal-centered reversible one-electron transfer. The metal-centered oxidation steps occur at lower potentials than the third oxidation steps of the free bases. UV/Visible spectral changes observed during oxidation confirm a metal-centered oxidation generating a cobalt(III) cation, which is rather unusual when compared with cobalt porphyrin complexes, in which the oxidation of the metal usually occurs before the oxidation of the ligand.

(© Wiley-VCH Verlag GmbH & Co. KGaA, 69451 Weinheim, Germany, 2004)

Introduction

The chemical and biological properties of vitamin B12 and its derivatives have generated considerable interest in the chemical investigation of cobalt complexes.[1]

Since functional mimics of multielectronic redox enzymes may involve two or more metal centers, numerous cofacial metalloporphyrins have been synthesized and cofacial cobalt porphyrins have been studied to evaluate their ability to carry out the tetraelectronic electrocatalytic reduction of O_2 to H_2O.[2]

Cobalt porphyrins are well-known systems and their redox behavior has been extensively studied;[3] however, cobalt complexes of larger polypyrrolic macrocycles have not yet been investigated. Although numerous macrocyclic polypyrrolic ligands have been synthesized,[4−10] their complexation properties with transition metals remain scarce in the literature[11−13] and only a few cobalt complexes have been characterized.[14,15]

Cyclooctapyrrolic ring systems have recently been synthesized.[16−18] They possess a "figure-eight" conformation delimiting two tetrapyrrolic complexation sites that are able to accommodate up to two divalent cations as shown in crystallographic structures.[19−21] However, due to their twisted geometry, the two tetrapyrrolic sites do not share the same plane. They are separated by a dihedral angle of approximately 60°. These cyclooctaphyrins (COP) have allowed the preparation and characterization of several cobalt complexes: Co_2L_1 with the ligand H_4L_1 [[34]COP(1.1.1.0.1.1.1.0)] as well as CoH_2L_2 and $CoCuL_2$ with the ligand H_4L_2 [[32]COP(1.0.1.0.1.0.1.0)] (Figure 1).

The aim of the present electrochemical investigation was to determine whether or not cyclooctaphyrins are able to stabilize cobalt(I) and/or cobalt(III), as is usually observed in porphyrins.[23−25] In order to study the solvent effects, electrochemical investigations were performed using rotating disk and cyclic voltammetry in two media differing in their solvation properties: benzonitrile (PhCN) and dichloromethane (CH_2Cl_2). Spectroelectrochemistry was used to identify the electron transfer sites (ligand versus metal).

The present results on cobalt cyclooctaphyrins can then be compared with our previous studies on three series of cyclooctaphyrin metallocomplexes for which only ligand-centered electron transfers were observed.[26,27]

Results and Discussion

Electrochemical Studies

The redox behavior of the three cobalt cyclooctaphyrin complexes were determined by cyclic voltammetry (CV) and rotating disk voltammetry (RDV) in dry PhCN + 0.1 M $TBAPF_6$ solutions at room temperature (25 °C).

[a] Laboratoire d'Electrochimie et de Chimie Physique du Corps Solide, UMR 7512 − CNRS, Université Louis Pasteur, 4, rue Blaise Pascal, 67000 Strasbourg, France
Fax: (internat.) + 33-3-90241431
E-mail: gross@chimie.u-strasbg.fr
[b] Institut für Organische Chemie, Universität zu Köln, Greinstrasse 4, 50939 Köln, Germany

 © 2004 Wiley-VCH Verlag GmbH & Co. KGaA, Weinheim DOI: 10.1002/ejic.200300499

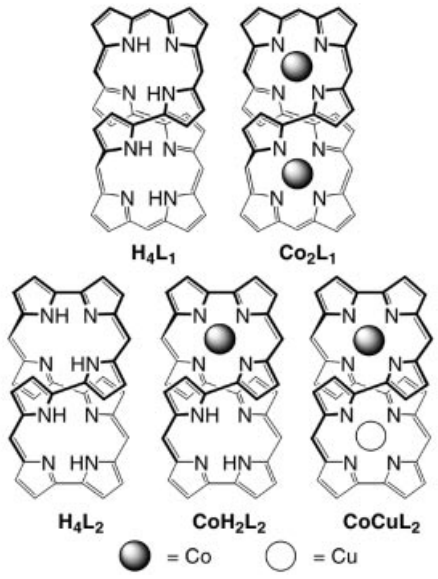

Figure 1. Free bases and complexes studied in the two cyclooctaphyrin series; the ethyl groups on the pyrroles are omitted for clarity; the compounds are named [−]COP(-.-.-.-.-.-.-) after the nomenclature proposed by Franck for polypyrrolic macrocycles[22]

RDV on Co_2L_1 presents two reduction (−1.96 and −1.33 V/Fc) and four oxidation waves (−0.42, 0.06, 0.30 and 0.63 V/Fc) (Figure 2). All waves are of similar amplitude and wave analysis using Tomeš criteria[28] give slopes close to 56.4 mV, the expected value for reversible one-electron processes, for the two reduction and the first three oxidation steps, whereas the fourth oxidation step has a slope of 90 mV (Table 1).

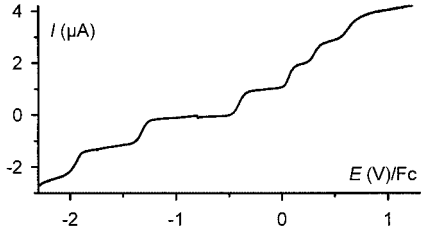

Figure 2. Rotating disk voltammetry on Co_2L_1 (≈10^{-4} M) in PhCN +0.1 M Bu_4NPF_6, at a Pt working electrode; scan rate: 0.05 V/s. N = 2000 rpm

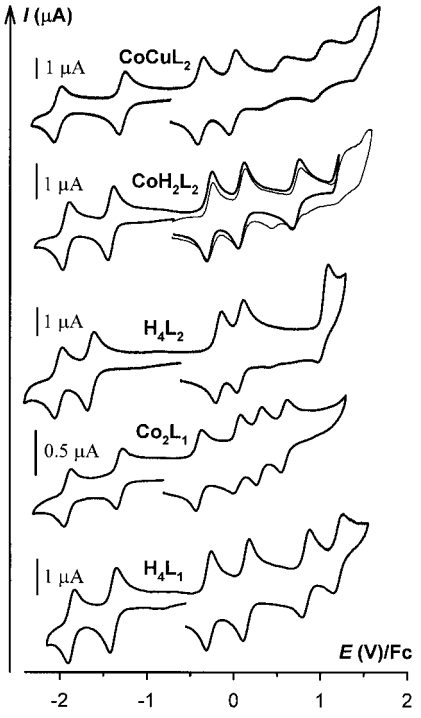

Figure 3. Cyclic voltammetry on H_4L_1, Co_2L_1, H_4L_2, CoH_2L_2 and $CoCuL_2$ in PhCN +0.1 M Bu_4NPF_6, at a Pt working electrode; scan rate: 1 V/s for H_4L_2 and 0.05 V/s for H_4L_1, Co_2L_1, CoH_2L_2 and $CoCuL_2$. c ≈10^{-4} M.

The results from the cyclic voltammetric study of Co_2L_1 (Figure 3) confirms the reversibility of each of the two one-electron reduction processes, as well as the first three one-electron oxidation steps. In contrast with the results from the rotating disk voltammetric study, the fourth oxidation step is also reversible. This reversibility was confirmed by monitoring the peak current (I_p) and the peak potentials (E_p) with increasing scan rates: E_p remained invariant with ν for sweep rates up to 5 V/s, the peak current ratio remained close to unity for all ν, and the peak potential difference ($\Delta E = E_{pc} - E_{pa}$) was approximately 60 mV.

A particular behavior is observed for the second oxidation step when the vertex potential is fixed after the third or fourth oxidation steps with sweep rates higher than 0.1 V/s. As shown in Figure 4 (a) the reverse peak of step II disappears on increasing the sweep rates and a new peak is observed at −0.11 V/Fc. Such behavior may be due to slow

Table 1. Redox potentials obtained by rotating disk voltammetry, in PhCN +0.1 M Bu_4NPF_6, at a Pt working electrode; scan rate: 0.05 V/s. $E = (E_{pc}+E_{pa})/2$; potentials vs. Fc

Compound	E red$_2$ ($E_{3/4} - E_{1/4}$)	E red$_1$ ($E_{3/4} - E_{1/4}$)	E ox$_1$ ($E_{3/4} - E_{1/4}$)	E ox$_2$ ($E_{3/4} - E_{1/4}$)	E ox$_3$ ($E_{3/4} - E_{1/4}$)	E ox$_4$ ($E_{3/4} - E_{1/4}$)	E ox$_5$ ($E_{3/4} - E_{1/4}$)
Co_2L_1	−1.96 V (62 mV)	−1.33 V (60 mV)	−0.42 V (62 mV)	0.06 V (56 mV)	0.30 V (54 mV)	0.63 V (90 mV)	–
CoH_2L_2	−1.95 V (63 mV)	−1.41 V (61 mV)	−0.29 V (57 mV)	0.09 V (60 mV)	0.74 V (68 mV)	1.37 V (89 mV)	–
$CoCuL_2$	−2.01 V (65 mV)	−1.28 V (62 mV)	−0.39 V (57 mV)	−0.03 V (61 mV)	0.57 V (73 mV)	1.08 V (84 mV)	1.47 V (77 mV)

 © 2004 Wiley-VCH Verlag GmbH & Co. KGaA, Weinheim

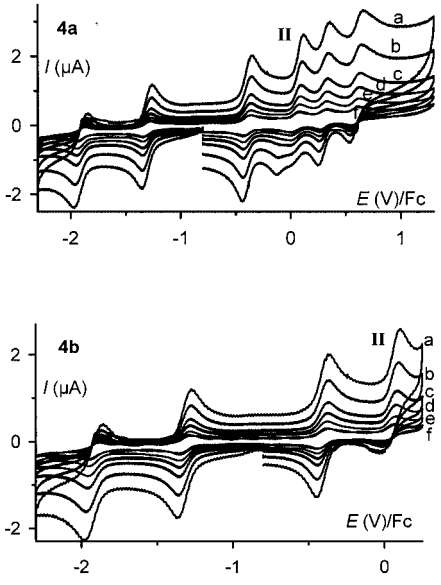

Figure 4. Series of cyclic voltammograms of Co_2L_1 ($\approx 10^{-4}$ M) with different scan rates in PhCN +0.1 M Bu_4NPF_6, performed at a Pt working electrode; scan rates for: a) 1 V/s; b) 0.5 V/s; c) 0.2 V/s; d) 0.1 V/s; e) 0.05 V/s; f) 0.02 V/s; for 4a potential range from −2.30 V to +1.30 V/Fc, and for 4b potential range from −2.30 V to +0.25 V/Fc.

geometric rearrangements occurring during the third oxidation process, preventing the molecule from returning to its initial structure again in the CV time scale ($\nu > 0.1$ V/s). The fact that the disappearance of a peak and the appearance of a new peak is not observed when the third oxidation has not been reached [Figure 4 (b)], confirms that these geometric rearrangements occur in the tricationic species.

It should be mentioned that the third and the fourth oxidation processes observed for Co_2L_1 using CV (Table 2) and rotating disk voltammetry (Table 1) occur at potentials that are less positive by 400 mV relative to those of the free bases, and by 200 mV relative to those of complexes with non-electroactive metals. This could be an indication of metal-centered electron transfers, which would explain the above hypothesis concerning the geometric changes that occur during the third oxidation process.

The two reduction and first two oxidation steps of the other two cobalt complexes, CoH_2L_2 and $CoCuL_2$, are similar to those of the free base H_4L_2.[26,27] After the second oxidation step, the complexes have a distinct behavior. When using RDV and CV, CoH_2L_2 presents a third one-electron oxidation that occurs at 0.73 V/Fc, which is 280 mV less positive than the third oxidation of the free base (Table 2). A fourth one-electron oxidation step is observed at +1.27 V/Fc (Figure 3). These data are in agreement with a metal-centered oxidation process for the third oxidation step of CoH_2L_2.

The complex $CoCuL_2$ presents three additional one-electron oxidation steps after the second oxidation. The third oxidation occurs at +0.57 V/Fc, 440 mV less positive than that of the free base (Table 2). This is consistent with the third oxidation process occurring at the cobalt center. The fourth and fifth oxidation steps are observed at +1.08 and +1.47 V/Fc (Figure 3).

It has been shown that in cobalt porphyrin complexes, the redox potential of the $Co^{III/II}$ couple is dependent on both the solvent and the supporting electrolyte. Indeed, strong coordinating solvents facilitate the oxidation of the metal, whereas in non-bonding solvents the redox potential is shifted towards positive potentials.[23−25,29−31] On the other hand, the redox potentials of ligand-centered electron transfers are less sensitive to solvation changes than metal-centered processes. For these reasons, a new set of measurements in non-coordinating CH_2Cl_2 was performed to study the solvent effects on the redox potentials when going from benzonitrile to dichloromethane.

In CH_2Cl_2, the reduction and first two oxidation steps of Co_2L_1 are similar to that described previously in PhCN. The third oxidation step is shifted to more positive potentials by 300 mV, while the fourth oxidation step is no longer observed under these experimental conditions. The addition of a strong axial ligand in dichloromethane is expected to shift the redox potential of a metal-centered electron transfer.[23−25] Therefore, pyridine was added to confirm that the third oxidation process is metal-centered. After the addition of pyridine, the third oxidation step shifts cathodically towards the value observed in PhCN (Figure 5). The

Table 2. Redox potentials obtained by cyclic voltammetry, in PhCN (at a Pt working electrode) and in CH_2Cl_2 (on a GC working electrode) +0.1 M Bu_4NPF_6; scan rate: 0.1 V/s. $E = (E_{pc}+E_{pa})/2$; potentials vs. Fc

Compound	Solvent	E red$_2$ (Volt)	E red$_1$ (Volt)	E ox$_1$ (Volt)	E ox$_2$ (Volt)	E ox$_3$ (Volt)	E ox$_4$ (Volt)	HL gap (Volt)
H_4L_1	PhCN	−1.88	−1.40	−0.30	0.13	0.83	1.21	1.10
	CH_2Cl_2	−1.78	−1.49	−0.38	0.14	0.87	1.19	1.11
Co_2L_1	PhCN	−1.92	−1.32	−0.41	0.03	0.29	0.58	0.91
	CH_2Cl_2 + Py	−1.89	−1.40	−0.45	0.07	0.39	0.69	0.95
	CH_2Cl_2	−1.96	−1.43	−0.48	0.08	0.59	−	0.95
H_4L_2	PhCN	−2.02	−1.64	−0.18	0.08	1.01	1.06	1.46
	CH_2Cl_2	−1.97	−1.66	−0.23	0.11	1.12	1.12	1.43
CoH_2L_2	PhCN	−1.93	−1.41	−0.28	0.09	0.73	1.27	1.13
	CH_2Cl_2	−2.02	−1.57	−0.41	0.05	0.78	−	1.16
$CoCuL_2$	PhCN	−2.01	−1.28	−0.39	−0.03	0.57	1.08/1.47	0.89
	CH_2Cl_2	−2.11	−1.39	−0.46	0.00	0.74	1.10/−	0.93

 © 2004 Wiley-VCH Verlag GmbH & Co. KGaA, Weinheim

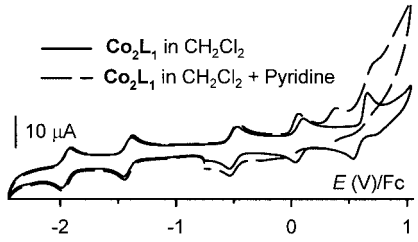

Figure 5. Cyclic voltammetry on Co_2L_1 ($5 \cdot 10^{-4}$ M) (solid line) and on Co_2L_1 +12 equivalents of pyridine (dashed line) in CH_2Cl_2 +0.1 M Bu_4NPF_6, at a Pt working electrode (scan rate: 0.1 V/s)

redox potentials determined are presented in Table 2. All of the above results demonstrate that the third oxidation step corresponds to the oxidation of Co^{II} to Co^{III}.

Under the same experimental conditions, a large potential shift (170 mV) is observed for the third oxidation step of $CoCuL_2$, and only a small shift (50 mV) is observed for CoH_2L_2 (Table 2). Such a small shift is characteristic of poor axial coordination by the cobalt ion. This can be explained in the following way: as this is a mononuclear complex of the smallest cyclooctaphyrin, it is possible that the ligand is more tightly wrapped around the cobalt cation, thus hindering the access for axial coordination to a greater extent relative to $CoCuL_2$.

Spectroelectrochemistry

In order to determine the electron transfer sites, spectroelectrochemical studies were carried out. Comparison of the spectral changes during electrolysis of the cobalt complexes with the spectra of the parent compounds (free base and complexes with non-electroactive metals) allowed us, in most cases, to assign the electron transfer sites in the cobalt complexes.

For each cobalt complex, the reduction processes produce spectral evolutions with well-defined isosbestic points. The spectra obtained after electrolysis revert quantitatively to the initial spectrum by stepwise electrochemical restoration of the starting cyclooctaphyrin. This result indicates that the two electroreduced species are stable in the time scale of the spectroelectrochemical experiments, i.e. about 30 min, which is a good indication of the high stability of the electrogenerated species under these experimental conditions. Spectral changes seen for the cobalt complexes are similar to those observed for the parent compounds [a blue shift for Co_2L_1; Figure 6 (a) and red shifts for CoH_2L_2 and $CoCuL_2$; Figure 6 (c and e)], which confirms that the reductions are ligand-centered. For complexes CoH_2L_2 and $CoCuL_2$, the presence of an intense and sharp absorption band (Soret-like) is observed after the second reduction process, as seen previously for metallocomplexes of cyclooctaphyrins with the same ligand.[27]

The three oxidation steps also produce spectral evolutions with well-defined isosbestic points, even for $CoCuL_2$ [Figure 6 (f)], for which the third oxidation process is quasi-reversible when using CV. The initial spectra could be quantitatively recovered by stepwise reduction of the electrogenerated species, which indicates the high stability of the generated species.

The fourth and further oxidations could not be studied for CoH_2L_2 and $CoCuL_2$ since their oxidation steps occur too close to the electrolyte discharge.

Spectral evolutions for the two first oxidations are similar to those of the free bases (blue shift for Co_2L_1 [Figure 6 (b)] and red shift for CoH_2L_2 and $CoCuL_2$ [Figure 6 (d and f)], which are characteristic of ligand-centered oxidations, thus generating the corresponding dications. Spectral evolutions for the third oxidation step differ for each complex studied.

For Co_2L_1 and CoH_2L_2, the spectral evolutions for the third oxidation step are quite different from those observed for the free base. The intensity of the band changes, while no changes are observed in the absorption wavelength. This is a good indication of a metal-centered oxidation process.

For $CoCuL_2$, the changes involving the third oxidation step are more significant; indeed the absorption bands at 388 and 646 nm decrease in intensity, whereas new bands appear at 331 and 424 nm.

The Unexpected Synthesis of the Radical Cation $CoH_2L_2^+$

As only a few cobalt complexes were available, we considered the possibility of the insertion of a second cobalt cation in the mononuclear complex by in situ complexation. As no spectroscopic data were available for the dinuclear cobalt complex of the ligand H_4L_2, in situ complexation in a mixture of methanol/dichloromethane (1:1) was tested with copper since the UV/Visible spectra of the mononuclear copper complex and the homodinuclear copper complex are already available. In situ complexation of copper to the ligand H_4L_2 confirmed the formation of the mononuclear complex [for 1 equiv. of $Cu(CF_3SO_3)_2$] and the dinuclear complex [for 2 equiv. of $Cu(CF_3SO_3)_2$]. The spectra shift to the red when going from the free base to the mono- and dinuclear copper complex, as shown in Figure 7 (a).

The same experiment was carried out with the cobalt salts $Co(CF_3SO_3)_2$ and $Co(OH)_2$. The first observation was that the complexation kinetics are much slower for cobalt than for copper. The characteristic spectrum of the mononuclear complex was observed eight hours after the introduction of the cobalt salt for a stoichiometric mixture. Further spectral changes were observed only when a large excess (saturated solution) of the cobalt(II) salt was added to the mononuclear complex. The observed spectrum indicated the presence of a new species X in solution [Figure 7 (b)]. Compound X was prepared by dissolving the free base H_4L_2 (5.3 mg) in 30 mL of a mixture of methanol/dichloromethane (1:1). 3000 equivalents of $Co(OH)_2$ were added to the solution, and the suspension was stirred overnight. The excess solid was removed by filtration. The solution was dried over $MgSO_4$ and then filtered. Finally, the solvent was removed under vacuum. A dark blue powder was obtained. The UV/Visible spectrum of X is identical to the spectrum observed when using spectroelectrochemistry after the first oxidation process of CoH_2L_2; this implies that the radical cation $CoH_2L_2^{\bullet+}$ is formed. Rotating disk voltammetry on the prepared compound shows potentials that are similar

 © 2004 Wiley-VCH Verlag GmbH & Co. KGaA, Weinheim

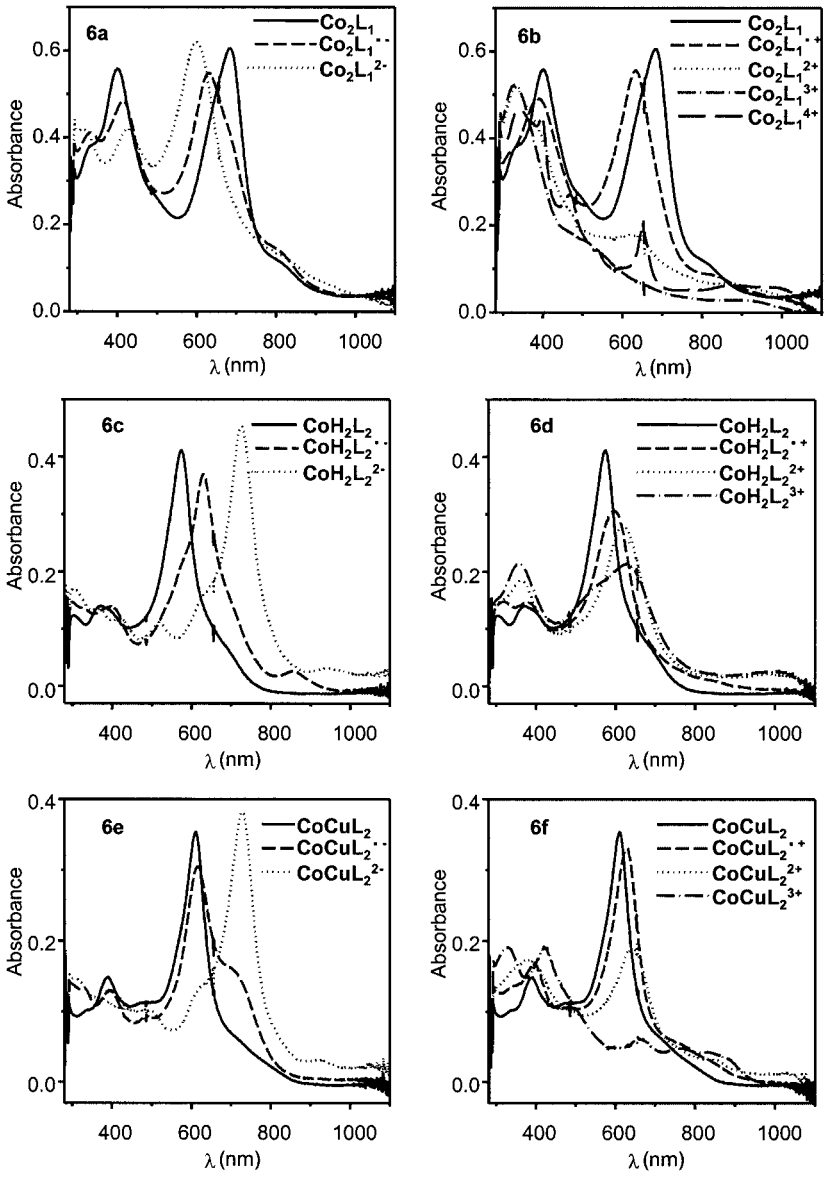

Figure 6. Spectroelectrochemistry on Co_2L_1, CoH_2L_2 and $CoCuL_2$, in PhCN +0.1 M Bu_4NPF_6; reduction [Figure 6 (a)] and oxidation processes [Figure 6 (b)] of Co_2L_1. Reduction [Figure 6 (c)] and oxidation processes [Figure 6 (d)] of CoH_2L_2; reduction [Figure 6 (e)] and oxidation processes [Figure 6 (f)] of $CoCuL_2$; $c \approx 10^{-5}$ M

to those observed for the complex CoH_2L_2; however, instead of an oxidation at −0.28 V/Fc, a reduction current is observed (Figure 8). The spectroelectrochemical reduction of X at −0.4 V/Fc produces spectral evolutions with well-defined isosbestic points that lead to the spectrum of neutral CoH_2L_2.

All these observations confirm that the prepared species X is in fact the radical cation of the complex CoH_2L_2. Mass spectrometry also confirms that X is a mononuclear cobalt complex (m/z = 537 $[M + H]^{2+}$, expected mass for $C_{68}H_{86}CoN_8$: 1073). In situ complexation did not allow us to prepare a new homodinuclear complex to extend our electrochemical studies. No explanation about the formation of this radical has been established. However, since the first oxidation step of the complex CoH_2L_2 occurs at a very low potential, the possible presence of an oxidizing agent as an impurity in the cobalt salt (3000 equiv.) used in excess or oxygen (even our experimental conditions are not suitable for this kind of reaction),[32] could be responsible for the chemical reaction generating the radical cation.

Discussion

The main difference between the free bases and the cobalt complexes (see Tables 1 and 2) that belong to the same COP ligand series involves the redox potentials beyond the second oxidation process. The third oxidations for the cobalt complexes occur at potentials much less positive than those observed for the free bases, and correspond to the oxidation of Co^{II} to Co^{III}. The redox potential of the latter step is solvent-dependent, as expected for metal-centered electron

 © 2004 Wiley-VCH Verlag GmbH & Co. KGaA, Weinheim

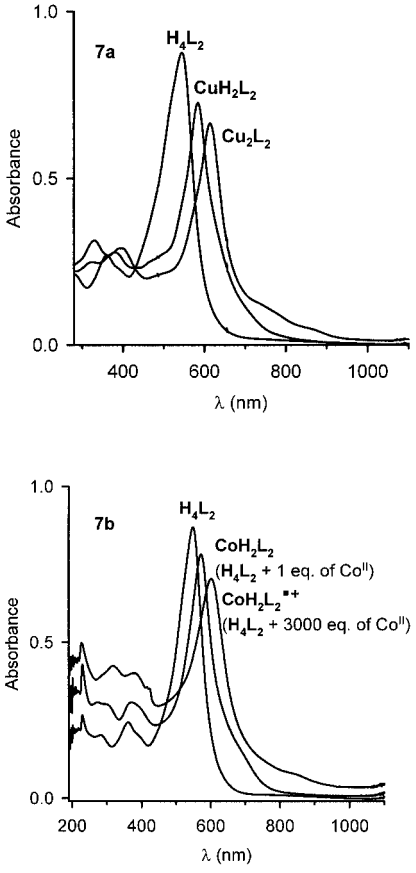

Figure 7. UV/Visible absorption spectra of H_4L_2 ($\approx 10^{-5}$ M) and spectral evolutions for in situ complexation in a mixture of methanol/dichloromethane (1:1) with metallic divalent salts; 7a for in situ complexation with Cu^{II} and 7b for in situ complexation with Co^{II}

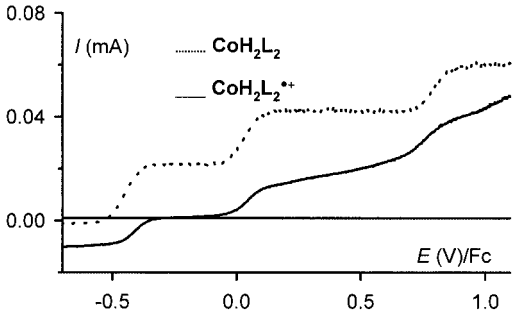

Figure 8. Rotating disk voltammetry on CoH_2L_2 and $CoH_2L_2^+$ in CH_2Cl_2 + 0.1 M Bu_4NPF_6, at a Glassy Carbon (GC) working electrode; scan rate: 0.01 V/s. N = 2000 rpm; $c \approx 10^{-4}$ M

transfers and as observed previously for porphyrins.[23,24] This behavior is due to the conversion of a preferred square-planar coordination for the Co^{II} to an octahedral coordination for the Co^{III} ion. Thus, a coordinating solvent like PhCN will be axially coordinated by metals, thus stabilizing the Co^{III} ion. This stabilization will facilitate the generation of Co^{III}, such that the potential will be cathodically shifted relative to the values determined in CH_2Cl_2.

All the studies undertaken confirm that COP do not stabilize the Co^{I} species at all. This is not the case for previously studied cobalt complexes.[24] COP behave like corrphycenes[33] and porphycenes,[34] and differ vastly from porphyrins, which usually stabilize cobalt(I) in the tetrapyrrolic ring system. The observed $Co^{II/III}$ redox potentials in COP are much more positive than those observed previously in tetrapyrrolic ring systems (−0.07 V/Fc for corrphycene,[33] +0.195 V/Fc for porphycene[34] and +0.30 V/Fc for porphyrins[35]). Such positive potentials are in agreement with the fact that cyclooctaphyrins destabilize Co^{III} in the corresponding "tetrapyrrolic" coordination site of COP. Within the COP series, Co_2L_1 stabilizes the cobalt(III) atom to a greater extent than other COP complexes such as CoH_2L_2 and $CoCuL_2$. Comparison with previously studied cobalt tetrapyrrolic macrocyclic complexes was not possible since the oxidation of the cobalt ion occurs before ring oxidation for these complexes. For the COP complexes, the oxidation of the cobalt ion occurs after the generation of the dication.

Spectral changes for the free base and the cobalt complex are similar during the two reduction and first two oxidation steps, indicating that these four redox steps occur on the ligand, generating the radical anion and the dianion during reduction, and the radical cation and the dication during oxidation. The free base presents a non-reversible behavior for the second reduction step for prolonged electrolysis: the spectral changes are similar to those observed for metal complexes for at least the first ten minutes. Thus, we can conclude that this electron transfer is also ligand-centered.

The third oxidation presents different spectral changes for the free base and the metal complex, which is consistent with a metal-centered electron transfer process. The spectral changes during this third oxidation for the cobalt complex mainly involve the intensity of the absorption bands. This type of behavior is also characteristic of a metal-centered electron transfer process, as generally it induces smaller geometric or topographic changes in the molecule.

For the other cobalt complexes similar conclusions are obtained from the spectroelectrochemical results. In addition, their behavior in two different solvents provides confirmation of the nature of the electron transfers.

Conclusion

All cyclooctaphyrin cobalt complexes undergo two reduction processes and a first and a second oxidation process, all one-electron, reversible and ligand-centered. Beyond the second oxidation, the redox behavior is different for each complex. They all possess a third one-electron reversible oxidation process centered at the metal ($Co^{2+} \rightarrow Co^{3+}$). The homodinuclear cobalt complex also undergoes a fourth oxidation step that is one-electron and reversible, and centered at the second cobalt cation; no further oxidations are observed. For the monocobalt complex, another oxidation is observed (ligand-centered), as well as two other oxidation steps observed in the case of the heterodinuclear cobalt-copper complex. Spectroelectrochemistry confirms the nature of the electron transfers. The metal-centered steps are affected by the solvent coordi-

 © 2004 Wiley-VCH Verlag GmbH & Co. KGaA, Weinheim

nation properties. A shift towards cathodic potentials is observed for these steps in PhCN, except in the case of the monocobalt complex. An attempt to obtain the homodinuclear cobalt complex of the COP(1.0.1.0.1.0.1.0) series[32] led to the formation of the monocobalt complex radical cation. Under our experimental conditions, no cobalt-centered reductions are observed.

Experimental Section

General Remarks: In most of the cases the electrochemical measurements were carried out in a glove box (less than 3 ppm of H_2O and less than 2 ppm of O_2) at room temperature (25 ± 2 °C) in PhCN containing 0.1 M $TBAPF_6$ in a classical three electrode cell, connected to a PAR (model 273) potentiostat, interfaced with a PC computer. The working electrode was a platinum (Pt) disk electrode (diameter: 2 mm), used either motionless as in cyclic voltammetry (v = 20 mV/s to 5 V/s) or as a rotating disk electrode. The auxiliary and the pseudo-reference electrodes were platinum wires. PhCN (Aldrich, 99 %) was dried for two days over $CaCl_2$ (anhydrous, Fluka, 97 %), and distilled on P_2O_5 (Prolabo) under reduced pressure in an inert atmosphere (Argon). Bu_4NPF_6 was dried in an oven (65 °C) under vacuum for two days. Bu_4NPF_6 was dissolved in PhCN inside the glove box and the solution was then percolated over activated alumina. The available potentials at a platinum working electrode ranged from −2.5 to +1.8 V/Fc.

Some measurements were carried out under classical conditions out of the glove box, in CH_2Cl_2 containing 0.1 M $TBAPF_6$ in a three electrode cell. The electrochemical cell was connected to a computerized multipurpose electrochemical device (Autolab PGSTAT T20) controlled by GPSE software. The working electrode was a glassy carbon (GC) disk electrode (diameter: 3 mm), used either motionless as in cyclic voltammetry (v = 20 mV/s to 5 V/s) or as a rotating disk electrode. The auxiliary electrode was a platinum wire, and the reference electrode was Ag/AgCl/KCl (sat.) electrode. All potentials are referred to the ferrocene/ferrocenium (Fc/Fc^+) couple used as internal standard.

Spectroelectrochemical measurements were carried out in PhCN in a home-made quartz cell, having an optical pathway of 1 mm. The working electrode was a platinum grid (1000 mesh) placed in the optical pathway. The reference and the auxiliary electrodes were platinum wires separated by cotton from the solution in individual compartments. The cell was filled in the glove box, and hermetically closed, then it was placed in a diode array spectrophotometer (Hewlett−Packard 8453), and the spectra were recorded during electrolysis.

2,3,7,8,12,13,16,17,21,22,26,27,31,32,35,36-Hexadecaethyloctaphyrin-(1.1.1.0.1.1.1.0)ato-dicobalt(II) (Co_2L_1): The dinuclear cobalt(II) complex Co_2L_1 was prepared by dissolving the free base H_4L_1 (52 mg, 0.05 mmol) in 50 mL of absolute DMF, by gently heating the solution under argon. A solution of cobalt(II) acetate tetrahydrate (125 mg, 0.5 mmol) dissolved in 15 mL of DMF was added to the ligand and the solution was refluxed for three hours. After cooling to room temperature, 50 mL of toluene was added to the solution as well as 150 mL of ice water. The organic layer was washed several times with water, dried over Na_2SO_4 and finally the solvent was removed under vacuum. Recrystallization under argon in a mixture of acetonitrile/t-butylmethyl ether (4:1) gave Co_2L_1 as a black powder. Yield 36 mg (65 %). MS (FAB): m/z = 1156 $[M^+]$ (100 %). $C_{70}H_{86}Co_2N_8$ (1157.4): calcd. C 72.64, H 7.49, N 9.68; found C 72.36, H: 7.49, N: 9.42. IR (CsI): $\tilde{\nu}$ = 2962, 2930, 2869, 1663, 1577, 1492, 1464, 1450, 1371, 1314, 1275, 1205, 1170, 1141, 1110, 1055, 1029, 1018, 986, 960, 925, 848, 835, 809, 746, 679 cm^{-1}. UV/Vis (CH_2Cl_2) λ_{max} (ε) = 347 sh (34400), 401 (51500), 682 nm (55600 M cm^{-1}). M.p. >300 °C.

2,3,6,7,11,12,15,16,20,21,24,25,29,30,33,34-Hexadecaethyloctaphyrin-(1.01.0.1.0.1.0)atocobalt(II) (CoH_2L_2): The mononuclear cobalt(II) complex CoH_2L_2 was prepared by dissolving the free base H_4L_2 (102 mg, 0.1 mmol) in a mixture of 30 mL of dichloromethane and 1 mL of triethylamine under an inert atmosphere. $Co(OAc)_2$ $4H_2O$ (55 mg, 0.22 mmol) in 15 mL of methanol was added to the solution. The mixture was stirred at room temperature for six hours and the solvent removed under vacuum. At all times the solution temperature was maintained below 25 °C. The remaining compound was chromatographically filtered through aluminum oxide (5 × 2 cm column) with a hexane/dichloromethane mixture (1:3) and finally recrystallized from an acetonitrile/dichloromethane/methanol mixture (1:1:1). CoH_2L_2 was obtained as green crystals. Yield 86 mg (80 %). MS (FAB): m/z = 1073 (100 %) $[M]^+$. $C_{68}H_{86}CoN_8$ (1074.4): calcd. C 76.02, H: 8.07, N 10.43; found C 76.07, H 8.10, N 10.40. IR (KBr): $\tilde{\nu}$ = 2962, 2929, 2869, 1570, 1531, 1507, 1464, 1389, 1270, 1224, 1210, 1187, 1153, 1122, 1109, 1056, 1004, 953, 873, 829, 764 cm^{-1}. UV/Vis (CH_2Cl_2): λ_{max} (ε) = 272 (34000), 370 (34000), 571 (91000), 674 nm (20000 M cm^{-1}). M.p. > 300 °C.

2,3,6,7,11,12,15,16,20,21,24,25,29,30,30,33,34-Hexadecaethyloctaphyrin-(1.01.0.1.0.1.0)atocobalt(II)copper(II) ($CoCuL_2$): The heterodinuclear cobalt copper complex $CoCuL_2$ was obtained by dissolving the mononuclear cobalt complex CoH_2L_2 (107 mg, 0.1 mmol) in 50 mL of CH_2Cl_2. $Cu(OAc)_2$ H_2O (20 mg) dissolved in methanol was added to the solution and the mixture was stirred for one hour at room temperature. The solvent was removed under vacuum and the compound purified by chromatographic filtration through aluminum oxide (5 × 1 cm column) with a mixture of toluene/hexane (1:2). The unique fraction was finally recrystallized from a hexane/dichloromethane (1:1) mixture yielding $CoCuL_2$. MS (FAB): m/z = 1134 (100 %) $[M]^+$, 1151 (20) $[M + 1/2O_2]^+$. $C_{68}H_{84}CoCuN_8$ (1136.0): calcd. C 71.9, H 7.45, N 9.86; found C 71.52, H 7.49, N 9.98. IR (CsI): $\tilde{\nu}$ = 2961, 2928, 2867, 1561, 1520, 1496, 1464, 1387, 1369, 1266, 1228, 1187, 1153, 1122, 1108, 1060, 1006, 954, 874, 833, 782 cm^{-1}. UV/Vis (CH_2Cl_2): λ_{max} (ε) = 389 (37000), 608 nm (87000 M cm^{-1}). M.p. > 300 °C.

[1] A. Eschenmoser, *Angew. Chem.* **1988**, *100*, 5−40; *Angew. Chem. Int. Ed. Engl.* **1988**, *27*, 5−39.
[2] J. P. Collman, P. S. Wagenknecht, J. E. Hutchison, *Angew. Chem.* **1994**, *106*, 1620−1639; *Angew. Chem. Int. Ed. Engl.* **1994**, *33*, 1537−1554 and references cited therein.
[3] K. M. Kadish, *Progress in Inorganic Chemistry* (Ed.: S. J. Lippard) Vol. 34, pp 435−605, J. Wiley & Sons, New York, **1986**.
[4] J. L. Sessler, M. J. Cyr, A. K. Burrell, *Synlett* **1991**, 127−134.
[5] J. L. Sessler, M. Cyr, A. K. Burrell, *Tetrahedron* **1992**, *48*, 9661−9672.
[6] T. D. Lash, *Angew. Chem.* **2000**, *112*, 1833−1837; *Angew. Chem. Int. Ed.* **2000**, *39*, 1763−1767.
[7] J. L. Sessler, A. K. Burrell, *Topics in Current Chemistry* **1991**, *161*, 177−273.
[8] A. Jasat, D. Dolphin, *Chem. Rev.* **1997**, *97*, 2267−2340.
[9] J. L. Sessler, S. J. Weghorn, *Expanded, Contracted & Isomeric Porphyrins*, Elsevier Science Ltd. Redwood Books, Wiltshire, **1997**.

 © 2004 Wiley-VCH Verlag GmbH & Co. KGaA, Weinheim

[10] J. L. Sessler, A. Gebauer, E. Vogel, *The Porphyrin Handbook*, vol. 2, 1, Academic Press, San Diego, **2000.**
[11] R. Charrière, T. A. Jenny, H. Rexhausen, A. Gossauer, *Heterocycles.* **1993**, *36*, 1561−1575.
[12] J. L. Sessler, S. J. Weghorn, Y. Hiseada, V. Lynch, *Chem. Eur. J.* **1995**, *1*, 56−67.
[13] V. J. Bauer, D. L. J. Clive, D. Dolphin, J. B. Paine, F. L. Harris, M. M. King, J. Loder, S. W. C. Wang, R. B. Woodward, *J. Am. Chem. Soc.* **1983**, *105*, 6429−6436.
[14] J. L. Sessler, S. J. Weghorn, Y. Hiseada, V. Lynch, *Chem. Eur. J.* **1995**, *1*, 56−67.
[15] H. Rexhausen, PhD Dissertation, University of Berlin, **1983**.
[16] M. Bröring, J. Jendrny, L. Zander, H. Schmickler, J. Lex, Y. D. Wu, M. Nendel, J. Chen, D. A. Plattner, K. N. Houk, E. Vogel, *Angew. Chem.* **1995**, *107*, 2709−2711; *Angew. Chem. Int. Ed. Engl.* **1995**, *34*, 2515−2517.
[17] E. Vogel, M. Bröring, J. Fink, D. Rosen, H. Schmickler, J. Lex, K. W. K. Chan, Y. D. Wu, D. A. Plattner, M. Nendel, K. N. Houk, *Angew. Chem.* **1995**, *107*, 2705−2709; *Angew. Chem. Int. Ed. Engl.* **1995**, *34*, 2511−2514.
[18] J. L. Sessler, D. Seidel, V. Lynch, *J. Am. Chem. Soc.* **1999**, *121*, 11257−11258.
[19] L. Zander, PhD dissertation, University of Köln, **1998**.
[20] M. Michels, PhD dissertation, University of Köln, **1999**.
[21] A. Werner, M. Michels, L. Zander, J. Lex, E. Vogel, *Angew. Chem.* **1999**, *111*, 3866−3870; *Angew. Chem. Int. Ed.* **1999**, *38*, 3650−3653.
[22] M. Gosmann, B. Franck, *Angew. Chem.* **1986**, *98*, 1107−1108; *Angew. Chem. Int. Ed. Engl.* **1986**, *25*, 1100−1101.
[23] L. A. Truxillo, D. G. Davis, *Anal. Chem.* **1975**, *47*, 2260−2267.
[24] F. A. Walker, D. Beroiz, K. M. Kadish, *J. Am. Chem. Soc.* **1976**, *98*, 3484−3489.
[25] D. K. Lavallee, M. J. Bain, *Inorg. Chem.* **1976**, *15*, 2090−2093.
[26] J. P. Gisselbrecht, J. Bley-Escrich, M. Gross, L. Zander, M. Michels, E. Vogel, *J. Electroanal. Chem.* **1999**, *469*, 170−175.
[27] J. Bley-Escrich, J. P. Gisselbrecht, E. Vogel, M. Gross, *Eur. J. Inorg. Chem.* **2002**, 2829−2837.
[28] J. Tomeš, *Collect. Czech. Chem. Commun.* **1937**, *9*, 150.
[29] D. K. Geiger, E. J. Pavlak, L. T. Kass, *J. Chem. Educ.* **1991**, *68*, 337−339.
[30] D. K. Geiger, *J. Chem. Educ.* **1991**, *68*, 340−342.
[31] M. J. M. Nesset, N. V. Shokhirev, P. D. Enemark, S. E. Jacobson, F. A. Walker, *Inorg. Chem.* **1996**, *35*, 5188−5200.
[32] Z. Dokuzovic, X. Ahmeti, D. Pavlovic, I. Murati, S. Asperger, *Inorg. Chem.* **1982**, *21*, 1576−1581.
[33] J. P. Gisselbrecht, M. Gross, E. Vogel, J. L. Sessler, *Inorg. Chem.* **2000**, *39*, 2850−2854.
[34] C. Bernard, J. P. Gisselbrecht, M. Gross, E. Vogel, M. Lausmann, *Inorg. Chem.* **1994**, *33*, 2393−2401.
[35] S. Kelly, D. Lançon, K. M. Kadish, *Inorg. Chem.* **1984**, *23*, 1451−1458.

Received July 23, 2003
Early View Article
Published Online December 12, 2003

 © 2004 Wiley-VCH Verlag GmbH & Co. KGaA, Weinheim

Yttrium β-Diketonate Glyme MOCVD Precursors: Effects of the Polyether Length on Stabilities, Mass Transport Properties and Coordination Spheres

Graziella Malandrino,[a] Raffaella Lo Nigro,[b] Ignazio L. Fragalà,*[a] and Cristiano Benelli[c]

Keywords: Yttrium / Thermogravimetry / Superconductors

The glyme adducts of trishexafluoroacetylacetonato yttrium, [Y(hfa)$_3$·monoglyme], [Y(hfa)$_3$·diglyme], [Y(hfa)$_3$·(H$_2$O)$_2$·triglyme] and [Y(hfa)$_2$·tetraglyme]$^+$[Y(hfa)$_4$]$^-$ {CH$_3$(OCH$_2$CH$_2$)$_n$-OCH$_3$, n = 1 monoglyme, 2 diglyme, 3 triglyme and 4 tetraglyme}, were synthesized and characterized by elemental analysis, mass spectrometry, and IR, ^{1}H and ^{13}C NMR spectroscopy. Additionally, [Y(hfa)$_3$·monoglyme] and [Y(hfa)$_3$·diglyme] were characterized by single-crystal X-ray diffraction studies. The mass-transport properties of these adducts were investigated by thermogravimetric analysis, differential scanning calorimetry, evaporation-rate measurements and chemical vapour-deposition experiments. There is evidence of high volatility and very good thermal stabilities with a residue lower than 2–4 %. Vaporization-rate experiments proved that all adducts are well-suited for metal-organic chemical vapour-deposition experiments. The [Y(hfa)$_3$·monoglyme] complex was successfully applied in the low-pressure MOCVD process of YBaCuO HTc superconductor using a multimetal molten single source.

(© Wiley-VCH Verlag GmbH & Co. KGaA, 69451 Weinheim, Germany, 2004)

Introduction

New lanthanide β-diketonate adducts with polyethers[1−13] have recently attracted particular attention because they have better properties than their parent β-diketonate precursors for MOCVD, in terms of thermal stability and volatility.

Although yttrium is not a 4f element, its chemistry resembles that of lanthanides and, in particular, similarities are observed either with neodymium and samarium or with holmium and erbium ions, depending on whether the nature of the bonds is predominantly covalent or ionic.[14] Yttrium ions are present in a wide variety of materials, ranging from yttria (Y_2O_3) and yttria-stabilized zirconia (YSZ), to optoelectronic materials such as yttrium aluminium or indium garnet (YGA and YIG respectively), or from yttrium aluminate ($YAlO_3$) to the superconducting metal oxide $YBa_2Cu_3O_{7-\delta}$ (YBCO). The synthesis of these materials in the form of thin films, using a friendly and low-cost technique, represents a great challenge. In this context, the Metal-Organic Chemical Vapour Deposition (MOCVD) technique offers a softer approach for all these applications, with lower processing temperatures and greater throwing power (versatility and adaptability) than other alternative methodologies.[15]

To date, the conventional yttrium precursors, such as Y(tmhd)$_3$ (Htmhd = 2,2,6,6-tetramethyl-3,5-heptandione), have had several drawbacks, most notably the high quantity of residue left in commercial evaporators/bubblers and their poor stability in the atmosphere.[16,17]

In this scenario, novel monomeric, thermally stable, volatile and water-free yttrium complexes are of strategic relevance due to the lack of MOCVD precursors with suitable mass-transport properties. This consideration prompted investigations on new, suitable, highly chelated molecular architectures that inhibit oligomerization and water-coordination processes and improve the thermal stability, volatility and mass-transport properties.

It has been already demonstrated that the combined use of fluorinated β-diketonates and of ancillary-coordinated polyethers provides monomeric, volatile and thermally stable precursors of a large variety of metal ions including rare-earth metals.[1−7,12,13,18] The same strategy was adopted for the yttrium ion, and the tailoring of the molecular architecture of the ligand framework yielded novel, very promising second-generation yttrium precursors.[19,20] However, there is no information on the thermal and mass-transport properties of all these adducts.

In this paper we report the synthesis and transport properties of the four yttrium adducts [Y(hfa)$_3$·L] [where

[a] Dipartimento di Scienze Chimiche and Unità INSTM of Catania, Università di Catania
Viale Andrea Doria 6, 95125 Catania, Italy
E-mail: lfragala@dipchi.unict.it
[b] IMM-CNR, sezione di Catania,
Stradale Primosole n 50, 95121 Catania, Italy
[c] Dipartimento di Chimica and Unità INSTM of Firenze, Università di Firenze, Italy

 © 2004 Wiley-VCH Verlag GmbH & Co. KGaA, Weinheim DOI: 10.1002/ejic.200300354

Hhfa = 1,1,1,5,5,5-hexafluoroacetylacetone, L = CH_3O-$(CH_2CH_2O)_nCH_3$ with n = 1 monoglyme (1,2-dimethoxyethane), 2 diglyme [bis(2-methoxyethyl)ether), [$Y(hfa)_3$·$(H_2O)_2$·triglyme] [triglyme = (2,5,8,11-tetraoxadodecane)], and [$Y(hfa)_2$·tetraglyme]$^+$[$Y(hfa)_4$]$^-$, [tetraglyme = (2,5,8,11,14-pentaoxatetradecane)]. The X-ray single crystal structure of [$Y(hfa)_3$·monoglyme] is reported and the current X-ray data of [$Y(hfa)_3$·diglyme] are compared with those previously reported. Thermal stabilities and volatilities of all the adducts were evaluated and compared with those of the first-generation yttrium precursors. The use of [$Y(hfa)_3$·monoglyme] in the deposition of YBCO thin films was also addressed in detail, and, finally, the effects of the polyether length on the coordination/structure, thermal stability, volatility and coordination sphere of the $Y(hfa)_3$ moiety are discussed.

The aim of the present study is, therefore, the functional validation of these "second-generation" yttrium precursors, in the perspective of MOCVD applications, also in terms of a multimetal molten single source.

Results

Synthesis

The adducts of $Y(hfa)_3$ with four different glymes were prepared through one-pot reactions from yttrium hydroxide, hexafluoroacetylacetone and polyether in hexane [see Equation (1)]:

$$Y(OH)_3{\cdot}nH_2O + 3Hhfa + L \rightarrow [Y(hfa)_3{\cdot}L] + (n+3)H_2O$$
$$\text{or } [Y(hfa)_3{\cdot}(H_2O)_2{\cdot}L'] \quad \text{or } [Y(hfa)_2{\cdot}L'']^+[Y(hfa)_4]^-$$
(L = monoglyme, diglyme; L' = triglyme; L'' = tetraglyme) (1)

A slight excess of yttrium hydroxide favours the isolation of the product, since the insoluble excess of $Y(OH)_3{\cdot}nH_2O$ can be easily filtered off. The present syntheses can be efficiently carried out in hexane with good yields thus avoiding the use of carcinogenic benzene or toluene, as in the alternative syntheses already reported.[19,20]

The adducts synthesised are very soluble in common organic solvents such as ethanol, chloroform, acetone, pentane, and toluene, and slightly soluble in cyclohexane. Adducts **1−3** have low melting points and evaporate quantitatively at low temperature under vacuum. They are nonhygroscopic and can be handled in air.

X-ray Single Crystal Structures of [$Y(hfa)_3$·monoglyme] and [$Y(hfa)_3$·diglyme]

The ORTEP drawing of the asymmetric unit [$Y(hfa)_3$·monoglyme] is shown in Figure 1. Selected bond lengths and angles are reported in Table 1. The crystal structure consists of monomeric units of molecules where an yttrium ion is in an eight coordination sphere formed by the six oxygen atoms of three hfa ligands and by two oxygen atoms of the monoglyme ligand. The coordination polyhedron around the yttrium atom is highly distorted and far from any idealized polyhedron. The average Y−O(hfa) distance is 2.34 Å, similar to the bond lengths observed in other $Y(hfa)_3$ derivatives.

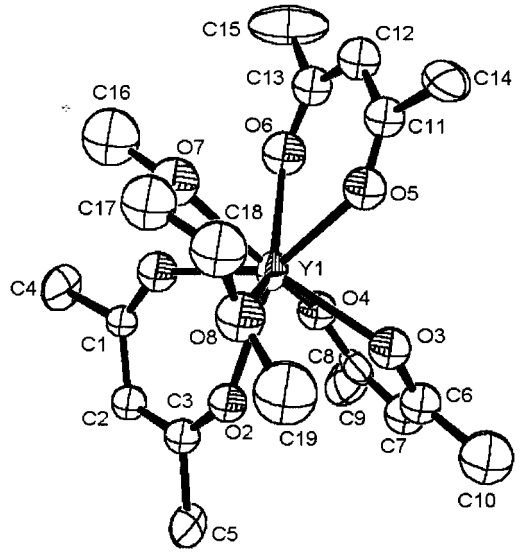

Figure 1. ORTEP drawing of the asymmetric unit of complex [$Y(hfa)_3$·monoglyme]; CF_3 groups have been omitted for clarity; probability of thermal ellipsoids is 50 %

The ORTEP drawing of the asymmetric unit [$Y(hfa)_3$·diglyme] is shown in Figure 2. Selected bond lengths and angles are reported in Table 2. The crystal structure consists of monomeric units of molecules where an yttrium ion is in a nine coordination sphere formed by the six oxygen atoms of three hfa ligands and by three oxygen atoms of the diglyme ligand. The [$Y(hfa)_3$·diglyme] complex possesses an orthorhombic structure. It should be noted that the structure of [$Y(hfa)_3$·diglyme] has been previously published by Pollard et al,[19] but in a monoclinic habit. The average Y−O(hfa) distance, observed in the current, more symmetrical structure, is 2.361 Å, 0.015 Å longer than the bond lengths observed in the monoclinic derivative (2.346 Å). Analogously, the average lenght of the Y−O(diglyme) bonds presently observed (2.510 Å) is 0.015 Å greater than that previously reported (2.495 Å).

It is interesting to compare the structures of these adducts with those of the analogous La,[1,4] Gd,[2] and Ho[20] derivatives. The average Y−O lenghts observed are similar to those reported for the Gd and Ho adducts. Moreover a large difference (0.150 Å) is observed between the average Y−O(diglyme) and the average Y−O(hfa) lenghts in the [$Y(hfa)_3$·diglyme], which is exactly the same as that observed for the Gd derivative and much larger than that reported (0.014 Å) for the La analogue. These data may be interpreted by considering the ionic radius values of the La^{3+} (1.13 Å), Gd^{3+} (1.02 Å), Y^{3+} (0.93 Å), and Ho^{3+} (0.97 Å) ions.

NMR Spectra

^1H and ^{13}C NMR spectra (see Table 3) were recorded in $CDCl_3$ for adducts **1−3**. In the case of adduct **4**, the lower

 © 2004 Wiley-VCH Verlag GmbH & Co. KGaA, Weinheim

Table 1. Selected bond lengths [A] and angles [°] for [Y(hfa)$_3$·monoglyme]

	Bonds
Y(1)−O(6)	2.322(12)
Y(1)−O(2)	2.325(11)
Y(1)−O(1)	2.344(10)
Y(1)−O(3)	2.346(10)
Y(1)−O(4)	2.353(10)
Y(1)−O(5)	2.365(12)
Y(1)−O(7)	2.456(12)
Y(1)−O(8)	2.476(11)
	Angles
O(6)−Y(1)−O(2)	145.9(4)
O(6)−Y(1)−O(1)	79.7(4)
O(2)−Y(1)−O(1)	72.3(4)
O(6)−Y(1)−O(3)	119.1(4)
O(2)−Y(1)−O(3)	76.4(4)
O(1)−Y(1)−O(3)	142.3(4)
O(6)−Y(1)−O(4)	77.9(4)
O(2)−Y(1)−O(4)	77.9(4)
O(1)−Y(1)−O(4)	78.9(3)
O(3)−Y(1)−O(4)	74.3(3)
O(6)−Y(1)−O(5)	73.9(4)
O(2)−Y(1)−O(5)	139.1(3)
O(1)−Y(1)−O(5)	145.4(4)
O(3)−Y(1)−O(5)	71.7(4)
O(4)−Y(1)−O(5)	116.0(4)
O(6)−Y(1)−O(7)	78.2(4)
O(2)−Y(1)−O(7)	111.3(4)
O(1)−Y(1)−O(7)	74.2(4)
O(3)−Y(1)−O(7)	138.3(4)
O(4)−Y(1)−O(7)	146.7(3)
O(5)−Y(1)−O(7)	78.7(4)
O(6)−Y(1)−O(8)	136.4(5)
O(2)−Y(1)−O(8)	72.7(4)
O(1)−Y(1)−O(8)	108.9(4)
O(3)−Y(1)−O(8)	80.6(4)
O(4)−Y(1)−O(8)	145.1(4)
O(5)−Y(1)−O(8)	77.3(4)
O(7)−Y(1)−O(8)	64.4(4)

solubility in $CDCl_3$ required $(CD_3)_2CO$ and C_6D_6 for ^1H and ^{13}C NMR spectroscopy, respectively. The ^1H NMR spectra always show a singlet around 6.0 ppm associated with the alkene proton of the hfa ligand. Different resonances are associated with the polyether framework and the related values are reported in Table 3. The spectrum of **3** contains a resonance (δ = 3.94 ppm) associated with the coordinated H_2O. The intensities of pertinent resonances point to a 3:2:1 (hfa:H_2O:triglyme) ratio.

The evaluation of the relative intensities of hfa and tetraglyme resonances of adduct **4** points to a 6:1 (hfa:tetraglyme) ratio. This observation may be accounted for by considering an ionic structure [Y(hfa)$_2$·tetraglyme]$^+$-[Y(hfa)$_4$]$^-$, as previously proposed by Pollard et al.[19]

The ^{13}C NMR ($CDCl_3$) spectra can be assigned by comparison with the data of related lanthanum complexes.[1,3,4] Details of associated resonances are reported in Table 3.

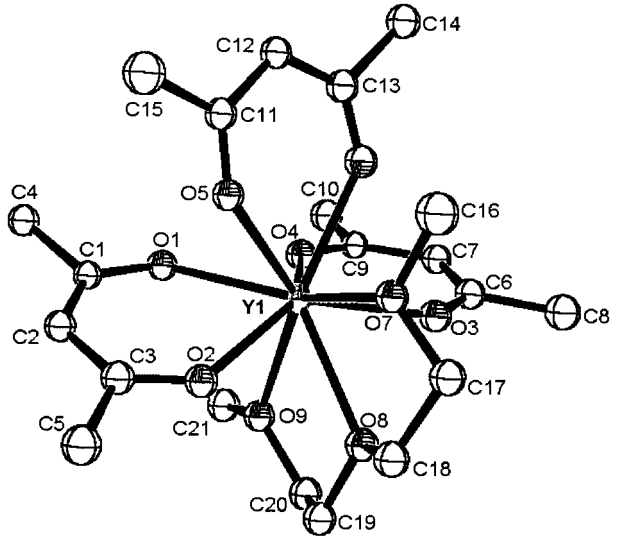

Figure 2. ORTEP drawing of the crystal structure of [Y(hfa)$_3$·diglyme]; CF_3 groups have been omitted for clarity; probability of thermal ellipsoids is 50 %

Mass Spectra

The FAB$^+$ spectra of the adducts **1**−**4** are reported in Table 4. The spectra show fragment peaks due to fragmentation of both the hfa and polyether ligands. In addition, there is evidence of the characteristic fluorine-transfer process, already observed in the spectra of the analogous alkaline-earth[18,21] and lanthanide (La, Gd, Eu) adducts.[2,4,6] The fluorine-transfer process preludes a fluoride phase formation that could contaminate the deposited films, unless appropriate conditions are used. No molecular ion peaks or peaks at higher mass were observed for the adducts. The major peak of all the adducts corresponds to the ion [Y(hfa)$_2$·L]$^+$. At lower mass values, the more abundant peaks correspond to the fragments [Y(hfa)·L + F]$^+$, [Y·L + 2F]$^+$, [Y(hfa)$_2$]$^+$, [Y(hfa) + F]$^+$.

Infrared Spectra

The IR spectra of the raw and sublimed adducts are identical. The absence of any bands around 3300−3600 cm^{-1} in the spectrum of **1**, **2** and **4** is indicative of H_2O-free species. In contrast, the broad bands at 3380 cm^{-1} and 3260 cm^{-1} in the spectrum of **3** are associated with coordinated water (see below). In addition all the spectra show the characteristic peaks at 1660 cm^{-1} and 1500−1550 cm^{-1} associated with C=O and C=C stretching, respectively. The characteristic trend of peaks at 1255, 1210, 1140 and 1100 cm^{-1} arises from the overlap of the band due to C−F stretching and those associated with C−O stretching. The peaks between 800 and 1050 cm^{-1} may be considered fingerprints of the glyme coordination to the yttrium hexafluoroacetylacetonate moiety.

Mass-Transport Properties

The thermal characteristics of the raw adducts were studied by atmospheric-pressure thermogravimetric (TG) analy-

 © 2004 Wiley-VCH Verlag GmbH & Co. KGaA, Weinheim

Table 2. Selected bond lengths [A] and angles [°] for [Y(hfa)$_3$·diglyme]

	Bonds
Y(1)−O(1)	2.334(7)
Y(1)−O(3)	2.335(6)
Y(1)−O(2)	2.347(8)
Y(1)−O(6)	2.352(8)
Y(1)−O(4)	2.384(7)
Y(1)−O(5)	2.415(8)
Y(1)−O(7)	2.477(6)
Y(1)−O(9)	2.487(7)
Y(1)−O(8)	2.522(7)
	Angles
O(1)−Y(1)−O(3)	142.7(2)
O(1)−Y(1)−O(2)	73.6(2)
O(3)−Y(1)−O(2)	135.1(3)
O(1)−Y(1)−O(6)	99.7(2)
O(3)−Y(1)−O(6)	72.6(3)
O(2)−Y(1)−O(6)	140.6(3)
O(1)−Y(1)−O(4)	70.5(2)
O(3)−Y(1)−O(4)	72.6(2)
O(2)−Y(1)−O(4)	136.6(2)
O(6)−Y(1)−O(4)	70.1(2)
O(1)−Y(1)−O(5)	69.6(2)
O(3)−Y(1)−O(5)	134.0(2)
O(2)−Y(1)−O(5)	72.0(3)
O(6)−Y(1)−O(5)	69.3(3)
O(4)−Y(1)−O(5)	115.6(2)
O(1)−Y(1)−O(7)	139.3(2)
O(3)−Y(1)−O(7)	76.3(2)
O(2)−Y(1)−O(7)	82.0(2)
O(6)−Y(1)−O(7)	79.2(2)
O(4)−Y(1)−O(7)	141.4(2)
O(5)−Y(1)−O(7)	72.1(2)
O(1)−Y(1)−O(9)	76.1(2)
O(3)−Y(1)−O(9)	87.2(2)
O(2)−Y(1)−O(9)	76.9(2)
O(6)−Y(1)−O(9)	140.4(2)
O(4)−Y(1)−O(9)	71.6(2)
O(5)−Y(1)−O(9)	138.8(2)
O(7)−Y(1)−O(9)	129.4(2)
O(1)−Y(1)−O(8)	129.1(2)
O(3)−Y(1)−O(8)	67.5(2)
O(2)−Y(1)−O(8)	67.7(2)
O(6)−Y(1)−O(8)	131.3(2)
O(4)−Y(1)−O(8)	120.4(2)
O(5)−Y(1)−O(8)	124.0(2)
O(7)−Y(1)−O(8)	65.3(2)
O(9)−Y(1)−O(8)	64.1(2)

sis, differential scanning calorimetry (DSC) and atmospheric pressure TG vaporization-rate experiments.[22] The TG curves of **1−4** are reported in Figure 3. Single sublimation steps are observed for the monoglyme, diglyme and tetraglyme adducts. The monoglyme adduct shows a 96 % weight loss in the 79−220 °C range with a 4 % residue left at 275 °C. Adducts **2** and **4** show a weight loss in the 90−260 °C (residue = 2 % to 300 °C) and 170−330 °C (residue = 4 % to 400 °C) temperature ranges, respectively. The triglyme adduct shows two distinct sublimation steps corresponding to weight losses of 29 % in the temperature range 80−230 °C and 60 % in the temperature range 230−300 °C. The first step is probably due to the loss of the triglyme and coordinated H_2O molecules, whose corresponding weight loss is about 22 %.

When TG atmospheric-pressure vaporization rates of adducts **1−4** are compared to the data of [Y(tmhd)$_3$·H_2O] in Figure 4, it becomes evident that adducts **1** and **2** are more volatile than the "first-generation" [Y(tmhd)$_3$·H_2O] precursor, and in particular, vaporize approximately four and two times faster than [Y(tmhd)$_3$·H_2O], respectively. Adduct **3** shows a nonlinear behaviour of the vaporization rate confirming that partial decomposition may occur during vaporization. The low volatility of adduct **4** is probably due to its ionic structure: [Y(hfa)$_2$tetraglyme]$^+$ [Y(hfa)$_4$]$^-$.

The DSC data (see Figure 5) of these adducts show some interesting features in addition to the melting and evaporation processes. The DSC curve of the monoglyme adduct shows two endothermic peaks at 75.7 °C associated with the melting of the product and at approximately 175 °C due to evaporation. Similarly the DSC curve of adduct **2** shows two endothermic peaks associated with melting (62.2 °C) and evaporation processes (about 150 °C), respectively. Moreover, there is evidence at 220 °C of an exothermic peak that is observed in the freshly prepared as well as in the aged (over 4 months) samples.

The DSC data of adduct **3** show an unusually broad endothermic peak at 53.8 °C, which can be mainly associated with the melting of the product. Nevertheless, it is likely that another kind of process, that is, a solid-phase transition peak, may be hidden under the same peak. A second endothermic peak (at around 250 °C) is associated with the evaporation of the adduct. Similarly to adduct **2**, an exothermic peak is observed at 235 °C.

Adduct **4** shows two endothermic peaks at 176.9 °C, associated with the melting process, and at approximately 275 °C, due to evaporation. An exothermic peak was also found at 248.6 °C.

MOCVD YBCO Deposition From a Molten Multimetal Single Source

The [Y(hfa)$_3$·monoglyme] adduct was successfully employed in a novel, strategic approach to grow $YBa_2Cu_3O_{7-\delta}$ (YBCO) films on $LaAlO_3$ (100) substrates by MOCVD.

The synthesis of any multielement oxide film always introduces complications in the growth process due to the different physico-chemical properties of each single precursor that, of course, requires specific optimization. Recently we reported a new, very simple, low-cost route to high quality $LaAlO_3$ (100) films on $SrTiO_3$ (100) substrates adopting a multimetal molten single source.[23] The novelty of the approach relies upon the use of the [La(hfa)$_3$·diglyme] complex as a solvent for the aluminum precursor Al(acac)$_3$ (Hacac = acetylacetone), thus affording a two-component molten source. The same approach was adopted in the current study and the [Y(hfa)$_3$·monoglyme] complex was used as a solvent for the Ba and Cu precursors. Deposition parameters were, therefore, optimized for the single multimetal source.

 © 2004 Wiley-VCH Verlag GmbH & Co. KGaA, Weinheim

Table 3. ^1H and ^{13}C NMR spectroscopy data of adducts **1, 2, 3** and **4**

Complex	^1H NMR			^{13}C NMR			
	$-CO-CH-CO$	H_2O	polyether[a]	$-CO-CH-CO$	$-CO-CH-CO$	$-CF_3$	polyether[a]
[Y(hfa)$_3$·monoglyme]	6.20 (s, 3 H)		**a** 3.63 (s, 6 H), **b** 3.83 (s, 4 H)	91.72 (s)	178.06 (q, ^2J = 35 Hz)	117.40 (q, ^1J = 283 Hz)	**a** 61.36, **b** 71.49
[Y(hfa)$_3$·diglyme]	6.10 (s, 3 H)		**a** 3.46 (s, 6 H), **b**, **c** 3.83 (m, 8 H)	90.71 (s)	176.82 (q, ^2J = 36 Hz)	117.60 (q, ^1J = 283 Hz)	**a** 60.46 **b** 70.72, **c** 71.11
[Y(hfa)$_3$·(H$_2$O)$_2$·triglyme]	6.10 (s, 3 H)	3.89 (s, 4 H)[b]	**a** 3.40 (s, 6 H), **b**, **c** 3.68 (m, 8 H), **d** 3.76 (s, 4 H)	90.85 (s)	177.08 (q, ^2J = 35 Hz)	117.54 (q, ^1J = 284 Hz)	**a** 59.07, **b** 70.24, **c** 70.48, **d** 71.67
[Y(hfa) tetraglyme]$^+$[Y(hfa)$_4$]$^-$[c]	6.17 (s, 6 H)		**a** 3.30 (s, 6 H), **b**, **c** 3.53 (m, 8 H), **d**, **e** 3.59 (s, 8 H)	89.60 (s)	177.20 (q, ^2J = 34 Hz)	117.79 (q, ^1J = 283 Hz)	**a** 58.46, **b** 70.74, **c** 70.92, **d** 72.34

[a] The following notation has been used from monoglyme (CH**a**$_3$-O-CH**b**$_2$)$_2$ through tetraglyme (CH**a**$_3$-O-CH**b**$_2$-CH**c**$_2$-O-CH**d**$_2$CH**e**$_2$)$_2$O. [b] The position of the water peak moves with concentration. [c] The ^1H NMR spectrum was recorded in acetone, while the ^{13}C NMR spectrum was recorded in C_6D_6.

Table 4. Major peaks in the mass spectra of adducts **1**, **2**, **3** and **4**

Assignment	[Y(hfa)$_3$·monoglyme]	[Y(hfa)$_3$·diglyme]	[Y(hfa)$_3$·(H$_2$O)$_2$·triglyme]	[Y(hfa)$_2$·tetraglyme]$^+$[Y(hfa)$_4$]$^-$
$[M-(hfa)]^+$	593 (100 %)	637 (100 %)	681 (100 %)	725 (100 %)
$[M - 2(hfa) + F]^+$	405 (50 %)	449 (46 %)	494 (80 %)	537 (54 %)
$[M - (hfa) - L]^+$	503 (11 %)			503 (20 %)
$[M - 2(hfa) - L + F]^+$	315 (10 %)	315 (27 %)		315 (22 %)
$[M - 3(hfa) + 2F]^+$	217 (85 %)	261 (78 %)		349 (75 %)
$[YF_2]^+$	126 (70 %)	126 (81 %)	126 (50 %)	

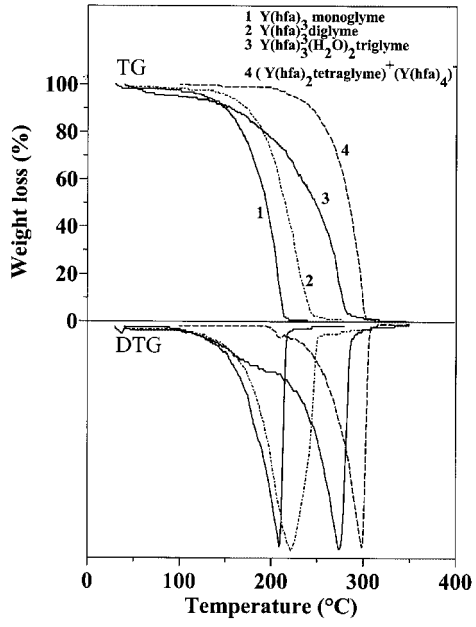

Figure 3. TG-DTG curves of adducts **1−4**

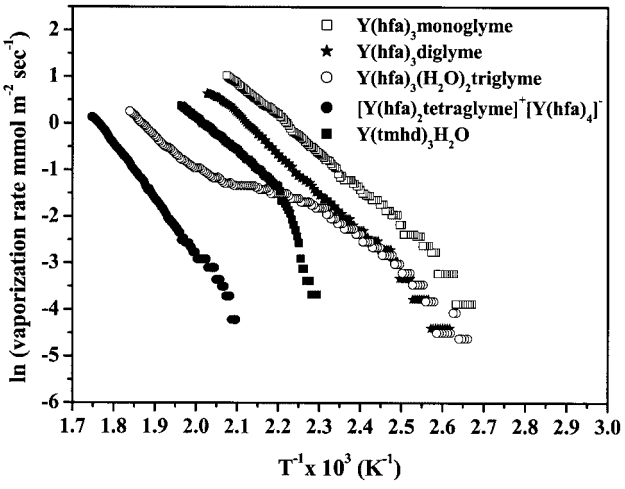

Figure 4. Atmospheric-pressure TG vaporization-rate data of adducts **1−4**

Systematic studies were carried out by changing operational parameters governing both deposition and cooling−annealing processes. The best operative parameters for the growth of high quality YBCO films are the following: i) a single molten multimetal source consisting of a mixture of [Y(hfa)$_3$·monoglyme], [Ba(hfa)$_2$·tetraglyme] and Cu(tmhd)$_2$ complexes (where Htmhd = 2,2,6,6-tetramethyl-3,5-heptanedione) in the 1:2:0.5 Y:Ba:Cu ratio; ii) argon carrier gas (300 sccm); iii) 200 sccm flow of water-saturated oxygen as a reaction gas; iv) deposition temperature of 800 °C; v) deposition time of 3 hours, and vi) annealing at 500 °C in oxygen ambient for 12 hours.

In Figure 6 the DSC curve of the 1:2:0.5 (Y:Ba:Cu) mixture is compared with the curves of each individual precur-

 © 2004 Wiley-VCH Verlag GmbH & Co. KGaA, Weinheim

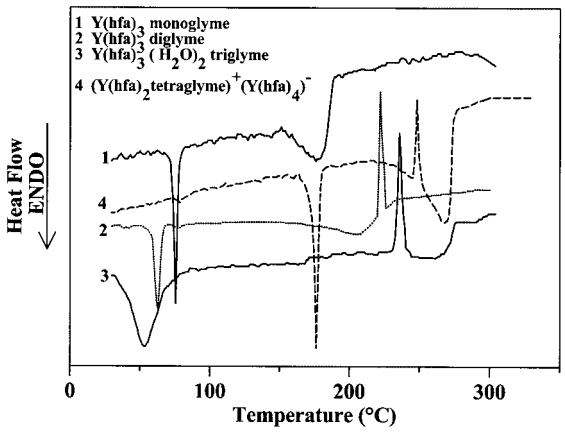

Figure 5. DSC curves of adducts **1**−**4**

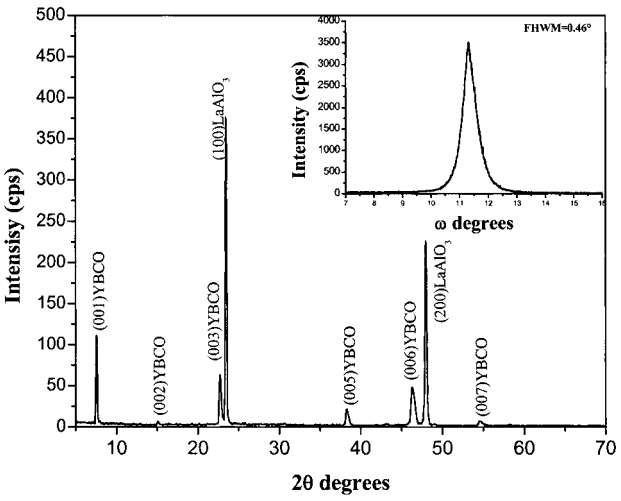

Figure 7. X-ray diffraction pattern of an MOCVD grown YBCO film on an $LaAlO_3$ (100) substrate; the inset shows the rocking curve of the YBCO (003) reflection

sor. The DSC scans of the single [Y(hfa)$_3$·monoglyme], [Ba(hfa)$_2$·tetraglyme] and Cu(tmhd)$_2$ precursors show evidence of the endothermic peaks due to melting {75.7 °C for [Y(hfa)$_3$·monoglyme], 153.6 °C for [Ba(hfa)$_2$·tetraglyme], and 196.3 °C for Cu(tmhd)$_2$} and to evaporation from the melts in the 150−190 °C, 260−290 °C, and 210−260 °C temperature ranges, respectively. The DSC scan of the multicomponent precursor mixture shows a lower temperature peak (73.5 °C) representing the melting of the [Y(hfa)$_3$·monoglyme] component. The following endothermic broad peak in the 110−160 °C temperature range clearly represents dissolution of [Ba(hfa)$_2$·tetraglyme] and Cu(tmhd)$_2$. Finally the endothermic process at the highest temperature (190−270 °C) is associated with the evaporation of the melted mixture. In this context the endothermic peaks expected for [Ba(hfa)$_2$·tetraglyme] and Cu(tmhd)$_2$ melting, at 153.6 °C and 196.3 °C, respectively, are not observed.

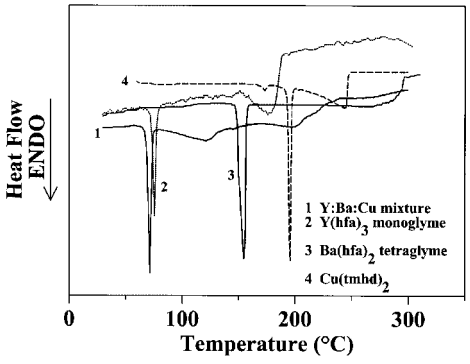

Figure 6. DSC curve of the 1:2:0.5 (Y:Ba:Cu) multimetal single source mixture compared with data of individual precursors [Y(hfa)$_3$·monoglyme], [Ba(hfa)$_2$·tetraglyme], and Cu(tmhd)$_2$

Great attention was devoted to the oxygen partial pressure during the cooling−annealing process, because of its influence on the phase transition from the tetrahedral to the orthorhombic phase. Thus, YBCO films were slowly cooled (3 °C/min) under low pressure (10 Torr) and then maintained at 500 °C under oxygen flow for 12 hours. The chemical composition of the YBCO samples, determined with a windowless EDX detector, indicates the correct 1:2:3 Y:Ba:Cu ratio. No fluorine atoms were detected. The X-ray diffraction pattern of a typical YBCO film deposited on $LaAlO_3$(100) substrates is shown in Figure 7. All the reflections are indexed as (00*l*) peaks, thus indicating that the films are strongly *c*-axis aligned. The degree of *c*-axis alignment was determined by ω-scans (rocking curve) of the (003) YBCO peak. The FWHM value of 0.46° indicates a high degree of texturing. The in-plane (*a*-and *b*-axes) alignment was established by recording the (103) pole figure. The intense four poles at $\Psi = 46°$ observed every 90° of φ in the (103) pole figure indicate a good in-plane orientation of the YBCO films on the $LaAlO_3$ (100) substrate.

Finally, the surface morphology of the YBCO films was observed by scanning electron microscopy. All the prepared samples show smooth surfaces with "platelike" grains. Preliminary measurements of electrical transport properties give a critical temperature (T_c) value of 83 K and a critical current density (J_c) of 10^5 A/cm.[2]

Discussion

The present syntheses reinforce our earlier assertion that this one-pot route is a "general" strategy for the preparation of alkaline-earth (M = Ba, Sr, and Ca)[18] and rare-earth[1−6] volatile and thermally stable metal adducts suitable for MOCVD applications. This synthetic procedure involves open-bench manipulations and yields, reproducibly, the water-free products **1**, **2** and **4**, despite Y(OH)$_3$·*n*H$_2$O being the reagent. Therefore, polyethers act as hard Lewis bases, which encapsulate the metal ion and favourably compete with H$_2$O in saturating the coordination sphere around the metal. Only in the case of the triglyme adduct, some H$_2$O molecules were found to be coordinated to the yttrium centre as indicated by the presence of the band at about 3600 cm^{-1} in the IR spectrum. The related X-ray single

 © 2004 Wiley-VCH Verlag GmbH & Co. KGaA, Weinheim

crystal structure (see Exp. Sect.) points to an outer-sphere complex [Y(hfa)$_3$·(H$_2$O)$_2$·triglyme]. In addition, the ^{1}H NMR integration is indicative of a 3:2:1 (hfa:H$_2$O:triglyme) ratio and the fingerprint region of the IR spectrum points to a different and probably weaker coordination. It is interesting to observe that the outer-sphere complex is immediately formed with the current synthetic strategy, while it is originated by sublimation from the ionic structure [Y(hfa)$_2$·triglyme]$^+$[Y(hfa)$_4$]$^-$ obtained by Pollard et al.[19]

The vaporization behaviour of adduct **3**, which depends on the coordinated H$_2$O, deserves some further comments. It was already mentioned (see above) that the triglyme adduct shows two thermogravimetric step losses, thus indicating evaporation accompanied by a partial decomposition of the precursor. This behaviour has already been observed in other hydrated compounds. Therefore, H$_2$O is not an "innocent" or "spectator" ligand, but it plays a key role in the chemistry of this MOCVD precursor, similarly to the previous behaviour reported by Luten et al. for [Y(tmhd)$_3$·H$_2$O]$_2$.[16]

The polyether length also plays a crucial role on the coordination sphere around the yttrium ion and, hence, on the thermal properties of the related adducts. In fact, there is evidence of an intriguing interplay between the polyether chain length and the yttrium ionic radius in determining the volatility of these adducts (see Figure 3). Therefore, small polyethers, such as the monoglyme or diglyme, form more volatile precursors. The longer triglyme and tetraglyme parent adducts have more complex coordination spheres and form the less volatile adducts **3** and **4**, which are not so thermally stable. The coordinated H$_2$O molecules in **3** are responsible for the two-step decomposition−evaporation, while the proposed ionic structure of **4** accounts for the higher melting point and consequent low volatility.

In this context, it becomes interesting to compare the measured melting points with those reported by Pollard et al.[19] The observed data indicate that only the melting point of adduct **4** is quite similar. The data of **3** cannot be compared, since its melting point was not reported in ref.[19] However, our melting point of **1** is about 20 °C higher while that of **2** is about 20 °C lower. It is important to note that adduct **2** has a slightly different X-ray single crystal structure but no explanation for the discrepancy observed in the case of **1** can be proposed. In any case, it is noteworthy that the melting point data were obtained by DSC measurement-curves and agree quite well with the Koeffler data.

Structural analogies between the yttrium adducts and those of the previously reported lanthanide homologues deserve further comments. This series of complexes is analogous to that observed for Eu[6] and Gd[2] but is different from that observed for La ions.[1,4] In fact, in the case of La, completely different coordination spheres were found for adducts **1**, **3** and **4**. This indicates that in these compounds yttrium behaves like a smaller ionic radio lanthanon.

Close analogies with the diglyme La homologous precursor were found for [Y(hfa)$_3$·monoglyme] in terms of its ability to act as a solvent for other precursors, thus forming a multimetal liquid single MOCVD source. In particular, it dissolves the [Ba(hfa)$_2$·tetraglyme] and Cu(tmhd)$_2$ precursors and the formed melt represents a suitable source for the growth of YBCO thin films. The resulting in-situ growth of YBCO films using a single molten multimetal source is an important result. The multimetal mixture can be easily and cleanly evaporated from the melt with constant mass-transport rates. On the contrary the sublimation of solid precursors suffers several drawbacks associated with sintering and surface passivation upon sublimation, which, in turn, render transport processes largely irreproducible.

Even more important, the use of precursors in a single liquid phase implies simpler reactor design and control of deposition parameters, since the interplay of control of different sublimation−evaporation parameters and carrier gas flows are no longer required.

In summary, the present procedure yields quantitatively nonhygroscopic adducts through a viable low-cost route. This represents an important issue for materials used in CVD applications, where low-cost chemicals that can be manipulated on open benches are an important objective.[24] Furthermore the obtained raw materials are pure and the final products (no impurities are introduced in the one-pot synthesis) do not require further sublimation steps.

Conclusions

The present one-pot synthetic strategy has proven an efficient route for the preparation of thermally stable and volatile yttrium second-generation adducts from commercially available products. Thermogravimetric and vaporization-rate experiments indicate that they can be used in MOCVD deposition at temperatures lower than 200 °C, with better mass-transport properties and thermal behaviour than conventional rare-earth metal CVD precursors. Furthermore because of their low melting points they can be used as thermally stable precursors in the liquid phase, hence under constant vaporization and mass-transport rates.

The effect of the polyether framework was widely investigated and the results emphasise the key role of the polyether length on the coordination sphere, which, in turn, affects the thermal stability and volatility of the adducts.

Finally, adduct **1** was tested as a solvent for a variety of precursors for YBCO deposition complexes, thus providing liquid single-sources, which simultaneously deliver all the metal components in the required stoichiometry. In the present work, the monoglyme yttrium adduct was used as a solvent for [Ba(hfa)$_2$·tetraglyme] and Cu(tmhd)$_2$. The resulting multimetal, molten single-source was employed for the growth of highly textured YBCO films having good surface morphologies.

The present approach, which adopts a monocomponent, simple and low-cost MOCVD reactor, is an attractive alternative to the classical multicomponent MOCVD processes.

 © 2004 Wiley-VCH Verlag GmbH & Co. KGaA, Weinheim

Experimental Section

Reagents: Hhfa, monoglyme, diglyme, triglyme and tetraglyme (Aldrich) were used without any further purification. Yttrium nitrate $[Y(NO_3)_3{\cdot}5H_2O]$ was purchased from Aldrich.

General Procedures: Elemental microanalyses were performed in the Analytical Laboratories of the University of Catania. ^{1}H NMR spectra were recorded on a Varian Inova 500 spectrometer. Infrared data were collected on a 684 Perkin−Elmer spectrometer as nujol mulls between NaCl plates. Thermal measurements were made using a Mettler 3000 system equipped with a TG 50 thermobalance, a TC 10 processor and DSC 30 calorimeter. The weights of the samples were between 10−15 mg (TGA) and 4−8 mg (DSC). Analyses were carried out under prepurified nitrogen using a 5 °C/min heating rate. FAB^+ mass spectra were obtained with a Kratos MS 50 spectrometer.

Synthesis of $Y(OH)_3{\cdot}nH_2O$: $Y(OH)_3{\cdot}nH_2O$ was precipitated from an aqueous solution of yttrium nitrate on addition of sodium hydroxide. The gelatinous precipitate was filtered and dried under vacuum over P_4O_{10}.

Synthesis of [Y(hfa)$_3$·monoglyme] (1): $Y(OH)_3{\cdot}nH_2O$ (1.482 g, 10.59 mmol) was first suspended in hexane (150 mL). Monoglyme (0.849 g, 9.42 mmol) was added to the suspension. Hhfa (5.881 g, 28.27 mmol) was added under vigorous stirring after 10 min and the mixture was refluxed whilst stirring for 1 hour. The excess of yttrium hydroxide was filtered off from the hot solution. White crystals precipitated after partial evaporation of the solvent. The colourless crystals were collected by filtration and dried under vacuum. The yield is 81 %. The melting point of the crude product is 74−77 °C. $C_{19}H_{13}F_{18}O_8Y$ (800.2): calcd. C 28.54, H 1.62; found C 28.24, H 1.56 %. The adduct sublimes quantitatively at 75−80 °C/10^{-3} Torr. IR (nujol or hexachlorobutadiene): $\tilde{\nu}$ = 2930 (vs), 1660 (s), 1610 (w), 1570 (m), 1540 (m), 1505 (m), 1455 (s), 1380 (m), 1250 (s), 1200 (s), 1150 (s), 1100 (m), 1040 (s), 1020 (m), 950 (w), 870 (m), 830 (vw), 800 (m), 770 (w), 740 (m), 660 (s), 600 (s), 530 (m) cm^{-1}. The NMR, MS and IR data of the raw and sublimed adduct are identical.

Synthesis of [Y(hfa)$_3$·diglyme] (2): Prepared as described for the monoglyme adduct from $Y(OH)_3{\cdot}nH_2O$ (1.152 g, 8.23 mmol), Hhfa (4.411 g, 21.21 mmol) and diglyme (0.948 g, 7.07 mmol). Yield 78 %. The melting point of the crude product was 60−63 °C. $C_{21}H_{17}F_{18}O_9Y$ (844.2): calcd. C 29.88, H 2.03; found C 29.25, H 2.25 %. The adduct sublimes quantitatively at 80−85 °C/10^{-3} Torr. IR (nujol or hexachlorobutadiene): $\tilde{\nu}$ = 2930 (s), 1660 (vs), 1605 (w), 1560 (w), 1530 (m), 1505 (s), 1460 (s), 1380 (m), 1260 (s), 1205 (s), 1140 (s), 1090 (s), 1055 (m), 1045 (s), 1010 (m), 950 (w), 870 (m), 835 (w), 800 (m), 770 (w), 740 (m), 660 (s), 600 (s), 535 (w) cm^{-1}. The NMR, MS and IR data of the raw and sublimed adduct are identical.

Synthesis of [Y(hfa)$_3$·(H$_2$O)$_2$·triglyme] (3): Prepared as described for the monoglyme adduct from $Y(OH)_3{\cdot}nH_2O$ (1.613 g, 11.52 mmol), Hhfa (6.615 g, 31.80 mmol) and triglyme (1.890 g, 10.60 mmol). Yield 88 %. Melting point of the crude product 52−55 °C. $C_{23}H_{25}F_{18}O_{12}Y$ (924.3): calcd. C 29.86, H 2.70; found: C 29.25, H 2.57 %. The adduct sublimes quantitatively at 95−105 °C/10^{-3} Torr. IR (nujol or hexachlorobutadiene): $\tilde{\nu}$ = 3370 (m), 3260 (m), 2930 (s), 1660 (s), 1560 (m), 1530 (m), 1505 (m), 1460 (s), 1370 (m), 1350 (w), 1255 (s), 1210(s), 1140 (s), 1100 (s), 1020 (w), 1005 (w), 940 (w), 840 (w), 800 (m), 740 (w), 720 (vw), 660 (m), 600 (m), 535 (w) cm^{-1}. The NMR, MS and IR data of the raw and sublimed adduct are identical.

Synthesis of [Y(hfa)$_2$·tetraglyme]$^+$[Y(hfa)$_4$]$^-$ (4): Prepared as described for the monoglyme adduct from $Y(OH)_3{\cdot}nH_2O$ (1.153 g, 8.24 mmol), Hhfa (4.410 g, 21.20 mmol) and tetraglyme(1.570 g, 7.067 mmol). Dichloromethane was used instead of hexane. Yield 65 %. The melting point of the crude product is 175−178 °C. $C_{40}H_{28}F_{36}O_{17}Y$ (1553.5): calcd. C 30.9, H 1.81; C 28.83, H 1.89 %. The adduct sublimes quantitatively at 130−140 °C/10^{-3} Torr. IR

Table 5. Crystal data and structure refinement for [Y(hfa)$_3$·monoglyme] and [Y(hfa)$_3$·diglyme]

Identification code	Y(hfa)$_3$Monoglyme	Y(hfa)$_3$Diglyme
Empirical formula	$C_{19}H_{13}F_{18}O_8Y$	$C_{21}H_{17}F_{18}O_9Y$
Molecular mass	800.20	844.26
Temperature	120(2) K	120(2) K
Wavelength	1.54052 Å	1.54184 Å
Crystal system	Orthorombic	Orthorombic
Space group	Pcab	$Pc2_1n$
Unit cell dimensions	a = 16.095(5) Å; α = 90.00(5)°	a = 11.151(5) Å; α = 90.00(5)°
	b = 17.983(5) Å; β = 90.00(5)°	b = 12.371(5) Å; β = 90.00(5)°
	c = 20.753(5) Å; γ = 90.00(5)°	c = 22.251(5) Å; γ = 90.00(5)°
Volume	6007(3) Å^3	3070 (2) Å^3
Z	8	4
Density (calculated)	1.770 Mg/m^3	1.827 Mg/m^3
Absorption coefficient	4.184 mm^{-1}	4.157 mm^{-1}
F(000)	3136	1664
Crystal size	0.385 × 0.502 × 0.235 mm	0.432 × 0.416 × 0.181 mm
Theta range for data collection	4.91 to 54.07°	4.44 to 58.03°
Index ranges	$0 \le h \le 16$, $0 \le k \le 18$, $0 \le l \le 21$	$-1 \le h \le 12$, $-1 \le k \le 19$, $-22 \le l \le 22$
Reflections collected	2906	8389
Independent reflections	2788 [R(int) = 0.0988]	3724 [R(int) = 0.0594]
Refinement method	Full-matrix least-squares on F^2	Full-matrix least-squares on F^2
Data/restraints/parameters	2788/18/312	3723/19/294
Goodness-of-fit on F^2	1.005	1.058
Final R indices [$I > 2\sigma(I)$]	$R1$ = 0.1152, $wR2$ = 0.2896	$R1$ = 0.0731, $wR2$ = 0.1919
R indices (all data)	$R1$ = 0.1700, $wR2$ = 0.3258	$R1$ = 0.0775, $wR2$ = 0.1992
Largest diff. peak and hole	1.307 and −1.626 eA^{-3}	2.192 and −1.737 eA^{-3}

 © 2004 Wiley-VCH Verlag GmbH & Co. KGaA, Weinheim

(nujol or hexachlorobutadiene): $\tilde{\nu}$ = 2930 (s), 1650 (vs), 1605 (w), 1565 (m), 1540 (m), 1515 (m), 1495 (w), 1460 (s), 1380 (m), 1350 (w), 1260 (s), 1220 (s), 1200 (s), 1140 (s), 1100 (m), 1060 (m), 1035 (m), 950 (m), 930 (w), 850 (m), 830 (vw), 800 (m), 770 (w), 740 (m), 720 (vw), 660 (s), 600 (s), 535 (m) cm^{-1}. The NMR, MS and IR data of the raw and sublimed adduct are identical.

X-ray Structure Determination:[25] Single crystal X-ray diffraction patterns of mono-, di-, and triglyme adducts were obtained at room temperature using an ENRAF NONIUS CAD 4 four-circle diffractometer equipped with Mo-K_α radiation (λ = 0.71069 Å). The triglyme derivative was found to be isomorphous with the outer-sphere complex already reported by K. D. Pollard et al.,[19] and, therefore, it was not analysed further. Diffraction data for the diglyme derivative were collected at 120 K using the same diffractometer and the unit-cell parameters were derived from least-squares refinements of setting angles of 25 reflections in the 9−15° range. Data are reported in Table 5 with other experimental parameters. No crystals were found to be isomorphous to the previously reported crystal structure. The new data for the monoglyme derivative single crystal were collected at 100 K using a diffractometer equipped with a CCD SMART 1 K area detector (Bruker) and a Cu rotating anode. Six series of ω scans were collected using the SMART software,[26] each one of 0.3° width and 10 s exposure time. The data were reduced using the software package SAINT.[27] Completeness of unique data to 54.2 θ were 97.4 % with 0.97 redundancy and 98.3 % with 3.31 redundancy for the mono- and diglyme derivatives, respectively. Cell parameters were determined from a nonlinear least square fit of the peaks collected in the first 620 frames.

Corrections were applied for Lorentz and polarization effects. The intensities of the diglyme adduct were corrected for absorption (ψ scan) while for the monoglyme derivative attempts to account for absorption were performed by using the DIFABS package without improvement in the refinements. The reflections were processed by the direct method program SIR97[28] which provided satisfactory sets of atomic parameters for yttrium and oxygen atoms. The other atomic parameters were determined by conventional Fourier difference synthesis by using the SHELX93 package[29] up to the final results. The conventional agreement factor for the monoglyme adduct remained not satisfactory and therefore several crystals from different batches were examined. The data reported in Table 5 represent parameters with the lowest *R* values. A residual thermal disorder prevented a better refinement of the data. Anisotropic displacement parameters were introduced for several non hydrogen atoms trying to maintain a good parameters/observable factor. The hydrogen atoms were included as idealized atoms riding on the respective carbon atoms with C−H bond lengths appropriate to the carbon atom hybridization. The isotropic displacement parameters for each H atom were fixed 1.5 times the equivalent values of the bound carbon.

MOCVD Experiments: Low pressure MOCVD deposition of pure (00*l*)-oriented YBCO films was carried out from the metal precursors [Y(hfa)$_3$·monoglyme], [Ba(hfa)$_2$·tetraglyme], and Cu(tmhd)$_2$ using a horizontal hot-wall reactor. In each experiment a suitable mixture (see below) of yttrium, barium and copper precursors was used. The volatile liquid mixture was contained in a resistively heated alumina boat at 120 °C and was transported to the deposition zone by a 300 sccm argon flow. YBCO thin films were deposited on $LaAlO_3$ (100) substrates heated at 800 °C. Water saturated O_2 flow (200 sccm) was used as the reaction gas and introduced near to the substrate. The water bubbler was maintained at room temperature. The mass flows were controlled with 1160 MKS flowmeters using an MKS 147 electronic control unit. The total pressure was maintained at 5 Torr during the growth process. The depositions were carried out for 180 minutes. YBCO thin films were slowly cooled to 500 °C at a low total pressure of 10 Torr (P_{O2} = 4 Torr). The annealing step at 500 °C was performed at atmospheric pressure in oxygen ambient for 12 hours.

X-ray diffraction θ-2θ scans of thin films were recorded with a Bruker-AXS D 5005 θ-θ X-ray diffractometer using Cu-K_α radiation operating at 40 kV/30 mA. The pole figures were recorded on a Bruker-AXS D-5005 Texture X-ray diffractometer using Cu-K_α radiation operating at 40 kV/30 mA.

The atomic composition of the films was analyzed by energy dispersive X-ray analysis (EDX) using an IXRF detector. The surface morphology was examined with a Leo Iridium 1450 scanning electron microscope (SEM).

Acknowledgments

The authors thank the MIUR for financial support under Progetto Cluster 14 P.E. 2.

[1] G. Malandrino, R. Licata, F. Castelli, I. L. Fragalà, C. Benelli, *Inorg. Chem.* **1995**, *34*, 6233−6234.
[2] G. Malandrino, O. Incontro, F. Castelli, I. L. Fragalà, C. Benelli, *Chem. Mater.* **1996**, *8*, 1292−1297.
[3] G. Malandrino, I. L. Fragalà, S. Aime, W. Dastrù, R. Gobetto, C. Benelli, *J. Chem. Soc., Dalton Trans.* **1998**, 1509−1512.
[4] G. Malandrino, C. Benelli, F. Castelli, I. L. Fragalà, *Chem. Mater.* **1998**, *10*, 3434−3444.
[5] G. Malandrino, R. Lo Nigro, F. Castelli, I. L. Fragalà, C. Benelli, *Chem. Vap. Deposition* **2000**, *6*, 233−238.
[6] G. Malandrino, M. Bettinelli, A. Speghini, I. L. Fragalà, *Eur. J. Inorg. Chem.* **2001**, 1039−1044.
[7] K. D. Pollard, H. A. Jenkins, R. J. Puddephatt, *Chem. Mater.* **2000**, *12*, 701−710.
[8] S. R. Drake, M. B. Hursthouse, K. M. Abdul Malik, S. A. S. Miller, D. J. Otway, *Inorg. Chem.* **1993**, *32*, 4464−4471.
[9] I. Baxter, J. A. Darr, M. B. Hursthouse, K. M. Abdul Malik, J. McAleese, D. M. P. Mingos, *Polyhedron* **1998**, *17*, 1329−1341.
[10] S. R. Drake, A. Lyons, D. J. Otway, A. M. Z. Slawin, D. J. Williams, *J. Chem. Soc., Dalton Trans.* **1993**, 2379−2386.
[11] I. Baxter, S. R. Drake, M. B. Hursthuose, K. M. Abdul Malik, J. McAleese, D. J. Otway, J. C. Plakatouras, *Inorg. Chem.* **1995**, *34*, 1384−1394.
[12] S. J. Kang, Y. S. Jung, Y. S. Sohn, *Bull. Korean Chem. Soc.* **1997**, *18*, 75−80.
[13] J. H. Lee, Y. S. Jung, Y. S. Sohn, S. J. Kang, *Bull. Korean Chem. Soc.* **1998**, *19*, 231−235.
[14] J. K. Marsh, *J. Chem. Soc.* **1947**, 1084−1086.
[15] M. L. Hitchman, K. F. Jensen, *Chemical Vapor Deposition: Principles and Applications* Academic Press, London, **1993**.
[16] H. A. Luten, W. S. Rees Jr., V. L. Goedken, *Chem. Vap. Deposition* **1996**, *2*, 149−161.
[17] A. Gleizes, S. Sans-Leinan, D. Medus, N. Hovnanian, P. Miele, J. D. Foulon, *Inorg. Chim. Acta* **1993**, *209*, 47−53.
[18] G. Malandrino, F. Castelli, I. L. Fragalà, *Inorg. Chim. Acta* **1994**, *224*, 203−207.
[19] K. D. Pollard, J. J. Vittal, G. P. A. Yap, R. J. Puddephatt, *J. Chem. Soc. Dalton Trans.* **1998**, 1265−1268.
[20] S. J. Kang, Y. S. Jung, I. H. Suh, *Bull. Korean Chem. Soc.* **1999**, *20*, 95−98.
[21] K. Timmer, C. I. M. A. Spee, A. Mackor, H. A. Meinema, A. L. Spek, P. van Der Sluis, *Inorg. Chim. Acta* **1991**, *190*, 109−117.
[22] Experiments were performed with a temperature ramp up of 5 °C/min under N_2 and with a 4 mm alumina sample pan.

 © 2004 Wiley-VCH Verlag GmbH & Co. KGaA, Weinheim

[23] G. Malandrino, I. L. Fragalà, P. Scardi, *Chem. Mater.* **1998**, *10*, 3765−3768.
[24] J. T. Spencer, *Progress in Inorganic Chemistry* (Ed.: K. D. Karlin), Wiley: New York, **1994**, *41*, 145.
[25] CCDC-207289 (**1**) and -207290 (**2**) contain the supplementary crystallographic data for this paper. These data can be obtained free of charge at www.ccdc.cam.ac.uk/conts/retrieving.html [or from the Cambridge Crystallographic Data Centre, 12 Union Road, Cambridge CB2 1EZ, UK; Fax: (internat.) +44-1223-336-033; E-mail: deposit@ccdc.cam.ac.uk].
[26] SMART: Area-Detector Integration Software.; Siemens Industrial Automation, Inc.: Madison, WI, **1995**.
[27] SAINT, Version 4.0, Siemens Industrial Automation, Inc.: Madison, WI, **1995**.
[28] A. Altomare, M. C. Burla, M. Camalli, G. L. Cascarano, C. Giacovazzo, A. Guagliardi, A. G. G. Molteni, G. Polidori, R. Spagna, *SIR97: A New Program for Solving and Refining Crystal Structures*, IRMEC-CNR, Bari, Italy, **1997**.
[29] G. M. Sheldrick, SHELX 97, University of Göttingen, Germany, **1997**.

Received June 9, 2003
Early View Article
Published Online November 28, 2003

 © 2004 Wiley-VCH Verlag GmbH & Co. KGaA, Weinheim

Comparative Electrochemical Study of Unsubstituted and Substituted Bis(phthalocyaninato) Rare Earth(III) Complexes

Peihua Zhu,[a] Fanli Lu,[a] Na Pan,[a] Dennis P. Arnold,*[b] Shuyong Zhang,[a] and Jianzhuang Jiang*[a,c]

Keywords: Phthalocyanines / Sandwich complexes / Rare earths / Electrochemistry

The electrochemistry of homoleptic substituted phthalocyaninato rare earth double-decker complexes $M(TBPc)_2$ and $M(OOPc)_2$ [M = Y, La...Lu except Pm; H_2TBPc = 3(4),12(13),21(22),30(31)-tetra-*tert*-butylphthalocyanine, H_2OOPc = 3,4,12,13,21,22,30,31-octakis(octyloxy)phthalocyanine] has been comparatively studied by cyclic voltammetry (CV) and differential pulse voltammetry (DPV) in CH_2Cl_2 containing 0.1 M tetra-*n*-butylammonium perchlorate (TBAP). Two quasi-reversible one-electron oxidations and three or four quasi-reversible one-electron reductions have been revealed for these neutral double-deckers of two series of substituted complexes, respectively. For comparison, unsubstituted bis(phthalocyaninato) rare earth analogues $M(Pc)_2$ (M = Y, La...Lu except Pm; H_2Pc = phthalocyanine) have also been electrochemically investigated. Two quasi-reversible one-electron oxidations and up to five quasi-reversible one-electron reductions have been revealed for these neutral double-decker compounds. The three bis(phthalocyaninato)cerium compounds display one cerium-centered redox wave between the first ligand-based oxidation and reduction. The half-wave potentials of the first and second oxidations and first reduction for double-deckers of the tervalent rare earths depend on the size of the metal center. The difference between the redox potentials of the second and third reductions for $M^{III}(Pc)_2$, which represents the potential difference between the first oxidation and first reduction of $[M^{III}(Pc)_2]^-$, lies in the range 1.08–1.37 V and also gradually diminishes along with the lanthanide contraction, indicating enhanced π–π interactions in the double-deckers connected by the smaller, lanthanides. This corresponds well with the red-shift of the lowest energy band observed in the electronic absorption spectra of reduced double-decker $[M^{III}(Pc')_2]^-$ (Pc' = Pc, TBPc, OOPc).

(© Wiley-VCH Verlag GmbH & Co. KGaA, 69451 Weinheim, Germany, 2004)

Introduction

Bis(phthalocyaninato) rare earth compounds have been extensively studied due to their potential applications for electronic devices.[1,2] Their electrochemical properties, especially those of lutetium compounds, have been intensively investigated in solutions or in aqueous $LiClO_4$, $KClO_4$, or KCl in cast, Langmuir–Blodgett, or spin-coated films by several research groups. These data are relevant to the use in electrochromic displays and molecular electronics of $Lu(Pc)_2$.[1–5] As noted by Simon and co-workers,[6] the gap between the first oxidation and first reduction processes of molecules is a good estimate of the thermal activation energy for the conduction of electric charges in the solid-state materials derived from these molecular precursors.

The spectroscopic properties, namely IR,[7] Raman,[8] and electronic absorption spectra,[9] of these sandwich-type (tetrapyrrole)metal compounds depend on the strong electronic interaction between the macrocycles, which in turn depends on the ring-to-ring distances in the molecules. Therefore it is worth studying systematically the electrochemical properties of the sandwich compounds of the complete series of rare earths for various ligands. So far, we have studied the molecular structures, NMR and vibrational spectroscopic characteristics of several series of tetrapyrrole compounds with the whole series of lanthanides from La to Lu.[7–10] The groups of Konami,[11] Iwase[12] and Homborg[13] have reported the NMR, electrochemical and electronic absorption properties of reduced double-deckers of the lanthanide series, namely $[Bu_4N][M(Pc)_2]$, $Li[M(Pc)_2]$ and $[N(C_nH_{2n+1})_4][M(Pc)_2]$, respectively. However, there is still no report on electrochemical investigations over the whole lanthanide series for the neutral bis(phthalocyaninato) species. The literature on any solution properties of the neutral unsubstituted bis-

[a] Department of Chemistry, Shandong University, Jinan 250100, China
Fax: (internat.) + 86-531-856-5211
E-mail: jzjiang@sdu.edu.cn
[b] School of Physical and Chemical Sciences, Queensland University of Technology, G. P. O. Box 2434, Brisbane 4001, Australia
Fax: (internat.) + 61-7-3864-1804
E-mail: d.arnold@qut.edu.au
[c] State Key Lab of Coordination Chemistry, Nanjing University, Nanjing 210093, China

 © 2004 Wiley-VCH Verlag GmbH & Co. KGaA, Weinheim DOI: 10.1002/ejic.200300509

(phthalocyaninato) rare earth complexes is not rich due to the limited solubility of $M(Pc)_2$ in common organic solvents such as CH_2Cl_2. Investigations of the electrochemical properties of substituted bis(phthalocyaninato) rare earth compounds are also scarce, being limited to $M(OPPc)_2$ (M = Eu, Gd),[14] $M(OHPc)_2$ (M = Eu, Gd),[14] $M(OBPc)_2$ (M = Yb, Lu)[4d] and $Lu(TBPc)_2$.[4c] The ligand abbreviations are given in Table 1.

Table 1. Abbreviations for ligands

Abbreviation	Ligand
H_2Por	general porphyrin
H_2TBPP	5,10,15,20-tetrakis(4-*tert*-butylphenyl)porphyrin
H_2OEP	2,3,7,8,12,13,17,18-octaethylporphyrin
H_2Pc	phthalocyanine
H_2TBPc	2(3),9(10),16(17),24(25)-tetra-*tert*-butylphthalocyanine
H_2OOPc	2,3,9,10,16,17,24,25-octakis(octyloxy)phthalocyanine
H_2OPPc	2,3,9,10,16,17,24,25-octakis(pentyloxy)phthalocyanine
H_2OHPc	2,3,9,10,16,17,24,25-octakis(heptyl)phthalocyanine
H_2OBPc	2,3,9,10,16,17,24,25-octakis(butyloxy)phthalocyanine
$H_2(2,3\text{-Nc})$	2,3-naphthalocyanine (linearly annulated tetrabenzophthalocyanine)
$H_2(2,3\text{-TBNc})$	3(4),12(13),21(22),30(31)-tetra-*tert*-butyl-2,3-naphthalocyanine

We report here on two series of substituted bis(phthalocyaninato)lanthanide compounds, $M(OOPc)_2$ and $M(TBPc)_2$, whose solubility in CH_2Cl_2 is significantly improved due to the introduction of extended or bulky substituents onto the Pc rings (Scheme 1). The electrochemical characterization of these substituted bis(phthalocyaninato) compounds of the whole series of lanthanides has been achieved using a glassy carbon disk working electrode. For comparison, the corresponding unsubstituted analogues $M(Pc)_2$ have also been prepared and investigated electrochemically. These unsubstituted counterparts also show recognizable and reproducible electrochemical features under the present conditions although the cyclic and differential pulse voltammograms are not resolved as clearly as those of the substituted analogues $M(TBPc)_2$ and $M(OOPc)_2$. By comparison between the electrochemical characteristics of unsubstituted and substituted bis(phthalocyaninato) compounds of the whole series of lanthanides, the effects of ionic radius of the rare earth metal and substituents (*tert*-butyl and octyloxy groups) on the electrochemical properties of double-decker compounds have been studied.

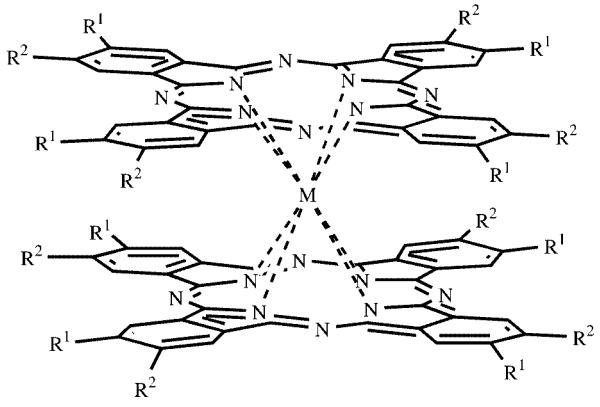

Scheme 1. Bis(phthalocyaninato) rare earth complexes $R^1 = R^2 = H$, $M(Pc)_2$ (**A**); $R^1 \neq R^2 = H$, *tert*-C_4H_9, $M(TBPc)_2$ (**B**); $R^1 = R^2 = OC_8H_{17}$, $M(OOPc)_2$ (**C**)

More redox couples can be revealed by using the glassy carbon disk due to the decreased interaction or affinity between the highly charged electrochemically generated complexes and the electrode.[12b,15] The same methodology has been applied here to render possible the first observation by DPV of the fifth one-electron reduction of $M(Pc)_2$ in solution.[15]

Results and Discussion

Electrochemical Characteristics of Bis(phthalocyaninato) Rare Earth Complexes $M(Pc)_2$ (M = Y, La...Lu except Pm)

The electrochemical behavior of all the double-decker sandwich complexes $M(Pc)_2$ was first investigated by cyclic voltammetry (CV) and then differential pulse voltammetry (DPV) in CH_2Cl_2. The half-wave redox potentials vs. SCE are summarized in Table 2. Figure 1 shows the cyclic voltammograms and differential pulse voltammograms of $Y(Pc)_2$ as a typical representative of this series of rare earth compounds. The cyclic voltammograms of other compounds in the same series are similar. Within the electrochemical window of CH_2Cl_2 and according to the CV and DPV results, all the double-decker compounds of tervalent rare earths except Lu undergo two quasi-reversible one-electron oxidations and up to five quasi-reversible one-electron reductions under the present conditions. The separation of the reduction and oxidation peak potentials for each process is 60−95 mV. Since the oxidation state of the central tervalent rare earth ion does not change (except for M = Ce), these processes are due to successive removal or addition of electrons from or to the ligand-based orbitals that are represented by the redox states illustrated in Scheme 2, where oxidations are labeled as Oxd_1 and Oxd_2 and the reductions as Red_1 to Red_5.

The electrochemistry of the unsubstituted double-deckers in CH_2Cl_2 seen here differs from that previously reported. For instance, only three or at most four reductions were observed for $Lu(Pc)_2$ in CH_2Cl_2 or benzonitrile (PhCN) containing $TBAPF_6$.[4] However, under our experimental conditions, the neutral bis(phthalocyaninato) compounds of tervalent rare earths undergo up to five one-electron reductions according to both the CV and, more clearly, the DPV results.

The effect of rare earth ion size is clearly demonstrated by the slight shift in the negative direction of the half-wave potentials of the first oxidation and first reduction of $M^{III}(Pc)_2$ with decreasing rare earth ion radius. Moreover, a linear correlation exists between the potentials of the first oxidation and first reduction and the tervalent rare earth ionic radii (Figure 2). The half-wave potentials of the second oxidation also depend on the ionic radius of the central rare earth metal (Figure 2). However, the slope of this

 © 2004 Wiley-VCH Verlag GmbH & Co. KGaA, Weinheim

Table 2. Half-wave redox potentials of $M(Pc)_2$ (V vs. SCE) in CH_2Cl_2 containing 0.1 M TBAP

	Oxd_2	Oxd_1	Red_1	Red_2	Red_3	Red_4	Red_5	$\Delta E^\circ_{1/2}$[a]	$\Delta E^{\circ\prime}_{1/2}$[b]
La	+1.34	+0.61	+0.27	−1.10	−1.31	−1.55[c]	−1.85[c]	0.34	1.37
Ce	+1.04[d]	+0.55[d]	+0.09[e]	−1.10[f]	−1.31[c] [f]			0.49[g]	1.19
Pr	+1.34	+0.58	+0.22	−1.15	−1.39	−1.68[c]	−1.80[c]	0.36	1.37
Nd	+1.49[c]	+0.56	+0.15	−1.12	−1.34	−1.63[c]	−1.74[c]	0.41	1.27
Sm	+1.56	+0.56	+0.14	−1.11	−1.33	−1.60[c]	−1.74[c]	0.42	1.25
Eu	+1.59	+0.55	+0.12	−1.07	−1.29	−1.54[c]	−1.70[c]	0.43	1.19
Gd	+1.57[c]	+0.52	+0.11	−1.08	−1.30	−1.53[c]	−1.72[c]	0.41	1.19
Tb	+1.60[c]	+0.51	+0.09	−1.08	−1.32	−1.53	−1.66[c]	0.42	1.17
Dy	+1.50	+0.47	+0.07	−1.09	−1.30	−1.57[c]	−1.83[c]	0.40	1.16
Y	+1.61	+0.47	+0.06	−1.11	−1.35	−1.66[c]	−1.81[c]	0.41	1.17
Ho		+0.47	+0.04	−1.10	−1.36	−1.70[c]	−1.88[c]	0.43	1.14
Er	+1.63	+0.47	+0.06	−1.09	−1.35	−1.60[c]	−1.75[c]	0.41	1.15
Tm	+1.54	+0.45	+0.05	−1.07	−1.29	−1.54[c]	−1.75[c]	0.40	1.12
Yb	+1.64[c]	+0.44	+0.02	−1.09	−1.32			0.42	1.11
Lu	+1.60[c]	+0.40	−0.02	−1.10[c]	−1.33[c]	−1.58[c]		0.42	1.08

[a] $\Delta E^\circ_{1/2}$ is the energy required to put a second electron in the semi-occupied HOMO of the neutral double-decker radical $M(Pc)_2$ or to remove one electron of the two from the HOMO of the reduced double-decker species $[M(Pc)_2]^-$: $\Delta E^\circ_{1/2} = Oxd_1 - Red_1$. [b] $\Delta E^{\circ\prime}_{1/2}$ is the potential difference between the first oxidation and first reduction processes, i.e. the HOMO−LUMO gap of $[M(Pc)_2]^-$: $\Delta E^{\circ\prime}_{1/2} = Red_1 - Red_2$. [c] Recorded by DPV. [d] This process involves an intermediate cerium Ce*X* species, where X is between III and IV. [e] Involves a cerium-centered redox process. [f] Involves a Ce^{III} species. [g] For $Ce(Pc)_2$: $\Delta E^\circ_{1/2} = Oxd_2 - Oxd_1$.

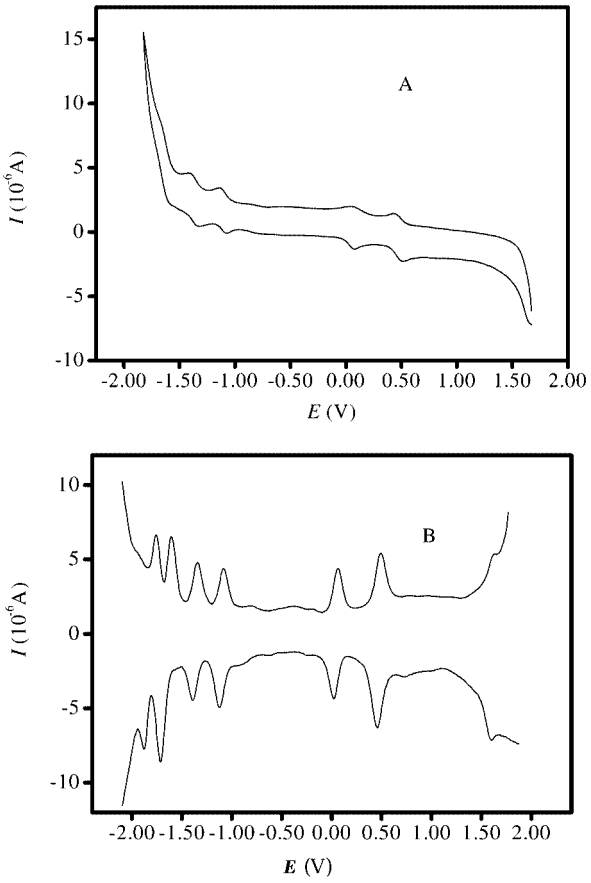

Figure 1. Cyclic voltammetry (A) and differential pulse voltammetry (B) of $Y(Pc)_2$ in CH_2Cl_2 containing 0.1 M $[Bu_4N][ClO_4]$ at scan rates of 20 and 10 mV s^{-1}, respectively

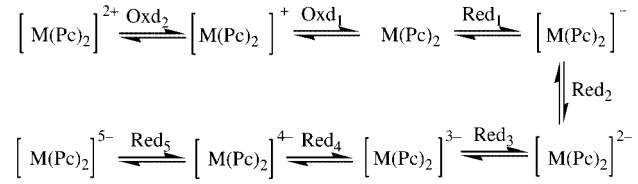

Scheme 2. The one-electron redox processes of $M(Pc)_2$

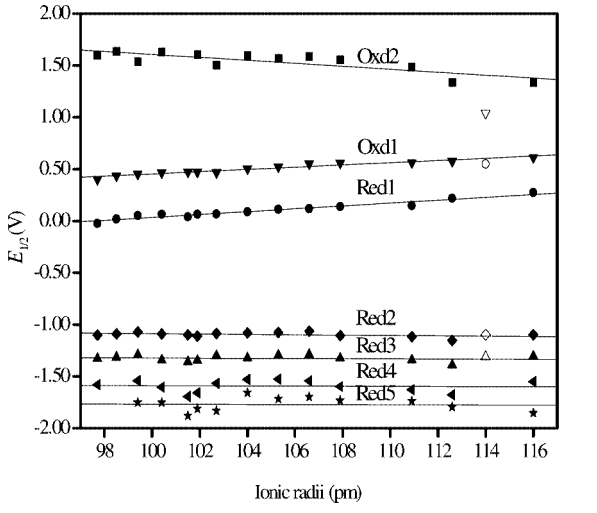

Figure 2. Half-wave potentials of redox processes of $M(Pc)_2$ as a function of the ionic radius of M^{III}

line is opposite to those of the first oxidation and first reduction waves (see below). The half-wave potentials of the second, third and fourth reductions for $M(Pc)_2$ are independent of the size of the central rare earth ions. This is also true for the half-wave potentials of the fifth reduction of $M^{III}(Pc)_2$ revealed here by DPV.

The potential difference between the first oxidation and first reduction process, $\Delta E^\circ_{1/2}$, for all double-decker compounds $M(Pc)_2$ spans a relatively narrow range, 0.34−0.43 V, which accords well with previously reported results for bis(phthalocyaninato)lutetium compounds.[4] This potential

 © 2004 Wiley-VCH Verlag GmbH & Co. KGaA, Weinheim

difference is important for molecular materials because it predicts electrical properties such as the thermal activation energy for conduction in the condensed phases derived from these molecular precursors.[6] As with $Lu(Pc)_2$, the unsubstituted bis(phthalocyaninato) rare earth compounds should be good molecular semi-conductors based on the small potential difference between their first oxidation and first reduction.

X-ray crystallographic studies of bis(phthalocyaninato) rare earth compounds show that the two isoindole N_4 planes are very close to each other (2.68−3.11 Å).[1a] This proximity of the two conjugated π-systems in a face-to-face configuration causes the monomer molecular orbitals to split, which can be demonstrated by studying the redox behavior and the optical properties (UV/Vis, near-IR and MCD spectra). Figure 3 shows a qualitative scheme for the frontier orbitals of $M(Pc)_2$ derived from the highest occupied and lowest unoccupied molecular orbitals (HOMO and LUMO) of $M(Pc)_2$.[16,17] The LUMO of mono(metallophthalocyanines) is doubly degenerate (e_g) and can accept up to four electrons; this is also true for the LUMO of the bis(phthalocyaninato) rare earth compounds. The HOMO of the homoleptic phthalocyaninato double-deckers results from a splitting of the $4a_u$ π-HOMO of the mono(phthalocyanines) due to the interactions between the rings. Thus, in the neutral complexes consisting of a tervalent metal ion sandwiched between (formally) a dianion and an anion radical, the HOMO is semi-occupied. These neutral bis(phthalocyaninato) compounds of tervalent rare earths are thus expected to be reducible by a total of five electrons as confirmed by the above-described electrochemical measurements. This orbital proposal is well supported by the optical properties, especially in the near-IR range of $M(Pc)_2$.[18] The bis(phthalocyaninato) tervalent rare earth complexes

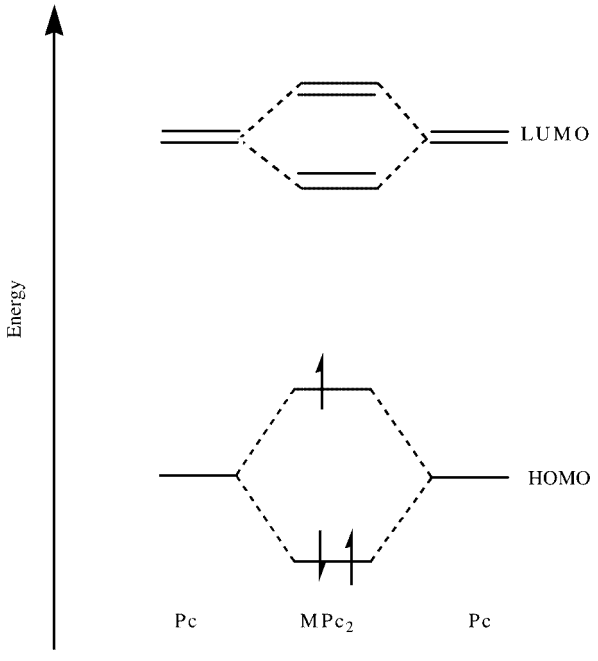

Figure 3. Frontier orbitals of $M(Pc)_2$

are known to be neutral radicals, the HOMO being semi-occupied. The absorption band at ca. 920 nm in the electronic spectrum, which shows an *A*-Faraday-type band in the MCD spectrum, is attributed to the electronic transition from the semi-occupied HOMO to the degenerate LUMO. The absorption to even lower energy at ca. 1400 nm is due to the transition from the second HOMO to the semi-occupied HOMO.[18] This energy represents the extent of electronic coupling between the macrocycles, since the electron correlation energy term vanishes due to the semi-occupation of the HOMO. This absorption band becomes increasingly blue-shifted with the lanthanide contraction, indicating that decreasing rare earth ionic size induces increasing ring-to-ring interaction and more profound splitting between the HOMO and second HOMO of double-deckers (Figure 3), and thus there is an increase in the energy of the HOMO and a decrease in that of the second HOMO. This is why the half-wave potentials of the second oxidation (Oxd_2) are shifted slightly in a more positive direction with decreasing rare earth ion radius, whereas those for the first oxidation and first reduction of $M^{III}(Pc)_2$, Oxd_1 and Red_1, are shifted slightly in the negative direction in the same order.

According to the orbital scheme depicted in Figure 3, $\Delta E^\circ_{1/2}$ (0.34−0.43 V) represents the energy for putting a second electron in the semi-occupied HOMO of the neutral double-decker radical $M(Pc)_2$ or to remove one electron of the two from the HOMO of the reduced double-decker species $[M(Pc)_2]^-$. In other words, it is the energy for pairing the two electrons in the HOMO of $[M(Pc)_2]^-$, and it remains almost unchanged for the whole series of lanthanides. The corresponding energy for removing one electron of the two from the HOMO of $Ce(Pc)_2$, 0.49 V, is slightly higher compared to that for $[M(Pc)_2]^-$ because of the smaller ionic size of the intermediate valence state of cerium and, thus, the more intense ring−ring interaction in $Ce(Pc)_2$. This is also true for substituted bis(phthalocyaninato)cerium complexes (Tables 3 and 4).

Furthermore, the difference of the redox potentials of Red_2 and Red_3 for $M(Pc)_2$ actually corresponds to the potential difference between the first oxidation and first reduction of $[M(Pc)_2]^-$, $\Delta E^{\circ\prime}_{1/2}$. The values range from 1.08 to 1.37 V across the series, and gradually diminish along with decreasing rare earth ion radius, clearly showing a size effect and indicating the enhanced π−π interactions in the double-deckers with smaller lanthanides compared with those connected by larger lanthanides (Table 2). The same general trend is also found for the substituted bis(phthalocyaninato) rare earth analogues $M(TBPc)_2$ and $M(OOPc)_2$ (see Table 4). As the first oxidation step and first reduction step, respectively, involve the HOMO and the LUMO of the molecule, the energy difference between these two redox processes for $[M(Pc)_2]^-$ corresponds to its electrochemical molecular band gap. Thus $\Delta E^{\circ\prime}_{1/2}$ should reflect the energy necessary for the transition of an electron from the HOMO to the LUMO of $[M(Pc)_2]^-$ and therefore should correlate with the lowest energy optical transition in the electronic absorption spectrum of $[M(Pc)_2]^-$. In fact, the diminished

 © 2004 Wiley-VCH Verlag GmbH & Co. KGaA, Weinheim

Table 3. Half-wave redox potentials of $M(TBPc)_2$ (V vs. SCE) in CH_2Cl_2 containing 0.1 M TBAP

	Oxd_2	Oxd_1	Red_1	Red_2	Red_3	Red_4	$\Delta E^\circ_{1/2}$[a]	$\Delta E^\circ_{1/2}$[b]
La	+1.36	0.52	0.14	−1.18	−1.43		0.38	1.32
Ce	+0.91[c]	+0.42[c]	−0.03[d]	−1.16[e]	−1.41[e]	−1.84[e] [f]	0.49[g]	1.13
Pr	+1.39	+0.49	+0.10	−1.14	−1.37	−1.76[f]	0.39	1.24
Nd	+1.46	+0.48	+0.08	−1.15[f]	−1.36[f]	−1.79[f]	0.40	1.23
Sm	+1.48	+0.46	+0.05	−1.13	−1.36[f]	−1.72[f]	0.41	1.18
Eu	+1.50	+0.45	+0.03	−1.13	−1.36	−1.74	0.42	1.16
Gd	+1.48	+0.42	+0.01	−1.15	−1.40[f]	−2.00[f]	0.41	1.16
Tb	+1.51	+0.41	−0.03	−1.20	−1.49[f]	−1.88[f]	0.44	1.17
Dy	+1.51	+0.39	−0.04	−1.15	−1.40[f]		0.43	1.11
Y	+1.57	+0.40	+0.01	−1.14	−1.44	−1.80[f]	0.41	1.14
Ho	+1.57	+0.37	−0.07	−1.20	−1.47[f]	−1.89[f]	0.44	1.13
Er	+1.56	+0.37	−0.05	−1.13	−1.38	−1.92[f]	0.42	1.08
Tm	+1.53[c]	+0.35	−0.08	−1.14	−1.40	−1.90[f]	0.43	1.06
Yb	+1.55	+0.35	−0.11	−1.19	−1.50[f]	−1.94[f]	0.46	1.08
Lu	+1.56	+0.35	−0.10	−1.19	−1.48	−1.80	0.45	1.09

[a] $\Delta E^\circ_{1/2}$ is the energy needed to put a second electron in the semi-occupied HOMO of the neutral double-decker radical $M(TBPc)_2$ or to remove one electron of the two from the HOMO of the reduced double-decker species $[M(TBPc)_2]^-$: $\Delta E^\circ_{1/2} = Oxd_1 - Red_1$. [b] $\Delta E^{\circ\prime}_{1/2}$ is the potential difference between the first oxidation and first reduction processes, i.e. the HOMO−LUMO gap of $[M(TBPc)_2]^-$: $\Delta E^{\circ\prime}_{1/2} = Red_1 - Red_2$. [c] This process involves an intermediate cerium Ce*X* species, where X is between III and IV. [d] Involves a cerium-centered redox process. [e] Involves a Ce^{III} species. [f] Recorded by DPV. [g] For $Ce(TBPc)_2$: $\Delta E^\circ_{1/2} = Oxd_2 - Oxd_1$.

Table 4. Half-wave redox potentials of $M(OOPc)_2$ (V vs. SCE) in CH_2Cl_2 containing 0.1 M TBAP

	Oxd_2	Oxd_1	Red_1	Red_2	Red_3	$\Delta E^\circ_{1/2}$[a]	$\Delta E^{\circ\prime}_{1/2}$[b]
La	+1.20	+0.46	+0.10	−1.31	−1.63	0.36	1.41
Ce	+0.78[c]	+0.33[c]	−0.18[d]			0.45[e]	
Pr	+1.23	+0.42	+0.01	−1.31	−1.64[f]	0.41	1.33
Nd	+1.25	+0.40	0.00	−1.28	−1.60[f]	0.40	1.28
Sm	+1.26	+0.40	−0.01	−1.29	−1.65[f]	0.41	1.28
Eu	+1.33	+0.36	−0.06	−1.29	−1.71	0.42	1.23
Gd	+1.40	+0.35	−0.07	−1.27	−1.56[f]	0.42	1.20
Tb	+1.38	+0.33	−0.10	−1.30	−1.60[f]	0.43	1.20
Dy	+1.35	+0.32	−0.11	−1.30	−1.66	0.43	1.19
Y	+1.40	+0.31	−0.12	−1.31	−1.69	0.43	1.19
Ho	+1.47	+0.31	−0.11	−1.29	−1.65[f]	0.42	1.18
Er		+0.30	−0.13	−1.30	−1.59[f]	0.43	1.17
Tm	+1.51[f]	+0.29	−0.15	−1.31[c]	−1.67[f]	0.44	1.16
Yb	+1.51[f]	+0.28	−0.15	−1.26	−1.62	0.43	1.12
Lu	+1.47	+0.27	−0.17	−1.30	−1.71	0.44	1.13

[a] $\Delta E^\circ_{1/2}$ is the energy needed to put a second electron in the semi-occupied HOMO of the neutral double-decker radical $M(OOPc)_2$ or to remove one electron of the two from the HOMO of the reduced double-decker species $[M(OOPc)_2]^-$: $\Delta E^\circ_{1/2} = Oxd_1 - Red_1$. [b] $\Delta E^{\circ\prime}_{1/2}$ is the potential difference between the first oxidation and first reduction processes, i.e. the HOMO−LUMO gap of $[M(OOPc)_2]^-$: $\Delta E^{\circ\prime}_{1/2} = Red_1 - Red_2$. [c] This process involves an intermediate cerium Ce*X* species, where X is between III and IV. [d] Involves a cerium-centered redox process. [e] For $Ce(OOPc)_2$: $\Delta E^\circ_{1/2} = Oxd_2 - Oxd_1$. [f] Recorded by DPV.

trend observed for $\Delta E^{\circ\prime}_{1/2}$ of bis(phthalocyaninato)metal complexes along with the rare earth contraction is in good agreement with the red-shift of the lowest electronic absorption band of $[M(Pc)_2]^-$, 682 nm for M = Sm to 705 nm for M = Lu, along with the same order.

The cerium double-decker is particularly interesting because of its anomalous electrochemical and spectroscopic properties. As indicated by electronic absorption, Raman and ^1H NMR studies, both phthalocyanine rings seem to exist as dianions in bis(phthalocyaninato)cerium, $Ce(Pc^{2-})_2$, while the valence state of the cerium ion appears to be intermediate between III and IV from XNAFS data. This anomaly is due to the strong hybridization of the 4f orbital of cerium with the π orbitals of conjugated phthalocyanine ligands.[19] The CV and DPV studies of $Ce(Pc^{2-})_2$ show five distinct redox waves that represent quasi-reversible single-electron processes. The second and third reduction peaks at −1.10 and −1.31 V, respectively, are related to the successive addition of electrons to the ligand-based orbitals that are represented by the redox states $[Ce(Pc)_2]^-/[Ce(Pc)_2]^{2-}$ and $[Ce(Pc)_2]^{2-}/[Ce(Pc)_2]^{3-}$, in which the cerium ion seems to be tervalent, because both potentials correspond with those of the rest of the series $M^{III}(Pc)_2$ [M ≠ Ce] (Table 2 and Figure 2). The anomalous reduction wave at +0.09 V thus appears to be metal-centered: $[Ce^{III}(Pc^{2-})_2]^-/[Ce^X(Pc^{n-})_2]$, where X is between III and IV, and *n* is an average formal charge such as to maintain the required net charge.[19] The anomalous (with respect to the other lanthanides) electronic structure of cerium and the strong hybridization of the 4f orbitals with the ligand orbitals make the metal-centered redox process (here either the addition, or the removal, of one electron to, or from, a 4f orbital of the cerium ion) dependent on the nature of the phthalocyanine rings. Therefore, the half-wave potential of the cerium-based redox process for $Ce(Pc)_2$ differs from that for $Ce(TBPc)_2$ and $Ce(OOPc)_2$ [Tables 3 and 4 (see below)], following the logical order 0.09, −0.03, −0.18 as the ligands become more electron-donating and thus the metal centre becomes harder to reduce. The first and second oxidation processes at +0.55 and +1.04 V for $Ce(Pc)_2$ involve successive removal of electrons from the ligand-based HOMO that are represented by the redox states: $[Ce^X(Pc)_2]/[Ce^X(Pc)_2]^+$ and $[Ce^X(Pc)_2]^+/[Ce^X(Pc)_2]^{2+}$

 © 2004 Wiley-VCH Verlag GmbH & Co. KGaA, Weinheim

(in which again a fractional average formal charge must be assigned to the ligands to maintain the overall charge). The cerium ion in these redox states has the same formal charge as in $[Ce(Pc)_2]^0$ because both potentials deviate significantly from the linear relationship established between the potentials of corresponding redox processes, actually the first reduction and first oxidation of $M^{III}(Pc)_2$, and the rare earth ion radii (Table 2 and Figure 2).

Electrochemical Characteristics of Bis[3(4),12(13),21(22),30(31)-tetra-*tert*-butylphthalocyaninato] Rare Earth Complexes $M(TBPc)_2$ (M = Y, La...Lu except Pm)

The bis[3(4),12(13),21(22),30(31)-tetra-*tert*-butylphthalocyaninato] rare earth complexes $M(TBPc)_2$, which are substituted by four *tert*-butyl groups on the periphery of each phthalocyanine macrocycle, are actually a mixture of isomers, all of which seem to have the same electrochemical properties. This has been confirmed by the electrochemical behavior of other bis(phthalocyaninato)lutetium or bis(naphthalocyaninato) rare earth compounds, tetrasubstituted on the periphery of each (na)phthalocyanine ring.[4c,9c]

Similar to the unsubstituted analogues, CV and DPV have revealed two ligand-centered quasi-reversible one-electron oxidations and up to four ligand-centered quasi-reversible one-electron reductions for $M^{III}(TBPc)_2$. The incorporation of the four electron-donating *tert*-butyl groups onto each phthalocyanine ring makes the compounds easier to oxidize and harder to reduce. This is well demonstrated by the lower oxidation and reduction half-wave potentials of the corresponding redox processes of $M(TBPc)_2$ compared with those of $M(Pc)_2$ (Table 3 and Figure 4). The cathodic shift of all the processes means that only four reductions were observed for $M(TBPc)_2$. The fifth reduction process observed for $M(Pc)_2$ under the same experimental conditions could not be seen. This is also the case for $M(OOPc)_2$ as discussed below. Moreover, since these *tert*-butyl-substituted bis(phthalocyaninato) rare earth complexes are more soluble in alkyl halides such as CH_2Cl_2 compared with $M(Pc)_2$, the measurement of their properties in solution is more favorable. This is verified by the improved resolution of the redox couples in most of the voltammograms. Figure 4 displays the CV and DPV diagrams of $Ce(TBPc)_2$, in which the sensitivity is seen to be better than for $M(Pc)_2$.

The dependence of the half-wave potentials of the redox processes on the ionic size of the central rare earth ion is similar for $M(TBPc)_2$ to that for $M(Pc)_2$ (Table 3). While the half-wave potentials of the second, third and fourth reductions of $M(TBPc)_2$ are independent of the size of the central rare earth ions, the potentials for the second and first oxidations and first reduction are size-sensitive, but the opposite slope is observed for the first process compared with the other two.

The small electron-pairing energy for $M(TBPc)_2$, $\Delta E^\circ_{1/2}$ (0.38−0.46 V), which corresponds well with those of corresponding $M(Pc)_2$ and $M(OOPc)_2$ (see below), indicates that

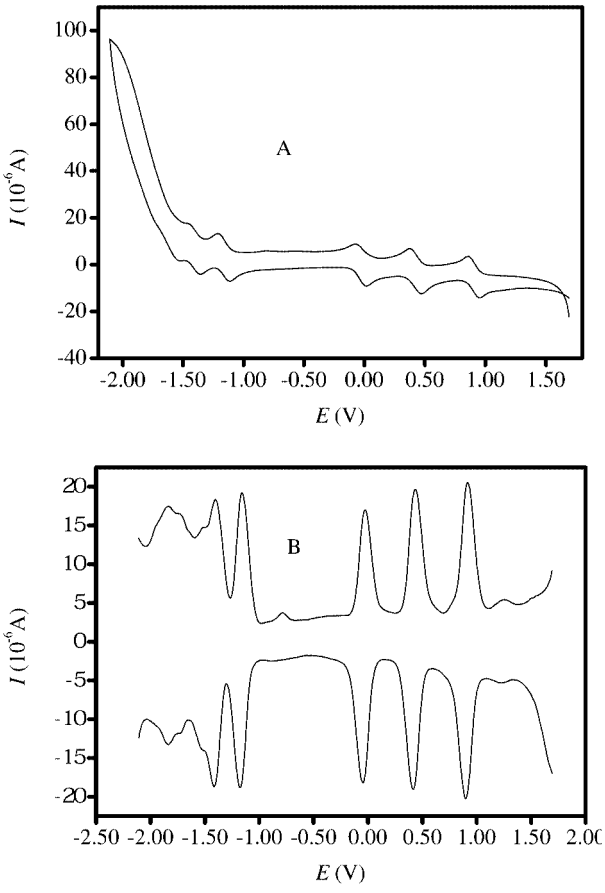

Figure 4. CV (A) and DPV (B) of $Ce(TBPc)_2$ in CH_2Cl_2 containing 0.1 M $[Bu_4N][ClO_4]$ at scan rates 20 and 10 mV s^{-1}, respectively

these substituted bis(phthalocyaninato) rare earth compounds should be good potential molecular semi-conductors, as expected for their unsubstituted analogues. Due to their increased solubility in common organic solvents, by virtue of the *tert*-butyl groups, these compounds would be more easily fabricated into electronic devices by solution fabrication methods. The similar $\Delta E^\circ_{1/2}$ values for $M(TBPc)_2$ to those of the unsubstituted counterparts indicates that the pairing energy in the HOMO of $[M(TBPc)_2]^-$ is quite similar to that for the HOMO of $[Mc(Pc)_2]^-$ although the redox potentials of the first oxidation and first reduction processes of $M(TBPc)_2$ shift cathodically due to the introduction of electron-donating *tert*-butyl groups. This is also true for $M(OOPc)_2$.

Furthermore, according to the decreasing $\Delta E^{\circ\prime}_{1/2}$ value of $M(TBPc)_2$ with decreasing rare earth ionic radius (Table 3), a red-shift in the lowest energy band of reduced tetra-*tert*-butyl-substituted bis(phthalocyaninato) rare earth compounds $[M(TBPc)_2]^-$ (M = Sm...Lu) should be expected to follow in the same order. In fact, the lowest energy band for $[M(TBPc)_2]^-$ shifts from 688 nm for M = Sm to 714 nm for M = Lu. This is also true for $[M(OOPc)_2]^-$.[9d]

As clearly shown in the CV and DPV spectra of $Ce(TBPc)_2$ (Figure 4) and on the basis of comparison between the electrochemical data of $Ce(TBPc)_2$ and those of

 © 2004 Wiley-VCH Verlag GmbH & Co. KGaA, Weinheim

$M^{III}(TBPc)_2$ (Table 3), the same Ce redox states apply here as for $Ce(Pc)_2$ [and also for $Ce(OOPc)_2$ (Table 4)].

Electrochemical Characteristics of Bis[3,4,12,13,21,22,30,31-octakis(octyloxy)phthalocyaninato] Rare Earth Complexes $M(OOPc)_2$ (M = Y, La...Lu Except Pm)

Very similar electrochemical behavior to that of $M(Pc)_2$ and $M(TBPc)_2$ has been revealed by CV and DPV methods for bis[3,4,12,13,21,22,30,31-octakis(octyloxy)phthalocyaninato] rare earth complexes $M(OOPc)_2$ (Table 4). The introduction of eight octyloxy groups, which are more electron-donating than the four *tert*-butyl groups, means that the double-deckers $M(OOPc)_2$ become easier to oxidize and harder to reduce, therefore showing lower first and second oxidation potentials and more negative first, second and third reduction potentials than the corresponding analogues $M(TBPc)_2$. Due to the additional shift of corresponding redox processes of $M(OOPc)_2$ to a more negative direction than those of $M(TBPc)_2$, only three reduction processes were observed within the electrochemical window of CH_2Cl_2 for the former. Under similar experimental conditions, only one one-electron oxidation and two one-electron reductions were observed by Takahashi[4d] for the butyloxy-substituted bis(phthalocyaninato) rare earth analogues $M(OBPc)_2$ (M = Yb, Lu).

As can be seen from Table 4, discussion for $Ce(OOPc)_2$ is prevented due to the failure to record the half-wave potential for the second reduction process by either CV or DPV.

Conclusions

The five quasi-reversible one-electron reductions observed within the electrochemical window of CH_2Cl_2 for the unsubstituted bis(phthalocyaninato) rare earth complexes $M^{III}(Pc)_2$ (M ≠ Ce, Pm, Yb, Lu) demonstrate again that the LUMO of bis(phthalocyaninato) rare earth compounds is doubly degenerate and can accept up to four electrons, while the HOMO of the bis(phthalocyaninato) tervalent rare earth complexes is semi-occupied and can accept one electron. However, only three and four quasi-reversible one-electron reductions were observed for $M^{III}(OOPc)_2$ and $M^{III}(TBPc)_2$, respectively, under the same experimental conditions, due to the shift of corresponding redox potentials in a negative direction induced by the introduction of electron-donating octyloxy or *tert*-butyl groups. As usual, the Ce complexes are exceptional due to the unique oxidation state of the central metal ion. One cerium-centered redox wave could easily be distinguished from the CV and DPV diagrams of these three bis(phthalocyaninato)cerium compounds. Systematic studies of the electrochemical characteristics of unsubstituted, tetra-*tert*-butyl- and octakis-(octyloxy)-substituted bis(phthalocyaninato) complexes of the whole tervalent lanthanide series clearly indicate that the half-wave potentials, in particular the first oxidation and first reduction processes, are all metal-ion-size-dependent. The change in the half-wave potentials of these redox processes is apparently due to stronger inter-ligand interactions and generally tighter bonding as the metal ion radius contracts across the series. In the next paper in this series the corresponding data for heteroleptic tris(phthalocyaninato) rare earth(III) triple-deckers are reported and analyzed.[20]

Experimental Section

Homoleptic bis(phthalocyaninato) rare earth double-decker compounds $M(Pc)_2$, $M(OOPc)_2$ and $M(TBPc)_2$ were prepared according to published procedures.[9d,14,21] CV and DPV measurements were carried out with a BAS CV-50 W voltammetric analyzer. The cell consists of inlets for a glassy carbon disk working electrode (2.0 mm diameter) and a silver-wire counter electrode. The reference electrode was Ag/Ag^+ connected to the solution by a Luggin capillary whose tip was placed close to the working electrode. Results are corrected for junction potentials by being referenced internally to the ferrocenium/ferrocene (Fe^+/Fe) couple [$E_{1/2}(Fe^+/Fe) = +0.50$ V vs. SCE]. The potentials in this paper are referenced to the SCE. Typically, a 0.1 M solution of $[Bu_4N][ClO_4]$ in CH_2Cl_2 containing 0.5 mM sample was purged with nitrogen for 10 min; the voltammograms were then recorded at ambient temperature with scan rates of 20 and 10 mV/s for CV and DPV, respectively.

Acknowledgments

The authors thank the National Natural Science Foundation of China (Grant No. 20171028), the National Ministry of Science and Technology of China (Grant No. 2001CB6105-04), The Science Committee of Shandong Province (Grant No. Z99B03), the National Educational Ministry of China, Shandong University, and Queensland University of Technology for financial support.

[1] [1a] J. Jiang, K. Kasuga, D. P. Arnold, in *Supramolecular Photosensitive and Electroactive Materials* (Ed.: H. S. Nalwa), Academic Press, New York, **2001**, chapter 2, pp. 113−210. [1b] D. K. P. Ng, J. Jiang, *Chem. Soc. Rev.* **1997**, *26*, 433−442. [1c] J. Jiang, W. Liu, D. P. Arnold, *J. Porphyrins Phthalocyanines* **2003**, *7*, 459−473.

[2] J. W. Buchler, D. K. P. Ng, in *The Porphyrin Handbook* (Eds.: K. M. Kadish, K. M. Smith, R. Guilard), Academic Press, New York, **1999**, chapter 20, pp. 245−294.

[3] [3a] M. M. Nicholson, in *The Phthalocyanines: Properties and Applications* (Eds.: C. C. Leznoff, A. B. P. Lever), VCH Publishers, New York, **1993**, vol. 3, pp. 76−117. [3b] P. M. S. Monk, R. J. Mortimer, D. R. Rosseinsky, in *Electrochromism: Fundamentals and Applications* (Eds.: P. Gregory, U. Anton), VCH Publishers, Weinheim, **1995**.

[4] [4a] M. L′Her, Y. Cozien, J. Courtot-Coupez, *J. Electroanal. Chem.* **1983**, *157*, 183−187. [4b] F. Castaneda, C. Piechocki, V. Plichon, J. Simon, J. Vaxiviere, *Electrochim. Acta* **1986**, *31*, 131−133. [4c] A. Pondaven, Y. Cozien, M. L′Her, *New J. Chem.* **1991**, *15*, 515−516. [4d] K. Takahashi, Y. Tomita, Y. Hada, K. Tsubota, M. Handa, K. Kasuga, K. Sogabe, T. Tokii, *Chem. Lett.* **1992**, 759−762. [4e] F. Guyon, A. Pondaven, P. Guenot, M. L′Her, *Inorg. Chem.* **1994**, *33*, 4787. [4f] M. L′Her, Y. Cozien, J. Courtot-Coupez, *C. R. Acad. Sci. Ser. 2* **1986**, *302*, 9−14.

[5] [5a] G. C. S. Collins, D. J. Schiffrin, *J. Electroanal. Chem.* **1982**, *139*, 335−369. [5b] S. Besbes, V. Pichon, J. Simon, J. Vaxiviere,

 © 2004 Wiley-VCH Verlag GmbH & Co. KGaA, Weinheim

J. Electroanal. Chem. **1987**, *237*, 61−68. [5c] F. Castaneda, V. Plichon, *J. Electroanal. Chem.* **1987**, *236*, 163−175. [5d] M. Bardin, E. Bertounesque, V. Plichon, J. Simon, V. Ahsen, O. Bekaroglu, *J. Electroanal. Chem.* **1989**, *271*, 173−180. [5e] Y. Liu, K. Shigehara, M. Hara, A. Yamada, *J. Am. Chem. Soc.* **1991**, *113*, 440−443. [5f] T. Toupance, V. Plichon, J. Simon, *New J. Chem.* **1999**, *23*, 1001−1006.

[6] [6a] J. Simon, J. J. Andre, *Molecular Semi-conductors*, Springer Verlag, Berlin, Germany, **1985**. [6b] M. Bouvet, J. Simon, *Chem. Phys. Lett.* **1990**, *172*, 299−302.

[7] [7a] J. Jiang, D. P. Arnold, H. and Yu, *Polyhedron* **1999**, *8*, 2129−2139. [7b] X. Sun, M. Bao, N. Pan, X. Cui, D. P. Arnold, J. Jiang, *Aust. J. Chem.* **2002**, *9*, 587−595. [7c] F. Lu, M. Bao, C. Ma, X. Zhang, D. P. Arnold, J. Jiang, *Spectrochim. Acta Part A*, in press.

[8] [8a] J. Jiang, L. Rintoul, D. P. Arnold, *Polyhedron* **2000**, *19*, 1381−1394. [8b] J. Jiang, U. Cornelissen, D. P. Arnold, X. Sun, H. Homborg, *Polyhedron* **2001**, *20*, 557−569. [8c] N. Pan, L. Rintoul, D. P. Arnold, J. Jiang, *Polyhedron* **2002**, *21*, 1905−1912. [8d] Y. Bian, L. Rintoul, D. P. Arnold, N. Pan, J. Jiang, *Vib. Spectrosc.* **2003**, *31*, 173−185. [8e] X. Sun, L. Rintoul, Y. Bian, D. P. Arnold, R. Wang, J. Jiang, *J. Raman Spectrosc.* **2003**, *34*, 306−314.

[9] [9a] J. Jiang, Y. Bian, F. Furuya, W. Liu, M. T. M. Choi, H. W. Li, N. Kobayashi, Q. Yang, T. C. W. Mak, D. K. P. Ng, *Chem. Eur. J.* **2001**, *7*, 5059−5069. **2003**, *27*, 844−849. [9b] J. Jiang, W. Liu, K. L. Cheng, K. W. Poon, D. K. P. Ng, *Eur. J. Inorg. Chem.* **2001**, 413−417. [9c] J. Jiang, W. Liu, K. W. Poon, D. Du, D. P. Arnold, D. K. P. Ng, *Eur. J. Inorg. Chem.* **2000**, 205−209. [9d] W. Liu, J. Jiang, D. Du, D. P. Arnold, *Aust. J. Chem.* **2000**, *53*, 131−136.

[10] Y. Bian, D. Wang, R. Wang, L. Wen, J. Dou, D. Zhao, D. K. P. Ng, J. Jiang, *New J. Chem.* **2003**, *27*, 844−849.

[11] [11a] H. Konami, H. Hatano, N. Kobayashi, T. Osa, *Chem. Phys. Lett.* **1990**, *165*, 397−400. [11b] H. Konami, H. Hatano, A. Tajiri, *Chem. Phys. Lett.* **1989**, *160*, 163−167.

[12] [12a] A. Iwase, C. Harnoode, Y. Kameda, *J. Alloys Compds.* **1993**, *192*, 280−283. [12b] C. Harnoode, F. Kitamura, T. Ohsaka, K. Tokuda, A. Iwase, *Denki Kagaku* **1993**, *61*, 767−769.

[13] [13a] M. S. Haghighi, H. Homborg, *Z. Anorg. Allg. Chem.* **1994**, *620*, 1278−1284. [13b] G. Ostendorp, H. Homborg, *Z. Anorg. Allg. Chem.* **1996**, *622*, 1222−1230.

[14] J. Jiang, R. C. W. Liu, T. C. W. Mak, T. W. D. Chan, D. K. P. Ng, *Polyhedron* **1997**, *16*, 515−520.

[15] K. M. Kadish, T. Nakanishi, A. Gürek, V. Ahsen, I. Yilmaz, *J. Phys. Chem. B* **2001**, *105*, 9817−9821.

[16] [16a] E. Orti, J. L. Bredas, *J. Chem. Phys.* **1990**, *92*, 1228−1235. [16b] R. Rousseau, R. Aroca, M. L. Rodriguez-Mendez, *J. Mol. Struct.* **1995**, *356*, 49−62. [16c] N. Ishikawa, *J. Porphyrins Phthalocyanines* **2001**, *5*, 87−101.

[17] [17a] A. Giraudeau, A. Louati, M. Gross, J. J. Andre, J. Simon, H. C. Su, K. M. Kadish, *J. Am. Chem. Soc.* **1983**, *105*, 2917−2919. [17b] A. Louati, M. El Meray, J. J. Andre, J. Simon, K. M. Kadish, M. Gross, A. Giraudeau, *Inorg. Chem.* **1995**, *24*, 1175−1179.

[18] N. Kobayashi, personal communication.

[19] [19a] W. Kuchle, M. Dolg, H. Stoll, *J. Phys. Chem.* **1997**, *101*, 7128−7133. [19b] Y. Bian, J. Jiang, Y. Tao, M. T. M. Choi, R. Li, A. C. H. Ng, P. Zhu, N. Pan, X. Sun, D. P. Arnold, Z. Zhou, H.-W. Li, D. K. P. Ng, *J. Am. Chem. Soc.* **2003**, *125*, 12257−12267. [19c] H. Homborg, personal communications.

[20] P. Zhu, N. Pan, C. Ma, X. Sun, D. P. Arnold, J. Jiang, *Eur. J. Inorg. Chem.*, accepted.

[21] J. Jiang, J. Xie, M. T. M. Choi, D. K. P. Ng, *J. Porphyrins Phthalocyanines* **1999**, *3*, 322−328.

Received July 28, 2003
Early View Article
Published Online December 12, 2003

 © 2004 Wiley-VCH Verlag GmbH & Co. KGaA, Weinheim

Electrochemistry of Heteroleptic Tris(phthalocyaninato) Rare Earth(III) Complexes

Peihua Zhu,[a] Na Pan,[a] Changqin Ma,[a] Xuan Sun,[a] Dennis P. Arnold,*[b] and Jianzhuang Jiang*[a,c]

Keywords: Phthalocyanines / Sandwich complexes / Rare earths / Electrochemistry

The electrochemical characteristics of a series of heteroleptic tris(phthalocyaninato) complexes with identical rare earths or mixed rare earths (Pc)M(OOPc)M(OOPc) [M = Eu...Lu, Y; H_2Pc = unsubstituted phthalocyanine, H_2(OOPc) = 3,4,12,13,21,22,30,31-octakis(octyloxy)phthalocyanine] and (Pc)Eu(OOPc)Er(OOPc) have been recorded and studied comparatively by cyclic voltammetry (CV) and differential pulse voltammetry (DPV) in CH_2Cl_2 containing 0.1 M tetrabutylammonium perchlorate (TBAP). Up to five quasi-reversible one-electron oxidations and four one-electron reductions have been revealed. The half-wave potentials of the first, second and fifth oxidations depend on the size of the metal center, but the fifth changes in the opposite direction to that of the first two. Moreover, the difference in redox potentials of the first oxidation and first reduction for (Pc)M(OOPc)M(OOPc), 0.85–0.98 V, also decreases linearly along with decreasing rare earth ion radius, clearly showing the rare earth ion size effect and indicating enhanced π–π interactions in the triple-deckers connected by smaller lanthanides. This order follows the red-shift seen in the lowest energy band of triple-decker compounds. The electronic differences between the lanthanides and yttrium are more apparent for triple-decker sandwich complexes than for the analogous double-deckers. By comparing triple-decker, double-decker and mononuclear [Zn^{II}] complexes containing the OOPc ligand, the HOMO–LUMO gap has been shown to contract approximately linearly with the number of stacked phthalocyanine ligands.
(© Wiley-VCH Verlag GmbH & Co. KGaA, 69451 Weinheim, Germany, 2004)

Introduction

Bis(phthalocyaninato) rare earth sandwich complexes have been extensively studied for potential applications in electronic devices.[1,2] The electrochemical properties of bis(phthalocyaninato) rare earth compounds have been systematically investigated from the viewpoint of electrochromic displays and to understand the nature of π−π interactions in the molecules.[3−5] Recently, triple-decker (na)phthalocyaninato rare earth analogues have aroused interest for the same reasons.[6−9] The expected relatively weaker electronic interaction in triple-deckers, which have a larger ring-to-ring separation than the double-decker analogues, has been revealed by spectroscopic studies. In 1986, Kasuga isolated traces of $Y_2(Pc)_3$ as a side-product in preparing double-decker $Y(Pc)_2$ and confirmed its triple-decker nature by mass spectrometry.[7a] Since 1993, Takahashi developed a new synthetic route for preparing homoleptic substituted tris(phthalocyaninato) rare earth compounds $M_2(OBPc)_3$ (M = La, Dy, Yb, Lu) using the reaction between free base phthalocyanine H_2(OBPc) and rare earth salt $M(OAc)_3{\cdot}nH_2O$[7b,7c] (for abbreviations of ligands, see Table 1). L'Her has detailed the synthesis, characterization, and electrochemical behavior of the tris(1,2-naphthalocyaninato)dilutetium compound $Lu_2(1,2\text{-Nc})_3$.[8] Ishikawa and co-workers have prepared homoleptic and heteroleptic

Table 1. Abbreviations for ligands

Abbreviation	Ligand
H_2TPP	5,10,15,20-tetraphenylporphyrin
H_2OEP	2,3,7,8,12,13,17,18-octaethylporphyrin
H_2Pc	phthalocyanine
H_2OOPc	2,3,9,10,16,17,24,25-octakis(octyloxy)phthalocyanine
H_2OBPc	2,3,9,10,16,17,24,25-octakis(butyloxy)phthalocyanine
H_2TBPc	2(3),9(10),16(17),24(25)-tetra-*tert*-butylphthalocyanine
H_2[Pc(15C5)$_4$]	phthalocyanine with four 15-crown-5 (1,4,7,10,13-pentaoxacyclopentadecane) voids at the 2,3-positions
H_2(1,2-Nc)	1,2-naphthalocyanine
H_2(2,3-TBNc)	3(4),12(13),21(22),30(31)-tetra-*tert*-butyl-2,3-naphthalocyanine

[a] Department of Chemistry, Shandong University, Jinan 250100, China
Fax: (internat.) + 86-531-856-5211
E-mail: jzjiang@sdu.edu.cn
[b] School of Physical and Chemical Sciences, Queensland University of Technology, G. P. O. Box 2434, Brisbane 4001, Australia
Fax: (internat.) + 61-7-3864-1804
E-mail: d.arnold@qut.edu.au
[c] Fujian Institute of Material Structure, Fuzhou 350002, P. R. China

 © 2004 Wiley-VCH Verlag GmbH & Co. KGaA, Weinheim DOI: 10.1002/ejic.200300510

phthalocyaninato triple-decker complexes $Lu_2(Pc)_3$ and (Pc)Lu[Pc(15C5)$_4$]Lu(Pc) and studied their electronic absorption and MCD spectra.[9] Our group have reported a novel, versatile route for preparing a series of heteroleptic phthalocyaninato rare earth triple-deckers containing unsubstituted phthalocyaninato and 2,3,9,10,16,17,23,24-octakis(octyloxy)phthalocyaninato (OOPc) ligands[6a] and have systematically studied their NMR properties.[6b] Using a similar synthetic methodology, Ishikawa has prepared a series of similar heteroleptic tris(phthalocyaninato) rare earth compounds (Pc)M(Pc)M′(OBPc) (M =/≠ M′ = Tb, Dy, Ho, Er, Tm, Yb, Y) and studied the interaction between the f-electronic systems and phthalocyanine ligands in the dinuclear complexes of paramagnetic tervalent lanthanide ions as well as the f−f interactions between the metal ions by magnetic measurements.[10a,10b] However, of the reported triple-decker tris[(na)phthalocyaninato] rare earth compounds only five, $M_2(OBPc)_3$ (M = La, Dy, Yb, Lu)[7b,7c] and $Lu_2(1,2\text{-}Nc)_3$,[8b] have been investigated by electrochemical methods. The ring-to-ring interaction in these triple-decker molecules is worthy of systematic study from both theoretical and experimental viewpoints. We report here the electrochemical properties of a series of heteroleptic phthalocyaninato rare earth triple-decker complexes (Pc)M(OOPc)M(OOPc) (M = Eu...Lu, Y) and (Pc)Tm(OOPc)Tm(Pc) (Scheme 1) by cyclic voltammetry (CV) and differential pulse voltammetry (DPV). For comparison, the electrochemistry of the substituted (phthalocyaninato)zinc complex Zn(OOPc) and double-decker rare earth compounds $M(Pc)_2$ and $M(OOPc)_2$ are also discussed. The latter two series and the analogues $M(TBPc)_2$ feature in our previous paper.[5]

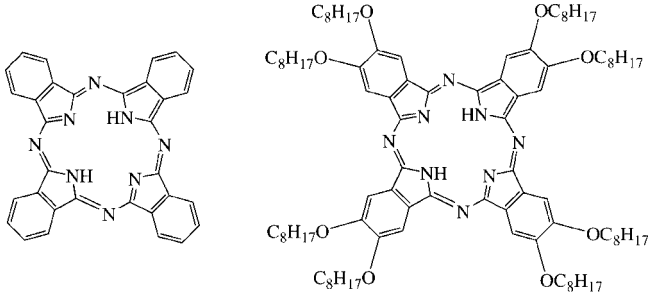

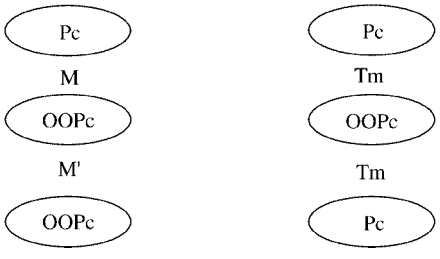

Scheme 1. Phthalocyanine ligands and schematic diagram of heteroleptic tris(phthalocyaninato) rare earth complexes (Pc)M(OOPc)M′(OOPc) (M = M′ = Eu...Lu, Y; M = Eu, M′ = Er) and (Pc)Tm(OOPc)Tm(Pc)

Results and Discussion

The electrochemical behavior of the triple-decker complexes together with monomeric Zn(OOPc) was investigated by cyclic voltammetry (CV) and differential pulse voltammetry (DPV) in CH_2Cl_2. While the monomeric compound Zn(OOPc) undergoes two reversible to quasi-reversible one-electron oxidations and two reversible to quasi-reversible one-electron reductions, the triple-decker compounds display up to five one-electron oxidations and up to four one-electron reductions within the electrochemical window of CH_2Cl_2 under the conditions employed. The reduction and oxidation peak potentials for each process are 60−90 mV apart. Since the oxidation state of the central zinc and tervalent rare earth ions in monomeric and triple-decker complexes, respectively, do not change, these processes are attributed to the successive removal, or addition, of one electron from, or to, the ligand-based orbitals of the redox states (Scheme 2). Oxidations are labeled Oxd_1 to Oxd_5 and the reductions Red_1 to Red_4. The half-wave redox potentials vs. SCE are summarized in Table 2. Representative cyclic voltammograms and differential pulse voltammograms for (Pc)Tm(OOPc)Tm(OOPc) are displayed in Figure 1. The observation of up to five cationic states for these triple-deckers supports the proposal of Lindsey that they are potential molecular materials for information storage.[11]

Our observations of the electrochemistry of these heteroleptic triple-deckers in CH_2Cl_2 differ slightly from those reported for homoleptic tris(phthalocyaninato) rare earth analogues.[7b,7c] For instance, up to four oxidation and three reduction processes were observed for $M_2(OBPc)_3$ in CH_2Cl_2 containing $TBAPF_6$.[7b,7c] However, under our experimental conditions, we observed two more oxidation states in some cases, particularly by DPV. Figure 2 shows the variation of the redox potentials of (Pc)M(OOPc)M(OOPc) with the ionic radius of the rare earth metal center. While the half-wave potentials of the third and fourth oxidations of (Pc)M(OOPc)M(OOPc) remain virtually unchanged, the half-wave potentials of the first, second and fifth oxidations of these triple-deckers correlate linearly with the ionic size of the rare earth metal center (Figure 2 and Table 2). The half-wave potentials of the first and second oxidations shift slightly in the cathodic direction with decreasing rare earth ion radius, while those of the fifth oxidation shift in the opposite direction.

As with bis(phthalocyaninato) rare earth compounds,[5] in the tris(phthalocyaninato) rare earth triple-decker molecules the close proximity of the three conjugated π-systems in a face-to-face configuration splits the doubly degenerate LUMO (e_g) and HOMO ($4a_u$) molecular orbitals derived from monophthalocyanines. This results in three pairs of doubly degenerate unoccupied frontier molecular orbitals (the bonding LUMO, second non-bonding LUMO and third anti-bonding LUMO) and three non-degenerate occupied frontier orbitals (the third bonding HOMO, second non-bonding HOMO and first anti-bonding HOMO) in the triple-deckers. The splitting of the filled MOs, actually the splitting between the first HOMO and second HOMO as

 © 2004 Wiley-VCH Verlag GmbH & Co. KGaA, Weinheim

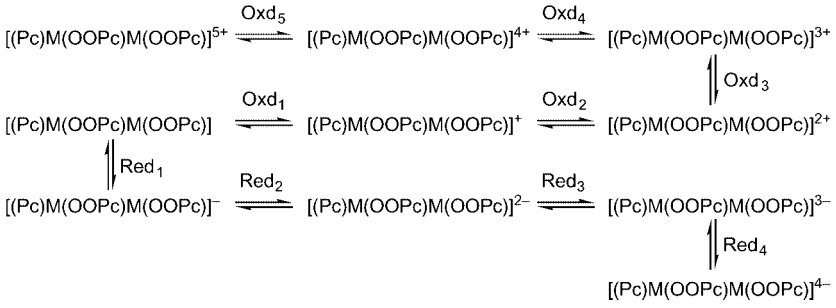

Scheme 2. One-electron redox processes of (Pc)M(OOPc)M(OOPc)

Table 2. Half-wave redox potentials of (Pc)M(OOPc)M′(OOPc) (M = M′ = Eu...Lu, Y; M = Eu, M′ = Er) together with (Pc)Tm(OOPc)Tm(Pc) and Zn(OOPc) (V vs. SCE) in CH_2Cl_2 containing 0.1 M TBAP

	Oxd_5	Oxd_4	Oxd_3	Oxd_2	Oxd_1	Red_1	Red_2	Red_3	Red_4	$\Delta E°_{1/2}$[a]
Eu	+1.45[b]	+1.30	+1.14	+0.63	+0.26	−0.72	−1.10	−1.41[b]		0.98
Gd	+1.49[b]	+1.32[b]	+1.18	+0.63	+0.25	−0.73	−1.09	−1.41[b]	−1.66[b]	0.98
Tb	+1.50[b]	+1.32[b]	+1.18	+0.62	+0.23	−0.75[b]	−1.08[b]	−1.43[b]	−1.76[b]	0.98
Dy	+1.66[b]	+1.35	+1.19	+0.61	+0.21	−0.78	−1.13	−1.51	−1.75[b]	0.99
Y	+1.50	+1.30	+1.14	+0.64	+0.27	−0.76	−1.06	−1.38		1.03
Ho			+1.19[b]	+0.60	+0.21	−0.72[b]	−1.05[b]	−1.38[b]		0.93
Er		+1.35	+1.19	+0.57	+0.18	−0.74	−1.06[b]	−1.41[b]	−1.60[b]	0.92
Tm		+1.34	+1.16	+0.54	+0.14	−0.77	−1.13	−1.55	−1.80[b]	0.91
Yb		+1.36	+1.18	+0.54	+0.14	−0.76	−1.09	−1.44	−1.62[b]	0.90
Lu		+1.38	+1.20	+0.53	+0.13	−0.72	−1.07	−1.39		0.85
Eu/Er[c]		+1.43	+1.19	+0.62	+0.22	−0.74	−1.07	−1.49[b]		0.96
Tm[d]	+1.76[b]	+1.46[b]	+1.28	+0.68	+0.27	−0.71	−0.97[b]	−1.37[b]	−1.67[b]	0.98
Zn[e]				+1.27	+0.50	−1.14	−1.22			1.64

[a] $\Delta E°_{1/2}$ is the potential difference between the first oxidation and first reduction processes, i.e. the HOMO−LUMO gap of corresponding molecules, namely (Pc)M(OOPc)M(OOPc), (Pc)Tm(OOPc)Tm(Pc) and Zn(OOPc). [b] Recorded by DPV. [c] (Pc)Eu(OOPc)Er(OOPc). [d] (Pc)Tm(OOPc)Tm(Pc). [e] Zn(OOPc).

well as the second HOMO and third HOMO of triple-decker, increases with the lanthanide contraction due to the increase in the ring-to-ring interaction. Therefore, there is an increase in the energy of the anti-bonding HOMO and a corresponding decrease in the energy of the third bonding HOMO in the same order, but no change in the energy of the non-bonding second HOMO. This is why the half-wave potentials of the first and second oxidations (Oxd_1 and Oxd_2) dealing with the first anti-bonding HOMO are shifted slightly to a more negative direction with decreasing rare earth radius, and those for the fifth oxidation of (Pc)M(OOPc)M(OOPc) (Oxd_5) involving the third bonding HOMO are shifted slightly in the positive direction, in the same order. Conversely, those for the third and fourth oxidations, which are related to the second non-bonding HOMO, are essentially unchanged. This proposal is also well supported by the optical properties of (Pc)M(OOPc)M(OOPc). Previous studies have revealed that the lowest energy electronic absorption band at 683−714 nm in the electronic spectra of triple-decker tris(phthalocyaninato) rare earth complexes (Pc)M(OOPc)M(OOPc) (M = Pr...Tm), which involves the electronic transition from the HOMO to the degenerate LUMO, is red-shifted with decreasing rare earth ionic size.[5] It is noteworthy that the first and second oxidation (HOMO-related) potentials of tris(phthalocyaninato) rare earth compounds depend in a similar way on the rare earth ionic size as do the first reduction and first oxidation (also involving the HOMO) of their double-decker counterparts. However, the sensitivity to ionic size is significantly less for the triple-deckers due to their larger inter-ring distances.[3−5]

The half-wave potentials of all the *reductions* for (Pc)M(OOPc)M(OOPc) appear to reveal no systematic trends with ionic size. These results also correspond well with those obtained for the bis(phthalocyaninato) rare earth double-deckers.[3−5]

The redox behavior of the heterodinuclear compound (Pc)Eu(OOPc)Er(OOPc) was also examined by CV and DPV, and parallels those of its counterparts with two identical metals (Table 2). The redox potentials, especially those involving the HOMO and LUMO of (Pc)Eu(OOPc)-Er(OOPc), i.e. the first and second oxidations and the first and second reductions, fit the linear correlation seen between the redox potentials and ionic radii for complexes with identical metals if the mean ionic radius of Eu and Er is employed. This corresponds well with the results of Weiss and co-workers on the electrochemistry of mixed (phthalocyaninato)(porphyrinato) rare earth triple-decker complexes containing mixed or identical rare earth metals, clearly indi-

 © 2004 Wiley-VCH Verlag GmbH & Co. KGaA, Weinheim

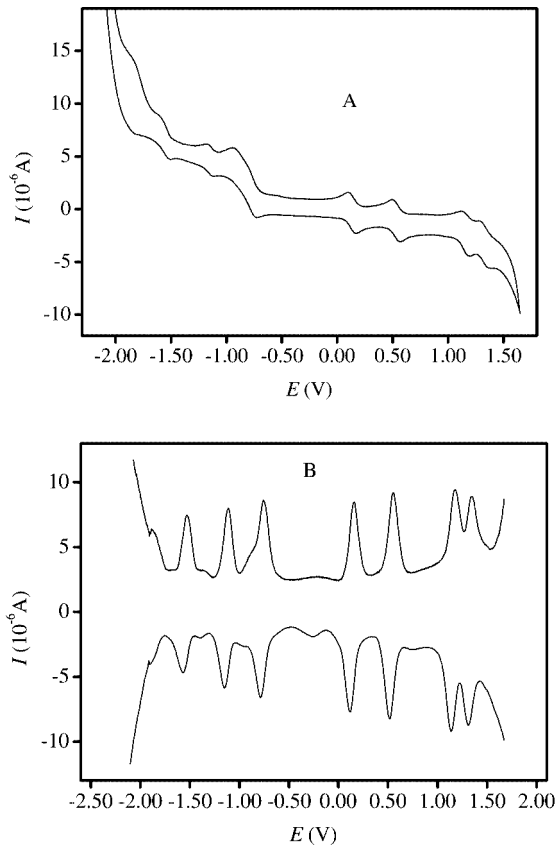

Figure 1. CV (A) and DPV (B) of (Pc)Tm(OOPc)Tm(OOPc) in CH_2Cl_2 containing 0.1 M $[Bu_4N][ClO_4]$ at scan rates of 20 and 10 $mV \cdot s^{-1}$, respectively

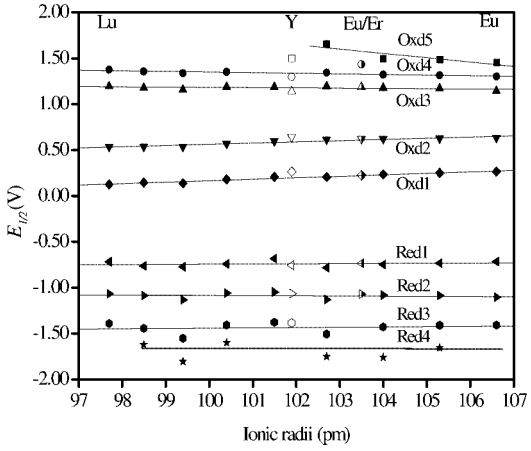

Figure 2. Half-wave potentials of redox processes of (Pc)M(OOPc)M(OOPc) (M = Eu...Lu) as a function of the ionic radius of M^{III}

cating the involvement of all three phthalocyanine rings in the frontier molecular orbitals of heteroleptic tris(phthalocyaninato) rare earth compounds.[12]

The potential difference between the first oxidation and first reduction, $\Delta E^\circ_{1/2}$, for all these triple-decker compounds (Pc)M(OOPc)M(OOPc) (M = Eu...Lu) spans the relatively narrow range 0.85−0.99 V, which corresponds well with results for $M_2(OBPc)_3$ (M = Dy, Yb, Lu)

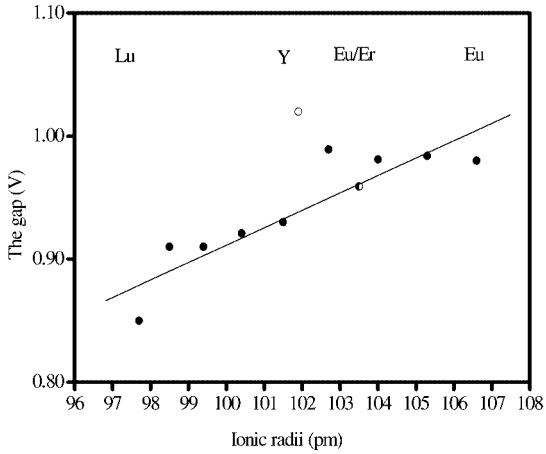

Figure 3. HOMO−LUMO gap between the half-wave potentials of the first oxidation and first reduction of (Pc)M(OOPc)M(OOPc) as a function of the ionic radius of M^{III}

(0.98−1.09 V)[7b,7c] and $Lu_2(1,2\text{-Nc})_3$[8b] (0.86 V). Figure 3 shows this potential gap for (Pc)M(OOPc)M(OOPc) as a function of the tervalent rare earth ionic radii. Clearly, the difference between the first oxidation and first reduction processes for (Pc)M(OOPc)M(OOPc) decreases more or less linearly with decreasing rare earth ion size. The clear outlier (Pc)Y(OOPc)Y(OOPc) is not unexpected as yttrium is not an f-series lanthanide, and so its interaction with the π orbitals of conjugated tetrapyrrole ligands is fundamentally different. Electrochemical investigations of a series of rare earth *double-decker* compounds with different tetrapyrrole ligands in either neutral or reduced form, namely $[M(Pc)_2]^-$ [3,4] and $M(Pc')_2$ (Pc′ = Pc, TBPc, OOPc),[5] $M(TBNc)_2$,[13] M(TPP)(Pc)[14] M(OEP)(Nc),[15] and $M(OEP)_2$,[16] have found that the gap between the first oxidation and the first reduction potentials of the monoanionic reduced form of all these tetrapyrrole double-deckers decreases linearly with the lanthanide contraction. The deviation for yttrium double-decker compounds $[Y(Pc')_2]^-$ (Pc′ = Pc, TBPc, OOPc) is not so obvious as in the triple-decker series studied here. This is due to the magnifying effects of the f−f interaction between the metal centers in the lanthanide triple-deckers. Of course, such interaction is absent for yttrium, so a large deviation is not unexpected.

As $\Delta E^\circ_{1/2}$ (Oxd_1 − Red_1), representing the electrochemical HOMO−LUMO gap, reflects the interactions among the tetrapyrrole rings in the sandwich molecules, the decrease in $\Delta E^\circ_{1/2}$ (Oxd_1 − Red_1) with the lanthanide contraction clearly suggests enhanced ring−ring interactions in the same order. This view is strongly supported as the HOMO−LUMO gap for the mixed-metal complex (Pc)Eu(OOPc)Er(OOPc) lies between those of the compounds with two identical metals (Pc)Eu(OOPc)Eu(OOPc) and (Pc)Er(OOPc)Er(OOPc) (Table 2 and Figure 3).

Furthermore, the electrochemical data for triple-deckers (Pc)M(OOPc)M(OOPc) and the mononuclear compound Zn(OOPc), together with those of the double-deckers $M(Pc)_2$ and $M(OOPc)_2$ obtained previously, render it pos-

 © 2004 Wiley-VCH Verlag GmbH & Co. KGaA, Weinheim

sible to compare the effect of the extension of the π-networks along an axis perpendicular to the phthalocyanine plane. It must be pointed out that in the neutral double-decker species $M(Pc')_2$ (Pc′ = Pc, OOPc), one of the two Pc′ rings is a monoanion radical ($Pc'^{\cdot -}$), therefore the reduced double-decker species $[M(Pc')_2]^-$ (Pc′ = Pc, OOPc) should be considered for comparison with the monomeric Zn(OOPc) and triple-decker (Pc)M(OOPc)M(OOPc), so that all the phthalocyanine rings are in the dianionic form Pc'^{2-}.[8b] Comparison of the HOMO−LUMO gap for (Pc)M(OOPc)M(OOPc) (M = Eu...Lu), 0.85−0.98 V, with that of 1.08−1.37 V for $[M(Pc)_2]^-$ (M = La...Lu) or 1.13−1.40 V for $[M(OOPc)_2]^-$ (La...Lu) from our previous work[5] and 1.64 V for Zn(OOPc) makes it clear that the extension of the bonding over more phthalocyanine rings has an obvious effect on the MO levels. Zn(OOPc) is used as a comparable representative mononuclear complex as its gap is the same as that for Lu(1,2-Nc)(OAc);[8b] likewise the gap for $[Lu(1,2\text{-}Nc)_2]^-$ lies in the range for our double-decker anions, and that for $Lu_2(1,2\text{-}Nc)_3$ is in the range for our triple-deckers.[8b] For a qualitative comparison, it therefore seems appropriate to use the Zn complex, and thus avoid recording the full series of mononuclear rare earth complexes. The increase in the number of macrocycles in the face-to-face stack from monomer to triple-decker via double-decker induces important modifications in the orbital systems of these complexes, manifested in the decrease in the HOMO−LUMO gap (Figure 4). Further axial extension of delocalization of the stacked π-conjugated molecules is therefore predicted to lead to corresponding molecular materials with narrower HOMO−LUMO gaps. According to Simon,[17] the potential difference between the first oxidation and first reduction processes, $\Delta E^\circ_{1/2}$, allows the prediction of electrical properties such as the thermal activation energy for the conduction process of the condensed phases derived from the corresponding molecular precursors. Therefore one can reasonably expect further improved electrical properties of stacked π-conjugated phthalocyanine-derived molecular systems, i.e. sandwich-type

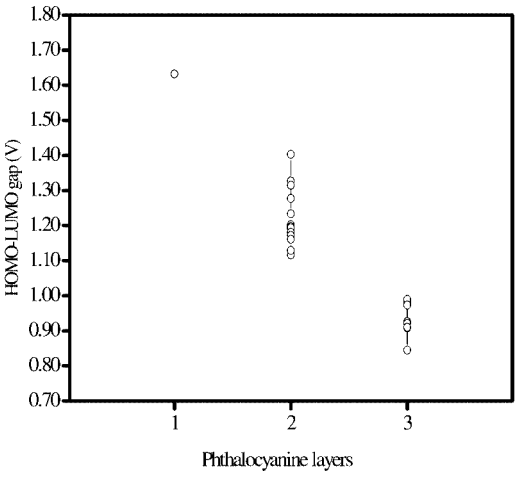

Figure 4. HOMO−LUMO gap of Zn(OOPc), $[M(OOPc)_2]^-$ (M = La...Lu; OOPc) and (Pc)M(OOPc)M(OOPc) (M = Eu...Lu) as a function of the number of phthalocyanine layers

(phthalocyaninato)metal oligomers or polymers, compared with those of double- and triple-deckers. So far no higher oligomers linked by metal ion connectors have been isolated, only systems linked by various axial ligands.[18]

CV and DPV studies revealed that (Pc)Tm(OOPc)-Tm(Pc), which is a representative of a series of more symmetrical heteroleptic tris(phthalocyaninato) rare earth compounds, also undergo five quasi-reversible one-electron oxidations and four quasi-reversible one-electron reductions (Table 2). In comparison with (Pc)Tm(OOPc)Tm(OOPc), the symmetrical compound clearly undergoes oxidations less readily, as shown by the higher oxidation potentials, whereas the reductions occur more readily, both effects being due to the incorporation of only one electron-rich OOPc ring in the molecule. However, the difference between the first oxidation and first reduction potentials of (Pc)Tm(OOPc)Tm(Pc), 0.97 V, is very similar to the 0.91 V for (Pc)Tm(OOPc)Tm(OOPc) and still lies in the range for the (Pc)M(OOPc)M(OOPc) series, indicating similar π−π interactions in the two series. Similar results have also been observed for heteroleptic and homoleptic bis(phthalocyaninato) rare earth compounds containing substituted phthalocyanine ring(s), namely M(Pc)(Pc*)[19] and $M(Pc^*)_2$ (Pc* = TBPc,[5,19a] OOPc,[5] OPPc,[19b] OHPc[19b]) when compared with the electrochemical properties of $M(Pc)_2$.[3−5]

Conclusions

Systematic studies of the electrochemical characteristics of heteroleptic tris(phthalocyaninato) rare earth complexes (Pc)M(OOPc)M(OOPc) have revealed that these compounds can undergo up to five quasi-reversible one-electron oxidations and up to four quasi-reversible one-electron reductions within the electrochemical window of CH_2Cl_2. The half-wave potentials of the first and second oxidations for these tervalent rare earth triple-deckers are metal-ion-size-dependent; the oxidations become easier with decreasing lanthanide ion size. Comparison among triple-deckers (Pc)M(OOPc)M(OOPc), reduced double-deckers $[M(Pc')_2]^-$ (Pc′ = Pc, OOPc)[5] and mononuclear Zn(OOPc) shows that the HOMO−LUMO gap is decreased by extension of the delocalized bonding along the axis perpendicular to the macrocycle plane.

Experimental

The monomeric (phthalocyaninato)zinc compound Zn(OOPc)[20] and heteroleptic phthalocyaninato rare earth triple-decker complexes (Pc)M(OOPc)M(OOPc) (M = Eu...Lu, Y), (Pc)Eu(OOPc)Er(OOPc), and (Pc)Tm-(OOPc)Tm(Pc) were prepared according to published procedures.[6a] Cyclic voltammetry (CV) and differential pulse voltammetry (DPV) were carried out with a BAS CV-50 W voltammetric analyzer. The cell consists of inlets for a glassy carbon disk working electrode (2.0 mm in diameter)

 © 2004 Wiley-VCH Verlag GmbH & Co. KGaA, Weinheim

and a silver-wire counter electrode. The Ag/Ag^+ reference electrode was connected to the solution by a Luggin capillary whose tip was placed close to the working electrode. Results were corrected for junction potentials by being referenced internally to the ferrocenium/ferrocene (Fe^+/Fe) couple [$E_{1/2}(Fe^+/Fe)$ = 0.50 V vs. SCE]. Potentials in this paper are referenced to the SCE. Typically, a 0.1 M solution of $[Bu_4N][ClO_4]$ in CH_2Cl_2 containing 0.5 mM of sample was purged with nitrogen for 10 min, and then the voltammograms were recorded at ambient temperature. The scan rate was 20 and 10 $mV \cdot s^{-1}$ for CV and DPV, respectively.

Acknowledgments

The authors thank the National Natural Science Foundation of China (Grant No. 20171028), the National Ministry of Science and Technology of China (Grant No. 2001CB6105-04), The Science Committee of Shandong Province (Grant No. Z99B03), the National Educational Ministry of China, Shandong University, and Queensland University of Technology for financial support.

[1] [1a] J. Jiang, K. Kasuga, D. P. Arnold, in: *Supramolecular Photosensitive and Electroactive Materials* (Ed.: H. S. Nalwa), Academic Press, New York, **2001**, chapter 2, pp. 113−210. [1b]D. K. P. Ng, J. Jiang, *Chem. Soc. Rev.* **1997**, *26*, 433−442. [1c] J. Jiang, W. Liu, D. P. Arnold, *J. Porphyrins Phthalocyanines* **2003**, *7*, 459−473.

[2] J. W. Buchler, D. K. P. Ng, in: *The Porphyrin Handbook* (Eds.: K. M. Kadish, K. M. Smith, R. Guilard), Academic Press, New York, **1999**, chapter 20, pp. 245−294.

[3] [3a] H. Konami, H. Hatano, N. Kobayashi, T. Osa, *Chem. Phys. Lett.* **1990**, *165*, 397−400. [3b] H. Konami, H. Hatano, A. Tajiri, *Chem. Phys. Lett.* **1989**, *160*, 163−167. [3c] A. Iwase, C. Harnoode, Y. Kameda, *J. Alloys Compds.* **1993**, *192*, 280−283. [3d] C. Harnoode, F. Kitamura, T. Ohsaka, K. Tokuda, A. Iwase, *Denki Kagaku* **1993**, *61*, 767−769.

[4] [4a] G. Ostendorp, H. W. Rotter, H. Homborg, *Z. Naturforsch., Teil B* **1996**, *51*, 567−573. [4b] M. S. Haghighi, C. L. Teske, H. Homborg, *Z. Anorg. Allg. Chem.* **1992**, *608*, 73−80.

[5] P. Zhu, F. Lu, N. Pan, D. P. Arnold, S. Zhang, J. Jiang, *Eur. J. Inorg. Chem.*, accepted.

[6] [6a] W. Liu, J. Jiang, D. P. Arnold, N. Pan, *Inorg. Chim. Acta* **2000**, *310*, 140−146. [6b] D. P. Arnold, J. Jiang, *J. Phys. Chem. A* **2001**, *105*, 7525−7533.

[7] [7a] K. Kasuga, M. Ando, H. Morimoto, M. Isa, *Chem. Lett.* **1986**, 1095−1098. [7b] K. Takahashi, M. Itoh, Y. Tomita, K. Nojima, K. Kasuga, M. Isa, *Chem. Lett.* **1993**, 1915−1918. [7c] K. Takahashi, J. Shimoda, M. Itoh, Y. Fujita, H. Okawa, K. Nojima, *Chem. Lett.* **1998**, 173−174.

[8] [8a] F. Guyon, A. Pondaven, M. L′Her, *J. Chem. Soc., Chem. Commun.* **1994**, 1125−1126. [8b] F. Guyon, A. Pondaven, J.-M. Kerbaol, M. L′Her, *Inorg. Chem.* **1998**, *37*, 569−576.

[9] [9a] N. Ishikawa, Y. Kaizu, *Chem. Phys. Lett.* **1994**, *228*, 625−632. [9b] N. Ishikawa, Y. Kaizu, *Chem. Phys. Lett.* **1995**, *236*, 50−56. [9c] N. Ishikawa, Y. Kaizu, *Mol. Cryst. Liq. Cryst.* **1996**, *286*, 585−590. [9d] N. Ishikawa, T. Okubo, Y. Kaizu, *Inorg. Chem.* **1999**, *38*, 3173−3181.

[10] [10a] N. Ishikawa, T. Iino, Y. Kaizu, *J. Am. Chem. Soc.* **2002**, *124*, 11440−11447. [10b] N. Ishikawa, T. Iino, Y. Kaizu, *J. Phys. Chem. A* **2002**, *106*, 9543−9550. [10c] X. Sun, X. Cui, D. P. Arnold, M. T. M. Choi, D. K. P. Ng, J. Jiang, *Eur. J. Inorg. Chem.* **2003**, 1555−1561. [10d] Y. Bian, J. Jiang, Y. Tao, M. T. M. Choi, R. Li, A. C. H. Ng, P. Zhu, N. Pan, X. Sun, D. P. Arnold, Z. Zhou, H.-W. Li, D. K. P. Ng, *J. Am. Chem. Soc.* **2003**, *125*, 12257−12267.

[11] [11a] J. Li, D. Gryko, R. B. Dabke, J. R. Diers, D. F. Bocian, W. G. Kuhr, J. S. Lindsey, *J. Org. Chem.* **2000**, *65*, 7379−7390. [11b] C. Clausen, D. T. Gryko, R. B. Dabke, N. Dontha, D. F. Bocian, W. G. Kuhr, J. S. Lindsey, *J. Org. Chem.* **2000**, *65*, 7363−7370. [11c] D. Gryko, J. Li, J. R. Diers, K. M. Roth, D. F. Bocian, W. G. Kuhr, J. S. Lindsey, *J. Mater. Chem.* **2001**, *11*, 1162−1180.

[12] D. Chabach, A. De Cian, J. Fischer, R. Weiss, M. E. M. Bibout, *Angew. Chem. Int. Ed. Engl.* **1996**, *35*, 898−899.

[13] J. Jiang, W. Liu, K.-W. Poon, D. Du, D. P. Arnold, D. K. P. Ng, *Eur. J. Inorg. Chem.* **2000**, 205−209.

[14] D. Chabach, M. Tahiri, A. De Cian, J. Fischer, R. Weiss, M. E. M. Bibout, *J. Am. Chem. Soc.* **1995**, *117*, 8548−8556.

[15] J. Jiang, Y. Bian, F. Furuya, W. Liu, M. T. M. Choi, H. W. Li, N. Kobayashi, Q. Yang, T. C. W. Mak, D. K. P. Ng, *Chem. Eur. J.* **2001**, *7*, 5059−5069.

[16] J. W. Buchler, B. Scharbert, *J. Am. Chem. Soc.* **1988**, *110*, 4272−4276.

[17] [17a] J. Simon, J. J. Andre, *Molecular semi-conductors*; Springer Verlag, Berlin, **1985**. [17b]M. Bouvet, J. Simon, *Chem. Phys. Lett.* **1990**, *172*, 299−302.

[18] [18a] H. Engelkamp, S. Middelbeek, R. J. M. Nolte, *Science* **1999**, *284*, 785−788. [18b] N. B. McKeown, *J. Mater. Chem.* **2000**, *10*, 1979−1995.

[19] [19a] A. Pondaven, Y. Cozien, M. L′Her, *New J. Chem.* **1991**, *15*, 515−516. [19b] J. Jiang, R. C. W. Liu, T. C. W. Mak, T. W. D. Chan, D. K. P. Ng, *Polyhedron* **1997**, *16*, 515−520.

[20] K. Kasuga, K. Asano, L. Lin, T. Sugimori, M. Handa, K. Abe, T. Kikkawa, T. Fujiwara, *Bull. Chem. Soc. Jpn.* **1997**, *70*, 1859−1865.

Received July 28, 2003
Early View Article
Published Online December 12, 2003

 © 2004 Wiley-VCH Verlag GmbH & Co. KGaA, Weinheim

Cyclopentadienyl Ru^{II} Complexes as Highly Efficient Catalysts for the *N*-Methylation of Alkylamines by Methanol

Alessandro Del Zotto,*[a] Walter Baratta,[a] Mauro Sandri,[a] Giancarlo Verardo,[a] and Pierluigi Rigo[a]

Keywords: Homogeneous catalysis / Ruthenium / Amines / *N*-methylation / Imines

The ruthenium(II) half-sandwich complex [RuCl(η^5-C_5H_5)(PPh_3)$_2$] (**1**) catalyses the reaction between methanol and alkylamines RNH_2 or R^1R^2NH to afford $RN(CH_3)_2$ and $R^1R^2NCH_3$ products, respectively. The reaction is quantitative and generally fast, at the methanol reflux temperature, for a wide spectrum of substrates. Starting from primary amines, the stepwise formation of $RN{=}CH_2$, $RNHCH_3$, and $RN(CH_3)_2$ has been observed. Both PPh_3 and Cl^- dissociation from **1** are key-steps in forming the effective catalytic species. The catalytic activity of several half-sandwich neutral or cationic complexes (**2**–**15**) related to **1** is also discussed.

(© Wiley-VCH Verlag GmbH & Co. KGaA, 69451 Weinheim, Germany, 2004)

Introduction

The efficient *N*-alkylation of primary or secondary amines by alcohols is an important synthetic route, the main advantage of which is that water is the only side-product. Thus, the reaction between amines and alcohols has been investigated in detail, particularly using homogeneous catalysts based on late transition metals;[1−12] those based on ruthenium have been the most widely investigated, including the ruthenium(II) complexes [$RuCl_2(PPh_3)_3$],[1,3,5−12] [$RuH_2(PPh_3)_4$],[2,4,5−7] [$RuHCl(CO)(PPh_3)_3$],[5,11] [$RuBr_2(PPh_3)_3$],[6] [$RuHCl(PPh_3)_3$],[6] [$RuH_2\{P(OEt)_3\}_4$],[7] [$RuCl_2(CO)_2(PPh_3)_2$],[8] [$RuCl_2(P{-}N)_2$],[8] (P−N = *o*-diphenylphosphanyl-*N*,*N*-dimethylaniline) [$RuH_2(CO)(PPh_3)_3$],[11] [$\{RuCl_2(\eta^5\text{-}C_5Me_5)\}_2$],[11] as well as those bearing terdentate NPN or NN′N type ligands,[12] the ruthenium(0) derivatives [$Ru(CO)_3(PPh_3)_2$],[5] [$Ru_3(CO)_{12}$],[11] and [Ru(cot)(cod)],[11] and, finally, "in situ" generated systems [$RuCl_3$/phosphane[6,7] or $RuCl_3/P(OR)_3$[6,7]] exhibit catalytic activity in the *N*-alkylation of amines by alcohols. Although the reaction is commonly performed in an autoclave at 120−215 °C, long reaction times are often required to obtain high yields of products.

During our studies[13−18] on the catalytic potential of the half-sandwich ruthenium(II) complex [RuCl(η^5-C_5H_5)(PPh_3)$_2$] (**1**), we found evidence that this readily available compound efficiently catalyses the *N*-methylation of both primary and secondary alkylamines by methanol, under milder conditions than previously reported for other ruthenium systems. Owing to the promising preliminary results obtained with **1**, we extended the investigation to a broad spectrum of half-sandwich ruthenium(II) complexes. In addition, as the *N*-alkylation of amines by alcohols is thought to proceed via an imine intermediate, which is then reduced to amine by a transfer hydrogenation process, useful information on the reduction of the C=N bond by transfer hydrogenation, a process of considerable importance, could also be obtained. The reduction of an imine intermediate is also a key-step in the reductive amination of aldehydes.

The results reported here demonstrate that complex **1** is the most active catalyst so far for the *N*-methylation of alkylamines by methanol.

Results and Discussion

N-Methylation of Amines

The amines employed in this work are shown in Table 1. When a primary (RNH_2) or secondary (R_2NH) alkylamine was refluxed in methanol in the absence of any catalyst, no *N*-methyl derivatives were observed. By contrast, when complex **1** was added to the boiling reaction mixture, the products $RN(CH_3)_2$ and R_2NCH_3, respectively, were quantitatively formed with rates that strongly depend on the nature of the R group. The reactions were carried out, under an argon atmosphere, with 1 mol % catalyst based on amine charged and methanol as solvent at reflux (oil bath 100 °C), with a methanol/amine molar ratio of ca. 100. Under the same experimental conditions, arylamines did not react over a 24 h period. Also, 1,2-ethylendiamine did not react with methanol, most probably owing to its chelation to the metal centre with formation of a catalytically inactive complex.

[a] Dipartimento di Scienze e Tecnologie Chimiche, Università di Udine
Via Cotonificio 108, 33100 Udine, Italy
Fax: (internat.) + 39-0432-558803
E-mail: alessandro.delzotto@dstc.uniud.it

 © 2004 Wiley-VCH Verlag GmbH & Co. KGaA, Weinheim **DOI: 10.1002/ejic.200300518**

Table 1. Substrates, reaction products and $t_{1/2}$s

Substrate	Product[a]	$t_{1/2}$ [b]
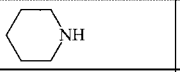	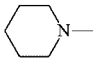	50 m
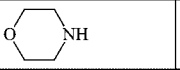	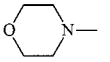	24 h 30 m
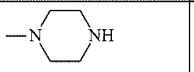	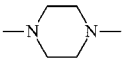	2 h 30 m
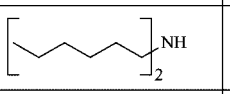	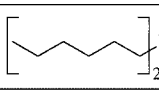	8 h
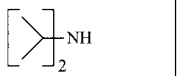	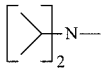	4 h 30 m
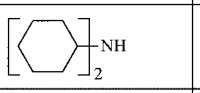	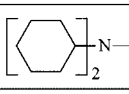	7 h
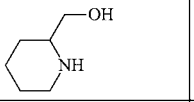	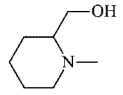	6 h 30 m
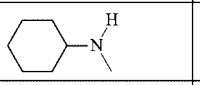	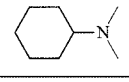	1 h
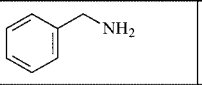	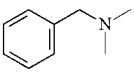	45 h
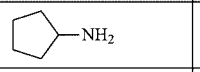	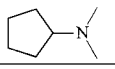	2 h 30 m
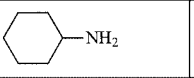	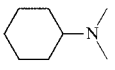	2 h 40 m
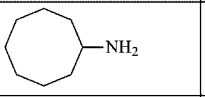	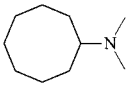	3 h
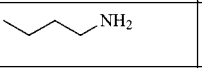	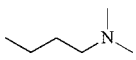	11 h
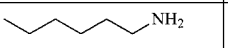	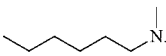	14 h
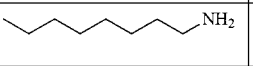	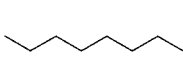	21 h
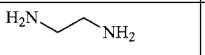	no reaction	
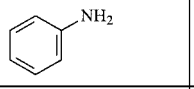	no reaction	
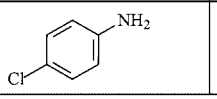	no reaction	

[a] For each substrate the yield is quantitative. Reaction conditions: T = 100 °C, 1 mol % complex **1**, solvent/amine molar ratio ≥ 100. [b] $t_{1/2}$ indicates the time necessary for the consumption of half of the starting amine.

To compare the reactivity of the various substrates, we chose the time needed to consume half of the starting amine ($t_{1/2}$) as a suitable parameter for both primary and secondary amines. The $t_{1/2}$s (Table 1) indicate that both basicity and steric crowding of the starting amine have an important influence on the reaction rate. No clear general trend was found, but the reaction rate usually increases on increasing the basicity of the substrate. For instance, the reaction rate decreased along the series piperidine (2.88), *N*-methylpiperazine (4.15), and morpholine (5.67) (the pK_bs in water solution are in parentheses). Furthermore, benzylamine, which has the highest pK_b (4.67) of the primary alkylamines examined here, shows the highest $t_{1/2}$. Within the series of *n*-alkyl primary amines ($C_xH_{2x+1}NH_2$; x = 4, 6, 8), whose pK_bs are 3.23, 3.44, 3.35 respectively, $t_{1/2}$ increases considerably on going from *n*-butyl- to *n*-octylamine.

To study in detail the *N*-methylation process promoted by **1**, the reaction between methanol and cyclohexylamine (**I**), chosen as a convenient substrate model, has been monitored by GC-MS (Figure 1). Apparently, the reaction proceeds stepwise (Scheme 1), the starting amine **I** being initially transformed into the imine *cyclo*-$C_6H_{11}-N=CH_2$ (**II**), whose concentration remains rather low (ca. 5 %) and almost constant throughout the reaction. A successive hydrogenation process converts **II** into the *N*-monomethyl derivative **III**, which is in turn transformed into the *N*,*N*-dimethyl product **IV**. For this final step, no intermediates could be detected in solution by GC-MS. The total conversion of **I** into **IV** is quantitative within ca. 6.5 h. The subsequent addition of **I** (100-fold excess with respect to **1**) to the reaction mixture requires about 7 h for its complete conversion into **IV**, indicating that the catalytic efficiency of **1** is maintained.

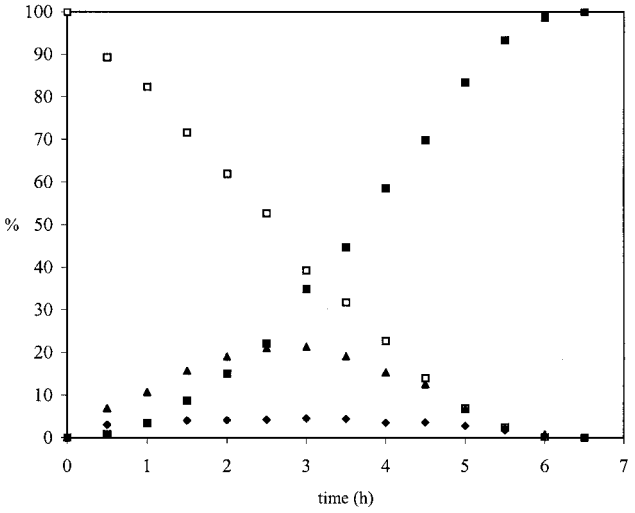

Figure 1. Variation in *cyclo*-$C_6H_{11}NH_2$ **I** (□), *cyclo*-$C_6H_{11}N=CH_2$ **II** (◆), *cyclo*-$C_6H_{11}NHCH_3$ **III** (▲), and *cyclo*-$C_6H_{11}NH(CH_3)_2$ **IV** (■) in the reaction between **I** and CH_3OH, at 100 °C with 1 mol % **1**

The rate of decay of **I** is virtually constant throughout the reaction, and several runs at different initial concentrations of **I** showed that the reaction is zero order for the amine, as reported by Watanabe and co-workers for the reaction between aniline and benzyl alcohol.[5] The effect of reaction time on the methylation of **I** (Figure 1) is similar

 © 2004 Wiley-VCH Verlag GmbH & Co. KGaA, Weinheim

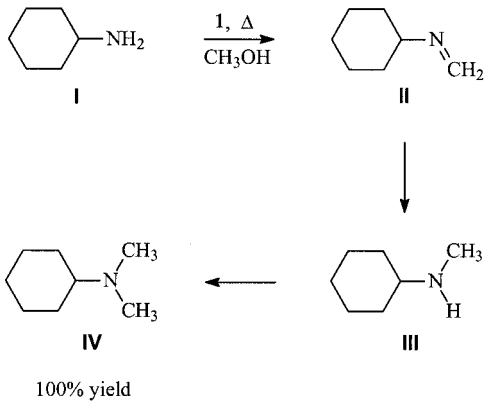

Scheme 1. Stepwise formation of *N*,*N*-dimethylcyclohexylamine **IV** from cyclohexylamine **I**

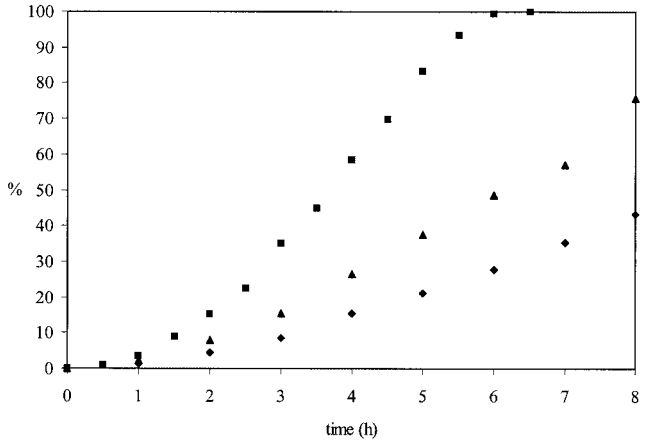

Figure 2. Amount of the product *cyclo*-$C_6H_{11}NH(CH_3)_2$ **IV** in the reaction between *cyclo*-$C_6H_{11}NH_2$ **I** and CH_3OH at 100 °C: with 1 mol % **1** (■); 1 mol % **1** and 5 mol % PPh_3 (▲); 1 mol % **1** and 20 mol % LiCl (◆)

to that reported for the alkylation of aminoarenes with alcohols in the presence of the complexes $[RuCl_2(PPh_3)_3]$[11] and $[RuCl_2(NN'N)(PPh_3)]$[12] {NN′N = $C_5H_3N[CH_2N(CH_3)_2]$-2,6}, for which no imine intermediates were detected in the reaction mixtures.

The reaction has also been carried out in the presence of 0.5 and 2 mol % catalyst, but at higher values complex **1** was not completely soluble in the reaction mixture. With 2 mol % **1**, **I** was converted completely into **IV** within 3.5 h. For the same reaction time 44.7 and 5.9 % of the product **IV** was obtained using 1 and 0.5 mol % catalyst, respectively. A nearly first-order dependence on the initial concentration of **1** was observed. In experiments at 20, 60, 70, and 80 °C, no catalytic activity was shown by **1** at 20 °C, while at 60 °C the reaction proceeded very slowly. At 80 °C the reaction rate was nearly the same as at 100 °C. At 70 °C no appreciable increase of the reaction rate with respect to 60 °C was observed.

Catalytic runs in the presence of different amounts of PPh_3 or Cl^- ions (LiCl) showed that both reagents strongly inhibit the reaction rate. Several experiments were run with PPh_3/**1** or LiCl/**1** molar ratios increasing from 1:1 to 20:1. In Figure 2 are reported the results obtained using a five-fold excess of PPh_3 and a 20-fold excess of LiCl, and, for comparison, that obtained with the catalyst only.

Catalytic Activity of Half-sandwich Complexes

To find the most efficient catalyst, several other half-sandwich ruthenium(II) complexes related to **1** (Table 2) were tested in the model reaction between cyclohexylamine and methanol. The aim was also to better understand the influence of both steric and electronic properties of the ancillary ligands on the catalytic activity of the complexes, and to get more information on the nature of the key-steps occurring at the metal centre.

The composition of the reaction mixtures after 6 h (100 °C, 1 mol % catalyst) (Table 2) clearly show that only complex **10**, bearing two P(*m*-Tolyl)$_3$ ligands, exhibits a catalytic activity similar to that of **1**. Complexes **9**, **12**, and **13**, containing the low sterically demanding ligands $PMePh_2$, $PHPh_2$ and CO, and **11** and **14**, bearing bidentate chelating ligands, are much less active than **1**, probably owing to a high activation barrier to neutral ligand dissociation. As regards the effect of the anionic ligand (X), the activity of the complexes decreases in the order **1** (Cl) > **2** (H) > **3** (I) > **4** (N_3) > **5** ($SnCl_3$). This trend apparently depends on both the size of X^- and the strength of the Ru−X bond, which can affect the tendency of half-sandwich ruthenium(II) complexes to dissociate a neutral ligand or the X^- ion to give a coordinatively unsaturated intermediate. Cationic complexes **6**−**8** show a catalytic activity that strongly decreases on increasing the number of coordinated acetonitrile ligands. The very low catalytic activity shown by the indenyl complex **15** is noteworthy since in the redox isomerisation of allyl alcohols to ketones[19b] complex **15** exhibits a higher catalytic activity than **1**, most probably due to the opening of a coordination site on the metal by haptotropic shift (from η^5 to η^3) of the indenyl ligand. Apparently, an analogous behaviour of complex **15** in the *N*-alkylation of amines is not operative.

NMR Measurements and Mechanistic Insights

The transition-metal-catalyzed *N*-alkylation reaction of primary amines with alcohols is generally thought to involve the hydrogenation of an imine intermediate, which results from the condensation of the starting amine with the aldehyde formed by deydrogenation of the alcohol.[1,5,8,11,12] The hydrogen produced in the dehydrogenation process is then transferred to the imine to give the alkylated secondary amine. With secondary amines, the condensation reaction with the aldehyde should give a transient immonium ion.

In the currently accepted mechanism, the ruthenium complex reacts with an alcohol molecule to give, via β-hydride elimination, a Ru−H(aldehyde) intermediate.[1,5,8,11,12] In a second step the condensation product of the aldehyde with the primary amine is hydrogenated by a Ru−H/Ru−H_2 system to the secondary amine. This product can re-enter the catalytic cycle to be converted into a

 © 2004 Wiley-VCH Verlag GmbH & Co. KGaA, Weinheim

Table 2. Reaction of *cyclo*-$C_6H_{11}NH_2$ with CH_3OH at 100 °C in the presence of 1 mol % of Ru^{II} complexes **1**−**15**; reaction mixture composition (%) after 6 h[a]

Catalyst	**I**	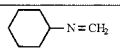 **II**	**III**	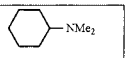 **IV**
[RuCl(Cp)(PPh_3)$_2$] **1**	0.2	0.3	0.6	98.9
[RuH(Cp)(PPh_3)$_2$] **2**	65.0	5.4	18.9	10.7
[RuI(Cp)(PPh_3)$_2$] **3**	59.5	15.7	18.3	6.5
[Ru(N_3)(Cp)(PPh_3)$_2$] **4**	79.1	5.3	12.5	3.1
[Ru($SnCl_3$)(Cp)(PPh_3)$_2$] **5**	96.8	3.2	0.0	0.0
[Ru(Cp)(CH_3CN)(PPh_3)$_2$]PF_6 **6**	37.6	8.5	20.7	33.2
[Ru(Cp)(CH_3CN)$_2$(PPh_3)]PF_6 **7**	56.1	11.7	17.0	15.2
[Ru(Cp)(CH_3CN)$_3$]PF_6 **8**	92.9	2.7	4.4	0.0
[RuCl(Cp)($PMePh_2$)$_2$] **9**	50.7	4.0	17.8	27.5
[RuCl(Cp){P(*m*-Tolyl)$_3$}$_2$] **10**	0.0	0.6	0.1	99.3
[RuCl(Cp)(dppe)][b] **11**	91.9	3.1	4.5	0.5
[RuCl(Cp)($PHPh_2$)(PPh_3)] **12**	90.0	2.8	7.0	1.2
[RuCl(Cp)(CO)(PPh_3)] **13**	87.6	12.4	0.0	0.0
[Ru(Cp)(Dipy)(PPh_3)]Cl[c] **14**	96.5	3.5	0.0	0.0
[RuCl(Indenyl)(PPh_3)$_2$] **15**	88.0	6.0	4.9	0.4

[a] Cp = η^5-C_5H_5. [b] dppe = 1,2-(diphenylphosphanyl)ethane. [c] dipy = 2,2′-dipyridyl.

tertiary amine. We tentatively propose that a similar mechanism also operates for the *N*-methylation catalysed by **1**.

$^{31}P\{^1H\}$ NMR studies indicate that the dissolution of **1** in CD_3OD occurs with Cl^- dissociation and formation of the cationic solvent complex [Ru(η^5-C_5H_5)(CD_3OD)(PPh_3)$_2$]$^+$ (**16**) (δ = 33.7 ppm). The analogous species containing CH_3OH has been isolated in low yield as the tetraphenylborate salt.[20] Addition of an excess of cyclohexylamine results in the formation of an equilibrium mixture of complexes **1**, **16**, and [Ru(η^5-C_5H_5)(*c*-$C_6H_{11}NH_2$)(PPh_3)$_2$]$^+$ (**17**) (δ = 45.4 ppm). No free PPh_3 is present in solution. Heating at 80 °C causes the catalytic formation of the imine **II** and the amines **III** and **IV**, while free PPh_3 appears in the reaction mixture. At this stage, the formation of the almost catalytically inactive [RuD(η^5-C_5H_5)(PPh_3)$_2$]$^+$ (**2-D**) [1:1:1 triplet, δ = 68.6, $J(^{31}P\text{-}^2H)$ = 4.9 Hz] is also observed (Scheme 2). Complex **17** has been isolated in the solid state in good yield as the perchlorate salt by treatment of complex **1** in THF with a slight excess of $AgClO_4$ in the presence of a tenfold excess of cyclohexylamine. Ru^{II} amino complexes analogous to **17** have been reported previously.[21] The $^{31}P\{^1H\}$ NMR chemical shift of complex **17** agrees with those found in related species with coordinated NH_3 and CH_3NH_2 (δ = 45.9 and 43.7 ppm, respectively).[21b] Prolonged heating of a CD_3OD solution of complex **17** results in its almost complete conversion into **16**.

The RuH(formaldehyde) intermediate, which is most probably the key-species of the catalytic cycle, might reasonably arise from complex **16** via PPh_3 dissociation that

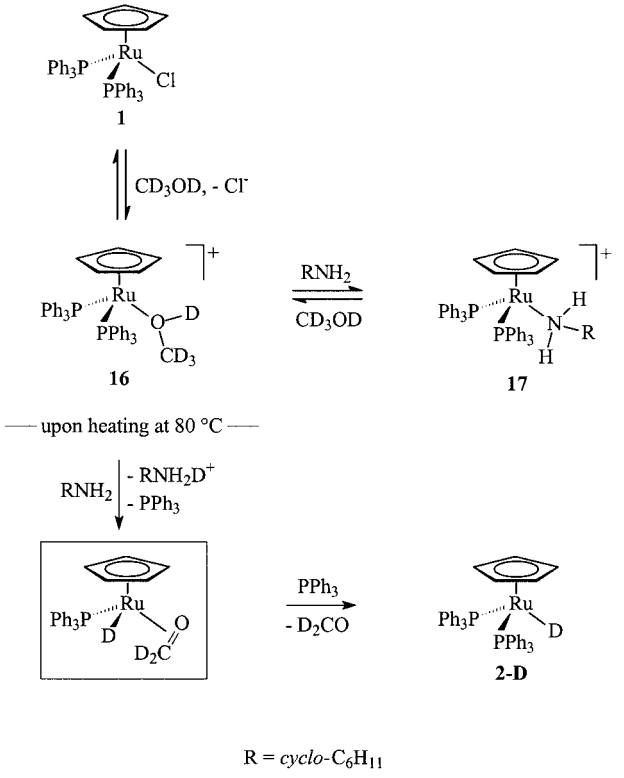

Scheme 2. Complexes detected in solution in CD_3OD on treatment of **1** with excess cyclohexylamine. The species in the square (spectroscopically not detectable) is assumed to be the key-intermediate that initiates the catalytic cycle. Most of **1** is converted into **2-D**, which has a low catalytic activity

 © 2004 Wiley-VCH Verlag GmbH & Co. KGaA, Weinheim

provides a vacant coordination site on the metal centre. This hypothesis agrees with the observed decrease in reaction rate in the presence of both free phosphane and chloride ions. In addition, the dissociation of both one PPh_3 and Cl^- from **1** has been previously proposed by Trost to account for the catalytic activity of this complex in other organic transformations.[19]

Finally, we found appreciable amounts of free imine in the reaction mixtures, unlike previous observations in which the imine is formed at the metal centre, by condensation between coordinated amine and aldehyde, and then, without decoordination, immediately hydrogenated to the corresponding amine.[1,5,8,11,12]

Conclusions

Complex **1** is confirmed as a homogeneous catalyst in several organic processes. The results indicate that it, as well as its P(*m*-Tolyl)$_3$ analogue **10**, exhibits the highest reported catalytic activity of ruthenium complexes for the *N*-methylation of primary and secondary alkylamines. Comparison of the literature data on the methylation of different alkylamines by methanol in the presence of Ru-based catalysts with those obtained here (Table 3) shows that **1** promotes a remarkably fast, quantitative conversion, under non-forcing conditions, of the starting amines into *N*-permethylated products. Such good results seem to indicate that complex **1** may also catalyze other organic processes that involve appropriate transformations of alkylamines or imines, such as the hydrogen transfer reduction of the latter.

Experimental Section

Caution! *Perchlorate salts of metal complexes with organic ligands are potentially explosive. These compounds must be handled with caution and should be prepared on a very small scale.*

Instrumentation and Analyses: The NMR spectra (^1H at 200.13, ^{13}C at 50.32, and ^{31}P at 81.02 MHz) in CD_3OD or CD_2Cl_2 solutions were run on a Bruker AC 200 F QNP spectrometer equipped with a variable-temperature probe. The chemical shifts were referenced to internal $SiMe_4$ for ^1H, residual $CHDCl_2$ for ^{13}C, and external 85 % H_3PO_4 for ^{31}P. High temperatures were calibrated with ethylene glycol 80 % in [D_6]DMSO. The GC-MS analyses were carried out with a Fisons TRIO 2000 gas chromatograph-mass spectrometer working in the positive ion 70 eV electron impact mode. The injector was kept at 250 °C and the column (Supelco® SE-54, 30 m long, 0.25 mm i.d., coated with a 0.5 μm phenyl methyl silicone film) was temperature programmed from 50 to 310 °C at 10 °C/min. GC analyses were run on a Fisons GC 8000 Series gas chromatograph equipped with a Supelco® PTA-5 column [30 m long, 0.53 mm i.d., coated with a 3.0 μm poly(5 % diphenyl/95 % dimethylsiloxane) film]; injector and column temperatures as indicated above.

Reagents and Catalysts: All amines (97−99.5 % purity) were purchased from Aldrich and used without further purification. Commercial methanol (Riedel) was purified on CaH_2 according to a standard method[22] and freshly distilled before use. However, the use of untreated solvent resulted in a negligible lowering of the reaction rate. The complexes [RuCl(η^5-C_5H_5)(PPh_3)$_2$] (**1**),[23] [RuH(η^5-C_5H_5)(PPh_3)$_2$] (**2**),[24] [RuI(η^5-C_5H_5)(PPh_3)$_2$] (**3**),[25] [RuN_3(η^5-C_5H_5)(PPh_3)$_2$] (**4**),[25] [Ru($SnCl_3$)(η^5-C_5H_5)(PPh_3)$_2$] (**5**),[26] [Ru(η^5-C_5H_5)(CH_3CN)(PPh_3)$_2$]PF_6 (**6**),[26] [Ru(η^5-C_5H_5)(CH_3CN)$_2$(PPh_3)]PF_6 (**7**),[27] [Ru(η^5-C_5H_5)(CH_3CN)$_3$]PF_6 (**8**),[28] [RuCl(η^5-C_5H_5)($PMePh_2$)$_2$] (**9**),[29] [RuCl(η^5-C_5H_5){P(*m*-Tolyl)$_3$}$_2$] (**10**),[15] [RuCl(η^5-C_5H_5)(dppe)] (**11**),[30] [RuCl(η^5-C_5H_5)($PHPh_2$)(PPh_3)] (**12**),[31] [RuCl(η^5-C_5H_5)(CO)(PPh_3)] (**13**),[32] [Ru(η^5-C_5H_5)(2,2′-dipyridyl)]Cl (**14**),[33] and [RuCl(Indenyl)(PPh_3)$_2$] (**15**)[34] were synthesised according to literature procedures.

Synthesis of Complex [Ru(η^5-C_5H_5)(*c*-$C_6H_{11}NH_2$)(PPh_3)$_2$]ClO_4 (17): Under an argon atmosphere, a mixture of complex **1** (181 mg, 0.25 mmol), $AgClO_4$ (62 mg, 0.30 mmol) and cyclohexylamine (248 mg, 2.5 mmol) was stirred in anhydrous THF (15 mL) for 30 min at room temperature. The resultant mixture was filtered through a glass-frit and then through a Celite® bed to eliminate traces of silver and silver compounds. *n*-Hexane (20 mL) was subsequently added to the solution and the THF pumped off. A yellow−green gum was obtained, which was slowly converted into a yellow solid by vigorous stirring in an ice-bath. The solid was recrystallised from THF/*n*-hexane in 73 % yield (162 mg).

Table 3. *N*-methylation of amines by methanol catalysed by ruthenium-based compounds. Comparison between literature data and the results herein reported[a]

Catalyst (mol %)	Starting amine	Product	Temperature	Time (h)	Yield (%)	Ref.
[$RuH_2(PPh_3)_4$] (5)			Reflux	48	15	[3]
[$RuCl_2(PPh_3)_3$] (1.3)			180 °C	7	95	[4]
$RuCl_3 \cdot nH_2O$ (2)			180 °C	15	3[a]	[8]
[RuCl(η^5-C_5H_5)(PPh_3)$_2$] (1)			100 °C	6.5	100	This work
[RuCl(η^5-C_5H_5)(PPh_3)$_2$] (1)			100 °C	3	100	This work

[a]14 % methylcyclohexylamine was also obtained. [b] 12 % *N*-methylaniline also obtained. [c] 6 % *N*-methylaniline also obtained. [d] cot = η^2-cyclooctene; cod = η^4-1,5-cyclooctadiene.

 © 2004 Wiley-VCH Verlag GmbH & Co. KGaA, Weinheim

$C_{47}H_{48}ClNO_4PRu$ (889.37): calcd. (%) C 63.47, H 5.44, N 1.57; found C 63.11, H 5.35, N 1.49 %. $^{31}P\{^1H\}$ NMR (CD_3OD): δ = 45.4 (s); $^{31}P\{^1H\}$ NMR (CD_2Cl_2): δ = 43.9 (s) ppm. ^1H NMR (CD_2Cl_2): δ = 0.60−2.32 (m, 11 H, *c*-C_6H_{11}), 4.39 (s, 5 H, C_5H_5), 6.88−7.71 (m, 30 H, C_6H_5) ppm. $^{13}C\{^1H\}$ NMR (CD_2Cl_2): δ = 24.4 (s), 25.2 (s), 34.9 (s), 61.4(t) J(^{13}C-^{31}P) = 2.3 Hz (*c*-C_6H_{11}), 80.6 (t) J(^{13}C-^{31}P) = 2.0 Hz (C_5H_5), 129.3 (*pseudo*-t), 131.0 (s), 133.7 (*pseudo*-t), 135.3 (*pseudo*-quintet) (C_6H_5) ppm.

General Procedure for the Catalytic *N*-Methylation of Amines: A 3-necked round-bottom flask (50 mL), equipped with a condenser and a rubber septum, was charged with catalyst (18.1 mg, $2.5 \cdot 10^{-2}$ mmol). Under an argon atmosphere, amine (2.5 mmol) and CH_3OH (10 mL, ca. 0.25 mol) were then added. After placing the flask in an oil-bath at a controlled temperature (60−100 °C) the initial orange mixture immediately turned into a clean yellow solution. Samples were extracted through the rubber septum with a syringe, diluted with diethyl ether and analysed by GC or GC-MS.

Acknowledgments

This research was financially supported by the Italian Ministero dell'Istruzione, dell'Università e della Ricerca (MIUR), Rome. MS thanks the Regione Autonoma Friuli-Venezia Giulia (Italy) for a postdoctoral fellowship.

[1] Y. Watanabe, Y. Tsuji, Y. Ohsugi, *Tetrahedron Lett.* **1981**, *22*, 2667−2670.
[2] R. Grigg, T. R. B. Mitchell, S. Sutthivaiyakit, N. Tongpenyai, *J. Chem. Soc., Chem. Commun.* **1981**, 611−612.
[3] A. Arcelli, B. Khai, G. Porzi, *J. Organomet. Chem.* **1982**, *235*, 93−96.
[4] S.-I. Murahashi, K. Kondo, T. Hakata, *Tetrahedron Lett.* **1982**, *23*, 229−232.
[5] Y. Watanabe, Y. Tsuji, H. Ige, Y. Ohsugi, T. Ohta, *J. Org. Chem.* **1984**, *49*, 3359−3363.
[6] Y. Tsuji, K.-T. Huh, Y. Watanabe, *J. Org. Chem.* **1987**, *52*, 1673−1680.
[7] K.-T. Huh, Y. Tsuji, M. Kobayashi, F. Okuda, Y. Watanabe, *Chem. Lett.* **1988**, 449−452.
[8] S. Ganguly, D. M. Roundhill, *Polyhedron* **1990**, 2517−2526.
[9] T. Kondo, S. Yang, K.-T. Huh, M. Kobayashi, S. Kotachi, Y. Watanabe, *Chem. Lett.* **1991**, 1275−1278.
[10] T. Kondo, S. Kotachi, S. Ogino, Y. Watanabe, *Chem. Lett.* **1993**, 1317−1320.
[11] Y. Watanabe, Y. Morisaki, T. Kondo, T. Mitsudo, *J. Org. Chem.* **1996**, *61*, 4214−4218.
[12] R. A. T. M. Abbenhuis, J. Boersma, G. van Koten, *J. Org. Chem.* **1998**, *63*, 4282−4290.
[13] W. Baratta, A. Del Zotto, P. Rigo, *Chem. Commun.* **1997**, 2163−2164.
[14] A. Del Zotto, W. Baratta, P. Rigo, *J. Chem. Soc., Perkin Trans. 1* **1999**, 3079−3081.
[15] W. Baratta, A. Del Zotto, P. Rigo, *Organometallics* **1999**, *18*, 5091−5096.
[16] A. Del Zotto, W. Baratta, G. Verardo, P. Rigo, *Eur. J. Org. Chem.* **2000**, 2795−2801.
[17] A. Del Zotto, W. Baratta, F. Miani, G. Verardo, P. Rigo, *Eur. J. Org. Chem.* **2000**, 3731−3735.
[18] A. Del Zotto, W. Baratta, F. Miani, G. Verardo, P. Rigo, *Inorg. Chim. Acta* **2003**, *349*, 249−252.
[19] [19a] B. M. Trost, R. J. Kulawiec, *J. Am. Chem. Soc.* **1992**, *114*, 5579−5584. [19b] B. M. Trost, R. J. Kulawiec, *J. Am. Chem. Soc.* **1993**, *115*, 2027−2036.
[20] R. J. Haines, A. L. Du Preez, *J. Organomet. Chem.* **1975**, *84*, 357−367.
[21] [21a] F. L. Joslin, M. Pontier Johnson, J. T. Mague, D. M. Roundhill, *Organometallics* **1991**, *10*, 41−43. [21b] F. L. Joslin, M. Pontier Johnson, J. T. Mague, D. M. Roundhill, *Organometallics* **1991**, *10*, 2781−2794. [21c] H. S. Chu, C. P. Lau, K. Y. Wong, W. T. Wong, *Organometallics* **1998**, *17*, 2768−2777. [21d] A. A. H. van der Zeijden, J. Jimenez, C. Mattheis, C. Wagner, K. Merzweiler, *Eur. J. Inorg. Chem.* **1999**, 1919−1930. [21e] J. A. Cabeza, I. del Rio, M. E. Navarro, S. Garcia-Granda, *Acta Crystallogr., Sect. E* **2001**, *57*, m162−m163.
[22] D. D. Perrin, W. L. Armarego, D. R. Perrin, *Purification of Laboratory Chemicals*, 2nd ed., Pergamon, Oxford, **1980**.
[23] M. I. Bruce, N. J. Windsor, *Aust. J. Chem.* **1977**, *30*, 1601−1604.
[24] T. Wilczewski, M. Bocheńska, J. F. Biernat, *J. Organomet. Chem.* **1981**, *215*, 87−96.
[25] M. M. T. Khan, M. M. Bhadbhade, M. R. H. Siddiqui, K. Venkatasubramanian, J. A. Tikhonova, *Acta Crystallogr., Sect. C* **1994**, *50*, 502−504.
[26] T. Blackmore, M. I. Bruce, F. G. A. Stone, *J. Chem. Soc., (A)* **1971**, 2376−2382.
[27] C. Slugovc, E. Rüba, R. Schmid, K. Kirchner, *Organometallics* **1999**, *18*, 4230−4233.
[28] T. P. Gill, K. R. Mann, *Organometallics* **1999**, *1*, 485−488.
[29] P. M. Treichel, D. A. Komar, P. J. Vincenti, *Synth. React. Inorg. Met.-Org. Chem.* **1984**, *14*, 383−400.
[30] G. S. Ashby, M. I. Bruce, J. B. Tomkins, R. C. Wallis, *Aust. J. Chem.* **1979**, *32*, 1003−1016.
[31] J. Geicke, I.-P. Lorenz, M. Engel, K. Polborn, *Inorg. Chim. Acta* **1998**, *269*, 157−161.
[32] S. G. Davies, S. J. Simpson, *J. Chem. Soc., Dalton Trans.* **1984**, 993−994.
[33] R. F. N. Ashok, M. Gupta, K. S. Arulsamy, U. C. Agarwala, *Inorg. Chim. Acta* **1985**, *98*, 161−167.
[34] L. A. Oro, M. A. Ciriano, M. Campo, C. Foces-Foces, F. H. Cano, *J. Organomet. Chem.* **1985**, *289*, 117−131.

Received July 28, 2003
Early View Article
Published Online November 28, 2003

 © 2004 Wiley-VCH Verlag GmbH & Co. KGaA, Weinheim

On the Reactivity of the Iminodiphosphane $C_6H_4(o\text{-}CN)N{=}PPh_2{-}PPh_2$: Fragmentation Versus Isomerisation

Zhaofu Fei,[a] Rosario Scopelliti,[a] and Paul J. Dyson*[a]

Keywords: N,P ligands / Palladium / Platinum / Reaction mechanisms / Structure elucidation

The reactivity of the iminodiphosphane $C_6H_4(o\text{-}CN)N{=}PPh_2{-}PPh_2$, which contains an N=P–P unit, has been investigated. Reaction with small molecules, [viz. H_2O/O_2, H_2O_2, CH_3OH, $C_6H_4(o\text{-}CN)NH_2$] and elemental sulfur result in cleavage of the P–P bond to give aminophosphane-derivatised compounds. The products from these reactions have been characterized spectroscopically, including two by single-crystal X-ray diffraction. The reactivity of the iminodiphosphane towards the transition metal complexes $[M(cod)Cl_2]$ (M = Pd or Pt) has also been investigated. In the reactions, the iminodiphosphane rearranges to form the more common diphosphonylamine (P–N–P) unit which chelates to the metal centres. Three different compounds were isolated from these reactions and they have all been fully characterised by spectroscopy and single-crystal X-ray diffraction.

(© Wiley-VCH Verlag GmbH & Co. KGaA, 69451 Weinheim, Germany, 2004)

Introduction

Iminophosphorus compounds such as iminophosphoranes $R_3P{=}NR'$ (I in Scheme 1) act as monodentate ligands using the lone pair at the N-centre.[1] Because the phosphorus centre is formally in the +5 oxidation state, it is rarely involved in coordination to transition metal centres, although the P=N unit has been observed to act as a π-donor.[2] Iminodiphosphanes with $PR_2{-}PR_2{=}NR'$(**II**) backbones are isoelectronic to oxodiphosphanes with $PR_2{-}PR_2{=}O$ (**III**) skeletons. Oxodiphosphanes are useful compounds, since they can rearrange on coordination to transition metals to give diphosphoxanes $PR_2{-}O{-}PR_2$ (**IV**), which act as bidentate ligands.[3] Diphosphoxanes are otherwise difficult to produce due to the Arbuzov rearrangement and their instability towards disproportionation. Iminodiphosphanes are the unstable isomers of diphosphonylamines, which have a $PR_2{-}NR'{-}PR_2$ (**V**) skeleton. Diphosphonylamines are widely used as ligands,[4] with the ability to chelate to various transition metal centres,[5] and such compounds have been reviewed in detail.[6] Some diphosphonylamine complexes have been evaluated as catalysts in, for example, asymmetric hydrogenation and hydroformylation reactions,[7] and much of the recent research has focused on either chiral ligands[8] or functionalized diphosphonylamines with additional donor centres.[9]

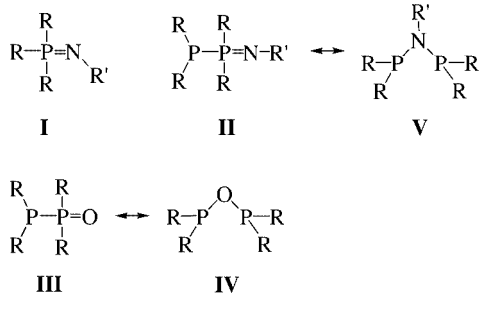

Scheme 1

Although iminodiphosphanes have been known for many decades,[10] they have not been studied to the same extent as oxodiphosphanes or diphosphonylamines. This could be because they are generally less stable than these other compounds; some iminodiphosphanes are pyrophoric.[11] Reactivity studies on iminodiphosphanes are essentially concerned with the rearrangement from N=P−P to P−N−P that takes place in the presence of organic bases.[12] Compared to a large number of reports on coordination chemistry of P−O−P and P−N−P ligands, we are not aware of any related studies with iminodiphosphanes, although one could envisage that the phorphorus(III) centre should enable a rich coordination chemistry. Following our recent report on the synthesis of the iminodiphosphane $C_6H_4(o\text{-}CN)N{=}PPh_2{-}PPh_2$ (**1**),[13] which was formed as the major product instead of the diphosphonylamine $C_6H_4(o\text{-}CN)N(PPh_2)_2$, we report herein on the reactivity of **1** towards different reagents ranging from small molecules to transition metal complexes, which lead to very different outcomes as those which we expected.

Results and Discussion

The reaction of **1** with small molecules and transition metal complexes leads to two different outcomes. In all re-

[a] Institut de Chimie Moléculaire et Biologique,
Ecole Polytechnique Fédérale de Lausanne, EPFL-BCH,
1015 Lausanne, Switzerland
Fax: (internat.) + 41-21-693-9885
E-mail: paul.dyson@epfl.ch

 © 2004 Wiley-VCH Verlag GmbH & Co. KGaA, Weinheim DOI: 10.1002/ejic.200300529

actions cleavage of the P−P bond takes place, but in the reactions with transition metal complexes P−P bond cleavage is accompanied by the formation of a new N−P bond.

Reactions of $C_6H_4(o\text{-CN})N{=}PPh_2{-}PPh_2$ (1) with Small Molecules

The iminodiphosphane **1** is stable in the solid state, but in solution it decomposes rapidly on exposure to air or moisture. In methanol, **1** decomposes immediately to form the aminophosphane precursor **2** and $Ph_2P{-}OMe$, as indicated by ^{31}P NMR spectroscopy which exhibits characteristic resonances at δ = 29.5 and 117.6 ppm, respectively.[14] Over a prolonged period, the only remaining phosphorus containing compound that is observed is $Ph_2P{-}OMe$ (Scheme 2). If a sample of **1** in CH_2Cl_2 is exposed to air or moisture, it slowly hydrolyses to the aminophosphane **2**, which reacts further to form the oxide [$C_6H_4(o$-CN)$NHPPh_2(O)$] (**3**). The other product observed in the reaction is $Ph_2P(O)PPh_2$, as evidenced by ^{31}P NMR spectroscopy, which exhibits two doublets centred at δ = −21.1 and 36.0 ppm ($^1J_{P,P}$ = 225 Hz).[14] The reaction of **1** with H_2O_2 is somewhat more complicated. In addition to the aminophosphane **2** and the oxide **3**, the ^{31}P NMR spectrum shows the presence of $Ph_2P(O)H$ and $Ph_2P(O)OH$ as indicated by signals at δ = 20 and 34 ppm, respectively.[14] Compound **1** also reacts with $C_6H_4(o\text{-CN})NH_2$ in $CDCl_3$ to form the aminophosphane **2** in quantitative yield; in this case, traces of HCl from the solvent may serve as catalysts leading to the cleavage of the P−P bond; a similar reaction has been previously reported.[12]

The reaction of **1** with elemental sulfur gave mixtures of several products. Attempts to isolate a pure product afforded [$C_6H_4(o$-CN)$NHPPh_2(S)$] (**6**; Scheme 3). Since it has previously been reported that treatment of iminodiphosphanes with elemental sulfur give N=P−P=S derivatives,[10] it is not unreasonable to assume that **6** and $Ph_2P(O)PPh_2$ could form via intermediates **4** or **5** (Scheme 3) by hydrolysis. The reaction was monitored by ^{31}P NMR spectroscopy over 24 hours. At the start of the reaction, two doublets at δ = 6.0 and 32.5 ppm ($^1J_{P,P}$ = 73.5 Hz) are observed. The coupling value is between that of an N=P−P=S intermediate similar to **4**, (ca. 30 Hz),[10] and that of type **5** compounds (ca. 100 Hz).[15] Few examples of related compounds are known[16] and it is therefore difficult to interpret the NMR spectroscopic data more fully. The intermediate could not be isolated. We must therefore speculate that while both could be involved, analogues of **5** are quite stable, and hence, **4** is more likely. It is worth noting that both **3** and **6** can be obtained in quantitative yield by reaction of **2** with H_2O_2 or elemental sulfur, respectively, using literature methods.[17]

The solid-state structures of **3** and **6** have been established by single-crystal X-ray diffraction and details of the structure determination are given in Table 1. Crystals of **3** were grown from diethyl ether and crystals of **6** were grown from dichloromethane/diethyl ether by slow evaporation. The structures of **3** and **6** are illustrated in Figures 1 and 2,

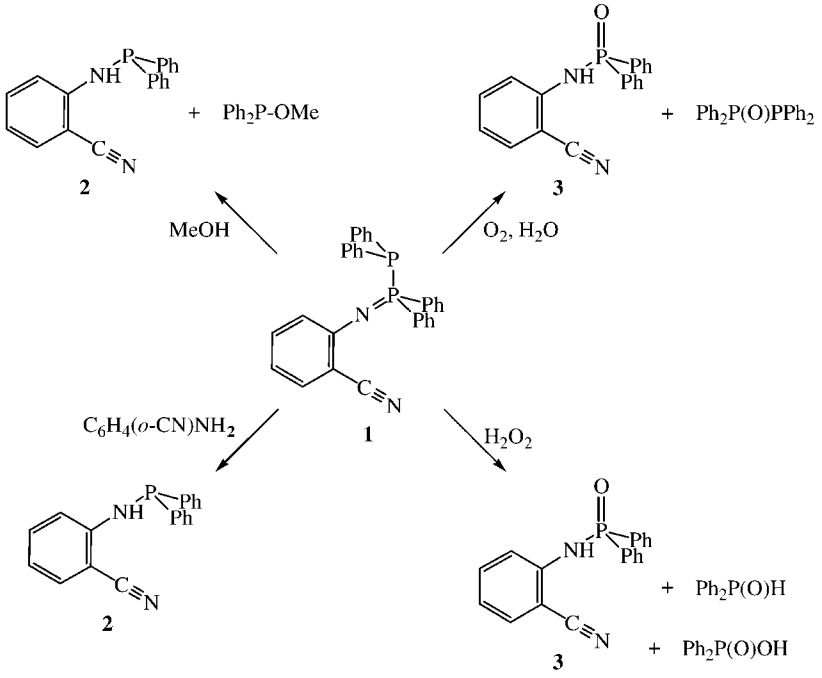

Scheme 2. Reaction of **1** with MeOH, O_2/H_2O, H_2O_2 and $C_6H_4(o\text{-CN})NH_2$

 © 2004 Wiley-VCH Verlag GmbH & Co. KGaA, Weinheim

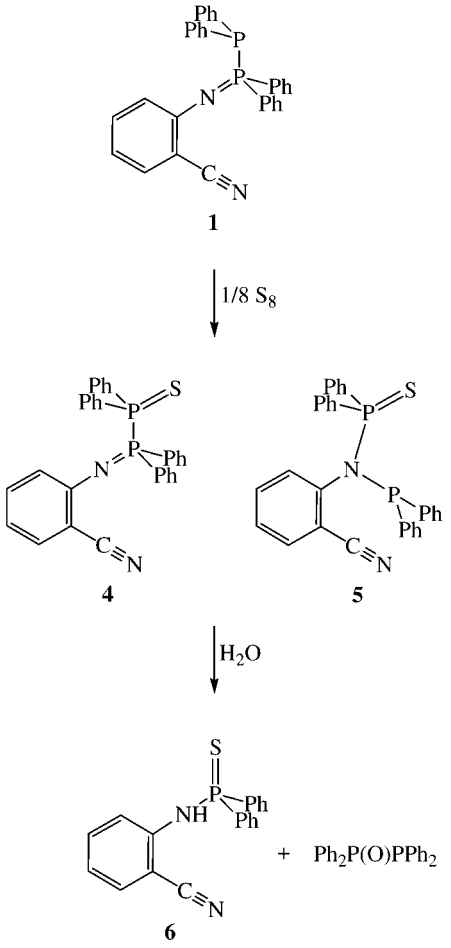

Scheme 3. Reaction of **1** with elemental sulfur showing the possible intermediates

respectively, and key bond parameters are given in the captions.

There are two independent molecules in the asymmetric unit of **3**. The P−N distances average 1.652(6) and 1.6773(15) Å in **3** and **6**, respectively, which is within the range usually found in related compounds.[18] The O-atom forms strong intermolecular N−H···O hydrogen bonds [N1A···O1B 2.788(7), N1B···O1AA 2.804(8) Å; N1A−H1A···O1B 161°, N1B−H1B···O1AA 152°], which, by symmetry, gives a polymeric one-dimensional chain along the base vector [1 0 1]. Interestingly, the N-atom of the CN group in **3** forms weak hydrogen bonds with the hydrogen atoms of a phenyl ring. In **6**, the hydrogen bond network similar to that observed in compound **2** (previously reported),[13] leads to a dimeric structure obtained through N−H···NC interactions [N···N, 3.098(2) Å; N−H···N, 151°]. The CN triple bond lengths in **3** and **6** are the same [1.140(10) versus 1.149(2) Å], and not significantly different from the free aminophosphane **2** [1.152(2) Å].

Reactions of C_6H_4(*o*-CN)N=PPh_2−PPh_2 (1) with Transition Metal Complexes

The reaction of **1** with [M(cod)Cl_2] (M = Pd or Pt, cod = cycloocta-1,5-diene) in equimolar quantities affords [M{C_6H_4(*o*-CN)N(PPh_2)$_2$}Cl_2], M = Pd (**7**), M = Pt (**8**), as the main products (Scheme 4). The synthesis of compounds **7** and **8** was followed by ^{31}P NMR spectroscopy, and in the reaction of **1** with [Pd(cod)Cl_2] in dichloromethane, for example, besides the main signal at δ = 39 ppm, another signal at δ = 64.2 ppm with low intensity was also observed. This peak probably corresponds to the free diphosphonylamine C_6H_4(*o*-CN)N(PPh_2)$_2$ (cf. the chemical shift of C_6H_4(*o*-OCH_3)N(PPh_2)$_2$ is δ = 65.6 ppm,[15] and C_6H_5N(PPh_2)$_2$ is δ = 67.7 ppm[19]). The ^{31}P NMR spectrum of **8** exhibits a signal at δ = 27.0 ppm ($^1J_{P,Pt}$ = 3377 Hz) typical of similar compounds, and there does not appear to be a significant influence on the chemical shift by virtue of the CN group.[20] The reaction of [M(cod)Cl_2] (M = Pd or Pt) with a series of iminodiphosphanes with electron-withdrawing groups[13b] have been followed by ^{31}P NMR spectroscopy. In one case, in the reaction between [Pt(cod)Cl_2] and C_6H_4(*o*-CF_3)N=PPh_2−PPh_2, the rate is sufficiently slow to reveal two doublets centred at δ = 65.0 ($J_{P\text{-}P}$ = 68 Hz) and 30.5 ($J_{P\text{-}P}$ = 68 Hz) ppm, which are tentatively ascribed to an intermediate in which the intact iminodiphosphane coordinates to the platinum. This assignment is based on the low value of the $J_{P\text{-}P}$ coupling constant and the short liftime, presumably because the coordinated iminodiphosphane rapidly rearranges to the diphosphonylamine, which initially coordinates through just one phosphorus centre before yielding the final product. Efforts to quench the reaction in order to analyse the intermediates in more detail failed. After 24 hours at room temperature the signals of the starting material and the two doublets at δ = 65.0 ppm and 30.5 ppm disappeared and only one main signal at δ = 25.5 ppm corresponding to the diphosphonylamine product remained.

The reaction of [Pt(cod)Cl_2] with two equivalents of **1** affords the cationic complex [Pt{C_6H_4(*o*-CN)N(PPh_2)$_2$}$_2$]Cl_2 (**9**) in high yield. ^{31}P NMR spectroscopy suggests that in the reaction complex, **8** forms initially, and reacts with further ligand to form **9**. The $^1J_{P\text{-}Pt}$ value of **9** is much lower than that of **8** and other mono-chelated platinum complexes, but is in keeping with structurally related bis-chelated compounds.[21] In the reaction mixture, low intensity signals at δ = 27.0 and 29.0 ppm are present, which correspond to **8** and the aminophosphane **2**. An additional signal at δ = 82.0 ppm with very low intensity is present, and possibly corresponds to Ph_2PCl. This would suggest that $Ph_2P^{\cdot}$ radicals are formed, which can be treated with [Pt(cod)Cl_2] starting material or CH_2Cl_2 solvent. The source of the chloride is more likely from [Pt(cod)Cl_2] as Ph_2PCl is also observed when the reaction is carried out in THF. The analogous reaction of **1** with [Pd(cod)Cl_2] does not give an analogous compound to **9**, possibly due to the smaller size of the palladium metal ion or the weaker Pd−P bond relative to platinum. Although we speculate that complexes **7**−**9** could be formed through the N=P−P−Pd or N=P−P−Pt intermediate, we were unable to obtain any evidence for their formation, even when the reactions were carried out at −20 °C.

 © 2004 Wiley-VCH Verlag GmbH & Co. KGaA, Weinheim

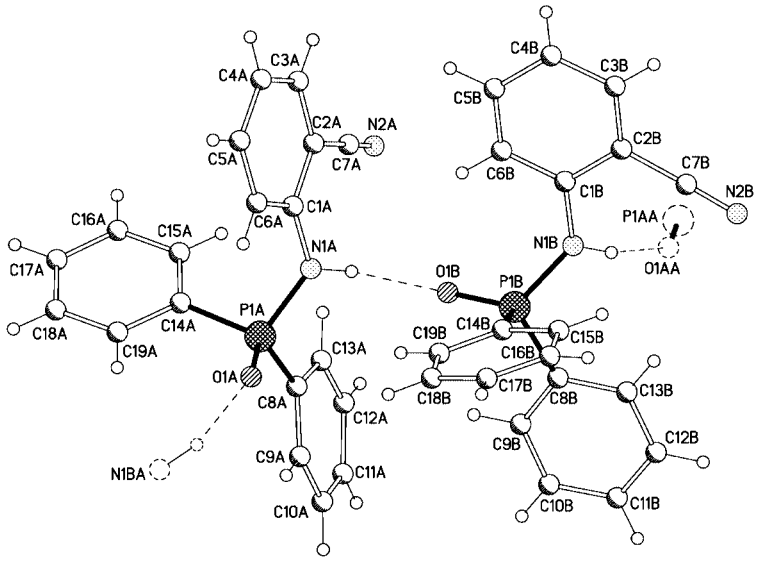

Figure 1. Molecular structure of **3** in the solid state; key bond lengths (Å) and angles (°) include: P1A−O1A 1.496(5), P1A−N1A 1.653(6), N1A−C1A 1.413(9), N2A−C7A 1.140(10), P1B−O1B 1.491(5), P1B−N1B 1.651(6), N1B−C1B 1.430(9), N2B−C7B 1.143(10); O1A−P1A−N1A 117.6(3), C1A−N1A−P1A 124.1(5), O1B−P1B−N1B 117.8(3), C1B−N1B−P1B 124.2(5); the second letter in the numbering scheme concerns the following symmetry transformation: $x - 1/2, -y + 1/2, z - 1/2$

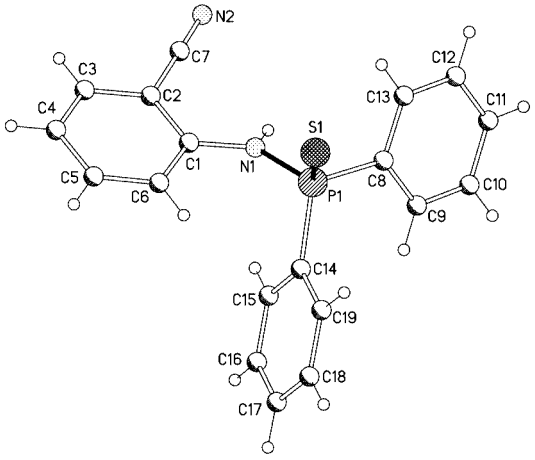

Figure 2. Molecular structure of **6** in the solid-state; key bond lengths (Å) and angles (°) include: S1−P1 1.9390(7), P1−N1 1.6773(15), N1−C1 1.399(2), N2−C7 1.149(2); N1−P1−S1 115.08(6), C1−N1−P1 126.84(13)

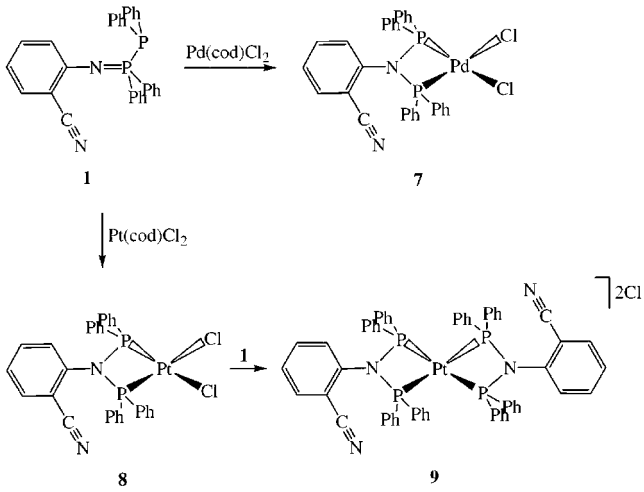

Scheme 4. Reaction of **1** with $[M(cod)Cl_2]$ (M = Pd or Pt)

Complex **7** forms good quality crystals suitable for X-ray determination from dichloromethane/thf solution at 0 °C. Crystals of complex **8** were obtained from dichloromethane/diethyl ether solution at 0 °C. Though the two structures could be isotypical, they have different space groups due to the cocrystallisation of different solvents with **7**. Two independent molecules lie within the asymmetric unit of **8**. There are close similarities between **7** and **8** shown in Figures 3 and 4, respectively. Both structures have a *cis*-chelating $C_6H_4(o\text{-}CN)N(PPh_2)_2$ ligand and two chloride ligands around the metal centres. The Pd−Cl/Pt−Cl and Pd−P/Pt−P bond lengths are all normal,[15,18,20] and the P1−N1−P2, and P1−Pd1−P2 angles as well as the P1···P2 distance in the palladium complex **7** compare very well with those found for **8** (see captions for details) and they are all within the range usually found in the related complexes.[15,18,20]

Compound **9** crystallises within a few minutes in a solvent mixture of dichloromethane and diethyl ether at −22 °C. The crystal architecture is composed of the dication, two chloride anions and eight dichloromethane molecules which form a *pseudo*-crown topology around the cation (Figure 5). The Pt metal centre lies on the inversion centre and this, in turn, imposes exact planar geometry at the metal centre although the bite angle of 71.51(3)° required by the chelating diphosphonylamine ligands causes a slight deviation from the idealised geometry. The phosphorus centres within each ligand are also close, the P1···P2 distance being 2.6919(11) Å, significantly longer than in **7** and **8**. The Pt−P bond lengths in **9** are equivalent with an aver-

 © 2004 Wiley-VCH Verlag GmbH & Co. KGaA, Weinheim

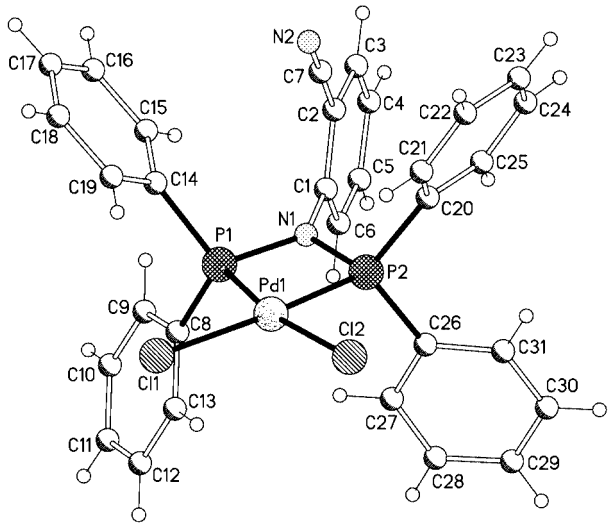

Figure 3. Molecular structure of **7** in the solid state; key bond lengths (Å) and angles (°) include: Pd1−P2 2.211(2), Pd1−P1 2.225(2), Pd1−Cl2 2.344(2), Pd1−Cl1 2.349(2), P1···P2 2.624(3), P1−N1 1.705(5), P2−N1 1.709(6), N1−C1 1.442(8), N2−C7 1.134(9); P2−Pd1−P1 72.53(8), Cl2−Pd1−Cl1 94.04(9), P1−N1−P2 100.4(3), C1−N1−P1 131.6(5), C1−N1−P2 127.9(5)

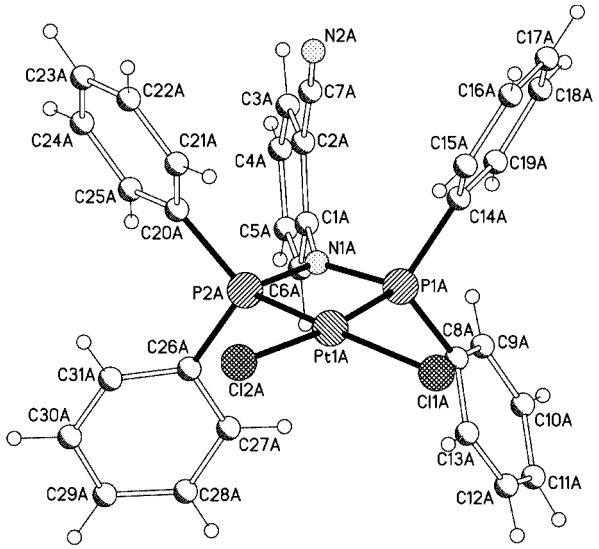

Figure 4. Molecular structure of **8** in the solid-state (showing one of the two independent molecules); key bond lengths (Å) and angles (°) include: Pt1A−P2A 2.208(5), Pt1A−P1A 2.217(4), Pt1A−Cl2A 2.325(4), Pt1A−Cl1A 2.357(5), P1A···P2A 2.639(6), P1A−N1A 1.716(15), P2A−N1A 1.692(14), N1A−C1A 1.45(3), N2A−C7A 1.16(2), Pt1B−P2B 2.200(5), Pt1B−P1B 2.205(5), Pt1B−Cl2B 2.336(5), Pt1B−Cl1B 2.345(5), P1B···P2B 2.620(7), P1B−N1B 1.709(15), P2B−N1B 1.687(15), N1B−C1B 1.42(2), N2B−C7B 1.14(2); P2A−Pt1A−P1A 73.24(17), Cl2A−Pt1A−Cl1A 91.8(2), P2A−N1A−P1A 101.5(8), C1A−N1A−P2A 126.9(11), C1A−N1A−P1A 131.4(11), P2B−Pt1B−P1B 73.00(18), Cl2B−Pt1B−Cl1B 91.48(19), P2B−N1B−P1B 101.0(8), C1B−N1B−P2B 126.4(12), C1B−N1B−P1B 132.2(12)

age length of 2.3035(9) Å. There is an extensive network of hydrogen-bonding interactions; the most important seem to comprise those between the chloride anions and dichloromethane solvent. Intra- and intermolecular hydrogen-bond-

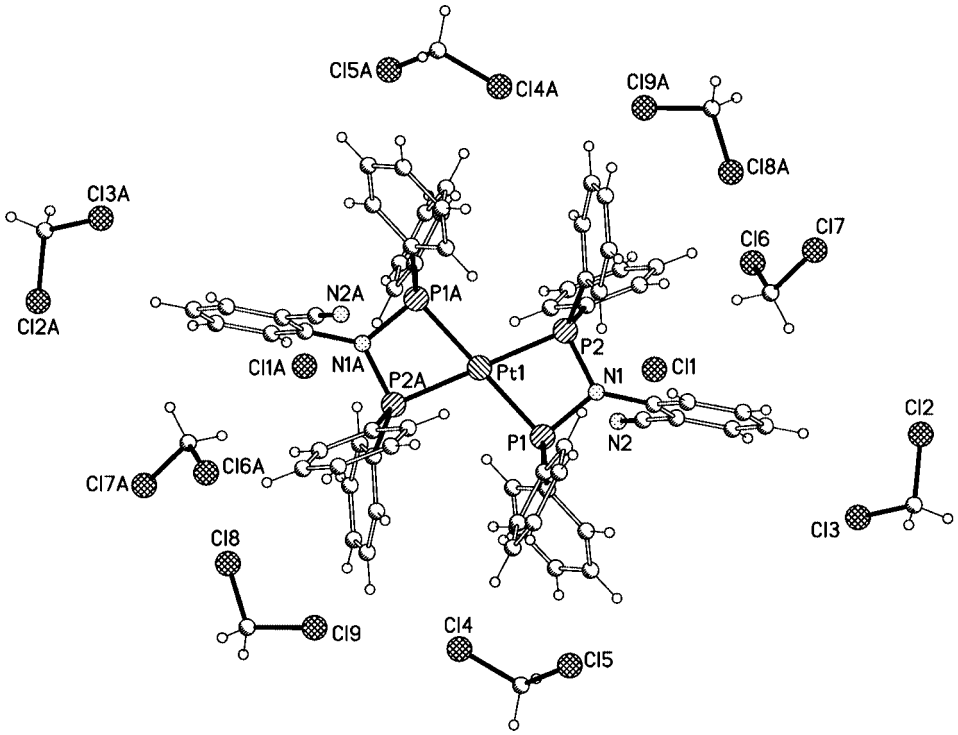

Figure 5. Molecular structure of **9**·8CH_2Cl_2 in the solid-state; key bond lengths (Å) and angles (°) include: Pt1−P1 2.3046(8), Pt1−P2 2.3025(8), P1−N1 1.718(2), P2−N1 1.713(3), N1−C1 1.445(4), N2−C7 1.148(4); P2A−Pt1−P1 108.49(3), P2−Pt1−P1 71.51(3), N1−P1−Pt1 92.33(9), N1−P2−Pt1 92.54(9), C1−N1−P2 126.95(19), C1−N1−P1 128.3(2), P2−N1−P1 103.34(14); letter A indicates the following symmetry transformation: $-x, -y, -z$

 © 2004 Wiley-VCH Verlag GmbH & Co. KGaA, Weinheim

ing interactions in a number of related platinum and palladium phosphane complexes have been reported previously.[22]

Concluding Remarks

In conclusion, we have examined the reactivity of $C_6H_4(o\text{-CN})N{=}PPh_2{-}PPh_2$ (**1**) towards small molecules and transition metal complexes. All the reactions carried out show that the P−P bond is easily cleaved. The reactions with small molecules give products with a P−NH backbone. In the presence of transition metals, rearrangements forming a P−N−P skeleton take place, a new type of reaction in this intensively explored field.

Experimental Section

All manipulations were performed under an inert atmosphere of dry nitrogen using standard Schlenk techniques. The iminodiphosphane $C_6H_4(o\text{-CN})N{=}PPh_2{-}PPh_2$ (**1**) and $C_6H_4(o\text{-CF}_3)N{=}PPh_2{-}PPh_2$ were prepared by the literature methods[13] and all other reagents were purchased from Aldrich and used as received. Solvents were dried using the appropriate reagents and distilled prior to use. NMR spectra were obtained at 20 °C on a Bruker DMX 200 instrument using $SiMe_4$ for ^1H and 85% H_3PO_4 for ^{31}P, as external standards. ESI-MS spectra were recorded on a Thermo-Finnigan LCQ™ Deca XP Plus quadrupole ion-trap instrument using literature methods[23] with samples infused directly into the source at 5 μL min^{-1} with a syringe pump. The spray voltage was set at 5 kV and the capillary temperature at 50 °C. Elemental analysis was carried out by the Institute of Molecular and Biological Chemistry (EPFL).

Reaction of 1 with MeOH: 1 (58 mg, 0.12 mmol) was added to MeOH (2.0 mL) at room temp. The ^{31}P NMR spectrum of the solution immediately showed the presence of two signals at δ = 29.5 and 117.6 ppm with equal intensity, corresponding to **2** and $Ph_2P{-}OMe$. After 24 h the signal at δ = 29.5 ppm disappeared leaving only the signal at δ = 117.6 ppm.

Reaction of 1 with O_2/H_2O: A sample containing **1** (195 mg, 0.40 mmol) in CH_2Cl_2 (5.0 mL) was exposed to air for two days. The resulting solid was then washed with diethyl ether (2 × 5.0 mL). The filtrates were collected and solvent was removed in vacuo. The remaining solid was washed with diethyl ether (2 × 2.0 mL). After slow evaporation of solvent, crystals of **3** were obtained, which were suitable for X-ray structure analysis. Yield 21 mg, 18 %. M.p. 168 °C. ^1H NMR (ppm in $CDCl_3$): δ = 6.70−8.15 (m, aromatic H), 5.50 (1 H, broad signal, NH) ppm. ^{31}P NMR (ppm in $CDCl_3$): δ = 20.5 (s) ppm. ESI-MS: *m/z*: 319 $[M + H]^+$. $C_{19}H_{15}N_2OP$ (318.3): calcd. C 71.69, H 4.75, N 8.80; found C 71.63, H 4.87, N 8.79.

Reaction of 1 with H_2O_2: An excess of H_2O_2 (0.20 mL, 30 %) was added at 0 °C to a solution of **1** (195 mg, 0.40 mmol) in CH_2Cl_2 (5.0 mL). The solvent was then removed and the resulting solid was recrystallised from dichloromethane and diethyl ether to give **3**. Yield 25.0 mg, 20 %.

Reaction of 1 with C_6H_4(o-CN)NH_2: A solution of **1** (486 mg, 1.0 mmol) and C_6H_4(o-CN)NH_2 (118 mg, 1.0 mmol) in $CDCl_3$ (5.0 mL) was stirred at room temp for 24 h. The ^{31}P NMR spectrum shows the full conversion of **1** into **2**. The solvent was removed in vacuo to give **2**. Yield 602 mg, 99 %. Spectroscopic data were in excellent agreement with that reported in ref.[13a]

Reaction of 1 with S_8: A sample containing **1** (195 mg, 0.40 mmol) and elemental sulfur (13 mg, 0.40 mmol) in CH_2Cl_2 (5.0 mL) was stirred at room temp for 24 h and then exposed to the air for 24 h. The resulting oily product was washed with diethyl ether (2 × 5.0 mL) to give a colourless solid. Recrystallisation from dichloromethane and diethyl ether gave compound **6** as colourless crystals suitable for X-ray analysis. Yield 50.0 mg, 15 %. M.p. 201 °C. ^1H NMR ($CDCl_3$): δ = 6.60−8.10 (m, aromatic H), 5.5 (1 H, broad signal, NH) ppm. ^{31}P NMR ($CDCl_3$): δ = 53.9 (s) ppm. ESI-MS: *m/z*: 335 $[M + H]^+$. $C_{19}H_{15}N_2PS$ (334.4): calcd. C 68.25, H 4.52, N 8.38; found C 68.63, H 4.57, N 8.29.

Reaction of 1 with [Pd(cod)Cl_2] in 1:1 Ratio: Pd(cod)Cl_2 (14.3 mg, 0.05 mmol) was added to a solution of **1** (24.3 mg, 0.05 mmol) in dichloromethane (5.0 mL) at room temp and stirred for 30 minutes. Thf (2.0 mL) was added and the sample was placed in a freezer at 0 °C. Crystals of **7** were collected by filtration. Yield 23.5 mg, 72 %. M.p. > 285 °C (decomp.). ^1H NMR ($CDCl_3$): δ = 6.65−8.15 (m, aromatic H) ppm. ^{31}P NMR ($CDCl_3$): δ = 39.0 (s) ppm. ESI-MS: *m/z*: 664 $[M - H + Li]^+$, $C_{31}H_{24}Cl_2N_2P_2Pd$ (663.8): calcd. C 56.09, H 3.64, N 4.22; found C 56.63, H 3.69, N 4.11.

An analogous procedure was used with $C_6H_4(o\text{-CF}_3)N{=}PPh_2{-}PPh_2$. Yield 68%. M.p. 220 °C. ^1H NMR (CD_3CN): δ = 6.65−8.15 (m, aromatic H) ppm. ^{31}P NMR (CD_3CN): δ = 44.80 (s) ppm. ESI-MS: *m/z*: $[M + H]^+$. $C_{31}H_{24}Cl_2F_3NP_2Pd$ (706.8): calcd. C 52.68, H 3.42, N 1.98; found C 52.73, H 3.49, N 2.00.

Reaction of 1 with [Pt(cod)Cl_2] in 1:1 Ratio: Pt(cod)Cl_2 (17.2 mg, 0.05 mmol) was added to a solution of **1** (24.3 mg, 0.05 mmol) in dichloromethane (5.0 mL) at room temp and stirred for 30 minutes. Thf (2.0 mL) was added and the sample was placed in a freezer at 0 °C. Crystals of **8** were collected by filtration. Yield 29.3 mg, 78 %. M.p. > 285 °C (decomp.). ^1H NMR ($CDCl_3$): δ = 6.60−8.10 (m, aromatic H) ppm. ^{31}P NMR $CDCl_3$): δ = 27.0 (s, ^1J(PPt) = 3377 Hz) ppm. ESI-MS: *m/z*: 754 $[M - H + Li]^+$. $C_{31}H_{24}Cl_2N_2P_2Pt$ (752.5): calcd. C 49.48, H 3.21, N 3.72; found H C 49.63, 3.30, N 3.68.

An analogous procedure was used with $C_6H_4(o\text{-CF}_3)N{=}PPh_2{-}PPh_2$. Yield 78 %. M.p. > 285 °C. ^1H NMR ($CDCl_3$): δ = 6.65−8.15 (several multiples, aromatic H) ppm. ^{31}P NMR ($CDCl_3$): δ = 25.43 (s, ^1J(PPt) = 3350.0 Hz) ppm. ESI-MS: *m/z*: 793 $[M + H]^+$. $C_{31}H_{24}Cl_2F_3NP_2Pt$ (795.5): calcd. C 46.81, H 3.04, N 1.76; found C 46.92, H 3.08, N 1.73.

Reaction of 1 with [Pt(cod)Cl_2] in 2:1 Ratio: Pt(cod)Cl_2 (18.7 mg, 0.05 mmol) was added to a solution of **1** (48.6 mg, 0.10 mmol) in dichloromethane (5.0 mL)and stirred for 30 min at room temp. Diethyl ether (2.0 mL) was added and the reaction mixture was placed in a freezer at −22 °C. X-ray suitable crystals of **9** were obtained within a few minutes. The crystals were collected by filtration. Yield 81.0 mg, 86 %. ^1H NMR ($CDCl_3$): δ = 6.60−8.10 (m, aromatic H), 5.32 (s, CH_2Cl_2) ppm. ^{31}P NMR ($CDCl_3$): δ = 39.5 (s, $^1J_{P,Pt}$ = 2399 Hz) ppm. ESI-MS^+ *m/z* = 1167 $[M]^+$. $C_{70}H_{64}Cl_{18}N_4P_4Pt$ (1918.4): calcd. C 43.83, H 3.36, N 2.92; found H 3.40, C 43.94, N 2.89.

An analogous procedure was used with $C_6H_4(o\text{-CF}_3)N{=}PPh_2{-}PPh_2$. Yield 51 %. M.p. 260 °C. ^1H NMR ($CDCl_3$): δ = 6.65−8.15 (m, aromatic H) ppm. ^{31}P NMR ($CDCl_3$): δ = 44.0 (s, ^1J(PPt) = 2400.0 Hz) ppm. ESI-MS: *m/z*: 1252 $[M]^+$. $C_{62}H_{48}Cl_2F_6N_2P_4Pt$ (1325.0): calcd. C 56.20, H 3.65, N 2.11; found C 56.32, H 3.68, N 2.13.

 © 2004 Wiley-VCH Verlag GmbH & Co. KGaA, Weinheim

X-ray Characterization: X-ray measurements were performed on a 4-circle kappa goniometer equipped with an Oxford Diffraction KM4 Sapphire CCD (**3**, **6**, **9**) and on a marresearch mar345 IPDS (**7**, **8**) at 140 K; **7** was collected at room temp. A summary of the crystallographic data and the structure refinements is listed in Table 1 and relevant geometrical parameters, including bond lengths and angles are included into the figure captions. Data reduction was carried out with CrysAlis RED, release 1.6.9.[24] Absorption correction[25] was applied to all data sets but **6**. Structure solutions of **3**, **8** and **9** by SIR92,[26] **6** by SHELXS-97[27] and **7** by SIR97.[28] Structure refinement as well as molecular graphics and geometrical calculations were performed for all structures with the SHELXTL software package, release 5.1.[29] The structures were refined using the full-matrix least-squares on F^2 with all non-H atoms anisotropically defined. H atoms were placed in calculated positions using the "riding model'. Some disorder problems were encountered during the refinement of **7** and **8**. In the case of **7**, THF molecules were disordered over the inversion centre with 50 % occupation and in order to get reasonable parameters some geometrical restraints were employed, whereas for **8** the whole structure has undergone "rigid bond'' restraints. CCDC-201872 (**9**) and -209134 ... -209137 (**3**, **6**, **7**, **8**) contain the supplementary crystallographic data for this paper. These data can be obtained free of charge at www.ccdc.cam.ac.uk/conts/retrieving.html [or from the Cambridge Crystallographic Data Centre, 12 Union Road, Cambridge CB2 1EZ, UK; Fax: (internat.) + 44-1223-336-033: E-mail: deposit@ccdc.cam.ac.uk].

Acknowledgments

We thank the EPFL and Swiss National Science Foundation for financial support.

[1] [1a] F. T. Edelmann, *Coord. Chem. Rev.* **1994**, *137*, 403. [1b] R. Fleischer, D. Stalke, *Coord. Chem. Rev.* **1998**, *176*, 431. [1c] A. Steiner, S. Zacchini, P. I. Richards, *Coord. Chem. Rev.* **2002**, *227*, 193.

[2] P. Imhoff, C. J. Elsevier, C. H. Stam, *Inorg. Chem. Acta* **1990**, *175*, 209.

[3] [3a] A. Burg, J. E. Griffiths, *J. Am. Chem. Soc.* **1960**, *82*, 1507. [3b] A. Burg, J. E. Griffiths, *J. Am. Chem. Soc.* **1960**, *84*, 3442. [3c] H. Wong, L. Prasad, E. J. Gabe, F. C. Bradley, *J. Organomet. Chem.* **1982**, *236*, 321. [3d] F. C. Bradley, E. H. Wong, E. J. Gabe, F. L. Lee, Y. Lepage, *Polyhedron* **1987**, *6*, 1103.

[4] [4a] P. Bhattacharyya, J. D. Woollins, *Polyhedron* **1995**, *20*, 993. [4b] J. T. Mague, *J. Cluster Sci.* **1995**, *6*, 217. [4c] A. Winkler, W. Bauer, F. W. Heinemann, V. Garcia-Montalvo, M. Moll, J. Ellermann, *Eur. J. Inorg. Chem.* **1998**, 437. [4d] J. Ellermann, M. Schütz, F. W. Heinemann, M. Moll, *Z. Anorg. Allg. Chem.* **1998**, *624*, 257. [4e] W. Bauer, J. Ellermann, M. Dotzler, D. Pohl, F. W. Heinemann, M. Moll, *Z. Anorg. Allg. Chem.* **2000**, *626*, 574.

[5] [5a] P. Battacharyya, J. D. Woollins, *Polyhedron* **1995**, *14*, 3367. [5b] S. M. Aucott, M. L. Clarke, A. M. Z. Slawin, J. D. Woollins, *J. Chem. Soc., Dalton Trans.* **2001**, 972. [5c] M. L. Clarke, A. M. Z. Slawin, J. D. Woollins, *Phosphorus, Sulfur Silicon* **2001**, *168*, 329. [5d] A. M. Z. Slawin, M. B. Smith, J. D. Woollins, *J. Chem. Soc., Dalton Trans.* **1997**, 1877. [5e] I. Bachert, P. Braunstein, R. Hasselbring, *New J. Chem.* **1996**, *20*, 993. [5f] I. Bachert, P. Braunstein, M. K. McCart, F. Fabrizi de Biani, F. Lashi, P. Zanello, G. Kickelbick, U. Schubert, *J. Organomet. Chem.* **1999**, *573*, 47. [5g] I. Bachert, I. Bartussek, P. Braunstein, E. Guillon, J. Rose, G. Kickelbick, *J. Organomet. Chem.* **1999**, *580*, 257. [5h] K. G. Gaw, M. B. Smith, J. W. Steed, *J. Organomet. Chem.* **2002**, *664*, 294.

[6] [6a] M. S. Balakrishna, V. S. Reddy, S. S. Krishnamurthy, J. F. Nixon, J. C. T. R. Burckett St. Laurent, *Coord. Chem. Rev.*

Table 1. Crystal data and details of the structure determination for **3**, **6**, **7**·2thf, **8** and **9**·8CH_2Cl_2

	3	**6**	**7**·2thf	**8**	**9**·8CH_2Cl_2
Chemical formula	$C_{19}H_{15}N_2OP$	$C_{19}H_{15}N_2PS$	$C_{39}H_{40}Cl_2N_2O_2P_2Pd$	$C_{31}H_{24}Cl_2N_2P_2Pt$	$C_{70}H_{64}Cl_{18}N_4P_4Pt$
Molecular weight	318.30	334.36	807.97	752.45	1918.32
Crystal system	monoclinic	monoclinic	triclinic	monoclinic	monoclinic
Space group	$P2_1/n$	$I2/a$	$P\bar{1}$	$P2_1$	$P2_1/n$
a (Å)	14.0346(18)	15.3909(12)	11.456(5)	10.957(4)	13.0331(6)
b (Å)	16.758(4)	9.3846(8)	11.481(4)	14.671(6)	21.2595(11)
c (Å)	14.748(3)	23.2452(13)	16.953(9)	17.6483(18)	15.7534(8)
α (°)	90	90	79.94(4)	90	90
β (°)	101.477(14)	95.181(6)	74.77(4)	96.912(19)	109.556(5)
γ (°)	90	90	61.87(5)	90	90
V (Å^3)	3399.4(12)	3343.7(4)	1893.9(15)	2816.4(15)	4113.1(3)
Z	8	8	2	4	2
$D_{calcd.}$ (g·cm^{-3})	1.244	1.328	1.417	1.775	1.549
F(000)	1328	1392	828	1464	1912
μ (mm^{-1})	0.167	0.289	0.751	5.310	2.410
T (K)	140	140	293	140	140
Wavelength (Å)	0.71073	0.71073	0.71070	0.71070	0.71073
Measured reflections	20002	9267	11515	16532	23617
Unique reflections	5686	2936	6262	9241	6869
Unique reflections [$I > 2\sigma(I)$]	1907	2462	2635	6194	5681
Data/parameters	5686/415	2936/208	6262/443	9241/686	6869/439
R_1 [a] [$I > 2\sigma(I)$]	0.0851	0.0354	0.0470	0.0571	0.0254
wR_2 [a] (all data)	0.1368	0.0957	0.1100	0.1522	0.0729
GooF[b]	0.943	1.072	0.812	1.053	1.102

[a] $R1 = \Sigma||F_o| - |F_c||/\Sigma|F_o|$; $wR_2 = [\Sigma w(F_o^2 - F_c^2)^2/\Sigma w(F_o^2)^2]^{1/2}$. [b] GooF $= [\Sigma w(F_o^2 - F_c^2)^2/(n\text{-}p)]^{1/2}$ where n is the number of data and p is the number of parameters refined.

 © 2004 Wiley-VCH Verlag GmbH & Co. KGaA, Weinheim

1994, *129*, 1. [6b] T. Appleby, J. D. Woollins, *Coord. Chem. Rev.* **2002**, *235*, 121.

[7] [7a] S. Naili, J.-F. Carpentier, F. Agbossou, A. Mortreux, *Organometallics* **1995**, *14*, 401. [7b] M. S. Balakrishna, K. Ramaswamy, R. M. Abhyankar, *J. Organomet. Chem.* **1998**, *560*, 131.

[8] [8a] A. M. Z. Slawin, J. D. Woollins, Q. Zhang, *J. Chem. Soc., Dalton Trans.* **2001**, 621. [8b] A. Badia, R. Navarro, E. P. Urriolabeitia, *J. Organomet. Chem.* **1998**, *554*, 105. [8c] L. Dahlenberg, R. Götz, *J. Organomet. Chem.* **2001**, *619*, 88.

[9] [9a] A. D. Burrows, M. F. Mahon, M. T. Palmer, *J. Chem. Soc., Dalton Trans.* **2001**, 3615. [9b] K. G. Gaw, M. B. Smith, A. M. Z. Slawin, *New J. Chem.* **2000**, *24*, 429.

[10] [10a] H. Rossknecht, A. Schmidtpeter, *Z. Naturforsch., Teil B* **1971**, *26*, 81. [10b] H. Rossknecht, W. P. Lehman, A. Schmidtpeter, *Phosphorus* **1975**, *5*, 195.

[11] O. Scherer, W. M. Janssen, *J. Organomet. Chem.* **1969**, *20*, 111.

[12] [12a] V. L. Foss, Yu. A. Veits, T. E. Tretyakova, I. F. Lutsenko, *Zh. Obshch. Khim.* **1977**, *47*, 954. [12b] V. L. Foss, Yu. A. Veits, T. E. Ghernykh, I. F. Lutsenko, *Zh. Obshch. Khim.* **1984**, *54*, 2670. [12c] Yu. A. Veits, E. G. Neganova, A. A. Borisenko, V. L. Foss, I. F. Lutsenko, *Zh. Obshch. Khim.* **1989**, *59*, 1733.

[13] [13a] Z. Fei, R. Scopelliti, P. J. Dyson, *Inorg. Chem.* **2003**, *42*, 2125. [13b] Z. Fei, R. Scopelliti, P. J. Dyson, *Dalton Trans.* **2003**, 2772.

[14] S. Berger, S. Braun, H.-O. Kalinowski, *NMR-Spektroskopie von Nichtmetallen, Band 3,* ^{31}*P NMR-Spektroskopie*, Georg Thieme Verlag, Stuttgart, New York, **1993**.

[15] K. G. Gaw, M. B. Smith, A. M. Z. Slawin, *New J. Chem.* **2000**, *24*, 429.

[16] Yu. G. Gololobov, E. A. Suvalova, T. I. Chudakova, *Zh. Obshch. Khim.* **1981**, *51*, 1433.

[17] Z. Fei, N. Kocher, C. J. Mohrschladt, H. Ihmels, D. Stalke, *Angew. Chem. Int. Ed.* **2003**, *42*, 783.

[18] [18a] A. M. Z. Slawin, J. D. Woollins, Q. Z. Zhang, *Chem. Commun.* **1999**, 386. [18b] T. Q. Ly, A. M. Z. Slawin, J. D. Woollins, *Angew. Chem. Int. Ed.* **1998**, *37*, 2501.

[19] W. Seidel, M. Alexiev, *Z. Anorg. Allg. Chem.* **1978**, *438*, 68.

[20] A. D. Burrows, M. F. Mahon, M. T. Palmer, *J. Chem. Soc., Dalton Trans.* **2000**, 1669.

[21] [21a] C. S. Browning, D. H. Farrar, *J. Chem. Soc., Dalton Trans.* **1995**, 521. [21b] C. S. Browning, D. H. Farrar, *J. Chem. Soc., Dalton Trans.* **1995**, 2005.

[22] [22a] J. W. Ellis, K. N. Harrison, P. A. T. Hoye, A. G. Orpen, P. G. Pringle, M. B. Smith, *Inorg. Chem.* **1992**, *31*, 3026. [22b] E. C. Alyea, G. Ferguson, S. Kannan, *Chem. Commun.* **1998**, 345. [22c] S. E. Durran, M. B. Smith, A. M. Z. Slawin, T. Gelbrich, M. B. Hursehouse, M. E. Light, *Can. J. Chem.* **2001**, *79*, 780. [22d] P. W. Dyer, P. J. Dyson, S. L. James, P. Suman, J. E. Davies, C. M. Martin, *Chem. Commun.* **1998**, 1375. [22e] P. Suman, P. W. Dyer, P. J. Dyson, S. L. James, J. W. Steed, *New J. Chem.* **1998**, *22*, 1311.

[23] W. Henderson, J. S. McIndoe, B. K. Nicholson, P. J. Dyson, *J. Chem. Soc., Dalton Trans.* **1998**, 519.

[24] Oxford Diffraction Ltd., Abingdon, Oxfordshire, UK, 2002.

[25] DELABS. N. Walker, D. Stuart, *Acta Crystallogr., Sect. A* **1983**, *39*, 158.

[26] SIR92 − A program for crystal structure solution. A. Altomare, G. Cascarano, C. Giacovazzo, A. Guagliardi, *J. Appl. Crystallogr.* **1993**, *26*, 343.

[27] SHELX97 − Programs for Crystal Structure Analysis (Release 97−2). G. M. Sheldrick, Institüt für Anorganische Chemie der Universität, Tammanstrasse 4, 3400 Göttingen, Germany, **1998**.

[28] SIR97 − A. Altomare, M. C. Burla, M. Camalli, G. L. Cascarano, C. Giacovazzo, A. Guagliardi, A. G. G. Moliterni, G. Polidori, R. Spagna, *J. Appl. Cryst.* **1999**, *32*, 115.

[29] Bruker AXS, Inc., Madison, Wisconsin, 53719, USA, **1997**.

Received July 31, 2003
Early View Article
Published Online November 28, 2003

 © 2004 Wiley-VCH Verlag GmbH & Co. KGaA, Weinheim

Syntheses, Crystal Structures and Magnetic Properties of Four Cu^{II}-Hg^{II} Mixed-Metal Halide Oligomers

Jun-Ling Song,[a] Jiang-Gao Mao,*[a] Hui-Yi Zeng,[a] and Zhen-Chao Dong[b]

Keywords: Copper / Mercury / Magnetic properties / Cluster compounds

Four heteronuclear Cu^{II}–Hg^{II} halides containing 2,2-bipyridine (bipy) ligands have been synthesized and structurally characterised by single-crystal X-ray diffraction studies. The dinuclear complex $[Cu(bipy)_2HgCl_2Br_2]$ (**1**) contains a five-coordinate copper(II) ion and a four-coordinate Hg^{II} ion, in which the two different types of metal ions are bridged by a pair of chloride anions. $[Cu_2(bipy)_4HgBr_4][Hg_2Br_6]$ (**2**) contains a trinuclear $[Cu_2(bipy)_4HgBr_4]^{2+}$ cation in which the two copper(II) ions are bridged by an $[HgBr_4]^{2-}$ tetrahedron via two Cu–Br bonds, and an edge-sharing tetrahedral $[Hg_2Br_6]^{2-}$ anion. The structure of $[Cu_2(bipy)_4Hg_2Br_6]$-$[Hg_4Br_{10}]$ (**3**) features a 1-D chain along the diagonal of the *a* and *c* axes constructed from tetranuclear $[Cu_2(bipy)_4Hg_2Br_6]^{2+}$ cations interconnected by $[Hg_4Br_{10}]^{2-}$ tetramers via elongated Hg–Br contacts (3.185 Å). Within the tetranuclear cationic unit, two $[Cu(bipy)_2]^{2+}$ units are bridged by an edge-sharing dimeric tetrahedral $[Hg_2Br_6]^{2-}$ anion. In the trinuclear complex $[Cu(bipy)_2Hg_2Cl_6]$ (**4**), each $[Hg_2Cl_6]^{2-}$ dimer bridges with a $[Cu(bipy)_2]^{2+}$ ion to form a trinuclear $[Cu(bipy)_2Hg_2Cl_6]$ unit, and each pair of such units is bridged by a pair of elongated Hg–Cl bonds [3.043(5) Å] to form a dimeric unit. The magnetic properties of **1**, **2**, and **4** have also been investigated.

(© Wiley-VCH Verlag GmbH & Co. KGaA, 69451 Weinheim, Germany, 2004)

Introduction

For several decades there has been considerable interest in polynuclear transition-metal complexes with linear-chain structures due to their unusual optical, electronic, and magnetic properties.[1] Such compounds are also ideal systems for the study of metal−metal interactions and in the search for molecular metal wires.[2] Low dimensional metal−organic halide networks have received considerable research attention in recent years due to their potential applications as electronic materials and catalysts.[3] Extensive studies on copper complexes are largely driven by their photochemical and photophysical properties. To date, numerous mononuclear metal coordination polymers with interesting structural motifs have been successfully synthesized. In contrast, the chemistry of bimetallic coordination polymers has received considerably less attention. Bimetallic coordination polymers have the potential to exhibit interesting physical properties such as electronic conductivity or magnetic ordering that result from interactions between two distinct metal centers connected by a suitable linker.[4] Homonuclear oligomers and chains of copper or mercury halogen compounds with polyamine ligands have been reported in the literature.[5−7] Their structures can be viewed as being built from polyamine (such as bipy) coordinated copper(II) moieties connected to copper(I) or copper(II) halides. Heteronuclear metal halides can exhibit not only new structural motifs that are unseen in homo-metallic systems, but also new or enhanced physical or chemical properties. However reports on heteronuclear metal halide compounds are relatively rare.[8−10] Several copper−zinc and copper−zirconium chlorides have been reported by the Martin group and[8] a series of nickel organoamine-halocadmates were reported by Zubieta and co-workers.[9] One, two, and three-dimensional mixed metal coordination polymers have been found in the Cu(prazinecarboxylate)$_2$/$CdCl_2$ system[10] and several Cu−Hg halides have been reported.[11] $[Cu(2\text{-pyrazinecarboxylato})_2HgI_2]\cdot HgI_2$ consists of an open framework constructed from Cu(2-pyrazinecarboxylato)$_2$ and HgI_2 building blocks, the other linear HgI_2 molecule is encapsulated in the cavity of the framework as a guest molecule.[11a] In $[Cu(en)_2][Hg_2Cl_6]$, the $[Cu(en)_2]^{2+}$ cations are bridged by dimeric Hg_2Cl_6 anions into a 1-D chain, whereas in $[Cu(en)_2][Hg_2Br_6]$, the $[Hg_2Br_6]^{2-}$ anions are interconnected through Hg−Br bonds to form an infinite chain and such chains are further bridged by $[Cu(en)_2]^{2+}$ cations into a 2-D layer. $[Cu(en)_2][HgBr_4]$ has a different chain structure in which the $[Cu(en)_2]^{2+}$ moieties are bridged by $[HgBr_4]$ tetrahedra.[11b] In $[Cu(bipy)_3]$-$[Hg_2I_6]$, the anions remain isolated due to the presence of a third chelating bipy ligand at the copper(II) ion.[11c]

We utilized the 2,2′-bipyridine ligand as a template to form the $[Cu(2,2'\text{-pyridine})_2]^{2+}$ cation. Reactions of the latter with Hg^{II} halides under different conditions (such as

[a] State Key Laboratory of Structural Chemistry, Fujian Institute of Research on the Structure of Matter, Chinese Academy of Sciences,
Fuzhou, Fujian 350002, P. R. China
[b] National Institute for Materials Science,
1-2-1 Sengen, Tsukuba, Ibaraki 305-0047, Japan

 © 2004 Wiley-VCH Verlag GmbH & Co. KGaA, Weinheim DOI: 10.1002/ejic.200300554

different Cu/Hg ratios and solvents) led to four new $Cu^{II}-Hg^{II}$ mixed-metal oligomers, namely binuclear $[Cu(bipy)_2HgCl_2Br_2]$ (**1**), $[Cu_2(bipy)_4HgBr_4][Hg_2Br_6]$ (**2**) containing a trinuclear $[Cu_2(bipy)_4HgBr_4]^{2+}$ cation and an isolated $[Hg_2Br_6]^{2-}$ anion, $[Cu_2(bipy)_4Hg_2Br_6][Hg_4Br_{10}]$ (**3**) featuring a 1-D chain built from tetranuclear $[Cu_2(bipy)_4Hg_2Br_6]^{2+}$ cations interconnected by $[Hg_4Br_{10}]^{2-}$ tetramers and the trinuclear $[Cu(bipy)_2Hg_2Cl_6]$ (**4**), in which two $[Cu(bipy)_2]^{2+}$ cations are bridged by an $[Hg_4Cl_{12}]^{2-}$ tetramer. Herein we report their syntheses, crystal structures, and characterization.

Results and Discussion

The structures of **1**−**4** feature linear heteronuclear $Cu^{II}-Hg^{II}$ halogen oligomers in which the two different types of metal ions are bridged by the halide anions.

As shown in Figure 1, the Hg^{II} ion in dinuclear $[Cu(bipy)_2HgCl_2Br_2]$ (**1**) is tetrahedrally coordinated by two chloride anions and two bromide anions, whereas the copper(II) ion is six-coordinate with two bidentate chelating bipy ligands and two chloride anions in a distorted octahedral geometry. The Cu−N distances range from 2.00(1) to 2.08(1) Å. The Hg−Cl, Hg−Br, and Cu−Cl distances are 2.670(3), 2.488(2), and 2.750(4) Å, respectively and these bond lengths are similar to those reported in other copper(II) and Hg^{II} halogen complexes.[5,6,11] Unlike in $[Cu(en)_2]HgBr_4$,[11b] the Cu^{II} and Hg^{II} ions in **1** are bridged by a pair of μ^2-chloride anions to form a dinuclear molecular unit. $[Cu(en)_2]HgBr_4$ has a 1-D chain structure in which the two metal centers are bridged by only one bromide anion.[11b] We suggest that the difference is mainly due to the much larger steric hindrance of the bipy ligand than that of ethylene diamine. The structure of **1** is also significantly different from that of binuclear $[Ni(bipy)_2CdCl_2I_2]$ in that the cadmium(II) ion has a square planar coordination geometry instead of a tetrahedral one for the Hg^{II} ion.[9]

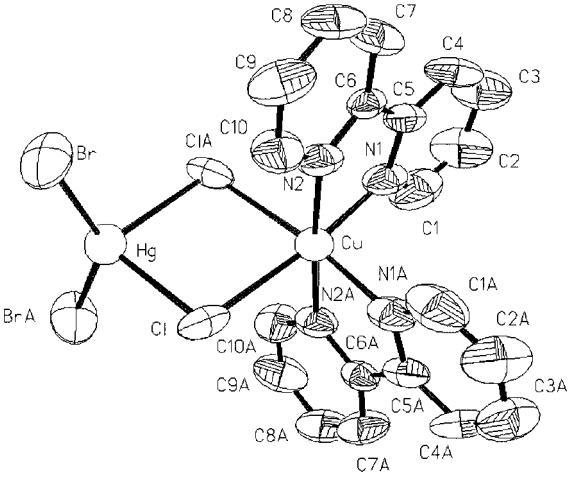

Figure 1. ORTEP representation of the asymmetric unit of $[Cu(bipy)_2HgCl_2Br_2]$ (**1**). Thermal ellipsoids are drawn at the 50% probability level. Symmetry code for the generated atoms: $1-x$, y, $3/2-z$

The Cu···Hg separation is 3.881(1) Å, indicating that there is no metal−metal bonding between the two metal centers.

These dinuclear molecular units in **1** are further interlinked via weak π-π interactions between neighboring pyridine rings to form a 1-D chain along the diagonal of the *a* and *c* axes (Figure 2). The distance between the centers of two such rings is 3.949 Å, and the dihedral angle between the two rings is 4.4°. Similar π-π interactions between pyridine rings have been reported in many phen-containing copper(II) complexes.[12] Such chains are held together via weak van der Waals forces.

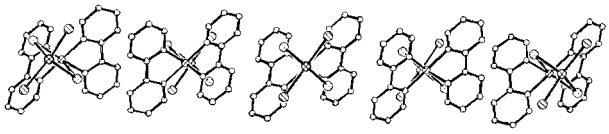

Figure 2. A 1-D chain formed from molecular units of complex **1** via π-π interactions between the pyridine rings

The copper(II) ions in **2**, **3**, and **4** are five-coordinate with two chelating bipy ligands and a halide anion. The coordination geometries around the Cu^{II} ions can be described as a slightly distorted square pyramidal with the square plane formed by 4 N atoms and the halogen atom occupying the axial position.

The structure of $[Cu_2(bipy)_4HgBr_4][Hg_2Br_6]$ (**2**) contains a trinuclear $[Cu_2(bipy)_4HgBr_4]^{2+}$ cation and a $[Hg_2Br_6]^{2-}$ anion (Figure 3). Within the trinuclear cationic unit, a pair of $[Cu(bipy)_2]^{2+}$ cations are bridged by an $HgBr_4$ tetrahedron. Hg(2) in the $[Hg_2Br_6]^{2-}$ anion is also four-coordinate and two $HgBr_4$ tetrahedra share an edge (Br5−Br5A) to form a dimeric unit. Such an $[Hg_2Br_6]^{2-}$ anion has been reported in other Hg^{II} bromide complexes.[11] The Cu−N, Cu−Br, and Hg−Br distances are similar to those in **1** (Table 1). The shortest Hg−Hg and Hg−Cu distances are 3.838(1) and 4.698(1) Å, respectively, thus there is no metal−metal interaction. The distance from Cu(1) in $[Cu_2(bipy)_4HgBr_4]^{2+}$ to the bromide of the nearest $[Hg_2Br_6]^{2-}$ anion is 3.838(2) Å, indicating that there are only electrostatic interactions between the two different building units. Similar to **1**, the neighboring $[HgCu_2(bipy)_4Br_4]^{2+}$ cations are further interlinked via weak π-π interactions between pyridine rings to form a 1-D double chain along the diagonal of the *a* and *c* axes. The

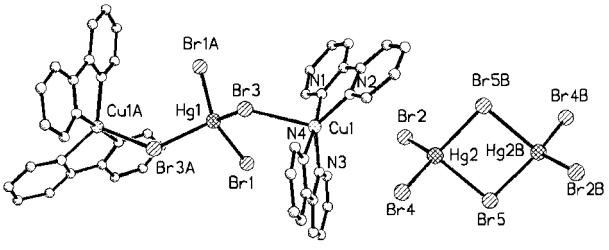

Figure 3. The structure of $[Cu_2(bipy)_4HgBr_4][Hg_2Br_6]$ (**2**). Symmetry codes for the generated atoms: a. $-x$, y, $1/2-z$; b. $-1/2-x$, $3/2-y$, $-1-z$

 © 2004 Wiley-VCH Verlag GmbH & Co. KGaA, Weinheim

Table 1. Selected bond lengths [Å] and angles [°] for **1**−**4**

1			
Hg−Br#1[a]	2.4882(16)	Hg−Br	2.4882(16)
Hg−Cl	2.670(3)	Hg−Cl#1	2.670(3)
Cu−N(2)#1	2.000(11)	Cu−N(2)	2.000(11)
Cu−N(1)#1	2.077(13)	Cu−N(1)	2.077(13)
Cu−Cl#1	2.750(4)	Cu−Cl	2.750(4)
2			
Hg(1)−Br(1)#1	2.539(3)	Hg(1)−Br(1)	2.539(3)
Hg(1)−Br(3)#1	2.707(2)	Hg(1)−Br(3)	2.707(2)
Hg(2)−Br(2)	2.520(3)	Hg(2)−Br(4)	2.525(3)
Hg(2)−Br(5)#2	2.663(3)	Hg(2)−Br(5)	2.814(3)
Br(3)−Cu(1)	2.778(4)	Cu(1)−N(1)	1.961(17)
Cu(1)−N(4)	1.987(17)	Cu(1)−N(3)	2.035(16)
Cu(1)−N(2)	2.058(17)		
3			
Hg(1)−Br(3)	2.514(2)	Hg(1)−Br(2)	2.526(2)
Hg(1)−Br(1)	2.626(2)	Hg(1)−Br(2)#1	3.108(2)
Hg(2)−Br(5)	2.403(3)	Hg(2)−Br(4)	2.411(3)
Hg(2)−Br(6)	3.043(3)	Hg(3)−Br(7)	2.528(2)
Hg(3)−Br(6)	2.531(3)	Hg(3)−Br(8)	2.653(2)
Hg(3)−Br(8)#2	2.802(2)	Cu−N(2)	1.972(15)
Cu−N(3)	1.990(14)	Cu−N(1)	2.000(15)
Cu−N(4)	2.025(15)	Cu−Br(1)	2.791(4)
4			
Hg(1)−Cl(3)	2.333(5)	Hg(1)−Cl(2)	2.334(5)
Hg(1)−Cl(1)	2.734(4)	Hg(1)−Cl(4)	2.889(5)
Hg(2)−Cl(6)	2.359(5)	Hg(2)−Cl(5)	2.386(5)
Hg(2)−Cl(4)	2.534(4)	Cu−N(2)	1.982(13)
Cu−N(3)	1.992(13)	Cu−N(1)	2.057(13)
Cu−N(4)	2.139(13)	Cu−Cl(1)	2.319(5)

[a] Symmetry transformations used to generate equivalent atoms: For **1**: #1 $-x + 1$, y, $-z + 3/2$. For **2**: #1 $-x$, y, $-z + 1/2$ #2 $-x - 1/2$, $-y + 3/2$, $-z - 1$. For **3**: #1 $-x$, $-y$, $-z + 2$ #2 $-x - 1$, $-y$, $-z + 1$.

distance between the centers of two such rings is 3.771 Å, and the dihedral angle between the two rings is 6.2°.

The structure of $[Cu_2(bipy)_4Hg_2Br_6][Hg_4Br_{10}]$ (**3**) features a novel one-dimensional chain along the diagonal of the *a* and *c* axes (Figure 4). The chain is built from tetranuclear $[Cu_2Hg_2(bipy)_4Br_6]^{2+}$ cations interconnected by $[Hg_4Br_{10}]^{2-}$ tetramers via elongated Hg−Br bonds [3.185(2) Å]. Within the tetranuclear $[Cu_2Hg_2(bipy)_4Br_6]^{2+}$ cation, the edge-sharing tetrahedral dimeric $Hg(1)_2Br_6$ unit bridges with two $[Cu(bipy)_2]^{2+}$ units via two Br(1) atoms. The $[Hg_4Br_{10}]^{2-}$ tetramer is composed of an edge-sharing $Hg(3)_2Br_6$ dimeric unit and two $Hg(2)Br_2$ units [Br−Hg−Br 160.7(1)°] that are interconnected via Hg−Br bonds [Hg(2)−Br(6) 3.043(3) Å]. The coordination geometries around Hg(1) and Hg(3) can be described as slightly distorted tetrahedral. The distortion of the $Hg(2)Br_4$ tetrahedron is even more severe, two of the Hg-Br distances are longer than the remaining two Hg−Br bonds by more than 0.64 Å (Table 1). Similar to the situation in **1** and **2**, there is no metal−metal bonding between the metal centers, the shortest Hg−Cu and Hg−Hg distances are 4.435(2) and 3.823(2) Å, respectively. The 1-D chains of $[Cu_2(bipy)_4Hg_2Br_6][Hg_4Br_{10}]$ (**3**) are further interconnected via weak π-π interactions between neighboring pyridine rings to form a <010> 2-D layer (Figure 5). The distance between the centers of two such rings is 4.153 Å, and the dihedral angle between the two rings is 1.9°.

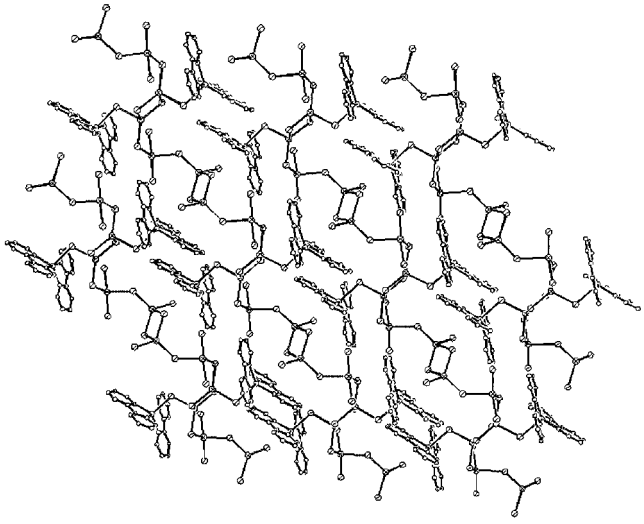

Figure 5. A <0 1 0> layer formed by 1-D chains of complex **3** through π-π interactions between the pyridine rings

In $[Cu(bipy)_2Hg_2Cl_6]$ (**4**), each $[Hg_2Cl_6]^{2-}$ dimeric unit bridges with a $[Cu(bipy)_2]^{2+}$ cation to form a trinuclear

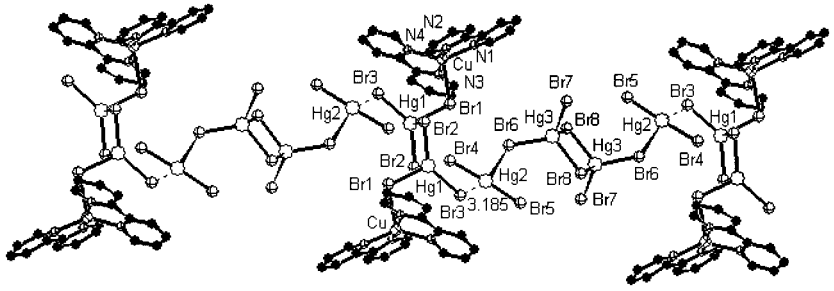

Figure 4. 1-D chain of $[Cu_2(bipy)_4Hg_2Br_6][Hg_4Br_{10}]$ (**3**) along the diagonal axis of *a* and *c*. Longer Hg−Br contacts are represented by dotted lines

 © 2004 Wiley-VCH Verlag GmbH & Co. KGaA, Weinheim

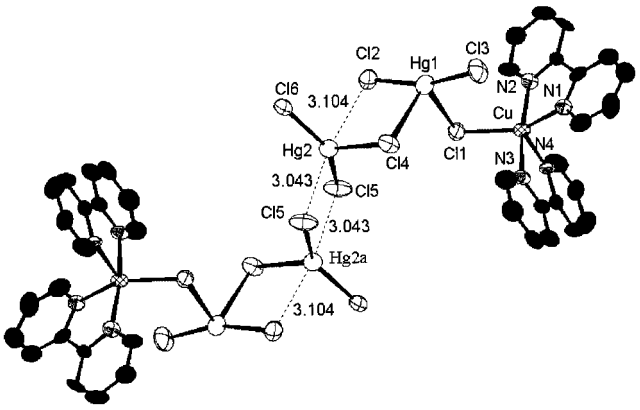

Figure 6. ORTEP representation of the structure of $[Cu(bipy)_2Hg_2Cl_6]_2$ (**4**). Thermal ellipsoids are drawn at the 50% probability level. Longer Hg−Cl contacts are represented by dotted lines. Symmetry code for the generated atoms: $1 - x, 2 - y, -z$

$[Cu(bipy)_2Hg_2Cl_6]$ unit (Figure 6). Two such neighboring units are interconnected by a pair of weak Hg−Cl bonds [Hg(2)−Cl(5) Å] into a hexanuclear $[Cu(bipy)_2Hg_2Cl_6]_2$ unit. The Hg(2)−Cl(2) distance of 3.104 Å is also much longer than the remaining Hg−Cl distance (Table 1). With all Hg−Cl bonds included, the coordination geometry around Hg(2) can be described as distorted trigonal bipyramidal with the two axial Hg−Cl bonds elongated. The coordination geometry of the Hg(1) center is severely distorted tetrahedral. The shortest Cu−Hg and Hg−Hg contacts are 4.053(1) and 4.0699(1) Å, respectively. The shortest Hg−Cl distance between two neighboring $[Hg_2Cu(bipy)_2Cl_6]_2$ units is more than 3.582(5) Å, thus these dimeric units are not further condensed. The structure of **4** is different from those of $[Cu(en)_2][Hg_2Cl_6]$ and $[Cu(en)_2][Hg_2Br_6]$ although they have a similar structural formula.[11b] In $[Cu(en)_2][Hg_2Cl_6]$, each $[Hg_2Cl_6]$ anion bridges with two $[Cu(en)_2]^{2+}$ cations to form a 1-D chain, and the Cu^{II} ion has a Jahn−Teller distorted octahedral coordination geometry. In $[Cu(en)_2][Hg_2Br_6]$, the copper(II) ion is also octahedrally coordinated, however the $[Hg_2Br_6]^{2-}$ anions are interconnected into a 1-D chain, and all Hg^{II} ions are five-coordinate with trigonal bipyramidal geometries. The anionic chains of $[Hg_2Br_6]^{2-}$ are cross-linked by bridging $[Cu(en)_2]^{2+}$ cations into a 1-D layer.[11b] Again we suggest the steric effect of the bipy group plays an important role in determining the structures of the so formed Cu^{II}−Hg^{II} halide compounds. Strong steric hindrance of two bipy ligands makes the octahedral coordination geometry unfavorable for the Cu^{II} ion.

The formula units of **4** are packed via π-π interactions between the pyridine rings to form a 1-D chain along the diagonal of the *a* and *c* axes. The distance from the pyridine ring center formed by N(3), C(11), C(12), C(13), C(14), and C(15) to that formed by N(4), C(16), C(17), C(18), C(19), and C(20) in neighboring formula units is 3.888 Å. The dihedral angle between these two pyridine rings is only 5.2°.

Results of magnetic measurements for **1**, **2**, and **4** indicate that the three compounds contain one, two, and one isolated single-spin d^9 Cu^{II} ion, respectively. Magnetic measurements for **3** were not performed due to an insufficient amount of samples. The measured μ_{eff} values are 1.766(3), 2.494(2), and 1.764(1) μ_B, respectively for **1**, **2**, and **4**. These values decrease very slightly with decreasing temperature and non-linear fitting of the data according to the Cuie−Weiss law [$\chi_M = C/(T - \theta) + \chi_0$] in the temperature range of 6−300 K gives θ vlues of −0.24(3), −0.27(1), and −0.15(6), and χ_0 values of $3.1(2)\cdot10^{-4}$, $-6.5(2)\cdot10^{-4}$, and $-3.9(2)\cdot10^{-4}$ emu/mol, for **1**, **2**, and **4** respectively. Thus there is little magnetic interaction between neighboring Cu^{II} ions, which is in good agreement with results from the X-ray structural analyses in which the nearest Cu···Cu separations are 8.112(2), 7.431(2), and 7.386(2) Å, for **1**, **2**, and **4** respectively.

Experimental Section

Materials and Methods: $CuCl_2\cdot2H_2O$, $CuBr_2$, $HgBr_2$, and 2,2′-bipyridine were purchased from the Fourth Factory of Shanghai Reagent and NH_4PF_6 was obtained from Acros. All chemicals and solvents were of reagent grade and used without further purification. Elemental analyses were performed on a Vario EL III elemental analyzer. IR spectra were recorded on a Magna 750 FT-IR spectrometer as KBr pellets in the 4000−400 cm^{-1}. Magnetic susceptibility measurements on polycrystalline samples were performed with a Quantum Design SQUID magnetometer at a field of 1 T over the range of 6 to 300 K. Raw data were corrected for the susceptibility of the container.

Synthesis of $[Cu(bipy)_2HgCl_2Br_2]$ (1): $CuCl_2\cdot2H_2O$ (0.09 g, 0.5 mmol), NH_4PF_6 (0.16 g,1.0 mmol, used for adjusting pH value of the solution), and 2,2′-bipyridine (0.16 g, 1.0 mmol) were dissolved in a solvent mixture of acetone (10.0 mL), ethanol (10.0 mL), and acetonitrile (10.0 mL) whilst stirring at room temperature. After 10 min, $HgBr_2$ (0.16 g, 0.5 mmol) was added and the solution was stirred for 20 hours. The resultant solution with a pH value close to 6.0 was filtered and allowed to evaporate slowly at room temperature. Blue crystals of **1** were obtained after five days in a yield of 40.2% (0.16 g). IR (KBr cm^{-1}): $\tilde{\nu}$ = 1601 m, 1570 w, 1495 m, 1444 s, 1317 m, 839 vs, 768 vs, 731 m, 557 m. $C_{20}H_{16}Br_2Cl_2CuHgN_4$ (807.22): found C 29.81, H 2.48, N 6.95%; calcd. C 29.76, H 2.00, N 6.94%.

Synthesis of $[Cu_2(bipy)_4HgBr_4][Hg_2Br_6]$ (2): $CuBr_2$ (0.16 g, 0.5 mmol), NH_4PF_6 (0.16 g, 1.0 mmol), and 2,2′-bipyridine (0.16 g, 1.0 mmol) were dissolved in a solvent mixture of acetone (10.0 mL), ethanol (10.0 mL), and acetonitrile (10.0 mL) at room temperature and stirred for 30 min. $HgBr_2$ (0.36 g, 1.0 mmol) was then added and the reaction was allowed to continue for a further 20 hours. The resultant solution with a pH value of 6.0 was filtered and the filtrate was allowed to evaporate slowly at room temperature. Green-blue crystals of **2** were obtained after one day in a yield of 78.1% (0.42 g). IR data (KBr cm^{-1}): $\tilde{\nu}$ = 1601s, 1495 m, 1473 s, 1444 vs, 1317 m, 1252 m, 1159 m, 1034 m, 764 vs, 732 s, 663 w. $C_{40}H_{32}Br_{10}Cu_2Hg_3N_8$ (2152.69): found C 22.54, H 3.20, N 5.12, Cu 6.26%. calcd. C 22.32, H 1.50, N 5.21, Cu 5.9%.

Synthesis of $[Cu_2(bipy)_4Hg_2Br_6][Hg_4Br_{10}]$ (3): A mixture of $CuBr_2$ (0.16 g, 0.5 mmol), NH_4PF_6 (0.08 g, 0.5 mmol), and 2,2′-bipyridine (0.16 g, 1.0 mmol) was dissolved in a solvent mixture of acetonitrile (5 mL) and methanol (5 mL) which was placed in one side of an H-shaped tube (total volume 35 mL). $HgBr_2$ (0.18 g, 0.5 mmol) dis-

 © 2004 Wiley-VCH Verlag GmbH & Co. KGaA, Weinheim

Table 2. Summary of crystal data and details of intensity collection and refinement for **1**−**4**

Compound	**1**	**2**	**3**	**4**
Formula	$C_{20}H_{16}Br_2Cl_2CuHgN_4$	$C_{40}H_{32}Br_{10}Cu_2Hg_3N_8$	$C_{40}H_{32}Br_{16}Cu_2Hg_6N_8$	$C_{20}H_{16}Cl_6CuHg_2N_4$
Molecular mass	807.22	2152.69	3233.92	989.79
Crystal system	monoclinic	monoclinic	monoclinic	triclinic
Space group	*C*2/*c*	*C*2/*c*	$P2_1/c$	$P\bar{1}$
Crystal size [mm]	0.30 × 0.18 × 0.14	0.32 × 0.24 × 0.06	1.00 × 0.10 × 0.08	0.46 × 0.40 × 0.24
a [Å]	21.7605(12)	25.5990(9)	13.904(3)	9.8091(2)
b [Å]	9.3851(5)	14.3303(4)	16.723(3)	11.5407(3)
c [Å]	15.6452(8)	15.2380(6)	14.272(3)	12.4901(2)
α [deg]	90	90	90	82.140(1)
β [deg]	132.187(2)	109.3850(10)	101.90(3)	71.099(1)
γ [deg]	90	90	90	85.734(1)
V [Å^3]	2367.5(2)	5273.0(3)	3247.3(11)	1324.45(5)
Z	4	4	4	2
Dc [gcm^{-3}]	2.2652.265	2.712	3.307	2.482
μ [cm^{-1}]	10.991	17.113	24.648	12.981
F(000)	1508	3904	2852	910
Reflections, total	3914	9306	6619	6805
Reflections, unique	2049(R_{int} = 5.63%)	4605(R_{int} = 7.15%)	6351(R_{int} = 8.41%)	4583(R_{int} = 4.74%)
No. of parameters refined	137	286	325	299
GOF on F^2	0.911	1.135	0.935	1.130
R[a] ($I > 2.00\sigma(I)$]	0.0537	0.0808	0.0681	0.0707
R_w[b] ($I > 2.00\sigma(I)$]	0.1125	0.1538	0.1472	0.1713
Residual extremes [e·Å^{-3}]	1.171, −1.188	1.615, −2.350 (1.02 and 1.33 Å from Hg2)	1.859 (1.20 Å from Hg2), −1.341	2.045, −2.964 (2.04 and 1.05 Å from Hg1)

[a] $R1 = \Sigma||F_o| - |Fc||/\Sigma|F_o|$ and $wR2 = \{\Sigma w(F_o^2 - F_c^2)^2/\Sigma w(F_o^2)^2\}^{1/2}$. [b] Data with $I > 4\sigma(I)$ for **3**.

solved in acetonitrile (10 mL) was added to the other side of the H-shaped tube. A solvent mixture of CH_2Cl_2 (5 mL) and hexane (5 mL) was then layered on the top of both ends of the H-shaped tube. The tube was sealed and the reaction allowed to proceed through diffusion of the two solutions over a period of six days. Air-stable green-blue crystals of **3** were collected from the $HgBr_2$-containing side of the H-tube in a very low yield of 5.6% (0.045 g). IR (KBr cm^{-1}): $\tilde{\nu}$ = 1601 s, 1568 m, 1477 m, 1444 vs, 1317 m, 1159 m, 1034 m, 764 vs, 729 s, 663 m. $C_{40}H_{32}Br_{16}Cu_2Hg_6N_8$ (3233.92): found C 14.92, H 2.60, N 3.34%; calcd. C 14.86, H 2.30, N 3.47%.

Synthesis of $[Cu(bipy)_2Hg_2Cl_6]_2$ (4): Compound **4** was synthesized by a similar procedure to that of **1** by reacting $CuCl_2{\cdot}2H_2O$ (0.09 g, 0.5 mmol), NH_4PF_6 (0.16 g, 1.0 mmol), 2,2′-bipyridine (0.16 g, 1.0 mmol), and $HgBr_2$ (0.27 g, 1.0 mmol) in a solvent mixture of acetone (10.0 mL) and methanol (10.0 mL) at room temperature. Yield 50.0%. IR (KBr): $\tilde{\nu}$ = 1599 cm^{-1} s, 1493 m, 1473 s, 1443 vs, 1317 m, 1250 m, 1157 m, 1028 m, 769 vs, 729 s, 650 w. $C_{20}H_{16}Cl_6CuHg_2N_4$ (989.79): found C 24.36, H 1.06, N 5.52%; calcd. C 24.25, H 1.62, N 5.65%.

Crystallography: Single crystals of **1**, **2**, and **4** were mounted on a Siemens Smart CCD diffractometer equipped with graphite-monochromated Mo-K_α radiation (λ = 0.71073 Å). Intensity data were collected by the narrow frame method at 293 K. The data sets were corrected for Lorentz polarization as well as for absorption using the SADABS program.[13] Data collection for **3** was performed on an Enraf−Nonius CAD4 diffractometer with graphite-monochromated Mo-K_α radiation (λ = 0.71073 Å) at 298 K using ω-2θ scan methods. The data set for **3** was corrected for Lorentz polarization and an empirical absorption correction was applied based on the ψ scan technique. All four structures were solved by direct methods and refined by full-matrix least-squares fitting on F^2 using SHELX-97.[13] All non-hydrogen atoms were refined with anisotropic thermal parameters. Hydrogen atoms were located in geometrically calculated positions. Crystallographic data and structural refinements for **1** to **4** are summarized in Table 2. Important bond lengths and angles are listed in Table 1.

CCDC-209447 to -209450 contain the supplementary crystallographic data for this paper. These data can be obtained free of charge at www.ccdc.cam.ac.uk/conts/retrieving.html [or from the Cambridge Crystallographic Data Centre, 12, Union Road, Cambridge CB2 1EZ, UK; Fax: (internat.) +44-1223-336-033; E-mail: deposit@ccdc.cam.ac.uk].

Acknowledgments

This work was supported by the Innovative Project, the Introduction of Overseas Elitists Program by the Chinese Academy of Sciences and the Scientific Research Foundation for the Returned Overseas Chinese Scholars, State Education Ministry.

[1] [1a] B. F. Abrahams, M. J. Hardie, B. F. Hoskin, R. Robson, E. E. Sutherland, *J. Chem. Soc., Chem. Commun.* **1994**, 1049−1050. [1b] B. F. Hoskins, R. Robson, N. V. Y. Scarlett, *Angew. Chem. Int. Ed. Engl.* **1995**, *34*, 1203−1204. [1c] M. Fujita, Y. J. Kwon, O. Sasaki, K. Yamaguchi, K. Ogura, *J. Am. Chem. Soc.* **1995**, *117*, 7287−7288. [1d] F. Robinson, M. J. Zaworotko, *J. Chem. Soc., Chem. Commun.* **1995**, 2413−2414. [1e] O. M. Yaghi, H. Li, *J. Am. Chem. Soc.* **1996**, *118*, 295−296.

[2] S. Y. Lai, T. W. Lin, Y. H. Chen, C. C. Wang, G. H. Lee, M. H. Yang, M. K. Leung, S. M. Peng, *J. Am. Chem. Soc.* **1999**, *121*, 250−251.

[3] [3a] J. R. D. Debord, Y.-J. Lu, C. J. Warren, R. C. Haushalter, J. Zubieta, *Chem. Commun.* **1997**, 1365−1366. [3b] S. S. Tandon, L. Q. Chen, L. K. Thompson, J. N. Bridson, *Inorg. Chem.* **1994**, *33*, 490−497.

 © 2004 Wiley-VCH Verlag GmbH & Co. KGaA, Weinheim

[4] [4a] P. C. Ford, E. Cariati, J. Bourassa, *Chem. Rev.* **1999**, *99*, 3625−3647. [4b] V. W.-W. Yam, K. K. W. Lo, *Chem. Soc. Rev.* **1999**, *28*, 323−334. [4c] H. O. Stumpf, L. Ouahab, Y. Pei, D. Grandjean, O. Kahn, *Science* **1993**, *261*, 447−449. [4d] H. O. Stumpf, L. Ouahab, Y. Pei, P. Bergerat, O. Kahn, *J. Am. Chem. Soc.* **1994**, *116*, 3866−3874.

[5] [5a] J. Kaiser, G. Brauer, F. A. Schroder, I. F. Tayor, S. E. Rasmussen, *J. Chem. Soc., Dalton Trans.* **1974**, 1490−1493. [5b] Y. Cui, J. Chen, G. Chen, J. Ren, W. Yu, Y. Qian, *Acta Crystallogr., Sect. C: Crystal. Struct. Commun.* **2001**, *57*, 349−351. [5c] J.-V. Folgado, P. Gomez-Romero, F. Sapina, D. Beltran-Porter, *J. Chem. Soc., Dalton Trans.* **1990**, 2325−2329.

[6] [6a] R. P. Hammond, M. CavaLuzzi, R. C. Haushalter, J. A. Zubieta, *Inorg. Chem.* **1999**, *38*, 1288−1292. [6b] S. Menon, M. V. Rajasekharan, J. P. Tuchagues, *Inorg. Chem.* **1997**, *36*, 4341−4346. [6c] R. D. Willett, G. Pon, C. Nagy, *Inorg. Chem.* **2001**, *40*, 4342−4352.

[7] [7a] T. Kajiwara, R. Murao, T. Ito, *J. Chem. Soc., Dalton Trans.* **1997**, 2537−2538. [7b] I. Ara, L. R. Falvello, J. Fornies, S. Sicilia, P. Villarroya, *Organometallics* **2000**, *19*, 3091−3099. [7c] Z. P. Zheng, C. B. Knobler, M. D. Mortimer, G. G. Kong, M. F. Hawthorne, *Inorg. Chem.* **1996**, *35*, 1235−1243. [7d] X. J. Zhang, Y. Xie, W. T. Yu, Q. R. Zhao, M. H. Jiang, Y. P. Tian, *Inorg. Chem.* **2003**, *42*, 3734−3737.

[8] J. D. Martin, A. M. Dattelbaum, T. A. Thornton, R. M. Sullivan, J. Yang, M. T. Peachey, *Chem. Mater.* **1998**, *10*, 2699−2713.

[9] D. J. Chesnut, R. C. Haushalter, J. Zubieta, *Inorg. Chim. Aata* **1999**, *292*, 41−51.

[10] D. M. Ciurtin, M. D. Smith, H. C. Zur Loye, *J. Chem. Soc., Dalton Trans.* **2003**, 1245−1250.

[11] [11a] Y.-B. Dong, M. D. Smith, H.-C. zur Loye, *Angew. Chem. Int. Ed.* **2000**, *39*, 4271−4273. [11b] A. Schunk, U. Thewalt, *Z. Anorg. Allg. Chem.* **2001**, *627*, 797−802. [11c] J.-L. Song, H.-Y. Zeng, B.-P. Yang, Z.-C. Dong, G.-C. Guo, J.-S. Huang, *Chinese J. Struct. Chem.* **2003**, *22*, 29−32.

[12] [12a] M. P. Gupta, R. D. Sahu, R. Ram, P. R. Maulik, *Z. Kristallogr.* **1983**, *163*, 155−156. [12b] Y.-Q. Zheng, J.-L. Lin, *Z. Kristallogr., NCS* **2000**, *215*, 157−158. [12c] M. Fleck, E. Tillmannse, L. Bohaty, *Z. Kristallogr., NCS* **2000**, *215*, 619−620. [12d] Y.-Q. Zheng, W.-H. Liu, J.-L. Lin, *Z. Anorg. Allg. Chem.* **2002**, *628*, 620−624.

[13] [13a] G. M. Sheldrick, *Program SADABS*; University of Göttingen, **1995**. [13b] G. M. Sheldrick, *SHELXTL, Crystallographic Software Package*, Version 5.1, Bruker-AXS, Madison, WI, **1998**.

Received August 10, 2003
Early View Article
Published Online December 12, 2003

 © 2004 Wiley-VCH Verlag GmbH & Co. KGaA, Weinheim

A Microporous Zinc Phosphonocarboxylate with a Zeolite ABW Framework via the Trialkyl Phosphonocarboxylate Route: In situ Synthesis and Characterization of $Na[Zn(O_3PC_2H_4CO_2)]\cdot H_2O$

Xian-Ming Zhang[a]

Keywords: Microporous materials / Organic-inorganic hybrid / Zeolites / Zinc

A new zinc phosphonocarboxylate $Na[Zn(O_3PC_2H_4CO_2)]\cdot H_2O$ (**1**) has been hydrothermally synthesized by base-catalyzed hydrolysis of trimethyl 3-phosphonopropionate. An X-ray crystallographic study revealed that **1** consists of parallel stacked inorganic hexagonal sheets which are connected by organic –C–C–C–O– pillars forming a three-dimensional framework with the same topology as ABW-type zeolites. The accessible channel of **1** consisting of 22 atoms is larger than those of ABW-type zeolites and the metal phosphonates $Zn(O_3PC_2H_4NH_2)$ and $Zn(O_3PC_2H_4CO_2H)\cdot 1.5H_2O$. TGA shows the trapped water molecules in **1** can be thermally removed without damage to the framework. Furthermore, dehydrated **1** is stable up to 340 °C.

(© Wiley-VCH Verlag GmbH & Co. KGaA, 69451 Weinheim, Germany, 2004)

Introduction

Zeolites are microporous aluminosilicates and have widespread applications as absorbents, for separations, as catalysts and for ion-exchange.[1–5] The desire to develop new microporous materials has led to increasing interest in the synthesis of metal phosphonate materials in recent years.[6–7] Metal phosphonates are organic-inorganic hybrid materials in which the nature of the organic phosphonic acid, H_2O_3P-R-Z, can be designed to confer specific properties to this class of solids.[8–10] The dimensionality of metal phosphonates can be directly influenced by the Z terminal functional and the R group. Thus, it is possible to manipulate the metal phosphonate framework by choosing a system with or without a Z terminal function and by changing the R group. In the absence of the Z function, metal phosphonates usually have layered or tubular structures[11–17]with an arrangement that strongly depends upon the nature and oxidation state of the metal. One of the exceptions is β-$Cu(CH_3PO_3)$ which exhibits a three-dimensional structure with a channel-type arrangement.[18] If the terminal Z functional is the -PO_3H_2 group which has three potential binding sites, the resultant metal phosphonates often show three-dimensional pillared layered structures.[19–25] If the Z functional end is the $-CO_2H$,[26–33] $-C(NH_2)CO_2H$,[34–36] or NH_2[37] group, the dimensionality of the metal phosphonates often relies on the length of the R group.

Although some progress has been made in the construction of microporous metal phosphonate materials as mentioned above, less progress has been achieved in the synthesis of microporous metal phosphonates with the topology of zeolites. One requirement for metal phosphonates with such a topology is that all metal ions and phosphonic acids must be rigidly 4-connected. This results in a structure like the (4;2) connected topology of zeolites.[38] To the best of our knowledge, only two metal phosphonates with the topology of zeolites have been reported namely $Zn(O_3PC_2H_4CO_2H)\cdot 1.5H_2O$[33] and $Zn(O_3PC_2H_4NH_2)$.[37] Therefore, the generation of metal phosphonates with the zeolite topology poses a significant synthetic challenge due to the high coordination tendency and flexibility of organic phosphonic acids. Another problem in metal phosphonate chemistry is that many metal phosphonates formed by traditional methods (direct reaction of phosphonic acid with metal source by the hydrothermal method, by heating to reflux appropriate solutions, or by making metal salts contact with molten phosphonic acid) are formed too rapidly to allow growth of crystals sufficiently large to enable single crystal structural determinations to be carried out.[19] In this paper we report the crystal structure and thermal behavior of a new microporous zinc phosphonocarboxylate $Na[Zn(O_3PC_2H_4CO_2)]\cdot H_2O$ (**1**) which has an open framework with the same topology as ABW-type zeolites.

Results and Discussion

Both the selection of trimethyl 3-phosphonopropionate as the 3-phosphonopropionic acid source and the maintaining of strongly basic conditions are very critical for the

[a] Department of Chemistry, Shanxi Normal University, Linfen, Shanxi 041004, China
Fax: (internat.) + 86-354-2051375
E-mail: zhangxm@dns.sxtu.edu.cn

 © 2004 Wiley-VCH Verlag GmbH & Co. KGaA, Weinheim DOI: 10.1002/ejic.200300563

formation of single crystals of **1**. For example, one similar reaction (keeping all other conditions unchanged except for 3-phosphonopropionic acid in place of trimethyl 3-phosphonopropionate) did not result in single crystals of **1** but instead, a colorless powder. The synthesis of metal phosphonocarboxylates directly from the relevant trialkyl phosphonocarboxylate appears to be an extremely productive adaptation of the traditional hydrothermal methods employed in the syntheses of these materials. The initial pH in the synthesis of **1** must be strongly basic in order to promote in situ hydrolysis of the trialkyl phosphonocarboxylate to the phosphonocarboxylic acid. Although some metal phosphonates have been prepared by acid-catalyzed hydrolysis of dialkyl phosphonates,[39−40] no metal phosphonate has been synthesized by base-catalyzed hydrolysis of trialkyl phosphonocarboxylate. The synthetic method in this work has two benefits 1) the use of the trialkyl phosphonocarboxylate rather than the phosphonocarboxylic acid removes the need to synthesize the acid because trialkyl phosphonocarboxylates are often far easier to purify (this can often be achieved simply by distillation) than the corresponding phosphonocarboxylic acids and 2) the slow in situ formation of phosphonocarboxylic acid by base-catalyzed hydrolysis of trimethyl 3-phosphonopropionate will ensure the growth of single crystals sufficiently large to allow a single crystal X-ray structural determination.

The IR spectrum of **1** shows one broad band centered at 3451 cm^{-1} confirming the presence of crystal lattice water. The coordination of the carboxylate is represented by strong bands at 1641 and 1562 cm^{-1} which arise from the asymmetric and symmetric stretching modes of the C−O bonds of the carboxylate group. The set of intense bands from 900 to 1100 cm^{-1} is due to the stretching vibrations of the tetrahedral CPO_3 group.

A single-crystal X-ray diffraction study revealed that **1** crystallizes in the monoclinic space group $P2_1/n$ and the asymmetric unit consists of one crystallographically independent zinc atom, one 3-phosphonopropionate unit, one sodium ion and one crystal lattice water molecule as shown in Figure 1. The Zn(1) site is tetrahedral, being coordinated by three PO_3 oxygen atoms originating from three different 3-phosphonopropionate ligands and one carboxylate oxygen atom from an additional 3-phosphonopropionate ligand. Each of the three oxygen atoms of the PO_3 group coordinates to only one zinc atom. The coordination mode of the PO_3 group in **1** is referred as a (1,1,1) connection[41] which in combination with one additional carboxylate oxygen furnishes a μ_4:η^1:η^1:η^1:η^1 coordination mode for the 3-phosphonopropionate unit which is also observed in $Zn(O_3PC_2H_4CO_2H)\cdot 1.5H_2O$.[33] The Zn(1)−O and P(1)−O bond lengths are in the ranges of 1.926(3)−1.947(3) Å and 1.519(3)−1.529(3) Å, respectively. The O−Zn(1)−O angles are in the range of 101.05(13)−114.59(12)° which shows some deviation from ideal angle of 109.5°.

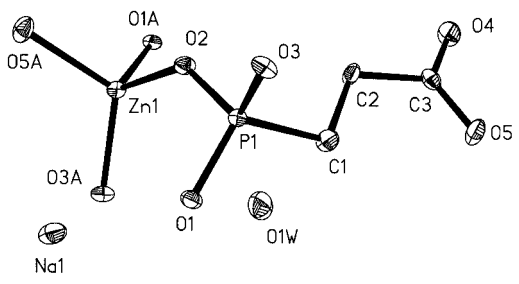

Figure 1. View of the coordination environment of the zinc atom in **1**

Within the *ac* plane, the corner-sharing connections of the CPO_3 and ZnO_4 tetrahedra result in a two-dimensional hexagonal sheet with a (6^3) topology as shown in Figure 2. The parallel stacking 2-D hexagonal sheets are held together by organic −C−C−C−O− pillars to form a 3-D pillared layered open framework (Figure 3). In each hexagonal sheet, one free corner of each tetrahedral atom can point up (U) or down (D) from the layer. The hexagonal sheets in **1** are arranged such that three adjacent tetrahedral

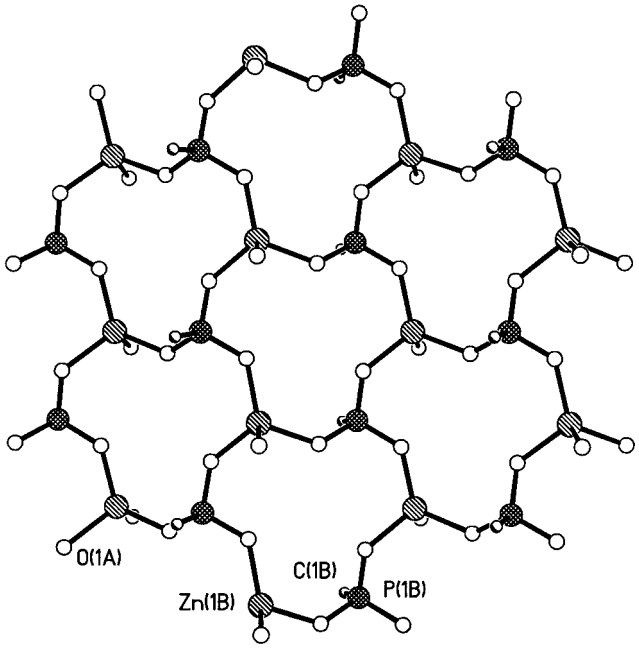

Figure 2. Perspective view of the 2-D hexagonal inorganic sheet

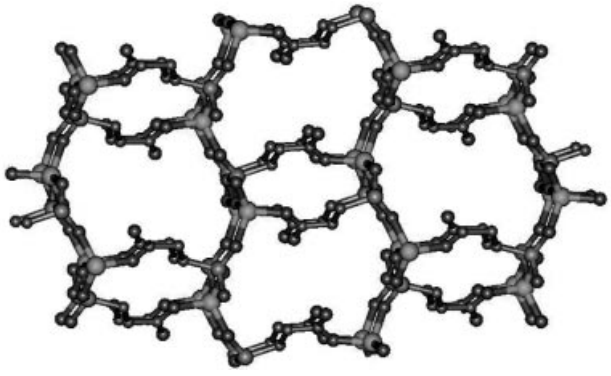

Figure 3. Perspective view of the 3-D zeolite structure of **1** showing the 22-atom channel. For clarity, the trapped sodium ions and water molecules have been omitted

 © 2004 Wiley-VCH Verlag GmbH & Co. KGaA, Weinheim

atoms all are directed up while the other adjacent three are directed down (UUUDDD),[38,42] which indicates that **1** has the topology of ABW-type zeolites. The Zn and P centers occupy 4-connected vertices of the ABW-type zeolite framework and the two-connected connectors are the O atoms and the C−C−C−O pillars. There are two types of channel along the *a* axis direction as shown in Figure 3. The larger one, sized ca. 3.4−7.2 Å, has roughly a dumbbell shape which is enclosed by 22 atoms with the sequence O−P−C−C−C−O−Zn−O−P−O−Zn−O−P−C−C−C−O−Zn−O−P−O−Zn. The guest sodium ions and water molecules are trapped in the channels in **1**. The smaller channel enclosed by 14 atoms is too small to contain guest molecules.

It is interesting to compare the structure of **1** with some ABW-type aluminosilicate and metal phosphate zeolites. Zeolite ABW structures can be viewed as being built from the stacking of hexagonal sheets. The unit cell of **1** was chosen so that the stacking direction is along the *b* axis, just as in hydrated ABW-type zeolites. The hexagonal layers in **1** and other ABW-type zeolites are similar because their repeat units in two directions within the hexagonal layers are close [8.797 Å and 5.462 Å in NH_4CoPO_4-ABW; 8.883 Å and 5.222 Å in **1**]. The repeat units along the hexagonal layer stacking direction in **1** is 15.519 Å which is significantly larger than those in hydrated ABW-type aluminosilicate and metal phosphate zeolites (10.313 Å for $LiAlSiO_4{\cdot}H_2O$ and 8.797 Å for NH_4CoPO_4-ABW).[42,43] The accessible channel along the layer stacking direction in zeolite ABW is composed of 16 atoms (8 corner-shared TO_4 tetrahedra, Scheme 1, B) but the accessible channel in **1** consists of 22 atoms. The accessible channel in **1** is also larger than those of the only other known metal phosphonates with the topology of zeolites i.e. $Zn(O_3PC_2H_4CO_2H){\cdot}1.5H_2O$[33] and $Zn(O_3PC_2H_4NH_2)$[37] in which the accessible channels also consist of 16 atoms with sizes close to those of ABW-type zeolites. Compared with ABW-type zeolites, the larger repeat unit along the hexagonal layer stacking direction and the larger channel size in **1** result from the longer connector. The connectors along the hexagonal layer stacking direction in ABW-type zeolites and **1** are O atoms and C−C−C−O groups, respectively. Compared with the only other known metal phosphonates with the topology of zeolites, $Zn(O_3PC_2H_4CO_2H){\cdot}1.5H_2O$ and $Zn(O_3PC_2H_4NH_2)$, the larger channel size in **1** mainly results from its unique architecture. Unlike $Zn(O_3PC_2H_4CO_2H){\cdot}1.5H_2O$ and $Zn(O_3PC_2H_4NH_2)$ which have inorganic (4.8^2) layers (Scheme 1, B), **1** is constructed from inorganic hexagonal (6^3) layers connected by organic pillars into a 3-D framework.

The TGA trace of **1** shows an initial mass loss of 7.5 % below 185 °C, attributable to loss of the trapped water molecules within the channels (Figure 4). The second mass loss starting at around 340 °C is thought to be due to the oxidation of the hydrocarbon part of the phosphonocarboxylate group. The total mass loss is 29.3 % upon heating to 600 °C in flowing air, which is consistent with the loss of the organic part of the material (calculated mass loss is 28.7 %). This value is also consistent with the CHN analysis. Control experiments confirm that the framework of **1** is maintained upon heating and removal of the trapped water molecules but it does not undergo exchange of the Na^+ ions by protons.

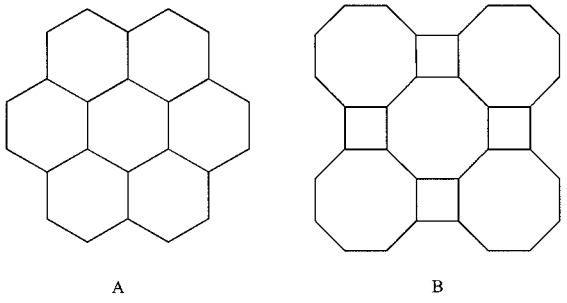

Scheme 1. Schematic view of 2-D (4.8^2) (A) and (6^3) (B) nets in zeolite ABW. For clarity, the oxygen atoms are represented by straight lines

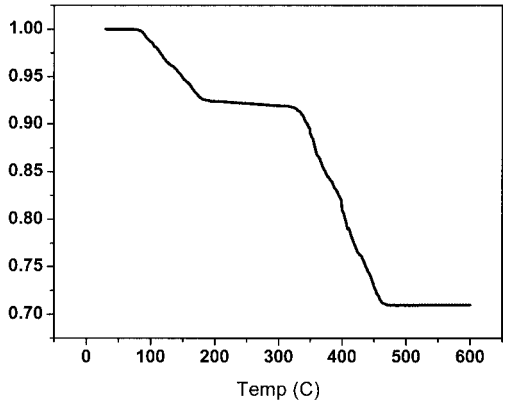

Figure 4. The TGA curve of **1**

In conclusion, we have synthesized a new microporous zinc phosphonocarboxylate with a zeolite ABW-type topology by base-catalyzed hydrolysis of trimethyl 3-phosphonopropionate. The use of the trialkyl phosphonocarboxylate as the phosphonocarboxylic acid source simplifies the traditional methods for metal phosphonocarboxylates and the in situ formation of phosphonocarboxylic acid guarantees the growth of single crystals of sufficient size for X-ray diffraction. The accessible channel in ABW-type zeolites consists of 16 atoms but partial replacement of O atoms with C−C−C−O groups as connectors in **1** generates same topological structure with a larger accessible channel consisting of 22 atoms.

Experimental Section

General Remarks The synthesis was carried out in a 15 mL volume Teflon-lined reactor under autogenous pressure with a filling capacity of 50 %. The CHN microanalysis was performed on a Perkin-Elmer 240 elemental analyzer. The FT-IR spectra were recorded in KBr pellets in the range of 4000−400 cm^{-1} on a Nicolet 5DX spectrometer. Thermal gravimetric analyses (TGA) were per-

 © 2004 Wiley-VCH Verlag GmbH & Co. KGaA, Weinheim

formed under a static air atmosphere from 30−600 °C using a Perkin-Elmer 7 thermogravimetric analyzer with a heating rate of 10 °C·min^{-1}.

Synthesis of Na[Zn($O_3PC_2H_4CO_2$)]·H_2O (1): A mixture of $Zn(MeCO_2)\cdot 2H_2O$ (0.220 g, 1 mmol), trimethyl 3-phosphonopropionate (0.228 g, 1 mmol), NaOH (0.18 g, 4.5 mmol), and H_2O (7 mL) in the molar ratio of 1:1:4.5:400 was stirred in air for 20 min (pH > 14) and transferred into a 15 mL Teflon-lined stainless steel reactor which was heated to 160 °C for 120 h. After cooling to room temperature, colorless needles **1** (65 %) in a single phase were recovered. The pH decreased to ca. 12 during the reaction. Elemental analysis for **1**: $C_3H_6O_6ZnNa$: calcd. C 14.00, H 2.35; found C 13.94, H 2.39. IR (KBr): $\tilde{\nu}$ = 3603 w cm^{-1}, 3451 br., 3088 w, 2968 w, 2927 w, 1641 s, 1608 m, 1562 s, 1454 m, 1418 m, 1257 m, 1124 m, 1094 s, 1011 s, 958 s, 832 m, 764 w, 721 w.

X-ray Crystallographic Study: Data collection was performed at 293 K on a Bruker Apex diffractometer (Mo-K_α, λ = 0.71073 Å). Lorentz-polarization and absorption corrections were applied. The structure was solved by direct methods and refined with the full-matrix least-squares technique (SHELX-97).[44] Analytical expressions of neutral-atom scattering factors were employed and anomalous dispersion corrections were incorporated. In all cases, all non-hydrogen atoms were refined anisotropically. Hydrogen atoms of organic ligands were geometrically placed. Hydrogen atoms of water were located from a difference Fourier map and refined with isotropic temperature factors. The crystallographic data for **1** are listed in Table 1 and selected bond lengths and bond angles are given in Table 2.

CCDC-216687 contains the supplementary crystallographic data for this paper. These data can be obtained free of charge at www.ccdc.cam.ac.uk/conts/retrieving.html [or from the Cambridge Crystallographic Data Center, 12 Union Road, Cambridge CB2 1EZ, UK; Fax: (internat.) + 44-1223-336-033; E-mail: deposit@ccdc.cam.ac.uk].

Table 1. Crystal and structure refinement for **1**

Empirical formula	$C_3H_6NaO_6PZn$
Molecular mass	257.41
Temperature [K]	293(2)
Wavelength [Å]	0.71073
Crystal system	Monoclinic
Space group	$P2_1/n$
a [Å]	5.222(1)
b [Å]	15.519(3)
c [Å]	8.883(2)
β [°]	90.63(3)
V [Å^3]	719.8(3)
Z	4
Density (calculated) [Mg·m^{-3}]	2.375
Absorption coefficient [mm^{-1}]	3.678
F(000)	512
Crystal size [mm]	0.40 × 0.03 × 0.03
Theta range for data collection [°]	2.62−27.69
Index ranges	$-6 \le h \le 6$; $-13 \le k \le 20$; $-11 \le l \le 11$
Reflections collected	3341
Independent reflections	1520 R_{int} = 0.0325
Max. and min. transmission	0.8977 and 0.3209
Refinement method	Full-matrix least-squares on F^2
Data/restrains/parameters	1520/0/110
Goodness-of-fit on F^2	1.030
Final R indices [$I > 2\sigma(I)$]	0.0395, 0.0811
R indices (all data)	0.0530, 0.0850
Extinction coefficient	0.0006(9)
Largest diff. peak and hole [e·A^{-3}]	0.600 and −0.491

Acknowledgments

The author thanks Mrs. Shu-Ping Huang for collection of the X-ray data.

Table 2. Bond lengths [Å] and angles [°] in **1**

Bond	Bond length	Bond	Bond length
Zn(1)−O(3)[a]	1.926(3)	P(1)−O(2)	1.519(3)
Zn(1)−O(2)	1.938(3)	P(1)−O(1)	1.525(3)
Zn(1)−O(1)[b]	1.944(3)	P(1)−O(3)	1.529(3)
Zn(1)−O(5)[c]	1.947(3)	P(1)−C(1)	1.795(4)
O(1)−Na(1)	2.421(3)	Na(1)−O(3)[a]	2.518(3)
O(2)−Na(1)[d]	2.345(3)	Na(1)−O(1W)[e]	2.343(4)
Na(1)−O(4)[c]	2.290(3)		
Bond	**Bond angle**	**Bond**	**Bond angle**
O(3)[a]−Zn(1)−O(2)	114.59(12)	O(1)−P(1)−O(3)	109.91(16)
O(3)[a]−Zn(1)−O(1)[b]	110.70(12)	O(2)−P(1)−C(1)	108.59(19)
O(2)−Zn(1)−O(1)[b]	109.80(12)	O(1)−P(1)−C(1)	110.21(18)
O(3)[a]−Zn(1)−O(5)[c]	117.18(13)	O(3)−P(1)−C(1)	107.26(19)
O(2)−Zn(1)−O(5)[c]	101.05(13)	P(1)−O(1)−Zn(1)[e]	125.85(16)
O(1)[b]−Zn(1)−O(5)[c]	102.49(12)	P(1)−O(2)−Zn(1)	133.80(17)
O(2)−P(1)−O(1)	110.60(16)	P(1)−O(3)−Zn(1)[f]	129.39(18)
O(2)−P(1)−O(3)	110.21(16)		

[a] Symmetry codes: $x - 1/2, -y + 3, z + 1/2$; [b] $x + 1/2, -y + 3/2, z + 1/2$; [c] $-x + 1/2, y - 1/2, -z + 1/2$; [d] $x + 1, y, z$; [e] $x - 1/2, -y + 3/2, z - 1/2$; [f] $x + 1/2, -y + 3/2, z - 1/2$.

 © 2004 Wiley-VCH Verlag GmbH & Co. KGaA, Weinheim

[1] D. W. Breck, *Zeolite Molecular Sieves*, Kreiger, Malabar, **1974**.
[2] R. M. Barrer, *Hydrothermal Chemistry of Zeolites*, Academic Press: London, **1982**.
[3] R. Szostak, *Molecular Sieves - Principles of Synthesis and Identification*, 2nd ed., Blackie: London, **1998**.
[4] A. K. Cheetham, G. Ferey, T. Loiseau, *Angew. Chem. Int. Ed.* **1999**, *38*, 3268.
[5] S. Cundy, P. A. Cox, *Chem. Rev.* **2003**, *103*, 663.
[6] J. Zhu, X. Bu, P. Feng, G. D. Stucky, *J. Am. Chem. Soc.* **2000**, *122*, 11563.
[7] A. Clearfield, *Chem. Mater.* **1998**, *10*, 2801.
[8] G. A. Neff, M. R. Helfrich, M. C. Clifton, C. J. Page, *Chem. Mater.* **2000**, *12*, 2363.
[9] V. V. Guliants, J. B. Benziger, S. Sundaresan, *Chem. Mater.* **1995**, *7*, 1493.
[10] J. C. Amicangelo, G. L. Rosenthal, W. R. Leenstra, *Chem. Mater.* **2003**, *15*, 390.
[11] B. Bujoli, O. Pena, P. Palvadeau, J. Le Bideau, C. Payen, J. Rouxelt, *Chem. Mater.* **1993**, *5*, 583.
[12] M. I. Khan, Y.-S. Lee, C. J. O'Connor, R. C. Haushalter, J. Zubieta, *Chem. Mater.* **1994**, *6*, 721.
[13] M. B. Doran, A. J. Norquist, D. O'Hare, *Chem. Mater.* **2003**, *15*, 1449.
[14] A. Altomare, C. Bellitto, S. A. Ibrahim, M. R. Mahmoud, R. Rizzi, *J. Chem. Soc., Dalton Trans.* **2000**, 3913.
[15] Y. Zhang, K. J. Scott, A. Clearfield, *Chem. Mater.* **1993**, *5*, 495.
[16] M. I. Khan, Y.-S. Lee, C. J. O'Connor, R. C. Haushalter, J. Zubieta, *J. Am. Chem. Soc.* **1994**, *116*, 4525.
[17] D. M. Poojar, D. Grohol, A. Clearfield, *Angew. Chem. Int. Ed. Engl.* **1995**, *34*, 1508.
[18] J. L. Bideau, C. Payen, P. Palvadeau, B. Bujoli, *Inorg. Chem.* **1994**, *33*, 4885.
[19] B. Zhang, D. M. Poojary, A. Clearfield, *Inorg. Chem.* **1998**, *37*, 1844.
[20] D. M. Poojary, B. Zhang, P. Bellinghausen, A. Clearfield, *Inorg. Chem.* **1996**, *35*, 5254.
[21] D. M. Poojary, B. Zhang, P. Bellinghausen, A. Clearfield, *Inorg. Chem.* **1996**, *35*, 4942.
[22] D. M. Poojary, B. Zhang, A. Clearfield, *Chem. Mater.* **1999**, *11*, 421.
[23] C. Serre, G. Ferey, *Inorg. Chem.* **2001**, *40*, 5350.
[24] C. Serre, G. Ferey, *Inorg. Chem.* **1999**, *38*, 5370.
[25] L.-M. Zheng, C.-Y. Duan, X.-R. Ye, L.-Y. Zhang, C. Wang, X.-Q. Xin, *J. Chem. Soc., Dalton Trans.* **1998**, 905.
[26] N. Stock, S. A. Frey, G. D. Stucky, A. K. Cheetham, *J. Chem. Soc., Dalton Trans.* **2000**, 4292.
[27] A. Distler, S. C. Sevov, *Chem. Commun.* **1998**, 959.
[28] T. Kijima, S. Watanabe, M. Machida, *Inorg. Chem.* **1994**, *33*, 2586.
[29] P. Rabu, P. Janvier, B. Bujoli, *J. Mater. Chem.* **1999**, *9*, 1323.
[30] F. Serpaggi, G. Ferey, *Inorg. Chem.* **1999**, *38*, 4741.
[31] M. Riou-Cavellec, M. Sanselme, N. Guillou, G. Ferey, *Inorg. Chem.* **2001**, *40*, 723.
[32] S. Ayyappan, G. D. Delgado, A. K. Cheetham, G. Férey, C. N. R. Rao, *J. Chem. Soc., Dalton Trans.* **1999**, 2905.
[33] S. Drumel, P. Janvier, P. Barbom, M. Bujoli-Doeuff, B. Bujoli, *Inorg. Chem.* **1995**, *34*, 148.
[34] J.-G. Mao, A. Clearfield, *Inorg. Chem.* **2002**, *41*, 2319.
[35] H. Jankovics, M. Daskalakis, C. P. Raptopoulou, A. Terzis, V. Tangoulis, J. Giapintzakis, T. Kiss, A. Salifoglou, *Inorg. Chem.* **2002**, *41*, 3366.
[36] S. J. Hartman, E. Todorov, C. Cruz, S. C. Sevov, *Chem. Commun.* **2000**, 1213.
[37] S. Drumel, P. Janvier, D. Deniaud, B. Bujoli, *J. Chem. Soc., Chem. Commun.* **1995**, 1051.
[38] J. V. Smith, *Chem. Rev.* **1988**, *88*, 149.
[39] G. B. Hix, B. M. Kariuki, S. Kitchin, M. Tremayne, *Inorg. Chem.* **2001**, *40*, 1477.
[40] P.-A. Jaffres, V. Caignaert, D. Villemin, *Chem. Commun.* **1999**, 1997.
[41] D. Massiot, S. Drumel, P. Janvier, M. Bujoli-Doeuff, B. Bujoli, *Chem. Mater.* **1997**, *9*, 6.
[42] P. Feng, X. Bu, S. H. Tolbert, G. D. Stucky, *J. Am. Chem. Soc.* **1997**, *119*, 2497.
[43] E. K. Anderson, G. Ploug-Sorensen, *Z. Kristallogr.* **1986**, *176*, 67.
[44] G. M. Sheldrick, *SHELX-97, Program for X-ray Crystal Structure Solution and Refinement*, Göttingen University, Germany, **1997**.

Received August 12, 2003
Early View Article
Published Online November 28, 2003

 © 2004 Wiley-VCH Verlag GmbH & Co. KGaA, Weinheim

Apparent Allyl Rotation in New Allylpalladium(II) Complexes with Pyrazolyl *N*-Donor Ligands

Ana Guerrero,[a] Félix A. Jalón,[a] Blanca R. Manzano,*[a] Ana Rodríguez,[a] Rosa María Claramunt,*[b] Pilar Cornago,[b] Viktor Milata,[c] and José Elguero[d]

Keywords: Fluxionality / N ligands / Allyl ligands / Palladium

The ligands 2,4,6-tris(pyrazol-1-yl)-1,3,5-triazine (TPzT), 2,4,6-tris(3,5-dimethyl-pyrazol-1-yl)-1,3,5-triazine (Me_2-TPzT), and 2,4,6-tris(3,4,5-trimethylpyrazol-1-yl)-1,3,5-triazine (Me_3-TPzT) have been synthesised and their reaction with $[Pd(\eta^3\text{-}C_4H_7)(THF)_2]X$ was explored. The reaction in a 1:3 molar ratio (ligand/solvate) leads to the new derivatives $[\{Pd(\eta^3\text{-}C_4H_7)\}_2(BPz'TO)]X$ (Pz′ = pyrazole, X = BF_4, **2a**; Pz′ = 3,5-dimethylpyrazole, X = PF_6, **2c**; Pz′ = 3,4,5-trimethylpyrazole, X = PF_6, **2d**) in which the N-donor ligand has been partially hydrolysed. The complexes exist in the form of two isomers, a *meso* form and a *d,l* pair. An apparent allyl rotation process leads to a *syn-syn/anti-anti* interconversion and also to an interchange between the two isomers. The values of $\Delta G_c^{\ddagger}$ at the coalescence temperature have been calculated. The results, which have also been compared with those previously obtained for the complex with the 4-methylpyrazole ligand, indicate that the activation barrier for the process is not affected by the change in the pyrazole group. Appreciable effects were not observed on changing the concentration or on the addition of water to the acetone solutions of **2c**. However, the influence of the solvent (acetone versus chloroform) is worth noting. A negative activation entropy has been found and a mechanistic proposal for the process is included. The molecular structure of **2c** has been determined by X-ray diffraction. The *meso* isomer, in which the two C–Me axes of the allylic groups are oriented in the same direction, is found in the solid state.

(© Wiley-VCH Verlag GmbH & Co. KGaA, 69451 Weinheim, Germany, 2004)

Introduction

The chemistry of (η^3-allyl)palladium complexes has been widely studied due to them acting as precursors or intermediates in different catalytic processes.[1] The fluxional behaviour of these systems, either directly related to the allyl group or to the ancillary ligands, has also attracted much attention.[2] Apart from the fundamental interest of these studies, the dynamics of the allylpalladium derivatives have important implications in a variety of catalytic processes, especially those involving nucleophilic attack on (η^3-allyl)palladium intermediates in enantioselective synthesis.[3] One process that the allyl group frequently undergoes is a mutual exchange of *syn* and *anti* groups, which can lead to isomer interconversions.[4−12] This interchange is normally believed to occur through an η^3-η^1-η^3 pathway that in some cases is selective[13−15] due to steric or electronic factors (a high *trans* influence of a group favours the opening of the allylic carbon atom situated in the *trans* position). Theoretical calculations concerning the mechanism of the η^3-η^1-η^3 isomerisation in (η^3-allyl)palladium complexes have led to the conclusion that the process involves tetracoordinate (η^1-allyl)palladium intermediates with coordination of a solvent molecule or an ancillary ligand.[16] A second dynamic process that is frequently observed in complexes with N-donor ligands is the apparent rotation of the allyl group.[17−27] In certain examples both of the aforementioned processes have been observed.[28−34] Depending on the molecular symmetry, the apparent rotation is observed as a *syn-syn*/*anti-anti* exchange and/or an isomerisation process. Different mechanisms have been proposed for the apparent allyl rotation and these may be classified into two groups: i) associative mechanisms[19,27,28,31,32] that involve pentacoordinate intermediates with coordination of the solvent, the anion or other molecules, ii) dissociative mechanisms[17,18,20−22,24,25,30,33] that involve formation of

[a] Departamento de Química Inorgánica, Orgánica y Bioquímica, Facultad de Químicas, Universidad de Castilla-La Mancha, Avda Camilo José Cela 10, 13071 Ciudad Real, Spain
Fax: (internat.) + 34-926-295318
E-mail: Blanca.Manzano@uclm.es
[b] Departamento de Química Orgánica y Biología, Facultad de Ciencias, UNED, Senda del Rey 9, 28040 Madrid, Spain
Fax: (internat.) + 34-91-3986697
E-mail: rclaramunt@ccia.uned.es
[c] Department of Organic Chemistry, Faculty of Chemical Technology, Slovak Technical University, Radlinskeho 9, 812 37 Bratislava, Slovak Republic
[d] Instituto de Química Médica, Centro de Química Orgánica "Manuel Lora-Tamayo", CSIC, Juan de la Cierva 3, 28006 Madrid, Spain

T-shaped three-coordinate intermediates after partial dissociation of a bidentate ligand, usually through Pd−N bond rupture. In some cases it has been reported that a ligand of higher basicity makes the apparent rotation more difficult,[20] while increased steric hindrance of the N-donor ligand facilitates the process.[19,28] In recent years we have been interested in the synthesis, structural characterisation and dynamic behaviour of (allyl)Pd^{II} complexes with N-donor ligands containing pyrazolyl substituents.[22−27,35] In most cases the process of apparent allyl rotation was observed and led to isomer interconversion. When the (allyl)-palladium fragment was treated with ligands of type **I** [2,4,6-tris(4-R-pyrazol-1-yl)-1,3,5-triazines; see Scheme 1; $R^3 = R^5 = H$, R^4 = Me, Br] it was found that during the course of the reaction one of the pyrazolyl residues was lost and, ultimately, the complexes formed were derived from the 4,6-bis(4-R-pyrazol-1-yl)-1,3,5-triazin-2-olate anion **II**[24] (see Scheme 1). The $\Delta G_c^{\ddagger}$ data led us to conclude that the main driving force of the hydrolysis process was the formation of a better coordinating ligand. In the work described here, we decided to explore the behaviour of similar ligands containing differently substituted pyrazolyl groups. In this way it was possible to analyse the influence (steric or electronic) of the pyrazolyl ring on the energy barrier of the apparent rotation process. We also decided to study the effect of concentration, the addition of water and a change in the solvent. Another aim was to determine whether the hydrolysis process was affected by differing basicity and consequently, the different leaving group character of the pyrazole moiety.

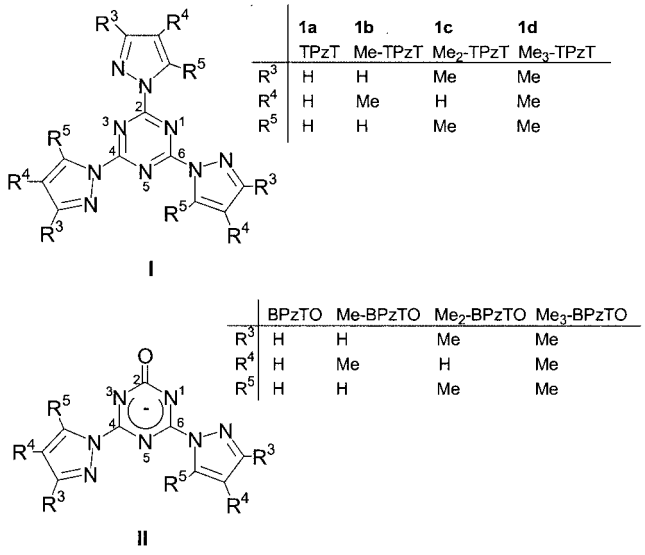

Scheme 1

The ligands used in this work were **1a**, **1c**, and **1d** (see Scheme 1). The ligand **1b**[24] is also included for the sake of comparison. The introduction of methyl substituents in positions 3 and 5 of the pyrazole rings increases the basicity and the steric hindrance, while the same substitution in position 4 would only be expected to cause an electronic change.

Results and Discussion

Synthesis of Ligands 1a−1d

Ligand **1a**,[36,37] ligand **1b** and its reaction with (allyl)palladium fragments,[24] and ligand **1c** and its X-ray molecular structure[38] have all been reported previously. The synthesis of **1d** is reported for the first time in this paper.

Synthesis of the Allyl Complexes

Reaction of the $[Pd(\eta^3\text{-}C_4H_7)(THF)_2]X$, X = BF_4^-, PF_6^- {obtained by mixing $[Pd(\eta^3\text{-}C_4H_7)(\mu\text{-}Cl)]_2$ and $AgBF_4$ or $AgPF_6$ in THF} with the ligands **1a**, **1c**, or **1d** gave complexes **2a**, **2c**, and **2d**, respectively, containing the hydrolysed ligand (see Scheme 2 and Exp. Sect.). Compounds **2b**·BF_4, **2b**·PF_6 and complexes with other anions have been described previously.[24]

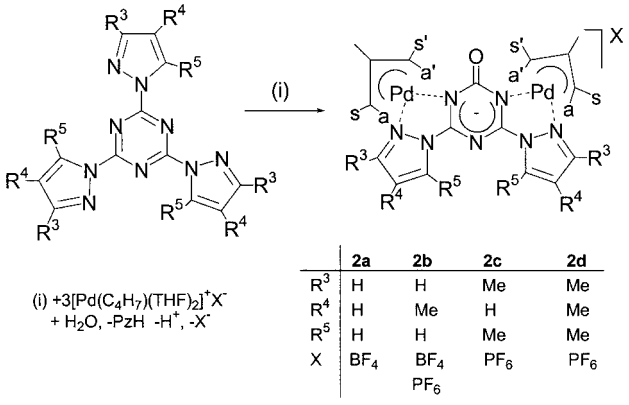

Scheme 2

We tried unsuccessfully to isolate the intermediate $[Pd(\eta^3\text{-}C_4H_7)_2\cdot\mathbf{1}]X$ but, although the work was carried out under anhydrous N_2 and with freshly distilled (under N_2) solvents, hydrolysis to **2** always took place. Indeed, the hydrolysed products **2** were isolated even when the reaction was carried out at low temperature. The water necessary for the hydrolysis must arise from the silver salts and also perhaps from traces in the solvent. It was attempted to completely remove all water from $AgPF_6$ but this unfortunately proved impossible, even after drying the salt over P_2O_5 with a vacuum lower than 10^{-2} Torr for 5 d. Similar problems have been reported previously.[39] Given that the more basic the pyrazole the worse it is as a leaving group, ligand **1d** was selected (pK_a values: pyrazole 2.48, 4-methylpyrazole 3.04, 3,5-dimethylpyrazole 4.06, 3,4,5-trimethylpyrazole 4.56)[40] but, in this case, the same result was obtained. This observation is in accordance with our previous results[24] where it was found that the methoxy group, which is a poorer leaving group than pyrazole, also underwent the hydrolysis process. This result also supports our previously reported conclusion that the hydrolysis of the R-TPzT ligands, in the presence of the allylpalladium fragment, may have its origin in the bond reinforcement of the triazin-2-olate anion with the palladium centres. Complexes **2** are soluble in acetone, THF and dichloromethane but insoluble

 © 2004 Wiley-VCH Verlag GmbH & Co. KGaA, Weinheim

in diethyl ether, pentane and hexane. This solubility behaviour was used to obtain crystals of **2c**.

Structural Characterisation of Complexes 2a, 2c, and 2d

The IR spectra of the complexes contain a ν(C=O) band at 1696 (**2a**), [1685 (**2b**)],[24] 1691 (**2c**), or 1687 cm^{-1} (**2d**). The most characteristic peak in the FAB^+/MS corresponds to $[M - X]^+$ and this appears at 552 (**2a**), [580 (**2b**)],[24] 608 (**2c**), or 636 Da (**2d**). These peaks are due to the loss of the counterion from the molecular mass of the ionic complex. Secondary peaks that correspond to the loss of one or two allyl groups are also observed.

The data from the ^1H NMR spectra are compiled in Table 1. The signals of the complexes were assigned by comparison with the data for the corresponding ligands and considering the information obtained from NOE studies. For example, ligand **1d** and complex **2d** exhibit an NOE between Me^4 and Me^3/Me^5. The resonance for Me^3 also showed NOEs with H_{anti} and H_{syn} signals. A shift towards higher energies is observed in the resonances of the complexes with respect to the non-coordinated N-donor ligands.

At room temperature, **2a** showed only one broad signal for the H_{syn} or H_{anti} protons while the corresponding spectra for **2c** and **2d** contained two signals for each kind of protons. In all cases, signals corresponding to one type of pyrazole group were observed at this temperature. When the ^1H NMR spectra of the complexes were registered at low temperature, splitting of the signals was detected. Evidence was seen for two types of pyrazole groups in different ratios along with four H_{anti} and four H_{syn} (two types of intensities) protons. If we consider these data and the information deduced for the similar complex **2b**,[24] the situation observed must be due to the presence of two isomers − a *d*,*l* pair and a *meso* form − that differ in the relative orientation of the two allyl groups (see Scheme 3). Each isomer contains two equivalent pyrazole rings and two asymmetric and equivalent allylic groups. In the case of complex **2d**, where the allylic signals at low temperature are more differentiated than in the other complexes, we performed NOE studies at 213 K. It can be seen from the data in Table 1 that it was possible to identify, from the NOEs observed with the Me^3 signal, the resonances due to the allylic group *cis* to the pyrazole ring in each isomer. The H_{syn} and H_{anti} atoms of the same allylic carbon atom also showed a mutual NOE.

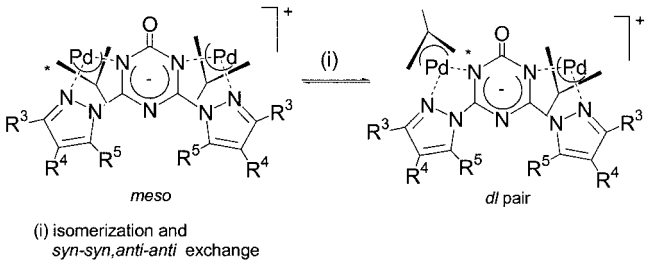

Scheme 3

The NOE studies at room temperature (and also in some cases at low temperature) showed a transfer of magnetisation within an allyl group between the two H_{syn} atoms on the one hand, and the two H_{anti} atoms on the other. This information, together with the observation of two isomers at low temperature that are seen as a single form at room temperature, is a clear indication of fluxional behaviour in the complexes. This possibility was further investigated by means of variable-temperature ^1H NMR spectroscopy studies and the results will be discussed in a separate section.

The $^{13}C\{^1H\}$ NMR spectroscopic data of the ligands and complexes at room temperature are reported in Table 2. The asymmetry of the 2-methylallyl group is apparent from the signals of the terminal carbon atoms at δ ≈ 60 ppm, one

Table 1. ^1H NMR spectroscopic data for ligands and complexes in [D_6]acetone (*M* = major isomer; *m* = minor isomer)

Compound	Temp. [K]	Pyrazole H^5/Me^5	Pyrazole H^3/Me^3	H^4/Me^4	Allyl H_{syn}	Allyl H_{anti}	Me
TpzT (**1a**)	293	8.80 (dd, J_{45} = 2.8 J_{35} = 0.7)	7.99 (dd, J_{34} = 1.5)	6.73 (dd)			
Me_2-TpzT (**1c**)	293	2.84 (s)	2.26 (s)	6.22 (s)			
Me_3-TpzT (**1d**)	293	2.69 (s)	2.28 (s)	1.96 (s)			
2a	293	9.0 (m)	8.4 (m)	6.99 (m)	4.5 (br. s)	3.33 (br. s)	2.20 (s)
2a *M* (56 %)	203	9.07 (dd, J_{45} = 2.9 J_{35} = 0.7)	8.45 (dd, J_{34} = 1.5)	6.99 (dd)	4.51 (s), 4.49 (s)	3.34 (s), 3.32 (s)	2.14 (s)
2a *m* (44 %)	203	9.12 (dd, J_{45} = 2.9 J_{35} = 0.5)	8.49 (dd, J_{34} = 1.5)	7.03 (dd)	4.57 (s), 4.49 (s)	3.35 (s), 3.29 (s)	2.18 (s)
2c	293	2.87 (s)	2.46 (s)	6.63 (s)	4.79 (br. s), 4.39 (br. s)	3.42 (s), 3.22 (s)	2.17 (s)
2c *M* (64 %)	213	2.87 (s)	2.45 (s)	6.83 (s)	4.67 (s), 4.41 (s)	3.40 (s), 3.17 (s)	2.19 (s)
2c *m* (34 %)	213	2.85 (s)	2.45 (s)	6.79 (s)	4.72 (s), 4.42 (s)	3.40 (s), 3.17 (s)	2.09 (s)
2d	293	2.81 (s)	2.44 (s)	2.11 (s)	4.79 (br. s), 4.39 (br. s)	3.41 (br. s), 3.21 (br. s)	2.17 (s)
2d *M* (56 %)	213	2.77 (s)	2.42 (s)	[a]	4.67 (br. s), 4.43[b] (br. s)	3.35 (s), 3.11[b] (s)	[a]
2d *m* (44 %)	213	2.74 (s)	2.42 (s)	[a]	4.72[b] (br. s), 4.48 (br. s)	3.37[b] (s), 3.17 (s)	2.16 (s)

[a] Overlapped with the solvent signal. [b] Resonances of the protons *cis* to the pyrazole ring.

 © 2004 Wiley-VCH Verlag GmbH & Co. KGaA, Weinheim

Table 2. $^{13}C\{^1H\}$ NMR chemical shifts (ppm) for ligand and complexes at 293 K (unless specified, the signals are singlets; n.o.: not observed)

Compd.	Solvent	Triazine	Pyrazolyl substituents			Allyl		
			C^3 [Me^3]	C^4 [Me^4]	C^5 [Me^5]	−C=	CH_2	CH_3
TPzT (**1a**)	[D_6]acetone	165.0	146.6	111.3	131.9			
Me_2-TPzT (**1c**)	$CDCl_3$	164.3	153.3 [14.0]	111.9	144.4 [15.5]			
Me_3-TPzT (**1d**)	$CDCl_3$	164.1	153.5 [12.5]	118.0 [8.1]	139.6 [13.7]			
2a	[D_6]acetone	162.2	149.5	112.9	133.6	133.1	61.5 (br. s), 63.5 (br. s)	23.7
2c	[D_6]acetone	165.2	157.3 [15.5]	112.9	148.0 [16.2]	131.0	59.0 65.0	23.3
2d	$CDCl_3$	n.o.	155.8 [12.4]	119.4 [8.5]	142.9 [14.3]	130.2	57.7 65.1	23.5

close to the C=O and the other to the pyrazole. A number of the allyl signals are broad, indicating the existence of the afore-mentioned fluxional process. Complexation produces small effects on the signals of the ligands. HMQC experiments, relating ^1H and ^{13}C signals, proved particularly useful in assigning the methyl groups of the pyrazole rings.

X-ray Structure of 2c

The molecular structure of **2c** was determined by X-ray diffraction. The molecular structure consists of a dinuclear Pd monocation and a PF_6 counteranion. The ORTEP plot of the cation is shown in Figure 1, the crystallographic data are given in Table 6 and a selected list of bond lengths and angles is reported in Table 3. The N-donor ligand adopts a practically planar conformation with three coplanar heterocycles. The Pd centres are also practically coplanar with the azolylazine molecule. The bite angle of this ligand is ca. 76° in both coordination positions. The Pd−N bond lengths are also almost identical [2.076(6) and 2.102(5) Å], with the distance being slightly longer for the Pd−N(triazinolate) than for the Pd−N(pyrazole) bonds. The Pd−C bond lengths with the allyl groups are in the range expected for these types of complexes,[24] with the longer distance measured for the Pd−C(central) than for the Pd−C(terminal) bonds. The dihedral angle between the allylic plane and the palladium coordination plane is ca. 114°, with the C(central)-to-CH_3 vector pointing away from the metal centre. If we define a plane containing the Pd centre and the corresponding N-donor atoms (coordination plane), the terminal allylic carbon atoms are practically in the plane and the central carbon atom is clearly above it. The C(7)−O(1) bond length is 1.207(8) Å, which is indicative of a certain degree of double-bond character. The triazinolate ring C−N distances at C(7) are typical single-bond values (ca. 1.39 Å), and the remaining four C−N distances are narrowly spread in the double-bond range [between 1.319(8) and 1.334(9) Å]. If one also considers the planarity of the heterocycle, this situation points to a pentadienide delocalization bonding of the five atoms N(1)−C(5)−N(2)−C(6)−N(3).

Table 3. Bond lengths [Å] and angles [°] for **2c**

Pd(1)−N(4)	2.076(6)	N(4)−Pd(1)−N(1)	75.8(2)
Pd(1)−C(1)	2.094(7)	C(1)−Pd(1)−C(3)	68.0(3)
Pd(1)−N(1)	2.102(5)	N(6)−Pd(2)−N(3)	76.3(2)
Pd(1)−C(3)	2.117(8)	C(15)−Pd(2)−C(13)	68.3(4)
Pd(1)−C(2)	2.147(8)		
Pd(2)−N(6)	2.079(7)		
Pd(2)−N(3)	2.099(6)		
Pd(2)−C(15)	2.109(9)		
Pd(2)−C(13)	2.118(8)		
Pd(2)−C(14)	2.133(8)		
O(1)−C(7)	1.207(8)		
N(1)−C(5)	1.319(8)		
N(1)−C(7)	1.396(8)		
N(2)−C(6)	1.332(9)		
N(2)−C(5)	1.334(9)		
N(3)−C(6)	1.330(9)		
N(3)−C(7)	1.393(9)		

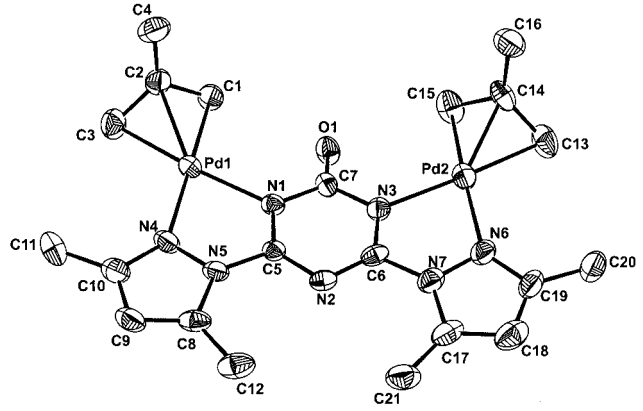

Figure 1. ORTEP view with atomic numbering of the cation of complex **2c**

Fluxional Behaviour of the Allyl Complexes

Variable-temperature ^1H NMR studies in [D_6]acetone were performed for **2a**, **2c**, and **2d** in the temperature range 183−323 K. As stated previously, low-temperature ^1H NMR spectra contain resonances corresponding to the presence of two isomers in a different ratio (a *d*,*l* pair, a *meso* form; see Scheme 3 and Table 1). Several coalescences were observed on increasing the temperature: the two signals due to each pyrazole proton and also the allylic methyl groups simplified to give one resonance and the four lines for the H_{syn} protons coalesced consecutively until finally only one resonance was observed (the same was seen for the H_{anti} signals). Consequently, a process was observed that involved an apparent allyl rotation that simultaneously

 © 2004 Wiley-VCH Verlag GmbH & Co. KGaA, Weinheim

Table 4. Coalescence temperatures and free energies of activation for complexes **2a**−**d**

Compd.[a]	T_c [K]	$\Delta G_c^{\ddagger}$ [kJ/mol^{-1}]	Interchanging groups	Compd.	T_c [K]	$\Delta G_c^{\ddagger}$ [kJ/mol^{-1}]	Interchanging groups
2a	243	51.8	H^3	**2c**	253	56.0	H_{anti} (3+4)
	249	53.2	H^5		267	57.3	H_{syn} (1+2)
	251	53.5	H^4		268	58.0	H^4
	255	54.1	Me-allyl		285	60.3	Me-allyl
	258	55.1	H_{syn} (1+2)	**2d**	205	46.0	Me^3
	286	60.3	H_{anti} (1+2) + (3+4)		227	49.4	H_{anti} (1+2)
	300	60.9	H_{syn} (1+2) + (3+4)		235	49.2	H_{anti} (3+4)
2b[24]	243	53.6	H^3		243	53.9	Me-allyl
	253	54.4	H^5		259	55.4	H_{syn} (1+2)
	253	54.6	H_{syn} (1+2)		259	54.7	H_{syn} (3+4)
	258	56.0	H_{anti} (1+2)		259	55.4	Me^5
	263	58.0	H_{syn} (3+4)		283	58.2	Me^4
	288	60.5	H_{anti} (1+2) + (3+4)	**2d**; $CDCl_3$	307	70.5	Me-allyl
	302	60.9	H_{syn} (1+2) + (3+4)				

[a] Unless specified, [D_6]acetone solutions with a concentration of $7.94\cdot10^{-3}$ M. See Scheme 1 for the labelling scheme. For the allylic protons 1−4 refer to the signals in the order of decreasing frequency.

leads to an isomerisation and to a *syn-syn/anti-anti* interchange. Interconversion between H_{anti} and H_{syn} protons was not seen in these studies. It is possible that the absence of a ligand of high *trans* influence increases the energy of this process. Free energies of activation were calculated from the coalescence temperatures and the δν values between the coalescing signals. The corresponding data are shown in Table 4 and in each case the interchanging groups are indicated. The data for complex **2b**[24] have also been included for the sake of comparison. When the free energy of activation values are plotted against the coalescence temperatures for **2a**−**2d** (see Figure 2), it can be seen that the values do not differ significantly from one complex to another. Consequently, the process of apparent allyl rotation is not markedly affected by a change in the basicity or steric hindrance of the pyrazolyl fragment.

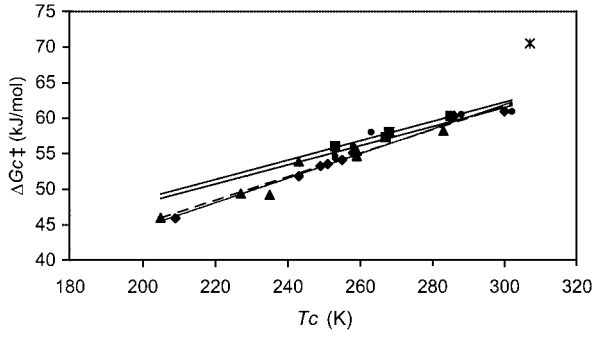

Figure 2. Linear plot of $\Delta G_c^{\ddagger}$ [kJ/mol] versus T_c [K] for complexes **2a**−**2d** in [D_6]acetone (see Table 4): **2a** (diamonds, -----), **2b** (dots, ——), **2c** (squares, ——), **2d** (triangles, ——), **2d** (star) in $CDCl_3$

In the case of complex **2d** a variable-temperature ^1H NMR spectroscopy study was also performed in $CDCl_3$. At low temperature (213 K) a splitting of the allylic methyl signal is observed. This enables the calculation of the corresponding free energy of activation (see Table 4). When the value obtained is compared with those calculated for complex **2d** in [D_6]acetone (see Figure 2), it is evident that in this poorly coordinating solvent the process of allyl rotation is clearly hindered. We must take into account that the anions in our complexes are also of low coordinating ability.

In the case of complex **2c**, variable-temperature studies were performed at different concentrations and also after the addition of water for one of the experiments. In this way, we tried to evaluate whether the presence of water in the deuterated solvent could influence the dynamic process. The $\Delta G_c^{\ddagger}$ values are collected in Table 5 and the appropriate plot is shown in Figure 3. The two lines corresponding to the studies with and without additional water are extremely similar. This means that in [D_6]acetone the addition of water does not affect the interconversion process. Moreover, the effect of the concentration, at least in the range studied, is also of minor importance.

It can be deduced unambiguously from Figures 2 and 3 that the value for the entropy of activation is negative. Con-

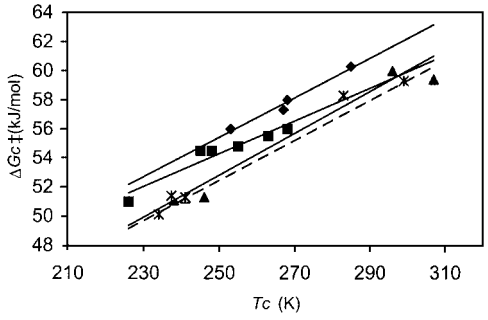

Figure 3. Linear plot of $\Delta G_c^{\ddagger}$ [kJ/mol] versus T_c [K] for complex **2c** in [D_6]acetone (see Tables 4 and 5): $7.94\cdot10^{-3}$ (diamonds, ——), $4.18\cdot10^{-3}$ (squares, ——); $2.10\cdot10^{-3}$ (triangles, -----); $2.10\cdot10^{-3}$ (stars, ——) with 15 μL of H_2O in 0.5 mL of solution

 © 2004 Wiley-VCH Verlag GmbH & Co. KGaA, Weinheim

Table 5. Coalescence temperatures and free energies of activation for complex **2c** at different concentrations in [D_6]acetone (see also the data of **2c** in Table 4; see Scheme 1 for the labelling scheme; for the allylic protons 1−4 refer to the signals in the order of decreasing frequency)

Conc.	T_c [K]	$\Delta G_c^{\ddagger}$ [kJ/mol^{-1}]	Interchanging groups	Conc.	T_c [K]	$\Delta G_c^{\ddagger}$ [kJ/mol^{-1}]	Interchanging groups
$4.18\cdot10^{-3}$ M	226	51.0	Me^3	$2.1\cdot10^{-3}$ M	238	51.1	H_{syn} (1+2)
	245	54.5	Me^5		241	51.2	H^4
	248	54.5	H_{anti} (3+4)		246	51.3	Me-allyl
	255	54.8	H_{syn} (1+2)		296	60.0	H_{anti} (1+2) + (3+4)
	263	55.5	H^4		307	59.4	H_{syn} (1+2) + (3+4)
	268	56.0	Me-allyl	$2.1\cdot10^{-3}$ M[a]	234	50.1	H_{syn} (1+2)
					237.3	51.4	H^4
					241	51.3	Me-allyl
					283	58.3	H_{anti} (1+2) + (3+4)
					299	59.3	H_{syn} (1+2) + (3+4)

[a] With the addition of 15 μL of H_2O in 0.5 mL of solution.

sidering all these data, we propose an associative mechanism involving the coordination of acetone. Such a situation is in accordance with the negative sign of the entropy and the effect of the solvent. Even in the more concentrated solutions, it is assumed that acetone coordination takes place without difficulty and that the concentration does not significantly influence the process. After coordination of the acetone molecule, the system could evolve through pseudorotation of the allyl group.[2a,28] We cannot rule out the participation of the bond breaking of Pd−N(triazine) in this process. However, there is evidence that the Pd−N(pyrazole) bond rupture does not influence this process because ligands with pyrazole groups that differ substantially in their electronic (and steric) characteristics practically have the same energetic barrier.

Experimental Section

General Comments: All manipulations were carried out under dry oxygen-free nitrogen using standard Schlenk techniques. Solvents were distilled from the appropriate drying agents and degassed before use. The derivative [Pd(η^3-C_4H_7)(μ-Cl)]$_2$[41] and ligands **1a**,[36,37] **1b**,[24] and **1c**[38] were prepared according to literature procedures. Elemental analyses were performed with a Perkin−Elmer 240 B microanalyser. IR spectra where recorded as nujol mulls with a Perkin−Elmer PE 883 IR spectrometer. Mass spectra (position of the peaks in Da) were recorded with a VG Autospec spectrometer (University of Zaragoza) using the FAB$^+$ technique and *m*-nitrobenzylic alcohol as matrix, and HPLC1100-MSD (Quadrupole analyzer) for the electrospray technique. ^{1}H and ^{13}C{^{1}H} NMR spectra were recorded with a Varian Unity 300 spectrometer using, unless specified, $(CD_3)_2CO$ as solvent and the chemical shifts are given in ppm. Standard experimental conditions were employed.[24,25] The ^{15}N NMR spectrum of compound **1d** was registered with a Bruker DRX 400 instrument with the chemical shifts in ppm, obtained by the heteronuclear-shift-correlation-spectra gs-HMQC and gs-HMBC with the standard pulse sequences[42] and referenced to an external sample of nitromethane. (^{1}H-^{1}H) COSY spectra: standard pulse sequence with an acquisition time of 0.214 s, pulse width 10 ms, relaxation delay 1 s, number of scans 16, number of increments 512. The NOE difference spectra were recorded with the following acquisition parameters: spectral width 5000 Hz, acquisition time 3.27 s, pulse width 18 ms, relaxation delay 4 s, irradiation power 5−10 dB, number of scans 240. For variable-temperature spectra the probe temperature (±1 K) was controlled by a standard unit calibrated with a methanol reference. Free energies of activation (kJ·mol^{-1}) were calculated[43] from the coalescence temperature (T_c) and the frequency difference between the coalescing signals (extrapolated at the coalescence temperature) with the formula $\Delta G_c^{\ddagger} = a\cdot T\cdot[9.972 + \log(T/\delta\nu)]$, $a = 1.914\cdot10^{-2}$. The estimated error in the calculated free energies of activation is ±1.1 kJ·mol^{-1}. *M* and *m* refer to the major or minor isomers, respectively.

Preparation of Compounds

(a) 2,4,6-Tris(3,4,5-trimethylpyrazol-1-yl)-1,3,5-triazine (1d): NaH (55.6 mg of 95 %, 2.2 mmol) was added to a solution of 3,4,5-trimethylpyrazole[44] (237 mg, 2.15 mmol) in freshly distilled dry THF (20 mL). After 1 h at 90 °C, the solution was cooled and 2,4,6-trichlorotriazine (cyanuric chloride) (99 % purity, Aldrich C9,550-1) (126.1 mg, 0.62 mmol) was added. The solution was heated at 90 °C for 10 h and at 70 °C for 18 h. The solvent was evaporated and the residue chromatographed on silica using $CHCl_3/CH_3OH$ (2:1) as eluent. Compound **1d** [R_f ($CHCl_3/CH_3OH$, 2:1) = 0.23], m.p. 295−297 °C, yield 49 % (135.7 mg). $C_{21}H_{27}N_9$ (405.24): calcd. C 62.20, H 6.71, N 31.09; found C 62.18, H 6.99, N 30.87. MS (FAB$^+$): *m*/*z* = 406.2 Da; (electrospray): *m*/*z* = 406.2 Da. ^{15}N NMR (40.56 MHz, $CDCl_3$, 25 °C): δ = −168.4 (N-1, pyrazole), −87.4 (N-2, pyrazole), −168.4 (N-triazine) ppm.

(b) [{Pd(η^3-C_4H_7)}$_2$(BPzTO)]BF_4 (2a): $AgBF_4$ (52.2 mg, 0.26 mmol) was added to a solution of [Pd(η^3-C_4H_7)(μ-Cl)]$_2$ (52.8 mg, 0.13 mmol) in THF (20 mL). The mixture was stirred for 2 h and protected from light. The solution was filtered through Celite to eliminate AgCl. The ligand TPzT (24.3 mg, 0.087 mol) was added and the mixture was stirred for 4 h. The solvent was evaporated to dryness and the pale yellow residue was washed with diethyl ether. The solid was crystallised in acetone/diethyl ether to obtain white crystals of **2a**. Yield: 36 % (20 mg). $C_{17}H_{20}BF_4N_7OPd_2$ (638.00): calcd. C 32.00, H 3.16, N 15.36; found C 31.75, H 3.28, N 15.24.

(c) [{Pd(η^3-C_4H_7)}$_2$(Me_2-BPzTO)]PF_6 (2c): A similar procedure to that used for **2a** was applied for **2c**. Amounts were as follows: $AgPF_6$ (145.6 mg, 0.58 mmol), [Pd(η^3-C_4H_7)(μ-Cl)]$_2$ (113.4 mg, 0.29 mmol), Me_2-TPzT (69.8 mg, 0.19 mmol). The solid was pale yellow in colour. Yield: 35 % (50 mg). $C_{21}H_{28}F_6N_7OPPd_2$ (752.27): calcd. C 33.53, H 3.75, N 13.03; found C 33.43, H 3.63, N 12.99.

 © 2004 Wiley-VCH Verlag GmbH & Co. KGaA, Weinheim

(d) [{Pd(η^3-C_4H_7)}$_2$(Me_3-BPzTO)]PF_6 (2d): A similar procedure to that used for **2a** was applied for **2d**. Amounts were as follows: $AgPF_6$ (60.7 mg, 0.24 mmol), [Pd(η^3-C_4H_7)(μ-Cl)]$_2$ (48.0 mg, 0.12 mmol), Me_3-TPzT (32.4 mg, 0.08 mmol). The solid was pale yellow in colour. Yield: 30 % (19 mg). $C_{24}H_{32}F_6N_7OPPd_2$ (792.34): calcd. C 36.38, H 4.07, N 12.37; found C 36.02, H 4.33, N 12.59.

Preparation of NMR Spectroscopic Samples of 2: Samples for the studies found in Table 4. The corresponding amount of the complexes (**2a**: 2.53 mg; **2c**: 2.99 mg; **2d**: 3.14 mg) was dissolved in 0.5 mL of the deuterated solvent. Samples for the studies found in Table 5. Complex **2c** (3.14 mg) was dissolved in 1 mL of [D_6]acetone. After recording the NMR spectra, 0.25 mL of this solution was mixed with 0.25 mL of [D_6]acetone and the spectra were recorded. Finally, 15 μL of H_2O was added.

X-ray Data Collection, Structure Determination, and Refinement of Complex 2c: The crystallographic data and experimental details are given in Table 6. Crystals of complex **2c** suitable for X-ray diffraction were obtained by slow diffusion of pentane into a saturated solution of the complex in acetone. Accurate unit cell parameters were determined by least-squares refinement of the setting angles of 25 randomly distributed and carefully centred reflections. The data collection was performed with a Nonius-Mach3 diffractometer equipped with a graphite monochromator [Mo-K_α radiation (λ = 0.71073 Å)] using an $\omega/2\theta$ scan technique to a maximum value of 56°. Data were corrected for Lorentz and polarisation effects. The structures were solved by direct methods (SIR92)[45] and refined first isotropically by full-matrix least squares using the SHELXL-97[46] program and then anisotropically by blocked full-matrix least squares for all the non-hydrogen atoms. The hydrogen atoms were included in calculated positions and refined "riding" on their parent carbon atoms. CCDC-212257 (**2c**) contains the supplementary crystallographic data for this paper. These data can be obtained free of charge at www.ccdc.cam.ac.uk/conts/retrieving.html or from the Cambridge Crystallographic Data Centre, 12 Union Road, Cambridge CB2 1EZ, UK [Fax: (internat.) + 44-1223-336-033; E-mail: deposit@ccdc.cam.ac.uk].

Table 6. Crystal data and structure refinement for **2c**

Empirical formula	$C_{21}H_{28}N_7OPd_2{\cdot}PF_6$
Formula mass	752.27 Da
Temperature	293(2) K
Wavelength	0.71073 Å
Crystal system, space group	triclinic, $P\bar{1}$
Unit cell dimensions	a = 8.815(5) Å, α = 106.560(5)°
	b = 12.936(5) Å, β = 102.890(5)°
	c = 13.074(5) Å, γ = 99.190(5)°
Volume	1352.6(11) Å^3
Z, calculated density	2, 1.847 g/cm^3
Absorption coefficient	14.59 cm^{-1}
F(000)	744
Crystal size	0.3 × 0.2 × 0.2 mm
Limiting indices	$-11 \le h \le 11$, $-17 \le k \le 16$,
	$0 \le l \le 17$
Reflections collected/unique	6808/6525 [R(int) = 0.0510]
Data/restraints/parameters	6525/37/398
Goodness-of-fit on F^2	0.951
Final R indices [$I > 2\sigma(I)$]	$R1$ = 0.0559, $wR2$ = 0.1100
R indices (all data)	$R1$ = 0.1814, $wR2$ = 0.1444
Largest diff. peak and hole	0.502 and −0.652 e·Å^{-3}

Acknowledgments

We are grateful to the Spanish DGES/MCyT (Project Nos. BQU-2000-0252 and BQU-2002-00286) for financial support.

[1] [1a] J. Tsuji, *Palladium Reagents and Catalysts, Innovation in Organic Synthesis*, Wiley & Sons, Chichester, **1996**. [1b] S. A. Godleski, in: *Comprehensive Organic Synthesis* (Eds.: B. M. Trost, I. Fleming), Pergamon Press, New York, **1991**, vol. 4, Chapter 3.3. [1c] P. J. Harrington, in: *Comprehensive Organometallic Chemistry II* (Eds.: E. W. Abel, F. G. A. Stone, G. Wilkinson, R. J. Puddephatt), Elsevier, New York, **1995**, vol. 12, p.797. [1d] J.-E. Bäckvall, *Metal-catalyzed Cross Coupling Reactions*, VCH, Weinheim, Germany, **1998**, p. 339. [1e] B. M. Trost, C. Lee, in: *Catalytic Asymmetric Synthesis*, 2nd ed. (Ed.: I. Ojima), Wiley-VCH, New York, **2000**, p. 593−649. [1f] A. Pfaltz, M. Lautens, in: *Comprehensive Asymmetric Catalysis* (Eds.: E. N. Jacobsen, A. Pfaltz, H. Yamamoto), Springer, Heidelberg, **1999**, p. 833−886.

[2] [2a] K. Vrieze, *Dynamic Nuclear Resonance Spectroscopy* (Eds.: L. M. Jackman, F. A. Cotton), Academic Press, New York, **1975**, chapter 11, p. 441. [2b]P. S. Pregosin, R. Salzmann, *Coord. Chem. Rev.* **1996**, *155*, 35−68. [2c] J. W. Faller, in: *Encyclopedia of Inorganic Chemistry* (Ed.: R. B. King), John Wiley and Sons, Chichester, **1994**, vol. 7, p. 3925−3926. [2d] F. A. Jalón, B. R. Manzano, F. Gómez-de la Torre, A. M. Guerrero, A. M. Rodríguez, in: *Targets in Heterocyclic Systems, Chemistry and Properties* (Eds.: O. A. Attanasi, D. Spinelli), Italian Society of Chemistry, Roma, **1999**, vol 3, 399−438.

[3] [3a] B. M. Trost, D. L. Van Vranken, *Chem. Rev.* **1996**, *96*, 395−422. [3b] B. M. Trost, *Pure Appl. Chem.* **1996**, *68*, 779−784. [3c] J. D. Oslob, B. Åkermark, P. Helquist, P. O. Norrby, *Organometallics* **1997**, *16*, 3015−3021. [3d] C. Larksarp, H. Alper, *J. Am. Chem. Soc.* **1997**, *119*, 3709−3715. [3e] H. Hagelin, B. Åkermark, P.-O. Norrby, *Organometallics* **1999**, *18*, 2884−2895. [3f] J. C. Anderson, R. J. Cubbon, J. D. Harling, *Tetrahedron: Asymmetry* **2001**, *12*, 923−935. [3g] P. J. Harrington, in: *Comprehensive Organometallic Chemistry* (Eds.: E. W. Abel, F. G. A. Stone, G. Wilkinson, L. S. Hegedus), Pergamon, Oxford, **1995**, vol. 12, p. 882−894 and references cited therein.

[4] [4a] P. W. N. M. van Leeuwen, P. W. Praat, *J. Chem. Soc., Chem. Commun.* **1970**, 365−366. [4b] F. G. A. Stone, N. M. Boag, M. Green, J. L. Spencer, *J. Organomet. Chem.* **1977**, *127*, C51−C54. [4c] R. E. Rülke, V. E. Raasjager, P. Wehman, C. J. Elsevier, P. W. N. M. van Leeuwen, K. Vrieze, J. Fraanje, K. Boubitz, A. L. Spek, *Organometallics* **1996**, *15*, 3022−3031.

[5] [5a] J. M. Brown, D. I. Hulmes, P. J. Guiry, *Tetrahedron* **1994**, *50*, 4493−4506. [5b] T. D. W. Claridge, J. M. Long, J. M. Brown, D. Hibbs, M. B. Hursthouse, *Tetrahedron* **1997**, *53*, 4035−4050.

[6] [6a] P. Barbaro, P. S. Pregosin, R. Salzmann, A. Albinati, R. W. Kunz, *Organometallics* **1995**, *14*, 5160−5170. [6b] T. Hosocawa, Y. Wakabayashi, K. Hosocawa, T. Tsuji, S. I. Murahashi, *Chem. Commun.* **1996**, 859−860. [6c] S. Ramdeehul, L. Barloy, J. A. Osborn, A. De Cian, J. Fischer, *Organometallics* **1996**, *15*, 5442−5444. [6d] H. A. Ankersmit, N. Veldman, A. L. Spek, K. Vrieze, G. Van Koten, *Inorg. Chim. Acta* **1996**, *252*, 339−354.

[7] L. Canovese, F. Visentin, P. Uguagliati, V. Lucchini, G. Bandoli, *Inorg. Chim. Acta* **1998**, *277*, 247−252.

[8] [8a] I. Schwarz, J. Rust, C. W. Lehmann, M. Braun, *J. Organomet. Chem.* **2000**, *605*, 109−116. [8b] F. Gómez-de la Torre, Y. Gutiérrez, F. A. Jalón, B. R. Manzano, A. Rodríguez, *Monatsh. Chem.* **2000**, *131*, 1267−1280.

[9] [9a] J. Krause, R. Goddard, R. Mynott, K-R. Pörschke, *Organometallics* **2001**, *20*, 1992−1999. [9b] P. Braunstein, F. Naud, A. Dedieu, M. M. Rohmer, A. De Cian, S. J. Rettig, *Organometallics* **2001**, *14*, 2966−2981.

[10] M. Kollmar, B. Goldfuss, M. Reggelin, F. Rominger, G. Helmchen, *Chem. Eur. J.* **2001**, *7*, 4913−4927.

[11] L. Canovese, G. Chessa, C. Santo, F. Visentin, P. Uguagliati, *Organometallics* **2002**, *21*, 4342−4349.

[12] M. Ogasawara, K. Takizawa, T. Hayashi, *Organometallics* **2002**, *21*, 4853−4861.

[13] [13a] C. Breutel, P. S. Pregosin, R. Salzmann, A. Togni, *J. Am. Chem. Soc.* **1994**, *116*, 4067−4068. [13b] P. S. Pregosin, R. Salz-

 © 2004 Wiley-VCH Verlag GmbH & Co. KGaA, Weinheim

mann, A. Togni, *Organometallics* **1995**, *14*, 842−847. [13c] J. Herrmann, P. S. Pregosin, R. Salzmann, A. Albinati, *Organometallics* **1995**, *14*, 3311−3318.
[14] R. Fernández-Galán, F. Jalón, B. R. Manzano, J. Rodríguez de la Fuente, M. Vrahami, B. Jedlicka, W. Weissensteiner, *Organometallics* **1997**, *16*, 3758−3768.
[15] P. Dotta, P. G. A. Kumar, P. S. Pregosin, *Magn. Reson. Chem.* **2002**, *40*, 653−658.
[16] N. Solin, K. J. Szabó, *Organometallics* **2001**, *20*, 5464−5471.
[17] A. Albinati, R. W. Kunz, C. J. Ammann, P. S. Pregosin, *Organometallics* **1991**, *10*, 1800−1806.
[18] A. Gogoll, J. Örnebro, J.-E. Bäckvall, *J. Am. Chem. Soc.* **1994**, *116*, 3631−3632.
[19] [19a] B. Crociani, F. Di Bianca, A. Giovenco, T. Boschi, *Inorg. Chim. Acta* **1987**, *127*, 169−182. [19b] B. Crociani, S. Antonaroli, M. Paci, F. Di Bianca, L. Canovese, *Organometallics* **1997**, *16*, 384−391.
[20] A. Gogoll, H. Grennberg, A. Axén, *Organometallics* **1997**, *16*, 1167−1178.
[21] Y. Takao, T. Takeda, J. Watanabe, J. Setsune, *Organometallics* **1999**, *18*, 2936−2938.
[22] J. Elguero, A. Fruchier, A. de la Hoz, F. A. Jalón, B. R. Manzano, A. Otero, F. Gómez-de la Torre, *Chem. Ber.* **1996**, *129*, 589−594.
[23] F. A. Jalón, B. R. Manzano, A. Otero, M. C. Rodríguez, *J. Organomet. Chem.* **1995**, *494*, 179−185.
[24] F. Gómez-de la Torre, A. de la Hoz, F. A. Jalón, B. R. Manzano, A. Otero, A. M. Rodríguez, M. C. Rodríguez-Pérez, A. Echevarría, J. Elguero, *Inorg. Chem.* **1998**, *37*, 6606−6614.
[25] F. Gómez-de la Torre, A. de la Hoz, F. A. Jalón, B. R. Manzano, A. M. Rodríguez, J. Elguero, M. Martínez-Ripoll, *Inorg. Chem.* **2000**, *39*, 1152−1162.
[26] N. Arroyo, F. Gómez-de la Torre, F. A. Jalón, B. R. Manzano, B. Moreno-Lara, A. M. Rodríguez, *J. Organomet. Chem.* **2000**, *603*, 174−184.
[27] M. C. Carrión, A. Díaz, A. Guerrero, F. A. Jalón, B. R. Manzano, A. Rodríguez, R. L. Paul, J. C. Jeffery, *J. Organomet. Chem.* **2002**, *650*, 210−222.
[28] S. Hansson, P-O. Norrby, M. P. T. Sjögren, B. Åkermark, M. E. Cucciolito, F. Giordano, A. Vitagliano, *Organometallics* **1993**, *12*, 4940−4948.
[29] J. Sprinz, M. Kiefer, G. Helmchen, M. Reggelin, G. Huttner, O. Walter, L. Zsolnai, *Tetrahedron Let.* **1994**, *35*, 1523−1526.
[30] [30a] J. G. P. Delis, J. H. Groeen, K. Vrieze, P. W. N. M. van Leeuwen, N. Veldman, A. L. Spek, *Organometallics* **1997**, *16*, 551−562. [30b] L. Canovese, F. Visentin, P. Uguagliati, G. Chessa, V. Lucchini, G. Bandoli, *Inorg. Chim. Acta* **1998**, *275−276*, 385−394.
[31] B. Crociani, S. Antonaroli, G. Bandoli, L. Canovese, F. Visentin, P. Uguagliati, *Organometallics* **1999**, *18*, 1137−1147.
[32] R. J. van Haaren, K. Goubitz, J. Fraanje, G. P. F. Van Strijdonck, H. Oevering, B. Coussens, J. N. H. Reek, P. C. J. Kamer, P. W. N. M. van Leeuwen, *Inorg. Chem.* **2001**, *40*, 3363−3372.
[33] J. W. Faller, H. L. Stokes-Huby, M. A. Albrizzio, *Helv. Chim. Acta* **2001**, *84*, 3031−3042.
[34] M. A. Pericàs, C. Puigjaner, A. Riera, A. Vidal-Ferran, M. Gómez, F. Jiménez, G. Muller, M. Rocamora, *Chem. Eur. J.* **2002**, *8*, 4164−4178.
[35] A. M. Guerrero, F. A. Jalón, B. R. Manzano, R. M. Claramunt, M. D. Santa María, C. Escolástico, J. Elguero, A. M. Rodríguez, M. A. Maestro, J. Mahía, *Eur. J. Inorg. Chem.* **2002**, 3178−3189.
[36] A. Echevarría, J. Elguero, A. L. Llamas-Saiz, C. Foces-Foces, G. Schultz, I. Hargittai, *Struct. Chem.* **1994**, *5*, 255−264.
[37] A. L. Llamas-Saiz, C. Foces-Foces, A. Echevarría, J. Elguero, *Acta Crystallogr., Sect. C* **1995**, *51*, 1401−1404.
[38] A. Guerrero, F. A. Jalón, B. R. Manzano, R. Claramunt, P. Cabildo, L. Infantes, F. H. Cano, J. Elguero, *J. Heterocycl. Comp.* **2003**, 1584−1591.
[39] E. Horn, M. R. Snow, *Aust. J. Chem.* **1980**, *33*, 2369−2376.
[40] J. Catalán, J.-L. M. Abboud, J. Elguero, *Adv. Heterocycl. Chem.* **1987**, *41*, 187−274.
[41] W. T. Dent, R. Long, G. Wilkinson, *J. Chem. Soc.* **1964**, 1585.
[42] S. Braun, H.-O. Kalinowski, S. Berger, *150 and More Basic NMR Experiments*, Wiley-VCH, **1998**.
[43] J. Sandström, *Dynamic NMR Spectroscopy*, Academic Press, London, **1982**.
[44] [44a] L. C. Behr, R. Fusco, C. H. Jarboe, *Pyrazoles, Pyrazolines, Pyrazolidines, Indazoles and Condensed Rings*, Interscience, **1967**, Table 10, p. 460. [44b]R. Goddard, R. M. Claramunt, C. Escolástico, J. Elguero, *New. J. Chem.* **1999**, 237−240. [44c] F. Aguilar Parrilla, F. Männle, H.-H. Limbach, J. Elguero, N. Jagerovic, *Magn. Reson. Chem.* **1994**, *32*, 699−702.
[45] A. Altomare, G. Cascarano, C. Giacovazzo, A. Guagliardi, M. C. Burla, G. Polidori, M. Camalli, *J. Appl. Crystallogr.* **1994**, 435−436.
[46] G. M. Sheldrick, *Program for the Refinement of Crystal Structures from Diffraction Data*, University of Göttingen, Göttingen, Germany, **1997**.

Received June 6, 2003
Early View Article
Published Online November 28, 2003

Formation of Cubic GaN Nanocrystals: A Study of the Thermal Stability of GaP Nanocrystals under Nitrogen

Shanmin Gao,[a] Liying Zhu,[a] Yi Xie,*[a] and Xiaobo Qian[a]

Keywords: Gallium / Phosphorus / Nitrides / Nanostructures / Thermochemistry

Cubic GaN nanoparticles and nanorods have been successfully synthesized from the nitridation of nanocrystalline GaP at 500 °C for 30 min, by manipulating different heating rates in nitrogen. The results of the thermal stability studies of nanocrystalline GaP under N_2 at different heating rates support the idea that cubic GaN can form from GaP via a N–P metathesis mechanism. The morphology of the cubic GaN can be controlled by variation of the external synthetic parameters such as the rate of heating. This work shows that it is very simple to synthesize cubic GaN nanoparticles or nanorods and opens a wide route towards detailed studies of the fundamental properties and potential applications of semiconductor nanocrystals.

(© Wiley-VCH Verlag GmbH & Co. KGaA, 69451 Weinheim, Germany, 2004)

Introduction

Nanostructures have potential for unique applications in electronics, optoelectronics and catalysis due to their high surface-to-volume ratios, quantum confinement effects and high fraction of chemically similar surface sites.[1,2] Wide band-gap semiconductor compound nanomaterials of the 13−15 group, such as GaN, GaP and GaAs are important in fundamental physics and are widely used for high-speed digital circuits, electronic and optoelectronic devices.[3] Over the past several years, considerable efforts have been made to explore new and simple synthetic routes to group 13−15 semiconductor nanocrystals.[4−7]

Of this group of semiconductors, the properties of GaN nanocrystals have received the least attention due to the difficulty involved in their preparation. Of the limited studies on GaN nanocrystals which have been reported, most have focused on hexagonal GaN with the wurtzite structure.[8−12] In comparison, cubic GaN nanocrystals have generally been studied in the form of thin films.[13−15] A recent report of cubic GaN powder synthesis via ammonolysis under thermal conditions required over 2700 atm of NH_3 pressure for over 24 h and the resultant product was generally found to be mixed with hexagonal phase GaN.[16] Moreover, cubic GaN has advantageous physical properties compared with those of the hexagonal phase, such as easier *p*-type doping, easier cleaving for laser facets, and a narrower energy band gap which means it is easier to reach the blue and green region.[17] Studies of the synthesis of cubic GaN nanocrystals is therefore of great importance.

Low-dimensional crystal structures, geometries such as wires, rods, and thin films are currently the focus of much attention due to their special properties.[18−20] These fascinating systems are expected to exhibit remarkable mechanical, electrical, optical and magnetic properties. Such low-dimensional crystalline materials have potential applications in molecular based electronic devices such as optical memory and in switches, displays and data records. Several approaches have been successfully developed for the fabrication of such nanowires and nanorods and their morphologies, microstructures and growth mechanisms have been studied.[21−25]

The synthesis, optical properties and catalytic reactivity of GaP nanocrystals have been studied in detail by our group.[26−28] The growth process and stability of GaP nanocrystals under thermal conditions in benzene have also been studied and a method for controlling the reaction process and uniformity of GaP grains has been reported.[29]

As is already known, the application of semiconductors depends on the change in the environmental conditions, so studying the influence of such conditions on the properties of semiconductor nanomaterials is also important. In this study, the thermal stability of GaP nanocrystals under a nitrogen atmosphere was investigated in detail and resulted in the establishment of a new preparative route to cubic GaN nanoparticles and nanorods.

Results and Discussion

XRD patterns were used to examine the crystal structures and phase purities of the products which were obtained by heating GaP nanoparticles at 500 °C for 30 min.

[a] Structure Research Laboratory and
Department of Chemistry,
University of Science and Technology of China,
Hefei, Anhui 230026, P. R. China
Fax: (internat.) +86-551-3603987
E-mail: yxielab@ustc.edu.cn

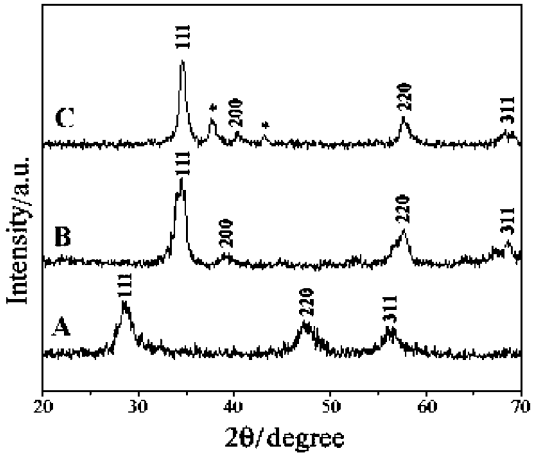

Figure 1. XRD patterns of (A) the starting GaP nanocrystals (B) the pure cubic GaN sample prepared from the heat treatment of GaP nanocrystals at 500 °C for 30 min with a heating rate of 5 °C/min and 10 °C/min (C) the cubic GaN sample prepared from the heat treatment of GaP nanocrystals at 500 °C for 30 min with a heating rate of 20 °C/min, the note * labels the residual elemental Ga

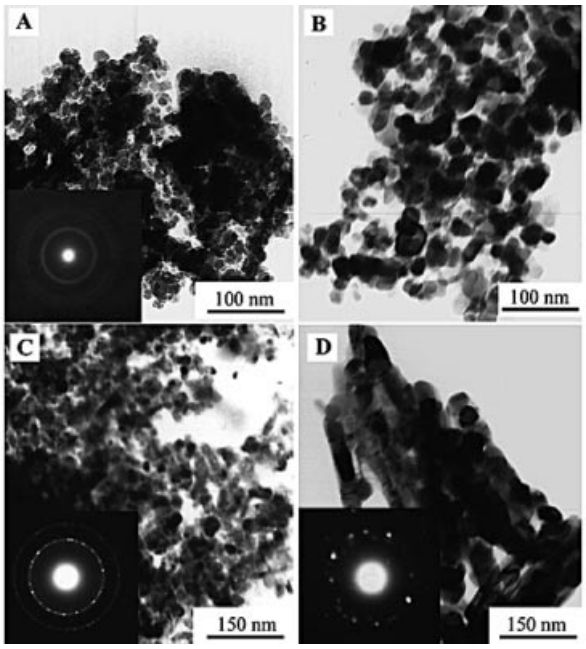

Figure 2. (A) TEM image of the starting GaP nanocrystals (B), (C) and (D) TEM images of cubic GaN obtained from heat treatment of GaP nanocrystals in N_2 at 500 °C for 30 min at heating rates of 5 °C/min, 10 °C/min and 20 °C/min, respectively; the picture insets are the SAED patterns of the corresponding materials

Figure 1 (A) displays the XRD pattern of the starting GaP nanocrystals. Pure cubic GaN was obtained from GaP nanocrystals at a low heating rate (≤10 °C/min) under N_2 at 500 °C for 30 min and the corresponding XRD pattern is shown in Figure 1 (B). All the reflections at $2\theta = 35.5$, 40.5, 58 and 68.5°, were indexed to the (111), (200), (220) and (311) lattice planes of cubic GaN, respectively. The calculated lattice parameter of cubic GaN using a computer simulation is $a_0 = 4.502 \pm 0.004$ Å, which is good agreement with the reported value.[17]

Figure 1 (C) shows the XRD pattern of the product prepared from the heat treatment of GaP nanocrystals under N_2 at 500 °C for 30 min at a heating rate of 20 °C/min, indicating that the product is cubic GaN coexisting with a minor amount elemental Ga (denoted as *, JC,PDF File, No. 31-0539). The minor elemental Ga can be easily removed by treatment using 1 N hydrochloric acid and pure cubic GaN can be obtained and its identity confirmed by its XRD pattern which is similar to that in Figure 1 (B). The XRD patterns of all the products are quite different from that of the starting GaP nanoparticles. The above results show that cubic GaN is formed by the heat treatment GaP nanocrystals under N_2 via a P−N metathesis reaction.

The morphology and structure of the prepared cubic GaN nanocrystallites were further characterized using transmission electron microscopy (TEM). Figure 2 (A) shows that the starting GaP nanocrystals are uniform spherical particles with a diameter of 8 ± 2 nm. Figure 2 (B and C) show that the cubic GaN obtained under N_2 at 500 °C for 30 min are uniform spherical particles with a diameter of 16 ± 2 nm for the product obtained with a heating rate of 5 °C/min and 22 ± 3 nm for the product obtained with a heating rate of 10 °C/min, in good agreement with the XRD result in which the average size can be calculated by employing the Scherrer equation. They exhibit the same morphology as the starting GaP nanocrystallites, the only difference being that the resultant GaN nanocrystals are larger than the starting GaP nanocrystallites due to the heat treatment at 500 °C. The SAED pattern [inset of Figure 2 (C)] shows diffraction rings consistent with the (111), (200), and (220) lattice plane of the cubic GaN phase. Except for the cubic GaN obtained at 500 °C for 30 min with a heating rate of 20 °C/min, the morphologies of the products [Figure 2 (D)] are different from the product obtained at 500 °C for 30 min with a heating rate of 10 °C/min in which nanorods are formed with diameters of 25 −30 nm and lengths of 200 −500 nm.

X-ray photoelectron spectroscopy (XPS) was used to investigate the elemental composition of the starting GaP nanocrystals and the above prepared GaN nanocrystals. The XPS results can provide evidence for the formation of GaN. Higher resolution spectra were taken of the Ga_{3d} and N_{1s} regions. The XPS spectra are shown in Figure 3. The binding energy values of the Ga_{3d} and N_{1s} core levels agree well with their chemical environments in cubic GaN. This clearly indicates that the N_2 molecules must be chemically bonded to Ga atoms, presumably forming N−Ga bonds.

The above results indicate that the P−N metathesis reaction occurred regardless of the heating rates used in our experiments . The replacement of P by N atoms is facilitated by the fact that P is more volatile than Ga and tends to escape from GaP upon thermal annealing. Traditionally, nitridation reactions using N_2 need high temperature (>1000 °C), since N_2 is very inert and stable. Small GaN crystals have been synthesized from molten gallium and N_2 at 700 °C in an alkali metal flux[30,31] and nanorod architectures have been prepared from catalyzed reactions between

 © 2004 Wiley-VCH Verlag GmbH & Co. KGaA, Weinheim

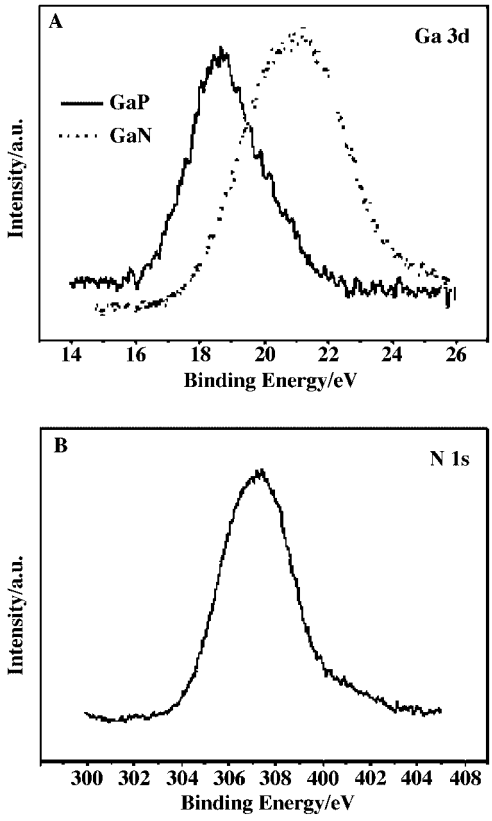

Figure 3. XPS spectra of the Ga_{3d} (A) and N_{1s} (B) core levels; the solid line represents the raw material GaP nanocrystals and the broken line represents the prepared cubic GaN obtained by heat treatment of GaP nanocrystals in N_2 at 500 °C for 30 min with a heating rate of 10 °C/min

gallium and NH_3 above 900 °C.[32,33] Our experiments indicate that cubic GaN can form at lower temperatures and shorter reaction times, an observation which is based on the high surface-to-volume ratio of nanocrystalline raw materials of GaP which can remarkably reduce the difficulty of nitridation. The GaP particles sizes significantly affect the nitridation reaction. The nitridation process may become more difficult or even incomplete and when the particle sizes reach the micron dimension, XRD results indicate that no GaN forms at all. Furthemore, at different heating rates the synthesized GaN exhibits different nanoscale morphologies, which leads us to believe that different heating rates cause different reaction mechanisms. The mechanisms of the surface adsorption reaction on GaP nanocrystals, and the formation of cubic GaN nanoparticles and nanorods are shown schematically in Scheme 1.

Regardless of the heating rates used in our experiments, the initial process involves the desorption of P atoms from the starting GaP nanocrystallites, adsorption of N atoms on the GaP surface and the further nitridation reaction [Scheme 1 (A)]. As is known, the surface area of nanocrystals is much larger than the bulk materials and there exist many vacancies and dangling bonds on the surface. In our experiments, the N_2 molecules are adsorbed onto the surface of the starting GaP nanocrystals during the initial stage of heating [Scheme 1 (A1)]. Firstly N_2 is adsorbed on

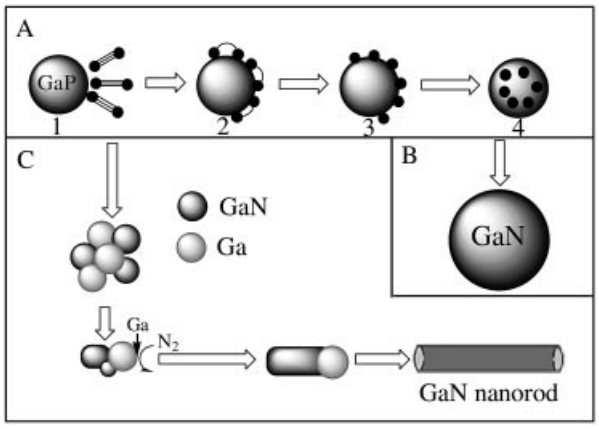

Scheme 1. The proposed mechanism for the formation of cubic GaN nanocrystals; (A) the surface adsorption reaction of N_2 on GaP nanocrystals and the nucleation of GaN; (B) the growth of GaN nanoparticles at lower heating rates; (C) step growth of GaN nanorods at higher heating rates

to the surface of the GaP nanocrystals (adsorbent), the physical adsorption depending on the van der Waals force. The vacancies and dangling bonds on the surface of the GaP nanocrystals provide a favorable environment for N_2 molecules to form bonds. Upon elevating the temperature, chemical bonding of N and Ga results, producing the activated adsorption. As a result, the N_2 molecules can be activated on the surface of GaP nanocrystals at a rather low temperature, remarkably weakening the strength of the N≡N bond on the surface of the GaP nanocrystals [Scheme 1 (A2)]. After the activated N atoms have formed [Scheme 1 (A3)] the N−P metathesis reaction can take place [Scheme 1 (A4)]. Since the metathesis reaction involves conversion of one zinc blende structure to another zinc blende structure this reaction can therefore be called a topotactic transformation.

At a lower heating rate (≤10 °C/min), the desorption of P, absorption of N and nitridation of GaP is a synchronous process on the GaP nanocrystals with no formation of excess Ga droplets, an observation which has been validated by the XRD pattern [as shown in Figure 1 (B)]. Thus GaN gradually forms on the surface of the GaP nanoparticles during this process. The total reaction can be described as in Equation (1).

$$GaP + N_2 \rightarrow GaN + P \quad (1)$$

The high surface area and reactivity of nanocrystalline GaP directly result in the formation of cubic GaN at lower temperature, lower pressure and shorter reaction times [Scheme 1 (B)]. The resultant GaN nanoparticles inherit the GaP matrixes in terms of structure and morphology which explains the similarity between the structures and morphologies of the resultant GaN and the starting GaP.

When the heating rate is higher (≥20 °C/min), however, the reaction is complicated and the initial chemical reaction is the desorption of P from the GaP nanocrystals, as described in Equation (2).

$$GaP \rightarrow Ga + P \quad (2)$$

 © 2004 Wiley-VCH Verlag GmbH & Co. KGaA, Weinheim

The desorption chemical reaction is dominant and rapid and so the newly formed gallium has high activity and can react with N_2 to produce GaN nuclei, Equation (3).

$$Ga + N_2 \rightarrow GaN \quad (3)$$

A higher heating rate also promotes gallium coalescence along with its nitridation resulting in the appearance of smaller droplets of Ga. GaN nuclei start to aggregate and act as the nucleation seeds, then, stepwise growth proceeds with Ga droplets being pushed outward by the descending GaN [Scheme 1 (C)]. The Ga droplets play a crucial role in the growth of GaN nanorods based on the vapor-solid (VS) mechanism which is widely used to explain the growth of fiber-like semiconductors.[34] VS growth is apparently supported by the large Ga surface area and high reactivity which increases the effective steady-state Ga vapor pressure. The system is not in equilibrium because the Ga vapor reacts to form GaN. The increased rate of evaporation afforded by the large surface area of Ga more than likely produces a larger *steady-state* vapor pressure than is present over larger and coarser Ga particles. Scheme 1 (C) schematically depicts the mechanism of the formation of cubic GaN nanorods. More evidence has been provided by the supplementary experiments undertaken with a heating rate of 50 °C/min. The crystal structures and phase purities of the products are shown in Figure 4 (A) and the morphologies of the nanocrystalline GaN samples are shown in Figure 4 (B). The XRD pattern of the product prepared from the heat treatment of GaP nanocrystals under N_2 at 500 °C for 30 min with a heating rate of 50 °C/min indicates that the product is cubic GaN coexisting with a minor amount of elemental Ga (denoted as *) supporting that idea that cubic GaN nanorods can be obtained at the higher heating rate and the growth of GaN nanorods is based on the vapor-solid (VS) mechanism.

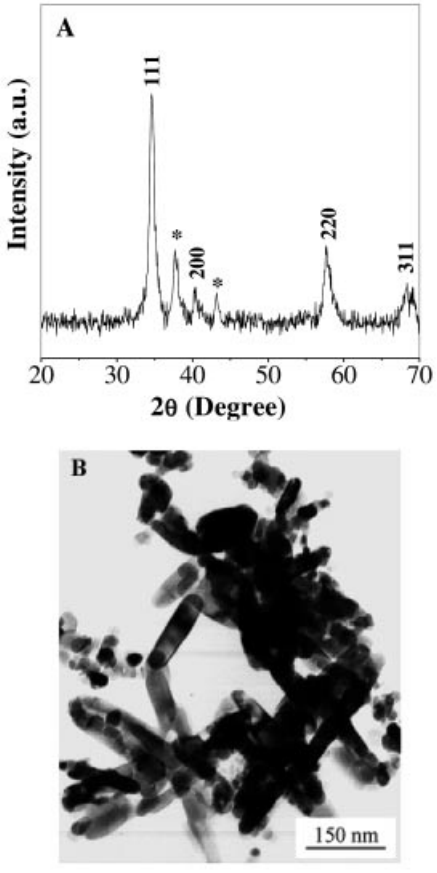

Figure 4. XRD pattern (A) and TEM image (B) of cubic GaN obtained from heat treatment of GaP nanocrystals at 500 °C for 30 min in N_2 with a heating rate of 50 °C/min

The above mechanism showing that cubic GaN can form in GaP via P−N metathesis is directly supported by the thermal stability study of GaP nanocrystals under nitrogen. At a lower heating rate, the desorption of P and nitridation are synchronous processes and, accordingly, the weight loss should be slow. At a higher heating rate, however, the desorption of P is preferential, so the weight loss should be rapid. In order to validate this, the thermogravimetric analysis (TGA) technique was used to analyze the thermal behavior of the GaP nanoparticles under N_2 at different heating rates. A typical TGA profile is shown in Figure 5, and the results are completely in accord with the above conclusion.

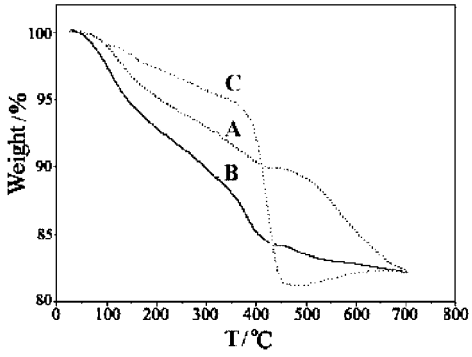

Figure 5. Thermogravimetric analyses of GaP nanocrystals in an N_2 flow at different heating rates; (A) 5 °C/min, (B) 10 °C/min, (C) 20 °C/min

One can see that at a heating rate of 5 °C/min [Figure 5 (A)], the weight loss is gradual, i.e. reaction (1) takes place during this process. The N and Ga atoms can be rendered miscible by an oxidation process since the N and Ga atoms can form a stable electrovalent bond, resulting in the final formation of GaN nanoparticles. At a heating rate of 10 °C/min, the weight loss is quicker than with a heating rate of 5 °C/min [Figure 5 (B)]. A precipitate line is obtained at a heating rate of 20 °C/min [Figure 5 (C)], indicating that the weight loss is much quicker than at the heating rates of 5 °C/min and 10 °C/min, namely, that reaction (2) takes place first followed by reaction (3) so the weight increases again later. The thermal stability results of GaP nanocrystalline under N_2 at different heating rates support the proposed mechanism that cubic GaN can form in GaP via a N−P metathesis mechanism.

Conclusion

In conclusion, a convenient, low-temperature technique has been established for the synthesis of cubic GaN nano-

 © 2004 Wiley-VCH Verlag GmbH & Co. KGaA, Weinheim

crystals based on the fact that the small size effect of the starting GaP can remarkably reduce the difficulty of nitridation. Cubic GaN nanoparticles and nanorods have been successfully synthesized from the nitridation of nanocrystalline GaP at 500 °C for 30 min using a range of different heating rates. The thermal stability results of GaP nanocrystalline under N_2 at different heating rates support the proposal that cubic GaN can form in GaP via a N−P metathesis mechanism.

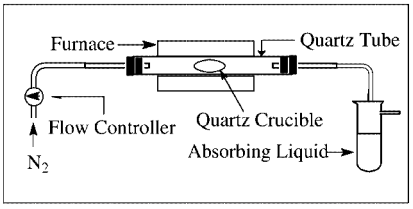

Figure 6. Schematic experimental setup for the formation of cubic GaN nanocrystals; GaP nanocrystals were placed in the quartz crucible

Experimental Section

Synthesis of Cubic GaN Nanocrystals: The starting GaP nanocrystals used in the present study were synthesized in the benzene-thermal route using Na_3P and $GaCl_3$ as the raw materials which has been described in detail elsewhere.[26] In a typical experiment, the starting GaP nanocrystals were loaded into a quartz crucible which was then horizontally placed in the quartz tube of a tubular furnace. The experimental setup for the formation of cubic GaN nanocrystals is described schematically in Figure 6. Firstly, the quartz tube was evacuated for 20 min. After this, the quartz tube was ventilated with high purity (99.999%) N_2 at a flow of about 20 sccm (standard cubic centimeters per minute) for several minutes, a unit mass flow controller was used to regulate the flow velocity of N_2 gas. The system was heated to 500 °C using different heating rates and then maintained at this temperature for 30 min. The samples were then allowed to cool to room temperature and were subsequently sealed in glass tubes for further characterization.

Characterization: Powder X-ray diffraction (XRD) patterns were obtained at room temperature using a Rigaku D/max-γA model X-ray diffractometer with Ni-filtered Cu-K_α radiation. TEM images of the samples were obtained from a Hitachi H800 transmission electron microscope using an accelerating voltage of 200 kV. Samples for TEM investigations were briefly ultra-sonicated in ethanol, and then a drop of suspension was placed on a holey copper grid with carbon film. X-ray photoelectron spectra (XPS) were measured on a VGESCALAB 220i-XL X-ray photo spectrometer with Al-K_α (1186.6 eV) radiation as the exciting source with measurements performed at pressures lower than 1×10^{-8} Torr. Thermogravimetric analyses (TGA) were performed on a Perkin−Elmer DC/2C type TG-DTA apparatus under a N_2 atmosphere at different heating rates. Fourier transform infrared spectra (FT-IR) of pellets of the samples mixed with KBr were recorded on a Nicolet Magna-IR 750 FTIR spectrometer at a resolution of 4 cm^{-1}.

Acknowledgments

We gratefully acknowledge financial support from the National Natural Research Foundation of China. We thank Dr. Y. W. Ding for his discuss of the TGA results.

[1] Y. Cui, C. M. Lieber, *Science* **2001**, *291*, 851.
[2] S. Sharma, M. K. Sunkara, *J. Am. Chem. Soc.* **2002**, *124*, 12288.
[3] X. F. Duan, Y. Huang, Y. Cui, J. F. Wang, C. M. Lieber, *Nature* **2001**, *409*, 66.
[4] S. J. Pearton, F. Ren, *Adv. Mater.* **2000**, *12*, 1571.
[5] G. P. Mitchell, C. A. Mirkin, R. L. Letsinger, *J. Am. Chem. Soc.* **1999**, *121*, 8122.
[6] D. L. Klein, R. Richard, A. K. L. Lin, A. P. Alivisatos, P. L. McEuen, *Nature* **1997**, *389*, 699.
[7] T. Somery, R. Werner, A. Forchel, M. Catalano, R. Cingolani, Y. Arakawa, *Science* **1999**, *285*, 1095.
[8] A. Argoitia, C. C. Hayman, J. C. Angus, L. Wang, J. S. Dyck, K. Kash, *Appl. Phys. Lett.* **1997**, *70*, 179.
[9] G. L. Wood, E. A. Pruss, R. T. Paine, *Chem. Mater.* **2001**, *13*, 12.
[10] J. A. Jegier, S. McKernan, A. P. Purdy, W. L. Gladfelter, *Chem. Mater.* **2000**, *12*, 1003 and references cited therein.
[11] J. L. Coffer, M. A. Johnson, B. L. Zhang, *Chem. Mater.* **1997**, *9*, 2671.
[12] A. Manz, A. Birkner, M. Kolbe, R. A. Fischer, *Adv. Mater.* **2000**, *12*, 569.
[13] D. Wang, S. Yoshida, M. Ichikawa, *Appl. Phys. Lett.* **2002**, *80*, 2472.
[14] D. Schikora, M. Hankeln, D. J. As, K. Lischka, T. Litz, A. Waag, T. Buhrow, F. Henneberger, *Phys. Rev. B* **1996**, *54*, R8381.
[15] T. Suski, H. Teisseyre, S. P. Lepkowski, P. Perlin, T. Kitamura, Y. Ishida, H. Okumura, S. F. Chichibu, *Appl. Phys. Lett.* **2002**, *81*, 232.
[16] A. P. Purdy, *Chem. Mater.* **1999**, *11*, 1648.
[17] W. Y. Wang, Y. P. Xu, D. F. Zhang, X. L. Chen, *Mater. Res. Bull.* **2001**, *36*, 2155.
[18] J. T. Hu, T. W. Odom, C. M. Lieber, *Acc. Chem. Res.* **1999**, *32*, 435.
[19] M. P. Azch, K. H. Ng, R. M. Penner, *Science* **2000**, *290*, 2120.
[20] Z. R. Dai, Z. W. Pan, Z. L. Wang, *J. Phys. Chem. B* **2002**, *106*, 902.
[21] W. S. Shi, Y. F. Zheng, N. Wang, C.-S. Lee, S.-T. Lee, *Adv. Mater.* **2001**, *13*, 591.
[22] X. Duan, J. Wang, C. M. Lieber, *Appl. Phys. Lett.* **2000**, *76*, 1116.
[23] X. Duan, C. M. Lieber, *Adv. Mater.* **2000**, *12*, 298.
[24] M. S. Gudiksen, C. M. Lieber, *J. Am. Chem. Soc.* **2000**, *122*, 8801.
[25] L. Grocholl, J. J. Wang, E. G. Gillan, *Chem. Mater.* **2001**, *13*, 4290.
[26] S. M. Gao, Y. Xie, J. Lu, G. A. Du, W. He, D. L. Cui, B. B. Huang, M. H. Jiang, *Inorg. Chem.* **2002**, *41*, 1850.
[27] S. M. Gao, J. Lu, Y. Zhao, N. Chen, Y. Xie, *Chem. Commun.* **2002**, 2880.
[28] S. M. Gao, J. Lu, N. Chen, Y. Zhao, Y. Xie, *Chem. Commun.* **2002**, 3064.
[29] S. M. Gao, J. Lu, Y. Zhao, N. Chen, Y. Xie, *Eur. J. Inorg. Chem.* **2003**, 1822.
[30] H. Yamane, M. Shimada, F. J. Disalvo, *Mater. Lett.* **2000**, *42*, 66.
[31] H. Yamane, T. Kajiwara, T. Sekiguchi, M. Shimada, *Jpn. J. Appl. Phys.* **2000**, *39*, L146.
[32] X. F. Duan, C. M. Lieber, *J. Am. Chem. Soc.* **2001**, *122*, 188.
[33] C. C. Chen, C. C. Yeh, *Adv. Mater.* **2000**, *12*, 738.
[34] J. A. Haber, P. C. Gibbons, W. E. Buhro, *J. Am. Chem. Soc.* **1997**, *119*, 5455.

Received June 2, 2003
Early View Article
Published Online December 4, 2003

 © 2004 Wiley-VCH Verlag GmbH & Co. KGaA, Weinheim

Multi-Dimensional Systems Built from Dichromate Anions − Syntheses, Crystal Structures, and Magnetic Properties

Xiao-Yan Chen,[a] Bin Zhao,[a] Peng Cheng,*[a] Bin Ding,[a] Dai-Zheng Liao,[a] Shi-Pin Yan,[a] and Zong-Hui Jiang[a]

Keywords: Chromium / Magnetic properties / N ligands / Self-assembly

Three novel compounds with bridging dichromate anions with the formulae $[Fe(4,4'\text{-bpy})_2Cr_2O_7]_n$ (**1**), $[Co(4,4'\text{-bpy})_2Cr_2O_7]_n$ (**2**), and $[Ni(dpa)_2Cr_2O_7]\cdot H_2O$ (**3**) (4,4′-bpy = 4,4′-bipyridine, dpa = 2,2′-dipyridylamine) have been synthesized and characterized. The isostructural compounds **1** and **2** belong to the monoclinic space group *C*2/*c* and have been shown to be three-dimensional polymers in which the dichromate anions connect neighboring layers formed by $[M(4,4'\text{-bpy})_2]^{2+}$ (M = Fe, Co) units. Compound **3** is a metallacrown type compound, crystallizing in the monoclinic space group $P2_1/n$. Two chromate anions link two Ni^{II} centers forming a dinuclear entity. The uncoordinated oxygen atom of the dichromate anion forms a hydrogen bond with the N–H unit of dpa resulting in a two-dimensional network. Measurements of magnetic susceptibilities indicate the presence of antiferromagnetic interactions in **1** and **2** whereas the exchange coupling between the Ni^{II} ions in **3** is ferromagnetic. The IR and UV/Vis spectra of the above complexes have also been investigated.

(© Wiley-VCH Verlag GmbH & Co. KGaA, 69451 Weinheim, Germany, 2004)

Introduction

Investigations of novel inorganic-organic hybrid framework assemblies constitute one of the most active areas of material science and chemical research. The intense interest in these materials has been driven, to a large extent, by their interesting properties such as electrical conductivity, magnetism, photo-mechanistic behavior, and shape specificity as well as their potential applications in areas such as catalysis.[1−3] Many important properties of supramolecular systems depend largely on their structures and topologies. Rational design and construction of new materials with specific networks has therefore become a particularly important and topical subject.[4,5]

The chromate ion has long been known to bridge metal centers forming oligomeric and polymeric systems and many chromate bridged polynuclear complexes have been characterized.[6−9] On the other hand we know that between the physiologically accessible pH values of 2−6 the $HCrO_4^-$ and $Cr_2O_7^{2-}$ ions are in equilibrium.[10] Whereas many structural studies of simple or double "inorganic" dichromates have been reported,[11] the use of the dichromate anion as a bridging ligand forming multi-dimensional networks needs to be explored more deeply.[12,13]

We started to design hybrid complexes with dichromate anions and the typical polypyridine system which is well-known to act as a rigid, rod-like organic building block. In this paper we report the synthesis and structural characterization of three dichromate polymers, $[Fe(4,4'\text{-bipy})_2Cr_2O_7]_n$ (**1**), $[Co(4,4'\text{-bipy})_2Cr_2O_7]_n$ (**2**), and $[Ni(dpa)_2Cr_2O_7]\cdot H_2O$ (**3**) (4,4′-bpy = 4,4′-bipyridine, dpa = 2,2′-dipyridylamine). Furthermore, their magnetic and spectroscopic properties have also been studied.

Results and Discussion

Crystal Structure of $[Fe(4,4'\text{-bpy})_2Cr_2O_7]_n$ (1)

The molecular structure of **1** is shown in Figure 1. The iron atom is in an octahedral environment. Besides the two coordinated *trans*-oxygen atoms of the dichromate [Fe1−O1, 2.137(4); Fe1−O4, 2.132(4) Å] with the O1−Fe1−O4 angle of 173.65(13)°, there are four coordinated nitrogen atoms from the 4,4′-bipyridine ligands [Fe1−N1, 2.122(3); Fe1−N2, 2.277(4); Fe1−N3, 2.135(4); Fe1−N4, 2.264(4) Å]. Compared with $[Fe(C_2O_4)$(4,4′-bipyridine)] and $[FeCl_2$(4,4′-bipyridine)], the Fe−O and Fe−N bond lengths are in the normal range.[14,15] The non-bridging Cr−O distances are shorter than those of the bridging Cr−O distances. The Cr^{VI} ion adopts an almost regular tetrahedral geometry with an average O−Cr−O bond angle 109.46° for each $[Cr_2O_7]^{2-}$ unit. The Cr−O−Cr bond angle deviates significantly from 180° and is 128.5(2)° in **1**. Surprisingly, there is a 22.4° difference in the two Fe−O−Cr angles [157.9(2)° at O1 vs. 135.5(2)° at O4], although the Fe−O bond lengths are not significantly differ-

[a] Department of Chemistry, Nankai University, Tianjin 300071, P. R. China
Fax: (internat.) + 86-22-23502458,
E-mail: pcheng@nankai.edu.cn

 © 2004 Wiley-VCH Verlag GmbH & Co. KGaA, Weinheim DOI: 10.1002/ejic.200300410

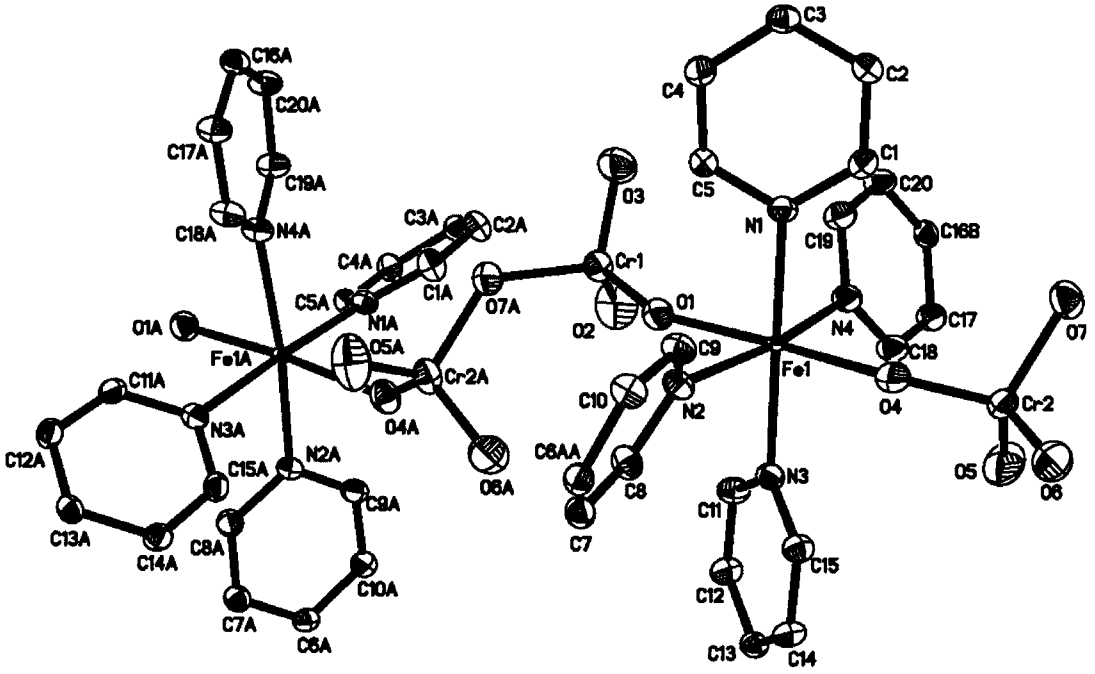

Figure 1. ORTEP diagram of $[Fe(4,4'\text{-bpy})_2Cr_2O_7]_n$ (**1**); the hydrogen atoms and parts of the pyridine rings have been omitted for clarity

ent (Table 1). As a result there are two distinct Fe···Cr distances of 3.702(7) and 3.497(5) Å, which are similar to those of some rare examples of Fe−Cr systems.[10,16]

The structure of **1** contains 2-D parallelogram sheets built upon $[Fe(4,4'\text{-bpy})_2]^{2+}$ building blocks which are cross-linked by dichromate anions like the pillars in clays to form a 3-D structure with two types of channels perpendicular to the (010) and (101) planes, respectively. The rhombic channels with dimensions of 8.859 × 11.472 Å (defined by neighboring Fe···Fe distances) perpendicular to the (010) plane are shown in Figure 2(a), and the square channels with dimensions of 11.436 × 11.472 Å perpendicular to the (101) plane are shown in Figure 2(b).

$[Co(4,4'\text{-bpy})_2Cr_2O_7]_n$ (2)

The structures of **1** and **2** are isostructural except that Fe atoms are replaced by Co atoms. Owing to the difference of the atomic radius, the coordination geometry around the Co^{II} ion is slightly different. The Co^{II} ion is also in an octahedral environment with two *trans*-oxygen atoms of the two dichromate anions in the apical position and four nitrogen atoms of the 4,4′-bpy ligand in the equatorial plane. Similarly, the bridging Cr−O bond lengths [average Cr−O: 1.711(5)Å] are longer than the non-bridging Cr−O bond lengths [average Cr−O: 1.598(5) Å]. The angle O−Co−O is 175.31(14)°. The Cr^{VI} also adopts an almost regular tetrahedral geometry with an average O−Cr−O bond angle of 109.46° for each $[Cr_2O_7]^{2-}$ unit and the Cr−O−Cr bond angle of 128.7(2)° in **2** is similar to that in **1**. There is a 17.6° difference in the two Co−O−Cr angles [157.7(2)° and 140.1(2)°] which is smaller than that observed in compound **1**. Consequently there are also two distinct Co···Cr distances of 3.623(5) and 3.480(4) Å.

In compound **2**, the Co^{II} ions are linked by 4,4′-bpy units in two orthogonal directions and dichromate ions in the third direction thus forming a 3-D structure with two types of channels, similar to **1**. The dimensions of the channels are slightly different: the rhombic channels perpendicular to the (010) plane are 8.790 × 11.436 Å, and the square channels are 11.383 × 11.436 Å perpendicular to the (101) plane.

$[Ni(dpa)_2Cr_2O_7]\cdot H_2O$ (3)

The structure of **3** contains a center of inversion with two $\mu_{1,5}$-dichromate bridges between the two nickel atoms forming a metalla-crown type compound. There has been considerable interest in metalla-crown chemistry owing to its potential applications in chemically modified electrodes, anion-selective separation agents, liquid-crystal precursors and magnetic materials.[17−21]

The Ni···Ni separation of 6.642(5) Å is relatively large, e.g. the Ni···Ni separation in $[Py_2Ni_2(HOOCCMe_3)_2(OOCCMe_3)_2(\mu\text{-}OOCCMe_2)(\mu\text{-}OH_2)]$ is 3.456(2) Å,[22] and two terminal dpa ligands on each nickel complete the ligation (Figure 3). The coordination geometry around the nickel atom is octahedral, the equatorial positions being occupied by three nitrogen atoms from two dpa ligands and one oxygen atom from one bridging dichromate anion [Ni1−O1, 2.071(3) Å]. The axial positions are occupied by the other nitrogen atom of the dpa ligand and one oxygen atom from the other dichromate anion [Ni1−O7A, 2.064(3) Å]. The Ni−N distances ranging from 2.054(4) to 2.075(3) Å are similar to those found in [(oxa)Ni(dpa)] [2.029(2) −2.062(2) Å].[23] Each dpa pyridyl ring is essentially planar and the dihedral angle between the two rings is 35.0°, which is clearly different from other dpa complexes, e.g. in com-

 © 2004 Wiley-VCH Verlag GmbH & Co. KGaA, Weinheim

Table 1. Selected bond lengths [Å] and angles [deg] for **1**, **2**, and **3**

Complex **1**			
Fe(1)−N(1)	2.122(3)	Fe(1)−O(4)	2.132(4)
Fe(1)−O(1)	2.137(4)	Fe(1)−N(3)	2.135(4)
Fe(1)−N(4)	2.264(4)	Fe(1)−N(2)	2.277(4)
Cr(1)−O(2)	1.600(4)	Cr(1)−O(3)	1.610(4)
Cr(1)−O(1)	1.634(4)	Cr(2)−O(6)	1.591(4)
Cr(2)−O(5)	1.603(4)	Cr(2)−O(4)	1.641(4)
Cr(2)−O(7)	1.791(4)		
N(1)−Fe(1)−O(4)	87.16(13)	N(1)−Fe(1)−O(1)	91.78(13)
O(4)−Fe(1)−O(1)	173.65(13)	N(1)−Fe(1)−N(3)	177.50(13)
O(4)−Fe(1)−N(3)	91.03(13)	O(1)−Fe(1)−N(3)	89.83(13)
N(1)−Fe(1)−N(4)	90.19(14)	O(4)−Fe(1)−N(4)	100.04(14)
O(1)−Fe(1)−N(4)	86.22(13)	N(3)−Fe(1)−N(4)	91.82(14)
N(1)−Fe(1)−N(2)	88.74(14)	O(4)−Fe(1)−N(2)	88.72(14)
O(1)−Fe(1)−N(2)	84.99(13)	N(3)−Fe(1)−N(2)	89.49(14)
N(4)−Fe(1)−N(2)	171.11(13)	O(2)−Cr(1)−O(3)	109.7(3)
O(2)−Cr(1)−O(1)	110.4(2)	O(3)−Cr(1)−O(1)	110.1(2)
Complex **2**[a]			
Co(1)−O(7)	2.051(4)	Co(1)−O(3)#1	2.053(3)
Co(1)−N(1)	2.116(4)	Co(1)−N(3)	2.139(4)
Co(1)−N(2)#2	2.207(4)	Co(1)−N(4)#3	2.213(4)
Cr(1)−O(1)	1.591(4)	Cr(1)−O(2)	1.599(4)
Cr(1)−O(3)	1.639(3)	Cr(1)−O(4)	1.780(4)
Cr(2)−O(6)	1.593(4)	Cr(2)−O(5)	1.611(4)
Cr(2)−O(7)	1.648(4)	Cr(2)−O(4)	1.779(4)
O(7)−Co(1)−O(3)#1	175.31(14)	O(7)−Co(1)−N(1)	87.04(14)
O(3)#1−Co(1)−N(1)	91.82(14)	O(7)−Co(1)−N(3)	91.20(14)
O(3)#1−Co(1)−N(3)	89.81(14)	N(1)−Co(1)−N(3)	177.57(15)
O(7)−Co(1)−N(2)#2	88.97(15)	O(3)#1−Co(1)−N(2)#2	86.47(14)
N(1)−Co(1)−N(2)#2	89.26(15)	N(3)−Co(1)−N(2)#2	89.05(14)
N(1)−Co(1)−N(4)#3	90.15(15)	N(3)−Co(1)−N(4)#3	91.74(15)
O(1)−Cr(1)−O(2)	109.2(2)	O(1)−Cr(1)−O(3)	109.7(2)
O(2)−Cr(1)−O(3)	110.3(2)	O(1)−Cr(1)−O(4)	109.8(2)
Cr(2)−O(4)−Cr(1)	128.7(2)	Cr(2)−O(7)−Co(1)	140.1(2)
Complex **3**[b]			
Ni(1)−N(6)	2.054(4)	Ni(1)−N(1)	2.062(3)
Ni(1)−O(7)#1A	2.064(3)	Ni(1)−N(4)	2.070(4)
Ni(1)−O(1)	2.071(3)	Ni(1)−N(3)	2.075(3)
Cr(1)−O(4)	1.597(4)	Cr(1)−O(2)	1.605(3)
Cr(1)−O(1)	1.620(3)	Cr(1)−O(3)	1.761(3)
N(6)−Ni(1)−N(1)	177.87(13)	N(6)−Ni(1)−O(7)#1A	91.85(17)
N(1)−Ni(1)−O(7)#1A	88.24(14)	N(6)−Ni(1)−N(4)	86.65(18)
N(1)−Ni(1)−N(4)	93.39(15)	O(7)#1A−Ni(1)−N(4)	176.10(13)
N(6)−Ni(1)−O(1)	89.39(14)	N(1)−Ni(1)−O(1)	92.74(13)
O(7)#1A−Ni(1)−O(1)	85.93(12)	N(4)−Ni(1)−O(1)	90.45(14)
N(6)−Ni(1)−N(3)	91.60(15)	N(1)−Ni(1)−N(3)	86.28(14)
O(7)#1A−Ni(1)−N(3)	91.36(13)	N(4)−Ni(1)−N(3)	92.28(14)
O(1)−Ni(1)−N(3)	177.15(13)	O(4)−Cr(1)−O(2)	110.1(2)
O(4)−Cr(1)−O(1)	110.28(19)	O(2)−Cr(1)−O(1)	111.31(19)
O(4)−Cr(1)−O(3)	108.20(19)	O(2)−Cr(1)−O(3)	105.76(18)
O(1)−Cr(1)−O(3)	111.02(16)		

[a] #1: $x - 1/2, y + 1/2, z - 1/2$; #2: $x, -y + 1, z - 1/2$; #3: $x, -y, z + 1/2$. [b] #1A: $-x + 2, -y + 1, -z$.

plex $[Cu(dpa)(dca)_2]_n$ the dihedral angle between two pyridine rings of 27.2° is very close to that of free dpa (23°).[24] One nickel atom is coordinated to two dpa units and the large twist serves to relieve the steric hindrance within the ligand.

Despite the fact that the Cr^{VI} adopts an almost regular tetrahedral geometry with an average O−Cr−O bond angle 109.46°, the geometric conformation of the $[Cr_2O_7]^{2-}$ unit in **3** is somewhat different: the Cr−O−Cr bond angle [134.39(19)°] is large compared with those seen in **1** and

 © 2004 Wiley-VCH Verlag GmbH & Co. KGaA, Weinheim

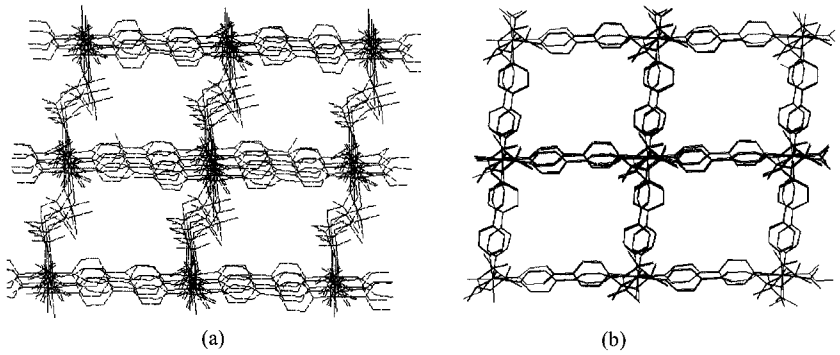

Figure 2. (a) Views of the structure of **1** perpendicular to the (010) plane, showing the rhombic channels; (b) views of the structure of **1** perpendicular to the (101) plane, showing the square channels

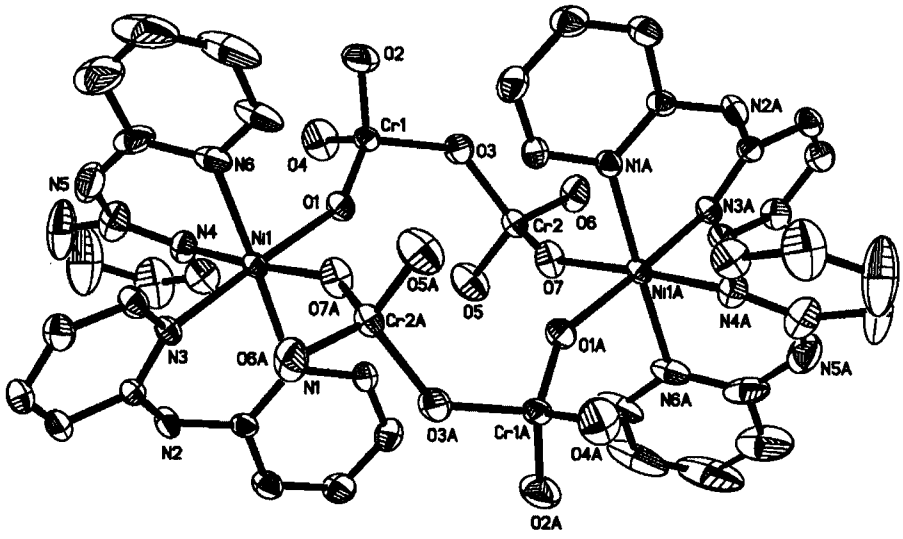

Figure 3. ORTEP diagram of $[Ni(dpa)_2Cr_2O_7]\cdot H_2O$ (**3**), the hydrogen atoms and water molecule have been omitted for clarity

2, and the Ni−O−Cr angles are equal to 151.59(18)°. The widening of the angle at the oxo center may be due to the steric requirements of forming this unusual 12-membered ring. Consequently the Ni···Cr distances are equal to 3.578(5) Å.

The hydrogen atoms of the water molecule in **3** form hydrogen bonds with the nitrogen atoms of neighboring dpa ligands [−H···N, 2.859(3) Å] and uncoordinated oxygen atoms of the bridging dichromate anions [O−H···O, 2.857(8) Å] leading to a 2-D network.

Spectroscopic Properties

The IR spectra of all the complexes show the stretching and bending frequencies of C−C and C−N bonds in the ranges of ca. 1650−1400 cm^{-1} and 1250−650 cm^{-1}, respectively. The ν_{Cr-O} stretching frequencies can be observed at 930−950 cm^{-1} which are in good agreement with those reported for $K_2Cr_2O_7$.[25]

The UV/Vis spectra are also similar. In the UV range, strong absorptions appears at ca. 270−285 nm, which can be assigned to ligand transitions. In the visible region weak absorptions can be observed at ca. 490 nm (spin-forbidden transitions $^5T_{2g}\rightarrow{}^3T_{1g}$, $^3T_{2g}$, ^3E_g) and a relatively stronger absorption at 880 nm ($^5T_{2g}\rightarrow{}^5E_g$) for high-spin Fe^{II} ion can be observed in the spectrum of **1**. A broad strong band centered at ca. 520 nm in the spectrum of **2** can be observed and may be attributed to the d-d transitions of Co^{II} ions in an octahedral environment [$^4T_{1g}\rightarrow{}^4A_{2g}$ and $^4T_{1g}\rightarrow{}^4T_{1g}(P)$]. For complex **3**, the electronic spectrum in the visible range contains a strong absorption band at 630 nm and a weaker one at 475 nm, which are characteristic of an octahedrally coordinated Ni^{II} ion and can be assigned to $^3A_{2g}\rightarrow{}^3T_{1g}$ and $^3A_{2g}\rightarrow{}^3T_{1g}(P)$ transitions, respectively.

Magnetic Properties

The molar magnetic susceptibilities χ_M were measured in the temperature range of 2 to 300 K in a field of 5 KOe for **1**, and 10 KOe for **2** and **3** (Figures 4−7).

As shown in Figure 4, the value of $\chi_M T$ for **1** at 300 K is 2.99 $cm^3\cdot K\cdot mol^{-1}$ (4.89 μ_B) which is close to that of an isolated high-spin Fe^{II} ion ($S = 2$). As the temperature is decreased, the value of $\chi_M T$ decreases gradually and then decreases rapidly in the lower temperature region indicating that a weak antiferromagnetic coupling exists between the

 © 2004 Wiley-VCH Verlag GmbH & Co. KGaA, Weinheim

Fe^{II} ions. In **1**, two exchange pathways are available: one is the inter-chain coupling (via 4,4′-bpy) and the other is the intra-chain interaction (via the dichromate anion). The system was therefore treated using a one-dimensional approach. The Heisenberg exchange theory was utilized, where the Hamiltonian in Equation (1) was employed. The molar magnetic susceptibility per ion is given by the polynomial expression in Equation (2).[26]

$$H = -2J\sum_{i=1}^{N-1} S_i \cdot S_{i+1} \quad (1)$$

$$\chi_{chain} = (Ng^2\mu_B^2)(kT)^{-1}[(A(s) + [B(s)]\,x^2) \times (1 + [C(s)]x + [D(s)]x^3)^{-1}] \quad (2)$$

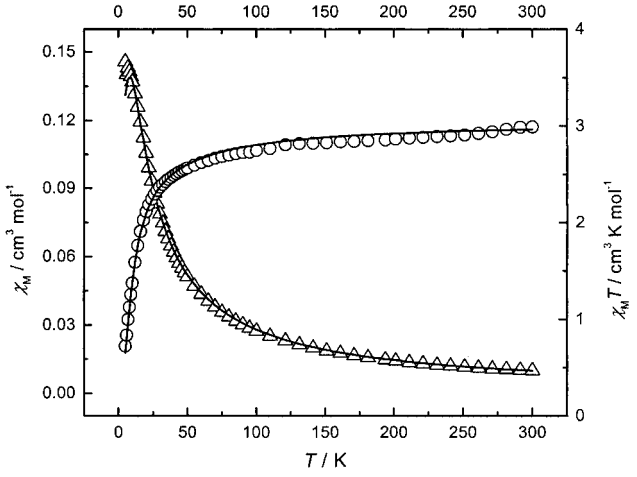

Figure 4. Plots of χ_M (Δ) and $\chi_M T$ (O) versus temperature for **1**; the solid line represents the theoretical curve with the best fit parameters

A molecular field approximation, Equation (3), was then used to modify the inter-chain interaction (zJ') giving the final susceptibility equations of the systems.[27] For the case of the $S = 2$ linear chain, $A = 2.000$, $B = 71.938$, $C = 10.428$, $D = 955.56$, and $x = J / kT$. The best fit of the magnetic susceptibility data yielded $J = -0.74$ cm^{-1}, $zJ' = -0.045$ cm^{-1} and $g = 2.02$. The agreement factor R is 3.65×10^{-4} $\{R = \Sigma[(\chi_M)^{obs} - (\chi_M)^{calc}]^2/[(\chi_M)^{obs}]^2\}$. This result indicates that there are weak antiferromagnetic interactions between the Fe^{II} ions within the chain which may be due to the large Fe···Fe distance and there also exist weak inter-chain antiferromagnetic interactions.

$$\chi_M = \chi_{chain} / [1 - \chi_{chain}(2zJ' / Ng^2\beta^2)] \quad (3)$$

For compound **2**, the high-spin octahedral Co^{II} ion has a $^4T_{1g}$ ground state and, as a consequence, exhibits unquenched spin-orbit coupling in addition to zero-field splitting, which dominates in the low-temperature region.[28]

Unfortunately, no expressions account for both factors simultaneously. Therefore, the data for **2** were fit using the expression in Equation (4) (with $x = \lambda/kT$) for spin-orbit coupling. The molecular field approximation which was further considered for the magnetic interactions between cobalt(II) ions and the magnetic susceptibilities is illustrated in Equation (5). The best fit (as shown in Figure 5) was obtained with values of $A = 1.5$, $\lambda = -170.8$ cm^{-1}, $g = 2.19$ and $zJ' = -0.09$ cm^{-1}, where A is a crystal field parameter ($A = 1.5$ is the weak-field limit), λ is the spin-orbit coupling constant ($\lambda = -176.0$ cm^{-1} is the free-ion value). The agreement factor $R = 4.71 \times 10^{-5}$. These are very similar to the published values for the related compound $[Ph_4P][Co\{N(CN)_2\}_3]$ (A = 1.5, $\lambda = -170.0$ cm^{-1}).[28] Thus, the fit suggests the presence of cobalt ions with slightly distorted octahedral geometries which is consistent with the crystal structure. The room-temperature magnetic moment of 5.13 μ_B is close to that expected for a weak-field ion (5.20 μ_B), with the slightly lower value indicative of the small perturbation from the ideal octahedral geometry as can be observed in the structure. The value of zJ' indicates a very weak antiferromagnetic exchange interaction between the Co^{II} ions.

$$\chi_M = \frac{N\beta^2}{3kT}\frac{\left[\frac{7(3-A)^2x}{5} + \frac{12(A+2)^2}{25A} + \left\{\frac{2(11-2A)^2x}{45} + \frac{176(A+2)^2}{675A}\right\}\exp\left(-\frac{5Ax}{2}\right) + \left\{\frac{(A+5)^2x}{9} - \frac{20(A+2)^2}{27A}\right\}\exp(-4Ax)\right]}{\frac{x}{3}\left[3 + 2\exp\left(-\frac{5Ax}{2}\right) + \exp(-4Ax)\right]} \quad (4)$$

$$\chi_M = \chi_{Co} / [1 - \chi_{Co}(2zJ' / Ng^2\beta^2)] \quad (5)$$

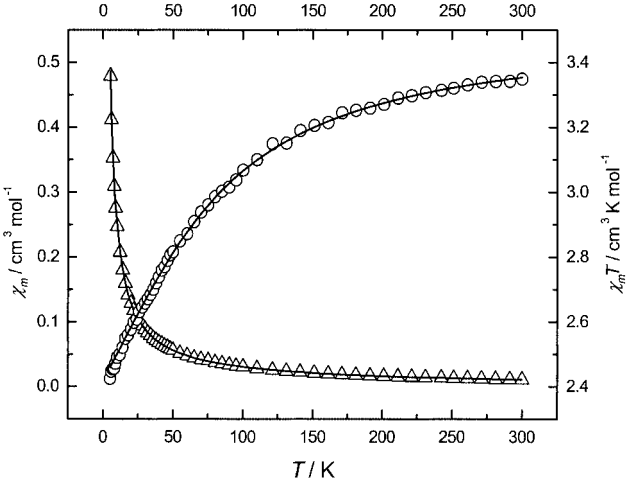

Figure 5. Plots of χ_M (Δ) and $\chi_M T$ (O) versus the temperature for **2**; the solid line represents the theoretical curve with the best fit parameters

The temperature dependence of $\chi_M T$ of **3** is shown in Figure 6. At room temperature $\chi_M T$ is 2.074 cm^3·K·mol^{-1} which is as expected for a spin-only Ni^{II} ion. It continuously increases upon cooling and reaches a maximum value of 2.172 cm^3·K·mol^{-1} at 24 K and further rapidly decreases to 1.85 cm^3·K·mol^{-1} at 2 K. This curve is in agreement with a significant ferromagnetic coupling between the nickel ions whereas in the published literature, most of the dimers with Ni^{II} (d^8) centers have been described as antiferromagnetic.[29–31] Zero-field splitting (D) and inter-

 © 2004 Wiley-VCH Verlag GmbH & Co. KGaA, Weinheim

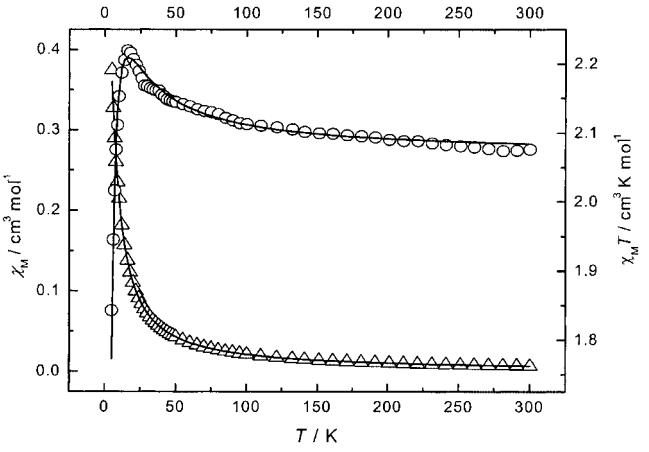

Figure 6. Plots of χ_M (Δ) and $\chi_M T$ (O) versus temperature for **3**; the solid line represents the theoretical curve with the best fit parameters

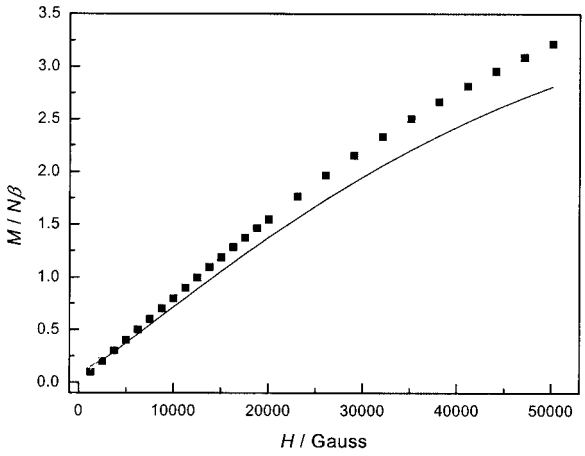

Figure 7. Magnetization curve of **3** (black squares) at 5 K; solid line: Brillouin function corresponding to two uncoupled Ni ions measured at 5 K supports the ferromagnetic interaction in this compound; the experimental values are higher than those calculated by Brillouin functions for two isolated centers with $S = 1$, which confirms the weak ferromagnetic correlation between the two Ni^{II} ions;[35] the effects of single-ion zero-field splitting and inter-dimer interactions cause the rapid low-temperature decrease in $\chi_M T$

molecular interactions could account for the decrease of $\chi_M T$ in the lower temperature region.

The nickel dimers contain "octahedrally" coordinated divalent nickel. Since the single-ion ground state is an orbital singlet state, it is appropriate to use the isotropic spin-coupling Hamiltonian [Equation (6)][32] where $\hat{H}_o$ is the Hamiltonian without considering the zero-field splitting and inter-dimer interactions, J is the exchange integral for the intra-dimer interaction between nickel atoms with spin operators $\hat{s}_1$ and $\hat{s}_2$. Since divalent nickel can have a large zero-field splitting parameter, it is necessary to evaluate the effect of single-ion zero-field splitting on the susceptibility. Allowing an external magnetic field H to be applied, the Hamiltonian can be described as shown in Equation (7).[33]

$$\hat{H}_o = -2J\hat{S}_1 \cdot \hat{S}_2 \quad (6)$$

$$\hat{H} = -2J\hat{S}_1 \cdot \hat{S}_2 - D(\hat{S}_{1z}^2 + \hat{S}_{2z}^2) - g\beta H\hat{S} \quad (7)$$

Taking $g_x = g_z = g$ (a very good approximation for Ni^{2+}), the temperature dependence of the magnetic susceptibilities was calculated using the equation derived from the above Hamiltonian operator.[33,34]

A temperature independent susceptibility term ($N\alpha$) was also include and was set as 2.0×10^{-4} cm^3·mol^{-1}.

A good fit, shown in Figure 6, was obtained for the following parameter set: $g = 2.04$, $J = 1.68$ cm^{-1}, $D = -2.86$ cm^{-1} and $R = 8.96 \times 10^{-5}$. Also the magnetization curve is shown in Figure 7 (0−50 kOe).

According to the above results, the two nickel(II) ions are weakly ferromagnetically coupled through the dichromate anions joining them [Ni···Ni, 6.642(5) Å].

Conclusion

The combined use of the polypyridine system and dichromate anion as ligands towards M^{II} ions [M = Fe (**1**), Co (**2**), Ni (**3**)] allowed us (i) to obtain three new dichromate bridged polymers with the dichromate exhibiting a $\mu_{1,5}$ bridging mode (ii) to study their spectroscopic properties, and (iii) to investigate the efficiency of this mode in mediating exchange interactions between the M^{II} ions. In conclusion, using the dichromate anion to form multi-dimensional systems is quite a useful method for building up multi-dimensional structures. It promises to open a new route for the formation of coordination polymers, which may exhibit interesting topologies and potential properties such as magnetic ordering and spectroscopic or electrical conductivity.

Experimental Section

General Remarks C, H, and N analyses were obtained at the Institute of Elemental Organic Chemistry, Nankai University. IR spectra were recorded in KBr disks on a Shimadzu IR-408 infrared spectrophotometer in the 4000−600 cm^{-1} region. UV/Vis spectra in DMF were recorded on a Shimadzu UV-2101 PC UV/Vis scanning spectrophotometer. Variable-temperature magnetic susceptibilities were measured on a Quantum Design MPMS-7 SQUID magnetometer. Diamagnetic corrections were made with Pascal's constants for all the constituent atoms.

Preparation of $[Fe(4,4'\text{-bipy})_2Cr_2O_7]_n$ (1): An aqueous solution of $(NH_4)_2Fe(SO_4)_2 \cdot 6H_2O$ (78.4 mg, 0.2 mmol) and 4,4′-bipyridine (62.5 mg, 0.4 mmol) was heated to reflux for a few minutes. $K_2Cr_2O_7$ (58.8 mg, 0.2 mmol) dissolved in water (5 mL) was then added. The resultant mixture was heated to reflux for 2 h and was then filtered. The filtrate was evaporated at room temperature. Red crystals suitable for X-ray analysis were obtained after a week. Yield: 40%. $C_{20}H_{16}Cr_2FeN_4O_7$: calcd. C 41.12, H 2.76, N 9.59; found C 41.45, H 2.72, N 9.43.

$[Co(4,4'\text{-bipy})_2Cr_2O_7]_n$ (2): The synthetic method here was similar to that used for the preparation of **1** except that

 © 2004 Wiley-VCH Verlag GmbH & Co. KGaA, Weinheim

Table 2. Data collection and processing parameters for **1**, **2**, and **3**.

	1	**2**	**3**
Formula	$C_{20}H_{16}Cr_2FeN_4O_7$	$C_{20}H_{16}CoCr_2N_4O_7$	$C_{20}H_{20}Cr_2N_6NiO_8$
Fw	584.22	587.30	635.13
K	273(2)	293(2)	273(2)
Space group	*C*2/*c*	*C*2/*c*	$P2_1/n$
a (Å)	21.656(9)	21.512(8)	10.158(9)
b (Å)	15.299(6)	15.328(6)	13.855(12)
c (Å)	17.050(7)	16.904(6)	18.475(16)
β (°)	127.130(5)	127.176(6)	102.884(15)
V (Å^3)	4504(3)	4441(3)	2535(4)
Z	8	8	4
ρ (g/cm^3)	1.723	1.757	1.664
μ (mm^{-1})	1.634	1.750	1.633
θ (°)	1.78−25.03	1.78−25.02	1.85−25.02
Index ranges	$-19 \le h \le 25$	$-21 \le h \le 25$	$-12 \le h \le 7$
	$-16 \le k \le 18$	$-17 \le k \le 18$	$-13 \le k \le 16$
	$-20 \le l \le 20$	$-20 \le l \le 9$	$-18 \le l \le 21$
Refl. collected	9026	8891	8835
Independent refl.	3090, R_{int} = 0.0313	3828, R_{int} = 0.0487	4391, R_{int} = 0.0396
Max/min transmission	0.7359 and 0.6400	0.7210 and 0.6218	0.7359 and 0.6400
Data/restraints/parameter	3930/0/307	3828/0/307	4391/0/334
Goodness-of-fit on F^2	1.067	1.020	1.010
R_1, wR_2 [$I>2\sigma(I)$]	0.0462, 0.1214	0.0514, 0.1119	0.0409, 0.0903
R_1, wR_2 (all data)	0.0586, 0.1305	0.0767, 0.1205	0.0778, 0.1029
Largest diff. peak and hole (e·Å^{-3})	1.176 and −0.933	0.915 and −0.623	0.644 and −0.312

$(NH_4)_2Fe(SO_4)_2{\cdot}6H_2O$ was replaced with $Co(ClO_4)_2{\cdot}6H_2O$. After several days, wine-colored crystals suitable for X-ray analysis were obtained. Yield: 55%. $C_{20}H_{16}CoCr_2N_4O_7$: calc. C 40.90, H 2.75, N 9.54; found C 40.76, H 2.67, N, 9.45.

$[Ni(dpa)_2Cr_2O_7]{\cdot}H_2O$ (3): The synthetic method here was similar to that used for the preparation of **1** except that $(NH_4)_2Fe(SO_4)_2{\cdot}6H_2O$ and 4,4′-bipyrydine were replaced by $Ni(ClO_4)_2{\cdot}6H_2O$ and dpa, respectively. Dark green crystals suitable for X-ray analysis were obtained after a week. Yield: 62%. $C_{20}H_{20}Cr_2N_6NiO_8$: calcd. C 37.82, H 3.17, N 13.23; found C 38.04, H 3.35, N 13.14.

Crystallographic Studies: Crystals of **1**, **2**, and **3** having the approximate dimensions of 0.30 mm × 0.25 mm × 0.20 mm were mounted on glass fibers. Determinations of the unit cells and data collection were performed with Mo-*Kα* radiation (λ = 0.71073 Å) on a Bruker SMART 1000 diffractometer equipped with a CCD camera. The ω − 2θ scan technique was employed. Crystal parameters and structural refinements for **1**, **2** and **3** are summarized in Table 2. Selected bond lengths and angles are listed in Table 1.

The structures were solved primarily by direct method and secondly by Fourier difference techniques and refined by the full-matrix least-squares method. Computations were performed with the SHELXL-97 program.[36,37] All non-hydrogen atoms were refined anisotropically. The hydrogen atoms were set in calculated positions and refined as riding atoms with a common fixed isotropic thermal parameter.

CCDC-194478 (for **1**), -187395 (for **2**), and -200551 (for **3**) contain the supplementary crystallographic data for this paper. These data can be obtained free of charge via www.ccdc.cam.ac.uk/conts/retrieving.html (or from the Cambridge Crystallographic Data Center, 12 Union Road, Cambridge CB2 1EZ, UK; Fax: + 44-1223-336-033; or E-mail: deposit@ccdc.cam.ac.uk).

Acknowledgments

This work was supported by the National Natural Science Foundation of China (No. 90101028, 50173011) and the Teaching and Research Award Program for Outstanding Young Teachers in Higher Education Institutions of MOE, P. R. C.

[1] O. Kahn, *Molecular Magnetism*; VCH Publishers: New York, **1993**.
[2] S. Kitagawa, M. Kondo, I. Furuchi, M. Munakata, *Angew. Chem. Int. Ed. Engl.* **1994**, *33*, 1759−1761.
[3] M. I. Khan, E. Yohannes, D. Powell, *Inorg. Chem.* **1999**, *38*, 212−213.
[4] S. R. Batten, R. Robson, *Angew. Chem. Int. Ed.* **1998**, *37*, 1461−1494.
[5] O. M. Yaghi, H. Li, T. L. Groy, *Inorg. Chem.* **1997**, *36*, 4292−4293.
[6] H. Oshio, T. Kikuchi, T. Ito, *Inorg. Chem.* **1996**, *35*, 4938−4941.
[7] H. Oshio, H. Okamoto, T. Kikuchi, T. Ito, *Inorg. Chem.* **1997**, *36*, 3201−3203.
[8] H. Oshio, T. Kikuchi, T. Ito, *Chem. Lett.* **2000**, 1138−1139.
[9] P. Chaudhuri, M. Winter, K. Wieghardt, S. Gehring, W. Haase, B. Nuber, J. Weiss, *Inorg. Chem.* **1998**, *37*, 1564−1569.
[10] S. Lorenzo, D. C. Craig, M. L. Scudder, I. G. Dance, *Polyhedron* **1999**, *18*, 3181−3185.
[11] J. T. Park, T. Nishioka, T. Suzuki, K. Isobe, *Bull. Chem. Soc. Jpn.* **1994**, *67*, 1968−1971.
[12] G. De Munno, T. Poerio, M. Julve, F. Lloret, J. Faus, A. Caneschi, *J. Chem. Soc., Dalton Trans.* **1998**, 1679−1685.
[13] A. J. Norquist, K. R. Heier, P. S. Halasyamani, C. L. Stern, K. R. Poeppelmeier, *Inorg. Chem.* **2001**, *40*, 2015−2019.
[14] J. Y. Lu, M. A. Lawandy, J. Li, *Inorg. Chem.* **1999**, *38*, 2695−2704.
[15] M. A. Lawandy, X. Y. Huang, R. J. Wang, J. Li, J. Y. Lu, T. Yuen, C. L. Lin, *Inorg. Chem.* **1999**, *38*, 5410−5414.

 © 2004 Wiley-VCH Verlag GmbH & Co. KGaA, Weinheim

[16] B. C. Dave, R. S. Czernuszewicz, *Inorg. Chem.* **1994**, *33*, 847−848.
[17] V. L. Pecoraro, A. J. Stemmler, B. R. Gibney, J. J. Bodwin, H. Wang, J. W. Kampf, A. Barwinski, *Progress in Inorganic Chemistry, Vol. 45* (Ed.: K. D. Karlin), John Wiley & Sons, New York, **1997**, pp. 83−177.
[18] S. X. Liu, S. Lin, B. Z. Lin, C. C. Lin, J. Q. Huang, *Angew. Chem. Int. Ed.* **2001**, *40*, 1084−1086.
[19] J. A. Halfen, J. J. Bodwin, V. L. Pecoraro, *Inorg. Chem.* **1998**, *37*, 5416−5417.
[20] B. Kurzak, E. Farkas, T. Glowiak, H. Kozlowski, *J. Chem. Soc., Dalton Trans.* **1991**, 163−167.
[21] A. J. Stemmler, A. Barwinski, M. J. Baldwin, V. Young, V. L. Pecoraro, *J. Am. Chem. Soc.* **1996**, *118*, 11962−11963.
[22] I. L. Eremenko, S. E. Nefedov, A. A. Sidorov, M. A. Golubnichaya, P. V. Danilov, V. N. Ikorskii, Y. G. Shvedenkov, V. M. Novotortsev, I. I. Moiseev, *Inorg. Chem.* **1999**, *38*, 3764−3773.
[23] J. Y. Lu, T. J. Schroeder, A. M. Babb, M. Olmstead, *Polyhedron* **2001**, *20*, 2445−2449.
[24] J. Carranza, C. Brennan, J. Sletten, F. Lloret, M. Julve, *J. Chem. Soc., Dalton Trans.* **2002**, 3164−3170.
[25] J. B. Bates, L. M. Toth, A. S. Quist, G. E. Boyd, *Spectrochim. Acta, Ser. A* **1973**, *29*, 1585.
[26] W. Hiller, J. Strahle, A. Datz, M. Hanack, W. E. Hatfield, L. W. ter Haar, P. Gutlich, *J. Am. Chem. Soc.* **1984**, *106*, 329−335.
[27] C. J. ÓConnor, *Prog. Inorg. Chem.* **1982**, *29*, 203−206.
[28] J. W. Raebiger, J. L. Manson, R. D. Sommer, U. Geiser, A. L. Rheingold, J. S. Miller, *Inorg. Chem.* **2001**, *40*, 2578−2581.
[29] M. I. Arriortua, A. R. Cortés, L. Lezama, T. Rojo, X. Solans, M. Font Bardía, *Inorg. Chim. Acta* **1990**, *174*, 263−269.
[30] R. Vicente, A. Escuer, J. Ribas, M. Salah el Fallah, X. Solans, M. Font-Bardia, *Inorg. Chem.* **1993**, *32*, 3557−3561.
[31] K. K. Nanda, R. Das, L. K. Thompson, K. Venkatsubramanian, P. Paul, K. Nag, *Inorg. Chem.* **1994**, *33*, 1188−1193.
[32] A. P. Ginsberg, *Inorg. Chim. Acta Rev.* **1971**, *5*, 45.
[33] A. P. Ginsberg, R. L. Martin, R. W. Brookes, R. C. Sherwood, *Inorg. Chem.* **1972**, *11*, 2884.
[34] J. Glerup, P. A. Goodson, D. J. Hodgson, K. Michelson, *Inorg. Chem.* **1995**, *34*, 6255−6264.
[35] Z. E. Serna, L. Lezama, M. K. Urtiaga, M. I. Arriortua, M. G. Barandika, R. Cortés, T. Rojo, *Angew. Chem. Int. Ed.* **2000**, *39*, 344−347.
[36] G. M. Sheldrick, *SHELXS 97, Program for the Solution of Crystal Structures*; University of Göttingen: Germany, **1997**.
[37] G. M. Sheldrick, *SHELXL 97, Program for the Refinement of Crystal Structures*; University of Göttingen: Germany, **1997**.

Received June 27, 2003
Early View Article
Published Online December 19, 2003

 © 2004 Wiley-VCH Verlag GmbH & Co. KGaA, Weinheim

Intercalation of γ-Butyrolactone into Vanadyl Phosphate and Niobyl Arsenate

Vítězslav Zima,*[a] Klára Melánová,[a] Ludvík Beneš,[a] Miroslava Trchová,[b] and Jiří Dybal[b]

Keywords: Intercalations / Powder X-ray diffraction / Vibrational spectroscopy / ab initio calculations

Intercalation compounds of vanadyl phosphate and isostructural niobyl arsenate with γ-butyrolactone, $VOPO_4{\cdot}C_4H_6O_2$ and $NbOAsO_4{\cdot}C_4H_6O_2$, respectively, were prepared from corresponding propanol intercalates by molecular exchange in a microwave field. The prepared intercalates were characterized using powder X-ray diffraction, density measurements, and thermogravimetric analysis. Infrared and Raman spectra indicate a coordination of the carbonyl oxygen atom of the γ-butyrolactone molecule to the vanadium or niobium atom of the host structure. Quantum mechanical calculations at the ab initio level confirm the proposed structure in which the γ-butyrolactone guest molecules are arranged with the plane of the ring perpendicular to the host layers and are anchored to the layers through the carbonyl oxygen atom coordinated to the transition metal atom of the host.

(© Wiley-VCH Verlag GmbH & Co. KGaA, 69451 Weinheim, Germany, 2004)

Introduction

Vanadyl phosphate dihydrate $VOPO_4{\cdot}2H_2O$ and other isostructural layered compounds are able to accommodate some types of organic molecules in the interlayer space.[1] Aliphatic alcohols and diols,[2−4] amines,[5] carboxylic acids,[6] carboxamides[7] and aliphatic nitriles[8] belong to the compounds which can be intercalated in such a way. Great attention has been devoted to the intercalation of heterocyclic N- and S-donors.[9−13] Recently, the intercalation of ketones,[14,15] aldehydes,[16] poly(ethylene glycol)s,[17,18] and heterocycles with O-donors[18−20] into vanadyl phosphates has been described. These guests are anchored to the host layers by donor−acceptor bonds of their carbonyl or ether oxygen atoms to the vanadium atoms. These intercalates, except aliphatic aldehyde intercalates, are generally very stable in air and the guest molecules are released at relatively high temperatures (for example, the tetrahydrofuran intercalate decomposes at about 160 °C[19]). It indicates that the host−guest interaction is very strong. The aliphatic aldehyde intercalates are unstable and the guests undergo aldol condensation and oxidation. On the other hand, aromatic aldehyde intercalates do not decompose in this way.[16] Some of these intercalates are crystalline solids and their diffractograms show, besides a series of sharp (00*l*) reflections, a number of (*hkl*) diffraction lines giving evidence for a regular structure.

This paper reports the results of the intercalation of γ-butyrolactone into vanadyl phosphate and isostructural niobyl arsenate.

Results and Discussion

γ-Butyrolactone cannot be intercalated directly in anhydrous vanadyl phosphate and replacement of water molecules in $VOPO_4{\cdot}2H_2O$ does not lead to an intercalation. The intercalate had to be prepared by replacing 1-propanol or 2-propanol in the corresponding $VOPO_4$ intercalate with the desired guest. The prepared intercalate was a yellow crystalline solid indicating that vanadium(v) had not been significantly reduced. Similarly, white niobyl arsenate intercalated with γ-butyrolactone was prepared from $NbOAsO_4{\cdot}2C_3H_7OH$. As follows from the results of elemental analyses, both intercalates contain one molecule of the guest per formula unit.

The diffractograms (see Figure 1) of both intercalates show a series of sharp (00*l*) reflections and also contain a number of (*hkl*) diffraction lines (Tables 1 and 2) giving evidence of a regular structure. The lattice parameters of the tetragonal structure are $a = 6.2163(8)$ Å and $c = 9.6681(9)$ Å for the $VOPO_4$ intercalate and $a = 6.6557(8)$ Å and $c = 9.805(3)$ Å for the $NbOAsO_4$ intercalate. The calculated density of 2.205 g/cm^3 for $VOPO_4{\cdot}C_4H_6O_2$ is in a good agreement with the experimental value of 2.21 g/cm^3. A new diffraction line with $d = 11.100$ Å was observed in the diffractogram of the $VOPO_4$ intercalate, measured using synchrotron radiation. This diffractogram can be in-

[a] Joint Laboratory of Solid State Chemistry of Institute of Macromolecular Chemistry of Academy of Sciences and University of Pardubice,
Studentská 84, 53210 Pardubice, Czech Republic
Fax: (internat.) + 420-40-603-6011
E-mail: vitezslav.zima@upce.cz
[b] Institute of Macromolecular Chemistry, Academy of Sciences of the Czech Republic,
Heyrovský Sq. 2, 16206 Prague 6, Czech Republic

 © 2004 Wiley-VCH Verlag GmbH & Co. KGaA, Weinheim **DOI: 10.1002/ejic.200300461**

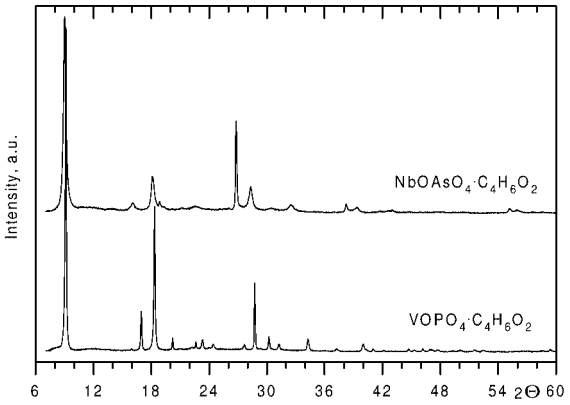

Figure 1. Diffractograms of the prepared intercalates

Table 1. Powder data for $VOPO_4$ intercalated with γ-butyrolactone [a = 6.2163(8) Å, c = 9.6681(9) Å]

2θ [°]	d [Å]	Intensity	h	k	l	$2\theta_{exp} - 2\theta_{calcd.}$ [°]
9.139	9.6680	96	0	0	1	0.000
16.943	5.2285	10	1	0	1	0.001
18.334	4.8349	100	0	0	2	−0.003
20.193	4.3937	2	1	1	0	0.009
22.185	4.0036	1	1	1	1	−0.012
23.287	3.8166	5	1	0	2	−0.004
27.652	3.2232	5	0	0	3	−0.005
28.699	3.1080	21	2	0	0	0.002
30.182	2.9586	6	2	0	1	0.005
31.238	2.8608	6	1	0	3	0.003
34.276	2.6139	8	2	0	2	0.007
37.191	2.4154	3	0	0	4	0.025
39.990	2.2526	12	1	0	4	0.002
41.033	2.1977	1	2	2	0	0.001
42.131	2.1430	1	2	2	1	0.003
42.652	2.1180	1	1	1	4	−0.001
44.691	2.0260	1	3	0	1	0.002
45.297	2.0003	1	2	2	2	0.011
46.122	1.9664	1	3	1	0	−0.016
46.958	1.9333	4	0	0	5	0.008
47.690	1.9053	1	3	0	2	−0.022
49.299	1.8469	2	1	0	5	−0.014
49.994	1.8228	1	2	1	4	0.036
			3	1	2	−0.053
51.591	1.7701	4	1	1	5	−0.004
52.445	1.7432	1	3	0	3	−0.010
57.112	1.6114	1	0	0	6	0.000
61.170	1.5138	1	1	1	6	−0.042
67.958	1.3782	2	3	1	5	0.017

dexed in the triclinic space group $P\bar{1}$ using a fourfold cell with shifted layers. Butyrolactone molecules form a superstructure in the interlayer space.[21]

Both intercalates are stable in air (at a relative humidity of ca. 50%) as are tetrahydrofuran or tetrahydropyran intercalates.[19]

The thermal stability of the $VOPO_4$ intercalate was monitored by X-ray diffraction and thermogravimetry. The position and the intensity of the diffraction lines did not change up to 160 °C. Above this temperature, the intensity of the

Table 2. Powder data for $NbOAsO_4$ intercalated with γ-butyrolactone [a = 6.6557(8) Å, c = 9.805(3) Å]

2θ [°]	d [Å]	Intensity	h	k	l	$2\theta_{exp} - 2\theta_{calcd.}$ [°]
9.010	9.8069	100	0	0	1	−0.002
16.080	5.5074	7	1	0	1	−0.002
18.112	4.8939	20	0	0	2	0.033
18.846	4.7049	8	1	1	0	0.006
22.515	3.9458	5	1	0	2	0.009
26.768	3.3278	56	2	0	0	0.000
28.283	3.1529	15	2	0	1	−0.015
30.441	2.9341	3	1	0	3	−0.003
32.497	2.7530	6	2	0	2	0.005
38.215	2.3532	7	2	2	0	−0.001
39.317	2.2897	4	2	2	1	−0.028
42.574	2.1218	1	2	2	2	−0.008
55.146	1.6641	2	4	0	0	−0.008
55.844	1.6450	1	3	0	4	−0.003
62.361	1.4878	1	4	2	0	0.020
63.135	1.4714	1	4	2	1	−0.001

diffraction lines decreases and the sample becomes green which means that vanadium(v) is reduced and butyrolactone starts to decompose as follows from the thermogravimetry. The total weight loss (34.8%) corresponds to the formula $VOPO_4{\cdot}C_4H_6O_2$. The $NbOAsO_4{\cdot}C_4H_6O_2$ intercalate was not monitored by thermogravimetry, because the host is decomposed at ca. 500 °C.

The character of the bonding between the guest and the host layers in the butyrolactone intercalates was studied by IR and Raman spectroscopy. The IR spectrum of liquid butyrolactone, its intercalates in $VOPO_4$ and $NbOAsO_4$ and the spectra of corresponding hosts in the region from 4000

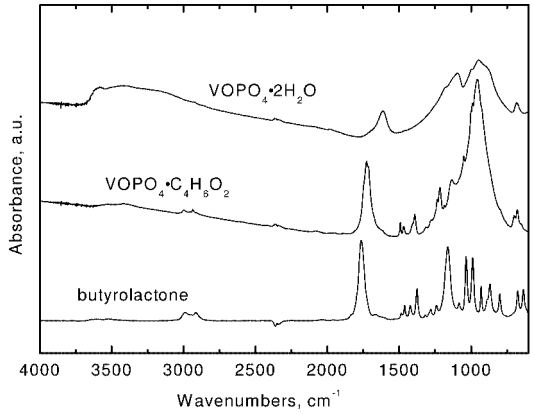

Figure 2. FT IR spectra of liquid butyrolactone (ATR on ZnSe crystal), vanadyl phosphate intercalated with butyrolactone and vanadyl phosphate dihydrate (in KBr pellets)

to 650 cm^{-1} are given in Figures 2 and 3. The Raman spectra of these compounds are given in Figures 4 and 5. The observed bands of the host compounds can be assigned properly, based on the previous studies of the $MOXO_4$ compounds.[22] The spectra have been interpreted in terms of the vibrations of the PO_4^{3-} and AsO_4^{3-} tetrahedrons. Positions of all of the arsenate bands are shifted to lower wavenumbers due to the mass effect of the As atom compared to the P atom.

 © 2004 Wiley-VCH Verlag GmbH & Co. KGaA, Weinheim

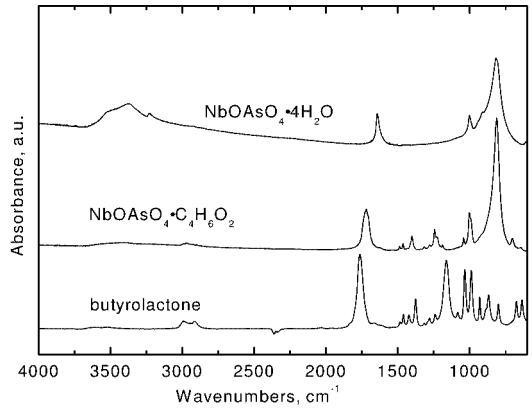

Figure 3. FT IR spectra of liquid butyrolactone (ATR on ZnSe crystal), niobyl arsenate intercalated with butyrolactone and niobyl arsenate tetrahydrate (in KBr pellets)

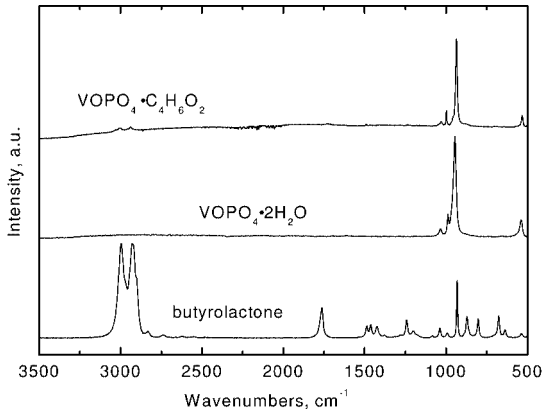

Figure 4. Raman spectra of liquid butyrolactone, vanadyl phosphate intercalated with butyrolactone and vanadyl phosphate dihydrate

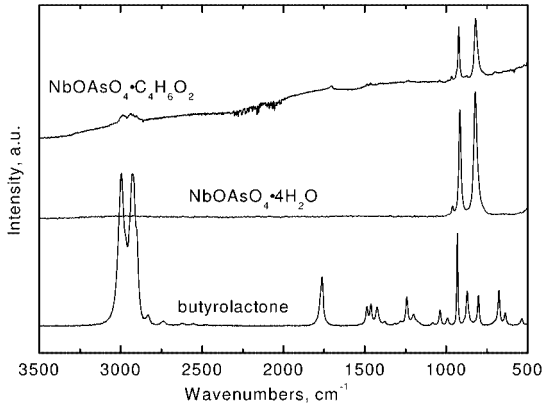

Figure 5. Raman spectra of liquid butyrolactone, niobyl arsenate intercalated with butyrolactone and niobyl arsenate tetrahydrate

The positions of the main spectral bands of the host structures in the vibration spectra of $VOPO_4$ and $NbOAsO_4$ intercalated with butyrolactone differ only slightly from those of vanadyl phosphate and niobyl arsenate hydrates. It confirms that the structures of the original $VOPO_4$ and $NbOAsO_4$ layers remain unchanged after the intercalation reaction. This conclusion is extremely important for the strategy of modeling.

The intense band at 937 cm^{-1} in the Raman spectrum of the $VOPO_4$ intercalate (see Figure 4) corresponds to the symmetric $\nu(PO_4)$ stretching vibration of the phosphate tetrahedron in the $(VOPO_4)_\infty$ layers and it is observed at 957 cm^{-1} in the IR spectrum of the intercalate (see Figure 2). Analogously the intense band at 820 cm^{-1} in the Raman spectrum of the $NbOAsO_4$ intercalate (see Figure 5) corresponds to the symmetric $\nu(AsO_4)$ stretching vibration of the arsenate tetrahedron in the $(NbOAsO_4)_\infty$ layers and it is observed at 817 cm^{-1} in the IR spectrum of the intercalate (see Figure 3). The positions of the V=O and Nb=O stretching vibrations appear to be especially sensitive to atoms coordinated to the vanadium atom within an octahedral arrangement in the host lattice structure. For instance, when water molecules are intercalated into $VOPO_4$, the position of this band at 1035 cm^{-1} in the IR spectrum of the anhydrous form of vanadyl phosphate changes to 995 cm^{-1} typical of mono- and dihydrates.[23] In the Raman spectrum of the vanadyl phosphate we can observe the V=O stretching vibration at 989 cm^{-1} corresponding to the hydrate form and also the vibration at 1035 cm^{-1} corresponding to the anhydrous form of vanadyl phosphate (see Figure 4). It is a result of the partial escape of the water molecules which occurs during the measurements due to the laser beam. In the Raman spectrum of niobyl arsenate, the Nb=O stretching vibration of the hydrate form is observed at 919 cm^{-1} and for the anhydrous form it is situated at 961 cm^{-1} (Figure 5). In the Raman spectrum of the vanadyl phosphate intercalate, the peak at 1000 cm^{-1} corresponds most probably to the V=O stretching vibration with an oxygen atom of butyrolactone coordinated to the vanadium atom (see Figure 4). Analogously, the peak at 924 cm^{-1} in the Raman spectrum of niobyl arsenate corresponds to the Nb=O stretching vibration with an oxygen atom of butyrolactone coordinated to the niobyl atom (see Figure 5). In the IR spectra of the intercalates these bands are overlapped by the spectrum of butyrolactone.

Comparing the positions of the stretching vibration bands of the C=O and C−O groups in the IR and Raman spectra of the pristine butyrolactone with these bands in the spectra of $VOPO_4$ and $NbOAsO_4$ intercalates we observed some shifts which indicate an interaction between the butyrolactone molecules and the host structure. The C=O stretching vibration observed at 1764 cm^{-1} in the IR spectrum of pure liquid butyrolactone is shifted to 1727 cm^{-1} in the IR spectrum of the $VOPO_4$ intercalate and to 1721 cm^{-1} in the IR spectrum of the $NbOAsO_4$ intercalate. In addition, a shoulder is clearly visible on the lower wavenumber side of the C=O stretch peak in the IR spectra. Its position changes from 1762 cm^{-1} in the Raman spectrum of pure butyrolactone to a small peak at 1726 cm^{-1} in the Raman spectrum of the $VOPO_4$ intercalate and at 1707 cm^{-1} of the $NbOAsO_4$ intercalate. The band due to the C−O stretching ring vibration of butyrolactone, observed at 1161 cm^{-1} in its IR spectrum is most probably shifted to the higher wavenumbers; to 1217 cm^{-1} in the IR spectrum

 © 2004 Wiley-VCH Verlag GmbH & Co. KGaA, Weinheim

of the vanadyl phosphate intercalate (see Figure 2) and to 1244 cm^{-1} in the IR spectrum of the niobyl arsenate intercalate (see Figure 3). In the Raman spectra, these peaks are very small.

When the carbonyl oxygen atom of an ester is the donor, a weakening of the C=O bond can be expected together with a strengthening of the adjacent C−O bond as a secondary effect. When forming adducts with Lewis acids in which the metal ion is hexacoordinated by the ester molecule, esters show a negative shift in their carbonyl stretching frequency and a positive shift in their C−O stretching frequency.[24] It was shown[25] that the lithium ions are bound through the oxygen atom of the carbonyl group of butyrolactone in $LiClO_4$/butyrolactone solution. Both the C−C and C=O stretch vibrations are sensitive to an interaction between the Li^+ ion and the butyrolactone molecule. The shifts observed in the spectra of the butyrolactone intercalates indicate a coordination of the O_{guest} of the C=O group of butyrolactone to the vanadium and niobium atoms of the hosts.

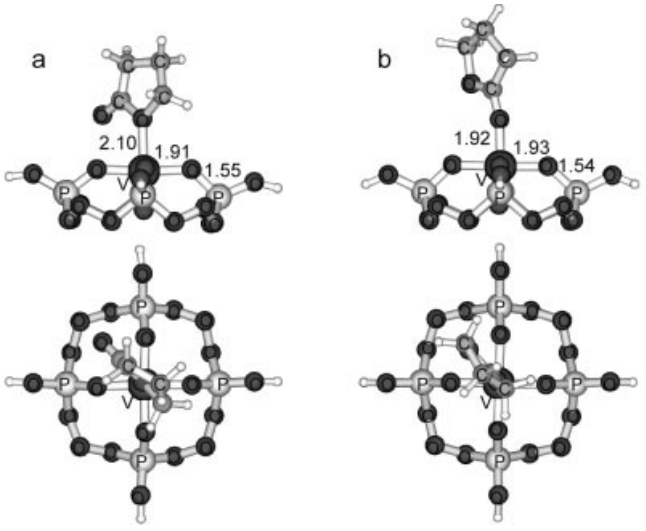

Figure 6. Two optimized HF/TZV structures of the molecular segment modeling the vanadyl phosphate−butyrolactone interaction with indicated bond lengths [A]

Figure 6 shows ab initio (HF/TZV) optimized structures of the molecular segment representing local interactions of vanadyl phosphate with butyrolactone. In order to preserve the overall planar structure of the segment during full geometry optimizations and at the same time make the electronic structure in the segment close to the conditions appearing in the intercalates, an oxygen atom had to be inserted between two neighboring PO_4 groups. Free terminal oxygen atoms have been replaced by OH groups and the total charge of the model compound was set to +3. It was found that all geometry optimizations with various starting orientations of butyrolactone with respect to the vanadyl group lead to the structures displayed in Figure 6 (a and b), which indicates that both C=O→V and C−O(−C)→V bonds can be formed. However, the structure shown in Figure 6 (b) is energetically more favorable by 22.7 kcal/mol and thus only the structure with the C=O→V bond is expected to be formed in the intercalates. This is also confirmed by the results of calculations of vibrational frequencies. While the calculated frequency of the C=O stretching vibration in the structure at Figure 6 (a) is shifted to higher wavenumbers compared to free butyrolactone, the C=O stretching vibration of the structure with the C=O→V bond [Figure 6 (b)] is shifted to lower wavenumbers as observed in the IR and Raman spectra.

Experimental Section

Preparation: The propanol intercalates were prepared by suspending microcrystalline $VOPO_4{\cdot}2H_2O$ or $NbOAsO_4{\cdot}4H_2O$ in dry propanol and monitored by a short exposure to a microwave field. The intercalation compounds were obtained by displacing propanol in $VOPO_4{\cdot}2C_3H_7OH$ or $NbOAsO_4{\cdot}2C_3H_7OH$ by γ-butyrolactone. The propanol intercalate (0.5 g) was dispersed in 15 mL of γ-butyrolactone and exposed to a microwave field for 5 min. The intercalates were filtered off, washed with diethyl ether, and dried in nitrogen. The composition of the intercalate was determined by elemental analyses. $C_4H_6O_7PV$ (248.0): calcd. C 19.37, H 2.44; found C 19.61 H 2.39. $C_4H_6AsNbO_7$ (333.9): calcd. C 14.39, H 1.81; found C 14.25, H 1.87.

XRD: Powder data were obtained with a D8-Advance diffractometer (Bruker AXE, Germany) using Cu-K_α radiation with a secondary graphite monochromator. Diffraction angles were measured from 7 to 80° (2θ).

Density: Density of the $VOPO_4$ intercalate was measured with an automated helium pycnometer (AutoPycnometer 1320, Micromeritics, USA) to 0.01 $g{\cdot}cm^{-3}$ accuracy.

Thermogravimetry: The TG analyses were performed using a Netzsch STA 449C instrument. The measurements were carried out in air between 30 and 800 °C at a heating rate of 5 $°C{\cdot}min^{-1}$.

IR Spectroscopy: IR measurements in the range 400−4000 cm^{-1} were made with a fully computerized Bruker IFS 55 EQUINOX FTIR spectrometer with DLATGS detector (256 scans per spectrum at 4 cm^{-1} resolution). Measurements of the intercalates were performed ex situ in the transmission mode using KBr pellets. The spectrum of the corresponding liquid butyrolactone was measured by the ATR technique on a ZnSe crystal. The spectra were corrected for the content of H_2O and CO_2 in the optical path.

Raman Spectroscopy: FT Raman spectra were collected using a Bruker IFS 55 EQUINOX FTIR spectrometer equipped with an FT Raman module FRA 106/S with diode-pumped, temperature-stabilized Nd YAG laser, and InGaAs detector (128 interferograms were co-added per spectrum in the range 4000 to −1000 cm^{-1} at 4 cm^{-1} resolution).

Calculations: Quantum chemical calculations were carried out at the ab initio level of theory employing the Gaussian 98[26] program package. Local interactions and structures in intercalates of vanadyl phosphate with the nitrile group were studied at the HF level using a TZV basis set.[27]

Acknowledgments

This study was supported by the Grant Agency of the Czech Republic (Grant No. 202/01/0520). The help of the Ministry of Education, Youth and Sports of the Czech Republic (VZ, 113200002)

 © 2004 Wiley-VCH Verlag GmbH & Co. KGaA, Weinheim

and the Academy of Sciences of the Czech Republic (Key project ASCR 205062 and grant AVOZ4050913) is also appreciated.

[1] J. Kalousová, J. Votinský, L. Beneš, K. Melánová, V. Zima, *Collect. Czech. Chem. Commun.* **1998**, *63*, 1−19.
[2] L. Beneš, K. Melánová, V. Zima, *Eur. J. Inorg. Chem.* **2001**, 1883−1887.
[3] L. Beneš, V. Zima, K. Melánová, *J. Incl. Phenom.* **2001**, *40*, 131−138.
[4] L. Beneš, K. Melánová, V. Zima, *J. Solid State Chem.* **2000**, *151*, 225−230.
[5] K. Beneke, G. Lagaly, *Inorg. Chem.* **1983**, *22*, 1503−1507.
[6] L. Beneš, J. Votinský, J. Kalousová, K. Handlíř, *Inorg. Chim. Acta* **1990**, *176*, 255−259.
[7] M. Martinez-Lara, L. Moreno-Real, A. Jimenez-Lopez, S. Bruque-Gamez, A. Rodriguez-Garcia, *Mater. Res. Bull.* **1986**, *21*, 13−23.
[8] L. Beneš, V. Zima, K. Melánová, M. Trchová, P. Matějka, *J. Incl. Phenom.* **2002**, *43*, 95−99.
[9] J. W. Johnson, A. J. Jacobson, J. F. Brody, S. M. Rich, *Inorg. Chem.* **1982**, *21*, 3820−3825.
[10] A. De Stefanis, S. Foglia, A. A. G. Tomlinson, *J. Mater. Chem.* **1995**, *5*, 475−483.
[11] H. Nakajima, G. Matsubayashi, *J. Mater. Chem.* **1994**, *4*, 1325−1329.
[12] T. Yatabe, G. Matsubayashi, *J. Mater. Chem.* **1996**, *6*, 1849−1852.
[13] R. Pozas-Tormo, L. Moreno-Real, S. Bruque-Gamez, M. Martinez-Lara, J. Ramos-Barado, *Mater. Sci. Forum* **1992**, *91−93*, 511−516.
[14] K. Melánová, L. Beneš, V. Zima, P. Čapková, M. Trchová, *Collect. Czech. Chem. Commun.* **1999**, *64*, 1975−1979.
[15] P. Čapková, M. Trchová, V. Zima, H. Schenk, *J. Solid State Chem.* **2000**, *150*, 356−362.
[16] K. Melánová, L. Beneš, V. Zima, J. Votinský, *J. Solid State Chem.* **2001**, *157*, 50−55.
[17] K. Melánová, L. Beneš, V. Zima, R. Vahalová, M. Kilián, *Chem. Mater.* **1999**, *11*, 2173−2178.
[18] K. Goubitz, P. Čapková, K. Melánová, W. Molleman, H. Schenk, *Acta Crystallogr., Sect. B* **2001**, *57*, 178−183.
[19] V. Zima, K. Melánová, L. Beneš, P. Čapková, M. Trchová, P. Matějka, *Chem. Eur. J.* **2002**, *8*, 1703−1709.
[20] L. Beneš, V. Zima, K. Melánová, M. Trchová, P. Čapková, B. Koudelka, P. Matějka, *Chem. Mater.* **2002**, *14*, 2788−2795.
[21] P. Čapková, unpublished results.
[22] S. D. Ross, *Inorganic Infrared and Raman Spectra*, McGraw-Hill, London, **1972**.
[23] M. Trchová, P. Čapková, P. Matějka, K. Melánová, L. Beneš, *J. Solid State Chem.* **1999**, *148*, 197−204.
[24] W. L. Driessen, W. L. Groeneveld, F. W. Van Der Wey, *Recl. Trav. Chim. Pays-Bas* **1970**, *89*, 353−367.
[25] J. J. Wang, X. P. Xuan, J. S. Lu, N. Pei, Y. J. Mo, *Z. Phys. Chem.* **2001**, *215*, 437−446.
[26] M. J. Frisch, G. W. Trucks, H. B. Schlegel, G. E. Scuseria, M. A. Robb, J. R. Cheeseman, V. G. Zakrzewski, J. A. Jr. Montgomery, R. E. Stratmann, J. C. Burant, S. Dapprich, J. M. Millam, A. D. Daniels, K. N. Kudin, M. C. Strain, O. Farkas, J. Tomasi, V. Barone, M. Cossi, R. Cammi, B. Mennucci, C. Pomelli, C. Adamo, S. Clifford, J. Ochterski, G. A. Petersson, P. Y. Ayala, Q. Cui, K. Morokuma, D. K. Malick, A. D. Rabuck, K. Raghavachari, J. B. Foresman, J. J. V. Cioslowski, A. G. Ortiz, B. B. Baboul, G. Stefanov, A. Liu, Liashenko, P. Piskorz, I. Komaromi, R. Gomperts, R. L. Martin, D. J. Fox, T. Keith, M. A. Al-Laham, C. Y. Peng, A. Nanayakkara, C. Gonzalez, M. Challacombe, P. M. W. Gill, B. Johnson, W. Chen, M. W. Wong, J. L. Andres, C. Gonzalez, M. Head-Gordon, E. S. Replogle, J. A. Pople, *Gaussian 98*, Revision A.9, Gaussian, Inc., Pittsburgh, PA, **1998**.
[27] A. Schaefer, C. Huber, R. Ahlrichs, *J. Chem. Phys.* **1994**, *100*, 5829−5835.

Received July 14, 2003
Early View Article
Published Online November 19, 2003

 © 2004 Wiley-VCH Verlag GmbH & Co. KGaA, Weinheim

Copper(I)-Assembled Pseudorotaxanes Bearing Bis(nitrile) Ligands: Selective Formation of Large Chelate Rings

Efstathia G. Sakellariou,[a] Jean-Paul Collin,*[a] Christiane O. Dietrich-Bucheker,[a] and Jean-Pierre Sauvage*[a]

Keywords: Copper / N ligands / Macrocycles / Chelates

The syntheses of two novel Cu^{I}-bis(benzonitrile) complexes of the type $[Cu(dCN_n)_2][PF_6]$ {where dCN_n = $NCPhO(CH_2)_n$-OPhCN, n = 3, 4} are described. Both compounds have been characterized by X-ray crystallography. To our surprise, and although the two complexes were quite similar, two very distinct structures were obtained. For the $[Cu(dCN_4)_2][PF_6]$ complex, a tetrahedral geometry was observed whereas for $[Cu(dCN_3)_2][PF_6]$, a polymeric assembly was formed. A further extension of this work involved the syntheses of two threaded species bearing the M30 macrocycle, Cu metal and a dCN_n ligand. The formation of the desired complexes was confirmed by means of mass spectrometry as well as 1-D and 2-D ^1H NMR spectroscopy. Finally, the cyclic voltammograms of all 4 new species were recorded giving rise to redox potentials ranging from +0.88 to +1.25 V. These new threaded complexes are of particular interest since they can form the basis of novel rotaxane structures.

(© Wiley-VCH Verlag GmbH & Co. KGaA, 69451 Weinheim, Germany, 2004)

Introduction

Nowadays rotaxanes and catenanes constitute an important class of compounds[1] exhibiting interesting properties such as photoinduced electron transfer[2] and controlled molecular motion.[3] Due to the various synthetic strategies developed during the course of the last 20 years, interest in these multi-component systems has experienced a spectacular revival. However, as some of the synthetic approaches employed for their preparation are based on a metal-templated strategy,[4] the metallic species involved should be carefully chosen as it plays an essential role in the actual assembling of such complex structures. In addition, the electronic properties of the metal in question are important in order to control intramolecular electron transfer processes, in relation to the modeling of the photosynthetic reaction center, or to trigger electrochemically driven motions in artificial molecular machines and motors.[5] Traditionally, tetrahedral copper(I) has been the metal of choice in order to induce the formation of entangled structures from two coordinating molecular threads or to drive the formation of a pseudo-rotaxane from a ring and a molecular string.[4] Moreover, the use of octahedrally coordinated metal centers in order to assemble and pre-organize the various organic fragments to be incorporated in the desired catenanes and rotaxanes has also been described.[6,7] A further extension of this work involved the use of a five-coordinate Zn^{2+} center bearing terpyridine and phenanthroline as the coordinating ligands thus giving rise to novel catenane structures.[8]

Although the bidentate chelate of choice has mainly been the 1,10-phenanthroline (phen) unit and its derivatives, other ligands can be envisaged which should also lead to intertwined or threaded species, precursors of the catenanes and rotaxanes to be synthesized. Since copper(I) forms relatively stable complexes with π-accepting ligands and, in particular, with acetonitrile, the possibility of using bidentate chelates consisting of two terminal benzonitrile groups has been explored. In the present article the coordination chemistry between copper(I) and the aforementioned ligands as well as the formation of threaded complexes containing the traditional phen-incorporating 30-membered ring (M30),[9] copper(I) and a bis(nitrile) ligand is described.

Results and Discussion

The bis-nitrile ligands, as well as the 30-membered ring (M30) used in the preparation of the threaded complexes are represented in Scheme 1.

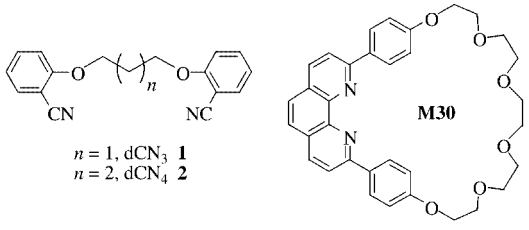

Scheme 1

[a] Laboratoire de Chimie Organo-minérale, UMR 7513 du CNRS
Université Louis Pasteur, Faculté de Chimie,
4 rue Blaise Pascal, 67070 Strasbourg Cedex, France
E-mail: sauvage@chimie.u-strasbg.fr

Surprisingly, chelates consisting of two or more nitrile groups as coordinating sites have been very scarcely used. Angelici and co-workers synthesized a series of interesting complexes with various metal centers in conjunction with such ligands or their isocyanide analogues.[10] Recently, our group also described the synthesis of ruthenium(II) benzonitrile complexes in relation to light-driven molecular machines and motors.[11]

1. Synthesis of $[Cu(dCN_n)_2][PF_6]$ (n = 3, 4) Complexes

The synthesis of the two novel copper(I)−bis(benzonitrile) complexes is depicted in Equation (1).

$$[Cu(CH_3CN)_4][PF_6] \xrightarrow{2\ dCN_n} [Cu(dCN_n)_2][PF_6] + 4\ CH_3CN \quad (1)$$

$n = 3$, $[Cu(dCN_3)_2][PF_6]$ **3**

$n = 4$, $[Cu(dCN_4)_2][PF_6]$ **4**

Reaction of $Cu(CH_3CN)_4{\cdot}PF_6$ with two equivalents of the corresponding dCN_n (n = 3, 4) ligand in dichloromethane results in the quantitative formation of compounds **3** and **4**. The novel complexes were obtained as solids and were characterized by mass spectrometry and ^1H NMR spectroscopy. Moreover, reversible cyclic voltammograms were recorded for both Cu−dCN_n complexes. In particular, $[Cu(dCN_3)_2]^{2+/+}$ showed a remarkably high redox potential of E° = +1.20 V vs. the SCE in CH_2Cl_2, similar to that of the tetrahedral complex $[Cu(dCN_4)_2]^{2+/+}$ (E° = +1.25 V vs. SCE) in the same solvent.

X-ray Structural Studies

In both cases, single crystals suitable for X-ray analysis were obtained by slow diffusion of *n*-hexane (for compound **3**) or diisopropyl ether (for compound **4**) into a degassed solution of the corresponding complex in dichloromethane. Although the only difference between the two Cu−dCN_n complexes resides in the number of carbon atoms incorporated in the chain connecting the two benzonitrile rings, it is sufficient to give rise to two distinct structures as shown in Figures 1 and 2. Thus, although for the $Cu(dCN_3)_2{\cdot}PF_6$ complex a polymeric structure was obtained, for the $Cu(dCN_4)_2{\cdot}PF_6$ compound a monomeric tetrahedral structure was quantitatively formed. In the latter case, a bis-macrocyclization was achieved resulting in the formation of two 15-membered rings assembled around the copper center. The stability of this complex is remarkable confirming the preference of Cu^I in a tetra-coordinated geometry, as well as the "chelate" effect that the two dCN_4 ligands are exerting on the metal atom. Moreover, the high yielding reaction leading to this complex shows that very large metallacycles can be strongly stabilized over ill-defined oligomers or polymers. This is consistent with the observation that cyclic assemblies are very often formed quantitatively from multisite ligands and appropriate metal centers, one of the archetypical examples being that of Fujita's squares consisting of 4 Pd^{II} atoms at the corners and four 4,4′-bipyridine units as edges.[12]

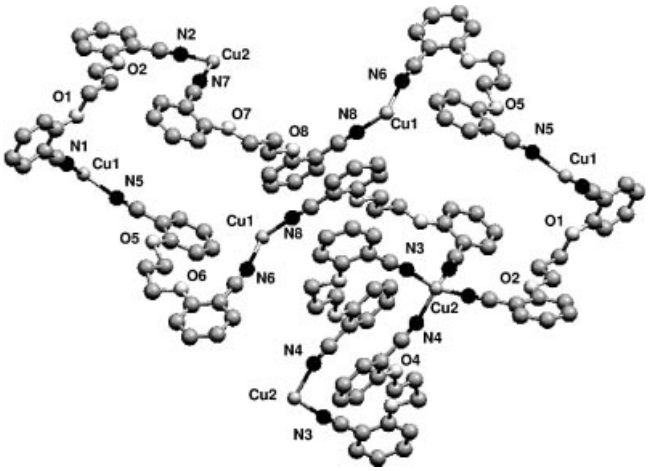

Figure 1. Repeating unit of the polymeric structure obtained for $[Cu(dCN_3)_2][PF_6]$. The assembly consists of 2 types of macrocycles of different size. Hence, the small cycle (28-membered ring) contains two Cu centers connected via two dCN_3 ligands whereas the larger cycle (84-membered ring) bears six Cu centers and the same number of dCN_3 ligands connected to each other in an alternating fashion (Cu-dCN_3−Cu-dCN_3···)

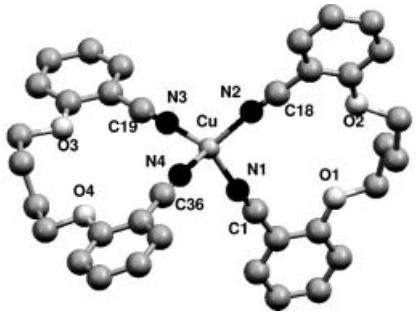

Figure 2. Crystal structure of $[Cu(dCN_4)_2][PF_6]$. A tetrahedral geometry around the Cu-center can be observed with the average Cu−N distances being 1.97 Å. Hydrogen atoms are omitted for clarity. The average N−Cu−N bond angle is 109.4 deg

It should be noted, however, that in the case of the polymeric structure **3** the average Cu^I−N bond length was found to be 1.99 Å which is not significantly different from that of the monomeric complex **4** (1.97 Å) and of the same order of magnitude as the average bond length found in $[Cu(CH_3CN)_4][PF_6]$ (1.99 Å).[13] On the other hand, a slightly longer Cu^I−N distance was measured in the tetrakis benzonitrile Cu^I complex $[Cu(PhCN)_4][SbCl_6]$ (2.05 Å).[14] Selected bond lengths and bond angles are given for both complexes in Tables 1 and 2.

2. Synthesis of $[Cu(M30)(dCN_n)][PF_6]$ (n = 3, 4) Threaded Complexes

Having successfully synthesized the two new Cu-dCN_n complexes, the threading reaction incorporating a ring, namely M30, the Cu metal and a dCN_n ligand was also attempted in order to see if the synthesis of pseudo-rotaxane structures based on such benzonitrile ligands was feasible.

Based on CPK models, the dCN ligand was found to fit comfortably within the cavity of the M30 ring which was therefore chosen as the macrocycle for the threading reac-

 © 2004 Wiley-VCH Verlag GmbH & Co. KGaA, Weinheim

Table 1. Selected bond lengths [Å] and bond angles [deg] for **3**

3	Length (Å)	**3**	Angle (deg)
$Cu(1)-N_{dCN(1)}$	2.01	$N_{dCN(1)}-Cu(1)-N_{dCN(5)}$	114.2
$Cu(1)-N_{dCN(5)}$	2.00	$N_{dCN(1)}-Cu(1)-N_{dCN(6)}$	113.2
$Cu(1)-N_{dCN(6)}$	2.00	$N_{dCN(1)}-Cu(1)-N_{dCN(8)}$	103.9
$Cu(1)-N_{dCN(8)}$	1.989	$N_{dCN(5)}-Cu(1)-N_{dCN(6)}$	101.2
$Cu(2)-N_{dCN(2)}$	2.001	$N_{dCN(5)}-Cu(1)-N_{dCN(8)}$	110.6
$Cu(2)-N_{dCN(2)}$	2.001	$N_{dCN(6)}-Cu(1)-N_{dCN(8)}$	114.1
$Cu(2)-N_{dCN(3)}$	1.997	$N_{dCN(2)}-Cu(2)-N_{dCN(3)}$	110.7
$Cu(2)-N_{dCN(4)}$	2.009	$N_{dCN(2)}-Cu(2)-N_{dCN(7)}$	107.4
$Cu(2)-N_{dCN(7)}$	1.99	$N_{dCN(3)}-Cu(2)-N_{dCN(7)}$	115.6
		$Cu(1)-N_{dCN(1)}-C_{(1)}$	178.0

Table 2. Selected bond lengths [Å] and bond angles [deg] for **4**

4	Length (Å)	**4**	Angle (deg)
$Cu(1)-N_{dCN(1)}$	2.004	$N_{dCN(1)}-Cu(1)-N_{dCN(2)}$	107.8
$Cu(1)-N_{dCN(2)}$	1.955	$N_{dCN(2)}-Cu(1)-N_{dCN(3)}$	116.7
$Cu(1)-N_{dCN(3)}$	1.982	$N_{dCN(3)}-Cu(1)-N_{dCN(4)}$	107.6
$Cu(1)-N_{dCN(4)}$	1.963	$N_{dCN(1)}-Cu(1)-N_{dCN(4)}$	110.7
		$N_{dCN(1)}-Cu(1)-N_{dCN(3)}$	104.9
		$N_{dCN(2)}-Cu(1)-N_{dCN(4)}$	109.0
		$Cu(1)-N_{dCN(1)}-C(1)$	173.7

tion. The synthetic strategy employed in order to prepare the desired threaded species is shown in Scheme 2.

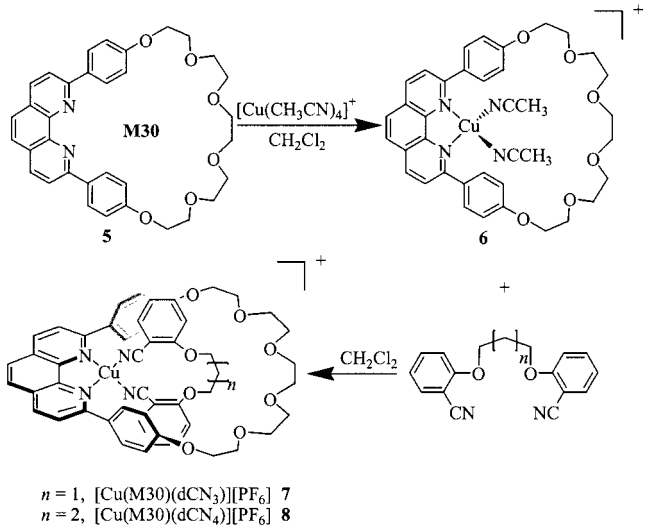

Scheme 2. Synthesis of the threaded complexes **7** and **8**

Thus, to a degassed solution of M30 in dichloromethane, a solution of the $Cu(CH_3CN)_4{\cdot}PF_6$ salt in the same solvent was added. Upon addition, a drastic change in color was observed from yellow to orange confirming the formation of complex **6**. To this complex, a solution of the corresponding dCN_n ligand was added and the reaction stirred overnight at ambient temperature under argon. The formation of the desired complexes **7** and **8** was confirmed by means of mass spectrometry and 1-D and 2-D ^{1}H NMR spectroscopy. In particular the 2-D NMR spectra were very informative, well-resolved and corresponded to the desired compounds. As shown in Figure 3, ^{1}H NMR spectroscopy confirmed the threaded structure of **8** and the entwining of the phen and dCN_4 units around the metal center. A similar spectrum was also obtained for compound **7**.

Hence, due to the intense ring current effect of the C_6H_4CN units, the resonance signals corresponding to the H_o and H_m protons of the phenoxy moieties in the threaded complex move to higher field compared with the free ligand M30. The same pattern was also observed for the $H_{1'}$ protons of the dCN_4 ligand which, upon threading, experience the ring current of the macrocycle and thus move to lower ppm values. This NMR behavior is in accord with previously described systems.[15] 2-D ^{1}H NMR spectroscopy was also employed in order to further elucidate both structures. The ROESY spectrum of complex **8** is given as a representative example in Figure 4. As expected, signals in the aromatic region showing the through space coupling of protons $H_{5,6}$ with $H_{4,7}$ and H_o with $H_{3,8}$ were observed. Moreover, interactions between the H_α protons of the dCN_4 ligand with $H_{4'}$ as well as coupling of the H_a protons of the M30 chain with H_m were present.

However, the threading reaction was mainly confirmed by the ROESY signals such as those between the $H_{4'}$ protons of dCN_4 and the $H_{b,c,d}$ protons of the M30 ring, as well as the signals between the H_α and H_β protons of dCN_4 and the H_a and $H_{b,c,d}$ protons of the macrocyclic chain. Two equally important signals stem from the interactions of both H_α and H_β protons of the dCN_4 ligand with the H_m protons of the phenoxy rings. All these observations are consistent with the interactions predicted based on the CPK model of the threaded structure in question.

Finally, the cyclic voltammograms of the pseudorotaxane structures **7** and **8** were also obtained. Hence, for the threaded complexes the $E°$ values were found to be +0.95 V and +0.88 V for $[Cu(M30)(dCN_3)]^{2+/+}$ and $[Cu(M30)(dCN_4)]^{2+/+}$, respectively. The less positive $E°$ values of compounds **7** and **8**, when compared with the $E°$ values of **3** and **4**, indicate a slight destabilization of the Cu^I oxidation state versus Cu^{II} upon formation of the pseudorotaxane structures. Unfortunately, all attempts to grow crystals suitable for X-ray analysis were unsuccessful for either of the two complexes.

However, both compounds are of particular interest since they could form the basis of novel rotaxane structures. Forming derivatives of the benzene rings could be envisaged in order to attach "stoppers" at each of the dCN fragments thus leading to the final rotaxanes.

Experimental Section

General: ^{1}H NMR spectra were acquired on either a Bruker AM 300 (300 MHz) or a Bruker AM 400 (400 MHz) spectrometer using the deuterated solvent as the lock and the residual solvent as the internal reference. Mass spectra were obtained using a VG ZAB-HF (FAB) spectrometer or a VG-BIOQ triple quadrupole, positive mode (ES-MS). Electrochemical experiments were performed using an EG&G PAR model 273A potentiostat with a standard three-

 © 2004 Wiley-VCH Verlag GmbH & Co. KGaA, Weinheim

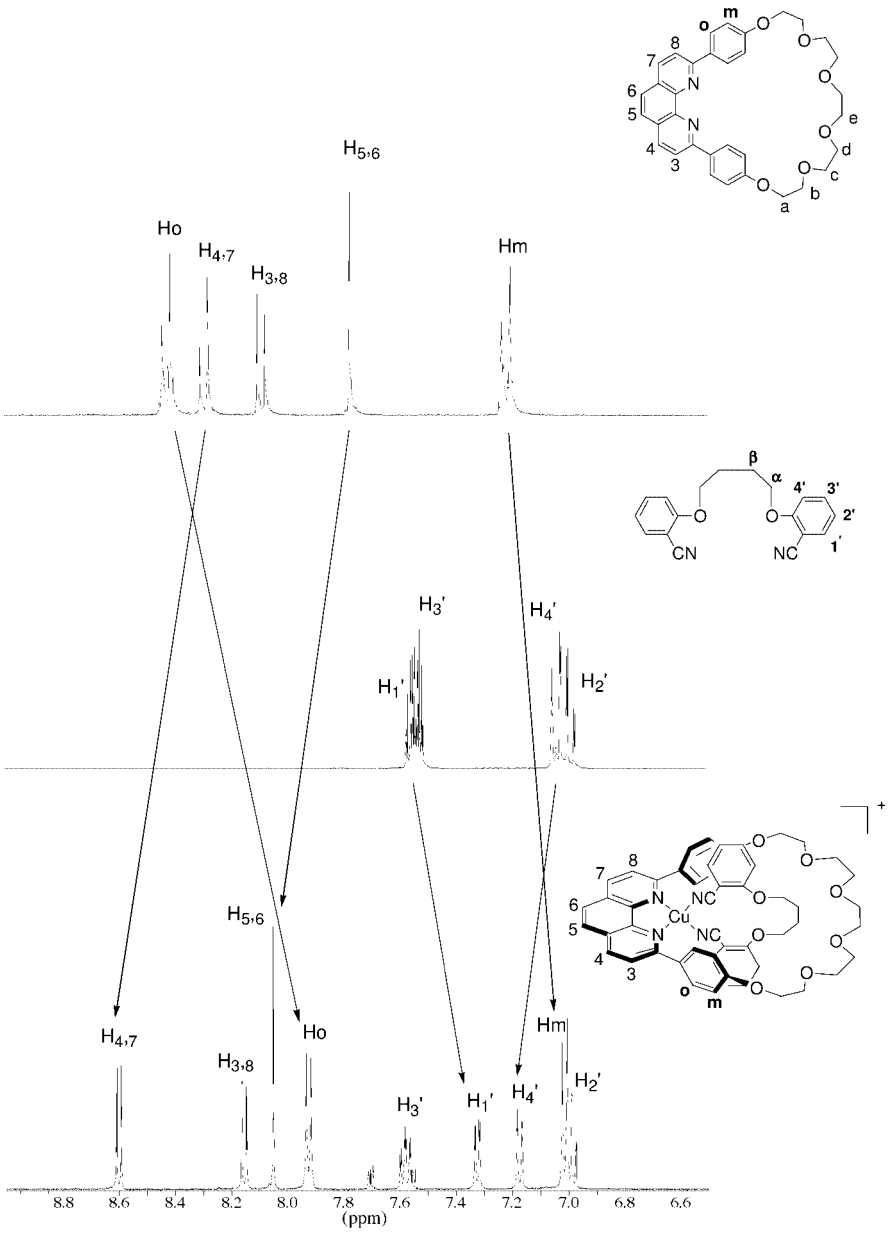

Figure 3. ^{1}H NMR spectra showing the aromatic regions of the macrocyclic ring **5**, the free ligand **3** and the corresponding threaded complex **8** in CD_2Cl_2

electrode configuration. Cyclic voltammetry was carried out in CH_2Cl_2, using as supporting electrolyte a Pt working electrode, a Pt counter-electrode, and an SCE as the reference electrode. The typical sweep rate was 100 mV/s, and the window used was from −2.0 V to +1.4 V. The following chemicals were prepared according to literature procedures: M30,[9] dCN_3,[11] dCN_4.[11] CH_2Cl_2 was dried by heating to reflux over CaH_2 followed by distillation.

[Cu(dCN$_3$)$_2$][PF$_6$] (3): To a degassed solution of $Cu(CH_3CN)_4{\cdot}PF_6$ (36.2 mg, 0.09 mmol) in CH_2Cl_2 (4 mL) was added a solution of dCN_3 (54.3 mg, 0.19 mmol) in the same solvent (4 mL) and the resultant reaction mixture was left stirring at 20 °C under argon for 24 h. Evaporation of the solvent gave complex **3** as a yellowish solid (69 mg). ^{1}H NMR (300 MHz, CD_2Cl_2, 25 °C): δ = 7.73−7.60 (m, 4 H), 7.18−7.06 (m, 4 H), 4.38 (t, J = 5.5 Hz, 4 H), 2.45 (q, J = 5.5 Hz, 2 H) ppm. MS: (ES-MS): m/z (%) = 619 (100) [M − H − PF_6^-], 341 (100) [M − dCN_3 − H − PF_6^-]. Redox potential (V vs. SCE): $E°$ ($Cu^{II/I}$) = 1.20 V.

[Cu(dCN$_4$)$_2$][PF$_6$] (4): To a degassed solution of $Cu(CH_3CN)_4{\cdot}PF_6$ (88.9 mg, 0.24 mmol) in CH_2Cl_2 (10 mL) was added a solution of dCN_4 (0.14 g, 0.48 mmol) in the same solvent (10 mL) and the resultant reaction mixture was left stirring at 20 °C under argon for 12 h. Evaporation of the solvent gave complex **4** as a white solid (187 mg, 98%). ^{1}H NMR (300 MHz, CD_2Cl_2, 25 °C): δ = 7.71−7.59 (m, 4 H), 7.11−7.01 (m, 4 H), 4.18 (br. s, 4 H), 2.13 (br. s, 4 H) ppm. MS: (ES-MS): m/z (%) = 647 (86) [M − H − PF_6^-], 355 (100) [M − dCN_4 − H − PF_6^-]. Redox potential (V vs. SCE): $E°$ ($Cu^{II/I}$) = 1.25 V.

[Cu(M30)(dCN$_3$)][PF$_6$] (7): A solution of $Cu(CH_3CN)_4{\cdot}PF_6$ (17 mg, 0.04 mmol) in degassed CH_2Cl_2 (6 mL) was added under argon and

 © 2004 Wiley-VCH Verlag GmbH & Co. KGaA, Weinheim

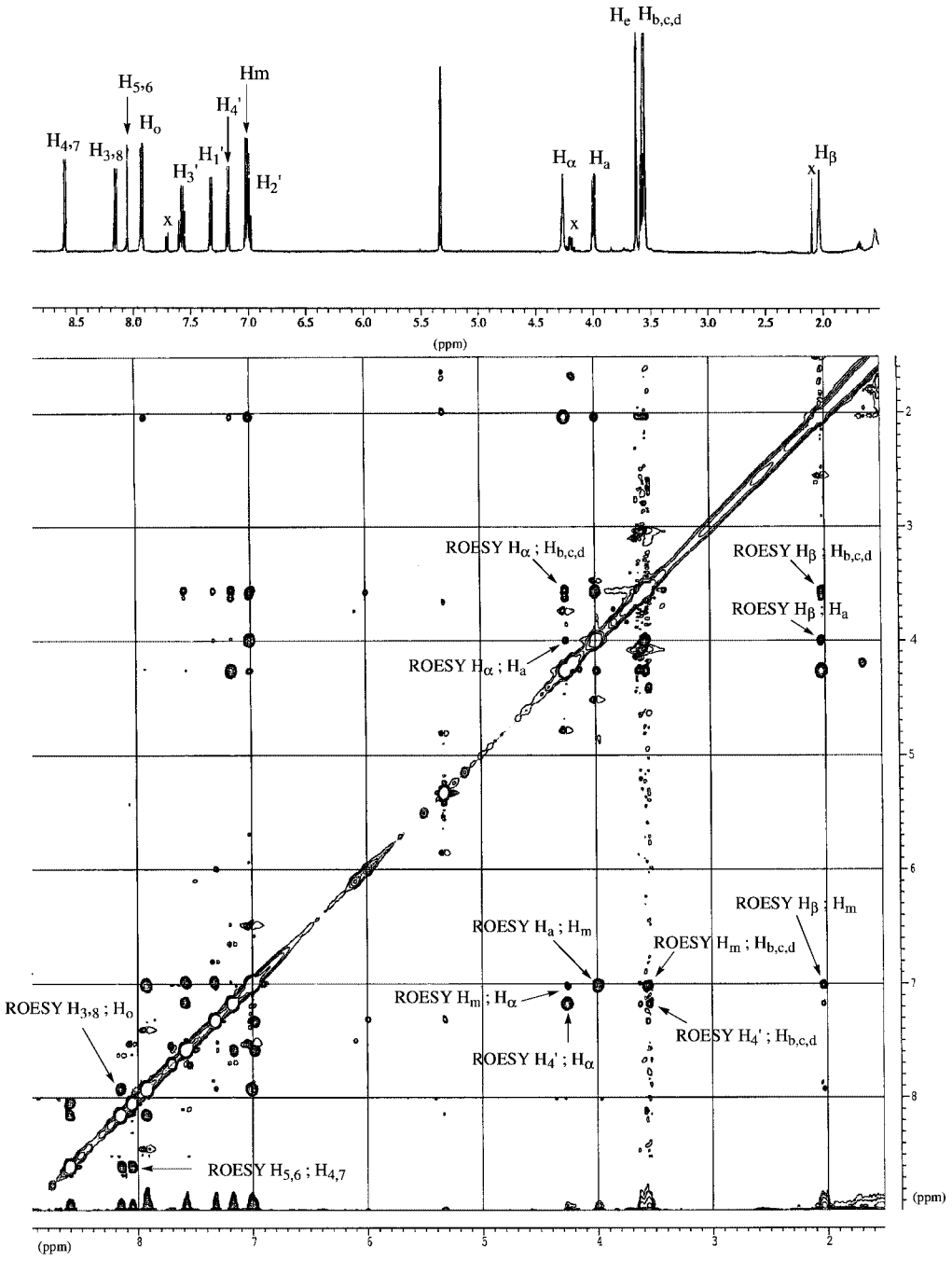

Figure 4. ROESY spectrum of the threaded complex **8** in CD_2Cl_2, (X denotes a small amount of impurity)

at 20 °C to a stirred degassed solution of M30 (25.8 mg, 0.04 mmol) in CH_2Cl_2 (5 mL) via a cannula. The instantaneous appearance of a deep orange color was ascribed to the formation of **6**. After 1 h at room temperature a solution of dCN_3 (12.7 mg, 0.04 mmol) in CH_2Cl_2 (5 mL) was added to **6**. The resultant reaction mixture was stirred for a further 2.5 h under argon. Evaporation of the solvent gave **7** as a brown solid (47 mg, 99.2%). ^{1}H NMR (400 MHz, CD_2Cl_2, 25 °C): δ = 8.63 (d, *J* = 8.2 Hz, 2 H), 8.19 (d, *J* = 8.4 Hz, 2 H), 8.07 (s, 2 H), 7.92 (d, *J* = 8.5 Hz, 4 H), 7.56 (ddd, *J* = 8.0, *J* = 1.7, *J* = 1.4 Hz, 2 H), 7.47 (dd, *J* = 7.8, *J* = 1.7 Hz, 2 H), 7.11 (d, *J* = 8.5 Hz, 2 H), 7.05 (d, *J* = 7.8 Hz, 4 H), 7.03 (dt, *J* = 7.5, *J* = 0.7 Hz, 2 H), 4.34 (t, *J* = 5.8 Hz, 4 H), 4.06 (t, *J* = 5.6 Hz, 4 H), 3.62 (t, *J* = 5.6 Hz, 8 H), 3.59 (s, 4 H), 3.54 (s, 4 H), 2.36 (q, *J* = 5.8 Hz, 2 H) ppm. MS: (ES-MS): *m/z* (%) = 907 (79) [M − H − PF_6^-], 629 (74) [M − dCN_3 − PF_6^-]. Redox potential (V vs. SCE): E° ($Cu^{II/I}$) 0.95 V.

[Cu(M30)(dCN$_4$)][PF$_6$] (8): A solution of $Cu(CH_3CN)_4{\cdot}PF_6$ (62.9 mg, 0.17 mmol) in degassed CH_2Cl_2 (15 mL) was added under argon and at 20 °C to a stirred degassed solution of M30 (96.1 mg, 0.17 mmol) in CH_2Cl_2 (15 mL) via a cannula. The instantaneous appearance of a deep orange color was ascribed to the formation of **6**. After 1 h at room temperature a solution of dCN_4 (49.6 mg, 0.17 mmol) in CH_2Cl_2 (10 mL) was added to **6**. The resultant reaction mixture was stirred for a further 2.5 h under argon. Evaporation of the solvent gave **8** as a brown solid (176 mg, 99%).

 © 2004 Wiley-VCH Verlag GmbH & Co. KGaA, Weinheim

^{1}H NMR (400 MHz, CD_2Cl_2, 25 °C): δ = 8.60 (d, *J* = 8.4 Hz, 2 H), 8.15 (d, *J* = 8.2 Hz, 2 H), 8.05 (s, 2 H), 7.92 (d, *J* = 8.7 Hz, 4 H), 7.58 (ddd, *J* = 8.0, *J* = 1.7, *J* = 1.4 Hz, 2 H), 7.32 (dd, *J* = 7.8, *J* = 1.7 Hz, 2 H), 7.17 (d, *J* = 8.5 Hz, 2 H), 7.01 (d, *J* = 8.8 Hz, 4 H), 6.98 (dt, *J* = 7.5, *J* = 0.9 Hz, 2 H), 4.26 (s, 4 H), 3.99 (t, *J* = 6.0 Hz, 4 H), 3.62 (s, 4 H), 3.54−3.60 (m, 12 H), 2.03 (s, 4 H) ppm. MS: (FAB-MS): *m*/*z* (%) = 921 (60) [M − H − PF_6^-], 629 (100) [M − dCN_4 − PF_6^-]. Redox potential (V vs. SCE): $E°$ ($Cu^{II/I}$) = 0.88 V.

X-ray Data Collection: Crystal data and details of data collection for both **3** and **4** are given in Table 3. The Mo1EN package was used for all computations.[16]

Table 3. Crystallographic data for **3** and **4**

	3	**4**
Empirical formula	$C_{68}H_{58}Cu_2F_{12}N_8O_9P_2$	$C_{72}H_{64}Cu_2N_8O_8{\cdot}2PF_6$
Formula mass	1548.28	1586.37
Crystal system	triclinic	monoclinic
Space group	$P\bar{1}$	$P1\ 2_1/c1$
a (Å)	15.3889(3)	15.7347(2)
b (Å)	16.1548(3)	14.2188(2)
c (Å)	16.9597(3)	32.8202(4)
α (deg)	62.249(5)	90
β (deg)	75.535(5)	91.868(5)
γ (deg)	73.918(5)	90
V (Å^3)	3548.9(1)	7338.9(2)
Z	2	4
Color	colorless	colorless
$D_{calcd.}$ (g cm^{-3})	1.45	1.44
μ (mm^{-1})	0.736	0.713
Temp. (K)	173	173
λ (Å)	0.71073	0.71073
R[a]	0.096	0.083
R_w[b]	0.113	0.097

CCDC-215999 and -216000 contain the supplementary crystallographic data for this paper. These data can be obtained free of charge at www.ccdc.cam.ac.uk/conts/retrieving.html [or from the Cambridge Crystallographic Data Center, 12, Union Road, Cambridge CB2 1EZ, UK; Fax: (internat.) +44-1223-336-033; E-mail: deposit@ccdc.cam.ac.uk].

Acknowledgments

We thank the CNRS (France) and the European Community for financial support. We would also like to thank André De Cian, Nathalie Kyritsakas and Jean Fischer for the X-ray structures as well as Patrice Staub for his technical assistance.

[1] [1a] D. B. Amabilino, J. F. Stoddart, *Chem. Rev.* **1995**, *95*, 2725−2828. [1b] G. Schill, *Catenanes, Rotaxanes and Knots*, Academic Press, New York, **1971**. [1c] C. O. Dietrich-Buchecker, J.-P. Sauvage, *Chem. Rev.* **1987**, *87*, 795−810. [1d] D. B. Amabilino, P. R. Ashton, L. Perez-Garcia, J. F. Stoddart, *Angew. Chem. Int. Ed. Engl.* **1995**, *34*, 2378−2380.

[2] [2a] A. M. Brouwer, C. Frochot, F. G. Gatti, D. A. Leigh, L. Mottier, F. Paolucci, S. Roffia, G. W. H. Wurpel, *Science* **2001**, *291*, 2124−2128. [2b] M. Andersson, M. Linke, J.-C. Chambron, J. Davidsson, V. Heitz, L. Hammarstroem, J.-P. Sauvage, *J. Am. Chem. Soc.* **2002**, *124*, 4347−4362. [2c] M.-J. Blanco, M. Consuelo Jimenez, J.-C. Chambron, V. Heitz, M. Linke, J.-P. Sauvage, *Chem. Soc., Rev.* **1999**, *28*, 293−305. [2d] M. Linke, J.-C. Chambron, V. Heitz, J.-P. Sauvage, *J. Am. Chem. Soc.* **1997**, *119*, 11329−11330.

[3] [3a] D. A. Leigh, J. K. Y. Wong, F. Dehez, F. Zerbetto, *Nature* **2003**, *424*, 174−179. [3b] B. L. Feringa (Ed.); *Molecular Switches*; Wiley-VCH, Weinheim, **2001**. [3c] J.-P. Sauvage (Ed.), *Molecular Machines and Motors*; in: *Structure & Bonding*; Springer-Verlag Berlin, vol. 99, **2001**. [3d] Special Issue of *Acc. Chem. Res.* **2001**, *34*, N° 6. [3e] J.-P. Sauvage, *Acc. Chem. Res.* **1998**, *31*, 611−619. [3f] V. Balzani, M. Gomez-Lopez, J. F. Stoddart, *Acc. Chem. Res.* **1998**, *31*, 405−414.

[4] [4a] P. D. Beer, A. S. Rothin, *Polyhedron* **1989**, *8*, 1251. [4b] M. Fujita, F. Ibukuro, H. Hagihara, K. Ogura, *Nature* **1994**, *367*, 720. [4c] C. O. Dietrich-Buchecker, J.-P. Sauvage, J.-M. Kern, *J. Am. Chem. Soc.* **1984**, *106*, 3043−3045. [4d] J.-C. Chambron, C. O. Dietrich-Buchecker, J.-P. Sauvage, *Comprehensive Supramolecular Chemistry*; Pergamon Press: Oxford, **1996**, vol. 9, p. 43. [4e]M. Fujita, S. Nagao, M. Iida, K. Ogata, K. Ogura, *J. Am. Chem. Soc.* **1993**, *115*, 1574. [4f] C. O. Dietrich-Buchecker, B. Colasson, M. Fujita, A. Hori, N. Geum, S. Sakamoto, K. Yamaguchi, J.-P. Sauvage, *J. Am. Chem. Soc.* **2003**, *125*, 5717.

[5] [5a] V. Balzani, A. Credi, F. M. Raymo, J. F. Stoddart, *Angew. Chem. Int. Ed.* **2000**, *39*, 3348−3391. [5b] A. Livoreil, C. O. Dietrich-Buchecker, J.-P. Sauvage, *J. Am. Chem. Soc.* **1994**, *116*, 9399−9400. [5c] R. A. Bissel, E. Còrdova, A. E. Kaifer, J. F. Stoddart, *Nature* **1994**, *369*, 133−137. [5d] L. Raehm, J.-M. Kern, J.-P. Sauvage, *Chem. Eur. J.* **1999**, *5*, 3310−3317. [5e] For a recent monograph on molecular machines, see: *Molecular Devices and Machines* (Eds.: V. Balzani, M. Venturi, A. Credi), Wiley-VCH, **2003**.

[6] [6a] P. Mobian, J.-M. Kern, J.-P. Sauvage, *J. Am. Chem. Soc.* **2003**, *125*, 2016−2017. [6b] J.-P. Collin, D. Pomeranc, D. Jouvenot, V. Heitz, J.-C. Chambron, J.-P. Sauvage, *Chem. Eur. J.* **2003**, *9*, 4247−4254.

[7] [7a] D. A. Leigh, P. J. Lusby, S. J. Teat, A. J. Wilson, J. K. Y. Wong, *Angew. Chem. Int. Ed.* **2001**, *40*, 1538−1543. [7b] C. A. Hunter, P. C. Mayers, *Nature* **2001**, *411*, 763.

[8] C. Hamann, J.-M. Kern, J.-P. Sauvage, *Inorg. Chem.* **2003**, *42*, 1877−1883.

[9] C. O. Dietrich-Buchecker, J.-P. Sauvage, *Tetrahedron* **1990**, *46*, 503−512.

[10] [10a] R. J. Angelici, M. H. Quick, G. A. Kraus, D. T. Plummer, *Inorg. Chem.* **1982**, *21*, 2178−2184. [10b] D. T. Plummer, G. A. Kraus, R. J. Angelici, *Inorg. Chem.* **1983**, *22*, 3492−3497.

[11] [11a] E. Baranoff, J.-P. Collin, Y. Furusho, A.-C. Laemmel, J.-P. Sauvage, *Chem. Commun.* **2000**, 1935−1936. [11b] E. Baranoff, J.-P. Collin, J. Furusho, Y. Furusho, A.-C. Laemmel, J.-P. Sauvage, *Inorg. Chem.* **2002**, *41*, 1215−1222.

[12] [12a] M. Fujita, J. Yazaki, K. Ogura, *J. Am. Chem. Soc.* **1990**, *112*, 5645−5646. [12b] M. Fujita, F. Ibukuro, K. Yamaguchi, K. Ogura, *J. Am. Chem. Soc.* **1995**, *117*, 4175−4176. [12c] M. Fujita, *Acc. Chem. Res.* **1999**, *32*, 53−61.

[13] L. A. Dakin, P. C. Ong, J. S. Panek, R. J. Staples, P. Stavropoulos, *Organometallics* **2000**, *19*, 2896−2908.

[14] S. Brownstein, N. F. Han, E. Gabe, Y. Le Page, *Can. J. Chem.* **1989**, *67*, 2222−2226.

[15] [15a] C. O. Dietrich-Buchecker, J.-P. Sauvage, J.-M. Kern, *J. Am. Chem. Soc.* **1990**, *111*, 7791−7800. [15b] D. J. Cardenas, P. Gaviña, J.-P. Sauvage, *J. Am. Chem. Soc.* **1997**, *119*, 2656−2664. [15c] L. Raehm, J.-M. Kern, J.-P. Sauvage, *Chem. Eur. J.* **1999**, *5*, 3310−3317.

[16] C. K. Fair, in: *MolEN, An Interactive Intelligent System for Crystal Structure Analysis*, Nonius, Delft, The Netherlands, **1990**.

Received July 25, 2003
Early View Article
Published Online December 19, 2003

 © 2004 Wiley-VCH Verlag GmbH & Co. KGaA, Weinheim

New Pentadentate Carboxylate-Derivatized Sulfur Ligands Affording Water Soluble Iron Complexes with [Fe(NS_4)] Cores that Bind Small Molecules (CO, NO, PMe_3) as Co-Ligands[‡]

Dieter Sellmann,[†][a] Kai P. Peters,*[a] and Frank W. Heinemann[a]

Keywords: Iron / Nickel / S ligands / P ligands / Water solubility

In the search for polydentate sulfur ligands that are able to form water-soluble iron complexes which can bind nitrogenase relevant molecules, the new pentadentate ligands py$CO_2Me$$S_4$–$H_2$ [2,6-bis[2-mercapto-3-(methoxycarbonyl)-phenylthio]dimethylpyridine] (**1**) and py$CO_2H$$S_4$–$H_2$ [2,6-bis(2-mercapto-3-carboxyphenylthio)dimethylpyridine] (**2**) having NS_4 donor atom sets and terminal thiolate donors have been synthesized. The starting material was $CO_2Me$$S_2$–$H_2$ (2,3-dimercapto benzoic acid methyl ester) which was alkylated with 2,6-bis[(tosyloxy)methyl]pyridine. The problem of specifically achieving regioselective monoalkylation of this 1,2-benzene-dithiol derivative was solved by carrying out the alkylation of $CO_2Me$$S_2$–$H_2$ at –78 °C in the presence of stoichiometric amounts of a base. Saponification of **1** afforded the carboxylic acid derivative. Coordination of py$CO_2Me$$S_4^{2-}$ to Fe^{II} in the presence of co-ligands (L = CO, PMe_3) yielded the complexes [Fe(L)(py$CO_2Me$$S_4$)] where L = CO (**5**) or PMe_3 (**4**). Upon treatment with $NOBF_4$, complex **5** afforded [Fe(NO)(py$CO_2Me$$S_4$)]$BF_4$ (**7**) which could be subsequently converted to the isolable 19 valence electron species [Fe(NO)(py$CO_2Me$$S_4$)] (**8**) upon reduction with N_2H_4. In the absence of potential co-ligands, coordination of py$CO_2Me$$S_4^{2-}$ to Fe^{II} afforded the dinuclear complex [Fe(py$CO_2Me$$S_4$)]$_2$ (**6**) whilst coordination to Ni^{II} gave [Ni(py$CO_2Me$$S_4$)]$_x$ (**3**). Solubility of these complexes in water could be achieved by replacing the CO_2Me groups with CO_2H substituents. The ligand py$CO_2H$$S_4^{2-}$ afforded the iron complexes [Fe(L)(py$CO_2H$$S_4$)] [L = CO (**10**) and PMe_3 (**12**)] and [Fe(NO)(py$CO_2H$$S_4$)]$BF_4$ (**11**). Both **10** and **12** could be reversibly deprotonated to give the corresponding water-soluble salts $(NMe_4)_2$[Fe(L)(*py*$CO_2$$S_4$)] with L = CO {$(NMe_4)_2$ [**9**]} and PMe_3 {$(NMe_4)_2$ [**13**]}. The complexes were characterized by elemental analysis, spectroscopic methods and X-ray structural determinations. The molecular structure of [Fe(PMe_3)(py$CO_2H$$S_4$)] (**12**) was found to exhibit inter- and intramolecular O–H···O and O–H···S hydrogen bonds which serve as models for proton transfer steps from external sources to the active sites of metal sulfur enzymes.
(© Wiley-VCH Verlag GmbH & Co. KGaA, 69451 Weinheim, Germany, 2004)

Introduction

Iron atoms in sulfur dominated coordination spheres constitute the active sites of numerous metal enzymes.[1] In the search for low-molecular weight complexes which are capable of modeling characteristic features of the active sites of FeMo, FeV or FeFe nitrogenases such as the sulfur environment of the iron centers, binding of small molecules, and redox-activity, we have recently discovered the [Fe(pyS_4)] fragment (see Figure 1).[2]

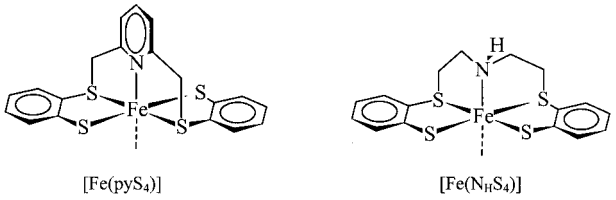

Figure 1. Schematic structure of [Fe(pyS_4)] and [Fe(N_HS_4)] fragments

This fragment binds small molecules, e.g. CO, N_2H_2, N_2H_4, NH_3.[3] The resultant complexes are redox-active and are formed diastereoselectively, always exhibiting the thiolate and thioether donors in *trans* positions. In contrast with related [Fe(L)(N_HS_4)][4] complexes of the pentadentate ligand $N_HS_4^{2-}$ [= dianion of 2,2′-bis(2-mercapto-phenylthio)diethylamine] which may contain low- or high-spin Fe^{II} depending on the σ or σ-π character of the ligand L, all 18 valence electron [Fe(L)(pyS_4)] complexes are diamagnetic. This was demonstrated, for example, by [Fe(CO)-

[‡] Transition Metal Complexes with Sulfur Ligands, 159. Part 158: D. Sellmann, A. Hille, F. W. Heinemann, M. Moll, A. Rösler, J. Sutter, G. Brehm, B. A. Hess, M. Reiher, S. Schneider, *Inorg. Chim. Acta* **2003**, *348*, 194-198.

[†] Deceased.
[a] Institut für Anorganische Chemie der Universität Erlangen-Nürnberg,
Egerlandstraße 1, 91058 Erlangen, Germany
Fax: (internat.) +49-9131-852-7367
E-mail: peters@anorganik.chemie.uni-erlangen.de

 DOI: 10.1002/ejic.200300519 © 2004 Wiley-VCH Verlag GmbH & Co. KGaA, Weinheim

(pyS_4)] and [Fe(N_2H_4)(pyS_4)] which are both diamagnetic.[3] [Fe(L)(pyS_4)] complexes are, however, usually soluble only in non-aqueous solvents thus preventing any investigations in water which is clearly the important solvent in biological systems. In order to resolve this problem and to obtain water-soluble complexes, we attempted to introduce carboxylic acid substituents into the pyS_4^{2-} ligand. This required new ligands, the design and synthesis of which are reported here together with some related iron and nickel complexes.

Results and Discussion

Ligand Synthesis

Figure 2 summarizes starting materials, notations and the target ligands **1** and **2**.

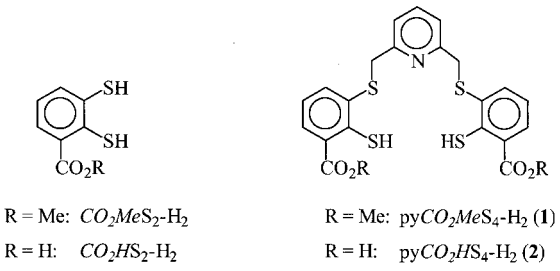

Figure 2. Starting materials, notations and the target ligands **1** and **2**

The notations $CO_2MeS_2{-}H_2$, $pyCO_2MeS_4{-}H_2$, $pyCO_2HS_4{-}H_2$, etc. have been used throughout in order to facilitate legibility and designation of the degrees of protonation/deprotonation of the individual ligands.

The starting material for the pentadentate target ligand **1** was $CO_2MeS_2{-}H_2$, and the major problem was to connect two of these molecules with 2,6-bis[(tosyloxy)methyl]-pyridine such that only one of the two SH functions in $CO_2MeS_2{-}H_2$ would be regioselectively alkylated.

All attempts to achieve a regioselective mono-alkylation using [$Fe^{II}(CO)_2$] or [Ni^{II}] complex fragments as templates remained unsuccessful, although such template reactions have afforded very good results in previous preparations of related ligands.[5] Analogous attempts with the acid derivative $CO_2HS_2{-}H_2$ also failed, as did direct alkylations of $CO_2MeS_2{-}H_2$ under ambient conditions in the absence of templates. In all cases an inseparable mixture of the three regioisomers **1**, **1a**, and **1b** was obtained (Figure 3).

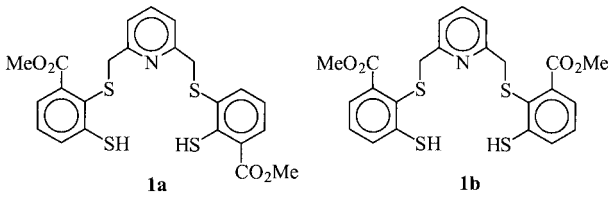

Figure 3. Isomers of $pyCO_2MeS_4{-}H_2$ (**1**)

After a number of laborious experiments, it was finally found that alkylation of $CO_2MeS_2{-}H_2$ in the presence of one equivalent of NMe_4OH at −78 °C afforded the target molecule **1** as the major product. Even then however, a purification step via the nickel complex [Ni($pyCO_2MeS_4$)]$_x$ was necessary. Acidic hydrolysis of [Ni($pyCO_2MeS_4$)]$_x$ afforded **1** as its HCl salt in isomeric purity after recrystallization. Saponification of the ester functions of **1** gave the acid derivative $pyCO_2HS_4{-}H_2$ (**2**) (Scheme 1).

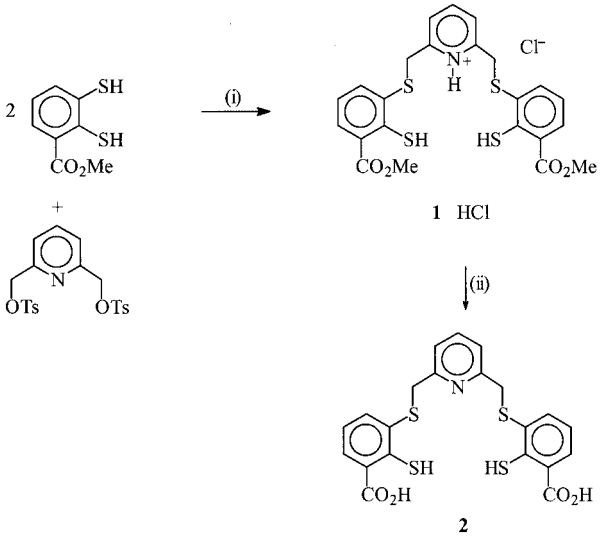

Scheme 1. Synthesis of the target ligands **1** and **2**: (i) 1) +2 NMe_4OH, −78 °C, THF/MeOH, 15 h; 2) $HCl_{aq.}$, CH_2Cl_2; 3) +2 LiOMe, + $Ni(OAc)_2{\cdot}4H_2O$, MeOH; 4) $HCl_{aq.}$, CH_2Cl_2. (ii) 1) +10 $NaOH_{aq.}$, THF, 72 h; 2) $HCl_{aq.}$, CH_2Cl_2

Neither ^1H nor ^{13}C NMR spectroscopy enabled us to unambiguous distinguish the target ligand **1** from its symmetrical regioisomer **1b**. This was possible only by an X-ray structural determination (vide infra).

Syntheses of Iron and Nickel Complexes

Straightforward coordination of the anion $pyCO_2MeS_4^{2-}$ to Fe^{II} and Ni^{II} afforded a series of complexes which are shown in Scheme 2.

Reaction of **1**·HCl with $Ni(OAc)_2{\cdot}4H_2O$ in the presence of three equivalents of LiOMe (for deprotonation of the pyridinium NH and thiol SH functions) afforded yellow-brown [Ni($pyCO_2MeS_4$)]$_x$ (**3**) which is presumably dinuclear like the analogous [Ni(pyS_4)]$_2$.[2] Complex **3** is moderately soluble in DMF and DMSO but only sparingly soluble in all other common solvents. Analogous reactions of **1**·HCl with $FeCl_2{\cdot}4H_2O$ in the presence of PMe_3 or CO gave red [Fe(PMe_3)($pyCO_2MeS_4$)] (**4**) and red [Fe(CO)($pyCO_2MeS_4$)] (**5**), respectively, with **5** showing a ν(CO) band at 1952 cm^{-1} in KBr. In the absence of potential co-ligands, dinuclear violet-red [Fe($pyCO_2MeS_4$)]$_2$ (**6**) was formed instead. Complex **6** is almost insoluble in all common solvents although THF suspensions of **6** react with gaseous CO to give **5** indicating that **6** partially dissociates into coordinatively unsaturated [Fe($pyCO_2MeS_4$)] monomers. Treatment of the carbonyl complex [Fe(CO)($pyCO_2MeS_4$)]

 © 2004 Wiley-VCH Verlag GmbH & Co. KGaA, Weinheim

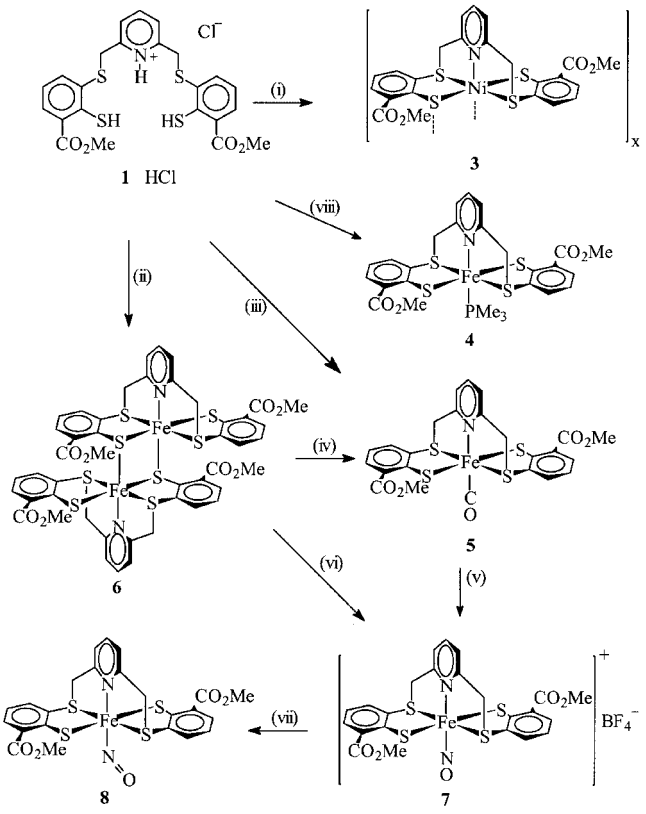

Scheme 2. Fe and Ni complexes with [M(pyCO_2MeS$_4$)] fragments: (i) +3 LiOMe, + $Ni(OAc)_2{\cdot}4H_2O$, MeOH; (ii) +3 LiOMe, + $FeCl_2{\cdot}4H_2O$, MeOH; (iii) +3 LiOMe, + $FeCl_2{\cdot}4H_2O$, + exc. CO, MeOH; (iv) + exc. CO, THF; (v) + $NOBF_4$, CH_2Cl_2; (vi) +2 $NOBF_4$, CH_2Cl_2; (vii) + exc. H_2N_4, MeOH; (viii) +3 LiOMe, + $FeCl_2{\cdot}4H_2O$, + exc. PMe_3, MeOH

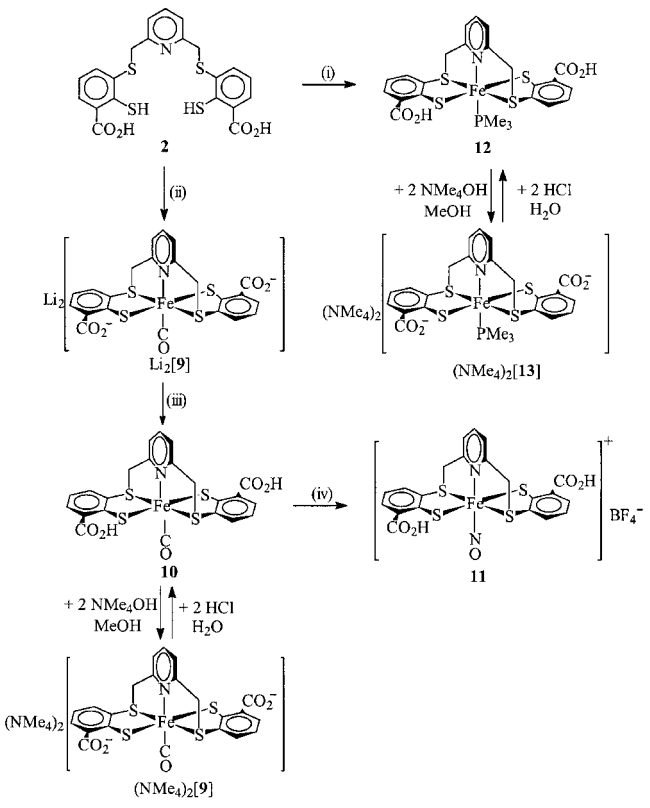

Scheme 3. Synthesis of acidic [Fe(L)(pyCO_2HS$_4$)] complexes and corresponding salts with [Fe(L)(pyCO_2S$_4$)]$^{2-}$ anions: (i) + $FeCl_2{\cdot}4H_2O$, + exc. PMe_3, MeOH; (ii) +4 LiOMe, + $FeCl_2{\cdot}4H_2O$, + exc. CO, MeOH; (iii) +2 HCl, H_2O (iv) + $NOBF_4$, CH_2Cl_2

(**5**) with $NOBF_4$ led to CO substitution and formation of the brown 18 valence electron nitrosyl derivative [Fe(NO)(pyCO_2MeS$_4$)]BF_4 (**7**) having a ν(NO) band at 1881 cm^{-1}. Complex **7** also formed when dinuclear **6** was treated with an excess of $NOBF_4$. Reduction of **7** with hydrazine gave the neutral red-brown [Fe(NO)(pyCO_2MeS$_4$)] (**8**) having a ν(NO) band at 1617 cm^{-1}.

Preparation of complexes with the acid derivative pyCO_2HS$_4$−H_2 (**2**) or its fully deprotonated anion pyCO_2S$_4^{4-}$ were generally achieved in the same way (Scheme 3). The resultant complexes enabled studies of the reversible deprotonations and the electronic influence of carboxylic acid vs. carboxylate functions. It proved difficult to obtain analytically pure samples of salts containing [Fe(pyCO_2S$_4$)]$^{2-}$ anions. Recrystallization attempts of these salts always afforded powders and, in fact, single crystals suitable for an X-ray diffraction study could not be obtained.

Reaction of pyCO_2HS$_4$−H_2 (**2**) with four equivalents of LiOMe and subsequent treatment with $FeCl_2{\cdot}4H_2O$ and CO afforded Li_2[Fe(pyCO_2S$_4$)] (Li_2[**9**]). This compound tenaciously retained varying amounts of LiCl, H_2O, and MeOH. Its identity, however, was confirmed by IR and NMR spectroscopy and by its reaction with aqueous HCl which afforded the neutral complex [Fe(CO)(pyCO_2HS$_4$)] (**10**). Complex **10** could be reversibly deprotonated with NMe_4OH to give $(NMe_4)_2$[Fe(CO)(pyCO_2S$_4$)] {$(NMe_4)_2$[**9**]} and treatment of **10** with $NOBF_4$ afforded the corresponding nitrosyl complex [Fe(NO)(pyCO_2HS$_4$)](BF_4) (**11**) (ν(NO): 1900 cm^{-1} in KBr). Complex **11** could not be isolated in an analytically pure form but its identity was established from a combination of NMR and IR spectroscopy. Surprisingly, the PMe_3 complex [Fe(PMe_3)(pyCO_2HS$_4$)] (**12**) formed directly from neutral pyCO_2HS$_4$−H_2 and $FeCl_2{\cdot}4H_2O$ in the presence of an excess of PMe_3. The excess PMe_3 presumably acts as base giving PMe_3H^+ cations which result in the appropriate proton concentration needed for formation of neutral **12**. Deprotonation of **12** with NMe_4OH gave the salt $(NMe_4)_2$[Fe(PMe_3)(pyCO_2S$_4$)] {$(NMe_4)_2$[**13**]}.

X-ray Structural Determinations

X-ray structural determinations were indispensable for confirming the regioselectivity of the alkylation reactions (vide supra). Figure 4 shows the molecular structures of pyCO_2MeS$_4$−H_2·HCl (**1**·HCl), [Fe(CO)(pyCO_2MeS$_4$)] (**5**), [Fe(pyCO_2MeS$_4$)]$_2{\cdot}H_2O{\cdot}$THF (**6**·H_2O·THF) and [Fe(PMe_3)(pyCO_2HS$_4$)]·0.25MeOH (**12**·0.25MeOH). Table 1 lists selected distances and angles.

The ligand **1**·HCl exhibits C_2 symmetry in the solid state. The carboxylic acid methyl ester substituents are located in positions *ortho* to the thiol functions. The Cl^- counterion

 © 2004 Wiley-VCH Verlag GmbH & Co. KGaA, Weinheim

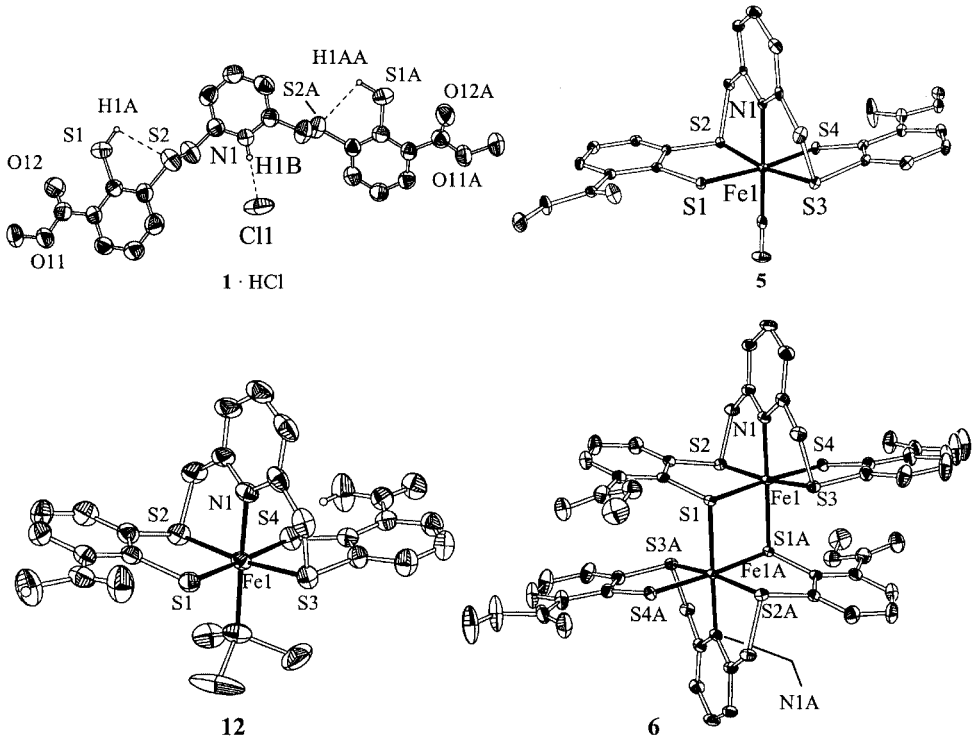

Figure 4. Molecular structures of pyCO_2MeS$_4$−H$_2$·HCl (**1**·HCl), [Fe(CO)(pyCO_2MeS$_4$)] (**5**), [Fe(pyCO_2MeS$_4$)]$_2$·H$_2$O·THF (**6**·H$_2$O·THF) and [Fe(PMe$_3$)(pyCO_2HS$_4$)]·0.25MeOH (**12**·0.25MeOH) (50% probability ellipsoids, C-bonded H atoms and solvent molecules omitted)

Table 1. Selected distances (pm) and angles (deg) of [Fe(CO)(pyCO_2MeS$_4$)] (**5**), [Fe(pyCO_2MeS$_4$)]$_2$·H$_2$O·THF (**6**·H$_2$O·THF) and [Fe(PMe$_3$)(pyCO_2HS$_4$)]·0.25MeOH (**12**·0.25MeOH)

Complex	**5**	**6**	**12**
Fe1−N1	201.0(2)	197.8(3)	200.4(3)
Fe1−S1	230.79(6)	227.7(1)	229.5(1)
Fe1−S2	220.05(6)	222.1(1)	220.9(1)
Fe1−S3	221.80(6)	220.9(1)	220.4(1)
Fe1−S4	228.41(6)	228.7(1)	227.7(1)
Fe1−L	174.1(2)	234.8(1)	223.4(1)
N1−Fe1−S3	84.83(5)	86.29(9)	85.02(8)
N1−Fe1−S4	90.12(6)	88.03(9)	89.84(7)
S1−Fe1−S4	174.19(2)	176.12(4)	176.53(4)
S2−Fe1−S4	85.35(2)	93.84(4)	88.95(3)
S2−Fe1−S1	89.75(2)	88.61(4)	89.03(3)
S3−Fe1−S4	90.05(2)	89.51(4)	88.89(3)
S2−Fe1−S3	169.86(2)	170.40(4)	170.05(4)

forms a hydrogen bond to the protonated pyridine N atom.

The metal centers of all the complexes are six-coordinate and exhibit pseudo octahedral geometries. The thiolate and thioether donors always adopt *trans* positions to each other with the pyridine N donors in apical positions such that square pyramidal [MNS$_4$] cores result. This indicates that the rigid bis-methylene-pyridine bridge connecting the 1,2-benzene-dithiol fragments exerts a stereochemical directing influence. The sixth positions of the pseudo-octahedral metal centers are occupied either by the co-ligand L (CO, PMe$_3$) or a thiolate donor of another [MNS$_4$] core. Dinuclear [Fe(pyCO_2MeS$_4$)]$_2$ possesses a crystallographically imposed inversion center and contains both enantiomers of the chiral [Fe(pyCO_2MeS$_4$)] fragment. **5** crystallizes in the chiral space group $P2_1$ and contains only one enantiomer.

Distances and angles show no anomalies and lie in the range observed for the parent complex [Fe(CO)(pyS$_4$)].[2] The Fe−N(pyridine) distances range from 197. 8(3) to 201.2(6) pm in **6** and **7** respectively. Fe−S(thioether) distances (≈221 pm) are always shorter than Fe−S(thiolate) distances (≈228 pm) within the [FeNS$_4$] cores. The Fe−S distances to the bridging thiolate donors in dinuclear **6** are distinctly longer (≈234 pm) indicating the tendency of **6** to dissociate into mononuclear [Fe(pyCO_2MeS$_4$)] fragments.

The structure of [Fe(PMe$_3$)(pyCO_2HS$_4$)] (**12**) deserves special interest because the crystal lattice contains chains of [Fe(PMe$_3$)(pyCO_2HS$_4$)] molecules which are connected by intermolecular O−H···O hydrogen bonds. Each [Fe(PMe$_3$)-(pyCO_2HS$_4$)] molecule exhibits an additional intramolecular O−H···S(thiolate) hydrogen bond. Figure 5 shows part

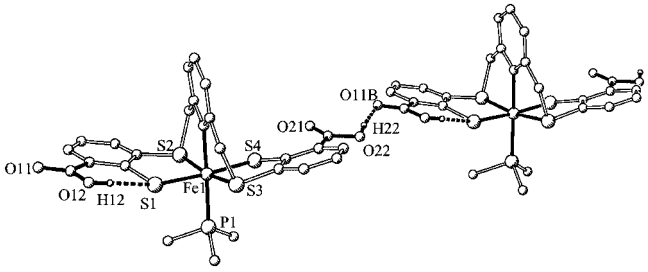

Figure 5. Intra- and intermolecular hydrogen bonds of [Fe(PMe$_3$)-(pyCO_2HS$_4$)] (**12**)

 © 2004 Wiley-VCH Verlag GmbH & Co. KGaA, Weinheim

of the crystal lattice consisting of chains that each contain only homochiral molecules.

The presence of intermolecular hydrogen bonds can be inferred from the distances *d*(O22−H22) = 82 pm, *d*(H22···O11B) = 193 pm, *d*(O22···O11b) = 274.1(4) pm and the angle [O22−H22···O11B] = 170.8°. The intramolecular O−H···S hydrogen bonds are indicated by the distances *d*(O12−H12) = 82 pm, *d*(H12···S1) = 211 pm, *d*(O12···S1) = 289.0(3) pm and the angle [O12−H12···S1] = 159.4°. In particular, the *d*(H12···S1) distance is considerably shorter than the sum of van der Waals radii of sulfur and hydrogen (r_H = 100 pm, r_S = 180 pm)[7] and suggests a strong S···H interaction. Such a strong S···H interaction is also indicated by an IR band in **12** at 2612 cm^{-1} (in KBr). This band can be assigned to a ν(OH) vibration strongly lowered in energy by hydrogen-bonding or alternatively to a ν(SH) vibration indicating protonation of the thiolate donor. The two types of hydrogen bonds in which the carboxylic acid groups are involved make these groups vibrationally inequivalent such that two different $\nu(CO)_{COOH}$ bands can be observed in the IR (KBr) spectrum of **12** at 1701 and 1668 cm^{-1}.

Inter- and intramolecular hydrogen bonds like those observed in **12** are of interest because they can serve as models for the transport of protons in metal sulfur enzyme proteins. Protons from an external source first bind to carboxylic acid/carboxylate side chains of the protein, migrate from there to Brønsted-basic sulfur sites and, if needed in an [H^+/e^-] coupled enzyme reaction, to a substrate molecule coordinated to a metal center.

General Properties and Spectroscopic Characterization of Complexes

A major goal of this work was to achieve water solubility of specific complexes by the rational design of ligands. This objective was successfully accomplished with lithium and ammonium salts of the anions $[Fe(CO)(py\mathit{CO_2}S_4)]^{2-}$ (**9**) and $[Fe(PMe_3)(py\mathit{CO_2}S_4)]^{2-}$ (**13**). The salts Li_2[**9**], $(NMe_4)_2$[**9**], and $(NMe_4)_2$[**13**] are soluble in H_2O and water-like solvents such as MeOH. All the other complexes are sparingly soluble or insoluble in H_2O or MeOH. The low solubility of neutral $[Fe(CO)(py\mathit{CO_2H}S_4)]$ (**5**) or $[Fe(PMe_3)(py\mathit{CO_2H}S_4)]$ (**12**) in H_2O corresponds to the insolubility in water of higher aliphatic or aromatic carboxylic acids.

All complexes were characterized by elemental analysis and common spectroscopic methods. The IR (KBr) spectra of the CO complexes exhibit characteristic ν(CO) bands in the region 1970−1949 cm^{-1} and those of the 18 VE nitrosyl complexes $[Fe(NO)(py\mathit{CO_2R}S_4)](BF_4)$ [R = Me (**7**), R = H (**11**)] display ν(NO) bands at 1881 and 1900 cm^{-1}. The ν(NO) band of the neutral 19 valence electron species appears at 1617 cm^{-1}, indicating that the unpaired electron occupies an antibonding orbital. As shown by DFT calculations for the related parent complex $[Fe(NO)(pyS_4)]$, this molecular orbital is antibonding with respect to all Fe−ligand interactions and has a large contribution from a π* type NO orbital.[8]

^{1}H NMR spectroscopy proved to be particularly suitable for quickly checking the purity and symmetry of the ligands and complexes. The ^{1}H and ^{13}C NMR spectra show typical signals for pyS_4 cores corroborating the two-fold symmetry for all compounds. Like $[Fe(PR_3)(pyS_4)]$ (R = PMe_3, $PnPr_3$), the PMe_3 complexes **4**, **12**, and $(NMe_4)_2$[**13**] show sharp ^{1}H NMR signals only in the presence of an excess of PMe_3. This has been previously explained by suggesting the occurrence of a reversible dissociation of the phosphane ligands in solution.[3]

Electronic Influence of Benzene Ring Substituents

CO_2R (R = alkyl, H) substituents are generally considered to withdraw electron density from benzene rings by inductive or mesomeric effects. It was therefore of interest to examine whether such an electron-withdrawing effect of the CO_2R substituents would reach beyond the thioether and thiolate donors and be detectable at the metal centers of the homologous complexes. This question was probed by examining the ν(CO) frequencies of the iron complexes listed in Table 2.

Table 2. ν(CO) Frequencies of iron carbonyl complexes with $[Fe(pyS_4)]$ cores [cm^{-1}]

Complex	In KBr	In solution
$[Fe(CO)(pyS_4)]$	1963	1974 (THF)[9]
$[Fe(CO)(pyS_4)]\cdot MeOH$	1955[2]	–
$[Fe(CO)(py\mathit{CO_2Me}S_4)]$	1952	1974 (THF)
$[Fe(CO)(py\mathit{CO_2H}S_4)]$	1962	1963 (DMF)
$Li_2[Fe(CO)(py\mathit{CO_2}S_4)]\cdot H_2O\cdot 3MeOH\cdot LiCl$	1969	1973 (MeOH)
$(NMe_4)_2[Fe(CO)(py\mathit{CO_2}S_4)]\cdot 2H_2O$	1949	1973 (MeOH)
$[Fe(CO)(py^{\mathit{bu}}S_4)]$	1969	1969 (THF)[9]

Table 2 demonstrates that all CO complexes show very similar or almost identical ν(CO) frequencies in solution indicating that different benzene ring substituents have practically no influence upon the electron density at the iron centers. In the solid state (KBr), the ν(CO) frequencies, although lying in the same range, show larger differences. As evidenced by both $[Fe(CO)(pyS_4)]$[9] and $[Fe(CO)(pyS_4)]\cdot MeOH$,[2] however, the presence of a lattice MeOH molecule can cause a wavenumber shift of 8 cm^{-1}. Conversely, $[Fe(CO)(py\mathit{CO_2H}S_4)]$ and $[Fe(CO)(py^{\mathit{bu}}S_4)]$[9] show practically identical ν(CO) frequencies in KBr, although two electron-withdrawing CO_2H substituents have been replaced by four electron donating tertiary butyl substituents. In conclusion, the results indicate that the benzene ring substituents have no significant influence upon the electron density at the metal center but, rather, the ν(CO) shifts observed are due to solvation or crystal packing effects. This conclusion is supported by cyclic voltammetry (CV) studies. The isoelectronic iron carbonyl complexes $[Fe(CO)(pyS_4)]$,[9] $[Fe(CO)(py\mathit{CO_2Me}S_4)]$, and $[Fe(CO)(py\mathit{CO_2H}S_4)]$ each show a reversible redox wave in the anodic region.

 © 2004 Wiley-VCH Verlag GmbH & Co. KGaA, Weinheim

Table 3 lists the redox potentials of the three complexes in either CH_2Cl_2 or DMF.

Table 3. Redox potentials of carbonyl complexes with [Fe(pyS_4)] cores [mV]

Complex	CH_2Cl_2	DMF
[Fe(CO)(pyS_4)]	460	468
[Fe(CO)(pyCO_2MeS_4)]	514	539
[Fe(CO)(pyCO_2HS_4)]	–	490

The potentials (Table 3) indicate that CO_2R substituents render complexes with [Fe(pyS_4)] cores more difficult to oxidize. Conversely, when changing from CO_2Me to CO_2H, the trend in redox potentials is reversed. In addition the overall shifts of the redox potentials in the range of 22−71 mV (in DMF) are small. Taking into account also the fact that redox potentials in solution are sensitive towards the nature of the solvent and solvation effects (cf. the values in CH_2Cl_2 and DMF), it can safely be assumed that the ν(CO) frequencies listed in Table 2 indeed confirm that CO_2R substituents do not have a significant influence upon the electron density at the metal centers or [Fe(L)(NS_4)] cores.

Concluding Discussion

Two new pentadentate ligands containing NS_4 donor atom sets and terminal thiolate donors have been synthesized and coordinated to Fe^{II} and Ni^{II} centers affording a series of new iron and nickel complexes. The general problem of achieving a regioselective and specific mono-alkylation of the nearly equivalent thiol functions in the 1,2-benzenedithiol derivative $CO_2MeS_2-H_2$ could be solved by carrying out the alkylation at low temperature in the presence of limited amounts of a base (1 NMe_4OH:1 $CO_2MeS_2-H_2$) affording the target ligand py$CO_2MeS_4-H_2$ (**1**). Saponification of py$CO_2MeS_4-H_2$ (**1**) gave the acid derivative py$CO_2HS_4-H_2$ (**2**) that enabled synthesis of [Fe(L)(pyCO_2HS_4)] complexes (L = CO, PMe_3). These complexes become water-soluble upon deprotonation of the CO_2H substituents and form salts of the type (cation)$_2$[Fe(L)(pyCO_2S_4)] which had been the primary goal of this work.

Spectroscopic, electrochemical and X-ray structural results indicate that introducing CO_2Me or CO_2H substituents into the benzene rings of [Fe(L)(pyS_4)] complexes does not change the electron density at the Fe centers significantly. This is important for further investigations since achieving water solubility of the [Fe(L)(pyS_4)] complexes was the major goal but without changing the coordination properties of the iron centers that bind a considerable number of small molecules relevant to nitrogenase.

The X-ray structure of [Fe(PMe_3)(pyCO_2HS_4)] (**12**) further revealed that such complexes can form inter- and intramolecular O−H···O and O−H···S(thiolate) bonds. These hydrogen bonds may serve as models for the transport of protons from external sources to the metal centers of enzymes when small molecules binding to these centers are reduced by coupled [H^+/e^-] transfer steps.

Experimental Section

General Methods: Unless noted otherwise, all procedures were carried out under nitrogen using standard Schlenk techniques at room temperature with stirring. Solvents were dried and distilled before use. As far as possible, reactions were monitored by IR or NMR spectroscopy. Spectra were recorded on the following instruments: IR (KBr discs or CaF_2 cuvettes, solvent bands were compensated): Perkin−Elmer 16PC FTIR. NMR: Jeol-JNM-GX 270, JNM-EX 270 and JNM-LA 400 with the residual signals of the deuterated solvent used as an internal reference. Spectra were recorded at 25 °C. Mass spectra: JEOL MSTATION 700 spectrometer. Elemental analysis: Carlo Erba EA 1106 or 1108 analyzer. Magnetic susceptibility: Johnson Matthey susceptibility balance. Cyclic voltammetry was performed with a Radiometer Copenhagen IMT 102 electrochemical interface using a three-electrode cell with a glassy carbon (Radiometer Copenhagen EDI) working electrode and Pt reference and counter electrodes. Solutions were 10^{-3} M; $NBu_4[PF_6]$ (10^{-1} M) was used as the supporting electrolyte. Potentials were referenced to the normal hydrogen electrode (NHE) using Fc/Fc^+ as an internal standard (E_{Fc/Fc^+} = 0.4 V vs. NHE).[11] "S_2"-H_2 (1,2-benzene-dithiol),[12] $CO_2MeS_2-H_2$ (2,3-dimercapto benzoic acid methyl ester),[13] and 2,6-bis[(tosyloxy)methyl]pyridine[14] were prepared as described in the literature.

py$CO_2MeS_4-H_2$ (1): A yellow solution of $CO_2MeS_2-H_2$ (17.38 mmol, 3.48 g) and NMe_4OH (17.38 mmol, 7.36 mL of a 25% solution in MeOH) in THF (100 mL) was combined with a solution of 2,6-bis[(tosyloxy)methyl]pyridine (3.89 g, 8.69 mmol) in THF (130 mL) at −78 °C. After 2 h at −78 °C and 15 h at room temperature the resultant white precipitate was separated by filtration and washed with THF (35 mL). The combined filtrates were evaporated and the remaining residue was dissolved in CH_2Cl_2 (100 mL). Concentrated hydrochloric acid (20 mL) was added and the resultant mixture was stirred vigorously for 5 min. The CH_2Cl_2 phase was separated from the aqueous phase, washed with water (5 × 25 mL) until a pH of 7 was attained, dried over Na_2SO_4 and the solvents evaporated. The resultant almost colorless solid foam was suspended in MeOH (75 mL), and LiOMe (17.33 mmol, 17.33 mL of a 1 M solution in MeOH) was added. The resultant solution was filtered and combined with a solution of $Ni(OAc)_2{\cdot}4H_2O$ (2.16 g, 8.68 mmol) in MeOH (40 mL). The yellow-brown precipitate thus obtained was separated by filtration after 1 h, washed with MeOH (30 mL), dried in vacuo and suspended in CH_2Cl_2 (120 mL). Concentrated hydrochloric acid (30 mL) was added and the mixture was stirred vigorously for 20 min. The CH_2Cl_2 phase was separated from the acidic green aqueous phase, dried over Na_2SO_4 and the solvents evaporated. The resultant yellow solid foam was recrystallized from CH_2Cl_2/*n*-hexane to give green-yellow crystals. Yield: 2.33 g py$CO_2MeS_4-H_2{\cdot}$HCl (**1**·HCl) (61%).^{1}H NMR ($CDCl_3$, 269.60 MHz): δ = 18.2 (br., 2 H, N*H*), 7.97 (vdd, 2 H, C_6H_3), 7.80 (vt, 1 H, H_γ, pyridine), 7.59 (vdd, 2 H, C_6H_3), 7.17 (vd, 2 H, H_β, pyridine), 7.06 (vt, 2 H, C_6H_3), 6.58 (s, 2 H, S*H*), 4.65 (s, 4 H, CH_2), 3.87 (s, 6 H, CO_2CH_3) ppm. $^{13}C\{^1H\}$ NMR ($CDCl_3$, 67.83 MHz): δ = 167.3 (CO_2CH_3), 154.2, 143.6, 139.4, 132.4, 132.3, 131.7, 127.2, 124.3 [*C*(aryl)], 52.6 (CO_2CH_3), 36.3 (CH_2) ppm. IR (KBr): $\tilde{\nu}$ = 2486 (br. m, N−H + S−H), 1714 cm^{-1} (s, C=O). MS (FD^+, CH_2Cl_2): *m*/*z* = 504 [py$CO_2MeS_4-H_3]^+$.

 © 2004 Wiley-VCH Verlag GmbH & Co. KGaA, Weinheim

$C_{23}H_{22}ClNO_4S_4$ (540.14): calcd. C 51.14, H 4.11, N 2.59, S 23.75; found C 51.36, H 4.10, N 2.61, S 23.62.

pyCO_2HS$_4$−H$_2$ (2): A suspension of **1**·HCl (1.00 g, 1.85 mmol) and NaOH (18.5 mmol, 18.5 mL of a 1 M solution in H_2O) in THF (20 mL) was stirred vigorously for 24 h, reduced to one half of its volume, stirred again for 48 h and then filtered. Concentrated hydrochloric acid (18.5 mmol, 18.5 mL) was added to the pale yellow filtrate. The resultant pale yellow precipitate was separated by filtration, washed with H_2O (60 mL) and dried in vacuo. Yield: 0.815 g pyCO_2HS$_4$−H$_2$ (**2**) (93%). ^{1}H NMR ([D$_8$]1,4-dioxane, 269.72 MHz): δ = 11.73 (br., 2 H, CO_2H), 7.95 (vdd, 2 H, C_6H_3), 7.54 (vdd, 2 H, C_6H_3), 7.50 (vt, 1 H, H_γ, pyridine), 7.13 (br., 2 H, S*H*), 7.07 (vd, 2 H, H_β, pyridine), 7.00 (vt, 2 H, C_6H_3), 4.23 (s, 4 H, CH_2) ppm. ^{13}C{^{1}H} NMR ([D$_8$]1,4-dioxane, 67.83 MHz): δ = 169.2 (*C*OOH), 157.8, 143.4, 138.3, 137.6, 135.5, 132.1, 127.6, 124.3, 122.5 [C(aryl)], 40.6 (*C*H$_2$) ppm. IR (KBr): $\tilde{\nu}$ = 2960 (br. m, O−H), 2490 (m, S−H), 1685 cm^{-1} (s, C=O). MS (FD$^+$; 1,4-dioxane): *m*/*z* = 476 [pyCO_2HS$_4$−H$_2$]$^+$. $C_{21}H_{17}NO_4S_4$ (475.63): calcd. C 53.03, H 3.60, N 2.94, S 26.97; found C 52.98, H 3.47, N 3.01, S 26.85.

[Ni(pyCO_2MeS$_4$)]$_x$ (3): To a suspension of **1**·HCl (0.400 g, 0.74 mmol) in MeOH (30 mL) and THF (10 mL) was added LiOMe (2.22 mmol, 2.22 mL of a 1 M solution in MeOH). The resultant yellow solution was filtered, and a solution of Ni(OAc)$_2$·4 H_2O (0.160 g, 0.64 mmol) in MeOH (12 mL) was added dropwise. The yellow-brown precipitate which formed was separated by filtration, washed with MeOH and dried in vacuo. Yield: 0.288 g [Ni(pyCO_2MeS$_4$)]$_x$ (**3**) (80%). IR (KBr): $\tilde{\nu}$ = 1721 cm^{-1} (s, C=O). MS (FD, DMF): *m*/*z* = 559 [Ni(pyCO_2MeS$_4$)]$^+$. $C_{23}H_{19}NNiO_4S_4$ (560.36): calcd. C 49.30, H 3.42, N 2.50, S 22.89; found C 49.39, H 3.42, N 2.29, S 22.64.

[Fe(PMe$_3$)(pyCO_2MeS$_4$)] (4): A solution of $FeCl_2$·4 H_2O (0.073 g, 0.37 mmol) in MeOH (8 mL) was added to a solution of **1**·HCl (0.199 g, 0.37 mmol), LiOMe (1.1 mmol, 1.1 mL of a 1 M solution in MeOH) and PMe_3 (0.073 mL, 0.74 mmol) in MeOH (25 mL). After 2 h the resultant red precipitate was separated by filtration, washed with MeOH (15 mL) and Et_2O (15 mL), and dried in vacuo. Yield: 0.170 g [Fe(PMe$_3$)(pyCO_2MeS$_4$)] (**9**) (73%). ^{1}H NMR (CD_2Cl_2, exc. PMe_3, 399.65 MHz): δ = 7.65 (vdd, 2 H, C_6H_3), 7.31 (vdd, 2 H, C_6H_3), 7.05 vt, 1 H, H_γ, pyridine), 6.92 (vd, 2 H, H_β, pyridine), 6.71 (vt, 2 H, C_6H_3), 4.70 (d, 2 H, CH*H*), 4.35 (d, 2 H, C*H*H), 3.63 (s, 6 H, CO_2CH_3), 0.96 [d, ^2J (P, H) = 9 Hz, 9 H, P(CH_3)$_3$], 0.87 [s, exc. P(CH_3)$_3$] ppm. ^{13}C{^{1}H} NMR (CD_2Cl_2, exc. PMe_3, 100.40 MHz): δ = 168.5 (*C*O$_2$CH$_3$), 159.4, 138.3, 135.3, 133.1, 132.9, 120.3, 120.1 [*C*(aryl)], 57.6 (d, *C*H$_2$), 51.9 (CO$_2$*C*H$_3$), 16.6 [exc. P(*C*H$_3$)$_3$], 16.3 [P(*C*H$_3$)$_3$] ppm. ^{31}P{^{1}H} NMR (CD_2Cl_2, exc. PMe_3, 161.70 MHz): δ = 22.1 [*P*(CH$_3$)$_3$], −61.3 [exc. *P*(CH$_3$)$_3$] ppm. IR (KBr): $\tilde{\nu}$ = 1718 (s, C=O), 948 (m, P−C−H) cm^{-1}. $C_{26}H_{28}FeNO_4PS_4$ (633.60): calcd. C 49.29, H 4.45, N 2.21, S 20.24; found C 49.10, H 4.67, N 2.21, S 19.99.

[Fe(CO)(pyCO_2MeS$_4$)] (5)

(a) from 6: A suspension of **6**·H_2O·THF (0.070 g, 0.06 mmol) in THF (20 mL) was saturated with CO gas for 3 h and kept under a CO atmosphere for a further 24 h. The resultant red solution was filtered and reduced to one third of its volume. After addition of MeOH (5 mL) the red precipitate which formed was separated by filtration, washed with MeOH (5 mL) and dried in vacuo. Yield: 0.060 g [Fe(CO)(pyCO_2MeS$_4$)] (**5**) (82%).

(b) from 1: A solution of $FeCl_2$·4H_2O (0.083 g, 0.42 mmol) in MeOH (15 mL) was added to a solution of **1**·HCl (0.225 g, 0.42 mmol) and LiOMe (1.25 mmol, 1.25 mL of a 1 M solution in MeOH) in THF (15 mL) under an atmosphere of CO. The mixture was kept under CO gas for a further 2 h. The resultant red precipitate was separated by filtration, washed with MeOH (10 mL) and Et_2O (10 mL) and dried in vacuo. Recrystallization from CH_2Cl_2/Et_2O afforded fine red needles. Yield: 0.174 g [Fe(CO)(pyCO_2MeS$_4$)] (**5**) (71%).^{1}H NMR ($CDCl_3$, 269.60 MHz): δ = 7.67 (m, 4 H, C_6H_3), 7.32 (vt, 1 H, H_γ, pyridine), 7.11 (vd, 2 H, H_β, pyridine), 6.91 (vt, 2 H, C_6H_3), 5.12 (d, 2 H, CH*H*), 4.48 (d, 2 H, C*H*H), 3.84 (s, 6 H, CO_2CH_3) ppm. ^{13}C{^{1}H} NMR ($CDCl_3$, 67.70 MHz): δ = 214.7 (*C*O), 167.5 (*C*O$_2$CH$_3$), 160.2, 157.3, 136.7, 135.6, 135.3, 132.2, 132.1, 121.6, 121.2 [C(aryl)], 56.6 (*C*H$_2$), 51.9 (CO$_2$*C*H$_3$) ppm. IR (KBr): $\tilde{\nu}$ = 1967 (sh, CO), 1952 (s, CO), 1718 (s, C=O) cm^{-1}. IR (THF): $\tilde{\nu}$ = 1974 (s, CO) cm^{-1}. MS (FD$^+$, CH_2Cl_2): *m*/*z* = 585 [Fe(CO)(pyCO_2MeS$_4$)]$^+$, 557 [Fe(pyCO_2MeS$_4$)]$^+$. C_{24} $H_{19}FeNO_5S_4$ (585.52): calcd. C 49.23, H 3.27, N 2.39, S 21.91; found C 49.46, H 3.21, N 2.37, S 21.66.

[Fe(pyCO_2MeS$_4$)]$_2$ (6): A solution of $FeCl_2$·4H_2O (0.320 g, 1.61 mmol) in MeOH (55 mL) was added dropwise to a solution of **1**·HCl (0.950 g, 1.76 mmol), LiOMe (5.28 mmol, 5.28 mL of a 1 M solution in MeOH) and a small amount of NaBH4 in THF (50 mL) over the course of 3 h. The violet microcrystalline solid which formed was separated by filtration after 45 min, washed with THF (40 mL), MeOH (25 mL) and again with THF (15 mL) and dried in vacuo. Yield: 0.925 g [Fe(pyCO_2MeS$_4$)]$_2$·H_2O·THF (**6**·H_2O·THF) (87%). IR (KBr): $\tilde{\nu}$ = 1711 (s, CO) cm^{-1}. MS (FD$^+$, DMF): *m*/*z* = 557 [Fe(pyCO_2MeS$_4$)]$^+$. Magnetic susceptibility (296 K): μ_{eff} = 0 μ_B. $C_{50}H_{48}Fe_2N_2O_{10}S_8$ (1205.16): calcd. C 49.83, H 4.01, N 2.32, S 21.29; found C 49.59, H 3.85, N 2.34, S 21.37.

[Fe(NO)(pyCO_2MeS$_4$)]BF$_4$ (7)

(a) from 6: $NOBF_4$ (0.023 g, 0.20 mmol) and **6**·H_2O·THF (0.119 g, 0.10 mmol) were suspended in CH_2Cl_2 (15 mL) for 2.5 h. The resultant brown precipitate was separated using a centrifuge, washed with CH_2Cl_2 (5 mL), and recrystallized from acetone. Yield: 0.070 g [Fe(NO)(pyCO_2MeS$_4$)]BF$_4$·0.5 acetone (**7**·0.5 acetone) (50%). $C_{24.5}H_{22}BF_4FeN_2O_{5.5}S_4$ (703.37): calcd. C 41.84, H 3.15, N 3.98, S 18.23; found C 41.95, H 2.93, N 3.96, S 18.18.

(b) from 5: Solid $NOBF_4$ (0.020 g, 0.17 mmol) was added to a solution of **5** (0.100 g, 0.17 mmol) in CH_2Cl_2 (40 mL). The resultant brown precipitate was separated by filtration after 18 h, washed with CH_2Cl_2 (15 mL) and dried in vacuo. Yield: 0.110 g [Fe(NO)(pyCO_2MeS$_4$)]BF$_4$·0.25CH_2Cl_2 (**7**) (93%). ^{1}H NMR (CD_3CN, 269.73 MHz): δ = 7.97 (m, 4 H, C_6H_3), 7.72 (vt, 1 H, H_γ, pyridine), 7.42 (vd, 2 H, H_β, pyridine), 7.39 (vt, 2 H, C_6H_3), 5.49 (d, 2 H, CH*H*), 4.95 (d, 2 H, C*H*H), 3.84 (s, 6 H, CO_2CH_3) ppm. ^{13}C{^{1}H} NMR (CD_3CN,, 67.83 MHz): δ = 166.8 (*C*O-OCH$_3$), 159.0, 154.1, 140.6, 137.1, 134.9, 133.7, 132.0, 127.2, 125.6 [C(aryl)], 56.2 (*C*H$_2$), 53.0 (CO$_2$*C*H$_3$) ppm. IR (KBr): $\tilde{\nu}$ = 1881 (s, NO), 1712 (s, C=O) cm^{-1}. MS (FD$^+$, CH_3CN): *m*/*z* = 557 [Fe(pyCO_2MeS$_4$)]$^+$. $C_{23.25}H_{19.5}BCl_{0.5}F_4FeN_2O_5S_4$ (695.56): calcd. C 40.15, H 2.82, N 4.03, S 18.44; found C 40.45, H 2.77, N 3.83, S 18.44.

[Fe(NO)(pyCO_2MeS$_4$)] (8): Hydrazine (0.02 mL, 0.66 mmol) was added to a brown solution of **7**·0.25CH_2Cl_2 (0.050 g, 0.07 mmol) in MeOH (15 mL). A red-brown precipitate formed which was separated using a centrifuge after 15 h, washed with MeOH (10 mL) and dried in vacuo. Yield: 0.025 g [Fe(NO)(pyCO_2MeS$_4$)] (**8**) (61%). IR (KBr): $\tilde{\nu}$ = 1720 (s, C=O), 1617 (s, NO) cm^{-1}. MS (FD$^+$, DMF): *m*/*z* = 557 [Fe(pyCO_2MeS$_4$)]$^+$. $C_{23}H_{19}FeN_2O_5S_4$ (587.53): calcd. C 47.02, H 3.26, N 4.77, S 21.83; found C 47.09, H 3.29, N 4.50, S 21.47.

 © 2004 Wiley-VCH Verlag GmbH & Co. KGaA, Weinheim

Li_2[Fe(CO)(pyCO_2S_4)] {Li_2[9]}: A solution of **2** (0.336 g, 0.71 mmol) and LiOMe (2.84 mmol, 2.84 mL of a 1 M solution in MeOH) in MeOH (20 mL) was combined with a solution of $FeCl_2{\cdot}4H_2O$ (0.141 g, 0.71 mmol) in MeOH (10 mL). The resultant dark red solution was saturated with CO gas for 1.5 h and filtered after addition of THF (15 mL). The solvent was then removed in vacuo. The so formed light red residue was suspended in THF (50 mL) for 2 h, separated by filtration, washed with THF (30 mL) and dried in vacuo. Yield: 0.497 g Li_2[Fe(CO)(pyCO_2HS_4)]·LiCl·H_2O·3MeOH (Li_2[**9**]·LiCl·H_2O·3MeOH) (96%). ^{1}H NMR (D_2O,): δ = 7.63 (vd, 2 H, C_6H_3), 7.31 (vt, 1 H, H_γ, pyridine), 7.14 (vd, 2 H, H_β, pyridine), 6.95 (m, 4 H, C_6H_3), 4.92 (vd, 2 H, CH*H*), 4.61 (vd, 2 H, C*H*H) ppm. ^{13}C{^{1}H} NMR (D_2O, 100.40 MHz): δ = 217.0 (*C*O), 178.1 (CO_2^{2-}), 158.0, 149.7, 142.5, 137.4, 135.7, 133.0, 127.9, 124.2, 122.7 [C(aryl)], 56.2 (CH_2) ppm. IR (KBr): $\tilde{\nu}$ = 1969 (s, CO), 1586 (s, CO_2^{2-}), 1392 (s, CO_2^{2-}) cm^{-1}. $C_{25}H_{27}ClFeLi_3NO_9S_4$ (725.85): calcd. C 41.37, H 3.75, N 1.93, S 17.67; found C 41.45, H 3.58, N 1.88, S 17.31.

[Fe(CO)(pyCO_2HS_4)] (10): Hydrochloric acid (1.92 mmol, 7 mL of a 1% solution in H_2O) was added dropwise to a solution of Li_2[**9**]·LiCl·H_2O·3MeOH (0.347 g, 0.48 mmol) in H_2O (25 mL). The resultant light red precipitate was separated using a centrifuge, washed with H_2O (30 mL) and MeOH (40 mL) and dried in vacuo. Yield: 0.255 g [Fe(CO)(pyCO_2HS_4)] (**10**) (95%). ^{1}H NMR ([D_6]DMSO, 269.73 MHz): δ = 12.67 (br., 2 H, COO*H*), 7.90 (vd, 2 H, C_6H_3), 7.61 (vt, 1 H, H_γ, pyridine), 7.44 (m, 4 H, H_β, pyridine + C_6H_3), 6.98 (vt, 2 H, C_6H_3), 4.90 (s, 4 H, CH_2) ppm. ^{13}C{^{1}H} NMR ([D_6]DMSO, 67.83 MHz): δ = 216.8 (*C*O), 168.1 (*C*OOH), 156.9, 156.7, 136.4, 135.7, 134.9, 133.3, 130.5, 121.7 [C(aryl)], 55.7 (CH_2) ppm. IR (KBr): $\tilde{\nu}$ = 2974 (m, O−H), 1962 (s, CO), 1681 (s, C=O) cm^{-1}. MS (FD^+, DMSO): *m*/*z* = 529 [Fe(pyCO_2HS_4)]$^+$. $C_{22}H_{15}FeNO_5S_4$ (557.48): calcd. C 47.40, H 2.71, N 2.51, S 23.01; found C 47.68, H 2.59, N 2.58, S 23.21.

[Fe(NO)(pyCO_2HS_4)]BF_4 (11): $NOBF_4$ (0.045 g, 0.39 mmol) and **10** (0.215 g, 0.39 mmol) were suspended in CH_2Cl_2 (40 mL) for 3 days. The resultant brown precipitate was separated by filtration, washed with CH_2Cl_2 (20 mL), dried partially in vacuo and dissolved in MeCN (10 mL). The resultant brown solution was filtered and the solvents evaporated. The brown residue thus formed was dried in vacuo for 60 h. Yield: 0.185 g [Fe(NO)(pyCO_2HS_4)]BF_4 (**11**) (73%). ^{1}H NMR (CD_3CN, 269.72 MHz): δ = 7.98 (vd, 4 H, C_6H_3), 7.70 (vt, 1 H, H_γ, pyridine), 7.38 (m, 4 H, H_β, pyridine + C_6H_3), 5.48 (d, 2 H, CH*H*), 4.93 (d, 2 H, C*H*H) ppm. ^{13}C{^{1}H} NMR (CD_3CN, 67.75 MHz): δ = 158.2, 153.8, 139.8, 136.5, 134.5, 133.1, 131.7, 130.8, 126.4, 124.8 [C(aryl)], 55.2 (CH_2) ppm. IR (KBr): $\tilde{\nu}$ = 2959 (br., O−H), 1900 (s, NO), 1711 (s, C=O) cm^{-1}. MS (FD^+, DMF): *m*/*z* = 529 [Fe(pyCO_2HS_4)]$^+$. $C_{21}H_{15}BF_4FeN_2O_5S_4$ (646.25): calcd. C 39.03, H 2.34, N 4.33; found C 37.94, 2.52 H, N 3.91.

$(NMe_4)_2$[Fe(CO)(pyCO_2S_4)] {$(NMe_4)_2$[9]}: NMe_4OH (0.36 mmol, 0.15 mL of a 25% solution in MeOH) was combined with a suspension of **10** (0.099 g, 0.18 mmol) in MeOH (15 mL) giving a red solution that was filtered and the solvents evaporated. The resultant red residue was dried in vacuo for 15 h. Yield 0.118 g $(NMe_4)_2$[Fe(CO)(pyCO_2S_4)]·$2H_2O$·MeOH [$(NMe_4)_2$[**9**]·$2H_2O$·MeOH) (85%). ^{1}H NMR (D_2O, 269.72 MHz): δ = 7.61 (vdd, 2 H, C_6H_3), 7.33 (vt, 1 H, H_γ, pyridine), 7.15 (vd, 2 H, H_β, pyridine), 6.92 (m, 4 H, C_6H_3), 4.88 (d, 2 H, CH*H*), 4.61 (d, 2 H, C*H*H), 2.96 [s, 24 H, N(CH_3)$_4^+$] ppm. ^{13}C{^{1}H} NMR (D_2O, 67.83 MHz): δ = 217.6 (*C*O), 178.7 (CO_2), 158.5, 150.2, 143.0, 137.9, 136.3, 133.6, 128.4, 124.8, 123.2 [C(aryl)], 57.1 (CH_2), 56.7 [N(CH_3)$_4^+$] ppm. IR (KBr): $\tilde{\nu}$ = 1949 (s, CO), 1580 (s, CO_2^{2-}), 1382 (s, CO_2^{2-}) cm^{-1}. $C_{31}H_{45}FeN_3O_9S_4$ (771.83): calcd. C 48.24, H 5.88, N 5.44, S 16.62; found C 48.09, H 6.13, N 5.64, S 16.59.

[Fe(PMe_3)(pyCO_2HS_4)] (12): A solution of $FeCl_2{\cdot}4H_2O$ (0.090 g, 0.46 mmol) in MeOH (5 mL) was added dropwise to a yellow solution of **2** (0.217 g, 0.46 mmol) and PMe_3 (0.365 mL, 3.65 mmol) in MeOH (10 mL). The resultant red precipitate was separated by filtration after 30 min, washed with MeOH (10 mL) and dried in vacuo. Yield: 0.200 g [Fe(PMe_3)(pyCO_2HS_4)] (**12**) (72%). ^{1}H NMR ([D_6]DMSO, 399.65 MHz, exc. PMe_3): δ = 12.47 (s, 2 H, COO*H*), 7.94 (vd, 2 H, C_6H_3), 7.34 (m, 5 H, C_6H_3 + H_γ, pyridine + H_β, pyridine), 6.89 (vt, 2 H, C_6H_3), 4.78 (d, 2 H, CH*H*), 4.66 (d, 2 H, C*H*H), 1.05 [d, ^2J (P, H) = 8 Hz, 9 H, P(CH_3)$_3$], 0.99 [s, exc. P(CH_3)$_3$] ppm. ^{13}C{^{1}H} NMR ([D_6]DMSO, 100.40 MHz, exc. PMe_3): δ = 168.7 (*C*OOH), 159.8, 158.80, 137.1, 134.9, 133.5, 133.2, 129.7, 120.3, 120.1 [C(aryl)], 56.3 (CH_2), 16.0 [exc. P(CH_3)$_3$], 15.7 [P(CH_3)$_3$] ppm. ^{31}P{^{1}H} NMR ([D_6]DMSO, 161.70 MHz, exc. PMe_3): δ = 24.1 [*P*(CH_3)$_3$], −61.8 [exc. *P*(CH_3)$_3$] ppm. IR (KBr): $\tilde{\nu}$ = 2966 (m, O−H), 2612 (w, S−H/O−H), 1701, 1668 (s, CO), 949 (m, P−C−H) cm^{-1}. MS (FD^+, DMSO): *m*/*z* = 529 [Fe(pyCO_2HS_4)]$^+$. $C_{24}H_{24}FeNO_4PS_4$ (605. 54): calcd. C 47.60, H 4.00, N 2.31, S 21.18; found C 47.35, H 4.28, N 2.33, S 20.93.

$(NMe_4)_2$[Fe(PMe_3)(pyCO_2S_4)] {$(NMe_4)_2$[13]}: NMe_4OH (0.19 mmol, 0.076 mL of a 25% solution in MeOH) was combined with a suspension of **12** (0.099 g, 0.18 mmol) in MeOH (15 mL) giving a red solution that was filtered after 10 min. The filtrate was evaporated in vacuo and the resultant dark red residue was dried in vacuo for 15 h. Yield: 0.062 g $(NMe_4)_2$[Fe(PMe_3)(pyCO_2S_4)]·H_2O {$(NMe_4)_2$[**13**]·H_2O} (88%). ^{1}H NMR (CD_3OD, 269.72 MHz, exc. PMe_3): δ = 7.63 (vd, 2 H, C_6H_3), 7.13 (m, 5 H, H_γ, pyridine + H_β, pyridine), 6.93 (vd, 2 H, C_6H_3), 6.79 (vt, 2 H, C_6H_3), 4.82 (br., 2 H, CH*H*), 4.56 (br., 2 H, C*H*H), 1.05 [d, ^2J (P, H) = 9 Hz, 9 H, P(CH_3)$_3$], 1.00 [exc. *P*(CH_3)$_3$] ppm. ^{13}C{^{1}H} NMR (CD_3OD, 67.83 MHz, exc. PMe_3): δ = 179.0 (CO_2), 161.2, 156.9, 144.7, 136.8, 133.8, 131.9, 126.2, 121.2, 120.7 [C(aryl)], 57.4 (CH_2), 56.1 [N(CH_3)$_4^+$], 17.0 [d, P(CH_3)$_3$], 16.4 [exc. *P*(CH_3)$_3$] ppm. ^{31}P{^{1}H} NMR (CD_3OD, 161.79 MHz, exc. PMe_3): δ = 22.3 [*P*(CH_3)$_3$], −61.7 [exc. *P*(CH_3)$_3$] ppm. $C_{32}H_{48}FeN_3O_5PS_4$ (769.84): calcd. C 49.93, H 6.28, N 5.46, S 16.61; found C 49.92, H 6.55, N 5.31, S 16.73.

X-ray Structural Determinations of pyCO_2MeS_4−H_2·HCl (1·HCl), [Fe(CO)(pyCO_2MeS_4)] (5), [Fe(pyCO_2MeS_4)]$_2$·H_2O·THF (6·H_2O·THF) and [Fe(PMe_3)(pyCO_2HS_4)]·0.25 MeOH (12·0.25MeOH): Green-yellow single crystals of **1**·HCl were grown by layering a solution of the ligand (0.560 g, 1.04 mmol) in CH_2Cl_2 (40 mL) with *n*-hexane (70 mL) over one week. Red plates of **6**·H_2O·THF were obtained by layering a solution of $FeCl_2{\cdot}4H_2O$ (0.021 g, 0.11 mmol) in H_2O (20 mL) successively with a solution of **1**·HCl (0.058 g, 0.11 mmol) in THF (20 mL), a layer of THF (8 mL), a layer of MeOH (20 mL) and 0.32 mL of a 1 M solution of LiOMe in MeOH. Orange prisms of **5** formed within one week from a saturated CH_2Cl_2 solution which had been layered with the same amount of MeOH. Red blocks of **12**·0.25MeOH were obtained by layering a solution of **1a**·HCl (0.080 g, 0.17) in THF (5 mL) with a solution of $FeCl_2{\cdot}4H_2O$ (0.033 g, 0.17 mmol) and PMe_3 (0.1 mL, 0.1 mmol) in MeOH (3 mL).

Suitable single crystals were embedded either in protective perfluoro polyalkyl ether oil or sealed in a glass capillary under N_2. Intensity data were collected using graphite monochromated Mo-K_α radiation (λ = 71.073 pm) on a Nonius−KappaCCD diffractometer (**6**, **5**) or a Siemens P4 diffractometer (**1**·HCl, **12**·0.25MeOH). Intensity data have been corrected for absorption

 © 2004 Wiley-VCH Verlag GmbH & Co. KGaA, Weinheim

Table 4. Crystallographic data for pyCO_2MeS$_4$−H_2·HCl (**1**·HCl), [Fe(CO)(pyCO_2MeS$_4$)] (**5**), [Fe(pyCO_2MeS$_4$)]$_2$·H_2O·THF (**6**·H_2O·THF) and [Fe(PMe_3)(pyCO_2HS$_4$)]·0.25MeOH (**12**·0.25MeOH)

Compound	**1**·HCl	**5**	**6**·H_2O·THF	**12**·0.25MeOH
Formula	$C_{23}H_{22}ClNO_4S_4$	$C_{24}H_{19}FeNO_5S_4$	$C_{50}H_{48}Fe_2N_2O_{10}S_8$	$C_{24.25}H_{25}FeNO_{4.25}PS_4$
M_r [g mol^{-1}]	540.11	585.49	1205.08	613.51
Crystal size [mm]	0.45×0.38×0.25	0.40×0.25×0.14	0.50×0.30×0.10	0.60×0.35×0.20
F(000)	2240	600	622	633
Crystal system	orthorhombic	monoclinic	triclinic	triclinic
Space group	$Fdd2$	$P2_1$	$P\bar{1}$	$P\bar{1}$
a [pm]	3868.1(4)	809.65(2)	972.42(6)	757.9(1)
b [pm]	1015.8(1)	1468.12(4)	1076.16(6)	1247.4(1)
c [pm]	1234.0(1)	1014.06(3)	1460.90(9)	1429.6(1)
α [°]	90	90	91.415(5)	87.76(1)
β [°]	90	100.614(2)	107.943(6)	79.64(1)
γ [°]	90	90	115.724(4)	86.67(1)
V [nm^3]	4.8487(8)	1.18475(6)	1.2877(2)	1.3267(2)
Z	8	2	1	2
$\rho_{calcd.}$ [g cm^{-3}]	1.480	1.641	1.554	1.536
μ [mm^{-1}]	0.534	1.028	0.948	0.977
T [K]	294(2)	100(2)	100(2)	200(2)
θ range [°]	2.11−25.99	4.06−28.00	3.44−26.37	2.22−27.00
Measured refl.	2494	12127	21722	7099
Unique refl.	2377	5145	5247	5780
$R_{int.}$	0.0342	0.0334	0.0573	0.0325
Observed refl.	1440	4881	4101	4348
σ criterion	$I > 2\sigma(I)$	$I > 2\sigma(I)$	$I > 2\sigma(I)$	$I > 2\sigma(I)$
Refl. parameters	154	373	364	362
R_1 [$I > 2\sigma(I)$]	0.0583	0.0260	0.0450	0.0455
wR_2 (all data)	0.1512	0.0584	0.1224	0.1165
Absorption correction T_{min}/T_{max}	0.759/0.816	0.770/0.900	0.747/1.000	0.380/0.430
Absolute structure parameters[18]	0.1(2)	0.00(1)	−	−

effects using either Psi-scans (**1**·HCl, **12**·0.25MeOH), multiple scans of equivalent reflections (SADABS,[15] **6**·H_2O·THF) or a numerical Gaussian integration (**5**). The structures were solved by direct methods, and full-matrix least-squares refinements were carried out on F^2 (SHELXTL NT 5.10[16] for **5**, **12** or SHELXTL NT 6.12[17] for **1**, **6**). All non hydrogen atoms were refined anisotropically. Ligand **1** crystallizes as an HCl adduct and the complexes **6** and **12** crystallize with solvent molecules (**6**·H_2O·THF, **12**·0.25MeOH). The MeOH solvate molecule in **12**·0.25MeOH is disordered on a crystallographic inversion center, as is the THF molecule in **6**·H_2O·THF, with two alternative sites for the O atom of the THF molecule. No hydrogen atoms have been taken into account for the structural model of the disordered MeOH of **12**·0.25MeOH and the solvent water of **6**·H_2O·THF. The PMe_3 group in **12** is disordered with two different sites having occupancies of 62(1)% and 38(1)%, respectively. The hydrogen atoms in **1**·HCl, **6**·H_2O·THF and **12**·0.25MeOH were geometrically positioned with isotropic displacement parameters fixed at 1.2 or 1.5 times the U(eq) of the corresponding carbon atom. The positions of the hydrogen atoms in **5** were taken from a difference Fourier synthesis. Their positional parameters were refined with a fixed common isotropic displacement parameter. Table 4 summarizes selected crystallographic data.[19]

Acknowledgments

We thank Prof. Dr. Horst Kisch for his helpful suggestions. Financial support of this work by the Deutsche Forschungsgemeinschaft (SFB, 583 "Redoxactive Metal Complexes") and the Fonds der Chemischen Industrie is gratefully acknowledged.

[1] [1a] H. Deng, R. Hoffmann, *Angew. Chem.* **1993**, *105*, 1125−1128; *Angew. Chem. Int. Ed. Engl.* **1993**, *32*, 1062−1065. [1b] I. G. Dance, *J. Biol. Inorg. Chem.* **1996**, *1*, 581−586. [1c] J. B. Howard, D. C. Rees, *Chem. Rev.* **1996**, *96*, 2965−2982. [1d] R. R. Eady, *Chem. Rev.* **1996**, *96*, 3013−3030. [1e] B. K. Burgess, D. J. Lowe, *Chem. Rev.* **1996**, *96*, 2983−3012. [1f] K. K. Stavrev, M. C. Zerner, *Chem. Eur. J.* **1996**, *2*, 83−87. [1g] D. Sellmann, J. Sutter, *J. Biol. Inorg. Chem.* **1996**, *1*, 587−593. [1h] D. C. Rees, J. B. Howard, *Current Opinion in Chemical Biology* **2000**, *4*, 559−566. [1k] M. D. Fryzuk, S. A. Johnson, *Coord. Chem. Rev.* **2000**, *200−202*, 379−409. [1m] D. Sellmann, A. Fürsattel, J. Sutter, *Coord. Chem. Rev.* **2000**, *200−202*, 545−561. [1n] O. Einsle, F. A. Tezcan, S. L. A. Andrade, B. Schmid, M. Yoshida, J. B. Howard, D. C. Rees, *Science* **2002**, *297*, 1696−1700. [1o] F. Barrière, *Coord. Chem. Rev.* **2003**, *236*, 71−89. [1p] B. Hinnemann, J. K. Nørskov, *J. Am. Chem. Soc.* **2003**, *125*, 1466−1467.

[2] D. Sellmann, J. Utz, N. Blum, F. W. Heinemann, *Coord. Chem. Rev.* **1999**, *190−192*, 607−627.

[3] D. Sellmann, N. Blum, F. W. Heinemann, *Z. Naturforsch., Teil B* **2001**, *56*, 581−588.

[4] [4a] D. Sellmann, W. Soglowek, F. Knoch, G. Ritter, J. Dengler, *Inorg. Chem.* **1992**, *31*, 3711−3717. [4b] D. Sellmann, W. Soglowek, F. Knoch, M. Moll, *Angew. Chem.* **1989**, *101*, 1244−1245; *Angew. Chem. Int. Ed. Engl.* **1989**, *28*, 1271−1272.

[5] [5a] D. Sellmann, U. Kleine-Kleffmann, *J. Organomet. Chem.* **1983**, *247*, 307−320. [5b] D. Sellmann, U. Kleine-Kleffmann, *J. Organomet. Chem.* **1983**, *258*, 315−329. [5c] D. Sellmann, H. Kunstmann, F. Knoch, M. Moll, *Inorg. Chem.* **1988**, *27*, 4183−4190.

[6] [6a] F. E. Hahn, W. W. Seidel, *Angew. Chem.* **1995**, *107*, 2938−2941; *Angew. Chem. Int. Ed. Engl.* **1995**, *34*, 2700−2703.

 © 2004 Wiley-VCH Verlag GmbH & Co. KGaA, Weinheim

[6b] W. W. Seidel, F. E. Hahn, T. Lügger, *Inorg. Chem.* **1998**, *37*, 6587−6596. [6c] W. W. Seidel, F. E. Hahn, *J. Chem. Soc., Dalton Trans.* **1999**, 2237−2241. [6d] H. V. Huynh, C. Schulze-Isfort, W. W. Seidel, T. Lügger, R. Fröhlich, O. Kataeva, F. E. Hahn, *Chem. Eur. J.* **2002**, *8*, 1327−1335.
[7] L. Pauling, *Die Natur der Chemischen Bindung*, VCH, Weinheim, **1973**, p. 249.
[8] D. Sellmann, N. Blum, F. W. Heinemann, B. A. Hess, *Chem. Eur. J.* **2001**, *7*, 1874−1880.
[9] N. Blum, PhD Dissertation, University of Erlangen-Nürnberg, **2000**.
[10] [10a] D. Sellmann, G. Mahr, F. Knoch, M. Moll, *Inorg. Chim. Acta* **1994**, *224*, 45−59. [10b] D. Sellmann, T. Becker, F. Knoch, *Chem. Eur. J.* **1996**, *2*, 1092−1098.
[11] [11a] H. M. Koepp, H. Wendt, H. Strehlow, *Z. Elektrochem.* **1960**, *64*, 483−491. [11b] G. Gritzner, J. Kuta, *Pure Appl. Chem.* **1984**, *56*, 461−466.
[12] J. Degani, R. Fochi, *Synthesis* **1976**, *7*, 471−472.
[13] D. Sellmann, T. Becker, F. Knoch, *Chem. Ber.* **1996**, *119*, 509−519.
[14] J. S. Bradshaw, P. Huszthy, C. W. McDaniel, J. Y. Zhu, N. K. Dalley, R. M. Izatt, *J. Org. Chem.* **1990**, *55*, 3129−3137.
[15] SADABS *Bruker-Nonius*, Inc., Madison, WI, USA, **2002**.
[16] SHELXTL 5.10 *Bruker AXS*, Inc., Madison, WI, USA, **1998**.
[17] SHELXTL 6.12 *Bruker AXS*, Inc., Madison, WI, USA, **2002**.
[18] H. D. Flack, *Acta Crystallogr., Sect. A* **1983**, *39*, 876−881.
[19] CCDC-214043 (**1**·HCl), -214045 (**5**), -214046 (**6**·H_2O·THF) and CCDC-214047 (**12**·0.25MeOH) contain the supplementary crystallographic data for this paper. These data can be obtained free of charge at www.ccdc.cam.ac.uk/conts/retrieving.html [or from the Cambridge Crystallographic Data Centre, 12 Union Road, Cambridge CB2 1EZ, UK; Fax: (internat.) + 44-1223/336-033; E-mail: deposit@ccdc.cam.ac.uk].

Received July 29, 2003
Early View Article
Published Online December 12, 2003

 © 2004 Wiley-VCH Verlag GmbH & Co. KGaA, Weinheim

Unusual Cu^{II} and Mn^{II} Complexes of Phenol-Based Ligands Containing Amine, Pyridine and Formyl Functions: Unexpected Structural Features and Solution Studies

Iryna A. Koval,[a] Mieke Huisman,[a] Arno F. Stassen,[a] Patrick Gamez,[a] Martin Lutz,[b] Anthony L. Spek,[b] and Jan Reedijk*[a]

Keywords: Copper / Manganese / Magnetic properties / EPR spectroscopy / Cyclic voltammetry

The phenol-based ligand Hpy2ald containing formyl, amine and pyridine functions reacts with copper(II) nitrate, copper(II) bromide and manganese(II) chloride to yield complexes with unexpected structures. In contrast to previously reported coordination compounds with similar ligands, the carbonyl group of the ligand in all complexes does not coordinate to the metal ions. The metal-to-ligand ratio is 2:1 in the case of the copper(II) nitrate complex and 1:1 in the case of the copper(II) bromide and manganese(II) chloride complexes. The copper(II) nitrate complex exhibits both donor-atom and coordination number asymmetry, as one copper ion is pentacoordinate with an N_3O_2 donor set, and the other one is hexacoordinate with an O_6 donor set. In the latter two complexes, the phenol group of the ligand remains protonated and fails to bridge the two metal ions; instead it is semi-coordinated to only one metal ion. This results in the formation of mononuclear complexes in which copper(II) or manganese(II) ions have a distorted square-pyramidal surrounding. All complexes were structurally, spectroscopically and magnetically investigated.
(© Wiley-VCH Verlag GmbH & Co. KGaA, 69451 Weinheim, Germany, 2004)

Introduction

Dinucleating phenol-based ligands, which are able to bind two metal ions simultaneously, have attracted significant attention from scientists in the past few years.[1−5] Interest in this topic is due partly to the presence of a dinuclear metal core in many proteins and enzymes. A large number of complexes with phenol-based ligands have been synthesized to mimic dimetallic biosites.[6−8] In addition, interest in this type of complex is also driven by their attractive catalytic[9,10] and magnetic[11−13] properties.

The recognition of the asymmetric nature of many dinuclear biosites has led to the synthesis of a variety of dinucleating ligands bearing adjacent, but dissimilar, donor sets. These ligands have been collectively termed "compartmental". Some time ago, Adams et al. reported an unexpected nickel-induced hydrolysis of unsymmetrical Schiff base compartmental ligands,[2,14] which resulted in the transformation of the imino group of the ligands into a formyl moiety. As this hydrolysis only occurred when nickel(II) salts with non- or weakly coordinating anions were used, it was suggested that the presence of such anions, as well as nickel ions, is crucial.[14]

All the dinuclear complexes obtained with these in situ generated ligands were found to have very similar crystal structures, comprising a dimetallic core with two bridging phenolato groups from two ligands. In all cases the metal-to-ligand ratio was found to be 2:2. The coordination environment around each metal ion was completed by three nitrogen donor atoms from an amino arm of the ligand and an oxygen atom of the formyl group, formed by hydrolysis, to give a distorted octahedron.

In the present study, three novel complexes of the phenol-based compartmental ligand Hpy2ald (Figure 1), containing formyl, amino and pyridine functions, with copper(II) nitrate and bromide, and manganese(II) chloride are reported. The ligand Hpy2ald was prepared as an intermedi-

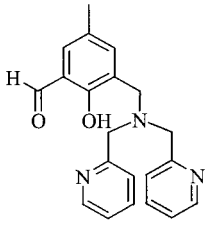

Figure 1. The phenol-based ligand Hpy2ald, containing the tridentate arm in the 2-position and the carbonyl group in the 6-position of the aromatic ring

[a] Leiden University, Leiden Institute of Chemistry,
P. O. Box 9502, 2300 RA Leiden, Netherlands
Fax: (internat.) + 31-71-527-4671
E-mail: reedijk@chem.leidenuniv.nl
[b] Bijvoet Center for Biomolecular Research, Crystal and Structural Chemistry, Utrecht University,
Padualaan 8, 3584 CH Utrecht, Netherlands

ate in the synthesis of asymmetric dinucleating ligands.[15] In contrast to the coordination compounds reported by Adams et al.,[2,14] the present complexes do not possess dinuclear cores comprised of two metal ions and two ligands. In all complexes, the carbonyl group of the ligand does not coordinate to the metal ions, which partly originates from the presence of a stronger nitrate, bromide or chloride donor anion. The metal-to-ligand ratio was found to be 2:1 for the nitrate complex and 1:1 for the bromide and chloride complexes. The crystal structures, spectroscopic and magnetic properties of all three complexes are reported.

Results and Discussion

General

The phenol-based ligand Hpy2ald contains a tridentate arm in the 6′-position, and a carbonyl group in the 2′-position of the phenol ring. Quite similar ligands and their Ni^{II} coordination compounds were previously described by Adams et al.[2] In the overwhelming majority of cases, the ligands reported by Adams were formed in situ by the hydrolysis of an imino arm of the initially dinucleating phenol-based ligands.[2] The structures of the previously described complexes with this type of ligand include dinuclear metal cores, where two metals are doubly bridged by two phenolato groups. In all cases, the C=O group of the ligand is coordinated to the metal ion.[2]

In the present study, three new copper(II) and manganese(II) complexes with the ligand Hpy2ald are reported, each possessing quite different structures. The reaction of Hpy2ald with copper(II) nitrate yields the asymmetric dinuclear complex $[Cu_2(py2ald)(\mu\text{-}NO_3)(NO_3)_2]\cdot CH_3CN$ (Figure 2), in which the two metal ions are doubly bridged by a deprotonated cresolate anion and a didentate nitrate anion. The metal-to-ligand ratio in this complex is 2:1, and the octahedral coordination environment of one of the copper ions is completed by chelating nitrate anions. The aldehyde group of the ligand remains non-coordinated.

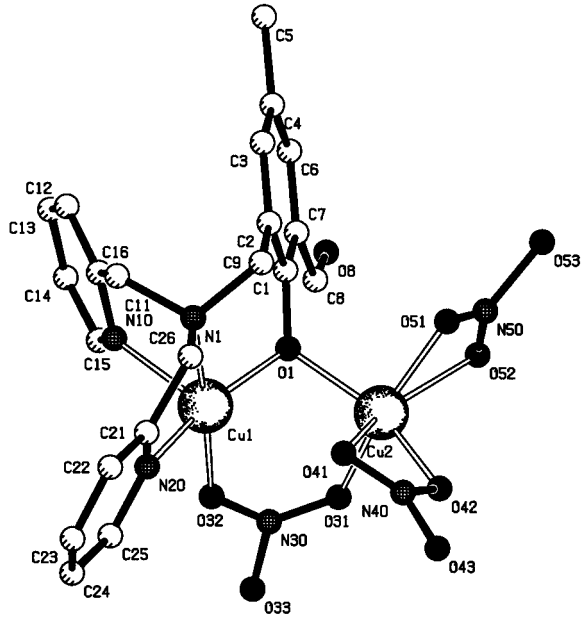

Figure 2. Platon[33] projection of the crystal structure of $[Cu_2(py2ald)(\mu\text{-}NO_3)(NO_3)_2]\cdot CH_3CN$; hydrogen atoms are omitted for clarity

The reaction of Hpy2ald with $CuBr_2$ yields a mononuclear complex with the formal composition $[Cu(Hpy2ald)Br_2]\cdot 0.5H_2O$. In the crystal, the copper complexes form dimers by hydrogen bonding with the lattice water molecules as hydrogen bond donors and the coordinated bromides as acceptors (Figure 3). The metal to ligand ratio within a mononuclear fragment is 1:1. In this complex, the phenol group of the ligand remains protonated, failing to bridge two metal ions and instead being only semi-coordinated to one metal. As in the case of the nitrate complex, the aldehyde group is not coordinated, but instead is hydrogen-bonded to the protonated phenol. The octahedral coordination environment around the metal ion is completed by nitrogen donor atoms of the tridentate arm from the ligand and two bromide anions.

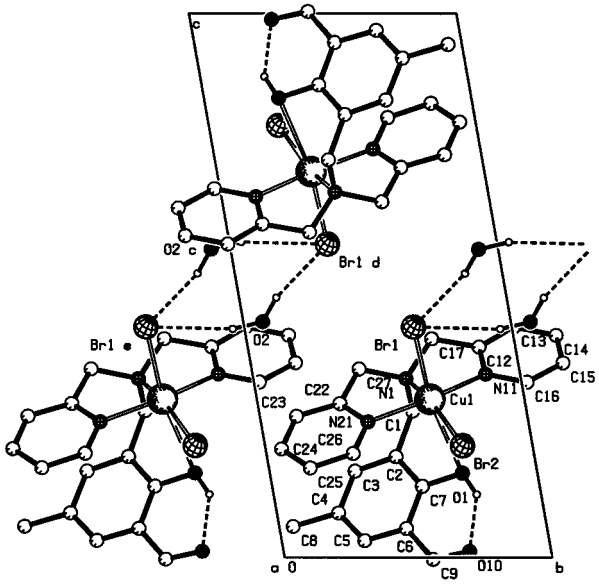

Figure 3. Platon[33] projection of the crystal structure of $[Cu(Hpy2ald)Br_2]\cdot 0.5H_2O$; the occupancy factor of each water molecule is 0.50; only the hydrogen atoms participating in hydrogen bonding are shown

Finally, the reaction of Hpy2ald with manganese(II) chloride yields the complex $[Mn(Hpy2ald)Cl]_2$. The molecular structure of this complex is very similar to the structure of the copper(II) bromide complex with intramolecular hydrogen bonding, but in the crystal lattice no intermolecular hydrogen bonding is present.

These unusual structural features of the three complexes open the possibility to speculate that the structure of complexes with carbonyl-containing phenol-based ligands is largely determined by the donor properties of the anion. Due to the presence of a very weak donor carbonyl group in the ligand, the counterions present in the solution may compete with the oxygen atom of the carbonyl group for a place in the coordination sphere of the metal ion. Thus, a dinuclear

 © 2004 Wiley-VCH Verlag GmbH & Co. KGaA, Weinheim

core comprised of two metal ions and two ligands, in which the carbonyl group is coordinated to the metal ions, can only be formed if non-coordinating, or very weakly coordinating, anions are present in the solution. This hypothesis is supported by the fact that reaction of Hpy2ald with perchlorate or tetrafluoroborate metal salts yields complexes with structures[16] very similar to those described by Adams.[2] At the same time, stronger donors, such as nitrate and halogen anions, prevent a weaker donor — the carbonyl group — from coordinating to the metal ion. In addition, in all cases, changing the initial ratio of the reactants did not influence the structure of the formed complexes.

Crystal Structure Descriptions

[Cu_2(py2ald)(μ-NO_3-O,O′)(NO_3-O,O′)$_2$]·CH_3CN (1)

A molecular plot of [Cu_2(py2ald)(μ-NO_3)(NO_3)$_2$]·CH_3CN is shown in Figure 2. Selected bond lengths and angles are given in Table 1. The dinuclear core consists of two copper ions [Cu···Cu distance 3.0652(6) Å], bridged on one side by an endogenous (μ-phenoxo) bridge and on the other side by an exogenous didentate nitrate anion. The complex shows both coordination-number and donor-atom asymmetry. Cu1 is five-coordinate with an almost ideal square-pyramidal geometry (the parameter τ, which is used to describe the percentage of trigonal distortion from a square-pyramidal geometry, is 0.07 for the Cu1 ion; τ is zero for an ideal square pyramid and one for an ideal trigonal bipyramid),[17] and an N_3O_2 donor set. The basal plane contains two *cis*-located oxygen atoms, O1 from the deprotonated cresolate and O32 from the bridging nitrate anion, and two *cis*-located nitrogen atoms, N1 of the tertiary amine group and N20 of the pyridine ring. The nitrogen atom N10 from the other pyridine ring occupies the apical position. The interior angles of the basal plane vary between 82.07(9)° and 93.06(8)°. The distance Cu1···O41 is 3.031(3) Å and is thus too long to consider the O41 atom as the sixth ligand for the Cu1 ion.

The Cu2 ion is six-coordinate with a very distorted octahedral geometry and an O_6 donor set. Only one of the oxygen atoms belongs to the ligand: the other five are from three different nitrate anions. Two oxygen atoms (O41 and O52) from the two didentate chelating nitrate ions occupy the axial positions, with long Cu−O bonds of 2.585(3) Å and 2.479(3) Å, respectively. The O41−Cu2−O52 angle is only 149.42(9)°, indicating a very large distortion from the regular octahedral geometry, apparently imposed by the small bite angle of the nitrate anions. The oxygen atoms (O42 and O51) of two didentate chelating nitrate anions, the oxygen atom (O1) of the deprotonated cresolate and the oxygen atom (O31) of the didentate bridging nitrate anion lie in the equatorial plane, with Cu−O distances of 1.945(2)−1.978(2) Å. The interior angles of the equatorial plane are somewhat larger than 90°, viz. 90.26(10)−95.55(10)°. One non-coordinated molecule of acetonitrile is present in the crystal lattice.

Table 1. Selected bond lengths and angles for [Cu_2(py2ald)(μ-NO_3)(NO_3)$_2$]·CH_3CN

Bond lengths (Å)			
Cu1−O1	1.9918(19)	Cu2−O1	1.959(2)
Cu1−O32	1.937(2)	Cu2−O31	1.945(2)
Cu1−N1	2.041(2)	Cu2−O41	2.585(3)
Cu1−N10	2.199(2)	Cu2−O42	1.946(2)
Cu1−N20	1.999(2)	Cu2−O51	1.978(2)
Cu1···O41	3.031(3)	Cu2−O52	2.479(3)
Bond angles (°)			
O1−Cu1−O32	92.46(8)	O1−Cu2−O31	90.63(9)
O1−Cu1−N1	93.06(8)	O1−Cu2−O41	96.70(8)
O1−Cu1−N10	89.20(8)	O1−Cu2−O42	151.99(9)
O1−Cu1−N20	163.73(9)	O1−Cu2−O51	93.75(9)
O32−Cu1−N1	174.17(9)	O51−Cu2−O52	57.90(8)
O32−Cu1−N10	99.34(9)	O1−Cu2−O52	101.69(8)
O32−Cu1−N20	92.11(9)	O31−Cu2−O41	103.36(8)
N1−Cu1−N10	82.59(9)	O31−Cu2−O42	90.26(10)
N1−Cu1−N20	82.07(9)	O31−Cu2−O51	158.59(9)
N10−Cu1−N20	105.44(9)	O31−Cu2−O52	100.68(8)
Cu1−O1−Cu2	101.75(9)	O41−Cu2−O42	55.99(10)
		O41−Cu2−O51	96.94(8)
		O41−Cu2−O52	149.42(9)
		O42−Cu2−O51	95.55(10)
		O42−Cu2−O52	105.63(10)

[Cu(Hpy2ald)Br_2]·0.5H_2O (2)

A molecular plot of the complex is shown in Figure 3. Selected bond lengths and angles are presented in Table 2. As can be evidenced from the picture, the unit cell contains two mononuclear formula units and one water molecule, which appears to be disordered over two positions with an occupancy factor of 0.50. These uncoordinated water molecules act as hydrogen bond donors with coordinated bromide anions as acceptors (see Table 3), thus resulting in the formation of centrosymmetric dimers with the formal composition [Cu(Hpy2ald)Br_2]$_2$·H_2O.

Table 2. Selected bond lengths and bond angles for [Cu(Hpy2ald)Br_2]·0.5H_2O

Bond lengths (Å)			
Cu1−Br1	2.7278(4)		
Cu1−Br2	2.4299(4)		
Cu1−O1	2.932(2)		
Cu1−N1	2.0815(19)		
Cu1−N11	2.0170(19)		
Cu1−N21	2.0246(19)		
Bond angles (°)			
Br1−Cu1−Br2	99.197(12)	Br2−Cu1−N21	97.42(6)
Br1−Cu1−O1	170.75(4)	O1−Cu1−N1	82.40(7)
Br1−Cu1−N1	100.65(5)	O1−Cu1−N11	78.43(7)
Br1−Cu1−N11	93.34(6)	O1−Cu1−N21	95.50(7)
Br1−Cu1−N21	93.63(5)	N1−Cu1−N11	81.03(8)
Br2−Cu1−O1	78.04(5)	N1−Cu1−N21	81.05(8)
Br2−Cu1−N1	160.15(5)	N11−Cu1−N21	161.69(8)
Br2−Cu1−N11	98.15(6)		

 © 2004 Wiley-VCH Verlag GmbH & Co. KGaA, Weinheim

Table 3. Selected bond lengths and angles for [Mn(Hpy2ald)Cl_2]

Bond lengths (Å)			
Mn1−Cl1	2.3737(9)		
Mn1−Cl2	2.4078(8)		
Mn1−O31	2.793(2)		
Mn1−N1	2.360(2)		
Mn1−N11	2.217(2)		
Mn1−N21	2.223(2)		
Bond angles (°)			
Cl1−Mn1−Cl2	106.07(3)	Cl2−Mn1−N21	94.92(6)
Cl1−Mn1−O31	76.21(5)	O31−Mn1−N1	75.92(7)
Cl1−Mn1−N1	151.89(5)	O31−Mn1−N11	78.07(7)
Cl1−Mn1−N11	104.33(6)	O31−Mn1−N21	88.15(7)
Cl1−Mn1−N21	102.28(6)	N1−Mn1−N11	73.27(8)
Cl2−Mn1−O31	175.64(5)	N1−Mn1−N21	73.22(7)
Cl2−Mn1−N1	101.98(5)	N11−Mn1−N21	145.95(8)
Cl2−Mn1−N11	97.70(6)		

The coordination environment around the copper(II) ion can best be described as either a very distorted octahedron with a Br_2N_3O donor set, or a square pyramid with a Br_2N_3 donor set and a loosely bound phenol group. The phenol group of the cresol ring remains protonated, which prevents it from forming a bridge between the two copper ions. This, in turn, results in the formation of a mononuclear complex. The oxygen atom (O1) from the phenol group can thus be best regarded as being only semi-coordinated to the Cu1 ion, with a very long Cu−O distance of 2.932(2) Å. It lies in one of the apical positions of an imaginary octahedron, with the second apical position being occupied by one of the bromide anions at a Cu1−Br1 distance of 2.7278(4) Å. The O1−Cu1−Br1 angle is 170.75(4)°. The equatorial plane is formed by the second bromide anion (Br2), the nitrogen atom (N1) from the tertiary amine group, and two nitrogen atoms (N11 and N21) from the pyridine rings. The pyridine rings are located on either side of the ligand plane, and are thus *trans* to each other. The interior angles N1−Cu1−N11 and N1−Cu1−N21 are smaller than 90° [81.03(8)° and 81.05(8)°, respectively], due to the constraints imposed by the three-bond ligand-bite.

Besides the intermolecular hydrogen bonding, an intramolecular hydrogen bond is realized between the cresolic proton and the oxygen atom from the formyl group (the O1···O10 distance is 2.645 Å, see also Table 4).

[Mn(Hpy2ald)Cl_2] (3)

A molecular plot of the complex is shown in Figure 4. Selected bond lengths and angles are presented in Table 3. The structure of the complex is very similar to that of complex **2**. However, in this case no intermolecular hydrogen bonding is present between the formula units. The coordination environment around the Mn1 ion can best be described as a very distorted octahedron. The chloride anion (Cl2) and the oxygen atom (O31) from the cresol group occupy the axial positions. Although the Mn1−O31 distance of 2.793(2) Å is shorter than the respective distance in complex **2** [2.932(2) Å], the oxygen atom can still be best regarded as being only semi-coordinated to the manganese ion. Similarly to the copper(II) bromide complex, the OH group of the cresolic moiety remains protonated. The Cl2−Mn1−O31 angle is 175.64(5)°. The basal plane of the octahedron is formed by two nitrogen atoms (N11 and N21) from two pyridine rings, the nitrogen atom (N1) from the tertiary amine group and the chloride anion (Cl1). The

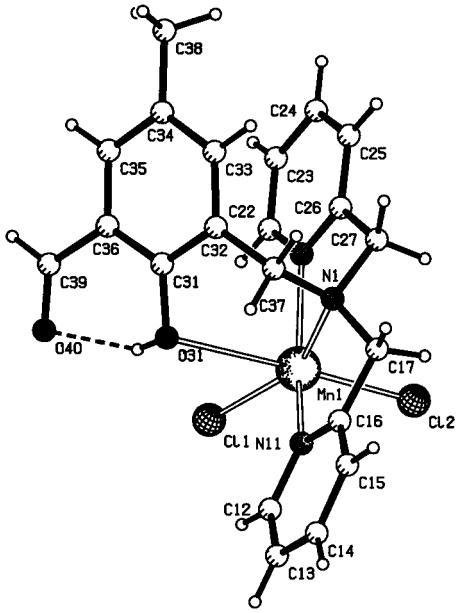

Figure 4. Platon[33] projection of the crystal structure of [Mn(Hpy2ald)Cl_2]

Table 4. Hydrogen bonds D−H···A for [Cu(Hpy2ald)Br_2]$_2$·H_2O and [Mn(Hpy2ald)Cl_2]

	Donor−H···Acceptor	D−H (Å)	H···A (Å)	D···A (Å)	D−H···A (°)
	O1−H10···O10	1.00(5)	1.82(5)	2.645(3)	137(4)
[Cu(Hpy2ald)Br_2]·0.5H_2O	O2−H20···Br1[a]	0.99	2.44	3.405(4)	164.2
	O2−H30···Br1	0.95	2.70	3.592(4)	155.3
[Mn(Hpy2ald)Cl_2]	O31−H1O···O40	0.72(3)	2.01(3)	2.660(3)	151(4)

[a] $2 - x, 1 - y, 1 - z$.

 © 2004 Wiley-VCH Verlag GmbH & Co. KGaA, Weinheim

Mn−N distances vary in the range 2.217(2)−2.360(2) Å, and the Mn1−Cl1 distance is 2.3737(9) Å. An intramolecular hydrogen bond is realized between the hydrogen atom of the cresolic group and the oxygen atom from the formyl group, with an O31···O40 distance of 2.660 Å (Table 4).

Physical Characterization

Mass Spectroscopy

The mass spectra (ESI-MS) of $[Cu(Hpy2ald)Br_2]\cdot H_2O$ and $[Mn(Hpy2ald)Cl_2]$, both recorded in methanol, are characterized by one major peak corresponding to the moiety $[M(Hpy2ald)X]^+$ (m/z = 491 for $[Cu(Hpy2ald)Br]^+$ and m/z = 437 for $[Mn(Hpy2ald)Cl]^+$). These results are as expected and indicate that the solid-state structures of both complexes are retained in solution. However, if the mass spectrum of $[Mn(Hpy2ald)Cl_2]$ is recorded again after one week in solution, two new peaks appear in the spectrum, at the expense of the original ones, at m/z = 362 and m/z = 451. The first of them was tentatively assigned to the product of an oxidation of the formyl group of the ligand to the respective carboxylate group. The theoretically calculated isotope pattern for the formula $C_{21}H_{20}N_3O_3$ (corresponding to the ligand with the carboxylic group instead of a formyl moiety) is in a good agreement with the experimentally observed one. Assuming the first assumption is correct, the peak at m/z = 451 should correspond to the complex of composition $[MnL'Cl]^+$, where L′ is the oxidized ligand. Interestingly, the oxidation of the ligand was only observed for the manganese complex, but not for the copper complexes.

The mass spectra of $[Cu_2(py2ald)(\mu\text{-}NO_3)(NO_3)_2]$ were recorded for comparison in two different solvents (acetonitrile and methanol). The spectrum of the complex in acetonitrile solution shows two major peaks. The most intense one, at m/z = 596, corresponds to the fragment $[Cu_2(py2ald)(NO_3)_2]^+$, in agreement with the solid-state structure of the complex. However, the second peak in the spectrum, whose intensity is only slightly lower (relative abundance 95%) at m/z = 472, corresponds to the mononuclear fragment $[Cu(Hpy2ald)NO_3]^+$. The discrimination between mononuclear and dinuclear fragments is unambiguous from the difference in observed isotopic patterns, caused by the presence of one or two copper ions. The structure of the latter complex can be expected to look similar to the structure of the copper bromide complex, with the phenol group of the ligand being still protonated. When the spectrum of the complex is recorded in methanol solution, the peak corresponding to the mononuclear fragment $[Cu(Hpy2ald)(NO_3)(CH_3OH)_2]^+$ becomes the most intense, while the intensity of the peak corresponding to the dinuclear moiety diminishes significantly (relative abundance 60%). The results of mass spectroscopy prompted us to suggest that, in solution, the dinuclear complex with the deprotonated ligand exists in equilibrium with the mononuclear complex with the protonated ligand, and this equilibrium is shifted towards the mononuclear complex in a methanol solution.

Ligand-Field Spectroscopy

Ligand-field spectra of all complexes were recorded in the solid state, as well as in solution (methanol for complexes **2** and **3** and acetonitrile and methanol for complex **1**). The ligand-field spectrum of complex **1** in the solid state (diffuse reflectance) is characterized by two major peaks. The first one, at 418 nm, corresponds to the LMCT transition of the phenolate group to the copper ions.[6] The second peak, at 640 nm, is in a normal range for d-d transitions of Cu^{II} ions.[18] In the diffuse reflectance spectrum of complex **2**, a fairly broad peak corresponding to a d-d transition is observed at 750 nm, with a shoulder around 940 nm. As shown previously, such spectroscopic behavior (high-energy absorption band in the visible region with a low-energy shoulder) is typical for square-pyramidal copper(II) complexes.[19] Thus the coordination sphere around the metal center can indeed be best described as square pyramidal. Another intense band is observed at 378 nm. Taking into account that the OH group of the ligand is only semi-coordinated to the copper ion, and thus the LMCT band from the OH group to the metal ions is unlikely to be visible, we were forced to assign this band to the charge transfer from the bromide anions to the copper ions. Similarly, in the diffuse reflectance spectrum of complex **3** a band is observed at 356 nm, which was assigned to the charge-transfer band from the chloride anions to the manganese ions. The d-d transition band in octahedrally surrounded Mn^{II} is known to be very weak, and must be hidden by the tail of the LMCT band, which is not uncommon.[18]

When the spectrum of complex **1** in acetonitrile solution is recorded, the position of the d-d transition band shifts only slightly to 672 nm. However, when the spectrum is recorded in methanol, this band shifts significantly (from 640 nm to 719 nm) towards higher wavelengths (“red shift”). These results suggest the change of the coordination sphere around the copper(II) ions in solution, presumably towards a square-pyramidal geometry.[20] This observation appears to be in agreement with the results of mass-spectroscopic measurements, which suggest the presence of significant amounts of mononuclear copper(II) species in methanol solution. The position of the d-d band in the spectrum of complex **1** in methanol solution is quite close to the position of the d-d band in complex **2**, which can be regarded as additional evidence for the presence of a mononuclear species similar in structure to complex **2**.

When the spectrum of complex **2** is taken in methanol solution, the position of the d-d band shifts somewhat towards the UV region (ca. 700 nm). Possible reasons for this shift are the solvation of the copper ions or partial exchange of the bromide anions with methanol molecules. The spectrum of $[Mn(Hpy2ald)Cl_2]$ remains unchanged if recorded in methanol. However, after a prolonged time in solution a shift of the LMCT band (ca. 100 nm) towards

 © 2004 Wiley-VCH Verlag GmbH & Co. KGaA, Weinheim

the IR region is observed, suggesting the oxidation of the ligand, as evidenced by mass-spectroscopic measurements.

EPR Spectroscopy

The EPR spectrum of complex **1**, recorded in the solid state at room temperature, exhibits one fairly broad isotropic signal with $g = 2.15$. No hyperfine splitting is resolved and no triplet signal is detected. The resolution does not improve upon cooling to liquid nitrogen temperature. A very similar spectrum is observed when the measurement is performed on a frozen acetonitrile solution. These data suggest an interaction between two copper(II) centers at relatively close positions, leading to exchange narrowing. However, when the spectrum is recorded in a methanol glass, it becomes much more complicated (Figure 5a). The spectrum obviously indicates the presence of two different species in solution, and can be best regarded as an overlapping superposition of two rhombic spectra. For both species, a ^{63,65}Cu hyperfine splitting can be observed in the g_z region, although some lines are partially hidden either due to the overlapping of two spectra with each other, or in $g_{x,y}$ region. The resulting spectrum was satisfactory simulated[21] (Figure 5b) considering two non-interacting Cu^{II}-containing species in an approximate 1:1 ratio. For the species X, the simulating parameters are $g_x \approx g_y = 2.10$, $g_z = 2.44$, $A_x = 1.1$ mT (11×10^{-4} cm^{-1}), $A_y = 0$, $A_z = 10.9$ mT (124×10^{-4} cm^{-1}), and for the species Y, $g_x \approx g_y = 2.14$, $g_z = 2.26$, $A_x = 0$, $A_y = 0.43$ mT (4×10^{-4} cm^{-1}), and $A_z = 17.2$ mT (182×10^{-4} cm^{-1}). Although the exact interpretation proved to be difficult, these parameters suggest a $d_{x^2-y^2}$ ground state for both species X and species Y. The simulation parameters for species X are characteristic for elongated rhombic octahedral CuO_6 chromophores,[20] and are very close to the values typical for Cu^{II} ions in a methanol glass. The origin of this species could be Cu^{II} ions coordinated by the nitrate anions and/or, at least partially, by methanol molecules. The simulation parameters for the species Y are close to those for square-planar CuN_2O_2 chromophores. Thus, these results are in good agreement with the presence in solution of a mononuclear species $[Cu(Hpy2ald)NO_3]^+$, as suggested by mass spectrometry and ligand-field spectroscopy. However, it should be noticed that neither EPR nor ligand-field measurements provide any direct evidence confirming the presence of dinuclear species in solution as well. Thus, although the presence of dinuclear species was evidenced during the mass-spectroscopic measurements, it cannot be directly deduced from other spectroscopic techniques. Therefore we cannot exclude another possibility — the complete dissociation of the dinuclear complex into mononuclear units of composition $[Cu(Hpy2ald)NO_3]^+$ in methanol solution.

The EPR spectrum of complex **2** in the solid state has a rhombic character, with $g_x = 2.05$, $g_y = 2.10$ and $g_z = 2.25$, suggesting a $d_{x^2-y^2}$ ground state. When the spectrum is recorded in a methanol glass, hyperfine splitting becomes obvious. Three of four lines are easily observed (Figure 6a), whereas the fourth is partially hidden in the $g_{x,y}$ region. The spectrum was simulated[21] (Figure 6b) using the parameters $g_x = 2.04$, $g_y = 2.06$, $g_z = 2.24$, $A_x \approx A_y \approx 0$ and $A_z = 18.4$ mT (192×10^{-4} cm^{-1}). These data suggest a distorted square-pyramidal environment for the Cu^{II} ions,[22] in agreement with the crystal structure of the complex.

One can also notice an additional peak at high field (approximately 330 mT), with a g-value below 2, in the spectrum of the complex. The appearance of this signal may indicate the presence of a small amount of dinuclear copper(II) species in solution. Although the solid-state structure of the complex is essentially mononuclear, the partial formation of dinuclear species in solution due to the presence of potentially bridging bromide anions can be imagined. In this case, this absorption should originate from a $\Delta M_s = \pm 1$ transition of the triplet spectrum.[6] No signal corresponding to a $\Delta M_s = \pm 2$ transition could be detected. As the structure of these presumably dinuclear species is unknown, the presence of this high-field signal was neglected during the simulation of the spectrum.

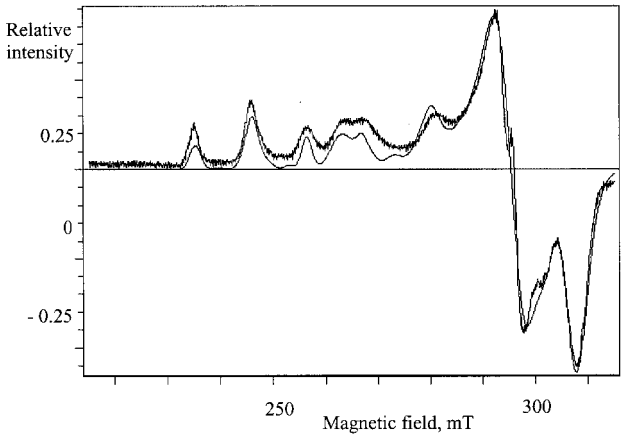

Figure 5. X-band EPR spectrum of: a) $[Cu_2(py2ald)(NO_3)_3]$ (frozen methanol solution, 77 K), and b) simulated curve[21] (see text for further details)

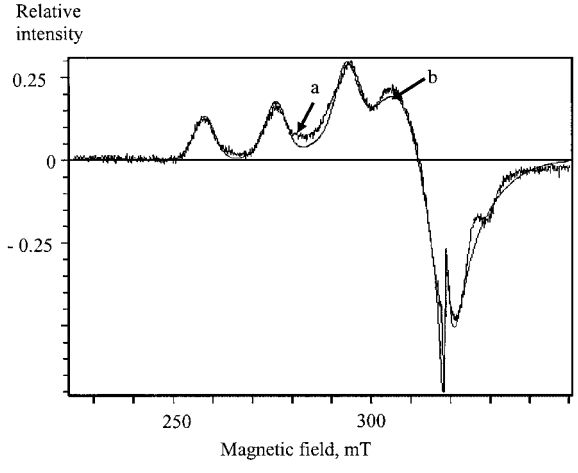

Figure 6. X-band EPR spectrum of: a) $[Cu(Hpy2lad)Br_2]_2 \cdot H_2O$ (frozen methanol solution, 77 K), and b) the simulated curve[21] (see text for further details); the sharp signal in the spectrum belongs to the reference DPPH ($g = 2.0036$)

 © 2004 Wiley-VCH Verlag GmbH & Co. KGaA, Weinheim

Table 5. Calculated equivalent conductances (ohm^{-1} cm^2 mol^{-1}) of the complexes, measured for 1 mM solutions in acetonitrile (**1**) and in methanol (**1**, **2** and **3**)

	$[Cu_2(py2ald)(NO_3)_3]\cdot CH_3CN$	$[Cu(Hpy2ald)Br_2]\cdot 0.5H_2O$	$[Mn(Hpy2ald)Cl_2]$
Acetonitrile	117	–	–
Methanol	160	73	78

The X-band EPR spectrum of the manganese complex **3** in the solid state shows a very broad pattern in the range 0−800 mT. The resolution does not improve upon cooling to 77 K. Such behavior of manganese complexes is not unusual and is caused by zero-field splitting effects.[23] No hyperfine splitting can be observed in the solid-state spectrum, due to dipole-dipole interactions between closely located manganese(II) ions. The spectrum recorded in a frozen methanol solution is much better resolved and shows the usual ^{55}Mn six-line pattern (A = 9.3 mT).

Conductivity Measurements

The specific conductivity of 1 mM solutions of the complexes was measured in acetonitrile and methanol for complex **1**, and in methanol for complexes **2** and **3**. The calculated values of equivalent conductances of all three complexes are presented in Table 5. As can be seen, the value of the equivalent conductance for complex **1** in acetonitrile (117 ohm^{-1} cm^2 mol^{-1}) suggests that the complex exists as a 1:1 electrolyte in acetonitrile solution.[24] However, in methanol solution the equivalent conductivity value of 160 ohm^{-1} cm^2 mol^{-1} falls in the range observed for 2:1 electrolytes.[24] These results seem to support the hypothesis about the complete dissociation of the dinuclear complex **1** into mononuclear units in methanol solution, as one would expect the resulting $[Cu(Hpy2ald)(NO_3)_2]$ complex to behave as a 1:2 electrolyte, due to relatively weak bonds between the copper ions and the nitrate groups. The values of the equivalent conductivities obtained for complexes **2** and **3** are very close (Table 5) and suggest that both complexes are 1:1 electrolytes.[24]

Cyclic Voltammetry

The cyclic voltammogram of complex **1**, recorded in an acetonitrile solution while scanning towards the negative region of potentials, is characterized by one quasi-reversible wave ($E_{1/2}$ = -0.31 V, ΔE = 0.19 V, v = 0.1 V), which was tentatively assigned to the $Cu^{II,II}/Cu^{II,I}$ redox couple, and one completely irreversible wave at E_{pc} = −0.60 V. On the reverse scan, a sharp stripping peak, caused by the redissolution of the copper metal deposited on the electrode, is present. It can therefore be concluded that the second metal-centered reduction is accompanied by the destruction of the complex. This is not surprising, as the coordination of three nitrate anions to the Cu^{I} ion is unlikely to be possible in this case. In the positive range of potentials, a reversible oxidation wave ($E_{1/2}$ = 0.81 V) is observed, corresponding to the one-electron oxidation of the ligand.[6] The cyclic voltammogram recorded in a methanol solution in the negative range of potentials is characterized as well by two successive partially overlapping electrochemical waves. However, they are shifted significantly towards the positive range of potentials and are completely irreversible (E_{pc} = −0.19 V and E_{pc} = −0.28 V). Similarly to the previous case, the reduction of the copper(II) ions to the copper(I) state is accompanied by the decomposition of the complex and the deposition of the metal on the electrode surface. The positive potential range does not change significantly when recording the voltammogram in a methanol solution.

The cyclic voltammogram of complex **2**, recorded in a methanol solution while scanning towards the negative range of potentials, is characterized by one fully reversible one-electron electrochemical wave, corresponding to the Cu^{II}/Cu^{I} complexed couple ($E_{1/2}$ = −0.12 V, ΔE = 0.18 V, v = 0.1 V/s). In the positive range of potentials, one irreversible electrochemical wave at E_{pa} = 1.17 V is observed, assigned to the ligand oxidation.

The cyclic voltammogram of complex **3** is characterized by only one irreversible oxidation wave at E_{pa} = 1.20 V. By comparing the results with the cyclic voltammogram of complex **2**, this electrochemical wave was assigned to the ligand oxidation. No metal-centered electrochemical waves can be observed up to +1.5 V vs. Ag/AgCl electrode, suggesting a very significant stability of the Mn^{II} oxidation state in the complex.

Magnetic Susceptibility

Magnetic susceptibility measurements have been performed on powdered crystals of **1** (m = 29.11 mg), **2** (m = 50.20 mg) and **3** (19. 04 mg) at 0.1 Tesla. Values for χ in the copper(II) complexes have been calculated for dinuclear species.

At 300 K, the χT value for complex **2** is 0.84 $cm^3\cdot K\cdot mol^{-1}$. This value remains almost constant, as the compound shows Curie−Weiss behavior over the entire temperature region. The Curie constant C_2 is 0.42 $cm^3\cdot K\cdot mol^{-1}$, indicating a g value of 2.12. The Curie temperature θ_2 is 0 K, as expected. Thus no magnetic coupling is present between two mononuclear fragments coupled by the disordered water molecule.

For complex **3**, χT is 4.40 $cm^3\cdot K\cdot mol^{-1}$ at 300 K, corresponding to a magnetic moment of 5.93 μ_B. This value is in perfect agreement with the theoretically expected value for a high-spin Mn^{II} ion (S = 5/2). It remains unchanged over the entire temperature range, indicating the paramagnetic behavior of the complex, as could be predicted from the structure of the complex. The Curie temperature θ is 0 K, as expected.

 © 2004 Wiley-VCH Verlag GmbH & Co. KGaA, Weinheim

A plot of χ^{-1} and χT vs. temperature for complex **1** between 5 and 150 K (with χ being the magnetization per dinuclear complex) is shown in Figure 7. From the increase of the magnetic susceptibility at low temperature (from $\chi_1 T$ = 0.89 $cm^3 \cdot K \cdot mol^{-1}$ at 150 K to $\chi_1 T$ = 1.05 $cm^3 \cdot K \cdot mol^{-1}$ at 5 K) ferromagnetic behavior is evidenced. By linear regression, the Curie constant has been determined to be 0.45 $cm^3 \cdot K \cdot mol^{-1}$, which results in a g value of 2.18. This value is in very good agreement with that determined from EPR measurements in the solid state (g = 2.15).

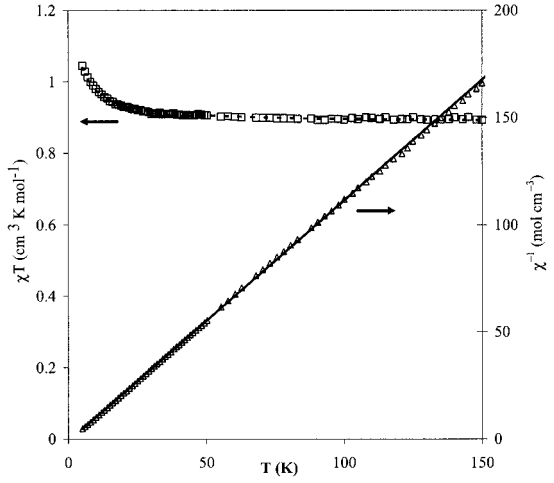

Figure 7. $\chi_1 T$ vs. T (Δ) and χ_1^{-1} vs. T curves ($\square$) of **1**; the solid line represents the linear fitting according to the Curie−Weiss law and the dashed line represents the calculated lines for the parameters J = 3.2 cm^{-1}, g = 2.17 and $R = 1.24 \times 10^{-5}$

A ferromagnetic interaction is usually observed when the magnetic orbitals of two metal ions have a negligible overlap, whereas an antiferromagnetic exchange is found when the magnetic orbitals are pointing towards each other in such a way that the overlap integral is reasonably large.[25,26] In complex **1**, two unpaired electrons of the Cu1 and Cu2 ions are both occupying $d_{x^2-y^2}$ orbitals. In a symmetrical complex, a bridging phenoxo group with an angle of 101.75(9)° between the copper centers would normally result in an antiferromagnetic interaction. However, due to the asymmetry of the penta- and hexacoordinate copper(II) ions, induced by the ligand Hpy2ald and the nitrate anions, an overlapping of two $d_{x^2-y^2}$ orbitals can be expected to be insignificant. In this case, a weak ferromagnetic exchange can be expected.

The magnetic behavior has been simulated using the Bleaney−Bowers equation[27,28] [see Equation (1)], in which $-J$ is the magnetic exchange parameter and all constants have their usual value.[27]

$$\chi = \frac{2Ng^2\beta^2}{kT[3 + \exp(-J/kT)]} \quad (1)$$

The best simulation is obtained with the values J = 3.2 cm^{-1} and g = 2.17. The reliability factor, defined as $R = n^{-1}[\Sigma(\chi_{obs} - \chi_{cal})^2/(\chi_{cal})^2]$ (n = number of data points) is 1.24×10^{-5}.

Conclusion

In the present study, three new complexes of copper(II) nitrate, copper(II) bromide and manganese(II) chloride with a phenol-based ligand containing a formyl group in the *ortho* position of the phenol ring have been prepared and structurally characterized. The structures of all compounds are very different from previously reported ones with similar ligands. In all cases, the carbonyl group of the ligand does not coordinate to the metal ions. The reaction of copper(II) nitrate with the ligand yields a dinuclear complex $[Cu_2(py2ald)(\mu\text{-}NO_3)(NO_3)_2]$, which possesses both donor-atom asymmetry and coordination-number asymmetry, whereas both copper(II) bromide and manganese(II) chloride form mononuclear complexes of formula [M(Hpy2-ald)X_2] (X = Cl or Br). The behavior of the complexes in the solid state and in solution was characterized by means of ligand field and EPR spectroscopy, mass spectrometry, conductivity measurements, cyclic voltammetry and magnetic susceptibility studies. Whereas the coordination environments of the metal ions for the mononuclear complexes appear to be mostly retained upon dissolution, we were able to observe the dissociation of the dinuclear nitrate complex in methanol. Although the results of mass-spectroscopic measurements suggest the existence of mononuclear, as well as dinuclear, species at equilibrium, other spectroscopic techniques, as well as conductivity measurements, do not offer direct evidence for the presence of an initial dinuclear complex in methanol solution. Therefore, the complete dissociation of the initial dinuclear complex into mononuclear units of composition $[Cu(Hpy2ald)(NO_3)_2]$, whose structure is expected to be similar to the copper(II) bromide and manganese(II) chloride complexes, can also be suggested. The magnetic susceptibility measurements indicate a ferromagnetic behavior for the nitrate complex and paramagnetic behavior for both the copper chloride and manganese bromide complexes.

Experimental Section

Materials and Methods: All starting materials are commercially available and were used as purchased. The ligand Hpy2ald was synthesized as described previously.[15] The infrared spectra of the complexes in the 4000−300 cm^{-1} range were recorded on a Bruker 330V IR spectrophotometer equipped with a Golden Gate Diamond. The ligand-field spectra of the solids (300−2000 cm^{-1}, diffuse reflectance) and in solution were taken on a Perkin−Elmer 330 spectrophotometer equipped with a data station. Electrospray mass spectra (ESI-MS) in acetonitrile or methanol solution were recorded on a Thermo Finnigan AQA apparatus. X-band electron paramagnetic resonance (EPR) measurements were performed at room temperature and at 77 K in the solid state, or at 77 K as frozen methanol solutions on a Jeol RE2x electron spin resonance spectrometer, using DPPH (g = 2.0036) as a standard. The conductivity measurements were performed using a Philips PW9526 digital

 © 2004 Wiley-VCH Verlag GmbH & Co. KGaA, Weinheim

conductivity meter and PW 9552/60 measuring cell with 1 mM solutions of the complexes in acetonitrile and/or methanol. Cyclic voltammetry measurements were performed with an Autolab PGSTAT 10 cyclic voltammeter, using a Pt working electrode and a Ag/AgCl reference electrode in acetonitrile or methanol (10^{-3} M), with tetrabutylammonium perchlorate as supporting electrolyte, at a scan rate of 0.1 mV/s. Bulk magnetizations of polycrystalline samples were measured in the range 5−300 K with a Quantum Design MPMS-5S SQUID magnetometer, in a 1 kG applied field. The data were corrected for the experimentally determined contribution of the sample holder. Corrections for the diamagnetic responses of the complexes, as estimated from Pascal's constants, were applied.[29]

The solution studies were performed with either acetonitrile or methanol as solvent in the case of complex **1**, and methanol for complexes **2** and **3**, due to the fact that neither of the two latter complexes is soluble in acetonitrile.

$[Cu_2(py2ald)(\mu\text{-}NO_3)(NO_3)_2]\cdot CH_3CN$ (1): 20 mL of an acetonitrile solution of the ligand (56 mg, 0.16 mmol) were added to an equal volume of a copper(II) nitrate solution (77 mg, 32 mmol) in acetonitrile. Slow evaporation of the solvent led to the appearance of green rectangular crystals, which were of sufficient quality for X-ray structure determination. The crystals were found to deteriorate rapidly when taken out of the mother liquor, due to the loss of an acetonitrile molecule. $C_{21}H_{20}Cu_2N_6O_{11}$ (659.5): calcd. C 38.2, H 3.1, N 12.7; found C 37.9, H 3.4, N 12.8. IR: 3047 cm^{-1} (C−H stretching), 1610 (C=O stretching), 1550 (C=C arom., C=N arom.), 1436 (chelating didentate NO_3^-, N=O stretching), 1283 [bridging didentate NO_3^-, $\nu_a(NO_2)$], 998 [bridging didentate NO_3^-, $\nu_s(NO_2)$].

$[Cu(Hpy2ald)Br_2]\cdot 0.5H_2O$ (2): 20 mL of a methanol solution of the ligand (56 mg, 0.16 mmol) were added to an equal volume of a copper(II) bromide solution (72 mg, 0.32 mmol). Green rectangular crystals appeared when the solvent was almost completely evaporated. Their quality was found to be suitable for X-ray diffraction analysis. $C_{42}H_{44}Br_4Cu_2N_6O_5$:calcd. C 43.5, H 3.8, N 7.3; found C 43.9, H 3.8, N 7.5. IR: ca. 3600 cm^{-1}, broad band (H_2O, asymmetric and symmetric OH stretching), 2980 (C−H stretching), 1654 (C=O stretching), 1608 (C=C arom., C=N arom.).

$[Mn(Hpy2ald)Cl_2]$ (3): 20 mL of a methanol solution containing manganese(II) chloride dihydrate (129 mg, 0.8 mmol) were added to an equal volume of a methanol solution of the ligand (56 mg, 0.16 mmol). Slow evaporation of the resulting bright-yellow solution gave colorless crystals of the product. These crystals were found to be of sufficient quality for X-ray crystal structure determination. $C_{21}H_{21}Cl_2MnN_3O_2$: calcd. C 53.3, H 4.5, N 8.9; found C 52.9, H 4.9, N 8.9. IR: 2968 cm^{-1} (C−H stretching), 1655 (C=O stretching), 1604 (C=C arom., C=N arom.)

X-ray Crystallographic Study: X-ray intensities were collected on a Nonius−KappaCCD diffractometer with rotating anode (λ = 0.71073 Å, graphite monochromator) at a temperature of 150(2)K up to a resolution of $(\sin\theta/\lambda)_{max}$ = 0.65 $Å^{-1}$. The structures were solved by direct methods (SHELXS-97,[30] compound **1**) or automated Patterson methods (DIRDIF99,[31] compounds **2** and **3**) and refined with SHELXL-97[32] against F^2 of all reflections. Non-hydrogen atoms were refined freely with anisotropic displacement parameters. The phenolic hydrogen atoms of compounds **2** and **3** were located in the difference Fourier map and refined freely with isotropic displacement parameters. The water hydrogen atoms of compound **2** were located in the difference Fourier map and kept fixed in these positions. All other hydrogen atoms were refined as rigid groups. Illustrations, structure calculations, and structure checking were performed with the PLATON software package.[33] Further crystallographic details are given in Table 6.
CCDC-216684 (**1**), -216685 (**2**), and -216686 (**3**) contain the supplementary crystallographic data for this paper. These data can be obtained free of charge at www.ccdc.cam.ac.uk/conts/retrieving.html [or from the Cambridge Crystallographic Data Center, 12 Union Road, Cambridge CB2 1EZ, UK; Fax: (internat.) + 44-1223/336-033; E-mail: deposit@ccdc.cam.ac.uk].

Table 6. Crystallographic details for complexes **1**, **2** and **3**

	1	**2**	**3**
Formula	$C_{21}H_{20}Cu_2N_6O_{11}\cdot C_2H_3N$	$C_{21}H_{21}Br_2CuN_3O_2\cdot 0.5H_2O$	$C_{21}H_{21}Cl_2MnN_3O_2$
Molecular mass	700.56	579.78	473.25
Crystal color	dark green	green	yellow
Crystal size [mm^3]	0.48 × 0.24 × 0.18	0.24 × 0.18 × 0.06	0.56 × 0.15 × 0.03
Crystal system	monoclinic	triclinic	triclinic
Space group	$P2_1/c$ (no. 14)	$P\bar{1}$ (no. 2)	$P\bar{1}$ (no. 2)
a (Å)	8.6632(7)	7.7651(1)	7.6829(14)
b (Å)	17.3510(10)	8.8800(1)	8.8364(11)
c (Å)	19.5299(17)	16.9099(2)	16.329(2)
α (deg.)	90	98.0365(6)	95.936(11)
β (deg.)	97.203(7)	93.0171(7)	92.005(14)
γ (deg.)	90	112.7805(6)	111.789(13)
V ($Å^3$)	2912.5(4)	1057.19(2)	1020.6(3)
Z	4	2	2
$D_{calcd.}$ (g/cm^3)	1.598	1.821	1.540
μ [mm^{-1}]	1.529	4.838	0.932
Absorption correction	SADABS[34]	PLATON (DELABS)[33]	SADABS[34]
Transmission range	0.61−0.76	0.38−0.79	0.64−0.97
Refl. collected/unique	51234/6695	14345/4758	16182/4640
Parameters/restraints	390/0	276/0	267/0
$R1/wR2$ [$I > 2\sigma(I)$]	0.0408/0.1091	0.0260/0.0595	0.0467/0.1098
$R1/wR2$ [all refl.]	0.0532/0.1172	0.0325/0.0625	0.0755/0.1225
GoF	1.043	1.036	1.037

 © 2004 Wiley-VCH Verlag GmbH & Co. KGaA, Weinheim

Acknowledgments

We would like to thank Dr. E. Bouwman for the helpful discussions concerning EPR spectroscopy. Support from the NRSC Catalysis (a Research School Combination of HRSMC and NIOK) is kindly acknowledged. Also, support and sponsorship concerted by COST Action D21/003/2001 is kindly acknowledged. This work was supported in part (M.L., A.L.S.) by The Netherlands Foundation for Chemical Sciences (CW) with financial aid from the Netherlands Organization for Scientific Research (NWO).

[1] J. Reim, B. Krebs, *J. Chem. Soc., Dalton Trans.* **1997**, 3793−3804.
[2] H. Adams, D. E. Fenton, S. R. Haque, S. L. Health, M. Ohba, H. Okawa, S. E. Spey, *J. Chem. Soc., Dalton Trans.* **2000**, 1849−1856.
[3] S. S. Tandon, L. K. Thompson, J. N. Bridson, V. McKee, A. J. Downard, *Inorg. Chem.* **1992**, *31*, 4635−4642.
[4] H. Adams, S. Clunas, D. E. Fenton, G. Handley, P. E. McHugh, *Inorg. Chem. Commun.* **2002**, *5*, 1044−1047.
[5] N. N. Murthy, M. Mahroof-Tahir, K. D. Karlin, *Inorg. Chem.* **2001**, *40*, 628−635.
[6] S. Torelli, C. Belle, I. Gautier-Luneau, J. L. Pierre, E. Saint-Aman, J. M. Latour, L. Le Pape, D. Luneau, *Inorg. Chem.* **2000**, *39*, 3526−3536.
[7] K. Abe, K. Matsufuji, M. Ohba, H. Okawa, *Inorg. Chem.* **2002**, *41*, 4461−4467.
[8] L. Dubois, D.-F. Xiang, X.-S. Tan, J. Pecaut, P. Jones, S. Baudron, L. Le Pape, J. M. Latour, C. Baffert, S. Chardon-Noblat, M.-N. Collomb, A. Deronzier, *Inorg. Chem.* **2003**, *42*, 750−760.
[9] P. Karsten, A. Neves, A. J. Bortoluzzi, M. Lanznaster, V. Drago, *Inorg. Chem.* **2002**, *41*, 4624−4626.
[10] K. D. Karlin, J. C. Hayes, Y. Gultneh, R. W. Cruse, J. W. McKown, J. P. Hutchinson, J. Zubieta, *J. Am. Chem. Soc.* **1984**, *106*, 2121−2128.
[11] C. J. O'Connor, D. Firmin, A. K. Pant, B. Ram Babu, E. D. Stevens, *J. Am. Chem. Soc.* **1986**, *25*, 2300−2307.
[12] B. Krebs, K. Schepers, B. Bremer, G. Henkel, E. Althaus, W. Muller-Warmuth, K. Griesar, W. Haase, *Inorg. Chem.* **1994**, *33*, 1907−1914.
[13] E. Lambert, B. Chabut, S. Chardon-Noblat, A. Deronzier, G. Chottard, A. Bousseksou, J.-P. Tuchagues, J. Laugier, M. Bardet, J.-M. Latour, *J. Am. Chem. Soc.* **1997**, *119*, 9424−9437.
[14] H. Adams, S. Clunas, D. E. Fenton, *Inorg. Chem. Commun.* **2001**, *4*, 667−670.
[15] I. A. Koval, D. Pursche, A. F. Stassen, P. Gamez, B. Krebs, J. Reedijk, *Eur. J. Inorg. Chem.* **2003**, 1669−1674.
[16] I. A. Koval, M. Huisman, A. F. Stassen, P. Gamez, M. Lutz, A. L. Spek, D. Pursche, B. Krebs, J. Reedijk, *Inorg. Chim. Acta*, in press.
[17] A. W. Addison, T. N. Rao, J. Reedijk, J. van Rijn, G. C. Verschoor, *J. Chem. Soc., Dalton Trans.* **1984**, 1349−1356.
[18] A. B. P. Lever, *Inorganic Electronic Spectroscopy, Vol. 33*, Elsevier, Amsterdam, **1984**.
[19] U. Rajendran, R. Viswanathan, M. Palaniandavas, N. Laskiminaraya, *J. Chem. Soc., Dalton Trans.* **1994**, 1219−1226.
[20] *Comprehensive Coordination Chemistry, Vol. 5*, (Ed.: G. Wilkinson), Pergamon Press, Toronto, **1987**.
[21] F. Neese, *The program EPR, a modeling approach, Version 1.0*, University of Konstanz, **1993**.
[22] B. J. Hathaway, D. E. Billing, *Coord. Chem. Rev.* **1970**, *5*, 143−207.
[23] S. T. Warzeska, F. Micchiche, M. Chiara Mimmi, E. Bouwman, H. Kooijman, A. L. Spek, J. Reedijk, *J. Chem. Soc., Dalton Trans.* **2001**, 3507−3512.
[24] W. J. Geary, *Coord. Chem. Rev.* **1971**, *7*, 81−122.
[25] P. J. Hay, J. C. Thibeault, R. Hoffmann, *J. Am. Chem. Soc.* **1975**, *97*, 4884−4899.
[26] O. Kahn, *Angew. Chem. Int. Ed. Engl.* **1985**, *24*, 834−850.
[27] O. Kahn, *Molecular Magnetism*, Wiley-VCH, New York, **1993**.
[28] B. Bleaney, K. D. Bowers, *Proc. R. Soc., London Ser. A* **1952**, *214*, 451−465.
[29] I. M. Kolthoff, P. J. Elving, *Treatise on Analytical Chemistry, Vol. 4*, Interscience Encyclopedia, Inc., New York, **1963**.
[30] G. M. Sheldrick, *SHELXS-97*, University of Gottingen, Germany, **1997**.
[31] P. T. Beurskens, G. Admiraal, G. Beurskens, W. P. Bosman, S. Garcia-Granda, R. O. Gould, J. M. M. Smits, C. Smykalla, *The DIRDIF99 program system, Technical Report of the Crystallography Laboratory, University of Nijmegen, The Netherlands*, **1999**.
[32] G. M. Sheldrick, *SHELXL-97, Program for the refinement of crystal structures*, University of Göttingen, Germany, **1997**.
[33] A. L. Spek, *J. Appl. Cryst.* **2003**, *36*, 7−13.
[34] G. M. Sheldrick, *SADABS*, University of Göttingen, Germany, **2003**.

Received August 13, 2003
Early View Article
Published Online December 12, 2003

Group 13 Complexes of 5-Methyl-1,3,5-dithiazinane[‡]

Juan Carlos Gálvez-Ruiz,[a] Carlos Guadarrama-Pérez,[a] Heinrich Nöth,[b] and Angelina Flores-Parra*[a]

Keywords: Aluminum / Halides / Indium / Conformational analysis

The synthesis of mono-N adducts of 5-methyl-1,3,5-dithiazinane (**1**) with $Al(CH_3)_3$, $Al(CH_3)_2Cl$, $AlCl_3$, $AlBr_3$ (**5**–**8**), a bis-N adduct with $InCl_3$ (**9**), and the corresponding dithiazinanium salts with the anions $AlBr_4^-$, $AlCl_4^-$, $GaCl_4^-$ and BCl_4^- (**10**–**14**) are reported. Compounds **5**–**7** adopt a preferred conformation in solution at room temperature and **8** at –10 °C. $\Delta G^{\neq}$ values for the ring inversion were calculated for **5**–**8**. Compounds **6**–**14** were studied by single-crystal X-ray diffraction. The solution and solid-state analyses showed that the rings are present in all cases in a chair conformation. In compounds **5**–**8** the tetrahedral aluminum atom is found in an equatorial position. In the indium compound **9** the metal atom has a tbp geometry. For dithiazinanium rings **10**–**14** dipolar intra- and intermolecular interactions between halogen atoms and C–H and N–H are reported. Two different conformations for the N–CH_3 were found in compound **14**.
(© Wiley-VCH Verlag GmbH & Co. KGaA, 69451 Weinheim, Germany, 2004)

Introduction

We are currently investigating the coordinating and conformational behavior of 5-methyl-1,3,5-dithiazinane (**1**).[1,2] This compound is in conformational equilibrium with the methyl group in an unexpected axial position and has five lone pairs available for coordination (Scheme 1). The geminal position of the heteroelements makes the CH protons relatively acidic,[2b] meaning that they could coordinate molecules bearing lone pairs through hydrogen bonding.

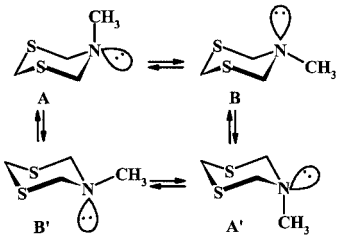

Scheme 1. A and A′ are the preferred conformers in the conformational equilibrium of 5-methyldithiazinane **1**; the processes from A to B and A′ to B′ involve nitrogen inversion and from A to B′ and A′ to B ring inversion

Dithiazinane rings are fragile in the presence of metals and moisture and, as a consequence, their coordination chemistry is practically unknown except for the results from our group.[1,2,3a]

Boron Lewis acids have been used as a probe for the basic sites of compound **1**, giving the N→BX_3 adducts **2**.[2] An excess of borane (BH_3 or $BHCl_2$) produces 6-borata-5-aza-1,3-dithiocyclohexanes **3**[1b,2d,2f] (Scheme 2). Nitrogen is always the preferred coordination site, and the S→B coordinative bond in **4** has been only observed when the borata heterocycle bearing a BH_2 group is treated with an excess of BH_3·THF; its weak S→BH_3 bond is readily broken upon removal of the solvent.[1c][2f]

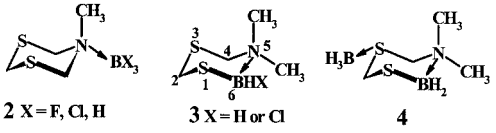

Scheme 2

An important discovery has been the fact that the conformational equilibrium of **1** is abruptly stopped by N-coordination to BH_3 or boron halides. This unexpected result was explained by significant proton-hydride and proton-halide intramolecular stabilizing interactions.[2a,3]

These findings stimulated us to continue the exploration of the coordinating properties of compound **1** with other group 13 compounds. Here, the synthesis of N adducts of dithiazinane **1** with $Al(CH_3)_3$, $Al(CH_3)_2Cl$, $AlCl_3$, $AlBr_3$

[‡] This work is part of the PhD thesis of J. C. G.-R. Chemistry Department of Cinvestav-Mexico, **2003**.
[a] Chemistry Department, Centro de Investigación y de Estudios Avanzados del I.P.N.,
A.P. 14-740, C.P. 07000, México D.F., México
Fax: (internat.) + 52-555-747-113
E-mail: aflores@mail.cinvestav.mx
[b] Department of Chemistry, Ludwig-Maximilians-Universität, Butenandt-Straβe 5−13,
(Haus D), 81377 München, Germany

and $InCl_3$ is reported, as well as variable-temperature NMR experiments in order to obtain the $\Delta G^{\neq}$ of the ring inversion and to understand the coordination effect in the conformational equilibrium. The study of the molecules **5**−**8** in solution is complemented by X-ray diffraction analysis of **6**−**9**. The corresponding dithiazinanium salts **10**−**14** bearing the anions $AlBr_4^-$, $AlCl_4^-$ $GaCl_4^-$ and BCl_4^- and Cl^-, respectively, are formed in the presence of traces of moisture. Their X-ray diffraction data disclosed interesting intermolecular interactions in the solid state.

Results and Discussion

5-Methyl-1,3,5-dithiazinane Complexes

The reaction of compound **1** with equimolar amounts of $Al(CH_3)_3$, $Al(CH_3)_2Cl$, $AlCl_3$ or $AlBr_3$ in toluene (or $CHCl_3$) at 4 °C gave exclusively the N→Al mono adducts **5**−**8**, as established by NMR spectroscopy, especially by ^{27}Al NMR studies, which showed the characteristic resonances (δ = 110−183 ppm) for tetracoordinate aluminum atoms at room temperature (reported range between 100 and 200 ppm)[4] (Scheme 3). In the ^{13}C NMR spectra, the coordination effect is readily noted at room or at low temperature for C-2, C-4 and C-6, which are shifted to lower frequencies by up to 3 ppm, while N−CH_3 presents only a modest effect (Δδ = 1 ppm), indicating that it remains in an axial position. At room temperature, the ^1H NMR spectra of compounds **5**−**7** (at −10 °C for **8**) in C_7D_8 present separated and coupled signals for all the ring protons, showing that the rings are present in a fixed conformation due to the N-coordination. By comparison with the ^1H NMR spectra of N-boron adducts of dithiazinane,[1b,1c,2e] it was also deduced that the aluminum is placed in an equatorial position (Table 1). Opening of the dithiazinane ring in the presence of an excess of $AlMe_3$ proceeds by the breaking of two C−S bonds and the formation of an $MeEt_2N$-$AlMe_3$ adduct (^{27}Al δ = 139 ppm, $\Delta_{1/2}$ = 866 Hz). The ^{13}C NMR spectrum for this adduct shows signals for N−Et at δ = 49.66 and 9.27 ppm and for N−Me at δ = 40.79 ppm.

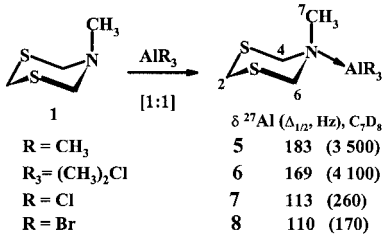

Scheme 3. Preferred conformation of compounds **5**−**8** and their ^{27}Al NMR data (in C_7D_8)

Variable temperature ^1H NMR experiments in C_7D_8 were performed in order to estimate the energies for ring inversion. The solutions were heated up to 75 °C without either a breaking of the Al−N bond or an opening of the ring, contrary to the situation observed for borane adducts.[1b,1c,2d] The ring-inversion energy is related to the size of the substituents at the nitrogen atom. A group with a big steric effect will be in an equatorial position, with a high ring-inversion energy.[5] On the other hand, a second effect — that the ring inversion energy is augmented by hydride-proton and halide-proton stabilizing interactions[2a,3a] — could be added to the anchorage of the ring conformation, as we have established for other boron adducts. The $\Delta G^{\neq}$ values for the ring inversion of compounds **5**−**8** are summarized in Table 1. All the aluminum groups

Table 1. ^1H NMR (400 MHz) data [δ (^nJ)] of anchored compounds **5**−**8** and their $\Delta G^{\neq}$ values (kJ/mol)

	Solvent	H-2eq	H-2ax	H-4eq and H-6eq	H-4ax and H-6ax	H-7	$\Delta G^{\neq}$
1 (25 °C)	[D_8]toluene	3.58 (s)	3.58 (s)	3.89 (s)	3.89 (s)	2.39(s)	−
1 (−90 °C)	[D_8]THF	3.60	4.60	3.93	4.95	2.60(s)	46.0[a]
	T_c, −41 °C	(dt, ^2J = 13.3, ^4J = 2.6 Hz)	(d, ^2J = 13.3 Hz)	(dd, ^2J = 13.3, ^4J = 2.6 Hz)	(d, ^2J = 12.7 Hz)		
5 (−10 °C)	[D_8]toluene	2.30	3.12	3.25	4.03	2.28 (s)	62.6 ± 0.5
	T_c, 59 °C	(dt, ^2J = 13.9, ^4J = 2.6 Hz)	(d, ^2J = 13.9 Hz)	(dd, ^2J = 13.6, ^4J = 2.6 Hz)	(d, ^2J = 13.6 Hz)		
6 (−15 °C)	[D_8]toluene	2.24	3.12	3.30	4.23	2.30 (s)	66.0 ± 0.5
	T_c, 75 °C	(d, ^2J = 13.9 Hz)	(d, ^2J = 13.9 Hz)	(d, ^2J = 13.9 Hz)	(d, ^2J = 13.9 Hz)		
7 (10 °C)	[D_8]toluene	1.93	2.73	3.45	4.24	2.44 (s)	68.5 ± 0.5
	T_c, 75 °C	(dt, ^2J = 13.3, ^4J = 2.2 Hz)	(d, ^2J = 13.3 Hz)	(dd, ^2J = 13.5, ^4J = 2.2 Hz)	(d, ^2J = 13.5 Hz)		
8 (−60 °C)	[D_8]toluene	1.65	2.50	3.45	4.24	2.37 (s)	51.7 ± 0.5
	T_c, −5 °C	(d, ^2J = 13.9 Hz)	(d, ^2J = 13.9 Hz)	(d, ^2J = 12.4 Hz)	(d, ^2J = 12.4 Hz)		
5 (−10 °C)	$CDCl_3$	3.48	4.26	3.88	4.62	2.83 (s)	−
		(dt, ^2J = 13.9, ^4J = 2.2 Hz)	(d, ^2J = 13.9 Hz)	(dd, ^2J = 13.0. ^4J = 2.2 Hz)	(d, ^2J = 13.9 Hz)		
6 (27 °C)	$CDCl_3$	3.47 (s br)	4.26 (s br)	3.99 (s br)	4.79 (s br)	2.96 (s)	−
7 (−10 °C)	$CDCl_3$	3.49	4.31	4.20	4.95	3.18 (s)	−
		(d, ^2J = 14.3 Hz)	(d, ^2J = 14.3 Hz)	(d, ^2J = 13.8 Hz)	(d, ^2J = 13.8 Hz)		
8 (−55 °C)	$CDCl_3$	3.48	4.32	4.29	5.03	3.19 (s)	−
		(d, ^2J = 14.3 Hz)	(d, ^2J = 14.3 Hz)	(d, ^2J = 13.6 Hz)	(d, ^2J = 13.6 Hz)		

[a] Same value was found in $CDCl_3$/$CFCl_3$.[7] δ (ppm) of $AlCH_3$: for **5**, −0.69 (s) in [D_8]toluene and −0.89 (s) in $CDCl_3$; for **6**, −0.47(s) in [D_8]toluene and −0.63(s) in $CDCl_3$.

 © 2004 Wiley-VCH Verlag GmbH & Co. KGaA, Weinheim

fix the dithiazinane conformation as is seen from their $\Delta G^{\neq}$ values when compared with data of the free dithiazinane ($\Delta G^{\neq}$ = 46.0 kJ/mol in [D_8]THF and in $CDCl_3/CFCl_3$ [6]). In compounds **5**−**8** the size of the coordinating group determines the inversion of the ring, as in the case of $AlMe_3$ and $AlClMe_2$ adducts. A second effect stabilizing the inversion could be the interactions between the halogen atoms and the acidic C−H protons. Therefore, it is expected that $AlClMe_2$, $AlCl_3$ and $AlBr_3$ need a higher energy for the ring inversion due to possible cooperative, weak H···X interactions. Analyses of the results shows that the highest ring-inversion energy was found for the $AlCl_3$ adduct **7**. The lowest energy corresponds to the $AlBr_3$ adduct **8** but there is no clear explanation for this behavior, because the low energy is observed despite the fact that $AlBr_3$ is a big group and the Al−N bond length in **8** (1.982 Å) is the shortest in the series (**5**−**8**) indicating a strong bond {the same trend was found in the dissociation energy of pyridine·$AlCl_3$ (77.3 kJ/mol) and pyridine·$AlBr_3$ (73.6 kJ/mol)[7]}. Therefore, we have carefully analyzed the halide-proton contacts in the solid state in order to find the reason for the conformational behavior of this adduct. An explanation could be that bromine atoms present a weaker interaction than chlorine with the hydrogen atoms as a consequence of their lower electronegativity and their larger size.[8]

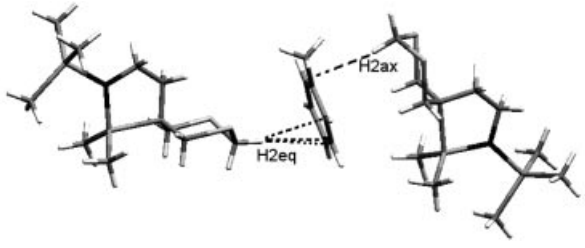

Figure 1. View of *O*-dimethylaluminum-*O*-trimethylaluminum-2(1,3,5)-dithiazinan-5-yl-ethanolate showing a polymeric array produced by π-interactions of toluene with SCH_2S protons (distances are: $H2_{eq}$−C_{ortho} 2.79 Å, $H2_{eq}$−C_{meta} 2.74 Å and $H2_{eq}$−C_{para} 2.80 Å, and $H2_{ax}$−C_{ipso} 2.75 Å)[9]

An interesting fact concerning the ^{1}H NMR chemical shifts of the C-2 protons in compounds **4**−**8** in toluene is that they are well shielded. This can be explained by an arrangement of the toluene aromatic ring density in front of the C-2 protons, as was observed in the solid state in the X-ray molecular structure of another derivative of dithiazinane[9] (Figure 1).

We were unable to obtain single crystals of compound **5,** in contrast to compounds **6** (obtained from $C_6H_5CH_3$ at −20 °C), **7** (from CH_2Cl_2 at 25 °C) and **8** (from $C_6H_5CH_3$ at 25 °C). In all cases the aluminum atoms are tetracoordinate and are found in equatorial positions. The angles at the nitrogen atoms deviate little from the ideal tetrahedral angles. The N−Al bond [**6**: 2.044(2) Å; **7**: 1.993(5) Å; **8**: 1.982(5) Å] is, in all cases, slightly shorter than the ideal covalent bond length (2.05 Å)[10] indicating a strong coordinative bond. The dithiazinane ring has a chair conformation. In all compounds one of the hydrogen atoms of the N-methyl group is pointing towards the space in the middle of the sulfur atoms where the sulfur orbitals (50% p character)[11] are also pointing. The C−H···S distances range from 2.76 to 2.85 Å. This is significantly shorter than the sum of the van der Waals radii (3.0 Å). The bond lengths and angles are given in Tables 2 and 3 and the crystallographic data and selected data collection in Table 4.

In compound **6** the chlorine atom is arranged in a staggered position between the methyl and a methylene group of the ligand (Figure 2a). Two short, weak contacts were found between Cl···H4eq (2.860 Å) and Cl···H7 (3.080 Å) (Σr_{VDW} = 3.1 Å). The Cl···H4eq interaction can be also

Table 2. Selected bond lengths [Å]

6		**7**		**8**		**9**		**10**		**12**	
Cl1−Al1	2.176(1)	S1−C6	1.797(6)	Cl1−Al1	2.136(1)	Al6−N5	1.982(5)	In1−Cl1A	2.376(1)	Ga1−Cl3	2.160(2)
S1−C6	1.807(3)	S3−C4	1.793(7)	Cl2−Al1	2.147(1)	Br1−Al6	2.272(2)	In1−Cl2	2.383(1)	Ga1−Cl4	2.174(2)
S2−C4	1.804(3)	Cl2−Al1	2.101(3)	Cl3−Al1	2.122(1)	Br3−Al6	2.272(2)	In1−N1A	2.413(3)	S1−C6	1.772(9)
Al1−C9	1.974(3)	Cl1−Al1	2.110(3)	Cl4−Al1	2.134(1)	Br2−Al6	2.270(2)	In1−Cl1	2.376(1)	S3−C2	1.777(7)
N5−C6	1.474(4)	N5−C4	1.492(8)	S1−C2	1.783(5)	S1−C2	1.813(7)	In1−N1	2.413(3)	N5−C4	1.499(9)
N5−C7	1.497(3)	N5−C6	1.495(7)	S3−C4	1.788(4)	S3−C2	1.808(7)	S3−C2	1.817(4)	N5−C7	1.514(10)
S1−C2	1.806(4)	S1−C2	1.806(7)	N5−C4	1.490(5)	S1−C6	1.793(7)	S3−C4	1.820(4)	Ga1−Cl2	2.174(1)
S2−C2	1.799(5)	S3−C2	1.806(7)	N5−C7	1.508(4)	S3−C4	1.799(6)	S5−C4	1.808(4)	Ga1−Cl1	2.185(2)
Al1−C8	1.955(3)	Cl3−Al1	2.112(3)	S1−C6	1.789(4)	N5−C4	1.509(7)	S5−C6	1.824(4)	S1−C2	1.812(8)
Al1−N5	2.044(2)	Al1−N5	1.993(5)	S3−C2	1.791(4)	N5−C6	1.506(7)	N1−C2	1.486(5)	S3−C4	1.792(8)
N5−C4	1.495(3)	N5−C7	1.493(7)	N5−C6	1.497(5)	N5−C7	1.512(8)	N1−C6	1.486(4)	N5−C6	1.509(8)

11		**13**				**14**					
S1−C6	1.791(5)	S1A−C6A	1.79(2)	Br2−Al1	2.309(5)	Cl2−B1	1.875(10)	S32−C22	1.807(8)		
S3−C2	1.792(6)	S1A−C2A	1.82(1)	Br3−Al1	2.275(5)	Cl3−B1	1.858(9)	S32−C42	1.786(6)		
F1−B1	1.368(7)	S3A−C2A	1.76(2)	Br4−Al1	2.275(5)	Cl4−B1	1.792(9)	N5−C4	1.496(7)		
F3−B1	1.349(7)	S3A−C4A	1.77(1)	S1−C2	1.79(1)	Cl5−B1	1.781(9)	N5−C6	1.521(8)		
N5−C7	1.495(6)	N5A−C6A	1.48(2)	S1−C6	1.81(2)	S1−C2	1.784(7)	N5−C7	1.474(9)		
N5−C4	1.501(6)	N5A−C7A	1.49(2)	S3−C4	1.79(2)	S1−C6	1.776(7)	N52−C42	1.481(7)		
		N5A−C4A	1.50(2)	S3−C2	1.82(2)	S3−C2	1.796(7)	N52−C62	1.482(8)		

 © 2004 Wiley-VCH Verlag GmbH & Co. KGaA, Weinheim

Table 3. Selected bond angles [°]

6		**7**		**8**		**9**		**13**	
C2−S1−C6	96.83(15)	C6−S1−C2	98.4(3)	N5−Al6−Br3	107.10(15)	Cl1A−In1−Cl1	119.65(5)	C6AS1AC2A	99.3(8)
C2−S2−C4	97.77(16)	C4−S3−C2	98.5(3)	N5−Al6−Br1	106.46(16)	Cl1A−In1−N5A	91.80(8)	C2A−S3A−C4A	99.1(8)
C8−Al1−C9	117.77(15)	N5−Al1−Cl1	106.28(17)	N5−Al6−Br2	106.35(15)	Cl1A−In1−N5	90.33(8)	C6A−N5A−C7A	109.6(11)
C9−Al1−N5	107.22(11)	N5−Al1−Cl2	105.91(18)	Br2−Al6−Br1	114.72(7)	Cl1A−In1−Cl2	120.17(3)	C6A−N5A−C4A	112.7(12)
C9−Al1−Cl1	110.17(12)	N5−Al1−Cl3	106.52(19)	Br2−Al6−Br3	110.53(8)	Cl1−In1−Cl2	120.17(3)	C7A−N5A−C4A	111.9(11)
C8−Al1−N5	107.24(11)	Cl1−Al1−Cl3	112.43(13)	Br3−Al6−Br1	111.20(8)	Cl1−In1−N5A	90.33(8)	S3A−C2A−S1A	113.1(8)
C8−Al1−Cl1	111.63(12)	Cl2−Al1−Cl1	112.84(13)	C6−S1−C2	97.5(3)	Cl1−In1−N5	91.80(8)	N5A−C4A−S3A	113.1(9)
N5−Al1−Cl1	101.35(8)	Cl2−Al1−Cl3	112.23(12)	C4−S3−C2	97.4(3)	Cl2−In1−N5	87.88(7)	N5A−C6A−S1A	113.9(11)
C4−N5−C7	110.8(2)	C4−N5−Al1	107.9(4)	C4−N5−Al6	108.5(4)	Cl2−In1−N5A	87.88(7)	C2−S1−C6	96.3(7)
C4−N5−Al1	109.02(16)	C4−N5−C6	110.5(5)	C6−N5−Al6	108.8(4)	N1−In1−N5A	175.8(1)	C4−S3−C2	96.3(7)
C6−N5−C7	112.0(2)	C4−N5−C7	110.9(5)	C7−N5−Al6	108.6(4)	C2−S3−C4	97.69(18)	Br1−Al1−Br3	111.8(2)
C6−N5−Al1	104.69(14)	C6−N5−Al1	108.6(4)	C4−N5−C7	110.9(5)	C4−S5−C6	98.34(18)	Br1−Al1−Br4	110.0(2)
C6−N5−C4	110.6(2)	C7−N5−Al1	108.0(4)	C6−N5−C4	109.1(4)	C2−N5−In1	106.8(2)	Br3−Al1−Br4	110.3(2)
C7−N5−Al1	109.54(17)	C7−N5−C6	110.7(5)	C6−N5−C7	110.9(5)	C6−N5−In1	108.0(2)	Br1−Al1−Br2	108.0(2)
S2−C2−S1	112.19(19)	S1−C2−S3	111.6(4)	S3−C2−S1	111.7(3)	C7−N5−In1	107.3(2)	Br3−Al1−Br2	106.1(2)
N5−C4−S2	115.79(19)	N5−C4−S3	116.9(5)	N5−C4−S3	116.9(4)	C2−N5−C6	111.0(3)	Br4−Al1−Br2	110.6(2)
N5−C6−S1	117.59(17)	N5−C6−S1	117.0(5)	N5−C6−S1	117.1(4)	C7−N5−C2	111.8(3)	C7−N5−C4	112.4(13)
						C7−N5−C6	111.7(3)	C7−N5−C6	114.6(13)
						N5−C2−S3	116.6(2)	C4−N5−C6	108.5(12)
						S5−C4−S3	112.7(2)	S1−C2−S3	112.5(8)
						N5−C6−S5	116.2(3)	N5−C4−S3	118.2(11)
								N5−C6−S1	117.6(10)

10		**11**		**12**		**14**			
Cl1−Al1−Cl2	106.98(5)	C6−S1−C2	98.5(2)	Cl3−Ga1−Cl2	111.28(9)	C6−S1−C2	98.8(3)	Cl3−B1−Cl2	102.7(5)
Cl3−Al1−Cl1	110.91(6)	C2−S3−C4	98.5(2)	Cl2−Ga1−Cl1	106.81(7)	C4−S3−C2	97.3(3)	Cl4−B1−Cl3	111.6(5)
Cl3−Al1−Cl2	110.83(6)	C6−N5−C4	111.7(4)	Cl2−Ga1−Cl4	109.46(7)	C62−S12−C22	98.0(3)	Cl5−B1−Cl2	110.5(5)
Cl3−Al1−Cl4	109.73(5)	C6−N5−H5	110.6(41)	Cl3−Ga1−Cl1	110.75(8)	C42−S32−C22	97.0(3)	Cl5−B1−Cl3	112.3(5)
Cl4−Al1−Cl1	109.69(6)	C7−N5−C4	110.8(4)	Cl3−Ga1−Cl4	110.02(8)	C4−N5−C6	110.9(5)	Cl5−B1−Cl4	114.0(5)
Cl4−Al1−Cl2	108.62(5)	C7−N5−C6	109.7(4)	Cl4−Ga1−Cl1	108.42(8)	C7−N5−C4	114.5(5)	S1−C2−S3	111.9(4)
C2−S1−C6	98.52(19)	F2−B1−F3	111.3(5)	C6−S1−C2	98.4(4)	C7−N5−C6	114.0(5)	N5−C4−S3	114.4(4)
C4−S3−C2	98.2(2)	F2−B1−F1	105.6(5)	C2−S3−C4	99.0(4)	C42−N52−C62	111.9(5)	N5−C6−S1	114.1(4)
C4−N5−C6	111.9(3)	F3−B1−F1	110.4(5)	C4−N5−C6	111.2(5)	C42−N52−C72	109.9(5)	S12−C22−S32	111.8(4)
C4−N5−C7	110.1(3)	F4−B1−F1	108.8(6)	C4−N5−C7	110.0(5)	C62−N52−C72	110.7(5)	N52−C42−S32	113.8(4)
C6−N5−C7	110.6(3)	F4−B1−F3	107.6(5)	C6−N5−C7	110.8(6)	Cl4−B1−Cl2	105.0(4)	N52−C62−S12	114.1(4)
S1−C2−S3	113.4(2)	F4−B1−F2	113.0(7)	S3−C2-S	112.9(4)				
N5−C4−S3	114.2(2)	S3−C2−S1	111.7(3)	N5−C4−S3	113.0(5)				
N5−C6−S1	113.2(3)	N5−C4−S3	113.2(3)	N5−C6−S1	114.0(5)				
		N5−C6−S1	112.7(3)						

deduced from the sharp Cl−Al−N angle (101.25°), which means that Cl approaches H4eq. Intermolecular interactions are confined to a Cl1′···H2eq distance of 2.774 Å (Figure 2b).

In the N→$AlCl_3$ adduct **7**, the N→Al bond length is 1.993(5) Å. There are six weak cooperative intramolecular van der Waals contacts of the Cl atoms with the hydrogen atoms of neighboring CH units (range 2.92−3.00 Å) leading to a rather symmetrical orientation of the $AlCl_3$ molecule to the $H_3CN(CH_2)_2$ group. The Cl−Al−N angles are slightly sharper [105.9(2), 106.3(2) and 106.5(2)°] than those of a regular tetrahedron and cause the CH and Cl atoms to approach each other (Figure 3). A weak intermolecular S···Cl interaction of 3.467 Å is also observed[8a,8b,12] (Σr_{VDW} = 3.70 Å).

In the solid state, compound **8** has an N→Al bond length of 1.982(5) Å, with Br−Al−N bond angles of 107.1(2)°, 106.5(2)° and 106.4(2)°. Six short, weak intramolecular contacts between bromine and the neighboring hydrogen atoms are found, with H···Br distances ranging from 2.97 to 3.12 Å [Σr_{VDW} H···Br = 3.2 Å] (Figure 4b).

In the crystal, each molecule has three intermolecular interactions with three neighboring molecules, through H···Br van der Waals contacts [2.89, 2.90 and 3.04 Å]. The interaction of two sulfur atoms of one molecule with two bromine atoms,[13] each from a different molecule, is shown in Figure 5, including a short Br···H contact (2.887 Å).

The equimolecular reaction of compound **1** with $InCl_3$ in toluene at room temperature gives a white solid that crystallized from $CHCl_3$. It proved to be the 2:1 adduct **9** (Scheme 4).

The structure of **9** in the solid state reveals a pentacoordinate indium atom bound to two molecules of dithiazinane **1** through its N atoms, which are placed at the apical positions of a trigonal bipyramidal arrangement about the indium center. The molecule has C_2 symmetry, the two-fold axis running through the In−Cl2 bond (Figure 6). The N−In bond lengths are 2.413(3) Å. The N atoms of both

 © 2004 Wiley-VCH Verlag GmbH & Co. KGaA, Weinheim

Table 4. Crystal data and data collection

	6	**7**	**8**	**9**	**10**	**11**	**12**	**13**	**14**
Formula	$C_6H_{15}AlClNS_2$	$C_4H_9AlCl_3NS_2$	$C_4H_9AlBr_3NS_2$	$C_8H_{18}Cl_3InN_2S_4$	$C_4H_{10}AlCl_4NS_2$	$C_4H_{10}BF_4NS_2$	$C_4H_{10}Cl_4GaNS_2$	$C_8H_{19}S_4N_2AlBr_4$	$C_8H_{20}BClN_2S_4$
Mol. wt.	227.74	268.57	401.95	491.65	305.05	223.06	347.77	618.11	460.59
Cryst. size (mm)	0.45 × 0.5 × 0.8	0.1 × 0.2 × 0.3	0.22 × 0.25 × 0.32	0.1 × 0.1 × 0.1	0.1 × 0.2 × 0.45	0.2 × 0.2 × 0.3	0.29 × 0.33 × 0.42	0.2 × 0.2 × 0.1	0.15 × 0.2 × 0.3
Cryst. system	Triclinic	Monoclinic	Monoclinic	Monoclinic	Monoclinic	Monoclinic	Monoclinic	Monoclinic	Triclinic
Space group	$P\bar{1}$	$P2_1/n$	$C2/c$	$C2/c$	$P2_1$	$P2_1/n$	$P2_1$	$P2_1/n$	$P\bar{1}$
a (Å)	6.629(2)	6.9685(11)	24.4453(19)	9.412(1)	6.3285(5)	6.3380(10)	6.3195(10)	8.1153(11)	9.240(2)
b (Å)	8.884(2)	15.507(3)	7.0171(6)	11.203(1)	11.4100(9)	11.709(2)	11.4084(16)	13.3781(16)	11.180(2)
c (Å)	10.371(2)	10.1903(14)	16.4329(13)	16.819(2)	8.7702(7)	12.742(3)	8.7657(14)	18.211(2)	11.560(2)
α (°)	99.655(2)	90	90	90	90	90	90	90	100.85(3)
β (°)	91.893(3)	91.132(3)	121.465(2)	90.162(2)	101.626(2)	96.17(3)	101.455(2)	95.448(2)	112.48(3)
γ (°)	109.986(3)	90	90	90	90	90	90	90	105.98(3)
V (Å^3)	563.2(2)	1101.0(3)	2404.3(3)	1773.5(3)	620.29(9)	940.1(3)	619.38(16)	1968.2(4)	1001.2(3)
Z	2	4	8	4	2	4	2	4	4
ρ(calcd.) (Mg/m^3)	1.343	1.620	2.221	1.841	1.438	1.576	1.865	2.086	1.528
μ (mm^{-1})	0.735	1.235	10.436	2.241	1.096	0.574	3.374	8.637	1.132
F(000)	240	544	1520	976	272	456	344	1192	472
Index range	$-5 \le h \le 8$	$-8 \le h \le 8$	$-22 \le h \le 31$	$-11 \le h \le 12$	$-7 \le h \le 6$	$-8 \le h \le 8$	$-7 \le h \le 7$	$-10 \le h \le 10$	$-11 \le h \le 11$
	$-11 \le k \le 11$	$-19 \le k \le 19$	$-8 \le k \le 8$	$-14 \le k \le 14$	$-13 \le k \le 13$	$-15 \le k \le 15$	$-15 \le k \le 8$	$-15 \le k \le 16$	$-14 \le k \le 14$
	$-12 \le l \le 12$	$-8 \le l \le 13$	$-19 \le l \le 19$	$-21 \le l \le 21$	$-10 \le l \le 10$	$-16 \le l \le 16$	$-10 \le l \le 10$	$-23 \le l \le 23$	$-15 \le l \le 14$
2θ (°)	58.32	58.42	58.06	57.70	58.12	55.00	57.78	3.78 to 59.48	55.08
Temp (K)	193(2)	193(2)	193(2)	193(2)	193(2)	293(2)	193(2)	193(2)	293(2)
Refl. collected	3226	6234	6790	4990	3603	4072	3686	11462	7734
Refl. unique	1693	1791	2186	1773	1892	2152	2103	3912	4458
Refl. observed 4σ	1532	783	1632	1455	1820	1463	1802	2037	3048
R (int.)	0.0262	0.1946	0.0596	0.0447	0.0269	0.0330	0.0550	0.1701	0.0335
No. variables	160	101	101	83	149	123	114	178	186
GOOF	1.087	0.905	0.998	0.9770	1.070	1.065	1.007	1.066	1.022
Final R (4σ)	0.0464	0.0610	0.0431	0.0320	0.0264	0.0845	0.0413	0.0909	0.0923
Final $wR2$	0.1228	0.0894	0.0972	0.0741	0.0694	0.2424	0.0923	0.2133	0.2476
Larg res peak e/Å^3	0.327	0.341	0.713	1.279	0.389	0.925	0.594	1.200	1.168

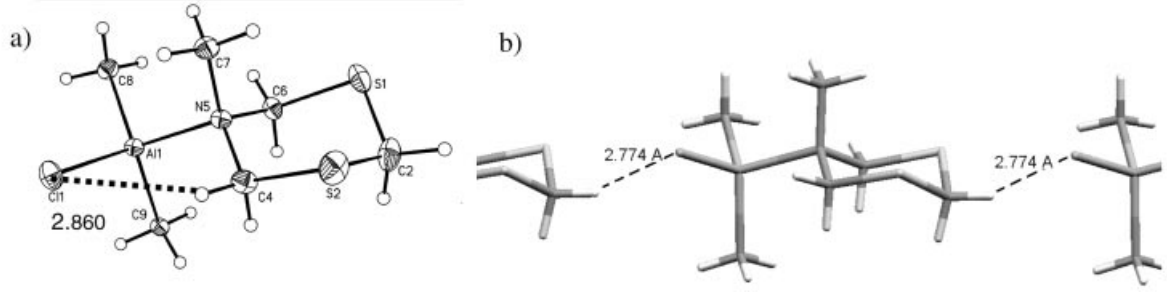

Figure 2. a) ORTEP representation of compound **6**; b) intermolecular Cl···H distances (Å)

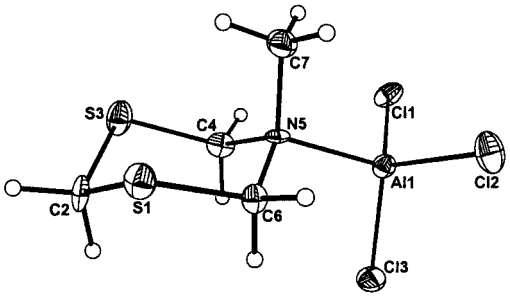

Figure 3. ORTEP representation of compound **7**

dithiazinane rings stand almost in orthogonal planes. The equatorial In−Cl bond lengths are 2.376(1) Å [Cl1 and Cl1A] and 2.383(3) Å [Cl2], the angles Cl−In−Cl are close to 120° and the N5−In1−N5A angle is 175.8(1)°. To the best of our knowledge, only two other similar structures corresponding to bis-adducts are reported in the Cambridge Crystallographic Database — bis(dibenzylamine)indium trichloride[14a] and bis(trimethylamine)indium trichloride.[14b] Similar structures have been found for ether adducts $[InCl_3(OR_2)_2]$.[14c] In the database, only one monoamine adduct $(Me_3Sn)_3N{\rightarrow}InCl_3$ is reported.[14d]

In compound **9**, the dithiazinane rings retain the chair conformation, with the methyl group in an axial position (Figure 6). Twelve H···Cl distances [three each of 2.630, 2.744, 2.800 and 2.885 Å] are shorter than the van der Waals contacts (Figure 7).

The orientation of the molecule **9** in the lattice is characterised by intermolecular interactions between sulfur atoms in a tail-to-tail arrangement (Figure 8). The S···S distances [3.429 and 3.433 Å; Σr_{VDW} = 3.60 Å] are similar to those found in elemental sulfur (3.502, 3.376 for monoclinic S_8).[15] Cl2 has two intermolecular hydrogen bonds (H···Cl = 2.684 Å)[16] with two axial C-2 hydrogen atoms of two different molecules.

 © 2004 Wiley-VCH Verlag GmbH & Co. KGaA, Weinheim

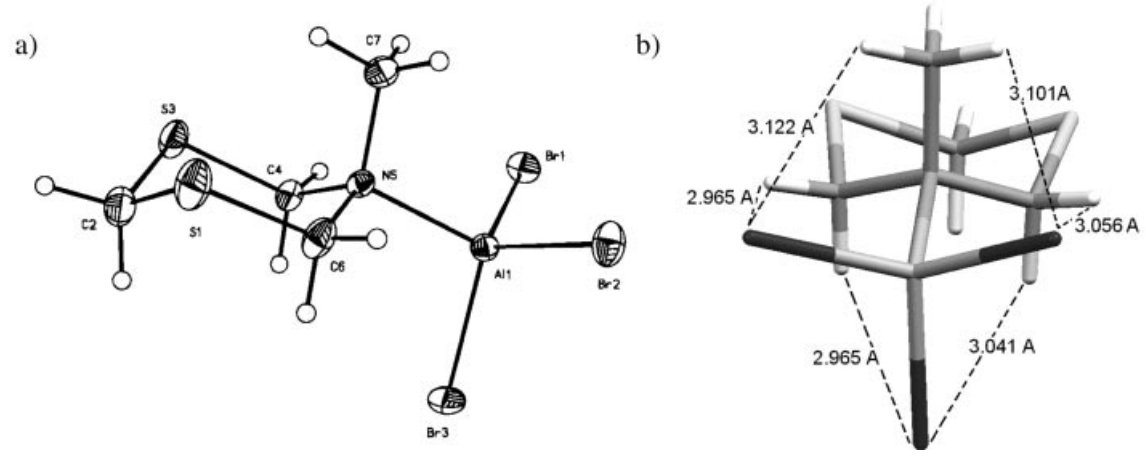

Figure 4. a) ORTEP representation of compound **8**; b) the six weak intramolecular dipolar van der Waals interactions found in **8** (Å)

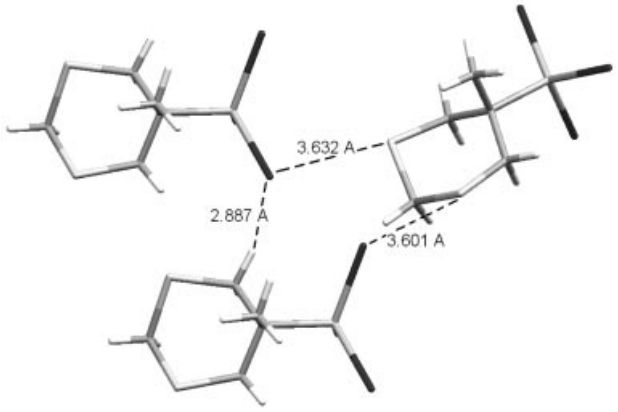

Figure 5. Arrangement of the unit cell of compound **8** showing the intermolecular contacts (Å) between three molecules

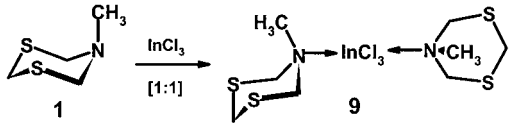

Scheme 4

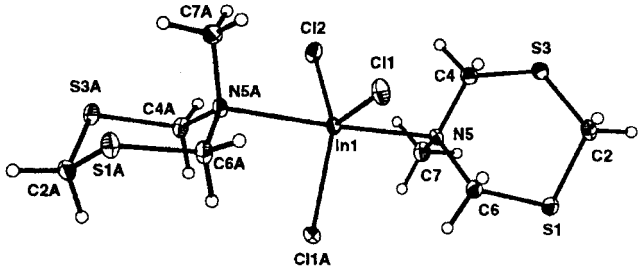

Figure 6. a) ORTEP representation of compound **9**

5-Methyl-1,3,5-dithiazinan-5-ium Cations with $AlCl_4^-$, $AlBr_4^-$, $GaCl_4^-$ BCl_4^- and Cl^- Anions (10−14)

The 5-methyl-1,3,5-dithiazinanium salts with MX_4^- anions [$AlCl_4^-$ **10**, BF_4^- **11**, $GaCl_4^-$ **12**, $AlBr_4^-$ **13**, BCl_4^- and Cl^- **14**] are formed by hydrolysis of the corresponding N→MX_3 adducts. They are crystalline solids that are insoluble in organic solvents (CH_2Cl_2, $CHCl_3$, C_7H_8); their structures were established by X-ray diffraction analysis. The molecular structure of the free dithiazinane ligand in the solid state shows that the methyl group adopts an axial position.[1d] Here it is very interesting to note that the dithiazinane rings present two conformations in the solid state, one with the methyl group in an equatorial position (**10**−**12**) and the other of a dithiazinanium salt with the methyl in an equatorial position and connected to one molecule of free dithiazinane with the N−Me group in an axial position (**13**); the actual structure is $L(LH^+)AlBr_4^-$. In another extraordinary case, conformations with methyl groups in equatorial or in axial positions were found in the same crystal (**14**). To the best of our knowledge this is the first solid-state structure of a dithiazinanium ring with the methyl group in an axial position.

In compounds **10**−**12** the dithiazinane is protonated, the methyl group is present in the equatorial position and the anion is placed on top of the heterocycle. The distances

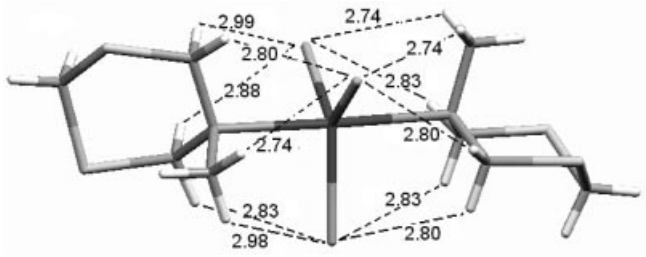

Figure 7. Short intramolecular H···Cl contacts (Å) in compound **9**

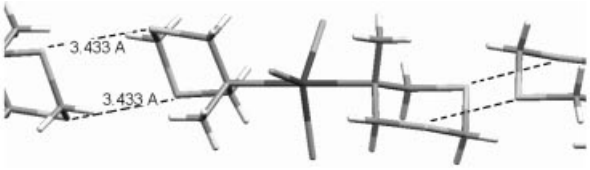

Figure 8. Intermolecular sulfur-sulfur interactions (Å) in the crystal of compound **9**

 © 2004 Wiley-VCH Verlag GmbH & Co. KGaA, Weinheim

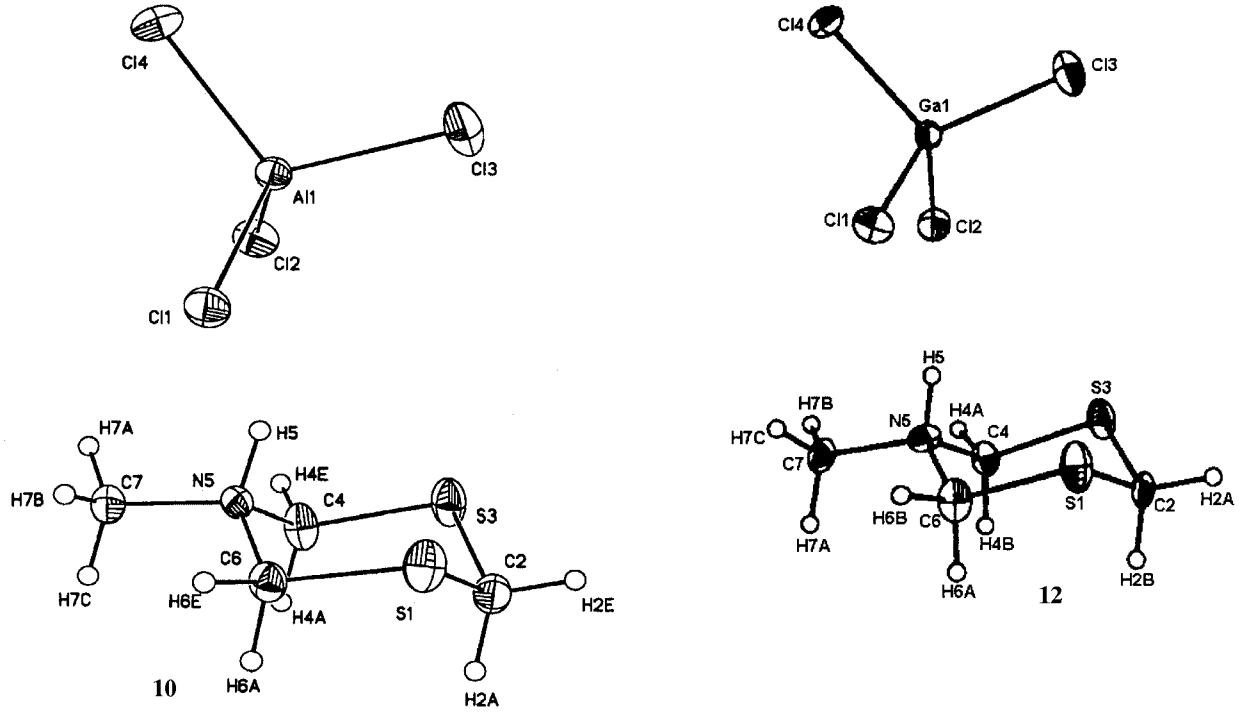

Figure 9. ORTEP representation of the crystal structures of **10** and **12**

between N−H5 and the halogen atoms of the anion are: for compound **10** 2.470 and 3.100 Å, for **11** 2.280 and 2.502 Å and for **12** 2.216 and 2.958 Å. Hydrogen bonding closes the X−M−X angle of the atoms near N−H5 [in **10**, 106.98(5)° in **11**, 105.6(5)° and in **12**, 106.81(7)°]. The angle C7−N5−H5 is sharp [101.03(1)° in **12**, 104.4(4)° in **11** and 108(3)° in **10**]. The tetrahedral geometry of the nitrogen atoms is distorted in **10** and **12** due to the hydrogen bonds between the N−H and the halogen atoms; the angles for **10** are C4−N5−H5 99(3)° and C6−N5−H5 116(3)° and for **12** 105.09(1)° and 118.36(1)° (Figures 9 and 10).

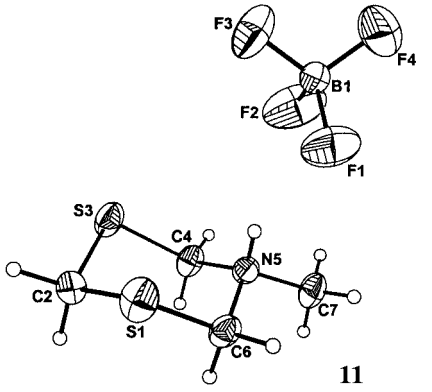

Figure 10. ORTEP representation of the crystal structure of **11**

In compounds **10**−**12** up to five dithiazinane hydrogen atoms participate in intermolecular interactions by

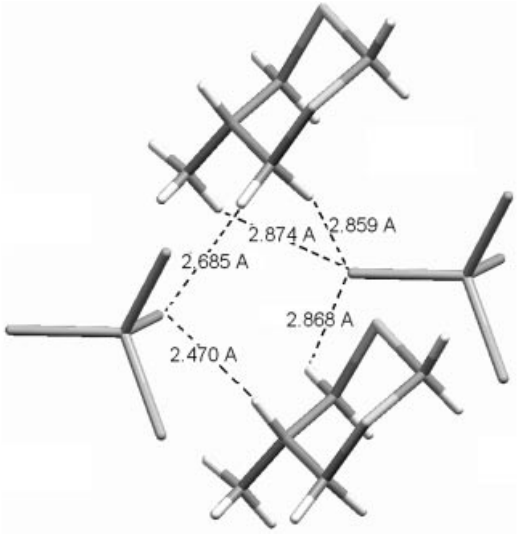

Figure 11. Arrangement (distances in Å) of anion and heterocyclic cations in compound **10**

hydrogen−halogen contacts. In Figure 11, the intermolecular interactions of anions and the heterocyclic cation in the lattice of **10** are shown. Around each anion five cycles are organized with five different interactions.

Compound **11** presents six intermolecular hydrogen bonds with six short distances (Figure 12). Compound **12** also has many intermolecular contacts in the unit cell, with seven intermolecular hydrogen halogen bonds for each molecular unit (Figure 13).

 © 2004 Wiley-VCH Verlag GmbH & Co. KGaA, Weinheim

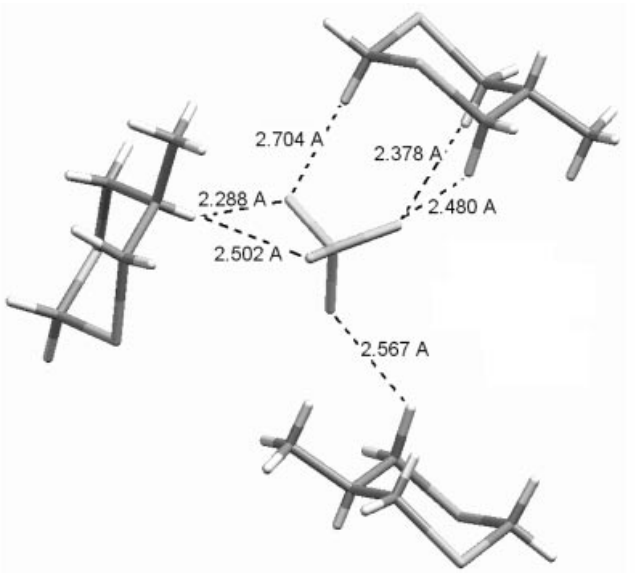

Figure 12. Arrangement of anions and heterocyclic cations in the cell of compound **11**

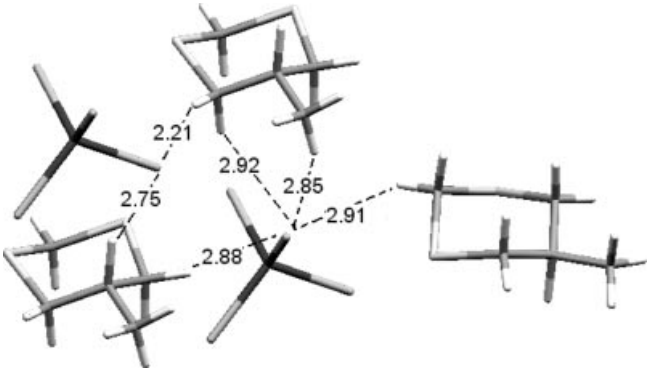

Figure 13. Arrangement of anions and heterocyclic cations in the unit cell of compound **12** (Å)

Compound **13** presents a very interesting molecular arrangement in the solid state because it co-crystallizes with a free dithiazinane molecule. In the asymmetric unit the free ligand has the methyl group in an axial position and the protonated ligand has the methyl group in an equatorial position (Figure 14). The heterocycles interact through a strong nitrogen-hydrogen bond N5H5A···N12 [2.068 Å] and one C−H···S hydrogen bond [2.974 Å].[6,17]

The unit cell of compound **14** is quite interesting because it shows a mixture of two different conformers of the protonated dithiazinane, one with the methyl group in an equatorial position and the other in an axial position. The cell also contains two different anions: BCl_4^- and Cl^-. The chloride ion is strongly bound to two N−H units (one axial and other equatorial) each one belonging to different conformers of the protonated dithiazinane. The corresponding H···Cl distances are H5···Cl1 (2.180 Å) and H5A···Cl1 (2.257 Å; Figure 15b). The interaction between the N−H and the chloride contributes to a significant distortion around the nitrogen atom. For the dithiazinanium with the axial methyl group, the C4−N5−H5 angle is 104(1)° and the C6−N5−H5 angle is 94(1)°. In the dithiazinanium with the equatorial methyl group the corresponding angles are 104(1)° and 103(2)°.

The position of the BCl_4^- group merits some comments: there are two face-to-face BCl_4^- anions, and the distance between the two Cl atoms of two BCl_4^- units (2.480 Å) is much shorter than the sum of the van der Waals radii (3.4−3.6 Å). This short distance, which, in principle, should produce a strong repulsive interaction between the chlorides, has no simple explanation, however, there are eight CH···Cl contacts altogether, and these may be responsible for stabilizing this molecular arrangement (Figure 16). Reports of Cl···Cl interactions in the solid state can be found in the literature.[18]

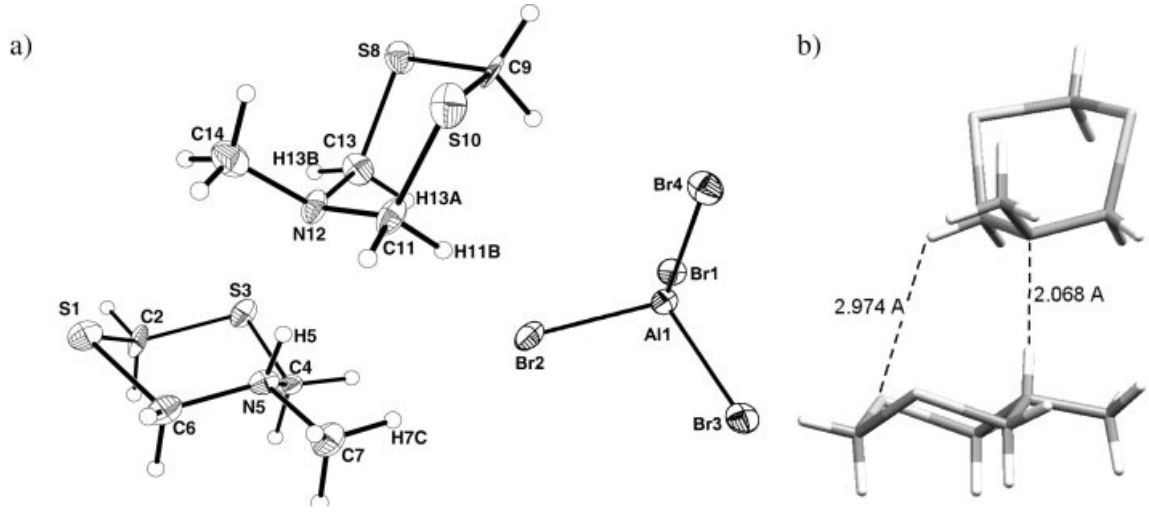

Figure 14. Crystal structure of compound **13**: a) ORTEP representation; b) interactions (Å) between dithiazinanium and dithiazinane molecules

 © 2004 Wiley-VCH Verlag GmbH & Co. KGaA, Weinheim

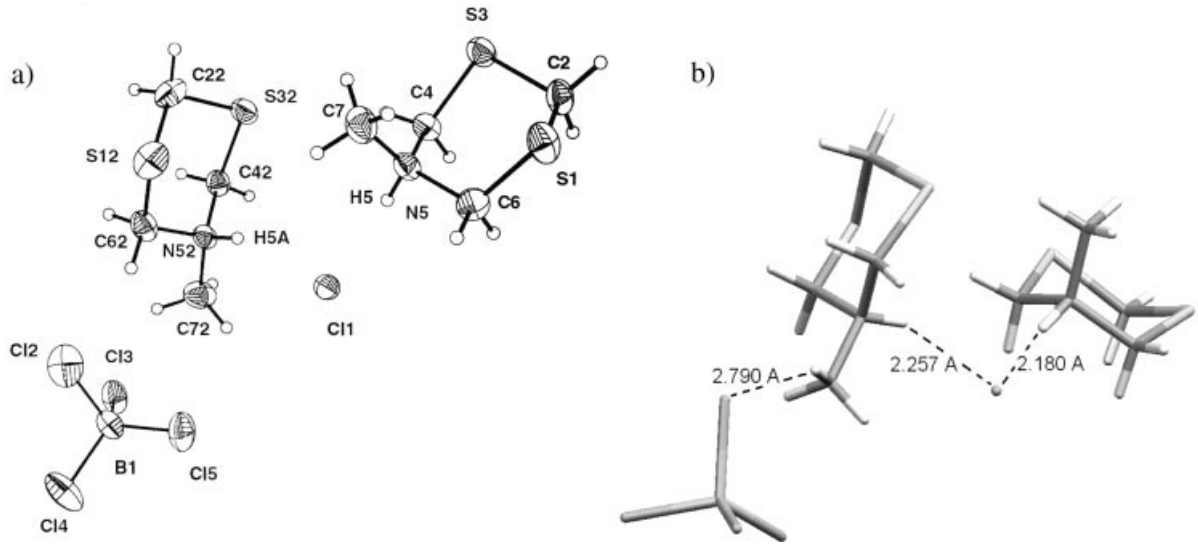

Figure 15. Crystal structure of compound **14**: a) ORTEP representation; b) distances (Å) between H5 and H5A with Cl^- and BCl_4^-.

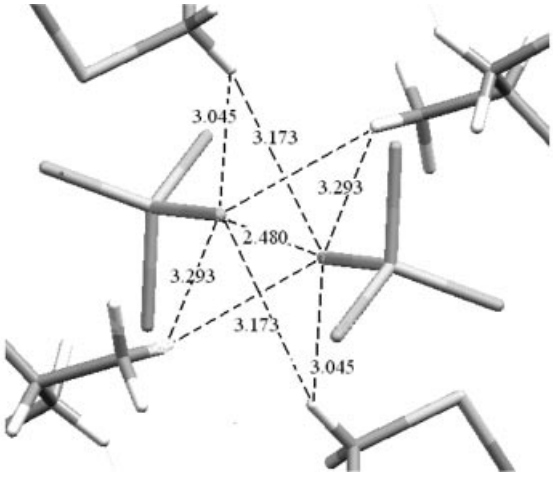

Figure 16. A projection showing the arrangement of anion and heterocycle fragments in the unit cell of **14**

Conclusion

Dithiazinane is an interesting ligand which forms coordination compounds with dimethylaluminum chloride, aluminum trihalides and indium trichloride. The coordination occurs only through the nitrogen atom. It was found by NMR spectroscopy in solution that coordination leads to preferred conformations for the dithiazinane cycle. The ring-inversion energies were calculated from NMR experiments in solution. Opening of the cycle by $AlMe_3$ was found to occur by C−S bond breaking. In the solid state these compounds show many intramolecular and intermolecular interactions, most of them of van der Waals type, but others appear to be weak intermolecular polar interactions, which determine the preferred conformations. CH···Hal and NH···Hal intermolecular interactions were observed in many cases. The sulfur atoms are also involved in short intermolecular S···S contacts in compound **9** and S···Br contacts in **8**. In solution and in the solid state, C2H···π interactions were detected.

The dithiazinanium ion interacts with anions rich in lone pairs, such as MX_4^- or X^-, through its acidic NH hydrogen atoms, in very versatile ways, and through different conformers.

Experimental Section

All anhydrous solvents were freshly distilled prior to use. ^1H, ^{13}C and ^{27}Al NMR spectra were recorded with 270 or 400 MHz ^1H Jeol instruments and are referenced to TMS (^1H and ^{13}C) and $Al(OH)_6^{3+}$ for ^{27}Al. Melting points were measured on a Gallenkamp apparatus and are uncorrected.

Crystal data and data collection are reported in Table 4. Enraf−Nonius Kappa and Siemens−P4 diffractometers with CCD detectors were used. Absorption correction was performed using the program SADABS. Computations for all compounds were done by using SHELXS-97 (Sheldrick 1990) and SHELXL-97 (Sheldrick 1997).[19] Atomic scattering factors for neutral C, N, O and H atoms were taken from ref.[20] Hydrogen atoms were found in difference electron density maps. The NH hydrogen atoms were freely refined isotopically.

CCDC-217486 to -217494 (for **6**−**14**) contain the supplementary crystallographic data for this paper. These data can be obtained free of charge at www.ccdc.cam.ac.uk/conts/retrieving.html [or from the Cambridge Crystallographic Data Centre, 12, Union Road, Cambridge CB2 1EZ, UK; Fax: (internat.) +44-1223-336-033; E-mail: deposit@ccdc.cam.ac.uk].

General Procedure for the Preparation of N→AlR$_{3-n}$X$_n$ (n = 3, 2, 0) Adducts: Two solutions in dry toluene and under an N_2 atmosphere containing equivalent stoichiometric amounts of the aluminum reagent $AlR_{3-n}X_n$ (n = 3,2,0) and compound **1** were slowly mixed at 4 °C and stirred for 20 min. A precipitate formed which was removed by filtration and recrystallized from toluene.

5-Methyl-1,3,5-dithiazinane(N-Al)trimethylalane (5): Compound **1** (225 mg, 1.66 mmol) in toluene (20 mL) and a solution of $AlMe_3$ in hexane (2 M, 1.66 mmol, 0.83 mL) were mixed. The white solid

 © 2004 Wiley-VCH Verlag GmbH & Co. KGaA, Weinheim

formed was isolated and crystallized from toluene (yield: 310 mg, 90%). The crystals were not adequate for X-ray diffraction studies, m.p. 76−78 °C. ^{13}C NMR ($CDCl_3$, −10 °C): δ = 56.9 (C4 and C6), 36.6 (*C*7), 31.7 (C2), −9.8 (Al*C*H$_3$) ppm. ^{13}C NMR ($C_6D_5CD_3$ at −10 °C): δ = 56.5 (C4 and C6), 35.6 (C*7*), 30.6 (C2), −6.9 (Al*C*H$_3$) ppm. $C_7H_{18}AlNS_2$ (215.29): calcd. C 40.55, H 8.75, N 6.76; found C 40.43, H 8.73, N 6.57.

5-Methyl-1,3,5-dithiazinane(N-Al)dimethylaluminum Chloride (6): A 1 M solution of $AlMe_2Cl$ in hexane (1.33 mmol, 1.33 mL) was slowly added at room temp. to a solution of compound **1** (180 mg, 1.33 mmol) in toluene (20 mL). A yellow solid separated which was isolated and crystallized from toluene at −20 °C (yield: 270 mg, 90%), m.p. 91−93 °C. ^{13}C NMR ($CDCl_3$, 27 °C): δ = 56.9 (C4 and C6), 36.2 (C7), 31.5 (C2), −10.0 (Al*C*H$_3$) ppm. ^{13}C NMR ($C_6D_5CD_3$ at −15 °C): δ = 56.2 (C4 and C6), 35.1 (C7), 30.4 (C2), −7.7 (Al*C*H$_3$) ppm. $C_6H_{15}AlClNS_2$ (235.72): calcd. C 31.64, H 6.64, N 6.15; found C 30.88, H 6.21, N 5.60.

5-Methyl-1,3,5-dithiazinane(N-Al)aluminum Trichloride (7): A solution of $AlCl_3$ (165 mg, 1.23 mmol) in CH_2Cl_2 (20 mL) and a solution of compound **1** (167 mg, 1.23 mmol) in CH_2Cl_2 (20 mL) were mixed. Compound **7** precipitated as a white solid which was isolated and crystallized from toluene at room temp. (260 mg, 80%), m.p. 104−106 °C. ^{13}C NMR ($CDCl_3$, −10 °C): δ = 57.0 (C4 and C6), 36.1 (C7), 31.1 (C2) ppm. ^{13}C NMR ($C_6D_5CD_3$, 10 °C): δ = 56.8 (C4 and C6), 35.3 (C7), 30.1 (C2) ppm. $C_4H_9AlCl_3NS_2{\cdot}C_7H_8$ (286.98): calcd. C 25.42, H 3.93, N 4.68; found C 25.64, H 4.60, N 4.80.

5-Methyl-1,3,5-dithiazinane(N-Al)aluminium Tribromide (8): $AlBr_3$ (210 mg, 0.78 mmol) in toluene (20 mL) and compound **1** (106 mg, 0.78 mmol) dissolved in toluene (20 mL) were mixed. Adduct **8** was obtained as a yellow solid which was crystallized from toluene at room temp. (yield: 230 mg, 75%) and m.p. 110−112 °C. ^{13}C NMR ($CDCl_3$, −55 °C): δ = 57.1 (C4 and C6), 36.3 (C7), 31.5 (C2) ppm. ^{13}C NMR ($CDCl_3$, −55 °C): δ = 56.5 (C4 and C6), 35.2 (C7), 29.7 (C2) ppm. $C_4H_9AlBr_3NS_2$ (401.94): calcd. C 11.95, H 2.26, N 3.48; found C 11.75, H 2.56, N 3.41.

Bis[5-Methyl-1,3,5-dithiazinane(N-Al)]indium Trichloride (9): A solution of **1** (100 mg, 0.74 mmol) in $CHCl_3$ (20 mL) was added to a suspension of $InCl_3$ (164 mg, 0.74 mmol) in $CHCl_3$ at room temp. The mixture was stirred for 30 min and the solid was isolated by filtration. Crystallization of the white solid from $CHCl_3$ at room temp. gave 160 mg (90%) of **9**. $C_8H_{18}Cl_3InN_2S_4{\cdot}2CHCl_3$ (657.14): calcd. C 15.84, H 2.91, N 4.26; found C 16.19, H 2.94, N 3.89.

General Procedure for the Preparation of 5-Methyl-1,3,5-dithiazinan-5-ium Salts 10−14: Two solutions under a N_2 atmosphere, one of the aluminum or borane reagent ($AlR_{3-n}X_n$, BX_3) and the other of compound **1** in the same solvent, were slowly mixed (in a 1:1 ratio) at 4 °C, and stirred for 20 min. The precipitate was removed by filtration and the filtrate was stirred for 20 min in an open system. The salts were obtained as crystalline solids.

5-Methyl-1,3,5-dithiazinan-5-ium Tetrachloroaluminate (10): Compound **10** was obtained as crystals (m.p. 84−86 °C) in 90% yield. $C_8H_{20}AlCl_5N_2S_4$ (476.47): calcd. C 15.43, H 2.54, N 3.33; found C 15.65, H 2.66, N 3.41.

5-Methyl-1,3,5-dithiazinan-5-ium Tetrafluoroborate (11): A solution of $BF_3{\cdot}OEt_2$ (11.6 M, 0.032 mL, 0.37 mmol) was added at −78 °C to compound **1** (50 mg, 0.37 mmol) in $CDCl_3$ (1 mL) under an N_2 atmosphere. After two weeks of storing at room temp., some white crystals were obtained (m.p. 79−80 °C). $C_4H_{10}AlBF_4NS_2$ (223.06): calcd. C 21.54, H 4.52, N 6.28; found C 21.15, H 4.66, N 6.13.

5-Methyl-1,3,5-dithiazinan-5-ium Tetrachlorogallate (12): $GaCl_3$ (240 mg, 1.36 mmol) in toluene and compound **1** (184 mg, 1.36 mmol) dissolved in toluene (20 mL) were mixed at 4 °C. Compound **12** was obtained as a white solid. It was crystallized from toluene at room temp. and proved to have the composition (**1**·H$^+$)$GaCl_4{\cdot}C_7H_8$ (420 mg, 90%); m.p. 54−56 °C. ^{1}H NMR ($CDCl_3$): δ = 4.5 (s, 4 H), 4.0 (s, 2 H), 3.0 (s, 3 H) ppm. ^{13}C NMR: δ = 58.4 (C4 and C6), 36.9 (C7), 32.4 (C2) ppm. $C_4H_{10}Cl_4GaNS_2{\cdot}C_7H_8$ (439.84): calcd. C 15.43, H 2.54, N 3.33; found C 15.65, H 2.66, N 3.41.

5-Methyl-1,3,5-dithiazinan-5-ium Tetrabromoaluminate (13): The white solid was recrystallized from toluene at room temp. (m.p. 83−85 °C). $C_8H_{19}AlBr_4N_2S_4$ (618.11): calcd. C 15.43, H 2.54, N 3.33; found C 15.65, H 2.66, N 3.41.

Bis(5-Methyl-1,3,5-dithiazinan-5-ium) Tetrachloroborate Chloride (14): A solution of $BCl_3{\cdot}$DMS (4 M, 0.09 mL, (0.37 mmol) was added to a solution of compound **1** (50 mg, 0.37 mmol) in $CDCl_3$. The mixture was stored for one week at room temp., after which time some white crystals had separated; m.p. 109−111 °C. $C_8H_{19}BCl_4N_2S_4$ (424.13): calcd. C 22.66, H 4.52, N 6.60; found C 22.43, H 4.50, N 6.00.

Acknowledgments

We thank Cinvestav-México and Conacyt-México for financial support and scholarships to J. C. G.-R. and C. G.-P., as well as Sonia A. Sanchez-Ruíz for recording the elemental analyses.

[1] [1a] A. Flores-Parra, S. A. Sánchez-Ruiz, *Heterocycles* **1999**, *51*, 2079−2090. [1b] A. Flores-Parra, S. A. Sánchez-Ruiz, C. Guadarrama-Pérez, *Eur. J. Inorg. Chem.* **1999**, 2063−2068. [1c] G. Cadenas-Pliego, M.-J. Rosales-Hoz, R. Contreras, A. Flores-Parra, *Tetrahedron: Asymmetry* **1994**, *5*, 633−640. [1d] G. Cadenas-Pliego, L. M. R. Martínez-Aguilera, A. M. Bello-Ramírez, M.-J. Rosales-Hoz, R. Contreras, J. C. Daran, S. Halut, A. Flores-Parra, *Phosphorus, Sulfur, and Silicon* **1993**, *81*, 111−123. [1e] G. Cadenas-Pliego, R. Contreras, A. Flores-Parra, J. C. Daran, S. Halut, *Phosphorus, Sulfur, and Silicon* **1993**, *84*, 9−15.

[2] [2a] A. Flores-Parra, S. A. Sanchez-Ruiz, C. Guadarrama-Pérez, H. Nöth, R. Contreras, *Eur. J. Inorg. Chem.* **1999**, 2069−2073. [2b] C. Guadarrama-Pérez, G. Cadenas-Pliego, L. M. R. Martínez-Aguilera, A. Flores-Parra, *Chem. Ber./Recueil* **1997**, *130*, 813−817. [2c] L. M. R. Martínez-Aguilera, G. Cadenas-Pliego, R. Contreras, A. Flores-Parra, *Tetrahedron: Asymmetry* **1995**, *6*, 1585−1592. [2d] A. Flores-Parra, G. Cadenas-Pliego, L. M. R. Martínez-Aguilera, M. L. García-Nares, R. Contreras, *Chem. Ber.* **1993**, *126*, 863−867. [2e] A. Flores-Parra, N. Farfán, A. I. Hernández-Bautista, L. Fernández-Sánchez, R. Contreras, *Tetrahedron* **1991**, *47*, 6903−6914. [2f] PhD thesis of G. Cadenas-Pliego, Cinvestav-México, Chemistry Department (**1995**).

[3] [3a] M. Güizado-Rodríguez, A. Flores-Parra, R. Tapia-Benavides, R. Contreras, V. I. Bakhmutov, *Inorg. Chem.* **2001**, *40*, 3243−3246. [3b] M. Güizado-Rodríguez, A. Ariza-Castolo, G. Merino, A. Vela, H. Nöth, V. I. Bakhmutov, R. Contreras, *J. Am. Chem. Soc.* **2001**, *123*, 9144−9152.

[4] [4a] J. W. Akitt, in *Ann. Rep. NMR Spectroscopy* (Ed.: E. F. Mooney), Academic Press Inc. (London), (**1972**), vol. 5A, p. 465. [4b] I. Krossing, PhD. thesis, Ludwig-Maximilians-Universität München, Fakultät für Chemie und Pharmazie (**1997**).

[5] E. L. Eliel, in *Stereochemistry of Carbon Compounds*, McGraw-Hill, Kogakusha, LTD., **1962**.

[6] L. Angiolini, R. P. Duke, R. A. Y. Jones, R. Katrizky, *J. Chem. Soc., Perkin Trans. 2* **1972**, 674−680.

 © 2004 Wiley-VCH Verlag GmbH & Co. KGaA, Weinheim

[7] J. C. Bailau, A. F. Trotman-Dickerson, in *Comprehensive Inorganic Chemistry*, Pergamon Press, **1973**, vol. 1, p. 1027.
[8] [8a] G. R. Desiraju, *Acc. Chem. Res.* **1996**, *29*, 441−449 and references cited therein. [8b] G. R. Desiraju, in *The Crystal as a Supramolecular Entity* (Ed.: John Wiley & Sons), Chichester, England, **1996**, vol. 2. [8c] J. W. Steed and J. L. Atwood, in *Supramolecular Chemistry* (Ed.: John Wiley & Sons), Chichester, England, **2000**. [8d] M. A. Viswamitra, R. Radhakrishnan, J. Bandekar, J. Desiraju, *J. Am. Chem. Soc.* **1993**, *115*, 4868−4869.
[9] J. C. Gálvez-Ruiz, H. Nöth, A. Flores-Parra, *Inorg. Chem.* (in press).
[10] J. E. Huheey, E. A. Keiter, R. L. Keiter, in *Inorganic Chemistry* (Ed.: Harper Collins), College Publishers, **1993**, 4th edition.
[11] C. Guadarrama-Pérez, results of ab initio calculation of dithiazinanes.
[12] M. R. Bryce, L. C. Murphy, *Nature* **1984**, *309*, 119−126.
[13] A. C. Legon, J. M. A. Thumwood, *Phys. Chem. Chem. Phys.* **2001**, *3*, 2758−2764.
[14] [14a] J. Pauls, S. Chitsaz, B. Neumüller, *Z. Anorg. Allg. Chem.* **2001**, *627*, 1723−1730. [14b] R. Karia, G. R. Willey, M. G. B Drew, *Acta Crystallogr., Sect. C* **1986**, *42*, 558−560. [14c] M. F. Self, A. T. McPhail, R. L. Wells, *Polyhedron* **1993**, 455−459. B. R. Whittlesey, I. P. Ittycheriah, *Acta Crystallogr.* **1994**, 693−695. [14d] Q. M. Cheng, O. Stark, K. Merz, M. Winteo, R. A. Fisher, *J. Chem. Soc., Dalton Trans.* **2002**, 2933−2936.
[15] [15a] D. B. Werz, T. H. Staeb, Ch. Benisch, B. J. Rausch, F. Rominger, R. Gleiter, *Org. Lett.* **2002**, *4*, 339−342. [15b] M. Munakata, T. Kuroda-Sowa, M. Maekawa, A. Hirota, S. Kitagawa, *Inorg. Chem.* **1995**, *34*, 2705−2710. [15c] D. B. Werz, R. Gleiter, F. Rominger, *J. Am. Chem. Soc.* **2002**, *124*, 10638−10639. [15d] A. J. Bridgeman, G. Cavigliasso, L. R. Ireland, J. Rothery, *J. Chem. Soc., Dalton Trans.* **2001**, 2095−2108. [15e] A. Cruz, M. Gayosso, R. Contreras, *Heteroatom Chem.* **2001**, *12*, 586−593. [15f] G. R. Desiraju, *J. Mater. Chem.* **1991**, *1*, 201−203.
[16] [16a] U. Koch, P. L. A. Popelier, *J. Phys. Chem.* **1995**, *99*, 9747−9754. [16b] T. Steiner, W. Saenger, *J. Am. Chem. Soc.* **1993**, *115*, 4540−4547.
[17] [17a] H. Borrmann, I. Persson, M. Sandström, C. M. V. SatÅlhandske, *J. Chem. Soc., Perkin Trans. 2* **2000**, 393−402. [17b] G. R. Desiraju, T. Steiner, *The Weak Hydrogen Bond in Structural Chemistry and Biology*, Oxford University Press, Inc., New York, **1999**. [17c]O. Kennad, *J. Am. Chem. Soc.* **1982**, *104*, 5063−5070. [17d] J. J. Novoa, M. C. Rovira, C. Rovira, J. Tarres, *Adv. Mater.* **1995**, *7*, 233−237.
[18] [18a] G. R. Desiraju, R. Parthasarathl, *J. Am. Chem. Soc.* **1989**, *111*, 8725−8726. [18b] V. R. Pedireddi, D. S. Reddy, B. S. Goud, D. C. Gaig, A. D. Rae, G. R. Desiraju, *J. Chem. Soc., Perkin Trans. 2* **1994**, 2353−2360. [18c] D. E. Williams, L.-Y. Hsu, *Acta Crystallogr., Sect. A* **1985**, *41*, 296−301. [18d] G. R. Desiraju, *Crystal Engineering: The Design of Organic Solids*, Elsevier, Amsterdam, **1989**.
[19] G. M. Sheldrick, in *SHELXL-97 Program for Crystal Structure Refinement*, University of Göttingen, Germany, **1997**, Release 97-2.
[20] *International Tables for X-ray Crystallography*; **1994**, *IV*, Kynoch Press, Birmingham, England.

Received June 20, 2003
Early View Article
Published Online November 28, 2003

 © 2004 Wiley-VCH Verlag GmbH & Co. KGaA, Weinheim

Synthesis, Structure, and Redox Properties of a New Aqua Ruthenium Complex Containing the Tridentate [9]aneS$_3$ and the Didentate 1,10-Phenanthroline Ligands

Xavier Sala,[a] Albert Poater,[a] Isabel Romero,[a] Montserrat Rodríguez,[a] Antoni Llobet,*[a] Xavier Solans,[b] Teodor Parella,[c] and Teresa M. Santos[d]

Keywords: Thioether compounds / Catalysis / Oxidations / Redox chemistry / Ruthenium

The synthesis of a new Ru–H_2O complex [Ru(phen)(H_2O)([9]aneS$_3$)](ClO_4)$_2$, **2**, (phen = 1,10-phenanthroline, [9]aneS$_3$ = 1,4,7-trithiacyclononane) is described. The complex is characterized by UV/Vis and 1-D and 2-D NMR spectroscopy in solution. The complex has been further characterized in the solid-state by X-ray diffraction analysis which displays a distorted octahedral coordination geometry around the Ru metal center. The cyclic voltammetric experiments of the complex show a pH-dependent chemically irreversible wave at $E_{p,a}$ = 0.82 V, at pH = 7.0, indicating the low stability of the higher oxidation states. Nevertheless, before the complex decomposes, it is capable of electrocatalytically oxidizing benzyl alcohol (BzOH) to benzaldehyde with a second-order rate constant of 19.8 $M^{-1}s^{-1}$.
(© Wiley-VCH Verlag GmbH & Co. KGaA, 69451 Weinheim, Germany, 2004)

Introduction

Over the last two decades a large number of ruthenium polypyridyl complexes containing a water molecule directly bonded to the metal has emerged.[1] The [Ru(trpy)(bpy)(H_2O)]$^{2+}$ (trpy = 2,2′:6′,2′′-terpyridine and bpy = 2,2′-bipyridine) complex described by Meyer et al.[1a] constitutes a paradigm of this type of complexes, both from a structural and a reactivity point of view.

The Ru^{II}–H_2O complexes are of interest since the corresponding higher oxidation states can be reached within a relatively narrow potential range by sequential electron and proton loss, as shown in Equations (1) and (2) for [Ru(trpy)(bpy)(H_2O)]$^{2+}$.

$$[Ru^{II}(trpy)(bpy)(H_2O)]^{2+} \underset{+1H^+,+1e^-}{\overset{-1H^+,-1e^-}{\rightleftharpoons}} [Ru^{III}(trpy)(bpy)(OH)]^{2+} \quad (1)$$

$$E_{1/2}(Ru^{III/II} \text{ at pH} = 7) = 0.49 \text{ V vs. SSCE}$$

$$[Ru^{III}(trpy)(bpy)(OH)]^{2+} \underset{+1H^+,+1e^-}{\overset{-1H^+,-1e^-}{\rightleftharpoons}} [Ru^{IV}(trpy)(bpy)(O)]^{2+} \quad (2)$$

$$E_{1/2}(Ru^{IV/III} \text{ at pH} = 7) = 0.62 \text{ V vs. SSCE}$$

These higher oxidation states, especially Ru^{IV}=O, are active catalysts for a variety of oxidative reactions such as the oxidation of alkenes to epoxides,[2] sulfides to sulfoxides,[3] phosphane to phosphane oxides,[4] alcohols to aldehydes,[5] and even saturated alkanes to alcohols.[6] Furthermore, from a bioinorganic perspective, they have also been shown to be able to selectively bind and cleave DNA molecules.[7]

A challenging aspect associated with the chemistry of Ru–H_2O type of complexes is the understanding of how electronic factors transmitted by the ligands can influence the stability of the different oxidation states, and as a consequence its reactivity.[8] With this purpose several Ru–H_2O complexes have been described containing electron-donating and electron-withdrawing substituents in the polypyridylic ligands,[9] as well those that have a variety of ancillary ligands containing oxygen donors such as picolinate or acetylacetonate and phosphorus donors such as phosphanes.[10]

In this paper we report on the synthesis, structural and spectroscopic characterization of the first example of a Ru–H_2O polypyridylic complex containing a thioether type ligand, [Ru(phen)(H_2O)([9]aneS$_3$)]$^{2+}$ (phen = 1,10-phen-

[a] Departament de Química, Universitat de Girona, Campus de Montilivi, 17071 Girona, Spain
E-mail: antoni.llobet@udg.es
[b] Departament de Cristallografia, Mineralogia i Dipòsits Minerals, Universitat de Barcelona, Martí i Franquès, s/n, 08028 Barcelona, Spain
[c] Departament de Química, Universitat Autònoma de Barcelona, Bellaterra, 08193 Barcelona, Spain
[d] Department of Chemistry, University of Aveiro, 3810–193 Aveiro, Portugal
Supporting information for this article is available on the WWW under http://www.eurjic.org or from the author.

 © 2004 Wiley-VCH Verlag GmbH & Co. KGaA, Weinheim DOI: 10.1002/ejic.200300137

anthroline. [9]aneS$_3$ = 1,4,7-trithiacyclononane). The electronic properties exerted by the thioether ligand to the metal center are discussed, together with its influence on the redox and catalytic properties.

Results and Discussion

Synthesis and Solid-State Structure

The synthesis of the complex [Ru(phen)(H$_2$O)([9]aneS$_3$)](ClO$_4$)$_2$ (**2**) is straight forward and consists of the addition of Ag^{I} to the corresponding Ru^{II}−Cl complex according to Equation (3).

$$[Ru(Cl)(phen)([9]aneS_3)]^+ + Ag^+ + H_2O \longrightarrow [Ru(phen)(H_2O)([9]aneS_3)]^{2+} + AgCl \quad (3)$$

The crystal structure of complex **2·2H$_2$O** was solved by means of single-crystal X-ray diffraction analysis and its crystallographic data, as well as selected bond lengths and angles are presented in Table 1 and Table 2, respectively. Figure 1 presents the ORTEP diagram for the cationic moiety of the molecule, including the corresponding labeling scheme.

The molecular structure of **2** shows that the Ru metal center has a distorted octahedral coordination environment. The [9]aneS$_3$ ligand coordinates facially through its sulfur atoms in an endodentate manner, while the phen ligand is chelated through its N atoms. The sixth coordination site is occupied by the oxygen atom of the aqua ligand. Bond lengths and angles are within the expected values for this type of complexes.[11,12] It is interesting to note here that the Ru−S bond lengths *trans* to the N atoms of the phen ligand are about 4 pm larger than the Ru−S distance *trans* to the aqua ligand, denoting the stronger *trans* effect of the former ligand with respect to the latter. The S−Ru−S *cis* angles are close to 90° indicating the good facial fit of the ligand for an octahedral type of geometry

Table 1. Crystal data for complex **2**

	2·2H$_2$O
Empirical formula	$C_{18}H_{26}Cl_2N_2O_{11}RuS_3$
Molecular mass	714.56
Crystal system, space group	triclinic, $P\bar{1}$
a, Å	8.143(3)
b, Å	9.137(8
c, Å	18.754(7)
α,°	99.46(5)
β,°	91.52(3)
γ,°	107.77(5)
V, Å^3	1306.3(13)
Formula units per cell	2
Temperature, K	298(2)
λ, Mo-K_α, Å	0.71073
$\rho_{calcd.}$, g cm^{-3}	1.817
μ, mm^{-1}	1.104
R_1[a]	0.0386
wR_2[b]	0.0580

[a] $R_1 = \Sigma F_o - F_c / \Sigma F_o$. [b] $wR_2 = [\Sigma\{w(F_o^2 - F_c^2)^2\}/\Sigma\{w(F_o^2)^2\}]^{1/2}$, where $w = 1/[\sigma^2(F_o^2) + (0.0042P)^2]$ and $P = (F_o^2 + 2F_c^2)/3$.

Table 2. Selected bond lengths [Å] and angles [°] for complex **2**

Ru1−N1	2.086(4)	N1−Ru1−N12	78.08(15)	O1−Ru1−S1	91.03(10)
Ru1−N12	2.101(4)	N1−Ru1−O1	85.97(14)	S2−Ru1−S1	88.61(6)
Ru1−O1	2.183(3)	N12−Ru1−O1	83.78(13)	N1−Ru1−S3	174.20(11)
Ru1−S2	2.2636(18)	N1−Ru1−S2	91.67(11)	N12−Ru1−S3	96.16(12)
Ru1−S1	2.2986(17)	N12−Ru1−S2	96.41(11)	O1−Ru1−S3	94.21(10)
Ru1−S3	2.300(2)	O1−Ru1−S2	177.54(10)	S2−Ru1−S3	88.21(7)
		N1−Ru1−S1	97.84(12)	S1−Ru1−S3	87.95(7)
		N12−Ru1−S1	173.59(12)		

Table 3. pK_a and Electrochemical data at pH = 7.0 in μ = 0.1 phosphate buffer solution or in acetonitrile for related Ru complexes

Complex[a][b]	$E_{1/2}$[c] (IV/III)	$E_{1/2}$[c] (III/II)	pK_a(II)	Ref.	Complex[d]	$E_{1/2}$[b] (III/II)	Ref.
[Ru^{II}(acac)(trpy) OH$_2$)]$^{2+}$	0.56	0.19	11.2	[8]	[Ru^{II}(phen)([9]aneS$_3$)(Cl)]$^+$	1.15	[e]
[Ru^{II}(bpea)(bpy)(OH$_2$)]$^{2+}$	0.46	0.34	11.1	[1g]	[Ru^{II}(tpm)(phen)(Cl)]$^+$	0.67	[1f]
[Ru^{II}(trpy)(tmen)(OH$_2$)]$^{2+}$	0.59	0.36	10.8	[8]	[Ru^{II}(py)(phen)([9]aneS$_3$)]$^{2+}$	1.62	[17]
[Ru^{II}(tpm)(bpy)(OH$_2$)]$^{2+}$	0.71	0.40	10.8	[1f]	[Ru^{II}(tpm)(py)(bpy)]$^{2+}$	1.15	[24]
[Ru^{II}(tpm)(phen)(OH$_2$)]$^{2+}$	0.71	0.41	10.7	[1f]	[Ru^{II}(py)$_3$([9]aneS$_3$)]$^{2+}$	1.44	[25]
[Ru^{II}(trpy)(bpy)(OH$_2$)]$^{2+}$	0.62	0.49	9.7	[1a]	[Ru^{II}(tpm)(py)$_3$]$^{2+}$	1.02	[26]
[Ru^{II}([9]aneS$_3$)(phen)(OH$_2$)]$^{2+}$	–	0.77	10.2	[e]			
[Ru^{II}(trpy)(dppene)(OH$_2$)]$^{2+}$	1.53	1.17	–	[8]			

[a] Ligand abbreviations used: acac = acetylacetonate; dppene = *cis*-1,2-bis(diphenylphosphanyl)ethylene; tmen = *N*,*N*,*N*′,*N*′-tetramethylethylenediamine; bpea = *N*,*N*-bis(2-pyridyl)ethylamine. tpm = tris(1-pyrazolyl)methane. [b] Complexes in H$_2$O at pH = 7, μ = 0.1 phosphate buffer solution. [c] Redox potentials are reported with respect to the SSCE reference electrode. [d] Complexes in acetonitrile with 0.1 M tetraalkylammonium hexafluorophosphate. [e] This work.

 © 2004 Wiley-VCH Verlag GmbH & Co. KGaA, Weinheim

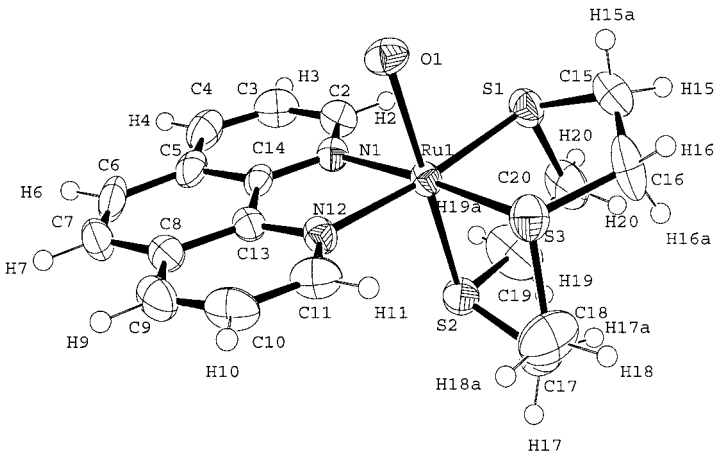

Figure 1. An ORTEP view (50% probability) of the molecular structure of cation **2**, including the atom labeling scheme

with no steric distortions from the other ligands.[13] In sharp contrast, the [9]aneS$_3$ ligand exerts a strong steric interaction over both the phen and the aqua ligands, which is clearly manifested, for instance, in the *trans* bonding angles that are all significantly smaller than 180°, ranging from 173.59(12)° to 177.54(10)°, thus producing a sort of umbrella folding [all *cis* X−Ru−S, X = N or O, angles are significantly larger than 90°, ranging from 91.03(10)° to 97.84(12)°, with a mean value for the six angles of 94.21(10)°]. Two disordered perchlorate anions balance the cationic charge. Finally, there are two waters of crystallization per complex that form an intricate network of hydrogen-bonds. O1w forms a strong hydrogen-bond with the aqua ligand bound to the Ru metal center and with the other crystallization water molecule (O2w). It also interacts weakly with one of the perchlorate counteranions. The other perchlorate ion interacts weakly with both the hydrogen atoms of the phen and the [9]aneS$_3$ ligands, whereas O2w interacts only with O1w and one of the perchlorate ions.

Spectroscopic Properties

The 1-D and 2-D NMR spectra for the aqua complex **2** were recorded in D_2O. The ^1H NMR spectrum of **2** is shown in Figure 2 (assignments are shown in the Exp. Sect.). The other NMR spectra are presented as supplementary information. All the resonances in the NMR spectra were unambiguously identified and are consistent with the same structure found in the solid-state. It is worth mentioning here that the cationic part of complex **2** is asymmetric. Nevertheless, from a magnetic point of view, at room temperature, it can be considered as having a plane of symmetry that bisects the [9]aneS$_3$ and the phen ligands in two halves, and which contains the Ru1, O1, and S2 atoms. The spectrum consists of a series of resonances in the δ = 2.4−3.6 ppm region that can be assigned to the thioether ligand, and a series of resonances in the δ = 5.8−9.6 ppm region arising from the phen ligand. There are three key NOESY effects together with the COSY map that allows for the unmistakable assignment of all the resonances observed in the ^1H NMR spectrum. The first two are interligand NOE effects observed between H11 (phen) and H17 (strong NOE effects, hydrogen atoms situated at a distance of 2.64 Å in the X-ray structure) and H18a (4.45 Å), which allows for the identification of the hydrogen atoms of the [9]aneS$_3$ ligand directed towards phen relative to those that are pointing away from the phen ligand. The third key NOE effect is also strong and is observed between H18 and H16a (2.47 Å), which allows for the clear differentiation of the H atoms of C17 from those of C18. Finally, the geminal protons can be assigned easily using the HETCOR ^1H-^{13}C map, and thus a complete assignment of the [9]aneS$_3$ ligand is achieved. With regard to the phen ligand, the resonances at δ = 7.95 and 8.15 ppm can be assigned to H10 and H7, respectively, based on their multiplicity. The doublet at 9.40 ppm is assigned to H11 based on the above-mentioned interligand NOE effects, and finally, the doublet at δ = 8.67 ppm is assigned to H9. The assignments for the phen ligand are consistent with the COSY map.

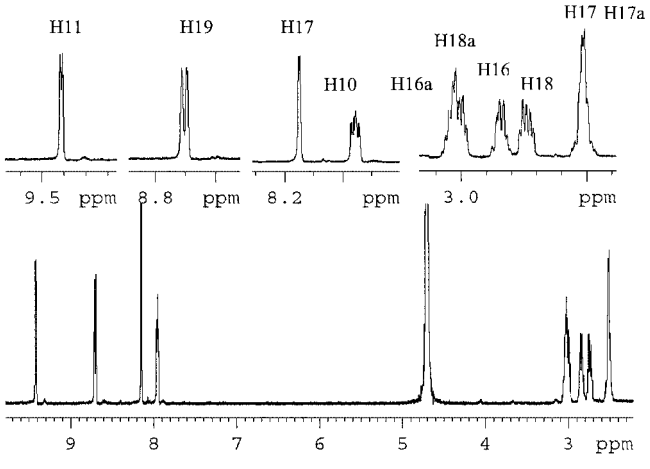

Figure 2. ^1H NMR spectrum of the complex **2** recorded in D_2O; amplifications of selected zones are displayed on top

 © 2004 Wiley-VCH Verlag GmbH & Co. KGaA, Weinheim

The electronic spectrum of the aqua complex **2** at pH 7.0 is shown in Figure 3. Below 300 nm two predominantly ligand based $\pi-\pi^*$ transitions appear at λ_{max} = 259 nm (ε = 39750 $cm^{-1}M^{-1}$) and 288 nm (15355 $cm^{-1}M^{-1}$); above 300 nm two bands appear at 353 nm (6766 $cm^{-1}M^{-1}$) and 410 nm (6578 $cm^{-1}M^{-1}$) that can be assigned to a series of MLCT $d\pi-\pi^*$(Ru−phen) transitions and their vibronic components, based on previous literature for related complexes.[1g,11,14] Under basic conditions complex **2** deprotonates generating the corresponding hydroxy derivative, $[Ru^{II}(OH)(phen)([9]aneS_3)]^+$ (**3**). For the hydroxo complex **3**, the two MLCT bands are shifted to higher wavelengths relative to those of the corresponding Ru−aqua complex **2** [410 nm (6816 $cm^{-1}M^{-1}$) and 432 nm (6811 $cm^{-1}M^{-1}$)] due to the relative destabilization of $d\pi$ (Ru) levels prompted by the hydroxo ligand.[1g,15] A pK_a of 10.1 is obtained from the acid-base spectrophotometric titration of **2** (shown as an inset in Figure 3), giving one isosbestic point at 379 nm, see Equation (4).

$$[Ru^{II}(phen)(H_2O)(9aneS_3)]^{2+} \longrightarrow [Ru^{II}(OH)(phen)(9aneS_3)]^{+} + H^{+} \quad (4)$$

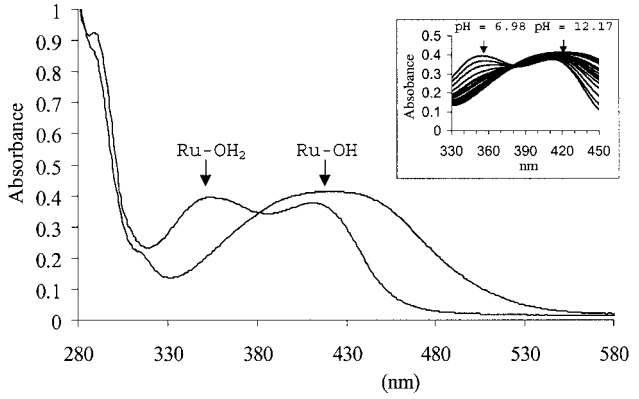

Figure 3. UV/Vis spectra of complex **2** at pH 7.0 phosphate buffer, and of complex **3** at pH 12.2. The inset shows the acid-base spectrophotometric titration of a $5\cdot10^{-5}$ M solution of **2** in the 330−450 nm region (the pH of the different spectra are 7.0, 9.2, 9.6, 9.9, 10.15, 10.3, 10.5, 10.7, 11.2, 11.3, 11.7, 10.05, 12.2)

Redox Chemistry and Catalytic Properties

The redox properties of the aqua complex **2** were investigated by means of cyclic voltammetric and coulometric techniques. Figure 4 shows the cyclic voltammograms of complex **2** at pH = 7.0, in the presence and absence of benzyl alcohol, BzOH, and their mathematical simulation has been performed using the software DIGISIM and is presented as Supporting Information.[16] As can be observed, a chemically irreversible wave is obtained at pH = 7.0 and at a scan rate of 100 mV/s, with $E_{p,a}$ = 0.82 V and a small returning wave at $E_{p,c}$ = 0.72 V ($E_{1/2}$ = 0.77 V; ΔE = 100 mV); these redox processes have been tentatively assigned to the Ru^{III}/Ru^{II} redox couple based on electronic arguments (vide infra) and whilst taking into consideration that the charge under the anodic wave is similar to that of the Ru^{III}/Ru^{II} couple of $[Ru^{II}(py)(phen)([9]aneS_3)]^{2+}$ [17] which behaves in a reversible manner. No further electrochemical processes are observed under these conditions for potentials up to 1.7 V. In sharp contrast, the homologous Ru−Cl complex **1**, displays a reversible wave due to the Ru^{III}/Ru^{II} couple with $E_{1/2}$ = 1.15 V ($E_{p,a}$ = 1.19 V, $E_{p,c}$ = 1.11 V, ΔE = 81 mV), in acetonitrile. For the Ru−OH_2 complex, **2**, the reduction potential observed varies with pH with a slope of 56.0 mV per pH unit, as expected for this type of compound. The corresponding Pourbaix diagram in the pH range from 6 to 10 is shown as supplementary information. Several attempts have been undertaken to further characterize the Ru^{III}/Ru^{II} couple by performing CV experiments at different temperatures and at different scan rates, but the results did not give further meaningful information. The instability of the Ru^{III}−OH species manifested in the CV is also displayed when it is oxidized using NaOCl as the oxidant at pH = 2.5, as expected. The process was followed spectrophotometrically and is shown as supplementary material. In the UV/Vis spectrum the initial bands of **2** at 353 and 410 nm progressively disappear on addition of NaOCl, generating a spectrum with new bands of low intensity at 320 and 370 nm, with two isosbestic points at 280 and 330 nm. Given this chemically irreversible behavior two possibilities arise: the formation of a μ-oxo species or disproportionation to Ru^{II} and Ru^{IV}, followed by the oxidation of the $[9]aneS_3$ ligand to the corresponding sulfoxide. The former is ruled out since Ru−O−Ru species have a very characteristic band in the 550−650 nm range[18] that is not observed in the present case, whereas strong evidence for the latter is obtained. The addition of NaOCl to **2** was also followed by NMR spectroscopy. A shift to lower field is observed for the signals of all the methylenic protons of $[9]aneS_3$, in agreement with the oxidation to their corresponding sulfoxide species. This statement is also supported by the fact that no electroactivity of the oxidized species is observed in the 0.0−1.2 V potential window at pH = 7.0, due to the strong electron-withdrawing capacity of the sulfoxide species which prevents further oxidations of the newly generated diamagnetic Ru^{II} complex.

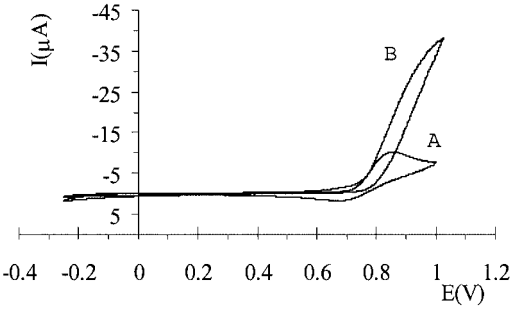

Figure 4. Cyclic voltammograms at a scan rate of 20 mV/s of complex **2** at pH = 7.0 in the absence (A) and presence of 0.2 M BzOH (B)

 © 2004 Wiley-VCH Verlag GmbH & Co. KGaA, Weinheim

Table 3 presents the pK_a and electrochemical information of several polypyridylic Ru−Cl, Ru−OH_2, and Ru−py (py = pyridine). As can be seen, the redox properties of the Ru−H_2O type of complexes are highly sensitive to the nature of the ancillary ligands. Strong σ-electron donors stabilize the Ru^{III} oxidation state and thus a decrease in the Ru^{III}/Ru^{II} reduction potential is observed. The opposite effect is observed with good π-electron acceptor ligands which increase the Ru^{III}/Ru^{II} redox potential due to the stabilization of Ru^{II} by dπ−π* back-bonding.[10]

For **2**, comparison of the redox potentials can be made with $[Ru(tpm)(N\text{-}N)(L)]^{2+}$ (tpm, tris(1-pyrazolyl)methane; N-N is bpy or phen; L = H_2O, Cl, or py). The tpm complexes are a convenient choice since, like [9]aneS_3, tpm is a tridentate facial ligand, and therefore the influence of geometrical aspects on redox potentials is minimized. Thus, when comparing the Ru^{III}/Ru^{II} redox potential of the aqua complexes, $[Ru(T)(N\text{-}N)(H_2O)]^{2+}$ (T = tpm or [9]aneS_3), it is found that the thioether ligand produces an increase of 360 mV with regard to the corresponding tpm complex, due to both a much weaker σ-donor capacity and a stronger π-acceptor ability of the former ligand.[19] A similar phenomenon is also found for the Ru−Cl and Ru−py complexes where, as shown in Table 3, an increase of 480 and 420−470 mV in the Ru^{III}/Ru^{II} redox potential is observed, respectively.

The combination of σ- and π-electronic perturbations exerted by the [9]aneS_3 ligand over the ruthenium metal center results in an increase in the Ru^{III}/Ru^{II} redox potential for the Ru−aqua complex **2**, that in turn is responsible for the instability of the corresponding Ru^{III}−OH species, which undergoes a decomposition process. This increase in the redox potentials is also manifested by the fact that the corresponding Ru^{IV}/Ru^{III} redox wave is not found throughout the entire pH range, on scanning up to 1.7 V. The high reactivity of the Ru^{III}−OH species is also shown by its ability to oxidize BzOH. This is illustrated in Figure 4, where the cyclic voltammograms are recorded both in the presence and absence of BzOH. When the alcohol is present, there is a strong enhancement of the anodic peak current due to the electrocatalytic oxidation of the alcohol forming benzaldehyde.[20] Meyer and co-workers[20b] have previously proposed a Ru^{III}−OH species that is capable of oxidizing BzOH, even though it is usually the Ru^{IV} species that is capable of carrying out such an oxidation reaction. In our study, the strong electron-withdrawing nature of the [9]aneS_3 ligand results in a high increase in the Ru^{III}/Ru^{II} redox potential, and thus it is plausible that the +3 oxidation state is sufficiently reactive so as to oxidize BzOH.

Increasing amounts of BzOH (0.10, 0.18, 0.20 M) were added to the solution and a series of cyclic voltammograms were recorded with a scan rate of 20 mV/s (see Figure 4 and the Supplementary Information). At this scan rate, the system behaves in a steady-state condition, and thus the limiting current is predicted to be independent of scan rate.[21] A second-order rate constant, k_{cat} = 19.3 $M^{-1}s^{-1}$, is experimentally determined using the equation described by Shain et al.[21] A similar value is also obtained, k_{cat} = 19.8 $M^{-1}s^{-1}$, from the mathematical simulation (See supplementary material) of the process using DIGISIM. This value is of the same order of magnitude as for the polypyridylic Ru^{IV}=O complexes described previously in the literature,[22] which are capable of oxidizing the same substrate under similar conditions, with k_{cat} values ranging from 6.0 to 30.8 $M^{-1}s^{-1}$. The formation of benzaldehyde as the only product was corroborated in a bulk experiment using the following conditions: 1.46 mM **2**/0.145 M BzOH/$9.09\cdot10^{-3}$ M NaOCl/pH 6.9 phosphate. This system yields 8.55 mM benzaldehyde after 15 minutes at 22.0 °C.

In summary, a new Ru−aqua complex, **2**, containing the soft [9]aneS_3 ligand has been prepared and its structural, spectroscopic and redox properties are described. The bonding of the facial thioether ligand by the Ru metal center results in a high anodic shift of the Ru^{III}/Ru^{II} couple relative to the complex $[Ru(tpm)(phen)(H_2O)]^{2+}$, due to the weaker σ- and stronger π-bonding capacities exerted by [9]aneS_3 over the Ru metal center relative to the pyrazolylic ligand. These electronic interactions are also responsible for the instability of the corresponding Ru^{III}−OH species. However, the decomposition reaction coupled to the Ru^{III}−OH species is slower than the oxidation of BzOH that yields the initial Ru^{II}−OH_2 and benzaldehyde, thus generating a catalytic cycle.

Experimental Section

Materials: All reagents used in the present work were obtained from Aldrich Chemical Co and were used without further purification. Reagent grade organic solvents were obtained from SDS, and high purity deionized water was obtained by passing distilled water through a nanopure Mili-Q water purification system. The complex $[Ru^{II}(Cl)(phen)([9]aneS_3)]Cl$, **1**, was prepared according to literature procedures and recrystallized twice from methanol prior to its use.[11]

Preparations: All synthetic manipulations were routinely performed under a nitrogen atmosphere using Schlenk tubes and vacuum line techniques in the dark. Electrochemical experiments were performed in the dark under a N_2 or Ar atmosphere with degassed solvents.

Caution! The complex described in this section contains the perchlorate ion as a counteranion; perchlorate salts are potentially explosive.

$[Ru^{II}(phen)(OH_2)([9]aneS_3)](ClO_4)_2\cdot2H_2O$ (2·2H_2O): A sample of **1** (35 mg, 0.051 mmol) was added to a solution of $AgClO_4$ (27.0 mg, 0.130 mmol) dissolved in water/acetone (1:1) (15 mL). The resulting mixture was refluxed for 2 h. AgCl was filtered through a frit containing celite and the volume was reduced using a rotary evaporator under reduced pressure until the solution started to become turbid. A pale orange solid the precipitated. The solid was washed with hexane and diethyl ether and dried under vacuum. Yield: 23.5 mg (53%). $C_{18}H_{22}Cl_2N_2O_9RuS_3\cdot2H_2O$: found (calcd.) C 30.47 (30.25), H 3.72 (3.64), N 4.03 (3.92), S 13.30 (13.44). ^{1}H NMR (500 MHz, D_2O, 25 °C): δ, 2.50 (m, H17, H17a), 2.75 (m, H18), 2.85 (m, H16), 3.00 (m, H18a), 3.05 (m, H16a), 7.95 (dd, J_{9-10} = 7.7, J_{10-11} = 3.8 Hz, H10), 8.15 (d, J_{7-9} = 0.5 Hz, H7), 8.67 (d, J_{9-10} = 7.7 Hz, H9), 9.40 (d, J_{11-10} = 3.8 Hz, H11) ppm. ^{13}C NMR (500 MHz,

 © 2004 Wiley-VCH Verlag GmbH & Co. KGaA, Weinheim

D_2O, 25 °C): δ, 32.5 (C18), 33.02 (C16), 35.07 (C17), 127.34 (C10), 129.07 (C7), 132.2 (C8), 139.8 (C9), 148 (C13), 155.1 (C11). For the NMR spectroscopic assignments we have used the same labeling scheme as those used in the X-ray structure shown in Figure 1. $E_{1/2}$ (pH, 7.0 phosphate buffer) = 0.77 V vs. SSCE. UV/Vis (pH, 7.0 phosphate buffer) $\lambda_{max,}$ nm (ε, $M^{-1}cm^{-1}$), assignment: 259 (39750) π−π*; 288 (15355) π−π*; 353 (6766) dπ−π*(phen); 410 (6578) dπ−π*(phen).

Instrumentation and Measurements: UV/Vis spectroscopy was performed on a Cary 50 Scan (Varian) UV/Vis spectrophotometer using 1 cm quartz cells. pH measurements were performed using a Micro-pH-2000 instrument from Crison. Cyclic voltammetric (CV) experiments were performed with a PAR 263A EG&G potentiostat or an IJ-Cambria IH-660 using a three electrode cell. A glassy carbon disc electrode (3 mm diameter) from BAS was used as the working electrode, platinum wire as auxiliary and SSCE as the reference electrode. All cyclic voltammograms presented in this work were recorded under a nitrogen atmosphere. The pH was adjusted from 0−2 with HCl, adding sodium chloride to keep a minimum ionic strength of 0.1 M. From pH 2−10, 0.1 M phosphate buffers were used, and from pH 10−12 diluted CO_2 free NaOH was used. All $E_{1/2}$ values reported in this work were estimated from cyclic voltammetry as the average of the oxidation and reduction peak potentials $(E_{p,a} + E_{p,c})/2$. Unless explicitly mentioned, the concentrations of the complexes were approximately 1 mM.

Catalytic studies at neutral pH have been performed in phosphate buffer solution. The conversion of benzyl alcohol to benzaldehyde was followed by GC using Shimadzu GC-17A gas chromatography apparatus in a TRA-5 Column (30 m × 0.25 mm diameter) incorporating a FID detector. GC conditions: initial temperature 80 °C for 1 min, ramp rate 10 °/min, final temperature 220 °C, injection temperature 220 °C, detector temperature 250 °C, carrier gas He at 25 mL/min. Under these conditions, the retention times for benzaldehyde and benzyl alcohol are 3.9 and 4.9 minutes, respectively.

NMR spectroscopy was performed on a Bruker 500 MHz or a Bruker DPX 200 MHz spectrometer. Samples were run in deuterium oxide. Elemental analyses were performed using a CHNS-O Elemental Analyser EA-1108 from Fisons.

X-ray Structure Determination: Suitable crystals of $[Ru(phen)(H_2O)([9]aneS_3)](ClO_4)_2{\cdot}2H_2O$ (**2·2H$_2$O**) were grown from water as yellow blocks. A prismatic crystal (0.1 × 0.1 × 0.2 mm) was selected and mounted on an Enraf−Nonius CAD4 four-circle diffractometer. Unit-cell parameters were determined from automatic centering of 25 reflections ($12 < \theta < 21°$) and refined by least-squares methods. Intensities were collected with graphite monochromatized Mo-*Kα* radiation, using the ω/2θ scan-technique. 7668 reflections were measured in the range $2.21 \leq \theta \leq 29.97°$, of which 7617 were independent ($R_{int} = 0.010$), and 3557 reflections were assumed as observed applying the condition $I > 2\sigma(I)$. Three reflections were measured every two hours as orientation and intensity controls, significant intensity decay was not observed. Lorentz-polarization but no absorption corrections were made.

The structure was solved by Patterson synthesis, using the SHELXS computer program[23a] and refined by full-matrix least-squares methods with the SHELXL-97 computer program[23a], using 7617 reflections. The function minimized was $\Sigma w\|F_o|^2 + |F_c|^2|^2$, where $w = [\sigma^2(I) + (0.0440P)^2]^{-1}$ and $P = (F_o^2 + 2F_c^2)/3$; f, f′, and f″ were taken from International Tables of X-ray Crystallography.[23b] All H atoms were computed and refined, using a riding model, with an isotropic temperature factor equal to 1.2 times the equivalent of the temperature factor of the atoms which are linked. The final R (on F) factor was 0.0386, wR (on F^2) = 0.0580 and the goodness of fit was 0.845 for all observed reflections. The number of refined parameters was 298. Max. shift/esd = 0.014, mean shift/esd = 0.002. Max. and min. peaks in the final difference synthesis was 0.538 and −0.677 $e{\cdot}Å^{-3}$, respectively.

Crystallographic data for the structure included in this paper have been deposited with the Cambridge Crystallographic Data Centre as supplementary publication no. CCDC-204307. These data can be obtained free of charge at http://www.ccdc.cam.ac.uk/conts/retrieving.html [or from the Cambridge Crystallographic Data Centre, 12 Union Road, Cambridge CB2 1EZ, UK; Fax: (internat.) +44-1223-336-033; E-mail: deposit@ccdc.cam.ac.uk].

Acknowledgments

This research has been financed by MCYT of Spain through project BQU2000−0458. AL is grateful to CIRIT Generalitat de Catalunya (Spain) for the Distinction award and the aid SGR2001-UG-291. AL also thanks Johnson and Matthey for a $RuCl_3{\cdot}xH_2O$ loan. X.S and A.P are grateful for the award of a doctoral grant from the University of Girona and from CIRIT, respectively.

[1] [1a] R. A. Binstead, T. J. Meyer, *J. Am. Chem. Soc.* **1987**, *109*, 3287. [1b] C. M. Che, T. F. Lai, K. Y. Wong, *Inorg. Chem.* **1987**, *26*, 2289. [1c] J. H. Muller, J. H. Acquaye, K. J. Takeuchi, *Inorg. Chem.* **1992**, *31*, 4552. [1d] A. Gerli, J. Reedijk, M. T. Lakin, A. L. Spek, *Inorg. Chem.* **1995**, *34*, 1836. [1e] X. Hua, M. Shang, A. G. Lappin, *Inorg. Chem.* **1997**, *36*, 3735. [1f] A. Llobet, P. Doppelt, T. J. Meyer, *Inorg. Chem.* **1998**, *27*, 514. [1g] M. Rodriguez, I. Romero, A. Llobet, A. Deronzier, M. Biner, T. Parella, H. Stoeckli-Evans, *Inorg. Chem.* **2001**, *40*, 4150. [1h] M. Shiotsuki, H. Miyai, Y. Ura, T. Suzuki, T. Kondo, T. Mitsudo, *Organometallics* **2002**, *21*, 4960. [1i] M. H. V. Huynh, L. M. Witham, J. M. Lasker, M. Wetzler, B. Mort, D. L. Jameson, P. S. White, K. J. Takeuchi, *J. Am. Chem. Soc.* **2003**, *125*, 308.

[2] [2a] J. C. Dobson, W. K. Seok, T. J. Meyer, *Inorg. Chem.* **1986**, *25*, 1513. [2b] A. S. Goldstein, R. H. Beer, R. S. Drago, *J. Am. Chem. Soc.* **1994**, *116*, 2424. [2c] L. K. Stultz, R. A. Binstead, M. S. Reynolds, T. J. Meyer, *J. Am. Chem. Soc.* **1995**, *117*, 2520. [2d] W. C. Cheng, W. Y. Yu, K. K. Cheung, S. M. Peng, C. K. Poon, C. M. Che, *Inorg. Chim. Acta* **1996**, *242*, 105. [2e] C. Ho, C. M. Che, T. C. Lau, *J. Chem. Soc., Dalton Trans.* **1990**, 967. [2f] D. Carmona, C. Cativiela, S. Elipe, F. J. Lahoz, M. P. Lamata, M. Pilar, M. L. R. Deviu, L. A. Oro, C. Vega, F. Viguri, *Chem. Commun.* **1997**, 2351. [2g] W. H. Fung, W. Y. Yu, C.-M. Che, *J. Org. Chem.* **1998**, *63*, 7715.

[3] [3a] L. Roecker, J. C. Dobson, W. J. Vining, T. J. Meyer, *Inorg. Chem.* **1987**, *26*, 779. [3b] J. H. Acquaye, J. G. Muller, K. J. Takeuchi, *Inorg. Chem.* **1993**, *32*, 160. [3c] X. Hua, A. G. Lappin, *Inorg. Chem.* **1995**, *34*, 992. [3d] L. F. Szczepura, S. M. Maricich, R. F. See, M. R. Churchill, K. J. Takeuchi, *Inorg. Chem.* **1995**, *34*, 4198. [3e] X. Hua, M. Shang, A. G. Lappin, *Inorg. Chem.* **1997**, *36*, 3735.

[4] [4a] B. A. Moyer, B. K. Sipe, T. J. Meyer, *Inorg. Chem.* **1981**, *20*, 1475. [4b] W. K. Seok, Y. J. Son, S. W. Moon, H. N. B. Lee, *Kor. Chem. Soc.* **1998**, *19*, 1084.

[5] [5a] M. S. Thompson, T. J. Meyer, *J. Am. Chem. Soc.* **1982**, *104*, 4106. [5b] L. E. Roecker, T. J. Meyer, *J. Am. Chem. Soc.* **1987**, *109*, 746. [5c] M. E. Marmion, K. J. Takeuchi, *J. Am. Chem. Soc.* **1988**, *110*, 1742. [5d] R. A. Binstead, M. E. MacGuire, A. Dovletoglou, W. K. Seok, L. E. Roecker, T. J. Meyer, *J. Am. Chem. Soc.* **1992**, *114*, 173. [5e] C. M. Che, C. Ho, T. C. Lau, *J. Chem. Soc., Dalton Trans.* **1991**, 1259. [5f] V. J. Catalano, R. A. Heck, C. E. Immoos, A. Ohman, M. G. Hill, *Inorg. Chem.*

 © 2004 Wiley-VCH Verlag GmbH & Co. KGaA, Weinheim

1998, *37*, 2150. [5g] C. M. Che, K. W. Cheng, M. C. W. Chan, T. C. Lau, C. K. Mak, *J. Org. Chem.* **2000**, *65*, 7996−8000.

[6] [6a] T. C. Lau, C. M. Che, W. O. Lee, C. K. Poonl, *J. Chem. Soc., Chem. Commun.* **1988**, 1406. [6b] C. M. Che, V. W. W. Yam, T. C. W. Mak, *J. Am. Chem. Soc.* **1990**, *112*, 2284. [6c] N. Grover, S. A. Ciftan, H. H. Thorp, *Inorg. Chim. Acta* **1995**, *240*, 335. [6d] C. Morice, P. Lemaux, C. Moinet, G. Simonneaux, *Inorg. Chim. Acta* **1998**, *273*, 142. [6e] K. Jitsukawa, Y. Oka, H. Einaga, H. Masuda, *Tetrahedron Letters* **2001**, *42*, 3467.

[7] [7a] A. H. Krotz, L. Y. Kuo, J. K. Barton, *Inorg. Chem.* **1993**, *32*, 5963. [7b] T. M. Santos, B. J. Goodfellow, M. G. B. Drew, J. Pedrosa de Jesus, V. Félix, *Metal Based Drugs* **2001**, *8(3)*, 125. [7c] S. Delaney, M. Pascaly, P. K. Bhattacharya, J. K. Barton, *Inorg. Chem.* **2002**, *41*, 1966. [7d] O. Schiemann, J. K. Barton, N. J. Turro, *J. Phys. Chem. B* **2000**, *104*, 7214.

[8] A. Dovletoglou, S. Ajao Adeyemi, T. J. Meyer, *Inorg. Chem.* **1996**, *35*, 4120.

[9] A. Llobet, *Inorg. Chim. Acta* **1994**, *221*, 125.

[10] [10a] R. A. Leising, K. J. Takeuchi, *Inorg. Chem.* **1987**, *26*, 4391. [10b] C. A. Bessel, R. A. Leising, K. J. Takeuchi, *J. Chem. Soc., Chem. Commun.* **1991**, 883.

[11] B. J. Goodfellow, V. Félix, S. M. Pacheco, J. Pedrosa de Jesus, M. G. B. Drew, *Polyhedron* **1997**, *16*, 393.

[12] [12a] C. Landgrafe, W. S. Sheldrick, *J. Chem. Soc., Dalton Trans.* **1994**, 1885. [12b] B. J. Goodfellow, S. M. Pacheco, J. Pedrosa de Jesus, V. Félix, M. G. B. Drew, *Polyhedron* **1997**, *16*, 3293. [12c] T. M. Santos, B. J. Goodfellow, J. Madureira, J. Pedrosa de Jesus, V. Félix, M. G. B. Drew, *New J. Chem.* **1999**, *23*, 1015. [12d] J. Madureira, T. M. Santos, B. J. Goodfellow, M. Lucena, J. Pedrosa de Jesus, M. G. Santana-Marques, M. G. B. Drew, V. Félix, *J. Chem. Soc., Dalton Trans.* **2000**, 4422.

[13] G. J. Grant, S. S. Shoup, C. L. Baucom, W. N. Setzer, *Inorg. Chim. Acta* **2001**, *317*, 91.

[14] [14a] J. Z. Wu, B. H. Ye, L. Wang, L. N. Ji, J. Y. Zhou, R. H. Li, Z. Y. Zhou, *J. Chem. Soc., Dalton Trans.* **1997**, 1395. [14b] B. J. Coe, S. Hayat, R. L. Bedoes, M. Helliwell, J. C. Jeffrey, S. R. Batten, P. S. White, *Dalton Trans.* **1997**, 591.

[15] K. J. Takeuchi, H. S. Thompson, D. W. Pipes, T. J. Meyer, *Inorg. Chem.* **1984**, *23*, 1845.

[16] DigiSim for Windows 95. Version 3.05. File type: CV. Bioanalytical Systems.

[17] X. Sala, I. Romero, M. Rodríguez, A. Llobet, unpublished work.

[18] [18a] A. Llobet, M. E. Curry, H. T. Evans, T. J. Meyer, *Inorg. Chem.* **1989**, *28*, 3131. [18b] T. R. Weaver, T. J. Meyer, S. A. Adeyemi, G. M. Brown, R. P. Eckberg, W. E. Hatfield, R. W. Murray, D. J. Untereker, *J. Am. Chem. Soc.* **1975**, *97*, 3039.

[19] [19a] G. J. Grant, T. Salupobryant, L. A. Holt, D. Y. Morrissey, M. J. Gray, J. D. Zubkowski, E. J. Valente, L. F. Mehne, *J. Organomet. Chem.* **1999**, *587*, 207. [19b] S. R. Cooper, *Acc. Chem. Res.* **1988**, *21*, 141.

[20] [20a] T. J. Meyer, *J. Electrochem. Soc.* **1984**, *131*, 221C. [20b] L. K. Stultz, M. H. V. Huynh, R. A. Binstead, M. Curry, T. J. Meyer, *J. Am. Chem. Soc.* **2000**, *122*, 5984.

[21] Under steady-state conditions, the limiting current is predicted to be independent of scan rate, and the second-order rate constant is given by the expression, $i_L = n{\cdot}F{\cdot}A{\cdot}C_o{\cdot}(D{\cdot}k_{cat}{\cdot}C_s)^{1/2}$ where i_L is the limiting current, n is the number of electrons transferred, A is the electrode area, C_o is the concentration of Ru^{II}, D is the diffusion coefficient, and C_s is the substrate concentration. [21a] D. S. Polcyn, I. Shain, *Anal. Chem.* **1966**, *38*, 376. [21b] A. J. Bard, L. R. Faulkner, in: *Electrochemical Methods; Wiley*; New York, **1980**.

[22] [22a] V. J. Catalano, R. A. Heck, C. E. Immoos, A. Ohman, M. Hill, *Inorg. Chem.* **1998**, *37*, 2150. [22b] E. L. Lebeau, T. J. Meyer, *Inorg. Chem.* **1999**, *38*, 2174. [22c] A. Gerli, J. Reedijk, M. T. Lakin, A. L. Spek, *Inorg. Chem.* **1995**, *34*, 1836.

[23] [23a] G. M. Sheldrick, **1997**. Univer. Göttingen, Germany. [23b] International Tables of X-ray Crystallography, **1974**, Ed. Kynoch Press, vol. IV, pp. 99−100 and 149.

[24] K. Barkawi, A. Llobet, T. J. Meyer, *J. Am. Chem. Soc.* **1988**, *110*, 7751.

[25] S. Roche, H. Adams, S. E. Spey, J. A. Thomas, *Inorg. Chem.* **2000**, *39*, 2385.

[26] F. Laurent, E. Plantalech, B. Donnadieu, A. Jimenez, F. Hernandez, M. Martinez-Ripoll, M. Biner, A. Llobet, *Polyhedron* **1999**, *18*, 3321.

Received March 13, 2003
Early View Article
Published Online December 4, 2003

 © 2004 Wiley-VCH Verlag GmbH & Co. KGaA, Weinheim

Electrochemical Behaviour of First Row Transition Metal Substituted Polyoxotungstates: A Comparative Study in Acetonitrile

Maria Salete Balula,[a,b] José A. Gamelas,[a,b] Helena M. Carapuça,[a] Ana M. V. Cavaleiro,*[a,b] and Walkiria Schlindwein[c]

Dedicated to Prof. Dr. João E. J. Simão on the occasion of his 75th birthday

Keywords: Polyoxometalates / Sandwich complexes / Transition metals / Electrochemistry

A comparative study of the electrochemical behaviour of several transition metal substituted polyoxotungstates in acetonitrile solution with tetra-*n*-butylammonium perchlorate as a supporting electrolyte is presented. Tetra-*n*-butylammonium salts of Keggin-type polyoxoanions, α-$[(C_4H_9)_4N]_4H_x[XW_{11}M(H_2O)O_{39}]\cdot nH_2O$, X = P, Si; M^{II} = Co, Ni, M^{III} = Fe, Mn, x = 0–2, n = 0–2, and sandwich-type polyoxoanions, α-B-$[(C_4H_9)_4N]_7H_3[M_4(H_2O)_2(PW_9O_{34})_2]$, M^{II} = Co, Mn, have been studied by cyclic voltammetry and spectroelectrochemistry. Under the conditions used, the tungsten-oxo framework of the metal substituted Keggin anions could accept up to three electrons in quasi-reversible one-electron consecutive processes. Comparison with the corresponding lacunary anions is presented. Redox processes at the metal centre have been detected for all metals M except Ni. For the anions α-$[XW_{11}M(H_2O)O_{39}]^{m-}$, the co-existence of species with a different degree of protonation was deduced from cyclic voltammetry results whenever protons were included in the molecular formula. The influence of the solids' composition on the electrochemical results is stressed. For the sandwich anions, cyclic voltammetry revealed redox processes occurring on the W atoms and also on the metallic belt. Two metal atoms in the belt of the α-B-$[Co^{II}_4(H_2O)_2(PW_9O_{34})_2]^{10-}$ anion could be electrochemically oxidised to Co^{III} in two separate steps. A similar result was observed for the Mn^{II} analogue, but the corresponding first step was not as well defined. Re-oxidation was only detected for the Co anion. This work is the first comparative study of the electrochemical behaviour of such transition metal substituted polyoxotungstates in an organic medium.
(© Wiley-VCH Verlag GmbH & Co. KGaA, 69451 Weinheim, Germany, 2004)

Introduction

Transition metal substituted polyoxotungstates have attracted special attention over the last two decades, due to their wide range of potential applications,[1–8] especially the Keggin-type polyoxoanions α-$[XW_{11}M(L)O_{39}]^{m-}$ (X = P, Si, etc., M = transition metal and L = monodentate ligand, abbreviated as $XW_{11}M$). These may be viewed as complexes where the lacunary anion α-$[XW_{11}O_{39}]^{n-}$ (XW_{11}) coordinates the transition metal ion M^{p+} in a pentadentate fashion.[9] A labile water molecule usually occupies the sixth coordination position, giving a pseudo-octahedral environment around the metal M (Figure 1, A). The inorganic tungsten-oxo framework is inert towards oxidation but can accept reversibly up to four electrons.[5,9] The metal M may also be involved in reversible redox processes. With this in mind, several metal substituted Keggin anions have been used as electrocatalysts to reduce pollutants such as NO_2^- or NO,[10,11] and also to reduce H_2O_2 and to oxidise alcohols or cleave aryl olefins.[12–16]

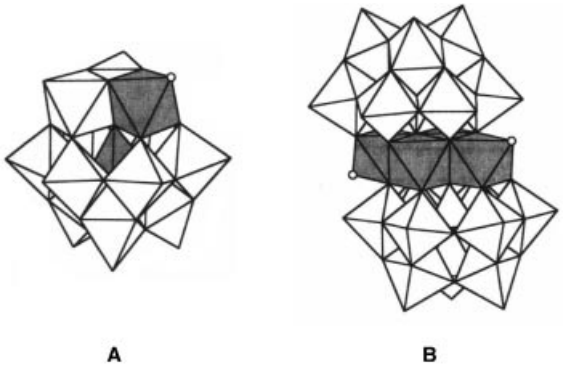

Figure 1. Structure of the complexes α-$[XW_{11}M(H_2O)O_{39}]^{m-}$ (A) and α-B-$[M_4(H_2O)_2(PW_9O_{34})_2]^{p-}$ (B). Each dashed octahedron represents a MO_6 group and the open circles represent the oxygen atom from a water molecule coordinated to M

[a] Department of Chemistry, University of Aveiro, 3810-193 Aveiro, Portugal
Fax: (internat.) + 351-234-370084
E-mail: ana@dq.ua.pt
[b] CICECO, University of Aveiro, 3810-193 Aveiro, Portugal
[c] Department of Chemistry, De Montfort University LE1 9BH, Leicester, England

Another interesting type of complex of general formula α-B-$[M_4(H_2O)_2(PW_9O_{34})_2]^{p-}$, abbreviated as $M_4(PW_9)_2$, has a sandwich structure in which two sub-units α-B-$[PW_9O_{34}]^{9-}$ are linked to a belt of four metal ions[9] (Figure 1, B). Because the several metal centres in these complexes could be activated separately in redox processes, studies on their potential as electrocatalysts are certainly needed.

In addition to electrocatalysis, the above metal substituted polyoxotungstates are, in general, active in liquid-phase oxidative catalysis, and several related reviews have appeared.[2−4] Their activity and selectivity depend on the type of substrate, experimental conditions (oxidant, solvent, temperature), and on the substituting metal.[2,3] Studies on the electrochemistry of such polyoxoanions in different solvents may help in understanding their behaviour as oxidative catalysts. Numerous electrochemical studies have been made, in aqueous media, of mono-substituted Keggin polyoxotungstates with X = P, Si, such as for Mn[16−19] and Fe,[10,12,20,21] among other metals.[5,22−24] Anions with X = Zn have also been examined.[25,26] Nevertheless, studies in organic solution are scarce. Cyclic voltammetry in acetonitrile has been reported for $[PW_{11}Cu^{II}O_{39}]^{5-}$,[27] $[H_xSiW_{11}(VO)O_{39}]^{(6-x)-}$,[28] $[XW_{11}M(H_2O)O_{39}]^{m-}$, X = P, Si, Ge, B, M = Ru^{III},[29] Ir^{IV},[11,30] $[PW_{11}TcO_{40}]^{4-}$,[31] and $[XW_{11}Re^{V,VI,VII}O_{40}]^{4-}$, X = P ($Re^{V}$), Si ($Re^{VI}$), B ($Re^{VII}$).[32] Also, co-solvent effects on the redox behaviour of the $[SiW_{11}Mn(H_2O)O_{39}]^{6-}$ anion have been analysed.[19] For the sandwich-type complexes $M_4(PW_9)_2$ in acetonitrile, studies on $[Cu_4(H_2O)_2(PW_9O_{34})_2]^{10-}$ and $[Fe_4(H_2O)_2(PW_9O_{34})_2]^{6-}$ have been published.[27,33] Studies of $Mn_4(PW_9)_2$ in aqueous solution have also been performed.[18,34] There is an obvious lack of information on the electrochemistry of these two kinds of polyoxoanions in organic solvents, considering that many redox catalysis experiments are, in fact, performed in non-aqueous media, such as acetonitrile or 1,2-dichloroethane.[2,3]

In this context, we have studied the electrochemical behaviour, in acetonitrile, of the anions $[XW_{11}O_{39}]^{n-}$ and $[XW_{11}M(H_2O)O_{39}]^{m-}$, X = P, Si, M^{II} = Co, Ni, M^{III} = Fe, Mn, and $[M_4(H_2O)_2(PW_9O_{34})_2]^{10-}$, M^{II} = Co, Mn. Experiments were performed using TBA salts. Determination of the diffusion coefficient in acetonitrile was attempted for several polyoxoanions. The electrochemical behaviour of the above-mentioned polyoxoanions in acetonitrile is, to our knowledge, described for the first time in a systematic way. In terms of catalysis, special interest has been paid to reactions at the metal centres (Co, Fe, Mn).

Results and Discussion

Characterisation of the Tetrabutylammonium Compounds

TBA salts with $[PW_{11}O_{39}]^{7-}$ and $[PW_{11}M(H_2O)O_{39}]^{m-}$ anions have been synthesised and characterised previously.[35−39] The compounds with the anions $[SiW_{11}M(H_2O)O_{39}]^{m-}$, M^{II} = Co, Ni, M^{III} = Fe, Mn, have four TBA cations in the molecular formula, and are isostructural. Their powder X-ray diffraction patterns were similar to those of the P analogues with metals like Co^{II}, Ni^{II} or Fe^{III},[39] indicating that the Si compounds crystallise with the same body-centred cubic structure as the P-anions.[39,40] Conversely, the X-ray diffraction powder pattern of $TBA_4H_4[SiW_{11}O_{39}]$ was identical to that of the tetragonal phase of the corresponding $TBA_4H_3[PW_{11}O_{39}]$.[39]

The infrared spectra of the compounds with the sandwich polyoxoanions, $TBA_7H_3[M_4(H_2O)_2(PW_9O_{34})_2]$, M^{II} = Co, Mn, were similar. The spectra of the present TBA salts differ from those of the corresponding potassium salts in the ν_{as}(P−O) and ν_{as}(W−O−W) region. The band due to the P−O stretching vibration, at 1030−1040 cm^{-1} for the potassium salts of the polyoxoanions $M_4(PW_9)_2$, M = Co, Mn,[41] presented a shoulder at higher wave-number in the spectra of the TBA salts (Figure 2, a,b). Therefore, the TBA counter-cations probably induce a larger distortion of the central phosphate groups of the α-B-$[PW_9O_{34}]^{10-}$ sub-units.[42,43]

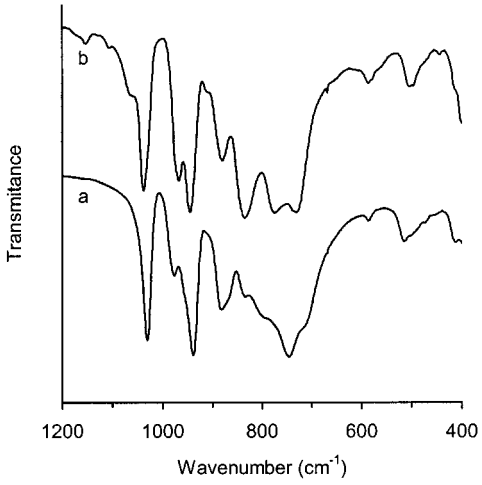

Figure 2. IR spectra of (a) $K_{10}[Mn_4(H_2O)_2(PW_9O_{34})_2]\cdot 23H_2O$ and (b) $[(C_4H_9)_4N]_7H_3[Mn_4(H_2O)_2(PW_9O_{34})_2]$

General Electrochemical Behaviour of the Keggin-Type Anions $XW_{11}M$ (X = P, Si) in Acetonitrile

Cyclic voltammograms (CV) of the $XW_{11}M$ anions in acetonitrile exhibited, in the negative potential region, one to three pairs of cathodic/anodic peaks corresponding to the redox processes of tungsten atoms (Figure 3). The substituting metal was reduced for Fe^{III} and Mn^{III} substituted anions. The voltammetric results, including those obtained for the lacunary XW_{11} anions, are summarised in Table 1. For comparison, results for $[XW_{12}O_{40}]^{3/4-}$, X = P, Si (XW_{12}), under the same experimental conditions, are included in Table 1. These are similar to previously published values.[11,29,44,45] Additionally, for M = Co^{II} (X = P, Si) and Mn^{III} (X = Si), anodic waves at positive potentials were observed, due to the oxidation of the metal M.

 © 2004 Wiley-VCH Verlag GmbH & Co. KGaA, Weinheim

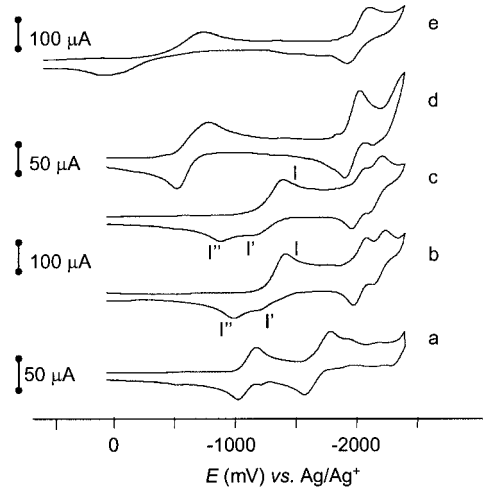

Figure 3. Cyclic voltammetry at a glassy carbon working electrode (scan rate = 100 mV/s) of acetonitrile solutions (10 mM) of (a) PW_{11}, (b) $PW_{11}Co^{II}$, (c) $PW_{11}Ni^{II}$, (d) $PW_{11}Fe^{III}$, (e) $PW_{11}Mn^{III}$

All the reduction processes of the W atoms in the metal substituted Keggin anions were quasi-reversible. The ΔE_p (anodic to cathodic peak separation) for the ferrocene/ferrocenium redox couple in acetonitrile was used as the reversibility reference (71 mV). There was an apparent decrease in the reversibility for the transition metal substituted heteropolyanions, relative to the parent structure XW_{12}. For the lacunary XW_{11} anions, the voltammetric behaviour is also consistent with W quasi-reversible reductions.

Controlled potential electrolysis revealed that each of the two first W reduction peaks corresponded to one-electron transfer processes. The number of electrons of the third W reduction (when observed) was estimated to be one, by comparison of the current of the corresponding voltammetric peak with those of the first and second reductions. Thus the tungsten-oxo framework of the heteropolyanions studied could accept one to three electrons, within the present experimental potential range.

The peak potentials of the two first W reductions were more negative for the substituted species than for the corresponding lacunary anions or for the parent Keggin anions. As found in aqueous solution,[5,21,22,46] there is no obvious correlation between the charge of lacunary or of the metal substituted anions and the reduction potentials of W (Figure 4), in contrast to the case of parent Keggin anions in aqueous[9] and non-aqueous systems[47] or for the anions $XW_{11}Ir^{IV}$, X = P, Si, Ge, B in acetonitrile.[11]

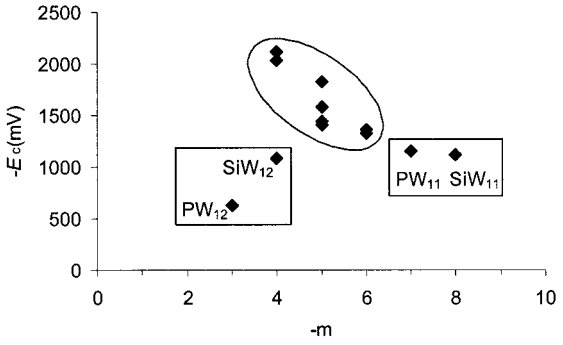

Figure 4. Potentials of the first tungsten reduction peaks of the cyclic voltammograms of XW_{12}, XW_{11}, and $XW_{11}M$ vs. the formal charge of the unprotonated anions

The redox potentials for the W atoms of the studied anions in acetonitrile were, in general, shifted towards more negative values than those reported in aqueous solution for the corresponding potassium salts.[10,18,21,22] This has been be explained by considering Lewis interactions between the polyoxoanions (bases) and the solvent molecules (acids). A correlation between the Guttmann acceptor number of the solvent[48] and the potential of the first one-electron re-

Table 1. Cyclic voltammetric data[a] for XW_{12}, XW_{11}, and $XW_{11}M$ anions in acetonitrile

Polyoxo anion	X = P				X = Si			
	$M^{III/II}$	1st W[b]	2nd W	3rd W	$M^{III/II}$ [b]	1st W	2nd W	3rd W
XW_{12}		−629 (65)	−1170 (73)	−1875 (72)		−1078 (70)	−1593 (78)	−2289 (92)
XW_{11}		−1150 (91)	−1702 (128)	−		−1119 (124)	−1626 (124)	−2284 (121)
$XW_{11}Co^{II}$		(I) −1440	−2098 (102)	−2257 (87)		−1328 (342)	−1921 (116)	−2166 (107)
		(I′) −1239				-1446 (110)		
		(I′′) −1035						
$XW_{11}Ni^{II}$		(I) −1411	−2116 (105)	−2261 (93)		−1358 (409)	−1959 (98)	−2148 (90)
		(I′) −1173				−1452 (119)		
		(I′′) −939						
$XW_{11}Fe^{III}$	−818 (251)	−2038 (119)			(I) −693	−1584 (220)	−1964 (130)	−2199 (141)
					(I′) −504			
					(I′′) −233			
$XW_{11}Mn^{III}$	−778 (762)	−2115 (165)			(I) −646	−1828 (290)	−2052 (98)	
					(I′) −103			
					(I′′) +228			

[a] Cathodic peak potentials and cathodic-to-anodic peak separation (in parentheses), both in mV vs. Ag/Ag^+; working electrode: glassy carbon; polyoxoanion concentration: $1.0 \cdot 10^{-2}$ M; supporting electrolyte: $TBAClO_4$ (0.1 M); scan rate: 100 $mV \cdot s^{-1}$. [b] I′ and I′′ are the anodic counterparts of peak I.

 © 2004 Wiley-VCH Verlag GmbH & Co. KGaA, Weinheim

duction has been found for α-$[SiW_{12}O_{40}]^{4-}$.[49] For redox processes at the substituting metals, the fact that the solvent may act as a donor ligand, substituting the labile water molecules coordinated to the metal M, must be considered. Recent studies have shown that for the XW_{12} anions the number of transferred electrons and the corresponding potentials are affected by various solution conditions besides the solvent, namely the acidity and the presence of different cations.[5,44,45] The influence of charge distribution on the redox behaviour of some lacunary and metal-substituted Keggin and Dawson-type species was referred by Keita et al.[46] For the $XW_{11}M$ anions the interplay of all these factors is far from being understood, preventing straightforward comparison of results obtained in different media.

Keggin-Type Anions with M^{II} = Co, Ni

The cyclic voltammograms of $XW_{11}Co$ and $XW_{11}Ni$ (X = P, Si) in acetonitrile exhibited three tungsten one-electron redox couples at negative potentials. Two anodic counterparts (I′ and I′′) were observed for the first reduction peak (Figure 3), even when the potential scan was reversed at ca. −1800 mV, i.e. after the first 1-e⁻ reduction of tungsten.

On increasing the scan rate (from 20 to 200 mV/s, Figure 5) the first W electron transfer with the P-anions (Figure 5, A), i.e. the first reduction peak I (around −1400 mV), was shifted to more negative potentials (ca. 38 and 50 mV, respectively, for $PW_{11}Co$ and $PW_{11}Ni$); the anodic peak I′′ became less negative and increased in intensity compared with peak I′; the position of I′ was unchanged. The W peaks at potentials more negative than −1800 mV were unchanged.

The above-mentioned splitting of the anodic counterpart of peak **I** and the observed variations with scan rate are attributed to the co-existence of distinct polyoxoanion species with different degrees of protonation. Protons were introduced in solution due to the molecular formula of the salts $TBA_4H[PW_{11}M(H_2O)O_{39}]\cdot nH_2O$. The first anodic peak (I′) corresponds to the oxidation of the less protonated species (namely $[PW_{11}M(H_2O)O_{39}]^{6-}$) whereas peak I′′, at more positive potentials, must correspond to the oxidation of a more protonated species, possibly $H[PW_{11}M(H_2O)O_{39}]^{5-}$. As the first 1-e⁻ tungsten reduction produced a single peak it was assumed that protonation occurred after reduction. Similar behaviour has been observed previously for $SiW_{11}Mn^{II}$, in aqueous solutions,[18] i.e. depending on scan rate, reoxidation scans showed two peaks attributed to species with different degrees of protonation.

$SiW_{11}Co$ and $SiW_{11}Ni$ anions showed similar electrochemical behaviour to that of the P analogues (Figure 5, B), except that the first cathodic process was split into two peaks of approximately equal height (as found by semi derivative deconvolution) whose position did not change significantly with scan rate. Nevertheless, these first reduction processes for the Si-polyoxoanions corresponded to overall 1-e⁻ reductions (determined by coulometry). The observed splitting of the first cathodic W peak may indicate the existence of two stable species in the initial solutions, possibly differing in protonation degree. Protons were again introduced in solution due to the molecular formula $TBA_4H_2[SiW_{11}M(H_2O)O_{39}]\cdot nH_2O$.

Additionally, Co^{II} was oxidised at positive potentials. The voltammograms were better defined at a Pt working electrode, where the oxidation peaks occurred at E_{pa} = +954 mV for the $SiW_{11}Co$ anion and at E_{pa} = +1003 mV for $PW_{11}Co$ (100 mV/s). Bulk electrolysis with coulometric determination at a Pt working electrode, performed at +1100 mV for the $SiW_{11}Co$ and at +1200 mV for the $PW_{11}Co$ anions, gave 1.0 and 1.1 electrons transferred, respectively. The in situ visible spectra of the oxidised solutions revealed

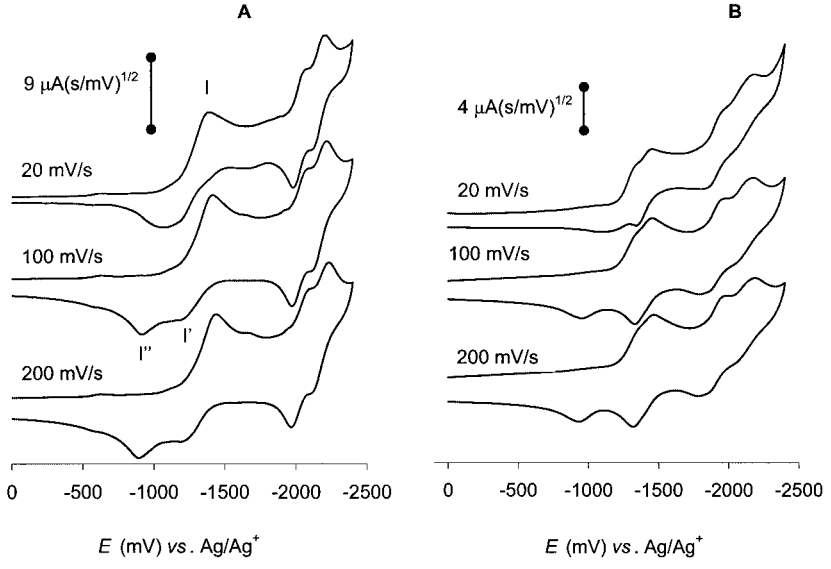

Figure 5. Effect of scan rate on normalized cyclic voltammograms obtained at a glassy carbon working electrode of (A) $PW_{11}Ni^{II}$ and (B) $SiW_{11}Ni^{II}$ (10 mM acetonitrile solutions)

 © 2004 Wiley-VCH Verlag GmbH & Co. KGaA, Weinheim

a new band around 670 nm, indicating a $Co^{III}O_6$ chromophore.[50]

Different waves in the cyclic voltammograms corresponding to species with different degrees of protonation are uncommon with Keggin-type polyoxoanions, but have been reported for the anion $[H_xSiW_{11}(V^{IV}O)O_{39}]^{(6-x)-}$ in acetonitrile[28] and for $SiW_{11}Mn^{II}$ in aqueous solution.[18] Their appearance depends on the interplay of equilibrium and kinetic factors, namely acidity constants of the protonated anions, amount of protons present in solution and kinetics of proton exchange. The conditions here reported seem to favour their appearance.

Cyclic voltammograms of $PW_{11}Ni$ and $SiW_{11}Co$ in acid aqueous solutions (pH = 2.2) also show two anodic peaks as counterparts of the first cathodic wave (in this case, a 2-electron wave) that are attributed to the α-and β-isomers of the reduced anion.[22] In those voltammograms, the corresponding peak positions were not significantly altered by changing the scan rate and the intensity of the anodic peak at more positive potentials increased as the scan rate decreased. In the present study, the position of peak I′′ altered, and the variation in relative peak heights $I_{pa}(I')/I_{pa}(I'')$ with scan rate was the opposite of that in aqueous solution. These findings, together with the observation of peaks I′ and I′′ for the 1-electron reduced polyoxometalates, may indicate that the two observed anodic peaks do not correspond to different isomers. So far, for Keggin-type anions, except $[XW_{12}O_{40}]^{5-}$, X = Al, Ga,[51,52] the formation of β-isomers by spontaneous isomerization of the corresponding α-anions has been reported to occur after the uptake of, at least, two electrons.[21,22,52]

Himeno et al. have prepared β-$[PW_{12}O_{40}]^{3-}$ in water/acetonitrile solutions,[44] showing that CH_3CN, as an auxiliary solvent, stabilized markedly this isomer. Nevertheless, both α and β isomers of that anion were kinetically inert in the water/acetonitrile medium.[44] Accordingly, the results obtained here do not indicate that the organic solvent may favour α→β isomerization.

Keggin-Type Anions with M^{III} = Mn, Fe

The CV of the anions $XW_{11}M^{III}$ showed, at negative potentials, waves corresponding to the reduction of W and of the metal M^{III}. Those of $PW_{11}Fe^{III}$ and $PW_{11}Mn^{III}$ polyoxoanions exhibited two redox couples (Figure 3, d,e). Controlled potential bulk electrolysis at −1000 mV for the Fe and at −1200 mV for the Mn polyoxoanion indicated that, in both cases, the first reduction step was an one-electron reaction (0.85 and 0.90 electrons were transferred, respectively). The solution of $PW_{11}Fe^{III}$ in acetonitrile changed from yellow to purple and a band with the maximum at 536 nm appeared in the visible region spectrum (Figure 6), corresponding to the $PW_{11}Fe^{II}$ anion.[10] For the $PW_{11}Mn^{III}$ anion the characteristic bands of the $Mn^{III}O_6$ chromophore,[17,53] at 493 and 524 nm (sh), disappeared during electrolyses and the electronic spectrum of the electrolysed solution showed only a charge-transfer band extending to the UV region, indicating a $Mn^{II}O_6$ chromophore.[53,54] These results clearly show that the first reduction peak in the voltammograms of $PW_{11}Fe^{III}$ and $PW_{11}Mn^{III}$ was due to the one-electron transfer at the substituting metal centre ($Fe^{III}\rightarrow Fe^{II}$ and $Mn^{III}\rightarrow Mn^{II}$, respectively). For the Mn^{III}/Mn^{II} couple, $E_{pa} - E_{pc}$ was quite large and increased with scan rate (ΔE_p near 760 mV at 100mV/s). As the normalised current intensity of the peaks did not vary noticeably with scan rate, the large irreversibility of the Mn^{III}/Mn^{II} couple seems to be due to slow electron transfer. This differs from aqueous solutions, in which the Mn^{III}/Mn^{II} couple for the different manganese substituted Keggin anions originated quasi-reversible waves with a peak separation in the 70−170 mV range.[16,17,19] Nevertheless, the particular kinetic inertness of the Mn^{III}/Mn^{II} couple has been referred to for other Mn complexes.[55]

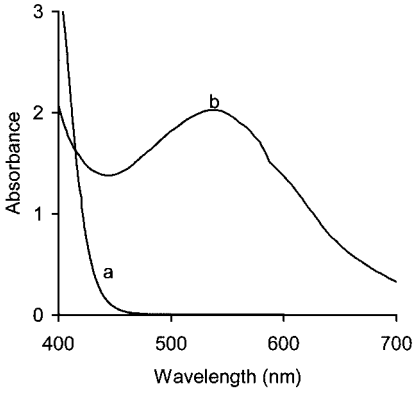

Figure 6. Visible electronic absorption spectra of the acetonitrile solution of $PW_{11}Fe^{III}$ before (a) and after bulk electrolyses at −1000 mV (b)

Except for the variation in ΔE_p corresponding to the M^{III}/M^{II} pairs (much larger for Mn than for Fe), the cyclic voltammograms of $PW_{11}Fe^{III}$ and $PW_{11}Mn^{III}$ did not change significantly with scan rate and the peaks were not split. As these polyoxoanions contain no protons in the molecular formula, no protonated species are expected. These results may further indicate that the behaviour described above for the $XW_{11}Co^{II}$ and $XW_{11}Ni^{II}$ anions is caused by protonated species.

The cyclic voltammetric data (Table 1) for the $XW_{11}Fe^{III}$ and $XW_{11}Mn^{III}$ compounds show more peaks for the Si-polyoxoanions than for the P-anions, as the tungsten atoms in the polyoxoanions containing Si are reduced at less negative potentials than the P analogues. This is another consequence of the presence of protons in solution. The voltammetric behaviour of the parent Keggin polyoxometalates in organic solvents is strongly sensitive to the presence of H^+.[45,56] In particular, the peak potentials of the W reduction waves shifted to less negative values as the amount of H^+ increased, to a point in which the one-electron reduction waves were changed into two-electron waves.[45,56] Of the compounds with metal substituted anions described in this work only $PW_{11}Fe$ and $PW_{11}Mn$ do not have protons in the molecular formula, and only for these anions is

 © 2004 Wiley-VCH Verlag GmbH & Co. KGaA, Weinheim

the first W reduction peak more negative than −2000 mV (Figure 3 and Table 1).

Another interesting feature in the CV of the Si anions is the unexpected splitting of the 1-e⁻ reduction process at the M atom. This is more clearly seen for the iron anion (Figure 7); the Mn^{III}/Mn^{II} couple gave less well-resolved waves. Thus, besides the main iron reduction peak at −693 mV (Table 1), another cathodic peak with low current intensity appeared near −1040 mV. Electrolysis at potentials near −1200 mV indicated that one 1-electron reduction took place, suggesting that both peaks correspond to one Fe atom. The observed splitting was interpreted in terms of an equilibrium between $SiW_{11}Fe(H_2O)$ and $SiW_{11}Fe(OH)$. Hydrolysis of Fe^{III} substituted Keggin anions has been reported,[20,57,58] with the formation of monomeric complexes and/or dimeric or other polynuclear species. The former seem to be obtained in the presence of non-aqueous solvents, whereas water leads to extensive dimerization. In particular, Kuznetsova et al. observed only the monomeric species $PW_{11}Fe(L)$, L = H_2O, OH^-, in acetonitrile solutions of TBA salts with $Fe:PW_{11}$ = 1:1.[57] The CV obtained in acetonitrile of the TBA salt of $PW_{11}Fe(OH)$, prepared as previously published,[39] also showed two reduction waves, cumulatively corresponding to the 1-electron reduction of Fe. In the CV of $SiW_{11}M^{III}$ anions, the anodic counterpart of the reduction peak at less negative potentials showed the same pattern as for $XW_{11}Co$ and $XW_{11}Ni$, i.e. two anodic peaks.

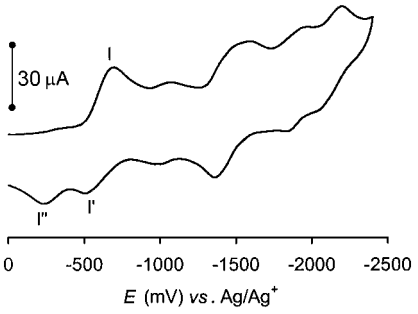

Figure 7. Cyclic voltammetry at a glassy carbon working electrode of $SiW_{11}Fe^{III}$ (10 mM acetonitrile solution, scan rate = 100 mV/s)

For the $SiW_{11}Mn^{III}$ anion, besides the $Mn^{III/II}$ redox couple, the oxidation of Mn^{III} to Mn^{IV} was observed at the Pt electrode at E_{pa} = +1046 mV (not observed for the analogue $PW_{11}Mn^{III}$). Electrolysis at +1200 mV gave 0.9 electrons transferred. Such Mn redox processes for $XW_{11}Mn^{III}$, X = P, Si, in acetonitrile are consistent with those reported for $XW_{11}Mn^{II}$ in aqueous solution.[16,17,19]

Lacunary Keggin-Type Anions

The lacunary polyoxotungstates XW_{11} (X = P, Si) gave well-defined cyclic voltammograms with two and three one-electron redox waves at negative potentials, respectively (Table 1). Under the conditions used the peak potentials of PW_{11} and SiW_{11} were similar, whereas, in the voltammogram of the parent Keggin anions, the W peak potentials in SiW_{12} were more negative than for PW_{12}, reflecting the higher charge of the anion. The different behaviour found for the parent and lacunary anions was again attributed to possible protonation of the latter, due to protons from the TBA salts (with formula $TBA_4H_3[PW_{11}O_{39}]$ and $TBA_4H_4[SiW_{11}O_{39}]$, respectively). These protons do not exist in the salts of XW_{12} anions.

Electrochemical Behaviour of the Sandwich-Type Polyoxoanions $M_4(PW_9)_2$

Cyclic voltammetry between 1300 and −2400 mV for the TBA salts of sandwich polyoxoanions in acetonitrile revealed no significant changes upon varying the scan rate from 20 to 200 $mV \cdot s^{-1}$. For potentials < −1000 mV three quasi-reversible waves, corresponding to tungsten reductions (Table 2), were observed. Figure 8 presents the voltammogram of the $Mn_4(PW_9)_2$ anion (the Co^{II} polyoxoanion showed similar electrochemical behaviour).

Oxidation processes at the metal M were clearly observed at a Pt working electrode. For the Co sandwich polyoxoanion, two oxidation peaks of identical intensity were detected at +811 and +1123 mV (Figure 9, a). In the corresponding reduction scan, the two cathodic peaks observed at less positive potentials are the counterparts of the first oxidation process (Figure 9, b). Electrolysis of the $Co_4(PW_9)_2$ solution at the Pt electrode with coulometric determination, performed at +950 mV, indicated the transfer of 0.8 electrons, meaning that each oxidation peak corresponds to a one-electron process (total loss of two electrons). Considering the structure of the polyoxoanion,[59,60] the oxidation processes might occur at the two more external Co atoms (atoms bound to a water molecule in Figure 1, B), more accessible for the electron transfer to the electrode surface. Previous studies of two salts of oxidized derivatives of the $Mn^{II}_4(PW_9)_2$ anion have suggested that oxidation occurred first at the more external Mn atoms.[34] From the above considerations the cobalt oxidation processes can be described as (L = H_2O and/or CH_3CN):

$$[Co^{II}_2(L)_2Co^{II}_2(PW_9)_2]^{10-} \rightarrow [Co^{III}(L)Co^{II}(L)Co^{II}_2(PW_9)_2]^{9-} + e^-$$

$$[Co^{III}(L)Co^{II}(L)Co^{II}_2(PW_9)_2]^{9-} \rightarrow [Co_2{}^{III}(L)_2Co^{II}_2(PW_9)_2]^{8-} + e^-$$

We could not explain unambiguously the two reduction peaks that are the cathodic counterparts of the first oxidation process. The shape of the cyclic voltammograms was not altered either by change of scan rate or by multiple successive scans.

The Mn sandwich polyoxoanion at the Pt working electrode showed two irreversible oxidation processes at the Mn centre (Figure 9, c), with the total electron transfer of two electrons (value obtained by electrolysis with coulometric determination at +860 mV using the Pt electrode). A similar irreversible behaviour had been observed in studies in aqueous solution, and attributed to slow electron transfer, possibly due to Jahn−Teller distortion of the $Mn^{III}O_6$ octahedra, rather than to chemical irreversibility.[34]

 © 2004 Wiley-VCH Verlag GmbH & Co. KGaA, Weinheim

Table 2. Cyclic voltammetric data[a] for $M^{II}_4(PW_9)_2$ anions in acetonitrile

Polyoxoanion	M[b]		1st W[c]	2nd W[c]	3rd W[c]
	E_c	E_a	E_c (ΔE_p)	E_c (ΔE_p)	E_c (ΔE_p)
$Mn_4(PW_9)_2$		500, sh; 749	−1604 (92)	−2078 (112)	−2248 (88)
$Co_4(PW_9)_2$	488; 716; 1018	811; 1123	−1593 (83)	−2045 (95)	−2219 (116)

[a] Cathodic (E_c) and anodic (E_a) peak potentials and cathodic-to-anodic peak separation (ΔE_p) in mV vs. Ag/Ag^+; polyoxoanion concentration: $3.0\cdot10^{-3}$ M; supporting electrolyte: $TBAClO_4$ (0.1 M); scan rate: 100 $mV\cdot s^{-1}$. [b] Platinum foil electrode. [c] Glassy carbon electrode.

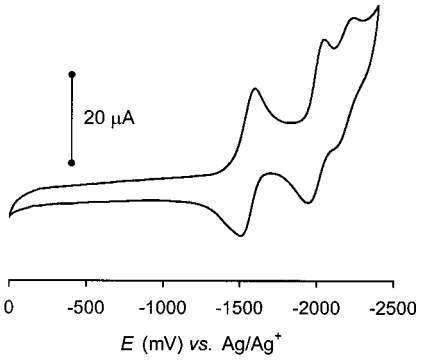

Figure 8. Cyclic voltammetry at a glassy carbon working electrode of an acetonitrile solution (3.0 mM) of $Mn^{II}_4(PW_9)_2$ (scan rate = 20 mV/s) in the negative potential region

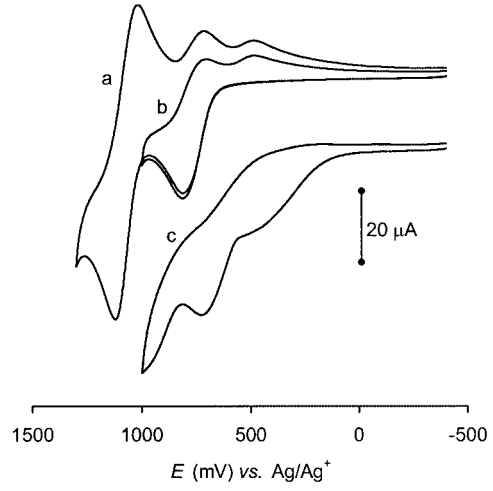

Figure 9. Cyclic voltammetry at a Pt foil working electrode of acetonitrile solutions (3.0 mM) of $Co^{II}_4(PW_9)_2$ (scan rate = 100 mV/s) (a, b) and $Mn^{II}_4(PW_9)_2$ (scan rate = 20 mV/s) (c) in the positive potential region

Diffusion Coefficients

Diffusion coefficients (D values) are not normally determined in mechanistic studies on electrochemical processes. However, the diffusion of species towards the electrode is important in the overall electrochemical reaction. The dependence of the cathodic and anodic peak currents on the square root of the scan rate indicates that the electrode processes are diffusion controlled. The diffusion coefficients may be estimated by applying the Randles-Sevcik equation, $|I_p| = 2.69\cdot A\cdot n^{3/2}\cdot C\cdot D^{1/2}\cdot v^{1/2}$; where A is the electrode area, C is the concentration, n is the number of electrons transferred and v is the scan rate. Here, we determined the electrode area to be $8.58\cdot10^{-2}$ cm^2, by chronoamperometry with a 4 mM $K_4Fe(CN)_6$ +2 M KCl solution at 25 °C, where $D = 6.29\cdot10^{-6}$ $cm^2\cdot s^{-1}$.[61] The diffusion coefficients were estimated only for the polyoxoanions where the reduction peak characteristics (ΔE_p and $E_p - E_{p/2}$)[61] were closer to what is expected for a reversible process. Within the scan rate range used for the Keggin-type anions (20 to 200 mV/s), all of the correlation coefficients determined were ca. 0.99. For the parent Keggin anions PW_{12} and SiW_{12} we obtained $6.0\cdot10^{-6}$ and $4.3\cdot10^{-6}$ cm^2/s, respectively. The reported $6.1\cdot10^{-6}$ for $[SiW_{12}O_{40}]^{4-}$ in aqueous solution (pH, 4.0),[62] is slightly higher than that obtained in acetonitrile. For the lacunary and metal substituted anions, the estimated values of $1.5\cdot10^{-7}$ to $1.3\cdot10^{-6}$ cm^2/s are lower than those reported in aqueous solution for identical anions of the same charge, e.g. $XW_{11}M$, X = P, Si, Ge, B; M = Cr, Fe, Ir,[11,14] (ca. $3-4\times10^{-6}$ cm^2/s) and others.[63] However, care must be taken in making direct comparisons with these literature values, since they were obtained not only with different solvent composition, but also with different countercations, which are important factors that affect D.[63]

Concluding Remarks

We have performed a comparative study by cyclic voltammetry and spectroelectrochemistry of the polyoxoanions $[XW_{11}M(H_2O)O_{39}]^{m-}$, and $[XW_{11}O_{39}]^{n-}$, X = P, Si, M^{II} = Co, Ni, M^{III} = Fe, Mn, in acetonitrile solutions obtained by solubilisation of the corresponding TBA salts. In general, cyclic voltammetry in acetonitrile revealed several differences between the electrochemical behaviour of the anions and previous results in aqueous solution.[10,18,21,22] Thus, tungsten one-electron reductions were detected in acetonitrile, with corresponding reduction potentials at more negative values than those in aqueous solution. These facts were not totally unexpected, as comparable results had been previously reported for other Keggin-type anions,[5] but had not been systematically observed for the transition-metal-substituted anions here reported, for which studies in organic solvents were unknown.

The preparative methods used here led to the TBA salts $TBA_4H_x[XW_{11}M(H_2O)O_{39}]$ and $TBA_4H_x[XW_{11}O_{39}]$. Because of this, protons were introduced in solution (except

 © 2004 Wiley-VCH Verlag GmbH & Co. KGaA, Weinheim

for $PW_{11}M^{III}$, with $x = 0$) with important consequences for redox behaviour observed by cyclic voltammetry in acetonitrile. The degree of protonation of the anions or of the corresponding reduced species in acetonitrile solution is not known, but the fact that the results reflected the composition of the solids used is worth noting. In summary, the different effects identified in the study of these compounds are:

(1) In the presence of protons, tungsten atoms were reduced at less negative potentials. Compounds for which, due to stoichiometry, protons were not added to the solution had a CV with fewer peaks in the potential range studied.

(2) For compounds with $x = 1$ or 2, equilibria established between species with different protonation degrees changed the general pattern of the voltammograms, splitting some waves (generally those at less negative potentials). However, for the lacunary anions, for which $x = 3$ or 4, no such splitting of the re-oxidation waves was observed.

Consequently, the CV of the $PW_{11}M^{III}$, presented only one tungsten redox pair, whereas, depending on the compound studied, two or three electrons were transferred to the tungsten-oxo framework of the other heteropolyanions upon reduction.

Redox processes were detected at the metal centre for all the studied metal substituted Keggin anions, except for $XW_{11}Ni$. Two of the chosen anions included reducible substituting metal ions (Mn^{III} and Fe^{III}), and the waves corresponding to the M^{III}/M^{II} redox pairs were identified. This contrasts with reported studies on Ru^{III} and Ir^{IV} complexes in acetonitrile, in which reduction of the metals was not detected by cyclic voltammetry.[11,29] Our results indicate that the oxidation $Mn^{II} \rightarrow Mn^{III}$ is more favourable in acetonitrile than in water.[17] This accords with the slow oxidation of Mn^{II} to Mn^{III} by atmospheric O_2 that is commonly found for these anions in acetonitrile solution. Further oxidation to Mn^{IV} was only observed for $SiW_{11}Mn$. Oxidation of cobalt(II), and the corresponding reduction, was observed for both $XW_{11}Co$ anions (X = P, Si). Nevertheless, oxidations at high potentials ($Mn^{III} \rightarrow Mn^{IV}$ and $Co^{II} \rightarrow Co^{III}$) were more conveniently studied at a Pt electrode.

We have performed the first electrochemical study of the Keggin-derived sandwich complexes $[M_4(H_2O)_2(PW_9O_{34})_2]^{10-}$, M^{II} = Co, Mn, in acetonitrile. Metal oxidation in two separate steps was observed for both anions, but only for cobalt could the corresponding reductions be detected by cyclic voltammetry. Thus, in acetonitrile, two atoms in the belt of the $[M^{II}_4(H_2O)_2(PW_9O_{34})_2]^{10-}$ anions (possibly the more external metal atoms) could be electrochemically oxidised in two separate steps to M^{III}.

Experimental Section

Reagents and Methods: All reagents were used as received, including tetra-*n*-butylammonium perchlorate (Sigma) and acetonitrile (Panreac, for instrumental analyses, HPLC grade). Elemental and thermogravimetric analysis, spectroscopic studies (infrared and visible), and powder X-ray diffraction analysis were performed as described previously.[64]

Electrochemical Measurements: Cyclic voltammetry measurements were carried out on a BAS 100BW electrochemical analyser using a conventional three-electrode single compartment cell supplied by BAS Inc. The working electrode was a glassy carbon disc electrode (BAS) or a homemade platinum foil electrode. The surface of the glassy carbon electrode was polished with 0.3 μm alumina and washed with distilled water and acetonitrile before each experiment. The auxiliary electrode was a Pt wire. The reference electrode comprised an Ag wire immersed in a solution of $AgNO_3$ (0.01 M) and $TBAClO_4$ (0.1 M) in acetonitrile. The Ag/Ag^+ reference electrode was calibrated against ferrocene/ferrocenium redox couple (1 mM) in the same solvent/electrolyte system. At scan rates between 20 and 200 mV/s, ferrocene presented $E_{1/2} = +0.087$ V vs. Ag/Ag^+, with a peak separation, ΔE_p, (anodic to cathodic) of 71 mV. All potentials quoted are relative to the Ag/Ag^+ reference electrode. The measurements were made at room temperature (ca. 20 °C), within the potential window +1300 to −2400 mV. The solutions were degassed with pure nitrogen for 5 minutes before use and blanketed with nitrogen gas during the voltammetric scans. Acetonitrile solutions (0.1 M $TBAClO_4$) were prepared for TBA salts of $XW_{11}M$ ($1.00 \cdot 10^{-2}$ M) or for TBA salts of $M_4(PW_9)_2$ ($3.00 \cdot 10^{-3}$ M).

Controlled potential electrolysis experiments were performed using a BAS 100BW electrochemical analyser or an AUTOLAB PGSTAT 30 Potentiostat. The reference electrode was the same as above. A carbon cloth or a platinum mesh was used as the working electrode. The counter electrode was a platinum mesh of large surface area placed in a glass tube chamber filled with the supporting electrolyte (0.2 M $TBAClO_4$ in acetonitrile) and separated from the working electrode compartment (electrolysis solution) by a porous vycor frit. To remove oxygen, nitrogen was constantly bubbled through the electrolysis solution, which was continuously stirred with a magnetic bar. All experiments were performed at room temperature.

Spectroelectrochemical experiments were performed on a UNICAM UV1 spectrophotometer connected to an AUTOLAB PGSTAT 30 potentiostat, using a quartz cuvette (4 cm optical path). The three-electrode system was inserted in the cell and kept under continuous nitrogen bubbling and stirring during electrolysis. The working electrode was a platinum foil. Experiments were performed at room temperature.

Synthesis of the Tetrabutylammonium Compounds: Published procedures were used to prepare $[(C_4H_9)_4N]_3[PW_{12}O_{40}]$,[65] $[(C_4H_9)_4N]_4[SiW_{12}O_{40}]$,[65] $[(C_4H_9)_4N]_4H_3[PW_{11}O_{39}]$,[38] $[(C_4H_9)_4N]_4H_x[PW_{11}M(H_2O)O_{39}]\cdot nH_2O$, M^{II} = Co, Ni, $x = 1$, $n = 1-2$; M^{III} = Fe, $x = 0$, $n = 0$.[38] The general procedure described in ref.[38] was also used to prepare $[(C_4H_9)_4N]_4[PW_{11}Mn^{III}(H_2O)O_{39}]$.

$[(C_4H_9)_4N]_4H_4[SiW_{11}O_{39}]$, $[(C_4H_9)_4N]_4H_2[SiW_{11}M(H_2O)O_{39}]\cdot nH_2O$, $n = 1-2$; M^{II} = Co, Ni, $[(C_4H_9)_4N]_4H[SiW_{11}M(H_2O)O_{39}]$, M^{III} = Fe, Mn, were obtained from potassium salts using a procedure adapted from the literature.[66] The potassium compounds of $SiW_{11}M$ (or SiW_{11}) were prepared by reported methods.[20,50,53,67] An aqueous solution of the potassium salt (0.5 mmol in 30 mL) and a solution of TBABr in 1,2-dichloroethane (4 mmol in 45 mL) were mixed and vigorously stirred. The organic phase was then collected and the 1,2-dichloroethane removed by evaporation. The so-obtained oil was then dissolved in acetonitrile (ca.

 © 2004 Wiley-VCH Verlag GmbH & Co. KGaA, Weinheim

20 mL) and the resultant tetrabutylammonium compound was precipitated by the addition of the minimum amount of water.

$[(C_4H_9)_4N]_7H_3[M_4(H_2O)_2(PW_9O_{34})_2]$, M^{II} = Co, Mn. An aqueous solution of the potassium salt[41,68] of the $M_4(PW_9)_2$ anion (2.7 mmol in 270 mL) and a solution of TBABr (42 mmol) in an identical volume of 1,2-dichloroethane were prepared and the polyoxoanion was extracted into the organic phase. A second organic extract was collected by a further addition of TBABr organic solution. The organic extracts were then left to evaporate and the so-formed crystals were filtered off and washed with water.

The TBA salts of $SiW_{11}M$ (or SiW_{11}) and $M_4(PW_9)_2$ were re-crystallised in acetonitrile. Dissolution in the minimum amount of acetonitrile followed by the addition of water (with vigorous stirring) then afforded pure samples of TBA compounds.

$[(C_4H_9)_4N]_4H_4[SiW_{11}O_{39}]$, analytical data [found (calculated), %]: W 54.5 (55.4), C 21.68 (21.07), N 1.53 (1.53), H 4.09 (4.09). IR (cm^{-1}): 1010, ν_{as}(W=O), 966, ν_{as}(Si−O)/ν_{as}(W−O_b−W), 919, 884, ν_{as}(W−O_c−W), 801.

$[(C_4H_9)_4N]_4H_2[SiW_{11}Co(H_2O)O_{39}].H_2O$, analytical data: W 51.9 (54.0), Co 1.38 (1.57), C 20.87 (20.55), N 1.49 (1.50), H 4.04 (4.04). IR (cm^{-1}): 1001, ν_{as}(W=O), 959, ν_{as}(Si−O)/ν_{as}(W−O_b−W), 907, 878 (sh), ν_{as}(W−O_c−W), 808, 792 (sh), 740 (sh).

$[(C_4H_9)_4N]_4H_2[SiW_{11}Ni(H_2O)O_{39}]\cdot 2H_2O$, analytical data: W 51.2 (53.8), C 20.10 (20.45), N 1.43 (1.49), H 3.92 (4.08). IR (cm^{-1}): 1001, ν_{as}(W=O), 958, ν_{as}(Si−O)/ν_{as}(W−O_b−W), 907, 885 (sh), ν_{as}(W−O_c−W), 807, 721, 699.

$[(C_4H_9)_4N]_4H[SiW_{11}Fe(H_2O)O_{39}]$, analytical data: W 53.5 (54.4), Fe 1.48 (1.50), C 20.38 (20.67), N 1.46 (1.51), H 3.87 (3.98). IR (cm^{-1}): 1005, ν_{as}(W=O), 960, ν_{as}(Si−O)/ν_{as} (W−O_b−W), 913, 878, ν_{as}(W−O_c−W), 796, 740 (sh).

$[(C_4H_9)_4N]_4H[SiW_{11}Mn(H_2O)O_{39}]$, analytical data: W 53.1 (54.4), Mn 1.36 (1.48), C 20.70 (20.67), N 1.57 (1.51), H 4.02 (3.98). IR (cm^{-1}): 1004, ν_{as}(W=O), 960, ν_{as}(Si−O)/ν_{as}(W−O_b−W), 915, 894 (sh), 875, ν_{as}(W−O_c−W), 793.

$[(C_4H_9)_4N]_7H_3[Co_4(H_2O)_2(PW_9O_{34})_2]$, analytical data: W 53.3 (51.5), P 1.02 (0.96), Co 3.74 (3.67), C 20.42 (20.92), N 1.38 (1.52), H 3.99 (4.06). IR (cm^{-1}): ν_{as}(P−O), 1063 (sh), 1042, ν_{as}(W=O), 966, 946, ν_{as}(W−O_b−W), 883, ν_{as}(W−O_c−W), 832, 776, 721. Visible spectrum [acetonitrile solution, in nm (ε in $mol^{-1}dm^3cm^{-1}$)]: 502 (ε = 114); 527 sh (ε = 132); 546 sh (ε = 153); 568 (ε = 163).

$[(C_4H_9)_4N]_7H_3[Mn_4(H_2O)_2(PW_9O_{34})_2]$, analytical data: W 49.9 (51.6), P 0.95 (0.97), Mn 3.08 (3.42), C 20.81 (20.97), N 1.42 (1.53), H 4.00 (4.07). IR (cm^{-1}): ν_{as}(P−O), 1065 (sh), 1037, ν_{as}(W=O), 966, 944, ν_{as}(W−O_b−W), 879, ν_{as}(W−O_c−W), 834, 774, 730.

Acknowledgments

Thanks are due to FCT and the University of Aveiro for financial support of this work. M. S. B. and J. A. G. are grateful to FCT and FEDER for their grants.

[1] *Polyoxometalates: From Platonic Solids to Antirectroviral Activity* (Eds.: M. T. Pope, A. Muller), Kluwer, Dordrecht, **1994**.
[2] C. L. Hill, C. M. Prosser-McCartha, *Coord. Chem. Rev.* **1995**, *143*, 407−455.
[3] R. Neumann, *Prog. Inorg. Chem.* **1998**, *47*, 317−370.
[4] I. V. Kozhevnikov, *Chem. Rev.* **1998**, *98*, 171−198.
[5] M. Sadakane, E. Steckhan, *Chem. Rev.* **1998**, *98*, 219−237.
[6] J. T. Rhule, C. L. Hill, D. A. Judd, *Chem. Rev.* **1998**, *98*, 327−357.
[7] D. E. Katsoulis, *Chem. Rev.* **1998**, *98*, 359−387.
[8] E. Coronado, C. J. Gomez-Garcia, *Chem. Rev.* **1998**, *98*, 273−296.
[9] M. T. Pope, *Heteropoly and Isopoly Oxometalates*, Springer Verlag, **1983**.
[10] J. E. Toth, F. C. Anson, *J. Am. Chem. Soc.* **1989**, *111*, 2444−2451.
[11] W. Sun, H. Liu, J. Kong, G. Xie, J. Deng, *J. Electroanal. Chem.* **1997**, *437*, 67−76.
[12] J. E. Toth, J. D. Melton, D. Cabelli, B. H. Bielski, F. C. Anson, *Inorg. Chem.* **1990**, *29*, 1952−1957.
[13] E. Steckhan, C. Kandzia, *Synlett* **1992**, 139−140.
[14] C. Rong, F. C. Anson, *Inorg. Chem.* **1994**, *33*, 1064−1070.
[15] J. C. Bart, F. C. Anson, *J. Electroanal. Chem.* **1995**, *390*, 11−19.
[16] M. Sadakane, E. Steckhan, *J. Mol. Catal. A* **1996**, *114*, 221−228.
[17] X. Zang, M. T. Pope, M. R. Chance, G. B. Jameson, *Polyhedron* **1995**, *14*, 1381−1392.
[18] A. Muller, L. Dloczik, E. Diemann, M. T. Pope, *Inorg. Chim. Acta* **1997**, *257*, 231−239.
[19] M. Sadakane, E. Steckhan, *Acta Chem. Scan.* **1999**, *53*, 837−841.
[20] F. Zonnevijlle, C. M. Tourné, G. F. Tourné, *Inorg. Chem.* **1982**, *21*, 2751−2757.
[21] J. E. Toth, F. C. Anson, *J. Electroanal. Chem.* **1988**, *256*, 361−370.
[22] F. A. Couto, A. M. V. Cavaleiro, J. D. Pedrosa de Jesus, J. E. Simão, *Inorg. Chim. Acta* **1998**, *281*, 225−228.
[23] A. M. V. Cavaleiro, J. D. Pedrosa de Jesus, H. I. S. Nogueira, in: *Metal Clusters in Chemistry* (Eds.: P. Braunstein, L. A. Oro, P. R. Raithbay), VCH, Weinheim, **1999**, vol. 1, p. 444−458.
[24] M. Sadakane, M. Higashijima, *Dalton Trans.* **2003**, 659−664.
[25] L. Cheng, H. Sun, B. Liu, J. Liu, S. Dong, *J. Chem. Soc., Dalton Trans.* **1999**, 2619−2625.
[26] L. Cheng, H. Sun, B. Liu, J. Liu, S. Dong, *Electrochem Commun.* **1999**, *1*, 155−158.
[27] J. A. F. Gamelas, M. S. Balula, H. M. Carapuça, A. M. V. Cavaleiro, *Electrochem Commun.* **2003**, *5*, 378−382.
[28] S. P. Harmalker, M. T. Pope, *J. Inorg. Biochem.* **1986**, *28*, 85−95.
[29] W. Sun, Y. Xie, H. Liu, J. Kong, S. Jin, G. Xie, J. Deng, *Indian J. Chem.* **1997**, *36A*, 1023−1030.
[30] H. Liu, W. Sun, B. Yue, S. Jin, J. Deng, G. Xie, *Synth. React. Inorg. Metal−Org. Chem.* **1997**, *27*, 551−566.
[31] M. J. Abrams, C. E. Costello, S. Shaikh, J. Zubieta, *Inorg. Chim. Acta* **1991**, *180*, 9−11.
[32] F. Ortega, M. T. Pope, *Inorg. Chem.* **1984**, *23*, 3292−3297.
[33] X. Zhang, Q. Chen, D. C. Duncan, R. J. Lachicotte, C. L. Hill, *Inorg. Chem.* **1997**, *36*, 4381−4386.
[34] X. Zhang, G. B. Jameson, C. J. O'Connor, M. T. Pope, *Polyhedron* **1996**, *15*, 917−922.
[35] E. Radkov, R. H. Beer, *Polyhedron* **1995**, *14*, 2139−2143.
[36] X. Zhang, M. T. Pope, *J. Mol. Catal. A* **1996**, *114*, 201−208.
[37] J. A. Gamelas, F. A. Couto, M. C. Trovão, A. M. V. Cavaleiro, J. A. S. Cavaleiro, J. D. Pedrosa de Jesus, *Thermochim. Acta* **1999**, *326*, 165−173.
[38] M. M. Q. Simões, C. M. M. Conceição, J. A. F. Gamelas, P. M. D. N. Domingues, A. M. V. Cavaleiro, J. A. S. Cavaleiro, A. J. V. Ferrer-Correia, R. A. W. Johnstone, *J. Mol. Catal. A* **1999**, *144*, 461−468.
[39] J. A. F. Gamelas, M. R. Soares, A. Ferreira, A. M. V. Cavaleiro, *Inorg. Chimica Acta* **2003**, *342*, 16−22.
[40] E. Coronado, J. R. Galan-Mascaros, C. Gimenez-Saiz, C. J. Gomez-Garcia, S. Triki, *J. Am. Chem. Soc.* **1998**, *120*, 4671−4681.

 © 2004 Wiley-VCH Verlag GmbH & Co. KGaA, Weinheim

[41] R. G. Finke, M. W. Droege, P. J. Domaille, *Inorg. Chem.* **1987**, *26*, 3886−3896.
[42] R. D. Peacock, T. J. R. Weakley, *J. Chem. Soc.(A)* **1971**, 1836−1839.
[43] C. Rocchiccioli-Deltcheff, R. Thouvenot, *J. Chem. Res. (S)* **1977**, 46−47; C. Rocchiccioli-Deltcheff, R. Thouvenot, *J. Chem. Res. (M)* **1977**, 546−571.
[44] S. Himeno, M. Takamoto, T. Ueda, *J. Electroanal. Chem.* **1999**, *465*, 129−135.
[45] S. Himeno, M. Takamoto, *J. Electroanal. Chem.* **2002**, *528*, 170−174.
[46] B. Keita, Y. W. Lu, L. Nadjo, R. Contant, *Eur. J. Inorg. Chem.* **2000**, 2463−2471.
[47] T. Osakai, A. Saito, T. Hori, *J. Electroanal. Chem.* **1994**, *364*, 149−154.
[48] V. Gutmann, *The Donor-Acceptor Approach to Molecular Interactions*, Plenum, New York, **1978**.
[49] B. Keita, D. Bouaziz, L. Nadjo, *J. Electrochem. Soc.* **1988**, *135*, 87−91.
[50] T. J. R. Weakley, S. A. Malik, *J. Inorg. Nucl. Chem.* **1967**, *29*, 2935−2944.
[51] I. A. Weinstock, J. C. Cowan, E. M. G. Barbuzzi, H. Zeng, C. L. Hill, *J. Am. Chem. Soc.* **1999**, *121*, 4608−4617.
[52] X. López, J. M. Maestre, C. Bo, J. M. Poblet, *J. Am. Chem. Soc.* **2001**, *123*, 9571−9576.
[53] C. M. Tourné, G. F. Tourné, S. A. Malik, T. J. R. Weakley, *J. Inorg. Nucl. Chem.* **1970**, *32*, 3875−3890.
[54] C. M. Tourné, G. F. Tourné, *Bull. Soc. Chim. Fr.* **1969**, 1124−1136.
[55] U. Kolle, U. Engler, *Eur. J. Inorg. Chem.* **2002**, 165−170.
[56] S. Himeno, M. Takamoto, T. Ueda, *J. Electroanal. Chem.* **2000**, *485*, 49−54.
[57] L. I. Kuznetsova, L. G. Detusheva, M. A. Fedotov, V. A. Likholobov, *J. Mol. Cat., A* **1996**, *111*, 81−90.
[58] L. I. Kuznetsova, L. G. Detusheva, N. I. Kuznetsova, M. A. Fedotov, V. A. Likholobov, *J. Mol. Cat., A* **1997**, *117*, 389−396.
[59] T. J. R. Weakley, H. T. Evans, J. S. Showell, G. F. Tourné, C. M. Tourné, *J. Chem. Soc., Chem. Commun.* **1973**, 139−140.
[60] H. T. Evans, C. M. Tourné, G. F. Tourné, T. J. R. Weakley, *J. Chem. Soc., Dalton Trans.* **1986**, 2699−2705.
[61] R. N. Adams, *Electrochemistry at Solid Electrodes*, Marcel Dekker, New York, **1969**.
[62] L. C. W. Baker, M. T. Pope, *J. Am. Chem. Soc.* **1960**, *82*, 4176−4179.
[63] V. Grigoriev, C. L. Hill, I. Weinstock, *J. Am. Chem. Soc.* **2000**, *122*, 3544−3545.
[64] J. A. F. Gamelas, A. M. V. Cavaleiro, E. M. Gomes, M. Belsley, E. Herdtweck, *Polyhedron* **2002**, *21*, 2537−2545.
[65] C. Rocchiccioli−Deltcheff, M. Fournier, R. Franck, R. Thouvenot, *Inorg. Chem.* **1983**, *22*, 207−216.
[66] D. K. Lyon, W. K. Miller, T. Novet, P. J. Domaille, E. Evitt, D. C. Johnson, R. Finke, *J. Am. Chem. Soc.* **1991**, *113*, 7209−7221.
[67] A. Tézé, G. Hervé, *Inorg. Synth.* **1990**, *27*, 85−96.
[68] C. J. Gomez-Garcia, E. Coronado, P. Gomez-Romero, N. Casan-Pastor, *Inorg. Chem.* **1993**, *32*, 3378−3381.

Received May 17, 2003
Early View Article
Published Online December 19, 2003

 © 2004 Wiley-VCH Verlag GmbH & Co. KGaA, Weinheim

*P**,*N*-Bidentate Amino Phosphoramidites: New Highly Effective Ligands for Pd-Catalysed Asymmetric Allylic Substitution

Konstantin N. Gavrilov,*[a] Vasily N. Tsarev,[b] Alexei A. Shiryaev,[a] Oleg G. Bondarev,[c] Sergey E. Lyubimov,[a] Eduard B. Benetsky,[a] Alexander A. Korlyukov,[b] Mikhail Yu. Antipin,[b] Vadim A. Davankov,[b] and Hans-Joachim Gais[c]

Keywords: Asymmetric catalysis / *P*,*N*-ligands / Allylation / Palladium / Rhodium

New chiral *P**,*N*-hybrid amino phosphoramidites have been obtained by one-step phosphorylation of amino alcohols. Complexation of the new ligands with $[Rh(CO)_2Cl]_2$ and $[Pd(allyl)Cl]_2$ gave the corresponding chelate complexes $[Rh(CO)Cl(\eta^2\text{-P,N})]$ and $[Pd(allyl)(\eta^2\text{-P,N})]^+BF_4^-$, which subsequently afforded up to 90% *ee* in the asymmetric Pd-catalysed sulfonylation of 1,3-diphenyl-2-propenyl acetate with sodium *p*-toluenesulfinate. In the enantioselective alkylation of 1,3-diphenyl-2-propenyl acetate with dimethyl malonate, up to 98% enantioselectivity was achieved with $[Pd(allyl)(\eta^2\text{-P,N})]^+BF_4^-$ complexes as chiral catalysts.

(© Wiley-VCH Verlag GmbH & Co. KGaA, 69451 Weinheim, Germany, 2004)

Introduction

Chiral ligands with three P−O and/or P−N bonds have become increasingly important because of their synthetic availability, high π-acidity of the phosphorus atom, high resistance to oxidative destruction,[1−3] and their low cost. For example, BINOL-based monophosphites, which are highly efficient in asymmetric hydrogenation, are only 2% of the price of the well-known diphosphane BINAP.[4] Further modified heterobifunctional chiral phosphites, especially *P*,*N*-bidentate ones, have been applied to good effect in a wide range of catalytic processes, such as Cu-catalysed conjugate addition, Ir-catalysed hydrogenation and Rh-catalysed hydrosilylation.[1−3,5,6] In Pd-catalysed allylic substitution, work has concentrated mainly on nonsymmetric and sterically hindered substrates,[5−9] with only moderate results for the most common test substrate, 1,3-diphenyl-2-propenyl acetate (**1**, Scheme 1).[10]

Thus, pyridinophosphite ligands derived from (*S*)-BINOL provided product **2** with an enantioselectivity of up to 37%,[11,12] and phosphitooxazolines based on (*S*)- or (*R*)-BINOL afforded up to 43% *ee*.[13] Even more modest results − less than 31% *ee* − were delivered by the quinoline-derived phosphite ligands based on (*R*)-BINOL, (1*R*,2*R*)-*N*,*N*′-dimethyl-1,2-diphenylethylene-1,2-diamine, *N*-methylephedrine, (1*R*,2*R*)-1,2-bis(methylamino)cyclohexane, and (*S*)-prolinol.[14] The most effective *P*,*N*-bidentate ligands applied so far in the Pd-catalysed allylic substitution of **1** with dimethyl malonate are the compounds **4**−**6**.

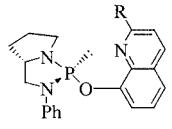

4 QUIPHOS (R=H)

85% *ee*[14-16]

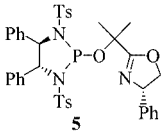

5

88% *ee*[7]

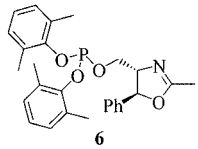

6

85% *ee*[17]

Notably, variation of R did not increase the enantioselectivity of ligand **4**.[14] Thus, more effective phosphite ligands are still needed. Indeed, the only phosphite ligands used in asymmetric allylic sulfonylation (Scheme 1) appear to be the phosphitooxazolines **7** and **8** recently reported by us.[18,19] They delivered up to 92% *ee* in the synthesis of **3**, which is very close to the efficiency of Helmchen's phosphanyloxazolines.[20]

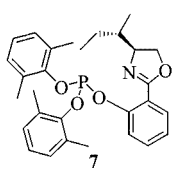

7

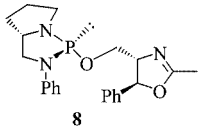

8

Here we describe the synthesis of new P*-chiral amino phosphoramidites, their complexation with Rh^I and Pd^{II} and application in Pd-catalysed enantioselective allylic substitution.

[a] Department of Chemistry, Ryazan State Pedagogic University, 46 Svoboda Str., Ryazan 390000, Russia
[b] Institute of Organoelement Compounds, Russian Academy of Sciences, 28 Vavilova Str., Moscow 119991, Russia
[c] Institut für Organische Chemie der Rheinisch-Westfälischen Technischen Hochschule Aachen, Professor-Pirlet-Straße 1, 52056 Aachen, Germany
Supporting information for this article is available on the WWW under http://www.eurjic.org or from the author.

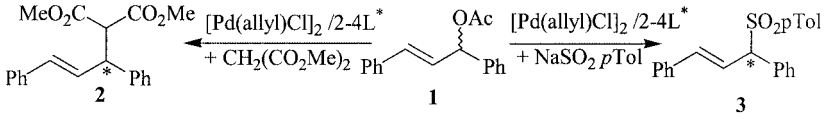

Scheme 1

Results and Discussion

The novel *P*,*N*-ligands were synthesized through the one-step phosphorylation of appropriate amino alcohols **10a**−**d** with (2*R*,5*S*)-2-chloro-3-phenyl-1,3-diaza-2-phosphabicyclo-[3.3.0]octane (**9**) (Scheme 2).

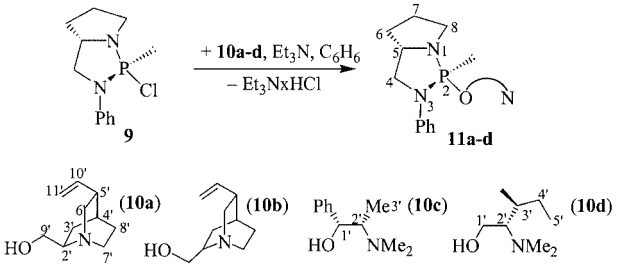

Scheme 2

Compounds **11a**−**d** are both stable and very soluble in common organic solvents. The synthesis is highly stereoselective, yielding only epimers with exocyclic substituents at the phosphorus atom in a pseudo-equatorial location. Therefore, the *P**-stereocenter has an (*R*) absolute configuration, which is proved by the characteristic[16,19] $^2J_{C\text{-}8,P}$ coupling (34.3−38.5 Hz) in the ^{13}C NMR spectra of **11a**−**d** (see Table 2 and Exp. Sect.). The magnitude of $^2J_{C\text{-}8,P}$ seems to be strongly controlled by the dihedral angle associated with the lone-pair orbital of the phosphorus atom and C-8.[21]

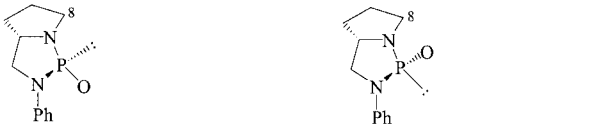

cis-location of C(8) and phosphorus lone pair; $^2J_{C(8),P} \sim 40$ Hz

trans-location of C(8) and phosphorus lone pair; $^2J_{C(8),P} \sim 0$ Hz

The pseudo-equatorial location of exocyclic functions was previously found for ligands **4**,[16] **8**,[19] and for (*S*)-prolinol-based phosphacyclanes.[21,22] According to the ^{31}P NMR spectroscopic data (Table 1), from ligands **11a**−**d**, only **11d** contains some minor stereoisomer with an (*S*) configuration of the *P**-stereocenter.

Complexation of **11a**−**d** with $[Rh(CO)_2Cl]_2$ and [Pd(allyl)Cl]$_2$ (in the presence of $AgBF_4$) produced neutral and cationic metal *cis*-chelates, respectively (Scheme 3).

Thus, the $^1J_{P,Rh}$, $^1J_{C,Rh}$, $^2J_{C,P}$ and ν(CO) data for complexes **12a**,**c**,**d** (Tables 1 and 2) agree well with the suggested structures (see ref.[8] and refs. cited therein); ν(CO) and $^1J_{P,Rh}$ are sensitive indicators that allow us to estimate the π-acceptor ability of the phosphorus center and the degree of electronic nonsymmetry of *P*,*N*-ligands.[8,9,23] Accordingly, amino phosphoramidites **11a**−**d** are intermediate between amino phosphanes and amino phosphites.[6,24]

Table 1. Selected spectroscopic data for **11a**−**d**, **12a**,**c**,**d**, and **13a**−**d** (in $CHCl_3$)

Compound	^{31}P NMR δ_P	^1J(P,Rh) [Hz]	IR ν(CO) [cm^{-1}]
11a	122.9		
11b	121.8		
11c	121.4		
11d	120.7 (98%), 114.4 (2%)[a]		
12a	129.4	235.3	2008
12c	128.0	232.4	2010
12d	124.7	234.0	2005
13a	126.9, 125.8		
13b	125.8		
13c	127.6, 125.6		
13d	124.9, 123.5		

[a] Percentage of each epimer.

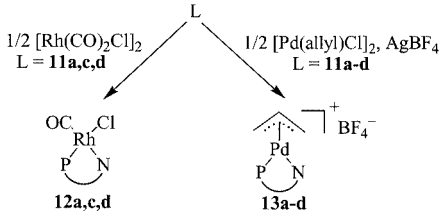

Scheme 3

Table 2. ^{13}C NMR spectroscopic data for **11a** and **12a** (in $CDCl_3$; $J_{C,P}$ in Hz)

Carbon atom	Compound **11a**	**12a**
CO		184.9 ($^1J_{C,Rh}$ = 70.9, $^2J_{C,P}$ = 21.9)
C_{Ar}	145.5−114.5	142.3−116.6
10′	140.4	137.4
11′	114.0	115.6
5	63.0 (^2J = 8.8)	62.4 (^2J = 11.7)
9′	62.9 (^2J = 4.6)	66.5 (^2J = 2.8)
2′	55.5 (^3J = 2.3)	59.6
4	54.6 (^2J = 7.3)	52.8 (^2J = 4.0)
7′	48.9	50.7
8	48.4 (^2J = 38.5)	49.6 (^2J = 19.7)
6′	47.4	48.0
5′	39.6	38.6
6	31.9	30.9
4′	27.3	26.4
8′	26.5	25.5
7	25.9 (^3J = 3.8)	25.1 (^3J = 4.4)
3′	24.4	25.3

 © 2004 Wiley-VCH Verlag GmbH & Co. KGaA, Weinheim

Besides chelate product **12d**, the reaction of **11d** with $[Rh(CO)_2Cl]_2$ afforded the *trans*-$[Rh(CO)Cl(\eta^1\text{-}L)_2]$ complex, where the ligands are coordinated in a *P*-monodentate manner. The complex clearly exhibits the characteristic doublet peak δ_P = 123.8 ppm, $^1J_{P,Rh}$ = 176.8 Hz (46%) in the ^{31}P NMR spectrum. Such side-products have been observed several times and arise from the sterically hindered nitrogen atom, which impedes chelation.[8,9,19]

In complex **12a**, the quinuclidine nitrogen atom is coordinated to the rhodium atom, as witnessed by the significant (up to 4 ppm) coordination shifts $\Delta\delta_C = \delta_C(\text{complex}) - \delta_C(\text{ligand})$ observed for C-2′, C-6′, and C-7′ (Table 2). Similar $\Delta\delta_C$ values have been observed for chelate Rh^I complexes with quincoridine-derived phosphites.[25] The large $^2J_{C\text{-}8,P}$ values in complex **12a** (19.7 Hz) clearly indicate that the quinuclidyl substituent is in a pseudo-equatorial position and, therefore, that the *P** atom had an (*R*) absolute configuration. This conclusion, and other findings on the structure of **12a**, agree well with the X-ray analysis data of its monocrystal. Thus, in the crystal of **12a** two independent molecules are characterized by (*S*) and (*R*) configurations of asymmetric N(1′) and P(2) atoms (without taking into account the formal priority of the metal atom). In one independent molecule, the phospholidine cycle has a twist conformation with deviations of C(4) and C(5) atoms of 0.27 and 0.20 Å, respectively, while in a second independent molecule this cycle is characterized by a slightly distorted envelope conformation with a deviation of N(3) of 0.29 Å. The pyrollidine cycles have envelope conformations [C(7) atoms deviate by 0.58 Å on average] with the phenyl substituent in a pseudo-equatorial position. The quincoridine substituent occupies a pseudo-equatorial position as related to the phospholidine cycle. In turn, the rhodium atom occupies an axial position.

Similarly to the compound described in ref.[16], the phosphorus atom in **12a** has a tetrahedral configuration (the sum basal N−P−O and N−P−N angles are 302 and 298°, respectively). The N(1)−P(2)−O(1) and N(3)−P(2)−O(1) angles are about 2−3° less than the analogous ones in ref.[16] The elongation of P−N bonds by up to 0.02 Å compared to those in ref.[16] may due to a *trans* effect of the chlorine substituent.

The rhodium atom has almost ideal square-planar coordination, with an average deviation from the mean plane of 0.02 Å. The bond lengths of coordination polyhedra of the rhodium atom are close to those in rhodium and palladium complexes with *P,N*-bidentate aryl phosphites[8] (Figure 1).

The principal structural difference between the two independent molecules is the geometry of the six-membered metallacycles, which are characterized by a distorted boat conformation. The C(2′) and P(2) atoms in the first molecule deviate from the basal plane by 0.62 and 0.50 Å, and C(2′A) and P(2A) in the second molecule deviate by 0.32 and 0.60 Å, respectively. Previously investigated rhodium and palladium complexes with the same type of coordination polyhedra have six-membered metallacycles with a chair conformation. However, the introduction of the bulky ferrocenyl moiety near the six-membered metallacycle[8] changed this conformation to a distorted boat. Thus, the distorted boat conformation of the metallacycles in **12a** can be attributed to steric overcrowding caused by the massive 1-azabicyclo[2.2.2]octane and 1,3-diaza-2-phosphabicyclo-[3.3.0]octane moieties.

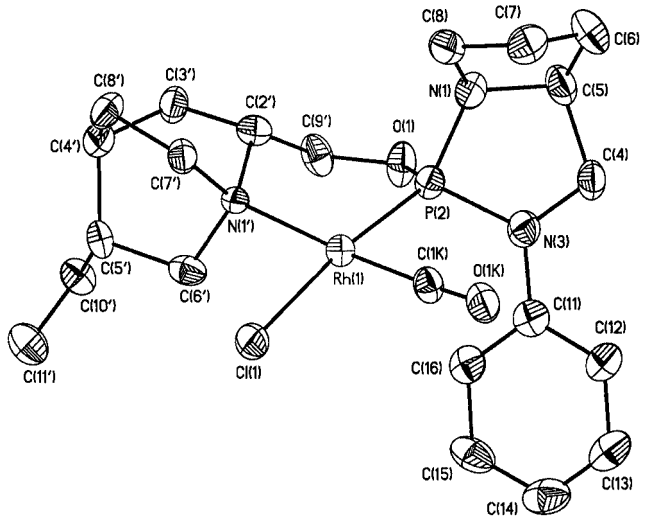

Figure 1. General view of one of the two independent molecules of **12a**; atoms are presented as thermal ellipsoids drawn at 50% probability level; selected averaged bond lengths [Å] and angles [°]: Rh(1)−P(2) 2.176(2), Rh(1)−Cl(1) 2.408(2), Rh(1)−N(1′) 2.174(6), Rh(1A)−C(1 K) 1.826(9), C(1 K)−O(1 K), O(1 K)−C(1 K) 1.11(1), P(2)−N(1) 1.656(8), P(2)−N(3) 1.706(7); P(2)−Rh(1)−C(1 K) 85.5(3), Cl(1)−Rh(1)−C(1 K) 89.4(3), Cl(1)−Rh(1)−N(1 K) 90.7(2), Cl(1)−Rh(1)−P(2) 172.29(8), N(1′)−Rh(1)−C(1 K) 176.0(3), N(1)−P(2)−N(3) 93.0(4)

Cationic palladium chelates **13a**−**d** are stable in air and very soluble in common organic media. There are two sets of peaks in the ^{31}P NMR spectra of **13a**, **13c**, and **13d** (Table 1), which indicate the existence of the *exo* and *endo* isomers of the compounds. Two peak sets are not seen for complex **13b**, because of either the fast interconversion of isomers or the absence of one of them (see refs.[8,9] and references cited therein).

Amino amidophosphites **12a**−**d** and the isolated complexes **13a**−**d** were tested in asymmetric Pd-catalysed allylic substitution processes (Scheme 1). For allylic sulfonylation (Table 3) moderate chemical (up to 66%) and good optical (up to 90% *ee*) yields of product **3** were achieved. For ligand **11a**, the enantioselectivity does not depend on the L*/[Pd] ratio (Entries 1−3). We suppose that the active catalytic particle here is represented by a cationic chelate $[Pd(allyl)(\eta^2\text{-}P,N)]^+X^-$ (X^- = Cl^-, BF_4^-). Indeed, its singlet peak δ_P = 125.0 ppm (28%) was found in the ^{31}P NMR spectrum of the $[Pd(allyl)Cl]_2$/4L* (L* = **11a**) solution in $CHCl_3$, together with signals of uncoordinated **11a** (δ_P = 122.9 ppm) and $[Pd(allyl)(\eta^1\text{-}P,N)(\eta^2\text{-}P,N)]^+Cl^-$ (AX system: δ_P = 100.3 ppm and δ_P = 61.4 ppm, $^2J_{P,P}$ = 87.7 Hz). With ligand **11d**, the L*/[Pd] ratio also did not influence the catalytic outcome (Entries 12,13,15). In contrast, when the ratio **11b**/[Pd] was increased from 1:1 to 2:1, the enantioselectivity improved sharply from 39 to 76% *ee* (Entries 4, 5). Most probably, here the palladium complex containing two molecules of the ligand possesses high catalytic activity

 © 2004 Wiley-VCH Verlag GmbH & Co. KGaA, Weinheim

Table 3. Enantioselective allylic sulfonylation of **1** with $NaSO_2pTol$ (in THF)

Entry	Catalyst precursor	Ligand	L*/[Pd]	Isolated yield [%]	*ee* [%][a]
1	$[Pd(allyl)Cl]_2$	**11a**	1:1	56	77 (*S*)
2	$[Pd(allyl)Cl]_2$	**11a**	2:1	50	73 (*S*)
3	**13a**		1:1	24	76 (*S*)
4	$[Pd(allyl)Cl]_2$	**11b**	1:1	45	39 (*S*)
5	$[Pd(allyl)Cl]_2$	**11b**	2:1	65	76 (*S*)
6	$[Pd_2(dba)_3] \times CHCl_3$	**11b**	1:1	57	67 (*S*)
7	**13b**		1:1	41	60 (*S*)
8	$[Pd(allyl)Cl]_2$	**11c**	1:1	13	74 (*S*)
9	$[Pd(allyl)Cl]_2$	**11c**	2:1	25	61 (*S*)
10	$[Pd_2(dba)_3] \times CHCl_3$	**11c**	1:1	17	10 (*R*)
11	**13c**		1:1	66	80 (*S*)
12	$[Pd(allyl)Cl]_2$	**11d**	1:1	39	87 (*S*)
13	**$[Pd(allyl)Cl]_2$**	**11d**	**2:1**	**40**	**90 (*S*)**
14	$[Pd_2(dba)_3] \times CHCl_3$	**11d**	1:1	15	20 (*S*)
15	**13d**		1:1	40	83 (*S*)

[a] Measured by HPLC [(*R*,*R*)-Whelk-01].

and is very stereoselective. In addition, a considerable counterion effect was observed for complexes with ligand **11b** (Entries 4, 7).[26]

As all the variations in the structures of both the N-containing fragment and the carbon bridge between the P and N atoms did not cause considerable changes in enantioselectivity, the catalytic performance of ligands **11a−d** is mostly determined by the bicyclic chiral phosphorus block.

With $[Pd_2(dba)_3] \times CHCl_3$ as a catalytic precursor, generally inferior results were obtained. For ligands **11c** and **11d** the enantioselectivity dropped very sharply (Entries 10, 14), and even a product with reversed absolute configuration was produced in one case (Entry 10).

Application of pre-formed palladium complexes **13a−d** in asymmetric allylic alkylation resulted in excellent chemical and optical yields (Table 4). The enantioselectivity of the reaction demonstrates a strong dependence on both the solvent (Entries 3 and 4) and the structure of the amino alcohol block (Entries 1 and 3). Comparison of the results (under identical reaction conditions) for sulfonylation (Table 3, Entries 3, 7, 11, 15) and for alkylation (Table 4, Entries 1, 3, 5, 7) reveals that the right choice of nucleophile is important in achieving high level of enantioselectivity in allylic substitution reactions.

Table 4. Enantioselective allylic alkylation of **1** with dimethyl malonate

Entry	Catalyst precursor	Solvent	Conv. [%][a]	*ee* [%][b]
1	**13a**	THF	> 99	95 (*S*)
2	**13a**	CH_2Cl_2	99	97 (*S*)
3	**13b**	THF	98	91 (*R*)
4	**13b**	CH_2Cl_2	72	52 (*R*)
5	**13c**	THF	83	89 (*S*)
6	**13c**	CH_2Cl_2	88	79 (*S*)
7	**13d**	THF	> 99	92 (*S*)
8	**13d**	**CH_2Cl_2**	**92**	**98 (*S*)**

[a] Measured by HPLC. [b] Determined by HPLC analysis using a Daicel Chiralcel OD-H column.

The enantioselectivity obtained with ligands **11a−d** in the Pd-catalysed allylic alkylation of **1** with dimethyl malonate (98% *ee*) is the highest reported for chiral phosphite ligands and approaches the best overall results.[5,6,10]

Experimental Section

General Remarks: All reactions were performed under argon in dehydrated solvents. IR spectra were recorded with a Specord M80 or Nicolet 750 instrument. ^{31}P and ^{13}C NMR spectra were recorded with a Bruker AMX 400 instrument (162.0 MHz for ^{31}P, 100.6 MHz for ^{13}C). Complete assignment of all the resonances in ^{13}C NMR spectra was achieved with DEPT techniques. Chemical shifts (ppm) are given relative to Me_4Si (^{13}C NMR) and 85% H_3PO_4 (^{31}P NMR). Mass spectra were recorded with a Kratos MS890 spectrometer (EI), an MSVKh TOF spectrometer with ionization by Cf-252 fission fragments (plasma desorption technique, PD), and an AMD 402 spectrometer (FAB). Elemental analyses were performed at the Laboratory of Microanalysis (Institute of Organoelement Compounds, Moscow). $[Rh(CO)_2Cl]_2$,[27] $[Pd(allyl)Cl]_2$,[28] $[Pd_2(dba)_3] \times CHCl_3$,[29] amino alcohol **10d**,[30] and (2*R*,5*S*)-2-chloro-3-phenyl-1,3-diaza-2-phosphabicyclo[3.3.0]-octane (**9**)[19] were synthesized by published procedures. Complexes **12a** and **13a−d** were synthesized by techniques similar to that reported.[9] Rhodium complexes **12c**,**d** were synthesized for the ^{31}P NMR and IR experiments in $CHCl_3$ medium analogously to the known procedures.[8] Compound **10c** was purchased from Aldrich and dried in vacuo (2 Torr, 3 h) immediately before use. Amino alcohols **10a**,**b** (quincoridine and quincorine, Buchler GmbH) and **10d** were azeotropically dried with benzene and distilled before use.

Synthesis and Characterization

Preparation of Ligands. General Technique: A solution of (2*R*,5*S*)-2-chloro-3-phenyl-1,3-diaza-2-phosphabicyclo[3.3.0]octane (**9**) (1 g, 4.2×10^{-3} mol) in benzene (15 mL) was added dropwise to a stirred solution of the appropriate amino alcohol **10a−d** (4.2×10^{-3} mol) and Et_3N (0.6 mL, 4.2×10^{-3} mol) in the same solvent (15 mL) at 0 °C. The reaction mixture was then heated to boiling point, allowed to cool, stirred at 50 °C for 1 h, allowed to cool to room temperature and then filtered. The solvent was removed in vacuo (40 Torr), and the residue was dissolved in hexane (25 mL), filtered, concentrated and dried in vacuo (1 Torr, 2 h).

(2*R*,5*S*,2′*R*,4′*S*,5′*R*)-3-Phenyl-2-[(5′-vinyl-2′-quinuclidyl)methoxy]-1,3-diaza-2-phosphabicyclo[3.3.0]octane (11a): Colourless oil, 1.41 g (91% yield). MS (EI, 70 eV): *m*/*z* (%) = 371 (29) $[M]^+$, 289 (50), 221 (34), 205 (100), 197 (72), 136 (91). $C_{21}H_{30}N_3OP$ (371.2): calcd. C 67.90, H 8.14, N 11.31; found C 68.24, H 8.35, N 11.17.

(2*R*,5*S*,2′*S*,4′*S*,5′*R*)-3-Phenyl-2-[(5′-vinyl-2′-quinuclidyl)methoxy]-1,3-diaza-2-phosphabicyclo[3.3.0]octane (11b): Colourless oil, 1.391 g (90% yield). MS (EI, 70 eV): *m*/*z* (%) = 371 (30) $[M]^+$, 289 (48), 221 (34), 205 (100). $C_{21}H_{30}N_3OP$ (371.2): calcd. C 67.90, H 8.14, N 11.31; found C 68.17, H 8.28, N 11.20.

(2*R*,5*S*,1′*R*,2′*S*)-2-(2′-Dimethylamino-1′-phenylpropoxy)-3-phenyl-1,3-diaza-2-phosphabicyclo[3.3.0]octane (11c): Colourless oil, 1.466 g (92% yield). ^{13}C NMR (100.6 MHz, $CDCl_3$): δ = 7.8 (s, C-3′), 26.5 (d, ^3J = 4.5 Hz, C-7), 31.4 (s, C-6), 40.6 (s, NMe_2), 46.7 (d, ^2J = 34.3 Hz, C-8), 53.7 (d, ^2J = 7.5 Hz, C-4), 62.3 (d, ^2J = 9.0 Hz, C-5), 64.8 (d, ^3J = 2.4 Hz, C-2′), 76.7 (s, C-1′),

 © 2004 Wiley-VCH Verlag GmbH & Co. KGaA, Weinheim

114.5−145.6 (C_{Ar}) ppm. MS (EI, 70 eV): *m*/*z* (%) = 312 (2), 222 (67), 205 (12), 117 (100). MS (PD): *m*/*z* (%) = 383 (10) $[M]^+$, 205 (60), 162 (85), 72 (100). $C_{22}H_{30}N_3OP$ (383.2): calcd. C 68.91, H 7.89, N 10.96; found C 69.13, H 8.00, N 11.18.

(2*R*,5*S*,2′*S*,3′*S*)-2-(2′-Dimethylamino-3′-methylpentyloxy)-3-phenyl-1,3-diaza-2-phosphabicyclo[3.3.0]octane (11d): Colourless oil, 1.291 g (89% yield). ^{13}C NMR (100.6 MHz, $CDCl_3$), δ = 11.0 (s, C-5′), 15.3 (s, CH_3), 26.0 (d, ^3J = 3.4 Hz, C-7), 26.5 (s, C-4′), 32.1 (s, C-6), 33.3 (s, C-3′), 41.9 (s, NMe_2), 48.4 (d, ^2J = 38.5 Hz, C-8), 54. 7 (d, ^2J = 7.2 Hz, C-4), 58.5 (s, C-1′), 63.4 (d, ^2J = 8.8 Hz, C-5), 67.5 (d, ^3J = 1.9 Hz, C-2′), 114.6−145.8 (C_{Ar}) ppm. MS (EI, 70 eV): *m*/*z* (%) = 334 (1), 205 (66), 114 (100). MS (PD): *m*/*z* (%) = 349 (15) $[M]^+$, 319 (27), 221 (34), 114 (100). $C_{19}H_{32}N_3OP$ (349.2): calcd. C 65.30, H 9.23, N 12.02; found C 65.54, H 9.35, N 11.88.

Rhodium(I) and Palladium(II) Complexes

[Rh(CO)Cl(11a−P⌒N)] (12a): Pale yellow solid, 0.180 g (93% yield). IR (Nujol): $\tilde{\nu}$ = 296 [ν(Rh−Cl)] cm^{-1}. $C_{22}H_{30}ClN_3O_2PRh$ (537.1): calcd. C 49.13, H 5.62, Cl 6.59, N 7.81; found C 49.40, H 5.78, Cl 6.82, N 8.03.

[Pd(allyl)(11a−P⌒N)]$^+BF_4^-$ (13a): Pale yellow solid, 0.232 g (96% yield). MS (FAB): *m*/*z* (%) = 518 (100) $[M - BF_4]^+$, 477 (21), 311 (42), 205 (96). $C_{24}H_{35}BF_4N_3OPPd$ (605.2): calcd. C 47.59, H 5.82, N 6.94; found C 47.33, H 5.98, N 7.16.

[Pd(allyl)(11b−P⌒N)]$^+BF_4^-$ (13b): Yellow solid, 0.213 g (88% yield). MS (FAB): *m*/*z* (%): 518 (100) $[M - BF_4]^+$, 477 (15), 311 (29), 205 (30). $C_{24}H_{35}BF_4N_3OPPd$ (605.2): calcd. C 47.59, H 5.82, N 6.94; found C 47.44, H 6.03, N 6.89.

[Pd(allyl)(11c−P⌒N)]$^+BF_4^-$ (13c): White solid, 0.222 g (90% yield). MS (FAB): *m*/*z* (%): 530 (32) $[M - BF_4]^+$, 489 (12), 162 (100). $C_{25}H_{35}BF_4N_3OPPd$ (617.2): calcd. C 48.61, H 5.71, N 6.80; found C 48.37, H 5.84, N 6.93.

[Pd(allyl)(11d−P⌒N)]$^+BF_4^-$ (13d): Beige solid, 0.220 g (94% yield). MS (FAB): *m*/*z* (%): 496 (8) $[M - BF_4]^+$, 455 (5), 128 (100). $C_{22}H_{37}BF_4N_3OPPd$ (583.2): calcd. C 45.27, H 6.39, N 7.20; found C 45.51, H 6.23, N 7.33.

Crystallographic Data for 12a: Crystals of $C_{22}H_{30}ClN_3O_2PRh$ are monoclinic, space group $P2_1$, *a* = 8.410(3) Å, *b* = 11.557(4) Å, *c* = 23.267(8) Å, *V* = 2261.1(14) $Å^3$, *Z* = 4, *M* = 537.82, $d_{calcd.}$ = 1.580 $g·cm^{-3}$, μ(Mo-K_α) = 9.68 cm^{-1}, *F*(000) = 1104. Intensities of 13120 reflections were collected at 120 K with a SMART CCD 1000 diffractometer using Mo-K_α radiation (λ = 0.71072 Å, ω-scans with 0.3° step and 10 s exposure for each frame) and 8058 independent reflections (R_{int} = 0.0365) were used in further refinement. An absorption correction was applied semi-empirically from equivalents. The structure of **12a** was solved by direct methods and refined by a full-matrix techniques against F^2 in anisotropic approximation using the SHELXTL-97 5.1 program package[31]. The positions of hydrogen atoms were calculated geometrically and included in the refinement using the rigid body approximation. The refinement converged to wR_2 = 0.1238 and *GOF* = 1.020 for all independent reflections [R_1 = 0.0567 was calculated for 6829 observed reflections with $I > 2\sigma(I)$]. The absolute configuration was determined by use of the Flack parameter. CCDC-215598 contains the supplementary crystallographic data for this paper. These data can be obtained free of charge at www.ccdc.cam.ac.uk/conts/retrieving.html [or from the Cambridge Crystallographic Data Centre, 12 Union Road, Cambridge CB2 1EZ, UK; Fax: (internat.) + 44-1223/336-033; E-mail: deposit@ccdc.cam.ac.uk].

Supporting Information: ^1H NMR spectroscopic data for compounds **11a−d** and the catalytic experimental procedures are provided (see also footnote on the first page of this article).

Acknowledgments

The authors gratefully acknowledge receiving quincoridine and quincorine from Buchler GmbH (Germany) and thank Dr. P.V. Petrovskii (Institute of Organoelement Compounds, Moscow) for assistance in characterizing the products and Dr. A.V. Korostylev (Leibniz-Institut für Organische Katalyse, Rostock, Germany) for assistance in preparation of the manuscript. This work was partially supported by the Russian Foundation for Basic Research (Grant No. 03-03-32181) and Grant of the President of RF for young scientists − doctors of sciences (No. MD-21.2003.03).

[1] J. Ansell, M. Wills, *Chem. Soc. Rev.* **2002**, *31*, 259−268.
[2] A. Alexakis, C. Benhaim, *Eur. J. Org. Chem.* **2002**, 3221−3236.
[3] O. Molt, T. Schrader, *Synthesis* **2002**, 2633−2670.
[4] M. T. Reetz, G. Mehler, A. Meiswinkel, T. Sell, *Tetrahedron Lett.* **2002**, *43*, 7941−7943.
[5] F. Fache, E. Schulz, M. L. Tommasino, M. Lemaire, *Chem. Rev.* **2002**, *100*, 2159−2231.
[6] K. N. Gavrilov, A. I. Polosukhin, *Russ. Chem. Rev.* **2002**, *65*, 661−682.
[7] R. Hilgraf, A. Pfaltz, *Synlett* **1999**, 1814−1816.
[8] K. N. Gavrilov, O. G. Bondarev, R. V. Lebedev, A. A. Shiryaev, S. E. Lyubimov, A. I. Polosukhin, G. V. Grintselev−Knyazev, K. A. Lyssenko, S. K. Moiseev, N. S. Ikonnikov, V. N. Kalinin, V. A. Davankov, A. V. Korostylev, H. J. Gais, *Eur. J. Inorg. Chem.* **2002**, 1367−1376.
[9] K. N. Gavrilov, O. G. Bondarev, R. V. Lebedev, A. I. Polosukhin, A. A. Shiryaev, S. E. Lyubimov, P. V. Petrovskii, S. K. Moiseev, V. N. Kalinin, N. S. Ikonnikov, V. A. Davankov, V. A. Korostylev, *J. Organomet. Chem.* **2002**, *655*, 204−217.
[10] B. M. Trost, C. Lee, in: *Catalytic Asymmetric Synthesis* (Ed.: I. Ojima), 2nd ed., Wiley-VCH, Inc., New York, **2000**, p. 593.
[11] C. Arena, D. Drommi, F. Faraone, *Tetrahedron: Asymmetry* **2000**, *11*, 2765−2779.
[12] C. Arena, D. Drommi, F. Faraone, *Tetrahedron: Asymmetry* **2000**, *11*, 4753−4759.
[13] S. Gladiali, G. Loriga, S. Medici, R. Taras, *J. Mol. Catal., A: Chemical.* **2003**, *196*, 27−38.
[14] G. Delapierre, J. M. Brunel, T. Constantieux, G. Buono, *Tetrahedron: Asymmetry.* **2001**, *12*, 1345−1352.
[15] J. M. Brunel, T. Constantieux, A. Labande, F. Lubatti, G. Buono, *Tetrahedron Lett.* **1997**, *38*, 5971−5974.
[16] J. M. Brunel, T. Constantieux, G. Buono, *J. Org. Chem.* **1999**, *64*, 8940−8942.
[17] A. I. Polosukhin, O. G. Bondarev, S. E. Lyubimov, V. A. Korostylev, K. A. Lyssenko, V. A. Davankov, K. N. Gavrilov, *Tetrahedron: Asymmetry* **2001**, *12*, 2197−2204.
[18] O. G. Bondarev, S. E. Lyubimov, A. A. Shiryaev, N. E. Kadilnikov, V. A. Davankov, K. N. Gavrilov, *Tetrahedron: Asymmetry.* **2002**, *13*, 1587−1588.
[19] K. N. Gavrilov, O. G. Bondarev, V. N. Tsarev, A. A. Shiryaev, S. E. Lyubimov, A. S. Kucherenko, V. A. Davankov, *Russ. Chem. Bull.* **2003**, *52*, 122−125.
[20] H. Eichelmann, H.-J. Gais, *Tetrahedron: Asymmetry* **1995**, *6*, 643−647.
[21] H. Arzoumanian, G. Buono, M. B. Choukrad, J.-F. Petrignani, *Organometallics* **1988**, *7*, 59−62.
[22] A. I. Polosukhin, O. G. Bondarev, S. E. Lyubimov, A. A. Shiryaev, P. V. Petrovskii, K. A. Lysenko, K. N. Gavrilov, *Russ. J. Coord. Chem.* **2001**, *27*, 591−597.
[23] A. Snyder, A. Togni, V. Weisli, *Organometallics* **1997**, *16*, 225−260.
[24] K. N. Gavrilov, *Russ. J. Inorg. Chem.* **1997**, *42*, 368−384.

 © 2004 Wiley-VCH Verlag GmbH & Co. KGaA, Weinheim

[25] A. I. Polosukhin, K. N. Gavrilov, O. G. Bondarev, V. A. Korostylev, P. V. Petrovskii, V. A. Davankov, *J. Organomet. Chem.* **2000**, *608*, 89−95.
[26] U. Burckhardt, M. Baumann, A. Togni, *Tetrahedron: Asymmetry* **1997**, *8*, 155−162.
[27] J. A. McCleverty, G. Wilkinson, *Inorg. Synth.* **1966**, *8*, 211−214.
[28] P. R. Auburn, P. B. McKenzie, B. Bosnich, *J. Am. Chem. Soc.* **1985**, *107*, 2033−2046.
[29] K. Moseley, P. M. Maitlis, *J. Chem. Soc., Dalton Trans.* **1974**, 169−175.
[30] T. Hayashi, M. Konishi, M. Fukushima, K. Kanehira, T. Hioki, M. Kumada, *J. Org. Chem.* **1983**, *48*, 2195−2202.
[31] G. M. Sheldrick, *SHELXTL-97*, V5.10, Bruker AXS, Inc., Madison, WI 53719, USA, **1997**.

Received May 5, 2003
Early View Article
Published Online December 4, 2003

 © 2004 Wiley-VCH Verlag GmbH & Co. KGaA, Weinheim

Flexidentate Behaviour of 2-Pyridylsulfonamides − Direct Electrochemical Synthesis and Spectroscopic and X-ray Characterisation of Neutral Copper(II) Complexes of *N*-(2-Pyridyl)sulfonamides

Inmaculada Beloso,[a] Joaquín Borrás,[b] Jesús Castro,*[a] José A. García-Vázquez,[c] Paulo Pérez-Lourido,[a] Jaime Romero,[c] and Antonio Sousa*[c]

Dedicated to the memory of Professor D. G. Tuck

Keywords: Copper / S ligands / Electrochemical synthesis / N ligands

Copper complexes with potentially bidentate *N*-(2-*p*yridyl)-sulfonylamide ligands have been synthesised by the electrochemical oxidation of the metal in an acetonitrile solution of the neutral amide and additional bidentate N–N coligands. The compounds have been characterised by microanalysis and EPR, vibrational and electronic spectroscopy. In representative cases the structures were also determined by X-ray diffraction methods. Various coordination behaviour is found for the ligands, which act in a *N*,*N*′-bidentate or *N*,*O*-bidentate manner, the latter giving abnormally short Cu–O bonds. (© Wiley-VCH Verlag GmbH & Co. KGaA, 69451 Weinheim, Germany, 2004)

Introduction

Metal complexes containing amide ligands are of great recent interest[1−4] because they are easily made, and the substituents can be readily amended so as to tune their bite angle and steric hindrance. The chemistry of metal complexes containing pyridine-functionalised amido ligands of the type shown in Scheme 1 has received much attention.[5−9] The bulky substituents on these ligands stabilise the metal complexes.

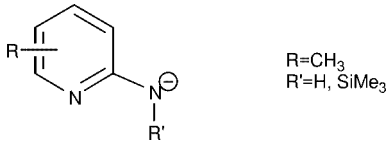

Scheme 1

Consequently, it was decided to study the chemistry of the metal complexes of sulfonyl-2-pyridine-amines. These ligands, Scheme 2, contain a bulky sulfonyl group as a substituent of the exocyclic nitrogen atom. In addition, its electron-withdrawing effect increases the acid character of the NH group and makes ligand deprotonation easier.[4]

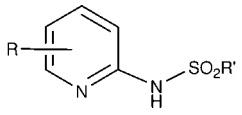

Scheme 2

These ligands can coordinate to the metal in several different ways (Scheme 3).

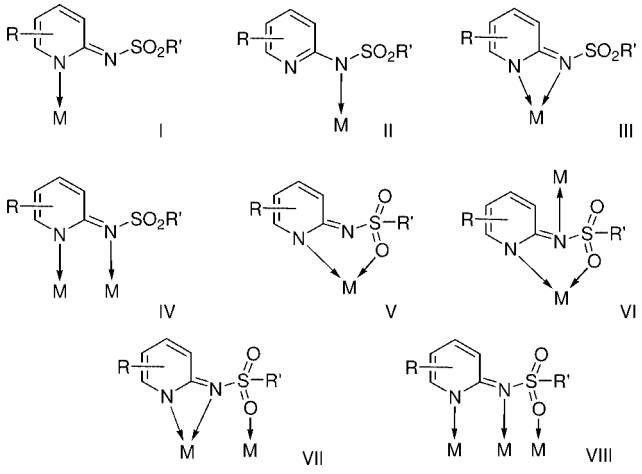

Scheme 3

[a] Departamento de Química Inorgánica, Universidade de Vigo, 36200 Vigo, Spain
Fax: (internat.) + 34-986-813-798
E-mail: fojo@uvigo.es
[b] Departamento de Química Inorgánica. Fac. Farmacia, Univ. Valencia
Vicent Andrés Estellés s/n, 46100 Burjassot, Valencia, Spain.
[c] Departamento de Química Inorgánica, Universidade de Santiago de Compostela,
15782 Santiago, Spain
Fax: (internat.) + 34-981-597-525
E-mail: qiansoal@usc.es

Coordination modes I and II have been found in zinc compounds. For complexes showing coordination mode I, a weak interaction between the metal and the exocyclic nitrogen atom is present,[10] while mode II exhibits a weak interaction between the zinc and the pyridine nitrogen atom.[11] Coordination mode III is the most common, and has been found in cobalt(II),[12] nickel(II),[13] and cadmium(II)[14,15] complexes. Coordination mode IV has only been found in copper(II)[9] and silver(I)[9,16] complexes, and coordination mode V has only been found in zinc(II)[11] and cadmium(II)[15] complexes. Coordination modes VI and VII have been found in a polymer compound of cadmium(II)[14] and the coordination mode VIII only occurs in silver(I) complexes.[16]

Coordination mode IV appears to have only been found with copper(II) and silver(I). When the ligand has no substituent on the pyridine ring (R = H) the compound is dinuclear.[9] To check if the nuclearity and the coordination mode could be modified, we introduced a methyl group at position 3 or 6 on the pyridine ring to determine the influence of the steric hindrance produced by such substitution on the coordination of the pyridine and the sulfonamide nitrogen atoms. Substitution at position 4 does not influence the coordination mode and a dinuclear compound is again obtained.[16] Therefore, and to continue similar studies on Zn^{II} [11] and Cd^{II},[15] we report here the electrochemical synthesis and characterisation of several heteroleptic copper(II) complexes with a number of benzenesulfonyl-2-pyridineamide ligands. The pyridine ring contains one methyl group and the benzene ring also contains one methyl group (*p*-toluene group) or, alternatively, three methyl groups (mesitylene group) (Scheme 4).

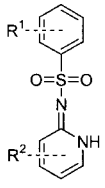

Code	R^1	R^2
HTs3mepy	4-Me	3-Me
HTs6mepy	4-Me	6-Me
HMs3mepy	2,4,6-Me_3	3-Me
HMs6mepy	2,4,6-Me_3	6-Me

Scheme 4. The sulfonamide ligands

Results and Discussion

Anodic oxidation of copper metal in a non-aqueous solution containing a weakly acidic ligand alone or as a mixture with a coligand, such as 2,2′-bipyridine (bipy) or 1,10-phenanthroline (phen), yields the products $[CuL_2H_2O]$ or $[CuL_2L']$, respectively, were L is the deprotonated form of the parent ligand and L′ the coligand (i.e. bipy or phen) (see Exp. Sect.). The compounds are obtained by air concentration of the resulting solution as green air-stable crystalline products. They are insoluble in water and in most common organic solvents.

The electrochemical efficiency, defined as the amount of metal dissolved per number of Faradays, was close to 1.0 $mol \cdot F^{-1}$ in all cases. This fact, along with the evolution of hydrogen at the cathode, is compatible with a reaction mechanism involving the anodic oxidation to copper(I) and the deprotonation of the ligand at the cathode.

Anode: $Cu + L^- \rightarrow [CuL] + e^-$

Cathode: $HL + e^- \rightarrow L^- + 1/2\ H_2$

$[CuL] + HL + L' \rightarrow [CuL_2L'] + 1/2\ H_2$

The oxidation of copper(I) by another HL molecule has been observed in other electrochemical processes involving copper anodes.[17]

Description of the Structures

The crystal and molecular structures of several complexes and the ligand HMs3mepy have been determined by single crystal XRD. The crystal data are collected in Tables 12 and 13.

Structure of HMs3mepy

HMs3mepy crystallizes in the monoclinic *C*2/*c* space group, $Z = 4$, and consists of molecules of [(2,4,6-trimethylphenyl)sulfonyl]imino-1*H*-3-methyl-2-pyridine associated two-by-two by intermolecular hydrogen bonds established between the pyridine nitrogen atom of one molecule and two sulfonamide oxygen atoms, one of which forms an intramolecular contact while the other is involved in an intermolecular contact with a neighbouring molecule. The imine nitrogen is not implicated in these bonds. This arrangement contrasts with the hydrogen network found in HTspy[13] and HTs6mepy,[15] where the hydrogen bonds involve the N_{py} and the $N_{sulfonamide}$ atoms. The methyl group in position 3 of the pyridine ring precludes the use of the $N_{sulfonamide}$ atom with HTs3mepy for steric reasons. This explanation is supported by the observed ligational mode of HTs3mepy (vide infra).

The structure of HTs3mepy and the atomic numbering scheme (Figure 1), and selected bond lengths and angles and hydrogen bond parameters (Table 1 and Table 2), are given here.

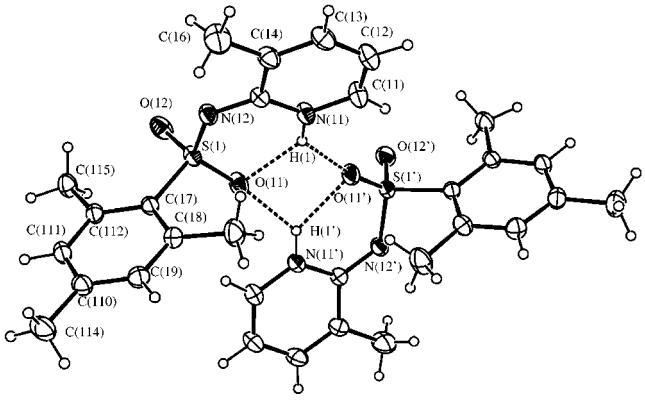

Figure 1. Structure of HMs3mepy

The bond lengths and bond angles are similar to those in other *N*-2-pyridinyl benzenesulfonamide derivatives.[11,13,15] The hydrogen atom on the *N*-pyridine ring shows that the free ligand is the imido tautomer (I) rather than the amido

 © 2004 Wiley-VCH Verlag GmbH & Co. KGaA, Weinheim

Table 1. Slected bond lengths [Å] and angles [°] for HMs3mepy

S−O(12)	1.4345(14)	S−O(11)	1.4517(12)
S−N(12)	1.5937(14)	S−C(17)	1.7821(16)
N(11)−C(15)	1.359(2)	N(11)−C(11)	1.364(2)
N(11)−H(1)	0.945(19)	N(12)−C(15)	1.326(2)
O(12)−S−O(11)	114.30(9)	O(12)−S−N(12)	108.89(8)
O(11)−S−N(12)	113.04(7)	O(12)−S−C(17)	109.76(8)
O(11)−S−C(17)	107.47(8)	N(12)−S−C(17)	102.71(7)

Table 2. Hydrogen bonds and short contacts for HMs3mepy (^{i}: symmetry transformations used to generate equivalent atoms: $-x$, y, $0.5 - z$)

D−H···A	*d*(D−H)	*d*(H···A)	*d*(D···A)	<(DHA)
N(11)−H(1)···O(11)	0.945(19)	2.00(2)	2.7209(18)	131.6(16)
N(11)−H(1)···O(11^{i})	0.945(19)	2.124(19)	2.8858(19)	136.7(16)
C(113)−H(11A)···N(12)	0.96	2.61	3.102(3)	112.2
C(113)−H(11B)···O(11)	0.96	2.47	3.086(3)	121.8
C(115)−H(11E)···O(12)	0.96	2.40	2.747(2)	100.9

tautomer (II). This situation is similar to that described for related compounds (Scheme 5).[11,13,15]

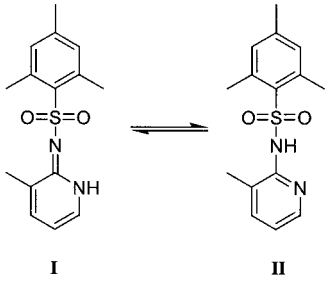

I **II**

Scheme 5

Structure of [Cu(Ts3mepy)$_2$H$_2$O]

This compound crystallizes in the monoclinic $P2_1/c$ space group, $Z = 4$. Its structure is shown in Figure 2 together with the atomic numbering scheme.

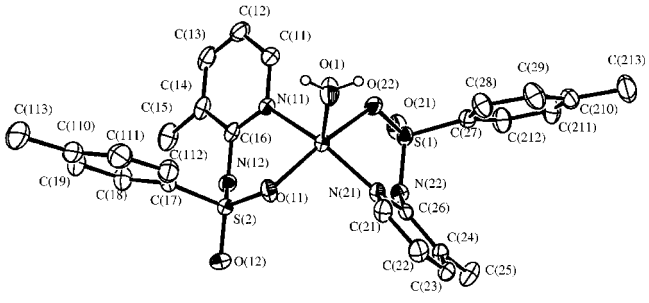

Figure 2. Molecular structure of [Cu(Ts3mepy)$_2$H$_2$O]

The crystal structure can be described as discrete molecules of [Cu(Ts3mepy)$_2$H$_2$O] associated by intermolecular interactions. The hydrogen atoms of the coordinated water molecule are involved in hydrogen bonds with the amide nitrogen atoms that are not coordinated to the metal in such a way that infinite chains are formed parallel to the *b* axis (Figure 3). Selected bond lengths and angles are given in Table 3 and Table 4.

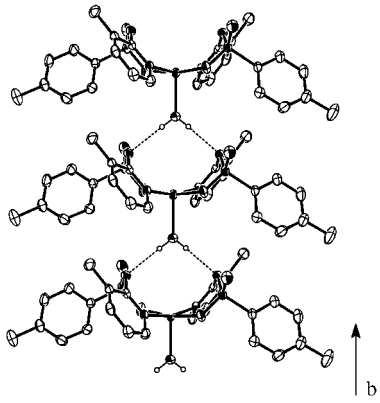

Figure 3. Supramolecular structure of [Cu(Ts3mepy)$_2$H$_2$O]

Table 3. Selected bond lengths [Å] and angles [°] for [Cu(Ts3mepy)$_2$(H$_2$O)]

Cu−N(21)	1.974(2)	Cu−N(11)	1.980(2)
Cu−O(11)	2.0018(18)	Cu−O(22)	2.0130(18)
Cu−O(1)	2.160(2)	S(1)−O(21)	1.428(2)
N(21)−Cu−N(11)	164.73(9)	N(21)−Cu−O(11)	88.69(8)
N(11)−Cu−O(11)	89.81(8)	N(21)−Cu−O(22)	88.86(8)
N(11)−Cu−O(22)	89.72(8)	O(11)−Cu−O(22)	168.98(8)
N(21)−Cu−O(1)	97.00(9)	N(11)−Cu−O(1)	98.27(10)
O(11)−Cu−O(1)	95.88(10)	O(22)−Cu−O(1)	95.08(10)

Table 4. Hydrogen bonds for [Cu(Ts3mepy)$_2$(H$_2$O)] (Å and °). (^{i}: symmetry transformations used to generate equivalent atoms: x, $y - 1$, z)

D−H···A	*d*(D−H)	*d*(H···A)	*d*(D···A)	∠(DHA)
O(1)−H(1)···N(12)^{i}	0.81(3)	2.11(3)	2.917(3)	175(3)
O(1)−H(2)···N(22)^{i}	0.85(3)	2.14(3)	2.984(3)	179(3)

The copper atom is coordinated by a molecule of water and two monoanionic (*N*,*O*)-bidentate ligands through the nitrogen of the pyridine ring and one oxygen atom of a sulfonic group. The sulfonamide nitrogen atoms are 3.039(2) and 3.093(2) Å, respectively, away from the copper atom, and so they are not bonded. Consequently, the coordination around the metal can be described as [CuN$_2$O$_3$]. This is quite surprising as sulfonyl oxygen atoms are not good donors, and copper(II) complexes containing ligands bonded through the sulfonamide oxygen donors are scarce.[18,19] The environment around the central atom is square pyramidal with a very small distortion towards a

 © 2004 Wiley-VCH Verlag GmbH & Co. KGaA, Weinheim

trigonal bipyramidal geometry ($\tau = 0.07$).[20] The apical position of the pyramid is occupied by the oxygen atom of the water molecule and the base consists of an (N_2O_2) arrangement in a *trans* disposition. This base is almost planar (*rms* = 0.0353). The copper atom is 0.2273(11) Å above the plane.

The Cu−N bond lengths are in the normal range found for $Cu-N_{py}$ bonds.[4,21] However, the Cu−O bonds [$Cu-O_{water}$ = 2.160(2); Cu−O(11) = 2.0018(18) and Cu−O(22) = 2.0130(18) Å] are unusually short for such O-donor atoms.[21,22] Firstly, the apical $Cu-O_{water}$ in pentacoordinate copper complexes are normally much longer than the Cu−O bonds in the basal plane.[23,24] In addition, the $Cu-O_{sulfonamide}$ bond is the shortest found so far in sulfonamide copper complexes.

Structures of the Complexes [Cu(Ts3mepy)$_2$bipy], [Cu(Ts3mepy)$_2$phen], [Cu(Ms3mepy)$_2$bipy] and [Cu(Ts3mepy)$_2$phen]

Complexes [Cu(Ts3mepy)$_2$bipy] and [Cu(Ts3mepy)$_2$phen] crystallize in the triclinic $P\bar{1}$ space group, $Z = 2$. Complexes [Cu(Ms3mepy)$_2$bipy] and [Cu(Ms3mepy)$_2$phen] crystallize in the monoclinic $P2_1/c$ space group, $Z = 4$. The compounds consist of discrete molecules without relevant intermolecular interactions.

The molecular structures are shown in Figures 4−7, together with the atomic numbering schemes. Selected bond lengths and angles are given in Table 5.

In all the compounds, one of the sulfonamide ligands behaves in a (*N*,*O*)-bidentate manner and the other one is *N*-monodentate. The coligand (2,2-bipyridine or 1,10 phenanthroline) acts as an (*N*,*N*′)-bidentate ligand. The different

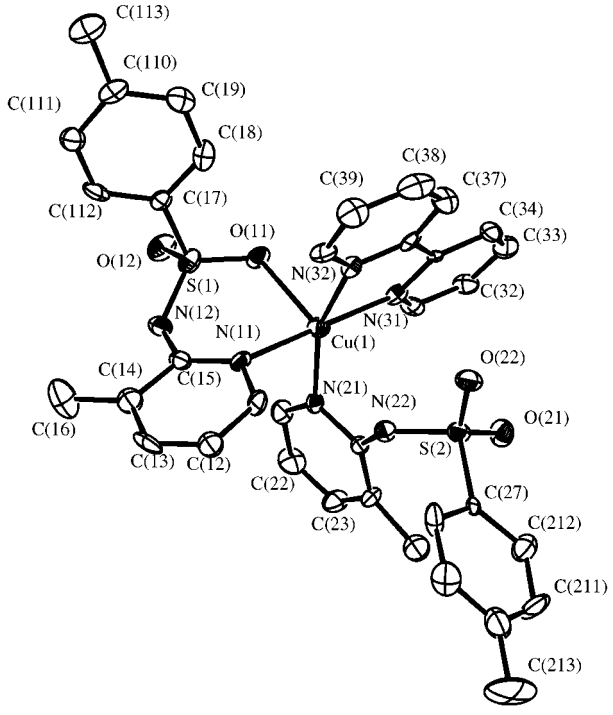

Figure 4. Molecular structure of [Cu(Ts3mepy)$_2$bipy]

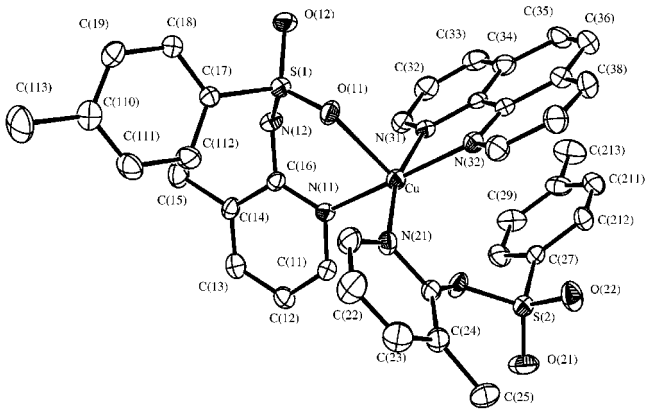

Figure 5. Molecular structure of [Cu(Ts3mepy)$_2$phen]

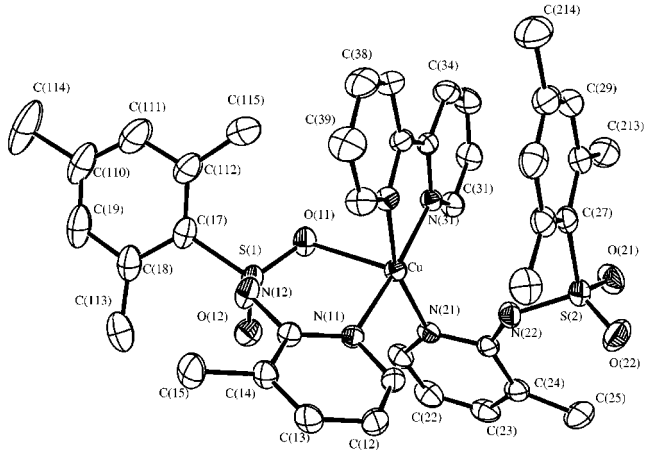

Figure 6. Molecular structure of [Cu(Ms3mepy)$_2$bipy]

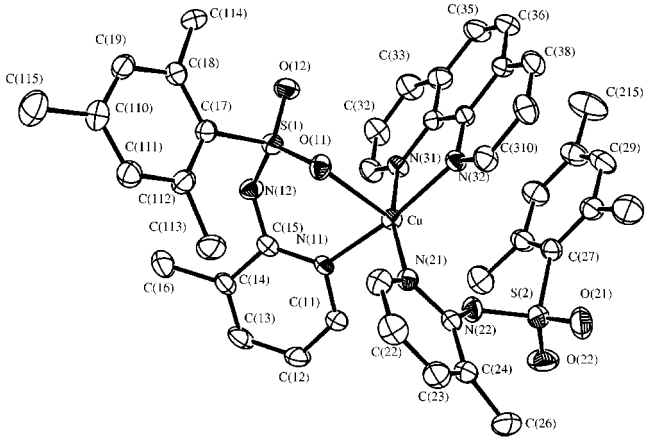

Figure 7. Molecular structure of [Cu(Ms3mepy)$_2$phen]

coordination behaviour of the two tosylamide ligands is the most significant feature of the structures.

The copper atom is in a pentacoordinate environment with four Cu−N bonds close to 2.0 Å, Cu−O bonds ranging from 2.209(6) to 2.291(2) Å and with another $Cu-N_{sulfonamide}$ interaction, not considered as a bond, ranging from 2.592(7) Å for [Cu(Ts3mepy)$_2$bipy] to 2.726(3) Å for [Cu(Ms3mepy)$_2$phen] (Table 5).

The coordination polyhedron is best described as square pyramidal with a distortion towards a trigonal bipyramidal

 © 2004 Wiley-VCH Verlag GmbH & Co. KGaA, Weinheim

Table 5. Selected bond lengths [Å] and angles [°] for the pentacoordinate compounds $[CuL_2L']$, L′ = bipy or phen

	[Cu(Ts3mepy)$_2$bipy]	[Cu(Ts3mepy)$_2$phen]	[Cu(Ms3mepy)$_2$bipy]	[Cu(Ms3mepy)$_2$phen]
Cu(1)−O(11)	2.209(6)	2.244(3)	2.2914(18)	2.263(2)
Cu(1)−N(11)	2.019(8)	2.004(4)	2.0259(19)	2.032(3)
Cu(1)−N(21)	2.020(7)	2.003(4)	1.984(2)	1.994(3)
Cu(1)−N(31)	1.999(8)	2.039(4)	2.0355(19)	2.018(3)
Cu(1)−N(32)	2.023(8)	2.029(4)	2.005(2)	2.039(3)
Cu(1)−N(22)	2.592(7)	2.665(4)	2.620(2)	2.726(3)
N(11)−Cu(1)−N(21)	89.9(3)	92.77(14)	93.61(8)	94.01(12)
N(11)−Cu(1)−N(32)	96.0(3)	175.90(17)	93.86(8)	172.36(13)
N(11)−Cu(1)−N(31)	175.8(3)	94.91(15)	173.69(9)	93.93(12)
N(11)−Cu(1)−O(11)	90.4(3)	87.64(14)	92.59(7)	86.77(10)
N(21)−Cu(1)−N(31)	92.4(3)	165.11(17)	92.63(8)	164.93(12)
N(21)−Cu(1)−N(32)	158.8(3)	90.98(16)	163.31(9)	92.38(12)
N(21)−Cu(1)−O(11)	103.7(3)	92.07(16)	104.56(8)	93.38(11)
N(31)−Cu(1)−O(11)	92.4(3)	100.97(14)	84.91(7)	99.84(10)
N(32)−Cu(1)−O(11)	96.6(3)	93.88(14)	89.98(8)	88.69(10)
N(31)−Cu(1)−N(32)	80.6(3)	81.07(17)	80.36(8)	80.79(12)

Table 6. Environment around the metal

[Cu(Ts3mepy)$_2$(H$_2$O)]	[Cu(Ts3mepy)$_2$bipy] [Cu(Ts3mepy)$_2$phen] [Cu(Ms3mepy)$_2$bipy] [Cu(Ms3mepy)$_2$phen]	[Cu(Ts6mepy)$_2$bipy] [Cu(Ts6mepy)$_2$phen] [Cu(Ms6mepy)$_2$bipy] [Cu(Ms6mepy)$_2$phen]
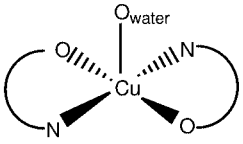	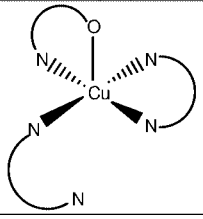	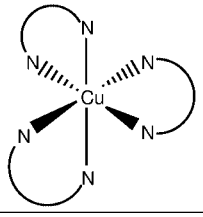

Table 7. Some short contacts between rings [Å] (stacking) for the pentacoordinate compounds $[CuL_2L']$, L′ = bipy or phen

[Cu(Ts3mepy)$_2$phen]		[Cu(Ms3mepy)$_2$phen]		[Cu(Ms3mepy)$_2$bipy]	
N(31)−C(28)	3.607(6)	N(31)−C(212)	3.585(6)	N(31)−C(37)	3.680(4)
C(29)−C(31)	3.652(7)	N(32)−C(27)	3.680(5)	N(32)−C(212)	3.446(4)
C(33)−C(210)	3.599(8)	C(2)−C(311)	3.651(4)	N(32)−C(27)	3.752(3)
C(34)−C(211)	3.477(8)	C(2)−C(312)	3.663(4)	C(210)−C(37)	3.386(4)
C(37)−C(212)	3.705(8)	C(28)−C(311)	3.679(6)	C(210)−C(38)	3.697(5)
C(34)−C(210)	3.508(8)	C(29)−C(37)	3.683(6)	C(211)−C(39)	3.681(5)
C(211)−C(312)	3.599(7)	C(210)−C(34)	3.729(7)	C(212)−C(310)	3.680(4)
C(212)−C(312)	3.600(7)	C(211)−C(312)	3.611(6)		
C(212)−C(311)	3.471(7)	C(212)−C(31)	3.968(7)		
C(35)−C(211)	3.555(8)				

between 12 and 28% (τ = 0.12−0.28, see Table 6).[20] The oxygen atom occupies the apical position of the pyramid and the four nitrogen atoms of the three ligands form the basal plane. The copper atoms lies 0.203(2), 0.122(2), 0.114(1), and 0.069(2) Å out of this basal plane, respectively.

The Cu−N bond lengths are as expected for such complexes and do not warrant further comment. However, the Cu−O bonds [2.209(6) to 2.291(2) Å], although slightly longer than in [Cu(Ts3mepy)$_2$H$_2$O], are shorter than the Cu−O(apical) distances normally found in copper(II) square-pyramid complexes.[18,23] This distance is remarkable since the sulfonamide groups are not good O-donors.

Complexes [Cu(Ts3mepy)$_2$bipy] and [Cu(Ts3mepy)$_2$phen] crystallize in the same space group, but their molecular arrangements are different due to a twist around the S(2)−N(22) bond (Figure 4 and Figure 5). Thus, in [Cu(Ts-3mepy)$_2$phen], the planes of the 1,10-phenanthroline and the benzene ring of the monoanionic monodentate sulfonamide ligand are almost parallel, with a dihedral angle of

 © 2004 Wiley-VCH Verlag GmbH & Co. KGaA, Weinheim

5.3(2)° and distances between rings of 3.471(7) Å. This disposition produces an intramolecular π,π-stacking interaction that stabilises the structure.[24] This interaction does not seem to be present at an intermolecular level. Some short distances between rings are indicated in Table 7.

Conversely, complexes [Cu(Ms3mepy)$_2$bipy] and [Cu(Ms3mepy)$_2$phen] crystallize in the same space group, $P2_1/c$, and a intramolecular π,π-stacking interaction is found in both cases; the dihedral angles between rings are 3.2(1) and 1.41(8)°, respectively. However, the complexes are not identical, showing differences related to the spatial position of the mesitylene group, which is directed towards the π,π-stacking axis, or is twisted outward (Figure 8). Other parameters are also indicated in Table 7.

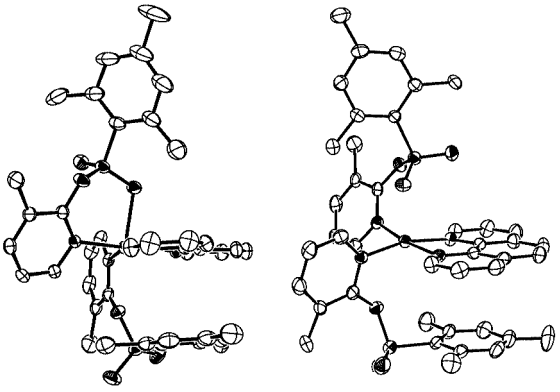

Figure 8. Spatial differences between [Cu(Ms3mepy)$_2$bipy] (left) and [Cu(Ms3mepy)$_2$phen] (right)

Structure of [Cu(Ms6mepy)$_2$phen]

This compound crystallizes in the triclinic $P\bar{1}$ space group with two chemically equivalent molecules in the asymmetric unit. Only one of the molecules is represented in Figure 9 (together with the atomic numbering pattern). Selected bond lengths and angles are given in Table 8.

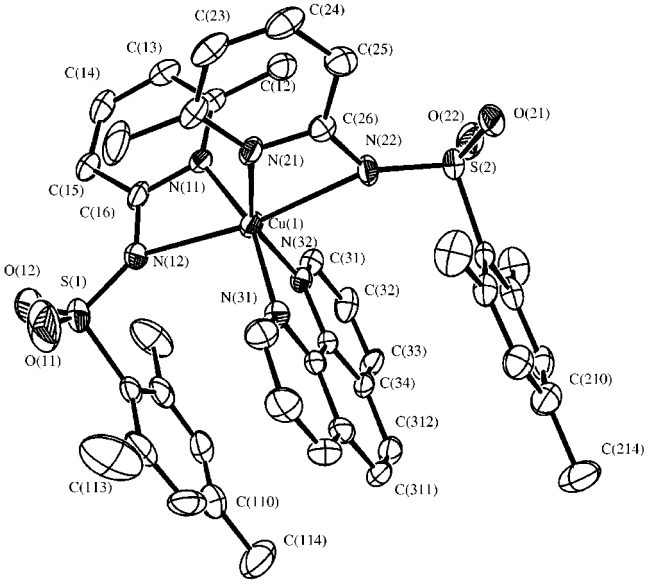

Figure 9. Molecular structure of [Cu(Ms6mepy)$_2$phen]

Table 8. Selected bond lengths [Å] and angles [°] for [Cu(Ms6mepy)$_2$phen]

Cu(1)−N(11)	1.985(6)	Cu(1)−N(31)	2.015(6)
Cu(1)−N(21)	2.023(6)	Cu(1)−N(32)	2.035(6)
Cu(1)−N(12)	2.357(6)	Cu(1)−N(22)	2.506(5)
Cu(2)−N(41)	1.983(6)	Cu(2)−N(51)	2.000(6)
Cu(2)−N(62)	2.001(6)	Cu(2)−N(61)	2.016(5)
Cu(2)−N(42)	2.413(6)	Cu(2)−N(52)	2.503(6)

N(11)−Cu(1)−N(31)	160.4(2)	N(11)−Cu(1)−N(21)	94.3(2)
N(31)−Cu(1)−N(21)	97.3(2)	N(11)−Cu(1)−N(32)	96.1(2)
N(31)−Cu(1)−N(32)	80.9(3)	N(21)−Cu(1)−N(32)	152.0(2)
N(11)−Cu(1)−N(12)	61.5(2)	N(31)−Cu(1)−N(12)	99.3(2)
N(21)−Cu(1)−N(12)	112.4(2)	N(32)−Cu(1)−N(12)	95.5(2)
N(11)−Cu(1)−N(22)	113.6(2)	N(31)−Cu(1)−N(22)	86.0(2)
N(21)−Cu(1)−N(22)	58.1(2)	N(32)−Cu(1)−N(22)	93.9(2)
N(12)−Cu(1)−N(22)	169.8(2)		
N(41)−Cu(2)−N(51)	93.1(2)	N(41)−Cu(2)−N(62)	158.9(3)
N(51)−Cu(2)−N(62)	97.6(2)	N(41)−Cu(2)−N(61)	95.6(2)
N(51)−Cu(2)−N(61)	156.5(3)	N(62)−Cu(2)−N(61)	81.7(2)
N(41)−Cu(2)−N(42)	60.0(2)	N(51)−Cu(2)−N(42)	115.1(3)
N(62)−Cu(2)−N(42)	99.0(2)	N(61)−Cu(2)−N(42)	88.1(2)
N(41)−Cu(2)−N(52)	115.4(2)	N(51)−Cu(2)−N(52)	58.3(3)
N(62)−Cu(2)−N(52)	85.6(2)	N(61)−Cu(2)−N(52)	98.3(2)
N(42)−Cu(2)−N(52)	172.7(2)		

The coordination behaviour of the anionic ligands in this complex is quite different from the other systems described here as the sulfonamide anionic ligands behave as (*N*,*N*)-bidentate ligands. A neutral 1,10-phenanthroline molecule acting as an (*N*,*N*)-donor completes the coordination sphere of the metal. Consequently, the coordination polyhedron around the copper(II) is best described as a highly distorted octahedron, CuN_6. There are several sources of distortion: Two Cu−N bond lengths are longer than the others, with a maximum of 2.506(5) Å. In addition, the anionic ligands form a four-membered chelate ring with angles of only 58.1(2) to 61.5(2)°. The theoretical equatorial plane is also highly distorted in that the dihedral angle between the planes formed by the central atom and the donors $N_{phen}-Cu-N_{phen}$ and $N_{py}-Cu-N_{py}$ is 32.66° [average values for the two molecules: 33.85(26) and 31.48(38)°].

Once again, significant intramolecular π,π stacking stabilisation is produced between the 1,10-phenanthroline unit and the benzene rings of the two sulfonamide ligands. This interaction does not seem to continue on an intermolecular level. The dihedral angles between the rings involved in this interaction are ∠6.2(4)° (average 3.6°). The centres of the three rings are ca. 3.704 and 3.651 Å apart. Some short distances between rings are indicated in Table 9.

Spectroscopic and Magnetic Studies

The IR spectra of the complexes do not show the band attributable to ν(N−H), which in the free ligand appears at 3248−3222 cm^{-1}. This change confirms that the hydrogen atom of the amide group is lost during electrolysis. The bands in the spectra of the ligands in the range 1594−1612 cm^{-1}, due to the ν(C=N) absorption, appear in similar po-

 © 2004 Wiley-VCH Verlag GmbH & Co. KGaA, Weinheim

Table 9. Selected short contacts between rings [Å] (stacking) for [Cu(Ms6mepy)$_2$phen]

N(31)−C(18)	3.775(10)	N(31)−C(17)	3.798(10)
N(31)−C(212)	3.895(9)	N(31)−C(27)	3.916(8)
N(32)−C(112)	3.623(9)	N(32)−C(17)	3.888(9)
C(18)−C(36)	3.655(10)	C(19)−C(37)	3.530(14)
C(111)−C(34)	3.521(11)	C(110)−C(312)	3.597(13)
C(112)−C(35)	3.634(10)	C(111)−C(35)	3.656(11)
C(28)−C(35)	3.667(10)	C(29)−C(312)	3.613(11)
C(211)−C(37)	3.692(11)	C(29)−C(311)	3.664(11)
N(62)−C(47)	3.706(9)	C(210)−C(311)	3.624(12)
C(48)−C(610)	3.625(10)	N(61)−C(512)	3.726(10)
C(49)−C(68)	3.559(13)	N(62)−C(48)	3.647(9)
C(410)−C(612)	3.688(14)	C(410)−C(67)	3.537(12)
C(412)−C(65)	3.630(10)	C(59)−C(612)	3.616(13)
C(511)−C(63)	3.616(13)	C(511)−C(64)	3.546(12)
C(510)−C(64)	3.548(11)	C(510)−C(611)	3.523(12)

sitions in the complexes except when the ligands Ts6mepy$^-$ and Ms6mepy$^-$ are present, in which case the bands are shifted to lower frequencies due to coordination through the sulfonamide nitrogen atom. The bands of the ligands at 1338−1369 cm^{-1}, attributable to ν_{as}(S =O), are also seen for the complexes with Ts3mepy$^-$ and Ms3mepy$^-$ but in these cases they are shifted to slightly lower frequencies due to the coordination.

In addition, the IR spectra of the mixed complexes show absorptions that are typical of coordinated 2,2′-bipyridine (764 and 736 cm^{-1}) and 1,10-phenanthroline (1520, 850, and 720 cm^{-1}).

The electronic reflectance spectrum of the pentacoordinate complex [Cu(Ts3mepy)$_2$H$_2$O] shows a very broad band, probably a multicomponent band, at 15800 with a shoulder at ca. 11800 cm^{-1}, a situation in accord with a pseudo-square planar pyramidal environment forming a [CuN$_2$O$_3$] chromophore.[25]

The electronic reflectance spectra of [Cu(Ts3mepy)$_2$phen], [Cu(Ts3mepy)$_2$bipy], [Cu(Ms3mepy)$_2$phen], and [Cu(Ms3mepy)$_2$bipy] show two broad bands in the range 16300−15900 cm^{-1} and 12300−10600 cm^{-1}. This is similar to the spectra of copper(II) complexes involving a [CuN$_4$O] chromophore.[26]

The electronic reflectance spectrum of [Cu(Ms6mepy)$_2$phen] shows two bands at 14430 and 10955 cm^{-1}, which are similar to those found for [Cu(Ms6mepy)$_2$bipy], [Cu(Ts6mepy)$_2$bipy], and [Cu(Ts6mepy)$_2$phen], suggesting an octahedral [CuN$_6$] chromophore for all these compounds.[27]

The magnetic moments at room temperature are close to 1.8 B.M. in all cases, as expected for d^9 systems.

The X-band spectra of polycrystalline samples of the complexes were recorded at room temperature. Table 10 show the EPR parameters of the ternary complexes obtained by simulation.[28] As an example, Figure 10 shows both the obtained and simulated EPR spectrum of [Cu(Ms6mepy)$_2$phen].

All the spectra are axial with similar EPR parameters so that it can be predicted due to the similarity of the sulfonamide ligands and the bipy and phen. Bertini[29] has suggested that $A_{\|}$ may be a measure of the coordination polyhedron around copper(II). Accordingly $A_{\|}$ from 120 to 150 G indicates a square-pyramidal geometry while values of 160−200 G correspond to a square planar or six-coordinate stereochemistry. The $A_{\|}$s of[Cu(Ts3mepy)$_2$(H$_2$O)], [Cu(Ts3mepy)$_2$bipy] and [Cu(Ms3mepy)$_2$bipy] suggest a square-pyramidal arrangement, in agreement with their crystal structures. The $A_{\|}$s of [Cu(Ms6mepy)$_2$phen] indicate a six-coordinate geometry, which agrees with the crystal structure. The complexes [Cu(Ts3mepy)$_2$phen] and [Cu(Ms3mepy)$_2$phen] are in the limit between the pentacoordinate and the six-coordinate environment; their crystal structures both show a distorted square-pyramidal geometry. From the $A_{\|}$s of [Cu(Ms6mepy)$_2$bipy] we propose a six-coordinate around copper(II). Similar conclusions were obtained from the spectroscopic data.

Table 10. EPR and RD parameters for the complexes (sh: shoulder)

Compound	$g_{\|}$	$g_{\perp}$	$A_{\|}$	$\tilde{\nu}$ [cm^{-1}]	
[Cu(Ts3mepy)$_2$(H$_2$O)]	2.25	2.11	140	15800	11820(sh)
[Cu(Ts3mepy)$_2$bipy]	2.26	2.06	150	15975	10640
[Cu(Ts3mepy)$_2$phen]	2.21	2.07	156	16315	12195
[Cu(Ms3mepy)$_2$bipy]	2.23	2.07	150	16130	11765
[Cu(Ms3mepy)$_2$phen]	2.26	2.07	155	16315	12300
[Cu(Ts6mepy)$_2$bipy]	2.26	2.08	−	13515	9320
[Cu(Ts6mepy)$_2$phen]	2.26	2.08	−	13280	10640
[Cu(Ms6mepy)$_2$bipy]	2.26	2.06	163	14165	11200
[Cu(Ms6mepy)$_2$phen]	2.26	2.08	166	14430	10955

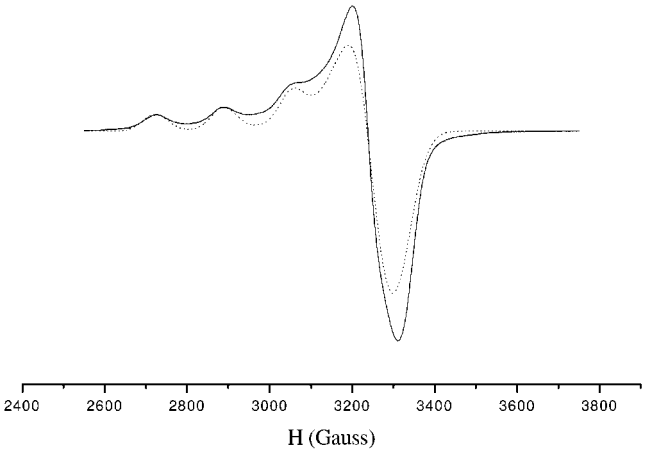

Figure 10. EPR Spectra in X-band of the complex [Cu(Ms6mepy)$_2$phen] (solid line) and its simulation (dotted line) as a powder at room temperature

Conclusion

The most important feature of these complexes is the coordinative behaviour of the anionic ligand and the presence or absence of π,π-stacking (Table 11).

The ligands behave in a (*N*,*O*) bidentate way with a substituent at position 3. However, for a substituent in position

 © 2004 Wiley-VCH Verlag GmbH & Co. KGaA, Weinheim

Table 11. Conclusions

Complex	Behaviour of the ligands L^1	L^2	Coligand	Environment around Cu atom	Geometry	π-π stacking
$[Cu(Ts3mepy)_2(H_2O)]$	bidentate-(N,O)	bidentate-(N,O)	monodentate-O	$[CuN_2O_3]$	Square pyramid ($\tau = 0.07$)	no
$[Cu(Ts3mepy)_2bipy]$	monodentate-N	bidentate-(N,O)	bidentate-(N,N)	$[CuN_4O]$	Square pyramid ($\tau = 0.28$)	no
$[Cu(Ts3mepy)_2phen]$	monodentate-N	bidentate-(N,O)	bidentate-(N,N)	$[CuN_4O]$	Square pyramid ($\tau = 0.18$)	yes
$[Cu(Ms3mepy)_2phen]$	monodentate-N	bidentate-(N,O)	bidentate-(N,N)	$[CuN_4O]$	Square pyramid ($\tau = 0.12$)	yes
$[Cu(Ms3mepy)_2bipy]$	monodentate-N	bidentate-(N,O)	bidentate-(N,N)	$[CuN_4O]$	Square pyramid ($\tau = 0.18$)	yes
$[Cu(Ts6mepy)_2bipy]$	bidentate-(N,N)	bidentate-(N,N)	bidentate-(N,N)	$[CuN_6]$	Octahedral	
$[Cu(Ts6mepy)_2phen]$	bidentate-(N,N)	bidentate-(N,N)	bidentate-(N,N)	$[CuN_6]$	Octahedral	
$[Cu(Ms6mepy)_2phen]$	bidentate-(N,N)	bidentate-(N,N)	bidentate-(N,N)	$[CuN_6]$	Octahedral	yes
$[Cu(Ms6mepy)_2bipy]$	bidentate-(N,N)	bidentate-(N,N)	bidentate-(N,N)	$[CuN_6]$	Octahedral	

6, they behave in a (*N*,*N*) bidentate way. Probably, the difference can be traced to a steric effect. A substituent in position 3 pushes the sulfonyl group towards the metal, and induces (*N*,*O*) bidentate behaviour.

In addition, when the coligand is 1,10-phenanthroline the third ring allows a π,π-stacking, either with the toluene ring or the mesytilene ring. When the coligand is 2,2′-bipyridine, π,π-stacking is only produced when the benzene ring is substituted by three methyl groups. This could be due to the electron-releasing effect of the three methyl groups in the ring, together with the increasing size of the group.

Experimental Section

Acetonitrile, dichloromethane, 2-amino-3-picoline, 2-amino-6-picoline, *p*-toluenesulfonyl chloride, 2-mesitylenesulfonyl chloride, 2,2′-bipyridine, 1,10-phenanthroline monohydrate, sodium carbonate, magnesium sulfate, and all other reagents were commercial products and were used as supplied. Copper (Aldrich) was used as 2 × 2 cm plates.

Preparation of the Ligands

Ligands were prepared by reaction of the corresponding amine and the sulfonyl chloride in a 1:1 ratio. Details are given for a representative example.

HMs3mepy: An aqueous solution of sodium carbonate (1.95 g, 18.4 mmol in 20 mL) was added dropwise to a solution of 2-amino-3-picoline (2.0 g, 18.4 mmol) and 2-mesitylenesulfonyl chloride (4.05 g, 18.4 mmol) dissolved in dichloromethane. The reaction mixture was then stirred overnight and water (100 mL) was added. The organic layer was then separated and dried over anhydrous magnesium sulfate. The solvent was evaporated and the crude product, an oil, was treated with ethanol. The resulting white solid was isolated by filtration and identified as HMs3mepy; yield 16.7%. $C_{15}H_{18}N_2O_2S$ (%): calcd. C 62.1, H 6.2, N 9.6, S 11.0; found C 61.3, H 6.0, N 9.3, S 11.2. ^{1}H NMR ($CDCl_3$, ppm): δ = 2.15 [s, 3 H, CH_3(py)]; 2.25 [s 3 H, CH_3(*p*-mesityl)]; 2.71 [s, 6 H, CH_3(*o*-mesityl)]; 6.47 (t, 1 H, py); 6.89 (s, 2 H, tolyl); 7.36 (d, 1 H, py); 7.42 (d, 1 H, py; 12.33 (b, 1 H, NH). IR (KBr, cm^{-1}): 3222 (m), 2940 (w), 1633 (w), 1595 (s), 1544 (s), 1375 (w), 1338 (s), 1259 (m), 1098 (s), 1047 (m), 780 (m), 676 (m). EI MS: *m*/*z* (%): 291 (100) [M^+]; 108 (10) [M^+ − {O_2S-mesityl}].

HMs6mepy: Yield 42.1%. $C_{15}H_{18}N_2O_2S$ (%): calcd. C 62.1, H 6.2, N 9.6, S 11.0; found C 61.3, H 6.4, N 9.5, S 10.9. ^{1}H NMR ($CDCl_3$, ppm): δ = 2.24 [s, 3 H, CH_3(*p*-mesityl)]; 2.37 [s, 3 H, CH_3(py)]; 2.69 [s, 6 H, CH_3(*o*-mesityl)]; 6.55 (d, 1 H, py); 6.74 (d, 1 H, py); 6.88 (s, 2 H, tolyl); 7.37 (t, 1 H, py); 9.40 (b, 1 H, NH). IR (KBr, cm^{-1}): 3236 (w), 2931 (w), 1617 (s), 1533 (m), 1457 (m), 1363 (vs), 1290 (m), 1136 (s), 1063 (w), 834 (m), 656 (m). EI MS: *m*/*z* (%): 291(4) [M^+]; 108 (13) [M^+ − {O_2S-mesityl}].

HTs3mepy: Yield 26.7%. $C_{13}H_{14}N_2O_2S$ (%): calcd. C 59.5, H 5.4, N 10.7, S 12.2; found C 58.7, H 5.7, N 10.2, S 11.8. ^{1}H NMR ($CDCl_3$, ppm): δ = 2.15 [s, 3 H, CH_3(py)]; 2.35 [s, 3 H, CH_3(tolyl)]; 6.50 (t, 2 H, tolyl); 7.21 (d, 1 H, py); 7.40 (d, 1 H, py); 7.49 (d, 1 H, py); 7.85 (d, 2 H, tolyl); 12.14 (b, 1 H, NH). IR (KBr, cm^{-1}): 3248 (m), 2920 (w), 1593 (s), 1543 (s), 1399 (m), 1371 (m), 1342 (s), 1255 (m), 1126 (s), 1080 (m), 963 (m), 767 (w), 683 (m), 570 (w). EI MS: *m*/*z* (%): 262 (8) [M^+]; 108 (20) [M^+ − {O_2S-tolyl}].

HTs6mepy: Yield 37.5%. $C_{13}H_{14}N_2O_2S$ (%): calcd. C 59.5, H 5.4, N 10.7, S 12.2; found C 58.8, H 5.6, N 10.6, S 12.3. ^{1}H NMR ($CDCl_3$, ppm): δ = 2.36 [s, 3 H, CH_3(tolyl)]; 2.41 [s, 3 H, CH_3(py)]; 6.60 (d, 1 H, py); 7.06 (d, 1 H, py); 7.22 (d, 2 H, tolyl); 7.46 (t, 1 H, py); 7.79 (d, 2 H, tolyl); 9.95 (b, 1 H, NH). IR (KBr, cm^{-1}): 3231 (w), 3052 (w), 2958 (w), 1613 (vs), 1534 (m), 1369 (s), 1252 (m), 1135 (s), 1089 (m), 855 (m), 787 (m), 661 (m), 572 (m). EI MS: *m*/*z* (%): 262 (6) [M^+]; 108 (3) [M^+ − {O_2S-tolyl}].

Preparation of Complexes. General Procedure: The complexes were obtained by an electrochemical procedure.[30] The cell consisted of a tall-form beaker (100 mL) fitted with a rubber bung through which the electrochemical leads entered. An acetonitrile solution of either the ligand or the ligand/coligand (1,10-phenanthroline·monohydrate or 2,2′-bipyridine) mixture containing tetraethylammonium perchlorate (ca. 20 mg) as electrolyte was electrolysed using a platinum wire as the cathode and a copper plate as the sacrificial anode. Direct current was supplied by a purpose-built d.c. power supply. The applied voltages (5−15 V) allowed sufficient current flow for smooth dissolution of the copper metal. The current was maintained at 10 mA for one hour. In all cases, hydrogen was evolved at the cathode. These cells can be summarised as $Cu_{(+)}/CH_3CN + HL + L'/Pt_{(-)}$ where L′ is 2,2′-bipyridine or 1,10-phenanthroline.

After one hour of electrolysis, the resultant clear green solutions were filtered to remove any particles of metal and then left to concentrate. This procedure afforded crystalline products in good yield. The solids were then washed with acetonitrile and diethyl ether and dried at room temperature.

[Cu(Ts3mepy)$_2$H$_2$O]: Electrochemical oxidation of a copper anode in a solution of the ligand *N*-(3-methyl-2-pyridyl)-*p*-toluenesulfonamide, (0.19 g, 0.75 mmol) in acetonitrile (50 cm^3), at 12 V and

 © 2004 Wiley-VCH Verlag GmbH & Co. KGaA, Weinheim

10 mA for 1 h, dissolved copper (25 mg), E_f = 1.05 mol·F^{-1}. $C_{26}H_{28}CuN_4O_5S_2$ (%): calcd. C 51.7, N 9.3, H 4.7, S 10.6; found C 51.2, N 9.4, H 4.5, S 10.3. IR (KBr, cm^{-1}): 3444 (m), 2922 (w), 1593 (s), 1419 (s), 1336 (w), 1265 (m), 1133 (s), 1090 (m), 853 (w), 814 (w), 665 (m), 587 (m), 546 (m).

[Cu(Ts3mepy)$_2$bipy]: Electrolysis of a solution of the ligand (0.19 g, 0.75 mmol) and 2,2′-bipyridine (0.58 g, 0.37 mmol) in acetonitrile, (50 cm^3) at 10 V and 10 mA for 1 h dissolved copper (26 mg) from the anode, E_f = 1.10 mol·F^{-1}. $C_{36}H_{34}CuN_4O_4S_2$ (%): calcd. C 58.3, N 11.3, H 4.6, S 8.6; found C 57.8, N 11.3, H 4.8, S 8.4. IR (KBr, cm^{-1}): 3441 (m), 2922 (w), 1606 (m), 1445 (w), 1416 (s); 1327 (m), 1247 (m), 1128 (m), 1085 (m), 772 (m), 737 (w), 659 (m), 587 (m), 550 (m).

[Cu(Ts3mepy)$_2$phen]: A solution of the ligand (0.19 g, 0.75 mmol) and 1,10−phenanthroline (0.07 g, 0.37 mmol) in acetonitrile (50 cm^3) was electrolyzed at 8 V and 10 mA for 1 hour; copper metal (22 mg) was dissolved from the anode, E_f = 0.93 mol·F^{-1}. $C_{38}H_{34}CuN_4O_4S_2$ (%): calcd. C 59.4, N 10.9, H 4.7, S 8.3; found C 59.5, N 11.1, H 4.7, S 8.3. IR (KBr, cm^{-1}): 34445 (m), 2918 (w), 1592 (m), 1414 (s), 1326 (m), 1243 (m), 1126 (m), 1096 (m), 988 (m), 848 (w), 720 (w), 588 (m), 545 (m).

[Cu(Ms3mepy)$_2$bipy]: A solution of the ligand *N*-(3-methyl-2-pyridyl)mesitylenesulfonamide (0.22 g, 0.75 mmol) and 2,2′-bipyridine (0.58 g, 0.37 mmol) in acetonitrile (50 cm^3) was electrolyzed at 14 V and 10 mA for 1 hour; copper (27 mg) was dissolved from the anode, E_f = 1.13 mol·F^{-1}. $C_{40}H_{42}CuN_4O_4S_2$ (%): calcd. C 60.1, N 10.5, H 5.3, S 8.0; found C, 59.5, N 10.2, H 5.3, S 8.1. IR (KBr, cm^{-1}): 3443 (m), 2931 (w), 1605 (m), 1416 (s), 1327 (m), 1228 (m), 1117 (s), 1057 (w), 770 (m), 728 (w), 687 (m), 593 (w), 521 (w).

[Cu(Ms3mepy)$_2$phen]: Electrochemical oxidation of a copper anode in a solution of the ligand (0.22 g, 0.75 mmol) and 1,10-phenanthroline (0.07 g, 0.37 mmol) in acetonitrile (50 cm^3), at 14 V and 10 mA for 1 h dissolved copper (22 mg), E_f = 0.93 mol·F^{-1}. $C_{42}H_{42}CuN_4O_4S_2$ (%): calcd. C 61.1, N 10.2, H 5.1, S 7.8; found C 61.1, N 10.4, H 5.2, S 7.6. IR (KBr, cm^{-1}): 3425 (m), 2930 (w), 1594 (m), 1512 (m), 1416 (s), 1319 (m), 1121 (s), 845 (m), 724 (m), 683 (w), 593 (w), 532 (w).

[Cu(Ts6mepy)$_2$bipy]: A similar experiment to those described above (10 V, 10 mA, 1 h) with *N*-(6-methyl-2-pyridyl)-*p*-toluenesulfonamide (0.19 g, 0.75 mmol) and 2,2′-bipyridine (0.58 g, 0.37 mmol) in acetonitrile (50 cm^3) led to the dissolution of 25 mg of metal, E_f = 1.05 mol·F^{-1}. $C_{36}H_{34}CuN_4O_4S_2$ (%): calcd. C 58.3, N 11.3, H 4.6, S 8.6; found C 57.9, N 11.6, H 4.4, S 8.5. IR (KBr, cm^{-1}): 3445 (m), 2922 (w), 1596 (m), 1457 (s), 1339 (s), 1135 (s), 1097 (m), 855 (m), 769 (w), 731 (w), 660 (w), 577 (w), 550 (w).

[Cu(Ts6mepy)$_2$phen]: A similar experiment to those described above (12 V, 10 mA, 1 h) with HTs6mepy (0.19 g, 0.75 mmol) and 1,10-phenanthroline (0.07 g, 0.37 mmol) in acetonitrile (50 cm^3) led to the dissolution of metal (22 mg), E_f = 0.93 mol·F^{-1}. $C_{38}H_{34}CuN_4O_4S_2$ (%): calcd. C 59.4, N 10.9, H 4.7, S 8.3; found C 58.8, N 11.4, H 4.5, S 7.9. IR (KBr, cm^{-1}): 3441 (m), 2924 (w), 1596 (m), 1518 (w), 1457 (m), 1339 (m), 1266 (m), 1134 (m), 1096 (m), 852 (w), 723 (w), 665 (m), 578 (m), 551 (w).

[Cu(Ms6mepy)$_2$bipy]: In similar fashion to above (12 V, 10 mA, 1 h), *N*-(6-methyl-2-pyridyl)-2-mesitylenesulfonamide (0.22 g, 0.75 mmol) and 2,2′-bipyridine (0.58 g, 0.37 mmol) in acetonitrile (50 cm^3) led to the dissolution of 28 mg of metal, E_f = 1.18 mol·F^{-1}. $C_{40}H_{42}CuN_4O_4S_2$ (%): calcd. C 60.1, N 10.5, H 5.3, S

Table 12. Summary of crystal data and structure refinement

Identification code:	HMs3mepy	[Cu(Ts3mepy)$_2$H$_2$O]	[Cu(Ts3mepy)$_2$bipy].	[Cu(Ts3mepy)$_2$phen]
Empirical formula	$C_{30}H_{36}N_4O_4S_2$	$C_{26}H_{28}N_4O_5S_2Cu$	$C_{36}H_{34}N_6O_4S_2Cu$	$C_{38}H_{34}N_6O_4S_2Cu$
Molecular mass	580.75	604.18	742.35	766.37
Temperature	293(2) K	293(2) K	293(2) K	293(2) K
Wavelength	0.71073 Å	0.71073 Å	0.71073 Å	0.71073 Å
Crystal system, space group	Monoclinic, *C*2/*c*	monoclinic, $P2_1/c$	triclinic, $P\bar{1}$	triclinic, $P\bar{1}$
Unit cell dimensions	*a* = 15.069(2) Å *b* = 8.0862(11) Å *c* = 24.651(3) Å α = 90° β = 102.765(3)° γ = 90°.	*a* = 16.6262(15) Å *b* = 6.0343(5) Å *c* = 27.530(3) Å α = 90° β = 103.112(2)° γ = 90°	*a* = 17.346(3) Å *b* = 9.2519(14) Å *c* = 24.083(3) Å α = 90° β = 114.640(8)° γ = 90°	*a* = 10.7185(12) Å *b* = 10.9915(13) Å *c* = 17.6002(19) Å α = 106.300(2)° β = 102.900(3)° γ = 97.734(2)°
Volume	2929.5(7) Å^3	2690.0(4) Å^3	3513.0(9) Å^3	1896.3(4) Å^3
Z, calculated density	4, 1.317 Mg/m^3	4, 1.492 Mg/m^3	2, 1.404 Mg/m^3	2, 1.342 Mg/m^3
Absorption coefficient	0.224 mm^{-1}	1.011 mm^{-1}	0.789 mm^{-1}	0.733 mm^{-1}
F(000)	1232	1252	1540	794
Crystal size	0.41 × 0.47 × 0.50 mm	0.8 × 0.46 × 0.62 mm	0.03 × 0.10 × 0.14 mm	0.9 × 0.1 × 0.16 mm
Theta range for data collection	2.77 to 28.05°.	1.52 to 28.01°	1.29 to 28.09°.	1.97 to 28.05°
Index ranges	−19 ≤ *h* ≤ 18, −9 ≤ *k* ≤ 10, −32 ≤ *l* ≤ 28	−21 ≤ *h* ≤ 21, −7 ≤ *k* ≤ 6, −29 ≤ *l* ≤ 36	−22 ≤ *h* ≤ 22, −12 ≤ *k* ≤ 12, −31 ≤ *l* ≤ 18	−13 ≤ *h* ≤ 14, −13 ≤ *k* ≤ 14, −23 ≤ *l* ≤ 17
Reflections collected/unique	8866/ 3441 [*R*(int) = 0.0279]	14844/6056 [*R*(int) = 0.0364]	17080/7613 [*R*(int) = 0.1615]	11011/7676 [*R*(int) = 0.0600]
Completeness to 2θ	96.5%	93.3%	83.9%	83.4%
Data/restraints/parameters	3441/0/209	6056/0/355	7613/0/426	7676/0/464
Goodness-of-fit on F^2	1.043	0.923	0.697	0.740
Final *R* indices [$I > 2\sigma(I)$]	R_1 = 0.0446, wR_2 = 0.1174	R_1 = 0.0404, wR_2 = 0.0911	R_1 = 0.0570, wR_2 = 0.1005	R_1 = 0.0572, wR_2 = 0.0900
R indices (all data)	R_1 = 0.0590, wR_2 = 0.1240	R_1 = 0.0797, wR_2 = 0.1017	R_1 = 0.3440, wR_2 = 0.1974	R_1 = 0.1689, wR_2 = 0.1089
Largest diff. peak and hole	0.256 and −0.422 e·Å^{-3}	0.397 and −0.312 e·Å^{-3}	0.426 and −0.343 e·Å^{-3}	0.266 and −0.269 e·Å^{-3}

 © 2004 Wiley-VCH Verlag GmbH & Co. KGaA, Weinheim

Table 13. Summary of crystal data and structure refinement

Identification code:	[Cu(Ms3mepy)$_2$bipy]	[Cu(Ms3mepy)$_2$phen]	[Cu(Ms6mepy)phen]$_2$
Empirical formula	$C_{40}H_{42}N_6O_4S_2Cu$	$C_{42}H_{42}N_6O_4S_2Cu$	$C_{42}H_{42}N_6O_4S_2Cu$
Molecular mass	798.46	822.48	822.48
Temperature	293(2) K	293(2) K	293(2) K
Wavelength	0.71073 Å	0.71073 Å	0.71073 Å
Crystal system, space group	monoclinic, $P2_1/c$	monoclinic, $P2_1/c$	triclinic, $P\bar{1}$
Unit cell dimensions	a = 17.1798(11) Å	a = 16.2855(12) Å	a = 15.370(5) Å
	b = 15.6081(10) Å	b = 15.8753(11) Å	b = 16.143(5) Å
	c = 15.5389(9) Å	c = 15.0249(11) Å	c = 17.532(5) Å
	α = 90°	α = 90°.	α = 109.564(5)°.
	β = 105.6420(10)°	β = 96.897(2) deg.	β = 92.724(5)°
	γ = 90°	γ = 90°.	γ = 98.831(5)°.
Volume	4012.4(4) Å^3	3856.4(5) Å^3	4027(2) Å^3
Z, calculated density	4, 1.322 Mg/m^3	4, 1.417 Mg/m^3	2, 1.357 Mg/m^3
Absorption coefficient	0.696 mm^{-1}	0.726 mm^{-1}	0.695 mm^{-1}
F(000)	1668	1716	1716
Crystal size	0.15 × 0.23 × 0.54 mm	0.44 × 0.12 × 0.12 mm	0.31 × 0.25 × 0.22 mm
Theta range for data collection	1.79 to 28.02°	1.80 to 28.02°	1.24 to 26.48°
Index ranges	$-22 \le h \le 22$,	$-20 \le h \le 21$,	$-17 \le h \le 19$,
	$-20 \le k \le 20$,	$-20 \le k \le 19$,	$-20 \le k \le 17$,
	$-14 \le l \le 20$	$-19 \le l \le 15$	$-21 \le l \le 21$
Reflections collected/unique	23177/9157 [R(int) = 0.0578]	22031/8786 [R(int) = 0.0599]	33835/16311 [R(int) = 0.0788]
Completeness to 2θ	94.3%	94.3%	97.9%
Data/restraints/parameters	9157/0/486	8786/0/496	16311/5/1007
Goodness-of-fit on F^2	0.862	0.871	0.934
Final R indices [$I > 2\sigma(I)$]	R_1 = 0.0443, wR_2 = 0.0893	R_1 = 0.0528, wR_2 = 0.1023	R_1 = 0.0703, wR_2 = 0.1779
R indices (all data)	R_1 = 0.0991, wR_2 = 0.1009	R_1 = 0.1505, wR_2 = 0.1222	R_1 = 0.2359, wR_2 = 0.2432
Largest diff. peak and hole	0.392 and −0.264 e·Å^{-3}	0.448 and −0.291 e·A^{-3}	0.891 and −0.628 e·A^{-3}

8.0; found C 59.7, N 10.4, H 5.2, S 7.8. IR (KBr, cm^{-1}): 3443 (m), 2931 (w), 1598 (s), 1457 (s), 1343 (s), 1251 (m), 1125 (s), 1083 (m), 843 (m), 768 (w), 732 (w), 671 (w), 587 (w), 535 (w).

[Cu(Ms6mepy)$_2$phen]: By a similar procedure (15 V, 10 mA, 1 h), HMs6mepy, (0.22 g, 0.75 mmol) and 1,10-phenanthroline (0.07 g, 0.37 mmol) in acetonitrile (50 cm^3) led to the dissolution of metal (25 mg), E_f = 1.05 mol·F^{-1}. $C_{42}H_{42}CuN_4O_4S_2$ (%): calcd. C 61.1, N 10.2, H 5.2, S 7.8; found C 60.8, N 10.1, H 5.2, S 7.6. IR (KBr, cm^{-1}): 3445 (m), 2931 (w), 1594 (m), 1519 (w), 1457 (m), 1344 (m), 1250 (w), 1124 (s), 1082 (m), 845 (m), 722 (w), 689 (w), 588 (w), 533 (w).

Physical Measurements: The C, N, H, and S contents of the compounds were determined on a Carlo−Erba EA 1108 microanalyser. IR spectra in the solid state were recorded as KBr mulls on a Bruker Vector-22 spectrophotometer. The ^{1}H NMR spectra of the ligands were recorded on a Bruker ARX-400 MHz spectrometer using $CDCl_3$ as solvent. Solid-state electronic spectra were recorded on a Shimadzu UV 3101 PC. Magnetic measurements were made using a DMS VSM 1160. EI (70 eV, 250 °C), and LSI mass spectra were recorded on a VG Autospec-M Micromass, using 2-nitrobenzyl alcohol (2-NBA) as matrix material. EPR measurements on solid samples were recorded on a Bruker EMX spectrometer, using frequencies between 9400 and 9800 MHz (X-band).

X-ray Crystallographic Study: Data collections were taken on a SIEMENS Smart CCD area-detector diffractometer with graphite-monochromated Mo-K_α radiation. Absorption corrections were carried out using SADABS.[31]

All the structures were solved by direct methods and refined by full-matrix least-squares based on F^2.[32] All non-hydrogen atoms were refined with anisotropic displacement parameters. For HMs3mepy the hydrogen atoms (except those of the methyl groups) were located on a difference electron density map and refined with isotropic displacement parameters. For the complexes, hydrogen atoms were included in idealised positions and refined with isotropic displacement parameters, except for those of the water molecule of [Cu(Ts3mepy)$_2$H$_2$O], which were located and refined with isotropic displacement parameters. Atomic scattering factors and anomalous dispersion corrections for all atoms were taken from International Tables for X-ray Crystallography.[33] Details of crystal data and structural refinements are given in Tables 12 and 13.

CCDC 187516 and 209128−209133 contain the supplementary crystallographic data for this paper. These data can be obtained free of charge at www.ccdc.cam.ac.uk/conts/retrieving.html [or from the Cambridge Crystallographic Data Centre, 12 Union Road, Cambridge CB2 1EZ, UK; Fax: (internat.) + 44-1223-336-033; E-mail: deposit@ccdc.cam.ac.uk].

Acknowledgments

This work was supported by the FLUNTA DE ALICIA, under the grant PGIDT00PXI20305PR, the Ministerio de Ciencia y Tecnología (Spain), under grant BQU2002−01819, and the Universidade de Vigo, under grant C221 122F 64102.

[1] [1a] G. Wilkinson, R. D. Gillard, J. A. McCleverty; *Comprehensive Coordination Chemistry*, Ed. Pergamon Press, Oxford, **1987**. [1b] H. E. Bryndza, W. Tam, *Chem. Rev.* **1988**, *88*, 1163−1188. [1c] M. D. Fryzuk, C. D. Montgomery, *Coord. Chem. Rev.* **1989**, *95*, 1−40.

[2] [2a] J. Casanova, G. Alzuet, J. Borrás, O. Carugo, *J. Chem. Soc., Dalton Trans.* **1996**, 2239−2244. [2b] L. Gutiérrez, G. Alzuet, J. A. Real, J. Cano, J. Borrás, A. Castiñeiras, *Inorg. Chem.* **2000**, *39*, 3608−3614. [2c] L. Gutiérrez, G. Alzuet, J. Borrás, A. Casti-

 © 2004 Wiley-VCH Verlag GmbH & Co. KGaA, Weinheim

ñeiras, A. Rodríguez-Fortea, E. Ruiz, *Inorg. Chem.* **2001**, *40*, 3089−3096. [2d] L. Gutiérrez, G. Alzuet, J. A. Real, J. Cano, J. Borrás, A. Castiñeiras, *Eur. J. Inorg. Chem.* **2002**, 2094−2102.
[3] D. Iacopino, L. Menabue, M. Saladini, *Aust J. Chem.* **1999**, *52*, 741−748 and references cited therein.
[4] C. A. Otter, S. M. Couchman, J. C. Jeffery, K. L. V. Mann, E. Psillakis, M. D. Ward, *Inorg. Chim. Acta* **1998**, *278*, 178−184, and references cited therein.
[5] R. Kempe, *Eur. J. Inorg. Chem.* **2003**, 791−803, and references cited therein.
[6] R. Clerac, F. A. Cotton, K. R. Dunbar, C. A. Murillo, I. Pascual, X. Wang, *Inorg. Chem.* **1999**, *38*, 2655−2657.
[7] L. M. Engelhardt, M. G. Gardiner, C. Jones, P. C. Junk, C. L. Raston, A. H. White, *J. Chem. Soc., Dalton Trans.* **1996**, 3053−3057.
[8] C. L. Raston, B. W. Skelton, V. A. Tolhurst, A. H. White, *Polyhedron* **1998**, *17*, 935−942.
[9] [9a] C.-F. Lee, S.-M. Peng, *J. Chin. Chem. Soc., (Taipei)* **1991**, *38*, 559−564. [9b] H.-Y. Cheng, P.-H. Cheng, C.-F. Lee, S.-M. Peng, *Inorg. Chim. Acta* **1991**, *181*, 145−147.
[10] S. Cabaleiro, J. Castro, E. Vázquez-López, J. A. García-Vázquez, J. Romero, A. Sousa, *Acta Cristallogr.* **1999**, *C56*, 293−295.
[11] I. Beloso, J. Castro, J. A. García-Vázquez, P. Pérez-Lourido, J. Romero, A. Sousa, *Polyhedron* **2003**, *22*, 1099−1111.
[12] S. Cabaleiro, J. Castro, J. A. García-Vázquez, J. Romero, A. Sousa, *Polyhedron* **2000**, *19*, 1607−1614.
[13] S. Cabaleiro, J. Castro, E. Vázquez-López, J. A. García-Vázquez, J. Romero, A. Sousa, *Polyhedron* **1999**, *18*, 1669−1674.
[14] S. Cabaleiro, J. Castro, E. Vázquez-López, J. A. García-Vázquez, J. Romero, A. Sousa, *Inorg. Chim. Acta* **1999**, *294*, 87−94, and references cited therein.
[15] I. Beloso, J. Castro, J. A. García-Vázquez, P. Pérez-Lourido, J. Romero, A. Sousa, *Z. Anorg. Allg. Chem.* **2003**, *629*, 275−284.
[16] I. Beloso, J. Castro, J. A. García-Vázquez, P. Pérez-Lourido, J. Romero, A. Sousa, unpublished results.
[17] J. Castro, J. Romero, J. A. García-Vázquez, A. Castiñeiras, M. L. Durán, A. Sousa, *Z. Anorg. Allg. Chem.* **1992**, *615*, 155−160.
[18] A. Nanthakumar, J. Miura, S. Diltz, C.-K. Lee, G. Aguirre, F. Ortega, J. W. Ziller, P. J. Walsh, *Inorg. Chem.* **1999**, *38*, 3010−3013.
[19] L. P. Battaglia, A. B. Corradi, L. Menabue, M. Saladini, M. Sola, *J. Chem. Soc., Dalton Trans.* **1987**, 1333−1339.
[20] A. W. Addison, T. N. Rao, J. van Reedijk, J. Van Rijn, G. C. Verschoor, *J. Chem. Soc., Dalton Trans.* **1984**, 1349−1356.
[21] G. B. Gavioli, M. Borsari, L. Menabue, M. Saladini, *J. Chem. Soc., Dalton Trans.* **1991**, 2961−2965.
[22] P. Comba, P. Jurisic, Y. D. Lampeka, A. Peters, A. I. Prikhod'ko, H. Pritzkow, *Inorg. Chim. Acta* **2001**, *324*, 99−107.
[23] [23a] R. L. Chapman, F. S. Stephens, R. S. Vagg, *Inorg. Chim. Acta* **1980**, *43*, 29−33. [23b] M. Mulqi, F. S. Stephens, R. S. Vagg, *Inorg. Chim. Acta* **1981**, *51*, 9−14. [23c] M. Mulqi, F. S. Stephens, R. S. Vagg, *Inorg. Chim. Acta* **1981**, *52*, 177−182. [23d] F. S. Stephens, R. S. Vagg, *Inorg. Chim. Acta* **1982**, *57*, 43−49.
[24] C. Janiak, *J. Chem. Soc., Dalton Trans.* **2001**, 3885−3896.
[25] [25a] S. Ferrer, J. G. Haasnoot, J. Reedijk, E. Müller, M. B. Cingi, M. Lanfranchi, A. M. M. Lanfredi, J. Ribas, *Inorg. Chem.* **2000**, *39*, 1859−1867. [25b] P. Gómez-Sainz, J. García-Tojal, M. A. Maestro, J. Mahía, F. J. Arnáiz, T. Rojo, *Polyhedron* **2002**, *21*, 2257−2263.
[26] [26a] Z. He, P. J. Chaimungkalanont, D. C. Craig, B. Colbran, *J. Chem. Soc., Dalton Trans.* **2000**, 1419−1429. [26b] G. Murphy, C. Murphy, B. Murphy, B. Hathaway, *J. Chem. Soc., Dalton Trans.* **1997**, 2653−2660.
[27] [27a] J. R. Hartman, R. W. Vachet, W. Pearson, R. J. Wheat, J. H. Callahan, *Inorg. Chim. Acta* **2003**, *343*, 119−132. [27b] I. Riggio, G. A. van Albada, D. D. Ellis, A. L. Spek, J. Reedijk, *Inorg. Chim. Acta* **2001**, *313*, 120−124.
[28] *WINEPR-Simfonia 1.25.* Bruker Analytik GmbH, Kalrsruhe, FRG, **1994−1996**.
[29] I. Bertini, in: *ESR and NMR of Paramagnetic Species in Biological and related Systems* (Eds.: I. Bertini, R. S. Drago), D. Reidel Publishing Co. Dordrecht (Holland), **1980**, chapter 11.
[30] [30a] M. C. Chakravorti, G. V. B. Subrahmanyam, *Coord. Chem. Rev.* **1994**, *135/136*, 65−92. [30b] A. M. Vecchio-Sadus, *J. Appl. Electrochem.* **1993**, *23*, 401−416. [30c] D. G. Tuck, *Pure Appl. Chem.* **1979**, *51*, 2005−2018. [30d] J. A. Davies, C. M. Hokensmith, V. Yu Kukushkin, Yu N. Kukushkin, in: *Synthetic Coordination Chemistry. Principles and Practice.* Word Scientific Publishing Co. Pte. Ltd., **1996**, chapter 7.
[31] G. M. Sheldrick, *SADABS*, An empirical absorption correction program for area detector data, University of Göttingen, Germany, **1996**.
[32] G. M. Sheldrick, *SHELX-97*, Program for the solution and refinement of crystal structures. University of Göttingen, Germany, **1997**.
[33] *International Tables for X-ray Crystallography, Vol C*, Ed. Kluwer, Dordrecht, **1992**.

Received June 4, 2003
Early View Article
Published Online December 19, 2003

 © 2004 Wiley-VCH Verlag GmbH & Co. KGaA, Weinheim

Glycosyl-Curcuminoids as Potential New Chelating Agents in Iron Overload Chelation Therapy

Beatrice Arezzini,[a] Marco Ferrali,[a] Erika Ferrari,[b] Romano Grandi,[b] Stefano Monti,[b] and Monica Saladini*[b]

Keywords: Chelates / Iron / Gallium / Redox chemistry / Bioinorganic chemistry

The iron(III) chelating ability of some glycosyl derivatives of curcuminoids is tested by means of UV, potentiometric and NMR studies. The pK_a of the ligands and the stability constants of their Fe^{3+} and Ga^{3+} complexes are evaluated by UV spectroscopy. The only metal binding site of the ligand is the β-dioxo moiety; the glycosyl moiety does not interact with the metal ion at acidic pH values but it helps to stabilise metal/ligand (1:2) complexes by means of hydrophilic interactions. By comparing the pFe^{3+} of our ligands with those reported for other chelating agents we suggest using these molecules as pro-drugs in iron overload treatment. Some of the more water-soluble derivatives are also tested for their antioxidant properties "in vitro" in biological systems and proved to act as free-radical scavengers inhibiting the iron redox cycle.

(© Wiley-VCH Verlag GmbH & Co. KGaA, 69451 Weinheim, Germany, 2004)

Introduction

Iron regulation in the human body follows complex mechanisms that tend to limit external exchange and make the re-utilisation from internal sources more efficient. However, although essential for the proper functioning of living cells, iron is toxic when present in excess. In the presence of oxygen, "loosely bound iron" is able to switch between its two more stable oxidation states (Fe^{3+}/Fe^{2+}), thereby generating hydroxyl radicals and favouring the so-called "Fenton Chemistry".[1,2] In healthy individuals, iron levels are under tight control and there is little or no opportunity for iron-catalysed free radical generating reactions. However, there are situations where the iron status can change, either locally, as in ischaemic tissue, or systematically, as with genetic haemochromatosis or transfusion-induced iron overload, as for patients suffering from β-thalassemia. So it is intuitively derived that metal — in this particular case iron — intoxication should be treated with chelating agents.

The main feature of the design of a chelating agent for iron should be its affinity and selectivity towards this metal. The most widely used iron chelator is Desferrioxamine B (Desferal®, DFO), a hexadentate ligand from the family of siderophores that shows great affinity for iron(III), giving rise to a 1:1 complex. The main drawback of DFO, apart from side effects with prolonged treatment, is that it has to be administered by intravenous injection. Consequently, there is an urgent need for an orally active chelating agent able to improve the way of life of patients.

The main target in designing an orally active sequestering agent is its bio-availability, which is related to an efficient gastrointestinal tract (GIT) absorption. The ligand needs to be quite lipo-soluble in order to be absorbed by the gastrointestinal tract, although this property also enables it to penetrate critical barriers such as the blood-brain barrier (BBB) and the blood-placental barrier (BPB). A possible way to overcome the negative aspects of lipophilicity is to use a lipophilic pro-drug that is easily absorbed by the GIT and reach the bloodstream, where it can be cleared by the liver and finally converted into an iron-selective chelator in the hepatocytes. The complex formed by iron scavenging inside the hepatocytes can be excreted by bile and/or urine.

Curcumin is spice and pigment from *Curcuma longa* L. (Zingiberaceae) and it is best known for its antioxidant,[3–6] anti-inflammatory[4,7] and anticancer[3,4,8,9] activities. We have recently investigated the iron-chelating ability of curcumin and its diacetyl derivative (Scheme 1), observing a lowering of the pK_a value of the β-dioxo moiety in the presence of iron(III), and the formation of mixed hydroxo species ($[Fe(CURH_2)(OH)_2]$ and $[Fe(DCUR)(OH)_2]$) in a methanol/water (1:1) solution, whose stability is close to that of the Desferrioxamine complex. The main drawback in the clinical use of curcumin is its low water solubility. To overcome this handicap, we have synthesised new glycosyl

[a] Department of Physiopathology and Experimental Medicine, University of Siena,
Via Aldo Moro, 53100 Siena, Italy
E-mail: ferrali@unisi.it
[b] Department of Chemistry, University of Modena and Reggio Emilia,
Via Campi 183, 41100 Modena, Italy
E-mail: saladini@unimore.it
Supporting information for this article is available on the WWW under http://www.eurjic.org or from the author.

 © 2004 Wiley-VCH Verlag GmbH & Co. KGaA, Weinheim DOI: 10.1002/ejic.200300463

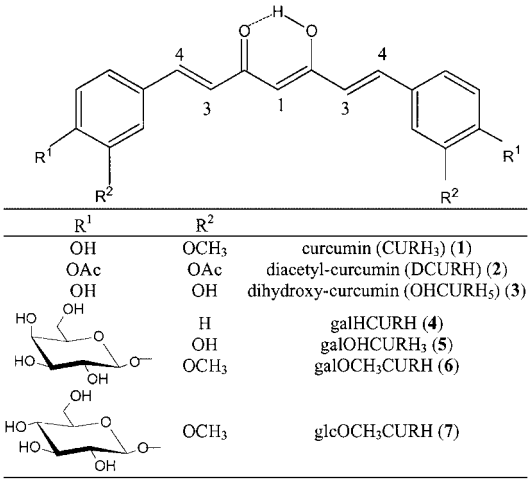

R^1	R^2	
OH	OCH_3	curcumin ($CURH_3$) (**1**)
OAc	OAc	diacetyl-curcumin (DCURH) (**2**)
OH	OH	dihydroxy-curcumin ($OHCURH_5$) (**3**)
	H	galHCURH (**4**)
	OH	$galOHCURH_3$ (**5**)
	OCH_3	$galOCH_3CURH$ (**6**)
	OCH_3	$glcOCH_3CURH$ (**7**)

Scheme 1

derivatives (Scheme 1). Apparently hexadentate ligands are the best iron chelators, and a recent study on a hydroxypyridinone derivative CP502 has shown good oral absorption and iron excretion, even though it is bidentate.[17] Glycosyl-curcuminoids have the great advantage of being administrated by oral formulation in their acetylated form, and even though their high molecular weight hinders the diffusion processes through the GIT, high dosages are completely safe. Acetyl-glycosyl-curcuminoids can probably be absorbed by the GIT thanks to their high lipophilicity. They then reach the liver where, through hydrolytic processes, the glycosyl-curcuminoids are set free to complex iron and then excreted in urine and/or bile.

Here we investigate by means of spectroscopic (UV/Vis and potentiometric) techniques the iron(III) and gallium(III) chelating ability of these ligands; NMR spectroscopic data are also useful in studying the metal complexation, therefore we substituted the paramagnetic iron(III) with diamagnetic gallium(III) as suggested in some recent works.[10−12] Some of the water-soluble derivatives were also tested for their antioxidant properties "in vitro" in a biological system.

Results and Discussion

Potentiometry

The low water solubility of compounds **1**−**6** ($\leq 5 \times 10^{-5}$ M) prevented the potentiometric analysis of these systems. The greater solubility of **7** (approx. 5×10^{-3} M) allowed us to perform a potentiometric study and the evaluated data are reported in Tables 1 and 2, together with the spectrophotometric data. Potentiometric analysis gives more accurate results than the other techniques but the stability constants' values are very similar to those calculated from the UV data, therefore we may consider spectrophotometric analysis a reliable probe in testing the chelating ability of slightly water soluble systems.

Table 1. Logarithm of stepwise protonation constant (estimated standard deviation 0.1, if not specified); T = 25 °C, I = 0.1 M $NaNO_3$

	3[a]	**4**	**5**	**6**	**7**
$\log K_{a1}$	7.8	8.8	7.9	9.2	9.2/9.22(3)[b]
$\log K_{a2}$	8.6		9.9		
$\log K_{a3}$	9.3		10.9		
$\log K_{a4}$	10.8				
$\log K_{a5}$	12.5				

[a] $\log K_a$ values are referenced to a methanol/water (1:1) system. [b] Potentiometric data.

Table 2. Logarithm of stability constants of complex species calculated from spectrophotometric and potentiometric data for iron(III) and gallium(III) complexes; all data recorded at 25 °C, I = 0.1 M $NaNO_3$; estimated standard deviation of 0.1 if not specified; L represents the ligand with the enolic group in the dissociated form

	4	**6**	**7**	**7**[a]	**5**	**3**[b]
$[FeL]^{2+}$	10.2	10.7	11.0	10.73(3)	10.3	17.1
$[FeL(OH)]^{+}$	1.7	2.8	2.4	2.98(2)	0.3	20.8
$[FeL_2]^{+}$	19.5	20.5	20.8	19.82(1)	22.7	
$[FeL_2(OH)]$	13.2	16.3	16.0	16.10(2)	13.5	
$[GaL]^{2+}$	9.8	12.1	11.8		11.2	
$[GaL(OH)]^{+}$	3.7	2.8	3.2		1.2	
$[GaL_2]^{+}$	19.0	22.9	22.5		19.0	
$[GaL_2(OH)]$	14.0	14.2	12.5		10.5	

[a] Potentiometric data. [b] $\log\beta$ values are referenced to a methanol/water (1:1) system.

UV/Vis Spectroscopy

Glycosyl-curcuminoids, similarly to curcuminoids, maintain their dye properties — they are all characterised by an absorbance at ca. 400 nm.

Upon plotting absorbance vs. pH, only one equivalent point is observed for each ligand; the pK_a values calculated from the spectrophotometric data are reported in Table 1. The presence of the sugar moiety does not affect the pK_{a1} value, while some electronic effect is due to the substituents on the aromatic ring: the electron-withdrawing effect of OH groups stabilizes the conjugate base, lowering the pK_{a1} value, and as a consequence ligand **5** is the most acidic one in aqueous solution.

The addition of an iron(III) solution to the free ligands causes an LMCT[13] band to appear at ca. 500 nm, typical of (β-diketonate)Fe^{3+} complexes, and by monitoring the changes in the spectra upon progressive addition of Fe^{3+} solution, the stoichiometry of the complexes can be proposed.

Figure 1 shows the absorbance increase with the M/L molar ratio, which reaches a maximum at an M/L value of 0.5, corresponding to an M/L (1:2) complex. Once the 1:2 complex has formed no more significant changes in ab-

 © 2004 Wiley-VCH Verlag GmbH & Co. KGaA, Weinheim

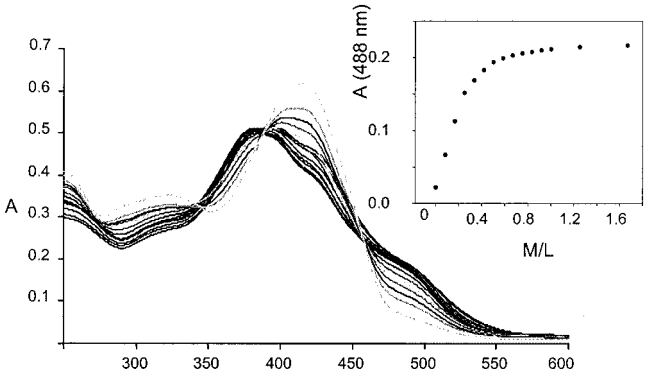

Figure 1. Spectrophotometric titration of **5** with Fe^{3+} solution and plot of absorbance vs. M/L at λ = 488 nm

sorbance are seen for the LMCT band, probably due to the small difference in the spectrophotometric curves of the 1:1 and 1:2 complexes. The addition of metal solution, causing a reduction in the pH value from 5 to 3, induces the formation of complex species even at a pH of about 3. The same experiments were carried out under buffered conditions (pH = 7), where the only difference is the increased intensity of the LMCT band. No differences were found in logβ values when taking into account the formation of a phosphate complex as its stability ($\log K[FeHL]^+ = 7.5$[14]) is significantly lower than those of our complexes.

Titration of the ligands with Ga^{3+} solution generates the same behaviour as observed in the presence of Fe^{3+}.

The pH-metric titration of the metal complexes was performed in aqueous solution for the glycosyl derivatives, while for the **3**/Fe^{3+} system a methanol/water (1:1) solution was used due to the poor solubility of the ligand in aqueous media. No hint of metal complex or metal hydroxide precipitation was observed.

The pH-metric titration of all L/Fe^{3+} (1:1) systems gives a typical UV spectral pattern and a plot of λ_{max} vs. pH, or *A* vs. pH at fixed λ gives a titration curve with two equivalent points (EP; Figure 2). The first EP (pH ≈ 4) is due to the deprotonation of the β-dioxo moiety, although it is several pH units lower than normal thanks to the great affinity for Fe^{3+}. The second one is probably due to the cleavage of

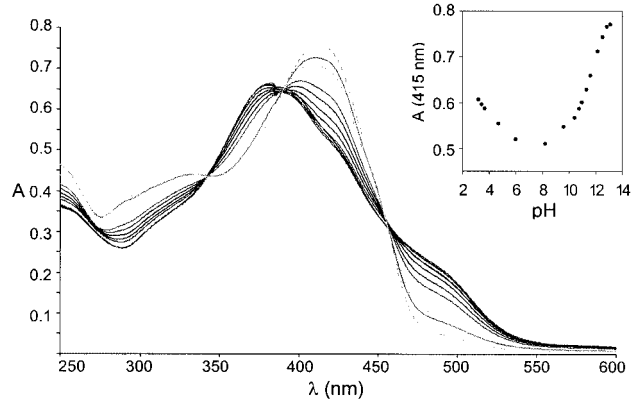

Figure 2. Spectrophotometric titration of a **7**/Fe^{3+} (1:1) system with NaOH and plot of absorbance vs. pH at λ = 415 nm

the metal complex under extremely basic conditions (pH > 10) and to the competition of hydroxide anions in metal complexation, although in **3**- and **5**-containing systems the involvement of dissociated catechol groups in metal coordination cannot be excluded.

The pH-metric titration of Ga^{3+}-glycosyl-curcuminoids parallels well the performance in the presence of Fe^{3+}.

The stability constants for Fe^{3+} and Ga^{3+} complexes are reported in Table 2. Comparison of the behaviour of glycosyl-curcuminoids with those of the parent curcuminoids shows that the former prefer M/L (1:2) complexes despite the steric hindrance of the saccharide units. This is because of the polar/non-polar character of the molecule. In aqueous solution the apolar core is tightly bound to the metal ion while the polar units form hydrophilic interactions (especially hydrogen bonds), giving a more stable structure and hindering the metal ion from coordinating additional ligands such as oxygen, therefore probably inhibiting oxidative processes.

In order to compare stability constants relative to the same kind of equilibrium, they need to be corrected by considering the ligand's protonation constants. It is more useful to consider the species distribution to understand which is the prevailing species under physiological conditions. In Figures 3−5 the species distribution curves for **7**/Fe^{3+}-, **5**/Fe^{3+}- and **3**/Fe^{3+}-containing systems are reported.

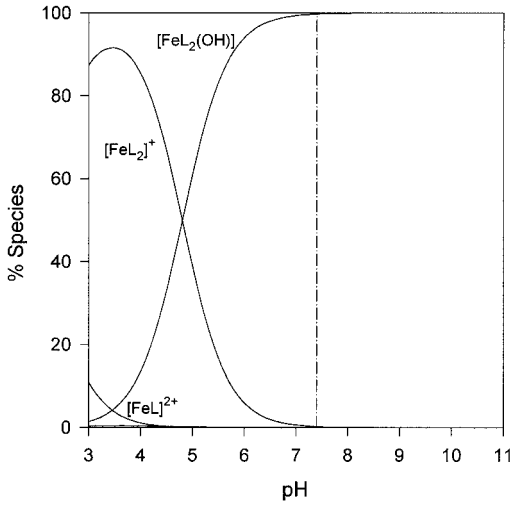

Figure 3. Species distribution curves for Fe/L systems in a 1:4 molar ratio; $[Fe^{3+}] = 5 \times 10^{-5}$ M, L = **7**

The prevailing species at physiological pH (7.4) have different stoichiometries for the three classes of ligands reported. Therefore a more proper comparison of the effective Fe^{3+}-chelating ability is represented by pFe^{3+}, defined as $-\log[Fe^{3+}]$.[15] This value is usually calculated with [L] = 10^{-5} M and $[Fe^{3+}] = 10^{-6}$ M, and, unlike stability constants, takes into account the effects of ligand protonation and denticity as well as differences in metal/ligand stoichiometry. A plot of pFe^{3+} versus pH provides a useful method for comparing the ability of chelators to bind iron(III) at different pH values as a high value of log*K* is not necessarily characterised by a high value of pFe^{3+}. Figure 6

 © 2004 Wiley-VCH Verlag GmbH & Co. KGaA, Weinheim

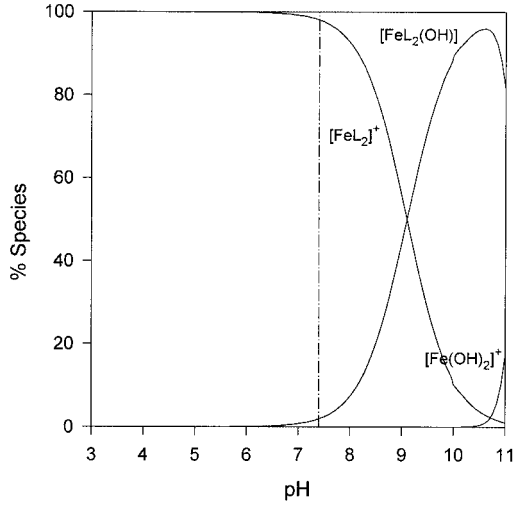

Figure 4. Species distribution curves for Fe/L systems in a 1:4 molar ratio; $[Fe^{3+}] = 5 \times 10^{-5}$ M, L = **5**

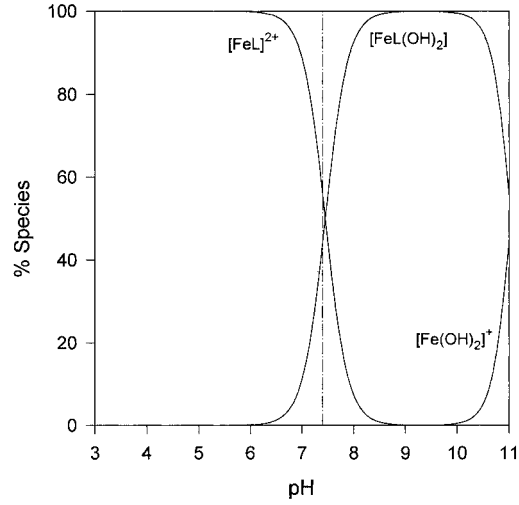

Figure 5. Species distribution curves for Fe/L systems in a 1:4 molar ratio; $[Fe^{3+}] = 5 \times 10^{-5}$ M, L = **3**

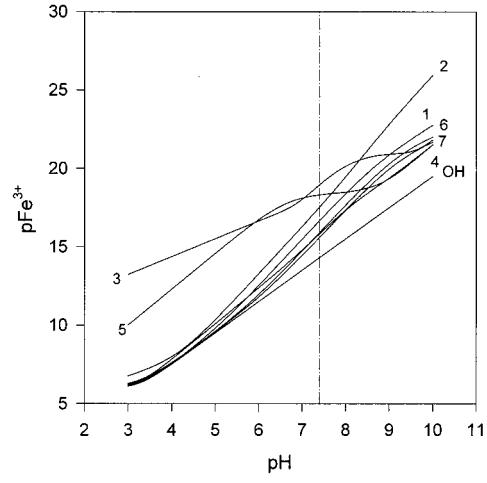

Figure 6. pFe^{3+} vs. pH for curcuminoids and glycosyl-curcuminoids; $[Fe^{3+}] = 10^{-6}$ M, [L] = 10^{-5} M; OH stands for Fe^{3+} aqueous solution

shows the plot of pFe^{3+} vs. pH for the curcuminoids and glycosyl-curcuminoids investigated in this work. Compounds **3** and **5** show the highest pFe^{3+} values at physiological and acidic conditions, despite their low $\log K_{a1}$ values; this behaviour may be due to the presence of phenolic functions that play an important role in the hydrogen bond network involving water molecules, and furthermore they are possibly involved in metal interactions. Table 3 shows the pFe^{3+} for different chelating agents. Notice how hexadentate ligands usually have higher pFe^{3+} values than bidentate one.

Table 3. pFe^{3+} values at pH = 7.4 for different Fe^{III}-chelating agents; DFO = Desferoxamine; DMB = 2,3-dihydroxy-*N*,*N*-dimethylbenzamide

	pFe^{3+}
MECAM[a]	28
DFO[a]	26
3-Hydroxypyridin-4-one[a]	20
3	19.0
5	18.3
2	17.6
1	16.7
6	15.9
4	15.8
7	15.6
DMB[a]	15
Acetohydroxamic acid[a]	13

[a] Values taken from ref.[33]

NMR Study

All spectra of glycosylated ligands are characterised by a sharp distinction between the pyranoside moiety and the aliphatic and aromatic ones; of particular interest are the protons on the double bond and the enolic proton, although the latter is quite mobile and tends to exchange in MeOD solution with D_2O. Gallium(III) can properly substitute iron(III) for the NMR study.[11−13] The study of its interactions in solution is useful in order to understand both the real chelating site and the stoichiometry of the complexes.

Titration of a solution of **5** with Ga^{III} (Figure 7) indicates the formation of new signals, in slow exchange on the NMR timescale, upon increasing the M/L molar ratio. The titration was performed without any buffer, since little changes are observed in the pH values (ca. 0.5 pH units). The formation of the new sets of signals is not a consequence of the pH decreasing induced by hydrolysis of Ga^{III}, but it is more reasonably attributed to the formation of complex species.

On increasing the Ga^{III} concentration the first kind of complex is formed; all of the ligand is complexed when the ratio mol of metal/mol of ligand is 0.5, therefore a 1:2 stoichiometry can be proposed for this species. The greatest downfield shift is for the 4-H signal; 4-H probably "feels" the positive charge in the resonance structure of the bis-

 © 2004 Wiley-VCH Verlag GmbH & Co. KGaA, Weinheim

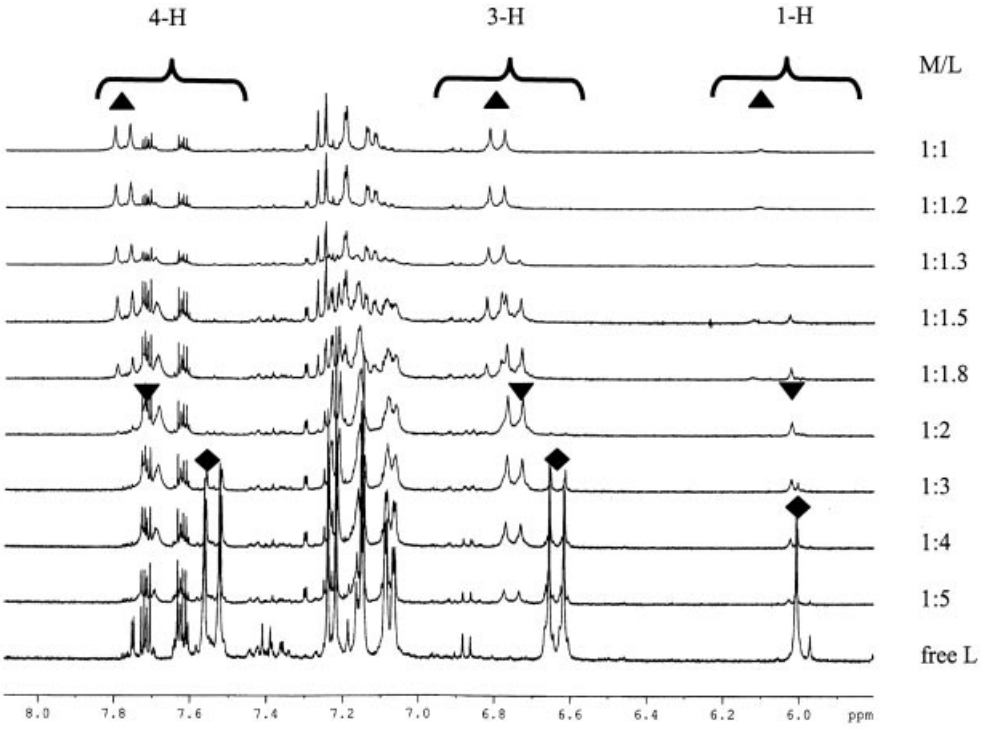

Figure 7. ^{1}H NMR titration of **5** with $Ga(NO_3)_3$ in MeOD solution; diamonds: free ligand signals; downward pointing triangles: M/L (1:2) complex signals; upward pointing triangles: M/L (1:1) complex signal

(chelate) complex, while a smaller shift is seen for the 3-H signal. Because of exchange processes with residual D_2O, the signal for 1-H is quite broad, making it difficult to follow its shift. Another important aspect of this titration is that the pH* value on the methanol scale is very low (ca. 2.5), and no addition of base is necessary to form the complexes, thus all these complex species are also present under very acidic conditions, and the affinity for metal ion is so high that it anticipates enolic deprotonation until pH* $\approx$ 3.

Upon increasing the quantity of metal further, the M/L (1:1) complex is formed. Its signals are more downfield shifted than those of the 1:2 complex, and this behaviour is in line with a more localised positive charge at the metal centre in the 1:1 complex than in the 1:2 complex. In line with the behaviour of curcumin, the phenolic groups in **5** do not interact with the metal ion, at least under the very acidic conditions that prevent catechol dissociation. Small changes are found for the aromatic protons due to the delocalisation of the metal charge along the aliphatic chain and aromatic rings. Finally, no evidence of an interaction between the sugar moiety and metal ion is observed by NMR spectroscopy in acid media, although we cannot exclude a possible glycoside interaction with the metal ion under physiological conditions, as reported in the literature in the solid state.[16−18]

The carbon atoms parallel the protons' behaviour. 2D inverse detection methods show a greater shift of the C-4 signal (δ = 4 ppm) followed by the C-3 signal (δ = 2 ppm) in the 1:1 complex, while in the 1:2 complex smaller shifts are observed.

Attempts to titrate the 1:1 complex solution with NaOH resulted in precipitation of the metal complex.

All glycosyl-curcuminoids share the same behaviour, confirming that the substituents on the aromatic rings and the nature of the sugar do not affect the metal coordination.

Effect of the Chelators on Lipid Peroxidation

Figure 8 shows the time-dependent formation of TBARS as a hint of iron-dependent lipid peroxidation in rat liver microsomes. Notice that the presence of the chelators **3** and **5** interferes — although to different extents — with the lipid peroxidation evolution. In particular, compound **3** almost completely inhibits TBARS formation even if it is present in the incubation mixture at one half or the same concentration as that of the metal. On the other hand, compound **5** completely prevents microsomal lipid peroxidation only when present at a concentration twice that of iron. As a consequence, compound **5** seems to prevent TBARS formation only when the M/L (1:2) complex is formed, while compound **3** is active independently of the complexation stoichiometry. This is due to the catecholic structure of compound **3**, which possibly also acts as a free-radical scavenger when iron is present in excess compared to the chelator. It therefore seems to have a double action: it blocks oxygen-active species generated by the iron redox cycle and inhibits its initiation in the iron-chelated form. Since compound **5** is a galactosyl ester of compound **3** it is possible that under in vivo conditions, after galactosidase action, it acquires the same properties as **3**. In conclusion, both compound **3** and its derivative esters appear to be useful anti-

 © 2004 Wiley-VCH Verlag GmbH & Co. KGaA, Weinheim

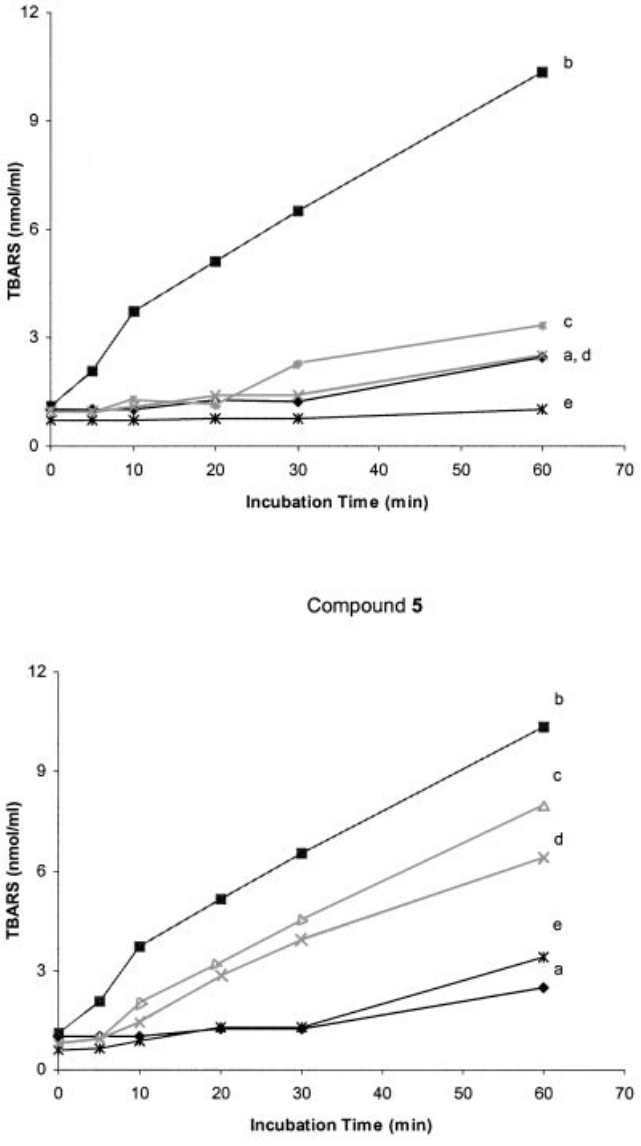

Figure 8. Iron-dependent TBARS evolution in a rat liver microsomal preparation (MC): a) control MC; b) MC plus 100 μM $FeCl_3$ and 2.5 mM ADP; c) as in b) plus 50 μM chelator; d) as in b) plus 100 μM chelator; e) as in b) plus 200 μM chelator; the microsomal protein concentration was 1.5 mg/mL in the incubation system; the values represent the mean of two or three experiments

oxidants preventing lipid peroxidation both in vitro and, presumably, in vivo.

Experimental Section

General: Compounds **4**−**7** were synthesised as reported in ref.[19], while compound **3** was synthesised according to the Pabon reaction.[20] $FeCl_3$ was used to avoid hydrolysis processes; standardisation of the stock methanolic solution was performed with a Spectroflame D ICP plasma spectrometer.

Potentiometry: Potentiometric measurements were performed in aqueous solution at 25 ± 0.1 °C according to the general procedures previously reported.[21] A constant ionic strength of 0.1 M (solid $NaNO_3$) and nitrogen gas were maintained in all experiments. The stability constants were refined with the Hyperquad program[22] taking into account the presence of $[Fe(OH)]^{2+}$ and $[Fe(OH)_2]^{+}$ species.[16] The protonation constant of the ligand was determined by the titration of 5×10^4 M solutions. The ligand/Fe system was investigated in 1:1, 1:2 and 1:4 molar ratios. Aqueous NaOH (5×10^{-3} M) was used as titrant in the pH range 3−10.

Spectroscopy: Spectrophotometric titrations were performed using a Perkin−Elmer Lambda 20 spectrophotometer at 25 ± 0.1 °C in the 200−600-nm spectral range, employing a 1-cm quartz cell. 2.5×10^{-5} M solutions of ligands **4**−**7** were investigated in aqueous solution while **3** was used in methanolic/aqueous (1:1, v/v) media; pH values were adjusted by adding small amounts of concentrated NaOH. In the titrations of **3** the glass electrode was calibrated using two appropriate buffers (pH = 5.57 and 8.02).[23] Constant additions (10 μL each time) of Fe^{III} solution (10^{-2} M) were performed using a micropipette in order to reach different M/L molar ratios. All the titrations were done also in a buffer solution (pH = 7.4, NaH_2PO_4/Na_2HPO_4). The pH-metric titration of the M/L (1:1) solutions was obtained varying the pH value by adding a small amount of concentrated NaOH. The protonation constants of the ligands and formation constants of metal complexes were evaluated from spectrophotometric titrations using the pHab2000 software.[24] ^1H NMR spectra were obtained with a Bruker Avance AMX-400 spectrometer at 400.13 MHz with a 5-mm broadband probe (inverse detection). Acquisition parameters were as follows: spectral bandwidth 17 ppm, pulse width 7.6 μs (90° pulse), pulse delay 1 s, number of scans 216−512. H,H COSY,[25] HMQC[26,27] and HMBC[28] were performed with typical averaged parameters: $^1J_{H,C} = 145$ Hz and $^3J_{H,C} = 7$ Hz, typical delay for inversion recovery optimised to give null for protons bound to ^{12}C, in BIRD sequence, is around 400 ms. The spectra of the ligands were recorded for mM solutions in CD_3OD, since their signals in D_2O solution were so broad that they could not be assigned, probably due to the formation of aggregate species. The combined electrode was standardised with CH_3OH buffers (pH = 5.79 and 7.53), pD values were then corrected by 0.4 units according to the relationship: pD = pH + 0.4.[25] All spectra were collected at 25 ± 0.1 °C and referenced to TMS. A solution of Ga^{III} was prepared by dissolving 2.5 mg of $Ga(NO_3)_3 \cdot 9H_2O$ in 0.1 mL of CD_3OD. Equimolar solutions of **3**−**7** in the same solvent were prepared. Constant additions (10 μL each time) of Ga^{III} solution were performed using a micropipette, the mixture was stirred and spectra were registered after a few minutes from the addition.

Biological Studies: Rat liver microsomes (MC) were prepared from fasted animals.[29] MC equivalent to 4 g of liver were resuspended in 36 mL of 50 mM trimaleate buffer (TM, pH = 7.4). The suspension was adjusted to 3 mg of microsomal protein per mL and 300 μM NADPH added just before the experimental procedure. A solution of 5 mM ADP plus 200 μM $FeCl_3$ was prepared in the same buffer. Solutions of ligands **3** and **5** (20 mM) in water/ethanol were prepared. To 3 mL of the microsomal suspension 0.6, 1.2, 2.4 μmol of the two chelators were added in separate flasks; then 3 mL of the ADP/iron solution was added and the incubation started at 37 °C in a shaking bath. After the indicated times, aliquots were withdrawn to measure the amount of TBARS formed.[30]

Supporting Information (see also footnote on the first page of this article): Figure showing the 2D heterocorrelated spectrum with evolution of the $^1J_{C,H}$ coupling constants for the free ligand **5**, the complex Ga^{III}-**5** (1:2) and the complex Ga^{III}-**5** (1:1); spectrophotometric titration of **5** (inset shows λ_{max} vs. pH).

 © 2004 Wiley-VCH Verlag GmbH & Co. KGaA, Weinheim

Acknowledgments

We are thankful to the "Centro Interdipartimentale Grandi Strumenti (CIGS)" of the University of Modena and Reggio Emilia, which supplied the NMR spectrometer.

[1] B. Halliwell, J. M. C. Gutteridge, *Methods Enzymol.* **1990**, *186*, 1−85.
[2] H. C. Sutton, C. C. Winterbourn, *Free Radical Biol. Med.* **1989**, *6*, 53−60.
[3] Sreejayan, M. N. A. Rao, *J. Pharm. Pharmacol.* **1994**, *46*, 1013−1016.
[4] Sreejayan, M. N. A. Rao, *Int. J. Pharm.* **1993**, *100*, 93−97.
[5] M. K. Unnikrishnan, M. N. A. Rao, *Pharmazie* **1995**, *50*, 490−492.
[6] H. P. T. Ammon, M. A. Wahl, *Planta Med.* **1991**, *57*, 1−7.
[7] R. J. Anto, G. Kuttan, K. V. D. Babu, K. N. Rajasenkaran, R. Kuttan, *Pharm. Pharmacol. Commun.* **1998**, *4*, 103−106.
[8] R. J. Anto, G. Kuttan, K. V. D. Babu, K. N. Rajasekharan, R. Kuttan, *Int. J. Pharm.* **1996**, *131*, 1−7.
[9] H. H. Tønnesen, H. De Vries, J. Karlsen, G. B. van Henegouwen, *J. Pharm. Sci.* **1987**, *76*, 371−3.
[10] M. Borsari, E. Ferrari, R. Grandi, M. Saladini, *Inorg. Chim. Acta* **2002**, *328*, 61−68.
[11] R. A. Atkinson, A. L. M. S. El Din, B. Kieffer, J. F. Lefevre, M. A. Abdallah, *Biochemistry* **1998**, *37*, 15965−15973.
[12] Y. Hara, L. Shen, A. Tsubouchi, M. Akiyama, K. Umemoto, *Inorg. Chem.* **2000**, *39*, 5074−5082.
[13] S. Kazanis, T. C. Pochapsky, *J. Biomol. NMR* **1997**, *9*, 337−346.
[14] R. L. Lintvedt, L. K. Kernitsky, *Inorg. Chem.* **1970**, *9*, 491−494.
[15] H. H. Tønnesen, J. V. Greenhill, *Int. J. Pharm.* **1992**, *87*, 79−87.
[16] NIST Standard Reference Database 46, Critically Selected Stability Constants, Version 5, webbook.nist.gov
[17] R. C. Hider, Z. D. Liu, S. Piyamongkol, *Transf. Sci.* **2000**, *23*, 201−209.
[18] K. Hegetschweiler, T. Kradolfer, V. Gramlich, R. D. Hancock, *Chem. Eur. J.* **1995**, *1*, 74−88.
[19] K. Hegetschweiler, L. Hausherr-Primo, W. H. Koppenol, V. Gramlich, L. Odier, W. Meyer, H. Winkler, A. X. Trautwein, *Angew. Chem. Int. Ed. Engl.* **1995**, *34*, 2242−2243.
[20] K. Hegetschweiler, M. Ghisletta, L. Hausherr-Primo, T. Kradolfer, *Inorg. Chem.* **1995**, *34*, 1950−1953.
[21] E. Ferrari, R. Grandi, S. Monti, M. Saladini, *Can. J. Chem.*, in press.
[22] H. J. J. Pabon, *Recl. Trav. Chim. Pay-Bas* **1964**, *83*, 379−386.
[23] M. Borsari, L. Menabue, M. Saladini, *Polyhedron* **1999**, *18*, 1983−1989.
[24] P. Gans, A. Sabatini, A. Vacca, *Talanta* **1996**, *43*, 1739−1753.
[25] D. D. Perrin, B. Dempsey, *Buffers for pH and Metal Ion Control*, Chapman and Hall, London, **1979**.
[26] P. Gans, A. Sabatini, A. Vacca, *Ann. Chim.* **1999**, *89*, 45−49.
[27] K. Nagayama, A. Kumar, K. Wuethrich, R. R. Ernst, *J. Magn. Reson.* **1980**, *40*, 321−334.
[28] A. Bax, R. H. Griffey, B. L. Hawkins, *J. Magn. Reson.* **1983**, *5*, 301−315.
[29] A. Bax, S. Subramanian, *J. Magn. Reson.* **1986**, *67*, 565−569.
[30] A. Bax, M. F. Summers, *J. Am. Chem. Soc.* **1986**, *108*, 2093−2094.
[31] M. Ferrali, S. Bambagioni, A. Ceccanti, D. Donati, G. Giorgi, M. Fontani, F. Laschi, P. Zanello, M. Casolaro, A. Pietrangelo, *J. Med. Chem.* **2002**, *45*, 5776−5785.
[32] M. Comporti, A. Hartman, N. R. Di Luzio, *Lab. Invest.* **1967**, *16*, 616−624.
[33] Z. D. Liu, R. C. Hider, *Coord. Chem. Rev.* **2002**, *232*, 151−171.

Received July 15, 2003
Early View Article
Published Online December 19, 2003

 © 2004 Wiley-VCH Verlag GmbH & Co. KGaA, Weinheim

Kinetics and Mechanism of Axial Ligand Substitution of Alkyl Cobaloximes by Substituted Pyridines in Different Solvents

Basam M. Alzoubi,[a] Mohamed S. A. Hamza,[a,b] Alessandro Felluga,[c] Lucio Randaccio,[c] Giovanni Tauzher,[c] and Rudi van Eldik*[a]

Keywords: Cobaloximes / Solvent effects / *trans* effect / Ligand-substitution reactions / Nitrogen heterocycles

Ligand-substitution reactions of *trans*-RCo(Hdmg)$_2$S (where R = $PhCH_2$ or CF_3CH_2, Hdmg = dimethylglyoximate, and S = H_2O or MeOH) were studied for the nucleophiles 4-aminopyridine (4-NH_2Py), pyridine (Py) and 4-cyanopyridine (4-CNPy). From the pressure and temperature dependence of the substitution of methanol by 4-NH_2Py, Py, and 4-CNPy, the activation parameters $\Delta H^{\neq}$, $\Delta S^{\neq}$, and $\Delta V^{\neq}$ were estimated for the cases where R = $PhCH_2$ and CF_3CH_2. The activation parameters for the substitution of H_2O by Py and 4-CNPy in the case where R = CF_3CH_2 were also found. The kinetic data and activation parameters show that the dissociative character of the reaction decreases on changing the R group from $PhCH_2$ to CF_3CH_2 and the solvent from MeOH to H_2O.
(© Wiley-VCH Verlag GmbH & Co. KGaA, 69451 Weinheim, Germany, 2004)

Introduction

The study of the chemical and physical properties of organocobalt compounds, which serve as models for vitamin B_{12}, is of interest both to inorganic and bioinorganic chemists. Various pseudo-octahedral organometallic complexes of Co^{III}, containing equatorial ligands such as dioximes,[1−9] imino groups/oximes[10] and Schiff bases derived from diamines and salicylaldehyde[11] or acetylacetonate[12] have been proposed as models for the vitamin B_{12} coenzyme. Some of us recently studied the reaction of cyanide with various alkylcobalamins (RCbl, where R = CN, $CNCH_2$, CF_3, CF_3CH_2, CF_2H, CH_3, $BrCH_2$) and found that the nature of the alkyl group has an important influence on the thermodynamic equilibrium constants, and the kinetics and mechanism of the substitution reactions of the axial ligand *trans* to the alkyl group.[13,14]

The nature of the axial alkyl group in cobaloximes[2] and in related $[RCo\{(DO)(DOH)pn\}H_2O]^+$ complexes[15] has an effect on the substitution of the ligand in the *trans* position. This substitution is very rapid and involves a dissociative activation mode, similar to the substitution of labile cobalamin complexes. Ligand-substitution reactions of vitamin B_{12} and its models in general follow a dissociative (I_d or D) type of mechanism.[16−28] In the case of the coenzyme, evidence was initially reported for an associative substitution mode, which was, however, recently reinterpreted and instead assigned to a subsequent Co−C heterolysis reaction.[29] An interchange mechanism may involve either associative or dissociative activation (I_a or I_d mechanism), according to the relative importance of bond making and bond breaking in the transition state. Evidence that usually leads to the assignment of a dissociative mechanism includes the absence of any relationship between the nature of the entering nucleophile and the rate constant, an increase in lability with an increase in the electron donating ability of the alkyl group R in the *trans* position, and positive values for both $\Delta V^{\neq}$ and $\Delta S^{\neq}$.

In general, kinetic studies are performed under pseudo first order conditions using a large excess of ligand over the complex. A linear dependence of the observed pseudo first-order rate constant on the concentration of the entering nucleophile has been observed in almost in all cases, both for aquacobalamin and synthetic models in aqueous solution. The first deviation from linearity was reported for the reaction of $[RCo\{(DO)(DOH)pn\}H_2O]^+$ complexes (R = Me and Et).[15] Curvature in the plot of k_{obs} versus ligand concentration generally characterizes multistep processes, such as a limiting dissociative mechanism (D), which involves a pentacoordinate intermediate, or a mechanism in which intermediate species are formed in a rapid pre-equilibrium which precedes the slow substitution step. In the above-mentioned complexes, linear relationships between

[a] Institute for Inorganic Chemistry, University of Erlangen-Nürnberg,
Egerlandstr. 1, 91058 Erlangen, Germany
[b] Department of Chemistry, Faculty of Science, Ain Shams University
Cairo, Egypt
[c] Dipartimento di Scienze Chimiche, Università degli Studi di Trieste,
34127 Trieste, Italy
Supporting information for this article is available on the WWW under http://www.eurjic.org or from the author.

k_{obs} and ligand concentration were found for the substitution of water by a number of nucleophiles. However, curvature was observed for L = imidazole, benzylamine, pyridine and 4-methylpyridine. Since the later four ligands all contain aromatic group, it was tentatively suggested that these are involved in forming the intermediate, perhaps through a π-π interaction with the conjugated system of the (DO)(DOH)pn equatorial ligand.

More recently, a non-linear dependence of k_{obs} on the concentration of the entering ligand has been reported for the reaction of aquacobalamin with substituted pyridines.[16] This was first incorrectly interpreted as evidence for the operation of a limiting dissociative mechanism, but later work clearly demonstrated that the observed deviation was due to the rapid formation of adducts involving the nucleophiles and cobalamin, preceding the slow substitution reaction according to a dissociative interchange mechanism.[17] This finding greatly enhanced our interest in mechanisms associated with the reactions of nucleophiles that contain an aromatic group because of the connection with the biochemistry of vitamin B_{12}. Therefore, in order to obtain a deeper understanding of this phenomenon, we extended the present study to cobaloximes, which are the most widely recognised model systems for the study of vitamin B_{12}. We report kinetic data for ligand-substitution reactions of $RCo(Hdmg)_2S$ with various pyridines, where R = $PhCH_2$ and CF_3CH_2, S = H_2O and MeOH and L = 4-NH_2Py, Py, and 4-CNPy, in order to study the kinetic *trans* effect in alkyl cobalt complexes as a function of nucleophile concentration, temperature and pressure.

Results and Discussion

The ligand-substitution reactions of *trans*-$RCo(Hdmg)_2S$ (where R = CF_3CH_2 and $PhCH_2$) with various nucleophiles L = 4-NH_2Py, Py, and 4-CNPy to form $RCo(Hdmg)_2L$, according to Equation (1), were studied with MeOH and H_2O as solvents.

$$RCo(Hdmg)_2S + L \rightarrow RCo(Hdmg)_2L + S \quad (1)$$

The results fall into two categories: (i) when the incoming ligand is Py or 4-NH_2Py, a non-linear concentration dependence is obtained for both $PhCH_2$ (S = MeOH) and CF_3CH_2 (S = MeOH or H_2O) derivatives, (ii) when the incoming ligand is 4-CNPy, a linear relationship is observed for both the $PhCH_2$ (S = MeOH) and CF_3CH_2 (S = MeOH or H_2O) derivatives. The reaction of $(4-10) \times 10^{-4}$ M *trans*-$RCo(Hdmg)_2(H_2O)$ with an excess of nucleophile (4-NH_2Py and Py) was studied at various temperatures in MeOH and H_2O. The results are shown in Figure 1 (R = CF_3CH_2, L = 4-NH_2Py in MeOH) and Figure 2 (R = CF_3CH_2, L = Py in H_2O); see also Figure S1 (R = $PhCH_2$, L = 4-NH_2Py in MeOH) and Figure S2 (R = CF_3CH_2, L = Py in MeOH) in the Supporting Information (see footnote on the first page of this article). The plots show significant curvature at high nucleophile concentration and negligible intercepts, which can be interpreted (see below) in terms of the interchange mechanism presented in Equations (2) and (3). The corresponding rate law is given in Equation (4), where K represents the equilibrium constant for precursor formation, and k the interchange rate constant. In these cases, k and K can be separated kinetically so that their values can be discussed individually.

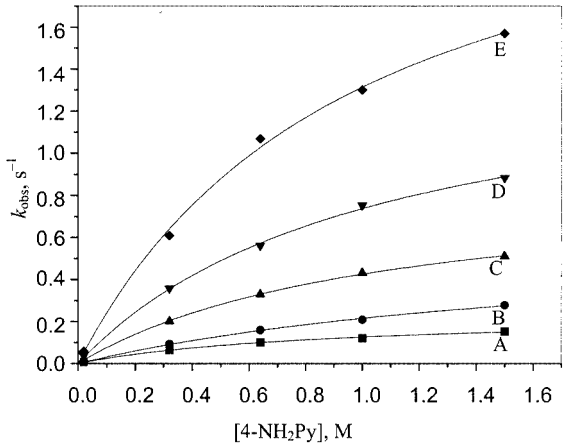

Figure 1. Plots of k_{obs} versus [4-NH_2Py] for the reaction with *trans*-$(CF_3CH_2)Co(Hdmg)_2(MeOH)$ as a function of temperature. Experimental conditions: $[Co^{III}] = 1 \times 10^{-3}$ M and temperature 20.0 (A), 25.0 (B), 30.0 (C), 35.0 (D), and 40.0 °C (E)

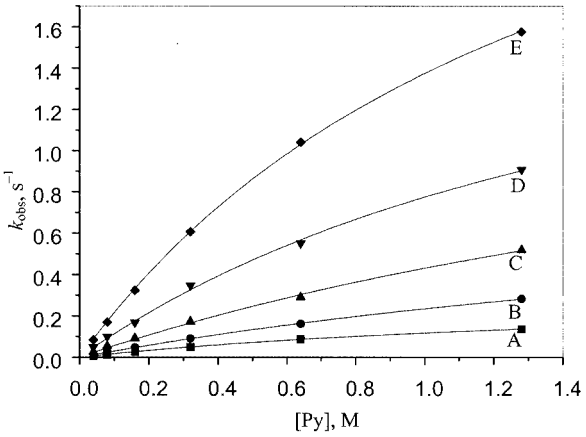

Figure 2. Plots of k_{obs} versus [Py] for the reaction with *trans*-$(CF_3CH_2)Co(Hdmg)_2(H_2O)$ as a function of temperature. Experimental conditions: $[Co^{III}] = 1 \times 10^{-3}$ M, pH = 8.0, I = 0.1 M $NaClO_4$ and temperature 20.0 (A), 25.0 (B), 30.0 (C), 35.0 (D), and 40.0 °C (E)

$$RCo(Hdmg)_2S + L \underset{}{\overset{K}{\rightleftharpoons}} [RCo(Hdmg)_2S.L] \quad (2)$$

$$[RCo(Hdmg)_2S.L] \xrightarrow{k} RCo(Hdmg)_2L + S \quad (3)$$

$$k_{obs} = kK[L]/(1 + K[L]) \quad (4)$$

Figures 3 and S3 (for the latter see the Supporting Information) show plots for k_{obs} versus [L] for the reaction of R = CF_3CH_2 with L = 4-CNPy in MeOH and H_2O, and

 © 2004 Wiley-VCH Verlag GmbH & Co. KGaA, Weinheim

R = $PhCH_2$ with L = Py and 4-CNPy in MeOH, respectively. The linear plots have negligible intercepts, which indicate that the back reactions do not contribute significantly and that no parallel reaction takes place. This behaviour can be expressed by the rate law given in Equation (5), from which it follows that the overall second-order rate constant (k_a) is a composite of k and K, and cannot be separated easily.

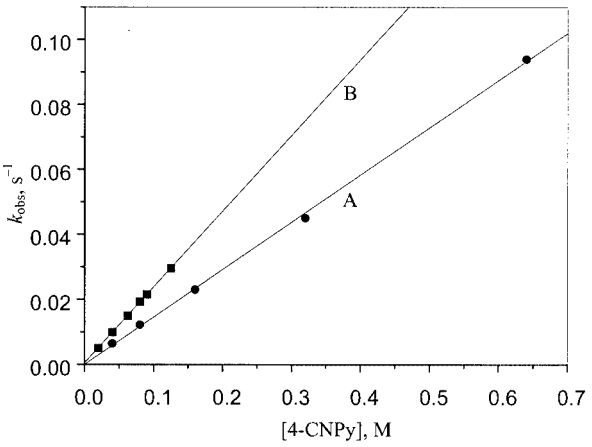

Figure 3. Plots of k_{obs} versus [4-CNPy] for the reaction with *trans*-$(CF_3CH_2)Co(Hdmg)_2S$ where S = MeOH (A) and H_2O (B) as a function of temperature. Experimental conditions: $[Co^{III}] = 1 \times 10^{-3}$ M, (pH = 8.0, I = 0.1 M $NaClO_4$ for S = H_2O) and temperature 25.0 °C

$$k_{obs} = k_a[L] = kK[L] \quad (5)$$

Tables 1, 2, 3, and 4 summarize the kinetic data obtained at different temperatures and pressures for the series of reactions investigated in this study. Plots of $\ln(k_a)$ versus pressure give good linear relationships as shown in Figure 4 for the reactions of *trans*-$(CF_3CH_2)Co(Hdmg)_2(MeOH)$

Table 1. Kinetic data for the reaction of *trans*-$RCo(Hdmg)_2(MeOH)$ with 4-NH_2Py as a function of temperature

R	T, °C	k, s^{-1}	K, M^{-1}	kK, $M^{-1}\,s^{-1}$
$PhCH_2$ [a]	5.0	127 ± 4	0.38 ± 0.02	48 ± 3
	10.0	187 ± 10	0.47 ± 0.03	88 ± 7
	15.0	228 ± 22	0.62 ± 0.07	141 ± 21
	20.0	458 ± 39	0.52 ± 0.06	238 ± 34
	25.0	1017 ± 135	0.35 ± 0.03	356 ± 56
	$\Delta H^{\neq}$, kJ·mol^{-1}			67 ± 2
	$\Delta S^{\neq}$, J·mol^{-1} K^{-1}			+28 ± 7
CF_3CH_2 [b]	20.0	0.24 ± 0.02	1.13 ± 0.16	0.27 ± 0.04
	25.0	0.61 ± 0.05	0.54 ± 0.07	0.33 ± 0.05
	30.0	0.88 ± 0.03	0.94 ± 0.05	0.83 ± 0.05
	35.0	1.50 ± 0.07	0.96 ± 0.09	1.44 ± 0.15
	40.0	2.60 ± 0.16	1.02 ± 0.12	2.65 ± 0.35
	$\Delta H^{\neq}$, kJ·mol^{-1}			90 ± 9
	$\Delta S^{\neq}$, J·mol^{-1} K^{-1}			+49 ± 29

[a] $[PhCH_2Co(Hdmg)_2MeOH] = 4 \times 10^{-4}$ M, [4-NH_2Py] = 0.01−0.64 M in MeOH. [b] $[CF_3CH_2Co(Hdmg)_2MeOH] = 1 \times 10^{-3}$ M, [4-NH_2Py] = 0.02−1.5 M in MeOH.

with 4-NH_2Py, Py and 4-CNPy. Similar plots are presented in Figures S4 and S5 (see the Supporting Information) for the reactions between $RCo(Hdmg)_2H_2O$ and the nucleophiles L = 4-NH_2Py, 4-CNPy, and Py, where R = $PhCH_2$ and S = MeOH, and the nucleophiles L = 4-CNPy and Py, where R = CF_3CH_2 and S = H_2O, respectively. The activation parameters for the substitution of methanol by 4-NH_2Py, Py, and 4-CNPy in the case where R = $PhCH_2$ were found to be $\Delta H^{\neq}$ = 67 ± 2, 77 ± 1 and 80 ± 2 kJ·mol^{-1}, $\Delta S^{\neq}$ = +28 ± 7, +57 ± 5 and +71 ± 6 J·mol^{-1} K^{-1}, and $\Delta V^{\neq}$ = +9.8 ± 0.1, +10.3 ± 0.3 and +13.0 ± 0.3 cm^3 mol^{-1}, respectively. The activation parameters in the case where R = CF_3CH_2 were found to be $\Delta H^{\neq}$ = 90 ± 9, 91 ± 5 and 89 ± 3 kJ·mol^{-1}, $\Delta S^{\neq}$ = +49 ± 29, +42 ± 17 and +36 ± 8 J·mol^{-1} K^{-1}, and $\Delta V^{\neq}$ = +7.5 ± 0.3, +8.6 ± 0.1 and +9.4 ± 0.1 cm^3 mol^{-1}, respectively. The activation parameters for substitution of H_2O by Py and 4-CNPy, where R = CF_3CH_2, were found to be $\Delta H^{\neq}$ = 94 ± 4 and 93 ± 1 kJ·mol^{-1}, $\Delta S^{\neq}$ = +62 ± 14 and +55 ± 4 J·mol^{-1} K^{-1}, and $\Delta V^{\neq}$ = +5.7 ± 0.4 and +7.4 ± 0.1 cm^3 mol^{-1}, respectively. These activation parameters, in particular the values of $\Delta V^{\neq}$, support the operation of a dissociative mechanism.

The discussion of the kinetic data will focus on the observed second-order rate constants for the overall reaction given in Equation (1), which is a composite of K and k, as given in Equations (2) and (3). Although for some systems k and K could be separated kinetically, the activation parameters were always determined for the combined value of kK, i.e. k_a. Little is presently known about the temperature and pressure dependence of the precursor formation step, and for that reason the thermodynamic contributions of K form part of the overall reported parameters. This complication should be kept in mind when interpreting the overall rate and activation parameters.

The reactivity of the cobaloxime complexes shows a strong dependence on the nature of the alkyl substituent R. The lability of these complexes was affected by the electronic and steric properties of the alkyl group. The second-order rate constants for the reaction of *trans*-$(PhCH_2)Co(Hdmg)_2(MeOH)$ with 4-NH_2Py, Py, and 4-CNPy were found to be 356, 182, and 296 $M^{-1}\,s^{-1}$ at 25.0 °C, respectively. However, those obtained for the reaction with *trans*-$(CF_3CH_2)Co(Hdmg)_2(MeOH)$ were 0.330, 0.147 and 0.153 $M^{-1}\,s^{-1}$ at 25.0 °C, respectively. The second-order rate constants for the reaction of *trans*-$(CF_3CH_2)Co(Hdmg)_2(H_2O)$ with Py and 4-CNPy in H_2O were found to be 0.317 and 0.214 $M^{-1}\,s^{-1}$ at 25.0 °C, respectively. This trend shows that the kinetic *trans* effect is greater for R = $PhCH_2$ than for R = CF_3CH_2, in accordance with the donor properties of the alkyl group. For the complexes *trans*-$[RCo(LNHpy)(HLNHpy)]^+$, where HLNHpy is the tridentate 2-(2-pyridylethyl)amino-3-butanone oxime ligand and $LNHpy^-$ its conjugate base, the second-order rate constants for substitution of 2-(pyridylethyl) were found to be 19.1, 0.25, 2.2 × 10^{-2}, and 1.7 × 10^{-2} $M^{-1}\,s^{-1}$ for R = Et, Me, CF_3CH_2, and $-CH_2-$, respectively.[30] The reaction between alkylcobalamins

 © 2004 Wiley-VCH Verlag GmbH & Co. KGaA, Weinheim

Table 2. Kinetic data for the reaction of *trans*-RCo(Hdmg)$_2$(S) with L in MeOH and H_2O as a function of temperature

	k_a, M^{-1} s^{-1}			
	R = $PhCH_2$, S = MeOH		R = CF_3CH_2,L = 4-CNPy	
T, °C	L = Py[a]	L = 4-CNPy[b]	S = MeOH[c]	S = H_2O[d]
5.0	18.3 ± 0.1	28 ± 2		
10.0	33.9 ± 0.3	49 ± 2		
15.0	64 ± 1	97 ± 1		
20.0	108 ± 1	173 ± 2	0.073 ± 0.001	0.112 ± 0.001
25.0	182 ± 1	296 ± 3	0.153 ± 0.001	0.214 ± 0.003
30.0			0.254 ± 0.001	0.393 ± 0.004
35.0			0.464 ± 0.003	0.739 ± 0.004
40.0			0.820 ± 0.004	1.390 ± 0.020
$\Delta H^{\neq}$, kJ·mol^{-1}	77 ± 1	80 ± 2	89 ± 3	93 ± 1
$\Delta S^{\neq}$, J·mol^{-1} K^{-1}	+57 ± 5	+71 ± 6	+36 ± 8	+55 ± 4

[a] [$PhCH_2Co(Hdmg)_2MeOH$] = 4 × 10^{-4} M, [Py] = 0.01 M. [b] [$PhCH_2Co(Hdmg)_2MeOH$] = 4 × 10^{-4} M, [4-CNPy] = 0.01 M. [c] [$CF_3CH_2Co(Hdmg)_2MeOH$] = 4 × 10^{-4} M, [4-CNPy] = 0.08 M. [d] [$CF_3CH_2Co(Hdmg)_2H_2O$] = 1 × 10^{-3} M, [4-CNPy] = 0.08 M, pH = 8 and I = 0.1 M $NaClO_4$.

Table 3. Kinetic data for the reaction of *trans*-(CF_3CH_2)Co(Hdmg)$_2$(S) with Py in MeOH and H_2O as a function of temperature

	T, °C	*k*, s^{-1}	*K*, M^{-1}	*kK*, M^{-1} s^{-1}
S = MeOH[a]	20.0	0.88 ± 0.05	0.07 ± 0.01	0.062 ± 0.010
	25.0	1.13 ± 0.05	0.13 ± 0.01	0.147 ± 0.013
	30.0	2.04 ± 0.14	0.12 ± 0.01	0.245 ± 0.026
	35.0	3.36 ± 0.40	0.12 ± 0.02	0.403 ± 0.083
	40.0	9.82 ± 0.89	0.08 ± 0.01	0.786 ± 0.121
	$\Delta H^{\neq}$, kJ·mol^{-1}			91 ± 5
	$\Delta S^{\neq}$, J·mol^{-1} K^{-1}			+42 ± 17
S = H_2O[b]	20.0	0.33 ± 0.01	0.57 ± 0.03	0.188 ± 0.011
	25.0	0.96 ± 0.08	0.33 ± 0.04	0.317 ± 0.047
	30.0	1.71 ± 0.25	0.34 ± 0.07	0.581 ± 0.147
	35.0	2.20 ± 0.19	0.54 ± 0.07	1.188 ± 0.185
	40.0	3.40 ± 0.08	0.68 ± 0.03	2.312 ± 0.117
	$\Delta H^{\neq}$, kJ·mol^{-1}			94 ± 4
	$\Delta S^{\neq}$, J·mol^{-1} K^{-1}			+62 ± 14

[a] [$CF_3CH_2Co(Hdmg)_2MeOH$] = 1 × 10^{-3} M and [Py] = 0.04−4.0 M. [b] [$CF_3CH_2Co(Hdmg)_2(H_2O)$] = 1 × 10^{-3} M, [Py] = 0.04−1.28 M, pH = 8 and I = 0.1 M $NaClO_4$.

(RCb1) and cyanide showed that the kinetic *trans* effect decreases in the order (R =) Pr > Me (ca. 10^4 $M^{-1}s^{-1}$) > CF_3CH_2 > CF_2H (10^3 M^{-1} s^{-1}) > CF_3 > $NCCH_2$ > CN (0.1 M^{-1} s^{-1}).[14] The substitution of H_2O by CN^- for various cobinamides (RCbi) increases in the order (R =) H_2O = DMBz < OH^- < CN^- < CH_2=CH, Me, and Et, with the corresponding rate constants ranging from about 10^3 to about 10^8 M^{-1} s^{-1}.[31]

The pK_{BH+} values for 4-NH_2Py, Py, and 4-CNPy are 9.17,[32] 5.23,[32] and 1.7[33] (estimated), respectively. Both in water and methanol, the second-order rate constants for the ligation of the pyridines are only slightly affected by their basicity. Such a weak sensitivity of the *kK* values is consistent with an I_d mechanism, which is controlled by the breaking of the Co−S bond. Analogously, the substitution rate constants of aquacobalamin by a variety of substituted pyridine ligands were found to be independent of their pK_{BH+} values.[25]

The second-order rate constants for substitution of H_2O in *trans*-(CF_3CH_2)Co(Hdmg)$_2$(H_2O) by Py and 4-CNPy are higher than that found for the corresponding reaction with cysteine,[34] and this was ascribed to metal-to-ligand π bonding. The range of rate constants for axial ligand binding to methylaquacobaloxime are 4.3−7.5 (RNH_2), 12.8−27.3 (RS^-), 49.6−55.2 (RSH), and 92−200 (X-py) M^{-1} s^{-1}.[35] That is, the π-acceptor ligands (X-Py, RS^- and RSH) react more rapidly than pure σ donors (RNH_2). In the ligand-substitution reactions of *trans*-MeCo(Hdmg)$_2$(H_2O), the higher reactivity of the substituted pyridines (as compared to neutral or anionic thiolates) stand in contrast to the opposite reactivity order for these same nucleophiles with various unsaturated carbon electrophiles.[35] The ratio of the second-order rate constants for the reaction of pyridine and 4-CNpy with alkylcobaloxime (R = CF_3CH_2) is 1.48, and that for R = Me is 1.24. The second-order rate constant in the case of R = Me is higher than for R = CF_3CH_2, which is due to the stronger labilization by R = Me.

The second-order rate constants for the substitution of H_2O in *trans*-RCo(Hdmg)$_2$(H_2O) by pyridine were found to

 © 2004 Wiley-VCH Verlag GmbH & Co. KGaA, Weinheim

Table 4. Kinetic data for the reaction of *trans*-$RCo(Hdmg)_2S$ with 4-NH_2Py, Py, and 4-CNPy as a function of pressure

	Pressure, MPa	k_{obs}, s^{-1}		
		4-NH_2Py	Py	4-CNPy
R = $PhCH_2$, S = MeOH[a]	10	2.28 ± 0.07	0.98 ± 0.03	1.28 ± 0.03
	50	1.94 ± 0.05	0.83 ± 0.01	1.01 ± 0.05
	90	1.63 ± 0.04	0.68 ± 0.01	0.81 ± 0.01
	130	1.37 ± 0.04	0.58 ± 0.01	0.66 ± 0.06
	$\Delta V^{\neq}$, $cm^3\ mol^{-1}$	+9.8 ± 0.1	+10.3 ± 0.3	+13.0 ± 0.3
R = CF_3CH_2, S = MeOH[b]	10	0.150 ± 0.006	0.107 ± 0.001	0.116 ± 0.006
	50	0.136 ± 0.007	0.093 ± 0.002	0.100 ± 0.006
	90	0.119 ± 0.002	0.082 ± 0.001	0.087 ± 0.001
	130	0.107 ± 0.003	0.072 ± 0.001	0.075 ± 0.004
	$\Delta V^{\neq}$, $cm^3\ mol^{-1}$	+7.5 ± 0.3	+8.6 ± 0.1	+9.4 ± 0.1
R = CF_3CH_2, S = H_2O[c]	10	–	0.135 ± 0.002	0.114 ± 0.003
	50	–	0.127 ± 0.003	0.101 ± 0.004
	90	–	0.115 ± 0.002	0.091 ± 0.002
	130	–	0.104 ± 0.002	0.081 ± 0.002
	$\Delta V^{\neq}$, $cm^3\ mol^{-1}$	–	+5.7 ± 0.4	+7.4 ± 0.1

[a] [$PhCH_2Co(Hdmg)_2MeOH$] = (4−7) × 10^{-4} M, {[4-NH_2Py], [Py] = 0.04 M and at 5.0 °C}, {[4-CNPy] = 0.0225 M and at 10.0 °C}. [b] [$CF_3CH_2Co(Hdmg)_2MeOH$] = 2 × 10^{-3}, [NH_2Py] = 0.08 M, {[Py], [4-CNPy] = 0.16 M}, and at 40.0 °C. [c] [$CF_3CH_2Co(Hdmg)_2H_2O$] = 2 × 10^{-3}, [Py] and [4-CNPy] = 0.08 M, pH = 8, at 40.0 °C and I = 0.1 M $NaClO_4$.

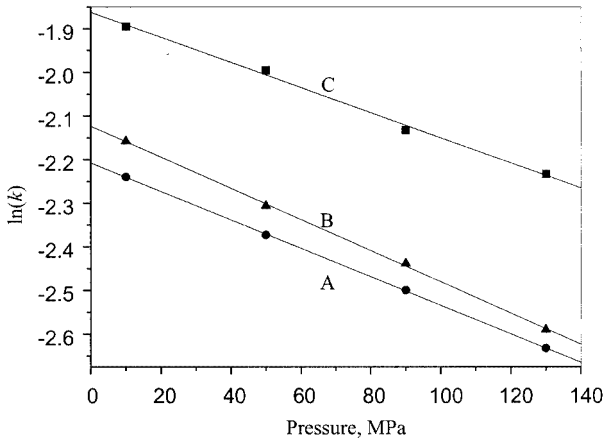

Figure 4. Plots of ln(k) versus pressure for the reaction between *trans*-$(CF_3CH_2)Co(Hdmg)_2(MeOH)$ and L, where L = Py (A), 4-CNPy (B) and 4-NH_2Py (C). Experimental conditions: [Co^{III}] = 2 × 10^{-3} M, [NH_2Py] = 0.08 M, [Py] and [4-CNPy] = 0.16 M, at 40.0 °C

be 1.49 × 10^4 (isopropyl), 1.17 × 10^3 (ethyl), 1.16 × 10^2 (methyl), 1.22 × 10^3 (phenylethyl), 1.64 × 10^2 (3-cyanopropyl), 1.65 × 10^2 (2-methoxyethyl), 2.34 × 10^1 (1-propenyl), 4.2 (iodomethyl), 3.17 × 10^{-1} (2,2,2-trifluoroethyl), 1.06 × 10^{-1} (chloromethyl), and 5.59 × 10^{-2} (cyanomethyl) $M^{-1}\ s^{-1}$ at 25 °C, respectively.[36] The second-order rate constants for substitution of methanol by pyridine in the complex *trans*-$(RSO_2)Co(Hdmg)_2(MeOH)$ were found to be 4.79 ± 0.01 and 3.56 ± 0.11 $M^{-1}\ s^{-1}$ for R = *p*-tolyl and methyl, respectively. Substitution of the solvent by pyridine in the complex $(CH_3C_6H_4SO_2)Co(Hdmg)_2S$ does have an effect on the second-order rate constants, which were found to be 1.12 × 10^{-1}, 4.79 × 10^{-2}, and 4.16 × 10^{-3} $M^{-1}\ s^{-1}$ for S = EtOH, MeOH, and H_2O, respectively.[37]

Ligand-substitution reactions of *trans*-$RCo(Hdmg)_2H_2O$, for R = $PhCH_2$ by Py and 4-CNPy in methanol, and also for R = CF_3CH_2 by 4-CNPy in H_2O and MeOH, are characterised by a linear dependence of the observed pseudo first-order rate constant on the concentration of the entering nucleophile as shown in Figures 3 and S3. In terms of the suggested dissociative interchange mechanism, this means that precursor formation is weak and does not show up in the kinetic data even at high concentrations of the entering ligand. The curvature observed in the nucleophile concentration dependence of k_{obs} for the substitution reactions of *trans*-$RCo(Hdmg)_2(H_2O)$ (R = $PhCH_2$ and CF_3CH_2) by 4-NH_2Py and Py suggests that an interchange mechanism involving a rapid pre-association of the complex with the incoming ligand is operating. The precursor-formation constant decreases when the electron donor ability of the alkyl group in the *trans* position is increased. It was found that the precursor-formation constants for the substitution of MeOH by 4-NH_2Py are 0.35 and 0.54 M^{-1} at 25.0 °C for R = $PhCH_2$ and CF_3CH_2, respectively. It is also apparent that the precursor-formation constant depends on the nature of the nucleophile. The π-electron density on the Py ring increases in the order 4-CNPy < Py < 4-NH_2Py,[38] which is also the order of increasing tendency for precursor formation.

It is generally known from the literature that a system must be sufficiently electron-rich in order that bonding through the π-electrons of pyridine can occur.[39] This π-interaction results in the effective binding of the nucleophile close to the metal centre during precursor formation, which is followed by an interchange of ligands controlled by

 © 2004 Wiley-VCH Verlag GmbH & Co. KGaA, Weinheim

breakage of the Co−OH_2 bond by an I_d mechanism.[25] The pre-equilibrium constants for the reaction of $[MeCo\{(DO)(DOH)pn\}H_2O]^+$ with L = imidazole, benzylamine, Py and 4-MePy at 25 °C were found to be 0.26, 0.12, 1.00, and 1.81 M^{-1}, respectively.[15] The pre-equilibrium constants for the reaction of aquacobalamin with Py, 4-MePy, and 2,4-DMePy were found to be 1.1, 2.5, and 4.9 M^{-1}, respectively.[25]

By way of comparison, the lability of *trans*-$RRh(Hdmg)_2(H_2O)$ is affected by the steric and electronic effects of the alkyl group R, and in all cases the reaction rate is almost independent of the nucleophilicity of the incoming ligand.[40,41] There is a definite trend in the $\Delta V^{\neq}$ data: the values are significantly positive for the faster substitution reactions (R = CH_3) but significantly negative for the slower substitution reactions (R = CF_3CH_2).[42] This trend correlates well with the *trans*-influence of the R groups in the ground state, as observed for a series of pyridine (py) complexes: the Rh−Py bond length decreases in the order CH_3 [2.220(3) Å] > $ClCH_2$ [2.178(3) Å] > CF_3CH_2 [2.145(3) Å].[40,41] A similar trend is expected for the Rh−O bond in the corresponding aqua complexes: faster reactions are thus associated with the stronger *trans* influence of the methyl group, and slower reactions with the weaker *trans* influence of $ClCH_2$ and CF_3CH_2. Furthermore, the nature of the R group directly determines the substitution mechanism. The strong donor properties of CH_3 result in a dissociative substitution process (I_d), characterised by the significantly positive $\Delta V^{\neq}$ value, whereas the weaker donor properties of CF_3CH_2 favour a more associative substitution mechanism (I_a), as indicated by the significantly negative value of $\Delta V^{\neq}$.[42] Thus, in the transition state the degree of bond breakage (Rh−OH_2) and bond formation (Rh−L) is controlled by the donor properties of R.

The $\Delta H^{\neq}$ values for substitution reactions of *trans*-$RCo(Hdmg)_2(H_2O)$ (for R = $PhCH_2$ and CF_3CH_2) by pyridine derivatives in H_2O and methanol are relatively independent of the nature of the incoming ligand. It is expected that the reactions involve a dissociative activation process, since the ligands are loosely bound in the transition state. The activation enthalpy for the substitution reaction with R = CF_3CH_2 is higher than for R = $PhCH_2$ due to the strong Co−OH_2 bond in the ground state. Hence, $\Delta H^{\neq}$ values appear to be affected by both the electron-withdrawing and steric effects of the R group. The influence of these factors on $\Delta S^{\neq}$, however, cannot be rationalised. The entropy values should be slightly more positive since the transition state should be less ordered than the initial state, owing to the relief of steric strain. The organocobaloximes are about 10^5 times more labile than the corresponding nitro and iodo-aqua complexes. This very high rate enhancement is due to both the decrease in the activation enthalpy and the increase in the activation entropy.[43]

The values of $\Delta V^{\neq}$ obtained for R = CF_3CH_2 in methanol were found to be +7.5, +8.6, and +9.4 $cm^3\ mol^{-1}$, respectively. The values of $\Delta V^{\neq}$ for substitution of the solvent by pyridine derivatives (4-NH_2Py, Py, and 4-CNPy) in the complex *trans*-$(PhCH_2)Co(Hdmg)_2(H_2O)$ were found to be +9.8, +10.3 and +13 $cm^3\ mol^{-1}$, respectively. This is consistent with an enhanced dissociative (limiting D) character in the mechanism on going from the CF_3CH_2 derivative to the $PhCH_2$ derivative. Interestingly, $\Delta V^{\neq}$ for substitution of H_2O by Py and 4-CNPy (R = CH_2CF_3 in H_2O) were found to be +5.7 and +7.4 $cm^3\ mol^{-1}$, respectively. In these cases the small positive values of $\Delta V^{\neq}$ suggest that the mechanism is of an I_d nature. Thus the substitution mechanism changes from limiting D to I_d along the series from R = $PhCH_2$ to R = CF_3CH_2, on decreasing the basicity of the nucleophiles, and on changing the solvent from MeOH to H_2O. This mechanistic changeover is clearly seen in the size of $\Delta V^{\neq}$, and can be directly correlated with the donor properties of R, which in turn control the magnitude of the rate constants. The greater donating properties of $PhCH_2$ result in a limiting dissociative process as characterized by the significantly positive $\Delta V^{\neq}$. Similarly, the weaker donor properties of CF_3CH_2 favour more a dissociative interchange mechanism, as shown by the $\Delta V^{\neq}$ data. The activation parameters for substitution of aquacobalamin by thiourea, substituted thiourea and pyridine for the forward and reverse reactions conclusively confirm that the mechanism of the substitution is a dissociative interchange. For instance, the volumes of activation for both the forward and reversible reactions have values between +6 and +10 $cm^3\ mol^{-1}$.[16,17]

We conclude that all the available data underline the operation of a limiting dissociative (D) mechanism for substitution of methanol by 4-CNPy when R = $PhCH_2$. However, when R = CF_3CH_2, the mechanism is I_d for substitution of the solvent by 4-CNPy in methanol or H_2O. The non-linear concentration dependence must therefore be due to the operation of an I_d mechanism, and involve the formation of a precursor complex. The strong precursor formation is ascribed to an interaction of the π system of the pyridine ligand with the coordination sphere of the complex. This π interaction results in the effective binding of the entering nucleophile close to the metal centre during precursor formation, which is followed by an interchange of ligands controlled by the breakage of the Co−solvent bond by an I_d mechanism.

Experimental Section

Materials: All chemicals were of p. a. grade and used as received. 4-Aminopyridine and 4-cyanopyridine were purchased from Acros, tricine buffer from Sigma and pyridine from Baker. Ultra pure water was used in the kinetic measurements. *trans*-$RCo(Hdmg)_2H_2O$ (R = CF_3CH_2, $PhCH_2$) were prepared as previously reported.[44] Because alkyl cobaloximes are light sensitive, their solutions were prepared and handled away from light.

Instrumentation: The pH of the solution was measured using a Mettler Delta 350 pH meter. The pH meter was calibrated with standard buffer solutions at pH 4 and 7. UV/Vis spectra were recorded on Shimadzu UV-2101 and Hewlett Packard 8452A spectrophotometers.

 © 2004 Wiley-VCH Verlag GmbH & Co. KGaA, Weinheim

Kinetic measurements were carried out on an Applied Photophysics SX 18MV stopped-flow instrument coupled to an online data acquisition system. At least eight kinetic runs were recorded under all conditions, and the reported rate constants represent the mean values. All kinetic measurements were carried out under pseudo-first order conditions, i.e. the entering nucleophile concentration was in at least a tenfold excess. Measurements at high pressure were carried out using a home-made high pressure stopped-flow unit.[45] Kinetic data were analyzed with the OLIS KINFIT program. All instruments used were thermostatted to the desired temperature (± 0.1 °C).

Acknowledgments

The authors gratefully acknowledge financial support from CNR (Rome), MIUR (Rome), PRIN No. MMO3185591, the Deutsche Forschungsgemeinschaft and the Max-Buchner Research Foundation (to R. v. E.).

[1] N. Bresciani-Pahor, M. Forcolin, L. G. Marzilli, L. Randaccio, M. F. Summers, P. J. Toscano, *Coord. Chem. Rev.* **1985**, *63*, 1.
[2] A. L. Crumbliss, W. K. Wilmarth, *J. Am. Chem. Soc.* **1970**, *92*, 2593.
[3] K. L. Brown, S. Satyanarayana, *J. Am. Chem. Soc.* **1992**, *114*, 5674.
[4] K. L. Brown, R. G. Kallen, *J. Am. Chem. Soc.* **1972**, *94*, 1894.
[5] L. G. Marzilli, P. J. Toscano, L. Randaccio, N. Bresciani-Pahor, M. Calligaris, *J. Am. Chem. Soc.* **1979**, *101*, 6754.
[6] L. Randaccio, N. Bresciani-Pahor, P. J. Toscano, L. G. Marzilli, *J. Am. Chem. Soc.* **1980**, *102*, 7372.
[7] N. Bresciani-Pahor, L. Randaccio, P. J. Toscano, A. Sandercock, L. G. Marzilli, *J. Chem. Soc., Dalton Trans.* **1982**, 129.
[8] M. F. Summers, P. J. Toscano, N. Bresciani-Pahor, G. Nardin, L. Randaccio, L. G. Marzilli, *J. Am. Chem. Soc.* **1983**, *105*, 6259.
[9] N. Bresciani-Pahor, L. G. Marzilli, L. Randaccio, P. J. Toscano, E. Zangrando, *J. Chem. Soc., Chem. Commun.* **1984**, 1508.
[10] G. Costa, G. Mestroni, E. de Savorgnani, *Inorg. Chim. Acta* **1969**, *3*, 323.
[11] G. Costa, G. Mestroni, L. Stefani, *J. Organomet. Chem.* **1967**, *7*, 493.
[12] G. Costa, G. Mestroni, G. Tauzher, L. Stefani, *J. Organomet. Chem.* **1966**, *6*, 181.
[13] M. S. A. Hamza, X. Zou, K. L. Brown, R. van Eldik, *Inorg. Chem.* **2001**, *40*, 5440.
[14] M. S. A. Hamza, X. Zou, K. L. Brown, R. van Eldik, *J. Chem. Soc., Dalton Trans.* **2002**, 3832.
[15] G. Tauzher, R. Dreos, G. Costa, M. Green, *J. Chem. Soc., Chem. Commun.* **1973**, 413.
[16] G. Stochel, R. van Eldik, *Inorg. Chem.* **1990**, *29*, 2075.
[17] M. Meier, R. van Eldik, *Inorg. Chem.* **1993**, *32*, 2635.
[18] B. M. Alzoubi, M. S. A. Hamza, C. Dücker-Benfer, R. van Eldik, *Eur. J. Inorg. Chem.* **2002**, 968.
[19] M. S. A. Hamza, C. Dücker-Benfer, R. van Eldik, *Inorg. Chem.* **2000**, *39*, 3777.
[20] G. Stochel, R. van Eldik, H. Kunkely, A. Vogler, *Inorg. Chem.* **1989**, *28*, 4314.
[21] A. G. Gergan, N. E. Brasch, R. van Eldik, *Inorg. Chem.* **2001**, *40*, 1430.
[22] F. Nome, J. H. Fendler, *J. Chem. Soc., Dalton Trans.* **1976**, 1212.
[23] H. M. Marques, J. C. Bradley, L. A. Campbell, *J. Chem. Soc., Dalton Trans.* **1992**, 2019.
[24] H. M. Marques, *J. Chem. Soc., Dalton Trans.* **1991**, 339.
[25] F. F. Prinsloo, M. Meier, R. van Eldik, *Inorg. Chem.* **1994**, *33*, 900.
[26] W. W. Reenstra, W. P. Jencks, *J. Am. Chem. Soc.* **1979**, *101*, 5780.
[27] F. F. Prinsloo, E. L. J. Breet, R. van Eldik, *J. Chem. Soc., Dalton Trans.* **1995**, 685.
[28] M. S. A. Hamza, *J. Chem. Soc., Dalton Trans.* **2002**, 2831.
[29] [29a] N. E. Brasch, M. S. A. Hamza, R. van Eldik, *Inorg. Chem.* **1997**, *36*, 3216. [29b] M. S. A. Hamza, A. G. Cregan, N. E. Brasch, R. van Eldik, *J. Chem. Soc.* **2003**, 596.
[30] B. M. Alzoubi, M. S. A. Hamza, A. Felluga, L. Randaccio, G. Tauzher, R. van Eldik, *Eur. J. Inorg. Chem.* **2003**, 3738−3744.
[31] D. A. Baldwin, E. A. Betterton, J. M. Pratt, *S. Afr. J. Chem.* **1982**, *35*, 173.
[32] A. Albert, E. P. Serjeant, *The Determination of Ionization Constants*, Chapman and Hall, London, **1984**.
[33] P. Moore, R. G. Wilkins, *J. Chem. Soc.* **1964**, 3454.
[34] M. S. A. Hamza, A. Felluga, L. Randaccio, G. Tauzher, R. van Eldik, *Dalton Trans.* submitted for publication.
[35] K. L. Brown, D. Chernoff, D. J. Keljo, R. G. Kallen, *J. Am. Chem. Soc.* **1972**, *94*, 6697.
[36] K. L. Brown, D. Lyles, M. Pencovici, R. G. Kallen, *J. Am. Chem. Soc.* **1975**, *97*, 7338.
[37] J. M. Palmer, E. Deutsch, *Inorg. Chem.* **1975**, *14*, 17.
[38] E. S. Gould, *Mechanism and Structure in Organic Chemistry*, Holt International, London, **1970**.
[39] K. Schofield, *Hetero-Aromatic Nitrogen Compounds: Pyrroles and Pyridines*, Butterworths, London, **1967**, 2213.
[40] N. B. Pahor, R. Dreos-Garlatti, S. Geremia, L. Randaccio, G. Tauzher, E. Zangrando, *Inorg. Chem.* **1990**, *29*, 3437.
[41] L. Randaccio, S. Geremia, R. Dreos-Garlatti, G. Tauzher, F. Asano, G. Pellizer, *Inorg. Chim. Acta* **1992**, *194*, 1.
[42] [42a] R. van Eldik, A. E. Merbach, *Comments, Inorg. Chem.* **1992**, *12*, 341. [42b] C. Dücker-Benfer, R. Dreos, R. van Eldik, *Angew. Chem. Int. Ed. Engl.* **1995**, *34*, 2245.
[43] R. Dreos-Garlatti, G. Tauzher, G. Costa, M. Green, *Inorg. Chim. Acta* **1981**, *50*, 95.
[44] G. N. Schrauzer, R. J. Windgassen, *J. Am. Chem. Soc.* **1966**, *88*, 3738.
[45] R. van Eldik, W. Gaede, S. Wieland, J. Kraft, M. Spitzer, D. A. Palmer, *Rev. Sci. Instrum.* **1993**, *64*, 1355.

Received October 14, 2003

 © 2004 Wiley-VCH Verlag GmbH & Co. KGaA, Weinheim

EurJIC
European Journal of Inorganic Chemistry

Issue 4/2004

Pages 661–914

Papers available ahead of print in Early View at www.interscience.wiley.com

Earliest available Table of Contents:
Automatically, free of charge by e-mail through
www.interscience.wiley.com/alerts

COVER PICTURE

The cover picture shows planar heterodinuclear phthalocyanine (Pc) dimers consisting of Pc and pyrazinoporphyrazine and of Pc and naphthalocyanine. In the picture, red spheres indicate nitrogen atoms. These dimers commonly show broad absorption bands between ca. 500 and 1000 nm, while the differential pulse voltammetry and molecular orbital calculations suggest that the dimers are unstable to oxidation, and that the two relatively independent chromophore units interact. Details are discussed in the article by N. Kobayashi and H. Ogata on p. 906 ff.

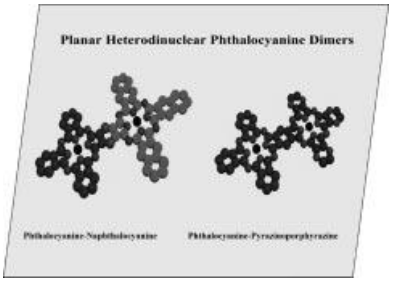

MICROREVIEW

Contents

675 **R. W. J. M. Hanssen, R. A. van Santen, H. C. L. Abbenhuis***

The Dynamic Status Quo of Polyhedral Silsesquioxane Coordination Chemistry

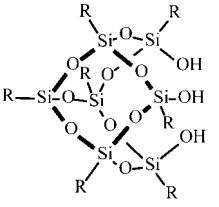

Keywords: Catalysis / Organometallic chemistry / Si ligands / Silsesquioxanes / Silanol

 © 2004 Wiley-VCH Verlag GmbH & Co. KGaA, Weinheim

SHORT COMMUNICATIONS

685 **F. Heirtzler,* S. Dias, M. Neuburger**

Dimeric Metallo-Organic Supramolecular Quinoxaline Stacking Synthons

Keywords: Supramolecular chemistry / Helical structures / Heterocycles / Stacking interactions / Self-assembly / Sandwich complexes

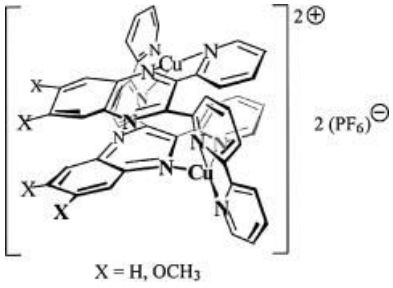

689 **B. Ronig, T. Bick, I. Pantenburg, L. Wesemann***

Stannaborate Chemistry: Nucleophilic Substitution at the Cluster Sphere

Keywords: Boranes / Boron / Tin / Nucleophilic substitution

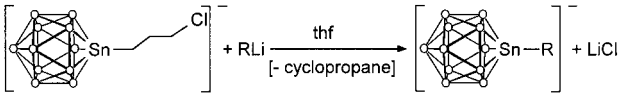

FULL PAPERS

695 **K. V. Axenov, V. V. Kotov, M. Klinga, M. Leskelä, T. Repo***

New Bulky Bis(amino)cyclodiphosph(III)azanes and Their Titanium(IV) Complexes: Synthesis, Structures and Ethene Polymerization Studies

Keywords: Phosphazenes / Titanium / Homogeneous catalysis / Polymerization

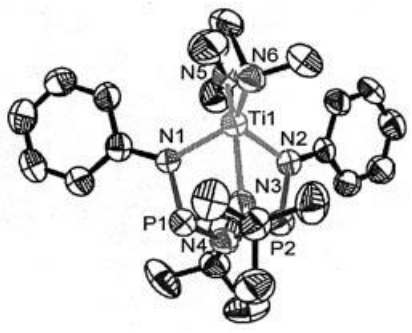

707 **A. Grirrane, A. Pastor, E. Álvarez, C. Mealli, A. Ienco, P. Rosa, F. Montilla, A. Galindo***

Manganese Oxydiacetate Complexes: Synthesis, Structure and Magnetic Properties

Keywords: Manganese / Tridentate ligands / Coordination modes / Magnetic properties

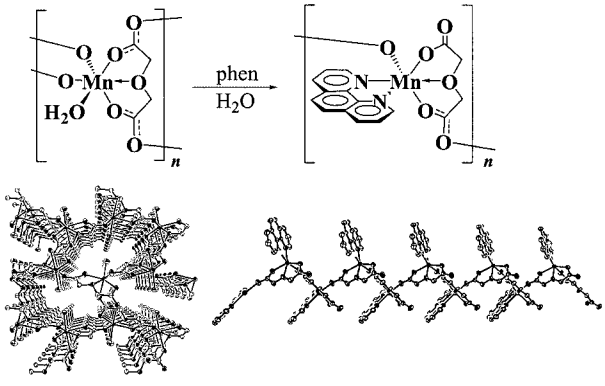

718 **V. Münchow, R. Steudel***

Preparation of 17 Sulfur-Rich Chain-Like Thiaalkanes R−S_x−R′−S_y−R and R−S_x−R′−S_y−R′−S_z−R (x, y, $z > 2$) from Titanocene Thiolate Complexes

Keywords: Alkanes / Ligand effects / Sandwich compounds / Sulfur / Titanium

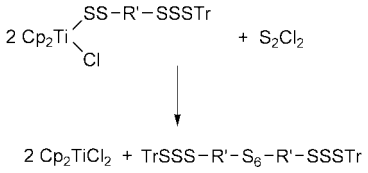

726 **F. Stoffelbach, B. Rebière, R. Poli***

A Bis(diazadiene) Adduct of $MoCl_2$: Mononuclear, Octahedral, Undistorted and Diamagnetic

Keywords: Density functional calculations / Magnetic properties / Molybdenum / N ligands / X-ray diffraction

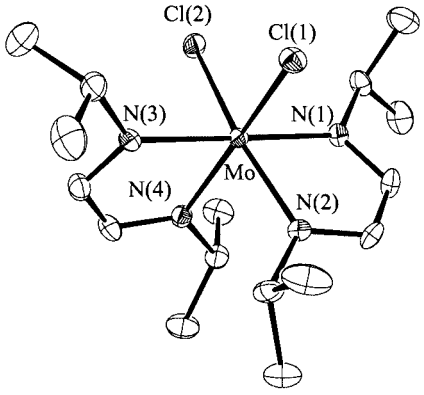

732 **B. Crociani,* S. Antonaroli, L. Canovese, P. Uguagliati, F. Visentin**

Kinetic Studies of the Oxidative Addition and Transmetallation Steps Involved in the Cross-Coupling of Alkynyl Stannanes with Aryl Iodides Catalysed by η^2-(Dimethyl fumarate)-(iminophosphane)palladium(0) Complexes

Keywords: Palladium / N,P ligands / Kinetics / Cross-coupling

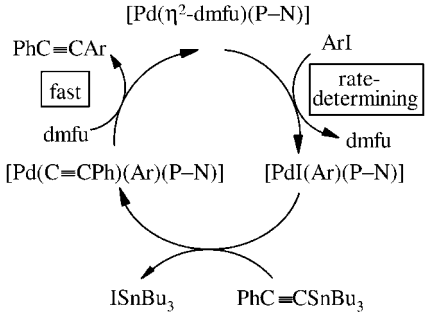

743 **M. Saito,* N. Henzan, M. Nitta, M. Yoshioka**

Synthesis, Structures and Reactions of Novel 9,10-Dihydro-9,10-distannaanthracenes

Keywords: Halogenation / Synthesis design / Tin

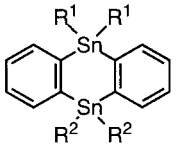

$R^1 = R^2 = Me$
$R^1 = R^2 = p\text{-}OMeC_6H_4$
$R^1 = Me$, $R^2 = t\text{-}Bu$
$R^1 = p\text{-}OMeC_6H_4$, $R^2 = Me$
$R^1 = R^2 = Cl$
$R^1 = R^2 = I$

749 **M. Fild, C. Thöne,* S. Tötös**

Synthetic and Structural Studies of Pd^{II} and Pt^{II} Complexes with Quincorine and Quincoridine Derivatives

Keywords: N,P ligands / Heterocycles / Palladium / Platinum / Bioinorganic chemistry

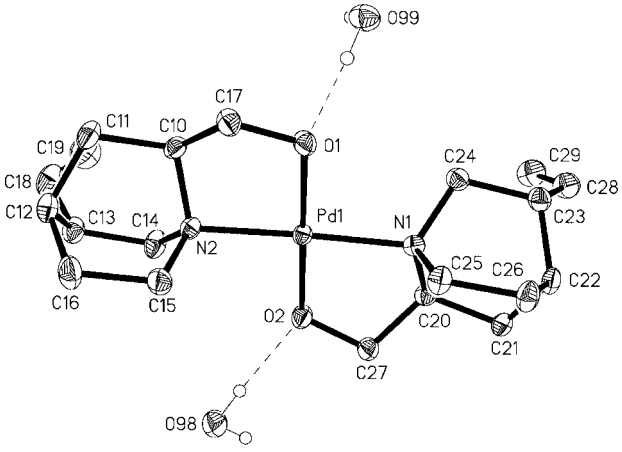

 © 2004 Wiley-VCH Verlag GmbH & Co. KGaA, Weinheim

762 **A. Thirumurugan, S. Natarajan***

Inorganic–Organic Hybrid Compounds: Synthesis and Structures of New Metal Organic Polymers Synthesized in the Presence of Mixed Dicarboxylates

Keywords: Carboxylate ligands / Coordination modes / Thermochemistry / Lanthanides

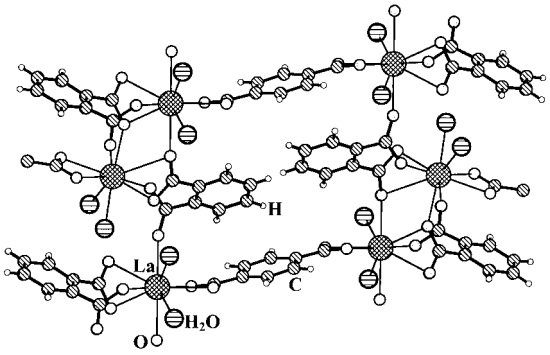

771 **K. Y. Dorogov, A. V. Churakov, L. G. Kuzmina, J. A. K. Howard, G. I. Nikonov***

Direct Hydride/Silyl Exchange – Synthesis and X-ray Study of the Bis(silyl) Complex [$Cp_2NbH(SiCl_3)_2$]

Keywords: Hydride ligands / Niobium / Si ligands / X-ray diffraction

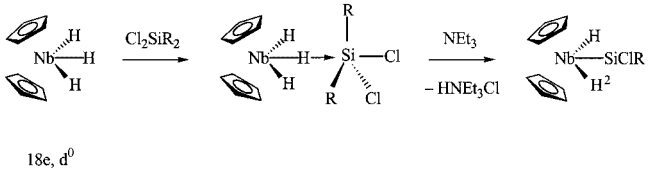

776 **D. Sturmayr, U. Schubert***

A Comparison of the Reactivity of Chloroalkanes and Chlorosilanes towards Activated Pt^{II} Complexes by DFT Calculations

Keywords: Hemilabile ligands / Oxidative addition / Reductive elimination / Density functional calculations / Silanes

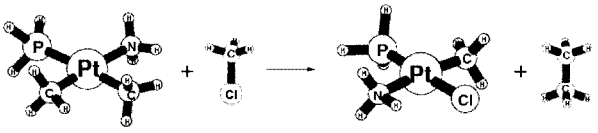

783 **M. Merkel, D. Schnieders, S. M. Baldeau, B. Krebs***

Structural Snapshots of a Dynamic Coordination Sphere in Model Complexes for Catechol 1,2-Dioxygenases

Keywords: Iron / Tripodal ligands / Coordination modes / Enzymes

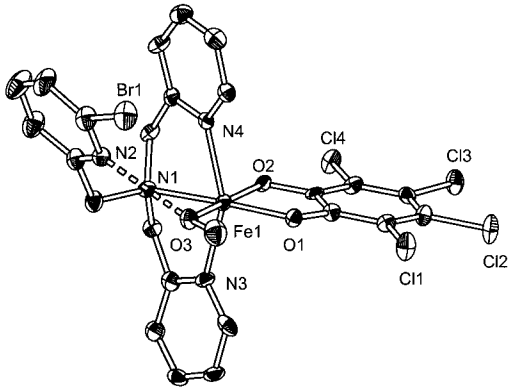

791 **G. Lenoble, C. Lacaze-Dufaure, M. Urrutigoïty, C. Mijoule, P. Kalck***

Tandem Palladium-Catalyzed Cyclocarbonylation of Isolimonene: A Mechanistic Investigation and Theoretical Calculations on the Fully Diastereoselective Step

Keywords: Asymmetric induction / Cyclocarbonylation / Density functional calculations / Homogeneous catalysis / NMR spectroscopy / Palladium

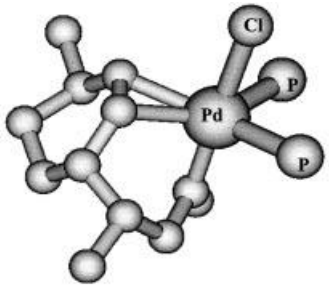

 © 2004 Wiley-VCH Verlag GmbH & Co. KGaA, Weinheim

798 **Y. Ohgo,* T. Ikeue, M. Takahashi, M. Takeda, M. Nakamura***

Anomalous Difference in Magnetic Behavior between Highly Saddled Iron(III) Porphyrin Complexes in the Solid State

Keywords: Iron / Porphyrinoids / Spin crossover / Magnetic properties

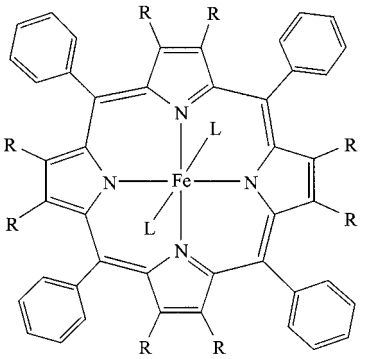

$[Fe(OMTPP)L_2]^+$ (R = Methyl)
$[Fe(OETPP)L_2]^+$ (R = Ethyl)
L = DMAP, Py

810 **N. d'Alessandro, M. Di Deo, M. Bonetti, L. Tonucci, A. Morvillo, M. Bressan***

Hydration of Propargylic Alcohols by Ruthenium Catalysts, with Dominant Anti-Markovnikov Regioselectivity, Formation of α,β-Unsaturated Products and Catalytic Decarbonylation to 1-Alkenes

Keywords: Ruthenium / Alkynes / Phthalocyanines / Hydration / Decarbonylation

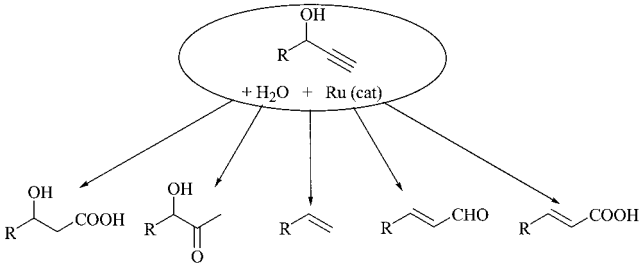

818 **A. F. Hill,* J. M. Malget, A. J. P. White, D. J. Williams**

Dihydrobis(pyrazolyl)borate Alkylidyne Complexes of Tungsten

Keywords: Borates / Carbyne ligands / Multiple bonds / N Ligands / Tungsten

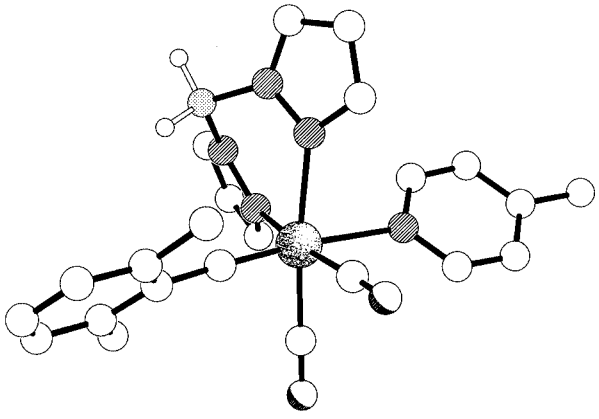

829 **W.-K. Wong,* H. Liang, J. Guo, W.-Y. Wong, W.-K. Lo, K.-F. Li, K.-W. Cheah, Z. Zhou, W.-T. Wong**

Template Synthesis, Crystal Structure and Luminescent Properties of Neutral N_4O_3 Tripodal $Ln^{III}L$ Complexes (Ln^{III} = La^{3+}, Eu^{3+}, Gd^{3+}, Tb^{3+}, Dy^{3+}, Ho^{3+}, Er^{3+}, Tm^{3+} or Lu^{3+}; H_3L = Tris{[3′-(2″-pyridyl)-5′-*tert*-butyl-2′-hydroxybenzylidene-2-imino]ethyl}amine)

Keywords: Lanthanides / Luminescence / Schiff bases / Tripodal ligands

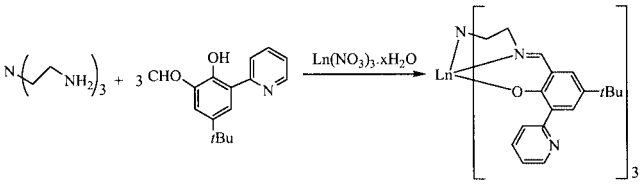

Ln = La **1**, Eu **2**, Gd **3**, Tb **4**, Dy **5**, Ho **6**, Er **7**, Tm **8**, Lu **9**

 © 2004 Wiley-VCH Verlag GmbH & Co. KGaA, Weinheim

837 **H. He, J. Guo, Z. Zhao, W.-K. Wong,* W.-Y. Wong, W.-K. Lo, K.-F. Li, L. Luo, K.-W. Cheah**

Synthesis, Characterization and Near-Infrared Photoluminescence of Monoporphyrinate Lanthanide Complexes Containing an Anionic Tripodal Ligand

Keywords: Lanthanides / Photoluminescence / Porphyrins / Tripodal ligands

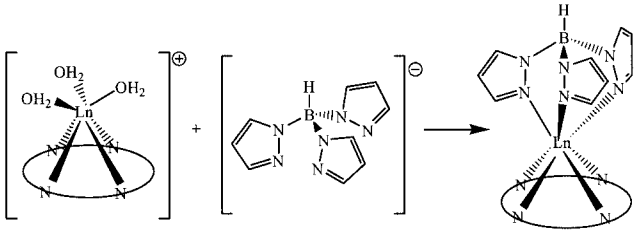

846 **M. Klopstra, G. Roelfes, R. Hage, R. M. Kellogg, B. L. Feringa***

Non-Heme Iron Complexes for Stereoselective Oxidation: Tuning of the Selectivity in Dihydroxylation Using Different Solvents

Keywords: Dihydroxylation / Enzyme models / Epoxidation / Iron / N ligands / Oxidation

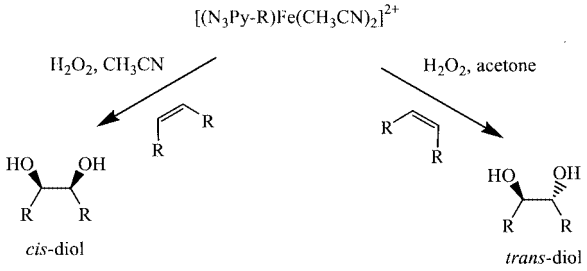

857 **M. Costas, C. Anda, A. Llobet,* T. Parella, H. Stoeckli Evans, E. Pinilla**

Synthesis, Structure and Hydrolytic Properties of a Family of New Zn Complexes Containing Hexaazamacrocyclic Ligands

Keywords: Zinc / Cooperative effects / Coordination chemistry / Fluxionality / Homogeneous catalysis / Macrocyclic ligands

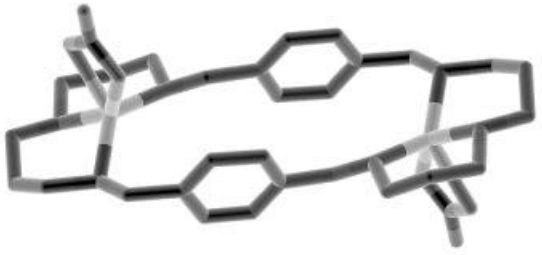

866 **L.-C. Song,* G.-A. Yu, H.-T. Wang, F.-H. Su, Q.-M. Hu, Y.-L. Song, Y.-C. Gao**

Synthesis, Characterization and Properties of Transition Metal Pd/Pt [60]Fullerene Complexes Containing Phosphane Ligands − Crystal Structure of [Pd(η^2-C_{60}){$Ph_2PCH_2(CH_2OCH_2)_2CH_2PPh_2$}]

Keywords: Fullerenes / Palladium / Phosphanes / Platinum

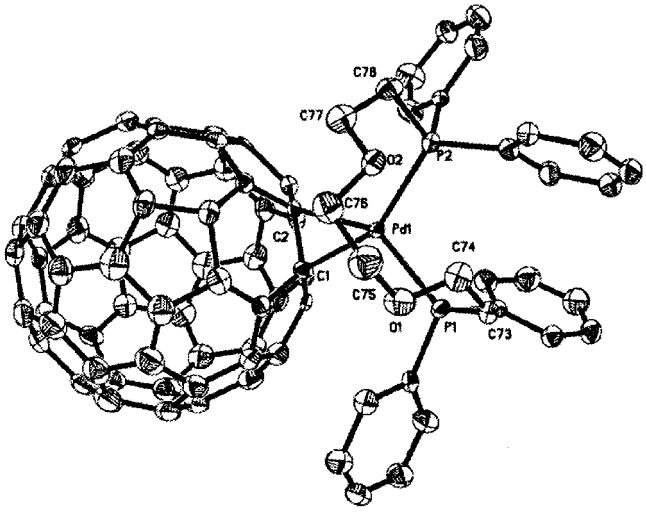

 © 2004 Wiley-VCH Verlag GmbH & Co. KGaA, Weinheim

872 **D. Saravanakumar, N. Sengottuvelan, V. Narayanan, M. Kandaswamy,* K. Chinnakali, G. Senthilkumar, H. K. Fun**

Synthesis, Structural, Magnetic and Electrochemical Studies of Antiferromagnetically Coupled Symmetric Oxamidate-Bridged Binuclear Copper(II) Complexes

Keywords: Magnetic properties / Electrochemistry / Copper / N,O ligands

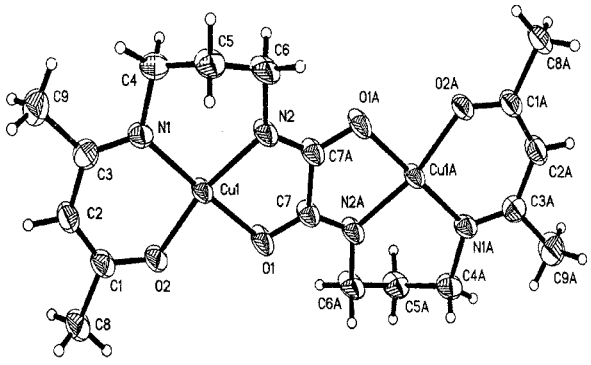

879 **N. Reddig, D. Pursche, M. Kloskowski, C. Slinn, S. M. Baldeau, A. Rompel***

Tuning the Catalase Activity of Dinuclear Manganese Complexes by Utilizing Different Substituted Tripodal Ligands

Keywords: Manganese / Tripodal ligands / Bioinorganic chemistry / Enzyme models

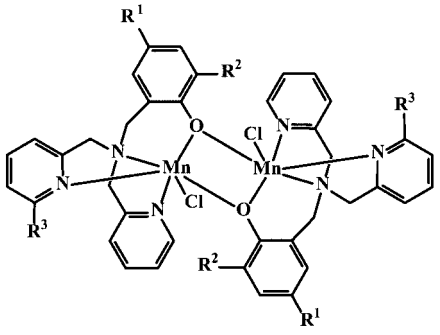

1 : $R^1 = R^2 = R^3 = H$ **4 : $R^1 = NO_2$; $R^2 = H$; $R^3 = Me$**
2 : $R^1 = NO_2$; $R^2 = R^3 = H$ **5 : $R^1 = R^3 = H$; $R^2 = OMe$**
3 : $R^1 = R^2 = H$; $R^3 = Me$

888 **L. Dahlenburg,* R. Götz**

Iridium Complexes with Chiral and Achiral β-Aminophosphane Ligands: Catalysts for >C=O Hydrogenation and H/D Exchange Involving both Homo- and Heterolytic H_2 Activation

Keywords: Chirality / Hydrogenations / Isotopic exchange / Iridium

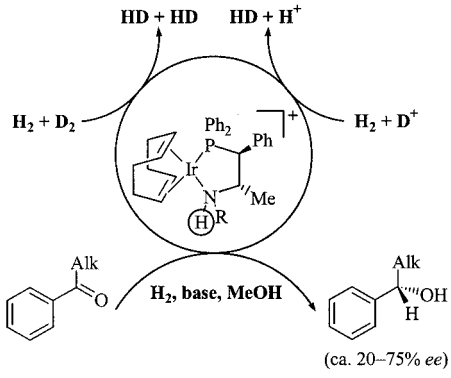

(ca. 20–75% *ee*)

906 **N. Kobayashi,* H. Ogata**

Some Properties and Molecular Orbitals of Planar Heterodinuclear Phthalocyanines

Keywords: Circular dichroism / Cyclic voltammetry / Phthalocyanines / UV/Vis spectroscopy

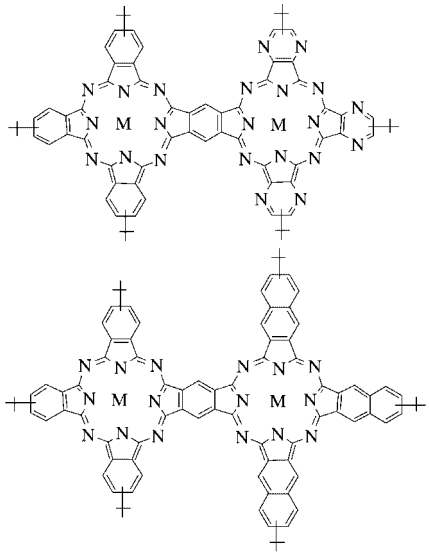

 © 2004 Wiley-VCH Verlag GmbH & Co. KGaA, Weinheim

The Dynamic Status Quo of Polyhedral Silsesquioxane Coordination Chemistry

Rob W. J. M. Hanssen,[a] Rutger A. van Santen,[a] and Hendrikus C. L. Abbenhuis*[a]

Keywords: Catalysis / Organometallic chemistry / Si ligands / Silsesquioxanes / Silanol

The chemistry of polyhedral oligomeric silsesquioxanes (POSS) has taken a tremendous leap over the past decade. New synthetic approaches have been developed, and new complexes based on elements throughout the periodic table have been synthesized and applied in catalytic processes such as alkene epoxidation, Oppenauer oxidation, alkene polymerization, Diels–Alders reactions and alkene metathesis. The use of silsesquioxane ligands as models for silica surface has provided an intimate knowledge of the reactions on the surface of this much-used support. New methods have been developed to incorporate silsesquioxanes into new materials. Encapsulation in siloxane polymers has provided precision supports for catalysts and controlled calcination has produced materials with well-defined metal oxide particles. This paper reviews the history and the latest developments of silsesquioxane chemistry.
(© Wiley-VCH Verlag GmbH & Co. KGaA, 69451 Weinheim, Germany, 2004)

Silsesquioxanes: Introduction and History

Polyhedral oligomeric silsesquioxanes (POSS), or simply silasesquioxanes or silsesquioxanes is the general IUPAC name for a family of polycyclic compounds consisting of silicon and oxygen (See Figure 1). The name sil(a)sesquioxane is derived from *sil-oxane* (compounds of silicon and oxygen) and *sesqui* (Latin, meaning one and a half), and the general name reflects the ratio of silicon and oxygen in the completely condensed silsesquioxanes $[RSiO_{3/2}]_{2n}$ (vide infra).

Silsesquioxanes are part of a larger family of silicon-oxygen compounds, called spherosilicates. The main feature of

[a] Schuit Institute of Catalysis, Eindhoven University of Technology,
P. O. Box 513, 5600 MB Eindhoven, The Netherlands
Fax: (internat.) + 31-40-245-5054
E-mail: H.C.L.Abbenhuis@tue.nl

Rob Hanssen studied Chemical Engineering at Eindhoven University of Technology and graduated on the heterogenisation of titanium-based silsesquioxane epoxidation catalysts in MCM-41 type materials. After his graduation, he continued his stay at the Laboratory of Inorganic Chemistry and Catalysis to do a Ph.D. on the formation and reactivity of multinuclear silsesquioxane metal complexes, which he successfully defended in May 2003.

Rutger van Santen is a Full Professor in Catalysis. He received his Ph.D. from Leiden University in 1971 with Prof. L. J. Oosterhoff as supervisor. In 1971/72 he was a postdoctoral fellow at SRI, Menlo, California in the Molecular Physics Department. Next he joined the Koninklijke/Shell Laboratorium Amsterdam where he had several functions in catalysis research. In 1982/84 he was assigned to Shell Development Company in Houston, Texas. In 1986 he was appointed part-time Professor in Surface Chemistry at Eindhoven University of Technology followed by the appointment as Full Professor in Catalysis in 1988. His research interests are in the field of the molecular aspects of heterogeneous catalysis following three main themes: computational studies of surface-chemical reactivity, mechanism in heterogeneous catalysis and physical chemistry of catalyst synthesis. He is recipient of the gold medal of the Royal Dutch Chemical Society (1981), the Ciapetta Lectureship of the North American Catalysis Association (1991) and the Bourke lectureship of the Royal Society of Chemistry (1996), Spinoza award (1997, NWO) and the Alwin-Mittasch Medal (Dechema, 2001). In 2001 he became chairman of the Royal Dutch Chemical Society and Rector Magnificus of the TUE.

In 1992, Erik Abbenhuis obtained his PhD thesis at Utrecht University having worked in the group of Prof. Dr. G. van Koten on "Intramolecular Coordination in Tantalum Alkylidene Chemistry". He continued with academic research as a postdoc, first in Strasbourg, then at the ETH Zürich, following his appointment as a fellow of the Royal Dutch Academy of Arts and Sciences in 1994. He now has his own research group at Eindhoven University of Technology, coached by Prof. Dr. D. Vogt, in which emphasis is put on molecular aspects of heterogeneous catalysis.

MICROREVIEWS: This feature introduces the readers to the author's research through a concise overview of the selected topic. Reference to important work from others in the field is included.

 DOI: 10.1002/ejic.200300412 © 2004 Wiley-VCH Verlag GmbH & Co. KGaA, Weinheim

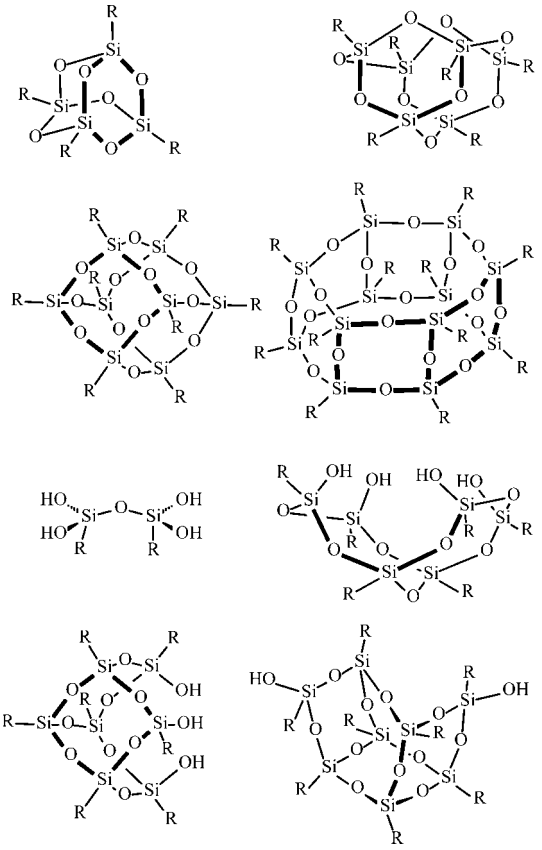

Figure 1. Overview of incompletely and completely condensed silsesquioxanes in the literature (typical R groups include: Me, Et, *i*Pr, *i*Bu, *i*Oc (isooctyl), Ph, *c*-C_5H_9, *c*-C_6H_{11}, *c*-C_7H_{13}, norbornyl)

silsesquioxanes is the presence of one non-silicate, organic group on the silicon atoms. The initial discovery of silsesquioxanes dates back to 1946, when Scott[1] described completely condensed methyl-substituted silsesquioxanes. Although he was not able to assign their exact structure, he was able to determine that the general formula was $[(CH_3)SiO_{3/2}]_{2n}$, in which n was an integer. Nine years later, the molecular structure of a series of organosilsesquioxanes was determined by single-crystal X-ray diffraction by Barry et al.[2] They first showed the cubic or hexagonal prismatic shape of the completely condensed molecules.

A major contribution to the synthesis of silsesquioxanes (completely and incompletely condensed) was published by Brown and Vogt in 1965.[3] They described the polycondensation of cyclohexyltrichlorosilane in an acetone/water mixture. The main products that were formed at the beginning of the reaction were incompletely condensed dimers [$RSi(OH)_2ORSi(OH)_2$, R = cyclohexyl] and higher oligomers, that still contained silanol groups. After some time (days to months), the cubic, incompletely condensed silsesquioxane trisilanol $(R_7Si_7O_9)(OH)_3$ was formed to a greater extent together with the completely condensed $R_6Si_6O_9$ with no residual silanol groups. In the 1990s, Feher described the same procedure for cyclopentyl- and cycloheptyltrichlorosilane. In this case no completely condensed products were isolated. The hydrolytic polycondensation of cyclopentyltrichlorosilane led exclusively to the formation of the trisilanol $(c\text{-}C_5H_9)_7Si_7O_9(OH)_3$, while polycondensation of cycloheptyltrichlorosilane led to a mixture of the trisilanol $(c\text{-}C_7H_{13})_7Si_7O_9(OH)_3$ and the tetrasilanol $(c\text{-}C_7H_{13})_6Si_6O_7(OH)_4$. The application of norbornyl as the organic side-group was explored by Hambley et al. A mixture of trisilanol and tetrasilanol was formed.[4]

The process of formation of the silsesquioxane compounds is thought to be a multi-step hydrolysis-condensation reaction (see Scheme 1). The first step is the hydrolysis of an alkylsilane precursor with water, forming organopolysilanol compounds (step *i*). In the right environment, depending on the concentration of water and solvent, and the pH, these precursors can condense with each other, leading to the formation of oligosiloxanes (step *ii*). The thermodynamics,[5–7] kinetics and solubility of the products will determine the resulting product mixture, ranging from lower oligosiloxane dimers or tetramers, to polyhedral oligomeric silsesquioxanes like the tetra- and trisilanol silsesquioxanes.

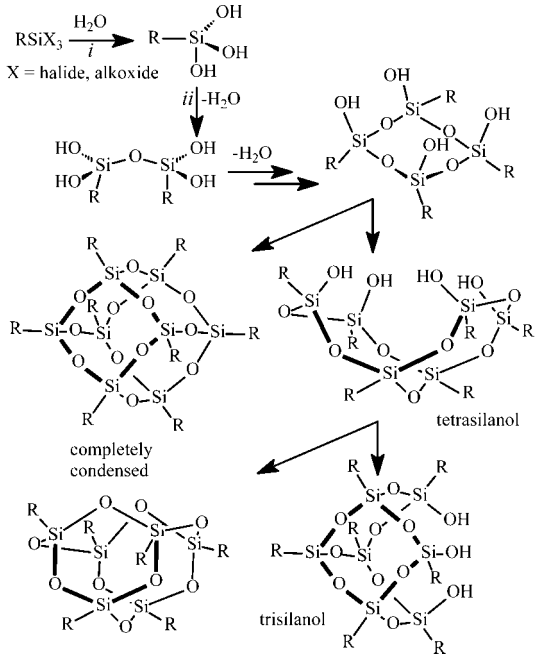

Scheme 1. Generalized formation scheme for siloxanes and silsesquioxane-type compounds

For a long time the major hurdle in the use of silsesquioxanes was the long preparation time (ranging from a few weeks to 36 months) and the limitation of the organic side-groups on the silicon atoms. New developments and ideas have shortened the preparation times considerably. The use of high-throughput experimentation and synthesis robots may accelerate the optimization of synthesis conditions.[8] Recently, base-catalyzed polycondensation reactions have proven to be an excellent way to prepare large quantities of silsesquioxanes. Lichtenhan and Abbenhuis have applied for patents on the preparation of completely condensed and incompletely condensed silsesquioxanes with isobutyl and

 © 2004 Wiley-VCH Verlag GmbH & Co. KGaA, Weinheim

isooctyl side-groups that can be prepared on large scales in a short time.

Until recently, functionalization of silsesquioxane silanols has been limited to either corner-capping of trisilanols with a trihaloorganosilane moiety, leaving no further reactive silanol group (*a*), or reaction of the trisilanol with mono- or dihaloorganosilane reactants, leaving two or one silanol groups, respectively (*b*). In the first case, a large number of possible side groups can be introduced, ranging from simple alkyl groups to reactive alcohols, amines and alkenyl groups. These groups allow the silsesquioxane cores to be included in polymeric materials. Furthermore, there is a substantial interest in octafunctional silsesquioxanes where all the side groups on the silicon atoms are identical and reactive. In these cases the functionality ranges from alkyls, alcohols, amides and carboxylates to halides, nitrates and phosphanes.[9−24] These can even be used as building blocks for dendrimers, as shown by Cole-Hamilton et al. for use in catalytic hydroformylation reactions (vide infra).[25−28] In the second case, the introduction of reactive functional groups besides the silsesquioxane's silanols has proved to be more complex. To date, the groups in the added functionality are limited to trialkyl- and triarylsilicon and -tin groups, and these groups are more often used for protection of one or more of the silanol groups than for functionalization. Selectivity in these reactions either arises from the different acidities of the silanols of the starting material or from steric hindrance of the silylating agent.

Metal Silsesquioxanes

Feher et al. initiated the research towards the use of silsesquioxane molecules as ligands for main group and transition metals at the end of the 1980s,[29] considering silsesquioxanes as models for industrially used silica supports. The resemblance of silsesquioxanes to silica supports is not only apparent from the molecular structure, but the electronic properties of silsesquioxane silanol groups mimic the behavior of silica as well.

In Figure 2, a few important structural similarities between silsesquioxanes and schematized silica surfaces are depicted. First of all, the defined orientation of the silanol groups, which is also present in silsesquioxanes, may ensure a strong multi-dentate bonding to metals. Furthermore, silsesquioxanes have enough residual siloxane bridges to resemble the silica surface and these residual siloxane bridges can interact with the metal.

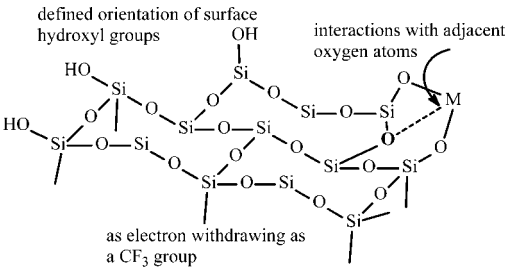

Figure 2. Schematic overview of a silica-based catalyst support, indicating important surface properties

Silsesquioxane silanols can be modified by silylation to resemble the different silanol sites that can be present on a silica surface. Dijkstra et al. performed an in-depth study on the synthesis and characterization of silsesquioxane models for silica silanol sites (see Figure 3).[30] By comparison of the relative ion-pair acidities in THF for the different silanol sites, they found that the geminal silanols are among the least acidic, and hence least reactive, silanol groups, closely followed by isolated silanol groups. Due to their ability for extensive hydrogen bonding, the Brønsted acidity of vicinal disilanol and trisilanol groups is orders of magnitude larger. These findings provide insight into the relative reactivity of species on a silica surface.

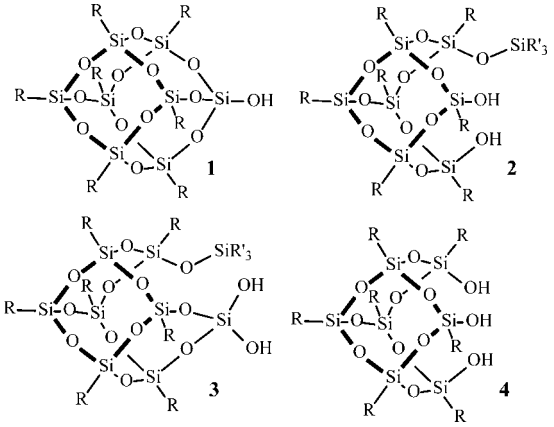

Figure 3. Silsesquioxane representations of silanol sites on silica surfaces: **1** isolated silanol; **2** vicinal disilanol; **3** geminal disilanol; **4** vicinal trisilanol

Since the discovery of silsesquioxanes, a rich coordination chemistry has been developed with elements throughout the periodic table; at present, these involve: Li, Na, K, Be, Mg, Sc, Y, La, U, Ti, Zr, Hf, V, Ta, Cr, Mo, W, Fe, Ru, Os, Co, Rh, Pt, Cu, Au, Zn, B, Al, Ga, Tl, Ge, Sn, Pb, N, P, As, Sb, Bi, S, F, Cl.

Group I (Li, Na, K)

Feher et al. have reported sodium complexes as intermediates in the synthesis of transition metal complexes.[31] These intermediates were either not isolated or found to be unstable out of solution. The groups of Aspinall, Edelmann and Abbenhuis have used lithium silsesquioxanes extensively as a transmetallation agent to prepare transition metal complexes.[32−34] In some cases the lithium ions remain present in the transition or main group metal complex.[32,34−36] Duchateau et al. reported a mixed boron-lithium silsesquioxane.[37] The group of Edelmann also reported a potassium silsesquioxane complex and gave a crystal structure, although no experimental details were provided.[34]

Group 2 (Be, Mg)

The chemistry of Group 2 elements has not been explored much in the past. Edelmann et al. published a crystal structure of a mixed beryllium-lithium silsesquioxane.[35]

 © 2004 Wiley-VCH Verlag GmbH & Co. KGaA, Weinheim

Smet et al. reported the use of a magnesium-substituted silsesquioxane as an intermediate in the reaction with epoxides.[38] Lichtenhan reported a polymeric material based on a silsesquioxane disilanol and dialkylmagnesium.[39] Liu and Feher reported the application of magnesium-substituted silsesquioxanes as model supports for titanium-based alkene polymerization catalysts.[40,41] Hanssen described the synthesis and reactivity studies of a tetranuclear magnesium complex, and Maxim subsequently used this complex to prepare microporous magnesium-containing silica materials.[42,43]

Group 3 (Sc, Y, La, Lanthanides and Actinides)

Hermann et al. first mentioned the synthesis and crystal structures of Nd and Y silsesquioxanes complexes.[44] Due to the high solubility of Group 3 silsesquioxanes they were not able to isolate a "naked' Y silsesquioxane, but addition of coordinating triphenylphosphane oxide yielded crystals suitable for X-ray crystal-structure analysis. The large ion-size and high electrophilicity of the ion induced a high degree of coordination of siloxide and siloxane groups from the ligand to the metal showing, for the first time, an interaction of a siloxane bridge with a metal ion. Aspinall et al. isolated a PMDTA adduct of an yttrium silsesquioxane.[45] By applying the method of lithium transmetallation they also synthesized a mixed lithium-ytterbium complex.[32] Edelmann et al. displayed a great interest in the synthesis of Group 3 and lanthanide complexes. They reported samarium and scandium complexes of the isolated silanol silsesquioxane **1** (Figure 3),[36] a seven-coordinate cerium(IV) silsesquioxane (starting from a Ce^{III} precursor),[46] and various mixed-metal lithium-lanthanide complexes.[34] They also reported the synthesis of the first known actinide silsesquioxane complex: a six-coordinate uranium(VI) complex that was formed regardless of the uranium precursor.[34] Although most of the papers deal with models for catalysts on silica surfaces, no catalytic experiments were performed.

Group 4 (Ti, Zr, Hf)

Much work has been done on Group 4 silsesquioxane complexes and the application of these complexes in catalytic processes such as ethylene polymerization,[40,41,47–54] alkene epoxidation[8,38,55–68] and Oppenhauer oxidations.[69] Most of the work in this area has been the topic of several excellent review articles.[34,52][65] A specific interest in the group of Abbenhuis is the heterogenization of active and selective epoxidation catalysts (Figure 4). Krijnen et al. reported the heterogenization of titanium silsesquioxane complexes in mesoporous MCM-41 type materials.[60][62][64][70] No leaching was observed for all-silica MCM-41 materials, while aluminum-containing MCM-41 had to be silylated after impregnation of the titanium silsesquioxane complex.

Skowronska-Ptasinski et al. described the copolymerization and cross-linking of vinyl-substituted silsesquioxane titanium complexes with siloxane oligomers.[58] The resulting materials proved to be active and selective catalysts

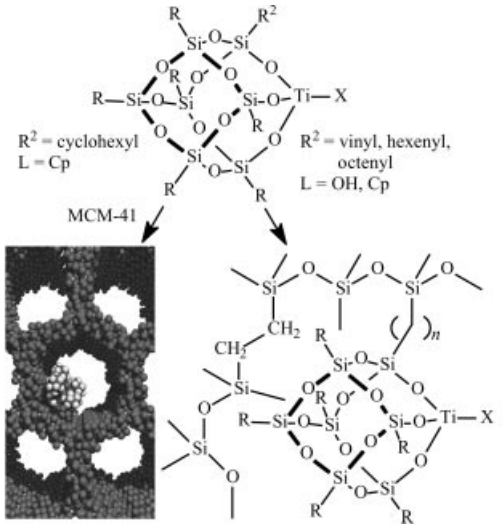

Figure 4. Immobilization of a titanium silsesquioxane complex by physisorption in a mesoporous MCM-41 host (left) or tethering to a 3D-netted siloxane polymer (right)

for the epoxidation of alkenes with the cheap oxidant hydrogen peroxide. A material obtained by physical encapsulation of a non-vinyl-functionalized titanium silsesquioxane complex was also active as a catalyst, while the titanium complex in solution could not activate hydrogen peroxide. This emphasies the importance of the physical surrounding of the catalytic center in epoxidation reactions, where one should avoid high concentrations of water and peroxide near the active metal center. More about Group 4 silsesquioxane complexes can be found in the literature.[29,31,39][71–76]

Group 5 (V, Ta)

Feher et al. explored the use of Group 5 metals ligated by silsesquioxanes by reacting vanadium(III) and vanadium(V) precursors with silsesquioxane trisilanol compounds.[76–79] The magnetic properties of the paramagnetic vanadium(III) silsesquioxanes were studied. The application of the diamagnetic vanadium(V) silsesquioxane complexes as precursors for ethylene polymerization was studied in-depth. Based on in situ NMR studies they were able to propose a catalytic model for the interaction of the vanadium systems with aluminium activators. One of the most important steps for the activation of the system was the breaking of metal-siloxy bonds in order for the metal to gain its catalytic activity, as shown in Scheme 2.

Wada et al. used the vanadium(V) complexes to prepare microporous vanadium silicates by controlled calcination of the complex in air at 723 K. The materials proved to be efficient catalysts for the photocatalytic oxidation of methane,[81] benzene and cyclohexane.[82]

The other metal in Group 5 that was investigated was tantalum. Basset et al. used a tantalum silsesquioxane complex as a model compound to explain the formation of tantalum alkylidene species on a silica surface.[83]

 © 2004 Wiley-VCH Verlag GmbH & Co. KGaA, Weinheim

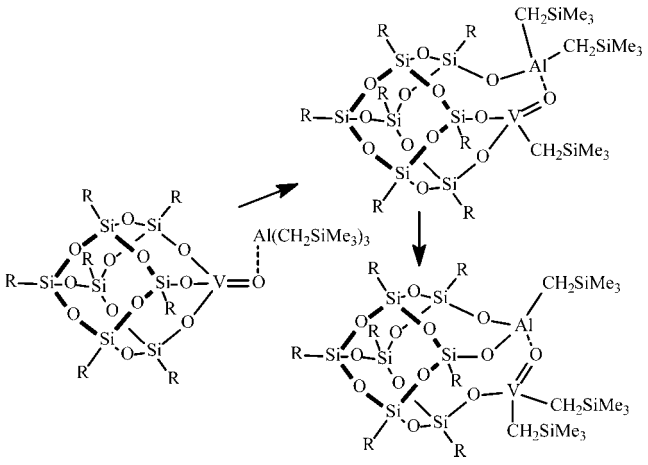

Scheme 2. Activation of a vanadium(V) silsesquioxane complex with an alkylaluminum compound

Group 6 (Cr, Mo, W)

Reaction of chromium oxide with a mono-protected trisilanol led to the formation of a bis-oxo chromium silsesquioxide ester (see Figure 5). Feher et al. tested this compound in the polymerization of ethylene as a surface model for the chromium-based Phillips catalyst.[80,84] It produced medium molecular weight polyethylene with a high polydispersity, indicating multiple active sites. Vorstenbosch et al. employed this type of chromium silsesquioxane ester for the catalytic epoxidation of alkenes with *tert*-butyl hydroperoxide. Although the respective epoxide was formed in high yield, it was found that the active species in the reaction was a non-silsesquioxane chromium species, an indication of metal leaching.[59] Maxim et al. used the chromium silsesquioxane for the synthesis of microporous-silica-supported chromium that was found to be active in the low-temperature catalytic oxidation of ammonia.[85,86]

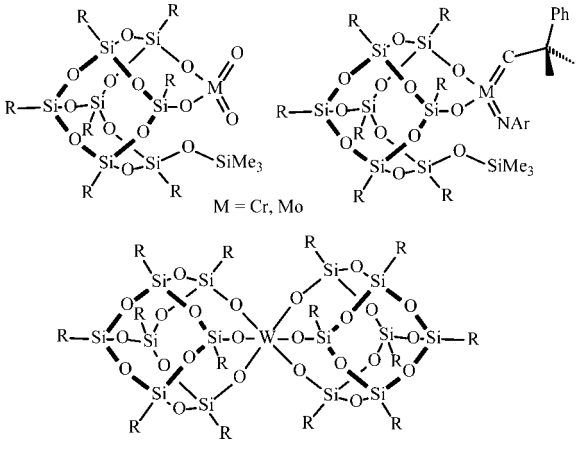

Figure 5. Examples of silsesquioxane group 6 metal complexes

Feher et al. also synthesized the corresponding molybdenum bis-oxo silsesquioxide ester by a thallium transmetallation route (vide infra).[87] A variant of the well-known molybdenum-based Schrock carbene complex showed high activity in olefin metathesis reactions (see Figure 5).[31] The high activity was attributed to the highly electron-withdrawing character of the silsesquioxane framework. Cross-metathesis of vinyl-substituted silsesquioxanes with the Schrock carbene complex $[Mo(CHCMe_2Ph)(NAr)\{OCMe(CF_3)_2\}_2]$ yielded a silsesquioxane with an alkylidene-metal fragment attached to the former vinyl side-group.[88] In an attempt to synthesize a model for silica-supported tungsten catalysts, Smet et al. synthesized a bis(silsesquioxane)-tungsten complex (Figure 5), for which the synthesis is atypical as no base is required to trap the HCl formed.[89] More reports of Group 6 metal silsesquioxanes can be found in the literature.[9,29,87,90–92]

Group 7

To date, no one has reported the synthesis of Group 7 metal silsesquioxanes where the metal is directly linked to the silanol groups. Attempts to synthesize rhenium silsesquioxane complexes resulted in either dehydration reactions of the silsesquioxane, or yielded complicated product mixtures.[93] Lücke et al. reported the synthesis of a octafunctionalized phosphorous silsesquioxane that was used a ligand for $[MnCp(CO)_2]$.[9]

Group 8 (Fe, Ru, Os)

Although the introduction of iron, in the form of ferrocene, as a side-group on the silicon was reported in 1993,[94–96] Ott et al.[97] and Edelmann et al.[98] have only recently reported the synthesis and application of iron silsesquioxanes where the iron atom is attached to the silanolate groups (Figure 6).

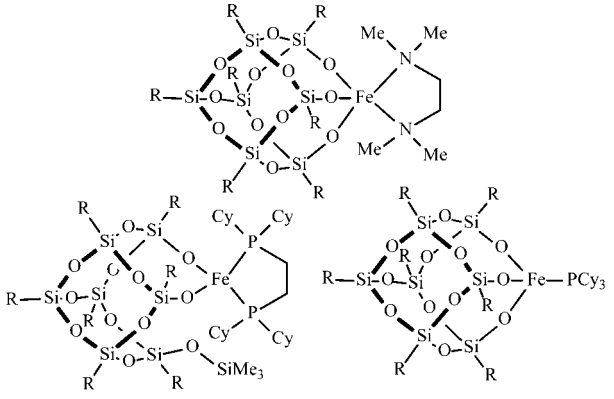

Figure 6. Iron silsesquioxanes reported by Ott et al. and Edelmann et al.

Ott et al. used monophosphanes and diphosphanes as stabilizing agents for the unfilled coordination space on the metal. Addition of small amounts of water to these compounds led to the loss of the phosphane ligand and the formation of anionic oxygen-bridged bis(iron-silsesquioxane) species. Because of structural similarities to the active center of iron found in zeolites, they applied the iron silses-

 © 2004 Wiley-VCH Verlag GmbH & Co. KGaA, Weinheim

quioxane complexes in the catalytic oxidation of benzene with N_2O to phenol. No conversion into phenol was observed, possibly due to the low temperature. Edelmann et al. used TMEDA instead of diphosphanes. The complex of Edelmann was used by Maxim et al. to prepare iron on microporous silica by controlled calcination of the complex.[33] The iron was well dispersed in the material and was present as nanosized metal oxide particles of about 2−8 nm. The addition of extra silsesquioxane trisilanol to the mixture before calcination enabled them to vary the iron content in the material, while keeping the material properties unchanged. Mixing a third component into the pre-calcination mixture — the chromium silsesquioxide ester (vide supra) — allowed Maxim et al. to synthesize silica-supported mixed-metal materials.[99] These materials were tested in catalytic decomposition of N_2O to N_2 and O_2, and were found to be more active than the iron-only systems, and more selective than the chromium-only systems. A mixed metal-oxide phase (Fe−Cr−Si−O) was identified by Raman spectroscopy.

Four examples of ruthenium attached to a silsesquioxane core have been reported. Feher et al. synthesized one complex by a cross-metathesis route as described for molybdenum.[88] Wada et al. used a phosphorus-functionalized silsesquioxane as a ligand for ruthenium.[100] Marsmann et al. used thiol-functionalized silsesquioxanes to bind to ruthenium and osmium carbonyl clusters.[101] Hong et al. published $Ru(terpy)_3$ complexes covalently linked to a silsesquioxane dendrimer.[102]

Liu et al. reported the crystal structure of a silsesquioxane-substituted osmium cluster in 1990 (Figure 7).[103]

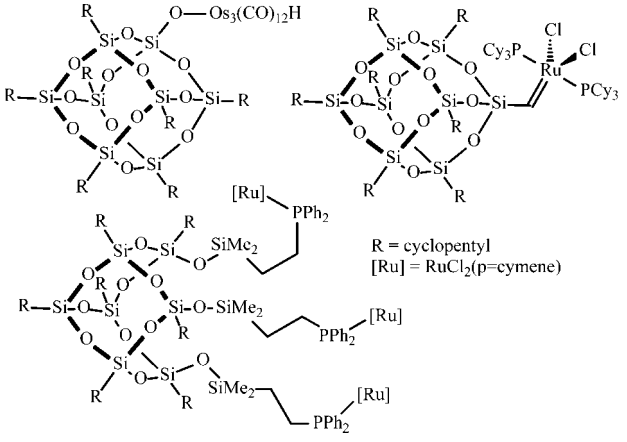

Figure 7. Examples of silsesquioxane complexes of osmium and ruthenium

Group 9−10 (Co, Rh, Pt)

The direct coupling of metals in this group to the silanol functionality of silsesquioxanes has been limited to platinum (see Figure 8). Abbenhuis et al. described the reaction of $Pt(CO_3)$(dppe) with trisilanol and mono-silylated disilanol silsesquioxane ligands.[104] Johnson et al.,[105] and Feher et al.[31] used mono-silylated thallium silsesquioxide complexes as a transmetallating agent to make silsesquioxane platinum compounds, although in some cases the use of thallium silsesquioxide complexes frustrated the synthesis of the complex due to residual thallium ions in the isolated materials.[105]

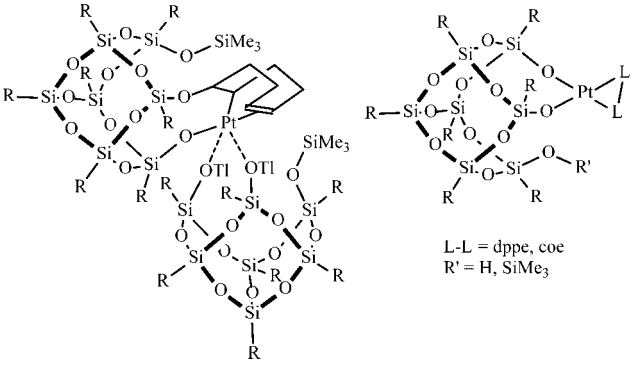

Figure 8. Pt silsesquioxane complexes by Abbenhuis, Feher and Johnson

Other reported ways of attaching Group 9−10 metals to silsesquioxanes are coordination of a donor group to the metal (S,[101][106] P[9,25,28,100,106−108]) and oxidative addition of a metal to Si−H (Co,[95,109] Rh[110]). Cole-Hamilton et al. used phosphorous-functionalized silsesquioxane-based dendrimers as ligands for rhodium to perform hydroformylation reactions.[25,28] They found a positive dendritic effect towards the linear product. Nowotny et al. used a phosphorous-functionalized silsesquioxane to chelate a Rh cluster to function as a model for a P-functionalized silica surface.[107] No catalytic tests were reported for the silsesquioxane compound.

Group 11−12 (Cu, Au, Zn)

Silsesquioxane complex chemistry has not been developed to a large extent for metals in these groups. Edelmann et al. treated $(CuO\mathit{t}Bu)_4$ with monosilylated disilanol and obtained a product with a crystal structure in which the tetrameric core of the copper alkoxide was maintained (see Figure 9). Pugin et al. used sulfur-functionalized silsesquioxanes as ligands for Au_{55} clusters and were able to correlate the increased Coulomb gap to the increased size of the cluster going from PPh_3 to the silsesquioxane-based ligand.[111] Abis et al. prepared di- and trisubstituted gold silsesquioxanes as a model for the interaction of gold carbamate precursors with silica surfaces (see Figure 9).[112]

Group 13 (B, Al, Ga, Tl)

Due to the high reactivity of the precursors from this group, particularly the alkyl complexes, with silanol groups, the silanolate coordination chemistry is well developed. Duchateau et al.,[113−115] Edelmann et al.,[116] and Feher et al.[117−119] prepared aluminum silsesquioxane complexes as models for aluminum sites in zeolites and on silica, and as models for methyl alumoxane compounds. Abbenhuis et al. applied aluminum-containing silsesquioxane polymers as heterogeneous catalysts for the acceleration of Diels−Alder reactions of enones.[120] Maxim et al. used aluminum silses-

 © 2004 Wiley-VCH Verlag GmbH & Co. KGaA, Weinheim

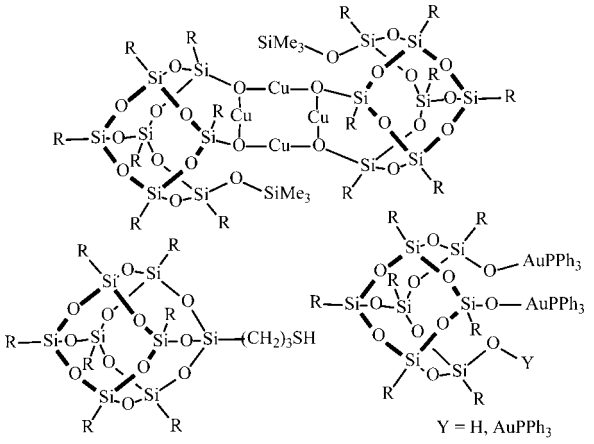

Figure 9. Examples of complexes of copper and gold and a thiol-functionalized ligand for gold clusters

quioxanes as precursors for microporous aluminosilicates by controlled calcination.[43]

Feher et al.[121] and Duchateau et al.[37] investigated the interaction of gallium precursors ($GaMe_3$ and $GaCl_3$).[122] Wada et al. used gallium silsesquioxane precursors to synthesize microporous gallium silicate materials with acidic sites by controlled calcination of the complexes in air.[123]

The interaction of boron with silsesquioxanes was the topic of research of Feher, Collins and Duchateau. Feher et al.[124] and Duchateau et al.[37] investigated the possible geometries that can be adopted by boron in a strained silsesquioxane environment. They found that boron can assume both trigonal-square and tetrahedral geometries. Collins[125] and Duchateau[50] synthesized silsesquioxane organoboranes and organoborates that could be used as models for silica-supported borane activators for Group 4 olefin polymerization catalysts (Figure 10). Reaction with bisalkylzirconocene complexes showed that both boranes and borates were susceptible to borane-zirconium exchange reactions, rendering the catalyst inactive. They concluded that the grafting of boranes on silica is not a useful method for subsequent immobilization of polymerization catalysts.

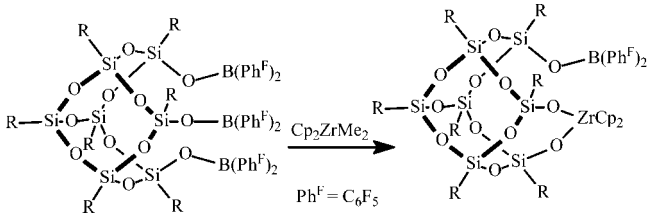

Figure 10. Interaction of dimethylzirconocene with a tris(organobora)silsesquioxane leading to borane-zirconocene exchange (Collins et al.)

Thallium silsesquioxane complexes have been mainly applied for transmetallation reactions where the thallium is replaced by high-valent transition metals.[31][87] Their ability to withstand dehydration reactions of the silsesquioxane framework, a common occurrence when using high-valent transition metals in combination with amine bases, make these complexes suitable for the synthesis of middle and late transition metal complexes, although the high toxicity is a serious disadvantage.

Outlook of Silsesquioxane Complex Chemistry

Besides extending the range of metals that can form complexes with silsesquioxane ligands, there are many challenges for the future of silsesquioxane chemistry. The introduction of functional groups besides the silanol groups could give new insights in the coordination chemistry of silsesquioxanes, and the introduction of coordinating groups like amines, thiols and phosphanes could have interesting effects on the catalytic performance of metal complexes. The introduction of silsesquioxane ligands and complexes in an approach as proposed by Skowronska-Ptasinski can revolutionize the way supported catalysts are made, due to the precise environment in which the metal center is incorporated. Controlled calcination of mixtures of silsesquioxane ligands and metal complexes yields highly dispersed, small metal oxide particles or even molecularly dispersed metal ions on a silica surface, with controllable multi-metallic content. Finally, the knowledge gained from the silsesquioxane model work should be transferred more to actual silica-supported systems or the ideas should be used to synthesize active and selective homogeneous catalysts, appropriate for industrial use.

[1] D. W. Scott, *J. Am. Chem. Soc.* **1946**, *68*, 356−358.
[2] A. J. Barry, W. H. Daud, J. J. Domicone, J. W. Gilkey, *J. Am. Chem. Soc.* **1955**, *77*, 4248−4252.
[3] J. F. Brown, L. H. Vogt, *J. Am. Chem. Soc.* **1965**, *87*, 4313−4317.
[4] T. W. Hambley, T. Maschmeyer, A. F. Masters, *Appl. Organomet. Chem.* **1992**, *6*, 253−260.
[5] T. Kudo, M. S. Gordon, *J. Am. Chem. Soc.* **1998**, *120*, 11432−11438.
[6] T. Kudo, M. S. Gordon, *J. Phys. Chem. A* **2000**, *104*, 4058−4063.
[7] K. Jug, D. Wichmann, *J. Comp. Chem.* **2000**, *21*, 1549−1553.
[8] P. P. Pescarmona, J. C. Van der Waal, I. E. Maxwell, T. Maschmeyer, *Angew. Chem. Int. Ed.* **2001**, *40*, 740−743.
[9] S. Lücke, K. Stoppek-Langner, J. Kuchinke, B. Krebs, *J. Organomet. Chem.* **1999**, *584*, 11−15.
[10] F. J. Feher, J. J. Schwab, D. M. Tellers, A. Burstein, *Main Group Chem.* **1998**, *2*, 169−181.
[11] E. Müller, F. T. Edelmann, *Main Group Met. Chem.* **2000**, 485.
[12] X. Zhang, K. J. Haxton, L. Ropartz, D. J. Cole-Hamilton, R. E. Morris, *J. Chem. Soc., Dalton Trans.* **2001**, 3261−3268.
[13] D. P. Fasce, R. J. J. Williams, R. Erra-Balsells, Y. Ishikawa, H. Nonami, *Macromol.* **2001**, *34*, 3534−3539.
[14] J. Choi, J. Harcup, A. F. Yee, Q. Zhu, R. M. Laine, *J. Am. Chem. Soc.* **2001**, *123*, 11420−11430.
[15] U. Dittmar, B. J. Hendan, H. C. Marsmann, *J. Organomet. Chem.* **1995**, *489*, 185−194.
[16] B. Hong, T. P. Thoms, H. J. Murfee, M. J. Lebrun, *Inorg. Chem.* **1997**, *36*, 6146−6147.
[17] F. J. Feher, K. D. Wyndham, D. J. Knauer, *Chem. Commun.* **1998**, 2393−2394.
[18] F. J. Feher, K. D. Wyndham, M. A. Scialdone, Y. Hamuro, *Chem. Commun.* **1998**, 1469−1470.
[19] F. J. Feher, K. D. Wyndham, *Chem. Commun.* **1998**, 323−324.

 © 2004 Wiley-VCH Verlag GmbH & Co. KGaA, Weinheim

[20] B. W. Manson, J. J. Morrison, P. I. Coupar, P. A. Jaffrés, R. E. Morris, *J. Chem. Soc., Dalton Trans.* **2001**, 1123−1127.
[21] P. I. Coupar, P. A. Jaffrés, R. E. Morris, *J. Chem. Soc., Dalton Trans.* **1999**, 2183−2187.
[22] B. J. Hendan, H. C. Marsmann, *J. Organomet. Chem.* **1994**, *483*, 33−38.
[23] E. Rikowski, H. C. Marsmann, *Polyhedron* **1997**, *16*, 3357−3361.
[24] M. C. Gravel, C. Zhang, M. Dindermann, R. M. Laine, *Appl. Organomet. Chem.* **1999**, *13*, 329−336.
[25] L. Ropartz, R. E. Morris, G. P. Schwarz, D. F. Foster, D. J. Cole-Hamilton, *Inorg. Chem. Commun.* **2000**, *3*, 714−717.
[26] L. Ropartz, R. E. Morris, D. F. Foster, D. J. Cole-Hamilton, *Chem. Commun.* **2001**, 361−362.
[27] L. Ropartz, K. J. Haxton, D. F. Foster, R. E. Morris, A. M. Z. Slawin, D. J. Cole-Hamilton, *J. Chem. Soc., Dalton Trans.* **2002**, 4323−4334.
[28] L. Ropartz, R. E. Morris, D. F. Foster, D. J. Cole-Hamilton, *J. Mol. Catal. A* **2002**, *182−183*, 99−105.
[29] F. J. Feher, *J. Am. Chem. Soc.* **1986**, *108*, 3850−3852.
[30] T. W. Dijkstra, R. Duchateau, R. A. Van Santen, A. Meetsma, G. P. A. Yap, *J. Am. Chem. Soc.* **2002**, *124*, 9856−9864.
[31] F. J. Feher, T. A. Budzichowski, *Polyhedron* **1995**, *14*, 3239−3253.
[32] J. Annand, H. C. Aspinall, A. Steiner, *Inorg. Chem.* **1999**, *38*, 3941−3943.
[33] N. Maxim, A. Overweg, P. J. Kooyman, J. H. M. C. Van Wolput, R. W. J. M. Hanssen, R. A. Van Santen, H. C. L. Abbenhuis, *J. Phys. Chem. B* **2002**, *106*, 2203.
[34] V. Lorenz, A. Fischer, S. Giessman, J. W. Gilje, Y. K. Gunko, K. Jacob, F. T. Edelmann, *Coord. Chem. Rev.* **2000**, *206−207*, 321−368.
[35] V. Lorenz, A. Fischer, F. T. Edelmann, *Inorg. Chem. Commun.* **2000**, *3*, 292−295.
[36] V. Lorenz, A. Fischer, F. T. Edelmann, *J. Organomet. Chem.* **2002**, *647*, 245−249.
[37] R. Duchateau, G. Gerritsen, R. A. Van Santen, G. P. Yap, *Organometallics* **2003**, *22*, 100−110.
[38] P. Smet, J. Riondato, T. Pauwels, L. Moens, L. Verdonck, *Inorg. Chem. Commun.* **2000**, *3*, 557−562.
[39] T. S. Haddad, J. D. Lichtenhan, *J. Inorg. Organomet. Polym.* **1995**, *5*, 237−246.
[40] J. C. Liu, *Chem. Commun.* **1996**, 1109−1110.
[41] L. J. C. Liu, *Appl. Organomet. Chem.* **1999**, *13*, 295−302.
[42] R. W. J. M. Hanssen, A. Meetsma, R. A. Van Santen, H. C. L. Abbenhuis, *Inorg. Chem.* **2000**, *40*, 4049−4052.
[43] N. Maxim, P. C. M. M. Magusin, P. J. Kooyman, J. H. M. C. Van Wolput, R. A. Van Santen, H. C. L. Abbenhuis, *Chem. Mater.* **2001**, *13*, 2958−2964.
[44] W. A. Hermann, R. Anwander, V. Dufaud, W. Scherer, *Angew. Chem.* **1994**, *106*, 1338−1340; *Angew. Chem. Int. Ed. Engl.* **1994**, *33*, 0000−0000 ?.
[45] H. C. Aspinall, J. Annand, *J. Chem. Soc., Dalton Trans.* **2000**, 1867−1871.
[46] Y. K. Gunko, R. Reilly, F. T. Edelmann, H. G. Schmidt, *Angew. Chem. Int. Ed.* **2001**, *40*, 1279−1281.
[47] R. Duchateau, H. C. L. Abbenhuis, R. A. Van Santen, A. Meetsma, S. K. Thiele, M. F. Van Tol, *Organometallics* **1998**, *17*, 5663−5673.
[48] R. Duchateau, H. C. L. Abbenhuis, R. A. Van Santen, S. K. Thiele, M. F. Van Tol, *Organometallics* **1998**, *17*, 5222−5224.
[49] R. Duchateau, U. Cremer, R. J. Harmsen, S. I. Mohamud, H. C. L. Abbenhuis, R. A. Van Santen, A. Meetsma, S. K. Thiele, M. F. Van Tol, M. Kranenburg, *Organometallics* **1999**, *18*, 5447−5459.
[50] R. Duchateau, R. A. Van Santen, G. P. Yap, *Organometallics* **2000**, *19*, 809−816.
[51] J. R. Severn, R. Duchateau, R. A. Van Santen, D. D. Ellis, A. L. Spek, *Organometallics* **2002**, *21*, 4−6.
[52] R. Duchateau, *Chem. Rev.* **2002**, *102*, 3525−3542.
[53] F. T. Edelmann, S. Giessman, A. Fischer, *Chem. Commun.* **2000**, 2153−2154.
[54] H. C. L. Abbenhuis, *Angew. Chem.* **1999**, *111*, 1125−1127; *Angew. Chem. Int. Ed.* **1999**, *38*, 1058−1060.
[55] H. C. L. Abbenhuis, S. Krijnen, R. A. Van Santen, *Chem. Commun.* **1997**, 331−332.
[56] T. Maschmeyer, M. C. Klunduk, C. M. Martin, D. S. Shephard, J. M. Thomas, B. F. Johnson, *Chem. Commun.* **1997**, 1847−1848.
[57] M. C. Klunduk, T. Maschmeyer, J. M. Thomas, B. F. Johnson, *Chem. Eur. J.* **1999**, *5*, 1481−1485.
[58] M. D. Skowronska-Ptaskinska, M. L. W. Vorstenbosch, R. A. Van Santen, H. C. L. Abbenhuis, *Angew. Chem. Int. Ed.* **2002**, *41*, 637−639.
[59] M. L. W. Vorstenbosch, Alkene epoxidation with silsesquioxane-based chromium and titanium complexes. Schuit Institute of Catalysis, Eindhoven, **2002**.
[60] S. Krijnen, H. C. L. Abbenhuis, R. W. J. M. Hanssen, J. H. C. Van Hooff, R. A. Van Santen, *Angew. Chem. Int. Ed.* **1998**, *37*, 356−358.
[61] R. A. Van Santen, H. C. L. Abbenhuis, M. L. W. Vorstenbosch, Method for producing silsasesquioxane metal complexes, novel silsesquioxane metal complexes and the use thereof. PCT/EP98/01932 (WO, 98/46352), 1−24, **1998**.
[62] S. Krijnen, B. L. Mojet, H. C. L. Abbenhuis, J. H. C. Van Hooff, R. A. Van Santen, *Phys. Chem. Chem. Phys.* **1999**, *1*, 361−365.
[63] S. Krijnen, R. J. Harmsen, H. C. L. Abbenhuis, J. H. C. Van Hooff, R. A. Van Santen, *Chem. Commun.* **1999**, 501−502.
[64] S. Krijnen, H. C. L. Abbenhuis, R. W. J. M. Hanssen, J. H. C. Van Hooff, R. A. Van Santen, *Mater. Res. Soc.* **1999**, 645−650.
[65] H. C. L. Abbenhuis, *Chem. Eur. J.* **2000**, *6*, 25−32.
[66] M. Crocker, R. H. Herold, A. G. Orpen, *Chem. Commun.* **1997**, 2411−2412.
[67] M. Crocker, R. H. Herold, A. G. Orpen, M. Overgaag, *J. Chem. Soc., Dalton Trans.* **1999**, 3791−3804.
[68] M. Crocker, R. H. Herold, Preparation of oxirane compounds with titanasilsesquioxane catalysts. PCT/EP96/05873 (WO, 97/24344). 1999.
[69] R. H. Meijer, The winding road from oppenhauer to sustainable catalytic oxidations of alcohols, Eindhoven, **2002**.
[70] R. A. Van Santen, S. Krijnen, R. W. J. M. Hanssen, H. C. L. Abbenhuis, Method for producing a supported catalyst. WO 99/03581 (PCT/EP98/040598).
[71] F. T. Edelmann, S. Giessman, A. Fisher, *J. Organomet. Chem.* **2001**, *620*, 80−89.
[72] K. Wada, M. Nakashita, M. Bundo, K. Ito, T. Kondo, T. Mitsudo, *Chem. Lett.* **1998**, *1998*, 659−660.
[73] K. Wada, M. Bundo, D. Nakabayashi, N. Itayama, T. Mitsudo, *Chem. Lett.* **2000**, 628−629.
[74] Y. K. Gunko, L. Nagy, W. Bruser, V. Lorenz, A. Fischer, S. Giessmann, F. T. Edelmann, K. Jacob, A. Vertes, *Monatsh. Chem.* **1999**, *130*, 45−54.
[75] F. J. Feher, S. L. Gonzales, J. W. Ziller, *Inorg. Chem.* **1988**, *27*, 3440−3442.
[76] F. J. Feher, J. F. Walzer, *Inorg. Chem.* **1990**, *29*, 1604−1611.
[77] F. J. Feher, J. F. Walzer, *Inorg. Chem.* **1991**, *30*, 1689−1694.
[78] F. J. Feher, J. F. Walzer, R. L. Blanski, *J. Am. Chem. Soc.* **1991**, *113*, 3618−3619.
[79] F. J. Feher, R. L. Blanski, *J. Am. Chem. Soc.* **1992**, *114*, 5886−5887.
[80] F. J. Feher, R. L. Blanski, *Makromol. Chem., Macromol. Symp.* **1993**, *66*, 95−107.
[81] K. Wada, M. Nakashita, A. Yamamoto, T. Mitsudo, *Chem. Commun.* **1998**, 133−134.
[82] K. Wada, M. Nakashita, A. Yamamoto, H. Wada, T. Mitsudo, *Chem. Lett.* **1997**, *12*, 1209−1210.
[83] M. Chabanas, E. A. Quadrelli, B. Fenet, C. Coperet, J. Thivolle-Cazat, J. M. Basset, A. Lesage, L. Emsley, *Angew. Chem. Int. Ed.* **2001**, *40*, 4493.

 © 2004 Wiley-VCH Verlag GmbH & Co. KGaA, Weinheim

[84] F. J. Feher, R. L. Blanski, *J. Chem. Soc., Chem. Commun.* **1990**, 1614−1616.
[85] N. Maxim, H. C. L. Abbenhuis, P. J. Stobbelaar, B. L. Mojet, R. A. Van Santen, *Phys. Chem. Chem. Phys.* **1999**, *1*, 4473−4477.
[86] N. Maxim, Metal Silsesquioxanes as Precursors to Microporous Metallosilicates, Schuit Institute of Catalysis, Eindhoven, **2002**.
[87] F. J. Feher, K. Rahimian, T. A. Budzichowski, *Organometallics* **1995**, *14*, 3920−3926.
[88] F. J. Feher, D. Soulivong, A. G. Eklund, K. D. Wyndham, *Chem. Commun.* **1997**, 1185−1186.
[89] P. Smet, B. Devreese, F. Verpoort, T. Pauwels, I. Svoboda, S. Foro, J. Van Beeumen, L. Verdonck, *Inorg. Chem.* **1998**, *37*, 6583−6586.
[90] T. A. Budzichowski, S. T. Chacon, M. H. Chisholm, F. J. Feher, W. Steib, *J. Am. Chem. Soc.* **1991**, *113*, 689−691.
[91] F. J. Feher, T. A. Budzichowski, K. Rahimian, J. W. Ziller, *J. Am. Chem. Soc.* **1992**, *114*, 3859−3866.
[92] M. H. Chisholm, T. A. Budzichowski, F. J. Feher, J. W. Ziller, *Polyhedron* **1992**, *11*, 1575−1579.
[93] H. C. L. Abbenhuis, personal communication, **1997**.
[94] M. Morán, C. M. Casado, I. Cuadrado, *Organometallics* **1993**, *12*, 4327−4333.
[95] C. Marcolli, G. Calzaferri, *Appl. Organomet. Chem.* **1999**, *13*, 213−226.
[96] C. M. Casado, I. Cuadrado, M. Morádo, B. Alonso, M. Barranco, J. Losada, *Appl. Organomet. Chem.* **1999**, *13*, 245−249.
[97] R. T. Baker, K. C. Ott, W. Tumas, F. Liu, K. D. John, B. L. Scott, *Angew. Chem. Int. Ed.* **2000**, *39*, 3127−3130.
[98] T. Edelmann, V. Lorenz, A. Fischer, *Z. Anorg. Allg. Chem.* **2000**, *626*, 1728−1730.
[99] N. Maxim, A. Overweg, P. J. Kooyman, R. A. Van Santen, H. C. L. Abbenhuis, *J. Mater. Chem.* **2002**, 3792−3798.
[100] K. Wada, D. Izuhara, M. Shiotsuki, T. Kondo, T. Mitsudo, *Chem. Lett.* **2001**, 734.
[101] P. Braunstein, J. R. Galsworthy, B. J. Hendan, H. C. Marsmann, *J. Organomet. Chem.* **1998**, *551*, 125−131.
[102] H. J. Murfee, T. P. Thoms, J. Greaves, B. Hong, *Inorg. Chem.* **2000**, *39*, 5209−5217.
[103] J. C. Liu, S. R. Wilson, J. R. Shapley, F. J. Feher, *Inorg. Chem.* **1990**, *29*, 5138−5139.
[104] H. C. L. Abbenhuis, A. D. Burrows, H. Kooijman, M. Lutz, M. T. Palmer, R. A. Van Santen, A. L. Spek, *Chem. Commun.* **1998**, 2627−2628.
[105] B. F. Johnson, E. A. Quadrelli, J. E. Davies, N. Feeder, *Chem. Commun.* **2000**, 1031−1032.
[106] B. J. Hendan, H. C. Marsmann, *Appl. Organomet. Chem.* **1999**, *13*, 287−294.
[107] M. Nowotny, T. Maschmeyer, B. F. Johnson, P. Lahuerta, J. M. Thomas, J. E. Davies, *Angew. Chem. Int. Ed.* **2001**, *40*, 955−958.
[108] R. Bahtiar, F. J. Feher, *Rapid. Commun. Mass. Spectr.* **1999**, *13*, 687−694.
[109] M. Rattay, D. Fenske, P. Jutzi, *Organometallics* **1998**, *17*, 2930−2932.
[110] P. G. Harrison, C. H. Hall, *J. Sol-gel. Sci. Tech.* **1998**, *13*, 391−396.
[111] G. Schmid, R. Pugin, J. O. Malm, J. Bovin, *Eur. J. Inorg. Chem.* **1998**, 813−817.
[112] L. Abis, L. Armelao, D. Belli Dell′Amico, F. Calderazzo, F. Garbassi, A. Merigo, E. A. Quadrelli, *J. Chem. Soc., Dalton Trans.* **2001**, 2709.
[113] R. Duchateau, R. J. Harmsen, H. C. L. Abbenhuis, R. A. Van Santen, A. Meetsma, S. K. Thiele, M. Kranenburg, *Chem. Eur. J.* **1999**, *5*, 3130−3135.
[114] M. D. Skowronska-Ptaskinska, R. Duchateau, R. A. Van Santen, G. P. A. Yap, *Organometallics* **2001**, *20*, 3519−3530.
[115] M. D. Skowronska-Ptaskinska, R. Duchateau, R. A. Van Santen, G. P. A. Yap, *Eur. J. Inorg. Chem.* **2001**, 133−137.
[116] F. T. Edelmann, K. Gun, S. Giessman, F. Olbrich, *Inorg. Chem.* **1999**, *38*, 210−211.
[117] F. J. Feher, T. A. Budzichowski, K. Weller, *J. Am. Chem. Soc.* **1989**, *111*, 153−163.
[118] F. J. Feher, K. Weller, *Organometallics* **1990**, *9*, 2638−2640.
[119] F. J. Feher, K. Weller, J. W. Ziller, *J. Am. Chem. Soc.* **1992**, *114*, 9686−9688.
[120] H. C. L. Abbenhuis, H. W. Van Herwijnen, R. A. Van Santen, *Chem. Commun.* **1996**, 1941−1942.
[121] F. J. Feher, T. A. Budzichowski, J. W. Ziller, *Inorg. Chem.* **1997**, *36*, 4082−4086.
[122] N. Maxim, H. C. L. Abbenhuis, P. C. M. M. Magusin, R. A. Van Santen, *Chin. J. Chem.* **2001**, *19*, 30−39.
[123] K. Wada, K. Yamada, T. Kondo, T. Mitsudo, *Chem. Lett.* **2001**, 12−13.
[124] F. J. Feher, T. A. Budzichowski, J. W. Ziller, *Inorg. Chem.* **1992**, *31*, 5100−5105.
[125] R. A. Metcalfe, D. I. Kreller, J. Tian, H. Kim, N. J. Taylor, J. F. Corrigan, S. Collins, *Organometallics* **2002**, *21*, 1719−17.

Received June 27, 2003

 © 2004 Wiley-VCH Verlag GmbH & Co. KGaA, Weinheim

Dimeric Metallo-Organic Supramolecular Quinoxaline Stacking Synthons

Fenton Heirtzler,*[a][‡] Sandra Dias,[a] and Markus Neuburger[b]

Keywords: Supramolecular chemistry / Helical structures / Heterocycles / Stacking interactions / Self-assembly / Sandwich complexes

Condensation of *ortho*-phenylene diamines with an unsymmetrical 2,6′-bipyridyl-2′′-pyridyl α-diketone (**2**) affords helical ligands **3a** and **3b** that self-assemble in the presence of copper(I) to produce the helical, dimeric metallo-organic complexes $[\mathbf{3a}_2Cu_2][PF_6]_2$ and $[\mathbf{3b}_2Cu_2][PF_6]_2$. These complexes have a flat, double-decker-like structure that results from atopomeric twisting in the ligand scaffolding, as confirmed by X-ray crystal structural analysis on $[\mathbf{3a}_2Cu_2][PF_6]_2$. This study also indicates a close parallel between the distances involved in inter- and intramolecular stacking phenomena. Detailed NMR spectroscopic analysis of both complexes indicates that their dications possess very closely related solution-state structures. Achieving this self-assembly program is an important step towards realizing dimerically self-assembled metallo-organic materials that have a discotic alignment.
(© Wiley-VCH Verlag GmbH & Co. KGaA, 69451 Weinheim, Germany, 2004)

Introduction

Oligopyridines and related compounds self-assemble in the presence of appropriate metal ions into tubular metallo-organic complexes with either a helical chirality[1] or a *meso*-configuration.[2] Ligands of less regular structure may form dimeric complexes with a flattened topology.[3] Our work concerns the synthesis[4] and metallo-organic supramolecular chemistry of hybrid pyrazine−pyridine ligands. These are 2,3-disubstituted with 2,6′-substituted oligopyridyl chains. In the presence of appropriate metal cations, they self-assemble to dimeric, intramolecularly stacked metallo-organic complexes.[5] Pyrazine derivatives of 2,5-disubstituted ligands with oligopyridyl chains undergo other metallo-organic self-assembly patterns.[6] Nevertheless, knowledge of the precise manner in which the structures of the 2,3-disubstituted ligands control their self-assembly behavior is limited. Solution- and solid-state studies have indicated that torsional congestion leads to helical twisting of the oligopyridyl strands about each other, and inter- and intramolecular π-stacking interactions occur in both the ligands and their complexes.[4b]

In the presence of copper(I), unsymmetrical ligand **1** forms a dimeric cation $[\mathbf{1}_2Cu_2]^{2+}$, which in principle may exist in either C_2-symmetric or *meso* configurations. In the C_2-form, pairs of pyrazine and pyridine rings overlap, whereas in the *meso* form two pyrazine−pyridine overlaps occur. However, only the chiral form of $[\mathbf{1}_2Cu_2]^{2+}$ has been detected. These double-decker dimers can also be arranged in stacked fashion in the crystal lattice.[5b] Thus, we were attracted to the use of related compounds to construct parallel metallo-organic π-stacking arrays, in particular those possessing discotic and lamellar ordering. Discotic macroscopic ordering is conductive to the formation of mesophase-forming, liquid-crystalline materials and facilitates their use in liquid-crystalline displays and electrically and photoelectrically conductive films.[7] The tetrahedral geometry of copper(I) hitherto has resulted in nematic (tubular) mesotropic ordering in oligopyridine-type metallo-organic complexes.[8]

Initial steps towards these goals include: (a) the preparation of ligands resembling **1** but containing long hydrophobic chains and (b) confirmation of the ligands' self-assembly pattern and stereochemistry {c.f. $[\mathbf{1}_2Cu_2]^{2+}$, C_2 or *meso*}. Ligand **1** is synthesized from α-diketone **2**, and we have presented a synthesis of **2** that is amenable to multigram amounts.[4b] Thus, simple condensation of **2** with aromatic 1,2-diamines already containing attachment points for hydrocarbon tails will afford quinoxaline-type ligands analogous to **1**. We chose attachment of alkyl groups through ether bonding because of this linkage's chemical robustness. An additional benefit of the overall strategy is the extension of the π-electronic stacking system to enhance graphite-like stacking interactions in the corresponding dimeric complexes.

[a] Chemical Laboratory, School of Physical Sciences, University of Kent,
Canterbury, Kent CT2 7NZ, UK
[b] Departement Chemie, Universität Basel,
Spitalstrasse 51, 4056 Basel, Switzerland
Fax: (internat.) +41-61-267-1005
E-mail: markus.neuburger@unibas.ch
[‡] New address: Department of Entomology, University of California,
Davis, CA 95616 USA.
Fax: (internat.) + 1-530-752-1537,
E-mail: Heirtzler@web.de
Supporting information for this article is available on the WWW under http://www.eurjic.org or from the author.

 DOI: 10.1002/ejic.200300531 © 2004 Wiley-VCH Verlag GmbH & Co. KGaA, Weinheim

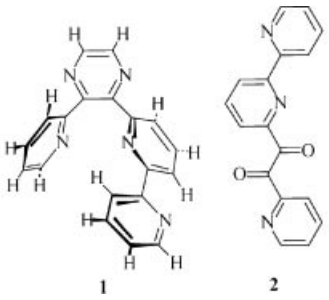

1 2

Results and Discussion

The α-diketone **2** was condensed under acidic conditions with *ortho*-phenylene diamine or 4,5-diaminoveratrole,[9] affording the unsymmetrical quinoxaline-pyridine **3a** and the dimethoxyquinoxaline homologue **3b** in 47 % and 48 % yields, respectively (Scheme 1).[10] The ^{1}H NMR spectra (Figure 1) of these two materials were completely assigned through combination of 2D techniques and comparison of the quinoxaline AA′BB′ systems. Just as for **1**, compounds **3a** and **3b** experience an upfield shifting of H-3′′′ attached to the terminal pyridine ring of the bipyridyl ring system (δ = 7.30 ppm), which is attributed to through-space interaction with the opposing solitary pyridine ring and a helical molecular conformation.

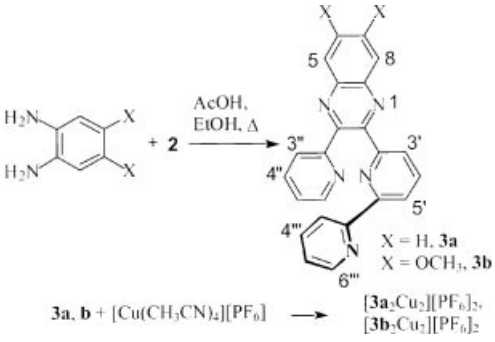

Scheme 1. Synthesis of quinoxaline-type ligands and their dimeric copper(I) complexes

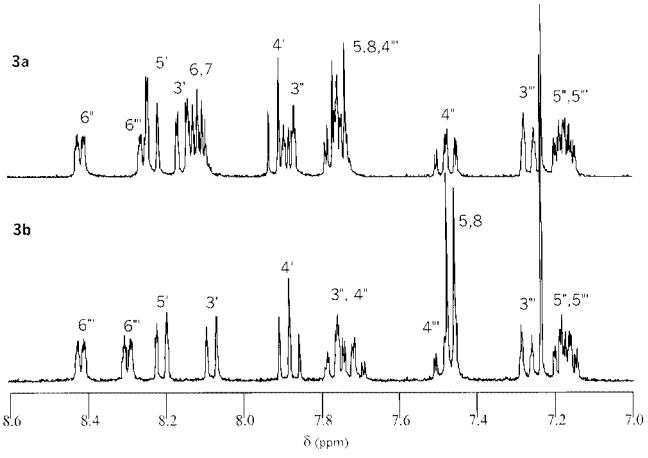

Figure 1. ^{1}H NMR spectra of ligands **3a** and **3b** ($CDCl_3$, 270 MHz)

Treatment of ligands **3a** and **3b** with one equivalent of copper(I)tetrakis(acetonitrilo) hexafluorophosphate in degassed methanol at room temperature gave purple-colored solutions, from which solids were deposited. Crystalline material resulted after slow diffusion of diethyl ether into concentrated acetonitrile solutions. Results of combustion analyses and electrospray mass spectrometry together indicated the presence of dimeric complexes $[\mathbf{3a}_2Cu_2][PF_6]_2$, and $[\mathbf{3b}_2Cu_2][PF_6]_2$.[11] The differential scanning calorimetric profiles of these two materials contain sharp endotherms at 329 and 250 °C, respectively, consistent with unitary compositions. Relative to the parent ligands, their UV-Vis spectra exhibit intensely absorbing, red- and blue-shifted maxima, as well as weak MLCT bands occurring at λ_{max} = 510 nm {$[\mathbf{3a}_2Cu_2][PF_6]_2$, ε = 4.000} and 479/580 nm {$[\mathbf{3b}_2Cu_2][PF_6]_2$, ε = 6.100/4.000}. The latter complex also displays strong adsorption bands at 353/368 nm, attributable to the dimethoxyquinoxaline chromophore (c.f. ligand **3b**: 362/387 nm). The presence of the MLCT bands in both complexes bespeaks of the existence of copper(I) centers surrounded by tetrahedral ligand fields. Yet, the lack of exceptional concentration dependence in the position of the λ_{max} values bespeaks of the absence of a pronounced solution-state aggregation.[12] The complexes were also investigated with cyclic voltammography (Figure 2). In particular, $[\mathbf{3a}_2Cu_2][PF_6]_2$ and $[\mathbf{3b}_2Cu_2][PF_6]_2$ display quasi-reversible Cu(I/II) processes centered at 0.44 V and 0.38 V, relative to the ferrocene/ferrocenium couple. Both metal centers within the same complex are active at identical potentials. Repeated redox cycling of the quinoxaline derivative complex resulted in the decomposition of this material, as evidenced by the appearance of additional redox processes at 1.04 V (reduction) and 0.48 V (oxidation). Gratifyingly, these processes were significantly less prominent in $[\mathbf{3b}_2Cu_2][PF_6]_2$. Since the introduction of electron-rich methyl ether groups into the ligand scaffolding should increase the ligand sensitivity to oxidative degradation, it is possible that greater ligand−metal interaction may account for the stability of $[\mathbf{3b}_2Cu_2][PF_6]_2$.

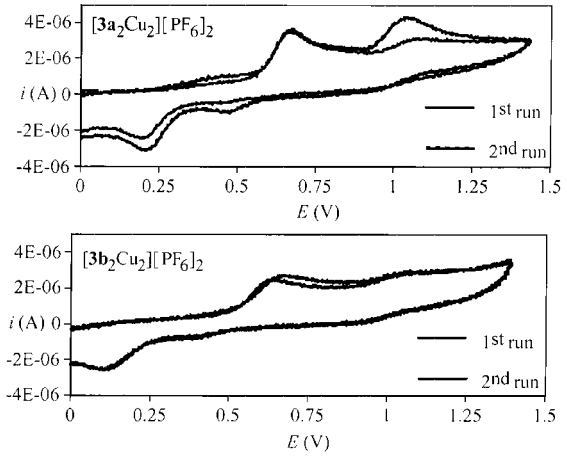

Figure 2. Cyclic voltammograms of dimeric dicopper(I) complexes in acetonitrile (supporting electrolyte: nBu$_4$PF$_6$; all potentials relative to the ferrocenium−ferrocene couple)

 © 2004 Wiley-VCH Verlag GmbH & Co. KGaA, Weinheim

The ^{1}H NMR spectra of both complexes were completely assigned through use of 2D NMR spectroscopy and by comparison to related compounds[13] (Figure 3). The chemical shifts of the flanking 2,6′-bipyridyl groups for both complexes are generally coincident. The proton shifts attributed to the pyridine ring participating in the metallophane "decks" appear upfield as expected from their local anisotropy. In $[\mathbf{3b}_2Cu_2][PF_6]_2$, the aromatic positions adjacent to the methoxy groups appear at δ = 6.6/6.8 ppm, which we tentatively interpret as evidence of a mutual shielding effect between the two equivalents of disubstituted quinoxaline-like complexes. Of special note in both complexes is the shielding effect on H-3′′, which is attributable to an orthogonal π-stacking interaction with the bipyridyl ring system (c.f. H-3′′′ in **3a** and **3b**). Variable temperature NMR spectra, recorded in $[D_3]$MeCN and non-coordinating $[D_3]MeNO_2$ [14] down to −40 °C, exhibited negligible decoalescence phenomena. It is thus reasonable to assume that $[\mathbf{3a}_2Cu_2][PF_6]_2$ and $[\mathbf{3b}_2Cu_2][PF_6]_2$ possess similar structures in solution.

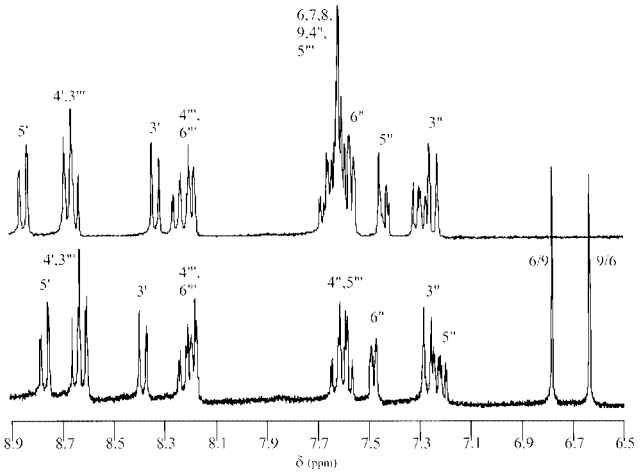

Figure 3. ^{1}H NMR Spectra of dicopper(I) metallophanes $[\mathbf{3a}_2Cu_2][PF_6]_2$ and $[\mathbf{3b}_2Cu_2][PF_6]_2$ (CD_3CN, 270 MHz)

A crystal structure analysis was undertaken on the complex $[\mathbf{3a}_2Cu_2][PF_6]_2$ to investigate its stereochemistry and lattice packing.[15] A double-decker geometry results from the combination of two bidentate sites (2,6′-bipyridyl and 2′,3"-pyridylquinoxalinyl) surrounding each tetrahedral metal center. Quinoxaline N adjacent to bipyridyl remains uncoordinated. While this arrangement is shared by both the C_2- and *meso*-diastereomers, the dication crystallizes in the C_2-symmetric form, that is, pyridyl quinoxaline moieties within the same dication are arranged in a parallel fashion. The overall crystal symmetry (space group *Pbca*) corresponds to a racemic crystal; one of the two equally likely enantiomers is displayed in Figure 4.

Intramolecularly, the quinoxaline ring fragments overlap in an offset fashion (Figure 5). This also results in classical parallel π-stacking overlap[16] between areas of low and high electron density. The geometrical center of the benzenoid subring on quinoxaline is separated from quaternary C(8a) by 3.45 Å, while the center of the pyrazinoid

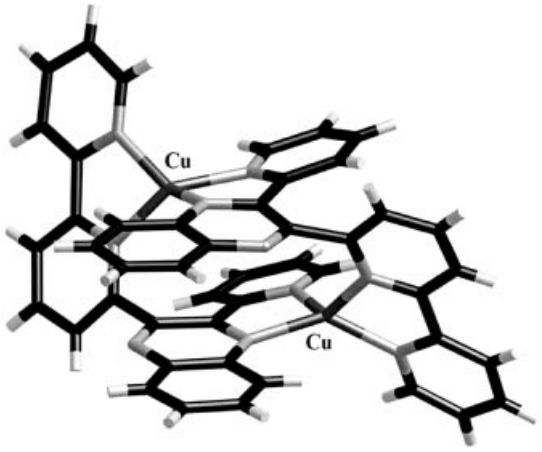

Figure 4. X-ray crystal structure of one of the two enantiomeric dicopper(I) cations from $[\mathbf{3a}_2Cu_2][PF_6]_2$

ring is closest to C(4a) at 3.40 Å. The stacked quinoxalinyl ring system is twisted by 18.67° relative to pyridyl. A consequence of this is that while the quinoxaline ring atoms are separated from the mean plane of the opposing quinoxaline ring by 3.36 ± 0.04 Å, the average atomic separation from the pyridylquinoxaline system to its opposing mean plane is 3.43 ± 0.16 Å. The two quinoxalinyl fragments deviate by 1.3° from coplanarity, while the two stacked pyridyl residues the deviation is 5.9°.

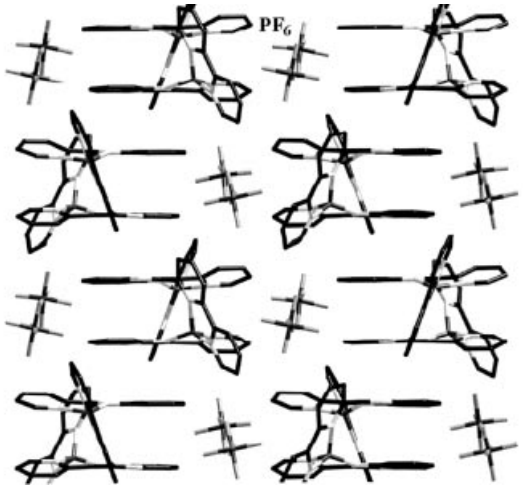

Figure 5. Crystal lattice of $[\mathbf{3a}_2Cu_2][PF_6]_2$

Homochiral dicationic complexes interact through offset stacking interactions involving the quinoxaline ring systems (average distance of quinoxaline atoms from the mean plane, 3.35 ± 0.09 Å; dihedral angle between planes: 3.90°); in particular those involving benzo and pyrazinyl domains overlap (distance between ring centers, 3.63 Å). Strata composed of Δ,Δ- and Λ,Λ−configured metallophane dimers are separated by weaker parallel edge-on contacts between 2,2′-bipyridyl flanks (ca. 4.8 Å) and the hexafluorophosphate counterions.

 © 2004 Wiley-VCH Verlag GmbH & Co. KGaA, Weinheim

Conclusion

The applicability of quinoxaline-pyridine hybrids for engineering highly stacked, self-assembling metallo-organic networks has been confirmed. It employs a combination of heterocyclic synthesis, a new metallo-organic supramolecular synthon and intramolecular π-stacking effects over extended arene surfaces. At least for smaller alkoxy chains, a consequence of the complexes' C_2-symmetry is the location of all four ether functionalities on the same side of the complex dication. The extension of this strategy to the preparation of mesotropic, liquid-crystalline materials is currently under investigation.

Acknowledgments

We thank the Engineering and Physical Sciences Research Council (EPSRC) for financial support (Grant R/R09138), the EPSRC Mass Spectroscopy Centre for mass spectra as well as Dr. D. Smith (University of Kent) for technical assistance.

[1] [1a] L. F. Lindoy, I. M Atkinson, in *Self-Assembly in Supramolecular Systems-Monographs* in *Supramolecular Chemistry* (Ed.: J. F. Stoddart), Royal Society of Chemistry, London, **2000**. [1b] J.-M. Lehn, *Supramolecular Chemistry, Concepts and Perspectives*, New York, VCH, **1995**.

[2] [2a] M. Albrecht, S. Kotila, *Chem. Commun.* **1996**, 2309−2310. [2b] A. Bilyk, M. M. Harding, P. Turner, T. W. Hambley, *J. Chem. Soc., Chem. Commun.* **1995**, 2549−2553. [2c] M. J. Hannon, C. L. Painting, W. Errington, *Chem. Commun.* **1997**, 307−308.

[3] [3a] P. Baxter, J.-M. Lehn, A. DeCian, J. Fischer, *Angew. Chem. Int. Ed. Engl.* **1993**, *32*, 69−72. [3b] M. Fujita, N. Fujita, K. Ogura, K. Yamaguchi, *Nature* **1999**, *400*, 52−55. [3c] A. H. Eisenberg, M. V. Ovchinnikov, C. A. Mirkin, *J. Am. Chem. Soc.* **2003**, *125*, 2836−2837.

[4] [4a] F. R. Heirtzler, M. Neuburger, M. Zehnder, E. C. Constable, *Liebigs Ann./Recueil* **1997**, 297−301. [4b] F. Heirtzler, M. Neuberger, K. Kulike, *J. Chem. Soc., Perkin Trans. 1* **2002**, 809−820.

[5] [5a] F. Heirtzler, T. Weyhermüller, *J. Chem. Soc., Dalton Trans.* **1997**, 3653−3654. [5b] T. Bark, T. Weyhermüller, F. Heirtzler, *Chem. Commun.* **1998**, 1475−1476.

[6] [6a] T. Bark, M. Duggeli, H. Stoeckli-Evans, A. v. Zelewsky, *Angew. Chem. Int. Ed.* **2001**, *40*, 2848−2851. [6b] D. Brown, S. Muranjan, Y. Jang, T. Thummel, *Org. Lett.* **2002**, *4*, 1253−1256.

[7] [7a] J.-P. Farges in *Organic Conductors -Fundamentals and Applications* (Ed.: A. M. Hermann), Marcel Dekker, New York, **1994**. [7b]E. O. Arikainen, N. Boden, J. Bushby, J. Clements, B. Movaghar, A. Wood, *J. Mater. Chem.* **1995**, *5*, 2161−2165. [7c] W. B. Euler in *Handbook of Organic Conductive Molecules and Polymers* (Ed.: H. S. Nalwa), Chichester, Wiley, **1997**, vol. 2, p 719. [7d] T. Ishiguro, K. Yamaji, G. Saito in *Organic Superconductors -Springer Series in Solid State Sciences*, vol. 88 (Ed.: P. Fulde), Springer-Verlag, Heidelberg, **1998**.

[8] [8a] L. Douce, A. El-ghayoury, A. Skoulios, R. Ziessel, *Chem. Commun.* **1999**, 2033−2034. [8b] K. E. Rowe, D. W. Bruce, *Liq. Cryst.* **1996**, *20*, 183−193. [8c] C. Tschierske, *Angew. Chem. Int. Ed.* **2000**, *39*, 2454−2458. [8d] E. Terazzi, J. M. Benech, J. P. Rivera, G. Bernardinelli, B. Donnio, D. Guillon, C. Piguet, *Dalton Trans.* **2003**, 769−772.

[9] M. M. G. Antonisse, B. H. M. Snellink-Ruel, I. Yigit, J. F. J. Engbersen, D. N. Reinhoudt, *J. Org. Chem.* **1997**, *62*, 9034−9038.

[10] Full experimental details for the preparation of **3a**, **3b**, $[\mathbf{3a}_2Cu_2][PF_6]_2$ and $[\mathbf{3b}_2Cu_2][PF_6]_2$, including ^1H and ^{13}C NMR, IR, UV-Vis spectroscopy (Figures, mass spectra and combustion analyses are provided as Supporting information).

[11] $[\mathbf{3a}_2Cu_2][PF_6]_2$: $C_{46}H_{30}Cu_2F_{12}N_{10}P_2\cdot 2H_2O$ (1175.86): calcd. C 46.99, H 2.91, N 11.91; found C 46.70, H 2.63, N 11.55. LSIMS (NOBA matrix, rel. intensity): *m/z* = 993 {$[M - PF_6]^+$, 25 %}, 849 {$[M - 2PF_6]^+$, 75 %}; $[\mathbf{3b}_2Cu_2][PF_6]_2$: $C_{50}H_{38}Cu_2F_{12}N_{10}O_4P_2\cdot H_2O$ (1277.95): calcd. C 46.99, H 3.16, N 11.96; found C 47.40, H 3.61, N 11.50. MALDI-TOF (MeOH/MeCN, rel. intensity): *m/z* = 1113 {$[M - PF_6]^+$, 25 %}, 484 {$[M/2 - 2PF_6]^+$, 100 %}.

[12] C. A. Hunter, P. Leighton, J. K. M. Sanders, *J. Chem. Soc., Perkin Trans. 1* **1989**, 547−552.

[13] The details of these studies will be reported shortly (I. Prokes, F. Heirtzler, *Chem. Commun.* **2003**, *in press*).

[14] W. A. E. McBryde, *IUPAC Chemical Data Series*, *no. 17*, Pergamon Press: Oxford, **1978**.

[15] X-ray Crystallographic Study on $[\mathbf{3a}_2Cu_2][PF_6]_2$: A sample was mounted on a KappaCCD area detector using the oil-drop method. Unit cell determination, data collection and integration was carried out with the programs Collect,[17] Denzo and Scalepack.[18] The structure was solved by direct methods using the program SIR92.[19] Anisotropic least-squares full-matrix refinement was carried out on all non-hydrogen atoms using the program CRYSTALS.[20] Positions of the hydrogen atoms were determined geometrically. Chebychev polynomial weights[21] were used to complete the refinements. Scattering factors have been taken from the International Tables, vol. IV, Table 2.2B. Crystallographic data for $[\mathbf{3a}_2Cu_2][PF_6]_2$ ($C_{46}H_{30}Cu_2N_{10}\cdot 2PF_6$): M_r = 1139.83 gmol^{-1}, brown needles (0.12 × 0.18 × 0.41 mm), space group *Pbca*, *a* = 13.4184(16), *b* = 24.736(6), *c* = 27.549(5) Å; α = β = γ = 90°; *V* = 9143.9 Å^3, *Z* = 8, $\rho_{calcd.}$ = 1.679 g·cm^{-3}, *F*(000) = 4464, radiation Mo-K_α (λ = 0.70173 Å), *T* = 173 °C, 78945 reflections measured (4.08 < θ < 27.50) of which 10477 were independent. *R*1 = 0.0686, *wR*2 = 0.0498, goodness-of-fit: 0.9872 for 6220 reflections with $I > 2\sigma(I)$ and 658 parameters. Residual electron density: −0.84/1.03 e·Å^{-3}. CCDC-216375 contains the supplementary crystallographic data for this paper. These data can be obtained free of charge at www.ccdc.cam.ac.uk/conts/retrieving.html [or from the Cambridge Crystallographic Data Centre, 12, Union Road, Cambridge CB2 1EZ, UK; Fax: (internat.) +44-1223/336-033; E-mail: deposit@ccdc.cam.ac.uk].

[16] C. A. Hunter, J. K. M. Sanders, *J. Am. Chem. Soc.* **1990**, *112*, 5525−5534.

[17] COLLECT Software, Nonius BV **1997**−**2001**.

[18] Z. Otwinowski and W. Minor, in *Methods in Enzymology* in *Macromolecular Crystallography*, vol. 276, Part A (Eds.: C. W. Carter, Jr. and R. M. Sweet) Academic Press, New York, **1997**, p 307.

[19] A. Altomare, G. Cascarano, G. Giacovazzo, A. Guagliardi, M. C. Burla, G. Polidori, M. Camalli, *J. Appl. Cryst.* **1994**, *27*, 435.

[20] D. J. Watkin, R. J. Carruthers, P. Betteridge, CRYSTALS, Chemical Crystallography Laboratory, Oxford, UK, **1985**.

[21] J. R. Carruthers, D. J. Watkin, *Acta Crystallogr., Sect. A* **1979**, 698−699.

Received July 31, 2003

 © 2004 Wiley-VCH Verlag GmbH & Co. KGaA, Weinheim

Stannaborate Chemistry: Nucleophilic Substitution at the Cluster Sphere

Benno Ronig,[b] Torsten Bick,[b] Ingo Pantenburg,[b] and Lars Wesemann*[a]

Keywords: Boranes / Boron / Tin / Nucleophilic substitution

Nucleophilic substitution at (γ-chloropropyl)stanna-*closo*-dodecaborate $[Cl(CH_2)_3SnB_{11}H_{11}]^-$ with RLi [R = Ph, $Me_2NC_6H_4$, ferrocenyl (Fc)] and RMgBr (R = vinyl, benzyl) affords the substitution products containing the anion $[RSnB_{11}H_{11}]^-$. The reaction products have been characterized by elemental analysis, NMR spectroscopy and in the cases where R = Ph, $Me_2NC_6H_4$, Fc and vinyl by X-ray structure analysis.
(© Wiley-VCH Verlag GmbH & Co. KGaA, 69451 Weinheim, Germany, 2004)

Introduction

The nucleophilic substitution at tin(IV) halides with organic derivatives of electropositive elements is a very important method for the formation of new tin−carbon bonds.[1] In another possible route, triorganylstannyl metal compounds find extensive use for the preparation of Sn−C units.[1] In this context, the nucleophilic substitution at tetraorganotin compounds with basic nucleophilic reagents such as alkyl- or phenyllithium is a less frequently used method and is more well-known in the case of the transmetallation reactions and the preparation of organolithium, organoboron or organocopper compounds. Thus, a straightforward procedure is the formation of vinyllithium by reaction between tetravinyltin and four equivalents of phenyllithium.[2] The equilibrium of this kind of reaction is driven completely to the right side when the stability of the formed organolithium compound is larger than that of the starting lithium reagent.

Currently we are exploring the chemistry of a heteroborate, the stanna-*closo*-dodecaborate $[SnB_{11}H_{11}]^{2-}$ dianion, which is accessible in amounts of about five grams following a two step procedure.[3] The investigation of the ligand abilities of this cluster with respect to its cocatalytic properties and use in metal cluster formation are of interest to us.[4,5] Furthermore, we are studying organic transformation reactions at the cluster sphere. So far it is well established that the dianion $[SnB_{11}H_{11}]^{2-}$ acts as a nucleophile with alkyl iodides or reactive alkyl bromides like propargyl bromide.[6] The reaction with alkyl iodides is equivalent to an oxidation of the tin nucleus deduced from ^{119}Sn NMR and Mössbauer spectroscopy studies.[7] In this publication, we present the nucleophilic substitution at the tin center in alkylated stanna-*closo*-dodecaborate derivatives.

[a] Institut für Anorganische Chemie II, Universität Tübingen, Auf der Morgenstelle 18, 72076 Tübingen, Germany
Fax: (internat.) + 49-7071-5306
E-mail: lars.wesemann@uni-tuebingen.de
[b] Institut für Anorganische Chemie, Universität zu Köln, Greinstr. 6, 50939 Köln, Germany

Results and Discussion

(γ-Benzenesulfonyloxy)alkyltributyltin derivatives (Scheme 1) have been used successfully for the synthesis of cyclopropane derivatives.[8] In the stereoselective reaction with *n*-butyllithium, the products are cyclopropane, tetrabutyltin and lithium phenylsulfonate (Scheme 1).[9]

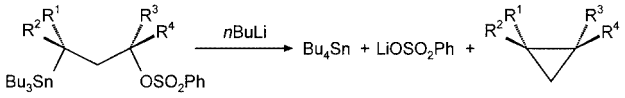

Scheme 1. Stereoselective formation of alkylated cyclopropane derivatives by nucleophilic attack at the tin atom in (γ-benzenesulfonyloxy)alkyltributyltin compounds (R^1−R^4 = alkyl substituent)

In analogy to this cyclopropane formation reaction, we have treated (γ-chloropropyl)stanna-*closo*-dodecaborate (**1**) with a variety of nucleophiles (Scheme 2 and 3). It turned out that the very reactive lithium reagents attack the tin center at room temperature and the desired products **2**, **3** and **4** can be isolated in high yield. Grignard reagents, however, have to be refluxed in THF in order to react successfully at the tin vertex.

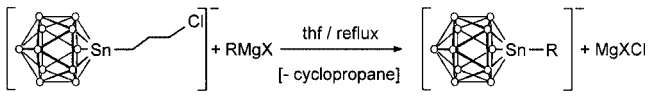

$[Bu_3MeN][Cl(CH_2)_3(SnB_{11}H_{11})]$ (1) $[Bu_3MeN][R(SnB_{11}H_{11})]$

Scheme 2. Nucleophilic substitution at the tin vertex in (γ-chloropropyl)stanna-*closo*-dodecaborate with lithium organic reagents: R = Ph **2**, $[p\text{-}Me_2NC_6H_4]$ **3**, Fc **4**

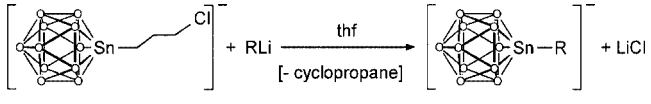

$[Bu_3MeN][Cl(CH_2)_3(SnB_{11}H_{11})]$ (1) $[Bu_3MeN][R(SnB_{11}H_{11})]$

Scheme 3. Nucleophilic substitution in refluxing THF: R = $CH_2C_6H_5$ **5**, H_2CCH **6**

Reaction of an alkyl-substituted stanna-*closo*-dodecaborate derivative $\{[RSnB_{11}H_{11}]^-\}$ with a nucleophile $[R']^-$ would lead to an equilibrium mixture between $\{[RSnB_{11}H_{11}]^- + [R']^-\}$ and $\{[R'SnB_{11}H_{11}]^- + [R]^-\}$ with the ratios dependent on the stability of the respective anions $[R']^-$ and $[R]^-$. On use of the γ-chloropropyl substituent, this reaction is driven completely to the right side, since the leaving group cyclopropane and the chloride anion are formed. In order to use the γ-chloropropyl substituent as a protecting group, we treated the alkylated cluster **1** with hydride as the nucleophile. From this reaction the unsubstituted cluster **7** was isolated in high yield (Scheme 4).

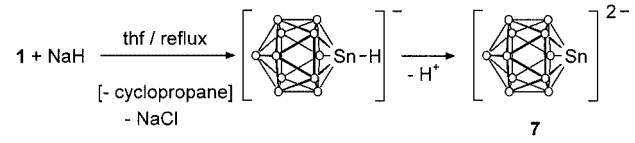

7

Scheme 4. Substitution reaction with a hydride nucleophile followed by deprotonation

However, so far we were not able to isolate the postulated, protonated cluster anion $[HSnB_{11}H_{11}]^-$ from this reaction or by treatment of **7** with a mineral acid. The air-stable substitution products **2**−**6** have been characterized by elemental analysis, NMR spectroscopy and in the cases of **2**−**4** and **6** by X-ray crystal structure analysis. In the ^1H NMR spectrum of the substitution products, the absence of the characteristic signals of the $Sn-(CH_2)_3-Cl$ group is a very good indicator for a successful reaction. The ^{11}B NMR spectrum of the starting materials and the products exhibit almost no change; two signals around δ = −11 and −16 ppm (B12, B2−B11) are characteristic for the substituted cluster. In order to confirm the geometry of the product salts, X-ray crystal structure determinations have been

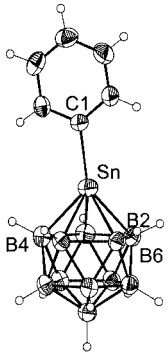

Figure 1. Molecular structure of the anion of $[Bu_3MeN][PhSnB_{11}H_{11}]$ (**2**) in the solid state; interatomic distances in [pm] (with estimated standard deviations in parentheses): Sn−C 210.7(3), Sn−B2 228.1(3), Sn−B3 228.4(3), Sn−B4 228.6(3), Sn−B5 228.7(3), Sn−B6 229.1(3); thermal ellipsoids are shown at the 50 % probability level

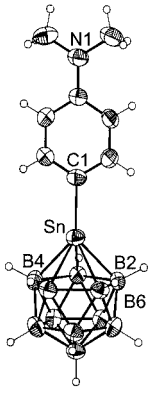

Figure 2. Molecular structure of the anion of $[Bu_3MeN][Me_2NC_6H_4SnB_{11}H_{11}]$ (**3**) in the solid state; interatomic distances in [pm] (with estimated standard deviations in parentheses): Sn−C 210.0(4), Sn−B2 228.7(5), Sn−B3 228.8(5), Sn−B4 229.0(5), Sn−B5 229.4(5), Sn−B6 229.7(5); thermal ellipsoids are shown at the 50 % probability level

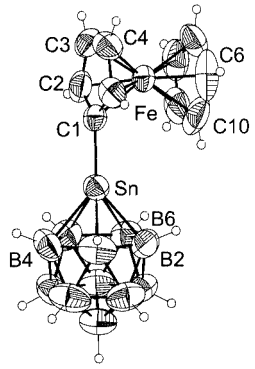

Figure 3. Molecular structure of the anion of $[Bu_3MeN][FcSnB_{11}H_{11}]$ (**4**) in the solid state; thermal ellipsoids are shown at the 50 % probability level; interatomic distances in [pm] (with estimated standard deviations in parentheses): Sn−C 206.8(3), Sn−B2 225.5(5), Sn−B3 227.4(5), Sn−B4 227.6(5), Sn−B5 228.1(5), Sn−B6 228.4(4), Fe−C1 202.9(4), Fe−C2 202.9(4), Fe−C3 203.6(4), Fe−C4 203.6(4), Fe−C5 204.0(4), Fe−C6 200.9(4), Fe−C7 201.3(4), Fe−C8 201.4(5), Fe−C9 201.8(4), Fe−C10 201.8(5)

 © 2004 Wiley-VCH Verlag GmbH & Co. KGaA, Weinheim

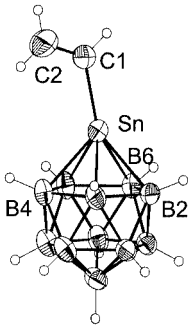

Figure 4. Molecular structure of the anion of $[Bu_3MeN][(H_2CCH)SnB_{11}H_{11}]$ (**6**) in the solid state; thermal ellipsoids are shown at the 50 % probability level; interatomic distances in [pm] (with estimated standard deviations in parentheses): Sn−C1 207.7(5), C1−C2 129.6(8), Sn−B2 229.1(5), Sn−B3 229.3(5), Sn−B4 229.5(6), Sn−B5 230.4(5), Sn−B6 230.3(5)

carried out. In Table 1, details of the X-ray structure solutions are listed and in Figures 1−4, the structures of the respective anions in the solid state are depicted.

The results of the crystal structure determinations are consistent with the findings of elemental analysis and NMR spectroscopy. The geometries of the substituted clusters exhibit no peculiarities and the Sn−B and B−B interatomic distances are in the range known from other derivatives. The deviation from linearity of the angle C−Sn−(antipodal)B (**2** 171.7°, **3** 175.8°, **4** 178.1°, **6** 167.2°) is a common effect in these substituted stannaborate derivatives and can be explained by packing forces in the solid state.

Conclusion

With this straightforward substitution at the tin center in γ-chloropropyl-substituted stanna-*closo*-dodecaborate, a method for the linkage of an aromatic cluster anion with π-systems like the phenyl, ferrocenyl or vinyl moiety has been found.

Experimental Section

General: All manipulations were carried out under dry N_2 in Schlenk glassware; solvents were dried and purified by standard methods and stored under N_2. NMR spectroscopy was performed on a Bruker AC 200 (^{1}H: 200 MHz, int. TMS; ^{11}B{^{1}H}: 64 MHz, ext. $BF_3{\cdot}Et_2O$). Elemental analysis was carried out by the Institut für Anorganische Chemie der Universität zu Köln, on a Heraeus C,H,N,O rapid elemental analyser.

$[Bu_3MeN][PhSnB_{11}H_{11}]$ (2): $[Bu_3MeN][H_{11}B_{11}SnC_3H_6Cl]$ (368 mg, M_r = 526.64 g/mol, 0.699 mmol) was dissolved in 20 mL THF and treated with an excess of phenyllithium (in Et_2O) at −78 °C. After stirring the solution overnight at room temperature, volatiles were removed in vacuo and the residue was washed with H_2O (20 mL). The product was dissolved in CH_2Cl_2, filtered and crystallized by slow diffusion of *n*-hexane to give **2** (234 mg, M_r = 526.21 g/mol, 0.445 mmol, 64 %). ^{1}H NMR (CD_2Cl_2): δ = 0.98 (t, 9 H, ^3J = 7.3 Hz, CH_2CH_3), 1.41 (m, 6 H, CH_2CH_3), 1.64 (m, 6 H, $CH_2CH_2CH_3$), 3.00 (s, 3 H, NCH_3), 3.16 (m, 6 H, NCH_2), 7.55 (m, 5 H, C_6H_5) ppm. ^{11}B{^{1}H} NMR (CD_2Cl): δ = −11.1 (s, B12), −16.4 (s, B2−B6 and B7−B11). $C_{19}H_{46}B_{11}NSn$ (526.21): calcd. C 43.37, H 8.81, N 2.66; found C 43.51, H 8.82, N 2.79.

$[Bu_3MeN][Me_2NC_6H_4SnB_{11}H_{11}]$ (3): $[Bu_3MeN][H_{11}B_{11}SnC_3H_6Cl]$ (477 mg, M_r = 526.64 g/mol, 0.906 mmol) was dissolved in 20 mL THF and treated with an excess of [*p*-$Me_2NC_6H_4Li$] in Et_2O at −78 °C. After stirring the solution overnight at room temperature, volatiles were removed in vacuo and the residue was washed with H_2O (20 mL). The product was dissolved in CH_2Cl_2, filtered and crystallized by slow diffusion of *n*-hexane to give **3** (186 mg, M_r = 569.28 g/mol, 0.327 mmol, 36 %). ^{1}H NMR (CD_2Cl_2): δ = 1.00 (t, 9 H, ^3J = 7.3 Hz, CH_2CH_3), 1.41 (m, 6 H, CH_2CH_3), 1.66 (m, 6 H, $CH_2CH_2CH_3$), 2.92 [s, 6 H, $C_6H_4N(CH_3)_2$], 3.01 (s, 3 H, NCH_3), 3.19 (m, 6 H, NCH_2), 7.20 (m, 4 H, C_6H_4) ppm. ^{11}B{^{1}H} NMR (CD_2Cl_2): δ = −12.1 (s, B12), −16.9 (s, B2−B6 and B7−B11). $C_{21}H_{51}B_{11}N_2Sn$ (569.28): calcd. C 44.31, H 9.03, N 4.92; found C 42.99, H 8.95, N 4.71.

$[Bu_3MeN][FcSnB_{11}H_{11}]$ (4): $[Bu_3MeN][H_{11}B_{11}SnC_3H_6Cl]$ (500 mg, M_r = 526.64 g/mol, 0.949 mmol) was dissolved in THF at −78 °C and treated with a solution of $Li[C_5H_4FeC_5H_5]$ (546 mg, M_r = 562.67 g/mol, 0.889 mmol) in THF (20 mL). After stirring the solution overnight at room temperature, volatiles were removed in vacuo and the residue was washed with H_2O (20 mL). The product was dissolved in CH_2Cl_2, filtered and crystallized by slow diffusion of *n*-hexane to give **4** (423 mg, M_r = 634.13 g/mol, 0.667 mmol, 75 %). ^{1}H NMR (CD_2Cl_2): δ = 1.02 (t, 9 H, ^3J = 7.8 Hz, CH_2CH_3), 1.48 (m, 6 H, CH_2CH_3), 1.66 (m, 6 H, $CH_2CH_2CH_3$), 3.01 (s, 3 H, NCH_3), 3.20 (m, 6 H, NCH_2), 4.37 (s, 5 H, FeC_5H_5), 4.52 [s, 2 H, SnC-$(CH)_2$-$(CH)_2$], 4.60 [s, 2 H, SnC-$(CH)_2$-$(CH)_2$] ppm. ^{13}C{^{1}H} NMR (CD_2Cl): δ = 13.8 (CH_2CH_3), 20.1 (CH_2CH_3), 24.7 ($CH_2CH_2CH_3$), 49.5 (NCH_3), 62.5 (NCH_2), 70.4 (FeC_5H_5), 72.1 [SnC-$(CH)_2$-$(CH)_2$], 75.1 [SnC-$(CH)_2$-$(CH)_2$] ppm. ^{11}B{^{1}H} NMR (CD_2Cl_2): δ = −12.6 (s, B12), −17.3 (s, B2−B6 and B7−B11). $C_{23}H_{50}B_{11}FeNSn$ (634.13): calcd. C 43.56, H 7.95, N 2.21; found C 43.35, H 8.05, N 2.25.

$[Bu_3MeN][PhCH_2SnB_{11}H_{11}]$ (5): $[Bu_3MeN][H_{11}B_{11}SnC_3H_6Cl]$ (670 mg, M_r = 526.64 g/mol, 1.27 mmol) was dissolved in THF (30 mL) and treated with $PhCH_2MgBr$ (0.95 mL, 2 M solution in THF, 1.90 mmol). After stirring overnight at reflux temperatures, the solution turned yellow and volatiles were removed in vacuo. The residue was washed with H_2O (20 mL). The remaining residue was dissolved in EtOH, filtered and crystallized to give **5** (0.61 g, M_r = 540.24 g/mol, 1.13 mmol, 89 %). ^{1}H NMR (CD_2Cl_2): δ = 1.01 (t, 9 H, ^3J = 7.3 Hz, CH_2CH_3), 1.41 (m, 6 H, CH_2CH_3), 1.62 (m, 6 H, $CH_2CH_2CH_3$), 3.01 (s, 3 H, NCH_3), 3.17 (m, 6 H, NCH_2), 3.98 (s, 2 H, -$SnCH_2Ph$), 7.32 (m, 4 H, C_6H_4) ppm. ^{11}B{^{1}H} NMR (CD_2Cl_2): δ = −12.5 (s, B12), −17.1 (s, B2−B6 and B7−B11). $C_{20}H_{48}B_{11}NSn$ (540.24): calcd. C 44.47, H 8.96, N 2.59; found C 43.93, H 9.16, N 2.67.

$[Bu_3MeN][(H_2CCH)SnB_{11}H_{11}]$ (6): $[Bu_3MeN][H_{11}B_{11}SnC_3H_6Cl]$ (850 mg, M_r = 526.64 g/mol, 1.61 mmol) was dissolved in THF (30 mL) and treated with vinylmagnesium bromide (1.93 mL, 1 M solution in THF). After stirring the reaction mixture under reflux overnight, all volatiles were removed in vacuo. The residue was washed with H_2O (20 mL). Crystallization from CH_2Cl_2 by diffusion of *n*-hexane affords **6** (0.71 g, M_r = 476.11 g/mol, 1.49 mmol, 87 %). ^{1}H NMR (CD_2Cl_2): δ = 1.01 (t, 9 H, ^3J = 7.1 Hz, CH_2CH_3), 1.46 (m, 6 H, CH_2CH_3), 1.68 (m, 6 H,

 © 2004 Wiley-VCH Verlag GmbH & Co. KGaA, Weinheim

Table 1. Crystal data and structure refinement parameters for $[Bu_3MeN][PhSnB_{11}H_{11}]$ (**2**), $[Bu_3MeN][Me_2NC_6H_4SnB_{11}H_{11}]$ (**3**), $[Bu_3MeN][FcSnB_{11}H_{11}]$ (**4**) and $[Bu_3MeN][(H_2CCH)\text{-}SnB_{11}H_{11}]$ (**6**)

	2	**3**	**4**	**6**
Empirical formula	$C_{19}H_{46}B_{11}NSn$	$C_{21}H_{51}B_{11}N_2Sn$	$C_{23}H_{50}B_{11}FeNSn$	$C_{15}H_{44}B_{11}NSn$
M_r [g/mol]	526.17	569.24	634.09	476.11
		Data Collection		
Diffractometer	STOE IPDS II	STOE IPDS II	STOE IPDS II	STOE IPDS II
Radiation	Mo-K_α (graphite monochromator, λ = 71.073 pm)			
T [K]	170(2)	170(2)	293(2)	170(2)
Index range	$-21 \le h \le 21$ $-22 \le k \le 20$ $-24 \le l \le 24$	$-14 \le h \le 14$ $-25 \le k \le 25$ $-22 \le l \le 22$	$-13 \le h \le 13$ $-15 \le k \le 15$ $-18 \le l \le 18$	$-18 \le h \le 20$ $-22 \le k \le 22$ $-21 \le l \le 24$
Rotation angle range	0° ≤ ω ≤ 180°; ψ = 0° 0° ≤ ω ≤ 180°; ψ = 90° 0° ≤ ω ≤ 180°; ψ = 135°	0° ≤ ω ≤ 180°; ψ = 0° 0° ≤ ω ≤ 122°; ψ = 90°	0° ≤ ω ≤ 180°; ψ = 0° 0° ≤ ω ≤ 114°; ψ = 90°	0° ≤ ω ≤ 180°; ψ = 0° 0° ≤ ω ≤ 58°; ψ = 90°
Increment	Δω = 2°	Δω = 2°	Δω = 2°	Δω = 2°
No. of images	270	151	147	119
Exposure time [min]	1	6	3	10
Detector distance [mm]	120	100	120	120
2θ Range [deg]	1.9−54.8	2.3−59.5	1.9−54.8	1.9−54.8
Total data collected	125815	36462	21249	47182
Unique data	6274	6080	7283	5243
Observed data	3595	3687	3931	2736
R_{merg}	0.0692	0.1324	0.0419	0.1132
Absorption correction	numerical, after crystal shape optimization[10,11]			
Transmission max/min	0.8191/0.5040	0.9435/0.5404	0.9119/0.6526	0.8904/0.7607
		Crystallographic data[12]		
Crystal size [mm]	0.3 × 0.3 × 0.2	0.2 × 0.2 × 0.1	0.5 × 0.3 × 0.05	0.5 × 0.15 × 0.15
Colour, habit	colourless, polyhedron	colourless, polyhedron	orange, plate	colourless, needle
Crystal system	orthorhombic	monoclinic	triclinic	orthorhombic
Space group	*Pbca* (no. 61)	$P2_1/n$ (no. 14)	$P\bar{1}$ (no. 2)	*Pcab* (no. 61)
a [pm]	1689.7(1)	1025.9(1)	1066.0(2)	1602.9(1)
b [pm]	1760.2(1)	1867.4(2)	1192.3(2)	1756.3(2)
c [pm]	1874.8(1)	1628.4(2)	1442.8(2)	1901.1(2)
α [°]	90	90	72.95(1)	90
β [°]	90	97.90(1)	79.51(1)	90
γ [°]	90	90	69.92(1)	90
V [nm^3]	5.5763(6)	3.0902(6)	1.6398(1)	5.3517(9)
Z	8	4	2	8
$\rho_{calcd.}$ [g·cm^{-3}]	1.253	1.224	1.284	1.182
μ [mm^{-1}]	0.925	0.841	1.218	0.957
F(000)	2176	1184	652	1968
		Structure analysis and refinement		
Structure determination	SHELXS-97[13] and SHELXL-93[14]			
No. of variables	474	317	338	258
R indexes [$I > 2\sigma(I)$][a]	R_1 = 0.0330 wR_2 = 0.0740	R_1 = 0.0480 wR_2 = 0.0941	R_1 = 0.0353 wR_2 = 0.0801	R_1 = 0.0420 wR_2 = 0.0822
R indexes [all data]	R_1 = 0.0634 wR_2 = 0.0800	R_1 = 0.0874 wR_2 = 0.1055	R_1 = 0.0774 wR_2 = 0.0900	R_1 = 0.1011 wR_2 = 0.0956
GooF [S_{obs}]	1.001	0.880	0.998	1.026
GooF [S_{all}]	0.796	1.023	0.808	0.842
Largest difference map hole/peak [e$^-$ 10^{-6} pm^{-3}]	−0.656/0.730	−0.731/0.784	−0.541/0.688	−0.500/0.531

[a] $R_1 = \Sigma| |F_o| - |F_c| | / \Sigma |F_o|$. [b] $wR_2 = [\Sigma w(F_o^2 - F_c^2)^2 / \Sigma w(F_o^2)^2]^{1/2}$, $S_2 = [\Sigma w(F_o^2 - F_c^2)^2/(n\text{-}p)]^{1/2}$, with $w = 1/[\sigma^2(F_o)^2 + (0.0529 \cdot P)^2]$ for **2**, $w = 1/[\sigma^2(F_o)^2 + (0.0573 \cdot P)^2]$ for **3**, $w = 1/[\sigma^2(F_o)^2 + (0.0512 \cdot P)^2]$ for **4** and $w = 1/[\sigma^2 (F_o)^2 + (0.0452 \cdot P)^2]$ for **6**, were $P = (F_o^2 + 2F_c^2)/3$. $F_c^* = k F_c [1 + 0.001 \cdot |F_c|^2 \lambda^3/\sin(2\theta)]^{-1/4}$.

$CH_2CH_2CH_3$), 3.02 (s, 3 H, NCH_3), 3.18 (m, 6 H, NCH_2), 6.28 (d, 1H *trans,* $^3J_{trans}$ = 19.4 Hz, CH=C*H*H), 6.52 (d, 1H *cis,* $^3J_{cis}$ = 11.7 Hz, CH=CH*H*), 6.80 (m, 1 H, C*H*=CHH) ppm. $^{11}B\{^1H\}$ NMR (CD_2Cl_2): δ = −12.4 (s, B12), −17.2 (s, B2−B6 and B7−B11). $C_{15}H_{44}B_{11}NSn$ (476.11): calcd. C 37.84, H 9.31, N 2.94; found C 37.41, H 9.61, N 2.21.

 © 2004 Wiley-VCH Verlag GmbH & Co. KGaA, Weinheim

Acknowledgments

We thank the Deutsche Forschungsgemeinschaft (Schwerpunktprogramm Polyeder) and the Fonds der Chemischen Industrie for financial support.

[1] J. L. Wardell in *Chemistry of Tin* (Ed.: P. J. Smith), Blackie Academic & Professional, **1998**, pp. 95−137.
[2] D. Seyferth, M. A. Weiner, *Chemistry & Industry* **1959**, 402.
[3] R. W. Chapman, J. G. Kester, K. Folting, W. E. Streib, L. J. Todd, *Inorg. Chem.* **1992**, *31*, 979−983.
[4] L. Wesemann, S. Hagen, T. Marx, I. Pantenburg, M. Nobis, B. Drießen-Hölscher, *Eur. J. Inorg. Chem.* **2002**, 2261−2265.
[5] S. Hagen, I. Pantenburg, F. Weigend, C. Wickleder, L. Wesemann, *Angew. Chem.* **2003**, *115*, 1539−1543; *Angew. Chem. Int. Ed.* **2003**, *42*, 1501−1505.
[6] T. Marx, B. Ronig, H. Schulze, I. Pantenburg, L. Wesemann, *J. Organomet. Chem.* **2002**, *664*, 116−122.
[7] T. Marx, B. Mosel, I. Pantenburg, S. Hagen, H. Schulze, L. Wesemann, *Chem. Eur. J.* **2003**, *9*, 4472−4478.
[8] A. Krief, M. Hobe, *Tetrahedron Lett.* **1992**, *43*, 6527−6528.
[9] A. Krief, M. Hobe, *Tetrahedron Lett.* **1992**, *43*, 6529−6532.
[10] X-RED 1.22, *Stoe Data Reduction Program (C)*, **2001**, Stoe & Cie GmbH, Darmstadt.
[11] X-Shape 1.06, Crystal Optimisation for Numerical Absorption Correction (C), **1999**, STOE & Cie GmbH, Darmstadt.
[12] CCDC-218253 (for **2**), -218254 (for **3**), -218255 (for **4**) and -218256 (for **6**) contain the supplementary crystallographic data for this paper. These data can be obtained free of charge at www.ccdc.cam.ac.uk/conts/retrieving.html [or from the Cambridge Crystallographic Data Centre, 12, Union Road, Cambridge CB2 1EZ, UK; Fax: (internat.) +44-1223/336-033; E-mail: deposit@ccdc.cam.ac.uk].
[13] G. M. Sheldrick, SHELXS-97-*Program for Structure Analysis*, Göttingen, **1998**.
[14] G. M. Sheldrick, SHELXL-93-*Program for Crystal Structure Refinement*, Göttingen, **1993**.

Received October 8, 2003

 © 2004 Wiley-VCH Verlag GmbH & Co. KGaA, Weinheim

New Bulky Bis(amino)cyclodiphosph(III)azanes and Their Titanium(IV) Complexes: Synthesis, Structures and Ethene Polymerization Studies

Kirill V. Axenov,[a] Vasily V. Kotov,[b] Martti Klinga,[a] Markku Leskelä,[a] and Timo Repo*[a]

Keywords: Phosphazenes / Titanium / Homogeneous catalysis / Polymerization

Bis(amino)cyclodiphosph(III)azanes *cis*-[(RNH)(PN-*t*Bu)]$_2$, R = 2,6-*i*Pr$_2$C$_6$H$_3$ (**2**), 2-*t*BuC$_6$H$_4$ (**3**), 2-CF$_3$C$_6$H$_4$ (**4**), 2,5-*t*Bu$_2$C$_6$H$_3$ (**5**), Ph$_2$CH (**6**), 2,4-Me$_2$C$_6$H$_3$ (**7**), 2,6-Et$_2$C$_6$H$_3$ (**8**), have been synthesized in the presence of Et$_3$N by a nucleophilic substitution reaction of *cis*-(ClPN-*t*Bu)$_2$ (**1**) with the corresponding bulky aryl and alkylamines. The bis(amino)-cyclodiphosph(III)azanes **2**–**8** adopt the thermodynamically stable *cis*-configuration – a prerequisite for efficient metal complex formation. Deprotonation of bis(amino)cyclodiphosph(III)azanes with *n*BuLi slowly afforded the corresponding salts, *cis*-[(2,4-Me$_2$C$_6$H$_3$N)(PN-*t*Bu)]$_2$Li$_2$(THF)$_2$. The crystal structure of *cis*-[(2,4-Me$_2$C$_6$H$_3$N)(PN-*t*Bu)]$_2$Li$_2$(THF)$_2$ (**9**) consists of a heterocube of two lithium atoms, two nitrogen atoms and a cyclodiphosph(III)azane ring. Transmetallation of Li compounds by TiCl$_4$ was unselective and led to a complex mixture of products. The direct reaction of *cis*-bis(amino)cyclodiphosph(III)azanes with Ti(NMe$_2$)$_4$ is the most efficient method to prepare the corresponding titanium(IV) bis-amido complexes *cis*-[(RN)(PN*t*Bu)]$_2$Ti(NMe$_2$)$_2$ (**11a**, **12a**, **14a**, **15a**). In the solid state, *cis*-[(PhN)(PN-*t*Bu)]$_2$Ti(NMe$_2$)$_2$ (**11a**) adopts a highly distorted trigonal-bipyramidal configuration at the metal center. These bis-amido titanium(IV) complexes have been subsequently transformed into the dichlorides *cis*-[(RN)(PN-*t*Bu)]$_2$TiCl$_2$ (**12**–**15**) with Me$_3$SiCl. After MAO activation the complexes possess moderate catalytic activity in ethene polymerization and produce linear polyethylene with molar masses of up to 2.6×10^6 g/mol and with narrow polydispersities. The catalytic activity and polymer properties depend strongly on the bulkiness of the ligand substituents; *cis*-[(2,6-*i*Pr$_2$C$_6$H$_3$N)(PN-*t*Bu)]$_2$TiCl$_2$ (**14**) gave the highest activity (231 kg PE/mol$_{cat}$ × bar × h).

(© Wiley-VCH Verlag GmbH & Co. KGaA, 69451 Weinheim, Germany, 2004)

Introduction

The highly efficient homogeneous α-olefin polymerization catalysts based on methylalumoxane (MAO) activated Group 4 metallocene dichlorides have stimulated intensive polymerization catalysis research over the past three decades.[1] The major focus has been on the preparation of various *ansa*-metallocenes, especially ones intended for the stereoselective polymerization of propene.[2] Numerous studies have also been made on late transition metal complexes,[3] constrained geometry catalysts[4] and complexes of Group 4 metals with non-cyclopentadienyl ligands. The substantial progress on non-metallocene polymerization catalysis has been achieved by both the "right" choice of a transition metal and the rational design of the ligand systems. Recent highly successful catalysts have been based on titanium and zirconium phenoxyimino-type complexes having novel polymerization properties,[5] as well as on highly efficient C_1-symmetric Group 4 pyridyl-amine catalysts aimed for isospecific propene polymerization.[6]

Ligands containing heteroatoms (e.g. phosphorus, nitrogen) are candidates for catalyst components because they bind strongly to the early transition metals and their mode of coordination as well as ligand hapticity can be varied.[7a] This allows the electronic character, geometric properties and steric protection of the catalytic center to be modified.[7] Bis(amido) complexes of titanium(IV) have attracted considerable attention because of their high activity in ethene polymerization after activation with MAO.[7,8] Thus, we found bis-amino type *cis*-2,4-bis(amino)cyclodiphosph(III)-azanes of the general formula *cis*-[(RNH)(PN-*t*Bu)]$_2$ to be interesting ligand precursors for olefin polymerization catalysts. The coordination chemistry of simple *cis*-2,4-bis(amino)cyclodiphosph(III)azanes, namely *cis*-[(*t*BuNH)(PN-*t*Bu)]$_2$ and *cis*-[(PhNH)(PN-*t*Bu)]$_2$ (structure A), has been described in the synthesis of both main group compounds[9] and titanium(IV), zirconium(IV) and hafnium(IV) complexes (structure B).[10,11,12] Their polymerization properties have not, to our knowledge, been published.

[a] Department of Chemistry, Laboratory of Inorganic Chemistry, P. O. Box 55, 00014 University of Helsinki, Finland
Fax: (internat.) + 358-9-19150198
E-mail: Timo.Repo@helsinki.fi
[b] Organisch-Chemisches Institut, Westfälische Wilhelms-Universität Münster,
Corrensstrasse 40, 48149 Münster, Germany
Supporting information for this article is available on the WWW under http://www.eurjic.org or from the author.

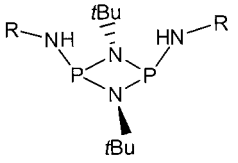

R = *t*Bu, Ph

A

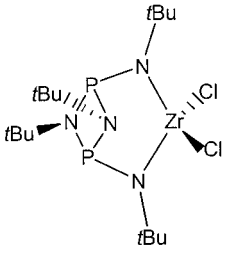

M - Ti, Zr, Hf

B

The relatively straightforward synthesis of various *cis*-2,4-bis(amino)cyclodiphosph(III)azanes make them attractive candidates to study the ligand's influence on the polymerization properties. In the present work, a synthetic approach to new *cis*-2,4-bis(amino)cyclodiphosph(III)azane ligands, *cis*-[(RNH)(PN-*t*Bu)]$_2$ (**2**–**8**), bearing bulky amino substituents and their titanium(IV) complexes has been developed and ethene polymerization studies carried out.

Results and Discussion

Ligand Synthesis

Phosphazanes, both cyclic and acyclic,[13] are stable P–N compounds that are easily synthesized. Cyclodiphosph(III)-azanes (containing a P_2N_2 moiety) were first reported by Michaelis and Schroeter in 1894[14] but were fully characterized only in the 1970s.[15,16] They have attracted most attention as precursors for hybrid (organic-inorganic) P–N polymeric materials,[16c] and as ligand precursors for the synthesis of main group element compounds[9] and some, still rare, early transition metal complexes.[10,11,12] They preparation, in good yield, is commonly based on the reaction of *cis*-(ClPN-*t*Bu)$_2$ (**1**) with either lithium amide or an excess of a free amine.[9] We investigated both of these methods to access the new, bulky bis(amino)cyclodiphosph(III)azanes.

However, some modifications of these general procedures became necessary as, for instance, 2,4-dimethylphenyllithiumamide in THF reacted with **1** nonselectively, and according to ^{31}P NMR data the cyclodiphosph(III)azane P_2N_2 ring was destroyed. Direct aminolysis of the P–Cl bond with free amines was then explored but, even under severe conditions, direct substitution was negligible. For example, **1** and 2,6-diisopropylphenylamine, failed to react under various conditions, even after refluxing in THF for one week; ^{31}P NMR data revealed only the starting compound **1** and the free amine. Apparently, the nucleophilic substitution did not take place because of the steric demand of the amine.

Another synthetic possibility is the application of Et_3N as a base in the reaction of **1** with bulky arylamines.[9] Thus, the reaction of **1** with 2,6-diisopropylphenylamine and an excess of Et_3N (4 equiv.), after refluxing for four days, gave, finally, the desired disubstituted compound *cis*-[(2,6-*i*Pr$_2$C$_6$H$_3$NH)(PN-*t*Bu)]$_2$ (**2**) in good yield. Further experiments with different ratios of reactants and reaction times showed the limitations of this reaction; the selectivity depends strongly on the ratio of arylamine to Et_3N, and on the refluxing time (Scheme 1). This optimized synthetic procedure was then applied to give various bis(amino)cyclodiphosph(III)azanes (**3**–**8** in Scheme 2).

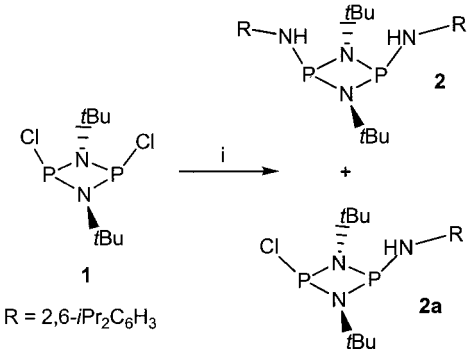

i - 2 equiv. RNH_2, 2 equiv. Et_3N in THF, 4 days refluxing (40% **2**, 60% **2a**)
or 2 equiv. RNH_2, 4 equiv. Et_3N in THF, 2 days refluxing (70% **2**, 30% **2a**)
or 2 equiv. RNH_2, 2 equiv. Et_3N in THF, 4 days refluxing (100% **2**, 0% **2a**)

Scheme 1

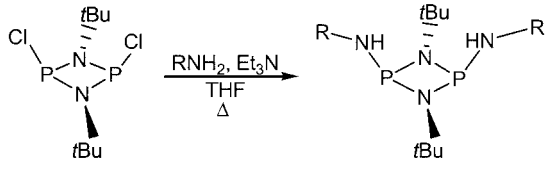

2, R = 2,6-*i*Pr$_2$C$_6$H$_3$
3, 2-*t*BuC$_6$H$_4$
4, 2-CF$_3$C$_6$H$_4$
5, 2,5-*t*Bu$_2$C$_6$H$_3$
6, Ph$_2$CH
7, 2,4-Me$_2$C$_6$H$_3$
8, 2,6-Et$_2$C$_6$H$_3$

Scheme 2

Et_3N acts as more than a simple Brönsted base that scavenges the generated HCl – at least four equivalents of it are required to obtain good yields. Some of the Et_3N can assist the nucleophilic substitution by coordination and polarization of the P–Cl bonds of (ClPN-*t*Bu)$_2$ (**1**), while the rest acts as a traditional Brönsted base.

Structure of the Bis(amino)cyclodiphosph(III)azanes

The obtained bis(amino)cyclodiphosph(III)azanes are colorless, air-sensitive oils or solids that are very soluble even in aliphatic hydrocarbon solvents. Despite the long refluxing times, the reactions proceed selectively and, according to ^{31}P NMR, yield only one product from each reaction. Bis(amino)cyclodiphosph(III)azanes can exist as *cis* and

 © 2004 Wiley-VCH Verlag GmbH & Co. KGaA, Weinheim

trans isomers; the differences in chemical shifts in the ^{31}P NMR spectra indicate which is present.[17] According to NMR spectroscopic data, the synthesized bis(amino)cyclodiphosph(III)azanes (**2**–**8**) adopt the synthetically more desirable, and thermodynamically more stable, *cis*-conformation (Exp. Sect.).

The single-crystal X-ray measurements of **3**–**5** also support the exclusive presence of the *cis*-isomer. The solid-state structures (Figures 1–3) and selected structural parameters (Table 1) are presented here. The solid-state structures reveal that the P_2N_2 cyclodiphosph(III)azane rings are bent from the mean plane. Such disturbance of the P_2N_2 rings accords with the results of earlier molecular orbital calculations for *cis*-cyclodiphosph(III)azanes with small amino substituents,[18] and may be caused by repulsive lone pair–bond pair electronic interactions.[9] Despite the sterically bulky aryl or alkyl substituents on these bis(amino)cyclodiphosph(III)azanes the basic structural features (bond lengths and angles) of the ligand backbone are rather similar to ones reported earlier (Table 1).

The solid-state structure of *cis*-[(2-*t*BuC_6H_4NH)(PN-*t*Bu)]$_2$ (**3**) (Figure 1), which has only monosubstituted aniline groups, resembles that established for *cis*-[(PhNH)(PN-*t*Bu)]$_2$.[9,12] In both structures, the *tert*-butyl groups on the P–N ring are bent towards the P_2N_2 mean plane [for **3**: C(1)–P_2N_2 plane 161.05(3)° and C(5)–P_2N_2 plane 170.94(3)°] and the orientation of the anilines gives an overall C_{2v} symmetry. The slight asymmetry of the P_2N_2 ring in **3** is reflected by the P–N endocyclic bond lengths, which vary from 1.707(3) to 1.728(3) Å.

The structural features of *cis*-[(2-$CF_3C_6H_4$NH)(PN-*t*Bu)]$_2$ (**4**) resemble those of **3** (Figure 2). The electron-with-

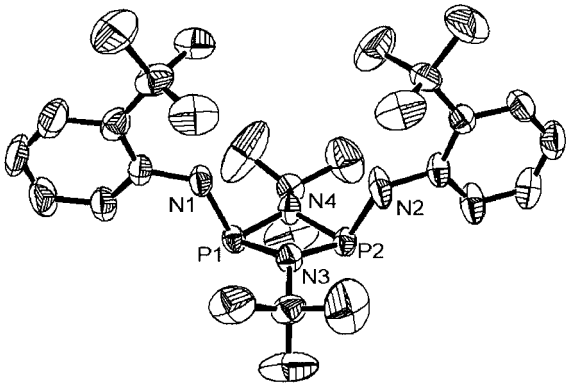

Figure 1. ORTEP diagram of *cis*-[(2-*t*BuC_6H_4NH)(PN-*t*Bu)]$_2$ (**3**)

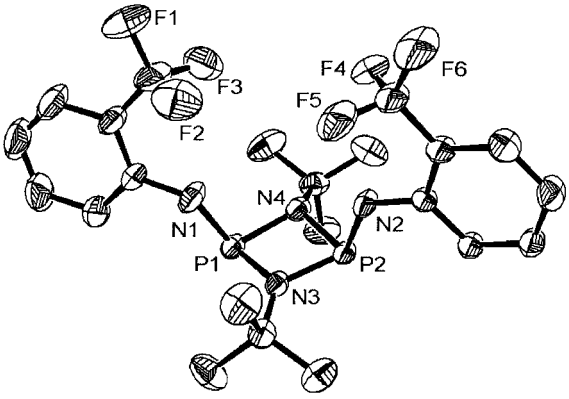

Figure 2. ORTEP diagram of *cis*-[(2-$CF_3C_6H_4$NH)(PN-*t*Bu)]$_2$ (**4**)

Table 1. Selected structural parameters for ligands **3**–**5**

	3	**4**	**5**	*cis*-[(*t*BuNH)(*t*BuNP)]$_2$ [20]	*cis*-[(PhNH)(*t*BuNP)]$_2$ [9]
Distances, Å					
P1–N3	1.728(3)	1.7063(15)	1.705(3)	1.721(2)	
P1–N4	1.707(3)	1.7256(17)	1.734(3)	1.730(2)	
P2–N3	1.726(3)	1.7072(16)	1.716(3)	1.730(2)	1.726(2)
P2–N4	1.715(3)	1.7184(16)	1.724(3)	1.721(2)	
P1–P2	2.5910(13)	2.5937(7)	2.5997(1)	2.600(2)	2.583(1)
P2–N2	1.680(3)	1.7064(15)	1.695(2)	1.664(2)	1.689(2)
N3–C1	1.485(5)	1.472(3)	1.473(4)	1.485(3)	
N4–C5	1.474(4)	1.481(3)	1.485(4)	1.485(3)	
N1–C9	1.403(4)	1.400(3)	1.411(4)	1.470(3)	
Angles, deg					
N3–P1–N4	80.56(14)	81.08(8)	80.67(13)	80.88(1)	
P1–N3–P2	97.20(15)	98.90(9)	98.92(14)	97.83(1)	
P1–N4–P2	98.43(15)	97.72(8)	97.50(14)	97.83(1)	
C1–N3–P1	125.5(2)	130.96(13)	129.8(2)	124.8(2)	
C5–N4–P1	128.5(2)	124.79(13)	124.9(2)	125.1(2)	
N2–P2–N4	105.01(18)	101.80(8)	101.60(13)	104.69(1)	
N2–P2–N3	101.15(16)	105.20(8)	106.21(13)	105.03(1)	
C9–N1–P1	128.1(3)	127.01(16)	125.8(2)	130.2(2)	
C23–N2–P2			127.3(2)		
C22–N2–P2					

 © 2004 Wiley-VCH Verlag GmbH & Co. KGaA, Weinheim

drawing CF_3 substituents on the aniline groups have a significant influence only on the P(2)−N(2) and P(1)−N(1) bond lengths, while the puckering of the P_2N_2 ring is fairly similar to that for **3**. Owing to the second *tert*-butyl group on the aniline moiety *cis*-[(2,5-di-*t*BuC_6H_3NH)(PN-*t*Bu)]$_2$ (**5**) (Figure 3) has lost its superfacial C_{2v} symmetry. The bond lengths and angles in the P_2N_2 ring are nevertheless similar to those of **3**.

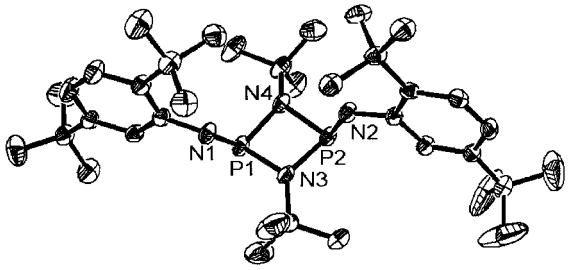

Figure 3. ORTEP diagram of *cis*-[(2,5-tBu$_2C_6H_3$NH)(PN-*t*Bu)]$_2$ (**5**)

Synthesis of Titanium(IV) Complexes

Of the various literature methods for the preparation of early transition metal complexes the general route is the transmetallation reaction between transition metal halides and alkali or alkaline earth metal salts of the ligand.[19] Applying a procedure described earlier,[20] the desired dilithium salts of *cis*-[(2,6-di-*i*PrC_6H_3NH)(PN-*t*Bu)]$_2$ (**2**) (see supporting information) and *cis*-[(2,4-di-MeC_6H_3NH)(PN-*t*Bu)]$_2$ (**7**) were prepared in THF (Scheme 3). According to the ^{1}H and ^{13}C NMR spectra, the lithium salts contains two coordinated THF molecules. The phosphorus signal at 163.01 ppm in the ^{31}P NMR spectrum confirms the formation of the lithium salt *cis*-[(2,4-di-MeC_6H_3N)(PN-*t*Bu)]$_2$-Li$_2$(THF)$_2$ (**9**).[21]

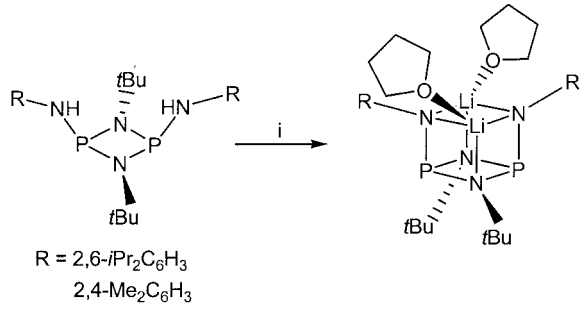

i - *n*BuLi, THF, reflux, 5h

Scheme 3

Recrystallization of the dilithium salt **9** from THF/hexane solution provided crystals suitable for X-ray study (Figure 4). Selected bond lengths and angles are collected in Table 2. The P_2N_2 ring is almost planar, which is also related to the symmetry of the molecule and to the equal bond lengths in the ring. The P_2N_2 ring, exocyclic N, and both Li atoms form an inorganic heterocube that is surrounded by the aniline groups of the ligand and two coordinated THF molecules. The exocyclic P−N bonds are shorter than the endocyclic ones [1.674(3) vs. 1.768(3) Å]. The bond lengths between Li and the exocyclic nitrogen atoms are almost equal [from 2.071(6)Å to 2.095(6)Å] and similar to those in related lithium amides [Li−N in {Li[N(SiMe$_3$)$_2$]OEt$_2$}$_2$ are 2.06(1) Å].[22] Thus, the solid-state structure of compound **9** has similar features to those described for *cis*-[(*t*BuN)(PN-*t*Bu)]$_2$Li$_2$(THF)$_2$,[21] but in **9** the lithium atom and endocyclic nitrogen atoms are further apart [2.133(6) Å] and can be considered typical for bonds between a coordinated lithium cation and a donor nitrogen atom.

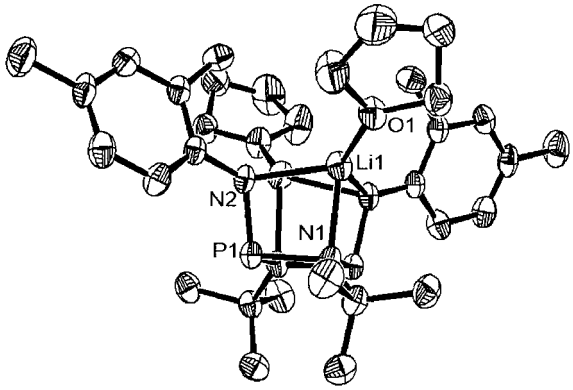

Figure 4. ORTEP diagram of *cis*-[(2,4-Me$_2C_6H_3$N)(PN-*t*Bu)]$_2$Li$_2$-(THF)$_2$ (**9**); one solvent molecule is omitted for clarity

Table 2. Selected structural parameters for compound **9**

Distances, Å			
P1−N1	1.768(3)	N2−Li1	2.133(6)
P1−N1a[a]	1.752(3)	N2−Li1a	2.095(6)
P1−N2	1.674(3)	Li1−Li1a	2.612(1)
P1−P1a	2.635(2)	Li1−O1	1.911(6)
N1−C1	1.492(4)	N2−C5	1.408(4)
N1−Li1	2.071(6)		
Angles, deg			
N1−P1−N1a	83.06(1)	N2−Li1−N2a	99.70(2)
P1−N1−P1a	96.92(1)	N1−Li1−N2	76.90(2)
N2−P1−N1	98.83(1)	Li1−N1−C1	123.80(2)
N2−P1−N1a	98.29(1)	C1−N1−P1	122.10(2)
Li1−N1−P1	91.76(2)	N1−Li1−O1	123.60(3)
Li1−N1−P1a	91.55(2)	O1−Li1−N2	121.80(3)
Li1−N2−Li1a	76.30(2)	C5−N2−Li1	127.10(2)
Li1−N2−P1	92.31(2)	C5−N2−Li1a	136.0(3)

[a] Label "a" means a symmetry equivalent atom at $-x$, y, $-z + 1/2$.

To synthesize titanium(IV) dichloride complexes from the *cis*-2,4-bis(amino)cyclodiphosph(III)azanes the above-described lithium salts were treated with $TiCl_4$. Surprisingly, the transmetallation reaction failed and led to a complex mixture of unidentified products. Only one complex, [(*t*BuN)$_2$(PN-*t*Bu)$_2$]$TiCl_2$ (**10**), previously synthesized by Stahl et al.[23] was obtained. This might be due either to the

 © 2004 Wiley-VCH Verlag GmbH & Co. KGaA, Weinheim

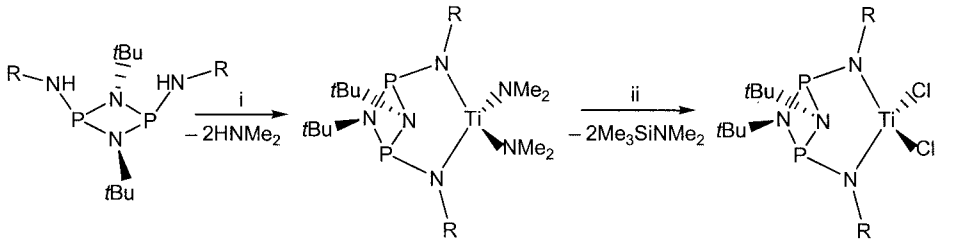

11, R = Ph
12a, Ph_2CH
13a, 2,6-$Et_2C_6H_3$
14a, 2,6-$iPr_2C_6H_3$
15a, 2,5-$tBu_2C_6H_3$

12, R = Ph_2CH
13, 2,6-$Et_2C_6H_3$
14, 2,6-$iPr_2C_6H_3$
15, 2,5-$tBu_2C_6H_3$

i - $Ti(NMe_2)_4$, toluene, reflux; ii - excess of Me_3SiCl

Scheme 4

steric demand of the obtained lithium {see the solid-state structure of [(2,4-di-MeC_6H_3N)(*t*BuNP)]$_2Li_2(THF)_2$ (**9**)} salts, which slow down the reaction, or to titanium tetrachloride, a strong Lewis acid, which may attack the P−N bond of the P_2N_2 cycle or the phosphorus lone pair more readily than a N−Li or N−Mg bond.

An alternative approach, the direct metallation of the ligand precursors through amine elimination,[24] turned out to be efficient. The reaction of the less Lewis-acidic $Ti(NMe_2)_4$ with [(RNH)(*t*BuNP)]$_2$ (**2**, **5**, **6**, **8**) occurred selectively, according to ^1H and ^{31}P NMR data, and the bis-amido complexes [(RNH)(*t*BuNP)]$_2Ti(NMe_2)_2$ (**11a**−**15a**) were formed (Scheme 4). Such bis-amido complexes are usually oils, and are highly soluble in aliphatic solvents, making their separation and purification difficult. Therefore, they were characterized on the basis of ^1H, ^{13}C and ^{31}P NMR spectroscopic data (see Supporting Information). Their ^1H NMR spectra revealed the C_{2v} symmetry expected for such titanium(IV) complexes and indicate the equivalence of all alkyl and aromatic substituents. Only the ligand precursor **4**, with electron-withdrawing CF_3 substituents, behaved differently, and complex formation under similar reaction conditions was incomplete.

With *cis*-[$(PhN)_2$(PN-*t*Bu)$_2$]$Ti(NMe_2)_2$ (**11a**), crystals suitable for X-ray analysis were obtained from a saturated hexane solution at −20 °C. The ORTEP diagram of **11a** (Figure 5) and selected bond lengths and angles (Table 3) are given here. In the solid state, four metal−amide bonds and an additional donor bond from one of the cyclophosph(III)azane ring nitrogen atoms define a highly distorted trigonal-bipyramidal coordination at the central titanium atom, reducing the symmetry of this molecule from C_2 to C_s in the solid state. In general, the coordination sphere of **11a** resembles previously described structures for Ti, Zr and Hf complexes based on the *cis*-[(*t*BuNH)(PN-*t*Bu)]$_2$ ligand.[10,11,12] The cyclophosph(III)azane ring is almost planar and the phenyl rings are almost perpendicular to the P_2N_2 plane and, hence, leave the metal center relatively open to nucleophilic attack.

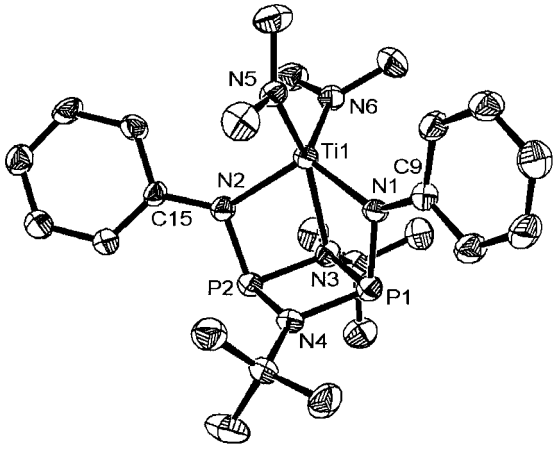

Figure 5. ORTEP diagram of *cis*-[(PhN)(PN-*t*Bu)]$_2Ti(NMe_2)_2$ (**11a**)

Table 3. Selected structural parameters for compound **11a**

Distances, Å			
Ti−N3	2.325(4)	P1−N3	1.791(4)
Ti−N1	2.020 (3)	P2−N3	1.770(4)
Ti−N2	2.011(3)	P1−N4	1.731(4)
Ti−N5	1.907(4)	P2−N4	1.728(4)
Ti−N6	1.884(4)	P1−P2	2.653(2)
P1−N1	1.708(4)		
Angles, deg			
N5−Ti−N6	98.66(2)	N5−Ti−N3	159.82(2)
N1−Ti−N2	111.80(1)	N6−Ti−N3	101.39(2)
N1−Ti−N5	101.26(2)	N1−P1−P2	101.73(1)
N1−Ti−N6	121.14(2)	N3−P1−N4	81.38(2)
N5−Ti−N2	98.67(2)	P1−N3−P2	96.32(2)
N6−Ti−N2	118.99(2)	P1−N4−P2	100.15(2)

The additional nitrogen is rather weakly coordinated, as indicated by the elongated bond length [2.325 (4) Å], which is significantly longer than the 2.267 (2) Å in the related

 © 2004 Wiley-VCH Verlag GmbH & Co. KGaA, Weinheim

compound $[(t\text{BuN})_2(\text{PN-}t\text{Bu})_2]\text{TiCl}_2$).[11] This may be due to NMe_2 substituents donating additional electron density from the sp^2-hybridized amido nitrogen atoms to the metal center, thereby decreasing the Lewis acidity of the titanium. Four amido nitrogen atoms are in a pseudo-tetrahedral environment around the metal center [N(1)−Ti−N(2) and N(5)−Ti−N(6) are 111.80 (1)° and 98.66 (2)° respectively] and the amido N−Ti bond lengths vary from 1.884 (4) to 2.020 (3) Å (Table 3).

Dichlorotitanium(IV) complexes are preferred as catalyst precursors in olefin polymerization due to their higher activity than the corresponding bis(amido) derivatives.[1a] The standard transformation of early transition metal bis(amido) complexes into their dichloride derivatives involves the reaction with an excess of Me_3SiCl.[25] Thus, we treated $[(RN)_2(\text{PN-}t\text{Bu})_2]\text{Ti}(NMe_2)_2$ (**11a**, **12a**, **14a**, **15a**) with an excess of Me_3SiCl (Scheme 4). The one-pot synthesis of $[(RN)_2(\text{PN-}t\text{Bu})_2]\text{TiCl}_2$ complexes is also possible, starting from a ligand precursor, tetrakis(dimethylamido)-titanium(IV) and Me_3SiCl (see Exp. Sect., **13**).

Evaporation of all solvents, followed by extraction with a mixture of CH_2Cl_2/hexane, gave the dichloro titanium(IV) complexes $[(RN)_2(\text{PN-}t\text{Bu})_2]\text{TiCl}_2$ (**12−15**) in good yield. All ^{1}H NMR spectra display a clear singlet at δ = 1.0−1.4 ppm for the imido *t*Bu groups, peaks at δ = 1.0-4.0 ppm for the alkyl substituents, and signals at δ = 7.0−7.8 ppm for the aromatic protons (see supporting information). Phosphorus signals in the ^{31}P NMR spectra appear in the same region as the peaks of the corresponding ligand. This indicates the covalent character of the Ti−amido bond, whereas in the lithium salts the Li−N bonds are strongly polarized.

With *cis*-$[(\text{PhN})_2(\text{PN-}t\text{Bu})_2]\text{Ti}(NMe_2)_2$ (**11a**), amine elimination by Me_3SiCl was unselective and led to the destruction of the parent bis-amido complex. This can be taken as a limitation of the synthetic route, since, without sufficient steric hindrance from the ligand side, breakage of the Ti−N phosphazane amido bond may occur instead of breakage of the Ti−N dimethylamido bond. Apparently, the phenyl group alone is not bulky enough to sufficiently protect the bonding between the metal center and ligand moiety and may be a reason for the lack of selectivity.

Ethene Polymerization

In addition to the preparative chemistry described above the ligand's influence on the titanium(IV) complexes in ethene polymerization was also investigated. After methylalumoxane (MAO) activation all dichloro titanium(IV) complexes $[(RN)_2(\text{PN-}t\text{Bu})_2]\text{TiCl}_2$ (**12−15**), regardless of polymerization temperature, produced high molar mass linear polyethylene. The polymerization results and the properties of the obtained polymers are summarized in Table 4.

Catalyst **10**/MAO bearing *tert*-butyl groups showed a remarkably high initial catalytic activity that severely declined after a few minutes (Figure 6, curve a). The polyethene produced had a high molar mass and a bimodal molar mass distribution, indicating at least two different active centers (run 1 in Table 4; M_w1 = 1 927 000 g/mol, M_w2 = 42 000 g/mol, for GPC curve see supporting information). After activation with MAO, complexes **12** with diphenylmethylamino substituents gave lower initial activities than **10**/MAO, but the steady state consumption of ethene was higher (run 2 in Table 4, curve b in Figure 6). Catalyst precursors **13** and **15** are slowly activated by MAO (Figure 6, curves c and e, respectively) but the high steady state of **15**/MAO is noteworthy. The polymers obtained with **12**/MAO and **13**/MAO exhibit a low molar mass shoulder in the GPC curve, which also explains the relatively large polydispersity (PD) values. **15**/MAO produces ultrahigh molar mass polyethene (M_w = 2.56 × 10^6 g/mol, M_w/M_n = 2.8).

Complex **14**/MAO displayed a combination of high initial activity and slow decline in productivity (Figure 6, d). After one hour of polymerization with the catalysts under similar conditions, the highest polymerization activity was recorded for **14**/MAO (121 kg of PE/(mol_{cat} × bar × h) (run 5 in Table 4). The polymer also exhibited a high molar mass (2.6 × 10^6 g/mol) and a narrow PD (2.17). In a further study, we examined the influence of catalyst concentration and polymerization temperature. Lower amounts of catalyst resulted in higher activities with no significant change in the molar mass of the polymers. For example, when the amount of catalyst **14**/MAO was halved (from 20 μmol to 10 μmol) and then to 5 μmol, the polymerization activity increased from 121 to 143 and 231 kg of PE/(mol_{cat} × bar

Table 4. Data for ethylene polymerization

Entry no.[a]	Catalyst	Concentration (μmol)	Reaction temp. (°C)	Time (min)	Yield (g)	Activity[b]	M_w (g/mol)	M_w/M_n	T_m (°C)
1	**10**	20	50	30	4.22	111	818 000	14.17	135.3
2	**12**	20	50	20	2.1	79	1 897 000	4.70	139.0
3	**13**	10	50	60	3.33	87.6	1 479 000	5.18	139.0
4	**14**	10	50	60	5.45	143.4	2 465 000	4.17	140.7
5	**14**	20	50	60	9.23	121	2 558 000	2.17	140.3
6	**14**	10	70	60	6.24	164.2	1 369 000	2.19	137.7
7	**14**	5	50	30	2.2	231.6	2 375 000	4.32	141.7
8	**15**	10	50	30	2.1	110.5	2 008 000	2.73	139.7
9	**15**	10	70	60	1.74	45.8	2 564 000	2.84	140.7
10	**15**	20	50	60	4.38	57.9	2 268 000	3.70	141.0

[a] MAO (Al/M = 1000), toluene (200 mL), ethylene (3.8 bar). [b] kg PE/(mol_{cat} × bar × h).

 © 2004 Wiley-VCH Verlag GmbH & Co. KGaA, Weinheim

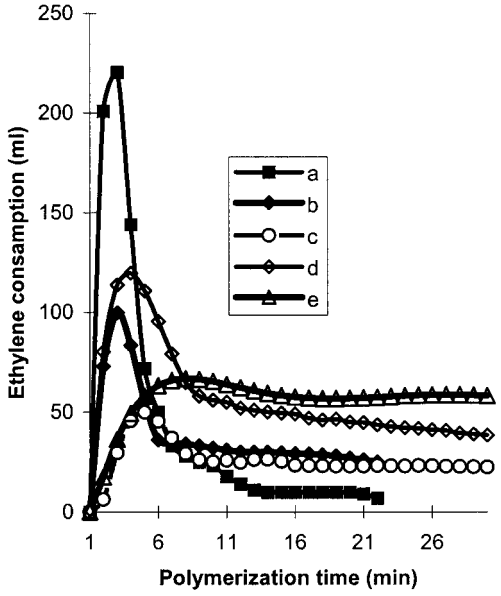

Figure 6. Ethylene consumption curves from polymerization experiments with (a) $[(t\text{BuN})(t\text{BuNP})]_2TiCl_2$ (**10**), (b) $[(Ph_2CHN)(t\text{BuNP})]_2TiCl_2$ (**12**), (c) $[(2,6\text{-}Et_2PhN)(t\text{BuNP})]_2TiCl_2$ (**13**), (d) $[(2,6\text{-}i\text{Pr}_2PhN)(t\text{BuNP})]_2TiCl_2$ (**14**), and (e) $[(2,5\text{-}t\text{Bu}_2PhN)(t\text{BuNP})]_2TiCl_2$ (**15**) as catalyst precursors

$\times$ h) (runs 5, 4 and 7, respectively, in Table 4). This indicates that mass transfer effects play an important role. On increasing the temperature from 50 to 70 °C (runs 5 and 6), the molar mass of the polymers clearly decreases, from 2.5 to 1.4 $\times$ 10^6 g/mol, while the PD is the same. This reveals that catalyst **14**/MAO is stable at higher temperatures.

From the results above, it appears that the catalytic performance of the bis(amido)cyclodiphosph(III)azane titanium(IV)dichlorides depends strongly on the ligand substituents. Activation with MAO was faster for the amido complexes $[(t\text{BuN})(t\text{BuNP})]_2TiCl_2$ (**10**) and $[(Ph_2CHN)(t\text{BuNP})]_2TiCl_2$ (**12**) than for the complexes **13**−**15** with aniline substituents. Moreover, the rate of decline of the polymerization and the steady state values depend on the catalyst precursors used. This indicates that the steric bulkiness of the ligand substituents can influence a sensitive equilibrium between active and dormant metal centers. The bulkiest aniline complex, **15**/MAO, exhibited the highest steady state activities followed by *cis*-$[(2,6\text{-}i\text{Pr}_2C_6H_3N)_2(PN\text{-}t\text{Bu})_2]TiCl_2$ (**14**) and *cis*-$[(2,6\text{-}Et_2C_6H_3N)_2(PN\text{-}t\text{Bu})_2]TiCl_2$ (**13**), i.e. in the order of steric bulkiness.

The polymerization behavior of **10**/MAO ($[(t\text{BuN})(t\text{BuNP})]_2TiCl_2$) is unique due to the bimodal molar mass distribution of the polymer. The relatively small *tert*-butyl groups not only leave the titanium center open for activation and polymerization but, at the same time, the catalyst is susceptible to side reactions. Coordination of the Lewis acidic cocatalyst (MAO) to the lone-pair electrons of phosphorus atoms can initiate destruction of the ligand,[11] which could explain the presence of different active centers and could also be one reason for the fast catalyst deactivation. Therefore, bulky aromatic groups attached directly to the amido nitrogen (**13**−**15**) have two roles: they protect the catalytic active center from side reactions and they prevent the phosphorus atoms of the ligand from destructive coordination to MAO.

Conclusion

New bis(amino)cyclodiphosph(III)azanes *cis*-$[(RNH)(PN\text{-}t\text{Bu})]_2$ **2**−**8** [R = 2,6-$i\text{Pr}_2C_6H_3$ (**2**), 2-$t\text{BuC}_6H_4$ (**3**), 2-$CF_3C_6H_4$ (**4**), 2,5-$t\text{Bu}_2C_6H_3$ (**5**), Ph_2CH (**6**), 2,4-$Me_2C_6H_3$ (**7**), 2,6-$Et_2C_6H_3$ (**8**)] bearing bulky substituents have been synthesized. According to NMR spectroscopic data and single-crystal X-ray analysis, all compounds adopt the thermodynamically more stable *cis*-configuration. Bis(amino)cyclodiphosph(III)azanes can be deprotonated with *n*BuLi, but an extended reaction time is required for complete formation of the lithium salts. The straightforward method of $TiCl_4$ transmetallation of these Li salts proceeded unselectively and gave a complex mixture of products. Direct reaction of $[(RNH)(t\text{BuNP})]_2$ (**2**, **5**, **6**, **8**) with the less Lewis acidic $Ti(NMe_2)_4$ and application of the amine elimination approach led to the desired bis(amido)cyclodiphosph(III)azane titanium(IV) dichloro complexes $[(RN)(t\text{BuNP})]_2TiCl_2$ (**12**−**15**) in high yield. According to the ^{31}P NMR spectra, the titanium(IV)-amido bonds in these complexes have covalent character.

MAO activated titanium(IV)dichloride complexes $[(RN)(t\text{BuNP})]_2TiCl_2$ (**12**−**15**) display moderate ethene polymerization activity. The polymerization behavior depends on the bulkiness of the ligand substituents. Large alkyl and aryl groups both protect the catalytically-active site from side reactions and prevent the phosphorus atoms of the ligand from destructive MAO coordination. Complex $[(t\text{BuN})(t\text{BuNP})]_2TiCl_2$ (**10**), bearing *t*Bu groups, exhibits an initially high polymerization activity, but ethene consumption falls off sharply after just a few minutes. $[(RN)(t\text{BuNP})]_2TiCl_2$ **12**−**15** produce very high molar mass polyethylene with a relatively narrow molar mass distribution. The bulky aromatic groups in **12**−**15** protect the metal center, which is seen in the slow decline of the catalytic activity during prolonged polymerization. The series of catalysts described here offers an efficient route toward very high or even ultrahigh molar mass linear polyethene. The focus of our future research is to introduce other early transition metals into the coordination chemistry of bis(amino)cyclodiphosph(III)azanes so as to enhance their catalytic performance.

Experimental Section

General Remarks: All manipulations were performed under an argon atmosphere using standard Schlenk techniques. The hydrocarbon and ethereal solvents were boiled under reflux over sodium and benzophenone, distilled, and stored under an inert atmosphere with pieces of sodium. Dichloromethane was boiled under reflux with CaH_2 powder and distilled before use. Mass spectra were measured on a JEOL SX102 spectrometer and the ^1H and ^{13}C

 © 2004 Wiley-VCH Verlag GmbH & Co. KGaA, Weinheim

NMR spectra were recorded on a Varian Gemini 200 MHz spectrometer. The ^1H and ^{13}C NMR spectra are referenced relative to $CHCl_3$ (δ = 7.24 and 77.0 ppm, respectively) or C_6D_5H (δ = 7.15 and 128.0 ppm, respectively). ^{31}P NMR spectra were collected with a Bruker AMX 400 spectrometer, with phosphorus signals referenced to an external 85 % H_3PO_4 solution. Elemental analyses were performed Analytische Laboratorien Prof. Dr. H. Malissa and G. Reuter GmbH, Lindlar, Germany. High-temperature gel permeation chromatography of polyethylene samples (GPC) was performed in 1,2,4-trichlorobenzene at 145 °C by using a Waters HPLC 150 C.

tert-Butylamine and phosphorus trichloride were purchased from Merck and purified by distillation under argon (*t*BuNH$_2$ over sodium hydroxide). Arylamines and diphenylmethylamine were obtained from Aldrich and distilled in vacuo over sodium hydroxide before use. Chlorotrimethylsilane was purchased from Fluka and used as received. Ti(NMe$_2$)$_4$ was purchased from Aldrich and used as solution in toluene. Methylalumoxane (MAO, 30 wt.% solution in toluene) was received from Borealis Polymers Oy. *cis*-[Cl(*t*BuNP)]$_2$ (**1**),[16] *cis*-[(*t*BuNH)(*t*BuNP)]$_2$,[21] *cis*-[(C$_6$H$_5$NH)(*t*BuNP)]$_2$ [12] and *cis*-[(*t*BuN)$_2$(*t*BuNP)$_2$]Li$_2$(THF)$_2$ [21] were prepared according to modified literature procedures.

***cis*-[(2,6-*i*Pr$_2$C$_6$H$_3$NH)(PN-*t*Bu)]$_2$ (2):** 2,6-Diisopropylaniline (5.5 mL, 5.15 g, 29 mmol) and Et$_3$N (8.1 mL, 5.87 g, 58 mmol) were added to a stirred solution of *cis*-(ClPN-*t*Bu)$_2$ (**1**) (4 g, 14.5 mmol) in THF (100 mL) and the reaction mixture was boiled under reflux for four days. After filtration, all volatile compounds were removed under vacuum and pentane (20 mL) was added to the residue. The mixture was then kept in a freezer (−20 °C) overnight. After additional filtration and removal of pentane the required product was obtained as a colorless oil (6.42 g, 80 %). $C_{32}H_{54}N_4P_2$ (556.8): calcd. C 69.03, H 9.78, N 10.06; found C 69.65, H 9.88, N 9.31. ^1H NMR (200 MHz, [D$_6$]benzene, 29 °C): δ_H = 1.17 (s, 18 H, *t*Bu), 1.27 (d, 24 H, C*H*$_3$, *i*Pr), 2.90 (m, 4 H, C*H*, *i*Pr), 4.63 (s, 2 H, N*H*), 7.05−7.18 (m, 6 H, Ar*H*) ppm. $^{13}C\{^1H\}$ NMR (50.3 MHz, [D$_6$]benzene, 29 °C): δ_C = 24.2 (*C*H$_3$, *i*Pr), 29.2 (m, *C*H, *i*Pr), 31.4 (t, *C*H$_3$C), 51.7 (t, CH$_3$*C*), 118.8 (Ar), 124.0 (Ar), 136.3 (Ar), 141.0 (d, Ar) ppm. $^{31}P\{^1H\}$ NMR (162 MHz, [D$_6$]benzene, 21 °C): δ_P = 114.8 (s) ppm. MS(EI): *m*/*z* (%) = 556 (48) [M$^+$], 380 (84), 204 (35), 176 (76), 57 (87).

***cis*-[(2-*t*BuC$_6$H$_4$NH)(PN-*t*Bu)]$_2$ (3):** Reaction of *cis*-(ClPN-*t*Bu)$_2$ (**1**) (0.65 g, 2.4 mmol), Et$_3$N (1.4 mL, 1.93 g, 9.6 mmol) and 2-*tert*-butylaniline (0.75 mL, 0.71 g, 4.7 mmol) and separation of the resulting crude product were carried out as for **2**. The obtained white solid was dissolved in pentane (10 mL) and the solution was concentrated to 3 mL and kept at −20 °C until colorless crystals appeared (0.90 g, 76 %). Crystals suitable for X-ray crystallography were obtained in this manner. $C_{28}H_{46}N_4P_2$ (500.6): calcd. C 67.17, H 9.26, N 11.19, P 12.37; found C 66.99, H 9.33, N 11.06, P 12.47. ^1H NMR (200 MHz, CDCl$_3$, 29 °C): δ_H = 1.29 (s, 18 H, *t*Bu), 1.50 (s, 18 H, *t*BuAr), 5.34 (br.s, 2 H, N*H*), 6.80 (td, 2 H, Ar*H*, ^1J = 7.8, ^2J = 1.5 Hz), 7.12 (t, 2 H, Ar*H*, ^1J = 7.8, ^2J = 1.5 Hz), 7.30 (dd, 2 H, Ar*H*, ^1J = 8.0, ^2J = 1.5 Hz), 7.71 (d, 2 H, Ar*H*, *J* = 8.0 Hz) ppm. $^{13}C\{^1H\}$ NMR (50.3 MHz, CDCl$_3$, 29 °C): δ_C = 31.1 (t, *C*H$_3$C, $J_{P,C}$ = 6.7 Hz), 30.6 (*C*H$_3$CAr), 34.2 (CH$_3$*C*Ar), 51.5 (t, CH$_3$*C*, $J_{P,C}$ = 13.7 Hz), 115.9 (Ar), 116.5 (Ar), 119.3 (Ar), 126.7 (Ar), 133.6 (Ar), 141.8 (d, Ar, *J* = 11.0 Hz) ppm. $^{31}P\{^1H\}$ NMR (162 MHz, CDCl$_3$, 21 °C): δ_P = 97.8 (s) ppm. MS(EI): *m*/*z* (%) = 500 (58) [M$^+$], 364 (94), 203 (10), 162(32), 57 (99).

***cis*-[(2-CF$_3$C$_6$H$_4$NH)(PN-*t*Bu)]$_2$ (4):** Reaction of *cis*-(ClPN-*t*Bu)$_2$ (**1**) (2.6 g, 9.5 mmol), Et$_3$N (5.3 mL, 3.80 g, 37.8 mmol) and 2-trifluoromethylaniline (2.4 mL, 3.05 g, 18.9 mmol) and separation of the obtained crude product were carried out as above. The resulting white solid was dissolved in pentane (20 mL). This solution was then concentrated to 8 mL and kept at −20 °C to yield colorless crystals of product (4.20 g; 85 %). Crystals suitable for X-ray crystallographic analysis were obtained in this manner. $C_{22}H_{28}F_2N_4P_2$ (524.4): calcd. C 50.39, H 5.38, N 10.68, P 11.81; found C 49.46, H 5.91, N 10.89, P 11.88. ^1H NMR (200 MHz, CDCl$_3$, 29 °C): δ_H = 1.29 (s, 18 H, *t*Bu), 5.49 (br.s, 2 H, N*H*), 6.90 (t, 2 H, Ar*H*, *J* = 7.7 Hz), 7.38 (t, 2 H, Ar*H*, *J* = 8.0 Hz), 7.48 (dd, 2 H, Ar*H*, ^1J = 7.7, ^2J = 1.4 Hz), 7.66 (d, 2 H, Ar*H*, *J* = 7.7 Hz) ppm. $^{13}C\{^1H\}$ NMR (50.3 MHz, CDCl$_3$, 29 °C): δ_C = 30.9 (t, *C*H$_3$C, $J_{P,C}$ = 6.5 Hz), 51.6 (t, CH$_3$*C*, $J_{P,C}$ = 12.5 Hz), 116.4 (*C*CF$_3$, $J_{C,F}$ = 29.0 Hz), 116.9 (Ar), 117.4 (Ar), 119.2 (Ar), 126.6 (q, Ar, $J_{C,F}$ = 5.0 Hz), 132.71 (Ar), 124.5 (q, *C*F$_3$, $J_{C,F}$ = 272.0 Hz) ppm. $^{31}P\{^1H\}$ NMR (162 MHz, CDCl$_3$, 21 °C): δ_P = 107.8 (s) ppm. MS(EI): *m*/*z* (%) = 524 (37) [M$^+$], 364 (94), 203(10), 161(32).

***cis*-[(2,5-*t*Bu$_2$C$_6$H$_3$NH)(PN-*t*Bu)]$_2$ (5):** 2,5-Di-*tert*-butylaniline (3.88 g, 18.9 mmol), *cis*-(ClPN-*t*Bu)$_2$ (**1**) (2.60 g, 9.5 mmol) and Et$_3$N (5.3 mL, 3.83 g, 37.8 mmol) were mixed in THF (80 mL) and then boiled under reflux for four days. After filtration, all volatile compounds were removed under vacuum. The resulting white solid was dissolved in CH$_2$Cl$_2$ (15 mL) and hexane (30 mL) was added. The resulting solution was then kept at 0 °C overnight. The suspension that formed was filtered off and all volatile components were removed from the filtrate. The white solid product was then recrystallized from CH$_2$Cl$_2$/hexane solution at −20 °C (colorless crystals; 3.94 g; 68 %). Crystals suitable for the X-ray analysis were obtained in this manner. $C_{36}H_{62}N_4P_2$ (612.9): calcd. C 70.55, H 10.20, N 9.14, P 10.11; found C 70.39, H 10.34, N 8.96, P 10.30. ^1H NMR (200 MHz, CDCl$_3$, 29 °C): δ_H = 1.33 (s, 18 H, *t*Bu), 1.30 (s, 18 H, *t*BuAr), 1.48 (s, 18 H, *t*BuAr), 5.30 (br.d, 2 H, N*H*, *J* = 7.0 Hz), 6.80 (dd, 2 H, Ar*H*, ^1J = 8.4, ^2J = 2.2 Hz), 7.20 (d, 2 H, Ar*H*, *J* = 8.4 Hz), 7.80 (dd, 2 H, Ar*H*, ^1J = 5.5, ^2J = 2.0 Hz) ppm. $^{13}C\{^1H\}$ NMR (50.3 MHz, CDCl$_3$, 29 °C): δ_C = 30.7 (*C*H$_3$CAr), 31.2 (t, *C*H$_3$C, $J_{P,C}$ = 6.8 Hz), 31.3 (*C*H$_3$CAr), 33.8 (CH$_3$*C*Ar), 34.3 (CH$_3$*C*Ar), 51.4 (t, CH$_3$*C*, $J_{P,C}$ = 13.5 Hz), 113.4 (Ar), 114.1 (Ar), 116.0 (Ar), 126.2 (Ar), 130.8 (Ar), 141.7 (d, Ar, *J* = 9.9 Hz) ppm. $^{31}P\{^1H\}$ NMR (162 MHz, CDCl$_3$, 21 °C): δ_P = 98.1 (s) ppm. MS(EI): *m*/*z* (%) = 612 (18) [M$^+$], 408 (96), 204(10), 57 (38).

***cis*-[(Ph$_2$CHNH)(PN-*t*Bu)]$_2$ (6):** The reaction of diphenylmethylamine (2.5 mL, 2.67 g, 18.9 mmol), *cis*-(ClPN-*t*Bu)$_2$ (**1**) (2.0 g, 7.3 mmol) and Et$_3$N (4.1 mL, 2.94 g, 29.1 mmol) and the separation of the crude product were carried out as for **5**. The resulting white solid was then dissolved in CH$_2$Cl$_2$ (20 mL), and hexane (20 mL) was added to give a solution that was kept at 0 °C overnight. The precipitate that formed was filtered off and solvents from the filtrate were removed. The white solid product was then recrystallized from CH$_2$Cl$_2$/hexane solution as colorless crystals (3.94 g; 72 %). $C_{34}H_{42}N_4P_2$ (568.7): calcd. C 71.81, H 7.44, N 9.85; found C 71.64, H 7.34, N 9.77. ^1H NMR (200 MHz, CDCl$_3$, 29 °C): δ_H = 0.97 (s, 18 H, *t*Bu), 3.44 (dd, 2 H, Ph$_2$C*H*), 5.60 (dd, 2 H, N*H*), 7.18 (m, 20 H, Ar*H*) ppm. $^{13}C\{^1H\}$ NMR (50.3 MHz, CDCl$_3$, 29 °C): δ_C = 30.5 (t, *C*H$_3$C), 51.6 (t, CH$_3$*C*), 59.7 (Ph$_2$*C*H), 126.8 (Ar), 127.3 (Ar), 128.3 (Ar), 145.5 (d) ppm. $^{31}P\{^1H\}$ NMR (162 MHz, CDCl$_3$, 21 °C): δ_P = 100.0 (br. s) ppm. MS(EI): *m*/*z* (%) = 568 (72) [M$^+$], 403 (48), 386 (95), 204(20), 183(99), 167 (98), 77 (47), 57 (32).

***cis*-[(2,4-Me$_2$C$_6$H$_3$NH)(PN-*t*Bu)]$_2$ (7):** Reaction of *cis*-(ClPN-*t*Bu)$_2$ (**1**) (5.15 g, 18.7 mmol), (11 mL, 7.58 g, 75 mmol) and 2,4-dimethylaniline (4.6 mL, 4.54 g, 37.4 mmol) and separation of the crude product were carried out as described for compound **2**. The crude

 © 2004 Wiley-VCH Verlag GmbH & Co. KGaA, Weinheim

product was then dissolved in pentane (20 mL) to give a solution that was kept in a freezer (−20 °C) overnight. After filtration and removal of solvent a colorless oil was obtained (7.46 g, 90 %) and used without further purification. ^{1}H NMR (200 MHz, $CDCl_3$, 29 °C): δ_H = 1.32 (s, 18 H, *t*Bu), 2.15 (s, 6 H, CH_3Ar), 2.27 (s, 6 H, CH_3Ar), 4.91 (br.d, 2 H, N*H*, *J* = 5.5 Hz), 6.96 (d, 4 H, Ar*H*), 7.50 (d, 2 H, Ar*H*) ppm. ^{13}C{^{1}H} NMR (50.3 MHz, $CDCl_3$, 29 °C): δ_C = 17.8 (*C*H_3Ar), 20.5 (*C*H_3Ar), 31.0 (t, *C*H_3C, $J_{P,C}$ = 6.5 Hz), 51.7 (t, CH_3*C*, $J_{P,C}$ = 13.7 Hz), 115.0 (Ar), 117.7 (Ar), 125.0 (Ar), 127.0 (Ar), 131.2 (Ar), 139.0 (d, Ar) ppm. ^{31}P{^{1}H} NMR (162 MHz, $CDCl_3$, 21 °C): δ_P = 99.0 (s) ppm.

***cis*-[(2,6-Et$_2$C$_6$H$_3$NH)(PN-*t*Bu)]$_2$ (8):** This was prepared in the same manner as **7**, starting from *cis*-(ClPN-*t*Bu)$_2$ (**1**) (2.6 g, 9.5 mmol), Et_3N (5.3 mL, 3.83 g, 37.8 mmol), and 2,6-diethylaniline (3.1 mL, 2.82 g, 18.9 mmol). A colorless oil (4.47 g; 94 %) was obtained and used without further purification. ^{1}H NMR (200 MHz, $CDCl_3$, 29 °C): δ_H = 1.38 (s, 18 H, *t*Bu), 1.50 (t, 12 H, CH_3, Et), 3.13 (q, *J* = 7.7 Hz, 8 H, CH_2, Et), 4.86 (s, 2 H, N*H*), 6.80−7.50 (m, 6 H, Ar*H*) ppm. ^{13}C{^{1}H} NMR (50.3 MHz, $CDCl_3$, 29 °C): δ_C = 15.3 (*C*H_3, Et), 26.7 (*C*H_2, Et), 31.8 (t, *C*H_3C, $J_{P,C}$ = 6.5 Hz), 52.1 (t, CH_3*C*, $J_{P,C}$ = 13.4 Hz), 123.2 (Ar), 130.0 (Ar), 136.1 (Ar), 141.2 (d, Ar) ppm. ^{31}P{^{1}H} NMR (162 MHz, $CDCl_3$, 21 °C): δ_P = 114.2 (s) ppm. MS (EI): *m*/*z* (%) = 500 (64) [M$^+$], 352 (83), 204 (20), 177(99), 57 (99).

[(2,4-Di-MeC$_6$H$_3$N)(*t*BuNP)]$_2$Li$_2$(THF)$_2$ (9): A solution of *n*BuLi in hexane (23 mL, 1.6 M, 35.5 mmol) was added dropwise to a stirred solution of **7** (7.46 g, 16.8 mmol) in THF (60 mL) at −30 °C. The reaction mixture was then stirred 20 min at −20 °C, allowed to warm to room temperature, and boiled under reflux for 5 h. The resulting yellow solution was then concentrated to 15 mL and pentane (40 mL) was added. This suspension was then stored overnight at −20 °C to give a white-yellow precipitate that was then separated and washed with several portions of pentane at −20 °C. The mother liquid was then concentrated to 8 mL and pentane (20 mL) was added. After two days at −20 °C a second lot of the white-yellow product was obtained (8.5 g in total; 84 %). Crystals suitable for X-ray analysis were obtained by crystallization from a THF/hexane mixture at −20 °C. ^{1}H NMR (200 MHz, [D$_6$]benzene, 29 °C): δ_H = 1.16 (m, 8 H, THF), 1.54 (s, 18 H, *t*Bu), 2.41 (d, 12 H, CH_3, Ar), 3.28 (m, 8 H, THF), 7.20 (m, 4 H, Ar*H*), 7.80 (d, *J* = 7.9 Hz, 2 H, Ar*H*) ppm. ^{13}C{^{1}H} NMR (50.3 MHz, [D$_6$]benzene, 29 °C): δ_C = 20.5 (*C*H_3, Ar), 23.1 (*C*H_3, Ar), 25.3 (THF), 30.7 (t, *C*H_3C, $J_{P,C}$ = 7.60 Hz), 53.3 (t, CH_3*C*, $J_{P,C}$ = 16.0 Hz), 68.3 (THF), 116.72 (Ar), 118.5 (Ar), 124.3 (Ar), 127.2 (Ar), 133.8 (Ar), 142.1 (d, Ar) ppm. ^{31}P{^{1}H} NMR (162 MHz, [D$_6$]benzene, 21 °C): δ_P = 163.01 (s) ppm.

[(*t*BuN)(*t*BuNP)]$_2$TiCl$_2$ (10): $TiCl_4$ (1.3 g, 0.75 mL, 6.84 mmol) was added dropwise to a solution of *cis*-[(*t*BuN)(*t*BuNP)]$_2$Li$_2$(THF)$_2$ (3.45 g, 6.84 mmol) in toluene at 0 °C. The reaction mixture was then stirred at 0 °C for 20 min and boiled under reflux overnight. The resulting brown suspension was filtered off and toluene was removed in vacuo. The obtained brown solid residue was then dissolved in CH_2Cl_2 (30 mL), and hexane was added until precipitation commenced. The solution then was cooled to −20 °C and left overnight. The resulting suspension was filtered through Celite and the solvents were removed. After a second recrystallization, an orange-brown powder (1.61 g; 50.6 %) was isolated. $C_{16}H_{36}Cl_2N_4P_2Ti$ (465.2): calcd. C 41.31, H 7.80; found C 41.58, H 8.01. ^{1}H NMR (200 MHz, [D$_6$]benzene, 29 °C): δ_H = 1.23 (s, 18 H, *t*Bu, P_2N_2 cycle), 1.66 (s, 18 H, *t*Bu) ppm. ^{13}C{^{1}H} NMR (50.3 MHz, [D$_6$]benzene, 29 °C): δ_C = 28.3 (t, $J_{P,C}$ = 7.25 Hz, *C*H_3, *t*Bu, P_2N_2 cycle), 33.7 (d, $J_{P,C}$ = 12.2 Hz, *C*H_3, *t*Bu), 54.6 (t, $J_{P,C}$ = 9.9 Hz, *C*, *t*Bu, P_2N_2 cycle), 60.2 (d, $J_{P,C}$ = 19.2 Hz, *C*, *t*Bu) ppm. ^{31}P{^{1}H} NMR (162 MHz, $CDCl_3$, 21 °C): δ_P = 117.4 (s) ppm. The complex was prepared earlier by a different procedure and the data given here are in good agreement with those reported.[21] MS(EI): *m*/*z* (%) = 465 (80) [M$^+$], 429 (40) [M$^+$ − Cl], 352 (98, ligand).

[(PhN)(*t*BuNP)]$_2$Ti(NMe$_2$)$_2$ (11a): A solution of Ti(NMe$_2$)$_4$ (1.3 g, 5.8 mmol) in toluene (10 mL) was added dropwise to a stirred solution of *cis*-[(PhNH)(*t*BuNP)]$_2$ (2.15 g, 5.5 mmol) in toluene (30 mL). The reaction mixture was then boiled under reflux overnight. All volatile components were removed in vacuo. The resultant red−brown residue was extracted with several portions of hexane. The extracts were then filtered, concentrated to 10 mL, and cooled to −20 °C to yield the product (1.34 g; 46.4 %) as a red-brown, crystalline solid. Crystals suitable for X-ray analysis were obtained by crystallization from hexane at −20 °C. $C_{24}H_{40}N_6P_2Ti$ (522.5): calcd. C 55.18, H 7.72, N 16.09; found C 55.53, H 8.00, N 15.53. ^{1}H NMR (200 MHz, $CDCl_3$, 29 °C): δ_H = 1.50 (s, 18 H, *t*Bu), 3.43 (s, 12 H, NMe$_2$), 7.03 (t, *J* = 7.33 Hz, 2 H, *p*-H-Ph) 7.20−7.50 (m, Ph) ppm. ^{13}C{^{1}H} NMR (50.3 MHz, $CDCl_3$, 29 °C): δ_C = 29.3 (t, $J_{P,C}$ = 7.2 Hz, *C*H_3, *t*Bu), 44.0 (NMe$_2$), 53.1 (t, $J_{P,C}$ = 11.1 Hz, *C*, *t*Bu), 117.7 (d, Ar), 119.5 (Ar), 128.6 (Ar), 151.0 (d, Ar) ppm. ^{31}P{^{1}H} NMR (162 MHz, $CDCl_3$, 21 °C): δ_P = 142.2 (s) ppm. MS(EI): *m*/*z* (%) = 522 (50) [M$^+$], 478 (64, M$^+$ − NMe$_2$), 434 (70, M$^+$ − 2NMe$_2$), 388 (90, ligand).

[(Ph$_2$CHN)(*t*BuNP)]$_2$TiCl$_2$ (12): *cis*-[(Ph$_2$CHNH)(*t*BuNP)]$_2$ (**6**) (2.23 g, 3.93 mmol) was dissolved in toluene and added via a syringe to a solution of Ti(NMe$_2$)$_4$ (0.87 g, 3.9 mmol) at 0 °C. The resultant mixture was boiled under reflux for 22 h to give the bis-dimethylamido titanium(IV) complex [(Ph$_2$CHN)(*t*BuNP)]$_2$-Ti(NMe$_2$)$_2$ (**12a**), which was analyzed by ^{1}H, ^{13}C and ^{31}P NMR. ^{1}H NMR (200 MHz, [D$_6$]benzene, 29 °C): δ_H = 1.22 (s, 18 H, *t*Bu), 1.82−2.40 (12 H, N*Me*$_2$), 3.54 (dd, 2 H, *J* = 14.0 Hz, C*H*, Ph$_2$CH), 7.11 (m, 16 H, *o*- and *m*-Ph), 7.25 (d, *J* = 7.1 Hz, 4 H, *p*-H-Ph) ppm. ^{13}C{^{1}H} NMR (50.3 MHz, [D$_6$]benzene, 29 °C): δ_C = 30.9 (t, $J_{P,C}$ = 7.2 Hz, *C*H_3C), 43.0 (NMe$_2$) 52.0 (t, $J_{P,C}$ = 15.0 Hz, CH_3*C*), 59.3 (d, *J* = 13.0 Hz, Ph$_2$*C*H), 126.8 (Ar), 127.7 (Ar), 128.6 (Ar), 146.1 (d, Ar) ppm. ^{31}P{^{1}H} NMR (162 MHz, $CDCl_3$, 21 °C): δ_P = 103.8 (s) ppm.

Subsequently, to form the dichloride, an excess of Me_3SiCl (5.2 mL, 4.48 g, 41.2 mmol) was added and the reaction mixture was stirred overnight at room temperature. The solvent was then removed and the product purified similarly to **10**, washed with pentane and dried in vacuo. The product was isolated as a brown powder (2.13 g, 72 %). $C_{34}H_{40}Cl_2N_4P_2Ti{\cdot}C_5H_{12}$ (757.6): calcd. C 61.83, H 6.92, N 7.40; found C 62.47, H 6.60, N 8.04. ^{1}H NMR (200 MHz, [D$_6$]benzene, 29 °C): δ_H = 1.20 (s, 18 H, *t*Bu), 3.50 (dd, 2 H, *J* = 14.1 Hz, C*H*, Ph$_2$CH), 7.00 (t, *J* = 7.3 Hz, 8 H, *o*-H-Ph), 7.10 (t, *J* = 7.4 Hz, 8 H, *m*-H-Ph), 7.27 (d, *J* = 7.7 Hz, 4 H, *p*-H-Ph) ppm ^{13}C{^{1}H} NMR (50.3 MHz, [D$_6$]benzene, 29 °C): δ_C = 30.8 (t, $J_{P,C}$ = 7.0 Hz, *C*H_3, *t*Bu), 52.0 (t, $J_{P,C}$ = 14.3 Hz, *C*, *t*Bu), 59.0 (Ph$_2$*C*H), 109.0 (Ar), 126.8 (Ar), 128.6 (Ar), 146.1 (Ar) ppm ^{31}P{^{1}H} NMR (162 MHz, $CDCl_3$, 21 °C): δ_P = 100.0 (s) ppm. MS (EI): *m*/*z* (%) = 684 (10) [M$^+$], 649 (15) [M$^+$ − Cl], 568 (95, ligand).

[(2,6-Et$_2$C$_6$H$_3$N)(*t*BuNP)]$_2$TiCl$_2$ (13): *cis*-[(2,6-Et$_2$C$_6$H$_3$NH)(*t*-BuNP)]$_2$ (**8**) (1.79 g, 3.58 mmol) in toluene and a toluene solution of Ti(NMe$_2$)$_4$ (0.8 g, 3.57 mmol) were treated as described above. To this solution Me_3SiCl (4.8 mL, 4.15 g, 38.2 mmol) was added and the reaction mixture was stirred overnight at room temperature. The solvent was removed then under vacuum to give a red-brown residue that was extracted first with hexane (30 mL) and then twice with a mixture of hexane (20 mL) and CH_2Cl_2 (7 mL).

 © 2004 Wiley-VCH Verlag GmbH & Co. KGaA, Weinheim

After filtration and evaporation of solvent, the product was dried in vacuo to give a red-brown oil (1.9 g, 86.4 %). $C_{28}H_{44}Cl_2N_4P_2Ti$ (617.4): calcd. C 54.47, H 7.18, N 9.07; found C 54.08, H 7.41, N 9.51. ^{1}H NMR (200 MHz, [D$_6$]benzene, 29 °C): δ_H = 1.41 (s, 18 H, *t*Bu), 1.45 (t, 12 H, C*H*$_3$, Et), 3.16 (q, *J* = 7.3 Hz, 8 H, C*H*$_2$, Et), 7.10−7.40 (6 H, H−Ar) ppm. ^{13}C{^{1}H} NMR (50.3 MHz, [D$_6$]benzene, 29 °C): δ_C = 14.9 (*C*H$_3$, Et), 26.3 (d, *J* = 9.9 Hz, *C*H$_2$, Et), 31.2 (t, $J_{P,C}$ = 6.5 Hz, *C*H$_3$, *t*Bu), 51.5 (t, $J_{P,C}$ = 14.5 Hz, *C,* *t*Bu), 123.3 (Ar), 127.1 (Ar), 135.7 (Ar), 138.1 (t, *J* = 1.9 Hz, Ar) ppm. ^{31}P{^{1}H} NMR (162 MHz, CDCl$_3$, 21 °C): δ_P = 114.6 (s) ppm. MS(EI): *m*/*z* (%) = 617 (55) [M$^+$], 583 (8) [M$^+$ − Cl], 500 (76, ligand).

[(2,6-*i*Pr$_2$C$_6$H$_3$N)(*t*BuNP)]$_2$TiCl$_2$ (14): A toluene solution of *cis*-[(2,6-*i*Pr$_2$C$_6$H$_3$NH)(*t*BuNP)]$_2$ (**2**) (3.65 g, 6.56 mmol) and Ti(NMe$_2$)$_4$ (1.47 g, 6.55 mmol) were treated as described above. The titanium(IV) bis-amido complex, generated in situ, [(2,6-*i*Pr$_2$C$_6$H$_3$N)(*t*BuNP)]$_2$Ti(NMe$_2$)$_2$ (**14a**) was then characterized by ^{1}H, ^{13}C, and ^{31}P NMR. ^{1}H NMR (200 MHz, [D$_6$]benzene, 29 °C): δ_H = 1.32 (s, 18 H, *t*Bu), 1.39 (d, 24 H, C*H*$_3$, *i*Pr), 3.00−3.23 (12 H, N*Me*$_2$), 3.91 (m, 4 H, C*H,* *i*Pr), 6.90−7.30 (6 H, H-Ar) ppm ^{13}C{^{1}H} NMR (50.3 MHz, [D$_6$]benzene, 29 °C): δ_C = 24.2 (*C*H$_3$, *i*Pr), 31.4 (t, $J_{P,C}$ = 6.5 Hz, *C*H$_3$, *t*Bu), 33.6 (d, *J* = 1 Hz, *C*H, *i*Pr), 45.7 (N*Me*$_2$), 51.6 (t, $J_{P,C}$ = 14.7 Hz, *C,* *t*Bu), 123.0 (Ar), 123.9 (Ar), 136.3 (t, *J* = 1.9 Hz, Ar), 140.9 (Ar) ppm. ^{31}P{^{1}H} NMR (162 MHz, CDCl$_3$, 21 °C): δ_P = 115.6 (s) ppm.

To obtain the dichloride complex, Me$_3$SiCl (9 mL, 7.47 g, 69 mmol) was added to the red-brown solution of [(2,6-*i*Pr$_2$C$_6$H$_3$N)(*t*BuNP)]$_2$Ti(NMe$_2$)$_2$ (**14a**) via syringe, and the reaction mixture was stirred overnight at room temperature. The so-obtained product was then purified similarly to **13** to afford a red-brown oil that was treated with Et$_2$O to give a red-brown solid after drying in vacuo (3.60 g, 81 %). $C_{32}H_{52}Cl_2N_4P_2Ti$ (673.5): calcd. C 57.07, H 7.78, N 8.32; found C 56.83, H 7.98, N 8.44. ^{1}H NMR (200 MHz, [D$_6$]benzene, 29 °C): δ_H = 1.32 (s, 18 H, *t*Bu), 1.39 (d, 24 H, C*H*$_3$, *i*Pr), 3.88 (m, 4 H, C*H,* *i*Pr), 7.10−7.60 (6 H, H−Ar) ppm. ^{13}C{^{1}H} NMR (50.3 MHz, [D$_6$]benzene, 29 °C): δ_C = 24.2 (*C*H$_3$, *i*Pr), 31.4 (t, $J_{P,C}$ = 6.7 Hz, *C*H$_3$, *t*Bu), 32.1 (d, *J* = 1 Hz, *C*H, *i*Pr), 51.3 (t, $J_{P,C}$ = 14.5 Hz, *C,* *t*Bu), 122.5 (Ar), 124.0 (Ar), 130.7 (Ar), 140.9 (Ar) ppm. ^{31}P{^{1}H} NMR (162 MHz, CDCl$_3$, 21 °C): δ_P = 115.6 (s) ppm. MS (EI): *m*/*z* (%) = 672 (10) [M$^+$], 639 (8) [M$^+$ − Cl], 556 (90, ligand).

[(2,5-*t*Bu$_2$C$_6$H$_3$N)(*t*BuNP)]$_2$TiCl$_2$ (15): A toluene solution of *cis*-[(2,5-*t*Bu$_2$C$_6$H$_3$NH)(*t*BuNP)]$_2$ (**5**) (2.73 g, 4.46 mmol) and Ti(NMe$_2$)$_4$ (1.0 g, 4.46 mmol) was treated in the same way as **13**. The resultant titanium(IV) bis-amido complex, generated in situ, [(2,5-*t*Bu$_2$C$_6$H$_3$N)(*t*BuNP)]$_2$Ti(NMe$_2$)$_2$ (**15a**) was characterized by ^{1}H, ^{13}C, and ^{31}P NMR. ^{1}H NMR (200 MHz, [D$_6$]benzene, 29 °C): δ_H = 1.44 (s, 36 H, *t*BuAr), 1.57 (s, 18 H, *t*Bu), 3.19 (12 H, N*Me*$_2$), 6.98 (dd, J_1 = 6.2, J_2 = 2.1 Hz, 2 H, 4-H−Ph), 7.36 (2 H, 3-H−Ph), 8.23 (dd, J_1 = 3.1, J_2 = 2.1 Hz, 2 H, 2-H−Ph) ppm. ^{13}C{^{1}H} NMR (50.3 MHz, [D$_6$]benzene, 29 °C): δ_C = 31.0 (*C*H$_3$, 5-*t*BuAr), 31.3 (t, $J_{P,C}$ = 6.5 Hz, *C*H$_3$, *t*Bu), 31.5 (*C*H$_3$, 2-*t*BuAr), 33.1 (*C,* 5-*t*BuAr), 34.0 (*C,* 2-*t*BuAr), 45.2 (N*Me*$_2$), 51.7 (t, $J_{P,C}$ = 13.7 Hz, *C,* *t*Bu), 113.8 (Ar), 114.5 (Ar), 117.1 (Ar), 131.2 (Ar), 141.9 (Ar), 150.0 (t, *J* = 1.2 Hz, Ar) ppm. ^{31}P{^{1}H} NMR (162 MHz, CDCl$_3$, 21 °C): δ_P = 98.86 (s) ppm.

To obtain the dichloride complex, Me$_3$SiCl (5.9 mL, 5.09 g, 46.8 mmol) was added to the red-brown solution of [(2,5-*t*Bu$_2$C$_6$H$_3$N)(*t*BuNP)]$_2$Ti(NMe$_2$)$_2$ (**15a**) and the reaction mixture stirred overnight at room temperature. All volatiles were then removed in vacuo and the residue was extracted three times with a mixture of hexane (30 mL) and CH$_2$Cl$_2$ (10 mL). After removal of the solvent, the product was washed with several portions (each 10 mL) of cold pentane and dried. A red−brown powder (2.40 g, 73.8%) was isolated. $C_{36}H_{60}Cl_2N_4P_2Ti$ (729.7): calcd. C 59.26, H 8.29, N 7.68; found C 58.94, H 8.41, N 7.86. ^{1}H NMR (200 MHz, [D$_6$]benzene, 29 °C): δ_H = 1.39 (s, 36 H, *t*BuAr), 1.52 (s, 18 H, *t*Bu), 6.93 (dd, ^1J = 6.2, ^2J = 2.1 Hz, 2 H2 Hz, 4-H−Ar), 7.32 (2 H, 3-H−Ar), 8.17 (dd, ^1J = 3.1, ^2J = 2.1 Hz, 2 H, 2-H−Ar) ppm. ^{13}C{^{1}H} NMR (50.3 MHz, [D$_6$]benzene, 29 °C): δ_C = 31.0 (*C*H$_3$, 5-*t*BuAr), 31.4 (t, $J_{P,C}$ = 6.0 Hz, *C*H$_3$, *t*Bu), 31.5 (*C*H$_3$, 2-*t*BuAr), 33.1 (*C,* 5-*t*BuAr), 34.5 (*C,* 2-*t*BuAr), 51.7 (t, $J_{P,C}$ = 13.7 Hz, *C,* *t*Bu), 113.8 (Ar), 114.5 (Ar), 117.1 (Ar), 131.1 (Ar), 137.8 (Ar), 150.0 (Ar) ppm. ^{31}P{^{1}H} NMR (162 MHz, CDCl$_3$, 21 °C): δ_P = 99.72 (s) ppm. MS (EI): *m*/*z* (%) = 728 (20) [M$^+$], 693 (10) [M$^+$ − Cl], 612 (40, ligand).

Polymerization Experiments: A 1-L glass autoclave (manufacturer Büchi) was charged with toluene (200 mL) and cocatalyst (MAO) (Al/Ti ratio was 1000), thermostatted (50 or 70 °C), saturated with ethene (3.8 bar), and the desired amount of complex solution was then added. The monomer pressure (±50 mbar) and temperature (±0.5 °C) were kept constant during each polymerization run. Monomer consumption, polymerization temperature and pressure were controlled by real-time monitoring. The polymerizations were quenched with 10 % HCl solution in methanol, and the polymer precipitated quantitatively by pouring the solution into methanol (400 mL) acidified with aqueous hydrochloric acid. The samples were washed several times with methanol and water, and dried at 60 °C.

X-ray Crystallographic Study: Crystal data of compounds **3**−**5** were collected with an Enraf−Nonius CAD-4 single-crystal diffractometer at 193(2) K using Cu-K_α radiation (graphite monochromator), 1.54179 Å (scan-type omega/2-theta). Intensities were corrected for Lorentz and polarization effects with XCAD4.[26,27]

The crystal data of compound **9** were collected with a Rigaku AFC-7S single-crystal diffractometer at 193(2) K using Mo-K_α radiation (graphite monochromator), 0.71073 Å (omega/2-theta scans). Intensities were corrected for Lorentz and polarization effects with TEXSAN.[28] A psi-scan absorption correction was made for each compound.[29]

The crystal data of compound **11a** were collected with a Nonius KappaCCD area-detector diffractometer at 173(2) K using Mo-K_α radiation (graphite monochromator), 0.71073 Å. Data reduction: COLLECT;[30] absorption correction: SADABS.[31]

Solution and refinement: SHELX-97,[32,33] direct methods. All non-hydrogen atoms were refined anisotropically. Hydrogen atoms were refined on calculated positions. The displacement factors of the H-atoms were 1.2× (1.5×) that of the host atom. Data relating to the structure determinations are collected in Table 5. CCDC-213508 to -213512 (for compounds **3**−**5**, **9**, **11a**) contain the supplementary crystallographic data for this paper. These data can be obtained free of charge at www.ccdc.cam.ac.uk/conts/retrieving.html [or from the Cambridge Crystallographic Data Centre, 12 Union Road, Cambridge CB2 1EZ, UK; Fax: (internat.) +44-1223/336-033; E-mail: deposit@ccdc.cam.ac.uk].

Acknowledgments

Financial support for this research by CIMO, University of Helsinki and the Academy of Finland is gratefully acknowledged.

Table 5. Crystallographic data for compounds **3**–**5**, **9**, **11a**

Compound	**3**	**4**	**5**	**9**	**11a**
Formula	$C_{28}H_{46}N_4P_2$	$C_{22}H_{28}F_6N_4P_2$	$C_{36}H_{62}N_4P_2$	$C_{36}H_{60}Li_2N_4O_3P_2$	$C_{24}H_{40}N_6P_2Ti$
Fw	500.63	524.42	612.84	672.70	522.46
Space group	$P2_1/n$	$P\bar{1}$	$P2_12_12_1$	$C2/c$	$P2_1/c$
a, Å	10.130(1)	9.251(1)	9.885(1)	14.761(5)	11.903(1)
b, Å	18.899(1)	11.010(1)	18.136(1)	15.070(3)	22.667(2)
c, Å	15.907(1)	13.790(1)	21.012(1)	17.815(3)	11.699(1)
α, deg	90	81.44(1)	90	90	90
β, deg	98.19(1)	82.66(1)	90	98.94(2)	115.808(1)
γ, deg	90	69.440(10)	90	90	90
V, Å^3	3014.3(4)	1296.1(2)	3766.9(5)	3914.8(17)	2841.6(4)
$d_{calcd.}$, g cm^{-3}	1.103	1.344	1.081	1.141	1.221
Z	4	2	4	4	4
μ, cm^{-1}	14.60	20.73	12.45	1.48	0.436
λ, Å	1.54179	1.54179	1.54179	0.71073	0.71073
T, K	193(2)	193(2)	193(2)	193(2)	173(2)
R[a]	0.0675	0.0486	0.0433	0.0835	0.0613
R_w[b]	0.1911	0.1417	0.1158	0.2345	0.1434

[a] $R = \Sigma F_o - F_c/\Sigma F_o$ for observed reflections [$I > 2\sigma(I)$]. [b] $Rw = \{\Sigma[w(F_o^2 - F_c^2)^2]/\Sigma[w(F_o^2)^2]\}^{1/2}$ for all data.

[1] [1a] C. Janiak, *Metallocenes* (Eds.: A. Togni, R. L. Haltermann) Wiley-VCH, Weinheim, **1998**, vol. 1 and 2. [1b] W. Kaminsky, M. Arndt, *Applied Homogeneous Catalysis with Organometallic Compounds* (Eds.: B. Cornils, W. A. Herrmann) VCH Verlagsgesellschaft, Weinheim, New York, Basel, Cambridge, Tokyo, **1996**, vol. 1 and 2.

[2] [2a] H. G. Alt, A. Köppl, *Chem. Rev.* **2000**, *100*, 1205. [2b] H. H. Brintzinger, D. Fischer, R. Mülhaupt, B. Rieger, R. M. Waymouth, *Angew. Chem.* **1995**, *107*, 1255; *Angew. Chem. Int. Ed. Engl.* **1995**, *34*, 1143. [2c] L. Resconi, L. Cavallo, A. Fait, F. Piemontesi, *Chem. Rev.* **2000**, *100*, 1253. [2d] G. W. Coates, *Chem. Rev.* **2000**, *100*, 1223. [2e] M. J. Bochmann, *J. Chem. Soc., Dalton Trans.* **1996**, 255.

[3] [3a] G. J. P. Britovsek, V. C. Gibson, B. S. Kimberley, P. J. Maddox, S. J. McTavish, G. A. Solan, A. J. P. White, D. J. Williams, *Chem. Commun.* **1998**, 849. [3b] B. L. Smal, M. Brookhart, J. Bennet, *J. Am. Chem. Soc.* **1998**, *120*, 4049. [3c] S. D. Ittel, L. K. Johnson, M. J. Brookhart, *Chem. Rev.* **2000**, *100*, 1169. [3d] P. M. Castro, K. Lappalainen, M. Ahlgren, M. Leskelä, T. Repo, *J. Polym. Science Part A: Polymer Chemistry* **2003**, *41*, 1380.

[4] [4a] Y.-X. Chen, T. J. Marks, *Organometallics* **1997**, *16*, 3649. [4b] T. K. Woo, P. M. Margl, J. C. W. Lohrenz, P. E. Blochl, T. Ziegler, *J. Am. Chem. Soc.* **1996**, *118*, 13021. [4c] Y.-X. Chen, C. L. Stern, S. Yang, T. J. Marks, *J. Am. Chem. Soc.* **1996**, *118*, 12451.

[5] [5a] L. Canali, D. C. Cherrington, *Chem. Soc. Rev.* **1999**, *28*, 85. [5b] S. Chang, L. Jones II, C. Wang, L. M. Henling, R. H. Grubbs, *Organometallics* **1998**, *17*, 3460. [5c] T. Repo, M. Klinga, P. Pietikäinen, M. Leskelä, A.-M. Uusitalo, T. Pakkanen, K. Hakala, P. Aaltonen, B. Löfgren, *Macromolecules* **1997**, *30*, 171. [5d] J. Saito, M. Mitani, J.-I. Mohri, Y. Yoshida, S. Matsui, S.-I. Ishii, S.-I. Kojoh, N. Kashiwa, T. Fujita, *Angew. Chem.* **2001**, *113*, 3002; *Angew. Chem. Int. Ed.* **2001**, *40*, 2918. [5e] M. Mitani, J. Mohri, Y. Yoshida, J. Saito, S.-I. Ishii, K. Tsuru, S. Matsui, R. Furuyama, T. Nakano, H. Tanaka, S. Kojoh, T. Matsugi, N. Kashiwa, T. Fujita, *J. Am. Chem. Soc.* **2002**, *124*, 3327. [5f] Y. Suzuki, N. Kashiwa, T. Fujita, *Chem. Let.* **2002**, 358.

[6] [6a] J. C. Stevens, H. Bonne, D. VanderLende, T. Boussie, G. M. Diamond, C. Goh, K. Hall, A. M. LaPointe, M. K. Leclerc, J. Longmire, V. Morphy, R. Rosen, J. Schoemaker, H. Turner, V. Busico, R. Cipullo, G. Talarico, *Book of abstracts, EUPOC 2003*, Milano, June 9–12, **2003**, 79. [6b] V. Busico, R. Cipullo, G. Talarico, J. C. Stevens, *Book of abstracts, EUPOC 2003*, Milano, June 9–12, **2003**, 81. [6c]T. R. Boussie, G. M. Diamond, C. Goh, K. A. Hall, A. M. LaPointe, M. Leclerc, C. Lund, V. Murphy, J. A. W. Shoemaker, U. Tracht, H. Turner, J. Zhang, T. Uno, R. K. Rosen, J. C. Stevens, *J. Am. Chem. Soc.* **2003**, *125*, 4306.

[7] [7a] G. J. P. Britovsek, V. C. Gibson, D. F. Wass, *Angew. Chem.* **1999**, *111*, 448; *Angew. Chem. Int. Ed.* **1999**, *38*, 428. [7b] V. C. Gibson, K. Spitzmesser, *Chem. Rev.* **2003**, *103*, 283.

[8] [8a] J. D. Scollard, D. H. McConville, *J. Am. Chem. Soc.* **1996**, *118*, 10008. [8b] J. D. Scollard, D. H. McConville, N. C. Payne, J. J. Vittal, *Macromolecules* **1996**, *29*, 5241. [8c] L. T. Armistead, P. S. White, M. R. Gagne, *Organometallics* **1998**, *17*, 216. [8d] S.-J. Kim, I. N. Jung, B. R. Yoo, S. H. Kim, J. Ko, D. Byun, S. O. Kang, *Organometallics* **2001**, *20*, 2136. [8e] C. Lorber, B. Donnadieu, R. Choukroun, *Organometallics* **2000**, *19*, 1963. [8f] Y. Schrodi, R. R. Schrock, P. J. Bonitatebus Jr., *Organometallics* **2001**, *20*, 3560.

[9] L. Stahl, *Coord. Chem. Rev.* **2000**, *210*, 203.

[10] L. P. Grocholl, L. Stahl, R. J. Staples, *Chem. Commun.* **1997**, 1465.

[11] D. F. Moser, C. J. Carrow, L. Stahl, R. J. Staples, *J. Chem. Soc., Dalton Trans.* **2001**, 1246.

[12] D. F. Moser, L. Grocholl, L. Stahl, R. J. Staples, *Dalton Trans.* **2003**, 1402.

[13] R. A. Shaw, *Phosphorus and Sulfur* **1978**, *4*, 99.

[14] A. Michaelis, G. Schroeter, *Ber. Dtsch. Chem. Ges.* **1894**, *27*, 490.

[15] R. Jefferson, J. F. Nixon, T. M. Painter, *J. Chem. Soc., Dalton Trans.* **1973**, 1415.

[16] [16a] G. Bulloch, R. Keat, D. G. Thompson, *J. Chem. Soc., Dalton Trans.* **1977**, 99. [16b] A. R. Davies, A. T. Dronsfield, R. N. Haszeldine, D. R. Taylor, *J. Chem. Soc., Perkin Trans.* **1973**, 379. [16c] T. G. Hill, R. C. Haltiwanger, M. L. Thompson, S. A. Katz, A. D. Norman, *Inorg. Chem.* **1994**, *33*, 1770. [16d] G. Bulloch, R. Keat, D. G. Thompson, *J. Chem. Soc., Dalton Trans.* **1977**, 1045.

[17] Based on published data, the δ_P of the *cis*-form is in the range 100–120 ppm while that of the *trans*-form is in the range 170–200 ppm, see ref.[15]

[18] I. Silaghi-Dumitrescu, I. Haiduc, *Phosphorus Sulfur Silicon* **1994**, *91*, 21.

[19] M. Bochmann, *Comprehensive Organometallic Chemistry II*

 © 2004 Wiley-VCH Verlag GmbH & Co. KGaA, Weinheim

(Ed.: M. F. Lappert), vol. 4, Pergamon Press, Oxford, UK, **1995**.
[20] I. Schranz, L. Stahl, R. J. Staples, *Inorg. Chem.* **1998**, *37*, 1493.
[21] As comparison, $[(PhN)(PN\text{-}t\text{Bu})]_2Li_2(THF)_2$ gives a signal at $\delta = 162.9$ ppm; see I. Schranz, D. F. Moser, L. Stahl, R. J. Staples, *Inorg. Chem.* **1999**, *38*, 5814.
[22] M. F. Lappert, M. J. Slade, A. Singh, *J. Am. Chem. Soc.* **1983**, *105*, 302.
[23] $[(t\text{BuN})(t\text{BuNP})]_2TiCl_2$ (**10**) was synthesized earlier by the direct reaction of $[(t\text{BuNH})(t\text{BuNP})]_2$ and $TiCl_4$ in the presence of Et_3N (see ref.[11]).
[24] F. Guerin, D. H. McConville, J. J. Vittal, *Organometallics* **1996**, *15*, 5586.
[25] R. R. Schrock, R. Baumann, S. M. Reid, J. T. Goodman, R. Stumpf, W. M. Davis, *Organometallics* **1999**, *18*, 3649.
[26] *CAD-4 Software (Updated 1998, Linux version)*; Enraf−Nonius, Delft, The Netherlands, **1985**.
[27] K. Harms, *Program for the Lp-correction of Enraf−Nonius CAD-4 Diffractometer Data*; University of Marburg, Marburg, Germany, **1996**.
[28] *TEXSAN*, *Single Crystal Structure Analysis Software, Version 1.6*. MSC, 3200 Research Forest Drive, Woodlands, TX 77381, USA, **1993**.
[29] A. C. T. North, D. C. Phillips, F. S. Mathews, *Acta Crystallogr., Sect. A* **1968**, *24*, 351−354.
[30] Nonius, *COLLECT*, Nonius BV, Delft, The Netherlands, **2002**.
[31] G. M. Sheldrick, *SADABS*, University of Göttingen, Germany, **1996**.
[32] G. M. Sheldrick, *SHELX-97*, *Program for the Solution and Refinement of Crystal Structures*, University of Göttingen: Göttingen, Germany, **1997**.
[33] G. M. Sheldrick, *SHELXTL/PC*, Siemens Analytical X-ray Instruments Inc., Madison, Wisconsin, USA, **1990**.

Received July 21, 2003
Early View Article
Published Online December 19, 2003

 © 2004 Wiley-VCH Verlag GmbH & Co. KGaA, Weinheim

Manganese Oxydiacetate Complexes: Synthesis, Structure and Magnetic Properties

Abdessamad Grirrane,[a] Antonio Pastor,[a] Eleuterio Álvarez,[b] Carlo Mealli,[c] Andrea Ienco,[c] Patrick Rosa,[d] Francisco Montilla,[a] and Agustín Galindo*[a]

Keywords: Manganese / Tridentate ligands / Coordination modes / Magnetic properties

The aerobic aqueous solution syntheses and structures of monomeric and polymeric Mn^{II} complexes containing the oxydiacetate ligand [$O(CH_2COO)_2^{2-}$ = oda] are reported. The magnetic properties of the polymeric products have also been investigated. The initially obtained species $[\{Mn(oda)(H_2O)\}\cdot H_2O]_n$ (**1**) has been reacted with bidentate or tridentate N-donor ligands such as *o*-phenanthroline (phen), 2,2′-bipyridine (bipy) and 2,2′:6,2′′-terpyridine (terpy) to give the complexes $[\{Mn(oda)(phen)\}\cdot 4H_2O]_n$ (**2**), $[Mn(oda)(bipy)(H_2O)]\cdot 2H_2O$ (**3**) and $[Mn(oda)(terpy)]\cdot 2H_2O$ (**4**), respectively. Species **1**–**4** are the first Mn-oda structures determined by X-ray methods. In all cases, the oda acts as a tridentate ligand toward one metal and adopts the typical planar arrangement. However, while the **3** and **4** are monomers, **2** and **1** are polymers as oda exploits both atoms of its carboxylate groups to coordinate other metals; **1** consists of a three-dimensional diamond-type network, while **2** is one-dimensional, consisting of an extended chain of {Mn(oda)(phen)} subunits. For both compounds, magnetic susceptibility measurements down to 2 K showed only weak antiferromagnetic interactions between high-spin Mn^{II} ions. Despite the expectedly similar coordinating capabilities of N-donor ligands, the bipy complex **3** is a monomer with the six-coordination completed by one water ligand. The tridentate nature of simultaneously present oda and terpy ligands excludes the coordination of water in complex **4**, the geometry of which is distorted from the octahedron, most likely due to a peculiar packing effect. Finally, the known five-coordinate complex $[MnCl_2(terpy)]$ (**5**), a side product of our synthetic experiments, has also been structurally characterized.
(© Wiley-VCH Verlag GmbH & Co. KGaA, 69451 Weinheim, Germany, 2004)

Introduction

As the active sites of several mononuclear enzymes are five- or six-coordinate manganese species containing coordinated carboxylate groups, water and nitrogen-donor molecules (for instance, imidazole groups),[1−5] research on the coordination compounds of manganese with such co-ligands has grown. In particular, model compounds may provide better insight into the manganese-based biological systems and, thus, most of this chemistry has been attempted in aqueous solution.

The oxydiacetate anion [oda = $O(CH_2COO)_2^{2-}$] features two carboxylate functions joined by a three-membered chain that is centred on an ethereal oxygen atom. The bonding capabilities of the ligand have been tested with most first-row transition metals, and mono-, bi- and polynucleating behaviours have been ascertained through several X ray structure determinations. Scheme 1 shows these coordination modes, without considering *syn* and *anti* isomers for the carboxylate bridge.

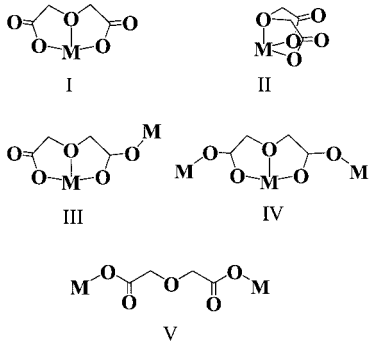

Scheme 1

The ligand usually behaves as tridentate monometallic. Two possible isomers, I or II, are known, for which the ligand oda is overall planar[6−12] or puckered, respectively.[10,13,14] In six-coordinate complexes, these isomers are referred to as *mer* or *fac*, respectively. Our previous DFT

[a] Departamento de Química Inorgánica, Universidad de Sevilla, Aptdo. 553, 41071 Sevilla, Spain
Fax: (internat.) + 34-95-4557153
E-mail: galindo@us.es
[b] Instituto de Investigaciones Químicas, CSIC, Avda. Américo Vespucio s/n, 41092 Sevilla, Spain
[c] ICCOM, CNR, Via Nardi 39, 50132 Firenze, Italy
[d] LAMM, Università degli Studi di Firenze, Via della Lastruccia 3, 50019 Sesto Fiorentino (FI), Italy

calculations for some nickel[12] and vanadium complexes,[15] as well as for the free oxydiacetic acid and the oxydiacetate anion,[12] all showed an energy difference between these isomers of a few kcal mol^{-1}. The highest ΔE of 8.5 kcal·mol^{-1} was found for the complex $[VO(oda)(H_2O)_2]$.[15] Our search in the Cambridge Database[16] on first row transition metals indicates that the most common binding mode for oda is planar (I in Scheme 1), with the external carboxylate oxygen atoms not involved in metal coordination. The residual nucleophilicity of the latter atoms is exerted usually through hydrogen bonding with crystallization water molecules.[6–12] There are other cases where the ligand oda still acts as tridentate toward one metal (in the overall planar arrangement), while the remaining carboxylate donors are also bound to one or two different metals (coordination modes III and IV, respectively, in Scheme 1). Two examples of these coordination modes are the complexes $[\{Co(oda)(H_2O)_2\}\cdot H_2O]_n$ [17] and $[\{Zn(oda)\}\cdot 0.3H_2O]_n$,[9] respectively. Finally, in some cases the ethereal oxygen atom of oda is uncoordinated and the whole ligand acts a μ-bridge between two equal metal centres, such as Ti^{IV} [7] and Zn^{II}, [18] (structure V, Scheme 1). Despite the widespread use of oda as a ligand with first row transition metals, there is still a paucity of data relative to chromium and manganese metals and, in particular, neither structural nor conformational data are available. For instance, only a potentiometric study of a Mn^{II}-oda system has been reported, without any stereochemical implication for the nature of the adduct investigated.[19]

We have recently found an interesting behaviour of the thio- analogue of oda [tda = $S(CH_2COO)_2^{2-}$] toward the Mn^{II} ion, with 2,2′-bipyridine as co-ligand. We have synthesized and documented the first example of a Mn^{II} dimer with the copper-acetate structure (sketch in Scheme 2).[20] $[Mn(tda)(bipy)]_n$, where the central sulfur atom of tda is not involved in coordination, is remarkable for at least three reasons: (i) the almost unobserved assembly of two local trigonal prisms through rectangular faces, (ii) the ascertained antiferromagnetism within the dimeric unit, (iii) the extended supramolecular arrangement formed in the solid state due to the interpenetration of the parallel bipyridine ligands in a gear-like arrangement. Encouraged by the above results, we have tested whether an aqueous solution of the ligand oda has an analogous reactivity pattern toward the Mn^{II} ion when associated with co-ligands such as 2,2′-bipyridine or other polydentate nitrogen bases. This chemistry is essentially unexplored and this paper presents the spectroscopic, magnetic and structural characterization of the synthesized products. The results are particularly interesting from the structural point of view as different stereochemical arrangements are observed for systems with components of similar nature.

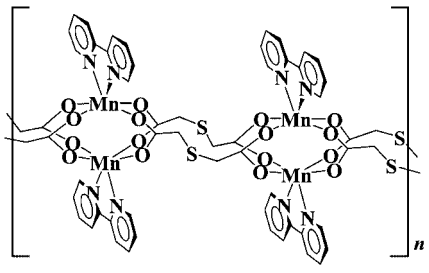

Scheme 2

Results and Discussion

A summary is given in Scheme 3 of the reactions and products studied. Beside routine spectroscopic analyses, the structures of compounds **1**–**5** have been determined by X-ray diffraction analysis. While species **1**–**4** represent the first examples of structurally characterized manganese oxydiacetate complexes, the oda-free compound **5** has been previously obtained,[21–23] and characterized by powder X-ray techniques[24] but its precise molecular structure was still unknown. All of the current work is illustrated in detail below.

Synthesis and Characterization

Treatment of aerobic aqueous solutions of manganese dichloride with a 1:1 mixture of Na_2CO_3 and oxydiacetic acid, $O(CH_2COOH)_2$, affords, after work up, colourless crystals of complex $[Mn(oda)(H_2O)_2]$ (**1**), in good yields. Related oxydiacetate complexes of nickel and cobalt were prepared by a similar procedure.[12] Only X-ray analysis (see below) could clearly show that **1** is a polymeric solid and that only one of the two water molecules is coordinated to the metal centre, so that the correct formulation is $[\{Mn(oda)(H_2O)\}\cdot H_2O]_n$. Subsequently, complex **1** was found react readily with each of three different N-donor ligands, *o*-phenanthroline (phen), 2,2′-bipyridine (bipy) and 2,2′:6,2′′-terpyridine (terpy) (Scheme 3), to give, almost invariably, good yields of yellow crystalline solids. Elemental analyses and the IR spectra indicated that additional water molecules were present in the so-obtained compounds but it was not possible to asses any difference between their coordination or simple crystallization roles. Again, only the subsequent X-ray determinations allowed us to assign formulae to the various products: $[\{Mn(oda)(phen)\}\cdot 4H_2O]_n$ (**2**), $[Mn(oda)(bipy)(H_2O)]\cdot 2H_2O$ (**3**), and $[Mn(oda)(terpy)]\cdot 2H_2O$ (**4**), respectively. Accordingly, while **3** and **4** are monomers, **2** is polymeric.

An alternative attempt to prepare complex **4** in a single step (i.e. by mixing in one pot $MnCl_2$ with a 1:1 mixture of Na_2CO_3 and $O(CH_2COOH)_2$ and by adding subsequently terpy) provided, after some work up, **4** and small amounts of a new yellow crystalline material that was analytically and structurally characterized as $[MnCl_2(terpy)]$ (**5**). Most probably, the obtainment of **5** was due to a small stoichiometric defect of $O(CH_2COOH)_2$ in the experimental procedure. In fact, as reported, complex **5** is easily obtainable by direct reaction between the water solutions of manganese dichloride with terpy.[21–23] Complex **4** is also formed from the reaction of the isolated complex **5** with one equivalent of sodium oxydiacetate (see Exp. Sect.). Evidently,

 © 2004 Wiley-VCH Verlag GmbH & Co. KGaA, Weinheim

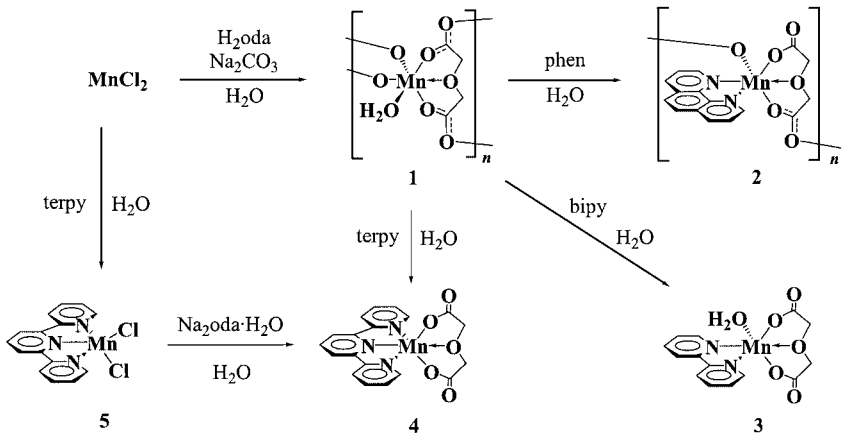

Scheme 3

species **5** is a sufficiently stable intermediate, which may or may not be isolated, in the reaction leading to **4**.

All of the synthesised compounds are air stable, both in solution and in the solid state. They may be dissolved in water but are not soluble in solvents of low polarity. The effective magnetic moments for **3** and **4** (solid state, room temperature) are in the range 5.7−5.9 μ_B, which are invariably consistent with five unpaired electrons in the ground-state configuration, and typical of high-spin mononuclear manganese(II) units. Similar manganese complexes that contain closely related ligands exhibit comparable μ_B values {e.g. 5.95 μ_B for [Mn(dipic)(bipy)]·2H_2O, dipic = pyridine-2,6-dicarboxylate}.[25] The magnetic behaviour of **1** and **2** is discussed below. Compounds **1**−**4** display the characteristic IR absorptions of oxydiacetate ligand. In particular, they feature a very strong, broad band at ca. 1600 cm^{-1}, which corresponds to the antisymmetric vibrations of the carboxylate groups, and a strong band at ca. 1430 cm^{-1}, which is assigned to the symmetric vibrations of the same groups. In many complexes of the first- and second-row[26,27] transition metals, and in all lanthanide and actinide complexes,[16] the ligand oda adopts a tridentate planar coordination mode. The non-planar arrangement of the ligand (II in Scheme 1) is uniquely found in some six-coordinate oxydiacetate compounds of nickel(II) and copper(II).[10,13,14] We have previously suggested and theoretically supported[12,15] the idea that the precise position of the C−O−C antisymmetric stretching band is diagnostic of the oda disposition in the various complexes. Thus, a planar oxydiacetate ligand is characterized by a sharp, strong band in the region 1150−1120 cm^{-1}, while the active IR band falls in the region around 1100 cm^{-1} when the arrangement is *fac*. Complexes **1**−**4** all display an absorption at ca. 1135 cm^{-1} that is attributable to C−O−C antisymmetric stretching; hence the planar disposition of oda is invariably assumed, and, indeed, is confirmed by the X-ray structural determinations.

Structural and Magnetic Studies

Compounds **1**−**5** have been structurally characterized by single-crystal X-ray diffraction analysis. In all cases, the Mn^{II} ion is high spin and, for **1**−**4**, the local coordination is pseudo-octahedral. Under these circumstances, the distribution of the five unpaired electrons in the 3d orbital shell is isotropic. Thus, the coordination bonds should be mainly due to the interaction of the ligands with the metal s and p orbitals, with a minor role for the d levels, as for d^0 (main group metals) and d^{10} configurations, i.e. the crystal field stabilization energy has little influence in these complexes, which have a good degree of hypervalency. This view is supported by the easy deformation of complex **4** from the octahedron (vide infra), and the stabilization of the five-coordinate compound **5** further confirms the minor role of the d orbitals in fixing the coordination sphere.

As discussed in textbooks,[28] the ease of substitution of one water ligand in Mn^{II} and Zn^{II} octahedral complexes, with respect to the Fe^{II}, Co^{II}, Ni^{II} and Cu^{II} analogues (Irving−Williams series), can be related to the ratio between the charge and the effective ionic radius (Shannon type[29]). In particular, the high-spin Mn^{II} ion has the largest radius in the series. Direct comparison between some of the present manganese structures and their equivalents with other metals allows a further check of the trends indicated. For instance, the complex [Mn(oda)(bipy)-(H_2O)]·2H_2O (**3**) has Co^{II}, Ni^{II} and Zn^{II} analogues. Similarly, [Mn(oda)(terpy)]·2H_2O (**4**) can be usefully compared with the Ni^{II} and Cu^{II} species. Detailed information is provided below when discussing the single structures.

None of the Mn^{II} complexes with the ligand oda and other N-donor chelates exhibit the unique features of the thiodiacetate complex $[Mn(tda)(bipy)]_n$ (Scheme 2), i.e. the two carboxylate functions of oda cannot be exploited to form a copper-acetate structural motif. This is probably because the affinity of the ethereal oxygen function for the manganese(II) ion is larger than with the thio-ethereal counterpart. The apparently difficult formation of $Mn^{II}-S_{ethereal}$ bonds (there are only a few structurally documented examples[30−34] favours the stretching of the tda chain and provides the best packing conditions to form the extended arrangement of the tetracarboxylate dimanganese units. Apparently, the $Mn^{II}-O_{ethereal}$ bond is readily

 © 2004 Wiley-VCH Verlag GmbH & Co. KGaA, Weinheim

formed for Mn^{II}-oda, and the reactivity follows alternative routes.

3D-Polymeric Complex $[\{Mn(oda)(H_2O)\}\cdot H_2O]_n$ (1)

Each manganese(II) ion of the parent compound $[\{Mn(oda)(H_2O)\}\cdot H_2O]_n$ (**1**) is six-coordinate by the tridentate oxydiacetate ligand in the *mer* configuration (planar arrangement), one coordinated water ligand and two additional oxygen atoms of carboxylic groups coming from symmetry repeated $\{Mn(oda)(H_2O)\}$ units (Figure 1). In this manner all of the five oda oxygen atoms are engaged in donations to the metal (coordination mode IV in Scheme 1). The overall structure of **1** is evidently a polymer that extends in three dimensions due to the four connections (two incoming and two outgoing dative bonds) that each $\{Mn(oda)(H_2O)\}$ fragment establishes with its neighbouring equivalents. Selected interatomic distances and angles for the local coordination of **1** are collected in Table 1. As usual, the Mn−O3 bond involving the ethereal oxygen atom [2.230(3) Å] is slightly longer than any other Mn−O(carboxylate) bond, either formed within one $\{Mn(oda)(H_2O)\}$ unit [2.208(3) and 2.194(3) Å for Mn−O1 and Mn−O2, respectively] or in the combination of different units [2.114(3) and 2.182(3) Å, for Mn−O4′ and Mn−O5′′, respectively].

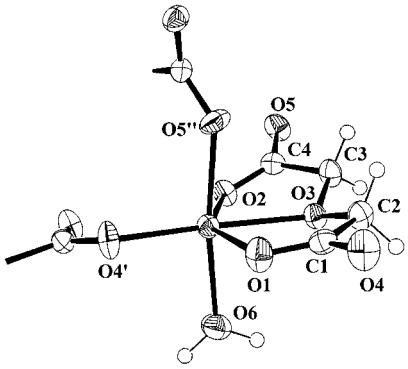

Figure 1. Local coordination environment about one Mn^{II} ion in $[\{Mn(oda)(H_2O)\}\cdot H_2O]_n$ (**1**). The atoms labelled with ′ and ′′ belong to two distinct $\{Mn(oda)(H_2O)\}$ units repeated by the symmetry operations $-x+2, y-1/2, -z+3/2$ and $x+1/2, -y+3/2, -z+2$, respectively

The overall topology of the polymeric system is a diamond-like network that is not interpenetrated, according to the useful schemes of O′Keeffe and co-workers.[35] Figure 2 (a) shows a scheme of such an arrangement limited to the manganese atoms. The arbitrary connections between them show apparent cavities occupied by the oxygen atoms of the solvate water molecules. The hydrogen bonding network is a key feature for this and the other manganese oda complexes described here and deserves a detailed analysis. As stated by Perec and co-workers,[9] the hydrogen bonding network due to the coordinated and solvent water molecules fixes the crystal packing of most oxydiacetate metal complexes. Complex **1** has channels that are parallel to the *a* axis (Figure 2, b). Inside these channels, the solvent water molecules

Table 1. Selected bond lengths and angles for **1**

Atoms[a]	Distance [Å]	Atoms	Angle [°]
Mn–O4'	2.114(3)	O4'–Mn–O6	92.58(12)
Mn–O6	2.173(3)	O4'–Mn–O5"	94.88(12)
Mn–O5"	2.182(3)	O6–Mn–O5"	172.15(12)
Mn–O2	2.194(3)	O4'–Mn–O2	120.39(10)
Mn–O1	2.208(3)	O6–Mn–O2	91.61(11)
Mn–O3	2.230(3)	O5"–Mn–O2	86.74(10)
O1–C1	1.235(4)	O4'–Mn–O1	95.40(10)
O2–C4	1.249(4)	O6–Mn–O1	89.47(12)
O3–C3	1.421(4)	O5"–Mn–O1	87.38(11)
O3–C2	1.423(4)	O2–Mn–O1	144.09(9)
O4–C1	1.266(4)	O4'–Mn–O3	167.98(9)
O5–C4	1.258(4)	O6–Mn–O3	88.58(11)
C1–C2	1.518(5)	O5"–Mn–O3	83.62(10)
C3–C4	1.511(5)	O2–Mn–O3	71.51(9)
		O1–Mn–O3	72.63(9)
		C1–O1–Mn	118.7(2)
		C4–O2–Mn	116.1(2)
		C3–O3–C2	115.0(3)
		C3–O3–Mn	115.4(2)
		C2–O3–Mn	116.6(2)
		C1–O4–Mn'''	121.5(2)
		C4–O5–Mn''''	135.9(2)
		O1–C1–O4	125.1(3)
		O1–C1–C2	120.6(3)
		O4–C1–C2	114.3(3)
		O3–C2–C1	109.1(3)
		O3–C3–C4	108.3(3)
		O2–C4–O5	123.4(4)
		O2–C4–C3	119.4(3)
		O5–C4–C3	117.2(3)

[a] Symmetry transformations used to generate equivalent atoms: ′ $-x+2, y-1/2, -z+3/2$; ′′ $x+1/2, -y+3/2, -z+2$; ′′′ $-x+2, y+1/2, -z+3/2$; ′′′′ $x-1/2, -y+3/2, -z+2$.

form a complicated structural pattern. For instance, the water molecule defined by O7 bridges two-coordinated water ligands (O6) of different $\{Mn(oda)(H_2O)\}$ units. The O7···O6 separations are as long as 2.760(4) and 2.843(5) Å, respectively. Additionally, O7 is involved in hydrogen bonding with O2 and O4 of oda carboxylate groups [O7···O2 and O7···O4 of 2.896(4) and 2.853(4) Å, respectively].

The molar magnetic susceptibility of complex **1** was measured in the range 1.9−300 K. Both the susceptibility, χ_{mol}, and its product with the temperature, $\chi_{mol}T$, (Figure 3) show typical paramagnetic behaviour. With 4.59 emu $K\cdot mol^{-1}$ at 300 K, $\chi_{mol}T$ is typical of uncorrelated high-spin Mn^{II} ions (theoretical value of 4.38 μ_B for five unpaired electrons and a Landé factor $g = 2$). On lowering the temperature, $\chi_{mol}T$ starts to decrease below 150 K, while χ_{mol} rises monotonically to a maximum at 5 K, revealing weak antiferromagnetic interactions between the Mn^{II} centers. A plot of the inverse susceptibility $1/\chi_{mol}$ versus temperature shows Curie−Weiss behaviour ($1/\chi_{mol} = (T - \theta)/C$) with a Curie constant $C = 4.705$ emu $K\cdot mol^{-1}$ and $\theta = -6.3$ K. The former magnitude corresponds to high-spin Mn^{II} with a *g*-factor of 2.074, which is far from the free-electron value expected for isotropic Mn^{II} and reflects experimental errors such as weighting. The θ value can be accounted for by the mean-field model. As described by Kahn,[36] $\theta = zJS(S+1)/3k$, where *J* is the interaction par-

 © 2004 Wiley-VCH Verlag GmbH & Co. KGaA, Weinheim

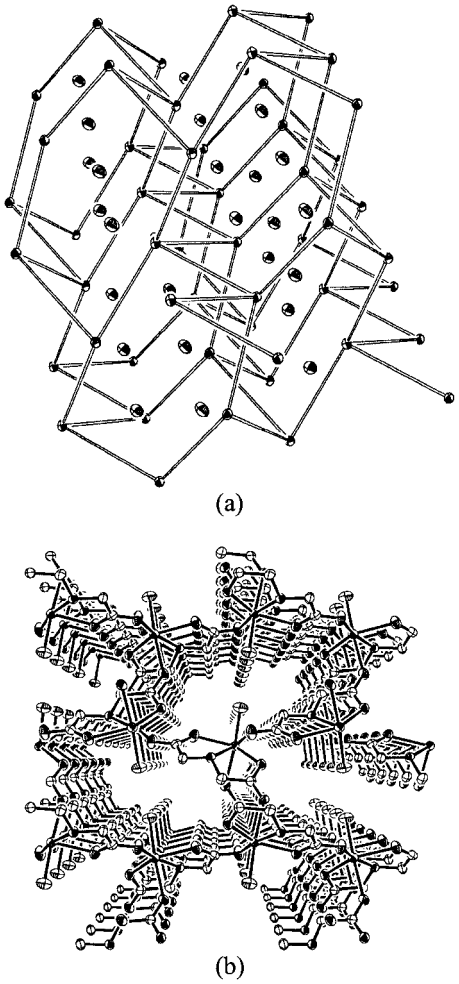

Figure 2. (a) Diamond-like three-dimensional pattern of $[\{Mn(oda)(H_2O)\}\cdot H_2O]_n$ (**1**) as highlighted by the network of Mn atoms alone (the lines interconnecting these atoms are not bonds). Oxygen atoms of the crystallization water molecules are shown within the cavities. (b) Complete packing diagram down the *a* axis (crystallization water and hydrogen atoms excluded)

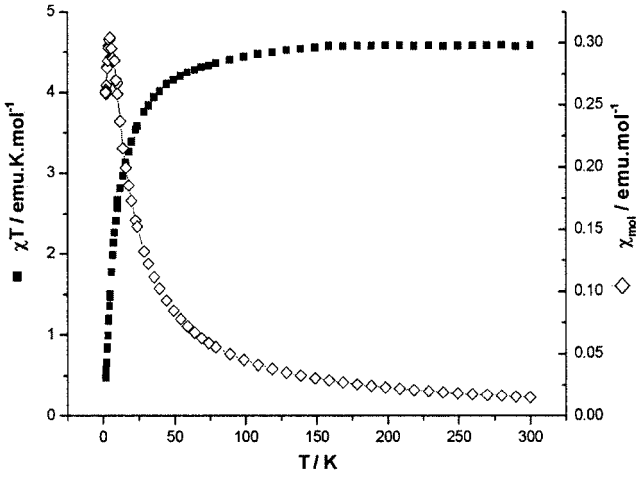

Figure 3. Molar magnetic susceptibility χ_{mol} (◆, cgs units) and its product with the temperature, $\chi_{mol}T$ (■, cgs units), of complex **1** between 1.9 and 300 K

ameter in the mean-field perturbation Hamiltonian $\hat{H} = -zJ\langle\hat{S}_z\rangle\cdot\hat{S}_z$, S is the spin of the interacting ion, and z is the number of nearest neighbours. For $z = 4$ (Figure 2, a) and $S = 5/2$, we find $J = -0.19$ cm^{-1} for this polymeric system. This weak interaction is thus in the -0.193 to -0.30 cm^{-1} range previously found for Mn^{II} complexes that are similarly bridged by a unique carboxylate moiety.[37]

1D-Polymeric Complex $[\{Mn(oda)(phen)\}\cdot 4H_2O]_n$ (2)

Compound **2** is also a polymer, in contrast with the related monomeric compounds $[M(oda)(phen)(H_2O)]$ (M = Ni,[10] Zn[9]). Each metal ion in **2** is six-coordinated by the three oxygen atoms of one oda ligand in the planar disposition, by the phen chelate and by an oxygen atom of a oda carboxylate group belonging to a symmetry repeated {Mn(oda)(phen)} unit (Figure 4, a). Here, the polymer extends as a one-dimensional chain (Figure 4, b) since each {Mn(oda)(phen)} unit acts both as an acceptor and as a donor with respect to its adjacent equivalents. The chains extend along the direction of the *a* axis. Selected bond lengths and angles for the local coordination of **2** are listed

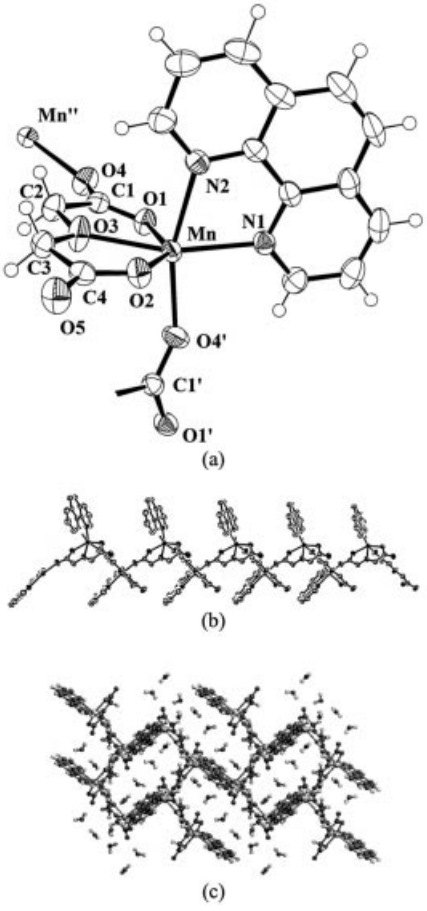

Figure 4. (a) Local coordination environment about Mn^{II} ion in complex $[\{Mn(oda)(phen)\}\cdot 4H_2O]_n$ (**2**). Primed and unprimed atoms are related by the symmetry operations x, y, z and x, $1/2 - y$, z, respectively. (b) ORTEP drawing showing a portion of the extended chain of {Mn(oda)(phen)} units in **2**; interspersed H_2O solvent molecules not shown. (c) View of the crystal packing of **2** that highlights the particular disposition of the solvent water molecules

 © 2004 Wiley-VCH Verlag GmbH & Co. KGaA, Weinheim

Table 2. Selected bond lengths and angles for complexes **2**−**4**

	2[a]	**3**	**4**
Distances [Å]			
Mn–O1	2.1798(17)	2.156(2)	2.1149(14)
Mn–O2	2.1680(17)	2.185(2)	2.1501(13)
Mn–O3	2.1876(17)	2.195(2)	2.1727(15)
Mn–N1	2.2184(19)	2.245(3)	2.2611(16)
Mn–N2	2.267(2)	2.242(3)	2.1950(15)
Mn–X[b]	2.1168(18)	2.165(3)	2.2845(16)
O1–C1	1.254(3)	1.253(3)	1.269(2)
O2–C4	1.262(3)	1.253(3)	1.259(2)
O4–C1	1.245(3)	1.249(3)	1.234(2)
O5–C4	1.241(3)	1.249(3)	1.237(2)
O3–C2	1.413(3)	1.416(3)	1.412(2)
O3–C3	1.417(3)	1.409(3)	1.404(2)
C1–C2	1.518(3)	1.515(4)	1.506(3)
C3–C4	1.513(3)	1.523(4)	1.513(3)
Angles [°]			
O1–Mn–O2	142.73(6)	142.51(8)	142.87(5)
O1–Mn–O3	71.03(6)	71.53(7)	72.18(5)
O1–Mn–X[b]	94.51(7)	99.29(10)	102.83(6)
O2–Mn–O3	71.70(6)	70.99(8)	71.78(5)
O2–Mn–X[b]	93.25(7)	87.30(10)	91.30(6)
O3–Mn–X[b]	103.25(8)	98.87(9)	99.03(7)
N1–Mn–N2	73.89(7)	72.35(9)	72.30(6)
N1–Mn–O1	96.61(7)	96.01(8)	90.70(6)
N1–Mn–O2	119.85(7)	121.17(8)	97.59(6)
N1–Mn–O3	162.56(7)	166.36(8)	116.72(7)
N1–Mn–X[b]	89.66(7)	88.42(9)	144.19(6)
N2–Mn–O1	95.68(7)	103.82(9)	120.34(5)
N2–Mn–O2	87.93(7)	84.79(9)	96.59(6)
N2–Mn–O3	94.64(8)	104.62(9)	165.64(6)
N2–Mn–X[b]	161.52(7)	151.17(10)	72.25(6)

[a] Symmetry transformations used to generate equivalent atoms: $' x - 1/2, -y + 1/2, z$. [b] The symbol "X" is atom O4′, O6, and N3 for **2**, **3**, and **4**, respectively.

in Table 2. Again, the coordination bond to the ethereal oxygen atom [Mn−O3 = 2.1876(17) Å] is slightly longer than any other Mn−O bond lengths. Amongst the latter, the distances within one {Mn(oda)(phen)} unit are longer than the corresponding inter-fragmental one [2.1680(17) and 2.1798(17) Å vs. 2.1168(18) Å, respectively]. There is no appreciable difference between the C−O bonds of the bidentate-dimetallic carboxylate group, but there is a minor asymmetry between the two C−O distances of the other carboxylate [compare the 1.241(3) and 1.262(3) Å for the C4−O5 and C4−O2 bonds, respectively]. At variance with **1**, one carboxylate oxygen atom (O5) of oda remains unused for metal coordination (coordination mode III in Scheme 1).

As with complex **1**, the hydrogen bonding network deserves a careful description. Solvent water molecules are interspersed between the parallel chains and participate to form a complicated hydrogen bonding network. In particular, the hydration molecules occupy the channels formed by the parallel disposition of the phenanthroline ligands (Figure 4, c). The carboxylate oxygen O5 forms two hydrogen bonds with two different water molecules centred at O7 and O9 [O5···O7 and O5···O9 are 2.812(3) and 2.851(3) Å, respectively]. A third water molecule (defined by O8) bridges the two previous ones [O8···O7 and O8···O9 of 2.940(4) and 2.775(4) Å, respectively]. A fourth hydration molecule, centred at O6, makes a hydrogen bonding with that at O7 [H71···O6 and H61···O7 of 2.00(5) and 1.86(5) Å, respectively]. Finally, the network features two similarly weak interactions between one water molecule and one-coordinated oxygen atom of ligand oda. In fact, O6 is 2.920(3) Å from O1, and O9 is 2.952(3) Å from O2.

The temperature dependence of the molar magnetic susceptibility of complex **2** was also measured. Both the susceptibility, χ_{mol}, and its product with the temperature, $\chi_{mol}T$, (Figure 5) again show typical paramagnetic behaviour. With 4.36 emu K·mol^{-1} at 300 K, the $\chi_{mol}T$ product corresponds to uncorrelated high-spin Mn^{II} ions. On lowering the temperature, $\chi_{mol}T$ starts to decrease below 50 K, while χ_{mol} rises monotonically without reaching a maximum. Though there are clearly antiferromagnetic interactions between the Mn^{II} centers, these are much weaker than those of complex **1**. The plot of the inverse susceptibility $1/\chi_{mol}$ versus temperature indicates Curie−Weiss behaviour with $\theta = -1.9$ K, and the expected theoretical value $C = 4.385$ emu K·mol^{-1}. For $z = 2$, for this polymeric chained system (Figure 4, b), and $S = 5/2$, we obtain $J = -0.11$ cm^{-1} through the mean-field model. Although weaker, this value is still close to the range previously cited for similarly bonded complexes.

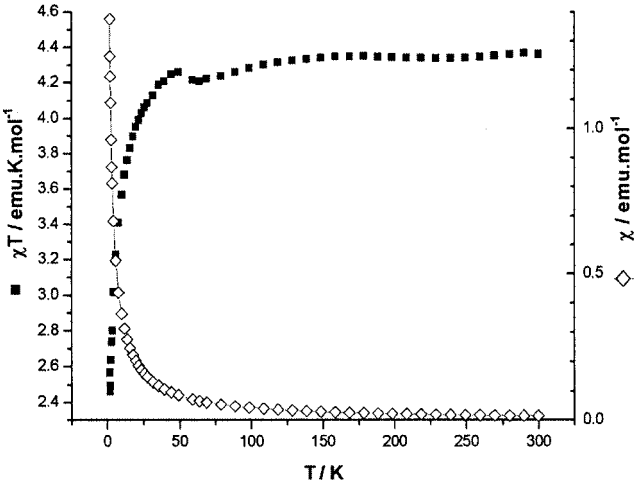

Figure 5. Molar magnetic susceptibility χ_{mol} (◇, cgs units) and its product with the temperature, $\chi_{mol}T$ (■, cgs units), of complex **2** between 1.9 and 300 K

Structure of [Mn(oda)(bipy)(H_2O)]·2H_2O (3)

Despite the expectedly similar coordinating capabilities of the phen and bipy ligands, the reaction of **1** with bipy affords the complex [Mn(oda)(bipy)(H_2O)]·2H_2O (**3**), which is monomer, in contrast to the polymeric character of **2**. There are other examples of similar metal-carboxylate complexes whose different structural motifs are imposed by the nature of the N-donor co-ligand. For example, a manganese succinato derivative that is a dimer when coordinated with 1,10-phenantroline[38,39] becomes polymeric (catena type) when 2,2′-bipyridine is used.[38−40] The manganese ion in **3**

 © 2004 Wiley-VCH Verlag GmbH & Co. KGaA, Weinheim

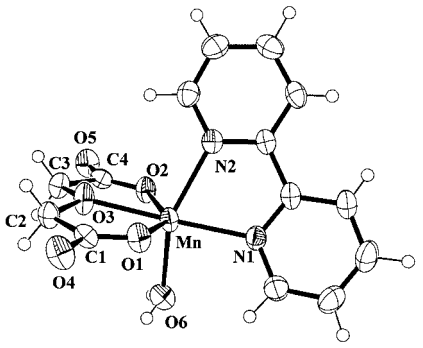

Figure 6. Molecular structure of the $[Mn(oda)(bipy)(H_2O)]\cdot 2H_2O$ complex (**3**); water molecules of crystallization not shown

is coordinated by the planar oxydiacetate anion, the bipy chelate and by one water molecule (Figure 6). The overall coordination mode is the most classic (I in Scheme 1) with only one oxygen atom per carboxylate group engaged as a donor towards the metal. Selected bond lengths and angles of complex **3** show no major differences in Mn-oda geometry compared with those of **2** (Table 2). However, even though only one oxygen atom per carboxylate is involved in metal coordination (O1 and O2), a delocalisation of the π bonding is observed, with all of the C−O distances being close to ca. 1.25 Å.

Although a monomer, compound **3** also has a peculiar hydrogen bonding network that certainly affects its crystal packing. The latter, described below, is certainly different from the one common to three isomorphous compounds that have the equivalent basic formula $[M(oda)(bipy)(H_2O)]$ (M = Ni,[12] Co[12] and Zn[9]). In fact, they, with 2.5 crystallization water molecules, belong to the space group *Fdd*2, while **3**, with only two hydration molecules, crystallizes in $P2_1/n$. In **3**, the O7 of one solvent water molecule forms two hydrogen bonds with the uncoordinated O4 and O5 of two carboxylate groups [O5···O7 and O4···O7 contacts are 2.83(4) and 2.85(4) Å, respectively]. The second H_2O molecule, centred at O8, acts as an hydrogen bonding acceptor from the metal-coordinated H_2O molecule (O6), while it is a donor with respect to both the carboxylate O5 atom and the O7 water atom. The three contacts projecting from O8 are 2.68(4), 2.76(4) and 2.83(5) Å, respectively. The Mn−O and Mn−N distances in **3** are the longest in the $[M(oda)(bipy)(H_2O)]$ series, the order being $Mn^{II} > Zn^{II} > Co^{II} > Ni^{II}$ (Table 3). As mentioned, the trend agrees with that of the Shannon radii and indirectly with the *q*/*r* ratios for these elements. The expanded coordination sphere of Mn^{II} also combines with larger distortions from the regular octahedral geometry. In particular, the O6−Mn−N2 angle deviates from linearity [151.17(10)°], a feature that, for instance, is much less evident for the other derivatives [cf. 170.4(1)° for nickel, 167.1(1)° for cobalt and 169.0(2)° for zinc].

Table 3. Comparison of selected bond lengths (Å) around the metal centre in $[M(oda)(bipy)(H_2O)]$ complexes

M	Mn	Ni[12]	Co[12]	Zn[9]
M–O1	2.156(2)	2.055(3)	2.050(3)	2.054(6)
M–O2	2.185(2)	2.054(3)	2.096(3)	2.084(5)
M–O3	2.195(2)	2.042(2)	2.115(3)	2.160(5)
M–N1	2.245(3)	2.046(3)	2.096(3)	2.102(5)
M–N2	2.242(3)	2.067(3)	2.115(3)	2.145(6)

Finally, the overall geometry of **3** resembles that of the closely relatable mononuclear complex [Mn(chedam)(bipy)-(H_2O)] (chedam = 4-hydroxypyridine-2,6-dicarboxylate).[25] The greater *trans* influence of the nitrogen donor of chedam with respect to that of the ethereal O3 atom of oda is evident. In fact, the Mn−N1 of 2.245(3) Å in **3** is significantly shorter than the corresponding Mn−N of 2.278(1) Å in the complex with the ligand chedam.

Structure of $[Mn(oda)(terpy)]\cdot 2H_2O$ (4)

The crystal structure of six-coordinate complex **4** is composed of discrete [Mn(oda)(terpy)] units (Figure 7, a), plus two water molecules of crystallization. Selected bond lengths and angles are given in Table 2. The connectivity requirements of both the oda and terpy ligands, both tridentate and planar arranged, prevents bite angles of 90° for any of the adjacent N−Mn−N or O−Mn−O. Accordingly, the geometry of the compounds is far from a regular octahedron. Moreover, the structure is distorted also from it highest possible symmetrical arrangement where the two oda and terpy planes could act as reciprocal mirror planes. These planes are still roughly almost perpendicular [the angle between the mean square planes is ca. 84.21(4)°] but the terpy molecule is significantly bent toward one of the lateral oxygen donors of oda (O2). Consider, for instance, the large difference between O2−Mn−N2 [96.59(6)°] and O1−Mn−N2 [120.34(5)°] (where N2 is the central donor of terpy). Interestingly, such a distortion does not seem to have an electronic origin but it is more likely due to the particular packing of [Mn(oda)(terpy)] molecules in the crystal. Figure 7 (b) shows that two terpy ligands of different molecules are clearly parallel (the planes are ca. 3.7 Å apart), but their π stacking involves only two of the three six-membered rings. Namely, only one central and one lateral ring of one terpy ligand eclipse precisely the equivalent rings of the other complex molecule. Furthermore, intermolecular hydrogen bonding also occurs (Figure 7, b). Generally, C−H groups of aromatic rings are not excellent hydrogen-bonding donors, but here one metal-coordinated carboxylate oxygen atom seems to be able to form such a bond [O2−H13′′ = 2.46(1) Å], and so causes the asymmetric orientation of oda, which should have a low energetic cost. This distortion is not so evident in the similar Ni and Cu complexes [M(oda)(terpy)]. In addition, these structures crystallize in different space groups ($P2_1/n$ and $P2_1/c$, respectively) and, as pointed out for **3**, the crystal packing and hydrogen bonding networks are, consequently, different. In particular, in **4** one lattice water molecule (O7) forms hydrogen bonds with the uncoordinated carboxylate oxygens O4 and O5 of two symmetry related [Mn(oda)(terpy)] molecules [O7···O4 and O7···O5 of 2.76(3) and 2.84(3) Å, respectively]. The second water molecule defined by O6 bridges, through two hydrogen bonds, the carboxylate oxy-

 © 2004 Wiley-VCH Verlag GmbH & Co. KGaA, Weinheim

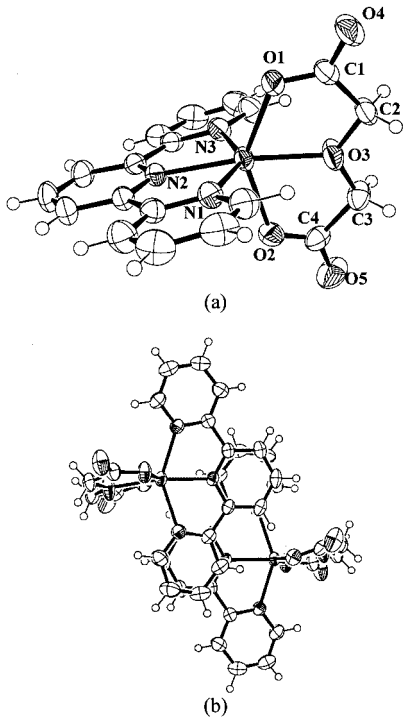

Figure 7. (a) Complex [Mn(oda)(terpy)]·2H_2O (**4**) (water molecules of hydration not shown). (b) Packing diagram of two symmetry related [Mn(oda)(terpy)] molecules, highlighting the hydrogen interaction

gens O1 and O5 of two [Mn(oda)(terpy)] units [O6···O1 and O6···O5 of 2.86(3) and 2.88(2) Å, respectively].

The bond to the ethereal oxygen atom [Mn−O3, 2.1727(15) Å] is again longer than the other two Mn−O1 and Mn−O2 lengths [2.1149(14) and 2.1501(14) Å, respectively]. This fact, although general for the manganese complexes discussed here, is in contrast with the equivalent structures of Ni^{II} [10] and Cu^{II} [6] ions (Table 4). In fact, the latter exhibit shorter $M-O_{ether}$ bonds than the other two M−O distances. Also, the Mn−N lengths in **4** are longer than the similar M−N in the Ni and Cu complexes, in agreement with the larger effective ionic radii,[29] as previously discussed.

Table 4. Comparison of selected bond lengths (Å) around the metal centre in [M(oda)(terpy)] complexes

M	Mn	Ni[10]	Cu[6]
M–O1	2.1149(14)	2.067(2)	2.202(5)
M–O2	2.1501(13)	2.074(2)	2.312(5)
M–O3	2.1727(15)	2.014(2)	2.070(5)
M–N1	2.2611(16)	1.985(3)	1.942(3)
M–N2	2.1950(15)	2.097(3)	2.031(4)
M–N3	2.2845(16)	2.105(3)	2.039(3)

Structure of [$MnCl_2$(terpy)] (5)

As mentioned, the complex [$MnCl_2$(terpy)] (**5**) has been previously reported,[21−23] and characterized by powder X-ray techniques,[24] but its molecular structure was unknown. Here, we observed that the manganese atom is five-coordinate and that the overall geometry is a distorted square pyramid (Figure 8). The only other example of a pentacoordinate manganese complex containing the terpy ligand is the compound [Mn(2,6-dimethoxybenzoato-*O*)$_2$(terpy)].[41]

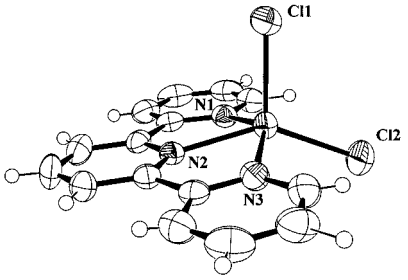

Figure 8. Molecular structure of [$MnCl_2$(terpy)] (**5**)

Selected bond lengths and angles of **5** are collected in Table 5. The Mn−Cl are similar [2.3611(15) and 2.3452(14) Å], whereas the three Mn−N compares well with those in complex **4**. The other structural parameters do not require further comments because they are unexceptional.

Table 5. Selected bond lengths and angles for **5**

Atoms	Distance [Å]	Atoms	Angle [°]
Mn1–Cl1	2.3611(15)	N2–Mn1–N1	72.07(12)
Mn1–Cl2	2.3452(14)	N2–Mn1–N3	71.90(13)
Mn1–N1	2.256(4)	N1–Mn1–N3	141.93(13)
Mn1–N2	2.203(3)	N2–Mn1–Cl2	144.16(10)
Mn1–N3	2.268(4)	N1–Mn1–Cl2	104.34(10)
		N3–Mn1–Cl2	97.66(10)
		N2–Mn1–Cl1	104.71(9)
		N1–Mn1–Cl1	97.79(10)
		N3–Mn1–Cl1	102.79(10)
		Cl2–Mn1–Cl1	111.07(5)

Conclusion

We have reported Mn^{II}-oda chemistry not previously explored. Four different types of compounds have been obtained and characterized that indicate the great propensity of this ligand to stabilize both monomeric and polymeric solid state compounds. Obviously, their characterization has required systematic X-ray diffraction studies that have allowed us to confirm the precise structural arrangements and also the easily deformable coordination sphere about the high-spin manganese(II) ion. The structural studies have highlighted the hydrogen bonding interactions in all the oda complexes studied, involving both the coordinated and the lattice water molecules and carboxylate oxygen atoms of oxydiacetate. These interactions may be fundamental in determining the crystal packing of various oda compounds. In particular, some of the manganese complexes have the same coordination sphere as other previously reported first-row transition metal compounds, but the overall crystal properties are different. Finally, the determined antiferromagnetic coupling constants for the present Mn^{II}-oda poly-

 © 2004 Wiley-VCH Verlag GmbH & Co. KGaA, Weinheim

meric systems are very small and fall in the lowest range reported for related carboxylate-bridged Mn^{II} complexes.[37]

Experimental Section

General Remarks: All preparations and other operations were carried out under aerobic conditions. Microanalyses (C, H, N) were carried out by the Microanalytical Service of the Instituto de Investigaciones Químicas (CSIC). Infrared spectra were recorded with a Perkin-Elmer Model 883 spectrophotometer (Nujol emulsion in NaCl plates). Magnetic moments were measured in the solid state, at room temperature, with a Sherwood Scientific (Cambridge Research Laboratory) magnetic balance, and between 1.9 and 300 K with a Cryogenic S600 SQUID magnetometer. Molar susceptibilities were then corrected using Pascal's constants.[42] Oxydiacetic acid and other chemicals were obtained from commercial sources and were used without further purification. The experimental procedure for the synthesis of **5** has also been included, although its preparation has been reported previously.[21−23]

[{Mn(oda)(H$_2$O)}·H$_2$O]$_n$ (1): Na_2CO_3 (1.28 g, 12 mmol) was added to a solution of $O(CH_2COOH)_2$ (1.61 g, 12 mmol) in water (20 mL). The mixture was then stirred until the evolution of CO_2 ceased and then added to a solution of $MnCl_2·4H_2O$ (2.37 g, 12 mmol) in water (25 mL). The resulting solution was stirred for 15 minutes and then concentrated. Acetone was added and the solution was then kept at room temperature overnight. Colourless crystals of complex **1** were formed, filtered off, washed with acetone and Et_2O and air dried (1.80 g, 65 %). IR (cm^{-1}): $\tilde{\nu}$ = 3350 br. ν(OH), 1587 s br. ν($COO_{asymm.}$), 1431 s ν($COO_{symm.}$), 1137 s ν($COC_{asymm.}$). μ = 5.8 μ_B at 24 °C. $C_4H_8MnO_7$ (223.04): calcd. C 21.52, H 3.59; found C 21.43, H 3.62.

[{Mn(oda)(phen)}·4H$_2$O]$_n$ (2): A solution containing *o*-phenanthroline·H_2O (0.10 g, 0.5 mmol) in hot water (20 mL) was added to a solution of **1** (0.12 g, 0.5 mmol) in water (15 mL). The resulting solution was then stirred for a few minutes. Subsequently, compound **2** crystallized upon evaporation of the solvent at room temperature after a few days; yellow crystals were filtered off, washed with water and acetone and dried in air (0.15 g, 70 %). IR (cm^{-1}): $\tilde{\nu}$ = 3478, 3368 br. ν(OH), 1601 s br. ν($COO_{asymm.}$), 1431 s ν($COO_{symm.}$), 1137 s ν($COC_{asymm.}$). μ = 5.7 μ_B at 24 °C. $C_{16}H_{20}MnN_2O_9$ (439.28): calcd. C 43.73, H 4.55, N 6.38; found C 43.81, H 4.60, N 6.74.

[Mn(oda)(bipy)(H$_2$O)]·2H$_2$O (3): Following a similar synthetic procedure as described for compound **2**, but using **1** (0.48 g, 2 mmol) and bipy (0.31 g, 2 mmol), **3** was obtained as yellow crystals in 70 % yield. IR (cm^{-1}): 3359 br. ν(OH), 1601 s br. ν($COO_{asymm.}$), 1449 s ν($COO_{symm.}$), 1137 s ν($COC_{asymm.}$). μ = 5.7 μ_B at 22 °C. $C_{14}H_{18}MnN_2O_8$ (397.24): calcd. C 42.32, H 4.53, N 7.05; found C 41.87, H 4.61, N 7.17.

[Mn(oda)(terpy)]·2H$_2$O (4): A solution of **1** (0.12 g, 0.5 mmol) in water (20 mL) was added to a suspension of terpy (0.12 g, 0.5 mmol) in water (30 mL). The mixture was then stirred until all the solid was dissolved and then it was concentrated. Slow evaporation of water afforded yellow crystals of **4**, which were collected by filtration, washed with water, acetone and diethyl ether and dried (0.18 g, 80 %). Re-crystallization of the product in water yielded yellow crystals suitable for an X-ray study. IR (cm^{-1}): $\tilde{\nu}$ = 3533, 3432, 3350 br. ν(OH), 1614 s br. ν($COO_{asymm.}$), 1426 s ν($COO_{symm.}$), 1133 s ν($COC_{asymm.}$). μ = 5.9 μ_B at 24 °C. $C_{19}H_{19}MnN_3O_7$ (456.31): calcd. C 49.97, H 4.16, N 9.2; found C 49.96, H 4.27, N 9.30. As an alternative route to this complex a solution of $O(CH_2COONa)_2·H_2O$ (0.03 g, 0.15 mmol) in water (5 mL) was added to a solution of [$MnCl_2$(terpy)] (**5**) (0.05 g, 0.15 mmol) in water (10 mL) . The resultant mixture was then stirred for 3 h. Slow evaporation of the solvent then gave yellow crystals of **4**, which were collected by filtration and air dried (0.03 g; 45 %).

[MnCl$_2$(terpy)] (5): A suspension of terpy (0.24 g, 1 mmol) in water (10 mL) was added to a solution of $MnCl_2·4H_2O$ (0.20 g, 1 mmol) in water (10 mL). The mixture was then stirred until a yellow solution formed, which was then concentrated. Yellow crystals of compound **5** were obtained after slow evaporation of the solvent (0.27 g, 75 %). $C_{15}H_{11}Cl_2MnN_3$ (359.12): calcd. C 50.12, H 3.06, N 11.69; found C 48.35, H 3.03, N 11.38.

X-ray Crystallographic Study: The crystal data and structural refinement of compounds **1**−**5** are summarized in Table 6. While the X-ray data of compound **1** were collected on a Bruker SMART diffractometer equipped with a 6000 CCD detector, all other data sets were collected on an Enraf−Nonius CAD4 diffractometer. Therefore, two distinct descriptions of the technical details are given.

In addition to the 6000 CCD detector, the Bruker SMART apparatus is equipped with a rotating anode generator, Goebel optics monochromated Cu-K_α radiation (λ = 1.54178 Å), and a Kryoflex low-temperature device.[43] Six sets of frames covering a hemisphere of the reciprocal space were recorded for a well-formed crystal of **1** (3 × 600 frames to ϕ = 0°, 120° and 240° respectively with the CCD detector placed to 2θ = −40°, and others 3 × 600 frames to ϕ = 60°, 180° and 300° respectively with the CCD detector placed to 2θ = −100°, ω-scans, Δω = 0.3°, time per frame 5 s). Data reduction up to θ = 81° was performed with the program SAINT+, and corrections for absorption with SADABS; of 4361 reflections measured 1417 were independent, R_{int} = 0.063.[43] The structure was solved by direct methods and refined by full-matrix least-squares on F^2 using the program SHELXL-97.[44] All non-hydrogen atoms were refined with anisotropic displacement parameters. The hydrogen atoms were located on a difference Fourier map and refined with isotropic displacement parameters. The highest residual peaks (three) 0.70−0.69 e·Å^{-3} were located close to the heavier atoms Mn and have no chemical sense.

Well-formed yellow crystals of the compounds **2**−**5** were mounted on a Enraf−Nonius CAD4 diffractometer equipped with a graphite monochromator and Mo-K_α radiation (λ = 0.71073 Å). In all cases, the cell dimensions were refined by least-squares refinement of 25 reflections in the 2θ range 10−20°. The intensity data were corrected for Lorentz and polarization effects and semiempirical absorption corrections (ψ scan). Three standard reflections were monitored every two hours during data collection. Atomic scattering factors are those reported by Cromer and Waber.[45] The structures were solved by direct methods using the SIR97[46] package of programs. Refinements were made by full-matrix least-squares on all F^2 data using SHELXL-97.[44] In general, ΔF Fourier maps, calculated at a later stage of refinement, allowed the localization of the hydrogen atoms. These atoms were assigned isotropic temperature factors and were refined in the final least-squares cycles. Anisotropic thermal parameters were allotted to all of the non-hydrogen atoms. No unusual trend in ΔF vs. F_o or ($sin\theta$)/λ was observed. In no case was a significant electron density residue detected from the final ΔF maps.

The molecular drawings were made using the program ORTEP-III for Windows[47,48] and SCHAKAL (Figure 3, c).[49] All crystallographic computational work was performed by using the user-friendly graphic interface of WINGX.[50]

 © 2004 Wiley-VCH Verlag GmbH & Co. KGaA, Weinheim

Table 6. Crystallographic data for complexes **1**−**5**

	1	**2**	**3**	**4**	**5**
Empirical formula	$C_4H_8MnO_7$	$C_{16}H_{20}MnN_2O_9$	$C_{14}H_{18}MnN_2O_8$	$C_{19}H_{19}MnN_3O_7$	$C_{15}H_{11}Cl_2MnN_3$
Molecular mass	223.04	439.28	397.24	456.31	359.11
Crystal system	orthorhombic	monoclinic	monoclinic	triclinic	monoclinic
Space group	$P2_12_12_1$ [a]	$P2_1/a$	$P2_1/n$	$P\bar{1}$	$P2_1/c$
a [Å]	6.9643(2)	9.639(4)	6.895(5)	8.5860(10)	10.9596(19)
b [Å]	9.9724(3)	18.144(2)	24.361(7)	10.5680(10)	8.232(4)
c [Å]	11.1951(3)	10.7654(11)	10.1538(13)	11.405(3)	16.289(3)
α [°]	90	90	90	79.38(2)	90
β [°]	90	95.633(19)	100.72(2)	82.360(10)	94.024(14)
γ [°]	90	90	90	75.040(10)	90
Volume [Å^3]	777.51(4)	1873.6(8)	1675.8(15)	978.7(3)	1465.9(7)
Z	4	4	4	2	4
Calculated density [g cm^{-3}]	1.905	1.557	1.575	1.548	1.627
Absorption coefficient (Mo-K_α) [mm^{-1}]	13.938[b]	0.758	0.833	0.723	1.259
$F(000)$	452	908	820	470	724
Reflections collected	4361	3284	3106	3618	2558
Unique reflections $I \geq 2\sigma(I)$	1417	3284	2938	3430	1979
R	0.035	0.036	0.038	0.029	0.046
wR	0.083	0.097	0.086	0.080	0.112

[a] Absolute structure parameter (Flack x parameter[51] = −0.005(7). [b] Cu-K_α radiation.

CCDC-206841, -206842, -206843, -206844 and -206845 contain the supplementary crystallographic data for this paper. These data can be obtained free of charge at www.ccdc.cam.ac.uk/conts/retrieving.html [or from the Cambridge Crystallographic Data Centre, 12 Union Road, Cambridge CB2 1EZ, UK; Fax: (internat.) +44-1223-336-033; E-mail: deposit@ccdc.cam.ac.uk].

Acknowledgments

Financial support from both the Ministerio de Ciencia y Tecnología (BQU2001−3715) and Junta de Andalucía is gratefully acknowledged. Thanks are expressed to Mr. Dante Masi for technical assistance with the X-ray work carried out at ICCOM and to Professor Davide Proserpio for providing the SCHAKAL picture. We are also grateful to Mr. César J. Pastor Montero (Laboratorio de Difracción de Rayos X, Facultad de Ciencias, Universidad Autónoma de Madrid) for the acquisition of the X-ray diffraction data of complex **1**.

Note Added in Proof (November 18, 2003): The X-ray structure of an Mn(oda) complex has been reported (C. Jiang, X. Zhu, Z.-P. Yu, Z.-Y. Wang, *Inorg. Chem. Commun.* **2003**, *6*, 706) while our work was in progress.

[1] *Manganese and Its Role in Biological Processes*, in *Metal Ions in Biological Systems* (Eds.: A. Sigel, H. Sigel), Marcel Dekker, New York, **2000**, vol. 37.
[2] N. A. Law, M. T. Caudle, V. L. Pecoraro, *Adv. Inorg. Chem.* **1999**, *46*, 305.
[3] *Manganese Redox Enzymes* (Ed.: V. L. Pecoraro), VCH, New York, **1992**.
[4] G. C. Dismukes, *Chem. Rev.* **1996**, *96*, 2909.
[5] V. K. Yachandra, K. Sauer, M. P. Klein, *Chem. Rev.* **1996**, *96*, 2927.
[6] N. Bresciani-Pahor, G. Nardin, R. P. Bonomo, E. Rizzarelli, *J. Chem. Soc., Dalton Trans.* **1983**, 1797.
[7] U. Thewalt, T. Guthner, *J. Organomet. Chem.* **1989**, *379*, 59.
[8] A. K. Powell, J. M. Charnock, A. C. Flood, C. D. Garner, M. J. Ware, W. Clegg, *J. Chem. Soc., Dalton Trans.* **1992**, 203.
[9] R. Baggio, M. T. Garland, M. Perec, *J. Chem. Soc., Dalton Trans.* **1996**, 2747.
[10] R. Baggio, M. T. Garland, M. Perec, *Inorg. Chim. Acta* **2000**, *310*, 103.
[11] D. del Río, A. Galindo, J. Tejedo, F. J. Bedoya, A. Ienco, C. Mealli, *Inorg. Chem. Commun.* **2000**, *3*, 32.
[12] A. Grirrane, A. Pastor, A. Ienco, C. Mealli, A. Galindo, *J. Chem. Soc., Dalton Trans.* **2002**, 3771.
[13] S. H. Whitlow, G. Davey, *J. Chem. Soc., Dalton Trans.* **1975**, 1228.
[14] R. P. Bonomo, E. Rizzarelli, N. Bresciani-Pahor, G. Nardin, *Inorg. Chim. Acta* **1981**, *54*, 17.
[15] D. del Río, A. Galindo, R. Vicente, C. Mealli, A. Ienco, D. Masi, *Dalton Trans.* **2003**, 1813.
[16] Cambridge Structural Database System, Cambridge Crystallographic data Centre, 12 Union Road, Cambridge, CB2 1EZ, UK: F. H. Allen, O. Kennard, *Chem. Des. Autom. News* **1993**, *8*, 31.
[17] W. E. Hatfield, J. H. Helms, B. R. Rohrs, P. Singh, J. R. Wasson, R. R. Weller, *Proc. Ind. Acad. Sci., Chem. Sci.* **1987**, *98*, 23.
[18] R. Baggio, M. T. Garland, M. Perec, D. Vega, *Inorg. Chim. Acta* **1999**, *284*, 49.
[19] S. N. Dubey, R. K. Beweja, D. M. Puri, *Indian J. Chem. Sect A* **1983**, *22*, 450.
[20] A. Grirrane, A. Pastor, A. Galindo, A. Ienco, C. Mealli, P. Rosa, *Chem. Commun.* **2003**, 512.
[21] M. K. Kabir, M. Kawahara, H. Kumagai, K. Adachi, S. Kawata, T. Ishii, S. Kitagawa, *Polyhedron* **2001**, *20*, 1417.
[22] B. Chiswell, D. S. Litster, *Inorg. Chim. Acta* **1978**, *29*, 25.
[23] C. M. Harris, T. N. Lockyer, N. C. Stephenson, *Aust. J. Chem.* **1966**, *19*, 1741.
[24] J. S. Judge, W. M. Reiff, G. M. Intille, P. Ballway, W. A. Baker Jr., *J. Inorg. Nucl. Chem.* **1967**, *29*, 1711.
[25] M. Devereux, M. McCann, V. Leon, V. McKee, R. J. Ball, *Polyhedron* **2002**, *21*, 1063.

 © 2004 Wiley-VCH Verlag GmbH & Co. KGaA, Weinheim

[26] R. Baggio, M. T. Garland, M. Perec, D. Vega, *Inorg. Chem.* **1995**, *34*, 1961.
[27] W. Ma, H. van Koningsveld, J. A. Peters, T. Maschmeyer, *Chem. Eur. J.* **2001**, *7*, 657.
[28] See for example: *Inorganic Chemistry: Principles of Structure and Reactivity*, J. E. Huheey, E. A. Keiter, R. L. Keiter, 4th ed., Harper Collins, New York, **1993**.
[29] R. D. Shannon, *Acta Crystallogr., Sect. A* **1976**, *32*, 751.
[30] N. Mangayarkarasi, M. Prabhakar, P. S. Zacharias, *Polyhedron* **2002**, *21*, 925.
[31] Y. Zhang, S. Wang, C. Bridges, J. E. Greedan, *Can. J. Chem.* **2000**, *78*, 1289.
[32] L. R. Gahan, V. A. Grillo, T. W. Hambley, G. R. Hanson, C. J. Hawkins, E. M. Proudfoot, B. Moubaraki, K. S. Murray, D. Wang, *Inorg. Chem.* **1996**, *35*, 1039.
[33] S. Karmakar, S. B. Choudhury, A. Chakravorty, *Inorg. Chem.* **1994**, *33*, 6148.
[34] P. Chakraborty, S. K. Chandra, A. Chakravorty, *Inorg. Chem.* **1993**, *32*, 5349.
[35] M. O′Keeffe, M. Eddaoudi, H. Li, T. Reineke, O. M. Yaghi, *J. Solid State Chem.* **2000**, *152*, 3.
[36] O. Kahn, *Molecular Magnetism*, VCH, New York, **1993**.
[37] H. Iikura, T. Nagata, *Inorg. Chem.* **1998**, *37*, 4702.
[38] M. McCann, M. T. Casey, M. Devereux, M. Curran, G. Ferguson, *Polyhedron* **1997**, *16*, 2547.
[39] Y.-Q. Zheng, J.-L. Lin, J. Sun, *Z. Anorg. Allg. Chem.* **2001**, *627*, 1059.
[40] M. J. Plater, M. R. St. J. Foreman, R. A. Howie, *J. Chem. Cryst.* **2000**, *30*, 445.
[41] L. S. Erre, G. Micera, E. Garribba, A. Cs. Benyei, *New J. Chem.* **2000**, *24*, 725.
[42] C. J. O′Connor, *Prog. Inorg. Chem.* **1982**, *29*, 20.
[43] Bruker, Programs SMART, version 5.054; SAINT, version 6.2.9; SADABS version 2.03; XPREP, version 5.1; SHELXTL, version 5.1. Bruker AXS Inc., Madison, WI, USA, **2001**.
[44] G. M. Sheldrick, Programs SHELXS-97 (crystal structure solution) and SHELXL-97 (crystal structure refinement), University of Göttingen, Germany, **1997**.
[45] D. T. Cromer, J. T. Waber, *Acta Crystallog.* **1965**, *18*, 104.
[46] SIR97, A. Altomare, M. C. Burla, M. Cavalli, G. L. Cascarano, C. Giacovazzo, A. Gagliardi, A. G. G. Moliterni, G. Polidori, R. Spagna, *J. Appl. Cryst.* **1999**, *32*, 115.
[47] ORTEP-III, M. N. Burnett, C. K. Johnson, Report ORNL-6895. Oak Ridge National Laboratory, Oak Ridge, TN, **1996**.
[48] L. J. Farrugia, *J. Appl. Chem.* **1997**, *30*, 565.
[49] E. Keller, *J. Appl. Crystallogr.* **1989**, *22*, 12.
[50] L. J. Farrugia, *J. Appl. Chem.* **1999**, *32*, 837.
[51] H. D. Flack, G. Bernardinelli, *Acta Crystallogr., Sect. A* **1999**, *55*, 908.

Received July 24, 2003
Early View Article
Published Online December 12, 2003

 © 2004 Wiley-VCH Verlag GmbH & Co. KGaA, Weinheim

Preparation of 17 Sulfur-Rich Chain-Like Thiaalkanes $R-S_x-R'-S_y-R$ and $R-S_x-R'-S_y-R'-S_z-R$ (x, y, $z > 2$) from Titanocene Thiolate Complexes[‡]

Vera Münchow[a] and Ralf Steudel*[b]

Keywords: Alkanes / Ligand effects / Sandwich compounds / Sulfur / Titanium

Two novel $Cp_2Ti(Cl)S_3R'S_3Tr$ complexes have been prepared by reaction of the six-membered metallacycles Cp_2TiS_4R' ($Cp = \eta^5$-C_5H_5, $R' = CMe_2$, 1,1-C_6H_{10}) with the sulfenyl chloride TrSCl ($Tr = CPh_3$) at 20 °C. These complexes were treated with: (a) sulfenyl chlorides (RSCl or RSSCl) to obtain 11 new thiaalkanes of the type $R–S_x–R'–S_y–R$ (R = Tr, 4-ClC_6H_4, 2-$C_{10}H_7$; $x = 3$, $y > 2$), or (b) with SO_2Cl_2, SCl_2 or S_2Cl_2 to prepare six sulfur-rich species of the type $Tr–S_x–R'–S_y–R'–S_z–Tr$ (x, z = 3, $y > 3$), as well as Cp_2TiCl_2. The thiaalkanes decompose upon heating to give mixtures of various linear and cyclic polysulfanes R_2S_n and $R'S_m$.

(© Wiley-VCH Verlag GmbH & Co. KGaA, 69451 Weinheim, Germany, 2004)

Introduction

Thiaalkanes are derivatives of alkanes (including cycloalkanes) in which some of the CH_2 groups have been replaced by sulfur atoms. Numerous compounds of this type are known, both chain-like and cyclic and mainly with a single sulfane unit $-S_x-$ ($x = 1, 2,...$) between two organic residues R.[1] In a narrower sense, thiaalkanes are compounds with two or more sulfane units separated by organic groups, for example $R-S_x-R'-S_y-R''$. In the following we restrict our discussion to chain-like species of this type. While thiaalkanes with single sulfur atoms or disulfane groups have been prepared in large numbers by the classical methods of organosulfur chemistry,[2] and are widely used as chemically resistant polymers,[3] almost no such species with either tri-, tetra-, penta- or hexasulfane units are known.[4] This is most surprising and unsatisfactory in the light of the biological activity of many thiaalkanes, in particular cyclic species, which makes them interesting to the pharmaceutical industry as well as for applications in agroscience.[1,5] In this work we report on the synthesis of chain-like sulfur-rich thiaalkanes with two and three polysulfane units from suitable titanocene thiolate complexes by ligand-transfer reactions.

In recent years a number of mono- and dinuclear titanocene thiolate complexes have been used to synthesize sulfur-rich homocycles, heterocycles and linear organic polysulfanes R_2S_n ($n > 2$) by reaction with organic or inorganic S−Cl compounds.[1,6] These reactions take place at 25 °C or below and often proceed quantitatively. A good example is the synthesis of the homocycles S_6 and S_{12} from titanocene pentasulfide Cp_2TiS_5 (**1**; $Cp = \eta^5$-C_5H_5) and sulfur dichloride[7] shown in Scheme 1.

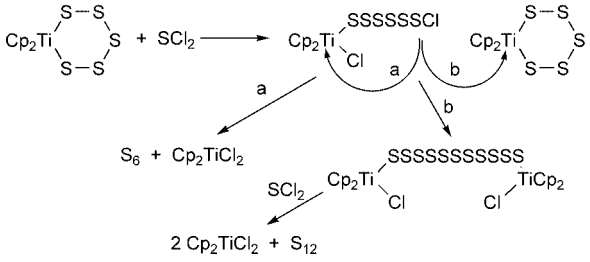

Scheme 1

The nucleophilic attack of the chlorine atoms of SCl_2 on the titanium atom opens the metallacycle producing an intermediate that either reacts intramolecularly by route (a) to give S_6 and Cp_2TiCl_2, or intermolecularly with another molecule of **1** to give a second linear intermediate which then reacts with SCl_2 to form S_{12} [route (b)]. While the reactive intermediates shown in Scheme 1 are hypothetical, the related dinuclear complex $(Cp_2TiCl)_2S_3$ has been isolated and characterized by X-ray crystallography.[8] Mononuclear complexes of the type $Cp_2TiX(S_xR)$ with sulfanido ligands containing more than one sulfur atom have also been isolated (e.g., X = Cl or SR with aryl or alkyl groups R; $x = 2, 3$[9]).

In this work we show how titanocene complexes with thiaalkane ligands can be used to prepare the title compounds containing up to 12 sulfur atoms. Most useful in

[‡] Sulfur Compounds, 236. Parts 229−235: R. Steudel et al., *Top. Curr. Chem.* **2003**, vols. *230* and *231*.

[a] Viale Regina Margherita 52/E, 36078 Valdagno (VI), Italy
E-mail: vera.anto@libero.it
[b] Institut für Chemie, Sekr. C2, Technische Universität Berlin, 10623 Berlin, Germany
Fax: (internat.) +49-30-3142-6519
E-mail: steudel@schwefel.chem.tu-berlin.de

 © 2004 Wiley-VCH Verlag GmbH & Co. KGaA, Weinheim DOI: 10.1002/ejic.200300591

this context were the two metallacycles $Cp_2TiS_4CMe_2$ (**2a**) and $Cp_2TiS_4C_6H_{10}$ (**2b**) first prepared by Giolando and Rauchfuss[10] from Cp_2TiS_5 and acetone or cyclohexanone, respectively (Scheme 2).

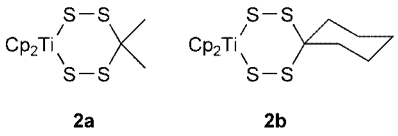

2a **2b**

Scheme 2

These air-stable compounds are soluble in organic solvents. Both complexes have been used before to synthesize heterocyclic sulfur compounds by reaction with dichlorosulfanes S_nCl_2.[11,12]

Results and Discussion

Ring-Opening Reaction with Ph_3CSCl

One aim of this work was to isolate the chain-like intermediates of the type shown in Scheme 1. To stabilize these reactive species we have chosen a particularly bulky substituent R on the sulfenyl chloride. Reaction of complexes **2a** or **2b** with triphenylmethylsulfenyl chloride Ph_3CSCl (tritylsulfenyl chloride, TrSCl) in a molar ratio of 1:1 at 20 °C in benzene produced the violet complexes **3a** and **3b** as shown in Scheme 3.

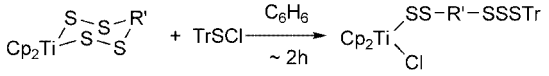

R': CMe_2 (**3a**), C_6H_{10} (**3b**)

Scheme 3

These reactions could easily be followed by HPLC analysis of the reaction mixtures since the retention times of **3a** and **3b** are higher than those of all other components in the mixture. Therefore, the corresponding peaks were well separated. Single crystals of **3a** and **3b** could not be obtained due to their instability in solution but the spectroscopic results (^1H and ^{13}C NMR, IR, Raman, UV/Vis) as well as their reactivity towards SCl compounds support the connectivities shown in Scheme 4 (see Exp. Sect.). In the ^1H NMR spectrum of **3a** there appears one singlet each for the

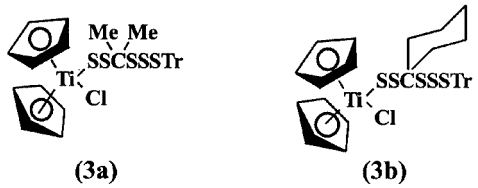

(3a) **(3b)**

Scheme 4

cyclopentadienyl (δ = 6.36 ppm) and methyl protons (δ = 1.69 ppm) besides the multiplet of the phenyl hydrogens near δ = 7.32 ppm. The violet color of the novel complexes in solution is caused by an absorption peaking at 560 ± 4 nm (in MeOH).

In the solid state complexes **3a** and **3b** are stable at 4 °C for several weeks but they decompose in solution at 20 °C, especially in the presence of air, with formation of Cp_2TiCl_2 and an ochre precipitate. Chlorinated solvents also initiate a slow decomposition. Therefore, the samples always contained a few percent of Cp_2TiCl_2 (probably with formation of mixed crystals) which also originates from the side reaction of TrSCl with **3a** or **3b**, respectively. However, for preparative purposes the purity was sufficient (see below). The content of Cp_2TiCl_2 can be determined by ^1H NMR spectroscopy (singlet at δ = 6.57 ppm). Complexes **3a** and **3b** are well soluble in benzene and carbon disulfide, but less so in *n*-hexane and methanol.

Attempts to isolate the corresponding complexes using other sulfenyl chlorides such as TrSSCl, 4-ClC_6H_4SCl and 2-$C_{10}H_7SCl$ failed due to rapid decomposition of the ring-opened complexes and their consecutive reactions with the sulfenyl chlorides.

Synthesis of Thiaalkanes

Treatment of complexes **3a** or **3b** with one equivalent of ClC_6H_4SCl in CS_2 at 20 °C expectedly yields the asymmetrical hexathiaalkanes **4a** and **4b** shown in Scheme 5. These reactions are rapid, as indicated by the immediate color change from violet to orange-red on addition of the sulfenyl chloride to the complexes **3a** and **3b**, respectively. The reactions are also very clean: only one peak was observed in the HPLC analysis of the isolated products **4a** and **4b** (besides the solvent peak).

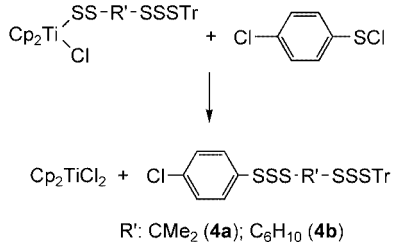

R': CMe_2 (**4a**); C_6H_{10} (**4b**)

Scheme 5

Both bis-trisulfanes **4a** and **4b** could be isolated in high purity as grayish-white powders in yields of 42% and 41%, respectively.

When we tried to synthesize the symmetrical bis-trisulfanes $Tr-S_3-R'-S_3-Tr$ by reaction of complexes **2a** and **2b** with *two* equivalents of TrSCl, according to Scheme 6, rather complex reaction mixtures were obtained regardless of whether the reaction was carried out in CS_2, CH_2Cl_2 or benzene at 20 °C.

 © 2004 Wiley-VCH Verlag GmbH & Co. KGaA, Weinheim

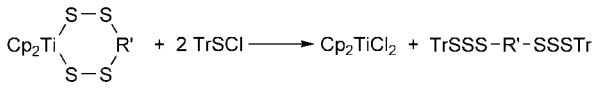

Scheme 6

The reaction times of more than 15 hours for complete, or nearly complete, disappearance of the starting materials evidently favor side reactions, for example a sulfur transfer between the intermediate sulfanido complexes as shown in Scheme 7.

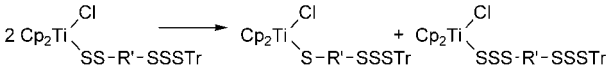

Scheme 7

As a consequence, three major thiaalkane products were detected by HPLC analysis, namely the expected $(TrS_3)_2R'$, the asymmetrical $TrS_3R'S_4Tr$ and the sulfur-rich $(TrS_3R')_2S_4$. The latter product most probably arises from the autoxidation of the intermediate $Cp_2TiCl(S_2R'S_3Tr)$ (see below). In addition, several minor products of similar retention time were detected but not identified. The identification of members of a homologous series is sometimes possible by inter- and extrapolation of the retention indices as they are linear functions of the sulfur content.[1,13] In other cases the independent preparation of the suspected species is necessary, and will be described below. Because of the complex composition of the reaction mixture no workup has been attempted since, even under an inert atmosphere, too many side-products were formed. Treatment of complexes **2a** and **2b** with TrCl also did not give the desired product $(TrS_2)_2R'$ since the reaction rate at 20 °C was very low, allowing parallel decomposition reactions.

More successful were the reactions of complexes **2a** and **2b** with the sulfur-rich derivatives TrS_xCl with $x = 2$ and 3 resulting in the bis-tetra- and -pentasulfanes **5a,b** and **6a,b** (Scheme 8).

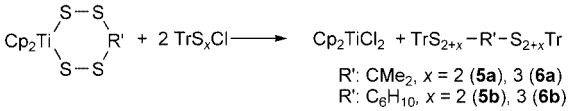

Scheme 8

The starting materials TrS_xCl were prepared according to published procedures[14] and the reaction took place in benzene at 20 °C. The reactivity of TrS_xCl ($x = 0-3$) towards titanocene polysulfido complexes evidently increases with increasing x. $Tr-S_4-CMe_2-S_4-Tr$ (**5a**) was isolated in 7% yield as a champagne-colored powder of m.p. 55 °C while the cyclohexylidene derivative $Tr-S_4-C_6H_{10}-S_4-Tr$ (**5b**) melts at 60 °C (yield 34%). The corresponding bis-pentasulfanes $Tr-S_5-R'-S_5-Tr$ (**6a,b**) were obtained analogously in 67% and 26% yields, respectively.

The two particularly sulfur-rich thiaalkanes $Tr-S_3-R'-S_4-R'-S_3-Tr$ (**7a,b**), mentioned above, were obtained as pure materials by oxidation of complexes **3a** and **3b**, respectively, with sulfuryl chloride in CS_2 solution at 20 °C (see Scheme 9; yields: 41% **7a**, 45% **7b**).

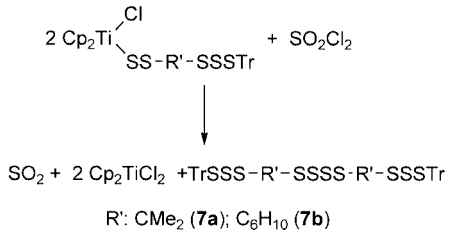

Scheme 9

Alternatively, **7a** could be obtained from **3a** by autoxidation with air in organic solvents at 20 °C (Scheme 10; yield 15%). Insoluble titanium-containing side products were observed as an ochre precipitate.

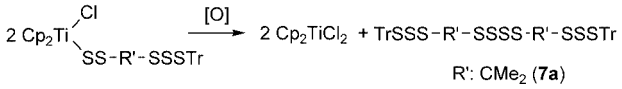

Scheme 10

Even more sulfur-rich derivatives were obtained by cleavage of complexes **3a** and **3b** with SCl_2 or S_2Cl_2 (Scheme 11), resulting in the corresponding penta- and hexasulfanes **8a,b** and **9a,b** (undecathia- and dodecathiaalkanes; yields: 19–36%).

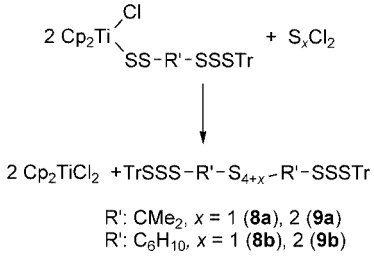

Scheme 11

These grayish-white or yellowish powder-like substances are soluble in methyl *tert*-butyl (MTB) ether.

Finally, we observed that various sulfenyl chlorides (RSCl) and disulfane chlorides (RSSCl) react with the complexes **3a** and **3b** to give the corresponding thiaalkanes. For

 © 2004 Wiley-VCH Verlag GmbH & Co. KGaA, Weinheim

example, TrSSCl and **3b** produced the heptathiaalkane Tr−S_3−C_6H_{10}−S_4−Tr **10** (Scheme 12).

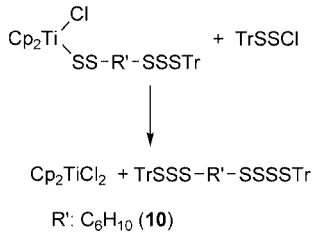

Scheme 12

The easily accessible aromatic sulfenyl chlorides ClC_6H_4SCl and $C_{10}H_7SCl$ produced the symmetrical bistrisulfanes **11a,b** and **12a,b** in 6−28% yield on reaction with complexes **2a** and **2b** (Scheme 13).

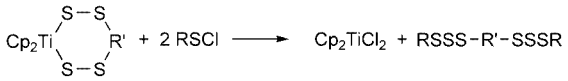

R \ R′	CMe_2	C_6H_{10}
ClC_6H_4	**11a**	**11b**
$C_{10}H_7$	**12a**	**11b**

Scheme 13

General Properties of the Novel Thiaalkanes

The thiaalkanes prepared in this work can be stored for several weeks at 4 °C without decomposition. They are readily soluble in carbon disulfide, benzene and MTB ether, but less so in *n*-hexane, *n*-pentane and methanol. As with other polysulfanes,[1] heating initiates decomposition reactions. This can best be seen from the mass spectra of compounds **11a,b** and **12a,b**, which are of the type R−S_3−R′−S_3−R. The temperatures required to evaporate these large molecules in a high vacuum (150−200 °C) result in complete decomposition, and no molecular ions were observed. However, all major peaks in the EI mass spectra could be assigned to cations of the following degradation and interconversion products: R_2S_n (n = 0−4), R′S_m (m = 1−5), RS_3R', RS_2, RS, and related smaller fragments. Some of these polysulfanes are known as pure compounds.[1] Evidently, the S−S bonds break homolytically on heating and the fragments recombine to form chain-like species R_2S_n and cyclic polysulfanes R′S_m. The observation of R_2, however, indicates that C−S bonds are also broken on electron impact.

During the HPLC analyses of the reaction mixtures it was once more observed that the retention time of the members of a homologous series, differing only in the number of sulfur atoms, systematically depends on the number of sulfur atoms. This can best be shown if the retention index (RS) is used which is independent of the chromatographic system and is therefore a characteristic property of these compounds (similar to the NMR chemical shift).[15] To determine RS values the sulfur homocycles S_x (x = 6, 8, 9, 10) are used as reference substances and their retention times t_R are measured under the same conditions. Then, their capacity factors $k' = (t_R - t_0)/t_0$ are calculated (t_0: dead time), the logarithms of which depend linearly on the number of sulfur atoms (n_S) as follows: $\ln k' = a + b \times n_S$. The latter relationship can be used to calculate a formal n_S value for any other substance by substituting its k' value into this equation. The formal n_S value obtained in this way defines the retention index of the novel substance as follows: RS = $100 \times n_S$. From the RS values of three members of the series Tr−S_x−CMe_2−S_x−Tr (x = 3, 4, 5) the following linear regression has been derived: RS = $568 + 128 \times x$ (r = 0.998). For the analogous cyclohexylidene species Tr-S_x-C_6H_{10}-S_x-Tr we obtained: RS = $662 + 134 \times x$ (r = 0.997). These relationships can be used to estimate the retention times of other members of these series by inter- and extrapolation. Pure methanol was used as the eluent in both cases.

Considerably longer homologous series have been observed for the species $(TrS_3CMe_2)_2S_x$ (x = 4−11) and $(TrS_3C_6H_{10})_2S_x$ (x = 4−12). In these cases the linear regressions are: RS = $965 + 60 \times x$ (r = 0.9997) and RS = $1147 + 61 \times x$ (r = 0.99986). The slopes of these functions are practically identical. The higher members of these series were prepared by reaction of complexes **3a** and **3b** with solutions of chlorosulfanes S_nCl_2 ($n > 2$) obtained by chlorination of elemental sulfur.[16]

The NMR and vibrational spectra of the novel thiaalkanes mainly show the presence of the corresponding organic groups R and R′ with little, if any, dependence on the number of sulfur atoms. Even the Raman spectra contain little information about the SS bonds, the stretching vibrations of which usually show up as strong lines in the 400−520 cm^{-1} region. However, compared to the strongest lines of the organic substituents (e.g. Tr: 1002 cm^{-1}, $C_{10}H_7$: 1380 cm^{-1}), the SS stretching vibrations often gave rise to only relatively weak signals in the indicated region. Therefore, the Raman spectra have not been listed in the Exp. Sect.[17]

Summary

We have synthesized two new titanocene polysulfido complexes $Cp_2TiCl(S_2R'S_3Tr)$ and 17 novel chain-like thiaalkanes by reaction of Ti−S bonds with S−Cl compounds (sulfenyl chlorides, sulfuryl chloride and sulfurchlorides). The thiaalkanes are of types R−S_x−R′−S_y−R (x, $y > 2$) and R-S_x−R′−S_y−R′−S_z−R (x, z = 3, $y > 3$) and have been isolated in moderate to low yields as colorless, grayish-white or grayish-yellow powder-like substances (R = CPh_3, 4-ClC_6H_4; R′ = CMe_2, 1,1-C_6H_{10}). To the best of our knowledge, these are the most sulfur-rich acyclic thiaalkanes of these types ever prepared. It has previously been shown that polysulfido ligands coordinated to a titanium atom can be utilized for ligand-transfer reactions with S−Cl compounds and other metals can also function as coordination centers (e.g. Zn[18]). Since a large number

 © 2004 Wiley-VCH Verlag GmbH & Co. KGaA, Weinheim

of thiolate complexes of main group and transition metals are known[19] the ligand-transfer method bears a tremendous potential for further research in synthetic sulfur chemistry.

Experimental Section

General:[17] The reactions were carried out with exclusion of moisture using carefully dried solvents. The chromatographic system has been described previously (HPLC with UV absorbance detector).[12] Octadecylsilane (C18) was used as the stationary phase throughout and pure methanol as the eluent. The following spectrometers were used: mass spectrometer AMD Intectra (based on Varian MAT 311A equipment) with 70 eV electron energy; NMR spectrometer WH 270 and ARX 200 by Bruker. FT-IR spectrometer Magna System 750 by Nicolet; Raman spectrometer Ramanor U 1000 by Jobin Yvon, equipped with krypton ion laser (647 nm), and FT-Raman spectrometer RFS 100 by Bruker with Nd-YAG laser (1064 nm). UV/Vis diode array spectrometer 990 by Waters (190−800 nm; on-line connected to the chromatographic system). With one exception (**12b**) NMR spectra were recorded at 200 MHz. ^{13}C NMR spectra are ^{1}H broad-band decoupled. Elemental analyses were performed using a Hewlett−Packard CHN analyzer 185 as well as a Perkin−Elmer Series II CHNS analyzer 2400.

Synthesis of Chloro(3,3-dimethyl-7,7,7-triphenyl-1,2,4,5,6-pentathiaheptyl)titanocene (3a): TrSCl (1.75 g, 5.63 mmol) and **2a** (1.57 g, 4.51 mmol) were stirred in benzene at 30−40 °C for 150 min. After removal of the solvent in vacuo the residue was dissolved in CS_2 (30 mL), *n*-pentane (70 mL) was added and the solution was cooled to −26 °C whereupon a mixture of **3a** and Cp_2TiCl_2 (ca. 10%) crystallized out, which was isolated, washed with *n*-pentane (30 mL) and dried in air (red-blue powder). Yield: 2.4 g (2.16 g of pure **3a**, 73%). The Cp_2TiCl_2 can be removed by stirring the solution with silica gel but the yield is then dramatically lower. M.p. (dec.): 133 °C. $C_{32}H_{31}ClS_5Ti$ (659.3): calcd. C 57.29, H 4.72, S 21.89 (Cp_2TiCl_2 content taken into account); found C 55.33, H 4.72, S 22.21. The low carbon value is explained by titanium carbide formation on combustion in the CHN analyzer. UV/Vis (methanol): λ_{max} (%) = 223 nm (100), 241 (87), 295 (23), 382 (7), 556 (9). ^{1}H NMR (CD_2Cl_2): δ = 7.32 (m, 15 H), 6.36 (s, 10 H), 1.69 (s, 6 H) ppm. Retention index (RS): 570.

Synthesis of Chloro(3-cyclohexylidene-7,7,7-triphenyl-1,2,4,5,6-pentathiaheptyl)titanocene (3b): TrSCl (1.00 g, 3.22 mmol) and **2b** (1.00 g, 2.57 mmol) were stirred in benzene at 30−40 °C for 180 min. After removal of the solvent in vacuo the residue was dissolved in CS_2 (20 mL), *n*-pentane (60 mL) was added and the solution was cooled to −26 °C for 15 h, whereupon a mixture of **3a** and Cp_2TiCl_2 (ca. 10%) crystallized out, which was isolated, washed with *n*-pentane (40 mL) and dried in air (red-blue powder). Yield: 0.77 g (0.69 g of pure **3b**, 39%). The Cp_2TiCl_2 can be removed by stirring the solution with silica gel but the yield is then dramatically lower. M.p. (dec.): 95−100 °C. $C_{35}H_{35}ClS_5Ti$ (699.3): calcd. C 58.92, H 4.94, S 20.64 (Cp_2TiCl_2 content taken into account); found C 58.42, H 4.64, S 18.72. UV/Vis (methanol): λ_{max} (%) = 209 nm (100), 240 (49), 288 (15), 383 (4), 564 (7). ^{1}H NMR (CD_2Cl_2): δ = 7.32 (m, 15 H), 6.37 (s, 10 H), 1.2−2.2 (multiplets, 10 H) ppm. ^{13}C NMR (CD_2Cl_2): δ = 23.0, 24.9, 35.4, 71.5, 73.3, 115.9, 127.2, 128.0, 130.4, 143.5 ppm. RS: 686.

Synthesis of 1-(4-Chlorophenyl)-3-{1-methyl-1-[(triphenylmethyl)-trisulfanyl]ethyl}trisulfane (4a): A mixture of 4-ClC_6H_4SCl (1 mL) and CS_2 (49 mL) was used to titrate a solution of **3a** (0.45 g, 0.68 mmol) in 50 mL of CS_2 dropwise until the violet color had changed to orange-red. After filtration the solution was shaken with ca. 0.5 g of silica gel for a few minutes to remove residual Cp_2TiCl_2 (color change to yellow).The gel was filtered off and washed with CS_2 (50 mL). Removal of the solvent produced an oil which was dissolved in a mixture of MTB ether (5 mL) and *n*-pentane (10 mL). The solvent was partly evaporated until a turbidity appeared, whereupon the solution was cooled to −78 °C. After decantation from the precipitated oil the solution was evaporated in vacuo and the residue dissolved in MTB ether (5 mL) and *n*-pentane (5 mL). Stepwise cooling of this solution to −50 °C produced a champagne-colored powder which was isolated and washed with *n*-pentane (35 mL). Yield: 0.17 g (42%). M.p. 90−95 °C. $C_{28}H_{25}ClS_6$ (589.4): calcd. C 57.06, H 4.28, S 32.65; found C 57.09, H 4.37, S 31.93. UV/Vis (methanol): λ_{max} (%) = 207 nm (100), 238 (44), 277 (12), 316 (6). ^{1}H NMR (CD_2Cl_2): δ = 7.55 (dm, 2 H), 7.33 (m, 17 H), 1.69 (s, 6 H) ppm. ^{13}C NMR (CD_2Cl_2): δ = 28.3, 64.9, 73.4, 127.3, 128.0, 129.3, 130.3, 131.9, 134.5, 135.6, 143.3 ppm. RS: 908.

Synthesis of 1-(4-Chlorophenyl)-3-{1-[(triphenylmethyltri)sulfanyl]cyclohexyl}trisulfane (4b): In analogy to the preparation of **4a**, complex **3b** (0.27 g, 0.39 mmol) was titrated. After removal of the silica gel the solvent was evaporated in vacuo producing an oil which was dissolved in a small amount of MTB ether followed by partial evaporation of the solvent until a sticky foam had formed. Upon addition of MTB ether (5 mL) this turned into a beige powder. After addition of *n*-pentane (25 mL) and cooling to −50 °C for 2 h a crystalline product was obtained which was filtered off and washed with *n*-pentane. Yield: 0.10 g (41%). M.p. 162 °C. $C_{31}H_{29}ClS_6$ (629.4): calcd. C 59.16, H 4.64, S 30.57; found C 59.32, H 4.86, S 29.25. UV/Vis (methanol): λ_{max} (%) = 207 nm (100), 238 (39), 278 (13), 315 (6). ^{1}H NMR (CD_2Cl_2): δ = 7.52 (dm, 2 H), 7.33 (m, 17 H), 1.2−2.2 (multiplets, 10 H) ppm. ^{13}C NMR (CD_2Cl_2): δ = 23.0, 25.0, 35.4, 70.8, 75.3, 127.3, 128.1, 129.3, 130.4, 131.9, 134.4, 135.9, 143.3 ppm. RS: 1080.

Synthesis of 1-{1-Methyl-1-[(triphenylmethyl)tetrasulfanyl]ethyl}-3-(triphenylmethyl)tetrasulfane (5a): Solid TrSSCl (1.50 g, 4.37 mmol) was added in portions and with stirring to a solution of **2a** (0.76 g, 2.18 mmol) in benzene (100 mL). Stirring for 30 min resulted in a color change to red. After evaporation of the solvent the residue was dissolved in CH_2Cl_2 (50 mL) and shaken with some silica gel (5 min). After filtration and evaporation of the solvent the residue was recrystallized from a CS_2/*n*-pentane mixture (5:25). Yield: 0.12 g (7%). M.p.: 55 °C. $C_{41}H_{36}S_8$ (785.3): calcd. C 62.71, H 4.62, S 32.67; found C 62.95, H 4.85, S 33.03. UV/Vis (methanol): λ_{max} (%) = 231 nm (100), 301 (22). ^{1}H NMR ($CDCl_3$): δ = 7.30 (m), 1.58 (s) ppm. ^{13}C NMR ($CDCl_3$): δ = 29.0, 64.3, 73.7, 127.3, 128.0, 130.3, 143.0 ppm. RS: 1071.

Synthesis of 1-(Triphenylmethyl)-3-{1-[(triphenylmethyl)tetrasulfanyl]cyclohexyl}tetrasulfane (5b): Preparation in analogy to the synthesis of **5a** from complex **2b** (0.25 g, 0.64 mmol), TrSSCl (0.44 g, 1.29 mmol) in benzene (30 mL) and using less CH_2Cl_2 (20 mL). Yield: 0.18 g (34%). M.p.: 60 °C. $C_{44}H_{40}S_8$ (825.3): calcd. C 64.03, H 4.89, S 31.08; found C 64.03, H 4.95, S 30.25. UV/Vis (methanol): λ_{max} (%) = 217 nm (100), 261 (22), 305 (13). ^{1}H NMR ($CDCl_3$): δ = 7.34 (m), 1.2−2.3 (multiplets) ppm. ^{13}C NMR ($CDCl_3$): δ = 22.7, 24.8, 26.9, 35.6, 70.4, 73.6, 127.2, 128.0, 130.2, 143.0 ppm. RS: 1186.

 © 2004 Wiley-VCH Verlag GmbH & Co. KGaA, Weinheim

Synthesis of 1-{1-Methyl-1-[(triphenylmethyl)pentasulfanyl]ethyl}-3-(triphenylmethyl)pentasulfane (6a): Solid **2a** (0.18 g, 0.52 mmol) was added in small portions with stirring to TrSSSCl (0.40 g, 1.07 mmol) in benzene (25 mL). After 10 min the solvent was evaporated, the residue was dissolved in CH_2Cl_2 (20 mL) and shaken with ca. 0.1 g of silica gel for a few minutes to remove Cp_2TiCl_2. After filtration and partial evaporation of the solvent excess *n*-pentane was added followed by complete evaporation of the solvent. The grayish-white residue was recrystallized from *n*-pentane. Yield: 0.30 g (67%). M.p.: 50 °C. $C_{41}H_{36}S_{10}$ (849.4): calcd. C 57.98, H 4.27; found C 58.51, H 3.75. UV/Vis (methanol): λ_{max} (%) = 240 nm (100), 294 (41). ^{1}H NMR (CD_2Cl_2): δ = 7.33 (m, 30 H), 1.71 (s, 6 H) ppm. ^{13}C NMR ($CDCl_3$): δ = 28.9, 64.8, 73.9, 127.3, 128.0, 130.3, 142.9 ppm. RS: 1212.

Synthesis of 1-(Triphenylmethyl)-3-{1-[(triphenylmethyl)pentasulfanyl]cyclohexyl}pentasulfane (6b): TrSSSCl (0.48 g, 1.28 mmol) was added in small portions with stirring to complex **2b** (0.25 g, 0.64 mmol) in benzene (30 mL). After 10 min the solvent was removed in vacuo, the residue dissolved in CH_2Cl_2 (20 mL) and shaken with some silica gel until the color had changed to yellow. After filtration and evaporation of the solvent the crude product was recrystallized twice from a CS_2/*n*-pentane mixture (5:25 mL) by cooling to −78 °C. Yield: 0.15 g (26%). M.p.: 60 °C. $C_{44}H_{40}S_{10}$ (889.5): calcd. C 59.42, H 4.53, S 36.05; found C 60.14, H 4.60, S 34.26. UV/Vis (methanol): λ_{max} (%) = 209 nm (100), 263 (19), 298 (11). ^{1}H NMR ($CDCl_3$): δ = 7.28 (m), 1.2−2.1 (multiplets) ppm. ^{13}C NMR ($CDCl_3$): δ = 22.8, 24.8, 35.4, 70.9, 73.8, 127.3, 128.0, 130.3, 143.0 ppm. RS: 1338.

Synthesis of Bis{1-methyl-1-[(triphenylmethyl)trisulfanyl]ethyl}-tetrasulfane (7a). Method A: A solution of 0.61 mL of SO_2Cl_2 in 9.4 mL of benzene was added rapidly but dropwise to complex **3a** (0.90 g, 1.37 mmol) in CS_2 (80 mL) until the color had changed from purple to orange-red. After filtration the solution was shaken with some silica gel to remove residual Cp_2TiCl_2. Filtration and evaporation of the solvent yielded a yellow oil which was dissolved in MTB ether (30 mL). Cooling to −78 °C gave an oily residue which was dissolved again in MTB ether and the solvent evaporated again. Yield: 0.25 g (41%).

Method B: Complex **3a** (0.41 g, 0.59 mmol) was dissolved in a mixture of benzene (150 mL), CS_2 (75 mL) and CH_2Cl_2 (25 mL) and stirred for 3 days resulting in a red-brown solution and an ochre precipitate. The filtered solution was stirred with little silica gel for 5 min. and this was then filtered off and washed with CS_2 (25 mL). Evaporation of the solvent gave an oily residue which was dissolved in a mixture of CH_2Cl_2 (3 mL), *n*-pentane (6 mL) and ethanol (15 mL). On cooling to −78 °C the product precipitated as a beige powder. Yield: 0.04 g (15%).%). M.p.: 54 °C. $C_{44}H_{42}S_{10}$ (891.5): calcd. C 59.28, H 4.75, S 35.97; found C 58.91, H 4.97, S 36.41. UV/Vis (methanol): λ_{max} (%) = 213 nm (100), 297 (9). ^{1}H NMR (CD_2Cl_2): δ = 7.31 (m, 30 H), 1.71 (s, 12 H) ppm. ^{13}C NMR (CD_2Cl_2): δ = 28.6, 64.8, 73.1, 127.3, 128.0, 130.3, 143.3 ppm. RS: 1217.

Synthesis of Bis{1-methyl-1-[(triphenylmethyl)trisulfanyl]cyclohexyl}tetrasulfane (7b): Preparation in analogy to **7a** (method A) from **3b** (0.77 g, 1.10 mmol) in 80 mL of benzene. After the color change from purple to orange-red the solvent was evaporated, the residue dissolved in 50 mL CS_2 and stirred with some silica gel. The solution was filtered and the residue washed with 20 mL of CH_2Cl_2. Evaporation of the solvent resulted in an oil which was dissolved in a mixture of 10 mL of CH_2Cl_2 and 50 mL of MTB ether. At −78 °C an oil precipitated which was isolated by decantation and dissolved in 50 mL of MTB ether. After complete evaporation of the solvent a champagne-colored powder was obtained. Yield: 0.24 g (45%). M.p.: 60 °C. $C_{50}H_{50}S_{10}$ (971.6): calcd. C 61.81, H 5.19; found C 59.93, H 5.47. UV/Vis (methanol): λ_{max} (%) = 208 nm (100), 297 (7). ^{1}H NMR (CD_2Cl_2): δ = 7.31 (m, 30 H), 1.2−2.2 (multiplets, 20 H) ppm. ^{13}C NMR (CD_2Cl_2): δ = 23.0, 25.0, 35.7, 70.8, 73.3, 127.3, 128.1, 130.4, 143.3 ppm. RS: 1397.

Synthesis of Bis{1-methyl-1-[(triphenylmethyl)trisulfanyl]ethyl}-pentasulfane (8a): A solution of SCl_2 (1 mL) in CS_2 (50 mL) was added dropwise and with stirring to a solution of **3a** (0.90 g, 1.37 mmol) in CS_2 (80 mL) until the color had changed from blue to red-orange. After filtration some silica gel was added with stirring. The solid was filtered off and washed with CS_2 (20 mL). The solvent of the combined solutions was evaporated and the oily residue dissolved in MTB ether (25 mL). Cooling yielded a precipitate which was isolated and dissolved again in MTB ether. Removal of the solvent produced a beige powder. Yield: 0.20 g (32%). M.p.: 52 °C. $C_{44}H_{42}S_{11}$ (923.5): calcd. C 57.22, H 4.58, S 38.19; found C 57.42, H 4.88, S 37.31. UV/Vis (methanol): λ_{max} (%) = 212 nm (100), 297 (9). ^{1}H NMR (CD_2Cl_2): δ = 7.34 (m, 30 H), 1.74 s, 12 H) ppm. ^{13}C NMR (CD_2Cl_2): δ = 28.6, 65.0, 73.6, 127.3, 128.1, 130.0, 143.3 ppm. RS: 1252.

Synthesis of Bis{1-[(triphenylmethyl)trisulfanyl]cyclohexyl}pentasulfane (8b): Preparation in analogy to **8a** from complex **3b** (0.83 g, 1.19 mmol). Yield: 0.14 g (23%). M.p.: 58 °C. $C_{50}H_{50}S_{11}$ (1003.67): calcd. C 59.84, H 5.02, S 35.14; found C 59.30, H 4.75, S 33.94. UV/Vis (methanol): λ_{max} (%) = 208 nm (100), 297 (8). ^{1}H NMR (CD_2Cl_2): δ = 7.32 (m, 30 H), 1.2−2.3 (multiplets, 20 H) ppm. ^{13}C NMR (CD_2Cl_2): δ = 23.0, 25.0, 35.6, 70.9, 75.3, 127.3, 128.1, 130.3, 143.3 ppm. RS: 1451.

Synthesis of Bis{1-methyl-1-[(triphenylmethyl)trisulfanyl]ethyl}-hexasulfane (9a): A solution of S_2Cl_2 (1 mL) in CS_2 (50 mL) was added dropwise and with stirring to a solution of **3a** (0.81 g, 1.23 mmol) in CS_2 (80 mL) until the color had changed from violet to orange-red. After stirring for 5 min the precipitated Cp_2TiCl_2 was filtered off and the filtrate was shaken with a small amount of silica gel for 5 min. The solids were filtered off and washed with CS_2 (50 mL); the combined filtrates were evaporated and the resulting oil was dissolved in a mixture of MTB ether and CS_2 (40:5 mL). Evaporation of the solvent gave a foam-like product which was pulverized, dissolved in CS_2/ethanol/MTB ether (10:10:5 mL) and cooled to −78 °C. Most of the solvents (CS_2 and ether) were removed on a rotary evaporator and the ethanolic solution was decanted off from the oily product. The latter was mixed with CH_2Cl_2/*n*-hexane/ethanol (7:20:20) and cooled to −78 °C whereupon a sticky precipitate was obtained. This was isolated, dissolved in a CH_2Cl_2/*n*-hexane/ethanol (7:20:10) mixture and this was cooled to −78 °C, resulting in a solid precipitate. Yield: 0.11 g (19%). M.p.: 55 °C. $C_{44}H_{42}S_{12}$ (955.6): calcd. C 55.30, H 4.43, S 40.27; found C 54.78, H 4.71, S 41.29. UV/Vis (methanol): λ_{max} (%) = 216 nm (100), 297 (12). ^{1}H NMR (CD_2Cl_2): δ = 7.32 (m, 30 H), 1.73 (s, 12 H) ppm. ^{13}C NMR (CD_2Cl_2): δ = 28.6, 65.0, 73.4, 127.3, 128.0, 130.3, 143.3 ppm. RS: 1334.

Synthesis of Bis{1-[(triphenylmethyl)trisulfanyl]cyclohexyl}-hexasulfane (9b): Preparation in analogy to **9a** from complex **3b** (0.72 g, 1.03 mmol) in 100 mL of CS_2 by titration with sulfur dichloride. Cp_2TiCl_2 was filtered off and the solution stirred with some silica gel which was then filtered off and the residue washed with 20 mL of CS_2. The solvent was evaporated and the remaining oil dissolved in a mixture of 5 mL of CS_2 and 20 mL of MTB ether. The solvents were evaporated until a turbidity appeared. Cooling to −78 °C resulted in a precipitate which was dissolved in 20 mL

 © 2004 Wiley-VCH Verlag GmbH & Co. KGaA, Weinheim

of MTB ether. Complete evaporation of the ether yielded a white powder. Yield: 0.19 g (36%). M.p.: 55 °C. $C_{50}H_{50}S_{12}$ (1035.7): calcd. C 57.98, H 4.87, S 37.15; found C 57.30, H 5.23, S 37.65. UV/Vis (methanol): λ_{max} (%) = 208 nm (100), 297 (10). ^{1}H NMR (CD_2Cl_2): δ = 7.33 (m, 30 H), 1.3−2.3 (multiplets, 20 H) ppm. ^{13}C NMR (CD_2Cl_2): δ = 23.0, 25.0, 35.5, 71.0, 73.3, 127.3, 128.1, 130.3, 143.3 ppm. RS: 1540.

Synthesis of 1-(Triphenylmethyl)-3-{1-[(triphenylmethyl)trisulfanyl]-cyclohexyl}tetrasulfane (10): TrSSCl (0.22 g, 0.64 mmol) was added in portions to a solution of **3b** (0.45 g, 0.64 mmol) in benzene (60 mL) until the color had changed from violet to orange-red. After evaporation of the solvent the residue was dissolved in CS_2 (50 mL) and stirred with some silica gel for 5 min. After filtration and washing the solid with CS_2 (10 mL) the combined solutions were partly evaporated. Some MTB ether and ethanol were added until a turbidity appeared, whereupon the mixture was cooled to −50 °C. The precipitated oil was isolated by decantation and dissolved in a small amount of CS_2 and excess MTB ether. The solvents were evaporated on a rotary evaporator until a foam appeared which was dried in vacuo (beige powder). Yield: 0.04 g (8%). M.p.: 60 °C. $C_{44}H_{40}S_7$ (793.3): calcd. C 66.62, H 5.08, S 28.30; found C 66.43, H 5.33, S 27.62. UV/Vis (methanol): λ_{max} (%) = 207 nm (100), 267 (10), 298 (5). ^{1}H NMR ($CDCl_3$): δ = 7.30 (m, 30 H), 1.2−2.1 (multiplets, 10 H) ppm. ^{13}C NMR ($CDCl_3$): δ = 22.78, 24.87, 35.28, 70.33, 73.15, 73.63, 127.16, 127.24, 127.97, 128.02, 130.33, 130.37, 143.12, 143.30 ppm. RS: 1125.

Synthesis of 3-(4-Chlorophenyl)-1-{1-methyl-1-[(4-chlorophenyl)trisulfanyl]ethyl}trisulfane (11a): Under nitrogen, a solution of ClC_6H_4SCl (0.50 g, 2.79 mmol) in CS_2 (10 mL) was added dropwise to complex **3a** (0.49 g, 1.41 mmol) in CS_2 (40 mL). Cp_2TiCl_2 was removed by filtration and stirring with a small amount of silica gel. The resulting clear solution was reduced to 5 mL, mixed with a little *n*-pentane and cooled to −78 °C. The precipitated beige powder was isolated and washed with *n*-pentane. Yield: 0.18 g (28%). M.p.: 49−54 °C. $C_{15}H_{14}Cl_2S_6$ (457.6): calcd. C 39.37, H 3.08, S 42.05; found C 39.15, H 2.89, S 41.87. UV/Vis (methanol): λ_{max} (%) = 214 nm (86), 241 (100), 275 (36), 306 (23). MS (150 °C): *m/z* (%) = 350 (1), 318 (17), 286 (73), 249 (21), 222 (9), 175 (45), 143 (100). ^{1}H NMR ($CDCl_3$): δ = 7.53 (dm, 4 H), 7.34 (dm, 4 H), 1.78 (s, 6 H) ppm. ^{13}C NMR ($CDCl_3$): δ = 28.5, 65.1, 129.3, 131.8, 134.7, 135.3 ppm. RS: 805.

Synthesis of 1-(4-Chlorophenyl)-3-{1-[(4-chlorophenyl)trisulfanyl]-cyclohexyl}trisulfane (11b): Under an atmosphere of nitrogen, a solution of ClC_6H_4SCl (0.37 g, 2.06 mmol) in CS_2 (20 mL) was added dropwise to **3b** (0.40 g, 1.03 mmol) in CS_2 (60 mL) resulting in a color change from violet to orange-red. After filtration, addition of a little silica gel and shaking for 5 min the yellow solution was filtered again and the solvent evaporated in vacuo. The residue was dissolved in MTB ether in an ultrasound bath. Reduction of the volume to 5 mL and cooling to −50 °C yielded a solid precipitate which was isolated and dried in vacuo. Yield: 0.03 g (6%). M.p.: 95 °C. $C_{18}H_{18}Cl_2S_6$ (497.6): calcd. C 43.44, H 3.65, S 38.66; found C 43.02, H 3.78, S 38.17. UV/Vis (methanol): λ_{max} (%) = 206 nm (100), 241 (82), 277 (27), 304 (19). MS (180 °C): *m/z* (%) = 350 (2), 318 (20), 289 (43), 286 (34), 254 (4), 222 (6), 210 (19), 178 (13), 175 (64), 145 (82), 143 (78), 114 (63), 108 (47), 81 (100). ^{1}H NMR ($CDCl_3$): δ = 7.53 (dm, 4 H), 7.33 (dm, 4 H), 1.3−2.2 (multiplets, 10 H) ppm. RS: 956.

Synthesis of 1-{1-Methyl-1-[(2-naphthyl)trisulfanyl]ethyl}-3-(2-naphthyl)trisulfane (12a): Solid $C_{10}H_7SCl$ (0.22 g, 1.15 mmol) was added to **3a** (0.20 g, 0.57 mmol) in CS_2 (50 mL) with stirring. After filtration some silica gel was added to remove dissolved Cp_2TiCl_2 and this was then filtered off and washed with CS_2 (10 mL). The combined solutions were evaporated and the oily residue was dissolved in MTB ether in an ultrasound bath. Cooling of the solution to −50 °C gave a white powder which was isolated and dried in air. Yield: 0.04 g (13%). M.p.: 55−57 °C. $C_{23}H_{20}S_6$ (488.8): calcd. C 56.52, H 4.12, S 39.36; found C 55.98, H 4.61, S 38.20. UV/Vis (methanol): λ_{max} (%) = 216 nm (85), 237 (100), 278 (28), 311 (15). MS (200 °C): *m/z* (%) = 382 (4), 350 (67), 318 (38), 286 (35), 265 (6), 254 (23), 234 (26), 202 (45), 191 (88), 170 (66), 159 (68), 138 (37), 128 (19), 115 (100), 106 (46). ^{1}H NMR (400 MHz, $CDCl_3$): δ = 8.05 (d, J_{meta} = 1.9 Hz, 2 H), 7.84 (m, 6 H), 7.67 (dd, J_{ortho} = 8.6 Hz, J_{meta} = 1.9 Hz, 2 H), 7.52 (m, 4 H), 1.78 (s, 6 H) ppm. RS: 952.

Synthesis of 1-(2-Naphthyl)-3-{1-[(2-naphthyl)trisulfanyl]-cyclohexyl}trisulfane (12b): Preparation in analogy to **12a** from **3b** (0.35 g, 0.90 mmol) and $C_{10}H_7SCl$ (0.35 g, 1.80 mmol). After dissolution in MTB ether a little ethanol and *n*-pentane were added and the volume was reduced in vacuo until a turbidity appeared. Stepwise cooling to −50 °C for precipitation and recrystallization from an MTB ether/*n*-hexane mixture with addition of a little ethanol to initiate the precipitation. Grayish-white powder. Yield: 0.09 g (19%). M.p.: 55−60 °C. $C_{26}H_{24}S_6$ (528.9): calcd. C 59.05, H 4.57, S 36.38; found C 58.26, H 4.18, S 35.66. UV/Vis (methanol): λ_{max} (%) = 216 nm (83), 238 (199), 277 (28), 309 (16). MS (160 °C): *m/z* (%) = 382 (3), 368 (10), 350 (58), 336 (48), 318 (21), 286 (26), 272 (21), 254 (9), 242 (15), 210 (34), 191 (100), 178 (19). ^{1}H NMR (CD_2Cl_2): δ = 8.06 (d, J_{meta} = 1.9 Hz, 2 H), 7.84 (m, 6 H), 7.69 (dd, J_{ortho} = 8.6 Hz, J_{meta} = 1.9 Hz, 2 H), 7.53 (m, 4 H), multiplets: 2.08−2.13 (4 H), 1.54−1.65 (4 H), 1.31−1.40 (2 H) ppm. ^{13}C NMR (CD_2Cl_2): δ = 22.93, 24.78, 35.47, 71.04, 126.80, 126.90, 127.68, 127.72, 127.78, 129.08, 129.54, 132.92, 133.36, 134.21 ppm. RS: 1070.

Acknowledgments

We are grateful to Dr. Yana Steudel for assistance with the graphics and the nomenclature. This work has been supported by the Deutsche Forschungsgemeinschaft.

[1] R. Steudel, *Chem. Rev.* **2002**, *102*, 3905−3945.
[2] D. Roberts, M. Born, J. L. Mieloszynski, D. Paquer, *Phosphorus Sulfur Silicon* **1993**, *83*, 49−51 and references cited therein.
[3] H. Lucke, *Aliphatische Polysulfide*, Hüthig & Wepf, Heidelberg, **1992**.
[4] Rubber vulcanized by sulfur may be considered as a thiaalkane containing sulfane bridges $-S_x-$ with x = 1, 2, 3.
[5] K. Morita, S. Kobayashi, *Chem. Pharm. Bull.* **1967**, *15*, 988−993; S. J. Wratten, D. J. Faulkner, *J. Org. Chem.* **1976**, *41*, 2465−2467; R. Gmelin, R. Susilo, G. R. Fenwick, *Phytochemistry* **1981**, *20*, 2521−2523; C.-C. Chen, C.-T. Ho, *J. Agric. Food. Chem.* **1986**, *34*, 830−833.
[6] R. Steudel, in *The Chemistry of Inorganic Ring Systems* (Ed.: R. Steudel), Elsevier, Amsterdam, **1992**, p. 233−253; M. Pridöhl, R. Steudel, F. Baumgart, *Polyhedron* **1993**, *12*, 2577−2585; K. Bergemann, M. Kustos, P. Krüger, R. Steudel, *Angew. Chem.* **1995**, *107*, 1481−1483, *Angew. Chem. Int. Ed. Engl.* **1995**, *43*, 1330−1331; M. Kustos, R. Steudel, *J. Org. Chem.* **1995**, *60*, 8056−8061; R. Steudel, U. Westphal, J. Pickardt, *Chem. Ber.* **1995**, *128*, 561−564; R. Steudel, K. Bergemann, J. Buschmann, P. Luger, *Inorg. Chem.* **1996**, *35*, 2184−2188; R. Steudel, M. Kustos, V. Münchow, U. Westphal, *Chem. Ber./Recueil* **1997**, *130*, 757−764; R. Steudel, K. Hassen-

 © 2004 Wiley-VCH Verlag GmbH & Co. KGaA, Weinheim

berg, V. Münchow, O. Schumann, J. Pickardt, *Eur. J. Inorg. Chem.* **2000**, 921−928.

[7] M. Schmidt, B. Block, H. D. Block, H. Köpf, E. Wilhelm, *Angew. Chem.* **1968**, *80*, 660−661, *Angew. Chem. Int. Ed. Engl.* **1968**, *7*, 632−633.

[8] R. Steudel, M. Kustos, A. Prenzel, *Z. Naturforsch., Teil B* **1997**, *52*, 79−82.

[9] A. Shaver, J. M. McCall, P. H. Bird, N. Ansari, *Organometallics* **1983**, *2*, 1894−1896; A. Shaver, S. Morris, *Inorg. Chem.* **1991**, *30*, 1926−1930.

[10] D. M. Giolando, T. B. Rauchfuss, *Organometallics* **1984**, *3*, 487−489.

[11] R. Steudel, R. Strauss, D. Jensen, *Chemikerztg.* **1985**, *109*, 349−350.

[12] R. Steudel, V. Münchow, J. Pickardt, *Z. Anorg. Allg. Chem.* **1996**, *622*, 1594−1600.

[13] H. J. Möckel, T. Freyholdt, J. Weiss, I. Molnar, in *Practical Aspects of Modern HPLC* (Ed.: I. Molnar), de Gruyter, Berlin, **1983**; R. Steudel, E.-M. Strauss, *Z. Naturforsch., Teil B* **1983**, *38*, 719−725.

[14] C. R. Williams, J. F. Britten, D. N. Harpp, *J. Org. Chem.* **1994**, *59*, 806−812. J. Albertsen, *Doctoral Dissertation*, Technical University Berlin, **1993**.

[15] R. Steudel, E.-M. Strauss, D. Jensen, *Z. Naturforsch., Teil B* **1990**, *45*, 1282−1290.

[16] R. Steudel, J. Steidel, T. Sandow, *Z. Naturforsch., Teil B* **1986**, *41*, 958−970.

[17] For further details including infrared and Raman spectroscopic data as well as figures of the NMR spectra of all compounds, see V. Münchow, Doctoral Dissertation, Technical University of Berlin, **1996**.

[18] A. K. Verma, T. B. Rauchfuss, *Inorg. Chem.* **1995**, *34*, 6199−6201; R. Steudel, O. Schumann, J. Buschmann, P. Luger, *Angew. Chem.* **1998**, *110*, 2502−2504, *Angew. Chem. Int. Ed.* **1998**, *37*, 2377−2378; R. Steudel, K. Hassenberg. J. Pickardt, *Eur. J. Org. Chem.* **2001**, 2815−2817.

[19] N. Takeda, N. Tokitoh, R. Okazaki, *Top. Curr. Chem.* **2003**, *231*, 153−202.

Received August 22, 2003
Early View Article
Published Online December 12, 2003

 © 2004 Wiley-VCH Verlag GmbH & Co. KGaA, Weinheim

A Bis(diazadiene) Adduct of $MoCl_2$: Mononuclear, Octahedral, Undistorted and Diamagnetic

François Stoffelbach,[a] Bertrand Rebière,[a] and Rinaldo Poli*[a,b]

Keywords: Density functional calculations / Magnetic properties / Molybdenum / N ligands / X-ray diffraction

The complex $[MoCl_2(i Pr_2dad)_2]$ ($i Pr_2dad$ = *i*PrN=CH–CH=N–*i*Pr) is obtained in one step by reduction of $[MoCl_3(THF)_3]$ in the presence of $i Pr_2dad$. The X-ray structure reveals a relatively undistorted octahedral coordination geometry with a relative *cis* configuration and points to a more appropriate description of the ligands as enediamides. The NMR investigation is in agreement with the same *cis* structure in solution and underlines the diamagnetism of the compound, at odds with previously reported very similar complexes. A bulk magnetic susceptibility measurement further confirms the compound's diamagnetism. No equilibrium with a dinuclear, metal-metal bonded species is apparent from the solution studies. A DFT calculation on the real molecule and on two R_2dad model systems with R = Ph and 4-HOC_6H_4 reveals how the ligand periphery delicately controls the magnetic and structural properties of this system.
(© Wiley-VCH Verlag GmbH & Co. KGaA, 69451 Weinheim, Germany, 2004)

Introduction

The coordination chemistry of diazadiene ligands (RN=CH−CH=NR; R_2dad) has attracted attention for quite some time,[1,2] because their high electronic and coordination mode flexibility (i.e. see **A**, **B** and **C**) imparts unusual electron-donor and -acceptor properties to these ligands, combining the useful features of N-based donors such as bipy and unsaturated acceptors such as dienes. Consequently, these ligands are generally compatible with metal centers in both high and low oxidation states. For some time, we have been investigating the coordination chemistry and the organometallic chemistry of molybdenum in intermediate oxidation states, mostly II, III and IV. Ligands with mild π-acidic properties, such as phosphanes, are quite compatible with these systems, but a wide range of ligands with extreme σ- and π-donor/acceptor properties also afford isolable and stable compounds. It was therefore of interest to probe the coordination of diazadiene ligands to these ions. We have recently shown[3] that a variety of R_2dad ligands easily add to $[CpMoCl_2]$ to yield $[CpMoCl_2(R_2dad)]$ complexes and a crystallographic study indicates that the dad ligand adopts a coordination mode closest to **B**. The metal center, therefore, is most appropriately described as formally Mo^V. In this contribution, we report the synthesis, the structural and physical characterization, and a DFT study of a compound resulting from the formal addition of two $i Pr_2dad$ ligands to $MoCl_2$. The product presents several unusual features when compared with other compounds that are very closely related to it.

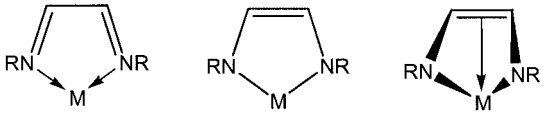

A **B** **C**

Results and Discussion

The complex $[MoCl_2(i Pr_2dad)_2]$ ($i Pr_2dad$ = *i*PrN=CH−CH=N*i*Pr) was prepared in one step from $[MoCl_3(THF)_3]$ by reduction with Zn in the presence of the diazadiene ligand. A similar strategy was previously used for the preparation of the related R_2dad complex with R = C_6H_4OMe-4,[4] and for the preparation of related $[MoCl_2(R_2dad)(CNMe)_2]$ complexes when conducted in the presence of methyl isocyanide, the main difference being the use of sodium as the reducing agent.[5] These other derivatives of $MoCl_2$, however, were not structurally characterized and no details of their stereochemistry (e.g. *cis* vs. *trans*) were evident from the spectroscopic studies.

The NMR properties unambiguously establish the diamagnetic nature of the compound and establish the cis stereochemistry of the molecule in solution. In fact, the four isopropyl methyl groups of an individual dad ligand are all inequivalent, as expected for the C_2 molecular symmetry, whereas they would all be equivalent for the C_{2v}-symmetric

[a] Laboratoire de Synthèse et d'Electrosynthèse Organométalliques, Faculté des Sciences "Gabriel", Université de Bourgogne,
6 Boulevard Gabriel, 21000 Dijon, France
[b] Laboratoire de Chimie de Coordination
205 Route de Narbonne, 31077 Toulouse Cedex, France
Fax: (internat.) + 33-5-61553003
E-mail: poli@lcc-toulouse.fr

 © 2004 Wiley-VCH Verlag GmbH & Co. KGaA, Weinheim DOI: 10.1002/ejic.200300168

trans isomer. Since the two dad ligands are symmetry related, four methyl peaks are observed overall in the ^1H NMR spectrum, each being split to a doublet by coupling with the corresponding methyne proton. The methyne protons correspondingly give rise to two different septets and the inner CH=N protons to two mutually coupled signals with a very small coupling constant (2.0 Hz).

Crystals of the [$MoCl_2$(*i*Pr$_2$dad)$_2$] derivative suitable for an X-ray structural study could be grown from diethyl ether at low temperature. The structural analysis confirms the identity of the molecule and establishes the cis stereochemistry (see Figure1). The geometry is essentially regular octahedral, the only slight deviations being attributable to the small bite of the chelating dad ligands [N(1)−Mo−N(2) = 75.55(8)° and N(3)−Mo−N(4) = 75.52(8)°]. The N(1) and N(3) ligands are essentially perfectly opposite to each other [N(1)−Mo−N(3) = 177.93(8)°] and at nearly right angles to both Cl atoms.

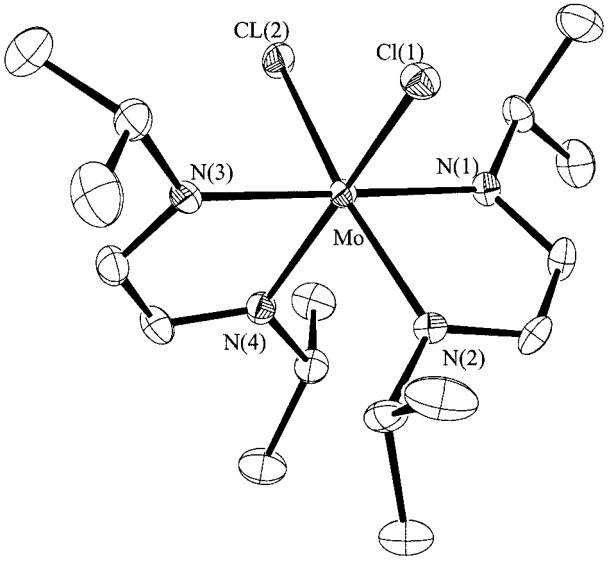

Figure 1. An ORTEP view of the geometry of [$MoCl_2$(*i*Pr$_2$dad)$_2$]

The Mo-dad five-membered rings are essentially planar [RMS deviation of fitted atoms = 0.0433 and 0.0256 for the MoN(1)C(1)C(2)N(2) and MoN(3)C(9)C(10)N(4) cycles, respectively; highest deviations from the plane: 0.0553(14) Å for atom N(2) and 0.0329(14) Å for atom N(3)]. The N−C distances average 1.338(8) Å and the C−C distances average 1.372(4) Å. These are considerably lengthened and shortened, respectively, when compared with those of free dad molecules such as *s-trans*-Cy$_2$dad [N−C: 1.258(2) Å; C−C: 1.457(2) Å] and also with those of complexes to which the bonding mode **A** can be clearly assigned (N−C: 1.26−1.30 Å; C−C: 1.40−1.46 Å).[1] The observed structural parameters are more consistent with a bonding description where the arrangement **B** plays a significant role and are very similar to those of our recently reported dad adduct of [$CpMoCl_2$].[3] Compounds such as the formally d^6 [$Mo(CO)_4$(R$_2$dad)] (R = *i*Pr or C$_6$H$_3$-*i*Pr$_2$-2,6),[6] d^4 [Mo(allyl)Br$(CO)_2$(R$_2$dad)] (R = *t*Bu, Ph),[7,8] and d^0 [MoO_2Cl_2(*t*Bu$_2$dad)],[9] on the other hand, show N−C and C−C parameters much closer to those of the free dad ligands, in better agreement with coordination mode **A**. Other Mo complexes with dad or dad-related ligands are also known.[10−13] We can advance the hypothesis that the dad ligand cannot operate as an effective π-acid in the above mentioned d^6 and d^4 complexes because of the competition with the stronger carbonyl ligands.

The Mo−N distances are slightly longer for the N(1) and N(3) atoms that are trans to each other, than for the N(2) and N(4) atoms located trans to the Cl atoms, reflecting the greater trans influence of the imino donors. The Mo−N distances are considerably shorter than in the structurally related complex [MoO_2Cl_2(*t*Bu$_2$dad)] [2.399(2) and 2.388(2) Å], where the two oxo ligands satisfy the maximum valence of the molybdenum center and therefore the dad ligand can only bind via the coordination mode **A**.[9] This is further supporting evidence for the description of the coordination geometry as **B** in the title compound. The Mo−Cl distances average 2.404(1) Å, these also being shorter than those found in other *cis*-dichloro complexes of Mo^{II} with strong *trans* ligands, for example 2.52(1) Å in [$MoCl_2$(dppe)$_2$],[14] and closer to typical Mo^{VI}−Cl distances, such as 2.356(1) Å in [MoO_2Cl_2(*t*Bu$_2$dad)][9] and 2.3251(7) Å in [(C$_5$H*i*Pr$_4$)MoO_2Cl],[15] in further agreement with the assignment of a higher formal oxidation state to the metal in compound **3**.

The compound's diamagnetism is the most surprising result concerning this compound, especially when compared with the paramagnetism (two unpaired electrons) measured for the very similar [$MoCl_2$(R$_2$dad)$_2$] and [$MoCl_2$(R$_2$dad)(CNMe)$_2$] (R = C$_6$H$_4$-OMe-4) complexes[4,5] and which is reasonably expected for low-spin octahedral d^4 Mo^{II} complexes, an example of which is [$MoCl_2$(PMe$_3$)$_4$].[16] Related W^{II} complexes with the same dad ligand are also paramagnetic.[4] The bulk diamagnetism of the title compound was confirmed by a magnetic susceptibility study. The striking difference between the two [$MoCl_2$(R$_2$dad)$_2$] compounds (diamagnetic for R = *i*Pr, paramagnetic for R = C$_6$H$_4$-OMe-4), under the assumption that the aryl derivative has a similar structure, leads to the hypothesis that the *i*Pr-substituted ligand is a better π-acceptor, delocalizing the metal electrons onto the ligand more effectively by adopting a binding mode closer to type **B** (as verified by the X-ray structural analysis), whereas the *p*-MeO-phenyl-substituted ligand leads to a molecule where the ligand adopts a binding mode closer to type **A** and which can be described more appropriately as a coordination compound of Mo^{II}. It seems rather surprising, however, that the 4-MeOC$_6$H$_4$ substitution would render the dad ligand a poorer π-acceptor than substitution by *i*Pr. This question has been addressed in more detail by a DFT investigation (see below).

Another peculiar feature of the title compound, given its diamagnetism, is the fact that no *major* distortion is revealed by the X-ray structural analysis. In fact, the large family of diamagnetic octahedral complexes of Mo^{II} (d^4) typically show rather severe distortions from the ideal octa-

 © 2004 Wiley-VCH Verlag GmbH & Co. KGaA, Weinheim

hedral geometry, with angles between bonds in relative cis positions as low as 72° and as high as 120°.[17] In the title compound, on the other hand, the only evident structural deformation is a straightforward consequence of the small bite of the two dad ligands. This phenomenon can again be rationalized on the basis of the extensive back-bonding to the dad ligands which is revealed by the solid-state structural data, so that the compound can no longer be assimilated as an octahedral d^4 dichlorobis(dad) complex of Mo^{II}. An electrochemical investigation of the title compound in THF shows two reversible one-electron processes, a reduction at $E_{1/2} = -1.27$ V and an oxidation at $E_{1/2} = -0.24$ V (Figure 2). Evidently, the orbitals involved in the electron addition and removal processes are more or less delocalized between the metal center and the ligands.

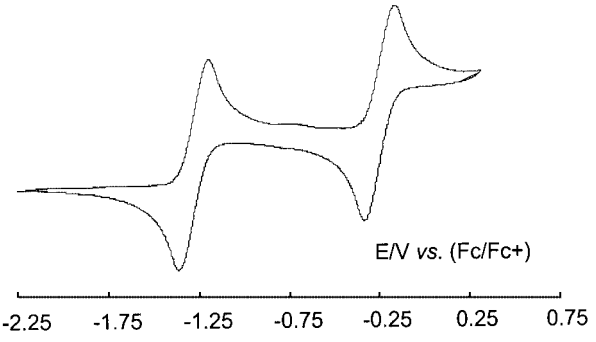

Figure 2. Cyclic voltammogram of a THF solution of [$MoCl_2(i\mathrm{Pr}_2\mathrm{dad})_2$]

In order to explore the details of the electronic structure for this compound and to understand the effect of the peripheral groups on the dad coordination mode, we have carried out DFT calculations on three different [$MoCl_2(R_2\mathrm{dad})_2$] systems with R = *i*Pr (the "real" system), Ph and 4-HOC_6H_4. The pairwise comparison between these three systems allows us to assess the electronic effect of aryl vs. alkyl groups on the dad ligand, as well as the effect of a para substituent with a mesomeric donating effect on the aryl groups. The computationally simpler OH substituent was used instead of the OMe substituent which is present in the literature compound,[4] since we only wish to probe the electronic effect of the OR conjugation with the aryl group. No major steric effect is expected to differentiate the electronic action of the *p*-OH and OMe groups.

All three systems have been fully optimized in both singlet and triplet states. The relative energies of the two spin states are reported in Table 1 together with relevant optimized geometrical parameters. First, it can be noted that the DFT-optimized structure for the real molecule in the spin singlet compares very closely with the experimentally determined structure (cf. first column of Table 1 with the data in Table 2). In particular, the C−N and C−C distances for the dad ligand are in close agreement with the experimental structure and with a description where the enediamido form **B** plays a significant role, whereas the triplet molecule shows longer C−N and shorter C−C distances, in agreement with reduced Mo-dad back-bonding. The angular parameters are not dramatically different in the two spin states. The opposite Cl−Mo−Cl and N−Mo−N(*cis*) angles become closer to the ideal octahedral values in the triplet state, whereas the N−Mo−N(*trans*) angle is less distorted in the singlet state. The optimized molecules with R = Ph and 4-HOC_6H_4 have geometrical features in close proximity to the R = *i*Pr system for both spin states.

The most interesting feature is the effect of R on the relative energy. For R = *i*Pr and Ph, the singlet state is more stable than the triplet by approximately the same amount (2−3 kcal mol^{-1}). Therefore, a change from an alkyl to an aryl group does not affect very much the electronic structure at the metal center. On the other hand, the addition of an OH substituent in the para position of the aryl group inverts the stability order in favor of the triplet state, in

Table 1. DFT optimized bond lengths [Å] and angles [deg], and relative energies in kcal mol^{-1}, for compounds $MoCl_2(R_2\mathrm{dad})_2$

	R = *i*Pr		R = Ph		R = 4-HOC_6H_4	
	Singlet	Triplet	Singlet	Triplet	Singlet	Triplet
Mo−Cl	2.495	2.522	2.461	2.498	2.467	2.507
Mo−N(*t*)	2.097	2.146	2.098	2.159	2.101	2.161
Mo−N(*c*)	2.060	2.111	2.082	2.146	2.081	2.146
N−C	1.356	1.337	1.361	1.343	1.361	1.344
C−C	1.396	1.422	1.392	1.416	1.391	1.415
Cl−Mo−Cl	105.54	92.51	111.24	93.84	110.12	93.57
N−Mo−N (chel)	75.70	75.45	75.30	75.38	75.40	75.51
N−Mo−N (*cis*)	83.97	95.05	81.16	84.20	81.18	84.01
N−Mo−N (*trans*)	173.84	168.42	173.39	169.23	174.45	168.64
E	0.00	2.85	0.00	2.09	0.00	−4.40

Table 2. Bond lengths [Å] and angles [deg] for [$MoCl_2(i\mathrm{Pr}_2\mathrm{dad})_2$]

Bond length	Bond length
Mo−N(1) 2.082(2)	Mo−N(2) 2.046(2)
Mo−N(3) 2.072(2)	Mo−N(4) 2.038(2)
Mo−Cl(1) 2.4046(7)	Mo−Cl(2) 2.4027(6)
N(1)−C(1) 1.338(3)	N(1)−C(6) 1.493(3)
N(2)−C(2) 1.326(3)	N(2)−C(3) 1.488(3)
N(3)−C(9) 1.345(3)	N(3)−C(14) 1.495(3)
N(4)−C(10) 1.342(3)	N(4)−C(11) 1.486(3)
C(1)−C(2) 1.369(4)	C(9)−C(10) 1.375(4)
Bond angle	**Bond angle**
N(1)−Mo−N(2) 75.55(8)	N(2)−Mo−N(3) 106.02(8)
N(1)−Mo−N(3) 177.93(8)	N(2)−Mo−N(4) 83.41(8)
N(1)−Mo−N(4) 103.43(8)	N(3)−Mo−N(4) 75.52(8)
N(1)−Mo−Cl(1) 91.66(6)	N(3)−Mo−Cl(1) 89.80(7)
N(1)−Mo−Cl(2) 89.23(6)	N(3)−Mo−Cl(2) 89.03(6)
N(2)−Mo−Cl(1) 87.07(6)	N(4)−Mo−Cl(1) 159.47(6)
N(2)−Mo−Cl(2) 162.47(6)	N(4)−Mo−Cl(2) 91.96(6)
Cl(2)−Mo−Cl(1) 102.22(2)	

 © 2004 Wiley-VCH Verlag GmbH & Co. KGaA, Weinheim

perfect agreement with the experimental results reported by Pombeiro et al.[4] We have attempted to pinpoint the reason for this unexpected result by inspecting the orbital interactions that are responsible for the Mo-dad bonding. As it turns out, the observed trend results from the combination of minor energy changes caused by the *p*-OH group on several bonding molecular orbitals in the deep energy region. From a qualitative point of view, we can argue that the *p*-OMe group, through its π-donating effect, makes the aryl group less capable of accepting electron density from the dad system and consequently renders the dad ligand a poorer π-acceptor, the ultimate effect being a relative destabilization of the singlet state. Some support for this statement comes from an analysis of the Mulliken charges (see Table 3). In the singlet state, the metal atom has a lower positive charge in the order 4-HOC_6H_4 < Ph < *i*Pr and, significantly, the HOC_6H_4 group has a greater positive charge relative to Ph.

Table 3. Mulliken charges for compounds $[MoCl_2(R_2dad)_2]$

	R = *i*Pr		R = Ph		R = 4-HOC_6H_4	
	Singlet	Triplet	Singlet	Triplet	Singlet	Triplet
Mo	0.706	0.668	0.681	0.727	0.668	0.671
N (total)	−1.343	−1.255	−1.619	−1.683	−1.602	−1.496
R (total)	0.719	0.783	1.026	1.042	1.058	1.077

The energies of the relevant frontier orbitals for the three calculated systems in both spin states are shown in Figure 3. The shape of the five orbitals for the singlet *i*Pr system, i.e. the title compound, are also shown. It can be seen that the overall trend of the MO energies is identical in all three cases, in particular on going from the Ph to the 4-HOC_6H_4 substituent. The Mo-dad back-bonding interaction is present with an approximately identical intensity in the HOMO and in the second highest occupied MO (SHOMO), as revealed by the contribution from the N atomic orbitals. For the SHOMO, this is quite evident from the contour plot included in Figure 3, whereas the HOMO maximizes its interaction with the dad ligand on the opposite side of the molecule (not visible). The LUMO is essentially a pure metal orbital, whereas the two higher energy empty orbitals are slightly Mo-dad antibonding (π*). The three lowest orbitals (SHOMO, HOMO and LUMO) also exhibit a small contribution from the Cl atoms which is Mo−Cl π* in nature.

The two Mo-dad π-interactions are responsible for the large splitting of the pseudo-octahedral "t_{2g}" set of orbitals and for the consequent adoption by the molecule of the singlet spin-state. It is to be noted that one of these two Mo-dad π bonding orbitals remains doubly occupied also in the triplet configuration, whereas one electron from the other orbital becomes Mo-dad nonbonding in the triplet state. Therefore, the overall Mo-dad π back-bonding interaction is only slightly reduced upon going from the singlet to the triplet. The MO analysis also shows that, in spite of the Mo-dad π-interaction, the major contribution to the

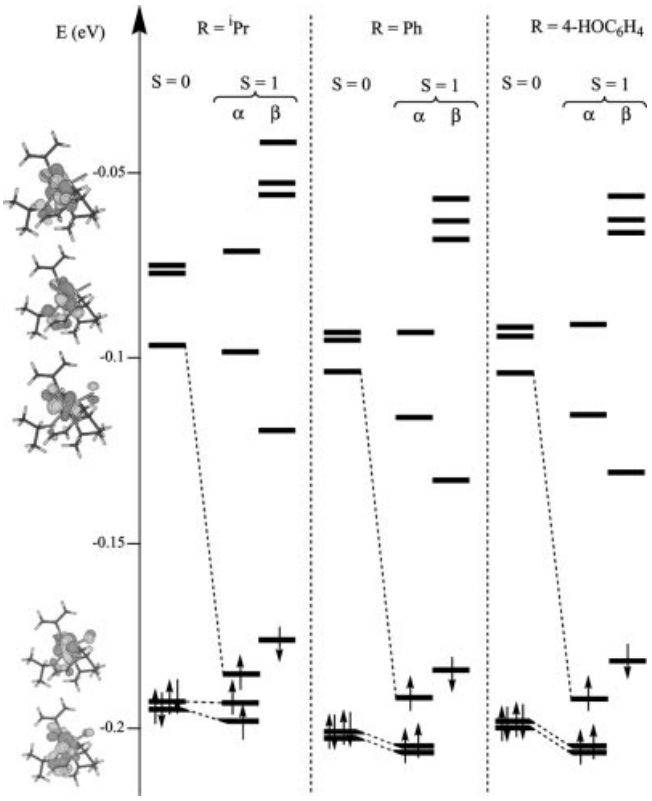

Figure 3. Energy diagram of the five 4d-derived frontier orbitals for singlet and triplet $[MoCl_2(R_2dad)_2]$ (R = *i*Pr, Ph, and 4-HOC_6H_4); on the left, MOLDEN views of the five orbitals for the singlet R = *i*Pr compound are also shown

HOMO remains that of the Mo atomic orbitals, while the Mulliken analysis shows that the majority of the spin density is localized on the Mo atom. Therefore, the one-electron oxidation process that is observed in the cyclic voltammetric study may be considered to be essentially a metal-based process. This observation serves to illustrate, once again, that the attribution of formal oxidation states has only a limited bookkeeping value when the ligands are able to adapt to their electronic environment via tunable π-interactions. This problem is commonplace in organometallic chemistry, for instance for M-olefin, M-diene, M-carbene complexes, and so forth.[18] The title compound may be described by the two limiting forms as a bis(diazadiene) Mo^{II} complex (bonding of type **A**), or as a bis(enediamido) Mo^{VI} complex (bonding of type **B**), or as anything in between. The real situation can only be revealed by the experimental observations (structural parameters, redox potentials, and so forth) and interpreted on the basis of the MO calculations.

A final interesting observation concerns the absence of any dinuclear product of formula $[Mo_2Cl_4(dad)_2]$, containing a quadruple Mo−Mo bond. There are numerous examples of $[Mo_2Cl_4L_4]$ compounds where the neutral ligands are N-based donors, mostly saturated amines,[19−24] but also nitriles,[25] pyridines,[26,27] bipyridines and other aromatic amines.[28] This observation may once again be rationalized by considering the strong π-accepting properties

 © 2004 Wiley-VCH Verlag GmbH & Co. KGaA, Weinheim

of the dad ligand. It is known, in fact, that strongly π-acidic ligands disfavor metal-metal bonds[29,30] and favor the establishment of mononuclear structures.

Conclusions

Compound $[MoCl_2(i\mathrm{Pr}_2\mathrm{dad})_2]$ is a remarkable coordination compound because of its diamagnetism, at odds with very similar complexes. The X-ray structure shows a relatively undistorted mononuclear octahedral coordination geometry for the complex, with bond lengths that are in better agreement with a bis(enediamido) Mo^{VI} model than with a bis(diazadiene) Mo^{II} model. The greater propensity of the di-*i*Pr-substituted dad ligand to adopt an enediamido coordination relative to the bis(C_6H_4OMe-4)-substituted dad ligands was not anticipated. The theoretical investigation shows the propensity of the dad ligands to accept electron density from the metal center in the HOMO and SHOMO and to reorganize to a coordination mode closer to that of enediamido ligands. These orbitals, however, retain a substantial metal contribution.

Experimental Section

General procedures: All manipulations were carried out under an atmosphere of dry and oxygen-free argon with standard Schlenk techniques. Toluene and diethyl ether were purified by reflux over sodium benzophenone ketyl and distilled under argon prior to use. The cyclic voltammogram was obtained with an EG&G 362 potentiostat connected to a Macintosh computer through MacLab hardware/software. The electrochemical cell was fitted with a Ag-AgCl reference electrode, a platinum disk working electrode and a platinum wire counter electrode. $[Bu_4N]PF_6$ (ca. 0.1 M) was used as supporting electrolyte in THF. All potentials are reported relative to ferrocene standard, which was added to the solution at the end of the experiment and measured at 100 mV/s. $[MoCl_3(THF)_3]$[31] and the $i\mathrm{Pr}_2$dad ligand[32] were prepared as described in the literature. The elemental analyses were carried out by the analytical service of the laboratory with a Fisons EA 1108 apparatus. NMR spectra were recorded in C_6D_6 at 25 °C on a Bruker DRX 500 spectrometer. The peaks positions are reported with positive shifts in ppm downfield of TMS, as calculated from residual solvent peaks.

Synthesis of $[MoCl_2(i\mathrm{Pr}_2\mathrm{dad})_2]$: $[MoCl_3(THF)_3]$ (1.25 g, 2.99 mmol), Zn (0.2 g, 3.05 mmol) and $i\mathrm{Pr}_2$dad (0.903 g, 6.44 mmol) were suspended in 15 mL of toluene at room temperature. The mixture was then stirred for three days at room temperature. The solution was filtered through Celite to remove an insoluble residue, evaporated to dryness, and warmed to 70 °C under vacuum in order to sublime the residual $i\mathrm{Pr}_2$dad. A crude product was obtained as a red dark microcrystalline solid. Yield: 0.92 g (69.2%). Recrystallization by cooling from Et_2O at −80 °C afforded X-ray quality crystals, one of which was used for the X-ray structural study. $C_{16}H_{32}Cl_2MoN_4$ (447.3): calcd. C 42.96, H 7.21, N 12.53; found C 43.19, H 7.30, N 12.21. Cyclic voltammetry (THF): reversible oxidation at $E_{1/2} = -0.24$ V ($\Delta E_p = 185$ mV) and reversible reduction at $E_{1/2} = -1.27$ V ($\Delta E_p = 177$ mV) (the ferrocene peak shows $\Delta E_p = 248$ mV). IR data (Golden gate): $\tilde{\nu}$ = 2968m cm^{-1}, 2926m, 2867m, 1490s, 1457m, 1363m, 1229s, 1219s, 1172s, 1121m, 1097m, 1024m, 795s. ^{1}H NMR (C_6D_6, 25 °C): δ = 0.32 (d, J = 6.6 Hz, CH_3), 0.47 (d, J = 6.7 Hz, CH_3), 1.12 (d, J = 6.7 Hz, CH_3), 1.54 (d, J = 6.6 Hz, CH_3), 4.18 (sept, J = 6.6 Hz, CH), 5.15 (sept, J = 6.7 Hz, CH), 6.02 (d, J = 2.0 Hz, CH=N), 6.52 (d, J = 2.0 Hz, CH=N) ppm. $\chi_M = -143.2 \times 10^{-6}$ cgs units (calculated correction for the ligand diamagnetism: $\chi_M = -259.6 \times 10^{-6}$ cgs units).

X-ray Analysis of $[MoCl_2(i\mathrm{Pr}_2\mathrm{dad})_2]$: Intensity data were collected on a Nonius−Kappa CCD at 110 K. The structure was solved via a Patterson search program[33] and refined with full-matrix least-squares methods based on F^2 (SHELX-97)[33] with the aid of the WINGX program.[34] All non-hydrogen atoms were refined with anisotropic thermal parameters. H atoms were found in a difference Fourier map and refined freely with their isotropic displacement parameters fixed at 1.2 or 1.5 (for CH_3) times the U_{eq} of their parent atoms. Refinement of the Flack parameter[35] showed that the crystal is an inversion twin[36] with a twin fraction of 0.54(3). The crystal data and refinement parameters are collected in Table 4, whereas selected bond lengths and angles are listed in Table 2.

Table 4. Crystal data and structure refinement for $[MoCl_2(i\mathrm{Pr}_2\mathrm{dad})_2]$

Formula	$C_{16}H_{32}Cl_2MoN_4$
Mol. mass	447.30
T (K)	110(2)
Crystal system	orthorhombic
Space group	$P2_12_12_1$
a (Å)	9.5125(2)
b (Å)	11.9721(2)
c (Å)	18.9856(4)
V (Å^3)	2162.17(7)
Z	4
F(000)	928
D_{calc} (g/cm^3)	1.374
Diffractometer	Enraf−Nonius KappaCCD
Scan type	mixture of φ rotations and ω scans
λ (Å)	0.71073
μ (mm^{-1})	0.858
Crystal size (mm^3)	0.3 × 0.175 × 0.125
sin(θ)/λ max (Å^{-1})	0.65
Index ranges	h: −10; 12 k: −15; 15 l: −24; 21
Absorption correction	SCALEPACK
RC = Refl. Collected	12354
IRC = independent RC	4861 [R(int) = 0.0343]
IRCGT = IRC and [$I > 2\sigma(I)$]	4380
Refinement method	full-matrix least-squares on $F2$
Data/restraints/parameters	4861/0/305
R for IRCGT	$R1$[a] = 0.0290, $wR2$[b] = 0.0497
R for IRC	$R1$[a] = 0.0367, $wR2$[b] = 0.0520
Goodness-of-fit[c]	1.013
Absolute structure parameter	0.54(3)
Largest diff. peak and hole (e·Å^{-3})	0.544 and −0.692

[a] $R1 = \Sigma(||F_o| - |F_c||)/\Sigma|F_o|$. [b] $wR2 = [\Sigma w(F_o^2 - F_c^2)^2/\Sigma[w(F_o^2)^2]^{1/2}$ where $w = 1/[\sigma^2(F_o^2) + 0.00*P + (0.0212*P)^2]$ and $P = [\mathrm{Max}(F_o^2,0) + 2*F_c^2)/3$. [c] Goodness of fit = $[\Sigma w(F_o^2 - F_c^2)^2/(N_o - N_v)]^{1/2}$.

CCDC-206713 contains the supplementary crystallographic data for this paper. These data can be obtained free of charge at www.ccdc.cam.ac.uk/conts/retrieving.html [or from the Cambridge

 © 2004 Wiley-VCH Verlag GmbH & Co. KGaA, Weinheim

Crystallographic Data Centre, 12 Union Road, Cambridge CB2 1EZ, UK; Fax: (internat.) + 44-1223/336-033; E-mail: deposit@ccdc.cam.ac.uk].

Computational Details: All calculations were performed using the Gaussian 98 program package.[37] The three-parameter form of the Becke, Lee, Yang and Parr functional (B3LYP),[38] was employed, in combination with the LanL2DZ library of basis functions, which includes both Dunning and Hay's D95 sets for H, C, O and N[39] and the relativistic Electron Core Potential (ECP) sets of Hay and Wadt for the 10 inner electrons of Cl and the 28 inner electrons of Mo.[40−42] All geometries were fully optimized without symmetry restrictions. For the open-shell species, the calculations used unrestricted open-shell methods. The mean value of the spin over the electronic density in an unrestricted calculations does not reproduce exactly the assigned spin multiplicity. In all our cases, though, it was considered to be suitable to identify unambiguously the spin state. Mean values of $<S^2>$ were in the narrow 2.097−2.174 range for triplets. In all cases, relative energies are given in kcal mol^{-1} and do not include a correction for zero-point energy.

Acknowledgments

We thank the CNRS and the French Ministry of Research for funding and Dr. P. Richard for assistance. F. S. thanks the CNRS and the Conseil Régional de Bourgogne for a BDI fellowship.

[1] G. Van Koten, K. Vrieze, *Adv. Organomet. Chem.* **1982**, *21*, 151−239.
[2] K. Vrieze, *J. Organomet. Chem.* **1986**, *300*, 307−326.
[3] F. Stoffelbach, R. Poli, P. Richard, *J. Organomet. Chem.* **2002**, *663*, 269−276.
[4] A. J. L. Pombeiro, M. F. N. N. Carvalho, *Rev. Port. Quim.* **1981**, *23*, 23−32.
[5] A. J. L. Pombeiro, R. L. Richards, *Transition Met. Chem.* **1981**, *6*, 255−258.
[6] H. tom Dieck, T. Mack, K. Peters, H. G. Vonschnering, *Z. Naturforsch., Teil B* **1983**, *38*, 568−579.
[7] A. J. Graham, D. Akrigg, B. Sheldrick, *Acta Crystallogr., Sect. C* **1983**, *39*, 192−194.
[8] A. J. Graham, D. Akrigg, B. Sheldrick, *Acta Crystallogr., Sect. C* **1985**, *41*, 995−996.
[9] K. Dreisch, C. Andersson, C. Stalhandske, *Polyhedron* **1993**, *12*, 303−311.
[10] R. Beckert, M. Doring, H. Gorls, F. Knoch, E. Uhlig, J. Wuckelt, *J. Prakt. Chem.* **1995**, *337*, 38−42.
[11] C. Kapplinger, R. Beckert, W. Imhof, *J. Prakt. Chem.* **1998**, *340*, 323−333.
[12] M. Doring, H. Gorls, R. Beckert, *Z. Anorg. Allg. Chem.* **1994**, *620*, 551−560.
[13] M. G. B. Drew, V. Félix, I. S. Gonçalves, F. E. Kühn, A. D. Lopes, C. C. Romão, *Polyhedron* **1998**, *17*, 1091−1102.
[14] G. Pelizzi, G. Predieri, *Gazz. Chim. Ital.* **1982**, *112*, 381−386.
[15] D. Saurenz, F. Demirhan, P. Richard, R. Poli, H. Sitzmann, *Eur. J. Inorg. Chem.* **2002**, 1415−1424.
[16] E. Carmona, J. M. Marín, M. L. Poveda, J. L. Atwood, R. D. Rogers, *Polyhedron* **1983**, *2*, 185−193.
[17] P. Kubácek, R. Hoffmann, *J. Am. Chem. Soc.* **1981**, *103*, 4320−4332.
[18] J. P. Collman, L. S. Hegedus, J. R. Norton, R. G. Finke, *Principles and Applications of Organotransition Metal Chemistry*, University Science Books, **1987**.
[19] F. A. Cotton, E. V. Dikarev, S. Herrero, *Inorg. Chem.* **1998**, *37*, 5862−5868.
[20] F. A. Cotton, E. V. Dikarev, S. Herrero, *Inorg. Chem.* **1999**, *38*, 490−495.
[21] F. A. Cotton, E. V. Dikarev, S. Herrero, *Inorg. Chem.* **1999**, *38*, 2649−2654.
[22] F. A. Cotton, E. V. Dikarev, S. Herrero, *Inorg. Chem.* **2000**, *39*, 609−616.
[23] M. Gerards, *Inorg. Chim. Acta* **1995**, *229*, 101−103.
[24] H. L. Chen, C. T. Lee, C. T. Chen, J. D. Chen, L. S. Liou, J. C. Wang, *J. Chem. Soc., Dalton Trans.* **1998**, 31−35.
[25] F. A. Cotton, R. Poli, *J. Am. Chem. Soc.* **1988**, *110*, 830−841.
[26] F. A. Cotton, E. V. Dikarev, S. Herrero, B. Modec, *Inorg. Chem.* **1999**, *38*, 4882−4887.
[27] F. A. Cotton, E. V. Dikarev, J. D. Gu, S. Herrero, B. Modec, *J. Am. Chem. Soc.* **1999**, *121*, 11758−11761.
[28] D. M. Baird, F. L. Yang, D. J. Kavanaugh, G. Finness, K. R. Dunbar, *Polyhedron* **1996**, *15*, 2597−2606.
[29] P. Brant, F. A. Cotton, J. C. Sekutowski, T. E. Wood, R. A. Walton, *J. Am. Chem. Soc.* **1979**, *101*, 6588−6593.
[30] F. A. Cotton, D. J. Darensbourg, B. W. S. Kolthammer, *J. Organomet. Chem.* **1981**, *217*, C14−C16.
[31] F. Stoffelbach, D. Saurenz, R. Poli, *Eur. J. Inorg. Chem.* **2001**, 2699−2703.
[32] J. M. Kliegman, R. K. Barnes, *Tetrahedron Lett.* **1969**, *24*, 1953−1956.
[33] G. M. Sheldrick, 'SHELX97 (Includes SHELXS-97 and SHELXL-97), Release 97−2, Programs for Crystal Structure Analysis', University of Göttingen, **1998**.
[34] L. J. Farrugia, *J. Appl. Crystallogr.* **1999**, *32*, 837−838.
[35] H. D. Flack, *Acta Crystallogr., Sect. A* **1983**, *39*, 876−881.
[36] H. D. Flack, G. Bernardinelli, *Acta Crystallogr., Sect. A* **1999**, *55*, 908−915.
[37] M. J. Frisch, G. W. Trucks, H. B. Schlegel, G. E. Scuseria, M. A. Robb, J. R. Cheeseman, V. G. Zakrzewski, J. Montgomery, J. A., R. E. Stratmann, J. C. Burant, S. Dapprich, J. M. Millam, A. D. Daniels, K. N. Kudin, M. C. Strain, O. Farkas, J. Tomasi, V. Barone, M. Cossi, R. Cammi, B. Mennucci, C. Pomelli, C. Adamo, S. Clifford, J. Ochterski, G. A. Petersson, P. Y. Ayala, Q. Cui, K. Morokuma, D. K. Malick, A. D. Rabuck, K. Raghavachari, J. B. Foresman, J. Cioslowski, J. V. Ortiz, A. G. Baboul, B. B. Stefanov, G. Liu, A. Liashenko, P. Piskorz, I. Komaromi, R. Gomperts, R. L. Martin, D. J. Fox, T. Keith, M. A. Al-Laham, C. Y. Peng, A. Nanayakkara, C. Gonzalez, M. Challacombe, P. M. W. Gill, B. Johnson, W. Chen, M. W. Wong, J. L. Andres, C. Gonzalez, M. Head-Gordon, E. S. Replogle, J. A. Pople, Gaussian 98, Revision A.9, Gaussian, Inc., **1998**.
[38] A. D. Becke, *J. Chem. Phys.* **1993**, *98*, 5648−5652.
[39] T. H. Dunning, Jr., P. J. Hay, *Modern Theoretical Chemistry* (Ed. H. F. Schaefer, III), Plenum, New York, **1976**.
[40] P. J. Hay, W. R. Wadt, *J. Chem. Phys.* **1985**, *82*, 270−283.
[41] W. R. Wadt, P. J. Hay, *J. Chem. Phys.* **1985**, *82*, 284−298.
[42] P. J. Hay, W. R. Wadt, *J. Chem. Phys.* **1985**, *82*, 299−310.

Received March 28, 2003
Early View Article
Published Online January 2, 2004

 © 2004 Wiley-VCH Verlag GmbH & Co. KGaA, Weinheim

Kinetic Studies of the Oxidative Addition and Transmetallation Steps Involved in the Cross-Coupling of Alkynyl Stannanes with Aryl Iodides Catalysed by η^2-(Dimethyl fumarate)(iminophosphane)palladium(0) Complexes

Bruno Crociani,*[a] Simonetta Antonaroli,[a] Luciano Canovese,[b] Paolo Uguagliati,[b] and Fabiano Visentin[b]

Keywords: Palladium / N,P ligands / Kinetics / Cross-coupling

The complexes [Pd(η^2-dmfu)(P–N)] {dmfu = dimethyl fumarate; P–N = 2-(PPh_2)C_6H_4–1-CH=NR, R = C_6H_4OMe-4 (**1a**), $CHMe_2$ (**2a**), $C_6H_3Me_2$-2,6 (**3a**), $C_6H_3(CHMe_2)_2$-2,6 (**4a**)} undergo dynamic processes in solution which consist of a P–N ligand site exchange through initial rupture of the Pd–N bond at lower energy and an olefin dissociation-association at higher energy. According to equilibrium constant values for olefin replacement, the complex [Pd(η^2-fn)(P–N)] (fn = fumaronitrile, **1b**) has a greater thermodynamic stability than its dmfu analogue **1a**. The kinetics of the oxidative addition of ArI (Ar = $C_6H_4CF_3$-4) to **1a** and **2a** lead to the products [PdI(Ar)(P–N)] (**1c**, **2c**) and obey the rate law, $k_{obs} = k_{1A} + k_{2A}$[ArI]. The k_{1A} step involves oxidative addition to a reactive species [Pd(solvent)(P–N)] formed from dmfu dissociation. The k_{2A} step is better interpreted in terms of oxidative addition to a species [Pd(η^2-dmfu)(solvent)(κ^1-P–N)] formed in a pre-equilibrium step from Pd–N bond breaking. The complexes **1c** and **2c** react with PhC≡$CSnBu_3$ in the presence of an activated olefin (ol = dmfu, fn) to yield the palladium(0) derivatives [Pd(η^2-ol)(P–N)] along with $ISnBu_3$ and PhC≡CAr. The kinetics of the transmetallation step, which is rate-determining for the overall reaction, obey the rate law: $k_{obs} = k_{2T}$[PhC≡$CSnBu_3$]. The k_{2T} values are markedly enhanced in more polar solvents such as CH_3CN and DMF. The solvent effect and the activation parameters suggest an associative S_E2 mechanism with substantial charge separation in the transition state. The kinetic data of the above reactions in various solvents indicate that, for the cross-coupling of PhC≡$CSnBu_3$ with ArI catalysed by **1a** or **2a**, the rate-determining step is represented by the oxidative addition and that CH_3CN is the solvent in which the highest rates are observed.

(© Wiley-VCH Verlag GmbH & Co. KGaA, 69451 Weinheim, Germany, 2004)

Introduction

The cross-coupling of organo-stannanes with carbon electrophiles catalysed by palladium complexes (Stille reaction) is a powerful synthetic method in organic chemistry.[1] The generally accepted catalytic cycle involves an initial oxidative addition of the organic electrophile to a palladium(0) species followed by transmetallation, *trans*-to-*cis* isomerisation if *trans*-diorganopalladium(II) intermediates are formed, and eventually reductive elimination of the coupled product.[1,2] As shown in previous studies,[3] for the complexity of the reactions involved the mechanism of the process can be variously affected by the nature of the ligand, the solvent, the reacting stannane and organic electrophile, and by the presence of additives such as LiCl or the free ligand. In fact, the rate-determining step of the cycle can either be the oxidative addition or the transmetallation or even the reductive elimination.[1c,2,4]

The mechanism described in Scheme 1 for the coupling of ArX (Ar = pentahalophenyl; X = halide, triflate) with $RSnBu_3$ (R = vinyl) has been recently proposed.[5]

In this mechanism, two transmetallation pathways may be present without any prior dissociation (or solvent displacement) of the ligand L in the intermediates *trans*-[$PdXArL_2$]. The associative S_E2 cyclic step (a) is favoured in weakly coordinating solvents of low polarity when X is a good bridging ligand such as a halide. It leads to a highly reactive *cis* species which undergoes an immediate reductive elimination and is strongly retarded by the presence of the free ligand L. The associative S_E2 open step (b) is favoured when L′ is a ligand or a polar coordinating solvent both of which lack bridging capability and when X is a good-leaving and poorly coordinating anionic ligand without bridging ability.

In contrast, the transmetallation of [{η^5-(1-Ph_2P)(2,4-Ph_2)C_5H_2}$(CO)_3$MoPdI(PPh_3)] by PhC≡$CSnBu_3$, leading to [{η^5-(1-Ph_2P)(2,4-Ph_2)C_5H_2}$(CO)_3$MoPd(C≡CPh)-

[a] Dipartimento di Scienze e Tecnologie Chimiche, Università di Roma "Tor Vergata",
Via della Ricerca Scientifica, 00133 Roma, Italy
Fax: (internat.) + 39-06-72594328
E-mail: crociani@stc.uniroma2.it
[b] Dipartimento di Chimica, Università di Venezia,
Dorsoduro 2137, 30123 Venezia, Italy
Fax: (internat.) + 39-041-2348517
E-mail:cano@unive.it

 © 2004 Wiley-VCH Verlag GmbH & Co. KGaA, Weinheim **DOI: 10.1002/ejic.200300376**

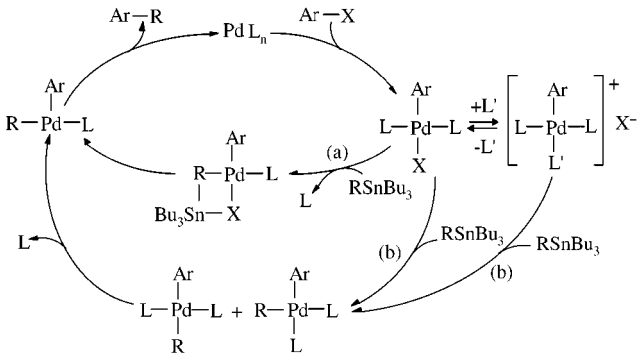

(L = PPh_3, $AsPh_3$; L' = ligand or solvent)

Scheme 1. Catalytic cycle for the cross-coupling reaction with palladium complexes containing monodentate ligands L

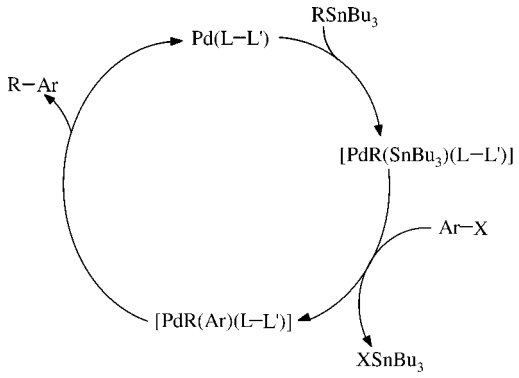

[L—L' = 2-(PPh_2)C_6H_4-1-CH=NC_2H_4Ph]

Scheme 2. Alternative catalytic cycle for the cross-coupling reaction with the system [PdCl(η^3-C_3H_5)]$_2$/L—L′ (1:2 molar ratio)

(PPh_3)] in dimethylformamide (DMF), was reported to proceed through a reactive species [{η^5-(1-Ph_2P)(2,4-Ph_2)C_5H_2}(CO)$_3$MoPdI(DMF)],formed in a displacement equilibrium of the ligand PPh_3 by the solvent when a low initial concentration of the starting complex was used.[6]

On the other hand, the complex *trans*-[PdIPh($AsPh_3$)$_2$] was also found to be in equilibrium with the species [PdIPh(solvent)($AsPh_3$)] (solvent = DMF) upon release of $AsPh_3$ in dimethylformamide,[7] in agreement with previous kinetic studies.[1b][3e] In a recent report, however, the concentration of [PdXR(solvent)($AsPh_3$)] (X = Cl, I; R = Ph, $C_6Cl_2F_3$) was found to be negligible in the presence of free arsane, indicating that under catalytic conditions the predominant transmetallation step involves the associative reaction of the stannane with the complex [PdXR($AsPh_3$)$_2$].[8]

In the coupling of pentahaloaryl triflates (ArX) with CH_2=CHSnBu$_3$ catalysed by [PdXAr(dppe)] [dppe = 1,2-bis(diphenylphosphanyl)ethane] the main intermediates, [PdAr(CH=CH_2)(dppe)] and [Pd(η^2-CH_2=CHAr)(dppe)], have been spectroscopically detected and characterised.[9]

The system [PdCl(η^3-C_3H_5)]$_2$/L—L′ (1:2 molar ratio) {L—L′ = 2-(PPh_2)C_6H_4—1-CH=NC_2H_4Ph}, was found to have a high catalytic efficiency in the coupling of 4-(trifluoromethyl)iodobenzene with PhC≡CSnBu$_3$.[10] From the detection of the labile complexes [PdI(SnBu$_3$)(L—L′)] and [Pd(C≡CPh)(SnBu$_3$)(L—L′)] in the ^{31}P NMR spectra of the reaction mixture, an alternative catalytic cycle was proposed involving the initial oxidative addition of PhC≡CSnBu$_3$ to an in situ generated palladium(0) species, Pd(L—L′) (Scheme 2).

The zero-valent complexes [Pd(η^2-dmfu)(P—N)] {dmfu = dimethyl fumarate; P—N = 2-(PPh_2)C_6H_4—1-CH=NR, R = alkyl and aryl group},[11] are quite active catalysts (or catalyst precursors) in the coupling of organostannanes with aryl halides.[12] The catalytic efficiency is retained for a prolonged period of time and increases considerably on going from alkyl to aryl *N*-substituents, and also in the presence of the free iminophosphane for a P—N/[Pd(η^2-dmfu)(P—N)] molar ratio ≥ 1. In a mechanistic investigation based mainly on IR and NMR spectroscopic data,[13] we have reported that the cross-coupling of PhC≡CSnBu$_3$ with $IC_6H_4CF_3$-4 proceeds through the classical cycle involving initial oxidative addition of the aryl iodide to [Pd(η^2-dmfu)(P—N)] {P—N = 2-(PPh_2)C_6H_4—1-CH=NR, R = C_6H_4OMe-4, $CHMe_2$}, or [Pd(η^2-dmfu)(P—N)$_2$] formed from the reaction of [Pd(η^2-dmfu)(P—N)] with one equivalent of the iminophosphane P—N, followed by trans-metallation of the product [PdI($C_6H_4CF_3$-4)(P—N)] and by fast reductive elimination of the alkyne PhC≡C$C_6H_4CF_3$-4 to regenerate the starting palladium(0) compound. With [Pd(η^2-dmfu)(P—N)] as the catalyst, the oxidative addition is the rate-determining step, while for [Pd(η^2-dmfu)(P—N)$_2$] the oxidative addition and transmetallation steps proceed at comparable rates.

We report herein the results of a kinetic investigation of the oxidative addition of $IC_6H_4CF_3$-4 to [Pd(η^2-dmfu)(P—N)] and the transmetallation of [PdI($C_6H_4CF_3$-4)(P—N)] by PhC≡CSnBu$_3$. The studies have been carried out using UV/Vis spectroscopic techniques in order to get a better understanding of the mechanism and of the factors which affect these fundamental steps of the catalytic cycle.

Results and Discussion

The structures of the palladium complexes used in the kinetic study are shown in Scheme 3.

According to the X-ray structural analyses of the iminophosphane derivatives [Pd(η^2-fn)(P—N)] (fn = fumaronitrile, **1b**)[14] and [PdI(Ph)(P—N)] {P—N = 2-(PPh_2)C_6H_4—1-CH=NR; R = Me, Et},[15] the olefin carbons are almost coplanar with the N—Pd—P coordination plane for the palladium(0) complexes, while in the palladium(II) complexes the iodide ligand is *trans* to the phosphorus atom.

In order to clarify the intimate mechanism governing the cross-coupling reaction between $IC_6H_4CF_3$-4 and PhC≡CSnBu$_3$ catalysed by the complexes **1a** and **2a**,[12,13]

 © 2004 Wiley-VCH Verlag GmbH & Co. KGaA, Weinheim

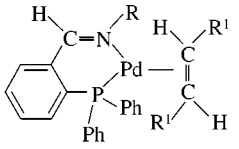

	1a	1b	2a	2b	3a	4a	5b
R	C_6H_4OMe-4	C_6H_4OMe-4	$CHMe_2$	$CHMe_2$	$C_6H_3Me_2$-2,6	$C_6H_3(CHMe_2)_2$-2,6	bornyl
R^1	CO_2Me	CN	CO_2Me	CN	CO_2Me	CO_2Me	CN

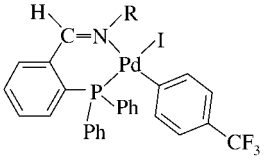

	1c	2c
R	C_6H_4OMe-4	$CHMe_2$

Scheme 3. Structures of the (iminophosphane)palladium complexes [bornyl = *endo*-(1*R*)-1,7,7-trimethylbicyclo[2.2.1]hept-2-yl]

we have chosen to break the problem down into separate studies, i.e. the oxidative addition and the transmetallation/reductive elimination reactions. Preliminary studies on the relative stability of the palladium(0) olefin complexes **1a** and **1b**, and on the solution behaviour of the palladium(0) and the palladium(II) complexes of Scheme 3 have been also carried out.

Relative Stability of Palladium(0) Olefin Complexes from Olefin Exchange Equilibria

Previous results on the oxidative addition of $IC_6H_4CF_3$-4 to [Pd(η^2-ol)(P−N)] (ol = dmfu, fn) involved in the catalytic cycle of the cross-coupling reaction[12,13] have shown that only the dmfu complexes display appreciable reactivity. Thus, we have tried to attribute this feature to a lower thermodynamic stability of such species with respect to their fn analogues by studying the equilibrium 1 of olefin exchange in THF and $CHCl_3$ by UV/Vis spectrophotometry [Equation (1)].

$$\underset{\mathbf{1a}}{[Pd(\eta^2\text{-dmfu})(P\text{—}N)]} + fn \underset{}{\overset{K_E}{\rightleftharpoons}} \underset{\mathbf{1b}}{[Pd(\eta^2\text{-fn})(P\text{—}N)]} + dmfu \quad (1)$$

The resultant K_E values of 8520±300 in $CHCl_3$ and 640±20 in THF indicate that the position of equilibrium is strongly shifted to the right. The much greater stability of complex **1b** is largely due to the greater π-accepting properties of fumaronitrile which increase the strength of the palladium-olefin bond as already observed for the olefin exchange equilibria in similar zero-valent complexes [Pd(η^2-ol)(L−L′)] {L−L′ = 2-(iminomethyl)pyridine[16] or 2-(methylthio)pyridine[17]}. A reduced electron density on the metal in **1b** will render the complex less susceptible to oxidative addition by the organic halide, thereby explaining its lack of reactivity.

The equilibrium constant in $CHCl_3$ is one-order of magnitude higher than in THF. We have confirmed the observed solvent effect by comparing the corresponding K_E values for the 2-(iminomethyl)pyridine complex [Pd(η^2-dmfu)(C_5H_4N-2-CH=NC_6H_4OMe-4)]. In THF, a value of 731±32 was obtained whereas in $CHCl_3$ a value of 4000±400 was previously determined.[16] We surmise that such an effect predominantly stems from a different stabilisation, by solvation, of the olefins in the two solvents examined even though they have comparable dielectric constants.

Solution Behaviour of the Palladium(0) and Palladium(II) Complexes

It is known that palladium(0) olefin complexes with *P,N*-chelating ligands undergo various dynamic processes in solution such as olefin rotation around its bond axis to the central metal, olefin dissociation, Pd−N bond rupture and exchange between the free and coordinated olefin.[11,18] The dissociative processes lead to unsaturated (or solvent-coordinated) species which may be of importance in the mechanism of the oxidative addition.[19] For instance, olefin dissociation leads to a species of the type Pd(P−N), which can be generated in situ also from the reaction of a mixture of [PdCl(η^3-C_3H_5)]$_2$/L−L′ (1:2 molar ratio) {L−L′ = 2-(PPh_2)C_6H_4−1-CH=NC_2H_4Ph} with $NaCH(CO_2Me)_2$.[10] Such a species undergoes oxidative addition with PhC≡C$SnBu_3$ or $IC_6H_4CF_3$-4 to give the products [Pd(C≡CPh)($SnBu_3$)(P−N)] or [PdI($SnBu_3$)(P−N)]. We have therefore examined the ^{1}H NMR spectra of the complexes **1a** and **2a** at 25 °C in $CDCl_3$ and [D_8]toluene and at variable-temperatures in [D_8]toluene (Table 1).

As can be seen, the signals of the imino proton appear at lower frequencies (δ = 0.6−0.7 ppm) in the aromatic solvent whereas those of the olefin protons appear at higher frequencies (δ = 0.4−0.7 ppm) relative to the corresponding signals in $CDCl_3$. The proton resonances of **1a** are fairly sharp in CD_3Cl but broader in [D_8]toluene indicating the occurrence of dynamic processes at increasing rates in the latter solvent. At higher temperatures in [D_8]toluene, the olefin H_{cis} and H_{trans} resonances (Δν = 260 Hz) coalesce at 56 °C, from which a $\Delta G^{\neq}$ value of 63.4 kJ·mol^{-1} can be evaluated.[20] The olefin methyl signals also coalesce at ca. 35 °C but in this case, however, a more precise measurement of the coalescence temperature was prevented by overlapping with the iminophosphane OCH_3 singlet (at δ = 3.31 ppm in the spectrum at 25 °C). The ^{1}H NMR spectra of **2a** at 25 °C are characterised by sharp olefin signals in the solvents examined. Upon heating the [D_8]toluene solution, the H_{cis} and H_{trans} signals (Δν = 129 Hz) coalesce at 75 °C ($\Delta G^{\neq}$ = 69.3 kJ·mol^{-1}). At approximately the same temperature the olefin methyl resonances are also in coalescence but overlap largely with the $CHMe_2$ septet (at δ = 3.22 ppm in the spectrum at 25 °C) of the iminophosphane. It is interesting to point out that the isopropyl Me groups remain diastereotopic at the various temperatures exam-

 © 2004 Wiley-VCH Verlag GmbH & Co. KGaA, Weinheim

Table 1. Selected ^{1}H NMR spectroscopic data of the palladium complexes

Complex	Solvent	Iminophosphane protons[a] N=CH	N−CH	CH_3	Olefin protons[a] CH_{cis}[b]	CH_{trans}[c]	CH_3
1a	[D$_8$]toluene	7.54 d [2.8]		3.31 s	4.85 br. s	4.20 br. s	3.30 br. s, 3.20 br. s
	$CDCl_3$[11]	8.11 d [4.0]		3.81 s	4.23 d (9.9)	3.55 dd (9.9)[9.9]	3.32 s, 3.14 s
2a	[D$_8$]toluene	7.54 d [3.6]	3.22 spt (6.4)	1.31 d, 1.28 d (6.4) (6.4)	4.65 dd (10.0) [2.8]	4.32 dd (10.0) [10.0]	3.52 s, 3.12 s
	$CDCl_3$	8.24 [3.2]	3.65 spt[d]	1.30 d, 1.29 d (6.3) (6.3)	4.13 dd (10.4) [2.4]	3.88 dd (10.4) [10.4]	3.65 s, 3.14 s
3a	[D$_8$]toluene	7.42 d [3.0]		2.14 s, 1.91 s	4.82 dd (10.2) [2.6]	3.94 dd (10.4) [10.4]	3.23 s, 3.17 s
	$CDCl_3$	8.06 d [3.2]		2.16 s, 1.90 s	4.24 dd (10.0) [2.4]	3.37 dd (10.2) [10.2]	3.18 s
4a	[D$_8$]toluene	7.73 d [3.2]		1.45 d, 1.19 d, (6.8) (6.8) 0.92 d, 0.59 d (6.8) (6.8)	4.82 dd (10.0) [3.0]	4.05 dd (10.0) [10.0]	3.15 s, 2.97 s
	$CDCl_3$	8.06 d [2.1]		1.45 d, 1.09 d, (6.8) (6.8) 0.98 d, 0.56 d (6.8) (6.8)	4.25 dd (10.4) [2.5]	3.49 dd (10.4) [10.4]	3.24 s, 2.93 s
5b[e]	[D$_8$]toluene	7.92 s	3.63 m	0.92 s, 0.72 s, 0.21 s	3.16 dd (9.5) [3.8]	2.82 dd (9.5) [9.5]	
5b[f]	[D$_8$]toluene	8.12 s	4.41 m	mk	mk	2.66 dd (9.7) [9.7]	
1c	CD_3CN	8.31 s		3.80 s			
2c	[D$_8$]toluene	7.54 s	5.93 spt (6.8)	1.05 d (6.8)			

[a] At 25 °C. Coupling constants $J_{H,H}$ in round brackets, $J_{P,H}$ in square brackets. br = broad, mk = masked. [b] *cis* to phosphorus. [c] *trans* to phosphorus. [d] Overlapping with the olefin CH_3 signal. [e] Major diastereoisomer, see text. [f] Minor diastereoisomer.

ined. Even at 75 °C, they are detected as two sharp doublets at δ = 1.27 and 1.24 ppm, respectively.

The fluxional behaviour of complexes **1a** and **2a** may be explained either by olefin rotation, by olefin dissociation-association or by P−N ligand site exchange through initial rupture of the Pd−N bond. In order to ascertain which is the actual process operating in solution, we have examined the variable-temperature ^{1}H NMR spectra of the complexes **3a** and **4a** which contain *N*-aryl substituents with increasing steric requirements, as well as those of complex **5b** which contains a chiral iminophosphane ligand. We have also compared the olefin ^{13}C NMR signals of **1a** and **2a** with those of **3a** and **4a** (Table 2).

The ^{1}H NMR spectrum of **5b** at 25 °C shows the presence of two diastereoisomers in a molar ratio of 6.0:1. The olefin H_{cis} and H_{trans} signals of the major diastereoisomer (Δν = 138 Hz) coalesce at 73 °C ($\Delta G^{\neq}$ = 68.7 kJ·mol^{-1}). At this temperature, the other resonances of the two diastereoisomers are distinct and sharp, although the molar ratio between the major and minor isomer decreases to 3.6:1. These findings indicate that the observed dynamic process does not involve olefin dissociation-association (which would cause interconversion of the diastereoisomers and eventually coalescence of their signals). However, the olefin dissociation-association process does occur at a lower rate (on the NMR time-scale) as indicated by the change in the isomer molar ratio when the temperature is increased.

The ^{1}H NMR spectra of **3a** and **4a** at 25 °C are characterised by the non-equivalence of the 2,6 groups on the *N*-aryl moieties: for **3a**, two singlets can be detected for the protons of the 2,6-Me groups (the singlet at δ = 2.14 ppm partially overlapping with the solvent signals) whereas for **4a**, four doublets can be detected for the Me protons and two septets (at δ = 3.38 and 2.83 ppm, respectively) for the CH protons of the 2,6-$CHMe_2$ groups. This is clearly a consequence of the asymmetric nature of the complexes and

 © 2004 Wiley-VCH Verlag GmbH & Co. KGaA, Weinheim

Table 2. Selected ^{13}C NMR spectroscopic data of the palladium(0) complexes

Complex	Iminophosphane carbons[a]			Olefin carbons[a]		
	N=CH	N−C	CH_3	C=O	CH_3	HC=CH
1a[11]	164.6	148.7	55.5	173.8, 173.5	50.4−50.0[b]	50.4−50.0[b]
2a	161.8	137.5	23.4, 22.1	174.2, 174.0	50.4, 50.3	48.2[c], 48.0 d[d] (32)
3a	167.3	151.9	18.6, 18.1	173.8, 173.3	50.6	50.2[c], 49.6 d[d] (30)
4a	166.9	150.5	24.2, 23.1, 22.6, 22.0	174.0, 172.6	50.5, 50.4	50.3[c], 49.8 d[d] (31)

[a] In $CDCl_3$ at 25 °C. Coupling constants $J_{P,H}$ in round brackets. [b] Overlapping signals. [c] *cis* to phosphorus. [d] *trans* to phosphorus.

of the restricted rotation around the N−aryl bond. When the [D_8]toluene solution of **4a** is warmed up, all the olefin and the $CHMe_2$ signals progressively broaden but at 95 °C (the highest temperature explored) only the coalescence of the olefin methyl signals ($\Delta\nu$ = 70 Hz) can be observed ($\Delta G^{\neq}$ = 75.3 kJ·mol^{-1}). In contrast, for the solution of **3a**, the olefin methyl signals ($\Delta\nu$ = 23 Hz) coalesce at 53 °C ($\Delta G^{\neq}$ = 69.4 kJ·mol^{-1}), the methyl signals of the *N*-$C_6H_3Me_2$-2,6 substituent ($\Delta\nu$ = 91 Hz) coalesce at 72 °C ($\Delta G^{\neq}$ = 69.7 kJ·mol^{-1}) and eventually the olefin H_{cis} and H_{trans} signals ($\Delta\nu$ = 351 Hz) coalesce at 93 °C ($\Delta G^{\neq}$ = 70.0 kJ·mol^{-1}). The close values of the activation free energies indicate that the same dynamic process is operating which interconverts simultaneously the two olefin methyl groups, the two methyl groups of the *N*-$C_6H_3Me_2$-2,6 substituent and the olefin H_{cis} and H_{trans} protons. Such a process cannot be the olefin rotation because it would lead to interconversion of only the olefin protons. The dynamic behaviour of **3a**, as well as that of the other complexes examined, is better rationalised by a process involving an initial solvent-assisted rupture of the Pd−N bond, followed by rotation around the N−aryl bond in the *P*-monodentate iminophosphane and ligand site exchange, as depicted in Scheme 4.

As can be seen by comparing structure **A** and the (rotated) structure **B**, this process brings about the simultaneous interconversions $R^1 \rightleftarrows R^2$, $Me^1 \rightleftarrows Me^2$, and $H^1 \rightleftarrows H^2$.

It is worth noting that the same mechanism applied to complex **2a** leads to the observed interconversions $R^1 \rightleftarrows R^2$ and $H^1 \rightleftarrows H^2$, but not to $Me^1 \rightleftarrows Me^2$ because the Me groups of the *N*-$CHMe_2$ substituent cannot interconvert by a simple rotation around the N−C bond in the *P*-monodentate iminophosphane. For such an interconversion, an inversion of configuration at the $N-C_{isopropyl}$ carbon atom would also be required.

According to this mechanism, the decreasing rate of the dynamic process in the complexes with *N*-aryl groups (**1a** > **3a** > **4a**) can be explained by the increasing steric hindrance exerted by the 2,6-substituents on the *N*-aryl group towards the incoming solvent molecule. Inspection of the ^{13}C NMR spectroscopic data in Table 2 shows that the olefin C=C carbons have comparable electron density in the complexes

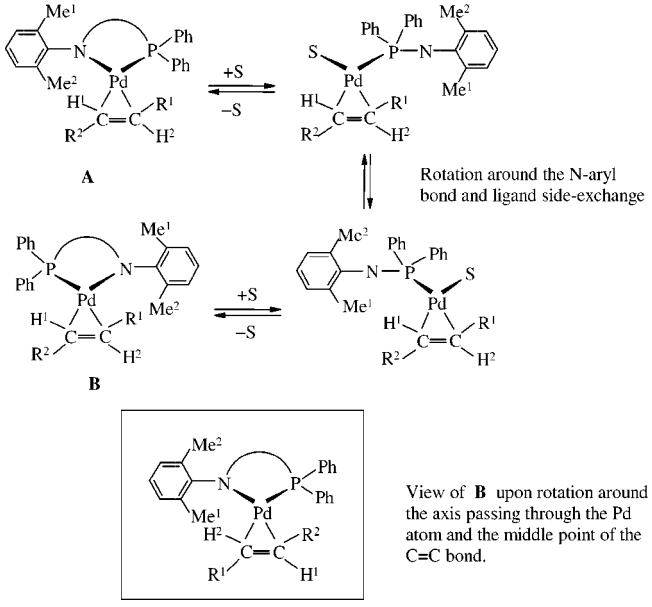

Scheme 4. Proposed mechanism for the dynamic behaviour of complex **3a** (R^1 = R^2 = CO_2Me; S = solvent)

1a, **3a**, and **4a** since they resonate in the narrow range of 50.4−49.6 ppm. In other words, this means that the extent of π back-donation in the Pd−η^2-dmfu bond and the electron donor properties of the P−N ligands (in essence, their bond strengths to the central metal) are comparable in this closely related series of complexes.

The different rate of the dynamic process observed for the complexes **1a** and **2a** (**1a** > **2a**) is essentially due to electronic factors since the *N*-C_6H_4OMe-4 and *N*-$CHMe_2$ groupings of the P−N ligands have similar steric requirements. From the data in Table 2 it appears that the olefin C=C carbons of **2a** are shielded by ca. 2 ppm relative to the corresponding carbons of **1a**, indicating a certain increase of π back-donation in the Pd−η^2-dmfu bond. This is clearly related to the electron-releasing isopropyl group which increases the σ donor properties of the imino nitrogen and, therefore, the strength of the Pd−N bond in **2a**. The imino ligands have been found to act more as σ-donors than as π-acceptors to palladium.[21] Conversely, the for-

 © 2004 Wiley-VCH Verlag GmbH & Co. KGaA, Weinheim

mally zero-valent complexes [Pd(η^2-ol)(N−N′)] (ol = activated olefin, N−N′ = α-diimine) and [Pd(η^2-ol)(P−N)] are better described as Pd^{II}-cyclopropane complexes on the basis of spectroscopic and crystallographic data.[11,14,21]

The ^1H spectra of **1c** (in CD_3CN) and **2c** (in [D_8]toluene) at 25 °C show that these palladium(II) complexes exist as single geometrical isomers in solution. No isomerisation or other dynamic process was observed in the variable-temperature ^1H NMR spectra of **2c** in [D_8]toluene in the range 25−90 °C.

As suggested by electrical conductivity measurements in acetonitrile, the complexes **1c** and **2c** undergo the solvolytic equilibrium 2 [Equation (2)].

$$[PdI(Ar)(P{-}N)] + CH_3CN \underset{}{\overset{K_S}{\rightleftharpoons}} [Pd(CH_3CN)(Ar)(P{-}N)]^+ + I^- \quad (2)$$

(Ar = $C_6H_4CF_3$-4)

The cationic complexes $[Pd(CH_3CN)(Ar)(P-N)]^+$ have been isolated as BF_4^- or $CF_3SO_3^-$ salts upon addition of $AgBF_4$ or $AgCF_3SO_3$ to the solution (see Exp. Sect.). The equilibrium constants K_S were determined by conductivity and checked by UV/Vis experiments at 25 °C (see Exp. Sect.). From the measured values [$K_S = (6.9\pm0.9)\times10^{-6}$ for **1c**; $K_S = (2.1\pm0.5)\times10^{-5}$ for **2c**] it appears that more than 20% and 35% of the cationic species $[Pd(CH_3CN)(Ar)\{2\text{-}(PPh_2)C_6H_4\text{-}1\text{-}CH{=}NC_6H_4OMe\text{-}4\}]^+$ and $[Pd(CH_3CN)(Ar)\{2\text{-}(PPh_2)C_6H_4\text{-}1\text{-}CH{=}NCHMe_2\}]^+$, respectively, are present in acetonitrile solution at 25 °C under kinetic conditions ([**1c**]$_0$ and [**2c**]$_0 = 1\cdot10^{-4}$ M). Conductivity measurements in other solvents ($CHCl_3$, THF, toluene, DMF) suggest that only in CH_3CN does the solvolytic equilibrium (2) take place.

Oxidative Addition Reactions

The oxidative addition of $IC_6H_4CF_3$-4 (ArI) to the complexes **1a** or **2a** proceeds according to Equation (3).

$$\underset{\textbf{1a, 2a}}{[Pd(\eta^2\text{-dmfu})(P{-}N)]} + ArI \rightarrow \underset{\textbf{1c, 2c}}{[PdI(Ar)(P{-}N)]} + dmfu \quad (3)$$

The progress of the reaction was monitored by ^1H and ^{31}P NMR spectroscopy at 25 °C in various solvents ($CDCl_3$, [D_8]THF, [D_7]DMF, and CD_3CN) using **1a** or **2a**/ArI molar ratios in the range of 1:5−1:10. The spectra at different times showed the presence of the reactants and products of Equation (3). No signal attributable to intermediates or side-products was detected. Under the same experimental conditions, no reaction was observed to occur between the fumaronitrile derivative **1b** and ArI.

For kinetic measurements, the oxidative addition to **1a** was monitored in different solvents and at different temperatures (in the range 15−45 °C) in the presence of an excess of ArI ([ArI] ≥ 10 × [**1a**]$_0$). The rate of any single reaction obeys the mono-exponential law:

$$D_t = D_\infty + (D_0 - D_\infty)\exp(-k_{obs}\,t)$$

where D_t, D_0, and D_∞ represent the absorbance of the system at time t, at time $t = 0$ and at the end of the reaction respectively, and k_{obs} is the pseudo-first-order rate constant.

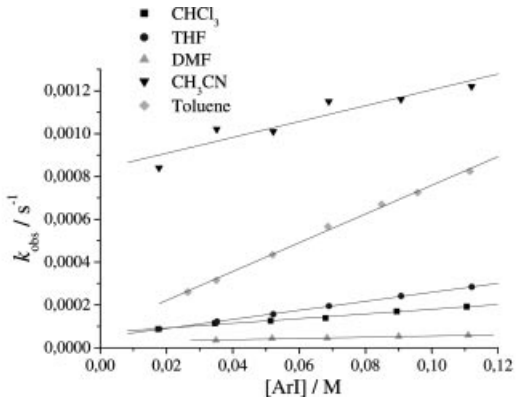

Figure 1. Plots of k_{obs} versus the aryl iodide concentration for the oxidative addition of ArI to complex **1a** in different solvents at 25 °C in the presence of dmfu ([**1a**]$_0 = 1\cdot10^{-4}$ M; [dmfu]$= 3\cdot10^{-3}$ M)

The ensuing k_{obs} values display a linear dependence on [ArI] in any solvent. As can be seen in Figure 1, a concentration independent (k_{1A}) and a concentration dependent (k_{2A}) path can always be detected so that the observed rate constants are represented by the following relationship:

$k_{obs} = k_{1A} + k_{2A}$[ArI]

The values of k_{1A} and k_{2A} in the solvents examined are reported in Table 3.

Table 3. Kinetic constants for the oxidative addition of ArI to **1a** in different solvents at 25 °C in the presence of dmfu ([**1a**]$_0 = 1\cdot10^{-4}$ M; [dmfu]$= 3\cdot10^{-3}$ M)

Solvent	k_{1A}/ s^{-1}	k_{2A}/ $M^{-1}s^{-1}$
DMF	$(2.6 \pm 0.2)\times10^{-5}$	$(2.9 \pm 0.3)\times10^{-4}$
THF	$(4.81 \pm 0.12)\times10^{-5}$	$(2.11 \pm 0.02)\times10^{-3}$
$CHCl_3$	$(7.1 \pm 0.4)\times10^{-5}$	$(1.09 \pm 0.06)\times10^{-3}$
Toluene	$(8.7 \pm 1.1)\times10^{-5}$	$(6.7 \pm 0.2)\times10^{-3}$
CH_3CN	$(8.3 \pm 0.5)\times10^{-4}$	$(3.8 \pm 0.7)\times10^{-3}$

The lowest k_{1A} and k_{2A} values were observed in DMF, while the highest k_{1A} value was observed in CH_3CN and the highest k_{2A} value in toluene. Such a reactivity clearly does not depend on the difference in dielectric constants, indicating that the transition states for both steps do not involve a substantial separation of electric charge. Furthermore, a radical mechanism can be ruled out since no diiodo derivative, which represents a typical by-product in the radical reactions, could be detected.

The kinetic constants were not appreciably influenced by different concentrations of free dmfu, as reported in Table 4.

From the kinetic data at different temperatures (Table 5), the activation parameters were determined using a re-parameterised Eyring equation.[22]

The negative activation entropies for the k_{1A} step suggest an essentially associative process. Negative $\Delta S^{\#}$ values were also obtained for the k_{2A} step, but these data should be regarded with caution (see further discussion).

 © 2004 Wiley-VCH Verlag GmbH & Co. KGaA, Weinheim

Table 4. Kinetic constants for the oxidative addition of ArI to **1a** in $CHCl_3$ at 25 °C in the presence of variable concentrations of added dmfu ($[\mathbf{1a}]_0 = 1\cdot10^{-4}$ M)

[dmfu]/M	k_{1A}/ s^{-1}	k_{2A}/ $M^{-1}s^{-1}$
0	$(5.4\pm0.3)\times10^{-5}$	$(1.24\pm0.05)\times10^{-3}$
$1\cdot10^{-3}$	$(5.9\pm0.1)\times10^{-5}$	$(1.20\pm0.02)\times10^{-3}$
$3\cdot10^{-3}$	$(7.1\pm0.4)\times10^{-5}$	$(1.09\pm0.06)\times10^{-3}$
$5\cdot10^{-3}$	$(7.4\pm0.2)\times10^{-5}$	$(1.08\pm0.04)\times10^{-3}$

Table 5. Kinetic constants and activation parameters ($\Delta H^{\neq}$/ kJ·mol^{-1}; $\Delta S^{\neq}$/J·mol^{-1}K^{-1}) for the oxidative addition of ArI to **1a** at variable temperature in different solvents in the presence of dmfu ($[\mathbf{1a}]_0 = 1\cdot10^{-4}$ M; [dmfu] = $3\cdot10^{-3}$ M)

Solvent	T / °C	k_{1A}/s^{-1}	k_{2A}/$M^{-1}s^{-1}$
CH_3CN	15	$(3.0\pm0.1)\times10^{-4}$	$(9\pm1)\times10^{-4}$
	25	$(8.3\pm0.5)\times10^{-4}$	$(3.8\pm0.7)\times10^{-3}$
	35	$(2.34\pm0.04)\times10^{-3}$	$(4.8\pm0.5)\times10^{-3}$
	45	$(5.2\pm0.2)\times10^{-3}$	$(1.6\pm0.4)\times10^{-2}$
		$\Delta H^{\neq} = 71\pm21$	$\Delta H^{\neq} = 59\pm12$
		$\Delta S^{\neq} = -63\pm8$	$\Delta S^{\neq} = -92\pm38$
Toluene	15	$(5.2\pm0.4)\times10^{-5}$	$(2.26\pm0.05)\times10^{-3}$
	25	$(1.57\pm0.04)\times10^{-4}$	$(5.97\pm0.05)\times10^{-3}$
	35	$(8.3\pm0.8)\times10^{-4}$	$(1.06\pm0.09)\times10^{-2}$
	45	$(1.39\pm0.03)\times10^{-3}$	$(3.87\pm0.17)\times10^{-2}$
		$\Delta H^{\neq} = 83\pm11$	$\Delta H^{\neq} = 67\pm2$
		$\Delta S^{\neq} = -38\pm4$	$\Delta S^{\neq} = -61\pm5$

On the basis of the above experimental data, the following mechanism can be proposed in which the reaction proceeds through two parallel pathways to yield the final product **1c**.

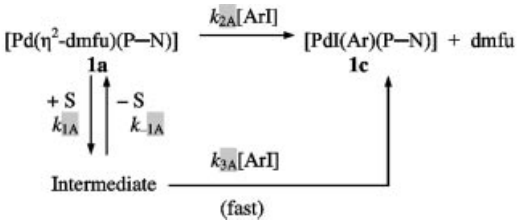

In the step k_{1A}, the interaction with the solvent produces a highly reactive intermediate which rapidly reacts with ArI to give **1c**. To a first approximation, step k_{2A} may be conceived as a bimolecular attack by the electrophile ArI on the starting complex **1a**. According to the solution behaviour of the complexes [Pd(η^2-dmfu)(P−N)] and to literature data on the mechanism of oxidative addition of iodobenzene to [Pd(η^2-dba)(L−L′)] (dba = dibenzylideneacetone; L−L′ = N, P ligand of the type aminophosphane or oxazolinophosphane),[19] the reactive intermediate may be formulated as a [Pd(solvent)(P−N)] species, resulting from the dissociation of the η^2-bound dmfu, or as a [Pd(η^2-dmfu)(solvent)(κ^1-P−N)] species, containing a P-monodentate iminophosphane and resulting from the Pd−N bond rupture (see Scheme 4). Under the steady state approach and with reasonable approximations,[23] the rate law:

$d[\mathbf{1a}]/dt = -[\mathbf{1a}](k_{1A} + k_{2A}[ArI])$

can be obtained which is identical to the experimental results irrespective of the nature of the reactive intermediate. However, a comparison of the $\Delta G^{\neq}$ value of 63.4 kJ·mol^{-1} {calculated at the coalescence temperature of 56 °C for the dynamic process of **1a** in [D_8]toluene, in which the intermediate [Pd(η^2-dmfu)(solvent)(κ^1-P−N)] is formed} and the $\Delta G^{\neq}$ value of 95.5 kJ·mol^{-1} (calculated at the same temperature from the activation parameters in Table 5 for step k_{1A} in toluene) rules out any intermediacy of [Pd(η^2-dmfu)(solvent)(κ^1-P−N)]. In the solvolytic pathway k_{1A}, a higher energy process is involved which is well represented by the solvent-assisted dissociation of the η^2-bound dmfu to form the intermediate [Pd(solvent)(P−N)] whose enhanced reactivity toward oxidative additions[10,13] is essentially due to the increased electron density on the central metal.

In order to get a better understanding of the second-order step k_{2A}, a kinetic study of the oxidative addition of ArI to the *N*-$CHMe_2$ complex **2a** was carried out in CH_3CN at 45 °C in the presence of dmfu ($[\mathbf{2a}]_0 = 1\cdot10^{-4}$ M; [dmfu] = $3\cdot10^{-3}$ M). The observed rate law is identical to that found for **1a**, with $k_{1A} = (2.71\pm0.03)\times10^{-4}$ s^{-1} and $k_{2A} = (6.3\pm0.4)\times10^{-4}$ $M^{-1}s^{-1}$. If compared with the corresponding rate constants for the reaction of **1a** under the same experimental conditions [$k_{1A} = (5.2\pm0.2)\times10^{-3}$ s^{-1} and $k_{2A} = (1.6\pm0.4)\times10^{-2}$ $M^{-1}s^{-1}$] one can see that for **2a** the k_{1A} value has decreased by one order of magnitude, while the k_{2A} value has decreased by two orders of magnitude. These changes are mainly related to electronic factors since the steric requirements of the *N*-substituents in these complexes are comparable. Thus, the decrease in k_{1A} can be explained by the presence of a stronger Pd−η^2-dmfu bond in **2a** due to the greater extent of π back-donation (see the ^{13}C NMR spectroscopic data in Table 2) which makes the olefin dissociation step more difficult. However, the marked decrease in k_{2A} is in contrast with the k_{2A} step, being a direct electrophilic attack on the palladium center of the complexes [Pd(η^2-dmfu)(P−N)]. The presence of a more electron-donating iminophosphane in **2a** increases the electron density on the central metal and, therefore, would favour such attack as reported for other palladium(0) complexes when the donor properties of the ancillary ligands are increased.[3f,24] The changes in the k_{2A} values can be rationalised if the oxidative addition of ArI in the path k_{2A} does not occur on the complexes [Pd(η^2-dmfu)(P−N)] but on the intermediates [Pd(η^2-dmfu)(solvent)(κ^1-P−N)] formed in a pre-equilibrium step (*K*).

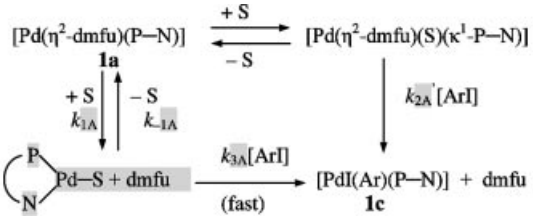

 © 2004 Wiley-VCH Verlag GmbH & Co. KGaA, Weinheim

In this case, the observed rate law becomes:

$k_{obs} = k_{1A} + k_{2A}'\cdot K[ArI]$

The measured k_{2A} term can now be represented by the product $k_{2A}'\cdot K$. Although the K constant cannot be experimentally determined due to the low, undetectable concentration of [Pd(η^2-dmfu)(solvent)(κ^1-P−N)] in the NMR solutions, its value is expected to decrease on going from **1a** to **2a** due to the presence of a stronger Pd−N bond in the latter complex. In contrast, it is reasonable to assume that the kinetic constants k_{2A}' are not particularly affected by the different electronic properties of the *N*-substituents in the intermediates with a *P*-monodentate iminophosphane.

Transmetallation and Reductive Elimination Reactions

The complexes **1c** and **2c** react with the stannane PhC≡CSnBu$_3$ in the presence of an activated olefin according to Equation (4).

$$\underset{\textbf{1c, 2c}}{[PdI(Ar)(P\!-\!N)]} + PhC{\equiv}CSnBu_3 + ol \rightarrow \underset{\substack{ol = dmfu : \textbf{1a, 2a}\\ ol = fn : \textbf{1b, 2b}}}{[Pd(\eta^2\text{-}ol)(P\!-\!N)]} + PhC{\equiv}CAr + ISnBu_3 \quad (4)$$

(Ar = $C_6H_4CF_3$-4)

As reported for palladium complexes with chelating bidentate ligands,[3d,9,10] the transmetallation of [PdI(Ar)(P−N)] by PhC≡CSnBu$_3$ leads to a labile intermediate [Pd(C≡CPh)(Ar)(P−N)] which undergoes reductive elimination of PhC≡CAr and η^2-coordination of the olefin to give the product [Pd(η^2-ol)(P−N)]. In the IR spectra (in THF) and in the ^{1}H, ^{119}Sn and ^{31}P spectra (in [D$_8$]THF) of the reaction mixtures at different times, only the starting materials and the final products were observed.[13] No side-product or intermediate of the type [Pd(C≡CPh)(Ar)(P−N)] was detected during the course of the reaction, indicating that the reductive elimination and η^2-coordination of the olefin are faster than the initial transmetallation step.

A kinetic study of reaction (4) was carried out under pseudo-first-order conditions using UV/Vis spectroscopy in different solvents and at different temperatures with an initial concentration [**1c**]$_0$ or [**2c**]$_0$ = $1\cdot10^{-4}$ M. Preliminary investigations in which the nature and the concentration of the activated olefin were changed (ol = dmfu, fn; [ol] in the range $2\cdot10^{-4}$ to $6\cdot10^{-4}$ M) led to the conclusion that the reaction rates are influenced neither by the different π-accepting properties nor by the concentration of the olefin. These findings along with the previous spectroscopic results[13] imply that i) transmetallation is the rate-determining step of the overall reaction (4) and ii) it is possible to choose the more π-accepting olefin fn that will impart a higher stability to the zero-valent products [Pd(η^2-fn)(P−N)] in order to asses unequivocally the mechanistic path without interference from side-reactions involving decomposition.

Irrespective of solvent and temperature, each reaction obeys the mono-exponential law:

$D_t = D_\infty + (D_0 - D_\infty)\cdot\exp(-k_{obs}\cdot t)$

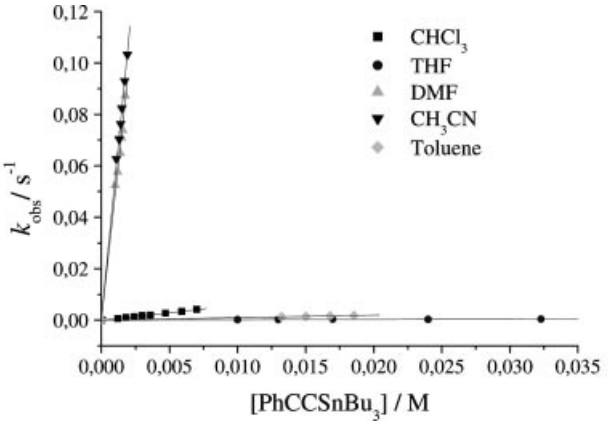

Figure 2. Plots of k_{obs} versus the stannane concentration for the transmetallation of **1c** with PhC≡CSnBu$_3$ in different solvents at 25 °C in the presence of fn ([**1c**]$_0$ = $1\cdot10^{-4}$ M; [fn]= $2\cdot10^{-4}$ M)

As reported in Figure 2 for the reactions of **1c**, the k_{obs} values at 25 °C depend on the stannane concentration in a linear manner so that the observed rate law can be represented by the relationship:

$k_{obs} = k_{2T}[PhC{\equiv}CSnBu_3]$

and the corresponding mechanism may be formulated as follows:

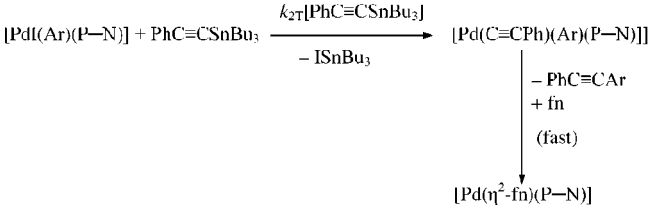

In all the solvents examined, the rate law does not display a solvolytic path, no intercept being detected in the plots in Figure 2. The measured k_{2T} values are listed in Table 6.

Table 6. Kinetic constants k_{2T} for the transmetallation of **1c** with PhC≡CSnBu$_3$ in different solvents at 25 °C in the presence of fn ([**1c**]$_0$ = $1\cdot10^{-4}$ M; [fn]= $2\cdot10^{-4}$ M)

Solvent	k_{2T}/ M^{-1}s^{-1}
THF	0.0107±0.0006
Toluene	0.10±0.01
$CHCl_3$	0.59±0.01
CH_3CN[a]	31±1
DMF	48±2

[a] In the presence of an excess of NEt_4I ([NEt_4I] = $1\cdot10^{-3}$ M).

As can be seen, a marked solvent effect is present with the highest k_{2T} values being observed in the more polar solvents CH_3CN and DMF. The kinetic measurements in CH_3CN were carried out in the presence of a large excess of NEt_4I in order to shift the position of equilibrium (2) completely to the left. In the absence of NEt_4I and with all other things being equal, the reaction in CH_3CN proceeds at a higher rate indicating that the cationic complex [Pd(Ar)(CH_3CN){2-(PPh_2)C_6H_4−1-CH=NC_6H_4OMe-4}]$^+$

 © 2004 Wiley-VCH Verlag GmbH & Co. KGaA, Weinheim

is a more reactive species than the neutral complex **1c**. Unfortunately, the reactivity of $[Pd(Ar)(CH_3CN)\{2\text{-}(PPh_2)C_6H_4\text{-}1\text{-}CH{=}NC_6H_4OMe\text{-}4\}]^+$ (as $CF_3SO_3^-$ salt) could not be determined because extensive decomposition occurred in the reaction mixture in the absence of the I^- ions.

From kinetic measurements at variable temperature, the activation parameters shown in Table 7 were evaluated.

Table 7. Kinetic constants k_{2T} and activation parameters for the transmetallation of **1c** with $PhC{\equiv}CSnBu_3$ in different solvents

Solvent	T / °C	k_{2T}/ $M^{-1}s^{-1}$	$\Delta H^{\neq}$/ $kJ{\cdot}mol^{-1}$	$\Delta S^{\neq}$/ $J{\cdot}mol^{-1}K^{-1}$
$CHCl_3$[a]	15	0.334±0.006	31±3	−146±12
	25	0.59±0.01		
	35	0.80±0.02		
	45	1.00±0.03		
CH_3CN[a][b]	15	27±1	23±1	−139±9
	25	55±1		
	35	68±4		
	45	108±4		

[a] In each kinetic run: $[\mathbf{1c}]_0 = 1{\cdot}10^{-4}$ M; [fn] = $2{\cdot}10^{-4}$ M. [b] In each kinetic run: $[NEt_4I] = 1{\cdot}10^{-3}$ M.

The markedly negative $\Delta S^{\neq}$ values clearly point to an associative S_E2 mechanism for the transmetallation step in both solvents. Because complex **1c** has an iodide ligand of good bridging ability, a cyclic four-center transition state may be operative in solvents of low polarity (toluene, THF, $CHCl_3$).[5] However, the strong acceleration observed in highly polar solvents (CH_3CN, DMF) is very much in favour of an open transition state with substantial charge separation.[5]

In the case of complex **2c**, the kinetic study of reaction (4) was carried out at 25 °C in $CHCl_3$ and CH_3CN under the same experimental conditions as for **1c**. In CH_3CN, an excess of NEt_4I was added ($[NEt_4I] = 1{\cdot}10^{-3}$ M). The observed kinetic law is identical to that found for **1c**, with $k_{2T} = 0.32{\pm}0.01$ $M^{-1}s^{-1}$ in $CHCl_3$ and $k_{2T} = 27{\pm}4$ $M^{-1}s^{-1}$ in CH_3CN. When compared with the corresponding values of **1c** in Table 6, one can see that the transmetallation step proceeds at comparable rates for both complexes. Presumably, the lower electrophilic character of the palladium center in **2c**, due to the greater electron-donating properties of the *N*-$CHMe_2$ substituent, is compensated for by the increased lability of the iodide ligand as can be inferred from the difference in the K_S constants of the equilibrium 2 for these complexes.

Conclusion

From the solution behaviour of the complexes $[Pd(\eta^2\text{-dmfu})(P{-}N)]$ and kinetic data for the oxidative addition of ArI (Ar = $C_6H_4CF_3$-4), a mechanism can be proposed consisting of (i) a solvolytic path the rate of which is zero-order with respect to ArI and involves the reactive species [Pd(solvent)(P−N)] formed in the olefin dissociation and (ii) a parallel path the rate of which is first-order with respect to ArI and involves the species $[Pd(\eta^2\text{-dmfu})(solvent)(\kappa_1\text{-}P{-}N)]$ formed in a pre-equilibrium dissociation of the Pd−N bond.

The reaction of [PdI(Ar)(P−N)] with $PhC{\equiv}CSnBu_3$ in the presence of activated olefins yields the complexes $[Pd(\eta^2\text{-ol})(P{-}N)]$. For this reaction, the rate-determining transmetallation step obeys a rate law which is first-order with respect to the stannane. The kinetic data suggest an associative S_E2 mechanism via an open transition state with substantial charge separation in highly polar solvents such as CH_3CN and DMF (path b of Scheme 1).

From the present study it clearly emerges that the oxidative addition represents the rate-determining step in the cross-coupling of $PhC{\equiv}CSnBu_3$ with ArI catalysed by $[Pd(\eta^2\text{-dmfu})(P{-}N)]$. The nature of the solvent is of great importance for increasing the overall rate of the catalysed reaction. In this respect, CH_3CN (a solvent with good coordinating properties and a high dielectric constant) proves to be the best suited medium since it enhances the rates of both the oxidative addition and transmetallation steps involved in the Stille process. Moreover, in the case of transmetallation in CH_3CN, the absence of added iodide allows the formation of a significant amount of the cationic species $[Pd(CH_3CN)(Ar)(P{-}N)]^+$ which increases the apparent rate of the reaction without leading to secondary decomposition products.

Experimental Section

^1H, $^{13}C\{^1H\}$, and $^{31}P\{^1H\}$ NMR spectra were recorded on a Bruker AM400 spectrometer operating at 400.13, 100.61, and 161.98 MHz, respectively, using solutions of the palladium complexes with concentrations in the range of $1{\cdot}10^{-2}$ to $2{\cdot}10^{-2}$ M. Chemical shifts are reported in ppm relative to TMS (^1H, ^{13}C) or external 85% H_3PO_4 (^{31}P). For the ^1H NMR spectra at variable temperature, the probe temperature was controlled by a standard unit calibrated with a methanol reference. Coalescence temperatures were determined to within an accuracy of 3 K. The estimated error in the calculated $\Delta G^{\neq}$ values is 0.6−0.8 $kJ{\cdot}mol^{-1}$. IR spectra were carried out using a Perkin−Elmer 983 spectrophotometer. UV/Vis spectra at variable temperature were recorded on a Peltier equipped Perkin−Elmer lambda 40 spectrophotometer. Conductivities were measured with CDM83 and Metrohm 660 conductimeters at 25 °C. All solvents were purified and dried before use according to standard methods.[25] The reactions were carried out under N_2 unless otherwise stated. The compounds $PhC{\equiv}CSnBu_3$, dimethyl fumarate, fumaronitrile, $AgBF_4$, and $AgCF_3SO_3$ were commercial samples and were used without further purification. The aryl iodide $IC_6H_4CF_3$-4 was distilled at reduced pressure before use. The iminophosphane $2\text{-}(PPh_2)C_6H_4\text{-}1\text{-}CH{=}NR$ [R = $CHMe_2$, C_6H_4OMe-4, $C_6H_3Me_2$-2,6, $C_6H_3(CHMe_2)_2$-2,6, bornyl] and the complexes $[Pd(\eta^2\text{-dmfu})(P{-}N)]$ (**1a**, **2a**), $[Pd(\eta^2\text{-fn})(P{-}N)]$ (**1b**, **2b**, **5b**), $[PdI(C_6H_4CF_3\text{-}4)(P{-}N)]$ (**1c**, **2c**) were prepared by published methods.[11,13,26] The complex $Pd_2(dba)_3{\cdot}CHCl_3$ was synthesised as described in the literature.[27]

Preparations

$[Pd(\eta^2\text{-dmfu})(P{-}N)]$ (3a, 4a): The required iminophosphane (1.0 mmol) and dmfu (173 mg, 1.2 mmol) were added to a stirred

 © 2004 Wiley-VCH Verlag GmbH & Co. KGaA, Weinheim

suspension of $Pd_2(dba)_3{\cdot}CHCl_3$ (1.035 g, 1 mmol) in dry acetone (30 mL). Stirring was continued for 2 h and the solution was then evaporated to dryness at reduced pressure. The solid residue was extracted with CH_2Cl_2 (20 mL) in the presence of activated charcoal. After filtration through celite, the clear red-brown solution was concentrated to a small volume (ca. 3 mL) and diluted with Et_2O to precipitate the products as yellow-orange solids. The complexes were purified by further precipitation from a toluene/*n*-hexane mixture.

3a: Yield 83% (535 mg). $C_{33}H_{32}NO_4PPd$ (644.0): calcd. C 61.54, H 5.01, N 2.17; found C 61.56, H 5.10, N 2.12%. IR (Nujol): $\tilde{\nu}$ = 1670 vs (C=O), 1615 ms (C=N) cm^{-1}. ^1H NMR ($CDCl_3$, 25 °C): δ = 8.06 (d, $J_{P,H}$ = 3.2 Hz, 1 H, N=CH), 7.6−6.9 (m, 17 H, C_6H_3 + C_6H_4 + C_6H_5), 4.24 (dd, $J_{H,H}$ = 10.0, $J_{P,H}$ = 2.4 Hz, 1 H, =CH *cis* to P), 3.77 (dd, $J_{H,H}$ = $J_{P,H}$ = 10.2 Hz, 1 H, =CH *trans* to P), 3.18 (s, 6 H, OCH_3), 2.16 (s, 3 H, CH_3), 1.90 (s, 3 H, CH_3) ppm. ^{31}P NMR ($CDCl_3$, 25 °C): δ = 19.69 (s) ppm.

4a: Yield 80% (560 mg). $C_{37}H_{40}NO_4PPd$ (700.1): calcd. C 63.47, H 5.76, N 2.00; found C 63.20, H 5.85, N 1.95%. IR (Nujol): $\tilde{\nu}$ = 1685 vs (C=O), 1622 ms (C=N) cm^{-1}. ^1H NMR ($CDCl_3$, 25 °C): δ = 8.06 (d, $J_{P,H}$ = 2.1 Hz, 1 H, N=CH), 7.6−6.9 (m, 17 H, C_6H_3 + C_6H_4 + C_6H_5), 4.25 (dd, $J_{H,H}$ = 10.4, $J_{P,H}$ = 2.5 Hz, 1 H, =CH *cis* to P), 3.49 (dd, $J_{H,H}$ = $J_{P,H}$ = 10.4 Hz, 1 H, =CH *trans* to P), 3.37 (spt, $J_{H,H}$ = 6.8 Hz, 1 H, $CHMe_2$), 3.24 (s, 3 H, OCH_3), 2.93 (s, 3 H, OCH_3), 2.64 (spt, $J_{H,H}$ = 6.8 Hz, 1 H, $CHMe_2$), 1.45 (d, $J_{H,H}$ = 6.8 Hz, 3 H, CH_3), 1.09 (d, $J_{H,H}$ = 6.8 Hz, 3 H, CH_3), 0.98 (d, $J_{H,H}$ = 6.8 Hz, 3 H, CH_3), 0.56 (d, $J_{H,H}$ = 6.8 Hz, 3 H, CH_3) ppm. ^{31}P NMR ($CDCl_3$, 25 °C): δ = 22.36 (s) ppm.

[Pd(CH_3CN)($C_6H_4CF_3$-4)[2-(PPh_2)C_6H_4−1-CH=NC_6H_4OMe-4)]CF_3SO_3: $AgCF_3SO_3$ (31 mg, 0.12 mmol) dissolved in CH_3CN (1 mL) was added to a solution of **1c** (93 mg, 0.12 mmol) in a CH_2Cl_2/CH_3CN mixture (7:1 v/v, 8 mL). After standing for 2 h in the dark, the insoluble AgI was removed by filtration and the resultant solution was evaporated to dryness at reduced pressure. The solid residue was redissolved in CH_2Cl_2 (10 mL). Addition of activated charcoal and filtration gave a clear solution which was concentrated to small volume (ca. 2 mL), then diluted with Et_2O to precipitate the product as a yellow microcrystalline solid. Yield 69% (69 mg). Λ_M ($1{\cdot}10^{-3}$ M, CH_3CN) = 134.4 $ohm^{-1}cm^2mol^{-1}$. $C_{36}H_{29}F_6N_2O_4PPdS$ (837.0): calcd. C 51.65, H 3.49, N 3.35; found C 51.81, H 3.55, N 3.45%. IR ($CHCl_3$): $\tilde{\nu}$ = 2289 ms (C≡N), 1636 m (C=N) cm^{-1}. ^1H NMR ($CDCl_3$, 25 °C): δ = 8.33 (s, 1 H, N=CH), 7.9−7.7 (m, 2 H, *o*-disubstituted C_6H_4), 7.59 (m, 1 H, *o*-disubstituted C_6H_4), 7.5−7.2 (m, 15 H, *o*-disubstituted C_6H_4 + *p*-disubstituted C_6H_4 + C_6H_5), 7.0−6.9 (m, 4 H, *meta* protons of *p*-disubstituted C_6H_4), 3.84 (s, 3 H, OCH_3), 2.30 (s, 3 H, CH_3CN) ppm. ^{31}P NMR ($CDCl_3$, 25 °C): δ = 34.74 (s) ppm.

[Pd(CH_3CN)($C_6H_4CF_3$-4)[2-(PPh_2)C_6H_4−1-CH=NCHMe_2)]BF_4: $AgBF_4$ (49 mg, 0.25 mmol) was added to a solution of **2c** (177 mg, 0.25 mmol) in CH_3CN (10 mL). The mixture was worked up as described above for the preparation of the analogous cationic complex to give the product as a yellow microcrystalline solid. Yield 73% (130 mg). Λ_M ($1{\cdot}10^{-3}$ M, CH_3CN) = 147.0 $ohm^{-1}cm^2mol^{-1}$. $C_{31}H_{29}BF_7N_2PPd$ (710.7): calcd. C 52.38, H 4.11, N 3.94; found C 52.15, H 4.02, N 3.86%. IR ($CHCl_3$): $\tilde{\nu}$ = 2316 mw, 2289 mw (C≡N), 1634 ms (C=N) cm^{-1}. ^1H NMR ($CDCl_3$, 25 °C): δ = 8.36 (s, 1 H, N=CH), 7.90 (m, 1 H, *o*-disubstituted C_6H_4), 7.78 (m, 1 H, *o*-disubstituted C_6H_4), 7.56 (m, 1 H, *o*-disubstituted C_6H_4), 7.5−7.2 (m, 13 H, *o*-disubstituted C_6H_4 + *p*-disubstituted C_6H_4 + C_6H_5), 6.95 (m, 2 H, *meta* protons of $C_6H_4CF_3$-4), 4.52 (spt, $J_{H,H}$ = 6.4 Hz, 1 H, $CHMe_2$), 2.30 (s, 3 H, CH_3CN), 1.37 (d, $J_{H,H}$ = 6.4 Hz, 6 H, CH_3) ppm. ^{31}P NMR ($CDCl_3$, 25 °C): δ = 32.70 (s) ppm.

Determination of the Equilibrium Constant K_E: To a thermostatically controlled (25 °C) solution of the complex under study (50 mL, ca. $1{\cdot}10^{-4}$ M) in the appropriate solvent were added successive micro-aliquots of the designated olefin and the absorbance changes were recorded in the range of 500−280 nm at 25 °C. The resultant array of absorbance data vs. the total concentration of added olefin was treated according to a published mathematical/statistical model.[16,17]

Determination of the Equilibrium Constant K_S: Several solutions of the complexes **1c** and **2c** at different concentrations (concentration intervals: $2.3{\cdot}10^{-5}$ to $2.4{\cdot}10^{-3}$ M, **1c**; $2.5{\cdot}10^{-5}$ to $2.6{\cdot}10^{-3}$ M, **2c**) in freshly distilled CH_3CN were prepared and thermostatically controlled at 25 °C. The specific conductivities were determined for each solution and the related molar conductivities were treated according to the method of Fuoss and Shedlovsky.[28]

A UV/Vis spectroscopic check was carried out as follows: the molar extinction coefficients (ε_k) of the starting complex (**1c** or **2c**) were determined from their solutions in the presence of a strong excess of NEt_4I, and those (ε_s) of the cationic species $[Pd(CH_3CN)(Ar)(P-N)]^+$ were determined from the solutions of their $CF_3SO_3^-$ or BF_4^- salts synthesised independently. The consistency of the conductivity determined K_S values and the reliability of the results was thus checked by a single spectrophotometric experiment by measuring the absorbance of a $1{\cdot}10^{-4}$ M solution of **1c** (or, **2c**) in CH_3CN. The ensuing absorbance values confirm, in both cases, the independently determined K_S constants.

Kinetic Measurements: The kinetics of the oxidative addition and transmetallation reactions were followed by UV/Vis spectroscopy upon addition of known micro-aliquots of a pre-thermostatically controlled solution of the appropriate reagent (ArI, or PhC≡CSnBu_3 and olefin) to a thermostatically controlled solution in the appropriate solvent of the complex under study {[Pd(η^2-dmfu)(P−N)] or [PdI(Ar)(P−N)} at the suitable temperature. The concentration of the reactant ensured in any case pseudo-first-order conditions and the reactions were followed by recording spectral changes in the suitable wavelength range or at a fixed wavelength. Mathematical and statistical data analysis was carried out on a PC equipped with a locally adapted non-linear regression procedure.

[1] [1a] J. K. Stille, *Angew. Chem. Int. Ed. Engl.* **1986**, *25*, 508−524. [1b] T. N. Mitchell, *Synthesis* **1992**, 803−815. [1c] V. Farina, in: *Comprehensive Organometallic Chemistry II* (Eds: E. W. Abel, F. G. A. Stone, G. Wilkinson), Pergamon, Oxford, **1995**, *12*, chapter 3.4, p. 161−240. [1d] V. Farina, G. P. Roth, *Adv. Metalorg. Chem.* **1996**, *5*, 1−53. [1e] T. N. Mitchell, in: *Metal-Catalyzed Cross-Coupling Reactions* (Eds. F. Diederich, P. J. Stang), Wiley-VCH, Weinheim, **1998**, p. 167−202. [1f] V. Farina, V. Krishnamurthy, V. J. Scott, *The Stille Reaction*, John Wiley & Sons, New York, **1998**.

[2] [2a] C. Amatore, A. Jutand, A. Suarez, *J. Am. Chem. Soc.* **1993**, *115*, 9531−9541. [2b] C. Mateo, D. J. Cardenas, C. Fernandez-Rivas, A. M. Echavarren, *Chem. Eur. J.* **1996**, *2*, 1596−1606.

[3] [3a] A. Gillie, J. K. Stille, *J. Am. Chem. Soc.* **1980**, *102*, 4933−4941. [3b] K. Tatsumi, R. Hoffmann, A. Yamamoto, J. K. Stille, *Bull. Chem. Soc. Jpn.* **1981**, *54*, 1857−1867. [3c] P. J. Stang, M. H. Kowalski, M. D. Schiavelli, D. J. Longford, *J. Am. Chem. Soc.* **1989**, *111*, 3347−3356. [3d] J. M. Brown, N. A. Cooley, *Organometallics* **1990**, *9*, 353−359. [3e] V. Farina, B. Krishnan, *J. Am. Chem. Soc.* **1991**, *113*, 9585−9595. [3f] V.

 © 2004 Wiley-VCH Verlag GmbH & Co. KGaA, Weinheim

Farina, B. Krishnan, D. R. Marshall, G. P. Roth, *J. Org. Chem.* **1993**, *58*, 5434−5444. [3g] J. Louie, J. F. Hartwig, *J. Am. Chem. Soc.* **1995**, *117*, 11598−11599. [3h] C. Amatore, E. Carré, A. Jutand, H. Tanaka, Q. Ren, S. Torii, *Chem. Eur. J.* **1996**, *2*, 957−966. [3i] C. Amatore, G. Broeker, A. Jutand, F. Khalil, *J. Am. Chem. Soc.* **1997**, *119*, 5176−5185. [3j] J. F. Hartwig, *Angew. Chem. Int. Ed.* **1998**, *37*, 2046−2067.

[4] E. Negishi, T. Takahashi, S. Baba, D. E. Van Horn, N. Okukado, *J. Am. Chem. Soc.* **1987**, *109*, 2393−2401.

[5] [5a] A. L. Casado, P. Espinet, *J. Am. Chem. Soc.* **1998**, *120*, 8978−8995. [5b] A. L. Casado, P. Espinet, A. M. Gallego, *J. Am. Chem. Soc.* **2000**, *122*, 11771−11782.

[6] A. Ricci, F. Angelucci, M. Bassetti, C. Lo Sterzo, *J. Am. Chem. Soc.* **2002**, *124*, 1060−1071.

[7] [7a] C. Amatore, A. Bucaille, A. Fuxa, A. Jutand, G. Meyer, A. N. Ntepe, *Chem. Eur. J.* **2001**, *7*, 2134−2142. [7b] C. Amatore, A. A. Bahsoun, A. Jutand, G. Meyer, A. Ndedi Ntepe, L. Ricard, *J. Am. Chem. Soc.* **2003**, *125*, 4212−4222.

[8] J. A. Casares, P. Espinet, G. Salas, *Chem. Eur. J.* **2002**, *8*, 4844−4853.

[9] A. L. Casado, P. Espinet, A. M. Gallego, J. M. Martìnez-Ilarduya, *Chem. Commun.* **2001**, 339−340.

[10] E. Shirakawa, T. Hiyama, *J. Organomet. Chem.* **1999**, *576*, 169−178, and references cited therein.

[11] S. Antonaroli, B. Crociani, *J. Organomet. Chem.* **1998**, *560*, 137−146.

[12] A. Scrivanti, U. Matteoli, V. Beghetto, S. Antonaroli, B. Crociani, *Tetrahedron* **2002**, *58*, 6881−6886.

[13] B. Crociani, S. Antonaroli, V. Beghetto, U. Matteoli, A. Scrivanti, *Dalton Trans.* **2003**, 2194− 2202.

[14] G. Bandoli, A. Dolmella, L. Crociani, S. Antonaroli, B. Crociani, *Transition Met. Chem.* **2000**, *25*, 17−25.

[15] L. Crociani, G. Bandoli, A. Dolmella, M. Basato, B. Corain, *Eur. J. Inorg. Chem.* **1998**, 1811−1820.

[16] L. Canovese, F. Visentin, P. Uguagliati, B. Crociani, *J. Chem. Soc., Dalton Trans.* **1996**, 1921−1925.

[17] L. Canovese, F. Visentin, G. Chessa, P. Uguagliati, A. Dolmella, *J. Organomet. Chem.* **2000**, *601*, 1−15.

[18] [18a] B. Jedlicka, R. E. Rülke, W. Weissensteiner, R. Fernández-Galán, F. A. Jalón, B. R. Manzano, J. Rodríguez-de la Fuente, N. Valdman, H. Kooijman, A. L. Spek, *J. Organomet. Chem.* **1966**, *516*, 97−110. [18b] R. Fernández-Galán, F. A. Jalón, B. R. Manzano, J. Rodríguez-de la Fuente, M. Vrahani, B. Jedlicka, W. Weissensteiner, *Organometallics* **1997**, *16*, 3758−3768. [18c] K. Selvakumar, M. Valentini, M. Wörle, P. S. Pregosin, A. Albinati, *Organometallics* **1999**, *18*, 1207−1215. [18d] F. A. Jalón, B. R. Manzano, F. Gómez-de la Torre, A. M. López-Agenjo, A. M. Rodríguez, W. Weissensteiner, T. Sturm, J. Mahía, M. Maestro, *J. Chem. Soc., Dalton Trans.* **2001**, 2417−2424. [18e] M. Zehnder, M. Neuburger, S. Schaffner, M. Jufer, D. A. Plattner, *Eur. J. Inorg. Chem.* **2002**, 1511−1517.

[19] C. Amatore, A. Fuxa, A. Jutand, *Chem. Eur. J.* **2000**, *6*, 1474−1482.

[20] The activation free energies have been estimated from the coalescence temperature (T_c) using the equation $\Delta G^{\neq} = -RT_c\ln[\pi h\Delta\nu/(2^{1/2}kT_c)]$. The palladium(0) species are fairly stable towards decomposition when the temperature is increased. A slight decomposition with formation of free dmfu is observed at the higher temperatures. The coalescence temperatures are, however, scarcely affected because the exchange between free and coordinated olefin is slow. Addition of free dmfu to the solution of **1a** at 56 °C actually caused only a slight broadening of the methyl signals of the free and coordinated olefin.

[21] R. van Asselt, C. J. Elsevier, W. J. J. Smeets, A. L. Spek, *Inorg. Chem.* **1994**, *33*, 1521−1531.

[22] [22a] D. M. Himmeblau, *Process Analysis by Statistical Methods*, John Wiley & Sons, New York, **1970**. [22b]P. Uguagliati, R. A. Michelin, U. Belluco, R. Ros, *J. Organomet. Chem.* **1979**, *169*, 115−122.

[23] The steady-state approach leads to the equation: $k_{obs} = k_{1A} + k_{2A}[ArI] - k_{1A}k_{-1A}/(k_{-1A} + k_{3A}[ArI])$ for [Pd(η^2-dmfu)(solvent)(κ^1-P−N)] as intermediate, or to the equation: $k_{obs} = k_{1A} + k_{2A}[ArI] - k_{1A}k_{-1A}[dmfu]/(k_{-1A}[dmfu] + k_{3A}[ArI])$ for [Pd(solvent)(P−N)] as intermediate. These equations become the observed rate law: $k_{obs} = k_{1A} + k_{2A}[ArI]$ when the reasonable approximations $(k_{-1A} + k_{3A}[ArI]) >> k_{1A}k_{-1A}$ or $(k_{-1A}[dmfu] + k_{3A}[ArI]) >> k_{1A}k_{-1A}[dmfu]$ are operative. On the other hand, the pre-equilibrium (K_1) condition:

$$[\text{Pd}(\eta^2\text{-dmfu})(\text{P—N})] \underset{-\text{S}}{\overset{+\text{S}}{\rightleftharpoons}} \text{Intermediate}$$
1a

was never taken into account since for both intermediates it leads to rate laws which do not correspond to the experimental one. As an example, for [Pd(η^2-dmfu)(solvent)(κ^1-P−N)] as the intermediate the rate law should become: $k_{obs} = (k_{2A}+k_{3A}K_1)[ArI]/(1+K_1)$.

[24] M. Huser, M.-T. Youinou, J. A. Osborn, *Angew. Chem. Int. Ed. Engl.* **1989**, *28*, 1386−1388.

[25] W. L. Armarengo, D. D. Perrin, *Purification of Laboratory Chemicals*, 3rd ed., Pergamon, New York, **1988**.

[26] B. Crociani, S. Antonaroli, L. Canovese, F. Visentin, P. Uguagliati, *Inorg. Chim. Acta* **2001**, *315*, 172−182.

[27] T. Ukai, H. Kawazura, Y. Ishii, J. J. Bonnet, J. A. Ibers, *J. Organomet. Chem.* **1974**, *65*, 253−266.

[28] [28a] R. M. Fuoss, T. Shedlovsky, *J. Am. Chem. Soc.* **1949**, *120*, 1496−1498. [28b] J. Barthel, *Angew. Chem. Int. Ed. Engl.* **1968**, *7*, 260−277. [28c] B. Crociani, F. Di Bianca, P. Uguagliati, L. Canovese, A. Berton, *J. Chem. Soc., Dalton Trans.* **1991**, 71−79.

Received June 18, 2003
Early View Article
Published Online January 2, 2004

 © 2004 Wiley-VCH Verlag GmbH & Co. KGaA, Weinheim

Synthesis, Structures and Reactions of Novel 9,10-Dihydro-9,10-distannaanthracenes

Masaichi Saito,*[a] Natsumi Henzan,[a] Minehiko Nitta,[a] and Michikazu Yoshioka[a]

Keywords: Halogenation / Synthesis design / Tin

A method for the synthesis of 9,10-dihydro-9,10-distannaanthracenes has been improved and applied to the synthesis of novel unsymmetrical 9,10-dihydro-9,10-distannaanthracenes. The first 9,9,10,10-tetrahalo-9,10-dihydro-9,10-distannaanthracenes were successfully synthesized by halogenation of 9,9,10,10-tetrakis(*p*-methoxyphenyl)-9,10-dihydro-9,10-distannaanthracene. The structures of the newly obtained 9,10-dihydro-9,10-distannaanthracenes were determined by X-ray analysis.

(© Wiley-VCH Verlag GmbH & Co. KGaA, 69451 Weinheim, Germany, 2004)

Introduction

Since the first synthesis of 9,9,10,10-tetraphenyl-9,10-dihydro-9,10-disilaanthracene,[1] studies of the synthesis, structures, and reactions of 9,10-dihydro-9,10-disilaanthracene have been developed.[2] The corresponding germanium analogs, 9,10-dihydro-9,10-digermaanthracenes, have also been synthesized and characterized.[3] One of the interesting features of 9,10-dihydro-9,10-dimetallaanthracenes is the conformations of their central six-membered rings which are dependent on substituents on the metal.[4−7] Although a few 9,10-dihydroanthracenes having a tin atom at the 10-position have been reported,[4,8] only one report on the 9,10-dihydro-9,10-distannaanthracene has appeared, but without synthetic or structural details.[9] During the course of our studies on tin-containing compounds with unique structures, we have already reported the first syntheses and structures of 9,9,10,10-tetramethyl- and 9,9,10,10-tetra-*tert*-butyl-9,10-dihydro-9,10-distannaanthracenes.[7,10] The tetramethyl derivative has a butterfly conformation, while the tetra-*tert*-butyl derivative has a planar structure. The dependence of conformation on substituents prompted us to investigate some other 9,10-dihydro-9,10-distannaanthracenes having aryl groups and those with unsymmetrical structures. The utility of 9,10-dihydro-9,10-dimetallaanthracene derivatives as potential precursors for metal-containing reactive species is also of interest. Recently, fascinating silicon-containing reactive species such as a bis(silyl anion)[11] and a relatively stable silyl radical[6] have been reported to be derived from 9,10-dihydro-9,10-disilaanthracenes. 9,9,10,10-Tetrahalogenated 9,10-dihydro-9,10-distannaanthracenes are expected to be good precursors for reactive tin-containing species having a 9,10-distannaanthracene skeleton. However, no report on such halogenated derivatives has appeared.

We report herein an improved method for the synthesis of aryl-substituted and unsymmetrical substituted 9,10-dihydro-9,10-distannaanthracenes. Halogenation of 9,9,10,10-tetrakis(*p*-methoxyphenyl)-9,10-dihydro-9,10-distannaanthracene to give the first 9,9,10,10-tetrahalo-9,10-dihydro-9,10-distannaanthracenes is also reported. The structures of the newly obtained 9,10-dihydro-9,10-distannaanthracenes are discussed.

Results and Discussion

Improved Method for the Synthesis of 9,10-Dihydro-9,10-distannaanthracenes

A previous publication reported the synthesis of 9,9,10,10-tetramethyl-9,10-dihydro-9,10-distannaanthracene (**1**) from the reaction of bis(*o*-bromophenyl)dimethylstannane (**2**) and dichlorodimethylstannane with magnesium in the presence of a catalytic amount of copper(I) cyanide in 25% yield.[7] By using *tert*-butyllithium for the lithiation of **2** in THF at −78 °C, the yield of **1** was increased to 51% (Scheme 1).

Introduction of *p*-methoxyphenyl groups on the tin was examined using *tert*-butyllithium. Bis(*o*-bromophenyl)bis(*p*-methoxylphenyl)stannane (**3**) was synthesized by the reaction of (2-bromophenyl)lithium with bis(*p*-methoxyphenyl)-dichlorostannane[12] in 48% yield. Lithiation of **3** using *tert*-butyllithium and subsequent reaction with bis(*p*-methoxyphenyl)dichlorostannane gave the 9,9,10,10-tetrakis(*p*-methoxyphenyl)-substituted compound **4** in 46% yield (Scheme 1).

[a] Department of Chemistry, Faculty of Science, Saitama University,
Shimo-okubo, Sakura-ku, Saitama City, Saitama, 338−8570 Japan
E-mail: masaichi@chem.saitama-u.ac.jp

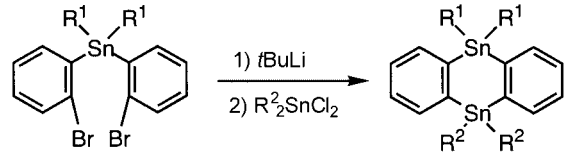

2 (R^1 = Me)
3 (R^1 = *p*-$OMeC_6H_4$)

1 (R^1 = R^2 = Me: 51%)
4 (R^1 = R^2 = *p*-$OMeC_6H_4$: 46%)
5 (R^1 = Me, R^2 = *t*Bu: 19%)
6 (R^1 = *p*-$OMeC_6H_4$, R^2 = Me: 14%)

	1	4	5	6	9	10
R^1	Me	*p*-$OMeC_6H_4$	Me	*p*-$OMeC_6H_4$	Cl	I
R^2	Me	*p*-$OMeC_6H_4$	*t*Bu	Me	Cl	I

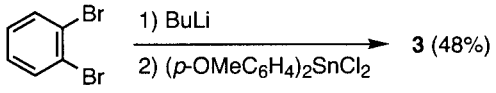

Scheme 1

Synthesis of Unsymmetrically-Substituted 9,10-Dihydro-9,10-distannaanthracenes

This improved method can be applied to the synthesis of unsymmetrically-substituted 9,10-dihydro-9,10-distannaanthracenes. Thus, lithiation of **2** and **3** with *tert*-butyllithium in THF at −78 °C and subsequent treatment with di-*tert*-butyldichlorostannane and dichlorodimethylstannane gave the 9,9-di-*tert*-butyl-10,10-dimethyl-substituted and 9,9-bis(*p*-methoxyphenyl)-10,10-dimethyl-substituted compounds **5** and **6** in yields of 19 and 14%, respectively (Scheme 1). The structures of **5** and **6** were determined using ^{1}H and ^{13}C NMR spectroscopy and elemental analysis.

Halogenation of 9,10-Dihydro-9,10-distannaanthracenes

In order to prepare further functionalized 9,10-dihydro-9,10-distannaanthracenes, the halogenations of the tetra-*tert*-butyl-substituted 9,10-dihydro-9,10-distannaanthracene **7**[7] and the 9,9,10,10-tetrakis(*p*-methoxyphenyl)-substituted 9,10-dihydro-9,10-distannaanthracene **4** were investigated. Reaction of **7** with bromine (1 equiv.) gave the dibromide **8** (77%) through the cleavage of a tin−phenyl bond because the ease of cleavage of the Sn−C bond is in the order of Sn−aromatic > −vinyl > −alkyl (Scheme 2).[13] Conversely, chlorination of **4** using acetyl chloride and aluminum chloride[14] gave 9,9,10,10-tetrachloro-9,10-dihydro-9,10-distannaanthracene (**9**), reflecting the ease of cleavage of an Sn−*p*-methoxyphenyl bond (Scheme 3). The *p*-methoxyphenyl group on tin is easily substituted by a halogen.[14] Reaction of **4** with iodine gave the tetraiodide **10** (Scheme 3). These haloganated 9,10-dihydro-9,10-distannaanthracenes, the first examples of a 9,9,10,10-tetrahalo-9,10-dihydro-9,10-distannaanthracene, are expected to be good precursors for reactive tin-containing species such as 9,10-distannaanthracene.

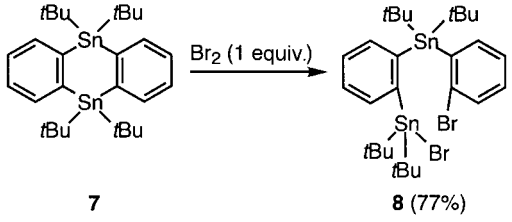

7 **8** (77%)

Scheme 2

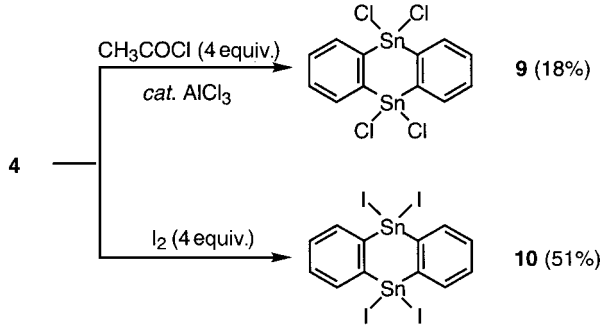

Scheme 3

X-ray Crystallographic Structures of the Newly Obtained 9,10-Dihydro-9,10-distannaanthracenes 4, 6, and 10

The X-ray crystallographic analyses were carried out at room temperature. The molecular structures of **4**, **6**, and **10** with selected bond lengths and angles are shown in Figures 1, 2, and 3, respectively. The central six-membered ring of

 © 2004 Wiley-VCH Verlag GmbH & Co. KGaA, Weinheim

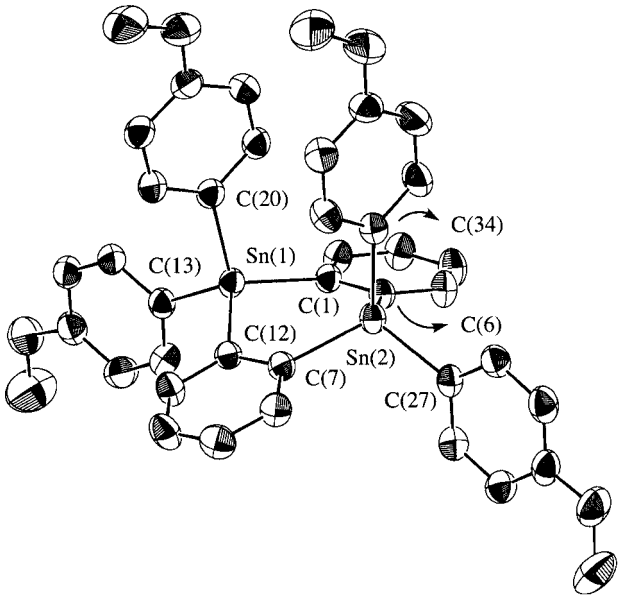

Figure 1. ORTEP drawing of **4** with thermal ellipsoids plots (40% probability for non-hydrogen atoms); selected bond lengths [Å] and angles (deg): Sn(1)−C(13) 2.127(3), Sn(1)−C(20) 2.127(3), Sn(2)−C(27) 2.135(3), Sn(2)−C(34) 2.130(3); C(1)−Sn(1)−C(12) 108.90(12), C(6)−Sn(2)−C(7) 109.07(12), C(13)−Sn(1)−C(20) 111.22(13), C(7)−Sn(2)−C(34) 109.00(13)

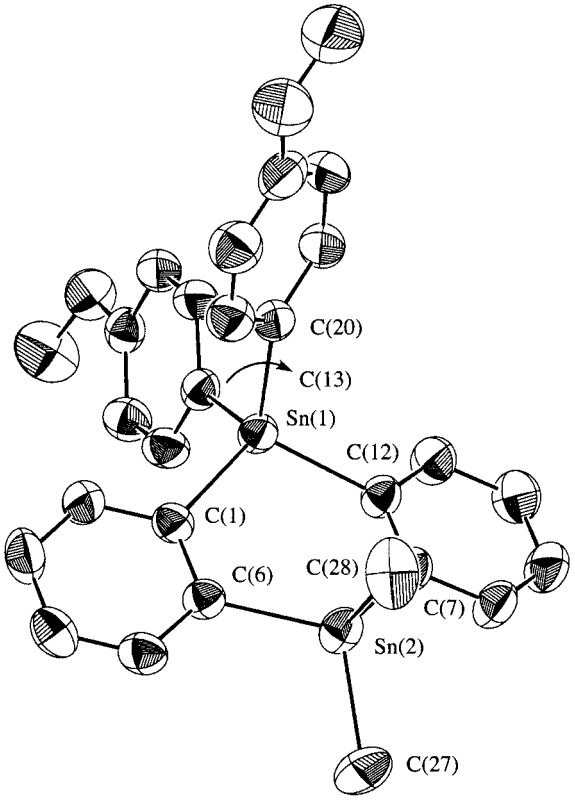

Figure 2. ORTEP drawing of **6** with thermal ellipsoids plots (40% probability for non-hydrogen atoms); selected bond lengths [Å] and angles (deg): Sn(1)−C(13) 2.137(3), Sn(1)−C(20) 2.146(4), Sn(2)−C(27) 2.145(5), Sn(2)−C(28) 2.128(5); C(1)−Sn(1)−C(12) 110.18(13), C(6)−Sn(2)−C(7) 108.63(13), C(13)−Sn(1)−C(20) 108.19(13), C(7)−Sn(2)−C(27) 112.3(2)

6 adopts a boat conformation and hence the tricyclic framework has a butterfly conformation with a dihedral angle of 156° as observed in the 9,9,10,10-tetramethyl derivative (143°).[7] Although 9,9,10,10-tetraphenyl-9,10-dihydro-9,10-disilaanthracene has a planar structure,[15] the central six-membered ring of **4** has a boat conformation with a dihedral angle of 149° due to the Sn−C_6H_4OMe-*p* bonds being longer than the Si−Ph bonds in the tetraphenyl compound so that the *p*-methoxyphenyl group can be orientated in a pseudoaxial position. The tetra-iodo derivative **10** has a planar structure, as observed in the 9,9,10,10-tetra-*tert*-butyl derivative,[7] probably due to the steric bulk of the iodine atom.

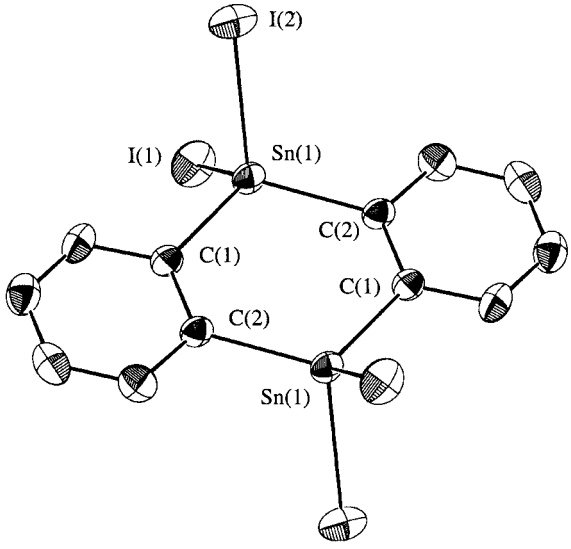

Figure 3. ORTEP drawing of **10** with thermal ellipsoids plots (40% probability for non-hydrogen atoms); selected bond lengths [Å] and angles (deg): Sn(1)−I(1) 2.6812(8), Sn(1)−I(2) 2.6795(8), Sn(1)−C(1) 2.129(7), Sn(1)−C(2) 2.124(8); C(1)−Sn(1)−C(2) 114.8(3), I(1)−Sn(1)−I(2) 104.76(3)

Conclusion

A novel method for the synthesis of 9,10-dihydro-9,10-distannanthracenes has been developed and novel 9,10-dihydro-9,10-distannanthracenes having unsymmetrical structures have been synthesized. Halogenation of 9,9,10,10-tetrakis(*p*-methoxyphenyl)-9,10-dihydro-9,10-distannaanthracene gave the first 9,9,10,10-tetrahalo-9,10-dihydro-9,10-distannaanthracenes. Although the 9,10-dihydro-9,10-distannanthracenes having *p*-methoxyphenyl groups on the tin have a butterfly conformation, the 9,9,10,10-tetraiodo derivative has a planar structure for steric reasons. Further investigations on the synthesis of reactive tin-containing species having a 9,10-distannaanthracene skeleton from 9,9,10,10-tetrahalo derivatives are currently in progress.

Experimental Section

General Procedure: All reactions were carried out under argon. THF and diethyl ether used in the syntheses were distilled from

 © 2004 Wiley-VCH Verlag GmbH & Co. KGaA, Weinheim

sodium benzophenone ketyl under an argon atmosphere before use. Magnesium (turnings) was purchased from Wako Pure Chemical Industries, Ltd. ^{1}H (400 MHz), ^{13}C NMR (101 MHz) and ^{119}Sn NMR (149 MHz) spectra were recorded on a Bruker AM-400 or an ARX-400 spectrometer in $CDCl_3$ with tetramethylsilane as an internal standard. Although ^nJ(Sn−^{13}C) couplings were observed in the ^{13}C NMR spectra as satellite signals, most of the ^nJ(^{119}Sn−^{13}C) and ^nJ(^{117}Sn−^{13}C) values could not be separately estimated because of broadening. The multiplicities of signals in the ^{13}C NMR spectra given in parentheses were deduced from DEPT spectra. Wet column chromatography (WCC) was carried out by using Merck Kieselgel 60 (SiO_2). All melting points were determined on a Mitamura Riken Kogyo MEL-TEMP apparatus and are uncorrected. Elemental analyses were carried out at the Microanalytical Laboratory of the Chemical Analysis Center, Saitama University. Data for the X-ray crystallographic analyses were collected on Mac Science Xdip or MXC18 K diffractometers with Mo-K_α radiation (λ = 0.71073 Å) and the structures were solved by direct methods.

Improved Synthesis of 9,9,10,10-Tetramethyl-9,10-dihydro-9,10-distannaanthracene (1): To a THF (10 mL) solution of bis(*o*-bromophenyl)dimethylstannnane[7] (**2**) (232 mg, 0.50 mmol) was added *t*BuLi (1.60 M in pentane; 1.25 mL, 2.00 mmol) at −78 °C and the resultant solution was stirred at this temperature for 1 h. After addition of a THF (5 mL) solution of dichlorodimethylstannane (110 mg, 0.50 mmol) at the same temperature, the reaction mixture was allowed to warm to room temperature. The resultant mixture was extracted with diethyl ether and the organic layer was washed with aqueous NH_4Cl. After removal of volatile components, the residue was subjected to WCC (SiO_2, hexane/ethyl acetate, 20:1) to afford 9,9,10,10-tetramethyl-9,10-dihydro-9,10-distannaanthracene[7] (**1**) (116 mg, 51%).

Preparation of Bis(*o*-bromophenyl)bis(*p*-methoxylphenyl)stannane (3): To a solution of butyllithium (1.56 M in hexane; 6.24 mL, 4.00 mmol) in a mixture of THF (10 mL) and diethyl ether (10 mL) was added 1,2-dibromobenzene (0.72 mL, 5.97 mmol) at −110 °C and the resultant solution was stirred at this temperature for 1.5 h. Subsequently, bis(*p*-methoxyphenyl)dichlorostannane[12] (1.304 g, 3.23 mmol) in THF (5 mL) and diethyl ether (5 mL) was added at −110 °C. The reaction mixture was allowed to warm to room temperature. The resultant mixture was extracted with diethyl ether and the organic layer was washed with aqueous NH_4Cl. After removal of volatile components, the residue was subjected to WCC (SiO_2, hexane/dichloromethane, 1:3) followed by recrystallization from dichloromethane and methanol to give bis(*o*-bromophenyl)bis(*p*-methoxylphenyl)stannane (**3**) (0.926 g, 48%). **3**: M.p. 142−145 °C (recrystallization from dichloromethane/methanol). ^{1}H NMR: δ = 3.82 (s, 6 H), 6.94−6.99 (m, 4 H), 7.25−7.27 (m, 4 H), 7.38−7.40 (m, 2 H), 7.52−7.68 (m, 6 H). ^{13}C NMR: δ = 55.0 (q), 114.4 [d, J(Sn−C) = 61 Hz), 126.9 [d, J(Sn−C) = 47 Hz), 128.4 (s), 130.9 (d), 132.1 [d, J(Sn−C) = 31 Hz), 132.5 [s, J(Sn−C) = 14 Hz], 138.6 [d, J(Sn−C) = 46 Hz], 139.3 [d, J(Sn−C) = 36 Hz), 144.5 (s), 160.4 (s). ^{119}Sn NMR: δ = −116.5 ppm. $C_{26}H_{22}Br_2O_2Sn$ (644.98): calcd. C 48.42, H 3.44; found C 48.54, H 3.35.

Preparation of 9,9,10,10-Tetrakis(*p*-methoxyphenyl)-9,10-dihydro-9,10-distannaanthracene (4): To a THF (10 mL) solution of **3** (1.006 g, 1.56 mmol) was added *t*BuLi (1.6 M in pentane; 3.0 mL, 4.8 mmol) at −78 °C and the resultant solution was stirred at this temperature for 20 min. After addition of a THF (5 mL) solution of bis(*p*-methoxyphenyl)dichlorostannane[12] (0.684 g, 1.69 mmol) at the same temperature, the reaction mixture was allowed to warm to room temperature. The resultant mixture was extracted with diethyl ether and the organic layer was washed with aqueous NH_4Cl. After removal of volatile components, the residue was subjected to WCC (SiO_2, hexane/dichloromethane, 1:4) followed by recrystallization from hexane and dichloromethane to give 9,9,10,10-tetrakis(*p*-methoxyphenyl)-9,10-dihydro-9,10-distannaanthracene (**4**) (0.584 g, 46%). **4**: M.p. 221−222 °C (recrystallization from hexane/dichloromethane). ^{1}H NMR: δ = 3.77 (s, 12 H), 6.79−6.83 (m, 8 H), 7.28−7.29 (m, 4 H), 7.34−7.36 (m, 8 H), 7.57−7.60 (m, 4 H). ^{13}C NMR: δ = 54.9 (q), 114.3 (d), 128.6 [s, ^1J(Sn−C) = 522, 546 Hz], 128.8 [d, J(Sn−C) = 49 Hz], 137.3 [d, J(Sn−C) = 45, 55 Hz], 138.4 [d, J(Sn−C) = 44 Hz], 150.8 [s, ^1J(Sn−C) = 520, 544, ^2J(Sn−C) = 52 Hz], 160.3 (s). ^{119}Sn NMR: δ = −173.6 [^3J(Sn−Sn) = 761 Hz] ppm. $C_{40}H_{36}O_4Sn_2$ (818.16): calcd. C 58.72, H 4.44; found C 58.63, H 4.29.

Preparation of 9,9-Di-*tert*-butyl-10,10-dimethyl-9,10-dihydro-9,10-distannaanthracene (5): To a THF (10 mL) solution of **2** (240 mg, 0.52 mmol) was added *t*BuLi (1.60 M in pentane; 1.30 mL, 2.08 mmol) at −78 °C and the resultant solution was stirred at this temperature for 30 min. To the reaction mixture was added a THF (5 mL) solution of di-*tert*-butyldichlorostannane (160 mg, 0.50 mmol) at the same temperature. After stirring for 2 h at −78 °C, the reaction mixture was gradually allowed to warm to room temperature. The resultant mixture was extracted with diethyl ether and the organic layer was washed with aqueous NH_4Cl. After removal of volatile components, the residue was subjected to WCC (SiO_2, hexane/ethyl acetate, 100:1) to afford 9,9-di-*tert*-butyl-10,10-dimethyl-9,10-dihydro-9,10-distannaanthracene (**5**) (52 mg, 19%). **5**: M.p. 77−79 °C (recrystallization from hexane/methanol). ^{1}H NMR: δ = 0.36 [s, 6 H, ^2J(Sn−H) = 52, 55 Hz], 1.30 [s, 18 H, ^3J(Sn−H) = 63, 65 Hz], 7.27−7.30 (m, 4 H), 7.54−7.56 (m, 4 H). ^{13}C NMR: δ = −7.7 [q, ^1J(Sn−C) = 329, 345 Hz], 29.9 [s, ^1J(Sn−C) = 365, 382 Hz], 31.5 (q), 127.6 (d), 128.1 (d), 136.3 [d, J(Sn−C) = 42, 48 Hz], 137.4 [d, J(Sn−C) = 42, 54 Hz], 152.0 [s, ^1J(Sn−C) = 362, 379, ^2J(Sn−C) = 53 Hz], 153.4 [s, ^1J(Sn−C) = 500, 523, ^2J(Sn−C) = 35 Hz]. ^{119}Sn NMR: δ = −156.3 [^3J(Sn−Sn) = 497, 546 Hz], −121.1 [^3J(Sn−Sn) = 497, 546 Hz] ppm. $C_{22}H_{32}Sn_2$ (533.94): calcd. C 49.49, H 6.04; found C 49.96, H 6.06.

Preparation of 9,9-Bis(*p*-methoxyphenyl)-10,10-dimethyl-9,10-dihydro-9,10-distannaanthracene (6): To a THF (5 mL) solution of **3** (196 mg, 0.30 mmol) was added *t*BuLi (1.60 M in pentane; 0.75 mL, 1.20 mmol) at −78 °C and the resultant solution was stirred at this temperature for 1 h. To the reaction mixture was added a THF (5 mL) solution of dichlorodimethylstannane (74 mg, 0.30 mmol) at the same temperature. After stirring for 1 h at −78 °C, the reaction mixture was gradually allowed to warm to room temperature. The resultant mixture was extracted with diethyl ether and the organic layer was washed with aqueous NH_4Cl. After removal of volatile components, the residue was subjected to WCC (SiO_2, hexane/ethyl acetate, 6:1) to afford 9,9-bis(*p*-methoxyphenyl)-10,10-dimethyl-9,10-dihydro-9,10-distannaanthracene (**6**) (27 mg, 14%). **6**: M.p. 115−118 °C (recrystallization from hexane/dichloromethane). ^{1}H NMR: δ = 0.32 [s, 6 H, ^2J(Sn−H) = 54, 56 Hz], 3.80 (s, 6 H), 6.93 (d, J = 9 Hz, 4 H), 7.24−7.28 (m, 2 H), 7.30−7.34 (m, 2 H), 7.38−7.50 (m, 4 H), 7.53−7.65 (m, 4 H). ^{13}C NMR: δ = −8.5 [q, ^1J(Sn−C) = 344 Hz], 55.0 (q), 114.5 [d, J(Sn−C) = 55 Hz], 128.3 (d), 128.6 (d), 128.9 (s), 136.1 [d, J(Sn−C) = 46, 56 Hz], 136.9 [d, J(Sn−C) = 55 Hz], 138.4 [d, J(Sn−C) = 44 Hz], 150.0 (s), 152.7 (s), 160.5 (s). ^{119}Sn NMR: δ = −171.6 [^3J(Sn−Sn) = 727, 796 Hz], −116.5 [^3J(Sn−Sn) = 727, 796 Hz] ppm. $C_{28}H_{28}O_2Sn_2$ (633.96): calcd. C 53.05, H 4.45; found C 53.32, H 4.38.

 © 2004 Wiley-VCH Verlag GmbH & Co. KGaA, Weinheim

Reaction of 9,9,10,10-Tetra-*tert*-butyl-9,10-dihydro-9,10-distannaanthracene (7) with Bromine: To a carbon tetrachloride (15 mL) solution of **7** (162 mg, 0.26 mmol) was added a carbon tetrachloride (5 mL) solution of bromine (42 mg, 0.26 mmol) at room temperature. After removal of the solvent, the residue was recrystallized from dichloromethane and methanol to give [2- (bromodi-*tert*-butylstannyl)](2-bromophenyl)di-*tert*-butylstannane (**8**) (133 mg, 77%). **8**: M.p. 182−184 °C (recrystallization from dichloromethane/methanol). ^{1}H NMR: δ = 1.26 [s, 18 H, ^3J(Sn−H) = 81, 84 Hz], 1.36 [br. s, 18 H, ^3J(Sn−H) = 68 Hz], 7.04−7.17 (m, 3 H), 7.20−7.24 (m, 1 H), 7.31−7.35 (m, 1 H), 7.50−7.55 (m, 1 H), 7.73−7.75 (m, 1 H). ^{13}C NMR: δ = 30.8 (q), 31.6 (br. q), 35.9 [s, ^1J(Sn−C) = 360, 377 Hz], 125.8 [d, J(Sn−C) = 34 Hz], 126.4 [d, J(Sn−C) = 11, 62 Hz], 127.5 [d, J(Sn−C) = 15, 40 Hz], 129.0 (d), 131.7 (s), 131.8 (d), 136.8 [d, J(Sn−C) = 48, 83 Hz], 139.2 [d, J(Sn−C) = 23 Hz], 141.0 [d, J(Sn−C) = 38, 61 Hz], 151.4 [s, J(Sn−C) = 43 Hz], 151.9 (s), 153.3 [s, J(Sn−C) = 50 Hz]. ^{119}Sn NMR: δ = −78.5 (br.), 3.9 ppm. $C_{28}H_{44}Br_2Sn_2$ (777.92): calcd. C 43.23, H 5.70; found C 43.45, H 5.72.

Preparation of 9,9,10,10-Tetrachloro-9,10-dihydro-9,10-distannaanthracene (9): To a toluene (5 mL) solution of **4** (183 mg, 0.22 mmol) was added acetyl chloride (0.063 mL, 0.84 mmol) in the presence of a catalytic amount of aluminum trichloride at 0 °C. After separation of insoluble materials in dichloromethane by filtration, the residue was crystallized from chloroform and dichloromethane to afford 9,9,10,10-tetrachloro-9,10-dihydro-9,10-distannaanthracene (**9**) (24 mg, 18%). **6**: M.p. 285−288 °C (decomp.) (recrystallization from dichloromethane/chloroform). ^{1}H NMR: δ = 7.63−7.69 (m, 4 H), 7.74−7.94 (m, 4 H). ^{13}C NMR: δ = 133.1 [d, J(Sn−C) = 92 Hz, C_β], 137.1 [d, J(Sn−C) = 84, 103 Hz, C_α], 152.4 (s, C_{ipso}) ppm. $C_{12}H_8Cl_4Sn_2$ (531.4): calcd. C 27.12, H 1.52; found C 27.28, H 1.42.

Preparation of 9,9,10,10-Tetraiodo-9,10-dihydro-9,10-distannaanthracene (10): A dichloromethane (50 mL) solution of iodine (700 mg, 2.76 mmol) was added to a dichloromethane (10 mL) solution of **4** (566 mg, 0.69 mmol). The mixture was heated to reflux for 1 day. After separation of insoluble materials in diethyl ether by filtration, the residue was crystallized from dichloromethane to afford 9,9,10,10-tetraiodo-9,10-dihydro-9,10-distannaanthracene (**10**) (316 mg, 51%). **10**: M.p. 278−280 °C (recrystallization from dichloromethane). ^{1}H NMR: δ = 7.52−7.55 (m, 4 H), 7.63−7.83 (m, 4 H). ^{13}C NMR: δ = 132.2 [d, J(Sn−C) = 14, 66 Hz, C_β], 136.9 [d, J(Sn−C) = 46, 76 Hz, C_α], 148.3 (s, C_{ipso}). ^{119}Sn NMR: δ = 189.1 ppm. $C_{12}H_8I_4Sn_2$ (897.2): calcd. C 16.06, H 0.90; found C 16.16, H 0.77.

Crystal and Experimental Data at 298 K for 4: $C_{40}H_{36}O_4Sn_2$, M = 818.104, crystal size 0.30 × 0.30 × 0.20 mm, monoclinic, a = 18.191(5), b = 11.400(2), c = 19.522(10) Å, β = 118.23(6) °, V = 3572(2) Å^3, D = 1.521 Mg·m^{-3}, μ(Mo-K_α) = 1.437 mm^{-1}, Z = 4, space group $P2_1/c$. Data were collected on a Mac Science MXC18 K diffractometer by using graphite-monochromated Mo-K_α radiation (λ = 0.71073 Å). The structure was solved by direct methods using SIR[16] and refined by full-matrix least-squares procedures (SHELXL-97)[17] on F^2 for all reflections (7777 reflections) for 416 variable parameters. $R_1(wR_2)$ = 0.037 (0.091) for all data, GOF = 1.158.

Crystal and Experimental Data at 298 K for 6: $C_{28}H_{28}O_2Sn_2$, M = 633.91, crystal size 0.30 × 0.30 × 0.10 mm, monoclinic, a = 17.2610(5), b = 9.4070(3), c = 28.0101(6) Å, β = 144.904(1)°, V = 2615.0(1) Å^3, D = 1.610 Mg·m^{-3}, μ(Mo-K_α) = 1.931 mm^{-1}, Z = 4, space group $P2_1/c$. Data were collected on a Mac Science DIP3000 diffractometer using graphite-monochromated Mo-K_α radiation (λ = 0.71073 Å). The structure was solved by direct methods using SIR[16] and refined by full-matrix least-squares procedures (SHELXL-97)[17] on F^2 for all reflections (5432 reflections) for 290 variable parameters. $R_1(wR_2)$ = 0.039 (0.090) for all data, GOF = 1.060.

Crystal and Experimental Data at 298 K for 10: $C_6H_4I_2Sn$, M = 448.596, crystal size 0.40 × 0.40 × 0.20 mm, triclinic, a = 7.407(5), b = 8.042(4), c = 9.203(7) Å, α = 102.42(5), β = 108.29(5), γ = 104.52(6)°, V = 477.4(5) Å^3, D = 3.121 Mg·m^{-3}, μ(Mo-K_α) = 9.066 mm^{-1}, Z = 2, space group $P\bar{1}$. Data were collected on a Mac Science MXC18 K diffractometer using graphite-monochromated Mo-K_α radiation (λ = 0.71073 Å). The structure was solved by direct methods using SIR[16] and refined by full-matrix least-squares procedures (SHELXL-97)[17] on F^2 for all reflections (2175 reflections) for 83 variable parameters. $R_1(wR_2)$ = 0.052 (0.145) for all data, GOF = 1.041.

CCDC-212959 (**4**), -212958 (**6**) -213182 (**10**) contain the supplementary crystallographic data for these compounds. These data can be obtained free of charge at www.ccdc.cam.ac.uk/conts/retrieving.html (or from the Cambridge Crystallographic Data Center, 12 Union Road, Cambridge CB2 1EZ, UK; Fax: (internat.) +44-1223/336-033; E-mail: deposit@ccdc.cam.ac.uk).

Acknowledgments

This work was partially supported by Grant-in-Aids for the Encouragement of Young Scientists, Nos. 10740288 (M. S.) and 13740349 (M. S.) from the Ministry of Education, Science, Sports and Culture, Japan and from the Japan Society for the promotion of Science, respectively. M. Saito also acknowledges a research grant from the Toray Science Foundation.

[1] [1a] H. Gilman, E. A. Zuech, *J. Am. Chem. Soc.* **1960**, *22*, 3605−3608. [1b] H. Gilman, E. A. Zuech, W. Steudel, *J. Org. Chem.* **1962**, *27*, 1836−1839.
[2] For a review, see: T. J. Barton, *Comprehensive Organometallic Chemistry*, 1st ed. (Eds.: G. Wilkinson, F. G. A. Stone, E. W. Abel) Pergamon Press, Elmsford, New York, **1982**, vol. 2, p. 273.
[3] O. A. D'yachenko, S. V. Soboleva, L. O. Atovmyan, *Zh. Strukt. Khim.* **1976**, *17*, 496−504.
[4] W. Z. McCarthy, J. Y. Corey, E. R. Corey, *Organometallics* **1984**, *3*, 255−263.
[5] See references cited in ref.[4]
[6] S. Kyushin, T. Shinnai, T. Kubota, H. Matsumoto, *Organometallics* **1997**, *16*, 3800−3804.
[7] M. Saito, M. Nitta, M. Yoshioka, *Organometallics* **2001**, *20*, 749−753.
[8] P. Jutzi, *Chem. Ber.* **1971**, *104*, 1455−1467.
[9] G. F. Lanthier, J. M. Miller, S. C. Cohen, A. G. Massey, *Org. Mass Spectrom.* **1974**, *8*, 235−246.
[10] 9,10-Distannatriptycene has been synthesized and characterized, see: M. A. Dam, O. S. Akkerman, F. J. J. de Kanter, F. Bickelhaupt, N. Veldman, A. L. Spek, *Chem. Eur. J.* **1996**, *2*, 1139−1142.
[11] [11a] W. Ando, K. Hatano, R. Urisaka, *Organometallics* **1995**, *14*, 3625−3627. [11b] K. Hatano, K. Morihashi, O. Kikuchi, W. Ando, *Chem. Lett.* **1997**, 293−294.
[12] B. N. Biddle, J. S. Gray, A. J. Crowe, *Appl. Organomet. Chem.* **1987**, *1*, 261−265.

 © 2004 Wiley-VCH Verlag GmbH & Co. KGaA, Weinheim

[13] [13a] W. P. Neumann, *The Organic Chemistry of Tin*, John Wiley & Sons, New York, **1970**. [13b] R. C. Poller, *The Chemistry of Organotin Compounds*, Logos Press, London, **1970**. [13c] A. K. Sawyer, *Organotin Compounds*, Marcel Dekker, New York, **1972**.
[14] L. R. Sita, *Acc. Chem. Res.* **1994**, *27*, 191−197.
[15] S. V. Soboleva, O. A. D'yachenko, L. O. Atovmyan, *Izv. Akad. Nauk. SSSR, Ser. Khim.* **1974**, 1443.
[16] A. Altomare, G. Cascarano, C. Giacovazzo, A. Guagliardi, *J. Appl. Crystallogr.* **1993**, *26*, 343−350.
[17] G. M. Sheldrick, SHELXL-97, Program for the Refinement of Crystal Structures; University of Göttingen, Göttingen, Germany, **1997**.

Received June 19, 2003
Early View Article
Published Online December 19, 2003

 © 2004 Wiley-VCH Verlag GmbH & Co. KGaA, Weinheim

Synthetic and Structural Studies of Pd^{II} and Pt^{II} Complexes with Quincorine and Quincoridine Derivatives

Manfred Fild,[a] Carsten Thöne,*[a] and Stefania Tötös[a]

Keywords: N,P ligands / Heterocycles / Palladium / Platinum / Bioinorganic chemistry

A series of Pd^{II}-quincorine and -quincoridine complexes in which the ligands are coordinated through *N*,*O*-donor atoms have been synthesised, and their structural features determined by X-ray crystallography. Additionally, new chiral tetradentate *N*,*P*-ligands containing two quinuclidine cores bridged through a *cis*-enediyne fragment have been obtained. The different coordinating properties of the new ligands, which contain two soft phosphorus and two hard nitrogen donors, to Pd^{II} and Pt^{II} are emphasised. Several typical complexes were structurally characterised by X-ray crystallography.

(© Wiley-VCH Verlag GmbH & Co. KGaA, 69451 Weinheim, Germany, 2004)

Introduction

The development of asymmetric catalysis using chiral organic compounds or chiral metal complexes has induced an increased interest in the synthesis of new optically active ligands.[1,2] In this context *cinchona* alkaloids, such as quinine and quinidine and their derivatives, readily available in both pseudo-enantiomeric forms, play an important role and are extensively used. Among asymmetric synthetic procedures in organic chemistry, one of the best known is the asymmetric dihydroxylation of olefins using various *cinchona* alkaloid derivatives as chiral monodentate amine ligands for OsO_4 as developed by Sharpless.[3] The mechanism of this reaction was also extensively analysed by Corey, and the most efficient ligands for promoting face-selective dihydroxylation of olefins were found to be bis-*cinchona* alkaloids such as the $(DHQD)_2PHAL$ system (Figure 1).[3−5]

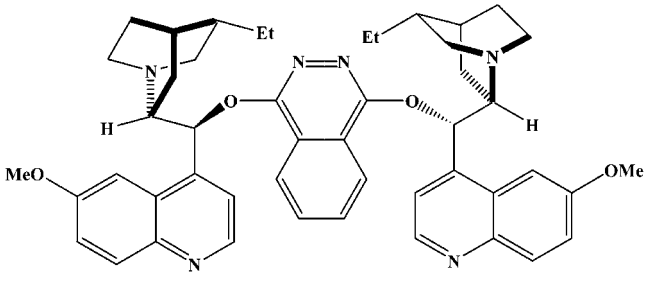

Figure 1. $(DHQD)_2PHAL$, a bis-*cinchona* alkaloid

Additionally, bidentate *N*,*P*-ligands have acquired a growing importance in the development of coordination chemistry and asymmetric catalysis.[6] A remarkable number of aminophosphane, -phosphite, -phosphonite and -phosphinite ligands have been developed and their complexes used for asymmetric catalytic reactions, such as cross-coupling, hydroformylation and hydrogenation.[7−9]

Beck et al. reported the first *N*,*O*-chelate complexes of cinchonidine and cinchonine, but only a few metal complexes of *cinchona* alkaloids have been described.[10] Quincoridine-based aminophosphite ligands and their Rh^{I} and Pd^{II} complexes have also been reported by Gavrilov and coworkers.[11] Recently, Lemaire et al. have developed a new family of *N*,*P*-ligands derived from quincorine (QCI) and quincoridine (QCD) with applications in hydroformylation, asymmetric hydrosilylation and asymmetric Grignard cross-coupling reactions.[12]

The chirality, in combination with the donor properties of QCI and QCD, should provide a useful ligand system for catalytic processes. QCI and QCD contain four stereogenic centres each, including the *N*-chiral 1*S*-configured bridgehead and also possess three potential donor sites: the OH group, a tertiary N-atom and an olefinic C=C bond (Figure 2).

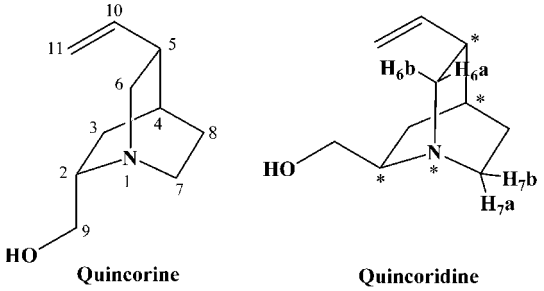

Figure 2. Atom numbering scheme and stereocentres in quincorine (QCI) and quincoridine (QCD)

[a] Institut für Anorganische und Analytische Chemie der Technischen Universität,
Hagenring 30, 38106 Braunschweig, Germany

 DOI: 10.1002/ejic.200300557 © 2004 Wiley-VCH Verlag GmbH & Co. KGaA, Weinheim

In the present work we report on new *N*,*O*-chelate and bis-*N*,*O*-chelate complexes of Pd^{II} with QCI and QCD and their corresponding saturated derivatives. New chiral aminophosphinites, containing two quinuclidine cores bridged through a *cis* enediyne fragment, are developed and their different coordination modes are described.

Results and Discussion

N,*O*-Chelate Complexes

In the course of this research program directed toward the synthesis and characterisation of new metal complexes, we have used QCI [(2*S*,4*S*,5*R*)-2-hydroxymethyl-5-vinyl-2-quinuclidine] (**1**) and QCD [(2*R*,4*S*,5*R*)-2-hydroxymethyl-5-vinyl-2-quinuclidine] (**2**) as ligands. The corresponding saturated derivatives [(2*S*,4*S*,5*R*)-5-ethyl-2-hydroxymethyl-2-quinuclidine] (**3**) and [(2*R*,4*S*,5*R*)-5-ethyl-2-hydroxymethyl-2-quinuclidine] (**4**) were prepared efficiently by hydrogenation, according to a known literature procedure (Scheme 1).[13]

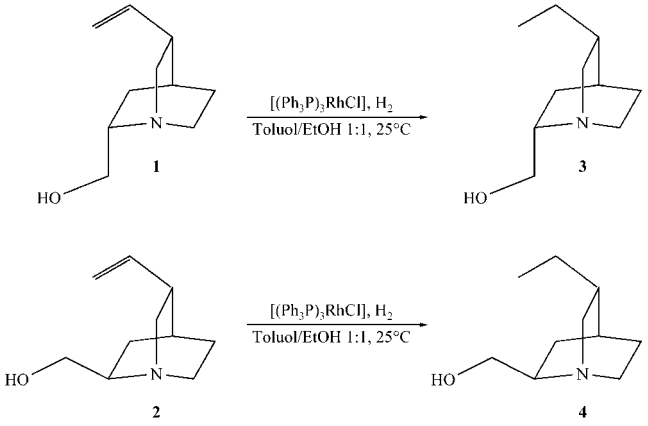

Scheme 1. The synthesis of dihydro-QCI (**3**) and dihydro-QCD (**4**)

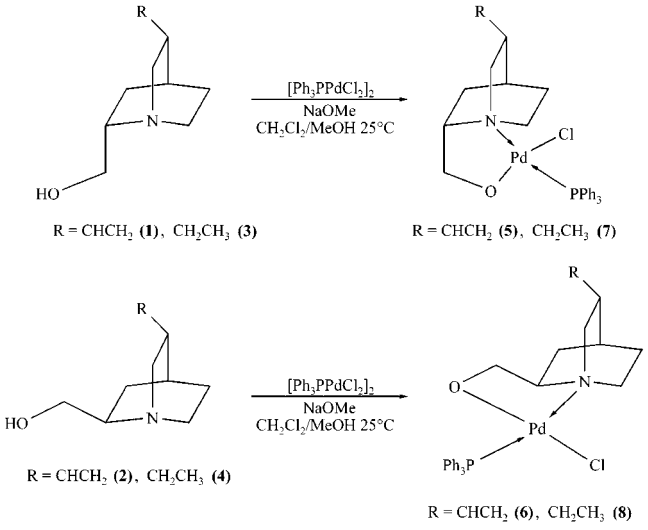

Scheme 2. The synthesis of phosphane Pd^{II}-QCI and -QCD complexes

Reactions of two equivalents of the ligands **1**−**4** with one equivalent of the chloro-bridged complex [$(Ph_3P)(Cl)Pd(\mu\text{-}Cl)_2Pd(Cl)(PPh_3)$] in the presence of NaOMe in CH_3OH/CH_2Cl_2 gave the corresponding five-membered ring chelate complexes **5**−**8** (Scheme 2).

All of the complexes **5**−**8** gave the expected fragmentation patterns in their positive FAB mass spectra. In the $^{31}P\{^1H\}$ NMR spectra of **5**−**8** all compounds display two singlets around δ = 26 (high intensity) and 23 ppm (low

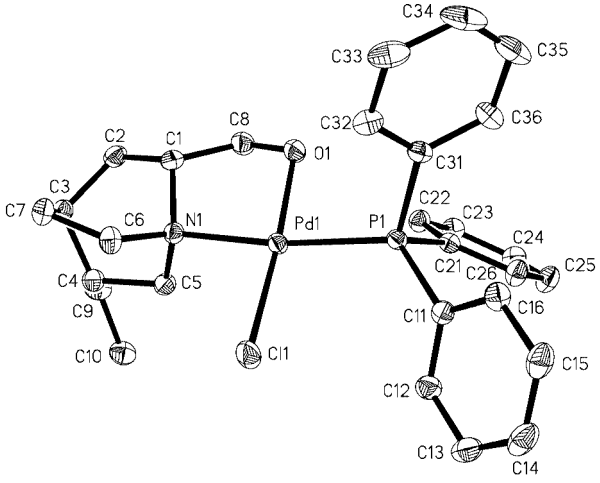

Figure 3. The molecular structure of **7**; H atoms omitted for clarity; ellipsoids at 50% probability level; selected bond lengths [Å] and angles [°]: Pd1−P1 2.2480(6), Pd1−Cl1 2.3020(6), Pd1−O1 1.9986(16), Pd1−N1 2.1043, O1−C8 1.407(3), N1−C1 1.496(3), N1−C5 1.495(3), N1−C6 1.494(3), C(aliph.)−C(aliph.) 1.508(3)−1.549(3); O1−Pd1−N1 84.69(7), N1−Pd1−Cl1 92.17(5), Cl1−Pd1−P1 95.99(2), P1−Pd1−O1 87.08(5), C8−O1−Pd1 108.87(13), O1−C8−C1 110.03(17), C8−C1−C2 115.78(18), C8−C1−N1 108.54(17), N1−C1−C2 109.90(17), C1−N1−C5 107.78(17), C1−N1−C6 110.55(17), C5−N1−C6 108.38(17), C3−C4−C5 107.86(18), C3−C4−C9 112.84(19), C5−C4−C9 112.99(18)

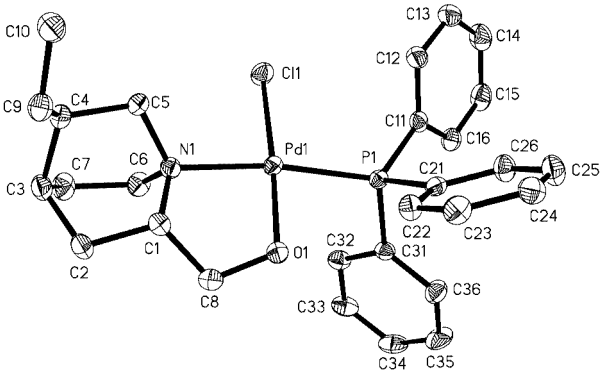

Figure 4. The molecular structure of **8**; H atoms omitted for clarity; ellipsoids at 50% probability level; selected bond lengths [Å] and angles [°]: Pd1−P1 2.2470(3), Pd1−Cl1 2.3082(3), Pd1−O1 2.0036(8), Pd1−N1 2.1101(9), O1−C8 1.4034(15), N1−C1 1.5103(14), N1−C5 1.4967(15), N1−C6 1.4940(15), C(aliph.)−C(aliph.) 1.5093(17)−1.5504(16); O1−Pd1−N1 85.27(4), N1−Pd1−Cl1 91.56(3), Cl1−Pd1−P1 97.409(11), P1−Pd1−O1 85.81(2), C8−O1−Pd1 107.79(7), O1−C8−C1 110.96(10), C8−C1−C2 116.19(10), C8−C1−N1 108.42(9), N1−C1−C2 109.30(10), C1−N1−C5 111.17(9), C1−N1−C6 106.98(9), C5−N1−C6 107.70(9), C3−C4−C5 106.62(10), C3−C4−C9 113.44(10), C5−C4−C9 111.40(10)

 © 2004 Wiley-VCH Verlag GmbH & Co. KGaA, Weinheim

intensity ≈ 5%). The signal with the high intensity was assigned to the *trans*-P−M−N isomer whereas the low intensity signal corresponds to the *cis*-P−M−N isomer. The formation of the five-membered chelate rings in **5**−**8** was also confirmed in the ^{1}H NMR spectra by the diastereotopicity of the 9-H atoms: an upfield shift of ca. 0.5 ppm was observed for one of them. The H-6 and H-7 atoms suffer a small downfield shift probably because of interaction with the d_z^2 orbital of the metal atom and the coordination of the tertiary N-atom.

Deep yellow crystals of the QCI-Pd^{II} complex **7** and the QCD-Pd^{II} complex **8**, suitable for X-ray analysis, were obtained from diethyl ether solutions by layering with hexanes. Single-crystal X-ray structure determinations (Figure 3 and 4) proved that the *trans*-P−M−N isomers were formed as the main products because of the steric demands of the bulky ligands. The chirality at C-2 is retained in the complexes. The coordination geometry around Pd is virtually square planar in both cases (mean dev. in **7**: 1.86 pm; **8**: 2.86 pm). The Pd atoms are incorporated into five-membered chelate rings. In the case of **7**, the ring adopts a twist conformation, and in **8** an envelope conformation, with C-8 as the flap. The similarity in the bonding situation around

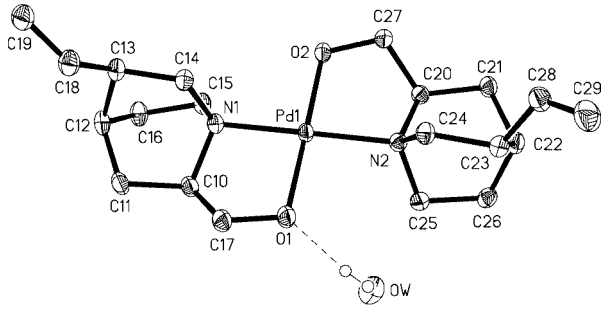

Figure 5. The molecular structure of **9** in the crystal; non-water hydrogens omitted for clarity; ellipsoids at 50% probability level; selected bond lengths [Å] and angles [°]: Pd1−O1 1.9852(14), Pd1−N1 2.0372(16), Pd1−O2 2.0006(14), Pd1−N2 2.0335(15), O1−C17 1.401(2), O2−C27 1.400(2), N1−C20 1.502(2), N1−C24 1.484(2), N1−C25 1.487(2), N2−C10 1.501(2), N2−C14 1.478(2), N2−C15 1.493(2), C13−C18 1.488(3), C18−C19 1.312(4), C23−C28 1.499(3), C28−C29 1.312(3), C(aliph.)−C(aliph.) 1.508(3)−1.556(3), O1···H99a 1.79(5), O2···H98a 1.92(3); O1−Pd1−N1 94.10(6), N1−Pd1−O2 85.24(6), O2−Pd1−N2 95.32(6), N2−Pd1−O1 85.49(6), C10−N2−Pd1 103.67(11), C14−N2−Pd1 115.40(11), C15−N2−Pd1 108.82(11), C20−N1−Pd1 106.48(11), C24−N1−Pd1 118.12(11), C25−N1−Pd1 104.60(11), C14−C13−C18 115.26(18), C24−C23−C28 117.56(16), C13−C18−C19 129.0(2), C23−C28−C29 129.2(2)

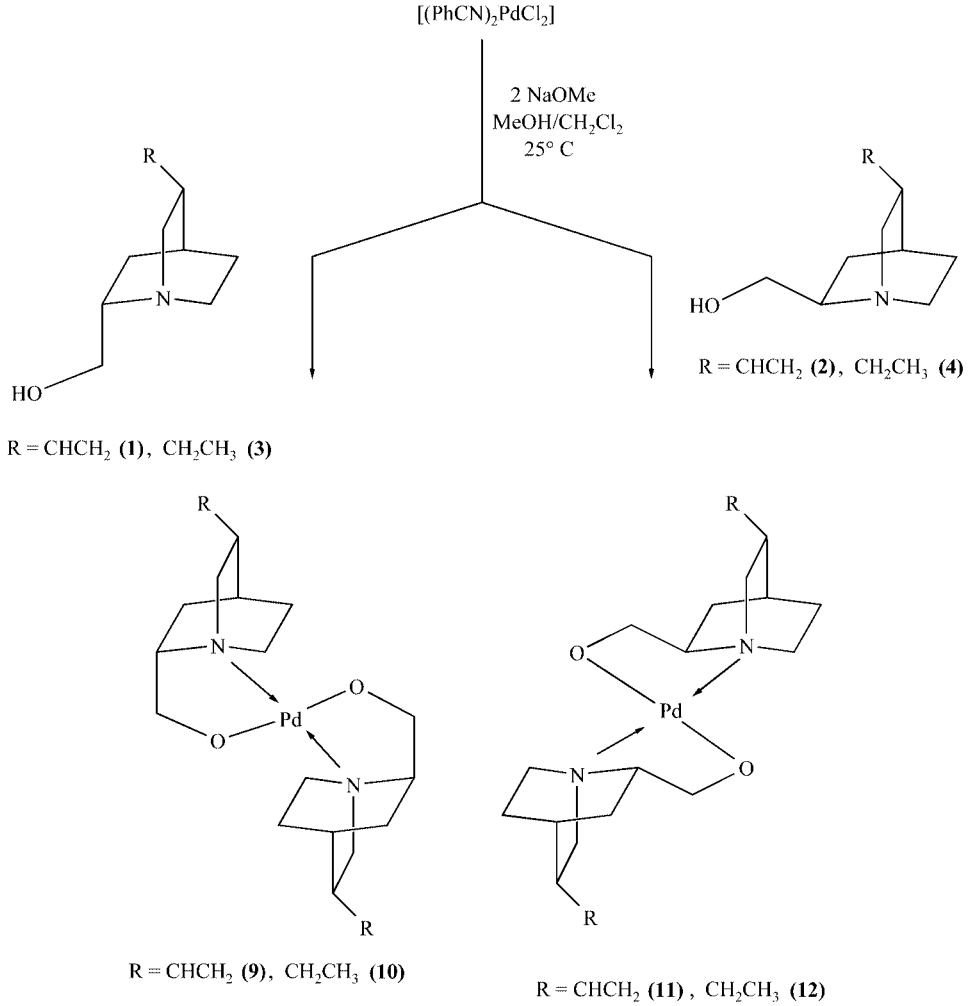

Scheme 3. The synthesis of homoleptic Pd^{II}-QCI and -QCD complexes

 © 2004 Wiley-VCH Verlag GmbH & Co. KGaA, Weinheim

Pd is also reflected in nearly identical bond lengths at Pd in both cases. They match the typically observed range for Pd−P, Pd−Cl and Pd−N bond lengths.

When one equivalent of *trans*-[$PdCl_2(PhCN)_2$] was reacted with two equivalents of **1**−**4** in the presence of NaOMe in methanol/dichloromethane, the bis-*N*,*O*-chelate complexes **9**−**12** were obtained in excellent yields (90%; Scheme 3).

All of the compounds **9**−**12** show the expected fragmentation patterns and the molecular ions in their EI mass spectra. Again, the ^{1}H NMR spectra confirmed the formation of the spiro complexes **9**−**12** because of the diastereotopicity of the 9-H atoms. These exhibit a downfield shift and an upfield shift associated with the different environment obtained through the closure of the five-membered chelate rings. The H-6 and H-7 atoms suffer a small downfield shift, perhaps because of the coordination of the tertiary N-atom to Pd and the interaction with the d_z^2 orbital of the metal.

Yellow crystals of **9** and **11** suitable for X-ray analysis were obtained from Et_2O by layering with hexanes. As shown in Figure 5 and 6, the coordination geometry around Pd is square planar (mean dev. **9**: 2.29 pm; **11**: 4.73 pm), with N(1) and N(2) occupying the *trans* positions. Because of the chelating ligands, Pd is in both cases the spiro atom and therefore part of two five-membered ring systems that display approximately envelope conformations, with the quinuclidine-bound carbon atoms in the flap positions.

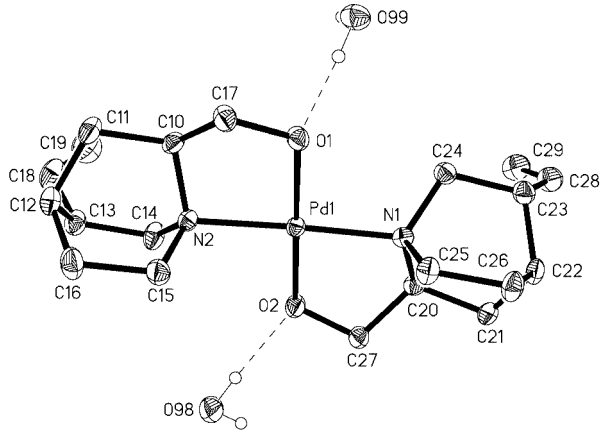

Figure 6. The molecular structure of **11** in the crystal; non-water hydrogens omitted for clarity; ellipsoids at 50% probability level; selected bond lengths [Å] and angles [°]: Pd1−O1 2.0054(10), Pd1−N1 2.0475(11), Pd1−O2 2.0037(10), Pd1−N2 2.0522(11), O1−C17 1.4048(17), O2−C27 1.4097(16), N1−C10 1.5149(17), N1−C14 1.4945(16), N1−C15 1.4915(19), N2−C20 1.5120(17), N2−C24 1.4978(18), N2−C25 1.4952(16), C13−C18 1.502(2), C18−C19 1.322(2), C23−C28 1.5070(19), C28−C29 1.311(2), C(aliph.)−(aliph.) 1.515(2)−1.5559(19), O1···Hw2 2.01(3); O1−Pd1−N1 85.99(4), N1−Pd1−O2 93.14(4), O2−Pd1−N2 85.94(4), N2−Pd1−O1 94.91(4), C10−N1−Pd1 104.87(8), C14−N1−Pd1 111.92(8), C15−N1−Pd1 114.12(8), C20−N2−Pd1 104.49(8), C24−N2−Pd1 111.81(8), C25−N2−Pd1 114.15(8), C14−C13−C18 112.03(12), C24−C23−C28 112.34(11), C13−C18−C19 125.93(19), C23−C28−C29 125.04(15)

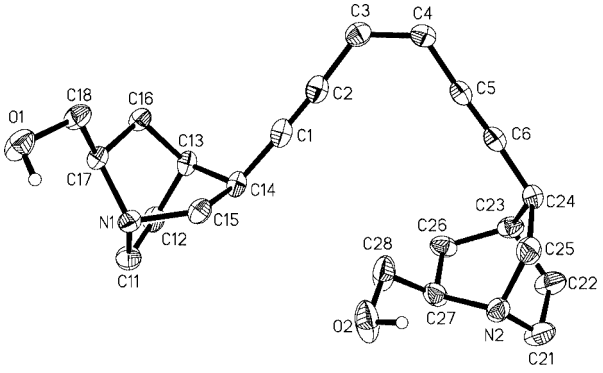

Figure 7. The molecular structure of **18** in the crystal; H-atoms omitted for clarity; ellipsoids at 50% probability level; selected bond lengths [Å] and angles [°]: C1−C2 1.199(2), C2−C3 1.429(2), C3−C4 1.343(2), C4−C5 1.428(2), C5−C6 1.197(2), C1−C14 1.467(2), C6−C24 1.467(2), N1−C11 1.4893(19), N1−C15 1.4732(18), N1−C17 1.4893(17), N2−C21 1.484(2), N2−C25 1.468(2), N2−C27 1.4804(19), C(aliph.)−C(aliph.) 1.507(3) to 1.573(2); C2−C1−C14 177.94(15), C1−C2−C3 176.98(15), C2−C3−C4 125.56(13), C3−C4−C5 125.16(13), C4−C5−C6 177.23(15), C5−C6−C24 176.72(15), C17−C18−O1 113.80(13), C27−C28−O2 113.97(16)

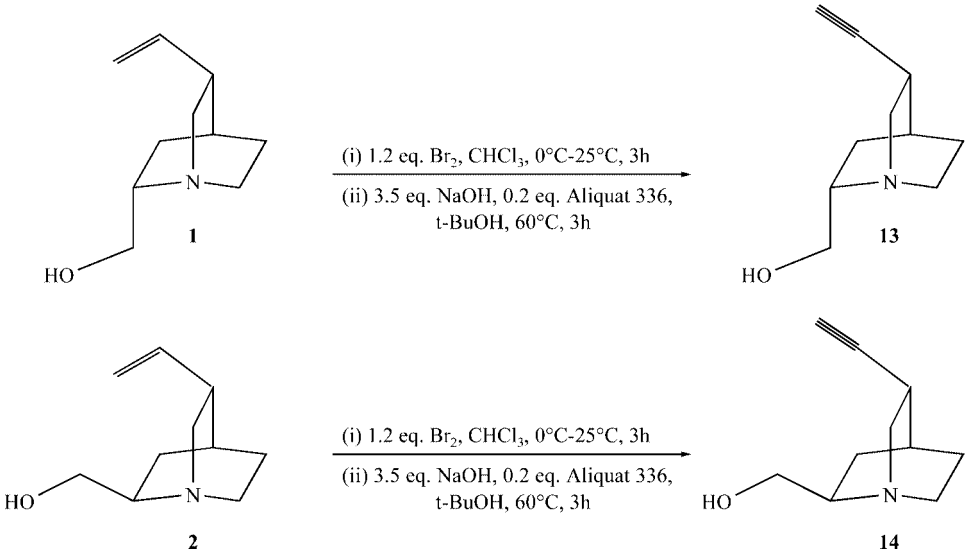

Scheme 4. The synthesis of didehydro-QCI (**13**) and didehydro-QCD (**14**)

 © 2004 Wiley-VCH Verlag GmbH & Co. KGaA, Weinheim

Both compounds crystallised with water molecules (**9**: one; **11**: two). In complex **9** intra- and intermolecular hydrogen-bonding [O−H···O: H···O 207(2)[i], 201(3) pm; [i] x, $y + 1$, z] forms chains, which are also connected by non-classical C−H···O hydrogen-bonding [H···O 266[ii], 248 pm[iii]; [ii] $-x + 2$, $y - 0.5$, $-z + 1$, [iii] $-x + 1$, $y + 0.5$, $-z + 1$]. The hydrogen-bonding scheme in **11** is similar, but with stronger classical O−H···O bonds [H···O 179(5), 192(3), 203(3)[i], 201(5) pm[ii]; [i] $-x$, $y - 0.5$, $-z + 1.5$, [ii] x, $y + 1$, z] and comparable non-classical C−H···O bonds [H···O: 263[i], 233[i], 254[iii], 251 pm[iv]; [iii] $-x + 1$, $y + 0.5$, $-z + 1.5$, [iv] $-x$, $y + 0.5$, $-z + 1.5$]. Again, the bond lengths in the molecules are unexceptional and match the usual observed ranges.

N,P-Ligand Synthesis

For the synthesis of *N,P*-ligands we used 10,11-didehydroquincorine (**13**) and 10,11-didehydroquincoridine (**14**) as precursors. The terminal alkynes **13** and **14** were prepared efficiently from **1** and **2** according to a known literature procedure (Scheme 4).[13]

The symmetrical (*Z*)-enediynes **17** and **18** were obtained in good yields in a two-step procedure[14,15] involving two sequential $[Pd(PPh_3)_4]$- and $[PdCl_2(PhCN)_2]$-catalysed coupling reactions from (*Z*)-1,2-dichloroethene and **13** and **14**. Colourless single crystals of **18** were obtained by layering a CH_2Cl_2 solution with hexanes. A structure determination revealed a *cis*-arrangement in the molecule (Figure 7).

Classical hydrogen-bonding of the type O−H···N [H···N: 196(3)[i], 203(3) pm[ii]; [i] $-x + 1$, $y - 0.5$, $-z + 0.5$; [ii] $-x + 1$, $y + 0.5$, $-z + 0.5$] together with non-classical C−H···O hydrogen-bonding [H···O: 257[iii], 245 pm[iv]; [iii] $x + 1$, y, z; [iv] $-x + 2$, $y + 0.5$, $-z + 0.5$] leads to the formation of zigzag chains parallel to the crystallographic *b*-axis in the crystal packing (Figure 8).5

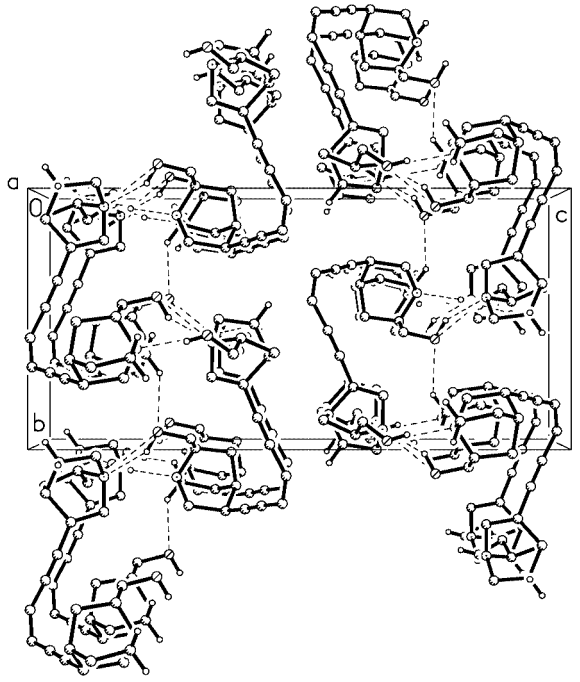

Figure 8. The packing of **18** in the crystal showing the hydrogen bonding; view along the *a* axis; molecules contain the OH group; other hydrogens omitted

Treatment of **17** and **18** with chlorodiphenylphosphane in dichloromethane, in the presence of triethylamine, gave the bis-aminophosphinites **19** and **20** in very good yields (Scheme 5).

These are pale yellow oils, which are stable under nitrogen atmosphere for a long time. In the $^{31}P\{^1H\}$ NMR spectra the resonances of the P atoms are found at $\delta = 115.29$ (**19**) and $\delta = 114.60$ ppm (**20**), respectively.

Platinum(II) and Palladium(II) Complexes

The bis-*N,P*-aminophosphinites **19** and **20**, having two soft electron-donating atoms and two hard electron-donating atoms, show different coordinating properties towards Pt^{II} and Pd^{II}. It is known that the formation of square-planar Pt^{II} complexes is strongly dependent on a number of factors, such as solvent polarity, the *trans* effect of the resident ligands, and the order of adding the reactants. When phosphorus is coordinated to ^{195}Pt, the geometry of the products can often be assigned from the magnitude of the coupling constants. These are strongly dependent on the

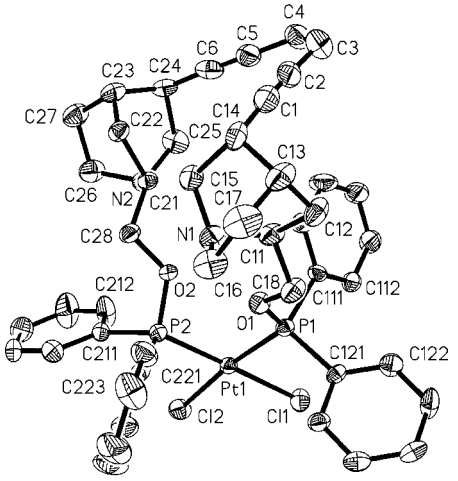

Figure 9. The molecular structure of **21**; hydrogen atoms and the disordered THF molecule are omitted for clarity; ellipsoids at 50% probability level; selected bond lengths [Å] and angles [°] (corresponding values of the second independent molecule in the asymmetric unit are given in brackets): Pt1−P1 2.2231(19) [2.2291(18)], Pt−1P2 2.229(2) [2.2349(18)], Pt1−Cl1 2.3642(19) [2.3564(18)], Pt1−Cl2 2.3532(19) [2.3536(18)], P1−O1 1.587(5) [1.597(5)], P2−O2 1.600(4) [1.601(4)], O1−C18 1.466(7) [1.459(6)], O2−C28 1.438(6) [1.442(6)], C1−C2 1.176(9) [1.204(9)], C2−C3 1.470(10) [1.473(11)], C3−C4 1.328(10) [1.299(14)], C4−C5 1.429(9) [1.363(15)], C5−C6 1.191(9) [1.227(15)], C1−C14 1.482(9) [1.459(8)], C6−C24 1.481(8) [1.415(15)], N1−C11 1.483(7) [1.456(6)], N1−C15 1.453(7) [1.461(7)], N1−C16 1.486(7) [1.490(8)], N2−C21 1.488(6) [1.515(8)], N2−C25 1.457(7) [1.478(10)], N2−C26 1.471(7) [1.501(12)], C(aliph.)−C(aliph.) 1.509(9)−1.580(7) [1.496(7)−1.583(11)]; P1−Pt1−P2 94.17(7) [93.23(7)], P1−Pt1−Cl1 85.41(7) [93.51(7)], P2−Pt1−Cl2 92.07(7) [85.85(7)], Cl1−Pt1−Cl2 88.29(7) [87.29(7)], C18−O1−P1 122.1(4) [116.2(3)], C28−O2−P2 127.5(4) [128.8(4)], O1−C18−C11 109.9(4) [111.0(4)], O2−C28−C21 107.9(4) [107.8(4)], C14−C1−C2 174.9(7) [177.3(7)], C1−C2−C3 176.0(7) [175.9(9)], C2−C3−C4 122.8(7) [126.3(10)], C3−C4−C5 128.6(7) [127.3(9)], C4−C5−C6 176.4(7) [176.9(10)], C5−C6−C24 175.9(6) [176.6(10)]

 © 2004 Wiley-VCH Verlag GmbH & Co. KGaA, Weinheim

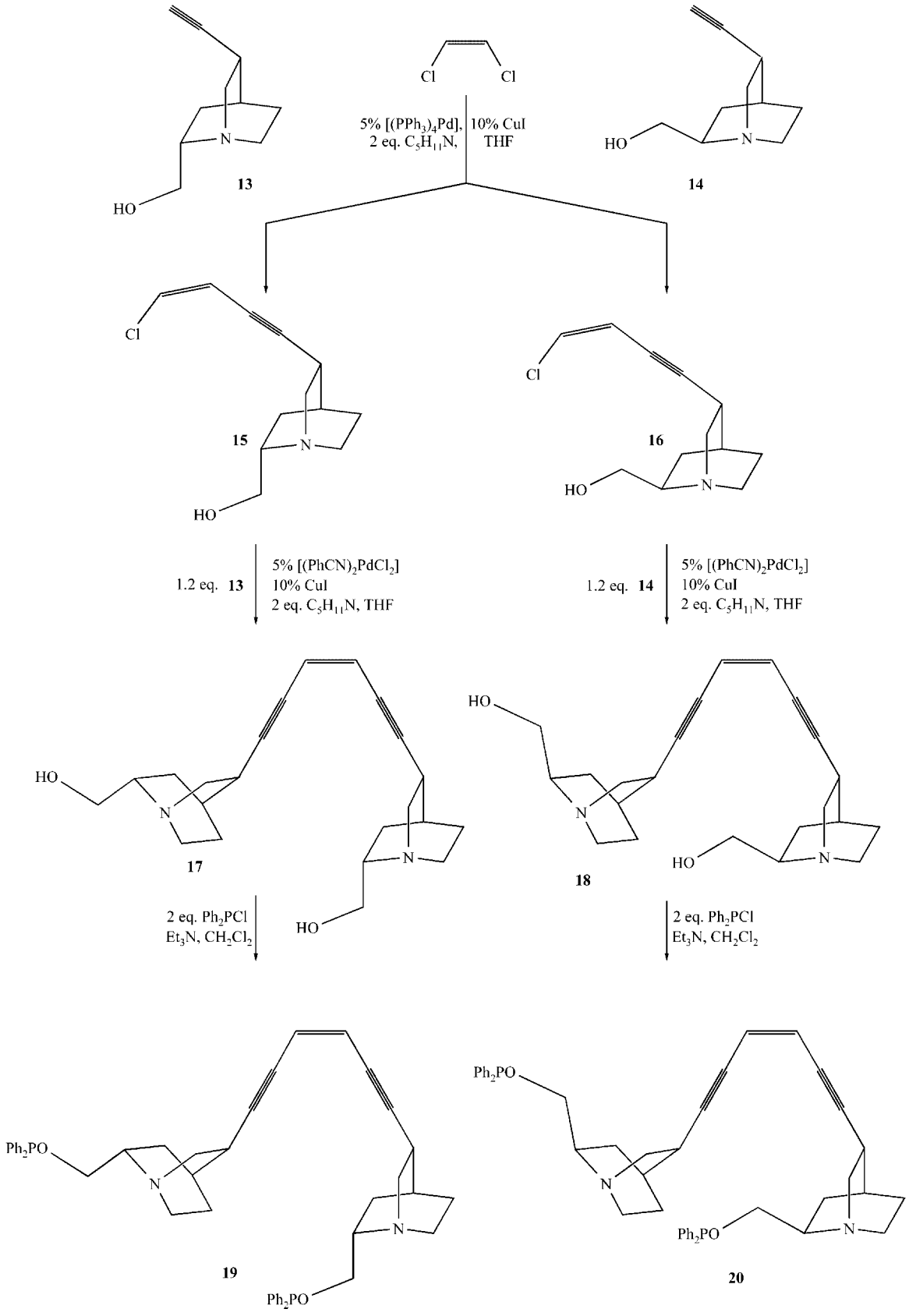

Scheme 5. The synthesis of the bis-*N*,*P*-aminophosphinites **19** and **20** from didehydro-QCI (**13**) and didehydro-QCD (**14**)

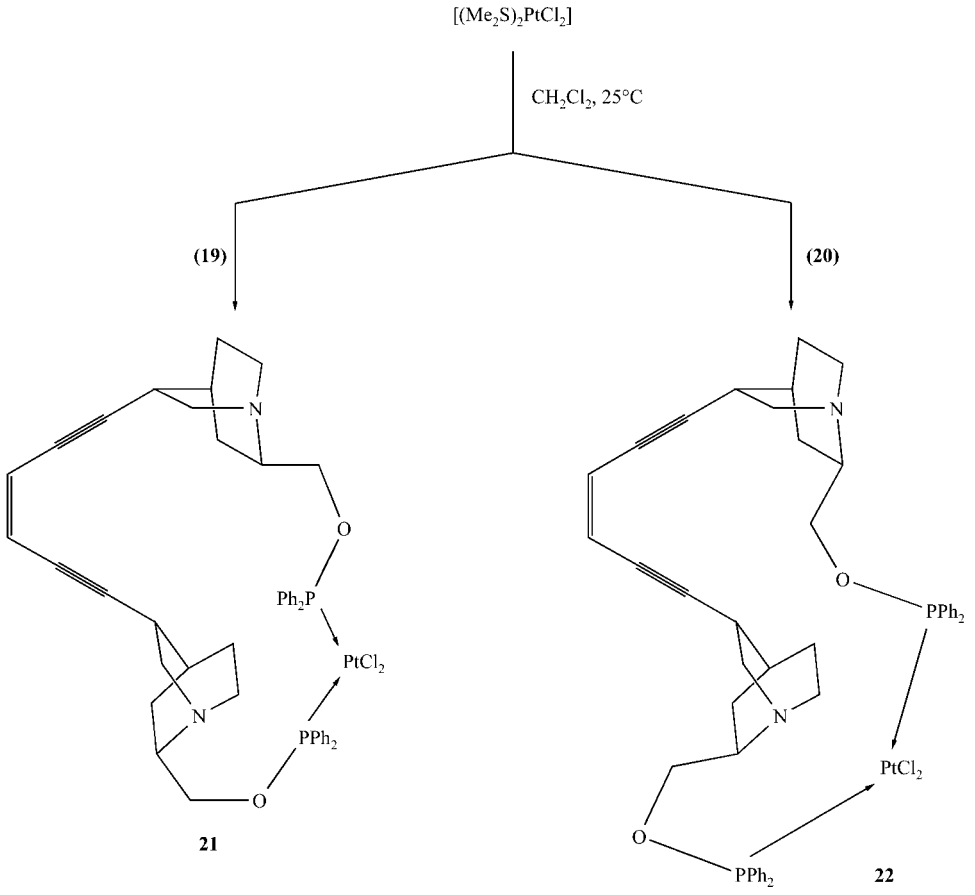

Scheme 6. Platinum(II) chelate complexes of the bis-*N*,*P*-aminophosphinites **19** and **20**

ligand *trans* to the phosphorus atom, because of the inductive effect of that ligand on the platinum-phosphorus bond. Ligands with a very strong σ-inductive character reduce the positive charge on the platinum atom and thus weaken the overlap of the phosphorus and the metal orbitals relative to the *trans*-ligands, which have weaker σ-inductive effects.[16]

When a solution of $[PtCl_2(SMe_2)_2]$ in dichloromethane was added to a solution of **19** or **20** in the same solvent, in a 1:1 molar ratio, the *cis* complexes **21** and **22** were obtained (Scheme 6).

In the $^{31}P\{^1H\}$ NMR spectra singlets, with ^{195}Pt satellites, at δ = 83.89 ppm ($^1J_{Pt,P}$ = 2099.28 Hz) (**21**) and δ = 85.10 ppm ($^1J_{Pt,P}$ = 2076.01 Hz) (**22**) are observed. The FAB mass spectra indicated that the complexes are monomeric. Slow diffusion of diethyl ether into a concentrated THF/dioxane solution of the complex **21** produced colourless crystals that crystallised in the non-centrosymmetric space group *P*1 with two independent molecules of **21** and one disordered and badly resolved THF molecule per formula unit (Figure 9).

The complex can be regarded as a 21-membered ring system with a $PtCl_2$ group that connects the phosphorus(III) ends of the ligand to form a macrocyclic complex with an essentially planar coordination geometry at platinum (mean dev. Pt1: 1.2; Pt2: 4.2 pm). Because of the steric demand of the aminophosphinite ligand, the bite angle at platinum is somewhat wider than 90° [94.17(7), 93.23(7)°]. The ligand is bound symmetrically with similar Pt−P bond lengths [222.31(19), 222.9(2); 222.91(18), 223.49(18) pm, respectively].

Attempts to synthesise the corresponding *trans* complex from **20** through the inverse addition of the reactants led, after 30 minutes at room temperature, to a complex mixture of products. The $^{31}P\{^1H\}$ NMR spectrum of this mixture displays many signals with different intensities and corresponding ^{195}Pt satellites, including the signal of the reactant. After 24 h at room temperature the *cis* complex **22** became the main product observed by ^{31}P NMR spectroscopy. Treatment of two equivalents of $[PtCl_2(SMe_2)_2]$ with one equivalent of **20**, in dichloromethane, again produced the *cis* complex **22**.

Armstrong and co-workers have reported recently that the bis-phosphane ligands 2,7-bis(3-diphenylphosphanylpropoxy)naphthalene (DPPN) and 2,7-bis(3-diphenylphosphanylethoxy)naphthalene (DPEN) form dimeric *cis*, *cis*/*trans* and *trans* complexes of platinum(II) depending on the conditions employed.[17] They have also demonstrated that an excess of the ligand catalyzes *trans*/*cis* isomerisation, either by adding an excess of the phosphane, or by having the excess present during the addition of the platinum precursor. Based on these and our results we conclude that the *cis* complexes **21** and **22** are the thermodynamic products.

 © 2004 Wiley-VCH Verlag GmbH & Co. KGaA, Weinheim

The complex mixture formed by the inverse addition of the reactants should be a mixture of kinetic and thermodynamic products and thus the free unchanged ligand has catalysed a *trans*/*cis* isomerisation. The ligands **19** and **20** show a marked preference to form *cis*-P−M−P-monomeric metallamacrocycles with Pt^{II} centres, even though a 1:2 molar ratio was employed.

In view of the interesting complexes **21** and **22** we tried to obtain the corresponding complexes with Pd^{II}. The results were completely different. The reaction of one equivalent of **20** with one equivalent of $[(\eta^4\text{-}C_7H_8)PdCl_2]$ in dichloromethane produced a yellow solid. The $^{31}P\{^1H\}$ NMR spectrum of the crude product shows many singlets up to $\delta = 103$ ppm. Attempts to isolate a pure complex from the mixture were unsuccessful.

When one equivalent of **19** or **20** was allowed to react with two equivalents of $[(\eta^4\text{-}C_7H_8)PdCl_2]$ in dichloromethane yellow solids were again obtained (Scheme 7).

The $^{31}P\{^1H\}$ NMR spectra of these products show only one signal around $\delta = 103$ ppm. The ESI mass spectra indicated that the compounds are the bis-*N*,*P*-chelate complexes **23** and **24** (Scheme 5). The formation of the six-membered chelate rings in **23** and **24** is also confirmed by ^1H NMR spectra. The 6b-H and 7a-H atoms undergo downfield shifts of more than 1.5 ppm in comparison with the free ligands because of the anisotropy of the phenyl groups. Secondly, in the $^1H,^1H$-COSY spectra of **23** and **24** the cross-peaks corresponding to the vicinal correlations of the 2-H atom with the 9-H atoms disappear due to the changing of the dihedral angles through the closure of the six-membered rings.

In contrast to platinum(II), palladium(II) shows a marked preference to form bis-*N*,*P*-chelate complexes with ligands **19** and **20**.

Conclusion

We have shown that the *N*,*O*-chelate complexes and bis-*N*,*O*-chelate complexes of Pd^{II} with QCI and QCD and their saturated derivatives are easy to prepare. The syntheses of two new bis-*N*,*P*-aminophosphinite ligands, derived from QCI and QCD, have been developed. Both ligands have two soft and hard donor-atoms that can be exploited to form mononuclear and binuclear chelate complexes. Platinum(II) forms P−M−P metallamacrocycle complexes, but palladium(II) prefers to form bis-*N*,*P*-chelate complexes with these ligands.

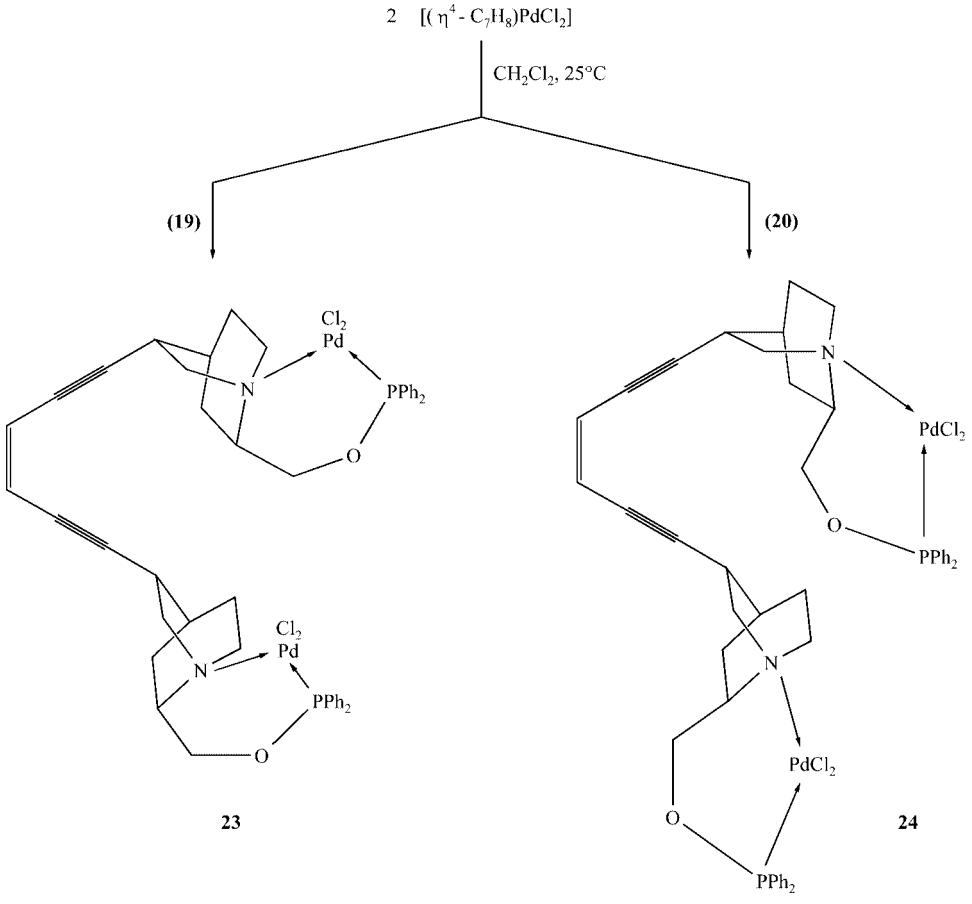

Scheme 7. Dinuclear palladium(II) complexes of the bis-*N*,*P*-aminophosphinites **19** and **20**

 © 2004 Wiley-VCH Verlag GmbH & Co. KGaA, Weinheim

Experimental Section

General Remarks: All reactions were performed under a dry nitrogen atmosphere using standard Schlenk techniques. CH_2Cl_2 was freshly distilled under nitrogen from P_4O_{10}, THF was dried over sodium/benzophenone and distilled prior to use. Et_3N was heated to reflux over sodium and distilled under nitrogen. Piperidine and nBuNH$_2$ were dried over NaOH and then distilled under nitrogen. Ph_2PCl and (*Z*)-1,2-dichloroethene were purchased from Aldrich. $Pd(PPh_3)_4$,[18] $[PdCl_2(PhCN)_2]$,[19] $[(\eta^4\text{-}C_7H_8)PdCl_2]$,[20] $[PdCl_2(PPh_3)]_2$ [21] and $[PtCl_2(SMe_2)_2]$[16] were prepared according to literature procedures. QCI (**1**) and QCD (**2**) were donated by Buchler GmbH. Dihydro-QCI (**3**), dihydro-QCD (**4**), didehydro-QCI (**13**), and didehydro-QCD (**14**) were prepared according to a literature procedure.[13] Preparative column chromatography was performed on Fluka silica gel (particle size 30−60 μm). Analytical TLC was carried out on Polygram Sil G/UV_{254} plates (0.2 mm silica gel). *tert*-Butyl methyl ether (MTBE) was purchased from Fluka.

NMR spectra were obtained from CD_2Cl_2, $CDCl_3$ and C_6D_6 solutions. ^{1}H, ^{13}C and ^{31}P NMR spectra were recorded using a Bruker DRX-400 spectrometer operating at 400, 100 and 162 MHz, respectively. Chemical shifts (δ) are given in ppm relative to residual $CHCl_3$ (δ = 7.27 ppm), CH_2Cl_2 (δ = 5.31 ppm) or C_6H_6 (δ = 7.16 ppm) for ^{1}H, $CDCl_3$ (δ = 77.0 ppm), CD_2Cl_2 (δ = 53.7 ppm) or C_6D_6 (δ = 128.7 ppm) for ^{13}C, and 85% H_3PO_4 (δ = 0.0 ppm, external) for ^{31}P. Coupling constants (*J*) are given in Hz. Mass spectra were obtained using a Finnigan MAT 90 spectrometer operating in FAB and ESI mode for coordination complexes (the isotope patterns matched calculated patterns in all cases), and in EI mode for the organic precursors. In all cases precision mass analyses confirmed the purity of the products. Melting points were determined on a Büchi 510 Melting Point apparatus and are uncorrected.

General Procedure for the Preparation of the Pd^{II}-Phosphane Complexes 5−8: A solution of ligand **1**−**4** and NaOMe in CH_2Cl_2/MeOH (1:1) was added dropwise to a suspension of $[PdCl_2(PPh_3)]_2$ in CH_2Cl_2 and the mixture was stirred for 3 h at room temperature. The solvent was then removed under vacuum and the residue was dissolved again in CH_2Cl_2 and stirred for 15 minutes. The suspension was filtered to removed NaCl and the resulting clear solution was concentrated to dryness. The crude product was recrystallised from diethyl ether and *n*-hexane.

5: From **1** (100 mg, 0.6 mmol), NaOMe (0.6 mmol) and $[PdCl_2(PPh_3)]_2$ (263 mg, 0.3 mmol). $C_{28}H_{31}ClNOPPd$ (570.41). M.p. 158−165 °C. ^{1}H NMR (400 MHz, $CDCl_3$): δ = 0.96−1.02 (m, 1 H, H-3), 1.55−1.67 (m, 2 H, H-8), 1.76−1.79 (m, 1 H, H-4), 1.80−1.87 (m, 1 H, H-3), 2.32−2.43 (m, 1 H, H-5), 3.06−3.12 (m, 2 H, H-6, H-9), 3.16−3.24 (m, 1 H, H-2), 3.36−3.43 (m, 1 H, H-7), 3.61−3.69 (m, 1 H, H-7), 3.74 (t, *J* = 11.44 Hz, 1 H, H-9), 3.81 (dd, *J* = 13.7, *J* = 10.62 Hz, 1 H, H-6), 5.00−5.07 (m, 2 H, 11), 5.77−5.86 (m, 1 H, 10), 7.26−7.38 (m, 9 H, Ph), 7.56−7.61 (m, 6 H, Ph) ppm. ^{13}C NMR (100 MHz, $CDCl_3$): δ = 22.26 (C-3), 27.13 (C-4), 27.72 (C-8), 39.62 (C-5), 43.50 (C-7), 58.09 (C-6), 67.96 (C-2), 73.57 (C-9), 115.22 (C-11), 128.03 (d, *J* = 10.85 Hz, Ph *o*-C), 129.51 (d, *J* = 51.52 Hz, Ph *i*-C), 130.56 (d, *J* = 2.63 Hz, Ph *p*-C), 134.67 (d, *J* = 10.98 Hz, Ph *m*-C), 140.57 (C-10) ppm. ^{31}P NMR (162 MHz, $CDCl_3$): δ = 26.84 (*trans* to N), 23.95 (*cis* to N) ppm. FAB: *m*/*z* = 570 $[M + H]^+$, 534 $[M - Cl]^+$.

6: From **2** (100 mg, 0.6 mmol), NaOMe (0.6 mmol) and $[PdCl_2(PPh_3)]_2$ (263 mg, 0.3 mmol). $C_{28}H_{31}ClNOPPd$ (570.41). M.p. 152−155 °C. ^{1}H NMR (400 MHz, $CDCl_3$): δ = 1.25−1.31 (m, 1 H, H-3), 1.49−1.56 (m, 1 H, H-3), 1.62−1.72 (m, 3 H, H-8, H-4), 2.38−2.45 (m, 1 H, H-5), 3.08 (dd, *J* = 11.98, *J* = 4.79 Hz, 1 H, H-9), 3.13−3.21 (m, 1 H, H-2), 3.24−3.31 (m, 2 H, H-7, H-6), 3.49−3.57 (m, 1 H, H-7), 3.65 (dd, *J* = 13.12, *J* = 10.23 Hz, 1 H, H-6), 3.73−3.79 (m, 1 H, 9), 5.00−5.04 (m, 2 H, 11), 5.70−5.79 (m, 1 H, 10), 7.26−7.38 (m, 9 H, Ph), 7.55−7.60 (m, 6 H, Ph) ppm. ^{13}C NMR (100 MHz, $CDCl_3$): δ = 21.56 (C-3), 26.03 (C-8), 27.39 (C-4), 39.45 (C-5), 48.94 (C-6), 52.57 (C-7), 67.50 (C-2), 73.01 (C-9), 115.64 (C-11), 128.03 (d, *J* = 10.85 Hz, Ph *o*-C), 129.45 (d, *J* = 51.47 Hz, Ph *i*-C), 130.56 (d, *J* = 2.64 Hz, Ph *p*-C), 134.65 (d, *J* = 1 1.00 Hz, Ph *m*-C), 138.43 (C-10) ppm. ^{31}P NMR (162 MHz, $CDCl_3$): δ = 26.83 (*trans* to N), 23.96 (*cis* to N) ppm. FAB: *m*/*z* = 570 $[M + H]^+$, 534 $[M - Cl]^+$.

7: From **3** (100 mg, 0.6 mmol), NaOMe (0.6 mmol) and $[PdCl_2(PPh_3)]_2$ (263 mg, 0.3 mmol). $C_{28}H_{33}ClNOPPd$ (572.42). M.p. 175−176 °C. ^{1}H NMR (400 MHz, $CDCl_3$): δ = 0.81−0.85 (t, *J* = 7.30 H, 3 H, CH_2CH_3), 0.95−1.00 (m, 1 H, H-3), 1.34−1.41 (m, 2 H, CH_2CH_3), 1.53−1.63 (m, 3 H, H-5, H-8), 1.72−1.81 (m, 2 H, H-3, H-4), 2.77−2.81 (m, 1 H, H-6), 3.07 (dd, *J* = 11.68, *J* = 4.32 Hz, 1 H, H-9), 3.13−3.24 (m, 1 H, H-2), 3.33−3.43 (m, 1 H, H-7), 3.61−3.68 (m, 1 H, H-7), 3.74 (t, *J* = 11.68 Hz, 1 H, H-9), 3.78 (dd, *J* = 13.38, *J* = 10.35 Hz, 1 H, H-6), 7.26−7.38 (m, 9 H, Ph), 7.56−7.62 (m, 6 H, Ph) ppm. ^{13}C NMR (100 MHz, $CDCl_3$): δ = 12.00 (CH_2CH_3), 21.98 (C-3), 24.84 (C-4), 27.92 (CH_2CH_3), 28.35 (C-8), 37.84 (C-5), 43.56 (C-7), 59.97 (C-6), 68.02 (C-2), 73.69 (C-9), 128.05 (d, *J* = 10.84 Hz, Ph *o*-C), 129.14 (d, *J* = 51.31 Hz, Ph *i*-C), 130.56 (d, *J* = 2.60 Hz, Ph *p*-C), 134.71 (d, *J* = 11.00 Hz, Ph *m*-C), ppm. ^{31}P NMR (162 MHz, $CDCl_3$): δ = 26.82 (*trans* to N), 26.74 (*cis* to N) ppm. FAB: *m*/*z* = 572 $[M + H]^+$, 536 $[M - Cl]^+$.

8: From **4** (100 mg, 0.6 mmol), NaOMe (0.6 mmol) and $[PdCl_2(PPh_3)]_2$ (263 mg, 0.3 mmol). $C_{28}H_{33}ClNOPPd$ (572.42). M.p. 130−132 °C. ^{1}H NMR (400 MHz, $CDCl_3$): δ = 0.80−0.84 (t, *J* = 7.39 Hz, 3 H, CH_2CH_3), 1.20−1.36 (m, 3 H, 3, CH_2CH_3), 1.45−1.52 (m, 1 H, H-3), 1.56−1.73 (m, 4 H, H-8, H-5, H-4), 2.99−3.26 (m, 4 H, H-7, H-2, H-9, H-6), 3.46−3.54 (m, 1 H, H-7), 3.58−3.64 (m, 1 H, H-6), 3.76 (t, *J* = 11.35 Hz, 1 H, H-9), 7.26−7.37 (m, 9 H, Ph), 7.56−7.61 (m, 6 H, Ph) ppm. ^{13}C NMR (100 MHz, $CDCl_3$): δ = 11.74 (CH_2CH_3), 21.35 (C-3), 25.13 (CH_2CH_3), 25.80 (C-4), 26.74 (C-8), 37.36 (C-5), 51.05 (C-6), 52.74 (C-7), 67.85 (C-2), 73.22 (C-9), 128.00 (d, *J* = 10.86 Hz, Ph *o*-C), 129.57 (d, *J* = 51.18 Hz, Ph *i*-C), 130.50 (d, *J* = 2.62 Hz, Ph *p*-C), 134.66 (d, *J* = 10.99 Hz, Ph *m*-C) ppm. ^{31}P NMR (162 MHz, $CDCl_3$): δ = 26.78 (*cis* to N) 26.64 (*trans* to N) ppm. FAB: *m*/*z* = 572 $[M + H]^+$, 536 $[M - Cl]^+$.

General Procedure for the Preparation of the Homoleptic Pd^{II} Complexes 9−12: A solution of ligand **1**−**4** and NaOMe in CH_2Cl_2/MeOH (1:1) was added dropwise to a solution of $[PdCl_2(PhCN)_2]$ in CH_2Cl_2 and the reaction mixture was stirred for 1 h at room temperature. The solvent was removed from the light yellow suspension under vacuum and the residue was dissolved again in CH_2Cl_2 and stirred for 15 minutes. The suspension was filtered to remove NaCl and the resulting yellow solution was concentrated to dryness. The crude product was recrystallised from diethyl ether and *n*-hexane.

9: From **1** (400 mg, 2.4 mmol), 2.4 mmol of NaOMe and $[PdCl_2(PhCN)_2]$ (460 mg, 1.2 mmol). $C_{20}H_{32}N_2O_2Pd$ (438.91). M.p. 152−155 °C. ^{1}H NMR (400 MHz, CD_2Cl_2): δ = 0.93−0.98 (m, 2 H, H-3), 1.55−1.63 (m, 4 H, H-8), 1.73−1.83 (m, 4 H, H-H-3, H-4), 2.38−2.42 (m, 2 H, H-5), 2.92 (dd, *J* = 11.21, *J* = 5.17 Hz, 2 H, H-9), 3.00−3.18 (m, 8 H, H-6, H-7, H-2), 3.44−3.49 (m, 2 H, H-9), 3.69−3.78 (m, 2 H, H-7), 5.07−5.13 (m, 4 H, H-11), 5.93−5.84 (m, 2 H, H-10) ppm. ^{13}C NMR (100 MHz, CD_2Cl_2): δ = 22.35 (C-3), 27.11 (C-4), 27.79 (C-8), 39.63 (C-5), 45.60 (C-7),

 © 2004 Wiley-VCH Verlag GmbH & Co. KGaA, Weinheim

58.89 (C-6), 69.38 (C-2), 70.95 (C-9), 115.14 (C-11), 140.96 (C-10). EI: *m/z* = 438 $[M]^+$, 408 $[M - CH_2O]^+$, 378 $[M - 2CH_2O]^+$.

10: From **3** (270 mg, 1.6 mmol), 1.6 mmol of NaOMe and $[PdCl_2(PhCN)_2]$ (300 mg, 0.8 mmol). $C_{20}H_{36}N_2O_2Pd$ (442.94). M.p. 144−147 °C. ^1H NMR (400 MHz, CD_2Cl_2): δ = 0.85−0.89 (t, *J* = 7.34 Hz, 6 H, CH_2CH_3), 0.90−0.95 (m, 2 H, H-3), 1.37−1.45 (m, 4 H, CH_2CH_3), 1.48−1.78 (m, 10 H, H-3, H-4, H-8, H-5), 2.68−2.73 (m, 2 H, H-6), 2.91 (dd, *J* = 11.1, *J* = 5.16 Hz, 2 H, H-9), 3.04−3.14 (m, 6 H, H-6, H-7, H-2), 3.44 (t, *J* = 11.1 Hz, 2 H, H-9), 3.76−3.68 (m, 2 H, H-7) ppm. ^{13}C NMR (100 MHz, CD_2Cl_2): δ = 11.98 (CH_2CH_3), 22.04 (C-3), 24.63 (C-4), 28.04 (CH_2CH_3), 28.38 (C-8), 37.76 (C-5), 45.65 (C-7), 60.88 (C-6), 69.34 (2), 70.99 (C-9). EI: *m/z* = 442 $[M]^+$, 412 $[M - CH_2O]^+$, 382 $[M - 2CH_2O]^+$.

11: From **2** (400 mg, 2.4 mmol), 2.4 mmol of NaOMe and $[PdCl_2(PhCN)_2]$ (460 mg, 1.2 mmol). $C_{20}H_{32}N_2O_2Pd$ (438.91). M.p. 155−160 °C. ^1H NMR (400 MHz, CD_2Cl_2): δ = 1.21−1.26 (m, 2 H, H-3), 1.45−1.52 (m, 2 H, H-3), 1.58−1.76 (m, 6 H, H-8, H-2), 2.36−2.42 (m, 2 H, H-5), 2.88−2.95 (m, 4 H, H-9, H-7), 2.98−3.07 (m, 2 H, H-9), 3.16−3.23 (m, 2 H, H-7), 3.33 (dd, *J* = 13.34, *J* = 10.21 Hz, 2 H, H-6), 3.38−3.44 (ddd, *J* = 13.34, *J* = 8.42, *J* = 2.18 Hz, 2 H, H-6), 3.50 (t, *J* = 10.96 Hz, 2 H, H-9), 5.05−5.10 (m, 4 H, H-11), 5.84−5.75 (m, 2 H, H-10) ppm. ^{13}C NMR (100 MHz, CD_2Cl_2): δ = 21.66 (C-3), 25.95 (C8), 27.84 (C-4), 39.78 (C-5), 50.93 (C-6), 53.34 (C-7), 69.20 (C-2), 70.88 (C-9), 115.45 (C-11), 138.97 (C-10). EI: *m/z* = 438 $[M]^+$, 408 $[M - CH_2O]^+$, 378 $[M - 2CH_2O]^+$.

12: From **4** (100 mg, 0.6 mmol), 0.6 mmol of NaOMe and $[PdCl_2(PhCN)_2]$ (113 mg, 0.3 mmol). $C_{20}H_{36}N_2O_2Pd$ (442.94). M.p. 180−182 °C. ^1H NMR (400 MHz, CD_2Cl_2): δ = 0.77−0.81 (t, *J* = 7.39 Hz, CH_2CH_3), 1.10−1.32 (m, 6 H, 3, CH_2CH_3), 1.36−1.42 (m, 2 H, H-3), 1.45−1.55 (m, 6 H, H-5, H-4, H-8), 1.61−1.68 (m, 2 H, H-8), 2.84−2.91 (m, 2 H, H-7), 2.95−3.10 (m, 6 H, H-6, H-2, H-9), 3.16−3.22 (m, 2 H, H-7), 3.3 (dd, *J* = 13.13, *J* = 9.84 Hz, 2 H, H-6), 3.5 (t, *J* = 12.43 Hz, 2 H, H-9) ppm. ^{13}C NMR (100 MHz, CD_2Cl_2): δ = 11.62 (CH_2CH_3), 21.21 (C-3), 25.12 (CH_2CH_3), 25.39 (C-4), 26.33 (C-8), 37.36 (C-5), 52.92 (C-6), 53.25 (C-7), 68.72 (C-2), 70.59 (C-9). EI: *m/z* = 442 $[M]^+$, 412 $[M - CH_2O]^+$, 382 $[M - 2CH_2O]^+$.

General Procedure for the Preparation of the Chloroenynes 15 and 16: A mixture of $[Pd(PPh_3)_4]$ (0.05 equiv.), (*Z*)-1,2-dichloroethene (3 equiv.), alkyne (1 equiv.), and piperidine or $nBuNH_2$ (2 equiv.) in absolute THF was stirred for 15 minutes at room temperature under a nitrogen atmosphere, and CuI (0.1 equiv.) was then added. The stirring was continued until TLC analysis indicated complete consumption of the alkyne (3−5 h). The reaction mixture was treated with a saturated aqueous solution of $NaHCO_3$ and extracted with CH_2Cl_2. The organic layer was dried over Na_2SO_4 and the solvent was removed in vacuo. The crude product was purified by column chromatography [MTBE/MeOH/NH_3(25%)] to yield the desired chloroenyne.

15: From **13** (2 g, 12 mmol), $[Pd(PPh_3)_4]$ (0.69 g, 0.59 mmol), CuI (0.23 g, 1.2 mmol), $nBuNH_2$ (1.75 g, 23.9 mmol) and (*Z*)-1,2-dichloroethene (3.49 g, 36 mmol). $C_{12}H_{16}ClNO$ (225.5). ^1H NMR (400 MHz, $CDCl_3$): δ = 0.74−0.80 (m, 1 H, H-3), 1.34−1.49 (m, 2 H, H-8), 1.89−1.93 (m, 1 H, H-4), 2.04−2.11 (m, 1 H, H-3), 2.49−2.57 (m, 1 H, H-7), 2.65−2.68 (m, 1 H, H-5), 2.85−2.93 (m, 2 H, H-7, H-6), 3.06−3.11 (m, 2 H, H-2, OH), 3.23 (dd, *J* = 13.17, *J* = 9.95 Hz, 1 H, H-6), 3.38−3.45 (m, 2 H, H-9), 5.79 (dd, *J* = 7.33, *J* = 2.23 Hz, 1 H, H-12), 6.26 (d, *J* = 7.33 Hz, 1 H, H-13) ppm. ^{13}C NMR (100 MHz, $CDCl_3$): δ = 24.91 (C-3), 26.18 (C-8), 26.56 (C-4), 28.95 (C-5), 39.55 (C-7), 56.82 (C-2), 56.88 (C-6), 62.61 (C-9), 75.09 (C-11), 102.02 (C-10), 112.20 (C-12), 127.39 (C-13) ppm. MS-EI (43 °C): *m/z* (%) = 227 (18) $[M^+]$, 225 (48) $[M^+]$, 194 (78), 190 (100), 162 (12), 159 (30), 132 (78), 126 (31), 103 (24), 82 (16), 77 (26), 72 (29), 63 (14), 55 (21), 51 (10), 44 (44). EI: *m/z* = 225 $[M]^+$, 194 $[M - CH_2OH]^+$, 190 $[M - Cl]^+$.

16: From **13** (2 g, 12 mmol), $[Pd(PPh_3)_4]$ (0.69 g, 0.59 mmol), CuI (0.23 g, 1.2 mmol), $nBuNH_2$ (2.06 g, 23.95 mmol) and (*Z*)-1,2-dichloroethene (3.49 g, 36 mmol). $C_{12}H_{16}ClNO$ (225.5). ^1H NMR (400 MHz, $CDCl_3$): δ = 1.38−1.62 (m, 4 H, H-8, H-3), 1.87−1.91 (m, 1 H, H-4), 2.59−2.63 (m, 1 H, H-5), 2.74−3.00 (m, 5 H, H-6, H-2, H-7), 3.31 (s, 1 H, OH), 3.57 (t, *J* = 11.24 Hz, 1 H, H-9), 5.78 (dd, *J* = 7.34, *J* = 2.23 Hz, 1 H, H-12), 6.26 (d, *J* = 7.34 Hz, 1 H, H-13) ppm. ^{13}C NMR (100 MHz, $CDCl_3$): δ = 24.19 (C-13), 25.45 (C-8), 27.28 (C-4), 29.33 (C-5), 47.83 (C-6), 48.42 (C-7), 57.23 (C-2), 62.03 (C-9), 75.60 (C-11), 101.37 (C-10), 112.14 (C-12), 127.46 (C-13) ppm. MS-EI (55 °C): *m/z* (%) = 227 (24) $[M^+]$, 225 (79) $[M^+]$, 208 (4), 194 (100), 190 (88), 158 (22), 132 (48), 126 (64), 117 (16), 112 (25), 103 (34), 82 (32), 77 (31), 72 (49), 63 (14), 55 (35), 51 (16), 44 (48), 42 (68). EI: *m/z* = 225 $[M]^+$, 194 $[M - CH_2OH]^+$, 190 $[M - Cl]^+$.

General Procedure for the Preparation of the Enediynes 17 and 18: $[PdCl_2(PhCN)_2]$ (0.05 equiv.), piperidine (2 equiv.) and terminal alkyne (1.2 equiv.) were added to a solution of pure chloroenyne (1 equiv.) in absolute THF, at room temperature, under a nitrogen atmosphere. CuI (0.1 equiv.) was then added to the stirred solution. The stirring was continued until TLC analysis indicated complete consumption of the chloroenyne. The reaction mixture was treated with a saturated aqueous solution of $NaHCO_3$ and extracted with CH_2Cl_2. The organic layer was dried over Na_2SO_4 and the solvent was removed in vacuo. The resulting crude product was purified by column chromatography [MTBE/MeOH/NH_3(25%)] to afford the desired enediyne.

17: From **15** (2.32 g, 10.28 mmol), $[PdCl_2(PhCN)_2]$ (197 mg, 0.5 mmol), CuI (196 mg, 1.02 mmol), piperidine (1.76 g, 20.46 mmol) and **13** (1.86 g, 11.27 mmol). $C_{22}H_{30}N_2O_2$ (354). ^1H NMR (400 MHz, $CDCl_3$): δ = 0.74−0.80 (m, 2 H, H-3), 1.34−1.49 (m, 4 H, H-8), 1.86−1.90 (m, 2 H, H-4), 2.03−2.10 (m, 2 H, H-3), 2.49−2.56 (m, 2 H, H-7), 2.66−2.68 (m, 2 H, H-5), 2.82−2.92 (m, 4 H, H-7, H-6), 3.02−3.10 (m, 2 H, H-2), 3.23 (dd, *J* = 13.15, *J* = 9.94 Hz, 2 H, H-6), 3.31−3.46 (m, 6 H, H-9, OH), 5.70 (s, 2 H, H-12) ppm. ^{13}C NMR (100 MHz, $CDCl_3$): δ = 25.08 (C-3), 26.18 (C-8), 26.65 (C-4), 29.03 (C-5), 39.64 (C-7), 56.95 (C-2), 57.12 (C-6), 62.76 (C-9), 78.69 (C-11), 100.91 (C-10), 118.96 (C-12) ppm. MS-EI (163 °C): *m/z* (%) = 354 (100) $[M^+]$, 337 (2), 323 (45), 297 (25), 295 (12), 277 (8), 265 (16), 242 (10), 238 (12), 224 (7), 210(17), 184 (14), 177 (7), 165 (11), 141 (8), 128 (13), 115 (12), 100 (9), 96 (10), 86 (12), 70 (14), 55 814), 44 (27), 42 (24). EI: *m/z* = 354 $[M]^+$, 323 $[M - CH_2OH]^+$.

18: From **16** (1.05 g, 4.65 mmol), $[PdCl_2(PhCN)_2]$ (90 mg, 0.2 mmol), CuI (88 mg, 0.46 mmol), piperidine (0.8 g, 9.3 mmol) and **14** (0.92 g, 5.57 mmol). $C_{22}H_{30}N_2O_2$ (354). ^1H NMR (400 MHz, $CDCl_3$): δ = 1.36−1.62 (m, 8 H, H-8, H-3), 1.87−1.88 (m, 2 H, H-4), 2.62−2.66 (m, 2 H, H-5), 2.74−3.00 (m, 10 H, H-6, H-2, H-7), 3.07 (s, 2 H, OH), 3.39 (dd, *J* = 11.1, *J* = 5 Hz, 2 H, H-9), 3.55 (t, *J* = 11.1 Hz, 2 H, H-9), 5.69 (s, 2 H, H-12) ppm. ^{13}C NMR (100 MHz, $CDCl_3$): δ = 24.35 (C-3), 25.55 (C-8), 27.43 (C-4), 29.45 (C-5), 48.01 (C-6), 48.43 (C-7), 57.13 (C-2), 62.14 (C-9), 79.24 (C-11), 100.17 (C-10), 118.99 (C-12), ppm. MS-EI (132 °C): *m/z* (%) = 354 (100) $[M^+]$, 323 (21), 297 (9), 295 (13), 279 (16), 268 (5), 252 (3), 242 (8), 222 (6), 210 (9), 196 (9), 182 (11), 167 (29), 149 (47), 126 (11), 115 (10), 108 (7), 96 (11), 86 (8), 71 (13), 57 (17), 44 (19), 42 (12). EI: *m/z* = 354 $[M]^+$, 323 $[M - CH_2OH]^+$.

 © 2004 Wiley-VCH Verlag GmbH & Co. KGaA, Weinheim

General Procedure for the Preparation of the Bis-*N*,*P*-aminophosphinites 19 and 20: A solution of Ph_2PCl (2.05 equiv.) in dry CH_2Cl_2 was cooled to 0 °C and then a solution of (*Z*)-enediyne (1 equiv.) and NEt_3 (4 equiv.) in the same solvent was added dropwise. After the addition, the reaction mixture was allowed to warm up to room temperature and stirred until TLC analysis indicated complete consumption of the reactant **17** and **18**. The solution was concentrated in vacuo and the residue was dissolved in CH_2Cl_2/*n*-hexane (1:2) and stirred for 15 minutes. The suspension was filtered to remove $Et_3N{\cdot}HCl$ and the resulting clear solution was concentrated to dryness. The crude product was purified by column chromatography under a nitrogen atmosphere (MTBE/acetonitrile/NEt_3) to afford the desired bis-aminophosphinite in very good yield.

19: From **17** (1.22 g, 3.44 mmol), Ph_2PCl (1.52 g, 6.8 mmol) and NEt_3 (13.7 mmol). $C_{46}H_{48}N_2O_2P_2$ (722.85). ^1H NMR (400 MHz, C_6D_6): δ = 0.75−0.80 (m, 2 H, H-3), 0.88−0.96 (m, 2 H, H-8), 1.00−1.08 (m, 2 H, H-8), 1.74−1.75 (m, 2 H, H-4), 2.13−2.18 (m, 2 H, H-3), 2.24−2.31 (m, 2 H, H-7), 2.43−2.45 (m, 2 H, H-5), 2.74−2.82 (m, 2 H, H-7), 2.92−3.04 (m, 4 H, H-6), 3.29−3.36 (m, 2 H, H-2), 3.64−3.70 (m, 2 H, H-9), 3.77−3.84 (m, 2 H, H-9), 5.59 (s, 2 H, H-12), 7.01−7.05 (m, 4 H, Ph), 7.09−7.13 (m, 8 H, Ph), 7.61−7.64 (m, 8 H, Ph) ppm. ^{13}C NMR (100 MHz, C_6D_6): δ = 25.75 (C-3), 26.46 (C-8), 27.65 (C-4), 29.32 (C-5), 41.04 (C-7), 56.68 (d, *J* = 7.23 Hz, C-2), 71.71 (d, *J* = 18.3 Hz, C-9), 57.81 (C-6), 79.41 (C-11), 101.79 (C-10), 119.47 (C-12), 128.43 (d, *J* = 6.97 Hz, Ph *m*-C), 128.50 (d, *J* = 6.97 Hz, Ph *m*-C), 129.21 (d, *J* = 3.35 Hz, Ph *p*-C), 130.62 (d, *J* = 8.32 Hz, Ph *o*-C), 130.83 (d, *J* = 8.14 Hz, Ph *o*-C), 143.31 (d, *J* = 8.40 Hz, Ph *i*-C), 143.49 (d, *J* = 7.83 Hz, Ph *i*-C) ppm. ^{31}P NMR (162 MHz, C_6D_6): δ = 115.29 ppm. EI: *m*/*z* = 722 $[M]^+$, 521 $[M - Ph_2PO]^+$, 201 $[Ph_2PO]^+$.

20: From **18** (1.36 g, 3.84 mmol), Ph_2PCl (1.78 g, 8.00 mmol) and NEt_3 (15.36 mmol). $C_{46}H_{48}N_2O_2P_2$ (722.85). ^1H NMR (400 MHz, C_6D_6): δ = 0.96−1.12 (m, 4 H, H-8), 1.18−1.25 (m, 2 H, H-3), 1.62−1.67 (m, 2 H, H-3), 1.74 (br. s, 2 H, H-4), 2.31−2.48 (m, 6 H, H-7, H-5), 2.86−2.93 (m, 4 H, H-6, H-2), 3.12 (ddd, *J* = 14.02, *J* = 6.68, *J* = 2.01 Hz, 2 H, H-6), 3.77−3.84 (m, 2 H, H-9), 4.05−4.12 (m, 2 H, H-9), 5.58 (s, 2 H, H-12), 7.01−7.05 (m, 4 H, Ph), 7.09−7.13(m, 8 H, Ph), 7.60−7.66 (m, 8 H, Ph) ppm. ^{13}C NMR (100 MHz, C_6D_6): δ = 25.22 (C-3), 25.53 (C-8), 28.31 (C-4), 29.96 (C-5), 48.58 (C-7), 49.63 (C-6), 56.78 (d, *J* = 6.28 Hz, C-2), 71.22 (d, *J* = 18.57 Hz, C-9), 79.94 (C-11), 101.20 (C-10), 119.39 (C-12), 128.37 (d, *J* = 6.70 Hz, Ph *m*-C), 128.46 (d, *J* = 6.55 Hz, Ph *m*-C), 129.10 (d, *J* = 1.80 Hz, Ph *p*-C), 130.55 (d, *J* = 11.36 Hz, Ph *o*-C), 130.76 (d, *J* = 11.32 Hz, Ph *o*-C), 143.63 (d, *J* = 14.51 Hz, Ph *i*-C), 143.82 (d, *J* = 14.69 Hz, Ph *i*-C) ppm. ^{31}P NMR (162 MHz, C_6D_6): δ = 114.60 ppm. EI: *m*/*z* = 722 $[M]^+$, 645 $[M - C_6H_5]^+$, 521 $[M - Ph_2PO]^+$, 201 $[Ph_2PO]^+$.

General Procedure for the Preparation of the Platinacycles 21 and 22: A solution of $[PtCl_2(SMe_2)_2]$ in CH_2Cl_2 (4 mL) was added dropwise to a stirred solution of **19** and **20** in CH_2Cl_2 (5 mL). After 15 minutes, the solvent was removed to give a pale-yellow solid. Recrystallisation from THF and toluene gave a white solid.

21: From **19** (370 mg, 0.51 mmol) and $[PtCl_2(SMe_2)_2]$ (200 mg, 0.51 mmol). M.p. 195−197 °C. $C_{46}H_{48}Cl_2N_2O_2P_2Pt$ (988.83). ^1H NMR (400 MHz, $CDCl_3$): δ = 0.86−0.91 (m, 2 H, H-3), 1.37−1.44 (m, 4 H, H-8), 1.97 (br. s, 2 H, H-4), 2.04−2.10 (m, 2 H, H-3), 2.24−2.32 (m, 2 H, H-7), 2.48−2.50 (m, 2 H, H-7), 2.71−2.74 (m, 2 H, H-5), 2.86−2.89 (m, 2 H, H-6), 3.07−3.11 (m, 2 H, H-2), 3.21 (dd, *J* = 13.22, *J* = 10.07 Hz, 2 H, H-6), 3.28 (br. s, 2 H, H-9), 3.47−3.49 (m, 2 H, H-9), 5.88 (s, 2 H, H-12), 7.37−7.53 (m, 12 H, Ph), 7.70−7.74 (m, 4 H, Ph), 8.04−8.09 (m, 4 H, Ph), ppm. ^{13}C NMR (100 MHz, $CDCl_3$): δ = 25.57 (C-8), 25.61 (C-3), 26.27 (C-4), 28.57 (C-5), 40.44 (C-7), 54.89 (d, *J* = 8.02 Hz, C-2), 56.86 (C-6), 68.42 (C-9), 78.42 (C-11), 100.81 (C-10), 118.77 (C-12), 127.85 (d, *J* = 11.73 Hz, Ph *m*-C), 128.25 (d, *J* = 12.05 Hz, Ph *m*-C), 131.40 (d, *J* = 69.43, Ph *i*-C), 131.56 (Ph *p*-C), 131.75 (Ph *p*-C), 132.41 (d, *J* = 12.34 Hz, Ph *o*-C), 132.45 (d, *J* = 77.80 Hz, Ph *i*-C), 132.70 (d, *J* = 11.58 Hz, Ph *o*-C) ppm. ^{31}P NMR (162 MHz, $CDCl_3$): δ = 83.89 ($^1J_{Pt,P}$ = 2099.28 Hz) ppm. FAB: *m*/*z* = 988 $[M]^+$, 953 $[M - Cl]^+$.

22: From **20** (250 mg, 0.346 mmol) and $[PtCl_2(SMe_2)_2]$ (135 mg, 0.346 mmol). M.p. 215 °C. $C_{46}H_{48}Cl_2N_2O_2P_2Pt$ (988.83). ^1H NMR (400 MHz, $CDCl_3$): δ = 1.46−1.56 (m, 8 H, H-8, H-3), 1.92 (br. s, 2 H, H-4), 2.28−2.32 (m, 2 H, H-2), 2.62−2.75 (m, 8 H, H-7, H-5, H-6), 2.94−3.01 (m, 2 H, H-6), 3.73−3.82 (m, 2 H, H-9), 4.07−4.09 (m, 2 H, H-9), 5.79 (s, 2 H, H-12), 7.25−7.36 (m, 12 H, Ph), 7.66−7.71 (m, 4 H, Ph), 7.81−7.86 (m, 4 H, Ph) ppm. ^{13}C NMR (100 MHz, $CDCl_3$): δ = 24.70 (C-8), 25.34 (C-3), 27.13 (C-4), 29.09 (C-5), 48.39 (C-7), 49.06 (C-6), 54.53 (d, *J* = 6.93 Hz, C-2), 70.27 (C-9), 79.12 (C-11), 100.10 (C-10), 119.03 (C-12), 127.84 (d, *J* = 12.06 Hz, Ph *m*-C), 128.10 (d, *J* = 11.89 Hz, Ph *m*-C), 131.40 (d, *J* = 7.15 Hz, Ph *p*-C), 131.90 (d, *J* = 11.86 Hz, Ph *o*-C), 132.47 (d, *J* = 11.56 Hz, Ph *o*-C), 132.56 (d, *J* = 74.00 Hz, Ph *i*-C), 133.47 (d, *J* = 75.00 Hz, Ph *i*-C) ppm. ^{31}P NMR (162 MHz, $CDCl_3$): δ = 85.10 ($^1J_{Pt,P}$ = 2076.01 Hz) ppm. FAB: *m*/*z* = 988 $[M]^+$, 953 $[M - Cl]^+$.

General Procedure for the Preparation of the Binuclear Pd^{II}-*N*,*P*-aminophosphinite Complexes 23 and 24: $[(\eta^4\text{-}C_7H_8)PdCl_2]$ was added to a solution of **19** or **20** in CH_2Cl_2 (20 mL) and the reaction mixture was stirred overnight at room temperature. The solvent of the clear yellow solution was removed under vacuum and the remaining yellow solid was washed twice with *n*-hexane and dried in vacuo for two days.

23: From **19** (160 mg, 0.22 mmol) and $[(\eta^4\text{-}C_7H_8)PdCl_2]$ (120 mg, 0.44 mmol). M.p. 210−214 °C. ^1H NMR (400 MHz, CD_2Cl_2): δ = 1.06−1.12 (m, 2 H, H-3), 1.49−1.67 (m, 4 H, H-8), 2.03 (br. s, 2 H, H-4), 2.25−2.31 (m, 2 H, H-3), 2.94−3.01 (m, 4 H, H-7, H-5), 3.19−3.24 (m, 4 H, H-6, H-2), 3.62−3.69 (m, 2 H, H-9), 3.84−3.95 (m, 2 H, H-9), 4.25−4.31 (m, 2 H, H-7), 5.09 (dd, *J* = 13.56, *J* = 10.4 Hz, 2 H, H-6), 5.80 (s, 2 H, H-12), 7.31−7.35 (m, 4 H, Ph), 7.42−7.47 (m, 6 H, Ph), 7.53−7.56 (m, 2 H, Ph), 7.59−7.65 (m, 4 H, Ph), 7.95−8.00 (m, 4 H, Ph) ppm. ^{13}C NMR (100 MHz, CD_2Cl_2): δ = 26.09 (C-4), 26.64 (C-8), 27.18 (C-3), 30.16 (C-5), 46.74 (C-7), 60.90 (d, *J* = 4.18 Hz, C-2), 62.07 (C-6), 67.85 (C-9), 79.83 (C-11), 98.95 (C-10), 119.87 (C-12), 128.39 (d, *J* = 12.46 Hz, Ph *m*-C), 128.96 (d, *J* = 12.07 Hz, Ph *m*-C), 130.85 (d, *J* = 62.07 Hz, Ph *i*-C), 131.86 (d, *J* = 49.16 Hz, Ph *i*-C), 132.42 (Ph *m*-C), 132.90 (d, *J* = 11.39 Hz, Ph *o*-C), 133.13 (Ph *p*-C), 134.61 (d, *J* = 13.04 Hz, Ph *o*-C) ppm. ^{31}P NMR (162 MHz, CD_2Cl_2): δ = 102.90 ppm. ESI: *m*/*z* = 1101 $[M + Na]^+$, 1043 $[M - Cl]^+$.

24: From **19** (200 mg, 0.27 mmol) and $[(\eta^4\text{-}C_7H_8)PdCl_2]$ (150 mg, 0.55 mmol). M.p. 238−240 °C. ^1H NMR (400 MHz, $CDCl_3$): δ = 1.44−1.50 (m, 2 H, H-3), 1.73−1.77 (m, 4 H, H-8), 1.85−1.92 (m, 2 H, H-3), 2.01 (br. s, 2 H, H-4), 2.78−2.83 (m, 2 H, H-6), 2.90−2.95 (m, 2 H, H-5), 3.05−3.09 (m, 2 H, H-2), 3.27−3.29 (m, 2 H, H-7), 3.91−4.01 (m, 2 H, H-9), 4.56−4.64 (m, 2 H, H-7), 4.86 (dd, *J* = 12.46, *J* = 10.40 Hz, 2 H, H-6), 5.64 (s, 2 H, H-12), 7.30−7.35 (m, 4 H, Ph), 7.37−7.47 (m, 6 H, Ph), 7.50−7.54 (m, 2 H, Ph), 7.66−7.71 (m, 4 H, Ph), 7.98−8.03 (m, 4 H, Ph) ppm. ^{13}C NMR (100 MHz, $CDCl_3$): δ = 25.64 (C-8), 26.16 (C-3), 27.27 (C-4), 30.02 (C-5), 52.96 (C-6), 54.79 (C-7), 61.02 (C-2), 67.40 (C-9), 80.14 (C-11), 96.91 (C-10), 119.45 (C-12), 128.27 (d, *J* = 12.50 Hz, Ph *m*-C), 128.61 (d, *J* = 12.10 Hz, Ph *m*-C), 131.32 (d, *J* = 78.90 Hz, Ph *i*-C), 131.85 (d, *J* = 60.71 Hz, Ph *i*-C), 132.16 (Ph *p*-C), 132.68 (d, *J* = 11.50 Hz, Ph *o*-C), 132.74 (Ph *p*-C), 134.30 (d,

 © 2004 Wiley-VCH Verlag GmbH & Co. KGaA, Weinheim

Table 1. Crystal data for the crystal structures of **7**, **8**, **9**, **11**, **18** and **21**

	7	**8**	**9**	**11**	**18**	**21**
Formula	$C_{28}H_{33}ClNOPPd$	$C_{28}H_{33}ClNOPPd$	$C_{20}H_{34}N_2O_3Pd$	$C_{20}H_{36}N_2O_4Pd$	$C_{22}H_{30}N_2O_2$	$C_{50}H_{56}Cl_2N_2O_3P_2Pt$
M_r	572.37	572.37	456.89	474.91	354.48	1060.90
Habit	yellow prism	yellow prism	yellow prism	yellow block	colourless prism	colourless tablet
Dimensions (mm)	0.46 × 0.22 × 0.16	0.43 × 0.26 × 0.17	0.35 × 0.21 × 0.12	0.38 × 0.37 × 0.27	0.46 × 0.26 × 0.14	0.25 × 0.21 × 0.1
Crystal system	orthorhombic	orthorhombic	monoclinic	orthorhombic	orthorhombic	triclinic
Space group	$P2_12_12_1$	$P2_12_12_1$	$P2_1$	$P2_12_12_1$	$P2_12_12_1$	$P1$
a (Å)	8.7380(14)	8.9083(6)	11.3948(6)	8.4067(14)	7.7902(9)	11.3323(10)
b (Å)	16.900(3)	16.6224(10)	7.3436(4)	10.0958(18)	10.9628(12)	12.8787(10)
c (Å)	17.208(3)	17.1522(10)	12.3835(8)	23.817(4)	22.772(2)	17.6247(14)
α (°)	90	90	90	90	90	92.556(3)
β (°)	90	90	99.917(3)	90	90	108.556(3)
γ (°)	90	90	90	90	90	104.543(3)
V (Å^3)	2541.3(7)	2539.9(3)	1020.75(10)	2021.4(6)	1944.8(4)	2338.6(3)
Z	4	4	2	4	4	2
D_x (Mg·m^{-3})	1.497	1.497	1.487	1.560	1.211	1.507
μ (mm^{-1})	0.92	0.92	0.93	0.95	0.08	3.23
F(000)	1176	1176	476	992	768	1072
T (°C)	−140	−140	−140	−140	−140	−140
$2\theta_{max}$	60	60	60	60	60	60
Transmission	0.56−0.83	0.69−0.86	0.74−0.89	0.43−0.75	no correction	0.59−0.80
No. of reflections:						
measured	53471	51018	18924	40178	22535	48900
independent	7430	7423	5947	5912	3225	25501
R_{int}	0.0686	0.0192	0.0177	0.0776	0.0329	0.0322
Parameters	299	299	243	260	243	1031
Restraints	0	0	1	0	0	952
wR (F^2, all refl.)	0.0699	0.0369	0.0397	0.0643	0.0934	0.0763
R (F, >4σ(F)]	0.0266	0.0139	0.0154	0.0245	0.0342	0.0333
S	1.07	1.05	1.04	1.03	1.02	0.98
Max. Δ/σ	<0.001	0.001	0.001	0.001	0.001	0.001
Max. Δρ (e·Å^{-3})	1.18	0.48	0.43	0.76	0.25	2.25
Flack parameter	−0.036(17)	−0.012(10)	0.011(13)	0.00(2)		0.005(4)

J = 12.97 Hz, Ph *o*-C) ppm. ^{31}P NMR (162 MHz, $CDCl_3$): δ = 103.76 ppm. ESI: m/z = 1101 [M + Na]$^+$, 1043 [M − Cl]$^+$.

Crystal Structure Analyses: The crystal-structure data for **7**, **8**, **9**, **11**, **18 and 21** were collected on a Bruker SMART 1000CCD area detector (graphite-monochromated Mo-K_α radiation, λ = 71.073 pm) at −140 °C in the ω- and φ-scan mode. Empirical absorption corrections were applied using the program SADABS. The structures were solved by direct methods using SHELXS-86/97,[22] and subjected to full-matrix least-squares refinement on F^2 using SHELXL-93/97,[23] with anisotropic displacement parameters for non-H atoms. The crystal structure of **21** contains one disordered THF molecule per formula unit, which could not be resolved satisfactorily. This led to a residual electron density of 2.25 e·Å^{-3}. The crystal structure was therefore refined using the restraints SIMU and DELU for the carbon, nitrogen and oxygen atoms. Additionally, the restraint FLAT was added to describe the local symmetry of the phenyl rings. Methyls were treated as rigid groups and O-bonded hydrogens were refined freely. All other hydrogen atoms were included using a riding model.

CCDC-216416 (**7**), -216417 (**8**), -216418 (**9**), -216419 (**11**), -216420 (**18**) and -216421 (**21**) contain the supplementary crystallographic data for this paper. These data can be obtained free of charge at www.ccdc.cam.ac.uk/conts/retrieving.html [or from the Cambridge Crystallographic Data Centre, 12, Union Road, Cambridge CB2 1EZ, UK; Fax: (internat.) +44-1223/336-033; E-mail: deposit@ccdc.cam.ac.uk].

[1] [1a] R. Noyori, *Asymmetric Catalysis in Organic Synthesis*; Wiley: New York, **1994**. [1b] I. Ojima, *Catalytic Asymmetric Synthesis*; VCH: New York, **1993**.

[2] [2a] M. Nógrádi, *Stereoselective Synthesis*; VCH: Weinheim, **1995**, p. 48ff. [2b] O. Červinka, *Enantioselective Reactions in Organic Chemistry*; Ellis Horwood: New York, **1995**, p. 68ff.

[3] [3a] P.-O. Norrby, H. C. Kolb, K. B. Sharpless, *J. Am. Chem. Soc.* **1994**, *116*, 8470−8478. [3b] For a very recent method for asymmetric desymmetrisation of *meso*-1,2-diols by phosphinite derivatives of *Cinchona* alkaloids see: S. Mizuta, M. Sadamori, T. Fujimoto, I. Yamamoto, *Angew. Chem.* **2003**, *115*, 3505−3507; *Angew. Chem. Int. Ed.* **2003**, *42*, 3383−3385.

[4] G. D. A. Dijkstra, R. M. Kellog, H. Wynberg, J. S. Svendsen, I. Marko, K. B. Sharpless, *J. Am. Chem. Soc.* **1989**, *111*, 8069−8076.

[5] E. J. Corey, M. C. Noe, *J. Am. Chem. Soc.* **1996**, *118*, 11038−11053.

[6] [6a] A. Albinati, F. Lianza, H. Berger, P. S. Pregosin, H. Rügger, R. W. Kunz, *Inorg. Chem.* **1993**, *32*, 478−486. [6b] A. de Renzi, G. Morelli, M. Scalone, *Inorg. Chim. Acta* **1982**, *65*, L119−L120. [6c] V. V. Dunina, E. B. Golovan, N. S. Gulyukina, Yu. K. Grishin, I. P. Beletskaya, *Russ. Chem. Bull.* **1997**, 1385.

[7] G. Chelucci, M. A. Cabras, C. Botteghi, M. Marchetti, *Tetrahedron: Asymmetry* **1994**, *5*, 299−302.

[8] I. D. Kostas, C. G. Screttas, *J. Organomet. Chem.* **1999**, *585*, 1−6.

[9] V. I. Tarorov, R. Kadyrov, T. H. Riermeier, J. Holz, A. Borner, *Tetrahedron: Asymmetry* **1999**, *10*, 4009−4015.

 © 2004 Wiley-VCH Verlag GmbH & Co. KGaA, Weinheim

[10] R. Hubel, K. Polborn, W. Beck, *Eur. J. Inorg. Chem.* **1999**, 471−482.
[11] A. I. Polosukhin, K. N. Gavrilov, O. G. Bondarev, A. V. Korostylev, P. V. Petrovskii, V. A. Davankov, *J. Organomet. Chem.* **2000**, *608*, 89−95.
[12] C. Salluzo, J. Breuzard, S. Pellet-Rostaing, M. Vallet, F. Le Guyader, M. Lemaire, *J. Organomet. Chem.* **2002**, 98−104.
[13] [13a] J. Frackenpohl, W. M. Braje, H. M. R. Hoffmann, *J. Chem. Soc., Perkin Trans. 1* **2001**, 47−65. [13b] O. Schrake, W. Braje, H. M. R. Hoffmann, R. Wartchow, *Tetrahedron: Asymmetry* **1998**, *9*, 3717−3722.
[14] D. Chemin, G. Linstrumelle, *Tetrahedron* **1994**, *50*, 5335−5344.
[15] M. Alami, B. Grousse, G. Linstrumelle, *Tetrahedron Lett.* **1994**, *35*, 3543−3544.
[16] F. R. Hartley, *The Chemistry of Platinum and Palladium*, ASP LTD London, **1973**.
[17] S. K. Armstrong, R. J. Gross, L. J. Farrugia, D. A. Nichols, A. Perry, *Eur. J. Inorg. Chem.* **2002**, 141−151.
[18] D. T. Rosevear, F. G. A. Stone, *J. Chem. Soc., (A)* **1968**, 164−167.
[19] J. R. Doyle, P. E. Slade, H. B. Jonassen, *Inorg. Synth.* **1960**, *6*, 218−219.
[20] D. Drew, J. R. Doyle, *Inorg. Synth.* **1972**, *13*, 48−49.
[21] F. R. Hartley, *Organomet. Chem. Rev.* **1970**, *A6*, 119−137.
[22] G. M. Sheldrick, SHELXS-86/97, A program for solving crystal structures, University of Göttingen, **1997**.
[23] G. M. Sheldrick, SHELXL-93/97, A program for refining crystal structures, University of Göttingen, **1997**.

Received August 11, 2003
Early View Article
Published Online December 19, 2003

 © 2004 Wiley-VCH Verlag GmbH & Co. KGaA, Weinheim

Inorganic−Organic Hybrid Compounds: Synthesis and Structures of New Metal Organic Polymers Synthesized in the Presence of Mixed Dicarboxylates

A. Thirumurugan[a] and Srinivasan Natarajan*[a]

Keywords: Carboxylate ligands / Coordination modes / Thermochemistry / Lanthanides

A hydrothermal reaction of a mixture of 1,2-dicyanobenzene (1,2-DCB), 1,4-benzene-dicarboxylic acid (1,4-BDC) along with the corresponding lanthanide salts at a pH of ≈ 5, gives rise to a new series of carboxylate coordination polymers, $[M_2(H_2O)_4\{(1,2BDC)_2(1,4BDC)\}]$, (M = La, Pr, Gd, Dy, and Y), which are three-dimensional in structure. The 1,2-DCB oxidized to the corresponding dicarboxylic acid, phthalic acid (1,2-BDC), during the reaction. The structures are of two types with the larger La and Pr lanthanides forming type-1 and the smaller ones, Gd, Dy, and Y, forming type-2. While La and Pr have an idealized D_{3h} triply capped trigonal prism coordination environment, Gd, Dy, and Y have a distorted dodecahedral arrangement with respect to the oxygen atoms. The three-dimensional structure consists of a column of M atoms connected through the 1,2-BDC, and is cross-linked through 1,4-BDC giving rise to rhombic one-dimensional channels. The water molecules, bound to the M atoms, project into the channels. The compounds also illustrate the lanthanide contraction principle. The compounds have been characterized using powder X-ray diffraction, TGA, IR, and photoluminescence measurements. Our continuing investigations clearly reveal that related compounds can be formed with all the rare earth metal ions.

(© Wiley-VCH Verlag GmbH & Co. KGaA, 69451 Weinheim, Germany, 2004)

Introduction

Design and synthesis of three-dimensional (3D) coordination polymers with well-defined pores is of current topical interest.[1−5] Large numbers of three-dimensional coordination polymers with porous structures and interesting adsorption properties have been prepared and characterized using a variety of benzene carboxylates.[6−25] Of these, benzene-1,4-dicarboxylic acid (H_2BDC) with a 180° separation between the two carboxylic groups and benzene-1,3,5-tricarboyxlic acid (H_3BTC) with a 120° separation have been proven to yield interesting structures. Recent studies have shown that it is profitable to explore mixed metal benzene dicarboxylates.[26–31] Hetero-bimetallic coordination polymers have traditionally been investigated for their many interesting properties, such as dimensionality and magnetism.[32] In addition, the variations in the coordination environment between the two different metals might also give rise to different structures. Though a large number of mixed metal carboxylates have been prepared, work on the use of mixed dicarboxylates is slow to emerge. Recently, H_2BDC and H_3BTC were used for the preparation of the first example of a Zn coordination polymer built-up from two different carboxylic acids.[21]

Most of the metal-organic frameworks reported in the literature have been prepared employing hydrothermal methods. The hydrothermal method, in some cases, gives rise to unexpected products due to side reactions.[33] We have been interested in the use of hydrothermal methods for the preparation of mixed carboxylate polymers, which invariably lead to uncharacterized dense precipitates. It is known that cyano groups on the phenyl ring are easily converted into carboxylic acid groups by hydrolysis.[34−36] Recently the use of 1,4-dicyanobenzene has been shown to give rise to a series of terephthalate coordination polymers under hydrothermal conditions.[36] In the present study, we have used 1,2-dicyanobenzene and 1,4-terephthalic acid in a hydrothermal system along with a series of lanthanide salts to produce new metal-organic polymers of the general formula, $[M_2(H_2O)_4\{(1,2BDC)_2(1,4BDC)\}]$, (M = La, Pr, Gd, Dy, and Y) with three-dimensional structures. In addition, the present system with the rare earth elements of different ionic radii provide us with an opportunity to examine the established lanthanide contraction, and its role on the coordination of the lanthanide ion and the structure. The 1,2-benzene dicarboxylate (isophthalate), found in the products, has been obtained by the hydrolysis of 1,2-dicyanobenzene, under hydrothermal conditions. This is only the second example of the preparation of a metal-organic framework containing two different multi-carboxylates as

[a] Framework Solids Laboratory, Chemistry and Physics of Materials Unit, Jawaharlal Nehru Centre for Advanced Scientific Research
Jakkur P. O., Bangalore 560 064, India
E-mail: raj@jncasr.ac.in (S. Natarajan)
Fax: (internat.) +91-80-846-2766

Supporting information for this article is available on the WWW under http://www.eurjic.org or from the author.

 © 2004 Wiley-VCH Verlag GmbH & Co. KGaA, Weinheim DOI: 10.1002/ejic.200300594

organic linkers. The first report was a Zn coordination polymer, $[Zn_3BDC{\cdot}2BTC{\cdot}2NH(CH_3)_2{\cdot}2NH_2(CH_3)_2]$, with three-dimensional connectivity.[21] In this paper, we report the synthesis, structure and characterization of the compounds.

Results

The title compounds, $[M_2(H_2O)_4\{(1,2BDC)_2(1,4BDC)\}]$, (M = La, Pr, Gd, Dy, and Y) can be grouped into two distinct classes based on the coordination environment around the central metal ion and the connectivity with the carboyxlate units. Thus, $[M_2(H_2O)_4\{(1,2BDC)_2(1,4BDC)\}]$, M = La and Pr, form type-1, and M = Gd, Dy, and Y, form type-2.

Structure of $[M_2(H_2O)_4\{(1,2BDC)_2(1,4BDC)\}]$ M = La and Pr (Type-1)

The asymmetric unit of type-1 compounds contains 44 non-hydrogen atoms, of which two M atoms are crystallographically independent (Figure 1, a). The structure is built up by the connectivity involving M (M = La and Pr) and the carboxylate units. Each M atom is coordinated by two carboxylate ligands [C(1) and C(31)] and [CC(11) and C(21)] in an *O,O′* manner and also coordinated in a monodendate way by three other carboxylate ligands. The M atoms also possess two terminal oxygen atoms, which are found to be water molecules. In addition, two oxygen atoms, [O(1) and O(9)], connect the M atoms through a three-coordinate bond, a μ_3 connection, leading to an effective nine-coordination for the central metal. The coordination environment around M atoms is an idealized D_{3h} triply capped trigonal prism (Figure 1, b). The M atoms have distances in the range 2.397(6)−2.923(5) Å (average 2.568 Å for La and 2.531 Å for Pr). The longer M−O distances are associated with the oxygen atoms, [O(1) and O(9)], having the μ_3 connection, which link the two M centers and a carbon atom. The other bond lengths, C−O, C−C, have the expected values observed in many similar compounds.[6−25] The O−M−O bond angles for M = La and Pr are in the range 46.81(15)−151.25(18)°. The various structural parameters observed in type-1 compounds are in the range expected for this type of bonding. Both the M atoms in the asymmetric unit have two terminal M−O linkages with an average distances of 2.521 Å, which are water molecules. Selected bond lengths are listed in Table 1.

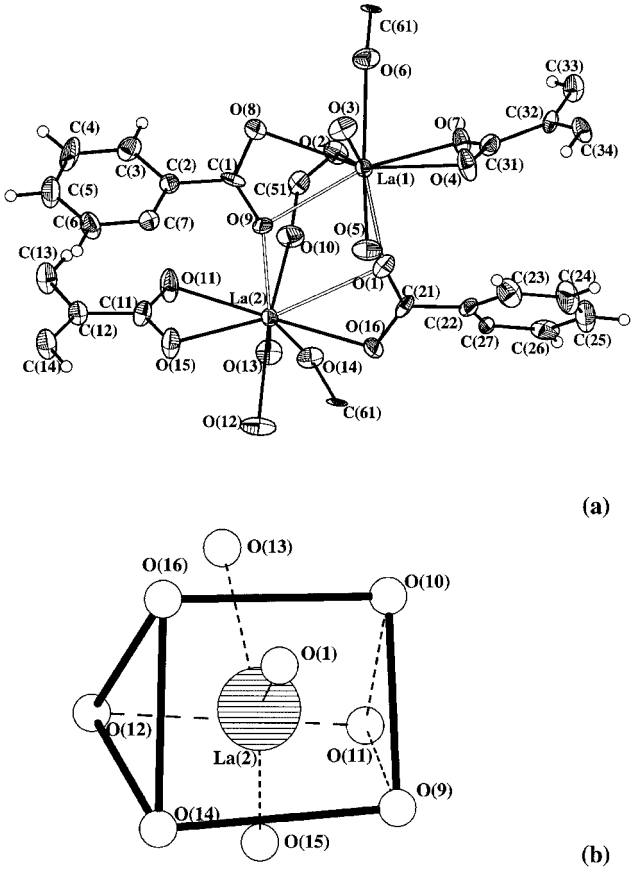

Figure 1. (a) ORTEP diagram showing the asymmetric unit for $[La_2(H_2O)_4\{(1,2BDC)_2(1,4BDC)\}]$. Thermal ellipsoids are given at 50% probability. The three-coordinate oxygen atoms connecting the La atoms are shown in open tubular bonds. (b) The coordination environment around La(2) showing the D_{3h} triply capped trigonal prism

Table 1. Selected bond lengths in $[M_2(H_2O)_4\{(1,2BDC)_2(1,4BDC)\}]$, (M = La, Pr). Symmetry transformations used to generate equivalent atoms: #1 $x-1, y+1, z$; #2 $x+1, y, z$; #3 $-x+2, -y+1, -z+1$; #4 $x-1, y, z$; #5 $-x, -y+2, -z$

Bond	Distance (Å) La	Pr	Bond	Distance (Å) La	Pr
M(1)−O(1)	2.475(6)	2.430(4)	M(2)−O(1)	2.923(5)	2.923(4)
M(1)−O(2)	2.527(5)	2.493(4)	M(2)−O(9)	2.563(5)	2.530(4)
M(1)−O(3)	2.516(5)	2.473(4)	M(2)−O(10)	2.397(6)	2.361(5)
M(1)−O(4)	2.561(5)	2.514(5)	M(2)−O(11)	2.519(6)	2.479(4)
M(1)−O(5)	2.572(6)	2.535(5)	M(2)−O(12)	2.523(6)	2.486(5)
M(1)−O(6)	2.522(6)	2.484(4)	M(2)−O(13)	2.547(5)	2.519(4)
M(1)−O(7)	2.597(5)	2.560(4)	M(2)−O(14)	2.526(5)	2.480(4)
M(1)−O(8)	2.643(5)	2.601(4)	M(2)−O(15)	2.555(5)	2.516(4)
M(1)−O(9)	2.681(5)	2.653(4)	M(2)−O(16)	2.571(5)	2.526(4)
O(1)−C(21)	1.257(9)	1.259(7)	O(9)−C(1)	1.260(9)	1.278(8)
O(2)−C(51)	1.261(9)	1.249(7)	O(10)−C(51)	1.253(10)	1.252(7)
O(4)−C(31)	1.257(10)	1.242(8)	O(11)−C(11)	1.250(10)	1.249(8)
O(6)−C(61)#1	1.259(9)	1.258(7)	O(14)−C(61)	1.264(9)	1.277(7)
O(7)−C(31)	1.261(9)	1.283(8)	O(15)−C(11)	1.267(10)	1.266(8)
O(8)−C(1)	1.265(9)	1.249(8)	O(16)−C(21)	1.267(9)	1.246(7)

The structure of the type-1 compounds, $[M_2(H_2O)_4\{(1,2BDC)_2(1,4BDC)\}]$ M = La and Pr, has two types of 1,2-BDC and 1,4-BDC acids. Thus, C2−C7 forms the benzene ring with C1 and C51 as the carboxylate units, and C22−C27 forms the benzene ring with C21 and C61 forming the carboxylate units completing the two 1,2-BDC. The 1,4-acid has an inversion center in the plane of the benzene ring (C12−C14 and C32−C34) with C11 and C31 being the carboxylate units. Of the carboxylate units, C1, C11, and C31 are bidentate and C51, C21, and C61 are monodentate, respectively, with respect to individual M ions. The framework structure of the type-1 compounds can

 © 2004 Wiley-VCH Verlag GmbH & Co. KGaA, Weinheim

be understood in terms of simpler building units. Thus, two three-coordinate oxygen atoms, [O(1) and O(9)], connect two M atoms to give rise to an edge-shared M_2O_{16} dimer. The 1,2-BDC connects the dimers giving rise to a sheet of

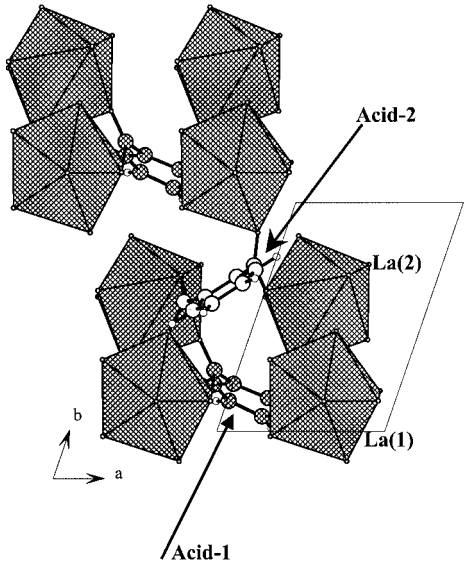

Figure 2. Figure showing the connectivity between La and the two 1,2BDC acids in the *ab* plane. Note that one of the 1,2BDC (acid 1) connects two La atoms forming an edge-shared La-dimer and the other (acid 2) connects the two such dimers together to form a column

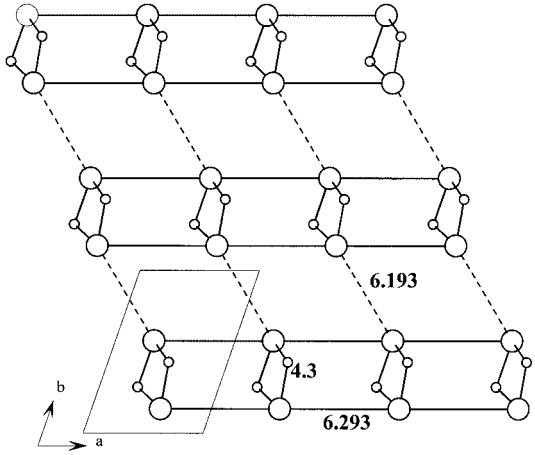

Figure 3. Figure shows the M-dimers, formed by the three-coordinate oxygen atoms, and its connectivity in the *ab* plane in Type-1 compounds. The connecting 1,2-BDC acids are not shown

M-carboxylate networks in the *ab* plane (Figures 2 and 3). While one 1,2-BDC connects a pair of M_2O_{16} dimers the second 1,2-BDC connects two different pairs forming a ladder-like arrangement. The arrangement of ladders and their connectivity gives rise to a corrugated sheet with steps in the *ab* plane. If we connect the M atom, the corrugated sheet is seen very clearly (Figure 3). The M−M atoms are separated by 4.3 Å within the dimer and 6.293 Å between the dimers in the same ladder. The distance between the two M dimers of different ladders is 6.193 Å (Figure 3). The corrugated sheets are cross-linked by the 1,4-BDC completing the three-dimensional structure as shown in Figure 4. The connectivity between the M, 1,2-BDC and 1,4-BDC gives rise to rhombic one-dimensional channels as shown in Figure 5. The two water molecules bound to the M ions (M = La and Pr) projects into the channels.

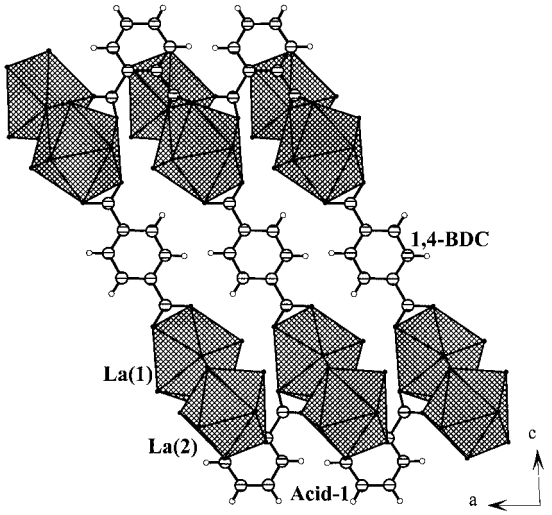

Figure 4. The view of the structure of the type-1 compound in the *ac* plane. The figure also shows the connectivity between two columns of dimers through 1,4-BDC. Only one of the 1,2-BDC acids is shown for clarity

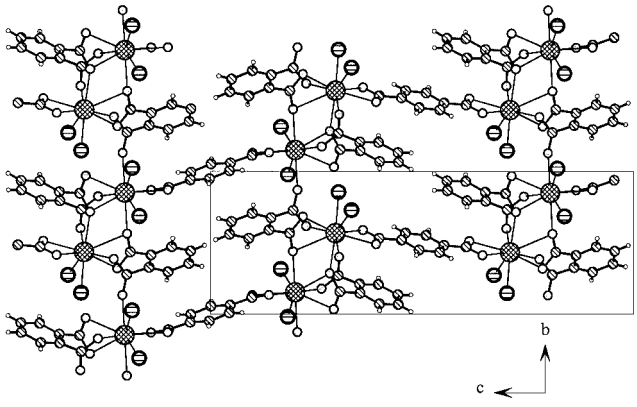

Figure 5. View of the structure of type-1 compound along the *bc* plane. The bonded water molecules are shown as large circles. Note that the bonded water molecule projects into the large channels

Structure of $[M_2(H_2O)_4\{(1,2BDC)_2(1,4BDC)\}]$ M = Gd, Dy, and Y (Type-2)

The asymmetric unit of the type-2 compounds $[M_2(H_2O)_4\{(1,2BDC)_2(1,4BDC)\}]$ M = Gd, Dy, and Y, have 21 non-hydrogen atoms, of which one M atom is independent (Figure 6, a). The M atoms are eight-coordinated with oxygen atoms that have M−O distances in the range 2.262(4)−2.509(4) Å (av. 2.381 for Gd, 2.411 Å for Dy, and 2.370 Å for Y). The coordination environment around the central M atom is a distorted dodecahedron. The C−O, C−C bond lengths show typical values.[6−25] The O−M−O bond angles for M = Gd, Dy, and Y are in the range

 © 2004 Wiley-VCH Verlag GmbH & Co. KGaA, Weinheim

52.50(12)−154.89(13)°. The various structural parameters observed in type-2 compounds are in the range expected for this type of bonding. The M atom has two terminal M−O linkages with an average distance of 2.405 Å, which are water molecules. Selected bond lengths are listed in Table 2.

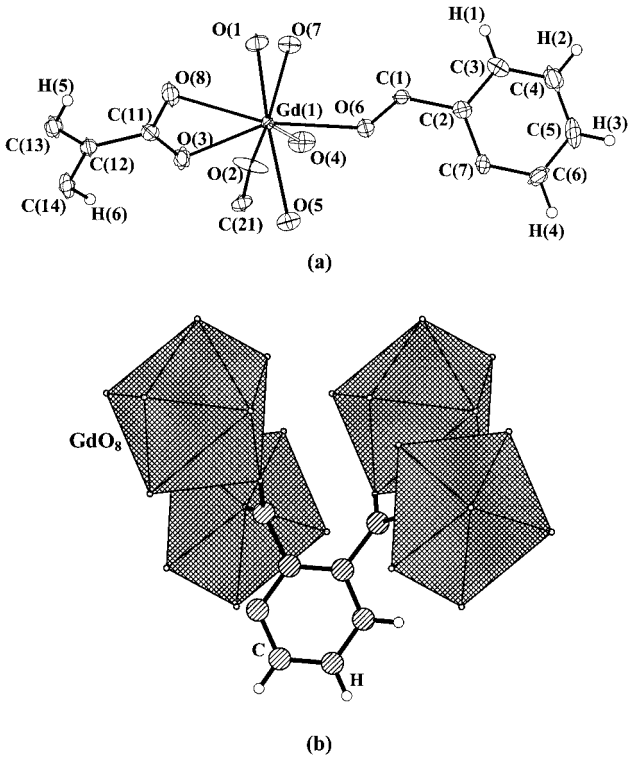

Figure 6.(a) ORTEP diagram showing the asymmetric unit for $[Gd_2(H_2O)_4\{(1,2BDC)_2(1,4BDC)\}]$. Thermal ellipsoids are given at 50% probability. (b) Figure showing the connectivity between the 1,2-BDC and Gd. Note that the acid has a monodendate connectivity with the distorted dodecahedrally coordinated Gd atoms

Table 2. Selected bond lengths for $[M_2(H_2O)_4\{(1,2BDC)_2(1,4BDC)\}]$ (M = Gd, Dy, and Y). Symmetry transformations used to generate equivalent atoms: #1 $-x, -y + 1, -z + 1$; #2 $-x, -y + 2, -z + 1$

Bond	Distance (Å)		
	Gd	Dy	Y
M(1)−O(2)	2.272(4)	2.314(4)	2.262(4)
M(1)−O(1)	2.306(4)	2.336(4)	2.285(4)
M(1)−O(6)	2.371(4)	2.409(3)	2.359(3)
M(1)−O(5)	2.398(4)	2.423(3)	2.389(3)
M(1)−O(4)	2.401(4)	2.426(4)	2.391(3)
M(1)−O(3)	2.406(4)	2.430(4)	2.395(3)
M(1)−O(7)	2.422(4)	2.441(3)	2.415(3)
M(1)−O(8)	2.475(4)	2.509(4)	2.461(4)
O(1)−C(1)#1	1.243(7)	1.244(7)	1.252(6)
O(2)−C(21)	1.247(7)	1.249(6)	1.238(6)
O(3)−C(11)	1.243(7)	1.242(7)	1.250(6)
O(6)−C(1)	1.263(6)	1.286(6)	1.261(6)
O(7)−C(21)#2	1.265(6)	1.258(6)	1.264(6)
O(8)−C(11)	1.289(7)	1.282(7)	1.276(6)

Unlike type-1, type-2 compounds have only one type of 1,2-BDC and 1,4-BDC acids. Thus, C2−C7 forms the benzene ring with C1 and C21 forming the carboxylate units for the 1,2-BDC, while the 1,4-BDC has an inversion center in the plane of the benzene ring (C12−C14) with C11 being part of the carboxylate unit. While 1,2-BDC only has monodendate connectivity through all the oxygen atoms, that of 1,4-BDC has bidentate bonding with respect to the M atoms. In Figure 6, b the monodendate connectivity between the M atoms and 1,2-BDC is shown. The connectivity between the M atoms and the 1,2-BDC acid, similar to type-1 compounds, gives rise to a corrugated step-like ladder arrangement. If the M atoms are connected, it gives

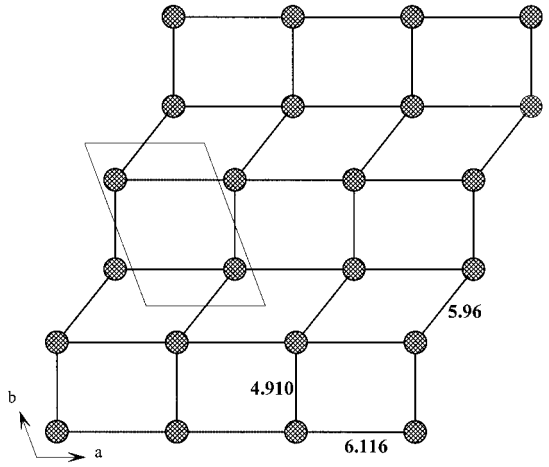

Figure 7. Figure shows the M atoms and its connectivity in Type-2 compounds. The connecting 1,2-BDC acids are not shown. Note that the M atom connectivity forms a corrugated four-connected net

rise to a four-connected network as shown in Figure 7. Similar to the type-1 compounds, the distance between the M atoms in the four-connected net varies between 4.910−6.116 Å (Figure 7). The connectivity between the 1,2-BDC, 1,4-BDC and the M atoms gives rise to rhombic one-dimensional channels (Figure 8). The two water mol-

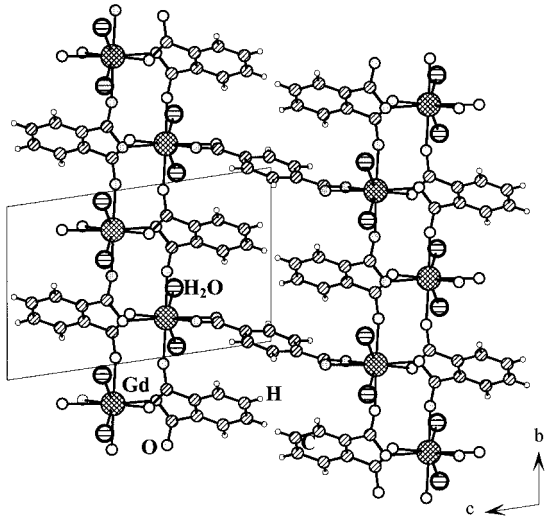

Figure 8. Structure of type-2 compound, $[Gd_2(H_2O)_4\{(1,2BDC)_2(1,4BDC)\}]$ in the *bc* plane. Note that the 1,2-acid and La form a ladder-like arrangement connected by 1,4-acids giving rise to rhombic-like channels. The bound water molecules are shown as large circles

 © 2004 Wiley-VCH Verlag GmbH & Co. KGaA, Weinheim

ecules bound to the M atoms project into these channels.

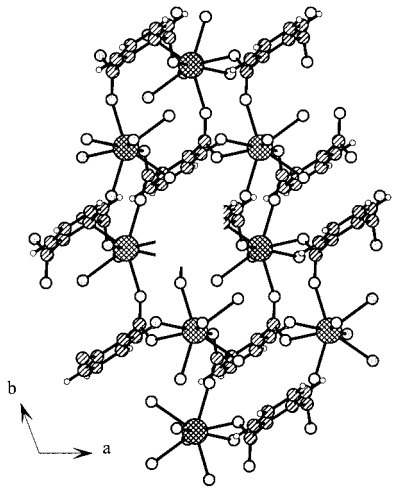

Figure 9. Structure of $[Gd_2(H_2O)_4\{(1,2BDC)_2(1,4BDC)\}]$ in the *ab* plane showing the arrangement of the benzene rings of the acid

The packing diagram in the *ab* plane is shown in Figure 9. The arrangement of the benzene carboxylates in the *ab* plane clearly indicates that direct π···π interactions have been avoided.

Discussion

Five new compounds have been synthesized with the general formula, $[M_2(H_2O)_4\{(1,2BDC)_2(1,4BDC)\}]$, M = La, Pr, Gd, Dy, and Y, employing mild condition hydrothermal reactions. The compounds have been prepared using 1,2-dicyanobenzene (1,2-DCB), but the final product contained benzene-1,2-dicarboxylic acid (phthalic acid). The 1,2-DCB compound has been hydrolyzed under the hydrothermal synthesis conditions to give rise to phthalic acid.

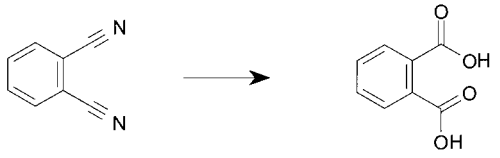

Since the product contained pthalic acid, we have made attempts to prepare the title compounds using pthalic acid in the starting synthesis mixture in place of 1,2-DCB. The experiments resulted in the desired product, but it was in the powder form with no single crystals being obtained. It is likely that the slow hydrolysis of 1,2-DCB to 1,2-BDC is needed to give rise to good quality single crystals of the coordination polymers described in this work.

All the compounds have been obtained as good quality single crystals and their structures were determined using single-crystal X-ray diffraction. Though the overall structure of the compounds appears to have close resemblance amongst them, there are minor differences between those formed with La and Pr and those formed with Gd, Dy, and Y. One of the differences is the absence of three-coordinate oxygen atoms (μ_3 connection) in the latter. The presence of three-coordinate oxygen atoms leads to the formation of M−O−M linkages and a dimer (M = La, Pr). Such a μ_3 connection of the oxygen atom in the M−O−M bridge is an electrostatic valence requirement of the bridging oxygen atoms. The μ_3 connections of the oxygen atoms are, probably, needed to accommodate the higher coordination of the large M ions.

The present study consists of a family of rare earth compounds with similar formulae and different structures. It appears that the size of the lanthanide ion possibly has a role in the final structure. In Figure 10, we have plotted the unit cell volume as a function of the covalent radii. We have considered the unit cell volume for the type-2 compounds to be double in order to be consistent with the formula. It is clear that there are two distinct slopes. The larger La and Pr appear to form a group while the smaller Gd, Dy, and Y belong to the other. This shows that there is a lanthanide contraction effect on the structure. Similar behavior has been noted in many compounds involving lanthanide ions, especially in intermetallic compounds.[37] The differences in the size of the lanthanide ions also results in different coordination for the M ions, which probably also leads to the observed differences in the structure.

From the TGA studies, it is clear that the bound water molecules leave at around 170−210 °C. In order to understand the thermal stability of these compounds, especially after the release of bound water molecules, we have performed careful experiments by heating the sample at different temperatures. For this purpose, we have selected the Y compound and heated the sample at each temperature in air for 120 min and the XRD patterns were recorded in the 2θ range of 5−30°. The results are shown in Figure 11. The samples appear to retain their structure only up to 150 °C, after which new peaks corresponding to yttrium oxide start appearing. From this, it is clear that the structure collapses after the loss of bound water of crystallization, unlike in

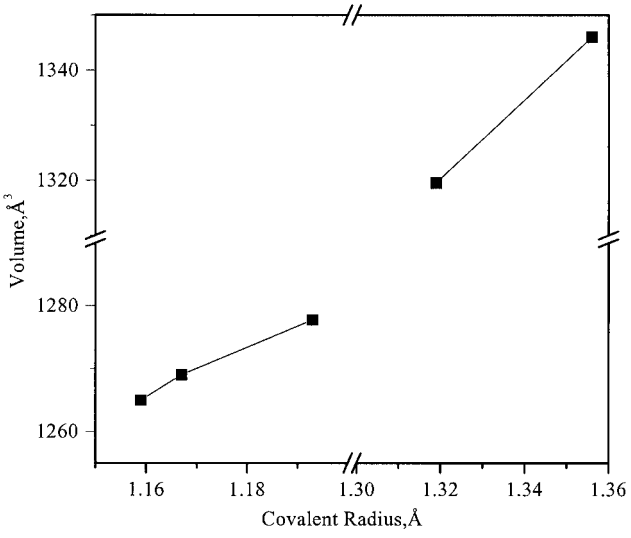

Figure 10. The variation of the crystal volume as a function of covalent radii of the lanthanide ions

 © 2004 Wiley-VCH Verlag GmbH & Co. KGaA, Weinheim

some of the lanthanide coordination polymers reported recently.[38]

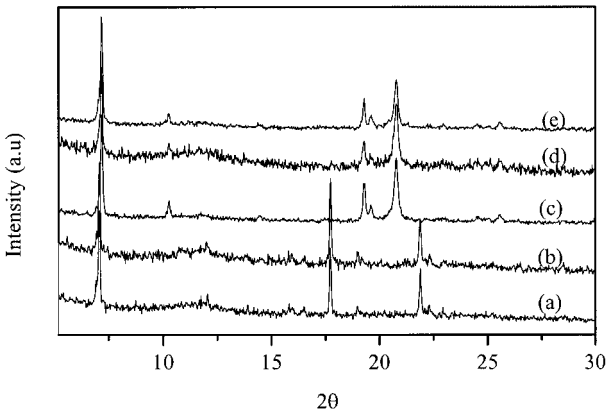

Figure 11. The XRD pattern of the $[Y_2(H_2O)_4\{(1,2BDC)_2$-$(1,4BDC)\}]$ as a function of temperature (a) 100, (b) 150, (c) 200, (d) 250, (e) 300 °C

The optical properties of the benzene carboxylates have been investigated since they involve the 4f orbitals, which are generally well shielded from their chemical environments by $5s^2$ and $5p^6$ electrons. The f-f transitions are parity forbidden, which leads to unfavorable excitation of the lanthanide ions. The photoluminescence studies indicate that both the acids, 1,2-BDC and 1,4-BDC, show photoluminescence (Figure 12). The main emission peak for the acids is located at the same position, at 240 nm. The emission bands for the acids, which also act as ligands in these compounds, may be attributable to the $\pi^* \rightarrow n$ transitions. Interestingly, the emission spectrum for the lanthanide coordination polymer shows a main peak at ≈ 400 nm. This peak corresponds to the intra-ligand fluorescent emission. In addition, the samples also exhibit additional emission bands when excited at 235 nm. These bands correspond to some of the expected $^5D_4 \rightarrow {}^7F_n$ transitions. The observed transitions are: $^5D_4 \rightarrow {}^7F_6$ = 508 (Gd), 494 (Dy), 483(Y); $^5D_4 \rightarrow {}^7F_5$ = 544 (Gd), 539 (weak, Dy), 542 (weak, Y); $^5D_4 \rightarrow {}^7F_4$ = 573, 592 (Gd), 584 (Dy), 574 (Y); $^5D_4 \rightarrow {}^7F_3$ = 616 (Gd). Similar behavior has been observed in many lanthanide coordination polymers.[8,39] As representative examples, the photoluminescence behavior for the acids along with Gd, Dy, and Y are given in Figure 12.

The pH of the initial reaction mixture also appears to play an important role in the formation of the compounds. A reaction mixture with a pH of ≈ 3 recrystallizes the 1,4-BDC acid and no other product was obtained. A reaction of a mixture of the 1,2-BDC and 1,4-BDC acids with a pH of ≈3 also recrystallizes only the acids. A starting reaction mixture containing both the acids at a pH of ≈ 5−6, however, gives rise to the desired product, but only in the powder form (very poor yield ≈ 5−10%) with no single crystals being obtained. In order to establish the pH conditions, we have also carried out reactions with piperidine and piperazine as the secondary base in place of NaOH, which resulted in the formation of the title compounds. From this, it appears that a pH of ≈ 5 is, probably, necessary to deprotonate the acid as the final product is devoid of any of the amine used in the synthesis, i.e., NaOH, piperidine, or piperazine.

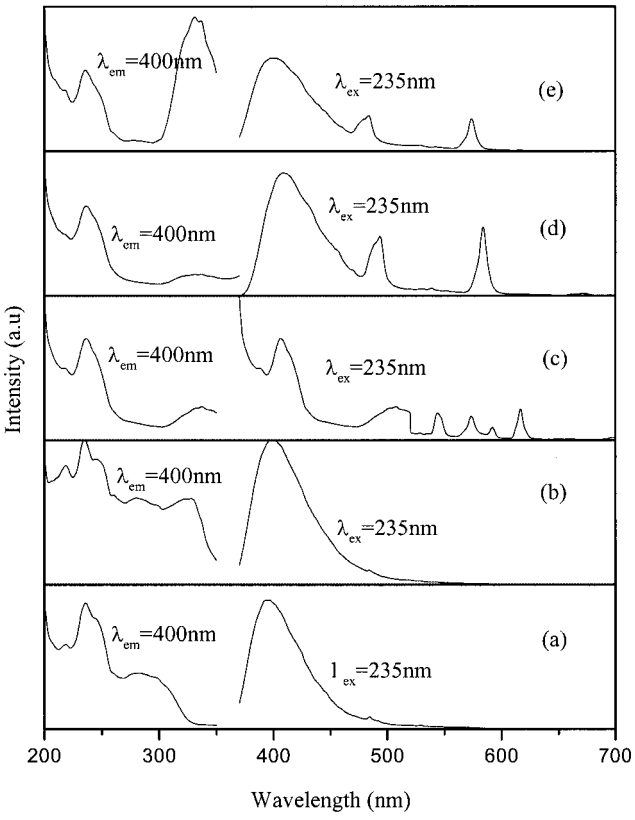

Figure 12. The photoluminescence spectra of the compounds along with the two acids. (a) 1,2-BDC, (b) 1,4-BDC, (c) Gd (d) Dy and (e) Y

Conclusions

A new series of coordination polymers of the general formula, $[M_2(H_2O)_4\{(1,2BDC)_2(1,4BDC)\}]$, M = La, Pr, Gd, Dy, and Y, have been prepared and characterized employing hydrothermal methods. The large lanthanides show a higher coordination compared with the smaller ones. The structure consists of a column of M−O formed by the connectivity between 1,2-BDC and M atoms and are interconnected by 1,4-BDC to give rise to the three-dimensional structure. The secondary coordinated water molecule does not appear to be reversibly adsorbed. The photoluminescence studies show some of the expected $^5D_4 \rightarrow {}^7F_n$ transitions. It is likely that related compounds encompassing other lanthanide ions with similar structures can be prepared. We are currently pursuing research in this direction.

Experimental Section

Synthesis and Initial Characterization: All the compounds have been prepared by employing hydrothermal methods. In a typical synthesis for the lanthanum coordination polymer, $LaCl_3$ (0.245 g)

 © 2004 Wiley-VCH Verlag GmbH & Co. KGaA, Weinheim

was dissolved in 5 mL of MilliQ water. 1,2-Dicyanobenzene (0.128 g) and terephthalic acid, [HOOC(C_6H_4)COOH; 1,4-BDC] (0.169 g) were then added to this under continuous stirring. Finally the pH was adjusted to ≈ 5 by the addition of 0.4 mL of 5 M NaOH and the mixture was homogenized for 30 min at room temperature. The final mixture with the composition, $LaCl_3$:1,2$(NC)_2C_6H_4$:1,4-BDC:2NaOH:278H_2O, was sealed in a 23 mL PTFE-lined acid digestion bomb and heated at 180 °C for 72 h under autogenous pressure. The pH after the reaction did not show an appreciable change. The resulting product contained rod-like crystals admixed with very small quantities of white powder were filtered under vacuum and dried at ambient temperature. The crystals were easily separated under an optical microscope and later by ultrasonification for further characterization. The yield of the single crystals was about ≈ 80% based on the La compound. The white powder was found to be amorphous by powder X-ray diffraction. The same compound can also be synthesized starting from other salts of La, [for ex. $La(NO_3)_3$], as well as by carrying our reactions in smaller capacity acid-digestion bombs (7 mL). Identical composition and synthesis conditions have been employed for the preparation of other compounds. In the case of the Gd and Dy compounds only good quality single crystals resulted from the reaction. The yield of the product in all the cases was 75−80%. The initial characterizations were carried out using elemental analysis, powder X-ray diffraction (XRD), thermogravimetric analysis (TGA) and Infra Red (IR) spectroscopy for all the compounds. Elemental analysis: for La, C 35.92% (34.20%), H 2.58% (2.37%); for Pr, C 34.38% (34.03%), H 2.47% (2.36%); for Gd, C 32.34% (32.76%), H 2.35% (2.27%); for Dy, C 32.61%(32.38%), H 2.11% (2.25%); and for Y, C 39.55% (38.80%), H 2.69% (2.94%). The powder XRD patterns were recorded on crushed single crystals in the 2θ range 5−50° using Cu *K*α radiation (Rich-Seifert, 3000TT). The XRD patterns indicated that the products were new materials; the patterns were entirely consistent with the structures determined using the single crystal X-ray diffraction.

Thermogravimetric analysis (TGA) has been carried out (Metler-Toledo) under an oxygen atmosphere (flow rate = 50 mL/min) in the temperature range 25 to 700 °C (heating rate = 10 °C/min). The studies show identical results for all the compounds with two sharp weight losses. The initial weight loss of 10% in the range 170−210 °C corresponds to the loss of four water molecules bound to La (calcd. 8.2%) and the second weight loss of 52.9% in the range 450−475 °C corresponds to the loss of the benzene carboxylates (calcd. 56%). The calcined sample was crystalline and the powder XRD lines match well with the corresponding pure oxides in all the cases.

Infra Red (IR) spectroscopic studies have been carried out in the mid-IR region as a KBr pellet (Bruker IFS-66v). The results indicate characteristic sharp lines with almost similar bands. Minor variations between the bands have been noticed between the compounds. The observed bands are: 3485−3620 (s) cm^{-1} − ν_{as}OH, 3292−3405 (s) cm^{-1} − ν_sOH, 3061 (w) cm^{-1} − ν_s(C−H)$_{aromatic}$, 1646−1669 (m) cm^{-1} − ν_s(C=O), 1605 (w) cm^{-1} − $\delta_s H_2O$, 1543(s) − (C−C)$_{skeletal}$, 1425 (s) cm^{-1} − δ_s(COO), 1405 (s) cm^{-1} − δ(OH), 1289−1294 (s) cm^{-1} − δ(CO), 1150 (s) cm^{-1} − δ(CH$_{aromatic}$)$_{in\text{-}plane}$, 750 (s) and 843 (s) cm^{-1} − δ(CH$_{aromatic}$)$_{out\text{-}of\text{-}plane}$.

Single Crystal Structure Determination: A suitable single crystal of each was carefully selected under a polarizing microscope and glued to a thin glass fiber. Crystal structure determination by X-ray diffraction was performed on a Siemen's Smart-CCD diffractometer equipped with a normal focus, 2.4 kW sealed tube X-ray source (Mo-*K*α radiation, λ = 0.71073 Å) operating at 40 kV and 40 mA. An empirical absorption correction based on symmetry equivalent reflections was applied using the SADABS program.[40] The structure was solved and refined using the

Table 3. Crystal data and structure refinement parameters for [$M_2(H_2O)_4${(1,2BDC)$_2$(1,4BDC)}] (M = La, Pr)

Structure parameter	La	Pr
Empirical formula	$C_{24}H_{20}La_2O_{16}$	$C_{24}H_{20}Pr_2O_{16}$
Molecular mass	842.16	846.22
Crystal system	triclinic	triclinic
Space group	$P\bar{1}$ (no. 2)	$P\bar{1}$, (no. 2)
a [Å]	6.2428(2)	6.2221(4)
b [Å]	8.9794(2)	8.9189(5)
c [Å]	25.3905(7)	25.2972(2)
α [°]	88.954(1)	88.730(1)
β [°]	86.896(1)	87.036(1)
γ [°]	70.920(1)	70.76(1)
V [Å^3]	1343.14(6)	1323.69(11)
Z	2	2
D (calc) [gcm^{-3}]	2.063	2.123
μ [mm^{-1}]	3.217	3.718
λ (Mo-K_α) [Å]	0.71073	0.71073
F(000)	796	820
2θ range [°]	1.6−46.6	1.6−46.6
Total data collected	5569	5637
Unique data	3748	3753
Observed data [$I > 2\sigma(I)$]	2868	3205
R_{merg}	0.041	0.0239
R indexes [$I > 2\sigma(I)$]	R_1 = 0.0351[a]; wR_2 = 0.0823[b][b]	R_1 = 0.0296[a]; wR_2 = 0.0820[b]
R indexes [all data]	R_1 = 0.0519[a]; wR_2 = 0.0928[b]	R_1 = 0.0364[a]; wR_2 = 0.0855[b]
Largest difference map peak and hole [e·Å^{-3}]	0.747 and −1.487	0.966 and −1.424

[a] $R_1 = \Sigma||F_o| - |F_c||/\Sigma|F_o|$. [b] $wR_2 = \{\Sigma[w(F_o^2 - F_c^2)^2]/\Sigma[w(F_o^2)^2]\}^{1/2}$. $w = 1/[\sigma^2(F_o)^2 + (aP)^2 + bP]$, $P = [\max(F_o^2,0) + 2(F_c)^2]/3$, where $a = 0.0089$ and $b = 0.0$ for La and $a = 0.00444$ and $b = 0.0$ for Pr.

 © 2004 Wiley-VCH Verlag GmbH & Co. KGaA, Weinheim

Table 4. Crystal data and structure refinement parameters for $[M_2(H_2O)_4\{(1,2BDC)_2(1,4BDC)\}]$ (M = Gd, Dy, and Y)

Structure parameter	Gd	Dy	Y
Empirical formula	$C_{12}H_{10}GdO_8$	$C_{12}H_{10}DyO_8$	$C_{12}H_{10}YO_8$
Molecular mass	439.45	447.50	371.11
Crystal system	triclinic	triclinic	triclinic
Space group	$P\bar{1}$, (no. 2)	$P\bar{1}$, (no. 2)	$P\bar{1}$, (no. 2)
a [Å]	6.1107(3)	6.1163(2)	6.1272(1)
b (Å)	8.8045(4)	8.8254(3)	8.8099(3)
c (Å)	12.8764(7)	12.9291(2)	12.8788(4)
α [°]	95.073(2)	94.752(2)	95.060(2)
β [°]	99.116(2)	99.311(2)	99.143(1)
γ [°]	109.958(2)	109.449(2)	110.302(2)
V [Å^3]	635.32(5)	642.36(2)	635.97(3)
Z	1	1	1
D (calcd.) [gcm^{-3}]	2.297	2.299	1.938
μ [mm^{-1}]	5.259	5.855	4.624
λ (Mo-K_α) [Å]	0.71073	0.71073	0.71073
F(000)	420	424	370
2θ range [°]	3.2−46.6	3.2−46.5	3.2−46.4
Total data collected	2677	2703	2652
Unique data	1791	1813	1773
Observed data [$I > 2\sigma(I)$]	1642	1696	1658
R_{merg}	0.0247	0.0215	0.0165
R indexes [$I > 2\sigma(I)$]	$R_1 = 0.0227$[a]; $wR_2 = 0.0564$[b]	$R_1 = 0.0228$[a]; $wR_2 = 0.0611$[b]	$R_1 = 0.0401$[a]; $wR_2 = 0.1073$[b]
R indexes [all data]	$R_1 = 0.0267$[a]; $wR_2 = 0.0572$[b]	$R_1 = 0.0253$[a]; $wR_2 = 0.0619$[b]	$R_1 = 0.0436$[a]; $wR_2 = 0.1092$[b]
Largest difference map peak and hole [e·Å^{-3}]	0.626 and −1.105	0.776 and −1.024	0.835 and −0.958

[a] $wR_1\ \Sigma||F_o|-|F_c||/\Sigma|F_o|$. [b] $wR_2 = \{\Sigma[w(F_o^2 - F_c^2)^2]/\Sigma[w(F_o^2)^2]\}^{1/2}$. $w = 1/[\sigma^2(F_o)^2 + (aP)^2 + bP]$, $P = [\max.(F_o^2,0) + 2(F_c)^2]/3$, where a = 0.0211 and b = 0.0 for Gd, a = 0.0348 and b = 0.1023 for Dy, and a = 0.0737 and b = 1.0849 for Y.

SHELXTL-PLUS suite of programs.[41] All the hydrogen atoms of the carboxylic acids were initially located in the difference Fourier maps and for the final refinement the hydrogen atoms were placed geometrically and held in the riding mode. The hydrogen atoms of the water molecules were not located in the difference Fourier maps. Final refinement included atomic positions for all the atoms, anisotropic thermal parameters for all the non-hydrogen atoms and isotropic thermal parameters for all the hydrogen atoms. Full-matrix least-squares refinement against $|F^2|$ was carried out using the SHELXTL-PLUS[41] suite of programs. Details of the structure solution and final refinements for the compounds $[M_2(H_2O)_4\{(1,2BDC)_2(1,4BDC)\}]$, (M = La and Pr) are given in Table 3 and for M = Gd, Dy, and Y are given in Table 4. The Selected bond lengths for $[M_2(H_2O)_4\{(1,2BDC)_2(1,4BDC)\}]$, M = La and Pr, are listed in Table 1 and for M = Gd, Dy, and Y in Table 2.

CCDC-214923 to -214927 contain the supplementary crystallographic data for this paper. These data can be obtained from the above, via www.ccdc.ac.uk/conts/retrieving.html (or from Cambridge Crystallographic Data Centre, 12 Union Road, Cambridge CB2 1EZ, UK, Fax: +44-1223-336-033, E-mail: deposit@ccdc.cam.ac.uk).

Acknowledgments

S. N. thanks the Department of Science and Technology (DST), Government of India for the award of a research project and A. T. the Council of Scientific and Industrial Research (CSIR) Government of India, for the award of a research fellowship.

[1] M. Eddaoudi, D. B. Moler, H. L. Li, B. L. Chen, T. M. Reineke, M. O'Keeffe, O. M. Yaghi, *Acc. Chem. Res.* **2001**, *34*, 319 and the references therein.
[2] P. J. Hagrman, D. Hargman, J. Zubieta, *Angew. Chem. Int. Ed.* **1999**, *38*, 2638.
[3] G. Ferey, *Chem. Mater.* **2001**, *13*, 3084 and the references therein.
[4] P. Day and A. E. Underhill, (Eds.); *Metal-Organic and Organic Molecular Magnets*, Philos. Trans. R. Soc., London, **1999**, 357 and the references therein.
[5] N. Snejko, E. Guitierrez-Puebla, J. L. Martinez, M. A. Monge, C. Ruiz-Valero, *Chem. Mater.* **2002**, *13*, 1879.
[6] N. L. Rosi, M. Eddaoudi, J. Kim, M. O'Keeffe, O. M. Yaghi, *CrystEngCommun.* **2002**, *4*, 401.
[7] H. L. Li, M. Eddaoudi, M. O'Keeffe, O. M. Yaghi, *Nature* **1999**, *402*, 276.
[8] H. L. Li, M. Eddaoudi, M. O'Keeffe, O. M. Yaghi, *J. Am. Chem. Soc.* **1998**, *122*, 11559.
[9] B. Chen, M. Eddaoudi, T. M. Reineke, J. W. Kampf, M. O'Keeffe, O. M. Yaghi, *Nature* **1999**, *402*, 276.
[10] K. Barthelet, J. Marrot, D. Riou, G. Ferey, *Angew. Chem. Int. Ed.* **2002**, *41*, 281.
[11] C. Serre, F. Millange, C. Thouvenot, M. Nogues, G. Marsolier, D. Louer, G. Ferey, *J. Am. Chem. Soc.* **2002**, *124*, 13519.
[12] S. O. H. Gutschke, D. J. Price, A. K. Powell, P. T. Wood, *Angew. Chem. Int. Ed.* **2001**, *40*, 1920.
[13] C. J. Kepert, T. Prior, M. J. Rosseinsky, *J. Am. Chem. Soc.* **2000**, *122*, 5158.
[14] J. W. Ko, K. S. Min, M. P. Suh, *Inorg. Chem.* **2002**, *41*, 2151.
[15] J. C. Dai, X. T. Wu, Z. Y. Fu, C. P. Cui, S. H. Hu, W. X. Du, L. M. Wu, H. H. Zhang, R. Q. Sun, *Inorg. Chem.* **2002**, *41*, 1391.
[16] B. G. Lor, E. G. Puebla, M. Iglesias, M. A. Monge, C. R. Valero, N. Snejko, *Inorg. Chem.* **2002**, *41*, 2429.
[17] C. D. Wu, C. Z. Lu, W. B. Yang, H. H. Zhuang, J. S. Huang, *Inorg. Chem.* **2002**, *41*, 3302.
[18] M. E. Braun, C. D. Steffek, J. Kim, P. G. Rasmussen, O. M. Yaghi, *Chem. Commun.* **2001**, 2532.

 © 2004 Wiley-VCH Verlag GmbH & Co. KGaA, Weinheim

[19] M. Edgar, R. Mitchell, A. M. Z. Slawin, P. Lightfoot, P. A Wright, *Chem. Eur. J.* **2001**, *7*, 5168.
[20] D. Cheng, M. A. Khan, R. P. Houser, *Inorg. Chem.* **2001**, *40*, 6858.
[21] W. Chen, J. Y. Wang, C. Chen, Q. Yue, H. M. Yuan, J. S. Chen, S. N. Wang, *Inorg. Chem.* **2003**, *42*, 944.
[22] S. S. Y. Chui, S. M. F. Lo, J. P. H. Charmant, A. G. Orpen, I. D. Williams, *Science* **1999**, *283*, 1148.
[23] [23a] M. Sanselme, J. M. Greneche, M. R. Cavellec, G. Ferey, *Chem. Commun.* **2002**, 2172. [23b] C. Serre, G. Ferey, *J. Mater. Chem.* **2002**, *12*, 3053. [23c] C. Serre, F. Millange, J. Marrot, G. Ferey, *Chem. Mater.* **2002**, *14*, 2409.
[24] Z. L. Huang, M. Drillon, N. Masciocchi, A. Sironi, J. T. Zhao, P. Rabu, P. Panissod, *Chem. Mater.* **2000**, *12*, 2805.
[25] T. B. Lu, H. Xiang, R. L. Luck, L. Jiang, Z. W. Mao, L. N. Ji, *New. J. Chem.* **2002**, *26*, 969.
[26] Y. B. Dong, M. D. Smith, H.-C. zur-Loye, *Angew. Chem. Int. Ed.* **2000**, *39*, 4271.
[27] E. Doedens, E. Yohannes, M. I. Khan, *Chem. Commun.* **2002**, 62.
[28] D. M. Curtin, M. D. Smith, H.-C. zur-Loye, *Chem. Commun.* **2002**, 74.
[29] Z. Shi, S.-H. Feng, S. Gao, L.-R. Zhang, G. Y. Yang, J. Hua, *Angew. Chem. Int. Ed.* **2000**, *39*, 2325.
[30] L.-C. Liang, R. Cao, W.-P. Su, M.-C. Hong, W.-J. Zhang, *Angew. Chem. Int. Ed.* **2000**, *39*, 3304.
[31] Y.-C. Liang, M.-C. Hong, W.-P. Su, R. Cao, W.-J. Zhang, *Inorg. Chem.* **2001**, *40*, 4574.
[32] D. M. J. Doble, C. H. Benison, A. J. Blake, D. Fenske, M. S. Jackson, R. D. Kay, W.-S. Li, M. Schroder, *Angew. Chem.* **1999**, *111*, 2042; *Angew. Chem. Int. Ed.* **1999**, *38*, 1915.
[33] R. Vaidhyanathan, S. Natarajan, C. N. R. Rao, *Inorg. Chem.* **2002**, *41*, 4496.
[34] H. K. Fun, S. S. S. Raj, R. G. Xiong, J. L. Zuo, Z. Yu, X. Z. You, *J. Chem. Soc., Dalton Trans.* **1999**, 1915.
[35] O. R. Evans, R. G. Xiong, Z. Wang, G. K. Wong, W. Lin, *Angew. Chem. Int. Ed.* **1999**, *38*, 536.
[36] D. Sun, R. Cao, Y. Liang, Q. Shi, W. Su, M. Hong, *J. Chem. Soc., Dalton Trans.* **2001**, 2335.
[37] [37a] G. V. Subba Rao, G. Balakrishnan, *Bull. Mater. Sci. (India)* **1984**, *6*, 283, and references therein. [37b] G. V. Subba Rao, *Proc. Ind. National Sci. Acad.* **1986**, *52A*, 292.
[38] L. Pan, K. M. Adams, H. E. Hernandez, X. Wang, C. Zheng, Y. Hattori, K. Kaneko, *J. Am. Chem. Soc.* **2003** (in press).
[39] G. F. Liu, Z. P. Qiao, H. Z. Wang, X. M. Chen, G. Yang, *New. J. Chem.* **2002**, *26*, 791.
[40] G. M. Sheldrick, *SADABS Siemens Area Detector Absorption Correction Program*, University of Göttingen, Göttingen, Germany, **1994**.
[41] G. M. Sheldrick, *SHELXTL-PLUS, Program for Crystal Structure Solution and Refinement*, University of Göttingen, Göttingen, Germany, **1997**.

Received August 25, 2003
Early View Article
Published Online December 12, 2003

 © 2004 Wiley-VCH Verlag GmbH & Co. KGaA, Weinheim

Direct Hydride/Silyl Exchange — Synthesis and X-ray Study of the Bis(silyl) Complex $[Cp_2NbH(SiCl_3)_2]$

Konstantin Yu. Dorogov,[a] Andrei V. Churakov,[b] Lyudmila G. Kuzmina,[b] Judith A. K. Howard,[c] and Georgii I. Nikonov*[a]

Keywords: Hydride ligands / Niobium / Si ligands / X-ray diffraction

Niobocene trihydride reacts directly with the chlorosilanes $SiCl_2R'R''$ (R′, R″ = Me, Ph) and $SiCl_3Me$ to give the dihydridomonosilyl derivatives $[Cp_2Nb(H)_2(SiCl_nR_{3-n})]$ (n = 1, 2), whereas the analogous reaction with $SiCl_4$ affords $[Cp_2Nb(H)_2(SiCl_3)]$ and the bis(silyl) complex $[Cp_2NbH(SiCl_3)_2]$, whose X-ray structure was determined.
(© Wiley-VCH Verlag GmbH & Co. KGaA, 69451 Weinheim, Germany, 2004)

Introduction

Silyl transition metal complexes are of great current interest as intermediates in silane dehydrogenative coupling reactions[1−3] and various hydrosilylation reactions.[4−6] It is therefore not surprising that a large number of silyl complexes have been prepared by oxidative addition of the H−Si bond.[7,8] We have been developing an alternative approach to main-group element substituted transition metal complexes L_nM-ER_m based on *direct interaction* of a basic transition metal hydride with the main-group element halides.[9−18] The niobocene trihydride Cp_2NbH_3 was a substrate of choice to test such reactivity because it possesses basic metal−hydride bonds but lacks any lone pair or a vacant coordination site, thus eliminating competing reaction pathways.[17] This approach works very well for the bond construction between metal atoms and group-5 (P, As, Sb, Bi)[9−15] and heavy group-4 (Ge, Sn, Pb)[16−18] atoms, but no such study has been done for silicon so far. In the literature there are only two reports dealing with the reactions of metal hydrides with halosilanes; both consider the reactivity of electron-rich metal centers bearing metal-centered lone pairs. Lemke et al. have recently reported that the reaction between the basic d^6 ruthenium complex $[CpRuH(PMe_3)_2]$ and chlorosilanes gives silyl derivatives by an anticipated *chloride/metal exchange* (Scheme 1).[19,20] Jutzi et al. have reported a similar reaction with the d^2 molybdenum complex $[Cp_2MoH_2]$, resulting in the silyl hydride derivatives $[Cp_2MoH(SiR_3)]$, although no mechanism was proposed.[21] There is also a practical aspect that motivated us to study the reactivity of metal−hydride bonds towards chlorosilanes: Chlorosilanes are precursors for industrially important silicones, but only a few are available by direct synthesis.[22] Metal-catalyzed hydrosilylation of unsaturated hydrocarbons,[4] which circumvents this problem, is believed to proceed by H−Si bond oxidative addition to metal atoms to generate metal hydride intermediates.[23,24] Therefore one can expect that any interaction of the resultant M−H bond with an excess of chlorosilane should have a significant impact on the overall process of hydrosilylation, for example by giving rise to side-products or deactivation of the catalyst.

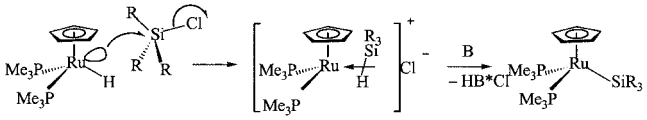

Scheme 1

Here we report our investigation of the reactions of niobocene trihydride $[Cp_2NbH_3]$ (**1**) with a series of chlorosilanes and present evidence for both a single and double silyl/hydride exchange. This synthetic approach has a potential for the preparation of silyl complexes not accessible by the silane oxidative addition route.

Results and Discussion

Synthesis of Mono- and Bis(silyl) Derivatives

The addition of dichlorosilanes $SiCl_2R'R''$ (R′, R″ = Me, Ph) to **1** in the presence of NEt_3 as an HCl sponge

[a] Chemistry Department, Moscow State University, Vorob'evy Gory, 119992 Moscow, Russia
Fax: (internat.) + 7-095-932-8846
E-mail: nikonov@org.chem.msu.su
[b] Institute of General and Inorganic Chemistry RAS
Leninskii Prosp. 31, 119991 Moscow, Russia
E-mail: kuzmina@igic.ras.ru
[c] Chemistry Department, University of Durham
South Road, Durham DH1 3LE, UK
E-mail: j.a.k.howard@durham.ac.uk

 DOI: 10.1002/ejic.200300134 © 2004 Wiley-VCH Verlag GmbH & Co. KGaA, Weinheim

gives the mono(silyl) complexes **2**−**4** in moderate to high yields. Compounds **2**−**4** are produced as an almost equimolar mixture of the central (**a**) and lateral (**b**) isomers, the latter being stabilized by nonclassical interligand hypervalent interactions (IHI) between the hydrido and silyl ligands.[25] The analogous reaction of **1** with the trichlorosilane $SiCl_3Me$ affords a mixture, the main component of which is the lateral isomer $[Cp_2Nb(H)_2(SiMeCl_2)]$ (**5b**) together with a small amount of **5a** and the monochloride $[Cp_2NbCl]_2$.[26] In contrast, the reaction of $HSiCl_2Me$ with **1** does not give the expected complex $[Cp_2Nb(H)_2(HSiClMe)]$. Instead, **5b** is formed in high yield as an Si−H addition product (this reaction apparently proceeds by conventional H_2 elimination to give the transient Cp_2NbH, amenable to oxidative addition[27,28]). Treatment of pure **5b** with $SiCl_3Me$ results in a partial isomerization to **5a**, but **5b** remains the main component of the mixture (65%). Complexes **2**−**4** were prepared independently by oxidative addition of silanes to **1** according to established procedures.[25] Reaction of **1** with bulkier ($SiCl_2Et_2$, $SiCl_2iPr_2$) or less acidic [$SiCl(OMe)Me_2$, $SiClMe_3$] silanes does not give any significant amount of $[Cp_2Nb(H)_2(SiR_3)]$. In this case, the reaction is accompanied by dihydrogen evolution and formation of a mixture of unidentified products, the main component of which is insoluble in non-polar solvents. One of the target complexes, $[Cp_2Nb(H)_2(SiCliPr_2)]$ (**6a**), was obtained by the reaction of Cp_2NbBH_4 with $HSiCliPr_2$ in the presence of NEt_3. Only the central isomer was obtained, the structure of which was determined by an X-ray diffraction study (vide infra).

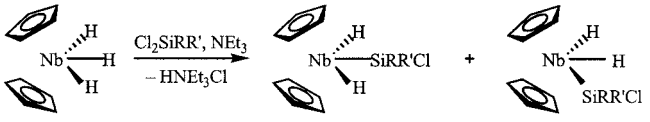

R = R' = Me **2**
R = R' = Ph **3**
R = Me, R = Ph **4**

Reaction of **1** with an excess of $SiCl_4$ is remarkable in that, in addition to the central and lateral mono(silyl) compounds $[Cp_2Nb(H)_2(SiCl_3)]$ (**7a**,**b**), the major product (60%) is the bis(silyl) complex $[Cp_2NbH(SiCl_3)_2]$ (**8**), which is formed by an unprecedented double hydride/silyl exchange. This compound was isolated from the more soluble **7a** and **7b** by washing the mixture with diethyl ether. The ^1H NMR spectrum of **8** shows the hydride resonance at $\delta = -3.29$ ppm, about 2 ppm downfield from the bis(silyl)-niobocene complexes with interligand hypervalent interactions (IHI),[25] suggesting a significantly reduced IHI. An X-ray diffraction study further confirmed this conclusion (vide infra). Compounds **7a** and **7b** were obtained independently by heating **1** with $HSiCl_3$ at 60 °C.

An important conclusion of this work is that the reactions of halosilanes with basic transition metal hydrides do not necessarily involve halogen/metal substitution/deprotonation steps because niobocene trihydride does not possess any metal-based lone-pair. Moreover, this molecule does not possess a vacant coordination site either, and the reaction occurs readily at temperatures below 25 °C, where dihydrogen elimination from pure $[Cp_2NbH_3]$ does not occur at any significant rate in the absence of silanes. Another thinkable pathway to **2**−**4** and **7** based on deprotonation of $[Cp_2NbH_3]$ by an amine, followed by nucleophilic substitution of the chloride of the silane can also be reliably ruled out, since it has previously been shown that amines cannot deprotonate $[Cp_2NbH_3]$.[17] The only reasonable option we are left with is that the reaction occurs by precoordination of the σ*-Lewis acid $Cl-SiR_3$ to the basic hydride center, forming a hypervalent $M-H\rightarrow SiR_3-Cl$ structure **9** (Scheme 2). Bridge formation is known to acidify the M−H−M′ bond drastically,[29] so that the hydride ion can now be abstracted from the complex **10** by a base as weak as an amine, affording eventually the silylated product. Several observations support this view. First, the hydrido ligands in **1** are Lewis bases of moderate strength (basicity factor $E_j = 0.93$).[30] Second, it is now recognized that even in the presence of metal-centered lone-pairs, the hydrido ligands are the kinetic sites for protonation,[31,32] and thus they are expected to be amenable for the interaction with other Lewis acids, too. It should be noted that Lewis acidity of silanes has precedents, for example, in the formation of hypervalent structures like $[H_2SiPh_3]^-$.[33] Third, the coordination of transition metal centers to M−H bonds is well established.[34] It is therefore reasonable to assume that this direct silyl/hydride exchange mechanism is general even for d^n ($n > 0$) systems, like the Ru and Mo complexes cited above. Complications can arise from the substitution of the silane in **10** by the chloride anion, leading (possibly) to the transient $[Cp_2Nb(H)_2Cl]$ and eventually to $[Cp_2NbCl]_2$ (as in the reaction with $SiCl_3Me$), and, in the case of bulkier or less acidic silanes [such as $SiCl_2Et_2$, $SiCl_2iPr_2$, $SiCl(OMe)Me_2$ and $SiClMe_3$], when Lewis acid induced dihydrogen elimination[35] occurs faster than deprotonation.

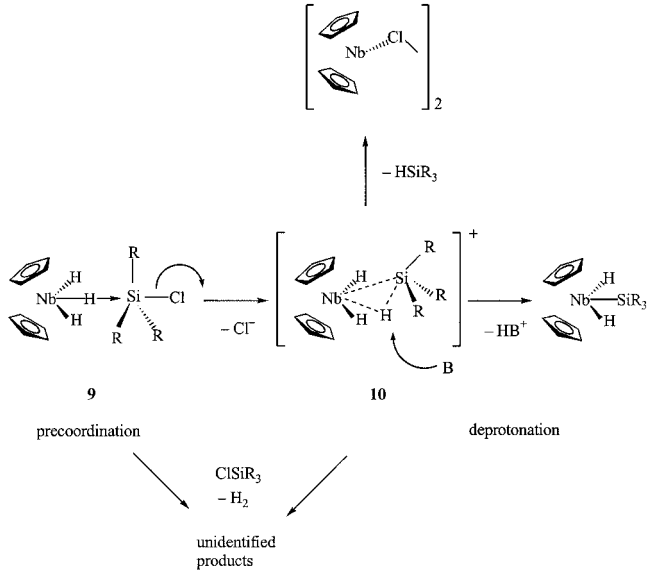

Scheme 2

 © 2004 Wiley-VCH Verlag GmbH & Co. KGaA, Weinheim

X-ray Studies

The molecular structure of **8** is shown in Figure 1, and selected bond lengths and angles are given in Table 1. The Nb−Si bonds for the two chemically equivalent silyl groups are very short [2.5597(5) and 2.5776(5) Å] due to the presence of three electron-withdrawing chlorine substituents at the silicon atom. The Si−Cl bond lengths fall within a narrow range [2.0835−2.0989(7) Å] without any significant difference between the chlorine atoms in and out of the niobocene bisectral plane. This fact, and the large Si−Nb−Si bond angle of 109.61(2)°, close to the values in classical bis(silyl) systems[25,27,28,36] and about 5° larger than in complexes with IHI, suggests the absence of any significant interligand Si−H interactions. This open Si−Nb−Si bond angle results in long Si−H contacts of 2.14(3) and 2.11(3) Å, about 0.1 Å longer than in complexes with IHI. This unexpected lack of Si−H interactions is either due to the low basicity of the Nb−H bond stemming from the presence of a large number of electron-withdrawing chlorine substituents on both the silyl centers, or due to hyperconjugation between the in-plane (Si−Cl)* antibonding orbital with the out-of-plane chlorine lone pairs of electrons. It should be emphasised that high basicity of the hydride ligand is a prerequisite for this type of interligand interaction tooccur because IHI stems from the interaction of an M−H bonding orbital with the (Si−X)* antibonding orbital.[25]

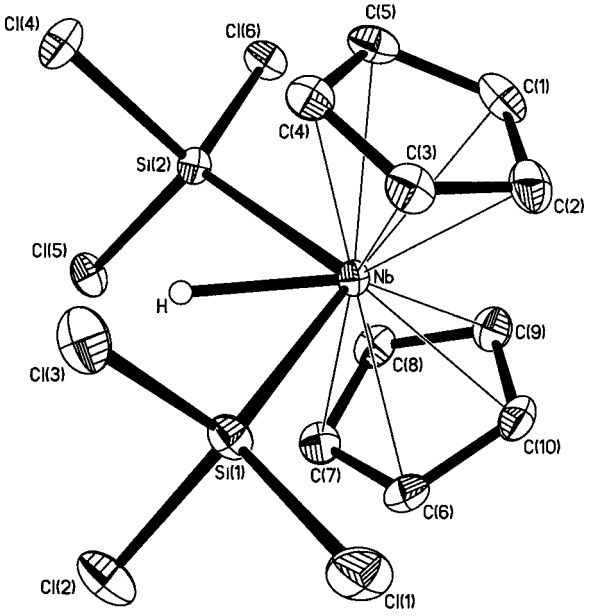

Figure 1. Molecular structure of $[Cp_2NbH(SiCl_3)_2]$ (**8**); displacement ellipsoids are shown at the 50% probability level; cyclopentadienyl hydrogen atoms are omitted for clarity

Table 1. Selected bond lengths [Å] and angles [°] for **8**

Nb−Si(1)	2.5776(5)	Nb−Si(2)	2.5597(5)
Si(1)−Cl(1)	2.0984(7)	Si(1)−Cl(2)	2.0835(7)
Si(1)−Cl(3)	2.0836(7)	Si(2)−Cl(4)	2.0841(7)
Si(2)−Cl(5)	2.0926(6)	Si(2)−Cl(6)	2.0988(7)
Nb−H	1.79(3)	Si(1)−H	2.14(3)
Si(2)−H	2.11(3)		
Si(2)−Nb−Si(1)	109.61(2)	H−Si(1)−Nb	43.4(8)
Cl(2)−Si(1)−Cl(1)	101.73(3)	H−Si(2)−Nb	43.8(8)
Cl(3)−Si(1)−Cl(1)	101.69(3)	Cl(2)−Si(1)−Cl(3)	101.69(3)
Cl(1)−Si(1)−Nb	116.57(3)	Cl(2)−Si(1)−Nb	116.55(3)
Cl(4)−Si(2)−Nb	116.67(2)	Cl(3)−Si(1)−Nb	116.17(3)
Cl(5)−Si(2)−Nb	116.50(3)	Cl(4)−Si(2)−Cl(5)	101.92(3)
Cl(5)−Si(2)−Cl(6	100.74(3)	Cl(4)−Si(2)−Cl(6)	101.77(3)
Cl(6)−Si(2)−Nb	116.67(2)		

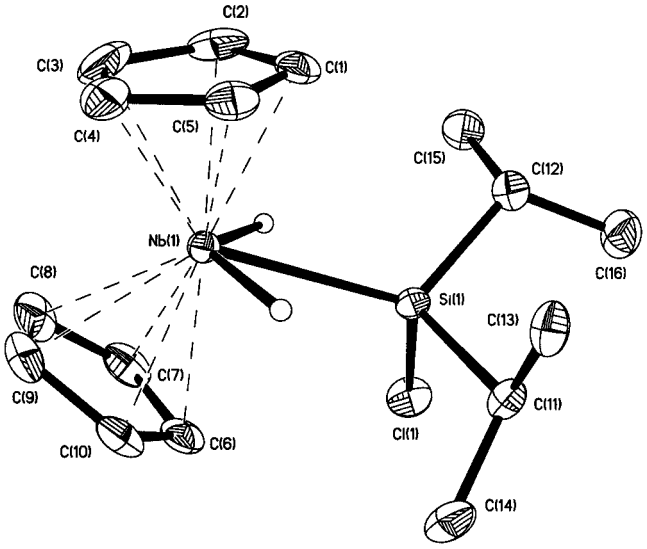

Figure 2. Molecular structure of $[Cp_2Nb(H)_2(SiCl\mathit{i}Pr_2)]$ (**6**); displacement ellipsoids are shown at the 50% probability level; all hydrogens apart from hydrides are omitted for clarity

The molecular structure of **6** is shown in Figure 2, and selected bond lengths and angles are given in Table 2. The silyl group is located in the central position in the niobocene bisectral plane, and two hydrides were found in the lateral positions with Nb−H distances of 1.65(3) Å. In spite of the presence of a chlorine substituent at silicon, the Nb−Si distance of 2.6496(7) Å is similar to the Nb−Si bond length in related alkyl- and aryl-substituted silyls.[25,27,28,36] Electron-withdrawing substituents X are known to diminish the M−Si bond lengths[37] due to the operation of Bent's rule.[38] Another exceptional feature in **6** is the long Si−Cl bond length of 2.1694(9) Å, which can be compared with the range 2.094−2.149 Å found in classical L_nMSiR_2Cl complexes (R = alkyl, aryl).[39−43] Apparently, these struc-

Table 2. Selected bond lengths [Å] and angles [°] for **6**

Nb(1)−Si(1)	2.6496(7)	Si(1)−C(11)	1.906(3)
Si(1)−Cl(1)	2.1694(9)	Si(1)−C(12)	1.922(3)
Nb(1)−H(1)	1.65(3)	Nb(1)−H(2)	1.65(3)
C(11)−Si(1)−C(12)	103.99(11)	C(11)−Si(1)−Cl(1)	101.02(8)
C(12)−Si(1)−Cl(1)	99.70(8)	C(11)−Si(1)−Nb(1)	117.37(8)
C(12)−Si(1)−Nb(1)	119.34(8)	Cl(1)−Si(1)−Nb(1)	112.55(3)
Si(1)−Nb(1)−H(2)	56.0(10)	Si(1)−Nb(1)−H(1)	64.5(10)
H(1)−Nb(1)−H(2)	120.4(14)		

 © 2004 Wiley-VCH Verlag GmbH & Co. KGaA, Weinheim

tural abnormalities are caused by the steric bulkiness of the two isopropyl groups at the silicon atom. Indeed, in the bulky silyl complex *fac*-[Ir(H)$_2$(Si*t*Bu$_2$Cl)(PMe$_3$)$_3$] both the Si−Cl bond of 2.187(4) Å and the Ir−Si bond of 2.392(3) Å are unusually long.[44] In the related complex [Ir(H)$_2${Si(H)Cl(C$_6$H$_3$-Mes$_2$-2,6)}(PEt$_3$)$_3$], with one very bulky substituent at the silicon atom, the Si−Cl bond length is 2.148(3) Å.[45]

Conclusion

This work has shown that halosilanes can interact with basic metal hydrides in the absence of metal-centered lone pairs, leading (depending on the silane) either to silyl derivatives or decomposition products. This reaction suggests new opportunities for the synthesis of silyl transition metal complexes and must be taken into account as a feasible (undesired) route during transition metal catalyzed hydrosilylation reactions of halosilanes.

Experimental Section

General Remarks: All manipulations were carried out using conventional Schlenk high vacuum and argon techniques. Solvents were dried with sodium or sodium benzophenone ketyl and distilled into the reaction vessel by high-vacuum gas-phase transfer. NMR spectra were recorded with a Varian VXR-400 spectrometer (^{1}H, 400 MHz; ^{13}C, 100.4 MHz). IR spectra were obtained in Nujol with an FTIR Perkin−Elmer 1600 series spectrometer. Silanes were purchased from Aldrich.

General Procedure for the Preparation of [Cp$_2$Nb(H)$_2$(SiClR$_2$)]: NEt$_3$ (2 mL, 6−7 equiv.) and 0.5 mL (ca. 2 equiv.) of the dichlorosilane were added to a solution of **1** (2−3 mmol) in diethyl ether (20 mL). A white voluminous precipitate formed immediately. The mixture was stirred for 3 h during which time a light-brown color developed. The solution was filtered and the residue washed with diethyl ether (10 mL). Volatiles were removed from the combined fractions in vacuo to give a brown solid. The material was recrystallized from a saturated diethyl ether solution at −26 °C to give the product as a mixture of two isomers. Yields: 29% (**2a**,**b**), 83% (**3a**,**b**), 35% (**4a**,**b**). **2a,b:** Characterization data as reported previously.[25] **3a:** ^{1}H NMR ([D$_6$]benzene): δ = −4.06 (s, 2 H, Nb−H), 4.53 (s, 10 H, Cp), 7.21−7.01 (Ph of **3a** and **3b**), 8.14 (d, $J_{H,H}$ = 7.1 Hz, 4 H, Ph) ppm. ^{13}C NMR ([D$_6$]benzene): δ = 148.39, 134.72 (Ph), 89.62 (s, Cp) ppm. **3b:** ^{1}H NMR ([D$_6$]benzene): δ = −3.93 (s, 1 H, Nb−H), −3.48 (s, 1 H, Nb−H), 4.62 (s, 10 H, Cp), 7.21−7.01 (Ph of **3a** and **3b**), 8.26 (d, $J_{H,H}$ = 7.4 Hz, 4 H, Ph) ppm. ^{13}C NMR ([D$_6$]benzene): δ = 145.78, 134.60 (Ph), 90.28 (s, Cp) ppm. C$_{22}$H$_{22}$ClNbSi (442.9): calcd. C 59.67, H 5.01; found C 59.34; H 5.14. **4a,b:** IR: ν(Nb−H) = 1725, 1694 cm^{-1}. **4a:** ^{1}H NMR ([D$_6$]benzene): δ = −4.15 (s, 2 H, Nb−H), 0.57 (s, 3 H, Me), 4.53 (s, 10 H, Cp), 7.20−7.02 (Ph of **4a** and **4b**), 8.26 (d, $J_{H,H}$ = 7.7 Hz, 4 H, Ph) ppm. ^{13}C NMR ([D$_6$]benzene): δ = 89.15 (s, Cp) ppm. **4b:** ^{1}H NMR ([D$_6$]benzene): δ = −4.50 (s, 1 H, Nb−H), −4.24 (s, 1 H, Nb−H), 0.91 (s, 3 H, Me), 4.50 (s, 5 H, Cp), 4.73 (s, 5 H, Cp), 7.20−7.02 (Ph of **4a** and **4b**), 8.15 (d, $J_{H,H}$ = 7.2 Hz, 4 H, Ph) ppm. ^{13}C NMR ([D$_6$]benzene): δ = 90.17 (s, Cp), 89.23 (s, Cp) ppm. C$_{17}$H$_{20}$ClNbSi (380.8): calcd. C 53.68, H 5.29; found C 53.47; H 4.90.

Preparation of [Cp$_2$Nb(H)$_2$(Si*i*Pr$_2$Cl)] (6): NEt$_3$ (2 mL) followed by HSi*i*Pr$_2$Cl (0.32 mL, 1.89 mmol) was added to a solution of Cp$_2$NbBH$_4$ (0.45 g, 1.89 mmol) in 40 mL of toluene. The mixture was stirred overnight. All volatiles were removed in vacuo and the residue was extracted with diethyl ether, filtered and concentrated under reduced vacuum until a yellow compound started to form. Keeping the mixture at −20 °C afforded **6** in the form of yellow crystals. The cold solution was further concentrated and decanted. Yield: 0.511 g (1.36 mmol, 72%). IR: ν(Nb−H) = 1736 cm^{-1}. ^{1}H NMR ([D$_6$]benzene): δ = −4.64 (s, 2 H, Nb−H), 1.35 (d, $J_{H,H}$ = 4.5 Hz, 6 H, Me), 1.32 (m, 2, CH), 1.19 (d, $J_{H,H}$ = 6.0 Hz, 6 H, Me), 4.66 (s, 10 H, Cp) ppm. ^{13}C NMR ([D$_6$]benzene): δ = 88.5 (s, Cp), 23.2 (CH), 18.9 (Me), 18.8 (Me) ppm. C$_{16}$H$_{26}$ClNbSi (374.8): calcd. C 51.27, H 6.99; found C 51.03; H 7.08.

Reactions of 1 with SiCl$_4$. Reaction a: NEt$_3$ (1.2 mL, 8.6 mmol, 2.5 equiv.) and SiCl$_4$ (0.42 mL, 3.66 mmol) were added to a solution of **1** (0.773 g, 3.42 mmol) in toluene (20 mL). A white precipitate formed immediately and the solution became amber, accompanied by gas evolution. The mixture was stirred overnight. The mixture was filtered and the residue washed with toluene (2 × 20 mL). Volatiles were removed from the combined fractions in vacuo to give a red crystalline substance. This was washed with diethyl ether (3 × 15 mL) and the volatiles were removed from the combined fractions affording a light amber crystalline solid, which according to the ^{1}H NMR spectrum was a mixture of **8**, **7a** and **7b**, along with some minor by-products. Yield: 0.361 g. The pink residue (0.100 g, 0.203 mmol, 6%) from the toluene-soluble fraction left after washing with diethyl ether was pure **8**. **Reaction b:** Compound **1** (0.77 g, 3.41 mmol) was added to a solution of NEt$_3$ (1.1 mL, 7.9 mmol, 1.1 equiv.) and SiCl$_4$ (0.8 mL, 7.0 mmol) in toluene (20 mL). Within 5 min, the solution became red-brown, accompanied by evolution of a gas that was not condensable by liquid nitrogen (apparently dihydrogen). After 0.5 h of stirring, a precipitate had formed. The mixture was then stirred overnight. The mixture was filtered and the residue washed with toluene (20 mL). The volatiles were removed from the combined fractions in vacuo to give an amber crystalline substance which, according to its ^{1}H NMR spectrum, was **8** along with a small amount of **7a** and **7b**. This material was recrystallized from diethyl ether. Yield: 0.21 g (0.43 mmol, 12%). **8:** IR: ν(Nb−H) = 1694 cm^{-1}. ^{1}H NMR ([D$_6$]benzene): δ = −3.29 (br. s, 1 H, Nb−H). 4.77 (s, 10 H, Cp) ppm. ^{13}C NMR ([D$_6$]benzene): δ = 96.6 (s, Cp) ppm. C$_{10}$H$_{11}$Cl$_6$NbSi$_2$ (492.98): calcd. C 24.36, H 2.25; found C 24.20, H 2.60. **7a:** IR: ν(Nb−H) = 1716 cm^{-1}. ^{1}H NMR ([D$_6$]benzene): δ = −3.86 (s, 2 H, Nb−H), 4.65 (s, 10 H, Cp) ppm. ^{13}C NMR ([D$_6$]benzene): δ = 90.4 ppm. **7b:** IR: ν(Nb−H) = 1766 cm^{-1}. ^{1}H NMR ([D$_6$]benzene): δ = −3.81 (s, 1 H, Nb−H), −3.69 (s, 1 H, Nb−H), 4.68 (s, 10 H, Cp) ppm. ^{13}C NMR ([D$_6$]benzene): δ = 92.2 ppm. C$_{10}$H$_{12}$Cl$_3$NbSi (359.58): calcd. C 33.41, H 3.36; found C 32.95, H 3.21.

X-ray Crystallographic Study. Crystal Data for 6: C$_{16}$H$_{26}$ClSiNb, M_r = 374.82, a = 9.32040(10), b = 11.8553(2), c = 15.60840(10) Å, β = 99.54°, V = 1700.82(4) Å^3, Z = 4, d = 1.464 g cm^{-3}, monoclinic, $P2_1/n$. Data collection: Bruker Smart three-circle diffractometer with CCD area detector with Mo-K_α radiation and graphite monochromator, μ(Mo-K_α) = 0.921 mm^{-1}, T = 120(2) °C, data-collection mode, 2.17° < Θ < 26.99°, 3706 reflections measured, 3041 symmetry-independent reflections with $I > 2\sigma(I)$. The structure was solved by direct methods and refined by full-matrix least-squares procedures with anisotropic approximation for all non-hydrogen atoms, using the SHELXTL software.[46] The hydrogen atoms were found from difference maps and refined isotropically, reflection/parameter ratio in the final refinement was

 © 2004 Wiley-VCH Verlag GmbH & Co. KGaA, Weinheim

13.4, $R_1 = 0.0290$, $wR_2 = 0.0578$ and GOF = 1.100. **Crystal Data for 8:** $C_{10}H_{11}Cl_6Si_2Nb$, $M_r = 492.98$, $a = 9.1658(2)$, $b = 14.3502(4)$, $c = 13.3894(4)$ Å, $\beta = 99.620(1)°$, $V = 1736.36(8)$ Å^3, $Z = 4$, $d = 1.886$ g cm^{-3}, monoclinic, $P2_1/n$. Data collection: Bruker Smart three-circle diffractometer with CCD area detector with Mo-K_α radiation and graphite monochromator, μ(Mo-K_α) = 1.737 mm^{-1}, crystal size 0.30 × 0.30 × 0.08 mm, $T = 120(2)$ °C, data-collection mode, $2.66° < \Theta < 30.15°$, 3984 reflections measured, 3678 symmetry-independent reflections with $I > 2\sigma(I)$, multi-scan absorption correction with maximum and minimum transmission equal to 0.8735 and 0.6238, respectively. The structure was solved by direct methods and refined by full-matrix least-squares procedures with anisotropic approximation for all non-hydrogen atoms, using SHELXTL software.[46] The hydrogen atoms were found from difference maps and refined isotropically, reflection/parameter ratio in the final refinement was 18.4, $R_1 = 0.0226$, $wR_2 = 0.0575$ and GOF = 1.041. CCDC-219856 (**6**) and -190915 (**8**) contain the supplementary crystallographic data for this paper. These data can be obtained free of charge at www.ccdc.cam.ac.uk/conts/retrieving.html [or from the Cambridge Crystallographic Data Centre, 12 Union Road, Cambridge CB2 1EZ, UK; Fax: (internat.) + 44-1223-336-033; E-mail: deposit@ccdc.cam.ac.uk].

Acknowledgments

Support from the Russian Foundation for Basic Research for GIN (grant no. 00-03-32850) and LGK (grant no. 01-03-32474) is gratefully acknowledged. A. V. C. thanks the Royal Society of Chemistry for an RSC Journal Grant for International Authors.

[1] J. Y. Corey, in *Advances in Silicon Chemistry* (Ed.: G. Larson), JAI Press, Greenwich, CT, **1991**, vol. 1, p.327.
[2] T. D. Tilley, *Acc. Chem. Res.* **1993**, *26*, 22.
[3] F. Gauvin, J. F. Harrod, H. G. Woo, *J. Organomet. Chem.* **1998**, *42*, 363.
[4] I. Ogima, in *The Chemistry of Organic Compounds* (Eds.: S. Patai, Z. Rapport), Wiley, New York, **1989**, chapter 25.
[5] P.-F. Fu, L. Brard, Y. Li, T. J. Marks, *J. Am. Chem. Soc.* **1995**, *117*, 7157.
[6] M. B. Carter, B. Schiott, A. Butierrez, S. L. Buchwald, *J. Am. Chem. Soc.* **1994**, *116*, 11667.
[7] J. Y. Corey, J. Braddock-Wilking, *Chem. Rev.* **1999**, *99*, 175.
[8] T. D. Tilley, in *The Chemistry of Organosilicon Compounds* (Eds.: S. Patai, Z. Rapport), Wiley, New York, **1989**, chapter 24.
[9] G. I. Nikonov, D. A. Lemenovskii, J. Lorberth, *Organometallics* **1994**, *13*, 3127.
[10] G. I. Nikonov, L. G. Kuzmina, P. Mountford, D. A. Lemenovskii, *Organometallics* **1995**, *14*, 3588.
[11] G. I. Nikonov, K. Harms, J. Lorberth, D. A. Lemenovskii, *Inorg. Chem.* **1995**, *34*, 2461.
[12] G. I. Nikonov, D. A. Lemenovskii, J. Lorberth, *Polyhedron* **1996**, *15*, 1565.
[13] G. I. Nikonov, A. J. Blake, J. Lorberth, D. A. Lemenovskii, S. Wocadlo, *J. Organomet. Chem.* **1997**, *547*, 235.
[14] G. I. Nikonov, L. G. Kuzmina, Yu. K. Grishin, D. A. Lemenovskii, N. B. Kazennova, *J. Organomet. Chem.* **1997**, *547*, 183.
[15] G. I. Nikonov, L. G. Kuzmina, J. A. K. Howard, *Organometallics* **1997**, *16*, 3723.
[16] G. I. Nikonov, E. V. Avtomonov, W. Massa, *Chem. Ber./Recueil* **1997**, *130*, 1629.
[17] G. I. Nikonov, L. G. Kuzmina, J. Lorberth, *Eur. J. Inorg. Chem.* **1999**, 825.
[18] G. I. Nikonov, A. V. Churakov, M. Y. Antipin, *Organometallics* **2003**, *22*, 2178.
[19] F. R. Lemke, *J. Am. Chem. Soc.* **1994**, *116*, 11183.
[20] F. R. Lemke, K. J. Galat, W. J. Youngs, *Organometallics* **1999**, *18*, 1419.
[21] P. Jutzi, S. H. A. Petri, in *Organosilicon Chemistry III: From Molecules to Materials* (Eds.: N. Auner, J. Weis), Wiley-VCH, Weinheim, **1998**, p.275.
[22] G. H. Wagner, in *Abstracts of the 34th Organosilicon Symposium*, White Plains, NY, May 3−5, **2002**, HR4-1.
[23] A. J. Chalk, J. F. Harrod, *J. Am. Chem. Soc.* **1965**, *87*, 16.
[24] A. K. Roy, R. B. Taylor, *J. Am. Chem. Soc.* **2002**, *124*, 9510 and references cited therein.
[25] G. I. Nikonov, L. G. Kuzmina, S. F. Vyboishchikov, D. A. Lemenovskii, J. A. K. Howard, *Chem. Eur. J.* **1999**, *5*, 2497.
[26] D. A. Lemenovskii, T. V. Baukova, V. P. Fedin, *J. Organomet. Chem.* **1977**, *132*, C14.
[27] M. D. Curtis, L. G. Bell, N. M. Buter, *Organometallics* **1985**, *4*, 701.
[28] A. Antiñolo, F. Carrillo, M. Fajardo, A. Otero, M. Lanfranchi, M. A. Pellingheli, *Organometallics* **1995**, *14*, 1518.
[29] K. W. Kramarz, J. R. Norton, *Prog. Inorg. Chem.* **1994**, *42*, 14.
[30] J. T. Amella, V. V. Bakhmutov, E. V. Bakhmutova, N. V. Belkova, L. M. Epstein, A. Lledos, G. I. Nikonov, E. S. Shubina, *Chem. Eur. J.*, accepted for publication.
[31] G. Parkin, J. E. Bercaw, *J. Chem. Soc., Chem. Commun.* **1990**, 255.
[32] E. T. Papish, F. C. Rix, N. Spetseris, J. R. Norton, R. D. Williams, *J. Am. Chem. Soc.* **2000**, *122*, 12235.
[33] M. J. Bearpark, G. S. McGrady, P. D. Prince, J. W. Steed, *J. Am. Chem. Soc.* **2001**, *123*, 7735 and references cited therein.
[34] See, for example: A. Antinolo, F. Carrillo-Hermosilla, B. Chaudret, M. Fajardo, J. Fernandez Baeza, M. Lanfranchi, H. H. Limbach, M. Maurer, A. Otero, M. A. Pellinghelli, *Inorg. Chem.* **1996**, *35*, 7873.
[35] S. Camanyes, F. Masera, M. Moreno, A. Lledós, J. M. Lluch, J. Bertrán, *Angew. Chem. Int. Ed. Engl.* **1997**, *36*, 265.
[36] I. Tanaka, T. Ohhara, N. Niimura, Y. Ohashi, Q. Jiang, D. H. Berry, R. Bau, *J. Chem. Res.* **1999**, 14.
[37] K. Hübler, P. A. Hunt, S. M. Maddock, C. E. F. Rickard, W. R. Roper, D. M. Salter, P. Schwerdtfeger, L. J. Wright, *Organometallics* **1997**, *16*, 5076.
[38] H. A. Bent, *Chem. Rev.* **1961**, *61*, 275.
[39] K. E. Lee, A. M. Arif, J. A. Gladysz, *Chem. Ber.* **1991**, *124*, 309.
[40] B. R. Jagirdar, R. Palmer, K. J. Klabunde, L. Radonovich, *Inorg. Chem.* **1995**, *34*, 278.
[41] M. K. Hays, R. Eisenberg, *Inorg. Chem.* **1991**, *30*, 2623.
[42] T. S. Koloski, D. C. Pestana, P. J. Carroll, D. H. Berry, *Organometallics* **1994**, *13*, 489.
[43] G. I. Nikonov, P. Mountford, S. R. Dubberley, *Inorg. Chem.* **2003**, *42*, 258.
[44] E. A. Zarate, V. O. Kennedy, J. A. McCune, R. S. Simons, C. A. Tessier, *Organometallics* **1995**, *14*, 1802.
[45] R. S. Simons, J. C. Gallicci, C. A. Tessier, W. J. Youngs, *J. Organomet. Chem.* **2002**, *654*, 224.
[46] G. M. Sheldrick, *SHELXTL 5.04/VMS, An integrated system for solving, refining and displaying crystal structures from diffraction data*, Siemens Analytical X-ray Instrument Inc., Madison, WI, **1995**.

Received March 10, 2003
Early View Article
Published Online December 12, 2003

 © 2004 Wiley-VCH Verlag GmbH & Co. KGaA, Weinheim

A Comparison of the Reactivity of Chloroalkanes and Chlorosilanes towards Activated Pt^{II} Complexes by DFT Calculations

Dietmar Sturmayr[a] and Ulrich Schubert*[a]

Keywords: Hemilabile ligands / Oxidative addition / Reductive elimination / Density functional calculations / Silanes

The pathways of the C–Cl bond activation of CCl_4 and CH_3Cl by the 14-electron Pt^{II} complexes $[PtMe_2(PH_3)]$ or the corresponding reactions of $SiCl_4$ and SiH_3Cl with $[PtMe(SiH_3)(PH_3)]$ were investigated by DFT calculations. The complexes $[Pt(EH_3)Me(PH_3)]$ (E = C, Si) are models for $[Pt(EH_3)Me\{(\kappa^2\text{-}P,N)\text{-}Ph_2PCH_2CH_2NMe_2\}]$, with hemilabile P,N chelating ligands, used in practical experiments. While the reaction of $[Pt(EH_3)Me(PH_3)]$ with ECl_4 results in an EH_3/ECl_3 exchange, reaction of $[Pt(EH_3)Me(PH_3)]$ with EH_3Cl results in the elimination of E_2H_6. Both reactions proceed via a five-coordinate Pt^{IV} intermediate. The elimination of Si_2H_6 is endothermic.
(© Wiley-VCH Verlag GmbH & Co. KGaA, 69451 Weinheim, Germany, 2004)

Introduction

Hemilabile chelating ligands (A∩B) are used in coordination chemistry to enhance the reactivity of metal complexes.[1] The activating effect of such ligands results from the different metal−ligand bond strengths: while one atom (A) remains coordinated to the metal, a more weakly bonded second center (B) decoordinates more easily and reversibly.

Coordinatively and electronically unsaturated complexes play a key role in many stoichiometric and catalytic reactions of Pt^{II} complexes based on oxidative addition/reductive elimination reactions. Three-coordinate Pt^{II} complexes are often required for the initial oxidative addition reactions.[2] They are generally transient species generated in situ by ligand elimination from the square-planar precursor complexes. After oxidative addition has occurred, five-coordinate Pt^{IV} complexes are key intermediates in the product-forming reductive elimination reactions.[3] The use of hemilabile chelating ligands should therefore promote both oxidative addition reactions starting from the Pt^{II} complexes and reductive elimination reactions from the corresponding Pt^{IV} intermediates.

In the chemistry of metal-silicon compounds hemilabile ligands have hardly been used. In a series of papers, we have recently shown that the reactivity of Pt^{II} complexes towards silanes is greatly enhanced by using hemilabile chelating ligands of the type $\kappa^2\text{-}Ph_2P-X-NR_2$ (denoted as P∩N).[4] Furthermore, these complexes were also found to activate C−Cl bonds.[5,6] The outcome of the reactions of $[PtMe_2\{(\kappa^2\text{-}P,N)\text{-}Ph_2PCH_2CH_2NMe_2\}]$ (**A**) with $CH_{4-n}Cl_n$ (n = 1−4) on one hand and with $PhMe_2SiCl$ on the other showed remarkable differences. In the reaction with CCl_4, the complexes $[Pt(Cl)Me(P\cap N)]$, $[Pt(Cl)Me_3(P\cap N)]$ and $[Pt(Cl)C(Cl)=CH_2(P\cap N)]$ were formed at room temperature. A suggested reaction mechanism is shown in Scheme 1 (the final products are drawn in bold). In this reaction, the complex $[Pt(Cl)Me(P\cap N)]$ can be formed by two different routes. At room temperature, this complex was only obtained by reaction of **A** with the HCl cleaved in the reaction forming the vinylidene complex. Ethane elimination from $[Pt(Cl)Me_3(P\cap N)]$ with concomitant formation of $[Pt(Cl)Me(P\cap N)]$ occurred only in boiling benzene.

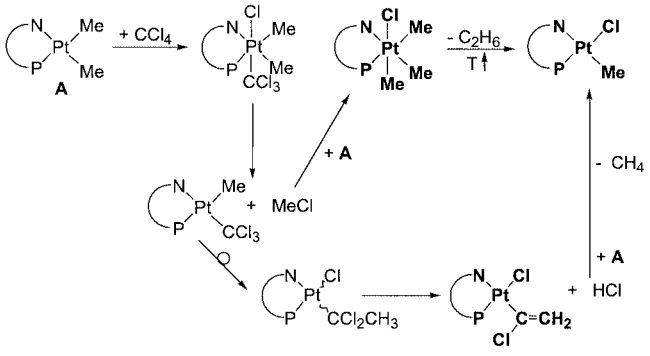

Scheme 1

The analogous reactions of $CHCl_3$ and CH_2Cl_2 with $[Pt(Cl)Me(P\cap N)]$ were much slower, but resulted in analogous products; CH_3Cl only reacts slowly with $[PtMe_2(P\cap N)]$ in a hot benzene solution to form $[Pt(Cl)Me_3(P\cap N)]$ and $[Pt(Cl)Me(P\cap N)]$, and thus does not fit into the sequence.

In contrast, when $[PtMe_2\{(\kappa^2\text{-}P,N)\text{-}Ph_2PCH_2CH_2NMe_2\}]$ was reacted with $PhMe_2SiCl$, the disilane $Ph_2Me_4Si_2$ was

[a] Institute of Materials Chemistry, Vienna University of Technology,
Getreidemarkt 9/165, 1060 Wien, Austria

 © 2004 Wiley-VCH Verlag GmbH & Co. KGaA, Weinheim DOI: 10.1002/ejic.200300418

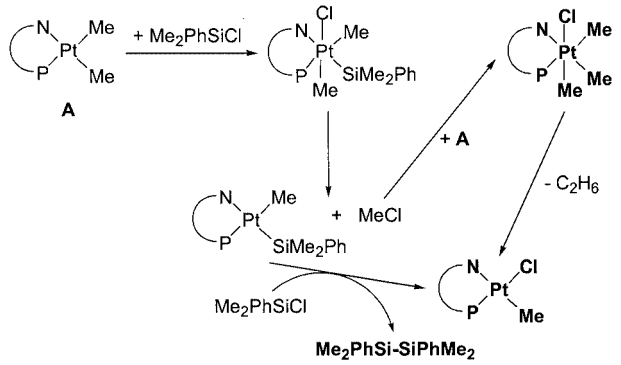

Scheme 2

formed quantitatively, together with the Pt^{IV} complex [Pt(Cl)Me_3(P∩N)] and the Pt^{II} complex [Pt(Cl)Me(P∩N)]. A possible reaction mechanism is shown in Scheme 2 (the final products are again drawn in bold).

The practical results suggested that the initial steps are the same in both the reaction of CCl_4 and $PhMe_2SiCl$. However, the [PtMe(SiMe$_2$Ph)(P∩N)] intermediate in the latter reaction reacted with another equivalent of $PhMe_2Si$-Cl to give the disilane, while the corresponding intermediate [Pt(CCl_3)Me(P∩N)] did not undergo C−C coupling.

These observations prompted us to investigate the pathways of the C−Cl and Si−Cl activation by the complexes [PtMe$_2$(P∩N)] using DFT calculations. While several theoretical calculations on the oxidative addition of silicon-element bonds to unsaturated PtL_2 (d^{10}) complexes have been performed,[7] little theoretical work has been carried out on such reactions with unsaturated d^8 $PtLX_2$ complexes.

Results and Discussion

As was already discussed in our earlier work,[8,9] at the key stage of the reaction the amino group of the chelating P∩N ligand was considered to be decoordinated, and therefore the chelate ligand was replaced by a PH_3 group in the calculations. In the four- and six-coordinate complexes, the chelating P∩N ligand was replaced by a PH_3 and NH_3 group. Further simplification was used in the reactions where the molecules $Me_2PhSiCl$ or Me_2PhSiH were involved. These were replaced by H_3SiCl and H_3SiH respectively.

Reaction of CCl_4 with [$PtMe_2(PH_3)$] (1)

As a first step in the reaction of [PtMe$_2$(P∩N)] with CCl_4, the oxidative addition of a C−Cl bond was suggested, followed by elimination of methyl chloride. The three-coordinate complex **1** and CCl_4 initially form the precursor complex $\mathbf{PC}_{1-2}$. This reaction requires 6.1 kcal/mol. In the distorted square-planar complex thus formed, the platinum atom interacts with CCl_4 through a weak Pt−Cl interaction (Pt−Cl 2.690 Å; Figure 1). The associated C−Cl bond is only slightly stretched from 1.793 Å in CCl_4 to 1.832 Å in $\mathbf{PC}_{1-2}$.

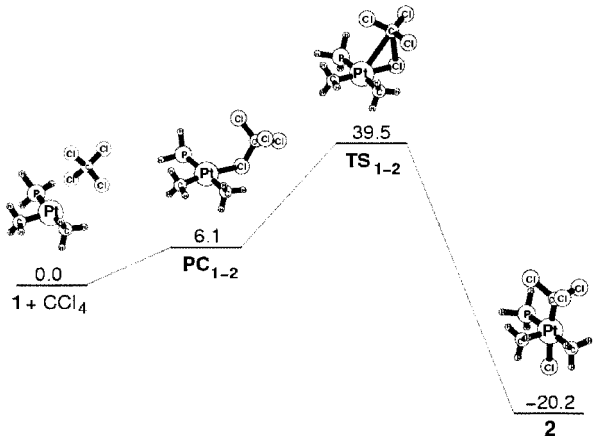

Figure 1. Reaction profile for the oxidative addition of CCl_4 to **1**; energies in kcal/mol

The transition state structure $\mathbf{TS}_{1-2}$ is formed by closing of the Pt−Cl−C angle from 118.7° in $\mathbf{PC}_{1-2}$ to 74.5° in $\mathbf{TS}_{1-2}$, corresponding to the formation of a new Pt−C bond. The C−Cl bond is now stretched to 2.788 Å, and the Pt−Cl bond is reduced to 2.481 Å. Additionally the C−Pt−Cl angle is increased from 170.9° in $\mathbf{PC}_{1-2}$ to 178.8° in $\mathbf{TS}_{1-2}$. The energy required for this change is 33.4 kcal/mol, which is quite high. On the other hand, the relaxation to [Pt(CCl_3)(Cl)$Me_2(PH_3)$] (**2**) liberates 59.7 kcal/mol. This high value is a result of the rearrangements during the relaxation to intermediate **2**, where the chlorine atom moves into the *trans* position to the CCl_3 group. The rearrangement of the chlorine is an effect of the stronger *trans* effect of the methyl group compared to the CCl_3 group.[8] The overall reaction of **1** with CCl_4 is best described as an oxidative addition via a three-center transition state. As expected from the different electronegativities, the Pt−Cl interaction develops faster than the Pt−C interaction.

The geometry optimization on the reactant side of $\mathbf{TS}_{3-4}$ leads to the square-pyramidal complex [Pt(CCl_3)(Cl)$Me_2(PH_3)$] (**3**) which is nearly equivalent to **2**. This shows that the two reaction profiles in Figure 1 and Figure 2 are connected. Hence the next stage of the reaction mechanism, which eventually leads to a reductive elimination of methyl chloride, begins with **3** (Figure 2). The energy required to form $\mathbf{TS}_{3-4}$ from intermediate **3** is 35.8 kcal/mol. The geometric changes on the way from **3** to **4** + $ClCH_3$ mirror those during the oxidative addition of CCl_4, i.e. the Cl−Pt−C angle closes from 96.1° in **3** to 53.9° in $\mathbf{TS}_{3-4}$, and the Pt−C bond is stretched from 2.072 Å to 2.603 Å. The change in the Pt−Cl bond length from 2.414 Å to 2.461 Å is much smaller. Through the changes in the geometry, a weak C−Cl interaction with 2.298 Å is formed.

The Pt−C bond is broken during the relaxation to $\mathbf{PC}_{3-4}$, and the C−Cl bond is fully formed. The bond length of 1.821 Å is close to the final C−Cl bond length of 1.806 Å in MeCl. The Pt−Cl bond length is increased to

 © 2004 Wiley-VCH Verlag GmbH & Co. KGaA, Weinheim

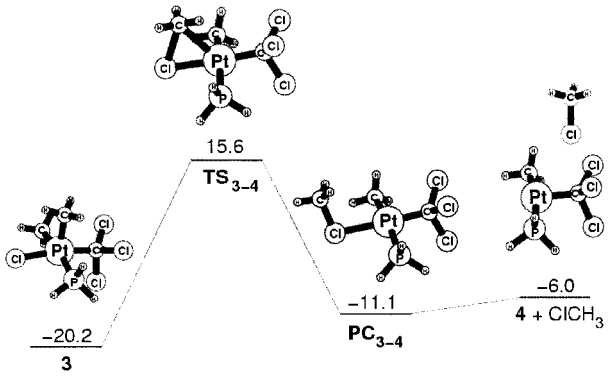

Figure 2. Continuing reaction profile for the reaction of **1** with CCl_4 (elimination of MeCl); energies in kcal/mol

2.617 Å and the energy released by the relaxation is 26.7 kcal/mol. MeCl is eventually fully dissociated. The last step is endothermic by +5.1 kcal/mol, but the whole reaction [Equation (1)] is exothermic by −6.0 kcal/mol.

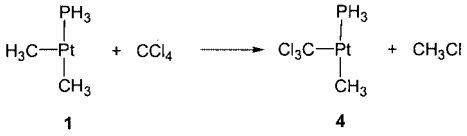

(1)

The formation of **4** is the key step for the reaction of CCl_4 with the dimethylplatinum complex **1**. This, in turn, allows further reactions to happen (Scheme 1), all of which are exothermic. Although there is a high activation energy barrier for the oxidative CCl_4 addition to **1**, these following exothermic reactions produce enough energy for this barrier to be overcome.[9]

Reaction of $SiCl_4$ with [Pt(SiH$_3$)Me(PH$_3$)] (5)

Though not yet practically investigated, the reaction between the three-coordinate complex **5** and $SiCl_4$ was also investigated for comparison. This is the silicon analogue to the previously discussed reaction, i.e. the SiH_3 group in the starting complex **5** is replaced by a $SiCl_3$ ligand [Equation (2)]. We have previously shown that the energetically preferred structure of the T-shaped complex **5** is the one where PH_3 and CH_3 are *trans* to each other.[8]

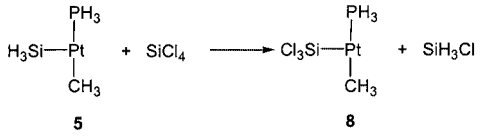

(2)

Complex **5** reacts with $SiCl_4$ to form the precursor complex $\mathbf{PC_{5-6}}$. The reaction requires 8.5 kcal/mol, and a weak Pt−Cl bond is formed. The Pt−Cl distance in $\mathbf{PC_{5-6}}$ (3.127 Å) is considerably longer than the corresponding distance in the reaction with CCl_4 (precursor complex $\mathbf{PC_{1-2}}$). This is due to the SiH_3 group in $\mathbf{PC_{5-6}}$ having a stronger *trans* effect than the methyl group in the *trans* position in $\mathbf{PC_{1-2}}$. The associated Si−Cl bond length (2.059 Å) is nearly unchanged relative to the free $SiCl_4$ molecule (2.047 Å).

As in the CCl_4 reaction, the Pt−Si bond forms by closing of the Pt−Cl−Si angle from 116.5° in $\mathbf{PC_{5-6}}$ to 65.2° in $\mathbf{TS_{5-6}}$, stretching of the Si−Cl bond to 2.205 Å and reducing the Pt−Cl bond length to 2.654 Å.

Compared to the reaction with CCl_4, the incoming $SiCl_4$ molecule is not as distorted in the transition-state structure as the CCl_4 molecule was. As a result, the energy required for this change is, at 11.8 kcal/mol, much lower than the 33.4 kcal/mol required for the reaction with CCl_4. On the other hand the relaxation to [Pt(Cl)Me(SiH$_3$)(SiCl$_3$)(PH$_3$)] (**6**) liberates only 18.9 kcal/mol. A rearrangement occurs during the relaxation to the intermediate **6**, where the chlorine atom moves *trans* to the $SiCl_3$ group, analogous to the CCl_4 reaction. This is again an effect of the stronger *trans* effect of the SiH_3 group compared to the $SiCl_3$ group. It is interesting to note that the formation of the intermediate **6** is slightly endothermic, in comparison to the analogous reaction with CCl_4, where the formation of the intermediate **2/3** was exothermic.

The geometry optimization on the reactant side of $\mathbf{TS_{7-8}}$ leads to the five-coordinate complex [Pt(Cl)Me(SiH$_3$)(SiCl$_3$)(PH$_3$)] (**7**) which is equivalent to **6**. Although the energy difference is 0.7 kcal/mol, the assumption that the two reaction profiles in Figure 3 and Figure 4 are connected is still valid. The energy required to form $\mathbf{TS_{7-8}}$ from **7** is

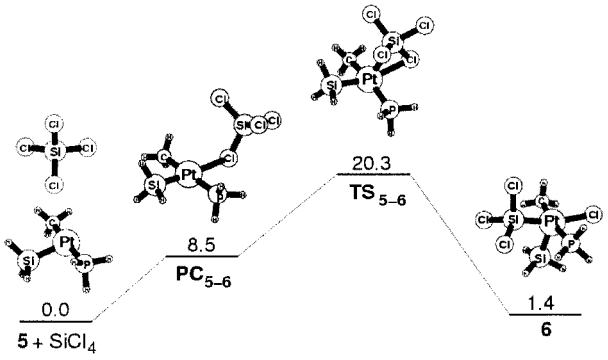

Figure 3. Reaction profile for the reaction of **5** with $SiCl_4$; energies in kcal/mol

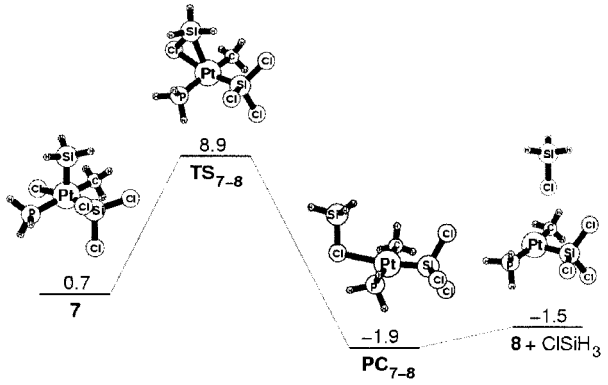

Figure 4. Continuing reaction profile for the reaction of **5** with $SiCl_4$ (elimination of H_3SiCl); energies in kcal/mol

 © 2004 Wiley-VCH Verlag GmbH & Co. KGaA, Weinheim

8.2 kcal/mol. This is again much less than in the CCl_4 reaction. The Cl−Pt−Si angle is changed from 101.5° in **7** to 52.8° in $\mathbf{TS}_{7-8}$, the Pt−Si bond is stretched from 2.360 Å to 2.644 Å, and a weak Si−Cl bond (2.318 Å) is formed. The change in the Pt−Cl bond length (from 2.439 Å to 2.567 Å) is much larger than for the case of CCl_4.

During the relaxation of $\mathbf{TS}_{7-8}$ to $\mathbf{PC}_{7-8}$, the Pt−C bond is broken and the Si−Cl bond is fully formed. The bond length of 2.114 Å is close to that of 2.081 Å in the H_3SiCl molecule. The Pt−Cl bond is lengthened to 2.849 Å and the energy released by the relaxation is 10.8 kcal/mol. Finally the H_3SiCl molecule is fully dissociated. The whole reaction [Equation (2)] is slightly exothermic by −1.5 kcal/mol.

Reaction of CH_3Cl with $[PtMe_2(NH_3)(PH_3)]$ (9)

Practical experiments have shown that a six-coordinate Pt^{IV} complex is formed in the reaction of $[PtMe_2(P\cap N)]$ with MeCl [Equation (3)] in contrast to the reaction with CCl_4.[5] For the calculation of the reaction profile (Figure 5), the four-coordinate complex **9** was taken as a starting point. The first step in the reaction with MeCl is the formation of the four-coordinate precursor $\mathbf{PC}_{9-10}$, which requires 14.5 kcal/mol. For the formation of this precursor complex the nitrogen must decoordinate, and a weak Pt−Cl bond (2.709 Å) must form.

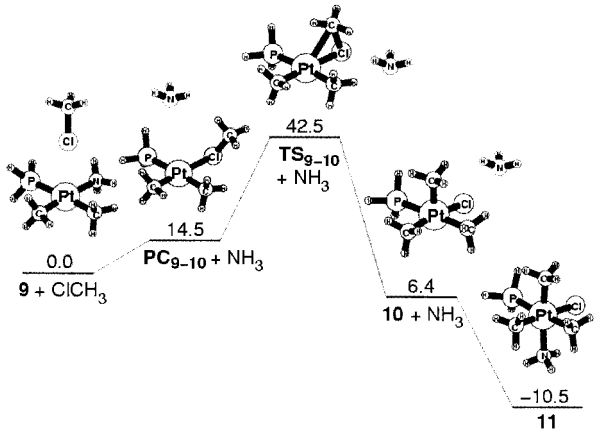

Figure 5. Reaction profile for the reaction of **9** with CH_3Cl; energies in kcal/mol

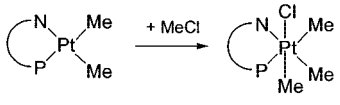

(3)

The energy required to form $\mathbf{TS}_{9-10}$ from $\mathbf{PC_{9-10}}$ is 28.0 kcal/mol, which is lower than the 33.4 kcal/mol for the case of CCl_4. In $\mathbf{TS}_{9-10}$ the carbon atom approaches the platinum atom (Pt−C 2.580 Å), while the corresponding C−Cl bond is stretched to 2.270 Å. The Pt−Cl bond is now 2.526 Å, and the Cl−Pt−C angle is 52.8°. During the relaxation to $[Pt(Cl)Me_3(PH_3)]$ (**10**) the Pt−C bond length is decreased to 2.063 Å while the C−Cl bond is broken. The Pt−Cl bond is now 2.466 Å and the Cl−Pt−C angle is 105.2°. Noticeably, the chlorine is not re-orientated as in the case of **2** (Figure 1). This is due to the fact that the incoming alkyl ligand is the same as the existing alkyl ligands (i.e. the chlorine is already *trans* to a methyl group).

The six-coordinate complex $[Pt(Cl)Me_3(NH_3)(PH_3)]$ (**11**) is formed through the re-coordination of the nitrogen. Here the platinum has an octahedral geometry as seen in the corresponding crystal structure of $[Pt(Cl)Me_3\{(\kappa^2\text{-}P,N)\text{-}Ph_2PCH_2CH_2NMe_2\}]$.[5] The reaction to form **11** is exothermic by −10.5 kcal/mol. The six-coordinate complex **11** is the only reaction product, because formation of a vinylidene complex is not possible. Elimination of MeCl would just reverse the reaction, but would not lead to the formation of a new complex.

Although the reaction to form **11** is exothermic, the practical results showed that ethane elimination can occur at elevated temperatures. The profile of this reaction is shown in Figure 6. Starting from the six-coordinate complex **11**, the five-coordinate intermediate $[Pt(Cl)Me_3(PH_3)]$ (**12**) is formed through the de-coordination of the nitrogen. This has a trigonal-bipyramidal geometry instead of a square-pyramidal geometry as in **10**. However, the trigonal-bipyramidal structure is only 0.4 kcal/mol higher in energy than the square-pyramidal structure. The formation of **12** needs 17.3 kcal/mol, and the C−C distance in **12** is 2.662 Å indicating that the two carbons approach each other.

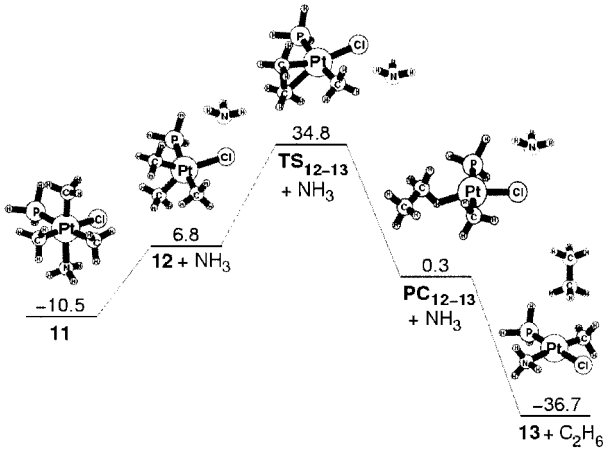

Figure 6. Elimination of ethane from **11**; energies in kcal/mol

An energy of 28.0 kcal/mol is required to form the transition state $\mathbf{TS}_{12-13}$. During this process both Pt−C bonds are lengthened, while a C−C bond (1.908 Å) is formed. On the other hand, the Pt−Cl bond is decreased from 2.443 Å in **12** to 2.367 Å in $\mathbf{TS}_{12-13}$. As shown in Figure 6, the vector of the outgoing C_2H_6 molecule is perpendicular to the plane of the remaining three-coordinate platinum complex. The C−C bond length of 1.530 Å and the Pt−C bond of 2.614 Å suggests that in the complex $\mathbf{PC}_{12-13}$ the ethane is fully formed. In the final step the nitrogen is re-coordinated, an energy of 37.0 kcal/mol is released and the complex $[Pt(Cl)Me(NH_3)(PH_3)]$ (**13**) is formed, where the chlorine is in the energetically favored *trans*-position to the phosphorus. Reductive elimination of ethane from the six-coor-

 © 2004 Wiley-VCH Verlag GmbH & Co. KGaA, Weinheim

dinate complex **11** releases an overall energy of 26.2 kcal/mol.

Reaction of SiH_3Cl with [PtMe(SiH_3)(PH_3)] (5)

For a further comparison with the carbon complexes, and due to interesting practical results (the formation of disilane), the corresponding reaction with SiH_3Cl and the platinum complex **5** [Equation (4)] was investigated. Starting from reactants **5** and SiH_3Cl the precursor $\mathbf{PC_{5-14}}$ is formed. This requires 1.3 kcal/mol (Figure 7).

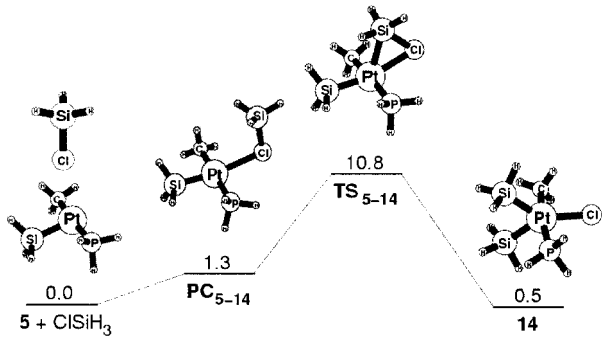

Figure 7. Reaction profile for the reaction **5** with SiH_3Cl; energies in kcal/mol

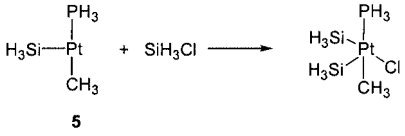

(4)

In the complex $\mathbf{PC_{5-14}}$, the chlorine of SiH_3Cl interacts weakly with the platinum (Pt−Cl 2.964 Å). Owing to the Pt−Cl interaction, the Si−Cl bond is weakened and stretched from 2.082 Å to 2.103 Å. The SiH_3Cl molecule approaches the platinum complex not quite perpendicularly to the Pt−Si bond but instead it tips slightly towards the carbon atom, giving a Si−Pt−Cl−Si dihedral angle of 27.7°.

In the transition state $\mathbf{TS_{5-14}}$ the Pt−Cl bond is further decreased to 2.608 Å, and the formation of a 2.599 Å long Pt−Si interaction can be observed. On the other hand, the Si−Cl bond is increased from 2.103 Å in $\mathbf{PC_{5-14}}$ to 2.316 Å in $\mathbf{TS_{5-14}}$. The energy required to form the transition state $\mathbf{TS_{5-14}}$ from the precursor $\mathbf{PC_{5-14}}$ is 9.5 kcal/mol.

The distorted trigonal-bipyramidal complex [Pt(Cl)Me(SiH_3)$_2$(PH_3)] (**14**) is formed from $\mathbf{TS_{5-14}}$, and 10.3 kcal/mol is released. During this process the Si−Cl bond is broken and the Pt−Si bond is fully formed. The final complex **14** consists of two equivalent SiH_3 groups. The geometry optimization on the reactant side of $\mathbf{TS_{15-16}}$ leads to the five-coordinate complex [Pt(Cl)Me(SiH_3)$_2$(PH_3)] (**15**), which is equivalent to **14**, with the SiH_3 and the Cl ligand in the trigonal plane.

The Si−Si distance of 3.026 Å in **15** is reduced to 2.492 Å in $\mathbf{TS_{15-16}}$ (Figure 8). In $\mathbf{TS_{15-16}}$ a 1.988 Å long Pt−H bond is formed, concurrently the corresponding Si−H bond increases from 1.488 Å to 1.564 Å and the Pt−Si bond is lengthened to 2.452 Å. The other Pt−Si bond (2.652 Å) is even longer. The energy required to form $\mathbf{TS_{15-16}}$, which can mainly be assigned to the formation of the Si−Si bond, is 30.1 kcal/mol. The five-coordinate complex [Pt(Cl)(H)Me(Si_2H_5)(PH_3)] (**16**) is formed freeing 19.9 kcal/mol. During the relaxation the Si−Si bond is reduced to 2.359 Å, and the Pt−H bond is fully formed with a bond length of 1.577 Å. The Si−Pt−H angle is 70.2° and the H−Pt−Cl angle 165.4°.

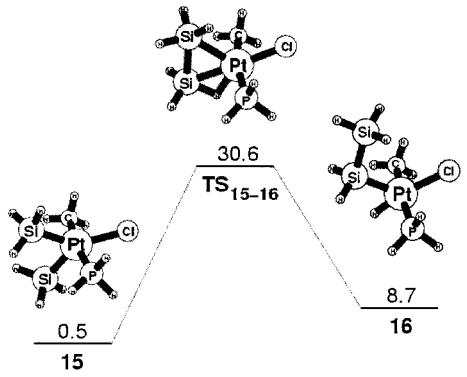

Figure 8. Continuing reaction profile for the reaction of **5** with $ClSiH_3$; energies in kcal/mol

The obvious final step would be the elimination of the disilane Si_2H_6. This step has not been calculated, but instead the comparable elimination of SiH_4 starting from [Pt(Cl)(H)Me(SiH_3)(PH_3)] (**17**) (Figure 9) was calculated.

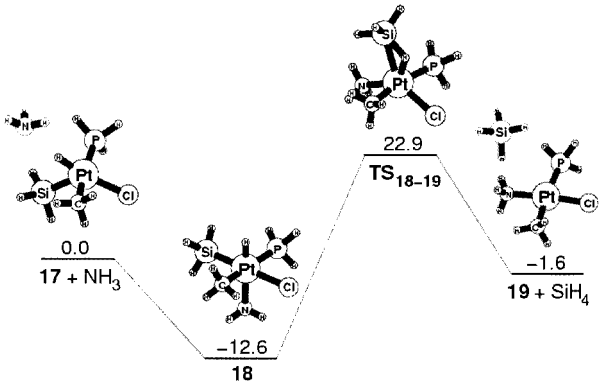

Figure 9. Reaction profile for the reaction of **17** with SiH_4; energies in kcal/mol

In the first step the nitrogen is re-coordinated to form the six-coordinate complex **18**, freeing 12.6 kcal/mol; 35.5 kcal/mol is required to form the transition state structure $\mathbf{TS_{18-19}}$. In $\mathbf{TS_{18-19}}$ the nitrogen is still coordinated, therefore the formation of the six-coordinate intermediate **18** is necessary to allow the reductive elimination of SiH_4. The elimination of SiH_4 and formation of [Pt(Cl)Me(NH_3)(PH_3)] (**19**) frees 24.5 kcal/mol. Although **19** is the energetically less favorable isomer (compared to **13**) the reaction energy is slightly exothermic at −1.6 kcal/

 © 2004 Wiley-VCH Verlag GmbH & Co. KGaA, Weinheim

mol. Rearrangement to the energetically favored isomer **13** would liberate an additional 9.0 kcal/mol. It is assumed that **16** can react in the same way as **17**, forming the disilane Si_2H_6.

In the practical experiment, the dimethylplatinum complex [$PtMe_2$(P∩N)] was reacted with $ClSiMe_2Ph$. In the first step of this reaction the methylsilylplatinum complex [PtMe($SiMe_2Ph$)(P∩N)] was formed, and the freed MeCl reacted with still available [$PtMe_2$(P∩N)] as described previously. The latter reaction is exothermic, which enables the total reaction to occur. It should be noted that in the reaction of [$PtMe_2$(P∩N)] with $ClSiMe_2Ph$ no hydrido silyl complex (corresponding to **16**) can be formed, because no hydrogen substituents are present. However, the energetics of the overall reaction for the elimination of the disilane directly from **15** (without the intermediacy of **16**) should be very similar to that calculated above.

Conclusions

A comparison of the chlorosilane and chloroalkane reactions with the three-coordinate Pt^{II} complexes shows that the reactions proceed in a geometrically very similar manner. A weak Pt−Cl interaction develops first, which then proceeds to a three-center transition state. The transition-state structures of incoming silanes are less disturbed than those of the corresponding carbon compounds. As a result the activation energies for CCl_4 and CH_3Cl (39.5 and 42.5 kcal/mol, respectively) are much higher than that for $SiCl_4$ and SiH_3Cl (20.3 and 10.8 kcal/mol). On the other hand, the product side relaxation of the transition state structures of the carbon compounds frees 59.7 kcal/mol for CCl_4 and 36.1 kcal/mol for CH_3Cl, which is much more than the 18.9 kcal/mol for $SiCl_4$, and 10.3 kcal/mol for SiH_3Cl.

For the distorted square-pyramidal intermediates **2**, **6**, **10** and **14** (Figures 1, 3, 5 and 7) the following points can be made: (i) When the substituents on the incoming alkyl or silyl group are different from that of the group in the T-shaped precursor complex (CCl_3 and $SiCl_3$ vs. CH_3 and SiH_3) then a rearrangement occurs, which puts the incoming groups (Cl and CCl_3 or $SiCl_3$) *trans* to each other in the square plane, i.e. the *axial* position of the square pyramid is occupied by a CH_3 or SiH_3 ligand, respectively; (ii) When the incoming alkyl or silyl group is the same as the ligand already present (CH_3 or SiH_3), then the incoming groups (Cl and CH_3 or SiH_3) are *cis* (axial/equatorial) in the square-pyramidal intermediate.

Starting from these intermediates (**2**, **6**, **10** and **14**), the reductive elimination of a C−Cl or Si−Cl bond is apparently preferred over the elimination of a C−C or Si−Si bond. When the incoming alkyl or silyl group is the same as the ligand already bonded to the T-shaped precursor complex, reductive C−Cl or Si−Cl elimination would only reverse the reaction.

The differences in the reactivity of CCl_4 and $Me_2PhSiCl$ found in the practical experiments (Scheme 1 and 2) can thus be traced back to the exothermic nature of the reaction leading from [Pt(CCl_3)Me(P∩N)] (corresponding to **4**) to the vinylidene complex [Pt(Cl)($CCl{=}CH_2$)(P∩N)] and HCl {which further reacts with [$PtMe_2$(P∩N)] in an exothermic reaction}. For the corresponding silyl complex (corresponding to **8**) this reaction is not possible, because it would lead to a highly energetic Si=C bond. This reaction is also not possible for [$PtMe_2$(P∩N)] (no chlorine present that can rearrange), therefore formation of **11** and elimination of ethane (at higher temperatures) is the only reaction possibility.

Computational Details

The geometry optimizations of the equilibrium geometries and transition structures were performed using the B3LYP version of DFT, which is comprised of Becke's hybrid three-parameter exchange functional and the correlation functional of Lee, Yang and Parr.[10,11] The 6-31G++(d) basis set was used an all atoms for the calculations. The relativistic effective core potential and basis set of Preuss and co-workers (which is available in the Gaussian 98 software package as SDD basis set) was used for platinum.[12] Vibrational mode analyses were carried out to confirm that on potential energy surfaces optimized geometries correspond to a local minimum without an imaginary frequency mode or a saddle point with only one imaginary mode. Corrections of zero-point vibrational energies were taken into account in stationary structures obtained. All of the calculations were carried out with the Gaussian 98 package of electronic structure programs.[13]

Acknowledgments

This work was supported by the Fonds zur Förderung der wissenschaftlichen Forschung (FWF).

[1] [1a] P. Braunstein, F. Naud, *Angew. Chem. Int. Ed.* **2001**, *40*, 680. [1b] C. S. Slone, D. A. Weinberger, C. A. Mirkin, *Prog. Inorg. Chem.* **1999**, *48*, 233. [1c] A. Buder, E. Lindner, *Coord. Chem. Rev.* **1991**, *108*, 27.
[2] J. P. Collman, L. S. Hegedus, J. R. Norton, R. G. Finke, *Principles and Applications of Organotransition Metal Chemistry*, University Science Books, Mill Valley, Ca., **1987**.
[3] U. Fekl, W. Kaminsky, K. I. Goldberg, *J. Am. Chem. Soc.* **2001**, *123*, 6423, and references cited therein.
[4] U. Schubert, J. Pfeiffer, F. Stöhr, D. Sturmayr, S. Thompson, *J. Organomet. Chem.* **2002**, *646*, 53, and references cited therein.
[5] F. Stöhr, D. Sturmayr, G. Kickelbick, U. Schubert, *Eur. J. Inorg. Chem.* **2002**, 2305.
[6] F. Stöhr, D. Sturmayr, U. Schubert, *Chem. Commun.* **2002**, 2222.
[7] S. Sakaki, M. Ieki, *J. Am. Chem. Soc.* **1993**, *115*, 2373. S. Sakaki, N. Mizoe, Y. Musashi, B. Biswas, M. Sugimoto, *J. Phys. Chem. A* **1998**, *102*, 8027. S. Sakaki, N. Mizoe, M. Sugimoto, *Organometallics* **1998**, *17*, 2510.
[8] D. Sturmayr, U. Schubert, *Monatsh. Chem.* **2003**, *134*, 791.
[9] D. Sturmayr, PhD Thesis, Vienna University of Technology, **2002**.
[10] A. D. Becke, *J. Chem. Phys.* **1993**, *18*, 5648.
[11] C. Lee, W. Yang, R. G. Parr, *Phys. Rev. B* **1988**, *37*, 785.

 © 2004 Wiley-VCH Verlag GmbH & Co. KGaA, Weinheim

[12] D. Andrae, U. Haeussermann, M. Dolg, H. Stoll, H. Preuss, *Theor. Chim. Acta* **1990**, *123*, 123.
[13] Gaussian 98, M. J. Frisch, G. W. Trucks, H. B. Schlegel, G. E. Scuseria, M. A. Robb, J. R. Cheeseman, V. G. Zakrzewski, J. A. Montgomery, R. E. Stratmann, J. C. Burant, S. Dapprich, J. M. Millam, A. D. Daniels, K. N. Kudin, M. C. Strain, O. Farkas, J. Tomasi, V. Barone, M. Cossi, R. Cammi, B. Mennucci, C. Pomelli, C. Adamo, S. Clifford, J. Ochterski, G. A. Petersson, P. Y. Ayala, Q. Cui, K. Morokuma, D. K. Malick, A. D. Rabuck, K. Raghavachari, J. B. Foresman, J. Cioslowski, J. V. Ortiz, B. B. Stefanov, G. Liu, A. Liashenko, P. Piskorz, I. Komaromi, R. Gomperts, R. L. Martin, D. J. Fox, T. Keith, M. A. Al-Laham, C. Y. Peng, A. Nanayakkara, C. Gonzalez, M. Challacombe, P. M. W. Gill, B. Johnson, W. Chen, M. W. Wong, J. L. Andres, C. Gonzalez, M. Head-Gordon, E. S. Replogle, J. A. Pople, Gaussian, Inc., Pittsburgh, PA, **1998.**

Received June 30, 2003
Early View Article
Published Online December 12, 2003

 © 2004 Wiley-VCH Verlag GmbH & Co. KGaA, Weinheim

Structural Snapshots of a Dynamic Coordination Sphere in Model Complexes for Catechol 1,2-Dioxygenases

Michael Merkel,[a] David Schnieders,[a] Sascha M. Baldeau,[a] and Bernt Krebs*[a]

Keywords: Iron / Tripodal ligands / Coordination modes / Enzymes

A series of mononuclear iron(III) complexes as models for intradiol cleaving catechol dioxygenases has been synthesized. In all six compounds, the iron(III) core is coordinated by the ligand [(6-bromo-2-pyridyl)methyl]bis[(2-pyridyl)methyl]amine (brtpa) which mimics the endogenous ligands of this enzyme class and their dynamic behavior. Its steric hindrance pushes the α-substituted pyridine arm of the ligand away from the coordination site in the presence of nucleophiles. This effect turns the iron-brtpa system into an excellent model system for the first step in the reaction mechanism of intradiol cleaving chatechol dioxygenases. The proton acceptor abilities of the bromopyridyl arm are underlined by a hydrogen bond to a coordinated methanol molecule in one of the new compounds and by base dependent kinetic investigations. The presented model system is an effective catalyst that requires between 0.5 and 1.0 fewer equivalents of external base than most other complexes due to the integration of an internal base.
(© Wiley-VCH Verlag GmbH & Co. KGaA, 69451 Weinheim, Germany, 2004)

Introduction

The metabolism of aromatic compounds by aerobic bacteria plays an important role in the global carbon cycle.[1,2] Catechol dioxygenases are mononuclear non-heme iron enzymes that can be isolated from bacteria. They catalyze the insertion of dioxygen into catechols with simultaneous ring cleavage. With regards to their regioselectivity they are divided into two major subgroups namely the intradiol and the extradiol cleaving enzymes.[3,4] Protocatechuate 3,4-dioxygenase (3,4-PCD) belongs to the class of intradiol cleaving catechol dioxygenases which catalyze the incorporation of dioxygen into catechols yielding derivatives of *cis,cis*-muconic acid. The X-ray crystal structure of this metalloenzyme reveals a trigonal bipyramidal geometry around the iron(III) core.[5,6] The first ligand sphere consists of two histidines and two tyrosines as endogenous protein ligands (His460, His462, Tyr408, Tyr447) and one solvent derived hydroxide ligand. Spectroscopic and electronic structure studies confirm that the axial Tyr447-Fe^{III} bond is weaker than the equatorial tyrosinate-iron(III) bond.[7]

The interaction of a substrate with Fe^{3+} causes the dissociation of the axial tyrosine and the hydroxide ligand leading to a substrate-iron(III) complex that is best described as octahedral with a vacant site (see Figure 1).[8,9] The departing ligands are believed to act as proton acceptors resulting in a dianionic coordination of the substrate. This enhances its ketonization, yielding a transient carbanion or Fe^{II}-semiquinone radical. The subsequent reaction with O_2 yields a peroxy intermediate which is coordinated to the iron through the remaining open coordination site. Decomposition of this peroxy adduct by a Criegee-type rearrangement affords muconic anhydride.

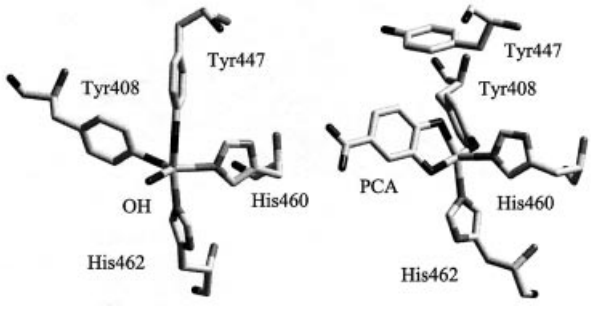

Figure 1. Active site of 3,4-PCD with hydroxide (left) and substrate (right)

In previous studies several functional models have been synthesized in order to gain insight in to the mechanism of catechol cleavage.[10] Whereas in models containing macrocyclic ligands no ligand exchange was observed,[11,12] partial substitutions were reported for coordinated tripodal ligands.[13] Herein we describe 6 crystal structures as well as functional investigations that demonstrate a weak bonding of the substituted arm of [(6-bromo-2-pyridyl)methyl]bis[(2-pyridyl)methyl]amine (brtpa) in iron complexes. The ability to act as an internal base and the replacement of the

[a] Institut für Anorganische und Analytische Chemie der Westfälischen Wilhelms-Universität,
Wilhelm-Klemm-Straße 8, 48149 Münster, Germany
Fax: (internat.) + 49-251-8338366
E-mail: krebs@uni-muenster.de

bromo-substituted pyridine arm by other ligands makes it an excellent functional model for Tyr447 in the enzyme.

Results and Discussion

We were able to characterize six new iron(III) coordination compounds containing the ligand brtpa. In five of these complexes tetrachlorocatecholate (tcc) or tetrabromocatecholate (tbc) was used as a substrate analog, respectively. These catecholates yield compounds that are good structural models for the substrate bound active site of the enzyme and that are not sensitive to air.[14−17]

$[Fe^{III}(brtpa)Br_3]$ (1)

The unit cell of compound **1** consists of four complex molecules, the structure of one such molecule is shown in Figure 2. The structure of **1** is closely related to that of $[Fe^{III}(brtpa)Cl_3]$ reported by Mandon et al.[18] The distorted octahedral coordination sphere of the iron(III) core is composed of three bromide ions and the brtpa ligand. The substituted pyridine does not coordinate, resulting in a tridentate facial coordination mode of the ligand. The three Fe−Br bonds are almost identical [2.447(1), 2.446(1), and 2.441(1) Å] and, as expected, significantly longer than the Fe−Cl bonds in the complex reported by Mandon et al. With respect to the nature of the N donor moieties, the largest Fe−N bond length with a value of 2.298(4) Å occurs between Fe(1) and the tertiary amine nitrogen N(1). Due to their ability to act as π-donors the distances between the nitrogens of the coordinated pyridines and the iron core are significantly shorter [2.197(4) Å and 2.183(4) Å].

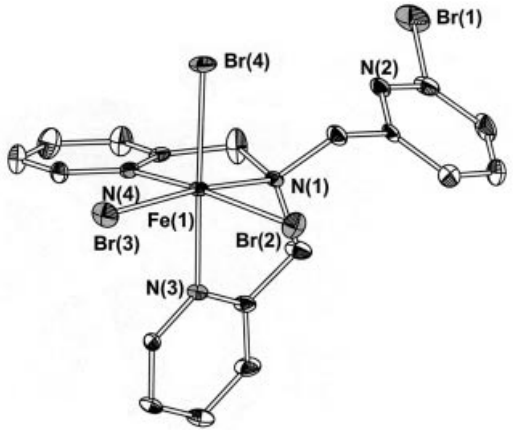

Figure 2. Ellipsoid plot of $[Fe^{III}(brtpa)Br_3]$ (50 % probability); hydrogen atoms omitted for clarity

The existence of five-membered chelate rings causes a distortion of the octahedron towards the tertiary amino group. This is reflected in the low values of the N−Fe−N angles [76.4(2) to 79.8(2)°]. Consequently the angles between the three bromide ligands are expanded [96.1(1) to 99.8(1)°].

$[Fe^{III}(brtpa)(tbc)]ClO_4·H_2O$ (2)

The monoclinic unit cell of compound **2** contains four complex cations, four disordered perchlorates and four water molecules. In contrast to Mandon's $[Fe(brtpa)Cl_3]$ complex[18] and the other iron complexes in this work, compound **2** is the first example of an iron(III) complex in which the brtpa ligand exhibits a tetradentate coordination mode. The remaining coordination sites are occupied by a tetrabromocatecholate dianion (tbc) resulting in a disordered octahedral coordination sphere (Figure 3).

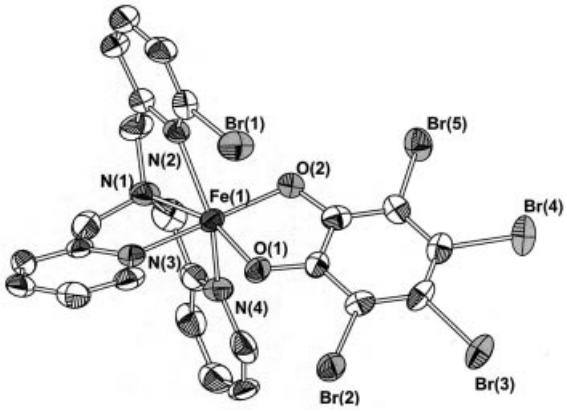

Figure 3. Ellipsoid plot of $[Fe^{III}(brtpa)(tbc)]^+$ (50 % probability); hydrogen atoms omitted for clarity

The similarity of the Fe−O bond lengths [Fe−O(1) = 1.941(5) Å and Fe−O(2) = 1.945(5) Å] demonstrates that the inhibitor substrate coordinates as a dianion rather than a semiquinone. The length of the Fe−N(2) bond [2.220(6) Å] which is the largest Fe−N distance in this complex indicates the weakness of this interaction. The character of this bond originates from the steric demand of the bromo substituent. As a result of this, the O(1)−Fe−N(2) angle is widened to 119.0(2)° which is the largest deviation from the ideal 90° angle and has two effects on the coordination of the catecholate. The first is a twist of 17.8° between the two planes through Fe, N(1), N(3) and Fe, O(1), O(2). Secondly the catecholate is bent down by 12.0° around the O(1)−O(2) axis (see Figure 4). Once again the preorganized five-membered chelate rings of the ligand lead to a significant contraction of the corresponding bond angles.

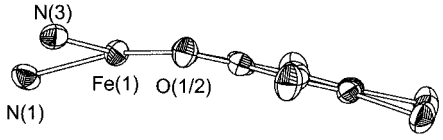

Figure 4. Ellipsoid plot of the catecholate binding in $[Fe^{III}(brtpa)(tbc)]^+$ (50 % probability)

$[Fe^{III}(brtpa)(tcc)(CH_3OH)]ClO_4·CH_3OH$ (3)

Four complex cations, four disordered perchlorate anions and four solvent molecules (methanol) form the unit cell of compound **3**. The iron(III) core is surrounded by the inhibitor substrate tetrachlorocatecholate (tcc), one methanol

 © 2004 Wiley-VCH Verlag GmbH & Co. KGaA, Weinheim

molecule and brtpa which coordinates as a tridentate meridional ligand. The bromo-substituted ligand arm has been displaced by the methanol molecule but participates in an intramolecular hydrogen bond with the proton of the coordinated alcohol function. Thus N(2) is tied at a distance of 2.675(6) Å from O(3) and 3.650(4) Å from the iron core. Although methanol is not a particularly good ligand, hydrogen bonds seem to stabilize its coordination to metal centers.[19] Similar intramolecular hydrogen bonds between metal bound solvent molecules and pyridyl moieties have been reported for copper(II) complexes[20,21] and recently for an iron(III) complex.[22] The Fe−O(3) distance of 2.050(4) Å indicates a weaker Fe−O bond compared with the anionic Fe−O_{tcc} interaction [1.924(3) Å and 1.975(4) Å]. The difference in the Fe−O_{tcc} bonds is a consequence of the *trans* effect of the opposing amine nitrogen and oxygen [O(3)] donors.

Due to the limited bite of five-membered chelate rings, the complex cation in **3** reflects the typical distortion of the octahedral coordination sphere. N(1)−Fe−N(3) [77.2(2)°], N(1)−Fe−N(4) [76.6(2)°], and O(1)−Fe−O(2) [83.3(2)°] are reduced, whereas O(1)−Fe−N(3) [97.8(2)°] and O(1)−Fe−N(4) [108.8(2)°] are widened (Figure 5).

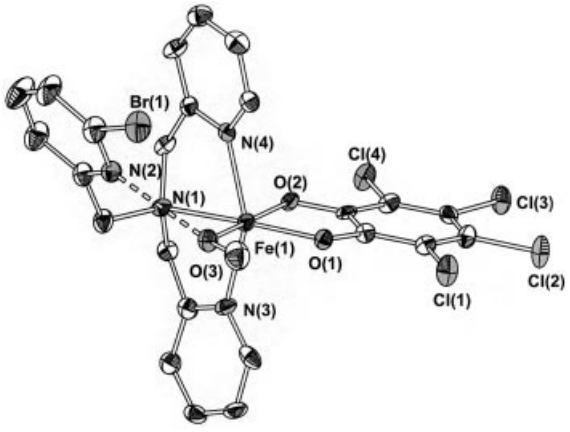

Figure 5. Ellipsoid plot of $[Fe^{III}(brtpa)(tcc)(CH_3OH)]^+$ (50 % probability); hydrogen atoms omitted for clarity

$[Fe^{III}(brtpa)(tcc)Cl]$ (4)

The monoclinic unit cell of compound **4** contains four complex molecules. As in compound **1** the brtpa ligand coordinates in a tridentate facial fashion. The equatorial plane of the octahedron is occupied by the two unsubstituted pyridine arms and the tcc dianion, whereas the axial positions are occupied by the tertiary amine nitrogen and a chloride ligand. As expected, the Fe−N(1) bond is the longest Fe−N bond in this complex [2.337(3) Å]. The slight difference in the Fe−O_{tcc} distance is caused by the asymmetry of the ligand's coordination. The N(1)−C(1) bond is almost in an eclipsed position towards the Fe(1)−O(2) bond, while the Fe(1)−O(1) bond is staggered between N(1)−C(1) and N(1)−C(7). This asymmetry also results in different O(1)−Fe−N(1) and O(2)−Fe−N(1) angles with values of 86.0(2) and 96.7(2)°, respectively. The non coordinating nitrogen atom N(2) of the bromo-substituted ligand arm lies at a distance of 5.278(4) Å from the iron core in this complex (Figure 6).

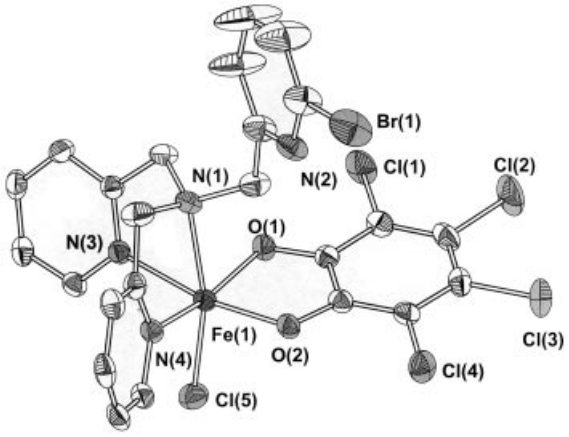

Figure 6. Ellipsoid plot of $[Fe^{III}(brtpa)(tcc)Cl]$ (50 % probability); hydrogen atoms omitted for clarity

$[Fe^{III}(brtpa)(tcc)NO_3]$ (5), $[Fe^{III}(brtpa)(tbc)NO_3]$ (6)

The crystal structures of compounds **5** and **6** show large resemblances to each other. In each of them the unit cell is composed of four iron(III) complexes. The brtpa ligand coordinates in a tridentate facial fashion with its two unsubstituted pyridine units. A nitrate anion and a dianionic catecholate (tcc in **5**; tbc in **6**) complete the octahedral coordination sphere.

The slight difference of 0.02 Å (**5**) and 0.03 Å (**6**) in the iron-catecholate bond lengths is a consequence of the orientation of the non-coordinating bromopyridine arm. This part of the ligand is orientated towards O(2) and thus the O(2)−Fe−N(1) angle is about 12° larger than O(1)−Fe−N(1) in both compounds. Characteristic for tripodal ligands are the long Fe−N(1) distances of 2.260(3) Å (**5**) and 2.252(4) Å (**6**), respectively, and the small angles along the five-membered chelate rings with values of less than 80°.

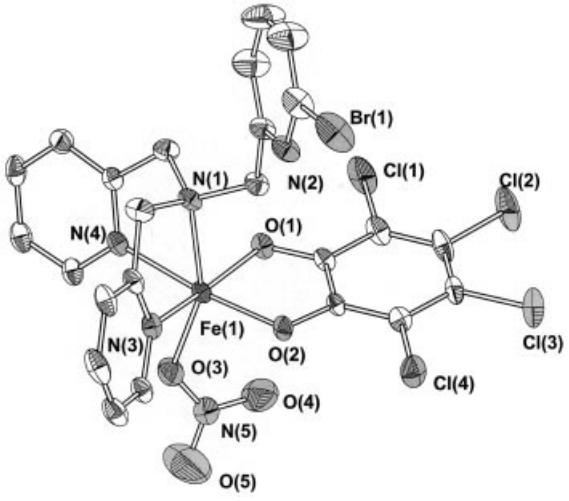

Figure 7. Ellipsoid plot of $[Fe^{III}(brtpa)(tcc)NO_3]$ (50 % probability); hydrogen atoms omitted for clarity

 © 2004 Wiley-VCH Verlag GmbH & Co. KGaA, Weinheim

Table 1. Selected bond lengths [Å] and angles [°] in **1**−**6**

1					
Fe(1)−Br(2)	2.447(1)	Br(2)−Fe(1)−Br(3)	96.1(1)	Br(3)−Fe(1)−N(4)	95.0(1)
Fe(1)−Br(3)	2.446(1)	Br(2)−Fe(1)−Br(4)	99.8(1)	Br(4)−Fe(1)−N(1)	90.9(1)
Fe(1)−Br(4)	2.441(1)	Br(2)−Fe(1)−N(1)	90.0(1)	Br(4)−Fe(1)−N(3)	164.3(1)
Fe(1)−N(1)	2.298(4)	Br(2)−Fe(1)−N(3)	89.5(1)	Br(4)−Fe(1)−N(4)	88.6(1)
Fe(1)−N(3)	2.197(4)	Br(2)−Fe(1)−N(4)	165.1(1)	N(1)−Fe(1)−N(3)	76.4(2)
Fe(1)−N(4)	2.183(4)	Br(3)−Fe(1)−Br(4)	97.4(1)	N(1)−Fe(1)−N(4)	77.5(2)
		Br(3)−Fe(1)−N(1)	168.7(1)	N(3)−Fe(1)−N(4)	79.8(2)
		Br(3)−Fe(1)−N(3)	94.1(1)		
2					
Fe(1)−O(1)	1.941(5)	O(1)−Fe(1)−O(2)	83.2(2)	O(2)−Fe(1)−N(4)	94.9(2)
Fe(1)−O(2)	1.945(5)	O(1)−Fe(1)−N(1)	160.7(2)	N(1)−Fe(1)−N(2)	75.4(2)
Fe(1)−N(1)	2.206(7)	O(1)−Fe(1)−N(2)	119.0(2)	N(1)−Fe(1)−N(3)	80.5(3)
Fe(1)−N(2)	2.220(6)	O(1)−Fe(1)−N(3)	87.7(2)	N(1)−Fe(1)−N(4)	75.4(3)
Fe(1)−N(3)	2.113(6)	O(1)−Fe(1)−N(4)	90.5(2)	N(2)−Fe(1)−N(3)	84.7(2)
Fe(1)−N(4)	2.150(7)	O(2)−Fe(1)−N(1)	110.7(2)	N(2)−Fe(1)−N(4)	150.4(3)
		O(2)−Fe(1)−N(2)	91.2(2)	N(3)−Fe(1)−N(4)	94.9(2)
		O(2)−Fe(1)−N(3)	166.7(2)		
3					
Fe(1)−O(1)	1.924(3)	O(1)−Fe(1)−O(2)	83.3(2)	O(2)−Fe(1)−N(4)	90.7(2)
Fe(1)−O(2)	1.975(4)	O(1)−Fe(1)−O(3)	91.7(2)	O(3)−Fe(1)−N(1)	97.0(2)
Fe(1)−O(3)	2.050(4)	O(1)−Fe(1)−N(1)	170.0(2)	O(3)−Fe(1)−N(3)	91.0(2)
Fe(1)−N(1)	2.245(4)	O(1)−Fe(1)−N(3)	97.8(2)	O(3)−Fe(1)−N(4)	87.7(2)
Fe(1)−N(3)	2.094(5)	O(1)−Fe(1)−N(4)	108.8(2)	N(1)−Fe(1)−N(3)	77.2(2)
Fe(1)−N(4)	2.108(4)	O(2)−Fe(1)−O(3)	173.9(2)	N(1)−Fe(1)−N(4)	76.6(2)
Fe(1)−N(2)	3.650(4)	O(2)−Fe(1)−N(1)	88.3(2)	N(3)−Fe(1)−N(4)	153.4(2)
O(3)−N(2)	2.675(6)	O(2)−Fe(1)−N(3)	93.1(2)		
4					
Fe(1)−Cl(5)	2.310(2)	Cl(5)−Fe(1)−O(1)	101.7(1)	O(1)−Fe(1)−N(4)	159.1(2)
Fe(1)−O(1)	1.954(3)	Cl(5)−Fe(1)−O(2)	95.4(1)	O(2)−Fe(1)−N(1)	96.7(2)
Fe(1)−O(2)	1.967(3)	Cl(5)−Fe(1)−N(1)	166.3(1)	O(2)−Fe(1)−N(3)	169.1(2)
Fe(1)−N(1)	2.337(3)	Cl(5)−Fe(1)−N(3)	94.4(1)	O(2)−Fe(1)−N(4)	89.0(2)
Fe(1)−N(3)	2.142(3)	Cl(5)−Fe(1)−N(4)	98.3(1)	N(1)−Fe(1)−N(3)	74.1(2)
Fe(1)−N(4)	2.141(3)	O(1)−Fe(1)−O(2)	83.1(2)	N(1)−Fe(1)−N(4)	75.6(2)
Fe(1)−N(2)	5.278(4)	O(1)−Fe(1)−N(1)	86.0(2)	N(3)−Fe(1)−N(4)	94.1(2)
		O(1)−Fe(1)−N(3)	90.4(2)		
5					
Fe(1)−O(1)	1.946(3)	O(1)−Fe(1)−O(2)	82.9(2)	O(2)−Fe(1)−N(4)	173.8(2)
Fe(1)−O(2)	1.967(3)	O(1)−Fe(1)−O(3)	107.2(2)	O(3)−Fe(1)−N(1)	155.8(2)
Fe(1)−O(3)	1.999(3)	O(1)−Fe(1)−N(1)	89.1(2)	O(3)−Fe(1)−N(3)	89.6(2)
Fe(1)−N(1)	2.260(3)	O(1)−Fe(1)−N(3)	161.9(2)	O(3)−Fe(1)−N(4)	85.7(2)
Fe(1)−N(3)	2.118(4)	O(1)−Fe(1)−N(4)	92.1(2)	N(1)−Fe(1)−N(3)	77.5(2)
Fe(1)−N(4)	2.146(4)	O(2)−Fe(1)−O(3)	99.1(2)	N(1)−Fe(1)−N(4)	75.6(2)
		O(2)−Fe(1)−N(1)	100.7(2)	N(3)−Fe(1)−N(4)	96.2(2)
		O(2)−Fe(1)−N(3)	87.7(2)		
6					
Fe(1)−O(1)	1.940(3)	O(1)−Fe(1)−O(2)	82.9(2)	O(2)−Fe(1)−N(4)	173.3(2)
Fe(1)−O(2)	1.970(3)	O(1)−Fe(1)−O(3)	107.7(2)	O(3)−Fe(1)−N(1)	155.5(2)
Fe(1)−O(3)	1.991(3)	O(1)−Fe(1)−N(1)	88.6(2)	O(3)−Fe(1)−N(3)	89.5(2)
Fe(1)−N(1)	2.252(4)	O(1)−Fe(1)−N(3)	161.9(2)	O(3)−Fe(1)−N(4)	85.6(2)
Fe(1)−N(3)	2.131(3)	O(1)−Fe(1)−N(4)	91.2(2)	N(1)−Fe(1)−N(3)	77.2(2)
Fe(1)−N(4)	2.146(4)	O(2)−Fe(1)−O(3)	99.0(2)	N(1)−Fe(1)−N(4)	75.6(2)
		O(2)−Fe(1)−N(1)	101.2(2)	N(3)−Fe(1)−N(4)	96.0(2)
		O(2)−Fe(1)−N(3)	88.9(2)		

 © 2004 Wiley-VCH Verlag GmbH & Co. KGaA, Weinheim

The large resemblances of **5** and **6** demonstrate that it is legitimate to compare compounds **2**, **3**, and **4** even though different inhibitor substrates are involved. As a representative of the two isostructural compounds the crystal structure of **5** is shown in Figure 7.

Selected bond lengths and angles for the iron(III) complexes are reported in Table 1.

Oxygenation of Bonded dbc in the Presence of Dioxygen

Stoichiometric Kinetic Studies

In order to gain information on the catechol cleavage activity, the decrease in the lower energy LMCT band was

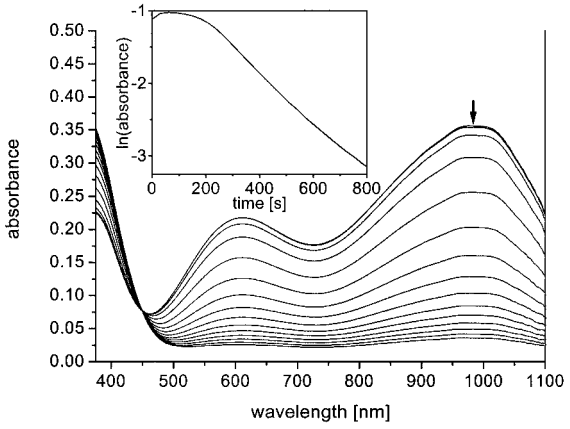

Figure 8. Progress of the reaction of $[Fe^{III}(brtpa)(dbc)]^+$ with dioxygen; inset: plot of ln(absorption)vs. time for this reaction (ambient temperature; 1.5 equiv. of base)

monitored by UV/Vis-spectroscopy. Figure 8 shows the decrease of this band during the reaction of in situ prepared $[Fe(brtpa)(dbc)]^+$ (where dbc = 3,5-di-*tert*-butylcatecholate) with dioxygen which is present in methanol saturated with air. A greater than tenfold excess of dioxygen ensures pseudo-first-order kinetics for the complete reaction and therefore a linear dependency of the plot of ln(absorbance) vs. time (inset in Figure 8) can be observed. By considering the concentration of dioxygen in air saturated methanol at ambient temperature, the reaction rate constant k can be obtained from the slope of this linear graph.

Different amounts of piperidine were added to the reaction mixture to ensure a dianionic binding of the substrate and thus a high reactivity. As can be seen from Figure 9, the highest reactivity was reached when 1.5 equivalents of base were added to the reaction mixture. Although complexes derived from similar tripodal ligands show catechol dioxygenase activity under the same conditions the highest activity can be observed upon addition of 2.0−2.5 equivalents of base in these systems.[14,16] The lower demand of base in the reaction of the new model compound can be explained by the peculiarity of the ligand and its weakly coordinated bromopyridine unit. As indicated by the intramolecular hydrogen bond in **3**, this unit can act as a proton acceptor and therefore as an internal base. Furthermore this behavior was confirmed by spectrophotometric titrations of a complex-catechol mixture with piperidine in which only 1.8 equivalents of the base were needed for an optimal dianionic binding of the catechol. The closely related me_1tpa system, where the bromine in brtpa is substituted by a methyl group, needs significantly more (2.4 equiv.) base to bind the catechol.[16]

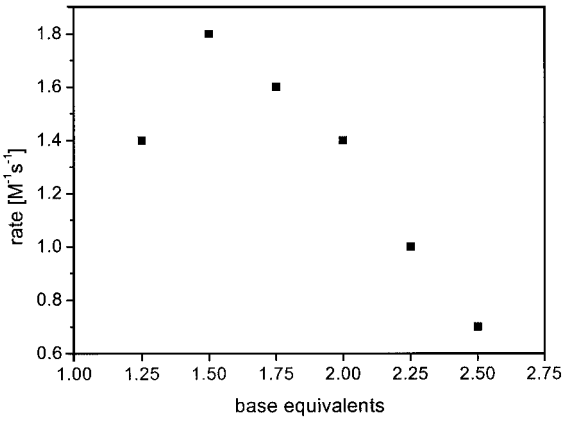

Figure 9. Correlation of reaction rates *k* and added equivalents of piperidine

As shown in Figure 9, a maximum reaction rate of 1.8 $M^{-1}s^{-1}$ was found for the iron brtpa system. This is of the same order of magnitude as those reported for other model compounds containing tripodal ligands. (For review articles see ref.[10])

Taking into consideration that Ogo et al. reported a model system in which coordinated acetylacetonate is used as an internal base,[23] it should be possible to generate the iron(III) complex $[Fe(brtpa)(acac)]^{2+}$ which allows cleavage of catechols without any further addition of base.

Identification of the Cleavage Products

The oxygenated products were characterized by GC/MS as well as ^1H NMR spectroscopy. Neither of these methods showed evidence for the undesired products of simple oxidation (quinones) or extradiol cleavage. The amount of external base in the reaction mixture (1.5 or 2.0 equiv.) had no effect on the product composition. In acetonitrile and dichloromethane, muconic anhydride was found as the exclusive reaction product whereas in methanol a mixture of muconic anhydride and its methanolysis product was detected by GC/MS. All results demonstrate that the present model system exclusively catalyzes the intradiol cleavage reaction.

Catalytic Reactions

The identification of the cleavage products was also performed for catalytic reactions. The substrate-catechol ratio in these experiments was 10:1 and 100:1, respectively. Even for the 100 fold excess of substrate, we observed complete conversion of the catechol. The GC/MS analysis revealed that only the desired intradiol cleavage products were formed in the reaction.

 © 2004 Wiley-VCH Verlag GmbH & Co. KGaA, Weinheim

Conclusion

With the crystal structures and functional investigations reported in this work we have established an excellent model system for the first steps in the reaction mechanism of catechol dioxygenases. The substituted pyridine moiety is a good mimic for the departing tyrosine ligand in the enzyme. This was demonstrated by the different positions of the ligand arm resulting in an increase of the corresponding Fe−N distance from 2.22 to 5.28 Å. Furthermore, the base dependent kinetic investigations revealed that the bromopyridine arm acts as an internal base. This behavior is confirmed by the presence of a hydrogen bond in **3**.

Experimental Section

Materials: All chemicals were purchased from commercial sources and used without any further purification.

Physical Measurements: ^{1}H and ^{13}C NMR spectra were measured on a Bruker WH 300 spectrometer. UV/Vis spectroscopy was performed on a Hewlett−Packard 8453 diode array spectrometer.

Syntheses

[(6-Bromo-2-pyridyl)methyl][(2-pyridyl)methyl]amine (brbpa): 6-Bromo-2-pyridine carboxaldehyde (20.0 g, 107.5 mmol) was stirred in methanol (100 mL). After slow addition of 2-(aminomethyl)pyridine (11.6 g, 107.5 mmol, 11.2 mL) the solution was stirred for a further 2 h. At 0 °C sodium borohydride (3.0 g, 79.3 mmol) was carefully added. The reaction mixture was stirred overnight and allowed to warm to room temperature. The mixture was acidified with hydrochloric acid to pH 1 and extracted with chloroform (5 × 40 mL) to separate impurities and side products. In order to neutralize the hydrochloride, the pH was adjusted to 8 with an aqueous solution of sodium hydroxide and the free amine was extracted with chloroform (5 × 40 mL). The combined organic layers were dried over $MgSO_4$ and the solvent was removed in vacuo yielding 24.62 g (88.5 mmol; 82 %) of a yellow oil which was used without further purification. ^{1}H NMR (400 MHz, $CDCl_3$): δ = 3.95 (s, 2 H, CH_2), 3.96 (s, 2 H, CH_2), 7.16 (m, 1 H, CH), 7.33 (m, 3 H, CH), 7.45 (t, 1 H, CH), 7.60 (m, 1 H, CH), 8.54 (d, 1 H, CH) ppm. ^{13}C NMR (100 MHz, $CDCl_3$): δ = 54.3, 54.7, 121.0, 122.0, 122.3, 126.2, 136.4, 138.8, 141.7, 149.4 159.6, 161.8.

[(6-Bromo-2-pyridyl)methyl]bis[(2-pyridyl)methyl]amine (brtpa): To a stirred mixture of brbpa (14.33 g, 51.5 mmol) and 2-picolyl chloride hydrochloride (8.45 g, 51.5 mmol) in THF (100 mL) was added triethylamine (14.4 mL, 10.5 g, 103 mmol). After heating to reflux for 48 h the mixture was cooled to room temperature and the resultant precipitate removed by filtration. The red solution was concentrated in vacuo. The residual red oil was extracted with boiling diethyl ether and upon cooling to −18 °C the off-white product precipitated. Yield 13.69 g (37.1 mmol; 72 %). NMR spectroscopic data have already been published.[24]

[Fe^{III}(brtpa)Br$_3$] (1): Iron(III) bromide (30 mg; 0.1 mmol) and brtpa (37 mg; 0.1 mmol) were stirred in acetone/methanol (6 mL, 1:1 mixture) for a few minutes. The mixture was then heated to reflux for a few seconds and filtered. Red crystals of complex **1** formed

Table 2. Crystallographic data and experimental details {$w = 1/[\sigma^2(F_o^2) + (xP)^2 + 0P]$, $P = (F_o^2 + 2F_c^2)/3$; **1**: $x = 0.0993$; **2**: $x = 0.0660$; **3**: $x = 0.0643$; **4**: $x = 0.0607$; **5**: $x = 0.1473$; **6**: $x = 0.0493$}

Compound	**1**	**2**	**3**	**4**	**5**	**6**
Empirical formula	$C_{18}H_{17}Br_4FeN_4$	$C_{24}H_{19}Br_5ClFeN_4O_7$	$C_{26}H_{25}BrCl_5FeN_4O_8$	$C_{24}H_{17}BrCl_5FeN_4O_2$	$C_{24}H_{17}BrCl_4FeN_5O_5$	$C_{24}H_{17}Br_5FeN_5O_5$
M_r	664.85	966.26	834.51	706.43	732.99	910.83
Temperature [K]	200(2)	100(2)	100(2)	183(2)	200(2)	193(2)
Radiation (λ [Å])	Cu-K_α (1.54178)	Cu-K_α (1.54178)	Cu-K_α (1.54178)	Cu-K_α (1.54178)	Cu-K_α (1.54178)	Cu-K_α (1.54178)
Crystal shape	red plate	dark blue rod	dark blue rod	red plate	red plate	red rod
Crystal size [mm]	0.32 × 0.15 × 0.05	0.34 × 0.12 × 0.09	0.29 × 0.08 × 0.08	0.30 × 0.20 × 0.20	0.45 × 0.34 × 0.10	0.35 × 0.11 × 0.06
Crystal system	monoclinic	monoclinic	monoclinic	monoclinic	monoclinic	monoclinic
Space group	$P2_1/c$ (No. 14)	$P2_1/c$ (No. 14)	$P2_1/n$ (No. 14)	$P2_1/n$ (No. 14)	$P2_1/n$ (No. 14)	$P2_1/n$ (No. 14)
a [Å]	7.42730(10)	19.6180(5)	8.4029(3)	11.9632(2)	12.1670(1)	12.4211(1)
b [Å]	19.4257(2)	9.1403(3)	19.6182(5)	15.5977(2)	15.3780(2)	15.5936(2)
c [Å]	14.86490(10)	17.4979(5)	19.1890(5)	15.1630(2)	15.2474(2)	15.4273(2)
β [°]	96.3360(10)	108.688(2)	95.286(2)	110.780(1)	107.089(1)	108.670(1)
V [Å^3]	2131.61(4)	2972.20(15)	3149.85(16)	2645.34(7)	2726.90(6)	2830.87(6)
Z	4	4	4	4	4	4
$\rho_{calcd.}$ [g·cm^{-3}]	2.072	2.155	1.760	1.774	1.785	2.137
μ [mm^{-1}]	14.547	13.220	9.712	11.260	10.167	12.936
F(000)	1276	1852	1676	1404	1460	1748
Scan range θ [°]	3.76 to 71.42	2.38 to 71.22	3.23 to 71.33	4.07 to 71.17	4.11 to 71.64	4.00 to 71.13
Index ranges	$-9 \le h \le 7$	$-21 \le h \le 23$	$-9 \le h \le 10$	$-14 \le h \le 13$	$-14 \le h \le 14$	$-13 \le h \le 14$
	$-23 \le k \le 23$	$-9 \le k \le 11$	$-22 \le k \le 23$	$-19 \le k \le 16$	$-18 \le k \le 17$	$-18 \le k \le 19$
	$-16 \le l \le 17$	$-21 \le l \le 21$	$-23 \le l \le 23$	$-18 \le l \le 15$	$-18 \le l \le 17$	$-18 \le l \le 17$
Reflections collected	12272	16319	17671	14982	15646	16001
Unique reflections	3994	5196	5820	4486	5046	5272
Reflections $I > 2\sigma(I)$	3668	3302	3712	3397	4264	4085
R_{int}	0.0793	0.0765	0.0708	0.0551	0.1187	0.0633
Data/restraints/parameters	3994/0/244	5196/0/398	5820/0/427	4486/0/334	5046/0/361	5272/0/371
Goodness-of-fit on F^2	1.032	0.966	0.952	0.984	1.032	0.944
Final R indices [$I > 2\sigma(I)$]	$R1 = 0.0491$	$R1 = 0.0533$	$R1 = 0.0554$	$R1 = 0.0425$	$R1 = 0.0708$	$R1 = 0.0395$
	$wR2 = 0.1312$	$wR2 = 0.1269$	$wR2 = 0.1280$	$wR2 = 0.1083$	$wR2 = 0.1885$	$wR2 = 0.0919$
R indices (all data)	$R1 = 0.0518$	$R1 = 0.0865$	$R1 = 0.0884$	$R1 = 0.0550$	$R1 = 0.0784$	$R1 = 0.0512$
	$wR2 = 0.1335$	$wR2 = 0.1373$	$wR2 = 0.1378$	$wR2 = 0.1126$	$wR2 = 0.1958$	$wR2 = 0.0957$
Largest diff. peak/hole [e·Å^{-3}]	1.138/−1.345	1.028/−1.095	0.790/−0.790	0.557/−0.639	1.015/−1.507	0.511/−1.108

 © 2004 Wiley-VCH Verlag GmbH & Co. KGaA, Weinheim

upon slow cooling. $C_{18}H_{17}Br_4FeN_4$ (664.82 g/mol). Crystal data are given in Table 2.

[Fe^{III}(brtpa)(tbc)]ClO_4·H_2O (2): To a stirred solution of iron(III) perchlorate hydrate (37 mg; 0.1 mmol) and brtpa (37 mg; 0.1 mmol) in of acetone (7 mL) was added tetrabromocatechol (42 mg; 0.1 mmol). After addition of triethylamine (20 mg, 28 μL, 0.2 mmol) the mixture was stirred for a few minutes and filtered. Upon slow diffusion of diethyl ether into the solution dark blue crystals of **2** preciptiated. $C_{24}H_{19}Br_5ClFeN_4O_7$ (966.26 g/mol). Crystal data are given in Table 2.

[Fe^{III}(brtpa)(tcc)(CH_3OH)]ClO_4·CH_3OH (3): $Fe(ClO_4)_3$·H_2O (37 mg; 0.1 mmol) and brtpa (37 mg; 0.1 mmol) were dissolved in methanol/acetone (9 mL, 3:1 mixture). After addition of tetrachlorochatechol monohydrate (26 mg; 0.1 mmol) and triethylamine (28 μL, 20 mg; 0.2 mmol) the mixture was stirred for a few minutes and filtered. Upon slow diffusion of diethyl ether into the solution dark blue crystals of compound **3** precipitated. $C_{26}H_{25}BrCl_5FeN_4O_8$ (834.52 g/mol). Crystal data are given in Table 2.

[Fe^{III}(brtpa)(tcc)Cl] (4): To a stirred solution of $FeCl_3$ (16 mg; 0.1 mmol), brtpa (37 mg; 0.1 mmol) and tetrachlorocatechol monohydrate (26 mg; 0.1 mmol) in methanol/acetone (7 mL, 1:3 mixture) was added triethylamine (20 mg, 28 μL, 0.2 mmol). After heating to reflux for a few seconds the mixture was filtered and slow diffusion of diethyl ether into the solution yielded red plates of complex **4**. $C_{24}H_{17}BrCl_5FeN_4O_2$ (706.44 g/mol). Crystal data are given in Table 2.

[Fe^{III}(brtpa)(tcc)NO_3] (5): To a stirred solution of $Fe(NO_3)_3$·$9H_2O$ (40 mg; 0.1 mmol), brtpa (37 mg; 0.1 mmol) and tetrachlorocatechol monohydrate (26 mg; 0.1 mmol) in methanol/acetone (7 mL, 3:1 mixture) was added triethylamine (20 mg, 28 μL, 0.2 mmol). After heating to reflux for a few seconds the mixture was filtered and slow diffusion of diethyl ether into the solution yielded red crystals of complex **5**. $C_{24}H_{17}Br_5FeN_5O_5$ (910.80 g/mol). Crystal data are given in Table 2.

[Fe^{III}(brtpa)(tbc)NO_3] (6) To a stirred solution of $Fe(NO_3)_3$·$9H_2O$ (40 mg; 0.1 mmol), brtpa (37 mg; 0.1 mmol) and tetrabromocatechol (42 mg; 0.1 mmol) in methanol/acetone (9 mL, 1:1 mixture) was added triethylamine (20 mg, 28 μL, 0.2 mmol). After heating to reflux for a few seconds the mixture was filtered and slow diffusion of diethyl ether into the solution yielded red plates of complex **6**. $C_{24}H_{17}BrCl_4FeN_5O_5$ (732.99 g/mol). Crystal data are given in Table 2.

Stoichiometric Kinetic Studies: The catechol cleavage activity of an in situ prepared complex solution was tested under addition of between 1.0 and 2.5 equivalents of piperidine as an external base. To a $2{\cdot}10^{-4}$ mol·L^{-1} methanolic solution (2 mL) consisting of $Fe(ClO_4)_3$·H_2O and the ligand was added a $2{\cdot}10^{-2}$ mol·L^{-1} (1 equivalent) solution of 3,5-H_2dbc (0.02 mL). The amount of base added to the reaction mixture was varied from 0.02 mL to 0.05 mL (1.0−2.5 equiv.; increment 0.005 mL; 0.25 equiv.) of a $2{\cdot}10^{-2}$ mol·L^{-1} solution. The decomposition of the complexes was followed at least three times by UV/Vis spectroscopy. Spectrophotometric titrations were carried out with the same solutions in a flow cell under an argon atmosphere.

Identification of the Cleavage Products

Stoichiometric Reactions: Identification of the reaction products was also carried out in presence of different amounts of base and in different organic solvents (dichloromethane, acetonitrile and methanol). To a stirred solution of $Fe(ClO_4)$·H_2O, the ligand brtpa and catechol (0.2 mmol) was added 1.5 or 2.0 equivalents of piperidine, respectively. After all catechol had reacted the solvent was evaporated under reduced pressure at ambient temperature. The iron complex was removed by silica gel filtration (CH_2Cl_2/$CHCl_3$, 1:2). After evaporation of the solvent (ambient temperature) the products were dried in vacuo and identified by GC/MS-coupling and ^{1}H NMR spectroscopy.

Catalytic Reactions: The reactions were carried out in acetonitrile solutions. To a stirred complex solution (0.1 and 0.01 mmol dissolved in 50 mL, respectively) were added 3,5-H_2dbc (222.3 mg, 1 mmol) and 1.5 equiv. of piperidine (relative to the iron complex). To ensure fast reactions, dioxygen was bubbled through the reaction mixture. Workup of the oxygenated products was done according to the procedure described for the stoichiometric reactions.

X-ray Crystal Structures

Intensity data of all complexes were collected on a Bruker AXS SMART 6000 CCD diffractometer (Cu-K_α, λ = 1.54178 Å, Göbel mirror) using the ω-scan technique. The collected reflections were corrected for absorption effects.[25] All structures were solved by direct methods and refined by full-matrix least-squares methods on F^2.[26] Further data collection parameters are summarized in Table 2.

CCDC-213838 to -213843 contain the supplementary crystallographic data for this paper. These data can be obtained free of charge at www.ccdc.cam.ac.uk/conts/retrieving.html [or from the Cambridge Crystallographic Data Center, 12, Union Road, Cambridge CB2 1EZ, UK; Fax: (internat.) +44-1223-336-033; E-mail: deposit@ccdc.cam.ac.uk].

Acknowledgments

Financial support from the Deutsche Forschungsgemeinschaft, the Fonds der Chemischen Industrie and the Bundesminsterium für Bildung und Forschung is gratefully acknowledged. M. M. thanks the University of Münster for a graduate fellowship.

[1] L. Que, Jr., R. Y. N. Ho, *Chem. Rev.* **1996**, *96*, 2607.
[2] T. D. H. Bugg, C. J. Winfield, *Nat. Prod. Rep.* **1998**, *15*, 513.
[3] E. F. Elstner, *Der Sauerstoff*, Wissenschaftsverlag, Mannheim, Wien, Zürich, **1990**.
[4] L. Que, Jr., *Bioinorganic Catalysis* (Eds.: J. Reedijk, E. Bouwman), 2nd ed., Marcel Dekker Inc., New York, Basel, **1999**.
[5] D. H. Ohlendorf, J. D. Lipscomb, P. C. Weber, *Nature* **1988**, *336*, 403.
[6] D. H. Ohlendorf, A. M. Orville, J. D. Lipscomb, *J. Mol. Biol.* **1994**, *244*, 586.
[7] M. I. Davis, A. M. Orville, F. Neese, J. M. Zaleski, J. D. Lipscomb, E. I. Solomon, *J. Am. Chem. Soc.* **2002**, *124*, 602.
[8] M. W. Vetting, D. A. D'Argenio, L. N. Ornston, D. H. Ohlendorf, *Biochemistry* **2000**, *39*, 7943.
[9] A. M. Orville, J. D. Lipscomb, D. H. Ohlendorf, *Biochemistry* **1997**, *36*, 10052.
[10] Review Articles: ref.[1]; R. Yamahara, S. Ogo, H. Masuda, Y. Watanabe, *J. Inorg. Biochem.* **2002**, *88*, 284.
[11] W. O. Koch, H.-J. Krüger, *Angew. Chem.* **1995**, *107*, 2928; *Angew. Chem. Int. Ed. Engl.* **1995**, *34*, 2671.
[12] N. Raffard, R. Carina, A. J. Simaan, J. Sainton, E. Rivière, L. Tchertanov, S. Bourcier, G. Bouchoux, M. Delroisse, F. Banse, J.-J. Girerd, *Eur. J. Inorg. Chem.* **2001**, 2249.
[13] R. R. Jacobson, Z. Tyeklar, A. Farooq, K. D. Karlin, S. Liu, J. Zubieta, *J. Am. Chem. Soc.* **1988**, *110*, 3690.

 © 2004 Wiley-VCH Verlag GmbH & Co. KGaA, Weinheim

[14] M. Pascaly, M. Duda, A. Rompel, B. H. Sift, W. Meyer-Klaucke, B. Krebs, *Inorg. Chim. Acta* **1999**, *291*, 289.
[15] F. Schweppe, H. Sirges, M. Pascaly, M. Duda, Ç. Nazikkol, W. Steinforth, B. Krebs, *Peroxide Chemistry. Mechanistic and Preparative Aspects of Oxygen Transfer* (Ed.: W. Adam), Wiley VCH, Weinheim, **2000**, 232.
[16] M. Pascaly, M. Duda, F. Schweppe, K. Zurlinden, F. K. Müller, B. Krebs, *J. Chem. Soc., Dalton Trans.* **2001**, 828.
[17] M. Merkel, F. K. Müller, B. Krebs, *Inorg. Chim. Acta* **2002**, *337*, 308.
[18] D. Mandon, A. Nopper, T. Litrol, S. Goetz, *Inorg. Chem.* **2001**, *40*, 4803.
[19] C. J. Boxwell, P. H. Walton, *Chem. Commun.* **1999**, 1647.
[20] S. P. Foxon, O. Walter, S. Schindler, *Eur. J. Inorg. Chem.* **2002**, 111.
[21] J. M. Rowland, M. M. Olmstead, P. K. Mascharak, *Inorg. Chem.* **2000**, *39*, 5326.
[22] S. Zhu, W. W. Brennessel, R. G. Harrison, L. Que, Jr., *Inorg. Chim. Acta*, in press.
[23] R. Yamahara, S. Ogo, Y. Watanabe, T. Funabiki, K. Jitsukawa, H. Masuda, H. Einaga, *Inorg. Chim. Acta* **2000**, *300*, 587.
[24] C.-L. Chuang, O. dos Santos, X. Xu, J. W. Canary, *Inorg. Chem.* **1997**, *36*, 1967.
[25] *Siemens Area Detector Absorption Correction,* Siemens.
[26] G. M. Sheldrick, *SHELX-97*, University of Göttingen, **1997**.

Received July 1, 2003
Early View Article
Published Online December 12, 2003

 © 2004 Wiley-VCH Verlag GmbH & Co. KGaA, Weinheim

Tandem Palladium-Catalyzed Cyclocarbonylation of Isolimonene: A Mechanistic Investigation and Theoretical Calculations on the Fully Diastereoselective Step

Géraldine Lenoble,[a] Corinne Lacaze-Dufaure,[b] Martine Urrutigoïty,[a] Claude Mijoule,[b] and Philippe Kalck*[a]

Keywords: Asymmetric induction / Cyclocarbonylation / Density functional calculations / Homogeneous catalysis / NMR spectroscopy / Palladium

Cyclocarbonylation of isolimonene catalyzed by complexes of the type $[HPd(SnCl_3)L_2]$ provides two cyclopentanone isomers (**2a** and **2b**) containing two new stereogenic centers with a good diastereomeric excess (up to 69 % with L_2 = dppf). These results show that chiral phosphane ligands are not necessary to ensure asymmetric induction. The diastereomeric excess is due, in fact, to the substrate itself, assisted by the steric hindrance of the diphosphanes. A full characterization of the two isomers by ^1H, ^{13}C and DPFGSE NOE NMR spectroscopy gives all the signal assignations and all the positions of the substituents of interest on the chiral carbon atoms. In order to have a better understanding of the catalytic process, we also present a density functional study of the crucial intermediate species **4** involved in the proposed catalytic cycle. Our calculations show that there is no coordination of the C=C bond in an *exo* mode. Conversely, we have found a pentacoordinate species with a trigonal bipyramidal geometry in which the C=C bond is coordinated in an *endo* mode. Selected bond lengths and bond orders are reported. The calculated net charge distribution supports the cyclization process, which proceeds through a C–C(O) and a C–Pd coupling. A β-hydride elimination reaction of **4** provides the two **2a** and **2b** isomers.

(© Wiley-VCH Verlag GmbH & Co. KGaA, 69451 Weinheim, Germany, 2004)

Introduction

Carbon monoxide is a very powerful building block in organic synthesis, provided it can be inserted into a framework with high selectivity. For several years we have used this strategy to functionalize monoterpenes.[1] Particularly interesting are the tandem reactions in which functionality already present on the terpene reacts with an active intermediate resulting from the insertion of carbon monoxide.[2] Recently, we have specially focused our attention on the cyclocarbonylation of isolimonene, where the endocyclic carbon-carbon double bond is involved in the process; preliminary results have been reported.[3] Rhodium and palladium play a central role in such carbonylation reactions and many papers have reported the catalytic activity of complexes such as $[HRh(CO)L_3]$ or $[PdCl_2L_2]$.[4] Palladium complexes, often with $SnCl_2$ as co-catalyst, are active in the alkoxycarbonylation of alkenes.[5] During the nineties, great effort went into developing enantio- or diastereoselective catalysts by introduction of chiral ligands into the coordination sphere of a metal.[6] Our studies on the carbonylation of (1*R*,2*S*,5*R*)-isopulegol, to provide the corresponding lactone, and our preliminary results on the carbonylation of (1*R*,4*R*)-isolimonene [(3*R*,6*R*)-3-isopropenyl-6-methylcyclohexene] have shown that the introduction of a chiral diphosphane ligand does not influence the diastereoselectivity of the two cyclocarbonylation reactions of interest.[2,3] Thus, the enantiofacial selectivity should be induced by the chiral substrate itself. The situation of isolimonene appeared to us particularly interesting because, of the three chiral centers present in the resulting product, two of them (C1 and C5 in Scheme 1) are obtained with exclusively one configuration (1*R* and 5*S*). Thus, the diastereomeric excess results in fact from an enantiomeric excess at C4 to provide **2a** and **2b** of Scheme 1.

In order to understand why the cyclization reaction catalyzed by palladium occurs exclusively at the C2 atom of isolimonene (which becomes C1 in the resulting product, see Scheme 1) and provides only the *R* configuration, we have performed quantum chemical calculations using the density functional theory (DFT) on the main intermediate which would give the enantioselective cyclization step.

[a] Laboratoire de Catalyse, Chimie Fine et Polymères, Ecole Nationale Supérieure des Ingénieurs en Arts Chimiques et Technologiques
118 route de Narbonne, 31077 Toulouse Cedex 4, France
Fax: (internat.) + 33-5-62885600
E-mail: Philippe.Kalck@ensiacet.fr
[b] CIRIMAT, Laboratoire des Interfaces et Matériaux, Ecole Nationale Supérieure des Ingénieurs en Arts Chimiques et Technologiques
118 route de Narbonne, 31077 Toulouse Cedex 4, France

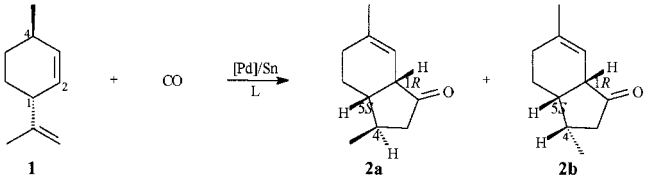

Scheme 1. Cyclocarbonylation of (1*R*,4*R*)-isolimonene (**1**) catalyzed by palladium

This paper deals with the complete identification of the two diastereomers **2a** and **2b** resulting from the carbonylation of (1*R*,4*R*)-isolimonene (**1**) based on DPFGSE NOE experiments[7] as well as the configuration at all the chiral carbon atoms. The analysis of the structure of these two isomers leads us to confirm that the active species contains a palladium-hydride bond. Calculations have been carried out on the two isomers **4a** and **4b**, and the two other possible diastereomers. DFT computations have been done on the crucial intermediate species, which contains an acyl group, and the fate of the endocyclic carbon-carbon double bond and the palladium center either in an *endo* or in an *exo* mode (Scheme 2); such calculations show that an enantioselective C1−C2 coupling in the *endo* mode is the only one possible. Finally, the full mechanism of the tandem carbonylation reaction is considered.

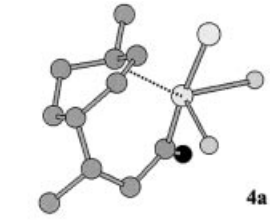

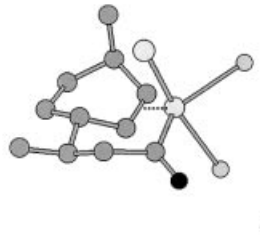

Scheme 2. Representation of two conceivable intermediates, **2a** resulting from an *endo* coordination mode and **2b** from an *exo* mode

Method of Calculation

As the complex $[PdCl_2(PPh_3)_2]$ reacts to give the same products in catalysis as $[PdCl(SnCl_3)(PPh_3)_2]$, although somewhat more slowly, we chose to model the species $[PdCl_2(PH_3)_2]$ in which PPh_3 has been replaced by the PH_3 ligand, as is normal in these types of calculations. The system contains a palladium atom, which is a transition metal and thus has strongly correlated *d* electrons. Consequently, we chose to carry out our study by using the density functional approach, which is well adapted to this type of problem.[8,9]

All structures presented here were fully optimized using conjugate gradient methods without constraints at the density functional theory (DFT) level with the Gaussian 98 software package release A.3.[10] The method has been described extensively elsewhere.[11−13] We used the B3LYP hybrid functional.[14,15] For all optimizations a valence basis-set of double-ξ quality was employed and relativistic effects were addressed implicitly by the use of relativistic effective core potentials for Pd, P and Cl.[16−18] For H, C and O the standard Dunning−Hay D95V basis was used.[19] A Mulliken population analysis, together with significant Mayer bond orders between palladium and its neighbors were thus determined. Finally, the charge-transfer effects arising between the metal atom and the ligands were examined.

Results and Discussion

Catalytic Experiments

Carbonylation of (1*R*,4*R*)-isolimonene (**1**; Scheme 1) at 40 bar (4 MPa) catalyzed by $[PdCl_2(PPh_3)_2]$ in the presence of $SnCl_2{\cdot}2H_2O$ and a slight excess of PPh_3, leads to a mixture of the two cyclopentanones **2a** and **2b** with good selectivity. These two products have been shown by mass spectrometry to contain a C11 framework and a ketone function; further strong evidence for the presence of a CO group results from the ν_{CO} band at 1740 cm^{-1} in the IR spectrum of both products. The mixture was enriched in one product to reach a **2a**/**2b** ratio of 90:10 by column chromatography on silica. ^1H and ^{13}C NMR characterizations confirmed that **2a** and **2b** are two diastereomers, and a complete assignment of the various configurations at the carbon atoms was obtained by NOE experiments, as discussed later.

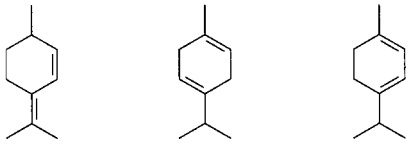

Scheme 3. Isomers of **1**

From Table 1 it can be seen that a 95 % conversion of the starting material can be obtained in 18 hours, giving a selectivity in **2a**+**2b** of 84 %, operating with a substrate-to-catalyst ratio of 50. The other products, which account for 16 %, were identified by GC-MS as isomers of **1**, the most abundant of which are shown in Scheme 3.

Addition of more substrate, as in runs 2 and 3, decreases the conversion but does not affect significantly the selectivity in **2**. The **2a**/**2b** ratio gives rise to a diastereomeric excess of 12 % in the three experiments.

We then introduced the classical chiral ligand (+)-DIOP into the coordination sphere of palladium and prepared the catalyst precursor $[PdCl_2\{(+)\text{-DIOP}\}]$ to carry out run 4.

 © 2004 Wiley-VCH Verlag GmbH & Co. KGaA, Weinheim

Table 1. Cyclocarbonylation reactions of (1*R*,4*R*)-isolimonene (**1**)[a]

	Catalytic precursor	Substrate/catalyst	Conversion (%)	Selectivity (%)	**2a/2b**[b]	*de*[b] (%)
1	$[PdCl_2(PPh_3)_2]$	50	95	84	56:44	12
2	$[PdCl_2(PPh_3)_2]$	80	78	80	55:45	10
3	$[PdCl_2(PPh_3)_2]$	100	62	82	56:44	12
4	$[PdCl_2\{(+)\text{-DIOP}\}]$	100	75	52	85:15	70
5	$[PdCl_2\{(-)\text{-DIOP}\}]$	100	75	52	85:15	70
6	$[PdCl_2(dppb)]$[c]	100	75	65	82:18	64
7	$[PdCl_2(dppf)]$[c]	100	71	68	84.5:15.5	69

[a] General conditions: Catalytic precursor = 1 mmol, $SnCl_2{\cdot}2H_2O$ = 2.5 mmol, P/Pd = 4, toluene = 25 mL, temp. = 70 °C, p_{CO} = 40 bar, t = 18 h. [b] Determined by GC. [c] Temp. = 97 °C.

Under the same catalytic conditions as in run 3, a 75 % conversion of **1** and a 52 % selectivity in **2** were observed. However, a diastereomeric excess of 70 % was calculated from the relative amounts of **2a** and **2b**. A similar experiment carried out with $[PdCl_2\{(-)\text{-DIOP}\}]$ led to the same results, especially the **2a**/**2b** ratio, which is still 85:15 and not the reverse. Therefore, whatever the configurations of the two chiral carbons of the diphosphane ligand, they have no influence on the diastereoselectivity and we suspected that the reaction could be governed by the chirality of the substrate itself.

Various experiments, not reported here, showed that a change in the temperature, pressure, or L*/Pd ratio did not affect significantly these performances, except maybe a higher pressure, which improved the conversion somewhat; for instance, at 80 bar, the yield is 82 %.

For this reason we have prepared two catalyst precursors containing the classical diphosphane ligands bis(diphenylphosphanyl)butane (dppb) and bis(diphenylphosphanyl)ferrocene (dppf). Runs 6 and 7 show that the performances of these two non-chiral catalysts are essentially the same as those of the DIOP-containing catalysts: the two diastereomeric excess values are 64 % and 69 % respectively. In experiments not described here, we also checked that shorter carbon chains in the ligands, like bis(diphenylphosphanyl)ethane and -propane, did not lead to any catalytic activity.[20] It can therefore be concluded that simple diphosphane ligands can play an important role, and thus assist the asymmetric catalysis, presumably through their electronic effects during the various steps of the catalytic cycle, but also thanks to their bulkiness during the asymmetric induction.

Stereochemistry Determination of 2a and 2b by NMR Spectroscopy

In previous studies, due to the isolation in the solid state of one isomer of the lactone obtained by cyclocarbonylation of (1*R*,2*S*,5*R*)-isopulegol and solved by an X-ray crystal structure, we have been able to determine all the configurations of the chiral centers present in the molecule and its diastereoisomers by NMR spectroscopy.[2d,3] With this knowledge, we have used NOE experiments to assign the positions of the various substituents of interest in **2a** and **2b**. NMR spectroscopic data for the two diastereomers **2a** and **2b** are displayed in Table 2, with the numbering system shown in Scheme 4, which differs from normal terpene nomenclature. These data were obtained from 1D ^1H and ^{13}C NMR spectra and COSY (^1H,^1H), HMQC (^1H,^{13}C) ^1J (see Figure 1) as well as long-range experiments. Due to the presence of a five-membered cycle and an endocyclic carbon-carbon double bond, most of the substituents are labeled as pseudo-equatorial in Schemes 5 and 6.

Table 2. NMR spectroscopic data for diastereomers **2a** and **2b** in $CDCl_3$

Atom	**2a**				**2b**			
	$\delta(^1H)$[a]	$^2J_{H,H}$[b]	$^3J_{H,H}$[b]	$\delta(^{13}C)$	$\delta(^1H)$[a]	$^2J_{H,H}$[b]	$^3J_{H,H}$[b]	$\delta(^{13}C)$
1	2.45 (dd)			49.3	2.35 (dd)			52.0
2				217.7				218.0
3pa	2.04 (dd)	18.3 (3pe)	6.8 (4)	45.0	1.92 (dd)	18 (3pe)	6 (4)	41.9
3pe	1.52 (dd)	18.3 (3pa)	8.1 (4)		1.52 (dd)			
4	1.70 (m)			31.0	2.00 (m)			31.4
5	1.70 (m)			41.1	1.90 (m)			38.2
6pa	1.54 (m)			21.8	1.55 (m)			19.8
6pe	1.35 (m)				1.35 (m)			
7pa	1.54 (m)			26.9	1.55 (m)			29.0
7pe	1.35 (m)				1.35 (m)			
8				135.6				135.7
9	4.90 (d)		1.4 (1)	116.1	5.16 (d)		1.5 (1)	116.4
10	0.76 (d)		6.4 (4)	18.7	0.76 (d)		6.4 (4)	15.1
11	1.30 (s)			23.6	1.30 (s)			23.2

[a] Resonance multiplicities in parentheses. [b] Coupled partners in parentheses.

 © 2004 Wiley-VCH Verlag GmbH & Co. KGaA, Weinheim

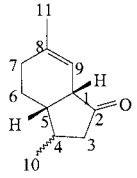

Scheme 4. Compound **2** (with IUPAC nomenclature)

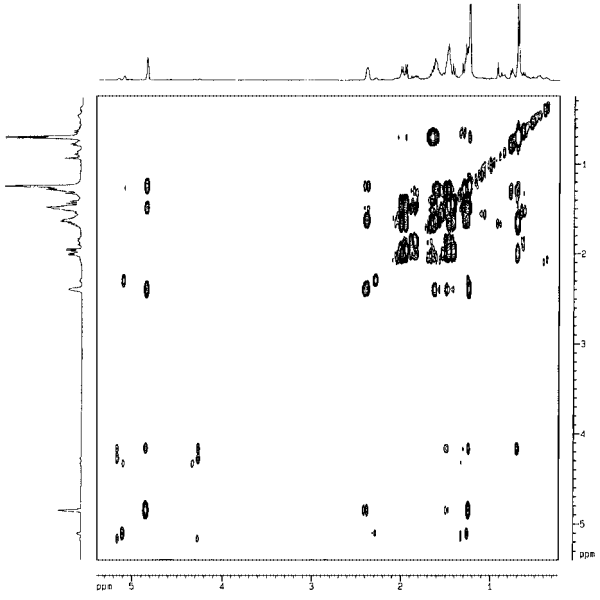

Figure 1. 2D COSY.DQF.GE ($^1H,^1H$) spectrum (400 MHz) of mixture of diastereomers **2a** and **2b** at 298 K in $CDCl_3$

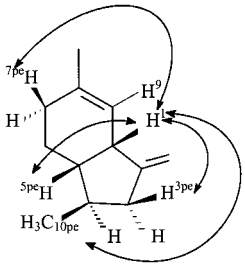

Scheme 5. Interactions observed for H1 in **2a**

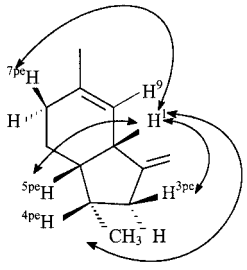

Scheme 6. Interactions observed for H1 in **2b**

The measurement of NOE effects by a 1D DPFGSE method appears to be much more selective for resonances that are not well resolved, especially when this is due to the overlap of several signals. As the spatial arrangement at C5 does not change during the reaction [C1 (*R*) in isolimonene becomes C5 (*S*) in cyclopentanone], irradiation of H1 on C1 in **2a** (Figure 2) allowed us to detect interactions with H9, H7 in a pseudo-equatorial position (pe), H5pe, H10pe, H11pe and H3pe (Scheme 5) indicating that all these atoms or groups are in the up position. Thus, C1 presents an *R* configuration, and C4 an *R* one.

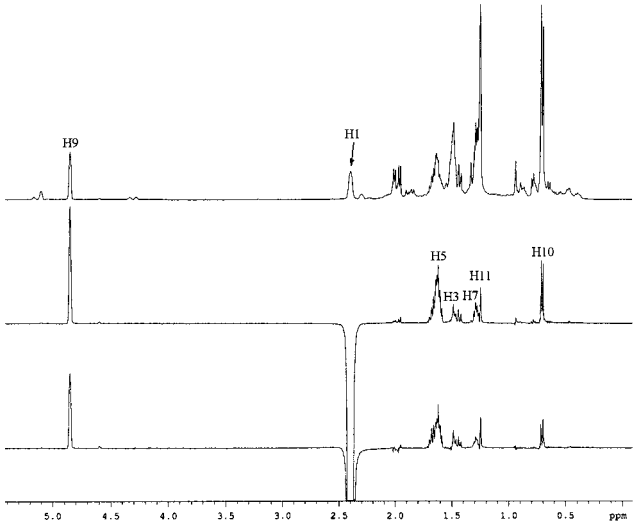

Figure 2. 1D NOESY-DPFGSE spectrum (400 MHz; irradiation of H1 on C1 in **2a**) of mixture of diastereomers **2a** and **2b** at 298 K in $CDCl_3$; top: full spectrum; middle: mixing time 800 ms; bottom: mixing time 400 ms

In the same 90:10 mixture of **2a**/**2b**, irradiation of H1 in **2b** (Figure 3) led us to assign the configurations C1 (*R*) and C4 (*S*; Scheme 6).

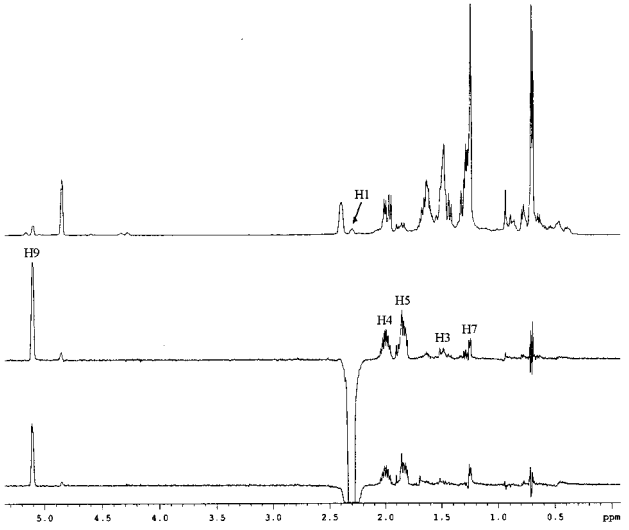

Figure 3. 1D NOESY-DPFGSE spectrum (400 MHz; irradiation of H1 on C1 in **2b**) of mixture of diastereomers **2a** and **2b** at 298 K in $CDCl_3$; top: full spectrum; middle: mixing time 800 ms; bottom: mixing time 400 ms

 © 2004 Wiley-VCH Verlag GmbH & Co. KGaA, Weinheim

This NMR study shows that in the two products obtained in the cyclocarbonylation reaction, the stereochemistry of C1 is unchanged in both isomers. The diastereomeric excess of 70 % results in fact from the two (*S* and *R*) configurations at the C4 atom (*R*/*S* = 85:15).

DFT Calculations

The shift of the endocyclic C=C bond from the substrate **1** to the resulting cyclopentanone **2** (Scheme 7) is indicative of a β-hydride elimination in an intermediate which affords a palladium hydride species. Thus, we have supposed the following sequence for the early steps of the catalytic cycle: formation of an alkylpalladium species by hydride transfer to the exocyclic C=C bond, and CO migratory insertion to afford the acyl intermediate **3**. During the cyclization process, which involves the carbon−carbon coupling of the two C1 and C2 atoms, we have considered that the stereoselectivity results from one privileged approach of the palladium center toward the endocyclic C=C bond in species **4** (Scheme 8). As the full system involves 39 atoms the potential hypersurface is rather complex, therefore we calculated only certain regions of this hypersurface, taking into account the classical geometries for d^8 complexes.

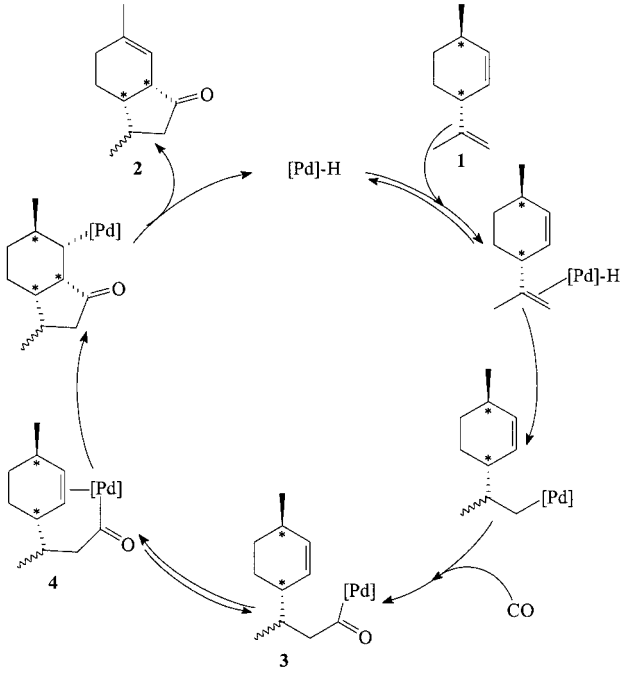

Scheme 7. Catalytic cycle of cyclocarbonylation of **1**

Our calculations show that there is no coordination of the C=C bond in an *exo* mode and we found two species with the C=C bond not coordinated to the metal center, which adopts a square-planar environment, at all (d_{Pd-C} = 4.75 and 5.63 Å for the more stable and 3.69 and 4.66 Å for the second one, which is 3 kcal·mol^{-1} higher in energy, as shown in Table 3). Moreover, we found a pentacoordinate species with a trigonal bipyramidal (TBP) geometry in which the C=C bond is coordinated in an *endo* mode (Scheme 9). Indeed, the two palladium−carbon bond lengths are 2.31 and 2.35 Å, corresponding to Mayer bond-orders of 0.36 and 0.31, respectively; in addition, the C−C bond length is 1.40 Å and its bond order is 1.53 (see Table 3). Among the various axial and/or equatorial positions for the ligands, the calculations seem to slightly favor (1.3 kcal·mol^{-1}) the Cl and CO-acyl ligands in the two axial positions.

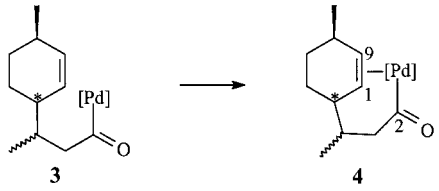

Scheme 8. Coordination of the endocyclic C=C bond of **1** to the palladium center

Concerning the Mulliken population analysis, our results show clearly that there are no significant differences between the net charges on each atom in both species.

Proposed Catalytic Cycle

Our calculations give strong evidence that the TBP intermediate in which the (*endo*)C=C double bond and the CO-acyl are in close vicinity allows the next step in the catalytic cycle. Indeed, the C2−C1 distance is 2.97 Å, whereas it is 3.58 and 4.41 Å in the less- and more-stable square-planar palladium species. The resulting C1 configuration is thus 100 % *R*.

A further analysis of the mechanism shows that the new intermediate **5**, in which the cyclopentanone has been formed and the palladium atom is still bonded to C9, presents the two palladium and H8 hydrogen atoms in mutual *cis* positions. Thus, a β-hydride elimination reaction, which re-forms the active palladium hydride species, is possible. In addition, the H1 atom is *trans* to Pd and cannot provide the β-H elimination required for the further step. Moreover, it is worth mentioning that a possible intermediate resulting from the coordination of the C=C bond in the *exo* mode would provide the two H1 and H8 hydrogen atoms in *trans* positions to the palladium atom; such a situation, in which no β-H elimination can occur, precludes any catalytic reaction. We did not detect these two isomers. Scheme 7 shows the catalytic cycle that we propose.

Conclusion

The main point of this study is related to an asymmetric induction that is caused by the substrate itself so that chiral ancillary phosphane ligands are not necessary in the catalytic reaction. Moreover, the steric hindrance of the diphosphane ligands plays an essential role in obtaining a large diastereomeric excess.

 © 2004 Wiley-VCH Verlag GmbH & Co. KGaA, Weinheim

Table 3. Absolute energies, representative bond lengths, selected Mayer bond orders and Mulliken net charges distribution in the intermediate species **4**

Complexes	Absolute energy (Hartree)	Distances (Å)	Bond order	Net charges
C=C uncoordinated species	−662.862124	Pd−C9: 5.63	Pd−C9: 0.00	Pd: −0.17
		Pd−C1: 4.75	Pd−C1: 0.00	C1: −0.25
		C1−C9: 1.35	C1−C9: 1.95	C9: −0.23
	−662.857868	Pd−C9: 4.66	Pd−C9: 0.00	Pd: −0.17
		Pd−C1: 3.69	Pd−C1: 0.00	C1: −0.26
		C1−C9: 1.35	C1−C9: 1.90	C9: −0.18
C=C coordinated species	−662.856565	Pd−C9: 2.35	Pd−C9: 0.31	Pd: −0.14
		Pd−C1: 2.31	Pd−C1: 0.36	C1: −0.23
		C1−C9: 1.40	C1−C9: 1.53	C9: −0.20

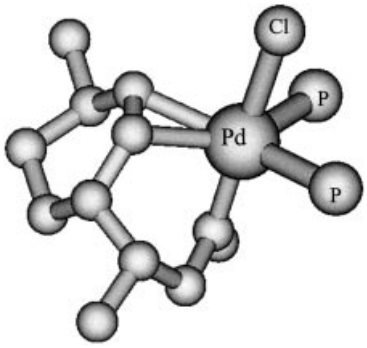

Scheme 9. Compound **4** (C=C *endo* coordination mode)

Experimental Section

Materials: Solvents with high purity, as well as (1*R*,4*R*)-isolimonene, were used as received from Dérivés Résiniques et Terpéniques (DRT SA). $SnCl_2{\cdot}2H_2O$ (Prolabo 98 %), triphenylphosphane (Aldrich 99 %), 1,4-bis(diphenylphosphanyl)butane (dppb) (Acros 98 %), 1,1′-bis(diphenylphosphanyl)ferrocene (dppf) (Aldrich 97 %), (−)-2,3-*O*-isopropylidene-2,3-dihydroxy-1,4-bis(diphosphanyl)butane [(−)-DIOP] and (+)-2,3-*O*-isopropylidene-2,3-dihydroxy-1,4-bis(diphosphanyl)butane [(+)-DIOP] (Janssen 98 %). Column chromatography was performed with SiO_2 (Merck).

Instrumentation: The ^1H, ^{13}C and ^{31}P NMR spectra were recorded with $CDCl_3$ solutions containing TMS as internal standard on a Bruker AMX 400 spectrometer operating at 400.13 MHz (^1H) and 100.62 MHz (^{13}C), and a Bruker AM 250 spectrometer operating at 250.13 MHz, 62.90 MHz and 101.26 MHz, respectively. Data are reported as follows: chemical shift in ppm (δ), multiplicity (s = singlet, d = doublet, t = triplet, q = quadruplet and m = multiplet), coupling constant (*J*) in Hz (n.d. = no determined), integration, and assignment (pa = pseudo-axial and pe = pseudo-equatorial). IR spectra were obtained on a Perkin−Elmer 1710 spectrometer; absorptions are reported in cm^{-1}. Analytical GC was carried out on a Carlo Erba MFC 500 apparatus equipped with a Econo-Cap FFAP (30 m; 0.53 mm; 1.2 μm) capillary column and a flame ionization detector. Products were identified by GC/MS on a Perkin−Elmer QMass 910 Mass Spectrometer with ionization voltage of 70 eV, with a Crompack CP WAX 52 CB (50 m; 0.32 mm; 0.2 μm) polar column.

General Procedure: A mixture of dichlorobis(triphenylphosphane)-palladium(II) (0.702 g, 1 mmol), hydrated tin(II) chloride (0.474 g, 2.5 mmol) and triphenylphosphane (0.524 g, 2 mmol) was introduced into a 250 mL stainless steel autoclave with mechanical stirring. A nitrogen-saturated mixture of isolimonene (13.624 g, 100 mmol) in toluene (25 mL) was introduced into the evacuated autoclave by aspiration. It was heated to 70 °C under 40 bar pressure of carbon monoxide at constant pressure. After 18 h, the autoclave was cooled and then slowly depressurized. The yellow-orange reaction mixture was analyzed by gas chromatography. The same procedure was followed for other ligands maintaining the P/Pd ratio at 4.

After the catalytic reaction, the organometallic compounds and the excess phosphane were separated from the crude solution by washing with CCl_4. The deeply colored oily layer was decanted. After concentration by rotary evaporation, the oily residue was purified by column chromatography on silica gel (petroleum ether/dichloromethane/ethyl acetate, 70:24:6).

Complexes: $[PdCl_2(PPh_3)_2]$ was prepared according to the literature procedure.[21] Yield 95 %. $^{31}P\{^1H\}$ NMR (250 MHz, $CDCl_3$, 25 °C): δ = 23.47 (s) ppm. IR (KBr): $\tilde{\nu}$ = 1481, 1436, 1099, 746, 693 cm^{-1}. Complexes containing diphosphanes were prepared by addition of the diphosphane to $[PdCl_2(PhCN)_2]$[22] in hot acetone.
[$PdCl_2$(dppb)]: Yield 90 %. $^{31}P\{^1H\}$ NMR (250 MHz, $CDCl_3$, 25 °C): δ = 63.75 (s) ppm.
[$PdCl_2$(dppf)]: Yield 88 %. $^{31}P\{^1H\}$ NMR (250 MHz, $CDCl_3$, 25 °C): δ = 36.14 (s) ppm.
[$PdCl_2$[(+)-DIOP)] and [$PdCl_2$[(−)-DIOP)]: Yield 85 %. $^{31}P\{^1H\}$ NMR (250 MHz, $CDCl_3$, 25 °C): δ = 16.47 (s) ppm.

(1*R*,4*R*,5*S*)-4,8-Dimethylbicyclo[4.3.0]non-8-en-2-one (2a): ^1H NMR (400 MHz, $CDCl_3$, 25 °C, TMS): δ = 4.90 (d, $^3J_{H,H}$ = 1.4 Hz, 1 H, H9), 2.45 (dd, n.d., 1 H, H1), 2.04 (dd, $^3J_{H,H}$ = 18.3, 6.8 Hz, 1 H, H3pa), 1.70 (m, 2 H, H4 and H5), 1.54 (m, 2 H, H6pa and H7pa), 1.52 (dd, $^3J_{H,H}$ = 8.1, 18.3 Hz, 1 H, H3pe), 1.35 (m, 2 H, H6pe and H7pe), 1.30 (s, 3 H, CH_3 11), 0.76 (d, $^3J_{H,H}$ = 6.4 Hz, 3 H, CH_3 10) ppm $^{13}C\{^1H\}$ NMR (400 MHz, $CDCl_3$, 25 °C): δ = 217.7 (C2), 135.6 (C8), 116.1 (C9), 49.3 (C1), 45.0 (C3), 41.1 (C5), 31.0 (C4), 26.9 (C7), 23.6 (C11), 21.8 (C6), 18.7 (C10) ppm. IR (KBr): $\tilde{\nu}$ = 1740 cm^{-1} (C=O). MS (70 eV, EI): *m*/*z* (%) = 79 (100) $[C_6H_7]^+$, 94 (100) $[C_7H_{10}]$, 164 (61) [M], 165 (9) $[M - H]^+$.

(1*R*,4*S*,5*S*)-4,8-Dimethylbicyclo[4.3.0]non-8-en-2-one (2b): ^1H NMR (400 MHz, $CDCl_3$, 25 °C, TMS): δ = 5.16 (d, $^3J_{H,H}$ = 1.5 Hz, 1 H, H9), 2.35 (dd, n.d., 1 H, H1), 2.00 (m, 1 H, H4), 1.92 (dd, $^3J_{H,H}$ = 6 and 18 Hz, 1 H, H3pa), 1.90 (m, 1 H, H5), 1.55 (m, 2 H, H6pa and H7pa), 1.52 (dd, n.d., 1 H, H3pe), 1.35 (m, 2 H, H6pe and H7pa), 1.30 (s, 3 H, CH3 11), 0.76 (d, $^3J_{H,H}$ = 6.4 Hz, 3 H, CH3 10) ppm. $^{13}C\{^1H\}$ NMR (400 MHz, $CDCl_3$, 25 °C): δ = 218.0 (C2), 135.7 (C8), 116.4 (C9), 52.0 (C1), 41.9 (C3), 38.2 (C5),

 © 2004 Wiley-VCH Verlag GmbH & Co. KGaA, Weinheim

31.4 (C4), 29.0 (C7), 23.2 (C11), 19.8 (C6), 15.1 (C10) ppm. IR (KBr): $\tilde{\nu}$ = 1740 cm^{-1} (C=O). MS (70 eV, EI): *m/z* (%) = 94 (100) $[C_7H_{10}]$, 79 (92) $[C_6H_7]^+$, 164 (61) [*M*], 165 (9) $[M - H]^+$.

Acknowledgments

We thank the Ministère de l'Education Nationale de la Recherche et de la Technologie for a Research Grant (L.G.). Acknowledgments are also due to Engelhard-CLAL for a generous loan of palladium, and DRT SA for the gift of (1*R*,4*R*)-isolimonene. We are indebted to CALMIP for computer resources with the GAUSSIAN 98 software package.

[1] [1a] I. Ciprès, J. Jenck, Ph. Kalck, *J. Mol. Catal.* **1990**, *58*, 387−392. [1b] I. Ciprès, Ph. Kalck, D. C. Park, F. Serein-Spirau, *J. Mol. Catal.* **1991**, *6*, 399−407. [1c] T. Chenal, I. Ciprès, J. Jenck, Ph. Kalck, *J. Mol. Catal.* **1993**, *78*, 351−366. [1d] R. Naigre, T. Chenal, I. Ciprès, Ph. Kalck, J-C. Daran, J. Vaissermann, *J. Organomet. Chem.* **1994**, *480*, 91−102. [1e] S. Sirol, Ph. Kalck, *New. J. Chem.* **1997**, *21*, 1129−1137.

[2] [2a] I. Ciprès, Ph. Kalck, D. C. Park, *J. Mol. Catal.* **1991**, *66*, 399−407. [2b] T. Chenal, R. Naigre, I. Ciprès, Ph. Kalck, J. C. Daran, J. Vaissermann, *J. Chem. Soc., Chem. Commun.* **1993**, 747−748. [2c] S. Sirol, J. P. Gorrichon, Ph. Kalck, P. M. Nieto, G. Commenges, *Magn. Reson. Chem.* **1999**, *37*, 127−132. [2d] G. Lenoble, R. Naigre, T. Chenal, M. Urrutigoïty, J. C. Daran, Ph. Kalck, *Tetrahedron: Asymmetry* **1999**, *10*, 929−936.

[3] C. Lacaze-Dufaure, G. Lenoble, M. Urrutigoïty, J. P. Gorrichon, C. Mijoule, Ph. Kalck, *Tetrahedron: Asymmetry* **2001**, *12*, 185−187.

[4] [4a] J. Tsuji, *Palladium Reagents and Catalysts*, John Wiley & Sons Ltd., Chichester, **1995**. [4b] *Applied Homogeneous Catalysis with Organometallic Compounds* (Eds.: B. Cornils, W. A. Herrmann), VCH, Weinheim, **1996**. [4c] *Transition Metals for Organic Synthesis* (Eds. M. Beller, C. Bolm), Wiley-VCH, Weinheim, **1998**.

[5] [5a] J. F. Knifton, *J. Org. Chem.* **1976**, *41*, 2885−2894. [5b] G. Cavinato, L. Toniolo, *J. Mol. Catal.* **1981**, *10*, 161−170. [5c] I. Cipres, J. Jenck, Ph. Kalck, *J. Mol. Catal.* **1990**, *58*, 387−392. [5d] L. L. da Rocha, A. O. Dias, E. N. dos Santos, R. Augusti, E. V. Gusevskaya, *J. Mol. Catal. A: Chem.* **1998**, *132*, 213−221.

[6] *Catalytic Asymmetric Synthesis* (Ed.: K. Nozaki, I. Ojima), Wiley-VCH, Weinheim, **2000**, pp.429−464.

[7] [7a] Q. N. Van, A. J. Shaka, *J. Magn. Reson.* **1996**, *119*, 295−302. [7b] K. Stott, J. Keeler, Q. N. Van, A. J. Shaka, *J. Magn. Reson.* **1997**, *125*, 302−309.

[8] I. Papai, D. R. Sahalub, C. Mijoule, *Surf. Sci.* **1990**, *236*, 241.

[9] J. Roques, C. Lacaze-Dufaure, C. Mijoule, *Surf. Sci.* **2001**, *479*, 231.

[10] M. J. Frisch, G. W. Trucks, H. B. Schlegel, G. E. Scuseria, M. A. Robb, J. R. Cheeseman, V. G. Zakrzewski, J. A. Montgomery, Jr., R. E. Stratmann, J. C. Burant, S. Dapprich, J. M. Millam, A. D. Daniels, K. N. Kudin, M. C. Strain, O. Farkas, J. Tomasi, V. Barone, M. Cossi, R. Cammi, B. Mennucci, C. Pomelli, C. Adamo, S. Clifford, J. Ochterski, G. A. Petersson, P. Y. Ayala, Q. Cui, K. Morokuma, D. K. Malick, A. D. Rabuck, K. Raghavachari, J. B. Foresman, J. Cioslowski, J. V. Ortiz, B. B. Stefanov, G. Liu, A. Liashenko, P. Piskorz, I. Komaromi, R. Gomperts, R. L. Martin, D. J. Fox, T. Keith, M. A. Al-Laham, C. Y. Peng, A. Nanayakkara, C. Gonzalez, M. Challacombe, P. M. W. Gill, B. Johnson, W. Chen, M. W. Wong, J. L. Andres, C. Gonzalez, M. Head-Gordon, E. S. Replogle, J. A. Pople, Gaussian 98, Revision A.3, Gaussian, Inc., Pittsburgh PA, **1998**.

[11] W. Kohn, L. J. Sham, *Phys. Rev.* **1965**, *140*, A1133.

[12] P. Hohenberg, W. Kohn, *Phys. Rev.* **1964**, *136*, B864.

[13] R. G. Parr, W. Yang, *Density functional Theory of Atoms and Molecules*, Oxford Press, **1989**.

[14] A. D. Becke, *J. Chem. Phys.* **1993**, *88*, 5648.

[15] J. P. Perdew, W. R. Wang, *Phys. Rev. B* **1992**, *45*, 13244.

[16] P. J. Hay, W. R. Wadt, *J. Chem. Phys.* **1985**, *82*, 270.

[17] W. R. Wadt, P. J. Hay, *J. Chem. Phys.* **1985**, *82*, 284.

[18] P. J. Hay, W. R. Wadt, *J. Chem. Phys.* **1985**, *82*, 299.

[19] T. H. Dunning Jr, P. J. Hay, in *Modern Theoretical Chemistry* (Ed.: H. F. Schaefer, III) Plenum, New York, **1976**.

[20] R. Naigre, PhD thesis, University of Toulouse (France), **1994**.

[21] D. R. Coulson, L. C. Satek, S. O. Orim, *Inorg. Synth.* **1972**, *13*, 121−124.

[22] J. M. Jenckins, J. C. Verkade, *Inorg. Synth.* **1968**, *11*, 108−111.

Received August 6, 2003
Early View Article
Published Online January 2, 2004

 © 2004 Wiley-VCH Verlag GmbH & Co. KGaA, Weinheim

Anomalous Difference in Magnetic Behavior between Highly Saddled Iron(III) Porphyrin Complexes in the Solid State

Yoshiki Ohgo,*[a] Takahisa Ikeue,[a] Masashi Takahashi,[b] Masuo Takeda,[b] and Mikio Nakamura*[a,c]

Dedicated to the late Professor Oyo Mitsunobu of Aoyama Gakuin University

Keywords: Iron / Porphyrinoids / Spin crossover / Magnetic properties

The spin states of microcrystalline samples of $[Fe(OMTPP)L_2]^+$ (L = DMAP or Py) have been examined and interpreted using Mössbauer spectroscopy, SQUID magnetometry and X-ray crystallography. The Mössbauer spectra of $[Fe(OMTPP)(DMAP)_2]^+$ and $[Fe(OMTPP)Py_2]^+$ showed that both of these complexes maintain the low-spin (S = 1/2) state over the 77–300 K temperature range. The spin states of these complexes were further confirmed by SQUID magnetometry. Thus, the magnetic behavior of $[Fe(OMTPP)Py_2]^+$ is quite different from that of the structurally related species $[Fe(OETPP)Py_2]^+$. The latter complex exhibits a novel spin crossover between the S = 3/2 and S = 1/2 states as revealed by the spectroscopic and magnetic measurements. In order to understand the reasons for the absence of the spin crossover process in $[Fe(OMTPP)Py_2]^+$, we have compared the crystal and molecular structures of $[Fe(OMTPP)Py_2]^+$ with those of the recently reported species $[Fe(OETPP)Py_2]^+$. In the case of $[Fe(OMTPP)Py_2]^+$, the Fe–N_{axial} bond lengths hardly change with temperature and are 2.058(6) and 2.024(4) Å at 298 and 80 K, respectively. These results are in sharp contrast to those of the spin crossover complex $[Fe(OETPP)Py_2]^+$, in which the Fe–N_{axial} bonds contract from 2.201(3) Å at 298 K to 1.993(3) Å at 80 K. We have ascribed the difference in magnetic behavior between $[Fe(OMTPP)Py_2]^+$ and $[Fe(OETPP)Py_2]^+$ to the difference in molecular packing; the former adopts a densely packed cubic crystal system while the latter shows a less condensed monoclinic system. A cavity calculation has further confirmed the above mentioned assumption. While the cavity sizes around the pyridine ligands in $[Fe(OETPP)Py_2]^+$ are 32.08 and 28.88 $Å^3$ at 298 K, that in $[Fe(OMTPP)Py_2]^+$ is only 19.81 $Å^3$. Furthermore, the cavities contract by 17.7% in $[Fe(OETPP)Py_2]^+$ when the temperature is lowered from 298 to 80 K whereas the contraction is only 5.3% in the case of $[Fe(OMTPP)Py_2]^+$. On the basis of these results, we have concluded that the loosely packed crystal system and the wide cavities around the axial ligands are the important requirements for the occurrence of the spin crossover process in the solid state.
(© Wiley-VCH Verlag GmbH & Co. KGaA, 69451 Weinheim, Germany, 2004)

Introduction

The spin states of iron(III) porphyrin complexes are controlled by several factors[1–3] the most important being the number and nature of the axial ligands. For example, axially bound strong field ligands such as cyanide, imidazole, and pyridine form low-spin (S = 1/2) six-coordinate complexes. In contrast, anionic ligands such as Cl^- and F^- lead to the formation of five-coordinate high-spin (S = 5/2) complexes. Maltempo discussed a quantum mechanically spin admixed S = 3/2, 5/2 state and suggested that the S = 3/2 state is an important contributor to the spin states of cytochromes c′, which are recognized as histidine ligated five-coordinate iron(III) complexes.[4–6] In fact, the mono(imidazole) complexes of iron(III) porphyrin exhibit the S = 3/2, 5/2 admixed intermediate-spin in a series of $[Fe(TMP)(R-Im)]^+$ complexes, where R–Im indicates alkyl-substituted imidazoles and benzimidazoles.[7–9] In general, the degree of the S = 3/2 contribution in five-coordinate complexes correlates with the ligand field of the anionic axial ligands - it increases as the ligand field of the axial ligands weakens. Reed and co-workers thus ranked the relative field strengths of weak anionic ligands (X) in [Fe(TPP)X] on the basis of spectroscopic and magnetic properties and called the resultant hierarchy a magnetochemical series.[10,11] We and others have recently reported that the deformation of the porphyrin ring is also an important factor which affects the spin states[12,13] and the electron configurations of iron(III) ions.[14–21] Thus, highly nonplanar six-coordinate com-

[a] Department of Chemistry, School of Medicine, Toho University,
Tokyo 143-8540, Japan
Fax: (internat.) + 813-5493-5430
E-mail: mnakamu@med.toho-u.ac.jp (M. N.)
yohgo@med.toho-u.ac.jp (Y. O.)
[b] Department of Chemistry, Faculty of Science, Toho University, Funabashi 274-8510, Japan
[c] Division of Biomolecular Science, Graduate School of Science, Toho University,
Funabashi 274-8510, Japan

 © 2004 Wiley-VCH Verlag GmbH & Co. KGaA, Weinheim **DOI: 10.1002/ejic.200300566**

plexes with weak field axial ligands such as the saddled $[Fe(OETPP)(THF)_2]^+$ and the ruffled $[Fe(T\textit{i}PrP)(THF)_2]^+$ exhibit an essentially pure intermediate spin state.[12] These results have been ascribed to the short $Fe-N_p$ (N_p: nitrogen atoms of porphyrin) bond lengths caused by the nonplanarity of the porphyrin rings[12,13,22–25] together with the weak coordinating ability of the axial ligands.[10,11] The strongly S_4 saddled OETPP ring stabilizes the intermediate spin state even in the presence of nitrogen bases. Thus the complexes $[Fe(OETPP)L_2]^+$ (L = Py and 4-CNPy) show the $S = 3/2$ state at room temperature and exhibit a novel spin transition from the $S = 3/2$ to the $S = 1/2$ state as the temperature is lowered.[26] In this paper, we report on the spin states of other saddle shaped complexes, namely $[Fe(OMTPP)L_2]^+$ (L = DMAP and Py) in the solid state on the basis of a combined analysis by Mössbauer spectroscopy, SQUID magnetometry, and X-ray crystallography. We also report on the anomalous difference in magnetic behavior between the structurally similar $[Fe(OMTPP)Py_2]^+$ and $[Fe(OETPP)Py_2]^+$ in the solid state and on the requirements for the occurrence of the spin crossover process (Scheme 1).

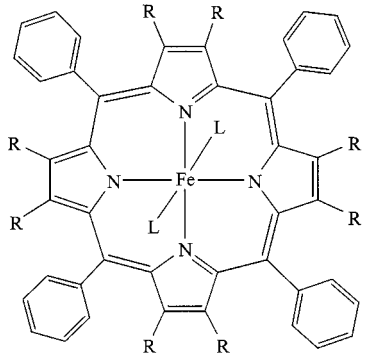

$[Fe(OMTPP)L_2]^+$ (R = Methyl)
$[Fe(OETPP)L_2]^+$ (R = Ethyl)
L = DMAP, Py

Scheme 1

Results and Discussion

Structural Characteristics

Figure 1 shows the molecular structure of $[Fe(OMTPP)(DMAP)_2]ClO_4 \cdot 4CHCl_3$ determined at 298 K. Two of the four solvent molecules and a counter anion (not shown) exhibit two disordered structures, A and B, in each site. The site-occupancy factors of the two solvent molecules and the counter anion for A:B are 0.85:0.15, 0.72:0.28, and 0.54:0.46, respectively. Figure 2 shows the molecular structure of $[Fe(OMTPP)Py_2]ClO_4 \cdot 1/3HClO_4 \cdot 4/3CHCl_3$ determined at 298 K. Because the Fe1, N2, and C16 atoms lie on the four-fold inverted axis, only a quarter of the molecule is crystallographically independent. Similarly, because Cl1, O2, C17, and H17 are on the three-fold axis, one-third of the counter anion and solvent molecules are in an asymmetric unit. The counter anion is disordered and the site-occupancy factors for the disordered O1A and O1B are 0.59 and 0.41, respectively, at 298 K. The structure of the counter anion at 80 K is, however, ordered as a consequence of the increase in the packing force and the decrease in the thermal movement of the molecule. Figure 3 shows the molecular structure of $[Fe(OETPP)(DMAP)_2]ClO_4$ determined at 298 K. This crystal turns out to be a polymorph of the crystal reported previously by Walker et al.[27] The present crystal, the polymorph A, with the space group $P3_121$ (#152) contains no solvent molecules, while the crystal reported by Walker et al., the polymorph B, with space group $Pna2_1$ (#33) contains four chloroform molecules in crystallographically independent space. Figure 4 shows the deviation of each atom in $[Fe(OMTPP)L_2]^+$ (L =

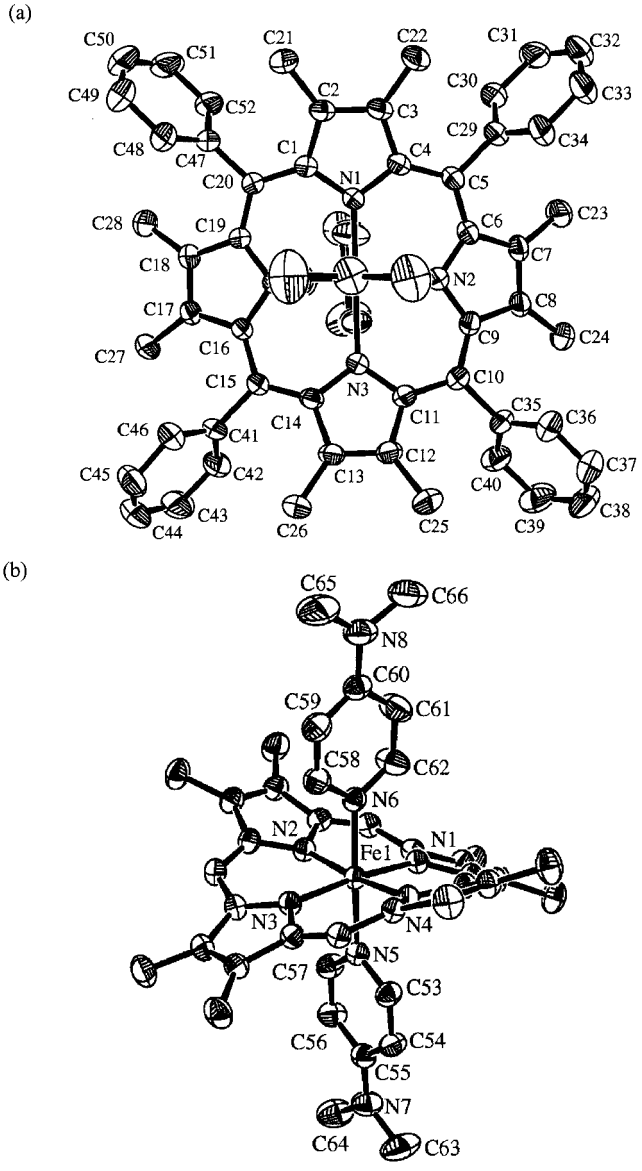

Figure 1. ORTEP diagrams of $[Fe(OMTPP)(DMAP)_2]^+$ together with the atom labeling; thermal ellipsoids are drawn at the 50% probability level: (a) top view (b) side view; phenyl rings are omitted for clarity in (b)

 © 2004 Wiley-VCH Verlag GmbH & Co. KGaA, Weinheim

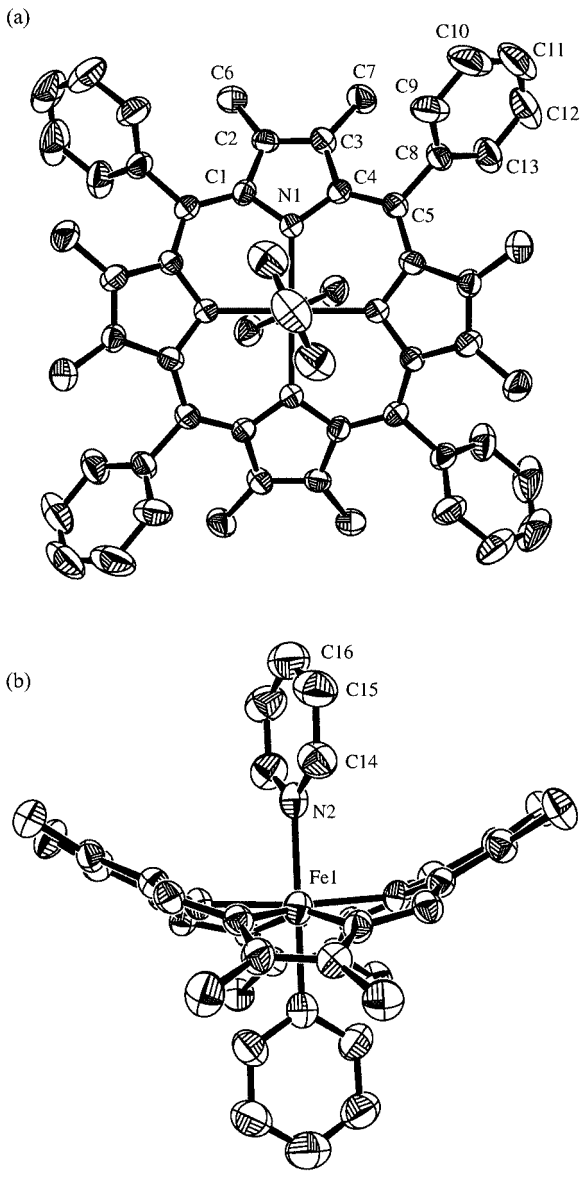

Figure 2. ORTEP diagrams of $[Fe(OMTPP)Py_2]^+$ together with the atom labeling for the unique quarter of the porphyrin; thermal ellipsoids are drawn at the 50% probability level: (a) top view (b) side view; phenyl rings are omitted for clarity in (b)

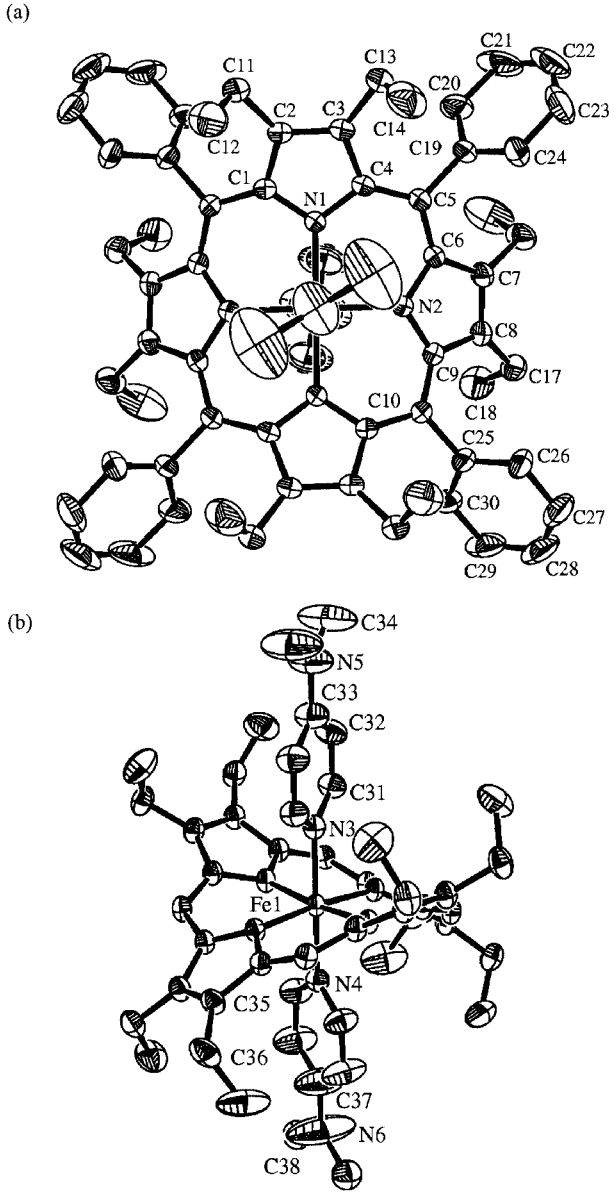

Figure 3. ORTEP diagrams of $[Fe(OETPP)(DMAP)_2]^+$ together with the atom labeling for the unique quarter of the porphyrin; thermal ellipsoids are drawn at the 50% probability level: (a) top view (b) side view; phenyl rings are omitted for clarity in (b)

DMAP, Py) and $[Fe(OETPP)L_2]^+$ (L = DMAP, Py[28]) from the average plane defined by the 24-atom porphyrin cores. Table 1 lists the crystal data for $[Fe(OMTPP)L_2]ClO_4$ (L = DMAP and Py) and $[Fe(OETPP)L_2]ClO_4$ (L = DMAP and Py[28]). Table 2 lists some structural parameters of the complexes[27,28] which are defined as follows: φ is the orientation angle of the axial ligand to the nearest N_P-Fe-N_P axis, θ is the dihedral angle between two axial ligands, τ is the dihedral angle between the average N4 plane and each pyrrole ring, ψ is the dihedral angle between two diagonal pyrrole rings, η is the twist angle between two diagonal pyrrole rings, ω is the dihedral angle between the phenyl group and the $C_\alpha-C_{meso}-C_{\alpha'}$ plane, and $|\Delta C_{meso}|$ and $|\Delta C_\beta|$ are the deviations of the *meso* and β-pyrrole carbon atoms from the mean porphyrin plane, respectively. They are also given in Scheme 2.

Figure 1 and Figure 4(a) clearly show that the porphyrin core of $[Fe(OMTPP)(DMAP)_2]^+$ is highly saddled. The average $Fe-N_p$ bond length of 1.979(3)Å is slightly shorter than that of 1.989 Å in the typical low-spin complex, $[Fe(TPP)(1\text{-}MeIm)_2]^+$.[29] The average $Fe-N_{axial}$ bond length of 2.009 Å is also quite close to the corresponding bond lengths of low-spin $[Fe(TPP)Py_2]^+$ and $[Fe(OEP)(DMAP)_2]^+$ which are 2.003 and 1.995 Å, respectively.[30,31] The β-pyrrole carbon atoms of each pyrrole ring are alternately displaced, on average, by ±0.94 Å from the 24-atom mean porphyrin plane. Because of the highly saddled structure, the complex has two mutually perpendicular clefts along the diagonal N_p-Fe-N_p axes. The DMAP ligands are situated almost exactly along these clefts. Thus, the φ values are only 1.3(3)° and 2.4(4)°. The

 © 2004 Wiley-VCH Verlag GmbH & Co. KGaA, Weinheim

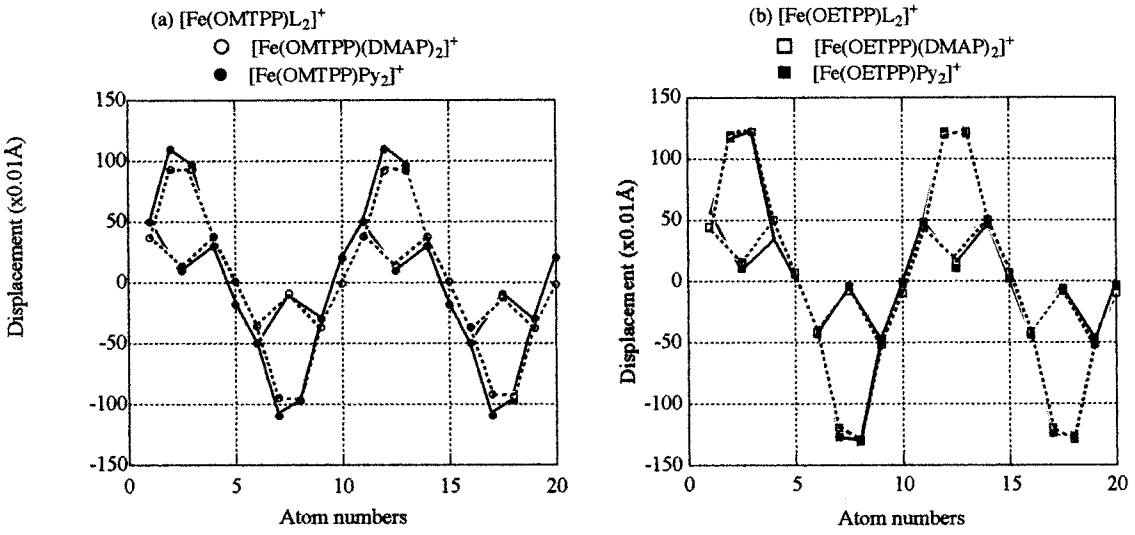

Figure 4. Perpendicular displacement of the peripheral carbon and nitrogen atoms of (a) $[Fe(OMTPP)L_2]^+$ and (b) $[Fe(OETPP)L_2]^+$ in units of 0.01 A, where L = DMAP and Py

Table 1. Crystal data of OMTPP and OETPP complexes

	$[Fe(OMTPP)(DMAP)_2]ClO_4$	$[Fe(OMTPP)(Py)_2]ClO_4$	$[Fe(OMTPP)(Py)_2]ClO_4$	$[Fe(OETPP)(DMAP)_2]ClO_4$
T(K)	298	298	80	298
Chemical Formula	$C_{66}H_{64}N_8O_4FeCl \cdot (CHCl_3)_4$	$C_{62}H_{54}N_6O_4FeCl \cdot (H_{0.33}Cl_{0.33}O_{1.33})$ $(C_{1.33}H_{1.33}Cl_4)$	$C_{62}H_{54}N_6O_4FeCl \cdot (H_{0.33}Cl_{0.33}O_{1.33})$ $(C_{1.33}H_{1.33}Cl_4)$	$C_{74}H_{80}N_8FeCl$
Crystal dimension(mm)	0.2 x 0.1 x 0.1	0.5 x 0.5 x 0.3	0.1 x 0.1 x 0.1	0.5 x 0.4 x 0.1
Crystal color	purple	purple	purple	purple
Crystal system	Monoclinic	Cubic	Cubic	Trigonal
Space group	$P2_1/c$ (#14)	I43d (#220)	I43d (#220)	$I3_121$(#152)
Mr	1602.02	1230.72	1230.72	1172.76
a (Å)	16.4556(5)	25.937(3)	25.609(1)	22.595(9)
b (Å)	23.7289(6)	25.937(3)	25.609(1)	22.595(9)
c (Å)	19.8424(6)	25.937(3)	25.609(1)	13.967(5)
α (°)	90	90	90	90
β (°)	91.924(1)	90	90	90
γ (°)	90	90	90	120
V (Å^3)	7743.6(4)	17448(3)	16795.5(9)	6175(4)
Z	4	12	12	3
Dx (Mg m^{-3})	1.374	1.406	1.460	0.946
Diffractometer	Rigaku RAXIS-RAPID Imaging Plate	Rigaku AFC-7R	Rigaku RAXIS-RAPID Imaging Plate	Rigaku RAXIS-RAPID Imaging Plate
Scan type	ω-scan	ω-scan	ω-scan	ω-scan
Absorption correction	multi-scan (T_{min} =0.869, T_{max} = 0.933)	ψ-scan (T_{min} =0.763, T_{max} = 0.845)	none	multi-scan (T_{min} =0.885, T_{max} = 0.975)
$2\theta_{max}$ (°)	55.0 (-19 < h < 21, -30<k<30, -25<l<25)	55.0 (-18 < h < 33, 0<k<23, -10<l<19)	55.0 (-33 < h < 33, -23<k<23, -17<l<18)	55.0 (-29 < h < 29, -29<k<29, -18<l<18)
No. of Indep. reflns.	17126	1948	3090	9164
No. of reflns with > 2σ(I)	11710	1290	2512	8884
No. of parameters	935	204	196	413
R_{int}	0.0546	0.0362	0.0960	0.0615
R1	0.0889	0.0423	0.0536	0.0594
wR^2	0.2543	0.1143	0.1144	0.1585
S	1.024	0.989	0.961	1.087
Weighting scheme	$w=1/[\sigma^2(Fo^2) + (0.01785P)^2+2.5869P]$ where $P = (Fo^2 +2Fc^2)/3$	$w=1/[\sigma^2(Fo^2) + (0.0623P)^2]$ where $P = (Fo^2 +2Fc^2)/3$	$w=1/[\sigma^2(Fo^2) + (0.0623P)^2]$ where $P = (Fo^2 +2Fc^2)/3$	$w=1/[\sigma^2(Fo^2) + (0.1236P)^2+0.4276P]$ where $P = (Fo^2 +2Fc^2)/3$
$(\Delta/\sigma)_{max}$	<0.001	<0.001	<0.001	<0.001
$\Delta\rho_{max}$ (eÅ^{-3})	0.906	0.192	0.819	0.991
$\Delta\rho_{min}$ (eÅ^{-3})	-0.725	-0.248	-0.527	-0.300

dihedral angle θ between the two DMAP ligands is 84.2°. The porphyrin core is ideally saddle shaped as indicated by the fairly small $|\Delta C_{meso}|$ and η values which are 0.01 Å and 1.3(4)°, respectively.

Replacement of the axially coordinated DMAP ligand by Py in $[Fe(OMTPP)L_2]^+$ causes some structural changes as shown in Figure 2 and Figure 4(a). The largest change is the elongation of the Fe−N_{axial} bonds from 2.009(3) to

 © 2004 Wiley-VCH Verlag GmbH & Co. KGaA, Weinheim

Table 2. Comparison of structural parameters $[Fe(OMTPP)L_2]^+$ and $[Fe(OETPP)L_2]^+$

Complexes	T/K	Fe-N_p /Å	Fe-N_{axial} /Å	ϕ / °	θ / °	τ / °	ψ / °	η / °	ω / °	$\lvert\Delta C_{meso}\rvert$ / 0.01Å	$\lvert\Delta C_\beta\rvert$ / 0.01Å	Cavity /Å^3	Ref
$[Fe(OMTPP)(DMAP)_2]^+$	298	1.979(3)	2.009	1.3(3) 2.4(4)	84.2	22.3(2)	143.0(2)	1.3(4)	56.0(2)	1	94	——	this work
$[Fe(OMTPP)Py_2]^+$	298	1.963(3)	2.058(6)	24.8(3)	90	26.1(1)	128.2(1)	10.0(3)	45.2(1)	19	104	19.81	this work
$[Fe(OMTPP)Py_2]^+$	80	1.973(3)	2.024(4)	23.4(2)	90	25.9(1)	128.5(1)	10.2(3)	45.4(1)	18	102	18.77	this work
$[Fe(OETPP)(DMAP)_2]^+$	298	1.977(2)	2.030(3)	10.6(2) 25.0(2)	53.2	30.8(1)	118.4(1)	4.0(2)	66.7(2)	8	122	——	this work
$[Fe(OETPP)(DMAP)_2]^+$	298	1.951	2.000	9 29	70	33[a]	114[a]	17[a]	66	28	122	——	[27]
$[Fe(OETPP)Py_2]^+$	298	1.985	2.201	1.1(4) 3.6(3)	82.3	32.4(1)[b]	115.2(2)[b]	1.2(3)[b]	40.6(1)	3	124	28.88 32.08	[28]
$[Fe(OETPP)Py_2]^+$	80	1.957	1.993	6.3(3) 11.6(3)	85.1	30.8(1)[b]	118.5(1)[b]	3.0(3)[b]	64.5(3)	6	121	23.19	[28]

[a] The angles are calculated on the basis of the molecular structure reported by Ogura et al.[27] [b] The angles are calculated on the basis of the molecular structure reported in our previous paper.

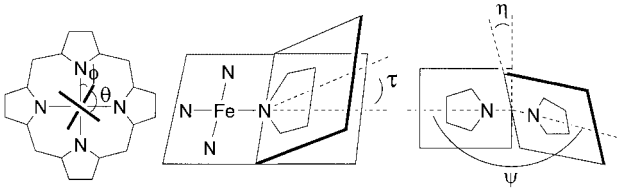

Scheme 2

2.058(6) Å. In contrast, the Fe−N_p bonds exhibit a small contraction of 0.016 Å. These results can be explained in terms of the difference in ligand field strength between DMAP and Py since DMAP is a much stronger field ligand than Py. Thus, the replacement of DMAP by Py weakens the axial coordination and lengthens the Fe−N_{axial} bonds, which in turn strengthens the equatorial coordination and causes concomitant contraction of the Fe−N_p bonds. The saddled motif in $[Fe(OMTPP)Py_2]^+$ is much deeper than that in $[Fe(OMTPP)(DMAP)_2]^+$ as indicated by the increase in the $|\Delta C_\beta|$ and τ values and the decrease in the ψ value; $|\Delta C_\beta|$ increases from 0.94 to 1.04 Å while ψ decreases from 143.0 to 128.2°. The $|\Delta C_{meso}|$ and η values are also different for two complexes - they are 0.01 Å and 1.3(4) ° for the DMAP, and 0.19 Å and 10.0(3)° for the Py complex. Such results indicate that, in contrast to the case of $[Fe(OMTPP)(DMAP)_2]^+$, the saddled structure of $[Fe(OMTPP)Py_2]^+$ contains some ruffling. Due to the mixing of the ruffled deformation, the mutually perpendicular clefts which are located along the diagonal N_p−Fe−N_p axes in the DMAP complex rotate to some extent about the Fe−N_{axial} axis. As a result, the axial ligands are aligned along the new clefts. This must be the reason why the φ value increased to 24.8(3)°.

As mentioned, $[Fe(OETPP)(DMAP)_2]^+$ has two polymorphs, A and B. Structural parameters of the polymorph A such as τ, ψ, and η are listed in Table 2. The same parameters of the polymorph B have been calculated on the basis of the molecular structure reported by Walker and co-workers[27] and these are also listed in Table 2. The average Fe−N_p and Fe−N_{axial} bond lengths are 1.977(2) and 2.030(3)Å in polymorph A, while those in polymorph B are 1.951Å and 2.000Å, respectively. The $|\Delta C_{meso}|$ and η values in A and B are also different from each other - they are 0.08 Å and 4.0° in A, and 0.28 Å and 17° in B. These data indicate that the saddled porphyrin ring in polymorph B contains some ruffling. The dihedral angles θ in A and B are 53.2° and 70°, respectively, which are much smaller than those of the other complexes.

The structural parameters of $[Fe(OMTPP)(DMAP)_2]^+$ can now be compared with those of polymorph A of $[Fe(OETPP)(DMAP)_2]^+$. As shown in Figure 3 and Figure 4(b), the saddled structure has increased on going from the OMTPP to the OETPP complex. The $|\Delta C_\beta|$ and ψ values are 0.94 Å and 143.0(2)° in $[Fe(OMTPP)(DMAP)_2]^+$ while they are 1.22 Å and 118.4(1)° in $[Fe(OETPP)(DMAP)_2]^+$. Although the average Fe−N_{axial} bond length has increased by 0.021 Å on going from OMTPP to OETPP, the average Fe−N_p bond lengths remain almost constant. In contrast to the ideally saddle shaped $[Fe(OMTPP)(DMAP)_2]^+$, the porphyrin core of $[Fe(OETPP)(DMAP)_2]^+$ exhibits a slight ruffling as revealed by the larger $|\Delta C_{meso}|$ and η values of 0.08 Å and 4.0(2)°. As a result, the φ values of the axial ligands have increased from 1.3(3)° and 2.4(4)° in $[Fe(OMTPP)(DMAP)_2]^+$ to 10.6(2) and 25.0(2)° in $[Fe(OETPP)(DMAP)_2]^+$.

Similarly, the structural parameters of $[Fe(OMTPP)Py_2]^+$ can be compared with those of $[Fe(OETPP)Py_2]^+$ reported in our previous communication.[28] The largest difference can be seen in the long Fe−N_{axial} bond lengths of 2.201Å in $[Fe(OETPP)Py_2]^+$. Even the Fe−N_p bonds show a small increase of 0.022 Å. As in the case of the DMAP complexes, the saddled structure has increased on going from the

 © 2004 Wiley-VCH Verlag GmbH & Co. KGaA, Weinheim

OMTPP to the OETPP complex. The $|\Delta C_\beta|$ and ψ values in $[Fe(OMTPP)Py_2]^+$ are 1.04 Å and 128.2(1)° compared with 1.24 Å and 115.2(2)° in $[Fe(OETPP)Py_2]^+$. While the porphyrin core of $[Fe(OMTPP)Py_2]^+$ exhibits some ruffling, that of $[Fe(OETPP)Py_2]^+$ shows quite a pure saddled structure. The $|\Delta C_{meso}|$ and η values are 0.03 Å and 1.2(3)°, respectively.[28] These results indicate that $[Fe(OETPP)Py_2]^+$ has two deep clefts along the diagonal N_p-Fe-N_p axes above and below the porphyrin ring. As a result, the pyridine ligands are situated almost exactly along the diagonal N_p-Fe-N_p axes and the φ values are only 1.1(4)° and 3.6(3)°. Thus, the orientation of planar axial ligands in highly saddled porphyrin complexes can be summarized as follows: the axial ligands are orientated along the diagonal N_p-Fe-N_p axes but they rotate toward the diagonal $C_{meso}-Fe-C_{meso}$ axes as the ruffling character increases.[32–34]

Table 3. Mössbauer parameters of $[Fe(OMTPP)L_2]^+$ and $[Fe(OETPP)L_2]^+$ (L = DMAP, Py)

L	T / K	IS / mm s^{-1}	QS / mm s^{-1}	Γ_1 / mm s^{-1}	Γ_2 / mm s^{-1}	Ref
OMTPP						
DMAP	290	0.16	1.86	0.30	0.33	this work
	70	0.23	1.89	0.38	0.54	
Py	299	0.19	2.18	0.23	0.26	this work
	78	0.25	2.18	0.33	0.42	
OETPP						
DMAP	290	0.19	2.21	0.27	0.32	[26]
	80	0.26	2.31	0.55	0.89	
Py	290	0.32	2.76	0.27	0.29	[26]
	70	0.25	2.29	0.47	0.64	

Spin States of $[Fe(OMTPP)L_2]^+$

(i) Mössbauer Spectra

Figure 5 shows the temperature dependence of the Mössbauer parameters such as isomer shift (IS) and quadrupole splitting (QS) for $[Fe(OMTPP)L_2]^+$ and $[Fe(OETPP)L_2]^+$ (L = DMAP, Py) determined for microcrystalline samples.[26] Table 3 lists the IS, QS and effective line widths (Γ_1 and Γ_2). The IS value increases from 0.16 to 0.23 mm·s^{-1} in the case of $[Fe(OMTPP)(DMAP)_2]^+$ as the temperature is lowered from 290 to 77 K. A similar increase has been observed for the IS values of $[Fe(OMTPP)Py_2]^+$ and $[Fe(OETPP)(DMAP)_2]^+$ which increase from 0.19 to 0.25 mm·s^{-1} and from 0.19 to 0.26 mm·s^{-1}, respectively. Only the IS value of $[Fe(OETPP)Py_2]^+$ shows a large decrease from 0.32 to 0.25 mm·s^{-1} as shown in Figure 5(a). The QS values of $[Fe(OMTPP)(DMAP)_2]^+$, $[Fe(OMTPP)Py_2]^+$, and $[Fe(OETPP)(DMAP)_2]^+$ are almost constant in the temperature range 290–77 K and are 1.86–1.90 mm·s^{-1} for $[Fe(OMTPP)(DMAP)_2]^+$, 2.13–2.18 mm·s^{-1} for $[Fe(OMTPP)Py_2]^+$, and 2.21–2.31 mm·s^{-1} for $[Fe(OETPP)(DMAP)_2]^+$. These three complexes thus maintain their low-spin states in the temperature ranges examined. The QS values of the low-spin complexes are in the range of 1.3–2.4 mm·s^{-1}.[26,35–37] In contrast, the QS value of 2.76 mm·s^{-1} for $[Fe(OETPP)Py_2]^+$ at 290 K is rather large and decreases to 2.29 mm·s^{-1} at 77 K. Since the S = 3/2 complexes are characterized by the large QS values,[10,12,13,24,26,38,39] this Mössbauer result suggests that $[Fe(OETPP)Py_2]^+$ exhibits a spin crossover from the predominantly S = 3/2 state at 290 K to the predominantly S = 1/2 state at 77 K.

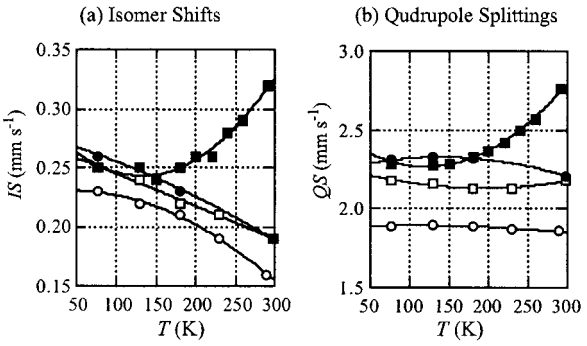

Figure 5. Temperature dependence of the Mössbauer parameters of $[Fe(OMTPP)L_2]ClO_4$ and $[Fe(OETPP)L_2]ClO_4$ measured on microcrystalline samples; open circles: $[Fe(OMTPP)(DMAP)_2]ClO_4$; open squares: $[Fe(OMTPP)Py_2]ClO_4$; filled circles: $[Fe(OETPP)(DMAP)_2]ClO_4$; filled squares: $[Fe(OETPP)Py_2]ClO_4$

(ii) SQUID Magnetometry

Figure 6 shows the temperature dependence of the effective magnetic moments of $[Fe(OMTPP)L_2]ClO_4$ (L = DMAP, Py) taken on microcrystalline samples using SQUID magnetometry. For comparison, the corresponding data for $[Fe(OETPP)L_2]ClO_4$ (L = DMAP, Py) reported in our previous communication are also given.[26] While the effective magnetic moments of $[Fe(OMTPP)(DMAP)_2]^+$, $[Fe(OMTPP)Py_2]^+$, and $[Fe(OETPP)(DMAP)_2]^+$ are 2.1–2.8 μ_B in the temperature range of 50–300 K, those of $[Fe(OETPP)Py_2]^+$ are 2.4–3.4 μ_B in the same temperature range. These results suggest that the former three complexes adopt mainly the S = 1/2 spin state while $[Fe(OETPP)Py_2]^+$ exhibits the spin transition from the predominantly S = 3/2 state to the predominantly S = 1/2 state as the temperature is lowered. The SQUID results are therefore consistent with the Mössbauer results.

Reasons for the Absence of the Spin Crossover Process in $[Fe(OMTPP)Py_2]^+$

In our previous communication, we reported the basis of the spectroscopic and magnetic results that are observed when a novel spin transition takes place from the S = 3/2 to the S = 1/2 spin state in $[Fe(OETPP)Py_2]^+$ both in solution and in the solid state as the temperature is lowered.[26] The X-ray crystallographic analysis of the same complex at three different temperatures revealed that the contraction of

 © 2004 Wiley-VCH Verlag GmbH & Co. KGaA, Weinheim

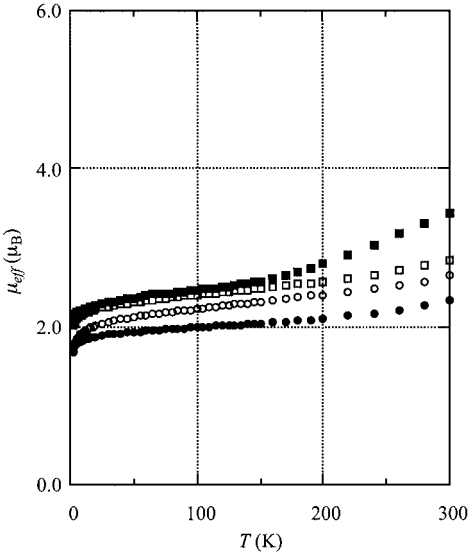

Figure 6. Temperature dependence of the effective magnetic moments of $[Fe(OMTPP)L_2]^+$ and $[Fe(OETPP)L_2]^+$ measured on microcrystalline samples using SQUID magnetometry; open circles: $[Fe(OMTPP)(DMAP)_2]ClO_4$; open squares: $[Fe(OMTPP)Py_2]ClO_4$; filled circles: $[Fe(OETPP)(DMAP)_2]ClO_4$; filled squares: $[Fe(OETPP)Py_2]ClO_4$

the Fe−N_{axial} bond is an important requirement for the spin crossover process to occur. The average Fe−N_{axial} bond length decreases from 2.201(3) to 1.993(3) Å as the temperature is lowered from 298 to 80 K.[28] Similar bond contractions have been reported by Scheidt and co-workers in $[Fe(OEP)(3\text{-}ClPy)_2]^+$, which could be ascribed to the spin transition from the $S = 5/2$ to the $S = 1/2$ state.[40,41] Thus, we expected such a spin transition should also occur in $[Fe(OMTPP)Py_2]^+$. Both the Mössbauer and SQUID measurements for the microcrystalline samples indicated, however, that such a phenomenon never occurs in the solid state. $[Fe(OMTPP)Py_2]^+$ maintains the $S = 1/2$ spin state over a wide range of temperatures. To understand the reasons for the absence of the spin crossover process in $[Fe(OMTPP)Py_2]^+$, we determined the crystal and molecular structures of this complex at 80 K. The crystal data and structural parameters are listed in Table 1 and Table 2, respectively. The data in Table 2 indicate that the Fe−N_{axial} bond in $[Fe(OMTPP)Py_2]^+$ shows only a slight decrease of 0.034 Å, as the temperature is lowered from 298 to 80 K whereas the corresponding decrease reaches as much as 0.208 Å in the case of the spin crossover complex, $[Fe(OETPP)Py_2]^+$. The data in Table 2 also indicate that the structural changes are fairly small in all respects including the values of φ, θ, τ, ω, ψ, and η. For example, while the axial ligands rotate by 5.2° and 8.0° as the temperature is lowered from 298 to 80 K in $[Fe(OETPP)Py_2]^+$, they rotate by only 1.4° in $[Fe(OMTPP)Py_2]^+$. These data are consistent with the Mössbauer and SQUID results, which indicate that $[Fe(OMTPP)Py_2]^+$ maintains the $S = 1/2$ spin state over a wide range of temperatures in the solid state.

The difference in the magnetic behavior can be ascribed to the difference in molecular packing between $[Fe(OMTPP)Py_2]^+$ and $[Fe(OETPP)Py_2]^+$ in the crystal lattices. The crystal data listed in Table 1 as well as those of $[Fe(OETPP)Py_2]^+$ reported in our previous communication indicate that the crystal systems for $[Fe(OMTPP)Py_2]^+$ and $[Fe(OETPP)Py_2]^+$ are different. The former adopts a cubic while the latter exhibits a monoclinic crystal system.[28] The monoclinic system is a less condensed packing form than the cubic system since the latter is the closest packing form as shown in Figure 7 (a and b). In fact, the density (D_x) of $[Fe(OMTPP)Py_2]^+$ with the cubic crystal system is 1.406 g cm^{-3}, while that of monoclinic $[Fe(OMTPP)(DMAP)_2]^+$ is 1.374 g cm^{-3} in spite of its larger molecular weight. It should be noted that the D_x value of the spin crossover complex, $[Fe(OETPP)Py_2]^+$, is only 1.296 g cm^{-3} at 298 K. Thus, $[Fe(OMTPP)Py_2]^+$ is the most densely packed among the three complexes. In other words, the Fe−N_{axial} bond contraction in $[Fe(OMTPP)Py_2]^+$ at lower temperature must be more difficult than that in $[Fe(OETPP)Py_2]^+$ since each molecule of $[Fe(OMTPP)Py_2]^+$ is placed in a densely packed crystal lattice even at ambient temperature. Consequently the spin crossover process, which requires a decrease in the Fe−N_{axial} bond length caused by the contrac-

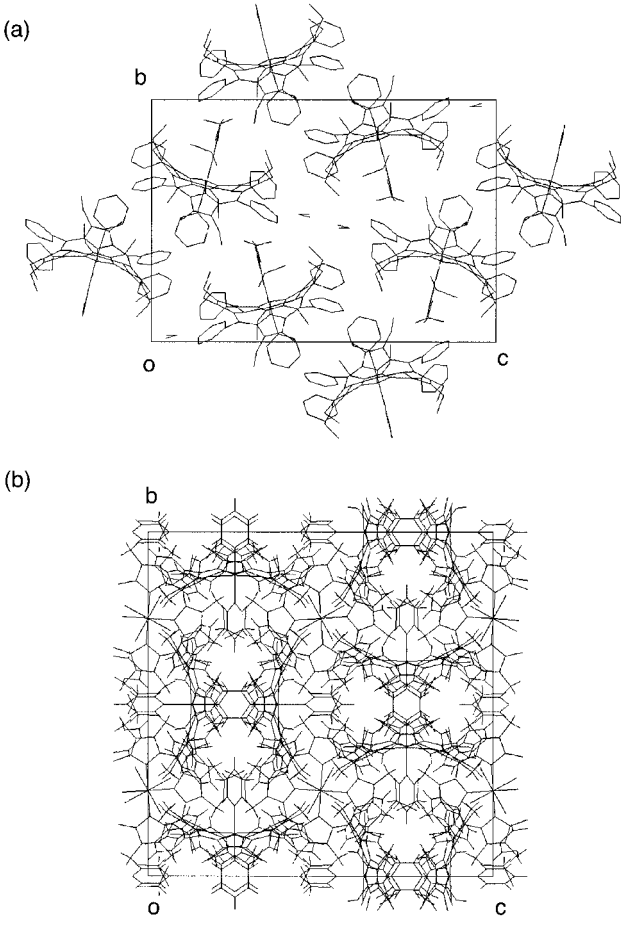

Figure 7. Crystal packing diagrams of (a) monoclinic $[Fe(OETPP)Py_2]^+$ and (b) cubic $[Fe(OMTPP)Py_2]^+$ viewed along the *a* axis

 © 2004 Wiley-VCH Verlag GmbH & Co. KGaA, Weinheim

tion of the unit cell, takes place only in $[Fe(OETPP)Py_2]^+$. It should also be noted that the decrease in the crystal lattice occurs differently between $[Fe(OMTPP)Py_2]^+$ and $[Fe(OETPP)Py_2]^+$ because of the difference in crystal systems. Since the structure of $[Fe(OMTPP)Py_2]^+$ adopts a cubic system, the contraction of the crystal lattice should occur isotropically as the temperature is lowered. In the case of $[Fe(OETPP)Py_2]^+$, however, an anisotropic contraction is expected at lower temperature because of its monoclinic system. In fact, we have observed quite a direction-dependent contraction as reported in our previous communication. The major contraction takes place along the *b*-axis, which is tilted by only 15° from the $Fe-N_{axial}$ axis.[28] Thus, the contraction of the unit cell along the b-axis specifically decreases the $Fe-N_{axial}$ bonds and, consequently, induces the spin crossover process.

As mentioned, the displacement and rotation of the axial ligands are the major driving forces for the spin-crossover process in $[Fe(OETPP)Py_2]^+$.[28] The degree of displacement and rotation should correlate closely with the shape and size of the cavity around the axial ligand. The axial ligands situated in a wide cavity could easily alter their positions when the external conditions such as temperature and pressure are changed. In this respect, quantitative elucidation of the cavities around the axial ligands is quite important for clarifying the mechanism of the spin-crossover process. To reveal the spatial environment around the axial ligands of $[Fe(OETPP)Py_2]^+$ and $[Fe(OMTPP)Py_2]^+$, we have carried out a CAVITY calculation developed by Ohashi and co-workers.[42,43] In this calculation, the cavity for the axial ligand is defined as the concave space limited by the surface of the spheres,[42,43] where each atom in the vicinity of the pyridine ligand is located in the center of the sphere with the radius of each sphere being greater than the van der Waals radius by 1.2 Å.[44] Figure 8 (a and b) exhibit the change in orientation of the pyridine ligand of $[Fe(OMTPP)Py_2]^+$ as the temperature is lowered from 298 to 80 K. In this complex, a quarter of the molecule is crystallographically independent. Thus, the cavity size and shape of each ligand is exactly the same in a single molecule. Figure 8 (c and d) illustrate the change in orientation of one of the pyridine ligands of $[Fe(OETPP)Py_2]^+$. Since the complex has two independent pyridine ligands in a single molecule, the cavities of the ligands are different from each other. The cavity sizes of these complexes are also listed in Table 2. The data in Table 2 clearly indicate that the cavity sizes are quite different between the two complexes. The OETPP complex showing the spin-crossover phenomenon has cavities of 32.08 and 28.88 $Å^3$ at 298 K, while the OMTPP complex has a much smaller cavity size of 19.81$Å^3$. Thus, the cavity size of the Py ligand in $[Fe(OMTPP)Py_2]^+$ is only 65% of that in $[Fe(OETPP)Py_2]^+$. Close inspection of the cavities in Figure 8 (c and d) reveals that the pyridine ligand in the OETPP complex, signified as a bold line, is aligned along the diagonal N1−N3 axis and makes contact with a convex surface created by the neighboring atoms at 298 K. When the temperature is lowered to 80 K, the $Fe-N_{axial}$ bond contracts. Concomitantly, the pyridine ligand rotates toward the diagonal $C_{meso}-C_{meso}$ axis to minimize the repulsion with the porphyrin core until it makes contact with another convex surface. In other words, each pyridine ligand of $[Fe(OETPP)Py_2]^+$ has room for rotation, which in turn enables the contraction of the $Fe-N_{axial}$ bond and makes the spin crossover possible. In contrast, the pyridine ligand in $[Fe(OMTPP)Py_2]^+$ is confined to a limited space of only 65% of that available in $[Fe(OETPP)Py_2]^+$. Furthermore, the cavity shape around the pyridine ligand does not allow any rotation of the ligand as shown in Figure 8 (a and b). Both sides of the pyridine ligand make contact with the convex surfaces. Another notable difference is the compression ratio of the cavity as the temperature is lowered from 298 to 80 K. Although the cavity of the OETPP complex decreases on average by 17.7%, that of the OMTPP complex shows a much smaller decrease of 5.25%. Thus, the absence of the spin crossover process in $[Fe(OMTPP)Py_2]^+$ can be attributed to the fact that the molecules are placed in a densely packed crystal lattice even at room temperature and that the axial ligands are confined to narrow cavities. In other words, a loosely packed crystal system and wide cavities around the axial ligands which allow their displacement and rotation are the important requirements for the spin transition to occur in the solid state.

Conclusions

Combined analysis using Mössbauer spectroscopy and SQUID magnetometry has revealed that the spin state of the saddle shaped complex $[Fe(OMTPP)Py_2]^+$ is quite different from that of the corresponding $[Fe(OETPP)Py_2]^+$. While $[Fe(OETPP)Py_2]^+$ exhibited a novel spin crossover process over 80−300 K, $[Fe(OMTPP)Py_2]^+$ maintained the $S = 1/2$ spin state in the same temperature range. The molecular structures of $[Fe(OMTPP)Py_2]^+$ determined at 298 and 80 K by X-ray crystallography further support the Mössbauer and SQUID results. The $Fe-N_{axial}$ bond contraction, which is one of the most important requirements for the spin crossover process to occur, is only 0.034 Å even if the temperature is lowered from 298 to 80 K whereas the bond contraction reaches as much as 0.208 Å in the case of $[Fe(OETPP)Py_2]^+$. To further understand the spin crossover process in the solid state, we have determined the cavity size of each ligand in $[Fe(OMTPP)Py_2]^+$ and $[Fe(OETPP)Py_2]^+$ by Ohashi's method.[42−44] While the OETPP complex has cavities of 32.08 and 28.88 $Å^3$, the OMTPP complex exhibits a much smaller cavity with a volume of 19.81 $Å^3$. Furthermore, the cavities of the OETPP complex decreased by 15.6 and 19.7% as the temperature was lowered from 300 to 80 K. In contrast, the contraction of the cavity in the OMTPP complex was only 5.3%. On the basis of these results, we conclude that the absence of the spin crossover process in $[Fe(OMTPP)Py_2]^+$ can be attributed to the densely packed crystal lattice together with the narrow cavities around the axial ligands. In other words, the molecules have to be placed in a loosely packed crystal

 © 2004 Wiley-VCH Verlag GmbH & Co. KGaA, Weinheim

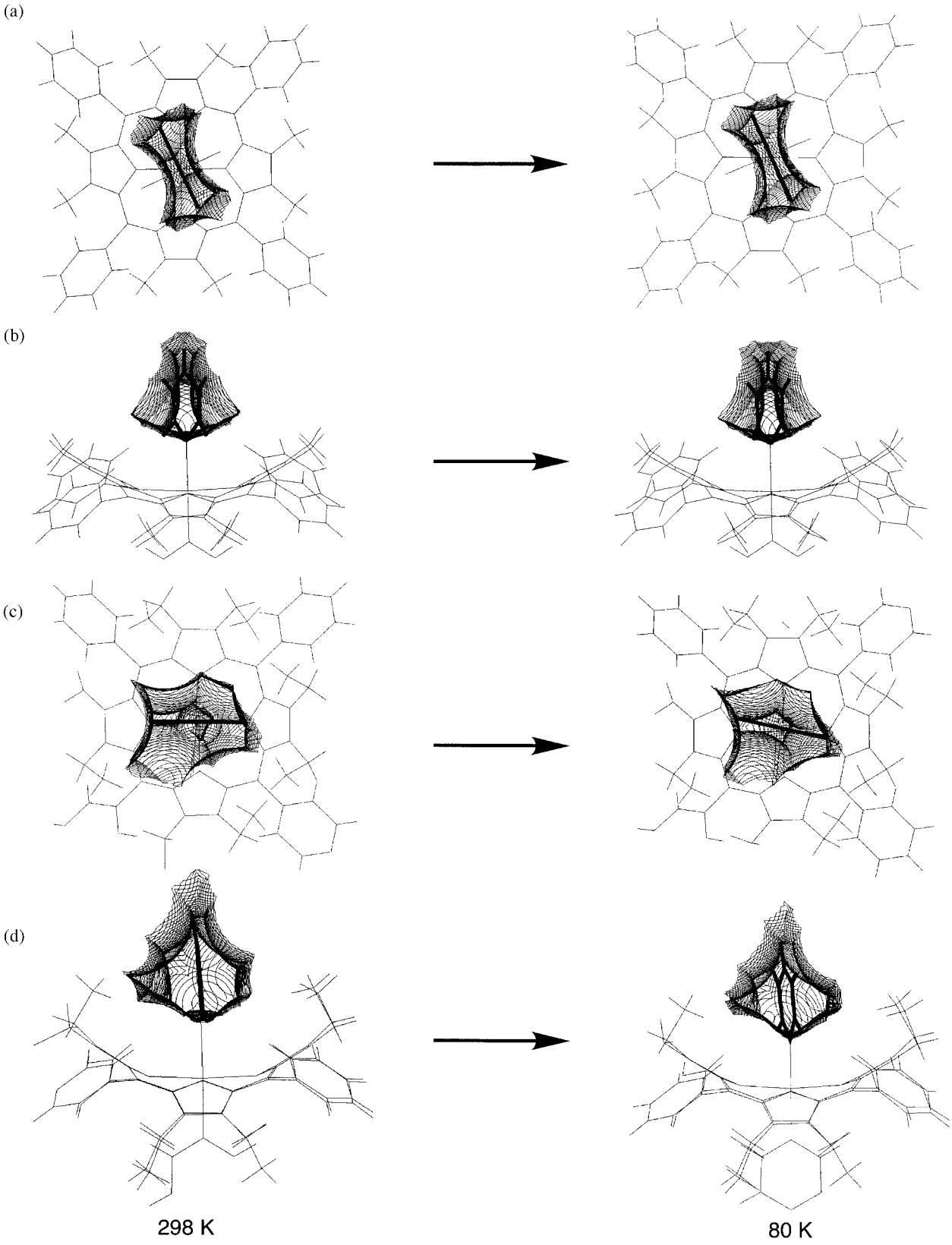

Figure 8. The orientation change of the pyridine ligands in the cavities of $[Fe(OMTPP)Py_2]ClO_4$ and $[Fe(OETPP)Py_2]ClO_4$ as the temperature is lowered from 298 K (left) to 80 K (right): (a) the cavity viewed along the normal to the average porphyrin plane of $[Fe(OMTPP)Py_2]ClO_4$, (b) the cavity viewed along the N2−N4 axis of $[Fe(OMTPP)Py_2]ClO_4$, (c) the cavity viewed along the normal to the average porphyrin plane of $[Fe(OETPP)Py_2]ClO_4$, and (d) the cavity viewed along the N1−N3 axis of $[Fe(OETPP)Py_2]ClO_4$

 © 2004 Wiley-VCH Verlag GmbH & Co. KGaA, Weinheim

lattice and the cavities around the axial ligands have to be wide for the occurrence of the spin crossover in the solid state.

Experimental Section

General Procedures: Iron-57 Mössbauer spectra were measured on a Wissel Mössbauer spectrometer system consisting of an MDU-1200 function generator, a DFG-1200 driving unit and an MVT-100 velocity transducer, incorporating a model 7800 multi-channel analyzer form Seiko EG&G Co. Ltd. The samples were kept in a Heli-Tran LT-3 gas-flow cryostat from Advanced Research System Inc. equipped with a 9620 digital temperature controller from Scientific Instruments Inc. and the ^{57}Co(Rh) source was kept at room temperature. The data were analyzed using the standard least-squares method. The isomer shifts (δ) are given relative to α-iron foil at room temperature. The solid state magnetic susceptibilities were measured over the temperature range 2−300 K in a magnetic field of 0.5 T with a SQUID magnetometer (Quantum Design MPMS-7). The measured data were corrected for diamagnetic contributions.

Synthesis: H_2(OMTPP) and the iron(III) chloride complex [Fe(OMTPP)Cl] were prepared according to the literature.[45−49] [Fe(OMTPP)(THF)$_2$]ClO_4 was prepared by the addition of a THF solution of $AgClO_4$ to a THF solution of [Fe(OMTPP)Cl].[49,50] The bis-ligated complexes, [Fe(OMTPP)L_2]ClO_4, were prepared by the addition of 10−15 equiv. of the ligand (DMAP or Py) to a $CHCl_3$ solution of [Fe(OMTPP)(THF)$_2$]ClO_4.[49]

Crystal Structure of [Fe(OMTPP)(Py)$_2$]ClO_4·1/3$HClO_4$·4/3$CHCl_3$ at 298 K

i) Preparation of Crystals: The purple solid [Fe(OMTPP)(THF)$_2$]ClO_4 was dissolved in $CHCl_3$ containing 10−15 equiv. of pyridine and allowed to stand at room temperature. One of the cubic crystals thus obtained was sealed within a glass capillary to prevent evaporation of solvent in the crystal lattice.

ii) X-ray Crystal Structure Analysis: All data were collected on a Rigaku AFC-7R diffractometer with filtered Mo-K_α radiation (λ = 0.71069Å) and a rotating anode generator. Cell constants and an orientation matrix for data collection were obtained from a least-squares refinement using the setting angles of 21 carefully centered reflections in the range $30.08 < 2\theta < 33.66°$ corresponded to an *I*-centered cubic cell. The data were collected at room temperature using the ω scan technique to a maximum 2θ value of 54.9°. Of the 1948 reflections which were collected, 1681 were unique (R_{int} = 0.0362). An empirical absorption correction based on azimuthal scans of several reflections was applied which resulted in transmission factors ranging from 0.80 to 0.98.[51] The structures were solved by direct methods with the program SIR97,[52] TEXSAN[53] and expanded using the program DIRDIF94.[54] The structure refinement was carried out by the full-matrix least-squares method with SHELXL-97.[55] All non-hydrogen atoms were refined anisotropically. All the hydrogen atoms were located in calculated positions. The positional parameters of the H atoms were constrained to have C−H distances of 0.96Å for primary, 0.97Å for secondary, and 0.93 Å for aromatic H atoms. The H-atom *U* values were constrained to have 1.2 times the equivalent isotropic *U* value of the atoms to which they are attached (1.5 for methyl groups). The atomic scattering factors were taken from the International Tables for Crystallography.

CCDC-208539 to -208542 contain the supplementary crystallographic data for this paper. These data can be obtained free of charge at www.ccdc.cam.ac.uk/conts/retrieving.html [or from the Cambridge Crystallographic Data Centre, 12, Union Road, Cambridge CB2 1EZ, UK; Fax: (internat.) +44-1223/336-033; E-mail: deposit@ccdc.cam.ac.uk].

iii) Crystal Data, Experimental and Refinement Details for Crystal Structure Determination: Crystal data: $C_{62}H_{54}N_6O_4Cl$·0.33$HClO_4$·1.33$CHCl_3$; M_r = 1230.72 g mol^{-1}; crystal color: purple; crystal dimensions: 0.5 × 0.5 × 0.3 mm; cubic, *I*43*d* (#220); $a = b = c$ = 25.937(3) Å; α = β = γ = 90°; *V*= 17448(3)Å^3; *Z* = 12; ρ = 1.406 gcm^{-3}; R_{int} = 0.0362, R_σ = 0.060; $-18 < h < 33$, $0 < k < 23$, $-10 < l < 19$; Refinement: Refinement on F^2; $R[F^2 > 2s(F^2)]$ = 0.0423, *R*(all data) = 0.0889, wR^2 = 0.1042; *S* = 0.988; 1948 reflections; 0 restraints; 204 parameters; $w = 1/[\sigma^2(F_o^2) + (0.0625\ P)^2]$ where $P = (F_o^2 + 2F_c^2)/3$; $(\Delta/\sigma)_{max} < 0.001$; $\Delta\rho_{max}$ = 0.19 eÅ^3; $\Delta\rho_{min}$ = −0.249 eÅ^3

Crystal Structure of [Fe(OMTPP)(DMAP)$_2$]ClO_4·4$CHCl_3$

i) Preparation of Crystals: The purple solid [Fe(OMTPP)(THF)$_2$]ClO_4 was dissolved in $CHCl_3$ containing 10−15 equiv. of DMAP and allowed to stand at room temperature. One of the prismatic crystals thus obtained was sealed within a glass capillary to prevent evaporation of solvent in the crystal lattice.

ii) X-ray Crystal Structure Analysis: All measurements were carried out on a Rigaku RAXIS-RAPID Imaging Plate diffractometer with graphite monochromated Mo-K_α radiation (λ = 0.71069Å) and a rotating anode generator. Indexing was performed from 3 oscillations which were exposed for 7.5 minutes. The camera radius was 127.40 mm. Readout was performed in the 0.100 mm pixel mode. The data were collected at 80 K to a maximum 2θ value of 55.0°. A total of 110 images, corresponding to 222.0° oscillation angles were collected with 3 different goniometer settings. Exposure time was 2.70 minutes per degree. Data were processed with the PROCESS-AUTO program package. Of the 106877 reflections which were collected, 17126 were unique (R_{int} = 0.039). The linear absorption coefficient, μ, for Mo-K_α radiation is 6.9 cm^{-1}. A symmetry related absorption correction using the ABSCOR program was applied which resulted in transmission factors ranging from 0.869−0.933. The data were corrected for Lorentz and polarization effects.[55] The structure was solved by a procedure similar to that described above.

iii) Crystal Data, Experimental and Refinement Details for Crystal Structure Determination: Crystal data: $C_{70}H_{67}N_8O_4ClFe$. 4$CHCl_3$; M_r = 1602.02 g mol^{-1}; crystal color: purple; crystal dimensions: 0.2 × 0.1 × 0.1 mm; monoclinic, $P2_1/c$ (#14); a= 16.4556(5)Å, b = 23.7289(6)Å, c = 19.8424(6)Å; β = 91.924(1)°; V = 7743.6(4) Å^3; Z = 4; ρ = 1.374 gcm^{-3}; R_{int} = 0.0546, R_σ = 0.0278; $-19 < h < 21$, $-30 < k < 30$, $-25 < l < 25$; Refinement: Refinement on F^2; $R[F^2 > 2\sigma(F^2)]$ = 0.0899, *R*(all data) = 0.1205, wR^2 = 0.2543; *S* = 1.024; 17126 reflections; 0 restraints; 935 parameters; $w = 1/[\sigma^2(F_o^2) + (0.01785P)^2 + 2.5869P]$ where $P = (F_o^2 + 2F_c^2)/3$; $(\Delta/\sigma)_{max} < 0.001$; $\Delta\rho_{max}$ = 0.906 eÅ^3; $\Delta\rho_{min}$ = −0.725 eÅ^3

Crystal Structure of [Fe(OETPP)(DMAP)$_2$]ClO_4

i) Preparation of Crystals: The purple solid [Fe(OETPP)(THF)$_2$]ClO_4 was dissolved in $CHCl_3$ containing 10−15 equiv. of DMAP and allowed to stand at room temperature. One of the prismatic crystals thus obtained was sealed within a glass capillary to prevent evaporation of solvent in the crystal lattice.

 © 2004 Wiley-VCH Verlag GmbH & Co. KGaA, Weinheim

ii) X-ray Crystal Structure Analysis: All measurements were carried out on a Rigaku RAXIS-RAPID Imaging Plate diffractometer with graphite monochromated Mo-K_α radiation (λ = 0.71069Å) and a rotating anode generator. Indexing was performed from 3 oscillations which were exposed for 1.5 minutes. The camera radius was 127.40 mm. Readout was performed in the 0.100 mm pixel mode. The data were collected at 298 K to a maximum 2θ value of 55.0°. A total of 110 images, corresponding to 386.5.0° oscillation angles were collected with 3 different goniometer settings. Exposure time was 1.70 minutes per degree. Data were processed using the PROCESS-AUTO program package. Of the 85871 reflections which were collected, 5022 were unique (R_{int} = 0.051). The linear absorption coefficient, μ, for Mo-K_α radiation is 5.1 cm^{-1}. A symmetry related absorption correction using the ABSCOR program was applied which resulted in transmission factors ranging from 0.885−0.975. The data were corrected for Lorentz and polarization effects.[56] The structure was solved by a procedure similar to that described above.

iii) Crystal Data, Experimental and Refinement Details for Crystal Structure Determination: Crystal data: $C_{74}H_{80}N_8ClFe$, M_r = 1172.76 g mol^{-1}; crystal color: purple; crystal dimensions: 0.5 × 0.4 × 0.1 mm; trigonal, $P3_121$(#152); $a = b$ = 22.595(9) Å, c = 13.967(5) Å; V = 6175(3) $Å^3$; Z = 3; ρ = 0.946 g cm^{-3}; R_{int} = 0.0615, R_σ = 0.0224; $-29 < h < 29$, $-29 < k < 29$, $-18 < l < 18$; Refinement: Refinement on F^2; $R[F^2 > 2\sigma(F^2)]$ = 0.0594, R(all data) = 0.0607, wR^2 = 0.1585; S = 1.087; 9164 reflections; 4 restraints; 413 parameters; $w = 1/[\sigma^2(F_o^2) + (0.1236\ P)^2 + 0.4276\ P]$ where $P = (F_o^2 + 2F_c^2)/3$; $(\Delta/\sigma)_{max} < 0.001$; $\Delta\rho_{max}$ = 0.991 $eÅ^3$; $\Delta\rho_{min}$ = −0.300 $eÅ^3$

Acknowledgments

We thank Professors Yuji Ohashi and Hidehiro Uekusa, Faculty of Science, Tokyo Institute of Technology for assistance with the X-ray measurements. This work was supported by the Grant in Aid (No. 14540521, M. N.) for Scientific Research from the Ministry of Education, Culture, Sports, Science and Technology, Japan. Thanks are due to the Research Center for Molecular-Scale Nanoscience, the Institute for Molecular Science (IMS).

[1] W. R. Scheidt, C. A. Reed, *Chem. Rev.* **1981**, *81*, 543−555.
[2] W. R. Scheidt, M. Gouterman, in *Iron Porphyrin, Part I* (Eds.: A. B. P. Lever, H. B. Gray), Addison-Wesley, Reading, MA, **1983**, pp. 89−139.
[3] W. R. Scheidt, in *The Porphyrin Handbook*, *Vol. 3* (Eds.: K. M. Kadish, K. M. Smith, R. Guilard), Academic Press, San Diego, **2000**, ch. 16, pp. 49−112.
[4] M. M. Maltempo, *J. Chem. Phys.* **1974**, *61*, 2540−2547.
[5] S. Fujii, T. Yoshimura, H. Kamada, K. Yamaguchi, S. Suzuki, S. Shidara, S. Takakuwa, *Biochim. Biophys. Acta* **1995**, *1251*, 161−169.
[6] H. Déméné, P. Tsan, P. Gans, D. Marion, *J. Phys. Chem. B.* **2000**, *104*, 2559−2569.
[7] Abbreviations: OMTPP or OETPP: dianions of 2,3,7,8,12,13,17,18-octamethyl- or 2,3,7,8,12,13,17,18-octaethyl-5,10,15,20-tetraphenylporphyrin. TMP, TPP, and T*i*PrP: dianions of 5,10,15,20-tetramesitylporphyrin, 5,10,15,20-tetraphenylporphyrin, and 5,10,15,20-tetraisopropylporphyrin. DMAP: 4-(dimethylamino)pyridine. Py: pyridine. 4-CNPy: 4-cyanopyridine dianion.
[8] A. Ikezaki, M. Nakamura, *Chem. Lett.* **2000**, 994−995.
[9] A. Ikezaki, M. Nakamura, *Inorg. Chem.* **2002**, *41*, 6225−6236.
[10] C. A. Reed, F. Guiset, *J. Am. Chem. Soc.* **1996**, *118*, 3281−3282.
[11] D. R. Evans, C. A. Reed, *J. Am. Chem. Soc.* **2000**, *122*, 4660−4667.
[12] T. Ikeue, T. Saitoh, T. Yamaguchi, Y. Ohgo, M. Nakamura, M. Takahashi, M. Takeda, *Chem. Commun.* **2000**, 1989−1990.
[13] J.-P. Simonato, J. Pecaut, L. Le Pape, J.-L. Oddou, C. Jeandey, M. Shang, W. R. Scheidt, J. Wojacynski, S. Wolowiec, L. Latos-Grazynski, J.-C. Marchon, *Inorg. Chem.* **2000**, *39*, 3978−3987.
[14] F. A. Walker in *The Porphyrin Handbook, Vol. 5* (Eds.: K. M. Kadish, K. M. Smith, R. Guilard), Academic Press, San Diego, **2000**, ch. 36, pp. 81−183.
[15] M. Nakamura, T. Ikeue, H. Fujii, T. Yoshimura, *J. Am. Chem. Soc.* **1997**, *119*, 6284−6291.
[16] M. Nakamura, T. Ikeue, H. Fujii, T. Yoshimura, K. Tajima, *Inorg. Chem.* **1998**, *37*, 2405−2414.
[17] T. Ikeue, Y. Ohgo, T. Saitoh, M. Nakamura, H. Fujii, M. Yokoyama, *J. Am. Chem. Soc.* **2000**, *122*, 4068−4076.
[18] S. Wolowiec, L. Latos-Grazynski, M. Mazzanti, J.-C. Marchon, *Inorg. Chem.* **1997**, *36*, 5761−5771.
[19] S. Wolowiec, L. Latos-Grazynski, D. Toronto, J.-C. Marchon, *Inorg. Chem.* **1998**, *37*, 724−732.
[20] M.-A. Pilard, M. Guillemot, L. Toupet, J. Jordanov, G. Simonneaux, *Inorg. Chem.* **1997**, *36*, 6307−6314.
[21] G. Simonneaux, V. Schünemann, C. Morice, L. Carel, L. Toupet, H. Winkler, A. X. Trautwein, F. A. Walker, *J. Am. Chem. Soc.* **2000**, *122*, 4366.
[22] Y. Ohgo, T. Saitoh, M. Nakamura, *Acta Crystallogr., Sect. C* **2001**, *57*, 233−234.
[23] Y. Ohgo, T. Saitoh, M. Nakamura, *Acta Crystallogr., Sect. C* **1999**, *55*, 1284−1286.
[24] M. Nakamura, T. Ikeue, Y. Ohgo, M. Takahashi, M. Takeda, *Chem. Commun.* **2002**, 1198−1199.
[25] K. M. Barkigia, M. W. Renner, J. Fajer, *J. Porhyrins and Phthalocyanins* **2000**, *5*, 415−418.
[26] T. Ikeue, Y. Ohgo, T. Yamaguchi, M. Takahashi, M. Takeda, M. Nakamura, *Angew. Chem. Int. Ed.* **2001**, *40*, 2617−2620.
[27] H. Ogura, L. Yatsunyk, C. J. Medforth, K. M. Smith, K. M. Barkigia, M. W. Renner, D. Melamed, F. A. Walker, *J. Am. Chem. Soc.* **2001**, *123*, 6564−6578.
[28] Y. Ohgo, T. Ikeue, M. Nakamura, *Inorg. Chem.* **2002**, *41*, 1698−1700.
[29] D. M. Collins, R. Countryman, J. L. Hoard, *J. Am. Chem. Soc.* **1972**, *94*, 2066−2072.
[30] D. Inniss, S. M. Soltis, C. E. Strouse, *J. Am. Chem. Soc.* **1988**, *110*, 5644−5650.
[31] M. K. Safo, G. P. Gupta, F. A. Walker, W. R. Scheidt, *J. Am. Chem. Soc.* **1991**, *113*, 5497−5510.
[32] W. R. Scheidt, J. L. Kirner, J. L. Hoard, C. A. Reed, *J. Am. Chem. Soc.* **1987**, *109*, 1963−1968.
[33] O. Q. Munro, H. M. Marques, P. G. Debrunner, K. Mohnrao, W. R. Scheidt, *J. Am. Chem. Soc.* **1995**, *117*, 935−954.
[34] Y. Ohgo, T. Ikeue, T. Saitoh, M. Nakamura, *Chem. Lett.* **2002**, 432−433.
[35] J. R. Sams, T. B. Tsin, in *The Porphyrins* (Ed.: D. Dolphin); Academic Press, New York, **1979**, vol. 4, ch. 9, pp 425−478.
[36] P. G. Debrunner, in *Iron Porphyrin Part III*, A (Eds. B. P. Lever, H. B. Gray), VCH, New York, **1989**, pp. 139−234.
[37] P. Gütlich, J. Ensling, in *Inorganic Electronic Structure and Spectroscopy*, *Vol. 1* (Eds.: E. I. Solomon, A. B. P. Lever), John Wiley & Sons, Inc., New York, **1999**, pp. 161−211.
[38] T. Ikeue, Y. Ohgo, M. Takahashi, M. Takeda, S. Neya, N. Funasaki, M. Nakamura, *Inorg. Chem.* **2001**, *40*, 3650−3652.
[39] H. Keutel, I. Käpplinger, E.-G. Jäger, M. Grodzicki, V. Schünemann, A. X. Trautwein, *Inorg. Chem.* **1999**, *38*, 2320−2327.
[40] W. R. Scheidt, D. K. Geiger, K. J. Haller, *J. Am. Chem. Soc.* **1982**, *104*, 495−499.
[41] M. K. Ellison, H. Nasri, Y.-M. Xia, J.-C. Marchon, C. E. Schulz, P. G. Debrunner, W. R. Scheidt, *Inorg. Chem.* **1997**, *36*, 4804−4811.

 © 2004 Wiley-VCH Verlag GmbH & Co. KGaA, Weinheim

[42] Y. Ohashi, K. Yanagi, T. Kurihara, Y. Sasada, Y. Ohgo, *J. Am. Chem. Soc.* **1981**, *103*, 5805−5812.
[43] A. Uchida, Y. Ohashi, Y. Sasada, *Nature (London)* **1986**, *320*, 51−52.
[44] A. Bondi, *J. Phys. Chem.* **1964**, *68*, 441−451.
[45] K. M. Barkigia, M. D. Berber, J. Fajer, C. J. Medforth, M. W. Renner, K. M. Smith, *J. Am. Chem. Soc.* **1990**, *112*, 8851−8857.
[46] L. D. Sparks, C. J. Medforth, M.-S. Park, J. R. Chamberlain, M. R. Ondrias, M. O. Senge, K. M. Smith, J. A. Shelnutt, *J. Am. Chem. Soc.* **1993**, *115*, 581−592.
[47] R.-J. Cheng, P.-Y. Chen, P.-R. Gau, C.-C. Chen, S.-M. Peng, *J. Am. Chem. Soc.* **1997**, *119*, 2563−2569.
[48] M. Nakamura, T. Yamaguchi, Y. Ohgo, *Inorg. Chem.* **1999**, *38*, 3126−3131.
[49] T. Ikeue, Y. Ohgo, T. Saitoh, T. Yamaguchi, M. Nakamura, *Inorg. Chem.* **2001**, *40*, 3423−3434.
[50] H. Ogoshi, H. Sugimoto, E. Watanabe, Z. Yoshida, Y. Maeda, H. Sakai, *Bull. Chem. Soc. Jpn.* **1981**, *54*, 3414−3419.
[51] A. C. T. North, D. C. Phillips, F. S. Mathews, *Acta Crystallogr., Sect. A* **1968**, *24*, 351−359.
[52] A. Altomare, M. C. Burla, M. Camalli, G. L. Cascarano, C. Giacovazzo, A. Guagliardi, A. G. G. Moliterni, G. Polidori, R. Spagna, *J. Appl. Cryst.* **1999**, *32*, 115−119.
[53] TEXSAN, *Crystal Structure Analysis Package, MSC/AFC Diffractometer Control Software*, Molecular Structure Corporation Houston; MSC, 3200 Research Forest Drive, The Woodlands, Texas 77381, USA, **1992**
[54] The DIRDIFß94 Program System, P. T. Beurskens, G. Admiraal, G. Beurskens, W. P. Bosman, R. de Gelder, R. Israel, J. M. M. Smits, Technical Report of the Crystallography Laboratory, University of Nijmegen, The Netherlands, **1994**.
[55] G. M. Sheldrick, SHELXL-97, *Program for the Refinement of Crystal Structures*, University of Göttingen, Germany, **1997**.
[56] T. Higashi, Program for Absorption Correction, Rigaku Corporation, Tokyo, Japan.

Received August 13, 2003
Early View Article
Published Online January 14, 2004

 © 2004 Wiley-VCH Verlag GmbH & Co. KGaA, Weinheim

Hydration of Propargylic Alcohols by Ruthenium Catalysts, with Dominant Anti-Markovnikov Regioselectivity, Formation of α,β-Unsaturated Products and Catalytic Decarbonylation to 1-Alkenes

Nicola d'Alessandro,[a] Milena Di Deo,[a] Monica Bonetti,[a] Lucia Tonucci,[a] Antonino Morvillo,[b] and Mario Bressan*[a]

Keywords: Ruthenium / Alkynes / Phthalocyanines / Hydration / Decarbonylation

Ruthenium catalysts — water-soluble ruthenium sulfophthalocyanine and heterogeneous ruthenium hydroxyapatite complexes — proved to be effective for the hydration of propargylic alcohols in entirely aqueous media. 1-Phenyl-2-propyn-1-ol underwent an unprecedented catalytic hydration-decarbonylation-dehydration reaction, giving rise to styrene and carbon monoxide; 2-propyn-1-ol and 3-butyn-2-ol gave predominantly the products of anti-Markovnikov addition, together with products of hydration-dehydration (α,β-rearrangement) and, to a minor extent, the decarbonylation products, ethene or propene, respectively. Hydrations were also conducted in D_2O, giving indications of the mechanism of the reactions and apparently ruling out the allenylidene route for the α,β-rearrangement.
(© Wiley-VCH Verlag GmbH & Co. KGaA, 69451 Weinheim, Germany, 2004)

Introduction

Alkynes are useful intermediates for the synthesis of carbonyl compounds through the well-known metal-catalyzed hydration reaction. Typically, the addition reactions of water to 1-alkynes are catalyzed by a variety of transition metal salts and complexes,[1−7] including $RuCl_3$,[8,9] all of which follow Markovnikov's rule to give ketones. Only very recently[10] has it been reported that the reaction can be regioselectively oriented to the formation of aldehydes (anti-Markovnikov addition) in the presence of catalytic amounts of some ruthenium(II) organometallic derivatives, containing either cyclopentadienyl[11,12] or indenyl[13] moieties, although temperatures of around 100 °C were still required. The accepted mechanism involves the rearrangement of the π-adduct deriving from the conventional interaction with the terminal alkynes at the metal center into a metal-vinylidene intermediate[13] or, alternatively, a hydrido-alkynyl complex,[12] the latter of which has recently been isolated as an intermediate in the activation of propargylic alcohols by [Cp*RuCl(dppe)];[14] both the proposed intermediates are prone to nucleophilic attack by water at the α-carbon atom. Previous results[15] showed the critical role played by the π-alkyne/vinylidene equilibrium in the regioselectivity of the hydration reactions, suggesting that addition of water to the π-adduct might follow Markovnikov's rule, eventually yielding methylketones, whereas addition to the vinylidene intermediate would lead to an acyl complex and, finally, aldehydes. However, only a few examples have reported good selectivity in the aldehyde formation,[11,13] as several alternative reaction pathways, not strictly dealing with conventional hydration, could become dominant. Among them, the catalytic cleavage of the carbon-carbon triple bond is particularly attractive, since it could represent an interesting topic from the synthetic point of view, if high selectivities can be attained in mild experimental conditions. So far, however, alkyne cleavage has also been demonstrated to work effectively in only a few cases.[16,17]

The potential for the use of both ruthenium catalysts and water as reagent prompted our interest in the subject. In the present work we tested the water-soluble ruthenium(II) complex ruthenium sulfophthalocyanine (RuPcS), previously studied by us as an effective catalyst for a variety of organic substrates in aqueous media,[18−22] and the heterogeneous ruthenium hydroxyapatite (RuHAP) catalyst, successfully tested for the aerobic oxidation of alcohols to aldehydes, reportedly via a metal-hydrido species,[23] which proved to work satisfactorily also in aqueous media.[24] This paper deals with the catalytic hydration of a number of propargylic (2-propyn-1-ol, 3-butyn-2-ol, 1-phenyl-2-propyn-1-ol and 1,1-diphenyl-2-propyn-1-ol) and non-propargylic alcohols (3-butyn-1-ol and 4-pentyn-1-ol). A variety of reaction pathways were observed, depending upon the nature of the substrate and the catalyst; among them, cleavage of

[a] Università "G. d'Annunzio" di Chieti-Pescara, Dipartimento di Scienze,
Viale Pindaro 42, 65127, Pescara, Italy
E-mail: bressan@sci.unich.it
[b] Università di Padova, Dipartimento di Chimica Inorganica and Centro C.N.R.,
Via Marzolo 1, 35100 Padova, Italy

 © 2004 Wiley-VCH Verlag GmbH & Co. KGaA, Weinheim **DOI: 10.1002/ejic.200300562**

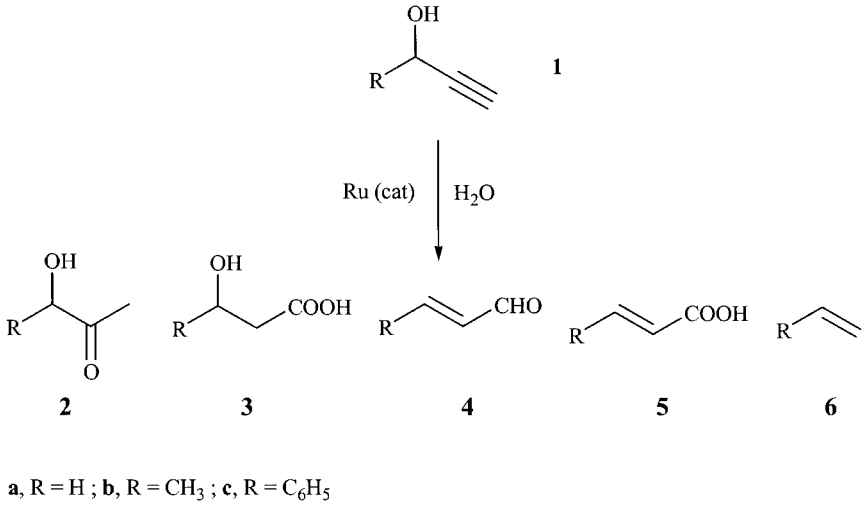

Scheme 1. Product distribution for the hydration of propargylic alcohols catalyzed by Ru^{II} derivatives

the triple bond, with formation of alkenes, was of particular interest (Scheme 1).

Results and Discussion

The RuHAP and RuPcS catalysts proved to be effective, at various selectivities, in the reaction of the terminal acetylenes 1-phenyl-2-propyn-1-ol, 2-propyn-1-ol, 3-butyn-2-ol and 4-pentyn-1-ol with water; no reaction took place in the absence of added catalyst or in the presence of calcium hydroxyapatite, whereas other simple ruthenium complexes, such as $[RuCl_2(DMSO)_4]$ (RuDMS) and $K_5[Ru(H_2O)PW_{11}O_{39}]$ (RuPW), behaved poorly. Very different and complex reaction patterns were found for each substrate examined, as reported in Table 1. The reactions were very slow below 80 °C.

In the presence of RuHAP and RuPcS, the non-propargylic alcohol 4-pentyn-1-ol was selectively transformed into 5-hydroxy-2-pentanone, the expected product of the conventional Markovnikov addition to the triple bond. The related substrate 3-butyn-1-ol (not shown) was poorly converted (about 10 %) during the 24 h reaction time and gave only minor amounts of products from both the Markovnikov and anti-Markovnikov addition, i.e. 4-hydroxy-2-butanone and 4-hydroxybutanoic acid, respectively, together with other unidentified compounds.

The propargylic alcohols behaved differently. Large amounts of 2-propyn-1-ol (**1a**) were converted, in the presence of both RuHAP and RuPcS, into hydroxyacetone (**2a**, the expected product of Markovnikov addition; Scheme 2), 3-hydroxy-propanoic acid (**3a**), acrylic acid (**5a**) and ethene (**6a**), together with minor amounts of glycolic and formic acid (Table 1), the latter likely arising from the oxidative cleavage of the substrate. No evidence was obtained for the presence of 3-hydroxypropanal, which should be the prod-

Table 1. Product analysis of the hydration reaction of propargylic alcohols by ruthenium catalysts[a]

Substrate	Catalyst	Conversion (mol %)	Yields (mol %) 2	3	4	5	6	By-products
1a	RuPcS	73	10	10	–	22	7[b]	8[c]
	RuHAP	70	12	20	–	12	8[b]	5[c]
	RuDMS	9	7	–	–	–	nd	1[c]
	RuPW	8	6	–	–	–	nd	1[c]
1b	RuPcS	70	2	7	–	15	15[b]	5[d]
	RuHAP	65	4	9	–	12	16[b]	5[d]
1c	RuPcS	70	2	–	3	–	16[e]	1[f]
	RuHAP	95	2	–	5	–	20[e]	1[f]
4-Pentyn-1-ol			5-hydroxy-2-pentanone					
	RuPcS	70	69					
	RuHAP	100	99					

[a] Substrate: 400 mM; catalysts: RuPcS, 10 mM; RuHAP, 40 mg/mL (78 mmol of Ru/L); water; 80 °C; 24 h reaction. [b] Measured as their 1,2-dibromo derivatives, after capturing the evolved gases into a bromine solution. [c] Glycolic and formic acid. [d] 2-Propanol. [e] Measured after extraction with diethyl ether; polystyrene and polymeric materials were also detected in not well-defined yields. [f] 1-Phenylethanol.

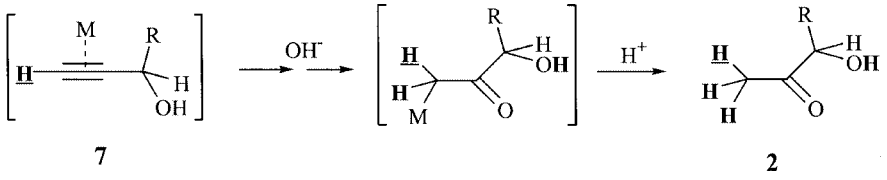

Scheme 2. Ruthenium-catalyzed Markovnikov hydration of propargylic alcohols (**H** coming from water; **H** coming from acetylenic proton)

 © 2004 Wiley-VCH Verlag GmbH & Co. KGaA, Weinheim

uct of anti-Markovnikov addition to the triple bond; instead, its oxidized product 3-hydroxy-propanoic acid, was detected in reasonable amounts. To avoid this undesired oxidation, we tried to conduct the reaction under an inert atmosphere (nitrogen), but the long times required for the formation of the products did not allow for a rigorous exclusion of oxygen and, indeed, only minor differences were observed with respect to the aerobic experiments, i.e. with no evidence for the aldehydic product. It should be noted here that aliphatic aldehydes, such as propionaldehyde and valeraldehyde, are easily oxidized to the corresponding carboxylic acids in the same reaction conditions and in the absence of added ruthenium catalysts. The third major reaction product, acrylic acid, could be conceivably attributed to a dehydration of 3-hydroxypropanoic acid. However, experiments conducted directly with β-propiolactone (a commercially available compound that rapidly hydrolyzes to 3-hydroxypropanoic acid in aqueous media) showed only minimal conversion into acrylic acid (less than 5 %) under these standard reaction conditions. The formation of the unsaturated product probably involves the well-known rearrangement of propargylic alcohols to α,β-unsaturated aldehydes, which is effectively catalyzed also by several ruthenium complexes.[25] More recently,[26] Wakatsuki has reported convincing evidence that the mechanism of the ruthenium-catalyzed rearrangement of propargylic alcohols to unsaturated aldehydes involves a series of organometallic intermediates, arising either by an initial anti-Markovnikov hydration of the vinylidene intermediate **8** (Scheme 3), followed by dehydration of the original OH group to **11** via **10**, or, alternatively, by an early dehydration of **8** to an allenylidene intermediate **9**, followed by the hydration step. Thus, the rearrangement of 2-propyn-1-ol was expected to produce acrolein; the observed formation of acrylic acid could again be due to the rapid oxidation of the aldehydic group, as in the case discussed previously. However, acrolein, as other α,β-unsaturated aldehydes, such as benzaldehyde and cinnamaldehyde, and contrary to the saturated aldehydes discussed above, is very difficult to oxidize under these reaction conditions. It is therefore reasonable to assume that acrylic acid is formed directly from the organometallic intermediate **11a** via a complex rearrangement-oxidation step. Finally, we also detected carbon monoxide and an appreciable amount of ethene (**6a**; see Exp. Sect.), which allowed a reasonable mass balance to be set for the overall transformation of **1a**.

The reaction of 3-butyn-2-ol (**1b**) with water closely resembles that of 2-propyn-1-ol and leads to all the expected products from the addition of water according to Markovnikov (hydroxybutanone, **2b**) and anti-Markovnikov rules (hydroxybutanoic acid, **3b**); we also detected the decarbonylated and dehydration/oxidation products, i.e. propene (**6b**) and 2-butenoic acid (**5b**), respectively, and carbon monoxide.

Hydration of 1-phenyl-2-propyn-1-ol (**1c**) reached 70 % and 95 % conversion (with RuPcS or RuHAP, respectively) of the starting material within 24 h (Table 1), but the reaction led to minimal amounts of the product of Markovni-

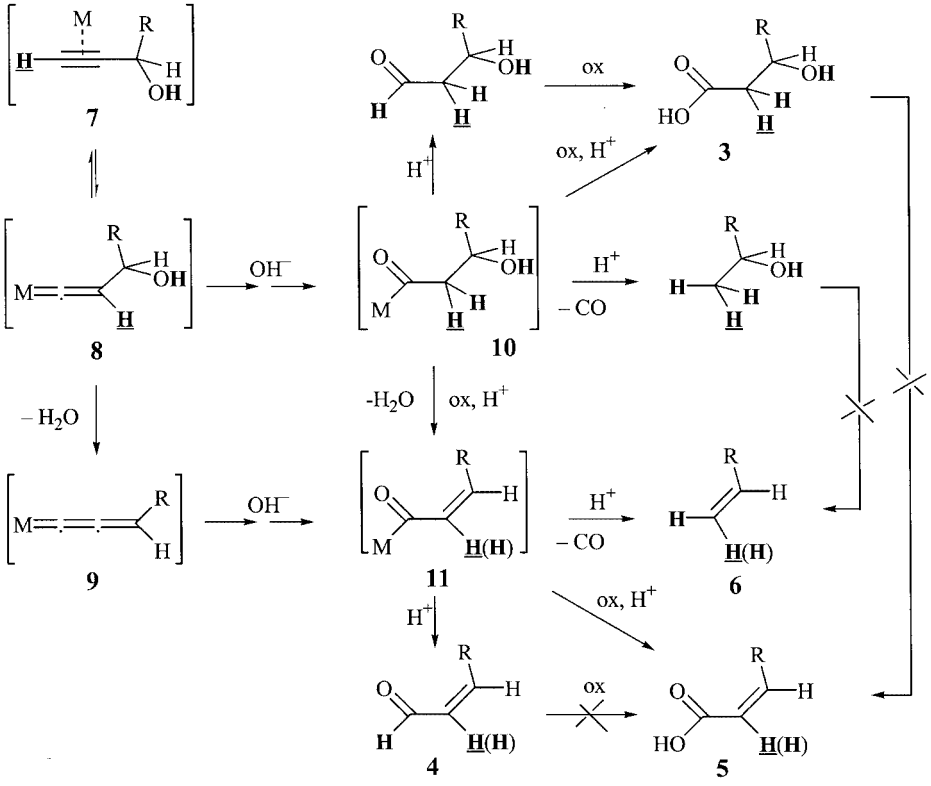

Scheme 3. Proposed pathway for ruthenium-catalyzed anti-Markovnikov hydration of propargylic alcohols (**H** coming from water; **H** coming from the acetylenic proton)

 © 2004 Wiley-VCH Verlag GmbH & Co. KGaA, Weinheim

kov addition [1-hydroxy-1-phenylpropanone (**2c**)] and no conventional products from the anti-Markovnikov addition, i.e. 3-hydroxy-3-phenylpropanal or the corresponding carboxylic acid. In addition, the α,β-unsaturated aldehyde [cinnamaldehyde (**4c**)], arising from the ruthenium-catalyzed rearrangement of the propargylic alcohol, was detected as a minor product. It should be recalled that in the reaction conditions cinnamaldehyde, as with other α,β-unsaturated aldehydes, does not undergo oxidation to the corresponding carboxylic acid and therefore the reported yields must be considered highly significant. Quite unexpectedly, the major product formed during the reaction was styrene (**6c**), which was detected after extraction of the reaction mixtures with diethyl ether (16−20 %; Table 1), together with carbon monoxide and large (but not quantified) amounts of styrene-based polymeric materials, likely accounting for the final mass balance. It should be noted that in the cases of ethene and propene discussed previously, no water-insoluble polymeric materials were detected. However, ethene and propene, unlike styrene, accumulate in the gas phase and therefore are expected to escape from the reaction mixture before they can be polymerised. Therefore the low mass-balance values for both **1a** and **1b** (Table 1) were attributed to some further unidentified products.

No reaction was observed for the other propargylic alcohol, 1,1-diphenyl-2-propyn-1-ol, when suspended in water as it is only slightly soluble. However, when the hydration was carried out in an organic solvent (toluene) with small amounts of added water and in the presence of the lipophilic ruthenium phthalocyanine derivative RuPc, instead of the water-soluble RuPcS, small amounts of 1,1-diphenylethene and of β-phenylcinnamaldehyde were formed, thus indicating a reactivity closely related to that of 1-phenyl-2-propyn-1-ol in the water/RuPcS system.

A simple explanation for the formation of $C_{(n-1)}$ alkenes (styrene, propene and ethene) from the corresponding propargylic alcohols (1-phenyl-2-propyn-1-ol, 3-butyn-2-ol and 2-propyn-1-ol, respectively) might involve decarbonylation of the anti-Markovnikov acyl-metal intermediate **10** to 1-substituted ethanol derivatives followed by a dehydration step (Scheme 3). 2-Propanol and 1-phenylethanol were detected in trace amounts in the case of 1-phenyl-2-propyn-1-ol and 3-butyn-2-ol, respectively. However, the fact that direct experiments conducted in the presence of ethanol, 2-propanol and 1-phenylethanol under the same reaction conditions showed minimal (or no) dehydration to ethene, propene and styrene (less than 2 % in the most favorable case, namely 1-phenylethanol), indicates that the alkenes are formed directly from an organometallic intermediate (likely **11**), in competition with the 1-substituted ethanol derivatives. The formation of alkenes also implies formation of carbon monoxide, which was always detected among the products of the hydration reactions. Decarbonylation of terminal acetylenes by hydration is indeed a known process, first reported by Bruce[27] and thoroughly investigated by Bianchini[28] in the case of phenylacetylene, which, in the presence of water and of the Ru^{II} complex $[RuCl_2(PNP)(PPh_3)]$, was quantitatively transformed into toluene and the stable mono-carbonyl adduct $[RuCl_2(CO)(PNP)]$. Wakatsuki[10] has also reported decarbonylation (likely stoichiometric) during the hydration of benzylacetylene in the presence of 10 % $[RuCl_2(C_6H_6)\{PPh_2(C_6F_5)\}]$. In the present case, decarbonylation turned out to be catalytic, thus indicating lability of the putative carbonylruthenium adducts with either RuHAP or RuPcS. Indeed, RuPcS was previously reported by us[21] to be able to add carbon monoxide, giving a carbonyl product possessing a strong band at 1960 cm^{-1}, but only under very severe conditions (100 atm) and after 24 h reaction.

Hydration Reactions in D_2O

Deuterium distribution in the products was evaluated by ^1H NMR spectroscopy and GC-MS measurements on the reaction mixtures from 2-propyn-1-ol (**1a**) and 1-phenyl-2-propyn-1-ol (**1c**). It has to be noted that acetylenic-proton exchange of the pure substrates in 99.9 % D_2O turned out to be slow even at 80 °C, with 100 % deuteration being reached only after 4 h (Figure 1). The rate of deuterium exchange in the presence of the RuPcS catalyst was similar for 1-phenyl-2-propyn-1-ol, at least at early reaction times, whereas in the case of 2-propyn-1-ol deuteration was much slower and never exceeded 40 % substitution, even after long reaction times (Figure 1). The observed different deuteration rates of the acetylenic proton must be compared with the hydration rates of the corresponding substrates (Figure 1), clearly indicating that 2-propyn-1-ol (**1a**) underwent hydration in D_2O mainly as the protonated RC≡CH

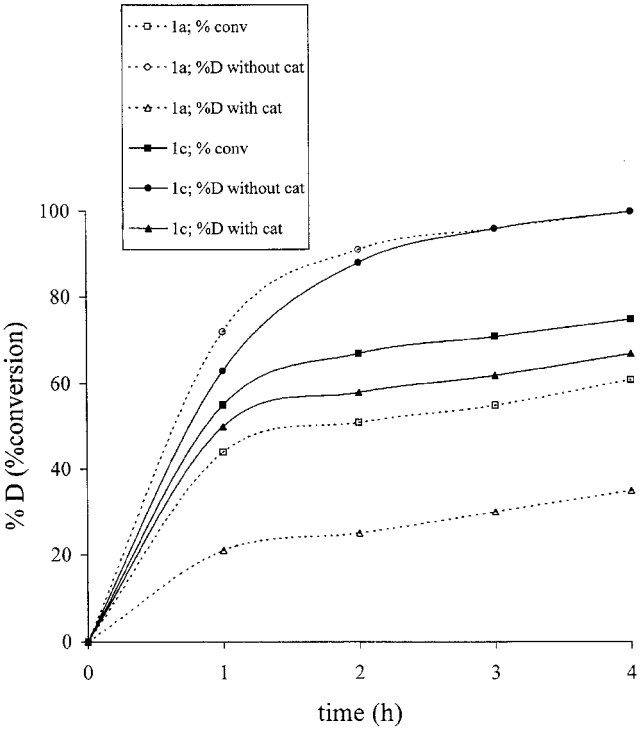

Figure 1. Incorporation of deuterium into 2-propyn-1-ol (**1a**; open squares and triangles, dotted lines) and 1-phenyl-2-propyn-1-ol (**1c**; filled squares and triangles, solid lines); % conversions of **1a** (open circles, dotted line) and **1c** (filled circles, solid line) are also reported

 © 2004 Wiley-VCH Verlag GmbH & Co. KGaA, Weinheim

species, while 1-phenyl-2-propyn-1-ol (**1c**) reacts as the deuterated RC≡CD species.

The rapid and almost complete deuteration of the acetylene proton of 1-phenyl-2-propyn-1-ol unfortunately precluded any significant conclusion about the possible mechanism of the hydration of this substrate (Scheme 2 and 3). The ^{1}H NMR spectrum of the product of Markovnikov addition — 1-hydroxy-1-phenylacetone (**2c**) — shows complete disappearance of the singlet arising from the methyl protons, in agreement with the dominant presence of the $CO-CD_3^+$ fragment (46 amu) in the mass spectrum; the molecular ion $CH_3COCH(Ph)OH^+$ is almost undetectable. The ^{1}H NMR spectrum of cinnamaldehyde (**4c**) lacks the signals of the aldehydic proton (doublet) and that of the proton bonded to the α-carbon, whereas the signals of the Ph*C*H=CH−CHO proton are covered by those of the phenyl protons. MS measurements clearly indicated that PhCH=CD−CDO was the dominant species. The ^{1}H NMR spectrum of styrene (**6c**) lacks the multiplets arising from the terminal methylene group, whereas the multiplet of the PhCH= proton collapses into a very broad signal, strongly indicative of an effective coupling with the two deuterium atoms in the α-position; the formula Ph−CH=CD_2 was fully confirmed by the GC-MS data.

Because of the slow deuterium exchange of the acetylenic proton, a selective deuterium distribution in the products was expected for 2-propyn-1-ol. Hydroxyacetone (**2a**, the product of Markovnikov addition) exhibits the $COC\underline{H}H_2$ (see Scheme 2) singlet in the ^{1}H NMR spectra considerably broadened and reduced in intensity, when compared with that of the singlet of the CH_2OH protons, but indicative of ca. 70 % deuteration (Figure 2). The mass spectrum shows the peak of the molecular ion shifted by +3 amu and that of the $COCH_3^+$ fragment by +2 amu (45 instead of 43 amu), in agreement with the dominant presence of the $CD_2H-CO-CH_2OD$ species. The dideuteration of the methyl group in the formed methylketone confirms the slow exchange of the terminal CH, since fast exchange would have yielded trideuteration, as found in 1-hydroxy-1-phenylacetone. The anti-Markovnikov addition of D_2O to RC≡CH probably involves the interconversion of an η^2-alkyne species to a vinylidene, therefore bringing the acetylenic hydrogen onto the carbon substituted with the R group and eventually giving RCHD−CDO (or RCHD−COOD;

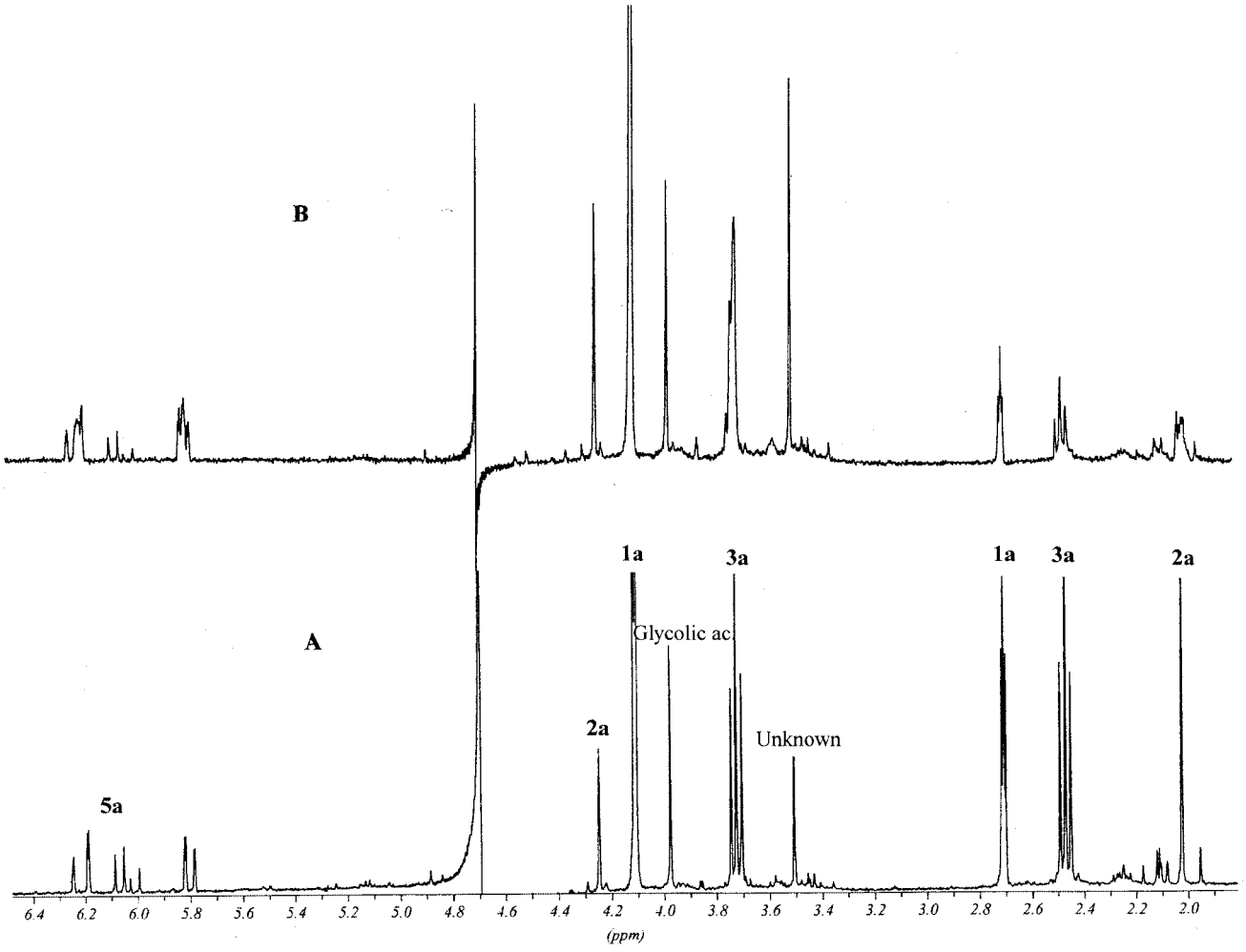

Figure 2. ^{1}H NMR spectra of the crude mixture of the hydration reaction of 2-propyn-1-ol (24 h, 80 °C) in H_2O (**A**) or in D_2O (**B**); the product numbers are the same as in Scheme 1

 © 2004 Wiley-VCH Verlag GmbH & Co. KGaA, Weinheim

Scheme 3), unless a rapid proton exchange is taking place on the vinylidene intermediate. We found that 3-hydroxypropanoic acid (**3a**) exhibits a distinctive deuteration at the methylene group next to the carbonyl carbon, with the ^{1}H NMR spectra showing a collapse of the two diagnostic triplets of the CH_2 signals at $\delta = 3.75$ and 2.50 ppm ($J = 6$ Hz) into a broad singlet and a triplet, respectively, in a roughly 2.5:1 intensity ratio (Figure 2) and therefore best fitting with an $HOCH_2-CHD-COOH$ species. No MS measurements were possible, since 3-hydroxypropanoic acid was not detectable in the GC. Acrylic acid (**5a**), arising from the hydration-dehydration reaction, shows the presence of both the $CH_2=CD-COOD$ ($m/z = 73$) and the $CH_2=CH-COOD$ species ($m/z = 72$), roughly in a 1:1 molar ratio. Accordingly, the ^{1}H NMR signals of the hydrogen atom bonded to the carbon atom next to the carboxylic function appear clearly weakened with respect to the signals of the methylene protons (ca. 50 % in intensity; Figure 2). Also ethene (**6a**), the decarbonylation product, exhibits only partial deuteration. The MS spectra of its dibromo adduct CH_2Br-CH_2Br shows an intense fragment arising from the loss of one Br atom as a series of peaks at 108 and 110 amu (^{79}Br) and at 109 and 111 amu (^{81}Br), in an intensity ratio of ca. 1:4, therefore suggesting the presence of both the dideuterated $C_2H_2D_2Br^+$ and monodeuterated $C_2H_3DBr^+$ ions. The latter two findings have some significance, since they apparently rule out the putative allenylidene route (i.e. **8a** → **9a** → **11a**, Scheme 3), for which complete deuteration of the carbon atom next to the metal-acyl function in **11a** was expected, thus eventually yielding exclusively the $CH_2=CD-COOH$ and $CD_2=CH_2$ species; the vinylidene route (i.e. **8a** → **10a** → **11a**, Scheme 3) is not contradictory with the observed formation of partially deuterated products.

Interaction of the Substrates with the Metal Complexes

The nature of the catalyst apparently influences the rate of the hydration more than it does the regioselectivity, which is strongly dependent upon the nature of the substrate. Since an attractive explanation of the observed behavior might be the different degree of stabilization of the π-adduct **7** in Scheme 2 vs. the metal-vinylidene intermediate **8** in Scheme 3, induced by the various substrates, we carefully analyzed an aqueous solution of RuPcS (10 mM) in the presence of increasing amounts of the substrates under investigation, and also, for comparison purposes, of other saturated and unsaturated alcohols (1-butanol, 2-propen-1-ol, ethanol). By increasing the substrate-to-metal ratios up to 20-fold, an enhancement of the measured acidity of the mixtures was generally observed, in some cases very sharp, but always irrespective of the nature of the substrates, and therefore hardly attributable to any significant metal/substrate interaction. Accordingly, ^{1}H NMR measurements of the propargylic alcohols/RuPcS systems in buffered solutions (with pHs varying between 0.5 and 9) exhibited only tiny and erratic shifts of the proton signals

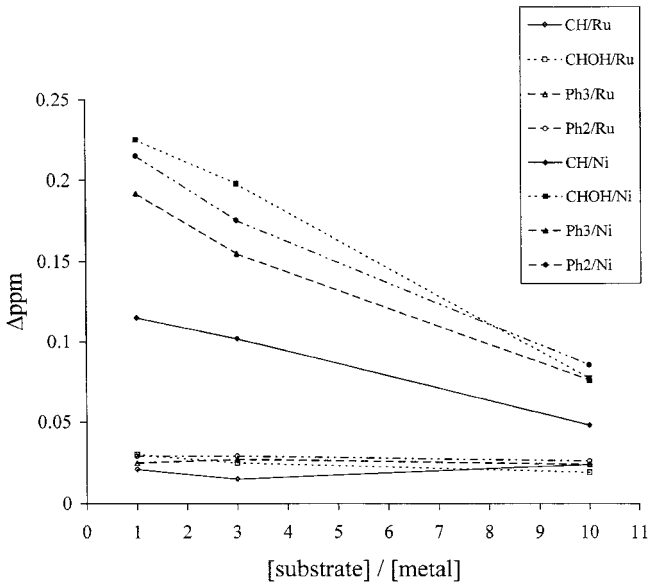

Figure 3. Differences in the ^{1}H NMR chemical shift for 1-phenyl-2-propyn-1-ol in the presence of MPcS's (10 mM), relative to the pure substrate: CH = acetylenic proton; CHOH = aliphatic proton; Ph_2 = *ortho* aromatic protons; Ph_3 = *meta* and *para* aromatic protons.

(±0.01 ppm), including the acetylenic one (Figure 3). For comparison purposes, we investigated other MPcS complexes (M = Fe, Co and Ni), all of them catalytically inactive for the reaction under investigation; for the 1-phenyl-2-propyn-1-ol/NiPcS system significant changes in the ^{1}H NMR spectra were detected by decreasing the substrate-to-metal ratios down to 1 to 1, with pronounced upfield shifts (up to 0.25 ppm) of the aromatic (Ph_2 and Ph_3) and aliphatic (CHOH) protons and less pronounced, but still significant, shifts of the acetylene proton (up to 0.15 ppm; Figure 3). This finding thus strongly suggests a substrate-metal interaction also involving the triple bond.

Conclusion

The first noteworthy finding in this paper is the different reactivity exhibited by the Ru^{II} derivatives in aqueous solution. Simple ruthenium complexes, like RuDMS and RuPW, gave almost exclusively products according to the Markovnikov rule and in very low yields (at least with 2-propyn-1-ol), whereas, when the metal is strongly complexed, i.e. with a phthalocyanine ring or a hydroxyapatite support, the reactivity was definitely enhanced. The regioselectivity was found to be strongly dependent upon the nature of the alkynol; in particular, only when the OH group is relatively close to the triple bond (propargylic alcohols) does the attack of water at the triple bond follow dominantly, if not exclusively, an *anti* Markovnikov pathway (in a broad sense), thus leading to aldehydic (or carboxylic acid) products, α,β-rearrangement of the substrate and/or decarbonylation. The selectivities in each of the above "anti-Markovnikov" products were however moderate and far lower

 © 2004 Wiley-VCH Verlag GmbH & Co. KGaA, Weinheim

than those reported with other ruthenium catalysts.[10,13] We have no data to support a real participation of the OH group in the π-adduct/vinylidene species equilibrium, but the fact that definite evidence of a metal−ligand interaction was obtained only for the catalytically inactive NiPcS species, suggests that the driving force of the RuPcS hydrations is essentially kinetic. The other important findings deal with the observed smooth decarbonylation of the propargylic alcohols to corresponding $C_{(n-1)}$ alkenes, which represents, to the best of our knowledge, the first catalytic decarbonylation process of terminal alkynes.

Experimental Section

Materials: Ruthenium tetrasulfophthalocyanine (RuPcS),[21] cobalt tetrasulfophthalocyanine (CoPcS),[29] *cis*-[$RuCl_2(DMSO)_4$] (RuDMS),[30] $K_5[Ru(H_2O)PW_{11}O_{39}]$ (RuPW)[31] and ruthenium hydroxyapatite (RuHAP; Ru 17 %, corresponding to 1.6 mmol/g)[23] were prepared by published procedures. Ruthenium phthalocyanine (RuPc) was prepared by the procedure of Weber and Bush,[29] starting from ruthenium trichloride, phthalic acid and urea. Other metal complexes, organic substrates, chromatographic and spectroscopic standards were purchased from Aldrich. D_2O (D ≥ 99 %) was obtained from Isotec Inc.

Apparatus: Organic analyses by GC were performed on aliquots withdrawn with a microsyringe from the aqueous reaction mixtures and diluted 1:20 with diethyl ether, on a HP 6890 GLC instrument equipped with FID, using a 30-m HP-5 (0.32 mm i.d.; 0.25 μm film thickness) or a 30 m HP-Innowax (0.25 mm i.d.; 0.25 μm film thickness) capillary column with the injection port kept at 250 °C (carrier gas: He). The identity of each product was confirmed by comparison of the fragmentation pattern in the mass spectrum obtained with an MD 800 Fisons mass spectrometer operating in the electron ionization mode at 70 eV. ^{1}H NMR measurements were performed on a Bruker Avance 300 MHz spectrometer equipped with a BBO 5 mm probe, by adding small amount of D_2O to the reaction mixtures (1:3); water suppression was carried out by a presaturation sequence using a composite pulse (zgcppr Bruker sequence). A co-axial capillary tube containing a 30 mM solution of 3-(trimethylsilyl)propionic-2,2,3,3-d_4 acid sodium salt (TSP) in water (D_2O) was used as reference. The identity of each product and their quantitation were confirmed by comparison of the position and intensity of suitable signals, by addition of measured amounts of pure compounds to the reaction mixtures.

Typical Procedure for the Hydration Reactions: The progress of the reactions was monitored by GC-MS and/or ^{1}H NMR spectroscopy; conversions, yields and rates were reproducible to within 10−15 %. We describe three different experimental procedures for the hydration reaction: (i) 2-propyn-1-ol, 3-butyn-2-ol, 1-phenyl-2-propyn-1-ol, 4-pentyn-1-ol, or 3-butyn-1-ol (equivalent to 400 mM of final solution) was added to an aqueous solution of RuPcS (10 mM) in a 5 mL vial in air or under a nitrogen atmosphere. The mixture was stirred for 24 h at 80 °C and analyzed by GC-MS and/or NMR spectroscopy. In the case of 1-phenyl-2-propyn-1-ol the reaction mixture was also treated with $CDCl_3$ (5 mL) and the extract analyzed by GC-MS and NMR spectroscopy; after the evaporation of the solvent, a polymeric film was obtained, which on the basis of IR analysis was shown to contain also polystyrene and/or styrene-based polymeric materials; (ii) the above substrates (400 mM) and RuHAP (78 mg/mL) in water were stirred at 80 °C for 24 h; the reaction mixtures were analyzed as above; (iii) 1,1-diphenyl-2-propyn-1-ol (400 mM) and RuPc (10 mM) in a water-saturated toluene solution were stirred at 80 °C for 24 h and directly analyzed by NMR spectroscopy and GC.

Hydration Reactions with D_2O: 2-Propyn-1-ol or 1-phenyl-2-propyn-1-ol (400 mM) and RuPcS (10 mM) or RuHAP (13.9 mg, 0.010 mmol) in D_2O (D ≥ 99.9 %) were reacted for 24 h at 80 °C. Hydroxyacetone, acrylic acid, 1-hydroxy-1-phenylacetone, cinnamaldehyde and styrene were detected by GC, GC-MS and NMR spectroscopy, either directly or, when necessary, after extraction with $CDCl_3$ from the reaction mixture; 3-hydroxypropanoic was directly analyzed only by NMR spectroscopy.

Detection of CO, Ethene and Propene: CO was captured by bubbling the evolved reaction gas through a CH_2Cl_2 solution of $[RuCl(dppp)_2]PF_6$; the amount of formed mono-carbonyl adduct $[RuCl(CO)(dppp)_2]PF_6$ was measured both by UV/Vis and IR analysis, by following the disappearance of the 460 nm band of the original complex or the appearance of the distinctive ν_{CO} absorption at 1930 cm^{-1} of the carbonyl adduct.[32] Although both UV and IR measurements might allow, in principle, the quantitation of the carbonyl adduct, and hence of the carbon monoxide produced, the quantitative results were erratic, probably due to the long reaction times required for the formation of the product. Ethene and propene were captured in a CH_2Cl_2 solution containing an excess of Br_2; the resulting 1,2-bromoalkane solutions were analyzed by GC, GC-MS and NMR spectroscopy, by comparing the results with those of the two commercial compounds (1,2-dibromoethane and 1,2-dibromopropane). Further qualitative data on the production of propene were obtained by headspace GC-MS analysis of the final reaction mixtures.

Acknowledgments

The authors thank Mr. Antonio Ravazzolo, C.N.R., Padova, for technical assistance.

[1] [1a] R. C. Laroci, W. W. Leong, in *Comprehensive Organic Synthesis* (Eds.: B. M. Trost, I. Fleming, M. F. Semmelhoci), Pergamon Press, Oxford, UK, **1991**, vol. 4, 269. [1b] J. March, *Advanced Organic Chemistry*, John Wiley & Sons, New York, US, **1992**, 762.
[2] Y. Fukuda, I. Utimoto, *J. Org. Chem.* **1991**, *56*, 3729−3731.
[3] J. Blum, H. Huminer, H. Alper, *J. Mol. Catal.* **1992**, *75*, 153−160.
[4] J. W. Hartman, W. C. Hiscox, P. W. Jennings, *J. Org. Chem.* **1993**, *58*, 7613−7614.
[5] I. I. Meier, J. A. Marsella, *J. Mol. Catal.* **1993**, *78*, 31−42.
[6] J. P. Damiano, M. Postel, *J. Organomet. Chem.* **1996**, *522*, 303−305.
[7] W. Baidossi, M. Lahav, J. Blum, *J. Org. Chem.* **1997**, *62*, 669−672.
[8] J. Halpern, B. R. James, A. L. W. Kemp, *J. Am. Chem. Soc.* **1966**, *88*, 5142−5146.
[9] T. M. M. Khan, S. B. Halligudi, S. Shuila, *J. Mol. Catal.* **1990**, *58*, 299−305.
[10] M. Tokunaga, Y. Wakatsuki, *Angew. Chem. Int. Ed.* **1998**, *37*, 2867−2869.
[11] T. Suzuki, M. Tokunaga, Y. Wakatsuki, *Org. Lett.* **2001**, *3*, 735−737.
[12] M. Tokunaga, T. Suzuki, N. Koga, T. Fukushima, A. Horiuchi, Y. Wakatsuki, *J. Am. Chem. Soc.* **2001**, *123*, 11917−11924.

 © 2004 Wiley-VCH Verlag GmbH & Co. KGaA, Weinheim

[13] P. Alvarez, M. Bassetti, J. Gimeno, G. Mancini, *Tetrahedron Lett.* **2001**, *42*, 8467−8470.
[14] E. Bustelo, M. Jimenez-Tenorio, M. C. Puerta, P. Valerga, *Eur. J. Inorg. Chem.* **2001**, 2391−2398.
[15] M. P. Gamasa, J. Gimeno, B. M. Martin-Vaca, J. Borge, S. Garcia-Granda, E. Perez-Carreno, *Organometallics* **1994**, *13*, 4045−4057.
[16] S. Datta, C.-L. Chang, K.-L. Yeh, R.-S. Liu, *J. Am. Chem. Soc.* **2003**, *125*, 9294−9295.
[17] C.-H. Jun, H. Lee, C. W. Moon, H.-S. Hong, *J. Am. Chem. Soc.* **2001**, *123*, 8600−8601.
[18] N. d'Alessandro, L. Tonucci, M. Bressan, L. K. Dragani, A. Morvillo, *Eur. J. Inorg. Chem.* **2003**, 1807−1814.
[19] N. d'Alessandro, L. Liberatore, L. Tonucci, A. Morvillo, M. Bressan, *New J. Chem.* **2001**, *25*, 1319−1324.
[20] N. d'Alessandro, L. Liberatore, L. Tonucci, A. Morvillo, M. Bressan, *J. Mol. Catal.* **2001**, *175*, 83−90.
[21] M. Bressan, N. Celli, N. d'Alessandro, L. Liberatore, A. Morvillo, L. Tonucci, *J. Organomet. Chem.* **2000**, *593−594*, 416−420.
[22] M. Bressan, N. d'Alessandro, L. Liberatore, A. Morvillo, *Coord. Chem. Rev.* **1999**, *185−186*, 385−402.
[23] K. Yamaguchi, K. Mori, T. Mizugaki, K. Ebitani, K. Kaneda, *J. Am. Chem. Soc.* **2000**, *122*, 7144−7145.
[24] K. Mori, I. Yamaguchi, T. Mizugaki, K. Ebitani, K. Kaneda, *Chem. Commun.* **2001**, 461−462.
[25] M. P. Picquet, A. Fernandez, C. Bruneau, P. H. Dixneuf, *Eur. J. Org. Chem.* **2000**, 2361−2366, and references cited therein.
[26] T. Suzuki, M. Tokunaga, Y. Wakatsuki, *Tetrahedron Lett.* **2002**, *43*, 7531−7533.
[27] M. I. Bruce, A. G. Swincer, *Aust. J. Chem.* **1980**, *33*, 1471−1483.
[28] C. Bianchini, J. A. Casares, M. Peruzzini, A. Romerosa, F. Zanobini, *J. Am. Chem. Soc.* **1996**, *118*, 4585−4594.
[29] J. H. Weber, D. H. Busch, *Inorg. Chem.* **1965**, *4*, 469−471.
[30] I. P. Evans, A. Spencer, G. Wilkinson, *J. Chem. Soc., Dalton Trans.* **1973**, 204−209.
[31] M. Bressan, L. Forti, F. Ghelfi, A. Morvillo, *J. Mol. Catal.* **1993**, *79*, 85−93.
[32] M. Bressan, P. Rigo, *Inorg. Chem.* **1975**, *14*, 2286−2288.

Received August 12, 2003
Early View Article
Published Online January 2, 2004

 © 2004 Wiley-VCH Verlag GmbH & Co. KGaA, Weinheim

Dihydrobis(pyrazolyl)borate Alkylidyne Complexes of Tungsten[‡]

Anthony F. Hill,*[a,b] John M. Malget,[a] Andrew J. P. White,[a] and David J. Williams[a]

Keywords: Borates / Carbyne ligands / Multiple bonds / N Ligands / Tungsten

$[W(\equiv CR)Br(CO)_2(NC_5H_4Me\text{-}4)_2]$ (R = $C_6H_3Me_2$-2,6 **1a**, $C_6H_2Me_3$-2,4,6 **1b**) react with $K[H_2B(pz)_2]$ (pz = pyrazol-1-yl) to provide two interconverting isomers of $[W(\equiv CR)(CO)_2(NC_5H_4Me\text{-}4)\{H_2B(pz)_2\}]$ (**2**), one isomer having been structurally characterised for R = $C_6H_3Me_2$-2,6 (**2a**). The reactions of $[W(\equiv CR)Br(CO)_2(CNR')_2]$ (**5**: R′ = $C_6H_3Me_2$-2,6, $CNMe_3$) with $K[H_2B(pz)_2]$ or of $[W(\equiv CR)Br(CO)_2(NC_5H_4Me\text{-}4)\{H_2B(pz)_2\}]$ (**2**) with isocyanides are more complex due to the facile formation of unstable ketenyl derivatives. In the absence of light, the reaction of $[W(\equiv CR)Br(CO)_2(CNR')_2]$ (**5**) with $K[H_2B(pz)_2]$ provides $[W(\equiv CR)(CO)_2(CNR')\{H_2B(pz)_2\}]$ (**3**) in moderate yield, similar yields were obtained from $[W(\equiv CR)(CO)_2(NC_5H_4Me\text{-}4)\{H_2B(pz)_2\}]$ (**2**) and CNR′. Under mild photolytic conditions both combinations provide primarily the thermally unstable ketenyl complex $[W(\eta^2\text{-}OCCR)(CO)(CNR')_2\{H_2B(pz)_2\}]$ (**4**). The picoline ligand in $[W(\equiv CR)Br(CO)_2(NC_5H_4Me\text{-}4)\{H_2B(pz)_2\}]$ (**2**) is readily replaced by PMe_2Ph to provide $[W(\equiv CR)(CO)_2(PMe_2Ph)\{H_2B(pz)_2\}]$ (structurally characterised for R = $C_6H_3Me_2$-2,6 **6a**). The reaction of either $[W(\equiv CR)(CO)_2(PMe_2Ph)\{H_2B(pz)_2\}]$ (**6**) or $[W(\equiv CR)(CO)_2(NC_5H_4Me\text{-}4)\{H_2B(pz)_2\}]$ (R = $C_6H_2Me_3$-2,4,6 **2b**) with excess PMe_2Ph provides $[W(\equiv CR)(CO)(PMe_2Ph)_2\{H_2B(pz)_2\}]$ (**7**). This complex is also obtained from $K[H_2B(pz)_2]$ and $[W(\equiv CR)Br(CO)(PMe_2Ph)_3]$ (**8**), the latter arising from the reaction of $[W(\equiv CR)Br(CO)_2(NC_5H_4Me\text{-}4)_2]$ (**1b**) with PMe_2Ph.
(© Wiley-VCH Verlag GmbH & Co. KGaA, 69451 Weinheim, Germany, 2004)

Introduction

The chemistry of alkylidyne complexes of tungsten[2] has been greatly enriched by use of hydrotris(pyrazolyl)borate ligands and their derivatives,[3] primarily from the works of Stone,[4] Angelici,[5] and Templeton.[6] The dihydrobis(pyrazolyl)borate chelate $[H_2B(pz)_2$; pz = pyrazol-1-yl; Scheme 1][3] is an intriguing ligand in its own right displaying a propensity for η^3-coordination through agostic and potentially hemilabile B−H−M interactions.

In the design of alkylidyne complexes for use in both stoichiometric and catalytic bond-forming processes, the incorporation of a vacant coordination site *cis* to the alkylidyne ligand remains a valuable goal, although this can present a challenge for low-valent metal centres which are typically more constrained by adherence to the 18-electron rule. Stone has described a range of tungsten alkylidyne complexes coligated by the $H_2B(pz)_2$ ligand and shown that they readily enter into bridge-assisted cluster-assembly reactions (Scheme 2).[7] The further observation that $[Mo(\equiv CC_6H_4OMe\text{-}2)(CO)\{P(OMe)_3\}_2\{H_2B(pz)_2\}]$ reacts stoichiometrically with $P\equiv CCMe_3$ under mild conditions

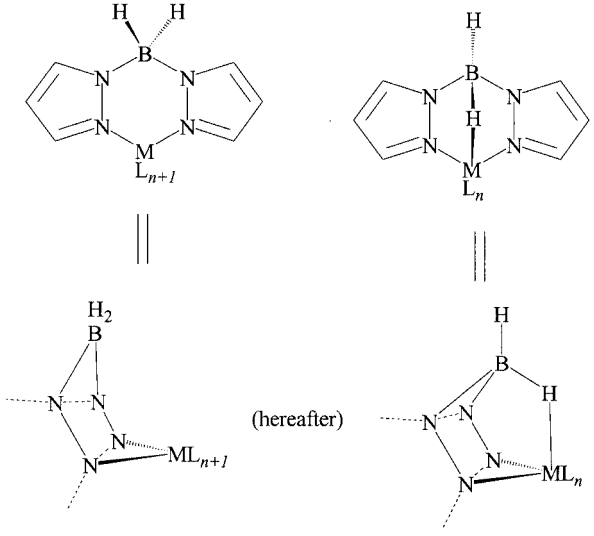

Scheme 1. Dihydrobis(pyrazolyl)borate coordination

to provide $[Mo(\equiv CCMe_3)(CO)\{P(OMe)_3\}_2\{H_2B(pz)_2\}]$[8] points toward the intermediacy of coordinatively unsaturated species, if an analogy with alkyne metathesis is entertained. However, no direct observation of the operation of the η^3-coordination mode was ever made in these processes. We considered that the $H_2B(pz)_2$ ligand might nevertheless, under suitably contrived circumstances, enter into η^3-coordination and thereby satisfy the above requirements by virtue of the hemilability of the agostic B−H−M interaction.

[‡] Poly(azotyl)chelate Chemistry, 11. Part 10: Ref.[1]

[a] Department of Chemistry, Imperial College London, South Kensington, SW7 2AZ, U.K.
E-mail: a.hill@rsc.anu.edu.au
[b] Research School of Chemistry, Institute of Advanced Studies, Australian National University, Canberra ACT, Australia

 © 2004 Wiley-VCH Verlag GmbH & Co. KGaA, Weinheim **DOI: 10.1002/ejic.200300444**

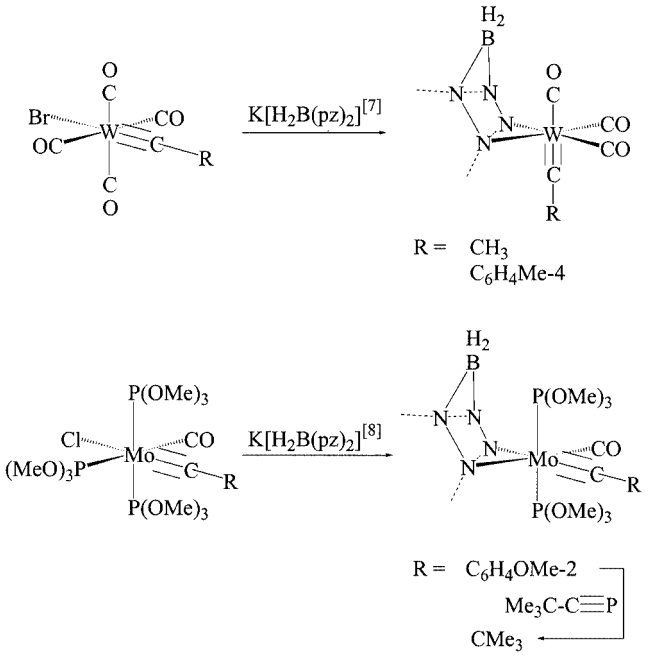

Scheme 2. Dihydrobis(pyrazolyl)borate alkylidynes[7,8]

The results described herein arise from an attempt to broaden the class of alkylidyne-$H_2B(pz)_2$ complexes in pursuit of such a situation. Although coordination of the $H_2B(pz)_2$ ligand has been structurally confirmed in the chemistry of chromium,[9] the Cambridge Crystallographic Data Centre contains no data for mononuclear $H_2B(pz)_2$ complexes of either molybdenum[10] or tungsten and accordingly, two crystallographic studies of complexes with the $H_2B(pz)_2W$ motif were undertaken.

Results and Discussion

Stone's original approach to alkylidyne complexes coligated by the $H_2B(pz)_2$ ligand, namely $[W(\equiv CR)(CO)_3\{\kappa^2\text{-}H_2B(pz)_2\}]$ (R = Me, C_6H_4Me-4; hereafter κ^2 implied unless otherwise indicated),[7] proceeded from Fischer's thermolabile precursors *trans*-$[W(\equiv CR)Br(CO)_4]$. Whilst the instability of the tetracarbonyl precursors did not preclude a detailed study of $[W(\equiv CR)(CO)_3\{H_2B(pz)_2\}]$, we sought a more convenient entry point. To this end, thermally stable bis(γ-picoline) precursor complexes were employed. We have previously employed the sterically congested xylylmethylidyne ligand to confer kinetic stability on alkylidyne complexes.[13] More recently, Berke employed the mesitylmethylidyne variant and this allowed the observation of rare examples of hydrido-alkylidyne complexes.[14]

The complexes *trans,cis,cis*-$[W(\equiv CR)Br(CO)_2(NC_5H_4Me\text{-}4)_2]$ (R = $C_6H_3Me_2$-2,6 **1a**, $C_6H_2Me_3$-2,4,6 **1b**) were readily obtained directly from $[W(CO)_6]$ in "one-pot" reactions by successive treatment with LiBr/LiR (from Li and RBr), $(CF_3CO)_2O$ and γ-picoline (Scheme 3), following a modification/combination of Mayr's syntheses of $[W(\equiv CPh)Cl(CO)_2(NC_5H_4)_2]$ and $[W(\equiv CPh)(O_2CCF_3)(CO)_2(tmeda)]$.[15,16] The 2-xylyl derivative **1a** has been previously employed for the preparation of various "half-sandwich" alkylidyne complexes, although its synthesis was not described.[13] The chloro(pyridine)mesitylmethylidyne complex $[W(\equiv CC_6H_2Me_3\text{-}2,4,6)Cl(CO)_2(NC_5H_5)_2]$ has recently been reported[14] by the Mayr synthesis from the reaction of Fischer's pre-isolated aroylate salt $[W\{C(=O)C_6H_2Me_3\text{-}2,4,6\}(CO)_5][NMe_4]$[17] with oxalyl chloride and pyridine. Whilst this salt would presumably also serve as a precursor for the subsequent introduction of the $H_2B(pz)_2$ ligand, the present high yielding "one-pot" synthesis of $[W(\equiv CC_6H_2Me_3\text{-}2,4,6)Br(CO)_2(NC_5H_4Me\text{-}4)_2]$ (**1a**) is both more convenient and atom efficient in a "green" sense. Specifically, by omitting the Li/NMe_4 metathesis step in the original Mayr synthesis, the bromide anion carried through from the original synthesis of the aryllithium replaces the trifluoroactetate ligand in the intermediate $[W(\equiv CR)(O_2CCF_3)(CO)_4]$. γ-Picoline was chosen to simplify the NMR data. Spectroscopic data for the complexes are unremarkable and conform to precedent.[2]

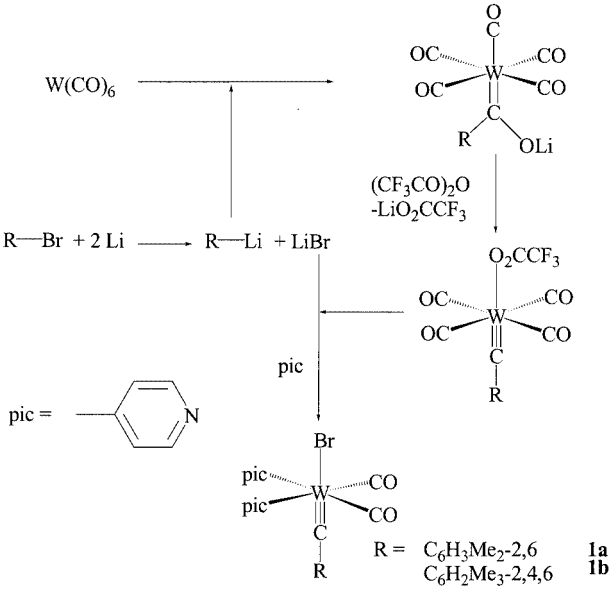

Scheme 3. One Pot Synthesis of alkylidyne tungsten precursors

The reactions of **1a** or **1b** with $K[H_2B(pz)_2]$ in propanone or dichloromethane provide high yields of the complexes formulated as $[W(\equiv CR)(CO)_2(NC_5H_4Me\text{-}4)\{H_2B(pz)_2\}]$ (R = $C_6H_3Me_2$-2,6 **2a**, $C_6H_2Me_3$-2,4,6 **2b**) on the basis of spectroscopic data and a crystallographic study (vide infra) of **2a**. Infrared (solution and solid-state) and ^1H NMR spectroscopic data for both **2a** and **2b** would appear to suggest the formation of one isomer, however, in this instance $^{13}C\{^1H\}$ NMR spectroscopic data appear more sensitive to the coordination environment around tungsten, revealing the coexistence of two isomers in solution (Scheme 4). Thus for **2b**, two carbyne associated resonances are observed at low field [δ = 294.5 (major), 284.5 (minor) ppm]. Similarly, the carbonyl resonances are observed in similar ratios; however, these latter data also allow the assignment of the

 © 2004 Wiley-VCH Verlag GmbH & Co. KGaA, Weinheim

stereochemistry at tungsten. Thus, the major isomer has only one carbonyl environment (δ = 225.3 ppm) whilst the minor isomer features two carbonyl resonances (δ = 227.5 and 221.5 ppm). Accordingly, the major isomer corresponds to the more symmetric geometry (i.e. with the picoline ligand *trans* to the alkylidyne substituent) which is also found in the solid state (Scheme 4, Figure 1). Similar behaviour was observed for **2b**.

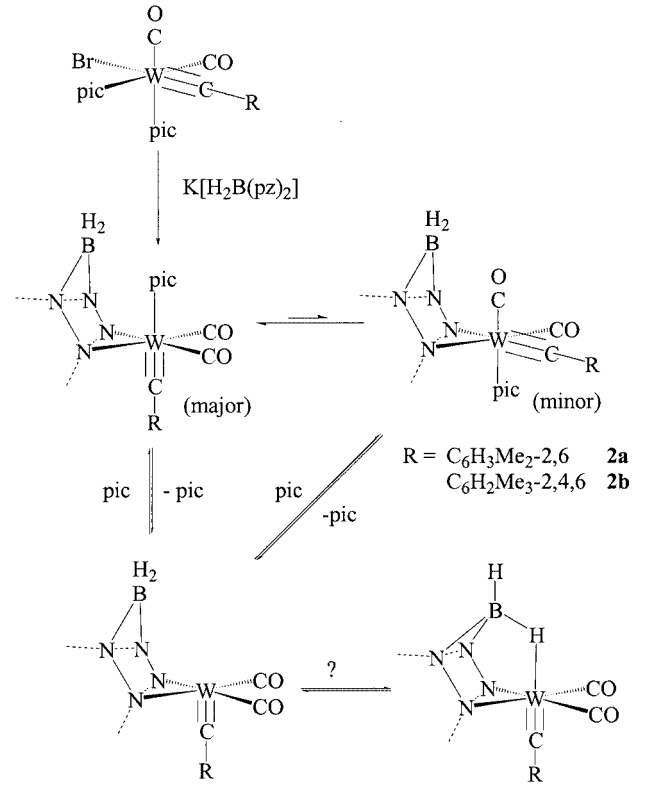

Scheme 4

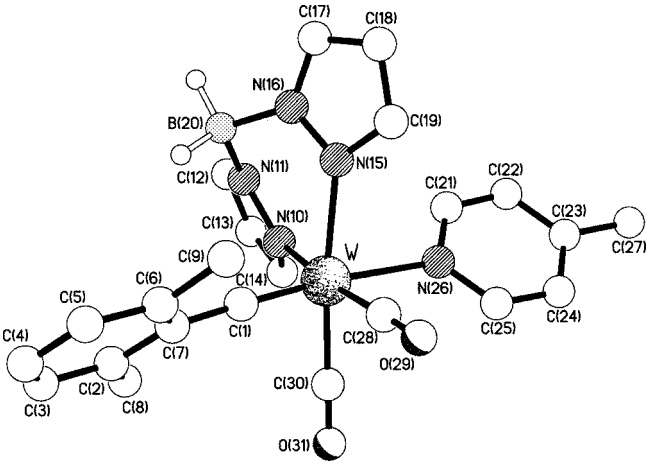

Figure 1. Molecular geometry of **2a**; hydrocarbon hydrogen atoms omitted

For both isomers to coexist and interconvert in solution, it may be surmised that the donor properties of the pyrazole and picoline groups are comparable. Since this equilibrium operates under mild conditions, it seems most likely that it occurs through dissociation of the picoline ligand, rearrangement of the five-coordinate complex and picoline recoordination, rather than unimolecular rearrangement of the octahedral complexes. The lability of the picoline ligand in **2** is also implicit in the ligand-substitution reactions discussed below. It might also be inferred that if tridentate coordination of the $H_2B(pz)_2$ ligand occurs to stabilize the five-coordinate intermediate, then this is easily replaced by picoline coordination since no spectroscopic evidence was obtained for such an intermediate.

The reactions of **2** with a range of ligands were investigated. Under ambient conditions neither **2a** nor **2b** appear to react with carbon monoxide within spectroscopically (IR) determinable limits. This is in contrast to the complex $[Mo(\equiv CC_6H_4OMe\text{-}2)(CO)\{P(OMe)_3\}_2\{H_2B(pz)_2\}]$[8] which equilibrates to a mixture with the complex $[Mo(\equiv CC_6H_4OMe\text{-}2)(CO)_2\{P(OMe)_3\}\{H_2B(pz)_2\}]$ under one atmosphere of CO in dichloromethane.[18] However, it is not surprising given that introduction of a further carbonyl ligand would be disfavored by the competitive π-acidity of the two carbonyl and alkylidyne ligands already present. The complex $[W(\equiv CC_6H_4Me\text{-}4)(CO)_3\{H_2B(pz)_2\}]$[7] has already been discussed (see above) and the synthesis proceeds in the absence of other potential donor ligands.

Isonitriles (CNR′: R′ = CMe_3, $C_6H_3Me_2$-2,6) which are more nucleophilic and less π-acidic ligands than CO do react with **2** by displacement of the picoline ligand. However, these reactions are complicated by the competitive formation of the ketenyl species. Thus, treating **2a** with either $CNCMe_3$ or $CNC_6H_3Me_2$-2,6 leads to complex mixtures. This was eventually traced to the competition of thermal and photochemical processes, each leading to thermally sensitive products. The major identifiable products of the thermal reaction were the alkylidyne complexes $[W(\equiv CC_6H_3Me_2\text{-}2,6)(CO)_2(CNR')\{H_2B(pz)_2\}]$ (**3**), whilst the major photo-products were the ketenyl complexes $[W(\eta^2\text{-}OCC_6H_3Me_2\text{-}2,6)(CO)(CNR')_2\{H_2B(pz)_2\}]$ (R′ = $C_6H_3Me_2$-2,6 **4a**, CMe_3 **4b**).

Kreiβl[19] studied the coupling of alkylidyne and carbonyl ligands to generate mononuclear ketenyl complexes in thermal reactions of $[W(\equiv CC_6H_4Me\text{-}4)(CO)_2(\eta\text{-}C_5H_5)]$ with PMe_3, whilst Stone showed similar couplings in dinuclear systems.[20] Subsequently, Geoffroy demonstrated that such processes could be photochemically induced.[21] Ketenyl formation through alkylidyne/carbonyl coupling has since been reviewed,[22] whilst the synthetic utility of ketenyl complexes has been amply demonstrated by Kreiβl.[23] The clarification of the processes involved in the reactions of **2** with isocyanides called for selective synthesis of the products since the reactions themselves were not synthetically useful in that the mixtures obtained required cryostatic chromatography (−40 °C) and the purified products were unstable at room temperature. The purple ketenyl complex $[W(\eta^2\text{-}OCC_6H_3Me_2\text{-}2,6)(CO)(CNCMe_3)_2\{H_2B(pz)_2\}]$ (**4b**) could most easily be obtained in modest yield (40 %) by the addition of $CNCMe_3$ to **2a** under irradiation (domestic sun

 © 2004 Wiley-VCH Verlag GmbH & Co. KGaA, Weinheim

lamp) followed by cryostatic chromatography. Although they could be retrospectively identified amongst the products of the reactions of **2** with CNR′, the alkylidyne complexes $[W(\equiv CC_6H_3Me_2\text{-}2,6)(CO)_2(CNR')\{H_2B(pz)_2\}]$ (R′ = $C_6H_3Me_2$-2,6 **3a**, CMe_3 **3b**) could most easily be obtained through the reactions of preformed $[W(\equiv CC_6H_3Me_2\text{-}2,6)Br(CO)_2(CNR')_2]$ (R′ = CMe_3 **5a**, $C_6H_3Me_2$-2,6 **5b**; Scheme 5)[24] with $K[H_2B(pz)_2]$, although exclusion of light was essential throughout their synthesis and isolation.

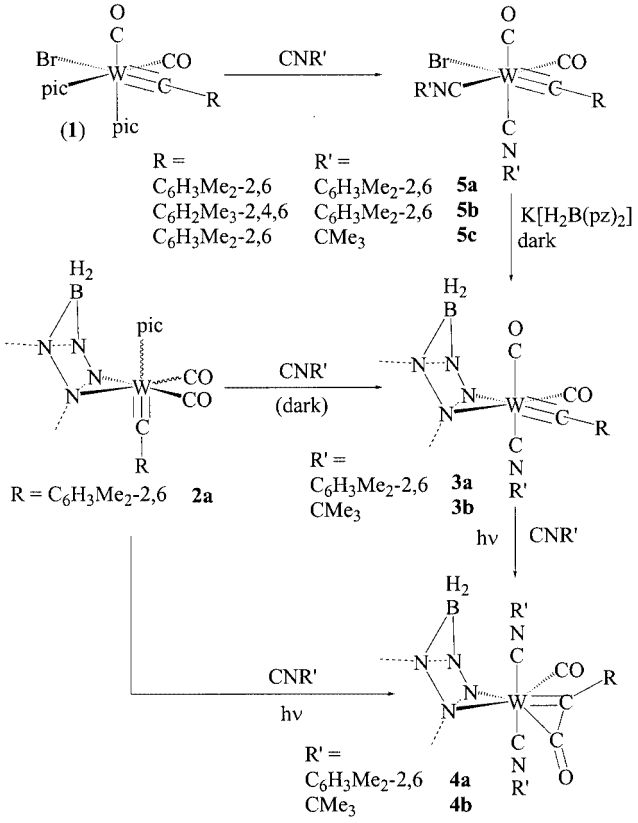

Scheme 5

The formulation of both the alkylidyne and ketenyl complexes rests upon spectroscopic and FAB-MS data, since their instability at ambient temperatures prevented us from obtaining either satisfactory elemental microanalysis or crystallographic grade crystals. Nevertheless, the spectroscopic data strongly support the formulations as do the unequivocal synthesis from bis(isocyanide) precursors. For the alkylidyne complex $[W(\equiv CC_6H_3Me_2\text{-}2,6)(CO)_2(CNCMe_3)\{H_2B(pz)_2\}]$ (**3b**), both ^1H and $^{13}C\{^1H\}$ NMR spectroscopic data confirm two distinct pyrazolyl environments, the latter also indicating chemically inequivalent carbonyl ligands. Taken together, these data are only consistent with the geometry shown in Scheme 5. Such arguments also support a similar geometry for **3a**. For the ketenyl complex $[W(\eta^2\text{-}OCCC_6H_3Me_2\text{-}2,6)(CO)(CNCMe_3)_2\{H_2B(pz)_2\}]$ (**4b**) the stereochemistry at tungsten also follows from a combination of IR and NMR spectroscopic data, the gross formulation being confirmed by FAB-MS data. Thus one isocyanide-associated absorption is observed in the infrared spectrum and one albeit broad resonance in the $^{13}C\{^1H\}$ NMR spectrum indicating a *trans*-$W(CNCMe_3)_2$ arrangement. The observation of a single isocyanide environment would suggest that either inversion of the $B(NN)_2W$ boat arrangement is rapid on the NMR timescale or that the BH_2 group does not sufficiently closely approach the *tert*-butyl groups to render these inequivalent. Molecular models and the related structural studies (vide infra) would argue for the former interpretation.

In contrast to the reactions with isocyanides, the reactions of **2** with dimethylphenylphosphane are straightforward and proceed through picoline substitution to provide a single isomer with no indication of ketenyl formation. Thus, treating **2** with one equivalent of PMe_2Ph in dichloromethane provided the complexes $[W(\equiv CR)(CO)_2(PMe_2Ph)\{H_2B(pz)_2\}]$ (R = $C_6H_3Me_2$-2,6 **6a**, $C_6H_2Me_3$-2,4,6 **6b**) each in only one isomeric form. The complex $[W(\equiv CC_6H_4Me\text{-}4)(CO)_3\{H_2B(pz)_2\}]$ has been reported to react with PPh_3 or PMe_3 to provide the complexes $[W(\equiv CC_6H_4Me\text{-}4)(CO)_2(PR_3)\{H_2B(pz)_2\}]$ by carbonyl substitution with no evidence for ketenyl formation.[7] The stereochemistry of **6a** in solution (Scheme 6, Figure 2) follows unequivocally from spectroscopic data and was confirmed by X-ray crystallography (vide infra). The diastereotopicity of the phosphane methyl groups confirms the absence of a molecular element of symmetry excluding the isomer with phosphane *trans* to the alkylidyne group. This possibility may also be discounted by the low value of $^2J_{P\text{-}C}$ (8.9 Hz) for the alkylidyne ^{13}C resonance. IR data

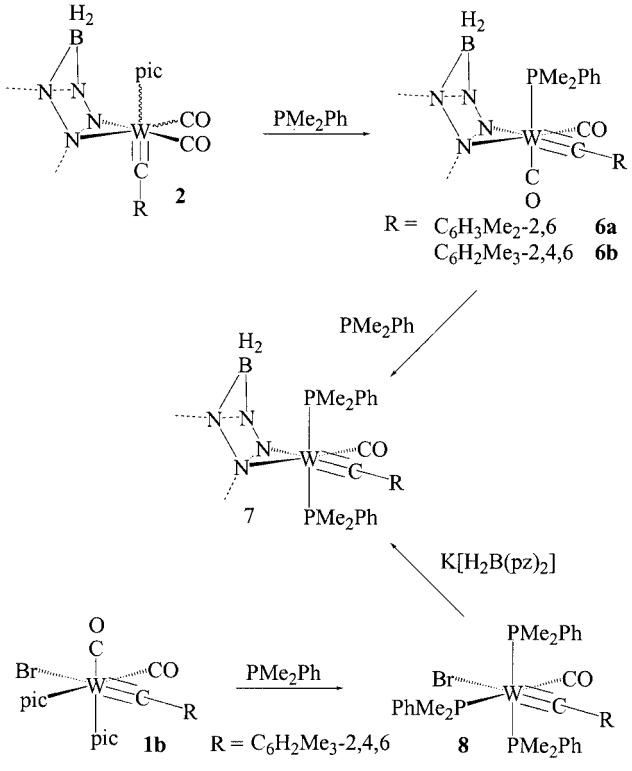

Scheme 6

 © 2004 Wiley-VCH Verlag GmbH & Co. KGaA, Weinheim

indicates a *cis*-$W(CO)_2$ arrangement whilst ^{13}C NMR spectroscopic data indicate that both the CO ligands and also the two pyrazolyl groups are chemically inequivalent. Similar arguments apply to the stereochemistry of **6b**.

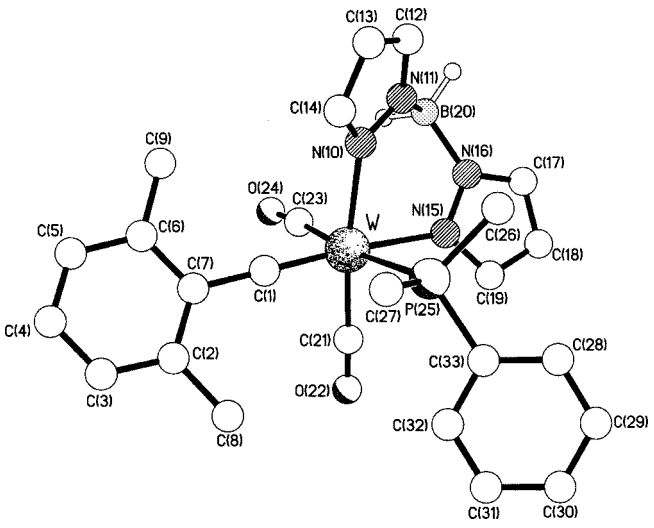

Figure 2. Molecular geometry of **6a**; hydrocarbon hydrogen atoms omitted

Treating the complex **6b** with excess PMe_2Ph leads to carbonyl substitution and formation of the *trans*-bis(phosphane) complex $[W(\equiv CC_6H_2Me_3\text{-}2,4,6)(CO)(PMe_2Ph)_2\{H_2B(pz)_2\}]$ (**7**). The stereochemistry at tungsten follows from ^1H, ^{31}P and ^{13}C NMR spectroscopic data. The chemical equivalence of the two phosphorus nuclei is manifest as a singlet resonance in the $^{31}P\{^1H\}$ NMR spectrum, whilst the *trans* arrangement is suggested by the virtual triplet nature of the ^{13}C resonance for the phosphane methyl groups. Notably this stereochemistry is equivalent to that proposed for $[Mo(\equiv CR)(CO)\{P(OMe)_3\}_2\{H_2B(pz)_2\}]$ (R = CMe_3, C_6H_4OMe-2).[8] The IR data [ν(CO) = 1992, 1903 cm^{-1}] for **6b** would suggest that the carbonyl ligands are not thermally labile. Accordingly, the facile formation of **7** from **6b** under mild conditions presumably proceeds through ketenyl formation followed by CO extrusion, as has been demonstrated in the synthesis of $[W(C\equiv CC_6H_4Me\text{-}4)(CO)(PMe_3)(\eta\text{-}C_5H_5)]$ from $[W(\equiv CC_6H_4Me\text{-}4)(CO)_2(\eta\text{-}C_5H_5)]$.[19] Notably, the reactions of $[W(\equiv CR)(CO)_2\{HB(pz)_3\}]$ (R = C_6H_4Me-4, SMe) with PMe_3 or PEt_3 stop at the ketenyl stage providing $[W(\eta^2\text{-}OCCC_6H_4Me\text{-}4)(CO)(PMe_3)\{HB(pz)_3\}]$[7] and $[W(\eta^2\text{-}OCCSMe)(CO)(PEt_3)\{HB(pz)_3\}]$,[5a] respectively.

An alternative synthesis of **7** was developed by the reaction of $[W(\equiv CC_6H_2Me_3\text{-}2,4,6)Br(CO)(PMe_2Ph)_3]$ (**8**) with $K[H_2B(pz)_2]$. The new precursor **8** was obtained from the reaction of **1b** with PMe_2Ph. The closely related complex $[W(\equiv CPh)Cl(CO)(PMe_3)_3]$ has been reported previously by Mayr, arising from the reaction of $[W(\equiv CPh)Cl(CO)_2(PMe_3)_2]$ with PMe_3 over a period of 7 days.[27] In the present case however the stoichiometric amount of phosphane suffices and the reaction is complete in 15 h. The *mer* geometry follows from ^1H, ^{13}C and $^{31}P\{^1H\}$ NMR spectroscopic data for the phosphane groups and the doublet-triplet fine structure of the carbonyl and alkylidyne group resonances in the $^{13}C\{^1H\}$ NMR spectrum. The complex **8** reacts cleanly with $K[H_2B(pz)_2]$ in tetrahydrofuran to provide **7**. In this case it is not necessary to invoke ketenyl intermediates.

Crystal Structure of $[W(\equiv CC_6H_3Me_2\text{-}2,6)(CO)_2(NC_5H_4Me\text{-}4)\{H_2B(pz)_2\}]\cdot 0.5CH_2Cl_2$ (2a·0.5CH_2Cl_2)

The complex crystallizes from a mixture of dichloromethane and petroleum ether as a dichloromethane hemisolvate, however, the solvent of crystallization which is disordered shows no directional interactions with the complex and neither are there any notable intermolecular interactions within the crystal lattice. The molecular geometry of the complex is depicted in Figure 1 and selected bond lengths and angles are presented in Table 1. The geometry at tungsten is distorted octahedral with angles between adjacent ligands lying in the range 82.9(2)−101.2(2)° such that the pyrazolyl groups bend away from the alkylidyne groups [C(1)−W−N(15) 100.5(2), C(1)−W−N(10) 101.2(2)°] whilst the carbonyl ligands bend less markedly towards it [C(1)−W−C(28) 85.6(3), C(1)−W−C(30) 87.9(3)°]. The bending of *cis* ligands away from metal−element multiple bonds is not uncommon and it has been suggested that this strengthens the multiple bonding.[28] The alkylidyne ligand is essentially linear at the carbyne carbon [W−C(1)−C(7) 178.0(5)°] and the W≡C separation of 1.810(6) Å falls within the range typical of alkylidyne tungsten complexes[2] and is similar to that found in, for example, $[W(\equiv CPh)(CO)_2(Ppy_3)]^+$ [1.811(7) Å].[29] The xylyl ring orientation is presumably dictated by steric effects as it places the *ortho* substituents between adjacent coligands, rather than allowing the aromatic π-system to conjugate with occupied metal t_{2g} orbitals. In a similar manner, the plane of the picoline ligand is approximately orthogonal (ca. 79°) to that of the alkylidyne, lying between the pyrazolyl rings of the $H_2B(pz)_2$ chelate and approximately bisecting the $W(CO)_2$ group. The octahedral γ-picoline complexes *trans*-$[W^{III}Cl_4(NC_5H_4Me\text{-}4)_2]^-$,[30] *cis,cis,trans*-$[W^{II}Br_2(bipy)(NC_5H_4Me\text{-}4)_2]$[31] and $[W^0(CO)_5(NC_5H_4Me\text{-}4)]$[32] have (mean) W−N bond lengths of 2.166, 2.176, and 2.257 Å, respectively, with a lengthening of the W−N bond on reduction of the metal centre (W^{III}, W^{II}, and W^0). For-

Table 1. Selected bond lengths (Å) and angles (°) for **2a**

W−C(1)	1.810(6)	W−C(28)	1.975(8)
W−C(30)	1.977(9)	W−N(15)	2.201(6)
W−N(10)	2.204(6)	W−N(26)	2.378(5)
C(1)−C(7)	1.416(9)		
C(1)−W−C(28)	85.6(3)	C(1)−W−C(30)	87.9(3)
C(28)−W−C(30)	87.6(3)	C(1)−W−N(15)	100.5(2)
C(28)−W−N(15)	94.3(3)	C(30)−W−N(15)	171.5(2)
C(1)−W−N(10)	101.2(2)	C(28)−W−N(10)	173.1(3)
C(30)−W−N(10)	93.6(3)	N(15)−W−N(10)	83.6(2)
C(1)−W−N(26)	173.8(2)	C(28)−W−N(26)	88.9(3)
C(30)−W−N(26)	88.9(2)	N(15)−W−N(26)	82.88(19)
N(10)−W−N(26)	84.30(18)	C(7)−C(1)−W	178.0(5)

 © 2004 Wiley-VCH Verlag GmbH & Co. KGaA, Weinheim

mal oxidation states have little meaning in compounds with metal−carbon multiple bonding. However, the sensitivity of the W−N bond lengths to the π-acidity of *trans*-disposed ligands has been demonstrated for the bis(pyridine) complex [W(≡CPh)Cl(CO)(ma)(py)$_2$][33] where the W−N bond *trans* to the strongly π-acidic maleic anhydride (ma) is longer (2.253 Å) than that *trans* to CO (2.233 Å). The W−N(26) bond length of 2.378(5) Å seen here for **2a** far exceeds those discussed above and is consistent with the lability demonstrated in reactions with CNR′ and PMe_2Ph and also its facile isomerism. This lengthening is also consistent with its location *trans* to an alkylidyne ligand which is generally considered to be strongest of all carbon π-acid ligands.

The W(pz)$_2$BH$_2$ metallacycle adopts a typical boat formation with both the tungsten and boron atoms lying ca. 0.65 Å out of the plane of the four nitrogen atoms which are coplanar to within 0.007 Å. This geometry is comparatively shallow and positions the BH_2 group well beyond any interaction with either the metal [BH···W 3.46 Å] or co-ligands. Thus, although the adopted conformation places the BH_2 adjacent to the alkylidyne, the BH···C(1) distance of 3.10 Å is probably too long to invoke any incipient nucleophilic interaction of the B−H bond with the carbyne carbon atom. The bite of the chelate at 83.6(2)° is somewhat contracted from 90° with the remaining angles within the chelate close to those expected for trigonal nitrogen [121.7(6)−125.0(4)°] and tetrahedral boron [107.9(6)°].

Crystal Structure of [W(≡CC$_6$H$_3$Me$_2$-2,6)(CO)$_2$(PMe$_2$Ph){H$_2$B(pz)$_2$}] (6a)

Yellow solvate-free needles were obtained by cooling a solution of the complex in a mixture of propanone and petroleum ether (40:60). The molecular geometry of the complex is depicted in Figure 2. As for complex **2a**, the tungsten center approximates octahedral geometry with angles between *cis*-ligands falling in the range 81.70(8)−100.00(11)° (Table 2). However, in contrast to **2a**, the $H_2B(pz)_2$ and alkylidyne groups assume a meridional disposition with the phosphane ligand *cis* to the alkylidyne group. The alkylidyne ligand displays a characteristically short W≡C separation [1.825(4) Å] (not significantly different from that in **2a**) and is slightly bent at the carbyne carbon atom [W−C(1)−C(7) 173.5(3)°], which lies within the range previously observed and generally attributed to crystal-packing effects.[2] The orientation of the xylyl group is such as to minimise steric interactions with *cis* coligands, which places the *ortho* substituents either side of the $W(CO)_2$ unit. The phosphane ligand has a W−P bond length of 2.564(1) Å which appears somewhat long. Limiting comparison to 6-coordinate tungsten complexes of PMe_2Ph with sterically modest co-ligands[34,35] there appears to be no obvious correlation between the oxidation state (d configuration) and the W−P bond length [d^6: 2.480−2.524; d^4: 2.484−2.512; d^3: 2.513−2.561; d^2: 2.481−2.538Å]. The dichotomy that clouds the assignment of oxidation states for alkylidyne complexes is shared by nitrosyl ligands and accordingly the most suitable structure for comparison is the complex *trans,cis,cis*-[W(NO)I(CO)$_2$(PMe$_2$Ph)$_2$] reported by Basolo[35] which also features particularly long W−P bond lengths [2.582(2), 2.554(2) Å].

The [H$_2$B(NN)$_2$W] chelate once again adopts a shallow boat conformation with here the tungsten and boron atoms that lie (0.54 and 0.65 Å, respectively) out of the N_4 plane which is coplanar to within 0.026 Å. The closest B−H hydrogen atom approach to the metal centre is 3.49 Å, too distant for any interaction. However, this hydrogen atom is positioned directly above one of the carbonyl ligands, the BH···C(23) distance being 2.87 Å, indicating a possible weak B−H···π* interaction. In contrast to **2a**, the low symmetry of **6a** allows the chelate to reveal the comparative *trans* influences of carbonyl and alkylidyne ligands. Thus the pyrazolyl group *trans* to the alkylidyne has a significantly (20σ) longer W−N bond length [2.292(3) Å] than that *trans* to the carbonyl [2.233(3) Å]. The difference in *trans* influence for the pyrazolyl and phosphane ligands is less obvious in the bonding of the carbonyl ligands with that *trans* to phosphorus [W−C(23) 2.014(5) Å], showing a smaller (7σ) lengthening relative to W−C(21) [1.980(4) Å]. The only intermolecular packing interaction of note is a parallel π−π stacking of the xylyl rings of centrosymmetrically related molecules with mean interplanar and centroid···centroid separations of 3.46 and 3.74 Å, respectively.

Table 2. Selected bond lengths (Å) and angles (°) for **6a**

W−C(1)	1.825(4)	W−C(21)	1.980(4)
W−C(23)	2.014(5)	W−N(10)	2.233(3)
W−N(15)	2.292(3)	W−P(25)	2.5644(10)
C(1)−C(7)	1.451(5)		
C(1)−W−C(21)	87.74(15)	C(1)−W−C(23)	86.64(16)
C(21)−W−C(23)	87.66(17)	C(1)−W−N(10)	99.92(13)
C(21)−W−N(10)	172.25(13)	C(23)−W−N(10)	93.91(14)
C(1)−W−N(15)	174.94(13)	C(21)−W−N(15)	87.35(14)
C(23)−W−N(15)	91.95(15)	N(10)−W−N(15)	85.02(11)
C(1)−W−P(25)	100.00(11)	C(21)−W−P(25)	95.61(12)
C(23)−W−P(25)	172.69(12)	N(10)−W−P(25)	82.00(8)
N(15)−W−P(25)	81.70(8)	C(7)−C(1)−W	173.5(3)

Experimental Section

General Procedures: All manipulations were carried out under an atmosphere of prepurified dinitrogen with conventional Schlenk-tube techniques. Solvents were purified by distillation from an appropriate drying agent [ethers and paraffins from sodium/potassium alloy with benzophenone as indicator; halocarbons from CaH_2]. Light petroleum ether refers to that fraction of boiling point 40−60 °C. Chromatographic separations were routinely performed using a cryostatically cooled column at −40 °C. ^{1}H, ^{13}C{^{1}H} and ^{31}P{^{1}H} NMR spectra were recorded with a Jeol JNM EX270 NMR spectrometer and referenced against internal Me_4Si (^{1}H), internal $CDCl_3$ (^{13}C) or external H_3PO_4 (^{31}P). Infrared spectra were recorded with a Perkin−Elmer 1720-X FT-IR spectrometer. FAB-Mass spectra were measured with an Autospec Q mass spectrometer using 3-nitrobenzyl alcohol as matrix ('pic' = γ-picoline). Photolyses were conducted with a domestic sun-lamp in cryo-

 © 2004 Wiley-VCH Verlag GmbH & Co. KGaA, Weinheim

statically cooled Schlenk-tubes. Commercial reagents were used as received and the salt $K[H_2B(pz)_2]$[3] prepared according to the following procedure. The original procedure involves heating $K[BH_4]$ and Hpz in a melt, with the progress of the reaction being monitored by the measurement of evolved hydrogen gas. In our laboratory, this usually provided samples of $K[H_2B(pz)_2]$ contaminated with both pyrazole and $K[HB(pz)_3]$. The following approach employs a solvent to moderate the reaction temperature and provide a homogeneous reaction mixture.

Synthesis of Potassium Dihydrobis(pyrazolyl)borate: Potassium tetrahydroborate (13.50 g, 0.25 mmol) and pyrazole (68.00 g, 1.00 mol), both finely ground, were suspended in toluene (250 mL) and gradually brought to reflux. After 12−16 h hydrogen gas evolution had effectively ceased. The clear solution was filtered whilst hot to remove any residual traces of unchanged $K[BH_4]$. The filtrate was allowed to cool with rapid stirring to about 40 °C whereupon a white precipitate formed that was filtered off. The finely divided white solid was washed with dichloromethane (3 × 50 mL), to remove any traces of unchanged pyrazole followed by diethyl ether (2 × 30 mL) and then dried in vacuo. Yield 32.60 g (70 % vs. $K[BH_4]$). The salt was characterised by comparison of spectroscopic data with those previously reported[3] and was found to be free of Hpz or $K[HB(pz)_3]$ within spectroscopically determinable limits (^{1}H NMR, IR).

Synthesis of $[W(\equiv CC_6H_3Me_2\text{-}2,6)Br(CO)_2(NC_5H_4Me\text{-}4)_2]$ (1a): This complex has been used previously for the preparation of various 2-xylyl methylidyne complexes, however, neither preparative details nor spectroscopic data were provided.[13a] Tungsten hexacarbonyl (4.25 g, 12 mmol) was suspended in diethyl ether (30 mL) to which 1.1 equivalents of $LiC_6H_3Me_2$-2,6·LiBr in 1 mL aliquots over 30 min were subsequently added. The pale yellow solution was cooled (dry ice/propanone) and trifluoroacetic anhydride (1.70 mL, 12.0 mmol) slowly added over a 5 min period. The mixture was stirred for 15 min after which γ-picoline (3.0 mL, 0.957 gcm^{-3}, 30 mmol) was added and allowed to warm to room temperature which resulted in evolution of carbon monoxide (CAUTION). After 12 h, a bright yellow precipitate was isolated from solution. This solid was redissolved in dichloromethane (20 mL) and the solution filtered under nitrogen through a plug of alumina (2 × 4 cm). The filtrate was diluted with diethyl ether (60 mL) and then cooled to −10 °C whereupon the bright orange solid which formed was isolated by filtration and dried in vacuo. Yield 6.38 g (85 %). IR (CH_2Cl_2): ν(CO) = 1984, 1895 cm^{-1}. Nujol: ν(CO) = 1980, 1888 cm^{-1}. ^{1}H NMR ($CDCl_3$, 25 °C): δ = 2.40, 2.45 [s × 2, 6 H × 2, $C_6H_3CH_3$ and $NC_5H_4CH_3$], 6.90 [d, 2 H, H3,5 (C_6H_3)], 7.03 [m, 1 H, H4 (C_6H_3)], 7.11, 8.97 [$(AB)_4$, 8 H, NC_5H_4, ^3J(AB) = 5.5 Hz] ppm. ^{13}C{^{1}H} NMR: δ = 266.4 [W≡C, ^1J (WC) = 207 Hz], 221.9 [WCO, ^1J (WC) = 171 Hz], 150.5−127.2 [C_6H_3 and NC_5H_4], 125.8 [C-3,5 (NC_5H_4)], 21.0, 20.5 ($C_6H_4CH_3$ and $NC_5H_4CH_3$) ppm. FAB-MS: *m*/*z* = 624 [M]$^+$, 596 [M − CO]$^+$, 568 [M − 2CO]$^+$, 543 [M − Br]$^+$, 529 [M − pic]$^+$, 503 [M − pic − CO]$^+$, 473 [M − pic − 2CO]$^+$, 450 [M − pic − Br]$^+$. $C_{23}H_{23}BrN_2O_2W$: calcd. C 44.33, H 3.72, N 4.50; found C 44.8, H 3.5, N 4.4.

Synthesis of *trans,cis,cis*-$[W(\equiv CC_6H_2Me_3\text{-}2,4,6)Br(CO)_2(NC_5H_4Me\text{-}4)_2]$ (1b): The synthesis follows the procedure described above, providing 6.74 g (88 %) of the desired complex from $[W(CO)_6]$ (4.25 g, 12.0 mmol). IR (CH_2Cl_2): ν(CO) = 1984, 1895 cm^{-1}. IR (nujol): ν(CO) = 1980, 1888 cm^{-1}. ^{1}H NMR ($CDCl_3$, 25 °C): δ = 2.20 [s, 3 H, $C_6H_2CH_3$-4], 2.40, 2.43 [s × 2, 12 H, $NC_5H_4CH_3$ and $C_6H_2CH_3$-2,6], 6.75 [s, 2 H, C_6H_2], 7.09, 8.95 [$(AB)_4$, 8 H, (NC_5H_4), ^3J(AB) = 5.6 Hz] ppm. ^{13}C{^{1}H} NMR: δ = 267.3 [W≡C, ^1J (WC) = 207.0 Hz], 222.2 [WCO, ^1J(WC) = 171.3 Hz], 153.2 [C-2,6 (NC_5H_4)], 150.6 [C-4 (NC_5H_4)], 143.8 [C-1 (C_6H_2)], 141.4 [C-2,6 (C_6H_2)], 137.7 [C-4(C_6H_2)], 128.1 [C-3,5 (C_6H_2)], 125.9 [C-3,5(NC_5H_4)], 21.4 ($C_6H_2CH_3$-4), 21.3, 20.6 ($NC_5H_4CH_3$ and $C_6H_2CH_3$-2,6) ppm. FAB-MS: *m*/*z* (%) = 638(29) [M]$^+$, 610(52) [M − CO]$^+$, 582(91) [M − 2CO]$^+$, 557(78) [M − Br]$^+$, 545(41) [M − pic]$^+$, 517(53) [M − pic-CO]$^+$, 487(63) [M − 2CO]$^+$, 464(37) [M − Br − pic]$^+$. $C_{24}H_{25}BrN_2O_2W$: calcd. C 45.24, H 3.95, N 4.40; found C 44.6, H 3.7, N 4.3.

Synthesis of *mer*- and *fac*-$[W(\equiv CC_6H_3Me_2\text{-}2,6)(CO)_2(NC_5H_4\text{-}Me\text{-}4)\{H_2B(pz)_2\}]$ (2a): The salt $K[H_2B(pz)_2]$ (1.77 g, 9.50 mmol, 1.1 equiv.) was added to *trans,cis,cis*-$[W(\equiv CC_6H_3Me_2\text{-}2,6)Br(CO)_2(NC_5H_4Me\text{-}4)_2]$ (**1a**, 5.00 g, 8.60 mmol) in propanone (30 mL) and the mixture was stirred for 12 h. The solution was concentrated in vacuo to about 10 mL and purified on an alumina-loaded column (2 × 30 cm) eluting with a mixture of propanone and hexane (1:2). The major orange fraction was collected, concentrated in vacuo to about 10 mL and diluted with *n*-hexane (50 mL). After cooling for 12 h at −10 °C a bright orange crystalline solid was isolated and dried in vacuo. Yield 4.20 g (87 %). Crystals of the *fac* isomer suitable for X-ray analysis were obtained upon recrystallization from a mixture of light petroleum and dichloromethane (4:1) at −10 °C (vide infra). IR (CH_2Cl_2): 1978, 1886 [ν(CO)] cm^{-1}. IR (nujol): 2437, 2405, 2284 [ν(BH_2)]; 1971, 1877 [ν(CO)] cm^{-1}. ^{1}H NMR ($CDCl_3$, 25 °C): δ = 2.24 [s, 3 H, $NC_5H_4CH_3$], 2.34 [s, 6 H, $C_6H_3(CH_3)_2$], 6.14−6.18 [m, 2 H, H-4($C_3H_3N_2$)], 6.85 [d, 2 H, H-3,5(C_6H_3)], 7.05 [t, 1 H, H-4(C_6H_3)], 7.20−8.00 [m, 10 H, H-3,5($C_3H_3N_2$) and H-2,3,5,6(NC_5H_4)] ppm. ^{13}C{^{1}H} NMR: δ = 294.5 (major W≡C), 284.5 (minor W≡C), 225.3 (major WCO), 227.5 (minor WCO), 221.5 (minor WCO), 150.8 [C-4(NC_5H_4)], 145.4 [C-3($C_3H_3N_2$)], 140.5 [C-4(C_6H_3)], 136.6 [C-5($C_3H_3N_2$)], 127.3 [C-2,6(C_6H_3)], 127.0 [C-3,5(C_6H_3)], 125.9 [C-3,5(NC_5H_4)], 105.4 [C-4($C_3H_3N_2$)], 21.2 [$NC_5H_4CH_3$], 20.6 [$C_6H_3CH_3$] ppm. FAB-MS: *m*/*z* (%) = 597(33) [M]$^+$, 569(80) [M − CO]$^+$, 541(35) [M − 2CO]$^+$, 503(41) [M − pic]$^+$, 446(19) [M − 2CO-pic]$^+$. $C_{23}H_{24}BN_5O_2W$: calcd. C 46.26, H 4.05, N 11.73; found C 45.6, H 3.9, N 10.9.

Synthesis of *fac*- and *mer*-$[W(\equiv CC_6H_2Me_3\text{-}2,4,6)(CO)_2(NC_5H_4\text{-}Me\text{-}4)\{H_2B(pz)_2\}]$ (2b): The compound *trans,cis,cis*-$[W\equiv CC_6H_2Me_3\text{-}2,4,6)Br(CO)_2(NC_5H_4Me\text{-}4)_2]$ (**1b**, 5.00 g, 7.80 mmol) was treated as above to afford an orange powder. Yield 4.20 g (88 %). IR (CH_2Cl_2): 1975, 1888 [ν(CO)] cm^{-1}. IR (nujol): 2425, 2351, 2287 [ν(BH_2)]; 1971, 1874 [ν(CO)] cm^{-1}. ^{1}H NMR ($CDCl_3$, 25 °C): δ = 2.16 (s, 3 H, $C_6H_2CH_3$-4), 2.29 (s, 3 H, $NC_5H_4CH_3$), 2.32 (s, 6 H, $C_6H_2CH_3$-2,6), 6.14−6.17 [m, 2 H, H-4($C_3H_3N_2$)], 6.67 [s, 2 H, H-3,5(C_6H_2)], 7.20−8.00 [m, 8 H, H-3,5($C_3H_3N_2$) and H-2,3,5,6(NC_5H_4)] ppm. ^{13}C{^{1}H} NMR: δ = 295.0 [major W≡C, ^1J(WC) = 200 Hz], 284.9 [minor W≡C, ^1J(WC) = 194 Hz], 225.5 [major WCO, ^1J(WC) = 169 Hz], 227.6 [minor WCO, ^1J(WC) = 169 Hz], 221.9 [minor WCO, ^1J(WC) = 169 Hz], 150.8 [C-4(NC_5H_4)], 145.4 [C-3($C_3H_3N_2$)], 136.5 [C-5($C_3H_3N_2$)], 127.8 [C-3,5(C_6H_3)], 125.9 [C-3,5(NC_5H_4), 125.6 [C-2,6(C_6H_2)], 105.4 [C-4($C_3H_3N_2$)], 21.2, 20.8 [$NC_5H_4CH_3$ and $C_6H_2CH_3$-4)], 20.6 [$C_6H_2CH_3$-2,6] ppm. FAB-MS: *m*/*z* (%) = 610 (33) [M]$^+$, 583 (41) [M − CO]$^+$, 555 (24) [M − 2CO]$^+$, 516 (100) [M − pic]$^+$, 488 (20) [M − CO − pic]$^+$, 460 (57) [M − pic − 2CO]$^+$. $C_{24}H_{26}BN_5O_2W$: calcd. C 47.17, H 4.29, N 11.46; found C 47.6, H 4.0, N 11.8.

Synthesis of $[W(\equiv CC_6H_3Me_2\text{-}2,6)(CO)_2(CNC_6H_3Me_2\text{-}2,6)\text{-}\{H_2B(pz)_2\}]$ (3a): The compound *trans,cis,cis*-$[W(\equiv CC_6H_3Me_2\text{-}2,6)Br(CO)_2(CNC_6H_3Me_2\text{-}2,6)_2]$ (**5a**, 0.20 g, 0.30 mmol) was dissolved in a mixture of diethyl ether and petroleum ether (9:1,

 © 2004 Wiley-VCH Verlag GmbH & Co. KGaA, Weinheim

30 mL) to which 1.1 equivalents of $K[H_2B(pz)_2]$ (0.06 g, 0.33 mmol) was subsequently added. The mixture was stirred for 4 h in the absence of light. The resulting red solution was concentrated under reduced pressure and purified on a silica-gel loaded column (2 × 30 cm, −40 °C) eluting with a mixture of dichloromethane and light petroleum (1:1). The red fraction was collected and the solvent removed in vacuo under the exclusion of light, to provide a glassy thermally sensitive red solid. Yield 0.16 g (84 %). IR (CH_2Cl_2): 2141 [ν(CN)]; 1998, 1923 [ν(CO)] cm^{-1}. ^1H NMR ($CDCl_3$, 25 °C): δ = 2.14 [s, 6 H, $NC_6H_3(CH_3)_2$], 2.66, 2.68 (s × 2, 6 H, $CC_6H_3CH_3$), 6.17 [m, 2 H, H-4($C_3H_3N_2$)], 6.96 [d, 2 H, H-3,5(CC_6H_3)], 7.00 [m, 3 H, H-3,5(NC_6H_3)], 7.09 [t, 1 H, H-4(C_6H_3)], 7.58−7.80 [m, 4 H, H-3,5($C_3H_3N_2$)] ppm. $^{13}C\{^1H\}$ NMR: δ = 287.5 (W≡C), 221.7, 210.6 (WCO), 168.0 (WCN), 146.8 [C-1(CC_6H_3)], 145.4 [C-1(NC_6H_3)], 145.0, 143.8 [C-5($C_3H_3N_2$)], 136.1, 135.2 [C-3($C_3H_3N_2$)], 127.9 [C-3,5(CC_6H_3)], 127.2 [C-3,5(NC_6H_3)], 105.2, 104.9 [C-4($C_3H_3N_2$)], 18.7, 18.2 [$NC_6H_3(CH_3)_2$ and $C_6H_3(CH_3)_2$] ppm. Satisfactory elemental and FAB-MS data not obtained due to thermal and photolytic lability.

Synthesis of [W(≡CC$_6$H$_3$Me$_2$-2,6)(CO)$_2$(CNCMe$_3$){H$_2$B(pz)$_2$}] (3b): The salt $K[H_2B(pz)_2]$ (0.06 g, 0.33 mmol, 1.1 equiv.) was added to *trans,cis,cis*-[W(≡$CC_6H_3Me_2$-2,6)Br$(CO)_2(CNCMe_3)_2$] (**5c**, 0.20 g, 0.30 mmol) in a mixture of diethyl ether and petroleum ether (9:1, 30 mL). The suspension was stirred for 4 h. under the exclusion of light. The resulting claret solution was concentrated under reduced pressure and purified on a silica gel loaded column (2 × 30 cm, −40 °C) eluting with a mixture of CH_2Cl_2 and light petroleum (1:1). The red fraction was collected and the solvent removed in vacuo (still in the absence of light). An amorphous red solid was obtained. Yield 0.12 g (67 %). IR (CH_2Cl_2): 2175 [ν(CN)]; 1998, 1918 [ν(CO)] cm^{-1}. ^1H NMR ($CDCl_3$, 25 °C): δ = 1.16 (s, 9 H, CMe_3), 2.50 (s, 6 H, $C_6H_3CH_3$), 5.99 [dd, 1 H, H-4($C_3H_3N_2$), $^3J_{H,H}$ = 2 Hz], 6.02 [dd, 1 H, H-4($C_3H_3N_2$), $^3J_{H,H}$ = 2 Hz], 6.80 (m × 2, 3 H, C_6H_3), 7.40−8.80 [m, 4 H, H-3,5($C_3H_3N_2$)] ppm. $^{13}C\{^1H\}$ NMR: δ = 285.6 (W≡C), 222.1, 211.2 (WCO), 144.3, 143.2 [C-5($C_3H_3N_2$)], 136.1, 135.5 [C-3($C_3H_3N_2$)], 126.9 [C-2,6(C_6H_3)], 126.6 [C-3,5(C_6H_3)], 147.8 [C-1(C_6H_3)], 139.6 [C-4(C_6H_3)], 104.8, 104.5 [C-4($C_3H_3N_2$)], 56.2 [$C(CH_3)_3$], 29.9 [$C(CH_3)_3$], 20.4 [$C_6H_3(CH_3)_2$] ppm. Satisfactory elemental analytical data not obtained due to thermal and photochemical lability.

Synthesis of [W(η^2-OCCC$_6$H$_3$Me$_2$-2,6)(CO)(CNCMe$_3$)$_2${H$_2$B(pz)$_2$}] (4b): *tert*-Butyl isocyanide (0.40, mL, 0.735 gcm^{-3}, 0.54 g, 6.50 mmol) was added to [W(≡$CC_6H_3Me_2$-2,6)$(CO)_2(NC_5H_4$Me-4){$H_2B(pz)_2$}] (**2a**, 0.50 g, 0.84 mmol) in dichloromethane (30 mL). The mixture was then irradiated for 3 h with stirring at 0 °C (ice bath). The resulting purple solution was concentrated to about 10 mL and purified on a silica-gel loaded column (2 × 30 cm, −40 °C) eluting initially with a mixture of CH_2Cl_2 and light petroleum (1:1) to remove orange [W(≡$CC_6H_3Me_2$-2,6)-$(CO)_2(CNCMe_3)${$H_2B(pz)_2$}] (**3b**, vide supra). The purple fraction containing **4b** was then eluted with tetrahydrofuran. The resulting eluate was concentrated under reduced pressure to about 2 mL, diluted with light petroleum (10 mL) and stored at −10 °C whereupon purple thermally sensitive microcrystals were obtained overnight. Yield 0.23 g (41 %). IR (CH_2Cl_2): 2162 [ν(CN)]; 1912 [ν(C≡O)]; 1699 [ν(C=O)] cm^{-1}. IR (nujol): 2405 [ν(BH)]; 2160 [ν(CN)]; 1917 [ν(C≡O)]; 1708 [ν(C=O)] cm^{-1}. ^1H NMR ($CDCl_3$, 25 °C): δ = 1.27 (s, 18 H, CMe_3), 2.02 [s, 6 H, $C_6H_3(CH_3)_2$], 6.02, 6.27 [dd × 2, 2 H, H-4($C_3H_3N_2$), $^3J_{H,H}$ = 2, 2 Hz], 7.00 [m, 3 H, C_6H_3], 7.58, 7.59, 7.64, 8.08 [d × 4, 4 H, H-3,5($C_3H_3N_2$)] ppm. $^{13}C\{^1H\}$ NMR: 247.3 (WCO), 217.2 (W=*C*CO), 208.8 (W=C*C*O), 153.0 (WCN), 144.9 [C-1(C_6H_3)], 147.0, 144.3 [C-3($C_3H_3N_2$)], 137.1, 135.9 [C-5($C_3H_3N_2$)], 127.1 [C-3,5(C_6H_3)], 126.2 [C-2,6(C_6H_3)], 104.8, 106.1 [C-4($C_3H_3N_2$)], 58.0 (CMe_3), 29.9 [$C(CH_3)_3$], 21.1 [$C_6H_3(CH_3)_2$] ppm. FAB-MS: *m*/*z* (%) = 671 (21) $[M]^+$, 641 (20) $[M - CO]^+$, 614 (100) $[M - 2CO]^+$, 588 (14) $[M - CNR']^+$, 559 (56) $[M - CO - CNR']^+$, 531 (16) $[M - 2CO - CNR']^+$. Satisfactory elemental data were not obtained due to the thermal instability. $C_{27}H_{35}BN_6O_2W$: calcd. C 48.38, H 5.26, N 12.54; found 45.5, H 4.4, N 11.3.

Synthesis of [W(≡CC$_6$H$_3$Me$_2$-2,6)Br(CO)$_2$(CNC$_6$H$_3$Me$_2$-2,6)$_2$] (5a): 2,6-Dimethylphenyl isocyanide (0.45 g, 3.4 mmol) was added to *trans,cis,cis*-[W(≡$CC_6H_3Me_2$-2,6)Br$(CO)_2(NC_5H_4$Me-4)$_2$] (**1a**, 1.00 g, 1.70 mmol) in diethyl ether (30 mL) and the mixture stirred for 15 h after which time the solvent was removed in vacuo. The resulting pale yellow solid was redissolved in *n*-hexane (10 mL) and filtered through diatomaceous earth. The filtrate was further diluted with hexane (15 mL) and cooled to −10 °C for 2 days during which time fine yellow needles formed which were isolated by decantation and dried in vacuo. Yield 0.98 g (89 %). IR (CH_2Cl_2): 2159, 2134 [ν(CN)]; 2021, 1974 [ν(CO)] cm^{-1}. IR (nujol): 2162, 2135 [ν(CN)]; 2005, 1959 [ν(CO)] cm^{-1}. ^1H NMR ($CDCl_3$, 25 °C): δ = 2.48 [s, 12 H, $NC_6H_3(CH_3)_2$], 2.58 [s, 6 H, $CC_6H_3(CH_3)_2$], 6.90, 6.92 [d × 2 H, H-3,5(C_6H_3)], 7.1 [m, 1 H, H-4(C_6H_3)] ppm. $^{13}C\{^1H\}$ NMR: δ = 269.7 [W≡C, ^1J(WC) = 189 Hz], 205.0 [WCO, ^1J(WC) = 136 Hz], 167.7 (br., C≡N), 161.8 (br., N-C), 150−124 (NC_6H_3 and CC_6H_3), 21.2 [$CC_6H_3(CH_3)_2$], 18.8 [$NC_6H_3(CH_3)_2$] ppm. FAB- MS: *m*/*z* (%) = 700 (12) $[M]^+$, 672 (58) $[M - CO]^+$, 644 (46) $[M - 2CO]^+$. Calcd for $C_{29}H_{27}BrO_2N_2W$: calcd. C 49.81, H 3.89, N 4.01; found C 50.0, H 4.1, N 3.9.

Synthesis of [W(≡CC$_6$H$_2$Me$_3$-2,4,6)Br(CO)$_2$(CNC$_6$H$_3$Me$_2$-2,6)$_2$] (5b): 2,6-Dimethylphenyl isocyanide (0.45 g, 3.40 mmol) was added to *trans,cis,cis*-[W(≡$CC_6H_2Me_3$-2,4,6)Br$(CO)_2(NC_5H_4$Me-4)$_2$] (**1b**, 1.00 g, 1.70 mmol) in diethyl ether (30 mL). The mixture was stirred for 15 h, after which time the solvent and γ-picoline were removed in vacuo. The resulting pale yellow solid was redissolved in hexane (10 mL) and filtered through diatomaceous earth. Light petroleum ether (15 mL) was added to the yellow filtrate and the mixture stored at −10 °C for 2 days, whereupon fine yellow crystalline needles were obtained and dried in vacuo. Yield 1.00 g (88 %). IR (CH_2Cl_2): 2158, 2132 [ν(CN)]; 2018, 1972 [ν(CO)] cm^{-1}. IR (nujol): 2162, 2134 [ν(CN)]; 2006, 1955 [ν(CO)] cm^{-1}. ^1H NMR ($CDCl_3$, 25 °C): δ = 2.18 (s, 3 H, $CC_6H_2CH_3$-4), 2.50 [s, 12 H, $NC_6H_3(CH_3)_2$], 2.56 [s, 6 H $CC_6H_2(CH_3)_2$-2,6] ppm. $^{13}C\{^1H\}$ NMR: δ = 270.5 [W≡C, ^1J(WC) = 189 Hz], 204.9 [WCO, ^1J(WC) = 136 Hz], 162.2 (br., WCN), 147.2 [C-1(C_6H_2)], 140.6 [C-2,6(C_6H_3)], 138.5[C-2,6(C_6H_2)], 135.6 [C-3,5(C_6H_2)], 129.3 [C-4(C_6H_3)], 128.0 [C-3,5(C_6H_3)], 126.6 [C-4(C_6H_2)], 21.6 [$C_6H_2CH_3$-4], 21.1, 19.0 [$NC_6H_3(CH_3)_2$-2,6 and $CC_6H_2(CH_3)_2$-2,6] ppm. FAB-MS: *m*/*z* (%) = 658 (100) $[M - 2CO]^+$. $C_{30}H_{29}BrN_2O_2W$: calcd. C 50.51, H 4.10, N 3.93; found C 50.2, H 4.0, N 3.9.

Synthesis of [W(≡CC$_6$H$_3$Me$_2$-2,6)Br(CO)$_2$(CNCMe$_3$)$_2$] (5c): *tert*-Butyl isocyanide (0.40 mL, 0.795 $gmol^{-1}$, 0.50 g, 6.0 mmol, excess) was added to *trans,cis,cis*-[W(≡$CC_6H_3Me_2$-2,6)Br$(CO)_2(NC_5H_4$Me-4)$_2$] (**1a**, 1.00 g, 1.70 mmol) in diethyl ether (30 mL) and the mixture stirred for 15 h. The resulting pale yellow solution was reduced to dryness in vacuo and light petroleum (50 mL) was added to the residue. The resulting solution was cooled to −10 °C for 12 h whereupon a bright yellow crystalline solid was isolated and dried in vacuo. Further crops were obtained by concentrating the supernatant liquor, though these were generally less pure. Yield 0.70 g (73 %). IR (CH_2Cl_2): 2158, 2132 [ν(CN)]; 2018, 1972 [ν(CO)] cm^{-1}. IR (nujol): 2162, 2134 [ν(CN)]; 2006, 1955 [ν(CO)] cm^{-1}. ^1H NMR ($CDCl_3$, 25 °C): δ = 1.57 [s, 18 H,

 © 2004 Wiley-VCH Verlag GmbH & Co. KGaA, Weinheim

CMe_3], 2.52 [s, 6 H, $C_6H_3(CH_3)_2$], 6.90 [d, 2 H, H-3,5(C_6H_3)], 7.10 [t, 1 H, H-4(C_6H_3)] ppm. $^{13}C\{^1H\}$ NMR: δ = 267.1 [W≡C, ^1J (WC) = 189 Hz], 206.8 [WCO, ^1J (WC) = 135 Hz], 147.0 (br., WC≡N), 146.1 [C-1(C_6H_3)], 140.3 [C-4(C_6H_3)], 127.4 [C-2,6(C_6H_3)], 127.2 [C-3,5(C_6H_3)], 57.4 [CMe_3], 30.5 [$C(CH_3)_3$], 20.8 [$C_6H_3(CH_3)_2$] ppm. FAB-MS: *m/z* = 606 $[M]^+$, 576 $[M - CO]^+$, 548 $[M - 2CO]^+$, 523 $[M - CNR]^+$, 492 $[M - CO - CNR]^+$. $C_{21}H_{27}BrN_2O_2W$: calcd. C 41.81, H 4.51, N 4.64; found C 41.7, H 4.4, N 4.5.

Synthesis of *fac*-[W(≡$CC_6H_3Me_2$-2,6)(CO)$_2$(PMe_2Ph){$H_2B(pz)_2$}] (6a): Dimethylphenylphosphane (0.12 mL, 0.97 gmL^{-1}, 0.12 g, 0.87 mmol) was added to *mer/fac*-[W(≡$CC_6H_3Me_2$-2,6)-(CO)$_2$(NC_5H_4Me-4){$H_2B(pz)_2$}] (**2a**, 0.50 g, 0.84 mmol) in dichloromethane (30 mL) and the mixture stirred for 12 h. The resulting orange solution was concentrated to about 10 mL and chromatographed on a silica-gel loaded column (2 × 30 cm, −30 °C) eluting with a mixture of dichloromethane and light petroleum ether (1:1). The major orange fraction was collected and concentrated under reduced pressure to about 10 mL and then diluted with diethyl ether (50 mL). This solution was cooled to −10 °C whereupon an orange microcrystalline solid was obtained. Yield 0.52 g (95 %). Crystals suitable for X-ray analysis were obtained upon recrystallization from hexane/propanone (4:1) at −10 °C. NB: The reaction is sufficiently clean that for most practical purposes the chromatography step may be omitted in which case, the solvent is simply removed and the resulting orange powder washed with light petroleum (10 mL) and dried thoroughly under high vacuum to remove liberated γ-picoline and unchanged phosphane. IR (CH_2Cl_2): 1992, 1903 [ν(CO)] cm^{-1}. IR (nujol): 2407, 2345, 2288 [ν(BH_2)]; 1974, 1885 [ν(CO)] cm^{-1}. ^1H NMR ($CDCl_3$, 25 °C): δ = 1.21, 1.31 [d × 2, 6 H, $^2J_{P,H}$ = 7.3 Hz, diastereotopic-PMe_2], 2.63 (s, 6 H, $C_6H_3CH_3$), 3.55 (br, BH_2), 6.12, 6.16 [dd × 2, 2 H, H-4($C_3H_3N_2$), $^3J_{H,H}$ = 2, 2 Hz], 6.96−7.10 [m, 3 H, H-4(C_6H_3)], 7.24−7.28 (m, 5 H, C_6H_5), 7.36, 7.56, 7.66, 7.89 [d × 4, 4 H, H-3,5($C_3H_3N_2$), $^3J_{H,H}$ = 2 Hz] ppm. $^{13}C\{^1H\}$ NMR: δ = 285.1 (d, W≡C, $^2J_{P,C}$ = 8.9 Hz), 227.0 (d, WCO, $^2J_{P,C}$ = 3.6 Hz), 213.4 (d, WCO, $^2J_{P,C}$ = 53.5 Hz), 144.9, 143.6 [C-3($C_3H_3N_2$)], 137.0, 136.8 [C-5($C_3H_3N_2$)], 135.7 [C-1(C_6H_5)], 130.8, 130.6 [C-2,6(C_6H_5)], 129.6−127.3 [C_6H_5 and C_6H_3], 105.4, 105.1 [C-4($C_3H_3N_2$)], 20.9 [$C_6H_3(CH_3)_2$], 15.7, 14.5 [d × 2, $^1J_{P,C}$ = 24 Hz, diastereotopic-$P(CH_3)_2$] ppm. $^{31}P\{^1H\}$ NMR: δ = −4.1 ppm [^1J(WP) = 230.6 Hz] ppm. FAB-MS: *m/z* (%) = 641 (14) $[M - H]^+$, 614 (90) $[M - CO]^+$, 584 (21) $[M - 2CO]^+$, 503 (11) $[M - PMe_2Ph]^+$. $C_{25}H_{28}BN_4O_2PW$: calcd. C 46.76, H 4.40, N 8.72; found C 46.2, H 4.2, N, 8.5.

Synthesis of *fac*-[W(≡$CC_6H_3Me_3$-2,4,6)(CO)$_2$(PMe_2Ph)-{$H_2B(pz)_2$}] (6b): This complex was prepared as described for **6a** (see above) from *mer/fac*-[W≡$CC_6H_2Me_3$-2,4,6)(CO)$_2$(NC_5H_4Me-4){$H_2B(pz)_2$}] (**2b**, 0.51 g, 0.84 mmol). Yield 0.53 g (95 %). IR (CH_2Cl_2): 1993, 1905 [ν(CO)]. IR (nujol): 2407, 2345, 2288 [ν(BH_2)]; 1976, 1882 [ν(CO)] cm^{-1}. ^1H NMR ($CDCl_3$, 25 °C): δ = 1.19, 1.34 [d × 2, 6 H, diastereotopic-PMe_2, $^2J_{P,H}$ = 7.1 Hz], 2.23 [s, 3 H, $C_6H_2CH_3$-4], 2.60 [s, 6 H, $C_6H_2(CH_3)_2$-2,6], 6.12, 6.16 [dd × 2, 2 H, H-4($C_3H_3N_2$), $^3J_{H,H}$ = 2, 2 Hz], 6.78 [s, 2 H, H-3,5(C_6H_2)], 7.28 (m, 5 H, C_6H_5), 7.34, 7.56, 7.66, 7.79 [d × 4, 4 H, H-3,5($C_3H_3N_2$), $^3J_{H,H}$ = 2 Hz] ppm. $^{13}C\{^1H\}$ NMR: δ = 284.4 [d, W≡C, $^2J_{P,C}$ = 8.6 Hz], 227.1 [WCO, $^2J_{P,C}$ = 3.6 Hz], 213.4 [d, WCO, $^2J_{P,C}$ = 53.1 Hz], 144.9, 143.6 [C-3($C_3H_3N_2$)], 137.0, 136.8 [C-5($C_3H_3N_2$)], 135.7 [C-1(C_6H_5), $^1J_{P,C}$ = 36 Hz], 130.7, 130.6 [C-2,6(C_6H_5)], 128.4, 128.2 [C-3,5(C_6H_5)], 127.7 [C-2,6(C_6H_2)], 127.3 [C-3,5(C_6H_3)], 105.4, 105.1 [C-4($C_3H_3N_2$)], 21.5 ($C_6H_2CH_3$-4), 20.9 [$C_6H_3(CH_3)_2$-2,6], 15.5, 14.5 [diastereotopic-$P(CH_3)_2$, $^1J_{P,C}$ = 24 Hz] ppm. $^{31}P\{^1H\}$ NMR: δ = −4.2 ppm [$^1J_{W,P}$ = 230.6 Hz]. FAB-MS: *m/z* (%) = 641 (8) $[M]^+$, 614 (75) $[M - CO]^+$, 584 (11) $[M - 2CO]^+$. Elemental microanalytical data not acquired.

Synthesis of *cis,trans,cis*-[W(≡$CC_6H_2Me_3$-2,4,6)(CO)(PMe_2Ph)$_2$-{$H_2B(pz)_2$}] (7): (a) Dimethylphenylphosphane (0.24 g, 1.60 mmol) was added to *mer/fac*-[W(≡$CC_6H_2Me_3$-2,4,6)(CO)$_2$(NC_5H_4Me-4){$H_2B(pz)_2$}] (**2b**, 0.50 g, 0.82 mmol) in dichloromethane (30 mL). The mixture was stirred for 12 h and the resulting red solution was then concentrated to about 10 mL under reduced pressure and purified on silica-gel (2 × 30 cm, −30 °C) eluting with a dichloromethane/light petroleum (1:1) mixture. The red eluate was concentrated in vacuo to about 10 mL and diluted with diethyl ether (50 mL). This solution was cooled to −10 °C whereupon a red crystalline solid was obtained, isolated by decantation and dried in vacuo. Yield 0.60 g (95 %). (b) A mixture of *mer*-[W(≡$CC_6H_2Me_3$-2,4,6)Br(CO)(PMe_2Ph)$_3$] (**8**, 0.50 g, 0.60 mmol) and K[$H_2B(pz)_2$] (0.12 g, 0.65 mmol) in dichloromethane (30 mL) was stirred for 1 h. The mixture was then purified as described in (a) (see above) to provide **7**. Yield 0.46 g (93 %). IR (CH_2Cl_2): 1860 [ν(CO)] cm^{-1}. IR (nujol): 2424, 2390, 2353, 2284 [ν(BH_2)]; 1857 [ν(CO)] cm^{-1}. ^1H NMR ($CDCl_3$, 25 °C): δ = 1.40, 1.47 [vt × 2, 12 H, *trans*-$(PMe_2)_2$, $^{2,4}J_{P,H}$ ca. 3 Hz], 2.19 [s, 3 H, $C_6H_2CH_3$-4], 2.49 [s, 6 H, $C_6H_2(CH_3)_2$-2,6], 5.98, 6.11 [dd × 2, 2 H, H-4($C_3H_3N_2$), $^3J_{H,H}$ = 2, 2 Hz], 6.69 (s, 2 H, C_6H_2), 7.08−7.26 (m, 10 H, C_6H_5), 7.36, 7.44, 7.58, 7.85 [d × 4, 4 H, H-3,5($C_3H_3N_2$), $^3J_{H,H}$ = 2 Hz] ppm. $^{13}C\{^1H\}$ NMR: δ = 278.2 (t, W≡C, $^2J_{P,C}$ = 11 Hz), 249.9 (t, WCO, $^2J_{P,C}$ = 5.3 Hz), 144.9, 143.6 [C-3($C_3H_3N_2$)], 136.5, 136.1 [C-5($C_3H_3N_2$)], 135.7 [C-1(C_6H_5), $^1J_{P,C}$ = 36.0 Hz], 130.6 [C-3,5(C_6H_2)], 130.5−127.5 [C-3,5(C_6H_5)], 104.9, 104.6 [C-4($C_3H_3N_2$)], 21.6 [$C_6H_2CH_3$-4)], 20.6 [$C_6H_2(CH_3)_2$-2,6], 17.9 [vt, $P(CH_3)_2$, $^{1,3}J_{P,C}$ = 13.4 Hz] ppm. $^{31}P\{^1H\}$ NMR: δ = 0.28 [$^1J_{W,P}$ = 281.4 Hz] ppm. FAB-MS: *m/z* (%) [assignment] = 766 (12) $[M]^+$, 738 (4) $[M - CO]^+$, 628 (100) $[M - PMe_2Ph]^+$, 598 (35) $[M - PMe_2Ph - CO]^+$, 459 (10) $[M - 2PMe_2Ph - CO]^+$. $C_{33}H_{41}BN_4OP_2W$: calcd. C 51.72, H 5.39, N 7.31; found C 52.1, H 5.7, N 6.8.

Synthesis of *mer*-[W(≡$CC_6H_2Me_3$-2,4,6)Br(CO)(PMe_2Ph)$_3$] (8): NB − the related complex *mer*-[W(≡CPh)Cl(CO)(PMe_3)$_3$] has been described previously by Mayr.[27] Dimethylphenylphosphane (0.70 g, 5.10 mmol) was added to *trans,cis,cis*-[W(≡$CC_6H_2Me_3$-2,4,6)Br(CO)$_2$(NC_5H_4Me-4)$_2$] (**1b**, 1.00 g, 1.70 mmol) in diethyl ether (30 mL) and the mixture stirred for 15 h. The resulting pale yellow solution was filtered though diatomaceous earth (20 × 30 mm). The yellow filtrate was then diluted with light petroleum (15 mL) and cooled to −10 °C for 2 days, whereupon a fine yellow powder was obtained which was isolated by decantation and dried in vacuo. Subsequent recrystallisation from a mixture of dichloromethane/petroleum ether (−20 °C) afforded bright yellow needles. Yield 1.01 g (90 %). IR (CH_2Cl_2): 1905 [ν(CO)] cm^{-1}. IR (nujol): 1900 [ν(CO)] cm^{-1}. ^1H NMR ($CDCl_3$, 25 °C): δ = 1.34−2.14 [m, 21 H, PMe_2 and $C_6H_2CH_3$-4], 2.19 [s, 6 H, $C_6H_2(CH_3)_2$-2,6], 6.68 [s, 2 H, H-3,5(C_6H_2)], 6.85−7.55 [m, 15 H, C_6H_5] ppm. $^{13}C\{^1H\}$ NMR: δ = 267.7 (dt, W≡C, $^2J_{P,C}$ = 7, 12 Hz), 233.3 [dt, WCO, *trans*- $^2J_{P,C}$ = 27, *cis*- $^2J(P_2C)$ = 7 Hz], 134.5−127.9 (C_6H_5 and, C_6H_2), 22.75 [vt, *trans*-diastereotopic-$W(PMe_2)_2$, $^{1,3}J(P_2C)$ = 15.1 Hz], 21.91 [$C_6H_2(CH_3)_2$-2,6], 21.41 ($C_6H_2CH_3$-4), 17.63 [vt, *trans*-diastereotopic-$W(PMe_2)_2$, $^{1,3}J(P_2C)$ = 13.4 Hz], 16.89 [d, unique-PMe_2, $^1J_{P,C}$ = 25.0 Hz] ppm. $^{31}P\{^1H\}$ NMR: δ = −15.0 [d, ^1J(WP) = 268, $^2J_{P,P}$ = 20], −22.5 [t, ^1J(WP) = 230, $^2J_{P,P}$ = 20 Hz] ppm. FAB-MS: *m/z* (%) = 700 (44) $[M - PMe_2Ph]^+$, 672 (100) $[M - CO - PMe_2Ph]^+$, 532 (14) $[M - CO - 2PMe_2Ph]^+$. $C_{35}H_{44}BrOP_3W \cdot 0.5CH_2Cl_2$: calcd. C 48.46, H 5.16; found C 48.6, H 5.0.

 © 2004 Wiley-VCH Verlag GmbH & Co. KGaA, Weinheim

Crystal Data, X-ray Data Collection and Structural Determination (a) [W(≡CC$_6$H$_3$Me$_2$-2,6)(CO)$_2$(NC$_5$H$_4$Me-4){H$_2$B(pz)$_2$}]·0.5CH$_2$Cl$_2$ (2a·0.5CH$_2$Cl$_2$): Orange/red blocks were grown by prolonged cooling of a saturated solution of the complex in a mixture of dichloromethane and petroleum ether (bp. 40−60 °C). Crystal data for **2a**: $C_{23}H_{24}BN_5O_2W·0.5CH_2Cl_2$, M_r = 639.6 g·mol^{-1}, monoclinic, $P2_1/c$ (no. 14), a = 9.463(3), b = 19.153(2), c = 16.228(3) Å, β = 105.41(2)°, V = 2835.6(10) Å^3, Z = 4, D_c = 1.498 g cm^{-3}, μ(Mo-K_α) = 4.19 mm^{-1}, T = 293 K, 3673 independent measured reflections, F^2 refinement, R_1 = 0.032, wR_2 = 0.087, 3081 independent observed absorption corrected reflections [$|F_o| > 4\sigma(|F_o|)$, 2θ ≤ 45°], 329 parameters.
(b) [W(≡CC$_6$H$_3$Me$_2$-2,6)(CO)$_2$(PMe$_2$Ph){H$_2$B(pz)$_2$}] (6a): Yellow needles were grown by cooling (−10 °C) a saturated solution of the complex in a mixture of propanone and light petroleum. Crystal data for **6a**: $C_{25}H_{28}BN_4O_2PW$, M_r = 642.1 g·mol^{-1}, monoclinic, $P2_1/n$ (no. 14), a = 9.982(1), b = 16.952(2), c = 15.970(2) Å, β = 103.31(1)°, V = 2629.6(5) Å^3, Z = 4, D_c = 1.622 g cm^{-3}, μ(Cu-K_α) = 8.94 mm^{-1}, T = 293 K, 3664 independent measured reflections, F^2 refinement, R_1 = 0.022, wR_2 = 0.054, 3385 independent observed absorption corrected reflections [$|F_o| > 4\sigma(|F_o|)$, 2θ ≤ 116°], 298 parameters. CCDC-219536 (**2a**) and −219537 (**6a**) contain the supplementary crystallographic data for this paper. These data can be obtained free of charge via internet at http://www.ccdc.cam.ac.uk/conts/retrieving.html or from the Cambridge Crystallographic Data Centre, 12 Union Road, Cambridge CB2 1EZ, UK; Fax (internat.) +44-1223/336-033; E-mail: deposit@ccdc.cam.ac.uk].

Acknowledgments

We wish to thank Professor F. G. A. Stone for helpful discussions and support. We are grateful to the S. E. R. C. (U.K.) for the provision of post-graduate studentships (to J. M. M.).

[1] M. R. St.-J. Foreman, A. F. Hill, A. J. P. White, D. J. Williams, *Organometallics* **2003**, *22*, 3831.
[2] [2a] H. S. Kim, R. J. Angelici, *Adv. Organomet. Chem.* **1987**, *27*, 51. [2b] A. Mayr, H. Hoffmeister, *Adv. Organomet. Chem.* **1991**, *32*, 227. [2c] A. Mayr, S. Ahn, *Adv. Trans. Metal Coord. Chem.* **1996**, *1*, 1. [2d] *Transition Metal Carbyne Complexes*, F. R. Kreißl (Ed.), NATO ASI Series *C392*, Kluwer, Dordrecht, **1992**.
[3] [3a] S. Trofimenko, *J. Am. Chem. Soc.* **1967**, *89*, 6288. [3b] S. Trofimenko, *Prog. Inorg. Chem.* **1986**, *34*, 115. [3c] S. Trofimenko, *Scorpionates: The Coordination Chemistry of Polypyrazolylborate Ligands*, Imperial College Press: London, **1999**.
[4] [4a] D. D. Ellis, J. M. Farmer, J. M. Malget, D. F. Mullica, F. G. A. Stone, *Organometallics* **1998**, *17*, 5540. [4b] J. C. Jeffery, F. G. A. Stone, G. K. Williams, *Polyhedron* **1991**, *10*, 215. [4c] S. H. F. Becke, M. D. Bermudez, N. H. Tran-Huy, J. A. K. Howard, O. Johnson, F. G. A. Stone, *J. Chem. Soc., Dalton Trans.* **1987**, 1229. [4d] M. D. Bermudez, E. Delgado, G. P. Elliott, N. H. Tran-Huy, F. Mayor-Real, F. G. A. Stone, M. J. Winter, *J. Chem. Soc., Dalton Trans.* **1987**, 1235. [4e] M. Green, J. A. K. Howard, A. P. James, A. N. De M. Jelfs, C. M. Nunn, F. G. A. Stone, *J. Chem. Soc., Dalton Trans.* **1986**, 1697. [4f] S. V. Hoskins, A. P. James, J. C. Jeffery, F. G. A. Stone, *J. Chem. Soc., Dalton Trans.* **1986**, 1709. [4g] J. C. Jeffery, F. G. A. Stone, G. K. Williams, *Polyhedron* **1991**, *10*, 215. [4h] I. J. Hart, A. F. Hill, F. G. A. Stone, *J. Chem. Soc., Dalton Trans.* **1989**, 2261. [4i] S. J. Davies, A. F. Hill, M. U. Pilotti, F. G. A. Stone, *Polyhedron* **1989**, *8*, 2265. [4j] M. K. Bermudez, F. G. A. Stone, *J. Organomet. Chem.* **1988**, *347*, 115. [4k] M. Green, J. A. K. Howard, A. P. James, C. M. Nunn, F. G. A. Stone, *J. Chem. Soc., Dalton Trans.* **1986**, 187. [4l] M. Green, J. A. K. Howard, A. P. James, A. N. De M. Jelfs, C. M. Nunn, F. G. A. Stone, *Chem. Commun.* **1984**, 1623.
[5] [5a] H. P. Kim, S. Kim, R. A. Jacobson, R. J. Angelici, *Organometallics* **1986**, *5*, 2481. [5b] H. P. Kim, R. J. Angelici, *Organometallics* **1986**, *5*, 2489. [5c] R. A. Doyle, R. J. Angelici, *J. Am. Chem. Soc.* **1990**, *112*, 194. [5d] R. A. Doyle, R. J. Angelici, F. G. A. Stone, *J. Organomet. Chem.* **1989**, *378*, 81. [5e] R. A. Doyle, R. J. Angelici, *J. Organomet. Chem.* **1989**, *375*, 73. [5f] W. W. Greaves, R. J. Angelici, *Inorg. Chem.* **1981**, *20*, 2983.
[6] [6a] A. E. Enriquez, J. L. Templeton, *Organometallics* **2002**, *21*, 852. [6b] K. C. Stone, G. M. Jamison, P. S. White, J. L. Templeton, *Inorg. Chim. Acta* **2002**, *330* 161. [6c] A. E. Enriquez, P. S. White, J. L. Templeton, *J. Am. Chem. Soc.* **2001**, *123*, 4992. [6d] D. S. Frohnapfel, P. S. White, J. L. Templeton, *Organometallics* **2000**, *19*, 1497. [6e] B. E. Woodworth, P. S. White, J. L. Templeton, *J. Am. Chem. Soc.* **1998**, *120*, 9028. [6f] B. E. Woodworth, D. S. Frohnapfel, P. S. White, J. L. Templeton, *Organometallics* **1998**, *17*, 1655. [6g] B. E. Woodworth, P. S. White, J. L. Templeton, *J. Am. Chem. Soc.* **1997**, *119*, 828. [6h] B. E. Woodworth, J. L. Templeton, *J. Am. Chem. Soc.* **1996**, *118*, 7418. [6i] G. M. Jamison, A. E. Bruce, P. S. White, J. L. Templeton, *J. Am. Chem. Soc.* **1991**, *113*, 5057. [6j] G. M. Jamison, P. S. White, J. L. Templeton, *Organometallics* **1991**, *10*, 1954. [6k] M. Etienne, P. S. White, J. L. Templeton, *J. Am. Chem. Soc.* **1991**, *113*, 2324. [6l] S. G. Feng, P. S. White, J. L. Templeton, *Organometallics* **1993**, *12*, 2131. [6m] S. G. Feng, J. L. Templeton, *Organometallics* **1992**, *11*, 2168. [6n] S. G. Feng, P. S. White, J. L. Templeton, *J. Am. Chem. Soc.* **1992**, *114*, 2951. [6o] G. M. Jamison, A. E. Bruce, P. S. White, J. L. Templeton, *J. Am. Chem. Soc.* **1991**, *113*, 5057. [6p] G. M. Jamison, P. S. White, J. L. Templeton, *Organometallics* **1991**, *10*, 1954. [6q] M. Etienne, P. S. White, J. L. Templeton, *J. Am. Chem. Soc.* **1991**, *113*, 2324. [6r] A. S. Gamble, P. S. White, J. L. Templeton, *Organometallics* **1991**, *10*, 693. [6s] D. C. Brower, M. Stoll, J. L. Templeton, *Organometallics* **1989**, *8*. 2786. [6t] A. E. Bruce, A. S. Gamble, T. L. Tonker, J. L. Templeton, *Organometallics* **1987**, *6*, 1350.
[7] M. D. Bermudez, F. P. E. Brown, F. G. A. Stone, *J. Chem. Soc., Dalton Trans.* **1988**, 1139.
[8] A. F. Hill, J. A. K. Howard, T. P. Spaniol, F. G. A. Stone, J. Szameitat, *Angew. Chem. Int. Ed. Engl.* **1989**, *28*, 210.
[9] [9a] A. Bencini, M. Di Vaira, F. Mani, *J. Chem. Soc., Dalton Trans.* **1991**, 41. [9b] P. Dapporto, F. Mani, C. Mealli, *Inorg. Chem.* **1978**, *17*, 1323.
[10] The B-functionalised ligands $Ph_2B(pz)_2$ [11] and $Et_2B(pz)_2$ [12] have been studied in molybdenum coordination chemistry. A recurrent feature is the stabilisation of coordinative unsaturation by nonclassical coordination of the organoboron substituent.
[11] $Ph_2B(pz)_2Mo$: [11a] S.-F. Lush, S.-H. Wang, G.-H. Lee, S.-M. Peng, S.-L. Wang, R.-S. Liu, *Organometallics* **1990**, *9*, 1862. [11b] F. A. Cotton, B. A. Frenz, C. A. Murillo, *J. Am. Chem. Soc.* **1975**, *97*, 2118.
[12] $Et_2B(pz)_2Mo$: [12a] F. A. Cotton, B. A. Frenz, A. G. Stanislowski, *Inorg. Chim. Acta* **1973**, *7*, 503. [12b] F. A. Cotton, T. LaCour, A. G. Stanislowski, *J. Am. Chem. Soc.* **1974**, *96*, 754. [12c] F. A. Cotton, V. W. Day, *J. Chem. Soc., Chem. Commun.* **1974**, 415. [12d] D. M. Collins, F. A. Cotton, C. A. Murillo, *Inorg. Chem.* **1976**, *15*, 1861. [12e] F. A. Cotton, B. W. S. Kolthammer, G. N. Mott, *Inorg. Chem.* **1981**, *20*, 3890. [12f] F. A. Cotton, G. N. Mott, *Inorg. Chem.* **1983**, *22*, 1136. [12g] F. A. Cotton, R. L. Luck, *Inorg. Chem.* **1989**, *28*, 3210.
[13] [13a] S. Anderson, A. F. Hill, B. A. Nasir, *Organometallics* **1995**, *14*, 2987. [13b] S. J. Dossett, A. F. Hill, J. A. K. Howard, B. A. Nasir, T. P. Spaniol, P. Sherwood, F. G. A. Stone, *J. Chem. Soc., Dalton Trans.* **1989**, 1871. [13c] A. F. Hill, F. Marken, B. A. Nasir, F. G. A. Stone, *J. Organomet. Chem.* **1989**, *363*, 311. [13d] A. F. Hill, H. D. Honig, F. G. A. Stone, *J. Chem. Soc., Dalton Trans.* **1988**, 3031. [13e] S. J. Dossett, A. F. Hill, J. C.

 © 2004 Wiley-VCH Verlag GmbH & Co. KGaA, Weinheim

Jeffery, F. Marken, P. Sherwood, F. G. A. Stone, *J. Chem. Soc., Dalton Trans.* **1988**, 2453.

[14] [14a] E. Bannwart, H. Jacobsen, F. Furno, H. Berke, *Organometallics* **2000**, *19*, 3605. [14b] F. Furno, T. Fox, H. W. Schmalle, H. Berke, *Organometallics* **2000**, *19*, 3630. [14c] E. Bannwart, H. Jacobsen, R. Hubener, H. W. Schmalle, H. Berke, *J. Organomet. Chem.* **2001**, *622*, 97. [14d] F. Furno, T. Fox, M. Alfonso, H. Berke, *Eur. J. Inorg. Chem.* **2001**, 1559.

[15] G. A. McDermott, A. M. Dorries, A. Mayr, *Organometallics* **1987**, *6*, 925.

[16] A. Mayr, G. A. McDermott, A. M. Dorries, *Organometallics* **1985**, *4*, 608.

[17] E. O. Fischer, A. Massböl, *Chem. Ber.* **1967**, *100*, 2445.

[18] A. F. Hill, unpublished observations.

[19] [19a] W. Uedelhoven, K. Eberl, F. R. Kreißl, *Chem. Ber.* **1979**, *112*, 3376. [19b] F. R. Kreißl, P. Friedrich, G. Huttner, *Angew. Chem. Int. Ed. Engl.* **1977**, *16*, 102.

[20] [20a] J. Martin-Gil, J. A. K. Howard, R. Navarro, F. G. A. Stone, *J. Chem. Soc., Chem. Commun.* **1979**, 1168. [20b] J. C. Jeffery, M. A. Ruiz, F. G. A. Stone, *J. Organomet. Chem.* **1988**, *355*, 231.

[21] [21a] J. B. Sheridan, D. B. Pourreau, G. L. Geoffroy, A. L. Rheingold, *Organometallics* **1988**, *7*, 289. [21b] J. B. Sheridan, G. L. Geoffroy, A. L. Rheingold, *Organometallics* **1986**, *5*, 1514. [21c] D. B. Pourreau, G. L. Geoffroy, *Adv. Organomet. Chem.* **1985**, *24*, 249.

[22] A. Mayr, C. M. Bastos, *Prog. Inorg. Chem.* **1992**, *40*, 1.

[23] [23a] J. Werner, M. Wolfgruber, N. H. Tran Huy, H. R. Schmidt, H. Heiss, P. Hofmann, F. R. Kreißl, *J. Organomet. Chem.* **1988**, *340*, 341. [23b] F. R. Kreißl, M. Wolfgruber, U. Thewalt, *J. Organomet. Chem.* **1986**, *317*, 175. [23c] F. R. Kreißl, G. Reber, G. Mueller, *Angew. Chem.* **1986**, *98*, 640. [23d] F. R. Kreißl, W. J. Sieber, P. Hofmann, J. Riede, M. Wolfgruber, *Organometallics* **1985**, *4*, 788. [23e] F. R. Kreißl, W. J. Sieber, H. G. Alt, *Chem. Ber.* **1984**, *117*, 2527. [23f] F. R. Kreißl, M. Wolfgruber, W. J. Sieber, K. Ackermann, *Organometallics* **1984**, *3*, 777. [23g] M. Wolfgruber, F. R. Kreißl, *J. Organomet. Chem.* **1983**, *258*, C9. [23h] F. R. Kreißl, W. J. Sieber, M. Wolfgruber, *Z. Naturforsch., Teil B* **1983**, *38*, 1419. [23i] F. R. Kreißl, M. Wolfgruber, W. Sieber, K. Ackermann, *J. Organomet. Chem.* **1983**, *252*, C39. [23j] F. R. Kreißl, W. Sieber, M. Wolfgruber, *Z. Naturforsch., Teil B* **1982**, *37*, 1485. [23k] K. Eberl, W. Uedelhoven, H. H. Karsch, F. R. Kreißl, *Chem. Ber.* **1980**, *113*, 3377.

[24] These precursor isocyanide complexes are analogues of $[W(\equiv CPh)Cl(CO)_2(CNCMe_3)_2]$[25] and $[Cr(\equiv CPh)Br(CO)_2(CNCMe_3)_2]$[26] which have been reported previously and were most conveniently prepared by the reactions of **1** with CNR′ in essentially quantitative yield.

[25] [25a] A. Mayr, S. M. Holmes, C. M. Bastos, *Organometallics* **1992**, *11*, 4358. [25b] A. C. Filippou, E. O. Fischer, *J. Organomet. Chem.* **1990**, *383*, 179.

[26] A. Frank, U. Schubert, G. Huttner, *Chem. Ber.* **1977**, *110*, 3020.

[27] A. Mayr, M. F. Asaro, M. A. Kjelsberg, K. S. Lee, D. Van Engen, *Organometallics* **1987**, *6*, 432.

[28] D. C. Brower, J. L. Templeton, D. M. P. Mingos, *J. Am. Chem. Soc.* **1987**, *109*, 5203.

[29] F.-W. Lee, M. C.-W. Chan, K.-K. Cheung, C.-M. Che, *J. Organomet. Chem.* **1998**, *563*, 191.

[30] J. Brencic, B. Ceh, I. Leban, *Z. Anorg. Allg. Chem.* **1987**, *549*, 233.

[31] I. Leban, J. V. Brencic, B. Ceh, *Acta Crystallogr., Sect. C* **1995**, *51*, 817.

[32] U. Klement, *Z. Kristallogr.* **1993**, *208*, 114.

[33] [33a] A. Mayr, A. M. Dorries, A. L. Rheingold, S. J. Geib, *Organometallics* **1990**, *9*, 964. [33b] A. Mayr, A. M. Dorries, G. A. McDermott, S. J. Geib, A. L. Rheingold, *J. Am. Chem. Soc.* **1985**, *107*, 7775.

[34] L = PMe_2Ph: [34a] *cis,trans,cis*-$[WCl_2(OCH_2CF_3)_2L_2]$ (2.489, 2.481 Å): H. Rothfuss, J. C. Huffman, K. G. Caulton, *Inorg. Chem.* **1994**, *33*, 187. [34b] *mer,cis*-$[WOCl_2L_3]$ (2.538, 2.508, 2.483 Å), *mer*-$[WCl_3L_3]$(2.513, 2.561, 2.542 Å): K. Yoon, G. Parkin, D. L. Hughes, G. J. Leigh, *J. Chem. Soc., Dalton Trans.* **1992**, 769. [34c] *fac*-$[W(CO)_3L_3]$ (2.515, 2.522, 2.524 Å): D. Rodewald, C. Schulzke, D. Rehder, *J. Organomet. Chem.* **1995**, *498*, 29. [34d] *trans*-$[WCl_2L_4]$ (2.496, 2.512, 2.493, 2.484 Å): H. Rothfuss, K. Folting, K. G. Caulton, *Inorg. Chim. Acta* **1993**, *212*, 165. [34e] *cis*-$[W(N_2)_2L_4]$ (2.480, 2.473, 2.281, 2.444 Å): H. Dadkhah, J. R. Dilworth, K. Fairman, C. T. Kan, R. L. Richards, D. L. Hughes, *J. Chem. Soc., Dalton Trans.* **1985**, 1523.

[35] Y. Sulfab, F. Basolo, A. L. Rheingold, *Organometallics* **1989**, *8*, 2139.

Received July 9, 2003
Early View Article
Published Online January 19, 2004

 © 2004 Wiley-VCH Verlag GmbH & Co. KGaA, Weinheim

Template Synthesis, Crystal Structure and Luminescent Properties of Neutral N_4O_3 Tripodal $Ln^{III}L$ Complexes (Ln^{III} = La^{3+}, Eu^{3+}, Gd^{3+}, Tb^{3+}, Dy^{3+}, Ho^{3+}, Er^{3+}, Tm^{3+} or Lu^{3+}; H_3L = Tris{[3′-(2′′-pyridyl)-5′-*tert*-butyl-2′-hydroxybenzylidene-2-imino]ethyl}amine)

Wai-Kwok Wong,*[a] Hongze Liang,[a] Jianping Guo,[a] Wai-Yeung Wong,[a] Wing-Kit Lo,[a] King-Fai Li,[b] Kok-Wai Cheah,[b] Zhongyuan Zhou,[c] and Wing-Tak Wong[d]

Keywords: Lanthanides / Luminescence / Schiff bases / Tripodal ligands

In the presence of Ln^{3+} (Ln = La, Eu, Gd, Tb, Dy, Ho, Er, Tm or Lu), tris(2-aminoethyl)amine condensed with three equivalents of 3-(2′-pyridyl)-5-*tert*-butyl-2-hydroxybenzaldehyde in methanol to give the neutral Schiff-base complex $Ln^{III}L$ (Ln = La **1**, Eu **2**, Gd **3**, Tb **4**, Dy **5**, Ho **6**, Er **7**, Tm **8** and Lu **9**; H_3L = tris{[3′-(2′′-pyridyl)-5′-*tert*-butyl-2′-hydroxybenzylidene-2-imino]ethyl}amine). The structures of compounds **4**–**7** were determined by X-ray crystallography. The crystal structure analyses revealed that the Schiff base behaves as a tri-deprotonated heptadentate ligand encapsulating the lanthanide metal ion within the N_4O_3 cavity, with all the pyridyl groups being pendant. Solution spectroscopic data suggest that the $Ln^{III}L$ complexes remain intact in methanol and exist as nine-coordinate non-electrolytes with the lanthanide metal ions coordinated to the N_4O_3 cavity of the tripodal Schiff base and two solvent molecules. The solution photoluminescent properties of these lanthanide Schiff-base complexes were also examined.
(© Wiley-VCH Verlag GmbH & Co. KGaA, 69451 Weinheim, Germany, 2004)

Introduction

The potential application of lanthanide complexes as magnetic resonance contrasting agents has led to the synthesis of a number of lanthanide(III) complexes with heptadentate tripodal Schiff-base ligands and amine phenol ligands.[1−4] Numerous lanthanide complexes with macrocyclic polydentate Schiff-base ligands[5−8] and acyclic tripodal heptadentate Schiff-base ligands have been reported in the literature.[1,2,9−12] Recently, the coordination chemistry of the decadentate Schiff base tris[4-(2-hydroxy-3-methoxyphenyl)-3-aza-3-butenyl]amine toward p- and f-block elements[13−17] has been examined. Dinuclear homo-[13] and heterometallic[14−17] complexes were obtained. Some lanthanide ions possess strongly emissive and long-lived excited states, such as Eu^{3+} and Tb^{3+}, but do not exhibit intense absorption bands. Therefore, considerable effort has been devoted to the design of lanthanide complexes where light is absorbed by the ligands and the corresponding electronic energy is then transferred onto the emitting metal ion. The use of a Zn^{2+} Schiff-base complex as a sensitizer for Nd^{3+}, Yb^{3+} and Er^{3+} near-infrared luminescence has been reported recently.[18] We are interested in the coordination chemistry of the decadentate Schiff base tris{[5′-*tert*-butyl-2′-hydroxy-3′-(2′′-pyridyl)benzylidene-2-imino]-ethyl}amine (H_3L) toward f-block metal ions, and particularly its sensitizing effect on lanthanide(III) metal ions. The design of the ligand strands of H_3L prevents the introduction of metal ions into the terminal nine-coordinate cavity, as this would result in the formation of fused chelating six-membered rings. Thus, H_3L is expected to behave as a heptadentate podate with the inner N_4O_3 cavity coordinating to the lanthanide ions and the terminal 2-pyridyl groups pendant, and will be an ideal ligand used for the preparation of heterometallic complexes. In this report, we describe a one-pot synthesis and the photoluminescent properties of stable, neutral, polydentate Schiff-base complexes of lanthanide(III) metal ions.

[a] Department of Chemistry, Hong Kong Baptist University
Waterloo Road, Kowloon Tong, Hong Kong, P. R. China
Fax: (internat.) + 852-3411-5862
E-mail: wkwong@hkbu.edu.hk
[b] Department of Physics, Hong Kong Baptist University
Waterloo Road, Kowloon Tong, Hong Kong, P. R. China
[c] Department of Applied Biology and Chemical Technology, Hong Kong Polytechnic University
Hung Hom, Hong Kong, P. R. China
[d] Department of Chemistry, The University of Hong Kong
Pokfulam Road, Hong Kong, P. R. China

Results and Discussion

Synthesis and Characterization

In the presence of one equivalent of $Ln(NO_3)_3{\cdot}5H_2O$ (Ln = La, Eu, Gd, Tb, Dy, Ho, Er, Tm or Lu), tris(2-

aminoethyl)amine (tren) undergoes condensation with three equivalents of 5-*tert*-butyl-2-hydroxy-3-(2′-pyridyl)benzaldehyde (Py-CHO) in methanol to give the neutral tripodal Schiff-base complexes $Ln^{III}L$ (Ln = La **1**, Eu **2**, Gd **3**, Tb **4**, Dy **5**, Ho **6**, Er **7**, Tm **8** and Lu **9**; H_3L = tris{[5′-*tert*-butyl-2′-hydroxy-3′-(2′′-pyridyl)benzylidene-2-imino]-ethyl}amine) in moderate to good yields (Scheme 1). Compounds **1**−**9** are remarkably stable towards air and moisture, are soluble in many organic solvents, and are even stable in protic solvents for weeks. They also show high thermal stability: when heated to as high as 200 °C, no discernible collapse of the crystals was observed. All these compounds gave satisfactory elemental analyses and exhibit a $\nu_{C=N}$ band at 1621−1623 cm^{-1} in their IR spectra and an $[M + H]^+$ peak in their positive FAB mass spectra. The structures of compounds **4**−**7** were determined by X-ray crystallography.

Compounds **4**−**7** are isomorphous and they all crystallized in the triclinic space group $P\bar{1}$ with two independent, but structurally similar, molecules per asymmetric unit. The crystal structure analyses reveal that the potentially decadentate tripodal ligand acts as a heptadentate ligand with the Ln^{3+} ion encapsulated within the N_4O_3 cavity of the Schiff base; all the pyridyl groups remain uncoordinated. A perspective drawing of **4** is shown in Figure 1.

For **4**, the Tb^{3+} ion is seven coordinate and its geometry can be considered as a mono-capped octahedron with the tertiary amine nitrogen N(4) capped on the triangular face formed by the three imino nitrogen atoms. The Tb−N distance of the capped tertiary nitrogen [Tb(1)−N(4) 2.686(4) Å] is longer than those of the imino nitrogens [Tb(1)−N(1) 2.456(4), Tb(1)−N(2) 2.475(4) and Tb(1)−N(3) 2.486(4) Å]. The Tb−O distances are 2.187(3) [Tb(1)−O(1)], 2.216(3) [Tb(1)−O(2)] and 2.205(3) Å [Tb(1)−O(3)]. The Tb−N(amino) distance and average Tb−N(imino) distance (2.472 Å) are slightly shorter than, whereas the average Tb−O (2.203 Å) distance is similar to, those of Pr(trensal)[9] [Pr−N(amino) 2.805(5), Pr−N(imino) 2.620 and Pr−O 2.282 Å] and Nd(trensal)[9] [Nd−N(amino) 2.799(4), Nd−N(imino) 2.601 and Nd−O 2.275 Å], after considering the influence of the lanthanide contraction. The carbon−nitrogen distances for the imino nitrogens [N(1)−C(1) 1.279(6), N(2)−C(32) 1.264(7) and N(3)−C(39) 1.258(8) Å] are in agreement with the C=N distance. All the pyridyl groups are pointing away from the metal and are not coplanar with the phenyl rings of the Schiff-base ligand. The torsion angles between the phenyl rings and the pyridyl groups are −33.4° [C(16)−C(10)−C(11)−C(15)], 37.7° [C(17)−C(18)−C(19)−C(23)] and 27.7° [C(54)−C(48)−C(49)−C(53)]. The

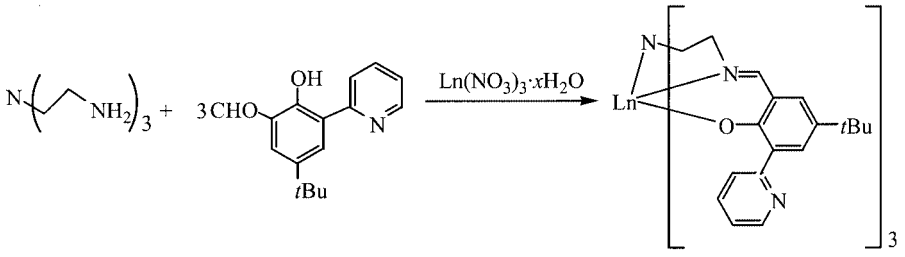

Ln = La **1**, Eu **2**, Gd **3**, Tb **4**, Dy **5**, Ho **6**, Er **7**, Tm **8**, Lu **9**

Scheme 1

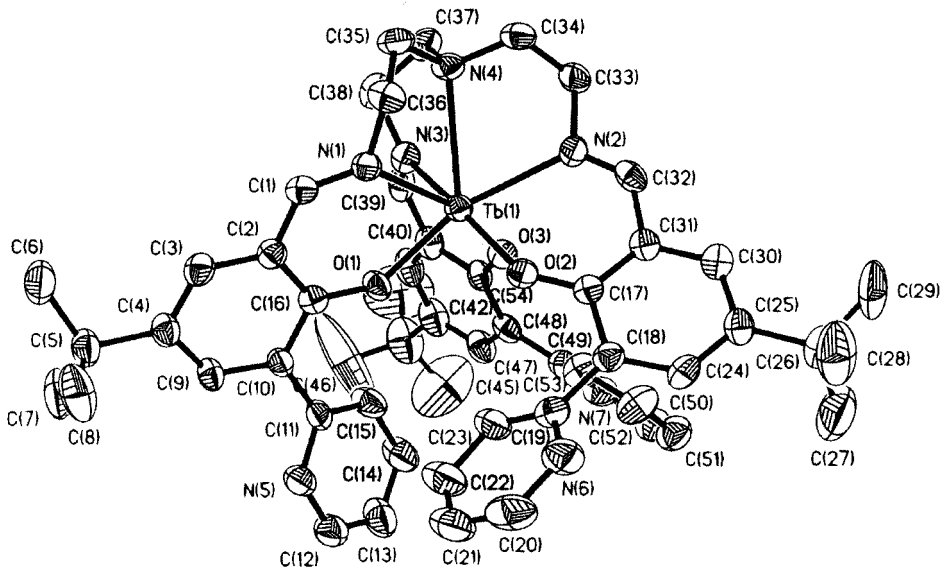

Figure 1. A perspective drawing of one molecule of compound **4**; hydrogen atoms are omitted for clarity

 © 2004 Wiley-VCH Verlag GmbH & Co. KGaA, Weinheim

Table 1. Selected bond lengths (Å) and bond angles (°) for compounds **4**−**7**

	4 (M = Tb)	**5** (M = Dy)	**6** (M = Ho)	**7** (M = Er)
M(1)−O(1)	2.187(3)	2.197(7)	2.1856(16)	2.180(5)
M(1)−O(2)	2.216(3)	2.198(7)	2.1858(18)	2.172(5)
M(1)−O(3)	2.205(3)	2.210(8)	2.1948(18)	2.189(5)
M(1)−N(1)	2.456(4)	2.437(8)	2.432(2)	2.662(6)
M(1)−N(2)	2.475(4)	2.476(10)	2.457(2)	2.455(6)
M(1)−N(3)	2.486(4)	2.474(9)	2.480(2)	2.410(6)
M(1)−N(4)	2.686(4)	2.685(8)	2.678(2)	2.468(7)
N(1)−C(imine)	1.279(6)	1.284(12)	1.285(3)	1.250(10)
N(2)−C(imine)	1.264(7)	1.289(14)	1.273(4)	1.292(8)
N(3)−C(imine)	1.258(8)	1.253(13)	1.274(3)	1.266(10)
O(1)−M(1)−O(2)	89.05(13)	90.8(3)	89.54(6)	88.8(2)
O(1)−M(1)−O(3)	90.70(12)	88.6(3)	88.97(7)	93.8(2)
O(2)−M(1)−O(3)	92.77(13)	93.7(3)	92.76(7)	89.8(2)
N(1)−M(1)−N(2)	114.86(14)	97.4(3)	95.98(7)	68.2(2)
N(1)−M(1)−N(3)	95.50(14)	114.0(3)	114.33(7)	67.5(2)
N(1)−M(1)−N(4)	66.50(12)	68.0(3)	66.88(6)	67.3(2)
N(2)−M(1)−N(3)	106.83(14)	107.4(3)	107.49(7)	112.3(2)
N(2)−M(1)−N(4)	68.17(13)	67.0(3)	67.54(8)	107.8(2)
N(3)−M(1)−N(4)	66.88(14)	67.9(3)	67.72(7)	99.2(2)
O(1)−M(1)−N(1)	72.58(13)	72.8(3)	73.58(6)	123.5(2)
O(1)−M(1)−N(2)	160.55(13)	89.6(3)	88.26(7)	73.3(2)
O(1)−M(1)−N(3)	89.63(14)	160.0(3)	160.81(7)	92.0(2)
O(1)−M(1)−N(4)	129.51(12)	130.3(3)	130.10(6)	167.2(2)

structures of compounds **5**−**7** are very similar to that of **4** and will not be discussed in detail here. Selected bond lengths and bond angles for compounds **4**−**7** are collectively listed in Table 1. Important structural properties of compounds **4**−**7** are given in Table 2. The M−N(imino), M−N(amino) and M−O(phenoxy) bond lengths decrease from **4** to **7**, reflecting the general rule of lanthanide contraction from the early to late f-elements.

Table 2. Structural properties of compounds **4**−**7**

	4	**5**	**6**	**7**
M−N(amino) (Å)	2.686	2.685	2.678	2.662
Average M−N(imino) (Å)	2.472	2.462	2.456	2.444
Average M−O (Å)	2.203	2.202	2.189	2.180
Torsion angle (°) [a]	**I** −33.4	**I** −33.0	**I** −34.8	**I** −35
	II 27.7	**II** 27.2	**II** 26.3	**II** 28
	III 37.7	**III** 36.0	**III** 36.8	**III** 35

[a] Torsion angles: **4** [**I** C(16)−C(10)−C(11)−C(15), **II** C(54)−C(48)−C(49)−C(53), **III** C(17)−C(18)−C(19)−C(23)]; **5** [**I** C(4)−C(5)−C(6)−C(7), **II** C(22)−C(23)−C(24)−C(25), **III** C(40)−C(41)−C(42)−C(43)]; **6** [**I** C(1)−C(2)−C(3)−C(4), **II** C(31)−C(30)−C(32)−C(33), **III** C(49)−C(48)−C(50)−C(51)]; **7** [**I** C(27)−C(26)−C(32)−C(33), **II** C(45)−C(44)−C(50)−C(51), **III** C(9)−C(8)−C(14)−C(15)].

Conductivity measurements show that compounds **1**−**9** behave as non-electrolytes in methanol solution. The electrospray ionization high-resolution mass spectrum (positive mode) of each complex in methanol shows a mass peak at *m*/*z* corresponding to $[M + H]^+$. For instance, the Eu^{3+} complex exhibits the mass peak at *m*/*z* = 1008.4032, which deviates less than 5 ppm from the theoretical peak value of 1008.4048 for the elemental composition $C_{54}H_{61}EuN_7O_3$. The observed isotopic distribution patterns of the $[M + H]^+$ peaks match well with the expected theoretical signals. The ^1H NMR spectrum of the Lu complex **9** in CD_3OD displays a single set of resonances attributed to the *tert*-butyl protons at δ = 1.35 (s, 27 H), the NCH_2CH_2N protons at δ = 2.82 (t, $J_{H,H}$ = 6.5 Hz, 6 H) and 3.10 ppm (t, $J_{H,H}$ = 6.5 Hz, 6 H), the 2-pyridyl protons at δ = 7.02 (t, $J_{H,H}$ = 6.5 Hz, 3 H), 7.15 (m, 3 H), 7.53 (m, 3 H) and 8.11 ppm (d, $J_{H,H}$ = 8.1 Hz, 3 H), the phenyl protons at δ = 7.63 (s, 3 H) and 8.00 ppm (s, 3 H) and the -N=C*H*- protons at δ = 8.47 ppm (s, 3 H). This indicates that there is only one species present in solution and the solution structure of the complex is similar to its solid-state structure, with the lanthanide ion coordinated in the N_4O_3 cavity of the ligand with pendant 2-pyridyl groups rotating freely in solution. Furthermore, luminescent studies (vide infra) on Eu^{3+} and Tb^{3+} complexes indicate that there are two methanol molecules coordinated to the lanthanide ions. The above data suggest that compounds **1**−**9** exist as nine-coordinate non-electrolytes in methanol solution, with the lanthanide metal ions coordinated in the N_4O_3 cavity of the tripodal ligand and also to two solvent molecules.

Photophysical Properties

At room temperature, compounds **1**−**9** exhibit similar solution absorption and emission spectra in the UV/Vis region. Their photophysical properties are summarized in Table 3. The absorptions between 255 and 383 nm can be assigned to $\pi \rightarrow \pi^*$ transitions of the tripodal Schiff-base ligand. The visible emission of compounds **1**−**9**, with lifetimes (τ) ranging from 3.8 to 9.4 ns and quantum yields (Φ_{em}) of 0.33−5.57 × 10^{-2}, can be assigned to the intra-

 © 2004 Wiley-VCH Verlag GmbH & Co. KGaA, Weinheim

Table 3. Photophysical data of compounds **1**−**9**[a]

Compound	Absorption λ_{max}/nm [log(ε/dm^3 mol^{-1} cm^{-1})]	Excitation λ_{exc}/nm	Emission λ_{em}/nm (τ/ns, $\Phi_{em} \times 10^2$)[b]
1	381 (3.99), 255 (4.39)	380	460 (9.4, 1.36)
2	380 (4.33), 255 (4.75)	380	470 (4.5, 0.46)
3	384 (4.09), 258 (4.53)	380	455 (3.8, 0.21)[c]
4	382 (4.30), 256 (4.68)	380	466 (4.7, 2.38)
5	382 (4.42), 257 (4.80)	380	466 (4.7, 1.27)
6	381 (4.29), 256 (4.70)	380	469 (4.6, 5.57)
7	383 (4.52), 256 (4.89)	380	466 (4.7, 2.29)
8	382 (4.33), 256 (4.71)	380	453 (4.5, 0.33)
9	378 (3.97), 256 (4.35)	380	460 (4.5, 3.62)[d]

[a] Photophysical measurements were made in $2 \cdot 10^{-5}$ M CH_3OH solution at room temperature. [b] Quantum yields were determined relative to quinine sulfate in 0.1 N H_2SO_4 ($\Phi = 0.55$). [c] Phosphorescence band was also observed at 508 nm ($\tau = 776$ μs). [d] Phosphorescence band was also observed at 500 nm ($\tau = 26.3$ ms).

ligand emission. The absorption, emission and excitation (monitored at 465 nm) spectra of **7** are shown in Figure 2. The photoluminescence excitation (PLE) spectrum reflects where the maximum contribution of the photoluminescence (PL) comes from. Under steady-state conditions, excited electrons relax from the highest excited states to the lowest excited states before they recombine radiatively or non-radiatively. In this case, the PLE spectrum shows exactly this situation; the maximum PL contribution comes from the lowest excited bands, with a decreasing contribution from the higher-energy band. Thus, although the absorption bands coincide with the excitation bands, as they should, the relative intensities of the energy bands by the two techniques can reveal the origin of the physical process measured. The emission spectra and decay time measurements for Gd^{3+} complexes allowed the identification of the lowest ligand triplet state in the complexes.[19−22] This is possible because the metal-centered (MC) electronic levels of Gd^{3+} are known to be located at 31000 cm^{-1}, typically well above the ligand-centered electronic levels of aromatic ligands.[23] Therefore, ligand-to-metal energy transfer and the consequent MC luminescence cannot be observed.

Figure 3 shows the variable temperature emission spectra of **3** in methanol. The time-resolved spectra of **3** show that at room temperature the lifetimes at 455 and 508 nm are

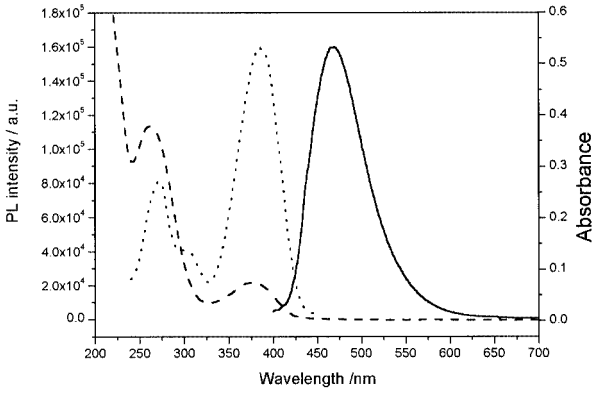

Figure 2. Room temperature absorption (− − − −), emission (———; excited at 380 nm) and excitation (·····; monitored at 465 nm) spectra of **7** in CH_3OH

both 3.8 ns, indicating that the emissions come from the same state and correspond to a ligand-centered (LC) short-lived fluorescence. At 77 K, on top of the weak LC fluorescence ($\tau = 4.1$ ns at 455 nm and 6.8 ns at 508 nm), an intense LC long-lived phosphorescence is also observed at 508 nm ($\tau = 776$ μs). This indicates that both LC singlet and triplet states exist at 77 K. The ligand-centered excited singlet state (^{1}LC) is estimated to be about 22000 cm^{-1} and the triplet state (^{3}LC) to be 19690 cm^{-1}.

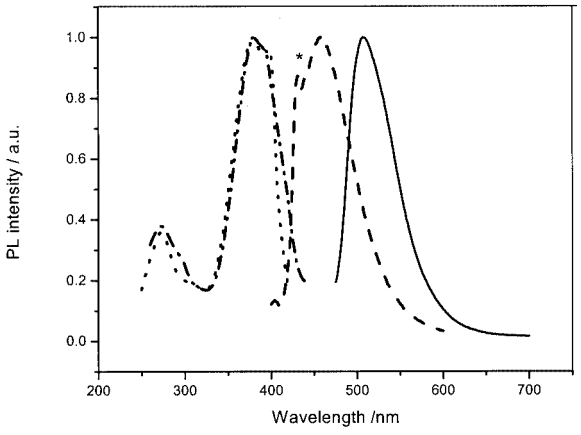

Figure 3. Variable-temperature emission and excitation spectra of **3** in CH_3OH; room temperature emission (− − −; excited at 380 nm) and excitation (·····; monitored at 455 nm) spectra, 77 K emission (———; excited at 380 nm) and excitation (−·−·−; monitored at 508 nm) spectra; the peak marked with an asterisk is due to scattering

The variable-temperature photoluminescent properties of compounds **2**, **4** and **7** in methanol have also been examined. Emission corresponding to the characteristic 4f−4f transitions of trivalent lanthanide metal ions was observed at 77 K but not at room temperature for **2** and **4**. Figure 4 and 5 show the room temperature and 77 K emission and excitation spectra of **2** and **4**, respectively. At room temperature, the time-resolved spectra of **2** and **4** taken at their emission peak ($\lambda_{max} = 470$ nm for **2**, $\tau = 4.5$ ns; $\lambda_{max} = 466$ nm for **4**, $\tau = 4.7$ ns) and 508 nm ($\tau = 4.5$ ns for **2** and 4.7 ns for **4**) show that the emission corresponds to a li-

 © 2004 Wiley-VCH Verlag GmbH & Co. KGaA, Weinheim

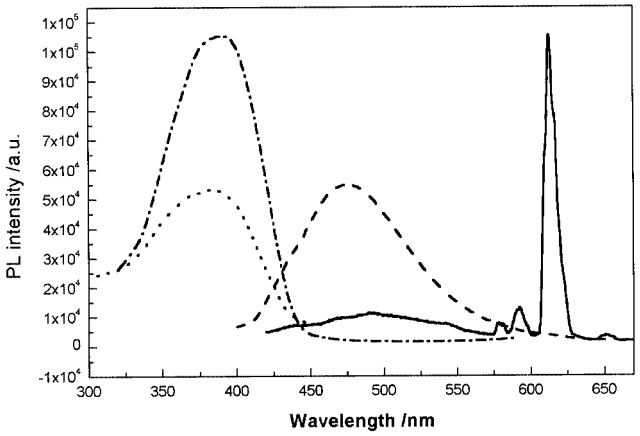

Figure 4. Variable-temperature emission and excitation spectra of **2** in CH_3OH; room temperature emission (– – –; excited at 380 nm) and excitation (·····; monitored at 465 nm) spectra, 77 K emission (———; excited at 380 nm) and excitation (–·–·–; monitored at 613 nm) spectra

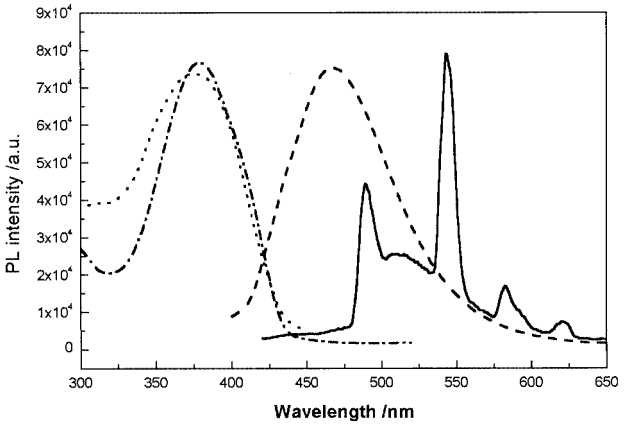

Figure 5. Variable-temperature emission and excitation spectra of **4** in CH_3OH; room temperature emission (– – –; excited at 380 nm) and excitation (·····; monitored at 465 nm) spectra, 77 K emission (———; excited at 380 nm) and excitation (–·–·–; monitored at 544 nm) spectra

gand-centered (^{1}LC) short-lived fluorescence. At 77 K, the lanthanide ion emission for compound **2**, which has a lifetime of 476 μs in CH_3OH and 787 μs in CD_3OD, corresponds to the $^5D_0 \rightarrow {}^7F_J$ transitions of Eu^{3+}, with the emission at 611 nm being assigned to the $^5D_0 \rightarrow {}^7F_2$ transition.[24] Other than the Eu^{3+} emission, a very broad and weak emission peak at around 470 nm was also observed at 77 K (Figure 4). Lifetime measurements confirmed that the emission was purely ^{1}LC fluorescence with no ^{3}LC phosphorescence (τ being 4.9 ns at 470 nm and 5.4 ns at 508 nm). The observation of ^{3}LC phosphorescence for the Gd^{3+} complex (**3**) but not for the Eu^{3+} complex (**2**) indicates that energy transfer from the ligand triplet ^{3}LC to Eu^{3+} excited states is quite efficient. The emission for compound **4** at 77 K, which has a lifetime of 572 μs in CH_3OH and 678 μs in CD_3OD, corresponds to the $^5D_4 \rightarrow {}^7F_J$ transitions of Tb^{3+}, with the emission centered at 551 nm arising from the $^5D_4 \rightarrow {}^7F_5$ transition.[24] Other than the Tb^{3+} emission, a very broad and weak emission centered around 466 nm and a medium-strong emission centered around 508 nm were also observed at 77 K (Figure 5). The time-resolved spectra show that there is only one lifetime at 466 nm (τ being 5.6 ns) and two different lifetimes at 508 nm (τ being 6.0 ns and 113 μs). This shows that the emission centered at 466 nm is due to ^{1}LC fluorescence and that at 508 nm to ^{3}LC phosphorescence. Unlike **2**, which does not show any ^{3}LC phosphorescence, **4** exhibits ^{3}LC phosphorescence, which is probably due to back energy-transfer from the metal excited state to the ^{3}LC. It has been shown that efficient back energy-transfer takes place in Tb^{3+} complexes when ΔE (^{3}LC – $^5D_4$) is less than 1850 cm^{-1}.[25] The energy of the ligand triplet state is about 2400 cm^{-1} higher than the energy of the $^5D_0$ Eu^{3+} luminescent level (17300 cm^{-1}) and lies at almost the same energy as the $^5D_4$ Tb^{3+} luminescent level (20450 cm^{-1}).[23] Thus, efficient ligand-to-metal energy transfer is observed for the Eu^{3+} complex and significant back energy-transfer for the Tb^{3+} complex. The excitation band of **2** (monitored at 613 nm for Eu^{3+}) and **4** (monitored at 545 nm for Tb^{3+}) is located around 380 nm in each case, and closely resembles their low-energy absorption band, indicative of their similar ori-

Table 4. Photophysical data of compounds **2** and **4** at 77 K[a]

Compound	Excitation (nm)	Emission (nm)	Transition	τ in CH_3OH[b] (μs)	τ in CD_3OD[b] (μs)
2	382	579	$^5D_0 \rightarrow {}^7F_0$		
		593	$^5D_0 \rightarrow {}^7F_1$		
		613	$^5D_0 \rightarrow {}^7F_2$		
		651	$^5D_0 \rightarrow {}^7F_3$	476	787
		681	$^5D_0 \rightarrow {}^7F_4$		
4	380	489	$^5D_4 \rightarrow {}^7F_6$		
		543	$^5D_4 \rightarrow {}^7F_5$	572	678
		582	$^5D_4 \rightarrow {}^7F_4$		
		621	$^5D_4 \rightarrow {}^7F_3$		

[a] Photophysical measurements were made in a $2 \cdot 10^{-5}$ M CH_3OH or CD_3OD solution at 77 K. [b] Measured in correspondence with the most intense emission band ($^5D_0 \rightarrow {}^7F_2$ for Eu^{3+} and $^5D_4 \rightarrow {}^7F_5$ for Tb^{3+}).

 © 2004 Wiley-VCH Verlag GmbH & Co. KGaA, Weinheim

gin. This clearly shows that the excitation of both Eu^{3+} and Tb^{3+} complexes originates from the $\pi \rightarrow \pi^*$ transitions of the Schiff-base antenna. Their low-temperature photophysical properties and assignments of the transitions are summarized in Table 4. Based on the different lifetimes of the lanthanide-ion emissions in CH_3OH and CD_3OD, the number of coordinated methanol molecules (*n*), which can be calculated from Horrocks equation,[26] is estimated to be 1.74 and 2.30 for Eu^{3+} and Tb^{3+}, respectively. This indicates that in methanol solution, there are two solvent molecules coordinated to the trivalent lanthanide metal ions.

However, even at 77 K, **7** exhibits no ^{3}LC emission in the visible region nor an emission corresponding to the $^4I_{13/2} \rightarrow {}^4I_{15/2}$ transition of Er^{3+} in the near-infrared region. This suggests that the Er^{3+} ion probably relaxes its energy, which it receives from the antenna, via vibrational modes to the environment.

Conclusion

In this paper, we have demonstrated that lanthanide Schiff-base complexes, $Ln^{III}L$, can be conveniently prepared by the condensation of tris(2-aminoethyl)amine with three equivalents of 5-*tert*-butyl-2-hydroxy-3-(2′-pyridyl)benzaldehyde in the presence of trivalent lanthanide metal ions. A photophysical study shows that the Schiff-base ligand can act as an antenna and transfer the absorbed light energy via its triplet state to the Eu^{3+} and Tb^{3+} metal ions.

Experimental Section

General Procedures: All reactions were carried out under an atmosphere of dry nitrogen. Solvents were dried by standard procedures, and distilled and deaerated prior to use. Hydrated lanthanide salts and tris(2-aminoethyl)amine (tren) were obtained from the Aldrich Chemical Company and used without further purification. 5-*tert*-Butyl-2-hydroxy3-(2′-pyridyl)benzaldehyde (Py-CHO) was prepared according to a literature method.[27] Microanalyses were performed by the Shanghai Institute of Organic Chemistry, Chinese Academy of Sciences, China. Electronic absorption spectra in the UV/Vis region were recorded on a Hewlett−Packard 8453 UV/Visible spectrophotometer, steady-state visible fluorescence and PL excitation spectra on a Photon Technology International (PTI) Alphascan spectrofluorimeter and visible decay spectra on a pico-N_2 laser system (PTI Time Master) with λ_{exc} = 337 nm. Quantum yields were computed according to a literature method[28] using quinine sulfate in 0.1 N H_2SO_4 as the reference standard (Φ = 0.55 in air-equilibrated water).[29] The number of coordinated solvent molecules (*n*) for the Eu^{3+} and Tb^{3+} complexes was calculated from the Horrocks equation $n = r(\tau_H^{-1} - \tau_D^{-1})$, where τ_H and τ_D are the excited-state lifetimes (in ms) in CH_3OH and CD_3OD, respectively, and the value of *r* is 2.1 and 8.4 for Eu^{3+} and Tb^{3+}, respectively.[26] Infrared spectra (KBr pellets) were recorded on a Nicolet Nagna-IR 550 spectrometer and NMR spectra on a JEOL EX270 spectrometer. Chemical shifts of ^{1}H NMR spectra were referenced to internal deuterated solvents and then recalculated to $SiMe_4$ (δ = 0.00 ppm). Low-resolution mass spectra (LRMS) were obtained on a Finnigan MAT SSQ-710 spectrometer in the positive FAB mode. Electrospray ionization high-resolution mass spectra (ESI-HRMS) were recorded on a QSTAR mass spectrometer. Conductivity measurements were carried out with a DDS-11 conductivity bridge for 10^{-4} mol dm^{-1} solutions in methanol.

Preparation of Lanthanide Schiff-Base Complexes: Compounds **1**−**9** were prepared using a similar method. A typical procedure for the preparation of the complexes is given for **1**.

Compound 1: A solution of $La(NO_3)_3{\cdot}6H_2O$ (0.044 g, 0.102 mmol) and Py-CHO (0.077 g, 0.304 mmol) in methanol (15 mL) was heated to 55 °C. Then, a solution of tren (0.015 g, 0.103 mmol) in methanol (10 mL) was added and the mixture was refluxed for an additional 2 h. The solution was then cooled to room temperature, filtered and the solvents evaporated to dryness in vacuo. The residue was re-dissolved in dichloromethane, filtered and slowly evaporated in air to give yellow crystals, which were filtered and dried in vacuo. Yield: 0.078 g, 74%; m.p. > 260 °C (decomp). ^{1}H NMR (in CD_3OD): δ = 1.36 (s, 27 H, *tert*-butyl), 2.82 and 3.10 (2 × t, $J_{H,H}$ = 6.5 Hz, 2 × 6 H, 3 × NCH_2CH_2N), 7.24 (t, $J_{H,H}$ = 6.2 Hz, 3 H, py-H), 7.55 (s, 3 H, Ar-H), 7.60 (m, 3 H, py-H), 7.86 (s, 3 H, Ar-H), 8.19 (m, 3 H, py-H), 8.28 (d, $J_{H,H}$ = 9.4 Hz, 3 H, py-H), 8.34 (s, 3 H, N=C*H*) ppm. IR (KBr): $\nu_{C=N}$ = 1623 cm^{-1}. ESI-HRMS (+ve mode, CH_3OH): *m*/*z* = 994.3854 [M + H]$^+$ ($C_{54}H_{61}LaN_7O_3$ requires 994.3899). $C_{54}H_{60}LaN_7O_3{\cdot}3.5H_2O$ (1057.06): calcd. C 61.35, H 6.40, N 9.28; found C 61.45, H 6.34, N 9.32.

Compound 2: $Eu(NO_3)_3{\cdot}6H_2O$ (0.045 g, 0.101 mmol), Py-CHO (0.077 g, 0.304 mmol) and tren (0.015 g, 0.103 mmol) were used. Yield: 0.064 g, 60%; light-yellow solid, m.p. > 210 °C (decomp). IR (KBr): $\nu_{C=N}$ = 1621 cm^{-1}. MS (FAB, +ve): *m*/*z* = 1008 [M + H]$^+$ for ^{153}Eu. ESI-HRMS (+ve mode, CH_3OH): *m*/*z* = 1008.4032 [M + H]$^+$ ($C_{54}H_{61}EuN_7O_3$ requires 1008.4048). $C_{54}H_{60}EuN_7O_3{\cdot}3.5H_2O$ (1070.12): calcd. C 60.60, H 6.26, N 9.16; found C 60.40, H 6.26, N 9.39.

Compound 3: $Gd(NO_3)_3{\cdot}6H_2O$ (0.045 g, 0.100 mmol), Py-CHO (0.077 g, 0.304 mmol) and tren (0.015 g, 0.103 mmol) were used. Yield: 0.072 g, 68%; light-yellow solid, m.p. > 250 °C (decomp). IR (KBr): $\nu_{C=N}$ = 1628 cm^{-1}. ESI-HRMS (+ve mode, CH_3OH): *m*/*z* = 1013.4004 [M + H]$^+$ ($C_{54}H_{61}GdN_7O_3$ requires 1013.4077). $C_{54}H_{60}GdN_7O_3{\cdot}2.5H_2O$ (1057.39): calcd. C 61.32, H 6.21, N 9.27; found C 61.36, H 6.10, N 9.29.

Compound 4: $Tb(NO_3)_3{\cdot}6H_2O$ (0.045 g, 0.099 mmol), Py-CHO (0.077 g, 0.304 mmol) and tren (0.015 g, 0.103 mmol) were used. Yield: 0.073 g, 69%, greenish-yellow solid, m.p. > 200 °C (decomp). IR (KBr): $\nu_{C=N}$ = 1623 cm^{-1}. MS (FAB, +ve): *m*/*z* = 1014 [M + H]$^+$ for ^{159}Tb. ESI-HRMS (+ve mode, CH_3OH): *m*/*z* = 1014.4061 [M + H]$^+$ ($C_{54}H_{61}N_7O_3Tb$ requires 1014.4089). $C_{54}H_{60}N_7O_3Tb{\cdot}2.5H_2O$ (1059.06): calcd. C 61.23, H 6.20, N 9.26; found C 61.24, H 6.06, N 9.28.

Compound 5: $DyCl_3$ (0.027 g, 0.100 mmol), Py-CHO (0.077 g, 0.304 mmol) and tren (0.015 g, 0.103 mmol) were used. Yield: 0.074 g, 71%, greenish-yellow solid, m.p. > 250 °C (decomp). IR (KBr): $\nu_{C=N}$ = 1622 cm^{-1}. MS (FAB, +ve): *m*/*z* = 1019 [M + H]$^+$ for ^{164}Dy. ESI-HRMS (+ve mode, CH_3OH): *m*/*z* = 1019.4180 [M + H]$^+$ ($C_{54}H_{61}DyN_7O_3$ requires 1019.4127). $C_{54}H_{60}DyN_7O_3{\cdot}H_2O$ (1035.61): calcd. C 62.62, H 6.05, N 9.47; found C 62.43, H 6.04, N 9.37.

Compound 6: $Ho(NO_3)_3{\cdot}5H_2O$ (0.044 g, 0.100 mmol), Py-CHO (0.077 g, 0.304 mmol) and tren (0.015 g, 0.103 mmol) were used. Yield: 0.071 g, 63%, yellow solid, m.p. > 170 °C (decomp). IR

 © 2004 Wiley-VCH Verlag GmbH & Co. KGaA, Weinheim

Table 5. Crystallographic data for compounds **4**−**7**

Compound	**4**·H_2O	**5**·CH_3OH·0.75H_2O	**6**·1.5H_2O	**7**·2CH_3OH
Empirical formula	$C_{54}H_{60}N_7O_3Tb·H_2O$	$C_{54}H_{60}N_7O_3Dy·CH_3OH·0.75H_2O$	$C_{54}H_{60}N_7O_3Ho·1.5H_2O$	$C_{54}H_{60}N_7O_3Er·2CH_3OH$
Molecular mass	1032.03	1063.15	1047.05	1086.46
Crystal size [mm]	0.36 × 0.25 × 0.18	0.10 × 0.10 × 0.05	0.20 × 0.10 × 0.10	0.22 × 0.18 × 0.17
Crystal system	triclinic	triclinic	triclinic	triclinic
Space group	$P\bar{1}$	$P\bar{1}$	$P\bar{1}$	$P\bar{1}$
a [Å]	15.700(3)	15.965(4)	15.6849(13)	15.967(1)
b [Å]	18.443(4)	18.320(5)	18.4880(14)	18.439(1)
c [Å]	19.035(4)	19.257(5)	19.0286(15)	19.456(1)
α [°]	81.692(4)	79.563(6)	81.6340(10)	80.24(1)
β [°]	85.099(4)	83.795(7)	85.1270(10)	84.300(9)
γ [°]	75.021(4)	74.440(6)	75.0850(10)	74.13(1)
V [Å^3]	5262(2)	5326(3)	5268.8(7)	5421.6(8)
Z	4	4	4	4
D_{calc} [g cm^{-3}]	1.300	1.319	1.316	1.331
T [K]	293	293	293	293
Absorption coefficient [mm^{-1}]	1.393	1.454	1.552	1.597
F(000)	2120	2172	2144	2244
θ range [°]	1.34−27.71	1.08−27.65	1.35−27.52	1.07−25.61
Reflections collected	31137	36293	30993	35189
Independent reflections	22778 (R_{int} = 0.0514)	24333 (R_{int} = 0.0800)	22558 (R_{int} = 0.0261)	18406 (R_{int} = 0.0440)
Goodness-of-fit	0.964 (on F^2)	0.838 (on F^2)	0.951 (on F^2)	0.950 (on F)
Final R indices [$I > n\sigma(I)$][a]	$R1$ = 0.0634 (n = 2.0)	$R1$ = 0.0668 (n = 2.0)	$R1$ = 0.0372 (n = 2.0)	R = 0.049 (n = 1.5)
	$wR2$ = 0.1609	$wR2$ = 0.1479	$wR2$ = 0.0864	R_w = 0.046

[a] $R = R1 = \Sigma\|F_o| - |F_c\|/\Sigma|F_o|$. $R_w = [\Sigma w(|F_o| - |F_c|)^2/\Sigma w(F_o)^2]^{1/2}$. $wR2 = \{\Sigma[w(F_o^2 - F_c^2)^2]/\Sigma[w(F_o^2)^2]\}^{1/2}$.

(KBr): $\nu_{C=N}$ = 1623 cm^{-1}. MS (FAB, +ve): m/z = 1020 [M + H]$^+$ for ^{165}Ho. ESI-HRMS (+ve mode, CH_3OH): m/z = 1020.4086 [M + H]$^+$ ($C_{54}H_{61}HoN_7O_3$ requires 1020.4139). $C_{54}H_{60}HoN_7O_3·CH_2Cl_2·H_2O$ (1122.98): calcd. C 58.82, H 5.75, N 8.73; found C 58.51, H 5.68, N 9.02.

Compound 7: $Er(NO_3)_3·5H_2O$ (0.045 g, 0.101 mmol), Py-CHO (0.077 g, 0.304 mmol) and tren (0.015 g, 0.103 mmol) were used. Yield: 0.088 g, 85%, yellow solid, m.p. > 340 °C (decomp). IR (KBr): $\nu_{C=N}$ = 1620 cm^{-1}. MS (FAB, +ve): m/z = 1021 [M + H]$^+$ for ^{166}Er. ESI-HRMS (+ve mode, CH_3OH): m/z = 1023.4086 [M + H]$^+$ ($C_{54}H_{61}ErN_7O_3$ requires 1023.4174). $C_{54}H_{60}ErN_7O_3·0.75H_2O$ (1035.87): calcd. C 62.60, H 6.00, N 9.47; found C 62.64, H 5.82, N 9.88.

Compound 8: $Tm(NO_3)_3·6H_2O$ (0.047 g, 0.102 mmol), Py-CHO (0.077 g, 0.304 mmol) and tren (0.015 g, 0.103 mmol) were used. Yield: 0.052 g, 50%, greenish-yellow solid, m.p. > 250 °C (decomp). IR (KBr): $\nu_{C=N}$ = 1623 cm^{-1}. MS (FAB, +ve): m/z = 1024 [M + H]$^+$ for ^{169}Tm. ESI-HRMS (+ve mode, CH_3OH): m/z = 1024.4192 [M + H]$^+$ ($C_{54}H_{61}N_7O_3Tm$ requires 1024.4178). $C_{54}H_{60}N_7O_3Tm·1.25H_2O$ (1046.55): calcd. C 61.96, H 6.03, N 9.37; found C 61.97, H 6.00, N 9.37.

Compound 9: $Lu(NO_3)_3·H_2O$ (0.036 g, 0.100 mmol), Py-CHO (0.077 g, 0.304 mmol) and tren (0.015 g, 0.103 mmol) were used. Yield: 0.066 g, 63%, yellow solid, m.p. > 220 °C (decomp). ^{1}H NMR (CD_3OD): δ = 1.35 (s, 27 H, *t*Bu), 2.81 and 3.10 (2 × t, $J_{H,H}$ = 6.5 Hz, 2 × 6 H, 3 × NCH_2CH_2N), 7.02 (t, $J_{H,H}$ = 6.5 Hz, 3 H, py-H), 7.15 (m, 3 H, py-H), 7.53 (m, 3 H, py-H), 7.63 (s, 3 H, Ar-H), 8.00 (s, 3 H, Ar-H), 8.11 (d, $J_{H,H}$ = 8.1 Hz, 3 H, py-H), 8.47 (s, 3 H, N=C*H*) ppm. IR (KBr): $\nu_{C=N}$ = 1623 cm^{-1}. ESI-HRMS (+ve mode, CH_3OH): m/z = 1030.4186 [M + H]$^+$ ($C_{54}H_{61}LuN_7O_3$ requires 1030.4243). $C_{54}H_{60}LuN_7O_3·H_2O$ (1048.08): calcd. C 61.87, H 5.97, N 9.36; found C 61.83, H 6.01, N 9.34.

X-ray Crystallography: Pertinent crystallographic data and other experimental details are summarized in Table 5. Crystals of **4**·H_2O, **5**·CH_3OH·0.75H_2O, **6**·1.5H_2O and **7**·2CH_3OH suitable for X-ray diffraction studies were grown by slow evaporation of a solution of the respective compound in methanol. The selected crystal of each complex was mounted on the top of a glass fiber for data collection. Intensity data were collected at 293 K on a Bruker Axs SMART 1000 CCD area-detector diffractometer (for **4**, **5** and **6**) and a Mar Research image plate scanner (for **7**) using graphite-monochromated Mo-K_α radiation (λ = 0.71073 Å). For **4** and **5**, the collected frames were processed with the software SAINT[30] and an absorption correction was applied (SADABS)[31] to the collected reflections. A self-consistent semi-empirical absorption correction based on Fourier coefficient fitting of symmetry-equivalent reflections was applied using the ABSCOR program for **6**. For **7**, interframe scaling was employed for the absorption correction. The space groups of each crystal were determined from the systematic absences and Laue symmetry checks and confirmed by successful refinement of the structures. The structures of all compounds were solved by direct method (SHELXTL^{TM})[32] and refined by full-matrix least-squares analysis. All non-hydrogen atoms were refined anisotropically. Hydrogen atoms were generated in their idealized positions and allowed to ride on their respective parent carbon atoms. CCDC-157465 (**4**), -190555 (**5**), -190556 (**6**) and -212141 (**7**) contain the supplementary crystallographic data for this paper. These data can be obtained free of charge at www.ccdc.cam.ac.uk/conts/retrieving.html [or from the Cambridge Crystallographic Data Centre, 12, Union Road, Cambridge CB2 1EZ, UK; fax: (internat.) +44-1223/336-033; E-mail: deposit@ccdc.cam.ac.uk].

Acknowledgments

Thanks are due to the Hong Kong Baptist University and the Hong Kong Research Grants Council (HKBU 2038/02P) for financial support.

 © 2004 Wiley-VCH Verlag GmbH & Co. KGaA, Weinheim

[1] A. Smith, S. J. Rettig, C. Orvig, *Inorg. Chem.* **1988**, *27*, 3929−3934.
[2] D. J. Berg, S. J. Rettig, C. Orvig, *J. Am. Chem. Soc.* **1991**, *113*, 2528−2532.
[3] S. Liu, L. Gelmini, S. J. Rettig, R. C. Thompson, C. Orvig, *J. Am. Chem. Soc.* **1992**, *114*, 6081−6087.
[4] S. Liu, L.-W. Yang, S. J. Rettig, C. Orvig, *Inorg. Chem.* **1993**, *32*, 2773−2778.
[5] P. Guerriero, S. Tamburini, P. A. Vigato, *Coord. Chem. Rev.* **1995**, *139*, 17−243.
[6] J.-C. G. Bünzli, C. Piguet, *Chem. Rev.* **2002**, *102*, 1897−1928.
[7] R. Rodríguez-Cortiñas, F. Avecilla, C. Platas-Iglesias, D. Imbert, J.-C. G. Bünzli, A. de Blas, T. Rodríguez-Blas, *Inorg. Chem.* **2002**, *41*, 5336−5349.
[8] P. Caravan, J. J. Ellison, T. J. McMurry, R. B. Lauffer, *Chem. Rev.* **1999**, *99*, 2293−2352.
[9] M. Kanesato, T. Yokoyama, O. Itabashi, T. M. Suzuki, M. Shiro, *Bull. Chem. Soc. Jpn.* **1996**, *69*, 1297−1302.
[10] M. Kanesato, T. Yokoyama, T. M. Suzuki, *Chem. Lett.* **1997**, 93−94.
[11] M. W. Essig, D. W. Keogh, B. L. Scott, J. G. Watkin, *Polyhedron* **2001**, *20*, 373−377.
[12] P. V. Bernhardt, B. M. Flanagan, M. J. Riley, *Aust. J. Chem.* **2001**, *54*, 229−232.
[13] P. Bhattacharyya, J. Parr, A. T. Ross, A. M. Z. Slawin, *J. Chem. Soc., Dalton Trans.* **1998**, 3149−3150.
[14] J.-P. Costes, F. Dahan, A. Dupuis, S. Lagrave, J.-P. Laurent, *Inorg. Chem.* **1998**, *37*, 153−155.
[15] J.-P. Costes, F. Dahan, A. Dupuis, J.-P. Laurent, *Chem. Eur. J.* **1998**, *4*, 1616−1620.
[16] J.-P. Costes, F. Dahan, A. Dupuis, *Inorg. Chem.* **2000**, *39*, 165−168.
[17] J.-P. Costes, F. Nicodème, *Chem. Eur. J.* **2002**, *8*, 3442−3447.
[18] W.-K. Wong, H. Liang, W.-Y. Wong, Z. Cai, K.-F. Li, K.-W. Cheah, *New J. Chem.* **2002**, *26*, 275−278.
[19] S. I. Klink, L. Grave, D. N. Reinhoudt, F. C. J. M. van Veggel, M. H. V. Werts, F. A. J. Geurts, J. W. Hofstraat, *J. Phys. Chem. A* **2000**, *104*, 5457−5468.
[20] Z. R. Reeves, K. L. V. Mann, J. C. Jeffery, J. A. McCleverty, M. D. Ward, F. Barigelletti, N. Armaroli, *J. Chem. Soc., Dalton Trans.* **1999**, 349−355.
[21] Y. Kawamura, Y. Wada, S. Yanagida, *Jpn. J. Appl. Phys.* **2001**, *40*, 350−356.
[22] G. F. de Sá, O. L. Malta, C. de Mello Donegá, A. M. Simas, R. L. Longo, P. A. Santa-Cruz, E. F. da Silva Jr., *Coord. Chem. Rev.* **2000**, *196*, 165−195.
[23] R. Reisfeld, C. K. Jorgensen. *Lasers and Excited States of Rare Earths*, Springer, Berlin, **1977**.
[24] W. T. Carnall, G. L. Goodman, K. Rajnak, R. S. Rana, *J. Chem. Phys.* **1989**, *90*, 3443−3457.
[25] M. Latva, H. Takalo, V. M. Mukkala, C. Matachescu, J.-C. Rodriguez-Ubis, J. Kankare, *J. Luminesc.* **1997**, *75*, 149−169.
[26] N. Sabbatini, M. Guardigli, J.-M. Lehn, *Coord. Chem. Rev.* **1993**, *123*, 201−228.
[27] F. Lam, J. X. Xu, K. S. Chan, *J. Org. Chem.* **1996**, *61*, 8414−8418.
[28] C. A. Parker, W. T. Rees, *Analyst (London)* **1960**, *85*, 587−600.
[29] S. R. Meech, D. C. Phillips, *J. Photochem.* **1983**, *23*, 193−217.
[30] *SAINT, Reference Manual*, Siemens Energy and Automation, Madison, WI, **1994−1996**.
[31] G. M. Sheldrick, SADABS, Empirical Absorption Correction Program, University of Göttingen, **1997**.
[32] G. M. Sheldrick, *SHELXTL*™, *Reference Manual*, v*er.5.1*, Siemens, Madison, WI, **1997**.

Received June 9, 2003
Early View Article
Published Online January 19, 2004

 © 2004 Wiley-VCH Verlag GmbH & Co. KGaA, Weinheim

Synthesis, Characterization and Near-Infrared Photoluminescence of Monoporphyrinate Lanthanide Complexes Containing an Anionic Tripodal Ligand

Hongshan He,[a,c] Jianping Guo,[a] Zhixin Zhao,[a] Wai-Kwok Wong,*[a] Wai-Yeung Wong,[a] Wing-Kit Lo,[a] King-Fai Li,[b] Li Luo,[b] and Kok-Wai Cheah[b]

Keywords: Lanthanides / Photoluminescence / Porphyrins / Tripodal ligands

Twelve neutral stable complexes of ytterbium(III) and erbium(III) coordinated by anionic hydridotris(pyrazol-1-yl)borate and *meso*-tetraphenylporphyrinate, and its derivatives with different substituents in the *para* position of the phenyl groups, were prepared and characterized. Crystal structure analyses revealed that seven nitrogen atoms, four from the porphyrinate dianion and three from the anionic tripodal ligand, are symmetrically coordinated to the lanthanide ions. Photophysical investigations of the complexes showed an enhancement of near-infrared photoluminescence as compared to aqua-coordinated monoporphyrinate lanthanide complexes. The solvent effect and substituent effects on the photoluminescent properties of the complexes were also investigated
(© Wiley-VCH Verlag GmbH & Co. KGaA, 69451 Weinheim, Germany, 2004).

Introduction

Recently, near-infrared (NIR) photoluminescence of three lanthanide ions, Nd^{3+}, Er^{3+} and Yb^{3+}, has attracted considerable attention for their potential application in optical amplification and fluoroimmunoassay.[1−8] Direct excitation of lanthanide ions is difficult because of the forbidden nature of their electronic transitions.[9] However, indirect excitation of an organic chromophore (antenna) that interacts closely with lanthanide the ions can make the energy of the triplet state of the ligand transfer efficiently to the excited state of the lanthanide ion and enable the ion to emit light;[10] the design of molecular systems with binding ability and photosensitizing properties for the construction of efficient photoluminescent lanthanide complexes is the key issue of this active area of research. Porphyrins are good candidates for this purpose because they can form stable complexes with lanthanide ions and have high absorbance.[11−15]

Several reports on NIR photoluminescent studies of porphyrinate lanthanide complexes have appeared in the literature during the past decades.[7,16−19] The results with Yb^{3+} and Er^{3+} complexes revealed that the porphyrin could indeed absorb the light and transfer the energy to lanthanide ions. However, the limited structural variation of the complexes tends to prohibit intensive investigation of the photophysical properties of lanthanide complexes, because most of them were prepared by the direct interaction of lanthanide β-diketonates with free porphyrin bases in 1,3,5-trichlorobenzene.[11−17] The lanthanide ion was therefore always coordinated by one porphyrinate dianion and one β-diketonate anionic ligand, which was very difficult to remove. Recently, we established a new method for the preparation of cationic lanthanide porphyrinate complexes of the general formula $[Ln(Por)(H_2O)_3]Cl$ (Ln = Yb^{3+}, Er^{3+} and Y^{3+}), in which one porphyrinate dianion and three aqua molecules are coordinated to the lanthanide ion.[18−21] The three aqua ligands in $[Ln(Por)(H_2O)_3]Cl$ can be substituted easily by other ligands, for example the (cyclopentadienyl)tris(diethylphosphito)cobaltate(I) anion, to form stable complexes.[18] This provides an opportunity for us to modify the monoporphyrinate lanthanide complexes for photoluminescent studies.

In this paper, we report the synthesis and characterization of a series of new stable ytterbium(III) and erbium(III) porphyrinate complexes coordinated by another anionic tripodal ligand, namely hydridotris(pyrazol-1-yl)borate (Scheme 1). The crystallographic analyses showed that seven N atoms, four from the porphyrinate dianion and three from the anionic tripodal ligand, are coordinated to the metal ions. The photoluminescence of lanthanide com-

[a] Department of Chemistry, Hong Kong Baptist University
Waterloo Road, Kowloon Tong, Hong Kong, P. R. China
Fax: (internat.) + 852-3411-5862
E-mail: wkwong@hkbu.edu.hk
[b] Department of Physics, Hong Kong Baptist University
Waterloo Road, Kowloon Tong, Hong Kong, P. R. China
[c] Department of Applied Chemistry, National Huaqiao University
Quanzhou 362011, P. R. China
Supporting information for this article is available on the WWW under http://www.eurjic.org or from the author.

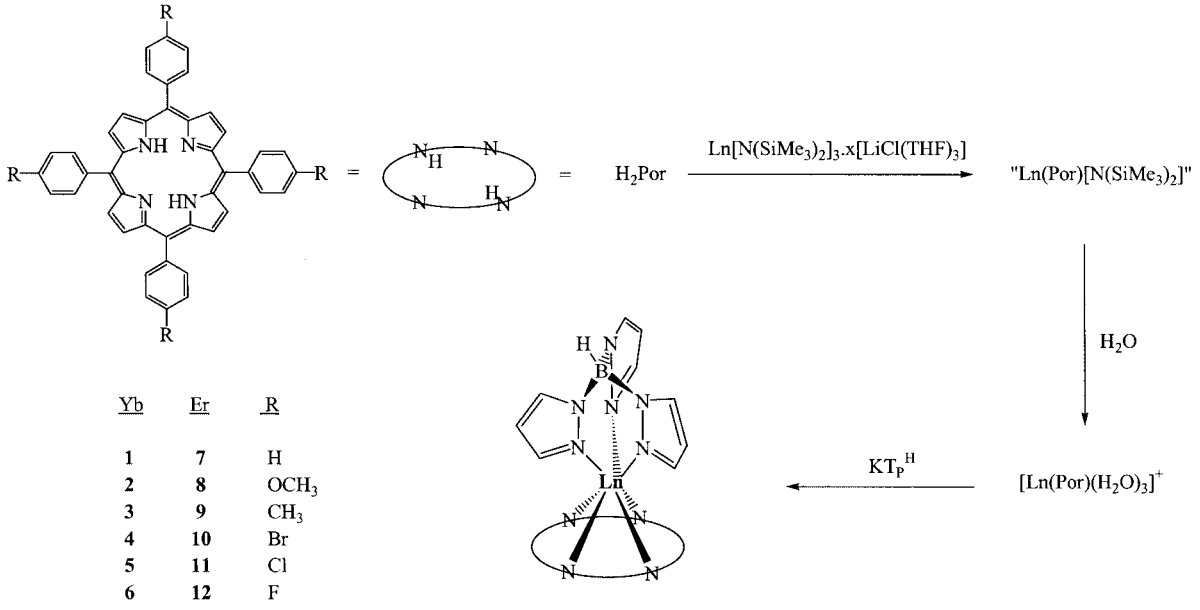

Yb	Er	R
1	**7**	H
2	**8**	OCH_3
3	**9**	CH_3
4	**10**	Br
5	**11**	Cl
6	**12**	F

Scheme 1

plexes was investigated in different solvents and the substituent effect on NIR luminescence will be discussed.

Results and Discussion

Synthesis and Characterization

The free porphyrin bases 5,10,15,20-tetraphenylporphyrin (H_2TPP), 5,10,15,20-tetrakis(*p*-tolyl)porphyrin (H_2TTP), 5,10,15,20-tetrakis(*p*-methoxyphenyl)porphyrin (H_2TMPP), 5,10,15,20-tetrakis(*p*-chlorophenyl)porphyrin (H_2TCPP), 5,10,15,20-tetrakis(*p*-bromophenyl)porphyrin (H_2TBPP), and 5,10,15,20-tetrakis(*p*-fluorophenyl)porphyrin (H_2TFPP), were prepared by direct condensation of the respective benzaldehyde with pyrrole in propionic acid according to the literature method[21] and purified by column chromatography using silica gel. The yields are 7−10%. Under a nitrogen atmosphere, refluxing of the free porphyrin base with a fivefold excess of $Ln[N(SiMe_3)_2]_3{\cdot}x[LiCl(THF)_3]$, generated in situ from the reaction of anhydrous $LnCl_3$ with three equivalents of $Li[N(SiMe_3)_2]$ in THF, in bis(2-methoxyethyl)ether for 48 h,[19−21] followed by stirring of the resulting mixture with a slight excess of potassium hydridotris(pyrazol-1-yl)borate (KT_p^H) in air at room temperature, gave the purple complexes $[Ln(Por)(T_p^H)]$ (Ln = Yb^{3+}, Por = TPP^{2-}, **1**; $TMPP^{2-}$, **2**; TTP^{2-}, **3**; $TBPP^{2-}$, **4**; $TCPP^{2-}$, **5** and $TFPP^{2-}$, **6**; Ln = Er^{3+}, Por = TPP^{2-}, **7**; $TMPP^{2-}$, **8**; TTP^{2-}, **9**; $TBPP^{2-}$, **10**; $TCPP^{2-}$, **11** and $TFPP^{2-}$, **12**) in high yields (Scheme 1). The complexes are quite stable in air and very soluble in chloroform, dichloromethane and *N*,*N*′-dimethylforamide. The electronic absorption spectra of complexes **1**−**12** are characteristic of normal metalloporphyrins.[23] The Soret band is observed at about 422 nm, while the Q bands are observed at 551 and 588 nm. After complexation, the number of Q bands of the porphyrin ring (four for free porphyrin base) is reduced to two. This is in agreement with Gouterman's four-orbital model,[24] which predicts that, due to an increase in symmetry, the four Q bands of the free porphyrin base will be reduced to two upon the formation of a metalloporphyrin. In the absorption spectra of regular metalloporphyrins there are two Q bands between 500 and 600 nm. The lower-energy band (α band) is the electronic origin Q(0,0) of the lowest singlet excited state S_1. The second band (β band) is its vibrational overtone and is labeled as Q(1,0). The relative intensities of these bands can be a qualitative yardstick of just how stable is the metal ion complexed to the four porphyrin nitrogen atoms. Thus, when the intensity of α is greater than that of β, the metal forms a stable complex with the porphyrin, whereas when α is less than β, the metal is easily displaced by protons.[25] The α/β relative intensity ratio for Yb^{3+} complexes **1**−**6** ranges from 0.12−0.44 and for Er^{3+} complexes **7**−**12** from 0.18−0.34. The typical N−H vibration for free porphyrin bases disappears from the IR spectra upon formation of the complexes. Complexes **1**−**12** exhibit similar fragmentation patterns in their mass spectra. Low-resolution (FAB-MS) and high-resolution mass spectra (ESI-HSMS) of the complexes confirmed that they are 1:1 adducts of monoporphyrinate and the anionic tripodal ligand. The electrospray ionization high-resolution mass spectra (positive mode) of the complexes in methanol show a mass peak corresponding to $[M + H]^+$. For instance, the Er^{3+} and Yb^{3+} complexes of $[Ln(TPP)(T_P^H)]$ exhibit mass peaks at m/z = 992.2815 and 1000.2788, respectively, which deviate by less than 5 ppm from the theoretical values of 992.2755 and 1000.2840 for the elemental composition of $C_{53}H_{39}BErN_{10}$ and $C_{53}H_{39}BN_{10}Yb$, respectively. The observed isotopic distribution patterns of the $[Ln(Por)(T_P^H) + H]^+$ peaks also match the expected theoretical signals.

 © 2004 Wiley-VCH Verlag GmbH & Co. KGaA, Weinheim

Crystals of **1**·2$CHCl_3$, **5**·$CHCl_3$·CH_3OH and **7**·2$CHCl_3$ suitable for X-ray diffraction studies were grown by slow evaporation of the solvents from solutions of the respective compounds in a chloroform/methanol (v/v, 1:1) solution. Compounds **1**, **5** and **7** are isomorphous and crystallized in the monoclinic space group $P2_1/n$ for **1** and **7**, and $P2_1/c$ for **5**. The selected bond lengths and bond angles of the complexes are given in the Supporting Information (Table S1). Perspective drawings of compounds **1** and **7** are shown in Figure 1 and 2, respectively. The structural analyses revealed that the lanthanide(III) ions are seven coordinate, surrounded by seven nitrogen atoms, four from the porphyrin dianion and three from the anionic tripodal ligand. The average bond length of Ln−N(porphyrin) is shorter than that of Ln−N(tripodal ligand), with Ln−N(porphyrin) and Ln−N(tripodal ligand) being 2.356 and 2.495 Å for **1**, 2.357 and 2.508 Å for **5**, and 2.373 and 2.518 Å for **7**, respectively.

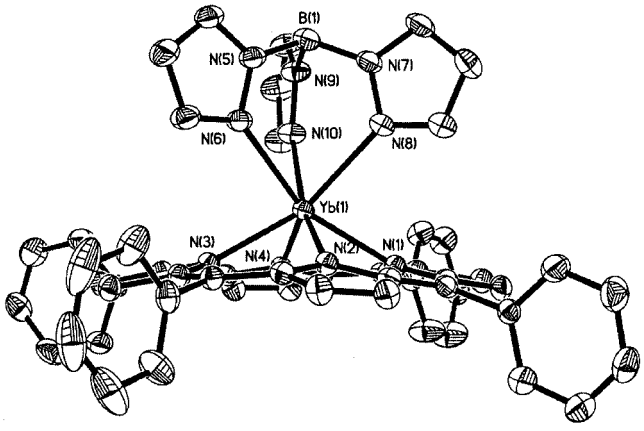

(a)

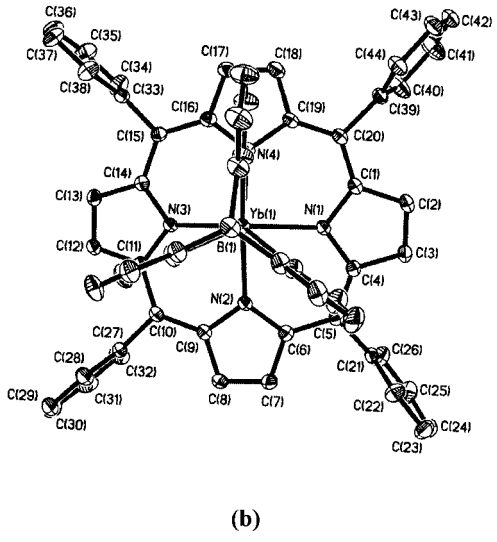

(b)

Figure 1. Perspective views of complex **1**: (a) side view; (b) top view

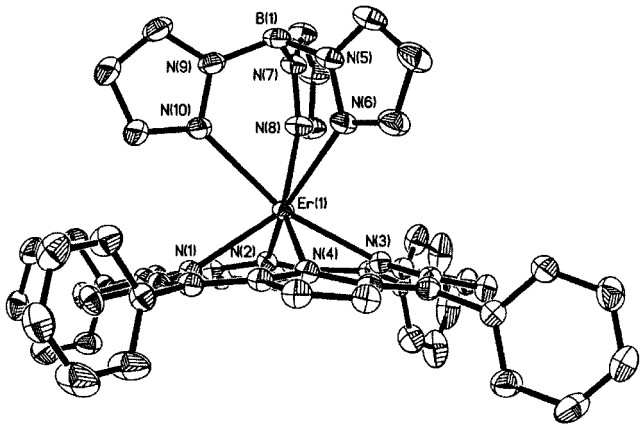

(a)

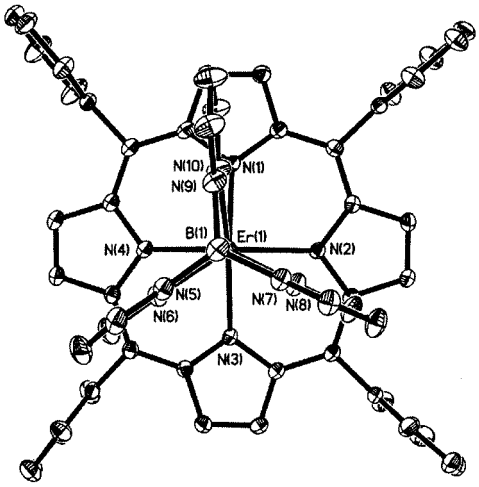

(b)

Figure 2. Perspective views of complex **7**: (a) side view; (b) top view

The mean nitrogen plane ($N_1N_2N_3N_4$) of the porphyrin dianion is almost parallel to the mean nitrogen plane ($N_6N_8N_{10}$) of the anionic tripodal ligand, forming a dihedral angle of 0.4°, 2.0° and 0.3° for **1**, **5** and **7**, respectively. The distance of the metal ion to the $N_1N_2N_3N_4$ mean plane is 1.172 Å for **1**, 1.167 Å for **5** and 1.195 Å for **7**, which is longer than that for [Ln(Por)$(H_2O)_3$]Cl[20] and shorter than that for [Ln(Por)(L_{OEt})] [L_{OEt} = cyclopentadienyltris(diethylphosphito)cobaltate(I)].[18] The distance of the metal ion to the $N_6N_8N_{10}$ mean plane is about 0.6 Å longer than that to the $N_1N_2N_3N_4$ mean plane, so the metal ion is much closer to the $N_1N_2N_3N_4$ mean plane. The substituents have little effect on the structural parameters except that the electron-withdrawing group (Cl) on the phenyl group gives a larger dihedral angle between the two planes (Table 1). The relative conformation of the tripodal ligand and the porphyrin dianion is slightly different between the Yb^{3+} and Er^{3+} complexes. A top view of their

 © 2004 Wiley-VCH Verlag GmbH & Co. KGaA, Weinheim

structures reveals that, for the Yb^{3+} complexes, one of the pyrazole planes of the tripodal ligand is just above one of the phenyl groups of the porphyrin dianion, while the other two pyrazole groups are above the pyrrole groups; for the Er^{3+} complex, all the three pyrazole groups are located above the pyrrole groups.

Table 1. Distance from the metal ion to the $N_1N_2N_3N_4$ and $N_6N_8N_{10}$ planes

Compound	d_1[a] (Å)	d_2[b] (Å)	A[c] (°)	Ref.
1	1.172	1.780	0.4	this work
5	1.167	1.790	2.0	this work
[Yb(TMPP)(H_2O)$_3$]Cl	1.08			[20]
7	1.195	1.800	0.3	this work
[Er(TMPP)(H_2O)$_3$]Cl	1.11			[20]
[Er(TPP)(L_{OEt})]	1.201			[18]

[a] Distance to the $N_1N_2N_3N_4$ mean plane. [b] Distance to the $N_6N_8N_{10}$ mean plane. [c] Dihedral angle formed between the $N_1N_2N_3N_4$ mean plane and the $N_6N_8N_{10}$ mean plane.

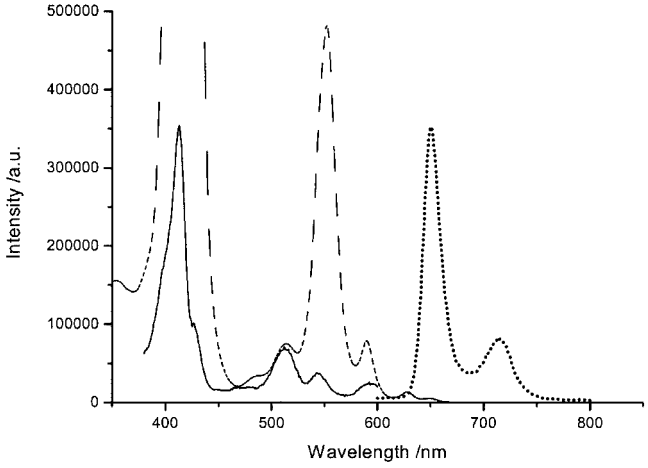

Figure 3. Room temperature absorption (– – –), emission (·····) (excited at 414 nm) and excitation (——) (monitored at 648 nm) spectra of **1** in $CHCl_3$

Photoluminescence Studies

The photophysical properties of compounds **1**−**12** were examined and the data are summarized in Table 2. The room temperature solution electronic absorption, excitation and emission spectra of compounds **1**−**12** in the UV/Vis region are almost identical and are characteristic of intra-ligand transitions of normal porphyrinate complexes.[13] Figure 3 shows the absorption, emission (excited at 414 nm) and excitation (monitored at 648 nm) spectra of **1**. The absorption bands at 421, 550 and 588 nm and emission peaks at 648 nm (τ = 12.9 ns and $\Phi_{em} = 0.11 \times 10^{-3}$) can be assigned to the intra-ligand $\pi \rightarrow \pi^*$ transitions of the porphyrinate ligand. The quantum efficiency of the metalloporphyrin is much lower than that of the corresponding free porphyrin base. For example, the quantum yield of **1** is less than 1% of the corresponding free porphyrin base H_2TMPP ($\Phi_{em} = 2.84 \times 10^{-2}$). Other than the visible emission, compounds **1**−**12** also exhibit typical emission corresponding to the lanthanide(III) ion in the near-infrared (NIR) region. Figure 4 shows the NIR emission and the excitation spectrum of **1**. The excitation bands of **1** in chloroform solution at 298 K (monitored at 980 nm) are observed at 560 and 596 nm, which almost coincide with its visible absorption bands at 550 and 588 nm. This clearly shows that the excitation of the Yb^{3+} ion is due to the $\pi \rightarrow \pi^*$ transitions of the porphyrinate antenna and excitation of the porphyrin is the photophysical pathway leading to the observable NIR luminescence. This is in agreement with our previous photoluminescent studies on related lanthanide porphyrinate complexes,[18,23] which show that the porphyrinate antenna transfers its absorbed visible energy of the Q band to the excited state of the metal ion, which then relaxes through emission in the NIR region. The NIR luminescence lifetime of **1**−**6** is about 20 μs and is much longer than the lifetime of the porphyrinate emission. Due to the limitation of our

Table 2. Photophysical data of compounds **1**−**12**[a]

Compound	Absorption: λ_{max}/nm [log(ε/dm^3 mol^{-1} cm^{-1})]	Excitation: λ_{exc}/nm	Emission: λ_{em}/nm (τ, $\Phi_{em} \times 10^3$)[b][c]
1	421 (5.55), 550 (4.15), 588 (3.22)	414	648 (12.9 ns, 0.11), 980 (20 μs)
2	424 (5.46), 552 (4.15), 592 (3.79)	418	647 (12.7 ns, 22.8), 980 (20 μs)
3	423 (5.58), 552 (4.23), 590 (3.87)	418	650 (13.2 ns, 0.22), 980 (20 μs)
4	423 (5.59), 551 (4.25), 588 (3.46)	417	650 (12.6 ns, 0.04), 980 (20 μs)
5	422 (5.62), 551 (4.27), 589 (3.48)	417	649 (12.4 ns, 0.31), 980 (20 μs)
6	421 (5.60), 550 (4.23), 587 (3.33)	415	650 (12.8 ns, 0.57), 980 (20 μs)
7	423 (5.72), 552 (4.31), 590 (3.57)	414	648 (9.1 ns, 0.16), 1540[d]
8	427 (5.52), 555 (4.14), 593 (3.67)	419	655 (9.1 ns, 0.03), 1540
9	424 (5.71), 553 (4.32), 592 (3.74)	418	651 (10.7 ns, 0.20), 1540
10	423 (5.63), 552 (4.18), 590 (3.48)	417	650 (10.5 ns, 0.26), 1540
11	424 (5.69), 552 (4.28), 590 (3.53)	416	650 (11.8 ns, 0.06), 1540
12	423 (5.63), 552 (4.22), 589 (3.49)	414	648 (11.7 ns, 0.17), 1540

[a] Photophysical measurements were made in $CHCl_3$ solution at room temperature. [b] Quantum yields were determined relative to [Ru(bipy)$_3$]Cl$_2$ in air-equilibrated water (Φ = 0.028). [c] Due to the limitation of the instrument, we were unable to determine the quantum yields of the NIR luminescence of compounds **1**−**12**. [d] Due to the limitation of the instrument, we were unable to measure the lifetime of the NIR luminescence of compounds **7**−**12**.

 © 2004 Wiley-VCH Verlag GmbH & Co. KGaA, Weinheim

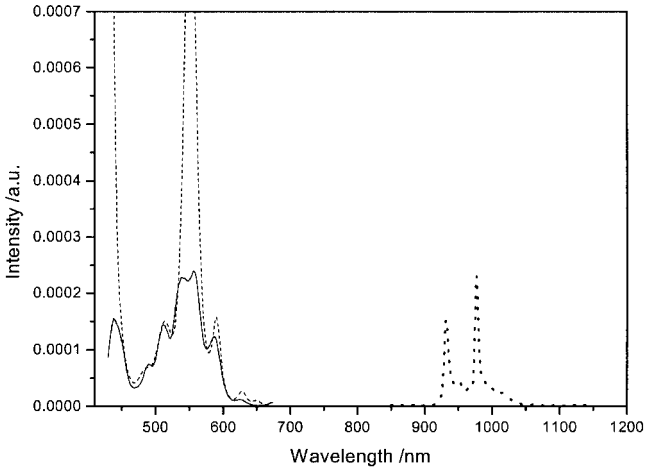

Figure 4. Room temperature absorption (– – –), NIR emission (·····) (excited at 420 nm) and excitation (——) (monitored at 980 nm) spectra of **1** in $CHCl_3$

equipment, we were unable to measure the excitation (monitored at 1540 nm) spectrum and the NIR luminescence lifetime of **7**–**12**.

The NIR emission spectra of the porphyrinate complexes are depicted in Figure 5. For the Yb^{3+} complexes, a strong emission due to the $^2F_{5/2} \rightarrow {}^2F_{7/2}$ transition is observed at 997 nm. This transition is split into six bands, one of these is sharp (980 nm) and the other five are weak (934, 953, 1002, 1020 and 1038 nm).For the Er^{3+} counterparts, two major peaks centered at 1018 and 1570 nm are observed. These can be attributed to the $^4I_{11/2} \rightarrow {}^4I_{15/2}$ and $^4I_{13/2} \rightarrow {}^4I_{15/2}$ transitions respectively. The first peak (1018 nm) splits into two others at 984 and 1020 nm, and the second peak (1570 nm) splits into five others at 1502, 1540, 1570, 1608 and 1634 nm.[2,4,8] The intensity of the emission of the complexes is enhanced relative to the aqua-coordinated monoporphyrinate complexes $[Ln(Por)(H_2O)_3]Cl$, as shown in Figure 6. Previously, we have investigated the photoluminescent properties of Yb^{3+} porphyrinate coordinated by L^-_{OEt}.[7] Well-split NIR emission peaks are also observed due to the strong bonding of the ligand to the Yb^{3+} ion. The present work further demonstrates that, upon coordination, the anionic tripodal ligand removes the degeneracy of the energy levels of the lanthanide ions by lowering the symmetry of these ions.

Figure 7 shows a simple, widely accepted photophysical model for the description of the sensitization process.[4,8] In this process, the porphyrin absorbs the light and is excited to its singlet state (S_1). The energy is then transferred to its triplet state (T_1), which is, in part, being transferred to the excited state of the lanthanide ion $(Ln^{3+})^*$ to produce the final luminescence. The overall NIR luminescence quantum yield (Φ) of the metal ion is the product of triplet yield (Φ_{ISC}), energy-transfer yield (Φ_{ET}) and the intrinsic luminescence quantum yield of the lanthanide ion (Φ_{Ln}). The structural and electronic variation of the porphyrin can disturb the excited energy level of the complexes and thus change the emission properties.[26,27] Therefore, we measured the NIR photoluminescence intensity of the complexes with different substituents in the *para* position of the phenyl groups of the porphyrin and found that both electron-do-

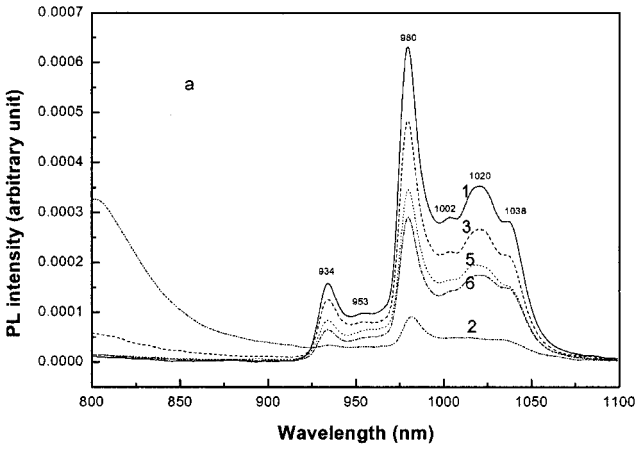

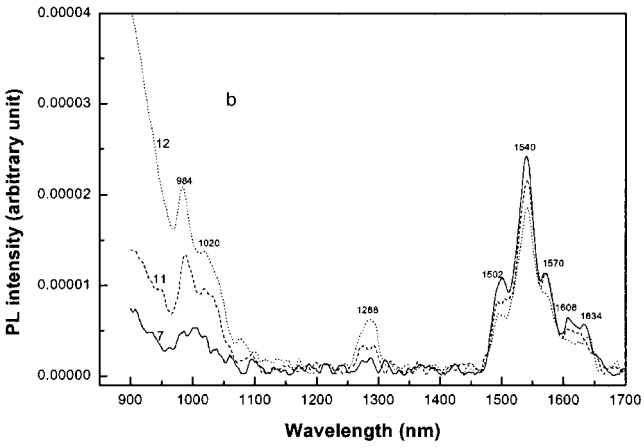

Figure 5. Luminescence of different (a) Yb^{3+} and (b) Er^{3+} complexes in chloroform at room temperature

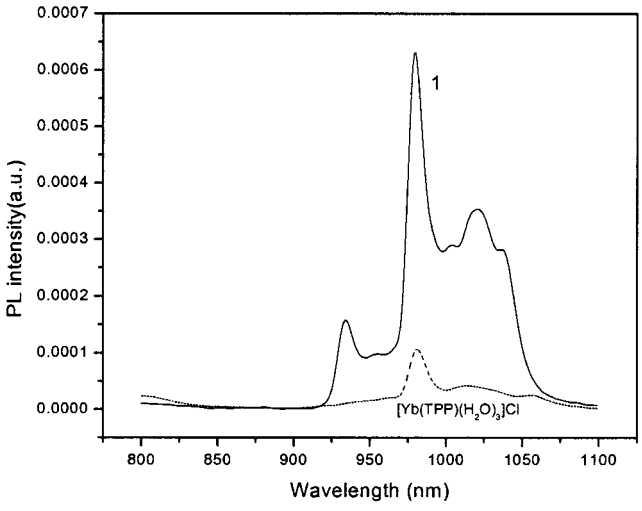

Figure 6. Luminescence of complex **1** and $[Yb(TPP)(H_2O)_3]Cl$ in chloroform at room temperature

 © 2004 Wiley-VCH Verlag GmbH & Co. KGaA, Weinheim

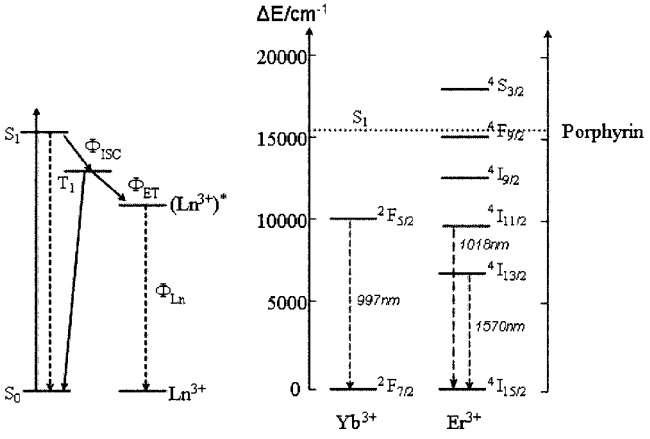

Figure 7. Schematic energy diagram of [Ln(Por)(T_p^H)] complexes; the arrows indicate the excitation mechanism of lanthanide ions by the porphyrin sensitizer ($S_0 \rightarrow S_1$ transition followed by intersystem crossing and energy transfer)

nating groups and halogen atoms are unfavorable for the NIR emission of Yb^{3+} complexes. For example, the unsubstituted complex **1** gave the strongest emission, with an intensity about six times higher than that of complex **2** and twice that of **6**. The reason for this is that electron donating groups (-OCH_3, -CH_3, etc.) allow the electrons on the phenyl groups to show greater π-conjugation with the porphyrin ring in the S_1 state, which results in an increase of the fluorescence quantum yield of the ligand and a decrease of the quantum yield of intersystem crossing Φ_{ISC}. Furthermore, the halogens can decrease the rate of intersystem crossing and thus make the Φ_{ISC} quite low.[26,28,29] The lower Φ_{ISC} leads to a weaker metal ion emission. As the emission of Er^{3+} complexes is much lower than that of Yb^{3+} complexes, the substituent effect was not apparent here.

We have also investigated the NIR photoluminescence of complex **7** in different solvents (Figure 8). The results showed that the NIR emission intensity of **7** is strongest in non-polar solvents such as benzene, gradually decreases as the polarity of the solvent increases and is completely quenched in methanol. According to the theory of non-radiative transitions in lanthanide complexes, the non-radiative relaxation between various J states may occur by interaction of the electronic levels of the lanthanide ion with suitable vibrational modes of the environment.[30] The presence of OH groups in methanol enhances the non-radiative deactivation of the lanthanide ion by vibronic coupling with the vibrational states of the O−H oscillators and thus quenches the emission.[31]

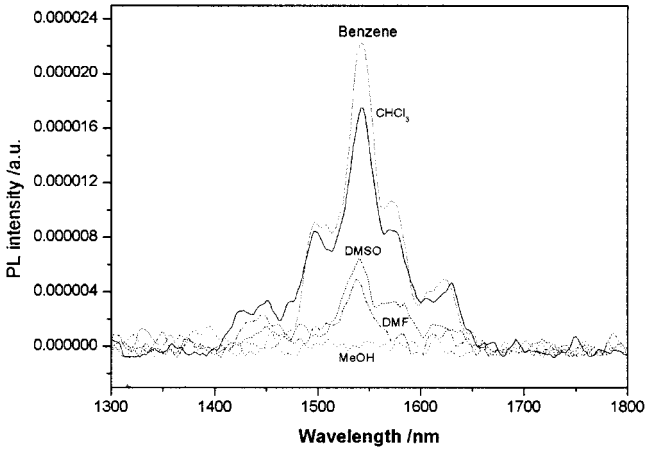

Figure 8. Luminescence of complex **7** in different solvents at room temperature

Concluding Remarks

In this paper, we have reported the synthesis of a series of lanthanide porphyrinate complexes of the general formula [Ln(Por)(T_P^H)] by the interaction of cationic porphyrinate complexes [Ln(Por)$(H_2O)_3$]Cl, generated in situ, with anhydrous KT_P^H and demonstrated that these complexes are good precursors for the preparation of other lanthanide porphyrinate complexes. We have also shown that porphyrinate ligands can behave as antennae by absorbing visible light and thus sensitize the NIR emission of lanthanide ions. Electron-donating groups and halogen atoms on the phenyl groups of the porphyrin ring are unfavorable for the emission of lanthanide ions.

Experimental Section

General: All reactions were carried out under an atmosphere of dry nitrogen. Solvents were dried by standard procedures, distilled and deaerated prior to use. All chemicals used were obtained from Aldrich Chemical Company. 5,10,15,20-Tetraphenylporphyrin (H_2TPP), 5,10,15,20-tetrakis(*p*-tolyl)porphyrin (H_2TTP), 5,10,15,20-tetrakis(*p*-methoxyphenyl)porphyrin (H_2TMPP), 5,10,15,20-tetrakis(*p*-chlorophenyl)porphyrin (H_2TCPP), 5,10,15,20-tetrakis(*p*-bromophenyl)porphyrin (H_2TBPP), 5,10,15,20-tetrakis(*p*-fluorophenyl)porphyrin (H_2TFPP) were prepared according to the literature methods by condensation of pyrrole and the corresponding aldehyde,[22] and characterized by TLC, ^{1}H NMR spectroscopy and FAB mass spectrometry. The IR spectra (KBr pellets) were recorded on a Nicolet Nagba-IR 550 spectrometer. NMR spectra were recorded on a Varian INOVA 400 spectrometer. Low-resolution mass spectra were obtained on a Finnigan MAT SSQ-710 in FAB (positive) mode. Electrospray ionization high-resolution mass spectra (ESI-HRMS) were recorded on a QSTAR mass spectrometer. Electronic absorption spectra in the UV/Vis region were recorded on a Hewlett−Packard 8453 UV/Visible Spectrophotometer, steady-state visible fluorescence and PL excitation spectra on a Photon Technology International (PTI) Alphascan spectro-fluorimeter and visible decay spectra on a pico-N_2 laser system (PTI Time Master) with λ_{exc} = 337 nm. NIR emission was detected by a liquid-nitrogen-cooled InSb IR detector (EG & G) with a preamplifier and recorded by a lock-in amplifier system as the third harmonic; the 355 nm line of an Nd:YAG laser (Quantel Brilliant B) was used as excitation light and also to pump the OPO (Opotek MagicPrism VIR) to provide a continuously tunable laser source from 410−670 nm with a pulse-width of 4 ns. NIR decay spectra were detected by an Oriel 77343 photomultiplier and monitored by a HP54522A 500 MHz oscilloscope. Quantum yields were computed according to the literature method[32] using [Ru(bipy)$_3$]Cl_2 as the reference standard (Φ = 0.028 in air-equilibrated

 © 2004 Wiley-VCH Verlag GmbH & Co. KGaA, Weinheim

water).[33] To avoid any second-order light reaching the detector, 710 and 830 nm cutoff filters were used where applicable. The complexes in different solution were analyzed in quartz cells at a concentration of 2×10^{-5} M. The power on the cell was 1 W and all spectra were corrected for the detector response.

Preparations of Precursor Complexes: Stock solutions of the precursor complexes, $Ln[N(SiMe_3)_2]_3{\cdot}x[LiCl(THF)_3]$ (Ln = Yb^{3+} and Er^{3+}), were prepared in a similar manner. A detailed description is given for the Yb^{3+} complex.

$Yb[N(SiMe_3)_2]_3{\cdot}x[LiCl(THF)_3]$ Solution (Solution A): *n*BuLi (31.0 mL, 1.6 M in hexane, 49.6 mmol) was added slowly over a period of 30 min to a solution of $(Me_3Si)_2NH$ (10.8 mL, 8.26 g, 51.2 mmol) in THF (20 mL) cooled in an ice bath. The reaction mixture was stirred, warmed up slowly to room temperature and stirred for another 12 h until a clear pale yellow solution was obtained. Then, the resultant solution was transferred slowly to a suspension of $YbCl_3$ (4.45 g, 15.9 mmol) in THF (20 mL). The reaction mixture was stirred for 24 h at room temperature until all of the $YbCl_3$ had been consumed. The resulting solution was centrifuged, filtered and the filtrate was made up to 100 mL with THF to give an approximately 0.16 M solution of $Yb[N(SiMe_3)_2]_3{\cdot}x[LiCl(THF)_3]$ (solution **A**).

$Er[N(SiMe_3)_2]_3{\cdot}x[LiCl(THF)_3]$ Solution (Solution B): The procedure for the preparation of solution **B** was the same as for solution **A**. *n*BuLi (15.5 mL, 1.6 M in hexane, 24.8 mmol), $(Me_3Si)_2NH$ (5.4 mL, 4.13 g, 25.6 mmol) and $ErCl_3$ (2.18 g, 8.0 mmol) were used. The resulting solution was then made up to 50 mL with THF to give an approximately 0.16 M solution of $Er[N(SiMe_3)_2]_3{\cdot}x[LiCl(THF)_3]$ (solution **B**).

Preparations of Compounds 1−12: Compounds **1**−**12** were prepared by the same procedure. A typical procedure is given for **1**.

[Yb(TPP)(Tp^H)] (1): Solution **A** (5.0 mL) was added to a solution of H_2TPP (0.10 g, 0.16 mmol) in bis(2-methoxyethyl)ether (6 mL) under a nitrogen atmosphere. The resulting solution was refluxed and the progress of the reaction was monitored by UV/Vis absorption spectroscopy until most of the free base had coordinated to the metal ion. Then, anhydrous KT^H_P (0.10 g, 0.40 mmol) was added and the resulting mixture was stirred in air for another 12 h. After the reaction was complete, the solvent was removed in vacuo and the residue redissolved in chloroform, filtered and chromatographed on silica gel using chloroform to elute the unchanged free porphyrin base first, and then chloroform/methanol (v/v, 10:1) to elute the product. The solvent was removed on a rotary evaporator. The product was dissolved in chloroform (5 mL) and the solution was filtered. Diffusion of methanol into the chloroform solution gave purple crystals of the desired complex. Yield: 0.14 g (87%). M.p. > 300 °C. IR (KBr): $\tilde{\nu}$ = 3420 m, 2965 m, 2453 w, 1159 m, 1439 m, 1331 s, 1263 s, 1201 m, 1048 s, 988 vs, 798 vs, 751 s, 700 s cm^{-1}. MS (+FAB): *m*/*z* = 999 $[M + H]^+$, 786 $[Yb(TPP)]^+$ for ^{174}Yb. ESI-HRMS (+ve mode, in CH_3OH): *m*/*z* = 1000.2788 {$[M + H]^+$, $C_{53}H_{39}BN_{10}Yb$ requires 1000.2840}.

[Yb(TMPP)(Tp^H)] (2): Solution **A** (5.0 mL), H_2TMPP (0.11 g, 0.16 mmol) and KT^H_P (0.10 g, 0.40 mmol) were used. Yield: 0.18 g (89%). M.p. > 300 °C. IR (KBr): $\tilde{\nu}$ = 3441 m, 2924 m, 2831 w, 1605 s, 1512 s, 1466 m, 1290 s, 1243 vs, 1171 vs, 1036 m, 1000 w, 798 m, 742 w, 607w cm^{-1}. MS (+FAB): *m*/*z* = 1121 $[M + H]^+$, 906 $[Yb(TMPP)]^+$ for ^{174}Yb. ESI-HRMS (+ve mode, in CH_3OH): *m*/*z* = 1120.3259 {$[M + H]^+$, $C_{57}H_{47}BN_{10}O_4Yb$ requires 1120.3263}.

[Yb(TTP)(Tp^H)] (3): Solution **A** (5.0 mL), H_2TTP (0.10 g, 0.16 mmol) and KT^H_P (0.10 g, 0.40 mmol) were used. Yield: 0.13 g (80%). M.p. > 300 °C. IR (KBr): $\tilde{\nu}$ = 3449 s, 2918 w, 2459 w, 1641 m, 1512 m, 1409 m, 1331 s, 1294 m, 1124 vs, 1059 s, 991 vs, 801 s, 762 s, 731 s cm^{-1}. MS (+FAB): *m*/*z* = 1056 $[M + H]^+$, 842 $[Yb(TTP)]^+$ for ^{174}Yb. ESI-HRMS (+ve mode, in CH_3OH): *m*/*z* = 1055.3377 {$[M + H]^+$, $C_{57}H_{46}BN_{10}Yb$ requires 1055.3388}.

[Yb(TBPP)(Tp^H)] (4): Solution **A** (5.0 mL), H_2TBPP (0.13 g, 0.14 mmol) and KT^H_P (0.10 g, 0.40 mmol) were used. Yield: 0.16 g (90%). M.p. > 300 °C. IR (KBr): $\tilde{\nu}$ = 3415 s, 2919 m, 2448 w, 1641 m, 1479 m, 1393 m, 1331 s, 1196 s, 1070 m, 1049 s, 990 vs, 799 vs, 725 m, 462 m cm^{-1}. MS (FAB, +ve): *m*/*z* = 1312 $[M + H]^+$, 1098 $[Yb(TBPP)]^+$ for ^{79}Br and ^{174}Yb. ESI-HRMS (+ve mode, in CH_3OH): *m*/*z* = 1311.9138 {$[M + H]^+$, $C_{53}H_{35}BN_{10}Br_4Yb$ requires 1311.9261}.

[Yb(TCPP)(Tp^H)] (5): Solution **A** (5.0 mL), H_2TCPP (0.10 g, 0.14 mmol) and KT^H_P (0.10 g, 0.40 mmol) were used. Yield: 0.12 g (81%). M.p. > 300 °C. IR (KBr): $\tilde{\nu}$ = 3420 m, 2918 w, 2459 m, 1641 m, 1479 s, 1387 m, 1331 s, 1212 m, 1090 s, 1048 s, 990 vs, 801 s, 760 m, 725 m, 496 m cm^{-1}. MS (+FAB): *m*/*z* = 1136 $[M + H]^+$, 922 $[Yb(TCPP)]^+$ for ^{35}Cl and ^{174}Yb. ESI-HRMS (+ve mode, in CH_3OH): *m*/*z* = 1138.1247 {$[M + H]^+$, $C_{53}H_{35}BN_{10}Cl_4Yb$ requires 1138.1267}.

[Yb(TFPP)(Tp^H)] (6): Solution **A** (5.0 mL), H_2TFPP (0.11 g, 0.17 mmol) and KT^H_P (0.10 g, 0.40 mmol) were used. Yield: 0.13 g (78%). M.p. > 300 °C. IR (KBr): $\tilde{\nu}$ = 3426 m, 2924 m, 2458 w, 1600 m, 1517 vs, 1520 vs, 1485 m, 1408 m, 1329 m, 1226 s, 1157 vs, 1048 s, 991 s, 804 vs, 726 m, 591 m, 534 m cm^{-1}. MS (FAB, +ve): *m*/*z* = 1072 $[M + H]^+$, 858 $[Yb(TFPP)]^+$ for ^{174}Yb. ESI-HRMS (+ve mode, in CH_3OH): *m*/*z* = 1072.2526 {$[M + H]^+$, $C_{53}H_{35}BN_{10}F_5Yb$ requires 1072.2464}.

[Er(TPP)(Tp^H)] (7): Solution **B** (5.0 mL), H_2TPP (0.10 g, 0.16 mmol) and KT^H_P (0.10 g, 0.40 mmol) were used. Yield: 0.14 g (88%). M.p. > 300 °C. IR (KBr): $\tilde{\nu}$ = 3449 s, 3143 m, 2464 m, 1605 m, 1409 s, 1297 s, 1129 s, 1050 s, 980 vs, 802 s, 753 s, 727 vs, 702 s cm^{-1}. MS (+FAB): *m*/*z* = 993 $[M + H]^+$, 779 $[Er(TPP)]^+$ for ^{167}Er. ESI-HRMS (+ve mode, in CH_3OH): *m*/*z* = 992.2815 {$[M + H]^+$, $C_{53}H_{39}BN_{10}Er$ requires 992.2755}.

[Er(TMPP)(Tp^H)] (8): Solution **B** (5.0 mL), H_2TMPP (0.12 g, 0.17 mmol) and KT^H_P (0.10 g, 0.40 mmol) were used. Yield: 0.14 g (80%). M.p. > 300 °C. IR (KBr): $\tilde{\nu}$ = 3452 m, 2966 m, 2831 w, 2459 w, 1606 m, 1521 s, 1509 s, 1296 s, 1250 vs, 1176 vs, 1050 m, 988 s, 804 s, 730 s, 597 m cm^{-1}. MS (+FAB): *m*/*z* = 1113 $[M + H]^+$, 899 $[Er(TMPP)]^+$ for ^{167}Er. ESI-HRMS (+ve mode, in CH_3OH): *m*/*z* = 1112.3141 {$[M + H]^+$, $C_{57}H_{47}BN_{10}O_4Er$ requires 1112.3177}.

[Er(TTP)(Tp^H)] (9): Solution **B** (5.0 mL), H_2TTP (0.12 g, 0.18 mmol) and KT^H_P (0.10 g, 0.40 mmol) were used. Yield: 0.16 g (86%). M.p. > 300 °C. IR (KBr): $\tilde{\nu}$ = 3441 m, 2929 w, 2459 w, 1528 s, 1409 m, 1331 s, 1296 m, 1128 vs, 1049 s, 990 vs, 800 s, 728 s cm^{-1}. MS (+FAB): *m*/*z* = 1046 $[M + H]^+$, 833 $[Er(TTP)]^+$ for ^{167}Er. ESI-HRMS (+ve mode, in CH_3OH): *m*/*z* = 1048.3425 {$[M + H]^+$, $C_{57}H_{47}BN_{10}Er$ requires 1048.3381}.

[Er(TBPP)(Tp^H)] (10): Solution **B** (5.0 mL), H_2TBPP (0.11 g, 0.12 mmol) and KT^H_P (0.10 g, 0.40 mmol) were used. Yield: 0.14 g (91%). M.p. > 300 °C. IR (KBr): $\tilde{\nu}$ = 3449 s, 2919 m, 2454 w, 1636 m, 1479 m, 1388 m, 1295 vs, 1131 s, 1071 m, 1049 s, 989 vs, 804 m, 727 m, 462 m cm^{-1}. MS (+FAB): *m*/*z* = 1305 $[M + H]^+$, 1091 $[Er(TBPP)]^+$ for ^{79}Br and ^{167}Er. ESI-HRMS (+ve mode, in

 © 2004 Wiley-VCH Verlag GmbH & Co. KGaA, Weinheim

Table 3. Crystallographic data for compounds **1**, **5** and **7**

Compound	**1**·2$CHCl_3$	**5**·$CHCl_3$·CH_3OH	**7**·2$CHCl_3$
Empirical formula	$C_{55}H_{40}BCl_6N_{10}Yb$	$C_{55}H_{39}BCl_7N_{10}OYb$	$C_{55}H_{40}BCl_6ErN_{10}$
Molecular weight	1237.52	1287.96	1231.74
Crystal size [mm]	0.40 × 0.20 × 0.18	0.80 × 0.60 × 0.50	0.50 × 0.30 × 0.20
Crystal system	Monoclinic	Monoclinic	Monoclinic
Space group	$P2_1/n$	$P2_1/c$	$P2_1/n$
a [Å]	18.5807(14)	14.0166(11)	18.5620(10)
b [Å]	14.7805(11)	27.385(2)	14.8096(8)
c [Å]	19.4796(15)	15.4285(12)	19.4955(11)
β [°]	98.8320(10)	114.0270(10)	98.8120(10)
V [Å^3]	5286.3(7)	5408.9(7)	5296.0(5)
Z	4	4	4
$D_{calcd.}$ [g cm^{-3}]	1.555	1.575	1.545
T [K]	293	293	293
μ(Mo-K_α) [mm^{-1}]	2.121	2.125	1.936
F(000)	2468	2544	2460
θ range [°]	1.65−27.50	1.76−27.51	1.73−27.51
Reflections collected	30049	30928	30301
Independent reflections	11829	12119	11818
R_{int}	0.0290	0.0233	0.0216
GOF on F^2	0.949	1.064	1.064
$R1$, $wR2$ [$I > 2\sigma(I)$][a]	0.0343, 0.0866	0.0419, 0.1188	0.0316, 0.0832
$R1$, $wR2$ (all data)	0.0524, 0.0922	0.0542, 0.1281	0.0428, 0.0877

[a] $R1 = \Sigma||F_o| - |F_c||/\Sigma|F_o|$; $wR2 = [\Sigma w(|F_o^2| - |F_c^2|)^2/\Sigma w|F_o^2|^2]^{1/2}$.

CH_3OH): m/z = 1229.9271 {$[M - HBr]^+$, $C_{53}H_{34}BN_{10}Br_3Er$ requires 1311.9261}.

[Er(TCPP)(Tp^H)] (11): Solution **B** (5.0 mL), H_2TCPP (0.12 g, 0.17 mmol) and KT_P^H (0.10 g, 0.40 mmol) were used. Yield: 0.16 g (89%). M.p. > 300 °C. IR (KBr): ṽ = 3448 m, 2459 m, 2360 w, 1647 m, 1478 s, 1409 m, 1300 s, 1090 s, 1050 s, 1003 s, 800 s, 760 m, 727 m, 496 m cm^{-1}. MS (+FAB): m/z = 1129 $[M + H]^+$, 915 $[Er(TCPP)]^+$ for ^{35}Cl and ^{167}Er. ESI-HRMS (+ve mode, in CH_3OH): m/z = 1128.1289 {$[M + H]^+$, $C_{53}H_{35}BN_{10}Cl_4Er$ requires 1128.1196}.

[Er(TFPP)(Tp^H)] (12): Solution **B** (5.0 mL), H_2TFPP (0.11 g, 0.17 mmol) and KT_P^H (0.10 g, 0.40 mmol) were used. Yield: 0.17 g (89%). M.p. > 300 °C. IR (KBr): ṽ = 3431 m, 2960 m, 2453 w, 1605 m, 1508 vs, 1409 m, 1295 s, 1221 s, 1158 vs, 1052 s, 988 s, 800 vs, 726 m, 591 m cm^{-1}. MS (+FAB): m/z = 1065 $[M + H]^+$, 851 $[Er(TFPP)]^+$ for ^{167}Er. ESI-HRMS (+ve mode, in CH_3OH): m/z = 1064.2468 {$[M + H]^+$, $C_{53}H_{35}BN_{10}F_4Er$ requires 1064.2378}.

X-ray Crystallography. Pertinent crystallographic data and other experimental details are summarized in Table 3. Crystals suitable for X-ray diffraction studies were grown by slow evaporation of solutions of the respective compounds in chloroform/methanol. No decay in intensity was encountered during the data collection. Intensity data for **1**, **5** and **7** were collected at 293 K on a Bruker Axs SMART 1000 CCD area-detector diffractometer using graphite-monochromated Mo-K_α radiation (λ = 0.71073 Å). The collected frames were processed with the software SAINT,[34] and an absorption correction was applied (SADABS)[35] to the collected reflections. The space groups of each crystal were determined from the systematic absences and Laue symmetry checks and confirmed by successful refinement of the structures. The structures of all compounds were solved by direct methods (SHELXTL)[36] and refined against F^2 by full-matrix least-squares analyses. All non-hydrogen atoms were refined anisotropically. Hydrogen atoms were generated in their idealized positions and allowed to ride on their respective parent carbon atoms.

CCDC-213538 (**1**), -213539 (**5**) and -213540 (**7**) contain the supplementary crystallographic data for this paper. These data can be obtained free of charge at www.ccdc.cam.ac.uk/conts/retrieving.html or from the Cambridge Crystallographic Data Centre, 12 Union Road, Cambridge CB2 1EW, UK [Fax: (internat.) + 44-1223/336-033; E-mail: deposit@ccdc.cam.ac.uk].

Acknowledgments

W.-K. Wong thanks the Hong Kong Baptist University (FRG/01-02/II-40) and the Hong Kong Research Grants Council (HKBU 2023/00P) for financial support.

[1] A. Beeby, R. S. Dickins, S. Faulkner, D. Parker, J. A. G. Williams, *Chem. Commun.* **1997**, 1401−1402.
[2] S. I. Klink, P. Oude Alink, L. Grave, F. G. A. Peters, J. W. Hofstraat, F. Geurts, F. C. J. M. van Veggel, *J. Chem. Soc., Perkin Trans. 2* **2001**, 363−372.
[3] M. H. V. Werts, J. W. Verhoeven, J. W. Hofstraat, *J. Chem. Soc., Perkin Trans. 2* **2000**, 433−439.
[4] M. H. V. Werts, J. W. Hofstraat, F. A. J. Geurts, J. W. Verhoeven, *Chem. Phys. Lett.* **1997**, *276*, 196−201.
[5] S. I. Klink, H. Keizer, F. C. J. M. van Veggel, *Angew. Chem.* **2000**, *112*, 4489−4491; *Angew. Chem. Int. Ed.* **2000**, *39*, 4319−4321.
[6] M. H. V. Werts, R. H. Woudenberg, P. G. Emmerink, R. van Gassel, J. W. Hofstraat, J. W. Verhoeven, *Angew. Chem.* **2000**, *112*, 4716−4718; *Angew. Chem. Int. Ed.* **2000**, *39*, 4542−4544.
[7] J. X. Meng, K. F. Li, J. Yuan, L. L. Zhang, W. K. Wong, K. W. Cheah, *Chem. Phys. Lett.* **2000**, *332*, 313−318.
[8] [8a] W. D. Horrocks Jr., J. P. Bolender, W. D. Smith, R. M. Supkowski, *J. Am. Chem. Soc.* **1997**, *119*, 5972−5973. [8b] G. F. de Sá, O. L. Malta, C. de Mello Donegá, A. M. Simas, R. L. Longo, P. A. Santa-Cruz, E. F. da Silva Jr., *Coord. Chem. Rev.* **2000**, *196*, 165−195. [8c] F. R. G. e Silva, O. L. Malta, C. Reinhard, H.-U. Güdel, C. Piguet, J. E. Moser, J.-C. G. Bünzli, *J. Phys. Chem. A* **2002**, *106*, 1670−1677. [8d] G. A. Hebbink, L. Grave, L. A. Woldering, D. N. Reinhoudt, F. C. J. M. van Veggel, *J. Phys. Chem. A* **2003**, *107*, 2483−2491.

[9] W. T. Carnall, *Handbook on the Physics and Chemistry of Rare Earths* (Ed.: K. A. Gschneidner, Jr., L. Eyring), Elsevier, Amsterdam, **1987**, vol. 3, p. 171.
[10] M. P. Oude Wolbers, F. C. J. M. van Veggel, B. H. M. Snellink-Ruel, J. W. Hofstraat, F. A. J. Geurts, D. N. Reinhoudt, *J. Chem. Soc., Perkin Trans. 2* **1998**, 2141−2150.
[11] C. P. Wong, R. F. Venteicher, W. D. Horrocks Jr., *J. Am. Chem. Soc.* **1974**, *96*, 7149−7150.
[12] G. A. Spyroulias, A. G. Coutsolelos, *Polyhedron* **1995**, *14*, 2483−2490.
[13] W. D. Horrocks Jr., R. F. Venteicher, C. A. Spilburg, B. L. Vallee, *Biochem. Biophys. Res. Commun.* **1975**, *64*, 317−322.
[14] W. D. Horrocks Jr., C. P. Wong, *J. Am. Chem. Soc.* **1976**, *98*, 7157−7162.
[15] W. D. Horrocks Jr., E. G. Hove, *J. Am. Chem. Soc.* **1978**, *100*, 4386−4392.
[16] M. I. Gaiduk, V. V. Grigoryants, A. F. Mironov, V. D. Rumyantseva, V. I. Chissov, G. M. Sukhin, *J. Photochem. Photobiol. B* **1990**, *7*, 15−20.
[17] Y. Korovin, Z. Zhilina, N. Kuzmin, S. Vodzinsky, Y. Ishkov, *J. Porphyrins Phthalocyanines* **2001**, *5*, 481−485.
[18] W. K. Wong, A. X. Hou, J. P. Gou, H. S. He, L. L. Zhang, W. Y. Wong, K. F. Li, K. W. Cheah, T. C. W. Mak, *J. Chem. Soc., Dalton Trans.* **2001**, 3092−3098.
[19] H. S. He, Z. X. Zhao, W. K. Wong, K. F. Li, J. X. Meng, K. W. Cheah, *Dalton Trans.* **2003**, 980−986.
[20] W. K. Wong, L. L. Zhang, W. T. Wong, F. Xue, T. C. W. Mak, *J. Chem. Soc., Dalton Trans.* **1999**, 615−622.
[21] W. K. Wong, L. L. Zhang, W. T. Wong, F. Xue, T. C. W. Mak, *J. Chem. Soc., Dalton Trans.* **1999**, 3053−3062.
[22] A. D. Adler, F. R. Longo, J. D. Finarelli, J. Goldmacher, J. Assour, I. Korsakoff, *J. Org. Chem.* **1967**, *32*, 476−477.
[23] K. Kalyanasundaram, *Photochemistry of Polypyridine and Porphyrin Complexes*, Academic Press, London, **1992**, p. 376.
[24] M. Gouterman, *The Porphyrins* (Ed.: D. Dolphin), Academic Press, New York, **1978**, vol. III, chapter 1.
[25] L. R. Milgrom, *The Colours of Life: An Introduction to The Chemistry of Porphyrins and Related Compounds*, Oxford University Press, Oxford, **1997**, p. 85.
[26] Z. Katona, A. Grofcsik, P. Baranyai, I. Bitter, G. Grabner, M. Kubinyi, T. Vidoczy, *J. Mol. Struct.* **1998**, *450*, 41−45.
[27] S. C. Jeoung, D. Kim, K. H. Ahn, D. W. Cho, M. Yoon, *Chem. Phys. Lett.* **1995**, *241*, 533−539.
[28] D. J. Quimby, F. R. Longo, *J. Am. Chem. Soc.* **1974**, *97*, 5111−5117.
[29] M. M. Nei, A. D. Adler, *J. Am. Chem. Soc.* **1974**, *97*, 5107−5111.
[30] N. Sabbatini, M. Guardigli, J.-M. Lehn, *Coord. Chem. Rev.* **1993**, *123*, 201−228 and references cited therein.
[31] A. Beeby, I. M. Clarkson, R. S. Dichins, S. Faulkner, D. Parker, L. Royle, A. S. de Sousa, J. A. G. Williams, M. Woods, *J. Chem. Soc., Perkin Trans. 2* **1999**, 493−504.
[32] C. A. Parker, W. T. Rees, *Analyst (London)* **1960**, *85*, 587−600.
[33] K. Nakamaru, *Bull. Chem. Soc. Jpn.* **1982**, *55*, 1639−1640.
[34] *SAINT*, Reference manual, Siemens Energy and Automation, Madison, WI, **1994−1996**.
[35] G. M. Sheldrick, *SADABS, Empirical Absorption Correction Program*, University of Göttingen, Germany, **1997**.
[36] G. M. Sheldrick, *SHELXTL*™ Reference manual, version 5.1, Siemens, Madison, WI, **1997**.

Received July 28, 2003
Early View Article
Published Online January 19, 2004

 © 2004 Wiley-VCH Verlag GmbH & Co. KGaA, Weinheim

Non-Heme Iron Complexes for Stereoselective Oxidation: Tuning of the Selectivity in Dihydroxylation Using Different Solvents

Marten Klopstra,[a] Gerard Roelfes,[a] Ronald Hage,[a] Richard M. Kellogg,[a] and Ben L. Feringa*[a]

Keywords: Dihydroxylation / Enzyme models / Epoxidation / Iron / N ligands / Oxidation

A new class of functional models for non-heme iron-based dioxygenases, including $[(N3Py\text{-}Me)Fe(CH_3CN)_2](ClO_4)_2$ and $[(N3Py\text{-}Bn)Fe(CH_3CN)_2](ClO_4)_2$ {N3Py-Me = [di(2-pyridyl)methyl]methyl(2-pyridyl)methylamine; N3Py-Bn = [di(2-pyridyl)methyl]benzyl(2-pyridyl)methylamine}, is presented here. NMR, UV and X-ray analyses revealed that six-coordinate low-spin Fe^{II} complexes with the pyridine N-atoms and the tertiary amine functionality of the ligand bound to Fe are formed. The two remaining coordination sites located *cis* to each other are occupied by labile CH_3CN groups that are easily exchanged by other ligands. We demonstrate that the reactivity and stereoselectivity of the complexes investigated depend on the choice of the solvent. The complexes have been examined as catalysts for the oxidation of both alkanes and olefins in CH_3CN. In this solvent alkanes are oxidized to alcohols and ketones and olefins to the corresponding *cis*-epoxides and *cis*-diols. In acetone as solvent a different reactivity pattern was found, with, as the most striking example, the *trans*-dihydroxylation of cis-olefins. ^{18}O-labeling studies in CH_3CN establish incorporation of ^{18}O from $H_2{}^{18}O_2$ and $H_2{}^{18}O$ in both the epoxide and the diol implicating an HO-Fe^{V}=^{18}O active intermediate originating from an $H_2{}^{18}O$-Fe^{III}OOH species. These results are in full agreement with mechanistic schemes derived for other dioxygenase model systems. Based on labeling studies in acetone an additional oxidation mechanism is proposed for this solvent, in which the solvent acetone is involved. This is the first example of a catalyst that can give *cis*- or *trans*-dihydroxylation products, just by changing the solvent.

(© Wiley-VCH Verlag GmbH & Co. KGaA, 69451 Weinheim, Germany, 2004)

Introduction

The catalytic oxidation of hydrocarbons using green oxidants like hydrogen peroxide or dioxygen is a topic of considerable interest.[1] Even though significant progress has been made, in particular with regard to epoxidation of alkenes using H_2O_2,[2−5] many challenges still remain. Among others, the hydroxylation of alkanes and the dihydroxylation of alkenes are highly interesting reactions from a synthetic point of view.

In nature an impressive variety of enzymes capable of performing these reactions with high selectivity under mild conditions exists. An important subset of this class of enzymes are the non-heme iron oxygenases, like, for example, methane monooxygenase,[6] which selectively oxidizes methane to methanol, the Rieske dioxygenases,[7,8] which are capable of stereospecifically dihydroxylating arenes, and iron-bleomycin, a metallo-glycopeptide that is capable of oxidative DNA cleavage,[9] but which can also oxidize a wide variety of organic substrates.[10]

The study of synthetic complexes that model the active site of these enzymes has been an important tool in the study of their functions. Some of these model complexes have proven to be very promising catalysts for the selective oxidation of organic substrates using H_2O_2 as the terminal oxidant. Stereoselective hydroxylation[11−14] epoxidation[4,14−16] and *cis*-dihydroxylation,[17−20] a reaction previously only available using osmium-,[21] ruthenium-[22] and manganese-based[23] catalysts, have been reported. Recently, even the first examples of enantioselective dihydroxylation have appeared in the literature.[24]

Recent studies have shed some light on the mechanism of these oxidation reactions. In the case of $[Fe(TPA)(CH_3CN)_2](ClO_4)_2$, a representative member of this class of catalysts, a strong and compelling case has been built in favor of the involvement of a formally HO-Fe^{V}O species that is formed by heterolysis of the O−O bond of a low spin Fe^{III}OOH intermediate.[13,20,25] This HO-Fe^{V}O species is postulated to be the active species responsible for the formation of both the epoxide and the *cis*-diol. The latter product is thought to be formed via a cyclic intermediate similar to reactions with $KMnO_4$.[15]

We have previously reported on the $[Fe(N4Py)(CH_3CN)](ClO_4)_2$ complex, which contains a pentadentate N ligand and reacts with H_2O_2 to form a well-defined and well-

[a] Department of Organic and Molecular Inorganic Chemistry, Stratingh Institute, University of Groningen, Nijenborgh 4, 9747 AG Groningen, Netherlands
Fax: (internat.) + 31-50-363-4296
E-mail: B.L.Feringa@chem.rug.nl

Supporting information for this article is available on the WWW under http://www.eurjic.org or from the author.

 © 2004 Wiley-VCH Verlag GmbH & Co. KGaA, Weinheim DOI: 10.1002/ejic.200300667

characterized $Fe^{III}OOH$ intermediate.[26−28] This intermediate was demonstrated to have an unusually weak O−O bond,[29,30] which is thought to be the reason for its high activity as an oxidation catalyst. Reactivity studies using a broad spectrum of mechanistic probes revealed that radical-type oxidizing species are involved and, consequently, a mechanism involving homolysis of the $Fe^{III}OOH$ species to give $Fe^{IV}O$ and ·OH was proposed.[31] This notion was later supported by calculations, which indeed showed homolysis to be the favored reaction pathway.[32] A strong effect of the solvent was observed. In acetone higher kinetic isotope effect (KIE) values of cyclohexane oxidation and higher C3/C2 ratios in adamantane oxidation were found compared to acetonitrile. This was attributed to the ability of acetone to act as an ·OH trap.

Following the TPA precedent we decided to redesign the N4Py ligand into a tetradentate ligand in order to obtain iron complexes capable of stereoselective oxidation. In this paper we present a new class of iron complexes with tetradentate ligands based on N4Py, in which one of the picolyl groups is replaced with a non-coordinating moiety like a methyl or a benzyl group (Figure 1). The properties of the corresponding iron complexes and their application as catalysts in oxidation reactions with H_2O_2 will be discussed, with particular emphasis on the effect of the solvent used, i.e. acetonitrile or acetone.

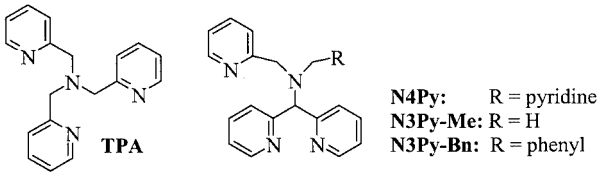

Figure 1. Ligands used for stereoselective epoxidation and *cis*-dihydroxylation of alkenes

Results and Discussion

Synthesis and Properties of Iron Complexes

Ligands **1** and **2** were prepared from a common precursor, N3Py (**3**).[33] N3Py-Me was obtained in high yield by reductive amination with formaldehyde and $NaBH(OAc)_3$ (Scheme 1).[34] N3Py-Bn was prepared by alkylation of N3Py with benzyl chloride in the presence of K_2CO_3.

Complexation of the ligands **1** and **2** with $Fe(ClO_4)_2·6H_2O$ in methanol/acetonitrile resulted in the formation of red crystals, characterized as $[(N3Py\text{-}R)Fe(CH_3CN)_2](ClO_4)_2$, based on ^1H NMR and ES/MS analysis and confirmed by X-ray analysis for this complex with an *N*-methyl substituent (Figure 2).

The six-coordinate Fe^{II} center has a distorted octahedral geometry, with the iron bound to the three pyridine N atoms, the tertiary amine functionality of the ligand and two acetonitrile molecules, originating from the solvent used for crystallization. The open coordination sites, where acetonitrile molecules are bound, are located *cis* with respect to each other, as was expected. The $Fe-N_{ligand}$ distances vary from 1.909(8) Å for Fe1−N5 to 1.965(9) Å for Fe1−N3. These distances are similar to those found for other low-spin iron(II) complexes like $[(N4Py)Fe(CH_3CN)](ClO_4)_2$,[19] and $[(TPA)Fe(CH_3CN)_2](ClO_4)_2$.[35]

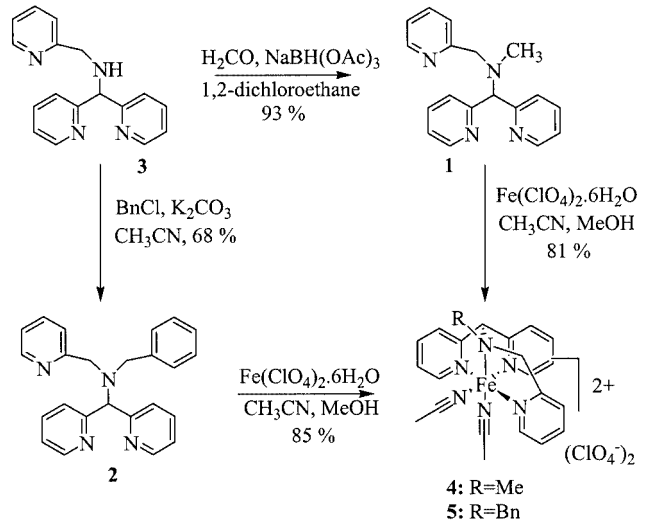

Scheme 1. Synthesis of ligands **1** and **2** and the corresponding iron(II) complexes **4** and **5**

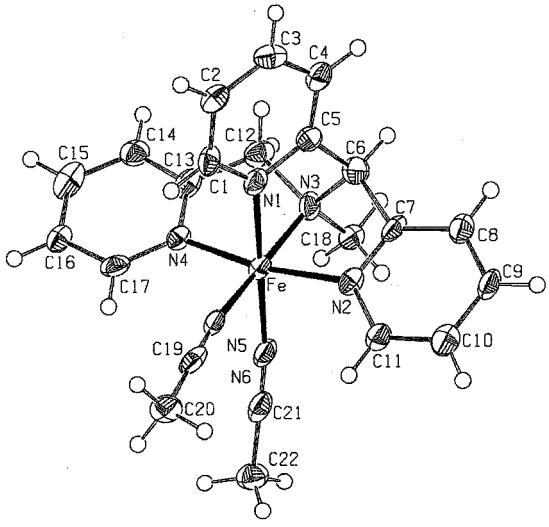

Figure 2. ORTEP plot of the cation of **4**

The ^1H NMR spectra in CD_3CN exhibit signals between $\delta = 0$ and 15 ppm, typical of a low-spin iron(II) complex. However, in contrast to the spectra of other low-spin iron(II) complexes like $[(TPA)Fe(CH_3CN)_2](ClO_4)_2$ and $[(N4Py)Fe(CH_3CN)_2](ClO_4)_2$,[28,35] which show very sharp signals, significant line broadening was observed for some of the signals of **4** and **5**. An example is the spectrum of **4** shown in Figure 3A. The line broadening is probably due to an equilibrium between the low-spin Fe^{II} bis-acetonitrile complex $[(N3Py\text{-}R)Fe(CH_3CN)_2]^{2+}$ and the paramagnetic high-spin Fe^{II} mono-acetonitrile complex $[(N3Py\text{-}R)Fe(CH_3CN)]^{2+}$, i.e. a reversible dissociation of one of the labile CH_3CN ligands. This was confirmed by the ^1H NMR

 © 2004 Wiley-VCH Verlag GmbH & Co. KGaA, Weinheim

spectrum in [D_6]acetone, in which dissociation of acetonitrile is irreversible and results in signals in the δ = 0−180 ppm range, characteristic for a high-spin Fe^{II} complex (Figure 3B).[28] A similar solvent effect was found in the UV/Vis spectra of **4** in CH_3CN and acetone. In CH_3CN **4** exhibits a UV/Vis spectrum with absorption peaks at 352 ($\varepsilon = 5.3 \times 10^3$ $M^{-1}cm^{-1}$) and 428 nm ($\varepsilon = 4.3 \times 10^3$ $M^{-1}cm^{-1}$), whereas in acetone the complex exhibits an absorption peak at 331 nm ($\varepsilon = 4.2 \times 10^3$ $M^{-1}cm^{-1}$) with shoulders at 459 ($\varepsilon = 3.2 \times 10^2$ $M^{-1}cm^{-1}$) and 506 nm ($\varepsilon = 2.2 \times 10^2$ $M^{-1}cm^{-1}$), suggesting the formation of a different species in acetone.

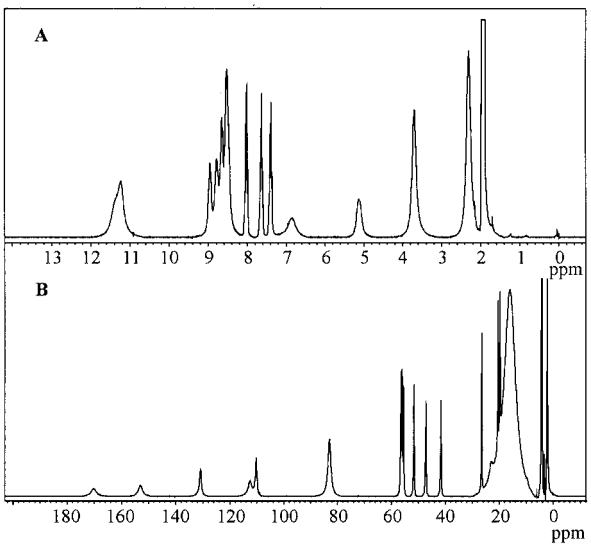

Figure 3. ^1H NMR spectrum of **4** (a) in CD_3CN and (b) in [D_6]-acetone

Cyclic voltammetry of **4** and **5** in CH_3CN showed one single quasi-reversible redox wave for the Fe^{II}/Fe^{III} couple at $E_{1/2}$ = 1180 mV (ΔE = 100 mV; i_a/i_p = 0.95) and 1200 mV vs. SCE (ΔE = 160 mV; i_a/i_p = 0.98), respectively. These values are significantly higher than those found for [(N4Py)Fe(CH_3CN)](ClO_4)$_2$ ($E_{1/2}$ = 1010 mV vs. SCE).[27] Apparently, in acetonitrile the low-spin iron(II) state is even more favored in the case of bis-acetonitrile complexes like **4** than mono-acetonitrile complexes like [(N4Py)-Fe(CH_3CN)](ClO_4)$_2$.

In acetone as solvent a different redox behaviour was observed for **4** (Figure 4). At a scan rate of 50 mV/s an oxidation wave was found at 1150 mV vs. SCE accompanied by a small reduction wave at 940 mV (i_a/i_p = 0.35) and a strong reduction wave at 350 mV vs. SCE. Increase of the scan rate leads to an increase of the reduction wave at 940 mV (i_a/i_p = 0.44 at 100 mV/s; i_a/i_p = 0.58 at 500 mV/s). When 600 mV vs. SCE was used as the vertex potential, i.e. without going through the oxidation at 1150 mV, no reduction wave was observed at 350 mV (Figure 4d). These results indicate that oxidation of the complex in acetone leads to an unstable species that decomposes to give a new species with a reduction potential at 350 mV.

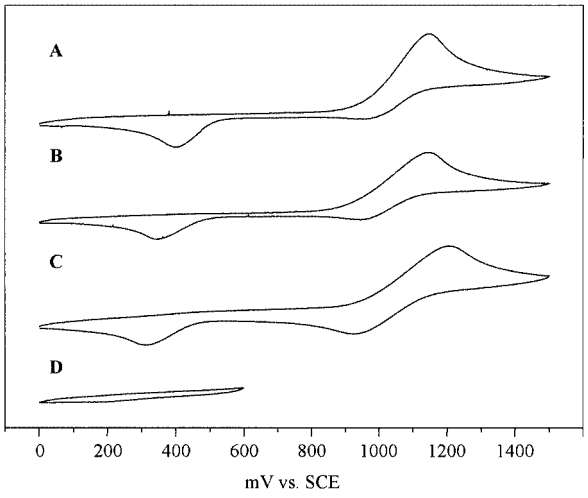

Figure 4. Cyclic voltammogram of 4 in acetone: (a) scan rate 50 mV/s; (b) Scan rate 100 mV/s; (c) scan rate 500 mV/s; (d) 600 mV used as vertex potential

Combined with the NMR spectroscopic data the results can be rationalized in the following manner (Scheme 2). In acetone loss of a labile acetonitrile ligand can occur affording **7**, which is assumed to have a redox potential of 940 mV. Oxidation of this complex will lead to the formation of the unstable mono-acetonitrile iron(III) complex **8**. Loss of the final acetonitrile ligand will result in the formation of an $[(N3Py\text{-}Me)Fe(X)]^{3+}$ species **9**, in which X can be acetone or water. This species will exhibit a different electrochemical behavior, presumably giving rise to the reduction wave at 350 mV.

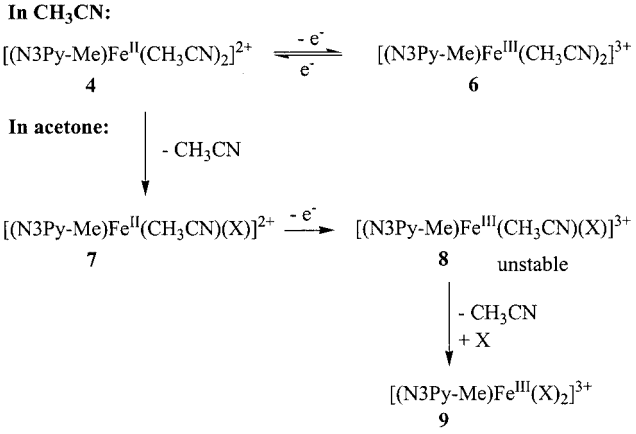

Scheme 2. Redox behavior of **4** in CH_3CN and acetone

Catalytic Oxidation with N3Py Iron Complexes

Complexes **4** and **5** were tested in catalytic oxidations of both alkanes and alkenes. The results are summarized in Table 1 and 2. In view of the different properties of the complexes in acetone and acetonitrile (vide supra), combined with the fact that it is known from catalytic oxidation with [(N4Py)Fe(CH_3CN)](ClO_4)$_2$ that the solvent can have a pronounced effect on the observed reactivity and selectivity,[31] both solvents were employed in catalytic oxidation.

 © 2004 Wiley-VCH Verlag GmbH & Co. KGaA, Weinheim

Table 1. Oxidation of alkanes by **4** and **5**; reactions performed under argon

Entry	Substrate	Products	Acetonitrile[a]		Acetone[a]	
			4	**5**	**4**	**5**
1	cyclohexane	cyclohexanol	7.9	8.1	8.8	5.7
		cyclohexanone	1.7	1.4	2.0	1.5
		A/K	4.6	5.8	4.4	3.8
2[b]	*cis*-1,2-dimethylcyclohexane	*trans*-1,2-dimethylcyclohexanol	2.3	2.7	4.8	4.1
		cis-1,2-dimethylcylcohexanol	0.4	0.6	1.8	1.9
		stereoselectivity (%)	85	73	82	68
3[b]	*trans*-1,2-dimethylcylohexane	*trans*-1,2-dimethylcyclohexanol	0.4	0.3	1.6	1.1
		cis-1,2-dimethylcylcohexanol	1.1	0.6	1.5	1.1
		stereoselectivity (%)	73	48	50	50
4	adamantane	1-adamantanol	13.1		13.3	
		2-adamantanol	2.5		1.1	
		2-adamantanone	1.3		0.5	
		tertiary/secondary	10.3		24.9	

[a] Turnover number = mol product/mol catalyst. [b] Secondary alcohols and ketones not quantified.

Table 2. Oxidation of alkenes by **4** and **5** with 50 equiv. H_2O_2; reactions carried out under air, unless noted otherwise

Entry	Complex	Substrate	Acetonitrile[a][b]				Acetone[a][c]			
			cis-epoxide	*trans*-epoxide	*meso*-diol	*rac*-diol	*cis*-epoxide	*trans*-epoxide	*meso*-diol	*rac*-diol
1	**4**	cyclooctene	14	–	22	1	17	–	0.2	4
2	**5**	cyclooctene	16	–	14	0	19	–	3	10
3	**4**	cyclohexene[d][e]	11[f]	–	13	0.7	0.8	–	0	2.4
4	**4**	*c*-stilbene	9[g]	0.7	8	0.6	7	3	6	7
		stereoselectivity (%)	93		93		70			54
5	**4**	*t*-stilbene	0[h]	8	0.5	7	0	6	11	3
		stereoselectivity (%)		>99		93		>99	79	
6	**4**	*c*-4-octene	19	1	17	1	11	3	0	1
		stereoselectivity (%)	95		94		79			>99
7	**4**	*t*-4-octene	2	4	1	1	2	6	1	1
		stereoselectivity (%)		67		50		75	50	
8	**4**	norbornene	36	–	*exo* 2 *endo* 1	2	2	–	*exo* 0 *endo* 1	43

[a] Turnover number = mol product/mol catalyst. [b] Reaction time 60 min. [c] Reaction time 30 min. [d] Reactions carried out under argon. [e] In acetone many other products were found, which were not identified. [f] 28 turnovers towards cyclohexenol and 7 turnovers towards cyclohexenone were observed. [g] 11 turnovers towards benzaldehyde were observed. [h] 13 turnovers towards benzaldehyde were observed.

Reactions were carried out under air, except in the case of substrates that are prone to undergo autoxidation in the presence of O_2, and an excess of substrate (1000 equiv.) was used to maximize turnover numbers. Hydrogen peroxide (50 equiv.) was introduced into the reaction mixture at 25 °C by syringe pump to reduce the loss of hydrogen peroxide due to catalase activity. Typical addition times are 60 and 30 min for acetonitrile and acetone, respectively. After the addition of H_2O_2 was complete the reaction mixture was stirred for another 5 min before a sample was taken and analyzed by GC.

Oxidation of Alkanes

Complexes **4** and **5** show a fair activity in the oxidation of cyclohexane in CH_3CN, with yields up to 19% based on hydrogen peroxide for complex **4** (Table 1, entry 1). These yields are slightly lower than those observed for $[(N4Py)Fe(CH_3CN)](ClO_4)_2$,[28] and $[(TPA)Fe(CH_3CN)_2](ClO_4)_2$,[36] and significantly lower than those found for $[(bpmen)Fe(CH_3CN)_2](ClO_4)_2$,[12,13] the most active non-heme iron cyclohexane oxidation catalyst known to date. The major product was cyclohexanol, with an alcohol/ketone (A/K) ratio of 3.8–5.8, significantly higher than those reported for radical chain autoxidation reactions (A/K ≈ 1).[37–39]

In acetone a similar reactivity and A/K ratio was obtained as in acetonitrile (Table 1, entry 1). However, one clear difference is seen with the KIE values for cyclohexanol formation, determined in a competition experiment between cyclohexane and $[D_{12}]$cyclohexane. In CH_3CN a k_H/k_D value of 3.5 was found for complex **4**, similar to the value observed for $[(TPA)Fe(CH_3CN)_2](ClO_4)_2$,[36] which was proposed to react via a formally Fe^VO species. Complex **5** gives a lower k_H/k_D value of 2.4. In acetone the k_H/k_D ratio increased significantly to 4.4 for **4** and 3.9 for **5**. The latter values are in the range of those typically observed in oxidations catalyzed by non-heme iron complexes using

 © 2004 Wiley-VCH Verlag GmbH & Co. KGaA, Weinheim

tert-butyl hydroperoxide as oxidant,[40] which were demonstrated to proceed via alkoxy radicals.[36−38]

The oxidation of *cis*- and *trans*-1,2-dimethylcyclohexane to the corresponding tertiary alcohols was studied to assess the stereoselectivity of the oxidation reaction. Although several isomeric secondary alcohols were also formed, these were not quantified. In CH_3CN the oxidation of *cis*-1,2-dimethylcyclohexane afforded rather low yields of tertiary alcohols with 85% and 82% retention of configuration at the tertiary carbon (i.e. formation of *trans*-1,2-dimethylcyclohexanol) for complexes **4** and **5**, respectively (Table 1, entry 2). Using *trans*-1,2-dimethylcyclohexane low yields of the tertiary alcohols, with 73% and 50% retention of configuration (i.e. *cis*-dimethylcyclohexanol) were also found for **4** and **5** (Table 1, entry 3). For comparison, more than 99% retention of stereochemistry was observed with $[(TPA)Fe(CH_3CN)_2](ClO_4)_2$,[41] $[(bpmen)Fe(CH_3CN)_2](ClO_4)_2$ [12] and cytochrome P-450 models,[42] whereas a complete lack of stereoselectivity was observed for $[(N4Py)Fe(CH_3CN)](ClO_4)_2$ [31] and in free-radical autoxidation.[43]

In acetone higher yields of tertiary alcohols were obtained, but generally with a lower degree of stereoselectivity. In the case of *cis*-1,2-dimethylcyclohexane 73% and 68% retention of configuration (Table 1, entry 2), and in the case of *trans*-1,2-dimethylcyclohexane 48% and 50% retention of configuration were obtained (Table 1, entry 3) with **4** and **5**, respectively.

Adamantane as substrate was oxidized both at the secondary and tertiary carbons. Using **4** a tertiary/secondary ratio (normalized on a per hydrogen basis) of 10.3 was obtained in acetonitrile (Table 1, entry 4). In acetone this ratio increased to 24.9 (Table 1, entry 4). For TPA and related tetradentate nitrogen-donor ligands values between 15 and 33 have been reported in CH_3CN as solvent.[13] For comparison, tertiary/secondary ratios of about 2 have been found for oxidation of alkanes by ·OH,[11] values of 3.1−3.3 for $[(N4Py)Fe(CH_3CN)](ClO_4)_2$,[31] 9.5−10 for oxidations by *t*BuOOH utilizing catalysts like $[Fe_2O(bipy)_4(H_2O)_2](ClO_4)_4$ and $[FeCl_2(TPA)](ClO_4)$,[44,45] and 11−48 for oxidations with PhIO catalyzed by P-450 mimics.[46]

Oxidation of Alkenes

The oxidation of symmetrical alkenes in CH_3CN with H_2O_2, catalyzed by **4** and **5**, gave both epoxidation and *cis*-dihydroxylation products (Table 2). Based on the results with Fe-TPA complexes this would be expected for iron complexes with two open coordination sites *cis* to each other.[15] All reactions could be carried out under air, except with cyclohexene as substrate, since this led to a strongly increased formation of the allylic alcohol and ketone. This indicates involvement of autoxidation pathways under air.[47]

Cyclooctene as a substrate afforded a very clean reaction giving only the epoxide and the *cis*-dihydroxylation product, i.e. the *meso*-diol (Table 2, entries 1 and 2). A small preference for *cis*-diol formation was observed with **4** whereas **5** displayed a small preference for epoxide formation.

Cyclohexene as substrate also gave the epoxide and the *meso*-diol as main products (Table 2, entry 3). However, with this substrate allylic oxidation products — cyclohexenol (28 turnovers) and cyclohexenone (seven turnovers) — were also formed.

With *cis*-stilbene and *cis*-4-octene the *cis*-oxide and *meso*-diol were also formed as major products, with a stereoselectivity of 93−95% (Table 2, entries 4 and 6). With *trans*-stilbene the *trans*-oxide, was the only detectable epoxidation product (Table 2, entry 5). The *cis*-dihydroxylation product, i.e. *rac*-1,2-diphenylethanediol, was obtained with a stereoselectivity of 94%. Besides the oxides and diols substantial amounts of benzaldehyde were also formed with the stilbenes — 11 and 13 turnovers for *cis*- and *trans*-stilbene, respectively. With *trans*-4-octene and norbornene a preference for epoxidation was found. For both substrates the corresponding diols were only formed in small amounts.

In acetone as solvent a very different reactivity pattern was observed. Generally, more side-products were found compared to oxidations in CH_3CN as solvent. Using cyclooctene as substrate, the epoxide and the 1,2-diols were obtained as major products (Table 2, entries 1 and 2). However, in contrast to the results in CH_3CN now the *trans*-dihydroxylation product, i.e. *rac*-1,2-cyclooctanediol, was obtained as major product, with a selectivity of 95% in the case of complex **4.** Complex **5** showed a little bit lower selectivity towards *rac*-diol (76%), but a significantly increased yield.

Cyclooctene oxide is known to be very robust so it is unlikely that the *rac*-diol is formed by epoxide ring-opening.[48] Furthermore, when cyclooctene oxide was subjected to the standard reaction conditions no diol formation was observed, which demonstrates that the *rac*-diol is formed independently and is not a decomposition product from the epoxide. Thus, by changing the solvent from acetonitrile to acetone the stereochemical outcome of the dihydroxylation reaction is changed from *cis* to *trans.*

With *cis*- and *trans*-4-octene and *cis*- and *trans*-stilbene the epoxides were formed in similar amounts as for the reaction in CH_3CN, with the *cis*-epoxidation product as major product (Table 2, entries 4−7). Hence, the stereochemistry of epoxidation is not dependent on the solvent.

With both *cis*- and *trans*-stilbene only small amounts of diol were found. However, substantial amounts of the corresponding acetonides were obtained, which are the products of the reaction of the diols with the solvent to form an acetal. Similar amounts of acetal were found by independent reaction of the corresponding diol under the same reaction conditions, indicating strongly that the acetonide is derived from the diol. When the acetonides are taken into account *cis*-stilbene gives the *trans*-dihydroxylation products — the *meso*-diol — as the main product and *trans*-stilbene affords mainly the corresponding *cis*-dihydroxylation products, i.e. the *rac*-diol.

With norbornene as substrate the main product was found to be *rac*-norbornanediol (Table 2, entry 8). When

 © 2004 Wiley-VCH Verlag GmbH & Co. KGaA, Weinheim

the epoxide was tested under these reaction conditions no diol formation was observed, again suggesting that the diol is not formed as a decomposition product of the epoxide. With cyclohexene as substrate many products were formed, including low yields of cyclohexene oxide and *rac*-1,2-cyclohexanediol (Table 2, entry 3). No evidence for *cis*-dihydroxylation products was found. However, many of the side-products that were formed have not been identified up to now, except the allylic oxidation products cyclohexenol (11 turnovers) and cyclohexenone (one turnover), which makes it difficult to compare the results for this substrate.

The most remarkable feature of the reactions in acetone is the fact that, in all cases, the *rac*-diol is the preferred product. For *cis*-alkenes like norbornene, cyclooctene, cyclohexene, and *cis*-stilbene, this amounts to a *trans*-dihydroxylation reaction. This is the first example of a catalyst that can give both *cis*- and *trans*-dihydroxylation just by changing the solvent. Catalytic *cis*-dihydroxylation is mostly achieved by OsO_4 complexes in the presence of a stoichiometric oxidant like $K_3Fe(CN)_6$ or *N*-methylmorpholine *N*-oxide.[21] *trans*-Diols are usually prepared from alkenes in two steps: first epoxidation followed by epoxide ring-opening.[49]

Labeling Studies

To obtain more information on the mechanism of the epoxidation and dihydroxylation reaction ^{18}O labeling experiments were performed. The oxidation of cyclooctene in acetonitrile was monitored by using 10 equivalents of a 2% solution of $H_2{}^{18}O_2$ in $H_2{}^{16}O$ under a N_2 atmosphere Table 3). Analysis was performed by GC/CI-MS. Only 50% of the epoxide contained ^{18}O. For the *meso*-diol predominantly the singly labeled product was found. In a complementary experiment using a 2% solution of $H_2{}^{16}O_2$ in $H_2{}^{18}O$ 28% of the epoxide contained an ^{18}O atom. For the *cis*-diol the main product was again singly labeled *cis*-cyclooctanediol. When a solution of 1% $H_2{}^{18}O_2$ in a 1:1 mixture of $H_2{}^{16}O$ and $H_2{}^{18}O$ was used, both singly and doubly labeled *cis*-cyclooctanediols were formed. These observations lend support to a proposed catalytically active species in which both oxygen atoms from hydrogen peroxide and water are present. Further evidence for such a mechanism was obtained by examining the incorporation of labeled oxygen as a function of concentration of water in the reaction mixture. The results are shown in Figure 5.

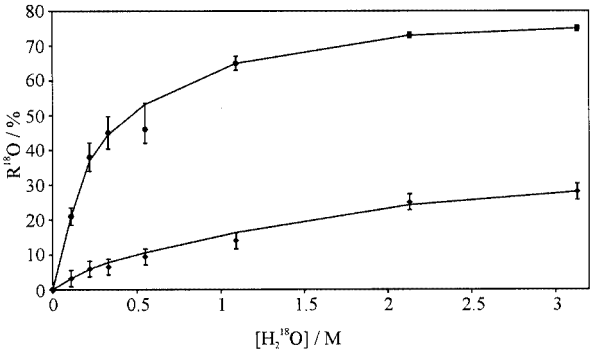

Figure 5. Incorporation of ^{18}O from $H_2{}^{18}O$: • diol; ◆ epoxide

At low concentration there is a more or less linear relationship between the concentration of water and the degree of incorporation of ^{18}O into the diol. At higher concentrations the extent of oxygen incorporation relative to the enhanced concentration decreases. This result is indicative of a pre-equilibrium between water and the active species of the catalyst. Similar results were found for the model systems $[(bpmen)Fe(CH_3CN)_2](ClO_4)_2$, $[(TPA)Fe(CH_3CN)_2](ClO_4)_2$, and several Fe-TPA derivatives for the oxidation of alkanes and alkenes.[50] Based on the cumulative data, which are in accordance with $[(TPA)Fe(CH_3CN)_2](ClO_4)_2$, the same mechanism for the oxidation in CH_3CN is proposed as was postulated for the oxidation with $[(TPA)Fe(CH_3CN)_2](ClO_4)_2$ (Scheme 3). In this mechanism the active $(HO)Fe^{V}{=}O$ species **13** is formed by heterolysis of the peroxide bond in intermediate **12**.

These labeling experiments were repeated in acetone, using *cis*-stilbene as substrate since it gives higher yields of *trans*-dihydroxylation products than cyclooctene. Here, incorporation of ^{18}O-oxygen into both epoxides and diols was investigated. The results are summarized in Table 4.

Even though a different substrate was used for the labeling studies and the level of ^{18}O incorporation is generally lower than in CH_3CN, the same pattern as in CH_3CN is discernible for the epoxidation and *cis*-dihydroxylation.

About one third of the label is built into the epoxide when $H_2{}^{18}O_2$ is used and about 40% incorporation is found when $H_2{}^{18}O$ is used. Also, in the case of the *cis*-diol the main fraction is singly labeled by $H_2{}^{18}O_2$. With $H_2{}^{18}O$ about one third of the product contains a single labeled oxygen, whereas with a combination of $H_2{}^{18}O_2$ and $H_2{}^{18}O$

Table 3. Incorporation of ^{18}O into the oxidation products of cyclooctene in acetonitrile[a]

Product	$H_2{}^{18}O_2$ in H_2O	H_2O_2 in $H_2{}^{18}O$	$H_2{}^{18}O_2$ in $H_2{}^{18}O/H_2O$ (1:1)
epoxide, labeled	50 (7)	28 (1)	53 (4)
cis-diol, not labeled	3 (1)	23 (1)	3 (1)
cis-diol, single labeled	94 (1)	76 (1)	37 (1)
cis-diol, double labeled	3 (1)	1 (1)	60 (1)

[a] Margins of error in parentheses.

 © 2004 Wiley-VCH Verlag GmbH & Co. KGaA, Weinheim

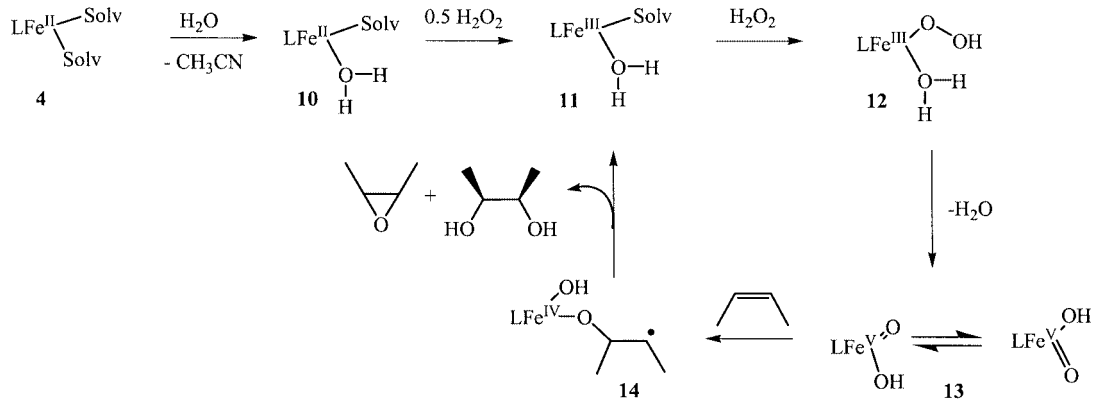

Scheme 3. Proposed mechanism for the catalytic oxidation by N3Py-MeFe$(ClO_4)_2(CH_3CN)_2$ in acetonitrile

Table 4. Incorporation of ^{18}O into the oxidation products of *cis*-stilbene in acetone[a]

Product	$H_2{}^{18}O_2$ in H_2O	H_2O_2 in $H_2{}^{18}O$	$H_2{}^{18}O_2$ in $H_2{}^{18}O/H_2O$ (1:1)
cis-epoxide, labeled	32 (1)	40 (1)	49 (6)
trans-epoxide, labeled	21 (1)	17 (5)	23 (5)
cis-diol, not labeled	10 (2)	70 (5)	15 (1)
cis-diol, single labeled	67 (8)	29 (5)	42 (4)
cis-diol, double labeled	23 (10)	1 (1)	43 (4)
trans-diol, not labeled	19 (8)	70 (3)	29 (1)
trans-diol, single labeled	63 (6)	17 (6)	49 (1)
trans-diol, double labeled	18 (2)	13 (3)	22 (1)

[a] Margins of error in parentheses.

about 40% of the product is singly labeled and 43% doubly labeled. Taken together the data suggest that the epoxide and the *cis*-diol are formed by the same mechanism as with CH_3CN as solvent, involving a catalytically active species in which oxygen atoms from both hydrogen peroxide and water are present.

The labeling data for the *rac*-diol are somewhat harder to interpret. One complication is the fact that the *rac*-diol was obtained in two forms, the "free" diol and the acetonide. Since the acetonide is a secondary product, derived from the diol, only the free diol was considered in the experiments. In the experiment with $H_2{}^{18}O_2$ 63% of the product contains a single label whereas roughly equal amounts of non-labeled and doubly labeled diol were found. This appears to suggest that at least one oxygen of the diol comes from H_2O_2. The use of $H_2{}^{18}O$ resulted mainly in a product without a label whereas the experiment with $H_2{}^{18}O_2$ and $H_2{}^{18}O$ gave only a marginally higher amount of doubly labeled product. Thus, the second oxygen in the *trans*-diol does not have a clear origin and can stem from multiple sources like H_2O_2, H_2O or, most probably, the solvent acetone.

Since the experiments were performed under an inert atmosphere, incorporation of oxygen from O_2 can be excluded.

Mechanistic Interpretation

N3Py-R Fe complexes (**4** and **5**) are clearly very promising catalysts for stereoselective catalytic oxidation with H_2O_2. The reactivity profile in acetonitrile, not unexpectedly, is very characteristic of an iron complex with two *cis* open coordination sites: stereoselective hydroxylation of alkanes and stereoselective epoxidation and dihydroxylation of alkenes. The reactivity pattern of alkane oxidation, including the observed KIE values in cyclohexane oxidation, the 3:2 ratio in adamantane oxidation and the high degree of stereoselectivity in the oxidation of *cis*- and *trans*-1,2-dimethylcyclohexane observed with **4** and **5** is strongly reminiscent of those reported for other iron complexes of tetradentate N ligands like [(TPA)Fe$(CH_3CN)_2$]$(ClO_4)_2$ [36] and [(bpmen)Fe$(CH_3CN)_2$]$(ClO_4)_2$.[12] Furthermore, the oxidation of alkenes gives rise to the corresponding epoxides and *cis*-dihydroxylation products with high stereoselectivity. These results are also similar to what was reported for [(TPA)Fe$(CH_3CN)_2$]$(ClO_4)_2$ in CH_3CN.[15,36] These findings suggest that a common mechanistic pathway for these complexes exists. A mechanism involving heterolysis of the O−O bond of a low-spin $Fe^{III}OOH$ intermediate **12** to give a formally $Fe^{V}O$ species **13** is proposed, similar to that for [(TPA)Fe$(CH_3CN)_2$]$(ClO_4)_2$-catalyzed hydroxylation[12][50a]

 © 2004 Wiley-VCH Verlag GmbH & Co. KGaA, Weinheim

and *cis*-dihydroxylation (Scheme 3).[15,17] Addition to a double bond presumably produces a radical species **14** that is too short lived to isomerize and thus rapidly reacts with the coordinated OH to form the *cis*-diol. The same mechanism is expected to apply to the N3Py-R complexes discussed here. This is clearly supported by the labeling experiments.

The oxidation results obtained in acetone as solvent are quite different from those in CH_3CN, and it is hard to rationalize them in a single mechanistic proposal. Based on the results it is more likely that several competing pathways exist.

Based on the labeling studies it appears that an active species similar to that proposed in the mechanism in CH_3CN, resulting from heterolysis of a $Fe^{III}OOH$ intermediate, is responsible for the formation of epoxide and *cis*-diol. The fact that the second O atom in the product is clearly not only derived from water molecules is presumably caused by scrambling with the solvent.

However, from the data it is clear that this cannot be the sole pathway. In particular, the fact that *rac*-diols are an important product of the oxidation of alkenes suggests that another mechanistic pathway exists as well. Furthermore, the higher KIE in the oxidation of cyclohexane and the stronger preference for oxidation at tertiary carbons in adamantane suggest the presence of a more selective oxidizing species but could also indicate the presence of alkoxy-type radicals (vide supra). The lower stereoselectivity in the hydroxylation of *cis*- and *trans*-1,2-dimethylcyclohexane, alkene epoxidation and alkene dihydroxylation, combined with the fact that generally more side products are formed in acetone than in CH_3CN as solvent, are certainly more indicative of the involvement of radical species.

One possibility for radical species to be formed is through the formation of an iron-acetonylperoxy intermediate (**15**), by reaction of the iron center with the hydrogen peroxide adduct of acetone, followed by homolysis of the O−O bond to generate an $Fe^{IV}O$ complex (**1**) and an acetonyloxy radical species **17** (Scheme 4). Iron-alkylperoxo complexes have been demonstrated to be particularly predisposed to undergo O−O bond homolysis.[51]

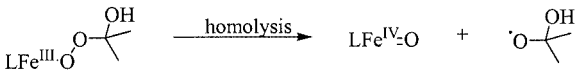

15 **16** **17**

Scheme 4. Proposed formation of radical species by homolysis of the O−O bond of a iron-acetonyl peroxy species

Such radical species could also explain the formation of *rac*-diols: analogous to the proposal for TMP-Fe complexes (TMP = tetramesitylporphyrin),[52] the $Fe^{IV}O$ species could add to the double bond, leaving a carbon radical intermediate that is sufficiently long-lived to undergo isomerization to the thermodynamically more stable *trans* form before formation of either the epoxide, which explains the reduced stereoselectivity in acetone, or the *rac*-diol by reaction with another oxygen radical species.

Conclusions

In this paper we have presented a new class of tetradentate N-ligands for application in iron-catalyzed oxidations using H_2O_2: N3Py-R, with R being Me or Bn. Compared to the parent ligand of this class of catalysts, TPA, the N3Py-R ligands presented here have the added advantage that the R group can be readily modified, for example by the introduction of chiral groups for use in catalytic asymmetric oxidations.

The electrochemistry, NMR features and UV/Vis spectra of the N3Py-Fe complexes are solvent dependent. In acetone the labile acetonitrile ligands are rapidly displaced, presumably by the solvent, leading to the formation of a high-spin complex with different spectroscopic and electrochemical behaviour.

In both solvents good oxidation activity with H_2O_2 as sacrificial oxidant was found, but the reactivity, and in particular the selectivity, are strongly solvent dependent.

Not surprisingly the reactivity pattern in acetonitrile is quite similar to that of $[(TPA)Fe(CH_3CN)_2](ClO_4)_2$. The N3Py-Fe complexes are capable of stereoselective hydroxylation, epoxidation and *cis*-dihydroxylation. Mechanistic studies support a mechanism similar to that described for TPA-Fe, involving formally $Fe^{V}O$ species.

A major finding reported in this paper is the very different reactivity pattern observed in acetone, a solvent never reported for $[(TPA)Fe(CH_3CN)_2](ClO_4)_2$. The most striking example is the oxidation of alkenes to give the corresponding epoxides and the *rac*-diol as the main products. Mechanistic studies revealed that most likely more than one competing mechanistic pathway is available in acetone. Besides the heterolysis of a tentative $Fe^{III}OOH$ intermediate to give formally $Fe^{V}O$ species — the dominant mechanism in CH_3CN — a pathway involving $Fe^{IV}O$ species and acetonyloxo radicals, formed by homolysis of an intermediate iron-acetonylperoxy species, is proposed. The $Fe^{IV}O$ species may be responsible for the formation of *trans*-diols, following the TMP-Fe precedent.

The work described here constitute the first examples of a new generation of iron-based oxidation catalysts that can give either *cis*-dihydroxylation or *trans*-dihydroxylation of alkenes, simply by switching from CH_3CN to acetone as solvent.

Experimental Section

General Information: Commercially available chemicals were used without further purification unless noted otherwise. $H_2{}^{18}O_2$ (90% ^{18}O-enriched, 2% solution in $H_2{}^{16}O$) and $H_2{}^{18}O$ (95% ^{18}O-enriched) was obtained from ICON Services Inc. N3Py[33] and *cis*-4-octene[53] were prepared according to literature procedures.

^1H NMR and ^{13}C NMR spectra were recorded on a Varian Gemini 300 spectrometer at ambient temperature (^1H at 300 MHz and ^{13}C

 © 2004 Wiley-VCH Verlag GmbH & Co. KGaA, Weinheim

at 75 MHz). Chemical shifts (in ppm) are referenced to the residual protic solvent peaks. X-band EPR spectra were obtained at liquid nitrogen temperature on a Bruker ECS106 instrument or at liquid helium temperatures on a Bruker E500 equipped with an Oxford Instruments ESR-10 cryostat. UV/Vis spectra were recorded on a Hewlett Packard 8453 diode array spectrophotometer, using a cell equipped with a home-built temperature-control device. Electrochemical studies were carried out with a PAR 273A potentiostat in acetonitrile with 0.1 M tetrabutylammonium perchlorate as the supporting electrolyte. Cyclic voltammograms (CV) were obtained by using a three-component system consisting of a glassy carbon working electrode, a platinum wire auxiliary electrode and a saturated calomel reference electrode. Mass spectra were recorded on a NERMAG R 3010 triple quadrupole mass spectrometer (Nermag, Argenteuil, France) equipped with a home-built atmospheric-pressure ionization source. GC analyses were performed on a Hewlett Packard 6890 Gas Chromatograph using a HP-1 dimethyl polysiloxane column or a HP-5 5%-phenyl methyl siloxane column, or a Hewlett Packard 5890 II Gas Chromatograph using a CP-wax 52 CB column or a CP-wax 57 CB column.

Caution: Perchlorate salts are potentially explosive and should be handled with care.

Crystallographic Studies. Crystal Structure Determination of 4: $(C_{22}H_{24}FeN_6)^{2+}\cdot(ClO_4^-)_2$, M_r = 627.22, triclinic, $P\bar{1}$, a = 10.504(8), b = 11.685(9), c = 12.449(9) Å, α = 77.20(1)°, β = 65.71(1)°, γ = 66.34(1)°, V = 1272.7(17) Å^3, Z = 2, D_x = 1.637 gcm^{-3}, λ(Mo-K_α) = 0.71073 Å, μ = 8.63 cm^{-1}, F(000) = 644, T = 90 K, $GooF$ = 0.970, $wR(F^2)$ = 0.2377 for 4307 reflections and 355 parameters and $R(F)$ = 0.0856 for 2378 reflections obeying $F_o \geq 4.0\ \sigma(F_o)$ criterion of observability.

The asymmetric unit consists of three moieties, a cationic Fe complex and two ClO_4^- anions. Crystals were obtained by recrystallization from a mixture of acetonitrile and pentane. The crystals were very fragile: contact with a glass fiber caused damage as crystal cracks. The recorded frames showed (broad) anisotropic mosaicity and duplicated reflections. A red parallelepiped-shaped crystal with the dimensions of 0.220 × 0.150 × 0.120 mm mounted on a glass fiber was aligned on a Bruker[54] SMART APEX CD diffractometer (Platform with full three-circle goniometer). The diffractometer was equipped with a 4 K CCD detector set 6.0 cm from the crystal. The crystal was cooled to 90 K using the Bruker KRYOFLEX low-temperature device. Intensity measurements were performed using graphite-monochromated Mo-K_α radiation from a sealed ceramic diffraction tube (SIEMENS). Generator settings were 50 kV/40 mA.

The structure was solved by Patterson methods (DIRDIF) and refined with SHELXL against F^2 of all reflections. Non-hydrogen atoms were refined freely with anisotropic displacement parameters. Hydrogen atoms were refined in rigid mode. Checking for higher symmetry and structure calculations were performed with the PLATON package.
CCDC-213726 contains the supplementary crystallographic data for this paper. These data can be obtained free of charge via www.ccdc.cam.ac.uk/conts/retrieving.html [or from the Cambridge Crystallographic Data Centre, 12 Union Road, Cambridge CB2 1EZ, UK; Fax: (internat.) +44-1223/336-033; E-mail: deposit@ccdc.cam.ac.uk].

***N*-[Di(2-pyridinyl)methyl]-*N*-methyl-*N*-(2-pyridinylmethyl)amine (N3Py-Me, 1):** Formaldehyde (37% solution in water, 0.45 mL, 6.0 mmol) was added to a solution of **3** (1.262 g, 4.59 mmol) in 1,2-dichloroethane (35 mL). $NaBH(OAc)_3$ (3.92 g, 18.5 mmol) was added in small portions. After stirring for 7 h at room temperature saturated $NaHCO_{3(aq)}$ (35 mL) was added and the 1,2-dichloroethane layer was separated. The aqueous layer was extracted with CH_2Cl_2 (3 × 20 mL). The combined organic layers were washed with 1 N NaOH (20 mL) and brine (20 mL), dried (Na_2SO_4) and the solvent removed in vacuo to give **1** (1.235 g, 4.27 mmol, 93%) as a slightly yellow oil. ^{1}H NMR ($CDCl_3$): δ = 2.19 (s, 3 H), 3.72 (s, 2 H), 4.96 (s, 1 H), 7.14 (m, 3 H), 7.71 (m, 6 H), 8.56 (m, 3 H) ppm. ^{13}C NMR ($CDCl_3$): δ = 40.32 (q), 61.04 (t), 77.87 (d), 121.76 (d), 122.10 (d), 122.92 (d), 123.21 (d), 136.29 (d), 136.43 (d), 148.86 (d), 149.22 (d), 159.37 (s), 160.59 (s) ppm. MS (CI): m/z = 291 [M + 1].

***N*-Benzyl-*N*-[di(2-pyridinyl)methyl]-*N*-(2-pyridinylmethyl)amine (N3Py-Bn, 2):** A mixture of benzyl chloride (0.46 mL, 3.8 mmol), **3** (740 mg, 2.7 mmol) and K_2CO_3 (370 mg, 2.7 mmol) in CH_3CN (20 mL) was stirred under an argon atmosphere. The mixture was heated under reflux overnight and benzyl chloride (0.23 mL, 1.9 mmol) was again added. After heating under reflux for 24 h the solvent was evaporated and water (20 mL) was added to the residue. The product was extracted with ethyl acetate (3 × 30 mL) and the combined ethyl acetate layers were washed with brine (15 mL) and dried (Na_2SO_4). Evaporation of the solvent followed by column chromatography (Alox. neutral, akt. I, ethyl acetate/hexane/triethylamine, 10:6:1) afforded **2** (670 mg, 1.83 mmol, 68%) as a yellow oil. ^{1}H NMR ($CDCl_3$): δ = 3.79 (s, 2 H), 3.90 (s, 2 H), 5.30 (s, 1 H), 7.14 (m, 4 H), 7.29 (m, 2 H), 7.40 (m, 2 H), 7.66 (m, 6 H), 8.48 (m, 1 H), 8.56 (m, 2 H) ppm. ^{13}C NMR ($CDCl_3$): δ = 54.93 (t), 56.47 (t), 71.24 (d), 121.62 (d), 121.90 (d), 122.60 (d), 123.75 (d), 126.77 (d), 128.14 (d), 128.70 (d), 136.11 (d), 136.23 (d), 138.94 (s), 148.81 (d), 149.15 (d), 160.04 (s) ppm. MS (CI): m/z = 367 [M + 1].

[(N3Py-Me)Fe(CH$_3$CN)$_2$](ClO$_4$)$_2$ (4): A solution of $Fe(ClO_4)_2\cdot 6H_2O$ (250 mg, 0.69 mmol) in CH_3CN (3 mL) was added to a solution of **1** (198 mg, 0.68 mmol) in MeOH (3 mL). The dark-red solution was placed in an ethyl acetate bath and after 3 days **4** (344 mg, 0.55 mmol, 81%) was isolated as dark-red crystals. ^{1}H NMR (CD_3CN): δ = 3.68, 5.12, 6.83, 7.40 (m, 1 H), 7.63 (m, 1 H), 8.02 (m, 1 H), 8.52, 8.65, 8.77, 8.95, 11.21 ppm. $C_{22}H_{24}Cl_2FeN_6O_8$: calcd. C 42.13, H 3.86, N 13.40; found C 41.98, H 3.78, N 13.27. UV/Vis (in CH_3CN): λ_{max} (ε) = 352 nm (5288 M^{-1}cm^{-1}), 428 (3261).

[(N3Py-Bn)Fe(CH$_3$CN)$_2$](ClO$_4$)$_2$ (5): Following the procedure as for **4**, starting from **2** (95 mg, 0.26 mmol) and $Fe(ClO_4)_2\cdot 6H_2O$ (105 mg, 0.29 mmol), **5** (152 mg, 0.22 mmol, 85%) was obtained as dark red crystals. ^{1}H NMR (CD_3CN): δ = 2.82, 4.44, 5.84, 6.98 (m, 3 H), 7.35 (m, 1 H), 7.49 (m, 3 H), 8.02 (m, 1 H), 9.40, 9.50, 9.64, 9.72, 9.79, 9.96, 10.78, 13.17 ppm. ES/MS: m/z = 521 [M − $(ClO_4)^-$ − 2(CH_3CN)]$^+$, 231.5 [M − 2(ClO_4)$^-$ − (CH_3CN)]$^{2+}$.

Catalytic Oxidations: All experiments were carried out under air, unless noted otherwise, in a water bath thermostatted at 25 °C. In a typical procedure cyclohexane (0.19 mL, 1000 equiv.) was added to a solution of **9** (8.75 × 10^{-4} M, 2 mL) and a known amount of bromobenzene (internal standard) in acetone. The reaction was started by syringe pump addition of 1 M H_2O_2 (88 μL, 50 equiv.) over 30 min. After the addition was complete the reaction mixture was stirred for an additional 5 min. An aliquot (1 mL) was taken from the reaction and filtered through a small silica column. The silica was thoroughly washed with diethyl ether or diethyl ether/10% methanol. The sample was concentrated to a volume of 2 mL by passing an Ar stream over the solution and then analyzed by GC.

 © 2004 Wiley-VCH Verlag GmbH & Co. KGaA, Weinheim

Kinetic Isotope Effect Determination: Essentially the same procedure was used as described above, but now a mixture of cyclohexane and [D_{12}]cyclohexane was used (ratio cyclohexane/[D_{12}]cyclohexane varied from 1:1 to 1:4). The KIE was determined by comparing the turnover numbers for cyclohexanol and [D_{11}]cyclohexanol (determined by GC using the CP-wax 52 CB column) and corrected for relative concentration of cyclohexane and [D_{12}]cyclohexane.

Labeling Experiments: In a typical procedure cyclooctene (0.23 mL, 1000 equiv.) was added to a solution of **4** ($8.75 \cdot 10^{-4}$ M, 2 mL) in acetonitrile under a N_2 atmosphere. The reaction was started by syringe pump addition of $H_2{}^{18}O_2$ (10 equiv., 30 μL of 2% $H_2{}^{18}O_2$ in $H_2{}^{16}O$, diluted with 220 μL acetonitrile) over 60 min. After the addition was complete the reaction mixture was stirred for an additional 5 min. The reaction mixture was filtered through a small silica column. The silica was thoroughly washed with diethyl ether or diethyl ether/10% methanol. The sample was concentrated to a volume of 2 mL by passing an Ar stream over the solution and then analyzed by GC/CI-MS.

In the $H_2{}^{18}O$ experiment, $H_2{}^{16}O_2$ (50% in $H_2{}^{16}O$, 2 μL) and $H_2{}^{18}O$ (90%, 48 μL) were dissolved in acetonitrile (50 μL) and used for the oxidation as mentioned above.

In the $H_2{}^{18}O_2/H_2{}^{18}O$ experiment, $H_2{}^{18}O_2$ (2% in $H_2{}^{16}O$, 25 μL) and $H_2{}^{18}O$ (90%, 25 μL) were dissolved in acetonitrile (50 μL) and used for the oxidation as mentioned above.

Acknowledgments

Financial support for this research from NWO-CW (project supramolecular catalysis) (M. K., B. L. F.) is gratefully acknowledged. We wish to thank Prof. L. Que Jr. (University of Minnesota) for helpful discussions and A. Meetsma for performing the X-ray analysis.

[1] [1a] R. A. Sheldon, J. K. Kochi, in *Metal Catalyzed Oxidations of Organic Compounds*, Academic Press, New York, **1981**. [1b] D. A. Goetsch, L. D. Schmidt, *Science* **1996**, *271*, 1560−1562. [1c] G. B. Shul'pin, *J. Mol. Catal. A* **2002**, *189*, 39−66.
[2] B. S. Lane, K. Burgess, *Chem. Rev.* **2003**, *103*, 2457−2473.
[3] [3a] J. Brinksma, R. Hage, J. Kerschner, B. L. Feringa, *Chem. Commun.* **2000**, 537−538. [3b] R. Hage, J. E. Iburg, J. Kershner, J. H. Koek, E. L. M. Lempers, R. J. Martens, U. S. Racherla, S. W. Russell, T. Swarthoff, M. R. P. van Vliet, J. B. Warnaar, L. van der Wolf, B. Krijnen, *Nature* **1994**, *369*, 637−639.
[4] M. C. White, A. G. Doyle, E. N. Jacobsen, *J. Am. Chem. Soc.* **2001**, *123*, 7194−7195.
[5] K. Kamata, K. Yonehara, Y. Sumida, K. Yamaguchi, S. Hikichi, N. Mizuno, *Science* **2003**, *300*, 964−966.
[6] M. Merkx, D. A. Kopp, M. H. Sazinsky, J. L. Blazyk, J. Muller, S. J. Lippard, *Angew. Chem. Int. Ed.* **2001**, *40*, 2782−2807.
[7] M. D. Wolfe, J. V. Parales, D. T. Gibson, J. D. Lipscomb, *J. Biol. Chem.* **2001**, *276*, 1945−1953.
[8] A. Karlsson, J. V. Parales, R. E. Parales, D. T. Gibson, H. Eklund, S. Ramaswamy, *Science* **2003**, *299*, 1039−1042.
[9] R. M. Burger, *Chem. Rev.* **1998**, *98*, 1153−1169.
[10] [10a] D. L. Boger, T. M. Ramsey, H. Cai, S. T. Hoehn, J. Stubbe, *J. Am. Chem. Soc.* **1998**, *120*, 9139−9148. [10b] D. C. Heimbrook, S. A. Carr, M. A. Mentzer, E. C. Long, S. M. Hecht, *Inorg. Chem.* **1987**, *26*, 3835−3836. [10c] N. Murugesan, S. M. Hecht, *J. Am. Chem. Soc.* **1985**, *107*, 493−500.
[11] M. Costas, K. Chen, L. Que Jr., *Coord. Chem. Rev.* **2000**, *200*, 517−544.
[12] K. Chen, L. Que Jr., *Chem. Commun.* **1999**, 1375−1376.
[13] K. Chen, L. Que Jr., *J. Am. Chem. Soc.* **2001**, *123*, 6327−6337.
[14] Y. Mekmouche, S. Ménage, C. Toia-Duboc, M. Fontecave, J.-B. Galey, C. Lebrun, J. Pécaut, *Angew. Chem. Int. Ed.* **2001**, *40*, 949−952.
[15] K. Chen, L. Que Jr., *Angew. Chem. Int. Ed.* **1999**, *38*, 2227−2229.
[16] W. Nam, R. Ho, J. S. Valentine, *J. Am. Chem. Soc.* **1991**, *113*, 7052−7054.
[17] K. Chen, M. Costas, J. Kim, A. K. Tipton, L. Que Jr., *J. Am. Chem. Soc.* **2002**, *124*, 3026−3035.
[18] J. Y. Ryu, J. Kim, M. Costas, K. Chen, W. Nam, L. Que Jr., *Chem. Commun.* **2002**, 1288−1289.
[19] M. Costas, L. Que Jr., *Angew. Chem. Int. Ed.* **2002**, *41*, 2179−2181.
[20] K. Chen, M. Costas, L. Que Jr., *J. Chem. Soc., Dalton Trans.* **2002**, 672−679.
[21] [21a] H. C. Kolb, M. S. VanNieuwenhze, K. B. Sharpless, *Chem. Rev.* **1994**, *94*, 2483−2548. [21b] I. E. Markó, J. S. Svendsen, in *Comprehensive Asymmetric Catalysis, Vol. II* (Eds.: E. N. Jacobsen, A. Pfaltz, H. Yamamoto), Springer-Verlag, Berlin, Heidelberg, **1999**, pp. 713−790.
[22] T. K. M. Shing, E. K. W. Tam, I. H. F. Chung, Q. Jiang, *Chem. Eur. J.* **1996**, *2*, 50−57.
[23] J. Brinksma, L. Schmieder, G. van Vliet, R. Boaron, R. Hage, D. E. de Vos, P. L. Alsters, B. L. Feringa, *Tetrahedron Lett.* **2002**, *43*, 2619−2622.
[24] M. Costas, A. K. Tipton, K. Chen, D.-H. Jo, L. Que Jr., *J. Am. Chem. Soc.* **2001**, *123*, 6722−6723.
[25] A. Bassan, M. R. A. Blomberg, P. E. M. Siegbahn, L. Que Jr., *J. Am. Chem. Soc.* **2002**, *124*, 11056−11063.
[26] M. Lubben, A. Meetsma, E. C. Wilkinson, B. Feringa, L. Que Jr., *Angew. Chem. Int. Ed. Engl.* **1995**, *34*, 1512−1514.
[27] G. Roelfes, M. Lubben, K. Chen, R. Y. N. Ho, A. Meetsma, S. Genseberger, R. M. Hermant, R. Hage, S. K. Mandal, V. G. Young Jr., Y. Zang, H. Kooijman, A. L. Spek, L. Que Jr., B. L. Feringa, *Inorg. Chem.* **1999**, *38*, 1929−1936.
[28] G. Roelfes, V. Vrajmasu, K. Chen, R. Y. N. Ho, J.-U. Rohde, C. Zondervan, R. M. la Crois, E. P. Schudde, M. Lutz, A. L. Spek, R. Hage, B. L. Feringa, E. Munck, L. Que Jr., *Inorg. Chem.* **2003**, *42*, 2639−2653.
[29] R. Y. N. Ho, G. Roelfes, B. L. Feringa, L. Que Jr., *J. Am. Chem. Soc.* **1999**, *121*, 262−265.
[30] N. Lehnert, R. Y. N. Ho, L. Que Jr., K. Fujisawa, E. I. Solomon, *J. Inorg. Biochem.* **2001**, *86*, 313.
[31] G. Roelfes, M. Lubben, R. Hage, L. Que Jr., B. L. Feringa, *Chem. Eur. J.* **2000**, *6*, 2152−2159.
[32] N. Lehnert, F. Neese, R. Y. N. Ho, L. Que Jr., E. I. Solomon, *J. Am. Chem. Soc.* **2002**, *124*, 10810−10822.
[33] G. Roelfes, M. E. Branum, L. Wang, L. Que Jr., B. L. Feringa, *J. Am. Chem. Soc.* **2000**, *122*, 11517−11518.
[34] A. F. Abdel-Magid, K. G. Carson, B. D. Harris, C. A. Maryanoff, R. D. Shah, *J. Org. Chem.* **1996**, *61*, 3849−3862.
[35] Y. Zang, J. Kim, Y. Dong, E. C. Wilkinson, E. H. Appelman, L. Que Jr., *J. Am. Chem. Soc.* **1997**, *119*, 4197−4205.
[36] C. Kim, K. Chen, J. Kim, L. Que Jr., *J. Am. Chem. Soc.* **1997**, *119*, 5964−5965.
[37] P. A. MacFaul, K. U. Ingold, D. D. M. Wayner, L. Que Jr., *J. Am. Chem. Soc.* **1997**, *119*, 10594−10598.
[38] P. A. MacFaul, I. W. C. E. Arends, K. U. Ingold, D. D. M. Wayner, *J. Chem. Soc., Perkin Trans. 2* **1997**, 135−145.
[39] S. Evans, J. R. Lindsay Smith, *J. Chem. Soc., Perkin Trans. 2* **2000**, *7*, 1541−1552.
[40] R. A. Leising, J. Kim, M. A. Pérez, L. Que Jr., *J. Am. Chem. Soc.* **1993**, *115*, 9524−9530.
[41] C. Kim, K. Chen, J. Kim, L. Que Jr., *J. Am. Chem. Soc.* **1997**, *119*, 5964−5965.
[42] J. R. Lindsay Smith, P. R. Sleath, *J. Chem. Soc., Perkin Trans. 2* **1983**, 1165−1169.
[43] S. Miyajima, O. Simamura, *Bull. Chem. Soc. Jpn.* **1975**, *48*, 526−530.

 © 2004 Wiley-VCH Verlag GmbH & Co. KGaA, Weinheim

[44] S. Ménage, J. M. Vincent, C. Lambeaux, G. Chottard, A. Grand, M. Fontecave, *Inorg. Chem.* **1993**, *32*, 4766−4773.
[45] T. Kojima, R. A. Leising, S. Yan, L. Que Jr., *J. Am. Chem. Soc.* **1993**, *115*, 11328−11335.
[46] J. T. Groves, T. E. Nemo, *J. Am. Chem. Soc.* **1983**, *105*, 6243−6248.
[47] H. Weiner, A. Trovarelli, R. G. Finke, *J. Mol. Catal. A: Chemical* **2003**, *191*, 217−252.
[48] [48a] J. Rudolph, K. L. Reddy, J. P. Chiang, K. B. Sharpless, *J. Am. Chem. Soc.* **1997**, *119*, 6189−6190. [48b] A. C. Cope, J. M. Grisar, P. E. Peterson, *J. Am. Chem. Soc.* **1959**, *81*, 1640−1642.
[49] [49a] M. Tokunaga, J. F. Larrow, F. Kakiuchi, E. N. Jacobsen, *Science* **1997**, *277*, 936−938. [49b] B. Rickborn, in *Comprehensive Organic Synthesis* (Ed.: B. M. Trost), Pergamon Press, Oxford, **1991**, pp. 733−775.
[50] [50a] J. Bernadou, B. Meunier, *Chem. Commun.* **1998**, 2167−2173. [50b] K. A. Lee, W. Nam, *Inorg. Chem.* **1998**, *37*, 606−607. [50c] W. Nam, J. S. Valentine, *J. Am. Chem. Soc.* **1993**, *115*, 1772−1778.
[51] [51a] S. J. Lange, H. Miyake, L. Que Jr., *J. Am. Chem. Soc.* **1999**, *121*, 6330−6331. [51b] M. P. Jensen, S. J. Lange, M. P. Mehn, E. L. Que, L. Que Jr., *J. Am. Chem. Soc.* **2003**, *125*, 2113−2128.
[52] [52a] J. T. Groves, Z. Gross, M. K. Stern, *Inorg. Chem.* **1994**, *33*, 5065−5072. [52b] Z. Gross, S. Nimri, *J. Am. Chem. Soc.* **1995**, *117*, 8021−8022. [52c] Z. Gross, *J. Biol. Inorg. Chem.* **1996**, *1*, 368−371. [52d] Z. Gross, *J. Org. Chem.* **1997**, *62*, 5514−5521.
[53] D. J. Hastings, A. C. Weedon, *Can. J. Chem.* **1991**, *69*, 1171−1182.
[54] Bruker (2000). *SMART, SAINT, SADABS, XPREP* and *SHELXTL/NT.* Smart Apex *Software Reference Manuals.* Bruker AXS Inc., Madison, Wisconsin, USA.

Received September 25, 2003
Early View Article
Published Online January 19, 2004

 © 2004 Wiley-VCH Verlag GmbH & Co. KGaA, Weinheim

Synthesis, Structure and Hydrolytic Properties of a Family of New Zn Complexes Containing Hexaazamacrocyclic Ligands

Miquel Costas,[a] Carmen Anda,[a] Antoni Llobet,*[a] Teodor Parella,[b] Helen Stoeckli Evans,[c] and Elena Pinilla[d]

Keywords: Zinc / Cooperative effects / Coordination chemistry / Fluxionality / Homogeneous catalysis / Macrocyclic ligands

The synthesis, structure and spectroscopic properties of a family of Zn complexes containing a dinucleating hexaazamacrocyclic ligand (L) and anionic ligands (X) of general formula $[Zn_2(X)_{4-n}(L)]^{n+}$ (**1**–**8**; L = H2p, H3p, Me2p, Me2m, Me3p, Me3m; X = Cl, n = 0; X = NO_3, n = 2) have been investigated. The solid-state structural characterisation has been performed by means of X-ray diffraction analysis for complexes **3**, **5**, **7·1/3CH$_2$Cl$_2$** and **8**. The Zn complexes **5**, **7·1/3CH$_2$Cl$_2$** and **8** containing chloride ligands present a distorted N_2Cl_2 tetrahedral coordination with two non-coordinated N atoms of the macrocyclic ligand. On the other hand, complex **3**, which contains nitrate ligands, displays an N_3O_2 pentacoordination with all the N atoms of the macrocyclic ligand bonded to the metal centres. The different factors governing the relative Zn–Zn disposition are discussed. NMR spectroscopy in solution reveals the presence of fluxional behaviour and a completely different structural arrangement than in the solid state. In particular, evidence for the formation and breaking of Zn–N bonds involving all the macrocyclic ligand aminic N atoms is obtained for the chloride complexes **2** and **4**–**8**. Finally, complexes **1**, **3**, **5** and **7** hydrolyse *p*-nitrophenyl acetate (NA) with second-order rate constants ranging from 0.045 to 0.193 $M^{-1}s^{-1}$, thus manifesting the influence of the ligands over the hydrolytic activity.
(© Wiley-VCH Verlag GmbH & Co. KGaA, 69451 Weinheim, Germany, 2004)

Introduction

Macrocyclic polyamines are well-known to participate in molecular recognition phenomena with different kinds of substrates, such as organic and inorganic cations, anions and neutral molecules.[1] Such interactions have attracted interest from environmental, catalytic and health-related domains.[2] Macrocyclic molecules containing two polyamine units linked by a spacer are also capable of ligating two metal atoms in close proximity. In some cases this leads to interactions between the two metallic centres that results in interesting magnetic,[3] electronic[4,5] and/or catalytic properties.[6–8] The ability of macrocyclic ligands to preorganise two metal centres at a particular distance has also been used in the design of Zn complexes that efficiently catalyse the hydrolysis of phosphate and carboxy esters[9–11] thus mimicking the activity of zinc enzymes that mediate hydrolytic reactions.[12–16] However, exhaustive characterisation of Zn complexes with macrocyclic polyamines is scarce. In this work we have synthesised and characterised a series of Zn complexes with hexaazamacrocyclic ligands where the metal coordination and the metal-metal relative disposition are modulated by the characteristics of the macrocyclic ligand. We have also studied the ability of these complexes to perform the hydrolysis of *p*-nitrophenyl acetate (NA). Our results demonstrate that small changes in the macrocyclic backbone lead to important changes in the Zn−Zn distance and in the hydrolytic ability manifested by the complexes.

[a] Departament de Química, Universitat de Girona,
Campus de Montilivi, 17071 Girona, Spain
Fax: (internat.) +34-972-418-150
E-mail: antoni.llobet@udg.es
[b] Servei de RMN, Universitat Autònoma de Barcelona,
Bellaterra 08193, Barcelona, Spain
Fax: (internat.) +34-93/581-2003
E-mail: teo@rmn4.uab.es
[c] Institut de Chimie, Université de Neuchâtel,
Av. Bellevaux 51, 2007 Neuchatel, Switzerland
Fax: (internat.) +41-32-718-2511
E-mail: Helen.Stoeckli-Evans@unine.ch
[d] Departamento de Quimica Inorgánica, Facultad de Ciencias Químicas, Universidad Complutense
Ciudad Universitaria, 28040 Madrid, Spain,
Fax: (internat.) +34-91-394-4284
E-mail: epinilla@quim.ucm.es
Supporting information for this article is available on the WWW under http://www.eurjic.org or from the author.

Results and Discussion

Synthesis and Solid-State Structure

The six macrocyclic ligands used in this work are shown in Scheme 1 and were prepared according to literature procedures.[17–20] This family of ligands comprises secondary amines and their hexamethylated analogues and is

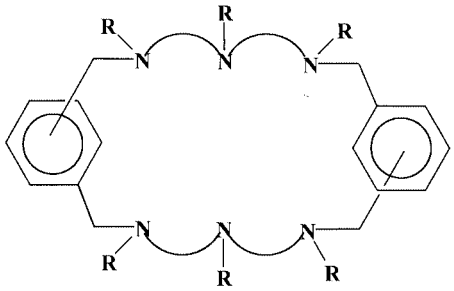

		= $(CH_2)_n$	
		$n = 2$	$n = 3$
R = H	*p*	**H2p**	**H3p**
R = Me	*p*	**Me2p**	**Me3p**
	m	**Me2m**	**Me3m**

Scheme 1. Macrocyclic ligands used in this work

characterised by the number of methylenic units linking the amines, which can be two or three, and by the aromatic substitution that takes place in the *meta* or *para* positions.

Reaction of those ligands at room temperature with two times the stoichiometric amount of the appropriate Zn^{II} salt in methanol affords the corresponding dinuclear Zn^{II} complexes **1**−**8** as white microcrystalline solids in modest to good yields (ranging from 34 to 77%), as shown in Equation (1) for the particular case of **5**.

$$\text{Me2p} + 2\ ZnCl_2 \xrightarrow{\text{MeOH}} [Zn_2Cl_4(\text{Me2p})] \quad (1)$$

The crystal structures of $[Zn_2(NO_3)_2(H3p)](NO_3)_2$ (**3**), $[Zn_2Cl_4(Me2p)]$ (**5**), $[Zn_2Cl_4(Me3p)]\cdot 1/3CH_2Cl_2$ (**7·1/3CH$_2$Cl$_2$**) and $[Zn_2Cl_4(Me3m)]$ (**8**) have been determined by means of single-crystal X-ray diffraction analysis. Table 1 contains their crystallographic data whereas Table 2 contains their selected bond lengths and angles. Figure 1 shows the ORTEP diagrams obtained for the cationic molecular structure of complex **3** (top left) and the neutral molecular structures of complexes **5** (top right), **7** (bottom left) and **8** (bottom right), together with the atom labelling system used.

The cationic part of **3** consists of the macrocyclic ligand, which binds to two zinc atoms, and an NO_3^- anion bonded to each metal adopting an (η^2-*O*,*O*-NO_3) chelating mode (Δr_{Zn-O} = 0.075 Å). The whole molecule has an inversion centre that relates the metal atoms and half of the macrocyclic ligand with the other half. The Zn metal centres are five-coordinate, binding to three N atoms from the macrocyclic ligand and two oxygens from the nitrate ligand. The Zn−N distances range from 1.992(6) to 2.054(7) Å and the two Zn−O bonds are significantly different [Zn−O1: 2.206(8) Å; Zn−O2: 2.281(9) Å], although all of them compare well with the observed values of complexes containing an N_3ZnO_2NO coordination environment.[21] The N−Zn−N bond angles range from 92.5(3)° to 128.1(3)° whereas the N−Zn−O angles range from 89.3(3)° to 141.0(3)°, reflecting the distortions imposed by the rigidity of the macrocyclic ligand and the asymmetry of the coordinated nitrate anion.

Table 1. Crystallographic data of **3**, **5**, **7** and **8**

Complex	**3**	**5**	**7·1/3CH$_2$Cl$_2$**	**8**
Empirical formula	$C_{28}H_{46}N_{10}O_{12}Zn_2$	$C_{30}H_{52}Cl_4N_6Zn_2$	$C_{34.33}H_{58.67}Cl_{4.67}N_6Zn_2$	$C_{34}H_{60}Cl_4N_6OZn_2$
Mol. mass (g/mol)	845.49	769.42	851.71	825.42
Crystal system	orthorhombic	monoclinic	hexagonal	monoclinic
Space group	Pbca	$P2_1/n$	$R\bar{3}$	$P2_1/c$
Crystal size (mm^3)	0.09 × 0.2 × 0.4	0.05 × 0.3 × 0.4	0.2 × 0.2 × 0.1	0.15 × 0.3 × 0.45
a (Å)	14.1458(12)	10.9716(7)	22.9991(14)	10.7508(9)
b (Å)	15.3309(13)	8.0318(5)	22.9991(14)	12.2409(8)
c (Å)	16.2605(14)	20.9911(13)	21.7424(15)	14.8889(13)
β (deg)	90	101.144(8)	120	95.772(10)
Volume (Å^3)	3526.4(5)	1814.9(2)	9960.0(11)	1949.4(3)
Z	4	2	9	2
Temperature (K)	296(2)	223(2)	223(2)	293(2)
λ(Mo-K_α) (Å)	0.71073	0.71073	0.71073	0.71073
$\rho_{calcd.}$ (g/cm^3)	1.593	1.408	1.278	1.406
μ (mm^{-1})	1.436	1.570	1.395	1.537
Meas. reflns.	17342	13530	23527	15306
Unique reflns.	3109	3513	4297	3579
Observed reflns. [$I > 2\sigma(I)$]	1713	2403	1823	1990
Parameters	216	194	211	211
$R1$ [$I > 2\sigma(I)$][a]	0.076	0.0298	0.0402	0.0332
$wR2$ (all data)[b]	0.24	0.0681	0.0949	0.0699

[a] $R1 = \Sigma(||F_o| - |F_c||)/\Sigma|F_o|$. [b] $wR^2 = \{\Sigma[w(F_o^2 - F_c^2)^2]/\Sigma(wF_o^4)\}^{1/2}$.

 © 2004 Wiley-VCH Verlag GmbH & Co. KGaA, Weinheim

Table 2. Selected bond lengths (Å) and bond angles (°) for **3**, **5**, **7** and **8**

	3	**5**	**7**·1/3CH_2Cl_2	**8**
Zn(1)−N(1)	2.042(6)	2.100(2)	2.088(4)	2.088(3)
Zn(1)−N(2)	2.054(7)	2.1194(19)	2.077(3)	2.108(2)
Zn(1)−N(3)	1.992(6)			
Zn(1)−Cl(1)		2.2153(7)	2.2395(15)	2.2103(9)
Zn(1)−Cl(2)		2.2092(7)	2.1888(14)	2.2266(9)
Zn(1)−O1	2.206(8)			
Zn(1)−O2	2.281(9)			
Zn(1)−Zn(1′)	8.73	12.395	10.744	6.743
N(1)−Zn(1)−N(2)	92.5(3)	87.38(7)	100.72(14)	100.95(10)
N(1)−Zn(1)−N(3)	128.1(3)			
N(2)−Zn(1)−N(3)	98.4(3)			
Cl(2)−Zn(1)−Cl(1)		121.19(3)	115.14(6)	119.12(4)
N(1)−Zn(1)−Cl(2)		112.49(6)	121.37(12)	105.49(7)
N(2)−Zn(1)−Cl(2)		111.02(6)	107.90(11)	108.70(7)
N(1)−Zn(1)−Cl(1)		108.58(6)	104.74(11)	113.59(7)
N(2)−Zn(1)−Cl(1)		111.08(5)	104.97(11)	107.42(7)
N(1)−Zn(1)−O(1)	94.9(3)			
N(1)−Zn(1)−O(2)	125.2(3)			
N(2)−Zn(1)−O(1)	141.0(3)			
N(2)−Zn(1)−O(2)	89.7(3)			
N(3)−Zn(1)−O(1)	106.6(3)			
N(3)−Zn(1)−O(2)	105.6(3)			
O(1)−Zn(1)−O(2)	55.3(3)			

Upon coordination, the macrocyclic ligand generates four six-membered rings containing the Zn metal, which, in all cases, adopt a chair conformation. The aromatic rings are oriented in a parallel manner and the coordinated nitrates are disposed in an *anti* configuration, as expected from a steric viewpoint. Finally the Zn···Zn distance is 8.73 Å. The structure is completed by two non-coordinating nitrate anions which could only be refined isotropically. Two oxygen atoms of each nitrate are within H-bond range (2.95−3.1 Å) of the N atoms of the macrocyclic ligand, on the opposite side of the $N_3Zn(\eta^2$-*O*,*O*)NO_3 unit.

The molecular structures of **5**, **7** and **8** consist of a neutral Zn_2Cl_4L unit. The macrocyclic molecules are again centrosymmetric. In sharp contrast to the previous structure and related complexes described in the literature — $[Pd_2Cl_2(Me2p)](ClO_4)_2{\cdot}H_2O$,[22] $[Cu_2Cl_2(Me2p)](BPh_4)(ClO_4){\cdot}CH_3CN$,[23] $[Cu_2(Me2p)(CO)_2](ClO_4)_2{\cdot}2H_2O$ and $[Cu_2(Me2m)(t\text{BuNC})_2](CF_3SO_3)_2$ [24] — the Zn atoms adopt a distorted tetrahedral geometry coordinated to only four of the six available N atoms of the macrocyclic ligand; each Zn coordinates to two chlorine atoms and two adjacent N atoms of the macrocycle, leaving two benzylic amines of the macrocycle as non-coordinating. Binding of the metal ion to only two N atoms of the macrocycle in **5**, **7** and **8** probably reflects that formation of the second Zn−Cl bond, in combination with the release of the strain imposed by the macrocyclic ligand, can overcome the breakage of a rather weak $Zn-N_{tertiary}$ bond.[25]

The coordination of Zn1 to two adjacent macrocyclic N atoms results in a five- (**5**), or six-membered (**7** and **8**) chelate ring where the six-membered ring always adopts a chair conformation. The Zn bond lengths and angles are within the expected range for Zn polyaza complexes previously reported in the literature.[26] The number of atoms that form the chelate cycle dramatically affects the N1−Zn−N2 and Cl1−Zn−Cl2 angles. The six-membered chelate rings of **7** and **8** result in N1−Zn−N2 angles of 100.72(14)° and 100.95(10)°, slightly smaller than the corresponding Cl1−Zn−Cl2 angles [115.14(6)° and 119.12(4)°, respectively], whereas the more constrained five-membered ring formed in the ethylene-based macrocycle **5** forces a more acute N1−Zn−N2 angle [87.38(7)°], remarkably smaller than the corresponding Cl1−Zn−Cl2 angle [121.19(3)°]. These parameters indicate a significant distortion from a tetrahedral geometry in **5**, which is further evidenced by the dihedral angle of 80.80° formed between the planes described by N2−Zn1−Cl2 and N1−Zn1−Cl1. It is interesting to note here that in all the structures described in the present work the aromatic rings are disposed in a parallel manner. Finally, complex **7** cocrystallises with a third of a molecule of severely disordered CH_2Cl_2.

For dinuclear complexes containing hexaazamacrocyclic ligands, such as the ones described here, the "internal cavity" of the complex can be defined as the smallest macrocycle containing the two metals. For complexes with all N atoms coordinated to the metal centre, as in **3**, the cavity dimension, expressed in terms of the number of member units, is dependent on the aromatic substitution (the *para* case having an internal cavity with two more units than the *meta*) and independent of the number of methylenic units within the amines. On the other hand, with a partial coordination of the macrocyclic ligand, such as that obtained in complexes **5**, **7** and **8**, the internal cavity will now depend on both factors. Thus, complex **7**, containing the Me3p ligand, will have a larger internal cavity than **3**, its H3p analogue, due to the enlargement produced by the partial coor-

 © 2004 Wiley-VCH Verlag GmbH & Co. KGaA, Weinheim

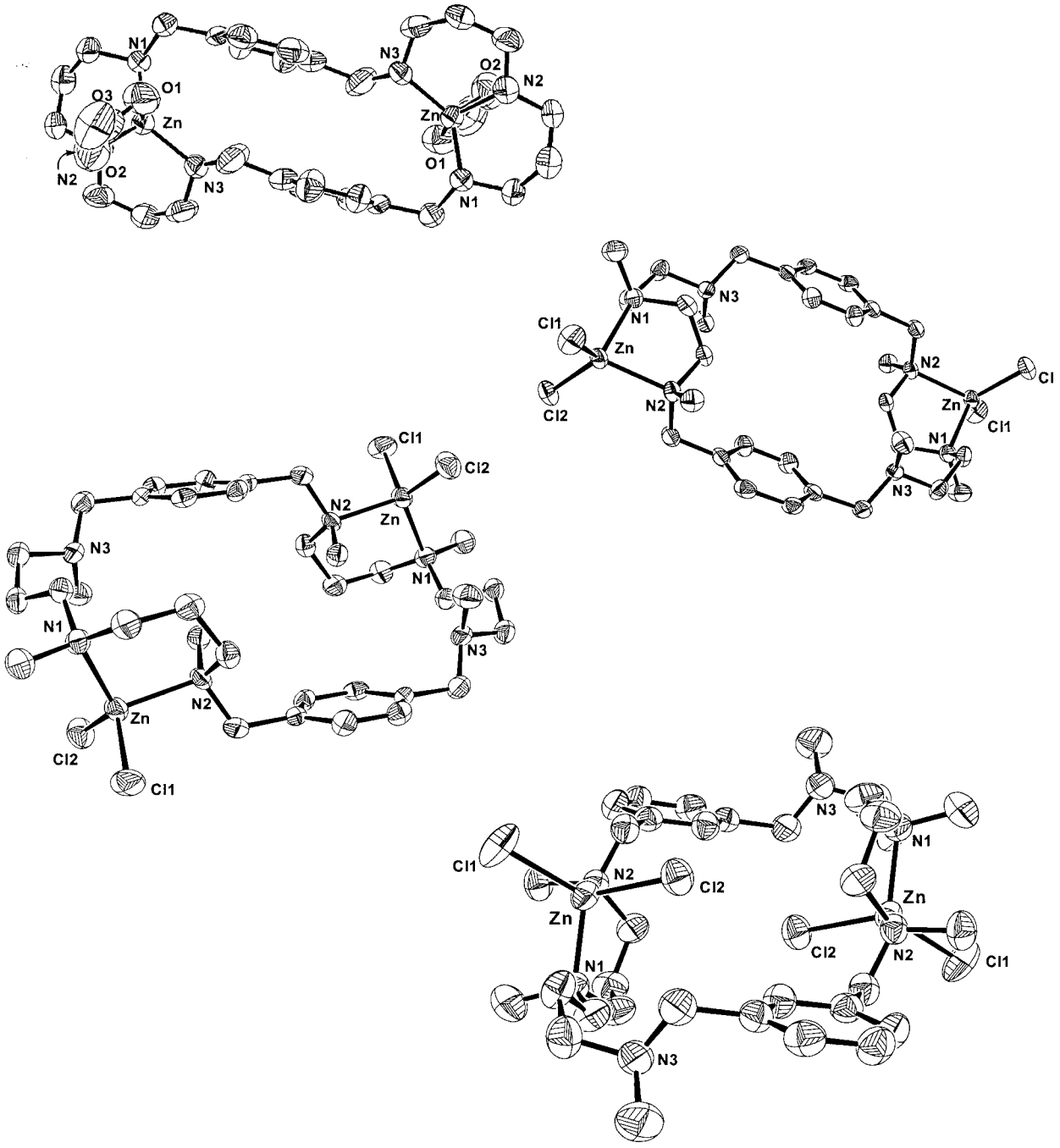

Figure 1. ORTEP diagram (50% probability) of the cationic part of complex **3** (top left), complex **5** (top right), complex **7** (bottom left) and **8** (bottom right)

dination of the former ligand. As a consequence the complex with the tertiary amine has a Zn···Zn distance larger than the corresponding secondary amine. Complex **5**, containing the Me2p ligand, has a smaller internal cavity than complex **7**, containing the analogous ligand but with propylene linkers instead of ethylene. In sharp contrast, **5** has a larger Zn···Zn distance than **7**, due to the relative disposition of the metal complexes produced by the methylene linkers. Finally, complex **8**, containing the Me3m ligand, which produces the largest internal cavity, presents the shortest Zn···Zn distance. This is due to the different arrangement that the *meta* aromatic substitution provokes with regard to the *para*, the former being more compact. As a consequence of this, in complex **8** (*meta* substitution) two of the Cl ligands bonded to the metal centres are directed towards the inside the cavity, whereas in complexes **5** and **7** (*para* substitution) all Cl ligands are clearly oriented outside the cavity and are pointing in opposite directions.

 © 2004 Wiley-VCH Verlag GmbH & Co. KGaA, Weinheim

NMR Spectroscopy and Solution Structure

The ^1H and ^{13}C NMR spectra of complexes **1**−**7** at room temperature in different deuterated solvents are presented as Supporting Information and are assigned in the Exp. Sect. No NMR spectra could be obtained for complex **8** due to its low solubility.

In the spectra, the resonances are shifted downfield relative to the free ligand demonstrating that the metal ion remains bound to the macrocycle in solution. However, it is interesting to point out here that the fine structure of the spectra of these complexes is not well resolved either due to poor resolution of multiple superimposed signals or, more likely (vide infra), the presence of fluxional behaviour. The latter may be attributed to fast exchange between different conformers in solution, although these phenomena alone cannot explain the apparent simplicity of the spectra, which is not consistent with the more asymmetric structure of the complexes in the solid state, as determined by X-ray crystallography. If retained in solution, the structure determined in the solid state should give rise to two different signals (assuming fast aromatic ring rotation) for the aromatic protons in the complexes containing *para*-substituted macrocycles (**5** and **7**). In addition, the benzylic protons in **5**, **6** and **7** should also give rise to at least two different signals in a 1:1 ratio. However, the ^1H NMR spectra of **5** in CD_2Cl_2 (D_2O) and **7** in DMSO (D_2O) show only one broad singlet at δ = 7.39 (7.56) and 7.24 (7.47) ppm, respectively, indicating that all the aromatic protons are equivalent on the NMR timescale. The benzylic protons also appear as a broad singlet at δ = 3.78 (3.99) for **5**, 3.77 for **6** and 3.46 (3.91) ppm for **7**, which implies that the four benzylic groups are again equivalent. Thus, these symmetric spectra could either indicate the presence of a symmetric structure in solution, where the six N atoms participate in the simultaneous binding of the Zn atoms, or, alternatively, it may suggest the presence of two or more species in solution, such as the one determined by X-ray crystallography, undergoing fast inter-exchange. This process supposes rapid Zn−N bond formation and breaking involving all the amino nitrogen atoms of the ligand. This type of behaviour is not uncommon for d^{10} metal ions probably due to the lack of ligand field stabilisation.[27] Further support for the fluxional behaviour of the complexes is provided by variable temperature NMR spectroscopy of **5** in CD_2Cl_2 (Figure S10). The initially simple room temperature ^1H NMR spectra become complicated upon lowering the temperature. For example, the aromatic and benzylic protons, which appear as singlets at 295 K, convert into multiple poorly resolved signals. The higher complexity of the low temperature spectra is consistent with the freezing-out of the fluxional processes, although even at 160 K the signals do not became completely resolved, thus precluding a complete assignment of the spectra.

The spectra of **3** and **4**, which show two broad singlet signals, with a 5:3 integration ratio that are assigned to the benzylic protons, are also unusual. The data are consistent with at least two dramatically different isomeric forms of the complex. However, the singlet structure of the signals strongly suggests again the presence of fluxional behaviour and that each of the signals does not belong to a single species but to a number of inter-exchanging isomers. The solvent strongly influences the nature of the fluxional behaviour, as deduced from the sharpening of the resonances when using D_2O instead of CD_2Cl_2 or [D_6]DMSO. Even though the signals do not totally resolve, it is obvious that in aqueous solution the speed of the process is enhanced. Another interesting aspect of the chemistry of these complexes emerges when comparing the ^1H NMR spectra of complex **2** or **4** with **5** or **7**, respectively, in the same solvent — the comparison of the spectra of Zn complexes bearing secondary or tertiary amine macrocyclic ligands, showing a sharp narrowing for the latter. This observation favours the description of the fluxional behaviour as bond formation and breaking rather than a unique structure since it indicates that the breaking of the weaker $Zn-N_{tertiary}$ bonds[25] requires lower activation energies. Thus $Zn-N_{tertiary}$ bonds can form and break faster than the stronger $Zn-N_{secondary}$ analogues, finally resulting in the narrowing of the resonances.

Hydrolytic Activity

The Zn complexes containing *para*-substituted ligands (**1**, **3**, **5** and **7**) described in the present work were tested in the hydrolysis of 4-nitrophenyl acetate (NA) [Equation (2)]. The *meta* derivatives could not be used due to their low solubility in water. Figure 2A shows the linear dependency of the initial rate constant k_{in} (defined as v_{in}/[NA]) with regard to [$ZnCl_4$(Me2p)] (**5**) at different pH values ranging from 7.31 to 8.40; more-detailed kinetic data related to the hydrolysis of NA in the presence of different Zn complexes is included as Supporting Information in Table S1. As expected, the increase in pH results in a monotonical increase of k_{in}. This behaviour can be interpreted in terms of the generation of the nucleophilic LZn−OH species which has been shown to be the active species in previous works with related ligands.[11,28] This behaviour also rules out the possibility of the free metal ion being the active species since, as the pH is increased, its concentration strongly decreases. On the other hand blank experiments with only free ligand or free metal ion under similar conditions display a much smaller hydrolytic capacity. Furthermore, the free ligand is not observed in the NMR spectra of the complexes reported here. It is interesting to point out here that the rate constants observed for [$ZnCl_4$(Me3p)] (**7**) and for its nitrate analogue [$Zn(NO_3)_2$(Me3p)]$(NO_3)_2$ (data not shown) are

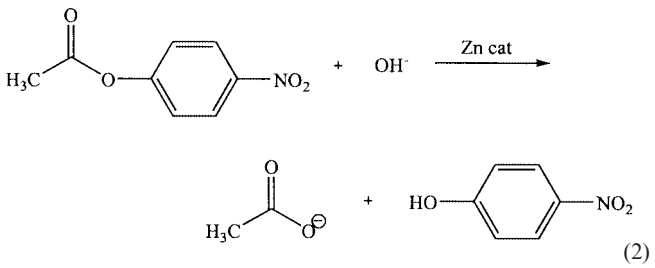

(2)

 © 2004 Wiley-VCH Verlag GmbH & Co. KGaA, Weinheim

virtually the same within experimental error. These results manifest the strong dependency of the rate constant with regard to the ligand system and, in contrast, the weak influence of the labile chloride and nitrate ligands.

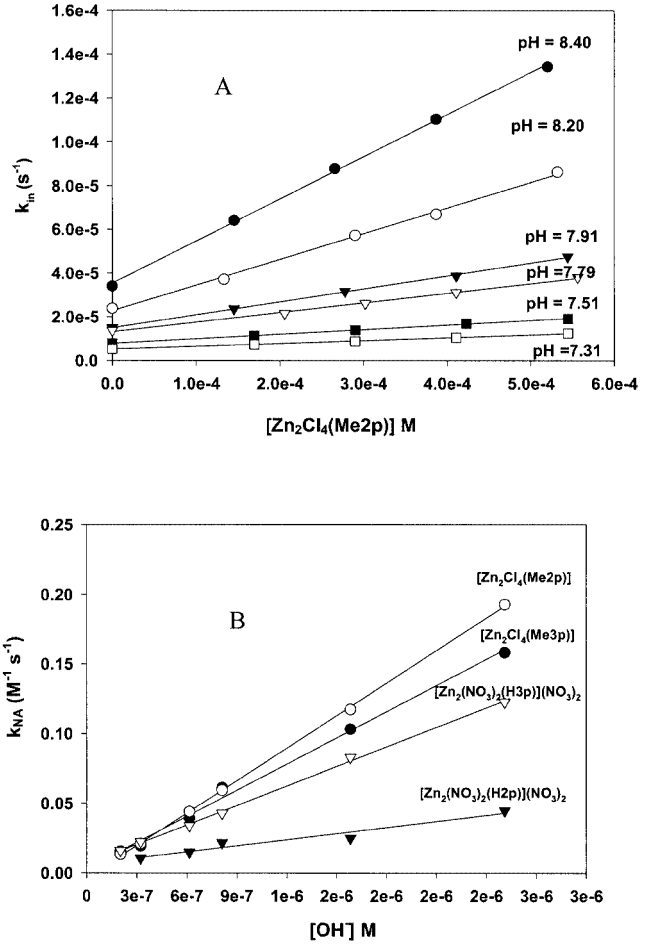

Figure 2. Kinetic data for the hydrolysis of 4-nitrophenyl acetate (NA) by the macrocyclic Zn complexes: A) initial rate constant k_{in} relative to [$ZnCl_4$(Me2p)] at different pH; B) second-order rate constants, k_{NA}, relative to [OH] for different macrocyclic Zn complexes

Unfortunately, in our case, at higher pH values the complexes start to precipitate out of the solution, preventing further kinetic analysis. A similar linear dependency is also found for complexes **1**, **3** and **7** and is presented as Supporting Information.

Second-order rate constants, k_{NA}, were obtained at a given pH from a plot of k_{in} vs. complex concentration. The linear dependency of this second-order rate constant against [OH] is shown in Figure 2B for the four *para* complexes. As can readily be seen, at a given pH complexes **5** (for instance at pH 8.4, k_{NA} = 0.193 $M^{-1}s^{-1}$) and **7** (0.158 $M^{-1}s^{-1}$), bearing tertiary amine ligands, give higher rate values than complexes **1** (0.045 $M^{-1}s^{-1}$) and **3** (0.123 $M^{-1}s^{-1}$) containing secondary amines. These values are about an order of magnitude lower than the best complexes reported in the literature for the same reaction under similar conditions,[28,29] although the low solubility of our complexes at pH's higher than 8.4 precludes a fair comparison.

Our results for the second-order rate constants are in agreement with tertiary amines generating more nucleophilic LZn−OH species than secondary amines due to the hydrophobicity of the former,[30] which precludes charge delocalisation among solvated species. When comparing complexes **5** and **7**, both with tertiary amines, at a given pH it is found that **5** has higher k_{NA} values than **7** even though the latter has four more methylenic groups. This is due to the fact that at the same pH the Me2p ligand generates a much higher concentration of LZn−OH species than Me3p, as has been previously shown in the literature for similar complexes.[31] Finally, for complexes bearing secondary amines the tendency is just the opposite than in the case of the tertiary amines just discussed. In particular, complex **1** presents significantly lower k_{NA} values than the rest of the studied complexes. At this moment it is not obvious to us why **1** has such a low hydrolytic activity, although, presumably, the structure of the ligand does not favour the interaction between the electrophile (Zn−OPO_2R) and nucleophile (Zn−OH) units.

Conclusion

A family of new dinuclear Zn complexes bearing hexaazamacrocyclic and chloride or nitrate ligands have been prepared and characterised from the corresponding metal salt and ligand as the starting materials. In the solid state, the metal coordination geometry as well as the ligand coordination mode are strongly dependent on the Zn starting material. Thus, $ZnCl_2$ generates a Cl_2N_2 tetrahedrally distorted environment for Zn with a coordination number (CN) of four whereas the $Zn(NO_3)_2$ salt generates an N_3O_2 environment with a CN of five. Furthermore the macrocyclic ligand in the former case coordinates through only four of the six possible N atoms, whereas in the latter case it coordinates through all its N atoms. These different coordination modes, together with the flexibility of the macrocyclic ligands, allows a certain control of the relative spatial Zn−Zn disposition.

NMR spectroscopy clearly indicates that the solution structure of these macrocyclic complexes is radically different from their structure in the solid state. In the case of the chloride complexes **2** and **4**−**8**, NMR spectroscopy reveals the presence of a fluxional behaviour that presumably involves exchange between conformational isomers and the formation and breaking of Zn−N bonds including all N atoms of the macrocyclic ligand.

Finally, complexes **1**, **3**, **5** and **7** have been shown to be capable of hydrolyzing *p*-nitrophenyl acetate (NA). Their different hydrolysis rates reveal how small variations in the ligand can significantly influence hydrolytic activity.

Experimental Section

Physical Methods: IR spectra were recorded on a Mattson-Galaxy Satellite FT-IR spectrophotometer as solid KBr pellets. Elemental

 © 2004 Wiley-VCH Verlag GmbH & Co. KGaA, Weinheim

analyses were conducted on a Carlo−Erba Instrument, Mod. CHNS 1108. UV/Vis spectra were recorded on a Varian Cary-50 spectrophotometer, using quartz cuvettes. NMR spectra were recorded at 298 K on a Bruker DPX200 Model Avance (4.7 T) operating at 200 MHz for proton. Spectra were referenced to the residual protio solvent peaks or TMS (tetramethylsilane).

Electrospray ionisation mass spectra were acquired using a Navigator quadrupole instrument (MassLab Group, Finnigan, Manchester, UK) equipped with an Aqua system for atmospheric pressure chemical ionisation (APCI) and electrospray (ESI). The samples were introduced either with a liquid chromatographic pump (P2000, Thermo Separation Products) at a flow rate of 0.3 mL/min using different proportions of H_2O/methanol as the mobile phase, or by direct infusion by the Aqua system. Positive ion spectra were acquired in full scan 2−1600 *m*/*z* in continuum mode.

Materials and Synthesis: Solvents were purchased from SDS as synthesis grade. Acetonitrile was distilled from over P_2O_5 (Prolabo) and stored over molecular sieves. Diethyl ether and THF were distilled from over Na (Panreac) or benzophenone (Fluka), respectively, just previously to their use. CH_2Cl_2 was distilled from over CaH_2 (Aldrich) and stored over molecular sieves. Methanol was distilled from over Mg (Aldrich) and stored in the dark over molecular sieves. Acetone was dried over $CaCl_2$ (Panreac) and stored over molecular sieves.

The macrocyclic ligands 3,6,9,16,19,22-hexaazatricyclo[22.2.2.2^{11,14}]-triaconta-1(27),11(30),12,14(29),24(28),25-hexaene (**H2p**), 3,7,11,18,22,26-hexaazatricyclo[26.2.2.2^{13,16}]tetratriaconta-1(31),13(34),14,16(33),28(32),29-hexaene (**H3p**), 3,6,9,16,19,22-hexamethyl-3,6,9,16,19,22-hexaazatricyclo[22.2.2.2^{11,14}]triaconta-1(27),11(30),12,14(29),24(28),25-hexaene (**Me2p**) 3,6,9,17,20,23-hexamethyl-3,6,9,17,20,23-hexaazatricyclo[23.3.1.1^{11,15}]triaconta-1(29),11,13,15(30),25,27-hexaene (**Me2m**), 3,7,11,18,22,26-hexamethyl-3,7,11,18,22,26-hexaazatricyclo[26.2.2.2^{13,16}]tetratriaconta-1(31),13(34),14,16(33),28(32),29-hexaene (**Me3p**) and 3,7,11,19,23,27-hexamethyl-3,7,11,19,23,27-hexaazatricyclo[27.3.1.1^{13,17}]tetratriaconta-1(33),13,15,17(34),29,31-hexaene (**Me3m**) were prepared according to the published procedures or slight modifications thereof.[17−20] (for structural drawing see Scheme 1).

[$Zn_2(NO_3)_2$(H2p)]$(NO_3)_2$·11/3H_2O (1·11/3H_2O): A methanol (3 mL) solution of $Zn(NO_3)_2$·6H_2O (179 mg, 0.60 mmol) was added dropwise to a vigorously stirred solution of H2p (123 mg, 0.30 mmol) in methanol (6 mL). A white precipitate rapidly appeared. The mixture was stirred for 30 min and then cooled down in an ice bath. The white solid that precipitated was then filtered, washed with methanol and dichloromethane and dried under vacuum. (168 mg, 0.21 mmol, 71%). FT-IR (KBr): ṽ, 3223, 2933, 2878 and 1383 cm^{-1}. $C_{24}H_{38}N_8O_6Zn_2$·11/3H_2O (855.5): calcd. C 33.70, H 5.34, N 16.37; found C 33.87, H 5.36, N 16.31. ^{1}H NMR (200 MHz, D_2O, 25 °C): δ = 2.50−3.20 (m, 16 H, NCH_2), 3.80−4.20 (m, 8 H, $ArCH_2$), 7.36 (s, 8 H, arom.) ppm. ^{13}C NMR (50 MHz, D_2O, 25 °C): δ = 45.9 (NCH_2), 52.0 ($ArCH_2$), 129.8 (arom. tert.), 136.6 (arom. quat.) ppm. MS: *m*/*z* = 727.56 [$Zn_2(NO_3)_2$(H2p)], 538.08 [$Zn(NO_3)$(H2p)].

[Zn_2Cl_4(H2p)]·4H_2O (2·4H_2O): A methanol (3 mL) solution of $ZnCl_2$ (28 mg, 0.20 mmol) was added dropwise to a vigorously stirred solution of H2p (41 mg, 0.10 mmol) in methanol (2.5 mL). A white precipitate rapidly appeared. The mixture was stirred for 30 min and then cooled down in an ice bath. The white solid that precipitated was then filtered, washed with methanol and dichloromethane and dried under vacuum. (25 mg, 0.04 mmol, 37%). $C_{24}H_{38}Cl_4N_6Zn_2$·4H_2O (755.3): calcd. C 38.17, H 6.14, N 11.13; found C 38.08, H 5.43, N 10.93. FT-IR (KBr): ṽ, 3217, 2930, 2874 and 1445 cm^{-1}. ^{1}H NMR (200 MHz, D_2O, 25 °C): δ = 2.50−3.20 (m, 16 H, NCH_2) 3.85 (m, 8 H, $ArCH_2$) 7.34 (s, 8 H, arom.) ppm. ^{13}C NMR (50 MHz, D_2O, 25 °C): δ = 47.8 (NCH_2), 55.3 ($ArCH_2$), 132.4 (arom. tert.), 139.3 (arom. quat.) ppm.

[$Zn_2(NO_3)_2$(H3p)]$(NO_3)_2$·4/3CH_3OH (3·4/3CH_3OH): A methanol (5 mL) solution of $Zn(NO_3)_2$·6H_2O (297 mg, 1 mmol) was added dropwise to a vigorously stirred solution of H3p (233 mg, 0.50 mmol) in methanol (10 mL). A white precipitate rapidly appeared. The mixture was stirred for 30 min and then cooled down in an ice bath. The white solid that precipitated was then filtered, washed with methanol and dichloromethane and dried under vacuum. (328 mg, 0.39 mmol, 77%). FT-IR (KBr): ṽ, 3223, 2933, 2878 and 1383 cm^{-1}. $C_{28}H_{46}N_8O_6Zn_2$·4/3CH_3OH (888.2): calcd. C 39.67, H 5.83, N 15.77; found C 39.84, H 5.86, N 15.73. ^{1}H NMR (200 MHz, D_2O, 25 °C): δ = 1.40−2.00 (m, 8 H, $CH_2CH_2CH_2$), 2.86 (s, 16 H, NCH_2), 3.31 (s, CH_3OH) 3.97 (s, 5 H, $ArCH_2$), 3.77 (s, 3 H, $ArCH_2$), 7.41 (s, 8 H, arom.) ppm. ^{13}C NMR (50 MHz, D_2O, 25 °C): δ = 22.9 (NCH_2) 44.7, 45.4 ($CH_2CH_2CH_2$), 49.5 (CH_3OH), 50.7 ($ArCH_2$) 129.9 (arom. tert.), 133.9, 136.1 (arom. quat.) ppm. MS: *m*/*z* = 783.66 [$Zn_2(NO_3)_3$(H3p)], 656.19 [$Zn(NO_3)_2$(H3p)], 594.19 [$Zn(NO_3)$(H3p)].

[Zn_2Cl_4(H3p)]·7/3H_2O (4·7/3H_2O): A methanol (5 mL) solution of $ZnCl_2$ (27 mg, 0.20 mmol) was added dropwise to a vigorously stirred solution of H3p (47 mg, 0.10 mmol) in methanol (3 mL). A white precipitate rapidly appeared. The mixture was stirred for 2 h and then cooled down in an ice bath. The white solid that precipitated was then filtered, washed with methanol and dried under vacuum. (25 mg, 0.34 mmol, 34%). FT-IR (KBr): ṽ, 3212, 2933, 2874 and 1431 cm^{-1}. $C_{28}H_{46}N_6Zn_2Cl_4$·7/3H_2O (781.3): calcd. C 43.04, H 6.54, N 10.76; found C 43.01, H 6.59, N 10.80. ^{1}H NMR (200 MHz, D_2O, 25 °C): δ = 1.74 (m, 8 H, $CH_2CH_2CH_2$), 2.89 (m, 16 H, NCH_2), 3.96 (s, 5 H, $ArCH_2$), 3.80 (s, 3 H, $ArCH_2$), 7.46 (s, 8 H, arom.) ppm. ^{13}C NMR (50 MHz, D_2O, 25 °C): δ = 22.2 ($CH_2CH_2CH_2$), 43.2, 43.9 (NCH_2), 50.5 ($ArCH_2$), 128.0, 128.2 (arom. tert.), 132.4, 133.5, 134.3 (arom. quat.) ppm. MS: *m*/*z* = 704.01 [Zn_2Cl_3(H3p)], 603.09 [$ZnCl_2$(H3p)], 567.64 [ZnCl(H3p)].

[Zn_2Cl_4(Me2p)] (5): Me2p (50 mg, 0.10 mmol) was dissolved in MeOH (2 mL). A solution of $ZnCl_2$ (28 mg, 0.20 mmol) dissolved in acetone (2 mL) was added to this solution. A white solid rapidly precipitated. The mixture was stirred for 30 min and the white solid filtered. The solid was collected and dissolved in CH_2Cl_2 (3 mL), filtered through celite and the solvent removed under vacuum. The residue that remained was washed with acetone and methanol to obtain the product as a white solid (56 mg, 0.07 mmol, 72%). FT-IR (KBr): ṽ = 1467 cm^{-1}. $C_{30}H_{50}Cl_4N_6Zn_2$ (767.3): calcd. C 46.96, H 6.57, N 10.95; found C 46.84, H 6.82, N 10.75. ^{1}H NMR (200 MHz, CD_2Cl_2, 25 °C): δ = 2.41 (s., 12 H, NCH_3), 2.50−3.10 (m, broad, 22 H, NCH_2 and NCH_3), 3.78 (s, 8 H, $ArCH_2$), 7.39 (s, 8 H, arom.) ppm. ^{13}C NMR (50 MHz, CD_2Cl_2, 25 °C): δ = 32.7, 44.9, 43.3 (NCH_3), 56.0 (NCH_2), 63.7 ($ArCH_2$), 131.2 (arom. tert.), 135.7 (arom. quat.) ppm. ^{1}H NMR (200 MHz, D_2O, 25 °C,): δ = 1.98 (s, 6 H, NCH_3), 2.68 (s, 12 H, NCH_3), 2.85 (m, 8 H, NCH_2), 2.99 (m, 8 H, NCH_2), 3.99 (s, 8 H, $ArCH_2$), 7.56 (s, 8 H, arom.) ppm. ^{13}C NMR (50 MHz, D_2O, 25 °C): δ = 42.0, 43.9, (NCH_3), 53.7, 54.4, (NCH_2), 63.0 ($ArCH_2$), 134.1 (arom. tert.), 136.4 (arom. quat.) ppm. MS: *m*/*z* = 631.14 [$ZnCl_2$(Me2p)], 595.69 [ZnCl(Me2p)].

[Zn_2Cl_4(Me2m)]·2H_2O·CH_3OH (6·2H_2O·CH_3OH): Me2m (78 mg, 0.16 mmol) was dissolved in MeOH (2 mL), and $ZnCl_2$ (43 mg, 0.32 mmol) dissolved in MeOH (2 mL) was added. A white precipi-

 © 2004 Wiley-VCH Verlag GmbH & Co. KGaA, Weinheim

tate rapidly appeared which redissolved upon stirring. The solvent was removed under vacuum and the residue was then dissolved in warm MeOH (5 mL). Upon standing, the product crystallised as white blocks (81 mg, 0.11 mmol, 67%). FT-IR (KBr): $\tilde{\nu}$, 1467 cm^{-1}. $C_{30}H_{50}N_6Zn_2Cl_4 \cdot 2H_2O \cdot CH_3OH$ (835.4): calcd. C 44.57, H 7.00, N 10.06; found C 44.44, H 6.89, N 10.23. ^1H NMR (200 MHz, [D$_6$]DMSO, 25 °C): δ = 2.32 (s, 12 H, NCH_3), 2.41 (s, 9 H, NCH_3 and DMSO) 2.50−2.571 (m, 16 H, NCH_2), 3.43 (s, CH_3OH), 3.77 (s, 8 H, $ArCH_2$), 4.16 (s, broad, OH), 7.38 (m, 6 H, arom.), 7.77 (s, broad, 2 H, arom.) ppm. ^{13}C NMR (50 MHz, [D$_6$]DMSO, 25 °C): δ = 42.8, 43.4 (NCH_3), 48.7 (CH_3OH), 53.3, 54.7 (NCH_2), 60.3 ($ArCH_2$), 127.8, 129.1 (arom. tert.), 136.4 (arom. quat.).

[Zn_2Cl_4(Me3p)]·1/3CH_2Cl_2 (7·1/3CH_2Cl_2): Me3p (65 mg, 0.12 mmol) was dissolved in MeOH/CH_2Cl_2 (2:1 v:v; 3 mL) and a solution of $ZnCl_2$ (32 mg, 0.24 mmol) in MeOH (3 mL) was added. A white precipitate rapidly appeared which was filtered, collected and dried under vacuum (65 mg, 0.08 mmol, 67%). FT-IR (KBr): $\tilde{\nu}$ = 1467 cm^{-1}. $C_{34}H_{58}Cl_4N_6Zn_2 \cdot 1.5CH_2Cl_2$ (950.8): calcd. C 44.84, H 6.47, N 8.84; found C 44.59, H 6.67, N 8.61. ^1H NMR (200 MHz, [D$_6$]DMSO, 25 °C): δ = 1.67 (m, 8 H, $CH_2CH_2CH_2$), 2.18 (s, 12 H, NCH_3), 2.28 (s, 6 H, NCH_3), 2.70−2.30 (m, 16 H, NCH_2), 3.46 (s, 8 H, $ArCH_2$), 7.24 (s, 8 H, arom.) ppm. ^{13}C NMR (50 MHz, [D$_6$]DMSO, 25 °C): δ = 23.3 ($CH_2CH_2CH_2$), 42.2 (NCH_3), 55.0, 55.2 (NCH_2 and CH_2Cl_2), 61.5, 79.6 ($ArCH_2$), 129.1 (arom. tert.),137.5 (arom. quat.) ppm. ^1H NMR (200 MHz, D_2O, 25 °C): δ = 1.89 (m., 8 H, $CH_2CH_2CH_2$), 2.53 (s, 12 H, NCH_3), 2.53 (s, 6 H, NCH_3), 2.83, (m, 16 H, NCH_2), 3.91 (s, 8 H, $ArCH_2$), 7.47 (s, 8 H, arom.) ppm. ^{13}C NMR (50 MHz, D_2O, 25 °C): δ = 23.4 ($CH_2CH_2CH_2$), 43.4 (NCH_3), 56.2, 56.9 (NCH_2), 62.8 ($ArCH_2$), 133.7 (arom. tert.), 136.8 (arom. quat.) ppm. MS: *m*/*z* = 687.25 [$ZnCl_2$(Me3p)], 651.80 [ZnCl(Me3p)].

[Zn_2Cl_4(Me3m)]·H_2O (8·H_2O): Me3m (142 mg, 0.26 mmol) was dissolved in MeOH (3 mL). $ZnCl_2$ (71 mg, 0.52 mmol) dissolved in MeOH (1 mL) was added to this solution. The solution was vigorously stirred until a fine white powder precipitated. The solid was filtered, collected and dried under vacuum (125 mg, 0.15 mmol, 59%). The product was recrystallised from $CHCl_3$ to obtain a white microcrystalline solid insoluble in most common solvents (42 mg, 0.05 mmol, 19.8%). FT-IR (KBr): $\tilde{\nu}$ = 1467 cm^{-1}. $C_{34}H_{58}Cl_4N_6Zn_2 \cdot H_2O$ (841.5): calcd. C 48.53, H 7.19, N 9.99; found C 48.61, H 6.85, N 9.94.

Kinetics of *p*-Nitrophenyl Acetate (NA) Hydrolysis: The hydrolysis rate of NA in the presence of the Zn complexes was measured in a H_2O/CH_3CN (90:10 v:v) solution by an initial-slope method, following the increase in the 402 nm absorption of the released *p*-nitrophenolate at 298 K (± 0.05 K). The molar absorbance of *p*-nitrophenolate was determined at the pH of each measurement. The qionic strength was adjusted to 0.1 with $NaNO_3$. pH was adjusted with Tris buffer (pH 7−9; 50 mM). In a typical experiment, after mixing NA (5.15×10^{-4} M) and the Zn complex (0.1−0.5 mM) in 10% CH_3CN solution at appropriate pH (the reference experiment uses only the Zn^{II} complex), the UV absorption decay was recorded immediately and was followed generally until 2% decay of NA. This provided v_{in} values from which pseudo-first-order rate constants, k_{in}, calculated according to the expression $k_{in} = v_{in}/[NA]$. Second-order rate constants, k_{NA}, were obtained at a given pH from the plot of k_{in} vs. complex concentration.

X-ray Crystallography: Single crystals of $[Zn_2(NO_3)_2(H3p)](NO_3)_2$ (**3**) suitable for X-ray analysis were obtained from a concentrated methanol solution of the complex upon standing. Suitable crystals of [Zn_2Cl_4(Me2p)] (**5**) were obtained as colourless plates by slow evaporation of a CD_2Cl_2 solution. Suitable crystals of [Zn_2Cl_4(Me3p)]·1/3CH_2Cl_2 (**7·1/3CH_2Cl_2**) were obtained as colourless blocks by slow evaporation of a CH_3OH/CH_2Cl_2 (1:1 v:v) solution. Suitable crystals of [Zn_2Cl_4(Me3m)] (**8**) were obtained as colourless blocks by recrystallisation of the crude reaction mixture from a $CHCl_3$/MeOH/benzene/THF (2:1:1:1 v:v) mixture.

For **3**, data were collected on a Bruker Smart CCD diffractometer, using Mo-K_α (λ = 0.71073 Å) radiation. A summary of the fundamental crystal data and refinement data are given in Table 1. Data were collected over a hemisphere of the reciprocal space by combination of three exposure sets. Cell parameters were determined and refined by a least-squares fit of all reflections collected (θ range = 2.33 to 25°, *hkl* from −16, −17, −19 to 13, 18, 19, respectively). Each frame exposure time was of 20 s, covering 0.3° in ω. The first 50 frames were recollected at the end of the data collection to monitor crystal decay. No appreciable decay in the intensities of standard reflections was observed. The structure was solved by direct methods and refined by full-matrix least-squares on F^2 (SHELXS-97).[32] Anisotropic parameters were used in the last cycles of refinement for all non-hydrogen atoms, with exceptions. For the NO_3^- counteranion, no resolvable positional disorder of these atoms was found, and they were isotropically refined. Hydrogen atoms were included in calculated positions and refined as riding on the respective carbon atoms, with the thermal parameters related to the bonded atoms, except H1, H2 and H3, bonded to nitrogen atoms, which were located in a Fourier synthesis, included and their parameters fixed. The largest residual peaks in the final difference map, maximum 1.052 e·$Å^{-3}$, are close to the non-coordinating NO_3^- anion.

The intensity data were collected at 298 K (**8**) or 223 K (**5** and **7·1/3CH_2Cl_2**) on a Stoe Image Plate Diffraction System[33] using Mo-K_α (λ = 0.71073 Å) graphite-monochromated radiation. Image plate distance: 70 mm; φ oscillation scans: 0−200°; step Δφ: 1.0°; 2θ range: 3.27−52.1°; $d_{max}-d_{min}$ = 12.45−0.81 Å. The structures were solved by direct methods using the program SHELXS-97.[34] The H-atoms were included in calculated positions and treated as riding atoms using the SHELXL default parameters. The refinement and all further calculations were carried out using SHELXL-97.[34] The non-H atoms were refined anisotropically, using weighted full-matrix least-squares on F^2. For **7·1/3CH_2Cl_2** a small amount of residual electron density was located in a final difference Fourier synthesis at the origin of the unit cell about a threefold inversion axis. The SQUEEZE routine in PLATON[35] indicated the presence of a solvent accessible region of ca. 100 electrons for a volume of 1507 $Å^3$. This was equated to be equal to one third (1/3) of a highly disordered CH_2Cl_2 molecule per molecule of complex, and the HKL file was modified accordingly. The molecular structure and crystallographic numbering scheme are illustrated in the ORTEP drawing (Figure 1).

Crystallographic data for the structure included in this paper have been deposited with the Cambridge Crystallographic Data Centre as supplementary publication nos. CCDC-212656 ... -212659, for the complexes **3**, **5**, **7·1/3** CH_2Cl_2 and **8**, respectively. These data can be obtained free of charge at http://www.ccdc.cam.ac.uk/conts/retrieving.html [or from the Cambridge Crystallographic Data Centre, 12 Union Road, Cambridge CB2 1EZ, UK; fax: (internat.) +44-1223/336-033; Email: deposit@ccdc.cam.ac.uk].

Supporting Information Available: NMR spectral characterisation data for the complexes described in the present work and VT-^1H NMR spectra of **5**. Kinetic data for the hydrolytic reactions.

 © 2004 Wiley-VCH Verlag GmbH & Co. KGaA, Weinheim

Acknowledgments

This research has been financed by MCYT of Spain through project BQU2000−0458. A. L. is grateful to CIRIT Generalitat de Catalunya (Spain) for a Distinction award and the aid SGR2001-UG-291. M. C. and C. A. are grateful for the award of a doctoral grant from CIRIT and the University of Girona, respectively.

[1] [1a] J. S. Bradshaw, *Aza-Crown Macrocycles*, Wiley: New York, **1993**. [1b]S. Aoki, E. Kimura, *Rev. Mol. Biotech.* **2002**, *90*, 129−155. [1c] C. Bazzicalupi, A. Bencini, E. Berni, S. Ciattini, A. Bianchi, C. Giorgi, P. Paoletti, B. Valtancoli, *Inorg. Chim. Acta* **2001**, *317*, 259−267. [1d] J. Nelson, M. Nieuwenhuyzen, I. M. Pál, R. Town, *Chem. Commun.* **2002**, 2266−2267. [1e] P. Dapporto, M. Formica, V. Fusi, M. Micheloni, P. Paoli, R. Pontellini, P. Romani, P. Rossi, *Inorg. Chem.* **2000**, *39*, 2156−2163. [1f] D. Kumar Chand, H.-J. Schneider, J. A. Aguilar, F. Escart, E. García-España, S. V Luis, *Inorg. Chim. Acta* **2000**, *316*, 71−78. [1g] F. Escarti, C. Miranda, L. Lamarque, J. LaTorre, E. García-España, M. Kumar, V. Arán, P. Navarro, *Chem. Commun.* **2002**, 936−937.

[2] [2a] R. M. Izatt, K. Pawlak, J. S. Bradshaw, R. L. Bruening, *Chem. Rev.* **1995**, *95*, 2529. [2b] J. M. Lehn, *Supramolecular Chemistry*, VCH: New York, **1995**. [2c]M. Formica, V. Fusi, M. Micheloni, R. Pontellini, P. Romani, *Coord. Chem. Rev.* **1999**, *184*, 347−363. [2d] X. Sun, M. Wuest, G. R. Weisman, E. H. Wong, D. P. Reed, C. A. Boswell, R. Motekaitis, A. E. Martell, M. J. Welch, C. J. Anderson, *J. Med. Chem.* **2002**, *45*, 469−477.

[3] M. Rodriguez, A. Llobet, M. Corbella, A. E. Martell, J. Reibenspies, *Inorg. Chem.* **1999**, *38*, 2328−2334.

[4] C. Harding, V. Macknee, J. Nelson, *J. Am. Chem. Soc.* **1991**, *113*, 9684−9685.

[5] C. Harding, J. Nelson, M. C. R. Symons, J. Wyatt, *J. Chem. Soc., Chem. Commun.* **1994**, 2499−2500.

[6] W. H. J. Chapman, R. Breslow, *J. Am. Chem. Soc.* **1995**, *117*, 5462−5469.

[7] G. K. Ragunathan, H.-J. Schneider, *Angew. Chem. Int. Ed. Engl.* **1996**, *35*, 1219−1221.

[8] M. Forconi, N. H. Williams, *Angew. Chem. Int. Ed.* **2002**, *41*, 849−852.

[9] C. Bazzicalupi, A. Bencini, A. Bianchi, V. Fusi, C. Giorgi, P. Paoletti, B. Valtancoli, D. Zanchi, *Inorg. Chem.* **1997**, *36*, 2784.

[10] C. Wendelstorf, S. Warzeska, E. Kövári, R. J. Kramer, *J. Chem. Soc., Dalton Trans.* **1996**, 3087.

[11] A. Bencini, E. Berni, A. Bianchi, V. Fedi, C. Giorgi, P. Paoletti, B. Valtancoli, *Inorg. Chem.* **1999**, *38*, 6323−6325.

[12] D. E. Wilcox, *Chem. Rev.* **1996**, *96*, 2435−2458.

[13] M. I. Page, A. P. Laws, *Chem. Commun.* **1998**, 1609−1617.

[14] R. B. Davies, E. P. Abraham, *Biochem. J.* **1974**, *143*, 129−135.

[15] W. N. Lipscomb, N. Sträter, *Chem. Rev.* **1996**, *96*, 2375−2433.

[16] N. Strater, W. N. Lipscomb, T. Klabunde, B. Krebs, *Angew. Chem. Int. Ed. Engl.* **1996**, *35*, 2024−2055.

[17] R. Menif, A. E Martell, P. J. Squattrito, A. Clearfield, *Inorg. Chem.* **1990**, *29*, 4723−4729.

[18] M. Pietraszkiewicz, R. Gasiorowski, *Chem. Ber.* **1990**, *123*, 405−406.

[19] A. Llobet, J. Reibenspies, A. E Martell, *Inorg. Chem.* **1994**, *33*, 5946−5951.

[20] T. Clifford, A. M. Danby, P. Lightfoot, D. T. Richens, R. W. Hay, *J. Chem. Soc., Dalton Trans.* **2001**, 240−247.

[21] [21a] K.-W. Yang, Y.-Z. Wang, Z.-X. Huang, J. Sun, *Polyhedron* **1997**, *16*, 109. [21b] J. A. Halfen, S. Mahapatra, E. C. Wilkinson, A. J. Gengenbach, V. G. Young Jr., L. Que Jr., W. B. Tolman, *J. Am. Chem. Soc.* **1996**, *118*, 763−776. [21c] R. Gregorzik, J. Wirbser, H. Vahrenkamp, *Chem. Ber.* **1992**, *125*, 157. [21d] A. Looney, G. Parkin, *Inorg. Chem.* **1994**, *33*, 1234−1237. [21e] C. Kimblin, W. E. Allen, G. Parkin, *J. Chem. Soc., Chem. Commun.* **1995**, 1813.

[22] A. Bencini, A. Bianchi, V. Fusi, C. Giorgi, P. Paoletti, J. A. Ramirez, B. Valtancoli, *Inorg. Chem.* **1999**, *38*, 2064.

[23] C. Bazzicalupi, A. Bencini, A. Bianchi, V. Fusi, C. Giorgi, P. Paoletti, A. Stefani, B. Valtancoli, *Inorg. Chem.* **1995**, *34*, 552−559.

[24] M. Costas, R. Xifra, A. Llobet, M. Solà, J. Robles, T. Parella, H. Stoeckli-Evans, M. Neuburger, *Inorg. Chem.* **2003**, *42*, 4456−4468.

[25] D. Meyerstein, *Coord. Chem. Rev.* **1999**, *185*, 141−147.

[26] [26a] S. Htoon, M. F. C. Ladd, *J. Cryst. Mol. Struct.* **1973**, *3*, 95. [26b] P. K. S. Gupta, L. W. Houk, D. Van der Helm, M. B. Hossain, *Acta Crystallogr., Sect. B* **1982**, *38*, 1818. [26c] F. Cariati, G. Ciani, L. Menabue, G. C. Pecallani, G. Rassu, A. Sironi, *Inorg. Chem.* **1983**, *22*, 1897−1902. [26d] U. Florke, H.-J. Haupt, *Acta Crystallogr., Sect. C* **1993**, *49*, 803. [26e] U. Florke, H.-J. Z. Haupt, *Kristallogr.* **1993**, *206*, 288. [26f] R. M. Zu. Kocker, G. Frenzen, B. Neumuller, K. Dehnicke, J. Magull, *Z. Anorg. Allg. Chem.* **1994**, *620*, 431. [26g] Y. Li, Y.-H. Lai, K. F. Mok, M. G. B. Drew, *Inorg. Chim. Acta* **1999**, *285*, 31−38. [26h] V. I. Ovcharenko, S. V. Fokin, G. V. Romanenko, I. V. Korobkov, P. Rey, *Izv. Akad. Nauk SSSR, Ser. Khim.* **1999**, 1539. [26i] A. Alexakis, A. Tomassini, C. Chouillet, S. Roland, P. Mangeney, G. Bernardinelly, *Angew. Chem. Int. Ed.* **2000**, *39*, 4093. [26j] H. Pfistner, D. Fenske, *Z. Anorg. Allg. Chem.* **2001**, *627*, 575.

[27] [27a] V. W.-W. Yam, Y.-L. Pui, K.-K. Cheung, *Inorg. Chem.* **2000**, *39*, 5741−5746. [27b] Q. Wu, J. A. Lavigne, Y. Tao, M. D′Iorio, S. Wang, *Inorg. Chem.* **2000**, *39*, 5248−5254. [27c] W. Yang, H. Schmider, Q. Wu, Y.-S. Zhang, S. Wang, *Inorg. Chem.* **2000**, *39*, 2397−2404. [27d] S. C. Goel, M. Y. Chiang, D. J. Rauscher, W. E. Buhro, *J. Am. Chem. Soc.* **1993**, *115*, 160−169. [27e] Y. Byun, D. Min, J. Do, Y. Hun, Y. Do, *Inorg. Chem.* **1996**, *35*, 3981−3989. [27f] S. J. Brudenell, L. Spiccia, D. C. R. Hockless, E. R. T. Tiekink, *J. Chem. Soc., Dalton Trans.* **1999**, *9*, 1475−1482. [27g] T. Kajiwara, S. Yokozawa, T. Ito, N. Iki, N. Morohashi, S. Miyano, *Angew. Chem. Int. Ed.* **2002**, *41*, 2076−2078.

[28] [28a] C. Bazzicalupi, A. Bencini, E. Berni, A. Bianchi, V. Fedi, V. Fusi, C. Giorgi, P. Paoletti, B. Valtancoli, *Inorg. Chem.* **1999**, *38*, 4115−4122. [28b] C. Bazzicalupi, A. Bencini, A. Bianchi, V. Fusi, C. Giorgi, P. Paoletti, B. Valtancoli, D. Zanchi, *Inorg. Chem.* **1997**, *36*, 2784−2790. [28c] T. Koike, M. Inoue, E. Kimura, M. Shiro, *J. Am. Chem. Soc.* **1996**, *118*, 3091−3099. [28d] K. G. Ragunathanm, H.-J. Scheneider, *Angew. Chem. Int. Ed. Engl.* **1996**, *35*, 1219−1220. [28e] W. H. Chapman Jr., R. Breslow, *J. Am. Chem. Soc.* **1995**, *117*, 5462−5469. [28f] T. Koike, E. Kimura, *J. Am. Chem. Soc.* **1991**, *113*, 8935−8941.

[29] L. Bonfá, M. Gatos, F. Mancin, P. Tecilla, U. Tonellato, *Inorg. Chem.* **2003**, *42*, 3943−3949.

[30] M. Ruf, K. Weis, H. Vahrenkamp, *J. Chem. Soc., Chem. Commun.* **1994**, 135−136.

[31] R. J. Motekaitis, Y. Li, Y. Murase, A. E. Martell, *J. Coord. Chem.* **1996**, *37*, 173.

[32] Stoe & Cie (**1998**). IPDS Software. Stoe & Cie GmbH, Darmstadt, Germany.

[33] G. M. Sheldrick, "SHELXS-97 Program for Crystal Structure Determination", *Acta Crystallogr., Sect. A* **1990**, *46*, 467−473.

[34] G. Sheldrick, "SHELXL-97", **1998**, University of Göttingen, Göttingen, Germany.

[35] A. L. Spek, "PLATON/PLUTON", *Acta Crystallogr., Sect. A* **1990**, *46*, C-34.

Received June 18, 2003
Early View Article
Published Online January 19, 2004

 © 2004 Wiley-VCH Verlag GmbH & Co. KGaA, Weinheim

Synthesis, Characterization and Properties of Transition Metal Pd/Pt [60]Fullerene Complexes Containing Phosphane Ligands − Crystal Structure of $[Pd(\eta^2\text{-}C_{60})\{Ph_2PCH_2(CH_2OCH_2)_2CH_2PPh_2\}]$

Li-Cheng Song,*[a] Guang-Ao Yu,[a] Hu-Ting Wang,[a] Fu-Hai Su,[a] Qing-Mei Hu,[a] Ying-Lin Song,[b] and Ya-Chen Gao[b]

Keywords: Fullerenes / Palladium / Phosphanes / Platinum

A solution of C_{60} in toluene reacts with $Pd(dba)_2$ or $Pd_2(dba)_3$ (dba = dibenzylideneacetone) and monophosphanes in a 1:1:2 molar ratio to give the corresponding Pd monophosphane fullerene derivatives $[Pd(\eta^2\text{-}C_{60})L_2]$ [L = $P(2\text{-Fu})_3$ (Fu = furyl) **1**; L = $P(2\text{-Fu})Ph_2$ **2**; L = PPh_2H **3**; L = $P(Fc)Ph_2$ (Fc = ferrocenyl) **4**; L = $P(Fc)_2Ph$ **5**], whereas reaction with $M(dba)_2$ (M = Pd, Pt) and subsequent treatment with diphosphanes in 1:1:1 molar ratio afforded the corresponding Pd/Pt diphosphane fullerene complexes $[Pd(\eta^2\text{-}C_{60})\{Ph_2PCH_2(CH_2OCH_2)_nCH_2PPh_2\}]$ (n = 1 **6**; n = 2 **7**; n = 3 **8**) and $[Pt(\eta^2\text{-}C_{60})\{Ph_2PCH_2(CH_2OCH_2)_nCH_2PPh_2\}]$ (n = 1 **9**; n = 2 **10**; n =3 **11**). All the new fullerene complexes **1**–**11** were characterized by elemental analysis, IR, ^1H NMR and ^{31}P NMR spectroscopy, as well as by X-ray diffraction analysis (for **7**). The optical limiting properties of **3**–**5** were determined and the possible pathways for the "one pot" reactions leading to **1**–**11** are briefly discussed.

(© Wiley-VCH Verlag GmbH & Co. KGaA, 69451 Weinheim, Germany, 2004)

Introduction

The synthesis, structural characterization, and properties of transition metal fullerene complexes have attracted great attention,[1] since the discovery of [60]fullerene[2] and its synthesis in macroscopic quantities.[3] These complexes may be classified into two major categories: exohedral metal complexes in which the fullerene behaves mainly as an electron-deficient alkene ligand directly π-bonded to transition metal center,[1] and endohedral compounds in which the metal atom is encapsulated by the fullerene cage.[4] We are interested in exohedral transition metal fullerene complexes[5] because it can be expected that the exohedral modification of the fullerene core using different metals with ancillary ligands may change the structure and properties of the fullerene itself and allow us to obtain new transition metal fullerene derivatives, possibly with novel structures and unique properties. In this article we will describe the synthesis and spectroscopic characterization of a series of new transition metal Pd/Pt [60]fullerene complexes containing mono- and diphosphane ligands. The nonlinear optical properties of some of the new derivatives and the crystal structure of one representative fullerene complex — $[Pd(\eta^2\text{-}C_{60})\{Ph_2PCH_2(CH_2OCH_2)_2CH_2PPh_2\}]$ — are also reported.

[a] Department of Chemistry, State Key Laboratory of Elemento-Organic Chemistry, Nankai University, Tianjin 300071, China
Fax: (internat.) +86-22-2350-4853
E-mail: lcsong@public.tpt.tj.cn
[b] Department of Physics, Harbin Institute of Technology, Harbin 150001, China

Results and Discussion

Synthesis and Characterization of $[Pd(\eta^2\text{-}C_{60})L_2]$

A toluene solution of C_{60} reacts with the mononuclear Pd complex $Pd(dba)_2$ (dba = dibenzylideneacetone) and the monophosphanes $P(2\text{-Fu})_3$ (Fu = furyl), $P(2\text{-Fu})_2Ph$, PPh_2H or $P(Fc)Ph_2$ in a 1:1:2 molar ratio at room temperature to give the corresponding monophosphane fullerene complexes **1**−**4**, respectively, in 63−93% yields, whereas it reacts with the dinuclear Pd complex $Pd_2(dba)_3$ and the monophosphane $P(Fc)_2Ph$ (Fc = ferrocenyl) under similar conditions to afford complex **5** in 76% yield (Scheme 1). Our attempts to prepare $[Pd(\eta^2\text{-}C_{60})\{P(Fc)_3\}_2]$ by the reac-

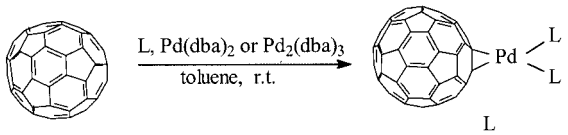

L	
1	$P(2\text{-Fu})_3$
2	$P(2\text{-Fu})Ph_2$
3	PPh_2H
4	$P(Fc)Ph_2$
5	$P(Fc)_2Ph$

Scheme 1

 © 2004 Wiley-VCH Verlag GmbH & Co. KGaA, Weinheim DOI: 10.1002/ejic.200300513

tion of a toluene solution of C_{60} with $Pd(dba)_2$ or $Pd_2(dba)_3$ followed by treatment with the monophosphane $P(Fc)_3$ under similar conditions were unsuccessful, probably due to the very low nucleophilicity of $P(Fc)_3$ caused by the three bulky ferrocenyl groups attached to the phosphorus atom.

It is believed that the sequential "one-pot" reactions leading to **1**−**5** include an intermediate fullerene complex $(C_{60}Pd)_n$ generated from C_{60} and $Pd(dba)_2$ or $Pd_2(dba)_3$, which reacts further with the monophosphanes to yield **1**−**5**. This pathway is suggested as C_{60} is known to react with $Pd_2(dba)_3$ to produce a black, insoluble polymer $(C_{60}Pd)_n$ ($n \approx 1$),[6] which can be depolymerized by monophosphanes to give the fullerene derivatives $[PdC_{60}L_2]$ (L = PPh_3, PEt_3).[7] This pathway is consistent with our observation that C_{60} reacts with $Pd(dba)_2$ or $Pd_2(dba)_3$ in toluene to give black suspensions.

Complexes **1**−**5** are air-stable solids that dissolve in polar solvents such as toluene, chlorobenzene, THF and CS_2, but do not dissolve in nonpolar solvents such as petroleum ether and hexane. In solution, **1**−**5** are air sensitive, and can release C_{60} completely within 1−2 days.

The IR spectra of **1**−**5** display four absorption bands in the range $\tilde{\nu}$ = 1435−521 cm^{-1} for their C_{60} cores,[8] while the ^{31}P NMR spectra of **1**−**5** each exhibit one singlet in the region δ = 7−30 ppm for the two identical P atoms. The ^1H NMR spectra of **1**−**5** show the corresponding signals for their respective hydrogen-containing groups. The UV/Vis spectra of **1**−**5** display two intense bands between 200 and 400 nm; the new weak broad band appearing at ca. 440 nm suggests that the C_{60} ligand is coordinated to palladium in an η^2-fashion in each of the compounds.[9]

The nonlinear optical properties of [60]fullerene and its derivatives are of considerable interest, largely because of their potential applications as optical limiting materials.[10−13] We recently studied the optical limiting properties of the fullerene derivatives **3**−**5**. Figure 1 shows the optical limiting curves of **3**−**5**, from which it can be seen that the optical limiting properties of **4** and **5** are virtually the same within the experimental accuracy. They display better optical limiting characteristics than **3**, probably due to both phenyl and ferrocenyl groups having stronger electron-donating ability than that of a hydrogen atom.[14]

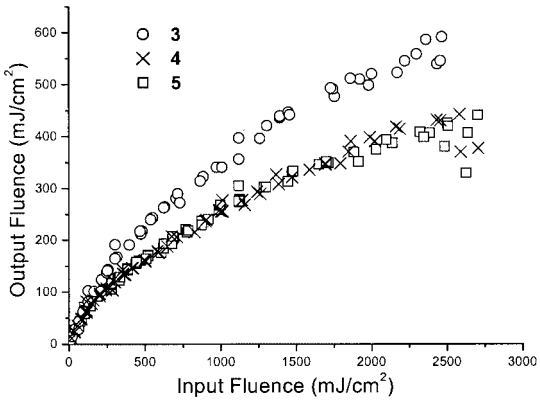

Figure 1. Optical limiting of **3**−**5** determined in toluene solution: **3** (6.26×10^{-5} mol/L); **4** (3.74×10^{-5} mol/L); **5** (5.10×10^{-5} mol/L)

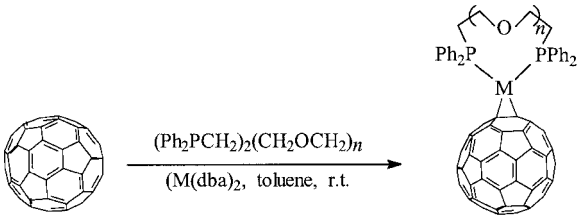

	M	n		M	n
6	Pd	1	**9**	Pt	1
7	Pd	2	**10**	Pt	2
8	Pd	3	**11**	Pt	3

Scheme 2

Synthesis and Characterization of $[Pd(\eta^2\text{-}C_{60})\{Ph_2PCH_2(CH_2OCH_2)_nCH_2PPh_2\}]$ and $[Pt(\eta^2\text{-}C_{60})\{Ph_2PCH_2(CH_2OCH_2)_nCH_2PPh_2\}]$

Similarly, C_{60} reacted with mononuclear complexes $M(dba)_2$ (M = Pd, Pt) in toluene, followed by in situ treatment with diphosphanes $Ph_2PCH_2(CH_2OCH_2)_nCH_2PPh_2$ (n = 1−3) in 1:1:1 molar ratio at room temperature to afford the first examples of the ether-chain-bridged diphosphane fullerene complexes **6**−**11** (M = Pd: n = 1 **6**, n = 2 **7**, n = 3 **8**; M = Pt: n = 1 **9**, n = 2 **10**, n = 3 **11**) in 61−94% yield (Scheme 2).

Presumably, these "one-pot" reactions for production of **6**−**11** also involve an intermediate polymer, either $(C_{60}Pd)_n$ or $(C_{60}Pt)_n$, generated from C_{60} and $M(dba)_2$ (M = Pd, Pt); the in situ reaction of $(C_{60}Pd)_n$ or $(C_{60}Pt)_n$ with the diphosphanes affords **6**−**11**. C_{60} is known to react with $Pt(dba)_2$ to give a black, insoluble polymer $(C_{60}Pt)_n$ ($n \approx 1$), and treatment of $(C_{60}Pt)_n$ with monophosphanes affords $[PtC_{60}L_2]$ (L = PPh_3, PEt_3).[15] Similarly, reaction of C_{60} with $Pd_2(dba)_3$ produces the polymer $(C_{60}Pd)_n$ ($n \approx 1$),[6] which reacts with dppe to yield $[PdC_{60}(dppe)]$.[7] We also observed the formation of black suspensions when C_{60} was reacted with $M(dba)_2$ (M = Pd, Pt) in toluene.

Similar to **1**−**5**, complexes **6**−**11** are air-stable solids, which are soluble in polar solvents, but insoluble in nonpolar solvents. In solution, **6**−**11** are air sensitive, but less so than **1**−**5**; they release C_{60} completely after two or three days. Compounds **6**−**11** were fully characterized by elemental analysis and spectroscopy, and **7** by X-ray crystallography. For instance, the IR spectra of **6**−**11** show four bands in the range $\tilde{\nu}$ = 1434−525 cm^{-1} for their C_{60} spheres,[8] whereas the UV/Vis spectra of **6**−**11** display two intense bands in the 200−400 nm range and one weak broad band at ca. 440 nm, indicating that the C_{60} ligand is coordinated to Pd or Pt in an η^2-mode in each of these complexes.[9] In addition, the ^{31}P NMR spectra of **6**−**8** show a singlet at about δ = 16 ppm for the two identical P atoms in each of **6**−**8**, whereas the spectra of **9**−**11** exhibit a singlet at about δ = 18 ppm, along with two satellite singlets due to ^{195}Pt-

 © 2004 Wiley-VCH Verlag GmbH & Co. KGaA, Weinheim

^{31}P coupling, attributed to the two identical P atoms in each of **9**−**11**.

Crystal Structure of 7

The molecular structure of **7** has been unequivocally confirmed by single-crystal X-ray diffraction techniques (Figure 2). Figure 3 displays its cell packing. Selected bond lengths and angles are listed in Table 1. As can be seen from Figure 2, complex **7** indeed consists of a C_{60} ligand bound to the Pd atom in an η^2-fashion by the C(1)−C(2) 6:6 bond, and a diphosphane ligand $Ph_2PCH_2(CH_2OCH_2)_2CH_2PPh_2$ chelated to the Pd atom through the P(1) and P(2) atoms. In addition, from Figure 3 it can be seen that each crystal cell contains two molecules of **7** and two molecules of MeOH. The closest contact between solvent MeOH and **7** [2.467 Å, from the oxygen atom of MeOH to C(10) of the C_{60} ligand] is less than the sum of the van der Waals radii of C and O (3.22 Å),[16] which might be due to disorder of the MeOH molecule. In addition, the disordered MeOH molecule could also give rise to the relatively high *R* value (0.1426) for the structure of **7**.

To the best of our knowledge, **7** is the first crystallographically characterized transition metal fullerene complex containing an ether-chain-bridged diphosphane ligand. The Pd coordination geometry of **7** is similar to that of its monophosphane PPh_3-containing analogue [Pd(η^2-C_{60})(PPh_3)$_2$].[17] Figure 4 shows that the corresponding bond lengths and angles within the coordination spheres of the Pd atoms of these two complexes are very similar.

It is noteworthy that the C(1)−C(2) bond lengths of **7** and [Pd(η^2-C_{60})(PPh_3)$_2$][17] are slightly longer than the 6:6 bond length in free C_{60},[1a] due to the metal-to-C_{60} π-back-

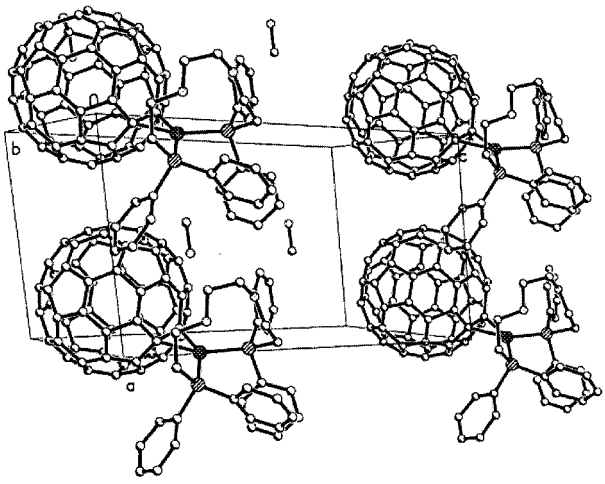

Figure 3. Cell packing of **7**

Table 1. Selected bond lengths (Å) and angles (°) for **7**

Pd(1)−C(1)	2.060(18)	P(1)−C(73)	1.80(2)
Pd(1)−C(2)	2.119(17)	P(1)−C(67)	1.83(2)
Pd(1)−P(1)	2.297(5)	P(2)−C(79)	1.77(2)
Pd(1)−P(2)	2.344(6)	P(2)−C(85)	1.81(2)
P(1)−C(61)	1.76(2)	C(1)−C(2)	1.43(3)
C(1)−Pd(1)−C(2)	40.1(7)	C(61)−P(1)−C(67)	102.8(9)
C(1)−Pd(1)−P(1)	103.2(5)	C(73)−P(1)−C(67)	100.7(9)
C(2)−Pd(1)−P(1)	143.2(5)	C(61)−P(1)−Pd(1)	117.9(6)
C(1)−Pd(1)−P(2)	150.5(5)	C(79)−P(2)−C(85)	102.1(9)
C(2)−Pd(1)−P(2)	110.4(5)	C(79)−P(2)−C(78)	101.7(10)
P(1)−Pd(1)−P(2)	106.27(19)	C(85)−P(2)−C(78)	106.9(10)
C(61)−P(1)−C(73)	103.5(10)	C(79)−P(2)−Pd(1)	113.7(6)

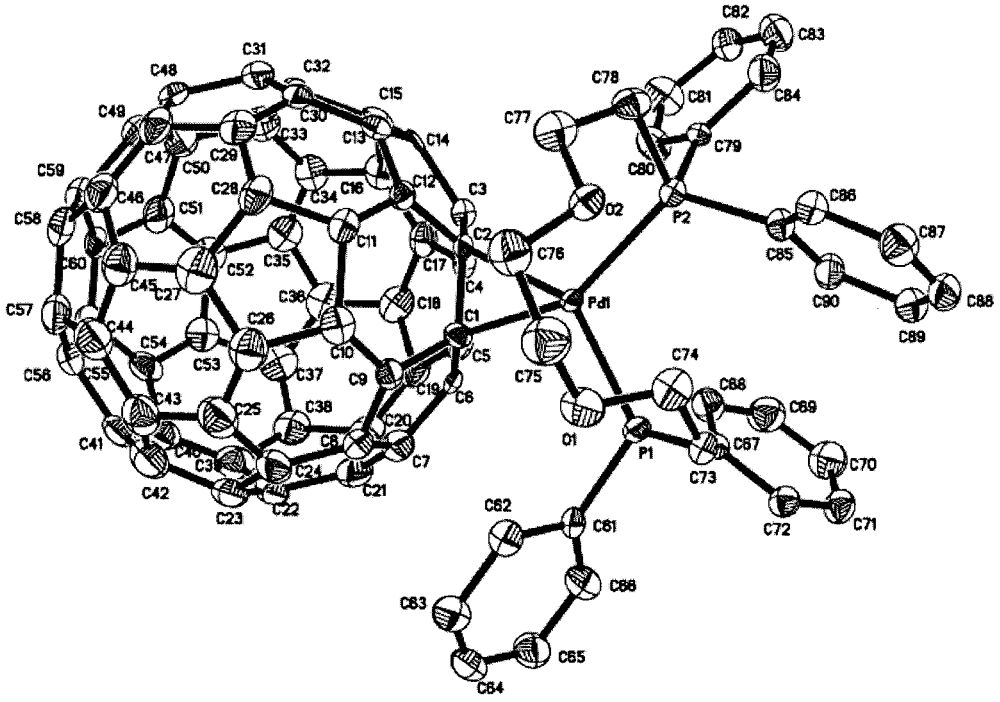

Figure 2. ORTEP diagram of **7**

 © 2004 Wiley-VCH Verlag GmbH & Co. KGaA, Weinheim

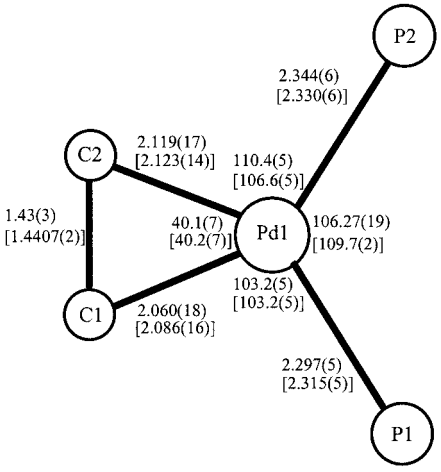

Figure 4. The Pd coordination sphere in **7** (lengths in angstroms and angles in degrees); values for its PPh_3 analogue[17] are given in brackets

donation.[1b] In addition, the Pd coordination geometries of **7** and $[Pd(\eta^2\text{-}C_{60})(PPh_3)_2]$ are square planar, the five atoms C(1), C(2), P(1), P(2) and Pd being coplanar, with deviations from the least-squares plane of less than 0.02 Å for **7** and 0.06 Å for $[Pd(\eta^2\text{-}C_{60})(PPh_3)_2]$.[17]

Interestingly, complex **7** could be regarded as a hybrid of a metallocrown ether and a fullerene, in which the Pd atom, part of an eleven-membered metallocrown ether ring [Pd(1)P(1)C(73)C(74)O(1)C(75)C(76)O(2)C(77)C(78)P(2)], is bound to the fullerene through the C(1)−C(2) 6:6 bond. In view of the unique structures and novel properties of both crown ether and fullerene, it can be expected that such modified hybrids might find practical applications in catalysis, molecular recognition and materials science.[1,18]

Experimental Section

General: All reactions were carried out under a highly purified nitrogen atmosphere using standard Schlenk or vacuum-line techniques. Toluene and hexane were distilled from Na/benzophenone ketyl. Other solvents were bubbled with nitrogen for at least 20 minutes before use. $Pd(dba)_2$,[19] $Pd_2(dba)_3$,[20] $P(Fc)_3$,[21] $P(Fc)_2Ph$,[22] $P(Fc)Ph_2$,[22] PPh_2H,[23] $P(2\text{-}Fu)_3$,[24] $P(2\text{-}Fu)Ph_2$ [25] and $Pt(dba)_2$ [26] were prepared according to literature methods. C_{60} (99.9%) is available commercially.

^1H NMR and ^{31}P NMR were recorded on a Bruker AC-P200 spectrometer, UV/Vis spectra on a Shimadzu UV-240 spectrometer and IR spectra on a Bio-Rad FTS 135 spectrometer. Elemental analysis was performed on an Elementar Vario EL analyzer. Melting points were determined on a Yanaco MP-500 apparatus.

Preparation of $[Pd(\eta^2\text{-}C_{60})\{P(2\text{-}Fu)_3\}_2]$ (1): A 50-mL three-necked flask equipped with a magnetic stir-bar, a rubber septum and a nitrogen inlet tube was charged with C_{60} (0.036 g, 0.05 mmol) and toluene (16 mL). $Pd(dba)_2$ (0.029 g, 0.05 mmol) was added to the purple toluene solution and then the mixture was stirred at room temperature for 0.5 h to give a black suspension. $P(2\text{-}Fu)_3$ (0.023 g, 0.10 mmol) was added to this suspension and the new mixture was stirred for another 0.5 h to produce a deep green solution. The solution was carefully layered with hexane (40 mL). After standing overnight, the mixture was filtered to give a precipitate, which was washed with (10 × 2 mL) of toluene and dried in vacuo. 0.054 g (84%) of **1** was obtained as a black solid. M.p. > 300 °C. ^1H NMR (200 MHz, $CDCl_3$, TMS): δ = 6.39 (s, 6 H, 6 H^4 of furan ring), 6.78 (s, 6 H, 6 H^3 of furan ring), 7.64 (s, 6 H, 6 H^5 of furan ring) ppm. ^{31}P NMR (81.0 MHz, $CDCl_3$, H_3PO_4): δ = 30.04 (s, 2 P) ppm. IR (KBr disk): $\tilde{\nu}$ = 2327 (m), 1458 (m), 1427 (m) (C_{60}), 1364 (m), 1213(m), 1183 (m) (C_{60}), 1159 (m), 1122(m), 1009 (s), 906 (m), 745 (s), 592 (m), 577(m) (C_{60}), 524 (s) (C_{60}), 490 (s), 438 (m) cm^{-1}. UV/Vis (PhCl): λ_{max} (log ε) = 285.0 (4.93), 333.3 (5.11), 406.7 (3.85), 435.5 (3.84) nm. $C_{84}H_{18}O_6P_2Pd$ (1291.43): calcd. C 78.12, H 1.40; found C 77.95, H 1.50.

Preparation of $[Pd(\eta^2\text{-}C_{60})\{P(2\text{-}Fu)Ph_2\}_2]$ (2): This complex was prepared similarly, with $P(2\text{-}Fu)Ph_2$ (0.025 g, 0.10 mmol) instead of $P(2\text{-}Fu)_3$; 0.042 g (63%) of **2** was obtained as a black solid. M.p. > 300 °C. ^1H NMR (200 MHz, $CDCl_3$, TMS): δ = 6.35 (s, 2 H, 2 H^4 of furan ring), 6.78 (s, 2 H, 2 H^3 of furan ring), 7.14−7.75 (m, 22 H, 4 C_6H_5, 2 H^5 of furan ring) ppm. ^{31}P NMR (81.0 MHz, $CDCl_3$, H_3PO_4): δ = 7.04 (s, 2 P) ppm. IR (KBr disk): $\tilde{\nu}$ = 1481 (m), 1434 (m) (C_{60}), 1356 (m), 1212 (m), 1183 (m) (C_{60}), 1120 (m), 1097 (m), 1009 (s), 904 (m), 874 (m), 742 (s), 693 (s), 577(m) (C_{60}), 524 (s) (C_{60}), 489 (m), 432 (m) cm^{-1}. UV/Vis (PhCl): λ_{max} (log ε) = 285.0 (4.91), 333.3 (4.93), 405.8 (4.17), 437.5(3.99) nm. $C_{92}H_{26}O_2P_2Pd$ (1331.58): calcd. C 82.98, H 1.97; found C 82.93, H 2.10.

Preparation of $[Pd(\eta^2\text{-}C_{60})(PPh_2H)_2]$ (3): This complex was prepared similarly, with PPh_2H (0.019 g, 0.10 mmol) in place of $P(2\text{-}Fu)_3$; 0.056 g (93%) of **3** was obtained as a black solid. M.p. 282−283 °C. ^1H NMR (200 MHz, $CDCl_3$, TMS): δ = 7.48−7.74 (m, 20 H, 4 C_6H_5), 8.08 (d, J = 484 Hz, 2 H, 2 HP) ppm. ^{31}P NMR (81.0 MHz, $CDCl_3$, H_3PO_4): δ = 22.50 (s, 2 P) ppm. IR (KBr disk): $\tilde{\nu}$ = 2923 (m), 1457 (m), 1435 (m) (C_{60}), 1183 (m) (C_{60}), 1107 (m), 1036 (m), 1000 (m), 821 (m), 746 (m), 696 (s), 577(m) (C_{60}), 524 (s) (C_{60}), 489 (m), 430 (m) cm^{-1}. UV/Vis (PhCl): λ_{max} (log ε) = 285.0 (4.50), 331.7 (4.42), 405.8 (3.85), 436.0 (3.92) nm. $C_{84}H_{22}P_2Pd$ (1199.47): calcd. C 84.11, H 1.85; found C 84.15, H 2.00.

Preparation of $[Pd(\eta^2\text{-}C_{60})\{P(Fc)Ph_2\}_2]$ (4): This complex was prepared similarly, with $P(Fc)Ph_2$ (0.037 g, 0.10 mmol) instead of $P(2\text{-}Fu)_3$; 0.053 g (68%) of **4** was obtained as a black solid. M.p. > 300 °C. ^1H NMR (200 MHz, $CDCl_3$, TMS): δ = 3.84 (s, 4 H, 2 H^3, 2 H^4), 4.01 (s, 10 H, 2 C_5H_5), 4.19 (s, 4 H, 2 H^2, 2 H^5), 7.25−7.75 (m, 20 H, 4 C_6H_5) ppm. ^{31}P NMR (81.0 MHz, $CDCl_3$, H_3PO_4): δ = 17.16 (s, 2 P) ppm. IR (KBr disk): $\tilde{\nu}$ = 3052 (m), 1570 (m), 1480 (m), 1458 (m), 1434 (m) (C_{60}), 1354 (m), 1306 (m), 1185 (m) (C_{60}), 1160(m), 1098 (m), 1028 (m), 1001 (m), 820 (s), 741 (s), 696 (s), 622 (m), 579(m) (C_{60}), 524 (s) (C_{60}), 485 (s), 430 (m) cm^{-1}. UV/Vis (PhCl): λ_{max} (log ε) = 287.0 (4.82), 333.0 (4.73), 405.6 (4.12), 432.5 (4.04) nm. $C_{104}H_{38}Fe_2P_2Pd$ (1567.51): calcd. C 79.69, H 2.44; found C 79.50, H 2.54.

Preparation of $[Pd(\eta^2\text{-}C_{60})\{P(Fc)_2Ph\}_2]$ (5): This complex was prepared similarly, with $Pd_2(dba)_3{\cdot}C_6H_6$ (0.026 g, 0.025 mmol) and $P(Fc)_2Ph$ (0.048 g, 0.10 mmol) instead of $Pd(dba)_2$ and $P(2\text{-}Fu)_3$; 0.068 g (76%) of **5** was obtained as a black solid. M.p. > 300 °C. ^1H NMR (200 MHz, $CDCl_3$, TMS): δ = 4.18 (s, 8 H, 4 H^3, 4 H^4), 4.38 (s, 20 H, 4 C_5H_5), 4.83, 5.03 (s, s, 8 H, 4 H^2, 4 H^5), 7.30−7.95 (m, 10 H, 2 C_6H_5) ppm. ^{31}P NMR (81.0 MHz, $CDCl_3$, H_3PO_4): δ = 13.84 (s, 2 P) ppm. IR (KBr disk): $\tilde{\nu}$ = 2923 (m), 2851(m), 1456 (m), 1434 (m) (C_{60}), 1185 (m) (C_{60}), 1161 (m), 1056 (m), 1106 (m), 1026 (m), 1002 (m), 821 (s), 740 (m), 697 (s), 578(m) (C_{60}),

 © 2004 Wiley-VCH Verlag GmbH & Co. KGaA, Weinheim

521 (s) (C_{60}), 438 (s), 431 (m) cm^{-1}. UV/Vis (PhCl): λ_{max} (log ε) = 285.0 (4.90), 333.3 (4.91), 405.8 (4.32), 435.6 (3.88) nm. $C_{112}H_{46}Fe_4P_2Pd$ (1783.35): calcd. C 75.43, H 2.59; found C 75.49, H 2.48.

Preparation of [Pd(η²-C_{60})($Ph_2PCH_2CH_2OCH_2CH_2PPh_2$)] (6): This complex was prepared similarly, with $Ph_2PCH_2CH_2OCH_2CH_2PPh_2$ (0.022 g, 0.05 mmol) instead of P(2-Fu)$_3$; 0.056 g (88%) of **6** was obtained as a black solid. M.p. > 300 °C. ^{1}H NMR (200 MHz, $CDCl_3$, TMS): δ = 2.63 (s, 4 H, 2 CH_2P), 3.78−4.03 (m, 4 H, 2 CH_2O), 7.08−7.78 (m, 20 H, 4 C_6H_5) ppm. ^{31}P NMR (81.0 MHz, $CDCl_3$, H_3PO_4): δ = 13.60 (s, 2 P) ppm. IR (KBr disk): ṽ = 2852 (m), 1570 (m), 1480 (m), 1459 (m), 1433 (s) (C_{60}), 1353 (m), 1183 (m) (C_{60}), 1101(s), 930 (s), 821 (m), 739 (s), 693 (s), 666 (m), 578(m) (C_{60}), 526 (s) (C_{60}), 499 (s), 438 (m) cm^{-1}. UV/Vis (PhCl): λ_{max} (log ε) = 290.0 (5.34), 333.3 (5.28), 405.5 (4.22), 437.5 (4.50) nm. $C_{88}H_{28}OP_2Pd$ (1269.56): calcd. C 83.25, H 2.22; found C 83.10, H 2.30.

Preparation of [Pd(η²-C_{60}){$Ph_2PCH_2(CH_2OCH_2)_2CH_2PPh_2$}] (7): This complex was prepared similarly, with $Ph_2PCH_2(CH_2OCH_2)_2CH_2PPh_2$ (0.024 g, 0.05 mmol) instead of P(2-Fu)$_3$; 0.040 g (61%) of **7** was obtained as a black solid. M.p. > 300 °C. ^{1}H NMR (200 MHz, $CDCl_3$, TMS): δ = 2.50−2.70 (m, 4 H, 2 CH_2P), 3.68−3.90 (m, 8 H, 4 CH_2O), 7.10−7.75 (m, 20 H, 4 C_6H_5) ppm. ^{31}P NMR (81.0 MHz, $CDCl_3$, H_3PO_4): δ = 17.95 (s, 2 P) ppm. IR (KBr disk): ṽ = 2858 (m), 1481 (m), 1460 (m), 1433 (s) (C_{60}), 1352 (m), 1184 (m) (C_{60}), 1127 (m), 1098(s), 994 (m), 739 (s), 695 (s), 578(m) (C_{60}), 525 (s) (C_{60}), 434 (m), 412 (m) cm^{-1}. UV/Vis (PhCl): λ_{max} (log ε) = 286.7 (5.24), 333.3 (5.13), 405.8 (4.37), 437.5 (4.24), nm. $C_{90}H_{32}O_2P_2Pd$ (1313.61): calcd. C 82.29, H 2.46; found C 82.42, H 2.45.

Preparation of [Pd(η²-C_{60}){$Ph_2PCH_2(CH_2OCH_2)_3CH_2PPh_2$}] (8): This complex was prepared similarly, with $Ph_2PCH_2(CH_2OCH_2)_3CH_2PPh_2$ (0.026 g, 0.05 mmol) instead of P(2-Fu)$_3$; 0.050 g (74%) of **8** was obtained as a black solid. M.p. > 300 °C. ^{1}H NMR (200 MHz, $CDCl_3$, TMS): δ = 2.46−2.60 (m, 4 H, 2 CH_2P), 3.70 (s, 12 H, 6 CH_2O), 7.12−7.65 (m, 20 H, 4 C_6H_5) ppm. ^{31}P NMR (81.0 MHz, $CDCl_3$, H_3PO_4): δ = 13.89 (s, 2 P) ppm. IR (KBr disk): ṽ = 2865 (m), 1571 (m), 1480 (m), 1459 (m), 1433 (s) (C_{60}), 1352 (m), 1183 (s) (C_{60}), 1099 (s), 974 (m), 739 (s), 695 (s), 577(m) (C_{60}), 525 (s) (C_{60}), 486 (m), 434 (m) cm^{-1}. UV/Vis (PhCl): λ_{max} (log ε) = 287.0 (5.27), 333.0 (5.28), 405.5 (4.10), 438.0 (4.15) nm. $C_{92}H_{36}O_3P_2Pd$ (1357.66): calcd. C 81.39, H 2.67; found C 81.35, H 2.56.

Preparation of [Pt(η²-C_{60})($Ph_2PCH_2CH_2OCH_2CH_2PPh_2$)] (9): This complex was prepared similarly, with Pt(dba)$_2$ (0.033 g, 0.05 mmol) and $Ph_2PCH_2CH_2OCH_2CH_2PPh_2$ (0.022 g, 0.05 mmol) instead of Pd(dba)$_2$ and P(2-Fu)$_3$; 0.064 g (94%) of **9** was obtained as a black solid. M.p. > 300 °C. ^{1}H NMR (200 MHz, $CDCl_3$, TMS): δ = 2.60−2.85 (m, 4 H, 2 CH_2P), 3.85−4.02 (m, 4 H, 2 CH_2O), 7.23−7.70 (m, 20 H, 4 C_6H_5) ppm. ^{31}P NMR (81.0 MHz, $CDCl_3$, H_3PO_4): δ = 16.59 (s, $J_{P,Pt}$ = 3876 Hz, 2 P) ppm. IR (KBr disk): ṽ = 2920 (m), 2853 (m), 1480 (m), 1459 (m), 1434 (s) (C_{60}), 1332 (m), 1280 (m), 1184 (m) (C_{60}), 1101(s), 928 (m), 906 (m), 823 (m), 741 (s), 694 (s), 577(m) (C_{60}), 527 (s) (C_{60}), 502 (s), 480 (m) cm^{-1}. UV/Vis (PhCl): λ_{max} (log ε) = 285.0 (4.62), 314.0 (5.10), 318.6 (5.11), 437.5(3.94) nm. $C_{88}H_{28}OP_2Pt$ (1358.22): calcd. C 77.82, H 2.08; found C 77.75, H 2.10.

Preparation of [Pt(η²-C_{60}){$Ph_2PCH_2(CH_2OCH_2)_2CH_2PPh_2$}] (10): This complex was prepared similarly, with Pt(dba)$_2$ (0.033 g, 0.05 mmol) and $Ph_2PCH_2(CH_2OCH_2)_2CH_2PPh_2$ (0.024 g, 0.05 mmol) instead of Pd(dba)$_2$ and P(2-Fu)$_3$; 0.066 g (94%) of **10** was obtained as a black solid, M.p. > 300 °C. ^{1}H NMR (200 MHz, $CDCl_3$, TMS): δ = 2.50−2.75 (m, 4 H, 2 CH_2P), 3.65−3.95 (m, 8 H, 4 CH_2O), 7.10−7.70 (m, 20 H, 4 C_6H_5) ppm. ^{31}P NMR (81.0 MHz, $CDCl_3$, H_3PO_4): δ = 19.34 (s, $J_{P\text{-}Pt}$ = 3949 Hz, 2 P) ppm. IR (KBr disk): ṽ = 2921 (m), 2853 (m), 1479 (m), 1459 (s), 1434 (s) (C_{60}), 1331 (m), 1279 (m), 1184 (m) (C_{60}), 1128 (s), 1099 (s), 994 (s), 743 (s), 696 (s), 673 (m), 577(m) (C_{60}), 527 (s) (C_{60}), 484 (m), 414 (m) cm^{-1}. UV/Vis (PhCl): λ_{max} (log ε) = 285.0 (4.69), 314.2 (5.15), 318.3 (5.16), 440 (3.84) nm. $C_{90}H_{32}O_2P_2Pt$ (1402.27): calcd. C 77.09, H 2.30; found C 76.99, H 2.38.

Preparation of [Pt(η²-C_{60}){$Ph_2PCH_2(CH_2OCH_2)_3CH_2PPh_2$}] (11): This complex was prepared similarly, with Pt(dba)$_2$ (0.033 g, 0.05 mmol) and $Ph_2PCH_2(CH_2OCH_2)_3CH_2PPh_2$ (0.026 g, 0.05 mmol) instead of Pd(dba)$_2$ and P(2-Fu)$_3$; 0.064 g (89%) of **11** was obtained as a black solid, M.p. > 300 °C. ^{1}H NMR (200 MHz, $CDCl_3$, TMS): δ = 2.60−2.85 (m, 4 H, 2 CH_2P), 3.50−3.95 (m, 12 H, 6 CH_2O), 7.11−7.70 (m, 20 H, 4 C_6H_5) ppm. ^{31}P NMR (81.0 MHz, $CDCl_3$, H_3PO_4): δ = 19.35 (s, $J_{P\text{-}Pt}$ = 3946 Hz, 2 P) ppm. IR (KBr disk): ṽ = 2910 (m), 2853 (m), 1481 (m), 1459 (m), 1434 (s) (C_{60}), 1332 (m), 1280 (m), 1183 (m) (C_{60}), 1141 (m), 1101(s), 976 (m), 903 (m), 740 (s), 694 (s), 577(m) (C_{60}), 526 (s) (C_{60}), 489 (m) cm^{-1}. UV/Vis (PhCl): λ_{max} (log ε) = 287.0 (5.09), 333.0 (5.09), 405.0 (4.25), 438.5 (4.17) nm. $C_{92}H_{36}O_3P_2Pt$ (1446.32): calcd. C 76.40, H 2.51; found C 76.42, H 2.54.

Determination of the Optical Limiting Properties: The investigation of the optical limiting properties of the fullerene derivatives was conducted at a wavelength of 532 nm. They were housed in quartz cells with a path 2 mm long with the same linear transmittance of 83%. The laser pulses used in experiments were supplied by a frequency-doubled, Q-switched, mode-locked Continuum ns/ps Nd:YAG laser system, which provides linearly polarized 8 ns (FWHM) optical pulses at 532 nm with a repetition of 1 Hz. The transverse mode of the laser pulses is nearly Gaussian. The input laser pulses adjusted by an attenuator were split into two beams. One was employed as reference to monitor the incident laser energy, and the other was focused onto the sample cell by using a lens with 30 cm focal length. The sample was positioned at the focus. The incidence and transmitting laser pulses were monitored by utilizing two energy detectors (818J-09B, Newport Corp). The optical limiting was studied by measuring the nonlinear fluence transmittance change with input fluence.

Crystal Structure Determination of 7: Single crystals of **7** suitable for X-ray diffraction analysis were obtained by slow diffusion of MeOH into a toluene solution of **7** at room temperature. A crystal of **7** was glued to a glass fiber and mounted on a Bruker SMART 1000 automated diffractometer. Data were collected at room temperature, using graphite monochromated Mo-K_α radiation (λ = 0.71073 Å) in the ω-2θ scanning mode. Absorption correction was performed with SADABS.[27] The structure was solved by direct methods using the SHELXS-97 program and refined by full-matrix least-squares techniques (SHELXL-97) on F^2.[28] Hydrogen atoms were located by using the geometric method. The crystal data and structural refinements details are listed in Table 2. CCDC-216076 contains the supplementary crystallographic data for this paper. These data can be obtained free of charge at www.ccdc.cam.ac.uk/conts/retrieving.html [or from the Cambridge Crystallographic Data Centre, 12, Union Road, Cambridge CB2 1EZ, UK; Fax: (internat.) +44-1223/336-033; E-mail: deposit@ccdc.cam.ac.uk].

 © 2004 Wiley-VCH Verlag GmbH & Co. KGaA, Weinheim

Table 2. Crystal data and structure refinements for **7**·MeOH

Empirical formula	$C_{91}H_{32}O_2P_2Pd$·MeOH
Formula mass	1345.54
Temperature (K)	293(2)
Crystal system	triclinic
Space group	$P\bar{1}$
a (Å)	9.986 (7)
b (Å)	13.934(10)
c (Å)	20.089(14)
α (°)	73.834(13)
β (°)	77.823(15)
γ (°)	80.527(15)
V (Å^3)	2608(3)
Z	2
$D_{calcd.}$(mg/mm^3)	1.714
μ (mm^{-1})	0.487
F (000)	1364
Unique reflections, R_{int}	10488, 0.0924
Observed reflections	6687
Goodness-of-fit on F^2	1.069
R [$I > 2\sigma(I)$]	$R_1 = 0.1426$, $wR_2 = 0.3314$

Acknowledgments

We are grateful to the National Natural Science Foundation of China and the Research Fund for the Doctoral Program of Higher Education of China for financial support of this work.

[1] For reviews see: [1a] A. L. Balch, M. M. Olmstead, *Chem. Rev.* **1998**, *98*, 2123−2165. [1b] P. J. Fagan, J. C. Calabrese, B. Malone, *Acc. Chem. Res.* **1992**, *25*, 134−142. [1c] W. Sliwa, *Transition Met. Chem.* **1996**, *21*, 583−592. [1d] A. H. Stephens, M. L. H. Green, *Adv. Inorg. Chem.* **1997**, *44*, 1−43.

[2] H. W. Kroto, J. R. Heath, S. C. O′Brien, R. F. Curl, R. E. Smalley, *Nature* **1985**, *318*, 162−163.

[3] W. Kräschmer, L. D. Lamb, K. Fostiropoulos, D. R. Huffman, *Nature* **1990**, *347*, 354−358.

[4] [4a] D. S. Bethune, R. D. Johnson, J. R. Salem, M. S. de Vries, C. S. Yannoni, *Nature* **1993**, *366*, 123−128. [4b] F. T. Edelmann, *Angew. Chem. Int. Ed. Engl.* **1995**, *34*, 981−985. [4c] S. Nagase, K. Koblayashi, T. Akasaka, *Bull. Chem. Soc. Jpn.* **1996**, *69*, 2131−2142.

[5] [5a] L.-C. Song, J.-T. Liu, Q.-M. Hu, G.-F. Wang, P. Zanello, M. Fontani, *Organometallics* **2000**, *19*, 5342−5351. [5b] L.-C. Song, Y.-H. Zhu, Q.-M. Hu, *J. Chem. Res. Synop.* **2000**, 316−317. [5c] P. Zanello, F. Laschi, M. Fontani, L.-C. Song, Y.-H. Zhu, *J. Organomet. Chem.* **2000**, *593−594*, 7−11. [5d] Y.-H. Zhu, L.-C. Song, Q.-M. Hu, C.-M. Li, *Org. Lett.* **1999**, *1*, 1693−1695. [5e] L.-C. Song, Y.-H. Zhu, Q.-M. Hu, *Polyhedron* **1997**, *16*, 2141−2143. [5f] L.-C. Song, Y.-H. Zhu, Q.-M. Hu, *Polyhedron* **1998**, *17*, 469−473. [5g] L.-C. Song, Y.-H. Zhu, Q.-M. Hu, *J. Chem. Res. Synop.* **1999**, 56−57. [5h] L.-C. Song, J.-T. Liu, Q.-M. Hu, L.-H. Weng, *Organometallics* **2000**, *19*, 1643−1647. [5i] L.-C. Song, J.-T. Liu, Q.-M. Hu, *J. Organomet. Chem.* **2002**, *662*, 51−58.

[6] H. Nagashima, A. Nakaoka, Y. Saito, M. Kato, T. Kawanishi, K. Itoh, *J. Chem. Soc., Chem. Commun.* **1992**, 377−379.

[7] H. Nagashima, H. Yamaguchi, Y. Kato, Y. Saito, M. Haga, K. Itoh, *Chem. Lett.* **1993**, 2153−2156.

[8] J. P. Hare, T. J. Dennis, H. W. Kroto, R. Taylor, A. W. Allaf, S. Balm, D. R. M. Walton, *J. Chem. Soc., Chem. Commun.* **1991**, 412−413.

[9] A. N. Chernega, M. L. H. Green, J. Haggitt, A. H. H. Stephen, *J. Chem. Soc., Dalton Trans.* **1998**, 755−767.

[10] L. W. Tutt, A. Kost, *Nature* **1992**, *356*, 225−226.

[11] Y. Wang, L.-T. Cheng, *J. Phys. Chem.* **1992**, *96*, 1530−1532.

[12] Y.-L. Song, G.-Y. Fang, Y.-X. Wang, S.-T. Liu, C.-F. Li, L.-C. Song, Y.-H. Zhu, Q.-M. Hu, *Appl. Phys. Lett.* **1999**, *74*, 332−334.

[13] G.-Y. Fang, Y.-L. Song, Y.-X. Wang, X.-R. Zhang, C.-F. Li, L.-C. Song, P.-C. Liu, *Opt. Commun.* **2000**, *183*, 523−527.

[14] Y.-Y. Liu, T.-X. He, X.-W. Cai, J.-G. Tian, L.-C. Song, Q.-M. Hu, W. Yan, *J. Optoelec. Las.* **1995**, *6*, 68−71.

[15] H. Nagashima, Y. Kato, H. Yamaguchi, E. Kimura, T. Kawanishi, M. Kato, Y. Saito, M. Haga, K. Itoh, *Chem. Lett.* **1994**, 1207−1210.

[16] A. Bondi, *J. Phys. Chem.* **1964**, *68*, 441−451.

[17] V. V. Bashilov, P. V. Petrovskii, V. I. Sokolov, S. V. Lindeman, I. A. Guzey, Y. T. Struchkov, *Organometallics* **1993**, *12*, 991−992.

[18] J.-M. Lehn, *Supramolecular Chemistry*, VCH, Weinheim, **1995**.

[19] Y. Takahashi, Ts. Ito, S. Sakai, Y. Ishii, *J. Chem. Soc., D* **1970**, 1065−1066.

[20] T. Ukai, H. Kawazura, Y. Ishii, J. J. Bonnet, J. A. Ibers, *J. Organomet. Chem.* **1974**, *65*, 253−266.

[21] G. P. Sollott, E. Howard Jr., *J. Org. Chem.* **1962**, *27*, 4034−4040.

[22] G. P. Sollott, H. E. Mertwoy, S. Portnoy, J. L. Snead, *J. Org. Chem.* **1963**, *28*, 1090−1092.

[23] W. Kuchen, H. Buchwald, *Chem. Ber.* **1958**, *91*, 2871−2877.

[24] D. W. Allen, B. G. Hutley, M. T. J. Mellor, *J. Chem. Soc., Perkin Trans. 2* **1972**, 63−67.

[25] D. W. Allen, B. G. Hutley, T. C. Rich, *J. Chem. Soc., Perkin Trans. 2* **1973**, 820−822.

[26] W. J. Cherwinski, B. F. G. Johnson, J. Lewis, *J. Chem. Soc., Dalton Trans.* **1974**, 1405−1409.

[27] G. M. Sheldrick, *SADABS, Program for Empirical Absorption Correction of Area Detector Data*, University of Göttingen, Germany, **1996**.

[28] G. M. Sheldrick, *SHELXTL, Structure Determination Software Programs*, Bruker Analytical X-ray System, Inc., Madison, WI, U.S.A., **1997**.

Received July 28, 2003
Early View Article
Published Online January 19, 2004

 © 2004 Wiley-VCH Verlag GmbH & Co. KGaA, Weinheim

Synthesis, Structural, Magnetic and Electrochemical Studies of Antiferromagnetically Coupled Symmetric Oxamidate-Bridged Binuclear Copper(II) Complexes

Duraisamy Saravanakumar,[a] Nallathambi Sengottuvelan,[a] Vengidusamy Narayanan,[a] Muthusamy Kandaswamy,*[a] Kandaswamy Chinnakali,[b] Gopal Senthilkumar,[b] and Hoong Kun Fun[c]

Keywords: Magnetic properties / Electrochemistry / Copper / N,O ligands

The new binuclear copper(II) complexes Cu_2L^{1-3} and $[Cu_2L^{4,5}](ClO_4)_2$ were synthesized by reaction of the monomeric *cis*-*N*,*N*′-bis(3-aminopropyl)oxamidatocopper(II) complex [Cu(oxpn)] with acetylacetone, benzoylacetone, salicylaldehyde, 2-pyridinecarboxaldehyde and diacetyl monoxime in the presence of copper(II) acetate or perchlorate owing to the *trans* isomerisation of the *cis*-oxamidato complex. The crystal structure of Cu_2L^1 consists of centrosymmetric binuclear copper(II) ions which are bridged by an oxamidato group in the *trans* conformation with a copper–copper distance of 5.121 Å. Each copper(II) ion occupies an inner site of the N_2O_2 donor with a distorted square-planar environment. Electrochemical studies showed that two quasireversible one-electron reduction waves are obtained in the cathodic region (E^1_{pc} = −0.48 to −1.02 V, E^2_{pc} = −1.08 to −1.34 V). The conproportionation constants K_{con} for the mixed-valence $Cu^{I}Cu^{II}$ complexes have been determined electrochemically. Room-temperature magnetic-moment studies of binuclear copper(II) complexes reveal the presence of a strong antiferromagnetic interaction (μ_{eff} = 1.14–1.24 μ_B) which is also observed from the broad spectra with g = 2.1. A variable-temperature magnetic-susceptibility study of the complexes **1** and **4** gives J values of −510 cm^{-1} and −497 cm^{-1} respectively.

(© Wiley-VCH Verlag GmbH & Co. KGaA, 69451 Weinheim, Germany, 2004)

Introduction

Inorganic chemists are interested in synthesizing bi- and polymetallic complexes to design new molecular materials with unusual magnetic and electrical properties[1−5] and these bi- and polymetallic systems are also attractive as synthetic models of metallo biomolecules[6−8] due to the close proximity of the metal centers. To prepare polynuclear complexes, the use of polynucleating ligands[9,10] and the use of metal complexes as ligands are the most commonly followed strategies.[11−14] Self-assembly of a mononuclear oxamidato complex with a metal ion leads to a novel coordination polymer.[15] Oxamide-based ligands such as *N*,*N*′-bis(3-aminopropyl)oxamide (H_2oxpn) have been of great interest due to their ability to form polynuclear complexes.[16] The oxamide bridge is known to be very efficient in transmitting the exchange interaction between magnetic ions.[17−19] Oxamide ligands with two distinct coordination sites are used in the design of ditopic receptors to allow the translocation of a metal ion driven by pH variation which can lead to mechanical work at the molecular level.[20,21] This possibility gives rise to a new class of potential artificial molecular machines.[22,23] It is also possible to use substituted oxamate and oxamide ligands in the stabilization of unusual high oxidation state transition metal ions.[24,25] Furthermore, the monomeric *cis*-oxamidato complex Cu(oxpn) easily yields binuclear[26,27] and polynuclear[28] complexes by changing its conformation from *cis* to *trans*. It has also been shown that the NH_2 group of *N*,*N*′-disubstituted oxamides can be condensed with a carbonyl group of several compounds to yield new binucleating ligands.[29,30]

The work reported here is concerned with the synthesis, structural, spectral, magnetic and electrochemical properties of disubstituted oxamidate-bridged binuclear copper(II) complexes. These complexes can be used to synthesize polynuclear complexes with suitable multidentate ligands. A schematic diagram of the ligand frames is given in Figure 1.

Results and Discussion

Binuclear complexes are synthesized by condensation between the terminal NH_2 group of [Cu(oxpn)] with acetyl-

[a] Department of Inorganic Chemistry, School of Chemical Sciences, University of Madras, Guindy Campus, Chennai 600025, India
Fax: (internat.) +91-44/2230-0488 or -/2235-2494
E-mail: mkands@yahoo.com
[b] Department of Physics, Anna University, Chennai 600025, India
[c] X-ray Crystallography Unit, School of Physics, Universiti Sains Malaysia, 11800 USM, Penang Malaysia

 © 2004 Wiley-VCH Verlag GmbH & Co. KGaA, Weinheim DOI: 10.1002/ejic.200300524

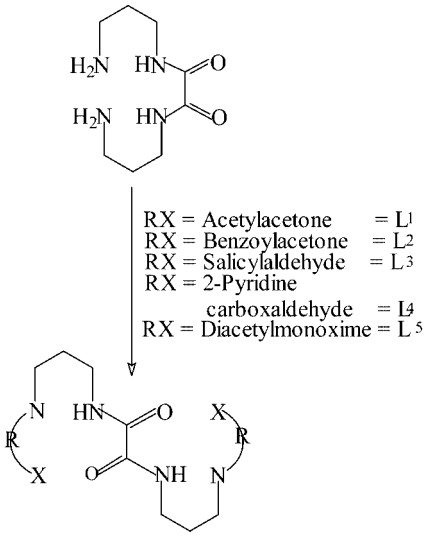

Figure 1. Schematic diagram of the ligand framework

acetone (L^1), benzoylacetone (L^2), salicylaldehyde (L^3), 2-pyridinecarboxaldehyde (L^4) or diacetyl monoxime (L^5) in the presence of copper(II) acetate (L^{1-3}) or copper(II) perchlorate ($L^{4,5}$). Complexes $[Cu_2L^{1-3}]$ contain N_2O_2 coordination sites, whereas complexes $[Cu_2L^{4,5}](ClO_4)_2$ have N_3O coordinating sites. The synthetic pathway of the complexes is shown in Scheme 1.

X-ray Structural Study of the Complex $[Cu_2L^1]$

$[Cu_2L^1]$ crystallizes from a methanol/chloroform solution in the space group *Pbca*. The ORTEP view of the binuclear copper(II) complex, which consists of centrosymmetric binuclear copper(II) ions, along with the atomic labeling scheme, is given in Figure 2. Crystal data and structure refinement details are given in Table 1, with selected bond lengths (Å) and angles (°) in Table 2. Within the binuclear molecule, an oxamidate group in the *trans* conformation bridges crystallographically equivalent copper(II) ions. Each copper(II) ion is four-coordinate, with an N_2O_2 coordination environment in a distorted square-planar geometry. The oxamidato bridge is planar within experimental uncertainties and has a dihedral angle of 5.7° with the N_2O_2 coordination plane, so that the whole centrosymmetric molecule can be considered as planar. The bridging group N2−O1−C7−C7A−N1A−O1A is planar, with the copper atom being displaced by −0.0084(3) Å from this plane. The Cu1−Cu1A separation within the binuclear unit is 5.121 Å. One alkylamino nitrogen, one oxamidato nitrogen, one oxamidato oxygen and one acetonato oxygen atom are coordinated to each Cu ion with distances of Cu1−N2 = 1.954(2) Å, Cu1−N1 = 1.960(2) Å, Cu1−O1 = 2.008(2) Å and Cu1−O2 = 1.8871(19) Å, respectively. The Cu1−O1 distance is 0.1211 Å longer than the Cu1−O2 distance. Both the nitrogen atoms N1 and N2 are present at nearly the same distance from the Cu atom, within experimental error. The copper−amidic nitrogen (Cu−N2) distance is

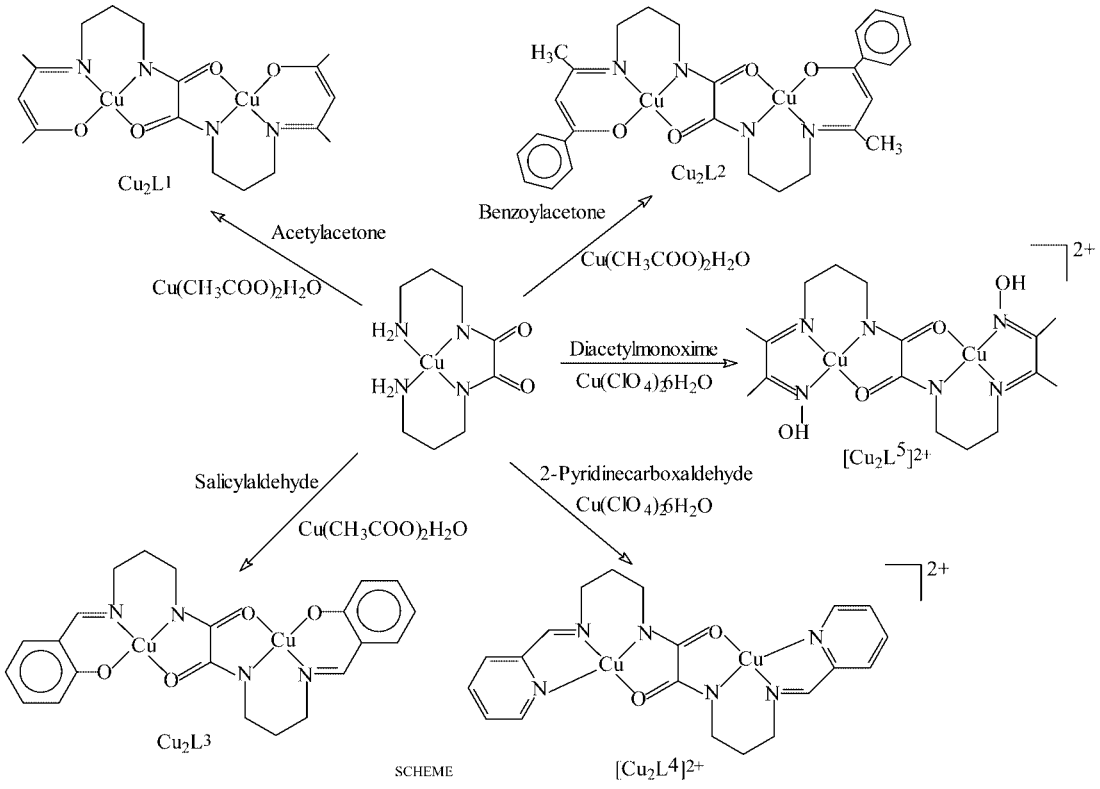

Scheme 1

 © 2004 Wiley-VCH Verlag GmbH & Co. KGaA, Weinheim

1.954 Å, which is close to those of several reported oxamidato complexes.[17,36] The copper−iminic nitrogen (Cu−N1) distance is 1.960 Å and the copper−oxamide oxygen (Cu−O1) bond length is 2.008 Å, which are comparable to those reported earlier.[17] The bond angles around the Cu atom show significant deviations from 90°, two of them – O1Cu1O2 [84.69°(9)] and N2Cu1O1 [82.98°(11)] – being narrower than the other two N1Cu1N2 [97.2°(11)] and N1Cu1O2 [95.41°(10)]. The sum of the angles around C7, O1and N2 is 360.0° indicating that these atoms are trigonal planar. This implies that Cu1−O−C−*N*−Cu1A is a delocalised unit as a result of conjugation of the electrons from the oxygen atoms and the lone pairs on the nitrogen atoms. This is further supported by the average O−C and C−N bond lengths [1.272(3) and 1.295(4) Å, respectively], which are shorter than expected for single O−C or C−N bonds (ca. 1.481 and 1.462 Å, respectively). From the molecular packing it is observed that there are no intermolecular contacts that are less than the sum of the corresponding van der Waals radii. This suggests that there are no forces other than van der Waals interactions stabilizing the structure.[30]

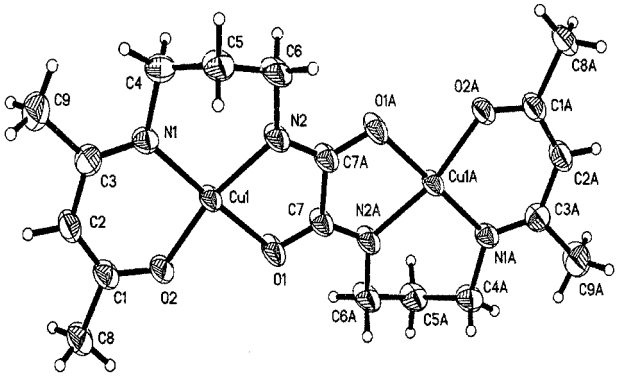

Figure 2. ORTEP diagram of complex $[Cu_2L^1]$ with atom labels and numbering scheme; hydrogen atoms are omitted for clarity

Table 1. Crystal data and structure refinement for $[Cu_2L^1]$

Empirical formula	$C_{18}H_{26}Cu_2N_4O_4$
Molecular mass	489.51
Temperature	183(2) K
Wavelength	0.71073 Å
Crystal system	orthorhombic
Space group	Pbca
Unit cell dimensions	a = 15.3679(5) Å
	b = 8.0448(3) Å
	c = 16.1903(6) Å
Volume	2001.63(12) Å^3
Z	4
Density (calculated)	1.718 g/cm^3
Absorption coefficient	2.160 mm^{-1}
F(000)	1072
Crystal size	0.50 × 0.46 × 0.10 mm
Theta range for data collection	2.65−28.26°
Index ranges	$-20 \le h \le 20$,
	$-10 \le k \le 10$, $-21 \le l \le 16$
Reflections collected	11341
Independent reflections	2461 [R(int) = 0.1099]
Completeness to theta	28.26° 99.0%
Absorption correction	empirical
Max. and min. transmission	0.8140 and 0.4133
Refinement method	full-matrix least-squares on F^2
Data/restraints/parameters	2461/0/132
Goodness-of-fit on F^2	0.991
Final R indices [$I > 2\sigma(I)$]	$R1$ = 0.0562, $wR2$ = 0.1426
R indices (all data)	$R1$ = 0.0738, $wR2$ = 0.1499
Extinction coefficient	0.0110(16)
Largest diff. peak and hole	0.800 and −1.078 e·Å^{-3}

Table 2. Selected bond lengths (Å) and angles (°) for complex $[Cu_2L^1]$

Cu1−O2	1.8871(19)	Cu1−N2	1.954(2)
Cu1−N1	1.960(2)	Cu1−O1	2.008(2)
O1−C7	1.272(3)	N2−C7	1.295(4)
C7−C7A	1.499(6)		
O2−Cu1−N1	95.41(10)	O2−Cu1−O1	84.69(9)
N2−Cu1−O1	82.98(11)	N2−Cu1−N1	97.20(11)
O2−Cu1−N2	166.73(11)	N1−Cu1−O1	176.50(12)
C7−O1−Cu1	110.88(18)	C1−O2−Cu1	125.8(2)
C6−N2−Cu1	128.0(2)	O1−C7−N2	128.0(3)
O1−C7−C7A	118.1(3)	N2−C7−C7A	113.9(3)

Spectral Studies

The IR spectra of all the complexes show sharp bands resulting from the C=N stretching vibration (1640 cm^{-1}) and the oximidato C=O stretching vibration (1590 cm^{-1}). The presence of an uncoordinated perchlorate anion in complexes Cu_2L^4 and Cu_2L^5 is inferred from a single broad band at 1100 cm^{-1} (ν_3 antisymmetric stretching), which is not split, and a medium band at 650 cm^{-1} (ν_4 antisymmetric bending). The absence of any band at 930 cm^{-1}(ν_2 symmetric stretching) indicates the lack of coordination of the perchlorate ion.[31−33] The UV/Vis spectrum of the mononuclear complex Cu(oxpn)[13] exhibits a d → d transition around 510 nm consistent with a tetracoordinate Cu atom in a nearly square-planar CuN_4 geometry. The binuclear complexes Cu_2L^{1-5} display a d-d band in the range 572−592 nm. The λ_{max} value of the binuclear complexes is higher than that of the mononuclear species; such a red shift implies that the conformation of the ligand is altered from *cis* to *trans*, which changes the environment of the Cu^{II} ions from N_4 to N_2O_2 and N_3O. This is consistent with a previously reported observation.[18] Besides the d → d transition, a moderately intense band in the range 300−400 nm is due to a ligand-to-metal charge transfer ($\pi \rightarrow d_\sigma$) transition and a band below 300 nm is assigned to an intraligand transition ($\pi \rightarrow \pi^*$). The absorptions around 570 nm are attributed to square-planar CuN_2O_2 and CuN_3O chromophores.[34] Therefore, it appears that there is a distorted square-planar geometry of the Cu centers in the copper(II) complexes. The solution X-band ESR spectrum of Cu_2L^1 is shown in Figure 3. The solution (10^{-3} M in DMF) ESR spectra of the complexes Cu_2L^{1-5} display one broad absorption at g = 2.10 centered at 3200 G at room temperature. The ESR spectra with no hyperfine splitting

 © 2004 Wiley-VCH Verlag GmbH & Co. KGaA, Weinheim

of the parallel component indicate that there is a strong antiferromagnetic interaction between the two copper(II) ions in the molecule.[16] Due to the favourable relative orientation of the magnetic orbitals a strong antiferromagnetic interaction is observed in spite of a Cu−Cu separation of about 5.121 Å. The fine structure of a triplet state for a Cu^{II} pair has two origins, namely the dipolar interaction and the combined effect of the local spin-orbit coupling and the exchange interaction, which leads to anisotropic and antisymmetric exchanges.[35] The above observation can be explained by earlier reports.[36,37]

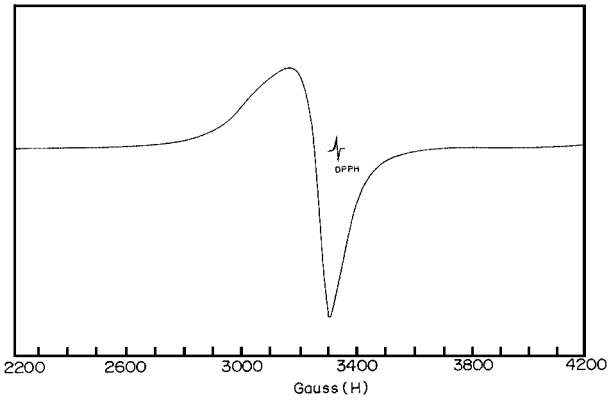

Figure 3. ESR spectrum of $[Cu_2L^1]$

Magnetic Susceptibility

The values of the magnetic moment for the binuclear copper(II) complexes measured at room temperature (298 K) are, at 1.14−1.24 μ_B, lower than the spin-only value and this clearly indicates that a strong antiferromagnetic exchange coupling is operating between the copper(II) ions. This behaviour shows a great similarity to that of binuclear Cu^{II} complexes involving bridging oxamido ligands and displaying a singlet−triplet energy gap of 500−600 cm^{-1}.[16,38−40] In order to determine the extent of magnetic interaction between the metal ions and to evaluate the singlet−triplet energy gap value $-2J$, magnetic susceptibilities at various temperatures (298−75 K) were measured. The temperature variation of $\chi_m T$ for the complexes $[Cu_2L^1]$ and $[Cu_2L^4](ClO_4)_2$ are shown in Figure 4. The experimental magnetic susceptibility values corrected for diamagnetism were fitted with the theoretical values defined by the modified Bleaney−Bowers equation.[41]

$$\chi_m = (Ng^2\beta^2)/(3kT)[3 + \exp(-2J/kT)]^{-1}(1 - P) + (0.45P/T) + N_\alpha$$

where χ_m is the molar magnetic susceptibility of the complex, P is the percentage of monomeric impurities, N is Avogadro's number, β is the Boltzmann constant, g is the average gyromagnetic ratio, $-2J$ is the singlet−triplet separation, and N_α is the temperature-independent paramagnetism (120×10^{-6} $cm^3 \cdot mol^{-1}$). A nonlinear least-square fitting program was employed to calculate $-J$, g and P. From the best fit of the susceptibility data with this equation, a J value of -510 cm^{-1} was obtained with $g = 2.10$ and $P = 0.0012$ for $[Cu_2L^1]$. $[Cu_2L^4]$ gave a J value of -497 cm^{-1} with $g = 2.12$ and $P = 0.0020$. Even though both complexes have the same bridging groups, $[Cu_2L^4]$ has a lower J value than $[Cu_2L^1]$ due to electronic effects. $[Cu_2L^1]$, containing an N_2O_2 coordination environment, has an enriched electron density facilitating the exchange interaction, whereas in the case of $[Cu_2L^4]$, the electron density at the N_3O site is lower than in $[Cu_2L^1]$ and hence the exchange interaction is also less. Electronic effects in symmetrical ligands have little influence on the magnetic exchange between copper(II) ions.[42] Higher J values are observed for $[Cu_2L^1]$ and $[Cu_2L^4]$, in which the oxamide bridge has the *trans* configuration and the two copper atoms have the same environment so that the two copper atoms are equal in energy. The large J values reveal that the strong antiferromagnetic interaction between two bridged Cu^{II} ions in complexes $[Cu_2L^1]$ and $[Cu_2L^4]$ is mainly due to the enhanced in-plane overlap of the oxamidato bridge.[43] The J value reported in this case is consistent with earlier reports[44−47] for *trans*-oxamidate-bridged binuclear copper(II) complexes.

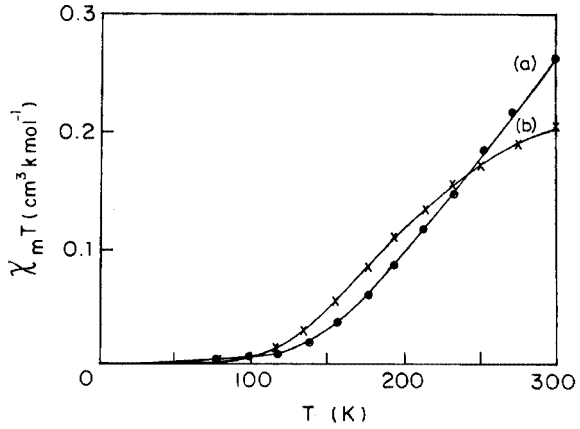

Figure 4. Temperature dependence of the magnetic properties for: (a) $[Cu_2L^1]$, and (b) $[Cu_2L^4](ClO_4)_2$

Electrochemical Studies

The molar conductivity of freshly prepared solutions of the complexes $[Cu_2L^{1-3}]$ in DMF falls in the range 10−15 Λ_m/S cm^2 mol^{-1}, indicating that the complexes are neutral. The molar conductance values of the complexes $[Cu_2L^{4,5}]$ are in the range 107−110 Λ_m/S $cm^2 \cdot mol^{-1}$ indicating that the complexes are 1:2 electrolytes.[48]

Cyclic Voltammetric Studies

The cyclic voltammograms for the copper(II) complexes at negative potential were recorded in the potential range 0 to −1.5 V; the data are summarized in Table 3. The cyclic voltammograms obtained for the complexes $[Cu_2L^1]$ and $[Cu_2L^5](ClO_4)_2$ in the cathodic region are shown in Figure 5. All the binuclear copper(II) complexes show two-step, one-electron, quasi-reversible reduction waves. Controlled potential electrolysis performed at a potential 100 mV more negative than the reduction wave indicates the consumption

 © 2004 Wiley-VCH Verlag GmbH & Co. KGaA, Weinheim

Table 3. Electrochemical data[a] of copper(II) complexes (reduction at cathodic potential)

Complex	E^1_{pc} (V)	E^1_{pa} (V)	$E^1_{1/2}$ (V)	ΔE (mV)	E^2_{pc} (V)	E^2_{pa} (V)	$E^2_{1/2}$ (V)	ΔE (mV)	K_{con}
$[Cu_2L^1]$	−0.82	−0.68	−0.75	140	−1.08	−0.97	−1.02	110	3.7×10^4
$[Cu_2L^2]$	−1.02	−0.91	−0.96	110	−1.34	−1.24	−1.29	100	3.8×10^5
$[Cu_2L^3]$	−0.52	−0.42	−0.47	100	−0.89	−0.80	−0.85	90	2.7×10^6
$[Cu_2L^4](ClO_4)_2$	−0.48	−0.39	−0.44	90	−0.68	−0.62	−0.65	60	3.6×10^3
$[Cu_2L^5](ClO_4)_2$	−0.55	−0.30	−0.43	250	−0.88	−0.77	−0.83	110	5.9×10^6

[a] Measured by CV at 50 mV/s. *E* vs. Ag/AgCl. Conditions: GC working and Ag/AgCl reference electrode; supporting electrolyte TBAP; [complex] = 1×10^{-3} M, [TBAP] = 0.1 M.

of one electron per molecule for both the first and second reduction wave. Cyclic voltammograms for all the complexes are similar and involve two quasi-reversible redox processes. Even though in all the complexes both the metal ions have the same geometry and same environment, two reduction waves are obtained in the cathodic region corresponding to stepwise one-electron reductions through a Cu^ICu^{II} intermediate to give a binuclear Cu^I species. In spite of the ligands being symmetrical, their dicopper(II) complexes show two quasi-reversible reduction waves.[49] The two redox processes are represented as follows:

$$Cu^{II}Cu^{II} \rightleftarrows Cu^{II}Cu^{I} \rightleftarrows Cu^{I}Cu^{I}$$

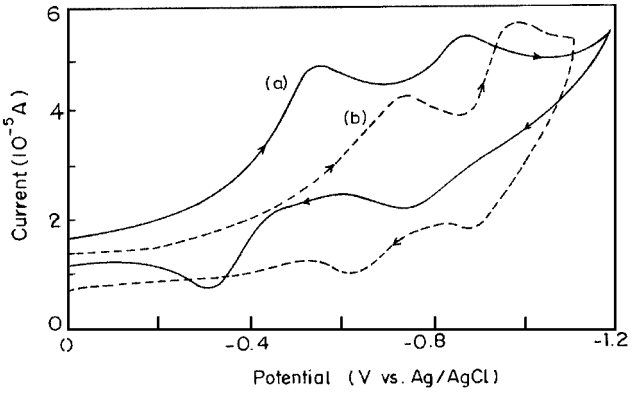

Figure 5. Cyclic voltammograms of: (a) $[Cu_2L^5](ClO_4)_2$, and (b) $[Cu_2L^1]$

The reason for the observation of two reduction waves may be due to electronic exchange between the metal ions: after the first one-electron reduction some of the electron density is transferred from the reduced metal ion to the other metal ion through the oxamidato bridge, and hence the second reduction appears at higher negative potential. The reduction waves are somewhat broad. This may be due to the equilibrium binding of solvent to the Cu^{II} center. The peak broadening diminishes as the scan rate increases.[50] The first reduction wave appears in the potential range −0.48 to −1.02 V. The second reduction wave occurs in the potential range −0.68 to −1.34 V. The potentials at the first reduction waves of the $[Cu_2L^{3-5}]$ are lower than for $[Cu_2L^{1,2}]$. This indicates that $[Cu_2L^{4,5}]$, with an N_3O coordination environment, are reduced more easily. Even though $[Cu_2L^3]$ possesses an N_2O_2 site like $[Cu_2L^{1,2}]$, the first reduction potential of $[Cu_2L^3]$ is lower than that of $[Cu_2L^{1,2}]$, possibly due to the combined effect of the phenoxide ion and unsaturation that reduce the electron density around the metal ion. The difference between the half-wave potentials of the two-redox processes is a measure of the relative stability of mixed-valence species. This approach used for symmetrical complexes with two metal ions in the same coordination environment. The stability of the mixed-valence species Cu^ICu^{II}, can be related to their conproportionation constants, K_{con}. The conproportionation constant for the equilibrium was calculated using the relationship $\log K_{con} = \Delta E/0.0591$. A greater K_{con} value indicates greater stability for the mixed-valence species or that the exchange interaction is greater with respect to the isovalent species.[51] This indicates that the enhanced stability for the Cu^ICu^{II} intermediate species is probably due to the exchange interaction between the metal centers[52] through the oxamido bridge. The larger the separation between the potentials of the couple, the greater the stability of mixed-valence species with respect to conproportionation.[53,54] Among the copper(II) complexes, $[Cu_2L^4]$ has a lower separation between the potentials than the other complexes, and the lower K_{con} value of $[Cu_2L^4]$ suggests easier access to the Cu^ICu^{II} species. This is because the exchange interaction is less due to distortion of the geometry, and the stability of the mixed-valence species is lower than that of the rest of the complexes. $[Cu_2L^3]$ and $[Cu_2L^5]$ have higher K_{con} values due to a larger separation between the potentials, and there may be a greater exchange interaction between the metal ions in $[Cu_2L^3]$ and $[Cu_2L^5]$. The conproportionation constant was calculated by following the equilibrium:

$$Cu^{II}\,Cu^{II} \rightleftharpoons Cu^{II}\,Cu^{I} \rightleftharpoons Cu^{I}\,Cu^{I}$$

$$Cu^{II}\,Cu^{II} + Cu^{I}\,Cu^{I} \overset{K_{con}}{\rightleftharpoons} 2Cu^{II}\,Cu^{I}$$

Conclusion

A series of *N*,*N*′-bis(disubstituted) oxamidato-bridged binuclear copper(II) complexes has been synthesized. The spectral, electrochemical and magnetic properties of the

 © 2004 Wiley-VCH Verlag GmbH & Co. KGaA, Weinheim

complexes were studied. From these studies it can be seen that a small variation in the ligand environment imposes an influence on the spectral, magnetic and electrochemical properties of the complexes.

Experimental Section

General: Elemental analysis was carried out on a Carlo Erba Model 1106 elemental analyzer. Electronic spectral studies were carried out on a Hitachi 320 model double beam spectrophotometer in the range 250−800 nm in DMF. IR spectra were recorded on a Hitachi 270−50 spectrophotometer as KBr disks in the range 4000−400 cm^{-1}. Cyclic voltammograms were obtained on a CH instruments electrochemical analyzer. The measurements were carried out at 50 mV/sec under oxygen-free conditions using a three-electrode cell with a glassy carbon electrode as the working electrode, a saturated Ag/AgCl electrode as the reference electrode and platinum wire as the auxiliary electrode. Tetra(*n*-butyl)ammonium perchlorate (TBAP) was used as the supporting electrolyte. The ferrocene/ferrocenium(1+) couple was used as an internal standard ($E_{1/2}$ of the Fc/Fc^+ couple under these experimental conditions is 470 mV in DMF and ΔE_p for Fc/Fc^+ is 70 mV at a 50 mV/sec scan rate). The conductivity measurements were carried out with an Elico digital conductivity bridge model CM-88 using freshly prepared 10^{-3} M solutions of the complexes in DMF. Room temperature magnetic moment and variable-temperature magnetic studies were performed on a PAR model 155 vibrating-sample magnetometer in the temperature range 77−300 K, and the instrument was calibrated using metallic nickel. All data were corrected for diamagnetism of the ligand estimated from Pascal's constants. X-band solution ESR spectra of the complexes (10^{-3} M in DMF) were recorded at 25 °C on a Varian EPR-E 112 spectrometer using diphenylpicrylhydrazine (DPPH) as the reference.

All the chemicals and solvents were of analytical grade and were used as received. The TBAP used as supporting electrolyte in electrochemical measurement was purchased from Fluka and recrystallised from hot methanol. (***Caution!*** *TBAP is potentially explosive, hence care should be taken in handling the compound*). DMF (HPLC) was obtained from Merck.

Preparation of [Cu(oxpn)]: The ligand H_2oxpn {*N*,*N*′-bis(3-aminopropyl) oxamide}[55] and its mononuclear copper(II) complex[18] were prepared following literature procedures.

Synthesis of [Cu_2L^1]: A methanolic solution (40 mL) of acetylacetone (0.40 mL, 3.8 mmol) and $Cu(CH_3COO)_2{\cdot}H_2O$ (0.38 g, 1.9 mmol) were added to a stirred suspension of Cu(oxpn) (0.5 g, 1.9 mmol) in methanol (20 mL). After stirring for an hour, the solution was heated to reflux for 20 min. The resulting solution was filtered and kept at room temperature. Green microcrystals were obtained on slow evaporation of the solution. Yield: 0.9 g (80%). Plate-shaped dark-green crystals suitable for XRD were obtained on recrystallisation from a methanol/chloroform mixture (1:1). $C_{18}H_{26}N_4Cu_2O_4$ (489.51): calcd. C 44.17, H 5.31, Cu 25.96, N 11.45; found C 44.15, H 5.28, Cu 25.43, N 11.42. Selected IR data (KBr): $\tilde{\nu}$ = 1618 (sh, I = 23.7%), 1598 (sh, 28.2%), 1552 (sh, 27.6%) cm^{-1} (sh = sharp, I = intensity). Conductance (Λ_m/S cm^2 mol^{-1}) in DMF 10. λ_{max} (nm) (ε/$M^{-1}{\cdot}cm^{-1}$) in DMF: 572 (200), 329 (18400), 263 (16500). g = 2.10; μ_{eff} = 1.15 μ_B; J = −510 cm^{-1}.

Synthesis of [Cu_2L^2]: This complex was synthesized by following the above procedure using benzoylacetone (0.61 g, 3.8 mmol) instead of acetylacetone. A dark-green crystalline compound was obtained. Yield: 0.75 g (67%). $C_{28}H_{30}Cu_2N_4O_4$ (613.66): calcd. C 54.81, H 4.89, Cu 20.71, N 9.13; found C 54.78, H 4.87, Cu 20.68, N 9.09. Selected IR data (KBr): $\tilde{\nu}$ = 1625 (sh, 7.6%), 1596 (sh, 20.5%), 1525 (sh, 17.6%) cm^{-1}. Conductance (Λ_m/S cm^2 mol^{-1}) in DMF: 14. λ_{max} (nm) (ε/$M^{-1}{\cdot}cm^{-1}$) in DMF: 581 (250), 344 (13600), 266 (11200). g = 2.10; μ_{eff} = 1.18 μ_B

Synthesis of [Cu_2L^3]: This complex was synthesized by following the above procedure using salicylaldehyde (0.39 mL, 3.8 mmol) instead of acetylacetone. A pale-green compound was obtained. Yield: 0.83 g (79%). $C_{22}H_{22}Cu_2N_4O_4$ (533.53): calcd. C 49.53, H 4.12, Cu 23.82, N 10.50; found C 49.52, H 4.10, Cu 23.75, N 10.49. Selected IR data (KBr): $\tilde{\nu}$ = 1615 (sh, 9.1%), 1593 (sh, 41.6%), 1530 (sh, 46.3%) cm^{-1}. Conductance (Λ_m/S cm^2 mol^{-1}) in DMF: 15. λ_{max} (nm) (ε/$M^{-1}{\cdot}cm^{-1}$) in DMF: 599 (240), 366 (47200), 261 (46100). g = 2.10; μ_{eff} = 1.14 μ_B

Synthesis of [Cu_2L^4] $(ClO_4)_2$: A methanolic solution (40 mL) of 2-pyridinecarboxaldehyde (0.36 mL, 3.8 mmol) and $Cu(ClO_4)_2{\cdot}6H_2O$ (0.7 g, 1.9 mmol) was added to a stirred suspension of Cu(oxpn) (0.5 g, 1.9 mmol) in methanol (20 mL). After stirring for an hour, the solution was heated to reflux for 20 min. The resulting solution was filtered and kept at room temperature. A brown crystalline compound was obtained on slow evaporation of the solution. Yield: 0.95 (71%). $C_{20}H_{22}Cl_2Cu_2N_6O_{10}$ (704.42): calcd. C 34.09, H 3.12, Cu 18.05, N 11.93; found C 34.02, H 3.15, Cu 17.92, N 11.89. Selected IR data (KBr): $\tilde{\nu}$ = 1624 (sh, 6.5%), 1590 (sh, 38.7%), 1098 (str, 4.3%), 650 (m, 24.2%) cm^{-1}. Conductance (Λ_m/S cm^2 mol^{-1}) in DMF: 110. λ_{max} (nm) (ε/$M^{-1}{\cdot}cm^{-1}$) in DMF: 592 (105), 345 (42400), 268 (47300). g = 2.10; μ_{eff} = 1.24 μ_B, J = −497 cm^{-1}.

Synthesis of [Cu_2L^5]$(ClO_4)_2$: This complex was synthesized by following the above procedure using diacetyl monoxime (0.61 g, 3.8 mmol) instead of 2-pyridinecarboxaldehyde. A green compound was obtained. Yield: 1 g (86%). $C_{16}H_{26}Cl_2Cu_2N_6O_{12}$ (692.41): calcd. C 27.74, H 3.75, Cu 18.36, N 12.73; found C 27.69, H 3.71, Cu 18.25, N 12.69. Selected IR data (KBr): $\tilde{\nu}$ = 2750 (str, 42.6%), 1622 (sh, 10.2%), 1591 (sh, 43.3%), 1102 (str, 7.6%), 1230 (str, 44.7%), 648 (m, 31.7%) cm^{-1}. Conductance (Λ_m/S cm^2 mol^{-1}) in DMF: 107. λ_{max} (nm) (ε/$M^{-1}{\cdot}cm^{-1}$) in DMF: 572 (140), 334 (48400), 262 (43800). g = 2.10; μ_{eff} = 1.21 μ_B

Crystal Structure Determinations: Accurate unit cell parameters and orientation matrices were obtained by a least-squares fit of high angle reflections with Mo-K_α radiation on a Siemens SMART CCD area detector in the ω-scan mode for [Cu_2L^1]. Cell refinement and data reduction were carried out using SAINT (Siemens, 1996). A total of 11341 reflections were collected, resulting in 2461 independent reflections of which 1805 had $I > 2\sigma(I)$ and these were considered as observed. The intensities were corrected for Lorentz and polarization effects. The structure was solved by direct methods as implemented in SHELXTL-97.[56] The positions of all non-hydrogen atoms were included in the full-matrix least-squares refinement using SHELXTL-97. The positions of all the hydrogen were geometrically fixed at calculated positions and they were allowed to ride on the corresponding non-hydrogen atoms. The final R factor was 0.0562, maximum and minimum values of the electron densities in the final electron density map were 0.800, −1.078 e·Å^{-3}. A dark-green crystal of [Cu_2L^1] of dimension 0.50 × 0.46 × 0.10 mm^3 was used for indexing and intensity data collection on a Siemens Smart CCD diffractometer equipped with a fine focus, 3 kW sealed tube X-ray source and graphite-monochromated Mo-K_α radiation (λ = 0.71073 Å) at 183(2) K. Empirical absorption corrections were applied for compound by using SADABS (Sheldrick, 1996) program for the Siemens area detector.

 © 2004 Wiley-VCH Verlag GmbH & Co. KGaA, Weinheim

CCDC-190328 contains the supplementary crystallographic data for this paper. These data can be obtained free of charge at www.ccdc.cam.ac.uk/conts/retrieving.html [or from the Cambridge Crystallographic Data Centre, 12, Union Road, Cambridge CB2 1EZ, UK; Fax: (internat.) +44-1223/336-033; E-mail: deposit@ccdc.cam.ac.uk].

Acknowledgments

The financial support received by D. S. and N. S. from ISRO is gratefully acknowledged.

[1] D. Gatteschi, O. Kahn, J. S. Miller, F. Palacio, *Magnetic Molecular Materials*, Kluwer Academic Publishers, Dordrecht, **1991**.
[2] R. L. Carlin, *Magnetochemistry*, Springer, Berlin, **1986**.
[3] M. Melnik, *Coord. Chem. Rev.* **1981**, *36*, 1−44.
[4] Y. Akhriff, J. Server-Carrio, A. Sancho, J. Garcia-Lozano, E. Escriva, J. V. Folgado, L. Soto, *Inorg. Chem.* **1999**, *38*, 1174−1185.
[5] E.-Q. Gao, J. K. Tang, D. Z. Liao, Z. H. Jiang, S. P. Yan, G. L. Wang, *Inorg. Chem.* **2001**, *40*, 3143−3140.
[6] K. D. Karlin, Z. Tyeklar, *Bioinorganic Chemistry of Copper*, Chapman & Hill, NewYork, **1993**.
[7] C. Belle, C. Beguin, I. G. Luneau, S. Hamman, C. Philouze, J. L. Pierre, F. Thomas, S. Torelli, *Inorg. Chem.* **2002**, *41*, 479−491.
[8] P. A. Vigato, S. Tamburini, D. E. Fenton, *Coord. Chem. Rev.* **1990**, *106*, 25−170.
[9] L. K. Thompson, L. Zhao, Z. Xu, D. O. Miller, W. M. Reiff, *Inorg. Chem.* **2003**, *42*, 128−139.
[10] Z. Xu, L. K. Thompson, V. A. Milvay, L. Zhao, T. Kelly, D. O. Miller, *Inorg. Chem.* **2003**, *42*, 2950−2959.
[11] En-Q. Gao, G. M. Yang, D. Z. Liao, Z. H. Jiang, S. P. Yan, G. L. Wang, *J. Chem. Res. (S)* **1999**, 278−279.
[12] J. M. Dominguez-Vera, N. Galvez, E. Colacio, R. Cuesta, J. P. Costes, J. P. Laurent, *J. Chem. Soc., Dalton Trans.* **1996**, 861−865.
[13] L. Cronin, A. R. Mount, S. Parsons, N. Robertson, *J. Chem. Soc., Dalton Trans.* **1999**, 1925−1927.
[14] C. Zhang, P. Zu, Z. Ma, D. Yan, *J. Coord. Chem.* **2000**, *50*, 159−167.
[15] S. Q. Zang, R. J. Tao, Q. L. Wang, N. H. Hu, Y. X. Cheng, J. Y. Niu, D. Z. Liao, *Inorg. Chem.* **2003**, *42*, 761−766.
[16] Y. Journaux, J. Sletten, O. Khan, *Inorg. Chem.* **1985**, *24*, 4063−4069.
[17] F. Lloret, M. Julve, J. Faus, R. Ruiz, I. Castro, M. Mollar, M. Philoche-Levisalles, *Inorg. Chem.* **1992**, *31*, 784−791.
[18] J. P. Costes, F. Dahan, J. P. Laurent, M. Drillon, *Inorg. Chim. Acta* **1999**, *294*, 8−13.
[19] M. Maekawa, S. Kitagawa, Y. Nakao, S. Sakamoto, A. Yatani, W. Mori, S. Kashino, M. Munakata, *Inorg. Chim. Acta* **1999**, *293*, 20−29.
[20] J.-M. Lehn, *Supramolecular Chemistry: Concepts and Perspectives*, VCH, Weinheim, **1995**.
[21] V. Amendola, L. Fabbrizzi, C. Mangano, P. Pallavicini, *Acc. Chem. Res.* **2001**, *34*, 488−493.
[22] V. Amendola, L. Fabbrizzi, C. Mangano, H. Miller, P. Pallavicini, A. Perotti, A. Taglietti, *Angew. Chem. Int. Ed.* **2002**, *41*, 2553−2556.
[23] V. Amendola, C. Brusoni, L. Fabbrizzi, C. Mangano, H. Miller, P. Pallavicini, A. Perotti, A. Taglietti, *J. Chem. Soc., Dalton Trans.* **2001**, 3528−3533.
[24] R. Ruiz, C. Surville-Barland, A. Aukauloo, E. Anxolabehere-Mallart, Y. Journaux, J. Cano, M. C. Munoz, *J. Chem. Soc., Dalton Trans.* **1997**, 745−752.
[25] B. Cervera, J. L. Sanz, M. J. Ibanez, G. Vila, F. Lloret, M. Julve, R. Ruiz, X. Ottenwaelder, A. Aukanloo, S. Poussereau, Y. Journaux, M. C. Munoz, *J. Chem. Soc., Dalton Trans.* **1998**, 781−790.
[26] F. Lloret, M. Julve, J. A. Real, J. Faus, R. Ruiz, M. Mollar, I. Castro, C. Bois, *Inorg. Chem.* **1992**, *31*, 2627−2633.
[27] R. Ruiz, J. Faus, F. Lloret, M. Julve, Y. Journaux, *Coord. Chem. Rev.* **1999**, *193*, 1069−1117.
[28] V. Mckee, *Adv. Inorg. Chem.* **1993**, *40*, 323−334.
[29] J. P. Laurent, J. P. Costes, G. Pradie, *Inorg. Chim. Acta* **1993**, *213*, 57−63.
[30] E. M. Opozda, E. Sledziewska, W. Lasocha, K. Goubitz, H. Schenk, *Polyhedron* **1998**, *17*, 281− 287.
[31] K. Nakamoto, *Infrared and Raman Spectra of Inorganic and Coordination Compounds*, Wiley- Interscience, New York, **1978**.
[32] J. Ribas, C. Diaz, R. Costa, J. Tercero, X. Solans, M. Font-Bardia, H. Stoeckli-Evans, *Inorg. Chem.* **1998**, *37*, 1575−1584.
[33] B. J. Hathway, A. E. Underhill, *J. Chem. Soc.* **1961**, 3091−3096.
[34] A. Bencini, C. Benelli, D. Gatteschi, C. Zanchini, A. C. Fabretti, G. C. Franchini, *Inorg. Chim. Acta* **1984**, *86*, 169−172.
[35] J. Owen, E. A. Harris, *Electron Paramagnetic Resonance* (Ed.: S. Geshind), Plenum Press, New York, **1972**.
[36] A. Bencini, M. Di Vaira, A. C. Fabretti, D. Gatteschi, C. Zanclini, *Inorg. Chem.* **1984**, *23*, 1620−1623.
[37] A. Bencini, C. Benelli, A. C. Fabretti, G. Franchini, D. Gatteschi, *Inorg. Chem.* **1986**, *25*, 1063−1066.
[38] J. P. Costes, F. Dahan, J. P. Laurent, *J. Chem. Soc., Dalton Trans.* **1989**, 1017−1025.
[39] R. Ruiz, F. Lloret, M. Julve, J. Faus, M. C. Munoz, X. Solans, *Inorg. Chim. Acta* **1993**, *213*, 261−268.
[40] J. P. Costes, F. Dahan, J. P. Laurent, *Inorg. Chim. Acta* **1995**, *230*, 199−203.
[41] B. Bleaney, K. D. Bowers, *Proc. R. Soc. London, Ser. A* **1952**, *214*, 451−463.
[42] P. Lacroix, O. Khan, F. Theobald, J. Leroy, C. Wakselman, *Inorg. Chim. Acta* **1988**, *142*, 129−134.
[43] O. Khan, *Angew. Chem. Int. Ed. Engl.* **1985**, *24*, 834−850.
[44] Z. N. Chen, J. Qiu, W. X. Tang, K. B. Yu, *Inorg. Chim. Acta* **1994**, *224*, 171−176.
[45] Z. N. Chen, D. G. Fu, K. B. Yu, W. X. Tang, *J. Chem. Soc., Dalton Trans.* **1994**, 1917−1921.
[46] J. A. Real, R. Ruiz, J. Faus, F. Lloret, M. Julve, Y. Journaux, M. Philoche-Levisalles, C. Bois, *J. Chem. Soc., Dalton Trans.* **1994**, 3769−3773.
[47] Z. N. Chen, W. X. Tang, K. B. Yu, *Polyhedron* **1994**, *13*, 783−789.
[48] W. J. Geary, *Coord. Chem. Rev.* **1971**, *7*, 81−122.
[49] S. S. Tandon, L. K. Thompson, J. N. Bridson, *Inorg. Chem.* **1993**, *32*, 32−39.
[50] M. Thirumavalavan, P. Akilan, M. Kandaswamy, K. Chinnakali, G. Senthilkumar, H. K. Fun, *Inorg. Chem.* **2003**, *42*, 3308−3317.
[51] R. Das, K. Nag, *Inorg. Chem.* **1991**, *30*, 2831−2833.
[52] B. Srinivas, N. Arulsamy, P. S. Zacharias, *Polyhedron* **1992**, *11*, 211−215.
[53] H. Liangren, *Polyhedron* **1992**, *11*, 941−946.
[54] P. K. Mandal, K. Nag, *J. Chem. Soc., Dalton Trans.* **1983**, 2429−2434.
[55] J. Chang, O. Vogl, *J. Polym. Sci.* **1977**, *15*, 311−322.
[56] G. M. Sheldrick, *SHELXTL-97. Program for the refinement of crystal structures* University of Göttingen, Germany, **1997**.

Received July 31, 2003
Early View Article
Published Online January 19, 2004

Tuning the Catalase Activity of Dinuclear Manganese Complexes by Utilizing Different Substituted Tripodal Ligands

Nicole Reddig,[a] Daniel Pursche,[a] Michael Kloskowski,[a] Caroline Slinn,[a] Sascha M. Baldeau,[a] and Annette Rompel*[a]

Keywords: Manganese / Tripodal ligands / Bioinorganic chemistry / Enzyme models

A series of five new dinuclear manganese(II/II) compounds with derivatives of 2-{[bis(pyridin-2-ylmethyl)amino]-methyl}phenol (HL_1) were synthesized and structurally characterized. All complexes crystallize in monoclinic space groups and exhibit Mn···Mn separations in the range of 3.392(8)–3.493(2) Å caused by bis(μ-phenoxo) bridging modes. The derivatives of HL_1 contain either electron-donating or -withdrawing substituents. A correlation between the electronic character of the different ring substituents, the redox potentials of the dinuclear transition metal complexes and the catalase activity has been revealed. In analogy to manganese catalase, all complexes show saturation kinetics at high substrate concentration. The investigated catalase activity places the compounds in the upper range of functional catalase mimics.

(© Wiley-VCH Verlag GmbH & Co. KGaA, 69451 Weinheim, Germany, 2004)

Introduction

The manganese catalases are the most intensively studied dinuclear manganese enzymes. By disproportionating hydrogen peroxide into water and dioxygen, manganese catalases protect cells from deleterious effects caused by this harmful by-product of respiration. In addition to heme-type catalases,[1] there is another class of manganese catalases that has been found in three bacterial organisms, *Lactobacillus plantarium*,[2,3] *Thermus thermophilus*,[4,5] and *Thermoleophilum album*.[6] The manganese catalase from *Thermus thermophilus* is the best characterized one. During the catalytic cycle the oxidation states of the dinuclear manganese center change between Mn_2(II/II) and Mn_2(III/III). There are also two inactive forms [Mn_2(II/III) and Mn_2(III/IV)], which are caused by one-electron transitions during the disproportionation of hydrogen peroxide.[7,8]

So far only three functional model systems for the catalase reaction have been described which employ Mn_2(II/II) and Mn_2(III/III) in their catalytic cycles. The first system, $[Mn_2(L^1)(\mu\text{-OAc})]^{2+}$, is based on a heptadentate ligand L^1 [*N*,*N*,*N*′,*N*′-tetrakis(2-methylenebenzimidazolyl)-1,3-diaminopropan-2-ol] and was the first functional catalase mimic.[9–12] The second model system is the [Mn_2(2-OHsalpn)$_2$] [2-OHsalpn = 1,3-bis(salicylideneamino)-2-propanol] system. It has been fully crystallographically and spectroscopically characterized in four different oxidation states and serves as both a structural and functional manganese catalase mimic.[13–15] At the moment the most efficient catalase mimic is based on the ligand bpia [bis(picolyl)-(*N*-methylimidazol-2-yl)amine], which belongs to the class of tripodal ligands. The [Mn_2(bpia)$_2$] system consists of four dinuclear complexes, that mimic structural, spectroscopic and functional features of manganese catalases. $[Mn_2(bpia)_2(\mu\text{-OAc})_2](ClO_4)_2$ and $[Mn_2(bpia)_2(\mu\text{-O})_2](ClO_4)_2$-$(PF_6)\cdot 2CH_3CN$ are the most efficient catalysts using the Mn_2(II/II) and Mn_2(III/IV) redox couple reported to date for the disproportion of hydrogen peroxide.[16]

In this paper we report the synthesis, characterization and catalase activity of five new dinuclear Mn_2(II/II) complexes. They are based on tripodal ligands featuring an N_3O donor set, where the parent ligand is 2-({bis[(pyridin-2-yl)-methyl]amino}methyl)phenol. The phenol moiety of the ligands leads to a bis(μ-phenoxo) bridging motif, leaving one vacant coordination site at each manganese center. These are occupied by two mutually *trans*-positioned chloride ions. The catalytic activity regarding the disproportionation of hydrogen peroxide depends on the ring substituents. It will be shown that electron-withdrawing groups decrease the ability to disproportionate hydrogen peroxide, whereas electron-donating groups increase this ability. The catalase activities of the model compounds described in this paper range between those of [Mn_2(bpia)$_2$] and [Mn_2(2-OHsalpn)$_2$] and place the five dinuclear manganese(II/II) complexes in second position for functional manganese catalase mimics.

Results and Discussion

Reaction of manganese(II) chloride tetrahydrate with the corresponding ligand under basic conditions yields the di-

[a] Institut für Anorganische und Analytische Chemie, Westfälische Wilhelms-Universität,
Wilhelm-Klemm-Str. 8, 48149 Münster, Germany
Fax: (internat.) + 49-251/833-8366
E-mail: rompela@uni-muenster.de

nuclear manganese complexes $[Mn_2(L_1)_2Cl_2]\cdot 2CH_2Cl_2$ (**1**), $[Mn_2(L_2)_2Cl_2]\cdot C_2H_5OH$ (**2**), $[Mn_2(L_3)_2Cl_2]\cdot 2CH_2Cl_2$ (**3**), $[Mn(L_4)_2Cl_2]\cdot 2CH_2Cl_2$ (**4**) and $[Mn_2(L_5)_2Cl_2]$ (**5**). All compounds crystallize in the monoclinic crystal system. Complexes **1**−**3** crystallize in the space group $P2_1/c$ (no.14), while **4** and **5** crystallize in $I2/a$ (no.15). Each unit cell consists of four complex molecules, except for compound **3**, where only two complex molecules can be found. Either eight (**1**), four (**2**, **3**, and **4**), or no (**5**) solvent molecules complete the unit cells. The manganese ions are in the oxidation state +II. They are bis(μ-phenoxo)-bridged by the ligands' phenol groups resulting in Mn···Mn-distances in the range from 3.392(8) Å (**5**) to 3.493(2) Å (**4**). The distorted octahedral coordination environment of each manganese center is formed by an N_3O_2Cl donor set, where, except for the chloride ions, all donor atoms are provided by the ligands. The crystal structure of the metal complexes are depicted below. Selected bonds and angles for all complexes are listed in Table 1.

Table 1. Selected distances [Å] and angles [°] of **1**−**5**

	1[a]	**2**[a]	**3**	**4**	**5**
Mn(1)···Mn(1a)[b]	3.411(1)	3.440(1)	3.406(2)	3.493(2)	3.392(8)
Mn(1)−Cl(1)	2.451(2)	2.426(1)	2.472(3)	2.425(9)	2.454(1)
Mn(1)−O(1)	2.119(4)	2.138(2)	2.147(3)	2.156(2)	2.138(2)
Mn(1)−O(1a)[b]	2.203(4)	2.199(2)	2.173(3)	2.205(2)	2.142(2)
Mn(1)−N(1)	2.367(5)	2.360(3)	2.330(4)	2.305(2)	2.372(2)
Mn(1)−N(2)	2.348(5)	2.263(3)	2.399(4)	2.313(2)	2.273(2)
Mn(1)−N(3)	2.254(5)	2.288(3)	2.338(4)	2.361(2)	2.312(2)
Mn(1)−O(1)−Mn(1a)[b]	105.2(2)	105.0(9)	104.1(1)	106.4(7)	104.8(7)
Cl(1)−Mn(1)−O(1)	111.2(1)	111.6(7)	117.5(1)	118.6(6)	114.7(5)
Cl(1)−Mn(1)−O(1a)[b]	105.2(1)	101.5(7)	97.0(1)	101.3(5)	101.5(6)
Cl(1)−Mn(1)−N(1)	155.7(1)	157.1(7)	154.9(1)	154.2(6)	152.9(7)
Cl(1)−Mn(1)−N(2)	88.1(1)	98.2(9)	96.3(1)	89.1(7)	93.2(6)
Cl(1)−Mn(1)−N(3)	96.0(1)	90.5(8)	90.6(2)	96.6(6)	88.5(8)
O(1)−Mn(1)−O(1a)[b]	76.0(1)	75.0(9)	75.9(1)	73.6(7)	75.2(7)
O(1)−Mn(1)−N(1)	85.4(2)	84.4(9)	85.0(1)	84.9(6)	84.4(7)
O(1)−Mn(1)−N(2)	92.9(2)	146.9(1)	88.5(1)	147.4(7)	150.6(8)
O(1)−Mn(1)−N(3)	151.1(2)	92.2(1)	148.5(2)	86.8(7)	87.8(7)
O(1a)−Mn(1)−N(1)[b]	95.8(2)	98.4(9)	99.5(1)	95.3(6)	102.0(8)
O(1a)−Mn(1)−N(2)[b]	165.0(2)	85.5(1)	163.0(1)	85.0(7)	90.8(7)
O(1a)−Mn(1)−N(3)[b]	87.9(2)	165.0(1)	87.4(2)	158.1(6)	162.6(7)
N(1)−Mn(1)−N(2)	73.0(2)	72.1(1)	71.9(1)	72.8(7)	73.2(8)
N(1)−Mn(1)−N(3)	72.3(2)	72.1(1)	71.4(2)	72.9(7)	72.5(9)
N(2)−Mn(1)−N(3)	97.8(2)	101.9(1)	103.1(2)	108.0(7)	102.9(8)

[a] Bond lengths and angles for Mn(2) are omitted for clarity. [b] Mn(1a) = Mn(2) and O(1a) = O(2) for **1**.

$[Mn_2(L_1)_2(Cl)_2]\cdot 2CH_2Cl_2$ (1; Figure 1): Mononuclear Cu,[17] Fe,[18] Re,[19] and Zn[20] complexes of HL_1 are known. In addition, dinuclear Fe,[21,22] Cu,[23] and Zn[20] complexes have also been published.

The Mn−N bond lengths around Mn(1) range from 2.254(5) for Mn(1)−N(3) to 2.367(5) Å for Mn(1)−N(1). The distances for the Mn(1)−O bonds are 2.119(4) [O(1)] and 2.203(4) Å [O(2)]. The longest bond to be found is Mn(1)−Cl(1) [2.451(2) Å]. Except for small deviations, the manganese−donor atom bonds for Mn(2) are in the same range as for Mn(1). The average N(1)−Mn(1)−N(X) (X = 2, 3) and N(4)−Mn(2)−N(Y) (Y = 5, 6) angles of 72.7 and 72.3° differ significantly from 90° and show the distortion from octahedral geometry due to constraints imposed by the ligand.

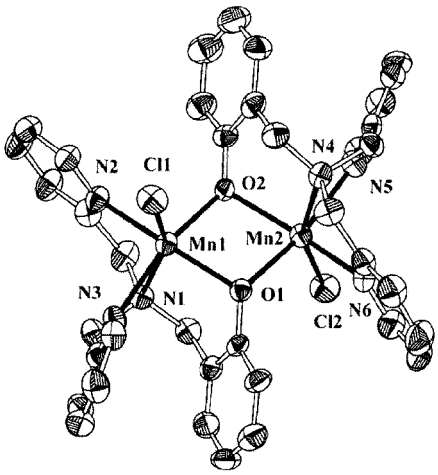

Figure 1. Ellipsoid plot of **1** showing 50% probability thermal ellipsoids; hydrogen atoms are omitted for clarity

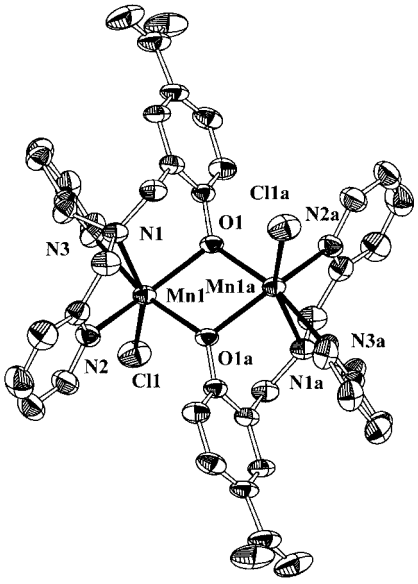

Figure 2. Ellipsoid plot of **2** showing 50% probability thermal ellipsoids; hydrogen atoms are omitted for clarity

$[Mn_2(L_2)_2(Cl)_2]\cdot C_2H_5OH$ (2; Figure 2): In 1987 an analogous structure of complex **2** was published by Nishida with NCS ligands instead of chloride ligands ($P2_1/n$).[24] In addition, mono- and dinuclear copper complexes[23,25−27] and mononuclear iron complexes[18,28] of HL_2 have been described in the literature.

There are two half complex molecules and one ethanol molecule in the asymmetric unit. Both manganese(II) centers of each independent complex molecule are related by a crystallographic inversion center. The coordination environment of Mn(1) is described as it is representative of both Mn(1) and Mn(2). The longest bond to be found is

 © 2004 Wiley-VCH Verlag GmbH & Co. KGaA, Weinheim

Mn(1)−Cl(1) [2.426(1) Å]. The chloride ion is bonded *trans* to the aliphatic nitrogen atom N(1), with a bond length of 2.360(3) Å. This is considerably longer than the manganese−pyridine distances Mn(1)−N(2) [2.263(3) Å] and Mn(1)−N(3) [2.288(3) Å]. The average distance for the Mn−O bonds is 2.168 Å.

The five-membered chelate rings containing Mn(1), N(1), N(2/3) cause a distortion from an ideal octahedral geometry. Hence, for the average N(1)−Mn(1)−N(X) (X = 2, 3) angles a deviation of 17.8° from the ideal 90° angle is observed. The distortion is shown best in the angles including *trans*-bonded donor atoms. The largest difference from linearity occurs in the angles O(1)−Mn(1)−N(2) [146.9(1)°].

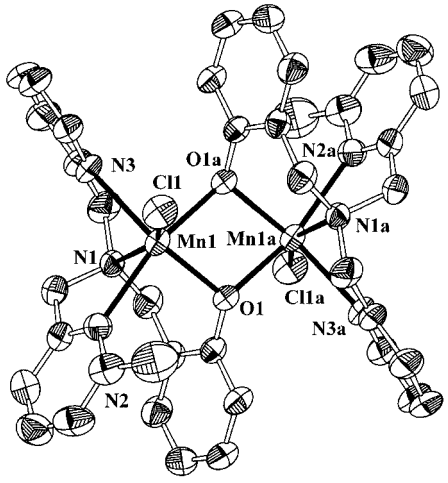

Figure 3. Ellipsoid plot of **3** showing 50% probability thermal ellipsoids; hydrogen atoms and a depiction of the chloride disorder are omitted for clarity

$[Mn_2(L_3)_2(Cl)_2]\cdot 2\ CH_2Cl_2$ (3; Figure 3): There is a crystallographic inversion center found in the middle of the dinuclear complex, rendering the two halves of the molecule crystallographically equivalent. The chloride ion is disordered. The occupation factors for both forms were refined to 0.71 and 0.29. The manganese−chlorine bonds show an average value of 2.407 Å. The aliphatic nitrogen atom N(1) is bonded *trans* to the chloride ion, with a bond length of 2.330(4) Å. This is shorter than the manganese−pyridine distances. The bond Mn(1)−N(2) [2.399(4) Å] is the longest manganese−nitrogen bond in the complex, which can be attributed to the steric effects of the methyl substituent in the *ortho* position of N(2). The Mn−O bond lengths are in the same range. The average N(1)−Mn(1)−N(X) (X = 2, 3) angle of 71.7° differs significantly from 90° and shows the distortion from octahedral geometry due to constraints imposed by the ligand.

$[Mn_2(L_4)_2(Cl)_2]\cdot 2CH_2Cl_2$ (4; Figure 4) and $[Mn_2(L_5)_2(Cl)_2]$ (5; Figure 4): A crystallographic inversion center in the middle of the complexes generates the corresponding symmetric equivalent half. Mn(1) is surrounded by an N_3O_2Cl donor set while the position of the chloride ion is slightly disordered. The occupation factors for both

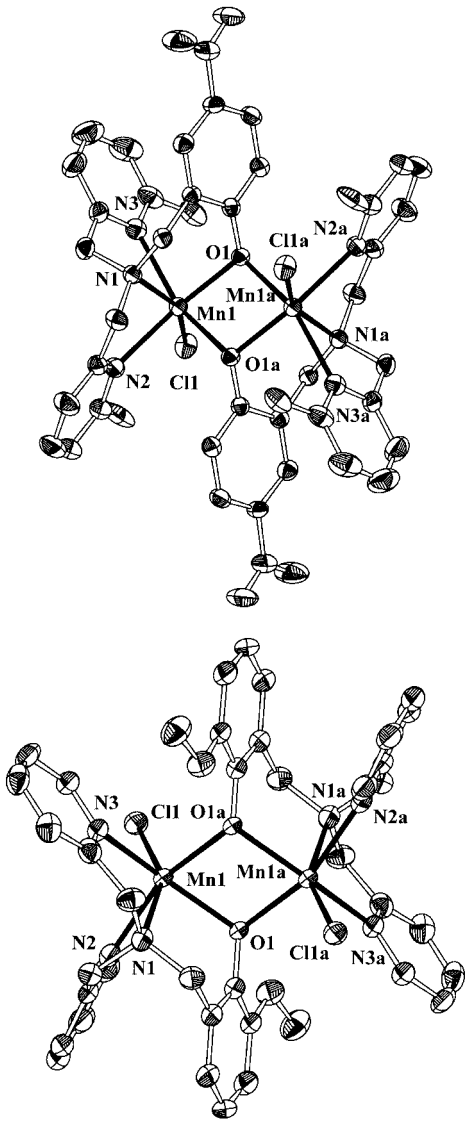

Figure 4. Ellipsoid plots of **4** (top) and **5** (bottom) showing 50% probability thermal ellipsoids; hydrogen atoms and a depiction of the chloride disorder are omitted for clarity

positions have been refined to 0.84 and 0.16 for complex **4** and 0.95 and 0.05 for **5**. In addition, compound **4** shows a disorder of the methyl substituent, where the occupation factors for both positions have been refined to 0.80 and 0.20.

The Mn(1)−Cl(1) bonds are the longest to be found in both compounds and show values of 2.425(9) Å (**4**) and 2.454(1) Å (**5**). The aliphatic nitrogen atom N(1) is bonded *trans* to the chloride ion with distances for **4** of 2.305(2) Å and for **5** of 2.372(2) Å to Mn(1). As expected, in **5** both pyridine nitrogen atoms N(2) and N(3) exhibit shorter bonds to the metal center with values of 2.273(2) Å and 2.312(2) Å, respectively. In complex **4** the Mn(1)−N(2, 3) distances are longer compared to Mn(1)−N(1) (see Table 1). This can be attributed to the steric effects of the disordered methyl substituent in the *ortho* position of N(2) and N(3), respectively. The two oxygen atoms O(1) and O(1a)

 © 2004 Wiley-VCH Verlag GmbH & Co. KGaA, Weinheim

are bonded *trans* to the aromatic nitrogen atoms N(2) and N(3). Distances of 2.156(2) Å (**4**) and 2.138(2) Å (**5**) for Mn(1)−O(1) and 2.205(2) Å (**4**) and 2.142(2) Å (**5**) for Mn(1)−O(1a) have been determined. The bis(μ-phenoxo)-bridging mode results in Mn···Mn separations of 3.493(2) Å for compound **4** and 3.392(8) Å for complex **5**. The distortion from ideal octahedral symmetry is best clarified by comparing the values for the two angles N(1)−Mn(1)−N(X) (X = 2, 3) and O(1)−Mn(1)−N(2) with their ideal values. The latter differs significantly from the ideal 180° with angles of 147.4(7)° (**4**) and 150.6(8)° (**5**), while the average angles for N(1)−Mn(1)−N(X) (X = 2, 3) deviate by around 17.2° from the ideal 90°.

There is a correlation between the Mn···Mn distances and the type of ring substituent. In particular, the influence of the electron-withdrawing effect of the NO_2 groups, that are *p*-bonded to the phenol oxygen atom in **2** and **4**, is conspicuous. Because of its −M effect the electron density of the phenolic oxygen atom is reduced through the aromatic π-system. This results in a weaker Mn−O bond, leading to larger Mn···Mn distances than in complexes **1**, **3**, and **5**. On the other hand electron-donating groups like methyl and methoxy moieties stabilize the Mn−O bonds resulting in shorter Mn···Mn separations than in the parent complex **1**.

Electrochemistry

The redox potentials of complexes **1**−**5** are summarized in Table 2. Figure 5 shows the cyclic voltammogram of compound **2** in acetonitrile as the most representative.

Table 2. Redox potentials of complexes **1**−**5**

Complex	$E_{1/2}$ (ΔE) [V] vs. Ag/AgCl $Mn_2^{II/II}/Mn_2^{II/III}$
1	0.44 (0.14)
2	0.76 (0.15)
3	0.45 (0.07)
4	0.64 (0.07)
5	0.45 (0.16)

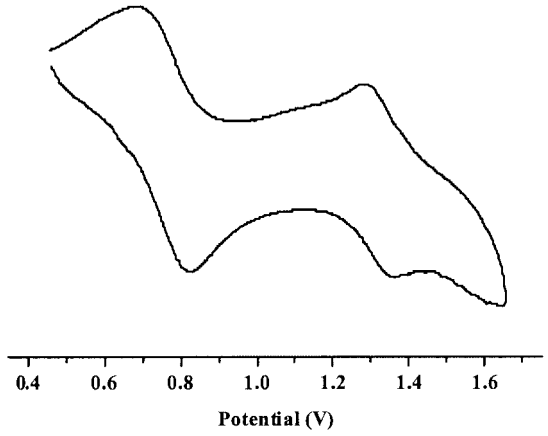

Figure 5. Cyclic voltammogram of **2** in acetonitrile

The observed redox potentials for the oxidation $Mn^{II}Mn^{II}/Mn^{II}Mn^{III}$ are in good agreement with data reported in the literature for similar dinuclear manganese compounds.[29−32]

For a reversible single-electron redox transition an ideal peak separation of 59 mV has to be detected. For compounds **3** and **4** the differences in peak potentials for the first redox transition show little difference from the ideal 59 mV (ΔE = 70 mV). This shift can be attributed to solvent effects.[33] Therefore these waves can clearly be attributed to a single-electron transfer in both complexes from Mn^{II}/Mn^{II} to Mn^{II}/Mn^{III}.

In the case of quasi-reversible electron transitions the determination of *n*, the number of electrons involved in the redox process, is more complicated. The large peak-separation for the first redox transition in the cyclic voltammogram of compounds **1**, **2**, and **5** (ΔE = 140−160 mV) indicates that the electron transfer is slow. For a system undergoing slow electron transfers it has been shown that the number of electrons can be determined using the following equation:[31,34] $\alpha n = 0.048/(|E_p - E_{p/2}|)$.

In the present case a value of 0.5 can be considered for the charge-transfer coefficient α due to the symmetrical shape of the corresponding wave. E_p is the peak potential of the considered wave and $E_{p/2}$ represents the potential value at half the intensity of the peak current. From the obtained data listed in Table 3 one can ascertain that $n = 1$ for the first redox transition.

Table 3. Potential peak values for the $Mn^{II}Mn^{II}/Mn^{II}Mn^{III}$ oxidation in **1**, **2**, and **5**

Compound	E_{pa} [V]	$E_{pa/2}$ [V]	E_{pc}	ΔE [V]
1	0.37	0.46	0.51	0.14
2	0.68	0.78	0.83	0.15
5	0.37	0.48	0.53	0.16

Thus, on the time scale of cyclic voltammetry (250 mV s^{-1}) our investigations lead to the following conclusion. For compounds **1**−**5** the first redox transition can clearly be attributed to a single-electron transfer from $Mn^{II}Mn^{II}$ to $Mn^{II}Mn^{III}$.

It is noteworthy that both oxidation waves in the cyclic voltammogram of **2** differ in intensity by a factor of 1.3. For the remaining complexes this difference is significantly smaller. To further investigate this second oxidation peak, additional electrochemical studies were performed on the pure ligand. In analogy to data reported by Blondin et al., oxidation of the phenolic part of the ligands occurs at higher potentials.[31] Those irreversible, ill-defined cyclic voltammetric traces overlay any supposed oxidation from $Mn^{II}Mn^{III}$ to $Mn^{III}Mn^{III}$.

However, there is a clear correlation between the revealed redox potentials and the type of ring substituent. As shown in Table 2, the increase of the redox potentials for the first transition is directly commensurate with the intensity of the

 © 2004 Wiley-VCH Verlag GmbH & Co. KGaA, Weinheim

electron-withdrawing effect of the ring substituents. This was observed before by Walton et al.[35] Their investigations on transition metal redox behavior were based on a series of mononuclear manganese compounds. Using different phenol-substituted triimine and triamine ligands an analogous influence on the redox potential was observed for CH_3O, CH_3, and NO_2 groups as *para*-substituents of the phenol group.

Catalase Activity

Compounds **1**−**5** are stable under ambient conditions and are not oxidized by atmospheric oxygen. All complexes are able to disproportionate hydrogen peroxide in aqueous solution. Like $[Mn(bpia)(\mu\text{-}OAc)]_2(ClO_4)_2$, they are examples of synthetic catalysts showing saturating kinetics at high substrate concentrations (see Figure 6).[16]

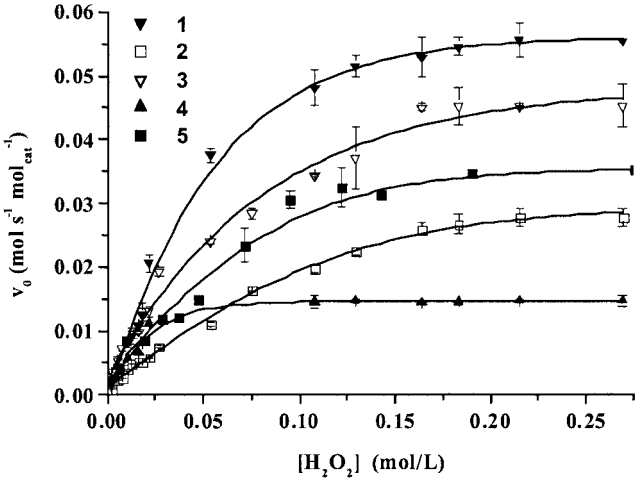

Figure 6. Initial rate of substrate consumption versus substrate concentration at constant concentration of **1**−**5**

Consequently, the data were fitted to the Michaelis−Menten equation, and the *turnover* number k_{cat}, the Michaelis constant K_M and k_{cat}/K_M were determined from the double reciprocal Lineweaver−Burk plot (Figure 7). The values of k_{cat}, K_M and k_{cat}/K_M are listed in Table 4.

Taking K_M as a measure of substrate affinity, the methoxy-substituted compound **5** exhibits the highest affinity for hydrogen peroxide (lowest value of K_M) while the parent complex **1** shows the lowest value for substrate binding (highest value of K_M). This is noteworthy if one considers that the unsubstituted ligand should allow easier access to the metal center, resulting in a higher affinity for hydrogen peroxide. Therefore electronic reasons must be the rate-determining effects for substrate binding. It is conceivable that the methoxy lone pairs interact with the substrate leading to higher substrate binding.

The *turnover number* k_{cat} can be interpreted as the rate of substrate conversion into the corresponding products. Once H_2O_2 is bonded to the metal center the rate of conversion is best for the parent complex **1**, followed by complex **3**

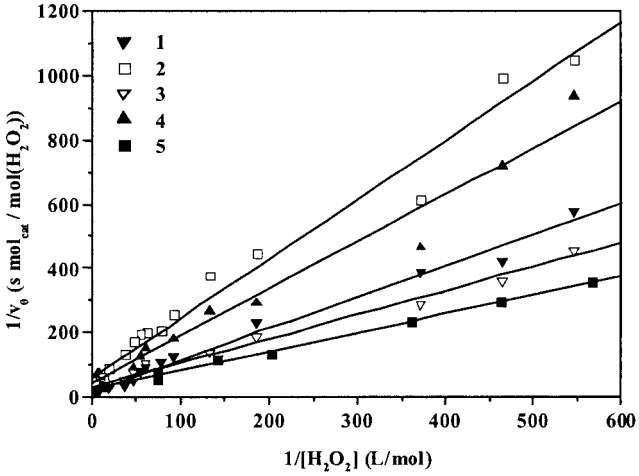

Figure 7. Lineweaver−Burk plots for **1**−**5**

(methyl substituted) and compound **5** (methoxy residue). The slowest complex in terms of *turnovers* is the *p*-nitro-substituted complex **2**, exhibiting a threefold slower catalytic conversion than **1**. The electron-withdrawing effect of the nitro group is presumably the decisive difference. This effect causes a reduction of the electron density of the manganese centers via the aromatic π-system. Since the disproportionation of hydrogen peroxide is a redox process this effect decreases the speed of substrate conversion.

In order to understand the observed kinetic data a comparison of k_{cat}/K_M as a criterion for catalytic efficiency and the determined redox potentials is necessary. By comparing the k_{cat}/K_M criteria of the five complexes a dependence of the rate of the hydrogen peroxide disproportionation on the ring substituents is also observed. Starting with complex **1**, which contains the unsubstituted parent ligand, the activity increases if electron-donating groups like methyl or methoxy substituents are bound to the pyridine or phenol arm (**2** and **5**). Although the methoxy group is bigger than the methyl group, complex **5** is more efficient than **2**. This can be attributed to the increased ability to donate electrons into the aromatic π-system compared to the methyl group. It seems to be that the complexes' catalase activity is more dependent on electronic than on steric effects. Therefore, by using a methoxy substituent k_{cat}/K_M of **5** is larger than for both **1** and **2**. On the other hand k_{cat}/K_M decreases if an NO_2 group is bonded in the *para* position to the bridging phenol oxygen atom. This is caused by its strong electron-withdrawing effect, which reduces the electron density of the manganese centers via the aromatic π-system. The use of both an electron-withdrawing and -donating group, as in **4**, leads to a higher k_{cat}/K_M than for **2**.

As shown by CV experiments (vide supra) the redox potentials correlate with the insertion of electron-withdrawing or -donating substituents. The cyclic voltammograms of compounds **1**, **3** and **5** exhibit lower values for the observed redox transitions, while the corresponding $E_{1/2}$ values for the remaining complexes are shifted to higher potentials. This coherence between the redox potentials and the utilized ring substituents underlines the determined catalase ac-

 © 2004 Wiley-VCH Verlag GmbH & Co. KGaA, Weinheim

Table 4. Catalytic activity of manganese catalase and synthetic catalase mimics

	k_{cat} [s^{-1}]	K_M [mM]	k_{cat}/K_M [$M^{-1}\cdot s^{-1}$]	Ref.
Thermus thermophilus catalase	2.6×10^5	83	3.1×10^6	[36]
Lactobacillus plantarum catalase	2.0×10^5	350	0.6×10^6	[7]
Thermoleophilum album catalase	2.6×10^4	15	1.7×10^6	[6]
$[Mn_2(bpia)_2(\mu\text{-}OAc)_2](ClO_4)_2$	1070	31.5	34000	[16]
5	140	18	7800	this work
3	165	24.2	6800	this work
1	283	54.3	5400	this work
4	115.6	33.2	3500	this work
2	87.7	31.8	2750	this work
$[Mn_2(salpn)_2O_2]$	2500	250	1000	[37,38]
$[Mn_2(2\text{-}OHsalpn)_2]$	4.2−21.9	10.2−118.0	160−990	[13,14]
$[Mn_2(tacn)(bipy)(\mu\text{-}O)_2(\mu\text{-}OAc)(MeOH)](ClO_4)_2\cdot MeOH$	13.2[a]	–	–	[39] [b]
$[Mn_2(bpia)_2(\mu\text{-}O)_2](ClO_4)_2(PF_6)\cdot 2CH_3CN$	8.1[a]	–	–	[16]
$[Mn_2(tacn)(\mu\text{-}O)_2(\mu\text{-}OAc)(OAc)_2]$	5.5[a]	–	–	[17] [b]
$[Mn_2(L^1)(\mu\text{-}OAc)(H_2)]^{2+}$	2.1[a]	0.3	700	[9−12] [c]
$[Mn_2(salpentO)(\mu\text{-}OAc)(\mu\text{-}OMe)(MeOH)_2]$	0.66	36	18	[40]
$[Mn(H_2O)_6](ClO_4)_2$	0.0063[a]	–	–	[13]

[a] No saturation kinetics observed/reported. [b] tacn = 1,4,7-trimethyl-1,4,7-triazacyclononane; bpy = 2,2′-bipyridine. [c] L^1 = *N*,*N*,*N*′,*N*′-tetrakis(2-methylenebenzimidazolyl)-1,3-diaminopropan-2-ol.

tivity. This is in good agreement with experiments reported previously concerning the binding efficiency of hydrogen peroxide to the manganese center,[13] where it has been reported that the manganese compounds donating the most electrons have the highest affinity for the substrate.

Since complexes **1**−**5** are hexacoordinate in the solid state it is most likely that at least one chloride ligand is replaced in solution by a solvent molecule that can easily be replaced by the substrate. This has been proved by MALDI experiments (see Exp. Sect.). This soft ionization method ensures that each species in solution is detected without further conversion into fragments. As is shown in the Exp. Sect. either an $[M^+ - Cl]$ or $[M^+ - HCl]$ species was detected in every spectrum. This is convincing evidence that the dinuclear structure is preserved in solution without the coordination of one chloride ion to the dinuclear metal core. Therefore one manganese ion provides a labile coordination site. This is sufficient to disproportionate H_2O_2 as it is postulated for the catalytic cycle of Mn catalase.[7]

The observed catalase activities place the complexes **1**−**5** within approximately three orders of magnitude of the three characterized manganese catalases in terms of both k_2 and k_2/K_M criteria.

Conclusion

The synthesis and structural characterization of five dinuclear manganese(II/II) compounds has been reported. The utilized tripodal ligands share two pyridine and one phenol moiety but differ in the type of substituents coordinated to the aromatic rings. It seems that the electronic character of the different ring substituents tunes the catalase activity, which correlates with the observed redox potentials of the dinuclear transition metal complexes. Groups donating electrons into the aromatic π-system lead to higher catalytic activity involving lower $E_{1/2}$ values while electron-withdrawing substituents cause the opposite effect, namely higher $E_{1/2}$ values and lower catalase activity. All compounds belong to the class of synthetic model complexes showing saturation kinetics at high substrate concentrations. The observed catalase activity places the complexes **1**−**5** within approximately three orders of magnitude of the three characterized manganese catalases in terms of both k_2 and k_2/K_M criteria. Compared to the two most efficient systems $[Mn_2(bpia)_2]$ and $[Mn_2(2\text{-}OHsalpn)_2]$, described by Triller et al.[16] and Gelasco et al.,[13] respectively, compounds **1**−**5** are the second best functional manganese catalase mimics.

Experimental Section

Physical Measurements: IR spectra were recorded with a Perkin−Elmer Spectrum GX FT-IR spectrometer in the range of 4000−400 cm^{-1}. Samples were prepared as KBr pellets. Elemental analyses were carried out with a Perkin−Elmer 2400 Series 2 analyzer. MALDI experiments were performed with a Bruker Daltonics MALDI Reflex IV spectrometer. The compounds were dissolved in the same solvent system as used for the kinetic measurements. Cyclic voltammetric experiments were performed with a BAS CV-27 voltammograph equipped with a BAS C-1B cell stand and a BAS RXY recorder. The concentration of the samples was 1×10^{-3} M in acetonitrile for **2**, 1×10^{-3} M in acetonitrile/DMF (15:1) for **4** and **5**, 3×10^{-3} M in acetonitrile/DMF (15:1) for **1** and **3**. Prior to use, solvents were purified by standard literature methods.[41] Tetrabutylammonium hexafluorophosphate (recrystallized from ethanol) was used as supporting electrolyte at a concentration of 0.1 M. A three-electrode array consisting of a glassy carbon working electrode, a platinum wire counter electrode and an Ag/AgCl reference electrode was used.

Kinetic Measurements: Catalase activities of all complexes were measured at 25 °C on the basis of fluorescence quenching using an oxygen sensor.[42] Hydrogen peroxide solution in water was placed in a vessel equipped with a thermostat (5 mL, prepared in different

 © 2004 Wiley-VCH Verlag GmbH & Co. KGaA, Weinheim

concentrations from 36.6% hydrogen peroxide solution in water, concentration determined iodometrically and manganometrically). Before each measurement, a calibration of the oxygen sensor was carried out by saturating the solution with dioxygen (100% dioxygen) and then with argon (0% dioxygen). The dioxygen concentration in dioxygen-saturated water has been determined to be 1.388 mM.[43] After a baseline had been established, 0.1 mL of a 0.01 M solution of the complex in degassed methanol was added, and the oxygen evolution was monitored. The average initial rate over three independent measurements, expressed as $mol(H_2O_2)\cdot s^{-1}\cdot[mol(catalyst)]^{-1}$,[12] was determined by linear regression from the slope of concentration versus time plots.

Syntheses: The ligands HL_3 and HL_4 were prepared according to the previously reported syntheses of HL_1 [21] and HL_2,[44] respectively, using *N*-[(6-methylpyridin-2-yl)methyl]-*N*-(pyridin-2-ylmethyl)amine instead of *N*,*N*-bis(pyridin-2-ylmethyl)amine.

2-[{[(6-Methylpyridin-2-yl)methyl](pyridin-2-ylmethyl)amino}-methyl]phenol (HL_3): Yield: 5.43 g (17 mmol, 75%). $C_{20}H_{21}N_3O$ (319.0): calcd. C 75.24, H 6.58, N 13.17; found C 75.13, H 6.34, N 13.15. ^{1}H NMR (300 MHz, $CDCl_3$): δ = 2.59 (s, 3 H, CH_3), 3.80 (s, 2 H, CH_2), 3.85 (s, 2 H, CH_2), 3.88 (s, 2 H, CH_2), 6.77−7.64 (m, 10 H, Ar-H), 8.57 (d, *J* = 4.8 Hz, 1 H, Ar-H) ppm. ^{13}C NMR (75 MHz, $CDCl_3$): δ = 24.2, 56.9, 59.2, 59.3, 116.6, 118.9, 120.1, 121.7, 122.2, 122.9, 123.3, 129.0, 130.2, 136.7, 137.0, 149.0, 157.6, 157.7, 158.0, 158.5 ppm. IR (KBr): $\tilde{\nu}$ = 3440 cm^{-1} (m, br), 3049 (s), 2956 (s), 2922 (s), 2855 (s), 2801 (s), 2708 (m), 2608 (m), 2256 (w), 2007 (w), 1979 (w), 1935 (w), 1905 (w), 1876 (w), 1789 (w), 1688 (w), 1612 (m), 1583 (vs), 1512 (w), 1488 (vs), 1465 (s), 1437 (s), 1428 (s), 1375 (s), 1362 (s), 1316 (w), 1289 (m), 1246 (w), 1204 (m), 1181 (w), 1161 (m), 1141 (m), 1122 (m), 1091 (m), 1039 (m), 1003 (m), 990 (w), 973 (m), 955 (w), 937 (w), 899 (w), 892 (w), 870 (w), 789 (s), 760 (vs), 717 (m), 646 (w), 604 (m), 558 (m), 542 (w), 479 (m), 444 (m).

2-[{[(6-Methylpyridin-2-yl)methyl](pyridin-2-ylmethyl)amino}-methyl]-4-nitrophenol (HL_4): Yield: 2.4 g (17 mmol, 57%). $C_{20}H_{20}N_4O_3$ (365.1): calcd. C 65.74, H 5.48, N 15.34; found C 65.60, H 5.39, N 15.26. ^{1}H NMR (300 MHz, $CDCl_3$): δ = 2.60 (s, 3 H, CH_3), 3.85 (s, 2 H, CH_2), 3.90 (s, 2 H, CH_2), 3.92 (s, 2 H, CH_2), 6.95−8.12 (m, 9 H, Ar-H), 8.58 (d, *J* = 4.8 Hz, 1 H, Ar-H) ppm. ^{13}C NMR (75 MHz, $CDCl_3$): δ = 24.0, 56.0, 58.8, 59.0, 117.2, 120.0, 122.0, 122.4, 123.2, 123.6, 125.6, 126.6, 137.0, 137.2, 137.9, 148.8, 156.8, 157.9, 161.2, 162.6 ppm. IR (KBr): $\tilde{\nu}$ = 3434 cm^{-1} (m, br), 3074 (m), 3049 (m), 3002 (m), 2930 (m), 2820 (m), 2717 (m), 2491 (w), 1736 (w), 1619 (m), 1600 (m), 1582 (s), 1511 (s), 1488 (s), 1460 (m), 1431 (m), 1377 (m), 1333 (vs), 1292 (s), 1262 (m), 1240 (s), 1178 (m), 1149 (m), 1133 (m), 1110 (m), 1088 (m), 1049 (m), 1009 (m), 976 (m), 931 (w), 904 (w), 878 (m), 839 (m), 823 (m), 750 (s), 733 (m), 641 (w), 610 (w), 566 (w), 511 (w), 494 (w), 450 (m).

The ligand 2-{[bis(pyridin-2-ylmethyl)amino]methyl}-6-methoxyphenol (HL_5) was synthesized as follows.

2-Methoxy-6-{[(pyridin-2-ylmethyl)amino]methyl}phenol: Equivalent amounts of 2-pyridylmethylamine (2.70 g, 25 mmol) and 2-hydroxy-3-methoxybenzaldehyde (3.80 g, 25 mmol) were dissolved in 100 mL of methanol and stirred for 2 h. After reduction with $NaBH_4$ (0.47 g, 12.5 mmol), the solution was stirred for a further 12 h. The mixture was acidified with hydrochloric acid to pH = 1 and, after concentrating under vacuum, extracted with chloroform (5 × 20 mL) to separate side products and impurities. In order to neutralize the hydrochloride, the pH was adjusted to 8 with an aqueous solution of NaOH and the free amine was extracted with chloroform (5 × 20 mL). The combined organic layers were dried ($MgSO_4$) and the solvent was removed under vacuum yielding the oily product. Yield: 5.73 g (23.6 mmol, 94%). ^{1}H NMR (300 MHz, $CDCl_3$): δ = 3.88 (s, 3 H, O-CH_3), 3.92 (s, 2 H, CH_2), 4.02 (s, 2 H, CH_2), 6.59−7.69 (m, 6 H, Ar-H), 8.56 (d, *J* = 4.8 Hz, 1 H, Ar-H).

2-{[Bis(pyridin-2-ylmethyl)amino]methyl}-6-methoxyphenol (HL_5): 2-Methoxy-6-{[(pyridin-2-ylmethyl)amino]methyl}phenol (4.88 g, 20.0 mmol) and 2-chloromethylpyridine hydrochloride (3.28 g, 20.0 mmol) were dissolved in 100 mL of methanol. A pH value of 9 was adjusted by adding solid potassium carbonate. The mixture was stirred at room temperature for 3 d while the pH value was controlled every 24 h. After the remaining K_2CO_3 was filtered off, the mixture was acidified carefully with hydrochloric acid to pH = 1. Further purification was performed with the method described above to yield an orange brown product. Yield: 3.99 g (11.9 mol, 50%). $C_{20}H_{21}N_3O_2$ (335.4): calcd. C 71.62, H 6.31, N 12.53; found C 71.50, H 6.19, N 12.76. ^{1}H NMR (300 MHz, $CDCl_3$): δ = 3.73 (s, 3 H, OCH_3), 3.89 (s, 2 H, CH_2), 3.90 (s, 4 H, CH_2), 6.71 (dd, *J* = 7.6 Hz, *J* = 7.9 Hz, 1 H, Ar-H), 6.74 (d, *J* = 7.9 Hz, 1 H, Ar-H), 6.83 (d, *J* = 7.6 Hz, 1 H, Ar-H), 7.13−7.66 (m, 6 H, Ar-H), 8.57 (d, *J* = 4.8 Hz, 2 H, Ar-H) ppm. ^{13}C NMR (75 MHz, $CDCl_3$): δ = 55.9, 56.7, 59.0, 111.3, 118.5, 122.3, 122.4, 123.2, 123.3, 134.9, 137.0, 146.9, 148.7, 158.2 ppm. IR (KBr): $\tilde{\nu}$ = 3434 cm^{-1} (m, br), 3054 (m), 3010 (m), 2935 (m), 2917 (m), 2835 (m), 2805 (m), 2750 (w), 2609 (w), 1947 (w), 1888 (w), 1586 (s), 1570 (m), 1486 (s), 1472 (s), 1433 (s), 1389 (m), 1372 (m), 1299 (m), 1250 (s), 1235 (s), 1160 (m), 1134 (m), 1073 (s), 1049 (m), 1006 (m), 994 (m), 976 (m), 954 (m), 933 (m), 886 (w), 837 (m), 777 (s), 761 (m), 737 (m), 631 (m), 617 (w), 561 (w), 539 (w), 510 (w), 483 (w), 467 (w).

Synthesis of the Dinuclear Complexes 1−5: All complexes were prepared according to the same method. Equivalent amounts of manganese(II) chloride tetrahydrate (0.25 mmol, 49.5 mg) and corresponding ligand were dissolved in 10 mL of ethanol and triethylamine (0.3 mmol, 42 μL) was added. After stirring the mixture for 12 h, the resulting precipitate was isolated and redissolved in 10 mL of dichloromethane. Crystals suitable for X-ray diffraction analysis were obtained by layering with hexane.

$[Mn_2(L_1)_2(Cl)_2]\cdot 2CH_2Cl_2$ (1): Yield:113.78 mg (0.12 mmol, 47%). $C_{38}H_{36}Cl_2Mn_2N_6O_2$ (789.52): calcd. C 57.81, H 4.60, N 10.64; found C 56.96, H 4.46, N 10.49. MS (MALDI): *m*/*z* = 754 [M^+ − Cl]. IR (KBr): $\tilde{\nu}$ = 3436 cm^{-1} (m, br), 3050 (m), 3021 (m), 3002 (m), 2982 (w), 2954 (m), 2913 (m), 2878 (m), 2830 (m), 2776 (w), 2604 (w), 2497 (w), 1885 (w), 1602 (vs), 1571 (s), 1476 (vs), 1452 (vs), 1396 (w), 1368 (w), 1349 (s), 1326 (w), 1308 (w), 1269 (vs), 1190 (w), 1150 (m), 1129 (m), 1095 (m), 1052 (m), 1037 (m), 1014 (m), 999 (m), 978 (m), 960 (m), 926 (m), 881 (s), 837 (m), 759 (vs), 737 (s), 660 (w), 638 (m), 576 (m), 517 (w), 493 (w), 477 (m).

$[Mn_2(L_2)_2(Cl)_2]\cdot EtOH$ (2): Yield: 155.41 mg (0.17 mmol, 67%). $C_{38}H_{34}Cl_2Mn_2N_8O_6$ (879.51): calcd. C 51.89, H 3.90, N 12.74; found C 51.46, H 3.86, N 12.24. MS (MALDI): *m*/*z* = 843 [M^+ − HCl]. IR (KBr): $\tilde{\nu}$ = 3427 cm^{-1} (s, br), 3056 (w), 2956 (w), 2848 (w), 1719 (m, br), 1600 (s), 1573 (m), 1477 (s), 1437 (m), 1395 (w), 1329 (w), 1286 (vs), 1180 (m), 1153 (m), 1126 (m), 1090 (s), 1051 (m), 1014 (m), 977 (w), 961 (w), 933 (m), 894 (w), 838 (w), 763 (m), 737 (s), 671 (m), 648 (s), 516 (w), 461 (m, br).

$[Mn_2(L_3)_2(Cl)_2]\cdot CH_2Cl_2$ (3): Yield: 106.27 mg (0.12 mmol, 47%). $C_{40}H_{40}Cl_2Mn_2N_6O_2$ (817.58): calcd. C 58.76, H 4.93, N 10.27; found C 58.40, H 4.23, N 9.67. MS (MALDI): *m*/*z* = 780 [M^+ − HCl]. IR (KBr): $\tilde{\nu}$ = 3399 cm^{-1} (s, br), 3054 (m), 3024 (m), 3001 (m), 2963 (m), 2923 (m), 2833 (m), 1907 (w), 1677 (s), 1602 (vs),

 © 2004 Wiley-VCH Verlag GmbH & Co. KGaA, Weinheim

Table 5. Details of structure determination, refinement and experimental parameters of compounds **1**−**5**

	1	**2**	**3**	**4**	**5**
Empirical formula	$C_{40}H_{40}Cl_6Mn_2N_6O_2$	$C_{40}H_{40}Cl_2Mn_2N_8O_7$	$C_{41}H_{42}Cl_4Mn_2N_6O_2$	$C_{41}H_{40}Cl_4Mn_2N_8O_6$	$C_{40}H_{42}Cl_2Mn_2N_6O_4$
Formula mass [g/mol]	959.36	925.58	902.33	992.33	851.56
Temperature [K]	213(2)	213(2)	213(2)	100(2)	100(2)
Wavelength [Å]	0.71073	0.71073	0.71073	0.71073	1.54178
Crystal system	monoclinic	monoclinic	monoclinic	monoclinic	monoclinic
Space group	$P2_1/c$ (No. 14)	$P2_1/c$ (No. 14)	$P2_1/n$ (No. 14)	$I2/a$ (No. 15)	$I2/a$ (No. 15)
a [Å]	11.104(2)	20.214(4)	11.870(2)	22.997(5)	21.8425(5)
b [Å]	15.394(3)	11.620(2)	13.171(3)	8.762(2)	8.7350(2)
c [Å]	25.306(5)	17.324(3)	15.417(3)	23.602(5)	21.9876(7)
β [°]	92.80(3)	96.94(3)	111.72(3)	101.37(3)	113.81(1)
V [Å^3]	4320.4(15)	4039.4(13)	2239.2(8)	4662.5(18)	3838.2(1)
Z	4	4	2	4	4
Density (calcd.) [g/cm^3]	1.475	1.522	1.459	1.526	1.470
μ [mm^{-1}]	0.998	0.818	0.965	0.941	7.040
Crystal size [mm]	0.31 × 0.20 × 0.12	0.48 × 0.40 × 0.24	0.40 × 0.40 × 0.32	0.13 × 0.11 × 0.09	0.12 × 0.10 × 0.08
θ range [°]	8.5 ≤ 2θ ≤ 52.0	8.8 ≤ 2θ ≤ 52.0	9.1 ≤ 2θ ≤ 52.0	3.52 ≤ 2θ ≤ 56.58	8.80 ≤ 2θ ≤ 142.36
Index ranges	−13 ≤ h ≤ 13	−24 ≤ h ≤ 24	−14 ≤ h ≤ 14	−30 ≤ h ≤ 30	−26 ≤ h ≤ 26
	−18 ≤ k ≤ 17	−14 ≤ k ≤ 14	−16 ≤ k ≤ 16	−11 ≤ k ≤ 11	−10 ≤ k ≤ 10
	−30 ≤ l ≤ 31	−21 ≤ l ≤ 21	−18 ≤ l ≤ 18	−31 ≤ l ≤ 31	−26 ≤ l ≤ 25
Reflections collected	30989	29776	15763	23512	10378
Independent reflections	8406	7886	4356	5795	3558
	[R(int) = 0.1966]	[R(int) = 0.1376]	[R(int) = 0.1474]	[R(int) = 0.0337]	[R(int) = 0.0342]
Data	8406	7886	4356	5795	3558
Parameters	505	518	292	339	335
Goodness-of-fit on F^2	1.033	1.025	1.084	1.007	0.998
Final R indices [$I > 2\sigma(I)$]	$R1$ = 0.0701	$R1$ = 0.0572	$R1$ = 0.0703	$R1$ = 0.0417	$R1$ = 0.0380
	$wR2$ = 0.1258	$wR2$ = 0.1363	$wR2$ = 0.1843	$wR2$ = 0.1105	$wR2$ = 0.0980
R indices (all data)	$R1$ = 0.1624	$R1$ = 0.0792	$R1$ = 0.0916	$R1$ = 0.0586	$R1$ = 0.0526
	$wR2$ = 0.1609	$wR2$ = 0.1510	$wR2$ = 0.2266	$wR2$ = 0.1134	$wR2$ = 0.1036
Largest diff. peak/hole [e$^-$/Å^3]	0.581/−0.382	0.585/−0.667	1.076/−1.018	0.570/−0.662	0.587/−0.220

1575 (w), 1478 (vs), 1455 (vs), 1396 (w), 1378 (w), 1349 (w), 1330 (w), 1297 (w), 1271 (s), 1163(s), 1156 (m), 1120 (m), 1092 (s), 1038 (m), 1009 (s), 979 (w), 965 (w), 888 (s), 844 (w), 787 (vs), 757 (w), 738 (w), 726 (w), 656 (w), 641 (m), 576 (w), 524 (w), 495 (w), 474 (w).

$[Mn_2(L_4)_2(Cl)_2]\cdot CH_2Cl_2$ (4): Yield: 141.63 mg (0.14 mmol, 57%). $C_{40}H_{38}Cl_2Mn_2N_8O_6$ (907.57): calcd. C 52.93, H 4.22, N 12.35; found C 53.59, H 4.05, N 11.31. MS (MALDI): m/z = 870 [M$^+$ − HCl]. IR (KBr): $\tilde{\nu}$ = 3436 cm^{-1} (s, br), 3054 (w), 2955 (m), 2922 (m), 2675 (w), 2492 (w), 1974 (w), 1595 (s), 1575 (s), 1477 (s), 1437 (w), 1327 (w), 1287 (s), 1180 (m), 1127 (w), 1091 (s), 1051 (w), 1011 (m), 966 (w), 935 (m), 895 (w), 880 (w), 834 (m), 782 (m), 764 (m), 736 (w), 671 (m), 646 (m), 558 (w), 514 (w), 488 (w), 455 (w).

$[Mn_2(L_5)_2(Cl)_2]$ (5): Yield: 131.51 mg (0.16 mmol, 62%). $C_{40}H_{40}Cl_2MnN_6O_4$ (848): calcd. C 56.55, H 4.75, N 9.89; found C 56.23, H 4.89, N 9.24. MS (MALDI): m/z = 813 [M$^+$ − Cl]. IR (KBr): $\tilde{\nu}$ = 3429 cm^{-1} (s, br), 3055 (w), 2921 (m), 2849 (m), 1603 (s), 1571 (m), 1478 (vs), 1456 (m), 1441 (m), 1388 (w), 1346 (w), 1308 (m), 1273 (m), 1237 (m), 1154 (w), 1126 (w), 1079 (m), 1051 (m), 1014 (m), 1000 (m), 970 (w), 897 (w), 849 (m), 767 (m), 736 (m), 638 (w), 618 (w), 494 (w), 442 (w), 410 (w).

X-ray Crystallographic Study: Single-crystal X-ray studies of complexes **1**−**3** were performed with a Stoe IPDS diffractometer with graphite-monochromated Mo-K_α radiation (λ = 0.71073 Å) at 213 K; studies on compound **4** were done with a Bruker AXS SMART APEX with graphite-monochromated Mo-K_α radiation (λ = 0.71073 Å) at 100 K; studies on compound **5** were done with a Bruker AXS SMART 6000 with Cu-K_α radiation (λ = 1.54178 Å) at 100 K. All structures were solved with direct methods and refined by full-matrix least-squares procedures on F_o^2 values (SHELXTL-Plus-97[45,46]). Anisotropic displacement parameters were used to refine the positions of all non-hydrogen atoms. Hydrogen atoms were placed at calculated positions according to a riding model with group isotropic temperature factors. The residual value wR_2 in Table 5 is defined as $[w(F_o^2 - F_c^2)^2/w(F_o^2)^2]^{1/2}$. Selected distances and angles are listed in Tables 1−4. CCDC-205842 (**1**), -205843 (**2**), -205844 (**3**), -205845 (**4**), and -205846 (**5**) contain the supplementary crystallographic data for this paper. These data can be obtained free of charge at www.ccdc.cam.ac.uk/conts/retrieving.html [or from the Cambridge Crystallographic Data Centre, 12 Union Road, Cambridge CB2 1EZ, UK; Fax: (internat.) + 44-1223/336-033; E-mail: deposit@ccdc.cam.ac.uk].

Acknowledgments

Financial support by the DFG (Deutsche Forschungsgemeinschaft, SPP 1118) and the FCI (Fonds der Chemischen Industrie) is gratefully acknowledged.

[1] M. J. Maté, G. Murshudov, J. Bravo, W. R. Melik-Adamyan, P. C. Loewen, I. Fita, in *Handbook of Metalloproteins* (Eds.: A. Messerschmidt, R. Huber, T. Poulos, K. Wieghardt), John Wiley & Sons, New York **2001**, p. 468.
[2] Y. Kono, I. Fridovich, *J. Biol. Chem.* **1983**, *258*, 6015.
[3] W. F. Beyer Jr., I. Fridovich, *Biochem.* **1985**, *24*, 6460.
[4] V. V. Barynin, A. A. Vagin, W. R. Melik-Adamyan, A. I. Grebenko, S. V. Khangulov, A. N. Popov, M. E. Andrianova, B. K.

 © 2004 Wiley-VCH Verlag GmbH & Co. KGaA, Weinheim

Vainshtein, *Dokl. Akad. Nauk SSSR* **1986**, *288*, 877; *Chem. Abstr.* **1986**, *105*, 74919q.
[5] V. V. Barynin, P. D. Hempstead, A. A. Vagin, S. V. Antonyuk, W. R. Melik-Adamyan, V. S. Lamzin, P. M. Harrison, P. Artymiuk, *J. Inorg. Biochem.* **1997**, *67*, 196.
[6] G. S. Allgood, J. J. Perry, *J. Bacteriol.* **1986**, *168*, 563.
[7] J. E. Penner-Hahn, in *Manganese Redox Enzymes* (Ed.: V. L. Pecoraro), VCH Publishers, Inc., New York, **1992**, p. 29.
[8] J. E. Penner-Hahn, *Struct. Bonding (Berlin, Ger.)* **1998**, *90*, 1.
[9] A. E. M. Boelrijk, G. C. Dismukes, *Inorg. Chem.* **2000**, *39*, 3020.
[10] P. Mathur, M. Crowder, G. C. Dismukes, *J. Am. Chem. Soc.* **1987**, *109*, 5227.
[11] P. J. Pessiki, S. V. Khangulov, D. M. Ho, G. C. Dismukes, *J. Am. Chem. Soc.* **1994**, *116*, 891.
[12] P. J. Pessiki, G. C. Dismukes, *J. Am. Chem. Soc.* **1994**, *116*, 898.
[13] A. Gelasco, S. Bensiek, V. L. Pecoraro, *Inorg. Chem.* **1998**, *37*, 3301.
[14] A. Gelasco, V. L. Pecoraro, *J. Am. Chem. Soc.* **1993**, *115*, 7928.
[15] A. Gelasco, M. L. Kirk, J. W. Kampf, V. L. Pecoraro, *Inorg. Chem.* **1997**, *36*, 1829.
[16] M. U. Triller, W.-Y. Hsieh, V. L. Pecoraro, A. Rompel, B. Krebs, *Inorg. Chem.* **2002**, *41*, 5544.
[17] S. Ito, S. Nishino, H. Itoh, S. Ohba, Y. Nishida, *Polyhedron* **1998**, *17*, 1637.
[18] S. Ito, M. Suzuki, T. Kobayashi, H. Itoh, A. Harada, S. Ohba, Y. Nishida, *J. Chem. Soc., Dalton Trans.* **1996**, 2579.
[19] H. Sugimoto, Y. Sasaki, *Chem. Lett.* **1997**, 541.
[20] A. Trösch, H. Vahrenkamp, *Eur. J. Inorg. Chem.* **1998**, 827.
[21] S. Yan, L. Que Jr., L. F. Taylor, O. P. Anderson, *J. Am. Chem. Soc.* **1988**, *110*, 5222.
[22] S. Yan, X. Pan, L. F. Taylor, J. H. Zhang, C. J. O'Connor, D. Britton, O. P. Anderson, L. Que Jr., *Inorg. Chim. Acta* **1996**, *243*, 1.
[23] H. Adams, N. A. Bailey, I. K. Campbell, D. E. Fenton, Q.-Y. He, *J. Chem. Soc., Dalton Trans.* **1996**, 2233.
[24] Y. Nishida, *Chem. Lett.* **1987**, *16*, 2151.
[25] U. Rajendran, R. Viswanathan, M. Palaniandavar, M. Lakshminarayanan, *J. Chem. Soc., Dalton Trans.* **1992**, 3563.
[26] R. Uma, R. Viswanathan, M. Palaniandavar, M. Lakshminarayanan, *J. Chem. Soc., Dalton Trans.* **1994**, 1219.
[27] M. Vaidyanathan, R. Viswanathan, M. Palaniandavar, T. Balasubramanian, P. Prabhaharan, T. P. Muthiah, *Inorg. Chem.* **1998**, *37*, 6418.
[28] R. Viswanathan, M. Palaniandavar, T. Balasubramanian, T. P. Muthiah, *Inorg. Chem.* **1998**, *37*, 2943.
[29] H.-R. Chang, S. K. Larsen, P. D. W. Boyd, C. G. Pierpont, D. N. Hendrickson, *J. Am. Chem. Soc.* **1988**, *110*, 4565.
[30] M. Marappan, V. Narayanan, M. Kandaswamy, *J. Chem. Soc., Dalton Trans.* **1998**, 3405.
[31] C. Hureau, E. Anxolabéhère-Mallart, M. Nierlich, F. Gonnet, E. Rivière, G. Blondin, *Eur. J. Inorg. Chem.* **2002**, 2710.
[32] D. P. Kessissoglou, W. H. Butler, V. L. Pecoraro, *Inorg. Chem.* **1987**, *26*, 495.
[33] J. Heinze, *Angew. Chem.* **1984**, *96*, 823; J. Heinze, *Angew. Chem. Int. Ed. Engl.* **1984**, *84*, 831.
[34] R. S. Nicholson, I. Shain, *Anal. Chem.* **1964**, *36*, 706.
[35] E. A. Lewis, J. R. Lindsay Smith, P. H. Walton, S. J. Archibald, S. P. Foxon, G. M. P. Giblin, *J. Chem. Soc., Dalton Trans.* **2001**, 1159.
[36] M. Shank, V. Barynin, G. C. Dismukes, *Biochemistry* **1994**, *33*, 15433.
[37] A. C. Rosenzweig, C. A. Frederick, S. J. Lippard, P. Nordlund, *Nature* **1993**, *366*, 537.
[38] E. J. Larson, V. L. Pecoraro, *J. Am. Chem. Soc.* **1991**, *113*, 7809.
[39] U. Bossek, M. Saher, T. Weyhermüller, K. J. Wieghardt, *J. Chem. Soc., Chem. Commun.* **1992**, 1780.
[40] C. Palopoli, B. Chansou, J.-P. Tuchagues, S. Signorella, *Inorg. Chem.* **2000**, *39*, 1458.
[41] J. F. Coetzee, in *Recommended Methods for Purification of Solvents*, Pergamon, Oxford, **1982**.
[42] R. Könecke, A. Comte, H. Jürgens, O. Kohls, H. Lam, T. Scheper, *Chem. Ing. Tech.* **1998**, *70*, 1611.
[43] *Handbook of Chemistry and Physics* (Ed.: R. C. Weast), 54th ed., CRC Press, Cleveland, **1973−1974**, B 116.
[44] Y. Nishida, H. Shimo, S. Kida, *J. Chem. Soc., Chem. Commun.* **1984**, 1611.
[45] G. M. Sheldrick, *SHELXS-97*, Universität Göttingen **1997**.
[46] G. M. Sheldrick, *SHELXL-97*, Universität Göttingen **1997**.

Received March 25, 2003
Early View Article
Published Online January 19, 2004

 © 2004 Wiley-VCH Verlag GmbH & Co. KGaA, Weinheim

Iridium Complexes with Chiral and Achiral β-Aminophosphane Ligands: Catalysts for >C=O Hydrogenation and H/D Exchange Involving both Homo- and Heterolytic H_2 Activation[‡]

Lutz Dahlenburg*[a] and Rainer Götz[a]

Dedicated to the memory of Professor Dieter Sellmann, who has shed much light!

Keywords: Chirality / Hydrogenations / Isotopic exchange / Iridium

Chiral and achiral *P,N*-chelated Ir^I complexes of the general type $[(COD)Ir(P\cap NR^1R^2)]BF_4$, where COD = η^4-1,5-C_8H_{12} and $P\cap NR^1R^2$ = (1*R*,2*R*)-, (1*S*,2*S*)-, or (1*R*,2*S*)-$Ph_2PC^1H(Ph)C^2H(Me)NR^1R^2$ (NR^1R^2 = NH_2, NHMe, $NHCH_2Ph$, $NHCHMe_2$, NMe_2), $Ph_2PCH_2CR_2NH_2$ (R = H, Me), or 2-$Ph_2PC_6H_4NHMe$, have been prepared by treating $[Ir(COD)_2]BF_4$ with the required β-aminophosphane in THF. The monolithiated ligands $Ph_2PCH_2CMe_2N(Li)H$ and 2-$Ph_2PC_6H_4N(Li)Me$ interacted with $[\{(COD)Ir(\mu\text{-}Cl)\}_2]$ to give the neutral alkyl- and arylamido compounds [(COD)-$Ir(Ph_2PCH_2CMe_2NH)$] and [(COD)Ir(2-$Ph_2PC_6H_4NMe$)]. All Ir^I complexes $[(COD)Ir(P\cap NR^1R^2)]BF_4$ acted as catalysts for the direct hydrogenation of alkyl aryl ketones to the corresponding 1-phenylalkanols, if combined with an alkaline or amine base in methanol under H_2 (10–50 bar) between 25 and 50 °C. The reaction occurred with modest to moderate enantioselectivity (ca. 20–75% *ee*) if chelate complexes bearing the various optically active β-aminophosphanes were used as catalysts. The base-free amido complexes [(COD)-$Ir(P\cap NR)$] displayed similar catalytic activity to the combined systems $[(COD)Ir(P\cap NHR)]BF_4$–KOH ($P\cap NHR$ = $Ph_2PCH_2CMe_2NH_2$, 2-$Ph_2PC_6H_4NHMe$). The ability of both the cationic β-amino- and the neutral β-amidophosphane Ir^I complexes to undergo oxidative H_2 addition and the observation of H_2/D^+ as well as H_2/D_2 exchange processes during catalysis provided evidence for a mechanism involving reversible "$[Ir^{III}(H)_2\text{–}P\cap NHR]^+ \rightleftarrows [(\eta^2\text{-}H_2)\text{–}Ir^{III}(H)\text{–}P\cap NR]^+$" proton-to-hydride transfer and heterolytic H_2 cleavage on amino–dihydride and amido–dihydrogen–monohydride tautomers. The crystal structures of [(COD)Ir{(1*S*,2*S*)-$Ph_2PCH(Ph)CH(Me)NHCH_2Ph$}]$BF_4$·2THF, [(COD)Ir{1*R*,2*S*-$Ph_2PCH(Ph)CH(Me)NHMe$}]BF_4·THF, and the orthometalated 18e Ir^I complex [(COD)Ir{(1*R*,2*S*)-$Ph_2PCH(C_6H_4\text{-}o)$-$CH(Me)NHCHMe_2$}], which resulted from treatment of [(COD)Ir{(1*R*,2*S*)-$Ph_2PCH(Ph)CH(Me)NHCHMe_2$}]$BF_4$ with excess KOH, have been determined by single crystal X-ray diffraction studies.

(© Wiley-VCH Verlag GmbH & Co. KGaA, 69451 Weinheim, Germany, 2004)

Introduction

Metal complexes containing both *P* and *N* donor ligands have been dominating the field of homogeneous catalytic hydrogenation of organic carbonyl compounds for several years. In particular, Noyori's ruthenium complexes $[RuCl_2\{bis(phosphane)\}(1,2\text{-diamine})]$ have been found to be excellent catalysts for the enantioselective reduction, by H_2, of simple ketones if activated by an excess of strong base.[1] Intramolecular heterolytic H_2 splitting across the polar metal−amide bond of initially formed amine-amido hydrido complexes, $[RuH(P\cap P)(HN\cap NH_2)]$, to reversibly give diamine dihydrides, $[RuH_2(P\cap P)(H_2N\cap NH_2)]$, has been shown to be a key step involved in the catalytic cycle. From the latter, $H^{\delta-}/H^{\delta+}$ equivalents are transferred simultaneously to the ketonic substrate once the carbonyl group has come into close contact with the second coordination sphere of the catalyst through an unconventional $Ru-H^{\delta-}\cdots>C^{\delta+}=O^{\delta-}\cdots H^{\delta+}-N$ "metal−ligand bifunctional" interaction.[2,3,4]

A different type of a highly enantioselective >C=O hydrogenation catalyst is exemplified by Zhang's Rh−PennPhos system, made up from in situ generated [(COD)Rh{(*R*,*S*,*R*,*S*)-Me-PennPhos}]Cl and a weakly coordinating base of moderate strength, such as 2,6-lutidine ["(*R*,*S*,*R*,*S*)-Me-PennPhos" denotes *P*,*P*′-1,2-phenylene-bis{(1*R*,2*S*,4*R*,5*S*)-2,5-dimethyl-7-phosphabicyclo[2.2.1]-heptane}].[5] Zhang's catalyst is believed to support the homogeneous hydrogenation of ketones following the classic Schrock−Osborn pathway,[6] i.e., homolytic scission of the H_2 molecule by oxidative addition with subsequent

[‡] Functional Phosphanes, XIII. Part XII: Ref.[7b].

[a] Institut für Anorganische Chemie der Universität Erlangen-Nürnberg,
Egerlandstrasse 1, 91058 Erlangen, Germany
Fax: (internat.) +49-9313-85-27387
E-mail: dahlenburg@chemie.uni-erlangen.de

 © 2004 Wiley-VCH Verlag GmbH & Co. KGaA, Weinheim **DOI: 10.1002/ejic.200300503**

>C=O/Rh−H insertion to produce an alkoxo hydrido rhodium(III) complex, in which the remaining hydride is *trans* to the alkoxo ligand so that reductive elimination of the product alcohol cannot easily occur. The authors speculated that the key function of the basic additive is to deprotonate the Rh−H bond forming baseH$^+$ as the conjugate acid, which in turn cleaves the Rh−alkoxo function by protonation.[5]

Based on this background, our recent activities have focussed on the catalytic potential in asymmetric >C=O hydrogenation of a class of optically active β-aminophosphane complexes of Ir^I and Rh^I, [(COD)M{Ph_2PCH-(Ph)CH(Me)NHR}]BF_4 (COD = η^4-1,5-C_8H_{12}; R = H, alkyl), having a chelated d^8 metal center (as found in Zhang's catalyst) embedded in a *P*,*N*-dominated coordination environment (which is an important characteristic of the Noyori systems).[7a,7b] An important further aspect of our work with these complexes arose from our interest in establishing whether the dihydrogen molecule is activated during catalysis by homolytic or heterolytic H−H bond breaking.[7b] Since it is well known that M−H derivatives of iridium, especially of Ir^{III}, are generally more stable and, hence, more readily accessible than those of rhodium, it has primarily been the family of iridium complexes that has been studied in detail up to now, notwithstanding a single observation that the Rh-based catalysts could be somewhat more selective than their iridium homologues (see below). Additional justification for the choice of aminophosphane-coordinated iridium complexes as potential >C=O hydrogenation catalysts arises from the observation that in situ systems composed of [{(COD)Ir(μ-Cl)}$_2$] or [Ir(COD)$_2$]BF_4 and 1,2-diphenylethylene-based chiral diamines can indeed catalyze the asymmetric reduction of ketones and α-keto esters with reasonable enantioselectivities.[8]

Results

Synthesis and Characterization of Ligands and Complexes

In earlier work[7a] we have worked out several useful procedures for the preparation of various optically active bidentate β-aminophosphanes, starting from commercially available (nor)ephedrine and pseudoephedrine diastereomers. In the first step of the syntheses, the different β-amino alcohols were stereospecifically converted into *cis* or *trans* aziridines using established synthetic organic methods.[9,10,11,12] Transformation of the aziridines into the desired *P*,*N* ligands was subsequently accomplished by regio- and stereospecific ring-opening with Ph_2PH in the presence of BF_3 as an activating additive. Enantiopure *P*,*N* ligands thus prepared included (+)-(1*S*,2*S*)-$Ph_2PCH(Ph)CH(Me)NH_2$ [(*S*,*S*)-**1**] hereafter, (−)-(1*R*,2*S*)-$Ph_2PCH(Ph)CH(Me)NH_2$ [(*R*,*S*)-**1**], and (−)-(1*R*,2*R*)-$Ph_2PCH(Ph)CH(Me)NHMe$ [(*R*,*R*)-**2**].[7a]

In a similar manner, (+)-(2*S*,3*S*)-*trans*-1,2-dimethyl-3-phenylaziridine[12] was used as a source of (−)-(1*R*,2*S*)-$Ph_2PCH(Ph)CH(Me)NHMe$ [(*R*,*S*)-**2**] for which a less direct four-step sequence had previously been described by Beck and Nagel[13] [Scheme 1, reaction (1)]. (−)-(2*S*,3*R*)-*cis*-1-benzyl-2-methyl-3-phenylaziridine analogously afforded (+)-(1*S*,2*S*)-$Ph_2PCH(Ph)CH(Me)NHCH_2Ph$ [(*S*,*S*)-**3**]. The required *N*-benzylaziridine had earlier been synthesized from (−)-norephedrine by consecutive reactions with PCl_5, benzaldehyde, and sodium borohydride[14] but was also readily accessible by alkylating the corresponding *N*-unsubstituted aziridine with *n*BuLi/benzyl chloride [Scheme 1, reaction (2)]. The (−)-(2*S*,3*R*)-*cis*- and (+)-(2*S*,3*S*)-*trans*-1-isopropyl-2-methyl-3-phenylaziridine isomers were obtained from (−)-*N*-isopropylnorephedrine[15] by the Gabriel method[9] or by reaction with the Horner reagent PPh_3/Br_2[11a] and nucleophilically opened with $Ph_2PH/F_3B{\cdot}OEt_2$ to furnish (+)-(1*S*,2*S*)-$Ph_2PCH(Ph)CH(Me)NHCHMe_2$ [(*S*,*S*)-**4**] and the corresponding (−)-(1*R*,2*S*) diastereomer (*R*,*S*)-**4** [Scheme 1, reaction (3)]. Conversion of (−)-*N*-methylephedrine with methanesulfonyl chloride to the *N*,*N*-dimethylaziridinium salt,[16] followed by treatment of the latter with Ph_2PH/NEt_3, cleanly afforded the *N*,*N*-dialkylated *P*,*N* ligand (−)-(1*R*,2*S*)-$Ph_2PCH(Ph)CH(Me)NMe_2$ [(*R*,*S*)-**5** Scheme 1, reaction (4)]. Additional β-aminophosphanes used in this study included the known achiral compounds $Ph_2PCH_2CH_2NH_2$ (**6**),[17] and 2-$Ph_2PC_6H_4NHMe$ (**7**)[18] and, as a new member of this family of ligands, $Ph_2PCH_2CMe_2NH_2$ (**8**) which resulted in the usual fashion from ring-opening of 2,2-dimethylaziridine, itself made from 2-amino-2-methylpropanol by the Wenker method[10,19] [Scheme 1, reaction (5)].

Similar to the procedures previously employed for the preparation of (−)-[(COD)Ir{(1*S*,2*S*)-$Ph_2PCH(Ph)$-$CH(Me)NH_2$}]BF_4 [**Ir**$^+$-(*S*,*S*)-**1**] and [(COD)M{(1*R*,2*R*)-$Ph_2PCH(Ph)CH(Me)NHMe$}]BF_4 [M = Rh: **Rh**$^+$-(*R*,*R*)-**2**; M = Ir: **Ir**$^+$-(*R*,*R*)-**2**],[7a] the new optically active chelate complexes [(COD)Ir{(1*S*,2*S*)-$Ph_2PCH(Ph)CH(Me)$-NHR}]BF_4 [R = CH_2Ph: **Ir**$^+$-(*S*,*S*)-**3**; R = $CHMe_2$: **Ir**$^+$-(*S*,*S*)-**4**] and [(COD)Ir{(1*R*,2*S*)-$Ph_2PCH(Ph)CH(Me)$-NR^1R^2}]BF_4 [R^1 = H, R^2 = Me: **Ir**$^+$-(*R*,*S*)-**2**; R^1 = H, R^2 = $CHMe_2$: **Ir**$^+$-(*R*,*S*)-**4**; R^1 = R^2 = Me: **Ir**$^+$-(*R*,*S*)-**5**] as well as their achiral analogues [(COD)Ir-($Ph_2PCH_2CR_2NH_2$)]BF_4 (R = H: **Ir**$^+$-**6**, R = Me: **Ir**$^+$-**8**) and [(COD)Ir(2-$Ph_2PC_6H_4NHMe$)]BF_4 (**Ir**$^+$-**7**) were isolated in high yield (>80%) from ligand exchange reactions between [Ir(COD)$_2$]BF_4 and equimolar quantities of the corresponding β-aminophosphane in THF (Scheme 2).

The monolithiated ligands 2-$Ph_2PC_6H_4N(Li)Me$ and $Ph_2PCH_2CMe_2N(Li)H$ interacted with [{(COD)Ir(μ-Cl)}$_2$] in hydrocarbon solution to give the neutral aryl- and alkylamido complexes [(COD)Ir(2-$Ph_2PC_6H_4NMe$)] [**Ir-7a**] and [(COD)Ir($Ph_2PCH_2CMe_2NH$)] [**Ir-8a**] as conjugate bases of their parent **Ir**$^+$-**7** and **Ir**$^+$-**8** cations (Scheme 3).

Crystallization of **Ir**$^+$-(*S*,*S*)-**3** and **Ir**$^+$-(*R*,*S*)-**2** from THF/pentane solvent mixtures afforded the two complexes as single-crystalline addition compounds, [(COD)Ir{(1*S*,2*S*)-$Ph_2PCH(Ph)CH(Me)NHCH_2Ph$}]$BF_4{\cdot}2$THF and [(COD)-Ir{(1*R*,2*S*)-$Ph_2PCH(Ph)CH(Me)NHMe$}]$BF_4{\cdot}$THF, respectively. The X-ray structural analyses of the two adduct complexes showed the presence of discrete ion pairs with the tetrafluoroborate anion hydrogen-bonded to the coordi-

 © 2004 Wiley-VCH Verlag GmbH & Co. KGaA, Weinheim

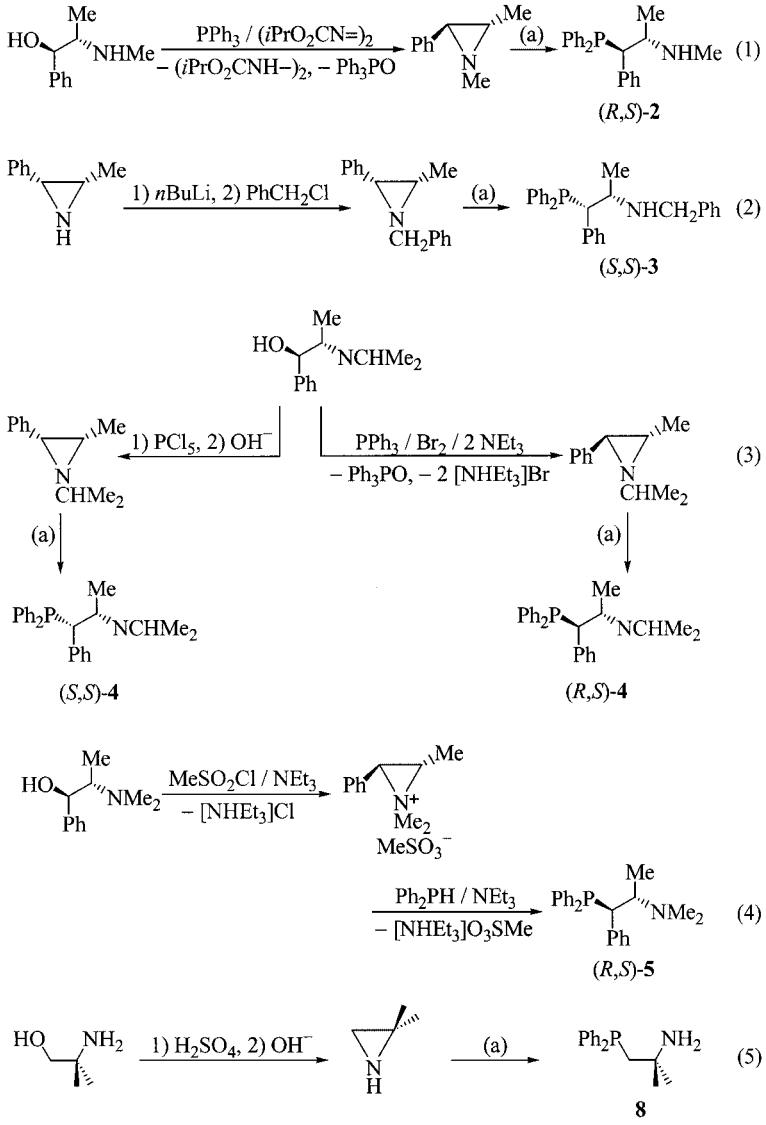

Scheme 1. Syntheses of new chiral and achiral β-aminophosphane ligands used in this work; step (a): 1. $F_3B{\cdot}OEt_2$, 2. Ph_2PH

nated amino functions (Figures 1 and 2). The Ir−P bond lengths of 2.279(7) and 2.298(4) Å, measured for the two compounds respectively, differ only slightly, if at all, and the same applies to the Ir−N distances which are 2.14 Å in both complexes. The chelate bite angles P−Ir−N are 83.0(6) and 83.7(3)° and thus compare well with the value of 82.3(2)° previously measured for the related rhodium cation $\mathbf{Rh}^+$-(*R*,*R*)-**2**.[7a] A common structural feature of the three complexes in the solid state is the equatorial alignment of the phenyl ring bonded to C-1 with respect to the five-membered chelate ring, causing the puckered metallacycle to adopt the δ conformation if the configuration at C-1 is *S* and, vice versa, to exist as a λ conformer if C-1 is in the *R* configuration. As a further consequence, the adjacent methyl group attached to C-2 is oriented equatorially if the two carbon atoms have like configuration (Figure 3; see also Figure 4 of ref.[7a]) but points to an axial direction if the configuration at C-2 is opposite to that at C-1 (Figure 4). Taking the surrounding of the coordinated nitrogen atom also into account, crystals of $\mathbf{Ir}^+$-(*S*,*S*)-**3**·2THF are seen to contain the chelate complex as a $\delta(S_{C\text{-}1},S_{C\text{-}2},S_N)$ diastereomer, the $\lambda(R_{C\text{-}1},S_{C\text{-}2},R_N)$ form being present in the solid state of $\mathbf{Ir}^+$-(*R*,*S*)-**2**·THF.

For $\mathbf{Rh}^+$-(*R*,*R*)-**2**, single crystals of which have been shown to be composed of the $\lambda(R_{C\text{-}1},R_{C\text{-}2},S_N)$ stereoisomer,[7a] and for its iridium homologue $\mathbf{Ir}^+$-(*R*,*R*)-**2** as well, ^{31}P NMR spectroscopic data indicated the presence in solution of three diastereomers in a roughly 10:3:1 distribution. Assuming that steric hindrance between the substituents attached to the chelate ring increases in the series $\lambda(R_{C\text{-}1},R_{C\text{-}2},S_N)$ (*C*-Ph, *C*-Me, and *N*-Me groups *all-trans-eq* aligned) < $\delta(R_{C\text{-}1},R_{C\text{-}2},S_N)$ (*all-trans-ax* conformer) ≈ $\lambda(R_{C\text{-}1},R_{C\text{-}2},R_N)$ (*C*-Ph/*C*-Me *trans-eq* oriented, *C*-Me/*N*-Me *cis-eq-ax* positioned) < $\delta(R_{C\text{-}1},R_{C\text{-}2},R_N)$ (*C*-Ph/*C*-Me in *trans-ax*, *C*-Me/*N*-Me in *cis-ax-eq* orientation), the observed isomers were previously assigned as sterically locked conformers $\lambda(R_{C\text{-}1},R_{C\text{-}2},S_N)$ (major), $\delta(R_{C\text{-}1},R_{C\text{-}2},S_N)$ (intermediate), and $\lambda(R_{C\text{-}1},R_{C\text{-}2},R_N)$ (minor).[7a] We have now ob-

 © 2004 Wiley-VCH Verlag GmbH & Co. KGaA, Weinheim

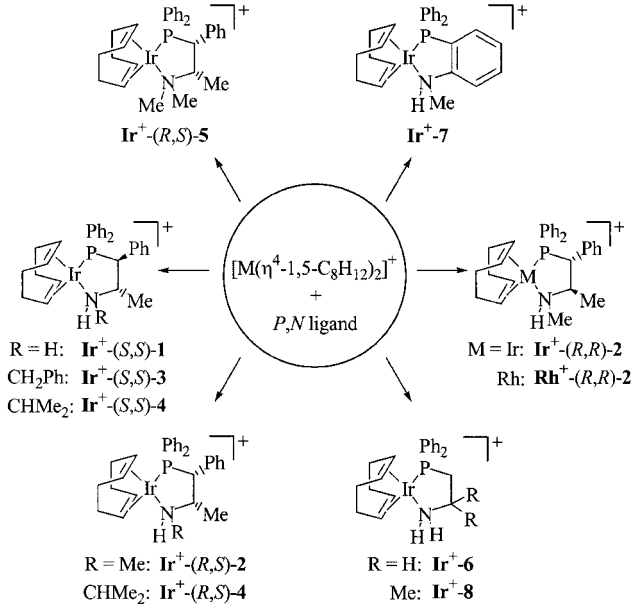

Scheme 2. Collection of cationic β-aminophosphane Ir^{I} complexes (all BF_4^- salts) and abbreviations

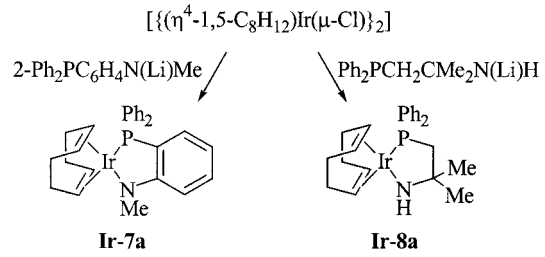

Scheme 3. Synthesis of β-amidophosphane Ir^{I} complexes

served that acetone solutions of the *N*-benzyl complex **Ir**$^+$-(*S*,*S*)-**3** exhibit NMR spectra (^{1}H, ^{13}C, ^{31}P) consistent with the existence of the cation in the dissolved state existing as only two ring conformers in an approximately 2:3 molar ratio (from ^{31}P{^{1}H} NMR; cf. Table 1). Assuming that the crystallographically established δ($S_{C\text{-}1}$,$S_{C\text{-}2}$,S_N) form contributes significantly to the isomeric distribution formed in solution, we can assign the NMR spectra displaying 40% relative intensity to that (*C*-Ph/*C*-Me)-*trans-eq*/(*C*-Me/*N*-Me)-*cis-eq-ax* conformer and ascribe the resonances showing up with 60% relative intensity to the sterically more favorable *all-trans-eq* δ($S_{C\text{-}1}$,$S_{C\text{-}2}$,R_N) isomeric cation. By implication, it becomes necessary to re-assign the conformers previously observed for the two Rh and Ir complexes M$^+$−(*R*,*R*)-**2** at intermediate concentration (vide supra)[7a] as λ($R_{C\text{-}1}$,$R_{C\text{-}2}$,R_N), i.e. enantiomeric to δ($S_{C\text{-}1}$,$S_{C\text{-}2}$,S_N), rather than δ($R_{C\text{-}1}$,$R_{C\text{-}2}$,S_N), which accordingly can be attributed to the conformational isomers formed at minor concentration (Table 1 and Scheme 4). By similar reasoning the conformers of **Ir**$^+$-(*S*,*S*)-**4** in a 1:3 distribution in solution can be formulated as δ($S_{C\text{-}1}$,$S_{C\text{-}2}$,S_N) and δ($S_{C\text{-}1}$,$S_{C\text{-}2}$,R_N), respectively.

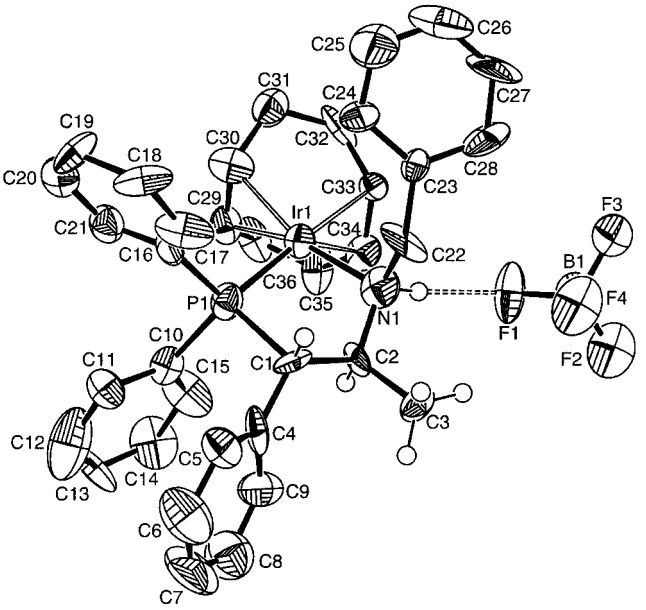

Figure 1. Perspective view of the [(COD)Ir{(1*S*,2*S*)-Ph_2PCH(Ph)CH(Me)NHCH$_2$Ph}]BF_4 ion pair; selected bond lengths [A] and angles [°]: Ir1−P1, 2.279(7); Ir1−N1, 2.14(2); Ir1−C29, 2.18(2); Ir1−C30, 2.13(2); Ir1−C33, 2.24(2); Ir1−C34, 2.24(2); N1−H···F1, 2.88(3). P1−Ir1−N1, 83.0(6); N1−H···F1, 166.7

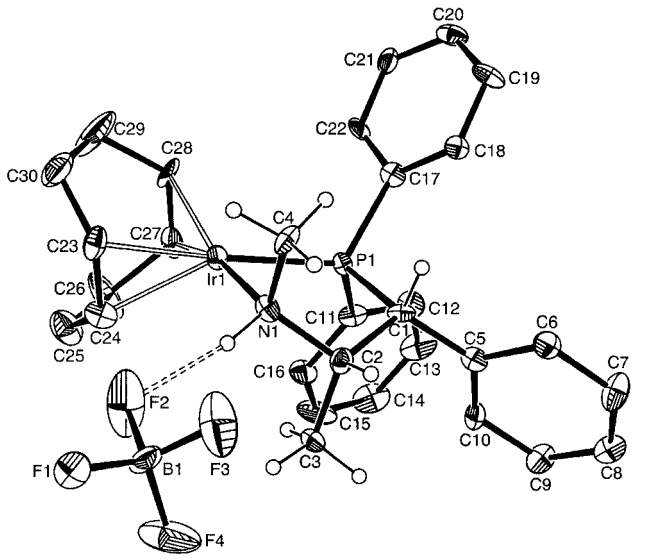

Figure 2. Perspective view of the [(COD)Ir{(1*R*,2*S*)-Ph_2PCH(Ph)CH(Me)NHMe}]BF_4 ion pair; selected bond lengths [A] and angles [°]: Ir1−P1, 2.298(4); Ir1−N1, 2.137(11); Ir1−C23, 2.224(14); Ir1−C24, 2.181(16); Ir1−C27, 2.165(16); Ir1−C28, 2.126(13); N1−H···F2, 2.925(16). P1−Ir1−N1, 83.7(3); N1−H···F2, 170.7

Solution ^{31}P NMR spectra of **Ir**$^+$-(*R*,*S*)-**2** and **Ir**$^+$-(*R*,*S*)-**4** indicate the presence of one exclusive [**Ir**$^+$-(*R*,*S*)-**4**] or at least one predominant [**Ir**$^+$-(*R*,*S*)-**2**] conformer. These can be assigned as λ($R_{C\text{-}1}$,$S_{C\text{-}2}$,R_N), i.e. identical with the isomeric form observed for **Ir**$^+$-(*R*,*S*)-**2** in the solid state. The favorable δ($S_{C\text{-}1}$,$S_{C\text{-}2}$) or λ($R_{C\text{-}1}$,$S_{C\text{-}2}$) foldings of the chelate rings with like or unlike configurations of the two bridging carbon atoms can also be ascribed to the single conformers

 © 2004 Wiley-VCH Verlag GmbH & Co. KGaA, Weinheim

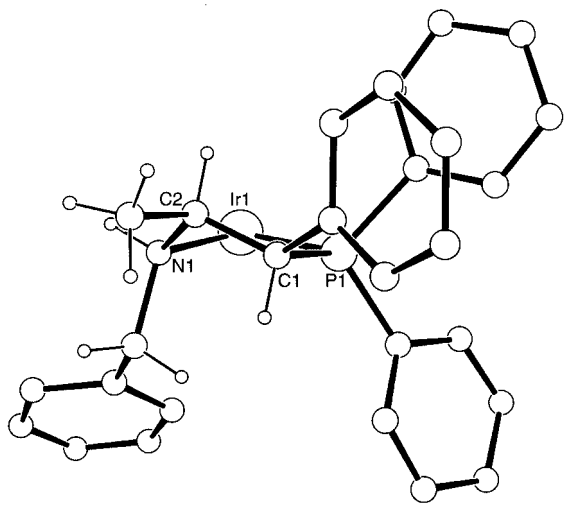

Figure 3. Schematic front view of the cation **Ir**$^+$-(*S*,*S*)-**3** emphasizing the $\delta(S_{C\text{-}1},S_{C\text{-}2},S_N)$ conformation of the chelate ring

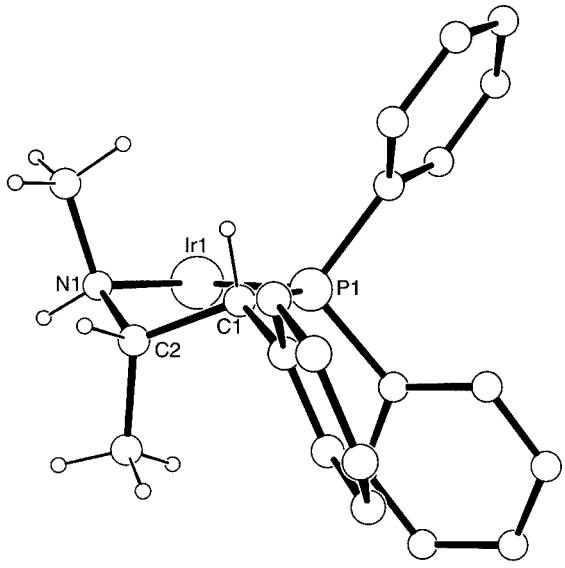

Figure 4. Schematic front view of the cation **Ir**$^+$-(*R*,*S*)-**2** emphasizing the $\lambda(R_{C\text{-}1},S_{C\text{-}2},R_N)$ conformation of the chelate ring

produced upon dissolution of the two complexes **Ir**$^+$-(*S*,*S*)-**1** and **Ir**$^+$-(*R*,*S*)-**5** possessing achiral amine functions (Table 1).

Catalytic >C=O Hydrogenation

If combined with an alkaline or amine base (1−5 equiv.) in methanol under H_2 (10−50 bar) between 25 and 50 °C, all the complexes shown in Scheme 2 act as catalysts for the hydrogenation of alkyl aryl ketones to the corresponding 1-phenylalkanols (Tables 2−4). The homogeneous >C=O reduction occurs enantioselectively if chelate complexes bearing the various (pseudo)ephedrine-based β-aminophosphanes are used as catalysts (Scheme 5).

The success of the hydrogenation reaction depends on the presence of an extra base in the catalytic system and the use of a protic reaction medium. Thus, virtually no catalytic

Table 1. ^{31}P NMR spectroscopic data of complex conformers observed in [D_6]acetone solution

Conformer[a]	δ(^{31}P)	Rel. conc. [%]
$\delta(S_{C\text{-}1},S_{C\text{-}2},R_N)$-**Ir**$^+$-(*S*,*S*)-**3**	46.65	60
$\delta(S_{C\text{-}1},S_{C\text{-}2},S_N)$-**Ir**$^+$-(*S*,*S*)-**3**	39.97	40
$\delta(S_{C\text{-}1},S_{C\text{-}2},R_N)$-**Ir**$^+$-(*S*,*S*)-**4**	45.44	75
$\delta(S_{C\text{-}1},S_{C\text{-}2},S_N)$-**Ir**$^+$-(*S*,*S*)-**4**	40.79	25
$\lambda(R_{C\text{-}1},R_{C\text{-}2},S_N)$-**Ir**$^+$-(*R*,*R*)-**2**	45.70[7a]	76
$\lambda(R_{C\text{-}1},R_{C\text{-}2},R_N)$-**Ir**$^+$-(*R*,*R*)-**2**	41.99[7a]	17
$\delta(R_{C\text{-}1},R_{C\text{-}2},S_N)$-**Ir**$^+$-(*R*,*R*)-**2**	38.07[7a]	7
$\lambda(R_{C\text{-}1},S_{C\text{-}2},R_N)$-**Ir**$^+$-(*R*,*S*)-**2**[b]	38.10	94
$\lambda(R_{C\text{-}1},S_{C\text{-}2},R_N)$-**Ir**$^+$-(*R*,*S*)-**4**	37.54	100
$\delta(S_{C\text{-}1},S_{C\text{-}2})$-**Ir**$^+$-(*S*,*S*)-**1**	46.44[7a]	100
$\lambda(R_{C\text{-}1},S_{C\text{-}2})$-**Ir**$^+$-(*R*,*S*)-**5**	35.70	100

[a] For stereochemical assignments, see text. [b] Low intensity singlets at δ = 38.01 and 41.27 are stereochemically unassigned.

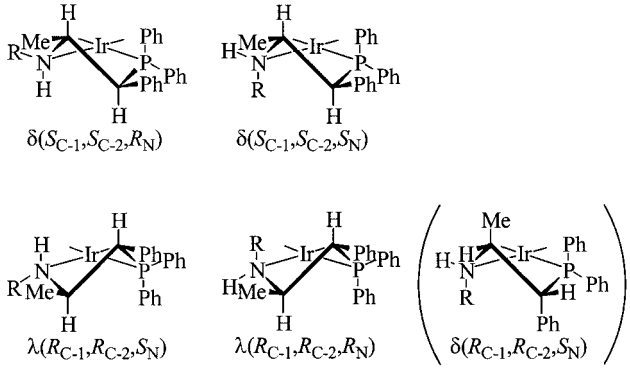

Scheme 4. Drawings of preferred (less preferred) conformers observed in solution (cf. Table 1)

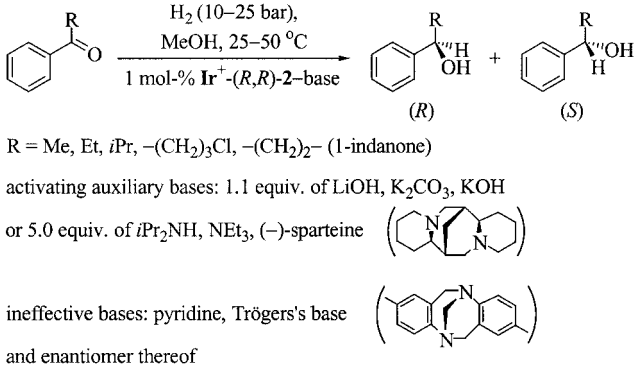

Scheme 5. Enantioselective hydrogenation of prochiral ketones using the **Ir**$^+$-(*R*,*R*)-**2** precatalyst in the presence of different bases

>C=O reduction occurred in methanol in the absence of an amine or an alkali metal hydroxide and, vice versa, in aprotic solvents, e.g. benzene, dichloromethane, or THF, containing such a basic additive. The likelihood of the ke-

 © 2004 Wiley-VCH Verlag GmbH & Co. KGaA, Weinheim

Table 2. Enantioselective hydrogenation of acetophenone using the **Ir**$^+$-(*R*,*R*)-**2** catalyst modified by different bases

Auxiliary base (equiv. rel. to c_{Ir})[a]	$p(H_2)$ [bar]	T [°C]	t [h]	yield [%]	*ee* [%] (polar.)	*ee* [%] (HPLC)
iPr$_2$NH (5.0)	25	50	40	100	46 (*S*)	41 (*S*)
NEt$_3$ (5.0)	25	50	40	100	39 (*S*)	30 (*S*)
(−)-sparteine (5.0)	25	50	16	100	53 (*S*)	47 (*S*)
(+)-Tröger's base (5.0)	25	50	16	–		
(−)-Tröger's base (5.0)	25	50	16	–		
pyridine (5.0)	25	50	40	–		
(*S*)-PhCH$_2$CH(NH$_2$)CH$_2$OH (5.0)	25	50	80	55	53 (*S*)	48 (*S*)
(*R*)-PhCH$_2$CH(NH$_2$)CH$_2$OH (5.0)	25	50	80	56	60 (*S*)	54 (*S*)
(1*R*,2*R*)-Ph$_2$PCH(Ph)CH(Me)NHMe (5.0)	25	50	80	69	48 (*S*)	41 (*S*)
LiOH (1.1)	10	25	22	100	58 (*S*)	52 (*S*)
K$_2$CO$_3$ (1.1)	10	25	16	100	43 (*S*)	40 (*S*)
KOH (1.1)	10	25	7	100	62 (*S*)	55 (*S*)

[a] 0.02 mmol of metal complex plus added base together with 2.0 mmol of acetophenone in 3 mL of methanol.

Table 3. Homogeneous hydrogenation of acetophenone using different KOH- and (−)-sparteine-activated [(COD)M(P∩NR^{1}R^2)]$^+$ catalyst complexes; M = Ir (Rh)

Complex	Base[a]	t [h]	yield [%]	*ee* [%] (polar.)	*ee* [%] (HPLC)
Ir$^+$-(*S*,*S*)-**1**	KOH[b]	7	100	42 (*R*)	38 (*R*)
	(−)-sparteine[c]	16	100	19 (*R*)	15 (*R*)
Ir$^+$-(*S*,*S*)-**3**	KOH	32	100	27 (*R*)	26 (*R*)
	(−)-sparteine	70	51	33 (*R*)	31 (*R*)
Ir$^+$-(*S*,*S*)-**4**	KOH	12	100	51 (*R*)	51 (*R*)
	(−)-sparteine	16	100	44 (*R*)	44 (*R*)
Rh$^+$-(*R*,*R*)-**2**	KOH	6	100	77 (*S*)	71 (*S*)
	(−)-sparteine	28	100	39 (*S*)	34 (*S*)
Ir$^+$-(*R*,*R*)-**2**	KOH	7	100	62 (*S*)	55 (*S*)
	(−)-sparteine	16	100	53 (*S*)	47 (*S*)
Ir$^+$-(*R*,*S*)-**2**	KOH	32	100	45 (*S*)	38 (*S*)
	(−)-sparteine	43	100	5 (*S*)	4 (*S*)
Ir$^+$-(*R*,*S*)-**4**	KOH	50	100	21 (*S*)	19 (*S*)
	(−)-sparteine	55	100	9 (*S*)	7 (*S*)
Ir$^+$-(*R*,*S*)-**5**	KOH	58	100	36 (*S*)	36 (*S*)
	(−)-sparteine	70	25	10 (*S*)	9 (*S*)
Ir$^+$-**6**	KOH	4	100		
	(−)-sparteine	40	92		
Ir$^+$-**7**	KOH[d]	65	100		
	(−)-sparteine[d]	65	82		
Ir$^+$-**8**	KOH	3	100		
	(−)-sparteine	35	92		

[a] 0.02 mmol of [(COD)M(P∩NR^{1}R^2)]$^+$−KOH or [(COD)M(P∩NR^{1}R^2)]$^+$−(−)sparteine (M/KOH = 1:1.1; M/(−)-sparteine = 1:5.0), and 2.0 mmol of acetophenone in 3 mL of methanol. [b] KOH-activated precatalysts: $p(H_2)$ = 10 bar, T = 25 °C. [c] (−)-Sparteine-modified complexes: $p(H_2)$ = 25 bar, T = 50 °C. [d] $p(H_2)$ = 50 bar, T = 50 °C.

tone reduction proceeding by metal-assisted direct transfer of $H^{\delta-}/H^{\delta+}$ equivalents from the H_2 molecule to the carbonyl function was substantiated by ruling out the alternative pathway involving $H^{\delta-}/H^{\delta+}$ transfer from the primary alcohol. No transformation of acetophenone to 1-phenylethanol was observed when the ketone and a catalytic system composed of **Ir**$^+$-(*R*,*R*)-**2** and (−)-sparteine in a 1:5 molar ratio (vide infra) were kept in a catalyst-to-substrate ratio of 1:100 in methanol at 50 °C for 40 h in the absence of hydrogen gas, although quantitative >C=O hydrogenation did occur if the same catalyst was combined with the ketone in a 1:100 stoichiometry under 25 bar of H_2 at 50 °C for 40 h in Me$_3$COH which, as a tertiary alcohol, cannot serve as a proton/hydride source.

The influence on the catalytic activity of the different oxygen and nitrogen bases depicted in Scheme 5 was qualitatively studied for a standard system composed of the acetophenone substrate and the **Ir**$^+$-(*R*,*R*)-**2**−base catalyst in question (Table 2). While pyridine and the two enantiomers of Tröger's base did not support the hydrogenation reaction, tertiary and secondary alkylamines such as NEt$_3$, (−)-sparteine, and iPr$_2$NH performed reasonably if added in fivefold excess relative to the **Ir**$^+$-(*R*,*R*)-**2** concentration. Reaction times required for complete transformation of the

 © 2004 Wiley-VCH Verlag GmbH & Co. KGaA, Weinheim

ketone at 50 °C under a pressure of 25 bar of H_2 were ≈ 40 h with triethyl and isopropylamine and only ca. 16 h with (−)-sparteine as auxiliary bases. It can therefore be concluded that the strength of the base which, compared with alkylamines, is low for heteroaromatic and arylamines,[20] exerts the important influence. In full agreement with this reasoning, strong oxygen bases such as LiOH, K_2CO_3, and particularly KOH were found to further decrease the times needed for quantitative hydrogenation, even if employed in a near equimolar **Ir**$^+$-(*R*,*R*)-**2**/base ratio at reduced temperature (25 °C) and H_2 pressure (10 bar). The addition of optically active chelating β-amino alcohols or -phosphanes had no significant influence on the selectivity of the catalysts but exerted a detrimental effect on their activity in that only reduced yields of the alcohol products were obtained after prolonged periods of time. Hence, for the catalytic runs described in the next section, potassium hydroxide or (−)-sparteine were employed as the "optimized" alkaline and amine bases.

The enantiomeric excesses of (*R*)- or (*S*)-PhCH(OH)Me that could be achieved in the hydrogenation of the standard acetophenone substrate in the presence of KOH-activated complexes ranged from 19−21% (*S*) for the iridium (pre)-catalyst **Ir**$^+$-(*R*,*S*)-**4** to 71−77% (*S*) for the rhodium system **Rh**$^+$-(*R*,*R*)-**2** (Table 3). Although the iridium homologue of the latter, **Ir**$^+$-(*R*,*R*)-**2**, was comparable in activity (≈ 7 vs. ≈ 6 h for quantitative >C=O reduction) it afforded a decidedly lower *ee* of only 55−62%. In the series of iridium complexes bearing chiral β-aminophosphanes with like configuration of their chelate backbone carbon atoms, viz. **Ir**$^+$-(*R*,*R*)-**2** and **Ir**$^+$-(*S*,*S*)-**1**,-**3**,-**4**, the *ee*'s were observed to increase in the order of their nitrogen substituents i.e. R = CH_2Ph < H < $CHMe_2$ < Me, suggesting that substitution by a medium sized methyl group is sufficient to afford the maximum enantioselectivity that can be achieved with these systems. Catalyst complexes bearing chiral *P*,*N* ligands with unlike stereochemistry of their backbone carbon atoms, i.e. **Ir**$^+$-(*R*,*S*)-**2**, **Ir**$^+$-(*R*,*S*)-**4**, and **Ir**$^+$-(*R*,*S*)-**5**, required much longer times for complete >C=O hydrogenation and also showed lower selectivities than their diastereomers with like carbon configurations in the C_2 linkages, viz. **Ir**$^+$-(*R*,*R*)-**2** and **Ir**$^+$-(*S*,*S*)-**4**. Furthermore, catalytically sluggish as *N*,*N*-dialkylated **Ir**$^+$-(*R*,*S*)-**5** proved to be, its mere ability to act as a catalyst gives unequivocal evidence that the presence of at least one NH function (which is met in all other complexes) is *not* a prerequisite for the particular compound to exhibit catalytic behavior. Nevertheless there exist major differences between the two classes of complexes with respect to their reactivity towards the dihydrogen molecule as will be shown below. Finally, the preferential formation of the product alcohol in the (*R*) configuration induced by complexes with δ($S_{C\text{-}1}$) stereochemistry of their chelate rings and, correspondingly, the predominance of the (*S*) enantiomer in the isomeric mixtures resulting from reactions promoted by all λ($R_{C\text{-}1}$) conformers shows that the hydrogenation catalysts described herein follow a λ/δ rule which predicts that λ chelates will give the (*S*) enantiomeric alcohol while δ chelates will produce the (*R*) enantiomer. Similar stereoselection has previously been documented for Ru^{II}-catalyzed >C=O hydrogenations.[3c][3d] The somewhat disappointing result that the product alcohols are generally formed, at best, in moderate optical yields either indicates an inherently low enantioselectivity of the systems or points to side reactions overriding the true selectivity of the complexes; e.g. the mixture of diastereomeric ring conformers detected in solution (Table 1) might act as interfering catalysts involved in competitive hydrogenation reactions.

Prochiral alkyl aryl ketones other than acetophenone which could be enantioselectively hydrogenated included propio- and isobutyrophenone, 3-chlorobutyrophenone, as well as 1-indanone (Table 4). Using the **Ir**$^+$-(*R*,*R*)-**2**-(−)-sparteine catalytic system, the product alcohols were formed as (*S*) enantiomers with optical yields between 29 and 68%, in full agreement with the empirical λ/δ rule formulated before. Attempts at the metal-assisted hydrogenation of dialkyl ketones such as 2-butanone, isopropyl methyl ketone, or pinacolone failed. Due to the basic conditions, these substrates underwent aldol reactions rather than reduction to give solids that were also isolated if the ketones were allowed to react in the presence of base but the absence of any added metal complex.

Table 4. Enantioselective hydrogenation of alkyl aryl ketones using the **Ir**$^+$-(*R*,*R*)-**2**−(−)-sparteine catalytic system[a]

Ketone	*t* [h]	yield [%]	*ee* [%] (polar.)
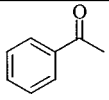	16	100	53 (*S*)
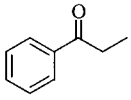	16	100	42 (*S*)
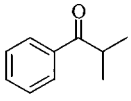	23	100	48 (*S*)
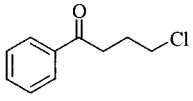	40	46[b]	68 (*S*)
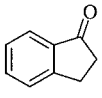	20	100	29 (*S*)

[a] 0.02 mmol of **Ir**$^+$-(*R*,*R*)-**2**, 0.1 mmol of (−)-sparteine, and 2.0 mmol of the ketonic substrate in 3 mL of methanol; $p(H_2)$ = 25 bar, *T* = 50 °C. [b] As a result of base-induced HCl elimination, the formation of 2-phenyltetrahydrofuran in low yield (≈4%) was also observed.

The mandatory presence of base in the catalytic systems suggests the intermediacy of in situ generated species that have lost H^+. For all catalysts derived from precursor complexes possessing *P*,*N* ligands with primary or secondary amine functions these could conceivably be amidoiridium(I) or -rhodium(I) complexes. In fact, the amides **Ir-7a** and **Ir-8a** (which were intentionally prepared for this specific pur-

 © 2004 Wiley-VCH Verlag GmbH & Co. KGaA, Weinheim

pose) did catalyze the hydrogenation of acetophenone to 1-phenylethanol without the addition of base, quantitatively transforming the ketone to the alcohol under the usual conditions in approximately the same periods of time as the combined catalytic systems **Ir**$^+$**-7**−KOH and **Ir**$^+$**-8**−KOH, respectively. Thus, with 1 mol % of **Ir-7a** and **Ir**$^+$**-7**−KOH as catalysts, the reactions were complete after 2 and 3 h under 10 bar of H_2 at 25 °C, while 60−65 h at 50 °C under 50 bar of H_2 were needed for the quantitative formation of the alcohol in the presence of 1 mol % of **Ir-8a** or **Ir**$^+$**-8**−KOH. The ability of the two base-free β-amidophosphane iridium(I) complexes to catalyze the homogeneous >C=O reduction by molecular hydrogen likewise depends on the use of alcohols (MeOH, *t*BuOH) as reaction media, wherein the iridium−amide bond remains unprotonated. The obviously low amide basicity can be attributed to the involvement of the nitrogen lone-pair in π bonding to the central metal[21] with resultant $sp^3 \rightarrow sp^2$ rehybridization, similar to the situation that has previously been encountered for the closely related anilide [Ir(CO)(PPh_3)(2-$Ph_2PC_6H_4NMe$)], where the nitrogen atom features a trigonal-planar rather than a pyramidal surrounding and can be protonated only by very strong acids such as hydrochloric[22a] or tetrafluoroboric.[22b]

In view of the catalytic efficacy of **Ir-7a** and **Ir-8a**, numerous attempts were made to obtain similar amides also by deprotonation of the *chiral* [(COD)Ir(P∩NHR]$^+$ precatalysts but they remained unsuccessful. Either the amine function stayed unattacked, e.g. by amines or dilute KOH/methanol, or complex reaction mixtures containing ketonic and/or imine-type components [IR (KBr): $\tilde{\nu}$ = 1685 and 1715 cm^{-1}] were produced, if the cationic aminophosphane complexes were treated with very strong bases such as excess alkoxide or *n*BuLi. Obviously, those amine complexes which are different from **Ir**$^+$**-7** and **Ir**$^+$**-8** and possess CH units adjacent to the amino group tend to undergo degradation of their *P*,*N* ligands in the presence of strong base − most probably by >C=NR elimination from initially formed β-H containing amides which decompose easily due to their coordinative unsaturation.

Only in a single and probably serendipitous case we were able to isolate a well-defined product from such reactions. Combination of **Ir**$^+$-(*R*,*S*)-**4** with concentrated methanolic KOH and subsequent crystallization of the crude product from hot acetone gave cyclometalated [(COD)Ir{(1*R*,2*S*)-$Ph_2PCH(C_6H_4$-*o*)CH(Me)NHCHMe$_2$}] [**Ir**-(*R*,*S*)-**4a**] (Figure 5); i.e. deprotonation had occurred at one of the *ortho* C−H bonds of the phenyl ring attached to chelate backbone rather than at the amino function; Scheme 6. Presumably because of the hemilabile nature of the extraordinarily long Ir−N bond, measured as 2.448(6) and 2.514(6) Å for the two crystallographically independent molecules, this coordinatively saturated complex does exhibit some catalytic activity, slowly transforming acetophenone in methanol under 10 bar of H_2 to racemic 1-phenylethanol. The formation of the product alcohol without any notable stereodiscrimination strongly suggests that the orthometalated complex is not an actual intermediate maintaining the catalytic cycle

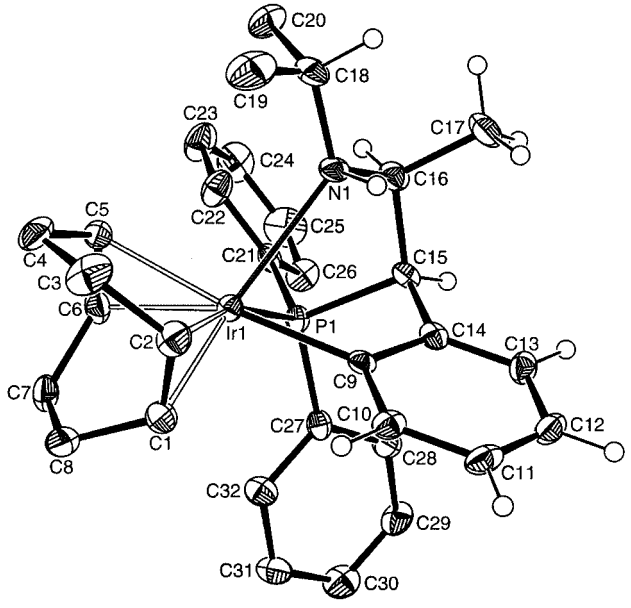

Figure 5. Perspective view of one of the two crystallographically independent molecules of orthometalated [(COD)Ir{(1*R*,2*S*)-$Ph_2PCH(C_6H_4$-*o*)CH(Me)NHCHMe$_2$] ("molecule 1"); selected bond lengths [Å] and angles [°]: Ir1−P1, 2.2917(18); Ir1−N1, 2.514(6); Ir1−C1, 2.099(7); Ir1−C2, 2.137(7); Ir1−C5, 2.183(7); Ir1−C6, 2.216(7); Ir1−C9, 2.104(7). P1−Ir1−N1, 78.86(14); P1−Ir1−C9, 77.13(19); N1−Ir1−C9, 75.3(2). Corresponding structural parameters for "molecule 2": Ir2−P2, 2.2942(18); Ir2−N2, 2.448(6); Ir2−C33, 2.213(7); Ir2−C34, 2.200(7); Ir2−C37, 2.119(7); Ir2−C38, 2.090(7); Ir2−C41, 2.119(7). P2−Ir2−N2, 80.50(14); P2−Ir2−C41, 77.11(19); N2−Ir2−C41, 75.3(2)

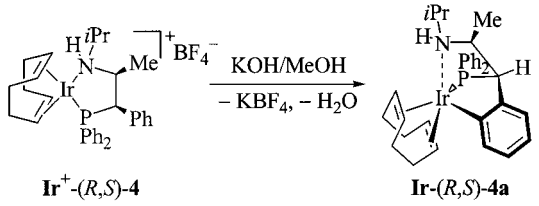

Scheme 6. KOH-assisted orthometalation

of enantioselective >C=O reduction but should rather be looked upon as a by-product resulting from a base-induced side reaction.

H/D Exchange Processes and H_2 Activation

When aceto- or benzophenone, dissolved in CH_3OD, were hydrogenated with H_2 employing either the base-free amide **Ir-8a** or the combined system **Ir**$^+$-(*R*,*R*)-**2**-(−)-sparteine as catalysts, the product alcohols were invariably characterized by NMR spectroscopy (^{1}H, ^{2}H, ^{13}C{^{1}H}; see Exp. Sect.) as mixtures containing the two isotopomers R^1R^2CHOD and R^1R^2CDOD in an almost 1:1 molar ratio. The evolution of *HD* gas was observed to be concomitant with the incorporation of solvent deuterons as $D^{\delta-}$ equivalents into the product carbinols [Scheme 7, reation (1)], as was the increasing formation of non-deuterated MeOH. No such uptake of D^+ as D^- by the ketonic substrate was noted if the hydrogenation was catalyzed by complex **Ir**$^+$-(*R*,*S*)-**5** possessing a tertiary amino donor group. Iridium-

 © 2004 Wiley-VCH Verlag GmbH & Co. KGaA, Weinheim

catalyzed H_2/D^+ exchange with concomitant formation of HD was similarly observed when MeOD solutions of all base-free aminophosphane complexes containing at least one N−H bond were pressurized in the absence of any ketonic substrate in an NMR tube to 5−10 bar of H_2 [Scheme 7, reation (2)], but again did not take place on attempted catalysis by the *N*,*N*-dialkylated cation **Ir**$^+$-(*R*,*S*)-**5**. Hence, the exchange of isotopes between the protic solvent and the hydrogen atmosphere, which is typical of heterolytic H−H cleavage during reaction,[3,23−30] neither depends on the presence of base nor is contingent on simultaneous >C=O hydrogenation but requires at least one acidic N−H bond in the coordination sphere of the catalyst complex.

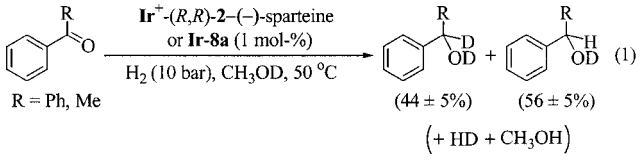

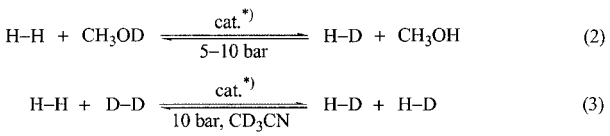

*) catalyzed by any NH-containing Ir^+ complex as well as by **Ir-7a** and **Ir-8a**

Scheme 7. Catalytic H_2/D^+ isotope exchange and H_2/D_2 scrambling in the presence [reation (1)] and absence of ketonic substrates [reations (2) and (3)]

Catalytic scrambling of isotopes with formation of HD was also detected when acetonitrile solutions of all NH-containing $[(COD)Ir(P\cap NHR)]^+$ complexes were exposed to 10 bar of an equimolar H_2/D_2 mixture [Scheme 7, reation (3)] but once more did not occur in the presence of the *N*,*N*-dialkylated derivative **Ir**$^+$-(*R*,*S*)-**5**. Control experiments in CD_3CN making use of a D_2-free hydrogen atmosphere ruled out the possibility that the observed HD did actually result from H_2/D^+ exchange between the H_2 component and the moderately acidic C−D bonds of the solvent molecules. The observed exchange of isotopes between the two gases implies the intermediate coordination of H_2 or D_2 to iridium, although the formation of any sufficiently long-lived Ir−H_2 adduct could not be traced by NMR spectroscopy down to −60 °C. Similar to the H_2/D^+ exchange described above, the observed H_2/D_2 scrambling process should involve heterolytic fission of the H−H and D−D bonds, respectively, since any isotope exchange brought about by homolytic cleavage of the two molecules would require simultaneous coordination of H_2 and D_2 to the same central metal, which is regarded as highly unlikely.[23c,23i,30]

Despite all failures to transform the iridium(I) amine complexes into their conjugate amides (vide supra), both the H_2/D_2 and the H_2/D^+ exchange processes were also catalyzed by the two amido complexes **Ir-7a** and **Ir-8a** [Scheme 7, reations (2) and (3)]. Furthermore, the initial product of the reaction between dihydrogen (5 bar) and **Ir-8a** in CD_3CN solution was unequivocally identified (see Exp. Sect.) as an *amido dihydride*, *cis*-[(CO-D)$IrH_2(Ph_2PCH_2CMe_2NH)$] (**Ir-9a**), originating from homolytic oxidative H_2 addition to the central metal (Scheme 8), rather than an *amino monohydride*, [(CO-D)$IrH(Ph_2PCH_2CMe_2NH_2)$] which would result from heterolytic H_2 addition to the N−H bond. The preference of **Ir-8a** to add the dihydrogen molecule by homolytic bond cleavage clearly contrasts with the heterolytic H−H fission concluded from the foregoing exchange experiments, notwithstanding that it corresponds to the low basicity of its amide function and also parallels the behavior of the related anilide $[Ir(CO)(PPh_3)(2\text{-}Ph_2PC_6H_4NMe)]$ described in previous work.[22a] As a further seemingly paradoxical result, the cationic aminophosphane complexes **Ir**$^+$**-8** and **Ir**$^+$-(*S*,*S*)-**1** were likewise seen to interact with molecular hydrogen by conventional oxidative addition, giving *cis*-[(CO-D)$IrH_2(Ph_2PCH_2CMe_2NH_2)]BF_4$ (**Ir**$^+$**-9**) and *cis*-$[(COD)IrH_2\{(1S,2S)\text{-}Ph_2PCH(Ph)CH(Me)NH_2\}]BF_4$ (**Ir**$^+$-**10**) as the first formed products (Scheme 8). Prolonged exposure of the iridium(I) precursors to H_2 at elevated pressures (> 10 bar) resulted in hydrogenic loss of the cyclooctadiene ligand with formation of solvate-stabilized adducts with *cis*,*cis*-$[(MeCN)_2IrH_2\{(1R,2S)\text{-}Ph_2PCH(Ph)CH(Me)NHMe\}]BF_4$ (**Ir**$^+$-**11**) being a representative example.

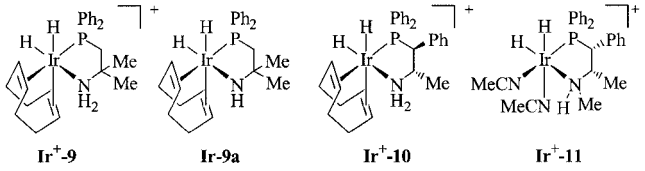

Scheme 8. Products of oxidative H_2 addition to β-amino- and β-amidophosphane iridium(I) precursors (cationic complexes: BF_4^- salts)

It was two important properties of the neutral amido and the cationic amino iridium(III) dihydrides that served to unravel the perplexing inconsistencies emerging, on the one hand, from the experimentally established homolytic H_2 addition by both the $[(COD)Ir(P\cap NHR)]^+$ and [(CO-D)$Ir(P\cap NR)$] complexes and, on the other hand, from the ability of the very same compounds to catalyze H_2/D_2 and H_2/D^+ scrambling processes.

Firstly, while the *amino*phosphane iridium(I) complex **Ir**$^+$**-8** and its (formally) conjugate *amide* **Ir-8a** do not coexist in alcoholic media in an acid−base equilibrium, the products of oxidative H_2 addition to these two d^8 substrates, **Ir**$^+$**-9** and **Ir-9a**, do so (Scheme 9). Pressurizing a solution of **Ir-8a** in methanol to 5 bar of H_2 which, as mentioned above, does not lead to any detectable **Ir**$^+$**-8**, not only gave the amido dihydride **Ir-9a** but also produced the conjugate amino dihydro complex **Ir**$^+$**-9** at spectroscopically

 © 2004 Wiley-VCH Verlag GmbH & Co. KGaA, Weinheim

detectable concentrations. The same result was obtained if a droplet of water was added to a solution of preformed **Ir-9a** in carefully dried CD_3CN. Vice versa, the latter amido dihydride was detected in addition to the predominantly formed amino dihydride $\mathbf{Ir^+}$**-9**, if a solution of $\mathbf{Ir^+}$**-8** in methanol containing dilute aqueous KOH at low concentration was pressurized with H_2 (Scheme 9). The basic properties of the amido function of the 18*e* complex **Ir-9a** can safely be attributed to its coordinative saturation which prevents the nitrogen lone-pair from engaging in π-bonding to the central metal. The reversible protonation of amido donor groups attached to an Ir^{III} center has some precedent in the literature: the amido-/aminophosphane complexes $[Ir(H)(Cl)(2\text{-}Ph_2PC_6H_4NR)(2\text{-}Ph_2PC_6H_4NHR)]$ (R = Et, CH_2Ph) react with protic acids HX (X = Cl, OH, O_2CMe) to yield cationic bis(aminophosphane) products, $[Ir(H)(Cl)(2\text{-}Ph_2PC_6H_4NHR)_2]^+$, from which the amido-/aminophosphane precursors can be restored by the addition of strong bases such as DABCO.[31]

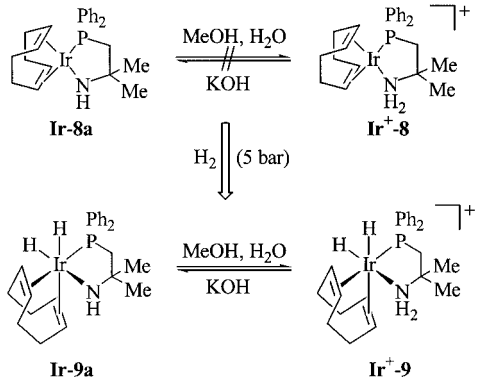

Scheme 9. Reversible (*de*)protonation of coordinatively saturated amino and amido dihydro Ir^{III} complexes

Secondly, cationic amino dihydrido complexes of the type $[(COD)IrH_2(P\cap NHR)]^+$ will undergo substitution of their hydride ligands by deuteride forming $[(COD)IrD_2(P\cap NHR)]^+$ (and presumably $[(COD)IrD_2(P\cap NDR)]^+$ as well) if treated with D_2. This behavior has been verified for $\mathbf{Ir^+}$**-9**, which was generated in situ by exposing an acetonitrile solution of $\mathbf{Ir^+}$**-8** at −60 °C in a high-pressure NMR tube to 5 bar of H_2. The diagnostic NMR signals of the H_2 adduct [δ(IrH) = −15.78 (d, *cis*-$^2J_{P,H}$ = 10.95 Hz), −12.60 (d, *cis*-$^2J_{P,H}$ = 15.91 Hz); δ(^{31}P) = 31.87] persisted when the excess pressure was released from the tube showing that $\mathbf{Ir^+}$**-9**, which at ambient conditions under an inert atmosphere reductively eliminates dihydrogen, remains stable if kept under 1 bar of hydrogen at low temperature. With constant cooling to −60 °C, the H_2 atmosphere was then replaced by D_2 under normal pressure, which was subsequently raised again to 5 bar. As a result, the original dihydride $[(COD)IrH_2(Ph_2PCH_2CMe_2NH_2)]^+$ was converted into the dideuteride $[(COD)IrD_2(Ph_2PCH_2CMe_2NH_2)]^+$ manifesting itself by (i) the disappearance of the IrH doublets in the ^{1}H NMR spectrum, (ii) the persistence of the ^{31}P singlet (δ = 31.4 for the deuterated compound) and (iii) the appearance of two high-field ^{2}H peaks at δ = −15.7 and −12.7, indicating an IrD_2 substructure with non-equivalent Ir−D bonds. As a particularly illuminating feature, the ^{2}H NMR spectrum furthermore displayed an HD doublet at δ = 4.37 ($^1J_{H,D}$ = 42.6 Hz) in addition to the D_2 singlet at δ = 4.33, demonstrating that catalytic H_2/D_2 scrambling goes together with $IrH_2 \rightarrow IrD_2$ exchange (Scheme 10). A comparatively broad resonance centered at δ = 2.3 and partly overlapping the CDH_2CN triplet at δ = 1.98, could not be assigned with certainty It may originate from deuterated amino functions which would then be consistent with the presence in solution of $[(COD)IrD_2(Ph_2PCH_2CMe_2NHD)]^+$ and $[(COD)IrD_2(Ph_2PCH_2CMe_2ND_2)]^+$ isotopomers as required by the equilibria shown in Scheme 10. However, the assignment to C−D bonds resulting from deuteration and de-coordination of the cyclooctadiene ligand, could not be excluded.

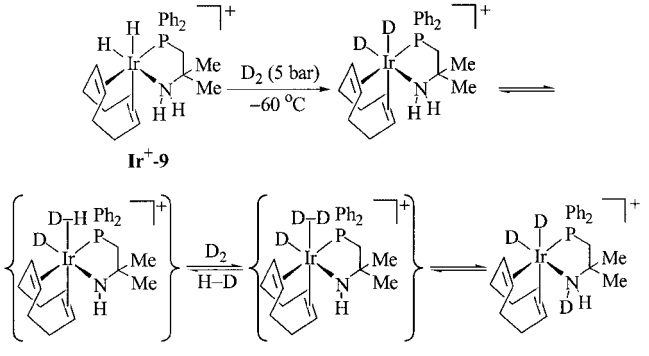

Scheme 10. Intermolecular D_2/Ir−H exchange and intramolecular Ir−D/N−H scrambling involving reversible "$[Ir^{III}(H)_2-P\cap NH_2]^+$" ⇄ "$[(\eta^2\text{-}H_2)\text{-}Ir^{III}(H)-P\cap NH]^+$" tautomerization

In an independent concluding experiment aiming at the unequivocal demonstration of the $[(COD)Ir(P\cap NHR)]^+$-catalyzed exchange of protons between the amino group and the gas, *N*-deuterated $[(COD)Ir\{(1R,2S)\text{-}Ph_2PCH(Ph)CH(Me)ND CHMe_2\}]^+$ [IR (KBr): $\tilde{\nu}$ = 2398 (ND) cm^{-1}] was first prepared from $\mathbf{Ir^+}$**-(*R*,*S*)-4** [IR (KBr): $\tilde{\nu}$ = 3209 (NH) cm^{-1}] and [D_1]methanol and then allowed to interact with H_2 under pressure in dry [D_8]THF. The solid that was recovered after removal of all volatile material displayed the characteristic N−H stretching vibration of the starting $\mathbf{Ir^+}$**-(*R*,*S*)-4**$^+$ complex, showing that an H_2/−NDR → HD/−NHR re-exchange of isotopes had occurred.

The formation of HD as a product obligatorily accompanying the hydride/deuteride exchange at the Ir^{III} center and the observation that both the catalyzed H_2/D_2 scrambling and the exchange of isotopes between dihydrogen molecules and solvent protons is only supported by complexes containing at least one N−H bond [Scheme 7, reactions (2) and (3)] are strongly suggestive of an equilibrium between two amino−dihydrido and amido−dihydrogen−monohydrido tautomers, "$[Ir^{III}(H)_2-$

 © 2004 Wiley-VCH Verlag GmbH & Co. KGaA, Weinheim

P∩NH$_2$]$^+$" and "[(η^2-H$_2$)-Ir^{III}(H)−P∩NH]$^+$", even if the η^2-H$_2$ isomeric form, which maintains the exchange of isotopes by intramolecular H/D scrambling (cf. Scheme 10),[23c,23e,23i,25] remained undetected by NMR spectroscopy down to −60 °C. Related equilibria that have previously been established, generally in an indirect fashion by the observation of H$_2$/D$^+$ exchange processes and/or isotopic scrambling between metal−hydride and protonated ligand sites, include the pairs of tautomers "H−M^{II}−S(H)R ⇄ (η^2-H$_2$)−M^{II}−SR" (M = Ru,[23h,27c,27d] Os,[28b,28c], Ni[27e,27f]) and "H−M^{III}−LH ⇄ (η^2-H$_2$)−M^{III}−L" (M = Rh: LH = RSH;[27a,27b] M = Ir: LH = NH$_3$,[26] OH$_2$,[25a,25b] RSH[28a]) as well as a family of Ir^{III} complexes containing a pendant basic aniline (acidic anilinium) function in addition to an acidic η^2-bound H$_2$ ligand (basic hydride).[25c,25d] Only in favorable cases where the pK_a of the coordinated dihydrogen molecule and the protonated ancillary ligand were similar[23i] was it possible to directly observe the equilibrium between the two tautomers.[28c] For the most part however, either the η^2-H$_2$ complex[25c,25d,26,27b,28] or the metal hydride containing the protonated N,[25c,25d] O,[25a] or S[27c] ligand remained undetected transients in the isotopic scrambling, depending on whether the coordinated H$_2$ molecule or the ligand bearing the proton was the stronger Brønsted acid or, vice versa, whether the ancillary deprotonated ligand or the metal−hydride bond[32] was the stronger Brønsted base.[25c,25d] With regard to the "[IrH$_2$(Ph$_2$PCH$_2$-CMe$_2$NH$_2$)]$^+$" ⇄ "[(η^2-H$_2$)(H)(Ph$_2$PCH$_2$CMe$_2$NH)]$^+$" tautomerization, we conclude that the amido−dihydrogen−monohydrido complex cannot be seen but resembles the undetected dihydrogen amide forms "[Ir^{III}(η^2-H$_2$)NH$_2$]$^{n+}$" of the long known hydrido ammine complexes [Ir^{III}(H)(NH$_3$)$_2$(PEt$_3$)$_2$L]$^{n+}$ (n = 1; L = Cl; n = 2: L = NH$_3$, PEt$_3$)[26] in being a transient species immediately yielding the other tautomer because the basicity of the coordinated amide by far exceeds that of the metal−hydride bond in the adjacent *cis* position.

Concluding Discussion

Putting all evidence together, we propose that H$_2$ activation as well as H$_2$/D$^+$ and H$_2$/D$_2$ exchange follow the cycle outlined in Scheme 11, which rests on the formation of either COD-coordinated or solvated *amino* and *amido* dihydro iridium(III) complexes, A and B, as the first key intermediates. Because of their coordinative saturation, amides B can act as bases toward the protic solvent to generate the conjugate amino complexes A at equilibrium concentrations (step a) and, equally important, are inert towards elimination of imine fragments from *P*,*N* ligands possessing β-hydrogen atoms. The readily occurring H$_2$/D$_2$ exchange processes, which require the presence of at least one acidic N−H function, points to a tautomeric equilibrium between A and the dihydrogen−hydrido−amido form F. Even if the tautomerization step f yields F only at spectroscopically undetectable transitory concentrations, these are sufficient to

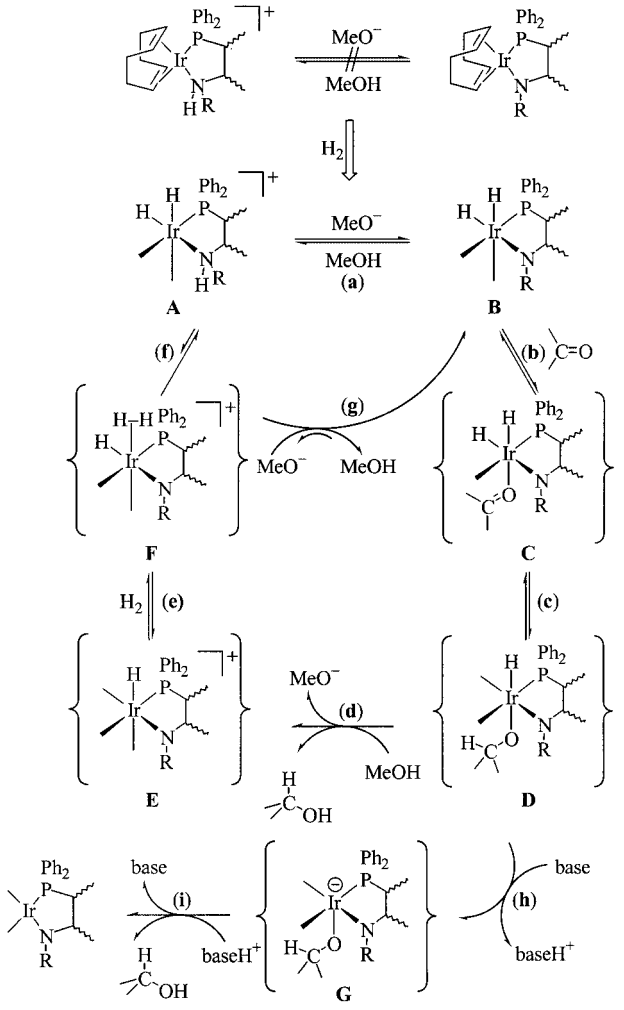

Scheme 11. Proposed catalytic cycle for >C=O hydrogenation and concomitant H$_2$/D$^+$ and H$_2$/D$_2$ exchange reactions (unlabeled coordination sites occupied by weakly bonded solvent molecules)

account for the observed H/D exchange processes since cationic Ir^{III}(μ-H$_2$)(H) complexes combine the possibility of facile *inter*molecular exchange between the bound H$_2$ ligand and free D$_2$ molecules (or molecules containing exchangeable protons) with low barriers to *intra*molecular exchange with the hydride ligand.[23c,23i]

The transient formation of tautomers F also explains the incorporation of solvent deuterons as D$^{\delta-}$ equivalents into the product alcohols that were obtained if the [(COD)Ir(P∩NHR)]$^+$−base-assisted hydrogenation of ketones was conducted in MeOD [Scheme 7, reaction (1)]. We propose that the catalysts described herein follow the classic Schrock−Osborn pathway[6] of >C=O/Ir−H insertion rather than the alternative Noyori−Morris mechanism of "metal−ligand bifunctional" interaction with the substrate,[2,3,4] mainly because the latter[5,6] does *not* depend on the use of protic reaction media but also occurs with comparable results in aprotic solvents such as benzene.[3] In the associated catalytic cycle the first formed amido dihydrides B are converted via ketone adducts C into alkoxo hydrides D, where the *trans* bond weakening H$^-$ ligand is expected

 © 2004 Wiley-VCH Verlag GmbH & Co. KGaA, Weinheim

to be bonded opposite to the alkoxide so that release of the alcohol by reductive elimination is impeded (steps b and c).[5] Protonation of the alkoxide ligand by the solvent with subsequent release of the product from the metal (step d) is a more feasible option which would also explain why the use of protic reaction media is essential for the catalysis. Addition of H_2 to the vacant (or weakly solvated) coordination site of the remaining cationic Ir^{III} species E (step e) leads back to F as the key transient that is able to connect the cycle of catalytic >C=O hydrogenation with the pathway of H_2/D^+ scrambling. *Intra*molecular deprotonation of the acidic H_2 ligand by the amide site (step f) will restore the amino dihydrido species A, which in turn can be converted into the conjugate amides B by the added base. Alternatively, *inter*molecular deprotonation (g) by the methoxide released during product formation (or even by the solvent itself) will directly regenerate the starting amido dihydrides B and, hence, can likewise serve to close the two interlinked cycles. An additional function of the mandatory base may be to deprotonate the alkoxo hydride D at the Ir−H bond forming G as a transient anionic Ir^{III} species which then is re-protonated by the conjugate acid baseH^+ at the alkoxo site[5,6] to release the product and regenerate the starting Ir^I amido complex (steps h and i). In this context, we briefly note that the proposed >C=O/Ir−H pathway can also explain the finding that *N*,*N*-dialkylated $[(COD)Ir\{(1R,2S)\text{-}Ph_2PCH(Ph)CH(Me)NMe_2\}]^+$ [**Ir**$^+$-(*R*,*S*)-**5**] in the presence of base *does* exhibit some catalytic activity for homogeneous ketone hydrogenation *but does not* act as a catalyst for either the H_2/D_2 or H_2/D^+ exchange processes. Oxidative addition of H_2, followed by coordination and insertion of the ketone, will give a *cationic* alkoxo hydrido intermediate in place of the *neutral* species D proposed in Scheme 11. Removal of the alcohol from the coordination sphere on the MeO^-/MeOH-driven pathway h → i therefore leads back to $[L_2Ir\{(1R,2S)\text{-}Ph_2PCH(Ph)CH(Me)NMe_2\}]^+$ as a solvated analogue of the starting compound **Ir**$^+$-(*R*,*S*)-**5**, thus maintaining the cycle of >C=O hydrogenation but barring the way to concomitant isotopic scrambling.

In summary, evidence has been presented for a mechanism of >C=O hydrogenation and H/D exchange catalyzed by iridium β-aminophosphane complexes which involves both homo- and heterolytic H_2 activation at the same metal center.[33]

Experimental Section

General Remarks: All manipulations were performed under nitrogen using standard Schlenk techniques. Solvents were distilled from the appropriate drying agents prior to use. IR: Mattson Polaris. NMR: Bruker DPX 300 (300.1 MHz for ^1H, 75.5 MHz for ^{13}C, 121.5 MHz for ^{31}P, and 46.1 MHz for ^2H) at 20±2 °C (if not stated otherwise) using $SiMe_4$ (or the solvent) or H_3PO_4 as internal or external standards, respectively (downfield positive; "m": deceptively simple multiplets); high-pressure experiments in Wilmad 528-PV-1 tubes (inner diameter: 2.2 mm). Polarimetry: Perkin−Elmer PE 241 (1 dm cells at room temperature). $[\alpha]_\lambda$ in 10 deg·cm^2·g^{-1} (estimated accuracy: ±3%), *c* in g 100 mL^{-1}. HPLC: Thermoquest P 4000 (UV detector).

(2-Aminoethyl)diphenylphosphane as well as the β-amino alcohols (−)-norephedrine, (−)-ephedrine, (−)-*N*-methylephedrine, (+)-pseudoephedrine, (−)-pseudoephedrine, and 2-amino-2-methylpropanol were used as obtained commercially (Fluka, Aldrich). Other starting materials, including (−)-*N*-isopropylnorephedrine,[15] diphenylphosphane,[34] the aziridines 2,2-dimethyl-,[19] (−)-(2*S*,3*R*)-*cis*-2-methyl-3-phenyl-,[7a][9b] (−)-(2*S*,3*S*)-*trans*-2-methyl-3-phenyl-,[7a][12c] (+)-(2*R*,3*S*)-*cis*-1,2-dimethyl-3-phenyl-,[7a] and (+)-(2*S*,3*S*)-*trans*-1,2-dimethyl-3-phenylaziridine,[12b][12c] the *P*,*N* ligands (2-diphenylphosphanyl)-*N*-methylaniline,[18] (+)-(1*S*,2*S*)-(2-amino-1-phenylpropyl)-, (−)-(1*R*,2*S*)-(2-amino-1-phenylpropyl)-, and (−)-(1*R*,2*R*)-(2-methylamino-1-phenylpropyl)diphenylphosphane[7a] as well as the iridium and rhodium complexes *trans*-$[IrCl(CO)PPh_3)_2]$,[35] $[\{(COD)Ir(\mu\text{-}Cl)\}_2]$,[36] $[Ir(COD)_2]BF_4$,[37] (−)-$[(COD)Ir\{(1S,2S)\text{-}Ph_2PCH(Ph)CH(Me)NH_2\}]BF_4$, and $[(COD)M\{(1R,2R)\text{-}Ph_2PCH(Ph)CH(Me)NHMe\}]BF_4$ (M = Rh, Ir)[7a] were prepared as described previously.

(−)-(2*S*,3*R*)-*cis*-1-Benzyl-2-methyl-3-phenylaziridine: A solution of (−)-(2*S*,3*R*)-*cis*-2-methyl-3-phenylaziridine (480 mg, 3.60 mmol) in THF (40 mL) was treated with *n*-butyllithium (2.25 mL of a 1.6 M solution in hexane) at 0 °C. After the addition of benzyl chloride (0.44 mL, 3.80 mmol) and stirring overnight, 2% aqueous citric acid (40 mL) and dichloromethane (50 mL) were added. The aqueous layer was saturated with NaCl and repeatedly extracted with CH_2Cl_2. The combined organic phases were thoroughly washed with $NaHCO_3$ and the solvents evaporated to dryness. The remaining colorless oil was purified by chromatography on a silica gel column with diethyl ether/*n*-pentane (1:8) as the eluent. Evaporation of the solvent from the eluate left the product as a colorless oil; yield 460 mg (57%). ^1H NMR ($CDCl_3$, ppm): δ = 0.87 (d, $^3J_{H,H}$ = 5.49 Hz, 3 H, CH_3), 1.82 ["qui", 1 H, C(2)-H)], 2.57 [d, $^3J_{H,H}$ = 6.57 Hz, 1 H, C(3)-H], 3.49, 3.66 (AB-dd, $^2J_{H,H}$ = 13.91 Hz, 2 H, CH_2), 7.1−7.5 (m, 10 H, C_6H_5). $^{13}C\{^1H\}$ NMR ($CDCl_3$, ppm): δ = 12.79 (CH_3), 41.72 (C-2), 46.18 (C-3), 64.42 (CH_2), 126.4−139.4 (C_6H_5). The NMR spectroscopic data corresponded to those reported in the literature in every respect.[14] $[\alpha]_{589}$ = −112.4 (*c* = 1.3, CH_2Cl_2).

(−)-(2*S*,3*R*)-*cis*-1-Isopropyl-2-methyl-3-phenylaziridine: (−)-(1*R*,2*S*)-*N*-Isopropylnorephedrine (830 mg, 3.97 mmol) was combined in chloroform (30 mL) at 0 °C with PCl_5 (1.10 g, 5.30 mmol). The mixture was heated to reflux for 1 h, then cooled in an ice bath and worked up by the cautions addition of methanol (15 mL). The residue remaining after evaporation to dryness, addition of ethanol (20 mL), and renewed removal of all volatile material was triturated with diethyl ether, separated by filtration and re-dissolved in chilled 5 M sodium hydroxide solution (40 mL). The resultant mixture was heated at 90 °C for 2 h, cooled to room temperature and extracted with diethyl ether. The combined organic layers were dried with Na_2SO_4, evaporated, and then distilled at 70 °C in the vacuum of an oil pump to give the product as a colorless liquid which solidified overnight forming tiny needle-shaped crystals; yield 375 mg (54%). ^1H NMR ($CDCl_3$, ppm): δ = 0.74 (d, $^3J_{H,H}$ = 5.67 Hz, 3 H, CH_3), 1.00, 1.02 [both d, $^3J_{H,H}$ = 5.85 Hz each, both 3 H, $CH(CH_3)_2$], 1.53 [sept, $CH(CH_3)_2$], 1.58 ["qui", 1 H, C(2)-H], 2.33 [d, $^3J_{H,H}$ = 6.75 Hz, 1 H, C(3)-H], 7.0−7.2 (m, 5 H, C_6H_5). $^{13}C\{^1H\}$ NMR ($CDCl_3$, ppm): δ = 13.70 (CH_3), 21.88, 22.08 [both $CH(CH_3)_2$], 40.51 (C-2), 45.87 (C-3), 61.34 [$NCH(CH_3)_2$], 125.4−138.0 (C_6H_5). $[\alpha]_{589}$ = −106.1 (*c* = 6.1, CH_2Cl_2).

(+)-(2*S*,3*S*)-*trans*-1-Isopropyl-2-methyl-3-phenylaziridine: A solution of bromine (255 μL, 4.95 mmol) in acetonitrile (5 mL) was

 © 2004 Wiley-VCH Verlag GmbH & Co. KGaA, Weinheim

added dropwise at 0 °C to triphenylphosphane (1.30 g, 4.95 mmol) dissolved in MeCN (15 mL). The resultant mixture was stirred for 2 h at room temperature, cooled in an ice bath, and then treated with an acetonitrile solution (5 mL) containing (−)-(1*R*,2*S*)-*N*-isopropylnorephedrine (1.035 g, 4.95 mmol) together with triethylamine (1.38 mL, 9.89 mmol). Stirring overnight caused a precipitate of triethylammonium bromide to separate from the solution, which was filtered off. The filtrate was thoroughly extracted with *n*-pentane and the combined extracts were concentrated to a small residual volume to deposit a white precipitate of triphenylphosphane oxide which was removed by filtration. The filtrate was evaporated in vacuo and then distilled with an oil pump generated vacuum at 70 °C to give 317 mg (43%) of the aziridine as a colorless liquid. ^{1}H NMR ($CDCl_3$, ppm): δ = 1.07, 1.10 [both d, $^3J_{H,H}$ = 6.21 Hz each, both 3 H, CH(C*H*$_3$)$_2$], 1.33 (d, $^3J_{H,H}$ = 5.85 Hz, 3 H, CH_3), 2.06 [d, $^3J_{H,H}$ = 2.91 Hz, 1 H, C(3)-H], 2.11 [m, 1 H, C(2)−H], 2.36 [sept, 1 H, C*H*(CH$_3$)$_2$], 7.0−7.3 (m, 5 H, C_6H_5). ^{13}C{^{1}H} NMR ($CDCl_3$, ppm): δ = 11.14 (CH_3), 22.87, 22.94 [both CH(*C*H$_3$)$_2$], 42.45 (C-2), 46.94 (C-3), 51.70 [N*C*H(CH$_3$)$_2$], 126.1−141.1 (C_6H_5). [α]$_{589}$ = +64.8 (*c* = 4.7, CH_2Cl_2).

(−)-(1*R*,2*S*)-(2-Methylamino-1-phenylpropyl)diphenylphosphane [(*R*,*S*)-2]: Boron trifluoride−diethyl etherate (2.32 mL, 18.50 mmol) was added dropwise to a $CHCl_3$ solution of (+)-(2*S*,3*S*)-*trans*-1,2-dimethyl-3-phenylaziridine (2.717 g, 18.45 mmol) and diphenylphosphane (3.20 mL, 18.50 mmol). The mixture was heated to reflux overnight, then hydrolyzed and adjusted to pH 8 by addition of $NaHCO_3$. The organic phase was separated, washed with 5% aqueous sodium hydrogencarbonate, dried over Na_2SO_4, and the solvents evaporated to leave a yellowish oily residue. The oil was re-dissolved in diethyl ether, filtered, evaporated again, and heated at 100 °C under a dynamic vacuum in order to remove any remaining diphenylphosphane; yield 289 mg (47%) of (*R*,*S*)-**2** as a colorless wax. ^{1}H NMR ($CDCl_3$, ppm): δ = 0.98 (d, $^3J_{H,H}$ = 6.39 Hz, 3 H, CCH_3), 1.83 [s (br), 1 H, NH], 2.30 (s, 3 H, NCH_3), 2.80 [m, 1 H, C(2)-H], 3.62 ["t", Σ|$^2J_{P,H}$ + $^3J_{H,H}$| = 11.70 Hz, 1 H, C(1)-H], 7.0−7.7 (m, 15 H, C_6H_5). ^{13}C{^{1}H} NMR ($CDCl_3$, ppm): δ = 18.60 (d, $^3J_{P,C}$ = 4.36 Hz, C*C*H$_3$), 34.11 (s, NCH_3), 51.89, 56.52 (both d, $J_{P,C}$ = 13.08, 16.72 Hz, C-1/*C*-2), 126.5−138.6 (C_6H_5). ^{31}P{^{1}H} NMR ($CDCl_3$, ppm): δ = −7.00. [α]$_{589}$ = −218 (*c* = 0.9, THF). $C_{22}H_{24}NP$ (333.4): calcd. C 79.25, H 7.26, N 4.20; found C 79.47, H 7.43, N 4.11.

(+)-(1*S*,2*S*)-(2-Benzylamino-1-phenylpropyl)diphenylphosphane [(*S*,*S*)-3]: The preparation was carried out as described for (*R*,*S*)-**2** by reacting BF_3-activated (−)-(2*S*,3*R*)-*cis*-1-benzyl-2-methyl-3-phenylaziridine (367 mg, 1.65 mmol) with diphenylphosphane (0.29 mL, 1.65 mmol); yield 325 mg (48%) of (*S*,*S*)-**3** as a white powder. ^{1}H NMR ($CDCl_3$, ppm): δ = 1.04 (d, $^3J_{H,H}$ = 6.57 Hz, 3 H, CCH_3), 1.41 [s (br), 1 H, NH], 2.81 [m, 1 H, C(2)-H], 3.64, 3.66 (AB-dd, $^2J_{H,H}$ = 13.45 Hz, 2 H, CH_2), 3.83 [dd, $^2J_{P,H}$/$^3J_{H,H}$ = 5.49/5.67 Hz, 1 H, C(1)-H], 6.9−7.5 (m, 20 H, C_6H_5). ^{13}C{^{1}H} NMR ($CDCl_3$, ppm): δ = 17.90 (d, $^3J_{P,C}$ = 9.45 Hz, C*C*H$_3$), 50.63 (s, NCH_2), 48.98, 53.54 (both d, $J_{P,C}$ = 14.53, 17.43 Hz, C-1/C-2), 119.5−140.2 (C_6H_5). ^{31}P{^{1}H} NMR ($CDCl_3$, ppm): δ = −8.05. [α]$_{589}$ = +64.5 (*c* = 6.7, CH_2Cl_2). $C_{28}H_{28}NP$ (409.5): calcd. C 82.12, H 6.89, N 3.42; found C 81.95, H 7.01, N 3.31.

(+)-(1*S*,2*S*)-(2-Isopropylamino-1-phenylpropyl)diphenylphosphane [(*S*,*S*)-4]: This material was obtained as outlined before by treating (−)-(2*S*,3*R*)-*cis*-1-isopropyl-2-methyl-3-phenylaziridine (263 mg, 1.50 mmol) in the presence of $F_3B{\cdot}OEt_2$ with diphenylphosphane (0.26 mL, 1.50 mmol); yield 421 mg (78%) of a colorless waxy solid. ^{1}H NMR ($CDCl_3$, ppm): δ = 0.63 (d, $^3J_{H,H}$ = 6.03 Hz, 3 H, CCH_3), 0.83, 1.00 [both d, $^3J_{H,H}$ = 6.21, 6.60 Hz, both 3 H, CH(C*H*$_3$)$_2$], 2.74 [m, 1 H, C(2)-H], 2.91 [sept, 1 H, C*H*(CH$_3$)$_2$], 3.81 [dd, $^2J_{P,H}$/$^3J_{H,H}$ = 3.84/6.60 Hz, 1 H, C(1)-H], 6.9−7.7 (m, 15 H, C_6H_5); NH not observed. ^{13}C{^{1}H} NMR ($CDCl_3$, ppm): δ = 18.20 (d, $^3J_{P,C}$ = 8.72 Hz, C*C*H$_3$), 22.24, 23.04 [both s, both CH(*C*H$_3$)$_2$], 43.94 [s, N*C*H(CH$_3$)$_2$], 47.70, 50.00 (both d, $J_{P,C}$ = 14.53, 16.71 Hz, C-1/C-2), 126.4−137.7 (C_6H_5). ^{31}P{^{1}H} NMR ($CDCl_3$, ppm): δ = −9.04. [α]$_{589}$ = +37.1 (*c* = 2.4, CH_2Cl_2). $C_{24}H_{28}NP$ (361.5): calcd. C 79.75, H 7.81, N 3.87; found C 79.63, H 7.99, N 3.79.

(−)-(1*R*,2*S*)-(2-Isopropylamino-1-phenylpropyl)diphenylphosphane [(*R*,*S*)-4]: The compound was prepared in a similar way to its (1*S*,2*S*) diastereomer above using BF_3-activated (+)-(2*S*,3*S*)-*trans*-1-isopropyl-2-methyl-3-phenylaziridine (371 mg, 2.12 mmol) together with an equimolar quantity of diphenylphosphane (0.37 mL) in $CHCl_3$; yield 669 mg (87%) of a colorless sticky solid. ^{1}H NMR ($CDCl_3$, ppm): δ = 0.64 (d, $^3J_{H,H}$ = 6.24 Hz, 3 H, CCH_3), 0.86, 0.88 (both d, $^3J_{H,H}$ = 6.39 Hz each, both 3 H, CH(C*H*$_3$)$_2$], 2.70 [sept, 1 H, C*H*(CH$_3$)$_2$], 2.99 [m, 1 H, C(2)-H], 3.52 [dd, $^2J_{P,H}$/$^3J_{H,H}$ = 4.84/6.60 Hz, 1 H, C(1)-H], 6.9−7.6 (m, 15 H, C_6H_5); NH not observed. ^{13}C{^{1}H} NMR ($CDCl_3$, ppm): δ = 20.32 (d, $^3J_{P,C}$ = 5.08 Hz, C*C*H$_3$), 22.01, 24.22 [both s, both CH(*C*H$_3$)$_2$], 45.34 [s, N*C*H(CH$_3$)$_2$], 51.41, 51.90 (both d, $J_{P,C}$ = 15.26, 12.35 Hz, C-1/C-2), 126.4−130.5 (C_6H_5). ^{31}P{^{1}H} NMR ($CDCl_3$, ppm): δ = −7.68. [α]$_{589}$ = −205 (*c* = 1.1, CH_2Cl_2). $C_{24}H_{28}NP$ (361.5): calcd. C 79.75, H 7.81, N 3.87; found C 79.52, H 8.02, N 3.73.

(−)-(1*R*,2*S*)-(2-Dimethylamino-1-phenylpropyl)diphenylphosphane [(*R*,*S*)-5]: Methanesulfonyl chloride (1.27 mL, 16.35 mmol) and triethylamine (3.50 mL, 24.52 mmol) were sequentially added to a chilled THF solution (40 mL) of (−)-*N*-methylephedrine (1.465 g, 8.17 mmol). The aziridinium methanesulfonate which was formed after stirring the mixture for 1 h at room temperature was further reacted by heating to reflux a toluene solution (50 mL) containing diphenylphosphane (1.42 mL, 8.17 mmol) and an additional amount of NEt_3 (2.30 mL, 16.35 mmol). After hydrolysis the product was isolated following the workup procedure described above for (*R*,*S*)-**2**; yield 1.11 g (39%) of the aminophosphane as a colorless wax. ^{1}H NMR ($CDCl_3$, ppm): δ = 0.87 (d, $^3J_{H,H}$ = 6.75 Hz, 3 H, CCH_3), 1.96 [s, 6 H, N(CH$_3$)$_2$], 3.04 [m, 1 H, C(2)-H], 3.55 [dd, $^2J_{P,H}$/$^3J_{H,H}$ = 6.03/7.68 Hz, 1 H, C(1)-H], 6.9−7.7 (m, 15 H, C_6H_5). ^{13}C{^{1}H} NMR ($CDCl_3$, ppm): δ = 18.60 (d, $^3J_{P,C}$ = 4.36 Hz, C*C*H$_3$), 34.11 [s, N(CH$_3$)$_2$], 51.89, 56.52 (both d, $J_{P,C}$ = 13.08, 16.72 Hz, C-1/C-2), 126.5−138.6 (C_6H_5). ^{31}P{^{1}H} NMR ($CDCl_3$, ppm): δ = −4.24. [α]$_{589}$ = −318 (*c* = 3.1, THF). $C_{23}H_{26}NP$ (347.4): calcd. C 79.51, H 7.54, N 4.03; found C 79.84, H 7.88, N 3.92.

(2-Amino-2-methylpropyl)diphenylphosphane (8): A mixture composed of 9.96 mmol in each case of 2,2-dimethylaziridine (708 mg), boron trifluoride diethyl etherate (1.26 mL), and diphenylphosphane (1.73 mL) in $CHCl_3$ (50 mL) was heated to reflux for 3 h. An oily precipitate resulting from polymerization of the aziridine was removed by decanting the supernatant liquid, which was worked up by hydrolysis as outlined before for (*R*,*S*)-**2** to give 870 mg (34%) of the *P*,*N* ligand as a clear colorless oil. ^{1}H NMR ($CDCl_3$, ppm): δ = 1.21 (s, 6 H, CH_3), 1.36 [s (br), 2 H, NH_2], 2.36 (d, $^2J_{P,H}$ = 3.66 Hz, CH_2), 7.2−7.6 (m, 10 H, C_6H_5). ^{13}C{^{1}H} NMR ($CDCl_3$, ppm): δ = 32.01 (d, $^3J_{P,C}$ = 7.99 Hz, CH_3), 45.83, 50.00 (both d, $J_{P,C}$ = 15.25, 15.26 Hz, C-1/C-2), 128.3−139.5 (C_6H_5). ^{31}P{^{1}H} NMR ($CDCl_3$, ppm): δ = −23.09. $C_{16}H_{20}NP$ (257.3): calcd. C 74.69, H 7.83, N 5.44; found C 74.79, H 7.98, N 5.21.

 © 2004 Wiley-VCH Verlag GmbH & Co. KGaA, Weinheim

[(COD)Ir(Ph$_2$PCH$_2$CH$_2$NH$_2$)]BF$_4$ [Ir$^+$-6]: To [Ir(COD)$_2$]BF$_4$ (472 mg, 0.95 mmol) suspended in THF (10 mL) was added dropwise a solution of **6** (220 mg, 0.96 mmol) in THF (15 mL). The dark red solution which formed on stirring overnight was reduced in vacuo to a small residual volume. Dilution with diethyl ether and *n*-pentane (20 mL each) caused the product to separate from solution as an orange microcrystalline precipitate which was collected by filtration, thoroughly washed with diethyl ether, and dried under a dynamic vacuum; yield 540 mg (91%). ^{1}H NMR (CDCl$_3$, ppm): δ = 1.7−2.3 (m, 8 H, diene CH$_2$), 2.85, 2.95 (both m, 2 H each, PCH$_2$/NCH$_2$), 3.36 [s (br), 2 H, NH$_2$], 4.7, 5.1 (both m, 2 H each, both diene CH), 7.1−7.7 (m, 10 H, C$_6$H$_5$). ^{13}C{^{1}H} NMR (CDCl$_3$, ppm): δ = 29.30 (s, 2 diene CH$_2$), 31.56 (d, $^1J_{P,C}$ = 32.69 Hz, PCH$_2$), 32.41 (s, 2 diene CH$_2$), 44.69 (d, $^2J_{P,C}$ = 5.09 Hz, NCH$_2$), 61.64 (s, CH=CH *trans* N), 93.33 (d, $^2J_{P,C}$ = 11.62 Hz, CH=CH *trans* P), 128.8−133.2 (C$_6$H$_5$). ^{31}P{^{1}H} NMR (CDCl$_3$, ppm): δ = 38.61. C$_{22}$H$_{28}$BF$_4$IrNP (616.5): calcd. C 42.86, H 4.58, N 2.27; found C 43.02, H 4.67, N 2.09.

The following complexes were prepared by a procedure analogous to that detailed before.

[(COD)Ir(2-Ph$_2$PC$_6$H$_4$NHMe)]BF$_4$ [Ir$^+$-7]: Yield, from [Ir(COD)$_2$]BF$_4$ (574 mg, 1.16 mmol) and the chelate ligand (338 mg, 1.16 mmol), 630 mg (80%) of **Ir$^+$-7** as a reddish brown solid. ^{1}H NMR (CDCl$_3$, ppm): δ = 1.6−2.5 (m, 8 H, diene CH$_2$), 2.85 (d, $^3J_{H,H}$ = 6.03 Hz, 3 H, CH$_3$), 3.1, 4.0, 5.2, 5.75 (all m, 1 H each, all diene CH), 7.2−8.0 (m, 14 H, C$_6$H$_5$ and C$_6$H$_4$); NH not observed. ^{13}C{^{1}H} NMR (CDCl$_3$, ppm): δ = 28.94, 31.13, 31.48, 34.77 (all s, all diene CH$_2$), 48.28 (s, CH$_3$), 61.92, 65.92 (both s, CH=CH *trans* N), 94.81, 98.99 (both d, $^2J_{P,C}$ = 13.08, 10.17 Hz, CH=CH *trans* P), 123.3−135.5 (C$_6$H$_5$ and C$_6$H$_4$), 157.83 (d, $^2J_{P,C}$ = 18.17 Hz, phenylene C-1). ^{31}P{^{1}H} NMR (CDCl$_3$, ppm): δ = 30.39. C$_{27}$H$_{30}$BF$_4$IrNP (678.6): calcd. C 47.79, H 4.46, N 2.06; found C 47.62, H 4.67, N 1.94.

[(COD)Ir(Ph$_2$PCH$_2$CMe$_2$NH$_2$)]BF$_4$ [Ir$^+$-8]: Yield, from [Ir(COD)$_2$]BF$_4$ (131 mg, 0.26 mmol) and the β-aminophosphane (68 mg, 0.26 mmol), 151 mg (88%) of **Ir$^+$-8** as a dark reddish brown solid. ^{1}H NMR (CDCl$_3$, ppm): δ = 1.40 (s, 6 H, CH$_3$), 1.7−2.4 (m, 8 H, diene CH$_2$), 2.51 (d, $^2J_{P,H}$ = 9.51 Hz, 2 H, PCH$_2$), 3.41 [s (br), 2 H, NH$_2$], 4.8, 5.3 (both m, 2 H each, both diene CH), 7.3−7.8 (m, 10 H, C$_6$H$_5$). ^{13}C{^{1}H} NMR (CDCl$_3$, ppm): δ = 28.88, 28.98, 29.28, 31.72 (all s, all diene CH$_2$), 32.31 (d, $^3J_{P,C}$ = 2.91 Hz, CH$_3$), 43.61 (d, $^1J_{P,C}$ = 30.52 Hz, PCH$_2$), 61.77 (d, $^2J_{P,C}$ = 5.09 Hz, NCH$_2$), 61.86 (s, CH=CH *trans* N), 93.73 (d, $^2J_{P,C}$ = 12.35 Hz, CH=CH *trans* P), 129.0−133.4 (C$_6$H$_5$). ^{31}P{^{1}H} NMR (CDCl$_3$, ppm): δ = 29.14. C$_{24}$H$_{32}$BF$_4$IrNP (644.6): calcd. C 44.73, H 5.00, N 2.17; found C 44.42, H 5.09, N 2.09.

[(COD)Ir{(1*S*,2*S*)-Ph$_2$PCH(Ph)CH(Me)NHCH$_2$Ph}]BF$_4$ [Ir$^+$-(*S*,*S*)-3]: Yield, from [Ir(COD)$_2$]BF$_4$ (235 mg, 0.48 mmol) and (*S*,*S*)-**3** (195 mg, 0.48 mmol), 314 mg (82%) of the complex as an orange solid containing the δ($S_{C\text{-}1}$,$S_{C\text{-}2}$,S_N) conformer (≈ 40%) together with the δ($S_{C\text{-}1}$,$S_{C\text{-}2}$,R_N) form (≈ 60%) as sterically locked ring conformers (isomeric distribution estimated from ^{1}H and ^{31}P{^{1}H} NMR). ^{1}H NMR ([D$_6$]acetone, ppm): δ[δ($S_{C\text{-}1}$,$S_{C\text{-}2}$,S_N)] = 1.32 (d, $^3J_{H,H}$ = 6.39 Hz, 3 H, CCH$_3$), 1.4−2.5 (m, 8 H, diene CH$_2$), 2.92 [m, 1 H, MeC(2)-H], 3.20, 3.39 (both m, 1 H each, both diene CH), 4.20, 4.22 (AB-dd, $^2J_{H,H}$ = 6.93 Hz, 2 H, CH$_2$), 4.58 [dd, $^2J_{P,H}$/$^3J_{H,H}$ = 6.39/3.63 Hz, 1 H, PhC(1)-H], 5.63 (m, 2 H, diene CH), 6.3 [s (br), 1 H, NH], 6.8−8.1 (m, 20 H, C$_6$H$_5$); δ[δ($S_{C\text{-}1}$,$S_{C\text{-}2}$,R_N)] = 1.19 (d, $^3J_{H,H}$ = 6.03 Hz, 3 H, CCH$_3$), 1.4−2.5 (m, 8 H, diene CH$_2$), 2.65 [m, 1 H, MeC(2)-H], 3.61, 3.67 (both m, 1 H each, both diene CH), 4.57 [dd, $^2J_{P,H}$/$^3J_{H,H}$ = 6.75/4.41 Hz, 1 H, PhC(1)-H], 4.71, 4.75 (AB-dd, $^2J_{H,H}$ = 6.48 Hz, 2 H, CH$_2$), 5.51 (m, 2 H, diene CH), 5.9 [s (br), 1 H, NH], 6.8−8.1 (m, 20 H, C$_6$H$_5$). ^{13}C{^{1}H} NMR ([D$_6$]acetone, ppm): δ[δ($S_{C\text{-}1}$,$S_{C\text{-}2}$,S_N)] = 17.37 (d, $^3J_{P,C}$ = 13.80 Hz, C*C*H$_3$), 26.1−37.6 (diene CH$_2$; partially obscured by solvent), 47.09 (d, $^1J_{P,C}$ = 24.71 Hz, PCH), 51.23 (s, CH$_2$), 64.40 (d, $^2J_{P,C}$ = 9.45 Hz, NCH), 64.52, 69.12 (both s, CH=CH *trans* N), 82.35, 94.20 (both d, $^2J_{P,C}$ = 16.72, 7.99 Hz, CH=CH *trans* P), 125.0−138.5 (C$_6$H$_5$); δ[δ($S_{C\text{-}1}$,$S_{C\text{-}2}$,R_N)] = 16.50 (d, $^3J_{P,C}$ = 13.80 Hz, C*C*H$_3$), 26.1−37.6 (diene CH$_2$; partially obscured by solvent), 53.45 (s, CH$_2$), 54.18 (d, $^1J_{P,C}$ = 25.43 Hz, PCH), 60.02 (d, $^2J_{P,C}$ = 9.45 Hz, NCH), 60.79, 65.65 (both s, CH=CH *trans* N), 92.89, 98.31 (both d, $^2J_{P,C}$ = 14.54, 8.72 Hz, CH=CH *trans* P), 125.0−138.5 (C$_6$H$_5$). ^{31}P{^{1}H} NMR ([D$_6$]acetone, ppm): δ = 39.97 [δ($S_{C\text{-}1}$,$S_{C\text{-}2}$,S_N) conformer], 46.65 [δ($S_{C\text{-}1}$,$S_{C\text{-}2}$,R_N) conformer]. C$_{36}$H$_{40}$BF$_4$IrNP (796.8): calcd. C 54.27, H 5.06, N 1.76; found C 54.52, H 5.21, N, 1.62.

[(COD)Ir{(1*S*,2*S*)-Ph$_2$PCH(Ph)CH(Me)NHCHMe$_2$}]BF$_4$ [Ir$^+$-(*S*,*S*)-4]: Yield, from [Ir(COD)$_2$]BF$_4$ (347 mg, 0.70 mmol) and (*S*,*S*)-**4** (300 mg, 0.76 mmol), 456 mg (87%) of the product as an orange solid composed of the two ring conformers δ($S_{C\text{-}1}$,$S_{C\text{-}2}$,S_N), ≈ 25%, and δ($S_{C\text{-}1}$,$S_{C\text{-}2}$,R_N), ≈ 75% (isomeric distribution estimated from the relative intensities of the ^{31}P resonances). ^{1}H NMR (CDCl$_3$, ppm): δ[δ($S_{C\text{-}1}$,$S_{C\text{-}2}$,R_N)] = 1.37 ["t", Σ|$^3J_{H,H}$ +$^5J_{H,H}$| = 13.14 Hz, 6 H, CH(C*H*$_3$)$_2$], 1.50 (d, $^3J_{H,H}$ = 6.78 Hz, 3 H, CCH$_3$), 1.5−2.4 (m, 8 H, diene CH$_2$), 3.22 [m, 1 H, MeC(2)-H], 3.34 [s (br), 1 H, NH], 3.63 (sept, $^3J_{H,H}$ = 6.57 Hz, 1 H, C*H*(CH$_3$)$_2$], 4.29 [dd, $^2J_{P,H}$ = 12.17, $^3J_{H,H}$ = 7.04 Hz, 1 H, PhC(1)-H], 4.87, 5.15, 5.37, 5.75 (all m, 1 H each, all diene CH), 6.8−7.6 (m, 15 H, C$_6$H$_5$). ^{13}C{^{1}H} NMR (CDCl$_3$, ppm): δ[δ($S_{C\text{-}1}$,$S_{C\text{-}2}$,R_N)] = 19.83 (d, $^3J_{P,C}$ = 13.08 Hz, C*C*H$_3$), 21.98, 24.23 [both s, CH(*C*H$_3$)$_2$], 26.10, 27.18, 31.81, 36.78 (all s, all diene CH$_2$), 54.71 (d, $^1J_{P,C}$ = 25.43 Hz, PCH), 55.03 [s, *C*H(CH$_3$)$_2$], 56.31, 62.88 (both s, CH=CH *trans* N), 60.75 (d, $^2J_{P,C}$ = 7.99 Hz, NCH), 93.90, 97.87 (both d, $^2J_{P,C}$ = 13.80, 9.44 Hz, CH=CH *trans* P), 124.5−136.9 (C$_6$H$_5$); ^{1}H and ^{13}C{^{1}H} spectra of the minor δ[δ($S_{C\text{-}1}$,$S_{C\text{-}2}$,S_N)] conformer not assigned. ^{31}P{^{1}H} NMR ([D$_6$]acetone, ppm): δ = 40.79 [δ($S_{C\text{-}1}$,$S_{C\text{-}2}$,S_N) conformer], 45.44 [δ($S_{C\text{-}1}$,$S_{C\text{-}2}$,R_N) conformer]. C$_{32}$H$_{40}$BF$_4$IrNP (748.7): calcd. C 51.34, H 5.39, N 1.87; found C 51.83, H 5.77, N 1.73.

[(COD)Ir{(1*R*,2*S*)-Ph$_2$PCH(Ph)CH(Me)NHMe}]BF$_4$ [Ir$^+$-(*R*,*S*)-2]: Yield, from [Ir(COD)$_2$]BF$_4$ (206 mg, 0.42 mmol) and the *P*,*N* ligand (153 mg, 0.46 mmol), 243 mg (81%) of **Ir$^+$**-(*R*,*S*)-**2** as a dark red precipitate containing the λ($R_{C\text{-}1}$,$S_{C\text{-}2}$,R_N) conformer (94%) in addition to two further sterically locked isomers of unassigned stereochemistry. ^{1}H NMR ([D$_6$]acetone, ppm): δ[λ($R_{C\text{-}1}$,$S_{C\text{-}2}$,R_N)] = 1.14 (d, $^3J_{H,H}$ = 6.54 Hz, 3 H, CCH$_3$), 1.4−2.6 (m, 8 H, diene CH$_2$), 2.67 (d, $^3J_{H,H}$ = 5.85 Hz, 3 H, NCH$_3$), 2.88 [m, 1 H, MeC(2)-H], 3.11 (m, 1 H, diene CH), 3.22 [s (br), 1 H, NH], 3.71 (m, 1 H, diene CH), 4.31 [dd, $^2J_{P,H}$ = 14.26, $^3J_{H,H}$ = 4.20 Hz, 1 H, PhC(1)-H], 5.27, 5.61 (both m, 1 H each, both diene CH), 6.7−8.2 (m, 15 H, C$_6$H$_5$). ^{13}C{^{1}H} NMR ([D$_6$]acetone, ppm): δ[λ($R_{C\text{-}1}$,$S_{C\text{-}2}$,R_N)] = 15.17 (d, $^3J_{P,C}$ = 11.62 Hz, C*C*H$_3$), 27.4−36.6 (diene CH$_2$; partially obscured by solvent), 40.13 (s, NCH$_3$), 56.76 (d, $^1J_{P,C}$ = 29.79 Hz, PCH), 60.07, 62.61 (both s, CH=CH *trans* N), 66.49 (d, $^2J_{P,C}$ = 9.45 Hz, NCH), 93.59, 96.20 (both d, $^2J_{P,C}$ = 10.17, 13.08 Hz, CH=CH *trans* P), 126.0−136.4 (C$_6$H$_5$). ^{31}P{^{1}H} NMR ([D$_6$]acetone, ppm): δ = 38.10 [94%; λ($R_{C\text{-}1}$,$S_{C\text{-}2}$,R_N)], 38.01 (≈ 4%), 41.27 (≈ 2%); both unassigned. C$_{30}$H$_{36}$BF$_4$IrNP (760.6): calcd. C 50.00, H 5.04, N 1.94; found C 50.24, H 5.32, N 2.01.

(−)-[(COD)Ir{(1*R*,2*S*)-Ph$_2$PCH(Ph)CH(Me)NHCHMe$_2$}]BF$_4$ [Ir$^+$-(*R*,*S*)-4]: Yield, from [Ir(COD)$_2$]BF$_4$ (863 mg, 1.74 mmol) and the β-aminophosphane (634 mg, 1.75 mmol), 1.070 g (82%) of the

 © 2004 Wiley-VCH Verlag GmbH & Co. KGaA, Weinheim

complex as an orange solid. ^{1}H NMR ([D$_6$]acetone, ppm): δ = 1.24, 1.32 [both d, $^3J_{H,H}$ = 6.78 Hz each, both 3 H, CH(CH_3)$_2$], 1.39 (d, $^3J_{H,H}$ = 6.57 Hz, 3 H, CCH$_3$), 1.7 (m, 1 H, diene CH$_2$), 1.9−2.3 (m, 5 H, diene CH$_2$), 2.3−2.6 (m, 2 H, diene CH$_2$), 3.12 [m, 1 H, MeC(2)-H], 3.4−3.6 (m, 2 H, diene CH), 3.65 [s (br), 1 H, NH], 4.51 [dd, $^2J_{P,H}$ = 12.99, $^3J_{H,H}$ = 4.95 Hz, 1 H, PhC(1)-H], 4.80 (sept, 1 H, CH(CH$_3$)$_2$], 5.41, 5.87 (both m, 1 H each, both diene CH), 6.8−7.9 (m, 15 H, C$_6$H$_5$). ^{13}C{^{1}H} NMR ([D$_6$]acetone, ppm): δ = 18.47 (d, $^3J_{P,C}$ = 7.99 Hz, CCH$_3$), 22.46, 23.71 [both s, CH(CH_3)$_2$], 26.37−35.90 (diene CH$_2$; partially obscured by solvent), 53.98 (d, $^1J_{P,C}$ = 27.61 Hz, PCH), 55.80 [s, CH(CH$_3$)$_2$], 61.67, 62.10 (both s, CH=CH *trans* N), 62.37 (d, $^2J_{P,C}$ = 7.99 Hz, NCH), 90.25, 93.91 (both d, $^2J_{P,C}$ = 14.54, 8.72 Hz, CH=CH *trans* P), 128.4−135.3 (C$_6$H$_5$). ^{31}P{^{1}H} NMR ([D$_6$]acetone, ppm): δ = 37.54. [α]$_{589}$ = −295 (*c* = 0.7, MeOH). C$_{32}$H$_{40}$BF$_4$IrNP (748.7): calcd. C 51.34, H 5.39, N 1.87; found C 51.65, H 5.30, N 2.00.

(−)-[(COD)Ir{(1*R*,2*S*)-Ph$_2$PCH(Ph)CH(Me)NMe$_2$}]BF$_4$ [Ir$^+$-(*R*,*S*)-5]: Yield, from [Ir(COD)$_2$]BF$_4$ (104 mg, 0.21 mmol) and the *P*,*N* ligand (80 mg, 0.23 mmol), 140 mg (83%) of **Ir$^+$-(*R*,*S*)-5** as an orange solid. ^{1}H NMR (CDCl$_3$, ppm): δ = 1.40 (d, $^3J_{H,H}$ = 6.60 Hz, 3 H, CCH$_3$), 1.5−2.4 (m, 8 H, diene CH$_2$), 2.90, 3.13 (both s, both NCH$_3$), 3.15 [m, 1 H, MeC(2)-H], 3.27, 3.37 (both m, 1 H each, both diene CH), 4.53 [dd, $^2J_{P,H}$ = 9.78, $^3J_{H,H}$ = 4.65 Hz, 1 H, PhC(1)-H], 4.71, 5.26 (both m, 1 H each, both diene CH), 6.8−7.6 (m, 15 H, C$_6$H$_5$). ^{13}C{^{1}H} NMR (CDCl$_3$, ppm): δ = 15.97 (d, $^3J_{P,C}$ = 6.54 Hz, CCH$_3$), 29.36, 29.69, 30.74, 32.63 (all s, all diene CH$_2$), 47.41 (d, $^1J_{P,C}$ = 23.25 Hz, PCH), 48.75, 50.15 (both s, both NCH$_3$), 59.00, 65.56 (both s, CH=CH *trans* N), 76.07 (d, $^2J_{P,C}$ = 7.26 Hz, NCH), 93.34, 97.34 (both d, $^2J_{P,C}$ = 12.35, 10.90 Hz, CH=CH *trans* P), 127.1−137.5 (C$_6$H$_5$). ^{31}P{^{1}H} NMR (CDCl$_3$, ppm): δ = 35.70. [α]$_{589}$ = −95.4, [α]$_{578}$ = −112 (both *c* = 0.3, MeOH). C$_{31}$H$_{38}$BF$_4$IrNP (734.7): calcd. C 50.68, H 5.21, N 1.91; found C 50.65, H 5.30, N 2.00.

[(COD)Ir(2-Ph$_2$PC$_6$H$_4$NMe)] (Ir-7a): A solution of **7** (318 mg, 1.09 mmol) in *n*-pentane (10 mL) was cooled to −70 °C and treated with *n*-butyllithium (0.44 mL, 1.10 mmol of a 2.5 M hexane solution). The resultant suspension of the monolithiated *P*,*N* ligand was allowed to warm to ambient temperature and then added to a stirred suspension of [{(COD)Ir(μ-Cl)}$_2$] (366 mg, 0.54 mmol) in benzene. Stirring for 3 h at ambient conditions caused the precipitation of lithium chloride which was separated by filtration. The filtrate was reduced in volume in vacuo to give 558 mg (87%) of a bright red solid retaining some residual solvent even after prolonged drying under a dynamic vacuum. ^{1}H NMR (CDCl$_3$, ppm): δ = 1.82, 2.18 (both m, 4 H each, both diene CH$_2$), 2.81 (m, 2 H, diene CH), 3.05 (s, 3 H, CH$_3$), 4.96 (m, 2 H, diene CH), 6.26, 6.53, 6.96, 7.08 (all m, 1 H each, all C$_6$H$_4$), 7.2−7.7 (m, 10 H, C$_6$H$_5$). ^{13}C{^{1}H} NMR (CDCl$_3$, ppm): δ = 30.47, 32.77 (both s, both diene CH$_2$), 39.24 (s, CH$_3$), 52.98 (s, CH=CH *trans* N), 91.62 (d, $^2J_{P,C}$ = 13.08 Hz, CH=CH *trans* P), 110.70, 114.29, (both d, $J_{P,C}$ = 12.82, 6.79 Hz, both phenylene C), 118.66 (d, $^1J_{P,C}$ = 54.34 Hz, phenylene C-2), 128.2−133.2 (C$_6$H$_5$ and 2 phenylene C), 171.84 (d, $^2J_{P,C}$ = 24.71 Hz, phenylene C-1). ^{31}P{^{1}H} NMR (C$_6$D$_6$, ppm): δ = 42.61. C$_{27}$H$_{29}$IrNP (590.7): calcd. C 54.90, H 4.95, N 2.73. C$_{27}$H$_{30}$IrNP·1/2C$_6$H$_6$ (629.8): calcd. C 57.21, H 5.12, N 2.22; found C 57.98, H 5.17, N 2.22.

[(COD)Ir(Ph$_2$PCH$_2$CMe$_2$NH)] (Ir-8a): The complex was prepared by analogy to the procedure outlined before employing ligand **8** (218 mg, 0.85 mmol), an equimolar portion of *n*BuLi in hexane, and [{(COD)Ir(μ-Cl)}$_2$](284 mg, 0.42 mmol); yield 385 mg (82%) of the amido complex as a dark red solid. ^{1}H NMR (C$_6$D$_6$, ppm): δ = 1.36 (s, 6 H, CH$_3$), 2.03, 2.24 (both m, 2 H each, both diene CH$_2$), 2.28 (d, $^2J_{P,C}$ = 10.23 Hz, 2 H, PCH$_2$), 2.40, 2.59 (both m, 2 H each, both diene CH$_2$), 2.99 (m, 2 H, diene CH), 4.5 [s (br), 1 H, NH], 4.90 (m, 2 H, diene CH), 7.15 (m, 6 H, C$_6$H$_5$), 7.74 (m, 4 H, C$_6$H$_5$). ^{13}C{^{1}H} NMR (C$_6$D$_6$, ppm): δ = 31.14, 35.60 (both s, both diene CH$_2$), 36.09 (d, $^3J_{P,C}$ = 7.99 Hz, CH$_3$), 46.89 (d, $^1J_{P,C}$ = 31.24 Hz, PCH$_2$), 47.62 (s, CH=CH *trans* N), 67.30 (d, $^2J_{P,C}$ = 9.45 Hz, NCH$_2$), 84.33 (d, $^2J_{P,C}$ = 14.54 Hz, CH=CH *trans* P), 128.7−134.1 (C$_6$H$_5$). ^{31}P{^{1}H} NMR (C$_6$D$_6$, ppm): δ = 49.85. C$_{24}$H$_{31}$IrNP (556.7): calcd. C 51.78, H 5.61, N 2.52; found C 52.55, H 5.97, N 2.12.

[(COD)Ir{(1*R*,2*S*)-Ph$_2$PCH(C$_6$H$_4$-*o*)CH(Me)NHCHMe$_2$] [Ir-(*R*,*S*)-4a]: A solution of potassium hydroxide (400 mg, 7.13 mmol) in methanol (10 mL) was combined with **Ir$^+$-(*R*,*S*)-4** (103 mg, 0.14 mmol) dissolved in MeOH (10 mL) to give an orange precipitate which was collected by filtration and washed with a few milliliters of methanol. Re-dissolution of the solid in hot acetone, followed by cooling to room temperature afforded the orthometalated complex as orange crystals which tenaciously retained some residual acetone solvent. ^{1}H NMR ([D$_6$]acetone, ppm): δ = 0.95, 1.08 [both d, $^3J_{H,H}$ = 6.24 each, both 3 H, CH(CH_3)$_2$], 1.20 (d, $^3J_{H,H}$ = 6.42 Hz, 3 H, CCH$_3$), 1.4−2.6 (m, 8 H, diene CH$_2$), 2.65 [m, 2 H, MeC(2)-H and CH(CH$_3$)$_2$], 3.95 [s (br), 1 H, NH], 4.05, 4.22 (both m, 1 H each, both diene CH), 4.39 [m, 1 H, PhC(1)-H], 5.21, 5.47 (both m, 1 H each, both diene CH), 6.81 (m, 2 H, C$_6$H$_4$), 7.08 (m, 1 H, C$_6$H$_4$), 7.26 (m, 3 H, C$_6$H$_5$), 7.29 (m, 1 H, C$_6$H$_4$), 7.44, 7.67 (both m, 7 H each, C$_6$H$_5$). ^{31}P{^{1}H} NMR ([D$_6$]acetone, ppm): δ = 44.99. C$_{32}$H$_{39}$IrNP (660.9): calcd. C 58.16, H 5.95, N 2.12. C$_{32}$H$_{39}$IrNP·C$_3$H$_6$O (718.9) calcd. C 58.47, H 6.31, N 1.95; found C 58.67, H 6.33, N 1.91.

***cis*-[(COD)IrH$_2$(Ph$_2$PCH$_2$CMe$_2$NH$_2$)]BF$_4$, (Ir$^+$-9):** A sample of **Ir$^+$-8** (20 mg) was dissolved in CD$_3$CN (2 mL), transferred into a high-pressure NMR tube and treated with 5 bar of H$_2$. ^{1}H NMR (CD$_3$CN, ppm): δ = −15.78 (d, *cis*-$^2J_{P,H}$ = 10.95 Hz, 1 H, IrH *trans* N), −12.60 (d, *cis*-$^2J_{P,H}$ = 15.91 Hz, 1 H, IrH *trans* >C=C<), 1.17 (s, 6 H, CH$_3$), 1.6−2.9 (m, 8 H, diene CH$_2$), 3.00 (d, $^2J_{P,H}$ = 9.33 Hz, 2 H, PCH$_2$), 3.89, 4.67 (both m, 1 H each, both diene CH), 4.93 [s (br), 2 H, NH$_2$], 5.58, 5.71 (both m, 1 H each, both diene CH), 7.1−8.2 (m, 10 H, C$_6$H$_5$). ^{31}P{^{1}H} NMR (CD$_3$CN, ppm): δ = 31.87.

***cis*-[(COD)IrH$_2$(Ph$_2$PCH$_2$CMe$_2$NH)] (Ir-9a):** A CD$_3$CN solution of **Ir-8a** was pressurized, in an NMR tube, to 5 bar of H$_2$. ^{1}H NMR (CD$_3$CN, ppm): δ = −18.13 (d, *cis*-$^2J_{P,H}$ = 8.79 Hz, 1 H, IrH *trans* N), −7.09 (d, *cis*-$^2J_{P,H}$ = 13.18 Hz, 1 H, IrH *trans* >C=C<), 1.13 (s, 6 H, CH$_3$), 1.5−2.7 (m, 10 H, diene CH$_2$ overlapping with PCH$_2$), 3.17 (m, 2 H, diene CH), 3.85 [s (br), 1 H, NH], 4.17 (m, 2 H, diene CH), 7.1−8.0 (m, 10 H, C$_6$H$_5$). ^{31}P{^{1}H} NMR (CD$_3$CN, ppm): δ = 17.68.

***cis*-[(COD)IrH$_2${(1*S*,2*S*)-Ph$_2$PCH(Ph)CH(Me)NH$_2$]BF$_4$ (Ir$^+$-10):** A sample of **Ir$^+$-(*S*,*S*)-1** (≈ 20 mg) in [D$_8$]THF (2 mL) was exposed to 1 bar of H$_2$ and immediately characterized by NMR spectroscopy. ^{1}H NMR ([D$_8$]THF, ppm): δ = −16.31 (d, *cis*-$^2J_{P,H}$ = 11.52 Hz, 1 H, IrH *trans* N), −12.44 (d, *cis*-$^2J_{P,H}$ = 14.82 Hz, 1 H, IrH *trans* >C=C<), 0.89 (d, $^3J_{H,H}$ = 6.03 Hz, 3 H, CH$_3$), 1.5−2.9 (m, 8 H, diene CH$_2$), 2.74 [m, 1 H, MeC(2)-H], 4.01 [dd, $^2J_{P,H}$ = 12.63, $^3J_{H,H}$ = 4.95 Hz, 1 H, PhC(1)-H], 4.16, 4.56, 4.77, 4.96, 5.27, 5.45 (all m, 1 H each, diene CH overlapping with NH$_2$), 6.9−7.7 (m, 15 H, C$_6$H$_5$). ^{31}P{^{1}H} NMR ([D$_8$]THF, ppm): δ = 46.03.

***cis*,*cis*-[(MeCN)$_2$IrH$_2${(1*R*,2*S*)-Ph$_2$PCH(Ph)CH(Me)NHMe]BF$_4$ (Ir$^+$-11):** A solution of **Ir$^+$-(*R*,*S*)-2** (90 mg, 0.12 mmol) in acetonitrile (2 mL) was stirred under 25 bar of H$_2$ for 2 h in an autoclave. The solid residue remaining after removal of all volatiles in vacuo

was re-dissolved in CD_2Cl_2 and immediately characterized by NMR spectroscopy. ^1H NMR (CD_2Cl_2, ppm): δ = −21.20, −21.14 (*AB*X m, *cis*-$^2J_{P,H}$ = 17.22, 22.11, *cis*-$^2J_{H,H}$ = 7.13 Hz, 1 H each, IrH_2), 1.09 (d, $^3J_{H,H}$ = 6.06 Hz, 3 H, $CHCH_3$), 1.73, 2.37 (both s, 3 H each, both CH_3CN), 2.87 (d, $^3J_{H,H}$ = 6.06 Hz, 3 H, NCH_3), 3.19 [m, 1 H, MeC(2)-H], 3.42 [s (br), 1 H, NH)], 4.01 [dd, $^2J_{P,H}$ = 13.71, $^3J_{H,H}$ = 4.38 Hz, 1 H, PhC(1)-H], 6.9−7.7 (m, 15 H, C_6H_5). $^{13}C\{^1H\}$ NMR (CD_2Cl_2, ppm): δ = 1.70, 2.97 (both s, CH_3CN), 15.27 (d, $^3J_{P,C}$ = 10.90 Hz, $CHCH_3$), 37.04 (s, NCH_3), 51.62, (d, $^1J_{P,C}$ = 34.15 Hz, PCH), 64.40 (d, $^2J_{P,C}$ = 5.81 Hz, NCH), 115.99 [s (br), CH_3CN *trans* H], 119.63 (d, $^3J_{P,C}$ = 18.90 Hz, CH_3CN *trans* P), 123.0−134.4 (C_6H_5). $^{31}P\{^1H\}$ NMR (CD_2Cl_2, ppm): δ = 32.27.

X-ray Structure Determinations: Single crystals of **Ir**$^+$-(*S*,*S*)-**3**·2THF (size 0.33 × 0.10 × 0.08 mm), **Ir**$^+$-(*R*,*S*)-**2**·THF (size 0.38 × 0.33 × 0.28 mm), and **Ir**-(*R*,*S*)-**4a** (size 0.50 × 0.45 × 0.23 mm) were grown from THF/*n*-pentane [**Ir**$^+$-(*S*,*S*)-**3**·2THF and **Ir**$^+$-(*R*,*S*)-**2**·THF] or acetone [**Ir**-(*R*,*S*)-**4a**]. Diffraction measurements were made at −90±2 °C [**Ir**$^+$-(*R*,*S*)-**2**·THF] and at −80±2 °C [**Ir**$^+$-(*S*,*S*)-**3**·2THF and **Ir**-(*R*,*S*)-**4a**] on an Enraf−Nonius CAD-4 MACH 3 diffractometer using graphite-monochromated Mo-K_α radiation (λ = 0.71073 Å); orientation matrices and unit cell parameters from the setting angles of 25 centered medium-angle reflections; collection of the diffraction intensities by ω scans (data corrected for absorption either empirically by ψ scans[38] [**Ir**$^+$-(*S*,*S*)-**3**·2THF: T_{min} = 0.406, T_{max} = 0.777; **Ir**$^+$-(*R*,*S*)-**2**·THF: T_{min} = 0.217, T_{max} = 0.316] or by refined absorption methods[39] [**Ir**-(*R*,*S*)-**4a**: T_{min} = 0.087, T_{max} = 0.318]. The structures were solved by direct methods and subsequently refined by full-matrix least-squares procedures on F^2 allowing for anisotropic thermal motion of all non-hydrogen atoms employing the WinGX package[40a] with the relevant programs (SIR-97,[41] SHELXL-97,[42] ORTEP-3[40b]) implemented therein. **Ir**$^+$-(*S*,*S*)-**3**·2THF: $C_{36}H_{40}IrNP$, BF_4, $2(C_4H_8O)$ (940.9); monoclinic, $P2_1$, a = 14.8593(15), b = 9.215(2), c = 15.108(2) Å, β = 93.506(9)°, V = 2064.8(5) Å^3, Z = 2, $d_{calcd.}$ = 1.513 g·cm^{-3}, μ(Mo-K_α) = 3.327 mm^{-1}; 2.59° ≤ Θ ≤ 22.48°, 6018 reflections collected (−15 ≤ h ≤ +15, −9 ≤ k ≤ +9, −16 ≤ l ≤ +16, including Friedel pairs), 5363 unique; wR = 0.1824 for all data and 488 parameters, R = 0.0835 for 3495 structure factors F_o > 4σ(F_o), absolute structure parameter[43] x = 0.00(3). **Ir**$^+$-(*R*,*S*)-**2**·THF: $C_{30}H_{36}IrNP$, BF_4, C_4H_8O (792.7); orthorhombic, $P2_12_12_1$, a = 9.268(2), b = 12.889(1), c = 27.147(6) Å, V = 3243(1) Å^3, Z = 4, $d_{calcd.}$ = 1.642 g·cm^{-3}, μ(Mo-K_α) = 4.218 mm^{-1}; 2.18° ≤ Θ ≤ 25.17°, 6122 reflections collected (−11 ≤ h ≤ +11, −15 ≤ k ≤ +15, −25 ≤ l ≤ +25, including Friedel pairs), 5418 unique; wR = 0.1328 for all data and 390 parameters, R = 0.0633 for 3963 structure factors F_o > 4σ(F_o), x = 0.02(2). **Ir**-(*R*,*S*)-**4a**: $C_{32}H_{39}IrNP$ (660.8); monoclinic, $P2_1$, a = 9.097(2), b = 19.312(4), c = 15.709(6) Å, β = 98.99(2)°, V = 2726(1) Å^3, Z = 4, $d_{calcd.}$ = 1.610 g·cm^{-3}, μ(Mo-K_α) = 4.978 mm^{-1}; 2.11° ≤ Θ ≤ 26.56°, 12154 reflections collected (−11 ≤ h ≤ +11, −24 ≤ k ≤ +24, −19 ≤ l ≤ +19, including Friedel pairs), 11382 unique; wR = 0.0734 for all data and 637 parameters, R = 0.0321 for 10345 structure factors F_o > 4σ(F_o), x = −0.012(6). CCDC-215609 [**Ir**$^+$-(*S*,*S*)-**3**·2THF], CCDC-215607 [**Ir**$^+$-(*R*,*S*)-**2**·THF], and CCDC-215608 [**Ir**-(*R*,*S*)-**4a**] contain the supplementary crystallographic data for this paper. These data can be obtained free of charge at www.ccdc.cam.ac.uk/conts/retrieving.html [or from the Cambridge Crystallographic Data Center, 12, Union Road, Cambridge CB2 1EZ, UK; Fax: (internat.) +44−1223/336-033; E-mail: deposit@ccdc.cam.ac.uk].

General Procedure for Catalytic >C=O Hydrogenation: A 10 mL capacity Schlenk tube equipped with a small magnetic stirring bar was charged with the catalyst complex dissolved in methanol (typically 0.02 mmol in 3.0 mL). The required equivalent of activating nitrogen or alkaline base (cf. Tables 2−4) and 2.0 mmol of acetophenone were added, the mixture was stirred for 10 min at ambient conditions, and the tube was inserted into an argon-filled stainless steel autoclave. The autoclave was sealed, pressurized and vented several times with H_2 (Messer-Griesheim; 99.999%), and subsequently pressurized (usually to 10−25 bar) and maintained with stirring at 25 or 50 °C. At the end of the reaction, the pressure was released, the solvent removed in vacuo, and the residue diluted with *n*-pentane to precipitate the catalyst as a red oil. The pentane solution was decanted and chromatographed on a silica gel column using diethyl ether/*n*-pentane (1:1) as the eluent. Volatiles were distilled off and the mixture of products was analyzed by ^1H NMR spectroscopy. Conversions and product compositions were determined on the basis of the integrations of the $PhC(O)CH_3$ and $PhCH(OH)CH_3$ signals. Enantiomeric excesses were measured either by HPLC using a Daicel Chiralcel OD column or by polarimetry as detailed elsewhere.[7a] Optical rotations were referenced to the following $[\alpha]_D$ values of the pure enantiomers taken from the literature: (*R*)-1-phenylethanol, +48.6 (*c* = 1, CH_2Cl_2);[44a] (*S*)-1-phenylpropanol, −47.7 (*c* = 6.8, Et_2O);[44b] (*S*)-2-methyl-1-phenylpropanol, +5.3 (*c* = 1.1, EtOH);[44c] (*S*)-1-indanol, +31.7 (*c* = 1, $CHCl_3$);[44d] (*S*)-4-chloro-1-phenylbutanol, −33 (*c* = 1, $CHCl_3$).[44e]

Representative Catalytic >C=O Hydrogenations and H_2/D^+ Exchange Experiments in CH_3OD: (a) A solution of of **Ir**$^+$-(*R*,*R*)-**2** (9.5 mg, 0.013 mmol), (−)-sparteine (14 μL, 0.065 mmol) and benzophenone (150 mg, 1.25 mmol) in CH_3OD (3 mL) was kept, in an autoclave, under 10 bar of H_2 at 50 °C for 10 h. The residue remaining after removal of the solvent was analyzed by NMR spectroscopy. ^1H NMR (CD_2Cl_2, ppm): δ = 5.76 (s with half intensity relative to 10 phenyl H, Ph_2CHOD), 7.2−7.5 (m, 10 H, C_6H_5). ^2H NMR (CH_2Cl_2, ppm): δ = 2.42 (br., OD), 5.78 (s, Ph_2CDOD). $^{13}C\{^1H\}$ NMR (CD_2Cl_2, ppm): δ = 76.52 (1:1:1 t, $^1J_{C,D}$ = 22.16 Hz, Ph_2CDOD), 76.93 (s, Ph_2CHOD). (b) The solution of catalyst complex, auxiliary base, and ketone in [D_1]methanol was prepared as before, transferred into a high-pressure NMR tube, exposed to 10 bar of H_2 at ambient conditions overnight, and then examined by ^1H NMR (ppm): δ = 4.37 (1:1:1 t, $^1J_{H,D}$ = 42.63 Hz, *H*D), 4.42 (s, H_2), 4.46 (s, OH), 5.92 (s, ≈ 0.6 H relative to 10 phenyl H, CH), 7.2−7.5 (m, 10 H, C_6H_5). (c) Experiment (b) was repeated in the absence of the base and the ketone. ^1H NMR: δ = 4.39 (1:1:1 t, $^1J_{H,D}$ = 42.63 Hz, *H*D), 4.42 (s, H_2), 4.46 (s with increasing intensity, OH).

General Procedure for H_2/D_2 Exchange Experiments: A high pressure NMR tube was charged with a solution of ≈0.01 mmol of any [(COD)Ir(P∩NHR]BF_4 complex in CD_3CN or CH_3CN. The solution was exposed to 10 bar of a 1:1 H_2/D_2 mixture and immediately analyzed by NMR spectroscopy. ^1H NMR (CD_3CN, ppm): δ = 4.37 (1:1:1 t, $^1J_{H,D}$ = 42.63 Hz, *H*D), 4.41 (s, H_2). ^2H NMR (CH_3CN, ppm): δ = 4.33 (s, D_2), 4.37 (d, $^1J_{H,D}$ = 42.5 Hz, H*D*).

Acknowledgments

We thankfully remember many fruitful and inspiring discussions with Professor Dieter Sellmann, initiator and first speaker of the Sonderforschungsbereich 583: Redox-Active Metal Complexes − Control of Reactivity via Molecular Architecture. Support of this work by the Deutsche Forschungsgemeinschaft (Bonn, SFB 583) and the Fonds der Chemischen Industrie (Frankfurt/Main) is gratefully acknowledged. We are also indebted to Mrs. S. Kammerer for her skilful assistance.

 © 2004 Wiley-VCH Verlag GmbH & Co. KGaA, Weinheim

[1] For leading overviews on enantioselective reduction of organic carbonyl compounds, see: [1a] R. Noyori, T. Ohkuma, *Angew. Chem.* **2001**, *113*, 40−75; *Angew. Chem. Int. Ed.* **2001**, *40*, 40−74. [1b] R. Noyori, *Angew. Chem.* **2002**, *114*, 2108−2123; *Angew. Chem. Int. Ed.* **2002**, *41*, 2008−2022 (2001 Nobel Lecture in Chemistry).

[2] [2a] M. Yamakawa, H. Ito, R. Noyori, *J. Am. Chem. Soc.* **2000**, *122*, 1466−1478. [2b] R. Noyori, M. Yamakawa, S. Hashiguchi, *J. Org. Chem.* **2001**, *66*, 7931−7944.

[3] [3a] K. Abdur-Rashid, A. J. Lough, R. H. Morris, *Organometallics* **2000**, *19*, 2655−2657. [3b] K. Abdur-Rashid, A. J. Lough, *Organometallics* **2001**, *20*, 1047−1049. [3c] K. Abdur-Rashid, M. Faatz, A. J. Lough, R. H. Morris, *J. Am. Chem. Soc.* **2001**, *123*, 7473−7474. [3d] K. Abdur-Rashid, S. E. Clapham, A. Hadzovic, J. N. Harvey, A. J. Lough, R. H. Morris, *J. Am. Chem. Soc.* **2002**, *124*, 15104−15118.

[4] R. Hartmann, P. Chen, *Angew. Chem.* **2001**, *113*, 3693−3697; *Angew. Chem. Int. Ed.* **2001**, *40*, 3581−3585.

[5] Q. Jiang, Y. Jiang, A. Xiao, P. Cao, X. Zhang, *Angew. Chem.* **1998**, *110*, 1203−1207; *Angew. Chem. Int. Ed.* **1998**, *37*, 1100−1103.

[6] R. R. Schrock, J. A. Osborn, *J. Chem. Soc., Sect. D: Chem. Commun.* **1970**, 567−658.

[7] [7a] L. Dahlenburg, R. Götz, *J. Organomet. Chem.* **2001**, *619*, 88−98. [7b] Preliminary communication: L. Dahlenburg, R. Götz, *Inorg. Chem. Commun.* **2003**, *6*, 443−446 (Paper presented at the XXXVth Int. Conf. Coord. Chem.; Heidelberg, July 21−26, 2002).

[8] [8a] M. L. Tommasino, C. Thomazeau, F. Touchard, M. Lemaire, *Tetrahedron Asymm.* **1999**, *10*, 1813−1819. [8b] C. Maillet, T. Praveen, P. Janvier, S. Minguet, M. Evain, C. Saluzzo, M. L. Tommasino, B. Bujoli, *J. Org. Chem.* **2002**, *67*, 8191−8196.

[9] [9a] S. Gabriel, *Ber. Dtsch. Chem. Ges.* **1888**, *21*, 1049. [9b] A. Galindo, L. Orea F., D. Gnecco, R. G. Enríquez, R. Toscano, W. F. Reynolds, *Tetrahedron Asymm.* **1997**, *8*, 2877−2879.

[10] [10a] H. Wenker, *J. Am. Chem. Soc.* **1935**, *57*, 2328. [10b] S. J. Brois, *J. Org. Chem.* **1962**, *27*, 3532−3534.

[11] [11a] L. Horner, H. Oediger, H. Hoffmann, *Justus Liebigs Ann. Chem.* **1959**, *626*, 26−34. [11b] I. Okada, K. Ichimura, R. Sudo, *Bull. Chem. Soc. Jpn.* **1970**, *43*, 1185−1189. [11c] W. Danzer, R. Höfer, H. Menzel, B. Olgemöller, W. Beck, *Z. Naturforsch. Teil B: Anorg. Chem. Org. Chem.* **1984**, *39*, 167−179.

[12] [12a] O. Mitsunobu, *Synthesis* **1981**, 1−28. [12b] J. R. Pfister, *Synthesis* **1984**, 969−970. [12c] M. A. Poelert, R. P. Hof, N. C. M. W. Peper, R. M. Kellog, *Heterocycles* **1994**, *37*, 461−475.

[13] [13a] W. Beck, U. Nagel, *Z. Anorg. Allg. Chem.* **1979**, *258*, 22−28. [13b] U. Nagel, H. Menzel, W. Beck, A. Guyot, M. Bartholin, *Z. Naturforsch. Teil B: Anorg. Chem. Org. Chem.* **1981**, *36*, 578−584.

[14] T. N. Van, N. De Kimpe, *Tetrahedron* **2000**, *56*, 7299−7304.

[15] J. E. Saavedra, *J. Org. Chem.* **1985**, *50*, 2271−2273.

[16] R. K. Dieter, N. Deo, B. Lagu, J. W. Dieter, *J. Org. Chem.* **1992**, *57*, 1663−1671.

[17] [17a] K. Issleib, A. Tzschach, *Chem. Ber.* **1959**, *92*, 1118−1126. [17b] K. Issleib, D. Haferburg, *Z. Naturforsch. Teil B: Anorg. Chem. Org. Chem.* **1965**, *20*, 916−918.

[18] [18a] A. B. van Oort, P. H. M. Budzelaar, J. H. G. Frijns, A. G. Orpen, *J. Organomet. Chem.* **1990**, *396*, 33−47. [18b] M. K. Cooper, J. M. Downes, P. A. Duckworth, E. R. T. Tiekink, *Aust. J. Chem.* **1992**, *45*, 595−609.

[19] T. L. Cairns, *J. Am. Chem. Soc.* **1941**, *63*, 871−872.

[20] $pK_A(BH^+)$ values: 3.2 (Tröger's base),[20a] 5.4 (pyridine),[20b] 10.6 (NEt_3),[20c] 11.0 (iP_2NH),[20c] and 11.3 (sparteine);[20d] with the exception of Tröger's base (50% aqueous alcohol) all in water. [20a] B. M. Wepster, *Recl. Trav. Chim. Pays-Bas Belg.* **1953**, *72*, 661−672. [20b] Th. J. Lane, M. G. Kappil, A. J. Kandathil, *J. Chem. Eng. Data* **1963**, *8*, 569−571. [20c] H. K. Hall Jr., *J. Am. Chem. Soc.* **1957**, *79*, 5441−5444. [20d] W. D. Crow, *Aust. J. Chem.* **1959**, *12*, 474−482.

[21] For ligand-to-metal p→p_z π interactions in square-planar d^8 complexes, see, for example: L. Dahlenburg, N. Höck, H. Berke, *Chem. Ber.* **1988**, *121*, 2083−2093.

[22] [22a] L. Dahlenburg, K. Herbst, *Chem. Ber./Recueil* **1997**, 1693−1698. [22b] K. Herbst, Dissertation, Universität Erlangen-Nürnberg, **1998**.

[23] For pertinent reviews on heterolytic H_2 activation, see: [23a] P. J. Bothers, *Progr. Inorg. Chem.* **1981**, *28*, 1−61. [23b] G. J. Kubas, *Acc. Chem. Res.* **1988**, *21*, 120−128. [23c] P. G. Jessop, R. H. Morris, *Coord. Chem. Rev.* **1992**, *121*, 121−284. [23d] D. M. Heinekey, W. J. Oldham Jr., *Chem. Rev.* **1993**, *93*, 913−926. [23e] R. H. Crabtree, *Angew. Chem.* **1993**, *105*, 828−845; *Angew. Chem. Int. Ed. Engl.* **1993**, *32*, 789−805. [23f] M. A. Esteruelas, L. A. Oro, *Chem. Rev.* **1998**, *98*, 577−588. [23g] G. Jia, C.-P. Lau, *Coord. Chem. Rev.* **1999**, *190−192*, 83−108. [23h] D. Sellmann, A. Fürsattel, J. Sutter, *Coord. Chem. Rev.* **2000**, *200−202*, 545−561. [23i] G. J. Kubas, *Metal Dihydrogen and σ-Bond Complexes*, Kluver Academic/Plenum Publishers, New York, **2001**, chapters 9 and 10.

[24] [24a] M. D. Fryzuk, P. A. MacNeil, *Organometallics* **1983**, *2*, 682−684. [24b] M. D. Fryzuk, C. D. Montgomery, S. J. Rettig, *Organometallics* **1991**, *10*, 467−472. [24c] M. D. Fryzuk, M. J. Petrella, R. C. Coffin, B. O. Patrick, *Compt. Rend. Chimie* **2002**, *5*, 451−460.

[25] [25a] R. H. Crabtree, M. Lavin, L. Bonneviot, *J. Am. Chem. Soc.* **1986**, *108*, 4032−4037. [25b] A. C. Albeniz, D. M. Heinekey, R. H. Crabtree, *Inorg. Chem.* **1991**, *30*, 3632−3635. [25c] D.-H. Lee, B. P. Patel, E. Clot, O. Eisenstein, R. H. Crabtree, *Chem. Commun.* **1999**, 297−298. [25d] K. Gruet, E. Clot, O. Eisenstein, D. H. Lee, B. Patel, A. Macchioni, R. H. Crabtree, *New. J. Chem.* **2003**, *27*, 80−87.

[26] R. Koelliker, D. Milstein, *J. Am. Chem. Soc.* **1991**, *113*, 8524−8525.

[27] [27a] D. Sellmann, J. Käppler, M. Moll, *J. Am. Chem. Soc.* **1993**, *115*, 1830−1836. [27b] D. Sellmann, G. H. Rackelmann, F. W. Heinemann, *Chem. Eur. J.* **1997**, *3*, 2071−2080. [27c] D. Sellmann, T. Gottschalk-Gauding, F. W. Heinemann, *Inorg. Chem.* **1998**, *37*, 3982−3988. [27d] D. Sellmann, A. Fürsattel, *Angew. Chem.* **1999**, *111*, 2142−2145; *Angew. Chem. Int. Ed.* **1999**, *38*, 2023−2026. [27e] D. Sellmann, F. Geipel, M. Moll, *Angew. Chem.* **2000**, *112*, 570−572; *Angew. Chem. Int. Ed.* **2000**, *39*, 561−563. [27f] D. Sellmann, J. Sutter, *Z. Anorg. Allg. Chem.* **2003**, *629*, 893−910.

[28] [28a] P. G. Jessop, R. H. Morris, *Inorg. Chem.* **1993**, *32*, 2236−2237. [28b] M. Schlaf, A. J. Lough, R. H. Morris, *Organometallics* **1993**, *12*, 3808−3809. [28c] M. Schlaf, A. J. Lough, R. H. Morris, *Organometallics* **1996**, *15*, 4423−4436.

[29] J. Huhmann-Vincent, B. L. Scott, G. F. Kubas, *Inorg. Chim. Acta* **1999**, *294*, 240−254.

[30] A. Llamazares, H. W. Schmalle, H. Berke, *Organometallics* **2001**, *20*, 5277−5288.

[31] [31a] S. Park, D. Hedden, D. M. Roundhill, *Organometallics* **1985**, *5*, 2151−2152. [31b] S. Park, M. P. Johnson, D. M. Roundhill, *Organometallics* **1989**, *8*, 1700−1707.

[32] R. Kuhlman, *Coord. Chem. Rev.* **1997**, *167*, 205−232.

[33] In the reviewing process, an alternate mechanism based on the intermediacy of [Ir(P∩NR)] and [IrH(P∩NHR)] as spectroscopically undetected but kinetically relevant transients was proposed for isotopic scrambling and >C=O reduction: [Ir(P∩NR)] + H_2 = [IrH(P∩NHR)]; [IrH(P∩NHR] + H_2 = [IrH_3(P∩NHR)]; [IrH_3(P∩NHR)] + MeOD = [IrH_3(P∩NDR)] + MeOH; [IrH_3(P∩NDR)] = [IrH(P∩NDR)] + H_2; [IrH(P∩NDR)] = [Ir(P∩NR)] + HD etc.; [IrH_3(P∩NHR)] + R_2CO = [IrH_2(P∩NR)] + R_2CHOH. This sequence does not, however, fit the experimental evidence in that it involves IrH_3 intermediates which should be quite stable and inert but were never met in the chemistry described in this communication. Furthermore, in order to make the suggested >C=O reduction step catalytic, the resulting amido dihydrides [IrH_2(P∩NR)] must regenerate the postulated [IrH_3(P∩NHR)] amino trihydrides either by hydrogen transfer

 © 2004 Wiley-VCH Verlag GmbH & Co. KGaA, Weinheim

from the solvent or by H_2 addition across the Ir−N bond. Again, no such chemistry was observed for amido dihydro complex **Ir-9a** reacting with MeOH under H_2 to reversibly produce $[IrH_2(P\cap NHR)]^+$ (**Ir**$^+$**-9**; Scheme 9) rather than H_2CO and/or $[IrH_3(P\cap NHR)]$.

[34] V. D. Bianco, S. Doronzo, *Inorg. Synth.* **1976**, *16*, 161−163.
[35] J. P. Collman, C. T. Sears Jr., M. Kubota, *Inorg. Synth.* **1990**, *28*, 92−94.
[36] J. L. Herde, J. C. Lambert, C. V. Senoff, *Inorg. Synth.* **1974**, *15*, 18−20.
[37] [37a] J. A. Osborn, R. R. Schrock, *J. Am. Chem. Soc.* **1971**, *93*, 3089−3091. [37b] T. G. Schenck, J. M. Downes, C. R. C. Milne, P. B. Mackenzie, T. G. Boucher, B. Bosnich, *Inorg. Chem.* **1985**, *24*, 2334−2337. [37c] M. J. Burk, J. E. Feaster, W. A. Nugent, R. L. Harlow, *J. Am. Chem. Soc.* **1993**, *115*, 10125−10138.
[38] A. C. T. North, D. C. Phillips, F. S. Mathews, *Acta Crystallogr., Sect. A* **1968**, *24*, 351−359.
[39] N. Walker, D. Stuart, *Acta Crystallogr., Sect. A* **1983**, *39*, 159−166.
[40] [40a] L. J. Farrugia, *J. Appl. Crystallogr.* **1999**, *32*, 837−838. [40b] L. J. Farrugia, *J. Appl. Crystallogr.* **1997**, *30*, 565.
[41] A. Altomare, M. C. Burla, M. Camalli, G. L. Cascarano, C. Giacovazzo, A. Guagliardi, A. G. G. Moliterni, G. Polidori, R. Spagna, *J. Appl. Crystallogr.* **1999**, *32*, 115−119.
[42] G. M. Sheldrick, *SHELXL-97* (Release 97−2), University of Göttingen, **1998**.
[43] H. D. Flack, *Acta Crystallogr., Sect. A* **1983**, *39*, 876−881.
[44] [44a] T. Hayashi, Y. Matsumoto, Y. Ito, *J. Am. Chem. Soc.* **1989**, *111*, 3426−3428. [44b] T. Sato, Y. Goto, T. Fujisawa, *Tetrahedron Lett.* **1982**, *23*, 4111−4112. [44c] S. Masamune, B. M. Kim, J. S. Petersen, T. Sato, S. J. Veenstra, T. Imai, *J. Am. Chem. Soc.* **1985**, *107*, 4549−4551. [44d] S. Top, G. Jaouen, *J. Organomet. Chem.* **1980**, *197*, 199−215. [44e] T. H. Chan, P. Pellon, *J. Am. Chem. Soc.* **1989**, *111*, 8737−8738.

Received July 24, 2003
Early View Article
Published Online January 19, 2004

 © 2004 Wiley-VCH Verlag GmbH & Co. KGaA, Weinheim

Some Properties and Molecular Orbitals of Planar Heterodinuclear Phthalocyanines

Nagao Kobayashi*[a] and Hiroshi Ogata[a]

Keywords: Circular dichroism / Cyclic voltammetry / Phthalocyanines / UV/Vis spectroscopy

The electronic absorption and magnetic circular dichroism (MCD) spectra, and differential pulse (DP) voltammograms of planar heterodinuclear phthalocyanine (Pc) dimers consisting of Pc and pyrazinoporphyrazine (PyZ), [Mt_2PcPyZ (Mt = H_2 and Zn)] and of Pc and naphthalocyanine (Nc), [Mt_2PcNc (Mt = H_2 and Co)] have been recorded. These dimers commonly show broad absorption bands between ca. 500 and 1000 nm, while the DP voltammograms suggest that the dimers are unstable towards oxidation, and that the two relatively independent chromophore units interact with one another. Molecular orbital (MO) calculations using the ZINDO/S Hamiltonian were performed in order to enhance the interpretation of the experimental results. Dimer orbitals were expressed by coupling the orbitals of the same symmetry, of the constituting mononucleates. It was suggested that for the HOMO of the dimers, the contribution of the more electron-rich moiety is large, while conversely for the LUMO, the contribution of the more electron-deficient moiety is large. The calculations suggested that there are three prominent transitions in the Q band region of the heterodimers. The intensity and position of these bands were suggested to be affected by the constituting mononucleates.
(© Wiley-VCH Verlag GmbH & Co. KGaA, 69451 Weinheim, Germany, 2004)

Introduction

For three quarters of a century, mononuclear phthalocyanines (Pcs) have been the subject of an intensive study in both the academic and applied fields.[1] Cofacial sandwich type Pc dimers have been known since1936,[2] while the first planar dimer was reported in 1987.[3] Since then, many papers have been published on both cofacial Pc dimers[4] and planar homodimers of Pc and Pc derivatives.[5] However, reports on heterodinuclear planar dimers are still rare.[6] In particular, the physicochemical and electrochemical properties have not been well elucidated.[7] We report here on some spectroscopic and electrochemical properties, together with the results of molecular orbital (MO) calculations on planar heterodinuclear phthalocyanine-pyrazinoporphyrazine (Pc-PyZ) and phthalocyanine-naphthalocyanine (Pc-Nc) complexes, which were not described in our preliminary communications (Figure 1).[6a,6b,6d]

Results and Discussion

(i) Electronic Absorption and MCD Spectra

In the cases of H_4PcPyZ and H_4PcNc, there is an ambiguity as to the position of the pyrrole protons, thus it is not appropriate to compare their spectra with the results of the MO calculations. Figure 2 therefore shows the absorption and MCD spectra of PcPyZ and PcNc obtained by the addition of $(Bu)_4NOH$, and of Co_2PcNc. All compounds show broad Q bands which stretch from ca. 500 to 1000 nm, and which are not a simple superimposition from those of the constituting mononuclear *tert*-butylated Pc and PyZ or Nc. The Q bands of PcPyZ and PcNc are similar in shape, having at least two peaks, of which those at the shorter wavelength are broader. The Q bands of PcNc and Co_2PcNc appeared at almost the same wavelength, which is longer than that of PcPyZ by ca. 10 nm. The absorption coefficients of the two Q peaks of PcNc are larger than those of PcPyZ, consistent with the results of MO calculations described later.

The Q band MCD spectra of the three complexes have common characteristics. Negative Faraday *B*-terms appeared corresponding to the absorption peaks at a longer wavelength,[5m] and dispersion type, Faraday *A*-term like curves were observed, associated with the Q band peak at a shorter wavelength. In these molecules, there is no degeneracy in the excited states so that the Faraday *B*-terms are expected, theoretically, to be associated with each absorption peak. Considering that the tendency towards cofacial aggregation is much more significant for larger Ncs than Pcs,[11] that the cofacial aggregation produces a broad Q absorption band as seen at ca. 600−750 nm in Figure 2, and that the Q band MCD of cofacial Pc analogues does not reflect the molecular symmetry of the constituting molecules,[12] the dispersion type Faraday *A*-term like MCD signal corresponding to the Q absorption band at shorter wavelength may imply that the species in Figure 2 contains

[a] Department of Chemistry, Graduate School of Science, Tohoku University,
Sendai 980-8578, Japan
Fax: (internat.) + 81-22-217-7719
E-mail: nagaok@mail.tains.tohoku.ac.jp

 © 2004 Wiley-VCH Verlag GmbH & Co. KGaA, Weinheim DOI: 10.1002/ejic.200300536

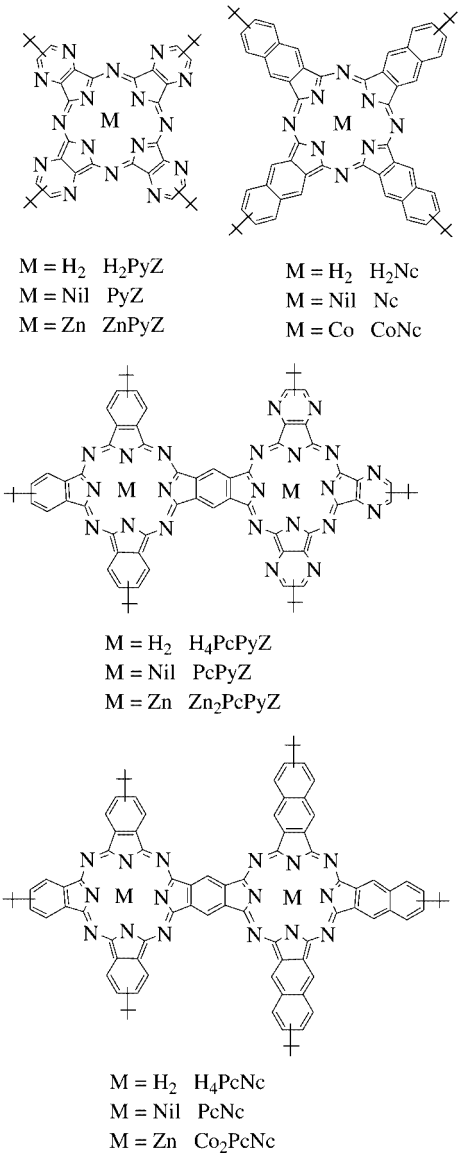

Figure 1. Structures and abbreviations of the compounds in this study

a certain amount of cofacially aggregated species. However, from our previous data[5m] in which the two Q_{00} bands of the homodinuclear planar Pc lie ca.1600−1800 cm^{-1} apart, together with the results of MO calculations on the compounds in the present study which will be discussed below, it is not unreasonable to expect the second Q_{00} band to appear at ca. 640−690 nm, since the other Q_{00} band lies at ca. 800−850 nm. Positive envelopes of the Faraday *B*-term superimposed with the pseudo Faraday *A*-terms at ca. 630−680 nm support this speculation. Another possibility for the interpretation of the dispersion type MCD curves at around 650−720 nm is that these are produced by two closely lying transitions, since MO calculations indicate two transitions in this region, differing from the case of the homodinuclear planar species [see section (iii)].

The apparent absorption coefficient of the B band of the Pc analogues is generally much smaller than that of the Q

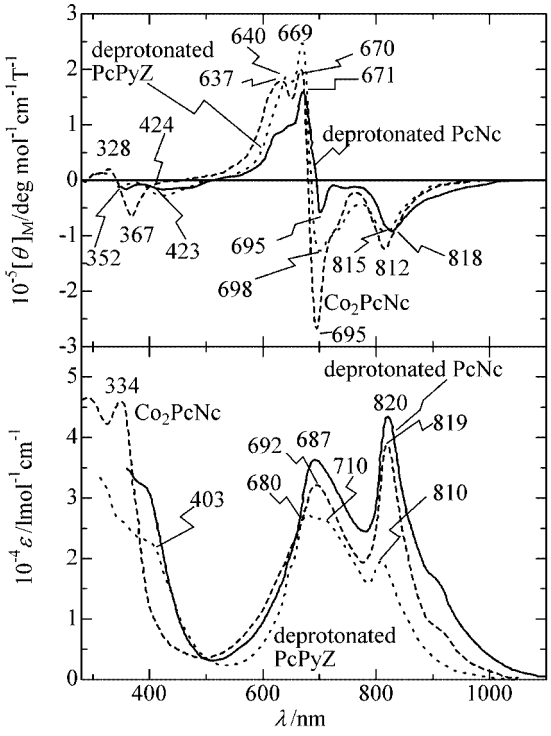

Figure 2. Electronic absorption (bottom) and MCD spectra (top) of (pyrrole proton-deprotonated) PcNc (solid lines), PcPyZ (dotted lines), and Co_2PcNc (broken lines)

band. Although we cannot directly compare the B band spectra of Zn_2PcPyZ and Co_2PcNc, since the central metal is different, the B bands of H_4PcPyZ and H_4PcNc appeared at 337 and 341 nm, and their relative intensity to the Q band is larger than in the monomeric species. When tetraammonium hydroxide was added to these metal-free species to form pyrrole-proton-deprotonated PcPyZ and PcNc, the intensity of the B band decreased and a shoulder appeared at ca. 400 nm for both compounds.

The MCD spectra show that the B band retains the characteristics of the Pc derivatives. Both H_4PcPyZ and H_4PcNc showed a dispersion type, pseudo Faraday *A*-term with a trough and peak at 372 and 320−321 nm, while their intensity was much smaller than that of the Q band, reflecting small angular momentum properties. In PcPyZ and PcNc, two weak pseudo Faraday *A*-terms appeared at around 403 and 366 nm, suggesting that many transitions are included in this region.

(ii) Voltammetry

Figure 3 shows differential pulse voltammograms of Zn_2PcPyZ, Co_2PcNc, and their constituting monomers in *o*-DCB. Unfortunately, we could not unify the type of central metal, since the compound which may be expressed as Co_2PcPyZ fragmented into the PyZ moiety in the cobalt insertion process, while the compound which is described as Zn_2PcNc fragmented during purification by column chromatography. The tetra-*tert*-butylated ZnPc showed two oxidation and reduction couples at 1.01, 0.21, −1.41, and −1.81 V, while ZnPyZ displayed the first oxidation poten-

 © 2004 Wiley-VCH Verlag GmbH & Co. KGaA, Weinheim

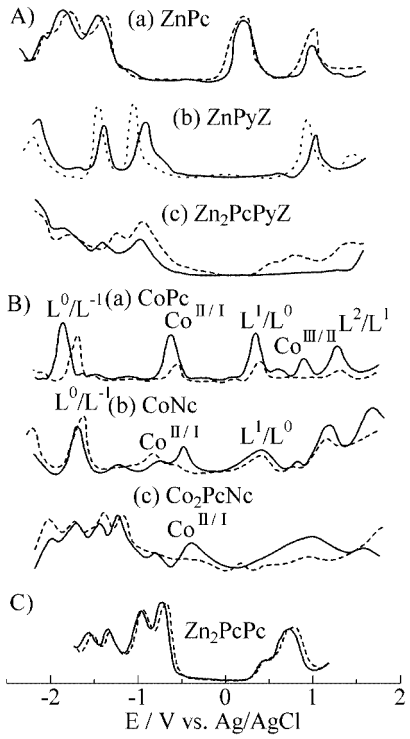

Figure 3. Differential pulse voltammograms of A) (a) ZnPc, (b) ZnPyZ, and (c) Zn_2PcPyZ, B) (a) CoPc, (b) CoNc, and (c) Co_2PcNc, and C) Zn_2PcPc (redrawn from ref.[5f]) in *o*-DCB containing 0.1 M TBAP. The sweep rate was 0.5 mV/s. The solid and broken lines are anodic and cathodic scans, respectively. L^0/L^{-1} and L^1/L^0 are the first reduction and oxidation of the ligand, respectively

tial at 1.03 V and three reduction couples at −0.97, −1.38, and −2.14 V due to the four electron-withdrawing pyrazine rings on the periphery. Zn_2PcPyZ, on the other hand, showed couples at ca. 1.36, 0.76, 0.50, −0.96, −1.34, −1.82, and ca. −2.2 V. Although the voltammograms are not clear, because of the instability of the compound in the positive potential region of the anodic scan, some of the other behavior (amount of current and splitting pattern) is similar to that of homodinuclear planar Pc dimers (voltammograms in C).[5f] That is, it appears as if the couples at 0.76 and 0.50 V correspond to the first oxidation, while those at −0.96 and −1.34, and −1.82 and −2.2 V correspond, respectively, to the first and second reductions of mononuclear species, suggesting that the voltammograms of Zn_2PcPyZ are caused by the interacting dipoles in the Pc and PyZ moieties.

The voltammograms of cobalt Pc derivatives differ from those of, for example, zinc, nickel, and copper derivatives in that they show couples due to the central metal, in addition to those of the ligand. On the basis of previous studies on cobalt Pcs,[13] the redox couples of *tert*-butylated CoPc and CoNc in this figure can be assigned as shown in the voltammograms. The voltammogram of Co_2PcNc is not as clear as that of the mononuclear species because of its low stability and small diffusion coefficient. However, four ligand redox couples characteristic of these types of compounds are explicitly seen at −1.22, −1.43, −1.73, and ca. −2.0 V, in addition to the $Co^{II/I}$ couple(s) which appeared at −0.36 (and −0.80) V, although the positive potential region is more irreversible and more ill-defined. Thus, the four ligand reduction redox couples strongly suggest that the dipoles in the CoPc and CoNc moieties are interacting without significant conjugation through the common benzene ring.

(iii) Molecular Orbital Calculations

In order to enhance our interpretation of the above spectroscopic and electrochemical properties, molecular orbitals (MOs) were calculated using the ZINDO/S Hamiltonian in the HyperChem. R5.1 program,[8] together with those of the constituting mononuclear molecules. The calculated electronic absorption spectra are shown in Figure 4 (all spectra were calculated for the zinc complexes, since Co^{II} in Pc, Nc, and PyZ is paramagnetic), with transition energies, oscillator strengths (*f*), and configurations summarized in Table 1. As detailed in previous publications,[14] in a one-electron description, the Q band of Pc analogues corresponds to a transition from the HOMO to the doubly degenerate LUMO. The B band is associated mainly with a transition from the HOMO-1 to the LUMO at the PPP level of calculations, while this is not clear at the ZINDO/S level of calculation since the B band is actually composed of two bands termed B1 and B2, and there is mixing of many configurations.[14f] For ZnPyZ and ZnPc, the present ZINDO/S calculations indicate the HOMO−LUMO transition and two prominent transitions in the B band region to be at 688 and 307/300 nm, and 699 and 292/278 nm, respectively, which is in approximate agreement with the experimental result (341 and 628 nm for ZnPyZ, and 349 and 671 nm for ZnPc in THF).[6a] This demonstrates the reliability of the calculations. As shown, in the case of mononuclear molecules, the Q band shifts to a longer wavelength in the order ZnPyZ, ZnPc, and ZnNc, with a con-

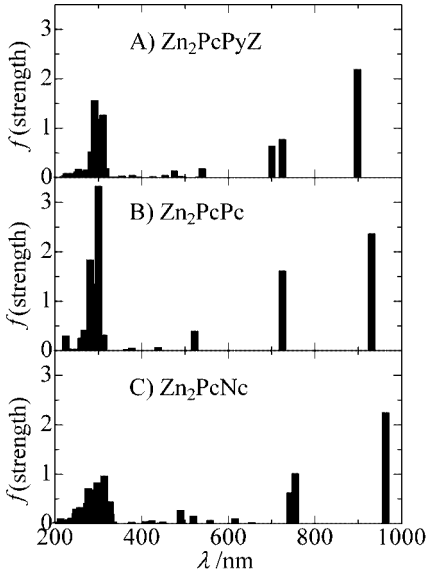

Figure 4. Calculated absorption spectra for A) Zn_2PcPyZ, B) Zn_2PcPc, and C) Zn_2PcNc

 © 2004 Wiley-VCH Verlag GmbH & Co. KGaA, Weinheim

Table 1. Calculated transition energies, oscillator strengths (*f*), and configurations

Energy [nm]	*f*	Configurations[a]
ZnPyZ		
688	0.80	93→94 (88%)
688	0.80	93→95 (88%)
307	1.65	91→94 (51%) 92→94 (34%)
307	1.65	91→95 (51%) 92→95 (34%)
300	1.04	92→94 (54%) 91→94 (36%)
300	1.04	92→95 (54%) 91→95 (36%)
278	0.15	93→102 (59%) 88→94 (25%)
278	0.15	93→103 (59%) 88→95 (25%)
254	0.11	88→94 (62%) 93→102 (15%)
254	0.11	88→95 (62%) 93→103 (15%)
Zn_2PcPyZ		
898	2.19	171→172 (88%)
725	0.78	171→173 (51%) 171→174 (24%) 170→173 (10%)
701	0.64	171→174 (43%) 171→173 (29%) 170→173 (18%)
539	0.19	170→173 (47%) 170→174 (21%) 171→174 (19%)
475	0.14	171→178 (42%) 170→178 (30%) 170→174 (17%)
318	0.19	166→172 (36%) 168→172 (32%) 169→172 (18%)
311	1.27	169→173 (33%) 168→174 (15%) 169→174 (12%) 167→173 (11%)
304	1.20	167→174 (15%) 169→173 (14%)
302	0.42	165→173 (29%) 165→174 (18%) 169→172 (14%) 169→175 (11%)
299	0.68	170→181 (25%) 168→173 (18%) 169→173 (13%)
298	0.95	163→172 (24%) 167→172 (16%)
298	0.32	164→173 (24%) 164→174 (23%) 163→172 (14%)
294	0.30	166→174 (17%) 164→172 (16%)
294	0.13	166→173 (17%)
291	1.57	167→172 (15%) 166→172 (12%) 165→173 (11%) 167→175 (11%)
287	0.22	171→186 (21%) 163→172 (12%)
283	0.53	171→189 (32%) 170→189 (14%)
282	0.15	171→186 (22%) 166→175 (11%) 170→187 (10%)
278	0.15	171→191 (37%) 171→189 (13%)
274	0.17	160→172 (25%)
269	0.14	171→190 (16%) 171→188 (12%) 161→173 (11%)
254	0.17	162→173 (25%) 159→172 (14%) 162→174 (12%) 158→172 (11%)
251	0.12	159→173 (20%) 162→172 (17%) 159→174 (12%)
ZnPc		
699	1.06	93→94 (87%)
699	1.06	93→95 (87%)
292	1.18	93→102 (36%) 92→94 (28%) 91→94 (13%) 91→95 (11%)
292	1.18	93→103 (36%) 92→95 (28%) 91→95 (13%) 91→94 (11%)
287	0.48	91→94 (53%) 93→102 (14%) 85→95 (11%)
287	0.48	91→95 (53%) 93→103 (14%) 85→94 (11%)
278	1.06	92→94 (50%) 93→102 (34%)
278	1.06	92→95 (50%) 93→103 (34%)
Zn_2PcNc		
964	2.25	198→199 (77%)
755	1.02	198→200 (59%) 197→200 (34%)
744	0.63	198→201 (81%)
616	0.11	197→199 (46%) 198→202 (33%) 198→199 (15%)
519	0.16	197→201 (64%) 198→203 (12%)
490	0.27	198→203 (34%) 197→203 (24%) 197→201 (21%)
328	0.20	195→199 (34%) 197→205 (24%) 198→205 (14%) 192→199 (11%)
326	0.44	196→199 (39%) 195→200 (21%) 194→199 (11%)
317	0.28	193→199 (28%) 196→199 (20%) 194→199 (14%)
315	0.13	198→210 (55%) 197→210 (33%)
313	0.97	196→200 (42%) 192→199 (30%)
298	0.19	195→200 (18%) 185→199 (18%) 196→199 (15%)
297	0.83	192→199 (19%) 198→219 (13%) 194→200 (12%)
295	0.44	194→202 (18%) 198→218 (14%) 193→199 (11%) 194→199 (11%) 193→202 (11%) 198→220 (10%)
295	0.15	187→199 (16%) 189→200 (14%) 195→199 (10%)
293	0.47	189→199 (42%) 187→200 (20%)
293	0.16	198→219 (32%) 193→201 (14%) 191→201 (13%)
292	0.62	190→201 (50%) 188→201 (17%)
288	0.50	195→200 (17%) 185→199 (16%) 192→200 (16%)
281	0.69	189→200 (26%) 187→199 (13%) 194→201 (13%) 195→199 (11%)

 © 2004 Wiley-VCH Verlag GmbH & Co. KGaA, Weinheim

Table 1. *(Continued)*

Energy [nm]	*f*	Configurations[a]
279	0.21	197→209 (32%) 1972→07 (11%)
277	0.72	198→222 (18%) 197→209 (13%) 191→199 (12%)
274	0.42	192→200 (44%) 185→199 (20%)
270	0.32	187→200 (43%) 189→199 (12%)
269	0.12	193→201 (24%) 198→221 (20%) 194→201 (10%)
261	0.10	187→199 (23%) 197→212 (20%)
258	0.33	185→200 (31%) 186→201 (18%)
249	0.13	183→202 (18%) 183→199 (14%) 186→199 (12%)
249	0.18	192→200 (14%) 192→203 (14%) 195→203 (11%) 186→199 (11%)
ZnNc		
771	1.34	129→130 (95%)
771	1.34	129→131 (95%)
324	0.54	129→138 (54%)
324	0.54	129→139 (54%)
316	0.26	128→130 (77%) 129→139 (10%)
316	0.26	128→131 (77%) 129→138 (10%)
285	2.09	124→131 (36%) 123→130 (18%) 124→130 (12%) 125→130 (11%)
285	2.09	124→130 (36%) 123→131 (18%) 124→131 (12%) 125→131 (11%)
246	0.12	120→130 (60%)
246	0.12	120→131 (60%)
242	0.77	128→134 (24%) 125→130 (20%) 127→133 (14%) 126→132 (11%)
242	0.77	128→135 (24%) 125→131 (20%) 126→133 (14%) 127→132 (11%)
Zn_2PcPc		
931	2.37	171→172 (89%)
726	1.62	171→173 (83%) 170→174 (10%)
522	0.40	170→174 (82%) 171→173 (12%)
312	0.32	167→172 (47%) 169→172 (43%)
309	0.14	170→178 (56%) 171→176 (15%) 170→184 (13%)
300	3.33	169→173 (60%) 168→174 (11%)
296	0.65	164→172 (46%) 165→175 (%)
294	0.12	166→173 (40%) 163→174 (40%)
290	1.35	171→188 (24%) 170→186 (16%) 164→172 (10%)
287	0.45	171→185 (44%) 170→187 (16%)
287	0.68	170→179 (40%) 171→180 (10%) 170→190 (10%)
280	1.84	169→172 (26%) 171→188 (25%) 167→172 (18%) 168→175 (11%)
267	0.42	160→173 (15%) 167→173 (14%) 161→174 (14%) 164→173 (12%)
260	0.26	155→172 (22%) 158→173 (20%) 162→173 (16%)

[a] Excited states with energy less than ca. 3.9 eV and *f* greater than 0.10 are shown.

comitant increase in the absorption coefficient, as has been substantiated by experiments[15] and reproduced by MO calculations[16] using the PPP method.[17] The purity of the Q band also increases in this order, since the configurations of the HOMO−LUMO transition increases.

Turning to the heterodinuclear Pc analogues in this study, the pair of orbitals comprising the lowest unoccupied level in a mononuclear unit split into two levels (Figure 5), so that two split Q bands are calculated at a longer wavelength: 898 and 725 for Zn_2PcPyZ and 964 and 755 nm for Zn_2PcNc (under the same conditions, the Q bands of the homodinuclear Zn_2PcPc were predicted at 931 and 726 nm). The calculated values lie in the correct direction, but fall towards somewhat longer wavelengths compared with the experimental values. In addition, the values indicate that the Q band position depends on that of the constituting units of the dimer. That is, the two Q bands estimated for Zn_2PcPyZ (898 and 725 nm) are at shorter wavelengths than those of Zn_2PcPc (931 and 726 nm), while those of Zn_2PcNc (964 and 755 nm) are calculated at even longer wavelengths. This, however, does not necessarily hold for the Q band intensity. The *f* values for the two Q bands for Zn_2PcPyZ, Zn_2PcPc, and Zn_2PcNc are 2.19 and 0.78, 2.37 and 1.62, and 2.25 and 1.02, respectively (the Q bands at longer wavelengths are always more intense), suggesting that the Q band of the homodimer may be stronger than that of the heterodimers. The values also suggest that in the heterodimers, the Q band of the dimers having larger π conjugation systems may be stronger. As shown by the configurations in Table 1, the calculations predict that for all the planar binucleates, in the one-electron description, the Q band to lower energy corresponds to a transition from the HOMO to LUMO, while that to higher energy is mainly associated with a transition from the HOMO to the LUMO+1. Of these, concerning configurations of the longer wavelength Q band, the contributions of the HOMO−LUMO transition for Zn_2PcPyZ, Zn_2PcPc, and Zn_2PcNc are 88, 89, and 77%, respectively, as for the above *f* values, suggesting that the contribution does not vary systematically with the structure of the constituting units.

 © 2004 Wiley-VCH Verlag GmbH & Co. KGaA, Weinheim

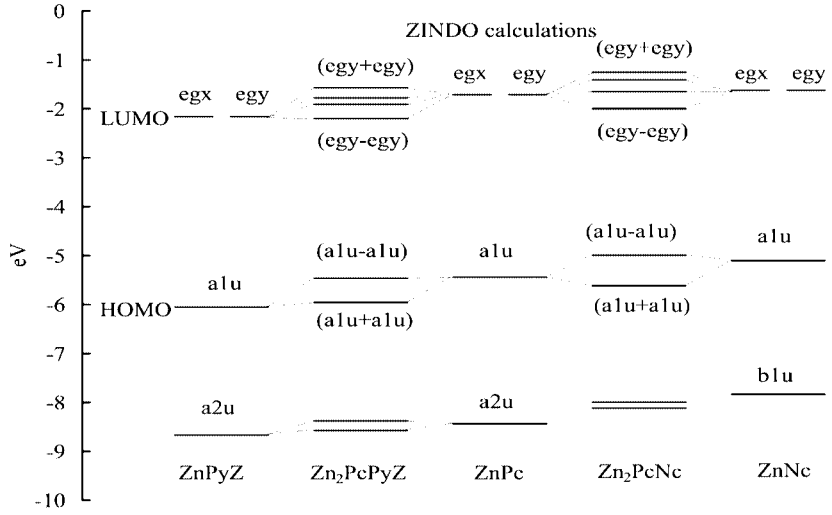

Figure 5. Partial molecular orbital energy diagram for Zn_2PcPyZ and Zn_2PcNc, and for ZnPyZ, ZnPc, and ZnNc, and their mutual relationships. The parentheses near each MO of the dimers indicate the expression of MO by the notation in D_{4h} symmetry, which is used for ZnPyZ, ZnPc, and ZnNc

From the configurational values for the HOMO to LUMO transition (Table 1), the purity of the transition at the longest wavelength of the dimers is similar to that of constituting monomers (88, 87, and 95% for ZnPyZ, ZnPc, and ZnNc, respectively) except for Zn_2PcNc.

Another notable point for the heterodimer spectra is the presence of a third transition lying closely in energy to the second transition (701 nm for Zn_2PcPyZ and 744 nm for Zn_2PcNc). This fairly intense band is ascribed mainly to the HOMO to LUMO+2 transition. It is possible, therefore, to consider that because of this transition, the experimental Q band at a shorter wavelength is much broader than that at a longer wavelength, since two closely lying transitions can produce a broad band due to superimposition. If this is the case, the dispersion type MCD associated with the second Q absorption peak can be considered to be produced by closely lying Faraday *B*-terms of opposite signs.

MO numbers 93, 171, 93, 198, and 129 are the HOMOs for ZnPyZ, Zn_2PcPyZ, ZnPc, Zn_2PcNc, and ZnNc, respectively. The data for the homodinuclear Zn_2PcPc are also shown for comparative purposes.

In the B band region, the calculated data of the constituting compounds are not complicated, particularly for ZnPyZ, although those of ZnNc are more complex because of the involvement of the transitions localized in the naphthalene ring. In contrast, the B band region of the dimers is very complex. The most intense region was predicted at 311 (f = 1.27) and 304 nm (f = 1.20) for Zn_2PcPyZ and 313 (f = 0.97) and 297 nm (f = 0.83) for Zn_2PcNc, implying that the more intense B band region of the two compounds would appear at a similar wavelength, if the two compounds could be prepared (we could not obtain Zn_2PcNc, since it fragmented during column chromatography).

Figure 5 shows how the four frontier orbitals in mononuclear constituting molecules split in the heterodimers. This figure indicates that two monomer orbitals having the same symmetry residing in different constituting units couple and produce two dimer orbitals, and that the extent of the splitting is larger for orbitals having a larger coefficient along the axis connecting the two constituting units (for the shape of orbitals, see Figure 6). That is, of the a_{1u} and a_{2u} orbitals, a_{1u} is larger, while of the e_{gx} and e_{gy} orbitals, the latter is larger. Furthermore, comparison of the orbital energies of the constituting monomers and the resulting dimers suggests that for the HOMO of the dimers the contribution of an electron-richer moiety is larger, while for the LUMO of the dimers the contribution of a more electron-deficient moiety is large. Indeed, if we compare the energy difference between the HOMO of Zn_2PcPyZ and those of ZnPc and ZnPyZ, the difference between Zn_2PcPyZ and ZnPc is much smaller than that between Zn_2PcPyZ and ZnPyZ. Similarly, the energy difference between the HOMO of Zn_2PcNc and ZnNc is much smaller than that between Zn_2PcNc and ZnPc. Accordingly, we can conclude that for the HOMO of Zn_2PcPyZ, the contribution of the Pc moiety is more significant than that of the PyZ moiety. In a similar manner, for the HOMO of Zn_2PcNc, the contribution of the Nc moiety is larger than that of the Pc moiety. In the case of the LUMO, the inverse relationship is observed for the energy difference between the LUMO of constituting monomers and the resultant dimers. Thus, the contribution of the PyZ moiety appears larger than that of the Pc moiety for the LUMO of Zn_2PcPyZ.

We can correlate the experimental redox potentials (Figure 3) with the calculated MO energies from Figure 5. Since relatively clear voltammetric curves were obtained in the negative potential region for all of the compounds, the reduction potentials of the two monomers and the resulting dimer complex can be discussed and compared with data in Figure 5. The first reduction in ZnPc and ZnPyZ corresponds to an addition of an electron to the e_g LUMO. A more negative potential (−1.41 V) is obtained for ZnPc

 © 2004 Wiley-VCH Verlag GmbH & Co. KGaA, Weinheim

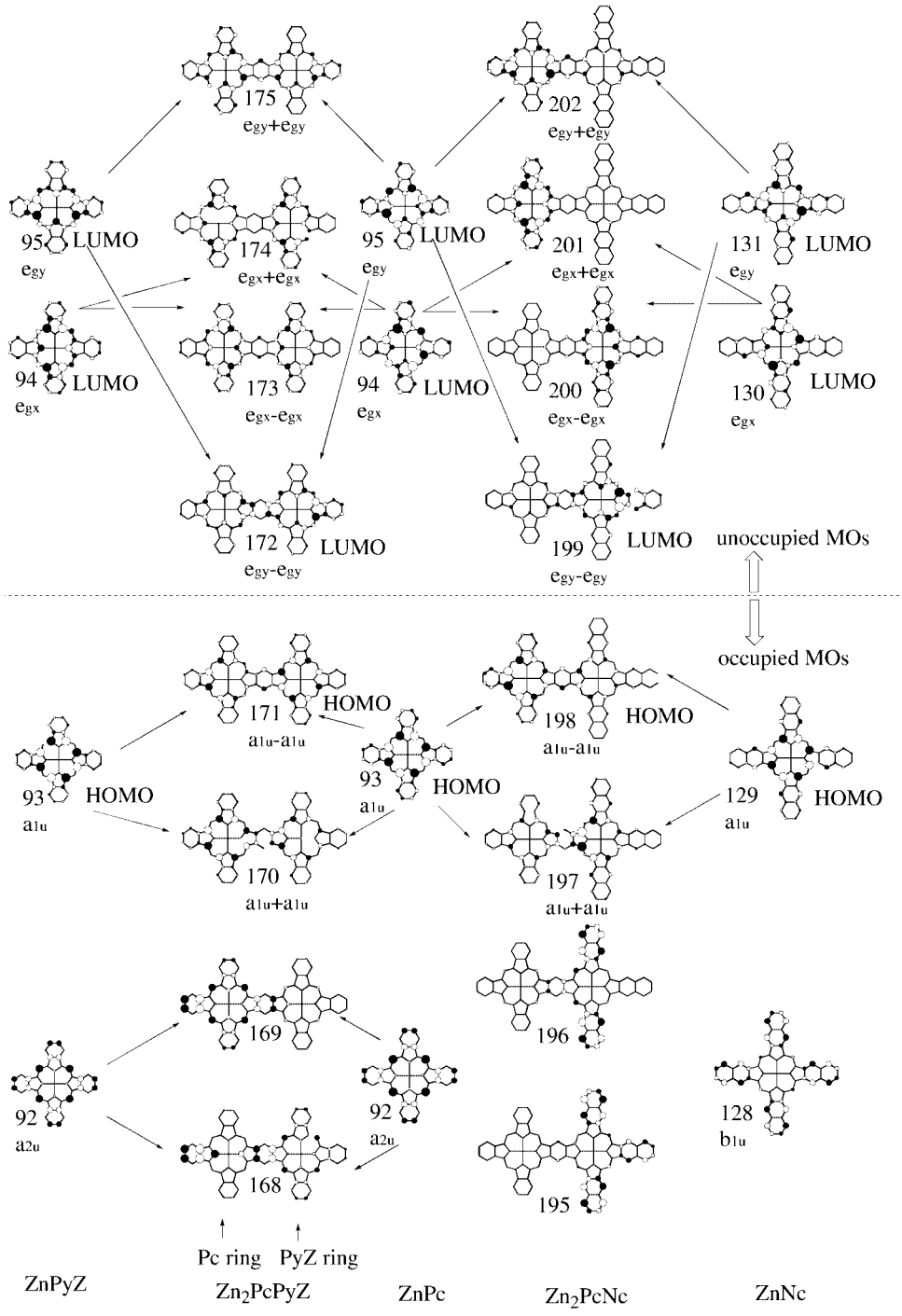

Figure 6. Eight frontier orbitals of Zn_2PcPyZ and Zn_2PcNc and four frontier orbitals of ZnPyZ, ZnPc, and ZnNc. The parentheses under each MO of the dimers indicate the expression of MO by the notation in D_{4h} symmetry, which is used for ZnPyZ, ZnPc, and ZnNc

than (−0.97 V) for ZnPyZ (Figure 3), as a result of the lower electron-density of ZnPyZ due to the electron-withdrawing property of the four peripheral pyrazine rings. Since the e_g orbital of ZnPc sits at a higher energy than that of ZnPyZ (Figure 5), the reduction of ZnPc is expected to require a higher potential. When ZnPc and ZnPyZ are laterally fused to form Zn_2PcPyZ, the calculated LUMO energy is very similar to that of ZnPyZ (Figure 5). As expected, the first reduction potentials of ZnPyZ and Zn_2PcPyZ are found to be very close [Figure 3, curves (b) and (c)]. The calculated LUMO energies of ZnPc and ZnNc are almost identical. The first reduction potentials of these compounds are therefore expected to be very similar. The LUMO energy of the resulting Zn_2PcNc dimer drops substantially, relative to that of ZnPc. As a result, the first reduction step for the Mt_2PcNc dimer occurs at a less negative potential than that of the corresponding MtPc or MtNc monomers. This feature is observed experimentally in the voltammograms of cobalt complexes in Figure 3 (curves in B). There is therefore clearly a close agreement

 © 2004 Wiley-VCH Verlag GmbH & Co. KGaA, Weinheim

between the calculated LUMO energies and the experimental reduction potentials. The HOMO energies and the oxidation potentials could not be compared in a similar manner, however, since the voltammograms are ill-defined in the positive potential region.

Figure 6 displays the four frontier orbitals of each mononuclear molecule and eight frontier orbitals of the resulting heterodimers. This figure clearly shows that the dimer orbitals are composed of the monomer orbitals with the same symmetry, since the dimer orbitals can be expressed as linear combinations of monomer orbitals of the same symmetry (see the notation below each MO). In addition, supporting the conclusions in Figure 5, for the HOMO of the dimer, the coefficient of the electron-richer moiety is large (i.e. in Zn_2PcPyZ, the coefficients in the Pc moiety are larger than those in the PyZ moiety, and similarly in Zn_2PcNc the coefficients in Nc are larger than those in the Pc moiety). Conversely, in the case of the LUMO, the coefficients in the more electron-deficient moiety is large (the PyZ moiety in Zn_2PcPyZ, and the Pc moiety in Zn_2PcNc).

Conclusion

The electronic absorption and magnetic circular dichroism (MCD) spectra, and differential pulse (DP) voltammograms of planar heterodinuclear phthalocyanine (Pc) dimers consisting of Pc and pyrazinoporphyrazine (PyZ) [Mt_2PcPyZ (Mt = H_2 and Zn)] and Pc and naphthalocyanine (Nc) [Mt_2PcNc (Mt = H_2 and Co)] have been recorded, and their properties interpreted by MO calculations using the ZINDO/S Hamiltonian. These dimers commonly show broad absorption bands between ca. 500 and 1000 nm, while the DP voltammograms suggest that the dimers are unstable to oxidation, and that, in these compounds, two relatively independent chromophore units interact. Dimer orbitals were found to be expressed by linear combinations of the orbitals of the constituting mononuclear orbitals of the same symmetry. It was suggested that for the HOMO of the dimers, the contribution of the electron-richer moiety is large, while, conversely, for the LUMO the contribution of the more electron-deficient moiety is large. The heterodimers showed two intense Q bands experimentally. Our calculations suggested that the position and intensity of these bands were affected by those of the constituting mononucleates. That is, PcPyZ dimers have a split Q band at shorter wavelengths than those of PcNc dimers. Of the two heterodimers, the Q band intensity of the PcNc dimer, i.e. the dimer consisting of larger π conjugation systems, appears larger than that of the PcPyZ dimer, since the calculated Q band of PyZ appears at a shorter wavelength and is weaker than that of Nc.

Experimental Section

(i) Measurements: Mass spectra were obtained with a JEOL JMS-HX110 mass spectrometer using *m*-nitrobenzyl alcohol (NBA) as a matrix (FAB mass). Electronic absorption spectra were recorded with a Hitachi U-3410 spectrophotometer using THF as a solvent. Magnetic circular dichroism (MCD) measurements were made with a JASCO J-725 spectrophotometer equipped with a JASCO electromagnet that produces magnetic fields of up to 1.09 T. Its magnitude was expressed in terms of molar ellipticity per tesla, $[\theta]_M$ (in $deg \cdot mol^{-1} \cdot dm^3 \cdot cm^{-1} \cdot T^{-1}$). The 400 MHz ^{1}H NMR spectral measurements were made with a JEOL-GSX-400 instrument. IR spectra were run on a Shimadzu FTIR-8100M spectrometer using KBr discs. Differential pulse voltammetry (DPV) experiments were carried out with conventional three-electrode cells, in which a platinum wire auxiliary electrode, a glassy carbon working electrode (0.07 cm^2), and an Ag/AgCl wire reference electrode were employed. The solvent for the electrochemical measurements, *o*-dichlorobenzene (*o*-DCB, Nacalai Tesque, specially prepared for HPLC) was used as supplied. Tetrabutylammonium perchlorate (TBAP) was used as an electrolyte. All electrochemical work was carried out under an atmosphere of dry nitrogen. DPV data were recorded with a Yanaco P-1100 polarographic analyzer connected to a Watanabe WX 4401 *XY* recorder.

(ii) Computational Method: MO calculations were performed using HyperChem. software[8] within the ZINDO/S level, in which the overlap weighting factors for σ-σ and π-π were 1.267 and 0.585, respectively. For the configuration interaction (CI) calculations, all singly excited configurations of up to 8 eV were included.

(iii) Materials: Deprotonation of the pyrrole proton in dinuclear metal-free species was affected by adding a small amount of tetra-*n*-butylammonium hydroxide. Tetra-*tert*-butylphthalocyaninatocobalt, CoPc, and tetra-*tert*-butylnaphthalocyaninatocobalt, CoNc, were used as in our previous paper.[9]

Tetra-*tert*-butylpyrazinoporphyrazinatozinc (ZnPyZ): This compound was obtained by zinc insertion using $Zn(OAc)_2$ to metal-free tetra-*tert*-butylpyrazinoporphyrazine[10] in EtOH/1,2-dichloroethane (1:1 v/v), and purified using a basic alumina column and CH_2Cl_2/MeOH as eluent in 71% yield. ^{1}H NMR (400 MHz, $CDCl_3$, TMS, ppm): δ = 9.87−9.67 (s, 4 H, Ar-H), 2.13−1.93 (m, 36 H, *t*Bu). $C_{40}H_{40}N_{16}Zn \cdot 3H_2O$: calcd. C 55.59, H 5.36, N 25.93; found C 55.02, H 5.56, N 25.27.

Tetra-*tert*-butylphthalocyaninatozinc (ZnPc): This compound was also obtained by zinc insertion to metal-free tetra-*tert*-butylphthalocyanine[6b] in EtOH/1,2-dichloroethane (1:1 v/v) in the dark for 15 h, and subsequent purification using a basic alumina and CH_2Cl_2. $C_{48}H_{48}N_8Zn$: calcd. C 71.85, H 6.03, N 13.97; found C 71.23, H 6.50, N 13.34.

Hexa-*tert*-butylphthalocyaninylpyrazinoporphyrazinatodizinc (Zn_2PcPyZ): A mixture of metal-free hexa-*tert*-butylphthalocyaninylpyrazinoporphyrazine,[6a] H_4PcPyZ (5.0 mg, 0.0039 mmol) and $Zn(OAc)_2$ (17 mg, 0.077 mmol) were refluxed in 1,2-dichloroethane/ EtOH (1:1 v/v) in the dark for 15 h, and after evaporating the solvent, the residue was chromatographed over a basic alumina column using a mixture of CH_2Cl_2 and MeOH, to give 5.0 mg (90% yield) of the desired dizinc complex, Zn_2PcPyZ as a blue powder. ^{1}H NMR (400 MHz, $CDCl_3$, TMS, ppm): δ = 9.5−7.0 (br, 14 H, Ar-H), 2.1−1.7 (m, 54 H, *t*Bu). MS (FAB, NBA): *m*/*z*: 1419 [M]. $C_{76}H_{68}N_{22}Zn_2 \cdot 2H_2O$: calcd. C 62.68, H 4.98, N 21.16; found C 62.35, H 5.41, N 20.77.

Hexa-*tert*-butylphthalocyaninylnaphthalocyaninatodicobalt (Co_2PcNc): A mixture of metal-free hexa-*tert*-butylphthalocyaninylnaphthalocyanine[6b] (4.0 mg, 0.0028 mmol) and $CoCl_2$ (7.2 mg, 0.056 mmol) was refluxed in DMF (2.0 mL) for 30 min. After evap-

 © 2004 Wiley-VCH Verlag GmbH & Co. KGaA, Weinheim

oration of the solvent, the residue was purified using a basic alumina column and CH_2Cl_2/MeOH as eluent, to give 3.8 mg (87.5% yield) of the desired Co_2PcNc as a blue powder. MS (FAB, NBA): *m/z*: 1550 [M]. $C_{94}H_{80}Co_2N_{16}{\cdot}H_2O$: calcd. C 71.93, H 5.27, N 14.28; found C 71.29, H 5.46, N 13.80.

Acknowledgments

This research was partially supported by the Ministry of Education, Science, Sports and Culture, a Grant-in-Aid for the COE project, Giant Molecules and Complex Systems, 2003.

[1] [1a] *Phthalocyanine. Properties and Applications* (Eds.: C. C. Leznoff, A. B. P. Lever), VCH Publications: New York. **1989, 1993, 1993, 1996**; Vols. I, II, III, and IV. [1b] *The Porphyrin Handbook* (Eds.: K. M. Kadish, K. M. Smith, R. Guilard), Academic Press: New York, **2003**, Vols. 15−20. [1c] *Phthalocyanine. Chemistry and Functions* (Eds.: H. Shirai, N. Kobayashi), IPC: Tokyo, **1997**. [1d] *The Phthalocyanines* (Eds.: F. H. Moser, A. H. Thomas), CRC Press, Boca Raton, FL, **1983**, Vols. 1 and 2.

[2] P. A. Barett, C. E. Dent, R. P. Linstead, *J. Chem. Soc.* **1936**, 1719−1736.

[3] C. C. Leznoff, H. Lam, S. M. Marcuccio, W. A. Nevin, P. Janda, N. Kobayashi, A. B. P. Lever, *J. Chem. Soc., Chem. Commun.* **1987**, 699−701.

[4] J. Jiang, K. Kasuga, D. P. Arnold, in: *Supramolecular Photosensitive and Electroactive Materials* (Ed.: H. S. Nalwa), Academic Press: New York, **2001**; Chapter 2, pp. 113−210.

[5] [5a] N. Kobayashi, M. Numao, R. Kondo, S. Nakajima, T. Osa, *Inorg. Chem.* **1991**, *30*, 2241−2244. [5b] N. Kobayashi, *J. Chem. Soc., Chem. Commun.* **1991**, 1203−1205. [5c] D. Lelievre, L. Bosio, J. Simon, J. J. Andre, F. Bensebaa, *J. Am. Chem. Soc.* **1992**, *114*, 4475−4479. [5d] D. Lelievre, O. Damette, J. Simon, *J. Chem. Soc., Chem. Commun.* **1993**, 939−940. [5e] J. Yang, M. R. Mark, *Tetrahedron Lett.* **1993**, *33*, 5223−5226. [5f] N. Kobayashi, H. Lam, W. A. Nevin, P. Janda, C. C. Leznoff, T. Koyama, A. Monden, H. Shirai, *J. Am. Chem. Soc.* **1994**, *116*, 879−890. [5g] T. F. Baumann, A. G. M. Barrett, B. M. Hoffman, *Inorg. Chem.* **1997**, *36*, 5661−5665. [5h] S. J. Lange, H. Nie, C. L. Stern, A. G. M. Barrett, B. M. Hoffman, *Inorg. Chem.* **1998**, *37*, 6435−6443. [5i] B. Hauschel, R. Jung, M. Hanack, *Eur. J. Inorg. Chem.* **1999**, 693−703. [5j] A. G. Montalban, W. Jarrel, E. Riguet, Q. J. McCubbin, M. E. Anderson, A. J. P. White, D. J. Williams, A. G. M. Barrett, B. M. Hoffman, *J. Org. Chem.* **2000**, *65*, 2472−2478. [5k] M. J. Cook, M. J. Heeney, *Chem. Eur. J.* **2000**, *6*, 3958−3967. [5l] E. M. Garcia-Frutos, F. Fernandez-Lazaro, E. M. Maya, P. Vazquez, T. Torres, *J. Org. Chem.* **2000**, *65*, 6841−6846. [5m] N. Kobayashi, T. Fukuda, D. Lelievre, *Inorg. Chem.* **2000**, *39*, 3632−3637. [5n] N. Kobayashi, A. Muranaka, V. N. Nemykin, *Tetrahedron. Lett.* **2001**, *42*, 913−915.

[6] [6a] N. Kobayashi, Y. Higashi, T. Osa, *J. Chem. Soc., Chem. Commun.* **1994**, 1785−1786. [6b] N. Kobayashi, Y. Higashi, T. Osa, *Chem. Lett.* **1994**, 1813−1816. [6c] G. Torre, M. V. Martinez-Diaz, P. R. Ashton, T. Torres, *J. Org. Chem.* **1998**, *63*, 8888−8893. [6d] K. Ishii, N. Kobayashi, Y. Higashi, T. Osa, D. Lelievre, J. Simon, S. Yamauchi, *Chem. Commun.* **1999**, 969−970.

[7] N. Kobayashi, *Coord. Chem. Rev.* **2002**, *227*, 129−152.

[8] *HyperChem. R5.1 Pro*, Hypercube Inc., Gainesville, FL, **1997**.

[9] N. Kobayashi, S. Nakajima, T. Osa, *Inorg. Chim. Acta* **1993**, *210*, 131−133.

[10] E. G. Gal'pern, E. A. Luk'yanets, *Acad. Nauk. SSSR. Bull. Chem. Sci.* **1973**, *22*, 1925.

[11] [11a] S. Tai, N. Hayashi, *J. Chem. Soc., Perkin Trans.2* **1991**, 1275−1279. [11b] S. Tai, N. Hayashi, M. Katayose, *Prog. Org. Coatings.* **1994**, *24*, 323−339.

[12] N. Kobayashi, M. Togashi, T. Osa, K. Ishii, S. Yamauchi, H. Hino, *J. Am. Chem. Soc.* **1996**, *118*, 1073−1085.

[13] [13a] W. A. Nevin, W. Liu, S. Greenberg, M. R. Hempstead, S. M. Marcuccio, M. Melnik, C. C. Leznoff, A. B. P. Lever, *Inorg. Chem.* **1987**, *26*, 891−899. [13b] N. Kobayashi, H. Lam, W. A. Nevin, P. Janda, C. C. Leznoff, A. B. P. Lever, *Inorg. Chem.* **1990**, *29*, 3415−3425.

[14] [14a] M. Gouterman, G. H. Wagniere, *J. Mol. Spectrosc.* **1963**, *11*, 108−127. [14b] B. W. Dale, *Trans. Faraday Soc.* **1969**, *65*, 331−339. [14c] A. Henriksson, B. Roos, M. Sundbom, *Theor. Chim. Acta* **1972**, *27*, 303−313. [14d] L. K. Lee, N. H. Sabelli, P. R. LeBreton, *J. Phys. Chem.* **1982**, *86*, 3926−3931. [14e] A. M. Schaffer, M. Gouterman, *Theor. Chim. Acta* **1972**, *25*, 62−82. [14f] J. Mack, M. J. Stillman, in: *The Porphyrin Handbook* (Eds.: K. M. Kadish, K. M. Smith, R. Guilard), Academic Press, New York, **2003**, Vols. 16, Chapter 103, pp. 43−116.

[15] E. A. Luk'yanets, *Electronic Spectra of Phthalocyanines and Related Compounds*, NIOPIK, Moscow, **1989**.

[16] [16a] S. Dong, B. Liu, J. Liu, N. Kobayashi, *J. Porphyrins Phthalocyanes.* **1997**, *1*, 333−340. [16b] N. Kobayashi, H. Konami, in: *Phthalocyanines-properties and Applications* (Eds.: C. C. Leznoff, A. B. P. Lever), VCH, New York, **1996**, Vol. 4, Chapter 9, pp. 343−404.

[17] [17a] R. Pariser, R. G. Parr, *J. Chem. Phys.* **1953**, *21*, 466−471, 767−776. [17b] J. A. Pople, *Trans. Faraday Soc.* **1953**, *49*, 1375−1385.

Received August 4, 2003
Early View Article
Published Online November 28, 2003

SHORT COMMUNICATIONS

943 **E. Kirillov, C. W. Lehmann, A. Razavi, J.-F. Carpentier***

[η^5:η^1-(3,6-*t*Bu$_2$Flu)SiMe$_2$N*t*Bu]Y(η^1-NC$_5$H$_6$)-(py)$_2$: A 1,4-Hydride-Addition Product to Pyridine that Provides Evidence for the First Fluorenyl(hydrido)metal (Group 3) Complex

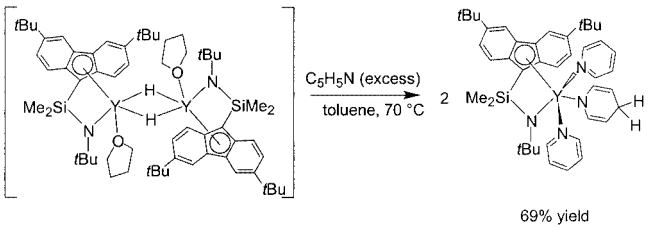

Keywords: Fluorenyl / Hydrides / Insertion / Pyridine / Yttrium

946 **X. Wang, J. Zhuang, Y. Li***

Pr_6O_{11} Single-Crystal Nanotubes from a Molten-Salt Synthetic Method

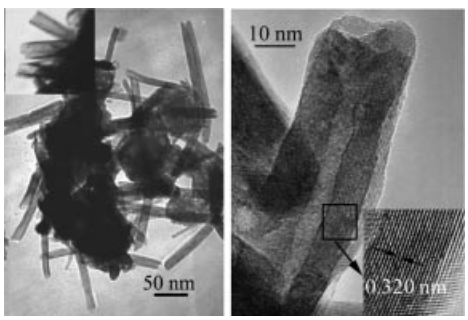

Keywords: Lanthanides / Molten salts / Nanotubes / Three-dimensional structures / X-ray diffraction

949 **A. Villanueva, M. C. Morales-Varela, E. Ruiz-Hitzky***

Microwave-Assisted Synthesis of MPS_3 Materials (M = Mn, Cd) Using a Dewar-Ampoule Device

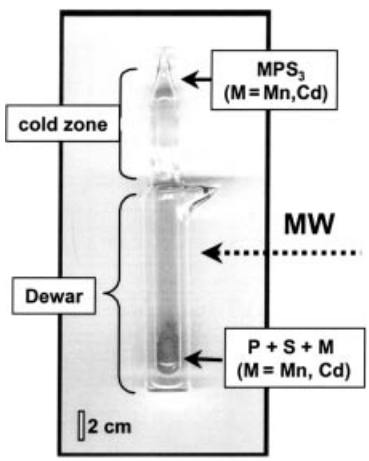

Keywords: Transition metals / Microwave-assisted reactions / Layered compounds / Synthesis design / Solid-phase synthesis

953 **Z.-E. Lin, J. Zhang, S.-T. Zheng, G.-Y. Yang***

A Novel Open-Framework Zinc Phosphite, $Zn_3(HPO_3)_4{\cdot}Ni(en)_2(H_2O)_2$, Templated by a Transition-Metal Complex

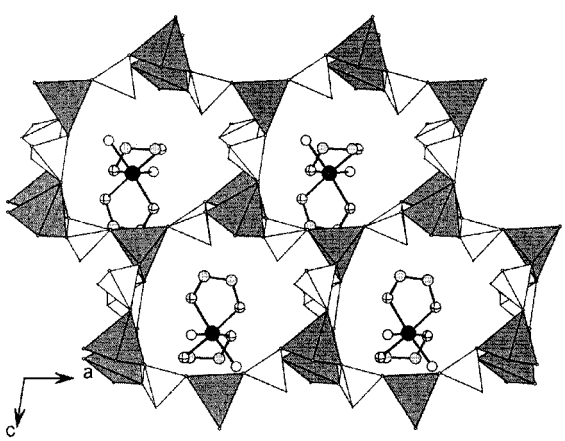

Keywords: Open framework / Inorganic solid / Zinc / Nickel / Template synthesis

956 **J. Zhang, S. Gao,* C.-M. Che***

A Blue Photoluminescent 2-D Coordination Polymer Constructed by Dinuclear Zinc(II) Subunits [$Zn_2(oz)_2$] [Hoz = 2-(2′-Hydroxyphenyl)-2-oxazoline] and Dicyanamide

Keywords: Zinc / Photoluminescence / Dinuclear subunit / Polymer / Thermal stability

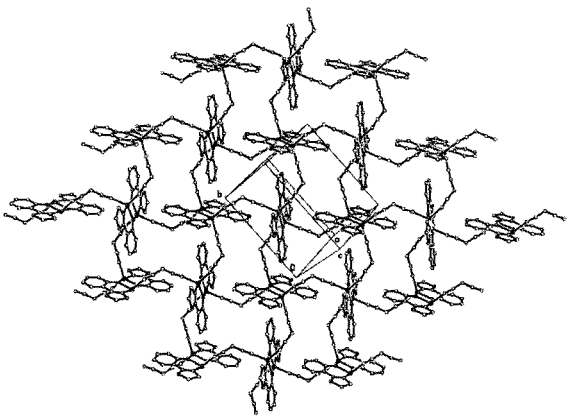

960 **F. Bigoli, M. C. Cabras, P. Deplano,* M. L. Mercuri, L. Marchió, A. Serpe, E. F. Trogu**

On the Use of the Bis(diiodine) Adduct of 1,4-Dimethylperhydro-1,4-diazepine-2,3-dithione (Me_2dazdt) to Recover Liquid Mercury Producing [Hg(Me_2dazdt)I_2] in a One-Step Reaction

Keywords: Mercury / S ligands / Iodine / Adducts / Oxidation

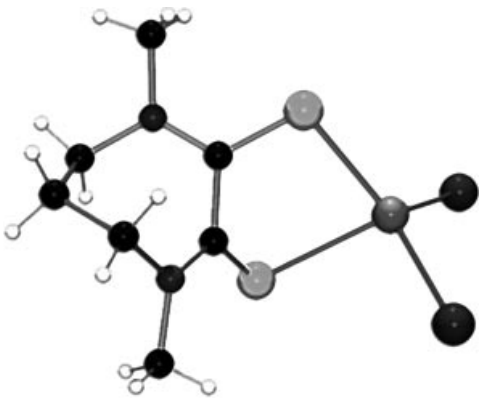

964 **T. Brasey, A. Buryak, R. Scopelliti, K. Severin***

Synthesis of a Metallamacrocyclic $Re(CO)_3$ Complex Using a Tridentate Bridging Ligand

Keywords: Host–guest chemistry / Metallamacrocycles / Rhenium / Silver

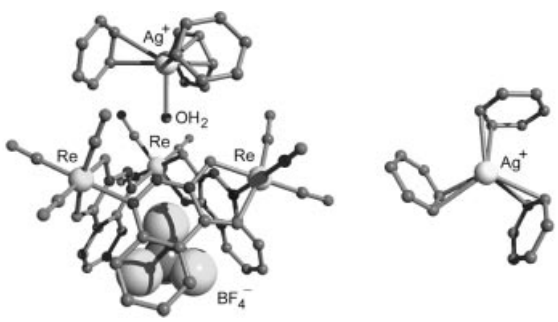

FULL PAPERS

969 **W. Uhl,* A. El-Hamdan**

Reactivity of Organoelement Subhalides of Gallium and Indium – Ga–Ga and In–In Bonds Bridged by Carboxylato Ligands

Keywords: Carboxylate ligands / Gallium / Indium / Subvalent compounds

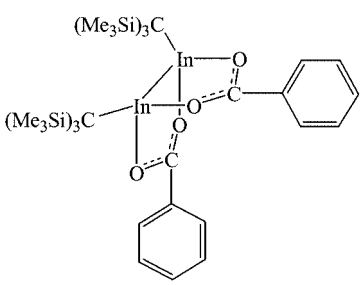

 © 2004 Wiley-VCH Verlag GmbH & Co. KGaA, Weinheim

973 **C. R. Mayer,* M. Hervé, H. Lavanant, J.-C. Blais, F. Sécheresse**

Hybrid Cyclic Dimers of Divacant Heteropolyanions: Synthesis, Mass Spectrometry (MALDI-TOF and ESI-MS) and NMR Multinuclear Characterisation

Keywords: Polyoxometalates / Bridging ligands / Mass spectrometry / Organic-inorganic hybrid composites

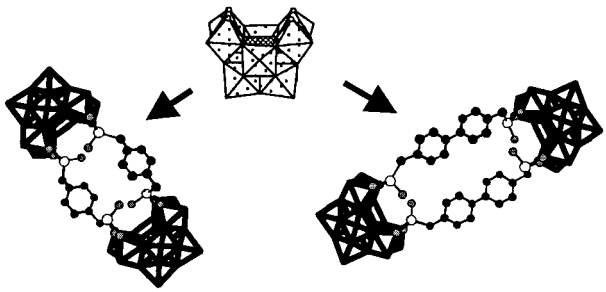

978 **P. P. Pescarmona, J. C. van der Waal, T. Maschmeyer***

Fast, High-Yielding Syntheses of Silsesquioxanes Using Acetonitrile as a Reactive Solvent

Keywords: Silsesquioxanes / NMR spectroscopy / Mass spectrometry / Solvent effects

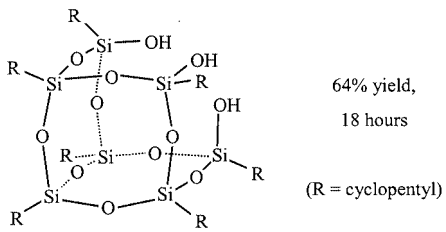

984 **S. Ross, T. Weyhermüller, E. Bill, E. Bothe, U. Flörke, K. Wieghardt, P. Chaudhuri***

Asymmetric Heterodinuclear $Fe^{III}M^{II}$ (M = Zn, Cu, Ni, Fe, Mn), $Co^{III}Fe^{II}$ and $Fe^{II}Co^{III}$ Species: Synthesis, Structure, Redox Behavior, and Magnetism

Keywords: Electrochemistry / Heterodinuclear complexes / Iron / Magnetic properties / Pyridine-2-aldoxime

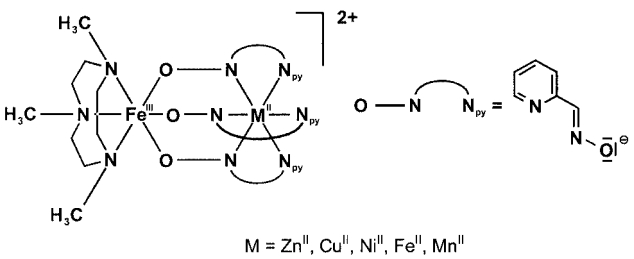

998 **R. C. Smith, J. D. Protasiewicz***

Systematic Investigation of PPV Analogue Oligomers Incorporating Low-Coordinate Phosphorus Centres

Keywords: Oligomers / Phosphorus / Phosphaalkenes

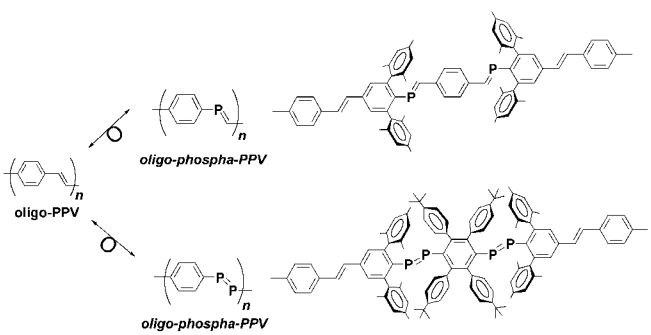

1007 **T. D. Keene, H. R. Ogilvie, M. B. Hursthouse, D. J. Price***

One-Dimensional Magnetism in New, Layered Structures: Piperazine-Linked Copper and Nickel Oxalate Chains

Keywords: Magnetic properties / Layered compounds / Hydrothermal synthesis / Coordination networks

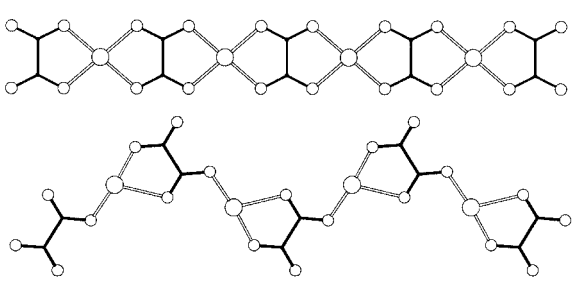

 © 2004 Wiley-VCH Verlag GmbH & Co. KGaA, Weinheim

1014 **K. Kandasamy, S. Kumar, H. B. Singh,* R. J. Butcher, K. T. Holman**

Synthesis, Structural Characterization and Fluorescence Properties of Organoselenium Compounds Bearing a Ligand Containing Both Bulky and Nonbonding Groups − The First Observation of Both Intramolecular Se···N and Se···O Interactions in a Diselenide Structure

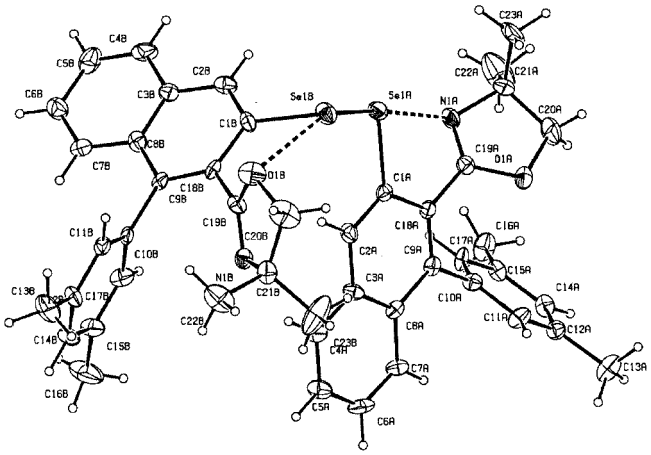

Keywords: Selenium / Intramolecular coordination / X-ray diffraction / Fluorescence

1024 **X.-C. Huang, S.-L. Zheng, J.-P. Zhang, X.-M. Chen***

Synthesis, Structure and Photoluminescent Studies of a Novel Supramolecular [Ag(phen)-(CN)]·(phen) Complex

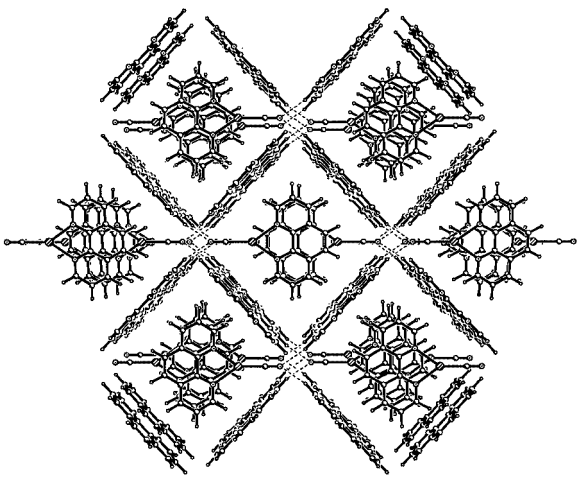

Keywords: Density functional calculations / N ligands / Pi interactions / Photoluminescence / Silver

1030 **A. Brunetta, G. Strukul***

Epoxidation versus Baeyer−Villiger Oxidation: The Possible Role of Lewis Acidity in the Control of Selectivity in Catalysis by Transition Metal Complexes

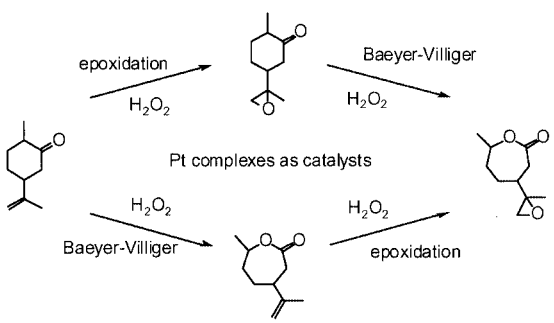

Can the Lewis acidity of the catalyst separate these steps?

Keywords: Lewis acids / Homogeneous catalysis / Oxidation / Peroxides

1039 **Y.-Q. Tian,* L. Xu, C.-X. Cai, J.-C. Wei, Y.-Z. Li, X.-Z. You***

Determination of the Solvothermal Synthesis Mechanism of Metal Imidazolates by X-ray Single-Crystal Studies of a Photoluminescent Cadmium(II) Imidazolate and Its Intermediate Involving Piperazine

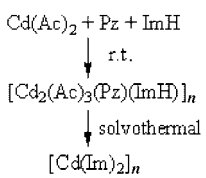

Keywords: Cadmium / Crystal engineering / Fluorescence / Nitrogen heterocycles / Zeolite analogues

 © 2004 Wiley-VCH Verlag GmbH & Co. KGaA, Weinheim

1045 **V. Kirin, P. W. Roesky***

Dinuclear Potassium-Chromium and Potassium-Tungsten Carbonyl Complexes

Keywords: Chromium / Coordination chemistry / N Ligands / Potassium / Tungsten

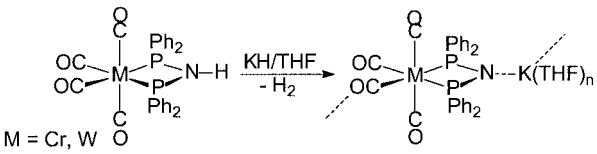

1051 **X.-B. Cui, J.-Q. Xu,* Y. Li, Y.-H. Sun, G.-J. Yang***

Hydrothermal Synthesis and Characterization of a Novel Sinusoidal Layer Structure Constructed From Polyoxometalates and Coordination Complex Fragments

Keywords: Hydrothermal synthesis / Magnetic properties / Polyoxometalates / X-ray diffraction

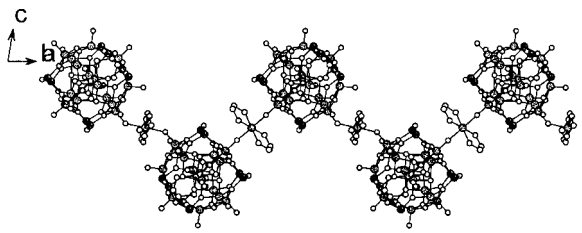

1056 **J. H. K. Yip,* J. Wu, K.-Y. Wong,* K. P. Ho, L. L. Koh, J. J. Vittal**

Electronic Interactions in Dinuclear Platinum and Palladium Ethynylferrocene and Ferrocenylvinylidene Complexes

Keywords: Platinum / Palladium / Ferrocene / Alkenes

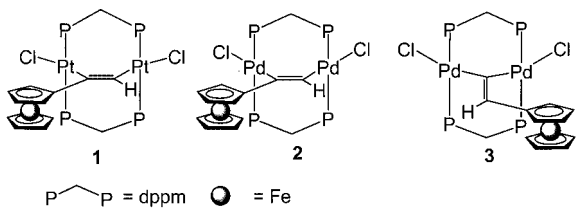

1063 **D. Cauzzi, C. Graiff, R. Pattacini, G. Predieri,* A. Tiripicchio, S. Kahlal, J.-Y. Saillard**

Cluster Growth Reactions with Selenido-Carbonyl Clusters − Synthesis, Characterisation and Theoretical Study of the Dimetallic *closo* Clusters $[WRu_3(\mu_4\text{-}Se)_2(\mu\text{-}CO)_4(CO)_6(L)_2]$ (L = Phosphane) and of the Donor-Acceptor Adduct $[(CO)_5W(\mu_4\text{-}Se)Ru_3(\mu_3\text{-}Se)(CO)_7\{P(CH_2Ph)Ph_2\}_2]$

Keywords: Ruthenium / Tungsten / Molybdenum / Cluster compounds / Selenium

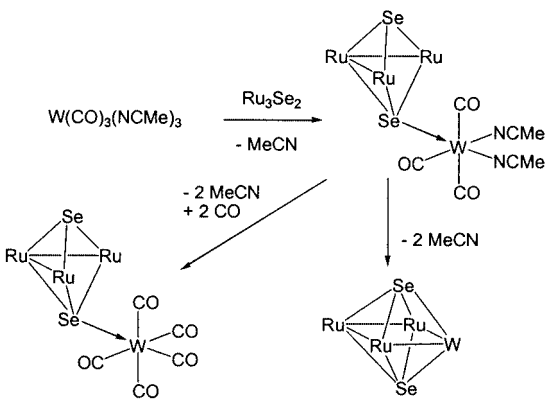

1073 **J. L. Shaw, T. B. Cardon, G. A. Lorigan, C. J. Ziegler***

Synthesis and Characterization of a Series of (Diphenyldipyrazolylmethane)copper Complexes as Possible Precursors to Type I Blue Copper Protein Active Site Models

Keywords: Copper / N ligands / Pyrazolylmethanes / Scorpionates

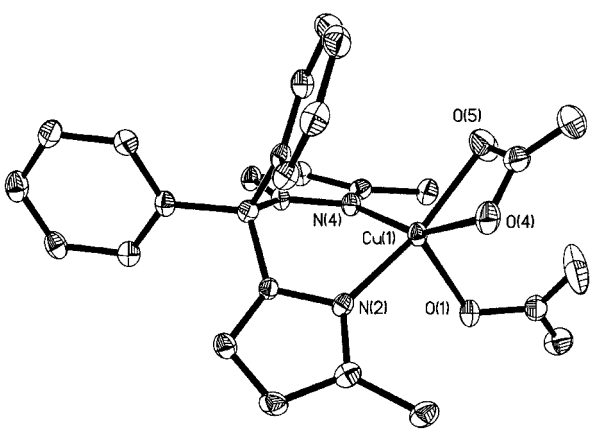

 © 2004 Wiley-VCH Verlag GmbH & Co. KGaA, Weinheim

1081 J.-M. Camus, J. Andrieu,* P. Richard, R. Poli

Allylpalladium(II) Complexes with Aminophosphane Ligands: Solution Behaviour and X-ray Structure of *cis*-[Pd(η^3-$CH_2CHCHPh$){Ph_2P-$CH_2CHPhNH(2,6$-$C_6H_3iPr_2)$}][PF_6]

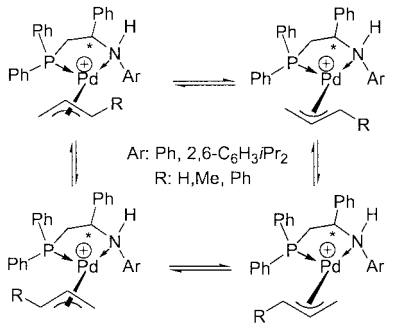

Keywords: Allyl ligands / N,P ligands / *syn-anti* exchange / Palladium

1092 B. Longato,* G. Bandoli, A. Dolmella

Hydroxo and Oxo Complexes of Platinum(II) Stabilized by Phosphanes: Synthesis and Characterization − X-ray Structures of *cis*-[L_2Pt-(μ-OH)]$_2(NO_3)_2$ (L = PMe_2Ph, $PMePh_2$) and [{*cis*-$(PMe_2Ph)_2Pt$}$_3$(μ-O)$_2$]Cl_2

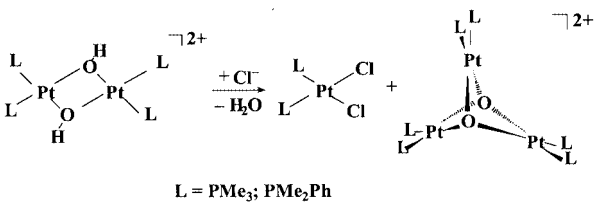

Keywords: Platinum / Oxo and hydroxo ligands / X-ray diffraction / Deprotonation reactions

1100 J. Olkowska-Oetzel, P. Sevillano, A. Eichhöfer, D. Fenske*

Binary and Ternary Cluster Complexes Containing Gold-Selenium, Gold-Indium-Selenium and Gold-Gallium-Tellurium − Synthesis and Structures of [$Au_5Se_2(PPh_3)_4$]Cl, [$(Au_3Se)_2${Ph_2P-$(CH_2)_6PPh_2$}$_3$]Cl_2, [$Au_{10}Se_4${$Ph_2P(CH_2)_5PPh_2$}$_4$]-$InCl_5$, [$Au_4(SeInCl_3)_2${$Ph_2P(CH_2)_5PPh_2$}$_2$], [Au_2-$(TeGaCl_3)${$Ph_2P(CH_2)_6PPh_2$}]$_2$ and [Au_8Se_4In-{$Ph_2P(CH_2)_2PPh_2$}$_4$]$(InCl_4)_3$

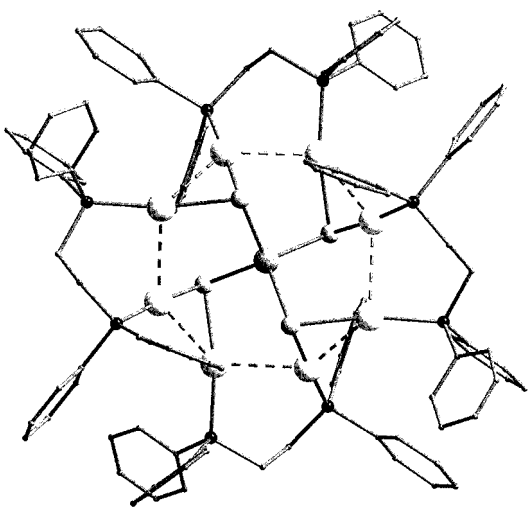

Keywords: Cluster compounds / Gallium / Gold / Indium / Selenium / Tellurium

1107 R. Kumar P., A. K. Singh,* R. J. Butcher, P. Sharma, R. A. Toscano

Tellurated Schiff Bases Formed from {2-[(4-Methoxyphenyl)telluro]ethyl}amine and Bis(2-aminoethyl) Telluride with *o*-Hydroxyacetophenone: Synthesis and Complexation Reactions with Hg^{II}, Pd^{II} and Ru^{II} − Crystal Structures of the Ligands, [Ru(*p*-cymene)Cl{$H_2NCH_2CH_2$-TeC_6H_4-4-OCH_3}]Cl·H_2O and [RuCl{4-Me-$OC_6H_4TeCH_2CH_2NHCH(CH_3)C_6H_4$-2-$O^-$}]

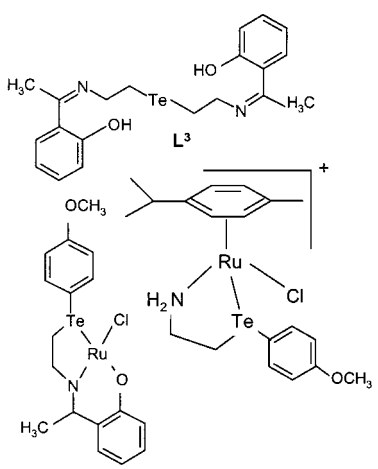

Keywords: Schiff bases / Ruthenium / Tellurium / X-ray diffraction / Synthetic methods

 © 2004 Wiley-VCH Verlag GmbH & Co. KGaA, Weinheim

1115 **H. Nöth,* M. Warchhold**

Sodium Hydro(isothiocyanato)borates: Synthesis and Structures

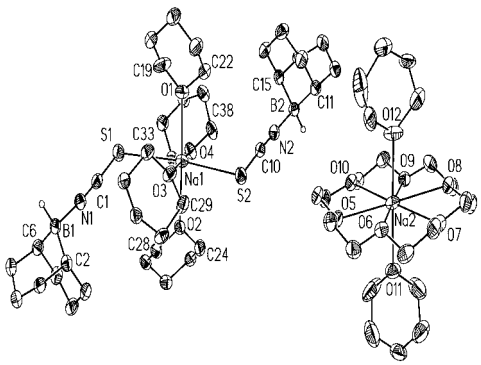

Keywords: Crown compounds / Sodium / NMR spectroscopy / Borates

1125 **P. Antoniotti, S. Borocci, F. Grandinetti***

Nitrogen Trifluoride as a Bifunctional Lewis Base: Implications for the Adsorption of NF_3 on Solid Surfaces

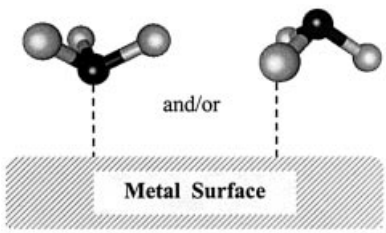

Keywords: Ab initio calculations / Nitrogen trifluoride / Lewis bases / Isomeric structures

 © 2004 Wiley-VCH Verlag GmbH & Co. KGaA, Weinheim

Multiproperty Molecular Materials: TTF-Based Conducting and Magnetic Molecular Materials

Lahcène Ouahab*[a] and Toshiaki Enoki[b]

Keywords: Conducting materials / Magnetic properties / Through-space interactions / Through-bond interactions

The chemistry and physics of molecule-based materials are exciting subjects, and due to potential applications this area is being extensively investigated. Considerable effort is currently being made to design and to investigate new materials involving interplay or synergy between multiple physical properties. This microreview examines materials combining magnetism and electrical properties. Some fundamental background material is covered, together with a discussion of constraints on the design of molecular materials with these physical properties. Some examples from the literature are then related, in order to illustrate the achievements in this area.
(© Wiley-VCH Verlag GmbH & Co. KGaA, 69451 Weinheim, Germany, 2004)

1. Introduction

Considerable effort is currently devoted to the synthesis and investigation of new molecule-based materials involving interplay and synergy between multiple physical properties.[1] The construction of molecule-based materials which possess two or more such properties is currently a challenging target. Optical properties in particular are of current interest (especially with respect to natural optical activity), but other combinations of properties have also been targeted both for their fundamental scientific interest and for their potential applications. These kinds of combinations of properties lead either to competition, coexistence, or cooperativity between the desired properties; the latter is much more difficult to achieve than the other two. It should be noted that the construction and control of the self-assembly of the molecular building blocks (so that the resulting supramolecular compound has the desired structure, stability and physical properties) is still a major challenge for synthetic chemists working in this area. Nevertheless, some significant achievements have been obtained, namely:
(i) *Light-induced magnetization*.[2] Direct applications of this technology would be photo-induced magnetic memory devices based on the choice of the laser wavelength. As an

[a] Laboratoire de Chimie du Solide et Inorganique Moléculaire, UMR 6511 CNRS-Université de Rennes 1, Groupe Matériaux Moléculaires, Institut de Chimie de Rennes, Campus de Beaulieu,
35042 Rennes cedex, France
E-mail: ouahab@univ-rennes1.fr
[b] Department of Chemistry, Tokyo Institute of Technology, Ookayama, Meguro-ku, Tokyo 152-8551, Japan
E-mail: tenoki@chem.titech.ac.jp

Lahcène Ouahab was born in 1953 in Setif Algeria, and received his Ph.D. from the University of Rennes 1 in 1985. He was Maître de Conférences at the University of Constantine (Algeria) and then associate Professor at the University of Rennes 1 before getting a permanent position in CNRS as "Chargé de Recherche". He is presently a CNRS Director of Research and leads the molecular materials research group. He is the director of the Laboratoire de Chimie du Solide et Inorganique Moléculaire at the Institut de Chimie (Université de Rennes 1). He was awarded the 1998 prize of the Coordination Chemistry Division of the French Chemical Society. His fields of research include molecular materials, and in particular, multifunctional materials, charge transfer complexes, radical ion salts, organic-inorganic hybrids, polymeric coordination complexes and polyoxometalates.

Toshiaki Enoki was born in 1946, and received his Ph.D. in 1974 from Kyoto University, Japan, under the supervision of Prof. Ikuji Tsujikawa. In 1987, he was appointed to the position of Associate Professor in the Department of Chemistry at Tokyo Institute of Technology, and is now a full Professor. His research interests include physical chemistry, especially molecular magnetism. He has been investigating molecular magnets on the basis of organic charge transfer complexes and carbon nano-materials. His pioneering work has contributed to the opening of the field of TTF-based molecular conducting magnets. He has also been leading work on magnetism in nanographites, which have recently been recognized as important spintronics materials.

MICROREVIEWS: This feature introduces the readers to the author's research through a concise overview of the selected topic. Reference to important work from others in the field is included.

example, some very interesting systems have been obtained by Hashimoto and co-workers, for example, a derivative of Prussian blue, namely the cobalt iron cyanide formulated as $K_{0.2}Co_{1.4}[Fe(CN)_6]6.9H_2O$,[2d,2e] which was found to exhibit photo-induced reversible magnetization. The critical temperature increases from 16 to 19 K under illumination with red light, as a result of oxidation state changes for the metal ions [Co^{III} ($S = 0$) and Fe^{II} ($S = 0$) to Co^{II} ($S = 3/2$) and Fe^{III} ($S = 1/2$)].

(ii) *Synergy between spin-crossover and magnetic interactions.*[3] To the best of our knowledge, $Fe(mnt)_2$-rad [or 2-(*para*-*N*-methylpyridinium)-4,4,5,5- tetramethylimidazoline-1-oxyl iron(III) bis(maleonitrile dithiolate)] is the only compound in which evidence has been found for synergy between the spin cross-over effect and intersite magnetic interactions. It was found the $[Fe(mnt)_2]^-$ moiety exhibits a spin cross-over between $S_{Fe} = 3/2$ at high temperature and $S_{Fe} = 1/2$ at low temperature. At the same time, an antiferromagnetic (AF) interaction operates between the spin of the $[rad]^+$ unit ($S = 1/2$) and the spin of the iron atom ($S_{Fe} = 1/2$) at low temperatures, giving rise to a singlet ground state.

(iii) *Electrical conductivity and magnetic interactions.*[4−13] Conducting materials incorporating localized spins are currently a subject of intense investigation. Numerous research groups are involved in this area, and many compounds of this kind have been isolated and characterized. Some important results obtained are the coexistence of paramagnetism and superconductivity,[5a,12] antiferromagnetism and superconductivity,[5c] ferromagnetism and metallic conductivity[5d] and also field-induced ferromagnetism and superconductivity.[12b,12c]

In this microreview, we focus on materials combining magnetic interactions and electrical properties.

2. Background to the Physics of π-d Interactions

Transition metals such as iron are widely known strong ferromagnetic materials. In such metal ferromagnets, the unpaired d-electrons, which stay in the inner shell, behave as localized electrons having magnetic moments, whereas the s- and p-electrons move freely in the crystal, acting as carriers of electrical charge. Thus, the d-electrons in the free electron jellium interact with the charge carriers through an s-d interaction, expressed by the following equation (when a conduction s-electron approaches a d-electron site):

$$2J_{s\text{-}d}\delta(r)\boldsymbol{sS} \quad (1)$$

where s and S are the spin operators for a conduction electron and a localized d-electron, respectively, $\delta(r)$ the delta function, and $J_{s\text{-}d}$ is the coupling constant for the exchange interaction between a conduction s-electron and a localized d-electron, and r is the distance between the conduction electron and the localized d-electron.

The interaction expressed by Equation (1) is termed the s-d interaction. In a crystal where the s-d interaction operates, the conduction carriers mediate the interaction between the magnetic moments of the localized d-electrons. Consequently, the mediation of conduction carriers results in a long-range interaction between localized magnetic moments of the d-electrons, expressed by Equation (2):

$$\frac{3N}{16\pi^2}\frac{J_{s-d}^2}{E_F}I(\boldsymbol{R}_{ij})S_{iz}S_{jz} \quad (2)$$

where R_{ij} is the distance between d-electrons having the z-components of spins S_{iz} at site i and S_{jz} at site j, E_F is the Fermi energy and $I(R_{ij})$ is the decaying function of R_{ij}, with a spatially oscillatory behavior which depends on the Fermi wave number k_F, as given by Equation (3):

$$I(\boldsymbol{R}_{ij}) = \frac{16\pi k_F^3}{(2k_F\boldsymbol{R}_{ij})^4}\left(2k_F\boldsymbol{R}_{ij}\cos 2k_F\boldsymbol{R}_{ij} - \sin 2k_F\boldsymbol{R}_{ij}\right) \quad (3)$$

The exchange interaction between localized magnetic moments in a metallic medium, described in Equation (2), is called the Rudermann−Kittel−Kasuya−Yoshida (RKKY) interaction, which is the origin of strong ferromagnetism in transition metals such as iron.

The RKKY interaction has strategic importance for the development of organic systems with magnetic interactions similar to the s-d interaction, and for the preparation of molecular versions of metal magnets. This could give new insights into phenomena related to the interplay between conduction carriers and localized magnetic moments.

Recently, a large variety of ''organic metal'' complexes and superconductors, modeled on organic charge-transfer complexes,[14] have been developed and their interesting novel properties uncovered. In such organic conductors, the constituent donor/acceptor molecules are planar, so that their π-electron orbitals (which protrude perpendicular to the molecular plane) overlap with each other, giving the π-electrons a small kinetic energy (transfer integral) in the 0.1−1 eV range. Therefore, these π-electrons play a role in the electron transport process, in contrast to conventional metals, in which the s- and p-electrons have a kinetic energy of several eV. In other words, organic conductors can be described as highly correlated electron systems, in which the kinetic energy of the π-electrons is smaller than or similar to the on-site Coulomb interaction. Moreover, one of the important features specific to organic complex crystals, associated with molecular stacking, is the one- or two-dimensionality of their lattices. As a consequence, organic conductors have electronic instabilities, resulting in the appearance of insulating states at low temperatures, such as charge density wave (CDW) and spin density wave states (SDW).[14]

The π-d interaction, which is the organic version of the s-d and s-f interactions, results from the introduction of d-electrons into organic conductors. It can be considered to possess a different nature from the s-d interaction, judging from the specific electronic and structural features men-

 © 2004 Wiley-VCH Verlag GmbH & Co. KGaA, Weinheim

tioned above. Here, we present a brief perspective on the magnetism emerging in π-d interaction systems, shown in Figure 1. In this regard, typical π-d based metal magnets appear in the regime where both the transfer integral and the π-d interaction $J_{\pi\text{-}d}$ govern the characteristics of the electronic structures. In the insulating regime, superexchange-mediated π-d composites are expected to provide ferrimagnets, weak ferromagnets or helical magnets, whereas metallic π-d systems only become organic magnetic superconductors if the π-d interaction is not strong enough to bring about pair-breaking against the superconducting state.

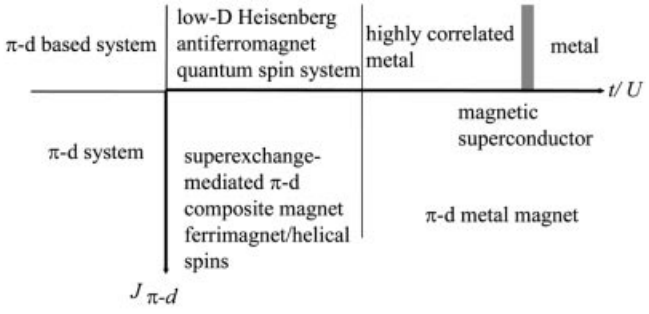

Figure 1. Overview of magnetism appearing in organic charge transfer complexes, depending on t, U and $J_{\pi\text{-d}}$

From the perspective of materials design, the π-d system model is based on the synergy between electrical conductivity and magnetic interactions. In this regard, a combination of TTF-based organic donors and magnetic anions having d-electrons could give rise to an interesting family of materials, classified as organic-inorganic hybrids, in which the spins are localized on the transition metals (d-electrons). In these materials, an interesting interplay between electron transport and magnetism could be produced by a long-range magnetic coupling between localized spins through the mobile π-electrons of the conducting networks (Scheme 1).

An alternative way of designing a molecule-based magnetic material would be to construct an organic compound in which the localized spins are borne by an organic radical.[11]

3. Conducting and Magnetic Materials

Conducting organic materials incorporating localized spin first appeared in the early 1980s.[4] In particular, (TMTSF)$FeCl_4$ and (TMTTF)$FeCl_4$ [4b] were the first compounds in which it was claimed that the weak antiferromagnetic interactions observed between the localized spins were mediated by the organic system. Since then, many compounds have been synthesized and characterized, but most of these materials show one of the following unfavorable situations between the two properties: (i) Stabilization of the superconducting state with paramagnetic anions, as in (BEDT-TTF)$_4$[$(H_2O)Fe(C_2O_4)_3$]C_6H_5CN (T_c = 8.5 K)[5a] and (BETS)$_2$($FeCl_4$)$_{0.5}$-($GaCl_4$)$_{0.5}$ (T_c = 4.6 K)[12] [BETS = bis(ethylene dithiotetraselenafulvalene)], (ii) Coexistence of two completely independent metallic and ferromagnetic sublattices, as in the recently-reported metal ferromagnets (BEDT-TTF)$_3$[$MnCr(C_2O_4)_3$][5d] and (BO)$_3$[$FeCr(C_2O_4)_3$],[5e] (iii) The presence of magnetic interactions not mediated by the conducting electrons, as found in some insulating salts of TTF derivatives containing $[Cr(NCS)_4(phen)]^-$,[8a] (phen = 1,10-phenanthroline). However, the following interesting examples are worthy of note.

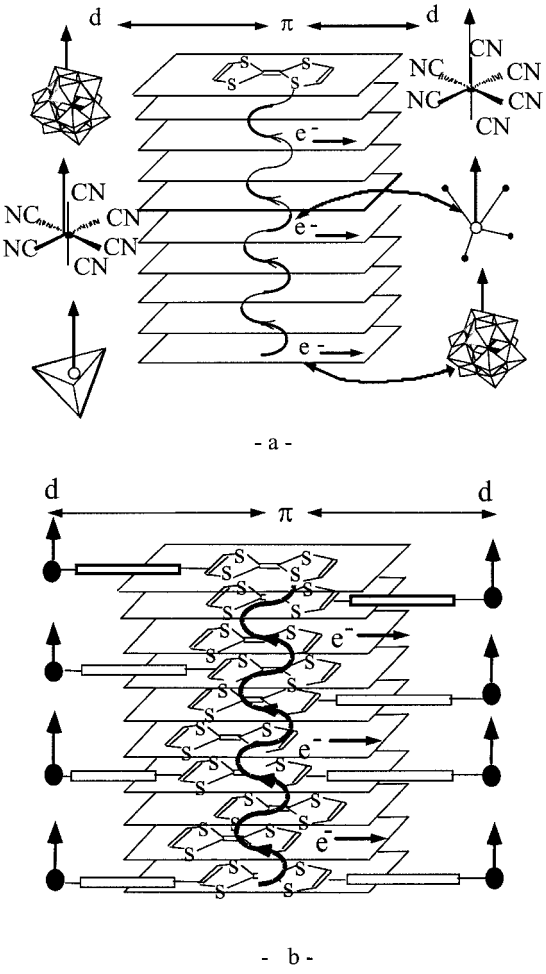

Scheme 1. Representation of the indirect exchange mechanism; (a) through space interaction, (b) through bridge interaction

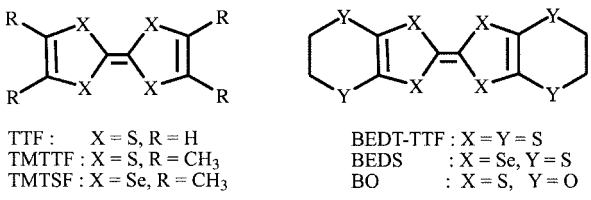

Scheme 2. Some typical organic donors; TTF = tetrathiafulvalene; TMTTF = tetramethyl-TTF; TMTSF = tetramethyltetraselenafulvalene; BEDT-TTF = bis(ethylenedithio)-TTF; BEDS = bis(ethylenedithio)tetraselenafulvalene; BO = bis(ethylenedioxo)-TTF

 © 2004 Wiley-VCH Verlag GmbH & Co. KGaA, Weinheim

3.1. $(BEDT\text{-}TTF)_3(CuCl_4)H_2O$

This compound was the first BEDT-TTF stable organic metal with a paramagnetic anion;[5f] it is metallic down to very low temperatures (200 mK). No superconductivity was observed under pressure (up to 12 kbar) at temperatures down to 2 K. The product of the susceptibility and the temperature ($\chi_M T$), obtained from ESR measurements, shows a gradual increase at low temperature, indicating short-range ferromagnetic interactions between the Cu^{II} atoms. The Cu···Cu distance was found to be greater than 8.5 Å, resulting in insignificant exchange interactions. A more probable explanation for this behavior is the possibility of indirect exchange through the free electrons of the conducting layer.

3.2. $(BETS)_2(MCl_4)$ ($M = Fe^{III}$, Ga^{III})

A series of BETS conductors with MX_4^- anions [$M = Fe^{III}$ ($S = 5/2$) and Ga^{III} ($S = 0$)] have been reported by Kobayashi et al.[12] These compounds [formulated as $(BETS)_2(MCl_4)$] revealed a rich polymorphism and some interesting properties, including superconductivity in the alloy $(BETS)_2(Fe_{0.5}Ga_{0.5}Cl_4)$. The compounds λ-$(BETS)_2(Fe^{III}Cl_4)$, containing a paramagnetic anion with $S = 5/2$, and its isomorphous salt λ-$(BETS)_2(Ga^{III}Cl_4)$, containing a diamagnetic anion are worthy of discussion. The crystal structures of these two compounds are identical, but their electrical conductivities are very different. Both salts are metallic between 300 K and 8 K, and have almost identical conductivities. But below 8 K, the Ga^{III}-containing salt has a superconducting transition, whereas the Fe^{III}-containing salt has a metal to insulator (MI) transition. It appears that the presence of paramagnetic species strongly influences the electrical conductivity in the donor layers. In agreement with this hypothesis, it was possible to restore the metallic state below 8 K at high magnetic fields.[12b,12c]

3.3 $(DMET)_2FeBr_4$ and $(EDTDM)_2FeBr_4$

These two compounds are isostructural.[15] They consist of alternately stacked donor conducting layers and square-lattice magnetic layers of Fe^{3+} with localized spins ($S = 5/2$). In each donor sheet, donor molecules form 1D chains subjected to weak inter-chain interactions, giving 3/4-filled quasi-1D π-electronic systems. The resistivity shows metallic features down to temperatures of about 40 K and 15 K for $(DMET)_2FeBr_4$ and $(EDTDM)_2FeBr_4$, respectively, below which the insulating SDW emerges. The magnetism is governed mainly by the Fe^{3+} ($S = 5/2$) localized spins. In $(DMET)_2FeBr_4$ and $(EDTDM)_2FeBr_4$, Fe^{3+} spins undergo 3D antiferromagnetic (AF) ordering at $T_N = 3.7$ and 3 K, respectively.

The magnetization curves are anomalous, as shown for $(DMET)_2FeBr_4$ in Figure 2 (a). Application of the external field along the spin-easy axis gives a spin-flop transition when B_{SF} is approximately 2 T. In addition, an anomaly appears around $B_2 \approx 5$ T in the hard axis direction. This feature cannot be explained only by Fe^{3+} spins, suggesting that donor electrons participate in the magnetization.

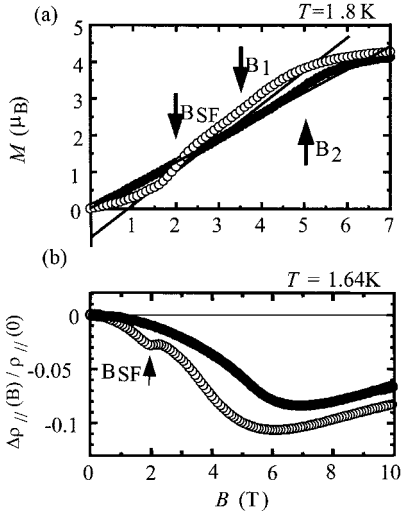

Figure 2. Field dependence of the magnetization; (a) and the in-plane magnetoresistance; (b) for $(DMET)_2FeBr_4$; open and closed circles denote the data for the field applied along the spin-easy and spin-hard axes, respectively; B_{SF} is the field of the spin-flop transition; B_1 and B_2 are the fields at which anomalies appear in the magnetization curves

Figure 2 (b) represents the magnetoresistance (MR) vs. field plot below T_N for the in-plane electron transport of $(DMET)_2FeBr_4$. The MR is negative in the whole field range up to 15 T with a minimum at around 6 T. Interestingly, an anomalous discontinuity exists at B_{SF}, when the field is applied in the spin-easy axis direction. For the field along the hard axis, the MR shows a discontinuity at $B_2 \approx 5$ T, at which the magnetization has an anomaly, as we can see by taking the derivative of the MR with respect to B.

The correlation between the magnetic behavior and the magnetoresistance features can be understood by the formation of SDW in the insulating phase. Below T_{MI}, localized magnetic moments generated in the donor electronic system are spatially ordered. A simple analysis gives the fourfold periodicity in the SDW state along the chain, since the donor is in the 3/4-filled electronic state. In the SDW state, in which the periodicity of the Fe^{3+} AF arrangement is well registered to the SDW, Fe^{3+} spins become antiferromagnetically ordered below T_N. This results in an enhancement of the SDW gap, compared to the case which has no internal magnetic field of Fe^{3+} spins. However, well above the field at which all the Fe^{3+} spins are ferromagnetically arranged, the potential of the Fe^{3+} magnetic lattice does not modify the SDW gap. Therefore, the elevation of the field strength gives negative MR up to the saturation field of Fe^{3+} spins. At fields higher than the field at which the SDW state is destroyed, individual electrons contribute to the transport, resulting in an increase in the MR. The anomaly at B_{SF} in the MR is the consequence of a subtle change in the magnetic energy, which modifies the SDW gap slightly.

 © 2004 Wiley-VCH Verlag GmbH & Co. KGaA, Weinheim

4. Current Developments

In order to establish magnetic or (at least) structural interactions between the organic and inorganic sublattices, some ideas are currently being explored in our groups. The first consists of using halogen-substituted organic donors and polycyanide anions.[5b,7b] The second uses an inorganic anion with π ligands[8] and the third (which is very recent) deals with coordination complexes containing TTF or its derivatives as ligands.[9,10,16]

4.1. Halogen-Substituted Donors

The nitrogen-halogen interaction is known from crystal engineering, and was used to construct the molecular pathway.[17] In our case, we used the unsymmetrical halogen-substituted organic donors DIETS [diiodo (ethylenedithio)-dithiadiselenafulvalene], DIEDO [diiodo(ethylenedioxo)-tetrathiafulvalene] and DIET [diiodo(ethylenedithio)tetrathiafulvalene],[18] which have two terminal iodine atoms with paramagnetic polycyanometalates such as $[M(CN)_6]^{3-}$ [7b] and $[Ni(mnt)_2]^{-}$ [7] as anions (Scheme 3). We describe here two types of compounds containing these anions.

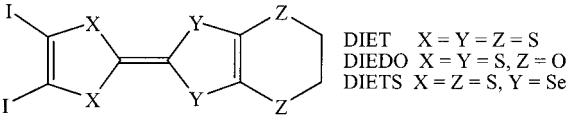

Scheme 3. Organic donors bearing iodine atoms

4.1(a). $(DIETS)_8[Cr(CN)_6]_{0.67}Cl_2 2H_2O$

This compound has a typical layered crystal structure with extremely short Donor···Anion (I···N) contacts.[7b] These distances (in the range 2.722 to 2.825 Å) are slightly shorter than the sum of van der Waals (vdW) separation of ca. 3.65 Å. From the physical properties (Figure 3) we concluded that this compound is semiconducting and paramagnetic. The dc. electrical conductivity measurements over the range 20−300 K show semiconducting behavior, with $\sigma_{RT} \approx 0.2\ Scm^{-1}$ and $E_A = 65$ K. The magnetic susceptibility (Figure 3) obeys the Curie−Weiss law ($C = 1.571$ emu K^{-1} mol^{-1}, $\Theta = -0.2$ K), and there is no magnetic ordering down to 1.7 K. The small Weiss temperature and the absence of any magnetic phase transition shows that the exchange interaction between the magnetic anions is small. The decrease of $\chi_M T$ at low temperature is attributed to AF interactions in the organic layer. Therefore, despite the very short contact attained in this compound, no magnetic interactions were observed between the conduction and magnetic systems.

4.1(b). $(EDO\text{-}TTFI_2)M(mnt)_2$ (M = Ni, Pt): An "Organic Metal" with a Ferromagnetic Interaction

$(EDO\text{-}TTFI_2)M(mnt)_2$ (M = Ni, Pt) complexes feature 1D metal chains (the donor EDO-$TTFI_2$ columns) and 1D magnetic chains [the $M(mnt)_2$ anion columns], which are

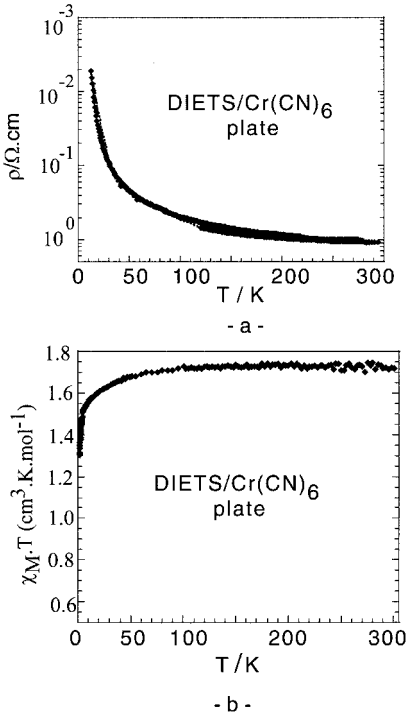

Figure 3. (a) Electrical conductivity and (b) magnetic properties of $(DIETS)_8[Cr(CN)_6]_{0.67}Cl_2 2H_2O$

aligned parallel to each other along the *c*-axis, as shown in Figure 4.[7a] The donor chain has a 3/4-filled state; the metal-insulator transition, T_{MI} = 88 and 96 K for M = Ni and Pt, respectively.

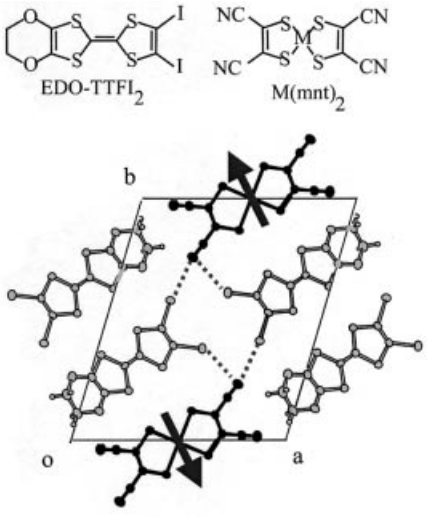

Figure 4. Crystal structure of $(EDO\text{-}TTFI_2)_2M(mnt)_2$ (M = Ni, Pt); dotted lines denote close CN−I atomic contacts between donor and anion; localized spins (S = 1/2) on acceptors are shown with arrows

The anion is in the half-filled state with a localized moment of S = 1/2. The temperature dependence of the magnetic susceptibility is shown in Figure 5. The susceptibility provides evidence for the presence of ferromagnetic interaction, as clearly seen from the increasing trend of χT at low

 © 2004 Wiley-VCH Verlag GmbH & Co. KGaA, Weinheim

temperatures for M = Ni and Pt. Actually, the observed susceptibility can be satisfactorily explained in terms of the Heisenberg model (for an $S = 1/2$ 1D ferromagnet), with $J = 18$ K for M = Ni, taking into account the absence of anisotropy in the susceptibility as shown in Figure 5 (a). The absence of 3D long-range order is the consequence of the 1D Heisenberg isotropic spin feature. For the Pt complex, the susceptibility has a large anisotropy dependent on the field direction [as shown in Figure 5 (b)], where the fitting is satisfactory with the Ising model (for an $S = 1/2$ 1D ferromagnet), with $J = 20$ K. From the peak in the susceptibility, it is clear that long-range 3D ordering takes place at $T_N = 5.5$ K; the weak inter-chain AF interaction ($J' \approx -0.05$), with the aid of the anisotropy, plays an important role, giving an antiparallel arrangement of ferromagnetic chains.

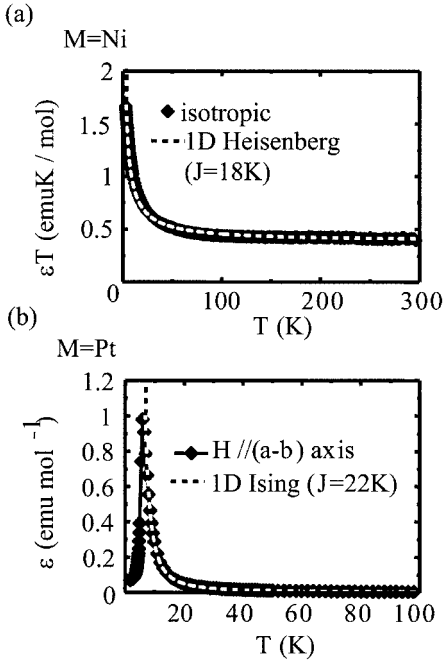

Figure 5. (a) χT vs. T plot for $(EDO\text{-}TTFI_2)_2Ni(mnt)_2$; the dashed line is the theoretical curve for the Heisenberg model (for a $S = 1/2$ 1D ferromagnet) ($J = 18$ K); (b) χ vs. T plot for $(EDO\text{-}TTFI_2)_2Pt(mnt)_2$; the solid line represents the curve for the Ising model (for a S = 1/2 1D ferromagnet) ($J = 20$ K).

The origin of the ferromagnetic interaction can be explained in terms of McConnell's theory,[19] namely, that the spin polarization effect causes the ferromagnetic interaction. The slipped metal-over-sulfur configuration of $M(mnt)_2$ molecules causes an AF interaction between the small negative spin density on the sulfur atom of an $M(mnt)_2$ unit and a large positive spin density on the metal atom of an adjacent $M(mnt)_2$ unit. Eventually, this local AF configuration produces a ferromagnetic interaction between the large positive spin densities on the metal atoms of adjacent $M(mnt)_2$ molecules.

The interaction between π-conduction carriers and localized spins is an important issue in the development of molecular versions of metal magnets. From this viewpoint, the ESR signal featuring a single Lorentzian shape for M = Ni and the absence of an ESR signal for M = Pt indicate the presence of a considerable interaction between conducting donors and magnetic anions.

4.2. Paramagnetic Anions with π Ligands

Recently, TTF- and TTP- (tetrathiapentalene) derived salts containing $[M(NCS)_4(L)_n]^-$ [where M = Cr^{III}, Fe^{III}, L = 1,10-phenanthroline (phen) or isoquinoline (isoq)] have been reported[8] (Scheme 4). In these compounds, magnetic interactions should be induced by both S···S contacts and π-stacking overlap between the paramagnetic anions and organic radicals. Indeed, a large number of the salts showed long-range ferrimagnetic and weak ferromagnetic order with T_c in the range 4.2−8.9 K.[8]

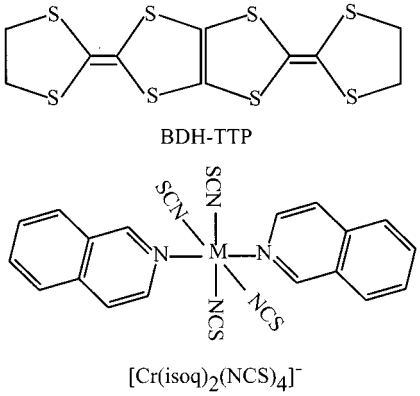

Scheme 4

As an example, we describe here (BDH-TTP)$[Cr(isoq)_2(NCS)_4]$ (**3**),[8c] where BDH-TTP = 2,5-bis(1,3-dithiolan-2-ylidene)-1,3,4,6-tetrathiapentalene. As shown in Figure 6, the crystal structure consists of one-dimensional chains parallel to the *c*-direction, with remarkably short intermolecular S···S distances (in the range 3.264−3.397 Å, vdW = 3.70 Å). The adjacent chains are connected through the π-π overlap of isoquinoline moieties [interplanar separation, $d = 3.600(5)$ Å] between the anions, and short S···S contacts [S(5)−S(5) = 3.640(2) Å] between the donors. In the [101] direction, neighboring anions are related by the *c*-glide plane, and therefore the orientation of these anions is different; the angle between the molecular axes (defined as isoq−M−isoq) is 6.0(3)°.

As expected from the 1:1 stoichiometry and the alternate stacking of donors and anions, the salt has a low conductivity [$\sigma(300\text{ K}) = 10^{-5}$ S cm^{-1}]. Its magnetic susceptibility [Figure 7 (a)] obeys the Curie−Weiss law above 50 K, with $\Theta = -20.4$ K and $C = 2.19$ emu K mol^{-1}, which is close to the corresponding spin-only value (2.25 emu K mol^{-1}) for non-interacting anion ($S = 3/2$) and donor ($S = 1/2$) spins, assuming $g = 2.0$ for each species. Below 50 K, $\chi_M T$ decreases with the temperature down to 8 K, but then it shows a steep increase at $T_C = 7.6$ K due to a magnetic transition. The insets of Figure 7 (a) present the field-cooled magnetization (FCM) measured at 10 mT, and the

 © 2004 Wiley-VCH Verlag GmbH & Co. KGaA, Weinheim

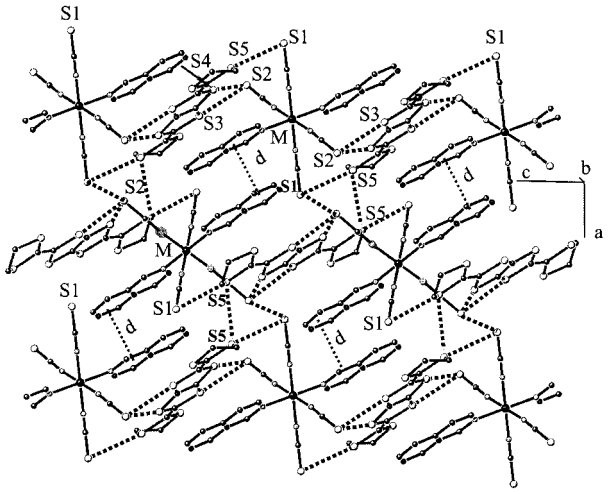

Figure 6. Projection of the crystal structure of (BDH-TTP)[Cr(isoq)$_2$(NCS)$_4$] in the *ac* plane, S···S contacts are shown

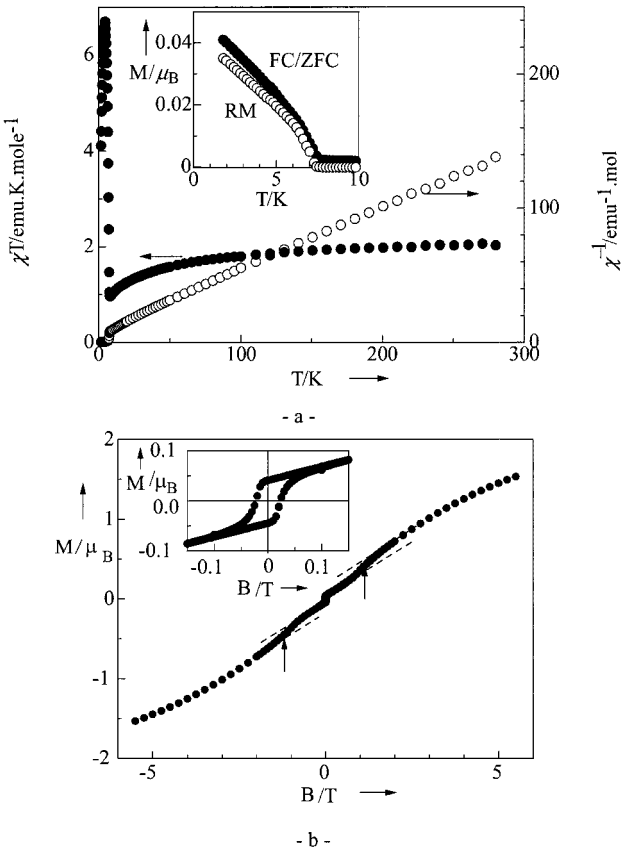

Figure 7. (a) Temperature dependence of $\chi_M T$ (filled circles) and χ_M^{-1} (open circles) for non-oriented samples, measured with an applied field of 10 mT for (BDH-TTP)[Cr(isoq)$_2$(NCS)$_4$]; inset: temperature dependence of the FCM (filled circles) and RM (open circles); (b) magnetization curves at 2 K measured on non-oriented samples; inset: hysteresis loop around B = 0 T

remnant magnetization (RM) observed after the external field of 10 mT is removed at 1.8 K. Below T_C = 7.6 K, the FCMs increase steeply and the RMs also emerge, indicating the presence of spontaneous magnetization. Moreover, in the magnetization curve a hysteresis loop is also observed around B = 0 T [Figure 7 (b)].

This salt has a bulk weak ferromagnetic state, originating from the angled alignment of the one-dimensional ferrimagnetic chains involving d-electrons and π-electrons. The origin of the intra-chain AF coupling are the short intermolecular S···S contacts between donors and anions, whereas the inter-chain coupling comes from the π-π overlap between anions and/or S···S contacts between donors.

4.3. Covalent Links Between Paramagnetic And Conducting Systems

As for the above-described compounds, the strategy commonly used in this area is the assembly of conducting organic sublattices and paramagnetic inorganic sublattices in salts comprising organic ions and paramagnetic inorganic counterions. In general, this yields materials with weak interactions (when they exist at all) between the two systems.

We are currently developing a strategy which consists in preparing new materials where the conducting and magnetic systems are covalently linked through a π-conjugated bridge, as shown in Scheme 1.[9,10] We have therefore synthesized and characterized new paramagnetic coordination complexes containing TTF or BEDT-TTF as ligands, as well as their radical cation salts. We present here as an example [Cu^{II}(hfac)$_2$](TTF-py)$_2$, where hfac = hexafluoroacetylacetonate[10] and TTF-py = 4-(2-tetrathiafulvalenylethenyl) pyridine. Its molecular and crystal structure are shown in Figure 8 (a). The Cu atom is bonded in the equatorial plane to the oxygen atoms of two bidentate hfac anions. The TTF-py ligands occupy the apical positions and are *trans* to each other; they are then bonded to the metal atom through the nitrogen atoms of the pyridyl ring. The crystal structure [Figure 8 (b)], consists of alternate organic (TTF-py) and inorganic [Cu(hfac)$_2$] layers, linked by a conjugated bridge. The two TTF moieties are neutral, and therefore this complex is insulating and paramagnetic, as expected.

The following step of this work was obviously the partial oxidation of these TTF-py ligands to introduce electrical conductivity. A part of this goal has now been achieved by the synthesis and the characterization of the unprecedented radical cation salt [Cu(hfac)$_2$(TTF-py)$_2$][PF$_6$][10] [Figure 9 (a)].

The bond lengths around the Cu atom are very close to those found in the neutral complex, but the central C=C bond length of the TTF-py moiety [1.369(8) Å], which is more sensitive to oxidation, is slightly larger than in the neutral complex [1.317(10) Å]. From the stoichiometry, we can deduce that the charge distribution is [Cu^{2+}(hfac)$_2^{2-}$(TTF-py)$_2^{+}$][PF$_6$]$^-$. This gives rise to a mixed valence state in the [Cu^{2+}(hfac)$_2^{2-}$(TTF-py)$_2^{+}$] radical unit. In the crystal structure [Figure 7 (a)], the TTF units form dimers separated by the PF$_6$ anions [Figure 9 (b)]; the isolated dimers are of course in the mixed valence state. Actually, this structural arrangement is not favorable for electrical conductivity, and therefore further work is needed to achieve electrical conductivity. Studies investiga-

 © 2004 Wiley-VCH Verlag GmbH & Co. KGaA, Weinheim

ting systematic changes in anions, metals and ligands are currently underway.

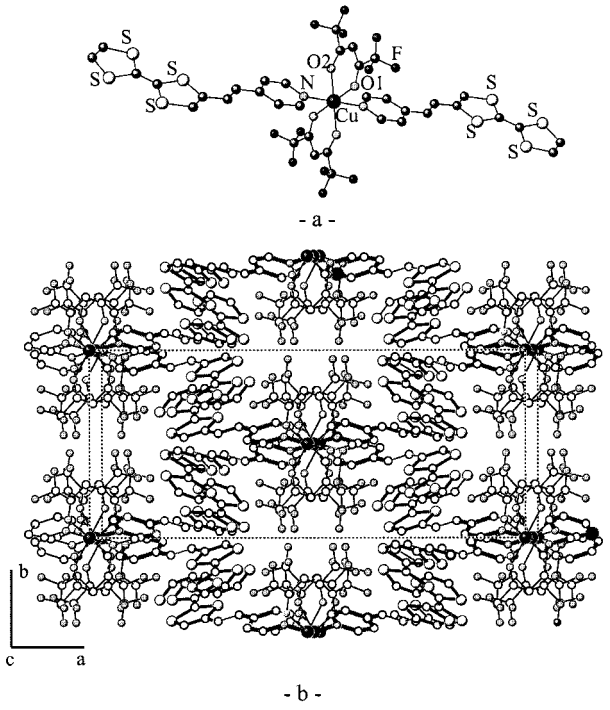

Figure 8. Molecular and crystal structure of $[Cu^{II}(hfac)_2](TTF\text{-}py)_2$, showing separate layers of organic and inorganic units linked by conjugated bridges

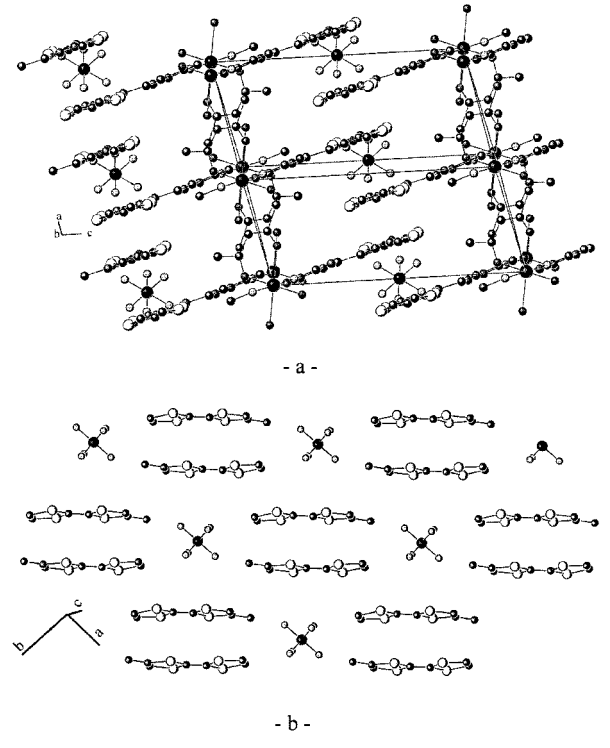

Figure 9. (a) Crystal structure of $[Cu^{2+}(hfac)_2^{2-}(TTF\text{-}py)_2^{+}][PF_6]^{-}$; (b) projection of the organic layer in the *ab* plane

5. Conclusions

In $(DIETS)_8(Et_4N)[Cr(CN)_6]_{0.66}Cl_2 2H_2O$, short I···N contacts were observed between donors and anions. This compound is semiconducting and paramagnetic. However, despite these very short contacts, no magnetic exchange interactions between donor π-electrons and anion d-electrons have been observed. $(EDO\text{-}TTFI_2)M(mnt)_2$ complexes (M = Ni, Pt) are metallic with ferromagnetic interactions, and $(BDH\text{-}TTP)[Cr(isoq)_2(NCS)_4]$ belongs to a series of insulating weak ferromagnets with T_c values in the range 5.8−8.9 K.

Finally, new transition metal complexes and their radical cation salts containing organic donor (TTF-py) as ligands covalently linked through π-conjugated bridges have been presented. These compounds are very promising and constitute a new approach for obtaining π-d interactions in bifunctional conducting and magnetic molecular materials.

From the present results, a combination of TTF-based donors and magnetic anions having d-electrons as building blocks should be expected to produce a large variety of molecular magnets having an unconventional interplay of electron transport and magnetism, owing to the hybrid structure of two components with different functions.

Acknowledgments

This work is supported by the French CNRS PICS program No 1433 and the University of Rennes 1. T. E. was partly supported by a Grant (Aids for Scientific Research, No. 15073211) from the Ministry of Education, Science, Sports, and Culture, Japan.

[1] O. Kahn, *Molecular Magnetism*, Verlag-Chemie, New York, **1993**. [1b]T. Enoki, J. I. Yamaura, A. Miyazaki, *Bull. Chem. Soc. Jpn.* **1997**, *70*, 2005−2023. [1c] L. Ouahab, *Chem. Mater.* **1997**, *9*, 1909−1926.

[2] [2a] P. Day, *Science* **1993**, *261*, 431−432. [2b] O. Kahn, *Comments Cond. Mat. Phys.* **1994**, *17*, 39−58. [2c] S. Decurtins, H. W. Schmalle, P. Schneuwly, L. Ensling, P. Gütlich, *J. Am. Chem. Soc.* **1994**, *116*, 9521−9528. [2d] O. Sato, T. Iyoda, A. Fujishima, K. Hashimoto, *Science* **1996**, *272*, 704−705. [2e] S. Ohkoshi, A. Fujishima, K. Hashimoto, *J. Am. Chem. Soc.* **1998**, *120*, 5349−5350. [2f] A. Bleuzen, C. Lomenech, A. Dolbecq, F. Villain, A. Goujon, O. Roubeau, M. Noguez, F. Varret, F. Baudelet, E. Dartyge, C. Giorgetti, J.-J. Gallet, C. Cartier dit Moulin, M. Verdaguer, *Mol. Cryst. Liq. Cryst.* **1999**, *335*, 253−262. [2g] M. Verdaguer, A. Bleuzen, V. Marvaud, J. Veissermann, M. Seuleiman, C. Desplanches, A. Cuiller, C. Train, R. Garde, G. Gelly, C. Lomenech, L. Rosenman, P. Veillet, C. Cartier dit Moulin, F. Villain, *Coord. Chem. Rev.* **1999**, *190−192*, 1023−1047.[2h] O. Kahn, O. Cador, J. Larionova, C. Mathonière, J. P. Sutter, L. Ouahab, *Mol. Cryst., Liq. Cryst.* **1997**, *305*, 1−16. [2i] S. Turner, C. Michaut, O. Kahn, L. Ouahab, A. Lecas, E. Amouyal, *New. J. Chem.* **1995**, *19*, 773−775.

[3] J. P. Sutter, M. Fettouhi, C. Michaut, L. Li, L. Ouahab, O. Kahn, *Angew. Chem. Int. Ed. Engl.* **1996**, *35*, 2113−2116.

[4] [4a] R. T. Henriques, L. Alcacer, J. P. Pouget, D. Jérôme, *J. Phys. C, Solid State Phys.* **1984**, *17*, 5197−5208. [4b] P. Batail, L. Ouahab, J. B. Torrance, M. L. Pylmann, S. S. P. Parkin, *Solid State Commun.* **1985**, *55*, 597−600. [4c] A. Aumuller, P. Erk, G. Klebe, S. Hunig, J. U. Shutz, H. P. Werener, *Angew. Chem. Int. Ed. Engl.* **1986**, *25*, 740−741. [4d] M. Y. Ogawa, J. Martinsen, S. M.

 © 2004 Wiley-VCH Verlag GmbH & Co. KGaA, Weinheim

Palmer, J. L. Stanton, J. Tanaka, R. L. Greene, B. M. Hoffman, J. A. Ibers, *J. Am. Chem. Soc.* **1987**, *109*, 1115−1121. [4e] M. Lequan, R. M. Lequan, C. Hauw, J. Gaultier, G. Maceno, P. Delhaès, *Synth. Metals* **1987**, *19*, 409−414. [4f] T. Mori, P. Wang, K. Imaeda, T. Enoki, H. Inokuchi, F. Sakai, G. Saito, *Synth. Metals.* **1988**, *27*, A451−456. [4g] T. Mallah, C. Hollis, M. Kurmoo, P. Day, M. Allan, R. H. Friend, *J. Chem. Soc., Dalton Trans.* **1990**, 859−865.

[5] [5a] A. W. Graham, M. Kurmoo, P. Day, *J. Chem. Soc., Chem. Commun.* **1995**, 2061−2062. [5b] P. Le Maguerès, L. Ouahab, N. Conan, C. J. Gomez-Garcia, P. Delhaès, J. Even, M. Bertault, *Solid State Commun.* **1996**, *97*, 27−32. [5c] H. Kobayashi, A. Kobayashi, P. Cassoux, *Chem. Soc. Rev.* **2000**, *29*, 325−333. [5d] E. Coronado, J. R. Galan-Mascaros, C. J. Gomez-García, V. N. Laukhin, *Nature* **2000**, *408*, 447−449. [5e] H. Yamochi, T. Kawasaki, Y. Nagata, M. Maesato, G. Saito, *Mol. Cryst. Liq. Cryst.* **2002**, *376*, 113−120. [5f] P. Day, M. Kurmoo, T. Mallah, I. R. Marsden, R. H. Friend, F. L. Pratt, W. Hayes, D. Chasseau, J. Gaultier, G. Bravic, L. Ducasse, *J. Am. Chem. Soc.* **1992**, *114*, 10722−10729.

[6] [6a] L. Ouahab, M. Bencharif, D. Grandjean, *C. R. Acad. Sci. Paris* **1988**, *Serie II. 307*, 749−752. [6b] L. Ouahab, M. Bencharif, A. Mhanni, D. Pelloquin, J. F. Halet, O. Peña, J. Padiou, D. Grandjean, C. Garrigou-Lagrange, J. Amiell, P. Delhaès, *Chem. Mater.* **1992**, *4*, 666−674. [6c] C. J. Gomez-Garcia, L. Ouahab, C. Gimenez-Saiz, S. Triki, E. Coronado, P. Delhaès, *Angew. Chem. Int. Ed. Engl.* **1994**, *33*, 223−226.

[7] [7a] J. Nishijo, E. Ogura, J. I. Yamaura, A. Miyazaki, T. Enoki, T. Takano, Y. Kuwatani, M. Iyoda, *Solid State Commun.* **2000**, *116*, 661−664. [7b] D. Thoyon, K. Okabe, T. Imakubo, S. Golhen, A. Miyazaki, T. Enoki, L. Ouahab, *Mol. Cryst. Liq. Cryst.* **2002**, *376*, 25−32.

[8] [8a] S. S. Turner, C. Michaut, S. Durot, P. Day, T. Gelbrich, M. B. Hursthouse, *J. Chem. Soc., Dalton Trans.* **2000**, 905−909. [8b] F. Setifi, S. Golhen, L. Ouahab, S. S Turner, P. Day, *Cryst. Eng. Commun.* **2002**, *4*, 1−6. [8c] F. Setifi, S. Golhen, L. Ouahab, A. Miyazaki, K. Okabe, T. Enoki, T. Toita, J. Yamada, *Inorg. Chem.* **2002**, *41*, 3786−3790. [8d] F. Setifi, L. Ouahab, S. Golhen, A. Miyazaki, T. Enoki, J. Yamada, *C. R. Acad. Sci. Paris, Chimie* **2003**, *6*, 309−316. [8e] A. Miyazaki, K. Okabe, T. Enoki, F. Setifi, S. Golhen, L. Ouahab, T. Toita, J. Yamada, *Synth. Met.* **2003**, *137*, 1195−1196.

[9] [9a] F. Iwahori, S. Golhen, L. Ouahab, R. Carlier, J. P. Sutter, *Inorg. Chem.* **2001**, *40*, 6541−6542. [9b] L. Ouahab, F. Iwahori, S. Golhen, R. Carlier, J. P. Sutter, *Synt. Metals* **2003**, *133−134*, 505−507.

[10] F. Setifi, L. Ouahab, S. Golhen, Y. Yoshida, G. Saito, *Inorg. Chem.* **2003**, *42*, 1791−1793.

[11] T. Sugawara, *Mol. Cryst. Liq. Cryst.* **1999**, *334*, 257−273.

[12] [12a] H. Kobayashi, H. Tomita, T. Naito, A. Kobayashi, F. Sakai, T. Watanabe, P. Cassoux, *J. Am. Chem. Soc.* **1996**, *118*, 368−377. [12b] A. Kobayashi, T. Udagawa, H. Tomita, T. Naito, H. Kobayashi, *Chem. Lett.* **1993**, 1559−1562. [12c] F. Goze, V. N. Laukhin, L. Brossard, A. Audouard, J. P. Ulmet, S. Askenazy, T. Naito, H. Kobayashi, A. Kobayashi, M. Tokumoto, P. Cassoux, *Europhys. Lett.* **1994**, *28*, 427−431.

[13] [13a] F. Setifi, S. Golhen, L. Ouahab, A. Miyazaki, K. Okabe, T. Enoki, T. Toita, J. Yamada, *Inorg. Chem.* **2002**, *41*, 3761−3768. [13b] F. Setifi, A. Ota, S. Golhen, L. Ouahab, H. Yamochi, G. Saito, *J. Solid State Chem.* **2002**, *168*, 450−456.

[14] [14a] T. Ishiguro, K. Yamaji, G. Saito, *Organic Superconductors*, **1998**, Springer, Berlin. [14b] J. M. Williams, J. R. Ferraro, R. J. Thorn, K. D. Carlson, U. Geiser, H. H. Wang, A. M. Kini, M. H. Whangbo, in *Organic Superconductors. Synthesis, Structure, Properties and Theory*, R. N. Grimes, (Ed.), Prentice Hall, Englewood Cliffs, New Jersey, **1992**.

[15] [15a] K. Enomoto, A. Miyazaki, T. Enoki, *Synth. Metals* **2001**, *120*, 977−978. [15b] K. Okabe, K. Enomoto, A. Miyazaki, T. Enoki, *Mol. Cryst. Liq. Cryst.* **2002**, *376*, 513−518. [15c] K. Enomoto, A. Miyazaki, T. Enoki, *Bull. Chem. Soc. Jpn.* **2003**, *76*, 945−959.

[16] [16a] S.-X. Liu, S. Dolder, M. Pilkington, S. Decurtins, *J. Org. Chem.* **2002**, *67*, 3160−3162. [16b] W. Xu, D. Zhang, H. Li, D. Zhu, *J. Mater. Chem.* **1999**, *9*, 1245−1249. [16c] S. Bouguessa, K. Hervé, S. Golhen, L. Ouahab, J. M. Fabre, *New J. Chem.* **2003**, *27*, 560−564. [16d] S-X. Liu, S. Dolder, P. Franz, A. Neels, H. Stoeckli-Evans, S. Decurtins, *Inorg. Chem.* **2003**, *42*, 4801−4803. [16e] S. Bouguessa, A. Gouasmia, S. Golhen, L. Ouahab, J. M. Fabre, *Tetrahedron Lett.* **2003**, *44*, 9275−9278.

[17] G. R. Desiraju, R. L. Harlow, *J. Am. Chem. Soc.* **1989**, *111*, 6757−6764.

[18] T. Imakubo, H. Sawa, R. Kato, *J. Chem. Soc., Chem. Commun.* **1995**, 1667−1668.

[19] H. M. McConnel, *J. Chem. Phys.* **1963**, *39*, 1910−1911.

Received November 11, 2003

 © 2004 Wiley-VCH Verlag GmbH & Co. KGaA, Weinheim

[η^5:η^1-(3,6-*t*Bu$_2$Flu)SiMe$_2$N*t*Bu]Y(η^1-NC$_5$H$_6$)(py)$_2$: A 1,4-Hydride-Addition Product to Pyridine that Provides Evidence for the First Fluorenyl(hydrido)metal (Group 3) Complex

Evgueni Kirillov,[a] Christian W. Lehmann,[b] Abbas Razavi,[c] and Jean-François Carpentier*[a]

Keywords: Fluorenyl / Hydrides / Insertion / Pyridine / Yttrium

Reaction of pyridine with the "constrained geometry" fluorenyl(hydrido)yttrium complex {[(3,6-*t*Bu$_2$Flu)SiMe$_2$N*t*Bu]Y(H)(THF)}$_2$ selectively gives the 1,4-addition product [η^5:η^1-(3,6-*t*Bu$_2$Flu)SiMe$_2$N*t*Bu]Y(η^1-NC$_5$H$_6$)(py)$_2$, which was characterized by single-crystal X-ray diffraction and ^{1}H and ^{13}C NMR spectroscopy.
(© Wiley-VCH Verlag GmbH & Co. KGaA, 69451 Weinheim, Germany, 2004)

Introduction

Activation of C−H bonds by (hydrido)metal (group 3) complexes is well known for a wide variety of substrates, including aromatic heterocycles.[1] In particular, [(C$_5$Me$_5$)$_2$Ln(H)]$_2$ (where Ln = Lu,[2] Sc,[3] Y[4]) and [(C$_5$H$_4$R)$_2$Y(H)(THF)]$_2$ (where R = H, Me)[5] readily react with 1 equiv. of pyridine (py) leading to *ortho*-metalated pyridine complexes, [(C$_5$R$_5$)$_2$Ln(η^2-(*C*,*N*)-C$_5$H$_4$N)]. In the presence of an excess of a strong Lewis base, such as THF or pyridine, the released dihydrogen may initiate the reductive transformation of the 2-pyridyl complexes to 1,2-hydride-addition products, eventually followed by isomerization to the 1,4-addition products upon heating.[4] Polar solvents promote direct addition of Ln−H to the pyridine ring.[5] Several yttrium hydrides bearing non-cyclopentadienyl ligands have been found to undergo such an insertion, giving directly both 1,2- and 1,4-addition products.[6] The structure of the 1,2-addition product, {[6,6′-Me$_2$-(C$_6$H$_3$)$_2$]-(2,2′-NSiMe$_2$*t*Bu)$_2$}Y(η-NC$_5$H$_6$)(py)$_2$, was established by X-ray diffraction.[7] In this contribution, we report the first structurally characterized example of a 1,4-addition pyridine product, which provides indirect evidence for the formation of the first (hydrido)metal (group 3) complex supported by a fluorenyl ligand.

[a] Organométalliques et Catalyse, UMR 6509 CNRS-Université de Rennes 1, Institut de Chimie de Rennes,
35042 Rennes Cedex, France
Fax: (internat.) + 33-2-23236939
E-mail: jean-francois.carpentier@univ-rennes1.fr
[b] Max-Planck-Institut für Kohlenforschung, Chemical Crystallography,
Postfach 101353, 45466 Mülheim/Ruhr, Germany
[c] Atofina Research,
Zone Industrielle C, 7181 Feluy, Belgium

Results and Discussion

Recently we have reported on the synthesis and characterization of the first "constrained geometry" (alkyl)yttrium complex [η^3:η^1-(3,6-*t*Bu$_2$Flu)SiMe$_2$N*t*Bu]Y(CH$_2$SiMe$_3$)(THF)$_2$ (**1**), stabilized by a fluorenyl-amido ligand.[8] In the course of these studies, we found that **1** reacts equally with H_2 or $PhSiH_3$ under ambient conditions (25 °C, 1 atm) to generate a yellow microcrystalline solid in high yield. Considering this reactivity and consistent with elemental analysis, the product was formulated as the putative hydride {[(3,6-*t*Bu$_2$Flu)SiMe$_2$-N*t*Bu]Y(H)(THF)}$_n$ (**2**). However, the surprising insolubility of the latter in common organic solvents (aromatic hydrocarbons, chlorinated solvents, THF), despite the presence of two *tert*-butyl substituents on the fluorenyl ligand, prevented its complete authentication. Complex **2** does not react with an equimolar amount of pyridine after one week at 25 °C but it completely dissolves in a toluene solution at 70 °C after 1 h in the presence of a 20-fold excess of [H$_5$]pyridine (vs. Y) (see Scheme 1). After evaporation of the solution and extraction of the residue with pentane, the new "constrained geometry" (amido)yttrium complex, **3**, was isolated in 69 % yield as an orange-brown crystalline material.

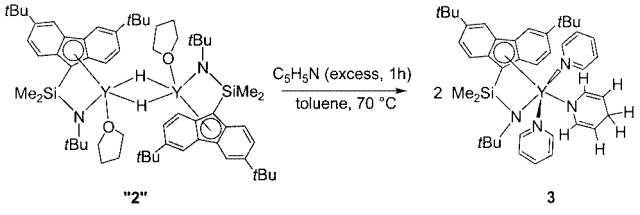

Scheme 1

 DOI: 10.1002/ejic.200300837 © 2004 Wiley-VCH Verlag GmbH & Co. KGaA, Weinheim

^{1}H and ^{13}C NMR spectroscopic data establish that **3** is the sole product of the reductive 1,4-addition of pyridine to the hydrido complex **2**. The ^{1}H NMR spectrum of **3** ([D$_6$]benzene, 25 °C) displays one set of sharp resonances consistent with C_v-symmetry that include one singlet and two doublets from the three pairs of equivalent fluorenyl protons, one singlet from the $SiMe_2$ moiety, and one singlet from each of the *tert*-butyl(fluorenyl) and *tert*-butyl(amido) groups. The 1,4-dihydropyridyl fragment is characterized by a doublet for the 2,6-protons (δ = 6.35 ppm, $^3J_{H,H}$ = 6.9 Hz), a multiplet for the 3,5-protons (δ = 4.59 ppm) and a broad singlet for the 4-methylene group (δ = 3.61 ppm).[5] The signals from the coordinated-pyridine molecules are broad at room temperature, which illustrates their fluxional behavior and suggests that they dissociate in solution. On the other hand, there is no evidence for exchange of the coordinated-pyridine molecules with the 1,4-dihydropyridyl fragment, which indicates that the reaction is not reversible at this temperature on the NMR time-scale.

An X-ray-diffraction study confirmed the structure of complex **3** and the coordination of two pyridine molecules in the solid-state (see Figure 1). The formal 18-electron yttrium center is coordinated in a distorted square-pyramidal geometry to four nitrogen atoms and to the centroid of the five-membered ring of the fluorenyl moiety, which occupies the apical position. Complex **3** and the parent alkyl complex **1** have a very similar pseudo-five-coordinate geometry: the THF molecules and the alkyl group in **1** are replaced in **3** by pyridine molecules and by a 1,4-dihydropyridinyl group, respectively. However, the coordination modes of the fluorenyl ligands in the solid-state structures are quite different; that is, in the alkyl complex **1**, the fluorenyl moiety is coordinated in an unusual non-symmetric, exocyclic η^3-coordination mode that involves the bridgehead atom and a neighboring atom of the central five-membered cycle, and the adjacent carbon atom of a phenyl ring.[8] In contrast, the molecular structure of **3** features a symmetric η^5-coordination. This observation is rather surprising considering that pyridine is a stronger base than THF and, therefore, should favor reduced hapticity of the fluorenyl moiety. This difference evidences that the variety of flexible coordination modes of fluorenyl ligands that we recently observed in a series of group 3 metal and lanthanide complexes[8,9] is strikingly dependent on minute electronic and steric factors. The solid-state structure of **3** has a plane of symmetry (non-crystallographic) that embraces the Flu(centroid) and the C(9), N(12), Si(1) and Y(1) atoms as well as the plane of the 1,4-dihydropyridine cycle. The bite angle Flu_{cent}−Y(1)−N(12) is 97.36° and resembles the corresponding Cp_{cent}−Y−N angles (97.1−97.8°) observed in half-sandwich yttrium complexes supported by Cp-amido ligands.[10] The average Y−C (C9, C9a, C8a, C4a, C4b) distance in **3** [2.701(2) Å] is in the range of values 2.646−2.719 Å, observed for other yttrium complexes with silylene-substituted fluorenyl fragments.[11] Similarly, the Y(1)−N(12) bond length of 2.232(2) Å is in the range of 2.208−2.253 Å, found in related "constrained geometry" Cp(amido)yttrium complexes.[10,12] The Y(1)−N(21) bond length between the yttrium and the nitrogen atom of the 1,4-dihydropyridine fragment [2.302(2) Å] is in agreement with the values observed in other yttrium complexes bearing terminal amido groups.[7,13] The bonds in the dihydropyridine fragment (see b in Figure 1) indicate reduction of pyridine via 1,4-insertion,[14] that is, the bond lengths C(22)−C(23) [1.332(3) Å] and C(25)−C(26) [1.338(3) Å] are significantly shorter than the other two C−C bonds in the ring [C(23)−C(24) 1.510(4), C(24)−C(25) 1.484(4) Å]. Also, the angle C(23)−C(24)−C(25) of 108.2(2)° is indicative of the sp^3-hybridization of the C(24) carbon atom.

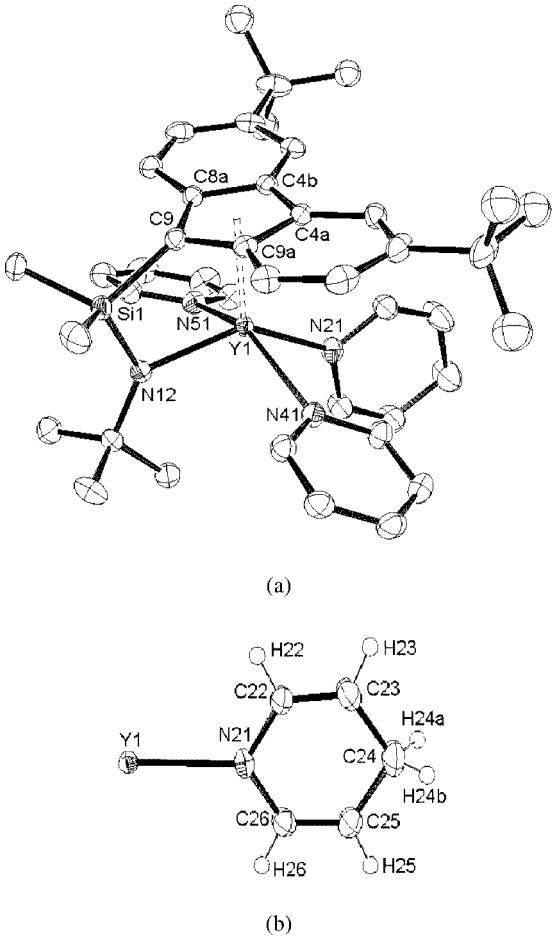

Figure 1. (a) ORTEP drawing of the molecular structure of **3**; thermal ellipsoids are drawn at the 50 % probability level; hydrogen and disordered carbon atoms from *tert*-butyl groups are omitted for the sake of clarity; selected bond lengths (Å) and angles (°) Y(1)−N(12) 2.2319(17), Y(1)−N(21) 2.3015(17), Y(1)−N(41) 2.5325(17), Y(1)−N(51) 2.5383(17), Y(1)−C(9) 2.6021(19), Y(1)−C(9A) 2.6883(18), Y(1)−C(8A) 2.6946(19), Y(1)−C(4B) 2.7588(19), Y(1)−C(4A) 2.7635(18), N(12)−Si(1)−C(9) 99.37(8), N(41)−Y(1)−N(51) 146.28(6), N(21)−Y(1)−N(41) 79.01(6), N(21)−Y(1)−N(51) 78.94(6), N(12)−Y(1)−N(21) 140.10(6); (b) view of the reduced pyridine fragment in **3**; selected bond lengths (Å) and angles (°) N(21)−C(22) 1.381(3), N(21)−C(26) 1.390(3), C(22)−C(23) 1.332(3), C(23)−C(24) 1.510(4), C(24)−C(25) 1.484(4), C(25)−C(26) 1.338(3), C(22)−C(23)−C(24) 123.3(2), C(23)−C(24)−C(25) 108.2(2), C(24)−C(25)−C(26) 123.3(2).

Two possibilities may account for the selective formation of the 1,4-hydride-addition product **3**: (i) although NMR monitoring showed no evidence for the formation of a tran-

 © 2004 Wiley-VCH Verlag GmbH & Co. KGaA, Weinheim

sient 1,2-addition product during the reaction course, the latter may rapidly isomerize to **3** due to the enforced conditions, which are required for completion of the reaction;[5,15] (ii) the reaction may involve direct 1,4-addition: nucleophilic attack on both the 2- and 4-positions is well known for pyridine rings.[16]

In conclusion, the isolation of the 1,4-addition product **3** brings indirect evidence of the hydrido nature of the complex formed by hydrogenolysis of the "constrained geometry" (fluorenyl-amido)yttrium alkyl complex **1**. Although its molecular structure and the reasons for its insolubility remain to be determined, complex **1** is, to the best of our knowledge, the first example of a hydrido complex of a group 3 metal supported by a fluorenyl ligand. The scope of this insertion reaction is currently under investigation.

Experimental Section

Crystallographic Data for 3: $C_{42}H_{55}N_4SiY$, M = 732.90, monoclinic, T = 100 K, space group $C2/c$, a = 23.3709(2), b = 13.03550(10), c = 26.4358(2) Å, α = 90, β = 104.75, γ = 90°, V = 7788.33(11) Å^3, Z = 8, D_c = 1.250 g·cm^{-3}, μ(Mo-K_α) = 1.562 mm^{-1}; 65290 reflections collected, 12419 unique (R_{int} = 0.0504), full-matrix least-squares on F^2 refinement, R_1 = 0.0442 [$I > 2\sigma(I)$], wR_2 = 0.1094 (all data). An orange crystal of dimensions 0.32 × 0.30 × 0.13 mm was coated in oil, mounted on a fibre and X-ray-diffraction data were collected using a Nonius−KappaCCD diffractometer employing CCD scans to cover reciprocal space up to 31.03° with 99.7 % completeness. Integration of raw data yielded a total of 65290 reflections, merged into 12412 unique reflections with R_{int} = 0.0504 after applying Lorentz, polarization and absorption correction. The structure was solved by Patterson methods using SHELXS-97.[17] Atomic positions and displacement parameters, on the anisotropic level for all non-hydrogen atoms, were refined using full-matrix least-squares based on F^2 using SHELXL-97.[17] Refinement of 446 parameters using all reflections converged at R_1 = 0.0442, wR_2 = 0.1094, with the highest residual electron-density peak of 1.2 Å^3. CCDC-219360 contains the supplementary crystallographic data for this paper. These data can be obtained free of charge at www.ccdc.cam.ac.uk/conts/retrieving.html [or from the Cambridge Crystallographic Data Centre, 12, Union Road, Cambridge, CB2 1EZ, UK; Fax: (internat.) +44-1223/336-033; E-mail: deposit@ccdc.cam.ac.uk].

Synthesis of 3: A solution of pyridine (0.668 g, 8.45 mmol, 20 equiv. vs. Y) in toluene (2 mL) was added to a suspension of **2** (0.240 g, 0.211 mmol of the dimer) in toluene (10 mL). The reaction mixture was stirred at 70 °C until complete dissolution of **2** was achieved (ca. 60 min). The resulting orange solution was evaporated under vacuum to give a brown residue, which was extracted with pentane (3 × 10 mL) to yield complex **3** as brown-orange crystals (0.210 g, 69 %) from combined pentane extracts. ^{1}H NMR (300 MHz, [D$_6$]benzene, 25 °C): δ = 8.36 (br. m, 4 H, 2,6-H, py), 8.08 (s, 2 H, 4,5-H, Flu), 7.93 (d, $^3J_{H,H}$ = 8.4 Hz, 2 H, 1,8-H, Flu), 6.88 (d, $^3J_{H,H}$ = 8.3 Hz, 2 H, 2,7-H, Flu), 6.78 (br. m, 2 H, 4-H, py), 6.51 (br. m, 4 H, 3,5-H, py), 6.35 (d, $^3J_{H,H}$ = 6.9 Hz, 2 H, NC*H*CHCH$_2$), 4.59 (m, 2 H, NCHC*H*CH$_2$), 3.61 (s, 2 H, NCHCHC*H*$_2$), 1.35 (s, 9 H, NCC*H*$_3$), 1.31 [s, 18 H, CC*H*$_3$(Flu)], 1.15 (s, 6 H, SiC*H*$_3$) ppm. ^{13}C{^{1}H} NMR (75 MHz, [D$_6$]benzene, 25 °C): δ = 150.8 (C-2,6, py), 140.8 (C-3,6, Flu), 137.4 (C-4, py), 135.9 (N*C*HCHCH$_2$), 126.3 (C-10,13, Flu), 123.5 (C-3,5, py), 123.4 (C-2,7, Flu), 123.1 (C-11,12, Flu), 121.8 (C-1,8, Flu), 116.8 (C-4,5, Flu), 94.7 (NCH*C*HCH$_2$), 82.8 (C-9, Flu), 54.3 (N*C*CH$_3$), 35.3 (NC*C*H$_3$), 33.7 (Flu-*C*CH$_3$), 31.9 (Flu-C*C*H$_3$), 24.9 (NCHCH*C*H$_2$), 7.4 (Si*C*H$_3$) ppm. $C_{42}H_{55}N_4SiY$ (732.92): calcd. C 68.83, H 7.56, N 7.64; found C 67.92, H 7.00, N 7.32.

Acknowledgments

We thank Total co. for financially supporting this research (post-doctoral fellowship to E. K.).

[1] M. Ephritikhine, *Chem. Rev.* **1997**, *97*, 2193.
[2] P. L. Watson, *J. Chem. Soc., Chem. Commun.* **1983**, 276.
[3] M. E. Thompson, S. M. Baxter, A. R. Bulls, B. J. Burger, M. C. Nolan, B. D. Santarsiero, W. P. Schaefer, J. E. Bercaw, *J. Am. Chem. Soc.* **1987**, *109*, 203.
[4] B.-J. Deelman, W. M. Stevels, J. H. Teuben, M. T. Lakin, A. L. Spek, *Organometallics* **1994**, *13*, 3881.
[5] W. J. Evans, J. H. Meadows, W. E. Hunter, J. L. Atwood, *J. Am. Chem. Soc.* **1984**, *106*, 1291.
[6] R. Duchateau, C. T. Van Wee, J. H. Teuben, *Organometallics* **1996**, *15*, 2291.
[7] T. I. Gountchev, T. D. Tilley, *Organometallics* **1999**, *18*, 2896.
[8] E. Kirillov, L. Toupet, C. W. Lehmann, A. Razavi, J.-F. Carpentier, *Organometallics* **2003**, *22*, 4467.
[9] E. Kirillov, L. Toupet, C. W. Lehmann, A. Razavi, S. Kahlal, J.-Y. Saillard, J.-F. Carpentier, *Organometallics* **2003**, *22*, 4038.
[10] [10a] K. C. Hultzsch, T. P. Spaniol, J. Okuda, *Angew. Chem.* **1999**, *111*, 163; *Angew. Chem. Int. Ed.* **1999**, *38*, 227. [10b] K. C. Hultzsch, P. Voth, K. Beckerle, T. P. Spaniol, J. Okuda, *Organometallics* **2000**, *19*, 228. [10c] S. Arndt, P. Voth, T. P. Spaniol, J. Okuda, *Organometallics* **2000**, *19*, 4690. [10d] P. Voth, S. Arndt, T. P. Spaniol, J. Okuda, *Organometallics* **2003**, *22*, 65.
[11] [11a] [η5:η5-(C13H8)SiMe2(C5Me4)]YN(SiMe3)2: M. H Lee, J.-W. Hwang, Y. Kim, J. Kim, Y. Han, Y. Do, *Organometallics* **1999**, *18*, 5124. [11b] [η5:η5-(C13H8)SiMe2(C5H4)]2{Y(μ-Cl)}2 and [η5:η5-(C13H8)SiPh2(3-tBu-C5H3)]2{Y(μ-Cl)}2: C. Qian, W. Nie, J. Sun, *Organometallics* **2000**, *19*, 4134.
[12] A. A. Trifonov, T. P. Spaniol, J. Okuda, *Organometallics* **2001**, *20*, 4869.
[13] [13a] L. Lee, D. J. Berg, G. W. Bushell, *Inorg. Chem.* **1994**, *33*, 5302. [13b] M. T. Gamer, S. Dehnen, P. W. Roesky, *Organometallics* **2001**, *20*, 4230. [13c] Y. Mu, W. E. Piers, M.-A. MacDonald, M. Zaworotko, *Can. Chem. J.* **1995**, *73*, 2233.
[14] For examples of 1,4-hydride-addition products of pyridine with group 12 and 13 metal complexes, see: [14a] Zn(η1-NC5H6)2(py)2: A. L. Spek, *Cryst. Struct. Commun.* **1982**, *11*, 1621. [14b] [Al(η1-NC5H6)4]+[Li(py)4]− and Al(η1-NC5H6)3(py): K. Hensen, A. Lemke, T. Stumpf, M. Bolte, H. Fleischer, C. R. Pulham, R. O. Gould, S. Harris, *Inorg. Chem.* **1999**, *38*, 4700.
[15] The reaction of **2** with [D$_5$]pyridine was also investigated in neat C$_5$D$_5$N as well as with a 20-fold excess (vs. Y) in toluene. In both cases the reaction proceeded only upon heating (70 °C), leading to the corresponding 1,4-addition-product **3**-d_5, without detection of ^{1}H NMR resonances for a possible transient 1,2-intermediate.
[16] J. A. Joule, G. F. Smith, *Heterocyclic Chemistry*, Van Nostrand Reinhold Co.: London, **1972**; chapter 4 and references cited therein.
[17] SHELXS-97 and SHELXS-97, Programs for crystal structure determination and refinement, G. M. Sheldrick, **1997**, University of Göttingen, Germany.

Received November 12, 2003

 © 2004 Wiley-VCH Verlag GmbH & Co. KGaA, Weinheim

Pr_6O_{11} Single-Crystal Nanotubes from a Molten-Salt Synthetic Method

Xun Wang,[a] Jing Zhuang,[a] and Yadong Li*[a]

Keywords: Lanthanides / Molten salts / Nanotubes / Three-dimensional structures / X-ray diffraction

Pr_6O_{11} single-crystal nanotubes with a typical 3-D crystal structure in the bulk have been successfully obtained through a template-free molten-salt synthetic method, the formation of which has been attributed to the periodical defect cluster distribution in the Pr_6O_{11} species. It is believed that the synthesis of this new type of 3-D nanotubes will be helpful to explore more rational synthetic methods to nanotubes of 3-D compounds.
(© Wiley-VCH Verlag GmbH & Co. KGaA, 69451 Weinheim, Germany, 2004)

Introduction

Nanotube materials have drawn continuous research attention because of their distinctive structural features combined with novel chemical and physical properties, which are of great research and application interest in electronic, energy and catalyst fields etc.[1−12] Various substances have been processed into nanotubes driven simply by one motivation: what if they are nanotubes?

It is generally believed that nanotubes are only thermodynamically stable when they have a similar layer structure to graphite.[1] Therefore, for many technologically and scientifically important compounds which do not possess layer structures, such as silicon,[5] GaN,[6] and metals,[7] templates are usually needed to confine and stabilize the growth of their nanotubes, including porous membranes,[8] carbon nanotubes,[9] nanorod arrays[5,6] and nanowires.[7] Some syntheses of nanotubes from 3-D compounds, such as ZnO and Te, have been achieved by melting Zn cores[10] or using Te[11] colloidal seeds as self templates, respectively. Meanwhile, stimulated by the possible rolling process in the formation of nanotubes, the thin-solid-film rolling method has been successfully developed by controlled release of polycrystalline layers from substrates.[12] These 3-D compounds, although restricted by large-scale preparation or crystalline quality, have undoubtedly enriched the nanotube categories and given us more inspiration on the exploration of new synthetic methods. Here, we demonstrate that single-crystal Pr_6O_{11} nanotubes, which have a typical 3-D crystal structure in the bulk, can be obtained through a template-free synthetic method. The formation of this nanotube is believed to be related to the periodical defect-cluster distribution in the Pr_6O_{11} species.

Results and Discussion

Our method was based on a molten-salt synthetic process, which has been widely adopted to prepare oxide nanowires by Wang et al.[13,14] and was recently expanded to the preparation of ZnO microtube arrays by us.[15]

The phase purity of the samples has been characterized on a Bruker D8-advance X-ray powder diffractometer with Cu-K_α radiation (λ = 1.5418 Å). As shown in Figure 1, all the reflections of the XRD patterns can be readily indexed to a pure face-centered cubic face of the Pr_6O_{11} crystal with lattice constants a = 5.4678 Å (JC,PDS 42−1121). The 2θ peaks at values of 28.26, 32.81, 47.04, 55.72, 58.46 and 68.64° correspond to the crystal planes of [111], [200], [220], [311], [222] and [400] of the crystalline Pr_6O_{11} species, respectively. The d values at 28.26° are calculated to be approximately 0.318 nm, corresponding to the [111] plane

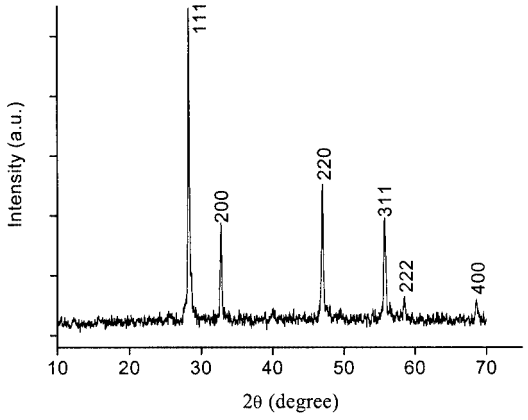

Figure 1. XRD patterns of the Pr_6O_{11} crystal after molten salt thermal treatment

[a] Department of Chemistry and the Key Laboratory of Atomic & Molecular Nanosciences (Ministry of Education, China), Tsinghua University,
Beijing 100084, P. R. China
Fax: (internat.) + 86-10-62788765
E-mail: ydli@tsinghua.edu.cn

 © 2004 Wiley-VCH Verlag GmbH & Co. KGaA, Weinheim **DOI: 10.1002/ejic.200300652**

spacing of the Pr_6O_{11} species. All the information from this XRD pattern indicates that the crystal structure of the Pr_6O_{11} species has been maintained after thermal treatment under current experimental conditions.

Thorough TEM analysis (Figure 2, a and b) has indicated that about 30 % of the raw Pr_6O_{11} microparticles have been converted into nanotubes. TEM analysis have shown that these nanotubes usually have diameters of approximately 10−20 nm and lengths of 100−500 nm; all of them have open ends. It is interesting to find that these nanotubes tend to aggregate together around the microparticles, which may serve as evidence for a possible exfoliation process for the formation of these nanotubes from the starting microparticles of the Pr_6O_{11} species.

HRTEM has provided further insight into the microstructure of these Pr_6O_{11} nanotubes. As shown in Figure 2 (c), the HRTEM image of an individual nanotube clearly demonstrates its multi-wall tubular structure with an outer diameter of approximately 20 nm and an inner diameter of about 6 nm; the interlayer spacing can be calculated to be about 0.320 nm, corresponding to the interlayer spacing of the [111] plane of the body-centered cubic Pr_6O_{11} species. The electron diffraction pattern of this nanotube (Figure 2, inset c) revealed its single-crystal nature and can be indexed as that of the [111] zone axis of the face-centered cubic Pr_6O_{11} species. EDS analysis (Figure 2, e) taken from an individual nanotube has indicated that only Pr and O atoms are present; no Na^+ or Cl^- ions were detected, indicating Pr_6O_{11} nanotubes.

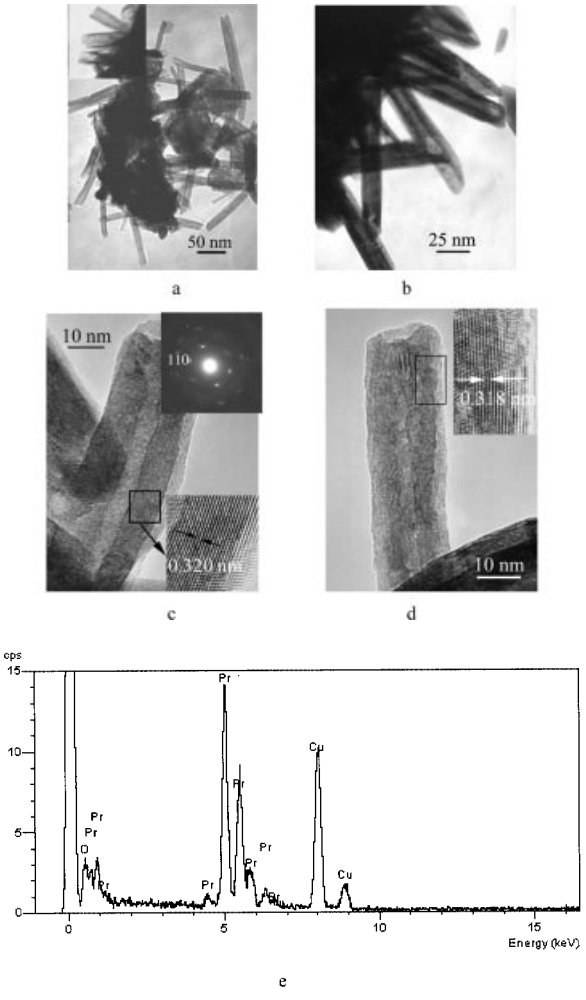

Figure 2. a) TEM images of Pr_6O_{11} nanotubes from NaCl melts; b) TEM images of Pr_6O_{11} nanotubes from KCl melts; c) HRTEM images of a single Pr_6O_{11} nanotube from NaCl melts; inset, electron-diffraction patterns of a single Pr_6O_{11} nanotube; d) HRTEM images of a single Pr_6O_{11} nanotube from KCl melts; e) EDS analysis of a single Pr_6O_{11} nanotube in Figure 2, c)

In contrast to previously reported nanotubes obtained under unrestricted conditions, Pr_6O_{11} nanotubes have no layer structure. Why then are the nanotube structures thermodynamically stable? A further insight into the crystal structure of the Pr_6O_{11} species may help us to illustrate the structure principle of these nanotubes.

The Pr_6O_{11} species is the most thermodynamically stable form of the PrO_x series. X-ray powder diffraction experiments of Pr_6O_{11} nanotubes show that it is related to PrO_2,[16] which has the fluorite structure (Figure 3, a).

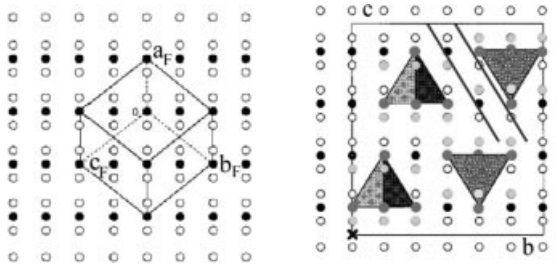

Figure 3. a) Model for the crystal structure of fluorite-type PrO_2; open circles, oxygen atoms; black circles, Pr atoms; b) model for the crystal structure of the Pr_6O_{11} sector viewed along [001] direction; open circles, oxygen atoms; black circles, Pr atoms with an oxidation state of +3; light gray circles, Pr atoms with an oxidation state of +4; dark gray circles, oxygen atoms in Pr_4O_6 vacancy cluster

It is believed that the structures of various intermediate praseodymium oxides are built from a simple basic defect cluster: Pr_4O_6. This defect cluster involves the vacant Pr_4 tetrahedron and its six edge-bridging oxygen atoms and is created when an oxygen atom is extracted from the parent fluorite structure PrO_2,[17,18] which results in two types of Pr cations in the Pr_6O_{11} species: Pr cations participating in the Pr_4O_6 vacancy cluster and those without an oxygen vacancy in their coordination sphere. The formal charge on these two types of Pr ions is +4 and +3, respectively. The result of the cation lattice relaxation is that the intracluster Pr−Pr distances have an average of 4.1 Å, while the intercluster Pr−Pr distances are about 0.4 Å shorter.[19] In other words, the Pr^{3+} ions are crowded into the region between the defect clusters. On the other hand, the dominant chemical force in the rare-earth oxides is ionic in nature, and the electrostatic repulsion between the defect clusters tends to separate them,[19] which may provide the possibility for the exfoliation process of Pr_6O_{11} single-molecule layers from the bulk. Among the different crystal planes of the Pr_6O_{11} structure, the [111] planes have the largest interlayer dis-

 © 2004 Wiley-VCH Verlag GmbH & Co. KGaA, Weinheim

tance (0.318 nm) and thus the weakest interaction between layers, so the [111] plane would be the preferred exfoliation direction, and the obtained Pr_6O_{11} nanotubes would grow along [1$\bar{1}$0] axis, which is consistent with our HRTEM and electron-diffraction analysis. Compared with the reported nanotubes of 2-D sheet structures, the interaction between layers is much stronger, so the crystal-lattice images are usually distorted to some extent (Figure 2, c and d).

The conditions of the exfoliation and the further tube-formation process would be critical considering that the following conditions must be met: 1) enough energy must be provided to overcome the strong electrostatic interaction between layers; 2) the provided energy should be moderate enough so that it cannot break all the layers to lead to the formation of irregular particles without a preferred direction; 3) once the layers have been exfoliated, appropriate hindrance should exist to avoid the recombination of the layers. Our experimental results show that NaCl and KCl melts meets these conditions.

Take NaCl as an example, at 840 °C (the melting point of NaCl is about 808 °C) NaCl will melt and ionize into Na^+ and Cl^- ions, which can attack the crowded $[Pr_x^{3+}O_y^{2-}]^{z-}$ anion and the positively charged $[Pr_4O_6]^{4+}$ vacancy cluster along all directions, so that combinations between layers can be loosened to some extent. Since the interaction between [111] layers is the weakest, exfoliation can occur first along the [111] planes, which can be then stabilized by the high viscosity of the NaCl flux and may lead to the formation of nanotubes.

Although the structural analysis is consistent with our experimental results, a thorough theoretical study is still needed to justify its reasonability. Nevertheless, for the first time, single-crystal nanotubes of Pr_6O_{11} with a typical 3-D crystal structure have been successfully obtained through this unrestricted molten-salt method, which we believe may be expanded to the synthesis of nanotubes with similar structures and will greatly encourage materials scientists to explore more rational synthetic methods for the formation of nanotubes from 3-D compounds.

Experimental Section

Synthesis of Pr_6O_{11} Nanotubes: In a typical synthesis procedure, analytical grade NaCl (1 g, or KCl) and Pr_6O_{11} (0.9 g, purity > 99.9 %) were mixed together, and ground in an agate mortar to form a homogeneous mixture, which was then transferred into a crucible, and calcined at 840 °C in air for 3 h. The system was allowed to cool to room temperature. The solidified NaCl-Pr_6O_{11} products obtained were immersed into fresh water for about ten hours to remove NaCl from the Pr_6O_{11} material, during which fresh water was constantly replaced. Aqueous solutions of $AgNO_3$ (0.1 mol/L) and HNO_3 (1 mol/L) were used to detect the remnant Cl^- ions present in the final products. The resultant black powders were filtered, and dried at 80 °C in air.

Acknowledgments

This work was supported by the NSFC (20025102, 50028201, 20151001), the Foundation for the Author of National Excellent Doctoral Dissertation of P. R. China, and the State Key Project of Fundamental Research for nanomaterials and nanostructures.

[1] R. Tenne, *Prog. Inorg. Chem.* **2001**, *50*, 269.
[2] G. R. Patzke, F. Krumeich, R. Nesper, *Angew. Chem. Int. Ed.* **2002**, 41, 2446.
[3] Y. D. Li, J. W. Wang, Z. X. Deng, Y. Y. Wu, X. M. Sun, D. P. Yu, P. D. Yang, *J. Am. Chem. Soc.* **2001**, *123*, 9904.
[4] [4a] X. Wang, Y. D. Li, *Angew. Chem. Int. Ed.* **2003**, *42*, 3497. [4b] X. Wang, X. Sun, D. Yu, B. Zou, Y. Li, *Adv. Mater.* **2003**, *15*, 1442. [4c] X. Wang, Y. D. Li, *Chem. Eur. J.* **2003**, *9*, 5627.
[5] R. Fan, Y. Y. Wu, D. Y. Li, M. Yue, A. Majumdar, P. D. Yang, *J. Am. Chem. Soc.* **2003**, *125*, 5254.
[6] J. Goldberger, R. R. He, Y. F. Zhang, S. W. Lee, H. Q. Yan, H. J. Choi, P. D. Yang, *Nature* **2003**, *422*, 599.
[7] Y. G. Sun, B. Mayers, Y. N. Xia, *Adv. Mater.* **2003**, 15, 641.
[8] C. R. Martin, *Science* **1994**, *266*, 1961.
[9] P. M. Ajayan, O. Stephan, P. Redlich, C. Colliex, *Nature* **1996**, *375*, 564.
[10] J. J. Wu, S. C. Liu, C. T. Wu, K. H. Chen, L. C. Chen, *Appl. Phys. Lett.* **2002**, *81*, 1312.
[11] B. Mayers, Y. N. Xia, *Adv. Mater.* **2002**, *14*, 279.
[12] O. G. Schmidt, K. Eberl, *Nature* **2001**, *410*, 168.
[13] W. Z. Wang, C. K Xu, G. H. Wang, Y. K. Liu, C. L. Zheng, *Adv. Mater.* **2002**, *14*, 837.
[14] W. Z. Wang, Y. K. Liu, C. K Xu, C. L. Zheng, G. H. Wang, *Chem. Phys. Lett.* **2002**, *362*, 119.
[15] X. H. Kong, Y. D. Li, *Arrays of ZnO Microtubes* **2003**, *11*, 1062.
[16] R. E. Ferguson, E. D. Guth, L. Eyring, *J. Am. Chem. Soc.* **1954**, *76*, 3890.
[17] R. L. Martin, *J. Chem. Soc., Dalton* **1974**, 1335.
[18] J. Zhang, R. B. von Dreele, L. Eyring, *J. Solid State Chem.* **1995**, *118*, 133.
[19] J. Zhang, R. B. von Dreele, L. Eyring, *J. Solid State Chem.* **1996**, *122*, 53.

Received September 17, 2003

 © 2004 Wiley-VCH Verlag GmbH & Co. KGaA, Weinheim

Microwave-Assisted Synthesis of MPS_3 Materials (M = Mn, Cd) Using a Dewar-Ampoule Device

A. Villanueva,[a] M. C. Morales-Varela,[a] and Eduardo Ruiz-Hitzky*[a]

Keywords: Transition metals / Microwave-assisted reactions / Layered compounds / Synthesis design / Solid-phase synthesis

We report on an easy procedure for the synthesis of inorganic solids such as MPS_3 materials (M = Mn, Cd) which uses a simple device consisting of a silica ampoule that is divided into a Dewar zone (*hot* zone) and a nonisolated part (*cold* zone), which is able to operate inside domestic microwave ovens. This is a rapid and advantageous method applied for the first time to the preparation of inorganic solids. It involves a heat concentration within the Dewar zone that allows the required temperature for the reaction between the components to be reached. In this way, a mixture of S, P, and a transition metal such as Mn or Cd, placed in the Dewar zone gives MPS_3 compounds. The temperature gradient assures the vapor phase transport to the *cold* zone. The resulting MPS_3 crystals are deposited within a few minutes in the *cold* area, in contrast to other conventional procedures requiring long periods of treatment or more complicated procedures for the synthesis of similar products.

(© Wiley-VCH Verlag GmbH & Co. KGaA, 69451 Weinheim, Germany, 2004)

Introduction

Microwave-assisted reactions are of increasing interest in different fields of synthetic chemistry to yield both inorganic materials (as in the solid-state synthesis of functional ceramics[1−5]) and organic compounds (as synthesis on supported phases[1,6]). Usually, the reactions developed under microwave (MW) heating show remarkable improvement over those carried out under conventional heating in an extraordinary acceleration of the processes. This is particularly true for solid-state reactions, as for instance, the synthesis of vanadates,[3] chromates,[4] and metal−chalcogenides.[5] In general, the MW treatment of mixtures of pure or combined elements such as metal oxides, nitrates, or carbonates, produces enough heat to induce a rapid transformation of the reagents, to give the corresponding inorganic materials through solid-state reactions, often with excellent yields. A successful control of these reactions depends on the intrinsic properties of the involved solids, mainly related to their conductivity behavior. The energy necessary for the MW-assisted solid-state reactions is given by the absorption of high frequency waves, related to the so-called tangent loss (tan δ), which is the ratio between the dielectric loss (ε′′) and the dielectric constant (ε′) of the material.[7] The tangent loss indicates the efficiency of the solid material towards the conversion of MW energy into thermal energy mainly associated with two mechanisms: dipole rotation and electrical conductivity (either ionic or electronic). In solid-state reactions, no relaxation process except for the conduction process of both electrons and ions, takes place because the molecular dipoles are fixed, leading to high loss tangent values.[1] This has been observed particularly for reactions involving semiconductors or ion-conducting solids, in which the increased temperature produces an increase of the electrical conductivity and therefore gives exponential MW energy absorption and rapid heating, that is, the so-called *thermal runaway.*[2]

Transition-metal phosphorus trisulfides (MPS_3; M = Mn, Cd) are the compounds selected in this paper to show the advantages of using the Dewar ampoule device. This is a family of layered compounds[8] with interesting properties as host lattices for intercalation of organic compounds,[9] and lithium insertion,[10] and is indeed useful as electrodes for lithium-batteries and in nonlinear optical devices. The structure of MPS_3 compounds derives from that of $CdCl_2$, and is closely related to the structure of transition-metal dichalcogenides.[11] Conventional synthesis of MPS_3 materials by ceramic methods needs a heating treatment program at temperatures in the 550−800 °C range, from one to several weeks[12] making the process too long for practical purposes. It is assumed that in these conditions a vapor phase transport mechanism occurs,[13] but the nature of the transported species is so far unknown. MPS_3 compounds can be alternatively prepared by coordination of $[P_2S_6]^{4-}$ anions to M^{2+} cations in aqueous solutions, as in the reaction at room temperature between $MnCl_2$ and sodium hexathiohypophosphate[14] [Equation (1)].

[a] Instituto de Ciencia de Materiales de Madrid, CSIC, Cantoblanco, 28049 Madrid, Spain
E-mail: eduardo@icmm.csic.es

$$2\,MnCl_2 + Na_4P_2S_6 \rightleftarrows 2\,MnPS_3 + 4\,NaCl \quad (1)$$

 DOI: 10.1002/ejic.200300654 © 2004 Wiley-VCH Verlag GmbH & Co. KGaA, Weinheim

This procedure is also long and tedious, because the sodium hexathiohypophosphate is a noncommercial product that needs to be prepared in the laboratory by reaction of sodium sulfide and phosphorus trichloride.[15] In addition, the reaction yield is lower than that of the ceramic method (about 67 %, from our experiments).

Results and Discussion

Figure 1. shows the apparatus developed for the MPS_3 synthesis, which essentially consists of a silica (quartz) ampoule with two different zones. One of the zones is furnished with a vacuum thermal barrier [i.e., it is a Dewar container (*hot* zone)], while the other zone is thermally deshielded (*cold* zone). Such a device was inspired by the typical two-zone furnace used to grow single crystals. The novelty of this design is that it operates inside a domestic MW oven, and this configuration allows the temperature to be reached so as to activate certain solid-state reactions. A sufficiently high temperature cannot be obtained in conventional reactors (e.g. standard sealed silica ampoules). For the first time, we have successfully applied this methodology to the preparation of well-crystallized MPS_3 layered solids, selected as an example in view of its difficult synthesis by the classical ceramic process. The attempts to produce these solid-state reactions using small amounts of metals inside conventional silica ampoules (i.e., classical quartz reactors) with MW irradiation always failed. Apparently, in an unshielded ampoule fast heat dissipation precludes the system from reaching a temperature high enough to afford the solid-state reaction. By contrast, the reaction is completed after a few minutes with MW irradiation when the Dewar ampoule apparatus is used, giving almost quantitative amounts of the corresponding metal phosphorus trisulfides. The driving idea to design such a device was to avoid the heat dissipation in the region of the reactor where the components are placed, thus assuring the increase of temperature required to produce the reaction. In our example, the MPS_3 compounds are deposited in the *cold* zone as relatively large crystals due to the temperature gradient that promotes the vapor-phase transport of the synthesized materials.

The nonmetallic elements, sulfur and phosphorus are insulators and practically transparent to MW, although theoretically they could be activated in the presence of a metal incorporated in the form of a fine powder. Under these conditions, the metal simultaneously acts as a reagent and as a MW absorber, because it couples very effectively with microwave radiation. This is the case for the reactions between sulfur and transition metals such as Ta, Cr, Fe, and Mn, which produces the corresponding sulfides.[16] In a similar way, we have tried to prepare MPS_3 compounds (M = Mn and Cd) by MW irradiation of a mixture of their three integrating elements using a conventional reactor (sealed, evacuated, single-quartz ampoule), using the same domestic MW oven. As indicated above, the reactions were always unsuccessful, even after a long time of treatment. It could

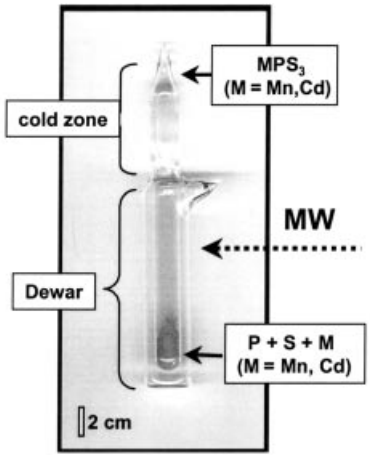

Figure 1. A picture of the Dewar ampoule highlighting its different parts and the process of MPS_3 crystallization

be maintained that under these conditions, the temperature reached is always lower than that required for the activation of the solid-state reaction. We have also unsuccessfully tried to carry out the $MnPS_3$ synthesis using mixtures of manganese metal and P_2S_5, or working under different conditions in a set of experiments involving conventional ampoules. In contrast, the Dewar ampoule offers a way to produce the phosphorus trichalcogenides quickly with excellent yields.

The details for the use of the Dewar ampoule with starting reagent mixtures of sulfur, phosphorus, and the selected transition metal (Mn or Cd), or alternatively mixtures of manganese, sulfur, and P_2S_5 (with stoichiometric MPS_3 ratios) are described in the Exp. Sect. Emission of very intense light of different colors is produced during the reactions, which are completed after 25−40 minutes of MW irradiation.

The MPS_3 resulting materials were characterized by XRD, FTIR spectroscopy and SEM-EDX analyses. Figure 2 shows the XRD patterns of $MnPS_3$ prepared by conventional procedures, that is, either from the ceramic method using a standard furnace (10 days, 700 °C, see A in Figure 2), or from soft conditions through a reaction involving various steps [Equation (1), see B in Figure 2], or by the MW-assisted synthesis using the Dewar ampoule (Figure 2, C and D). The XRD diagram of the reaction product obtained from the aqueous solution method [Equation (1)] corresponds to an ill-crystallized solid in view of the broad and low intensity *hkl* reflections attributed to $MnPS_3$ materials. All the diffraction peaks of the compound prepared by the ceramic method (Figure 2 A) fit very well with the corresponding ASTM file (No. 33−903), the diffractogram being very similar to the sample resulting from 25 minutes of MW irradiation of stoichiometric mixtures of Mn, P, and S (see D in Figure 2). Small differences in the relative intensities of the reflections of the two materials are attributed to preferred orientation effects: the [00 l] reflections of $MnPS_3$ (in particular for $l = 2$) are increased with respect to other reflections in the sample prepared by conventional techniques, while in the material prepared by

 © 2004 Wiley-VCH Verlag GmbH & Co. KGaA, Weinheim

the method reported here other reflections are relatively enhanced (like the [$\bar{1}$30] and [200] reflections, see Figure 2). The sample prepared from 30 minutes MW irradiation of Mn, P_2S_5, and S stoichiometric mixtures shows additional low intensity peaks identified as P_2S_5, MnP_4, and other by-products of variable P, S, and Mn composition.

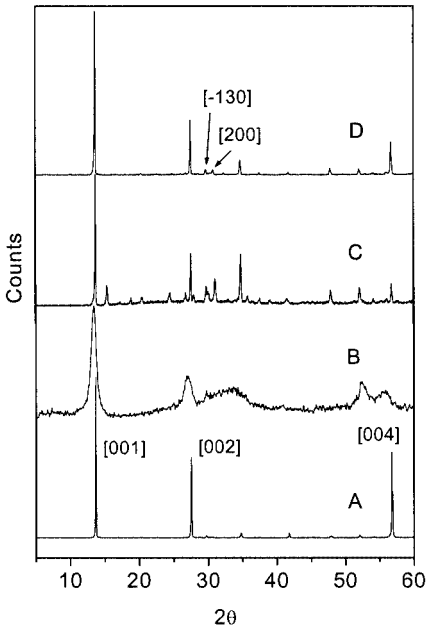

Figure 2. XRD diffraction patterns of $MnPS_3$ synthesized by: A) conventional heating of Mn + P + 3S (700 °C, 10 days); B) reaction of $Na_4P_2S_6$ with $MnCl_2$ in aqueous solution; C) MW-assisted reaction of 2Mn + P_2S_5 + S (30 min); D) MW-assisted reaction of Mn + P + 3S (25 min); traces A and D correspond to pure and highly crystalline $MnPS_3$, the differences between them being related to preferred orientations

Figure 3 shows the IR spectra (800−400 cm^{-1} region) of the reaction products obtained by the two methods that give the best results, that is, conventional heating and MW-assisted reactions involving the Mn + P + 3S mixture. The similarity between the compounds prepared by the two procedures is again evidenced by their coincidence in frequency and intensity of the IR absorption bands, the most characteristic of them appearing in the 700−400 cm^{-1} spectral region. According to Mathey and co-workers,[17] and Joy and Vasudevan,[18] the strong intensity band that appears at 573 cm^{-1} is attributed to P−S stretching vibrations $\nu_{P-S}(PS_3)$, whereas the ν_{P-P} vibration band appears at 440 cm^{-1}.

SEM images of the $MnPS_3$ products obtained by both procedures, the conventional ceramic method, and MW-assisted reactions show crystals of lamellar shape and average particle sizes of about 100 and 20 μm, respectively (Figure 4). The differences in the crystal size can be attributed to the different nucleation and crystal growth rates achieved by MW or conventional heating.

The method of preparation of $MnPS_3$ compounds, with MW's and the Dewar ampoule reported above has also been successfully applied to the synthesis of $CdPS_3$ materials. This result indicates the ability to extend the procedure to other members of the MPS_3 family.

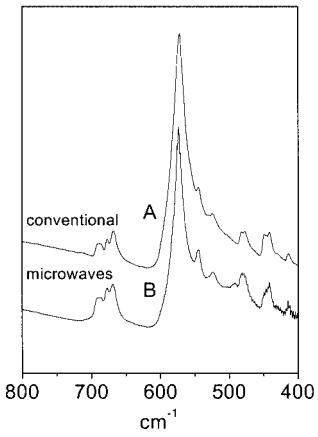

Figure 3. IR spectra (800−400 cm^{-1} region) of $MnPS_3$ obtained by: A) conventional heating of Mn + P + 3S (700 °C, 10 days); B) MW-assisted reaction of Mn + P + 3S (25 min)

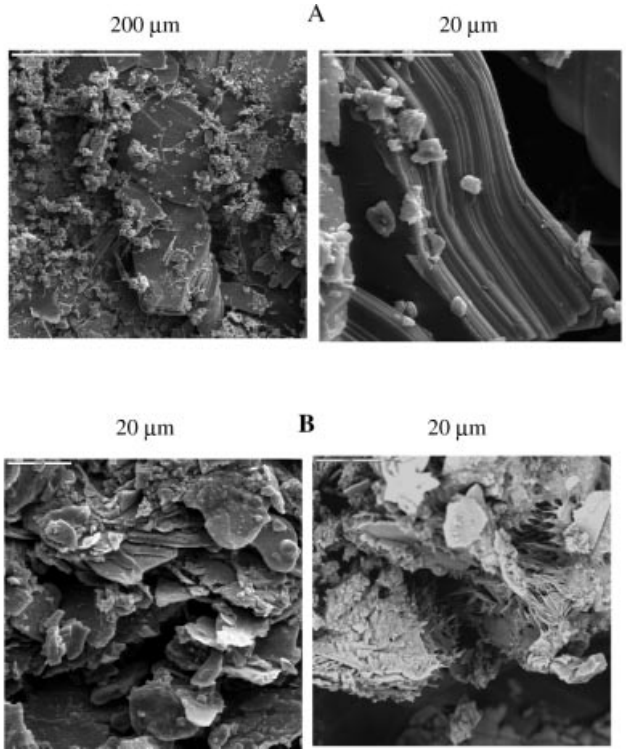

Figure 4. SEM images of $MnPS_3$ obtained by: A) conventional heating of Mn + P + 3S (700 °C, 10 days); B) MW-assisted reaction of Mn + P + 3S (25 min)

Conclusions

We have shown that a simple device such as the Dewar ampoule reported here, when used with an unmodified MW domestic oven, offers a new procedure to reach suitable temperatures(at least when small amounts of powdered metals are used) to allow the efficient and rapid synthesis of solids that are difficult to prepare by other routes, as it is the case of the MPS_3 compounds.

 © 2004 Wiley-VCH Verlag GmbH & Co. KGaA, Weinheim

Table 1. MW synthesis of MPS_3 compounds (M = Mn, Cd) under different experimental conditions

Reactor	Starting reagents	Resulting products	Irradiation time	Emitted light
Conventional ampoule	Mn + P + 3 S	no reaction	1−60 min	no emission
Conventional ampoule	Cd + P + 3 S	no reaction	1−60 min	no emission
Conventional ampoule	2 Mn + P_2S_5 + S	no reaction	1−60 min	no emission
Dewar ampoule	Mn + P + 3 S	$MnPS_3$	25 min	purple-blue
Dewar ampoule	2 Mn + P_2S_5 + S	$MnPS_3$	30 min	pink-orange
Dewar ampoule	Cd + P + 3 S	$CdPS_3$	40 min	white-yellow

In addition, the method developed here could be extended to the preparation of other materials with similar synthetic problems, that is, in the cases where the dielectric component prevails over the metallic or semiconducting elements involved in the starting mixture lowering the efficiency of microwave-assisted procedures. This could be the case of different metal oxides, nitrides, carbides, etc.

Experimental Section

General: Conventional ceramic syntheses of MPS_3 materials were carried out as follows: a mixture of S, P and the transition-metal elements was ground in an glove box (Ar) and sealed in a classical quartz ampoule under a vacuum of 10^{-2} Torr. The ampoule was heated to 700 °C at 1 °C/min and maintained at this temperature for 10 days.[12]

Synthesis of MPS_3 Compounds: MPS_3 (M = Mn, Cd) crystals were also prepared by the Dewar ampoule method as follows: 0.3 g of the starting reagents, either as Mn (Aldrich, 99.9 %) or Cd (Aldrich, 99.5 %), P (Aldrich, 99.99 %) and S [(Aldrich) sublimed, 100 mesh, mixture, or as Mn, P_2S_5 (Aldrich, 99 %)] and S were thoroughly mixed in 1:1:3 or 2:1:1 molar ratios, respectively. The mixture was then transferred to the Dewar zone inside a glove box (Ar atmosphere). After vacuum degassing and hermetic flame sealing, the reactor was surrounded by quartz wool to provide insulation for high temperatures and protection against possible explosions (CAUTION!). In this manner, the mixture was MW-treated in a Moulinex Optiquick model (900 W, 2.45 GHz) during various periods of time (from 5 to 40 minutes) by steps of 1−2 minutes to avoid overheating effects that could produce damage. During the reaction, flashes of very intense visible light are produced, their color depending on the nature of the starting reagents (Table 1). The end of the reaction, which occurs after about 25−40 minutes, is clearly indicated by the extinction of the emitted light. At this time, only traces of residual reagents remain coating the bottom of the hot zone of the Dewar ampoule. The resulting MPS_3 compounds were characterized by X-ray diffraction (Siemens D-500 instrument with a Cu anode and Ni filter), IR spectroscopy (Nicolet 20SXC spectrophotometer), and electron microscopy (SEM) (ZEISS DSM-960 microscope working at 20 kV).

Acknowledgments

The financial support from the CICYT, Spain, (MAT2000−1585-C03−01) is gratefully acknowledged. We would like to express our gratitude to Tomás García-Somolinos for his helpful technical assistance in the Dewar ampoule development. We are indebted to Dr. M. A. Camblor for his helpful discussion and comments incorporated to this article.

[1] (Eds.) M. M. Kingston, S. J. Haswell, *Microwave-Enhanced Chemistry*, ACS, Washington, **1997**.
[2] [2a] D. M. P. Mingos, R. Baghurst, *Br. Ceram. Trans. J.* **1992**, *91*, 124. [2b] D. M. P. Mingos, *Adv. Mater.* **1993**, *5*, 857. [2c] D. M. P. Mingos, D. R. Baghurst, *Chem. Soc. Rev.* **1991**, *20*, 1.
[3] B. Vaidhyanathan, K. Balaji, K. J. Rao, *Chem. Mater.* **1998**, *10*, 3401.
[4] M. Iwasaki, H. Takizawa, K. Uheda, T. Endo, M. Shimada, *J. Mater. Chem.* **1998**, *8*, 2765.
[5] [5a] B. Vaidhyanathan, M. Ganguli, K. J. Rao, *Mater. Res. Bull.* **1995**, *30*, 1173. [5b] A. G. Whittaker, M. P. Mingos, *J. Chem. Soc., Dalton Trans.* **1995**, 2073.
[6] [6a] E. Gutiérrez, A. Loupy, G. Bram, E. Ruiz-Hitzky, *Tetrahedron Lett.* **1989**, *30*, 945. [6b] G. Bram, A. Loupy, M. Majdoub, E. Gutiérrez, E. Ruiz-Hitzky, *Tetrahedron* **1990**, *46*, 5167. [6c] R. S. Varma, *Green Chemistry* **1999**, *1*, 43.
[7] (Eds.) W. S. Cheung, F. H. Levien, *Microwaves Made Simple: Principles and Applications*, Artech House, Inc., Norwood, **1985**.
[8] R. Brec, *Solid State Ionics* **1986**, *22*, 3.
[9] [9a] D. O'Hare, *Inorganic Intercalation Compounds* in *Inorganic Materials*, 2nd ed., (Eds: D. W. Bruce and D. O'Hare), John Wiley & Sons, Chichester, **1996**. [9b] R. Clement, *J. Chem. Soc., Chem. Commun.* **1980**, 647. [9c] I. Lagadic, P. G. Lacroix, R. Clement, *Chem. Mater.* **1997**, *9*, 2004. [9d] R. Clement, *J. Am. Chem. Soc.* **1981**, *103*, 6998.
[10] A. H. Thompson, M. S. Whittingham, *Mat. Res. Bull.* **1977**, *12*, 741.
[11] G. Ouvrad, R. Brec, J. Rouxel, *Mat. Res. Bull.* **1985**, *20*, 1181.
[12] [12a] W. Klingen, R. Ott, H. Hahn, *Z. Anorg. Allg. Chem.* **1973**, *396*, 271. [12b] W. Klingen, G. Eulenberger, H. Hahn, *Z. Anorg. Allg. Chem.* **1973**, *401*, 97. [12c] B. E. Taylor, J. Steger, A. Wold, *J. Solid State Chem.* **1973**, *7*, 461.
[13] [13a] A. R. Wildes, M. J. Harris, K. W. Godfrey, *J. Magnet. Magnetic Mater.* **1998**, *177−181*, 143. [13b] A. R. Wildest, S. J. Kennedy, T. J. Hickst, *J. Phys.: Condens. Matter* **1994**, *6*, L335.
[14] R. Clement, P. Garnier, J. Jegoudez, *Inorg. Chem.* **1986**, *25*, 1404.
[15] H. von Falius, *Z. Anorg. Allg. Chem.* **1968**, *356*, 189.
[16] A. G. Whittaker, M. P. Mingos, *J. Chem. Soc., Dalton Trans.* **1995**, 2073.
[17] Y. Mathey, R. Clement, C. Sourisseau, G. Lucazeau, *Inorg. Chem.* **1980**, *19*, 2773.
[18] P. A. Joy, S. Vasudevan, *J. Phys. Chem. Solids* **1993**, *54*, 343.
Received September 17, 2003

 © 2004 Wiley-VCH Verlag GmbH & Co. KGaA, Weinheim

A Novel Open-Framework Zinc Phosphite, $Zn_3(HPO_3)_4{\cdot}Ni(en)_2(H_2O)_2$, Templated by a Transition-Metal Complex

Zhi-En Lin,[a] Jie Zhang,[a] Shou-Tian Zheng,[a] and Guo-Yu Yang*[a]

Keywords: Open framework / Inorganic solid / Zinc / Nickel / Template synthesis

A new three-dimensional zinc phosphite, $Zn_3(HPO_3)_4{\cdot}Ni(en)_2(H_2O)_2$, which is the first example of an open-framework metal phosphite templated by a transition-metal complex, was hydrothermally synthesized. The connectivity of the strictly alternating ZnO_4 and HPO_3 units results in a three-dimensional framework with intersecting 8-ring and 12-ring channels, in which the transition-metal complexes reside.
(© Wiley-VCH Verlag GmbH & Co. KGaA, 69451 Weinheim, Germany, 2004)

Introduction

The research in the area of inorganic solids with regular-pore architectures is very intense due to the potential applications of these materials in ion-exchange, separation and catalysis.[1] Since the discovery of crystalline aluminophosphate molecular sieves in 1982,[2] much interest has been focused on open-framework metal phosphates because of their compositional diversity and rich structural chemistry.[3] The replacement of the tetrahedral phosphate group by a pyramidal phosphite unit has resulted in the preparation of a new class of compounds with interesting architectures, such as clusters,[4] chains, ladders,[5,6] or layers[7−9] and three-dimensional frameworks.[10−13] Clearfield reported $ZnCa(HPO_3)_2(H_2O)_2$ and $ZnSr(HPO_3)_2(H_2O)_2$ as the first members of open-framework metal phosphites.[14] Harrison reported the synthesis and structure of $[NH_2(CH_2)_2NH_2]_{0.5}{\cdot}ZnHPO_3$, which possesses an unprecedented architecture of two interpenetrated, independent, mixed inorganic-organic networks.[15] Very recently, a ladderlike chromium phosphite, $(C_2H_{10}N_2)[Cr(HPO_3)F_3]$, which is the first organically templated M−P−O compound containing Cr^{III}, has been successfully isolated by Rojo and co-workers.[16] Generally, these materials are synthesized from organic templates under mild hydrothermal conditions to avoid the formation of dense phases.

The employment of metal complexes as structure-directing agents is promising for the design and synthesis of new open-framework compounds with unusual architectures. Compared with organic molecules, metal complexes possess several unique features. First, they can adopt conformations that are difficult to achieve with organic molecules. Second, the wide range of oxidation states of metal ions endows the complexes with properties that are not found in organic molecules. In addition, the use of a chiral metal complex as a templating agent may give rise to a chiral open-framework compound. However, open-framework solids templated by metal complexes are rare.[17−26] This is in part due to the inadequate stability of metal complexes under the hydrothermal conditions needed for framework synthesis. Here we describe the synthesis and structure of a novel open-framework zinc phosphite, $Zn_3(HPO_3)_4{\cdot}Ni(en)_2(H_2O)_2$ (denoted FJ-8; FJ: Fujian Institute of Research on the Structure of Matter), which is the first example of an open-framework metal phosphite templated by a metal complex.

Results and Discussion

FJ-8 was synthesized under hydrothermal conditions in the presence of $Ni(en)_3^{2+}$ complexes as structure-directing agents. Single-crystal X-ray analysis indicates that FJ-8 possesses a three-dimensional open framework containing 8-ring and 12-ring channels along the [101] and [010] directions, respectively. The asymmetric unit of FJ-8 contains 30 non-hydrogen atoms, of which 19 belong to the host network and 11 to the guest-metal complex (see Figure 1). There are three crystallographically distinct Zn atoms and four crystallographically distinct P atoms. The zinc atoms are tetrahedrally coordinated by oxygen atoms with Zn−O bond lengths in the range of 1.905(6)−1.965(6) Å. The O−Zn−O angles are in the range of 96.9(3)−116.5(3)°. Each phosphorus atom shares three oxygen atoms with adjacent Zn atoms [P−O: 1.485(7)−1.529(6) Å] and the fourth ligand is a terminal P−H bond. The existence of

[a] Coordination and Hydrothermal Chemistry Group, State Key Laboratory of Structural Chemistry, Fujian Institute of Research on the Structure of Matter, Chinese Academy of Sciences,
Fuzhou, Fujian 350002, China
Fax: (internat.) + 86-591-371-0051
E-mail: ygy@ms.fjirsm.ac.cn
Supporting information for this article is available on the WWW under http://www.eurjic.org or from the author.

 DOI: 10.1002/ejic.200300601 © 2004 Wiley-VCH Verlag GmbH & Co. KGaA, Weinheim

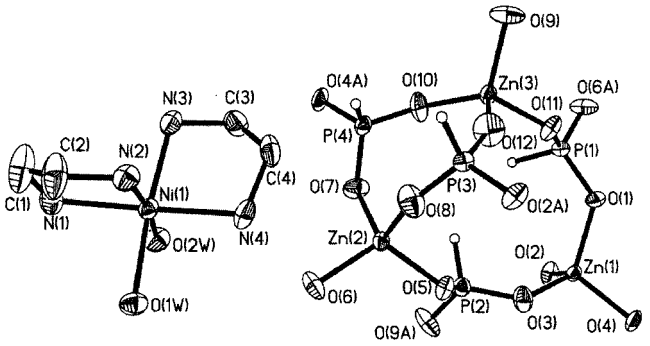

Figure 1. ORTEP view of the asymmetric unit of FJ-8, showing the labeling scheme and the 50 % probability displacement ellipsoids; atom labels with "A" refer to symmetry-generated atoms

P−H bonds is also confirmed by the band in the IR spectrum, which is characteristic of phosphite groups [ν(H−P) 2380 cm^{-1}]. The stoichiometry of $[Zn_3(HPO_3)_4]$ results in a net charge of −2, which is balanced by one $[Ni(en)_2(H_2O)_2]^{2+}$ cation.

The structure of FJ-8 is constructed from strictly alternating ZnO_4 tetrahedra and HPO_3 pseudopyramids that form a three-dimensional framework. There are two types of intersecting channels with different ring-aperture. The smaller one has an eight-membered ring and runs along the [101] direction with a diameter of 6.1 × 7.5 Å (see Figure 2). This channel is intersected by a larger channel with a 12-membered ring. The 12-membered window is somewhat puckered and the diameter of the channel is nearly 8.1 × 9.9 Å (see Figure 3).

The "openness" of a structure is defined in terms of its polyhedral-atom density (framework density, FD), defined as the number of polyhedral atoms per 1000 $Å^3$. The FD value in the structure of FJ-8 is 13.2, which indicates that the openness of this structure is similar to aluminosilicate molecular sieves such as ZSM-3 and ZSM-20.[27]

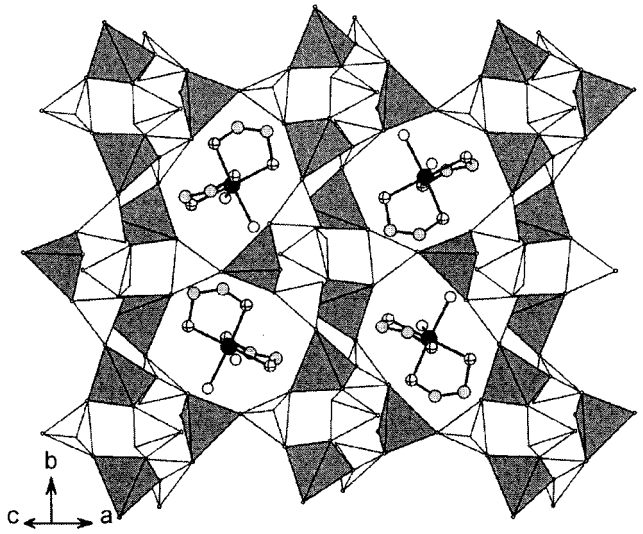

Figure 2. Polyhedral view of the structure of FJ-8 along the [101] direction showing the 8-ring channels; ZnO_4, medium-gray tetrahedra; HPO_3, white pseudopyramids

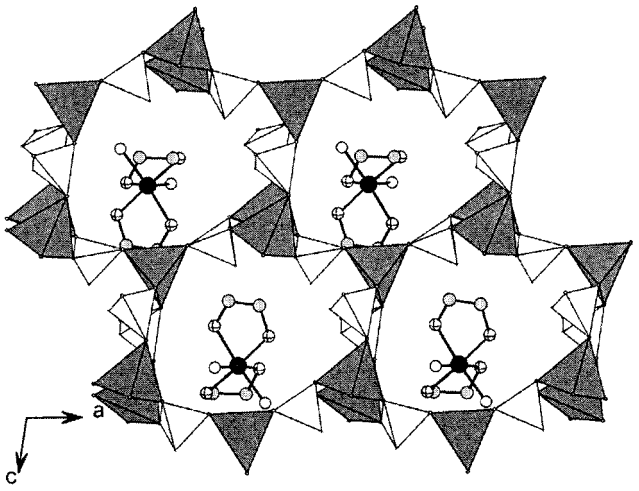

Figure 3. Polyhedral view of the structure of FJ-8 along the [010] direction showing the 12-ring channels; ZnO_4, medium gray tetrahedra; HPO_3, whitepseudo pyramids

The $[Ni(en)_2(H_2O)_2]^{2+}$ cations reside in the "free" space of the intersecting channels. This nickel complex is formed under hydrothermal conditions by the replacing one ethylenediamine ligand in $[Ni(en)3]^{2+}$ with two water molecules. Interestingly, the $[Ni(en)_2(H_2O)_2]^{2+}$ complex possesses two kinds of ligands: ethylenediamine and water. This structural feature is quite different from that of other metal complexes used in the synthesis of open-framework phosphates, as the latter contain only one type of ligand in a particular structure. There is extensive hydrogen bonding in the structure. The complex cations interact with the inorganic framework through strong H-bonds such as O(1 W)-H(5)···O(5) 2.24 Å, O(1 W)-H(6)···O(2) 2.17 Å, O(2 W)-H(7)···O(7) 2.23 Å, O(2 W)-H(8)···O(1) 2.08 Å, N(1)-H(9)···O(9) 2.61 Å, N(2)-H(12)···O(4) 2.30 Å, N(3)-H(13)···O(11) 2.17 Å, N(3)-H(14)···O(4) 2.48 Å, and N(4)-H(16)···O(6) 2.22 Å.

The initial thermogravimetric analysis, performed under flowing N_2, shows a three-step weight loss. The initial weight loss, between 160 and 230 °C, corresponds to the release of water ligands (observed 4.83 %; expected 4.92 %). The second step, occurring between 300 and 500 °C, is due to the partial departure of the ethylenediamine ligands (observed 9.62 %; expected 16.44 %). The lower value is probably due to the retention of ethylenediamine molecules in the solid residue. The last step, at 760 °C, with a mass loss of 7.18 %, is assigned to the removal of the residual ethylenediamine species. To examine the thermal stability of FJ-8 in the absence of water ligands, a sample of FJ-8 was heated in a thermal gravimetric apparatus at 230 °C for 1 h. Powder X-ray diffraction measurements for the dehydrated product showed that the structure collapsed and an unidentified phase was formed.

Conclusion

The hydrothermal synthesis of a novel three-dimensional open-framework zinc phosphite with the formula

$Zn_3(HPO_3)_4{\cdot}Ni(en)_2(H_2O)_2$ and its crystal structure were described. The structure consists of ZnO_4 and HPO_3 units, which are linked through their vertices to form a three-dimensional framework with intersecting 8-ring and 12-ring channels, in which the structure-directing agents reside. This compound is unusual because it is the first instance of an open-framework metal phosphite templated by a transition-metal complex. The use of other transition-metal complexes, such as $[Co(en)_3]^{2+}$ and $[Ni(1,3\text{-}DAP)_3]^{2+}$, in similar hydrothermal systems may result in other novel open-framework metal phosphites. Further work on this subject is in progress.

Experimental Section

Synthesis and Initial Characterization: FJ-8 was hydrothermally synthesized under autogenous pressure. In a typical synthesis, a mixture of ZnO (0.093 g, 1.14 mmol), H_3PO_3 (0.3 mL, 50 wt %), $Ni(en)_3Cl_2{\cdot}2H_2O$ (0.395 g, 1.14 mmol) and H_2O (2.5 mL) in a molar ratio of 1·2·1·130 was stirred under ambient conditions. The resulting gel was sealed in a Teflon-lined steel autoclave and heated at 160 °C for 7 days and then cooled to room temperature. The resulting product, consisting of single crystals in the form of light-purple prisms, was recovered by filtration, washed with distilled water and air-dried. Yield: 0.064 g, (23 % yield based on ZnO). The XRD powder pattern is in accord with the structure simulated on the basis of the single-crystal X-ray analysis, indicating phase purity. Inductively coupled plasma (ICP) spectrometric analysis gave the contents of Zn (calcd. 26.83 wt %; found 25.17 wt %), P (calcd. 16.95 wt %; found 15.41 wt %) and Ni (calcd. 8.03 wt %; found 7.86 wt %) and indicated a Zn:P:Ni ratio of 3:4:1. $C_4H_{24}N_4NiO_{14}P_4Zn_3$ (731.0): calcd. C 6.57, H 3.31, N 7.66; found C 6.48, H 3.26, N 7.61. IR (KBr): $\tilde{\nu}$ = 3345 s, 3280 s, 3274 s, 2960 m, 2890 m, 2380 s, 1680 m, 1605 m, 1465 m, 1095 s, 1020 s, 617 m, 590 m, 518 w cm^{-1}.

X-ray Crystallography: $C_4H_{24}N_4NiO_{14}P_4Zn_3$ (= FJ-8), M = 730.97, monoclinic, space group $P2_1/n$ (no.14), a = 9.9144(3), b = 14.4414(4), c = 14.9785(3) Å, β = 98.8870(10)°, V = 2118.84(10) $Å^3$, Z = 4, d = 2.291 g cm^{-3}, μ = 4.603 mm^{-1}, Mo-K_α radiation, λ = 0.71073 Å, 1.97 < θ < 25.09°. Crystal structure determination by X-ray diffraction was performed on a Siemens SMART CCD diffractometer with graphite-monochromated Mo-K_α (λ = 0.71073 Å) radiation in the ω and φ scanning mode at room temperature. An empirical absorption correction was applied using the SADABS program. The structure was solved by direct methods using the SHELXL-97 software package and refined with full-matrix least-squares, leading to a convergence with final $R1$ = 0.0557, $wR2$ = 0.1186 and S = 1.152 for 287 parameters and 3713 unique reflections with $I \geq 2\sigma(I)$ [R(int) = 0.0336].

CCDC-211514 contains the supplementary crystallographic data for this paper. These data can be obtained free of charge at www.ccdc.cam.ac.uk/conts/retrieving.html [or from the Cambridge Crystallographic Data Centre, 12 Union Road, Cambridge CB2 1EZ, UK; Fax: (internat.) + 44-1223/336-033; E-mail: deposit@ccdc.cam.ac.uk].

Acknowledgments

This work was supported by the NSF of China (Grant No. 20271050), the SRF for ROCS of State Education Ministry, the Ministry of Finance of China and the Talents Program of Chinese Academy of Sciences, and State Key Laboratory of Inorganic Synthesis and Preparative Chemistry of Jilin University.

[1] M. E. Davis, R. F. Lobo, *Chem. Mater.* **1992**, *4*, 756−768.
[2] S. T. Wilson, B. M. Lok, C. A. Messina, T. R. Cannan, E. M. Flanigen, *J. Am. Chem. Soc.* **1982**, *104*, 1146−1147.
[3] A. K. Cheetham, G. Férey, T. Loiseau, *Angew. Chem. Int. Ed.* **1999**, *38*, 3268−3292.
[4] W. T. A. Harrison, R. M. Yeates, M. L. F. Phillips, T. M. Nenoff, *Inorg. Chem.* **2003**, *42*, 1493−1498.
[5] W. T. A. Harrison, M. L. F. Phillips, J. Stanchfield, T. M. Nenoff, *Inorg. Chem.* **2001**, *40*, 895−899.
[6] S. Fernandez, J. L. Mesa, J. L. Pizarro, L. Lezama, M. I. Arriortua, T. Rojo, *Chem. Mater.* **2003**, *15*, 1204−1209.
[7] G. Bonavia, J. DeBord, R. C. Haushalter, D. Rose, J. Zubieta, *Chem. Mater.* **1995**, *7*, 1995−1998.
[8] S. Fernandez, J. L. Mesa, J. L. Pizarro, L. Lezama, M. I. Arriortua, R. Olazcuaga, T. Rojo, *Chem. Mater.* **2000**, *12*, 2092−2098.
[9] J. Liang, Y. Wang, J. Yu, Y. Li, R. Xu, *Chem. Commun.* **2003**, 882−883.
[10] W. T. A. Harrison, M. L. F. Phillips, T. M. Nenoff, *J. Chem. Soc., Dalton Trans.* **2001**, 2459−2461.
[11] W. T. A. Harrison, *J. Solid State Chem.* **2001**, *160*, 4−7.
[12] M. L. F. Phillips, T. M. Nenoff, C. T. Thompson, W. T. A. Harrison, *J. Solid State Chem.* **2002**, *167*, 337−343.
[13] Z. Shi, G. Li, D. Zhang, J. Hua, S. Feng, *Inorg. Chem.* **2003**, *42*, 2357−2361.
[14] M. Shieh, K. J. Martin, P. J. Squattrito, A. Clearfield, *Inorg. Chem.* **1990**, *29*, 958−963.
[15] J. A. Rodgers, W. T. A. Harrison, *Chem. Commun.* **2000**, 2385−2386.
[16] S. Fernandez, J. L. Mesa, J. L. Pizarro, L. Lezama, M. I. Arriortua, T. Rojo, *Angew. Chem. Int. Ed.* **2002**, *41*, 3683−3685.
[17] K. R. Morgan, G. Gainsford, N. B. Milestone, *J. Chem. Soc., Chem. Commun.* **1995**, 425−426.
[18] D. A. Bruce, A. P. Wilkinson, M. G. White, J. A. Bertrand, *J. Chem. Soc., Chem. Commun.* **1995**, 2059−2060.
[19] D. A. Bruce, A. P. Wilkinson, M. G. White, A. Bertrand, *J. Solid State Chem.* **1996**, *125*, 228−233.
[20] S. M. Stalder, A. P. Wilkinson, *Chem. Mater.* **1997**, *9*, 2168−2173.
[21] K. R. Morgan, G. J. Gainsford, N. B. Milestone, *Chem. Commun.* **1997**, 61−62.
[22] M. J. Gray, J. D. Jasper, A. P. Wilkinson, J. C. Hanson, *Chem. Mater.* **1997**, *9*, 976−980.
[23] D. J. Williams, J. S. Kruger, A. F. McLeroy, A. P. Wilkinson, J. C. Hanson, *Chem. Mater.* **1999**, *11*, 2241−2249.
[24] J. Yu, Y. Wang, Z. Shi, R. Xu, *Chem. Mater.* **2001**, *13*, 2972−2978.
[25] G.-Y. Yang, S. C. Sevov, *Inorg. Chem.* **2001**, *40*, 2214−2215.
[26] Y. Wang, J. Yu, Z. Shi, R. Xu, *J. Solid State Chem.* **2003**, *170*, 176−181.
[27] Ch. Baerlocher, W. M. Meier, D. H. Olson, *Atlas of Zeolite Framework Types*, 5th edn., Elsevier, Amsterdam, **2001**.

Received August 28, 2003

 © 2004 Wiley-VCH Verlag GmbH & Co. KGaA, Weinheim

A Blue Photoluminescent 2-D Coordination Polymer Constructed by Dinuclear Zinc(II) Subunits $[Zn_2(oz)_2]$ [Hoz = 2-(2′-Hydroxyphenyl)-2-oxazoline] and Dicyanamide

Jing Zhang,[a,b] Song Gao,*[a] and Chi-Ming Che*[b]

Keywords: Zinc / Photoluminescence / Dinuclear subunit / Polymer / Thermal stability

Substitution of the terminal oz group of the dinuclear $[Zn(oz)_2]_2$ complex (**1**) with dicyanamide [where Hoz = 2-(2′-Hydroxyphenyl)-2-oxazoline] results in the formation of a 2-D coordination polymer $[Zn(oz)N(CN)_2]_n$ (**2**) based on $[Zn_2(oz)_2]$ subunits. Both compounds exhibit strong blue photoluminescence but the coordination polymer **2** has greater thermal stability than the dinuclear complex **1**.

(© Wiley-VCH Verlag GmbH & Co. KGaA, 69451 Weinheim, Germany, 2004)

Introduction

Blue luminescent compounds have received considerable attention in recent years because of their potential applications in electroluminescent (EL) devices or light-emitting diodes (LED).[1] Since the realization of blue electroluminescence using poly(9,9-dihexylfluorene)[3a][3b] and poly(*p*-phenylene),[3c] intensive research in this area has been reported.[3d] Most of the reported examples are aromatic organic molecules, conjugated organic polymers,[1,2] organometallic compounds or metal−chelate compounds of Al^{III}, B(III), Zn^{II} or Cd^{II} based on 8-hydroxyquinoline,[4] methylquinolin-8-ol,[5] azomethine,[6] azaindole,[7] oxadiazole[8] and bipyridyl[9] ligands, while cases of condensed coordination polymers exhibiting blue luminescence are still rare. With the advantages of high thermal stability, good mechanical properties, versatile structures and relatively high emitting intensity (with respect to pure organic materials), blue luminescent coordination polymers have recently attracted significant interest.[10] Inspired by the electroluminescence research on the mononuclear complex of bis[2-(2-hydroxyphenyl)benzothiazolate]zinc $[Zn(BTZ)_2]$,[8a] we started using the ligand 2-(2′-hydroxyphenyl)-2-oxazoline, (Hoz), and dicyanamide anions as structural motifs to develop new blue luminescent coordination-polymers. Hoz has a smaller conjugated system than 2-(2-hydroxyphenyl)benzothiazolate, which may shift the emission wavelength of complexes with such a ligand to blue luminescence since fluorescent emission is dominated by the coordinated ligand. We herein describe the preparation, structural characterization and preliminary luminescence study of a dinuclear zinc complex $[Zn(oz)_2]_2$ (**1**) and a 2-D coordination polymer $[Zn(oz)N(CN)_2]_n$ (**2**) with the dinuclear $[Zn_2(oz)_2]$ fragment as subunit. The two dimer-based compounds may provide a model for studying the influence of the polymerization process upon luminescence and thermal stability.

[a] State Key Laboratory of Rare Earth Materials Chemistry and Applications & PKU-HKU Joint Laboratory on Rare Earth Materials and Bioinorganic Chemistry, College of Chemistry and Molecular Engineering,
Peking University, Beijing 100871, P. R. China
Fax: (internat.) + 86-10-62751708
E-mail: gaosong@pku.edu.cn
[b] Department of Chemistry, and HKU-CAS Joint Laboratory on New Materials, The University of Hong Kong,
Pokfulam Road, Hong Kong, China
Fax: (internat.) +852-2857-1586
E-mail: cmche@hku.hk

Results and Discussion

Complex **1** was prepared by mixing $Zn(ClO_4)_2$, Hoz, and triethylamine in methanol in a 1:2:2 molar ratio. Colorless single crystals were obtained after the reaction solution was left to stand overnight at room temperature. Complex **2** was prepared by dissolving equimolar amounts of sodium dicyanamide, Hoz and triethylamine in methanol (20 mL) and then adding $Zn(ClO_4)_2$ in methanol (5 mL) to the solution. The reaction mixture was filtered and after one week colorless crystals appeared in the filtrate. The ORTEP drawing of **1** is shown in Figure 1. Complex **1** is dimeric with two discrete molecules per unit cell. The zinc atom is five-coordinate with three oxygen and two nitrogen atoms. One chelated terminal ligand provides one oxygen and one nitrogen atom, and the two bridging ligands provide a total of two oxygen and one nitrogen atom. The coordination sphere can be described as distorted trigonal-bipyramidal. The two zinc atoms in a discrete molecule are symmetrically related and connected by the O1 atoms of the bridging ligands. Compared with the previously reported mononuclear com-

 © 2004 Wiley-VCH Verlag GmbH & Co. KGaA, Weinheim **DOI: 10.1002/ejic.200300719**

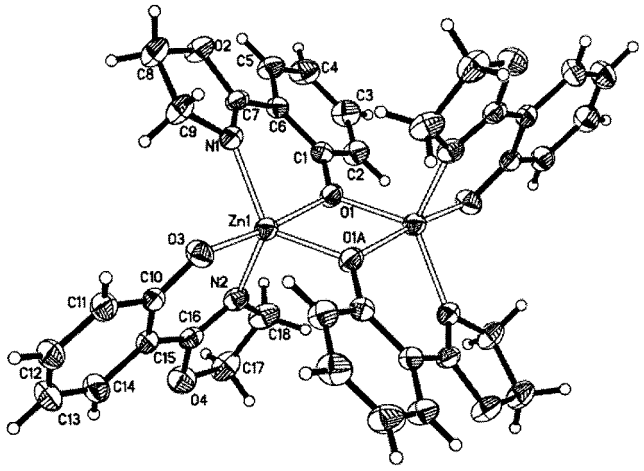

Figure 1. Perspective view of **1** (30% thermal ellipsoids except for hydrogen) and atom-numbering scheme; significant bond lengths (Å) and angles (°): Zn(1)−O(1) 2.118(2); Zn(1)−O(1A) 2.026(2); Zn(1)−O(3) 1.985(2); Zn(1)−N(1) 2.041(3); Zn(1)−N(2) 2.019(3); O(3)−Zn(1)−N(2) 90.14(11); O(3)−Zn(1)−O(1A) 102.50(10); N(2)−Zn(1)−O(1A) 106.12(11) O(3)−Zn(1)−N(1) 90.36(11); N(2)−Zn(1)−N(1) 125.00(12); O(1A)−Zn(1)−N(1) 127.28(11); O(3)−Zn(1)−O(1) 174.09(10); N(2)−Zn(1)−O(1) 95.31(11); O(1)−Zn(1)−O(1A) 78.22(10); N(1)−Zn(1)−O(1) 84.64(10)

plex $Zn(BTZ)_2$,[8a] the formation of the dinuclear motif in **1** may be caused by the smaller oz ligand and the existence of oxygen atoms acting as μ_2 bridges.

The zinc atoms in **2** display trigonal-bipyramidal geometry, as in **1**, with three nitrogen atoms, two of which are provided by terminal N atoms of different $[N(CN)_2]^-$ ligands and the other by the chelating oz ligand, and two oxygen atoms from two oz ligands. Hence, two oxygen atoms from two ligands bridging two symmetrically related zinc atoms form the dinuclear subunit. The ORTEP drawing of the dinuclear subunit is shown in Figure 2. Each subunit is further linked to four subunits through $\mu_{1,5}$ bridges of $[N(CN)_2]^-$ and each $[N(CN)_2]^-$ moiety acts as a bidentate spacer to coordinate to two zinc atoms with two nitrile nitrogen atoms. If the dinuclear units are viewed as connecting points, the structure can be simplified into a 2-D square-grid network (see **a** in Figure 3). Each square grid shares four $\mu_{1,5}$ $[N(CN)_2]^-$ groups as rhombic sides and four dimers as connecting nodes. The average distance between two parallel ligands from adjacent layers is 3.54 Å, indicating the existence of π−π stacking in the 3-D supramolecular architecture (see **b** in Figure 3).

The two complexes were further studied by thermogravimetric analysis, which showed that **1** began to lose weight at around 320 °C (see **a** in Figure 4) while **2** exhibited a higher decomposition temperature at 374 °C (see **b** in Figure 4).

The absorption spectrum of **1** in methanol at 298 K shows an intense low-energy band at λ_{max} = 337 nm, which is similar in energy to the absorption band (λ_{max} = 323 nm) of the deprotonated ligand oz^- in a KOH/MeOH solution (ca. 0.2 M; see Figure 5). Complex **1** is highly luminescent in methanol solution at 298 K and the emission maximum and quantum yield are 404 nm and 0.28 (quinine sulfate in

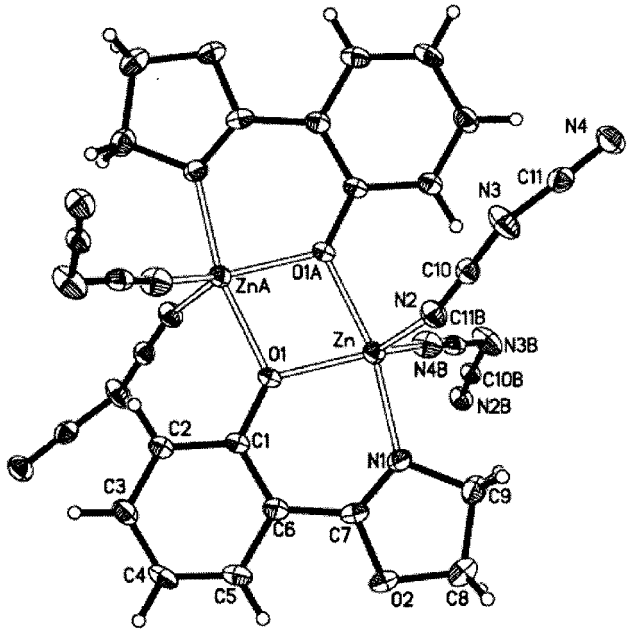

Figure 2. Perspective view of **2** (30% thermal ellipsoids except for hydrogen) and atom-numbering scheme: Zn−O(1) 1.9971(19); Zn−N(2) 2.029(2); Zn−N(1) 2.046(2); Zn−N(4B) 2.047(3); Zn−O(1A) 2.122(2); O(1)−Zn−N(2) 119.54(9); O(1)−Zn−N(1) 89.26(9); N(2)−Zn−N(1) 97.52(10); O(1)−Zn−N(4B) 127.02(10); N(2)−Zn−N(4B) 112.70(10); N(1)−Zn−N(4B) 92.35(11); O(1)−Zn−O(1A) 78.02(8); N(2)−Zn−O(1A) 92.26(9); N1−Zn−O(1A) 166.68(9); N(4B)−Zn−O(1A) 92.20(10)

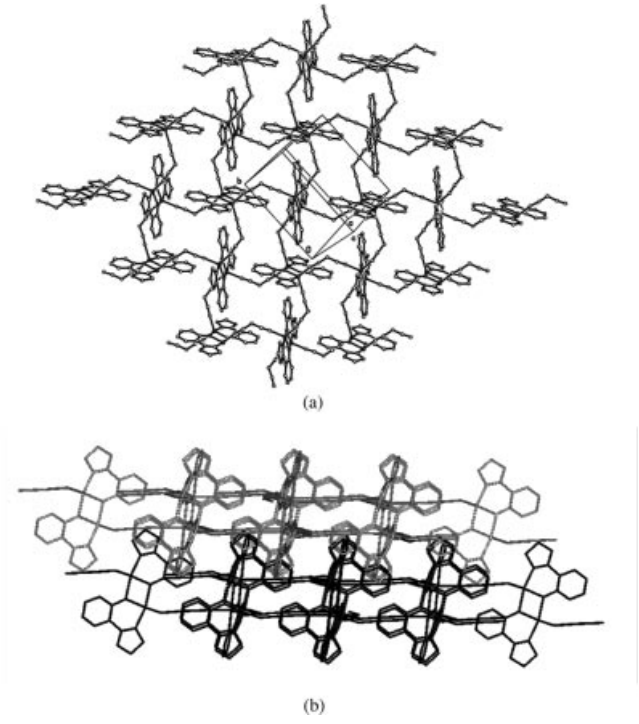

Figure 3. (a) 2-D square-grid network of **2**; (b) π-π stacking between adjacent layers

0.1 N sulfuric acid as reference), respectively. The lifetime for this emission is too short to be measured accurately by our instrument with a threshold of 100 ns. This emission is

 © 2004 Wiley-VCH Verlag GmbH & Co. KGaA, Weinheim

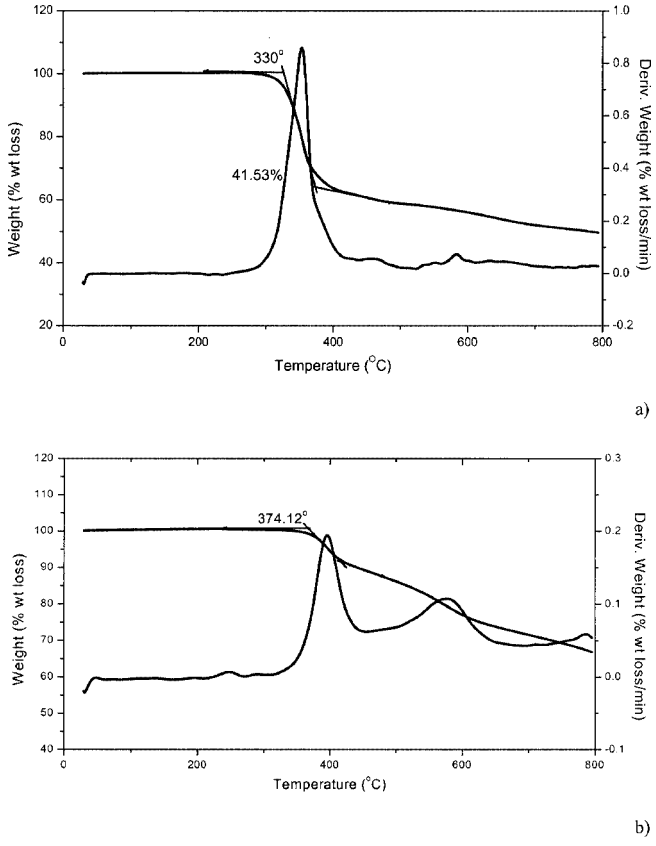

Figure 4. (a) TGA and DTGA curves of complex **1**; (b) TGA and DTGA curves of **2**

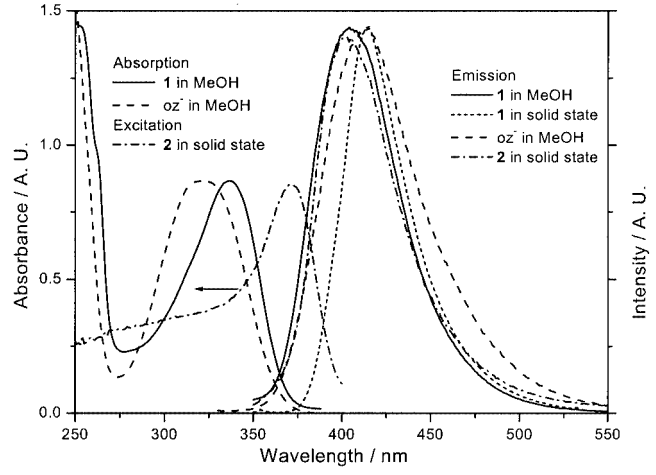

Figure 5. Absorption of the deprotonated oz^- ligand (λ_{ex} = 325 nm) and **1**, excitation of **2** (λ_{ex} = 430 nm) (left, the low-energy bands are normalized for comparison), and normalized emission (right) of the deprotonated oz^- ligand and **1** and **2** at 298 K (λ_{ex} = 325 nm)

similar in energy to that (emission maximum 415 nm, quantum yield 0.09) recorded for the deprotonated ligand oz^- in a KOH/MeOH solution (ca. 0.2 M; see Figure 5) but with a significantly higher quantum yield. These results indicate that the emission from complex **1** originates from the oz^- ligand and an intraligand charge-transfer excited-state is tentatively assigned. The emission enhancement from oz^- to complex **1** could be attributed to the coordination at the zinc atom, which presumably increases the structural rigidity and hence reduces the non-radiative decay-pathway for the excited state. The solid-state emission spectra of dimeric **1** and polymeric **2** (which is not soluble in common organic solvents) have also been recorded at 298 K and depicted in Figure 5. The emission energies (λ_{max} = 415 nm for **1** and 402 nm for **2**) are similar to that recorded for **1** in methanol solution at 298 K, suggesting that no new emissive species such as a $\pi-\pi^*$ excimer or exciplex are formed in the solid states.

Conclusion

Herein we reported the synthesis and photoluminescence study of a dinuclear zinc complex and a 2-D zinc coordination polymer containing dinuclear subunits. The two complexes exhibit similar ligand-centered fluorescence in the blue region. Incorporation of the dinuclear $[Zn_2(oz)_2]$ unit into a coordination polymer appears to improve the thermal stability while luminescence properties are not significantly modified.

Experimental Section

Synthesis of $[Zn(oz)_2]_2$ (1): $Zn(ClO_4)_2$ (0.5 mmol) was added to a methanol solution (20 mL) containing Hoz (1 mmol) and triethylamine (1 mmol). Colorless single crystals were obtained after the reaction solution was left to stand overnight at room temperature. $C_{36}H_{32}N_4O_8Zn_2$ (779.40): calcd. C 55.48, H 7.19, N 4.14; found C 55.24, H 7.25, N 4.17. IR (KBr): 2978(w), 2907(w), 1624(s), 1535(m), 1469(m), 1390(m), 1359(m), 1324(m), 1241(s), 1157(m), 1073(m), 951(m), 930(m), 847(m), 757(m), 689(m), 575(w), 535(w), 433(w) cm^{-1}.

Synthesis of $[Zn(oz)N(CN)_2]_n$ (2): Equimolar amounts of sodium dicyanamide, Hoz and triethylamine were dissolved in methanol (20 mL) and then $Zn(ClO_4)_2$ in methanol (5 mL) was added and the solution was filtered. After the filtrate was left at room temperature for one week, colorless crystals appeared. $C_{11}H_8N_4O_2Zn$ (293.58): calcd. C 45.00, H 2.75, N 19.08; found C 44.89, H 2.84, N 19.01. IR (KBr): 2977 (w), 2907 (w), 2339 (m), 2267 (m), 2198 (s), 1639 (s), 1555 (m), 1483 (s), 1384 (m), 1371 (m), 1323 (m), 1242 (s), 1159 (m), 1067 (m), 944 (m), 930 (m), 840 (m), 758 (m), 688 (m), 575 (w), 508 (w), 433 (w) cm^{-1}.

X-ray Crystallographic Determinations of 1 and 2: All the data collections were carried out on a Nonius Kappa CCD diffractometer with graphite-monochromated Mo-K_α radiation (0.71073 Å) at 293 K. Empirical absorption correction was applied to both cases. The structures were solved by direct methods and refined by a full-matrix least-squares technique based on F^2 using the SHELXL 97 program. All non-hydrogen atoms were refined anisotropically and hydrogen atoms were placed by calculation positions and refined isotropically (see Table 1).

CCDC-221016 (**1**) and CCDC-221015 (**2**) contains the supplementary crystallographic data for this paper. These data can be obtained free of charge at www.ccdc.cam.ac.uk/conts/retrieving.html [or from the Cambridge Crystallographic Data Centre, 12 Union Road, Cambridge CB2 1EZ, UK; Fax: (internat.) + 44-1223/336-033; E-mail: deposit@ccdc.cam.ac.uk].

 © 2004 Wiley-VCH Verlag GmbH & Co. KGaA, Weinheim

Table 1. Crystal data and structure refinement for complexes **1** and **2**

	1	**2**
Formula	$C_{36}H_{32}N_4O_8Zn_2$	$C_{11}H_8N_4O_2Zn$
M_R	779.400	293.58
λ (Å)	0.71073	0.71073
T (K)	293	293
Crystal system	Monoclinic	Monoclinic
Space group	$P2_1/c$	$P2_1/n$
a (Å)	8.9417(18)	9.5703(3)
b (Å)	9.851(2)	12.2372(4)
c (Å)	18.920(4)	9.7463(3)
α (°)	90	90
β (°)	96.181(3)	98.7230(10)
γ (°)	90	90
V (Å^3)	1656.8(6)	1128.22(6)
Z	2	4
ρ_{cacld} (Mg·m^{-3})	1.562	1.728
μ(Mo-K_α) (mm^{-1})	1.508	2.175
F(000)	800	592
Index ranges	$-11 \le h \le 11$, $-11 \le k \le 12$, $-24 \le l \le 23$	$-12 \le h \le 12$, $-15 \le k \le 15$, $-12 \le l \le 12$
Reflections collected	25062	19938
Independent reflections	3763	2479
Refinement method	Full-matrix least-squares on F^2	Full-matrix least-squares on F^2
Parameters	227	163
Goodness-of-fit	1.024	1.004
Final R indices [$I > 2\sigma(I)$]	$R1 = 0.046$, $wR2 = 0.08$	$R1 = 0.036$, $wR2 = 0.068$
Largest diff. peak/hole (e·Å^{-3})	0.57/−0.44	0.49/−0.47

Acknowledgments

This work was supported by the National Science Fund for Distinguished Young Scholars (20125104 and 20221101), the Research Fund for the Doctoral Program of Higher Education (20010001020), the Hong Kong Research Grants Council, and The Hong Kong University Foundation. We thank Dr. Lu Wei and Dr. Hui Zheng for photophysical measurements and helpful discussions on the photophysical properties.

[1] A. Kraft, A. C. Grimsdale, A. B. Holmes, *Angew. Chem. Int. Ed.* **1998**, *37*, 402−428.

[2] [2a] H. Mochizuki, T. Hasui, M. Kawamoto, T. Ikeda, C. Adachi, Y. Taniguchi, Y. Shirota, *Macromolecules* **2003**, *36*, 3457−3464. [2b] Y. H. Kim, D. C. Shin, S. K. Kwon, J. H. Lee, *J. Mater. Chem.* **2002**, *12*, 1280−1283.

[3] [3a] M. Fukuda, K. Sawada, K. Yoshino, *Jpn. J. Appl. Phys. 2.* **1989**, *28*, L1433−L1435. [3b] M. Fukuda, K. Sawada, K. Yoshino, *J. Polym. Sci. Polym. Chem. Ed.* **1993**, *31*, 2465−2471. [3c] G. Grem, G. Leditzky, B. Ullrich, G. Leising, *Adv. Mater.* **1992**, *4*, 36−37. [3d] D. L. Gin, V. P. Conticello, *Trends Polym. Sci.* **1996**, *4*, 217−223.

[4] [4a] M. Cölle, J. Gmeiner, W. Milius, H. Hillebrecht, W. Brütting, *Adv. Funct. Mater.* **2003**, *13*, 108−112. [4b] M. Cölle, R. E. Dinnebier, W. Brütting, *Chem. Commun.* **2002**, *23*, 2908−2909. [4c] Q. G. Wu, M. Esteghamatian, N. X. Hu, Z. Popovic, G. Enright, Y. Tao, M. D′Iorio, S. N. Wang, *Chem. Mater.* **2000**, *12*, 79−83.

[5] [5a] S. A. Van Slyke, *US Patent* **1992**, 5.151. 629. [5b] P. S. Bryan, F. V. Lovecchio, S. A. Van Slyke, *US Patent* **1992**, 5.141.671. [5c] S. F. Liu, C. Seward, H. Aziz, N. X. Hu, Z. Popovic, S. N. Wang, *Organometallics* **2000**, *19*, 5709−5714.

[6] [6a] K. Y. Ho, W. Y. Yu, K. K. Cheung, C. M. Che, *Chem. Commun.* **1998**, *19*, 2101−2102. [6b] K. Y. Ho, W. Y. Yu, K. K. Cheung, C. M. Che, *J. Chem. Soc., Dalton Trans.* **1999**, 1581−1586. [6c] W. Liu, A. Hassan, S. N. Wang, *Organometallics* **1997**, *16*, 4257−4259. [6d] S. N. Wang, *Coord. Chem. Rev.* **2001**, *215*, 79−98.

[7] [7a] W. Liu, A. Hassan, S. N. Wang, *Organometallics* **1997**, *16*, 4257−4259. [7b] S. N. Wang, A. Hassan, W. Liu, *Abstr. Pap. − Am. Chem. Soc.* **1997**, *214*, 343. [7c] A. Hassan, S. N. Wang, *Chem. Commun.* **1998**, 211−212. [7d] Y. G. Ma, H. Y. Chao, Y. Wu, S. T. Lee, W. Y. Yu, C. M. Che, *Chem. Commun.* **1998**, *22*, 2491−2492.

[8] [8a] Y. Hamada, T. Sano, H. Fujii, Y. Nishino, K. Shibata, *Jpn. J. Appl. Phys.* **1996**, *35*, L1339−L1341. [8b] G. Wang, Y. G. Zhang, Y. X. Cheng, D. G. Ma, L. X. Wang, X. B. Jing, F. S. Wang, *Synthetic Met.* **2003**, *137*, 1119−1120.

[9] L. Y. Zhang, G. F. Liu, S. L. Zheng, B. H. Ye, X. M. Zhang, X. M. Chen, *Eur. J. Inorg. Chem.* **2003**, *16*, 2965−2971.

[10] [10a] R. G. Xiong, J. L. Zuo, X. Z. You, B. F. Abrahams, Z. P. Bai, C. M. Che, H. K. Fun, *Chem. Commun.* **2000**, 2061−2062. [10b] Z. F. Chen, R. G. Xiong, J. Zhang, X. T. Chen, Z. L. Xue, X. Z. You, *Inorg. Chem.* **2001**, *40*, 4075−4077. [10c] J. Zhang, Y. R. Xie, Q. Ye, R. G. Xiong, Z. L. Xue, X. Z. You, *Eur. J. Inorg. Chem.* **2003**, 2572−2577.

Received December 10, 2003

 © 2004 Wiley-VCH Verlag GmbH & Co. KGaA, Weinheim

On the Use of the Bis(diiodine) Adduct of 1,4-Dimethylperhydro-1,4-diazepine-2,3-dithione (Me_2dazdt) to Recover Liquid Mercury Producing [Hg(Me_2dazdt)I_2] in a One-Step Reaction

Francesco Bigoli,[a] Maria Cristina Cabras,[b] Paola Deplano,*[b] Maria Laura Mercuri,[b] Luciano Marchiò,[a] Angela Serpe,[b] and Emanuele F. Trogu[b]

Keywords: Mercury / S ligands / Iodine / Adducts / Oxidation

Diiodine adducts with cyclic dithio-oxamides, where complexing and oxidising properties coexist in the same molecule, have been shown to be powerful oxidising reagents towards selected metals. Here we describe the reaction of Me_2dazdt·$2I_2$ [Me_2dazdt = 1,4-dimethylperhydro-1,4-diazepine-2,3-dithione (**1**)] with highly toxic liquid mercury which gives the complex [Hg(Me_2dazdt)I_2] (**2**) in a one-step reaction. X-rays analysis of **2** shows that the Hg^{II} centre is coordinated by two sulfur atoms of the chelating ligand and by two iodine atoms in a distorted tetrahedral geometry. The molecule is asymmetric and crystallizes in the chiral space group $P2_12_12_1$. In the unit cell only the M enantiomer is present [τ (S1–C1–C2–S2) = –61.1(5)°].

(© Wiley-VCH Verlag GmbH & Co. KGaA, 69451 Weinheim, Germany, 2004)

Introduction

Many efforts are currently devoted to find safe, non-polluting reagents which are effective for the dissolution of noble and heavy metals. The recovery of these metals has both environmental and economic relevance because of waste accumulation and simultaneous decrease of raw materials due to their extensive usage in novel technologies.[1] Diiodine adducts with appropriate donors, where complexing and oxidizing properties coexist in the same molecule, have a high potential to dissolve the above-cited metals under mild conditions.[2–4] Successful results have been obtained by our group using the bis(diiodine) adduct of 1,4-dimethylperhydro-1,4-diazepine-2,3-dithione [Me_2dazdt·$2I_2$ = (**1**)] to dissolve elemental gold in a one-step reaction, under mild conditions and in a short time.[5] Moreover, it is inert towards air and moisture and does not exhibit cytotoxicity.[6] These properties make this reagent an optimal candidate for such applications.[7] We are now employing this dissolution method towards highly toxic and heavy metals, with the view to remove them from waste from electronic equipment before disposal in order to prevent the metal dispersion into the soil. In this paper we show the reactivity of **1** towards liquid mercury which exhibits extremely high toxicity,[8] as well as great affinity for sulfur-donors.

Results and Discussion

[Hg(Me_2dazdt)I_2]

Me_2dazdt·$2I_2$ (**1**)[5] has been reacted with liquid mercury according to Scheme 1. Liquid mercury (24 mg) was consumed under the experimental conditions shown in Scheme 1 (2:1 adduct excess, room temperature, THF solvent) in approximately two hours. By Et_2O diffusion into the THF solution, well-formed, shiny, pale-yellow crystals precipitated in an almost quantitative yield.

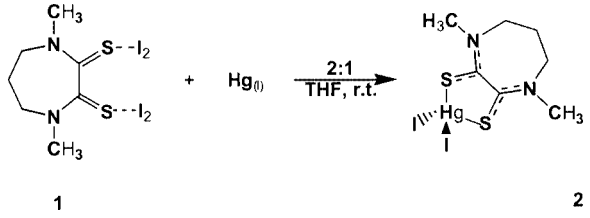

1 2

Scheme 1

These crystals have been isolated and characterised as [Hg(Me_2dazdt)I_2] (**2**). The use of Me_2dazdt·$2I_2$ has allowed the oxidation and complexation of liquid mercury producing **2** in a very easy and convenient route, under mild conditions and through a one-step reaction. An X-ray dif-

[a] Dipartimento di Chimica Generale ed Inorganica, Chimica Analitica, Chimica Fisica, Università di Parma, Parco Area delle Scienze 17/A, 43100 Parma, Italy
[b] Dipartimento di Chimica Inorganica ed Analitica, Università di Cagliari, 09042 Monserrato, Cagliari, Italy
Fax: (internat.) + 39-070-6754456
E-mail: deplano@unica.it

 © 2004 Wiley-VCH Verlag GmbH & Co. KGaA, Weinheim DOI: 10.1002/ejic.200300525

fractometric study on **2** has been performed. The molecular structure and the atomic-labelling scheme for **2** are shown in Figure 1. Bond lengths and angles are reported in Table 1.

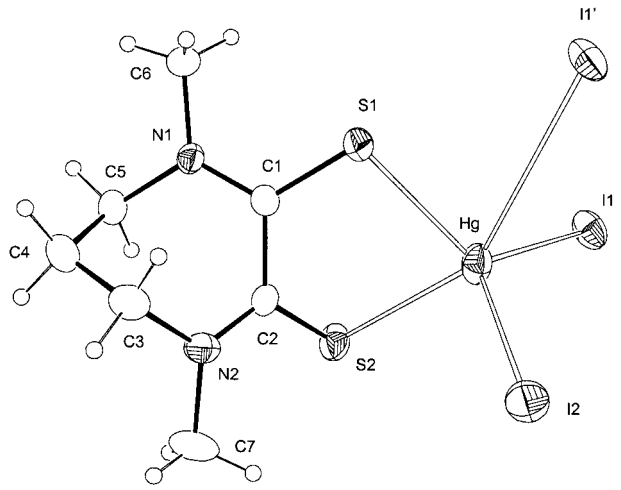

Figure 1. Perspective view of $[Hg(Me_2dazdt)I_2]$; thermal ellipsoids are drawn at the 30 % probability level

Table 1. Bond lengths [Å] and angles [deg] for $[HgI_2(Me_2dazdt)]$ (**2**)

Hg−I1	2.6931(4)	N1−C6	1.456(6)
Hg−I2	2.7091(5)	N1−C5	1.468(6)
Hg−S1	2.554(1)	N2−C2	1.326(6)
Hg−S2	2.776(1)	N2−C7	1.471(6)
Hg−I1[a]	3.8188(5)	N2−C3	1.474(6)
S1−C1	1.692(5)	C1−C2	1.507(6)
S2−C2C2	1.674(5)	C3−C4	1.507(8)
N1−C1	1.323(6)	C4−C5	1.508(7)
I1−Hg−I2	116.55(2)	C2−N2−C7	120.7(5)
I1−Hg−S1	119.89(4)	C3−N2−C7	118.0(4)
I1−Hg−S2	108.81(3)	N1−C1−C2	117.1(4)
I2−Hg−S1	119.18(4)	N1−C1−S1	121.8(4)
I2−Hg−S2	99.74(4)	C2−C1−S1	121.1(3)
S1−Hg−S2	82.37(4)	N2−C2−C1	116.8(4)
C1−S1−Hg	100.3(2)	N2−C2−S2	124.4(4)
C2−S2−Hg	89.4(2)	C1−C2−S2	118.7(4)
C1−N1−C5	120.8(4)	N2−C3−C4	111.4(5)
C1−N1−C6	121.1(4)	C3−C4−C5	111.6(4)
C5−N1−C6	118.0(4)	N1−C5−C4	110.7(4)
C2−N2−C3	121.1(4)		

[a] Symmetry = $-x + 1$, $y - 1/2$, $-z + 1/2$.

The mercury atom is in a severely distorted tetrahedral environment, coordinated by two iodine and two sulfur atoms of the chelating ligand. However, the Hg−S interatomic distances are significantly different [Hg−S1 = 2.554(1), Hg−S2 = 2.776(1) Å] as a consequence of a long contact between the metal and an iodine atom of an adjacent molecule [Hg−I1′ = 3.8188(5) Å] that renders the overall coordination geometry nearly trigonal bipyramidal with the equatorial positions occupied by the S1, I1 and I2 atoms. The lengthening of the Hg−S2 bond length is in accordance with the apical position occupied by S2 and by the *trans* influence of the iodine atom I1′. The I1′−Hg−S2 angle is significantly bent [150.07(3)°] and the S1−Hg−S2 angle is forced to be 82.37(4)° due to ligand chelation. The metal lies out of the S1−I1−I2 plane by 0.322(1) Å and is directed toward the S2 atom (cf. 0 Å for trigonal bipyramidal geometry and ca. 0.9 Å for tetrahedral coordination with average Hg−X bond lengths of ca. 2.7 Å). These main structural features are similar to those found in the complex $[Hg(bzimtH_2)_2I_2]$ ($bzimtH_2$ = benzo-1,3-imidazole-2-thione) where the mercury atom is similarly coordinated but the two sulfur atoms belong to two monothionic donors.[9] In other similarly coordinated complexes with heterocyclic thiones, shorter Hg−S interatomic distances and longer Hg−I interatomic distances were found and explained by considering the existence of different intermolecular interactions.[10,11] In the case of complex $[Hg(bzimtH_2)_2I_2]$, the long Hg−S interatomic distances were ascribed to the presence of NH···S interactions which were absent in complexes with shorter Hg−S interatomic distances.

In complex **2**, the C−S and the C−N interatomic distances of the two NCS fragments (Table 1) are in agreement with a strong electron delocalisation inside the thioamidic moieties as has been reported for similar systems.[12−15] Furthermore, no extension of the electron delocalization between the two planar thioamide groups is observed [C1−C2 1.507(6) Å]. The molecule is asymmetric and is therefore chiral. The S1−C1−C2−S2 torsion angle [−61.1(5)°] can be used to define the chirality of the molecular entity.[16]

The IR and Raman bands that are most significant in investigating the coordination mode of the Me_2dazdt ligand are ν(CN) and ν(C=S). In fact, sulfur donation should be accompanied by a shift to lower frequencies of ν(C=S) and simultaneously to higher frequencies of ν(CN).[17] Conflicting literature assignments of ν(C=S)[18−20] reflect difficulty in identifying this vibration, which may be extensively coupled with other vibrations and in several cases, this peak is not very sensitive to coordination.[21] Instead, the assignment of the ν(CN) is well established and can give useful information on the coordination of the ligand. Accordingly, the strong peak at $\tilde{\nu}$ = 1532 cm^{-1} in **2** ($\tilde{\nu}$ = 1530 cm^{-1} in **1**, 1493 cm^{-1} in the free ligand) is assigned to the ν(CN) vibration. A medium weak band ($\tilde{\nu}$ = 826 cm^{-1}) in **2** ($\tilde{\nu}$ = 824 cm^{-1} in **1**, 836 cm^{-1} in the free ligand) is tentatively assigned to ν(C=S). Thus, in accordance with X-ray results, vibrational spectroscopy shows that mesomeric forms involving CN double bonds contribute more than in the free ligand to the description of the structure of Me_2dazdt both in the adduct [ν(CN) = 1532 cm^{-1}] and in **2**. Therefore, when the sulfur atoms function as donors, the polar form of Me_2dazdt is favoured. Also, this contribution is very similar in the adduct and in the complex. Vibrational spectra of **2** in the Far-IR region are shown in Figure 2.

In **2**, a broad, very strong band centred ($\tilde{\nu}$ = 139 cm^{-1}) with shoulders (ca. $\tilde{\nu}$ = 150 and 125 cm^{-1}) appears in the Raman spectrum and in the IR spectrum ($\tilde{\nu}$ = 150 with a shoulder at 139 cm^{-1}). These overlapping bands are assigned to Hg−I vibrations (ν_{as} = 150 and 139 cm^{-1} and

 © 2004 Wiley-VCH Verlag GmbH & Co. KGaA, Weinheim

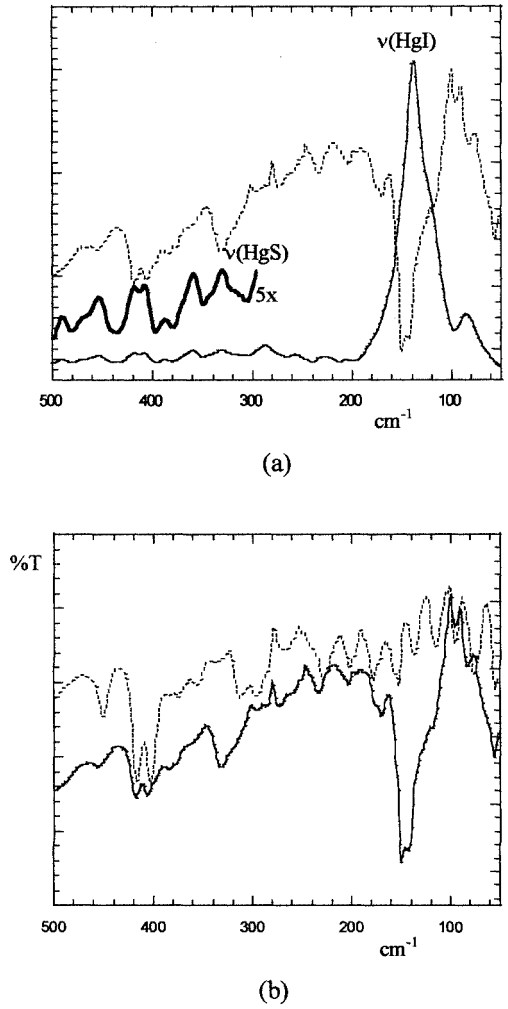

Figure 2. (a) Superimposed FT-Raman (continuous line), 5 times amplified FT-Raman (thick line) and FT-IR spectra (dotted line) of [Hg(Me$_2$dazdt)I$_2$]; (b) Far-IR spectra of polyethylene pellets of Me$_2$dazdt (dotted line) and [Hg(Me$_2$dazdt)I$_2$] (continuous line); transmittance is reported in arbitrary units

ν_s = 125 cm^{-1}; Figure 2, a).[22] The two weak Raman peaks ($\tilde{\nu}$ = 333 and 318 cm^{-1}; the spectrum is dominated by very strong Hg−I vibrations) which appear in the Far-IR spectrum as a broad peak ($\tilde{\nu}$ = 332 cm^{-1} with a shoulder at 318 cm^{-1}) and are not present in the free ligand's spectrum, (Figure 2, b) are tentatively assigned to Hg−S vibrations.

Conclusion

Me$_2$dazdt·2I$_2$, [the bis(diiodine) adduct of 1,4-dimethylperhydro-1,4-diazepine-2,3-dithione] was shown to be a valuable reagent towards liquid mercury, capable of dissolving the highly polluting metal in a one-step reaction to form the complex [Hg(Me$_2$dazdt)I$_2$] under mild conditions and has been fully characterised. The effectiveness and ease of the reaction coupled with the low environmental impact of the reagent and the extremely high toxicity of the metal make the reported dissolution technique relevance to Hg-recovery.

Experimental Section

General: Reagents and solvents of reagent grade quality were used as furnished by Aldrich. The adduct Me$_2$dazdt·2I$_2$ (**1**) and the ligand Me$_2$dazdt were prepared according to literature procedures.[23,4]

Synthesis of [Hg(Me$_2$dazdt)I$_2$]: A Me$_2$dazdt·2I$_2$ solution (0.170 g, 0.24 mmol in 100 mL of THF) and liquid mercury (0.024 g, 0.12 mmol; 2:1 molar ratio) were mixed in a heterogeneous phase and allowed to react while stirring at room temperature for 2 h. The red-brown solution of the adduct developed into a clear orange-yellow solution. Shiny yellow crystals of [Hg(Me$_2$dazdt)I$_2$], suitable for X-ray analysis, were obtained by slow crystallization from THF/Et$_2$O, with quantitative yield referred to Hg. $C_7H_{12}HgI_2N_2S_2$ (642.7): calcd. C 13.08, H 1.88, N 4.36, S 9.98; found C 13.42, H 1.62, N 4.40, S 9.86. Mid-IR (KBr pellets, cm^{-1}): $\tilde{\nu}$ = 2955 vw, 2923 w, 2852 vw, 1532 vs, 1458 ms, 1440 w, 1398 s, 1358 w, 1331 w, 1287 ms, 1278 s, 1255 m, 1212 vw, 1184 w, 1118 s, 1074 w, 1028 w, 967 w, 826 w, 751 w, 695 vw, 613 mw, 591 w, 538 vw, 417 vw. Far-IR (Polyethylene pellets, cm^{-1}): $\tilde{\nu}$ = 418 ms, 406 ms, 383 mw, 377 mw, 332 ms, 296 w, 273 w, 234 w, 203 w, 170 m, 150 vs, 142 vs, 96 vw, 83 w, 56 m. Raman (cm^{-1}): $\tilde{\nu}$ = 2983 w, 2926 mw, 1526 mw, 1458 w, 1439 vw, 1400 mw, 1358 w, 1287 w, 1256 w, 1213 vw, 1184 vw, 1108 vw, 887 vw, 696 vw, 614 vw, 540 mw, 419 w, 334 w, 283 w, 164 sh, 150 sh, 139 vs, 127 sh, 121 sh, 86 m, 75 mw. UV-Vis (ε = L·mol^{-1}·cm^{-1}): λ = 290 sh (ca. 600) nm, 340 sh (ca. 500).

Measurements: Microanalyses were performed on a Carlo−Erba CHNS elemental analyser model EA1108. IR spectra (4000−50 cm^{-1}) were recorded as KBr (Mid-IR) and polyethylene (Far-IR) pellets with a spectrometer Bruker Equinox-55 (resolution 4 cm^{-1}). FT-Raman spectra were recorded on a Bruker RFS100/S FT-spectrometer, fitted with an InGaAs detector (room temperature) and operating with an excitation frequency of 1064 nm (Nd:YAG laser). The power level of the laser source was 100 mW. The solid samples were introduced into a capillary tube and then fitted into the compartment designed for a 180° scattering geometry (resolution 4 cm^{-1}). No sample decomposition was observed during data collection. Electronic spectra (1500−300 nm) were recorded on a Cary 5 spectrophotometer by using CH_3CN solvent. Polarimetric measurements were performed on a Polax-D instrument using a 10 cm cell.

X-ray Crystallographic Study: A summary of data collection and structure refinement for **2** are reported in Table 2. Single-crystal data were collected with a Bruker AXS Smart 1000 area detector diffractometer (Mo-K_α, λ = 0.71073 Å). Cell parameters were refined from the observed setting angles and detector positions of selected strong reflections. Intensities were integrated from several series of exposure frames covering a hemisphere of reciprocal space.[24] No crystal decay was observed. Absorption correction using the program SADABS[25] was applied and resulted in transmission factors ranging from 0.408−1.000. The space group ($P2_12_12_1$) was chosen on the basis of the systematic extinction and intensity statistics, the absolute configuration has been confirmed at the 3σ level of the Flack parameter [−0.012(4)].[26] The structure was solved by direct methods (SIR97)[27] and refined with full-matrix least-squares (SHELXL-97),[28] using the Wingx software package.[29] Non-hydrogen atoms were refined anisotropically; hydrogen atoms were placed at their calculated positions. The maximum and minimum peaks on the final difference Fourier maps corresponded to 0.806 and −1.040 e·Å^{-3}. The programs Parst [30,31] and ORTEP3 for Windows[32] were also used. CCDC-199303 con-

 © 2004 Wiley-VCH Verlag GmbH & Co. KGaA, Weinheim

tains the supplementary crystallographic data for this paper. This data can be obtained free of charge at www.ccdc.cam.ac.uk/conts/retrieving.html [or from the Cambridge Crystallographic Data Centre, 12 Union Road, Cambridge CB2 1EZ, UK; Fax: (internat.) +44-1223/336-033; E-mail: deposit@ccdc.cam.ac.uk].

Table 2. Crystallographic data of compound $[HgI_2(Me_2dazdt)]$ (**2**)

Empirical Formula	$C_7H_{12}HgI_2N_2S_2$
M_r [g·mol^{-1}]	642.70
Crystal system	orthorhombic
Space group	$P2_12_12_1$ (No.19)
a [Å]	9.047(1)
b [Å]	9.216(1)
c [Å]	18.139(1)
V [Å^3]	1512.4(2)
Z	4
D [Mg·m^{-3}]	2.823
Wavelength [Mo-K_α]	λ = 0.71073 Å
T [K]	293
μ [mm^{-1}]	14.507
R_f collected/unique	16959/3485
R_{int}	0.0435
No. of parameters refined	130
GooF	1.017
R_1[a], wR_2[b]	0.0231, 0.417
R_1, wR_2 (all data)	0.0291, 0.427

[a] $R_1 = ||F_o| - |F_c||/|F_o|$. [b] $wR_2 = [w(F_o^2 - F_c^2)^2/wF_o^4]^{1/2}$.

Acknowledgments

The Università degli Studi di Cagliari is acknowledged for financial support in this research.

[1] Council Directive 2002/96/EC on waste electrical and electronic equipment (Jan. 27, **2003**).
[2] Y. Nakao, *Chem. Commun.* **1997**, 1765, and references cited therein.
[3] S. M. Godfrey, N. Ho, C. A. McAuliffe, R. G. Pritchard, *Angew. Chem. Int. Ed. Engl.* **1996**, *35*, 2344.
[4] F. Bigoli, P. Deplano, F. A. Devillanova, V. Lippolis, M. L. Mercuri, M. A. Pellinghelli, E. F. Trogu, *Inorg. Chim. Acta* **1998**, *267*, 115.
[5] F. Bigoli, P. Deplano, M. L. Mercuri, M. A. Pellinghelli, G. Pintus, A. Serpe, E. F. Trogu, *Chem. Commun.* **1998**, 2351.
[6] L. Pompei et al., unpublished work.
[7] M. Vanzi, A. Bonfiglio, P. Salaris, P. Deplano, E. F. Trogu, A. Serpe, G. Salmini, R. De Palo, *Microelectronics Reliability* **1999**, *39*, 1043.
[8] T. Suzuki, N. Imura, T. C. Clarkson, *Advances in Mercury Toxicology*, Plenum Press, New York, **1991**.
[9] Z. Popovic, Ž. Soldin, D. Matkovic-Calogovic, G. Pavlovic, M. Rajic, G. Giester, *Eur. J. Inorg. Chem.* **2002**, 171.
[10] N. A. Bell, T. N. Branston, W. Clegg, J. R. Creighton, L. Cucurull-Sánchez, M. R. J. Elsegood, E. S. Raper, *Inorg. Chim. Acta* **2000**, *303*, 220.
[11] Z. Popovic, G. Pavlovic, D. Matkovic-Calogovic, |142. Soldin, M. Rajic, D. Vikic-Topic, D. Kovacek, *Inorg. Chim. Acta* **1999**, *285*, 208.
[12] N. A. Bell, T. N. Branston, W. Clegg, J. R. Creighton, E. S. Raper, *Inorg. Chim. Acta* **2000**, *303*, 12.
[13] E. S. Raper, J. R. Creighton, R. E. Oughtred, *Acta Crystallogr., Sect. B* **1983**, *39*, 335.
[14] N. Trinajstic, *Tetrahedron Lett.* **1968**, 1529.
[15] K. Eichorn, *Acta Crystallogr., Sect. B* **1987**, *43*, 111.
[16] The negative sign of this *fiducial* torsion allows the definition of the molecular entity as the enantiomer M (minus) (Basic Terminology of Stereochemistry, *Pure Appl. Chem.* **1996**, *68*, *12*, 2193). As the space group is also chiral ($P2_12_12_1$), a polarimetric analysis has been performed in order to assess if a spontaneous resolution has occurred during the crystallization (acetonitrile as solvent). The zero value obtained by the measurement indicates that a racemic conglomerate (with distinct enantiomorphic crystals) may be present.
[17] B. Slootmaekers, E. Manessi-Zoupa, S. P. Perlepes, H. O. Desseyn, *Spectrochimica Acta Part A* **1996**, *52*, 1255.
[18] D. J. Williams, P. H. Poor, G. Ramirez, B. H. Heyl, *Inorg. Chim. Acta* **1988**, *147*, 221.
[19] G. Mille, J. Kister, G. Assef, J. Chouteau, *C. R. Acad. Sci., Ser. IIc: Chim.* **1978**, *286*, 477.
[20] J. R. Creighton, D. S. Gardiner, A. C. Gorvin, C. Gutteridge, A. R. W. Jackson, E. S. Raper, P. M. A. Sherwood, *Inorg. Chim. Acta* **1985**, *103*, 195.
[21] H. O. Desseyn, B. Slootmaekers, G. Lemière, *Spectrochimica Acta Part A* **2002**, *58*, 1785.
[22] K. Nakamoto, *Infrared and Raman Spectra of Inorganic and Coordination Compounds*, John Wiley & Sons, 14th ed., **1986**, p. 130.
[23] R. Isaksson, T. Lijefors, J. Sandstrom, *J. Chem. Res. Miniprint* **1981**, 664.
[24] SMART (control) and SAINT (integration) software for CCD systems, Bruker AXS, Madison, WI, USA, **1994**.
[25] Area-Detector Absorption Correction, Siemens Industrial Automation Inc., Madison, WI, **1996**.
[26] H. G. Flack, G. Bernardinelli, *J. Appl. Cryst.* **2000**, *33*, 1143.
[27] A. Altomare, M. C. Burla, M. Camalli, G. L. Cascarano, C. Giacovazzo, A. Guagliardi, A. G. G. Moliterni, G. Polidori, R. Spagna, *J. Appl. Cryst.* **1999**, *32*, 115.
[28] G. M. Sheldrick, SHELX-97. *Programs for Crystal Structure Analysis*, **1997**, (Release 97−2). University of Göttingen, Germany.
[29] L. J. Farrugia, *J. Appl. Crystallogr.* **1999**, *32*, 837.
[30] M. Nardelli, *Comput. Chem.* **1983**, *7*, 95.
[31] M. Nardelli, *J. Appl. Crystallogr.* **1995**, *28*, 659.
[32] L. J. Farrugia, *J. Appl. Crystallogr.* **1997**, *30*, 565.

Received July 31, 2003

 © 2004 Wiley-VCH Verlag GmbH & Co. KGaA, Weinheim

Synthesis of a Metallamacrocyclic $Re(CO)_3$ Complex Using a Tridentate Bridging Ligand

Thomas Brasey,[a] Andrey Buryak,[a] Rosario Scopelliti,[a] and Kay Severin*[a]

Keywords: Host−guest chemistry / Metallamacrocycles / Rhenium / Silver

The reaction of $[ReBr_3(CO)_3][NEt_4]_2$ with 3-hydroxy-1,2,3-benzotriazine-4(3*H*)-one in the presence of base gave the ionic rhenium complex $[ReBr(C_7H_4N_3O_2)(CO)_3][NEt_4]$ (**2**) which was crystallographically characterized. A neutral metallamacrocycle **3** was obtained upon abstraction of $[NEt_4]Br$ from complex **2**. This complex cocrystallizes with an unusual C_3-symmetric $[Ag(\eta^2\text{-benzene})_3(OH_2)][BF_4]$ complex as evidenced by single-crystal X-ray diffraction.
(© Wiley-VCH Verlag GmbH & Co. KGaA, 69451 Weinheim, Germany, 2004)

Introduction

The *fac*-$Re^I(CO)_3$ fragment has frequently been used as a building block for the construction of self-assembled metallomacrocycles,[1] some of which have found applications in the field of sensing[2] or catalysis.[3] For the synthesis of these macrocycles, bidentate ligands with N-heterocycles as donor groups were employed almost exclusively. We have recently shown that simple tridentate ligands with N,O,O′-donor atoms such 2,3-dihydroxypyridine[4] or 3,4-dihydroxy-2-methyl-pyridine[5] are well suited for the assembly of organometallic half-sandwich complexes of Ru^{II}, Rh^{III} and Ir^{III}.[6] In continuation of these studies, we have investigated the reaction of $[ReBr_3(CO)_3][NEt_4]_2$[7] (**1**) with 3-hydroxy-1,2,3-benzotriazine-4(3*H*)-one. Complex **1** was chosen as the starting material because the three bromo ligands can easily be replaced. When **1** is dissolved in water, for example, the thermodynamically stable[8] but kinetically labile[9] aqua complex $[Re(CO)_3(OH_2)_3]^+$ is formed. The benzotriazine derivative appeared to be a suitable reaction partner for the construction of a neutral metallamacrocycle because it can occupy the three available coordination sites by acting as a monoanionic, bridging chelate ligand.

Results and Discussion

A mixture of complex **1**, the ligand 3-hydroxy-1,2,3-benzotriazine-4(3*H*)-one and one equivalent of KOH was dissolved in methanol. After 12 h, the solvent was evaporated and the product was separated from the bromide salts by Soxhlet extraction with benzene. In this way we were able to obtain the adduct **2** in 72 % yield (Scheme 1). The infrared spectrum of **2** was characteristic of a $Re(CO)_3$ complex with strong bands in the carbonyl region at ν_{CO} = 2007 and 1855 cm^{-1}. The NMR spectra of **2** confirmed the presence of the benzotriazine ligand and the tetraethylammonium cation.

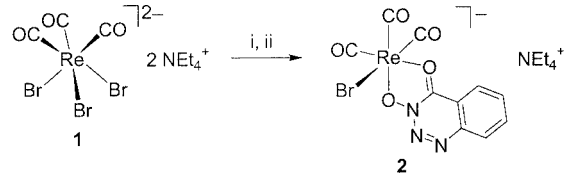

1 2

Scheme 1. Synthesis of complex **2**; (i) 3-hydroxy-1,2,3-benzotriazine-4(3*H*)-one, KOH (1 equiv.), MeOH, 12 h, r.t.; (ii) evaporation of MeOH and extraction with benzene

The structure of **2** was established by single-crystal X-ray analysis. The deprotonated benzotriazine derivative is coordinated by the two oxygen atoms to the Re atom (Figure 1). This is different from what has been observed for Ru- and Os-carbonyl complexes with this ligand; here a N−N′- or a N−O-coordination mode was found.[10] The third coordination site in **2** is still occupied by one bromo ligand, which is positioned *trans* to a carbonyl ligand, resulting in a negatively charged $Re(CO)_3$ complex. Due to the small bite angle of the chelate ligand, the octahedral geometry around the Re atom is slightly distorted.

In order to induce macrocyclization, the remaining bromo ligand of complex **2** was abstracted with $AgBF_4$ in methanol (Scheme 2). After crystallization from benzene/pentane, a product of the empirical formula $[Re(CO)_3(C_7H_4N_3O_2)]_n$ (**3**) was obtained. An alternative and simpler way to synthesize this complex is by suspending **2** in water followed by extraction of the product with diethyl ether (NEt_4Br remains in the aqueous phase).

The presence of the $Re(CO)_3$ fragment was confirmed by IR spectroscopy (ν_{CO} = 2026 and 1882 cm^{-1}). ^1H NMR

[a] Institut des Sciences et Ingénierie Chimiques, École Polytechnique Fédérale de Lausanne,
1015 Lausanne, Switzerland
Fax: (internat.) + 41-(0)21-693-9305
E-mail: kay.severin@epfl.ch

 © 2004 Wiley-VCH Verlag GmbH & Co. KGaA, Weinheim **DOI: 10.1002/ejic.200300880**

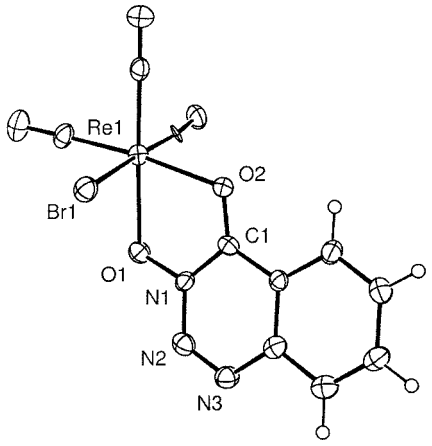

Figure 1. Molecular structure of complex **2** in the crystal; the $[NEt_4]^+$ cation and the CH_2Cl_2 molecule are not shown for clarity; selected bond lengths [Å] and angles [°]: Re1−O1 2.168(10), Re1−O2 2.163(9), Re1−Br1 2.6544(15), N1−O1 1.359(14), C1−O2 1.251(16); O1−Re1−O2 75.2(4), Br1−Re1−O1 83.9(3), Br1−Re1−O2 83.6(3)

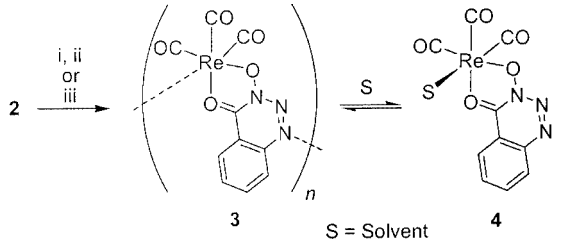

Scheme 2. Synthesis of the metallamacrocycle **3**; (i) $AgBF_4$ (1.1 equiv.), MeOH, 1 h, r.t.; (ii) crystallization from benzene/pentane; alternatively: (iii) separation with Et_2O/H_2O (yield: 80 %); in polar solvents such as methanol, the monomeric adducts **4** are formed

spectroscopic investigations in C_6D_6 were indicative of a highly symmetrical structure due to the presence of only one set of signals for the ligand. Unfortunately, we were not able to determine unequivocally the aggregation number of **3** with either mass spectrometry or single-crystal X-ray analysis, but based on the coordinate vectors of the benzotriazine ligand, a trimeric (see below) or tetrameric macrocycle seemed to be the most likely geometry.

When complex **3** is dissolved in coordinating polar solvents, both the NMR spectra as well as the UV-Vis spectroscopic data change substantially. In benzene, the macrocyclic complex **3** displays a maximum at $\lambda = 426$ nm, whereas in methanol the value is shifted to $\lambda = 373$ nm. A similar value is found in acetonitrile ($\lambda = 376$ nm). In C_6D_6, the signals for the benzotriazine ligand range from $\delta = 6.62-8.68$ ppm, whereas in CD_3OD the signals are confined to a region between $\delta = 7.92$ and 8.31 ppm (CD_3CN: 7.88−8.25 ppm). A plausible explanation of this data is that in coordinating solvents, we generate the monomeric solvent adducts **4** (Scheme 2). Such behaviour is not unprecedented: a solvent-dependent equilibrium between a dimer and a monomer has been described for $Re(CO)_3$ complexes with chelating $[NO]^-$ ligands.[11]

As a side product of the reaction between **2** and $AgBF_4$ (2 equiv.), we were able to isolate crystals of the macrocyclic compound **5** (ca. 5 % yield). As evidenced by X-ray crystallography, complex **5** contains an unusual C_3-symmetric $[Ag(\eta^2\text{-benzene})_3(OH_2)][BF_4]$ guest. A graphical representation of the structure is shown in Figure 2. The Re complex forms a trimeric metallamacrocycle. The $Re(CO)_3$ fragments are connected by the two O-atoms and the N1-atom of the benzotriazine ligand with the metal atoms being 7.066(2) Å apart from each other. To the best of our knowledge, this is the first structurally characterized macrocyclic $Re(CO)_3$ complex built with a tridentate chelate ligand. The noncovalent interactions with the guest molecule are of special interest. The metallamacrocycle forms a slightly concave cavity which has exactly the right size and symmetry to encapsulate the $[BF_4]^-$ anion.[12] On the other side of the macrocycle — and well shielded from the $[BF_4]^-$ anion — a $[Ag(\eta^2\text{-}C_6H_6)_3(OH_2)]^+$ complex is located. This cation represents one of the rare cases in which a $[Ag]^+$ ion is bound to three free arene ligands.[13] There are several examples of complexes containing the $[Ag(\eta^{1/2}\text{-arene})_3]^+$ structural motif, but here, chelating arene ligands such as cyclophane-type macrocycles were used to increase the stability of the complex.[14] The compound $[Ag(C_6H_6)_3][BF_4]$ on the other hand, is highly unstable: out of solution, it decomposes instantaneously even in an inert atmosphere (Figure 2).[13a]

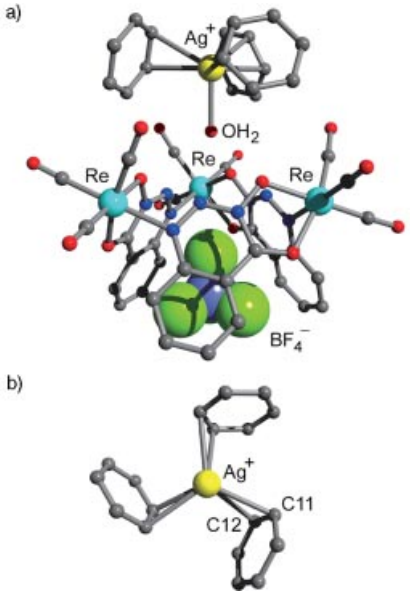

Figure 2. a) Graphic representation of the molecular structure of **5** in the crystal; the hydrogen atoms and a cocrystallized benzene molecule are not shown for clarity; b) view along the C_3-symmetry axis on the $[Ag(\eta^2\text{-benzene})_3]^+$ complex

The $[Ag]^+$ ion in complex **5** is situated on the symmetry axis and is thus coordinated to three benzene solvent molecules in a highly symmetrical fashion (Figure 2 b). In this context, it is interesting to note that the threefold symmetry was claimed to be unfavorable for $Ag(arene)_3$ coordination.[15] In view of our results, this statement appears to

 © 2004 Wiley-VCH Verlag GmbH & Co. KGaA, Weinheim

be questionable. At least the energy difference between a symmetrical and a distorted geometry must be small since there are only weak packing effects, which can influence the geometry of the $[Ag]^+$ complex in **5**. The Ag−C distances found for **5** are within the expected range [Ag−C11: 2.623(18); Ag−C12: 2.612(17) Å]. A water molecule is bound to the fourth coordination site of the silver ion [Ag−O: 2.297(3) Å]. It is within expected hydrogen-bond lengths to the oxo-groups of the bridging benzotriazine ligand [O···O′: 3.112(18) Å] thereby connecting the silver complex with the $Re(CO)_3$-macrocycle.

Conclusions

In summary, we have described the synthesis and the structure of a new $Re(CO)_3$-containing metallamacrocycle which is able to act as a host for the unusual silver complex $[Ag(\eta^2\text{-}C_6H_6)_3(OH_2)][BF_4]$. In elaboration of previous approaches to construct $Re(CO)_3$ macrocycles, an anionic, tridentate chelate ligand was used to bridge the rhenium centers. It seems likely that this synthetic concept can be expanded by employing other organometallic fragments such as *fac*-$[M^{II}(allyl)(CO)_2]$ (M = Mo, W) or *fac*-$[Pt^{IV}(CH_3)_3]$ and/or by using structurally related anionic ligands. The synthesis and the host-guest chemistry of such complexes is currently being investigated in our laboratory.

Experimental Section

General: All reactions were performed under dry dinitrogen, using standard Schlenk techniques. Complex $[ReBr_3(CO)_3][NEt_4]_2$ (**1**) was prepared according to a literature procedure.[7] The ^1H and ^{13}C spectra were recorded on a Bruker Advance DPX 400 or a Bruker Advance 200 spectrometer with the residual protonated solvents (^1H, ^{13}C) as internal standards. All spectra were recorded at room temperature.

Synthesis of Complex 2: Complex $[ReBr_3(CO)_3][NEt_4]_2$ (770 mg, 1.0 mmol) was added to a solution of the ligand 3-hydroxy-1,2,3-benzotriazine-4(3*H*)-one (163 mg, 1.0 mmol) and KOH (2.0 mL of 0.496 M, 1.0 mmol) in methanol (25 mL). After 12 h, the solvent was removed under reduced pressure and the product was separated by Soxhlet extraction with benzene. Evaporation of the solvent gave 465 mg of complex **2** (72 %). IR: $\tilde{\nu}$ = 2007 (CO), 1855 (CO) cm^{-1}. ^1H NMR ($CDCl_3$): δ = 1.30 (t, ^3J = 7 Hz, 12 H, CH_3, NEt_4), 3.32 (q, ^3J = 7 Hz, 8 H, CH_2, NEt_4), 7.68 (t, ^3J = 8 Hz, 1 H, aromatic CH), 7.78 (t, ^3J = 8 Hz, 1 H, aromatic CH), 8.08 (d, ^3J = 8 Hz, 1 H, aromatic CH), 8.24 (d, ^3J = 8 Hz, 1 H, aromatic CH) ppm. ^{13}C NMR ($CDCl_3$): δ = 10.7 (CH_3), 55.7 (CH_2), 121.4, 126.0, 130.8, 135.4, 137.0, 146.5, 157.8 (aromatic carbon atoms), 194.2, 198.6, 198.8 (CO) ppm. Crystals were obtained by slow diffusion of pentane into a solution of **2** in CH_2Cl_2. $C_{18}H_{24}BrN_4O_5Re{\cdot}1/3\ C_6H_6$ (668.56 g·mol^{-1}): calcd. C 35.93, H 3.92, N 8.38; found C 35.69, H 4.69, N 7.91.

Synthesis of Complex 3. Method A: A mixture of complex **2** (50 mg, 78 μmol) and $AgBF_4$ (17 mg, 88 μmol) was stirred in methanol (10 mL). After 1 h, the precipitate was filtered off and the solvent was evaporated. The product was then extracted with benzene. After evaporation of the solvent, the product was dried in vacuo (21 mg, 63 %). Crystals of complex **5** were obtained as a side product from benzene/pentane in reactions using a twofold excess of $AgBF_4$ with respect to complex **2**.

Method B: Complex **2** (50 mg, 78 μmol) is dissolved in a mixture of diethyl ether (10 mL) and H_2O (10 mL). The Et_2O phase was separated and washed two more times with H_2O (10 mL). After evaporation of the organic phase, the product was dried in vacuo (27 mg, 80 %). IR: $\tilde{\nu}$ = 2026 (CO) cm^{-1}, 1882 (CO). ^1H NMR (C_6D_6): δ = 6.62 (t, ^3J = 8 Hz, 1 H, aromatic CH), 6.82 (t, ^3J = 8 Hz, 1 H, aromatic CH), 7.63 (d, ^3J = 8 Hz, 1 H, aromatic CH), 8.68 (d, ^3J = 8 Hz, 1 H, aromatic CH) ppm. ^{13}C NMR ($C_6D_5CD_3$): δ = 122.12, 129.07, 130.03, 135.12, 138.09, 148.65 (aromatic carbon atoms; CO: n.o.) ppm. $C_{30}H_{12}N_9O_{15}Re_3{\cdot}H_2O{\cdot}Et_2O$ (1389.23 g·mol^{-1}): calcd. C 29.40, H 1.74, N 9.07; found C 29.13, H 2.04, N 9.14.

Crystallographic Data: Complex **2** × 0.5 CH_2Cl_2: $C_{18.5}H_{25}BrClN_4O_5Re$, M_r = 684.98 g·mol^{-1}, monoclinic, space group $P2_1/c$, a = 12.2500(8), b = 10.3793(5), c = 18.3764(14) Å; β = 96.137(6)°, V = 2323.1(3) Å^3, T = 140(2) K, Z = 4, μ = 7.102 mm^{-1}, λ = 0.71073 Å, 12362 measured reflections, 3865 independent reflections, R_{int} = 0.0499, R_1 [$I > 2\sigma(I)$] = 0.0697, wR_2 (all data) = 0.1662. Complex **5** × 3 C_6H_6: $C_{66}H_{50}AgBF_4N_9O_{16}Re_3$, M_r = 1978.43 g·mol^{-1}, rhombohedral, space group $R3c$, a = 20.8533(16), c = 26.492(3) Å, V = 9976.8(15) Å^3, T = 140(2) K, Z = 6, μ = 5.819 mm^{-1}, λ = 0.71073 Å, 19101 measured reflections, 3875 independent reflections, R_{int} = 0.1648, R_1 [$I > 2\sigma(I)$] = 0.0662, wR_2 (all data) = 0.1542. The benzene molecules have been constrained to regular hexagons with d(C−C) = 1.39 Å. Diffraction data were collected at 140 K, using Mo-K_α radiation and a Oxford Diffraction diffractometer with a kappa geometry and equipped with a Sapphire CCD detector. Data reduction was performed with CrysAlis RED 1.6.9.[16] Absorption correction was applied to all data sets using an empirical method (DIFABS).[17] Structure solutions were determined with ab initio direct methods.[18] All structures were refined using the full-matrix least-squares on F^2 with all non-H atoms anisotropically defined. The hydrogen atoms were placed in calculated positions using the "riding model" with $U_{iso} = a{\cdot}U_{eq}$(C) (where a is 1.5 for methyl hydrogen atoms and 1.2 for others, C is the parent carbon atom). Space group determination, structure refinement and geometrical calculations were carried out on all structures with the SHELXTL software package, release 5.1.[19] The graphical representation of the molecular structures of **2** was generated with the program ORTEP.[20] CCDC-216353 (for **2**) and -216354 (for **5**) contain the supplementary crystallographic data for this paper. These data can be obtained free of charge at www.ccdc.cam.ac.uk/const/retrieving.html (or from the Cambridge Crystallographic Data Centre, 12 Union Road, Cambridge CB21EZ, UK; Fax: (internat.) + 44-1223-336-033; or deposit@ccdc.cam.ac.uk).

Acknowledgments

We gratefully acknowledge support of this work by the Swiss National Science Foundation.

[1] For reviews see: [1a] S.-S. Sun, A. J. Lees, *Coord. Chem. Rev.* **2002**, *230*, 171−192. [1b] P. H. Dinolfo, J. T. Hupp, *Chem. Mat.* **2001**, *13*, 3113−3125.

[2] [2a] M. H. Keefe, J. L. O′Donnell, R. C. Bailey, S. T. Nguyen, J. T. Hupp, *Adv. Mat.* **2003**, *15*, 1936−1939. [2b] P. de Wolf, S. L. Heath, J. A. Thomas, *Chem. Commun.* **2002**, 2540−2541. [2c] G. A. Mines, B.-C. Tzeng, K. G. Stevenson, J. Li, J. T. Hupp,

 © 2004 Wiley-VCH Verlag GmbH & Co. KGaA, Weinheim

Angew. Chem. **2002**, *114*, 162−165; *Angew. Chem. Int. Ed.* **2002**, *41*, 154−157. [2d] S. J. Lee, W. Lin, *J. Am. Chem. Soc.* **2002**, *124*, 4554−4555. [2e] D. Xu, K. T. Khin, W. E. van der Veer, J. W. Ziller, B. Hong, *Chem. Eur. J.* **2001**, *7*, 2425−2434. [2f] S. Bélanger, J. T. Hupp, *Angew. Chem.* **1999**, *111*, 2360−2362; *Angew. Chem. Int. Ed.* **1999**, *38*, 2222−2224. [2g] S. Bélanger, J. T. Hupp, C. L. Stern, R. V. Slone, D. F. Watson, T. G. Carrell, *J. Am. Chem. Soc.* **1999**, *121*, 557−563.

[3] M. L. Merlau, M. del Pilar Mejia, S. T. Nguyen, J. T. Hupp, *Angew. Chem.* **2001**, *113*, 4369−4372; *Angew. Chem. Int. Ed.* **2001**, *40*, 4239−4242.

[4] [4a] Z. Grote, R. Scopelliti, K. Severin, *Angew. Chem.* **2003**, *115*, 3951−3955; *Angew. Chem. Int. Ed.* **2003**, *42*, 3821−3825. [4b] M.-L. Lehaire, R. Scopelliti, H. Piotrowski, K. Severin, *Angew. Chem.* **2002**, *114*, 1477−1480; *Angew. Chem. Int. Ed.* **2002**, *41*, 1419−1422. [4c] M.-L. Lehaire, R. Scopelliti, K. Severin, *Chem. Commun.* **2002**, 2766−2767. [4d] M.-L. Lehaire, R. Scopelliti, K. Severin, *Inorg. Chem.* **2002**, *41*, 5466−5474. [4e] H. Piotrowski, K. Severin, *Proc. Natl. Acad. Sci. USA* **2002**, *99*, 4997−5000. [4f] H. Piotrowski, K. Polborn, G. Hilt, K. Severin, *J. Am. Chem. Soc.* **2001**, *123*, 2699−2700. [4g] H. Piotrowski, G. Hilt, A. Schulz, P. Mayer, K. Polborn, K. Severin, *Chem. Eur. J.* **2001**, *7*, 3196−3208.

[5] T. Habereder, M. Warchhold, H. Nöth, K. Severin, *Angew. Chem.* **1999**, *111*, 3422−3425; *Angew. Chem. Int. Ed.* **1999**, *38*, 3225−3228.

[6] For a review see: K. Severin, *Coord. Chem. Rev.* **2003**, *245*, 3−10.

[7] R. Alberto, A. Egli, U. Abram, K. Hegetschweiler, V. Gramlich, P. A. Schubinger, *J. Chem. Soc., Dalton Trans.* **1994**, 2815−2820.

[8] A. Egli, K. Hegetschweiler, R. Alberto, U. Abram, R. Schibli, R. Hedinger, V. Gramlich, R. Kissner, P. A. Schubinger, *Organometallics* **1997**, *16*, 1833−1840.

[9] B. Salignac, P. V. Grundler, S. Cayemittes, U. Frey, R. Scopelliti, A. E. Merbach, R. Hedinger, K. Hegetschweiler, R. Alberto, U. Prinz, G. Raabe, U. Kölle, S. Hall, *Inorg. Chem.* **2003**, *42*, 3516−3526.

[10] S. Kumaresan, K.-L. Lu, J.-T. Hung, F.-Y. Lee, Y.-S. Wen, J. R. Hwu, *J. Organomet. Chem.* **1997**, *549*, 155−161.

[11] [11a] R. Czerwieniec, A. Kapturkiewicz, R. Anulewicz-Ostrowska, J. Nowacki, *J. Chem. Soc., Dalton Trans.* **2002**, 3434−3441. [11b] R. Czerwieniec, A. Kapturkiewicz, R. Anulewicz-Ostrowska, J. Nowacki, *J. Chem. Soc., Dalton Trans.* **2001**, 2756−2761.

[12] For supramolecular coordination compounds which act as hosts for the $[BF_4]^-$ anion see: [12a] L. Raehm, L. Mimassi, C. Guyard-Duhayon, H. Amouri, *Inorg. Chem.* **2003**, *42*, 5654−5659. [12b] O. V. Dolomanov, A. J. Blake, N. R. Champness, M. Schröder, C. Wilson, *Chem. Commun.* **2003**, 682−683. [12c] C.-Y. Su, Y.-P. Cai, C.-L. Chen, F. Lissner, B.-S. Kang, W. Kaim, *Angew. Chem.* **2002**, *114*, 3519−3523; *Angew. Chem. Int. Ed.* **2002**, *41*, 3371−3375. [12d] H. Amouri, M. N. Rager, F. Cagnol, J. Vaissermann, *Angew. Chem.* **2001**, *113*, 3748−3750; *Angew. Chem. Int. Ed.* **2001**, *40*, 3636−3638. [12e] F. Fochi, P. Jacopozzi, E. Wegelius, K. Rissanen, P. Cozzini, E. Marastoni, E. Fisicaro, P. Manini, R. Fokkens, E. Dalcanale, *J. Am. Chem. Soc.* **2001**, *123*, 7539−7552. [12f] K. M. Kim, J. S. Park, Y.-S. Kim, Y. J. Jun, T. Y. Kang, Y. S. Sohn, M.-J. Jun, *Angew. Chem.* **2001**, *113*, 2524−2526; *Angew. Chem. Int. Ed.* **2001**, *40*, 2458−2460.

[13] [13a] A. S. Batsanov, S. P. Crabtree, J. A. K. Howard, C. W. Lehmann, M. Kilner, *J. Organomet. Chem.* **1998**, *550*, 59−61. [13b] M. Munakata, L. P. Wu, T. Kuroda-Sowa, M. Maekawa, Y. Suenaga, G. L. Ning, T. Kojima, *J. Am. Chem. Soc.* **1998**, *120*, 8610−8618.

[14] For some selected examples see: [14a] T. Lahtines, E. Wegelius, K. Rissanen, *New. J. Chem.* **2001**, *25*, 905−911. [14b] T. Seppälä, E. Wegelius, K. Rissanen, *New J. Chem.* **1998**, 789−791. [14c] F. R. Heirtzler, H. Hopf, P. G. Jones, P. Bubenitschek, *Chem. Ber.* **1995**, *128*, 1079−1082. [14d] F. R. Heirtzler, H. Hopf, P. G. Gones, P. Bubenitschek, *Tetrahedron Lett.* **1995**, *36*, 1239−1242. [14e] F. R. Heirtzler, H. Hopf, P. G. Gones, P. Bubenitschek, V. Lehne, *J. Org. Chem.* **1993**, *58*, 2781−2784. [14f] H. C. Kang, A. W. Hanson, B. Eaton, V. Boekelheide, *J. Am. Chem. Soc.* **1985**, *107*, 1979−1985.

[15] S. V. Lindeman, R. Rathore, J. K. Kochi, *Inorg. Chem.* **2000**, *39*, 5707−5716.

[16] Oxford Diffraction Ltd, Abingdon, Oxfordshire, UK, **2001**.

[17] N. Walker, D. Stuart, *Acta Crystallogr., Sect. A* **1983**, *39*, 158−166.

[18] G. M. Sheldrick, *Acta Crystallogr., Sect. A* **1990**, *46*, 467−473.

[19] G. M. Sheldrick, *University of Göttingen*, **1997**; Bruker AXS, Inc., Madison, Wisconsin, 53719, USA, **1997**.

[20] L. J. Farrugia, *J. Appl. Crystallogr.* **1997**, *30*, 565.

Received November 27, 2003

 © 2004 Wiley-VCH Verlag GmbH & Co. KGaA, Weinheim

Reactivity of Organoelement Subhalides of Gallium and Indium — Ga−Ga and In−In Bonds Bridged by Carboxylato Ligands

Werner Uhl*[a] and Abdelhakim El-Hamdan[a]

Keywords: Carboxylate ligands / Gallium / Indium / Subvalent compounds

The organoelement subhalides $R_2Ga_2I_2$ (**5**) and $R_3In_3I_2$ [**6**; R = $C(SiMe_3)_3$] reacted with silver benzoate $AgOOCC_6H_5$ to yield the dicarboxylato dielement compounds $R_2E_2(\mu\text{-}OOCC_6H_5\text{-}O,O')_2$ (**7**, E = Ga; **8**, E = In). Both compounds possess E–E single bonds bridged by the chelating carboxylato ligands. The chelating groups are arranged perpendicular to one another. Owing to the small bite of the carboxylato group very short E–E bond lengths of 240.5 pm (Ga–Ga) and 265.4 pm (In–In) were observed.

(© Wiley-VCH Verlag GmbH & Co. KGaA, 69451 Weinheim, Germany, 2004)

Introduction

Careful oxidation of the tetrahedral tetraelement clusters $Ga_4[C(SiMe_3)_3]_4$ (**1**)[1] and $In_4[C(SiMe_3)_3]_4$ (**2**)[2] (Scheme 1) with halogens or organic halogen donors yielded the corresponding subhalides still containing the elements gallium and indium in low oxidation states. The transfer of only one bromine molecule by the reaction of **2** with 1,2-dibromoethane gave the tetraindium compound **3** (Scheme 1), in which the overall tetrahedral arrangement of the In atoms is retained.[3] One face of the tetrahedron is bridged by a μ_3-Br atom, while the second Br atom is located above an edge of that particular face. Reaction with hexachloroethane, or mixtures of $AlBr_3$ and Br_2, yielded the diindium(II) compounds **4**, which contain localized In−In single bonds and form dimers through chlorine or bromine bridges.[3,4] The corresponding digallium(II) compound **5** was obtained by the reaction of **1** with ICl in the presence of AlI_3.[5] In contrast to the diindium compounds **4** it remains monomeric, even in the solid state. An average oxidation state of +1.66 was found for the central atoms of the triindium compound **6**, which possesses a chain of three In atoms connected by In−In single bonds and was obtained by the treatment of **2** with I_2/AlI_3.[6]

These subhalides should be suitable starting compounds for the generation of secondary products by salt-elimination reactions. In a first investigation, which is described here in detail, we employed silver benzoate as a reagent. The driving force of silver halide formation should favor these reactions, and the chelating carboxylato ligand should stabilize any secondary product by coordinative saturation of the Ga or In atoms. Dicarboxylatodigallium compounds containing a Ga−Ga single bond should result from the use of **5**.

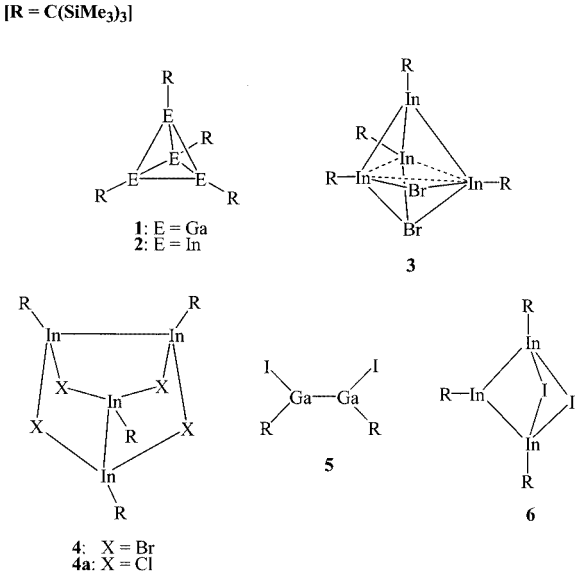

Scheme 1

Similar products have previously been obtained in our group by another route when we treated tetraalkyldigallane(4) $R_2Ga-GaR_2$ [R = $CH(SiMe_3)_2$] with carboxylic acids. Two equivalents of bis(trimethylsilyl)methane were released in the course of these reactions, and two alkyl substituents were replaced by the chelating acid residues.[7,8] In contrast, similar diindium dicarboxylates are not accessible by such a reaction, which instead resulted in the quantitative cleavage of the In−In bond by oxidation of the In atoms.[9] Owing to the singular structure of the digallium compounds, which is discussed in detail below, the synthesis and characterization of the corresponding diindium derivatives was of particular interest. Indium subhalides seemed to be suitable starting compounds for their generation.

[a] Fachbereich Chemie der Philipps Universität, Hans-Meerwein-Straße, 35032 Marburg, Germany
Fax: (internat.) +49-(0)6421-282-5653

Results and Discussion

Syntheses of the Dicarboxylatodigallium and -diindium Compounds 7 and 8

Treatment of the digallium(II) diiodide $R_2Ga_2I_2$ (**5**) with a suspension of silver benzoate in toluene at low temperature yielded colorless crystals of **7**, after recrystallization of the crude product from cyclopentane, in an almost quantitative yield. The integration ratio of the ^1H NMR spectrum showed one phenyl group per alkyl substituent, as expected for the complete replacement of both iodine atoms by benzoato groups. The resonance of the methyl protons appears at $\delta = 0.52$ ppm, which is in the characteristic range of compounds containing a Ga−Ga single bond. The molecular structure of **7**, possessing an intact Ga−Ga bond, was verified by an X-ray crystal-structure determination (see below) and is shown schematically in Equation (1). Compound **7** is thermally rather stable, with a melting point of 222 °C.

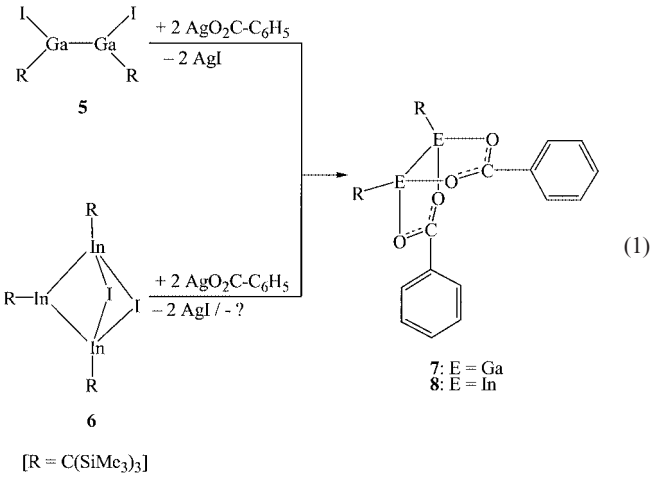

(1)

We hoped to synthesize the corresponding diindium(II) carboxylate **8** by the treatment of the dimeric subhalide $(R_2In_2Br_2)_2$ (**4**) with silver benzoate under similar reaction conditions. However, elemental indium precipitated, and the course of the reaction was more complicated. Crystals of the colorless product **8** could be obtained in very small quantities only. Interestingly, the diindium dicarboxylate **8** was finally isolated in 74% yield when we treated the triindium diiodide $R_3In_3I_2$ (**6**) with silver benzoate at low temperature [Equation (1)]. The silver iodide precipitate became black even at low temperature and in the dark, which may be caused by the formation of elemental indium as a by-product. However, tris(trimethylsilyl)methane, a possible second product of a disproportionation reaction, could not be detected by NMR spectroscopy. Formation of the tetraindium cluster **2** as another possible side product could not be verified by NMR spectroscopy or its characteristic violet color, either. The crude product of the reaction shows two further $SiMe_3$ resonances at $\delta = 0.45$ and 0.41 ppm, which may result from secondary products of the disproportionation but could not be assigned unambiguously. Compound **8** is less stable than its digallium analogue and decomposes already at 158 °C with the formation of a red-brown solid.

Molecular Structures

Compounds **7** and **8** (Figure 1 and 2, respectively) contain a Ga−Ga or an In−In single bond terminally coordinated by two tris(trimethylsilyl)methyl groups and bridged by two carboxylato ligands. The bridging of metal-metal bonds by carboxylato groups is a quite common structural motif in transition metal compounds,[10] however, it is extraordinarily rare in main-group chemistry.[11] While Ga−Ga bonds bridged by carboxylato groups have been reported by our group previously,[7,8] the bridging of an In−In bond is observed for the first time in compound **8**. Owing to the relatively long In−In bonds compared to Ga−Ga distances, and the small bite of the chelating ligand, such a structure was totally unexpected. According to quantum-chemical calculations the terminal coordination of carboxylato groups is very unfavorable because of the rather high energy required for the deformation of the inner OCO angle.[8] Because of this inflexibility, a terminal arrangement, with the coordination of only one metal atom, leads to a relatively short distance between the inner carbon atom of the chelate and the Ga or In atoms, which results in considerable steric and electrostatic repulsion.

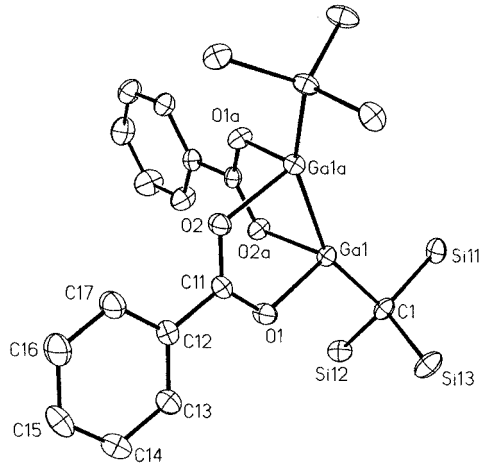

Figure 1. Molecular structure and numbering scheme of compound **7**; the thermal ellipsoids are drawn at the 40% probability level; methyl groups are omitted for clarity; selected bond lengths (pm) and angles (°): Ga1−Ga1′ 240.48(7), Ga1−C1 198.9(2), Ga1−O1 200.6(1), Ga1−O2′ 202.9(1); C1−Ga1−Ga1′ 156.38(6), O1−Ga1−O2′ 91.90(6), O1−Ga1−Ga1′ 88.95(4), O2′−Ga1−Ga1′ 85.95(4); Ga1′ and O2′ generated by $-x, y, -z + 3/2$

The rigidity of the CO_2 backbone results in almost indistinguishable C−O bond lengths [127.1 pm (**7**) and 126.8 pm (**8**), on average] and O−C−O bond angles [124.7° (**7**) and 124.9° (**8**)]. Thus, the bite of the carboxylato ligands [225.2 pm (**7**) and 224.9 pm (av., **8**)] is almost the same in both compounds despite the very different covalent radii of gallium and indium. A strong strain must result, which causes short E−E bond lengths. While that of the digallium compound **7** (240.5 pm) is in the lower range of Ga−Ga single-

 © 2004 Wiley-VCH Verlag GmbH & Co. KGaA, Weinheim

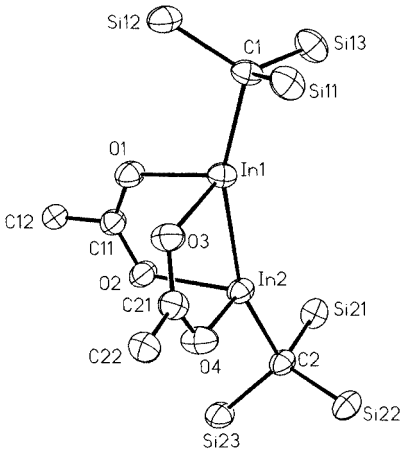

Figure 2. Molecular structure and numbering scheme of compound **8**; the thermal ellipsoids are drawn at the 40% probability level; methyl groups are omitted for clarity; only the *ipso*-carbon atoms of the phenyl groups are shown; selected bond lengths (pm) and angles (°) [the atoms In3, In4, C3, C4, O5, O6, O7 and O8 belong to the second independent molecule not shown here]: In1−In2 265.44(9), In3−In4 265.38(8), In1−C1 217.2(2), In2−C2 216.7(2), In3−C3 217.0(2), In4−C4 216.9(2), In1−O1 222.8(2), In1−O3 222.8(2), In2−O2 221.6(2), In2−O4 221.1(2), In3−O5 221.4(2), In3−O7 222.8(2), In4−O6 222.4(2), In4−O8 221.3(2); C1−In1−In2 158.74(6), C2−In2−In1 161.07(6), C3−In3−In4 160.43(6), C4−In4−In3 160.50(6), O1−In1−O3 89.93(6), O2−In2−O4 90.77(7), O5−In3−O7 90.38(7), O6−In4−O8 90.79(7), O1−In1−In2 85.13(4), O3−In1−In2 83.58(4), O2−In2−In1 83.99(4), O4−In2−In1 85.53(5), O5−In3−In4 85.15(4), O7−In3−In4 83.41(4), O6−In4−In3 84.01(4), O8−In4−In3 85.63(5)

bond lengths reported for digallium(II) halides $Ga_2X_4(L)_2$,[12] for instance, and is similar to that of the starting subhalide **5** (240.1 pm), the bridging of the In−In bond forces a very close In−In contact in **8** of 265.4 pm, which, to the best of our knowledge, is the shortest value reported so far.[13] The In−In single bonds in the starting subhalides **4** and **6** (Scheme 1) are considerably longer (282 pm on average).[3,6] The longer E−E bond in **8** compared to **7** causes slightly more acute E−E−O angles of 84.6° (versus 87.5° in **7**) and larger E−O−C angles of 122.3° (119.3° in **7**). The carboxylato ligands of both compounds are arranged almost ideally perpendicular to one another (O−E−O 91.9° and 90.5°, respectively). In accordance with the almost linear C−E−E groups (156.4° and 160.2°), the particular bonding situation of these compounds is described by sp-hybridized Ga or In atoms[8] so that both E−O bonds are mainly formed by two *p*-orbitals of each central atom. The phenyl substituents in both compounds are almost ideally co-planar with the carboxylato groups (angles between the normals of the corresponding planes 2.1° in **7** and 1.4 to 6.9° in **8**).

Experimental Section

General: All procedures were carried out under purified argon in dried solvents (toluene and diisopropyl ether over Na/benzophenone; cyclopentane over $LiAlH_4$). The compounds $R_2Ga_2I_2$ (**5**)[5] and $R_3In_3I_2$ (**6**)[6] were synthesized according to literature procedures. Commercially available silver benzoate (99%; Aldrich) was employed without further purification.

Synthesis of $R_2Ga_2(\mu\text{-}O_2CC_6H_5\text{-}O,O')_2$ [7; R = $C(SiMe_3)_3$]: A suspension of silver benzoate (69 mg, 0.301 mmol) in 20 mL of toluene was cooled to −90 °C and treated with a solution of the diiodide **5** (129 mg, 0.151 mmol) in 10 mL of toluene. The mixture was stirred and slowly warmed to −65 °C. The precipitate was filtered off at −70 °C, and subsequently the solvent was removed in vacuo at room temperature. The yellowish solid residue was recrystallized from cyclopentane, cooling from 20 to −15 °C. Yield: 124 mg (97%), colorless crystals, m.p. (argon, sealed capillary): 222 °C. ^{1}H NMR (C_6D_6, 400 MHz, 298 K): δ = 0.52 (s, 27 H, $SiMe_3$), 6.99 (m, 3 H, phenyl), 8.30 (m, 2 H, phenyl) ppm. ^{13}C NMR (C_6D_6, 100.6 MHz, 298 K): δ = 5.0 (GaC), 5.5 ($SiMe_3$), 128.7 and 130.8 (*m*- and *p*-C of phenyl), 131.4 and 133.7 (*ipso*- and *p*-C of phenyl), 177.6 (CO_2) ppm. IR (CsBr, nujol): $\tilde{\nu}$ = 1597 w phenyl; 1526 m νCO_2; 1462 vs. paraffin; 1411 s δCH_3; 1377 vs. paraffin; 1306 w, 1260 s δCH_3; 1174 vw, 1126 m, 1096 s, 1025 s δCH, νCC; 858 vs, 805 s, 754 vw, 718 m ρCH_3(Si); 699 w, 684 w ν_{as}SiC; 639 vw, 625 vw ν_sSiC; 513 w, 468 w, 373 vw νGaC, νGaO.

Synthesis of $R_2In_2(\mu\text{-}O_2CC_6H_5\text{-}O,O')_2$ [8; R = $C(SiMe_3)_3$]: Silver benzoate (50 mg, 0.218 mmol) was suspended in 20 mL of toluene and cooled to −90 °C. The suspension was treated with a solution of the triindium diiodide **6** (138 mg, 0.107 mmol) in 15 mL of toluene. A black precipitate was formed immediately, which was filtered off at −70 °C. The solvent was removed in vacuo at room temperature. The colorless residue was recrystallized from diisopropyl ether, cooling from 20 to 8 °C. Yield: 82 mg (74%; **8**·O*i*Pr_2); colorless crystals which include up to one molecule of diisopropyl ether per formula unit of **8**; m.p. (argon, sealed capillary): 158 °C (dec.). ^{1}H NMR (C_6D_6, 400 MHz, 298 K): δ = 0.49 (s, 27 H, $SiMe_3$), 1.06 (d, $^3J_{H,H}$ = 6 Hz, 6 H, Me of *i*Pr_2O), 3.43 (sept, $^3J_{H,H}$ = 6 Hz, 1 H, CH of *i*Pr_2O), 7.03 (m, 3 H, phenyl), 8.33 (m, 2 H, phenyl) ppm. ^{13}C NMR (C_6D_6, 100.6 MHz, 298 K): δ = 5.6 ($SiMe_3$), 15.5 (InC), 23.0 (Me of *i*Pr_2O), 68.1 (CH of *i*Pr_2O), 128.5 and 130.6 (*m*- and *p*-C of phenyl), 132.8 and 133.1 (*ipso*- and *p*-C of phenyl), 176.6 (CO_2) ppm. IR (CsBr, paraffin): $\tilde{\nu}$ = 1592 w phenyl; 1528 m νCO_2; 1460 vs. paraffin; 1377 vs. paraffin; 1306 vw, 1260 s δCH_3; 1124 m, 1086 m, 1025 s δCH, νCC; 859 vs, 843 s, 804 m, 718 m ρCH_3(Si); 699 w, 680 w ν_{as}SiC; 654 vw, 614 vw ν_sSiC; 515 w, 460 m νGaC, νGaO.

Crystal-Structure Determinations: Single crystals of compounds **7** and **8** were obtained by cooling solutions in cyclopentane (−15 °C, **7**) or diisopropyl ether (8 °C, **8**). Crystal data and structure-refinement parameters are given in Table 1. The molecules of compound **7** reside on a crystallographic twofold rotation axis. They crystallize with two cyclopentane molecules per formula unit, which can easily be removed on evacuation. A slight disorder was observed for the $C(SiMe_3)_3$ group; owing to the small occupation factor of 0.055, only the silicon atoms were refined on split positions. Compound **8** crystallizes with two independent molecules in the asymmetric unit, which further comprises two diisopropyl ether molecules. A disorder was observed for the $C(SiMe_3)_3$ group at C4, all atoms were refined at split positions with occupation factors of 0.76 and 0.24. A minor disorder was further detected for the $C(SiMe_3)_3$ group at C2; owing to the small occupation of the second position (0.07), only the silicon atoms of the minor component were refined.

CCDC-218887 (**7**) and -218888 (**8**) contain the supplementary crystallographic data for this paper. These data can be obtained free of charge at www.ccdc.cam.ac.uk/conts/retrieving.html [or from the Cambridge Crystallographic Data Centre, 12, Union Road, Cam-

 © 2004 Wiley-VCH Verlag GmbH & Co. KGaA, Weinheim

Table 1. Crystal data, data collection parameters, and structure refinement of compounds **7** and **8**[a]

	7	**8**
Formula	$C_{34}H_{64}Ga_2O_4Si_6 \cdot 2C_5H_{10}$	$C_{34}H_{64}In_2O_4Si_6 \cdot OC_6H_{14}$
Crystal system	Monoclinic	Monoclinic
Space group	$C2/c$ no. 15[14]	$P2_1/c$ no. 14[14]
Z	4	8
Temperature [K]	193(2)	193(2)
$d_{calcd.}$ [g/cm^3]	1.211	1.295
a [pm]	2224.6(2)	2260.3(5)
b [pm]	1452.01(10)	2814.9(6)
c [pm]	1774.3(2)	1782.8(4)
β [°]	109.47(3)	110.31(3)
V [10^{-30} m^3]	5403.6(9)	10638(4)
μ [mm^{-1}]	1.166	1.037
Crystal size [mm]	0.4 × 0.3 × 0.3	0.4 × 0.3 × 0.12
Diffractometer	STOE IPDS	
Radiation	Mo-K_α radiation; graphite monochromator	
θ range [°]	1.90 to 25.93	1.42 to 26.24
Index ranges	$-27 \le h \le 27$	$-28 \le h \le 28$
	$-17 \le k \le 17$	$-34 \le k \le 32$
	$-21 \le l \le 21$	$-22 \le l \le 22$
Independent reflections	5238 [R(int) = 0.0495]	21356 [R(int) = 0.0415]
Reflections $I > 2\sigma(I)$	4040	16776
Parameters	275	1131
$R = \Sigma\|\|F_o\| - \|F_c\|\|/\Sigma\|F_o\|$ [$I > 2\sigma(I)$]	0.0307	0.0272
$wR^2 = \{\Sigma w(F_o^2 - F_c^2)^2 / \Sigma w(F_o^2)^2\}^{1/2}$ (all data)	0.0758	0.0863
Max./min. residual [10^{30} e/m^3]	0.604/−0.480	0.804/−0.783

[a] Program: SHELXTL-Plus, SHELXL-97;[15] solutions by direct methods; full-matrix refinement with all independent structure factors.

bridge CB2 1EZ, UK; Fax: (internat.) +44-1223/336-033; E-mail: deposit@ccdc.cam.ac.uk].

Acknowledgments

We are grateful to the Deutsche Forschungsgemeinschaft and the Fonds der Chemischen Industrie for generous financial support.

[1] W. Uhl, W. Hiller, M. Layh, W. Schwarz, *Angew. Chem.* **1992**, *104*, 1378; *Angew. Chem. Int. Ed. Engl.* **1992**, *31*, 1364; W. Uhl, A. Jantschak, *J. Organomet. Chem.* **1998**, *555*, 263.
[2] W. Uhl, R. Graupner, M. Layh, U. Schütz, *J. Organomet. Chem.* **1995**, *493*, C1; W. Uhl, A. Jantschak, W. Saak, M. Kaupp, R. Wartchow, *Organometallics* **1998**, *17*, 5009.
[3] W. Uhl, S. Melle, *Chem. Eur. J.* **2001**, *7*, 4216.
[4] Similar dimeric silylgallium(II) halides have been reported: N. Wiberg, T. Blank, M. Westerhausen, S. Schneiderbauer, H. Schnöckel, I. Krossing, A. Schnepf, *Eur. J. Inorg. Chem.* **2002**, 351; G. Linti, W. Köstler, *Angew. Chem.* **1996**, *108*, 593; *Angew. Chem. Int. Ed. Engl.* **1996**, *35*, 550; A. Schnepf, E. Weckert, G. Linti, H. Schnöckel, *Angew. Chem.* **1999**, *111*, 3578; *Angew. Chem. Int. Ed.* **1999**, *38*, 3381. See also: H. Schnöckel, C. Klemp, in *Inorganic Chemistry Highlights* (Eds.: G. Meyer, D. Naumann, L. Wesemann), Wiley-VCH, Weinheim, **2002**, p. 245−257.
[5] W. Uhl, A. El-Hamdan, M. Prött, P. Spuhler, G. Frenking, *Dalton Trans.* **2003**, 1360.
[6] W. Uhl, S. Melle, G. Geiseler, K. Harms, *Organometallics* **2001**, *20*, 3355.
[7] W. Uhl, I. Hahn, H. Reuter, *Chem. Ber.* **1996**, *129*, 1425; W. Uhl, R. Graupner, I. Hahn, T. Spies, W. Frank, *Eur. J. Inorg. Chem.* **1998**, 355; W. Uhl, T. Spies, W. Saak, *Eur. J. Inorg. Chem.* **1998**, 1661; W. Uhl, T. Spies, D. Haase, R. Winter, W. Kaim, *Organometallics* **2000**, *19*, 1128; W. Uhl, L. Cuypers, M. Prött, K. Harms, *Polyhedron* **2002**, *21*, 511.
[8] W. Uhl, T. Spies, R. Koch, *J. Chem. Soc., Dalton Trans.* **1999**, 2385.
[9] W. Uhl, R. Graupner, S. Pohl, W. Saak, W. Hiller, M. Neumayer, *Z. Anorg. Allg. Chem.* **1997**, *623*, 883.
[10] F. A. Cotton, L. M. Daniels, C. Lin, C. A. Murillo, *J. Am. Chem. Soc.* **1999**, *121*, 4538.
[11] H. Binder, B. Brellochs, B. Frei, A. Simon, B. Hettich, *Chem. Ber.* **1989**, *122*, 1049; S. Adams, M. Dräger, B. Mathiasch, *J. Organomet. Chem.* **1987**, *326*, 173.
[12] Some examples: J. C. Beamish, A. Boardman, R. W. H. Small, I. J. Worrall, *Polyhedron* **1985**, *4*, 983; C. E. F. Rickard, M. J. Taylor, M. Kilner, *Acta Crystallogr.* **1999**, *C55*, 1215; E. M. Gordon, A. F. Hepp, S. A. Duraj, T. S. Habash, P. E. Fanwick, J. D. Schupp, W. E. Eckles, S. Long, *Inorg. Chim. Acta* **1997**, *257*, 247; W. Hönle, G. Miller, A. Simon *J. Solid State Chem.* **1988**, *75*, 147; H. J. Cumming, D. Hall, C. E. Wright, *Cryst. Struct. Commun.* **1974**, *3*, 107.
[13] In_2X_4 adducts: F. P. Gabbaï, A. Schier, J. Riede, H. Schmidbaur, *Inorg. Chem.* **1995**, *34*, 3855; R. J. Baker, R. D. Farley, C. Jones, M. Kloth, D. M. Murphy, *Chem. Commun.* **2002**, 1196; S. M. Godfrey, K. J. Kelly, P. Kramkowski, C. A. McAuliffe, R. G. Pritchard, *Chem. Commun.* **1997**, 1001; M. Scholten, R. Dronskowski, T. Staffel, G. Meyer, *Z. Anorg. Allg. Chem.* **1998**, *624*, 1741; H. Bärnighausen, *Z. Kristallogr.* **1989**, *186*, 16.
[14] *International Tables for Crystallography, Space Group Symmetry* (Ed.: T. Hahn), Kluwer Academic Publishers, Dordrecht, Boston, London, **1989**, vol. A.
[15] *SHELXTL-Plus, Release 4.2* for Siemens R3 Crystallographic Research Systems, Siemens Analytical X-ray Instruments Inc., Madison, USA, **1990**; G. M. Sheldrick, *SHELXL-97, Program for the Refinement of Structures*, University of Göttingen, **1997**.

Received September 8, 2003
Early View Article
Published Online January 28, 2004

 © 2004 Wiley-VCH Verlag GmbH & Co. KGaA, Weinheim

Hybrid Cyclic Dimers of Divacant Heteropolyanions: Synthesis, Mass Spectrometry (MALDI-TOF and ESI-MS) and NMR Multinuclear Characterisation

Cédric R. Mayer,*[a] Maryline Hervé,[a] Hélène Lavanant,[c] Jean-Claude Blais,[b] and Francis Sécheresse[a]

Keywords: Polyoxometalates / Bridging ligands / Mass spectrometry / Organic-inorganic hybrid composites

In the field of organic-inorganic hybrid composites, functionalized polyoxometalates constitute a special class of inorganic nanobuilding blocks (NBBs). This study represents a first approach related to the formation of new oligomeric hybrid species based on the reaction of bis(electrophilic) groups with a divacant heteropolyanion as the NBB. Bis(phosphonates) such as *para*-$H_2O_3PCH_2(C_6H_4)_nCH_2PO_3H_2$ (n = 1 or 2) have been treated with the divacant heteropolyanion $[\gamma\text{-}SiW_{10}O_{36}]^{8-}$ to form the hybrid cyclic dimer $[H_2\{(SiW_{10}O_{36})(O{=}PCH_2(C_6H_4)_nCH_2P{=}O)\}_2]^{6-}$. MALDI-TOF and ESI mass spectrometry have been used as essential analytical techniques for the characterization of such composite systems.

(© Wiley-VCH Verlag GmbH & Co. KGaA, 69451 Weinheim, Germany, 2004)

Introduction

"Hybrid organic-inorganic" is an old concept but still represents a current challenge because it allows combination of the specific properties of organic and inorganic components in a unique system.[1] This concept has experienced a notable expansion, especially since soft inorganic chemistry processes have been applied to new inorganic nanobuilding blocks (NBBs) such as oligosilsesquioxane derivatives,[2] organotin−oxo clusters,[3] transition metal−oxo clusters,[4] functionalized polyoxometalates and functionalized nanoparticles.[5] These NBBs have been chosen to cover a large domain of sizes and structures. The degree of organization and properties that can be obtained for such composites closely depends on the synergy between and the chemical nature of the organic and inorganic moieties. Thus, these hybrids can be categorized into two main classes depending on the nature of the interface and interactions shared by both components.[6] Class I corresponds to systems where no covalent or iono-covalent bonds exist between the inorganic and organic moieties, and class II refers to systems linked through strong chemical bonds (covalent bonds). For both classes, the chemical strategy depends largely on the functionalization of the NBBs.

Among these inorganic NBBs, polyoxometalates (POMs) based on Mo or W constitute a special class. In fact, these metallic oxo clusters play a great role in important areas such as catalysis, electro- and photochromism, magnetism, and medicine. Recently, the development of ordered assemblies of POMs within hybrid organic-inorganic materials has undergone considerable expansion, due to a large variety of electronic, magnetic, redox and photonic properties.[7] The main hybrid materials described in the literature belong to class I, being of anionic character and most of them are derived from Keggin heteropolyanions.[8] On the other hand, the materials of class II have appeared only very recently.[9] Indeed, their synthesis requires a prior covalent functionalization. Three different methods can be used to functionalize POM blocks. The first one proceeds by surface activation of POMs, resulting in the localization of the charge density at the oxygen atoms on the surface which permits covalent bonding with organometallic fragments.[10] In the second method, (organoimido)polyoxometalates[11] are used while the last one is based on multivacant polyoxotungstates showing an increased anionic charge density at the oxygen atoms on the lacunary surface. The highly nucleophilic character of the oxygen atoms permits

[a] IREM, Institut Lavoisier, UMR CNRS 8637, Université de Versailles St Quentin,
45 Avenue des Etats-Unis, 78035 Versailles, France
Fax: (internat.) + 33-1-39254381
E-mail: cmayer@chimie.uvsq.fr
[b] Laboratoire de Chimie Structurale Organique et Biologique, CNRS,UMR 7613, Université Pierre et Marie Curie,
4 Place Jussieu, 75252 Paris Cedex 05, France
Fax: (internat.) + 33-1-44273180
E-mail: blaisjc@ccr.jussieu.fr
[c] Laboratoire de Spectrométrie de Masse Bio-Organique, UMR CNRS 6014, INSERM-IFRMP23
CRUS, Bâtiment IRCOF, Université de Rouen,
76821 Mont St. Aignan Cedex
Fax: (internat.) + 33-2-35522441
E-mail: helene.lavanant@univ-rouen.fr

the covalent binding of electrophilic groups such as organotin groups[12] or organophosphorus groups.[13] A few hybrid materials have recently been described in class II by Maatta and co-workers who have reported (organoimido)-POMs as polystyrene pendants by co-polymerization of the monofunctional $[Mo_6O_{18}(NC_6H_4CH{=}CH_2)]^{2-}$ with a styrene monomer.[14] Mayer et al. have described the covalent entrapment in an organic matrix of [γ-$SiW_{10}O_{36}$(OSi−propyl methacrylate)$_4$]$^{4-}$ by radical co-polymerization resulting in the formation of a hybrid gel.[15]

This work is focused on the formation of a new cyclic hybrid POM by reaction of the divacant heteropolyanion $[\gamma\text{-}SiW_{10}O_{36}]^{8-}$ with two bis(phosphonate) groups, *para*-$H_2O_3PCH_2(C_6H_4)_nCH_2PO_3H_2$, where n = 1, 2. These systems have been characterized by a combination of multinuclear NMR spectroscopy (^{183}W, ^{29}Si and ^{31}P) and mass spectrometry (MALDI-TOF and ESI-MS).

Results and Discussion

Linear or cyclic hybrid polymers can be obtained in three main ways as shown in Scheme 1. The first path is the most commonly used and corresponds to the radical co-polymerization of monofunctional inorganic NBBs with an organic monomer. The second way concerns the polycondensation of bifunctional inorganic NBBs with a bifunctional organic precursor. A third possibility could be to treat an inorganic NBB containing two nucleophilic sites with a bis(electrophilic) group.

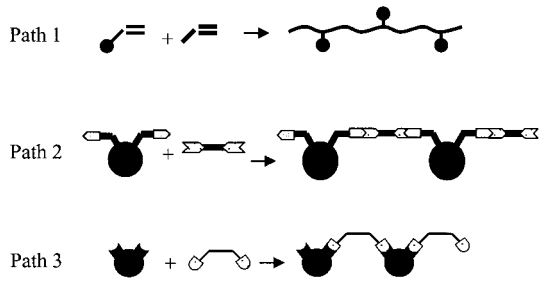

Scheme 1. Schematic structure of polymer hybrids: Path 1: radical co-polymerization of monofunctional inorganic NBBs with an organic monomer; Path 2: polycondensation of bifunctional inorganic NBBs with a bifunctional organic precursor; Path 3: reaction of an inorganic NBB containing two nucleophilic sites with a bis-electrophilic group

We have focused our attention on the last method, starting from the divacant heteropolyanion $[\gamma\text{-}SiW_{10}O_{36}]^{8-}$ and two types of bis(phosphonates). The choice of divacant POM was motivated by the ability of the four oxygen atoms of the vacancy to react with electrophilic phosphonate groups. This reaction was expected to lead to only one bifunctionalized POM.[16] Moreover, in recent works, this POM has been shown to be a good inorganic NBB precursor.[17,18] The choice of two bis(phosphonate) precursors, *para*-xylylenebis(phosphonate) (**LI**) and the homologue with a supplementary aromatic group (**LII**), was selected in order to check the influence of their organic chain lengths and to prevent the attachment of the two ending {$-PO_3$} groups to the same POM. The synthesis of these bis(phosphonates) proceeds through an Arbuzov reaction, the two terminal halide ligands are first transformed into {$-PO_3Et_2$} groups,[19] then hydrolyzed into acid functions. Hybrid systems have been obtained from the reaction of 1 equiv. of $[\gamma\text{-}SiW_{10}O_{36}]^{8-}$ suspended in acetonitrile with 1 equiv. of bis(phosphonate) previously dissolved in a mixture of dimethylformamide and hydrochloric acid. Tetrabutylammonium bromide was used as transfer agent. After subsequent purification, the oligomer was characterized by several techniques including multinuclear NMR spectroscopy (^{183}W, ^{29}Si and ^{31}P) and mass spectrometry (MALDI-TOF and ESI-MS). Matrix-assisted laser desorption ionization time-of-flight mass spectrometry (MALDI-TOF), in particular, has been already used with success for the characterization of two organosilyl derivatives of POMs.[20] To the best of our knowledge, however, electrospray ionization mass spectrometry (ESI-MS) has never been performed on these types of inorganic NBBs although it has recently been utilized for lacunary Keggin-type POMs.[21]

Upon proton decoupling each ^{31}P NMR spectrum showed only one resonance attributable to the RPO groups. These single lines display satellites corresponding to the heteronuclear couplings $^2J(^{183}W\text{-}^{31}P)$ = 10.1 Hz for **LI** and 10.3 Hz for **LII**, respectively, as expected for the symmetric attachment of phosphonates groups to the polyanionic surface. No free phosphonate ligands were observed in the solution NMR spectra. The ^{183}W NMR spectra each exhibit three lines with relative intensities of 1:2:2 (Figure 1). The most shielded resonances appear as doublets due to the heteronuclear phosphorus-tungsten couplings $^2J(^{183}W\text{-}^{31}P)$ = 10.2 Hz (for **LI**) and 10.8 Hz (for **LII**), respectively, as already observed in the ^{31}P NMR spectra. These features confirm that the $[\gamma\text{-}SiW_{10}O_{36}]^{8-}$ framework has retained its original C_{2v} symmetry after two organophosphonate units have been attached to the surface. Moreover, the shifting of the lines is quite close to that already observed for [γ-$SiW_{10}O_{36}(RPO)_2]^{4-}$ species.[16] Homonuclear tungsten-tungsten couplings were also observed and are presented in

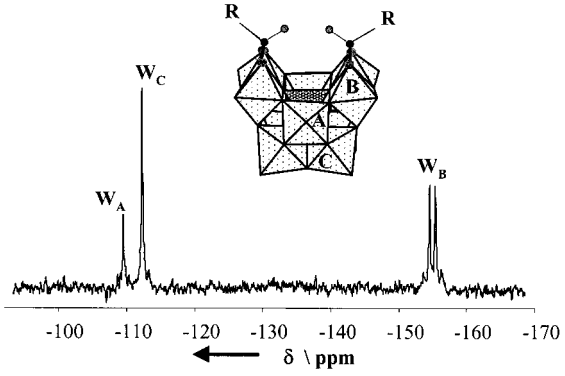

Figure 1. ^{183}W NMR (12.5 MHz) spectrum of **DII**, with a polyhedral representation of the polytungstate framework showing the three types of equivalent tungsten atoms

 © 2004 Wiley-VCH Verlag GmbH & Co. KGaA, Weinheim

the Exp. Sect. Here, for simplification purposes, we use the symbolism used in previous works for these types of functionalized POMs, as illustrated in Figure 1.[16,20] The line with a relative intensity of 1 was assigned to the W(C) atoms, the most shielded line with heteronuclear coupling to the W(B) atoms and the last line to W(A) atoms. ^{31}P and ^{183}W NMR spectroscopic data suggest that a cyclic species has been obtained, containing at least two POMs interlinked by bis(phosphonate) ligands. Thus, two RPO groups could be covalently attached on the lacunary surface through P−O−W bridges, the C_{2v} symmetry of the starting POM being conserved. At this stage, however, nothing is known about the degree of oligomerization of the hybrid.

In order to check whether ESI-MS could be used reliably to determine the structures of the composites, we first performed analyses on $[Bu_4N]_3[\gamma\text{-}SiW_{10}O_{36}(PhPO)_2]$ (noted **$[H(NBu_4)_3M]$**) used as a standard since it has already been fully characterized by X-ray diffraction methods.[16] The mass spectrum obtained from a 10^{-4} M solution in acetonitrile in the negative ion mode is shown in Figure 2 (a). Two signals have been detected at *m*/*z* = 896.7 and 1468.6 which have been attributed to **$[HM]^{3-}$** (calcd. *m*/*z* = 897.2) and **$[H(NBu_4)_1M]^{2-}$** (calcd. *m*/*z* = 1467.1), respectively. Although the presence of many tungsten atoms leads to a wide isotopic distribution with a Gaussian shape, in our case the resolution of the mass analyzer did not allow this distribution to be resolved and only rather large peaks representing an envelope of this distribution could be detected. The *m*/*z* values measured thus correspond to the centroid of the distribution which roughly amounts to an average molecular weight. Noticeably, no M^{4-} species were detected since a proton seemed to be strongly bound, probably through a P−O−H−O−P bridge between two terminal oxygen atoms of two {−P=O} groups. The presence of such a bound proton was also deduced from X-ray diffraction data.[16] It is quite usual in ESI-MS to detect a collection of multiply charged ions of different charge states corresponding to the attachment of various counterions. Here, the presence of two signals confirms the charge states as well as a double determination of the mass of the compound analyzed. In fact, in spite of the multiplicity of the signals, the interpretation of the mass spectrum remained straightforward, particularly since no fragmentation was observed.

The negative ion mass spectrum of the oligomer synthesized in this study is presented in Figure 2 (b), showing for the system based on **LII** three peaks at *m*/*z* = 905.5, 1135.5 and 1481.7. These signals were attributed to **$[H_2D]^{6-}$** (exp. *m*/*z* = 905.5, calcd. *m*/*z* = 905.9), **$[H_2(NBu_4)_1D]^{5-}$** (exp. *m*/*z* = 1135.5, calcd. *m*/*z* = 1135.6) and **$[H_2(NBu_4)_2D]^{4-}$** (exp. *m*/*z* = 1481.7, calcd. *m*/*z* = 1480.1), respectively, where D corresponds to the dimeric anion $[\{(SiW_{10}O_{36})[O=PCH_2(C_6H_4)_2CH_2P=O]\}_2]^{8-}$. The highest charge state detected was 6−, *two* protons are necessarily bound to the polyanion. The sterically improbable monomeric ions **$[HM]^{3-}$** and **$[H_2(NBu_4)M]^{2-}$**, where M is $\{(SiW_{10}O_{36})[O=PCH_2(C_6H_4)_2CH_2P=O]\}^{4-}$, would have the same *m*/*z* values of 905.5 and 1480.1, respectively. The presence of a peak at *m*/*z* = 1135.5 undoubtedly confirms the charge states to be from 6− to 4− rather than 3− and 2−.

MALDI-TOF mass spectrometry was also performed to seek confirmation of the dimerization as it usually yields mostly singly-charged species. The mass spectrum obtained in the positive ion mode presents several peaks in the region of *m*/*z* = 6000−8000 [Figure 3 (a) and (b)], regularly spaced with 242.5 u, corresponding to the mass of the Bu_4N^+ counterion. These peaks were therefore assigned to the cationic entities $[D + x\ Bu_4N + (8 - x)\ H]^+$, with D corresponding to the mass of *two* $\{SiW_{10}O_{36}\}$ units and *two* $\{O=PCH_2(C_6H_4)_nCH_2P=O\}$ units (*n* = 1, 2). These observed experimental values are consistent, within the experimental accuracy estimated as ±2 u in the *m*/*z* = 6000−8000 range, with the calculated masses for the different cations as shown

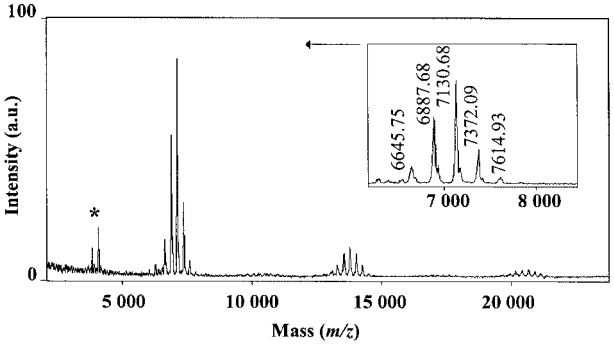

Figure 3. Positive ion MALDI-TOF mass spectra of **DII** and expansion of the *m*/*z* = 6000−8000 region, the asterisk indicates $[SiW_{12}O_{40}]^{4-}$ impurity

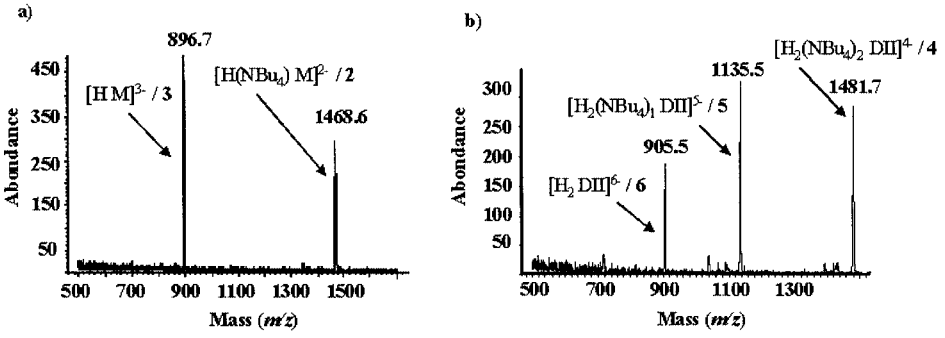

Figure 2. Negative ESI mass spectra of a) $[H\{\gamma\text{-}SiW_{10}O_{36}(PhPO)_2\}]^{3-}$ (**$[HM]^{3-}$**) and b) $[H_2\{(SiW_{10}O_{36})[O=PCH_2(C_6H_4)_2CH_2P=O]\}_2]^{6-}$ (**$[H_2DII]^{6-}$**)

 © 2004 Wiley-VCH Verlag GmbH & Co. KGaA, Weinheim

Table 1. MALDI-TOF MS data collected for $[\{(SiW_{10}O_{36})[O{=}PCH_2(C_6H_4)_1CH_2P{=}O]\}_2]^{8-}$ (**DI**) and $[\{(SiW_{10}O_{36})[O{=}PCH_2(C_6H_4)_2CH_2P{=}O]\}_2]^{8-}$ (**DII**) and calculated values

DI	+ 4 Bu_4N	+ 5 Bu_4N	+ 6 Bu_4N	+ 7 Bu_4N	+ 8 Bu_4N	+ 9 Bu_4N
Observed value	6249.4	6494.8	6734.7	6978.2	7220.4	7461.6
Calculated value	6251.2	6493.7	6736.1	6978.6	7221.1	7463.5
DII						
Observed value	–	6645.7	6887.7	7130.7	7372.1	7614.9
Calculated value	6403.4	6645.9	6888.3	7130.8	7373.3	7615.7

in Table 1. Other less intense signals were detected at higher *m*/*z* values (*m*/*z* = 12000−15000 and 19000−21000) as shown in Figure 3. These signals were most probably non-specific noncovalent aggregates of the dimeric compound D which are often produced during the desorption process in MALDI-TOF mass spectrometry.

Both the MALDI-TOF and ESI-MS results undoubtedly point to the presence of cyclic species and indicate the degree of oligomerization, in this case dimeric species are indicated.

Conclusion

The synthesis of hybrid oligomers from inorganic NBBs has undergone considerable developments in the last few years. In this context, the $[\{(SiW_{10}O_{36})[O{=}PCH_2(C_6H_4)_nCH_2P{=}O]\}_2]^{8-}$ (n = 1, 2) species, as represented in Figure 4, constitute an alternative approach for obtaining hybrids with a high degree of oligomerization. Moreover, this work has shown that mass spectrometry (combination of MALDI-TOF and ESI-MS) was more than just an alternative tool, but an essential technique in the characterization of these hybrid systems. Other bis(phosphonates) with larger sizes and different topologies are in preparation and their reactivity towards POMs will be reported very shortly.

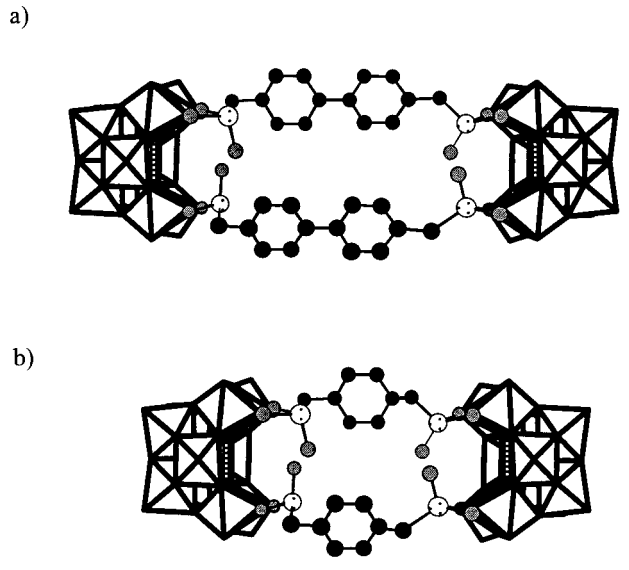

Figure 4. Proposed structures of a) $[H_2\{(SiW_{10}O_{36})[O{=}PCH_2(C_6H_4)_2CH_2P{=}O]\}_2]^{6-}$ and b) $[H_2\{(SiW_{10}O_{36})[O{=}PCH_2(C_6H_4)_1CH_2P{=}O]\}_2]^{6-}$

Experimental Section

General Procedures and Chemicals: $K_8[\gamma\text{-}SiW_{10}O_{36}]\cdot 12H_2O$ was prepared according to ref.[22] Other reagents and solvents were purchased from Aldrich and used as received. IR spectra (4000−250 cm^{-1}) were recorded with a Nicolet Magna 550 spectrometer in KBr pellets.

ESI-MS: The measurements were carried out using an HP 5989B single quadrupole mass spectrometer equipped with an electrospray source from Analytica of Branford. The instrument was operated in the negative ion mode. Source parameters were as follows: U_{needle} = 0 V, $U_{cyl.}$ = 3500 V, $U_{end.}$ = 3000 V, $U_{cap.}$ = 3500 V. Purified air was used as the nebulizing and drying gas, the presence of oxygen helping to prevent corona discharge which is often a problem during negative ion operation. The pressures of the nebulizing and drying gases were 0.34 and 1.70 bar, respectively, the nebulizing gas was heated to approximately 100 °C. Mass spectra were obtained by direct infusion with a Harvard Apparatus syringe pump of 10^{-4}, 5×10^{-5}, or 10^{-5} M sample solutions in pure distilled acetonitrile at a flow rate of 5 μL min^{-1}. The cone voltage U_c was varied, but was mostly set at low values of 10−40 V relative to the capillary exit voltage. Raising the cone voltage improves the ion transmission through the analyzer. It also increases the kinetic energy, which in turn enhances the formation of daughter ions by collisions with solvent and gas molecules within the region of primary stage pumping between the capillary exit and the sampling cone. The mass spectra shown are the result of approximately 20 scans summed from *m*/*z* = 50 to 1650. The mass axis was calibrated using the cluster ions observed from a 50 ng/μL solution of SDS (sodium dodecylsulfate) in acetonitrile.

MALDI-TOF MS: The spectra were recorded using a Voyager Elite Time-of-Flight Mass Spectrometer (PerSeptive Biosystems, Boston, MA, USA). In this apparatus, the pulsed N_2 laser beam (337 nm, 3 ns pulse duration, repetition rate 2 Hz) was focused onto the target with an angle of incidence of 45°. In all experiments the mass spectrometer was tuned in the linear mode using delayed extraction and a beam wire guide. The target voltage was set to +20 kV. The extraction delay and pulse voltage were adjusted to obtain the best mass resolution and the wire guide voltage was adjusted to obtain the best transmission. All mass spectra were recorded and averaged over 256 laser shots with a Tektronix TDS 520 oscilloscope (Beaverton, OR, USA). The samples were prepared as follows: the com-

 © 2004 Wiley-VCH Verlag GmbH & Co. KGaA, Weinheim

pound (2 mg) was dissolved in acetonitrile (500 μL; solution A), and dithranol (12 mg) was dissolved in CH_2Cl_2 (500 μL; matrix solution). 1 μL of solution A was then added to 50 μL of the matrix solution. An external calibration of the instrument with a POE 5000 standard was used.

NMR: The ^1H (300 MHz) NMR spectra were obtained at room temperature in 5-mm (o.d.) tubes with a Bruker AC 300 spectrometer equipped with a QNP probe head. Chemical shifts are given according to the IUPAC convention with respect to $SiMe_4$. The 12.5 MHz ^{183}W NMR spectra were recorded at 300 K in almost saturated DMF/CD_3CN (90:10, v/v) solutions in 10-mm (o.d.) tubes with the same spectrometer equipped with a low-frequency special VSP probe head. Chemical shifts are given with respect to 2 M aqueous Na_2WO_4 and were determined by the substitution method using a saturated D_2O solution of tungstosilicic acid $H_4SiW_{12}O_{40}$ as secondary standard (δ = −103.8 ppm).

***para*-Xylylenebis(phosphonic acid) (LI):** α,α′-Dibromo-*p*-xylene (2.084 g, $7.9.10^{-3}$ mol) was suspended in deaerated triethyl phosphite (25 mL) and the mixture was heated to reflux at 138 °C with stirring for 3 h. The unreacted triethyl phosphite was removed in vacuo at 80 °C. Crystalline products were obtained by dissolving the yellow oil in diethyl ether and cooling to −35 °C overnight. *para*-Xylylenebis(diethyl phosphonate) (1 g, $2.64.10^{-3}$ mol) was then dissolved in HCl (60 mL, 12 M) and heated to reflux overnight. The pure phosphonic acid was obtained by removing hydrochloric acid with a rotary evaporator. Yield: 0.65 g, 31%. ^1H NMR (300.13 MHz, [D_6]DMSO, TMS): δ = 2.90 (d, 2 H), 7.14 (s, 2 $H_{arom.}$) ppm. ^{31}P NMR (121.5 MHz, [D_6]DMSO, H_3PO_4): δ = 22.57 ppm.

1,1′-Biphenylene-4,4′-bis(methylene)bis(phosphonic acid) (LII): The procedure was similar except that the starting material was 4,4′-bis(chloromethyl)-1,1′-biphenyl (0.6 g, $2.39.10^{-3}$ mol). Yield: 0.33 g, 40.3%. ^1H NMR (300.13 MHz, [D_6]DMSO, TMS): δ = 2.97 (d, 2 H), 7.31 (d, 2 $H_{arom.}$), 7.54 (d, 2 $H_{arom.}$) ppm. ^{31}P NMR (121.5 MHz, [D_6]DMSO, H_3PO_4): δ = 22.38 ppm.

$(NBu_4)_6H_2[\{(SiW_{10}O_{36})[O{=}PCH_2(C_6H_4)CH_2P{=}O]\}_2]$ (DI): A homogeneous mixture of **LI** (0.089 g, 0.333 mmol) and 12 M hydrochloric acid (0.35 mL) in dimethylformamide (2 mL) was added dropwise to a suspension of solid $K_8[\gamma\text{-}SiW_{10}O_{36}]\cdot 12H_2O$ (1 g, 0.333 mmol) and Bu_4NBr (0.35 g, 1 mmol) in acetonitrile (30 mL). The resultant mixture was heated to reflux with stirring overnight. Acetonitrile was then removed by evaporation, and the crude product was precipitated from the dimethylformamide solution by diffusion of diethyl ether through the gas phase. The precipitate was filtered and washed with ethanol and diethyl ether. Yield: 1.3 g (0.180 mmol, 54%). ^{31}P NMR (121.5 MHz, DMF/CD_3CN, H_3PO_4): δ = 23.23 [$^2J(^{183}W,^{31}P)$ = 10.1 Hz] ppm. ^{183}W NMR (12.5 MHz, DMF/CD_3CN, Na_2WO_4): δ = −109.1 [s, 2 W, $^2J(^{183}W,^{183}W)$ = 21.6, 12.1 Hz], −113.0 [s, 4 W, $^2J(^{183}W,^{183}W)$ = 12.7, 16.5 Hz], −155.3 [d, 4 W, $^2J(^{183}W,^{183}W)$ = 21.35, 16.5, $^2J(^{183}W,^{31}P)$ = 10.2 Hz] ppm. IR (KBr): $\tilde{\nu}$ = 1160 (vw), 1060 (vw), 1006 (vw), 975 (s), 939 (m), 907 (vs), 885 (vs), 835 (m), 763 (vs), 552 (vw), 363 (w), 331 (w) cm^{-1}.

$(NBu_4)_6H_2[\{(SiW_{10}O_{36})[O{=}PCH_2(C_6H_4)_2CH_2P{=}O]\}_2]$ (DII): The synthesis followed the same procedure, using **LII** (0.114 g, 0.333 mmol). Yield: 1.5 g (0.203 mmol, 61.1%). ^{31}P NMR (121.5 MHz, DMF/CD_3CN, H_3PO_4): δ = 22.80 [$^2J(^{183}W,^{31}P)$ = 10.3 Hz] ppm. ^{183}W NMR (12.5 MHz, DMF/CD_3CN, Na_2WO_4): δ = −109.6 [s, 2 W, $^2J(^{183}W,^{183}W)$ = 7, 21.6 Hz], −112.3 [s, 4 W, $^2J(^{183}W,^{183}W)$ = 7, 20.3 Hz], −155.0 [d, 4 W, $^2J(^{183}W,^{183}W)$ = 20.35, 21.6, $^2J(^{183}W,^{31}P)$ = 10.8 Hz] ppm. IR (KBr): $\tilde{\nu}$ = 1160 (vw), 1060 (vw), 1006 (vw), 975 (s), 939 (m), 907 (vs), 885 (vs), 835 (m), 763 (vs), 552 (vw), 363 (w), 331 (w) cm^{-1}.

[1] H. Schmidt, B. Seiferling, *Mater. Res. Soc., Symp. Proc.* **1986**, *73*, 739.
[2] C. Zhang, F. Babonneau, C. Bonhomme, R. M. Laine, C. L. Soles, H. A. Hristo, A. F. Yee, *J. Am. Chem. Soc.* **1998**, *120*, 8380.
[3] C. Eychenne-Baron, F. Ribot, N. Steunou, C. Sanchez, F. Fayon, M. Biesemans, J. C. Martins, R. Willem, *Organometallics* **2000**, *19*, 1940.
[4] G. Kickelbick, U. Schubert, *Eur. J. Inorg. Chem.* **1998**, *2*, 159.
[5] C. R. Mayer, S. Neveu, V. Cabuil, *Adv. Mater.* **2002**, *14*, 595.
[6] C. Sanchez, F. Ribot, *New J. Chem.* **1994**, *18*, 1007.
[7] [7a] T. Yamase, *Chem. Rev.* **1998**, *98*, 307. [7b] C. Sanchez, G. J. de A. A. Soler-Illia, F. Ribot, T. Lalot, C. R. Mayer, V. Cabuil, *Chem. Mater.* **2001**, *13*, 3061. [7c] L. Xu, M. Lu, B. Xu, Y. Wie, Z. Peng, D. R. Powell, *Angew. Chem. Int. Ed.* **2002**, *41*, 4129.
[8] D. E. Katsoulis, *Chem. Rev.* **1998**, *98*, 359.
[9] R. C. Schroden, C. F. Blanford, B. J. Melde, B. J. Johnson, A. Stein, *Chem. Mater.* **2001**, *13*, 1074 and references therein.
[10] H. Zeng, G. R. Newkome, C. L. Hill, *Angew. Chem. Int. Ed.* **2000**, *39*, 1771.
[11] P. Gouzerh, A. Proust, *Chem. Rev.* **1998**, *98*, 77.
[12] F. Xin, M. T. Pope, *Inorg. Chem.* **1996**, *35*, 5693.
[13] C. R. Mayer, R. Thouvenot, *J. Chem. Soc., Dalton Trans.* **1998**, 7.
[14] A. R. Moore, H. Beatty, E. A. Maatta, *Chem. Commun.* **2000**, 1793.
[15] C. R. Mayer, R. Thouvenot, T. Lalot, *Macromolecules* **2000**, *33*, 4433.
[16] C. R. Mayer, P. Herson, R. Thouvenot, *Inorg. Chem.* **1999**, *38*, 6152.
[17] C. R. Mayer, S. Neveu, V. Cabuil, *Angew. Chem. Int. Ed.* **1999**, *38*, 3672.
[18] C. R. Mayer, R. Thouvenot, T. Lalot, *Chem. Mater.* **2000**, *12*, 257.
[19] A. K. Bhattacharya, G. Thyagarajan, *Chem. Rev.* **1981**, *81*, 415.
[20] C. R. Mayer, I. Fournier, R. Thouvenot, *Chem. Eur. J.* **2000**, *6*, 105.
[21] M. Bonchio, O. Bortolini, V. Conte, A. Sartorel, *Eur. J. Inorg. Chem.* **2003**, *4*, 699.
[22] J. Canny, A. Tézé, R. Thouvenot, G. Hervé, *Inorg. Chem.* **1986**, *25*, 2114.

Received July 21, 2003
Early View Article
Published Online January 28, 2004

 © 2004 Wiley-VCH Verlag GmbH & Co. KGaA, Weinheim

Fast, High-Yielding Syntheses of Silsesquioxanes Using Acetonitrile as a Reactive Solvent

Paolo P. Pescarmona,[a] Jan C. van der Waal,[a] and Thomas Maschmeyer*[a]

Keywords: Silsesquioxanes / NMR spectroscopy / Mass spectrometry / Solvent effects

New and efficient methods for the synthesis of cyclopentyl- and cyclohexylsilsesquioxanes are described. In the case of cyclopentylsilsesquioxane, pure trisilanol $(c\text{-}C_5H_9)_7Si_7O_9(OH)_3$ was obtained selectively within 18 h in an isolated yield of 64%. The synthesis of cyclohexylsilsesquioxanes also gives high yields, but it is not selective towards a particular structural type [main products: $(c\text{-}C_6H_{11})_6Si_6O_9$, $(c\text{-}C_6H_{11})_6Si_6O_8(OH)_2$, $(c\text{-}C_6H_{11})_7Si_7O_{10}OH$ and $(c\text{-}C_6H_{11})_7Si_7O_9(OH)_3$]. We discuss the crucial role of acetonitrile as a reactive solvent in these syntheses.
(© Wiley-VCH Verlag GmbH & Co. KGaA, 69451 Weinheim, Germany, 2004)

Introduction

Silsesquioxanes are hybrid inorganic/organic compounds that have an increasing number of applications in the field of catalysis[1,2] and materials science.[3,4] In particular, the incompletely condensed silsesquioxanes $R_7Si_7O_9(OH)_3$ (where R is an organic group, commonly cyclopentyl or cyclohexyl, cf. Figure 1) have been used both as soluble model compounds for silica surface sites and as precursors for active homogeneous catalysts.[5−9] The synthesis of this silsesquioxane was first reported by Brown and Vogt;[10] more recently it was optimised and studied in detail by Feher et al.[11,12] The trisilanol $R_7Si_7O_9(OH)_3$ [structural coding *a*7*b*3, cf. Equations (1) and (2)] can be obtained by the slow hydrolytic condensation of the corresponding trichlorosilane $RSiCl_3$ with acetone as the solvent [Equation (1), Equation (2) with $a + b = 2n$, where a, b and n are integers ($a = 1, 2, 3, \ldots$; $b = 0, 1, 2, 3, \ldots$; $n = 1, 2, 3, \ldots$) and $b \leq a + 2$].

$$RSiCl_3 + 3\,H_2O \rightarrow RSi(OH)_3 + 3\,HCl \quad (1)$$

$$a\,RSi(OH)_3 \rightleftarrows (RSiO_{1.5})_a(H_2O)_{0.5b} + (1.5a - 0.5b)\,H_2O \quad (2)$$

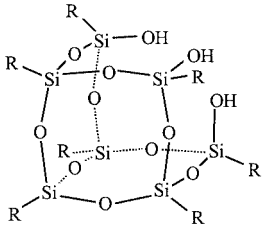

*a*7*b*3

Figure 1. Silsesquioxane *a*7*b*3 [R = cyclopentyl, cyclohexyl]

In the case of R = cyclopentyl, silsesquioxane *a*7*b*3 was the only product of the hydrolytic condensation and was obtained after 3 d of reaction in a yield of 29%.[12] When R = cyclohexyl, the hydrolytic condensation proceeded more slowly and produced a mixture of three silsesquioxanes: *a*6*b*0, *a*7*b*3 and *a*8*b*2.[11] Silsesquioxane *a*7*b*3 was the main product, but in a low yield (8% after a reaction of 12 weeks).

Recently, we reported a study of the synthesis of silsesquioxanes as precursors for Ti catalysts that are active in the epoxidation of alkenes, which we realised by means of High-Speed Experimentation (HSE) techniques.[13,14] We investigated the effects of the various parameters that influence the hydrolytic condensation and identified some general trends. Since one of our purposes was to find a faster way to prepare silsesquioxane precursors suitable for active catalysts, the reaction time was set at 18 h, which is a much shorter time than is required usually for the synthesis of silsesquioxanes. The best catalysts were obtained with R = cyclopentyl and cyclohexyl, using acetonitrile as the solvent. In this article, we report a follow-up study of these HSE leads by means of conventional laboratory techniques

[a] Laboratory of Applied Organic Chemistry and Catalysis, DelftChemTech, Technische Universiteit Delft, Julianalaan 136, 2628 BL Delft, The Netherlands
Fax: (internat.) + 31-152784289
E-mail: th.maschmeyer@tnw.tudelft.nl
[b] Avantium Technologies B.V., Zekeringstraat 29, 1014 BV, P. O. Box 2915, 1000 CX Amsterdam, The Netherlands

 © 2004 Wiley-VCH Verlag GmbH & Co. KGaA, Weinheim **DOI: 10.1002/ejic.200300494**

with the aim of fully characterising the silsesquioxane products and understanding the role of the solvent.

Results and Discussion

Synthesis of Cyclopentylsilsesquioxanes

The hydrolytic condensation of trichloro(cyclopentyl)silane in acetonitrile in the presence of an excess of water led to the formation of a white precipitate. After a reaction time of 18 h at 50 °C, a crude precipitate was obtained in 54% yield,[15] which contained mainly silsesquioxane *a*7*b*3 [$(c\text{-}C_5H_9)_7Si_7O_9(OH)_3$], as determined on the basis of ^{29}Si NMR and MS analyses. Small amounts of impurities were present in the precipitate, predominantly the cubic, completely condensed silsesquioxane ($c\text{-}C_5H_9)_8Si_8O_{12}$ [structural code *a*8*b*0, cf. Equations (1) and (2)]. If the reaction time was extended from 18 h to 2 weeks,[14] the yield of precipitated silsesquioxanes was nearly quantitative with the main fraction still being silsesquioxane *a*7*b*3. The synthesis was further optimised, on the basis of the observation of Feher et al., that the yield of the synthesis of cyclopentylsilsesquioxane *a*7*b*3 in acetone can be significantly improved by heating the reaction mixture under reflux.[12] Therefore, we modified our synthetic method by increasing the reaction temperature from 50 °C to reflux conditions. This modification led to an increase in the yield to 81% after a reaction time of 18 h and the high selectivity towards silsesquioxane *a*7*b*3 was preserved. Silsesquioxane *a*7*b*3 was then purified by extraction with pyridine[11,12] and the pure compound (as determined by ^{29}Si NMR spectroscopy, cf. Figure 2) was isolated in an overall yield of 64%, which is a significant improvement over the previously reported yield of 29% after 3 d of reaction.[12]

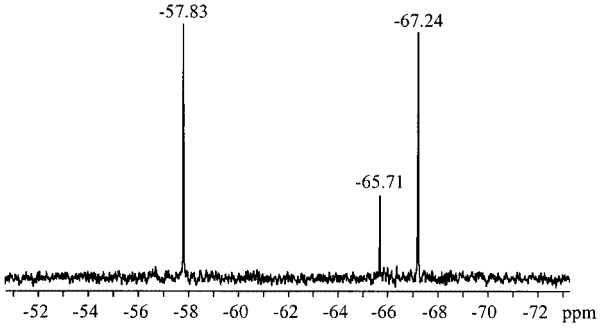

Figure 2. ^{29}Si NMR spectrum of cyclopentylsilsesquioxane *a*7*b*3

This improved synthetic procedure differs from that reported by Feher et al.[12] in regard to a number of parameters: the lower initial trichlorosilane concentration, the higher solvent/water ratio and, above all, the nature of the solvent (acetonitrile), which proved to be a dominant parameter that influences the synthesis of silsesquioxanes.[1,13,14]

After the hydrolytic condensation had proceeded for 18 h under reflux, the reaction mixture separated into two layers: a water phase (bottom) and an acetonitrile phase (top). This liquid-liquid phase separation is related to the hydrolysis of acetonitrile, a side reaction that is favoured by the presence of an acid [cf. Equation (3)],[16,17] which, in this case, was the hydrochloric acid produced during the hydrolysis of $(c\text{-}C_5H_9)SiCl_3$ [see Equation (3)].

$$CH_3CN + 2\,H_2O + HCl \rightarrow CH_3COOH + NH_4Cl \quad (3)$$

The ammonium chloride obtained is much more soluble in water than it is in acetonitrile, which causes the phase separation [only 0.41 g of ammonium chloride is necessary to induce phase separation of a mixture of water (12.5 mL) and acetonitrile (37.5 mL)]. The preferential solvation of ammonium chloride by water, relative to that of silsesquioxanes or acetonitrile, drives the reaction according to Equation (2) more towards the formation of condensed species. This effect is very pronounced towards the end of the experiment, i.e., when phase separation is actually observed. At the same time, the hydrolysis of acetonitrile in the presence of an acid plays an important role in that the formation of ammonium chloride (partially) neutralises the reaction mixture. A detrimental effect of the acidity of the solution has already been observed in the synthesis of silsesquioxane as Ti catalyst precursors.[13] Since silsesquioxanes undergo fast hydrolysis/condensation reactions under acidic conditions,[1] the species formed might be partially decomposed or further condensed before they begin to precipitate from the solution. Partial neutralisation of the reaction mixture could have the effect of slowing down the rates of the hydrolysis/condensation reactions and, thus, favour the precipitation of species that are only poorly soluble in this medium, like the incompletely condensed silsesquioxane *a*7*b*3.[18]

A further contributing factor regarding the improved yield when using acetonitrile as the solvent is its higher polarity relative to acetone, the solvent reported in the literature for the synthesis of silsesquioxane *a*7*b*3.[12] A highly polar solvent can better stabilise the incompletely condensed species by its interactions with their silanol groups, which, therefore, favours the synthesis of these silsesquioxanes over the completely condensed structures. Moreover, it has been proposed that the activation barrier for the condensation reactions towards the formation of silsesquioxanes is reduced in the presence of a polar molecule and that, therefore, the rate of product formation is increased.[19,20]

In this context, it is also relevant to note that acetonitrile has a higher boiling point than acetone (82 °C vs. 56 °C). Since the reaction is performed under reflux, the synthesis is accelerated further.

Synthesis of Cyclohexyl Silsesquioxanes

The hydrolytic condensation of trichloro(cyclohexyl)-silane in acetonitrile, in the presence of an excess of water, produced a white precipitate in 42% yield[15] after a reaction time of 18 h at 50 °C. The crude precipitate contained a mixture of silsesquioxane species, as determined by ^{29}Si NMR spectroscopy. The formation of the precipitate was

 © 2004 Wiley-VCH Verlag GmbH & Co. KGaA, Weinheim

accelerated by performing the synthesis under reflux, by analogy to the synthesis of cyclopentylsilsesquioxanes. This modification caused an increase of the yield to 79% after a reaction time of 18 h, with the precipitate still being a complex mixture of silsesquioxanes (see Figure 3 for the ^{29}Si NMR spectrum and the MS plot). MS analysis indicated that the silsesquioxanes present in the mixture mainly constituted 6, 7 or 8 siloxane units [$6 < a < 8$, cf. Equations (1) and (2)]. The most-intense peak in the ^{29}Si NMR spectrum ($\delta = -56.72$ ppm, 40% of the crude precipitate)[21] belongs to the completely condensed silsesquioxane (c-$C_6H_{11})_6Si_6O_9$ (*a6b*0, see Figure 4), which can be separated readily from the incompletely condensed species by extraction with pyridine, in which only the latter silsesquioxanes are soluble.[11] The main species present in the remaining mixture of incompletely condensed silsesquioxanes were assigned by combining ^{29}Si NMR spectroscopic and MS data: (c-$C_6H_{11})_6Si_6O_8(OH)_2$ (*a6b*2, 11% of the crude precipitate,[21] see Figure 4), (c-$C_6H_{11})_7Si_7O_{10}OH$ (*a7b*1, 29%, see Figure 4) and (c-$C_6H_{11})_7Si_7O_9(OH)_3$ (*a7b*3, 7%, see Figure 1). Silsesquioxane *a7b*3 can be separated by precipitation from a THF solution of the incompletely condensed silsesquioxane mixture by the slow addition of acetonitrile, in which it has a very low solubility. Silsesquioxane *a6b*2 is, on the other hand, the compound having the highest solubility in acetonitrile among those present in the mixture. Therefore, it can be separated by adding more acetonitrile slowly to the THF/acetonitrile solution, which, thus, induces the precipitation of all the other silsesquioxane structures. The solid obtained after removing silsesquioxanes *a6b*2 and *a7b*3 still contained a mixture of incompletely condensed silsesquioxanes that have very similar solubilities in many organic solvents and, therefore, resisted all attempts of further purification. The main component of this mixture was assigned to an *a7b*1 silsesquioxane structure (two isomers are possible for this silsesquioxane, see Figure 4).

The assignments were confirmed by silylation of the silanol groups of the incompletely condensed silsesquioxanes by means of their reaction with chlorotrimethylsilane $(CH_3)_3SiCl$.[22] The mixture of incompletely condensed structures obtained after separation of silsesquioxane *a6b*0 was treated with an excess of $(CH_3)_3SiCl$. The MS analysis of the products of the silylation reaction clearly shows the presence of four main species: disilylated *a6b*2, monosilylated *a7b*1, disilylated *a7b*3 and disilylated *a8b*2 (Figure 5). The monosilylated *a7b*1 was the species present in the highest concentration. On the basis of these experiments, the assignment of *a7b*1 as the main incompletely condensed species appears unequivocal. The ^{29}Si NMR spectroscopic peaks belonging to this silsesquioxane *a7b*1, both silylated or not, did not, however, correspond to those of the analogous silsesquioxane reported in the literature.[11] The peaks corresponding to the silylated *a7b*1 reported by Feher were present in the ^{29}Si NMR spectrum only as the second main species. This observation suggests that the two isomers of silsesquioxane *a7b*1 (Figure 4) were formed by our synthetic method, with the one known from the literature being the less abundant ($\alpha/\beta = 1:2$). The two isomers differ only in the spatial orientations of their silanol groups. They are both possible products of the hydrolytic condensation of trichloro(cyclohexyl)silane, while only the α-isomer of sil-

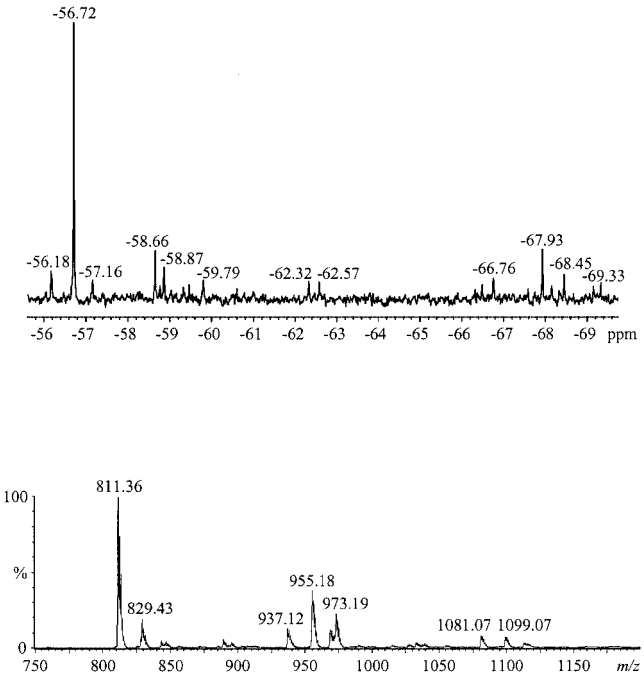

Figure 3. ^{29}Si NMR spectrum (top) and MS plot (bottom) of the cyclohexylsilsesquioxane mixture obtained after the hydrolytic condensation of trichloro(cyclohexyl)silane in acetonitrile

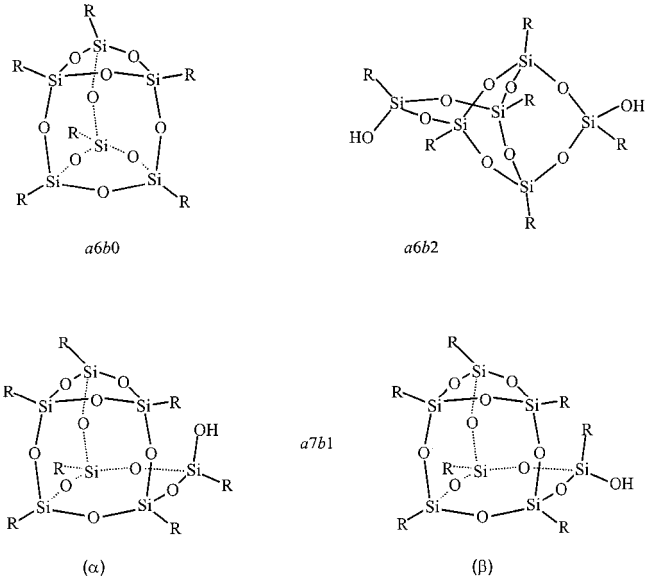

Figure 4. Silsesquioxanes *a6b*0, *a6b*2 and *a7b*1 (α and β isomers) (R = cyclohexyl)

sesquioxane *a7b*1 is obtained by the dehydration of silsesquioxane *a7b*3 reported by Feher.[11]

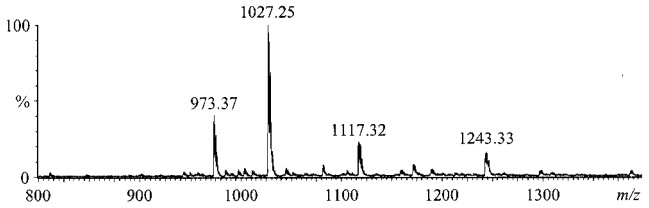

Figure 5. MS analysis of the incompletely condensed cyclohexylsilsesquioxanes, after silylation with $(CH_3)_3SiCl$

After hydrolytic condensation for 18 h under reflux and removal of the precipitate, the reaction was left at room temperature for 20 weeks: more white precipitate was formed (additional 10% yield).[15] The crude product was a mixture of three silsesquioxane species, with some impurities, as determined by ^{29}Si NMR spectroscopy: *a6b*0 (21%),[21] *a6b*2 (27%) and *a7b*3 (51%). Feher et al. have reported a similar increase in the ratio of silsesquioxane *a7b*3 among the products as the reaction time is increased.[11]

The synthesis procedure described here is the first reported method for obtaining silsesquioxanes *a6b*2 and *a7b*1 (both isomers) by the hydrolytic condensation of trichloro(cyclohexyl)silane. Cyclohexylsilsesquioxane *a6b*2 has been synthesised previously by the acid-mediated cleavage and rearrangement of silsesquioxane *a6b*0.[23] The α-isomer of cyclohexylsilsesquioxane *a7b*1 has been obtained formerly by dehydration of silsesquioxane *a7b*3.[11] The synthesis also afforded cyclohexylsilsesquioxane *a7b*3 in significant yields, although its separation from the rest of the mixture is not straightforward. This new method presents a number of differences from those reported previously,[11] namely: the solvent (acetonitrile), the lower initial trichlorosilane concentration and the higher solvent/water ratio. Additionally, performing the reaction under reflux caused a noticeable increase in yield of precipitate in our synthesis, while the rate of silsesquioxane formation could not be improved for the reaction reported in literature. Comparing the two synthetic methods, it is evident that the formation of silsesquioxanes is much faster with the new method, albeit less selective. Such an increase in the rate of formation of silsesquioxanes suggests that the conditions for the precipitation of silsesquioxanes are met more readily and for a larger number of different structures. This fact points to the relevance of using acetonitrile as the solvent, in agreement with the situation observed for the synthesis of cyclopentylsilsesquioxanes (vide supra). Analogously, after a reaction time of 18 h under reflux, the hydrolysis of acetonitrile and the consequent formation of NH_4Cl caused a liquid-liquid phase separation of the reaction mixture. To further study the effect of the presence of NH_4Cl, two additional experiments were performed:

1) Some NH_4Cl (0.073 M) was added to the starting mixture and led, after a reaction time of 18 h under reflux, to a silsesquioxane precipitate in a yield of 82%.[15] ^{29}Si NMR spectroscopic analysis showed that the amount of *a6b*0 increased relative to the other (incompletely condensed) silsesquioxanes. Thus, the addition of NH_4Cl not only increased the yield, but also drove the reaction towards the completely condensed species, which confirms the influence that the preferential solvation of NH_4Cl by water has on the silsesquioxane synthesis.

2) The hydrolytic condensation of trichloro(cyclohexyl)silane was performed in acetone (the solvent used by Brown[10] and Feher[11]) in the presence of NH_4Cl (0.15 M) as an additive: no precipitate was formed after a reaction time of 18 h under reflux (as is the case when no NH_4Cl is added). This finding indicates that the preferential solvation of NH_4Cl by water alone is not sufficient to accelerate the formation of silsesquioxanes.

The lower selectivity of the synthesis of cyclohexylsilsesquioxanes relative to that of cyclopentylsilsesquioxanes seems to be connected to the nature of the organic group.[1] The relatively larger steric hindrance of a cyclohexyl unit might account for the formation of the completely condensed silsesquioxane *a6b*0. The Si−O framework of this molecule is more strained than in the case of silsesquioxane *a7b*3 and, therefore, its formation might be expected to be unfavourable. On the other hand, the organic groups on the silicon atoms in this structure point away from each other: this arrangement may favour the formation of this molecule for bulkier organic groups, like cyclohexyl. Another effect of the organic group is to influence the solubility of the silsesquioxanes.[1] Cyclohexylsilsesquioxane *a7b*3 has been reported to be more soluble in organic solvents than cyclopentylsilsesquioxane *a7b*3.[11,12] The lower solubility of the cyclopentyl structure can account for its selective formation as a precipitate.

Conclusions

New methods for the synthesis of cyclopentyl- and cyclohexylsilsesquioxanes have been developed. In both cases, acetonitrile plays a strong role in accelerating the formation of a silsesquioxane precipitate. The influence of the hydrolysis of acetonitrile on the synthesis has been ascertained.

In the case of cyclopentylsilsesquioxanes, the synthesis is very selective towards the formation of structure *a7b*3, which can be obtained in 64% yield after a reaction time of 18 h. This fast and high-yielding method for preparing silsesquioxane *a7b*3, therefore, makes this compound more readily available for its many applications.

In the case of the synthesis of cyclohexylsilsesquioxanes, four silsesquioxane structures were produced in significant yields: *a6b*0, *a6b*2, *a7b*1 (both isomers) and *a7b*3. This method offers a facile way to synthesise the silsesquioxane structures *a6b*2 and *a7b*1, which are not readily accessible. The lower selectivity of this reaction seems to be connected to the higher solubility of cyclohexylsilsesquioxanes relative to that of cyclopentylsilsesquioxanes.

Experimental Section

General: ^{29}Si NMR spectroscopic characterisation of the silsesquioxanes was performed with a Varian VXR-400S (79.5 MHz, ^{1}H-

 © 2004 Wiley-VCH Verlag GmbH & Co. KGaA, Weinheim

decoupled, 25 °C) and with a Varian Inova-300 (59.6 MHz, ^{1}H-decoupled, 25 °C); pulse width = 30°; pulse delay = 10 s; ^{1}H decoupling during acquisition only. The positions of the silsesquioxanes' peaks in the ^{29}Si NMR spectra are influenced by the solvent in which they are dissolved. Spectra were recorded in THF and $CDCl_3$, with TMS as a reference. Mass spectrometric characterisation of the silsesquioxanes was performed with a Micromass Quattro LC-MS using ESI+ and APCI+ as ionisation techniques. Mass spectrometric analysis allows the identification of the number of siloxane units constituting the silsesquioxane structures (i.e., the value of *a*), but not their level of condensation (i.e., the value of *b*); this phenomenon is due to the fact that silsesquioxanes can coordinate or lose water molecules during the ionisation process.

Synthesis of Cyclopentyl Silsesquioxanes: Typically, deionised water (37.5 mL) was added carefully into a 500-mL round-bottom flask containing a solution of trichloro(cyclopentyl)silane (97% purity, 5.6 mL, 3.3×10^{-2} mol) in acetonitrile/water (4:1, v/v; 150 mL). This homogeneous solution was then heated to 50 °C or under reflux while stirring vigorously for 18 h; a white precipitate formed. The crude precipitate was dissolved in 20 times its weight of pyridine and stirred overnight. Next, the solution was filtered to remove the insoluble completely condensed species (traces) and poured into an equal volume of ice-cold aqueous HCl (37%); a white precipitate formed. The solid was filtered, carefully washed with water and dried overnight at 45 °C. An NMR spectrum of pure cyclopentylsilsesquioxane *a7b3* was obtained. ^{29}Si{^{1}H} NMR (THF): δ = −57.83 [s, 3 Si, (*c*-C_5H_9)SiO(OH)], −65.71 [s, 1 Si, (*c*-C_5H_9)$SiO_{1.5}$], −67.24 [s, 3 Si, (*c*-C_5H_9)$SiO_{1.5}$] ppm. MS (ESI+, cone voltage = 60 V, THF 78%, CH_3CN 20%, HCO_2H 0.1 M, 2%): *m/z* (%) = 875.04 [*a7b3* + H]$^+$ (100), 839.00 [*a7b3* − 2 H_2O + H]$^+$ (41), 897.08 [*a7b3* + Na]$^+$ (16), 911.09 [*a7b3* + 2 H_2O + H]$^+$ (16), 857.03 [*a7b3* − H_2O + H]$^+$ (11).

Synthesis of Cyclohexyl Silsesquioxanes: Typically, deionised water (125 mL) was added carefully into a 1-L round-bottom flask containing a solution of trichloro(cyclohexyl)silane (97% purity, 15 mL, 8.2×10^{-2} mol) in acetonitrile/water (4:1, v/v; 500 mL). This homogeneous solution was then heated to 50 °C or under reflux while stirring vigorously for 18 h.[24] The crude precipitate formed was dissolved in 20 times its weight of pyridine and stirred overnight. The solution was then filtered to remove the insoluble completely condensed species (*a6b0*) and poured into an equal volume of ice-cold aqueous HCl (37%) to precipitate the incompletely condensed silsesquioxanes. The solid mixture of silsesquioxanes was filtered, carefully washed with water and dried overnight at 45 °C. Silsesquioxane *a7b3* was separated by dissolving the mixture of incompletely condensed species in 5 times its weight of THF and then by slowly layering an equal weight of acetonitrile over the THF solution. Under these conditions, a white precipitate was obtained that mainly constituted silsesquioxane *a7b3*. The remaining solution was partially dried under reduced pressure and more acetonitrile was added slowly until a precipitate deposited. The solid was separated by filtration and the solution dried under reduced pressure to afford silsesquioxane *a6b2*. The silylation of the mixture of incompletely condensed silsesquioxanes was performed by adding chlorotrimethylsilane (200 μL) to a solution of the silsesquioxanes (0.3 g) in toluene (30 mL) and triethylamine (1.5 mL). The turbid solution was stirred overnight at room temperature. Next, the solvent and triethylamine were evaporated under reduced pressure to afford a white solid. The solid was extracted with pentane, the solution was filtered to remove the insoluble $(C_2H_5)_3N{\cdot}HCl$ and then concentrated under reduced pressure to give a solid containing the silylated silsesquioxanes. ^{29}Si{^{1}H} NMR: *a6b0* (THF): δ = −56.72 [s, 6 Si, (*c*-C_6H_{11})$SiO_{1.5}$] ppm; *a6b2* (THF): δ = −57.16 [s, 2 Si, (*c*-C_6H_{11})SiO(OH)], −62.32 [s, 2 Si, (*c*-C_6H_{11})$SiO_{1.5}$], −62.57 [s, 2 Si, (*c*-C_6H_{11})$SiO_{1.5}$] ppm; ($CDCl_3$): δ = −55.20 [s, 2 Si, (*c*-C_6H_{11})SiO(OH)], −61.72 [s, 2 Si, (*c*-C_6H_{11})$SiO_{1.5}$], −61.92 [s, 2 Si, (*c*-C_6H_{11})$SiO_{1.5}$]; *a7b1* (THF): δ = −56.18 [s, 1 Si, (*c*-C_6H_{11})$SiO_{1.5}$], −58.66 [s, 2 Si, (*c*-C_6H_{11})$SiO_{1.5}$], −58.87 [s, 1 Si, (*c*-C_6H_{11})SiO(OH)], −66.76 [s, 1 Si, (*c*-C_6H_{11})$SiO_{1.5}$], −67.93 [s, 2 Si, (*c*-C_6H_{11})$SiO_{1.5}$] ppm; ($CDCl_3$): δ = −56.23 [s, 1 Si, (*c*-C_6H_{11})$SiO_{1.5}$], −57.95 [s, 1 Si, (*c*-C_6H_{11})SiO(OH)], −58.58 [s, 2 Si, (*c*-C_6H_{11})$SiO_{1.5}$], −66.82 [s, 1 Si, (*c*-C_6H_{11})$SiO_{1.5}$], −67.66 [(s, 2 Si, (*c*-C_6H_{11})$SiO_{1.5}$)] ppm; silylated *a7b1* isomers ($CDCl_3$): (α): δ = 9.06 [s, 1 Si, $(CH_3)_3SiO_{0.5}$], −56.32 [s, 1 Si, (*c*-C_6H_{11})$SiO_{1.5}$], −59.02 [s, 2 Si, (*c*-C_6H_{11})$SiO_{1.5}$], −66.67 [s, 1 Si, (*c*-C_6H_{11})$SiO_{1.5}$], −68.74 {s, 1 Si, (*c*-C_6H_{11})SiO[OSi$(CH_3)_3$]}, −68.83 [s, 2 Si, (*c*-C_6H_{11})$SiO_{1.5}$] ppm; (β): δ = 8.20 [s, 1 Si, $(CH_3)_3SiO_{0.5}$], −56.28 [s, 1 Si, (*c*-C_6H_{11})$SiO_{1.5}$], −58.70 [s, 2 Si, (*c*-C_6H_{11})$SiO_{1.5}$], −66.89 [s, 1 Si, (*c*-C_6H_{11})$SiO_{1.5}$], −67.35 {s, 1 Si, (*c*-C_6H_{11})Si[OSi$(CH_3)_3$]}, −68.14 [s, 2 Si, (*c*-C_6H_{11})$SiO_{1.5}$] ppm; *a7b3* (THF): δ = −59.79 [s, 3 Si, (*c*-C_6H_{11})SiO(OH)], −67.86 [s, 1 Si, (*c*-C_6H_{11})$SiO_{1.5}$], −69.33 [s, 3 Si, (*c*-C_6H_{11})$SiO_{1.5}$] ppm. MS of crude precipitate (APCI+, cone voltage = 15 V, CH_2Cl_2; see Figure 3), for *a* = 6: *m/z* (%) = 811.36 [*a6b0* + H]$^+$ (100), 829.43 [*a6b2* + H]$^+$ (20); for *a* = 7: *m/z* (%) = 937.12 [*a7b1* − H_2O + H]$^+$ (14), 955.18 [*a7b1* + H]$^+$ (38), 973.19 [*a7b3* + H]$^+$ (23); for *a* = 8: *m/z* (%) = 1081.07 [*a8b0* + H]$^+$ (8), 1099.07 [*a8b2* + H]$^+$ (7); silylated incompletely condensed silsesquioxanes (APCI+, cone voltage = 15 V, toluene/acetonitrile, 2:1, few drops of CH_3CO_2H; see Figure 5): *m/z* (%) = 973.37 [disilylated *a6b2* + H]$^+$ (40), 1027.25 [monosilylated *a7b1* + H]$^+$ (100), 1117.32 [disilylated *a7b3* + H]$^+$ (22), 1243.33 [disilylated *a8b2* + H]$^+$ (15).

Acknowledgments

Anton Sinnema and Kristina Djanashvili are kindly acknowledged for the measurement of the NMR spectra.

[1] P. P. Pescarmona, T. Maschmeyer, *Aust. J. Chem.* **2001**, *54*, 583.
[2] H. C. L. Abbenhuis, *Chem. Eur. J.* **2000**, *6*, 25.
[3] P. G. Harrison, *J. Organomet. Chem.* **1997**, *542*, 141.
[4] C. Sanchez, J. de A. A. Soler-Illia, F. Ribot, T. Lalot, C. R. Mayer, V. Cabuil, *Chem. Mater.* **2001**, *13*, 3061.
[5] I. E. Buys, T. W. Hambley, D. J. Houlton, T. Maschmeyer, A. F. Masters, A. K. Smith, *J. Mol. Cat.* **1994**, *86*, 309.
[6] J.-C. Liu, *Chem. Commun.* **1996**, 1109.
[7] M. Crocker, R. H. M. Herold, A. G. Orpen, *Chem. Commun.* **1997**, 2411.
[8] T. Maschmeyer, M. C. Klunduk, C. M. Martin, D. S. Shephard, J. M. Thomas, B. F. G. Johnson, *Chem. Commun.* **1997**, 1847.
[9] J. M. Thomas, G. Sankar, M. C. Klunduk, B. F. G. Johnson, T. Maschmeyer, M. P. Attfield, R. G. Bell, *J. Phys. Chem. B* **1999**, *103*, 8809.
[10] J. F. Brown, L. H. Vogt, *J. Am. Chem. Soc.* **1965**, *87*, 4313.
[11] F. J. Feher, D. A. Newman, J. F. Walzer, *J. Am. Chem. Soc.* **1989**, *111*, 1741.
[12] F. J. Feher, T. A. Budzichowski, R. L. Blanski, K. J. Weller, J. W. Ziller, *Organometallics* **1991**, *10*, 2526.
[13] P. P. Pescarmona, J. C. van der Waal, I. E. Maxwell, T. Maschmeyer, *Angew. Chem. Int. Ed.* **2001**, *40*, 740.
[14] P. P. Pescarmona, T. Maschmeyer, *NATO Sci. Ser., II* **2002**, *69*, 173.
[15] Relative to silsesquioxane *a7b3* (the yield is calculated by dividing the mass of product by the mass of silsesquioxane *a7b3* that would be obtained if the reaction gave silsesquioxane *a7b3* quantitatively).

 © 2004 Wiley-VCH Verlag GmbH & Co. KGaA, Weinheim

[16] V. K. Krieble, C. I. Noll, *J. Am. Chem. Soc.* **1939**, *61*, 560.
[17] A. J. Belsky, T. B. Brill, *J. Phys. Chem. A* **1999**, *103*, 3006.
[18] While the partial neutralisation of the HCl formed during the hydrolysis of trichlorosilanes might have a role in accelerating the formation of silsesquioxane precipitates, complete neutralisation is detrimental. A decrease of the yield (from 79 to 44%, as crude precipitate) was observed by performing the synthesis of cyclohexylsilsesquioxanes in the presence of triethylamine. This result indicates that the hydrolysis/condensation reactions in the absence of HCl are significantly slowed down from the beginning of the synthesis.
[19] T. Kudo, M. S. Gordon, *J. Am. Chem. Soc.* **1998**, *120*, 11432.
[20] T. Kudo, M. S. Gordon, *J. Phys. Chem. A* **2000**, *104*, 4058.
[21] Percentages based on the integrals of the peaks present in the ^{29}Si NMR spectrum of the crude product.
[22] F. J. Feher, D. A. Newman, *J. Am. Chem. Soc.* **1990**, *112*, 1931.
[23] Peaks corresponding exactly to the ^{29}Si{^{1}H} NMR spectrum of the α-isomer of *a7b*1 reported by Feher[11] (assumed to have been measured in C_6D_6, although reported to be in $CDCl_3$) were found as the second main species in the ^{29}Si{^{1}H} NMR spectrum of the mixture of incompletely condensed silsesquioxanes measured in C_6D_6 {δ = −55.12 [s, 1 Si, (*c*-C_6H_{11})$SiO_{1.5}$], −57.05 [s, 1 Si, (*c*-C_6H_{11})SiO(OH)], −57.15 [s, 2 Si, (*c*-C_6H_{11})$SiO_{1.5}$], −66.06 [s, 1 Si, (*c*-C_6H_{11})$SiO_{1.5}$], −66.40 [s, 2 Si, (*c*-C_6H_{11})$SiO_{1.5}$)] ppm}. In the ^{29}Si{^{1}H} NMR spectra measured in THF or $CDCl_3$, only the two most intense peaks due to the α-isomer of *a7b*1 could be assigned [(THF): δ = −59.47 [s, 2 Si, (*c*-C_6H_{11})$SiO_{1.5}$], −68.45 (s, 2 Si, [*c*-C_6H_{11})$SiO_{1.5}$] ppm; ($CDCl_3$): δ = −57.76 [s, 2 Si, (*c*-C_6H_{11})$SiO_{1.5}$], −67.12 [s, 2 Si, (*c*-C_6H_{11})$SiO_{1.5}$)] ppm]; the three less-intense peaks could not be assigned unambiguously among the remaining peaks of the silsesquioxane mixture.
[24] F. J. Feher, F. Nguyen, D. Soulivong, J. W. Ziller, *Chem. Commun.* **1999**, 1705.
[25] The synthesis conducted under reflux was performed on both 100- and 1000-mL scales, resulting in the formation of the same silsesquioxane mixture each time.

Received July 22, 2003
Early View Article
Published Online January 28, 2004

 © 2004 Wiley-VCH Verlag GmbH & Co. KGaA, Weinheim

Asymmetric Heterodinuclear $Fe^{III}M^{II}$ (M = Zn, Cu, Ni, Fe, Mn), $Co^{III}Fe^{II}$ and $Fe^{II}Co^{III}$ Species: Synthesis, Structure, Redox Behavior, and Magnetism

Sylvia Ross,[a] Thomas Weyhermüller,[a] Eckhard Bill,[a] Eberhard Bothe,[a] Ulrich Flörke,[b] Karl Wieghardt,[a] and Phalguni Chaudhuri*[a]

Keywords: Electrochemistry / Heterodinuclear complexes / Iron / Magnetic properties / Pyridine-2-aldoxime

Reactions of an LFe^{III} unit with an $M(PyA)_3^{n-}$ ion prepared in situ, where L represents 1,4,7-trimethyl-1,4,7-triazacyclononane and PyA^- is the monoanion of pyridin-2-aldoxime, yield heterodinuclear cations of the general formula $[LFe^{III}(PyA)_3M]^{2+}$, where M = Zn^{II} (**1**), Cu^{II} (**2**), Ni^{II} (**3**), low-spin Fe^{II} (**4**) and Mn^{II} (**5**). Additionally, we also prepared the diamagnetic species $[LCo^{III}(PyA)_3Fe^{II}]^{2+}$ (**6**). The $Fe^{III}Co^{II}$ species could not be isolated because a facile intramolecular electron transfer leads to complex **7**, $[LFe^{II}(PyA)_3Co^{III}]^{2+}$. Compounds **1**–**7** contain three oximato anions as bridging ligands and are isostructural in the sense that they all contain a terminal metal(III) ion in a distorted octahedral environment (e.g., FeN_3O_3) and a second six-coordinate metal ion M in a mostly trigonal-prismatic MN_6 geometry. Complexes **1**–**7** were characterized on the basis of elemental analyses, mass spectrometry, IR, UV/Vis, Mössbauer, and EPR spectroscopy, and variable-temperature (2–295 K) magnetic susceptibility measurements. The solid-state structures of **1**–**7** have also been determined by X-ray crystallography. The cyclic voltammograms of the complexes reveal both ligand-centered and metal-centered redox processes. Analysis of the susceptibility data indicates the presence of antiferromagnetic exchange interactions that decrease in the following order: $Fe^{III}Cu^{II}$ (**2**) > $Fe^{III}Ni^{II}$ (**3**) > $Fe^{III}Mn^{II}$ (**5**), as is expected. We have used X-band EPR spectroscopy of **3** ($Fe^{III}Ni^{II}$) at 2–6 K to establish the electronic ground state in great detail and to complement the magnetic susceptibility measurements.

(© Wiley-VCH Verlag GmbH & Co. KGaA, 69451 Weinheim, Germany, 2004)

Introduction

The field of research on heteropolynuclear complexes having different paramagnetic centers is still limited today by the small number of known and structurally fully characterized compounds and by the relative difficulty in synthesizing new compounds. Hence, the preparation of heteropolymetallic complexes has been a challenge for coordination chemists for many years.[1−3] Exchange-coupled heterometallic complexes are relevant to many different research areas, ranging from chemistry to solid-state physics and biology, because of their potential impact in material science, catalysis, and metallobiochemistry. Such exchange interactions in metalloproteins that involve more than one metal center have elicited the interest of bioinorganic chemists.[4−8]

We have adopted a synthetic strategy of using metal oximates as ligands for paramagnetic centers to increase the nuclearity and to synthesize heterometallic complexes. Thus, we have described a series of oximato-bridged (diatomic N,O-bridging) symmetrical and asymmetrical cores: M_AM_B,[9] $M_AM_BM_A$,[10] and $M_AM_BM_BM_A$[11] (M_A, M_B being two different metal ions). In addition, we have synthesized asymmetric heterotrinuclear complexes with cores $M_AM_BM_C$[12] and butterfly cores[13] $(M_A)_2(\mu\text{-}O)_2(M_B)_2$. Thus, we have synthesized linear heterotrinuclear complexes of general formula **A** and asymmetric dinuclear motifs $Cr^{III}\mu(O-N)_3M^{II}$ by using [tris(pyridinealdoximato)-metallate]$^-$ anions, $[M^{II}(PyA)_3]^-$, as ligands for the LCr^{III} unit, where L represents the tridentate cyclic amine 1,4,7-trimethyl-1,4,7-triazacyclononane.[9,10]

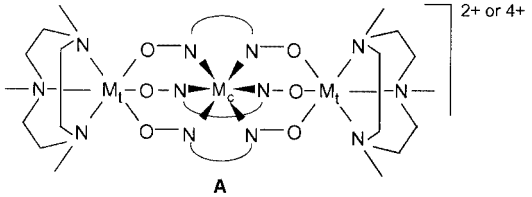

A

M_t = Fe^{III}, Mn^{III}, Mn^{IV}, Cr^{III}, Co^{III}

M_c = Zn^{II}, Cu^{II}, Ni^{II}, Fe^{II}, Mn^{II}

O−N N−O represents dioximate dianion

In this paper, we explore the effects of using Fe^{III} as the LM^{III} unit, i.e., $[LFe^{III}(PyA)_3M^{II}]^{2+}$ complex cations that are isostructural with the $[LCr^{III}(PyA)_3M^{II}]^{2+}$ centers. We

[a] Max-Planck-Institut für Bioanorganische Chemie, Stiftstraße 34−36, 45470 Mülheim an der Ruhr, Germany
E-mail: Chaudh@mpi-muelheim.mpg.de
[b] Universität − Paderborn, Warburgerstraße 100, 33098 Paderborn, Germany

 © 2004 Wiley-VCH Verlag GmbH & Co. KGaA, Weinheim DOI: 10.1002/ejic.200300533

report the synthesis, magnetic, spectroscopic, and other physical properties of the following compounds, where M = Zn (**1**), Cu (**2**), Ni (**3**), Fe (**4**) and Mn (**5**).

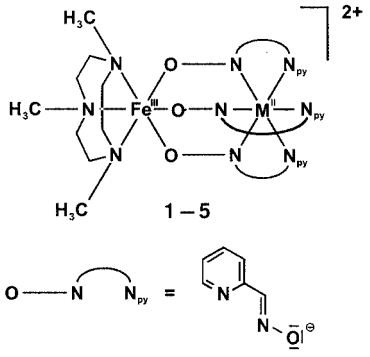

Additionally, we report the preparation and structural characterization of complexes $[LCo^{III}(PyA)_3Fe^{II}]^{2+}$ (**6**) and $[LFe^{II}(PyA)_3Co^{III}]^{2+}$ (**7**). Throughout this paper the compounds **1**–**7** are denoted by their metal centers only. Such isostructural series are not available for any other bridging ligands.

Results and Discussion

We utilized the high thermodynamic stability of the complex between Fe^{III} and the macrocycle 1,4,7-trimethyl-1,4,7-triazacyclononane together with the lability of the first transition series divalent metal ions to synthesize $Fe^{III}M^{II}$ dinuclear complexes. It is interesting to note that isolation of the intermediates $[M(PyA)_3]^-$ was not necessary during this synthetic route. Although no scrambling was observed, all attempts to strictly synthesize the cation $[LFe^{III}(PyA)_3Co^{II}]^{2+}$ under argon led to the isolation of **7**, $[LFe^{II}(PyA)_3Co^{III}]^{2+}$, as a result of facile intramolecular electron transfer. On the other hand, complex **6**, $[LCo^{III}(PyA)_3Fe^{II}]^{2+}$, was readily isolated starting from its respective materials. The colors of the heterometal dinuclear complexes **1**–**7** are light-to-deep-red/brown and they are air-stable in the solid state and also in solution for a few days, except for **7**.

Since the relevant bands in the IR spectra of comparable oxime-containing heteronuclear $Cr^{III}M^{II}$ complexes have been described earlier,[9] and the spectra of complexes **1**–**7** are also very similar, we refrain from discussing them in detail. The bands, together with their tentative assignments, are given in the Exp. Sect.

The electronic spectral results indicate that the complexes **1**–**7** are stable and retain their discrete dinuclear entities also in acetonitrile solution. Only complexes **3** and **7** exhibit lowest-energy spin-allowed d–d transitions at the Ni^{II} and Co^{III} centers, respectively. On the basis of their high extinction coefficients and transitions similar to those reported in the literature,[14] all bands below 350 nm (see Exp. Sect.) for complexes **1**–**7** are assigned to $\pi\rightarrow\pi^*$ transitions of the oxime ligand, whereas the bands above 400 nm, except at ca. 628, 729, and 891 nm for **3** and at 925 nm for **7**, are assigned to the MLCT and LMCT transitions indicating strong interactions of d orbitals with the conjugated π system of the oxime.[15] Judged on the basis of their low extinction coefficients, we tentatively ascribe the bands at ca. 628, 729, and 891 nm for **3** (Ni^{II}) and 925 nm for **7** (Co^{III}) to d–d transitions at the Ni^{II} and Co^{III} centers, respectively.

Electrospray-ionization mass spectrometry (ESI-MS) in the positive-ion mode proved to be a very useful analytical tool for characterizing complexes **1**–**7**. The major peaks are listed in the Exp. Sect. The ESI-MS results for **1**–**7** are very similar and show that, in most cases, there are only two peaks, which correspond to the monocation $[LFe(PyA)_3M(ClO_4)]^+$ and the dication $[LFe(PyA)_3M]^{2+}$. Interestingly, all the complexes show the doubly charged species $[LFe(PyA)_3M]^{2+}$ as the base peak (100%). There is practically no indication in the spectra for ligand fragmentation or cleavage of the dimer, which indicates the robustness of the clathrochelates,[16] i.e., multicyclic ligand systems that completely encapsulate a metal ion, derived from the pyridinealdoxime and the iron-containing capping agent. The data summarized in the Exp. Sect. show that mass spectrometry of the complexes demonstrates the nuclearity of all the complexes unambiguously and also provides a means for identification of the metal centers and the composition of the complexes. Complexes **1**–**7** are not fragile and can withstand the conditions of the ESI(pos)-MS ionization.[17]

Electrochemistry

Cyclic voltammograms (CV) of complexes **1**–**7** were measured at a glassy-carbon working electrode at ambient

Table 1. Cyclic voltammetric data in CH_3CN solutions: the reversible metal-centered oxidations and reductions of $[LM_A(PyA)_3M_B](ClO_4)_2$ **1**–**7**

Complex M_AM_B	$E_{1/2}^{ox}$ (M_A)	$E_{1/2}^{ox}$ (M_B)	$E_{1/2}^{red}$ (M_A)	$E_{1/2}^{red}$ (M_B)
1 $Fe^{III}Zn^{II}$		(+0.83)[a]	−0.80	
2 $Fe^{III}Cu^{II}$		+0.89	−0.62	
3 $Fe^{III}Ni^{II}$		+0.89	−0.72	
4 $Fe^{III}Fe^{II}$		+0.76	−0.62	
5 $Fe^{III}Mn^{II}$		+0.45, +0.73	−0.85, −1.07	
6 $Co^{III}Fe^{II}$		+0.53	−0.68	
7 $Fe^{II}Co^{III}$	+0.65	–	–	−0.63

[a] Ligand-centered oxidation; potentials in volts vs. Fc^+/Fc.

 © 2004 Wiley-VCH Verlag GmbH & Co. KGaA, Weinheim

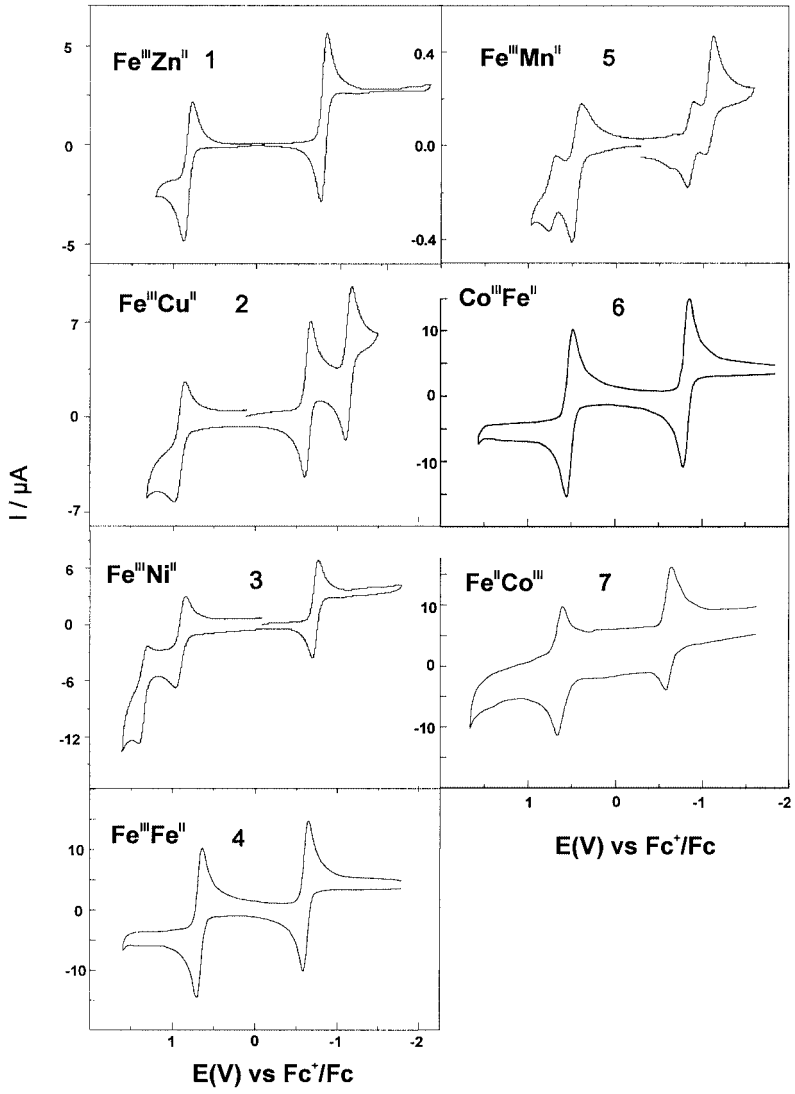

Figure 1. Cyclic voltammograms showing the reversible redox waves of complexes **1**−**7** in CH_3CN solutions containing 0.1 M nBu_4NPF_6; scan rates are 0.1 V/s, except for **5** where a scan rate of 1 V/s was used to achieve full reversibility of the first oxidative wave; working electrode: 2-mm glassy carbon or Pt disk; counter electrode: Pt; reference electrode: Ag/0.01 M $AgNO_3$ and referenced vs. Fc^+/Fc, added as an internal standard after each set of measurements

temperature in CH_3CN containing 0.1 M tetrabutylammonium hexafluorophosphate as the supporting electrolyte. The results are summarized in Table 1 and Figure 1. All redox potentials are referenced in V versus the ferrocenium/ferrocene couple (Fc^+/Fc) used as an internal standard, which is usually located at 0.09 V vs. Ag/0.01 M $AgNO_3$.

Each of the cyclic voltammograms of **1**−**7** (Figure 1) exhibits two reversible waves: one for an oxidation (in the range from +0.53 to +0.93 V) and one for a reduction (in the range from −0.62 to −0.85). The CV of **5** displays a particular feature: the oxidation and reduction are both split symmetrically into two components of unequal heights that are practically independent of the scan rate (0.3−3 V/s). The reason for this behavior is presently unknown. Apart from this exception, the heights of the peaks for oxidation and reduction of each complex are the same. Therefore, we conclude that they represent one-electron redox processes, since simultaneous, reversible two-electron oxidation *and* reduction of a mononuclear complex is not feasible. The two redox potentials for each complex, obtained from the voltammograms, are compiled in Table 1.

The reversible reductions observed for **1**−**7** in a relatively narrow potential range are assigned to the reduction of Fe^{III} (with **1**−**5**) or Co^{III} (with **6** and **7**) metal ions to their respective M^{II} forms. Complex **2** displays, in addition, a further reversible reduction wave at −1.14 V, which we assign to the Cu^{II}/Cu^{I} couple. At more negative potentials (ca. −2.0 V), further (irreversible) reductions occur for **3** and **5** (results not shown). These processes are assigned to ligand-centered reduction processes at the pyridin-2-aldoxime ligand in accordance with earlier observations[18] and results obtained with the analogous $Co^{III}Zn^{II}$ complex,[9] which exhibits *three* reversible reductions, with the one hav-

 © 2004 Wiley-VCH Verlag GmbH & Co. KGaA, Weinheim

ing the lowest reduction potential (−1.83 V) being ligand-centered.

The reversible oxidations could be due either to oxidation of the M^{II} metal ions (M_B for **1**−**6** and M_A for **7**) to their M^{III} forms or to ligand oxidation. Clearly with complex **1**, which bears the "redox-inactive" metal ion $M_B = Zn^{II}$, the oxidation must be ligand-centered. The similarity of the redox potentials for all complexes **1**−**7**, irrespective of the nature of the M^{II} metal ions, could suggest that this phenomenon applies to all the complexes **1**−**7**. Nevertheless, we assign these reversible oxidations to the oxidations of the M^{II} metal ions M_B (for **2**−**6**) or M_A (for **7**) to their respective M^{III} forms, since ligand oxidation was observed only at potentials higher than +1.1 V for the analogous $Co^{III}M^{II}$, $Mn^{III}M^{II}$, and $Cr^{III}M^{II}$ complexes,[9] after metal-centered oxidation. Also, irreversible oxidation of this ligand in Ni^{II} complexes has been described in the literature,[18] again at potentials > 1.0 V. With **3** and **5**, we also observed such oxidation peaks at more positive potentials — at +1.42 and +1.36 V for **3** and **5**, respectively — and these processes are indeed assignable to oxidation of the pyridin-2-aldoxime ligand.

Mössbauer Isomer Shifts and Quadrupole Splittings

The Mössbauer spectra for **1**−**7** were measured at 80 K in zero field to determine the spin and oxidation states of the iron centers. The iron coordination environments are also different, i.e., $Fe^{III}N_3O_3$ for **1**−**5**, $Fe^{II}N_6$ for **4** and **6**, and $Fe^{II}N_3O_3$ for **7**. Each spectrum, except for that of **4**, was fitted with a single quadrupole split doublet, whose isomer shifts (δ_{Fe}) and quadrupole splitting (ΔE_Q) values are listed in Table 2. Mössbauer results, except for **4**, indicate a single quadrupole splitting in accordance with only one type of iron coordination sphere in the solid-state structure, namely the iron site coordinated to the cyclic amine, 1,4,7-trimethyl-1,4,7-triazacyclononane. An isomer shift of δ_{Fe} = 1.07 mm·s^{-1} and a quadrupole splitting of ΔE_Q = 3.66 mm·s^{-1} for **7** are consistent with those observed for high-spin iron(II) ions in octahedral and distorted octahedral environments.[19] The spectrum of **4** is a best fit to two equal-area doublets, which imply two iron sites having different coordination spheres, in agreement with the molecular structure of **4**, and, thus, they are assigned to the Fe^{III} and Fe^{II} ions. A comparison of the Mössbauer data for **1**−**5** with those for **6** and **7** indicates clearly the d^5 high-spin electron configuration for the iron centers coordinated to the cyclic amine. This assignment is also confirmed by the X-ray structures of **1**−**7**. The Mössbauer parameters of complexes **4** and **6** containing the $Fe^{II}N_6$ core are completely in agreement with those observed for low-spin iron(II) ions in octahedral and distorted octahedral environments. Summarily, the Mössbauer spectra[19] show unambiguously the high-spin nature of the Fe^{III} centers in complexes **1**−**5** and of the Fe^{II} center in complex **7**, containing FeN_3O_3 coordination environments, and the low-spin character of the Fe^{II} centers bonded to the nitrogen donor atoms of pyridin-2-aldoxime in complexes **4** and **6**.

Table 2. Mössbauer parameters at 80 K in zero-field

Complex	δ_{Fe} [mm·s^{-1}]	ΔE_Q [mm·s^{-1}]
1 $Fe^{III}Zn^{II}$	0.40	0.16
2 $Fe^{III}Cu^{II}$	0.45	0.01
3 $Fe^{III}Ni^{II}$	0.47	0.12
4 $Fe^{III}Fe^{II}$	0.41	0.39
	0.26	0.33
5 $Fe^{III}Mn^{II}$	0.46	0.43
6 $Co^{III}Fe^{II}$	0.30	0.40
7 $Fe^{II}Co^{III}$	1.07	3.66

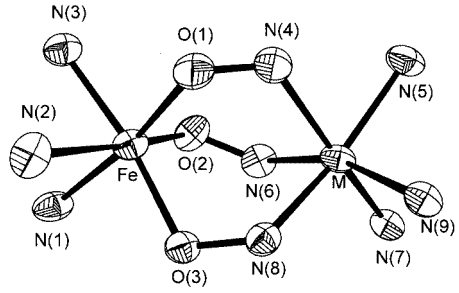

Figure 2. First coordination sphere of **3**, $Fe^{III}Ni^{II}$; the atom connectivities are identical for all complexes **1**−**7**

Table 3. Selected bond lengths [Å] for complexes $Fe^{III}Zn^{II}$ (**1**), $Fe^{III}Cu^{II}$ (**2**), $Fe^{III}Ni^{II}$ (**3**), $Fe^{III}Fe^{II}$ (**4**), and $Fe^{III}Mn^{II}$ (**5**)

	$Fe^{III}Zn^{II}$ (**1**)	$Fe^{III}Cu^{II}$ (**2**)	$Fe^{III}Ni^{II}$ (**3**)	$Fe^{III}Fe^{II}$ (**4**)	$Fe^{III}Mn^{II}$ (**5**)
Fe−N(1)	2.201(4)	2.187(3)	2.192(6)	2.202(6)	2.209(2)
Fe−N(2)	2.206(4)	2.201(3)	2.186(6)	2.174(8)	2.219(1)
Fe−N(3)	2.196(4)	2.186(3)	2.190(6)	2.195(8)	2.198(1)
Fe−O(1)	1.973(3)	1.950(2)	1.971(4)	1.963(5)	1.954(1)
Fe−O(2)	1.967(3)	1.993(2)	1.967(5)	1.970(7)	1.967(1)
Fe−O(3)	1.949(4)	1.967(2)	1.989(5)	1.976(7)	1.966(1)
$M^{II}-N(5)_{py}$	2.149(4)	2.293(3)	2.108(6)	1.977(7)	2.239(1)
$M^{II}-N(7)_{py}$	2.159(4)	2.114(3)	2.116(6)	1.990(8)	2.271(1)
$M^{II}-N(9)_{py}$	2.160(4)	2.023(3)	2.093(6)	2.001(8)	2.255(1)
$M^{II}-N(6)_{ox}$	2.155(4)	2.002(3)	2.052(6)	1.926(8)	2.243(1)
$M^{II}-N(8)_{ox}$	2.155(4)	2.129(3)	2.071(6)	1.907(8)	2.261(2)
$M^{II}-N(4)_{ox}$	2.205(4)	2.150(3)	2.063(6)	1.922(8)	2.242(1)

 © 2004 Wiley-VCH Verlag GmbH & Co. KGaA, Weinheim

Molecular Structures of $[LFe^{III}(PyA)_3M^{II}](ClO_4)_2$ [M = Zn (1), Cu (2), Ni (3), Fe (4), Mn(5)]

The X-ray structures confirm that mixed-metal $Fe^{III}M^{II}$ complexes have indeed been formed with geometries in which two pseudooctahedral polyhedra are joined by three oximato N−O groups. The coordinated ligand L exhibits no unexpected features.[10,20] The N−O (average 1.355 ± 0.008 Å) and C=N_{ox} (average 1.287 ± 0.017 Å) bond lengths and C−N−O bond angle (average 117.8 ± 1.6°) of the bridging pyridinaldoximate ligand are very similar to those of other comparable structures.[9,21−24] Figure 2 illustrates the thermal ellipsoid plot of the $N_3Fe(O-N_{ox})_3M(N_{py})_3$ core for the $Fe^{III}Ni^{II}$ compound **3**. Table 3 lists bond lengths of the first coordination sphere of the $Fe^{III}M^{II}$ compounds **1**−**5**. As expected, the donor atoms for the metal ions of the cations in **1**−**5** are identical [FeN_3O_3 and $M^{II}(N_{ox})_3(N_{py})$], but the coordination geometry of the divalent metal centers are not. Perspective views of the cations are shown in Figure 3 for **1** and **2** and in Figure 4 for **3**, **4**, and **5**.

The iron coordination geometry is distorted octahedral with three nitrogen atoms, N(1), N(2), and N(3), from the facially coordinated tridentate macrocyclic amine L and three oxygen atoms, O(1), O(2), and O(3), from the bridging oximate group (Figure 2). The Fe−N (average 2.197 ±

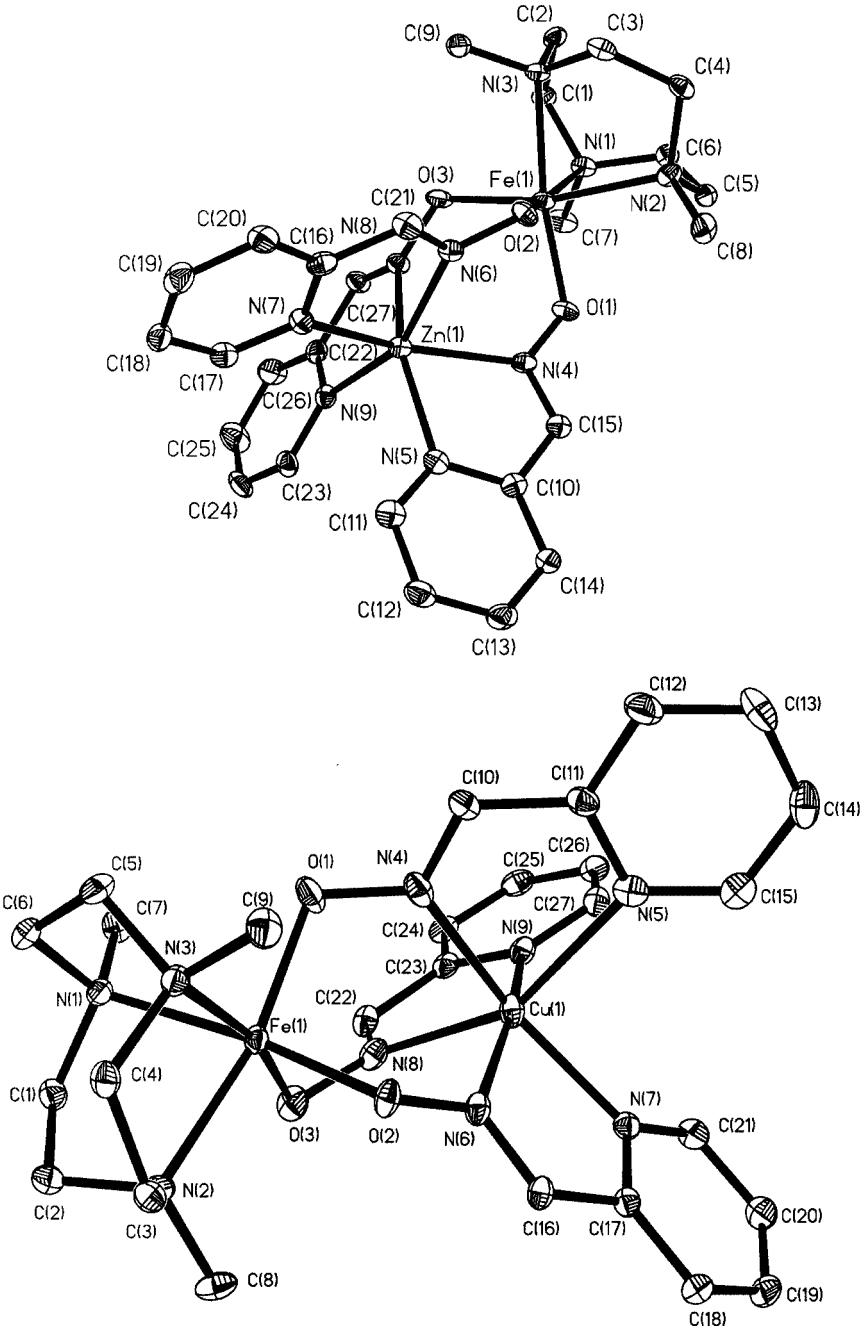

Figure 3. Molecular structures of the dications $Fe^{III}Zn^{II}$ in **1** (top) and $Fe^{III}Cu^{II}$ in **2** (bottom)

 © 2004 Wiley-VCH Verlag GmbH & Co. KGaA, Weinheim

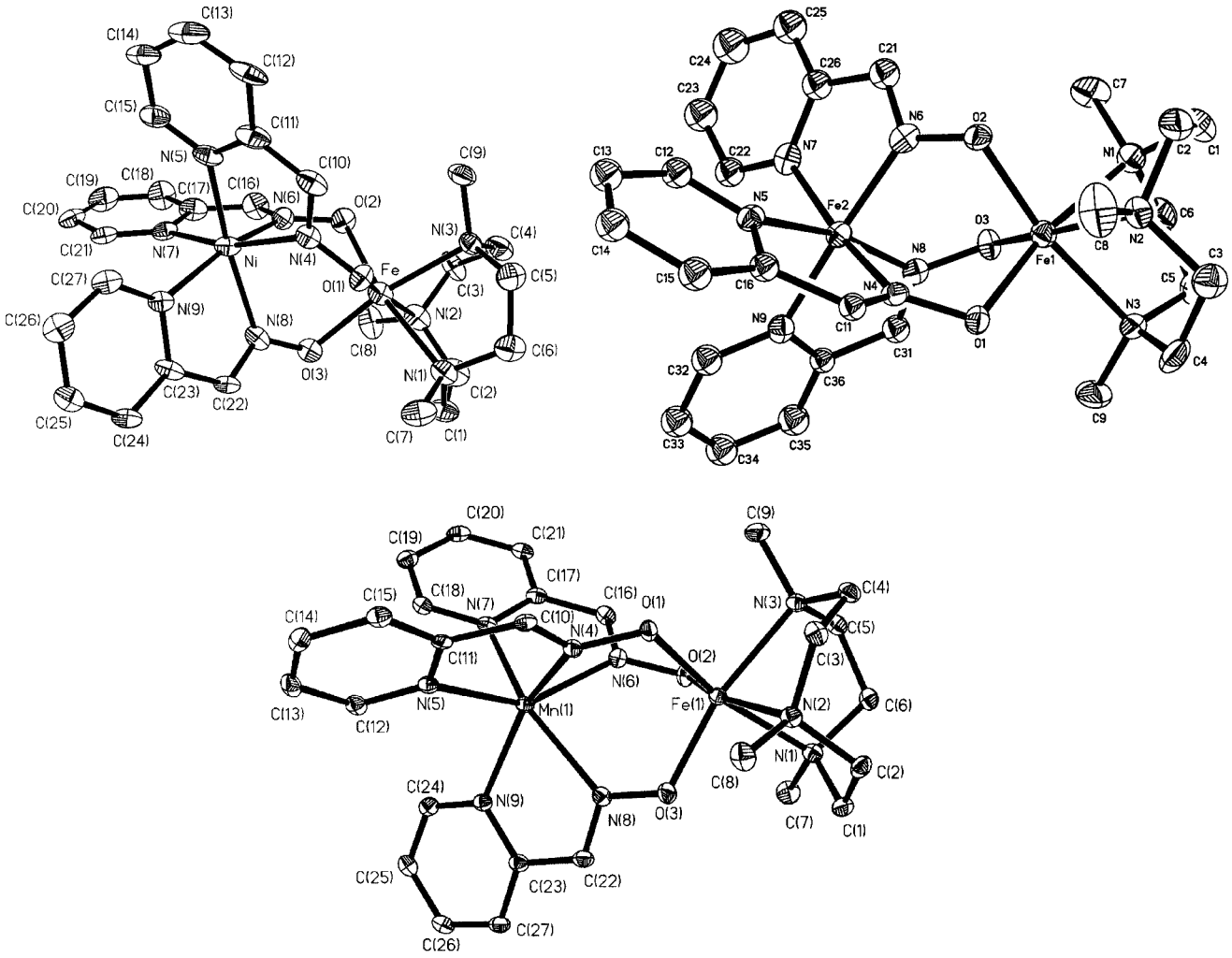

Figure 4. ORTEP diagrams of the complex cations showing the atom labeling schemes for $Fe^{III}Ni^{II}$ (**3**) (top, left), $Fe^{III}Fe^{II}$ (**4**) (top, right), and $Fe^{III}Mn^{II}$ (**5**) (bottom)

0.021 Å) and Fe−O (average 1.968 ± 0.020 Å) distances for complexes **1**−**5** correspond to those of known values[20,23] for Fe^{III} complexes with this macrocyclic amine, and are in agreement with a d^5 high-spin electronic configuration of the Fe^{III} centers, which is in complete agreement with the Mössbauer results. The largest deviation from the idealized 90° interbond angles is 12°, which occurs within the six-membered O−Fe−O chelate rings, the O−Fe−O angles ranging between 101.8(2) and 95.3(2)°, whereas the N−Fe−N angles fall between 78.95(5) and 81.1(3)°. The divalent second metal atom, which is separated from the ferric center at a distance 3.36−3.67 Å, does not affect the geometry of the ferric center. A similar observation has been made earlier for the analogous series of complexes featuring Cr^{III} ions.[9]

The crystal structure of complex **1** ($Fe^{III}Zn^{II}$) indicates the presence of two independent molecules crystallized with two molecules of solvent (methanol), which are hydrogen-bonded to two oxygen atoms of a perchlorate anion with O···O distances of 2.852 and 3.107 Å. We have found no substantial differences in the metrical parameters for the two independent molecules of **1**.

The second metal center, either Zn^{II}, Cu^{II}, Ni^{II}, Fe^{II}, or Mn^{II}, is also sixfold coordinated, yielding an MN_6 core. Coordination occurs facially through pyridine nitrogen atoms, $N_{py}(5)$, $N_{py}(7)$, and $N_{py}(9)$, and three azomethine nitrogen atoms, $N_{ox}(4)$, $N_{ox}(6)$, and $N_{ox}(8)$, from the pyridinaldoxime (PyA) ligand (Figure 2). The average M−N bond lengths fall within the ranges that are considered as normal covalent bonds for M^{II} centers with a high-spin configuration for Mn^{II} (d^5) (**5**), Ni^{II} (d^8) (**3**), and Cu^{II} (d^9) (**2**) and a d^6 low-spin electronic configuration for Fe^{II} (**4**). The low-spin electronic state of Fe^{II} in **4** has also been confirmed by the Mössbauer data.

The Cu−N distances and the angles N−Cu−N for **2** indicate that the resultant coordination sphere around the copper center in $Fe^{III}Cu^{II}$ is highly distorted. The smallest acute bite angle for *cis*-N−Cu−N occurs for the N(4)−Cu(1)−N(5) unit [73.3(1)°], where N(4) and N(5) atoms represent the oxime and pyridine nitrogen atoms, respectively, of the same pyridin-2-aldoximato ligand. On the other hand, the nitrogen atoms of the N(8)−Cu(1)−N(5) unit [154.3(1)°] belong to two different pyridinaldoximato ligands and the angle is the smallest

 © 2004 Wiley-VCH Verlag GmbH & Co. KGaA, Weinheim

Table 4. Selected structural parameters for complexes **1**−**7**

Complex	$Fe^{III}\cdots M^{II}$ or $Co^{III}\cdots Fe^{II}$ or $Fe^{II}\cdots Co^{III}$ [Å]	Av. twist angle φ [°][a]	Dihedral angle θ [°][b]
1 $Fe^{III}Zn^{II}$	3.593(1)	30.3	34.9/39.4/35.4
2 $Fe^{III}Cu^{II}$	3.507(1)	35.2	40.0/34.4/43.9
3 $Fe^{III}Ni^{II}$	3.476(1)	39.2	43.5/37.4/37.5
4 $Fe^{III}Fe^{II}$	3.359(2)	46.3	39.6/43.7/43.9
5 $Fe^{III}Mn^{II}$	3.665(1)	22.3	28.7/36.2/31.3
6 $Co^{III}Fe^{II}$	3.389(1)	45.7	45.0/46.3/41.0
7 $Fe^{II}Co^{III}$	3.389(2)	50.4	50.8/51.1/49.9

[a] The trigonal twist angle φ is the angle between the triangular faces comprising N(4)N(6)N(8) and N(5)N(7)N(9) (Figure 2) and has been calculated as the mean of the Newman projection angles viewed along the centroids of focus. For an ideal trigonal prismatic arrangement, φ is 0° and 60° for an octahedron (or trigonal-antiprismatic arrangement). [b] That the core Fe(O−N)M is not linear is shown by the dihedral angles θ between the planes comprising Fe(O−N) and M(N−O) atoms.

among the *trans*-N−Cu−N angles, which indicates the severe deviation of the copper geometry from octahedral. No substantial differences in bond lengths and angles are found between the two crystallographically independent molecules of **2**.

For comparison, the important structural parameters are given in Table 4. It is clear from the data in Table 4 that the geometries of the metal ions Mn^{II} (**5**), Fe^{II} (**4**), Ni^{II} (**3**), Cu^{II} (**2**), and Zn^{II} (**1**) are distorted from octahedra toward trigonal prisms, as is evident from the twist angles; these distortions can be ascribed to both electronic (LFSE) and size effects, as has been discussed earlier.[9,10,25]

Molecular Structures of $[LCo^{III}(PyA)_3Fe^{II}](ClO_4)_2$ (6) and $[LFe^{II}(PyA)_3Co^{III}](PF_6)_2$ (7)

Figure 5 displays two perspective views of the cations in **6** and **7** and their atom labeling schemes. Selected bond lengths and angles are listed in Tables 5 and 6. The structural data concerning the ligand parts of the complex are in good agreement with the findings of previous studies dealing with compounds having the same ligands and do not warrant any additional comments. The X-ray structures confirm that the heterodinuclear complexes **6** and **7** have indeed been formed with a Co···Fe distance of 3.389 Å. The cobalt center in **6** and the iron center in **7** are distorted octahedra coordinated with three nitrogen atoms from the facially coordinated tridentate macrocyclic amine L and three oxygen atoms from the bridging oximate groups. The distances Co−N [average 2.011(3) Å] and Co−O [average 1.942(4) Å] in **6** and Fe−N [average 2.178(12) Å] and Fe−O [average 2.101(1) Å] in **7** correspond well with literature values for low-spin Co^{III} and high-spin Fe^{II} complexes, respectively.[20,26] The high-spin d^6 electronic configuration of the iron(II) center in **7** has also been confirmed by the Mössbauer and susceptibility measurements.

The second metal center, iron in **6** or cobalt in **7**, is also sixfold coordinated yielding an MN_6 core. Coordination occurs through three pyridine nitrogen atoms and three azomethine nitrogen atoms (Figure 5). The Fe−N (in **6**) and Co−N (in **7**) bond lengths (Tables 5 and 6) are consistent with a d^6 low-spin electron configuration for the metal centers, which was confirmed also by the magnetochemical measurements. Some pertinent structural parameters are listed in Table 4.

Magnetic Susceptibility and EPR Measurements

Magnetic susceptibility data for polycrystalline samples of the complexes were collected in the temperature range 2−290 K in an applied magnetic field of 1 T. We use the Heisenberg spin Hamiltonian in the form $H = -2J\cdot S_{Fe}\cdot S_M$ for an isotropic exchange coupling with $S_{Fe} = {}^5/_2$ and $S_M = 0$ for Zn^{II} (**1**), low-spin Fe^{II} (**4**), $S_M = {}^1/_2$ for Cu^{II} (**2**), $S_M = 1$ for Ni^{II} (**3**), and $S_M = {}^5/_2$ for Mn^{II} (**5**); for complex **7**, the spin states used are $S_{Fe} = {}^4/_2$ for a high-spin Fe^{II} ion and $S_{Co} = 0$ for a low-spin d^6 Co^{III} ion. The experimental data for **2**, **3**, and **5** for the effective magnetic moments (μ_{eff}) versus temperature (T) are displayed in Figure 6. The experimental magnetic data for the complexes (**1**−**5** and **7**) were simulated using a least-squares fitting program and the solid lines in Figure 6 represent the simulations for **2**, **3**, and **5**. Table 7 summarizes selected magnetic parameters with the observed spin ground states.

Complex **6** is diamagnetic indicating that both the cobalt and iron centers are in low-spin d^6 electron configurations, which is a finding that is also in full accord with the Mössbauer and structural parameters. Above $T \approx 25$ K, complexes **1** and **4**, which are magnetically mononuclear, exhibit essentially temperature-independent μ_{eff} values of 5.90 ± 0.02 and 5.80 ± 0.05 μ_B, respectively. Simulations of the experimental magnetic moment data yield g_{Fe} values of 2.0 for **1** and 1.96 for **4** with $S_{Fe} = {}^5/_2$ and $S_M = 0$. We note that the value of $g_{Fe} = 1.96$ for a high-spin ferric ion is comparatively low.

The magnetic moment μ_{eff}/molecule for **7**, Fe^{II}(h.s.)-Co^{III}(l.s.), of 5.30 μ_B ($\chi_M\cdot T = 3.517$ $cm^3\cdot K\cdot mol^{-1}$) at 290 K decreases monotonically with decreasing temperature until it reaches a value of 4.90 μ_B ($\chi_M\cdot T = 3.002$ $cm^3\cdot K\cdot mol^{-1}$) at 30 K and then starts to further decrease rapidly and reaches a value of 2.57 μ_B ($\chi_M\cdot T = 0.827$ $cm^3\cdot K\cdot mol^{-1}$) at 2 K. This temperature dependence is in agreement with a high-spin ferrous ion having an orbital T ground term. A least-squares fit results in a g_{Fe} value of 2.12.

The experimental magnetic moment for **2**, Fe^{III}(h.s.)Cu^{II}, is 5.55 μ_B ($\chi_M\cdot T = 3.853$ $cm^3\cdot K\cdot mol^{-1}$) at 290 K, which is

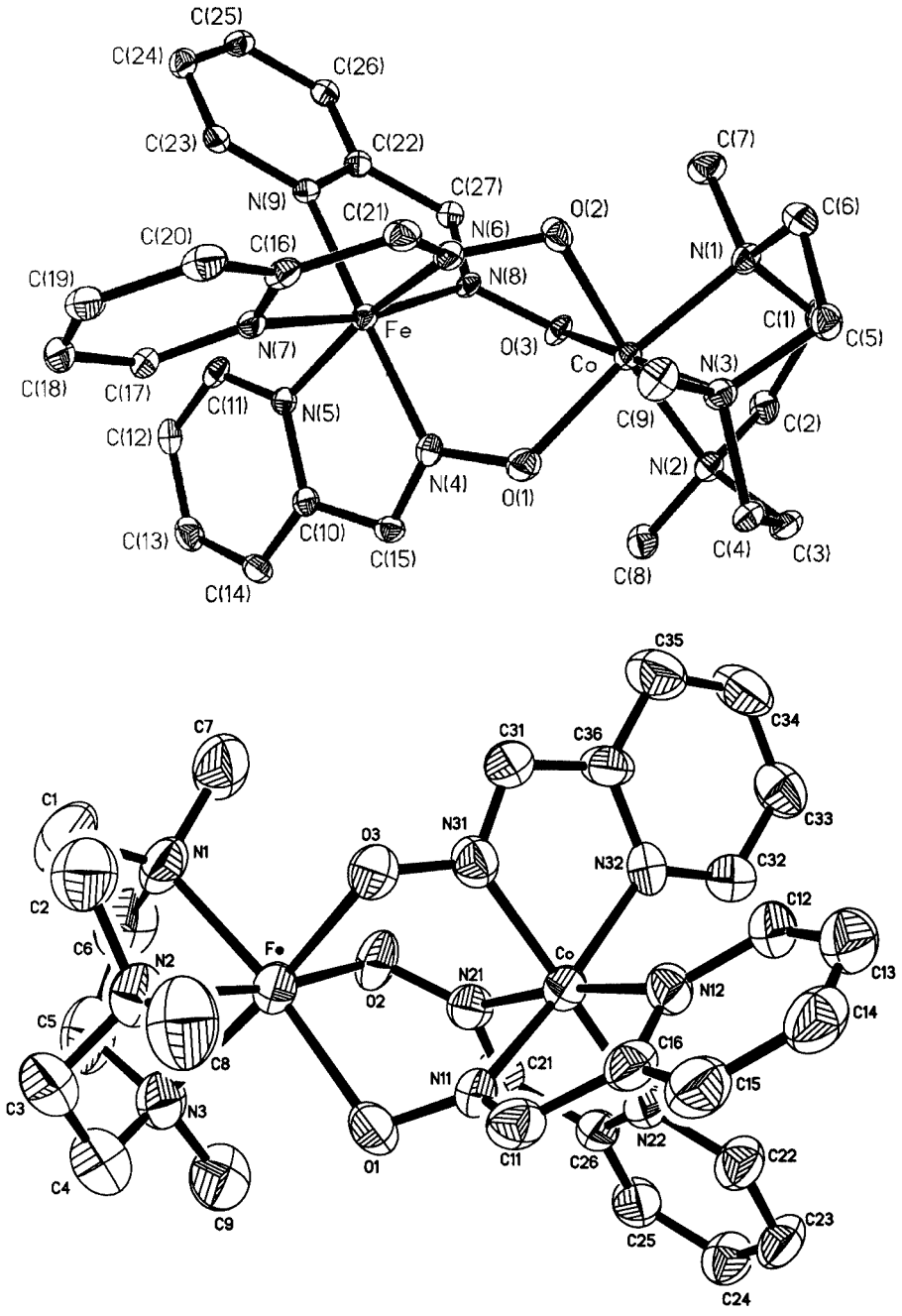

Figure 5. Perspective views of the cations in **6** ($Co^{III}Fe^{II}$) (top) and in **7** [Fe^{II}(h.s.)Co^{III}] (bottom)

significantly smaller than the theoretical value of μ_{eff} = 6.168 μ_B for two uncoupled spins of $S_{Fe} = {}^5/_2$ and $S_{Cu} = {}^1/_2$ with $g = 2.0$. Upon lowering the temperature, μ_{eff} decreases until a plateau is reached in the temperature range 80−40 K with a μ_{eff} value of ca. 4.88 μ_B ($\chi_M{\cdot}T$ = 2.974 $cm^3{\cdot}K{\cdot}mol^{-1}$), which is very close to the theoretical "spin-only" value of 4.90 μ_B for $S = 2$ expected as the ground state for an antiferromagnetically coupled $Fe^{III}Cu^{II}$ compound. Below 40 K, there is a decrease in μ_{eff} reaching a value of 3.27 μ_B ($\chi_M{\cdot}T$ = 1.341 $cm^3{\cdot}K{\cdot}mol^{-1}$) at 2 K. This deviation from the theoretical value is attributable to either zero-field splitting of the ground state $S_t = 2$ and/or intermolecular interactions. We have modeled this decrease with respect to the Weiss constant, θ. The least-squares fitting, shown as the solid line in Figure 6, of the experimental data leads to $J = -42.5\ cm^{-1}$, $g_{Fe} = 2.00$, $g_{Cu} = 2.05$, and θ = −0.4 K. The observed antiferromagnetic coupling ($J = -42.5\ cm^{-1}$) agrees well with the comparable exchange coupling constants reported earlier.[27]

The magnetic behavior of **3**, $Fe^{III}Ni^{II}$, is characteristic of an antiferromagnetically coupled dinuclear complex. At 290 K, the μ_{eff} value of 5.46 μ_B ($\chi_M{\cdot}T$ = 3.729 $cm^3{\cdot}K{\cdot}mol^{-1}$) decreases monotonically with decreasing temperature until it reaches a value of 3.53 μ_B ($\chi_M{\cdot}T$ =

 © 2004 Wiley-VCH Verlag GmbH & Co. KGaA, Weinheim

Table 5. Selected bond lengths [Å] and angles [°] for $[LCo^{III}(PyA)_3Fe^{II}](ClO_4)_2$ in **6**

Co−O(3)	1.939(3)	Co−O(2)	1.941(3)
Co−O(1)	1.947(3)	Co−N(2)	2.001(3)
Co−N(3)	2.001(3)	Co−N(1)	2.011(3)
Fe−N(4)	1.889(3)	Fe−N(8)	1.894(3)
Fe−N(6)	1.898(3)	Fe−N(9)	1.967(3)
Fe−N(7)	1.979(3)	Fe−N(5)	1.984(3)
O(1)−N(4)	1.352(4)	O(2)−N(6)	1.350(4)
O(3)−N(8)	1.355(4)		
O(3)−Co−O(2)	93.29(12)	O(3)−Co−O(1)	94.74(11)
O(2)−Co−O(1)	94.74(12)	O(3)−Co−N(2)	88.22(12)
O(2)−Co−N(2)	174.61(12)	O(1)−Co−N(2)	90.29(12)
O(3)−Co−N(3)	174.60(12)	O(2)−Co−N(3)	91.69(13)
O(1)−Co−N(3)	86.92(12)	N(2)−Co−N(3)	86.63(13)
O(3)−Co−N(1)	91.95(12)	O(2)−Co−N(1)	88.34(12)
O(1)−Co−N(1)	172.46(12)	N(2)−Co−N(1)	86.44(13)
N(3)−Co−N(1)	86.11(13)	N(4)−Fe−N(8)	89.44(13)
N(4)−Fe−N(6)	89.49(14)	N(8)−Fe−N(6)	89.56(13)
N(4)−Fe−N(9)	167.26(13)	N(8)−Fe−N(9)	81.16(13)
N(6)−Fe−N(9)	98.97(14)	N(4)−Fe−N(7)	97.88(13)
N(8)−Fe−N(7)	168.01(13)	N(6)−Fe−N(7)	81.06(14)
N(9)−Fe−N(7)	92.87(13)	N(4)−Fe−N(5)	80.90(14)
N(8)−Fe−N(5)	96.60(13)	N(6)−Fe−N(5)	168.50(13)
N(9)−Fe−N(5)	91.59(13)	N(7)−Fe−N(5)	93.93(13)

Table 6. Selected bond lengths [Å] and angles [°] for $[LFe^{II}(PyA)_3Co^{III}](PF_6)_2$ in **7**

Co−N(21)	1.901(9)	Co−N(31)	1.911(9)
Co−N(11)	1.912(8)	Co−N(32)	1.964(8)
Co−N(22)	1.972(8)	Co−N(12)	1.985(8)
Fe−O(1)	2.099(7)	Fe−O(3)	2.101(8)
Fe−O(2)	2.102(7)	Fe−N(1)	2.166(9)
Fe−N(2)	2.179(9)	Fe−N(3)	2.190(10)
O(1)−N(11)	1.328(10)	O(2)−N(21)	1.322(10)
O(3)−N(31)	1.315(10)		
N(21)−Co−N(31)	90.34(4)	N(21)−Co−N(11)	91.4(4)
N(31)−Co−N(11)	90.9(3)	N(21)−Co−N(32)	93.5(4)
N(31)−Co−N(32)	81.8(3)	N(11)−Co−N(32)	171.3(4)
N(21)−Co−N(22)	82.7(4)	N(31)−Co−N(22)	171.9(4)
N(11)−Co−N(22)	93.3(3)	N(32)−Co−N(22)	94.5(3)
N(21)−Co−N(12)	171.8(4)	N(31)−Co−N(12)	94.0(3)
N(11)−Co−N(12)	81.6(3)	N(32)−Co−N(12)	94.1(3)
N(22)−Co−N(12)	93.5(3)	O(1)−Fe−O(3)	91.3(3)
O(1)−Fe−O(2)	92.1(3)	O(3)−Fe−O(2)	90.8(3)
O(1)−Fe−N(1)	171.7(4)	O(3)−Fe−N(1)	97.0(3)
O(2)−Fe−N(1)	87.6(3)	O(1)−Fe−N(2)	98.2(3)
O(3)−Fe−N(2)	89.8(3)	O(2)−Fe−N(2)	169.7(3)
N(1)−Fe−N(2)	82.2(4)	O(1)−Fe−N(3)	89.6(3)
O(3)−Fe−N(3)	171.4(4)	O(2)−Fe−N(3)	97.8(4)
N(1)−Fe−N(3)	82.2(4)	N(2)−Fe−N(3)	81.6(4)

1.561 $cm^3 \cdot K \cdot mol^{-1}$) at 10 K. A plateau in $\mu_{eff}(T)$ observed at 10−50 K indicates the presence of an energetically isolated ground state with total spin $S_t = {}^3/_2$ (spin-only value $\mu_{eff} = 3.87\ \mu_B$) according to a dominating exchange interaction between Fe^{III} ($S_{Fe} = {}^5/_2$) and Ni^{II} ($S_{Ni} = 1$). Below 10 K, there is a further decrease in μ_{eff} beyond what is expected from usual saturation due to zero-field splitting of the ground-state quadruplet. Magnetic susceptibility data were analyzed on the basis of a spin-Hamiltonian description of the electronic ground state of the single ions and their exchange interaction according to Equation (1), where $\mathbf{S}_i$ ($i = 1, 2$) are the spins of the metal ions in the dimers, D_i, E/D_i, and g_i are the local axial and rhombic zero-field parameters and g values, respectively, and J represents the exchange coupling constant.

$$H = \Sigma\{D_i[S_{z,i}^2 - S_i(S_i + 1)/3 + (E/D_i)(S_{x,i}^2 - S_{y,i}^2)] + \mu_B\mathbf{B}\cdot g_i\cdot\mathbf{S}_i\} - 2J\, S_1\cdot S_2 \quad (1)$$

The temperature dependence of μ_{eff} was well simulated by Equation (1) with parameters $J_{FeNi} = -34\ cm^{-1}$, $g_{Fe} = 2.0$ (fixed), $g_{Ni} = 2.12$ (fixed), $D_{Fe} = -1.1\ cm^{-1}$, $D_{Ni} = 5\ cm^{-1}$ (fixed), and 5.8% paramagnetic impurity with $S = {}^1/_2$. In the corresponding fitting procedure, the axial zfs parameter for nickel D_{Ni} was fixed to the value obtained from an isostructural $Co^{III}Ni^{II}$ complex having diamagnetic Co^{III} (not shown)[9] and the sign of D_{Fe}, as well as the value for g_{Ni}, was fixed according to the constraints derived from the EPR data (see below).

Solutions of compound **3** in BuCN/toluene (75:25, 0.4 mM) show resolved X-band EPR spectra (Figure 7). The derivative lines at $g \approx 4$ and 2 are typical of $S_t = {}^3/_2$ with strong axial zero-field splitting ($D_t > h\nu$) and low rhombicity ($0 > E/D_t > 0.1$). The presence of a distinct sharp peak at $g \approx 6$, which increases at lower temperatures, indicates the $|m_s = \pm{}^3/_2 >$ Kramers doublet to be the ground

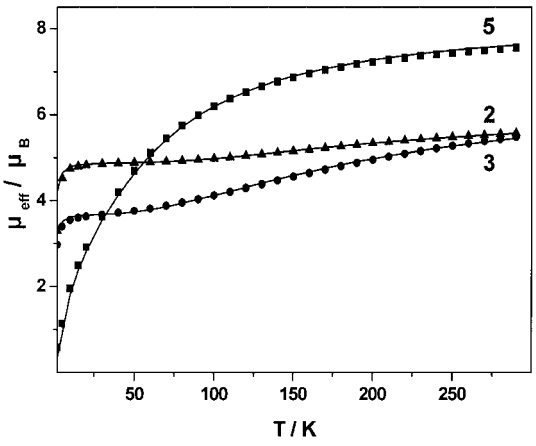

Figure 6. Plots of μ_{eff} vs. T for solid **2**, **3**, and **5**; the solid lines represent the best fit of the data to the Heisenberg−Dirac−van Vleck model (see text)

Table 7. Selected magnetic parameters for heterodinuclear complexes **1**−**7**

Complex	J [cm^{-1}]	g_{Fe}	g_M	Ground state (S_t)
1 $Fe^{III}Zn^{II}$	5.90 ± 0.02 μ_B	2.00	−	$S_t = {}^5/_2$
2 $Fe^{III}Cu^{II}$	−42.5	2.00	2.05	$S_t = 2$
3 $Fe^{III}Ni^{II}$ [a]	−34.0	2.00	2.12	$S_t = {}^3/_2$
4 $Fe^{III}Fe^{II}$(l.s.)	5.80 ± 0.05 μ_B	1.96	−	$S_t = {}^5/_2$
5 $Fe^{III}Mn^{II}$(h.s.)	−6.1	2.00	2.00	$S_t = 0$
6 Co^{III}(l.s.)Fe^{II}(l.s.)	diamagnetic			
7 Fe^{II}(h.s.)Co^{III}(l.s.)	5.1 ± 0.20 μ_B	2.12	−	$S_t = 2$

[a] $D_t = -1.8\ cm^{-1}$ (EPR), $D_t = -1.7\ cm^{-1}$ (susceptibility).

state, as a result of the negative zfs parameter D_t. The spectrum could be simulated reasonably well by using Equation (2) (see Exp. Sect.) for total spin $S_t = {}^3/_2$ with parameters $D_t = -1.8\ cm^{-1}$, $E/D_t = 0.078$, $g_t = (1.954, 1.954, 1.95)$, and isotropic g value $g_{t,iso} = 1.953$. The characteristic line shape of the powder spectrum was achieved by using a Gaussian distribution of the rhombicity parameter with a half-width $\sigma(E/D) = 0.078$.

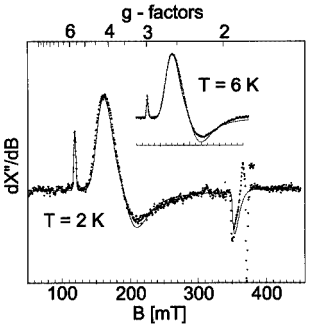

Figure 7. X-band EPR spectra of the $Fe^{III}Ni^{II}$ dimer **3** in BuCN/toluene solution recorded at 2 and 6 K (inset); experimental parameters: frequency = 9.4775 GHz, power = 2 μW (2 K)/20 μW (6 K), modulation = 1 mT/100 kHz; the solid lines are spin Hamiltonian simulations obtained using Equation (2) for total spin $S_t = {}^3/_2$ with parameters $D_t = -1.8\ cm^{-1}$, $E/D_t = 0.078$, $\sigma(E/D) = 0.078$, and $g_t = (1.954, 1.954, 1.95)$

The EPR parameter complements the interpretation of the magnetic data as given above. According to the spin projection properties, the ground-state parameters of complex **3** are related to the local single-ion values for iron and nickel by $D_t = (28/15)D_{Fe} + (1/15)D_{Ni}$ (neglecting dipolar contributions) and $g_t = 7/5\ g_{Fe} - 2/5\ g_{Ni}$. This finding indicates the dominant influence of the iron on the properties of the ground-state spin quadruplet. With the zfs value $D_{Fe} = -1.1\ cm^{-1}$ derived from the magnetic data (using fixed $D_{Ni} = 5\ cm^{-1}$), one obtains for the spin quadruplet $D_t = -1.7\ cm^{-1}$, which is strikingly close to the experimental value obtained from the EPR simulations ($-1.8\ cm^{-1}$). Hence, the complementary EPR and magnetic measurements determine the electronic properties of iron(III) and nickel(II) in **3** in great detail.

The μ_{eff} value for **5**, $Fe^{III}Mn^{II}$, decreases continuously from 7.64 μ_B ($\chi_M \cdot T = 7.299\ cm^3 \cdot K \cdot mol^{-1}$) at 290 K to 1.63 μ_B ($\chi_M \cdot T = 0.3304\ cm^3 \cdot K \cdot mol^{-1}$) at 2 K; this temperature dependence of μ_{eff} is a clear indication of an antiferromagnetic exchange coupling between two paramagnetic centers Fe^{III} ($S = {}^5/_2$) and Mn^{II} ($S = {}^5/_2$) with a resulting singlet ($S_t = 0$) ground state. Simulation of the experimental data (solid line in Figure 5) results in $J = -6.1\ cm^{-1}$, $g_{Fe} = g_{Mn} = 2.00$, and a paramagnetic impurity PI ($S = {}^5/_2$) = 0.3%.

Because a qualitative rationale for the trend of the antiferromagnetic exchange interactions between the spin carriers in the $Fe^{III}M^{II}$ pairs [M = Cu (**2**), Ni (**3**), and Mn (**5**)], on the basis of the established Goodenough−Kanamori rules[28] for superexchange as presented concisely by Ginsberg[29] and later by Kahn,[7] has been reported earlier,[3] we refrain from discussing it again in detail. Qualitatively, it can be said that the strength of exchange interactions increases upon decreasing the number of unpaired electrons, i.e., $Fe^{III}Mn^{II}$ (**5**) < $Fe^{III}Ni^{II}$ (**3**) < $Fe^{III}Cu^{II}$ (**2**), as the number of ferromagnetic paths operating in the interacting spin system decreases along the series shown above.

Several examples of structurally similar heterodimetallic complexes $Fe^{III}M^{II}$ (M = Zn, Cu, Ni, Co, or Mn) containing (μ-OR)bis(μ-carboxylato)-bridging ligands have been described in the literature[30−34] as models for dinuclear metal centers in proteins. Although the present exchange-coupled complexes **2**, **3**, and **5** having diatomic (−N−O) oximato bridges differ from the reported complexes,[30−34] it would be appropriate here to make a comparison of the efficacy of different bridging ligands with regard to the nature and magnitude of exchange couplings in the $Fe^{III}M^{II}$ pairs. The doubly or triply bridged $Fe^{III}M^{II}$ complexes exhibit exchange coupling varying from weakly ferromagnetic ($+4.2\ cm^{-1}$) to moderately antiferromagnetic ($-25\ cm^{-1}$). The bridging angle Fe−O(R)−M has been invoked[31] to rationalize this wide variation. In contrast, the tris(oximato)-bridged complexes **2**, **3**, and **5** are antiferromagnetically coupled, irrespective of the nature of the divalent metal center,[3,23,35] and, for comparable metal centers, they exhibit stronger exchange coupling than those reported in the literature,[31−35] although the Fe···M distances are significantly longer (ca. 0.2 Å) for the present complexes, which indicates that the oximato bridge is a better spin-coupler than either phenoxo or alkoxo groups.

Conclusions

In summary, we have synthesized and structurally characterized triply oximato-bridged heterodimetallic $Fe^{III}M^{II}$ complexes by using tris(pyridinaldoximato)metalates as ligands. This study confirms the essentially σ nature of the exchange interaction and applicability of the Goodenough−Kanamori rules in general to predict the nature of exchange interactions for different heterometal compounds containing the ferric ion in high-spin state. The strength of the antiferromagnetic interaction decreases in the following order: $Fe^{III}Cu^{II} > Fe^{III}Ni^{II} > Fe^{III}Mn^{II}$, as is expected.

The $Fe^{III}Co^{II}$ species could not be isolated because of facile intramolecular electron transfer leading to complex **7** ($Fe^{II}Co^{III}$). This finding is also in agreement with the cyclic voltammetric data.

The observation of the doubly charged species $[LFe(PyA)_3M]^{2+}$ as the base peak in each ESI-MS (positive) for all the complexes studied allowed the unambiguous characterization of these heterodimetal complexes.

Experimental Section

Materials and Physical Measurements: Reagent- or analytical-grade materials were obtained from commercial suppliers and used without further purification, except those for electrochemical measurements. Elemental analyses (C, H, N) were performed by the Micro-

 © 2004 Wiley-VCH Verlag GmbH & Co. KGaA, Weinheim

analytical Laboratory, Dornis & Kolbe, Mülheim, Germany. Quantitative determination of manganese, iron, and cobalt was performed spectrophotometrically as their dipicolinic acid complexes.[36] Copper and nickel were determined gravimetrically by using *N*-benzoyl-*N*-phenylhydroxylamine and dimethylglyoxime, respectively. The perchlorate anion was determined gravimetrically as tetraphenylarsonium perchlorate. Fourier transform IR spectra of the samples in KBr disks were recorded with a Perkin−Elmer 2000 FT-IR instrument. Electronic absorption spectra in solution were measured with a Perkin−Elmer Lambda 19 spectrophotometer. Magnetic susceptibilities of powdered samples were recorded with a SQUID magnetometer in the temperature range 2−295 K with an applied field of 1 T. Experimental susceptibility data were corrected for the underlying diamagnetism using Pascal's constants and for the TIP contributions. Cyclic voltammetric and coulometric measurements were performed using EG & G equipment (potentiostat/galvanostat model 273A). Mass spectra were recorded with either a Finnigan MAT 8200 (electron ionization, EIMS) or a MAT 95 (electrospray, ESI-MS) instrument. A Bruker DRX 400 instrument was used for NMR spectroscopy. The Mössbauer spectrometer worked in the conventional constant-acceleration mode with a ^{57}Co/Rh source. Isomer shifts are given relative to α-Fe at room temperature. X-band EPR spectra were recorded with a Bruker ELEXSYS E500 spectrometer equipped with a helium flow cryostat (Oxford Instruments ESR 910). The spectra were simulated on the basis of a spin Hamiltonian description of the spin ground state manifold of the dimer molecules according to Equation (2), where S_t is the manifold and D_t and E/D_t are the axial and rhombic zero-field parameters.

$$H_e = D[S_{t,z}^2 - S_t(S_t+1)/3 + (E/D)(S_{t,x}^2 - S_{t,y}^2)] + \mu_B \mathbf{B}\cdot g\cdot \mathbf{S}_t \qquad (2)$$

The simulation program was developed from the $S = {}^5/_2$ routines of Gaffney and Silverstone and specifically makes use of the calculation of transition fields based on a Newton−Raphson iterative method as described.[38]

Preparations

$LFeCl_3$: This complex was prepared as described previously.[37]

$[LFe^{III}(PyA)_3M^{II}](ClO_4)_2$ [M^{II} = Zn (1), Ni (3), Fe (4), Mn (5)]: As complexes **1** and **3**−**6** were prepared in very similar manners, only a representative method is described. An argon-scrubbed solution of *syn*-pyridin-2-aldoxime (0.36 g, 3 mmol) in methanol (75 mL) was stirred with $M(ClO_4)_2\cdot 6H_2O$ (1 mmol) and triethylamine (0.5 mL) under argon for 0.5 h. Solid $LFeCl_3$ (0.33 g, 1 mmol) was added to the resulting solution and the stirring was continued under argon for a further 1 h before the mixture was filtered to remove any solid particles. The volume of the filtrate was reduced by passing argon over the surface of the solution until crystals began to separate. The crystals were collected by filtration and washed with diethyl ether.

Complex 1, $Fe^{III}Zn^{II}$: Red-violet crystals. Yield 0.33 g (39%). $C_{27}H_{36}Cl_2FeN_9O_{11}Zn$ (854.8): calcd. C 37.94, H 4.25, N 14.75, Fe 6.53, ClO_4 23.16; found: C 39.1, H 4.4, N 15.1, Fe 6.7, ClO_4 23.4. IR (KBr): $\tilde{\nu}$ = 1636 (CN), 1005 (NO), 1605, 1554, 1480, 1441 (pyridine) cm^{-1}. UV/Vis (CH_3CN): λ_{max} (ε) = 257 (25720), 303 (27300), 390 sh (ca. 4500) nm ($M^{-1}\cdot cm^{-1}$). ESI-MS: *m*/*z* (%) = 753, 654, 327 (100).

Complex 3, $Fe^{III}Ni^{II}$: Red-brown crystals. Yield 0.36 g (42%). $C_{27}H_{36}Cl_2FeN_9NiO_{11}$ (848.1): calcd. C 38.07, H 4.26, N 14.81, Fe 6.56, Ni 6.90, ClO_4 23.37; found C 38.0, H 4.2, N 14.7, Fe 6.7, Ni 6.8, ClO_4 23.5. IR (KBr): $\tilde{\nu}$ = 1636 (CN), 1007 (NO), 1605, 1584 1476, 1444 (pyridine) cm^{-1}. UV/Vis (CH_3CN): λ_{max} (ε) = 220 (33600), 255 (31910), 305 (29910), 513 sh (ca. 2100), 628 sh (ca. 102), 729 (40) nm ($M^{-1}\cdot cm^{-1}$). ESI-MS: *m*/*z* (%) = 747, 324 (100).

Complex 4, $Fe^{III}Fe^{II}$: Deep-red crystals. Yield 0.35 g (40%). $C_{27}H_{36}Cl_2Fe_2N_9O_{11}$ (845.2): calcd. C 38.37, H 4.29, N 14.91, Fe 13.21, ClO_4 23.43; found C 38.6, H 4.3, N 14.8, Fe 13.6, ClO_4 23.6. IR (KBr): $\tilde{\nu}$ = 1635 (CN), 1006 (NO), 1604, 1563 1467, 1435 (pyridine) cm^{-1}. UV/Vis (CH_3CN): λ_{max} (ε) = 202 (35660), 252 (23660), 294 (27550), 512 (8280) nm ($M^{-1}\cdot cm^{-1}$). ESI-MS: *m*/*z* (%) = 745, 323 (100).

Complex 5, $Fe^{III}Mn^{II}$: Deep-red crystals. Yield 0.34 g (40%). $C_{27}H_{36}Cl_2FeMnN_9O_{11}$ (844.3): calcd. C 38.41, H 4.30, N 14.93, Fe 6.61, Mn 6.51, ClO_4 23.56; found C 38.8, H 4.3, N 14.8, Fe 6.7, Mn 6.6, ClO_4 23.7. IR (KBr): $\tilde{\nu}$ = 1636 (CN), 1007 (NO), 1601, 1549 1466, 1437 (pyridine) cm^{-1}. UV/Vis (CH_3CN): λ_{max} (ε) = 257 (44670), 306 (43750), 393 (ca. 10880), 515 sh (ca. 2750) nm ($M^{-1}\cdot cm^{-1}$). ESI-MS: *m*/*z* (%) = 744, 322.5 (100).

$[LFe^{III}(PyA)_3Cu](ClO_4)_2$ (2): A sample of anhydrous copper(II) chloride (0.14 g, 1 mmol) and triethylamine (0.5 mL) was added with stirring under argon to a degassed solution of methanol (75 mL) containing *syn*-pyridin-2-aldoxime (0.36 g, 3 mmol). After 0.5 h, the stirred solution was charged with solid $LFeCl_3$ (0.33 g, 1 mmol) and the stirring was continued at ambient temperature for a further 1 h. After addition of $NaClO_4\cdot H_2O$ (0.75 g, 6 mmol), the volume of the solution was reduced by passing argon over the surface of the solution. The brown-red microcrystalline product was collected by filtration. X-ray-quality crystals were obtained from an acetonitrile solution. Yield 0.5 g (59%). $C_{27}H_{36}Cl_2CuFeN_9O_{11}$ (852.9): calcd. C 38.02, H 4.25, N 14.78, Fe 6.55, Cu 7.45, ClO_4 23.32; found C 38.1, H 4.4, N 14.6, Fe 6.6, Cu 7.6, ClO_4 23.5. IR (KBr): $\tilde{\nu}$ = 1635 (CN), 1006 (NO), 1606, 1583 1475, 1444 (pyridine) cm^{-1}. UV/Vis (CH_3CN): λ_{max} (ε) = 207 (31930), 240 (30390), 302 (26960), 525 sh (ca. 1640) nm ($M^{-1}\cdot cm^{-1}$). ESI-MS: *m*/*z* (%) = 752, 326.5 (100).

$[LCo^{III}(PyA)_3Fe^{II}](ClO_4)_2$ (6): Solid $Co(CH_3COO)_2\cdot 4H_2O$ (0.25 g, 1 mmol) was added to a degassed methanolic solution (25 mL) of 1,4,7-trimethyl-1,4,7-triazacyclononane (0.17 g, 1 mmol) under argon; the solution was stirred further for 1 h. A methanolic solution (50 mL) of (0.36 g, 3 mmol) of *syn*-pyridin-2-aldoxime and $Fe(ClO_4)_2\cdot 6H_2O$ (0.36 g, 1 mmol) was added to the cobalt-containing solution and then stirred at room temperature for 0.5 h. The precipitated black-violet microcrystalline substance was collected by filtration. X-ray-quality crystals were obtained by recrystallization from CH_3CN. Yield 0.42 g (50%). $C_{27}H_{36}Cl_2CoFeN_9O_{11}$ (848.3): calcd. C 38.23, H 4.28, N 14.86, Co 6.95, Fe 6.58, ClO_4 23.45; found C 38.2, H 4.1, N 14.5, Co 6.7, Fe 7.0, ClO_4 23.6. IR (KBr): $\tilde{\nu}$ = 1636 (CN), 1016 (NO), 1602, 1563 1467, 1434 (pyridine) cm^{-1}. UV/Vis (CH_3CN): λ_{max} (ε) = 209 (46500), 247 (42900), 270 sh (ca. 32400), 326 (23400), 527 (4100) nm ($M^{-1}\cdot cm^{-1}$). ESI-MS: *m*/*z* (%) = 748, 324.5 (100).

$[LFe^{II}(PyA)_3Co^{III}](ClO_4)_2$ (7): Methanol (25 mL) containing Et_3N (0.5 mL) was degassed at room temperature. Solid $Co(CH_3COO)_2\cdot 4H_2O$ (0.25 g, 1 mmol) and *syn*-pyridin-2-aldoxime (0.36 g, 3 mmol) were added to the methanol solution with continuous stirring over 0.5 h. $LFeCl_3$ (0.33 g, 1 mmol) was added to this clear solution and the stirring was continued for a further 1 h. Addition of $NaClO_4\cdot H_2O$ (0.5 g, 4 mmol) afforded a deep-red microcrystalline solid, which was collected by filtration and washed with diethyl ether. Yield 0.31 g (37%). $C_{27}H_{36}Cl_2CoFeN_9O_{11}$ (848.3): C 38.23, H 4.28, N 14.86, Fe 6.58, Co 6.95, ClO_4 23.45; found C 38.2,

 © 2004 Wiley-VCH Verlag GmbH & Co. KGaA, Weinheim

Table 8. Crystallographic data for $[LFe(PyA)_3Zn](ClO_4)_2 \cdot CH_3OH$ (**1**), $[LFe(PyA)_3Cu](ClO_4)_2 \cdot CH_3CN$ (**2**), $[LFe(PyA)_3Ni](ClO_4)_2 \cdot CH_3OH$ (**3**), $[LFe(PyA)_3Fe](ClO_4)_2$ (**4**), and $[LFe(PyA)_3Mn](ClO_4)_2$ (**5**)

	$Fe^{III}Zn^{II}$ **1**	$Fe^{III}Cu^{II}$ **2**	$Fe^{III}Ni^{II}$ **3**	$Fe^{III}Fe^{II}$ **4**	$Fe^{III}Mn^{II}$ **5**
Empirical formula	$C_{28}H_{40}Cl_2FeN_9O_{12}Zn$	$C_{29}H_{39}Cl_2CuFeN_{10}O_{11}$	$C_{28}H_{40}Cl_2FeN_9NiO_{12}$	$C_{27}H_{36}Cl_2Fe_2N_9O_{11}$	$C_{27}H_{36}Cl_2FeMnN_9O_{11}$
Formula mass	886.81	893.99	880.15	845.2	844.34
Temperature [K]	100(2)	100(2)	100(2)	293(2)	100(2)
λ(Mo-K_α) [Å]	0.71073	0.71073	0.71073	0.71073	0.71073
Crystal system	monoclinic	monoclinic	monoclinic	triclinic	triclinic
Space group	$P2_1/c$	$P2_1/c$	$C2/c$	$P\bar{1}$	$P\bar{1}$
Unit cell dimensions [Å, °]	a = 20.050(4)	a = 19.7893(6)	a = 20.072(4) Å	a = 12.320(3) Å	a = 12.040(2) Å
	b = 24.346(4)	b = 24.6014(6)	b = 24.397(5)	b = 12.659(3)	b = 12.694(2)
	c = 15.079(3)	c = 15.1403(3)	c = 14.984(3)	c = 12.717(3)	c = 12.837(2)
				α = 100.02(1)	α = 110.62(2)
	β = 94.79(2)	β = 94.78(1)	β = 93.01(3)	β = 113.70(1)	β = 101.88(2)
				γ = 98.60(1)	γ = 101.25(2)
Volume [Å]^3; Z	7335(2), 8	7345.3(3), 8	7328(3), 8	1734.6(8), 2	1718.5(5), 2
Density (calcd.) [Mg/m^3]	1.606	1.617	1.596	1.618	1.632
Absorp. coeff. [mm^{-1}]	1.267	1.191	1.128	1.06	1.016
F(000)	3656	3680	3640	870	868
Crystal size [mm]	0.21 × 0.28 × 0.42	0.21 × 0.12 × 0.06	0.42 × 0.32 × 0.25	0.09 × 0.15 × 0.20	0.98 × 0.32 × 0.18
Diffractometer used	Siemens SMART	CAD 4	Siemens SMART	Siemens R3m/V	Siemens SMART
θ range for data collection [°]	1.59−25.51	2.07−30.0	1.67−23.24	1.5−27.5	1.78−34.02
Reflections collected	31266	157116	14222	8400	19767
Independent reflections	12364 (R_{int} = 0.0569)	21416 (R_{int} = 0.0964)	5218 (R_{int} = 0.1432)	8025 (R_{int} = 0.045)	11669 (R_{int} = 0.0171)
Data/restraints/parameters	12364/0/957	21387/0/975	5213/0/510	8025/0/373	11669/0/460
Goodness-of-fit on F^2	1.017	1.169	0.921	0.973	1.019
Final R indices [$I > 2\sigma(I)$]	R_1 = 0.0597,	R_1 = 0.0703,	R_1 = 0.0711,	R_1 = 0.099,	R_1 = 0.0364,
	wR_2 = 0.1481	wR_2 = 0.1143	wR_2 = 0.1433	wR_2 = 0.246	wR_2 = 0.0919
R indices (all data)	R_1 = 0.0945,	R_1 = 0.0992,	R_1 = 0.1315,	R_1 = 0.197,	R_1 = 0.0452,
	wR_2 = 0.1679	wR_2 = 0.1228	wR_2 = 0.1770	wR_2 = 0.332	wR_2 = 0.0978

Table 9. Crystallographic data for $[LCo^{III}(PyA)_3Fe^{II}](ClO_4)_2$ (**6**) and $[LFe^{II}(PyA)_3Co^{III}](PF_6)_2$ (**7**)

	$Co^{III}Fe^{II}$ **6**	$Fe^{II}Co^{III}$ **7**
Empirical formula	$C_{27}H_{36}Cl_2CoFeN_9O_{11}$	$C_{27}H_{36}CoF_{12}FeN_9O_3P_2$
Formula mass	848.33	939.37
Temperature [K]	100(2)	293(2)
λ(Mo-K_α) [Å]	0.71073	0.71073
Crystal system	triclinic	orthorhombic
Space group	$P\bar{1}$	$P2_12_12_1$
Unit cell dimensions [Å, °]	a = 12.020(3)	a = 12.283(3)
	b = 12.346(3)	b = 16.373(4)
	c = 12.693(3)	c = 18.387(5)
	α = 99.80(3)	
	β = 99.08(3)	
	γ = 113.43(3)	
Volume [Å^3], Z	1649.3(7), 2	3698(2), 4
Density (calcd.) [Mg/m^3]	1.708	1.687
Absorption coeff. [mm^{-1}]	1.179	1.032
F(000)	872	1904
Crystal size [mm]	0.32 × 0.20 × 0.38	0.30 × 0.17 × 0.14
Diffratometer used	Siemens SMART	Siemens R3m/V
θ range for data collection [°]	1.68−23.25	2.72−27.56
Reflections collected	6642	4734
Independent reflections	4665 (R_{int} = 0.0347)	4734 (R_{int} = 0.00)
Data/restraints/params	4664/0/463	4734/30/497
Goodness-of-fit on F^2	0.958	0.960
Final R indices [$I > 2\sigma(I)$]	R_1 = 0.0410,	R_1 = 0.055,
	wR_2 = 0.0993	wR_2 = 0.123
R indices (all data)	R_1 = 0.0542,	R_1 = 0.127,
	wR_2 = 0.1058	wR_2 = 0.169
Absolute structure parameter	−	0.07(4)

 © 2004 Wiley-VCH Verlag GmbH & Co. KGaA, Weinheim

H 4.3, N 14.8, Fe 6.7, Co 7.0, ClO_4 23.6. IR (KBr): $\tilde{\nu}$ = 1620 (CN), 1010 (NO), 1602, 1560 1470, 1444 (pyridine) cm^{-1}. UV/Vis (CH_3CN): λ_{max} (ε) = 208 (37900), 243 (29370), 317 (16050), 516 (1710), 925 (20) nm ($M^{-1}\cdot cm^{-1}$). ESI-MS: *m*/*z* (%) = 748, 324.5 (100). X-ray-quality crystals of $[LFe(PyA)_3Co](PF_6)_2$ were obtained by addition of $NaPF_6$ as the anion source, instead of $NaClO_4$, from a methanolic solution.

CAUTION: Although we experienced no difficulties with the compounds isolated as their perchlorate salts, the unpredictable behavior of perchlorate salts necessitates extreme caution in their handling.

X-Ray Crystallographic Data Collection and Refinement of the Structures: The crystallographic data for **1**−**7** are summarized in Tables 8 and 9. Graphite-monochromated Mo-K_α radiation (λ = 0.71073 Å) was used throughout. X-ray diffraction data were collected at 293(2) K using a Siemens R3m/V diffractometer for **4** and **7**. Dark-red/brown to red crystals of **1**, **2**, **3**, **5**, and **6** were fixed with perfluoropolyether onto glass fibers and mounted on a Siemens SMART diffractometer (CAD 4 for **2**) equipped with a cryogenic nitrogen cold stream, and intensity data were collected at 100(2) K. Final cell constants were obtained from a least-squares fit of the setting angles of several strong reflections. Intensity data were corrected for Lorentz and polarization effects. An empirical absorption correction by ψ scans was applied for **4** and **7**. The data set for **2** was not corrected for absorption. The program SADABS (G. M. Sheldrick, Universität Göttingen, **1994**) was used for absorption corrections on data sets for **1**, **3**, **5**, and **6**. The Siemens ShelXTL software package (G. M. Sheldrick, Universität Göttingen) was used for solution, refinement, and artwork of the structures; the neutral atom scattering factors of the program were used. All structures were solved and refined by direct methods and difference Fourier techniques. Non-hydrogen atoms were refined anisotropically and hydrogen atoms were placed at calculated positions and refined as riding atoms with isotropic displacement parameters. For **4**, the aldoximic carbon atoms were refined isotropically. The methanol molecule and a perchlorate anion in **1** were found to be disordered and, therefore, a split-atom model was used. The two positions of the oxygen atom of the methanol molecule, O(70), were refined with two occupancies; O(70)/O(70X) = 0.8:0.2. CCDC-214728 (**1**), -214729 (**2**), -214730 (**3**), -214731 (**5**), -214732 (**6**), -212949 (**4**), and -212950 (**7**) contain the supplementary crystallographic data for this paper. These data can be obtained free of charge at www.ccdc.cam.ac.uk/conts/retrieving.html [or from the Cambridge Crystallographic Data Centre, 12 Union Road, Cambridge CB2 1EZ, UK; Fax: (internat.) + 44-1223-336-033; E-mail: deposit@ccdc.cam.ac.uk].

Acknowledgments

This work was initiated in Bochum. Our thanks are due to M. Winter (Bochum), H. Schucht, P. Höfer, A. Göbels, and B. Mienert for their skilful technical assistance. Support from the Max Planck Society and Fonds der Chemischen Industrie is gratefully acknowledged.

[1] O. Kahn, *Adv. Inorg. Chem.* **1995**, *43*, 179.
[2] K. S. Murray, *Adv. Inorg. Chem.* **1995**, *43*, 261.
[3] P. Chaudhuri, *Coord. Chem. Rev.* **2003**, *243*, 143.
[4] See, for example: R. H. Holm, E. I. Solomon (Guest Eds.), *Chem. Rev.* **1996**, *96 (7)*; A. L. Feig, S. J. Lippard, *Chem. Rev.* **1994**, *94*, 759; L. Que, A. E. True, *Progr. Inorg. Chem.* **1990**, *38*, 98; S. J. Lippard, J. M. Berg, *Principles of Bioinorganic Chemistry*, University Science Books, Mill Valley, CF, **1994**; W. Kaim, B. Schwederski, *Bioanorganische Chemie*, B. G. Teubner, Stuttgart, **1991**; *Bioinorganic Chemistry of Copper* (Eds.: K. D. Karlin, Z. Tyeklár), Chapman & Hall, New York, **1993**; *Mechanistic Bioinorganic Chemistry* (Eds.: H. Holden Thorp, V. L. Pecoraro), American Chemical Society, Washington, **1995**.
[5] *Magneto-Structural Correlations in Exchange Coupled Systems* (Eds.: R. D. Willett, D. Gatteschi, O. Kahn), Kluwer Academic Publishers, Dordrecht, **1985**.
[6] *Magnetic Molecular Materials* (Eds.: D. Gatteschi, O. Kahn, J. S. Miller, F. Palacio), Kluwer Academic Publishers, Dordrecht, **1991**.
[7] O. Kahn, *Molecular Magnetism*, VCH-Verlagsgesellschaft, Weinheim, **1993**.
[8] *Research Frontiers in Magnetochemistry* (Ed.: C. J. O'Connor), World Scientific, Singapore, **1993**.
[9] [9a] S. Ross, T. Weyhermüller, E. Bill, K. Wieghardt, P. Chaudhuri, *Inorg. Chem.* **2001**, *40*, 6656. [9b] S. Ross, Dissertation, Bochum, **1998**.
[10] D. Burdinski, F. Birkelbach, T. Weyhermüller, U. Flörke, H.-J. Haupt, M. Lengen, A. X. Trautwein, E. Bill, K. Wieghardt, P. Chaudhuri, *Inorg. Chem.* **1998**, *37*, 1009 and references cited therein.
[11] C. Krebs, M. Winter, T. Weyhermüller, E. Bill, K. Wieghardt, P. Chaudhuri, *J. Chem. Soc., Chem. Commun.* **1995**, 1913.
[12] C. N. Verani, T. Weyhermüller, E. Rentschler, E. Bill, P. Chaudhuri, *Chem. Commun.* **1998**, 2475; C. N. Verani, E. Rentschler, T. Weyhermüller, E. Bill, P. Chaudhuri, *J. Chem. Soc., Dalton Trans.* **2000**, 4263.
[13] P. Chaudhuri, E. Rentschler, F. Birkelbach, C. Krebs, E. Bill, T. Weyhermüller, U. Flörke, *Eur. J. Inorg. Chem.* **2003**, 541 and references cited therein.
[14] K. Burger, I. Ruff, F. Ruff, *J. Inorg. Nucl. Chem.* **1965**, *27*, 179.
[15] P. Krumholz, *Struct. Bonding* **1971**, *9*, 139.
[16] D. H. Busch, *Rec. Chem. Prog.* **1964**, *25*, 107.
[17] H. Budzikiewicz, *Mass Spectrometry*, Wiley-VCH, Weinheim, **1998**.
[18] M. Orama, H. Saarinen, J. Korvenranta, *Acta Chem. Scand.* **1989**, *43*, 407.
[19] [19a] P. Gütlich, R. Link, A. X. Trautwein, *Mössbauer Spectroscopy and Transition Metal Chemistry*, Springer-Verlag, Berlin, **1978**. [19b] P. Gütlich, in *Mössbauer Spectroscopy* (Ed.: U. Gonser), Springer-Verlag, Berlin, **1975**, chapter 2.
[20] P. Chaudhuri, K. Wieghardt, *Prog. Inorg. Chem.* **1987**, *35*, 329.
[21] [21a] R. Beckett, B. F. Hoskins, *J. Chem. Soc., Dalton Trans.* **1972**, *291*, 2527. [21b] M. Nasakkala, H. Saarinen, J. Korvenranta, M. Orama, *Acta Crystallogr., Sect. C* **1989**, *45*, 1511. [21c] G. A. Pearse, P. R. Raithby, J. Lewis, *Polyhedron* **1989**, *8*, 301. [21d] E. O. Schlemper, J. Stunkel, C. Patterson, *Acta Crystallogr., Sect. C* **1990**, *46*, 1226. [21e] K. W. Nordquest, D. W. Phelps, W. F. Little, D. J. Hodgson, *J. Am. Chem. Soc.* **1976**, *98*, 1104.
[22] P. Chaudhuri, M. Winter, U. Flörke, H.-J. Haupt, *Inorg. Chim. Acta* **1995**, *232*, 125.
[23] P. Chaudhuri, M. Winter, B. P. C. Della Vedova, P. Fleischhauer, W. Haase, U. Flörke, H.-J. Haupt, *Inorg. Chem.* **1991**, *30*, 4777.
[24] [24a] M. R. Churchill, A. H. Reis, Jr., *Inorg. Chem.* **1972**, *11*, 1811 [24b] M. R. Churchill, A. H. Reis, Jr., *Inorg. Chem.* **1972**, *11*, 2299. [24c] J. W. Faller, C. Blankenship, B. Whitmore, S. Sena, *Inorg. Chem.* **1985**, *24*, 4483. [24d] M. R. Churchill, A. H. Reis, Jr., *Inorg. Chem.* **1973**, *12*, 2280.
[25] [25a] R. A. D. Wentworth, *Coord. Chem. Rev.* **1972/73**, 9, 171. [25b]R. M. Kirchner, C. Meali, M. Bailey, N. Howe, L. P. Torre, L. J. Wilson, L. C. Andrews, N. J. Rose, E. C. Lingafelter, *Coord. Chem. Rev.* **1987**, *77*, 89. [25c] S. A. Kunow, K. J. Takeuchi, J. J. Grzybowski, A. J. Tircitano, V. L. Goedken, *Inorg. Chim. Acta* **1996**, *241*, 21.
[26] [26a] P. Chaudhuri, K. Wieghardt, B. Nuber, J. Weiss, *Angew. Chem. Int. Ed. Engl.* **1985**, *24*, 778. [26b] P. Chaudhuri, M. Win-

ter, H.-J. Küppers, K. Wieghardt, B. Nuber, J. Weiss, *Inorg. Chem.* **1987**, *26*, 3302.

[27] P. Chaudhuri, M. Winter, P. Fleischhauer, W. Haase, U. Flörke, H.-J. Haupt, *J. Chem. Soc., Chem. Commun.* **1993**, 566.

[28] [28a] J. B. Goodenough, *Magnetism and the Chemical Bond*, Wiley, New York, **1963**. [28b] J. B. Goodenough, *J. Phys. Chem. Solids* **1958**, *6*, 287. [28c] J. Kanamori, *J. Phys. Chem. Solids* **1959**, *10*, 87.

[29] [29a] A. P. Ginsberg, *Inorg. Chim. Acta Rev.* **1971**, *5*, 45. [29b] R. L. Martin, in *New Pathways in Inorganic Chemistry* (Eds.: Ebsworth, Maddock, Sharpe), Cambridge University Press, Cambridge, U. K., **1968**.

[30] S. K. Dutta, R. Werner, U. Flörke, S. Mohanta, K. K. Nanda, W. Haase, K. Nag, *Inorg. Chem.* **1996**, *35*, 2292.

[31] [31a] A. S. Borovik, L. Que, Jr., V. Papaefthymiou, E. Münck, L. F. Taylor, O. P. Anderson, *J. Am. Chem. Soc.* **1988**, *110*, 1986. [31b] T. R. Holman, K. A. Andersen, O. P. Anderson, M. P. Hendrich, C. Juarez-Garcia, E. Münck, L. Que, Jr., *Angew. Chem. Int. Ed. Engl.* **1990**, *29*, 921. [31c] T. R. Holman, C. Juarez-Garcia, M. P. Hendrich, L. Que, Jr., E. Münck, *J. Am. Chem. Soc.* **1990**, *112*, 7611. [31d] T. R. Holman, Z. Wang, M. P. Hendrich, L. Que, Jr., *Inorg. Chem.* **1995**, *34*, 134.

[32] R. M. Buchanan, M. S. Mashuta, J. F. Richardson, K. J. Oberhausen, R. J. Webb, M. A. Nanny, *Inorg. Chem.* **1990**, *29*, 1301.

[33] [33a] S. Albedyhl, M. T. Averbuch-Pouchot, C. Belle, B. Krebs, J. L. Pierre, E. Saint-Aman, S. Torelli, *Eur. J. Inorg. Chem.* **2001**, 1383. [33b] K. Schepers, B. Bremer, B. Krebs, G. Henkel, E. Althaus, B. Mosel, W. Müller-Warmuth, *Angew. Chem. Int. Ed. Engl.* **1990**, *29*, 531.

[34] [34a] L. Yin, P. Cheng, S.-P. Yan, X.-Q. Fu, J. Li, D.-Z. Liao, Z.-H. Jiang, *J. Chem. Soc., Dalton Trans.* **2001**, 1398. [34b] P. Karsten, A. Neves, A. J. Bartoluzzi, M. Lanznaster, V. Drago, *Inorg. Chem.* **2002**, *41*, 4624.

[35] [35a] P. Chaudhuri, M. Winter, P. Fleischhauer, W. Haase, U. Flörke, H.-J. Haupt, *J. Chem. Soc., Chem. Commun.* **1990**, 1728. [35b] M. Lengen, E. Bill, C. Butzlaff, A. X. Trautwein, M. Winter, P. Chaudhuri, *Hyperfine Interact.* **1994**, *94*, 1849.

[36] H. Hartkamp, *Z. Anal. Chem.* **1964**, *199*, 183.

[37] P. Chaudhuri, M. Winter, K. Wieghardt, S. Gehring, W. Haase, B. Nuber, J. Weiss, *Inorg. Chem.* **1988**, *27*, 1564.

[38] B. J. Gaffney, H. J. Silverstone, "Simulation of the EMR Spectra of High-Spin Iron in Proteins", in *Biological Magnetic Resonance* (Eds.: L. J. Berliner, J. Reuben), Plenum Press, New York, London, **1993**, vol. 13.

Received August 1, 2003

 © 2004 Wiley-VCH Verlag GmbH & Co. KGaA, Weinheim

Systematic Investigation of PPV Analogue Oligomers Incorporating Low-Coordinate Phosphorus Centres

Rhett C. Smith[a] and John D. Protasiewicz*[a]

Keywords: Oligomers / Phosphorus / Phosphaalkenes

Sterically-encumbered ligands tethered to conjugated segments have been developed and employed in concert with existing bulky ligands to prepare a series of *phospha*-PPV oligomers. A study of the variation of $\lambda_{\pi\text{-}\pi^*}$ values along this series indicates that low-coordinate phosphorus centres can support conjugation across extended systems, and generally confirms the expected red shift across the series from all-carbon oligomers to phosphaalkenes to diphosphenes. These findings provide experimental evidence that low-coordinate phosphorus centres are in fact capable of supporting electronic communication across extended π conjugated systems.

(© Wiley-VCH Verlag GmbH & Co. KGaA, 69451 Weinheim, Germany, 2004)

Introduction

Since the discovery that selected polymers featuring extended π conjugation may exhibit conductivity[1] and other fascinating properties and the subsequent integration of such materials into devices such as OLEDs,[2] an explosion of research has emerged in the search for new systems with specifically desired properties.[3] Efforts in this area have focused particularly on tuning the band gap (and therefore absorption and emission wavelengths and conductivity) by varying substitution patterns or exploring different conjugated linkers along the conjugated polymer chain.[4] One of the most technologically promising classes of conjugated polymers are poly(*p*-phenylenevinylene)s (PPV)s.[3] Hence, numerous efforts have been undertaken to create new polymers that incorporate the basic PPV framework with other conjugated linkers. However, comparatively little work has been carried out in this area in which heavier main group elements have been incorporated along the main chain, despite the success that has been achieved with polythiophene and polyaniline, in which accessible lone pairs may participate in π conjugation (n−pπ interactions) giving rise to unique properties compared with their all carbon analogues.[3d]

The success of PPV's and variations thereof, along with the established analogy between the chemistry of carbon and phosphorus (phosphorus is often referred to as a "carbon copy"[5]) and the predicted π conjugative ability of phosphorus[6] led to our interest in the synthesis and study of "*phospha*-PPV's" in which olefinic bonds are replaced by P=C or P=P bonds to yield main group pπ−pπ conjugated materials. Such substitution may have a significant impact on the properties of the polymers. The recent synthesis of the first poly(*p*-phenylenephosphaalkene), **P1**, did indeed provide evidence for π-conjugation involving P=C functional groups in a polymer.[7]

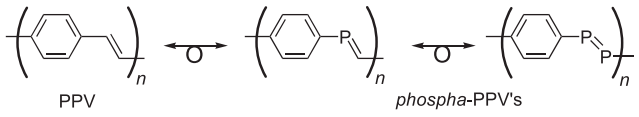

Another poly(*p*-phenylenephosphaalkene), **P2**, not only showed evidence for conjugation, but also revealed that such systems may also exhibit fluorescence,[8] a property critical for LEDs. Particularly noteworthy is the very exciting breakthrough that phosphole-containing oligomers have been successfully used in LEDs.[9] Several other investigations related to the incorporation of phosphorus into materials featuring possible π conjugation (in which phosphorus may contribute via n−pπ interactions) have also been reported.[10] Examples include polyarylphosphanes,[11] blue emitting polymers incorporating phosphole units,[12] poly(ferrocenylphosphanes),[13,14] and oligomers incorporating phosphirenes[15] or phospholes.[16−18]

Substitution of the sp^2 carbon atoms along the path of conjugation in PPV's by heavier elements such as phosphorus thus has a significant impact on the properties of polymers. For example, simple differences in polarizability and electron affinity will effect the hole and electron transport properties. In addition, the HOMO−LUMO gaps may become increasingly smaller upon substitution with low-coordinate (formally sp^2) P atoms along the path of conjugation. One approach to gaining a fuller understanding of how molecular properties affect properties displayed by polymeric systems is the so-called "oligomer approach" that has been used for studying PPV and related organic

[a] Department of Chemistry, Case Western Reserve University, Cleveland, Ohio 44106-7078, USA

 © 2004 Wiley-VCH Verlag GmbH & Co. KGaA, Weinheim DOI: 10.1002/ejic.200300551

conjugated materials.[19] In this approach studies of discrete model oligomers of increasing size can yield correlations between small molecules and polymers.

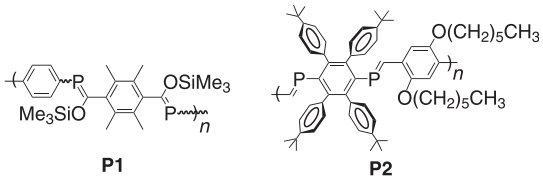

P1 **P2**

Some work has been carried out towards developing such an analogy for phosphaalkenes and diphosphenes, and towards drawing parallels between them and their all-carbon analogues. For example, discrete phosphaalkenes and diphosphenes are more easily reduced than olefin analogues. Studies of the reduction of bifunctional conjugated phosphaalkenes and diphosphenes have already revealed the additional possibilities of producing high-spin materials[20] and even molecular switches.[21] Further extensions of these studies require oligomers having longer conjugation paths and an increased phosphorus content. The longest π conjugated PPV-like molecules featuring phosphaalkene or diphosphene units reported prior to this particular investigation were analogues of distyrylbenzene[22,23] and stilbene.[24,25]

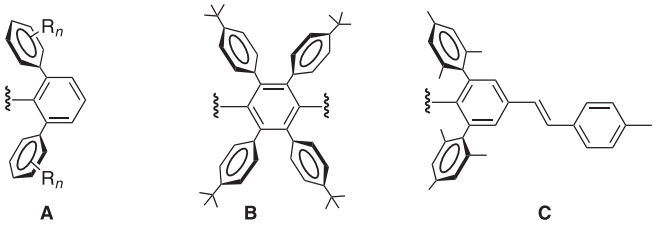

A **B** **C**

The absence of more (pπ−pπ conjugated) extended systems with (P=P) and (P=C) linkages can possibly be attributed to difficulties associated with the synthesis of suitably bulky ligands required to prevent the redistribution reactions that phosphaalkenes and diphosphenes are susceptible to in the absence of steric protection.[26] The extent of steric bulk required can be illustrated by the fact that it was not until the 2,4,6-tri-*tert*-butylphenyl (Mes*) ligand was employed that the first isolable diphosphene (Mes*P=PMes*) was reported.[25] More recently, *m*-terphenyl ligands **A** have also been extensively employed in the steric shielding of multiple bonds between heavier main group elements.[27]

In this report, routes to *m*-terphenyl ligands with conjugated groups tethered to the position *para* to the steric cleft (**C**) are detailed. These ligands, along with the existing ligands **A** and **B**, have enabled the preparation of a series of *phospha*-PPV oligomers as models for polymeric systems. The synthesis of this series of oligomers has allowed us to begin a systematic study of the effect of conjugation length and phosphorus for carbon substitution in PPV oligomers, the results of which are reported herein.

Results and Discussion

The protection of main group multiple bonds with *m*-terphenyl ligands featuring substitution *para* to the steric cleft is an underdeveloped area. Only a few 4-substituted 2,6-diarylphenyl ligands have been developed for use in low-coordinate phosphorus chemistry. Two relevant molecules bearing novel ligands have been pioneered by the Yoshifuji group.[28] While compound **D** could not be fully purified, diphosphene **E**, having a greater degree of steric protection, was isolated in 11 % yield.

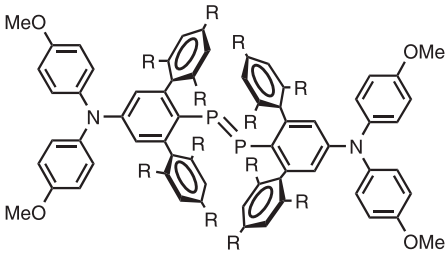

R = Me, **D**
λ = 446, 504 nm

R = *i*Pr, **E**
λ = 460, 530 nm

Both of these materials display impressive red shifts in their absorption spectra with data for **E** showing λ_{max} = 460 and 530 nm for the π−π* and n−π* bands, respectively. The approach to the amino functionalized terphenyl ligands was based upon introduction of the diarylamino functionality into preformed 1,4-diiodo-2,6-diarylbenzenes by a copper coupling step.

Our approach to functionalised terphenyls introduces functionality earlier in the synthesis. Specifically, 1,3-dichlorobenzene, the starting material for the simplest route to *m*-terphenyls (Scheme 1, top),[29] was replaced with substituted 1,3-dichlorobenzenes (**v**, **xi**, Scheme 1).

These materials should enable common access to terphenyl ligands bearing different aromatic groups on the periphery of the ligand. Synthesis of precursor **v** has been previously reported and we have been able to effect its synthesis in an overall yield of 71 % in 4 steps from the commercially available 1,3-dichlorobenzoyl chloride.[30,31] The more extended precursor **xi** could be prepared from the known intermediate phosphonium salt in an overall yield of 22 % in 6 steps starting with *p*-*tert*-butyltoluene.[32,33] The syntheses of **v** and **xi** are summarized in Scheme 2.

The substituted 1,3-dichloroarenes were thus employed for the synthesis of Dmp′I (Scheme 1, middle) and Dmp′′I (Scheme 1, bottom) using essentially the same conditions employed in the synthesis of the DmpI ligand (Scheme 1, top), although yields became increasingly lower as the length of the conjugated tether was increased. The decrease in yield with increased conjugation length may be due to decreased reactivity of the intermediate arynes. Alternatively, aryne formation may be inhibited due to an increase in stability of the 2-chlorolithio (or magnesio) benzene and subsequent difficulty of metal halide elimination. Longer reaction times for Dmp′I and Dmp′′I (10 and 16 hours, respectively) relative to DmpI (4 hours, ca. 60 % yield) partially compensate for less reactive substrates. Further increases in reaction times, however, did not provide increased

 © 2004 Wiley-VCH Verlag GmbH & Co. KGaA, Weinheim

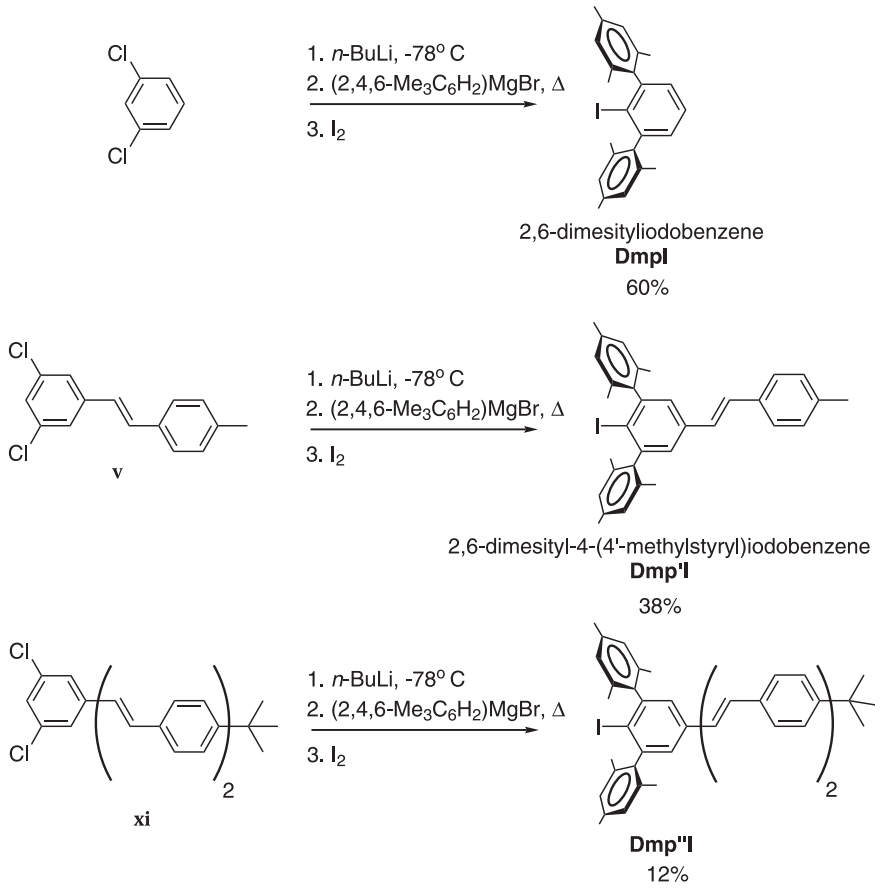

Scheme 1

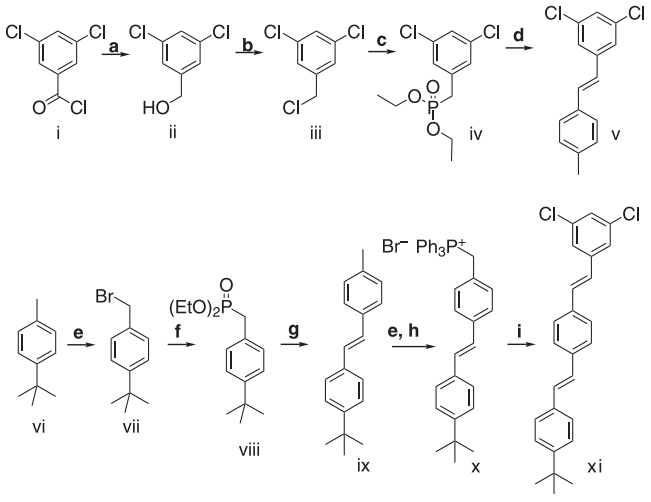

Scheme 2. Reagents and conditions: a) 1. $LiAlH_4$, 0 °C, 2. H^+; b) $SOCl_2$; c) $P(OEt)_3$, 160 °C; d) *p*-tolualdehyde, KO*t*Bu; e) NBS, BPO, reflux, 3 h; f) $P(OEt)_3$, 160 °C; g) *p*-tolualdehyde, KO*t*Bu; h) PPh_3, toluene, reflux; i) 3,5-dichlorobenzene, KO*t*Bu

yields for Dmp′ and Dmp′′I beyond 38 % and 12 %, respectively. Due to the significant decrease in yield and time consuming preparation of more complex starting materials required to access Dmp′′I compared with Dmp′I (Schemes 1 and 2), only the latter material has been pursued for utility in the current study.

The olefinic units in precursor materials (Scheme 2) were either prepared in the *E* form directly (via the Horner−Wittig reaction) or isomerized to the all-(*E*) conformation subsequent to synthesis. The retention of the all-(*E*) form in the course of the *m*-terphenyl synthesis and all subsequent steps was confirmed by the characteristic chemical shifts and coupling constants in ^{1}H NMR spectra. These diagnostic features were not resolved in the ^{1}H NMR spectrum of compound **9** (vide infra), however. Therefore the structural assignment of **9** was deduced using the known orientation of the starting material and the fact that a single species was observed in both ^{1}H and ^{31}P NMR spectra. The *E* forms were highly desired for a useful comparison with organic PPV oligomers and derivatives in which the *E* forms are technologically far more relevant than corresponding *Z* isomeric materials.[3]

Some differences in the general properties of Dmp′ derivatives compared with those of known Dmp analogues are of note. For example, the conjugated segment tethered to the Dmp′ ligand affords much greater solubility compared with analogous compounds featuring the simple Dmp ligand. Interesting colour differences can also be observed not only in the *phospha*-PPV oligomers that are the focus of the current study (vide infra), but also in the precursors. For example, while DmpLi is a white material,[34] Dmp′Li is a red-brown colour, probably indicating that the

 © 2004 Wiley-VCH Verlag GmbH & Co. KGaA, Weinheim

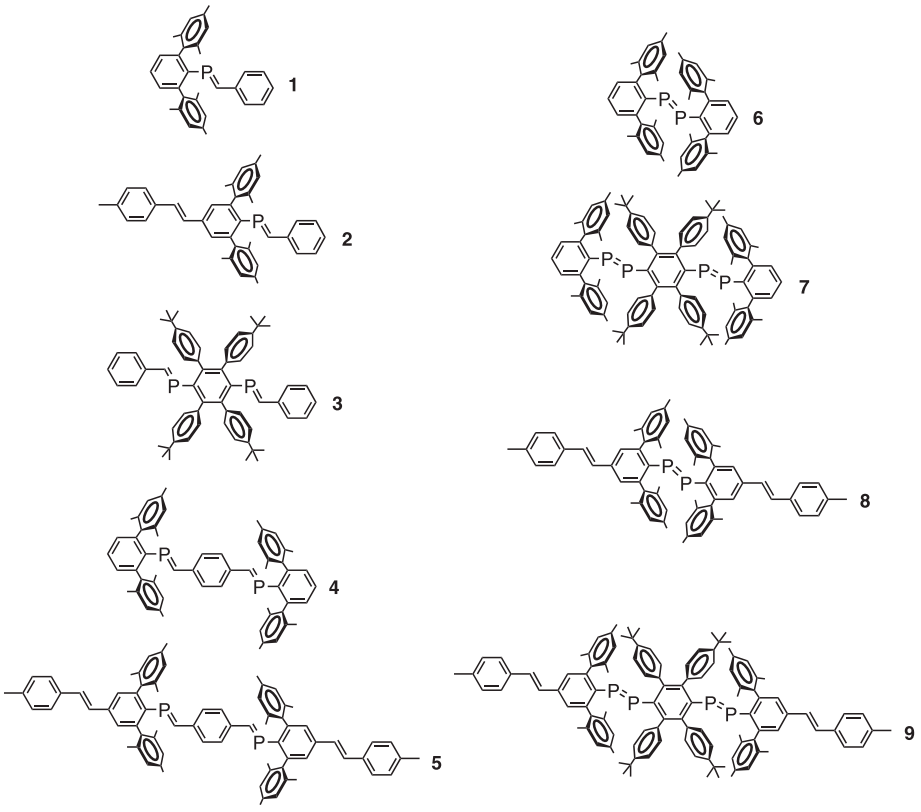

Scheme 3

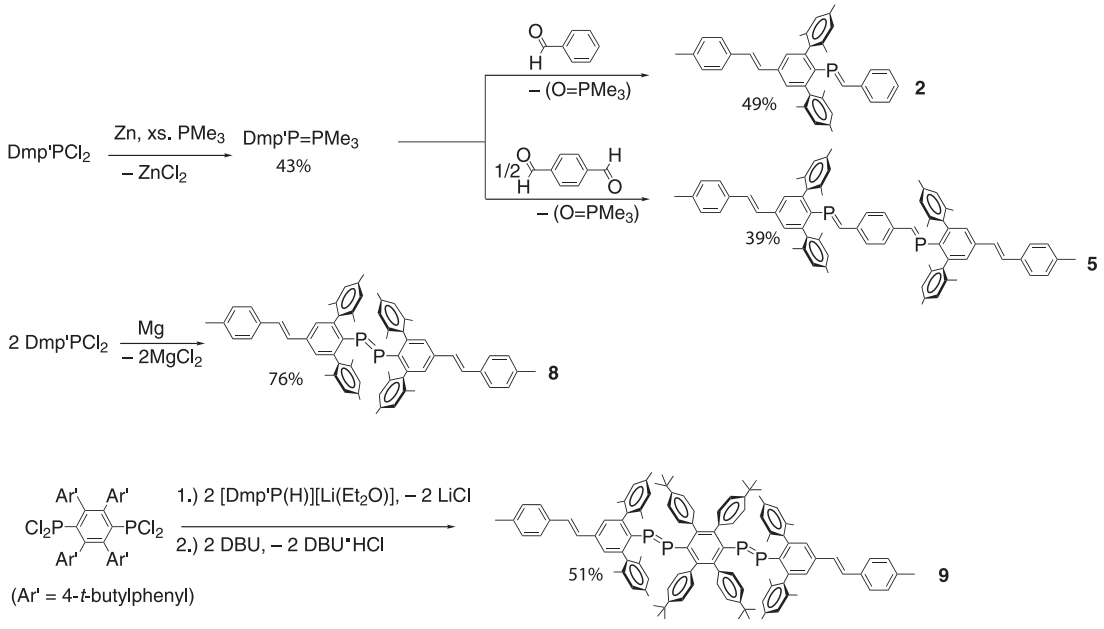

Scheme 4

extended conjugated system allows for delocalization of the anionic charge or possibly an ionic or charge separated structure. $DmpPCl_2$ (white) and $Dmp'PCl_2$ (pale yellow) (prepared from ArLi by known methods[45]), however, differ only slightly in colour. Interestingly, a notable colour change is noted for the air- and moisture-sensitive phospha-Wittig reagents $ArP{=}PMe_3$. Whereas $DmpP{=}PMe_3$ is yellow (λ = 348 nm, ε = 6021 $M^{-1}cm^{-1}$; λ = 390 nm, ε = 2998 $M^{-1}cm^{-1}$), $Dmp'P{=}PMe_3$ is deep red (λ = 332 nm, ε = 34,800 $M^{-1}cm^{-1}$; λ = 432 nm, ε = 10,600 $M^{-1}cm^{-1}$).

The Dmp′ ligand was thus used to produce a series of (P=C)- (Scheme 3, left) and (P=P)- (Scheme 3, right) containing *phospha*-PPV oligomers via the routes summarised in Scheme 4. These materials exhibit diagnostic bands in

 © 2004 Wiley-VCH Verlag GmbH & Co. KGaA, Weinheim

Table 1. Absorption data ($CHCl_3$) for **1**−**9** and comparison to organic models

C=C model	$\lambda_{\pi\text{-}\pi^*}$ (nm) (log ε)	P=C	$\lambda_{\pi\text{-}\pi^*}$ (nm) (log ε)	P=P	$\lambda_{\pi\text{-}\pi^*}$ (nm) (log ε)	$\lambda_{n\text{-}\pi^*}$ (nm) (log ε)
M1	317 (4.53)	**1**	334 (4.59)	**6**	372 (3.63)	456 (2.56)
M2 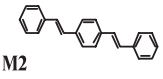	354 (4.77)[a]	**2**	341 (4.54)	**7**	398 (3.88)	476 (2.94)
		3	349 (4.60)			
		4	411 (4.68)			
M3 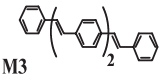	384 (4.92)[b]			**8**	407 (4.68)	470 (3.72)
M4 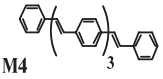	385 (5.10)[b,c]	**5**	417 (4.30)	**9**	422 (4.64)	481 (3.74)

[a] R. Erckel, H. Z. Fruehbeis, *Z. Naturforsch., Teil B* **1982**, *37*, 1472−1480. [b] G. Drefahl, G. Plotner, *Chem. Ber.* **1961**, *93*, 907−914. [c] Dioxane as solvent.

their visible absorption spectra. Phosphaalkenes commonly display a single characteristic absorption in the visible region normally assigned to a π−π* transition.[5,6] Diphosphenes exhibit similar bands due to π−π* transitions but these are accompanied by a second absorption band of significantly lower intensity at higher wavelengths that have been assigned to n−π* transitions.[24,25] The n−π* transition should be forbidden and therefore less intense. Following this convention, assignments of bands for **1**−**9** were made as summarized in Table 1. In accord with previous reports, the higher wavelength n−π* transitions for diphosphenes **6**−**9** have absorptivities approximately one order of magnitude lower than those of the corresponding π−π* transitions. This specific ordering has been the subject of some discussion, however.[24,35] The most recent experimental (electron density deformation) and computational results (DFT) give most credence to the above ordering, that is, the HOMO of a diphosphenes is more than likely the phosphorus lone pair orbital and the HOMO-1 is the π bond.[36]

The set of diphosphene oligomers **6**−**9** enables one to test this ordering in a different fashion. Figure 1 portrays two qualitative models for how the energies of pertinent frontier molecular orbitals should vary with increasing conjugation length. For the first model (Figure 1, left), the HOMO is assumed to be the π orbital and in the second model (Figure 1, right), the HOMO is assumed to be the phosphorus lone pair (n_+ combination). For both models the difference between the π and π* orbitals is diminished with increasing conjugation length and the lone pairs are assumed to be relatively unaffected. The first model predicts that as the conjugation length increases, the HOMO−HOMO−1 gap (described by Δ in Figure 1) should increase. The second model predicts the exact opposite. The very crude model given in the right of Figure 1 fits the observed trends for compounds **6**−**9** nicely, as well as agreeing with the most recent computational and experimental data for simple diphosphenes.[36]

A simple comparison of the absorption maxima ($\lambda_{\pi\text{-}\pi^*}$) for the all-carbon oligomers **M1**−**M4**, phosphaalkenes **1**−**5**, and diphosphenes **6**−**9** with central π-conjugated cores of equal length (Table 1) generally demonstrates the intended red shifts for the electronic transitions as either the phosphorus content or maximum conjugation length in-

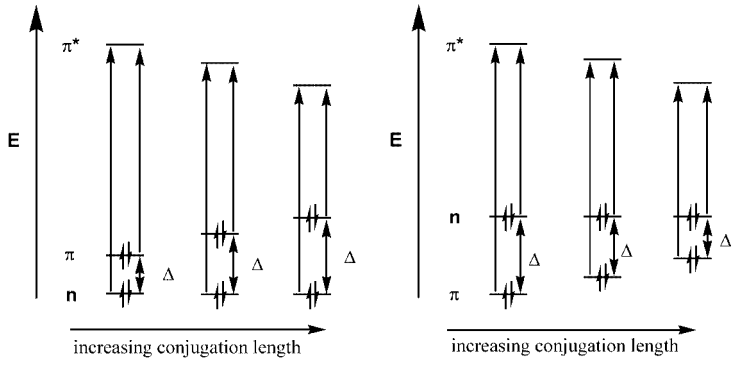

Figure 1. Simple MO diagrams for conjugated materials assuming the HOMO involves P=E π bonds (left) or n orbitals (right)

 © 2004 Wiley-VCH Verlag GmbH & Co. KGaA, Weinheim

creases. A more detailed evaluation, however, reveals some discrepancies in these general trends. For example, although the $\lambda_{\pi\text{-}\pi^*}$ values for compounds **2** and **3** are consistent with the anticipated red shift with increasing P content (one P=C in **2** versus two P=C units in **3**), the values might also be expected to be red shifted with respect to the all-carbon analogue, distyrylbenzene (**M2**). The $\lambda_{\pi\text{-}\pi^*}$ values for compounds **2** and **3** are actually *blue* shifted by 13 nm and 5 nm, respectively, relative to distyrylbenzene. Compound **4**, however, which is also of the same geometric conjugation length, is quite significantly red shifted by 57 nm. These large differences exhibited by molecules of equal conjugation length demonstrate the striking effects that steric influences can produce. Specifically, such deviations can be attributed to deflections of some portions of the conjugated system out of ideal coplanarity with one another in response to steric clashes. In this manner, the *effective* conjugation length is lowered relative to that expected for an entirely coplanar conjugated core. A simple example of this effect is the observed 33 nm blue shift in the $\lambda_{\pi\text{-}\pi^*}$ value of (*E*)-2,6-dimethylstilbene with respect to (*E*)-stilbene.[37]

Steric disruptions to coplanarity have in fact been intentionally incorporated into organic conjugated polymers and have been observed to provide a significant enhancement of electroluminescent efficiency.[38] In other cases, steric distortions induced by binding events along conjugated polymer backbones have led to significant changes in absorption maxima, a property routinely taken advantage of in the design of molecular sensors.[39] Such steric effects were also discussed in the analysis of the properties of a poly(*p*-phenylenephosphaalkene),[7] and we have previously observed this effect (at least in the solid state) by X-ray crystallographic analysis of diphosphene **7** and phosphaalkene **3**.[22]

The effect of such sterically-induced noncoplanarity may not have as great an impact on the $\lambda_{\pi\text{-}\pi^*}$ of **4** since, in that case, the steric bulk is located on the outer rings rather than on the central ring such that the latter may easily maintain conjugation with at least the two flanking P=C units without steric interference. A direct comparison of **4** can also be made with 1,4-[Mes*P=C(H)]$_2$C$_6$H$_4$ (Mes* = 2,4,6-tri-*tert*-butylphenyl),[40] in which the only difference is the replacement of Dmp with Mes* ligands. The Mes*-containing system has a $\lambda_{\pi\text{-}\pi^*}$ of only 326 nm, closer to that of stilbene than the all-carbon analogue, distyrylbenzene. Distortions of the phosphorus centre from the plane of the attached phenyl ring in the Mes* components are common due to the extreme steric pressure in such systems[41] and such distortions may complicate comparisons of the type made here. Regardless of the explanation, similar large differences can be observed when comparing $\lambda_{\pi\text{-}\pi^*}$ values for other materials featuring the two sets of ligands such as **6** (372 nm) with Mes*P=PMes* (340 nm) or **1** (334 nm) with Mes*P=C(H)Ph (259 nm).[38]

Another example of steric effects on effective conjugation is evident from the observed $\lambda_{\pi\text{-}\pi^*}$ value in **7**. Whereas a red shift of **7** with respect to **2**, **3**, or **4** might be expected, the observed value is actually within the range spanned by these three materials (390 nm for **7**, compared with 341 nm, 349 nm, and 411 nm for **2**, **3**, and **4**, respectively). This observation may not be altogether surprising in light of the much greater steric bulk about the P=P units in **7** compared with that about the P=C units in **2**–**4**.

Such minor and explainable deviations do not, however, detract from the overall trend observed when comparing systems with comparable steric positioning. For example, a comparison of **1** with **2**, **4** with **5**, **6** with **8** or **7** with **9**, where the pairs of compounds differ only by the addition of simple styryl units, all exhibit red shifts with increased conjugation length (15, 6, 35, and 32 nm, respectively). These data indicate that the incorporation of low-coordinate phosphorus centres into conjugated materials is a viable strategy for accessing materials featuring smaller band gaps than those observed in all-carbon analogues. Indeed, the $\lambda_{\pi\text{-}\pi^*}$ of 426 nm observed for simple (*E*)-PPV[42] is practically equalled by the comparatively small (P=P)-containing analogue **9** ($\lambda_{\pi\text{-}\pi^*}$ = 422 nm) despite steric influences.

In addition to changes in $\lambda_{\pi\text{-}\pi^*}$ with increasing length or P content, observed differences in absorptivity (given as logε, Table 1) are also noteworthy. For instance, while ε for **1** is similar to that of stilbene, the diphosphene analogue **6** has a value approximately eight times lower, and whereas ε increases uniformly with oligomer length for the organic models, the same trend does not hold for *phospha*-PPV analogues. These observations may again be due to steric factors. The sterically-induced perturbations from coplanarity which lead to a truncated effective conjugation length, as previously discussed, are synonymous with decreasing the cross section of the chromophore responsible for the $\pi-\pi^*$ transition, and the molar absorptivity of the band associated with this transition will therefore diminish (in the event that all else is held fairly constant). This proposition is supported by previously reported data on 2,6-disubstituted stilbenes.[37] For example, simple 2,6-dimethyl substitution leads to approximately half as much absorptivity as unsubstituted stilbene, along with the aforementioned blue shift in the absorption maximum. Even a single bulky subsistent, as in (*E*)-2-*tert*-butylstilbene ($\lambda_{\pi\text{-}\pi^*}$ = 285 nm, ε = 22,650 $M^{-1}cm^{-1}$), has a significant impact.[43] Clearly such an effect would be more pronounced in diphosphenes **6**–**9** than in phosphaalkenes **1**–**5** due to the greater steric crowding in the former. Based on such a steric argument, it would also be expected that for molecules of the same approximate *geometric* size there should be a correlation between $\lambda_{\pi\text{-}\pi^*}$ and ε. This premise is qualitatively demonstrated by the series of phosphaalkene distyrylbenzene analogues **2**–**4** in which $\lambda_{\pi\text{-}\pi^*}$ and ε both increase across from **2**–**4**. Certainly many more complex factors, such as polarity/polarizability and solvation effects of both ground and excited states (to mention a few), are involved in determining the absorptivity of a given system as well. Although the perhaps oversimplified steric arguments presented here are merely qualitative assessments based on rational conjecture, they seem in line with data on substituted stilbenes.

In summary, we have developed novel sterically-encumbered ligands tethered to conjugated segments and have employed these ligands in concert with existing bulky ligands

 © 2004 Wiley-VCH Verlag GmbH & Co. KGaA, Weinheim

to prepare a series of *phospha*-PPV oligomers. A study of the variation of $\lambda_{\pi\text{-}\pi^*}$ values along this series indicates that low-coordinate phosphorus centres can support conjugation across extended systems, and generally confirms the expected red shift across the series from carbon oligomers **M1**−**M4** (Table 1) to phosphaalkenes **1**−**5** to diphosphenes **6**−**9**. Importantly, these findings provide experimental evidence that such low-coordinate phosphorus centres are in fact capable of supporting electronic communication across extended π conjugated systems, a criterion required of any moiety viable in the type of materials of interest in the current investigation. Some noteworthy differences between the optical properties of these *phospha*-PPV oligomers and those of related organic systems may be explainable in terms of their inherent steric bulk.

Experimental Section

All manipulations were carried out in a dry box under an atmosphere of N_2. Acetonitrile was distilled from CaH_2 under nitrogen and all other solvents were distilled from sodium benzophenone ketyl prior to use. Compounds **1** and **4**,[44] **3** and **7**,[22] and **6**[45] were prepared as previously reported. Absorption spectra were carried out in degassed HPLC grade $CHCl_3$ on a Lambda 25 spectrophotometer. NMR spectra were recorded on a Varian Gemini instrument operating at 300 MHz for proton and 121.5 MHz for phosphorus. Proton and phosphorus spectra are referenced to residual solvent signals and 85 % phosphoric acid, respectively.

(*E*)-3,5-Dichloro-4′-methylstilbene (v): To a suspension of potassium *tert*-butoxide (18.7 g, 165 mmol) and 18-crown-6 (ca. 0.4 g) in THF (150 mL) was added dropwise over 30 minutes a solution of diethyl(3,5-dichlorobenzyl)phosphonate (44.6 g, 150 mmol) and 4-tolualdehyde (18.0 g, 150 mmol) in THF (300 mL). The mixture was then stirred for 24 hours at room temperature, after which time the reaction was quenched by pouring into 10 % methanolic HCl (500 mL). The mixture was filtered and diethyl ether (300 mL) and water (300 mL) were added to the filtrate. The organic layer that separated was washed with water (2 × 300 mL aliquots), neutralized (determined using pH paper) by addition of 5 % sodium hydrogencarbonate solution then rinsed with water (300 mL). Removal of volatiles from the organic solution yielded a sticky yellow solid. Triturating this solid in hexanes followed by filtration and drying of the solid in vacuo yielded the product as a pale yellow powder (30.2 g, 76.4 %). ^{1}H NMR ($CDCl_3$, ppm): δ = 2.36 (s, 3 H), 6.88 (d, *J* = 16 Hz, 1 H), 7.07 (d, *J* = 16 Hz, 1 H), 7.17 (d, *J* = 8 Hz, 2 H), 7.20 (t, *J* = 2 Hz, 1 H), 7.34 (d, *J* = 2 Hz, 2 H), 7.38 (d, *J* = 8 Hz, 2 H); m.p. 78−80 °C (ref.[30] 80−82 °C).

(*E*)-4-Iodo-3,5-dimesityl-4′-methylstilbene (Dmp′I): A solution of (*E*)-3,5-dichloro-4′-methylstilbene (**v**) (10.0 g, 38.0 mmol) in THF (125 mL) was cooled to −78 °C whereupon *n*-butyllithium (16.0 mL, 2.5 M in hexanes, 39.9 mmol) was added dropwise via cannula. After 1 hour of stirring at −78 °C, a solution of mesitylmagnesium bromide [prepared by the reaction of 2-bromomesitylene (26.5 g, 133 mmol) and Mg turnings (4.26 g, 190 mmol) in THF (150 mL)] was added dropwise via cannula at −78 °C. After warming to room temperature over a 3 hour period, the solution was heated to reflux for an additional 10 hours. After cooling to room temperature, the flask was placed in an ice bath and iodine (19.3 g, 76.0 mmol) was added in 5 g portions. After the exothermic reaction was complete and the characteristic iodine colour persisted in solution for 15 minutes, 5 % Na_2SO_3 (250 mL) was added to quench excess iodine and the solution became yellow. The organic layer was extracted with diethyl ether (250 mL), rinsed with water (2 × 250 mL aliquots) and volatiles removed to yield a sticky solid. The solid was dissolved in boiling hexanes and precipitated at −7 °C to yield the product as an off-white powder (8.15 g, 38.5 %). ^{1}H NMR ($CDCl_3$, ppm): δ = 2.12 (s, 3 H), 2.14 (s, 12 H), 2.23 (s, 6 H), 6.85 (d, *J* = 16 Hz, 1 H), 6.92 (s, 4 H), 6.97 (d, *J* = 16 Hz, 1 H), 6.98 (d, *J* = 8 Hz, 2 H), 7.13 (s, 2 H), 7.27 (d, *J* = 8 Hz, 2 H); m.p. 165−168 °C. HRMS(FAB, *m*/*z*): calcd. for $C_{33}H_{33}I$, 556.1627; found, 556.1628.

Dmp′PCl$_2$: A solution of Dmp′I (4.0 g, 7.2 mmol) in THF (125 mL) was cooled to −78 °C whereupon *n*-butyllithium (3.0 mL, 2.5 M in hexanes, 7.5 mmol) was added dropwise via cannula. After 1 hour of stirring at −78 °C, PCl_3 (1.9 mL, 22 mmol) was added rapidly with a syringe. After the resultant solution was allowed to warm to room temperature over three hours, volatiles were removed in vacuo. The resultant orange solid was stirred with acetonitrile (150 mL) for 15 minutes and filtered. Removal of volatiles in vacuo gave a yellow solid which was dissolved in diethyl ether and filtered to remove salts. Removal of the diethyl ether in vacuo gave the product as a pale yellow powder (0.93 g, 24 %). ^{1}H NMR ($CDCl_3$, ppm): δ = 2.01 (s, 12 H), 2.09 (s, 6 H), 2.36 (s, 3 H), 6.96 (s, 4 H), 7.03 (d, *J* = 16 Hz, 1 H), 7.13 (d, *J* = 16 Hz, 1 H), 7.17 (d, *J* = 8 Hz, 2 H), 7.25 (d, 2 H, $^4J_{H,P}$ = 3 Hz), 7.39 (d, *J* = 8 Hz, 2 H). ^{31}P NMR ($CDCl_3$, ppm): δ = 162.0.

Dmp′P=PDmp′ (8): Magnesium turnings (15 mg, 0.62 mmol) were added to a solution of Dmp′PCl_2 (0.30 g, 0.56 mmol) and the resultant mixture sonicated for approximately 3 hours during which time the solution became an orange-red colour. The solution was decanted from a small amount of remaining magnesium and volatiles were removed in vacuo. The crude solid was extracted with hexanes and filtered. Removal of the solvent in vacuo gave the product as a red-orange powder (0.26 g, 76 %). ^{1}H NMR ($CDCl_3$, ppm): δ = 1.73 (s, 24 H), 2.33 (s, 18 H), 6.77 (s, 8 H), 6.95 (d, *J* = 16 Hz, 2 H), 7.07 (d, *J* = 16 Hz, 2 H), 7.09 (s, 4 H), 7.13 (d, *J* = 8 Hz, 4 H), 7.33 (d, *J* = 8 Hz, 4 H). ^{31}P NMR ($CDCl_3$, ppm): δ = 490.8. HRMS (FAB, *m*/*z*): calcd. for $C_{66}H_{67}P_2$, 921.4718; found, 921.4672.

Dmp′P=PMe$_3$: To a stirred suspension of zinc dust (0.030 g, 0.46 mmol) and Dmp′PCl_2 (0.20 g, 0.38 mmol) was added trimethylphosphane (0.11 g, 1.4 mmol). The mixture was stirred for 3 hours during which time a red colour developed. The mixture was filtered, volatiles removed in vacuo and the crude solid dissolved in hexanes. The solution was then filtered and solvent removed in vacuo. The product was precipitated from a saturated *n*-pentane solution at −35 °C as a red solid (0.087 g, 43 %). ^{1}H NMR ($CDCl_3$, ppm): δ = 1.07 (d, 9 H, *J* = 12 Hz), 2.08 (s, 12 H), 2.34 (s, 9 H), 6.95 (s, 4 H), 6.94 (d, *J* = 16 Hz, 1 H), 7.01 (d, *J* = 16 Hz, 1 H), 7.05 (s, 2 H), 7.12 (d, *J* = 8 Hz, 2 H), 7.32 (d, *J* = 8 Hz, 2 H). ^{31}P NMR ($CDCl_3$, ppm): δ = −0.7 (d, *J* = 560 Hz), −110.4 (d, *J* = 560 Hz).

Dmp′P=C(H)Ph (2): Trimethylphosphane (0.11 g, 1.4 mmol) was added to a mixture of zinc dust (0.03 g, 0.46 mmol), Dmp′PCl_2 (0.20 g, 0.38 mmol) and benzaldehyde (0.042 g, 40 mmol). A yellow colour developed almost immediately and after stirring for 6 hours the mixture was filtered and the solvent removed in vacuo. The crude solid was dissolved in hexanes, filtered and the solvent removed from the filtrate in vacuo. The product was precipitated from a saturated *n*-pentane solution at −35 °C as a yellow solid (0.10 g, 49 %). ^{1}H NMR ($CDCl_3$, ppm): δ = 2.03 (s, 12 H), 2.21

 © 2004 Wiley-VCH Verlag GmbH & Co. KGaA, Weinheim

(s, 6 H), 2.28 (s, 3 H), 6.81 (s, 4 H), 6.97 (d, J = 16 Hz, 1 H), 6.81 (d, J = 16 Hz, 1 H), 7.04 (m, 5 H), 7.08 (d, J = 8 Hz, 2 H), 7.18 (s, 2 H), 7.31 (d, J = 8 Hz, 2 H), 8.59 (d, 1 H, $J_{H,P}$ = 25 Hz). ^{31}P NMR ($CDCl_3$, ppm): δ = 239.2 ppm. HRMS (FAB, MH^+, m/z): calcd. for $C_{40}H_{40}P$, 551.2868; found, 551.2864.

1,4-[Dmp′P=C(H)]$_2$C$_6$H$_4$ (5): Trimethylphosphane (0.17 g, 2.3 mmol) was added to a mixture of zinc dust (0.074 g, 1.1 mmol), Dmp′PCl_2 (0.30 g, 0.56 mmol), and terephthalaldehyde (0.038 g, 0.28 mmol). A yellow-orange colour developed almost immediately and after stirring for 10 hours the mixture was filtered and the solvent removed in vacuo. The crude solid was dissolved in boiling hexanes, filtered, and the solvent removed in vacuo. The resultant solid was then rinsed with a small amount of warm acetonitrile and the final product was precipitated from diethyl ether/hexanes solution at −35 °C as a yellow-orange solid (0.11 g, 39 %). ^{1}H NMR ($CDCl_3$, ppm): δ = 1.98 (s, 24 H), 2.18 (s, 12 H), 2.26 (s, 6 H), 6.77 (s, 8 H), 6.94 (d, J = 16 Hz, 2 H), 7.02−7.08 (m, 10 H), 7.15 (s, 4 H), 7.29 (d, J = 8 Hz, 4 H), 8.40 (d, 2 H, $J_{H,P}$ = 19 Hz). ^{31}P NMR ($CDCl_3$, ppm): δ = 242.3. MS (FAB, MH^+, m/z): calcd. for $C_{74}H_{73}P_2$, 1024; found, 1024.

Dmp′PH$_2$: To a stirred suspension of $LiAlH_4$ (0.18 g, 4.7 mmol) in THF (25 mL) was added solid Dmp′PCl_2 (1.2 g, 2.3 mmol) in small portions over 5 minutes. After stirring for 6 hours the mixture was filtered and volatiles removed in vacuo to give an off-white solid. This material was then dissolved in diethyl ether and filtered through alumina twice. Removal of volatiles in vacuo gave the product as an off-white powder (0.89 g, 85 %). ^{1}H NMR (C_6D_6, ppm): δ = 2.12 (s, 3 H), 2.14 (s, 12 H), 2.23 (s, 6 H), 3.31 (d, 2 H, J_{PH} = 212 Hz), 6.92 (s, 4 H), 6.98 (d, J = 7 Hz, 2 H), 7.02 (d, J = 16 Hz, 1 H), 7.16 (d, J = 16 Hz, 1 H), 7.18 (d, 2 H, $^4J_{H,P}$ = 2 Hz), 7.28 (d, J = 7 Hz, 2 H). ^{31}P NMR (C_6D_6, ppm): δ = −146.3 (t, J = 212 Hz).

1,4-[Dmp′P=P]$_2$C$_6$Ar$_4$ (Ar = 4-*tert*-butylphenyl) (9): A solution of [Li(Et_2O)][P(H)Dmp′][45] (0.19 g, 0.35 mmol) in diethyl ether (20 mL) was added at room temperature to a rapidly stirred suspension of Cl_2P-(p-C_6Ar_4)-PCl_2[22] (0.14 g, 0.17 mmol) in diethyl ether (20 mL) over a 10 min period. During this time a fine white precipitate formed. The solvent was reduced in volume to 20 mL and a solution of DBU (0.053 g, 0.35 mmol) in diethyl ether (5 mL) was added. Upon addition, the solution became orange and eventually nearly red over a 1 h period after which time the reaction mixture was filtered and the solvent removed in vacuo. The solid material was precipitated from n-pentane at −35 °C to give 0.18 g of red powder (51 %). ^{1}H NMR (C_6D_6, ppm): δ = 1.13 (s, 36 H), 1.93 (s, 24 H), 2.09 (s, 6 H), 2.33 (s, 12 H), 6.65 (d, J = 8 Hz, 8 H), 6.86 (d, J = 8 Hz, 8 H), 6.91−6.95 (m, 16 H), 7.11 (s, 4 H), 7.20 (d, J = 8 Hz, 4 H). ^{31}P NMR ($CDCl_3$, ppm): δ = 479.7 (d, J = 570 Hz), 524.8 (d, J = 570 Hz).

(*E*,*E*)-3,5-Dichloro-4′-(4-*tert*-butylstyryl)stilbene (xi): A solution of (*E*)-4-bromomethyl-4′-*tert*-butylstilbene (29.6 g, 89.9 mmol)[32] and triphenylphosphane (25.8 g, 98.2 mmol) was heated to reflux in toluene (200 mL) for four hours. The resultant suspension was cooled to room temperature and the fine white precipitate collected by filtration. The solid was rinsed with n-pentane and dried, giving 49.9 g (67.4 %) (*E*)-4-(4-*tert*-butylstyryl)benzyltriphenylphosphonium bromide. A suspension of this material (35.0 g, 59.2 mmol) and 3,5-dichlorobenzaldehyde (11.4 g, 65.1 mmol) in THF (200 mL) was added over 30 minutes to a THF (50 mL) solution of tBuOK (7.36 g, 65.1 mmol) containing 18-crown-6 (0.160 g, 0.605 mmol). The mixture was then stirred for 12 hours, and quenched by pouring into an equal volume of 10 % methanolic HCl, upon which a pale yellow solid precipitated. The precipitate was collected by filtration, rinsed with ethanol and dried. Proton NMR spectroscopic analysis of the crude solid indicated a mixture of *E* and *Z* isomers. Complete isomerization to the *E* form was successfully carried out by heating a toluene solution of the crude solid to reflux for 3 hours in the presence of a crystal of iodine, followed by rinsing with 5 % Na_2SO_3 and removal of volatiles in vacuo. Compound **xi** was isolated as a yellow powder (12.5 g, 51.9 %). ^{1}H NMR ($CDCl_3$, ppm): δ = 1.34 (s, 9 H), 6.95, d, 1 H, J = 16 Hz), 7.05 (d, J = 16 Hz, 1 H),7.09 (d, J = 16 Hz, 1 H), 7.14 (d, J = 16 Hz, 1 H), 7.22 (s, 1 H), 7.36−7.40 (m, 4 H), 7.45−7.52 (m, 6 H); m.p. 139−141 °C.

(*E*,*E*)-4-Iodo-3,5-dimesityl-4′-(4-*tert*-butylstyryl)stilbene (Dmp′′I): A solution of (*E*,*E*)-3,5-dichloro-4′-(4-*tert*-butylstyryl)stilbene (**xi**) (10.0 g, 24.5 mmol) in THF (125 mL) was cooled to −78 °C and n-butyllithium (10.3 mL, 2.5 M in hexanes, 25.8 mmol) was added dropwise via cannula. After 1 hour of stirring at −78 °C, a solution of mesitylmagnesium bromide [prepared by reaction of 2-bromomesitylene (17.1 g, 85.9 mmol) and Mg turnings (2.98 g, 123 mmol) in THF (85 mL)] was added dropwise via cannula at −78 °C. After warming to room temperature over a 3 hour period, the solution was then heated to reflux for an additional 10 hours. After cooling to room temperature the flask was placed in an ice bath and iodine (15.6 g, 61.4 mmol) was added in 3 g portions. After the exothermic reaction was complete and the characteristic iodine colour persisted in solution for 15 minutes, 5 % Na_2SO_3 (200 mL) was added to quench excess iodine and the solution became yellow. The organic layer was extracted with diethyl ether (200 mL), rinsed with water (2 × 200 mL aliquots) and volatiles removed to yield a viscous oil. Three precipitations of the material from a boiling ethanol solution subsequently cooled to −7 °C gave the product as a pale yellow powder (2.05 g, 11.8 %). ^{1}H NMR ($CDCl_3$, ppm): δ 1.35 (s, 9 H), 2.05 (s, 12 H), 2.39 (s, 6 H), 6.90 (s, 4 H), 7.03−7.14 (m, 4 H), 7.39−7.42 (m, 4 H), 7.46−7.52 (m, 6 H).

Acknowledgments

The authors thank Prof. Christoph Weder and Prof. Malcolm E. Kenney for use of instrumentation and the National Science Foundation (CHE-0202040) for support.

[1] [1a] H. Shirakawa, E. J. Louis, A. G. MacDiarmid, C. K. Chiang, A. J. Heeger, *J. Chem. Soc., Chem. Commun.* **1977**, 578. [1b] C. K. Chiang, C. R. Fincher, Y. W. Park, A. J. Heeger, H. Shirakawa, E. J. Louis, *Phys. Rev. Lett.* **1977**, *39*, 1098.
[2] J. H. Burroughes, D. D. C. Bradley, A. R. Brown, R. N. Marks, K. MacKay, R. H. Friend, P. L. Burn, A. B. Holmes, *Nature* **1990**, *347*, 539−541.
[3] [3a] H. Shirakawa, *Angew. Chem. Int. Ed.* **2001**, *40*, 2574−2580. [3b] A. G. MacDiarmid, *Angew. Chem. Int. Ed.* **2001**, *40*, 2581−2590. [3c] A. J. Heeger, *Angew. Chem. Int. Ed.* **2001**, *40*, 2591−2611. [3d] *Handbook of Conductive Materials and Polymers* (Ed.: H. S. Nalwa); John Wiley & Sons: New York, **1997**. [3f] *Handbook of Conducting Polymers, 2 ed.* (Eds.: T. A. Skotheim, R. L. Elsenbaumer, J. R. Reynolds); Dekker: New York, **1998**.
[4] A. Kraft, A. C. Grimsdale, A. B. Holmes, *Angew. Chem. Int. Ed.* **1998**, *37*, 402−428, and references cited therein.
[5] *Phosphorus: The Carbon Copy* (Eds.: K. B. Dillon, F. Mathey, J. F. Nixon); John Wiley & Sons: New York, **1998**.
[6] [6a] *Multiple Bonds and Low Coordination in Phosphorus Chemistry* (Eds.: M. Regitz, O. J. Scherer); Thieme Verlag: Stuttgart, **1990**. [6b] L. Nyulaszi, T. Veszpremi, J. Reffy, *J. Phys. Chem.* **1993**, *97*, 4011−4015. [6c] P. P. Power, *Chem. Rev.* **1999**, *99*, 3463−3503.

 © 2004 Wiley-VCH Verlag GmbH & Co. KGaA, Weinheim

[7] V. A. Wright, D. P. Gates, *Angew. Chem. Int. Ed.* **2002**, *41*, 2389−2392.
[8] R. C. Smith, X. Chen, J. D. Protasiewicz, *Inorg. Chem.* **2003**, *42*, 5468−5470.
[9] C. Fave, T.-Y. Cho, M. Hissler, C.-W. Chen, T.-Y. Luh, C.-C. Wu, R. Reau, *J. Am. Chem. Soc.* **2003**, *125*; 9254−9255.
[10] F. Mathey, *Angew. Chem. Int. Ed.* **2003**, *42*, 1578−1604.
[11] J. Zhou, B. L. Lucht, *J. Organomet. Chem.* **2002**, *653*, 167−176.
[12] [12a] S. S. H. Mao, T. D. Tilley, *Macromolecules* **1997**, *30*, 5566−5569. [12b] This group has also incorporated germoles into conjugated polymers: B. L. Lucht, M. A. Buretea, T. D. Tilley, *Organometallics* **2000**, *19*, 3469−3475.
[13] H. P. Withers, D. Seyferth, *Organometallics* **1982**, *1*, 1283−1288.
[14] C. H. Honeyman, D. A. Foucher, F. Y. Dahmen, R. Rulkens, A. J. Lough, I. Manners, *Organometallics* **1995**, *14*, 5503−5512.
[15] N. H. T. Huy, L. Ricard, F. Mathey, *Angew. Chem. Int. Ed.* **2001**, *40*, 1253−1255.
[16] E. Deschamps, L. Ricard, F. Mathey, *Angew. Chem. Int. Ed. Engl.* **1994**, *33*, 1158−1161.
[17] [17a] M.-O. Bevierre, F. Mercier, L. Ricard, F. Mathey, *Angew. Chem. Int. Ed. Engl.* **1990**, *29*, 655−657. [17b] M.-O. Bevierre, F. Mercier, L. Ricard, F. Mathey, A. Jutland, C. Amatore, *New J. Chem.* **1991**, *15*, 545−550.
[18] [18a] C. Hay, C. Fischmeister, M. Hissler, L. Toupet, R. Reau, *Angew. Chem. Int. Ed.* **2000**, *39*, 1812−1815. [18b] C. Hay, M. Hissler, C. Fischmeister, J. Rault-Berthelot, L. Toupet, L. Nyulaszi, R. Reau, *Chem. Eur. J.* **2001**, *7*, 4222−4236. [18c] C. Hay, M. Sauthier, M. Hissler, L. Nyulaszi, R. Reau, *Phosphorus, Sulfur, and Relat Elem.* **2002**, *177*, 1423−1425.
[19] [19a] K. Müllen, G. Wegner, (Eds.) *Electronic Materials. The Oligomer Approach*; Wiley-VCH: New York, **1998**. [19b] J. M. Tour, *Chem. Rev.* **1996**, *96*, 537−553. [19c] P. F. van Hutten, V. V. Krasnikov, G. Hadziioannou, *Acc. Chem. Res.* **1999**, *32*, 257−265.
[20] [20a] A. A. Badri, A. Jouaiti, M. Geoffroy, *Mag. Res. Chem.* **1999**, *37*, 735−742. [20b] M. Geoffroy, M. J. Cattani-Lorente, *Chem. Phys. Phys.-Chim. Biol.* **1991**, *88*, 1159−1166. [20c] A. Jouaiti, A. A. Badri, M. Geoffroy, G. Bernardinelli, *J. Organomet. Chem.* **1997**, *529*, 143−149.
[21] C. Dutan, S. Shah, R. C. Smith, S. Choua, T. Berclaz, M. Geoffroy, J. D. Protasiewicz, *Inorg. Chem.* **2003**, *42*, 6241−6251.
[22] S. Shah, T. Concolino, A. L. Rheingold, J. D. Protasiewicz, *Inorg. Chem.* **2000**, *39*, 3860−3867.
[23] H. Kawanami, K. Toyota, M. Yoshifuji, *J. Organomet. Chem.* **1997**, *535*, 1−5.
[24] L. Weber, *Chem. Rev.* **1992**, *92*, 1839−1906.
[25] M. Yoshifuji, I. Shima, N. Inamoto, K. Hirotsu, T. Higuchi, *J. Am. Chem. Soc.* **1981**, *103*, 4587−4589.
[26] [26a] N. Burford, J. A. C. Clyburne, M. S. W. Chan, *Inorg. Chem.* **1998**, 3204−3206. [26b] K. W. Klinkhammer, *Angew. Chem. Int. Ed. Engl.* **1997**, 2320−2322.
[27] [27a] P. P. Power, *Adv. Organomet. Chem.* **1999**, *32*, 1−65. [27b] G. H. Robinson, *Acc. Chem. Res.* **1999**, *32*, 773. [27c] J. A. C. Clyburne, N. McMullen, *Coord. Chem. Rev.* **2000**, *210*, 73−99.
[28] [28a] K. Tsuji, S. Sasaki, M. Yoshifuji, *Tetrahedron Lett.* **1999**, *40*, 3203−3206. [28b] S. Sasaki, H. Aoki, K. Sutoh, S. Hakiri, K. Tsuji, M. Yoshifuji, *Helv. Chim. Acta* **2002**, *85*, 3842−3847.
[29] A. Saednya, H. Hart, *Synthesis* **1996**, 1455−1458.
[30] R. M. Letch, *Org. Magn. Reson.* **1981**, *16*, 220−223.
[31] [31a] J. S. Cha, H. C. Brown, *J. Am. Chem.* **1993**, *58*, 4727−4731. [31b] I. F. Cottrell, D. H. Hands, G. Peter, G. R. Humphrey, S. H. B. Wright, *J. Heterocycl. Chem.* **1991**, *28*, 301−304. [31c] H. Irngartinger, B. Stadler, *Eur. J. Org. Chem.* **1998**, *4*, 605−626.
[32] S. Younes, G. Tchani, G. Baziard-Mouysset, J. L. Stigliani, M. Payard, *Eur. J. Med. Chem. Chim. Ther.* **1994**, *29*, 87−94.
[33] [33a] T. Sawada, M. Wakabayashi, H. Takeo, A. Miyazawa, M. Tashiro, *J. Chem. Soc., Perkin Trans. 1* **1999**, 403−408. [33b] C. Bellucci, G. Gualtieri, A. Chiarini, *Eur. J. Med. Chem. Chim. Ther.* **1987**, *22*, 473−478.
[34] K. Ruhlandt-Senge, J. J. Ellison, R. J. Wehmschulte, F. Pauer, P. P. Power, *J. Am. Chem. Soc.* **1993**, *115*, 11353−11357.
[35] [35a] T. L. Alan, A. C. Scheiner, Y. Yamaguchi, H. F. Schaefer III, *J. Am. Chem. Soc.* **1986**, *108*, 7579−7588. [35b] S. Elbel, A. Ellis, E. Nieke, H. Egsgaard, L. Carlsen, *J. Chem. Soc., Dalton Trans.* **1985**, 879−884. [35c] A. H. Cowley, *Polyhedron* **1984**, *3*, 389−432. [35d] S. Nagase, S. Suzuki, T. Kurakake, *Chem. Commun.* **1990**, 1724−1726.
[36] A. H. Cowley, A. Decken, N. C. Norman, C. Kruger, F. Lutz, H. Jacobsen, T. Ziegler, *J. Am. Chem. Soc.* **1997**, *119*, 3389−3390.
[37] D. Cao, D. Schollmeyer, H. Meier, *Eur. J. Org. Chem.* **1999**, 791−796.
[38] S.-J. Chung, D. W. Lee, O. Dong-Keun, J.-I. Jin, *Acta Polym.* **1999**, *50*, 298−303.
[39] D. T. McQuaid, A. E. Pullen, T. M. Swager, *Chem. Rev.* **2000**, *100*, 2537−2574, and references cited therein.
[40] [40a] H. Kawanami, K. Toyota, M. Yoshifuji, *J. Organomet. Chem.* **1997**, *535*, 1−5. [40b] H. Kawanami, K. Toyota, M. Yoshifuji, *Chem. Lett.* **1996**, *7*, 533−534.
[41] R. C. Smith, S. Shah, E. Urnezius, J. D. Protasiewicz, *J. Am. Chem. Soc.* **2003**, *125*, 40−41.
[42] W. W. Simmons, *The Stadtler Handbook of Ultraviolet Spectra*, Stadtler Research Laboratories, Philadelphia, **1979**.
[43] R. F. Heck, *J. Organomet. Chem.* **1972**, *37*, 389−396.
[44] [44a] S. Shah, J. D. Protasiewicz, *Chem. Commun.* **1998**, 1585−1586. [44b] S. Shah, J. D. Protasiewicz, *Coord. Chem. Rev.* **2000**, *210*, 181−201.
[45] E. Urnezius, J. D. Protasiewicz, *Main Group Chemistry* **1996**, *1*, 369−372.

Received August 8, 2003
Early View Article
Published Online December 12, 2003

 © 2004 Wiley-VCH Verlag GmbH & Co. KGaA, Weinheim

One-Dimensional Magnetism in New, Layered Structures: Piperazine-Linked Copper and Nickel Oxalate Chains

Tony D. Keene,[a] Helen R. Ogilvie,[a] Michael B. Hursthouse,[a] and Daniel J. Price*[a]

Keywords: Magnetic properties / Layered compounds / Hydrothermal synthesis / Coordination networks

Two new coordination network materials with the composition M(pip)(ox) (pip = piperazine; ox = oxalate; M = Ni, Cu) have been synthesised under ambient and hydrothermal conditions. These compounds adopt related structures, both consisting of intersecting $[M(pip)]_\infty$ and $[M(ox)]_\infty$ chains, which result in layered structures. The nickel compound crystallises in $P\bar{1}$. The metal ions are octahedrally coordinated and are linked by symmetric chelating bridging oxalate ions. In contrast, the copper compound crystallises in the chiral space group $P2_12_12_1$. Here the copper atom displays square pyramidal coordination geometry and the oxalate ions bridge metals in an unsymmetric fashion resulting in a polar metal-oxalate chain structure. The magnetic behaviour is determined by the nature of the exchange-coupled network. Only the antiferromagnetic interaction mediated by the bridging oxalate group is significant and the compounds are well modelled as 1-D antiferromagnetically coupled chains. For the copper compound ($S = {}^1/_2$) we determined J/k_B to be −25.9 K, while the nickel compound ($S = 1$) shows a larger exchange coupling ($J/k_B = -42.2$ K). In the nickel compound we see a significant deviation between the observed and calculated magnetic susceptibilities at the lowest experimental temperatures. This may be due either to the formation of a Haldane quantum antiferromagnetic ground state or to single-ion zero-field splitting effects.

(© Wiley-VCH Verlag GmbH & Co. KGaA, 69451 Weinheim, Germany, 2004)

Introduction

Structurally, the oxalate anion is well-known for its chelating coordination mode and for its symmetric bis-chelating bridging mode. The prevalence of this linking mode provides a degree of predictability with regard to the structural motifs and the architectures found in oxalate coordination networks.[1] Electronically, the oxalate anion is very good at mediating an exchange interaction between bridged paramagnetic metal ions. Consequently, many 1-D,[2] 2-D[3] and 3-D[4] magnetic networks have been characterised that contain just this bridging mode.

Magnetostructural correlations in oxalate-bridged homometallic Ni^{II} [5] and Cu^{II} [6] compounds are well-known. For Ni^{II}, the most common geometry; octahedral coordination and a symmetric bis-chelating oxalate bridge, results in antiferromagnetic coupling interactions in the range;(J/k_B = −32 to −56 K). The variation can be correlated with the coordination environment of the nickel ion. By comparison, oxalate-bridged copper-containing compounds show a greater range of coupling constants (0 to −500 K). Here the d^9 configuration means that only one magnetic orbital on each metal is involved in the coupling interaction. Thus, the symmetry of the crystal field and the relative orientations of the local crystal field axis of neighbouring metals to the bridging group orbitals are the key in determining the sign and magnitude of the magnetic interaction. The range of coupling constants is related to the variety of coordination geometries adopted by Cu^{II} ions.

In terms of structure, while many dinuclear oxalate-bridged nickel compounds are known, relatively few infinite chain structures have been reported.[7] This may be in part due to the difficulty in crystallising low solubility network materials. Similarly, symmetrically bridged dinuclear copper compounds are much more prevalent than other mono or polynuclear complexes. However, there are many more extended copper oxalate chain structures than analogous nickel structures.[8] In addition we see examples of 2-D networks[9] in solid-state copper oxalate chemistry. Although the symmetric bridging mode is dominant, there is a much greater variability in the oxalate coordination by copper, resulting in a greater range of oxalate bridging modes.

We have initiated a program of research to use structure-directing amines and ammonium cations in the synthesis of new oxalate network structures. Here we present the synthesis, structure and magnetic properties of two new compounds both with the composition M(pip)(ox) (e.g. where M is either Ni (**1**) or Cu (**2**), pip is the neutral cyclic diamine, piperazine and ox is the oxalate dianion. Our choice of oxalate and piperazine as distinct types of predominantly linear bridging ligands result in straight-forward network topologies in **1** and **2**. Despite the similarity in composition and overall structure, **1** and **2** crystallise in different space

[a] School of Chemistry, University of Southampton, Highfield, Southampton, SO17 1BJ, United Kingdom
Fax: (internat.) + 44-2380-596805
E-mail: daniel.price@soton.ac.uk

groups with different structures and very different metal and oxalate coordination environments.

Results and Discussion

Crystal Structures

Crystallographic data for both compounds are given in Table 1. The asymmetric unit of **1** (Figure 1) contains one half of a nickel atom, one half of a piperazine molecule and one half of an oxalate dianion. All of these components lie on crystallographic inversion centres. The nickel ion is approximately octahedrally coordinated with a *trans*-N_2O_4 coordination sphere. The oxalate ions chelate and bridge adjacent nickel ions in a normal fashion resulting in linear chains of metal oxalate running parallel to the *a*-axis [Figure 2 (a)]; thus the Ni···Ni separation in these chains is the *a*-parameter [5.3613(11) Å]. Two nickel ions are linked by a piperazine molecule, in the low-energy chair form, with bonds to the equatorial position. Thus the nickel ions and the piperazines form another 1-D motif, this time running parallel to the [01$\bar{1}$] direction with a Ni···Ni separation of 7.225(41) Å. Together the bridging oxalate and piperazine groups connect the nickel ions into a 2-D net in the (011) plane [Figure 2 (b)]. While the shortest Ni···Ni separation

Table 1. Crystallographic data for Ni(pip)(ox) (**1**) and Cu(pip)(ox) (**2**)

Compound	**1**	**2**
Formula	$C_6H_{10}N_2NiO_4$	$C_6H_{10}CuN_2O_4$
Crystal system	triclinic	orthorhombic
Space group	$P\bar{1}$ (no. 2)	$P2_12_12_1$ (no. 19)
a (Å)	5.3632(11)	6.8678(3)
b (Å)	5.9848(14)	10.3459(5)
c (Å)	6.4997(16)	10.6329(6)
α (°)	70.584(8)	90
β (°)	85.498(9)	90
γ (°)	78.176(12)	90
V (Å^3)	192.57(72)	755.51(7)
ρ (g cm^{-3})	2.008	2.090
T (K)	120	298
μ (mm^{-1})	2.500	2.872
Reflections collected	1271	5587
Unique data/parameters	776/63	1733/128
R_{int}	0.0765	0.0470
Goodness of fit (*S*)	1.040	1.185
*R*1/*wR*2 [$I > 2\sigma(I)$]	0.0562/0.1253	0.03760.0932
*R*1/*wR*2 [all data]	0.0760/0.1253	0.0436/0.1156

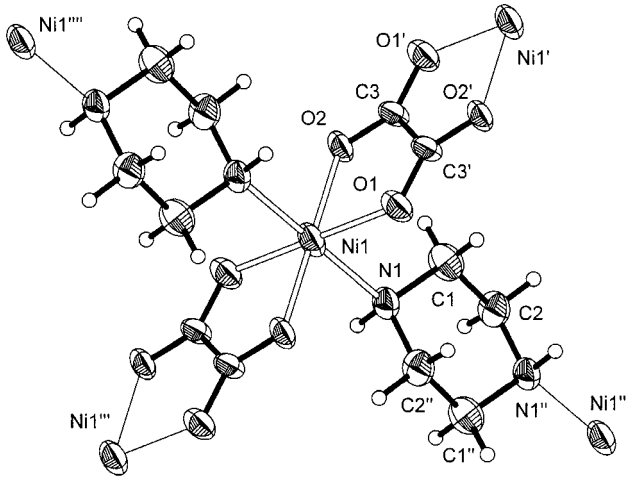

Figure 1. The asymmetric unit and selected symmetry equivalents of Ni(pip)(ox) (**1**) showing the nickel coordination sphere and the bridging modes of both ligands; thermal ellipsoids are at the 90 % probability level; selected bond lengths (Å) and angles (°): Ni1−O1 2.060(11), Ni1−O2 2.065(8), Ni1−N1 2,184(13), C3−C3′ 1.555(5), C3−O1′ 1.257(4), C3−O2 1.253(5) Å; O1−Ni1−O2 81.49(1), O1−Ni1−N1 88.69(1), O2−Ni1−N1 90.80(1)°; symmetry codes: ′ $(1-x, -y, -z)$; ′′ $(-x, 1-y, -1-z)$; ′′′ $(-1+x, y, z)$; ′′′′ $(x, -1+y, 1+z)$

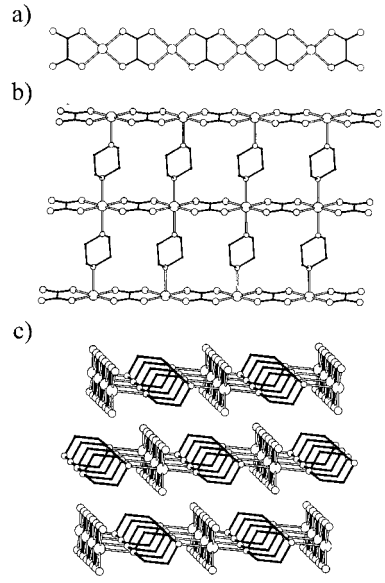

Figure 2. a) The symmetric oxalate bridging mode in the $[Ni(ox)]_\infty$ chains of **1**; b) the 2-D network formed by the intersection of metal-oxalate and metal-piperazine chains in **1**, viewed from an angle just off the *c*-axis; c) the packing of layers, viewed just off of the *a*-axis (hydrogen atoms omitted for clarity)

Table 2. Hydrogen bonds and short contacts: all hydrogen atom positions were fixed in an appropriate geometry and refined in riding mode

	D−H (Å)	H···A (Å)	D···A (Å)	D−H−A (°)
1				
N1−H1···O1[a]	0.910	2.67(2)	2.97(2)	100.4(3)
C2−H2b···O2[a]	0.970	2.47(1)	3.03(2)	116.7(3)
C1−H1a···O2	0.970	2.51(2)	2.99(2)	109.9(4)
C2−H2a···O2[b]	0.970	2.52(1)	3.28(2)	135.7(3)
C1−H1a···O1[c]	0.970	2.56(1)	3.31(1)	133.8(4)
2				
N2−H2···O2[d]	0.910	2.111(3)	2.904(5)	145.1(3)
N1−H1···O2[e]	0.910	2.158(3)	3.065(5)	175.1(3)
C5−H5a···O1[e]	0.971	2.398(3)	3.134(6)	132.2(3)
C5−H5a···O4[f]	0.971	2.453(3)	2.995(5)	114.9(3)
C3−H3b···O1	0.971	2.441(3)	2.981(6)	114.8(3)

[a] $-x, -y, -z$). [b] $(-x, -y, 1-z)$. [c] $(-x, -1-y, -z)$. [d] $(-1/2+x, 1/2-y, -z)$. [e] $(-x, 1/2+y, 1/2-z)$. [f] $(-1/2-x, 1-y, 1/2+z)$.

is through the bridging oxalate group, the next shortest Ni···Ni distances connect nickel ions in neighbouring layers along the *b* and *c* directions [5.9848(14) and 6.4997(16) Å, respectively]. The packing of these layers is shown in Figure 2 (c). There are several short C−H···O and N−H···O contacts between adjacent layers of Ni(pip)(ox) (Table 2). However, the very significant deviation from linearity of the N−H···O interaction and the fact that there are shorter C−H···O contacts suggests that hydrogen bonding to the amine proton is not significant in determining the overall structure of **1**.

The crystal structure of **2** contains one copper atom, one oxalate anion and one piperazine molecule in the asymmetric unit (Figure 3). The Cu^{II} cations are five-coordinate with a *trans*-N_2O_2 + O donor set in a square pyramidal geometry. The apical atom, O3, shows an elongated Cu−O bond of 2.413(3) Å, while the copper−ligand distances in the square base range from 1.954(3) to 2.060(4) Å. The oxalate anion bridges two neighbouring Cu atoms in an unsymmetrical manner, with one side of the oxalate unit in chelating mode through O1 (basal) and O3 (apical) while the other side is monodentate coordinating to a neighbouring copper atom through a basal site in a *syn*-geometry. This leaves one oxygen atom (O2) on the oxalate unit that is not involved in copper coordination. This oxalate bridging results in a polar ribbon of coplanar copper and oxalate ions running along the *c*-axis [Figure 4 (a)]. Within this ribbon, the copper ions form a zigzag chain with a Cu···Cu separation of 5.414(1) Å and a Cu−Cu−Cu angle of 158°. The piperazine molecule again adopts the low energy chair conformation with the hydrogen atoms on both nitrogen atoms, in an axial conformation. The piperazine groups also link neighbouring Cu atoms coordinating through *trans* sites on the square base of the pyramid to form a linear chain running parallel to the *a*-axis. Here the Cu···Cu separation is the *a*-parameter [6.8678(3) Å]. Together these two bridging units link copper ions into a 2-D array in the *ac*-plane [Figure 4 (b)]. Within a given layer all the $[Cu(ox)]_\infty$ chains have the same polarity, but between adjacent layers this polarity is reversed. Each amine proton is involved in hydrogen bonding to the oxygen atom O2 (not involved in copper coordination). In addition there are a large number of short C−H···O contacts (Table 2). The packing of these layers is shown in Figure 4 (c).

Although **1** and **2** have the same generic composition — M(pip)(ox) — the different stereoelectronic preferences of d^8 and d^9 configurations result in different metal coordination geometries and a change in the bridging mode of the oxalate. Despite these substantial local differences in the vicinity of the metal ions the overall structures show remarkable similarity. In both cases we can view the structures as intersecting chains of $[M(ox)]_\infty$ and $[M(pip)]_\infty$ resulting in a 2-D approximately "square" lattice of metal ions. These electrically neutral layers are then held together through a combination of Van der Waals and weak hydrogen bonding interactions.

Only three other nickel oxalate compounds display a linear chain motif; $[Ni(C_2O_4)(H_2O)_2]$,[7a−7c] [Ni(4-aminopyridine)$_2$(ox)][7d] and [Ni(4,4′-bipy)(ox)].[7e] The latter material

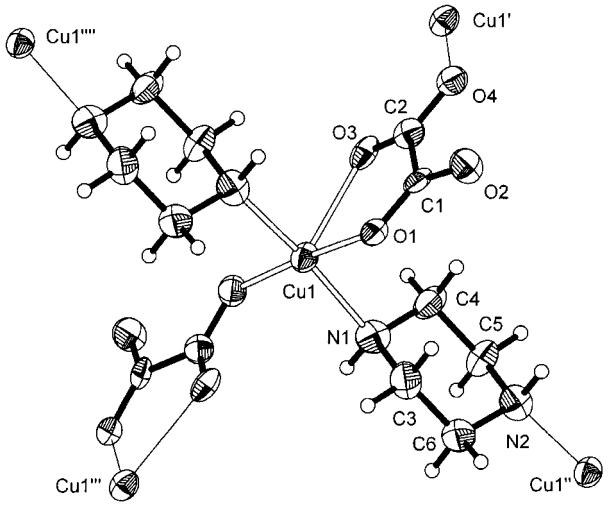

Figure 3. The asymmetric unit and selected symmetry equivalents of Cu(pip)(ox) (**2**) showing the copper coordination sphere and the bridging modes of both ligands; thermal ellipsoids are at the 90 % probability level; selected bond lengths (Å) and angles (°): Cu1−N1 2.058(4), Cu1−O1 1.954(3), Cu1−O3 2.413(3), Cu1′′−N2 2.043(4), Cu1′−O4 1.959(3), C1−C2 1.573(6), C1−O1 1.263(5), C1−O2 1.237(6), C2−O3 1.240(5), C2−O4 1.273(5) Å; N1−Cu1−O1 89.30(14), N1−Cu1−O4′′′′ 89.52(14), N2′′′′−Cu1−O4′′′ 90.65(14), N2′′′′−Cu1−O1 89.92(14), O3−Cu1−N1 99.55(15), O3−Cu1−O1 75.78(12), O3−Cu1−N2′′′′ 86.68(15), O3−Cu1−O4′′′ 109.54(12)°; symmetry codes: ′ ($^1/_2 - z$, $1 - y$, $-^1/_2 + z$); ′′ ($-1 + x$, y, z); ′′′ ($^1/_2 - x$, $1 - y$, $^1/_2 + z$); ′′′′ ($1 + x$, y, z).

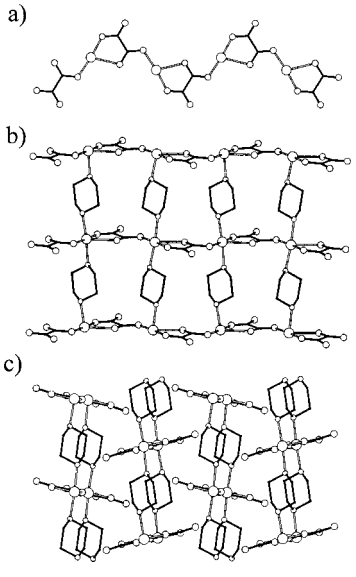

Figure 4. a) The unsymmetric oxalate bridging mode in **2**, resulting in a polar copper oxalate chain structure; b) the bridging mode of the oxalate ions and the linking of these chains by piperazine to form a 2-D net in **2**; view from just off the *b*-axis; c) the 3-D structure showing how layers pack together, viewed along the *c*-axis (hydrogen atoms omitted for clarity)

 © 2004 Wiley-VCH Verlag GmbH & Co. KGaA, Weinheim

displays remarkable structural similarity to **1** with essentially the same 2-D network topology. Other chain-containing materials are known where the oxalate ions coordinate to the nickel atom with *cis* geometry resulting in a zigzag chain structure.[7d,7f,7g] As with nickel, the majority of known compounds containing copper(II), oxalate and alkyl or aryl-amine ligands form dinuclear structures in which the oxalate-bridge metal ions in a symmetric bis-chelating fashion. However, there are a significant number of chain structures, which again contain bridging symmetric bis-chelating oxalate ions. Different amines have been used to stabilise linear chains[8a] (with *trans*-amine coordination), and zigzag chains[8b] (through *cis* coordination of the amine). Few copper(II) oxalate chain structures with a similar asymmetric oxalate bridging mode are known.[8c−8e] In all these cases the monodentate oxalate mode forms an axial coordination to the copper ion, resulting in a noncoplanar copper oxalate chain.

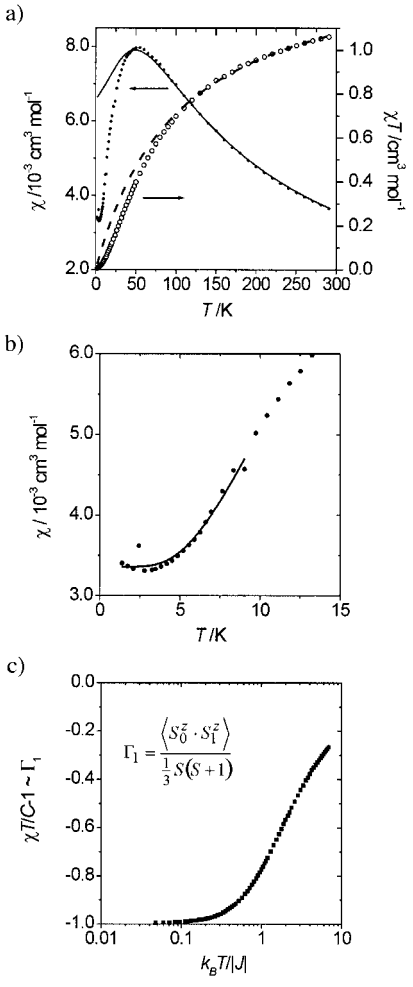

Figure 5. a) The thermal variation in the susceptibility (filled circles) of **1** and the best fit for an isotropic 1-D, (S = 1) model using Weng's equation for the data between 26 and 290 K; also shown in the product χT (open circles) and the Curie−Weiss fit to this data; b) fit of the low temperature data of **1** to an exponential function [Equation (3)] to estimate the energy gap; c) the nearest neighbour pair correlation function, Γ_1, derived from the susceptibility data plotted on a normalised axis scales

Electronic and Magnetic Properties

The approximately octahedral coordination of the Ni^{II} ion in **1** results in a $^3A_{1g}$ ground state, and the electronic spectra of **1** is consistent with this. We determined the crystal field splitting parameter, Δ_{oct} = 9440 cm^{-1}, the energy of the higher lying ^3P term to be at 11450 cm^{-1}, which results in β° = 27.7 %. We note also the presence of a spin-forbidden transition to a ^1E_g state at 14400 cm^{-1}. The enhanced intensity of this transition is due to mixing with the nearby $^3T_{1g}(F)$ state.

The magnetic susceptibility of **1** follows a Curie−Weiss law for data above 100 K [C = 1.446(7) $cm^3 \cdot K \cdot mol^{-1}$ and θ = −104(1) K]. A plot of $\mu_{eff}(T)$ shows the moment to increase monotonically on heating. It is clear that at the highest experimental temperature (290 K), the observed moment of 2.91 μ_B has not reached the asymptotic limit. A plot of $\chi(T)$ shows a broad maximum at 53(1) K with $\chi(T_{max})$ = 7.99(2) × $10^{-3} \cdot cm^3 \cdot mol^{-1}$ [Figure 5 (a)], on further cooling $\chi(T)$ tends to a value of 3.3(1) × 10^{-3} $cm^3 \cdot mol^{-1}$ as T approaches 0 K. The decrease in $\mu_{eff}(T)$ on cooling and the large negative Weiss constant suggest a significant antiferromagnetic exchange interaction between neighbouring nickel ions. From the crystallographic structure of **1** we expect the system to be well described as a 1-D "chain" of antiferromagnetically interacting spin moments. While typically spin-orbit coupling of the ground term to the low lying $^3T_{2g}$ state raises the g-value to about 2.25, g-values for Ni^{II} are usually isotropic, thus the system may be described by a Heisenberg Hamiltonian [Equation (1)]. The behaviour of an antiferromagnetically coupled chain of quantum spins was calculated by Weng,[10] and can be modelled by a polynomial approximation[11] [Equation (2)].

$$\hat{H} = -J \sum_i \mathbf{S}_i \cdot \mathbf{S}_{i+1} \tag{1}$$

$$\chi = \frac{N\mu_B^2 g^2}{k_B T}\left(\frac{A + Bx^2}{C + Dx + Ex^3}\right) \tag{2}$$

where $x = |J| / k_B T$

For $S = {}^1/_2$: A = 0.2500, B = 0.045743, C = 1.000, D = 0.77335, E = 0.43038

For S = 1: A = 0.6667, B = 0.64558, C = 1.000, D = 1.8018, E = 4.9448.

Least-squares fitting of the data over the whole of the measured temperature range (2−290 K) does not give a satisfactory agreement. The model underestimates the data at high temperatures and overestimates in the low temperature regime. If this model is applied to data over the limited region from 26 to 290 K a vastly improved fit is obtained [Equation (2); g = 2.31(1) and J/k_B = −42.2(3) K; Figure 5 (a)]. These couplings are in good agreement with reported values for a similarly bridged nickel oxalate compounds.[5,12]

 © 2004 Wiley-VCH Verlag GmbH & Co. KGaA, Weinheim

The discrepancy between the observed and calculated susceptibility at low temperatures may have one of several origins. Most likely either: a) the zero-field-splitting commonly observed in octahedral Ni^{II} complexes may be responsible; or b) we are seeing the formation of a "Haldane" quantum antiferromagnetic state. It is well-known that integer-spin chains are theoretically expected to display a gap[13] (known as the Haldane gap) immediately above a nonmagnetic ground state with novel quantum order. Theoretically this would result in an exponential increase in χ as T is increased from 0 K. In fact the low temperature susceptibility of **1** can be fitted to just such a model[14] [Equation (3); Figure 5 (b)] that results in a gap [Eg/k_B = 32(3) K]. This is in reasonable agreement with the expectation[15] that Eg is approximately $0.4|J|$ and is directly comparable to values reported for similarly coupled Ni^{II} chains.[16] We can use the measured susceptibility to derive an approximate value for the nearest-neighbour pair correlation function, Γ_1, from the susceptibility measurement.[17] The thermal evolution of Γ_1, which is proportional to the magnetic energy of the system, is shown in Figure 5 (c). For $\Gamma_1 = 0$ there is no correlation between neighbouring moments, while $\Gamma_1 = -1$ corresponds to perfect antiparallel alignment.

$$\chi = \chi_0 + C\exp\left(-\frac{Eg}{k_B T}\right) \tag{3}$$

The measured magnetic susceptibility of **2** shows a broad feature centred at about 13(2) K (determined by the derivative curve) although at the lowest experimental temperatures the susceptibility is seen to increase just as in a non-coupled paramagnetic material (Figure 6). A plot of reciprocal susceptibility vs. temperature showed approximately linear behaviour for data above 50 K. This could be fit to a Curie−Weiss law giving $C = 0.418(2)$ $cm^3 \cdot K \cdot mol^{-1}$ and $\theta = -44(1)$ K. The negative value for the Weiss constant θ, suggests a significant antiferromagnetic exchange interaction between neighbouring copper ions. From a plot of $\mu_{eff}(T)$, we can see that μ_{eff} increases on heating and by room temperature, the observed moment of 1.71(1) μ_B has not yet reached the asymptotic limit.

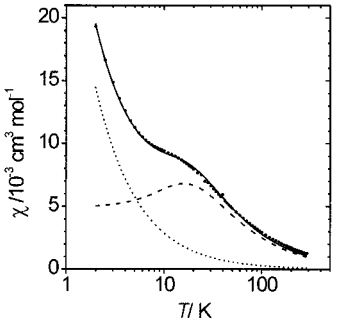

Figure 6. The thermal variation in the susceptibility (filled circles) of **2** and the best fit (solid line) for an isotropic 1-D, ($S = {}^1/_2$) model using Weng's equation plus a component due to a paramagnetic impurity (a logarithmic scale is used to highlight the good fit over a wide range of temperatures); each of these components is shown separately: contribution for **2** (dashed line), contribution due to paramagnetic impurity (dotted line)

Although consideration of the Cu···Cu separations suggests a 3-D network, the only likely magnetic superexchange pathway is through the bridging oxalate anion; thus we may anticipate 1-D magnetic behaviour. The observed broad maximum in the susceptibility at low temperature is consistent with this expectation. As with **1**, the magnetic interactions in compound **2** can be described by the Heisenberg Hamiltonian [Equation (1)], for which approximate solutions are known. Fitting the data to the quantum model[10,11] [Equation (2); Figure 6], plus a contribution due to a paramagnetic impurity gives a good fit [J/k_B = −25.9(1) K, g = 1.9 and 5.3 % paramagnetic impurity]. However, since the model clearly underestimates the high-temperature data it is likely that here g has been underestimated.

The coupling interaction between paramagnetic copper(II) ions is particularly well-studied, because the d^9 configuration always provides a simple spin ($S = {}^1/_2$) moment, free from orbital contributions and zero-field splitting effects which always complicate the analysis. Furthermore, the overwhelming tendency of Cu^{II} ions to form tetragonally elongated octahedra, square pyramid or square-planar coordination geometries results in a $d_{x^2-y^2}$ magnetic orbital and a clearly defined set of crystal field axis. The magnitude of the exchange coupling between Cu^{II} ions bridged by an oxalate ion depends crucially on the relative orientations of the magnetic $d_{x^2-y^2}$ orbitals of neighbouring cations and on the relative orientation of the oxalate group. Two different orbital orientations for the common symmetric bis-chelating mode are shown in Figure 7 (a and b).

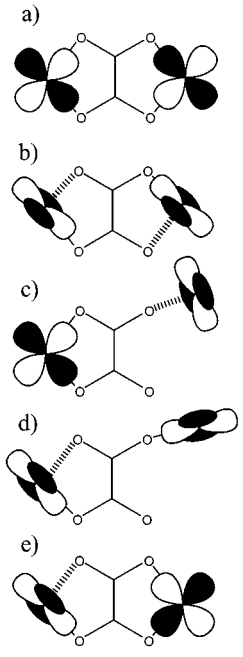

Figure 7. Some of the possible orbital topologies found in oxalato-bridged copper(II) compounds, see main text for details

 © 2004 Wiley-VCH Verlag GmbH & Co. KGaA, Weinheim

These different orbital topologies have antiferromagnetic couplings of approximately −500 and −9 K, respectively.[6,18] The unsymmetric μ-1,2,3-oxalato bridging mode is much less common[19] and in all previously reported compounds it appears that the magnetic orbital adopts the relative geometry shown in Figure 7 (c). This configuration supports exchange couplings in the range −0.50 to −3.9 K. To the best of our knowledge the disposition of the magnetic orbitals in **2** [Figure 7 (d)] is unique. This mode is related to an orbital topology seen occasionally in bis-chelating coordination geometries[8a,20] [Figure 7 (e)]. The larger exchange coupling observed in **2** compared to other unsymmetric μ-1,2,3 oxalato bridging modes is easily reconciled with the better spatial overlap of both metal $d_{x^2-y^2}$ orbitals and the oxalate orbitals.

Thermal Analysis

Thermogravimetric analysis of **1** under an O_2 atmosphere shows a single-stage decomposition at 400 °C to give a dark grey powder. The corresponding mass loss of 66.6 % agrees well with that expected upon formation of NiO. Compound **2** follows a similar single-step decomposition at about 220 °C with an observed weight loss of 38.9 %, consistent with the formation of CuO.

Conclusions

We have used two distinct bridging ligands to form a network with a topology that may have been anticipated. The difference in the structures of the Ni^{II} **1** and Cu^{II} **2** derivatives can be wholly attributed to the different stereoelectronic preferences of the d^8 and d^9 configurations. Both materials display 1-D antiferromagnetic behaviour consistent with the 1-D metal-oxalate structure. While the coupling constant in **1** is as expected the small value for **2** is due to the unusual orientations of the $d_{x^2-y^2}$ orbital on neighbouring metal ions relative to the oxalate bridge. The low temperature magnetism of **1** is consistent with the formation of a Haldane state, predicted for such a 1-D ($S = 1$) Heisenberg quantum antiferromagnet. However, these preliminary measurements do not rule out similar effects from zero-field splitting. If the low temperature state is a Haldane phase then **1** is an excellent material for further physical study. The fact that there is only one single spin carrier and one single coupling pathway per unit cell, and that both of these lie on crystallographic inversion centres greatly simplifies the interpretation of more sophisticated magnetic measurements. We are currently engaged in more detailed studies to better understand the magnetism of this ($S = 1$) material.

Experimental Section

Reagents: Nickel(II) hydroxide (97 %), oxalic acid (99 %), potassium oxalate monohydrate (99 %), and tetramethoxysilane (98 %) were all purchased from Aldrich, piperazine (99 %) from Acros, copper(I) chloride (96 %) from Fisher and copper(II) sulfate pentahydrate (99.5 %) from BDH. All used without further purification.

Physical Measurements: IR spectra were recorded on a Perkin−Elmer Spectrum One FT-IR machine as diffuse reflectance measurements between 4000 and 400 cm^{-1} using a KBr matrix. Elemental analysis for, C H and N was carried out commercially by Medac Ltd. UV-Vis/NIR spectra were recorded on a Perkin−Elmer Lambda 19 spectrometer in diffuse reflectance mode with the samples embedded in a $BaSO_4$ matrix. Thermogravimetric analysis was performed on a Metller Toledo TGA/SDTA851^e equipped with a T50800GCI gas control system and a T50801RD sample robot. Measurements were carried out under an atmosphere of approximately 60 % O_2 between 30 and 600 °C with a heating rate of 10 °C·min^{-1}. Single-crystal X-ray data was collected with monochromated Mo-K_α radiation (λ = 0. 71073 Å) on an Enraf−Nonius−Kappa CCD area detector as φ and ω scans to fill the Ewald sphere. Data collection and cell refinement were managed by DENZO,[21] absorption corrections were applied using SORTAV,[22] structure solution and refinement by SHELXS-97[23] and SHELXL-97[24] in the WinGX environment (Table 1).[25] CCDC-213878 **1** and CCDC-213879 **2** contain the supplementary crystallographic data for this paper. These data can be obtained free of charge at www.ccdc.cam.ac.uk/conts/retrieving.html [or from the Cambridge Crystallographic Data Centre, 12 Union Road, Cambridge CB2 1EZ, UK; Fax: (internat.) + 44-1223-336-033; E-mail: deposit@ccdc.cam.ac.uk].

Powder X-ray diffraction using a Siemens D5000 diffractometer was performed to confirm the purity and identity of all microcrystalline samples. Field-cooled magnetisation measurements were made between 2 and 290 K using a Quantum Design MPMS SQUID magnetometer in applied fields of 200 G. The powdered samples were held in an eicosane matrix to prevent reorientation effects. A diamagnetic correction of -119×10^{-6} cm^3·mol^{-2} was determined from Pascal's constants[26] and applied to both samples.

Synthesis of Ni(pip)(ox) (1): Nickel hydroxide (100 mg, 1.07 mmol), oxalic acid dihydrate (254 mg, 2.25 mmol), piperazine (689 mg, 8.00 mmol) and distilled water (10 mL) were placed into a 23 mL capacity Teflon lined autoclave and heated to 180 °C under autogenous pressure for 72 h. The green microcrystalline product was collected by filtration and dried in air (30 mg, 12 %). $C_6H_{10}N_2NiO_4$ (232.9): C 30.95, H 4.33, N 12.03; found C 31.23, H 4.61, N 12.08. IR: $\tilde{\nu}$ = 3250 cm^{-1} m, 3108 w, 3072 w, 3004 m, 2975 w, 2918 m, 2880 m, 2825 w, 2679 w, 2554 w, 2509 w, 2420 w, 2420 w, 2274 w, 2031 w, 1972 w, 1895 w, 1619 s, 1457 s, 1439 m, 1420 s, 1362 m, 1342 m, 1314 s, 1249 m, 1098 m, 1069 s, 1019 s, 992 s, 905 m, 881 s, 804 s, 647 m, 488 s, 414 s. UV-Vis: λ_{max} /cm^{-1} (ε/relative) = 9500 (0.423) $^3A_{2g} \rightarrow {}^3T_{2g}$(F), 14400 (0.315) $\rightarrow {}^1E_g$, 15600 (0.292) $\rightarrow {}^3T_{1g}$(F), 24700 (0.162) $\rightarrow {}^3T_{2g}$(P), 37900 (1.000).

Synthesis of Cu(pip)(ox) (2): A mixture of copper(I) chloride (1.000 g, 10.10 mmol), potassium oxalate monohydrate (2.000 g, 10.86 mmol), piperazine (1.000 g, 11.61 mmol) and distilled water (15 mL) was allowed to react in air for a period of 6 days. During the course of the reaction Cu^I both disproportionates and is slowly oxidised by air to Cu^{II}. The product is formed as a purple precipitate. The major contaminant $K_2Cu(ox)_2$·$2H_2O$ is removed by dissolution in H_2O and the product is collected by filtration. Yield 85 %. $C_6H_{10}CuN_2O_4$ (237.7): calcd. C 30.32, H 4.24, N 11.78; found C 28.54, H 4.44, N 10.81. IR: $\tilde{\nu}$ = 3189 cm^{-1} s, 3167 s, 2996 m, 2950 m, 2884 m, 2798 m, 2379 w, 2191 w, 1657 s, 1631 s, 1606 s, 1443 m, 1372 m, 1347 m, 1306 s, 1239 m, 1151 s, 1092 s, 1028 m, 1008 m, 892 s, 833 m, 789 s, 675 m, 596 m, 517 s, 421 m. UV-Vis: λ_{max} /cm^{-1} (ε/relative) = 14700 (0.684), 17500 (0.772), 27000 (0.930), 29100 (0.965), 33800 (1.000).

 © 2004 Wiley-VCH Verlag GmbH & Co. KGaA, Weinheim

Crystallisation of 2: Single crystals of **2** were obtained by a gel crystallisation method. Tetramethoxysilane (2 mL) was added to a solution of piperazine (0.500 g, 5.81 mmol) and potassium oxalate monohydrate (1.00 g, 5.43 mmol) in distilled water (18 mL), and the mixture allowed to react. This gel was transferred to a test tube. A solution of copper sulfate pentahydrate (1.25 g, 4.81 mmol) in distilled water (5 mL) was added to the top and allowed to diffuse slowly into the gel. After three days small, purple crystals of **2** formed.

Acknowledgments

We are grateful to Dr. H. J. Blythe (The University of Sheffield) for assistance with the magnetisation measurements and Dr. A. L. Hector (University of Southampton) for measurement of the TGA data. D. J. P. thanks the EPSRC for the award of an Advanced Research Fellowship.

[1] [1a] T. O. Salami, K. Marouchkin, P. Y. Zavillij, S. R. J. Oliver, *Chem. Mater.* **2002**, *14*, 4851. [1b] R. Vaidhyanathan, S. Natarajan, C. N. R. Rao, *J. Chem. Soc., Dalton Trans.* **2001**, 699. [1c] R. Vaidhyanathan, S. Natarajan, A. K. Cheetham, C. N. R. Rao, *Chem. Mater.* **1999**, *11*, 3636. [1d] S. Natarajan, R. Vaidhyanathan, C. N. R. Rao, S. Ayyappan, A. K. Cheetham, *Chem. Mater.* **1999**, *11*, 1633. [1e] S. Ayyappan, A. K. Cheetham, S. Natarajan, C. N. R. Rao, *Chem. Mater.* **1998**, *10*, 3746.

[2] Z. A. D. Lethbridge, A. F. Congreve, E. Esslmont, A. M. Z. Slawin, P. Lightfoot, *J. Solid State Chem.* **2003**, *172*, 212.

[3] [3a] P. Rabu, M. Drillon, *Adv. Eng. Mater.* **2003**, *5*, 189 and the references therein. [3b] S. Natarajan, *Solid State. Sci.* **2003**, *4*, 1331. [3c] R. Pellaux, H. W. Schmalle, R. Huber, P. Fischer, T. Hauss, B. Ouladdiaf, S. Decurtins, *Inorg. Chem.* **1997**, *36*, 2301. [3d] S. Decurtins, H. W. Schmalle, H. R. Oswald, A. Linden, J. Ensling, P. Gütlich, A. Hauser, *Inorg. Chim. Acta* **1994**, *216*, 65.

[4] [4a] R. Clément, S. Decurtins, M. Gruselle, C. Train, *Monats. Chem.* **2003**, *134*, 117 and references therein. [4b] E. Coronado, J. R. Galan-Mascaros, C. J. Gomez-Garcia, J. M. Martinez-Agudo, *Inorg. Chem.* **2001**, *40*, 113. [4c] K. P. Mortl, J.-P. Sutter, S. Golhen, L. Ouahab, O. Kahn, *Inorg. Chem.* **2000**, *39*, 1626. [4d] R. Andres, M. Gruselle, B. Malezieux, M. Verdaguer, J. Vaissermann, *Inorg. Chem.* **1999**, *38*, 4637. [4e] S. Decurtins, *Phil. Trans. Roy. Soc. Sect A* **1999**, *357*, 3025 and references therein.

[5] [5a] A. Escuer, R. Vicente, J. Ribas, J. Jaud, B. Raynaud, *Inorg. Chim. Acta* **1994**, *216*, 139. [5b] P. Román, C. Guzmán-Miralles, A. Luque, J. I. Beitia, J. Cano, F. Lloret, M. Julve, S. Alvarez, *Inorg. Chem.* **1996**, *35*, 3741. [5c] R. Wen, I. Bernal, S. S. Massoud, R. K. Thalji, D. R. Billodeaux, F. R. Fronczek, *Inorg. Chim. Acta* **1999**, *295*, 91.

[6] J. Cano, E. Ruiz, P. Alemany, F. Lloret, S. Alvarez, *J. Chem. Soc., Dalton Trans.* **1999**, 1669.

[7] [7a] H. Schmittler, *Monats. Dtsch. Akad. Wiss. Ber.* **1967**, *9*, 445. [7b] J.-P. Lagier, H. Pezerat, J. Dubernat, *Rev. Chim. Miner.* **1969**, *6*, 1081. [7c] R. Deyrieaux, C. Berro, A. Peneloux, *Bull. Soc. Chim. Fr.* **1973**, 25. [7d] O. Castillo, A. Luque, P. Román, F. Lloret, M. Julve, *Inorg. Chem.* **2001**, *40*, 5526. [7e] J. Y. Lu, M. A. Lawandy, J. Li, T. Yuen, C. L. Lin, *Inorg. Chem.* **1999**, *38*, 2695. [7f] O. Castillo, A. Luque, F. Lloret, P. Román, *Inorg. Chim. Acta* **2001**, *324*, 141. [7g] J. Y. Lu, T. J. Schrieder, A. M. Babb, M. Olmstead, *Polyhedron* **2001**, *20*, 2445.

[8] [8a] O. Castillo, A. Luque, F. Lloret, P. Román, *Inorg. Chem. Commun.* **2001**, *4*, 350. [8b] O. Castillo, A. Luque, M. Julve, F. Lloret, P. Román, *Inorg. Chim. Acta* **2001**, *315*, 9. [8c] J. Novosad, A. C. Messimeri, C. D. Papadimitriou, P. G. Veltsistas, J. D. Woolins, *Transition Met. Chem.* **2000**, *25*, 664. [8d] H. Oshio, U. Nagashima, *Inorg. Chem.* **1992**, *31*, 3295. [8e] U. Geiser, B. L. Ramakrishna, R. D. Willett, F. B. Hulsbergen, J. Reedijk, *Inorg. Chem.* **1987**, *26*, 3750.

[9] [9a] L. Cavalca, A. C. Vila, A. G. Manfredotti, A. A. G. Tomlinson, *J. Chem. Soc., Dalton Trans.* **1972**, 391. [9b] M. R. Sundberg, R. Kivekas, J. K. Koskimies, *J. Chem. Soc., Chem. Commun.* **1991**, 526. [9c] M. Hernandez-Molina, P. A. Lorenzo-Luiz, C. Ruiz-Perez, *Cryst. Eng. Commun.* **2001**, 16.

[10] C. Y. Weng, *PhD Thesis*, Carneige-Mellon University, Pittsburg, PA, **1969**.

[11] W. Hiller, J. Strähle, A. Datz, M. Hanack, W. E. Hatfield, L. E. ter Haar, P. Gütlich, *J. Am. Chem. Soc.* **1984**, *106*, 329.

[12] [12a] J. Glerup, P. A. Goodson, D. J. Hodgson, K. Michelsen, *Inorg. Chem.* **1995**, *34*, 6255. [12b] F. Brezina, Z. Smekal, Z. Travnicek, Z. Sindelar, R. Pastorek, J. Marek, *Polyhedron* **1997**, *16*, 1331. [12c] Z. Smekal, P. Thornton, Z. Sindelar, R. Klicka, *Polyhedron* **1998**, *17*, 1631. [12d] R. W. Wen, I. Bernal, S. S. Massoud, R. K. Thalji, D. R. Billodeaux, F. R. Fronczek, *Inorg. Chim. Acta* **1999**, *295*, 91. [12e] I. Muga, J. M. Gutiérrez-Zorrilla, P. Vitoria, A. Luque, M. Insausti, P. Román, F. Lloret, *Eur. J. Inorg. Chem.* **2000**, 2541.

[13] [13a] F. D. Haldane, *Phys. Lett. Sect A* **1983**, 464. [13b] F. D. Haldane, *Phys. Rev. Lett.* **1983**, *50*, 1153.

[14] T. Ishii, N. Aizawa, H. Hara, M. Yamashita, H. Matsuzaka, *Polyhedron* **2001**, *20*, 1297.

[15] M. P. Nightingale, H. W. J. Blöte, *Phys. Rev. B.* **1986**, *33*, 659.

[16] M. S. El Fallah, A. Escuer, R. Vicente, X. Solans, M. Font-Bardia, M. Verdaguer, *Inorg. Chim. Acta* **2003**, *344*, 133.

[17] L. J. de Jongh, A. R. Miedema, *Adv. Phys.* **2001**, *50*, 947.

[18] [18a] J. J. Girerd, O. Kahn, M. Verdauger, *Inorg. Chem.* **1980**, *19*, 274. [18b] O. Castillo, I. Muga, A. Luque, J. M. Gutiérrez-Zorrilla, J. Sertucha, P. Vitoria, P. Román, *Polyhedron* **1999**, *18*, 1235. [18c] J. Cano, P. Alemany, S. Alvarez, M. Verdaguer, E. Ruiz, *Chem. Eur. J.* **1998**, *4*, 476.

[19] H. Núñez, J.-J. Timor, J. Server-Carrió, L. Soto, E. Escrivà, *Inorg. Chim. Acta* **2001**, *318*, 8 and references therein.

[20] [20a] M. Julve, M. Verdaguer, O. Kahn, A. Gleizes, O. Philoche-Levisalles, *Inorg. Chem.* **1984**, *23*, 3808. [20b] S. Kitagawa, T. Okubo, S. Kawata, M. Kondo, M. Katada, H. Kobayashi, *Inorg. Chem.* **1995**, *34*, 4790.

[21] Z. Otwinoski, W. Minor, in *Methods in Enzymology*, vol. 276: *Macromolecular Crytstallography* (Eds.: C. W. Carter Jr., R. M. Sweet), Academic Press, **1997**, *Part A*, p. 307.

[22] [22a] R. H. Blessing, *Acta Crystallogr., Sect. A* **1995**, 33. [22b] R. H. Blessing, *J. Appl. Cryst.* **1997**, *30*, 421.

[23] G. M. Sheldrick, *Acta Crystallogr., Sect. A* **1990**, 467.

[24] G. M. Sheldrick, University of Göttingen, Germany, **1997**.

[25] L. J. Farrugia, *J. Appl. Cryst.* **1999**, *32*, 837.

[26] O. Kahn, *Molecular Magnetism*, VCH, Weinheim, **1993**.

Received August 22, 2003
Early View Article
Published Online January 28, 2004

 © 2004 Wiley-VCH Verlag GmbH & Co. KGaA, Weinheim

Synthesis, Structural Characterization and Fluorescence Properties of Organoselenium Compounds Bearing a Ligand Containing Both Bulky and Nonbonding Groups − The First Observation of Both Intramolecular Se···N and Se···O Interactions in a Diselenide Structure

Karuppasamy Kandasamy,[a] Sangit Kumar,[a] Harkesh B. Singh,*[a] Ray J. Butcher,[b] and K. Travis Holman[c]

Keywords: Selenium / Intramolecular coordination / X-ray diffraction / Fluorescence

The synthesis of bis[3-(4,5-dihydro-4,4-dimethyl-1,3-oxazol-2-yl)-4-(3,5-dimethylphenyl)-2-naphthyl] diselenide, R_2Se_2 (**4**), was achieved by a facile ortholithiation route. Further reaction of the diselenide with a stoichiometric amount of SO_2Cl_2 or Br_2 afforded the corresponding selenenyl halides RSeX [X = Cl (**5**), X = Br (**6**)]. The novel selenenyl iodide RSeI (**7**), in which the selenium and iodine are covalently bonded to each other, was obtained by treatment of the diselenide with an equimolar amount of iodine. The stable aryl benzyl selenide **8** was prepared by the reaction of benzyl chloride with lithium areneselenolate (**3**) at low temperature. Surprisingly, the reaction of the diselenide with 1,2-dibromo-*o*-xylene gave the selenenyl bromide (**6**) instead of the arylselenium derivative **9**. Elemental analysis, multinuclear (^1H, ^{13}C, ^{77}Se) NMR spectroscopic and mass spectrometric techniques were used for the identification of products. Compounds **4**, **6**, **7**, and **8** were also characterized by single-crystal X-ray diffraction studies.
(© Wiley-VCH Verlag GmbH & Co. KGaA, 69451 Weinheim, Germany, 2004)

Introduction

In recent years organoselenium chemistry has been receiving much attention from the whole chemical community because of its potential applications in various fields. Selenium reagents have been extensively used in a variety of organic reactions.[1] Other major applications are: i) ligand chemistry,[2] ii) precursors for the preparation of thin films in metal-organic chemical vapor deposition (MOCVD),[3] and iii) biochemistry.[4] Nevertheless, organoselenium compounds are known to be very unstable, highly reactive and very difficult to synthesize. Recent studies show that the use of sterically more hindered groups and intramolecularly coordinating groups has been successful in synthesizing some stable organoselenium compounds. Arnold et al.[5] and Bochmann et al.[6] have used sterically more hindered groups to stabilize unstable organoselenium compounds. Intramolecular Se···X (X = H,[7] S,[8] O,[9] F,[10] N,[4i,11] Cl and Br[10b,12]) interactions have also been successfully used for the same purpose. Ramasubbu et al.,[13] Goldstein et al.,[14] and Barton et al.[15] have analyzed the nature of the intramolecular interactions, and the electronic structure around the selenium atom has been interpreted in terms of a three center, four electron X···Se−R bond (hypervalent bond). These interactions are also expected to be responsible for the specific redox reactivity of organoselenium compounds[16] as well as stabilization of selenenic acid, the key intermediate in the glutathione peroxidase catalytic cycle.[4]

Although intramolecular coordination and steric effects have been employed individually for the synthesis of stable organoselenium compounds, to the best of our knowledge there are no reports of their combined use for the stabilisation of organoselenium compounds. The use of (4,4-dimethyl-2-phenyl)oxazoline for the preparation of some novel organoselenium compounds has been reported recently by our group.[11d] Metal thiolates[17] and selenolates[2k] incorporating the same substrate have also been synthesized and characterized. In zinc thiolate and selenolate complexes, chirality was observed as a result of the diastereotopic methylene protons of the oxazoline ring, which arises from the strong "hard-hard" interactions between the zinc and the imine nitrogen atoms. However, attempts to

[a] Department of Chemistry, Indian Institute of Technology, Bombay,
Powai, Mumbai 400 076, India
Fax: (internat.) + 91-22/2572-3480
E-mail: chhbsia@chem.iitb.ac.in
[b] Department of Chemistry, Howard University,
Washington, DC 20059, USA
Fax: (internat.) + 1-202-806-5442
E-mail: rbutcher@fac.howard.edu
[c] Department of Chemistry, Georgetown University,
Washington, DC 20057, USA
Fax: (internat.) + 1-202-687-6209
E-mail: kth7@georgetown.edu

 © 2004 Wiley-VCH Verlag GmbH & Co. KGaA, Weinheim **DOI: 10.1002/ejic.200300603**

obtain crystals of group 12 tellurolates[18] were unsuccessful due to the facile decomposition of the complexes in common solvents. In this context, we thought it worthwhile to use a ligand that can induce both steric and intramolecular coordination effects together as it could provide greater stability than ligands having either an *o*-chelating group or a sterically more demanding group. This would also provide an opportunity to study Se···N interactions in the presence of sterically more demanding group.

We report here the synthesis and characterization of some novel organoselenium complexes of 2-[1-(3,5-dimethylphenyl)-2-naphthyl]-4,5-dihydro-4,4-dimethyl-1,3-oxazole. This substrate has been synthesized as one of the intermediates in the preparation of mevanolactones, which are used as inhibitors in cholesterol biosynthesis.[19] A comparison of structural and spectroscopic properties with similar compounds derived from the sterically less hindered 4,4-dimethyl-2-phenyloxazoline and other ligands is also described.

Results and Discussion

Synthesis

The synthesis of the synthetically important diselenide **4** was achieved by an ortholithiation route. The lithium areneselenolate **3** was prepared by the direct metalation of 2-[1-(3,5-dimethylphenyl)-2-naphthyl]-4,5-dihydro-4,4-dimethyl-1,3-oxazole (**1**) with a 1.6 M solution of *n*BuLi in hexane followed by the addition of finely ground selenium powder. Oxidative work up gave the desired diselenide. Treatment of the diselenide with sulfuryl chloride gave the stable selenenyl chloride **5**. The stable bromo derivative **6** was obtained as a yellow crystalline solid by the reaction of diselenide with a stoichiometric amount of bromine. Isolation of the stable binary compounds containing selenium and iodine was difficult because of their similar electronegativity and their tendency to form charge-transfer adducts.[20] Although isolation has been possible using more hindered groups, like the 2,4,6-tri-*tert*-butylphenyl group,[21] a slight

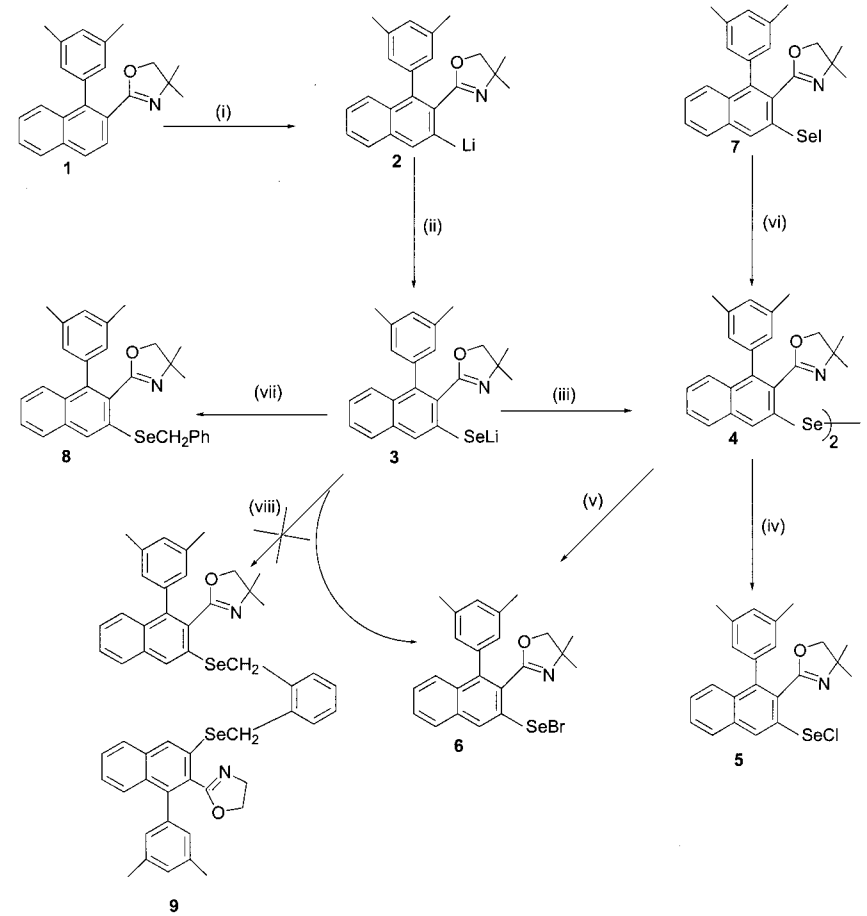

i). n-BuLi, Et_2O, 0°C, ii) Se°, Et_2O, 0°C iii). [O]/H_2O, iv) SO_2Cl_2, CCl_4, 0°C, v). Br_2, CCl_4, 0°C, (vi) I_2, CCl_4, 0°C, vii) $PhCH_2Cl$, (viii)1, 2 - dibromo-o-xylene, 0°C

Scheme 1. Synthetic route for the synthesis of organoselenium derivatives

 © 2004 Wiley-VCH Verlag GmbH & Co. KGaA, Weinheim

reduction of their steric bulkiness again led to the formation of the charge-transfer adduct.[22] However, our group has succeeded in isolating stable binary compounds containing selenium and iodine using ligands such as 4,4-dimethyl-2-phenyl-1,3-oxazoline,[11d] *N*,*N*-dimethylbenzylamine,[11e] and *N*,*N*-dimethylnaphthylamine.[11c] Here also, the reaction of the diselenide with stoichiometric amounts of iodine led to the formation of the novel mono-iodide **7**. This consistent isolation of stable Se−I bonded compounds regardless of bulkiness proves that the intramolecular approach is a more effective method for the isolation of unstable compounds than the steric approach. In general, aryl benzyl and allyl aryl selenides are unstable and decompose readily to give coupled hydrocarbon products and free selenium.[23] Treatment of the lithium areneselenolate **3** with equimolar amounts of benzyl chloride gave the stable benzylselenium derivative **8**. All these reactions are shown in Scheme 1.

The treatment of α,α-dibromo-*o*-xylene with the lithium areneselenolate **3** gave, unexpectedly, the selenenyl bromide **6** instead of the expected compound **9**. The reaction of $Se(dtc)_2$ with the lithiated product **2** was expected to give a stable symmetrical selenide. The yellow-colored product formed in this reaction decomposed immediately to give the starting material. It is worth mentioning that the reaction of 4,4-dimethyl-2-phenyl-1,3-oxazoline with $Se(dtc)_2$ afforded the expected bis(4,4-dimethyl-2-phenyl-1,3-oxazolin-2-yl) selenide.[24] Hence, the decomposition may be due to the steric crowding around the selenium atom. All attempts to synthesize a stable bis{2-[1-(3,5-dimethylphenyl)-2-naphthyl]-4,5-dihydro-4,4-dimethyl-1,3-oxazol-2-yl} selenide, lithium selenolate and selenol were unsuccessful.

Spectroscopic Studies

The ^{1}H NMR spectra of the diselenide **4** and aryl benzyl selenide **8** are not particularly informative as the peaks are only shifted slightly downfield (ca. 0.09 ppm) from those in the free ligand **1**, thus indicating the presence of a weak Se···N interaction. However, much larger downfield shifts (ca. 0.7 ppm for the methylene proton and ca. 0.4 ppm for the methyl protons) were observed for the selenenyl halides **5**, **6**, and **8**. This indicates a strong Se···N interaction. These ^{1}H NMR chemical shifts are in good agreement with those in other intramolecularly stabilized organoselenium compounds.[11c−11e]

The ^{77}Se NMR chemical shifts are quite informative about the Se···N nonbonding interactions. The ^{77}Se NMR spectrum of **4** exhibits a single peak at δ = 450 ppm, which is more downfield shifted than systems having sp^3 nitrogen atoms.[11c,11e] However, it is close to the diselenide of 4,4-dimethyl-2-phenyl-1,3-oxazoline.[11d] Interestingly, the crystal structure of the diselenide reveals that only one of the nitrogen atoms interacts with the Se atom, with the other being much further away (vide infra). The ^{77}Se NMR chemical shift of compound **8** lies upfield (δ = 351 ppm) from that of the corresponding diselenide (**4**; δ = 450 ppm). This may be due to the presence of the benzyl group, which cannot accept electron density from the selenium; the Se···N interaction may also be very weak. The crystal structure of **8** confirmed this very weak Se···N interaction (vide infra). The ^{77}Se NMR chemical shifts of compounds **5**, **6**, and **7** are very close to each other and downfield of the diselenide. This shows that their Se···N interactions are almost equal and stronger than Se···N interaction of **4**. This is also confirmed by the crystal structures of **6** and **7** (vide infra).

In the IR spectra, the $\nu_{C=N}$ vibrations for compounds **4**−**8** are found in the range 1670−1760 cm^{-1} and are shifted by 20−100 cm^{-1} to higher frequency relative to the free ligand, indicating that the nitrogen of the oxazoline ring is coordinated to the selenium atom. These shifts to higher frequencies may be due to the presence of negative hyperconjugation between the selenium and the nitrogen atom. The $\nu_{C=N}$ frequencies of compounds **5** and **6** are observed at higher frequencies than compounds **4** and **8**, indicating the stronger coordination of nitrogen in the selenenyl halides than in the diselenide or benzyl selenide.

Compounds **4**, **6**, **7**, and **8** exhibit similar absorption spectra, with a strong peak in the 280−310 nm region and an absorption maximum at 295 nm due to the ligand core. Fluorescence emission spectra for compounds **4**, **5**, **6**, **8**, and free ligand **1** were recorded to probe their fluorescence emission properties in methanol at an excitation wavelength of 285 nm. The quantum yield of fluorescence emission was determined with naphthalene (Φ_f = 0.23) as a standard.[25] From the quantum yield of the fluorescence emission of selenium derivatives **4** (Φ_f = 0.038), **5** (Φ_f = 0.018), **6** (Φ_f = 0.021), and **8** (Φ_f = 0.043) compared to the fluorescence emission of free ligand **1** (Φ_f = 0.067) it is clear that the fluorescence emissions are quenched in the selenium compounds compared to the ligand **1** due to the substitution of heavy metal atoms.[26]

Mass spectra were recorded for compounds **4**−**6**, and **8** to identify the constitution of the product under mass spectrometric conditions. The presence of seven isotopes of selenium leads to a highly characteristic group of selenium fragments. Molecular ion peaks were observed in low intensities for all compounds. In all cases except **5**, the base peaks observed at *m*/*z* = 402−412 with high intensity can be assigned to RSe^+ fragments. This strongly suggests a weakening of the Se−X (X = SeR, Br, CH_2Ph) bond *trans* to the Se···N fragment.

X-ray Crystallographic Studies

The significant bond lengths and bond angles of compounds **4**, **6**, **7**, and **8** are listed in Table 1.

Molecular Structure of 4

The X-ray crystal structure of **4** is shown in Figure 1. The coordination geometry around the selenium atom is distorted T-shaped with each selenium atom bonded to selenium, carbon and a nitrogen/oxygen atom. The most interesting feature of the structure is the existence of both Se···N and Se···O interactions between selenium and nitrogen/oxygen in the same molecule. This is the first structure, to the best of our knowledge, to be reported where both intramolecular Se···N and Se···O interactions exist in the same mol-

 © 2004 Wiley-VCH Verlag GmbH & Co. KGaA, Weinheim

Table 1. Important bond lengths (Å) and bond angles (°) for **4**, **6**, **7**, and **8**

Compound **4**			
Se(1A)···N(1A)	2.976(8)	Se(1B) ···O(1B)	2.9815(5)
Se(1A)−Se(1B)	2.3216(15)	N(1A)···Se(1A)−Se(1B)	173.88(17)
O(1B) ···Se(1B)−Se(1A)	152.28(2)	C(24C)−Se(1C)−N(1C)	164.3(2)
N(1B) ···Se(1B)−Se(1A)	118.28(12)	C(1A)−Se(1A)−Se(1B)	101.9(3)
C(1B)−Se(1B)−Se(1A)	101.5(3)		
Compound **6**		Compound **7**	
Se···N	2.052(3)	Se···N	2.059(5)
Se−Br	2.6485(7)	Se−I	2.8297(8)
O−C(11)	1.353(5)	O−C(11)	1.337(7)
N−C(11)	1.288(5)	N−C(11)	1.289(7)
N···Se−Br	175.15(10)	N···Se−I	175.26(14)
C(1)−Se−Br	95.91(12)	C(1)−Se−I	97.51(15)
C(1)−Se···N	81.03(15)	C(1)−Se···N	80.8(2)
Compound **8**			
Se(1A)−C(1A)	1.916(5)	Se(1A)−C(24A)	1.979(7)
Se(1B)−C(1B)	1.903(6)	Se(1B)−C(24B)	1.952(7)
Se(1C)−C(24C)	1.911(7)	Se(1C)−C(1C)	1.918(5)
Se(1D)−C(1D)	1.935(5)	Se(1D)−C(24D)	1.944(7)
C(1A)−Se(1A)−C(24A)	98.0(2)	C(1B)−Se(1B)−C(24B)	98.4(3)
C(24C)−Se(1C)−C(1C)	98.1(3)	C(1D)−Se(1D)−C(24D)	98.0(2)
C(1A)−C(10A)−C(11A)−N(1A)	−72.6(7)	C(1A)−C(10A)−C(11A)−O(1A)	106.7(6)
C(1B)−C(10B)−C(11B)−N(1B)	73.1(8)	C(1B)−C(10B)−C(11B)−O(1B)	104.9(6)
C(1C)−C(10C)−C(11C)−N(1C)	−77.8(7)	C(1C)−C(10C)−C(11C)−O(1C)	102.6(6)
C(1D)−C(10D)−C(11D)−N(1D)	75.2(7)	C(1D)−C(10D)−C(11D)−O(1D)	104.9(6)

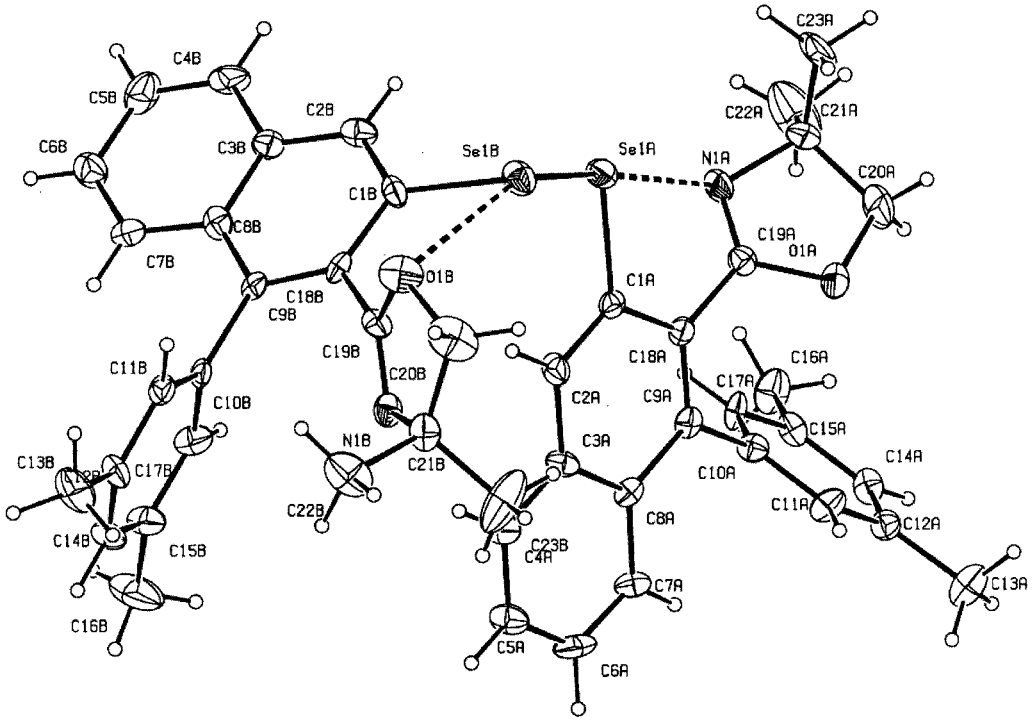

Figure 1. Molecular structure of **4**

ecule. Several structures of selenium compounds incorporating 4,4-dimethyl-2-phenyloxazoline,[2k,4i,17,18,24,27] have been reported by our group. In all cases only Se···N interactions were observed. Thus, the unusual observation of an intramolecular Se···O interaction in the structure of **4** may be explained by the orientation of the oxazoline rings.

 © 2004 Wiley-VCH Verlag GmbH & Co. KGaA, Weinheim

These rings are twisted about the C(18)−C(19) axis in opposite orientations such that in one oxazoline ring the nitrogen atom is directed towards the selenium [C(1A)−C(18A)−C(19A)−N(1A) = −48.27(14)° vs. C(1A)−C(18A)−C(19A)−O(1A) = 131.72(8)°], whereas in the other ring the oxygen atom is directed towards the selenium [C(1A)−C(18A)−C(19A)−O(1A) = 53.69(12)° vs. C(1A)−C(18A)−C(19A)−N(1A) = −127.58(10)°]. The orientation of the oxazoline rings may be due to the influence of steric crowding imposed by the sterically bulkier substituents present in the system. The Se(1A)···N(1A) [2.976(8) Å] and Se(1B)···O(1B) [2.9815 Å)] distances are similar to the respective distances in other related diselenides.[4i,28] The observed Se−Se distance [2.3216(16) Å] is also shorter than in bis(4,4-dimethyl-2-phenyl-1,3-oxazolin-2-yl) diselenide [2.354(8) Å],[11d] bis{2-[(dimethylamino)methyl]-phenyl} diselenide [2.357(1) Å][11e] and bis[2-(dimethylamino)naphthyl] diselenide[11c] [2.383(2) Å]. Another interesting feature in this structure is the "*cisoid*" conformation of the diselenide. Sandman et al.[29] have reported the crystal structures of two conformational polymorphs of bis(2-naphthyl) ditelluride. The "*cisoid*" conformations have a C−Se−Se−C torsion angle of less than 90° and the "*transoid*" conformations have a C−Se−Se−C torsion angle greater than 90°. In the case of **4** the C(1A)−Se(1A)−Se(1B)−C(1B) torsion angle is 81.42° and thus has a "*cisoid*" conformation. From the unusual intramolecular Se···N and Se···O interactions, the shorter Se−Se distance, and the "*cisoid*" conformation it may be concluded that the Se−Se and Se···N bond lengths are lengthened to minimize the steric crowding imposed by the sterically more demanding group present in this system. There are no significant intermolecular Se···Se contacts. The shortest intermolecular Se···Se distance [8.618 Å] is much longer than the sum of the van der Waals radii (3.8 Å). However, intermolecular Se···H [Se1A···H13AA: 3.1096 Å; Se1A···H2BA: 3.2678 Å; Se1B···H2AA: 2.7981 Å; Se1B···H13BB: 2.8697 Å] contacts exist that are much shorter than the sum of the van der Waals radii (3.35 Å). These short Se···H contacts may be a result of optimized dense packing of the molecules.

Molecular Structure of 6

An ORTEP view of **6** is shown in Figure 2. The geometry around Se is T-shaped and the methyl groups attached to the oxazoline are disordered. The strong nonbonded Se···N interaction [2.052(3) Å] is very close to the corresponding distance in [2-(4,4-dimethyl-1,3-oxazolin-2-yl)phenyl]selenium bromide [2.063(3) Å][11d] and shorter than in {2-[(dimethylamino)methyl]phenyl}selenium bromide [2.143(6) Å].[11e] The Se−Br bond length [2.6485(7) Å] is longer than the sum of the single-bond covalent radii of Se and Br (2.31 Å). The lengthening of the Se−Br bond length can be attri-

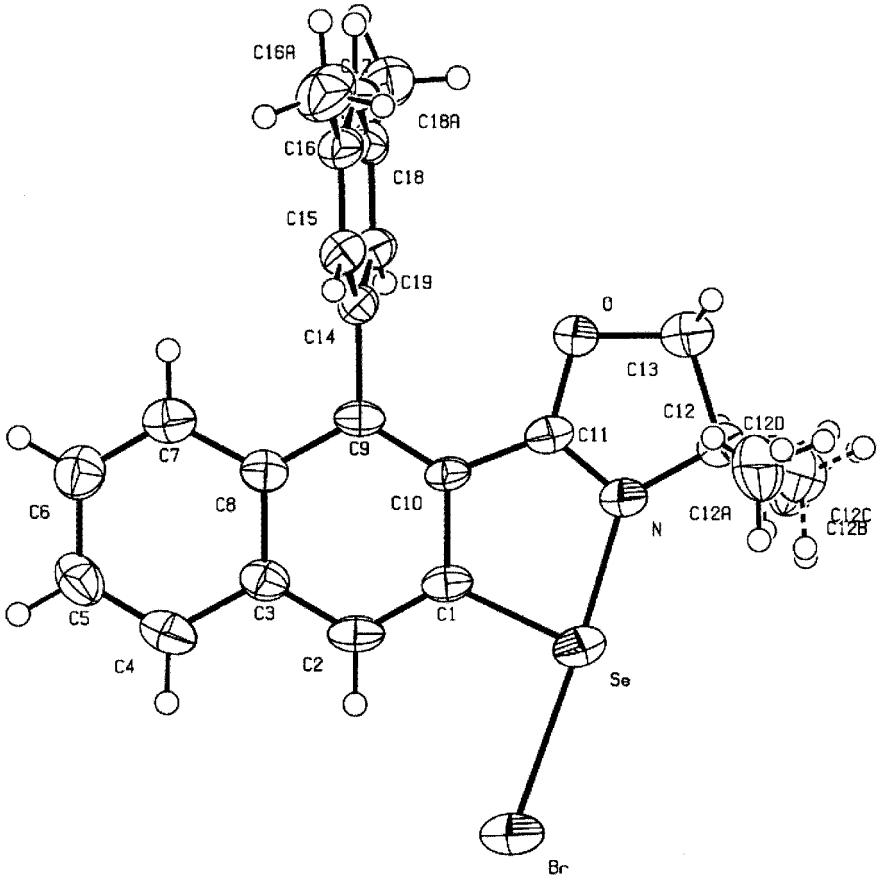

Figure 2. Molecular structure of **6**

 © 2004 Wiley-VCH Verlag GmbH & Co. KGaA, Weinheim

buted to the strong *trans* influence of the Se···N interaction. A similar observation has been made for the molecular structure of 2-formylbenzeneselenenyl bromide.[30] The Se−Br bond length in **6** [2.6485(7) Å] is also similar to the reported values for [2-(4,4-dimethyl-1,3-oxazolin-2-yl)phenyl]selenium bromide [2.631(9) Å] and {2-[(dimethylamino)methyl]phenyl}selenium bromide [2.634(1) Å]. The Se···N−Br angle [175.16 (10)°] is close to linear. From the C(1)−Se−Br [95.91(12)°] and C(1)−Se···N [81.03(15)°] bond angles the coordination around selenium can be regarded as trigonal bipyramidal if the lone pairs are taken into account. However, the packing pattern of this structure is significantly different from the other intramolecularly stabilized organoselenium bromides, including [2-(4,4-dimethyl-2-phenyloxazolinyl)phenyl]selenium bromide. In all the organoselenium bromides the formation of weak dimers by intermolecular interactions between selenium and bromine were observed.[11c−11e,31] However, in the case of **6** such intermolecular Se···Br interactions are absent. The shortest intermolecular Se···Br contact [4.8914 Å] is greater than the sum of the van der Waals radii (3.9 Å). The absence of intermolecular Se···Br interactions clearly suggests that the sterically more demanding group present in this system prevents the formation of weak dimers and thus confirms the formation of a truly monomeric selenium bromide. Intermolecular Br···H (Br···H2A: 2.7190 Å; Br···H19Aa: 3.1953 Å; Br···H4Ab: 3.1463 Å; Br···H5Ab: 3.0838 Å) and Se···H12C (3.1405 Å) contacts are observed in the packing diagram. The Br···H and Se···H distances are shorter than the sum of their van der Waals radii, at 3.45 Å and 3.35 Å, respectively. The short Se···H contacts may be a result of optimized dense packing of molecules as for the above structure.

Molecular Structure of 7

The molecular structure of **7** is given in Figure 3. This is isostructural with **6**. In this structure the methyl groups attached to the oxazoline rings are disordered. The observed intramolecular Se···N distance [2.059(5) Å] is considerably shorter than the corresponding distances in [2-(4,4-dimethyl-2-oxazoline)phenyl]selenium iodide [2.133(4) Å],[11d] and [8-(dimethylamino)-1-naphthyl]selenium iodide [2.242(5) Å],[11c] whereas the Se−I distance [2.8297(8) Å] is considerably longer than the corresponding distance in [2-(4,4-dimethyl-1,3-oxazolin-2-yl)phenyl]selenium iodide [2.7773(7) Å] and [8-(dimethylamino)-1-naphthyl]selenium iodide [2.742(9) Å]. The Se−I distance is also longer than in 2,4,6-tri-*tert*-butylphenyl iodo selenide [2.529(1) Å].[21] The elongation of the Se−I bond length may be attributed to the presence of a shorter (strong) Se···N interaction *trans* to the Se−I fragment. The N···Se−I bond angle

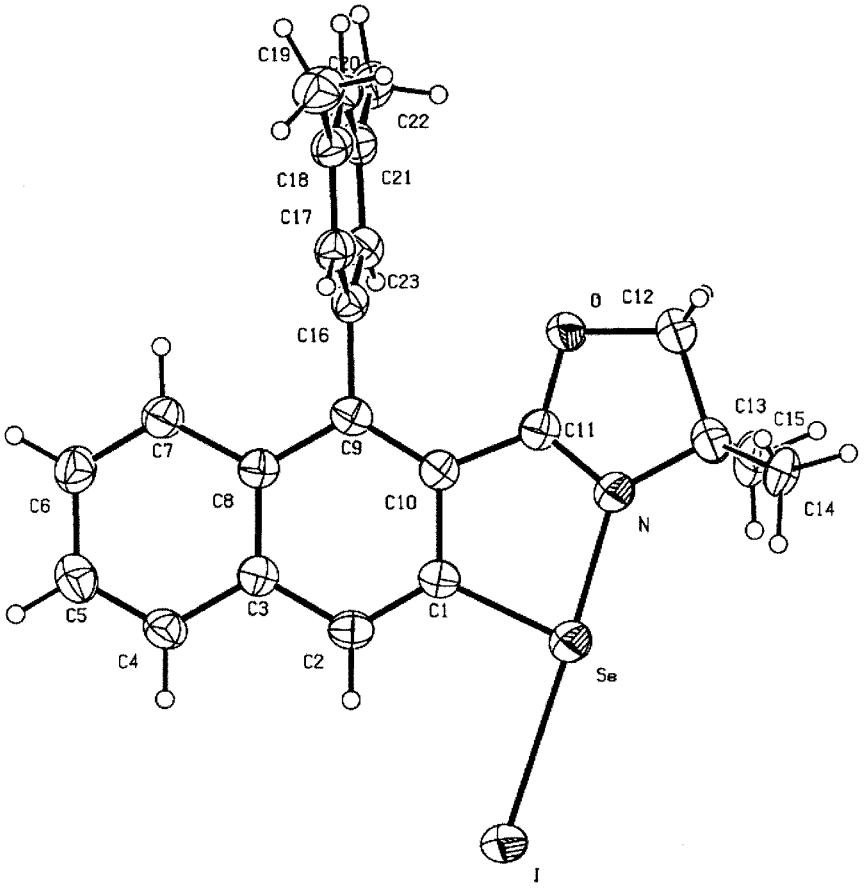

Figure 3. Molecular structure of **7**

 © 2004 Wiley-VCH Verlag GmbH & Co. KGaA, Weinheim

[175.26(14)°] is close to linear. In the packing diagram of **7** the shortest intermolecular contact between the selenium and iodine is 4.811 Å, about 0.8 Å greater than the sum of the van der Waals radii (4.02 Å). Intermolecular Se···H and Se···H contacts are also observed here that are shorter than the sum of the van der Waals radii, which may be due to the optimized dense packing of the molecules.

Molecular Structure of 8

The molecular structure of **8** is shown in Figure 4 as an ORTEP view. This compound crystallizes in the monoclinic system with four symmetry-independent molecules in the asymmetric unit cell. The geometry around the selenium atom is V-shaped. The selenium atom is bonded to two carbon atoms derived from two different organic substituents. It is worth noting that the C(1)−Se(1) [C(1A)−Se(1A): 1.916(5) Å; C(1B)−Se(1B): 1.903(6) Å; C(1C)−Se(1C): 1.918(5) Å; C(1D)−Se(1D): 1.935(5) Å] and C(24)−Se(1) [C(24A)−Se(1A): 1.979(7) Å; C(24B)−Se(1B): 1.952(7) Å; C(24C)−Se(1C): 1.911(7) Å; C(1D)−Se(1D): 1.944(7) Å] bond lengths, and the C(1)−Se(1)−C(24) [C(1A)−Se(1A)−C(24A): 98.0(2)°; C(1B)−Se(1B)−C(24B): 98.4(3)°; C(1C)−Se(1C)−C(24C): 98.1(3)°; C(1D)−Se(1D)−C(24D): 98.0(2)°] bond angle are significantly different for all four independent molecules. The Se−C(Ph) and Se−CH_2Ph bond lengths are in good agreement with the corresponding distances reported for the related systems.[11d,32] One of the interesting features is the longer Se−CH_2Ph [Se(1A)−C(24A): 1.979(7) Å] distance compared to that in the sterically less hindered benzyl 2-(4,4-dimethyl-1,3-oxazolin-2-yl)phenyl selenide [1.966(3) Å], even though the intramolecular Se···N interaction (3.3842 Å) was found to be much weaker than in the latter case [2.798(3) Å]. The lengthening of the Se−CH_2Ph distance even in the presence of a weak Se···N interaction suggests that the sterically more demanding group present in the system plays an important role. The very weak Se···N interaction may be a result of the perpendicular orientation of the oxazoline ring, which is twisted about the C(10)−C(11) bond axis such that the nitrogen atom is slightly away from the selenium. Figure 4 shows that Se and N atoms lie in a different plane, in contrast to the benzyl (4,4-dimethyl-1,3-oxazolin-2-yl)phenyl selenide where both the selenium and nitrogen are in same plane.

Conclusion

Novel organoselenium compounds, including a diselenide, with both intramolecular Se···N and Se···O interactions, incorporating a ligand with steric and intramolecularly coordinating groups, have been prepared and characterized. From the current results and their comparison with intramolecularly stabilized organoselenium compounds derived from sterically less-hindered ligands, it is apparent that the strength of the Se···N interaction also depends on the nature of the substituents (steric groups) present in the system, in addition to the nature of the nitrogen atom used as an *ortho* chelating group and the electronegativity of the group attached to the selenium atom. The Se···N nonbonding interactions are considerably stronger than in organoselenium

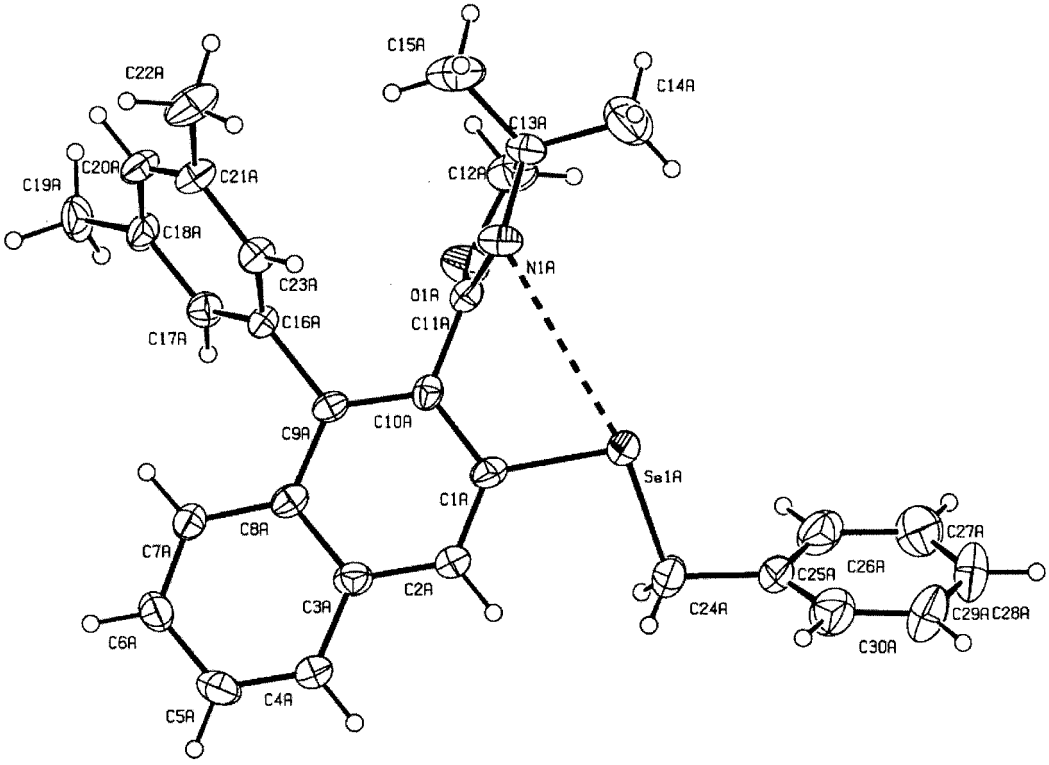

Figure 4. Molecular structure of **8**

 © 2004 Wiley-VCH Verlag GmbH & Co. KGaA, Weinheim

compounds derived from the sterically less-hindered ligands. The Se···N nonbonding interactions lengthen the Se···X bond (X = −Se, Br, I, or CH_2) and enhance the possibility of nucleophilic attack at the selenium atom. The intermolecular Se···X (X = Cl, Br, I) interactions generally observed in the other reported organoselenium halides are absent, possibly due to the presence of the sterically more-demanding group. Thus, selenium halides derived from this substrate can be considered as true monomers in the solid state. Although the intermolecular Se···X interactions of the organoselenium halides described here are not within the sum of the van der Waals radii, the intermolecular Se···X contacts decrease (strong interaction) as the size of the halogen atom increases. This may be attributed to the decrease of ligand-ligand repulsions (steric repulsions) as the size of the atom increases.

Experimental Section

General: All reactions were carried out in an inert atmosphere using nitrogen or argon with standard vacuum-line techniques. All solvents were purified by following the literature method and freshly distilled prior to use.[33] 2-[1-(3,5-Dimethylphenyl)-2-naphthyl]-4,5-dihydro-4,4-dimethyloxazole (Aldrich) and *n*-butyllithium (E. Merck) were reagent grade and used as received. $Se(dtc)_2$ was prepared by a reported procedure.[34] Melting points were recorded in capillary tubes and are uncorrected. ^1H, ^{13}C and ^{77}Se NMR were obtained at 300, 75.42 and 57.22 MHz, respectively, in $CDCl_3$ on a Varian VXR 300S spectrometer. Chemical shifts are cited with respect to $SiMe_4$ as internal (^1H and ^{13}C) and Me_2Se (^{77}Se) as external standard. Elemental analyses were determined with a Carlo−Erba model EA 1112 CHNS analyzer. Infrared spectra were recorded in the range of 4000−400 cm^{-1} on a Nicolet Impact 400 FT-IR spectrometer. UV/Vis spectra were recorded on a Shimadzu UV-160A spectrophotometer and fluorescence spectra on a Perkin−Elmer LS-55 Luminescence spectrometer. Fast atomic bombardment (FAB) mass spectra were recorded at room temperature on a JEOL SX 102/DA-6000 mass spectrometer/data system with xenon (6 kV, 10 mV) as the bombarding gas. The accelerating voltage was 10 kV. *m*-Nitrobenzyl alcohol was used as the matrix with cation detection. For isotopes the value given is for the most intense peak.

Synthesis of Diselenide 4: Addition of 1.6 M solution of *n*BuLi in hexane (3.45 mL, 5.5 mmol) to a diethyl ether (50 mL) solution of 2-[1-(3,5-dimethylphenyl)-2-naphthyl]-4,5-dihydro-4,4-dimethyloxazole (1.647 g, 5 mmol) under N_2 at 0 °C resulted in a dark brown solution of the lithiated compound. After 2 hours, finely ground selenium powder (0.4 g, 5 mmol) was added at 0 °C and the temperature maintained for 2 hours to give the lithium areneselenolate. The reaction mixture was then poured into a beaker containing cold aqueous $NaHCO_3$ and O_2 was passed at a moderate rate for 30 min and the mixture extracted with diethyl ether (50 mL). The organic phase was washed with water, and dried over Na_2SO_4. The filtrate was concentrated to give a yellow oil, which solidified upon addition of hexane. The compound was recrystallized from a hexane/dichloromethane (4:1) mixture to give yellow crystals of **4**. Yield: 0.97 g, 25%. M.p. 196−198 °C. $C_{46}H_{44}N_2O_2Se_2$ (816.2): calcd. C 67.83, H 5.44, N 3.44; found C 67.52, H 5.41, N 3.22. UV/Vis (dichloromethane): λ_{max} (ε) = 303.5 nm (18000 dm^3 mol^{-1} cm^{-1}), 350 (8000). ^1H NMR (300 MHz, $CDCl_3$, 298 K): δ = 1.29 (s), 2.37 (s), 3.78 (s), 1.29 (s), 2.37 (s), 3.78 (s), 7.05 (s), 7.35 (t), 7.65 (t), 7.75 (t), 8.3 (s) ppm. ^{13}C NMR (300 MHz, $CDCl_3$, 298 K): δ = 21.2, 28.0, 68.1, 79.4, 126.1, 127.0, 127.6, 127.8, 128.0, 129.0, 129.4, 131.2, 134.6, 137.1, 137.6, 140.9, 160.1 ppm. ^{77}Se NMR (300 MHz, $CDCl_3$, 298 K): δ = 450 ppm. IR (KBr): $\tilde{\nu}$ = 1670 cm^{-1} ν(C=N). FAB-MS: *m*/*z* = 816 [M^+].

Synthesis of Selenenyl Chloride 5: Treatment of a solution of the diselenide (0.16 g, 0.2 mmol) in carbon tetrachloride (25 mL) with a carbon tetrachloride solution of SO_2Cl_2 (0.6 mL of 2.1 g, 50 mL, 0.2 mmol) at room temperature gave a yellow precipitate after 1 hour. The mixture was evaporated to dryness under vacuum in order to give the desired compound. The yellow crystalline product was obtained after recrystallization from methanol/chloroform (2:1). Yield: 0.083 g, 93%. M.p. (decomp.) > 200 °C. $C_{23}H_{22}ClNOSe$ (443.05): calcd. C 62.39, H 5.01, N 3.16; found C 62.33, H 5.33, N 3.23. ^1H NMR (300 MHz, $CDCl_3$, 298 K): δ = 1.63 (s), 2.39 (s), 4.45 (s), 6.92 (s), 7.13 (s), 7.45 (t), 7.59 (d), 7.7 (t), 8.05 (d), 9.36 (s) ppm. ^{13}C NMR (300 MHz, $CDCl_3$, 298 K): δ = 21.3, 27.9, 65.3, 84.9, 115.8, 126.4, 127.4, 127.6, 128.2, 129.0, 129.9, 131.0, 134.9, 135.8, 137.2, 141.9, 143.8, 167.1 ppm. ^{77}Se NMR (300 MHz, $CDCl_3$, 298 K): δ = 839 ppm. IR (KBr): $\tilde{\nu}$ = 1755 cm^{-1} ν(C=N). FAB-MS: *m*/*z* = 443 [M^+].

Synthesis of Selenenyl Bromide 6: The procedure followed was the same as that used for the preparation of compound **5**, except the addition of Br_2/CCl_4 was carried out for 4 hour at 0 °C. The compound was recrystallized from a dichloromethane/hexane mixture to give yellow crystals. Yield: 0.06 g, 68%. M.p. (decomp.) > 216 °C. $C_{23}H_{22}BrNOSe$ (487.0): calcd. C 56.70, H 4.55, N 2.87; found C 56.51, H 4.39, N 2.70. UV/Vis (dichloromethane): λ_{max} (ε) = 399.5 nm (9540 dm^3 mol^{-1} cm^{-1}), 303.5 (11950). ^1H NMR (300 MHz, $CDCl_3$, 298 K): δ = 1.64 (s), 2.39 (s), 4.47 (s), 6.9 (s), 7.13 (s), 7.43 (t), 7.53 (d), 7.63 (t), 8.01 (d), 9.4 (s) ppm. ^{13}C NMR (300 MHz, $CDCl_3$, 298 K): δ = 21.3, 27.9, 65.2, 84.7, 115.9, 126.4, 127.6, 128.2, 129.1, 129.5, 129.8, 131.2, 134.9, 135.9, 137.2, 139.7, 143.8, 166.7 ppm. ^{77}Se NMR (300 MHz, $CDCl_3$, 298 K): δ = 836 ppm. IR (KBr): $\tilde{\nu}$ = 1660 cm^{-1} ν(C=N). FAB-MS: *m*/*z* = 488 [M + 1]$^+$, 487 [M^+].

Synthesis of Selenenyl Iodide 7: Here the procedure used for the preparation of compound **6** was also followed, with the addition of I_2 instead of SO_2Cl_2. The solution obtained was concentrated to give a yellow crystalline product. The compound was recystallized from a dichloromethane/hexane mixture (1:2). Yield: 0.42 g, 79%. M.p. (decomp.) > 240 °C. $C_{23}H_{22}INOSe$ (535.0): calcd. C 51.71, H 4.15, N 2.62; found C 51.68, H 4.12, N 2.46. UV/Vis (dichloromethane): λ_{max} (ε) = 400 nm (7890 dm^3 mol^{-1} cm^{-1}), 303 (17760). ^1H NMR (300 MHz, $CDCl_3$, 298 K): δ = 1.59 (s), 2.4 (s), 3.8 (s), 4.3 (s), 6.9 (s), 7.4 (m), 7.6 (m), 7.72 (d), 8.0 (d), 9.31 (s) ppm. ^{13}C NMR (300 MHz, $CDCl_3$, 298 K): δ = 21.6, 28.4, 65.4, 84.2, 117.0, 126.4, 127.5, 127.7, 127.9, 128.8, 129.7, 131.6, 132.3, 134.9, 136.2, 137.1, 143.5 ppm. ^{77}Se NMR (300 MHz, $CDCl_3$, 298 K): δ = 782 ppm.

Synthesis of Aryl Benzyl Selenide 8: The benzyl chloride (0.635 mL, 5 mmol) was added to the lithium selenolate at 0 °C and stirring continued for 2 hours. The usual work up followed by evaporation under reduced pressure gave the desired yellow compound, which was recrystallized from an acetonitrile/dichloromethane mixture (2:1). Yield: 0.7 g, 28%, M.p. 158−160 °C. $C_{30}H_{29}NOSe$ (500.2): calcd. C 72.29, H 5.86, N 2.81; found C 72.59, H 5.95, N 2.66. UV/Vis (dichloromethane): λ_{max} (ε) = 350 nm (3000 dm^3 mol^{-1} cm^{-1}), 303.5 (18420). ^1H NMR (300 MHz, $CDCl_3$, 298 K): δ = 1.12 (s), 2.35 (s), 3.83 (s), 4.22 (s), 7.02 (s), 7.39 (t), 7.6−7.49 (t),

 © 2004 Wiley-VCH Verlag GmbH & Co. KGaA, Weinheim

Table 2. Crystal data and structure refinement for **4**, **6**, **7** and **8**

Compound	**4**	**6**	**7**	**8**
Empirical formula	$C_{46}H_{44}N_2O_2Se_2$	$C_{23}H_{22}BrNOSe$	$C_{23}H_{22}INOSe$	$C_{30}H_{29}NOSe$
Molecular mass	814.75	487.29	534.28	498.50
Crystal system	Monoclinic	Monoclinic	Monoclinic	Monoclinic
Space group	$P2_1/c$	$P2_1/c$	$P2_1/c$	Cc
a (Å)	24.394(5)	11.3367(15)	11.4446(14)	14.6082(12)
b (Å)	8.1678(16)	9.8765(13)	9.8991(12)	14.6368(11)
c (Å)	21.307(5)	18.873(2)	18.675(2)	47.449(4)
β (deg)	106.944(17)	93.826(2)	91.865(7)	92.7850(10)
V (Å^3)	4061.0(15)	2108.5(5)	2114.6(4)	10133.5(14)
Z	4	4	4	16
D(calcd.) (Mg/m^3)	1.333	1.535	1.678	1.307
Abs coeff (mm^{-1})	1.860	3.688	3.248	1.504
Obsd. refls. [$I > 2\sigma(I)$]	5310	5066	2885	22326
Final $R(F)$ [$I > 2\sigma(I)$][a]	0.0732	0.0556	0.0515	0.0539
$wR(F^2)$ [$I > 2\sigma(I)$]	0.1073	0.1222	0.1510	0.1193
Data/restraints/parameters	5310/0/ 521	5066/6/270	2885/4/ 270	22326/2/1206
Goodness of fit on F^2	1.002	0.874	1.173	1.024

[a] $R(F_o) = ||F_o| - |F_c||/|F_o|$ and $wR(F_o^2) = \{[w(F_o^2 - F_c^2)^2]/[w(F_c^2)^2]\}^{1/2}$.

7.72 (d), 7.87 (s) ppm. ^{13}C NMR (300 MHz, $CDCl_3$, 298 K): δ = 21.2, 27.7, 67.9, 126.4, 126.7, 127.4, 128.2, 129.0, 130.4, 131.4, 133.3, 134.0, 137.0, 137.5, 138.3, 141.1, 161.7 ppm. ^{77}Se NMR (300 MHz, $CDCl_3$, 298 K): δ = 351 ppm. IR (KBr): $\tilde{\nu}$ = 1670 cm^{-1} ν(C=N). FAB-MS: m/z = 500 [M$^+$].

Attempted Synthesis of 9: A solution of α,α-dibromo-*o*-xylene (2.5 mmol) in 5 mL of diethyl ether was added dropwise at 0 °C to a diethyl ether solution of arenelithium selenolate (5 mmol). The mixture was stirred at 0 °C for 2 hours. The resulting mixture was washed with water, dried and the solvents evaporated to give a yellow solid which was characterized as the selenenyl bromide **6**.

X-ray Crystallography: The diffraction measurements for compounds **4**, **6**, and **7** were performed on a Siemens R3m/V diffractometer and compound **8** on a Bruker SMART diffractometer with graphite-monochromated Mo-K_α radiation (λ = 0.7170 Å). The structures were determined by routine heavy-atom and Fourier methods using SHELXS-86[35] and refined by full-matrix least-squares with the non-hydrogen atoms anisotropic and hydrogens with fixed isotropic thermal parameters of 0.07 Å^2 by means of the SHELXL-97 program.[36] Hydrogens were partially located from difference electron-density maps and the rest were fixed at predetermined positions. Scattering factors were from common sources. Some details of the structural refinement are given in Table 2.
CCDC-217082 to -217085 (**4**, **6**, **7**, and **8**, respectively) contain the supplementary crystallographic data for this paper. These data can be obtained free of charge at www.ccdc.cam.ac.uk/conts/retrieving.html [or from the Cambridge Crystallographic Data Centre, 12 Union Road, Cambridge CB2 1EZ, UK; Fax: (internat.) + 44-1223-336-033; E-mail: deposit@ccdc.cam.ac.uk].

Acknowledgments

We are grateful to the Department of Science and Technology (DST), New Delhi. Additional help from the Regional Sophisticated Instrumentation Center (RSIC), Indian Institute of Technology (IIT), Bombay, for 300 MHz NMR Spectroscopy, and the Tata Fundamental Research Institute (TIFR), Bombay, for 500 MHz NMR spectroscopy is gratefully acknowledged. Thanks are due to RSIC, Central Drug Research Institute (CDRI), Lucknow, for providing mass spectra.

[1] [1a] T. Wirth, *Angew. Chem.* **2000**, *112*, 3890; *Angew. Chem. Int. Ed.* **2000**, *39*, 3740. [1b] T. Wirth, *Organoselenium Chemistry*, Springer-Verlag, Berlin, **2000**, vol. 208. [1c] T. G. Back, *Organoselenium Chemistry*, Oxford University Press, Oxford, **1999**. [1d] S. Patai, Z. Rappoport, *The Chemistry of Organic Selenium and Tellurium Compounds*, Wiley, Chichester, **1986**, vol. 1; **1987**, vol. 2. [1e]N. Petragnani, H. A. Stefani, C. J. Valduga, *Tetrahedron* **2001**, *57*, 1411−1448. [1f] T. G. Back, Z. Moussa, M. Parvez, *J. Org. Chem.* **2002**, *67*, 499−508. [1g] L. Uehlin, G. Fragale, T. Wirth, *Chem. Eur. J.* **2002**, *8*, 1125−1133.

[2] [2a] W. Levason, S. D. Orchard, G. Reid, *Coord. Chem. Rev.* **2002**, *225*, 159−199. [2b] W. Levason, G. Reid, *J. Chem. Soc., Dalton Trans.* **2001**, 2953−2960. [2c] U. Englich, K. Ruhlandt-Senge, *Coord. Chem. Rev.* **2000**, *210*, 135−179. [2d] G. G. Briand, N. Burford, *Adv. Inorg. Chem.* **2000**, *50*, 285−357. [2e] J. Arnold, *Prog. Inorg. Chem.* **1995**, *43*, 353−417. [2f] L. Henriksen, N. Stuhr-Hansen, *J. Chem. Soc., Perkin Trans. 1* **1999**, 1915−1916. [2g] V. W.-W. Yam, Y.-L. Pui, K. M.-C. Wong, K.-K. Cheung, *Chem. Commun.* **2000**, 1751−1752. [2h] U. Englich, K. Ruhlandt-Senge, *Chem. Eur. J.* **2000**, *6*, 4063−4070. [2i] U. Englich, K. Ruhlandt-Senge, *Z. Anorg. Allg. Chem.* **2001**, *627*, 851−856. [2j] J. Laube, S. Jäger, C. Thöne, *Eur. J. Inorg. Chem.* **2001**, *2001*, 1983−1992. [2k] G. Mugesh, H. B. Singh, R. P. Patel, R. J. Butcher, *Inorg. Chem.* **1998**, *37*, 2663−2669. [2l] R. Kaur, H. B. Singh, R. P. Patel, S. K. Kulshreshtha, *J. Chem. Soc., Dalton Trans.* **1996**, 461−466.

[3] [3a] M. Bochmann, *Chem. Vap. Deposition* **1996**, *2*, 85−96. [3b] A. C. Jones, *Chem. Soc. Rev.* **1997**, 101−110. [3c] A. N. Gleizes, *Chem. Vap. Deposition* **2000**, *6*, 155−173. [3d] G. C. Bwembya, X. Song, M. Bochmann, *Chem. Vap. Deposition* **1995**, *1*, 78−80. [3e] J. McAleese, P. O'Brien, D. J. Otway, *Chem. Vap. Deposition* **1998**, *4*, 94−96.

[4] [4a] T. G. Chasteen, R. Bentley, *Chem. Rev.* **2003**, *103*, 1−26. [4b] G. Mugesh, W. W. du Mont, H. Sies, *Chem. Rev.* **2001**, *101*, 2125−2180. [4c] G. Mugesh, W. W. du Mont, *Chem. Eur. J.* **2001**, *7*, 1365−1370. [4d] G. Mugesh, H. B. Singh, *Chem. Soc. Rev.* **2000**, *29*, 347−357. [4e] Y. You, K. Ahsan, M. R. Detty, *J. Am. Chem. Soc.* **2003**, *125*, 4918−4927. [4f] G. Mugesh, W. W. du Mont, C. Wismach, P. G. Jones, *ChemBioChem* **2002**, *3*, 440−447. [4g] G. E. Arteel, H. Sies, *Environ. Toxicol. Pharmacol.* **2001**, *10*, 153−158. [4h] J. N. Commandeur, M. Rooseboom, N. P. Vermeulen, *Adv. Exp. Med. Biol.* **2001**, *500*, 105−112. [4i] G. Mugesh, A. Panda, N. S. Punekar, H. B. Singh, R. J. Butcher, *J. Am. Chem. Soc.* **2001**, *123*, 839−850. [4j] K. Goto, M. Nagahama, T. Mizushima, K. Shimada, T. Kawashima, R.

 © 2004 Wiley-VCH Verlag GmbH & Co. KGaA, Weinheim

Okazaki, *Org. Lett.* **2001**, *3*, 3569−3572. [4k] H. Sies, G. E. Arteel, *Free Radical Bio. Med.* **2000**, *28*, 1451−1455. [4l] Y. Xu, E. T. Kool, *J. Am. Chem. Soc.* **2000**, *122*, 9040−9041. [4m] X. Ren, J. Liu, G. Luo, Y. Zhang, Y. Luo, G. Yan, J. Shen, *Bioconjugate Chem.* **2000**, *11*, 682. [4n] H. Frisell, L. Engman, *J. Mol. Struct.* **2000**, *526*, 103−114. [4o] A. A. Vasil'ev, L. Engman, *J. Org. Chem.* **1998**, *63*, 3911−3917. [4p] S. C. Gamble, A. Wiseman, P. S. Goldfarb, *J. Chem. Tech. Biotechol.* **1997**, *68*, 123−134.

[5] [5a] D. R. Cary, G. E. Ball, J. Arnold, *J. Am. Chem. Soc.* **1995**, *117*, 3492−3501. [5b] C. P. Gerlach, V. Christou, J. Arnold, *Inorg. Chem.* **1996**, *35*, 2758−2766 and references cited therein.

[6] [6a] M. Bochmann, G. Bwembya, K. J. Webb, *Inorg. Synth.* **1997**, *31*, 19−24. [6b] M. Bochmann, A. K. Powell, X. Song, *J. Chem. Soc., Dalton Trans.* **1995**, 1645−1648 and references cited therein.

[7] [7a] R. Michalczyk, J. G. Schmidt, E. Moody, Z. Li, R. Wu, R. B. Dunlap, J. D. Odom, L. A. Silks III, *Angew. Chem.* **2000**, *112*, 3200−3203; *Angew. Chem. Int. Ed.* **2000**, *39*, 3067−3070. [7b] M. Iwaoka, H. Komatsu, S. Tomoda, *Bull. Chem. Soc. Jpn.* **1996**, *69*, 1825−1828. [7c] M. Iwaoka, S. Tomoda, *J. Am. Chem. Soc.* **1994**, *116*, 4463−4464.

[8] M. Tiecco, L. Testaferri, C. Santi, C. Tomassini, F. Marini, L. Bagnoli, A. Temperini, *Chem. Eur. J.* **2002**, *8*, 1118−1124.

[9] H. Komatsu, M. Iwaoka, S. Tomoda, *Chem. Commun.* **1999**, 205−206.

[10] [10a] W. Nakanishi, S. Hayashi, N. Itoh, *Chem. Commun.* **2003**, 124−125. [10b] M. Iwaoka, H. Komatsu, T. Katsuda, S. Tomoda, *J. Am. Chem. Soc.* **2002**, *124*, 1902−1909. [10c] W. Nakanishi, S. Hayashi, *J. Org. Chem.* **2002**, *67*, 38−48.

[11] [11a] M. Iwaoka, S. Tomoda, *J. Am. Chem. Soc.* **1996**, *118*, 8077−8084. [11b] M. Iwaoka, S. Tomoda, *Phosphorous Sulfur Silicon Relat. Elem.* **1992**, *67*, 125. [11c] A. Panda, G. Mugesh, H. B. Singh, R. J. Butcher, *Organometallics* **1999**, *18*, 1986−1993. [11d] G. Mugesh, A. Panda, H. B. Singh, R. J. Butcher, *Chem. Eur. J.* **1999**, *5*, 1411−1421. [11e] R. Kaur, H. B. Singh, R. P. Patel, *J. Chem. Soc., Dalton Trans.* **1996**, 2719−2726.

[12] M. Iwaoka, T. Katsuda, S. Tomoda, J. Harada, K. Ogawa, *Chem. Lett.* **2002**, *31*, 518−519.

[13] N. Ramasubbu, R. Parthasarathy, *Phosphorous Sulfur* **1987**, *31*, 221.

[14] B. M. Goldstein, S. D. Kennedy, W. J. Hennen, *J. Am. Chem. Soc.* **1990**, *112*, 8265−8268.

[15] D. H. R. Barton, M. B. Hall, Z. Lin, S. I. Parekh, J. Reibenspies, *J. Am. Chem. Soc.* **1993**, *115*, 5056−5059.

[16] [16a] S. R. Wilson, P. A. Zucker, R. R. C. Huang, A. Spector, *J. Am. Chem. Soc.* **1989**, *111*, 5936−5939. [16b] L. Engman, D. Stern, I. A. Cotgreave, C. M. Andersson, *J. Am. Chem. Soc.* **1992**, *114*, 9737−9743. [16c] V. Galet, J.-L. Bernier, J.-P. Henichart, D. Lesieur, C. Abadie, L. Rochette, A. Lindenbaum, J. Chalas, J.-F. R. de la Faverie, B. Pfeiffer, P. Renard, *J. Med. Chem.* **1994**, *37*, 2903−2911. [16d] M. Iwaoka, S. Tomoda, *J. Am. Chem. Soc.* **1994**, *116*, 2557−2561. [16e] T. Saiki, K. Goto, R. Okazaki, *Angew. Chem.* **1997**, *109*, 2320−2321; *Angew. Chem. Int. Ed. Engl.* **1997**, *36*, 2223−2224.

[17] G. Mugesh, H. B. Singh, R. J. Butcher, *Eur. J. Inorg. Chem.* **1999**, 1229−1236.

[18] G. Mugesh, H. B. Singh, R. J. Butcher, *J. Organomet. Chem.* **1999**, *577*, 243−248.

[19] L. P. Anderson, *DE* 3 525 256, 1986; *US Pat.* 633 809, **1984**.

[20] T. Klapoetke, J. Passmore, *Acc. Chem. Res.* **1989**, *22*, 234−240.

[21] W. W. du Mont, S. Kubiniok, K. Peters, H.-G. Von Schnering, *Angew. Chem.* **1987**, *99*, 820−821; *Angew. Chem. Int. Ed. Engl.* **1987**, *26*, 780−781.

[22] W. W. du Mont, A. Martens, S. Pohl, W. Saak, *Inorg. Chem.* **1990**, *29*, 4847−4848.

[23] H. Higuchi, M. Kugimiya, T. Otsubo, Y. Sakata, S. Misumi, *Tetrahedron Lett.* **1983**, *24*, 2593−2594.

[24] S. D. Apte, H. B. Singh, R. J. Butcher, *J. Chem. Res. (S)* **2000**, 160−161; (*M*), **2000**, 0559−0569.

[25] H. Du, R.-C. A. Fuh, J. Li, L. A. Corkan, J. S. Lindsay, *Photochem. Photobiol.* **1998**, *68*, 141−142.

[26] V. Balzani, V. Carassiti, *Photochemistry of Coordination Compounds*, London Academic Press, **1970**, p. 432.

[27] [27a] G. Mugesh, H. B. Singh, R. J. Butcher, *J. Chem. Res. (S)* **1999**, 416−417; (*M*) **1999**, 1801−1810. [27b] G. Mugesh, H. B. Singh, R. J. Butcher, *Tetrahedron: Asymmetry* **1999**, *10*, 237−242.

[28] G. Fragale, M. Neuburger, T. Wirth, *Chem. Commun.* **1998**, 1867−1868.

[29] D. J. Sandman, L. Li, S. Tripathy, J. C. Stark, L. A. Acampora, B. M. Foxman, *Organometallics* **1994**, *13*, 348−353.

[30] M. Baiwir, G. Llabres, O. Dideberg, L. Dupont, J. L. Piette, *Acta Crystallogr., Sect. B* **1975**, *31*, 2188−2191.

[31] S. M. Godfrey, C. A. McAuliffe, R. G. Pritchard, S. Sarwar, *J. Chem. Soc., Dalton Trans.* **1997**, 1031−1036.

[32] S. A. Mbogo, W. R. McWhinnie, T. S. Lobana, E. R. T. Tiekink, *J. Organomet. Chem.* **1990**, *388*, 273−277.

[33] D. D. Perrin, W. L. F. Armargo, D. R. Perrin, *Purification of Laboratory Chemicals*, Pergamon, New York, **1980**.

[34] O. Foss, *Inorg. Synth.* **1953**, *4*, 88.

[35] G. M. Sheldrick, *SHELXS-86, Program for Crystal Structures solution*, University of Göttingen, **1986**.

[36] G. M. Sheldrick, *SHELX 97, Program for Crystal Structure Refinement*, University of Göttingen, Germany, **1997**.

Received August 28, 2003
Early View Article
Published Online February 3, 2004

 © 2004 Wiley-VCH Verlag GmbH & Co. KGaA, Weinheim

Synthesis, Structure and Photoluminescent Studies of a Novel Supramolecular [Ag(phen)(CN)]·(phen) Complex

Xiao-Chun Huang,[a,b] Shao-Liang Zheng,[a] Jie-Peng Zhang,[a] and Xiao-Ming Chen*[a]

Keywords: Density functional calculations / N ligands / Pi interactions / Photoluminescence / Silver

A novel Ag^{I} complex [Ag(phen)(CN)]·(phen) (phen = 1,10-phenanthroline) has been solvothermally synthesized and characterized by X-ray diffraction. The crystal packing reveals unprecedented threefold interpenetrating three-dimensional four-connected networks self-assembled through C-H···N hydrogen bonds and π···π stacking interactions, which are stabilized by strong C-H···π interactions between the three independent networks. The photoluminescent properties have been investigated by molecular orbital (MO) calculations, showing that the luminescent properties of the complex in the solid state are due to both a $\pi_L \rightarrow \pi_L^*$ transition of the uncoordinated phen species and metal-to-ligand charge transfer (MLCT), admixed with the cyanide-to-ligand charge transfer (XLCT) of the [Ag(phen)(CN)] species.
(© Wiley-VCH Verlag GmbH & Co. KGaA, 69451 Weinheim, Germany, 2004)

Introduction

In the field of crystal engineering, many attempts have been made to control the molecular arrangement in a crystal using hydrogen bonds and π···π stacking interactions. The unique strength and direction of these interactions play important roles in the generation of a variety of molecular architectures.[1−8] Non-conventional hydrogen bonds with weak proton donor C-H groups are of great theoretical interest, especially for C-H···N hydrogen bonding interactions.[9−12] Many novel supramolecular structures have been constructed using these weak interactions, such as the supramolecular graphyne-like network structure of 2,4,6-triethynyl-1,3,5-triazine.[6]

1,10-Phenanthroline (phen) is a suitable ligand to study these supramolecular interactions since it contains a large π-system and rich C−H donors. Various novel structures have been constructed with phen and such interactions in our previous work.[13,14] Phen and its derivatives have also been widely used for synthesizing materials with interesting photoluminescence properties. Over the past two decades the photochemical and photophysical properties of d^{10} metal-phen complexes have been extensively investigated.[15−17] Most reported d^{10} metal-phen complexes are cationic, whereas their neutral complexes are rarely documented.[18] Recently, we have synthesized a variety of neutral d^{10} complexes with an unsymmetrical hydroxylated phen ligand; molecular orbital (MO) calculations of these compounds give an effectual proof in the analysis of their interesting photoluminescent mechanism.[19] Herein we describe the synthesis and crystal structure of a novel molecular adduct of a neutral silver(I) complex with a solvate phen molecule, [Ag(phen)(CN)]·(phen) (**1**), which exhibits interesting supramolecular interactions in the solid state. The photoluminescent properties of complex **1** have been investigated and the mechanisms have also been validated by MO calculations on the experimental geometries.

[a] School of Chemistry and Chemical Engineering, Sun Yat-Sen University,
Guangzhou 510275, China
Fax: (internat.) +86-20-8411-2245
E-mail: cescxm@zsu.edu.cn
[b] Department of Chemistry, Shantou University,
Shantou, Guangdong 515063, China

Results and Discussion

Synthesis and Characterization

Complex **1** was prepared by a solvothermal reaction from silver oxide and excess phen in a concentrated aqueous ammonia and acetonitrile mixture. The existence of a cyanide group in complex **1** may be due to the decomposition of acetonitrile at the relatively high temperature (140 °C) and autogenous pressure of the reaction, which is somewhat similar to the process of acetonitrile decomposition under physiological conditions.[20] The formation of the stable mononuclear species [Ag(phen)(CN)] may be ascribed to the slow release of the cyanide ligand from acetonitrile and the multiple weak interactions between [Ag(phen)(CN)] and excess phen ligand, since direct addition of the cyanide salt usually yielded polymeric products.[21]

The IR spectrum of complex **1** shows one band at 2128 cm^{-1}, which can be assigned to the ν(CN) stretching vibration of the terminal CN^- species, taking into account that it is close to the recorded value for $K[Ag(CN)_2]$ (2140

 © 2004 Wiley-VCH Verlag GmbH & Co. KGaA, Weinheim DOI: 10.1002/ejic.200300616

cm^{-1}).[22] The ν(CN) stretching vibration for terminally bound CN^- complexes shifts to higher energy than that (2080 cm^{-1})[23] of free cyanide ion in water due to the strong σ donation of the weakly anti-bonding lone pair on CN^- to the metal, but to lower energy than those found for linear M−CN−M complexes such as $[Ag_2(L^2)_2(\mu\text{-}CN)][BF_4]$ [L^2 = 4,7-bis(2-cyanomethyl)-1-thia-4,7-diazacyclononane] (2150 cm^{-1})[24] where the two metal centres are coupled.

Crystal Structure

The X-ray single-crystal structure analysis shows that complex **1** is a 1:1 molecular adduct of mononuclear [Ag(phen)(CN)] and an uncoordinated phen ligand. The [Ag(phen)(CN)] molecule is bisected by a crystallographic mirror plane. The silver(I) atom assumes a Y-shaped planar geometry in which the metal ion is ligated by two nitrogen atoms of a phen and one carbon atom of the terminal cyanide, as shown in Figure 1. The Ag(1)−N(2) distance is 2.301(2) Å, while the Ag(1)−C(1) bond length is 2.026(5) Å. The observed Ag−N distances are similar to the corresponding values [2.283(6) and 2.300(5) Å] found for $Ag(dmp)NO_3{\cdot}2H_2O$ (dmp = 2,9-dimethyl-1,10-phenanthroline),[25] while the Ag−C distance is typical of silver cyanide, and is shorter than that [2.083(2) Å] found for $[Ag_2(L^2)_2(\mu\text{-}CN)][BF_4]$ [L^2 = 4,7-bis(2-cyanomethyl)-1-thia-4,7-diazacyclononane].[24] In complex **1**, the N(2)−Ag(1)−C(1) bond angle is 143.4(1)°, whereas the N(2)−Ag(1)−N(2A) angle is 73.3(1)°.

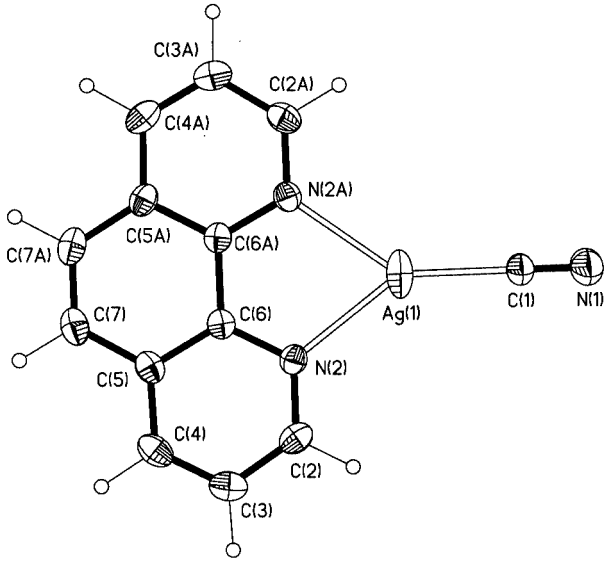

Figure 1. Perspective view of [Ag(phen)(CN)] (30 % thermal ellipsoids) with atom-numbering scheme; selected bond lengths (Å) and bond angles (°): Ag(1)−N(2) 2.301(2); Ag(1)−C(1) 2.026(5); N(2)−Ag(1)−C(1) 143.4(1); N(2)−Ag(1)−N(2A) 73.3(1); symmetry code: A) 1/2 − *x*, *y*, *z*

Cyanometallates are useful building blocks for the construction of supramolecular structures. Such supramolecular assemblies are usually achieved through bridging linear covalent M−CN−M bonding interactions.[23] In contrast, successful attempts to use a cyanide as a terminal ligand, especially for a hydrogen-bond acceptor, are rare.[26] The most intriguing feature in the structure of complex **1** is its unusual supramolecular interactions, including C-H···N hydrogen bonds, π···π stacking and C-H···π interactions involving the terminal cyanide and phen ligands, generating a unique supramolecular architecture in the solid state (Figure 2).

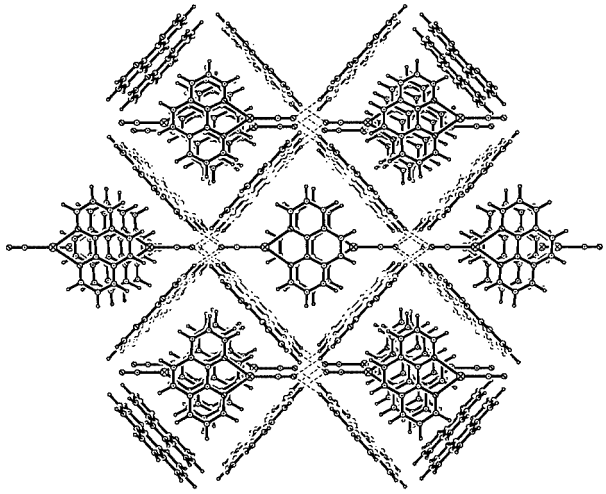

Figure 2. Crystal packing pattern of **1** viewed along the *a* axis

Adjacent [Ag(phen)(CN)] molecules in complex **1** are stacked in an inverse fashion through strong offset π···π aromatic stacking interactions, with a face-to-face distance of about 3.40 Å, forming a one-dimensional array (Figure 3, top),[3] whereas the uncoordinated phen molecules are arranged to give extended one-dimensional ribbons with relatively long C-H···N(phen) contacts (C···N 3.61 Å, H···N 2.60 Å, C-H···N 155°; Figure 3, bottom), where the H···N distance is still shorter than the van der Waals radii sum of 2.75 Å.[27] It is very interesting that the arrays and the ribbons are extended into a novel three-dimensional structure by strong C-H···N(CN) hydrogen bonds (C···N 3.41 Å, H···N 2.35 Å, C-H···N 164.4°). There are a few reported networks built from both weak C-H···X hydrogen bonds and π···π interactions.[13,14,28,29] A noteworthy example is the diamondoid network made up of C-H···O hydrogen bonds and π···π interactions in the structure of tetrakis(4-nitrophenyl)methane·G (G = THF, dioxane, nitrobenzene, 4-bromoanisole, anisole, ethoxybenzene, *p*-xylene, chlorobenzene).[28] The C-H···N hydrogen bonds are consistent with the previous report of this type of interactions, for example, the short C-H···N hydrogen bonds (C···N 3.27 Å, H···N 2.31 Å, C-H···N 180° and C···N 3.30 Å, H···N 2.34 Å, C-H···N 172.1°) in the structure of 2,4,6-triethynyl-1,3,5-triazine.[6] It should be noted that the acidity of $C_{(phen)}$−H is significantly weaker than $C_{(sp)}$−H or Cl_3C-H, which are

 © 2004 Wiley-VCH Verlag GmbH & Co. KGaA, Weinheim

involved in the most reported short and linear C-H···N hydrogen bonds.[5]

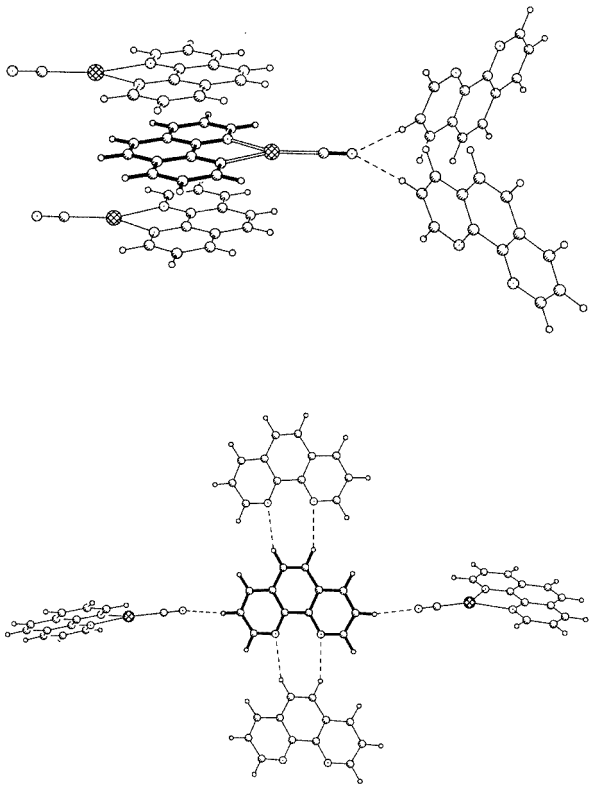

Figure 3. (top) The tetrahedral node defined by an [Ag(phen)(CN)] molecule connected to two other [Ag(phen)(CN)] molecules by π···π stacking interactions and two uncoordinated phen molecules by C-H···N hydrogen bonds; (bottom) the square-planar node defined by an uncoordinated phen molecule connected to two [Ag(phen)(CN)] moieties and two uncoordinated phen molecules by C-H···N hydrogen bonds

As shown in Figure 3, each [Ag(phen)(CN)] molecule forms hydrogen bonds and π···π interactions with its adjacent molecules in a tetrahedral arrangement (Figure 3, top), which can be regarded as a tetrahedral node; each uncoordinated phen molecule forms hydrogen bonds with its adjacent molecules in a square-planar arrangement, which can be regarded as a square-planar node (Figure 3, bottom). The three-dimensional structure of complex **1** linked by hydrogen bonds and π···π interactions can therefore be rationalized to contain equal numbers of tetrahedral nodes and square-planar nodes, where every node is connected to two nodes of the same type and two nodes of the other type (Figure 4, top). The resulting unprecedented binodal four-connected $(5^5 6)(5^4 8^2)$ topology is related to the well-known PtS net since it contains equal numbers of tetrahedral and square-planar nodes. However, the nodes of the PtS net are arranged in such a way that every node is connected to four nodes of the other type, in contrast to the topology found in complex **1**.[30] There is threefold interpenetration, with the networks being linked through edge-to-face C-H···π interactions between the coordinated ligands and uncoordinated phen molecules of the three nets, as illustrated in Figure 4 (bottom). Other examples of interpenetrating three-dimensional hydrogen-bonding networks linked by weak interactions include the structures of 4-(carboxamindo)-1-cubanecarboxylic acid, $[Zn(Him)_2(tpa)]\cdot H_2O$ (Him = imidazole, tpa = terephthalate) and $NH_4(bpedo)_2PF_6\cdot 3H_2O$ [bpedo = *trans*-bis(4-pyridyl)ethylene dioxide].[31–33] The pattern of C-H···π hydrogen bonds is very interesting in **1**, as there are two sets of contacts, with the short one having an H···π interaction of about 2.39 Å (C-H···π ca. 163°) and the longer one an H···π interaction of about 2.82 Å (C-H···π ca. 163°), which results in every coordinated phen species containing four C−H donors and every uncoordinated phen species being an acceptor for four C−H donors from two coordinated phen ligands (Figure 5).

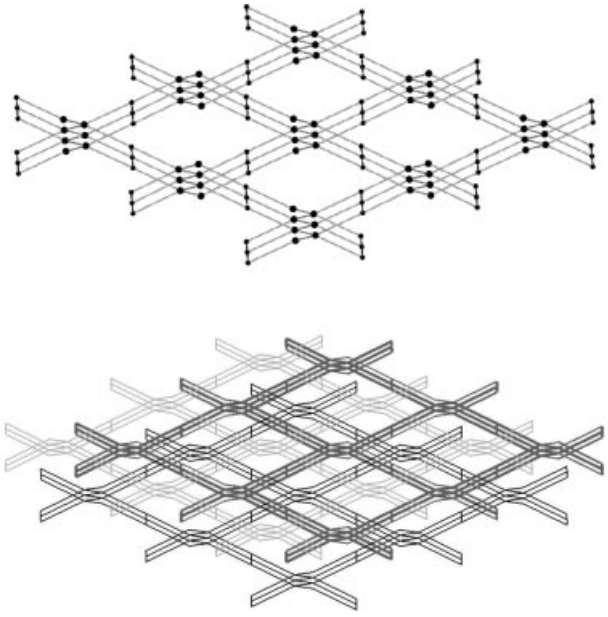

Figure 4. (top) The four-connected net constructed by the tetrahedral ([Ag(phen)(CN)], larger spheres) and square-planar (phen, smaller spheres) nodes, as well as (bottom) the threefold interpenetrating nets in **1**

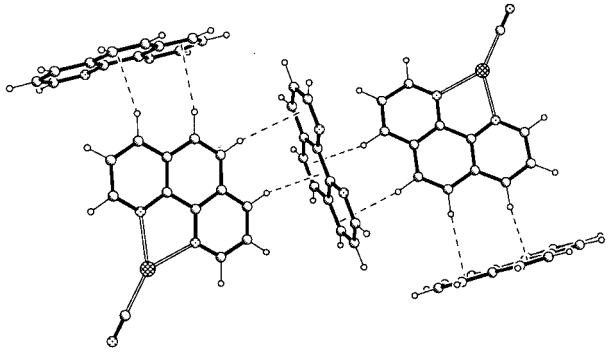

Figure 5. Perspective view of the C-H···π interactions

Luminescent Properties

Most luminescent Ag^I compounds exhibit emission at low temperature. Some important examples are organometallic silver(I) compounds containing bridging acetylide ligands,[34] silver(I) diisocyanide[35] and other silver(I) cyan-

 © 2004 Wiley-VCH Verlag GmbH & Co. KGaA, Weinheim

ide compounds.[36] Only a few monomeric and polymeric Ag^I complexes exhibit luminescence at room temperature.[37−41] Interestingly, solid **1** is luminescent at ambient temperature. Upon excitation at 325 nm, complex **1** displays an intense blue photoluminescence with three emission maxima at 406, 420 and 529 nm. The first two emission bands resemble the π-π* transition bands (385 and 403 nm) observed for solid phen (see Figure 6) due to the presence of uncoordinated phen molecules in **1**.

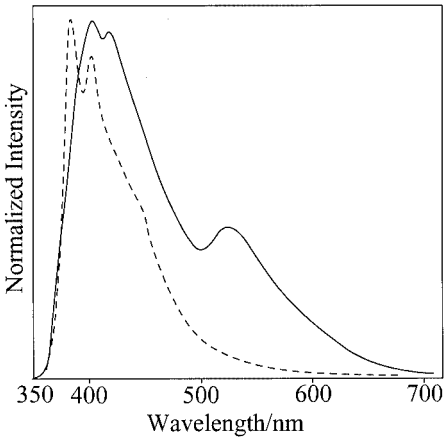

Figure 6. Photoluminescent spectra of solid **1** (−) and phen (---) (excited at 325 nm) in the solid state at room temperature

It has been suggested that the emission bands in the reported silver(I) complexes originate from dσ*-pσ or 4d−5s transitions, the excited states of a metal-to-ligand charge transfer (MLCT), or have an MMLCT character.[42−45] To assign the emission bands, we carried out molecular orbital (MO) calculations on the mononuclear [Ag(phen)(CN)] species and the phen molecule with the experimental geometries. The relevant HOMOs and LUMOs for [Ag(phen)(CN)] and phen, together with the orbital energies, are shown in the contour plots in Figure 7. For uncoordinated phen, the HOMOs are associated with the π-bonding orbital from the phen rings, while the LUMOs are mainly associated with the π-antibonding orbital; for [Ag(phen)(CN)], the HOMOs are mainly composed of σ(Ag−C≡N) orbitals, localized more on the metal center (namely the d_z^2 orbit), while the LUMOs are mainly composed of the π-antibonding orbital from the phen rings. There are deviations between the HOMO−LUMO analysis derived from our calculations (HOMO−LUMO gaps for [Ag(phen)(CN)] 3.74 eV; for phen 4.84 eV) and the experimentally measured emission energy (ca. 2.34 and 3.10 eV), since only the ground states were taken into consideration in the MO calculations. Moreover, extensive transverse interactions, such as π···π stacking, C−H···π interactions and C−H···N hydrogen bonds, exist in the real solid state and play an essential role in decreasing the HOMO−LUMO gaps.[19,46,47] These supramolecular interactions may also account for the decrease of the HOMO−LUMO gap of the phen groups in complex **1** compared to that of solid phen, resulting in a red-shift of the higher energy emission bands for complex **1**. Moreover, it is worthy to mention that the trend derived from the calculations is in accordance with the experimental results. As a characteristic of large heterocyclic aromatic ligands, the conjugated system can effectively decrease the π*-orbital energies, therefore the LUMO may not be contributed by the metal atom, as demonstrated by the MO calculation results of [Ag(phen)(CN)]. The ligation of a d^{10} metal atom to the heterocyclic aromatic ligand will further decrease the LUMO energy contributed by the π*-orbital, resulting in a much lower-energy emission band for the [Ag(phen)(CN)] species in complex **1**. It can therefore be concluded from the MO calculations that, for the adduct compound **1** in the solid state, the high-energy emission bands can mainly be assigned to the $\pi_L \rightarrow \pi_L^*$ transition of the uncoordinated phen molecules, whereas the low-energy transition is expected to be the metal-to-ligand charge transfer (MLCT), admixed with the cyanide-to-ligand charge transfer (XLCT) band.

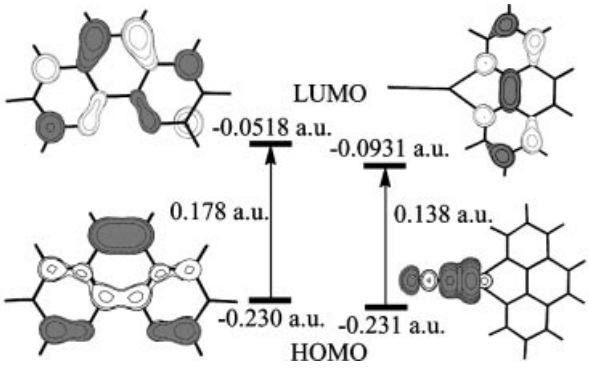

Figure 7. Contour plots and orbital energies of the HOMOs and LUMOs for phen (left) and [Ag(phen)(CN)] (right)

Conclusion

In summary, complex **1** shows an unprecedented four-connected three-dimensional network through cooperative π···π stacking interactions and C-H···N hydrogen bonds; the threefold interpenetrating net is connected by C-H···π interactions between the coordinated phen and uncoordinated phen species. The photoluminescence mechanism of **1** has been studied by molecular orbital calculations, showing that the photoluminescent properties are due to both the $\pi_L \rightarrow \pi_L^*$ transition of the uncoordinated phen molecule and metal-to-ligand charge transfer (MLCT), admixed with the cyanide-to-ligand charge transfer (XLCT) of the [Ag(phen)(CN)] molecule.

Experimental Section

General Remarks: The reagents and solvents employed are commercially available and were used as received without further purification. The C, H, and N microanalyses were carried out with a Perkin−Elmer 240 elemental analyser. The FT-IR spectra were recorded from KBr pellets in the range 4000−400 cm^{-1} on a Nicolet Magna 750 FT-IR spectrometer. The emission spectra were re-

 © 2004 Wiley-VCH Verlag GmbH & Co. KGaA, Weinheim

corded on a Perkin−Elmer LS50B fluorescence spectrophotometer, and the excitation source used was the 325 nm line of He-Cd laser (Kimmon IK5352R-D) with maximum power of 4 mW.

Synthesis of [Ag(phen)(CN)]·(phen) (1): Single crystals of complex **1** were obtained by a solvothermal method. In a typical procedure, silver oxide (0.5 mmol, 0.116 g), phen (2 mmol, 0.400 g), concentrated aqueous ammonia (5 mL) and acetonitrile (5 mL) were mixed sufficiently with stirring and placed into a 25-mL Teflon-lined steel autoclave and heated at 140 °C for 72 h, then cooled to 5 °C/h to 80 °C and held at that temperature for 10 h, followed by slow cooling to room temperature. Pale-yellow crystals (0.101 g) were collected in 20 % yield based on Ag_2O. $C_{25}H_{16}AgN_5$ (494.30): calcd. C 60.75, H 3.26, N 14.17; found C 60.43, H 3.78, N 14.15. FT-IR (KBr): $\tilde{\nu}$ = 3415 cm^{-1} (br. s), 3044 (m), 2925 (m), 2128 (m), 1683 (w), 1646 (m), 1618 (m), 1565 (m), 1503 (s), 1417 (s), 1136 (m), 1091 (m), 837 (m), 792 (w), 723 (m), 621 (w), 461 (w), 433 (w).

X-ray Crystallographic Study: A pale-yellow crystal (0.40 × 0.30 × 0.30 mm^3) of complex **1** suitable for X-ray analysis was selected and data collection was performed at 21 °C on a Bruker Smart Apex CCD diffractometer with graphite-monochromated Mo-K_α radiation (λ = 0.71073 Å). Data were corrected for Lorentz and polarization effects and empirical absorption corrections were applied using the SADABS program.[48] The structure was solved by direct methods and refined with full-matrix least-squares technique using the SHELXTL software suite.[49] Anisotropic thermal parameters were applied to all non-hydrogen atoms. The organic hydrogen atoms were generated geometrically with a restricted bond length (C−H 1.083 Å). The crystallographic data are listed in Table 1.
CCDC-216802 contains the supplementary crystallographic data for this paper. These data can be obtained free of charge at www.ccdc.cam.ac.uk/conts/retrieving.html [or from the Cambridge Crystallographic Data Centre, 12 Union Road, Cambridge CB2 1EZ, UK; Fax: (internat.) + 44-1223/336-033; E-mail: deposit@ccdc.cam.ac.uk].

Table 1. Crystal and structure refinement for complex **1**

Empirical formula	$C_{25}H_{16}AgN_5$
Molecular mass	494.30
Temperature (K)	293(2)
Wavelength (Å)	0.71073
Crystal system	orthorhombic
space group	Pnna
a (Å)	7.186(1)
b (Å)	18.599(4)
c (Å)	15.177(3)
V (Å^3)	2028.4(7)
Z	4
Calculated density (Mg/m^3)	1.619
Absorption coefficient (mm^{-1})	1.017
F(000)	992
Crystal size	0.40 × 0.30 × 0.30 mm^3
θ range for data collection (°)	1.73 to 26.00
Limiting indices	$-8 \le h \le 8$, $-22 \le k \le 17$, $-17 \le l \le 18$
Reflections collected/unique	10063/1990 [R_{int} = 0.033]
Completeness to θ = 26.00°	99.5 %
Absorption correction	Semi-empirical from equivalents
Max. and min. transmission	0.7502 and 0.6866
Refinement method	Full-matrix least-squares on F^2
Data/restraints/parameters	1990/0/143
Goodness-of-fit on F^2	1.068
Final *R* indices [$I > 2\sigma(I)$]	R_1 = 0.0410, wR_2 = 0.1004
R indices (all data)	R_1 = 0.0542, wR_2 = 0.1079
Extinction coefficient	0.0005(4)
Largest diff. peak and hole (*e*·Å^{-3})	0.380 and −0.425

Calculational Details: Density functional calculations were performed with the Gaussian 98 suite of programs,[50] at the B3LYP level. The basis set used for C, O, N and H atoms was 6−31G while effective core potentials with a LanL2DZ basis set were employed for transition metals. The contour plots of MOs were obtained with the Molden 3.5 graphic program.[51]

Acknowledgments

This work was supported by the National Natural Science Foundation of China (No. 20001008), the Ministry of Education of China (key project grant 01134) and a Doctorate Program Fund (No. 20020558024). The authors thank Prof. Kang-Cheng Zheng for his help in the MO calculations.

[1] J.-M. Lehn, *Supramolecular Chemistry*, VCH, Weinheim, **1995**.
[2] Y. Umezawa, S. Tsuboyama, K. Honda, J. Uzawa, M. Nishio, *Bull. Chem. Soc. Jpn.* **1998**, *71*, 1207−1213.
[3] C. Janiak, *J. Chem. Soc., Dalton Trans.* **2000**, 3885−3896.
[4] S. V. Lindeman, D. Kosynkin, J. K. Kochi, *J. Am. Chem. Soc.* **1998**, *120*, 13268−13269.
[5] T. Steiner, *Angew. Chem. Int. Ed.* **2002**, *41*, 48−76.
[6] M. Ohkita, M. Kavano, T. Suzuki, T. Tsuji, *Chem. Commun.* **2002**, 3054−3055.
[7] G. R. Desiraju, *J. Chem. Soc., Dalton Trans.* **2000**, 3745−3751.
[8] C. B. Aakeröy, A. M. Beatty, K. R. Lorimer, *J. Chem. Soc., Dalton Trans.* **2000**, 3869−3872.
[9] A. Cotton, L. M. Daniels, G. T. Jordan IV, C. A. Murillo, *Chem. Commun.* **1997**, 1673−1674.
[10] M. Mascal, *Chem. Commun.* **1998**, 303−304.
[11] I. Alkorta, I. Rozas, J. Elguero, *Chem. Soc. Rev.* **1998**, *27*, 163−170.
[12] M. Muthuraman, Y. L. Fur, M. B. Beucher, R. Masse, J.-F. Nicoud, S. George, A. Nangia, G. R. Desiraju, *J. Solid State Chem.* **2000**, *152*, 221−228.
[13] G.-F. Liu, B.-H. Ye, Y.-H. Ling, X.-M. Chen, *Chem. Commun.* **2002**, 1442−1443.
[14] X.-M. Chen, G.-F. Liu, *Chem. Eur. J.* **2002**, *8*, 4811−4817.
[15] N. Armaroli, *Chem. Soc. Rev.* **2001**, *30*, 113−124.
[16] C. T. Cunningham, J. J. Moore, K. L. H. Cunningham, P. E. Fanwick, D. R. McMillin, *Inorg. Chem.* **2000**, *39*, 3638−3644.
[17] A. J. Pallenberg, K. S. Koenig, D. M. Barnhart, *Inorg. Chem.* **1995**, *34*, 2833−2840.
[18] D. Rais, D. M. P. Mingos, R. Vilar, A. J. P. White, D. J. Williams, *Organometallics* **2000**, *19*, 5209−5217.
[19] S.-L. Zheng, J.-P. Zhang, X.-M. Chen, Z.-L. Huang, Z.-Y. Lin, W.-T. Wong, *Chem. Eur. J.* **2003**, *9*, 3888−3896.
[20] N.-L. Cheng, *Solvents Handbook*, 2nd ed., Chemistry Industry Press, Beijing, China, **1994**, p. 650.
[21] D. L. Bryce, R. E. Wasylishen, *Inorg. Chem.* **2002**, *41*, 4131−4138.
[22] T. M. Loehr, T. V. Long, *J. Chem. Phys.* **1970**, *53*, 4182−4186.
[23] K. R. Dunbar, R. A. Heintz, *Prog. Inorg. Chem.* **1997**, *45*, 283−391.
[24] V. Lippolis, A. J. Blake, P. A. Cooke, F. Isaia, W.-S. Li, M. Schröder, *Chem. Eur. J.* **1999**, *5*, 1987−1991.
[25] G. Swarnabala, M. V. Rajasekharan, *Polyhedron* **1996**, *15*, 3197−3201.
[26] K.-Y. Ho, W.-Y. Yu, K.-K. Cheung, C.-M. Che, *Chem. Commun.* **1998**, 2101−2102.
[27] A. Bondi, *J. Phys. Chem.* **1964**, *68*, 441−451.
[28] R. Thaimattam, F. Xue, J. A. R. P. Sharma, T. C. W. Mak, G. R. Desiraju, *J. Am. Chem. Soc.* **2001**, *123*, 4432−4445.
[29] X.-M. Zhang, M.-L. Tong, M.-L. Gong, X.-M. Chen, *Eur. J. Inorg. Chem.* **2003**, 138−142.

 © 2004 Wiley-VCH Verlag GmbH & Co. KGaA, Weinheim

[30] S. R. Batten, R. Robson, *Angew. Chem. Int. Ed.* **1998**, *37*, 1461−1494.
[31] S. S. Kuduva, D. C. Craig, A. Nangia, G. R. Desiraju, *J. Am. Chem. Soc.* **1999**, *121*, 1936−1944.
[32] J.-H. Yang, S.-L. Zheng, J. Tao, G.-F. Liu, X.-M. Chen, *Aust. J. Chem.* **2002**, *55*, 741−744.
[33] B.-Q. Ma, H.-L. Sun, S. Gao, *Chem. Commun.* **2003**, 2164−2165.
[34] V. W.-W. Yam, K. K.-W. Lo, W. K.-M. Fung, C.-R. Wang, *Coord. Chem. Rev.* **1998**, *171*, 17−41.
[35] P. D. Harvey, D. Fortin, *Coord. Chem. Rev.* **1998**, *171*, 351−354.
[36] M. A. Omary, H. H. Patterson, *J. Am. Chem. Soc.* **1998**, *120*, 7696−7705.
[37] M.-L. Tong, X.-M. Chen, B.-H. Ye, L.-N. Ji, *Angew. Chem. Int. Ed.* **1999**, *38*, 2237−2240.
[38] S.-L. Zheng, M.-L. Tong, S.-D. Tan, Y. Wang, J.-X. Shi, Y.-X. Tong, H. K. Lee, X.-M. Chen, *Organometallics* **2001**, *20*, 5319−5325.
[39] V. W.-W. Yam, K. K.-W. Lo, C.-R. Wang, K.-K. Cheung, *Inorg. Chem.* **1996**, *35*, 5116−5117.
[40] V. J. Catalano, H. M. Kar, J. Garnas, *Angew. Chem. Int. Ed.* **1999**, *38*, 1979−1982.
[41] D. Fortin, M. Drouin, M. Turcotte, P. D. Harvey, *J. Am. Chem. Soc.* **1997**, *119*, 531−541.
[42] C.-M. Che, M.-C. Tse, M. C. W. Chan, K.-K. Cheung, D. L. Phillips, K.-H. Leung, *J. Am. Chem. Soc.* **2000**, *122*, 2464−2468.
[43] P. C. Ford, A. Vogler, *Acc. Chem. Res.* **1993**, *26*, 220−226.
[44] M. Henary, J. I. Zink, *Inorg. Chem.* **1991**, *30*, 3111−3112.
[45] A. Vogler, H. Kunkely, *Chem. Phys. Lett.* **1988**, *150*, 135−137.
[46] B. Valeur, *Molecular Fluorescence:* P*rinciples and Applications*, Wiley-VCH, Weinheim, **2002**.
[47] S.-L. Zheng, J.-P. Zhang, W.-T. Wong, X.-M. Chen, *J. Am. Chem. Soc.* **2003**, *125*, 6882−6883.
[48] G. M. Sheldrick, *SADABS. Program for Scaling and Correction of Area Detector Data.* University of Göttingen, Göttingen, Germany, **1996**.
[49] G. M. Sheldrick, *SHELXTL*, Version 6.10, Bruker Analytical X-ray Systems, Madison, WI, USA, **2000**.
[50] M. J. Frisch, G. W. Trucks, H. B. Schlegel, G. E. Scuseria, M. A. Robb, J. R. Cheeseman, V. G. Zakrzewski, J. A. Jr. Montgomery, R. E. Stratmann, J. C. Burant, S. Dapprich, J. M. Millam, A. D. Daniels, K. N. Kudin, M. C. Strain, O. Farkas, J. Tomasi, V. Barone, M. Cossi, R. Cammi, B. Mennucci, C. Pomelli, C. Adamo, S. Clifford, J. Ochterski, G. A. Petersson, P. Y. Ayala, Q. Cui, K. Morokuma, D. K. Malick, A. D. Rabuck, K. Raghavachari, J. B. Foresman, J. Cioslowski, J. V. Ortiz, B. B. Stefanov, G. Liu, A. Liashenko, P. Piskorz, I. Komaromi, R. Gomperts, R. L. D. Martin, J. Fox, T. Keith, M. A. Al-Laham, C. Y. Peng, A. Nanayakkara, C. Gonzalez, M. Challacombe, P. M. W. Gill, B. Johnson, W. Chen, M. W. Wong, J. L. Andres, C. Gonzalez, M. Head-Gordon, E. S. Replogle, J. A. Pople, *Gaussian 98*, Revision A.5, Gaussian, Inc., Pittsburgh, PA, **1998**.
[51] G. Schaftenaar, *Molden*, Version 3.5, CAOS/CAMM Center Nijmegen, Toernooiveld, Nijmegen (Netherlands), **1999**.

Received September 2, 2003
Early View Article
Published Online January 28, 2004

 © 2004 Wiley-VCH Verlag GmbH & Co. KGaA, Weinheim

Epoxidation versus Baeyer−Villiger Oxidation: The Possible Role of Lewis Acidity in the Control of Selectivity in Catalysis by Transition Metal Complexes

Agostino Brunetta[a] and Giorgio Strukul*[a]

Keywords: Lewis acids / Homogeneous catalysis / Oxidation / Peroxides

The synthesis of a series of cationic complexes of Pt^{II} containing triphos or triphosPO and either a solvent, a hydroxo or a hydroperoxo as the fourth ligand is reported. The complexes are characterized by IR and $^{31}P\{^1H\}$ NMR spectroscopy and by molar conductivity data, and their Lewis acid characteristics determined by NMR techniques. All complexes are good catalysts for the epoxidation of olefins and the Baeyer–Villiger oxidation of ketones under mild conditions using hydrogen peroxide as oxidant. The latter reaction is more Lewis-acid demanding in terms of the electronic characteristics of the catalysts. The use of Lewis-acidic metal centers allows the selective oxidation of unsaturated ketones to the corresponding unsaturated esters without oxidation of the carbon-carbon double bond, indicating that a strong Lewis-acid character of the catalyst can be an important feature in the design of catalysts capable of separating the two processes.

(© Wiley-VCH Verlag GmbH & Co. KGaA, 69451 Weinheim, Germany, 2004)

Introduction

In transition metal chemistry, the idea of Lewis acidity is generally associated with electron-deficient metal centers such as the early metals in their highest oxidation state or the first row late metals such as Cu^{II} and Zn^{II}. This simple notion is supported by a huge number of applications in organic synthesis.[1] Within this framework, the idea of associating Lewis acidity with electron-rich metal centers like Pd^{II} and Pt^{II} for catalytic applications is a relatively recent one, the necessary condition to exploit the Lewis acidity of the latter systems being the presence of at least one positive charge on the complex. In the past few years, the number of applications of these systems in catalysis has been increasing, although, among the examples reported,[2] none refers to oxidation reactions.

Several years ago we reported the first example of transition metal catalysis in the Baeyer−Villiger (BV) oxidation of ketones, with H_2O_2 as the oxidant, and using a cationic complex of Pt^{II} as the catalyst.[3] The mechanism of the reaction[3b] (Figure 1) clearly indicates that, having no role in the activation of the oxidant, the major function of Pt in the catalytic cycle is to behave as a Lewis acid for the activation of the ketone. This view is strengthened by the analogies (Figure 1) between the quasi-peroxymetallacyclic intermediate **1** and the Criegee intermediate involved in the purely organic reaction using peracids (Pt replaces H^+). More recently, typical Lewis acids such as Al^{III},[4] Mg^{II},[5] and Sn^{IV} [6] have also been reported in the BV oxidation of ketones, emphasizing the importance of having a Lewis-acid center to promote the reaction by activation of the ketone.

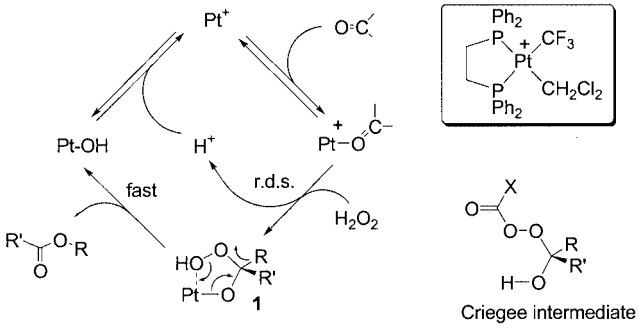

Figure 1. Reaction mechanism for the Baeyer−Villiger oxidation of ketones with hydrogen peroxide catalyzed by $[Pt(CF_3)(P\text{-}P)(solv)]^+$-type complexes

The same complex reported in Figure 1 was also recognized to be an efficient catalyst for the epoxidation of olefins with H_2O_2 under mild conditions,[7] although in this case the mechanism of the reaction (Figure 2) indicates that the function of the catalyst is more complex[7d] as it activates both the olefin towards nucleophilic attack and, at the

[a] Department of Chemistry, University of Venice
Dorsoduro 2137, 30123 Venezia, Italy
Fax: (internat.) + 39-041-257-8517
E-mail: strukul@unive.it

 © 2004 Wiley-VCH Verlag GmbH & Co. KGaA, Weinheim **DOI: 10.1002/ejic.200300584**

same time, hydrogen peroxide, increasing its nucleophilicity by coordination.

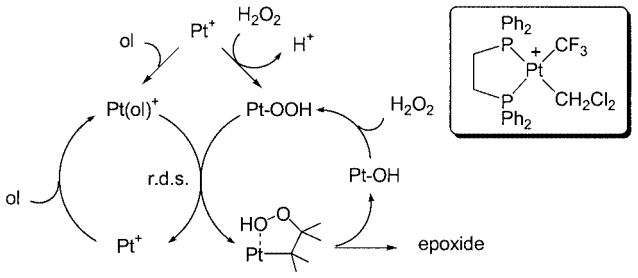

Figure 2. Reaction mechanism for the epoxidation of olefins with hydrogen peroxide catalyzed by $[Pt(CF_3)(P\text{-}P)(solv)]^+$-type complexes

Platinum complexes are the only catalysts known in the literature that catalyze both the BV and the epoxidation reactions with high activity. Moreover, they do so using hydrogen peroxide as the oxidant, i.e. a cheap, environmentally friendly oxidant, but also an elusive one for selective, non-radical-type oxidations. The versatility of these systems offers a unique opportunity to investigate in more detail the electronic properties of the metal center that allow us to separate the BV reaction from the epoxidation reaction. This aspect is crucial for selectivity whenever a bifunctional molecule is oxidized, and may have an important impact in organic synthesis, as both the BV and the epoxidation reactions are widely used as intermediate steps in complex synthetic procedures, leading to the preparation of pharma, agro and fine chemicals. As an example, Scheme 1 shows the theoretical case of dihydrocarvone where both parallel and consecutive reactions are possible leading to the unselective formation of the epoxy lactone. The aim of the present work is to establish whether the Lewis acidity of the metal center is of importance for controlling the relative rates of the BV and epoxidation reactions.

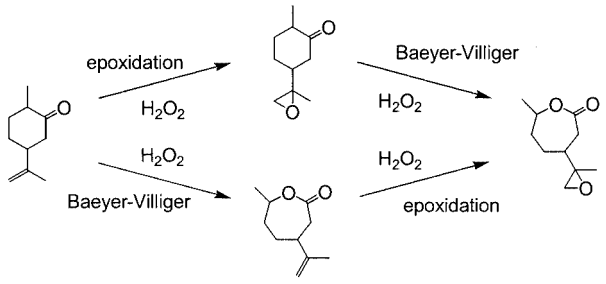

Scheme 1

Results and Discussion

Synthesis of Complexes

To address the problem exposed above, one has to design a class of cationic homologous complexes of platinum(II) with very similar geometric constraints, but differing in the electron density of the metal. Since the presence of a coordinated diphosphane seems to be a crucial requirement to promote the activity of these complexes,[3,7,8] to achieve this goal we chose tridentate ligands of the type P-P-P and P-P-P=O, bearing, respectively, three P donors and two P and one O donors. This would ensure the formation of bis-cationic complexes possessing, in principle, a significant Lewis acidity.

Square planar Pt^{II} complexes such as **2** and **3** containing tridentate ligands (Scheme 2) were synthesized following the procedure outlined in Scheme 3. This was already published for solvento complexes by Bergamini et al.[9] although the species were characterized in situ (NMR evidence) but never isolated. The isolation of the hydroxo and hydroperoxo complexes of **2** could be easily accomplished by addition of, respectively, OH^- to the corresponding solvento complex or H_2O_2 to the hydroxo complex. Conversely, in the case of **3**, given the lability of the oxygen donor, the same procedure led to the formation of a different species that was characterized in situ by NMR spectroscopy. Attempts to isolate this species synthetically using the procedure adopted for **2b** (i.e. addition of a stoichiometric amount of OH^- in acetone/H_2O) led to the formation of a complex mixture showing a different NMR spectrum. Isolation of a species (albeit in moderate yield) with the same NMR spectrum as observed in the in situ experiment could be accomplished in CH_2Cl_2 by adding an excess of OH^- in water. This species is most likely a neutral bis-hydroxo complex of the type $[Pt(OH)_2(P\text{-}P\text{-}P{=}O)]$ (**4**) as seems to be indicated by the full spectroscopic characterization (see below).

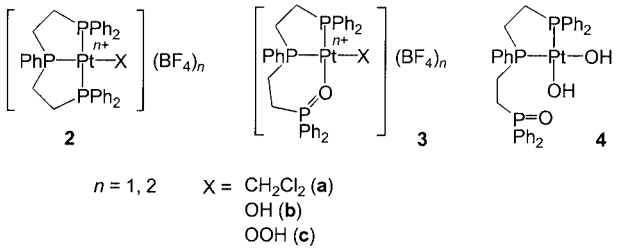

Scheme 2

Characterization of Complexes

All complexes were characterized by IR and $^{31}P\{^1H\}$ NMR spectroscopy, and molar conductivity measurements. A summary of the characterization data is reported in Table 1. For the purpose of simplicity, and with reference to Scheme 2, in reporting the NMR spectroscopic data P_a refers to the phosphorus *trans* to P (or to O in complexes **3**), P_b to the phosphorus *trans* to X and (only in complexes **3**) P_c to the oxidized phosphorus. As shown in Table 1, in the IR spectrum all complexes display the broad band characteristic of non-coordinated BF_4^- in the 1100−960 cm^{-1} range. Additionally, complexes **2b** and **2c** show typical weak O−H stretching frequencies at 3620 and 3483 cm^{-1}, respectively, in agreement with previously reported hydroxo

 © 2004 Wiley-VCH Verlag GmbH & Co. KGaA, Weinheim

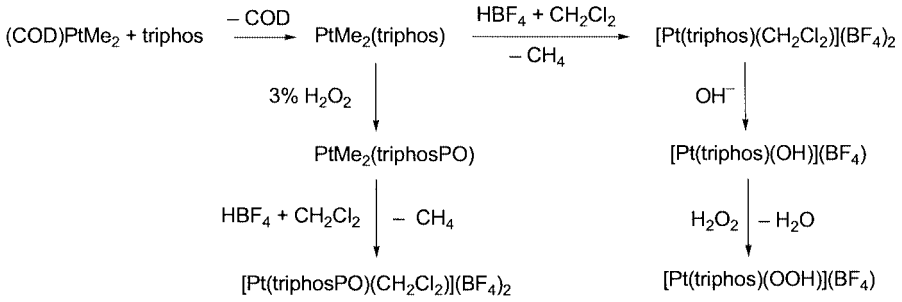

Scheme 3

Table 1. Characterization data for complexes **2** and **3**[a]

Complex	IR (cm^{-1})	$^{31}P\{^1H\}$ NMR (δ in ppm, J in Hz)	Molar conductivity ($\Omega^{-1}mol^{-1}cm^2$)
2a	1100–960 (b)	P_a 50.6 (s), $^1J_{P,Pt}$ = 2452 P_b 80.2 (s), $^1J_{P,Pt}$ = 3475	115–120
2b	3620 (w) 1100–960 (b)	P_a 77.7 (d), $^2J_{P,P}$ = 3.7, $^1J_{P,Pt}$ = 2575 P_b 39.6 (t), $^2J_{P,P}$ = 3.7, $^1J_{P,Pt}$ = 2625	79.6
2b[b]		P_a 75.2 (d), $^2J_{P,P}$ = 4.1, $^1J_{P,Pt}$ = 2592 P_b 39.2 (t), $^2J_{P,P}$ = 4.1, $^1J_{P,Pt}$ = 2620	
2c	3483 (w) 1100–960 (b)	P_a 70.9 (d), $^2J_{P,P}$ = 4.3, $^1J_{P,Pt}$ = 2385 P_b 42.4 (t), $^2J_{P,P}$ = 4.3, $^1J_{P,Pt}$ = 2811	90.3
3a	1100–960 (b) 1124 (s)	P_a 38.2 (s), $^1J_{P,Pt}$ = 3753 P_b 42.9 (s), $^1J_{P,Pt}$ = 3890 P_c 55.1 (d), $^3J_{Pb,Pc}$ = 9.0	172
4[b]	1178 (s) 3599 (w)[c]	P_a 33.4 (d), $^2J_{Pa,Pb}$ = 11.0, $^1J_{P,Pt}$ = 3477 P_b 39.4 (dd), $^2J_{Pa,Pb}$ = 11.0, $^3J_{Pb,Pc}$ = 52.5, $^1J_{P,Pt}$ = 3480 P_c 31.2 (d), $^3J_{Pc,Pb}$ = 52.5	8–10
2d[d]		P_a 48.4 (s), $^1J_{P,Pt}$ = 2459 P_b 82.2 (s), $^1J_{P,Pt}$ = 3434	
3d[d]		P_a 37.9 (d), $^2J_{Pa,Pb}$ = 6.8, $^1J_{P,Pt}$ = 3900 P_b 43.2 (s), $^1J_{P,Pt}$ = 3714 P_c 55.1 (d), $^3J_{Pb,Pc}$ = 11.1	

[a] IR in nujol; NMR in [D_6]acetone at 25 °C; molar conductivity: 10^{-3} M solution in EtOH. [b] NMR spectrum recorded in CD_2Cl_2. [c] In 1,2-dichloroethane solution. [d] NMR spectra recorded in acetone at −70 °C.

and hydroperoxo complexes of Pt^{II}.[7e,10] Similarly, in complex **3a** the P=O stretching frequency of the oxygen-coordinated ligand is observed at 1124 cm^{-1}.[11]

The NMR spectroscopic data were taken in [D_6]acetone. Complexes **2a** and **3a** give very broad signals in CD_2Cl_2 so a more coordinating solvent was necessary in order to observe a relatively static spectrum at room temperature. The signals are moderately broad so that P–P coupling constants cannot be determined. In general, P_b when it is *trans* to a solvent (as in **2a** and **3a**), displays higher P–Pt coupling constants. The same happens to P_a in **3a** where it is *trans* to the labile oxygen ligand. It should be noted that the P_b–Pt coupling constants for **2b** and **2c** are significantly smaller than in the case of mononuclear diphosphane complexes of platinum[7e,10a,12] where they fall in the 3000–3400 Hz range, reflecting the moderate *trans* effect of the -OH (-OOH) ligand, as was suggested by Appleton and Bennett.[12] The data reported for **2a**, **2b** and **3a** are identical to those observed in situ by Bergamini et al.[9]

Conductivity data for **2a**, **3a**, and **2b**, **2c** taken in 10^{-3} M MeOH solutions are in the range generally accepted for 1:2 and 1:1 electrolytes, respectively.[13]

At variance with the NMR spectra mentioned above, the addition of an excess of OH^- to **3a** results in the formation of a more static species (**4**) in which P–P coupling constants can be observed. The signal assigned to P_c is strongly shifted (about 20 ppm) to higher fields with respect to the parent compound, indicating that the O donor is probably no longer in the coordination sphere of the metal. This view seems to be confirmed by the observation that in the IR spectrum of the isolated species the P=O stretching frequency shifts from 1124 cm^{-1} in **3a** to 1178 cm^{-1} in **4**.[11] Additionally, the P_a–Pt and P_b–Pt coupling constants are practically identical (3477 and 3480 Hz respectively). The IR spectrum of **4** in dichloroethane solution also shows a weak band at 3599 cm^{-1}, typical of hydroxo complexes of Pt^{II}.[7d,7e,8a,10a] On this basis two possibilities are possible, both in agreement with the NMR spectroscopic data but neither corresponding to **3b**: the complex might be either a mononuclear bis-hydroxo complex or a dinuclear μ-hydroxo complex. The latter class of complexes is very stable and is relatively common in the literature in the case of Pt^{II}.[14] A possible formulation of **4** as a dinuclear μ-hydroxo complex might be supported by the values of the $^1J_{P,Pt}$ coupling con-

 © 2004 Wiley-VCH Verlag GmbH & Co. KGaA, Weinheim

stants that fall in the 3200−3600 Hz range typical for this class of complexes.[14] Addition of an excess (4:1) of HBF_4 in Et_2O (Scheme 4) allows us to observe the corresponding solvento complex **3a**, while the further addition of an excess of water leads to the formation of the aquo complex (see below and **3d** in Table 1). These observations would be consistent with **4** being both a bis-hydroxo complex (as formulated in Scheme 4) and also a dinuclear μ-hydroxo complex. Conclusive evidence for the nature of **4** as a mononuclear bis-hydroxo complex comes from IR spectroscopy, where the broad strong BF_4^- band is not observed, and from molar conductivity data. As shown in Table 1, the conductivity of a 10^{-3} M solution of **4** in MeOH is practically negligible, indicating that the complex is neutral.

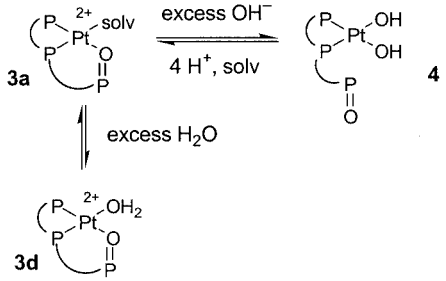

Scheme 4

Acidity Measurements

A critical point for the purpose of the present work is the determination of the Lewis acid characteristics of the homologous complexes **2a** and **3a**. This was initially investigated by IR spectroscopy, following addition to solutions of **2a** and **3a** of CO, acetonitrile and 2,6-dimethylphenyl isocyanide, all of which can easily displace the CH_2Cl_2 from the coordination sphere of the metal. It is well-known that both the CO, CN and NC stretching frequencies of the above coordinated molecules are sensitive to the electron density of the metal[14] and hence might be a valuable tool for understanding the Lewis acid nature of the metal center. Experiments were carried out in 1,2-dichloroethane (DCE). In the case of CO, solutions of the complexes were saturated with the gas prior to recording the IR spectrum, while with acetonitrile or 2,6-dimethylphenyl isocyanide variable amounts of reactant could be added. This allowed us to distinguish between the free and coordinated ligand. Table 2 summarizes the results obtained. As can be seen, in all cases the coordinated ligand vibrates at higher frequencies with respect to the free ligand (CO 2143 cm^{-1}; MeCN 2255 cm^{-1}; 2,6-dimethylphenyl isocyanide 2121 cm^{-1}), which is a good indication that the complexes are indeed Lewis acids. However, the addition of CO or CH_3CN results in negligible differences between the complexes, only with 2,6-dimethylphenyl isocyanide could a 5 cm^{-1} shift to higher frequency be observed in the case of **3b**. It has to be pointed out that with the latter complex the addition of an excess of isocyanide determines a further shift of the band maximum to higher frequencies as a result of the formation of a shoulder at about 2225 cm^{-1}, indicative of the presence of a second ligand in the coordination sphere of the metal causing the likely displacement of the labile O donor. Since the above IR data did not provide a clear answer as to which of the complexes was more Lewis acidic (common chemical sense would indicate **3a**) it was decided to turn to a different technique.

Table 2. IR data of **2a** and **3a** after reaction with CO, acetonitrile or 2,6-dimethylphenyl isocyanide[a]

Complex	ν(CO) (cm^{-1})	ν(CN) (cm^{-1})	ν(NC) (cm^{-1})
2a	2150	2295, 2324	2204
2b	2152	2296, 2326	2209

[a] In DCE solution; resolution 0.5 cm^{-1}.

Recently, Zhong et al.[16] have faced a similar problem in the study of a homologous series of cationic bis(aryl)diimine-ligated methyl complexes of Pt^{II} where the substituents on the aromatic rings were varied systematically. The aim of these authors was to determine the electronic effects of the ligands on the metal center and possibly find a correlation with respect to their properties in the C−H activation of alkanes. The problem was addressed by studying the equilibrium shown in Scheme 5 by ^1H NMR spectroscopy, where water is used as a Lewis base. The extent of this equilibrium can be taken as a measure of the Lewis acidity of the metal center. Although this method was developed for a different class of homologous complexes of Pt^{II}, it seems reasonable to apply it, at least semi-quantitatively, also to the present case. The ratio between Pt-solv and $Pt-OH_2$ complexes can be easily determined by $^{31}P\{^1H\}$ NMR spectroscopy at −70 °C {NMR spectroscopic data for $[Pt(H_2O)(P\text{-}P\text{-}P)](BF_4)_2$ (**2d**) and $[Pt(H_2O)(P\text{-}P\text{-}P{=}O)](BF_4)_2$ (**3d**) are reported in Table 1}. By applying mass balance to Pt and H_2O one can easily solve a four-equation system, which allows us to calculate the equilibrium constant (Scheme 5). This was found to be 110 for **2a** and 1400 for **3a** indicating that the latter is considerably more Lewis acidic than the former. Indeed, as the NMR experiments were carried out in acetone the solvento species are not exactly **2a** and **3a**, as in Scheme 2, but more correctly the corresponding acetone derivatives. The limitations of these

$$\text{Pt-solv} + H_2O \underset{-70\,^\circ C}{\overset{K_a}{\rightleftharpoons}} \text{Pt-OH}_2 + \text{solv}$$

solv = [D$_6$]acetone

$$\begin{cases} [Pt(H_2O)] / [Pt(solv)] = n \\ [H_2O] + [Pt(H_2O)] = C^\circ_b \\ [Pt(H_2O)] + [Pt(solv)] = C^\circ_a \\ [solv] = 15.2\ M \end{cases}$$

$$K_a = \frac{[Pt(H_2O)]\,[solv]}{[Pt(solv)]\,[H_2O]}$$

$$K_a = \frac{n\,(n+1)\,[solv]}{n\,(C^\circ_b - C^\circ_a) + C^\circ_b}$$

Scheme 5

 © 2004 Wiley-VCH Verlag GmbH & Co. KGaA, Weinheim

NMR experiments when used for the interpretation of the catalytic reactions that will be considered below are numerous: (i) the technique was developed for a different class of complexes, although the principle is quite general; (ii) the equilibrium constants are determined at −70 °C, while the catalysis is carried out at higher temperatures; (iii) the solvento complexes considered are actually Pt(acetone) instead of Pt(dichloromethane). Even with these limitations we believe that the overall meaning of the experiment is quite clear, i.e. **3a** is more acidic than **2a**.

Catalytic Activity

Having ascertained that **2a** and **3a** differ significantly in their Lewis acidity, their activity in the BV oxidation and in the epoxidation of olefins with hydrogen peroxide was compared. 2-Methylcyclohexanone and cyclooctene were chosen as prototype substrates and a substrate/H_2O_2/catalyst ratio equal to 100:100:1 was chosen. Reactions were carried out in DCE.

In both processes **2a** was found to be inactive at 20 °C, whereas at 70 °C a moderate activity was observed. In Figure 3 a comparison between **2a**, **2b** and **2c** in the epoxidation of cyclooctene is reported. As can be seen the homologous complexes display a very similar catalytic behavior: their maximum activity (expressed as zero-order rate constant) is essentially the same: a very short induction time is observed with **2b** and **2c**, indicating a relatively quick conversion into the catalytically active species, and only the amount of epoxide formed seems to differ markedly. The reactions are in any case very selective as the epoxide was the only product observed, with no evidence for glycol or further oxidation products. It has to be pointed out that under these experimental conditions a certain degree of irreproducibility was observed (approximately ±10% of the maximum activity and ±25% of the maximum conversion) as the result of a deactivation process that will be considered more thoroughly below. Similar results (Table 3) were observed for the oxidation of 2-methylcyclohexanone (2-heptalactone was the only oxidation product) both in terms of activity and conversion. Like in epoxidation, the reaction must be carried out at 70 °C, and deactivation of the catalyst is evident.

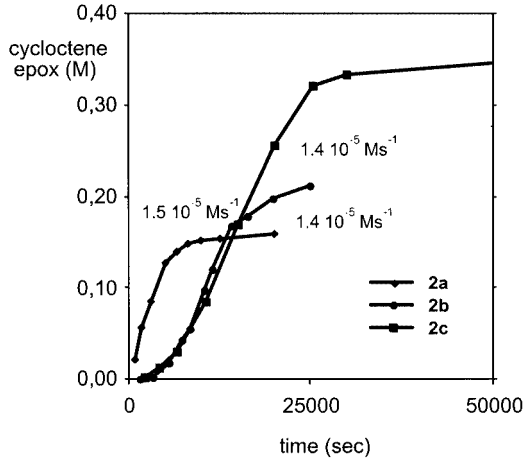

Figure 3. Reaction profiles for the epoxidation of cyclooctene with hydrogen peroxide catalyzed by homologous Pt^{II} complexes: [(triphos)Pt(solv)]$^{2+}$ (**2a**), diamonds; [(triphos)Pt(OH)]$^{+}$ (**2b**), circles; [(triphos)Pt(OOH)]$^{+}$ (**2c**), squares; numbers on the curves indicate the rate expressed as a zero-order rate constant; reaction conditions: catalyst 0.017 mmol; substrate 1.7 mmol; 35% H_2O_2 1.7 mmol; DCE 3 ml; N_2 1 atm.

The activity of **3a** is significantly different, although the reaction profile has the same shape as that shown for **2a** in Figure 3. As can be seen from Table 3, this catalyst is already active at 20 °C especially in the oxidation of 2-methylcyclohexanone, while the activity is very poor in the epoxidation of cyclooctene. At 70 °C it is approximately as active as **2a** in the epoxidation reaction and more active in the BV oxidation (Table 3), but seems to deactivate more quickly.

The reactivity shown by **2a** with respect to cyclooctene is observed also in the epoxidation of other olefins (Table 4). Even in this case a similar activity between **2a** and **2b** is observed. However, by the end of the epoxidation reactions, some epoxide hydrolysis occurs with formation of the corresponding glycol, probably promoted by the acid catalyst and due to the lower stability of these epoxides with respect to cyclooctene epoxide. Internal olefins are epoxidized more efficiently than terminal olefins (1-octene) and this contrasts with the behavior observed for other cationic Pt^{II} complexes {e.g. [Pt(CF_3)(P-P)(solv)]$^{+}$}, which are specific for the epoxidation of terminal olefins.[7] The α,β-unsatu-

Table 3. Catalytic activity of complexes **2** and **3** in the epoxidation of cyclooctene and the Baeyer−Villiger oxidation of methylcyclohexanone[a]

Catalyst	Substrate	Temp. (°C)	10^5 × max. rate (Ms^{-1})	Max. conv. (%)
2a	cyclooctene	70	1.5	20
2b		70	1.4	40
2c		70	1.4	25
2a	2-methylcyclohexanone	70	1.5	11
2b		70	1.6	13
3a	cyclooctene	20	0.05	2
3a		70	1.2	11
3a	2-methylcyclohexanone	20	2.0	40
3a		70	7.0	25

[a] Experimental conditions: catalyst 0.017 mmol; substrate 1.7 mmol; 35% H_2O_2 1.7 mmol; DCE 3 ml; N_2 1 atm.

 © 2004 Wiley-VCH Verlag GmbH & Co. KGaA, Weinheim

Table 4. Catalytic activity of complexes **2** and **3** in the oxidation of other substrates[a]

Catalyst	Substrate	Temp. (°C)	$10^5 \times$ max. rate (Ms^{-1})	Max. conv. (%)
2a	cyclohexene	70	1.0	20
2b		70	1.3	20
2a	1-octene	70	0.3	10
2b		70	0.4	15
2b	4-methyl-2-pentene	70	1.0	10
2a	2-cyclohexen-1-one	70	2.0	15
2b		70	1.5	12
3a	cyclopentanone	20	0.5	5
3a		70	4.5	15
3a	cyclohexanone	20	0.5	5
3a		70	6.2	11
3a	3,3-dimethyl-2-butanone	20	0.2	5
3a		70	5	6
3a	2-allylcyclohexanone	20	0.8	11

[a] Experimental conditions: catalyst 0.017 mmol; substrate 1.7 mmol; 35% H_2O_2 1.7 mmol; DCE 3 ml; N_2 1 atm.

rated ketone 2-cyclohexen-1-one is selectively epoxidized in agrement with previous findings with Pt^{II} complexes.[17]

Complex **3a** is less effective than **2a** in the epoxidation of olefins, but far more efficient in the BV oxidation of ketones (Table 4). Notably, the oxidation of open-chain ketones is also possible, a unique ability among the BV oxidation catalysts known in the literature, that is shared only with $[Pt(\mu\text{-}OH)(P\text{-}P)]_2^{2+}$ complexes.[8a]

Competition Reactions and the Possible Role of Lewis Acidity

The overall picture that emerges from an analysis of the catalytic activity of **2a** and **3a** is that the latter is far more active in the BV oxidation, whereas **2a** is probably a better epoxidation catalyst, although in this case the differences are less evident. This seems to confirm the considerations made in the Introduction, where the reactions were compared mechanistically and indicate that the BV oxidation is more Lewis acid demanding as far as the catalyst properties are concerned.

To clarify this point and possibly answer the main question raised — "can we exploit the Lewis acidity of the catalyst to control the selectivity of the reaction?" — some competition experiments and reactions on bifunctional substrates were carried out.

Table 5. Competition experiments in the oxidation of a mixture of cyclooctene and 2-methylcyclohexanone[a]

Catalyst	Product	Temp. (°C)	$10^5 \times$ max. rate (Ms^{-1})	Max. conv. (%)
2a	cyclooctene epoxide	20	–	–
	2-heptalactone			
2a	cyclooctene epoxide	70	0.8	20
	2-heptalactone		1.5	20
3a	cyclooctene epoxide	20	0.05	2
	2-heptalactone		1.5	30
3a	cyclooctene epoxide	70	1.0	10
	2-heptalactone		7.0	25

[a] Experimental conditions: catalyst 0.017 mmol; substrates 0.85 +0.85 mmol; 35% H_2O_2 1.7 mmol; DCE 3 ml; N_2 1 atm.

Initially, **2a** and **3a** were tested in the oxidation of a 1:1 mixture of cyclooctene and 2-methylcyclohexanone; the results are collected in Table 5. As can be seen, in the case of **3a** the reactivity observed seems to be simply the addition of the results observed in the reactions with the individual substrates. Conversely, the behavior of **2a** is somehow surprising and in contrast to the results observed with the individual substrates. In fact, some preference for the BV reaction seems to be evident at 70 °C. This trend becomes quite clear in the oxidation of unsaturated ketones. Scheme 6 summarizes the results observed with dihydrocarvone and 2-allylcyclohexanone. In both cases the exclusive product is the lactone, independently of the catalyst used. This might

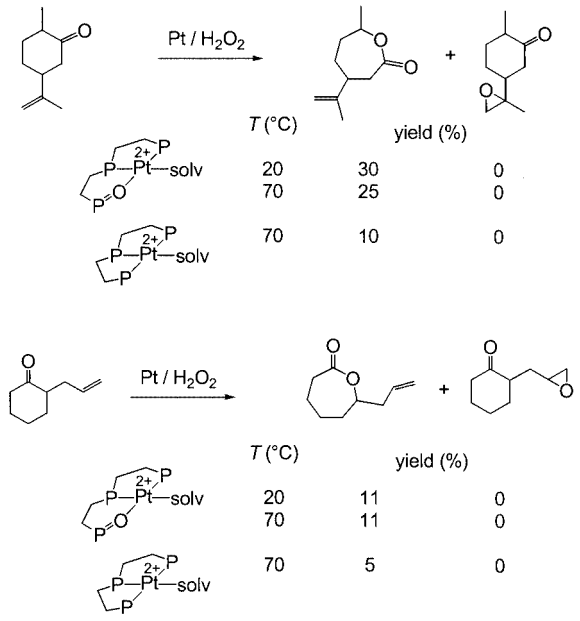

Scheme 6

 © 2004 Wiley-VCH Verlag GmbH & Co. KGaA, Weinheim

be partly due to the moderate activity of **2a** observed with terminal olefins. However, we believe that other factors might cooperate to explain the results of this competitive experiment. For example, if the complex is sufficiently Lewis acidic, even a metal center like Pt^{II} becomes more oxophilic and, in the presence of a molecule containing a C=C double bond and a C=O double bond, it becomes more prone to interact with a simple donor like oxygen and more reluctant to undergo back-bonding to the olefin. In other words, the discrimination may arise both from the intrinsic catalytic activity and from the coordinating ability of the metal, both properties being determined by the Lewis acidity of the central metal atom.

Deactivation of the Catalyst

As was mentioned above, a deactivation process is evident when reactions are carried out at 70 °C. This limits significantly the reproducibility of the catalytic experiments and seems to be independent both of the catalyst and of the oxidation reaction studied. When the metal species are isolated at the end of a catalytic reaction they can be recognized either as [PtCl(P-P-P)](BF_4) (from **2a**) or, at least partly, as [$PtCl_2$(P-P-P=O)] (from **3a**). In the case of **3a** the situation is more complex as some free, fully oxidized phosphane is also observed in the $^{31}P\{^1H\}$ NMR spectrum of the isolated material and therefore some phosphorus-free Pt species must also be formed. The most likely source of chloride is the solvent and it was demonstrated that the same chloro derivatives could be obtained by simply boiling the starting complexes in DCE, $CHCl_3$ or CH_2Cl_2. In the case of **3a** the observation that only the chloro complex is formed is a good indication that the other decomposed species are most likely generated in the catalytic reactions by hydrogen peroxide, which is responsible for the full oxidation of the phosphane. These observations imply that during the catalytic processes there is a parallel reaction between the catalyst and the solvent that leads to the complete conversion into catalytically inactive chloro derivatives. The inactivity of the chloro complexes was demonstrated by blank catalytic tests. The moderate stability of boiling DCE or chloroform and their tendency to form traces of HCl, which would explain our results, are quite well-known, although we have used DCE as solvent in Pt^{II}-catalyzed oxidations with hydrogen peroxide for the past 20 years and never observed such problems. The case of dichloromethane is less straightforward as this solvent boils at 42 °C and is recognized to be quite stable. We may speculate that a possible explanation for the above behavior may rely on a direct attack on the C−Cl bond by the strongly Lewis acidic Pt^{2+} metal centers.

Conclusions

In this work we have synthesized two classes of homologous cationic complexes of Pt^{II} containing tridentate ligands and bearing only one potentially vacant coordination site: one class contains three phosphorus donors while the other contains two phosphorus and one oxygen donors. Spectroscopic characterization indicates that the solvento derivative of the latter class of complexes (**3a**) is a stronger Lewis acid than its counterpart **2a**, although both are rather strong. Their use as catalysts in the BV oxidation of ketones and in the epoxidation of olefins has shown that the former reaction is quite Lewis-acid demanding with respect to the properties of the catalyst. This has allowed the complete control of the parallel oxidation processes in the oxidation of bifunctional substrates such as dihydrocarvone or 2-allylcyclohexanone, where the exclusive formation of the BV oxidation product was observed. The views presented in this work may probably be generalized and could be of help in the design of a new generation of selective, more active catalysts.

Experimental Section

Apparatus: IR spectra were recorded on a Nicolet 750 spectrophotometer either in nujol mulls using KBr plates or in CH_2Cl_2 solution using CaF_2 windows. $^{31}P\{^1H\}$ and ^1H NMR spectra were recorded on a Bruker AC200 spectrometer, operating in FT mode, using as external reference 85% H_3PO_4 and TMS, respectively. Negative chemical shifts are upfield from the reference. GLC measurements were taken on a Hewlett−Packard 5890A gas chromatograph equipped with a FID detector (gas carrier He). Identification of products was made by GLC by comparison with authentic samples. Molar conductivity measurements were made on 10^{-3} M solutions in MeOH with a CDM 83 Radiometer Copenhagen instrument, equipped with a CDC 334 immersion cell.

Materials: Solvents were dried and purified according to standard methods. Substrates were purified by passing through neutral alumina and stored in the dark at low temperature. Hydrogen peroxide (35% Fluka), triphos (Aldrich), HBF_4 (54% in diethyl ether; Aldrich) are commercial products and were used without purification.

The following compounds were prepared according to literature procedures: [$PtCl_2$(COD)],[18] [$PtMe_2$(COD)],[19] [$PtMe_2$(triphos)],[9] [$PtMe_2$(triphosPO)].[9] The preparation of new complexes was performed under dry N_2 by using Schlenk techniques, although all of them were found to be air stable once isolated.

Preparation of Complexes: Some of the complexes reported here were previously observed by in situ NMR spectroscopy, but never isolated and fully characterised.

[(triphos)Pt(CH_2Cl_2)](BF_4)$_2$ (2a): Triphos (0.3 g, 0.56 mmol) was dissolved in dry N_2-saturated CH_2Cl_2 (5 mL) and a solution of [$PtMe_2$(COD)] (0.19 g, 0.57 mmol) in dry N_2-saturated CH_2Cl_2 (5 mL) was added to this solution. The mixture was stirred for 2 hours under N_2 and then 200 μL of 54% HBF_4 was slowly added to the solution. This was stirred for 20 minutes, during which time rapid CH_4 evolution was observed. Water was added to the solution to eliminate traces of acid, the two phases were separated and the organic one was dried with anhydrous Na_2CO_3. The solvents were slowly evaporated from the solution in vacuo to give a white-yellow solid. This was recrystallized from CH_2Cl_2/Et_2O (0.46 g, yield 82%). $C_{35}H_{35}B_2Cl_2F_8P_3Pt$: calcd. C 42.54, H 3.57; found C 42.27, H 3.39.

[(triphosPO)Pt(CH_2Cl_2)](BF_4)$_2$ (3a): Triphos (0.80 g, 1.50 mmol) was dissolved in dry N_2-saturated CH_2Cl_2 (10 mL) and a solution

 © 2004 Wiley-VCH Verlag GmbH & Co. KGaA, Weinheim

of $[PtMe_2(COD)]$ (0.48 g, 1.44 mmol) in dry N_2-saturated CH_2Cl_2 (5 mL) was added to this solution. The mixture was stirred for 2 hours under N_2 and then a 3% solution of H_2O_2 (5 mL, 2 mmol) was added; after vigorously stirring for one hour the mixture was filtered. The two phases were separated and the organic phase was washed with water and dried with anhydrous Na_2CO_3, filtered and reduced to a small volume. 500 μL of 54% HBF_4 was then slowly added to the solution. This was stirred for 20 minutes during which rapid time CH_4 evolution was observed. Water was added to the solution to eliminate traces of acid, the two phases were separated and the organic one was dried with anhydrous Na_2CO_3. The solvents were slowly evaporated from the solution in vacuo to obtain a white-yellow solid. This was recrystallized from CH_2Cl_2/Et_2O (1.15 g, yield 80%). $C_{35}H_{35}B_2Cl_2F_8OP_3Pt$: calcd. C 41.86, H 3.51; found C 41.57, H 3.42.

[(triphos)Pt(OH)]BF_4 (2b): Compound **2a** (0.50 g, 0.51 mmol) was suspended in $CDCl_3$ (15 mL). A solution of NaOH (0.1 M) was added (15 mL) and the mixture was vigorously stirred for 30 minutes. The organic phase was separated, washed with water and dried with anhydrous Na_2CO_3, filtered and slowly evaporated in vacuo to obtained a white solid. This was recrystallized from CH_2Cl_2/Et_2O (0.37 g, yield 87%). $C_{34}H_{34}BF_4OP_3Pt$: calcd. C 49.00, H 4.11; found C 49.17, H 4.03.

[(triphos)Pt(OOH)]BF_4 (2c): Compound **2b** (0.62 g, 0.74 mmol) was suspended in $CDCl_3$ (5 mL). A 3.5% solution of H_2O_2 (1.5 mL, 1.5 mmol) was added and the mixture was vigorously stirred for 30 minutes. The white precipitate obtained was filtered off, washed with Et_2O and recrystallized from CH_2Cl_2/Et_2O (0.35 g, yield 55%). $C_{34}H_{34}BF_4O_2P_3Pt$: calcd. C 48.07, H 4.03; found C 48.15, H 4.11.

[(triphosPO)Pt$(OH)_2$] (4): Compound **3a** (0.30 g, 0.30 mmol) was dissolved in CH_2Cl_2 (4 mL) under N_2. A 4 M solution of NaOH (3 mL) in water was added and the mixture was stirred for one hour. The organic phase was separated, washed with water and dried with anhydrous Na_2CO_3. The solvents were slowly evaporated from the solution in vacuo to obtain a white solid. This was redissolved in warm acetone and kept at −15 °C for 24 hours. The white solid obtained was washed with diethyl ether and dried (0.070 g, yield 30%). $C_{34}H_{35}O_3P_3Pt$: calcd. C 52.38, H 4.52; found C 52.12, H 4.33.

Determination of the Acidity of the Complexes. NMR Method: In these experiments **1a** and **2a** were generated in an NMR tube from a known amount of precursor. The use of the isolated complexes **2a** and **3a** was found to be less reproducible as they contain traces of water. Typically 4.5×10^{-5} mol of $[PtMe_2(triphos)]$ or $[PtMe_2(triphosPO)]$ were dissolved in dry $[D_6]$acetone (0.7 mL). A stoichiometric quantity of 54% HBF_4 (12 μL, 0.9×10^{-4} mol) was added and, after evolution of methane, the $^{31}P\{^1H\}$ NMR spectrum was registered at −70 °C. Then, increasing volumes of H_2O (1, 1.5, 2, 3 μL) were introduced into the tube, and the $^{31}P\{^1H\}$ NMR spectrum at −70 °C was registered each time. A new species formed (**2d** or **3d**). By comparing the intensity of the signals at δ = 56 (**3a**, at −70 °C the signal shifts to lower fields) and 55 ppm (**3d**) and at δ = 51 (**2a**) and 48.5 ppm (**2d**) the equilibrium constant could be calculated as shown in Scheme 5.

Catalytic Reactions: These were carried out in a 10 mL round-bottomed flask equipped with a stopcock for vacuum/N_2 operations and a sidearm fitted with a screw-capped silicone septum to allow sampling. Stirring was performed by a Teflon-coated bar driven externally by a magnetic stirrer. Reactions at 70 °C were carried out using an oil bath connected with a thermostat. The concentration of the commercial 35% H_2O_2 solution was checked iodometrically prior to use.

The following general procedure was followed: the required amount of catalyst was placed in solid form (0.017 mmol) in the reactor, which was evacuated and filled with N_2. Purified, N_2-saturated olefin/ketone was added under N_2 flow, followed by the required amount of 1,2-dichloroethane (3 mL). After thermostating at the required temperature for a few minutes, the H_2O_2 solution in the appropriate amount was injected through the septum and the time was started.

All reactions were monitored by GLC by direct injection of samples taken periodically from the reaction mixtures with a microsyringe. Separation of the products was performed on a 25 m HP-5 capillary column using a flame ionization detector. The maximum rate was expressed as a zero-order rate constant from analysis of conversion vs. time curves.

[1] *Lewis Acids in Organic Synthesis* (Ed.: H. Yamamoto), Wiley-VCH: Weinheim, **2000**.

[2] [2a] K. Hori, J. Ito, T. Ohta, I. Furukawa, *Tetrahedron* **1998**, *54*, 12737. [2b] D. Ferraris, B. Young, T. Dudding, T. Lectka, *J. Am. Chem. Soc.* **1998**, *120*, 4548. [2c] A. K. Ghosh, H. Matsuda, *Org. Lett.* **1999**, *1*, 2157. [2d] S. Oi, E. Terada, K. Ohuchi, T. Kato, Y. Tachibana, I. Inoue, *J. Org. Chem.* **1999**, *64*, 8660. [2e] K. Hori, H. Kodama, T. Ohta, I. Furukawa, *J. Org. Chem.* **1999**, *64*, 5017. [2f] K. Pignat, J. Vallotto, F. Pinna, G. Strukul, *Organometallics* **2000**, *19*, 5160. [2g] J. Hao, M. Hatano, K. Mikami, *Org. Lett.* **2000**, *2*, 4059. [2h] T. Hattori, Y. Suzuki, O. Uesugi, S. Oi, S. Miyana, *Chem. Commun.* **2000**, 73. [2i] A. Fürstner, D. Voigtländer, W. Schrader, D. Giebel, M. Reetz, *Org. Lett.* **2001**, *3*, 417. [2j] N. M. Brunkan, P. S. White, M. R. Gagné, *Organometallics* **2002**, *21*, 1565. [2k] N. M. Brunkan, M. R. Gagné, *Organometallics* **2002**, *21*, 1576.

[3] [3a] M. Del Todesco Frisone, R. Giovanetti, F. Pinna, G. Strukul, *Stud. Surf. Sci. & Catal.* **1991**, *66*, 405. [3b] M. Del Todesco Frisone, F. Pinna, G. Strukul, *Organometallics* **1993**, *12*, 148.

[4] C. Bolm, O. Beckmann, C. Palazzi, *Can. J. Chem.* **2001**, *79*, 1593.

[5] C. Bolm, O. Beckmann, A. Cosp, C. Palazzi, *Synlett* **2001**, 1461.

[6] A. Corma, L. T. Nemeth, M. Renz, S. Valencia, *Nature* **2001**, *412*, 423.

[7] [7a] G. Strukul, R. A. Michelin, *J. Chem. Soc., Chem. Commun.* **1984**, 1538. [7b] G. Strukul, R. A. Michelin, *J. Am. Chem. Soc.* **1985**, *107*, 7563. [7c] R. Sinigalia, R. A. Michelin, F. Pinna, G. Strukul, *Organometallics* **1987**, *6*, 728. [7d] A. Zanardo, F. Pinna, R. A. Michelin, G. Strukul, *Inorg. Chem.* **1988**, *27*, 1966. [7e] A. Zanardo, F. Pinna, R. A. Michelin, G. Strukul, *Inorg. Chem.* **1989**, *28*, 1648.

[8] [8a] R. Gavagnin, M. Cataldo, F. Pinna, G. Strukul, *Organometallics* **1998**, *17*, 661. [8b] C. Paneghetti, R. Gavagnin, F. Pinna, G. Strukul, *Organometallics* **1999**, *18*, 5057.

[9] [9a] G. Annibale, P. Bergamini, V. Bertolasi, E. Bosco, M. Cattabriga, R. Rossi, *Inorg. Chim. Acta* **2002**, *333*, 116. [9b] G. Annibale, P. Bergamini, M. Cattabriga, *Inorg. Chim. Acta* **2001**, *316*, 25.

[10] [10a] G. Strukul, R. Ros, R. A. Michelin, *Inorg. Chem.* **1982**, *21*, 495. [10b] M. T. Atlay, M. Preece, G. Strukul, B. R. James, *J. Chem. Soc., Chem. Commun.* **1982**, 406.

[11] [11a] K. Nakamoto, *Infrared Spectra of Inorganic and Coordination Compounds*, 2nd edition, Wiley, New York, **1970**, p. 115. [11b] R. M. Silverstein, F. X. Webster, *Spectrometric Identification of Organic Compounds*, 6th ed., Wiley, New York, **1998**, p. 109.

[12] T. G. Appleton, M. A. Bennett, *Inorg. Chem.* **1978**, *17*, 738.

[13] W. J. Geary, *Coord. Chem. Rev.* **1971**, *7*, 81.

[14] [14a] G. W. Bushnell, K. R. Dixon, R. G. Hunter, J. J. McFarland, *Can. J. Chem.* **1972**, *50*, 3694. [14b] B. Longato, B. Corain,

 © 2004 Wiley-VCH Verlag GmbH & Co. KGaA, Weinheim

G. M. Bonora, G. Pilloni, *Inorg. Chim. Acta* **1987**, *137*, 75. [14c] A. L. Bandini, G. Banditelli, F. Demartin, M. Manassero, G. Minghetti, *Gazz. Chim. Ital.* **1993**, *23*, 417. [14d] J. J. Li, P. R. Sharp, *Inorg. Chem.* **1996**, *35*, 604.
[15] J. P. Collman, L. S. Hegedus, J. R. Norton, R. G. Finke, *Principles and Applications of Transition Metal Chemistry*, University Science Books, Mill Valley, **1987**, p. 110.
[16] H. A. Zhong, J. A. Labinger, J. E. Bercaw, *J. Am. Chem. Soc.* **2002**, *124*, 1378.
[17] C. Baccin, A. Gusso, F. Pinna, G. Strukul, *Organometallics* **1995**, *14*, 1161.
[18] J. X. McDermott, J. F. White, G. M. Whitesides, *J. Am. Chem. Soc.* **1976**, *98*, 6521.
[19] R. Bassan, K. H. Bryars, L. Judd, A. W. G. Platt, P. G. Pringle, *Inorg. Chim. Acta* **1986**, *121*, L41.

Received August 20, 2003
Early View Article
Published Online February 3, 2004

 © 2004 Wiley-VCH Verlag GmbH & Co. KGaA, Weinheim

Determination of the Solvothermal Synthesis Mechanism of Metal Imidazolates by X-ray Single-Crystal Studies of a Photoluminescent Cadmium(II) Imidazolate and Its Intermediate Involving Piperazine

Yun-Qi Tian,*[a,b] Li Xu,[a] Chen-Xin Cai,[a] Ji-Chong Wei,[a] Yi-Zhi Li,[a] and Xiao-Zeng You*[a]

Keywords: Cadmium / Crystal engineering / Fluorescence / Nitrogen heterocycles / Zeolite analogues

Cadmium(II) imidazolate (**3**), with a twofold interpenetrating diamondoid net, was obtained in a manner similar to cobalt(II) imidazolate. In the process, a crystallized intermediate involving piperazine (**2**), which was suitable for X-ray single crystal study, was isolated. Based on the composition of **2**, a mechanism for the solvothermal synthesis of metal imidazolates was proposed. **3**: a = 9.931(2), b = 10.739(2), c = 14.622(3) Å, $\alpha = \beta = \gamma = 90°$, orthorhombic, *Pcab*; **2**: a = 8.243(2), b = 9.883(2), c = 12.471(3) Å, α = 107.89(3)°, β = 92.56(3)°, γ = 100.87(3)°, triclinic, $P\bar{1}$. Both compounds are photoluminescent with λ_{max} = 459 nm for **3** and 444 nm for **2**; they also display quenching of the fluorescence with $\tau \approx 5$ ns. (© Wiley-VCH Verlag GmbH & Co. KGaA, 69451 Weinheim, Germany, 2002)

Introduction

The search for crystalline solids with unusual electrochemical, magnetic, photophysical and porous properties[1] has attracted an increasing amount of attention from materials scientists and has made the subjects of molecular design and crystal engineering grow almost exponentially in recent years.[2] Because of this, polymorphism, or supramolecular isomerism, has been found to be more general than was previously expected according to the Cambridge Structural Database (CSD).[3] Nevertheless, the phenomenon of extended polymorphism[4] is still rare, although it has been demonstrated that the frequency of occurrence of polymorphic modifications is not necessarily uniform in all categories of substances and it is probably more common in molecules that have conformational flexibility and/or multiple groups capable of hydrogen bonding or coordination.[2]

More recently, in our investigations of metal-organic frameworks with zeolitic topologies, we have found that extended polymorphism also exists in cobalt(II) imidazolate frameworks that show zeolite-like flexibility with variable T−T−T angles.[5] Unlike the flexibility mentioned above, the flexibility of the T−T−T angles can allow extended polymorphism in many zeolite varieties. Because of this we believe that there should be even more supramolecular isomers (or framework polymorphs) of cobalt(II) imidazolate than we have so far obtained. Although cobalt(II) imidazolate isomers have been prepared by a solvothermal method, an apparently successful synthetic strategy,[5] to create more isomers other synthetic strategies have to be developed. In order to do this, however, more details of the mechanism of the formation of cobalt(II) imidazolates are needed. In the synthesis of cobalt(II) imidazolate we noticed that piperazine plays a more important role than other organic bases, such as trialkylamines.[5b] Therefore, it is essential to understand the effect of the piperazine in the solvothermal synthesis in order to determine the synthetic mechanism.

According to the IR spectrum and the element analysis of the intermediate of cobalt(II) imidazolate involving piperazine, which separated as a powder after 12 h reaction at room temperature, and X-ray single crystal studies on the final solvothermal product of cobalt(II) imidazolates, a mechanism for the solvothermal synthesis of cobalt(II) imidazolates was proposed (Scheme 1), in which the piperazine serves not only as a base to deprotonate the imidazole, but also as a ligand that can coordinate to the metal center in cooperation with the imidazolate. Nevertheless, this is only a proposal since the intermediate is formed at room temperature while the nature of the relevant species under solvothermal conditions are still unknown.

Fortunately, during the synthesis of cadmium(II) imidazolate, besides the intermediate involving piperazine (Pz), $[Cd(OAc)_2(Pz)(im\text{-}H)]_n$ (**1**), which is similar to the cobalt(II) imidazolate intermediate that separated at room tempera-

[a] State Key Laboratory of Coordination Chemistry, Institute of Coordination Chemistry, Nanjing University, 210093 Nanjing, China
Fax: (internat.) +86-25-359-3522
E-mail: xyz@nju.edu.cn
[b] Department of Chemistry, Liaoning University, 210036 Shenyang, China
Fax: (internat.) +86-24-6220-2053
E-mail: ytian588@sina.com.cn

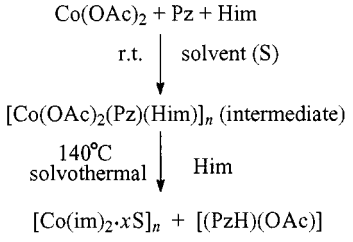

Scheme 1. Proposed reaction scheme for the solvothermal formation of cobalt imidazolate polymers

ture, we also obtained another compound with piperazine, $[Cd_2(OAc)_3(Pz)(im)]_n$ (**2**), which was obtained as single crystals under solvothermal conditions. To prepare the piperazine-free polymer, $[Cd(im)_2]_\infty$ (**3**), an even higher solvothermal temperature has to be used. Therefore, the solvothermal synthesis of the cadmium(II) imidazolate could be suitable for demonstrating the effect of the piperazine, and also for determining the solvothermal synthetic mechanism of metal imidazolates. In this paper, we present the crystal structures and photoluminescent properties of the cadmium imidazolate (**3**) and its intermediate(**2**), which are used to support the supposed solvothermal synthetic mechanism of cadmium(II) imidazolate and its cobalt analogues.

Results and Discussion

X-ray Crystal Structures

X-ray single crystal studies showed that **2** is a 2D quaternary coordination polymer (i.e., one with four different chemical components). In the asymmetric unit (Figure 1, top) of **2**, there are two Cd^{II} atoms, three acetates, two halves of different piperazine molecules and one imidazolate; the Cd1···Cd2 distance is 4.39 Å. In order to understand this complicated crystal structure easily, we can view the 2D coordination polymer as an assembly of cadmium(II) acetate chains (Figure 1, bottom) with piperazine and imidazolates. The chains are composed of two different cadmium-acetate links: (i) $[(OAc)Cd1(\mu\text{-}OAc)_2Cd1'(OAc)]$ (simplified as link A−A′, in which each cadmium is chelated by two acetates; Cd1 and Cd1′, separated by 3.74 Å, are doubly bridged by two oxygen atoms of the two inner acetates), and (ii) $[Cd2(\mu\text{-}OAc)_2Cd2']$ (simplified as link B−B′, in which each cadmium is chelated by one acetate; the two cadmiums Cd2 and Cd2′ are separated by a distance of 3.87 Å and doubly bridged by two oxygen atoms of the carboxylic groups). Subsequently, the two kinds of links, A−A′ and B−B′, are alternately connected to each other by the single oxygen bridges of the outside carboxylic groups of the A−A′ links in the [1 0 −1] direction. In the chains, the carboxylic oxygen atoms are all coordinated to the equatorial positions of the cadmium ions, while the axial positions of the metals are occupied alternately by imidazolate and piperazine within the chains along the [1 0 −1] axis and between the chains along the [3 0 1] axis, forming a 2D sheet that parallels the (0 1 0) plane (Figure 2, top).

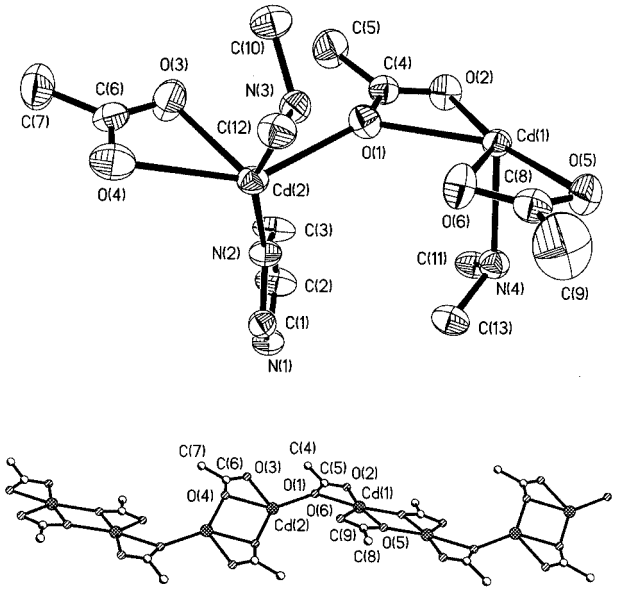

Figure 1. Top: ORTEP drawing of the asymmetric unit of **2** with thermal ellipsoids at 50% probability; bottom: ball and stick diagram of **2** showing the cadmium acetate chain of alternate connected links A−A′ ($[(OAc)Cd1(\mu\text{-}OAc)_2Cd1'O(OAc)]$) and B−B′ ($[Cd2(\mu\text{-}OAc)_2\ Cd2']$)

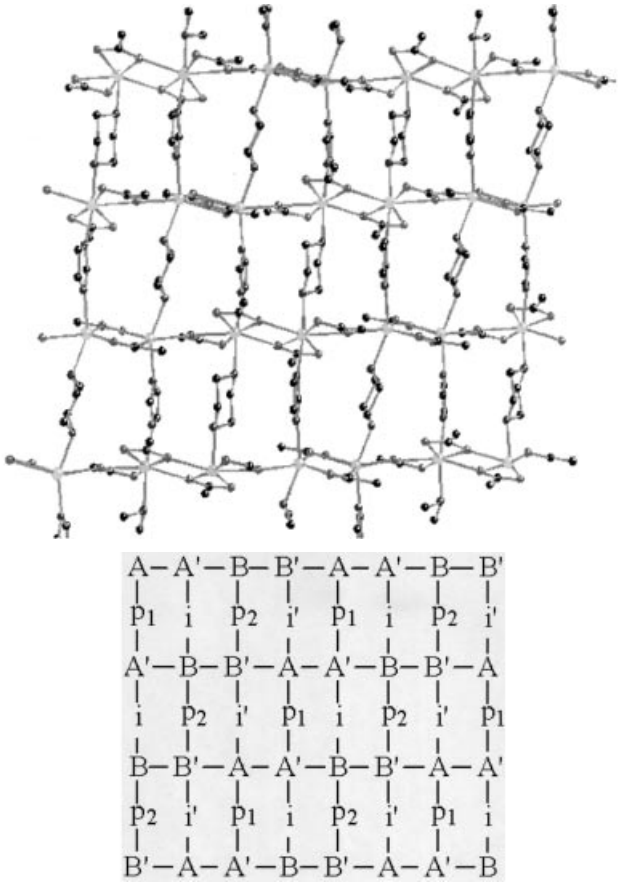

Figure 2. Top: View of the 2D structural layer of compound **2** along the [0 1 0] axis; top: ball and stick diagram of **2** (the hydrogen atoms are omitted for clarity); bottom: symbolized representation of the supramolecular 2D assembly of the quaternary coordination polymer (p = piperazine, i = imidazolate, A to A′, B to B′ and i to i′ are symmetry-related)

 © 2004 Wiley-VCH Verlag GmbH & Co. KGaA, Weinheim

Thus, the Cd^{II} ions in A−A′ are seven coordinate while the Cd^{II} ions in links B−B′ are six coordinate. For a distinct view of the supramolecular assembly of compound **2**, a 2D structure of symbolized components is illustrated as Figure 2, bottom. In the crystal of **2** such sheets are stacked parallel to the (010) plane with an interlayer distance of 9.883 Å, equal to the value of the crystal unit-cell parameter *b*.

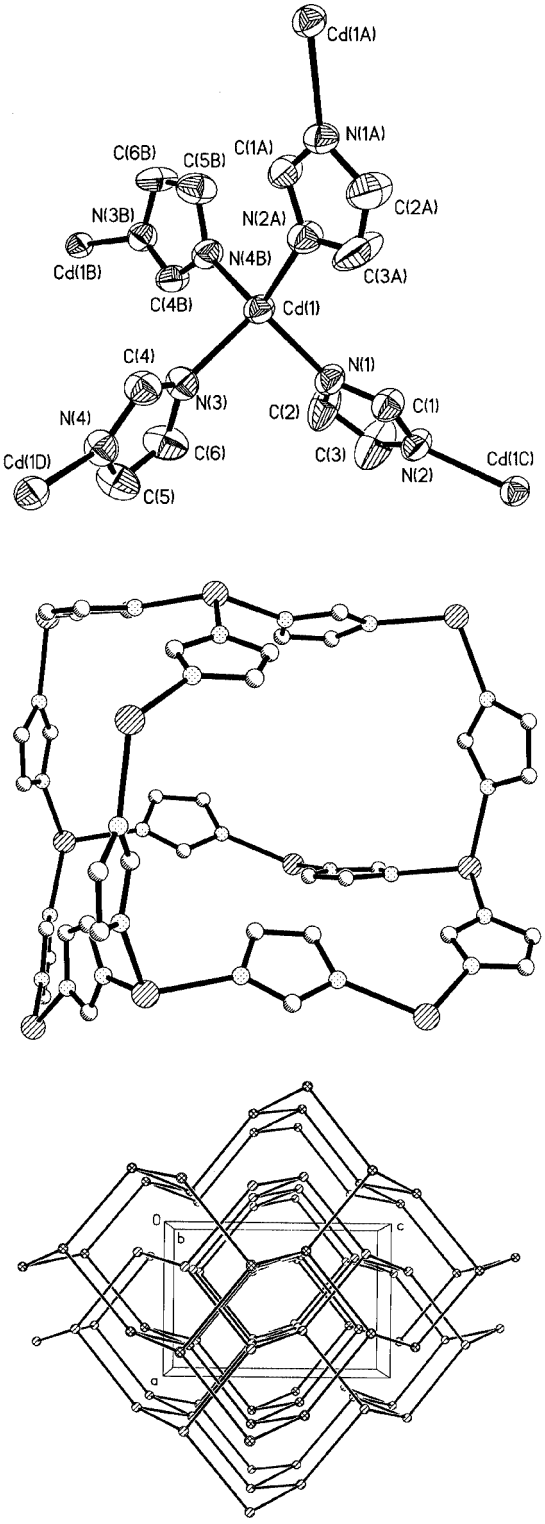

Figure 3. Top: ORTEP drawing of the Cd coordination environment in **3**, with thermal ellipsoids of 50% probability; middle: ball and stick diagram of the diamondoid-cage unit of **3**; bottom: ball and stick representation of the twofold parallel interpenetrating nets of **3** (ball = Cd^{II}, stick = imidazolate)

X-ray single-crystal studies on compound **3** show that this compound contains one Cd^{II} atom and two imidazolates in its asymmetric unit. In the structure, the Cd^{II} is four coordinate (Figure 3, top) like Co^{II} in all of the cobalt imidazolate isomers.[5b] The MN_4 tetrahedra exhibit almost the same deviations from a regular tetrahedron as those in $[Co_5(im)_{10}\cdot 2MB]_\infty$.[5a] However, the deviation of the T−T−T angles from a regular tetrahedron are much smaller than those in any of the cobalt(II) imidazolate isomers prepared so far (Table 1). It is known that a 3D net with regular tetrahedral nodes is likely to have a diamondoid structure,[6] and $[Cd(im)_2]_\infty$ indeed forms such a net with a cristobalite-like structure (Figure 3, middle). As an expanded diamondoid framework, compound **3** exhibits a "normal" mode[7] of twofold interpenetrating nets (Figure 3, bottom), in each of which the shortest Cd···Cd distance is ca. 6.4 Å. Compound **3** is, to the best of our knowledge, the first structurally characterized cadmium imidazolate homopolymer and is also the only metal imidazolate with a diamondoid topology that responds to the problem raised by Masciocchi et al.[4] The preparation of other structures of cadmium imidazolate has not yet been successful. The absence of polymorphism for this substance might be due to the limited flexibility of the Cd···Cd···Cd angles, which suffer from restrained Cd−N bond rotation.

Photoluminescent Properties

The diffuse-reflectance absorption and photoluminescence spectra of pure compounds **2** and **3** in the solid state at room temperature are shown in Figure 4. Compound **2** displays an intense photoluminescence emission at 444 nm (22523 cm^{-1}) that is red-shifted by about 1630 cm^{-1} from the 0−0 transition band (414 nm, 24155 cm^{-1}), while that of **3** is found at 459 nm (21786 cm^{-1}) and is red-shifted by about 1800 cm^{-1} from the 0−0 transition band (424 nm, 23585 cm^{-1}). It is well-known that the lowest excited state of imidazole is an n→π* transition that displays no photoluminescence;[8] therefore the increase in the rigidity of the imidazolate ligand upon forming the polymeric complexes should not cause the fluorescent emission of these compounds, especially considering that $[Zn(im)_2]_n$ displays almost no photoluminescence. It has also been shown that $[Cd(Him)_6](NO_3)_2$ and the intermediate $[Cd(OAc)_2(Pz)(imH)]$ (**1**) are also not photoluminescent. All this evidence suggests that the fluorescence must be due to the deprotonated imidazoles and/or the cadmium(II) centers. Therefore the fluorescent emissions in the two compounds are proposed to be ligand-to-metal charge-transfer (LMCT) in

 © 2004 Wiley-VCH Verlag GmbH & Co. KGaA, Weinheim

Table 1. Deviations of bond and angle parameters in the cobalt(II) and cadmium(II) imidazolates

	$Co(im)_2$ (1)	$Co(im)_2$ (2)	$Co(im)_2$ (3)	$Co(im)_2$ (4)	$Co(im)_2$ (5)	**3**
$(M-N)_{max} - (M-N)_{min}$ (Å)	0.045	0.020	0.059	0.116	0.042	0.031
$(M\cdots M)_{max} - (M\cdots M)_{min}$ (Å)	0.172	0.172	0.258	0.098	0.233	0.052
$(N-M-N)_{max} - (N-M-N)_{min}$ (°)	10.1	7.7	12.4	13.9	14.8	14.5
$(M\cdot\cdot M\cdot\cdot M)_{max} - (M\cdot\cdot M\cdot\cdot M)_{min}$ (°)	67.5	57.8	94.0	57.3	88.4	25.9

nature. It is also noticeable that compounds **2** and **3** display quenching of the fluorescence with $\tau = 4.8$ ns and 4.5 ns, respectively, which may mean that the substances are excellent candidates for potential photoactive materials.

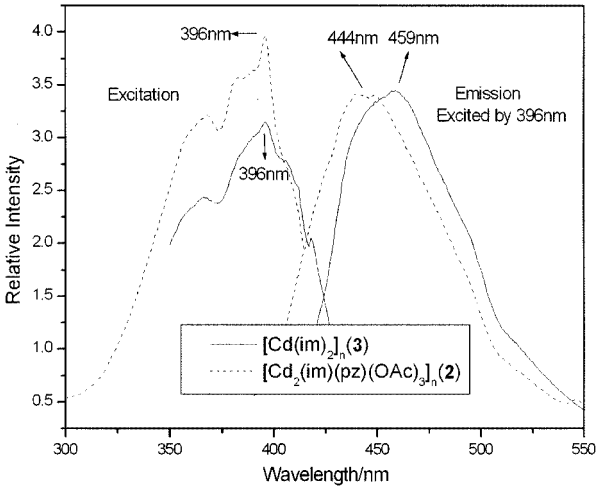

Figure 4. Solid-state excitation and emission spectra of $[Cd(im)_2]_n$ (**3**) and $[Cd_2(pz)(im)(OAc)_3]_n$ (**2**) at room temperature

The Coordination Buffering Effect of Piperazine

In the hydrothermal synthesis of inorganic zeolites, the organic amines play very important roles[9] in (i) structure-direction or templation, (ii) gel modification, and (iii) gel-PH alteration or buffering. Although organic amines are also necessary for the solvothermal synthesis of metal imidazolates, they are seemingly restricted to amines that are able to coordinate to metals. Nevertheless, the coordinating ability of the amines to metals should not be so strong that they cannot be replaced by imidazolates, and their basicity should not be so low that they are unable to deprotonate the imidazoles under solvothermal conditions. Our experiments show that piperazine is an ideal amine to act as both the ligand and the base (Scheme 1). Although we had managed to isolate a single crystal of the intermediate, a cobalt imidazolate involving piperazine formed at a lower solvothermal temperature, to support this proposed mechanism, all our attempts to isolate such an intermediate under the experimental conditions were in vain. However, in the cadmium imidazolate (**3**) synthesis, such a mass crystalline intermediate $[Cd_2(OAc)_3(Pz)(im)]_\infty$ (**2**), the intermediate II in Scheme 2, was separated and showed a different composition from $[Cd(OAc)_2(Pz)(im\text{-}H)]_n$ (**1**), the intermediate I, separated after 24 hours reaction at room temperature (the composition of **1** was determined according to the IR and elemental analyses as well as the charge balance principle. Although the mass spectrum was measured, no significant mass signals were observed due to the insolubility of the polymeric substances).

In order to confirm **2** as a real intermediate of **3**, we separated **2** and then allowed it to react with imidazole in a ratio of 1:3 under the same solvothermal conditions for another 24 hours. As expected, the product was as same as that of the one-pot reaction at 160 °C. Therefore, the solvothermal synthetic route of cadmium(II) imidazolate could be as depicted in Scheme 2, similar to that of the cobalt(II) imidazolate. However, in the latter case, the intermediate under solvothermal conditions is still unknown and it may not be the same as that of the cadmium imidazolate, although the fact that piperazine has taken part in the intermediate formation is undeniable. It is the buffering effect on the concentration of free metal ions by piperazine under solvothermal conditions that gives the template solvent enough time to direct the metal imidazolate to the default or the non-default structures[11] and allows the substance to crystallize with sufficient crystal size. So far, there have been six different topological structures[5,10] of cobalt imidazolates prepared by using piperazine as organic base and buffering ligand.

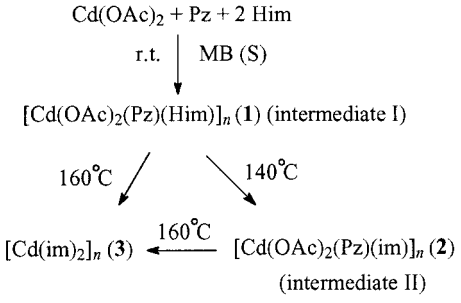

Scheme 2. Solvothermal synthetic route of cadmium(II) imidazolate

NB: During the writing of this paper the structure of **3** was published.[12] However, as the powdery product resulted from a different synthetic procedure, its structure had to be determined by an ab initio XRPD method.

Conclusion

The solvothermal synthesis of metal imidazolates is regarded as similar to the hydrothermal synthesis of inorganic

 © 2004 Wiley-VCH Verlag GmbH & Co. KGaA, Weinheim

zeolites or molecular sieves. However, depending on the effects of the organic bases in both of the above mentioned syntheses, the reaction mechanism of metal imidazolates should be different from that of zeolites or molecular sieves:[9] An amine with a certain coordinating ability can form coordination compounds with metals at room temperature and then release the metals steadily under the solvothermal conditions, thus facilitating the crystallization of porous structures of metal imidazolates. Therefore, it is understandable why the trialkylamines commonly used in the hydrothermal synthesis of zeolites are useless for the synthesis of metal imidazolates. As for an amine with strong coordinating ability, such as ethylenediamine, the use of such an organic base in the synthesis of metal imidazolates may lead to the need for a higher solvothermal temperature that will not facilitate a porous structure, or sometimes, due to the high stability of the metal-amine complexes, the metal imidazolate polymers may even not be realizable. Although the use of piperazine as the organic base was initially a random choice, it should now be seen as inevitable, although the search for other suitable organic amines, as synthetic variables is encouraged.

Experimental Section

General Remarks: Imidazole, cadmium acetate dihydrate and anhydrous piperazine were obtained from commercial sources and used without further purification. Elemental analyses for C, H and N were performed at the Materials Analysis Center of Nanjing University with a Perkin−Elmer 240 analyzer. Fourier Transform Infrared (FT-IR) Spectra were measured from KBr pellets by using a Nicolet FT-IR 17SX. The diffuse-reflection absorption UV/Vis spectra were performed on a Perkin−Elmer Lambda35 UV/Vis Spectrometer (No. 101N1102201). The fluorescence spectroscopic studies were conducted on an AMINCO Bowman Series 2 Luminescence Spectrometer, whilst the fluorescent quenching was measured on an SLM48000DSCF System.

$[Cd(OAc)_2(Pz)(Him)]$ (1): $Cd(OAc)_2{\cdot}2H_2O$ (1.33 g, 5 mmol), anhydrous piperazine (0.43 g, 5 mmol) and imidazole (0.68 g, 10 mmol) were added to 30 mL of 3-methyl-1-butanol, and this heterogeneous mixture was then stirred at room temperature for 24 h. The resulting powder was separated by filtration, washed with ethanol and diethyl ether, and dried in vacuo to give 1.34 g of **1**; yield ca. 70%. $C_{11}H_{20}CdN_4O_4$ (384.4): calcd. C 34.34, H 5.20, N 14.57; found C 35.01, H 5.86, N 13.27. IR (KBr pellet): $\tilde{\nu}$ = 3117 (vs, sh), 3059 (m), 2952 (m), 2885 (m), 2849 (m), 1579 (vs), 1464 (s), 1417 (vs), 1338 (m), 1329 (m), 1076 (s), 1058 (s), 941 (m), 835 (m), 791 (s), 667−621 (s) cm^{-1}.

$[Cd_2(OAc)_3(Pz)(im)]_\infty$ (2): $Cd(OAc)_2{\cdot}2H_2O$ (1.33 g, 5 mmol), anhydrous piperazine (0.43 g, 5 mmol) and imidazole (0.68 g, 10 mmol) were added to 30 mL of 3-methyl-1-butanol, and after being stirred at room temperature for 12 h, this heterogeneous mixture was placed into a Teflon-lined autoclave (34 mL). The autoclave was then sealed and heated at 140 °C for 24 hours. After cooling to room temperature, colorless crystals were collected and washed with 3 × 15 mL of ethanol and dried in vacuo to give 0.83 g of **2**; yield ca. 60%. $C_{13}H_{22}Cd_2N_4O_6$ (554.8): calcd. C 28.14, H 3.96, N 10.09; found C 27.89, H 3.68, N 9.67. IR (KBr pellet): $\tilde{\nu}$ = 3227 (s, sh), 3136 (m, sh), 3112 (m, sh), 3058 (m), 2967 (m), 2858 (m), 1562 (vs), 1498 (m), 1411 (s), 1340 (m), 1329 (m), 1073 (s), 1015 (m), 943 (m), 882 (s), 822 (m), 772 (m), 670−621 (m) cm^{-1}.

$[Cd(im)_2]_\infty$ (3): $Cd(OAc)_2{\cdot}2H_2O$ (1.33 g, 5 mmol), anhydrous piperazine (0.43 g, 5 mmol) and imidazole (0.68 g, 10 mmol) were added to 30 mL of 3-methyl-1-butanol, and after being stirred at room temperature for 12 h, this heterogeneous mixture was placed into a Teflon-lined autoclave (34 mL). The autoclave was sealed and heated at 160 °C for 24 hours. After cooling to room temperature, colorless crystals were collected and washed with 3 × 15 mL of ethanol and dried in vacuo to give 0.50 g of **3**; yield 40%. $C_6H_6CdN_4$ (246.4): calcd. C 29.22, H 2.44, N 22.73; found C 29.60, H 2.20, N 22.38. IR (KBr pellet): $\tilde{\nu}$ = 3130 (w), 1586 (w), 1482 (vs, sh), 145 (s, sh), 1315 (m), 1244 (s, sh), 1164 (m, sh), 1087 (vs, sh), 943 (s, sh), 818 (m), 756 (s, sh), 746 (s, sh), 664 (vs, sh) cm^{-1}.

X-ray Crystallographic Study: The X-ray single-crystal structure determination was carried out using an Enraf Nonius-CAD4SDP44 diffractometer with graphite-monochromated Mo-K_α radiation (λ = 0.71073 Å). The unit-cell parameters were based on 25 carefully centered reflections in the range $4.42° < 2\theta < 51.96°$. An absorption correction was applied using ψ-scan data. The structures were solved by direct methods and refined by full-matrix least-squares on F^2 using SHELXS-97 (version 5.1).[13] All non-hydrogen atoms were refined anisotropically. Hydrogen atoms were generated and included in the structure-factor calculations with assigned isotropic thermal parameters but were not refined. For the full-matrix least-squares refinements [$I > 2\sigma(I)$], the unweighted and weighted agreement factors $R = (||F_o| - |F_c||)/|F_o|$ and $wR = \{w[(|F_o|^2 - |F_c|^2)^2]/w[(|F_o|^2)^2]\}^{1/2}$ $\{w = 1/[\sigma^2(|F_o|^2) + (aP)^2 + bP]$, where $P = (|F_o|^2 + 2|F_c|^2)/3\}$ were used. The crystallographic data are summarized in Table 2, and selected bond lengths and bond angles of the compound **2** and **3** are listed in Table 3. CCDC-149555 (**2**) and -212355 (**3**) contain the supplementary crystallographic data for this paper. These data can be obtained free of charge at www.ccdc.cam.ac.uk/conts/retrieving.html [or from the Cambridge Crystallographic Data Centre, 12 Union Road, Cambridge CB2 1EZ, UK; Fax: (internat.) +44-1223/336-033; E-mail: deposit@ccdc.cam.ac.uk].

Table 2. Crystal data collection and structure refinement

	2	**3**
Empirical formula	$C_{13}H_{22}N_4O_6Cd_2$	$C_6H_6N_4Cd$
Mol. mass	555.51	246.55
Crystal system	triclinic	orthorhombic
Space group	$P\bar{1}$	*Pcab*
a (Å)	8.2430(16)	9.931(2)
b (Å)	9.883(2)	10.739(2)
c (Å)	12.471(3)	14.622(3)
α (°)	107.89(3)	90.00
β (°)	92.56(3)	90.00
γ (°)	100.87(3)	90.00
V (Å^3)	943.7(3)	1559.4(5)
Z	2	8
F (000)	544	944
$\rho_{calcd.}$ (g cm^{-3})	1.954	2.100
μ (mm^{-1})	2.288	2.735
R_1 [$I > 2\sigma(I)$]	0.0245	0.0296
wR_2 [$I > 2\sigma(I)$]	0.0631	0.0639
R_1 [all data]	0.0410	0.0700
wR_2 [all data]	0.0680	0.0732
GOF	1.064	1.035

 © 2004 Wiley-VCH Verlag GmbH & Co. KGaA, Weinheim

Table 3. Selected bond lengths [Å] and angles [°] for **2** and **3**[a]

2			
Cd(1)−N(4)	2.315(4)	Cd(1)−N(1)\$1	2.237(3)
Cd(1)−O(2)	2.389(3)	Cd(1)−O(5)\$2	2.378(3)
Cd(1)−O(1)	2.434(3)	Cd(1)−O(5)	2.414(3)
Cd(1)−C(4)	2.750(4)	Cd(1)−O(6)	2.543(4)
Cd(2)−N(3)	2.277(4)	Cd(2)−N(2)	2.192(3)
Cd(2)−O(4)\$3	2.373(3)	Cd(2)−O(3)	2.349(3)
Cd(2)−O(4)	2.490(4)	Cd(2)−O(1)	2.409(3)
N(1)\$1−Cd(1)−N(4)	171.87(13)	N(1)−Cd(1)\$4	2.237(3)
N(1)\$1−Cd(1)−O(2)	88.64(12)	N(4)−Cd(1)−O(5)\$2	80.82(13)
O(5)\$2−Cd(1)−O(2)	89.13(11)	N(4)−Cd(1)−O(2)	96.97(12)
N(4)−Cd(1)−O(5)	83.86(12)	N(1)\$1−Cd(1)−O(5)	89.30(12)
O(2)−Cd(1)−O(5)	166.35(11)	O(5)\$2−Cd(1)−O(5)	77.53(13)
N(4)−Cd(1)−O(1)	94.68(12)	N(1)\$1−Cd(1)−O(1)	93.38(12)
O(3)−Cd(2)−O(1)	98.20(11)	N(3)−Cd(2)−O(1)	74.44(13)
N(3)−Cd(2)−O(4)	93.43(13)	N(2)−Cd(2)−O(4)	110.74(13)
O(1)−Cd(2)−O(4)	145.95(11)	O(3)−Cd(2)−O(4)	52.79(12)
N(2)−Cd(2)−O(4)\$3	88.56(13)	N(3)−Cd(2)−O(3)	102.77(14)
O(3)−Cd(2)−O(4)\$3	125.42(9)	N(3)−Cd(2)−O(4)\$3	93.00(13)
O(5)−Cd(1)−O(6)	52.26(11)	N(2)−Cd(2)−O(1)	87.48(9)
N(2)−Cd(2)−N(3)	155.26(14)	O(1)−Cd(1)−O(6)	87.59(10)
O(2)−Cd(1)−O(1)	53.93(10)	N(2)−Cd(2)−O(3)	96.31(14)
N(4)−Cd(1)−O(6)	91.01(12)	O(5)−Cd(1)−O(1)	139.69(10)
O(2)−Cd(1)−O(6)	141.11(11)		
3			
Cd(1)−N(4)#1	2.188(4)	Cd(1)−N(1)	2.190(4)
Cd(1)−N(2)#2	2.199(5)	Cd(1)−N(3)	2.219(5)
N(1)−C(1)	1.327(7)	N(1)−C(2)	1.342(8)
N(2)−C(1)	1.308(7)	N(2)−C(3)	1.334(8)
N(4)#1−Cd(1)−N(1)	111.80(18)	N(1)−Cd(1)−N(2)#2	114.27(9)
N(4)#1−Cd(1)−N(3)	106.06(9)	N(1)−Cd(1)−N(3)	99.80(17)
N(2)#2−Cd(1)−N(3)	113.24(9)		

[a] Symmetry transformations used to generate equivalent atoms: **2:** \$1 $x-1, y, z$; \$2 $-x, -y+1, -z+1$; \$3 $-x+1, -y+1, -z$; \$4 $x+1, y, z$; \$5 $-x, -y+1, -z$; \$6 $-x+1, -y+1, -z+1$; **3:** #1 $x-1/2, -y+1, -z+3/2$; #2 $-x+1/2, y+1/2, -z+1$; #3 $-x+1/2, y-1/2, -z+1$; #4 $x+1/2, -y+1, -z+3/2$.

Acknowledgments

This work was supported by the State Key Project of Fundamental research (No. G200077500) and the National Science Foundation of China (No. 90101028).

[1] [1a] J. M. Lehn, *Supramolecular Chemistry*; VCH: Weinheim,**1995**. [1b]S. R. Batten, R. Roberson, *Angew. Chem. Int. Ed.* **1998**, *37*, 1460−1494. [1c] C. N. R. Rao and B. Raveau, in *Colossal Magnetoresistance, Charge Ordering and Related Properties of Rare Earth Manganese Oxides*, World Scientific: Singapore, **1998**. [1d]A. K. Cheetham, G. Férey, T. Loiseau, *Angew. Chem. Int. Ed.* **1999**, *38*, 3268−3292. [1e] O. M. Yaghi, H. Li, C. Davis, D. Richardson, T. L. Groy, *Acc. Chem. Res.* **1998**, *31*, 474−484. [1f] Z.-Y. Fu, X.-T. Wu, J.-C. Dai, S.-M. Hu, W.-X. Du, H.-H. Zhang, R.-Q. Sun, *Eur. J. Inorg. Chem.* **2002**, 2730−2735.

[2] B. Moulton, M. Zaworotko, *Chem. Rev.* **2001**, *101*, 1629−1658.

[3] L. Yu, G. A. Stephenson, C. A. Mitchell, C. A. Bunnell, S. V. Snorek, J. J. Bowyer, T. B. Borchardt, J. G. Stowell, S. R. Byrn, *J. Am. Chem. Soc.* **2000**, *122*, 585−591.

[4] N. Masciocchi, S. Bruni, E. Cariati, F. Cariati, S. Galli, A. Sironi, *Inorg. Chem.* **2001**, *40*, 5897−5905.

[5] [5a] Y.-Q. Tian, C.-X. Cai, Y. Ji, X.-Z. You, S.-M. Peng, G.-H. Lee, *Angew. Chem. Int. Ed.* **2002**, *41*, 1384−1386. [5b] Y.-Q. Tian, C.-X. Cai, X.-M. Ren, C.-Y. Duan, Y. Xu, S. Gao, X.-Z. You, *Chem. Eur. J.* **2003**, *9*, 5673−5685.

[6] M. O'Keeffe, M. Eddaoudi, H. Li, T. Reineke, O. M. Yaghi, *J. Solid State Chem.* **2000**, *152*, 3−20.

[7] S. R. Betten, R. Robson, *Angew. Chem. Int. Ed.* **1998**, *37*, 1460−1494.

[8] D. Rendell, *Fluorescence and phosphorescence*, John Wiley & Sons, New York, **1987**.

[9] R. Szostak, in *Molecular Sieves*, **1998**, 2nd Ed., Blackie Academic & Professional, imprint of Thomson Science, London, UK.

[10] The unpublished results of two isomorphic coordination polymers of cobalt imidazolate: $[Co_2(im)_4 \cdot DMA]_\infty$ (**6** in space group *Pbca* and **7** in space group $P2_1/n$; DMA = *N*,*N*-dimethylacetylamide).

[11] O. M. Yaghi, M. O'Keffee, N. W. Ockwig, H. K. Chae, M. Eddaoudi, J. Kim, *Nature* **2003**, *423*, 705−714.

[12] N. Masciocchi, G. A. Ardizzoia, S. Brenna, F. Castelli, S. Galli, A. Maspero, A. Sironi, *Chem. Commun.* **2003**, 2018−2019.

[13] G. M. Sheldrick, *SHELXTL-Plus V5.1 Software Reference Manual*; Bruker AXS Inc.: Madison, WI. **1997**.

Received August 12, 2003
Early View Article
Published Online January 29, 2004

 © 2004 Wiley-VCH Verlag GmbH & Co. KGaA, Weinheim

Dinuclear Potassium-Chromium and Potassium-Tungsten Carbonyl Complexes

Vladimir Kirin[a] and Peter W. Roesky*[a]

Keywords: Chromium / Coordination chemistry / N Ligands / Potassium / Tungsten

The tetracarbonyl complexes $[M(CO)_4\{\eta^2\text{-}(Ph_2P)_2NH\}]$ [M = Cr (**1a**), W (**1b**)] have been synthesised by reaction of $M(CO)_6$, $Me_3NO{\cdot}2H_2O$, and $(Ph_2P)_2NH$. Subsequent treatment of complexes **1a**,**b** with an excess of KH in THF at room temperature yields the potassium salts $[Cr(CO)_4\{\eta^2\text{-}(Ph_2P)_2N\}K(THF)_3]_n$ (**2a**) and $[W(CO)_4\{\eta^2\text{-}(Ph_2P)_2N\}K(THF)_2]_n$ (**2b**), respectively, in almost quantitative yields. The ionic compounds **2a**,**b** are stable at room temperature. All four compounds **1a**,**b** and **2a**,**b** were characterised by single-crystal X-ray diffraction. Compounds **2a**,**b** form infinite chains via isocarbonyl bridges in the solid state.

(© Wiley-VCH Verlag GmbH & Co. KGaA, 69451 Weinheim, Germany, 2004)

Introduction

Anionic P−N systems such as phosphinimides (R_2PNR'),[1,2] diphosphinoamides $[(Ph_2P)_2N]$,[3−6] phosphoraneiminates (R_3PN),[7−9] phosphiniminomethanides $[(RNPR'_2)CH]$,[10] phosphiniminomethandiides $[(RNPR'_2)C]$[11] and diiminophoshphinates $[(R_2P(NR'))]$[12] have been known for a long time and their chemistry has been intensively studied over the years. Today there are numerous papers describing the synthesis, structure and reactivity of these anions.[13] The P−N anions are frequently used as ligands in main group and transition metal chemistry.[7,14−16] Even sodium and potassium have sometimes been used as counterions for the P−N anions, although the vast majority of these compounds are lithium salts. These alkali-metal salts are generally generated by deprotonation of the corresponding neutral P−N system, for example an aminophosphane, with butyllithium,[1] sodium[4] or potassium hydride,[6] KO*t*Bu,[5] or by other methods.[8] Ellermann et al. have reported the deprotonation of a neutral P−N ligand that is coordinated to a transition metal fragment.[17,18] This work was performed in situ by deprotonation of bis(diphenylphosphanyl)aminechromium, -molybdenum or -tungsten tetracarbonyl, $[M(CO)_4\{\eta^2\text{-}(Ph_2P)_2NH\}]$ (M = Cr, Mo, W) with *n*-butyllithium. Due to its high sensitivity towards moisture and air the obtained intermediate was not isolated or characterised but further reacted at dry-ice temperature with, for example, chlorophosphanes (Scheme 1). A similar reaction has been performed on metal clusters having the $(Ph_2P)_2NH$ ligand in the coordination sphere.[19] Again, the corresponding alkali metal species was not isolated. Other groups have reported the deprotonation of cationic complexes ligated by $(Ph_2P)_2NH$, which led to zwitterionic compounds.[20]

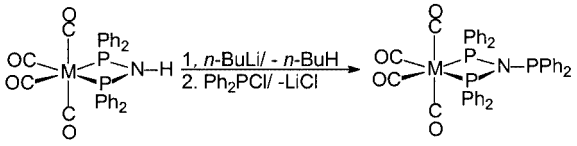

Scheme 1

In this article we report on the synthesis and structural characterisation of bis(diphenylphosphanyl)aminechromium and -tungsten tetracarbonyl, $[M(CO)_4\{\eta^2\text{-}(Ph_2P)_2NH\}]$ [M = Cr (**1a**), W (**1b**)], along with details of further reactions of these complexes with potassium hydride. These reactions lead, in a deprotonation reaction, to the corresponding amidopotassium compounds $[M(CO)_4\{\eta^2\text{-}(Ph_2P)_2N\}K(THF)_x]_n$ [M = Cr (**2a**), W (**2b**); x = 2, 3], which have been isolated and fully characterised by standard analytical/spectroscopic techniques. The structures of **2a**,**b** have been confirmed by single-crystal X-ray diffraction in the solid state. Compounds **2a**,**b** form infinite chains via isocarbonyl bridges in the solid state.

Results and Discussion

Synthesis

The tetracarbonyl complexes $[M(CO)_4\{\eta^2\text{-}(Ph_2P)_2NH\}]$ [M = Cr (**1a**), W (**1b**)] have been synthesised previously by reaction of $M(CO)_6$ with $(Ph_2P)_2NH$ in boiling dodecane.[18,21] We made compounds **1a**,**b** by reaction of $M(CO)_6$, $Me_3NO{\cdot}2H_2O$, and $(Ph_2P)_2NH$ in good yield at room temperature (Scheme 2). Compound **1a** was obtained without significant amounts of by-product, whereas the synthesis of **1b** also yielded the pentacarbonyl complex $[W(CO)_5\{\eta^1\text{-}(PhP_2)_2NH\}]$. Both **1a** and **1b** were character-

[a] Institut für Chemie, Freie Universität Berlin, Fabeckstraße 34−36, 14195 Berlin, Germany

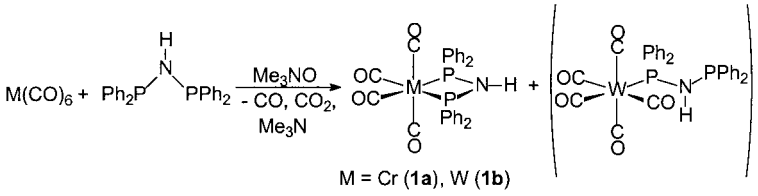

Scheme 2

ised by standard spectroscopic techniques. The observed chemical shifts in the NMR spectra are in good agreement with the literature data.[18,21]

The solid-state structures of both compounds were established by single-crystal X-ray diffraction in order to learn how further reactions at the ligand alter the complex framework.

The potassium salts $[Cr(CO)_4\{\eta^2\text{-}(Ph_2P)_2N\}K(THF)_3]_n$ (**2a**) and $[W(CO)_4\{\eta^2\text{-}(Ph_2P)_2N\}K(THF)_2]_n$ (**2b**) were obtained in almost quantitative yield by treatment of the neutral complexes **1a**,**b** with an excess of KH in THF at room temperature (Scheme 3). The ionic compounds **2a**,**b** are stable at room temperature even after several weeks the only sign of decomposition in the solid state is the loss of THF from the crystals. In solution we did not observe a possible intermolecular reaction of the amido group with the carbonyl ligand.

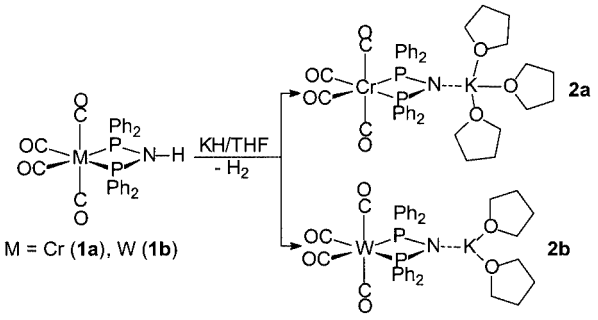

Scheme 3

Compounds **2a** and **2b** were characterised by Raman, ^1H, $^{13}C\{^1H\}$, and $^{31}P\{^1H\}$ NMR spectroscopy and elemental analysis. The $^{31}P\{^1H\}$ NMR resonances of **2a**,**b** [δ = 58.7 ppm (**2a**), 8.07 ppm (**2b**)] are significantly shifted upfield relative to **1a**,**b** [δ = 96.9 ppm (**1a**), 46.1 ppm (**1b**)]. Furthermore, an expected $^1J_{P,W}$ coupling in **2b** of 168.7 Hz is observed, which is about 40 Hz smaller than in **1b**. Based on earlier measurements of $(Ph_2P)_2CH_2$ and $[M(CO)_4\{\eta^2\text{-}(Ph_2P)_2CH_2\}]$ the signals in the $^{13}C\{^1H\}$ NMR spectra could be clearly assigned in the phenyl and in the carbonyl region.[22]

Solid-State Structures

The solid-state structures of **1a**,**b** (Figures 1 and 2, respectively) and **2a**,**b** (Figures 3 and 4, respectively) were established by single-crystal X-ray diffraction. The bond lengths and angles of **1a**,**b** are in the expected range. The complex framework is similar to the structurally characterised molybdenum compound $[Mo(CO)_4\{\eta^2\text{-}(Ph_2P)_2NH\}]\cdot CH_3CN$.[23] In contrast to compound **1a**, in **1b** one molecule of acetone is bound via a hydrogen bond to the N−H function of the ligand.

The ionic complexes **2a**,**b** show some surprising aspects in the solid state. Both complexes form polymeric one-dimensional chains in the crystal. In Figure 5 a cutout of the infinite chain of **2a** is shown. The potassium cations are bound to the amido nitrogen atom of one anion and to the oxygen atom of a carbonyl group of a neighbouring anion. Thus, a potassium isocarbonyl compound is formed. The K−N bond lengths are 271.1(2) pm (**2a**) and 273.6(3) pm (**2b**) and the K−O bond lengths are 264.9(2) pm (**2a**) and 270.2(3) pm (**2b**). There are no other structurally characterised K−W and only a few K−Cr isocarbonyl complexes

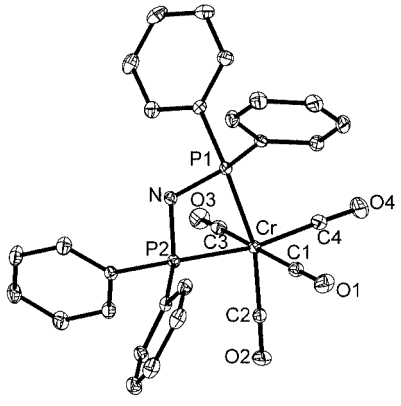

Figure 1. Perspective ORTEP view of the molecular structure of **1a**; thermal ellipsoids are drawn to encompass 50% probability; hydrogen atoms are omitted for clarity; selected distances [pm] and angles [°]: Cr−C1 189.1(2), Cr−C2 189.6(2), Cr−C3 185.2(2), Cr−C4 186.4(2), Cr−P1 236.33(6), Cr−P2 234.50(6), N−P1 169.6(2), N−P2 168.8(2), O1−C1 114.4(2), O2−C2 113.9(2), O3−C3 115.7(2), O4−C4 115.0(2); C1−Cr−C2 174.18(9), C1−Cr−C3 90.39(9), C1−Cr−C4 86.62(9), C2−Cr−C3 86.08(9), C2−Cr−C4 89.08(9), C3−Cr−C4 95.18(9), C1−Cr−P1 92.34(6), C2−Cr−P1 92.25(6), C3−Cr−P1 165.00(6), C4−Cr−P1 99.70(7), C1−Cr−P2 92.66(7), C2−Cr−P2 92.35(6), C3−Cr−P2 96.57(6), C4−Cr−P2 68.23(7), P1−Cr−P2 68.58(2), P1−N−P2 103.24(9)

 © 2004 Wiley-VCH Verlag GmbH & Co. KGaA, Weinheim

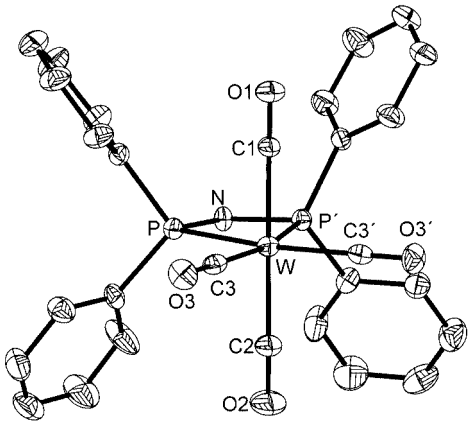

Figure 2. Perspective ORTEP view of the molecular structure of **1b**; thermal ellipsoids are drawn to encompass 50% probability; hydrogen atoms are omitted for clarity; selected distances [pm] and angles [°]: W−C1 205(2), W−C2 200(2), W−C3 201.4(15), W−P 249.2(4), N−P 167.3(10), O1−C1 113(2), O2−C2 118(3), O3−C3 114(2); C1−W−C2 176.8(9), C1−W−C3 87.6(6), C2−W−C3 90.3(6), C3−W−C3′ 97.9(8), C1−W−P 92.3(5), C2−W−P 90.3(6), C3−W−P 98.7(4), C1−W−P′ 92.3(5), C2−W−P′ 90.3(6), C3−W−P′ 163.4(4), P−W−P′ 64.7(2), P−N−P′ 105.7(9)

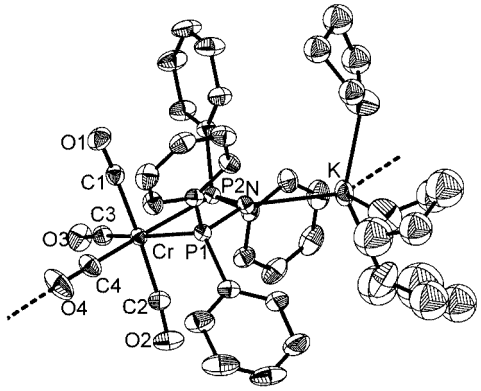

Figure 3. Perspective ORTEP view of the molecular structure of **2a**; thermal ellipsoids are drawn to encompass 50% probability; hydrogen atoms are omitted for clarity; selected distances [pm] and angles [°]: Cr−C1 189.2(2), Cr−C2 188.0(2), Cr−C3 185.5(2), Cr−C4 182.2(2), Cr−P1 236.74(7), Cr−P2 239.80(6), P1−N 166.4(2), P2−N 167.3(2), C1−O1 114.2(3), C2−O2 114.2(3), C3−O3 115.8(3), C4−O4 116.4(3), K−N1 271.1(2), K−O4′ 264.9(2), K−O5 266.8(3), K−O6 266.3(3), K−O7 270.3(3); C1−Cr−C2 174.72(10), C1−Cr−C3 93.88(10), C1−Cr−C4 88.46(11), C2−Cr−C3 88.55(10), C2−Cr−C4 86.68(11), C3−Cr−C4 94.07(11), C1−Cr−P1 90.05(7), C2−Cr−P1 88.86(7), C3−Cr−P1 164.31(7), C4−Cr−P1 101.23(8), C1−Cr−P2 87.50(7), C2−Cr−P2 96.63(7), C3−Cr−P2 101.53(7), C4−Cr−P2 164.12(8), P1−Cr−P2 63.43(2), O4′−K−O5 74.58(8), O4′−K−O6 115.56(10), O4′−K−O7 85.35(10), O4′−K−N 130.54(8), P1−N−P2 97.30(9), P1−N−K 138.73(9), P2−N−K

reported in the literature.[24] Furthermore, in **2a** the potassium atom is coordinated by three THF molecules and no π-coordination of the phenyl rings is observed. In contrast, the potassium atom of compound **2b** is surrounded by only two THF molecules. Due to the vacant coordination sites π-coordination of one phenyl ring of the $(Ph_2P)_2N$ group is seen. The different coordination modes of the potassium atoms in **2a** and **2b** cause significantly different O−K−N bond angles [130.54(8)° (**2a**) and 92.24(10)° (**2b**)] in both compounds. Furthermore, the M−C and the C−O bond

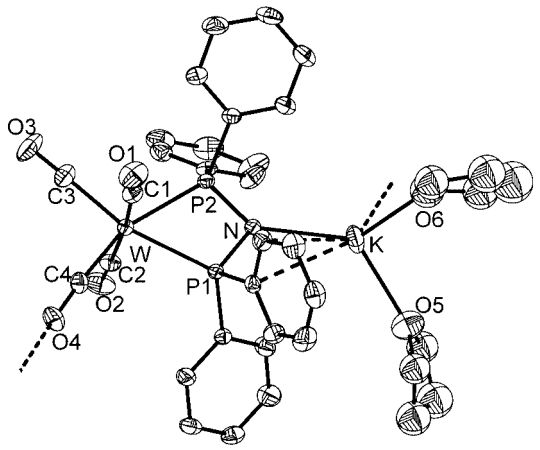

Figure 4. Perspective ORTEP view of the molecular structure of **2b**; thermal ellipsoids are drawn to encompass 50% probability; hydrogen atoms are omitted for clarity; selected distances [pm] and angles [°]: W−C1 202.3(4), W−C2 202.0(4), W−C3 200.2(4), W−C4 196.0(4), W−P1 251.80(8), W−P2 254.20(9), P1−N 166.0(3), P2−N 167.1(3), C1−O1 114.5(5), C2−O2 114.2(5), C3−O3 113.9(5), C4−O4 117.3(5), K−N1 273.6(3), K−O4′ 270.2(3), K−O5 260.4(6), K−O6 255.0(7); C1−W−C2 174.16(15), C1−W−C3 87.0(2), C1−W−C4 89.7(2), C2−W−C3 90.03(2), C2−W−C4 85.56(15), C3−W−C4 94.5(2), C1−W−P1 94.23(12), C2−W−P1 89.99(12), C3−W−P1 164.14(14), C4−W−P1 101.34(11), C1−W−P2 96.49(12), C2−W−P2 89.10(11), C3−W−P2 103.78(14), C4−W−P2 160.99(11), P1−W−P2 60.37(3), O4′−K−O5 94.85(15), O4′−K−O6 82.4(2), O4′−K−N 92.24(10), P1−N−P2 99.62(14), P1−N−K 107.04(12), P2−N−K 142.99(15)

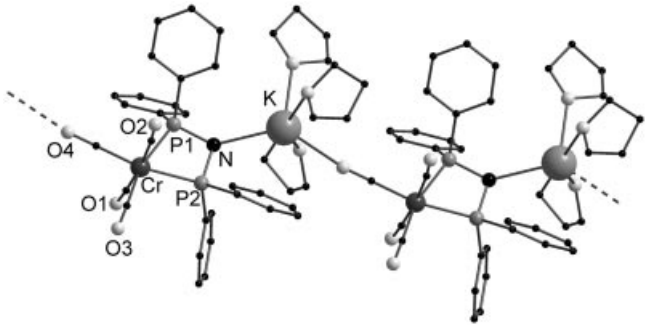

Figure 5. Solid-state structure of **2a** showing the atom labelling scheme, omitting hydrogen atoms; two units of infinite chain are shown

lengths are also influenced. In the CO group (C4O4) that forms the isocarbonyl bridge in **2a**,**b**, the M−C bond lengths are shortened, whereas the C−O bond lengths are lengthened [M−C: 186.4(2) pm (**1a**), 201.4(15) pm (**1b**), 182.2(2) pm (**2a**), 196.0(4) pm (**2b**); C−O: 115.0(2) pm (**1a**), 114(2) pm (**1b**), 116.4(3) pm (**2a**), 117.3(5) pm (**2b**)].

Due to the deprotonation of the $(Ph_2P)_2NH$ ligand in **2a**,**b** the geometry of the $(Ph_2P)_2N$ group is significantly different to that in **1a**,**b**. The P−N−P angles of **2a**,**b** [97.30(9)° (**2a**) and 99.62(14)° (**2b**)] are narrower than in $(Ph_2P)_2NH$ [118.9(2)°][25] and **1a**,**b** [103.24(9)° (**1a**) and 105.7(9)° (**1b**)]. The P−N distances of **2a**,**b** [166.4(2) pm, 167.3(2) pm (**2a**); 166.0(3) pm 167.1(3) pm (**2b**)], are slightly shorter than those observed in **1a,b** [169.6(2) pm, 168.8(2) pm (**1a**); 167.3(10) pm (**1b**)] and $(Ph_2P)_2NH$ (168.2 pm). All

 © 2004 Wiley-VCH Verlag GmbH & Co. KGaA, Weinheim

the P−N distances indicate a partial P−N multiple-bond character.[1a] Since the deprotonation does not significantly influence the P−N bond length we suggest that the negative charge in **2a**,**b** is basically located on the nitrogen atom. This is supported by the N−K contact in the solid state. To the best of our knowledge only three other structurally characterised heterobimetallic transition metal−alkali metal P−N complexes have been reported in the literature,[26] and none of them was generated by deprotonation of the corresponding phosphinoamine compound.

The Raman spectra of compounds **1a**,**b** and **2a**,**b** were recorded in the solid state. The spectrum of **1b** (without acetone) has been reported previously.[18] For **1b** we observe the same number of vibration modes, but at slightly different wavenumbers. This may be a result of the additional molecule of acetone. Based on earlier measurements on $[M(CO)_4\{\eta^2\text{-}(Ph_2P)_2CH_2\}]$ (M = Cr, W) the vibration modes could be clearly assigned.[27] For the C−O stretching vibration in **2a**,**b** a noticeable shift to lower wavenumbers is seen. This effect is especially noticeable for the symmetric and asymmetric stretching vibration of the equatorial CO groups (up to 56 cm^{-1} for **2a**). The weakening of the C−O bond observed in the Raman spectra is in agreement with the data of the single-crystal X-ray structures.

Conclusions

The $(Ph_2P)_2N^-$ anion, which was previously generated by a deprotonation reaction of $(Ph_2P)_2NH$, has been used to build alkali metal[3−6] titanium,[28] lanthanide,[6] and late transition metal complexes and clusters.[19,20] Now we have shown that the deprotonation of the tetracarbonyl complexes $[M(CO)_4\{\eta^2\text{-}(Ph_2P)_2NH\}]$ (M = Cr, W) with potassium hydride leads to bimetallic amidopotassium−isocarbonyl complexes $[Cr(CO)_4\{\eta^2\text{-}(Ph_2P)_2N\}K(THF)_3]_n$ (**2a**) and $[W(CO)_4\{\eta^2\text{-}(Ph_2P)_2N\}K(THF)_2]_n$ (**2b**), in which the transition metal is bound to the phosphorous atom and the alkali metal is coordinated to the nitrogen atom. Complexes **2a**,**b** form polymeric one-dimensional chains in the solid state. The new amido compounds are stable at room temperature and no intermolecular reaction of the amido function with carbonyl group is observed. Based on the results of the single-crystal X-ray structures we suggest that the negative charge is basically localised on the nitrogen atom.

Experimental Section

General: All manipulations of air-sensitive materials were performed with the rigorous exclusion of oxygen and moisture in flame-dried Schlenk-type glassware either on a dual manifold Schlenk line, interfaced to a high vacuum (10^{-3} Torr) line, or in an argon-filled M. Braun glove box. Ether solvents (tetrahydrofuran and diethyl ether) were predried over Na wire and distilled under nitrogen from Na/K alloy benzophenone ketyl prior to use. Hydrocarbon solvents (toluene and *n*-pentane) were distilled under nitrogen from $LiAlH_4$. All solvents for vacuum-line manipulations were stored in vacuo over $LiAlH_4$ in resealable flasks. CH_2Cl_2 and CH_3CN were distilled from over P_2O_5. Deuterated solvents were obtained from Aldrich Inc. (all 99 atom% D). NMR spectra were recorded on a Jeol JNM-LA 400 FT NMR spectrometer. Chemical shifts are referenced to internal solvent resonances and are reported relative to tetramethylsilane (^1H and ^{13}C) or 85% phosphoric acid (^{31}P NMR). Raman spectra were performed on a Bruker RFS 100. Elemental analyses were carried out with an Elementar vario EL. $(Ph_2P)_2NH$ was prepared according to a literature procedure.[29]

$[Cr(CO)_4\{\eta^2\text{-}(Ph_2P)_2NH\}]$ (1a): a) A solution of $Me_3NO{\cdot}2H_2O$ (1.14 g) in 11 mL of MeOH was added dropwise over 3 h to a suspension of $(Ph_2P)_2NH$ (1.78 g, 4.62 mmol) and $Cr(CO)_6$ (1.08 g, 4.91 mmol) in 25 mL of CH_2Cl_2. After this time the reaction mixture was stirred at room temperature for 18 h, filtered through silica gel and the solvents evaporated under reduced pressure. The solid residue was crystallised from hexane/CH_2Cl_2 mixture. Yield: 2.15 g (84.6%).

b) Upon addition of $Me_3NO{\cdot}2H_2O$ (0.23 g, 2.07 mmol) to a suspension of $Cr(CO)_6$ (0.42 g, 1.9 mmol) in 30 mL of MeCN at 0 °C, a yellow colour steadily developed. After 10 min of vigorous stirring, solid $(Ph_2P)_2NH$ (0.75 g; 1.95 mmol) was added to the reaction mixture. The resulting solution was stirred for 18 h at room temperature and then at 70 °C for 5 h. The solvent was removed under reduced pressure and the residue was chromatographed on silica gel using hexane/acetone (4:1) as eluent. The bright-yellow fraction ($R_f \approx 0.3$) was isolated and recrystallised from hexane/CH_2Cl_2 mixture. Yield: 0.63 g (60.3%). Raman (solid): $\tilde{\nu}$ = 3323 cm^{-1} (w, νN−H), 3058 (m, νC=C-*H*), 2018 (m, νCO_{ax}), 1915 (m, $\nu_{sym}CO_{eq}$), 1859 (m, $\nu_{asym}CO_{eq}$), 1583 (w, νC=C), 998 (s, νPC), 644 (w, δCO), 470 (m, νMC), 415 (m, νMC), 187 (s, νMP). ^1H NMR ($CDCl_3$, 400 MHz, 25 °C): δ = 7.51−7.23 (m, 20 H, Ph), 4.88 (t, $^2J_{P,H}$ = 6.9 Hz, 1 H, NH) ppm. ^{13}C NMR (C_6D_6, 100.4 MHz, 25 °C): δ = 228.8 (t, $^2J_{P,C}$ = 8.7 Hz, CO_{ax}), 221.7 (t, $^2J_{P,C}$ = 13.2 Hz, CO_{eq}), 139.3 (m, $J_{P,C}$ = 19.9 Hz, C_{ipso}), 130.5 (s, C_{para}), 130.3 (m, $^2J_{P,C}$ = 6.6 Hz, C_{ortho}), 128.7 (m, $J_{P,C}$ = 4.9 Hz, C_{meta}) ppm. ^{31}P NMR ($CDCl_3$, 161.7 MHz, 25 °C): δ = 96.9 ppm. $C_{28}H_{21}CrNO_4P_2$ (549.47) C 61.21, H 3.85, N 2.55; found C 60.99, H 3.80, N 2.43.

$[W(CO)_4\{\eta^2\text{-}(Ph_2P)_2NH\}]$ (1b) and $[W(CO)_5\{\eta^1\text{-}(Ph_2P)_2NH\}]$: A mixture of $W(CO)_6$ (2.7 g, 7.67 mmol), $Me_3NO{\cdot}2H_2O$ (0.86 g, 7.75 mmol), and $(Ph_2P)_2NH$ (2.86 g, 7.43 mmol) in 100 mL of MeCN was stirred at room temperature for 20 h and then heated at 60 °C for 18 h. The resulting yellow-green solution was evaporated to dryness and the residue was chromatographed on silica gel using hexane/acetone/ethyl acetate (4:1:1) as eluent. The colourless ($R_f \approx 0.7$) and bright-yellow ($R_f \approx 0.7$) fractions were isolated. Recrystallisation of the first fraction from hexane/acetone gave $[W(CO)_5\{\eta^1\text{-}(Ph_2P)_2NH\}]{\cdot}Me_2CO$ (0.9 g, 17.1%). A second fraction was recrystallised from hexane/ethyl acetate. The obtained crystals were dissolved in toluene and the solution was evaporated in vacuo to give $[W(CO)_4\{\eta^2\text{-}(Ph_2P)_2NH\}]$.

1b: Yield: 2.52 g (49.8%). Raman (solid, **1b**·acetone): $\tilde{\nu}$ = 3054 cm^{-1} (m, νC=C-*H*), 2018 (m, νCO_{ax}), 2923 (m, νCH), 1896 (m, νCO), 1884 (m, νCO), 1872 (m, νCO), 1859 (m, νCO), 1699 (m, νCO), 1586 (w, νC=C), 998 (s, νPC), 456 (sh νMC), 441 (sh, νMC), 180 (s, νMP). ^1H NMR (C_6D_6, 400 MHz, 25 °C): δ = 7.46 (m, 8 H), 6.95 (m, 12 H, Ph), 5.13 (t, $^2J_{P,H}$ = 5 Hz, 1 H, NH) ppm. ^{13}C NMR (C_6D_6, 100.4 MHz, 25 °C): δ = 210.7 (dd, $^2J_{P,C}$ = 22.7 Hz and 7.0 Hz, CO_{eq}), 202.7 (t, $^2J_{P,C}$ = 7.0 Hz, CO_{eq}), 138.6 (dd, $^1J_{P,C}$ = 38.2 Hz; $^3J_{P,C}$ = 6.8 Hz, C_{ipso}), 130.7 (d, $^2J_{P,C}$ = 15.6 Hz, C_{ortho}), 130.6 (s, C_{para}), 128.7 ($^2J_{P,C}$ = 4.9 Hz, C_{meta}) ppm. ^{31}P NMR (C_6D_6, 161.7 MHz, 25 °C): δ = 46.1 (s, $^1J_{P,W}$ = 208.1 Hz) ppm.

 © 2004 Wiley-VCH Verlag GmbH & Co. KGaA, Weinheim

$W(CO)_5\{\eta^1\text{-}(Ph_2P)_2NH\}$]: ^{1}H NMR ($C_6D_6$, 400 MHz, 25 °C): δ = 7.55 (m), 7.26 (m), 6.91 (m) (20 H, Ph); 3.48 (t, $^2J_{P,H}$ = 6.5 Hz, 1 H, NH), 1.54 (s, 6 H, Me_2CO) ppm. ^{13}C NMR (C_6D_6, 100.4 MHz, 25 °C): δ = 203.9 (Me_2CO), 199.8 (d, $^2J_{P,C}$ = 23.2 CO_{trans}), 197.6 (dd, $^2J_{P,C}$ = 7.83, $^4J_{P,C}$ = 2.9 Hz, CO_{cis}), 141.0 (dd, $^1J_{P,C}$ = 15.1, $^3J_{P,C}$ = 6.0 Hz), 139.1 (dd, $^1J_{P,C}$ = 46.5, $^3J_{P,C}$ = 3.9 Hz) (C_{ipso}); 131.7 (dd, $^2J_{P,C}$ = 12.8, $^4J_{P,C}$ = 2.1 Hz), 131.4 (d, $^2J_{P,C}$ = 21.5 Hz) (C_{ortho}); 130.6 (d, $^3J_{P,C}$ = 1.7 Hz), 129.36 (s) (C_{para}); 128.7 (d, $^4J_{P,C}$ = 7.4 Hz), 128.6 (d, $^4J_{P,C}$ = 9.9 Hz) (C_{meta}); 30.1 (Me_2CO) ppm. ^{31}P NMR (C_6D_6, 161.7 MHz, 25 °C): δ = 64.7 (d, $^2J_{P,P}$ = 71, $^1J_{P,W}$ = 267 Hz, coordinated P), 33.84 (d, uncoordinated P).

$[Cr(CO)_4\{\eta^2\text{-}(Ph_2P)_2N\}K(THF)_x]$ (x = 2−3) (2a): Solid **1a** (0.50 g, 0.91 mmol) was added to a suspension of KH (70 mg, 1.75 mmol) in 25 mL of THF. After stirring for 4 h at room temperature the solvent was removed in vacuo and the resulting yellow powder was crystallised from THF/*n*-pentane (1:4). After one day yellow crystals were obtained. Yield: 0.69 g (95%). Raman (solid): 3056 cm^{-1} (m, νC=C-*H*), 2983 (w, νCH), 2878 (w, νCH), 1986 (m, νCO_{ax}), 1879 (m, $\nu_{sym}CO_{eq}$), 1802 (m, $\nu_{asym}CO_{eq}$), 1584 (w, νC=C), 998 (s, νPC), 917 (w, νC−C), 483 (m, νMC), 420 (m, νMC), 184 (m, νMP). ^{1}H NMR ([D$_8$]THF, 400 MHz, 25 °C): δ = 7.73 (m, 8 H, Ph), 7.17 (m, 8 H, Ph) 7.09 (m, 4 H, Ph), 3.61 (m, 4 H, THF), 1.76 (m, 4 H, THF) ppm. ^{13}C NMR ([D$_8$]THF, 100.4 MHz, 25 °C): δ = 226.7 (CO_{ax}), 221.4 (t, $^2J_{P,C}$ = 13.2 Hz, CO_{eq}), 149.4 ($J_{P,C}$ = 19.4 Hz, C_{ipso}), 130.7 (s, C_{para}), 130.4 (C_{ortho}), 127.7 ($J_{P,C}$ = 5.8 Hz, C_{meta}), 68.21 (s, THF), 26.36 (s, THF) ppm. ^{31}P NMR ([D$_8$]THF, 161.7 MHz, 25 °C): δ = 58.7 ppm. $C_{36}H_{36}CrKNO_6P_2$ (x = 2; 731.72): calcd. C 59.09, H 4.96, N 1.91; found C 58.04, H 4.77, N 1.86.

$[W(CO)_4\{\eta^2\text{-}(Ph_2P)_2N\}K(THF)_2]$ (2b): Solid **1b** (2.5 g; 3.67 mmol) was added to a suspension of KH (237 mg, 5.92 mmol) in 50 mL THF. After stirring at room temperature for 4 h the solvent was removed in vacuo and the resulting yellow powder was crystallised from THF/*n*-pentane (1:4). After one day yellow crystals were obtained. Yield: 2.98 g (94%). Raman (solid): $\tilde{\nu}$ = 3055 cm^{-1} (m, νC=C-*H*), 2983 (w, νCH), 2877 (w, νCH), 1997 (m, νCO_{ax}), 1877 (m, $\nu_{sym}CO_{eq}$), 1802 (m, $\nu_{asym}CO_{eq}$), 1584 (w, νC=C), 997 (s, νPC), 918 (w, νC−C), 483 (w, νMC), 442 (m, νMC), 184 (m, νMP). ^{1}H NMR ([D$_8$]THF, 400 MHz, 25 °C): δ = 7.69 (m, 8 H, Ph), 7.18 (m, 8 H, Ph) 7.08 (m, 4 H, Ph), 3.61 (m, 4 H, THF), 1.76 (m, 4 H, THF) ppm. ^{13}C NMR (C_6D_6, 100.4 MHz, 25 °C): δ = 228.5 (CO_{ax}), 221.63 (CO_{eq}), 148.8 (m, $J_{P,C}$ = 23.09 Hz, C_{ipso}), 127.9 (s, C_{para}), 130.8 (m, $J_{P,C}$ = 6.4 Hz, C_{ortho}), 127.7 (m, $J_{P,C}$ = 5.2 Hz, C_{meta}), 68.2 (s, THF), 26.4 (s, THF). ^{31}P NMR ([D$_8$]THF, 161.7 MHz, 25 °C): δ = 8.07 ($^1J_{P,W}$ = 168.7 Hz) ppm. $C_{36}H_{36}KNO_6P_2W$ (863.58): calcd. C 50.07, H 4.20, N 1.62; found C 49.95, H 4.17, N 1.54.

X-ray Crystallographic Studies of 1a, 1b, 2a and 2b: Crystals of **1a** and **1b** were obtained from hexane/CH_2Cl_2 and hexane/acetone, respectively. Crystals of **2a** and **2b** were grown from THF/*n*-pentane (1:4). A suitable crystal was covered in mineral oil (Aldrich) and mounted onto a glass fibre. The crystal was transferred directly to the −73 °C cold N_2 stream of a Stoe IPDS or a Bruker CCD SMART 1000 diffractometer. Subsequent computations were carried out on an Intel Pentium III PC.

Data Collection and Refinement: SHELXS-97,[30] SHELXL-97.[31]

1a: Triclinic, space group $P\bar{1}$ (no. 2); lattice constants a = 982.50(14), b = 1160.8(2), c = 1278.0(2) pm, α = 106.368(4)°, β = 94.523(4)°, γ = 113.016(3)°, V = 1257.3(3) × 10^6 pm^3, Z = 2; μ(Mo-K_α) = 0.618 mm^{-1}; $2\theta_{max.}$ = 60.00°; 7271 (R_{int} = 0.0316) independent reflections measured, of which 4618 were considered observed with $I > 2\sigma(I)$; max. residual electron density 0.428 and −0.466 e/A^{-3}; 325 parameters (all non-hydrogen atoms were calculated as anisotropic; the positions of the H atoms were calculated for idealised positions) $R1$ = 0.0368; $wR2$ = 0.0874.

1b: Orthorhombic, space group *Pbcm* (no. 57); lattice constants a = 938.84(4), b = 1680.60(7), c = 1920.77(7) pm, V = 3030.6(2) × 10^6 pm^3, Z = 4; μ(Mo-K_α) = 3.956 mm^{-1}; $2\theta_{max.}$ = 56.00°; 3046 (R_{int} = 0.0526) independent reflections measured, of which 2830 were considered observed with $I > 2\sigma(I)$; max. residual electron density 4.760 and −3.408 e/A^{-3}; 183 parameters (all non-hydrogen atoms were calculated as anisotropic; the positions of the H atoms were calculated for idealised positions) $R1$ = 0.0801; $wR2$ = 0.2098.

2a: Monoclinic, space group *Cc* (no. 9); lattice constants a = 1601.3(3), b = 1328.9(3), c = 2056.8(4)pm, β = 111.046(4)°, V = 4084.9(13) × 10^6 pm^3, Z = 4; μ(Mo-K_α) = 0.508 mm^{-1}; $2\theta_{max.}$ = 61.00°; 11604 (R_{int} = 0.0156) independent reflections measured, of which 10574 were considered observed with $I > 2\sigma(I)$; max. residual electron density 0.814 and −0.405 e/A^{-3}; 325 parameters (all non-hydrogen atoms were calculated as anisotropic; the positions of the H atoms were calculated for idealised positions) Flack parameter 0.005(13), $R1$ = 0.0403; $wR2$ = 0.1118.

2b: Triclinic, space group $P\bar{1}$ (no. 2); lattice constants a = 969.1(2), b = 1113.5(2), c = 1804.1(3) pm, α = 94.348(3)°, β = 97.122(3)°, γ = 113.016(3)°, V = 108.075(3) × 10^6 pm^3, Z = 2; μ(Mo-K_α) = 3.415 mm^{-1}; $2\theta_{max.}$ = 60.00°; 10514 (R_{int} = 0.0240) independent reflections measured, of which 9368 were considered observed with $I > 2\sigma(I)$; max. residual electron density 2.229 and −1.569 e/A^{-3}; 379 parameters (all non-hydrogen atoms were calculated anisotropic; the positions of the H atoms were calculated for idealised positions) $R1$ = 0.0335; $wR2$ = 0.0975.

CCDC-217820 (**1a**), -217821 (**1b**), -217822 (**2a**), and -217823 (**2b**) contain the supplementary crystallographic data for this paper. These data can be obtained free of charge at www.ccdc.cam.ac.uk/conts/retrieving.html [or from the Cambridge Crystallographic Data Centre, 12, Union Road, Cambridge CB2 1EZ, UK; Fax: (internat.) +44-1223/336-033; E-mail: deposit@ccdc.cam.ac.uk].

Acknowledgments

This work was supported by the Deutsche Forschungsgemeinschaft (Graduiertenkolleg: Synthetische, mechanistische und reaktionstechnische Aspekte von Metallkatalysatoren) and the Fonds der Chemischen Industrie. Additionally, generous support from Prof. Dr. H. Krautscheid (Universität Leipzig) and PD Dr. W.-D. Hunnius is gratefully acknowledged.

[1] [1a] M. T. Ashby, Z. Li, *Inorg. Chem.* **1992**, *31*, 1321−1322. [1b] N. Poetschke, M. Nieger, M. A. Khan, E. Niecke, M. T. Ashby, *Inorg. Chem.* **1997**, *36*, 4087−4093. [1c] Z. Fei, R. Scopelliti, P. J. Dyson, *Inorg. Chem.* **2003**, *42*, 2125−2130.
[2] S. Wingerter, M. Pfeiffer, F. Baier, T. Stey, D. Stalke, *Z. Anorg. Allg. Chem.* **2000**, *626*, 1121−1130.
[3] [3a] J. Ellermann, M. Lietz, *Z. Naturforsch., Teil B* **1980**, *35b*, 64−67. [3b] H. Schmidbaur, S. Lautenschläger, F. H. Köhler, *J. Organomet. Chem.* **1984**, *271*, 173−180.
[4] J. Ellermann, M. Schütz, F. W. Heinemann, M. Moll, *Z. Anorg. Allg. Chem.* **1998**, *624*, 257−262.
[5] J. Ellermann, M. Schütz, F. W. Heinemann, M. Moll, *Chem. Ber./Recl.* **1997**, *130*, 141−143.
[6] P. W. Roesky, M. T. Gamer, M. Puchner, A. Greiner, *Chem. Eur. J.* **2002**, *8*, 5265−5271.
[7] K. Dehnicke, F. Weller, *Coord. Chem. Rev.* **1997**, *158*, 103−169.
[8] T. Gröb, K. Harms, K. Dehnicke, *Z. Anorg. Allg. Chem.* **2000**, *626*, 1065−1072.

 © 2004 Wiley-VCH Verlag GmbH & Co. KGaA, Weinheim

[9] S. Chitsaz, B. Neumüller, K. Dehnicke, *Z. Anorg. Allg. Chem.* **1999**, *625*, 9−10.
[10] [10a] M. T. Gamer, P. W. Roesky, *Z. Anorg. Allg. Chem.* **2001**, *627*, 877−881. [10b] R. P. Kamalesh Babu, K. Aparna, R. McDonald, R. G. Cavell, *Inorg. Chem.* **2000**, *39*, 4981−4984.
[11] [11a] C. M. Ong, D. W. Stephan, *J. Am. Chem. Soc.* **1999**, *121*, 2939. [11b] A. Kasani, R. P. Kamalesh Babu, R. McDonald, R. G. Cavell, *Angew. Chem.* **1999**, *111*, 1580; *Angew. Chem. Int. Ed.* **1999**, *38*, 1438.
[12] F. T. Edelmann, *Top. Curr. Chem.* **1996**, *179*, 113−148.
[13] O. J. Scherer, *Multiple Bonds and Low Coordination in Phosphorous Chemistry*, Georg Thieme Verlag, Stuttgart, **1990**.
[14] K. Dehnicke, M. Krieger, W. Massa, *Coord. Chem. Rev.* **1999**, *182*, 19−65.
[15] T. Appleby, J. D. Woolins, *Coord. Chem. Rev.* **2002**, *235*, 121−140.
[16] T. G. Wetzel, S. Dehnen, P. W. Roesky, *Angew. Chem.* **1999**, *111*, 1155−1158; *Angew. Chem. Int. Ed.* **1999**, *38*, 1086−1088.
[17] J. Ellermann, W. Wend, *J. Organomet. Chem.* **1985**, *281*, C29−C32.
[18] J. Ellermann, W. Wend, *New. J. Chem.* **1986**, *10*, 313−320.
[19] M. Knorr, C. Strohmann, *Eur. J. Inorg. Chem.* **1998**, 495−499.
[20] [20a] I. Bachert, I. Bartusseck, P. Braunstein, E. Guillon, J. Rosé, G. Kickelbick, *J. Organomet. Chem.* **1999**, *588*, 144−151. [20b] J. Geicke, I. P. Lorenz, P. Murschel, K. Polborn, *Z. Naturforsch., Teil B* **1997**, *52*, 593−603.
[21] J. Ellermann, W. H. Gruber, *Z. Naturforsch., Teil B* **1973**, *28*, 310−313.
[22] [22a] I. J. Colquhoun, W. Mc Farlane, *J. Chem. Soc., Dalton Trans.* **1982**, 1915−1921. [22b] G. T. Andrews, I. J. Colquhoun, W. J. Mc Farlane, *Polyhedron* **1983**, *2*, 783−790.
[23] M. Knorr, C. Strohmann, *Organometallics* **1999**, *18*, 248−257.
[24] [24a] D. J. Wink, J. R. Fox, N. J. Cooper, *J. Am. Chem. Soc.* **1985**, *107*, 5012−5014. [24b] M. D. Grillone, F. Benetollo, G. Bombieri, A. Del Pra, *J. Organomet. Chem.* **1999**, *575*, 193−199. [24c] L. Xu, A. Ugrinov, S. C. Sevov, *J. Am. Chem. Soc.* **2001**, *123*, 4091−4092. [24d] W.-q. Weng, A. M. Arif, R. D. Ernst, *Cluster Sci.* **1996**, *7*, 629−641. [24e] J. W. Freeman, A. M. Arif, R. D. Ernst, *Inorg. Chim. Acta* **1995**, *240*, 33−40.
[25] H. Nöth, E. Fluck, *Z. Naturforsch., Teil B* **1984**, *39*, 744−753.
[26] [26a] D. Fenske, B. Maczek, K. Maczek, *Z. Anorg. Allg. Chem.* **1997**, *623*, 1113−1120. [26b] G. Bai, H. W. Roesky, M. Noltemeyer, H.-G. Schmidt, *J. Chem. Soc., Dalton Trans.* **2002**, 2437−2440. [26c] G. Bai, H. W. Roesky, M. Noltemeyer, H.-G. Schmidt, *Organometallics* **2002**, *21*, 2789−2792.
[27] H. Gäbelein, J. Ellermann, *J. Organomet. Chem.* **1978**, *156*, 389−402.
[28] O. Kühl, T. Koch, F. B. Somoza, P. C. Junk, E. Hey-Hawkins, D. Plat, M. S. Eisen, *J. Organomet. Chem.* **2000**, *604*, 116−125.
[29] H. Noeth, L. Meinel, *Z. Anorg. Allg. Chem.* **1967**, *349*, 225−240.
[30] G. M. Sheldrick SHELXS-97, *Program for Crystal Structure Solution*, University of Göttingen, Germany, **1997**.
[31] G. M. Sheldrick, SHELXL-97 *Program for Crystal Structure Solution*, University of Göttingen, Germany, **1997**.

Received August 20, 2003
Early View Article
Published Online January 28, 2004

 © 2004 Wiley-VCH Verlag GmbH & Co. KGaA, Weinheim

Hydrothermal Synthesis and Characterization of a Novel Sinusoidal Layer Structure Constructed From Polyoxometalates and Coordination Complex Fragments

Xiao-Bing Cui,[a,b] Ji-Qing Xu,*[a] Yong Li,[a] Ying-Hua Sun,[a] and Guo-Yu Yang*[b]

Keywords: Hydrothermal synthesis / Magnetic properties / Polyoxometalates / X-ray diffraction

A novel polyoxometalate compound, $[As_8V_{14}O_{42}(SO_4)][Ni(en)_2]_3{\cdot}4.5H_2O$ (**1**), has been synthesized by a hydrothermal method and characterized by X-ray crystallography, showing that the compound **1** is the first example of a sinusoidal layer structure constructed from polyoxometalates and coordination complex fragments.
(© Wiley-VCH Verlag GmbH & Co. KGaA, 69451 Weinheim, Germany, 2004)

Introduction

Polyoxometalates (POMs) are a fascinating class of metal-oxygen cluster compounds with a wide structural variety and interesting properties, which are of use in fields as diverse as catalysis, sorption, molecular electronics, and medicine, amongst others.[1−3] Despite the fundamental and practical importance of polyoxometalates, the preparation of these complexes still remains elusive and is often described as self-assembly. Recently, a novel approach to the synthesis of polyoxometalate chemistry has been to find some novel units as building blocks and then to connect them up into one-, two-, or even three-dimensional extended solid frameworks in appropriate ways. This method is quite attractive and appears to hold the key to the development of a rational synthesis for tailor-made materials based on polyoxometalates with desirable features. The crucial requirement for the success of this approach is to find suitable polyoxometalates that could be readily assembled. Polyoxometalates and their derivatives provide an exciting opportunity to explore the potential of this approach. Hydrothermal synthesis techniques, in combination with organic templates, have been demonstrated to be useful in the preparation of metal oxide materials.[4,5] A number of extended solid framework materials based on polyoxometalates as building blocks have been synthesized hydrothermally.[6−17]

Arsenic-vanadium clusters, one of the most important subclasses of polyoxometalates, have been thoroughly investigated, and typical examples include $[As_8V_{14}O_{42}(X)]^{6-}$ ($X = SO_3^{2-}$ or SO_4^{2-}),[18] $[N(Me)_4]_4[As_8V_{14}O_{42}(H_2O)_{0.5}$ [18] and $K_6[As_6V_{15}O_{42}(H_2O)]{\cdot}8H_2O$.[18] Most of them exhibit discrete cluster structures and are able to function as building blocks. However, compared with the abundance of compounds based on the $[V_{18}O_{42}]$ cluster,[8−11,14] the linking of arsenic-vanadium clusters into one-, two-, and three-dimensional structures remains relatively unexplored.[12,13] We have therefore extended our search for solid framework complexes by exploiting arsenic-vanadium clusters as building blocks — the successful use of the $[As_8V_{14}O_{42}(SO_4)]^{6-}$ [18] cluster results in the formation of a two-dimensional structural compound $[As_8V_{14}O_{42}(SO_4)][Ni(en)_2]_3{\cdot}4.5H_2O$ (**1**), which is the first example of a two-dimensional sinusoidal layer structure constructed from polyoxometalates and coordination complex fragments.

Results and Discussion

A novel metal-oxygen cluster polymer, $[As_8V_{14}O_{42}(SO_4)][Ni(en)_2]_3{\cdot}4.5H_2O$, has been hydrothermally synthesized and structurally characterized. Selected bond lengths for **1** are given in Table 1. It crystallizes in the triclinic space group $P\bar{1}$ with a unit cell containing two units. There are four crystallographically independent nickel atoms in an asymmetric unit, Ni(2) and Ni(3) are located on inversion centers with occupancy factors of 0.5, and all other atoms are at general positions.

The X-ray crystal structural analysis suggests that compound **1** is a novel, sinusoidal layered compound containing $[As_8V_{14}O_{42}(SO_4)]^{6-}$ clusters, $[Ni(en)_2]^{2+}$ cations and waters of crystallization. The building block unit, shown in Figure 1, consists of fourteen distorted VO_5 square pyramids and eight AsO_3 triangular units, with a disordered SO_4^{2-} anion at its center. Every two AsO_3 groups are joined to-

[a] College of Chemistry and State Key Laboratory of Inorganic Synthesis and Preparative Chemistry,
Jilin University, Changchun 130023, P. R. China
E-mail: xjq@mail.jlu.edu.cn
[b] State Key Laboratory of the Structural Chemistry, Fujian Institute of Research on the Structure of Matter,
Chinese Academy of Sciences, Fuzhou, Fujian 350002, China
E-mail: ygy@ms.fjirsm.ac.cn

Table 1. Selected bond lengths (Å) for compound **1**

As(1)−O(31)	1.759(11)	V(5)−O(49)	2.009(9)
As(1)−O(47)	1.770(10)	V(5)−O(48)	2.024(10)
As(1)−O(32)	1.789(9)	V(6)−O(16)	1.600(11)
As(2)−O(23)	1.749(10)	V(6)−O(41)	1.934(10)
As(2)−O(11)	1.782(10)	V(6)−O(25)	1.956(10)
As(2)−O(42)	1.766(10)	V(6)−O(36)	2.016(10)
As(3)−O(44)	1.778(10)	V(6)−O(28)	2.032(10)
As(3)−O(26)	1.799(11)	V(7)−O(39)	1.571(11)
As(3)−O(32)	1.804(9)	V(7)−O(22)	1.943(10)
As(4)−O(49)	1.751(10)	V(7)−O(30)	1.968(10)
As(4)−O(38)	1.755(11)	V(7)−O(26)	2.003(10)
As(4)−O(11)	1.806(9)	V(7)−O(38)	2.035(11)
As(5)−O(33)	1.763(9)	V(8)−O(21)	1.639(10)
As(5)−O(8)	1.775(10)	V(8)−O(26)	1.945(10)
As(5)−O(40)	1.780(12)	V(8)−O(38)	1.978(10)
As(6)−O(48)	1.761(10)	V(8)−O(42)	2.014(10)
As(6)−O(9)	1.764(10)	V(8)−O(31)	2.009(10)
As(6)−O(19)	1.782(11)	V(9)−O(34)	1.601(10)
As(7)−O(28)	1.758(9)	V(9)−O(37)	1.937(10)
As(7)−O(45)	1.782(10)	V(9)−O(17)	1.947(10)
As(7)−O(40)	1.783(12)	V(9)−O(23)	2.008(10)
As(8)−O(29)	1.756(10)	V(9)−O(33)	2.012(9)
As(8)−O(36)	1.763(9)	V(10)−O(10)	1.630(9)
As(8)−O(19)	1.793(12)	V(10)−O(46)	1.910(10)
V(1)−O(24)	1.618(10)	V(10)−O(37)	1.932(10)
V(1)−O(46)	1.939(9)	V(10)−O(33)	2.006(10)
V(1)−O(25)	1.958(10)	V(10)−O(45)	2.008(10)
V(1)−O(45)	1.987(11)	V(11)−O(15)	1.599(12)
V(1)−O(47)	2.002(10)	V(11)−O(17)	1.955(10)
V(2)−O(35)	1.596(10)	V(11)−O(18)	1.952(10)
V(2)−O(22)	1.925(10)	V(11)−O(9)	2.014(11)
V(2)−O(41)	1.938(10)	V(11)−O(8)	2.042(10)
V(2)−O(44)	1.981(9)	V(12)−O(13)	1.607(11)
V(2)−O(29)	2.018(11)	V(12)−O(8)	1.956(11)
V(3)−O(14)	1.599(10)	V(12)−O(9)	1.961(11)
V(3)−O(46)	1.964(9)	V(12)−O(28)	1.971(11)
V(3)−O(37)	1.981(10)	V(12)−O(36)	1.981(11)
V(3)−O(42)	2.042(10)	V(13)−O(27)	1.634(11)
V(3)−O(31)	2.037(11)	V(13)−O(41)	1.934(9)
V(4)−O(20)	1.629(9)	V(13)−O(25)	1.934(10)
V(4)−O(22)	1.908(10)	V(13)−O(47)	1.981(9)
V(4)−O(30)	1.905(10)	V(13)−O(44)	1.978(10)
V(4)−O(29)	2.007(10)	V(14)−O(12)	1.604(11)
V(4)−O(48)	2.012(10)	V(14)−O(17)	1.936(10)
V(5)−O(43)	1.626(10)	V(14)−O(18)	1.963(10)
V(5)−O(30)	1.947(10)	V(14)−O(23)	1.998(9)
V(5)−O(18)	1.942(10)	V(14)−O(49)	2.023(9)

gether by an oxygen bridge, forming a handle-like As_2O_5 moiety. In the cluster, eight vanadium [V(1), V(2), V(4), V(5), V(9), V(10), V(13) and V(14)] oxygen square pyramids are linked to one another into a ring by sharing edges. In addition, three vanadium [V(6), V(11) and V(12)] oxygen square pyramids form a trimer by sharing edges. This trimer is connected across the ring by sharing edges with V(13)- and V(14)-containing square pyramids. Vanadium[V(3), V(7) and V(8)] oxygen square pyramids form another trimer by sharing edges, and this trimer is similarly connected on the opposite side of the ring to V(4)- and V(10)-containing square pyramids. Therefore, fourteen VO_5 square pyramids are arranged to form a cage, the overall chemical composition of which is $[(VO)_{14}O_{24}]$. Clearly there are twenty-four oxygen atoms occupying the vertices of the cage, which has a total of eighteen square faces. Fourteen of them are formed by the bases of the VO_5 square pyramids, and the remaining square faces are formed by the bases of the As_2O_5 units to give a total composition of $[As_8V_{14}O_{42}]^{4-}$. The V−O and the As−O distances are all similar to those in reported compounds.[18]

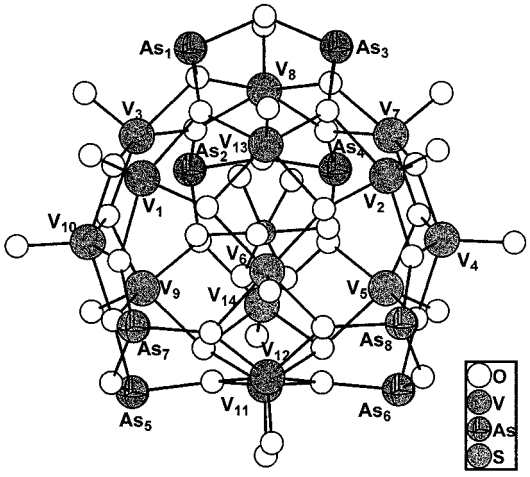

Figure 1. Ball-and-stick representation of the $[As_8V_{14}O_{42}(SO_4)]^{6-}$ cluster

There are two different types of $[Ni(en)_2]^{2+}$ cations in **1**. The first type contains $[Ni(2)(en)_2]^{2+}$, $[Ni(3)(en)_2]^{2+}$ and $[Ni(4)(en)_2]^{2+}$ cations, in which each octahedrally coordinated nickel atom bridges two clusters. The nickel site is defined by four nitrogen donors from two en ligands and *trans*-oxo atoms from two adjacent clusters, and these nickel atoms exhibit very strong covalent attachments to adjacent clusters, with Ni−O distances in the range 2.082(10)−2.110(10) Å. Four surface oxygen atoms of one cluster coordinate to four bridging nickel atoms [Ni(2), Ni(3) and two Ni(4)], so each cluster is connected to four neighboring ones into a two-dimensional network of $[-\{As_8V_{14}O_{42}(SO_4)\}-\{Ni(en)_2\}-\{As_8V_{14}O_{42}(SO_4)\}-]_n$ arrays, as shown in Figure 2 (a). This layer is arranged parallel to the crystallographic *ab* plane. In the layer, through the connection of each Ni(4) atom, the clusters are linked to one another along the $a - b$ axis into a novel straight chain, as shown in Figure 2 (b), while through the connections alternatively at Ni(2) and Ni(3), each chain is connected with the adjacent ones along the $a + b$ axis, forming a novel sinusoidal layer. Figure 2c clearly shows that the layer displays a beautiful sinusoidal ruffling look, with an amplitude of about 20.8 Å, which is larger than those in $[M(bpy)_2]_2V_6O_{17}$ (M = Zn, Ni, about 13 Å)[19,20] and $[Ni(Phen)_2]_2V_4O_{11}$ (about 18.5 Å),[21] whereas the period (about 25.9 Å) is also far larger than those in $[M(bpy)_2]_2V_6O_{17}$ (M = Zn, Ni, about 15 Å)[19,20] and $[Ni(Phen)_2]_2V_4O_{11}$ (about 9.7 Å).[21] These differences clearly originate from the fact that the layer of compound **1** is constructed from coordination complexes and bulky sphere-like $[As_8V_{14}O_{42}(SO_4)]^{6-}$ clusters, which makes the amplitude and period larger. The structure of compound **1**

 © 2004 Wiley-VCH Verlag GmbH & Co. KGaA, Weinheim

can be described as being built up from $[As_8V_{14}O_{42}(SO_4)]^{6-}$ clusters linked into a two-dimensional sinusoidal layer structure. It is the most unusual feature of compound **1**, and, to the best of our knowledge, such a feature has not been found in any other structures of polyoxometalates.

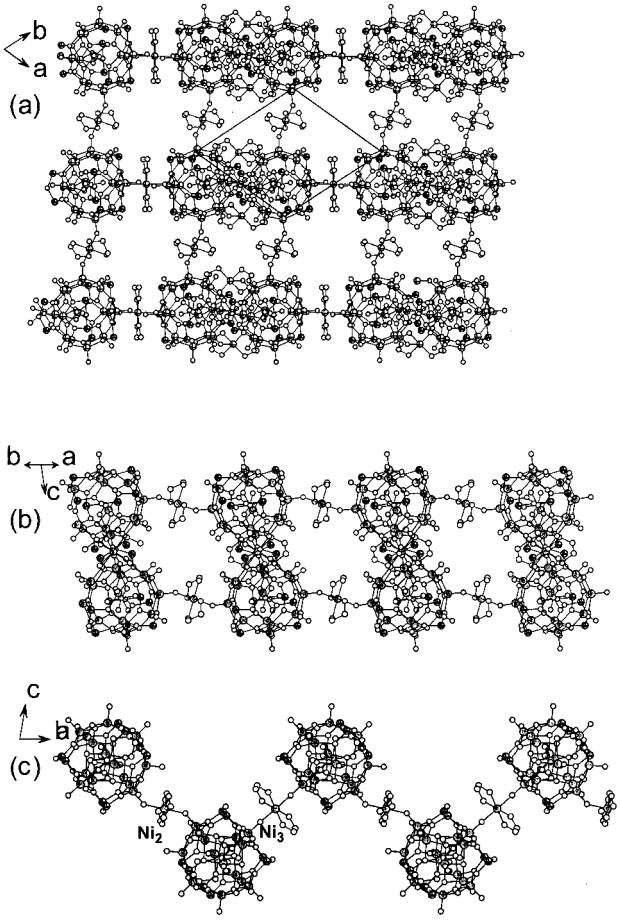

Figure 2. (a) A view of the sinusoidal layer of compound **1** down the *c* axis; (b) the sinusoidal layer of compound **1** extending along the $a - b$ axis; (c) the sinusoidal layer of compound **1** extending along the $a + b$ axis

The $[Ni(1)(en)_2]^{2+}$ cation is the second type of Ni atom, and it serves as a charge-compensating component. The $[Ni(en)_2]^{2+}$ cations of this type occupy the regions between the adjacent sinusoidal layers. In contrast to the bridging $[Ni(en)_2]^{2+}$ cations of the first group, the nickel atoms of the second group exhibit only weak interactions with the clusters, with Ni···O distances of 2.852(11)−3.145(11) Å.

The assignments of the oxidation states for the vanadium and arsenic atoms are consistent with the electric charge and confirmed by bond valence sum (BVS) calculations.[22] The BVS values for vanadium and arsenic atoms vary from 3.767 to 4.237 and from 2.997 to 3.240, respectively, indicating that the oxidation state for each vanadium atom and each arsenic atom is +4 and +3, respectively. The oxidation states of the vanadium atoms and the arsenic atoms are consistent with the formula of compound **1**.

Preliminary magnetic studies have been performed on a powered sample of **1** in the range 2−300 K. Plots of χ_m^{-1} and μ_{eff} vs. T for **1** are shown in Figure 3. The product μ_{eff} decreases continuously as the temperature is lowered, indicating the presence of an antiferromagnetic exchange interaction. The room-temperature value ($\mu_{eff} = 6.84\ \mu_B$) is smaller than the expected value ($\mu_{eff} = 7.83\ \mu_B$) for the 14 uncoupled $S = 1/2$ spins of the V^{4+} atoms and the two uncoupled $S = 1$ spins of the Ni^{2+} atoms (two nickel atoms of the first type are octahedrally coordinated, with $S = 1$, and the nickel atom of the second type displays a square-planar environment, with $S = 0$, assuming $g = 2.0$ for V^{4+} and $g = 2.20$ for Ni^{2+}), indicative of antiferromagnetic coupling. These antiferromagnetic coupling interactions are related to electron delocalization of high-nuclearity metal clusters.[23] Unfortunately, it is too difficult to fit the experimental magnetic data of this two-dimensional heteropolymetallic spin system using a suitable theoretical model.[24] However, the magnetic data of **1** obey the Curie−Weiss law in the high-temperature regions, and the fitting in the range 80−300 K gives values of $C = 5.26$ emu·mol^{-1}·K and $\theta = -1.11$ K, characteristic of an overall antiferromagnetic interaction.

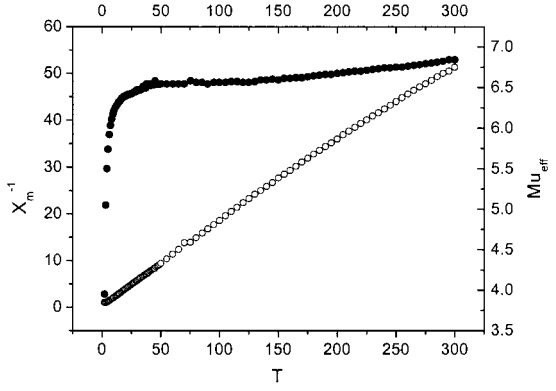

Figure 3. The effective magnetic moment μ_{eff} (filled circles) and inverse molar susceptibility (open circles) vs. temperature for **1**

The ESR spectrum of **1** at room temperature shows no signals for V^{4+}. This lack of signals indicates that the electrons of the cluster are spin-spin coupled. Figure 4 (a) shows the XPS[25] spectrum of **1** in the V 2p region, with the peak at 516.2 eV being ascribed to V^{4+}. Figure 4 (b) shows the spectrum of **1** in the As 3d region, with the peak at 45 eV being attributed to As^{3+}. The XPS estimation of the valence-state values seems to be in reasonable agreement with those calculated from the bond valence sum calculations. These results further confirm the valences of the arsenic and vanadium atoms.

Conclusion

Complex **1** is synthesized from V_2O_5 by exploiting the reducing ability of $H_2C_2O_4{\cdot}2H_2O$ and en. The presence of $H_2C_2O_4{\cdot}2H_2O$ and en is absolutely essential to the product formation. The successful synthesis of compound **1** provides another example of connecting arsenic-vanadium

 © 2004 Wiley-VCH Verlag GmbH & Co. KGaA, Weinheim

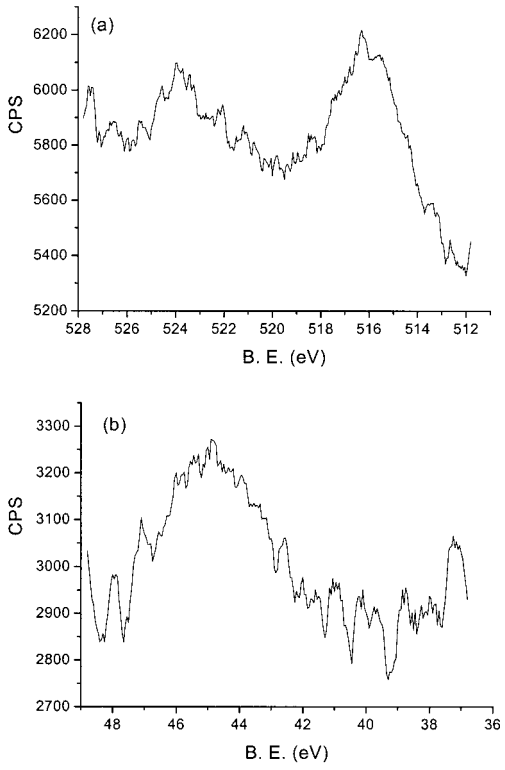

Figure 4. (a) XPS spectrum of V $2p_{3/2}$ for compound **1**; (b) XPS spectrum of As $3d_{5/2}$ for compound **1**

clusters by transition metal coordination complexes. It suggests that further condensation of clusters into higher dimensional solids through the linkage of the coordination complexes could be feasible. The bridging center may be replaced by other metal ions (Cu, Co, Mn etc.), and the building block clusters may be substituted by other arsenic-vanadium clusters, such as $[As_8V_{14}O_{42}(H_2O)_{0.5}]^{4-}$ [18] and $[As_6V_{15}O_{42}(H_2O)]^{6-}$.[18]

Experimental Section

General Remarks: All reagents were purchased commercially and used without further purification. The content of vanadium, nickel and arsenic was determined on a Perkin−Elmer Optima 3300DV spectrometer. Elemental analyses (C, H and N) were performed on a Perkin−Elmer 2400 Series II CHNS/O elemental analyzer. The infrared spectrum was obtained on an Perkin−Elmer spectrophotometer in the 200−4000 cm^{-1} region with pressed KBr pellet. Measurement of the electron-spin resonance (ESR) spectrum carried out on a Bruker ER 200D-SRC diffractometer. XPS measurements were performed on single crystals with an Escalab Mark II apparatus, using Mg-K_α X-ray radiation as the excitation source ($E_{Mg\text{-}K_\alpha}$ = 1253.6 eV). Variable-temperature magnetic susceptibility measurements for **1** were performed on a MPMS-XL magnetometer over the range 2−300 K.

Synthesis of 1: Compound **1** was hydrothermally synthesized in 73% yield (based on V). A mixture of As_2O_3 (0.40 g), V_2O_5 (0.36 g), $H_2C_2O_4{\cdot}2H_2O$ (0.25 g), en (0.24 g), $NiSO_4{\cdot}6H_2O$ (0.53 g), and distilled water (21.6 mL) in a molar ratio of 1:1:1:2:1:600 was stirred for ca. 10 min and then transferred to a Teflon-lined reactor and heated at 160 °C for three days. $H_2C_2O_4{\cdot}2H_2O$ was used as reducing agent and it was necessary to maintain the pH value of the reaction system. After cooling to room temperature, black block crystals were isolated. The compound **1** is stable to air in water, and in acetone. Elemental analysis (%): calcd. As 22.21, V 26.43, S 1.19, Ni 6.53, C 5.34, H 2.13, N 6.23; found As 22.18, V 26.41, S 1.14, Ni 6.54, C 5.33, H 2.07, N 6.21. IR: 3451(w) cm^{-1}, 2925(w), 1587(m), 1139(m), 1016(m), 969(s), 704(s).

X-ray Crystallographic Study: $C_{12}H_{57}As_8N_{12}Ni_3O_{50}SV_{14}$ (**1**), M_r = 2698.41, triclinic space group $P\bar{1}$, a = 12.9318(6) Å, b = 13.4441(7) Å, c = 21.2885(13) Å, α = 87.260(3)°, β = 77.637(2)°, γ = 68.699(3)°, V = 3366.5(3) $Å^3$, Z = 2, ρ = 2.662 $mg{\cdot}m^{-1}$, μ(Mo-K_α) = 6.704 mm^{-1}, $F(000)$ = 2606, R [$I \geq 2\sigma(I)$] = 0.0707, $wR2$ = 0.2161 for all reflections, goodness-of-fit = 0.883.
A black crystal (dimensions 0.447 × 0.367 × 0.273 mm^3) was carefully chosen from the batch sample and mounted on a glass fiber for data collection at 293 K on a Rigaku RAXIS-RAPID diffractometer equipped with Mo-K_α radiation. A total of 16168 reflections were measured, 9572 of which were unique. Structure solution was performed with SHELXS-97 by direct methods. All atoms except C(1) were refined anisotropically. The Ni(1) atom is disordered over two positions, with occupancy factors of 0.63 and 0.37, respectively. The hydrogen atoms were positioned with an idealized geometry and refined with fixed isotropic-displacement parameters using a riding model.
CCDC-210956 (**1**) contains the supplementary crystallographic data for this paper. These data can be obtained free of charge at www.ccdc.cam.ac.uk/conts/retrieving.html [or from the Cambridge Crystallographic Data Centre, 12 Union Road, Cambridge CB2 1EZ, UK; Fax: (internat.) + 44-1223/336-033; E-mail: deposit@ccdc.cam.ac.uk].

Acknowledgments

This work was supported by the National Natural Science Foundation of China (No. 20271021 and No. 20333070).

[1] M. T. Pope, A. Müller, *Angew. Chem. Int. Ed. Engl.* **1991**, *30*, 34−48.
[2] M. T. Pope, *Heteropoly- and Isopolyoxometalates*, Springer, Berlin, **1983**.
[3] P. Gouzerh, A. Proust, *Chem. Rev.* **1998**, *98*, 77−111.
[4] [4a] V. Soghomonian, Q. Chen, R. Haushalter, J. Zubieta, *Chem. Mater.* **1993**, *5*, 1595−1597. [4b] P. Zapf, R. Haushalter, J. Zubieta, *Chem. Mater.* **1997**, *9*, 2019−2024.
[5] T. Gier, G. Stucky, *Nature* **1991**, *349*, 508−510.
[6] B. Yan, Y. Xu, X. Bu, N. K. Goh, L. S. Chia, G. D. Stucky, *J. Chem. Soc., Dalton Trans.* **2001**, 2009−2014.
[7] X. Wang, L. Liu, G. Zhang, A. J. Jacobson, *Chem. Commun.* **2001**, 2472−2473.
[8] M. I. Khan, *J. Solid State Chem.* **2000**, *152*, 105−112.
[9] M. I. Khan, E. Yohannes, R. J. Doedens, *Angew. Chem. Int. Ed.* **1999**, *38*, 1292−1294.
[10] M. I. Khan, E. Yohannes, D. Powell, *Chem. Commun.* **1999**, 23−24.
[11] M. I. Khan, E. Yohannes, D. Powell, *Inorg. Chem.* **1999**, 212−213.
[12] X. Cui, Y. Sun, G. Yang, *Inorg. Chem. Commun.* **2003**, *6*, 259−261.
[13] W.-M. Bu, G.-Y. Yang, L. Ye, J.-Q. Xu, Y.-G. Fan, *Chem. Lett.* **2000**, 462−463.
[14] C. Pan, J. Xu, G. Li, X. Cui, Y. Le, G. Yang, *Dalton Trans.* **2003**, 517−518.

 © 2004 Wiley-VCH Verlag GmbH & Co. KGaA, Weinheim

[15] J. Lu, Y. Xu, N. K. Goh, L. S. Chia, *Chem. Commun.* **1998**, 2733−2734.
[16] L. Zhang, X. Zhao, J. Xu, T. Wang, *J. Chem. Soc., Dalton Trans.* **2002**, 3275−3276.
[17] C. Liu, D. Zhang, M. Xiong, D. Zhu, *Chem. Commun.* **2002**, 1416−1417.
[18] [18a] A. Müller, J. Döring, *Z. Anorg. Allg. Chem.* **1991**, *595*, 251−274. [18b] A. Müller, J. Doring, *Angew. Chem. Int. Ed. Engl.* **1988**, *27*, 1721. [18c] G. Huan, M. A. Greaney, A. J. Jacobson, *J. Chem. Soc., Chem. Commun.* **1991**, 260−261.
[19] Y. Zhang, J. R. D. Debord, C. J. O'Connor, R. C. Haushalter, A. Clearfield, J. Zubieta, *Angew. Chem. Int. Ed. Engl.* **1996**, *35*, 989−991.
[20] C. Liu, S. Gao, H. Hu, X. Jin, H. Kou, *J. Chem. Soc., Dalton Trans.* **2002**, 598−601.
[21] C. Liu, Y. Hou, J. Zhang, S. Gao, *Inorg. Chem.* **2002**, *41*, 140−143.
[22] D. Altermatt, I. D. Brown, *Acta Crystallogr., Sect. B* **1985**, *41*, 240−244.
[23] A. Müller, R. Sessoli, E. Krickemeyer, H. Bögge, J. Meyer, D. Gatteschi, L. Pardi, J. Westphal, K. Hovermeier, R. Rohlfing, J. Döring, F. Hellweg, C. Beugholt, M. Schmidtmann, *Inorg. Chem.* **1997**, *36*, 5239−5250.
[24] O. Kahn, *Molecular Magnetism*, VCH, Weinheim, Germany, **1993**.
[25] C. D. Wagner, W. M. Riggs, L. E. Davis, J. F. Moulder, and G. E. Muilenberg, *Handbook of X-ray Photoelectron Spectroscopy*, Perkin−Elmer Corp., MI, **1978**.

Received August 25, 2003
Early View Article
Published Online February 3, 2004

 © 2004 Wiley-VCH Verlag GmbH & Co. KGaA, Weinheim

Electronic Interactions in Dinuclear Platinum and Palladium Ethynylferrocene and Ferrocenylvinylidene Complexes

John H. K. Yip,*[a] Jianguo Wu,[a] Kwok-Yin Wong,*[b] Kam Piu Ho,[b] Lip Lin Koh,[a] and Jagadese J. Vittal[a]

Keywords: Platinum / Palladium / Ferrocene / Alkenes

The complex $[Pd_2(dppm)_2(\mu\text{-}\eta^1{:}\eta^1\text{-}H\text{–}C{=}C\text{–}Fc)Cl_2]$ (**2**) and its vinylidene isomer $[Pd_2(dppm)_2(\mu\text{-}C{=}CH\text{–}Fc)Cl_2]$ (**3**) [dppm = bis(diphenylphosphanyl)methane, Fc = ferrocenyl unit, $CpFeC_5H_4$] have been synthesized and characterized by single-crystal X-ray diffraction. Both **2** and **3** are A-frame structures with long Pd–Pd distances of 3.2055(9) Å (**2**) and 3.1002(2) Å (**3**), respectively, and square-planar metal coordination. The cyclic voltammograms (CV) of the complexes are measured and compared with that of $[Pt_2(dppm)_2(\mu\text{-}\eta^1{:}\eta^1\text{-}H\text{–}C{=}C\text{–}Fc)Cl_2]$ (**1**). The CV of **2** and **3** consist of a nearly reversible Fc-oxidation, an irreversible oxidation and a small reversible couple. The $E_{1/2}$ values (vs. Cp_2Fe^+/Cp_2Fe) of the Fc-groups in complexes **1**–**3** follow the order **2** (–75±8 mV) > **1** (–108±10 mV) > **3** (–124±8 mV). The difference in the $E_{1/2}$ values is explained by the orbital interactions between the acetylene and vinylidene groups with Pt_2 and Pd_2 cores. Our analysis shows that the metal-to-ligand π back-bonding and ligand-to-metal σ-donation have determining effects on the electronic interactions between the dimetallic centers and the bridgehead ligands.
(© Wiley-VCH Verlag GmbH & Co. KGaA, 69451 Weinheim, Germany, 2004)

Introduction

Understanding ligand-mediated electronic interactions is pertinent to the design of organometallic-based advanced materials. Special attention has been given to alkynyl (−C≡C−) and polynyl ligands because of the potential applications of their metal complexes in areas such as molecular electronics and photonic materials.[1] While many complexes containing acetylene (R−C≡C−R′)[2] and vinylidene (C=CRR′)[3] have been synthesized, the emphasis of the studies is mostly on the reactivity and structures of the compounds and the knowledge of the electronic interactions in these metal complexes is rather limited. Similar to the alkynyl group, acetylene and vinylidene can participate in π-conjugation with metal centers. However, there are differences between metal−acetylene/−vinylidene bonding and the metal−alkynyl bonding, which is expected to have pronounced effects on the electronic interactions mediated by these ligands. Apparently, a better understanding of the electronic interactions between the metal and the two organic linkages is essential for the exploitation of metal−acetylene and −vinylidene complexes in organometallic materials.

Dinuclear d^9−d^9 $[M_2(L)_2(L')_2]$ complexes (M = Ir^0, Rh^0, Pd^I, Pt^I; L = bridging diphosphane or diarsane, L′ = terminal ligands) are known to react with various groups (X) i.e. CO, acetylene, isocyandide, halides to form the so-called A-frame complexes $[M_2(L)_2(L')_2(\mu\text{-}X)]$ in which the two metal atoms are bridged by the X group in the apical position.[4] The complexes have been studied intensively, mainly for their intriguing structures and reactivity.[4,5] The first comprehensive theoretical study of the bonding of A-frame complexes was given by Hoffmann.[6] The optical spectroscopy and electronic structures of a series of A-frame vinylidene $[Ni_2(dppm)_2(\mu\text{-}C{=}CH_2)X_2]$ (X = Cl, Br, SCN)[7] and the luminescent properties of the distorted A-frame $[Pt_2(\mu\text{-}AuCl)(dppm)_2Cl_2]$ were reported.[8] In view of their structural simplicity and the theoretical underpinning, it is believed that the A-frame acetylene and vinylidene complexes could serve as models in probing the electronic communications mediated by the two unsaturated groups. Our recent study showed that the redox-active ethynylferrocene can be anchored onto an A-frame complex $[Pt_2(dppm)_2(\mu\text{-}\eta^1\text{-}\eta^1\text{-}HC{=}C{-}Fc)Cl_2]$ (**1**) (Fc = ferrocenyl $CpFeC_5H_4$) via the oxidative addition reaction with $[Pt^I{}_2(dppm)_2Cl_2]$.[9] The cyclic voltammogram (CV) of the complex shows a cathodic shift of the reduction potential of the Fc^+/Fc couple, indicating the existence of electronic interactions between the Fc group and the Pt_2 center. In order to further elucidate the electronic interactions between the dimetallic

[a] Department of Chemistry, The National University of Singapore,
10 Kent Ridge Crescent, 119260 Singapore
Fax: (internat.) + 65-67791691
E-mail: chmyiphk@nus.edu.sg
[b] Department of Applied Biology and Chemical Technology, Hong Kong Polytechnic University,
Hunghom, Kowloon, Hong Kong SAR, People's Republic of China

 © 2004 Wiley-VCH Verlag GmbH & Co. KGaA, Weinheim **DOI: 10.1002/ejic.200300595**

center and Fc group, we prepared the palladium analog of compound **1**, $[Pd_2(dppm)_2(\mu\text{-}\eta^1\text{-}\eta^1\text{-}HC{=}C{-}Fc)Cl_2]$ (**2**), and its vinylidene isomer $[Pd_2(dppm)_2(\mu\text{-}C{\equiv}CH{-}Fc)Cl_2]$ (**3**) (Scheme 1). Apart from showing the effects of the metal ion and the bridging ligand on the electronic interactions, our results also provide insights into the metal−acetylene and −vinylidene bonding.

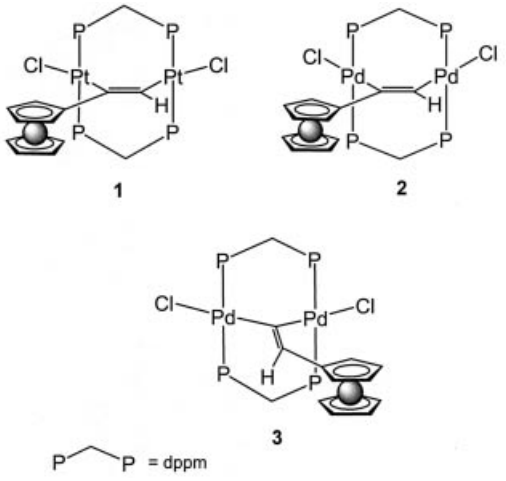

Scheme 1

Results and Discussion

Synthesis and Structures

Like other A-frame dipalladium-acetylene complexes,[10] $[Pd_2(dppm)_2(\mu_2\text{-}\eta^1{:}\eta^1\text{-}H{-}C{\equiv}C{-}Fc)Cl_2]$ (**2**) was synthesized from a reaction between $[Pd_2(dppm)_2Cl_2]$ and ethynylferrocene. The synthesis of the vinylidene complex $[Pd_2(dppm)_2(\mu\text{-}C{\equiv}CH{-}Fc)Cl_2]$ (**3**) is different from the conventional method which involves acid catalyzed isomerization of the dipalladium-acetylene complex[11] or reaction of $[Pd_2(dppm)_2Cl_2]$ with diiodoalkenes.[12] Refluxing a methanol solution of compound **2** with HBF_4 failed to transform complex 2 into its vinylidene isomer. We discovered that the vinylidene complex can be synthesized in moderate yield by the reaction between $[Pd_2(dppm)_2Cl_2]$ and ferrocenylacetylide ($Fc{-}C{\equiv}C^-$), which was generated from the deprotonation of $Fc{-}C{\equiv}C{-}H$ by NaOMe generated in situ. The formation of complex **3** may involve the reduction of $Fc{-}C{\equiv}C^-$ by the Pd−Pd bond (Scheme 2).

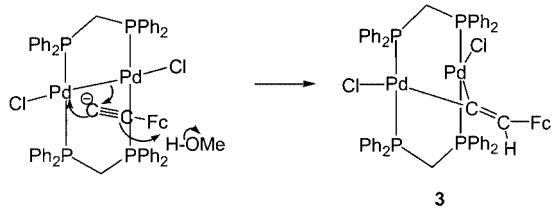

Scheme 2

The Pt-vinylidene complex, $[Pt_2(dppm)_2(\mu\text{-}C{=}CHFc)Cl_2]$, cannot by synthesized by this method or acid-catalyzed isomerization of compound **1**. As reported earlier, the reaction between $[Pt_2(dppm)_2Cl_2]$ and $FcC{\equiv}C^-$ led to the formation of $[Pt_2(dppm)_2(C{\equiv}C{-}Fc)_2]$.[13]

The complex **2** is isostructural to its Pt analog $[Pt_2(dppm)_2(\mu_2\text{-}\eta^1{:}\eta^1\text{-}H{-}C{\equiv}C{-}Fc)Cl_2]$, the structure of which was recently reported by us.[9] The X-ray crystal structure of compound **2** shows two nearly square-planar Pd ions bridged by two *trans* oriented dppm groups and one ethynylferrocene (Figure 1 and Table 1). Two chloride ions are coordinated *trans* to the two acetylene carbon atoms [C(1)−Pd(1)−Cl(1) = 170.1(3)°, C(2)−Pd(2)−Cl(2) 171.4(3)°]. As observed in many other dppm-bridged dinuclear compounds, the $Pd_2(P{-}C{-}P)_2$ metallocycle in **2** adopts a boat conformation. The Pd−P and Pd−Cl bond lengths are normal.[10,11,12] The Pd−C bond lengths, which are slightly different [Pd(1)−C(1) = 2.010(1) Å and Pd(2)−C(2) = 2.038(1) Å], are similar to the ones found in similar complexes such as $[Pd_2(dppm)_2(\mu_2\text{-}\eta^1{:}\eta^1\text{-}F_3C{-}C{=}C{-}CF_3)Cl_2]$ [Pd−C = 1.994(12) and 2.014(12) Å].[10] The long Pd−Pd distance of 3.2055(9) Å indicates the absence of a metal−metal bond; in other words, the two d^9 Pd^I ions in $[Pd_2(dppm)_2Cl_2]$ are formally oxidized to d^8 Pd^{II} ions in **2**. The distorted square-planar coordination geometry of the Pd ions is characteristic of d^8 metals. Accordingly the bridging ligand should be regarded as a dianionic ethylene $(H{-}C{=}C{-}Fc)^{2-}$, as suggested by the theoretical study.[6] In line with the assignment of the bridging acetylene as a dianionic ethylene $(H{-}C{=}C{-}Fc)^{2-}$ is the acetylene C(1)−C(2) bond length [1.309(14) Å], which is significantly longer than the averaged C≡C bond length (1.19 Å) but falls into the range of an average C=C bond. In addition, the angles between the bridging acetylene and the Pd atoms [Pd(1)−C(1)−C(2) = 117.2(8)° and Pd(2)−C(2)−C(1) = 118.4(8)°] are close to 120° expected for an sp^2 carbon. Similar bond angles and acetylene C−C distances are found in complex **1** [Pt−C−C = 120.4(7)° and 116.8(7)°, C−C = 1.293(1) Å]. The angles θ, which measure the deviation of

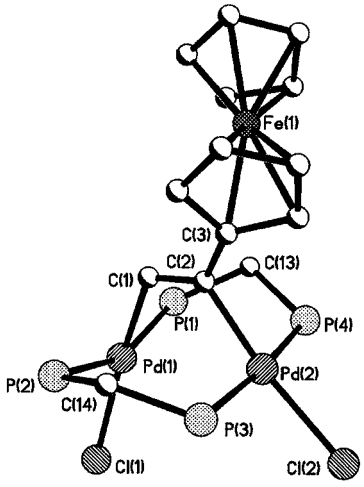

Figure 1. Molecular structure of compound **2**·CH_2Cl_2. All the H-atoms and solvent molecules are omitted for clarity

 © 2004 Wiley-VCH Verlag GmbH & Co. KGaA, Weinheim

the Pd−Cl bonds from the Pd−Pd vector (Scheme 3), are 52.74(9)° and 69.83(9)°. Similar angles θ [53.30(9)°, 69.44(9)°] were observed in the complex **1**. The $^{31}P\{^{1}H\}$ NMR spectrum of the complex is second-order showing two multiplets (AA′BB′)[10] at δ = 4.80 and 10.58.

Table 1. Selected bond length [Å] and angles [deg] for **2**·CH_2Cl_2

Pd(1)−C(1)	2.010(1)	Pd(2)−C(2)	2.038(1)
Pd(1)−Cl(1)	2.396(3)	Pd(2)−Cl(2)	2.407(2)
Pd(1)−Pd(2)	3.2055(9)	C(2)−C(3)	1.452(1)
C(1)−C(2)	1.309(1)	P(3)−Pd(2)−P(4)	173.34(9)
P(1)−Pd(1)−P(2)	157.29(9)	P(2)−Pd(1)−Cl(1)	95.72(1)
P(1)−Pd(1)−Cl(1)	105.08(1)	P(4)−Pd(2)−Cl(2)	91.66(9)
P(3)−Pd(2)−Cl(2)	171.4(3)	C(2)−Pd(2)−Cl(2)	171.4(3)
C(1)−Pd(1)−Cl(1)	170.1(3)	C(1)−C(2)−Pd(2)	118.4(8)
C(2)−C(1)−Pd(1)	117.2(8)		
C(1)−C(2)−C(3)	126.2(9)		

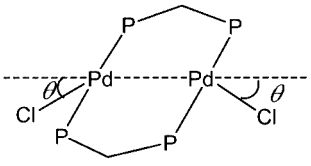

Scheme 3

The X-ray crystal structure $[Pd_2(dppm)_2(\mu\text{-}C{\equiv}CH{-}Fc)Cl_2]$ (**3**) (Figure 2 and Table 2) features a $[Pd_2(dppm)_2Cl_2]$ core similar to that of complex **2**. The two metal ions are bridged by the α-carbon atom of the ferrocenylvinylidene. The Fc group is disordered over two positions (50% occupancy for each position) which are symmetric with respect to the two Pd atoms. The α-carbon atom is equidistant from the two metal ions [Pd(1)−C(2) = 19.18(11) Å]. Although the Pd−Pd distance [3.1002(17) Å] is shorter than those reported in other A-frame Pd_2−vinylidene complexes, it is still too long to assign any formal bonding between the metal ions; accordingly, the Pd and the bridging ligand should be formulated as Pd^{II} and $Fc{-}CH{=}C^{2-}$, respectively. The bridging angle, Pd(1)−C(1)−Pd(1A), 107.8(9)°, is smaller than the 120° of an sp^2 carbon. This is by no means unique to the present complex, as a similar bridging angle is found in related compounds, i.e. $[Pd_2(dppm)_2(\mu\text{-}C{=}CH_2)Cl_2]$ [Pd−C−Pd = 109.2(8)°]. Due to their high thermal parameters, the distance between the two vinylidene carbon atoms C(2)−C(3) cannot be determined accurately. The angle θ, 38.16(2)°, is smaller than that in complex **2**. No ν(C≡C) vibration is observed in the IR spectrum of **3**. The $^{31}P\{^{1}H\}$ NMR spectrum is in accordance with the molecular structure of the complex as it shows two second-order multiplets centered at δ 13.5 which display a splitting pattern ascribable to the AA′BB′ system.[10]

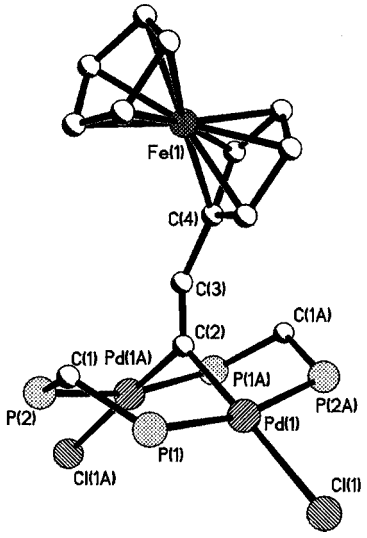

Figure 2. Molecular structure of compound **3**. All the H-atoms and solvent molecules are omitted for clarity

Table 2. Selected bond length [Å] and angles [deg] for **3**

Pd(1)−C(2)	1.918(1)	Pd(1A)−C(2)	1.918(11)
Pd(1)−Cl(1)	2.408(4)	Pd(1)−Pd(1A)	3.1002(2)
C(2)−C(3)	1.20(3)	C(3)−C(4)	1.44(3)
P(1)−Pd(1)−P(2A)	166.89(2)	P(2A)−Pd(1)−C(2)	84.12(11)
C(2)−Pd(1)−P(1)	86.78(8)	C(2)−Pd(1)−Cl(1)	177.9(5)
P(2A)−Pd(1)−Cl(1)	96.01(2)	P(1)−Pd(1)−Cl(1)	93.43(12)
C(3)−C(2)−Pd(1A)	126.1(4)	P(1)−Pd(1)−Pd(1A)	141.84(2)
C(4)−C(2)−C(3)	152.7(6)	Pd(1A)−C(2)−Pd(1)	107.8(9)

Electrochemistry of the Complexes

The electrochemical data of the complexes **1**−**3** are summarized in Table 3. Our previous study showed that, at room temperature, the cyclic voltammogram (CV) of **1** shows a reversible Fc^+/Fc-couple (ΔE_p = 60 mV, i_c/i_a = 1) at −108±10 mV vs. Cp_2Fe^+/Cp_2Fe.[9] There is an irreversible oxidation at 583±10 mV attributable to the oxidation of the Pt metal center. The corresponding Pt reduction occurs at 343±10 mV. No reduction wave was observed when the initial scan direction was made towards the cathodic side.

The CV of **2** measured in CH_2Cl_2 at room temperature (Figure 3) displays a reversible couple at $E_{1/2}$ = −75±8 mV (vs. Cp_2Fe^+/Cp_2Fe, $i_{pc}/i_{pa} \approx 1$, ΔE_p = 77 mV), an irreversible oxidation peak II at +487±8 mV, and a reversible couple III at $E_{1/2}$ = +833±8 mV ($i_{pc}/i_{pa} \approx 1$). Couple I at $E_{1/2}$ = −75±8 mV is attributable to the one-electron oxidation of the Fc group as its reduction potential is close to the Fc^+/Fc-couple of **1**. The peak-to-peak splitting (ΔE_p) of 77 mV is slightly larger than the 60 mV expected for a reversible one-electron couple. This is likely to be caused by the resistance of the dichloromethane electrolyte and the liquid junction potential between the reference electrode and the electrolyte. The reversible oxidation of the Fc group is followed by an irreversible oxidation wave II at +487±8 mV. The size of this irreversible oxidation wave is close to that of the Fc^+/Fc-couple, indicating that it too is a one-electron process. Reversing the voltammetric scan at 550 mV did not

 © 2004 Wiley-VCH Verlag GmbH & Co. KGaA, Weinheim

Table 3. Electrochemical data of compounds **1**, **2**, and **3**[a]

Complex[a]	Fc^+/Fc-couple I[b] $E_{1/2}$	Irreversible oxidation peak II[b] (reduction peak)	Reversible couple III[b] $E_{1/2}$
1	−108±10	+583±10 (343±10)	
2	−75±8	+487±8 (+330±8)	+833±8
3	−124±8	+679±8 (+623±8)	+969±8

[a] Measured in CH_2Cl_2 (0.1 M nBu_4NPF_6), working electrode: glassy carbon electrode (0.07 cm^2), reference electrode: $Ag/AgNO_3$ (0.1 M in CH_3CN), counter electrode: platinum wire. [b] mV vs. Cp_2Fe^+/Cp_2Fe.

result in the observation of the corresponding reduction wave for this oxidation. A small reduction peak, however, was observed at +311±8 mV in the reverse scan. This indicates that **2**, once oxidized at this potential, rapidly undergoes an irreversible 'chemical reaction'. Theoretical calculations on the isoelectronic and isostructural A-frame Rh^I_2(μ-acetylene) showed that the HOMO of the complex is mostly metal-based.[6] This suggests that the oxidation process at 487±8 mV could correspond to the one-electron oxidation of $Pd^{II}Pd^{II}$ to $Pd^{II}Pd^{III}$. Since Pd^{III} and Pd^{II} ions prefer different coordination geometries, the oxidation brings about drastic structural changes, which could account for the 'chemical reaction' following the electron transfer. The small reduction wave at 311±8 mV could be due to the product after the structural rearrangement has occurred. The irreversible oxidation at 487±8 mV is followed by a smaller but reversible couple III at $E_{1/2}$ = +833±8 mV. The smaller size of this couple compared to the Fc^+/Fc-couple is consistent with the structural rearrangement of the complex preceding the electron transfer. Tentatively the couple is assigned to the oxidation of $Pd^{III}Pd^{II}$ to $Pd^{III}Pd^{III}$.

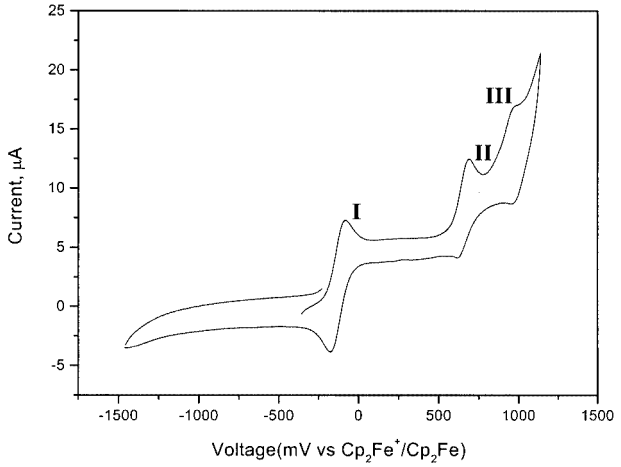

Figure 3. CV of **2** measured in CH_2Cl_2 (0.1 M nBu_4NPF_6), working electrode: glassy carbon electrode (0.07 cm^2), reference electrode: $Ag/AgNO_3$ (0.1 M in CH_3CN), counter electrode: platinum wire, concentration of complex = 1.2 mM, scan rate = 10 mV/s

Similar to compound **2**, the CV of the vinylidene complex **3** (Figure 4) exhibits a reversible couple I at $E_{1/2}$ = −124 ± 8 mV ($i_{p,c}/i_{p,a} \approx 1$; ΔE_p = 74 mV), an irreversible oxidation peak II at +679±8 mV and a smaller reversible couple at $E_{1/2}$ = +969±8 mV ($i_{p,c}/i_{p,a} \approx 1$). The reversible couple I $E_{1/2}$ = −124 mV is assigned to the Fc^+/Fc-couple. The size of the irreversible wave II at +679±8 mV is similar to that of the Fc^+/Fc-couple and is therefore assigned to the one-electron oxidation of Pd^{II} Pd^{II} to $Pd^{II}Pd^{III}$. A small reduction peak appeared at +623±8 mV, which is attributed to reduction of the rearranged product after the oxidation process has occurred. The smaller reversible couple III at +969±8 mV could be due to the oxidation of $Pd^{II}Pd^{III}$ to $Pd^{III}Pd^{III}$.

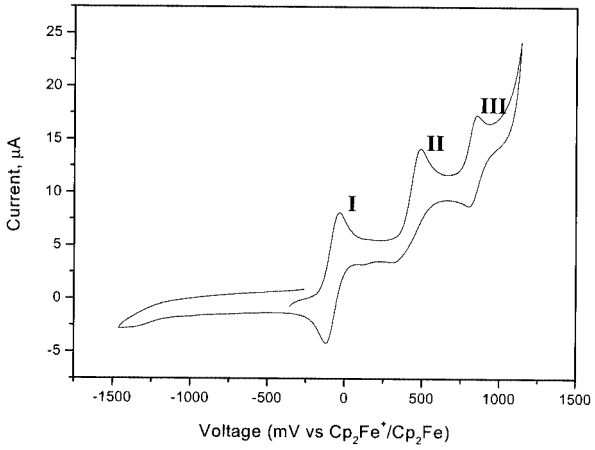

Figure 4. CV of **3** measured in: CH_2Cl_2 (0.1 M nBu_4NPF_6), working electrode: glassy carbon electrode (0.07 cm^2), reference electrode: $Ag/AgNO_3$ (0.1 M in CH_3CN), counter electrode: platinum wire, concentration of complex = 1.2 mM, scan rate = 10 mV/s

Electronic Interactions

A common electrochemical feature of the complexes is the low $E_{1/2}$ of their Fc^+/Fc-couples in comparison with the reported $E_{1/2}$ of ethynylferrocene (Fc^+−C≡CH/Fc−C≡CH = +254 mV vs. Cp_2Fe^+/Cp_2Fe).[14] In other words, the Fc groups in the three dinuclear complexes are more reducing or electron-rich than the one in the uncomplexed Fc−C≡C−H. This is consistent with the formal assignment of the bridgehead ligands as the dianionic $(H-C=C-Fc)^{2-}$ and $Fc-CH=C^{2-}$ species. Since the Fc groups in these complexes are connected to the acetylene and vinylidene groups via σ- and π-bonds, transfer of electron density from the dimetallic cores onto the linkage would lower the potential of the Fc^+/Fc-couple via π-conjugation and an inductive effect.

 © 2004 Wiley-VCH Verlag GmbH & Co. KGaA, Weinheim

Comparing the $E_{1/2}$ of the Fc^+/Fc-couples of the isostructural compounds **1** and **2** shows that the Fc group in the Pd_2 complex (−75±8 mV) is less reducing than the one in the Pt_2 complex (−108±10 mV). The interactions between the dianionic $(H-C{\equiv}C-Fc)^{2-}$ and the dinuclear M_2 centers (M = Pd^{II} and Pt^{II}) consist of σ- and π-donations from the ligand π-orbitals and the metal-to-ligand π back-bonding (Scheme 4). The bending of the $(H-C{\equiv}C-Fc)^{2-}$ unit lifts the degeneracy of the π- and π*-orbitals, with the energy in the order: $\pi_x^2 < \pi_z^2 < \pi^*_z{}^2 < \pi^*_x$ (*x* axis is parallel to the meridian of the complex).[6] In addition, the π_z- and π_z*-orbitals are hybridized with the 2s-orbital. The ligand(π_x)-to-metal π-donation is secondary as there is no low-lying accepting orbital in the metals to interact with the deep-seated π_x-orbital. In first-order approximation, the ligand-to-metal σ-donation involves, primarily, interactions between the filled bonding π_z- and antibonding π_z*-orbitals of $(H-C{\equiv}C-Fc)^{2-}$ and the empty dσ- and dσ*-orbitals, respectively. The latter orbitals arise from the bonding and antibonding combinations of the two $nd_{x^2-y^2}$-orbitals (*n* = 4 for M = Pd and 5 for M = Pt). While electron density drifts from $(H-C{\equiv}C-Fc)^{2-}$ to the M_2 core as a result of σ-donation, the metal-to-ligand π back-bonding, which involves the nd_{xy}-orbitals of M_2 and the π_x*-orbital of $(H-C{\equiv}C-Fc)^{2-}$, transfers electron density from the metal to the $(H-C{\equiv}C-Fc)^{2-}$ unit. The importance of the ligand-to-metal σ-donation in the interactions is obvious but the significance of the metal-to-ligand π back-bonding in the electronic interactions is rather uncertain. In view of the general conception that third row transition metals form stronger π back-bonding than their second row congeners, one would expect the $Pt_2 \rightarrow (H-C{\equiv}C-Fc)^{2-}$ π back-bonding to be stronger than the $Pd_2 \rightarrow (H-C{\equiv}C-Fc)^{2-}$ π back-bonding. This is consistent with the $E_{1/2}$ values of the Fc^+/Fc-couples in **1** and **2**.

The $E_{1/2}$ of the Fc^+/Fc-couple of the vinylidene complex (−124±8 mV) is lower than the corresponding $E_{1/2}$ of its acetylene isomer **2** (−75±8 mV). The Fc group of **3** is even more reducing than that of **1**, which suggests the metal-to-ligand π back-bonding is not the main cause for the low reduction potential. We believe that this difference in the reduction potentials could be interpreted as a weaker $Fc-CH{=}C^{2-} \rightarrow Pd_2$ σ-donation in complex **3**. Notably, the peak potential of the irreversible metal oxidation of complex **2** (+487±8 mV) is lower than that of complex **3** (+679±8 mV), suggesting that Pd_2 in **2** is more electron-rich than that in **3**. This is consistent with the argument that the $(H-C{\equiv}C-Fc)^{2-} \rightarrow Pd_2$ donation is stronger than the $Fc-CH{=}C^{2-} \rightarrow Pd_2$ donation. The σ-bonding in complex **3** involves the interactions between (i) the filled antibonding π*-orbital (vinylidene) and the dσ*-orbital (Pd_2) and (ii) an admixture of 2s- and $2p_y$-orbitals (vinylidene) and the dσ-orbital (Pd_2) (Scheme 5). The splitting of the dσ- and dσ*-orbitals would be increased by a better overlap of the two $d_{x^2-y^2}$-orbitals.[6] This can be achieved by shortening the Pd−Pd distance or reducing the angle θ. Comparing the structures of the two isomers shows that the Pd−Pd distance [3.1002(17) Å] and the angle θ [38.16(2)°] are shorter and smaller than the ones in complex **2** [Pd−Pd = 3.2055(9) Å; θ = 52.74(9)°, 69.83(9)°]. These structural features suggest that the dσ*-orbital in complex **3** is more destabilized than the one in complex **2**. The larger energy separation between the π_y*- and dσ*-orbitals weaken the σ-donation. On the other hand, one would expect the 2s/2p−dσ interaction to be enhanced as the dσ-orbital is now more stabilized. Nonetheless, the $E_{1/2}$ of the Fc group should be determined mainly by the π_y*−dσ* interaction since the π_y*-orbital is higher in energy than it is in π-conjugation with the Cp-ring of the Fc group. Another possibility for the poorer σ-donation in complex **3** is the relatively in-

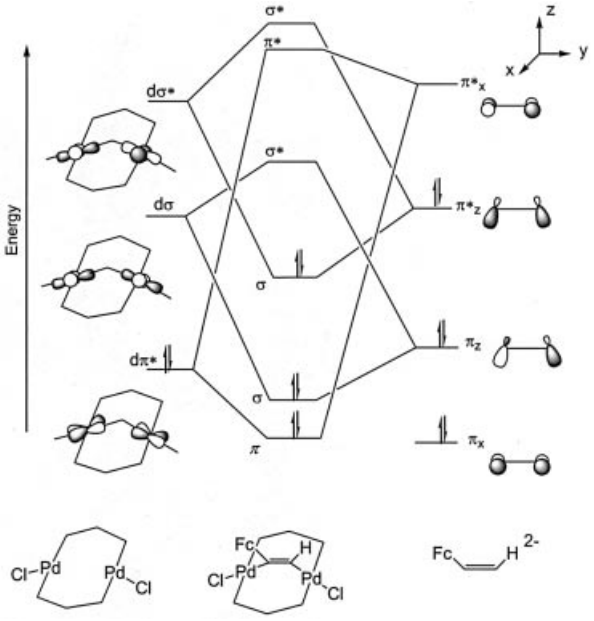

Scheme 4

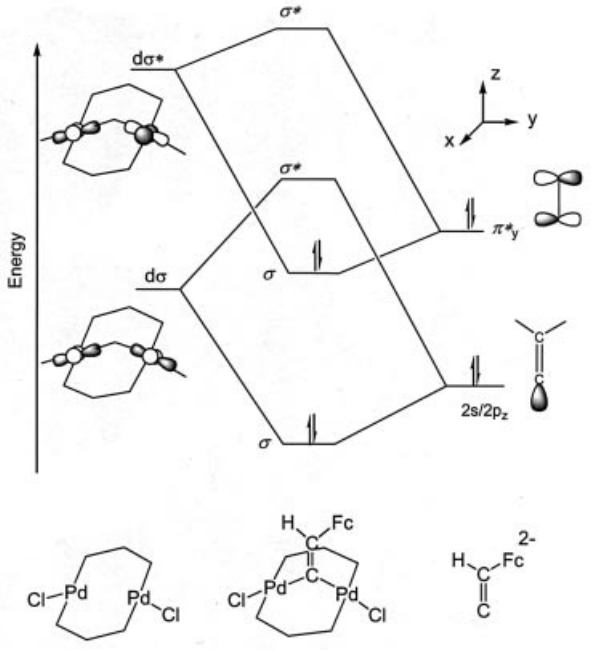

Scheme 5

 © 2004 Wiley-VCH Verlag GmbH & Co. KGaA, Weinheim

sufficient overlap between the apical carbon sp^2-hybridized orbital and the metal orbitals; suggested by the fact that the bridging angle Pd−C−Pd [107.8(9)°] is smaller than 120°. On the other hand, the orbital overlap between $(H-C{=}C-Fc)^{2-}$ and Pd_2 in complex **2** is better as the Pd(1)−C(1)−C(2) and Pd(2)−C(2)−C(1) angles [117.2(8)° and 118.4(8)°] are close to the ideal angle of an sp^2-hybridized carbon atom. This poor σ-donation would retain more electron density in the vinylidene from which the inductive effect would be transmitted via the σ-bonds to the ferrocenyl group, leading to a lower Fc^+/Fc potential as observed.

Concluding Remarks

In summary, our work demonstrated the presence of electronic interactions between the ferrocenyl group and the metal centers in the complexes $[Pd_2(dppm)_2(\mu\text{-}\eta^1{:}\eta^1\text{-}H-C{=}C-Fc)Cl_2]$ and $[Pd_2(dppm)_2(\mu\text{-}C{=}CH-Fc)Cl_2]$. Comparing the $E_{1/2}$ of the Fc^+/Fc-couples of $[Pd_2(dppm)_2(\mu\text{-}\eta^1{:}\eta^1\text{-}H-C{=}C-Fc)Cl_2]$ and its Pt-analog shows that the Pt has stronger metal-to-ligand π backbonding than the Pd. It is rather unexpected that the ligand-to-metal σ-donation in the Pd_2−μ-vinylidene complex is weaker than the one in the acetylene isomer. This is attributed to the destabilization of the dσ*-orbital and the poor orbital overlap between the bridging vinylidene and the metal ions.

Experimental Section

General Methods: All syntheses were carried out using standard Schlenk techniques. All solvents used in syntheses and electrochemical measurements were purified according to the literature methods. The supporting electrolyte $n\text{Bu}_4\text{NPF}_6$ (TBAH) obtained from Aldrich was recrystallized from ethanol and dried at 100 °C for 24 h before being used. Ethynylferrocene[15] and $[Pd_2(dppm)_2Cl_2]$[16] were prepared according to reported procedures. Dichloromethane used for the voltammetric measurements was distilled over P_2O_5.

Physical Measurements: NMR spectra were recorded at 25 °C on a Bruker ACF 300 spectrometer. Elemental analyses of the complexes were carried out in the microanalysis laboratory in the department of chemistry, the National University of Singapore. Solution infrared spectra of the complexes were recorded on a Bio-Rad TFS 156 spectrometer. A Bioanalytical Systems (BAS) model 100 W electrochemical analyzer was used in all electrochemical measurements. $n\text{Bu}_4\text{NPF}_6$ (0.1 M) was used as the supporting electrolyte unless otherwise stated. Cyclic voltammetry was performed in a conventional two-compartment electrochemical cell. The platinum disc working electrode (area 0.02 cm^2) was treated by polishing it with 0.05 μm alumina using a microcloth and then sonicated for 5 minutes in deionized water followed by rinsing with the solvent used in the electrochemical studies. An $Ag/AgNO_3$ (0.1 M in CH_3CN) electrode was used as reference electrode. The potential of the $Ag/AgNO_3$ reference electrode was calibrated against the $Cp_2Fe^{+/0}$ couple before and after each set of experiments to ensure the accuracy of the potential measured;[17] the $E_{1/2}$ of $Cp_2Fe^{+/0}$ was found to be 0.06±0.01 V vs. the $Ag/AgNO_3$ reference. The $E_{1/2}$ values are the average of the cathodic and anodic peak potentials for the oxidative and reductive waves of reversible couples.[18]

Synthesis of $[Pd_2(dppm)_2(\mu\text{-}\eta^1{:}\eta^1\text{-}HC{=}C-Fc)Cl_2]\cdot CH_2Cl_2$ ($2\cdot CH_2Cl_2$): A methanol suspension of $[Pd_2(dppm)_2Cl_2]$ (0.3 g, 0.29 mmol) and ethynylferrocene (0.06 g, 0.29 mmol) was stirred at room temperature for 24 h and the orange precipitate that formed was filtered. The solid was dissolved in dichloromethane and filtered. Excess diethyl ether was added to the filtrate to precipitate the product as an orange solid. The product was purified by diffusing diethyl ether into a dichloromethane solution. Yield 59%. $C_{63}H_{56}Cl_4FeP_4Pd_2$: calcd. C 56.11, H 4.16; found C 56.00, H 4.12 (%). ^{1}H NMR (300 MHz, CD_2Cl_2, δ/ppm): 5.42 (m, 1 H, H−C=), 3.06 (m, 2 H, PCH_2P), 3.41 (s, 5 H, C_5H_5), 3.41 (s, 4 H, C_5H_4), 3.25 (m, 2 H, PCH_2P), 6.94−7.98 (m, 40 H, Ph). $^{31}P\{^1H\}$ NMR (300 MHz, CD_2Cl_2, δ/ppm): 4.80 (m, 2 P), 10.58 (m, 2 P).

Synthesis of $[Pd_2(dppm)_2(\mu\text{-}C{\equiv}CH-Fc)Cl_2]$ (3): Sodium (0.02 g, 0.855 mmol) was added to a methanol solution (10 mL) of ethynylferrocene (0.18 g, 0.86 mmol). After 20 min of stirring hexane (60 mL) was introduced, followed by the addition of $[Pd_2(dppm)_2Cl_2]$ (0.30 g, 0.29 mmol). The mixture was stirred at room temperature for 12 h and then filtered. The solid was dissolved in dichloromethane and filtered. Excess diethyl ether was added to the filtrate to precipitate the product as an orange solid. The product was purified by diffusing diethyl ether into a dichloromethane solution. Yield 45%. $C_{62}H_{54}Cl_2FeP_4Pd_2$: calcd. C 58.93, H 4.28; found C 58.46, H 4.12 (%). ^{1}H NMR (300 MHz, CD_2Cl_2, δ/ppm): 5.56 (m, 1 H, H−C=C), 2.60 (m, 2 H, PCH_2P), 3.67 (s, 5 H, C_5H_5), 4.02 (s, 4 H, C_5H_4), 3.10 (m, 2 H, PCH_2P), 6.95−7.92 (m, 40 H, Ph). $^{31}P\{^1H\}$ NMR (300 MHz, CD_2Cl_2, δ/ppm): 12.7−14.5 (m).

X-ray Crystallography: The diffraction experiments were carried out on a Bruker AXS SMART CCD 3-circle diffractometer at T = 223 K, 2θ−ω scan with a sealed tube using graphite-monochromated Mo-K_α radiation (λ = 0.71073 Å). The following software was used: SMART[19] for collecting frames of data, indexing reflection and determination of lattice parameters; SAINT[19] for integration of intensity of reflections and scaling; SADABS[20] for empirical absorption correction; and SHELXTL[21] for space group determination, structure solution and least-squares refinements on $|F|^2$. The crystals were mounted at the end of glass fibers. Anisotropic thermal parameters were refined for the non-hydrogen atoms. The hydrogen atoms were placed in their ideal positions. A brief summary of crystal data and experimental details are given in Table 4. Crystallographic data for (i) **$[Pd_2(dppm)_2(\mu\text{-}\eta^1{:}\eta^1\text{-}HC{=}CFc)Cl_2]\cdot CH_2Cl_2$** ($2\cdot CH_2Cl_2$): of the 16441 reflections collected, 10837 were independent (R_{int} = 0.0466). Index range: $-15 \le h \le 17$, $-17 \le k \le 16$, $-21 \le l \le 19$. Refinement of F^2 converged with R_1 = 0.0982 for $I > 2\sigma(I)$ and wR_2 = 0.2672. The residual electron density is 3.142 and −2.392 e·Å^{-3}, (ii) **$[Pd_2(dppm)_2(\mu\text{-}C{=}CH-Fc)Cl_2]$ (3)**: of the 25934 reflections collected, 5298 were independent (R_{int} = 0.0747). Index range: $-19 \le h \le 18$, $-18 \le k \le 18$, $-24 \le l \le 15$. Refinement of F^2 converged with R_1 = 0.0611 for $I > 2\sigma(I)$ and wR_2 = 0.1648. The residual electron density is 0.394 and −0.239 e·Å^{-3}. The ferrocenyl unit is disordered over two positions with 50% occupancy. One of the phenyl groups is disordered and is modeled with two orientations, each with 50% occupancy.

CCDC-217655 (for **2**), and -217656 (for **3**) contain the supplementary crystallographic data for this paper. These data can be obtained free of charge at www.ccdc.cam.ac.uk/conts/retrieving.html [or from the Cambridge Crystallographic Data Centre, 12, Union

 © 2004 Wiley-VCH Verlag GmbH & Co. KGaA, Weinheim

Table 4. Crystal data and structure refinements for **2**·CH_2Cl_2 and **3**

	2·CH_2Cl_2	**3**
Formula	$C_{63}H_{56}Cl_4FeP_4Pd_2$	$C_{62}H_{54}Cl_2FeP_4Pd_2$
Molecular mass	1347.41	1262.48
Crystal system	triclinic	trigonal
Space group	$P\bar{1}$	$P3(1)21$
Z	2	3
Crystal size [mm^3]	0.6 × 0.6 × 0.56	0.56 × 0.46 × 0.16
Lattice parameters [Å]	a = 14.3059(2), b = 14.4442(2), c = 17.8761(3)	a = 16.017(4), b = 16.017(4), c = 20.353(7)
[deg]	α = 80.544(1), β = 71.517(1), γ = 67.986(1)	α = 90(1), β = 90(1), γ = 120(1)
V [A^3]	3236.29(8)	4522(2)
Density (calcd.) [$g \cdot cm^{-3}$]	1.383	1.391
Abs. coeff. [mm^{-1}]	1.070	1.058
$F(000)$	1360	1914
No. of parameters varied	670	335
Final R indices[a]	$R1$ = 0.0982. $wR2$ = 0.2672	$R1$ = 0.0611. $wR2$ = 0.1648
Goodness of fit[b]	1.122	0.904

[a] $R1 = (||F_o| - |F_c||)/(|F_o|)$; $wR2 = [w(F_o^2 - F_c^2)/w(F_o^4)]^{1/2}$. [b] GOF = $[w(F_o^2 - F_c^2)^2/(n - p)]^{1/2}$.

Road, Cambridge CB2 1EZ, UK; Fax: (internat.) +44-1223/336-033; E-mail: deposit@ccdc.cam.ac.uk].

Acknowledgments

J. H. K. Y. thanks The National University of Singapore for financial supports. K.Y.W. acknowledges the support from the Hong Kong Polytechnic University. We are grateful to Ms Tan Geok Kheng (NUS) for her assistance with the X-ray crystal structure determination.

[1] [1a] I. R. Whittal, A. M. McDonagh, M. G. Humphrey, *Adv. Organomet. Chem.* **1998**, *42*, 291. [1b] J. Manna, K. J. John, M. D. Hopkins, *Adv. Organomet. Chem.* **1995**, *38*, 79. [1c] S. R. Marder, in: *Inorganic Materials* (Eds.: D. W. Bruce, D. O'Hare), Wiley, Chichester, **1996**, p. 121. [1d] N. J. Long, C. K. Williams, *Angew. Chem. Int. Ed.* **2003**, *42*, 2586. [1e] C. R. Horn, J. A. Gladysz, *Eur. J. Inorg. Chem.* **2003**, 2211.

[2] [2a] P. K. Baker, *Adv. Organomet. Chem.* **1996**, *40*, 45. [2b] R. D. Adams, B. Qu, *Organometallics* **2000**, *19*, 2411. [2c] P. J. Low, R. Rousseau, P. Lam, K. A. Udachin, G. D. Enright, J. S. Tse, D. D. M. Wayner, A. J. Carty, *Organometallics* **1999**, *18*, 3885.

[3] [3a] C. Bruneau, P. H. Dixneuf, *Acc. Chem. Res.* **1999**, *32*, 311. [3b] M. Knorr, G. R. Schmitt, M. M. Kubicki, E. Vigier, *Eur. J. Inorg. Chem.* **2003**, 514. [3c] E. Bustelo, J. J. Carbo, A. Lledos, K. Mereiter, M. C. Puerta, P. Valerga, *J. Am. Chem. Soc.* **2003**, *125*, 3311. [3d] S. Hartmann S, R. F. Winter, B. M. Brunner, B. Sarkar, A. Knodler, I. Hartenbach, *Eur. J. Inorg. Chem.* **2003**, 876. [3e] K. Ilg, H. Werner, *Angew. Chem. Int. Ed.* **2000**, *39*, 1632.

[4] [4a] R. J. Puddephatt, *Chem. Soc. Rev.* **1983**, *12*, 99. [4b] C. F. J. Barnard, M. J. H. Russeh, in: *Comprehensive Coordination Chemistry* (Ed.: G. Wilkinson), vol. 5. Pergamon Press, Oxford, **1987**, chapter 51, p. 1099−1130. [4c]G. K. Anderson, *Adv. Organomet. Chem.* **1993**, *35*, 1.

[5] [5a] M. P. Brown, R. J. Puddephatt, M. Rashidi, K. R. Seddon, *J. Chem. Soc., Dalton Trans.* **1978**, 1540. [5b] A. L. Balch, L. S. Benner, M. M. Olmstead, *Inorg. Chem.* **1979**, *18*, 2996. [5c] M. C. Grossel, R. P. Moulding, K. R. Seddon, *Inorg. Chim. Acta* **1983**, *64*, L275. [5d] K. R. Grundy, K. N. Robertson, *Organometalics* **1983**, *2*, 1736.

[6] D. M. Hoffman, R. Hoffmann, *Inorg. Chem.* **1981**, *20*, 3543.

[7] J. D. Heise, J. J. Nash, P. E. Fanwick, C. P. Kubiak, *Organometallics* **1996**, 15, 1690.

[8] D. V. Toronto, A. L. Balch, D. S. Tinti, *Inorg. Chem.* **1994**, *33*, 2507.

[9] J. H. K. Yip, J. Wu, K.-Y. Wong, K.-W. Yeung, J. J. Vittal, *Organometallics* **2002**, *21*, 1612.

[10] C.-L. Lee, C. T. Hunt, A. L. Balch, *Inorg. Chem.* **1981**, *20*, 2498.

[11] [11a] J. A. Davis, K. Kirschbaum, C. Kluwe, *Organometallics* **1994**, *13*, 3664. [11b] C. Kluwe, J. Muller, J. A. Davis, *J. Organomet. Chem.* **1996**, *526*, 385. [11c] C. Kluew, J. A. Davis, *Organometallics* **1995**, *14*, 4257.

[12] J. A. Davis, A. A. Pinkerton, R. Syed, M. Vilmer, *J. Chem. Soc., Chem. Com.* **1988**, 47.

[13] J. H. K. Yip, J. Wu, K.-Y. Wong, K. P. Ho, C. S.-N. Pun, J. J. Vittal, *Organometallics* **2002**, *21*, 5292−5233.

[14] H. Nock, H. Schottenberger, *J. Org. Chem.* **1993**, *58*, 7048.

[15] J.-G. Rodriquez, A. Oñate, R. M. Martin-Villami, I. Fonseca, *J. Organomet. Chem.* **1996**, *513*, 71.

[16] P. G. Pringle, B. L. Shaw, *J. Chem. Soc., Dalton Trans.* **1983**, 889.

[17] G. Gritzner, J. Kúta, *Pure and Appl. Chem.* **1982**, *54*, 1527.

[18] R. R. Gagné, C. A. Koval, G. C. Lisensky, *Inorg. Chem.* **1980**, *19*, 2855.

[19] *SMART & SAINT Software Reference Manuals*, Version 4.0, Siemens Energy & Automation, Inc., Analytical Instrumentation, Madison, Wisconsin, USA, **1996**.

[20] G. M. Sheldrick, *SADABS a software for empirical absorption correction*, University of Gottingen, Gottingen, Germany, **1996**.

[21] *SHELXTL Reference Manual*, Version 5.03, Siemens Energy & Automation, Inc., Analytical Instrumentation, Madison, Wisconsin, USA, **1996**.

Received August 25, 2003
Early View Article
Published Online January 28, 2004

 © 2004 Wiley-VCH Verlag GmbH & Co. KGaA, Weinheim

Cluster Growth Reactions with Selenido-Carbonyl Clusters − Synthesis, Characterisation and Theoretical Study of the Dimetallic *closo* Clusters $[WRu_3(\mu_4\text{-}Se)_2(\mu\text{-}CO)_4(CO)_6(L)_2]$ (L = Phosphane) and of the Donor-Acceptor Adduct $[(CO)_5W(\mu_4\text{-}Se)Ru_3(\mu_3\text{-}Se)(CO)_7\{P(CH_2Ph)Ph_2\}_2]$

Daniele Cauzzi,[a] Claudia Graiff,[a] Roberto Pattacini,[a] Giovanni Predieri,*[a] Antonio Tiripicchio,[a] Samia Kahlal,[b] and Jean-Yves Saillard[b]

Keywords: Ruthenium / Tungsten / Molybdenum / Cluster compounds / Selenium

The open-triangular, *nido* clusters of the type $[Ru_3(\mu_3\text{-}Se)_2(CO)_7(L)_2]$ (L = PPh_3, $PPh_2(OMe)$, $PPh_2(Me)$, $P(p\text{-}MeOC_6H_4)_3$] react at room temperature with $[W(CO)_3(MeCN)_3]$ to give the dimetallic *closo* clusters $[WRu_3(\mu_4\text{-}Se)_2(\mu\text{-}CO)_4(CO)_6(L)_2]$. When L is $P(CH_2Ph)Ph_2$ the donor-acceptor adduct $[(CO)_5W(\mu_4\text{-}Se)Ru_3(\mu_3\text{-}Se)(CO)_7\{P(CH_2Ph)Ph_2\}_2]$ is obtained where the *nido* cluster $[Ru_3(\mu_3\text{-}Se)_2(CO)_7(L)_2]$ interacts with the fragment $W(CO)_5$ through a selenido ligand. DFT calculations, performed on the model species $[WRu_3(\mu_4\text{-}Se)_2(\mu\text{-}CO)_4(CO)_6(PH_3)_2]$ and $[(CO)_5W(\mu_4\text{-}Se)Ru_3(\mu_3\text{-}Se)(CO)_7(PH_3)_2]$, showed that the computed total energy of the latter is 1.1 eV lower than that of the former.
(© Wiley-VCH Verlag GmbH & Co. KGaA, 69451 Weinheim, Germany, 2004)

Introduction

In recent years we have carried out systematic investigations on the selenium-transfer reactions of tertiary phosphane and diphosphane selenides with carbonyl clusters $M'_3(CO)_{12}$ (M′ = Fe or Ru).[1−9] These reactions take advantage of the frailty of the P=Se bond and provide a simple, sometimes selective,[2] synthetic route to phosphane-substituted, mono- and diselenido clusters. When the starting phosphane contains heterocyclic groups, such as the 2-pyridyl and 2-thienyl moieties, P−C bond cleavage is observed, affording selenido-phosphido clusters coordinating to heterocyclic fragments.[5−7]

The synthesis of phosphane-substituted mixed-metal selenido clusters has also been investigated as the presence of different metals can influence the selectivity of certain processes,[8,9] leading to the formation of compounds with new and not always easily predictable structures. For the synthesis of dimetallic substituted selenido-carbonyl clusters two different synthetic strategies have been developed: (a) M′M + PSe, i.e. reactions between preformed dimetallic clusters and tertiary phosphane selenides,[10] and (b) M′Se + M, i.e. cluster growth reactions between preformed chalcogenide metal clusters and suitable organometallic fragments.

As regards route (b), selenido clusters $[Ru_3(\mu_3\text{-}Se)_2(CO)_7(L)_2]$ were considered to be ideal candidates for growth reactions. These starting compounds are open-triangular, *nido* clusters with seven skeletal electron pairs (SEPs), according to the requirements of the polyhedral skeletal electron pair (PSEP) theory. As a consequence they could be prone to add a zero SEP fragment, such as $M(CO)_3$, derived from $[M(CO)_3(CH_3CN)_3]$ (M = Mo or W), giving the corresponding *closo* clusters $[MRu_3(\mu_4\text{-}Se)_2(CO)_{10}(L)_2]$. In this regard Adams[11] and co-workers obtained the monophosphane sulfur derivative of formula $[WRu_3(\mu_4\text{-}S)_2(CO)_{11}(PMe_2Ph)]$ upon irradiating a solution of $[Ru_3(\mu_3\text{-}S)_2(CO)_9]$ and $[W(CO)_5(PMe_2Ph)]$.

In a preliminary communication,[12] the products of the reactions between $[Ru_3(\mu_3\text{-}Se)_2(CO)_7(PPh_3)_2]$ and $[M(CO)_3(CH_3CN)_3]$ were erroneously identified as the unexpected, centrosymmetric *closo* clusters $[M_2Ru_2(\mu_4\text{-}Se)_2(\mu\text{-}CO)_4(CO)_6(PPh_3)_2]$ (M = W or Mo) on the basis of misinterpreted X-ray structural analyses. However, preliminary MO calculations, mass spectral and accurate elemental analysis data stimulated further crystallographic studies, which revealed that a disorder exists in the crystals of these compounds involving the mutually opposite Ru and W atoms of the *closo* core of the cluster. This results in a disordered $Ru_3M(\mu_4\text{-}Se)_2$ cluster core instead of a centrosymmetric $M_2Ru_2(\mu_4\text{-}Se)_2$ one. Definitive evidence for this was provided by the solution of the crystal structure of $[WRu_3(\mu_4\text{-}Se)_2(\mu\text{-}CO)_4(CO)_6\{P(OMe)Ph_2\}_2]$ which does not

[a] Dipartimento di Chimica Generale ed Inorganica, Chimica Analitica, Chimica Fisica, Università di Parma,
Parco Area delle Scienze 17/A, 43100 Parma, Italy
Fax: (internat.) + 39-0521/905-557
E-mail: predieri@unipr.it
[b] LCSIM-UMR 6511, Institut de Chimie de Rennes, Université de Rennes 1,
35042 Rennes-Cedex, France

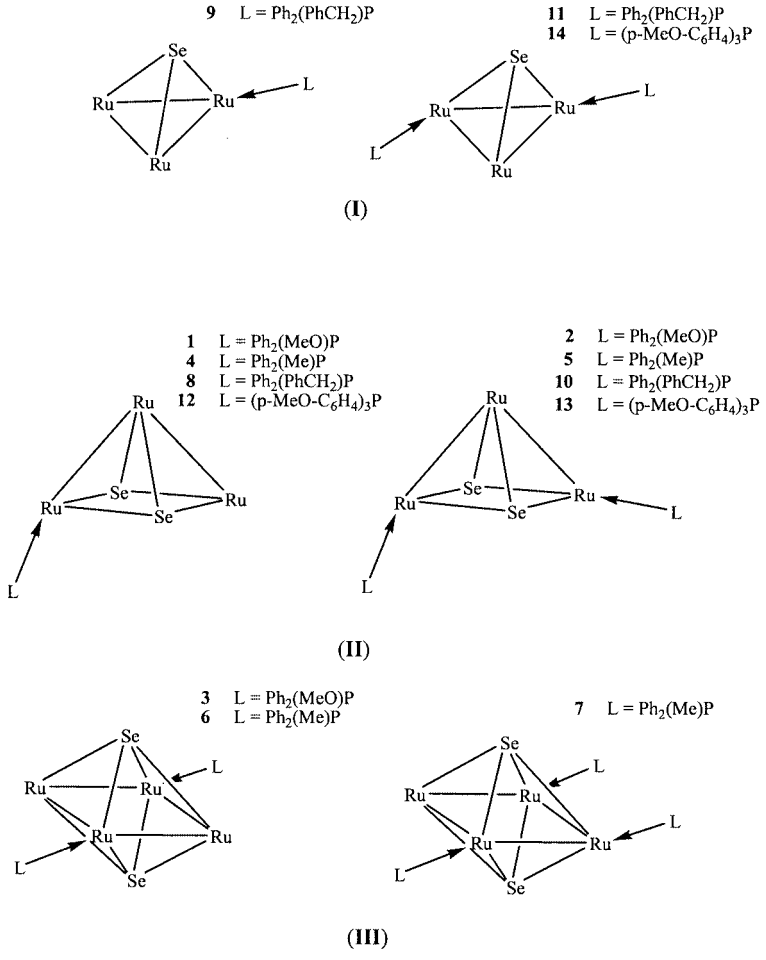

Scheme 1. (Carbonyl groups omitted)

exhibit the disorder described above. Consequently, this paper deals with the synthesis of five $[MRu_3(\mu_4\text{-}Se)_2(\mu\text{-}CO)_4(CO)_6(L)_2]$ clusters [M = Mo, L = PPh_3; M = W, L = $PPh_2(Me)$, $PPh_2(OMe)$, $P(p\text{-}MeO\text{-}C_6H_4)_3$] and the structural characterisation of four of them. In the case of the reaction involving $P(CH_2Ph)Ph_2$, we obtained $[(CO)_5W(\mu_4\text{-}Se)Ru_3(\mu_3\text{-}Se)(CO)_7\{P(CH_2Ph)Ph_2\}_2]$, which can be considered as the product of a donor-acceptor interaction between $[Ru_3(\mu_3\text{-}Se)_2(CO)_7\{P(CH_2Ph)Ph_2\}_2]$ and the $W(CO)_5$ fragment through a selenido ligand. Moreover, DFT calculations have been performed on the model compounds $[WRu_3(\mu_4\text{-}Se)_2(\mu\text{-}CO)_4(CO)_6(PH_3)_2]$ and $[(CO)_5W(\mu_4\text{-}Se)Ru_3(\mu_3\text{-}Se)(CO)_7(PH_3)_2]$. Besides these major results, some new phosphane selenides have been characterised, and used to produce the selenido clusters shown in Scheme 1. They can be grouped in three different families according to the cluster cores: Ru_3Se (I), Ru_3Se_2 (II) and Ru_4Se_2 (III). The crystal structures of two of them, $[Ru_3(\mu_3\text{-}Se)_2(CO)_7(L)_2]$ [L = $PPh_2(OMe)$ or $P(CH_2Ph)Ph_2$], have been determined by X-ray methods.

Results and Discussion

The new tertiary phosphane selenides $Ph_2(Me)PSe$, $Ph_2(MeO)PSe$, $(p\text{-}MeOC_5H_4)_3PSe$ and $Ph_2(PhCH_2)PSe$ were obtained in quantitative yield by selenium transfer from elemental Se to the parent phosphane. They exhibit a characteristic P=Se IR stretching band in the range 520−530 cm^{-1} and a ^{31}P NMR signal with ^{77}Se satellites, $^1J_{P,Se}$ being in the range 710−740 Hz as normally found in similar species.[13]

The reaction between $[Ru_3(CO)_{12}]$ and the tertiary phosphane selenides in hot toluene and in the presence of Me_3NO gave a number of substituted selenidoruthenium carbonyl clusters (some of them, **8**−**14**, already known) belonging to three different families: the monoselenido trinuclear species with a $Ru_3(\mu_3\text{-}Se)$ core (**9**, **11**, **14**; type I), the diselenido trinuclear species with a $Ru_3(\mu_3\text{-}Se)_2$ core (**1**, **2**, **4**, **5**, **8**, **10**, **12**, **13**; type II), and the diselenido tetranuclear species with a $Ru_4(\mu_4\text{-}Se)_2$ core (**3**, **6**, **7**; type III. See Scheme 1). As the reaction conditions are the same for all phosphanes, it appears that the product distribution is influenced by the nature of the phosphane.

Clusters belonging to the type I family could be regarded as the primary product of the attack of one molecule of the phosphane selenide on the starting reagent $[Ru_3(CO)_{12}]$, resulting in the transfer of a selenium atom to the metal triangle and the substitution of one or two carbonyl groups. These clusters undergo a second attack by another phos-

 © 2004 Wiley-VCH Verlag GmbH & Co. KGaA, Weinheim

phane selenide molecule affording, under appropriate conditions, the corresponding diselenido derivatives (clusters of type II). Mono- and disubstituted diselenido species are always present even if the starting Ru_3/PSe molar ratio is 1:1. Type II clusters can be described as square pyramids with two ruthenium and two selenium atoms alternating in the basal plane and the third ruthenium atom at the apex of the pyramid. Mono- and disubstitution by phosphanes occurs only at the base of the pyramid.

Type III clusters belong to the family of tetranuclear *closo* clusters with seven SEPs. They can be described as octahedral clusters with four ruthenium atoms in the equatorial plane and two selenium atoms at the apices. Two (**3**, **6**) or three (**7**) phosphane ligands substitute the same number of carbonyl groups. The coordination around each ruthenium atom is completed by carbonyl groups.

Slow crystallisation of compounds **2** and **10** from dichloromethane solutions afforded well-formed crystals suitable for an X-ray diffraction analysis. ORTEP views of **2** and **10** are shown in Figure 1 and 2, respectively. The most important bond lengths and angles are given in Table 1 together with those of a cluster of formula $[Ru_3(\mu_3\text{-}Se)_2(CO)_7(PPh_3)_2]$.[2]

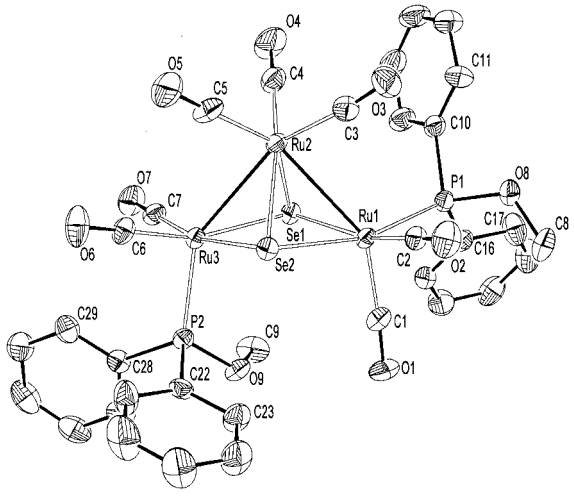

Figure 1. View (ORTEP, 30% probability level) of the molecular structure of **2** with the atom numbering scheme

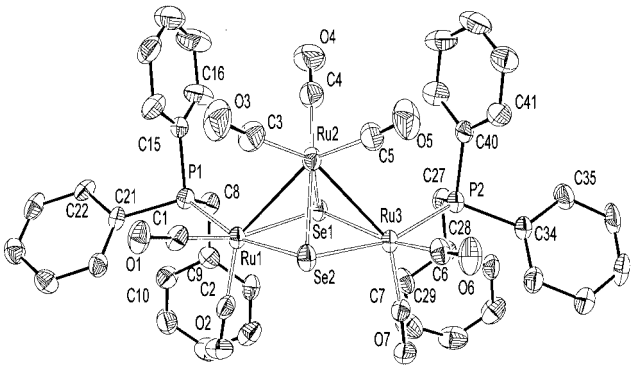

Figure 2. View (ORTEP, 30% probability level) of the molecular structure of **10** with the atom numbering scheme

The cluster cores are similar to that of the analogous compound $[Ru_3(\mu_3\text{-}Se)_2(CO)_7(PPh_3)_2]$[2] in which the Ru−Ru bond lengths are 2.801(2) and 2.855(2) Å; those of the six Ru−Se bonds range from 2.491(1) to 2.536(2) Å. The Ru−Ru bond lengths are 2.831(2) and 2.847(2) Å in **2** and 2.799(2) and 2.806(2) Å in **10**, whereas the Ru−Se bond lengths range from 2.485(1) to 2.529(2) Å in **2** and from 2.449(2) to 2.500(2) Å in **10**. In **10** the two diphenylbenzylphosphane ligands coordinate to two ruthenium atoms, substituting two carbonyl groups in *pseudo*-equatorial positions [the P1−Ru1 and P2−Ru3 bond lengths are 2.309(2) and 2.306(3) Å]. In **2** the two diphenylmethoxyphosphane ligands substitute two carbonyls in a *pseudo*-equatorial and *pseudo*-axial position. The P1−Ru1 and P2−Ru3 bond lengths [2.327(2) and 2.274(3) Å] differ remarkably because of the different *trans* influence of the Ru−Ru and Ru−Se bonds.

Clusters **2** and **10** show the same NMR behaviour in solution despite the different coordination of the phos-

Table 1. Comparison of selected bond lengths (Å) and angles (°) for compounds **2**, **10** and $[Ru_3(\mu_3\text{-}Se)_2(CO)_7(PPh_3)_2]$

	2	**10**	$[Ru_3(\mu_3\text{-}Se)_2(CO)_7(PPh_3)_2]$
Ru(1)−Ru(2)	2.8312(15)	2.8061(15)	2.855(2)
Ru(2)−Ru(3)	2.847(2)	2.7991(17)	2.801(2)
Ru(1)−Se(1)	2.4853(12)	2.4491(16)	2.514(2)
Ru(1)−Se(2)	2.5143(15)	2.4761(16)	2.491(2)
Ru(2)−Se(1)	2.5240(12)	2.4757(18)	2.523(2)
Ru(2)−Se(2)	2.5290(15)	2.500(2)	2.536(2)
Ru(3)−Se(1)	2.4872(16)	2.4497(15)	2.514(2)
Ru(3)−Se(2)	2.4987(12)	2.4704(16)	2.505(2)
Ru(1)−P(1)	2.327(2)	2.309(2)	2.371(4)
Ru(3)−P(2)	2.274(2)	2.306(3)	2.326(3)
Ru(1)−Ru(2)−Ru(3)	83.59(5)	83.96(6)	85.6(1)
Se(1)−Ru(3)−Se(2)	80.98(4)	80.30(6)	79.4(1)
Se(1)−Ru(1)−Se(2)	80.71(4)	80.20(6)	79.7(1)
Se(1)−Ru(2)−Se(2)	79.69(5)	79.23(7)	78.7(1)
Ru(1)−Se(1)−Ru(3)	99.11(4)	99.87(6)	100.6(1)
Ru(3)−Se(2)−Ru(1)	98.03(4)	98.56(6)	99.7(1)

 © 2004 Wiley-VCH Verlag GmbH & Co. KGaA, Weinheim

phane ligands in the solid state (eq-ax and eq-eq respectively). The room temperature ^{31}P NMR spectra of clusters **2** and **10**, as well as **5** and **13**, show two broad peaks which collapse at a temperature higher than 40 °C, together with two sharp singlets (see Figure 3 for **13**).

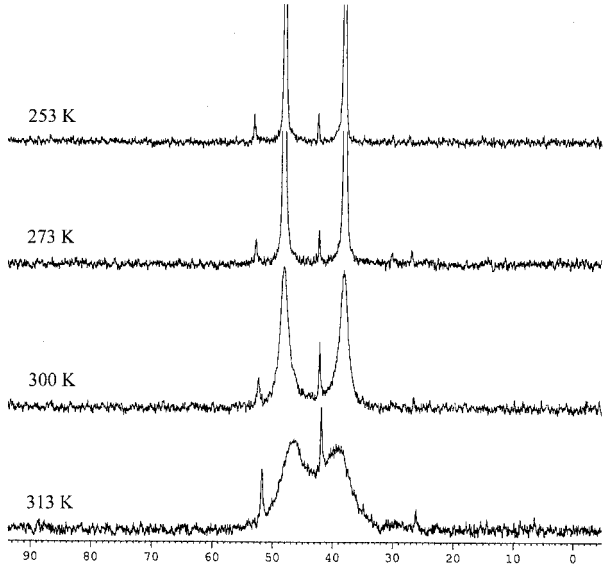

Figure 3. $^{31}P\{^{1}H\}$ NMR spectra of compound **13** recorded at different temperatures evidencing the incipient coalescence of the broad signals due to the different coordination modes of the phosphane ligands; the presence of four signals confirms the existence of the two isomeric forms A (broad peaks) and B (sharp peaks) depicted in Scheme 2

The two sets of peaks suggest the existence of two isomers A and B, indicated below in Scheme 2, as observed for $[Ru_3(\mu_3\text{-}Se)_2(CO)_7(\mu\text{-dppm})]$ (dppm = $Ph_2PCH_2PPh_2$).[14] They should be involved in an exchange process as occurs for the dppm derivative, consisting of the migration of a Ru−Ru bond from one side of the open Ru_3 triangle to the basal plane of the square pyramid (see Scheme 2). For all these complexes, an equilibrium takes place in solution starting from pure crystals of isomers A. The prevalence of isomer A (broader peaks) in solution is suggested by the fact that the basal metal sites are the preferred ones for phosphane substitution.[1] For both isomers the presence of two peaks suggests that the two P ligands are not equivalent. In fact, in B the two phosphanes occupy two different Ru sites, whereas in A (where the two Ru sites are equivalent) the presence of two peaks is probably the consequence of the fact that one phosphane ligand is coordinated in an axial position and the other in an equatorial position. As one ligand moves from the axial to the equatorial position, the other moves from equatorial to axial. This concerted movement of both ligands is responsible for the observed broadening of the major peaks.

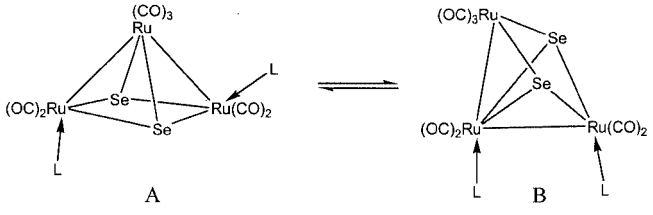

Scheme 2

Cluster Growth Reactions

Type II compounds are open-triangular, *nido* clusters with seven SEPs, according to the PSEP rules. As a consequence they could be prone to add a zero SEP fragment, such as $M(CO)_3$ (M = Mo or W), giving the *closo* clusters $MRu_3(\mu_4\text{-}Se)_2(CO)_{10}(L)_2$. We reacted clusters **2**, **5**, **10** and **13** with an excess of $W(CO)_3(CH_3CN)_3$ in dichloromethane. The reactions take place in a few hours, at room temperature, giving compounds $[WRu_3(\mu_4\text{-}Se)_2(\mu\text{-}CO)_4(CO)_6\{P(OMe)Ph_2\}_2]$ (**15**), $[WRu_3(\mu_4\text{-}Se)_2(\mu\text{-}CO)_4(CO)_6\{P(Me)Ph_2\}_2]$ (**16**), $[WRu_3(\mu_4\text{-}Se)_2(\mu\text{-}CO)_4(CO)_6\{P(p\text{-}MeO\text{-}C_6H_4)_3\}_2]$ (**17**) and $[(CO)_5W(\mu_4\text{-}Se)Ru_3(\mu_3\text{-}Se)(CO)_7\{P(CH_2Ph)Ph_2\}_2]$ (**20**) as the only isolable products. The IR spectra of **15**−**17**, in the carbonyl region are superimposable with $[WRu_3(\mu_4\text{-}Se)_2(\mu\text{-}CO)_4(CO)_6(PPh_3)_2]$ (**18**) and $[MoRu_3(\mu_4\text{-}Se)_2(\mu\text{-}CO)_4(CO)_6(PPh_3)_2]$ (**19**), suggesting the same molecular structure for all five compounds.

Clusters **15**, **17**, **18** and **19** were unequivocally identified by X-ray diffraction methods (**18** and **19** are isomorphous). Three of these clusters, namely **17**, **18** and **19**, show a crystallographically imposed C_i symmetry, so the mutually opposite Ru and M (M = W or Mo) atoms of the *closo* core of the cluster must be disordered and distributed in the two positions with the same occupancy factor in such a way that a disordered $[Ru_3M(\mu_4\text{-}Se)_2]$ cluster core forms instead of a centrosymmetric $[M_2Ru_2(\mu_4\text{-}Se)_2]$ core. Differently from the clusters **17**, **18** and **19**, cluster **15** does not show this type of disorder.

The structural diagrams of clusters **15**−**20** are shown in Scheme 3.

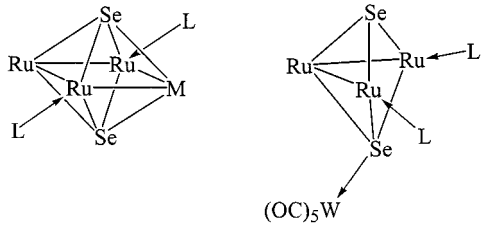

15 L = $P(OMe)Ph_2$ M = W
16 L = $P(Me)Ph_2$ M = W
17 L = $P(p\text{-}MeO\text{-}C_6H_4)_3$ M = W
18 L = PPh_3 M = W
19 L = PPh_3 M = Mo
20 L = $P(CH_2Ph)Ph_2$

Scheme 3. (Carbonyl groups omitted)

Because of the disorder, compounds **18** and **19** were previously identified as the six SEP species $[M_2Ru_2(\mu_4\text{-}Se)_2(\mu\text{-}CO)_4(CO)_6(L)_2]$ (M = W or Mo).[12] According to the PSEP theory, the observed *closo* arrangement is predicted to be unstable for electron-deficient species. This was con-

 © 2004 Wiley-VCH Verlag GmbH & Co. KGaA, Weinheim

firmed by DFT calculations on the isoelectronic models $[Mo_2Ru_2(\mu_4\text{-}Se)_2(\mu\text{-}CO)_4(CO)_6(L)_2]$ (L = CO, PH_3) assuming the observed *closo* architecture (geometry optimisation carried out assuming C_{2h} and C_i symmetry for L = CO and PH_3, respectively). Indeed, small HOMO-LUMO gaps were computed for these models (0.24 and 0.44 eV for L = CO and PH_3, respectively). Consistently, the excited triplet state was found to lie close to the singlet ground state (by 0.12 eV and 0.26 eV for L = CO and PH_3, respectively). All these results are indicative of a thermal and kinetic instability for $[M_2Ru_2(\mu_4\text{-}Se)_2(\mu\text{-}CO)_4(CO)_6(L)_2]$ (M = W or Mo), a result at variance with the behaviour of **18** and **19**. On the other hand, calculations on $[Mo_2Ru_2(\mu_4\text{-}Se)_2(\mu\text{-}CO)_4(CO)_6(L)_2]^{2-}$ and $[Mo_2Ru_2(\mu_4\text{-}SeH)_2(\mu\text{-}CO)_4(CO)_6(L)_2]$ (L = CO, PH_3) indicated thermal stability for the regular seven SEP count (HOMO-LUMO gap 1.92 eV (L = CO) and 1.81 eV (L = PH_3) for the former and 1.69 eV (L = CO) and 1.61 eV (L = PH_3) for the latter). Consistently, further crystallographic studies revealed that the correct formula for **18** and **19** is $[MRu_3(\mu_4\text{-}Se)_2(\mu\text{-}CO)_4(CO)_6(L)_2]$ (M = W or Mo).

ORTEP views of **15**, **17**, **18** and **19** are shown in Figure 4, 5, 6 and 7, respectively. The most important bond lengths and angles are given in Table 2 together with those calculated for the complex $[WRu_3(\mu_3\text{-}Se)_2(CO)_{10}(PH_3)_2]$.

The four *closo* seven SEP complexes can be described as distorted octahedra in which the three ruthenium and the M atoms lie in the basal plane with two selenium atoms at the apices. The Ru−Ru bond lengths span from 2.676(7) to 2.835(1) Å. The M−Ru bond lengths range from 2.852(6) to 2.939(2) Å for M = W and from 2.938(8) to 3.027(5) Å for M = Mo. Two phosphane ligands coordinate two nonbonded rutheniums through the phosphorus atoms. Four carbonyls asymmetrically bridge the Ru−Ru and Ru−M edges. The coordination around each metal atom is completed by terminal carbonyl groups.

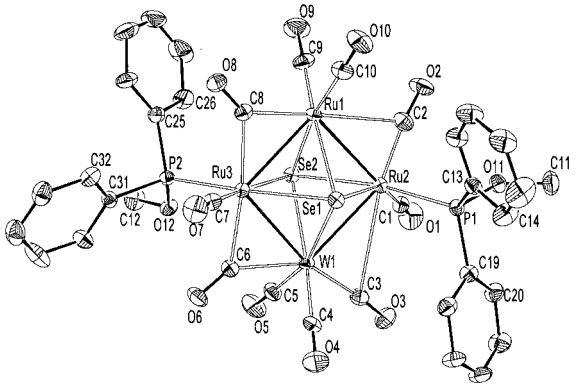

Figure 4. View (ORTEP, 30% probability level) of the molecular structure of **15** with the atom numbering scheme

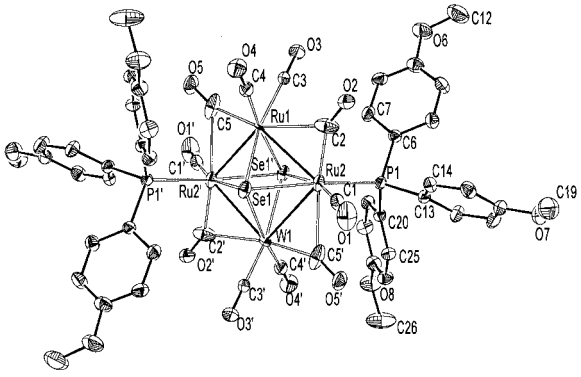

Figure 5. View (ORTEP, 30% probability level) of the molecular structure of one of the two disordered complexes **17** with the atom numbering scheme

DFT calculations on the $[WRu_3(\mu_4\text{-}Se)_2(\mu\text{-}CO)_4(CO)_6(PH_3)_2]$ model (assuming C_1 symmetry) lead to a large HOMO-LUMO gap (1.65 eV), as expected for a *closo*

Table 2. Comparison of selected bond lengths (Å) and angles (°) found for compounds **15**, **17**, **18**, **19** and calculated for complex $[WRu_3(\mu_3\text{-}Se)_2(CO)_{10}(PH_3)_2]$

	15	**17**	**18**	**19**	$WRu_3(\mu_3\text{-}Se)_2(CO)_{10}(PH_3)_2$
Ru(1)−Ru(2)	2.8349(11)	2.792(10)	2.826(4)	2.720(5)	2.878
Ru(1)−Ru(2′)[a]	2.7894(16)	2.676(7)	2.792(3)	2.781(7)	2.870
Ru(2)−M(1)[b]	2.9399(16)	2.935(4)	2.814(2)	2.938(8)	2.940
Ru(2′)−M(1)	2.8639(9)	2.851(6)	2.855(2)	3.027(5)	2.992
M(1)−Se(1)	2.6736(13)	2.658(5)	2.614(3)	2.855(5)	2.775
M(1)−Se(1′)	2.7028(10)	2.679(5)	2.626(2)	2.729(8)	2.775
Ru(1)−Se(1)	2.5841(13)	2.512(9)	2.614(4)	2.581(7)	2.650
Ru(1)−Se(1′)	2.540(4)	2.5894(10)	2.569(4)	2.505(5)	2.620
Ru(2)−Se(1)	2.6196(14)	2.5967(14)	2.5793(14)	2.5782(17)	2.686
Ru(2′)−Se(1′)	2.5878(14)	2.5967(14)	2.5793(14)	2.5782(17)	2.686
Ru(2)−Se(1′)	2.6067(13)	2.5894(10)	2.5976(15)	2.5971(17)	2.685
Ru(2′)−Se(1)	2.5644(11)	2.5894(10)	2.5976(15)	2.5971(17)	2.685
Ru(1)−Ru(2)−M(1)	90.29(4)	87.46(19)	90.73(8)	94.2(2)	92
Ru(1)−Ru(2′)−M(1)	92.81(3)	87.46(19)	90.73(8)	94.2(2)	93
Ru(2)−Ru(1)−Ru(2′)	90.18(4)	93.8(2)	89.88(11)	91.72(16)	86
Ru(2)−M(1)−Ru(2′)	86.67(3)	87.27(11)	88.83(7)	82.87(14)	85

[a] Symmetry transformations used to generate equivalent atoms: $-x + 1, -y, -z + 2$ (for **17**); $-x, -y, -z$ (for **18** and **19**); Ru(2′) = Ru(3) (for **15**), Se(1′) = Se(2) (for **15**). [b] M = W for **15**, **17** and **18**, Mo for **19**.

 © 2004 Wiley-VCH Verlag GmbH & Co. KGaA, Weinheim

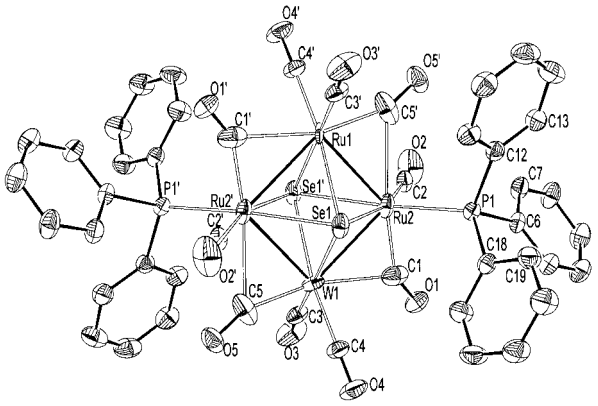

Figure 6. View (ORTEP, 30% probability level) of the molecular structure of one of the two disordered complexes **18** with the atom numbering scheme

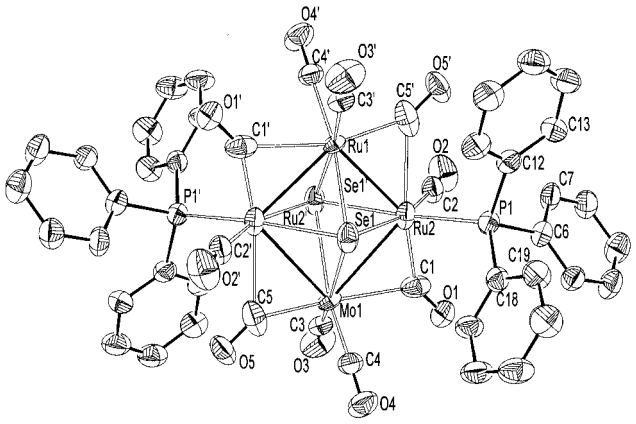

Figure 7. View (ORTEP, 30% probability level) of the molecular structure of one of the two disordered complexes **19** with the atom numbering scheme

seven SEP species. The major optimised bond lengths and angles are given in Table 2. Taking into account that such calculations are known to overestimate the bond lengths between heavy atoms by approximately 2−6%,[15] the optimised geometry of $[WRu_3(\mu_4\text{-}Se)_2(\mu\text{-}CO)_4(CO)_6(PH_3)_2]$ is in good agreement with the X-ray structures of **15**, **18** and **19**.

Surprisingly, in the case of the reaction between $[W(CO)_3(MeCN)_3]$ and **4**, we obtained the compound $[(CO)_5W(\mu_4\text{-}Se)Ru_3(\mu_3\text{-}Se)(CO)_7\{P(CH_2Ph)Ph_2\}_2]$ (**20**) as the only isolable product identified by X-ray diffraction methods. It could be considered as the product of a donor-acceptor interaction between a $W(CO)_5$ fragment and a selenido ligand of **10**. The presence of similar products is detectable on the preparative TLC plates in all the growth reactions described above, as red bands attributable to adducts (which decompose during elution) are always observed. In the case of $PPh_2(OMe)$, it was even possible to isolate and recognize, by FT-IR spectroscopy, a cluster analogous to **20**, which, however, rapidly decomposed. The decomposition product was identified as the starting disubstituted *nido* cluster **2**.

A view of cluster **20** is given in Figure 8. A list of the most important bond lengths and angles are given in Table 3.

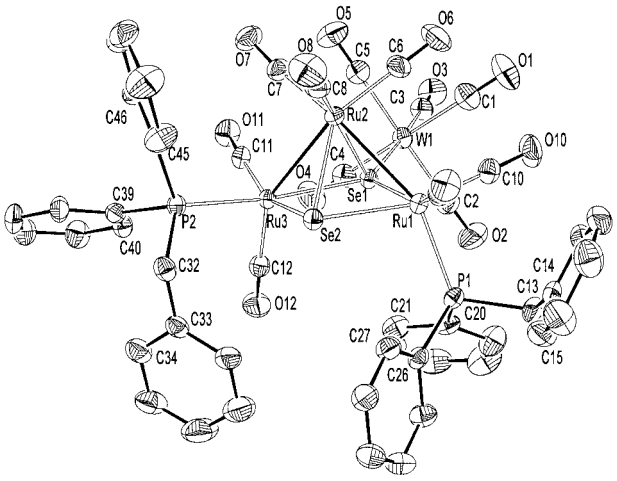

Figure 8. View (ORTEP, 30% probability level) of the molecular structure of **20** with the atom numbering scheme

Table 3. Selected bond lengths (Å) and angles (°) found for compound **20** compared with those calculated for the complex $[(CO)_5W(\mu_4\text{-}Se)Ru_3(\mu_3\text{-}Se)(CO)_7(PH_3)_2]$

	20	$[(CO)_5W(\mu_4\text{-}Se)Ru_3(\mu_3\text{-}Se)(CO)_7(PH_3)_2]$
Ru(1)−Ru(2)	2.802(2)	2.907
Ru(2)−Ru(3)	2.8526(13)	2.902
W(1)−Se(1)	2.6852(10)	2.757
Ru(1)−Se(2)	2.5008(15)	2.607
Ru(1)−Se(1)	2.5215(13)	2.582
Ru(2)−Se(2)	2.5379(13)	2.608
Ru(2)−Se(1)	2.5390(12)	2.698
Ru(3)−Se(2)	2.4950(13)	2.618
Ru(3)−Se(1)	2.5203(15)	2.649
Ru(1)−Ru(2)−Ru(3)	87.01(6)	87
Ru(1)−Se(1)−Ru(3)	101.09(5)	100
Ru(1)−Se(2)−Ru(3)	102.38(5)	100
Se(1)−Ru(1)−Se(2)	77.13(5)	81
Se(1)−Ru(3)−Se(2)	78.25(5)	80

It consists of a $[Ru_3(\mu_3\text{-}Se)_2(CO)_7\{P(CH_2Ph)Ph_2\}_2]$ moiety linked to a $W(CO)_5$ unit through a coordinative interaction between a selenido ligand and the tungsten atoms [Se1−W1 = 2.685(1) Å]. The $[Ru_3(\mu_3\text{-}Se)_2]$ core unit, described as a square pyramid with two ruthenium and two selenium atoms at the base of the pyramid and a ruthenium atom at the apex, is similar to those of **10** and **2** with similar Ru−Ru [2.802(2) and 2.853(1) Å], and Ru−Se bond lengths [ranging from 2.495(1) to 2.539(1) Å]. The two diphenylbenzylphosphane ligands substitute two ruthenium atoms at the base of the pyramid in a *pseudo*-equatorial and *pseudo*-axial position [P1−Ru1 and P2−Ru3 bond lengths of 2.315(1) and 2.345(2) Å]. The quadruply bridging selenido ligand (μ_4-Se) acts as a six-electron donor, two of which serve to attain an 18-electron configuration at the tungsten

 © 2004 Wiley-VCH Verlag GmbH & Co. KGaA, Weinheim

atom. An analogous unsubstituted compound of formula $[Os_3(\mu_3\text{-}S)(\mu_4\text{-}S)(CO)_9W(CO)_5]$ was previously reported by Adams et al.[16] In contrast to this osmium derivative, the heptacoordinate Ru2 atom is bound to a carbonyl group essentially *trans* with respect to the (μ_4-Se) ligand [Se1−Ru2−C8 176.9(2)°]. In the parent Os compound the carbonyl group is almost *trans* to the (μ_3-S) ligand [S−Os−C 166.4(2)°] and in that case the better donor character of the μ_3-ligand with respect to the μ_4-ligand has been invoked. In the case of **20** the steric hindrance of the two phosphane ligands predominates over the electronic factors and forces the system to be disposed in the observed way.

As regards the mechanism for the production of **20**, we are far from a unique solution, but it could involve a labile intermediate of formula $[Ru_3(\mu_3\text{-}Se)(\mu_4\text{-}Se)(CO)_7\{P(CH_2Ph)Ph_2\}_2W(CO)_3(CH_3CN)_2]$, formed from $[W(CO)_3(MeCN)_3]$ by loss of one acetonitrile ligand. Subsequently, two MeCN ligands could be substituted by two carbonyls. On the other hand, if the labile intermediate loses two acetonitrile ligands, the anchored $W(CO)_3$ fragment can approach the Ru_2Se_2 basal plane of the pyramid (i.e. the cavity of the *nido* polyhedron), leading to the previously described *closo* clusters. These reaction sequences are depicted in Scheme 4. In the case of $PPh_2(CH_2Ph)$, the corresponding dimetallic *closo* cluster has not been obtained, probably because of the steric hindrance of the benzyl group, which does not facilitate the approach of the $W(CO)_3$ moiety.

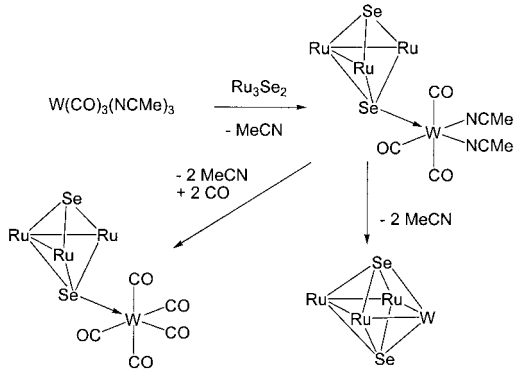

Scheme 4. (Carbonyl groups omitted)

DFT calculations on the $[(CO)_5W(\mu_4\text{-}Se)Ru_3(\mu_3\text{-}Se)(CO)_7(PH_3)_2]$ model (assuming C_1 symmetry) lead to the optimised bond lengths and angles given in Table 3. They are consistent with those computed for $[WRu_3(\mu_4\text{-}Se)_2(\mu\text{-}CO)_4(CO)_6(PH_3)_2]$. It is noteworthy that the computed total energy of $[(CO)_5W(\mu_4\text{-}Se)Ru_3(\mu_3\text{-}Se)(CO)_7(PH_3)_2]$ is 1.1 eV lower than that of $[WRu_3(\mu_4\text{-}Se)_2(\mu\text{-}CO)_4(CO)_6(PH_3)_2]$ + 2CO. Although this value has to be considered as a rough approximation of the enthalpy of the reaction $[(CO)_5W(\mu_4\text{-}Se)Ru_3(\mu_3\text{-}Se)(CO)_7(PH_3)_2] \rightarrow [WRu_3(\mu_4\text{-}Se)_2(\mu\text{-}CO)_4(CO)_6(PH_3)_2]$ + 2CO it is indicative of thermal stability of **20**. However, the adduct compounds are labile and prone to decompose over silica gel in the air in such a way that they cannot be obtained by TLC as mentioned above. Only in the case of $P(CH_2Ph)Ph_2$ were we able to isolate and characterise the corresponding adduct **20**. Moreover, the yield of these adducts, which does not exceed 40%, is influenced by the scarcity of free CO, which could be the limiting factor in the process of formation of the adduct molecules. Adams et al. observed that these adduct species can be prepared by UV irradiation of solutions of $[Os_3(CO)_9(\mu_3\text{-}S)_2]$ and $W(CO)_6$, giving $[Os_3(CO)_9(\mu_3\text{-}S)(\mu_4\text{-}S)\{W(CO)_5\}]$ in 70% yield.[16] This could be a more convenient route to obtain higher yields of similar adducts.

Experimental Section

General Procedures: The starting reagents $[Ru_3(CO)_{12}]$, elemental selenium, phosphanes and Me_3NO are pure commercial products (Aldrich and Fluka) and were used as received. The solvents (C. Erba) were dried and distilled by standard techniques before use. $[Ru_3Se_2(CO)_7(PPh_3)_2]$[2] $M(CO)_3(CH_3CN)_3$ (M = W or Mo)[17] and clusters **8**−**14**[18] were prepared according to literature procedures. All manipulations (prior to the TLC separations) were carried out under dry nitrogen by means of standard Schlenk-tube techniques. Elemental (C, H) analyses were performed with a Carlo Erba EA 1108 automated analyzer. IR spectra (KBr discs or CH_2Cl_2 solutions) were recorded on a Nicolet "Nexus" spectrometer. ^1H (300 MHz) and ^{31}P (162.0 MHz, 85% H_3PO_4 as external reference) NMR spectra ($CDCl_3$ solutions) were recorded on Bruker instruments, AC 300 (^1H) and AMX 400 (^{31}P). NICI Mass spectra (Negative-Ion Chemical Impact) were recorded on a Fennigan MAT SSQ710; *m*/*z* values are reported as the average of the isotopic distributions.

Synthesis of the Phosphane Selenides: The phosphane selenides were obtained as white powders by reacting the corresponding phosphanes with elemental selenium (in excess) in toluene at 90 °C with vigorous stirring. The solutions were dried in vacuo and the residues were extracted with dichloromethane. All products gave satisfactory elemental analysis. Their purity was checked by ^1H NMR spectroscopy.

$Ph_2(PhCH_2)PSe$: Yield 95%. FT-IR (KBr) $\nu_{(P=Se)}$: 526s cm^{-1}. ^{31}P NMR ($CDCl_3$): δ = 34.3 ppm (s, with ^{77}Se satellites, $^1J_{P,Se}$ = 715 Hz).

$Ph_2(MeO)PSe$: Yield 93%. FT-IR (KBr) $\nu_{(P=Se)}$: 520s cm^{-1}. ^{31}P NMR ($CDCl_3$): δ = 88.0 ppm (s, with ^{77}Se satellites, $^1J_{P,Se}$ = 715 Hz).

(p-MeO-$C_6H_4)_3PSe$: Yield 97%. FT-IR (KBr) $\nu_{(P=Se)}$: 526s cm^{-1}. ^{31}P NMR ($CDCl_3$): δ = 31.5 ppm (s, with ^{77}Se satellites, $^1J_{P,Se}$ = 718 Hz).

$Ph_2(Me)PSe$: Yield 97%. FT-IR (KBr) $\nu_{(P=Se)}$: 528s cm^{-1}. ^{31}P NMR ($CDCl_3$): δ = 23.3 ppm (s, with ^{77}Se satellites, $^1J_{P,Se}$ = 731 Hz).

Reaction of Phosphane Selenides with $[Ru_3(CO)_{12}]$

Reaction with $Ph_2(MeO)PSe$: $[Ru_3(CO)_{12}]$ (300 mg, 0.47 mmol) was reacted in a 1:2 ratio with $Ph_2(MeO)PSe$ (277 mg, 0.94 mmol) in toluene at 70 °C for 1.5 h in the presence of Me_3NO (35 mg, 0.47 mmol) until the solution turned deep reddish brown. The solvents were evaporated to dryness and the residue was redissolved in a small amount of dichloromethane. TLC separation on silica, using a 2:1 dichloromethane/hexane as eluent, yielded three bands

 © 2004 Wiley-VCH Verlag GmbH & Co. KGaA, Weinheim

together with some minor decomposition. The three bands contained clusters $[Ru_3(\mu_3\text{-}Se)_2(CO)_8\{P(OMe)Ph_2\}]$ (orange, **1**; yield 15%), $[Ru_3(\mu_3\text{-}Se)_2(CO)_7\{P(OMe)Ph_2\}_2]$ (red, **2**; yield 30%) and $[Ru_4(\mu_4\text{-}Se)_2(\mu\text{-}CO)_2(CO)_7\{P(OMe)Ph_2\}_2]$ (deep red, **3**; yield 25%) in order of elution.

1: FT-IR (CH_2Cl_2): ν(CO): 2077s, 2045vs, 2027s, 2005s, 1984sh cm^{-1}. ^1H NMR ($CDCl_3$, 298 K): δ = 3.60 (d, $^2J_{H,P}$ = 14.1 Hz, 3 H, CH_3), 7.4−7.9 (m, 10 H, 2Ph) ppm. $^{31}P\{^1H\}$ NMR ($CDCl_3$, 298 K): δ = 140.0 (br. s) ppm. $C_{21}H_{13}O_9PRu_3Se_2$: calcd. C 28.0, H 1.46; found C 27.9, H 1.41.

2: FT-IR (CH_2Cl_2): ν(CO): 2047s, 2015vs, 1973s, 1954sh cm^{-1}. ^1H NMR ($CDCl_3$, 298 K): δ = 3.42 (d), 3.59 (d) and 3.61 (d, $^2J_{H,P}$ = 12.1 Hz, 6 H, CH_3), 7.85−7.20 (m, 20 H, 4Ph) ppm. $^{31}P\{^1H\}$ NMR ($CDCl_3$, 298 K): δ = 146 (s), 141 (s) (isomer B); 139 (br), 137 (br) (isomer A) ppm. $C_{33}H_{26}O_9P_2Ru_3Se_2$: calcd. C 36.4, H 2.41; found C 36.3, H 2.41.

3: FT-IR (CH_2Cl_2): ν(CO): 2041w, 2012vs, 2000s, 1966m, 1844w, 1807w cm^{-1}. ^1H NMR ($CDCl_3$, 298 K): δ = 3.58 and 3.66 (d, $^2J_{H,P}$ = 13.2 Hz, 6 H, CH_3), 7.26−7.64 (m, 20 H, 4Ph). $^{31}P\{^1H\}$ NMR ($CDCl_3$, 298 K): δ = 139 (s) ppm. $C_{35}H_{26}O_{11}P_2Ru_4Se_2$: calcd. C 33.8, H 2.11; found C 33.5, H 2.12.

Reaction with $Ph_2(Me)PSe$: $[Ru_3(CO)_{12}]$ (300 mg, 0.47 mmol) was reacted in a 1:2 ratio with $Ph_2(Me)PSe$ (260 mg, 0.94 mmol) in toluene at 70 °C for 2 h in the presence of Me_3NO (35 mg, 0.47 mmol) until the solution turned deep reddish brown. The solvents were evaporated to dryness and the residue was redissolved in a small amount of dichloromethane. TLC separation on silica gel, using 3:1 dichloromethane/hexane as eluent, yielded four bands: an orange, a red, a brown and a deep red one in order of elution. The four bands contained compounds $[Ru_3(\mu_3\text{-}Se)_2(CO)_8\{P(Me)Ph_2\}]$ (**4**; yield 15%), $[Ru_3(\mu_3\text{-}Se)_2(CO)_7\{P(Me)Ph_2\}_2]$ (**5**; yield 30%), $[Ru_4(\mu_4\text{-}Se)_2(\mu\text{-}CO)_2(CO)_7\{P(Me)Ph_2\}_2]$ (**6**; yield 10%) and $[Ru_4(\mu_4\text{-}Se)_2(\mu\text{-}CO)(CO)_7\{P(Me)Ph_2\}_3]$ (**7**; yield 25%).

4: FT-IR (CH_2Cl_2): ν(CO): 2077s, 2043vs, 2025s, 2066s, 1975m cm^{-1}. ^1H NMR ($CDCl_3$, 298 K): δ = 2.49 (br., 3 H, CH_3), 7.4−7.8 (m, 10 H, 2Ph) ppm. $^{31}P\{^1H\}$ NMR ($CDCl_3$, 298 K): δ = 37.2 (s) ppm. $C_{21}H_{13}O_8PRu_3Se_2$: calcd. C 28.6, H 1.48; found C 28.6, H 1.47.

5: FT-IR (CH_2Cl_2): ν(CO): 2045vs, 2009vs, 1967m, 1946w cm^{-1}. ^1H NMR ($CDCl_3$, 298 K): δ = 2.20 (br), 2.32 (d) and 2.52 (d, $^2J_{H,P}$ = 9.3 Hz, 6 H, CH_3), 7.3−7.7 (m, 20 H, 4Ph) ppm. $^{31}P\{^1H\}$ NMR ($CDCl_3$, 298 K): δ = 52 (s), 43 (s) (isomer B); 47 (br), 40 (br) (isomer A) ppm. $C_{33}H_{26}O_7P_2Ru_3Se_2$: calcd. C 37.6, H 2.48; found C 37.3, H 2.41.

6: FT-IR (CH_2Cl_2): ν(CO): 2056w, 2038w, 2010vs, 1992sh, 1961sh, 1839w, 1800w cm^{-1}. ^1H NMR ($CDCl_3$, 298 K): δ = 2.07 (d) and 2.12 (d, $^2J_{H,P}$ = 9 Hz, 6 H, CH_3), 7.3−7.6 (m, 20 H, 4Ph) ppm. $^{31}P\{^1H\}$ NMR ($CDCl_3$, 298 K): δ = 35.15 (s), 25.1 (s) (3:2). $C_{35}H_{26}O_9P_2Ru_4Se_2$: calcd. C 34.7, H 2.16; found C 34.5, H 2.14.

7: FT-IR (CH_2Cl_2): ν(CO): 2017s, 1995vs, 1984s, 1955m, 1789w cm^{-1}. ^1H NMR ($CDCl_3$, 298 K): δ = 2.02 (d) and 2.30 (d, $^2J_{H,P}$ = 8.4 Hz, 9 H, CH_3), 7.2−7.9 (m, 30 H, 6Ph) ppm. $^{31}P\{^1H\}$ NMR ($CDCl_3$, 298 K): δ = 23.3 (s), 30.0 (s) (2:1). $C_{47}H_{39}O_8P_3Ru_4Se_2$: calcd. C 40.8, H 2.84; found C 40.3, H 2.81.

Synthesis of $[WRu_3(\mu_4\text{-}Se)_2(\mu\text{-}CO)_4(CO)_6\{P(OMe)Ph_2\}_2]$ (15): Compound **2** (50 mg, 0.089 mmol) and $[W(CO)_3(CH_3CN)_3]$ (50 mg, 0.128 mmol) were stirred in dry CH_2Cl_2 for 1 h at room temperature under N_2. The resulting dark solution was evaporated to dryness and the residue was dissolved in CH_2Cl_2 (10 mL). The product (cluster **15**, yield 40%) was separated and purified by TLC on silica gel, using diethyl ether/light petroleum (b.p. 40−60 °C) (2:1) as eluent mixture. FT-IR (CH_2Cl_2): ν(CO): 2043m, 2007vs, 1987vs, 1894m, 1910m, 1831w, 1799w cm^{-1}. ^1H NMR ($CDCl_3$, 298 K): δ = 3.49 (d), 3.58 (d), 3.66 (d) and 3.73 (d, 6 H, $^3J_{H,P}$ = 13.5 Hz, CH_3) (8:4:1:1); 7.10−7.80 (m, 20 H, 4Ph) ppm. $^{31}P\{^1H\}$ NMR ($CDCl_3$, 298 K): δ = 130.0 (s) ppm. MS (NICI): *m/z* (%) = 1356 (95) $[Ru_3W(\mu_4\text{-}Se)_2(CO)_{10}\{P(OMe)Ph_2\}_2]^+$, 1300 (100) $[Ru_3W(\mu_4\text{-}Se)_2(CO)_8\{P(OMe)Ph_2\}_2]^+$, 1272 (42) $[Ru_3W(\mu_4\text{-}Se)_2(CO)_7\{P(OMe)Ph_2\}_2]^+$, 1244 (15) $[Ru_3W(\mu_4\text{-}Se)_2(CO)_6\{P(OMe)Ph_2\}_2]^+$, 1216 (21) $[Ru_3W(\mu_4\text{-}Se)_2(CO)_5\{P(OMe)Ph_2\}_2]^+$, 1188 (16) $[Ru_3W(\mu_4\text{-}Se)_2(CO)_4\{P(OMe)Ph_2\}_2]^+$, 1160 (28) $[Ru_3W(\mu_4\text{-}Se)_2(CO)_3\{P(OMe)Ph_2\}_2]^+$, 1104 (25) $[Ru_3W(\mu_4\text{-}Se)_2(CO)\{P(OMe)Ph_2\}_2]^+$, 1076 (10) $[Ru_3W(\mu_4\text{-}Se)_2\{P(OMe)Ph_2\}_2]^+$. $C_{36}H_{26}O_{12}P_2Ru_3Se_2W$: calcd. C 31.9, H 1.93; found C 31.8, H 2.00.

Synthesis of $[WRu_3(\mu_4\text{-}Se)_2(\mu\text{-}CO)_4(CO)_6\{P(Me)Ph_2\}_2]$ (16): Compound **5** (80 mg, 0.076 mmol) and $[W(CO)_3(CH_3CN)_3]$ (60 mg, 0.153 mmol) were stirred in dry CH_2Cl_2 for 1.5 h at room temperature under N_2. The resulting dark solution was evaporated to dryness and the residue was dissolved in CH_2Cl_2 (10 mL). The product (cluster **16**, yield 45%) was separated and purified by TLC on silica gel, using diethyl ether/light petroleum (b.p. 40−60 °C) (2:1) as eluent mixture. FT-IR (CH_2Cl_2): ν(CO): 2043m, 2007vs, 1978vs, 1894m, 1910m, 1831w, 1800w cm^{-1}. ^1H NMR ($CDCl_3$, 298 K): δ = 2.08 (d), 2.03 (d) and 2.01 (d, $^2J_{H,P}$ = 8.5 Hz, 6 H CH_3) (1:3:9), 7.4−7.5 (m, 20 H, 4Ph) ppm. $^{31}P\{^1H\}$ NMR ($CDCl_3$, 298 K): no observable signals. MS (NICI): *m/z* (%) = 1324 (100) $[Ru_3W(\mu_4\text{-}Se)_2(CO)_{10}\{P(Me)Ph_2\}_2]^+$, 1296 (17) $[Ru_3W(\mu_4\text{-}Se)_2(CO)_9\{P(Me)Ph_2\}_2]^+$, 1268 (38) $[Ru_3W(\mu_4\text{-}Se)_2(CO)_8\{P(Me)Ph_2\}_2]^+$, 1240 (35) $[Ru_3W(\mu_4\text{-}Se)_2(CO)_7\{P(Me)Ph_2\}_2]^+$, 1212 (32) $[Ru_3W(\mu_4\text{-}Se)_2(CO)_6\{P(Me)Ph_2\}_2]^+$, 1184 (31) $[Ru_3W(\mu_4\text{-}Se)_2(CO)_5\{P(Me)Ph_2\}_2]^+$, 1156 (33) $[Ru_3W(\mu_4\text{-}Se)_2(CO)_4\{P(Me)Ph_2\}_2]^+$, 1128 (28) $[Ru_3W(\mu_4\text{-}Se)_2(CO)_3\{P(Me)Ph_2\}_2]^+$, 1100 (20) $[Ru_3W(\mu_4\text{-}Se)_2(CO)_2\{P(Me)Ph_2\}_2]^+$, 1072 (25) $[Ru_3W(\mu_4\text{-}Se)_2(CO\{P(Me)Ph_2\}_2]^+$, 1044 (27) $[Ru_3W(\mu_4\text{-}Se)_2\{P(Me)Ph_2\}_2]^+$. $C_{36}H_{26}O_{10}P_2Ru_3Se_2W$: calcd. C 32.7, H 1.98; found C 32.8, H 2.00.

Synthesis of $[WRu_3(\mu_4\text{-}Se)_2(\mu\text{-}CO)_4(CO)_6\{P(p\text{-}MeO\text{-}C_6H_4)_3\}_2]$ (17): Compound **13** (100 mg, 0.073 mmol) and $[W(CO)_3(CH_3CN)_3]$ (57.3 mg, 0.147 mmol) were stirred in dry CH_2Cl_2 for 1.5 h at room temperature under N_2. The resulting dark solution was evaporated to dryness and the residue was dissolved in CH_2Cl_2 (10 mL). The product (cluster **17**, yield 45%) was separated and purified by TLC on silica gel, using diethyl ether/light petroleum (b.p. 40−60 °C) (2:1) as eluent mixture. FT-IR (CH_2Cl_2): ν(CO): 2039m, 2005vs, 1976s, 1888m, 1831w, 1800w cm^{-1}. ^1H NMR ($CDCl_3$, 298 K): δ = 3.87 (s, 18 H, CH_3), 6.92 (dd, $^3J_{H_\alpha,H_\beta}$ = 9, $^4J_{H_\beta,^{31}P}$ = 1.8 Hz, 12 H, H_βAr), 7.29 (dd, $^3J_{H_\alpha,H_\beta}$ = 9, $^3J_{H_\alpha,^{31}P)}$ = 10.8 Hz, 12 H, H_αAr) ppm. $^{31}P\{^1H\}$ NMR ($CDCl_3$, 298 K): δ = 39.0 (s) ppm. MS (NICI): *m/z* (%) = 1361 (95) $[Ru_3W(\mu_4\text{-}Se)_2(CO)_{10}\{P(p\text{-}MeO\text{-}C_6H_4)_3\}_2]^-$, 1574 (100) $[Ru_3W(\mu_4\text{-}Se)_2(CO)_8\{P(p\text{-}MeO\text{-}C_6H_4)_3\}_2]^+$, 1546 (86) $[Ru_3W(\mu_4\text{-}Se)_2(CO)_7\{P(p\text{-}MeO\text{-}C_6H_4)_3\}_2]^+$, 1518 (72) $[Ru_3W(\mu_4\text{-}Se)_2(CO)_6\{P(p\text{-}MeO\text{-}C_6H_4)_3\}_2]^+$, 1490 (63) $[Ru_3W(\mu_4\text{-}Se)_2(CO)_5\{P(p\text{-}MeO\text{-}C_6H_4)_3\}_2]^+$, 1462 (62) $[Ru_3W(\mu_4\text{-}Se)_2(CO)_4\{P(p\text{-}MeO\text{-}C_6H_4)_3\}_2]^+$, 1432 (43) $[Ru_3W(\mu_4\text{-}Se)_2(CO)_2\{P(p\text{-}MeO\text{-}C_6H_4)_3\}_2]^+$, 1410 (32) $[Ru_3W(\mu_4\text{-}Se)_2(CO\{P(p\text{-}MeO\text{-}C_6H_4)_3\}_2]^+$, 1382 (24) $[Ru_3W(\mu_4\text{-}Se)_2\{P(p\text{-}MeO\text{-}C_6H_4)_3\}_2]^+$. $C_{52}H_{42}O_{16}P_2Ru_3Se_2W$: calcd. C 38.4, H 2.60; found C 38.0, H 2.60.

Mass Spectroscopic data of $[MRu_3(\mu_4\text{-}Se)_2(\mu\text{-}CO)_4(CO)_6(PPh_3)_2]$ [M = W (18), Mo (19)]: The synthesis of the *closo* clusters $[WRu_3(\mu_4\text{-}Se)_2(\mu\text{-}CO)_4(CO)_6(PPh_3)_2]$ (**18**) and $[MoRu_3(\mu_4\text{-}Se)_2(\mu\text{-}CO)_4(CO)_6(PPh_3)_2]$ (**19**) has been reported previously.[12]

18: MS (NICI): *m/z* (%) = 1449 (100) $[Ru_3W(\mu_4\text{-}Se)_2(CO)_{10}\{PPh_3\}_2]^+$, 1421 (20) $[Ru_3W(\mu_4\text{-}Se)_2(CO)_9\{PPh_3\}_2]^+$,

 © 2004 Wiley-VCH Verlag GmbH & Co. KGaA, Weinheim

1393 (33) $[Ru_3W(\mu_4\text{-}Se)_2(CO)_8\{PPh_3\}_2]^+$, 1365 (37) $[Ru_3W(\mu_4\text{-}Se)_2(CO)_7\{PPh_3\}_2]^+$, 1337 (31) $[Ru_3W(\mu_4\text{-}Se)_2(CO)_6\{PPh_3\}_2]^+$, 1309 (32) $[Ru_3W(\mu_4\text{-}Se)_2(CO)_5\{PPh_3\}_2]^+$, 1281 (35) $[Ru_3W(\mu_4\text{-}Se)_2(CO)_4\{PPh_3\}_2]^+$, 1253 (22) $[Ru_3W(\mu_4\text{-}Se)_2(CO)_3\{PPh_3\}_2]^+$, 1225 (25) $[Ru_3W(\mu_4\text{-}Se)_2(CO)_2\{PPh_3\}_2]^+$, 1197 (27) $[Ru_3W(\mu_4\text{-}Se)_2(CO)\{PPh_3\}_2]^+$, 1169 (21) $[Ru_3W(\mu_4\text{-}Se)_2\{PPh_3\}_2]^+$. $C_{46}H_{30}O_{10}P_2Ru_3Se_2W$: calcd. C 38.1, H 2.07; found C 38.2, H 2.10.

19: MS (NICI): *m/z* (%) = 1361 (100) $[Ru_3Mo(\mu_4\text{-}Se)_2(CO)_{10}\{PPh_3\}_2]^+$, 1333 (18) $[Ru_3Mo(\mu_4\text{-}Se)_2(CO)_9\{PPh_3\}_2]^+$, 1305 (43) $[Ru_3Mo(\mu_4\text{-}Se)_2(CO)_8\{PPh_3\}_2]^+$, 1277 (41) $[Ru_3Mo(\mu_4\text{-}Se)_2(CO)_7\{PPh_3\}_2]^+$, 1249 (37) $[Ru_3Mo(\mu_4\text{-}Se)_2(CO)_6\{PPh_3\}_2]^+$, 1221 (33) $[Ru_3Mo(\mu_4\text{-}Se)_2(CO)_5\{PPh_3\}_2]^+$, 1193 (22) $[Ru_3Mo(\mu_4\text{-}Se)_2(CO)_4\{PPh_3\}_2]^+$, 1165 (34) $[Ru_3Mo(\mu_4\text{-}Se)_2(CO)_3\{PPh_3\}_2]^+$, 1137 (18) $[Ru_3Mo(\mu_4\text{-}Se)_2(CO)_2\{PPh_3\}_2]^+$, 1109 (31) $[Ru_3Mo(\mu_4\text{-}Se)_2(CO)\{PPh_3\}_2]^+$, 1081 (23) $[Ru_3Mo(\mu_4\text{-}Se)_2\{PPh_3\}_2]^+$. $C_{46}H_{30}MoO_{10}P_2Ru_3Se_2$: calcd. C 40.5, H 2.20; found C 40.6, H 2.22.

Synthesis of the Adduct $[(CO)_5W(\mu_4\text{-}Se)Ru_3(\mu_3\text{-}Se)(CO)_7\{P(CH_2Ph)Ph_2\}_2]$ (20): Compound **10** (100 mg, 0.083 mmol) and $[W(CO)_3(CH_3CN)_3]$ (65 mg, 0.166 mmol) were stirred in dry CH_2Cl_2 for 1 h at room temperature under N_2. The resulting dark solution was evaporated to dryness and the residue was dissolved in CH_2Cl_2 (10 mL). The product (cluster **20**, yield 40%) was separated and purified by TLC on silica gel, using dichloromethane/light petroleum (b.p. 40−60 °C) (1:1) as eluent. FT-IR (CH_2Cl_2): ν(CO): 2071m, 2050vs, 2022vs, 1987m, 1972m, 1931s, 1895w cm^{-1}. ^1H NMR: δ = 3.81 (br., 4 H, CH_2 Bz), 7.7−6.5 (m, 24 H, Ph) ppm. $^{31}P\{^1H\}$ NMR: δ = 43.5 (br.) ppm. $C_{50}H_{34}O_{12}P_2Ru_3Se_2W$: calcd. C 39.2, H 2.24; found C 39.1, H 2.23.

Crystal Structure Determination of 2, 10, 15, 17, 18, 19 and 20·2CH$_2$Cl$_2$: Suitable crystals for the X-ray analysis for all complexes were obtained by layering methanol on dichloromethane solutions. The intensity data, at room temperature, of **2**, **10** and **20·2CH$_2$Cl$_2$** were collected on a Bruker AXS Smart 1000 single crystal diffractometer (equipped with an area detector using a graphite monochromated Mo-K_α radiation, λ = 0.71073 Å), those of **15**, **17**, and **18** on a Philips PW 1100 single-crystal diffractometer (graphite monochromated Mo-K_α radiation, λ = 0.71073 Å) and those of **19** on an Enraf Nonius CAD 4 single-crystal diffractometer (graphite monochromated Cu-K_α radiation, λ = 1.54184 Å). Crystallographic and experimental details for the structures are summarised in Table 4. An empirical correction for absorption was made for **15**, **17**, **18** and **19** [maximum and minimum value for the transmission coefficient was 1.000 and 0.7262 (**15**), 1.000 and 0.6872 (**17**), 1.000 and 0.5947 (**18**) and 1.000 and 0.460 (**19**)].[19a,19b] For complexes **2**, **10** and **20·2CH$_2$Cl$_2$** [maximum and minimum effective transmission value was 1.000 and 1.000 (**2**), 1.000 and 0.8532 (**10**) and 1.000 and 0.5104 (**20·2CH$_2$Cl$_2$**)] the raw frame data were processed using SAINT and SADABS to yield the reflection data file and the Bruker software was used for the absorption correction.[19c−19e] The structures were solved by Patterson and Fourier methods and refined by full-matrix least-squares procedures (based on F_o^2) (SHELX-97)[20] first with isotropic thermal parameters and then with anisotropic thermal parameters in the last cycles of refinement for all the non-hydrogen atoms. In the crystals of **20** dichloromethane molecules of solvation were found. The hydrogen atoms were introduced into the geometrically calculated positions and refined as riding on the corresponding parent atoms.

In the crystals of **17**, **18** and **19** a disorder exists which involves the mutually opposite Ru and W atoms of the *closo* core of the cluster, resulting in a disordered $[Ru_3M(\mu_4\text{-}Se)_2]$ core, distributed in two positions with the same occupancy factor, instead of the centrosymmetric $[M_2Ru_2(\mu_4\text{-}Se)_2]$ core.

CCDC-208915 (**2**), -208916 (**10**), -208917 (**15**), -208920 (**17**), -208918 (**18**), -208919 (**19**) and -208921 (**20·2CH$_2$Cl$_2$**) contain the supplementary crystallographic data for this paper. These data can be obtained free of charge at www.ccdc.cam.ac.uk/conts/retrieving.html [or from the Cambridge Crystallographic Data Centre, 12, Union Road, Cambridge CB2 1EZ, UK; Fax: (internat.) +44-1223/336-033; E-mail: deposit@ccdc.cam.ac.uk].

Table 4. Crystal data and structure refinement for **2**, **10**, **15**, **17**, **18**, **19** and **20·2CH$_2$Cl$_2$**

	2	**10**	**15**	**17**	**18**	**19**	**20·2CH$_2$Cl$_2$**
Formula	$C_{33}H_{26}O_9P_2Ru_3Se_2$	$C_{45}H_{34}O_7P_2Ru_3Se_2$	$C_{36}H_{26}O_{12}P_2Ru_3Se_2W$	$C_{52}H_{42}O_{16}P_2Ru_3Se_2W$	$C_{46}H_{30}O_{10}P_2Ru_3Se_2W$	$C_{46}H_{30}MoO_{10}P_2Ru_3Se_2$	$C_{52}H_{38}Cl_4O_{12}P_2Ru_3Se_2W$
Mol. wt.	1089.61	1209.79	1357.49	1629.78	1449.62	1361.71	1703.54
Crystal system	triclinic	triclinic	monoclinic	monoclinic	triclinic	triclinic	triclinic
Space group	$P\bar{1}$	$P\bar{1}$	$P2_1/n$	$P2_1/c$	$P\bar{1}$	$P\bar{1}$	$P\bar{1}$
a (Å)	8.792(3)	11.804(5)	14.533(4)	12.054(3)	10.102(5)	10.229(5)	13.819(3)
b (Å)	10.701(4)	14.109(5)	29.729(5)	15.643(5)	11.156(5)	11.147(5)	18.333(5)
c (Å)	21.163(5)	14.885(5)	9.572(3)	14.458(4)	11.205(5)	11.151(5)	13.259(3)
α (°)	79.90(5)	65.23(5)	90	90	95.86(2)	95.56(2)	77.36(5)
β (°)	85.36(5)	77.34(5)	98.76(5)	94.29(5)	97.33(2)	97.55(2)	66.38(5)
γ (°)	71.63(5)	72.54(5)	90	90	110.16(2)	110.29(2)	80.49(5)
V (Å^3)	1860(1)	2135(1)	4087(1)	2719(1)	1161(1)	1168(1)	2992(1)
Z	2	2	4	2	1	1	2
D_{calcd} (g cm^{-3})	1.946	1.882	2.206	1.991	2.073	1.935	1.891
F(000)	1052	1180	2568	1572	690	658	1636
Crystal size	0.11 × 0.12 × 0.20	0.18 × 0.22 × 0.25	0.15 × 0.21 × 0.19	0.12 × 0.15 × 0.11	0.14 × 0.31 × 0.15	0.12 × 0.21 × 0.09	0.22 × 0.11 × 0.20
μ, cm^{-1}	32.96	28.79	58.11	43.92	51.18	127.59	41.64
Reflns. collected	19813	8705	7629	5945	5606	4393	43030
Reflns. unique	9941 (R_{int} = 0.0545)	7003 (R_{int} = 0.0527)	7183 (R_{int} = 0.0456)	5945 (R_{int} = 0.0245)	5606 (R_{int} = 0.000)	4393 (R_{int} = 0.000)	16317 (R_{int} = 0.0690)
Obs. reflns. [$I > 2\sigma(I)$]	5117	3367	5539	3914	4072	2991	9452
R indices[a]	*R*1 = 0.0436	*R*1 = 0.0416	*R*1 = 0.0480	*R*1 = 0.0372	*R*1 = 0.0588	*R*1 = 0.0634	*R*1 = 0.0395
[$I > 2\sigma(I)$]	*wR*2 = 0.0754	*wR*2 = 0.0684	*wR*2 = 0.1229	*wR*2 = 0.0943	*wR*2 = 0.1248	*wR*2 = 0.1718	*wR*2 = 0.0882
R indices (all data)	*R*1 = 0.1152	*R*1 = 0.1129	*R*1 = 0.0671	*R*1 = 0.0719	*R*1 = 0.0847	*R*1 = 0.0936	*R*1 = 0.0946
	*wR*2 = 0.0927	*wR*2 = 0.0823	*wR*2 = 0.1386	*wR*2 = 0.1145	*wR*2 = 0.1405	*wR*2 = 0.2210	*wR*2 = 0.1034

[a] $R1 = \Sigma||F_o| - |F_c||/\Sigma|F_o|$; $wR2 = \{\Sigma[w(F_o^2 - F_c^2)^2]/\Sigma[w(F_o^2)^2]\}^{1/2}$.

 © 2004 Wiley-VCH Verlag GmbH & Co. KGaA, Weinheim

Computational Details: Density functional theory (DFT) calculations were carried out using the Amsterdam density functional (ADF) program[21] developed by Baerends and co-workers.[22] The Vosko−Wilk−Nusair parameterization[23] was used for the local density approximation (LDA) with gradient correction for exchange (Becke88)[24] and correlation (Perdew86).[25] Relativistic corrections were added using the ZORA (Zeroth Order Regular Approximation) scalar Hamiltonian.[26] The atom electronic configurations were described by a triple-ξ Slater-type orbital (STO) basis set for H 1s, C, O 2s and 2p, P 3s and 3p and Se 4s and 4p augmented with a 3d single-ξ polarisation function for C, O, P, with a 2p single-ξ polarisation function for H and 4d single-ξ polarisation function for Se. A triple-ξ STO basis set was used for Mo, Ru 4d and 5s and for W 5d and 6s augmented with a single-ξ 5p for Mo and Ru and 6p for W. A double-ξ STO basis set was used for W 5s and 5p. A frozen-core approximation was used to treat the core electrons of C, O, P, Se, Mo, Ru and W.

Acknowledgments

Financial support from Ministero dell'Università e della Ricerca Scientifica e Tecnologica (Cofin 2000) is gratefully acknowledged. The facilities of the Centro Interfacoltà di Misure "G. Casnati" (Università di Parma) were used to record the NMR and mass spectra. Computing facilities were provided by the Centre de Ressources Informatiques (CRI) of Rennes and the Institut de Développement et de Ressources en Informatique Scientifique du Centre National de la Recherche Scientifique (IDRIS-CNRS).

[1] D. Cauzzi, C. Graiff, G. Predieri, A. Tiripicchio, in *Metal Clusters in Chemistry* (Eds.: P. Braunstein, L. Oro, P. Raithby), vol. 1, VCH, Weinheim **1999**, 193.
[2] P. Baistrocchi, D. Cauzzi, M. Lanfranchi, G. Predieri, A. Tiripicchio, M. Tiripicchio Camellini, *Inorg. Chim. Acta* **1995**, *235*, 173.
[3] D. Cauzzi, C. Graiff, C. Massera, G. Predieri, A. Tiripicchio, D. Acquotti, *J. Chem. Soc., Dalton Trans.* **1999**, 3515.
[4] D. Cauzzi, C. Graiff, M. Lanfranchi, G. Predieri, A. Tiripicchio, *J. Chem. Soc., Dalton Trans.* **1995**, 2321.
[5] D. Cauzzi, C. Graiff, C. Massera, G. Predieri, A. Tiripicchio, *Inorg. Chim. Acta* **2000**, *300−302*, 471.
[6] D. Cauzzi, C. Graiff, C. Massera, G. Predieri, A. Tiripicchio, *J. Cluster Sci.* **2001**, *12*, 259.
[7] D. Cauzzi, C. Graiff, C. Massera, G. Predieri, A. Tiripicchio, *Eur. J. Inorg. Chem.* **2001**, 721.
[8] P. Braunstein, J. Rosé, Heterometallic Clusters in Catalysis, in *Metal Clusters in Chemistry* (Eds.: P. Braunstein, L. A. Oro, P. R. Raithby), VCH, Weinheim, **1999**, pp. 616−677.
[9] P. Braunstein, E. Sappa, A. Tiripicchio, *Coord. Chem. Rev.* **1985**, *65*, 219.
[10] [10a] C. Graiff, A. Ienco, C. Massera, C. Mealli, G. Predieri, A. Tiripicchio, F. Ugozzoli, *Inorg. Chim. Acta* **2002**, *330*, 95. [10b] P. Braunstein, C. Graiff, C. Massera, G. Predieri, J. Rosé, A. Tiripicchio, *Inorg. Chem.* **2002**, *41*, 1372.
[11] R. D. Adams, T. A. Wolfe, W. Wu, *Polyhedron* **1991**, *10*, 447.
[12] D. Cauzzi, C. Graiff, C. Massera, G. Mori, G. Predieri, A. Tiripicchio, *J. Chem. Soc., Dalton Trans.* **1998**, 321.
[13] D. Cauzzi, C. Graiff, M. Lanfranchi, G. Predieri, A. Tiripicchio, *J. Organomet. Chem.* **1997**, *536−537*, 497.
[14] D. Cauzzi, C. Graiff, G. Predieri, A. Tiripicchio, C. Vignali, *J. Chem. Soc., Dalton Trans.* **1999**, 237.
[15] M. T. Garland, J.-F. Halet, J.-Y. Saillard, *Inorg. Chem.* **2001**, *40*, 3342.
[16] R. D. Adams, I. T. Horvath, S. Wang, *Inorg. Chem.* **1985**, *24*, 1728.
[17] H. Werner, K. Dechelmann, U. Schoenenbergher, *Helv. Chim. Acta* **1970**, *53*, 2002.
[18] D. Belletti, D. Cauzzi, C. Graiff, A. Minarelli, R. Pattacini, G. Predieri, A. Tiripicchio, *J. Chem. Soc., Dalton Trans.* **2002**, 3160.
[19] [19a] N. Walker, D. Stuart, *Acta Crystallogr., Sect. A* **1983**, *39*, 158. [19b] F. Ugozzoli, *Comput. Chem.* **1987**, *11*, 109. [19c] *SMART Software Users Guide, Version 5.0*; Bruker Analytical X-ray Systems, Madison, WI, **1999**. [19d] *SAINT Software Users Guide*; Bruker Analytical X-ray Systems, Madison, WI, **1999**. [19e] G. M. Sheldrick, *SADABS*, Bruker Analytical X-ray Systems, Madison, WI, **1999**.
[20] [20a] G. M. Sheldrick, *SHELXL-93*, a program for crystal structure determination; University of Göttingen, Germany, **1993**. [20b] G. M. Sheldrick, *SHELXL-97, Program for crystal structure refinement*; University of Göttingen, Germany, **1997**.
[21] Amsterdam Density Functional program (ADF, 2000.02); Division of Theoretical Chemistry, Vrije Universiteit, De Boelelaan 1083, 1081 HV Amsterdam, The Netherlands; http://www.scm.com.
[22] [22a] E. J. Baerends, D. E. Ellis, P. Ros, *Chem. Phys.* **1973**, *2*, 41. [22b] E. J. Baerends, P. Ros, *Int. J. Quantum Chem.* **1978**, *S12*, 169. [22c] P. M. Boerringter, G. te Velde, E. J. Baerends, *Int. J. Quantum Chem.* **1988**, *33*, 87. [22d] G. te Velde, E. J. Baerends, *Int. J. Quantum Chem.* **1992**, *99*, 84.
[23] S. H. Vosko, L. Wilk, M. Nusair, *Can. J. Phys.* **1980**, *58*, 1200.
[24] [24a] A. D. Becke, *J. Chem. Phys.* **1986**, *84*, 4524. [24b] A. D. Becke, *Phys. Rev. A* **1988**, *38*, 3098.
[25] J. P. Perdew, *Phys. Rev. B* **1986**, *33*, 8822.
[26] [26a] E. van Lenthe, E. J. Baerends, J. G. Snijders, *J. Chem. Phys.* **1993**, *99*, 4597. [26b] E. van Lenthe, E. J. Baerends J. G. Snijders, *J. Chem. Phys.* **1994**, *101*, 9783. [26c] E. van Lenthe, R. van Leeuwen, E. J. Baerends, *Int. J. Quantum Chem.* **1996**, *57*, 281. [26d] E. van Lenthe, E. J. Baerends, J. G. Snijders, *J. Chem. Phys.* **1996**, *105*, 6505. [26e] E. van Lenthe, A. Ehlers, E. J. Baerends, *J. Chem. Phys.* **1999**, *110*, 8943.

Received June 21, 2003
Early View Article
Published Online February 3, 2004

Synthesis and Characterization of a Series of (Diphenyldipyrazolylmethane)copper Complexes as Possible Precursors to Type I Blue Copper Protein Active Site Models

Janet L. Shaw,[a] Thomas B. Cardon,[b] Gary A. Lorigan,[b] and Christopher J. Ziegler*[a]

Keywords: Copper / N ligands / Pyrazolylmethanes / Scorpionates

A series of copper complexes employing the neutral, bidentate, pyrazole-based ligand diphenyldipyrazolylmethane was synthesized and fully characterized by various techniques, including elemental analysis, EPR, and structure elucidation by single-crystal X-ray diffraction. The structures of compounds **3**–**8** reveal variable coordination environments at the copper center, ranging from square pyramidal to tetrahedral, depending on the steric bulk at the pyrazole periphery and on the identity of the counterion. Cyclic voltammetry data on these compounds show a positively shifted reduction potential as compared to those observed employing the negatively charged pyrazolylborates or β-diketiminates. These results indicate that these compounds may lead to (thiol)copper complexes that more accurately reproduce the reduction potentials observed during electron-transfer processes in blue copper proteins.
(© Wiley-VCH Verlag GmbH & Co. KGaA, 69451 Weinheim, Germany, 2004)

Introduction

Small models of the active sites of metalloenzymes remain important for understanding the structure−function relationships that exist between immediate metal-ion coordination environments and activities such as electron transport or dioxygen activation. Scorpionate ligands, such as the sterically hindered pyrazolylborates (see Figure 1), have been successful in mimicking many of the coordination geometries observed in the active sites of metalloproteins.[1−3] In addition to numerous zinc complexes,[4−6] pyrazolylborates have been employed for generating models of both type I blue copper proteins[7−10] and type III dicopper proteins,[11] such as plastocyanin and hemocyanin, respectively.[12−13] The ease of synthesis, the ability to add additional bulk to the pyrazole moieties, and the favorable multidentate binding mode are all responsible for the continued interest in pyrazolylborates as ligands for small model complexes. However, pyrazolyborates are negatively charged and can lead to complexes with higher oxidation states than those of the metal sites in native proteins.[14] Therefore, work continues toward the development of model complexes that can more accurately model the geometry and electronic structure of metal ions in proteins.

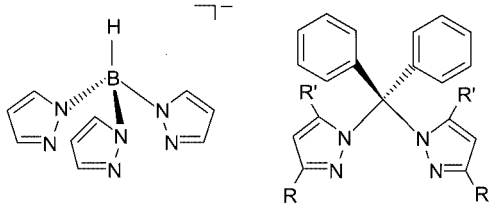

Figure 1. Schematic drawings of the ligands tris(pyrazolyl)borate (left) and diphenyldipyrazolylmethane (right) where R = R′ = H (**1**), R = R′ = CH_3 (**2**) and R = CH_3, R′ = H (**3**)

We have begun to explore the synthesis of active site models for copper proteins using the ligand diphenyldipyrazolylmethane, shown in Figure 1. Synthesized previously for use in polymerization catalysis,[15−16] this ligand is neutral and contains two pyrazole moieties available for bidentate metal-ion coordination. Like the pyrazolylborates, the pyrazole rings may be functionalized to incorporate more steric bulk around the copper center. This can be exploited to enforce desired geometries, inhibit the formation of bridging species, or promote low-coordination-number end products. Once synthesized, these compounds may be useful as starting materials in reactions with thiol or carboxylate-containing ligands to produce small model complexes of copper-enzyme active sites. Since these models incorporate a neutral ligand, we believe that they will exhibit redox potentials that more closely resemble those observed in nature

[a] University of Akron, Department of Chemistry, Akron, OH 44325, U.S.A.
Fax: (internat.) +1-330-972-7370
E-mail: ziegler@uakron.edu
[b] Miami University, Department of Chemistry, Oxford, OH 45056, U.S.A.
Supporting information for this article is available on the WWW under http://www.eurjic.org or from the author.

for type I blue copper proteins. Here we report our results on the synthesis and characterization of some (diphenyldipyrazolylmethane)copper complexes including crystal structures, cyclic voltammetry, and electron paramagnetic resonance spectra. We observe high potentials for the Cu^{II}/Cu^{I} redox couple, and increased steric bulk at the periphery of the pyrazole ring enforces lower coordination numbers.

Results and Discussion

The diphenyldipyrazolylmethanes (Figure 1, right) were synthesized using a modified procedure reported by Trofimenko that involves the generation of a pyrazolide ion and subsequent reaction with a dihalomethane.[17] These ligands have previously been employed in molybdenum[15] and palladium[16] complexes for use as catalysts. Figure 2 shows the crystal structures elucidated for ligands **1** and **2**. The C(1)−N(1,3) bond lengths in **1** are 1.490(4) Å and 1.484(4) Å, respectively, while in **2** they are 1.4753(17) Å and 1.4754(16) Å. The angle formed by N3−C1−N1 in **1** is 108.0(2)°, while in **2** it is 104.85(10)°. Based on their structural characteristics, these ligands should act as bidentate chelators. A comparison of the bond angles and lengths for these two ligands can be found in Table 1.

The copper complexes were synthesized by a reaction of either copper(II) nitrate or copper(I) chloride with the appropriate ligand in a number of organic solvents. In most cases the final product remained soluble throughout the reaction and was isolated by recrystallization from the appropriate solvent. All reactions produce X-ray quality crystals with little purification required.

A survey of the literature uncovers few examples of 1:1 complexes forming between dipyrazolyalkanes and either copper(I) or copper(II),[18−21] with the preference instead being 2:1 ligand-to-metal complexation.[22−23] Of these, less crystallographic information is available and the compounds have instead been characterized by other techniques such as IR spectroscopy, magnetic susceptibility, EPR, and ^{1}H NMR spectroscopy. The stoichiometry of the observed final products in the literature appears to depend on the starting copper salt (chloride salt vs. nitrate salt) and the degree of steric hindrance at the pyrazole periphery.

Unlike in the dipyrazolylalkane complexes, the majority of the compounds reported here form 1:1 complexes. The geometries of compounds **4**−**8** range from square pyramidal to tetrahedral, depending on the steric bulk at the pyrazole periphery and the counterion identity. Table 2 and Table 3 present relevant bond lengths and angles and the crystallographic data for compounds **4**−**8**, respectively. Compound **4** (see Figure 3) is best described as having a distorted square-pyramidal geometry. The copper(II) center is ligated by one bidentate **1** ligand, two nitrates and one water molecule in the axial position. The methanol employed in this reaction was not dried prior to use, and the

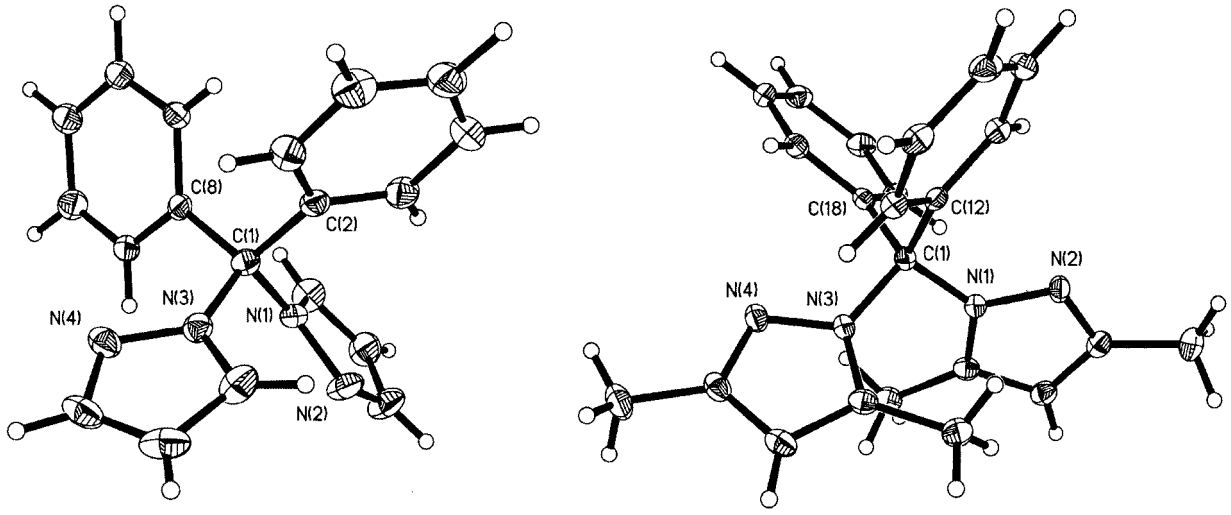

Figure 2. Structures of compounds **1** and **2** with thermal ellipsoids drawn at 50 % probability

Table 1. Comparison of bond lengths (Å) and angles (°) in **1** and **2**

	1		**2**	
C−N	C1−N1 1.490(4)	C1−N3 1.484(4)	C1−N1 1.4753(17)	C1−N3 1.4754(16)
C−C	C1−C2 1.535(4)	C1−C8 1.521(4)	C1−C12 1.5459(18)	C1−C18 1.5455(18)
N−C−N	N1−C1−N3 108.0(2)		N1−C1−N3 104.85(10)	
C−C−C	C2−C1−C8 113.3(3)		C12−C1−C18 107.26(10)	
N−C−C	N1−C1−C2 109.0(2)	N3−C1−C2 108.6(3)	N1−C1−C12 112.68(10)	N3−C1−C12 109.53(10)

 © 2004 Wiley-VCH Verlag GmbH & Co. KGaA, Weinheim

ligated water molecule may have come from residual water in the reaction solvent. The nitrates bind in a monodentate fashion with Cu−O distances of 1.971(3) Å and 1.975(3) Å. Within the literature, the modes of nitrate bonding can vary. For example, in the similar compound $Cu(bmpp)(NO_3)_2$ the two nitrates coordinate to the copper in an unsymmetrical bidentate fashion with Cu−O distances of 2.026(2) Å.[24] The Cu−O distance for the coordinating water molecule is 2.256(4) Å and the Cu−N bond lengths are both around 1.986(4) Å.

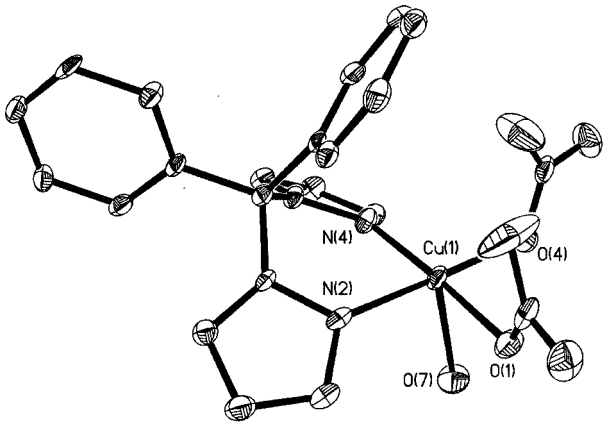

Figure 3. Structure of compound **4** with hydrogens omitted for clarity and thermal ellipsoids drawn at 50 % probability

Compound **5** (Figure 4) exhibits a similar geometry to complex **4**, but the water molecule in the coordination sphere is absent and one of the nitrates binds in a bidentate fashion with Cu−O distances of 1.9959(16) Å and 2.0110(19) Å. These distances are somewhat longer than those seen in **4** for the nitrates bound in a monodentate fashion. The lack of a coordinating water molecule may be due to the increase in steric bulk at the 3 position of the pyrazole ring in **5**. The coordination sphere of **5** is completed with a bidentate **3** ligand [Cu−N4 1.9344(18) and Cu−N2 1.9610(18)] and one monodentate nitrate group [Cu−O1 2.1361(17) Å]. Increasing the steric bulk at the pyrazole periphery in compound **5** alters the geometry from square pyramidal to pseudotetrahedral. In addition, the coordination geometry at the copper center is affected by the binding mode of the nitrate counterion. Whereas in compound **4** both nitrates ligate in a monodentate fashion, in compound **5** one nitrate is bidentate and the other is monodentate. This variable coordination mode of the nitrate counterion is not uncommon.

Unlike the Cu^{II} compounds, the Cu^{I} compound **7**, shown in Figure 5, forms a product with a 2:1 ratio of ligand to metal ion. The copper ion is in a distorted tetrahedral environment with two bidentate **1** ligands with Cu−N distances ranging from 2.007(3) Å to 2.045(3) Å and with N−Cu−N angles ranging from 91.38(10)° to 128.05(10)°. The intraligand N−Cu−N angles are closer to 90° while the interligand N−Cu−N angles are both near 120°. The bond lengths compare nicely to those reported for other 2:1 complexes $[Cu(bpp)_2](BF_4)$ (about 2.031 Å)[23] and $[CuL_2](ClO_4)$ (about 2.037 Å), where L = bis[2,2′-bis(2-imidazolyl)-biphenyl].[25] The bond angles in compound **7** show a slight compression along the intraligand axes. These bond angles compare well with those observed in the copper(II) complexes α- and β-$[Cu(bpp)_2](BF_4)_2$ (95.23−127.20° and 91.34−135.66°, respectively).[23] It is unclear as to why **7** exists as a 2:1 complex, but similar results have been observed in the literature: the ligand-to-metal ratio was found to depend not only on the steric bulk at the pyrazole periphery but also on the identity of the counterion.[21,26]

Table 2. Comparison of bond lengths (Å) and angles (°) in compounds **4**−**8**

	4	**5**	**6**	**7**	**8**
Cu−N	Cu−N2 1.985(4) Cu−N4 1.986(4)	Cu−N2 1.9610(18) Cu−N4 1.9344(18)	Cu−N1 2.008(5) Cu−N3 1.978(5) Cu−N5 1.991(5)	Cu−N2 2.032(3) Cu−N4 2.007(3) Cu−N5 2.045(3) Cu−N7 2.007(3)	Cu−N2 1.961(4) Cu−N4 2.011(4)
Cu−X	Cu−O1 1.975(3) Cu−O4 1.971(3) Cu−O7 2.256(4)	Cu−O1 2.1361(17) Cu−O4 1.9959(16) Cu−O5 2.0110(19)	Cu−O2 2.310(5) Cu−O4 2.025(4)		Cu−Cl1 2.2071(15) Cu−Cl2 2.2388(16)
N−Cu−N	N2−Cu−N4 87.59(15)	N2−Cu−N4 90.25(8)	N1−Cu−N3 92.10(2) N3−Cu−N5 89.9(2) N1−Cu−N5 176.1(2)	N2−Cu−N4 91.38(10) N5−Cu−N7 91.54(10) N2−Cu−N5 105.03(9) N4−Cu−N7 119.18(8) N2−Cu−N7 124.26(10) N4−Cu−N5 128.05(10)	N2−Cu−N4 88.72(16)
X−Cu−X	O4−Cu−O1 93.53(15) O4−Cu−O7 82.03(15) O1−Cu−O7 81.85(16)	O4−Cu−O5 64.12(7) O4−Cu−O1 105.44(7) O1−Cu−O5 105.00(7)	O2−Cu−O4 84.84(15) O4−Cu−N1 85.55(17)		Cl1−Cu−Cl2 95.82(6)
X−Cu−N	O4−Cu−N2 176.82(16) O1−Cu−N4 176.71(16) O1−Cu−N2 89.33(15) O4−Cu−N4 89.53(15) O7−Cu−N2 97.00(16) O7−Cu−N4 97.37(16)	O4−Cu−N2 101.43(7) O5−Cu−N2 158.02(8) O1−Cu−N2 94.59(7) O1−Cu−N4 96.42(7) O4−Cu−N4 154.12(7) O5−Cu−N4 97.23(7)	O2−Cu−N1 88.39(17) O4−Cu−N3 170.72(19) O4−Cu−N5 91.95(18) O2−Cu−N3 104.08(17) O2−Cu−N5 94.33(18)		Cl1−Cu−N2 153.42(13) Cl1−Cu−N4 95.66(12) Cl2−Cu−N2 91.36(12) Cl2−Cu−N4 153.99(12)

 © 2004 Wiley-VCH Verlag GmbH & Co. KGaA, Weinheim

Table 3. Crystallographic data for compounds **1**−**2** and **4**−**8**.

	1	**2**	**4**	**5**	**6**	**7**	**8**
Molecular formula	$C_{19}H_{16}N_4$	$C_{23}H_{24}N_4$	$C_{19}H_{18}CuN_6O_7$	$C_{21}H_{20}CuN_6O_6$	$C_{15}H_{24}CuN_8O_6$	$C_{38}H_{32}N_8Cl_2Cu_2$	$C_{19}H_{16}Cl_2CuN_4$
Fw	300.36	356.46	505.93	515.97	475.96	798.70	434.80
Crystal system	Ortho-rhombic	Monoclinic	Monoclinic	Orthorhombic	Orthorhombic	Monoclinic	Triclinic
Space group	*Pna*2$_1$	*P*2$_1$/*n*	*P*2$_1$/*n*	*P*2$_1$2$_1$2$_1$	Pbca	*Cc*	$P\bar{1}$
Cell constants							
a (Å)	14.857(5)	10.5405(11)	10.1001(15)	8.7650(8)	12.488(3)	21.0687(15)	7.461(3)
b (Å)	14.343(5)	10.5904(11)	12.7917(19)	9.4840(9)	11.531(3)	11.5004(8)	9.126(3)
c (Å)	7.113(2)	16.9489(18)	15.494(2)	26.280(2)	29.564(7)	17.2606(12)	13.938(5)
α (deg)	90	90	90	90	90	90	81.098(7)
β (deg)	90	93.549(2)	90.176(2)	90	90	115.806(10)	76.729(7)
γ (deg)	90	90	90	90	90	90	89.966(7)
Z	4	4	5	4	8	4	2
V (Å^3)	1515.8(9)	1888.3(3)	2001.8(5)	2184.6(4)	4257.1(17)	3765.1(5)	912.0(6)
Abs. coeff. μ_{calc} (mm^{-1})	0.081	0.076	1.437	1.052	1.075	1.310	1.501
δ_{calc} (Mg/m^3)	1.316	1.254	2.098	1.569	1.485	1.409	1.583
F(000)	632	760	1295	1060	1976	1632	442
Cryst. dimens. (mm)	0.2 × 0.1 × 0.05	0.3 × 0.2 × 0.05	0.4 × 0.1 × 0.1	0.4 × 0.3 × 0.2	0.1 × 0.03 × 0.03	0.1 × 0.2 × 0.2	0.1 × 0.1 × 0.05
No. of reflcns. collcd.	12699	16284	16932	18485	34627	16313	6670
No. of unique reflcns.	3612	4468	4651	5198	5131	8483	3185
No. of params.	272	340	370	387	289	451	299
R(*F*)	0.0702	0.0469	0.0723	0.0325	0.1180	0.0383	0.0576
$R_w(F^2)$	0.1317	0.1044	0.1321	0.0739	0.1786	0.0919	0.1020
GOF	1.035	1.044	1.267	1.074	1.280	1.033	1.037
Ratio min/max trans.	0.730155	0.906570	0.632826	0.776535	0.460436	0.892294	0.826543

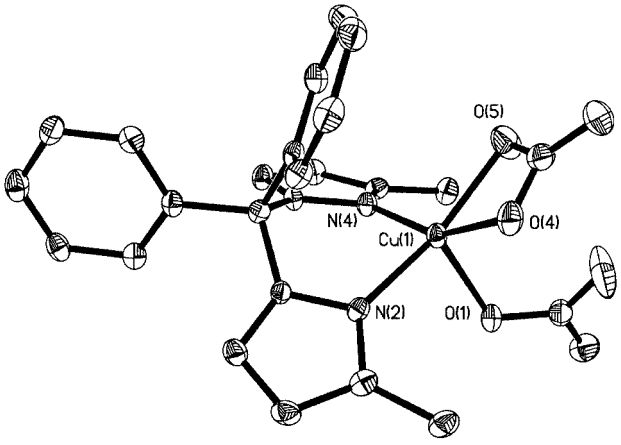

Figure 4. Structure of compound **5** with hydrogens omitted for clarity and thermal ellipsoids drawn at 50 % probability

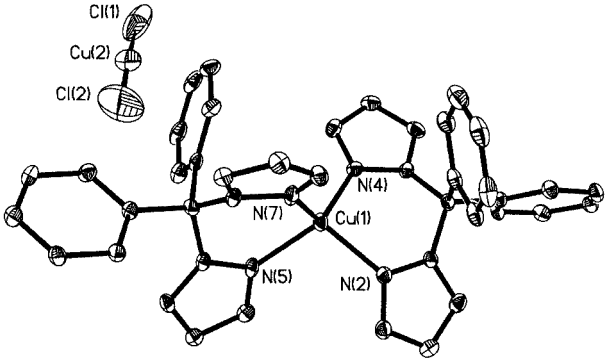

Figure 5. Structure of compound **7** with hydrogens omitted for clarity and thermal ellipsoids drawn at 50 % probability

Exposing an acetonitrile solution of compound **7** to air causes the clear solution to turn green over a 12 hour period. This color change is due to the oxidation of the d^{10} copper(I) compound (**7**) to the d^9 copper(II) compound (**8**). Crystals of the green solid **8** (see Figure 6) were grown from the air-exposed product by layering a solution of CH_2Cl_2 with hexane at room temperature. The crystal structure was elucidated and was found to contain a Cu^{II} ion in a tetrahedral-coordination environment with one bidentate **1** ligand and two ligated chloride ions. The average Cu−N and Cu−Cl bond lengths are 1.986(4) Å and 2.223(16) Å, respectively. These lengths are in close agreement with those reported for the tetrahedral complex Cu(bdpp)Cl_2, where bdpp is 1,3-bis(3′,5′-dimethylpyrazol-1′-yl)propane.[24] The N−Cu−N bond angle is 88.72(16)° and the N−Cu−Cl bond angles range from 91.36(12)−153.99(12)°, thus exhibiting a distorted tetrahedral environment at the copper center.

Unlike in the synthesis of compounds **4**−**8**, something unanticipated occurs upon reacting **2** with copper nitrate: the ligand decomposes. The product that forms (compound **6**) is a five-coordinate, distorted, square-pyramidal copper(II) complex with three ligating 3,5-dimethylpyrazole moieties and two monodentate nitrates (Figure 7). Relevant bond angles and lengths are listed in Table 2. The Cu−N bond-length values compare nicely to those reported for the polymeric $[Cu(pyrazole)_2]_x$ complex [1.992(6) Å vs. 1.957(2) Å].[27]

Similar examples have been documented in the literature for the decomposition of pyrazole-based ligands upon reac-

 © 2004 Wiley-VCH Verlag GmbH & Co. KGaA, Weinheim

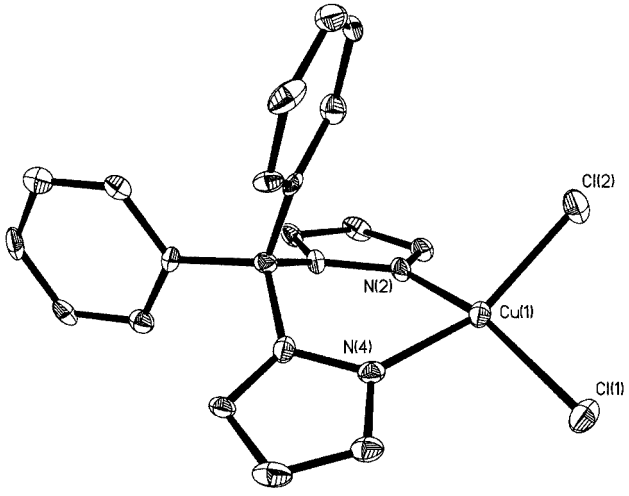

Figure 6. Structure of compound **8** with hydrogens omitted for clarity and thermal ellipsoids drawn at 50 % probability

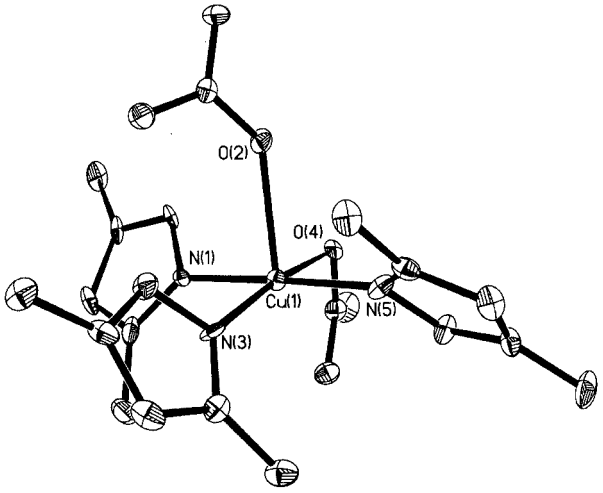

Figure 7. Structure of compound **6** with hydrogens omitted for clarity and thermal ellipsoids drawn at 50 % probability

tion with metal salts.[28,29] The proposed mechanism involves metal-mediated cleavage of the pyrazole nitrogen−X bond, where X may be boron, as is the case with pyrazolylborates, or carbon, as is the case in this report. We do not believe that compound **6** is a product of pyrazole impurity from the previous ligand synthesis because complete characterization of the Pz''_2CPh_2 ligand, prior to use in this metallation reaction, indicates purity. Attempts are currently under way to synthesize the $Cu(Pz''_2CPh_2)$ derivative under anaerobic conditions using dry solvents.

The low-temperature solution state EPR spectra of compounds **4**, **5**, **6** and **8** are shown in Figure 8. Changes in the features of such spectra result from the coordinated ligands, the compound geometry, and the compound charge, in decreasing order of importance.[30,31] Because the ligands used here are nearly identical, varying only by one methyl substituent, and because the coordination geometry of each complex is similar, as seen in Figures 3 4, 5 and 6, one would expect little change in the EPR spectrum of each compound, as is seen in Figure 8. Calculated $g_{\|}$, $g\perp$ and $A_{\|}$ values are shown in Table 4 and these values are similar to those recorded in the literature for compounds with similar structures.[24,32−34] The hyperfine splitting pattern for a Cu 3/2 spin is observed but there are no observable superhyperfine interactions. Calculated $A_{\|}$ values for **5** reveal a slight compression in this region of the spectra.

Table 4. Selected EPR parameters for **4**, **5**, **6** and **8**

	$g_{\|}$	$g_{\perp}$	$A_{\|}$
4	2.492	2.074	160 G
5	2.312	2.079	149 G
6	2.298	2.063	158 G
8	2.287	2.068	164 G

The cyclic voltammogram of **4** is shown in Figure 9. The quasi-reversible wave at 0.55 V vs. SCE (E_{pc} at 0.48 V, E_{pa} at 0.62 V, 0.31 V vs. NHE) is attributed to the Cu^{II}/Cu^{I} redox couple. A scan rate of 50 mv/s afforded optimal reversible behavior. A cyclic voltammogram was also acquired for compound **5** and is shown in Figure 9. The reversible wave at 0.63 V vs. SCE (E_{pc} at 0.55 V, and E_{pa} at 0.71 V, 0.39 V vs. NHE) is also ascribed to the Cu^{II}/Cu^{I} redox pair and is shifted by +0.1 V as compared to that observed for **4**. Once again, the best spectra resulted when

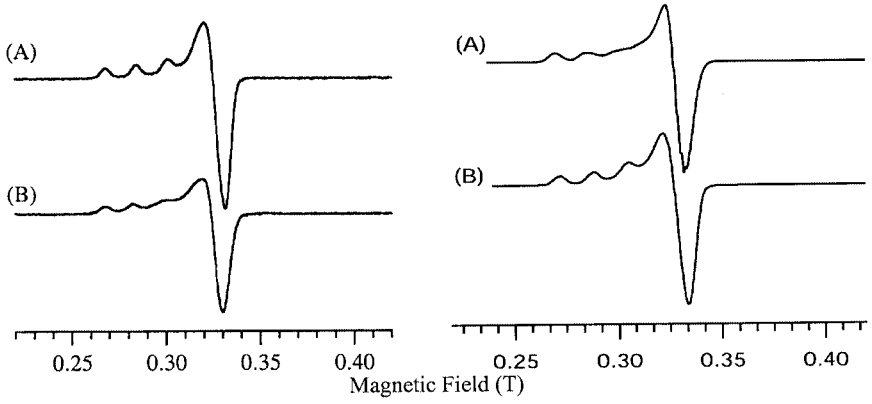

Figure 8. EPR spectra of compounds **4** (top, left), **5** (bottom, left), **6** (top, right) and **8** (bottom, right) (9.42 GHz) in MeOH at 120 K

 © 2004 Wiley-VCH Verlag GmbH & Co. KGaA, Weinheim

a scan rate of 50 mv/s was used. Altering this scan speed resulted in a decreased intensity of the voltammogram half-wave features.

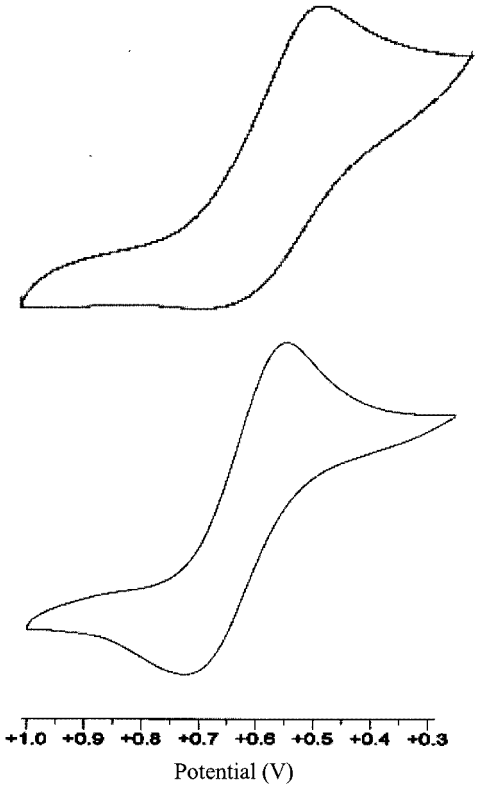

Figure 9. Cyclic voltammograms of compounds **4** (top) and **5** (bottom) at a scan rate of 50 mV/s in CH_3CN with 0.1 M $[Bu_4N]BF_4$ vs. SCE; y-axis is current measured in uA

These potentials are more positive than those of other copper-model complexes in the literature. For instance, in the β-diketiminate copper complex, LCuCl, where L is 2,4-bis(2,6-diisopropylphenylimido)pentane, a half-potential of −0.78 V vs. ferrocene (0.02 V vs. NHE) was reported in CH_2Cl_2.[33] This shift to a more negative potential results, in part, from the negative charge on the diketiminate ligand. The charge shifts the preference toward a +2 oxidation state at the copper center, thus resulting in a more negative potential for the Cu^{II}/Cu^{I} redox couple. Subsequent thiol complexes that incorporate either the above mentioned β-diketiminate or the popular tris(pyrazolyl)borate ligands also have reduction potentials that are significantly lower than those observed in copper-active sites in biology.[7,14]

Attempts were made to isolate thiol complexes by reacting complexes **3** and **4** with bulky aryl thiols such as triphenylmethanethiol or bidentate thiols such as 1,2-benzenedithiol. Each time decomposition occurs forming a reduced metal compound, indicative of colorless copper(I), and the disulfide. A reaction of compound **5** with 1,2-benzenedithiol did lead to a stable green complex in DMF, but crystals were not of X-ray quality. Further work is being done to determine the identity of this product. In addition, attempts are currently under way to further protect the copper ion from reduction chemistry, by increasing the steric bulk at the pyrazole periphery from a methyl to a *tert*-butyl group.

Conclusion

Diphenyldipyrazolylmethane reacts with commercially available copper salts to form low-coordination-number copper complexes. Reactions with copper(II) nitrate produce 1:1 complexes, while the reaction with copper(I) chloride yields a 2:1 complex. Similar compounds presented in the literature, employing dipyrazolylalkanes, produce mainly 2:1 complexes and it is therefore believed that the phenyl rings employed here provide additional protection to the copper ion. Also, the ability of the nitrate counterion to coordinate in different modes (monodentate or bidentate) influences the coordination environment of the copper ion. Additional counterions may be studied in order to affect changes in the copper ion-coordination environment. The geometry of these compounds in the solution state can be further studied by performing conductivity experiments in alcoholic solutions.

We hope that the diphenyldipyrazolyl ligands will produce more biologically relevant model complexes than those that currently exist in the literature because the neutrality of our ligand produces copper complexes with more positive reduction potentials than those observed employing negatively charged ligands, such as the pyrazolylborates. We find that increasing the steric bulk on the pyrazole ring, from compound **4** to compound **5**, leads to a slight preference for copper(I) rather than copper(II), based on the reduction potentials, because of the nearly tetrahedral geometry supported by this ligand. A delicate balance between these two oxidation states is necessary in order to adequately replicate the redox behavior observed in biology in type I blue copper proteins.

Experimental Section

All solvents and starting materials were obtained from commercially available sources and were used without further purification. Mass spectra were recorded using an ES MS Bruker Esquire-LC ion-trap mass spectrometer. ^{1}H NMR spectra were measured on a Gemini 300 MHz spectrometer. The elemental analysis was performed on a CE440 analyzer at the School of Chemical Sciences Microanalysis Laboratory at the University of Illinois at Urbana-Champaign. EPR data were collected at the University of Miami in Ohio. UV/Visible spectra were obtained using a Hitachi U-3010 instrument.

Synthesis of Diphenyldipyrazolylmethane Pz_2CPh_2 (1): All three ligands were synthesized using a slight modification of the procedure by Trofimenko.[17] After isolation of the yellow solid, the ligand was washed with hexanes to yield 1.13 g of white solid (47.7 % yield). Recrystallization by slow evaporation of a saturated toluene solution yielded crystals suitable for single-crystal X-ray diffraction. ^{1}H NMR (300 MHz, $CDCl_3$, 25 °C): δ = 7.65 (d, 2 H, 3-pz), 7.52 (d, 2 H, 5-pz), 7.43−7.33 (m, 6 H, ph), 7.06−7.03 (m, 4 H, ph), 6.31 (dd, 2 H, 4-pz). ES MS (+ ion, MeOH) 323.1 *m*/*z* [M +

 © 2004 Wiley-VCH Verlag GmbH & Co. KGaA, Weinheim

Na]. $C_{19}H_{16}N_4$ (300.36): calcd. C 75.97, H 5.38, N 18.64; found C 75.04, H 5.30, N 18.20.

Synthesis of Diphenylbis(3,5-dimethylpyrazolyl)methane Pz''_2CPh_2 (2): Ligand **2** was prepared similarly to ligand **1**. After workup, 1.06 g of yellow solid (43.0 % yield) were obtained. Crystals suitable for X-ray structural elucidation were grown from a THF/CH_3CN solvent mixture. ^1H NMR (300 MHz, $CDCl_3$, 25 °C): δ = 7.30−7.20 (m, 6 H, ph), 7.05−6.95 (m, 4 H, ph), 6.01 (s, 2 H, 4-pz), 2.22 (s, 6 H, 3-methyl), 1.58 (s, 6 H, 5-methyl). ES MS (+ ion, $CHCl_3$/MeOH) 379.2 *m*/*z* [M + Na]. $C_{23}H_{24}N_4$ (356.46): calcd. C 77.49, H 6.80, N 15.71; found C 77.04, H 6.75, N 15.45.

Synthesis of Diphenylbis(3-methylpyrazolyl)methane Pz'_2CPh_2 (3): Ligand **3** was prepared similarly to ligands **1** and **2**. The resulting yellow-orange solution was filtered and reduced under vacuum to afford a yellow oil. Hexanes were added to precipitate out a small amount of brown solid. A yellow solid resulted upon evaporation of the hexanes. This was washed with hexanes and deionized water to yield 1.70 g of a light yellow solid (58.7 %). ^1H NMR (300 MHz, $CDCl_3$, 25 °C): δ = 7.4 (s, 2 H, 5-pz), 7.4−7.3 (m, 6 H, ph), 7.2−7.1 (m, 4 H, ph), 6.05 (d, 2 H, 4-pz), 2.3 (s, 6 H, 3-methyl). ES MS (+ ion, $CHCl_3$/MeOH) 351.2 *m*/*z* [M + Na]. $C_{21}H_{20}N_4$ (328.41): calcd. C 76.80, H 6.15, N 17.05; found C 76.79, H 6.17, N 16.43.

Synthesis of $Cu(Pz_2CPh_2)(NO_3)_2\ H_2O$ (4): $Cu(NO_3)_2$ (0.082 g, 0.44 mmol) in MeOH (10 mL) was combined with a methanol solution of **1** (0.131 g, 0.44 mmol). The blue copper solution darkened upon combining the two reagents. The reaction was allowed to stir for 2 hours at room temperature. This solution was then reduced under vacuum to yield a blue solid. Recrystallization by layering of CH_2Cl_2 and hexane at −42 °C yielded crystals suitable for single-crystal X-ray diffraction (79.1 % yield). UV/Vis (CH_2Cl_2), λ (ε) = 716.0 nm (68 $M^{-1}cm^{-1}$). ES MS (+ ion, MeOH) 425.0 *m*/*z* [M − NO_3]. $C_{19}H_{16}CuN_6O_6$ (505.93): calcd. C 46.77, H 3.31, N 17.22; found C 46.38, H 3.18, N 16.85. $E_{1/2}$ (CH_3CN) 0.55 V vs. SCE (E_{pc} at 0.48 V, E_{pa} at 0.62 V).

Synthesis of $Cu(Pz'_2CPh_2)(NO_3)_2$ (5): $Cu(NO_3)_2$ (0.106 g, 0.56 mmol) dissolved in THF (10 mL) was added to a solution of **3** (0.185 g, 0.56 mmol) in THF (10 mL). The resulting green solution was stirred for 2 hours at room temperature. This solution was then reduced under vacuum to yield a green-blue solid. Crystals were obtained by layering CH_2Cl_2 with hexane at room temperature (75.3 % yield). Two crystal morphologies of this compound formed: blue needles that do not diffract X-rays well, and green blocks that were suitable for single-crystal X-ray diffraction. UV/Vis (CH_2Cl_2), λ (ε) = 779.0 nm (70 $M^{-1}cm^{-1}$). ES MS (+ ion, THF/MeOH) 453.0 *m*/*z* [M − NO_3]. $C_{21}H_{20}CuN_6O_6$ (515.97): calcd. C 48.89, H 3.92, N 16.28; found C 49.61, H 4.11, N 15.94. $E_{1/2}$ (CH_3CN) 0.63 V vs. SCE (E_{pc} at 0.55 V, and E_{pa} at 0.71 V).

Synthesis of $Cu(Pz'')_3(NO_3)_2$ (6): $Cu(NO_3)_2$ (0.264 g, 1.4 mmol) in MeOH (10 mL) was combined with a methanol solution of **2** (0.501 g, 1.4 mmol). The ligand was only partially soluble in methanol. The murky reaction was stirred for 12 hours and then allowed to evaporate down to afford a bluish-green solid. The solid was redissolved in CH_2Cl_2 and filtered to yield two products: a green solid and a blue solid (63.2 % yield crude product). Crystals of the blue solid were grown by layering CH_2Cl_2 and hexane at −42 °C. UV/Vis (CH_2Cl_2), λ (ε) = 633.0 nm (56 $M^{-1}cm^{-1}$). ES MS (+ ion, THF/MeOH) 317.1 *m*/*z* [M − NO_3 − Pz″]. $C_{15}H_{24}CuN_8O_6$ (475.96): calcd. C 37.86, H 5.09, N 23.53; found C 37.99, H 4.95, N 22.59. $E_{1/2}$ (CH_3CN) 0.70 V vs. SCE (E_{pc} at 0.63 V, E_{pa} at 0.77 V).

Syntheses of $[Cu(Pz_2CPh_2)_2]CuCl_2$ (7) and $Cu(Pz_2CPh_2)Cl_2$ (8): In a dry box with a nitrogen atmosphere, CuCl (0.052 g, 0.52 mmol) and **1** (0.155 g, 0.52 mmol) were combined in CH_3CN (10 mL). The resultant clear solution was left to stir for 6 hours. Slow evaporation of the reaction solution yielded clear crystals of compound **7** suitable for single-crystal X-ray diffraction (quantitative yield). The crystal structure was solved in the *Cc* space group. The literature reports that this space group can be problematic[35,36] so attempts were also made to solve the structure using the suggested *C*2/*c* space group, which incorporates a center of symmetry. However, refinement using *C*2/*c* was poor (R_1 ca. 20 %) as compared to *Cc* (R_1 = 3.83 %) and it was determined that the correct space group for structural elucidation was, in fact, *Cc*. In addition, the structure solved using *Cc* has C−C phenyl ring bond lengths [1.373(5)−1.404(4) Å] closer to the literature value of 1.397 Å, as compared to those for the elucidated structure in *C*2/*c* (1.305−1.434 Å). ES MS (+ ion, MeOH) 663.3 *m*/*z* [M − $CuCl_2$]. $C_{38}H_{32}Cl_2Cu_2N_8$ (798.70): calcd. C 57.14, H 4.05, N 14.02; found C 57.22, H 3.91, N 14.22.

A portion of compound **7** was redissolved in CH_3CN and exposed to air. The white solution of **7** gradually turned green over a 12 hour period. Crystals of the final oxidized green product (**8**) were grown by layering CH_2Cl_2 and hexane at room temperature. Additionally, compound **8** was synthesized by the reaction of $CuCl_2$ (0.158 g, 1.1 mmol) in THF (5 mL) with a THF solution of **1** (0.352 g, 1.2 mmol). Upon combining the two solutions a green precipitate formed immediately. The precipitate was removed via filtration and washed with additional THF (59.9 % yield). UV/Vis (CH_2Cl_2), λ (ε) = 417.0 nm (644 $M^{-1}cm^{-1}$), 677.0 (86 $M^{-1}cm^{-1}$). ES MS (+ ion, $CHCl_3$) 398.2 *m*/*z* [M − Cl]. $C_{19}H_{16}Cl_2CuN_4$ (434.80): calcd. C 52.47, H 3.72, N 12.88; found C 52.10, H 3.72, N 12.37. $E_{1/2}$ (CH_3CN) 0.37 V vs. SCE (E_{pc} at 0.26 V, E_{pa} at 0.47 V).

X-ray crystallography: X-ray intensity data were measured at 100 K (Bruker KRYO-FLEX) on a Bruker SMART APEX CCD-based X-ray diffractometer system equipped with a Mo-target X-ray tube (λ = 0.71073 Å) operated at 2000 watts power. Crystals were mounted on a cryoloop using Paratone N-Exxon oil and placed under a stream of nitrogen. The detector was placed at a distance of 5.009 cm from the crystals. Analyses of the data sets showed negligible decay during data collection. The data were corrected for absorption with the SADABS program. The structures were refined using the Bruker SHELXTL Software Package (Version 6.1), and were solved by direct methods until the final anisotropic full-matrix, least-squares refinement of F^2 converged.[37] Experimental details for all of the structures are provided in Table 3.

EPR experiments on compounds were carried out using a Bruker EMX X-band CW-EPR spectrometer consisting of an ER 041XG microwave bridge and a TE102 cavity coupled with a BVT 3000 nitrogen gas temperature controller (temperature stability of 0.2 K). EPR spectra were acquired by taking a 168 s field-swept scan with the center field set to 3200 G, a sweep width of 2000 G, a microwave frequency of 9.42 GHz, the modulation frequency was set to 100 kHz, and a modulations amplitude of 10.0 G. The spectra were acquired at a temperature of 120 K. The samples were dissolved in methanol to a final concentration of 1 mg/mL and transferred to 4 mm 707-SQ-250M fused quartz EPR tubes (Wilmad, Buena, NJ).

Cyclic voltammetry measurements were carried out on compounds **4**, **5**, **6** and **8** using a BAS 100B/W electrochemical workstation from Bioanalytical Systems, Inc. in West Lafayette, Indiana. HPLC grade acetonitrile (< 0.02 % H_2O) was used without further purification. A three-electrode setup with a platinum working electrode, a platinum wire electrode, and a saturated calomel reference elec-

 © 2004 Wiley-VCH Verlag GmbH & Co. KGaA, Weinheim

trode was employed. Copper complexes were prepared at 1 mM concentration using 0.1 M tetrabutylammonium tetrafluoroborate as the supporting electrolyte in CH_3CN. A scan rate of 50 mV/s afforded optimal reversible behavior. Solutions were degassed with nitrogen prior to use and all experiments were run under a blanket of inert gas.

CCDC-216892 to -216898 contain the supplementary crystallographic data for this paper. These data can be obtained free of charge at www.ccdc.cam.ad.uk/conts/retrieving.html [or from the Cambridge Crystllographic Data Centre, 12 Union Road, Cambridge CB21EZ, UK; Fax: (internat.) + 44-1223/336-033; E-mail: deposit@ccdc.cam.ac.uk].

Acknowledgments

J. L. S. acknowledges the GAANN fellowship for financial support. C. J. Z. acknowledges the University of Akron for a faculty research grant (FRG-1524). We also wish to acknowledge NSF Grant CHE-0116041 for funds used to purchase the Bruker-Nonius diffractometer and the Kresge Foundation and donors to the Kresge Challenge Program at the University of Akron for funds used to purchase the NMR instrument used in this work.

[1] S. Trofimenko, J. C. Calabrese, J. Domaille, J. S. Thompson, *Inorg. Chem.* **1989**, *28*, 1091−1101.
[2] A. L. Rheingold, L. N. Zakharov, S. Trofimenko, *Inorg. Chem.* **2003**, *42*, 827−833.
[3] S. Trofimenko, J. C. Calabrese, J. S. Thompson, *Inorg. Chem.* **1987**, *26*, 1507−1514.
[4] M. Ruf, H. Vahrenkamp, *Inorg. Chem.* **1996**, *35*, 6571−6578.
[5] H. Vahrenkamp, *Acc. Chem. Res.* **1999**, *32*, 589−596.
[6] H. Boerzel, M. Koeckert, W. Bu, B. Spingler, S. J. Lippard, *Inorg. Chem.* **2003**, *42*, 1604−1615.
[7] N. Kitajima, *Adv. Inorg. Chem.* vol. 39 (Synthetic approach to the structure and function of copper proteins) (Ed.: A. G. Sykes), Academic Press, New York, **1992**, 1−77.
[8] N. Kitajima, K. Fujisawa, M. Tanaka, Y. Moro-oka, *J. Am. Chem. Soc.* **1992**, *114*, 9232−9233.
[9] D. Qiu, L. Kilpatrick, N. Kitajima, T. G. Spiro, *J. Am. Chem. Soc.* **1994**, *116*, 2585−2590.
[10] D. W. Randall, S. Debeer George, B. Hedman, K. O. Hodgson, K. Fujisawa, E. I. Solomon, *J. Am. Chem. Soc.* **2000**, *122*, 11620−11631.
[11] N. Kitajima, K. Fujisawa, C. Fujimoto, Y. Moro-oka, S. Hashimoto, T. Kitagawa, K. Toriumi, K. Tatsumi, A. Nakamura, *J. Am. Chem. Soc.* **1992**, *114*, 1277−1291.
[12] E. T. Adman, *Adv. Protein Chem.* **1991**, *42*, 144−197.
[13] E. I. Solomon, M. J. Baldwin, M. D. Lowery, *Chem. Rev.* **1992**, *92*, 521−542.
[14] S. Mandal, G. Das, R. Singh, R. Shukla, P. K. Bharadwaj, *Coord. Chem. Rev.* **1997**, *160*, 191−235.
[15] K. Shiu, L. Yeh, S. Peng, M. Cheng, *J. Organomet. Chem.* **1993**, *460*, 203−211.
[16] S. Tsuji, D. C. Swenson, R. F. Jordan, *Organometallics* **1999**, *18*, 4758−4764.
[17] S. Trofimenko, *J. Am. Chem. Soc.* **1970**, *92*, 5118−5126.
[18] M. A. Mesubi, F. O. Anumba, *Transition Met. Chem.* **1985**, *10*, 5−8.
[19] C. Pettinari, G. G. Lobbia, G. Sclavi, D. Leonesi, *Polyhedron* **1995**, *14*, 1709−1723.
[20] C. Pettinari, F. Marchetti, A. Cingolani, D. Leonesi, M. Colapietro, S. Margadonna, *Polyhedron* **1998**, *17*, 4145−4154.
[21] C. Pettinari, R. Pettinari, M. Pellei, G. G. Lobbia, *Polyhedron* **1999**, *18*, 1941−1951.
[22] J. Reedijk, J. Verbiest, *Transition Met. Chem.* **1979**, *4*, 239−243.
[23] K. Flinzner, A. F. Stassen, A. M. Mills, A. L. Spek, J. G. Haasnoot, J. Reedijk, *Eur. J. Inorg. Chem.* **2003**, 671−677.
[24] A. M. Schuitema, M. Engelen, I. A. Koval, S. Gorter, W. L. Driessen, J. Reedijk, *Inorg. Chim. Acta* **2001**, *324*, 57−64.
[25] S. Knapp, T. P. Keenan, X. Zhang, R. Fikar, J. A. Potenza, H. J. Schugar, *J. Am. Chem. Soc.* **1990**, *112*, 3452−3464.
[26] D. Martini, M. Pellei, C. Pettinari, B. W. Skelton, A. White, *Inorg. Chim. Acta* **2002**, *333*, 72−82.
[27] M. K. Ehlert, S. J. Rettig, A. Storr, R. C. Thompson, J. Trotter, *Can. J. Chem.* **1989**, *67*, 1970−1974.
[28] J. L. Schneider, V. G. Young, W. B. Tolman, *Inorg. Chem.* **2001**, *40*, 165−168.
[29] C. H. Dungan, W. Maringgele, A. Meller, K. Niedenzu, H. Nöth, J. Serwatowska, J. Serwatowska, *Inorg. Chem.* **1991**, *30*, 4799−4806.
[30] H. Yokoi, A. W. Addison, *Inorg. Chem.* **1977**, *16*, 1341−1349.
[31] J. S. Thompson, T. J. Marks, J. A. Ibers, *J. Am. Chem. Soc.* **1979**, *101*, 4180−4192.
[32] W. B. Tolman, *Inorg. Chem.* **1991**, *30*, 4880−4882.
[33] P. L. Holland, W. B. Tolman, *J. Am. Chem. Soc.* **1999**, *121*, 7270−7271.
[34] B. Kozlevčar, P. Gamez, R. Gelder, W. L. Driessen, J. Reedijk, *Eur. J. Inorg. Chem.* **2003**, 47−50.
[35] R. E. Marsh, *Acta Crystallogr., Sect. B* **1997**, *53*, 317−322.
[36] F. H. Herbstein, R. E. Marsh, *Acta Crystallogr., Sect. B* **1998**, *54*, 677−686.
[37] G. M. Sheldrick, *SHELXTL, Crystallographic Software Package*, version 6.10; Bruker-AXS: Madison, WI, 2000.

Received August 7, 2003
Early View Article
Published Online January 28, 2004

 © 2004 Wiley-VCH Verlag GmbH & Co. KGaA, Weinheim

Allylpalladium(II) Complexes with Aminophosphane Ligands: Solution Behaviour and X-ray Structure of *cis*-[Pd(η^3-$CH_2CHCHPh$)-{$Ph_2PCH_2CHPhNH(2,6\text{-}C_6H_3iPr_2)$}][$PF_6$]

Jean-Michel Camus,[a] Jacques Andrieu,*[a] Philippe Richard,[a] and Rinaldo Poli[a][‡]

Keywords: Allyl ligands / N,P ligands / *syn-anti* exchange / Palladium

A new β-aminophosphane L^2 [$Ph_2PCH_2CH(Ph)NH(2,6\text{-}C_6H_3iPr_2)$], bearing an asymmetric carbon atom and a vicinal prochiral nitrogen centre and (η^3-allyl)palladium complexes of general formula [Pd(η^3-C_3H_4R){η^2-$Ph_2PCH_2CH(Ph)NHAr$}][PF_6] (**1**–**6**) (R = H, Me or Ph and Ar = Ph or 2,6-$C_6H_3iPr_2$) have been synthesised. NMR spectroscopic studies and a crystal structure analysis of complex **6** (R = Ph, Ar = 2,6-$C_6H_3iPr_2$) confirmed the highly diastereoselective coordination of the nitrogen atom. Because of the allyl fluxionality and the presence of asymmetric centres, all the complexes exist in solution as mixtures of up to four diastereomers. For the monosubstituted allyl complexes [Pd(η^3-C_3H_4R){$Ph_2PCH_2CH(Ph)NHAr$}][PF_6] (**3**–**6**, R = Me or Ph) only *cis*/*trans*-P and *endo*/*exo* isomers with *syn*-oriented allyl substituents have been observed in solution. The diastereomeric distribution is subject to a steric control since a modification of the steric bulk of the allyl substituents and/or N-aryl groups strongly affect the isomers ratio. An X-ray diffraction study of compound **6** reveals a mixture of *endo* and *exo cis*-P *syn* isomers and corresponds to the first *cis*-P isomer crystal structure for an N,P-ligand allyl complex. A phase-sensitive 2-D NOESY NMR analysis showed that complex **1** undergoes a selective *syn-anti* exchange isomerisation, involving exclusively a *trans*-P opening of the η^3-allyl moiety. Therefore, η^3-η^1-η^3 rearrangements in allylic complexes **1**–**6** were assumed to occur via the regioselective formation of a σ-allyl intermediate.

(© Wiley-VCH Verlag GmbH & Co. KGaA, 69451 Weinheim, Germany, 2004)

Introduction

Palladium-catalysed allylic substitution is a powerful methodology for the formation of new C−C or C−N bonds, with the potential to achieve high levels of enantioselectivity in the presence of chiral ligands.[1−4] In particular, the use of N,P-ligands provides very high enantioselectivities in the allylic alkylation of 1,3-diphenylpropenyl substrates.[5−10] One major advantage of hybrid ligands over ditopic ligands consists in the electronic differentiation of the coordinating atoms, inducing a nucleophilicity discrimination of the terminal allylic carbon atoms. Therefore, other chiral hybrid ligands such as O,P,[11,12] P,S[13,14] or N,S[15,16] have been studied in order to benefit from these electronic effects. Cationic allylic [Pd(η^3-allyl)L_2]$^+$ complexes with bidentate L_2 ligands are thought to be the key intermediate in the catalytic cycle and there is a growing interest in understanding their dynamic behaviour in solution and in elucidating mechanistic details related to the enantiocontrol.[17−19] For complexes containing ditopic N,P-ligands, the nucleophilic attack is assumed to occur at the carbon atom *trans* to the phosphorus[17,27,28] and the selectivities strongly depend on the relative abundance of diastereomeric allylic complexes. In comparison to extensive investigations of complexes with symmetric allyl ligands, few studies have been devoted to monosubstituted allyl complexes.[17,20−26] In the case of the allylic alkylation of asymmetric substrates, such as cinnamyl acetate or crotyl acetate, only the *trans*-P diastereomers lead to the product containing the new chiral centre; the *cis*-P isomers lead to achiral linear *Z* or *E* products (see Figure 1). The enantiocontrol is therefore subordinate to the regiocontrol.

In a previous contribution, we have described the synthesis and the coordinative behaviour of a chiral aminophosphane $Ph_2PCH_2CH(Ph)NHPh$ (L^1), in allylpalladium(II) complexes.[29] This study highlighted a diastereoselective N-coordination in the cationic complex [Pd(η^3-C_3H_5)(L^1)]+, and an N−H···Cl−M intramolecular interaction involving the dangling N−H moiety for the neutral complex [PdCl(η^3-C_3H_5)(κ1:P,L^1)]+ (see Figure 2) which is a feature of P-coordinated aminophosphanes with a secondary amine function.[30]

We report here the extension of our synthetic procedure to a new β-aminophosphane and to its cationic allylpalladium complexes, including ones with asymmetric mono-

[a] Laboratoire de Synthèse et d'Electrosynthèse Organométalliques, UMR 5188 CNRS, Université de Bourgogne, Faculté des Sciences "Gabriel", 6 Boulevard Gabriel, 21000 Dijon, France
E-mail: Jacques.Andrieu@u-bourgogne.fr
[‡] Current address: Laboratoire de Chimie de Coordination, UPR CNRS 8241, 205 route de Narbonne, 31077 Toulouse Cedex, France

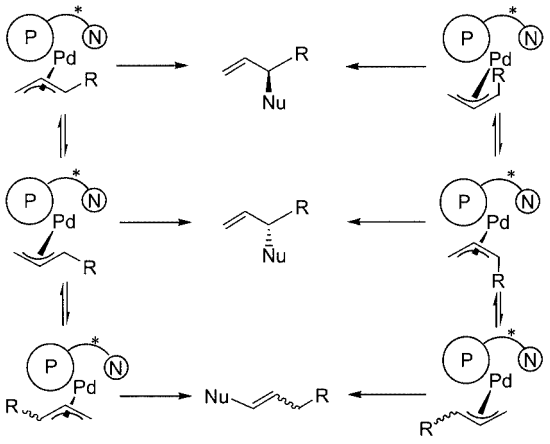

Figure 1. Regioselectivity and enantioselectivity in palladium-catalysed allylic alkylation arising from different diastereomeric η^3-allyl complexes

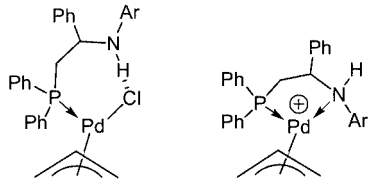

Figure 2. Coordinative features of aminophosphane L^1 in neutral and cationic allyl palladium complexes

substituted allyl ligands, as well as a detailed 2-D NOESY NMR investigation of the mechanism of interconversion of the various diastereomers. The diastereomeric ratio is strongly dependent on the steric bulk of the allyl N-substituents. The first X-ray structure of a *cis*-P allyl complex is also presented.

Results and Discussion

Synthesis of the Aminophosphane Ligand L^2 and Cationic Allylpalladium Complexes

The new aminophosphane ligand L^2 was synthesised by the same one-step procedure previously described for ligand L^1 (Scheme 1).[29] It consists of the nucleophilic attack of an imine moiety by the diphenylphosphinomethyl anion. After hydrolysis and workup, the aminophosphane was isolated in good yield as a light-yellow, microcrystalline powder and was characterised by ^1H, ^{13}C and ^{31}P NMR spectroscopy and by elemental analysis (see Exp. Sect.). The ^{31}P NMR spectroscopic data are in agreement with those of other β-N,P ligands bearing an sp^3 nitrogen centre and an ethylenic backbone linking the heteroatoms.[29,31,32]

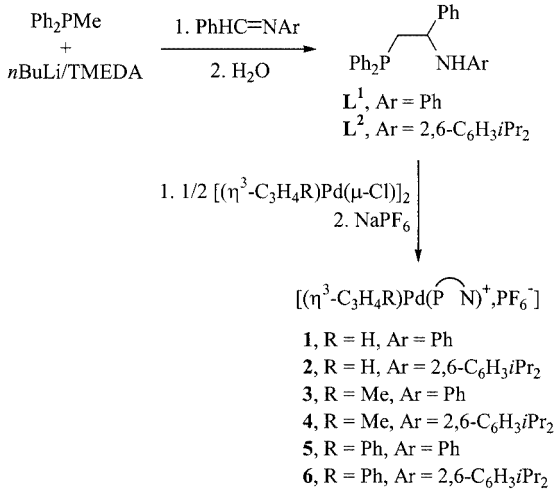

Scheme 1

The cationic allyl complexes **1**−**6** were synthesised by treatment of the chloro-bridged allylpalladium dimer with the appropriate ligand in the presence of an excess of the halide-scavenger $NaPF_6$ in dichloromethane. They were obtained in high yields as air-stable, white or yellow powders that are soluble in organic solvents, except alkanes and Et_2O. The ^{31}P NMR chemical shifts for compounds **1**−**6** are characteristic of the aminophosphane bidentate coordination. Since the ligands contain an asymmetric centre, the complexes may exist as different diastereomers arising from the different face coordination (*endo* or *exo*) of the allyl moiety with respect to the ligand. The *endo* isomer is defined as having the C−H bond of the internal allylic carbon atom pointing in the same direction as the N−H bond (see Scheme 2). For the monosubstituted allyl complexes, the allyl substituents can be in a *cis*-P or *trans*-P position and can be positioned *syn* or *anti* with respect to the internal allyl proton. Furthermore, the nitrogen atom becomes a new asymmetric centre upon coordination. However, because of the induction by the vicinal chiral carbon atom, its coordination is expected to be highly diastereoselective, as previously reported.[29,33] Therefore, only eight different diastereomers may arise, in principle, from the possible orientations of the allyl fragment. The diastereomeric distribution in solution at room temperature was determined in each case by NMR spectroscopy (except for **1**, which has already been reported[29]) and is presented below.

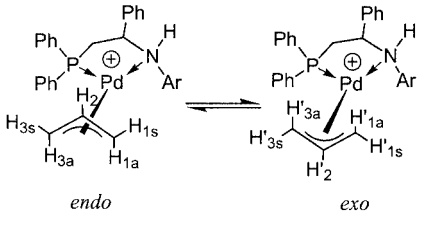

Scheme 2

 © 2004 Wiley-VCH Verlag GmbH & Co. KGaA, Weinheim

NMR Spectroscopic Studies on Allylic Compounds 1 and 2

The $^{31}P\{^1H\}$ NMR spectra of complexes **1** and **2** display two singlets in a 1:1 and 6.8:3.2 ratio, respectively. Because of the diastereoselective *N*-coordination and the allyl symmetry, compounds **1** and **2** may only afford two diastereomers (*endo* and *exo*, see Scheme 2). The diastereomeric ratio was confirmed by integration of the ^1H NMR spectra. The steric bulk of the N-substituents affects the isomeric proportion, as observed for other allyl compounds (see below). This seems to be an important key for the enantiocontrol in allylic substitution of 1,3-propenyl acetate derivatives.[8,18,19,34] For allylic complexes, the *endo*/*exo* ratio can be tuned by adjusting the steric constraints either around the donor atoms or on the allyl moiety.[14,19,35] You et al. have observed that, for a complex containing the 2-(phenylthio)-1-(4-*tert*-butyloxazolinyl)ferrocene ligand, an inversion of the configuration of the oxazoline ring asymmetric carbon slightly affects the *endo*/*exo* ratio (3.1:1 vs. 2.1:1), whereas introducing two benzylic groups at the 4-position of the oxazoline ring strongly displaces the equilibrium in favour of the *endo* diastereomer.[36]

The preferential nucleophilic attack at one specific allyl carbon atom is another way to achieve high enantioselectivity. The difference between the ^{13}C NMR chemical shifts of the external allyl carbon atoms ($\Delta\delta = \delta C_1 - \delta C_3$) is a measure of the difference between their electronic environments.[14,23,28,37] For complexes **1** and **2**, $\Delta\delta$ lies between 35.7 and 27.2 ppm depending on the isomer (see Table 1). Such a high $\Delta\delta$ is usual for N,P ligands, given the very different *trans* influence of the phosphorus and nitrogen atoms,[26] and reveals a higher electrophilicity for the C-1 atom (*trans*-P) than for the C-3 atom (*cis*-P; see Scheme 2). This feature has also been observed in the solid state, since the Pd−C distances are longer for $C_{trans\text{P}}$ than those for $C_{cis\text{P}}$.[19,38−40] It should be noted that the orientation of the allyl fragment induces slight differences in $\Delta\delta$ (35.7:32.5 for **1** and 29.9:27.2 for **2**). This feature probably arises from the steric hindrance caused by the N-substituents onto the allylic *trans*-P carbon atom, affecting its electrophilicity. Similar observations have been made for allylic complexes with phosphinoxazoline ligands.[41] Therefore, there is a close relation between the bulk of the N-substituents and (*i*) the *endo*/*exo* ratio, and (*ii*) the electrophilicity of the external carbon atoms.

Table 1. ^{13}C NMR spectroscopic data for allylic carbon atoms in complexes **1** and **2**

	$\delta^{13}C$ ($^2J_{H,P}$ in Hz) C-1 *trans*P	C-2	C-3 *cis*P	$\Delta\delta^{13}C$ (δC-1 − δC-3)
1a	87.1 (27)	120.6	51.4	35.7
1b	84.6 (28)	123.0	52.1	32.5
2a	82.3 (27)	120.3 (5)	52.4	29.9
2b	80.6 (29)	122.2 (5)	53.4	27.2

NMR Characterisation of Monosubstituted Allylic Compounds 3−6

As detailed above, the introduction of one substituent at an external allyl carbon atom increases the number of possible isomers from two to eight. NMR investigations for complexes **3**−**6** revealed that all of them exist as mixtures of four diastereomers in solution in different equilibrium ratios. The coupling constants and chemical shifts for the allyl moieties are reported in Table 2. The $^3J_{H,P}$, $^2J_{C,P}$ and $\delta^{13}C$ values are helpful for the assignment of each isomer as *trans*-P or *cis*-P, since the coupling constants to the phosphorus nucleus are greater for the *trans* than for the *cis*

Table 2. Selected ^{13}C and ^1H NMR spectroscopic data for allylic complexes **3**−**6** (n.d. = not determined)

Complexes	$\delta^{13}C$ ($J_{P,C}$ in Hz) C-1	C-2	C-3	CH_3	δ^1H ($J_{H,P}$ in Hz) 1-H*anti*	1-H*syn*	2-H	3-H*syn*	3-H*anti*	CH_3
3a (53%)	102.9 (26)	116.2 (5)	46.7 (4)	14.1 (4)	4.98 (n.d.)	−	5.23	3.79	2.56	0.66 (9.3)
3b (30%)	101.7 (26)	118.9 (5)	47.5 (3)	14.2 (4)	3.92 (n.d.)	−	5.58	3.54	2.82	1.04 (9.1)
3c (11%)	78.3 (23)	123.5 (6)	72.3 (5)	17.2	4.17 (n.d.)	2.72 (n.d.)	5.73	−	3.85	1.09 (9.1)
3d (6%)	74.2 (25)	n.d.	69.2 (4)	18.0	n.d.	2.81 (n.d.)	5.68	−	n.d.	1.46 (9.1)
4a (78%)	99.5 (26)	119.3 (5)	49.3 (4)	15.7 (4)	4.75 (n.d.)	−	5.34	4.10	2.83	0.67 (9.4)
4b (9%)	103.3 (27)	119.2 (6)	49.1	16.9 (5)	4.05 (n.d.)	−	5.72	3.67	2.92	1.26 (9.5)
4c (9%)	76.3 (27)	122.5 (5)	72.6 (4)	19.6	3.84 (9.4)	3.52 (n.d.)	5.61	−	4.16	1.62 (9.0)
4d (4%)	n.d.	n.d.	n.d.	19.0	n.d.	n.d.	5.83	−	n.d.	n.d.
5a (55%)	104.7 (24)	111.3 (5)	48.8	−	5.82 (n.d.)	−	5.82	3.88	2.77	−
5b (22%)	104.6 (24)	115.0 (5)	49.8	−	4.67 (9.9)	−	6.20	3.62	3.04	−
5c (12%)	80.7 (26)	116.7 (5)	73.9 (5)	−	4.47 (9.2)	4.25 (7.2)	6.19	−	4.81	−
5d (11%)	82.0 (25)	119.6 (5)	74.6 (5)	−	3.08 (9.3)	3.85 (n.d.)	5.83	−	4.62	−
6a (9%)	n.d.	n.d.	n.d.	−	5.95 (9.0)	−	5.68	3.62	2.79	−
6b (7%)	n.d.	n.d.	n.d.	−	4.92 (9.9)	−	6.40	n.d.	2.84	−
6c (62%)	79.4(25)	116.4(5)	74.6(6)	−	4.41(8.8)	3.83(7.8)	6.20	−	4.79	−
6d (22%)	76.6 (27)	118.8 (6)	76.1 (5)	−	2.99 (n.d.)	4.23 (7.3)	6.40	−	4.86	−

 © 2004 Wiley-VCH Verlag GmbH & Co. KGaA, Weinheim

nuclei.[26,42] For the 1-butenyl complexes, the coupling constants involving the external methyl moiety, $^4J_{H,P}$ and $^3J_{C,P}$, enable the establishment of the *cis*-P/*trans*-P ratio, whereas δ^1_H is not diagnostic of the relative orientation. Indeed, for 1-butenyl (R = Me) complexes based on other types of N,P ligands, van Leeuwen has proposed that the signal for the methyl group should be found at $\delta > 1.3$ ppm when in the *trans*-P position and at $\delta < 0.6$ ppm when in the *cis*-P position.[43] However, several ^{1}H NMR resonances for the methyl substituents in complexes **3**−**6** and other known allyl complexes transgress this "rule".[19,20,44] For instance, the isomers of complexes **3** show resonances at δ = 0.66, 1.04, 1.09 and 1.46 ppm (Figure 3). In spite of this difficulty, the *cis*/*trans*-P orientation could be established unambiguously from other NMR characteristics.

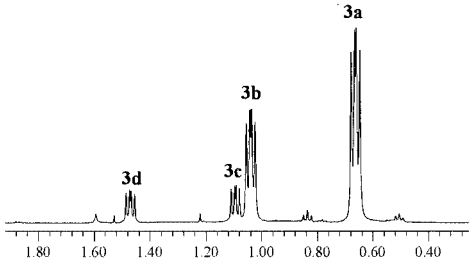

Figure 3. High field ^{1}H NMR spectrum ($CDCl_3$, 500 MHz, 283 K) of the CH_3 terminal group of complex **3**, showing the presence of four isomers

The analysis of the $^3J_{H_2,H_1}$ coupling constants allowed us to determine the relative positions of each allyl proton, revealing the exclusive presence of the *syn* isomers, i.e. having the protons 1-H and 2-H in *anti* positions. This contrasts with 1,3-disubstituted allylic complexes, for which minor amounts of isomers with the allylic substituents in the *anti* position are present in solution.[28,45] The *syn*/*anti* ratio could be affected by tuning the steric bulk between the ligand substituents and the allyl moiety.[18,19,43] The four isomers and their relative proportions are depicted in Figure 4. Compounds **3** and **4** have been identified as 53:30:11:6 and 78:9:9:4 mixtures, respectively, with the two major isomers (a and b) having a *syn trans*-P orientation. The two minor isomers were assigned to the *syn cis*-P diastereomers (c and d). Concerning the *trans*-P isomers, it can be observed that

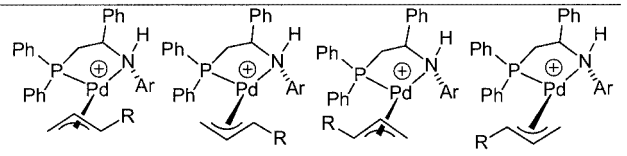

	endo/*exo syn trans*-P (**a**/**b** or **b**/**a**)	*endo*/*exo syn cis*-P (**c**/**d** or **d**/**c**)
3	53/30	11/6
4	78/9	9/4
5	55/22	12/11
6	9/7	62/22

Figure 4. Schematic representation and distribution of complexes **3**−**6** isomers

the greater steric bulk introduced by the addition of the two isopropyl groups at the *ortho* positions of the *N*-phenyl substituent induces a strong variation of the *endo*/*exo* (or *exo*/*endo*) ratio (from 53:30 for **3** to 78:9 for **4**), whereas the global *cis*/*trans*-P ratio is only slightly affected (around 85:15). The geometry of the least abundant isomer of **4** (4% relative abundance) could not be unambiguously elucidated because of its very low concentration, coupled with the partial overlap of its resonances with those of the other isomers. Therefore, it was assumed to correspond to the second *cis*-P isomer of the **c**/**d** couple.

An influence of the steric bulk on the diastereomeric proportion is also present for the 1-phenylpropenyl complexes **5** and **6**, which were observed as 55:22:12:11 and 62:22:9:7 isomeric mixtures in solution, respectively. Contrary to the observations for compounds **3** and **4**, introducing a bulky N-substituent leads to a strong variation of the *cis*/*trans*-P ratio, whereas the global *endo*/*exo* ratio is only slightly affected. Nevertheless, the most remarkable observation is that the major isomer in solution is a *cis*-P isomer for complex **6**. Indeed, the major isomers for most[47] monosubstituted allyl complexes reported in the literature present a

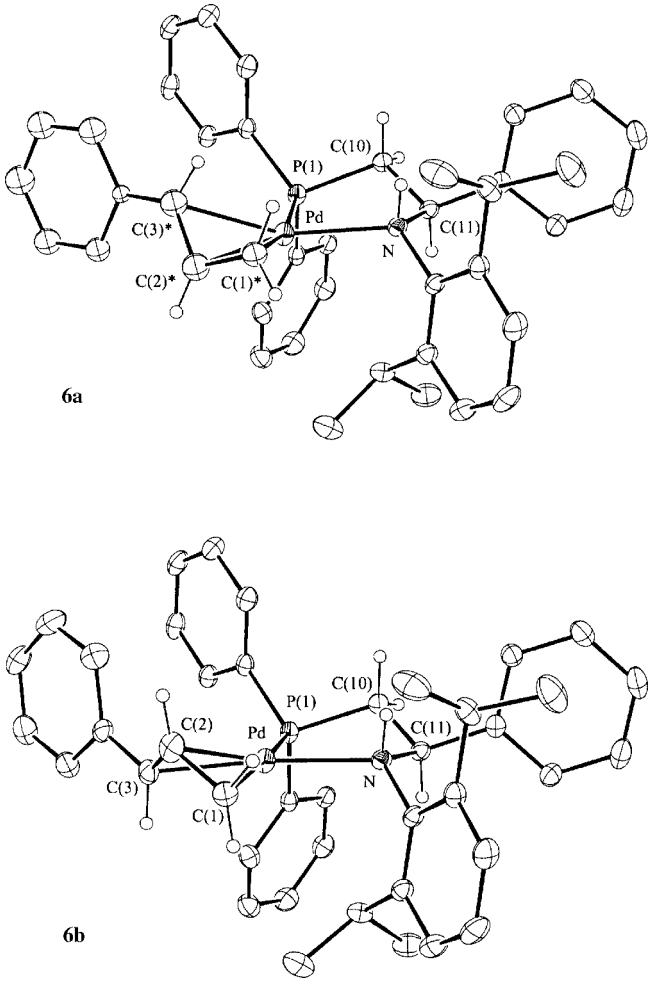

Figure 5. ORTEP views of the *exo*-**6c** and *endo*-**6d** isomers; only relevant hydrogen atoms are shown; for clarity, the CH_2Cl_2 solvent and the hexafluorophosphate anion are omitted.

 © 2004 Wiley-VCH Verlag GmbH & Co. KGaA, Weinheim

trans-P orientation.[17,20,23,43,44,46] To confirm this unexpected observation, suitable crystals were therefore grown and used for an X-ray crystallographic study.

The solid-state structure (discussed in more detail later) highlights the *cis*-P orientation of the phenyl group and corresponds to a solid solution of both *endo* and *exo* isomers in a 78:22 ratio (see Figure 5). To the best of our knowledge, this represents the first solid-state structural determination of an allylic complex with an N,P ligand in a *cis*-P position. The crystals were redissolved in $CDCl_3$ and the resulting solution was monitored by ^{31}P NMR spectroscopy (see Figure 6). The spectrum displays four singlets whose relative intensities evolved slowly from a 7:9:55:21 ratio (5 min) to the equilibrium 7:9:22:62 ratio after 24 hours. Therefore, the configuration of the two major isomers is completely established: the major isomer in the solid state (*endo cis*-P, **6d**) displays the ^{31}P NMR resonance at $\delta = 29.68$ ppm, whereas the major one in solution (^{31}P resonance at $\delta = 21.85$ ppm, **6c**) corresponds to the *exo cis*-P species.

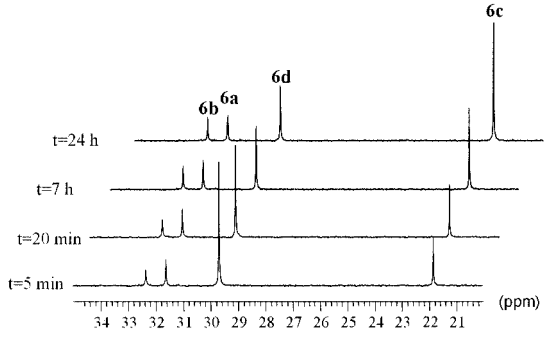

Figure 6. Kinetic ^{31}P NMR monitoring of crystals of **6** dissolved in $CDCl_3$

As already shown for complexes **3** and **4**, the addition of *i*Pr groups to the aryl *ortho* positions induces dramatic changes in the isomeric ratios on going from **5** to **6**, since it approximately inverts the *trans*-P/*cis*-P ratio from 77:23 to 16:84. The free rotation around the $C_{Ar}-N$ bond and the sterically demanding *i*Pr group destabilize the *trans*-P orientation of the allylic phenyl substituents. A similar behaviour was already observed by Helmchen and co-workers.[17,19,27] Therefore the subtle combination of steric repulsions between the allyl substituent and the N group allows a higher discrimination between the diastereomers. For the 1-butenyl complexes **3** and **4**, the *N*-isopropyl groups favour the *endo* isomer over the *exo* (or vice versa) and destabilize the *cis*-P vs. the *trans*-P isomers. The trend of tuning the *endo*/*exo* ratio has been reported mainly for symmetrically disubstituted allyl complexes, while very few papers have mentioned *cis*/*trans* control.[17,23,43] All the complexes studied in this paper provide evidence of the influence of the steric bulkiness of the nitrogen substituent on the diastereomeric ratio.

Crystal Structure of $[Pd(\eta^3\text{-}CH_2CHCHPh)\{Ph_2PCH_2\text{-}CHPhNH(2,6\text{-}C_6H_3iPr_2)\}][PF_6]$ (6)

Yellow crystals of compound **6** were grown from dichloromethane/pentane. As already mentioned above, the structure is quite interesting because it exhibits a solid mixture of two different *cis*-P diastereomeric cations within the same unit cell. Indeed, due to disorder around the allyl carbon atoms, accompanied by a slight tilting of the phenyl substituent, both *endo* and *exo cis*-P isomers have been identified in the solid state and their relative occupancies refined to afford a 78:22 ratio in favour of the *endo* isomer (**6d**, see Figure 5). Such a cocrystallisation phenomenon has many literature precedents for asymmetric allyl complexes[17,41,48–51] and allowed us to fully determine the major diastereomers not only in the solid state but also in solution, as detailed in the previous section. An ORTEP view of the *endo* and *exo* diastereomers and selected bond lengths and angles are reported in Figure 5 and Table 3, respectively. Both isomers **6c** and **6d** exhibit a typical distorted square-planar arrangement of the (η^3-allyl)Pd-P,N moiety.[17–19,28,41] The P–Pd–N bite angle of 84.89(6)° falls in the range observed for other compounds with five-membered rings containing N,P ligands and the Pd–P [2.284(1) Å] and Pd–N [2.165(2) Å] bond lengths are similar to other reported values.[44,52–55] As a result of the different *trans* influence of the N and P atoms, the Pd–C(1) bond [2.187(4) Å] is longer than the Pd–C(3) bond [2.156(4) Å]. The tilt angle α between the C(1)–C(2)–C(3) and P–Pd–N planes is 107.6°, which is in the wide range (100–120°) reported for other allylic compounds. The envelope conformation of the five-membered chelate ring is characteristic of this kind of ligand in the solid state.[29,33,56]

Table 3. Selected bond lengths (Å) and bond angles (°) for **6c** and **6d** (* denotes *exo* isomer atoms)

endo		*exo*	
Pd–N	2.165(2)		
Pd–P(1)	2.2839(7)		
Pd–C(1)	2.187(4)	Pd–C(1*)	2.223(16)
Pd–C(2)	2.153(4)	Pd–C(2*)	2.11(2)
Pd–C(3)	2.156(4)	Pd–C(3*)	2.214(15)
C(1)–C(2)	1.418(6)	C(1*)–C(2*)	1.461(16)
C(2)–C(3)	1.413(6)	C(2*)–C(3*)	1.415(15)
N–Pd–P(1)	84.89(6)		
C(1)–Pd–C(3)	67.31(16)	C(1*)–Pd–C(3*)	65.0(5)
N–Pd–C(1)	101.91(13)	N–Pd–C(1*)	101.6(4)
P(1)–Pd–C(3)	105.82(10)	P(1)–Pd–C(3*)	104.5(3)
C(1)–C(2)–C(3)	116.5(5)	C(1*)–C(2*)–C(3*)	111.9(15)
C(2)–C(3)–C(4)	123.9(4)	C(2*)–C(3*)–C(4*)	129.2(16)

NMR NOESY Studies of the Dynamic Behaviour of Complex 1

The fluxional behaviour of the isomeric forms of $[Pd(\eta^3\text{-allyl})(L\text{-}L')]^+$ complexes in solution has been established as

 © 2004 Wiley-VCH Verlag GmbH & Co. KGaA, Weinheim

a consequence of different possible allyl isomerisation pathways or of the dissociation of the L-L′ ligand.[4] The existence of a dynamic equilibrium between the two diastereomers of complex **1** in a 1:1 ratio has already been reported by us[29] and we then wished to clarify the allyl isomerisation pathway by recurring to 2-D NMR experiments. Therefore, a phase-sensitive 2-D NOESY experiment was carried out in $CDCl_3$ solution. Similar experiments have previously been described for related compounds.[37,41,57] Figure 7 shows the results of this experiment and the most relevant exchange cross-peaks are labelled from *a* to *d*. The allyl ^1H NMR resonances are labelled on the 1D spectrum for isomers **a** (*endo*) and **b** (*exo*) following the nomenclature of Scheme 2, the primed labels corresponding to the *exo* isomer.

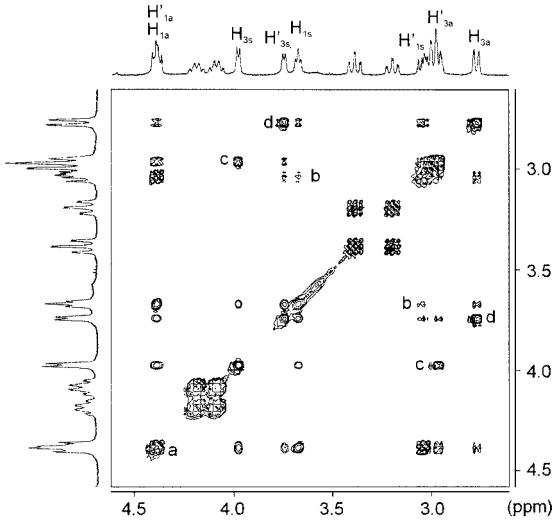

Figure 7. The ^1H-^1H phase-sensitive NOESY spectrum ($CDCl_3$, 500 MHz, 293 K) of complex **1**, showing the exchange cross-peaks (labelled *a* to *d*) in the isomers **1a** and **1b**

The spectrum shows exchange cross-peaks for all the external allylic protons belonging to the *same* C atom, indicating an η^3-η^1-η^3 isomerisation pathway. No exchange was observed between the H atoms on C_1 (*trans* to P) in **1a** and those on C_3 (*trans* to N) in **1b**, or vice versa, thereby excluding an apparent allyl rotation. At the C_1 position, the H_{1s} proton in **1a** exchanges with the H'_{1s} proton in **1b** (Figure 8). Correspondingly, the H_{1a} proton in **1a** exchanges with the H'_{1a} proton in **1b**. Thus, each terminal allyl proton *trans* to P keeps its relative position with respect to the internal allyl proton during the epimerisation process. At the C_3 position, on the other hand, cross-peaks between the 3-H_s (and 3-H_a) proton in **1a** and 3-H'_a (and 3-H'_s) proton in **1b** are observed. Thus, only the two terminal allyl protons *trans* to N trade places in the process. These two latter observations are in agreement with a *syn-anti* exchange, which implies the formation of an η^1-allyl intermediate by selective decoordination at the position *trans* to the phosphorus donor atom, followed by a C−C bond rotation and recoordination of the η^1-allyl double bond (see Scheme 3). This is consistent with the absence of any *anti cis*-P isomers for the monosubstituted complexes **3**−**6**. Other exchange cross-peaks were not observed. Notably, exchange peaks between 3-H_s and 3-H'_s and between 3-H_a and 3-H'_a are clearly absent. Because of the extensive overlap between the 1-H_a and 1-H'_a resonances, the absence of cross peaks between 1-H_a and 1-H'_s or between 1-H_s and 1-H'_a could not be unambiguously established, because any peak of this kind would be masked by the NOE peaks. However, we trust that we have sufficient evidence to conclude that a site-selective *syn-anti* exchange occurs at the C-3 atom.

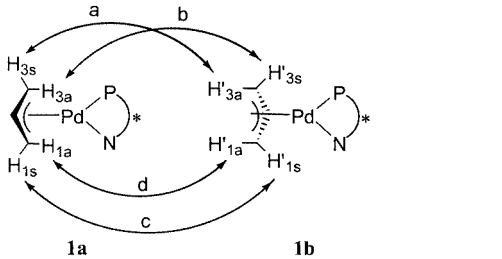

Figure 8. Exchange allyl protons between isomers **1a** and **1b**

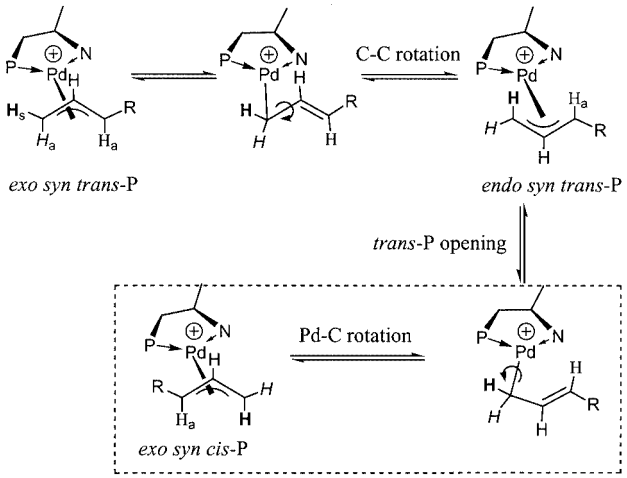

Scheme 3. η^3-η^1-η^3 isomerisation pathways involving a selective *trans*-P opening; dotted square: only for substituted allyl complexes **3**−**6**

Therefore, we can conclude that a selective opening of the η^3-allyl *trans* to the phosphorus atom occurs that leads exclusively to a *cis*-P σ-allyl intermediate during the η^3-η^1-η^3 isomerisation process. Such a selective process has already been described for chiral allyl complexes with P-based hybrid ligands resulting from the stronger *trans* influence of the P donor atom.[8,19,39,44] The only exception to this rule seems to involve a *cis*-P opening for a P,S ligand system.[14] For the other complexes reported here (**2**−**6**), we can as-

 © 2004 Wiley-VCH Verlag GmbH & Co. KGaA, Weinheim

sume a similar η^3-η^1-η^3 rearrangement by an exclusive *trans*-P opening. For the monosubstituted allyl compounds **3**−**6**, a second isomerisation pathway is necessary in order to interconvert the *cis*-P and *trans*-P isomers and this could involve an apparent allyl rotation. It seems likely that this pathway involves a Pd−C bond rotation after the selective *trans*-P opening (see Scheme 3). The same proposal was made by Krishnamurthy et al. to explain the *cis*/*trans* isomerisation of the minor isomers in [Pd(η^3-1-PhC_3H_4){$Ph_2PN(iPr)PPh(3,5\text{-}N_2C_3HMe_2)$}] complexes.[20]

Conclusion

The β-aminophosphane ligands $Ph_2PCH_2CH(Ph)NHAr$ [Ar = Ph L^1, (2,6-$C_6H_4iPr_2$) L^2] bearing a prochiral nitrogen atom display a bidentate coordination mode in allylpalladium complexes. Because of the presence of an asymmetric centre vicinal to the weakly basic amine function, the metal coordination is highly diastereoselective. Different (η^3-allyl)palladium complexes of formula [Pd(η^3-1-C_3H_4R)L][PF_6] (R = H, Me, Ph; L = L^1, L^2) have been synthesised and characterised in solution and in the solid state. In solution, they display a dynamic behaviour between the diastereomers because of a regioselective η^3-η^1-η^3 isomerisation of the allyl moiety interconverting *endo*/*exo* (for **1**−**6**) and *cis*/*trans*-P (for **3**−**6**) isomers. Complexes **3**−**6** show exclusively the *syn* orientation of the allylic substituents and therefore give rise to a mixture of four diastereomers. The isomeric proportion depends on the steric bulk of the allylic and/or N-substituents. The dynamic behaviour of **1** was studied by 2-D NOESY experiments. These prove that the *syn*-*anti* exchange process occurs via a regioselective η^3-allyl opening *trans* to the phosphorus position. On the basis of these results, the exclusive formation of *cis*-P η^1-allyl intermediates was assumed to occur by an apparent allyl rotation which equilibrates the *cis* and *trans*-P isomers for the monosubstituted allyl complexes **3**−**6**. Work aimed at obtaining enantiomerically pure forms of these aminophosphane ligands is in progress permitting the study of palladium-catalysed allylic alkylation of monosubstituted 1-propenyl substrates in order to correlate (or not) the regio-, stereo- and enantioselectivities with the observations described herein.

Experimental Section

All reactions were performed in Schlenk-type flasks under an argon atmosphere and solvents were purified and dried by conventional methods and distilled under argon. The ^1H, $^{13}C\{^1H\}$ and $^{31}P\{^1H\}$ NMR spectra were recorded in $CDCl_3$ on a Bruker 300 Advance or a Bruker 500 DRX instrument. Complete assignment was achieved by use of COSY, DEPT and HMQC experiments. All chemical shifts are relative to $SiMe_4$ (^1H and ^{13}C NMR) or 85% H_3PO_4 (^{31}P NMR) and are given in ppm. Numbering scheme used for the L^2 ligand: H^a, H^b and H^c are the non-equivalent PCH_2 and the NCH protons, respectively. Numbering scheme used for the allyl ligand: C^1, C^2 and C^3 are *trans* to P atom, central carbon and *cis* to P atom, respectively, and H^s and H^a are in the *syn* and *anti* positions, respectively, relative to the internal proton H^2. For complexes **1** and **2**, the carbon and proton chemical shifts are noted C, H and C′, H′ respectively, for the *endo* and *exo* diastereomers (see Scheme 2). The elemental analyses were performed on a Fisons EA 1108 apparatus at the L.S.E.O. in Dijon. The reagents *n*BuLi (1.6 M in hexane), Ph_2PCH_3 and $NaPF_6$ are commercial products from Aldrich, and were used as received. *N*-benzylidene-2,6-diisopropylaniline[58] and the chloro-bridged allylpalladium dimers[59] [Pd(η^3-C_3H_5)(μ-Cl)]$_2$, [Pd(η^3-MeC_3H_4)(μ-Cl)]$_2$, [Pd(η^3-PhC_3H_4)(μ-Cl)]$_2$ were prepared as described previously. Compound **1** and the ligand L^1 have already been described in a previous publication.[29]

Synthesis of Ligand L^2: According to Peterson's method,[60] 5.0 mL of *n*BuLi (1.6 M in hexane, 8 mmol) was slowly added to 1.2 mL of TMEDA (8 mmol) and the mixture was stirred at room temperature for 20 minutes. Methyldiphenylphosphane (1.5 mL, 8 mmol) was then slowly added. The mixture was stirred further leading within 30 minutes to a bright yellow precipitate, which was dissolved by addition of a few mililiters of THF. The solution was further stirred for half an hour and a solution of *N*-benzylidene-2,6-diisopropylaniline (1.65 g, 6.2 mmol) in 10 mL of THF was slowly added. The mixture was then stirred overnight, followed by hydrolysis with 20 mL of water. The water phase was separated and extracted three times with 20 mL of Et_2O. The combined organic phases were dried over $MgSO_4$ and the solvents were removed in vacuo. The product was recrystallised from ethanol and yellowish needles were isolated by filtration and dried in vacuo. Yield: 1.59 g (59%). $C_{32}H_{36}NP$ (465.6): calcd. C 82.55, H 7.79, N 3.01; found C 82.25, H 8.05, N 3.48. ^1H NMR ($CDCl_3$, 300.13 MHz): δ = 0.89 [d, $^3J_{H,H}$ = 6.5 Hz, 6 H, CH-(CH_3)$_2$], 1.02 [d, $^3J_{H,H}$ = 6.5 Hz, 6 H, CH-(CH_3)$_2$], 2.77 (ddd, $^2J_{H,P}$ = 1.0, $^3J_{H,H}$ = 8.0, $^2J_{H,H}$ = 13.5 Hz, 1 H, PCH^a), 2.91 (ddd, $^2J_{H,P}$ = 1.0, $^3J_{H,H}$ = 8.0, $^2J_{H,H}$ = 13.5 Hz, 1 H, PCH^b), 3.00 [septet, $^3J_{H,H}$ = 6.7 Hz, 2 H, CH-(CH$_3$)$_2$], 3.44 (broad s, 1 H, exchange with D_2O, NH), 3.93 (dt, $^3J_{H,H}$ = $^3J_{H,H}$ = 6.7, $^3J_{H,P}$ = 8.2 Hz, 1 H, NCH), 7.00 (m, 3 H, $H_{m,p}$ N-*Ph*), 7.14 (dd, $^4J_{H,H}$ = 1.4, $^3J_{H,H}$ = 7.9 Hz, 2 H, H_m C-*Ph*), 7.25−7.35 (m, 15 H, H_{arom}), 7.40 (dt, $^4J_{H,H}$ = 1.8, $^3J_{H,H}$ = 7.0 Hz, 1 H, H_o P-*Ph*), 7.45 (dt, $^4J_{H,H}$ = 1.8, $^3J_{H,H}$ = 7.0 Hz, 1 H, H_o P-*Ph*) ppm. $^{13}C\{^1H\}$ NMR (75.5 MHz, $CDCl_3$): δ = 24.3 [2C, 2 CH(CH_3)$_2$], 24.5 [2C, 2 CH(CH_3)$_2$], 28.2 [2C, 2 CH(CH$_3$)$_2$], 36.1 (d, $^2J_{C,P}$ = 14 Hz, PCH_2), 62.7 (d, $^3J_{C,P}$ = 17 Hz, NCH), 123.7 (2C, 2 C_m N-*Ph*), 124.0 (C_p N-*Ph*), 127.5 (2C, 2 C_m C-*Ph*), 127.9 (C_p C-*Ph*), 128.75 (2C, 2 C_o C-*Ph*), 128.85 (2C, 2 C_m P-*Ph*), 128.9 (2C, 2 C_m P-*Ph*), 129.0 (C_p P-*Ph*), 129.2 (C_p P-*Ph*), 132.9 (d, $^2J_{C,P}$ = 19 Hz, 2 C, 2 C_o P-*Ph*), 133.5 (d, $^2J_{C,P}$ = 21 Hz, 2 C, 2 C_o P-*Ph*), 138.9 (d, $^2J_{C,P}$ = 12 Hz, 1 C, 2 C_i P-*Ph*), 139.0 (d, $^2J_{C,P}$ = 12 Hz, 1 C, 2 C_i P-*Ph*), 141.1 (C_i C-*Ph*), 143.0 (2C, C_o N-*Ph*), 143.1 (C_i N-*Ph*) ppm. $^{31}P\{^1H\}$ NMR (121.5 MHz, $CDCl_3$): δ = −23.2 ppm.

[Pd(η^3-C_3H_5){$Ph_2PCH_2CHPhNH(2,6\text{-}C_6H_3iPr_2)$}][$PF_6$] (2): A dichloromethane solution (5 mL) of ligand L^2 (0.202 g, 0.53 mmol) was progressively added to a solution of [Pd(η^3-C_3H_5)Cl]$_2$ (97 mg, 0.26 mmol) in 5 mL of dichloromethane. The solution was stirred for 30 minutes at room temperature and then added to a suspension of $NaPF_6$ (0.223 g, 1.3 mmol) in 2 mL of dichloromethane. The mixture was stirred for a further 2 hours and filtered through Celite. The resulting yellow filtrate was concentrated in vacuo to ca. 1 mL. Addition of 15 mL of pentane caused the precipitation of the product, which was washed with pentane (2 × 20 mL). The white powder was filtered and dried under vacuum. Yield: 0.315 g (89%). $C_{35}H_{41}F_6NP_2Pd$ (758.1): calcd. C 55.45, H 5.45, N 1.84; found C 55.34, H 5.70, N, 2.11. Major isomer (**2a**, 68%): ^1H NMR

 © 2004 Wiley-VCH Verlag GmbH & Co. KGaA, Weinheim

($CDCl_3$, 500.13 MHz): δ = 0.34 [d, $^3J_{H,H}$ = 4.9 Hz, 3 H, CH-(CH_3)$_2$], 0.62 [d, $^3J_{H,H}$ = 4.9 Hz, 3 H, CH-(CH_3)$_2$], 0.95 [d, $^3J_{H,H}$ = 4.9 Hz, 3 H, CH-(CH_3)$_2$], 1.15 [d, $^3J_{H,H}$ = 4.9 Hz, 3 H, CH-(CH_3)$_2$], 2.86 [m, 1 H, C*H*-(CH$_3$)$_2$], 3.00 (dd, $^3J_{H,P}$ = 3.7, $^3J_{H,H}$ = 13.8 Hz, 1 H, H^{3a}), 3.14 (dt, $^3J_{H,H}$ = 2.9, $^2J_{H,P}$ = $^2J_{H,H}$ = 15.0 Hz, 1 H, PC*H*), 3.24 [m, 1 H, C*H*-(CH$_3$)$_2$], 3.66 (dt, $^3J_{H,H}$ = 3.6, $^2J_{H,P}$ = $^2J_{H,H}$ = 15.0 Hz, 1 H, PC*H*), 3.84 (t, $^3J_{H,P}$ = $^3J_{H1s,H2}$ = 5.9 Hz, 1 H, H^{1s}), 4.03(m, 1 H, NC*H*), 4.16 (d, $^3J_{H,H}$ = 6.8 Hz, 1 H, H^{3s}), 4.21 (dd, $^3J_{H,P}$ = 8.9, $^3J_{H,H}$ = 14.1 Hz, 1 H, H^{1a}), 5.51 (apparent tt, $^3J_{H2,H1s}$ = $^3J_{H2,H3s}$ = 6.9, $^3J_{H2,H1a}$ = $^3J_{H2,H3a}$ = 13.8 Hz, 1 H, H^2), 6.68 (d, $^3J_{H,H}$ = 10.8 Hz, 1 H, N*H*), 6.91−7.76 (m, merged with second diastereomer aromatic protons, H_{arom}) ppm. $^{13}C\{^1H\}$ NMR (125.7 MHz, $CDCl_3$): δ = 23.9 [CH-(*C*H$_3$)$_2$], 24.2 [CH-(*C*H$_3$)$_2$], 24.5 [CH-(*C*H$_3$)$_2$], 24.8 [CH-(*C*H$_3$)$_2$], 28.3 [2 *C*H-(CH$_3$)$_2$], 35.7 (d, $^2J_{C,P}$ = 25 Hz, P*C*H$_2$), 52.4 (C^3), 66.9 (d, $^3J_{C,P}$ = 7 Hz, N*C*H), 82.3 (d, $^2J_{C,P}$ = 27 Hz, C^1), 120.3 (d, $^2J_{C,P}$ = 5 Hz, C^2), 124.6−140.4 (m, 24 C, C_{arom}) ppm. $^{31}P\{^1H\}$ NMR (202.5 MHz, $CDCl_3$): δ = 30.71 (s), −142.75 (sept, $^1J_{F,P}$ = 716 Hz, PF_6^-) ppm. Minor isomer (**2b**, 32%): ^1H NMR: δ = 0.28 [d, $^3J_{H,H}$ = 5.3 Hz, 3 H, CH-(CH_3)$_2$], 0.69 [d, $^3J_{H,H}$ = 5.3 Hz, 3 H, CH-(CH_3)$_2$], 1.09 [d, $^3J_{H,H}$ = 5.3 Hz, 3 H, CH-(CH_3)$_2$], 1.13 [d, $^3J_{H,H}$ = 5.3 Hz, 3 H, CH-(CH_3)$_2$], 2.77 [m, 1 H, C*H*-(CH$_3$)$_2$], 2.96−3.00 (m, 2 H, H^{1s} and H^{3a}), 3.10 (dt, $^3J_{H,H}$ = 3.0, $^2J_{H,P}$ = $^2J_{H,H}$ = 14.8 Hz, 1 H, PC*H*), 3.46 (dt, $^3J_{H,H}$ = 4.0, $^2J_{H,P}$ = $^2J_{H,H}$ = 14.8 Hz, 1 H, PC*H*), 3.61 [m, 1 H, C*H*-(CH$_3$)$_2$], 3.90 (d, $^3J_{H,H}$ = 5.9 Hz, 1 H, H^{3s}), 4.19 (m, NC*H*), 4.35 (dt, $^2J_{H,H}$ = 2.1, $^3J_{H,P}$ = $^3J_{H,H}$ = 8.1 Hz, 1 H, H^{1a}), 6.02 (apparent tt, $^3J_{H2,H1s}$ = $^3J_{H2,H3s}$ = 6.4, $^3J_{H2,H1a}$ = $^3J_{H2,H3a}$ = 12.9 Hz, 1 H, H^2), 6.47 (d, $^3J_{H,H}$ = 9.8 Hz, 1 H, N*H*), 6.88−7.76 (m, merged with major diastereomer aromatic proton, H_{arom}) ppm. $^{13}C\{^1H\}$ NMR: δ = 23.4 [CH-(*C*H$_3$)$_2$], 23.7 [CH-(*C*H$_3$)$_2$], 24.2 [CH-(*C*H$_3$)$_2$], 24.4 [CH-(*C*H$_3$)$_2$], 28.2 [2 *C*H-(CH$_3$)$_2$], 35.7 (d, $^2J_{C,P}$ = 25 Hz, P*C*H$_2$), 53.4 (C^3), 66.9 (d, $^3J_{C,P}$ = 5 Hz, N*C*H), 80.6 (d, $^2J_{C,P}$ = 29 Hz, C^1), 122.2 (d, $^3J_{C,P}$ = 5 Hz, C^2), 124.4−139.8 (m, 24C, C_{arom}) ppm. $^{31}P\{^1H\}$ NMR: δ = 29.61 (s) ppm.

Complexes **3**−**6** were synthesised by following the same procedures as described above for the preparation of complex **2**.

[Pd(η^3-CH$_2$CHCHMe)(Ph$_2$PCH$_2$CHPhNHPh)][PF$_6$] (3): Starting materials: [Pd(η^3-MeC$_3$H$_4$)Cl]$_2$ (54 mg, 0.14 mmol), L^1 (104 mg, 0.27 mmol) and $NaPF_6$ (95 mg, 0.56 mmol). Yield: 0.164 g (88%). $C_{30}H_{31}F_6NP_2Pd$ (687.9): calcd. C 52.37, H 4.54, N 2.04; found C 52.23, H 4.89, N 2.34. Major *trans*-P isomer (**3a**, 53%): ^1H NMR ($CDCl_3$, 500.13 MHz): δ = 0.66 (dd, $^3J_{H,H}$ = 6.3, $^4J_{H,P}$ = 9.3 Hz, 3 H, C$^4H_3$), 2.56 (dd, $^2J_{H,H}$ = 2.1, $^3J_{H,H}$ = 11.8 Hz, 1 H, H^{3a}), 2.96 (dt, $^3J_{H,H}$ = 2.9, $^2J_{H,P}$ = $^2J_{H,H}$ = 14.6 Hz, 2 H, PC*H* and PC*H*′), 3.32 (dt, $^3J_{H,H}$ = 2.6, $^2J_{H,P}$ = $^2J_{H,H}$ = 14.3 Hz, 1 H, PC*H*), 3.79 (dd, $^2J_{H,H}$ = 2.6, $^3J_{H,H}$ = 6.8 Hz, 1 H, H^{3s}), 3.94 (m, 1 H, NC*H*), 4.98 (m, 1 H, H^{1a}), 5.23 (dt, $^3J_{H,H}$ = 6.3, $^3J_{H,H}$ = $^3J_{H,H}$ = 14.6 Hz, 1 H, H^2), 6.21 (d, $^3J_{H,H}$ = 11.4 Hz, 1 H, N*H*), 6.87−7.83 (m, merged with others diastereomers aromatic protons, H_{arom}) ppm. $^{13}C\{^1H\}$ NMR (125.7 MHz, $CDCl_3$): δ = 14.1 (d, $^3J_{C,P}$ = 4 Hz, C^4). 35.9 (d, $^2J_{C,P}$ = 23 Hz, P*C*H$_2$), 46.7 (d, $^2J_{C,P}$ = 4 Hz, C^3), 68.4 (d, $^3J_{C,P}$ = 10 Hz, N*C*H), 102.9 (d, $^2J_{C,P}$ = 26 Hz, C^1), 116.2 (d, $^2J_{C,P}$ = 5 Hz, C^2), 121.4−144.1 (m, 24C, C_{arom}) ppm. $^{31}P\{^1H\}$ NMR (202.5 MHz, $CDCl_3$): δ = 32.95 (s), −142.69 (sept, $^1J_{F,P}$ = 716 Hz, PF_6^-) ppm. Minor *trans*-P isomer (**3b**, 30%): ^1H NMR: δ = 1.04 (dd, $^3J_{H,H}$ = 6.3, $^4J_{H,P}$ = 9.1 Hz, 3 H, C$^4H_3$), 2.82 (d, $^3J_{H,H}$ = 10.1 Hz, 1 H, H^{3a}), 3.18 (dt, $^3J_{H,H}$ = 3.2, $^2J_{H,P}$ = $^2J_{H,H}$ = 14.6 Hz, 1 H, PC*H*), 3.54 (dd, $^2J_{H,H}$ = 2.2, $^3J_{H,H}$ = 6.8 Hz, 1 H, H^{3s}), 3.92 (m, 1 H, H^{1a}), 4.08 (m, 1 H, NC*H*), 5.58 (dt, $^3J_{H,H}$ = 6.9, $^3J_{H2,H1a}$ = $^3J_{H,H}$ = 13.8 Hz, 1 H, H^2), 5.87 (d, $^3J_{H,H}$ = 11.3 Hz, N*H*), 6.96−7.91 (m, merged with others diastereomers aromatic protons, H_{arom}) ppm. $^{13}C\{^1H\}$ NMR: δ = 14.2 (d, $^3J_{C,P}$ = 4 Hz, C^4), 35.5 (d, $^2J_{C,P}$ = 23 Hz, P*C*H$_2$), 47.5 (d, $^2J_{C,P}$ = 3 Hz, C^3), 68.8 (d, $^3J_{C,P}$ = 10 Hz, N*C*H), 101.7 (d, $^2J_{C,P}$ = 26 Hz, C^1), 118.9 (d, $^2J_{C,P}$ = 5 Hz, C^2), 144.4−121.5 (m, 24C, C_{arom}) ppm. $^{31}P\{^1H\}$ NMR: δ = 32.05 (s) ppm. Isomer *cis*-P (**3c**, 11%). ^1H NMR: δ = 1.09 (dd, $^3J_{H,H}$ = 6.3, $^4J_{H,P}$ = 9.1 Hz, 3 H, C$^4H_3$), 2.72 (broad d, $^3J_{H,H}$ = 6.9 Hz, H^{1s}), 4.17 (m,1 H, H^{1a}), 5.73 (m, 1 H, H^2), 6.25 (d, $^3J_{H,H}$ = 11.1 Hz, 1 H, N*H*) ppm. $^{13}C\{^1H\}$ NMR: δ = 17.2 (C^4), 72.3 (d, $^2J_{C,P}$ = 5 Hz, C^3), 78.3 (d, $^2J_{C,P}$ = 23 Hz, C^1), 123.5 (d, $^2J_{C,P}$ = 6 Hz, C^2) ppm. $^{31}P\{^1H\}$ NMR: δ = 32.10 (s) ppm. Isomer *cis*-P (**3d**, 6%): ^1H NMR: δ = 1.46 (dd, $^3J_{H,H}$ = 6.3, $^4J_{H,P}$ = 9.1 Hz, 3 H, C$^4H_3$), 2.81 (m, 1 H, H^{1s}), 5.68 (m, 1 H, H^2), 6.40 (d, $^3J_{H,H}$ = 11.0 Hz, 1 H, N*H*) ppm. $^{13}C\{^1H\}$ NMR: δ = 18.0 (C^4), 69.2 (d, $^2J_{C,P}$ = 4 Hz, C^3), 74.2 (d, $^2J_{C,P}$ = 25 Hz, C^1) ppm. $^{31}P\{^1H\}$ NMR: δ = 28.63 (s) ppm.

[Pd(η^3-CH$_2$CHCHMe){Ph$_2$PCH$_2$CHPhNH(2,6-C$_6$H$_3$*i*Pr$_2$)}][PF$_6$] (4): Starting materials: [Pd(η^3-MeC$_3$H$_4$)Cl]$_2$ (47 mg, 0.12 mmol), L^2 (112 mg, 0.24 mmol) and $NaPF_6$ (48 mg, 0.29 mmol). Yield: 0.149 g (81%). $C_{36}H_{43}F_6NP_2Pd$ (772.1): calcd. C 56.00, H 5.61, N 1.81; found C 55.81, H 5.77, N 2.14%. Major *trans*-P isomer (**4a**, 78%): ^1H NMR ($CDCl_3$, 500.13 MHz): δ = 0.36 [d, $^3J_{H,H}$ = 6.6 Hz, 3 H, CH-(CH_3)$_2$], 0.67 (dd, $^3J_{H,H}$ = 6.6, $^4J_{H,P}$ = 9.4 Hz, 3 H, C$^4H_3$), 0.69 [d, $^3J_{H,H}$ = 6.6 Hz, 3 H, CH-(C**H**$_3$)$_2$], 1.03 [d, $^3J_{H,H}$ = 6.6 Hz, 3 H, CH-(CH_3)$_2$], 1.17 [d, $^3J_{H,H}$ = 6.6 Hz, 3 H, CH-(CH_3)$_2$], 2.68 [sept, $^3J_{H,H}$ = 6.6 Hz, 1 H, C*H*-(CH$_3$)$_2$], 2.83 (dd, $^2J_{H,H}$ = 1.9, $^3J_{H,H}$ = 12.2 Hz, 1 H, H^{3a}), 3.20 [sept, $^3J_{H,H}$ = 6.4 Hz, 1 H, C*H*-(CH$_3$)$_2$], 3.27 (dt, $^3J_{H,H}$ = 3.0, $^2J_{H,P}$ = $^2J_{H,H}$ = 15.0 Hz, 1 H, PC*H*), 3.55 (dt, $^3J_{H,H}$ = 3.5, $^2J_{H,P}$ = $^2J_{H,H}$ = 14.8 Hz, 1 H, PC*H*), 4.10 (dd, $^2J_{H,H}$ = 2.6, $^3J_{H3s,H2}$ = 7.0 Hz, 1 H, H^{3s}), 4.14 (m, 1 H, NC*H*), 4.75 (m, 1 H, H^{1a}), 5.34 (dt, $^3J_{H2,H3s}$ = 7.0, $^3J_{H2,H1a}$ = $^3J_{H2,H3a}$ = 12.4 Hz, 1 H, H^2), 6.26 (d, $^3J_{H,H}$ = 10.9 Hz, 1 H, N*H*), 6.94−7.47 (m, merged with other diastereomers aromatic protons, H_{arom}) ppm. $^{13}C\{^1H\}$ NMR (125.7 MHz, $CDCl_3$): δ = 15.7 (d, $^3J_{C,P}$ = 4 Hz, C^4), 23.1 [CH-(*C*H$_3$)$_2$], 24.3 [CH-(*C*H$_3$)$_2$], 24.9 [CH-(*C*H$_3$)$_2$], 25.2 [*C*H-(*C*H$_3$)$_2$], 28.2 [*C*H-(CH$_3$)$_2$], 29.2 [*C*H-(CH$_3$)$_2$], 35.4 (d, $^2J_{C,P}$ = 25 Hz, P*C*H$_2$), 49.3 (d, $^2J_{C,P}$ = 4 Hz, C^3), 66.6 (d, $^3J_{C,P}$ = 8 Hz, N*C*H), 99.5 (d, $^2J_{C,P}$ = 26 Hz, C^1), 119.3 (d, $^2J_{C,P}$ = 5 Hz, C^2), 124.2−141.5 (m, 24C, C_{arom}) ppm. $^{31}P\{^1H\}$ NMR (202.5 MHz, $CDCl_3$): δ = 30.74 (s), −142.74 (sept, $^1J_{F,P}$ = 716 Hz, PF_6^-) ppm. Minor *trans*-P Isomer (**4b**, 9%): ^1H NMR: δ = 1.26 (dd, $^3J_{H,H}$ = 6.6, $^4J_{H,P}$ = 9.5 Hz, 3 H, C$^4H_3$), 2.92 (br. d, $^3J_{H,H}$ = 10.5 Hz, H^{3a}), 3.67 (dd, $^2J_{H,H}$ = 2.4, $^3J_{H3s,H2}$ = 6.2 Hz, 1 H, H^{3s}), 4.05 (m, 1 H, H^{1a}) 5.72 (dt, $^3J_{H2,H3s}$ = 6.8, $^3J_{H2,H1a}$ = $^3J_{H2,H3a}$ = 12.4 Hz, 1 H, H^2), 6.22 (d, $^3J_{H,H}$ = 10.9 Hz, 1 H, N*H*) ppm. $^{13}C\{^1H\}$ NMR: δ = 16.9 (d, $^3J_{C,P}$ = 5 Hz, C^4), 30.6 (d, $^2J_{C,P}$ = 24 Hz, P*C*H$_2$), 49.1 (broad, C^3), 66.8 (d, $^3J_{C,P}$ = 7 Hz, N*C*H), 103.3 (d, $^2J_{C,P}$ = 27 Hz, C^1), 119.2 (d, $^2J_{C,P}$ = 6 Hz, C^2) ppm. $^{31}P\{^1H\}$ NMR: δ = 28.90 (s) ppm. *cis*-P isomer (**4c**, 9%): ^1H NMR: δ = 1.62 (dd, 3 H, $^3J_{H,H}$ = 6.6, $^4J_{H,P}$ = 9.0 Hz, C$^4H_3$), 3.52 (masked, H^{1s}), 3.84 (dd, $^3J_{H,P}$ = 9.5, $^3J_{H1a,H2}$ = 13.5 Hz, 1 H, H^{1a}), 4.16 (masked, H^{3a}), 5.61 (dt, $^3J_{H2,H3s}$ = 7.7, $^3J_{H2,H1a}$ = $^3J_{H2,H3a}$ = 12.2 Hz, 1 H, H^2), 6.41 (d, $^3J_{H,H}$ = 10.9 Hz, 1 H, N*H*) ppm. $^{13}C\{^1H\}$ NMR: δ = 19.6 (C^4), 66.3 (d, $^3J_{C,P}$ = 7 Hz, N*C*H), 72.6 (d, $^2J_{C,P}$ = 4 Hz, C^3), 76.3 (d, $^2J_{C,P}$ = 27 Hz, C^1), 122.5 (d, $^2J_{C,P}$ = 5 Hz, C^2) ppm. $^{31}P\{^1H\}$ NMR: δ = 28.35 (s) ppm. *cis*-P isomer (**4d**, 4%): ^1H NMR: δ = 2.80 (masked, *H*), 4.03 (masked, *H*), 5.78 (dt, $^3J_{H2,H3s}$ = 7.7, $^3J_{H2,H1a}$ = $^3J_{H2,H3a}$ = 12.2 Hz, 1 H, H^2), 5.83 (d, $^3J_{H,H}$ = 10.9 Hz, 1 H, N*H*) ppm. $^{31}P\{^1H\}$ NMR: δ = 25.44 (s) ppm.

[Pd(η^3-CH$_2$CHCHPh)(Ph$_2$PCH$_2$CHPhNHPh)][PF$_6$] (5): Starting materials: [Pd(η^3-PhC$_3$H$_4$)Cl]$_2$ (54 mg, 0.10 mmol), L^1 (80 mg, 0.21 mmol) and $NaPF_6$ (43 mg, 0.26 mmol). Yield: 0.133 g (85%).

 © 2004 Wiley-VCH Verlag GmbH & Co. KGaA, Weinheim

$C_{35}H_{33}F_6NP_2Pd$ (750.0): calcd. C 56.06, H 4.40, N 1.90; found C 55.92, H 4.79, N 2.41. Major *trans*-P isomer (**5a**, 55%): ^{1}H NMR ($CDCl_3$, 500.13 MHz): δ = 2.77 (d, $^3J_{H,H}$ = 8.1 Hz, 1 H, H^{3a}), 2.90 (t, $^2J_{H,P}$ = $^2J_{H,H}$ = 14.6 Hz, 1 H, PC*H*), 3.40 (t, $^2J_{H,P}$ = $^2J_{H,H}$ = 13.9 Hz, 1 H, PC*H*), 3.88 (m, 2 H, NC*H* and H^{3s}), 5.82 (m, 2 H, H^2 and H^{1a}), 5.93 (d, $^3J_{H,H}$ = 11.1 Hz, 1 H, N*H*), 6.23−7.92 (m, merged with other diastereomers aromatic protons, H_{arom}) ppm. ^{13}C{^{1}H} NMR (125.7 MHz, $CDCl_3$): δ = 37.1 (d, $^2J_{C,P}$ = 24 Hz, PCH_2), 48.8 (C^3), 69.7 (d, $^3J_{C,P}$ = 10 Hz, NC*H*), 104.7 (d, $^2J_{C,P}$ = 24 Hz, C^1), 111.3 (d, $^2J_{C,P}$ = 5 Hz, C^2), 120.8−142.9 (m, 30 C, C_{arom}) ppm. ^{31}P{^{1}H} NMR (202.5 MHz, $CDCl_3$): δ = 35.50 (s), −142.70 (sept, $^1J_{F,P}$ = 716 Hz, PF_6^-) ppm. Minor *trans*-P isomer (**5b**, 22%): ^{1}H NMR: δ = 3.04 (d, $^3J_{H,H}$ = 10.8 Hz, 1 H, H^{3a}), 3.32 (m, 2 H, PCH_2), 3.62 (d, $^3J_{H,H}$ = 5.9 Hz, 1 H, H^{3s}), 3.99 (m, NC*H*), 4.67 (t, $^3J_{H,P}$ = $^3J_{H,H}$ = 9.9 Hz, 1 H, H^{1a}), 5.38 (d, $^3J_{H,H}$ = 10.9 Hz, 1 H, N*H*), 6.20 (m, H^2), 6.19−7.88 (m, merged with other diastereomers aromatic protons, H_{arom}) ppm. ^{13}C{^{1}H} NMR: δ = 37.8 (d, $^2J_{C,P}$ = 24 Hz, PCH_2), 49.8 (C^3), 69.7 (d, $^3J_{C,P}$ = 10 Hz, NC*H*), 104.6 (d, $^2J_{C,P}$ = 24 Hz, C^1), 115.0 (d, $^2J_{C,P}$ = 5 Hz, C^2), 121.4−147.3 (C_{arom}) ppm. ^{31}P{^{1}H} NMR: δ = 33.45 (s) ppm. Isomer *cis*-P (**5c**, 12%): ^{1}H NMR: δ = 4.25 (t, $^3J_{H,P}$ = $^3J_{H,H}$ = 7.2 Hz, 1 H, H^{1s}), 4.47 (dd, $^3J_{H,H}$ = 9.9, $^3J_{H,P}$ = 13.6 Hz, 1 H, H^{1a}), 4.81 (d, $^3J_{H,H}$ = 11.5 Hz, 1 H, H^{3a}), 6.19 (masked, H^2) ppm. ^{13}C{^{1}H} NMR: δ = 36.3 (d, $^2J_{C,P}$ = 25 Hz, PCH_2), 67.7 (d, $^3J_{C,P}$ = 10 Hz, NC*H*), 73.9 (d, $^2J_{C,P}$ = 5 Hz, C^3), 80.7 (d, $^2J_{C,P}$ = 26 Hz, C^1), 116.7 (d, $^2J_{C,P}$ = 5 Hz, C^2) ppm. ^{31}P{^{1}H} NMR: δ = 25.86 (s) ppm. Isomer *cis*-P (**5d**, 11%): ^{1}H NMR: δ = 3.08 (dd, $^3J_{H,H}$ = 9.4, $^3J_{H,P}$ = 13.7 Hz, 1 H, H^{1a}), 3.85 (masked, H^{3s}), 4.62 (d, $^3J_{H,H}$ = 11.5 Hz, 1 H, H^{3a}), 5.83 (masked, H^2) ppm. ^{13}C{^{1}H} NMR: δ = 36.3 (d, $^2J_{C,P}$ = 25 Hz, PCH_2), 68.1 (d, $^3J_{C,P}$ = 10 Hz, NC*H*), 74.6 (d, $^2J_{C,P}$ = 5 Hz, C^3), 82.0 (d, $^2J_{C,P}$ = 25 Hz, C^1), 119.6 (d, $^2J_{C,P}$ = 5 Hz, C^2) ppm. ^{31}P{^{1}H} NMR: δ = 25.61 (s) ppm.

[Pd(η^3-$CH_2CHCHPh$){$Ph_2PCH_2CHPhNH(2,6\text{-}C_6H_3iPr_2)$}][$PF_6$] (6): Starting materials: [Pd(η^3-PhC_3H_4)Cl]$_2$ (64 mg, 0.12 mmol), L^2 (115 mg, 0.25 mmol) and $NaPF_6$ (81 mg, 0.48 mmol). Yellow crystals suitable for X-ray diffraction were obtained from dichloromethane solution by layering with pentane. Yield: 0.172 g (82%). $C_{41}H_{46}F_6NP_2Pd$ (835.2): calcd. C 58.96, H 5.55, N 1.67; found C 59.19, H 5.78, N 1.94%. Major *cis*-P isomer (**6c**, 63%): ^{1}H NMR ($CDCl_3$, 500.13 MHz): δ = 0.32 [d, $^3J_{H,H}$ = 6.4 Hz, 3 H, CH-(CH_3)$_2$], 0.61 [d, $^3J_{H,H}$ = 6.7 Hz, 3 H, CH-(CH_3)$_2$], 1.11 [d, $^3J_{H,H}$ = 6.7 Hz, 3 H, CH-(CH_3)$_2$], 1.17 [d, $^3J_{H,H}$ = 6.5 Hz, 3 H, CH-(CH_3)$_2$], 2.86 [sept, $^3J_{H,H}$ = 6.7 Hz, 1 H, C*H*-(CH$_3$)$_2$], 3.02 (dt, $^3J_{H,H}$ = 2.8, $^2J_{H,P}$ = $^2J_{H,H}$ = 14.8 Hz, 1 H, PC*H*), 3.41 [m, 1 H, C*H*-(CH$_3$)$_2$], 3.66 (dt, $^3J_{H,H}$ = 3.4, $^2J_{H,P}$ = $^2J_{H,H}$ = 14.8 Hz, 1 H, PC*H*), 3.83 (dd, $^3J_{H,P}$ = 6.1, $^3J_{H,H}$ = 7.8 Hz, 1 H, H^{1s}), 3.97 (m, 1 H, NC*H*), 4.41 (dd, $^3J_{H,P}$ = 8.8, $^3J_{H1a,H2}$ = 13.8 Hz, 1 H, H^{1a}), 4.79 (d, $^3J_{H,H}$ = 11.8 Hz, 1 H, H^{3a}), 6.20 (ddd, $^3J_{H2,H1s}$ = 7.9, $^3J_{H2,H3a}$ = 11.8, $^3J_{H2,H1a}$ = 13.7 Hz, 1 H, H^2), 6.62 (d, $^3J_{H,H}$ = 10.8 Hz, 1 H, N*H*), 6.79−7.79 (m, merged with other diastereomers aromatic protons, H_{arom}) ppm. ^{13}C{^{1}H} NMR (125.7 MHz, $CDCl_3$): δ = 23.0 [CH-(CH_3)$_2$], 23.8 [CH-(CH_3)$_2$], 25.8 [CH-(CH_3)$_2$], 25.9 [CH-(CH_3)$_2$], 27.9 [CH-(CH_3)$_2$], 29.5 [CH-(CH$_3$)$_2$], 35.2 (d, $^2J_{C,P}$ = 24 Hz, PCH_2), 67.0 (d, $^3J_{C,P}$ = 8 Hz, NC*H*), 74.6 (d, $^2J_{C,P}$ = 6 Hz, C^3), 79.4 (d, $^2J_{C,P}$ = 25 Hz, C^1), 116.4 (d, $^2J_{C,P}$ = 5 Hz, C^2), 124.7−140.8 (m, 30 C, C_{arom}) ppm. ^{31}P{^{1}H} NMR (202.5 MHz, $CDCl_3$): δ = 21.85 (s), −142.62 (sept, $^1J_{F,P}$ = 716 Hz, PF_6^-) ppm. Minor *cis*-P isomer (**6d**, 22%): ^{1}H NMR: δ = 0.28 [d, $^3J_{H,H}$ = 6.4 Hz, 3 H, CH-(CH_3)$_2$], 0.70 [d, $^3J_{H,H}$ = 6.7 Hz, 3 H, CH-(CH_3)$_2$], 1.20 [d, $^3J_{H,H}$ = 6.6 Hz, 3 H, CH-(CH_3)$_2$], 1.27 [d, $^3J_{H,H}$ = 6.7 Hz, 3 H, CH-(CH_3)$_2$], 2.80 [sept, $^3J_{H,H}$ = 6.7 Hz, 1 H, C*H*-(CH$_3$)$_2$], 2.99 (m, 2 H, PC*H* and H^{3s}), 3.52 (dt, $^3J_{H,H}$ = 3.6, $^2J_{H,P}$ = $^2J_{H,H}$ = 14.7 Hz, 1 H, PC*H*), 3.78 [m, 1 H, C*H*-(CH$_3$)$_2$], 4.05 (m, 1 H, NC*H*), 4.23 (t, $^3J_{H,P}$ = $^3J_{H,H}$ = 7.3 Hz, 1 H, H^{1s}), 4.86 (d, $^3J_{H,H}$ = 11.8 Hz, 1 H, H^{3a}), 6.40 (m, 1 H, H^2), 6.44 (d, $^3J_{H,H}$ = 10.7 Hz, 1 H, N*H*), 6.85−7.79 (m, merged with other diastereomers aromatic protons, H_{arom}) ppm. ^{13}C{^{1}H} NMR: δ = 23.3 [CH-(CH_3)$_2$] 24.6 [CH-(CH_3)$_2$], 25.6 [CH-(CH_3)$_2$], 25.9 [CH-(CH_3)$_2$], 28.0 [CH-(CH$_3$)$_2$], 29.4 [CH-(CH$_3$)$_2$], 35.5 (d, $^2J_{C,P}$ = 21 Hz, PCH_2), 66.5 (d, $^3J_{C,P}$ = 8 Hz, NC*H*), 76.1 (d, $^2J_{C,P}$ = 5 Hz, C^3), 76.6 (d, $^2J_{C,P}$ = 27 Hz, C^1), 118.8 (d, $^2J_{C,P}$ = 6 Hz, C^2), 124.8−141.0 (C_{arom}) ppm. ^{31}P{^{1}H} NMR: δ = 29.68 (s) ppm. Isomer *trans*-P (**6a**, 9%): ^{1}H NMR: δ = 2.79 (d, $^3J_{H,H}$ = 11.9 Hz, 1 H, H^{3a}), 3.62 (d, $^3J_{H,H}$ = 6.8 Hz, 1 H, H^{3s}), 5.68 (dt, $^3J_{H,H}$ = 7.0, $^3J_{H,H}$ = 11.9 Hz, 1 H, H^2), 5.95 (dt, $^3J_{H,H}$ = 8.9, $^3J_{H,P}$ = 13.7 Hz, 1 H, H^{1a}) ppm. ^{31}P{^{1}H} NMR: δ = 31.60 (s) ppm. Isomer *trans*-P (**6b**, 7%): ^{1}H NMR: δ = 2.84 (masked, H^{3a}), 4.92 (dt, $^3J_{H,H}$ = 9.9, $^3J_{H,P}$ = 13.7 Hz, 1 H, H^{1a}), 6.40 (masked, H^2) ppm. ^{31}P{^{1}H} NMR: δ = 32.33 (s) ppm.

Crystal Structure Determination for 6: Crystal and refinement data are reported in Table 4. The data set was collected on an Enraf−Nonius KappaCCD diffractometer at 110 K using Mo-K_α radiation. The structure was solved with a Patterson search program[61] and refined with full-matrix least-squares methods[62] based on $|F^2|$ with the aid of the WINGX program.[63] The allylic fragment (CH_2···CH···CHPh) was found to be disordered with two different orientations (*endo*/*exo*). The occupation factors refined to m1 = 0.78 (*endo* isomer) and m2 = 1 − m1 = 0.22 (*exo* isomer).

Table 4. Crystallographic and refinement data for complexes **6**

Formula	$C_{41}H_{45}NPPd{\cdot}PF_6{\cdot}0.5(CH_2Cl_2)$
Mol. mass	876.58
T (K)	110(2)
Crystal system	monoclinic
Space group	*C*2/*c*
a (Å)	13.8841(2)
b (Å)	17.5047(2)
c (Å)	33.1026(5)
β (deg)	95.590(1)
V (Å^3)	8006.9(2)
Z	8
F(000)	3592
$D_{calcd.}$ (g/cm^3)	1.454
Diffractometer	Enraf−Nonius KappaCCD
Scan type	mixture of φ rotations and ω scans
λ (Å)	0.71073
μ (mm^{-1})	0.669
Crystal size (mm^3)	0.35 ∞ 0.25 ∞ 0.20
sin(θ)/λ max (Å^{-1})	0.65
Index ranges	h: −17; 18 k: −21; 22 l: −42; 42
Absorption correction	SCALEPACK
RC = Refl. Collected	16441
IRC = independent RC	9042 [R(int) = 0.032]
IRCGT = IRC and [$I > 2\sigma(I)$]	6538
Refinement method	Full-matrix L.S. on F^2
Data/restraints/parameters	9042/9/506
R for IRCGT	$R1$[a] = 0.0419, $wR2$[b] = 0.0938
R for IRC	$R1$[a] = 0.0697, $wR2$[b] = 0.1032
Goodness-of-fit[c]	1.067
Largest diff. peak and hole (e·Å^{-3})	0.80 and −1.10

[a] $R1 = \Sigma(||F_o| - |F_c||)/\Sigma|F_o|$. [b] $wR2 = [\Sigma w(F_o^2 - F_c^2)^2/\Sigma[w(F_o^2)^2]]^{1/2}$, where $w = 1/[\sigma^2(F_o^2) + (0.045P)^2 + 4.95P]$ and $P = [\text{Max}(F_o^2,0) + 2*F_c^2)/3$. [c] Goodness of fit = $[\Sigma w(F_o^2 - F_c^2)^2/(N_o - N_{H2,H3a})]^{1/2}$.

 © 2004 Wiley-VCH Verlag GmbH & Co. KGaA, Weinheim

All non-hydrogen atoms were refined with anisotropic thermal parameters except for the atoms belonging to the minor allylic fragment (*exo*) and the terminal carbon atom, C(1), of the major allylic fragment. The positions of the hydrogen atoms were either calculated or located in final Fourier difference maps and refined, after idealisation, with a riding model with isotropic temperature factors fixed to 1.5- or 1.2-times those of the corresponding parent atoms. CCDC-218899 contains the supplementary crystallographic data for this paper. These data can be obtained free of charge at www.ccdc.cam.ac.uk/conts/retrieving.html [or from the Cambridge Crystallographic Data Centre, 12 Union Road, Cambridge CB2 1EZ, UK; Fax: (internat.) +44-1223/336-033; E-mail: deposit@ccdc.cam.ac.uk].

Acknowledgments

We are grateful to the Ministère de la Recherche et de la Technologie for support and for a PhD fellowship (to J.-M. C.), the Centre National de la Recherche Scientifique (C.N.R.S.) and the Conseil Régional de Bourgogne for financial support of this work. We thank Dr. Bernard Hanquet (L.S.E.O.) for his assistance with the NOESY NMR experiments and Mr. Cédric Balan for technical assistance.

[1] A. Pfaltz, M. Lautens, in *Comprehensive Asymmetric Catalysis* (Eds.: E. N. Jacobsen, A. Pfaltz, H. Yamamoto), Springler, Heidelberg, **1999**, pp. 833−886.
[2] J. M. J. Williams, in *Catalysis in Asymmetric Synthesis*, Sheffield Academic Press, Sheffield, **1999**.
[3] M. Johannsen, K. A. Jorgensen, *Chem. Rev.* **1998**, *98*, 1689−1708.
[4] B. M. Trost, D. L. van Vranken, *Chem. Rev.* **1996**, *96*, 395−422.
[5] G. Helmchen, A. Pfaltz, *Acc. Chem. Res.* **2000**, *33*, 336−345.
[6] G. Helmchen, *J. Organomet. Chem.* **1999**, *576*, 203−214.
[7] A. Saitoh, T. Uda, T. Morimoto, *Tetrahedron: Asymmetry* **1999**, *10*, 4501−4511.
[8] A. Togni, U. Burckhardt, V. Gramlich, P. S. Pregosin, R. Salzmann, *J. Am. Chem. Soc.* **1996**, *118*, 1031−1037.
[9] H. Kubota, K. Koga, *Tetrahedron Lett.* **1994**, *35*, 6689−6692.
[10] G. J. Dawson, C. G. Frost, J. M. J. Williams, S. J. Coote, *Tetrahedron Lett.* **1993**, *34*, 3149−3150.
[11] W.-M. Dai, K. K. Y. Yeung, J.-T. Liu, Y. Zhang, I. D. Williams, *Org. Lett.* **2002**, *4*, 1615−1618.
[12] S. R. Gilbertson, P. Lan, *Org. Lett.* **2001**, *3*, 2237−2240.
[13] D. A. Evans, K. R. Campos, J. S. Tedrow, F. E. Michael, M. R. Gagné, *J. Am. Chem. Soc.* **2000**, *122*, 7905−7920.
[14] J. Herrmann, P. S. Pregosin, R. Salzmann, A. Albinati, *Organometallics* **1995**, *14*, 3311−3318.
[15] H. Adams, J. C. Anderson, R. J. Cubbon, D. S. James, J. P. Mathias, *J. Org. Chem.* **1999**, *64*, 8256−8262.
[16] A. Voituriez, E. Schultz, *Tetrahedron: Asymmetry* **2003**, *14*, 339−346.
[17] M. Kollmar, H. Steinhagen, J. P. Jansenn, B. Goldfuss, S. A. Malinovskaya, J. Vasquez, F. Rominger, G. Helmchen, *Chem. Eur. J.* **2002**, *8*, 3103−3114.
[18] M. Widhalm, U. Nettekoven, H. Kalchhauser, K. Mereiter, M. J. Calhorda, V. Felix, *Organometallics* **2002**, *21*, 315−325.
[19] M. Kollmar, B. Goldfuss, M. Reggelin, F. Rominger, G. Helmchen, *Chem. Eur. J.* **2001**, *7*, 4913−4927.
[20] S. K. Mandal, G. A. N. Gowda, S. S. Krishnamurthy, C. Zheng, S. Li, N. S. Hosmane, *Eur. J. Inorg. Chem.* **2002**, 2047−2056.
[21] R. J. van Haaren, C. J. M. Druijven, G. P. F. van Strijdonck, H. Oevering, J. N. H. Reek, P. C. J. Kamer, P. W. N. M. van Leeuwen, *Eur. J. Inorg. Chem.* **1999**, 1237−1241.
[22] R. Prétôt, A. Pfaltz, *Angew. Chem. Int. Ed.* **1998**, *37*, 323−325.
[23] R. Malet, M. Moreno-Manas, T. Parella, R. Pleixats, *J. Org. Chem.* **1996**, *61*, 758−763.
[24] P. Sennhenn, B. Gabler, G. Helmchen, *Tetrahedron Lett.* **1995**, *35*, 8595−8598.
[25] G. J. Dawson, J. M. J. Williams, S. J. Coote, *Tetrahedron Lett.* **1995**, *36*, 461−462.
[26] B. Akermark, B. Krakenberger, S. Hansson, A. Vitagliano, *Organometallics* **1987**, *6*, 620−628.
[27] G. Helmchen, S. Kudis, P. Sennhenn, H. Steinhagen, *Pure Appl. Chem.* **1997**, *69*, 513−518.
[28] U. Burckhardt, V. Gramlich, P. Hofmann, R. Nesper, P. S. Pregosin, R. Salzmann, A. Togni, *Organometallics* **1996**, *15*, 3496−3503.
[29] J. Andrieu, J.-M. Camus, J. Dietz, P. Richard, R. Poli, *Inorg. Chem.* **2001**, *40*, 1597−1605.
[30] J.-M. Camus, J. Andrieu, P. Richard, R. Poli, C. Baldoli, S. Maiorana, *Inorg. Chem.* **2003**, *42*, 2384−2390.
[31] J. Barluenga, F. López, F. Palacios, *Synthesis* **1989**, 298−300.
[32] T. Hayashi, M. Konishi, M. Fukushima, K. Kanehira, T. Hioki, M. Kumada, *J. Org. Chem.* **1983**, *48*, 2195−2202.
[33] J. Andrieu, P. Richard, J.-M. Camus, R. Poli, *Inorg. Chem.* **2002**, *41*, 3876−3885.
[34] H. Steinhagen, M. Reggelin, G. Helmchen, *Angew. Chem. Int. Ed. Engl.* **1997**, *36*, 2108−2110.
[35] M. Gomez, S. Jansat, G. Muller, M. A. Maestro, J. M. Saavedra, M. Font-Bardia, X. Solans, *J. Chem. Soc., Dalton Trans.* **2001**, 1432−1439.
[36] S.-L. You, X.-L. Hou, L.-X. Dai, Y.-H. Yu, W. Xia, *J. Org. Chem.* **2002**, *67*, 4684−4695.
[37] P. S. Pregosin, R. Salzmann, A. Togni, *Organometallics* **1995**, *14*, 842−847.
[38] J. P. Cahill, D. Cunneen, P. J. Guiry, *Tetrahedron: Asymmetry* **1999**, *10*, 4157−4173.
[39] R. Fernández-Galán, F. A. Jalón, B. R. Manzano, J. Rodríguez de la Fuente, *Organometallics* **1997**, *16*, 3758−3768.
[40] J. Sprinz, M. Kiefer, G. Helmchen, M. Reggelin, G. Huttner, O. Walter, L. Zsolnai, *Tetrahedron Lett.* **1994**, *35*, 1523−1526.
[41] K. Selvakumar, M. Valentini, M. Wörle, P. S. Pregosin, A. Albinati, *Organometallics* **1999**, *18*, 1207−1215.
[42] H. C. Clark, M. Hampden-Smith, H. Ruegger, *Organometallics* **1988**, *7*, 2085−2093.
[43] R. J. van Haaren, C. J. M. Druijven, G. P. F. van Strijdonck, H. Oevering, J. N. H. Reek, P. C. J. Kamer, P. W. N. M. van Leeuwen, *J. Chem. Soc., Dalton Trans.* **2000**, 1549−1554.
[44] B. Crociani, S. Antonaroli, G. Bandoli, L. Canovese, F. Visentin, P. Uguagliati, *Organometallics* **1999**, *18*, 1137−1147.
[45] P. Barbaro, P. S. Pregosin, R. Salzmann, A. Albinati, R. Kunz, *Organometallics* **1995**, *14*, 5160−5170.
[46] J. M. Brown, D. I. Hulmes, P. J. Guiry, *Tetrahedron* **1994**, *50*, 4493−4506.
[47] B. Crociani, S. Antonaroli, L. Canovese, F. Visentin, P. Uguagliati, *Inorg. Chim. Acta* **2001**, *315*, 172−182.
[48] A. Albinati, J. Eckert, P. Pregosin, H. Rueegger, R. Salzmann, C. Stoessel, *Organometallics* **1997**, *16*, 579−590.
[49] S. Schaffner, J. F. K. Mueller, M. Neuburger, M. Zehnder, *Helv. Chim. Acta* **1998**, *81*, 1223−1232.
[50] E. Pena-Cabrera, P.-O. Norrby, M. Sjoegren, A. Vitagliano, V. De Felice, J. Oslob, S. Ishii, D. O′Neill, B. kermark, P. Helquist, *J. Am. Chem. Soc.* **1996**, *118*, 4299−4313.
[51] S. Ramdeehul, L. Barloy, J. A. Osborn, A. De Cian, J. Fischer, *Organometallics* **1996**, *15*, 5442−5444.
[52] M. Sauthier, F. Leca, L. Toupet, R. Réau, *Organometallics* **2002**, *21*, 1591−1602.
[53] P. Braunstein, M. D. Fryzuk, M. Le Dall, F. Naud, S. J. Rettig, F. Speiser, *J. Chem. Soc., Dalton Trans.* **2000**, 1067−1074.
[54] M. Yamaguchi, M. Yabuki, T. Yamagishi, M. Kondo, S. Kitagawa, *J. Organomet. Chem.* **1997**, *538*, 199−202.
[55] P. von Matt, G. C. Lloyd-Jones, A. B. E. Minidis, A. Pfaltz, L.

 © 2004 Wiley-VCH Verlag GmbH & Co. KGaA, Weinheim

Macko, M. Neuburger, M. Zehnder, H. Rueegger, P. S. Pregosin, *Helv. Chim. Acta* **1995**, *78*, 265−284.
[56] A. Albinati, F. Lianza, H. Berger, P. S. Pregosin, H. Rüegger, R. W. Kunz, *Inorg. Chem.* **1993**, *32*, 478−486.
[57] A. Albinati, R. W. Kunz, C. J. Ammann, P. S. Pregosin, *Organometallics* **1991**, *10*, 1800−1806.
[58] B. E. Love, T. S. Boston, B. T. Nguyen, J. R. Rorer, *Org. Prep. Proc. Int.* **1999**, *31*, 399−405.
[59] P. R. Auburn, P. B. Mackenzie, B. Bosnich, *J. Am. Chem. Soc.* **1985**, *107*, 2033−2046.
[60] D. J. Peterson, *J. Organomet. Chem.* **1967**, *8*, 199−208.
[61] SHELXS-97, Programs for Crystal Structure Solution (Release 97-2). Sheldrick, G. M., Institüt für Anorganische Chemie der Universität, Tammanstrasse 4, 3400 Göttingen, Germany, **1998**.
[62] SHELXL-97, Programs for Crystal Structure Refinement (Release 97-2). Sheldrick, G. M., Institüt für Anorganische Chemie der Universität, Tammanstrasse 4, 3400 Göttingen, Germany, **1998**.
[63] L. J. Farrugia, *J. Appl. Crystallogr.* **1999**, *32*, 837−838.

Received September 4, 2003
Early View Article
Published Online February 5, 2004

 © 2004 Wiley-VCH Verlag GmbH & Co. KGaA, Weinheim

Hydroxo and Oxo Complexes of Platinum(II) Stabilized by Phosphanes: Synthesis and Characterization − X-ray Structures of *cis*-$[L_2Pt(\mu\text{-}OH)]_2(NO_3)_2$ (L = PMe_2Ph, $PMePh_2$) and $[\{cis\text{-}(PMe_2Ph)_2Pt\}_3(\mu\text{-}O)_2]Cl_2$

Bruno Longato,*[a,c] Giuliano Bandoli,[b] and Alessandro Dolmella[b]

Keywords: Platinum / Oxo and hydroxo ligands / X-ray diffraction / Deprotonation reactions

The dinuclear hydroxo complexes *cis*-$[L_2Pt(\mu\text{-}OH)]_2(NO_3)_2$ (L = PMe_2Ph and $PMePh_2$) have been characterized by single-crystal X-ray analysis, and their reactivity towards chloride ions has been investigated. Reaction of *cis*-$[L_2Pt(\mu\text{-}OH)]_2X_2$ (L = PMe_3, PMe_2Ph; X = NO_3^-, ClO_4^-) with $(NEt_4)Cl\cdot H_2O$ or $(AsPh_4)Cl$, in a 1:2 molar ratio, afforded a mixture of *cis*-$[L_2PtCl_2]$ and $[\{cis\text{-}L_2Pt\}_3(\mu\text{-}O)_2]^{2+}$ in ca. equimolar amounts. The trinuclear oxo compounds, separated by fractional crystallization of the reaction mixtures, were fully characterized by spectroscopic techniques, and the derivative $[\{cis\text{-}(PMe_2Ph)_2Pt\}_3(\mu\text{-}O)_2]Cl_2$ was also characterized by X-ray diffraction methods. Under the same experimental conditions, the structurally analogous hydroxo complex, stabilized by the less basic and more hindered $PMePh_2$ ligand, reacted with Cl^- to give *cis*-$[(PMePh_2)_2PtCl_2]$ as the only isolable species. The ^{31}P NMR spectroscopic analysis of the reaction mixtures allowed the detection of a moderately stable product, which is most likely to be the neutral hydroxo complex *cis*-$[L_2PtCl(OH)]$.

(© Wiley-VCH Verlag GmbH & Co. KGaA, 69451 Weinheim, Germany, 2002)

Introduction

Oxo complexes of platinum(II) stabilized by phosphanes of the type $[L_2Pt(\mu\text{-}O)]_2$ (L = PPh_3, PMe_2Ph; L_2 = bidentate phosphanes) have recently been described by P. R. Sharp.[1] They were obtained by deprotonation of the corresponding hydroxo bridged complexes $[L_2Pt(\mu\text{-}OH)]_2^{2+}$ with strong bases such as $LiN(SiMe_3)_2$. A common feature of the bridging oxo ligands, and their chalcogenide analogues,[2] is the ability to bind ions such as Li^+, Ag^+, Cu^+, and other metal centers, thus affording stable and well-characterized heteropolymetallic complexes. An exception is represented by the adduct $[cis\text{-}L_2Pt(\mu\text{-}O)]_2\cdot 2LiBF_4$ (L = PMe_2Ph), which decomposes in THF to give $[\{cis\text{-}L_2Pt\}_3(\mu\text{-}O)_2](BF_4)_2$ (Scheme 1), the trinuclear species in which each oxygen atom is symmetrically coordinated to three $[L_2Pt]^{2+}$ units.[3]

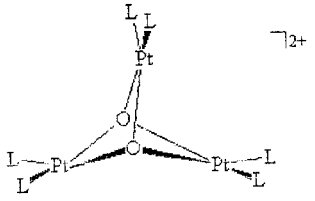

Scheme 1

We have now found that oxo complexes of this type are also formed when the hydroxo complexes *cis*-$[L_2Pt(\mu\text{-}OH)]_2^{2+}$ (L = PMe_3 and PMe_2Ph) react with chloride ions in aprotic solvents. The nucleophilic attack of Cl^- at the metal center affords a mixture of the mononuclear dichloro *cis*-$[L_2PtCl_2]$ species and the trinuclear $[\{cis\text{-}L_2Pt\}_3(\mu\text{-}O)_2]^{2+}$ species in which the relative quantity of the two compounds is strongly dependent on the amount of added chloride. A large excess of Cl^- ions leads to the formation of *cis*-$[L_2PtCl_2]$ as the main product, whereas relatively good yields of the oxo complex are formed when the molar ratio $n_{(Cl^-)}/n_{(\text{hydroxo complex})}$ approaches the value of 2:1. This finding contrasts the observations reported by Bushnell for the strictly related hydroxo complex stabilized by PEt_3.[4] In that case, addition of LiCl to a solution of $[cis\text{-}(PEt_3)_2Pt(\mu\text{-}OH)]_2^{2+}$, in a 2:1 molar ratio, gave the substitution product *cis*-$[(PEt_3)_2PtCl_2]$ and about half of the starting hydroxo complex remained unreacted.

[a] Dipartimento di Chimica Inorganica, Metallorganica ed Analitica, Università di Padova,
Via Marzolo 1, 35131 Padova, Italy
Fax: (internat.) +39-049-8275161
E-mail: longato@chin.unipd.it
[b] Dipartimento di Scienze Farmaceutiche, Università di Padova, Via Marzolo 5, 35131 Padova, Italy
[c] Istituto di Scienze e Tecnologie Molecolari, CNR, c/o Dipartimento di Chimica Inorganica, Metallorganica ed Analitica, Università di Padova, Via Marzolo 1, 35131 Padova, Italy.

 © 2004 Wiley-VCH Verlag GmbH & Co. KGaA, Weinheim **DOI: 10.1002/ejic.200300446**

In this paper, in addition to the X-ray structures of *cis*-$[L_2Pt(\mu\text{-}OH)]_2(NO_3)_2$ (L = PMe_2Ph, $PMePh_2$), we report on the details of the reaction of this class of dinuclear compounds with chloride ions. The facile deprotonation of the bridging hydroxo ligands, induced by the presence of the nucleophile Cl^-, offers an alternative route for the synthesis of the oxo compounds $[\{cis\text{-}L_2Pt\}_3(\mu\text{-}O)_2]^{2+}$ (L = PMe_2Ph, and PMe_3), one of which has not previously been described. The products have been isolated as pure compounds and characterized by spectroscopic methods, and the species $[\{cis\text{-}(PMe_2Ph)_2Pt\}_3(\mu\text{-}O)_2]Cl_2$ has also been characterized by single-crystal X-ray diffraction analysis. Moreover, the study of the reaction by ^{31}P NMR spectroscopy allowed the detection of unstable products, which are tentatively attributed to the mononuclear complexes *cis*-$[L_2PtCl(OH)]$ (L = PMe_3, PMe_2Ph, $PMePh_2$).

Results and Discussion

Synthesis and Characterization of the Hydroxo Complexes *cis*-$[(PMe_2Ph)_2Pt(\mu\text{-}OH)]_2X_2$ [X = NO_3^- (1a), ClO_4^- (1b)] and *cis*-$[(PMePh_2)_2Pt(\mu\text{-}OH)]_2(NO_3)_2$ (2)

We have already shown that the removal of the chloride ligands from the trimethylphosphane complex *cis*-$[(PMe_3)_2PtCl_2]$ with $AgNO_3$, followed by neutralization of the resulting solution, afforded the hydroxo compound *cis*-$[L_2Pt(\mu\text{-}OH)]_2(NO_3)_2$ (L = PMe_3). This compound is a dinuclear cationic complex, which is very soluble in water when the anion is the nitrate group.[5] More recently, we have prepared the complex *cis*-$[(PMe_2Ph)_2Pt(\mu\text{-}OH)]_2(NO_3)_2$ (**1a**) using the same procedure. This compound is still moderately soluble in water.[6] As previously observed for the PMe_3 analogue, the conversion of **1a** into the perchlorate salt results in a drastic decrease in the solubility. The compound *cis*-$[(PMe_2Ph)_2Pt(\mu\text{-}OH)]_2(ClO_4)_2$ (**1b**) can be obtained in a quantitative yield from **1a** by metathetical exchange. The complex *cis*-$[(PMePh_2)_2Pt(\mu\text{-}OH)]_2(NO_3)_2$ (**2**), which was prepared in a good yield using a slightly modified procedure, is virtually insoluble in water.

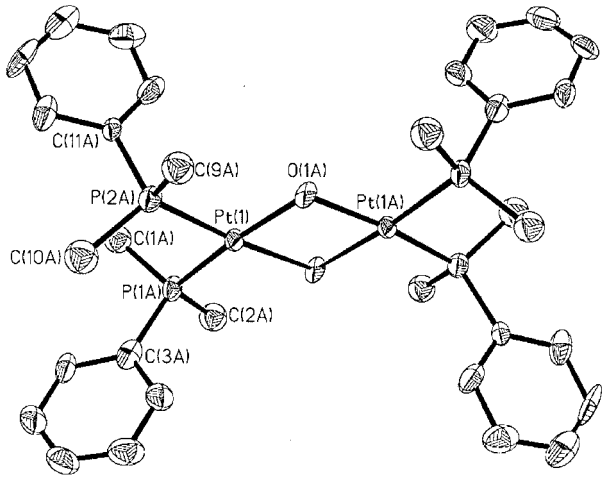

Figure 1. ORTEP drawing of **1a** showing 40% probability thermal ellipsoids and the essential atom numbering scheme; for clarity, the nitrate anions are omitted and only unit **I** is shown

The dinuclear nature of **1a** and **2** has been confirmed by single-crystal X-ray analysis. The ORTEP drawings of the two cations, *cis*-$[L_2Pt(\mu\text{-}OH)]_2^{2+}$, are shown in Figures 1 and 2, while the relevant bond lengths and angles are reported in Table 1. The unit cell of **1a** comprises two moieties denoted as **I** and **II**.

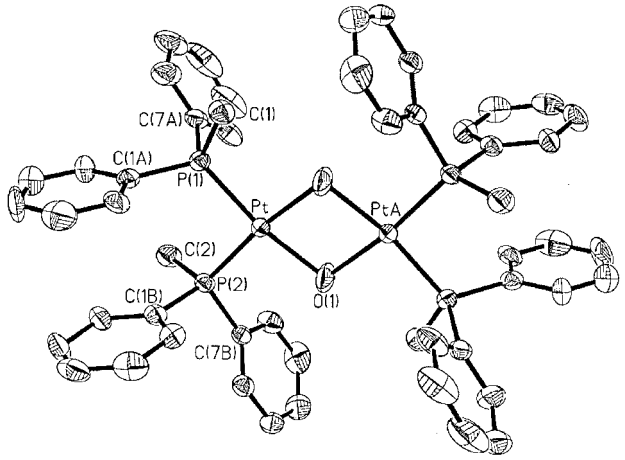

Figure 2. ORTEP drawing of **2** showing 40% probability thermal ellipsoids and the essential atom numbering scheme; for clarity, the nitrate anions are omitted

Table 1. Selected bond lengths [Å] and angles [°] for the complexes **1a** and **2**

	1a		**2**
	Unit I	Unit II	
Pt−P(1)	2.217(4)	2.234(4)	2.211(3)
Pt−P(2)	2.236(4)	2.219(4)	2.219(2)
Pt−O(1)	2.06(1)	2.08(1)	2.053(9)
Pt−O(1)[a]	2.08(1)	2.07(1)	2.073(8)
Pt···Pt[a]	3.233(1)	3.211(1)	3.174(1)
P(1)−Pt−P(2)	93.6(2)	94.9(2)	96.5(1)
P(1)−Pt−O(1)	172.3(3)	171.7(3)	170.0(2)
P(2)−Pt−O(1)[a]	171.4(3)	171.5(3)	172.4(3)
O(1)−Pt−O(1)[a]	77.5(4)	78.5(4)	79.4(4)
P(2)−Pt−O(1)[a]	95.0(3)	93.6(3)	91.1(2)
P(2)−Pt−O(1)	94.0(3)	93.1(3)	93.0(2)
Pt−O(1)−Pt[a]	102.5(4)	101.5(4)	100.6(2)

[a] At *x*, *y*, 1 − *z* in **1a**; at *x*, 1 − *y*, *z* in **2**.

The $P_4Pt_2O_2$ skeleton is essentially planar, within 0.03, 0.04, and 0.05 Å in **1a**−**I**, **1a**−**II**, and **2**, respectively. Comparison of the structural parameters of **1a** and **2** with those of the PMe_3 analogue shows only minor differences. In particular, the P−Pt−P and O−Pt−O angles are 93.6(2) and 77.5(4), 94.9(2) and 78.5(4), and 96.5(1)° and 79.4(4)° in **1a**−**I**, **1a**−**II**, and **2**, respectively, while the corresponding values in the PMe_3 analogue are 95.4(1) and 75.9(4)°. However, more significant changes are observed in the O···O and Pt···Pt distances. The O···O distance is relatively short in the PMe_3 derivative (2.54 Å), however, this distance is longer in

 © 2004 Wiley-VCH Verlag GmbH & Co. KGaA, Weinheim

1a and **2**, 2.61 Å and 2.64 Å, respectively; the latter value is the same as that observed for the structurally analogous complex that is stabilized by NH_3 ligands,[7] and only slightly shorter than that found in the PPh_3 derivative (2.66 Å).[3] An increase in the O···O separation is accompanied by a decrease in the Pt···Pt distance; 3.222 Å (average) in **1a**, 3.174(1) Å in **2** and 3.261 Å in the PMe_3 complex. This trend probably reflects the different repulsion effects at the metal centers due to the diverse basicity of the PR_3 ligands.[3]

As found in the PMe_3 analogue, in **1a** the hydroxo ligands interact via hydrogen-bonding with the nitrate anions. In particular, the atoms that are involved in this hydrogen-bonding interaction are O(6) (at x, y, $1 - z$) in unit **I** (O···O separation of 2.74 Å and an O−H···O angle of 167°) and O(2) (at x, $y + 1$, z) in unit **II** (separation of 2.79 Å and an angle of 178°). This hydrogen-bonding system is not present in the crystal packing of **2**, where the shortest O···O distance is 3.18 Å.

The spectroscopic characterization of compounds **1** and **2** has been carried out in [D_6]DMSO. In the ^{1}H NMR spectra, the OH resonances are observed as broad singlets at $\delta = 4.11$ (L = PMe_2Ph) and 3.53 (L = $PMePh_2$), values similar to that observed for the PMe_3 analogue ($\delta = 3.46$).[5] The ^{31}P NMR spectra, obtained at 36.23 MHz, exhibit a singlet flanked by the typical pattern due to the ^{195}Pt satellites. Each component of the doublet, which is assigned to the isotopomer $[L_2{}^{195}Pt(OH)_2PtL_2]^{2+}$ ($^1J_{P,Pt} = 3457$ Hz for **1** and 3571 Hz for **2**), is flanked by a couple of very weak resonances, separated by 304 Hz for **1** and 232 Hz for **2**, due to the contribution of the less abundant isotopomer $[L_2{}^{195}Pt(OH)_2{}^{195}PtL_2]^{2+}$ (relative abundance 11.4%). As previously noticed for *cis*-$[(PMe_2Ph)_2Pt(\mu\text{-}OH)]_2(BF_4)_2$,[3] the main resonance does not show resolved satellites, which are assigned to the $^3J_{P,Pt}$ coupling, indicating that the magnetic interaction between the ^{31}P and ^{195}Pt nuclei through three bonds is presumably too small to be observed.

Lability of the Bridging Hydroxo Ligands in *cis*-$[L_2Pt(\mu\text{-}OH)]_2^{2+}$ (L = PMe_3, PMe_2Ph, and $PMePh_2$)

The ^{1}H and ^{31}P NMR spectroscopic parameters of **1** and **2** do not exhibit appreciable changes with the concentration (in the 10^{-2} to 10^{-3} M range), suggesting that these dinuclear hydroxo-bridged complexes do not dissociate significantly in DMSO solution. However, the lability of the Pt−O bonds becomes evident when solutions of **1** and **2** are mixed. The ^{31}P NMR spectrum of a freshly prepared mixture shows, after a few minutes, the growth of two new singlets, symmetrically flanked by ^{195}Pt satellites at $\delta = -5.15$ ($^1J_{P,Pt} = 3541$ Hz) and −16.15 ($^1J_{P,Pt} = 3478$ Hz). These values for the chemical shifts and the coupling constants are intermediate between those found for the pure compounds (Table 2), and are consistent with the formation of the mixed complex *cis*-$[(PMe_2Ph)_2Pt(\mu\text{-}OH)_2Pt(PMePh_2)_2]^{2+}$. A similar exchange also occurs when **1** or **2** are mixed with *cis*-$[(PMe_3)_2Pt(\mu\text{-}OH)]_2(NO_3)_2$.

Table 2. ^{1}H and ^{31}P NMR spectroscopic data for *cis*-$[L_2Pt(\mu\text{-}OH)_2PtL'_2](NO_3)_2$ in [D_6]DMSO at 27 °C

L,L	δ_p [ppm]	$^1J_{P,Pt}$ [Hz]	δ_{OH} [ppm]
L = L′ = PMe_3	−24.5	3358	3.46
L = L′ = PMe_2Ph	−15.5	3457	4.11
L = L′ = $PMePh_2$	−5.32	3571	3.53
L = PMe_3 L′ = PMe_2Ph	−24.30 −15.73	3363 3446	3.40
L = PMe_3 L′ = $PMePh_2$	−24.87 −4.94	3377 3522	4.01
L = PMe_2Ph L′ = $PMePh_2$	−16.15 −5.15	3478 3541	3.90

In all the cases, the NMR spectrum of the resulting mixture shows the resonances of the starting complexes and two new singlets which are assigned to the species *cis*-$[L_2Pt(\mu\text{-}OH)_2PtL'_2]^{2+}$ (L = PMe_3, L′ = PMe_2Ph or $PMePh_2$). After a few hours at room temperature, the relative intensities of the signals due to the mixed complexes are approximately the same as those expected for a statistical distribution of the *cis*-$[L_2Pt(OH)]^+$ units according to the equilibrium reaction [Equation (1)].

$$cis\text{-}[L_2Pt(\mu\text{-}OH)]_2{}^{2+} + cis\text{-}[L'_2Pt(\mu\text{-}OH)]_2{}^{2+} \rightleftarrows 2\ cis\text{-}[L_2Pt(\mu\text{-}OH)_2PtL'_2]^{2+} \quad (1)$$

This exchange reaction is followed by a further redistribution of the neutral ligands around the metal center as indicated by the appearance of additional doublets due to the {*cis*-LL′Pt} moieties in the ^{31}P NMR spectra.[8] The lability of the bridging hydroxo ligands has previously been observed in the structurally related Ni^{II} complexes $[NiR(PMe_3)(\mu\text{-}OH)]_2$ (R= CH_2Ph; CH_2CMe_2Ph).[9]

Synthesis and Characterization of the Oxo Complexes [{*cis*-$L_2Pt\}_3(\mu\text{-}O)_2]X_2$ (L = PMe_3, X= ClO_4^-, 3; L = PMe_2Ph, X = Cl^-, 4)

When chloride ions were added to solutions of *cis*-$[L_2Pt(\mu\text{-}OH)]_2X_2$ (X = NO_3^-, ClO_4^-; L = PMe_3, PMe_2Ph) in DMSO or CH_2Cl_2/DMSO, at room temperature, a mixture of the species *cis*-$[L_2PtCl_2]$ and $[\{cis\text{-}L_2Pt\}_3(\mu\text{-}O)_2]^{2+}$ (L = PMe_3, **3**; PMe_2Ph, **4**) was formed. {^{1}H}^{31}P NMR analysis of the resulting pale yellow solutions shows that the relative quantity of the two products is strongly dependent on the stoichiometric ratio of the reactants. A large excess of Cl^- ions (molar ratio > 10), added as solid $(NEt_4)Cl{\cdot}H_2O$ or $(PPh_4)Cl$, affords the corresponding *cis*-$[L_2PtCl_2]$ as the only detectable species. At lower concentrations of the chloride ions, the solutions contain increasing amounts of the oxo complexes $[\{cis\text{-}L_2Pt\}_3(\mu\text{-}O)_2]^{2+}$.

 © 2004 Wiley-VCH Verlag GmbH & Co. KGaA, Weinheim

When the molar ratio $n_{(Cl^-)}/n_{(Pt\ complex)}$ is in the range 1−2, the relative intensity of the ^{31}P resonances which are assigned to the dichloro and oxo complexes approach the value expected from the following reaction [Equation (2)].

$$2\ cis\text{-}[L_2Pt(\mu\text{-}OH)]_2^{2+} + 2\ Cl^- \rightleftarrows cis\text{-}[L_2PtCl_2] + [\{cis\text{-}L_2Pt\}_3(\mu\text{-}O)_2]^{2+} + 2\ H_2O \quad (2)$$

The trinuclear complexes were obtained as pure compounds (^{31}P NMR spectroscopy) after precipitation with Et_2O, followed by fractional crystallization. The elemental analysis of the product isolated from the reaction of *cis*-$[(PMe_3)_2Pt(\mu\text{-}OH)]_2(ClO_4)_2$ with $(NEt_4)Cl$ was consistent with the separation of the oxo species as the perchlorate salt, $[\{cis\text{-}(PMe_3)_2Pt\}_3(\mu\text{-}O)_2](ClO_4)_2$ (**3**). The presence of the ClO_4^- ion was clearly evidenced by the typical absorption at 1093 cm^{-1} in the IR spectrum of the solid.

The crystallization of the product obtained from the reaction of *cis*-$[(PMe_2Ph)_2Pt(\mu\text{-}OH)]_2(ClO_4)_2$ with Cl^- gave crystals of $[\{cis\text{-}(PMe_2Ph)_2Pt\}_3(\mu\text{-}O)_2]Cl_2$ (**4**), i.e. the chloride salt of the oxo species, as established by single-crystal X-ray analysis. The structure of the dication of **4** is shown in Figures 3 and 4, while the relevant data are presented in Table 3.

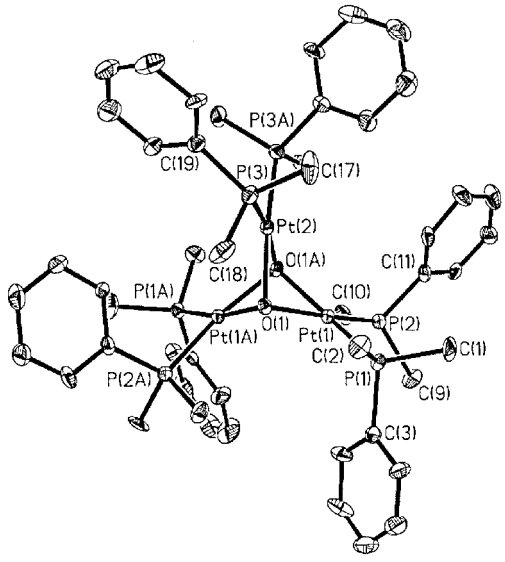

Figure 3. ORTEP drawing of **4** showing 35% probability thermal ellipsoids and the essential atom numbering scheme; for clarity, the chloride anions are omitted

The oxygen atoms cap a triangle formed by three $(PMe_2Ph)_2Pt$ units in which the average Pt···Pt distance is 2.884 Å. Comparison of this structure with that containing BF_4^- as the counterion[3] does not reveal any significant differences. For example, the Pt−O distances and the angles around the oxygen atoms are almost equal, averaging 2.087(5) Å and 87.4(2)° in **4** and 2.083(8) Å and 87.4(3)° in that previously determined. The three dihedral angles formed by the three P_2PtO_2 mean planes are 61.3, 58.7, and 61.3° in **4** and compare with the values of 61.8, 59.1, and 59.5° in the BF_4^- derivative.

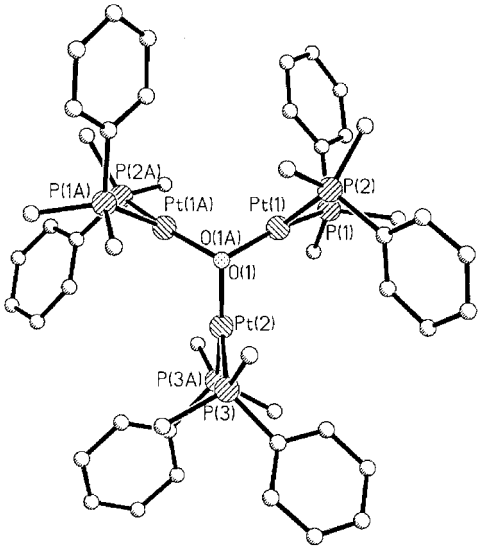

Figure 4. The dication of **4** viewed along the O(1)···O(1A) line

Table 3. Selected bond lengths [Å] and angles [°] for complex **4**

Pt(1)−O(1)	2.089(5)	Pt(1)−P(1)	2.229(2)
Pt(1)−O(1A)[a]	2.078(5)	Pt(1)−P(2)	2.230(2)
Pt(2)−O(1)	2.094(5)	Pt(2)−P(3)	2.233(2)
Pt(1)···Pt(2)	2.883(1)	Pt(2)···Pt(1A)	2.883(1)
Pt(1)···Pt(1A)	2.886(1)		
		P(3)−Pt(2)−O(1)	94.2(2)
P(1)−Pt(1)−P(2)	97.1(1)	P(3)−Pt(2)−P(3A)	97.9(1)
P(1)−Pt(1)−O(1)	94.8(1)	O(1)−Pt(2)−O(1A)	73.9(3)
O(1)−Pt(1)−O(1A)	74.3(2)	P(3)−Pt(2)−O(1A)	167.6(2)
O(1A)−Pt(1)−P(2)	94.2(1)	Pt(1)−O(1)−Pt(2)	87.1(2)
P(1)−Pt(1)−O(1A)	167.5(1)	Pt(1)−O(1)−Pt(1A)	87.7(2)
P(2)−Pt(1)−O(1)	167.7(1)	Pt(2)−O(1)−Pt(1A)	87.4(2)

[a] At $1/2 - x$, $y - 1/2$, $1/2 - z$.

Attempts to determine the structure of **3** by X-ray analysis were unsuccessful. However the ^{31}P NMR spectrum of this complex shows a pattern that is very similar to that shown in the spectrum of **4**. Both complexes are characterized by a singlet (at $\delta = -30.3$ and −19.5 ppm for **3** and **4**, respectively, in $[D_6]DMSO$) that is symmetrically flanked by satellites which can be assigned to the $^3J_{P,Pt}$ (ca. 13 Hz) and $^1J_{P,Pt}$ couplings (in the range 3356−3396 Hz for **3** and 3410−3460 Hz for **4**).

Dinuclear oxo complexes of platinum(II) stabilized by phosphanes are obtained by reacting the corresponding hydroxo compounds with strong bases [Equation (3)].

$$cis\text{-}[L_2Pt(\mu\text{-}OH)]_2(BF_4)_2 + 2\ LiNR_2 \rightleftarrows [cis\text{-}L_2Pt(\mu\text{-}O)]_2{\cdot}2LiBF_4 + 2\ HNR_2 \quad (3)$$

The bridging oxo ligands generally associate one or two molecules of $LiBF_4$, depending on the type of phosphane used. In solution, when L is PMe_2Ph, the dinuclear oxo complex decomposes to form the stable species $[\{cis\text{-}(PMe_2Ph)_2Pt\}_3(\mu\text{-}O)_2](BF_4)_2$ in a high yield.[3] In the reaction of **1**, and its PMe_3 analogue, with Cl^- ions [Equa-

 © 2004 Wiley-VCH Verlag GmbH & Co. KGaA, Weinheim

tion (2)], the ^{31}P NMR spectra obtained immediately after the addition of the chloride ions do not show signals which can be assigned to the dinuclear oxo complex. The formation of *cis*-$[L_2PtCl_2]$ and $[\{cis\text{-}L_2Pt\}_3(\mu\text{-}O)_2]^{2+}$ instead is accompanied by the formation of a relatively stable species; it has tentatively been suggested that this species is the mixed complex *cis*-$[L_2PtCl(OH)]$, although a dinuclear species of the type $[\{cis\text{-}L_2Pt\}_2(\mu\text{-}Cl)(\mu\text{-}OH)]^{2+}$ cannot be ruled out.[10] In a typical experiment, increasing amounts of $(AsPh_4)Cl$ as a solid were added to a CD_2Cl_2 solution of **1a** and the ^{31}P NMR spectrum of the resulting solution immediately obtained. Figure 5(a) shows the spectrum that is observed when the molar ratio $n_{(\mathbf{1a})}/n_{(Cl^-)}$ is 1.0. The main resonance signal is the singlet, whose chemical shift and coupling constant are very similar to those of unchanged **1a**. The signals of the oxo species (at $\delta = -19.5$) and the dichloro complex (at $\delta = -14.4$) exhibit relative intensities of 5.6:1, whereas the resonances assigned to *cis*-$[L_2PtCl(OH)]$, characterized by an AX multiplet, (at ca. $\delta = -12$ and -24 ppm; $^2J_{P,P} = 24$ Hz) are only just detectable.

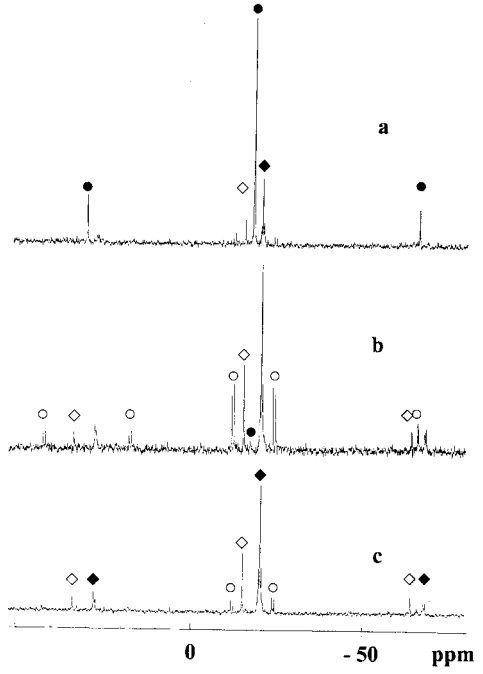

Figure 5. $\{^1H\}^{31}P$ NMR spectrum (at 36.23 MHz) of a solution ($3.73\cdot10^{-2}$ M) of **1a** in CD_2Cl_2 at 27 °C: (**a**) immediately after the addition of $(AsPh_4)Cl$ (molar ratio **1a**/Cl^- = 1:1); the labels (solid circle and solid diamond) refer to the complexes *cis*-$[(PMe_2Ph)_2Pt(\mu\text{-}OH)]_2^{2+}$ and *cis*-$[\{(PMe_2Ph)_2Pt\}_3(\mu\text{-}O)_2]^{2+}$, respectively; (**b**) ca. half an hour after (a), following the addition of a further amount of $(AsPh_4)Cl$ (molar ratio **1a**/Cl^- = 1:2); (**c**) after 12 h at 33 °C); the labels (open circle and open diamond) refer to the complexes *cis*-$[(PMe_2Ph)_2PtCl_2]$ and *cis*-$[(PMe_2Ph)_2PtCl(OH)]$, respectively

The further addition of chloride ions ($n_{(\mathbf{1a})}/n_{(Cl^-)}$ = 1:2), carried out after ca. 0.5 h, leads to the almost complete disappearance of the resonances due to the starting complex, whereas the AX multiplet became more intense to allow the detection of the platinum-195 satellites (Figure 5, b). The doublet at lower field ($\delta = -11.97$, $^1J_{P,Pt}$ 3930 Hz) is assigned to the PMe_2Ph molecule *trans* to the chloride ion, and the resonance at -23.86 ppm, with a lower P−Pt coupling constant (3020 Hz), is assigned to the phosphane *trans* to the hydroxo ligand. The intensities of these signals slowly decrease, whereas the relative intensities of the signals at $\delta = -19.5$ and -14.4 ppm remain apparently unchanged as shown in Figure 5(c), which represents the spectrum of the same solution left for 12 h at 33 °C.

A similar behavior was observed with the hydroxo complex stabilized by PMe_3. The spectrum of a mixture containing *cis*-$[(PMe_3)_2Pt(\mu\text{-}OH)]_2X_2$ and Cl^- in a 1:2 molar ratio shows, in addition to the resonances assigned to the oxo complex **3** (52% of relative intensity) and *cis*-$[(PMe_3)_2PtCl_2]$ (relative intensity 20%), an AX multiplet ($^2J_{P,P}$ = 20 Hz) at $\delta = -21.0$ and -34.0 ppm which disappears after 24 h. These results lead to conclusion that the species responsible for the AX multiplet, the mononuclear hydroxo complex *cis*-$[(PMe_3)_2PtCl(OH)]$, slowly decomposes leaving a pale yellow solution in which the only detectable resonances are those of the colorless species *cis*-$[L_2PtCl_2]$ and $[\{cis\text{-}L_2Pt\}_3(\mu\text{-}O)_2]^{2+}$.

Once formed, the species $[\{cis\text{-}L_2Pt\}_3(\mu\text{-}O)_2]^{2+}$ are unreactive towards an excess of Cl^- ions. In fact, the ^{31}P NMR spectrum of the isolated complex **3** (in **4**) in DMSO is unaffected by the addition of $AsPh_4Cl$ (molar ratio 1:3), after several days at room temperature. The stability of the Pt−O bonds in these trinuclear oxo complexes is confirmed by the observation that they do not undergo intermolecular exchange. Unlike their hydroxo precursors, when mixed in DMSO, **3** and **4** maintain their structure as is observed by the absence of new resonances in the ^{31}P NMR spectrum of the resulting mixture.

Reactivity of *cis*-$[(PMePh_2)_2Pt(\mu\text{-}OH)]_2^{2+}$ with Cl^-

Under the same conditions as those used for the PMe_3 and PMe_2Ph analogues, complex **2** does not form stable oxo species when treated with Cl^-. The ^{31}P NMR spectrum of a solution of **2** in $CDCl_3$ (or CH_2Cl_2/[D_6]DMSO mixtures) containing $(NEt_4)Cl\cdot H_2O$ (or $AsPh_4Cl$) in a 1:2 molar ratio, exhibit an intense singlet at $\delta = -1.08$ ($^1J_{P,Pt}$ = 3634 Hz) and an AX multiplet (δ = 1.97, $^1J_{P,Pt}$ = 4030 Hz and -9.03 ppm, $^1J_{P,Pt}$ = 3100 Hz, with $^2J_{P,P}$ = 23 Hz) as the main resonance signals. These signals are assigned to *cis*-$[(PMePh_2)_2PtCl_2]$ and to the neutral complex *cis*-$[(PMePh_2)_2PtCl(OH)]$. Two relatively weak signals are seen at $\delta = -8.85$ (singlet, $^1J_{P,Pt}$ = 3602 Hz) and at $\delta = -5.72$ (broad singlet). After 12 h at room temperature, the AX multiplet disappears, the resonance at $\delta = -5.72$ ppm also disappears and is replaced by a very weak singlet at $\delta = -5.92$ due to unchanged complex **2**. A further change in the ^{31}P NMR spectrum occurs after several days, leading to the complete disappearance of the resonance at $\delta = -8.85$. The low concentration and the moderate stability of the species responsible for this singlet prevents better characterization. The absence of the fine structure observed for **3** and **4**, however, seems to exclude the formation of the anal-

 © 2004 Wiley-VCH Verlag GmbH & Co. KGaA, Weinheim

ogous trinuclear species *cis*-$[\{(PMePh_2)_2Pt\}_3(\mu\text{-}O)_2]^{2+}$. On the other hand, the formation of a mononuclear species of the type *cis*-$[(PMePh_2)_2Pt(OH)_2]$, (the analogue *cis*-$[(PMe_3)_2Pt(OH)_2]$ (known to be unstable in chlorinated solvents) as has been seen before),[11] is not supported by the value of $^1J_{P,Pt}$ coupling constant. The observed value (3602 Hz), in fact, is only slightly lower than that of the dichloro complex, *cis*-$[(PMePh_2)_2PtCl_2]$ ($^1J_{P,Pt}$ = 3627 Hz); however, the difference between the observed value and those for *cis*-$[(PMe_3)_2Pt(OH)_2]$ (3254 Hz, in CD_2Cl_2) and *cis*-$[(PMe_3)_2PtCl_2]$ (3470 Hz) is large.[11] Similar considerations seem to exclude the formation of *cis*-$[(PMePh_2)_2Pt(\mu\text{-}O)]_2$ since such oxo species should have a $^1J_{P,Pt}$ value that is much lower than that of the precursor hydroxo complex.[3]

Conclusions

The structures of complexes **1** and **2** reported here represent further examples of the preference for the $\{L_2Pt(OH)\}^+$ moiety (L = phosphanes or diphosphanes) to form dinuclear species. This feature is in common with most of the monohydroxo complexes of Pt^{II} with N-donor ligands, although examples of the formation of hydroxo complexes with higher nuclearity from some diamines are known.[12]

An interesting feature of the phosphano-based complexes *cis*-$[L_2Pt(\mu\text{-}OH)]_2^{2+}$ (L = PMe_3, PMe_2Ph, and $PMePh_2$) is their reactivity towards Cl^- ions. Unlike the isostructural hydroxo compounds containing the chelate ligands 2,2′-bipyridine or phenanthroline, which are inert towards LiCl even at 100 °C,[13] they react with Cl^- ions under very mild conditions. When an excess of chloride ions is used, the substitution of the OH^- ligands, to give *cis*-$[L_2PtCl_2]$, is the predominant process. At lower concentrations of Cl^- ions, however, other reaction pathways become competitive, leading to the concomitant formation of the stable complexes $[\{cis\text{-}L_2Pt\}_3(\mu\text{-}O)_2]^{2+}$ when L is PMe_3 or PMe_2Ph, but an unstable and not yet fully characterized species when L is $PMePh_2$.

Experimental Section

Reagent and Chemicals: Reagent grade chemicals $(NEt_4)Cl\cdot H_2O$ (Ega-Chemie) and $(AsPh_4)Cl$ (Fluka) were used as received. The complexes *cis*-$[(PMePh_2)_2PtCl_2]$,[14] *cis*-$[(PMe_3)_2Pt(\mu\text{-}OH)]_2X_2$ (X = NO_3,[5] ClO_4),[15] and *cis*-$[(PMe_2Ph)_2Pt(\mu\text{-}OH)]_2(NO_3,)_2$ [6] were synthesized as previously reported.

Instrumentation: ^1H and $\{^1H\}^{31}P$ spectra were obtained with JEOL 90Q and/or Bruker 300AVANCE spectrometers. ^1H chemical shifts are referred to the residual peak of the deuterated solvent ($[D_6]$DMSO), whereas the external reference for ^{31}P is H_3PO_4 (85% w/w in H_2O). IR spectra in the range 4000−400 cm^{-1} were recorded as KBr pellets with a Perkin−Elmer 283 spectrophotometer.

Syntheses of the Complexes

Preparation of *cis*-$[(PMe_2Ph)_2Pt(\mu\text{-}OH)]_2(ClO_4)_2$ (1b): A solution of $AgNO_3$ (1.15 g, 6.77 mmol) in H_2O (20 mL) was added to a suspension of *cis*-$[(PMe_2Ph)_2PtCl_2]$ (1.84 g, 3.38 mmol) in H_2O (200 mL). The AgCl precipitate formed immediately was removed by filtration, and the resulting solution was neutralized with NaOH (0.092 M). Addition of $NaClO_4\cdot H_2O$ (0.48 g, 3.4 mmol) led to the immediate precipitation of a white microcrystalline solid, which was collected by filtration, washed with H_2O, EtOH, and Et_2O. The yield of the dry product **1b** was 1.29 g (92%). $C_{16}H_{23}ClO_5P_2Pt$ (587.8): calcd. C 32.69, H 3.94; found C 32.41, H 4.01. ^1H NMR at 89.55 MHz in $[D_6]$DMSO: δ = 7.5−7.7 (5 H, Ph), 4.09 (broad s, 1 H, OH), 1.54 (apparent doublet, J_{PH} = 11.7, $^3J_{PtH}$ = 35.6 Hz, 6 H, CH_3) ppm. $\{^1H\}^{31}P$ NMR at 36.23 MHz in $[D_6]$DMSO: δ = −14.50 (s, $^1J_{P,Pt}$ = 3456 Hz; $^2J_{Pt,Pt}$ = 304 Hz) ppm.

Caution*: *The above perchlorate is a potential explosive!

Preparation of *cis*-$[(PMePh_2)_2Pt(\mu\text{-}OH)]_2(NO_3)_2$ (2): A solution of $AgNO_3$ (0.794 g, 4.67 mmol) in EtOH (10 mL) and H_2O (2 mL) was added to a solution of *cis*-$[(PMePh_2)_2PtCl_2]$ (1.56 g, 2.34 mmol) in CH_2Cl_2 (20 mL). The AgCl precipitate formed immediately was filtered, and an aqueous solution (25.4 mL) of NaOH (0.092 M) was added to the resulting solution. The solution was concentrated under vacuum, and a white precipitate was obtained, which was recovered by filtration, washed twice with H_2O (10 mL) and dried under vacuum. The yield of the pure product **2** was 1.11 g (70%). $C_{26}H_{27}NO_4P_2Pt$ (674.5): calcd. C 46.29, H 4.03, N 2.08; found C 45.73, H 3.96, N 1.99. ^1H NMR at 89.55 MHz in $[D_6]$DMSO: δ = 7.5−7.8 (10 H, Ph), 3.53 (s broad, 1 H, OH), 1.62 [apparent doublet, J_{PH} = 10.7 Hz, 3 H, CH_3] ppm. $\{^1H\}^{31}P$ NMR in $[D_6]$DMSO: δ = −5.32 (s, $^1J_{P,Pt}$ = 3578, $^2J_{Pt,Pt}$ = 232 Hz) ppm.

Preparation of $[\{cis\text{-}(PMe_3)_2Pt\}_3(\mu\text{-}O)_2](ClO_4)_2$ (3): A solution of $(NEt_4)Cl\cdot H_2O$ (228 mg, 1.24 mmol) in CH_2Cl_2 (20 mL) was added to a stirred solution of *cis*-$[(PMe_3)_2Pt(\mu\text{-}OH)]_2(ClO_4)_2$ (576 mg, 0.62 mmol) in DMSO (15 mL), and the resulting pale yellow solution was left at room temperature for 18 h. Addition of Et_2O (100 mL) afforded a white precipitate which was recovered by filtration, dissolved in a minimum amount of CH_2Cl_2 and precipitated by addition of Et_2O. The crude solid (265 mg) was further purified from CH_2Cl_2/Et_2O, and a microcrystalline product was obtained which was recovered by filtration, washed with EtOH and dried under vacuum. The yield of the pure compound **3** was 91 mg [23%, based on Equation (2)]. $C_{18}H_{54}Cl_2O_{10}P_6Pt_3$ (1272): calcd. C 16.99, H 4.28; found C 16.78, H 4.16. ^1H NMR in $[D_6]$DMSO: δ = 1.59 (d, $J_{H,P}$ = 10.3, $^3J_{H,Pt}$ = 34 Hz) ppm. $\{^1H\}^{31}P$ NMR in CD_2Cl_2 (at 36.23 MHz): δ = −31.7 ($^1J_{P,Pt}$ = 3376−3406 Hz) ppm. Crystallization of the solid from $CH_2Cl_2/CHCl_3$ (1:1) gave needle-shaped colorless crystals unsuitable for X-ray diffraction analysis.

Preparation of $[\{cis\text{-}(PMe_2Ph)_2Pt\}_3(\mu\text{-}O)_2]Cl_2$ (4): A solution of $(NEt_4)Cl\cdot H_2O$ (166 mg, 0.90 mmol) in CH_2Cl_2 (10 mL) was added dropwise to a stirred solution of **1b** (533 mg, 0.49 mmol) in DMSO (6 mL). The resulting pale yellow solution was left at ca. 20 °C for 24 h. Addition of Et_2O (120 mL) gave a waxy solid which was rapidly washed with H_2O and then with Et_2O. The dried solid (360 mg) was purified twice by dissolution in CH_2Cl_2 and precipitation with toluene. The yield of **4**, free of the perchlorate salt, was 126 mg [yield 34%, based on Equation (2)]. $C_{48}H_{66}Cl_2O_2P_6Pt_3$ (1517.0): calcd. C 38.00, H 4.38; found C 37.85, H 4.29. ^1H NMR in $[D_6]$DMSO: δ = 7.96−7.53 (complex multiplets, 5 H, Ph), 1.52 (d, $J_{H,P}$ = 10.2 Hz with unresolved ^{195}Pt satellites) ppm. $\{^1H\}^{31}P$ NMR in CD_2Cl_2: δ = −20.1 ($^1J_{P,Pt}$ = 3460−3487 Hz) ppm.

 © 2004 Wiley-VCH Verlag GmbH & Co. KGaA, Weinheim

Table 4. Crystal and refinement data for complexes **1a**, **2**, and **4**

Complex	**1a**	**2**	**4**
Formula	$C_{32}H_{46}N_2O_8P_4Pt_2$	$C_{52}H_{54}N_2O_8P_4Pt_2$	$C_{48}H_{66}Cl_2O_2P_6Pt_3$
Molecular mass	1100.8	1349.0	1517.0
Color	colorless	colorless	colorless
Crystal system	triclinic	monoclinic	monoclinic
Space group	$P\ -1$ (No. 2)	$P\ 2_1/n$ (No. 14)	$C\ 2/c$ (No. 15)
a [Å]	10.642(2)	9.772(2)	23.160(2)
b [Å]	11.830(2)	16.292(3)	13.404(4)
c [Å]	16.129(3)	16.040(4)	17.996(4)
α [°]	105.66(1)		
β [°]	93.78(1)	100.48(2)	99.36(2)
γ [°]	94.75(1)		
V [Å^3]	1940.3(5)	2510.9(9)	5512(2)
Z	2	2	4
D_{calc} [g cm^{-3}]	1.884	1.784	1.828
$F(000)$	1064	1320	2912
μ (Mo-K_α) [mm^{-1}]	7.41	5.75	7.90
Crystal dimensions [mm]	0.20·0.20·0.30	0.15·0.25·0.20	0.30·0.15·0.08
Θ limits [°]	2.0 / 21.0	2.0 / 22.5	1.8 / 25.0
No. of independent data	4186	3286	4549
No. of data with $I > 2\sigma\ (I)$	3162	2815	3779
No. of variables	366	308	286
$R(F)$[a]	0.050	0.049	0.031
$wR(F^2)$[b]	0.121	0.131	0.066
Largest peak in ΔF [e·Å^{-3}]	1.3	1.7	0.8
GOF[c]	1.004	1.193	1.011

[a] $R(F) = \Sigma||F_o| - |F_c||/\Sigma|F_o|$. [b] $wR(F^2) = [\Sigma w(|F_o|^2 - |F_c|^2)^2/\Sigma w(|F_o|^2)^2]^{1/2}$. [c] GOF $= [\Sigma w(|F_o|^2 - |F_c|^2)^2/(n - p)]^{1/2}$.

X-ray Data Collection, Structure Solution and Refinement of 1a, 2, and 4:[16] The X-ray data collections were performed at room temperature with a Nicolet−Siemens four-circle R3m/V diffractometer on single-crystals mounted in thin-walled glass capillaries with graphite-monochromated Mo-K_α radiation (λ = 0.71073 Å).

Crystals of **1a** and **2** were obtained by slow diffusion of vapors of Et_2O into a saturated solution of the corresponding compound in ethanol, whereas crystals of **4** were obtained by slow evaporation of a $CH_2Cl_2/C_6H_5CH_3$ solution of the complex, at room temperature.

A summary of the X-ray analyses carried out on the complexes is listed in Table 4. The cell dimensions for the complexes were determined from the setting angles of 50 centered reflections. Intensity data were collected for unique portions of reciprocal space to the limit of observable diffraction. Corrections for X-ray absorption effects were applied on the basis of azimuthal scan data.[17] The absorption effects have been noticeable only in complex **4**, the transmission factors ranging from 0.637 to 0.996.

The unit cell of **1a** comprises two moieties denoted as **I** and **II**. The structures were solved by heavy-atom methods and refined by full-matrix least-squares against F^2. Pt, P, and phenyl C atoms of **1a** and all non-hydrogen atoms of **2** and **4** were assigned anisotropic displacement parameters. As expected, the nitrate groups of **1a** and **2** endure high thermal motions and they have been treated isotropically.

Final difference syntheses showed no chemically significant features, the largest maxima being close to the platinum. Refinements converged smoothly to residuals given in Table 4. All calculations were made with programs of the SHELXTL/PC[18] system and SHELXL-93[19] program.

Acknowledgments

This work was financially supported by the Ministero dell'Università e della Ricerca Scientifica e Tecnologica (PRIN 2001).

[1] P. R. Sharp, *J. Chem. Soc., Dalton Trans.* **2000**, 2647−2657.
[2] J. S. L. Yeo, J. J. Vittal, W. Henderson, T. S. A. Hor, *Inorg. Chem.* **2002**, *41*, 1194−1198.
[3] J. J. Li, W. Li, P. R. Sharp, *Inorg. Chem.* **1996**, *35*, 604−613.
[4] G. W. Bushnell, K. R. Dixon, R. G. Hunter, J. J McFarland, *Can. J. Chem.* **1972**, *50*, 3694−3699.
[5] G. Trovò, G. Bandoli, U. Casellato, B. Corain, M. Nicolini, B. Longato, *Inorg. Chem.* **1990**, *29*, 4616−4621.
[6] B. Longato, L. Pasquato, A. Mucci, L. Schenetti, *Eur. J. Inorg. Chem.* **2003**, 128−137.
[7] R. Faggiani, B. Lippert, C. J. L. Lock, B. Rosenberg, *J. Am. Chem. Soc.* **1977**, *99*, 777−781.
[8] D. G. Cooper, J. Powell, *J. Am. Chem. Soc.* **1973**, *95*, 1102−1108.
[9] E. Carmona, J. M. Marin, P. Palma, M. Paneque, M. L. Poveda, *Inorg. Chem.* **1989**, *28*, 1895−1900.
[10] M. E. Fakley, A. Pidcock, *J. Chem. Soc., Dalton* **1977**, 1444−1448.
[11] T. K. Miyamoto, Y. Suzuki, H. Ichida, *Chem. Lett.* **1992**, 839−842; T. K. Miyamoto, Y. Suzuki, H. Ichida, *Bull. Chem. Soc. Jpn.* **1992**, *65*, 3386−3397.
[12] R. Faggiani, B. Lippert, C. J. L. Lock, B. Rosenberg, *Inorg. Chem.* **1977**, *16*, 1192−1196; F. D. Rochon, A. Morneau, R. Melanson, *Inorg. Chem.* **1988**, *27*, 10−13.

 © 2004 Wiley-VCH Verlag GmbH & Co. KGaA, Weinheim

[13] S. Wimmer, P. Castan, F. L. Wimmer, N. P. Johnson, *J. Chem. Soc., Dalton Trans.* **1989**, 403−412.
[14] S. O. Grim, R. L. Keiter, W. Mc Farlane, *Inorg. Chem.* **1967**, *6*, 1133−1137.
[15] B. Longato, G. Bandoli, A. Mucci, L. Schenetti, *Eur. J. Inorg. Chem.* **2001**, 3021−3029.
[16] CCDC-168694 (for **1a**), -168695 (for **2**), and -168696 (for **4**) contain the supplementary crystallographic data for this paper. These data can be obtained free of charge at www.ccdc.cam.ac.uk/conts/retrieving.html [or from the Cambridge Crystallographic Data Centre, 12 Union Road, Cambridge CB2 1EZ, UK; Fax: (internat.) +44-1223/336-033; E-mail: deposit@ccdc.cam.ac.uk].
[17] A. C. T. North, D. C. Phillips, F. S. Mathews, *Acta Crystallogr., Sect. A* **1968**, *24*, 351−359.
[18] G. M. Sheldrick, *SHELXTL/PC*, Version 5.03, Siemens Analytical X-ray Instruments Inc., Madison, WI, **1994**.
[19] G. M. Sheldrick, *SHELXL-93*, Program for the Refinement of Crystal Structures, University of Göttingen, Germany, **1993**.

Received July 9, 2003
Early View Article
Published Online February 5, 2004

 © 2004 Wiley-VCH Verlag GmbH & Co. KGaA, Weinheim

Binary and Ternary Cluster Complexes Containing Gold-Selenium, Gold-Indium-Selenium and Gold-Gallium-Tellurium − Synthesis and Structures of $[Au_5Se_2(PPh_3)_4]Cl$, $[(Au_3Se)_2\{Ph_2P(CH_2)_6PPh_2\}_3]Cl_2$, $[Au_{10}Se_4\{Ph_2P(CH_2)_5PPh_2\}_4]InCl_5$, $[Au_4(SeInCl_3)_2\{Ph_2P(CH_2)_5PPh_2\}_2]$, $[Au_2(TeGaCl_3)\{Ph_2P(CH_2)_6PPh_2\}]_2$ and $[Au_8Se_4In\{Ph_2P(CH_2)_2PPh_2\}_4](InCl_4)_3$

Jolanta Olkowska-Oetzel,[a] Paloma Sevillano,[b] Andreas Eichhöfer,[c] and Dieter Fenske*[a,b,c]

Keywords: Cluster compounds / Gallium / Gold / Indium / Selenium / Tellurium

Reactions of gold phosphane complexes $[(AuX)(PR_3)]$ (X = Cl, Br, I; R = organic moiety) with $Se(SiMe_3)_2$ lead to the formation of gold complexes with chalcogenide bridges. The reaction of the complex $[Ph_3PAuCl]$ and *t*BuSe($SiMe_3$) gives the cluster $[Au_5Se_2(PPh_3)_4]Cl$ (**1**). The in situ preparation of the complex $[(AuCl)_2dpph]$ [dpph = $Ph_2P(CH_2)_6PPh_2$] by reaction of dpph with $[Me_2SAuCl]$, and subsequent reaction with $Se(SiMe_3)_2$, leads to the formation of $[(Au_3Se)_2(dpph)_3]Cl_2$ (**2**). Reactions of the gold(I) complex $[(AuCl)_2dpppe]$ [dpppe = $Ph_2P(CH_2)_5PPh_2$] with $Se(SiMe_3)_2$ and $InCl_3$ in different molar ratios lead to the formation of $[Au_{10}Se_4(dpppe)_4]InCl_5$ (**3**) and $[Au_4(SeInCl_3)_2(dpppe)_2]$ (**4**). The reaction of $[(AuCl)_2dpph]$ with $Te(SiMe_3)_2$ and $GaCl_3$ produces the isostructural cluster compound $[Au_4(TeGaCl_3)_2(dpph)_2]$ (**5**). From the reaction of $Se(SiMe_3)_2$ with $[(AuCl)_2dppe]$ [dppe = $Ph_2P(CH_2)_2PPh_2$] and $InCl_3$ $[Au_8Se_4In(dppe)_4](InCl_4)_3$ **6** can be isolated. The structures of **1**–**6** were determined by X-ray diffraction.
(© Wiley-VCH Verlag GmbH & Co. KGaA, 69451 Weinheim, Germany, 2004)

Introduction

Due to the important photophysical and photochemical properties of gold(I) complexes, many investigations have been undertaken towards the synthesis and structural analysis of gold complexes and clusters.[1−5] However, only a few examples of gold complexes with selenium or tellurium bridges are known.[2,6]

For the preparation of this kind of cluster complex, a reaction has been developed using metal halides MX_n (M = metal; X = Cl, Br, I) and silylated main group element derivatives, R−E−$SiMe_3$ (R = organic group, $SiMe_3$; E = S, Se, Te), in the presence of a tertiary phosphane PR_3. The driving force of this reaction is the formation of the corresponding trimethylsilyl halide, $XSiMe_3$.[7] The phosphane ligands stabilize the metal cluster complex and avoid theformation of the binary phases.[8] The first results in this kind of preparations, using silylated derivatives of S, Se and Te, were reported by Abel et al. and Schmidbaur et al.[9]

The use of polyphosphanes leads to the formation of large cluster complexes containing copper[10] and silver[11] atoms bridged by chalcogenides. Polyphosphanes were also successfully applied in analogous reactions with gold(I) salts, resulting in the formation of several gold cluster complexes which have been characterized, for example $[Au_{18}Se_8(dppe)_6]Br_2$,[12] $[Au_{10}Se_4(dpppe)_4]Br_2$,[13] $[Au_{34}Se_{14}(tpep)_6(tpep^{Se})_2]Cl_6$ [tpep = $P(PCH_2CH_2PPh_3)_3$ and $tpep^{Se}$ = $Ph_2P(Se)CH_2CH_2P(PCH_2CH_2PPh_3)_2$].[14] Some have been found to have luminescent properties, for example $[Au_{10}Se_4(dpppe)_4]Br_2$,[13] $[Au_{10}(\mu_3\text{-}S)_4(PNP)_4][PF_6]_2$ [PNP = $Ph_2PN(Pr)PPh_2$][15] and $[Au_{12}Se_4(dppm)_6](PF_6)_4$ (dppm = $Ph_2PCH_2PPh_2$).[16]

In contrast to the well-known binary chalcogenide cluster complexes of group 11 metals,[17,18] ternary chalcogenide compounds containing metals of group 11 and 13 are rare and of special interest due to their promising properties. For example, the ternary compounds $CuInSe_2$ or $CuGaSe_2$ have important potential in thin film technology for solar cells.[19] Recently, some ternary cluster compounds, for example $[Cu_{11}In_{15}Se_{16}(SePh)_{24}(PPh_3)_4]$,[20] $[Cu_6In_8S_{13}Cl_4(PEt_3)_{12}]$[21] and $[Ag_6In_8S_{13}Cl_4(PPh_3)_{12}]$[22] have been synthesized. Ternary In-Au and Ga-Au chalcogenide cluster

[a] DFG Center for Functional Nanostructures (CFN) Universität Karlsruhe
76128 Karlsruhe, Germany
Fax: (internat.) +49-721-608-8440
E-mail: Dieter.Fenske@chemie.uni-karlsruhe.de
[b] Institut für Anorganische Chemie der Universität Karlsruhe
76128 Karlsruhe, Germany
[c] Institut für Nanotechnologie im Forschungszentrum Karlsruhe
76128 Karlsruhe, Germany

 © 2004 Wiley-VCH Verlag GmbH & Co. KGaA, Weinheim **DOI: 10.1002/ejic.200300774**

$$[Ph_3PAuCl] + 0.5\ t\text{BuSe}(SiMe_3) \xrightarrow[CH_2Cl_2]{25^\circ C} [Au_5Se_2(PPh_3)_4]Cl\ \mathbf{1}$$

$$Ph_2P(CH_2)_6PPh_2 + 2\ [Me_2SAuCl] + 0.5\ Se(SiMe_3)_2 \xrightarrow[CH_2Cl_2]{25^\circ C} [(Au_3Se)_2(Ph_2P(CH_2)_6PPh_2)_3]Cl_2\ \mathbf{2}$$

$$[(AuCl)_2Ph_2P(CH_2)_5PPh_2] + 2\ Se(SiMe_3)_2 + InCl_3 \xrightarrow[CH_2Cl_2/THF]{25^\circ C} [Au_{10}Se_4(Ph_2P(CH_2)_5PPh_2)_4]InCl_5\ \mathbf{3}$$

$$[(AuCl)_2Ph_2P(CH_2)_5PPh_2] + Se(SiMe_3)_2 + 2\ InCl_3 \xrightarrow[CH_2Cl_2/THF]{25^\circ C} [Au_4(SeInCl_3)_2(Ph2P(CH_2)_5PPh_2)_2]\ \mathbf{4}$$

$$[(AuCl)_2Ph_2P(CH_2)_6PPh_2] + Te(SiMe_3)_2 + GaCl_3 \xrightarrow[CH_2Cl_2/THF]{25^\circ C} [Au_4(TeGaCl_3)_2(Ph2P(CH_2)_6PPh_2)_2]\ \mathbf{5}$$

$$[(AuCl)_2Ph_2P(CH_2)_2PPh_2] + InCl_3 + Se(SiMe_3)_2 \xrightarrow[CH_2Cl_2/THF]{25^\circ C} [Au_8Se_4In(Ph_2P(CH_2)_2PPh_2)_4](InCl_4)_3\ \mathbf{6}$$

Scheme 1. Preparation reactions of compounds **1**−**6**

compounds have, to the best of our knowledge, not yet been prepared.

In this work we report the preparation and X-ray characterization of some Au-chalcogenide, In-Au and Ga-Au chalcogenide cluster compounds.

Results and Discussion

Compounds **1**−**6** were prepared as shown in Scheme 1. From the reaction of $[Ph_3PAuCl]$ with tBuSe($SiMe_3$) in CH_2Cl_2 at room temperature a pale yellow solution was obtained. Layering of the solution with *n*-pentane produced yellow crystals of $[Au_5Se_2(PPh_3)_4]Cl$ (**1**). Crystals of the compound $[(Au_3Se)_2(dpph)_3]Cl_2$ [**2**; dpph = $Ph_2P(CH_2)_6PPh_2$] were obtained from the reaction of the corresponding phosphane ligand with $[Me_2SAuCl]$ and $Se(SiMe_3)_2$ in CH_2Cl_2. The final yellow solution was layered with *n*-pentane and, after a few days, yellow crystals were isolated.

Reaction of the gold(I) complex $[(AuCl)_2dpppe]$ [dpppe = $Ph_2P(CH_2)_5PPh_2$][23] with two equivalents of $Se(SiMe_3)_2$ and one equivalent of $InCl_3$ in CH_2Cl_2/THF gave the formation of small yellow crystals of **3**. If the reaction is carried out using an Se:In molar ratio of 1:2, cubic crystals of **4** are formed. Colorless crystals of the isostructural cluster compound **5** were obtained from the reaction of $[(AuCl)_2dpph]$ with $Te(SiMe_3)_2$ and $GaCl_3$ in CH_2Cl_2/THF, and from the reaction of $Se(SiMe_3)_2$ with $[(AuCl)_2dppe]$ [dppe = $Ph_2P(CH_2)_2PPh_2$] and $InCl_3$ (1:1:1) in CH_2Cl_2/THF colorless needles of **6** could be isolated.

The structures of the six compounds were determined by single-crystal X-ray crystallography.

$[Au_5Se_2(PPh_3)_4]Cl$ (1)

Complex **1** crystallizes in the triclinic space group $P\bar{1}$ with four molecules per unit cell and two molecules per asymmetric unit (Figure 1). These are identical within the standard deviations therefore only one of them will be discussed. Two molecules of dichloromethane are present as lattice-bound solvent in the crystal.

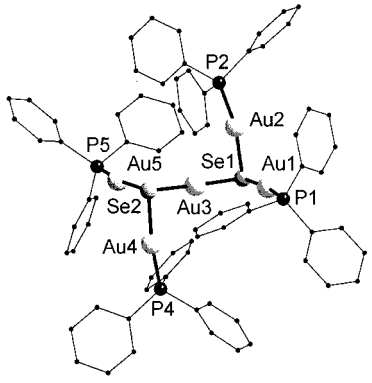

Figure 1. Crystal structure of the cation in **1**; selected distances (pm) and angles (°): Au1−Au2 305.94(9), Au2−Au3 299.56(10), Au3−Au4 304.87(10), Au3−Au5 327.04(11), Au1−Se1 245.17(12), Au2−Se1 245.58(14), Au3−Se1 246.43(12), Au3−Se2 245.75(12), Au4−Se2 243.48(14), Au5−Se2 243.83(12), Au1−P1 227.4(2), Au2−P2 226.6(3), Au4−P4 226.4(3), Au5−P5 226.6(3); Au1−Se1−Au2 77.13(4), Au1−Se1−Au3 78.64(4), Au2−Se1−Au3 75.01(4), Au4−Se2−Au5 79.89(4), Au4−Se2−Au3 77.09(4), Au5−Se2−Au3 83.82(4), Se2−Au3−Se1 177.87(4), P1−Au1−Se1 171.15(7), P2−Au2−Se1 167.65(7), P4−Au4−Se2 170.93(7), P5−Au5−Se2 170.27(7)

The Au_5Se_2 units in **1** are composed of two Au_3Se tetrahedra which share a corner; there are no bonds between the gold atoms inside the Au_5Se_2 unit (see Figure 1). The observed Au−Au distances are within the range 299.56(10)−327.04(11) pm. All selenium atoms act as μ_3-bridges above and below the plane defined by the gold atoms Au1 to Au5, with Au−Se−Au angles between 75.01(4)° and 83.82(4)°. Au−Se distances range from 243.48(14) to 246.43(12) pm, and are within the range of commonly observed distances in other Au−Se cluster complexes.[12−16]

The central gold atom has an almost linear coordination to two selenium atoms (Se1, Se2) with an angle of 177.87(4)°. The peripheral gold atoms also show a linear

 © 2004 Wiley-VCH Verlag GmbH & Co. KGaA, Weinheim

coordination geometry. The Se−Au−P angles are between 167.65(7) and 171.15(7)°, and the Au−P distances range from 226.4(3) to 227.4(2) pm. An isostructural compound $[Au\{S(AuPPh_3)_2\}_2][(CH_3)_3SnCl_2]$, prepared using a different procedure, has already been reported by Jones et al.[24]

Au_5Se_2 units are known building blocks in other Au−Se cluster cations. Some examples are $[Au_{10}Se_4(dppm)_4]^{2+}$, $[Au_{10}Se_4(dpppe)_4]^{2+}$ and $[Au_{10}Se_4(depe)_4]^{2+}$ [depe = $Et_2P(CH_2)_2PEt_2$].[13,14] In these cases, the complex cations are formed by two Au_5Se_2 units bridged by the phosphane ligands. In the complexes containing dppm and depe, the phosphane carbon chains are shorter, resulting in the formation of more-distorted Au_3Se tetrahedra. In the case of dpppe, the phosphane bridge is longer, resulting in an almost regular Au_3Se tetrahedron. In **1**, however, where a monodentate phosphane ligand was used for the preparation, almost regular Au_3Se tetrahedra are observed as there is no distortion due to the formation of bridges (see above).

$[(Au_3Se)_2(dpph)_3]Cl_2$ (2)

Complex **2** crystallizes in the monoclinic space group $P2_1/c$ with four molecules per unit cell. One molecule of *n*-pentane and one of dichloromethane are present as lattice-bound solvent in the crystal. The bond lengths and angles are within the expected range.[12−16] The cation $[(Au_3Se)_2(dpph)_3]^{2+}$ is composed of two Au_3Se tetrahedra bridged by dpph ligands (see Figure 2).

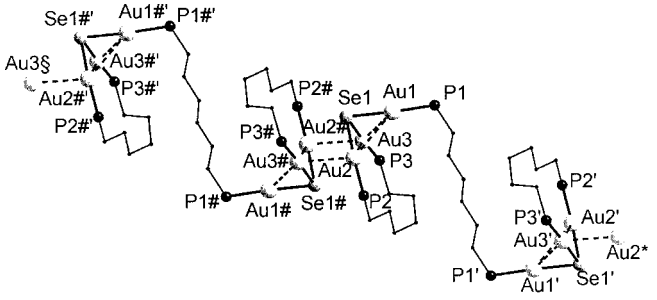

Figure 2. Crystal structure showing two cations in **2**; phenyl rings are omitted for clarity; symmetry transformations for the generation of equivalent atoms: $-x + 1, -y + 1, -z + 1$; selected distances (pm) and angles (°): Au1−Au2 326.19(10), Au1−Au3 301.66(8) Au2−Au3# 304.27(7), Au3−Au2# 304.27(7), Au1−Se1 242.47(10), Au2−Se1 245.38(11), Au3−Se1 247.35(11), Au1−P1 226.2(2), Au2−P2 227.6(3), Au3−P3 227.3(2); P1−Au1−Se1 175.10(7), P2−Au2−Se1 176.10(9), P3−Au3−Se1 177.58(7), Au1−Se1−Au3 76.02(3), Au2−Se1−Au3 82.58(3), Au3−Au2−Au1 55.18(2), Au3−Au1−Au2 62.23(2), Au3#−Au2−Au3 84.98(2), Au3#−Au2−Au1 124.55(1), Au1−Au3−Au2# 135.04(2), Au2#−Au3−Au2 95.02(2)

Selenium atoms act as μ_3-bridges to three gold atoms, building slightly distorted Au_3Se tetrahedra. The Se−Au distances are between 242.47(10) and 247.35(11) pm, and the Au−Se−Au angles range from 76.02(3) to 82.58(3)°.

All gold atoms exhibit an almost linear coordination geometry and are coordinated by a phosphorus and a selenium atom. The P−Au−Se angles are within the range 175.10(7)−177.58(7)° and the Au−P distances are between 226.2(2) and 227.6(3) pm.

Within the Au_3Se tetrahedra, the non-bonding Au−Au distances range from 301.66(8) to 326.19(10) pm. The intermolecular Au−Au distances between two Au_3Se units are relatively short, with a value of 304.27(7) pm. This shows that the short interactions, probably due to the "aurophilic attraction", lead to the formation of a polymeric chain of cations in the solid state.[25] Other examples of gold cluster complexes with secondary Au−Au bonding and solid-state polymers can be found in the literature.[14,26,27]

$[Au_{10}Se_4(dpppe)_4]InCl_5$ (3)

Complex **3** crystallizes in the monoclinic space group $C2/c$ with four molecules per unit cell. The Au_5Se_2 units within the cation of **3** are bridged by dpppe ligands (see Figure 3). The Au−Au distances between the Au_5Se_2 units are 312.3(2) and 333.2(2) pm. The Au_5Se_2 units consist of two Au_3Se tetrahedra sharing a corner (see above). In these tetrahedra, the selenium atoms are acting as μ_3-bridges to three gold atoms, being placed above and below the plane formed by the gold atoms (Au1−Au5 and symmetry equivalents) with Au−Se−Au angles of 74.02(9)° and 82.61(8)°. The Au−Se distances range between 245.2(3) and 247.4(3) pm (Figure 3).

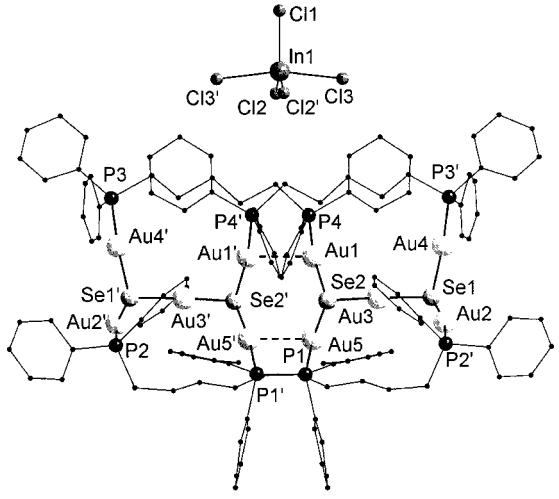

Figure 3. Crystal structure of **3**; symmetry transformations for the generation of equivalent atoms: $-x + 1, y, -z + 1/2$; selected distances (pm) and angles (°): Au1−Se2 244.9(3), Au1−Au3 302.32(16), Au1−Au1′ 312.3(2), Au1−Au5 323.47(19), Au2−Se1 247.4(3), Au2−Au3 294.72(14), Au3−Se1 242.2(3), Au3−Se2 242.7(3), Au3−Au5 306.18(15), Au3−Au4 328.29(16), Au4−P3′ 225.6(8), Au4−Se1 244.5(3), Au4−Au2′ 314.27(18), Au5−P1 226.4(7), Au5−Se2 245.2(3), Au5−Au5′ 333.2(2); P4−Au1−Se2 171.9(2), P4−Au1−Au1′ 108.9(2), Se2−Au1−Au1′ 78.70(7), Au3−Au1−Au1′ 130.03(4), P4−Au1−Au5 132.0(2), Se2−Au1−Au5 48.73(7), Au3−Au1−Au5 58.47(4), Au3−Au2−Au4 64.92(4), Se1−Au3−Se2 175.17(9), Au2−Au3−Au1 160.88(5), P1−Au5−Au1 131.6(2), Se2−Au5−Au1 48.66(8), Au3−Au5−Au1 57.31(4), Au3−Se1−Au2 74.02(9), Au1−Se2−Au5 82.61(8)

A distorted linear coordination geometry is found for the central gold atom (Au3 and symmetry equivalents), bonded to two selenium atoms with an Se−Au−Se angle of

 © 2004 Wiley-VCH Verlag GmbH & Co. KGaA, Weinheim

175.17(9)° and Au−Se distances of 242.2(3) and 242.7(3) pm. All non-central gold atoms also display a linear geometry and are coordinated to a selenium and a phosphorus atom, with Au−P bond lengths between 225.6(8) and 227.7(7) pm and P−Au−Se angles ranging from 169.06(8)° to 175.28(19)°.

An isostructural cation was found in the complex $[Au_{10}Se_4(dpppe)_4]Br_2$.[13,14] However, the Au−Au distances between the Au_5Se_2 units in **3** [312.3(2) and 333.2(2) pm] are longer than those in $[Au_{10}Se_4(dpppe)_4]Br_2$ [300.2(3) and 326.0(4) pm]. The Au−Au distances within the Au_5Se_2 units are shorter in **3** [range from 294.7(30) to 328.3(8) pm] than the ones found in the isostructural cluster $[Au_{10}Se_4(dpppe)_4]Br_2$ [298.0(3) to 334.1(3) pm].

$[Au_2(SeInCl_3)dpppe]_2$ (4)

Cluster **4** crystallizes in the triclinic space group $P\bar{1}$ with two molecules per unit cell. In **4** two gold atoms (Au1, Au2′) are coordinated to a selenium atom (Se1) and two phosphorous atoms (P1′, P2) of the bidentate phosphane ligand (see Figure 4), leading to a distorted linear coordination at gold (P−Au−Se from 173.59(4)° to 178.39(4)°]. The μ_3-Se^{2-} ligand is also coordinated to an In atom (In1) of an $InCl_3$ molecule. In the crystal lattice, two $[Au_2(SeInCl_3)dpppe]$ units form a dimer by inversion symmetry, with a planar square of gold atoms (Au1′−Au2−Au1 83.94(3) and Au2′−Au1−Au2 96.06(3)°]. The Au−Au distances within the Au_2Se units [Au1−Au2′ 320.88(9) pm] are slightly longer than the ones found between both Au_2Se-units [(Au1−Au2 311.67(10) pm]. Related Au_4 arrangements have been observed before in the ionic complex $[(PPh_3Au)_2(SCH_2Ph)](NO_3)$, with values of 307.7 and 319.4 pm for the non-bridged Au−Au distances and distances of 307.7 and 314.2 pm for the bridged ones,[28] and also in $[(PPh_3Au)_2(SC_6H_4CH_3)_2](PF_6)$, which has Au−Au distances of 317.3 pm for the free edges and 315.2 pm for the sulfur-bridged ones.[28] In analogy to these sulfur-bridged complexes, the selenium atoms in **4** are placed above and below the plane of the four-membered ring of gold atoms (Au1−Au2−Au1′−Au2′) with an Au1′−Se1′−Au2 angle of 78.83(3)°. With the $InCl_3$ directly bonded to the selenium atom, compound **4** represents the first step in the build-up of ternary gold indium chalcogenide complexes.

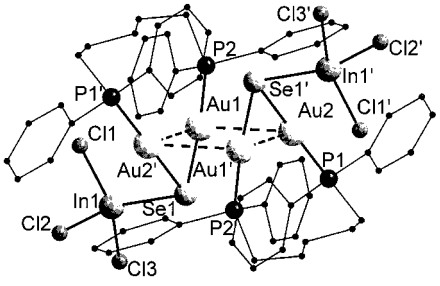

Figure 4. Crystal structure of **4**; symmetry transformations for the generation of equivalent atoms: $-x + 2, -y + 1, -z$; selected distances (pm) and angles (°): In1−Se1 254.74(11), Se1−Au1 244.60(8), Se1−Au2′ 244.95(8), Au1−P2 226.07(16), Au1−Au2 311.67(10), Au1−Au2′ 320.88(9), Au2−Se1′ 244.95(8); Au1−Se1−Au2′ 81.91(3), Au1−Se1−In1 93.95(4), P2−Au1−Se1 173.59(4), P2−Au1−Au2 100.64(5), Se1−Au1−Au2 85.61(4), Se1−Au1−Au2′ 49.09(2), Au2−Au1−Au2′ 96.06(3), P1−Au2−Se1′ 178.39(4), P1−Au2−Au1′ 130.20(4), Au1−Au2−Au1′ 83.94(3)

$[Au_2(TeGaCl_3)dpph]_2$ (5)

Compound **5** crystallizes in the monoclinic space group $P2_1/c$ with two molecules per unit cell. This cluster shows the same structural motif as **4**, with a central arrangement of four gold atoms, bridged by tellurium atoms, which are also coordinated to a $GaCl_3$ molecule (see Figure 5). A distorted linear geometry at each of the gold atoms is observed, with P−Au−Te angles ranging from 171.45(4)° to 176.42(4)°. The μ_3-Te^{2-} ligands are also coordinated to a Ga atom (Ga1, Ga1′) of a $GaCl_3$ molecule. The Au−Au distances are Au1−Au2 305.03(9) and Au2−Au1′ 340.8(1) pm with Au1−Au2−Au1′ and Au2′−Au1′−Au2 angles of 92.10(1)° and 87.90(1)°, respectively.

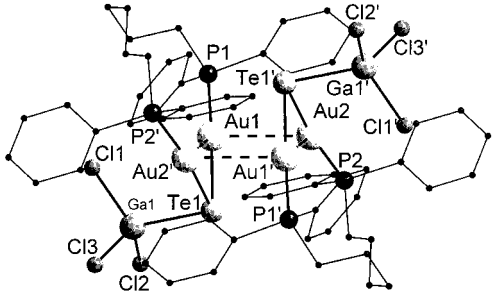

Figure 5. Molecular structure **5**; symmetry transformations for the generation of equivalent atoms: $-x + 1, -y + 1, -z$; selected distances (pm) and angles (°): Ga1−Te1 258.92(12), Te1−Au1 259.43(6), Te1−Au2′ 260.69(6), Au1−Au2 305.03(9), Au2−P2 228.66(14), Au2−Te1′ 260.69(6); Ga1−Te1−Au1 93.96(3), Ga1−Te1−Au2′ 88.89(2), Au1−Te1−Au2′ 81.87(2), P1−Au1−Te1 171.45(4), P1−Au1−Au2 107.21(4), Te1−Au1−Au2 81.34(2), P2−Au2−Te1′ 176.42(4), P2−Au2−Au1 98.32(4), Te1′−Au2−Au1 84.145(19)

$[Au_8Se_4In(dppe)_4](InCl_4)_3$ (6)

Compound **6** crystallizes in the monoclinic space group $C2/c$ (Figure 6). The hydrogen atoms were not calculated for this crystal structure. One molecule of dichloromethane is present as lattice-bound solvent in the crystal. The cation consists of a central indium atom (In1) enclosed within a distorted tetrahedron of four selenium atoms (Se1, Se2, Se1′, Se2′). The In−Se distances range from 258.5(3) to 259.5(3) pm with Se−In−Se angles ranging between 107.10(14)° and 110.85(8)°. Each of these μ_3-Se atoms coordinates to two Au atoms (Au1−Au4 and symmetry equivalent atoms) forming four Au_2Se units with Au−Se bond lengths ranging from 244.7(3) to 244.8(3) pm and Au−Se−Au angles within the range 77.12(7)−78.29(8)°. All the bidentate phosphane ligands (P1−P4 and symmetry equivalent atoms) bridge two Au atoms belonging to two different Au_2Se units, resulting in a distorted linear coordination environment for all Au atoms. Each gold atom is

 © 2004 Wiley-VCH Verlag GmbH & Co. KGaA, Weinheim

coordinated by one Se and one P atom [Se−Au−P: 167.52(9)−177.75(18)°; Au−P: 226.7(6)−228.2(7) pm]. A distorted eight-membered ring in the boat conformation is formed by the Au atoms, with Au−Au distances ranging from 301.41(15) (Au3−Au4) to 309.04(17) pm (Au4−Au1′). A similar Au−Au distance of 305.1(1) pm is found in $[(PPh_3Au)_2Se]$.[29] The structure of the cation in **3** can be rationalized as an In atom tetrahedrally coordinated by four $dppeAu_2Se$ units, where phosphane ligands connect neighbouring Au_2Se units. Similar Au_2Se units have been stabilized and crystallized before by the use of either monodentate phosphane ligands like PPh_3 in monomeric $[(PPh_3Au)_2Se]$[21] or bidentate phosphanes, such as $Ph_2PC_6H_4PPh_2$ (dppbe), in the polymeric $[Au_2Se(dppbe)]_\infty$.[14]

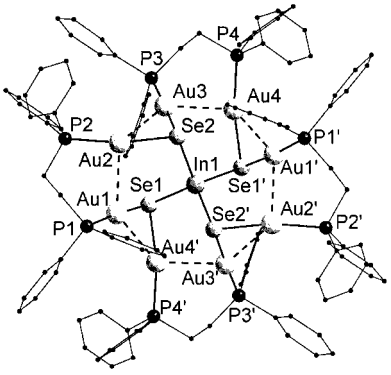

Figure 6. Molecular structure of the cation in **6**; symmetry transformations for the generation of equivalent atoms: $-x + 1$, y, $-z + 0.5$; selected distances (pm) and angles (°): Au1−P1 228.2(7), Au1−Se1 244.8(3), Au1−Au4′ 309.04(17), Au2−P2 226.7(6), Au2−Se2 244.7(3), Au2−Au3 305.06(15), Au3−P3 227.9(7), Au3−Se2 244.7(3), Au3−Au4 301.41(15), Au4−P4 227.4(8), In1−Se1 258.5(3), In1−Se2 259.5(3); P1−Au1−Se1 175.7(2), P1−Au1−Au2 92.62(19), Se1−Au1−Au2 91.61(7), P1−Au1−Au4′ 125.01(19), Se1−Au1−Au4′ 50.85(7) Au2−Au1−Au4′ 137.92(5), P2−Au2−Se2 167.52(19), P2−Au2−Au1 92.49(18), Se1−In1−Se2 110.85(8), Se2−In1−Se2′ 107.10(14), Au4′−Se1−Au1 78.29(8), Au4′−Se1−In1 97.73(9)

Experimental Section

All experiments with chalcogenide ligands were carried out under a dry nitrogen atmosphere. THF was dried over sodium-benzophenone, and CH_2Cl_2 over P_2O_5 followed by distillation of the solvents under nitrogen. Anhydrous $InCl_3$ was obtained from Aldrich.

Preparation of $[Ph_3PAuCl]$: A solution of [Au(thiodiglycol)Cl][30] (0.51 g Au, 2.59 mmol) in MeOH (5 mL) was added to a solution of PPh_3 (0.68 g, 2.59 mmol) in CH_2Cl_2 (20 mL). The mixture was stirred for 2 hours. The volume was reduced to a few milliliters and water (50 mL) was added to produce a white solid. The solid was filtered off, washed with water and dried in vacuo. Yield 85% (1.09 g).

Preparation of $[(AuCl)_2(phosphane)]$:[23,26] A solution of [Au(thiodiglycol)Cl][30] (0.40 g Au, 2.04 mmol) in MeOH (5 mL) was added to a solution of phosphane (phosphane = dppe, dpppe, dppph; 1.02 mmol) in CH_2Cl_2 (10 mL). The final mixture was stirred for 24 hours. The solvents were removed in vacuo and water (50 mL) added. The white precipitate was filtered off, washed with water and Et_2O, and dried in vacuo. Yield 70−85% (dppe 0.62 g, dpppe 0.74 g, dpph 0.80 g).

Preparation of $[Au_5Se_2(PPh_3)_4]Cl$ (1): tBuSe($SiMe_3$) (0.02 mL, 0.022 g, 0.107 mmol) was added at room temperature to a solution of $[Ph_3PAuCl]$ (0.10 g, 0.21 mmol) in CH_2Cl_2 (10 mL),. The final mixture was stirred for 14 hours to give a light yellow solution. This solution was layered with n-pentane and, after a few days, light yellow crystals of **1** had formed (see Table 1). Yield 60% (0.06 g). $C_{74}H_{48}Au_5Cl_5P_4Se_2$ (2396.6): calcd. C 37.05, H 2.67; found C 37.17, H 2.71.

Preparation of $[(Au_3Se)_2(dpph)_3]Cl_2$ (2): A solution of $[Me_2SAuCl]$ (19) (0.1 g, 0.35 mmol) in CH_2Cl_2 (5 mL) was added to a solution of dpph (0.08 g, 0.18 mmol) in CH_2Cl_2 (5 mL). The solutions were stirred for 30 minutes and $Se(SiMe_3)_2$ (0.04 mL, 0.039 g, 0.18 mmol) was added to give a yellow solution. This solution was layered with n-pentane and, a few days later, crystals of **2** had formed (see Table 1). Yield 40% (0.07 g). $C_{102}H_{96}Au_6Cl_2P_6Se_2$ (2916.9): calcd. C 41.96, H 3.29; found C 41.82, H 3.25.

Preparation of $[Au_{10}Se_4(dpppe)_4]InCl_5$ (3): $Se(SiMe_3)_2$ (0.10 mL, 0.44 mmol) was added to a solution of $[(AuCl)_2dpppe]$ (0.20 g, 0.22 mmol) in CH_2Cl_2 (25 mL) to give a yellow solution. A solution of $InCl_3$ (0.05 g, 0.22 mmol) in THF (2 mL) was added and a yellow precipitate was formed. The solid was filtered off and a few days later small yellow crystals of **3** were isolated (see Table 1). Yield 10% (0.02 g). $C_{116}H_{120}Au_{10}Cl_5InP_8Se_4$ (4339.6): calcd. C 32.11, H 2.79; found C 29.96, H 2.78.

Preparation of $[Au_4(SeInCl_3)_2(dpppe)_2]$ (4): $Se(SiMe_3)_2$ (0.05 mL, 0.22 mmol) was added to a solution of $[(AuCl)_2dpppe]$ (0.20 g, 0.22 mmol) in CH_2Cl_2 (25 mL). The solution became yellow. After five days $InCl_3$ (0.10 g, 0.44 mmol) in THF (2 mL) was added to the former solution, to produce colourless cubic crystals of **4** (see Table 1). Yield 65% (0.16 g). $C_{58}H_{60}Au_4Cl_6In_2P_4Se_2$ (2269.2): calcd. C 30.70, H 2.67; found C 29.56, H 2.48.

Preparation of $[Au_4(TeGaCl_3)_2(dpph)_2]$ (5): $Te(SiMe_3)_2$ (0.05 mL, 0.21 mmol) was added to a solution of $[(AuCl)_2dpph]$ (0.19 g, 0.21 mmol) in CH_2Cl_2 (25 mL). A solution of $GaCl_3$ (0.04 g, 0.22 mmol) in THF (2 mL) was then added to the resultant dark brown mixture After a few days colourless crystals of **5** had formed (see Table 1). Yield 40% (0.10 g). $C_{60}H_{64}Au_4Cl_6Ga_2P_4Te_2$ (2304.3): calcd. C 31.27, H 2.80; found C 30.48, H 2.75.

Preparation of $[Au_8Se_4In(dppe)_4](InCl_4)_3$ (6): A solution of $InCl_3$ (0.03 g, 0.12 mmol) in THF (2 mL) was added to a suspension of $[(AuCl)_2dppe]$ (0.10 g, 0.12 mmol) in CH_2Cl_2 (25 mL). $Se(SiMe_3)_2$ (0.03 mL, 0.12 mmol) was added. The mixture was stirred for 2 hours. After 2 days colourless needles of **6** started to grow in the flask (see Table 1). Complete crystallization was achieved by reducing the volume in vacuo. Yield 85% (0.09 g). $C_{104}H_{96}Au_8Cl_{12}In_4P_8Se_4$ (4370.0): calcd. C 28.58, H 2.21; found C 28.15, H 2.21.

X-ray Analyses: STOE-IPDS II (Mo-K_α); data collection and refinement (SHELXTL-97).[31] CCDC-214542 to -214547 (for **1**−**6**) contain the supplementary crystallographic data for this paper. These data can be obtained free of charge at www.ccdc.cam.ac.uk/conts/retrieving.html [or from the Cambridge Crystallographic Data Centre, 12, Union Road, Cambridge CB2 1EZ, UK; Fax: (internat.) + 44-1223-336-033; E-mail: deposit@ccdc.cam.ac.uk].

 © 2004 Wiley-VCH Verlag GmbH & Co. KGaA, Weinheim

Table 1. Crystallographic data for compounds **1**−**6**

	1·2CH_2Cl_2	**2**·CH_2Cl_2·C_5H_{12}	**3**	**4**	**5**	**6**·CH_2Cl_2
Formula	$C_{148}H_{128}Au_{10}Cl_{10}P_8Se_4$	$C_{204}H_{192}Au_{12}Cl_4P_{12}Se_4$	$C_{116}H_{120}Au_{10}Cl_5InP_8Se_4$	$C_{29}H_{30}Au_2Cl_3InP_2Se$	$C_{60}H_{64}Au_4Cl_6Ga_2P_4Te_2$	$C_{105}H_{98}Au_8Cl_{16}In_4P_8Se_4$
Space group	$P\bar{1}$	$P2_1/c$	$C2/c$	$P\bar{1}$	$P2_1/c$	$C2/c$
Z	2	4	4	2	2	4
Temperature (K)	203(2)	203(2)	150(2)	190(2)	180(2)	180(2)
a (pm)	1750.4(4)	1446.8(3)	1870.3(4)	1020.4(2)	1298.7(3)	3660.2(7)
b (pm)	2014.7(4)	1475.9(3)	2169.5(4)	1224.9(2)	1463.6(3)	1102.8(2)
c (pm)	2027.5(4)	2322.9(5)	3112.5(6)	1350.5(3)	1856.9(4)	3733.0(8)
α (°)	89.99(3)	90	90	73.29(3)	90	90
β (°)	89.98(3)	94.76(3)	97.87(3)	84.94(3)	105.39(3)	116.01(3)
γ (°)	86.57(3)	90	90	78.19(3)	90	90
Volume (10^6 pm^3)	7140(1)	4943.1(17)	12510(4)	1581.7(5)	3403.2(12)	13542(5)
Density (calcd.) (g/cm^3)	2.231	1.961	2.304	2.380	2.249	2.185
Theta range for data collection $2\theta_{max}$ (°)	1.54 to 28.33	1.97 to 28.29	1.53 to 27.16	3.63 to 31.69	1.63 to 24.92	1.24 to 23.97
Refl. collected	53765	30257	15551	11852	16894	26799
Ind. reflections	32153	12146	9086	6823	5895	10370
R_{int}	0.0979	0.1409	0.1085	0.0519	0.0635	0.0621
Refl. with $F_o > 4\sigma(F_o)$	14113	10698	5226	6627	4993	8336
Refined parameters	981	490	650	343	352	473
R_1	0.0595	0.0848	0.0755	0.0495	0.0305	0.0841
wR_2	0.1750	0.2172	0.1806	0.1456	0.0791	0.1939
Goodness of fit	1.040	1.042	1.026	1.298	0.655	1.230

Acknowledgments

This work was supported by the Deutsche Forschungsgemeinschaft (Centrum für funktionelle Nanostrukturen) and the Fonds der Chemischen Industrie.

[1] H. Schmidbaur, *Chem. Soc. Rev.* **1995**, *24*, 391−400; V. W.-W. Yam, K. K.-W. Lo, *Chem. Soc. Rev.* **1999**, *28*, 323−334; V. W.-W. Yam, E. C.-C. Cheng, *Angew. Chem.* **2000**, *112*, 4410−4414; *Angew. Chem. Int. Ed.* **2000**, *39*, 4240−4244.

[2] P. G. Jones, G. M. Sheldrick, E. Hädicke, *Acta Crystallogr., Sect. B* **1980**, *36*, 2777−2779; C. Lensch, P. G. Jones, G. M. Sheldrick, *Z. Naturforsch.* **1982**, *37b*, 944−9449; P. G. Jones, C. Thöne, *Chem. Ber.* **1990**, *123*, 1975−1978; I. Schröter, J. Strähle, *Chem. Ber.* **1991**, *123*, 2161−2164; S. P. Huang, M. G. Kanatzidis, *Angew. Chem.* **1992**, *104*, 799−801; *Angew. Chem. Int. Ed. Engl.* **1992**, *31*, 787−789; H. Schmidbaur, A. Kolb, E. Zeller, A. Schier, H. Beruda, *Z. Anorg. Allg. Chem.* **1993**, *619*, 1575−1579; S. Hofreiter, M. Paul, H. Schmidbaur, *Chem. Ber.* **1995**, *128*, 901−905; F. Canales, M. C. Gimeno, A. Laguna, P. G. Jones, *J. Am. Chem. Soc.* **1996**, *118*, 4839−4845; V. W. W. Yam, E. C. C. Cheng, K. K. Cheung, *Angew. Chem.* **1999**, *111*, 193−195; *Angew. Chem. Int. Ed.* **1999**, *38*, 197.-199.

[3] F. Canales, M. C. Gimeno, P. G. Jones, A. Laguna, *Angew. Chem.* **1994**, *106*, 811−812; *Angew. Chem. Int. Ed. Engl.* **1994**, *33*, 769−770.

[4] H. K. Yip, A. Schier, J. Riede, H. Schmidbaur, *J. Chem. Soc., Dalton Trans.* **1994**, 2333−2334.

[5] G. Marbach, J. Strähle, *Angew. Chem.* **1984**, *96*, 695.-696; *Angew. Chem. Int. Ed. Engl.* **1984**, *23*, 715−716.

[6] R. C. Haushalter, *Inorg. Chim. Acta* **1985**, *102*, L37−38; *Angew. Chem. Int. Ed. Engl.* **1985**, *24*, 432−435, E. Schulz Lang, C. Maichle-Mössmer, J. Strähle, *Z. Anorg. Allg. Chem.* **1994**, *620*, 1678−1685; D. Fenske, N. Zhu, T. Langetepe, *Angew. Chem.* **1998**, *110*, 2783−2787, *Angew. Chem. Int. Ed.* **1998**, *37*, 2640−2644; T. Langetepe, D. Fenske, *Z Anorg. Allg. Chem.* **2001**, *627*, 820−826.

[7] D. Fenske, J. Ohmer, J. Hachgenei, *Angew. Chem.* **1985**, *97*, 993−995; *Angew. Chem. Int. Ed. Engl.* **1985**, *24*, 993−995; D. Fenske, J. Ohmer, J. Hachgenei, K. Merzweiler, *Angew. Chem.* **1988**, *100*, 1300−1320; *Angew. Chem. Int. Ed. Engl.* **1988**, *27*, 1277−1296.

[8] S. Dehnen, A. Schäfer, D. Fenske, R. Ahlrichs, *Angew. Chem.* **1994**, *106*, 786−790; *Angew. Chem. Int. Ed. Engl.* **1994**, *33*, 746−748; A. Schäfer, R. Ahlrichs, *J. Am. Chem. Soc.* **1994**, *116*, 10686−10692; S. Dehnen, A. Schäfer, R. Ahlrichs, D. Fenske, *Chem. Eur. J.* **1996**, *2*, 429−435.

[9] E. W. Abel, C. R. Jenkins, *J. Organomet. Chem.* **1968**, *14*, 285−289; H. Schmidbaur, R. Franke, J. Eberlein, *Chem. Ztg.* **1975**, *99*, 91−92; K. Angermaier, H. Schmidbaur, *Z. Naturforsch.* **1996**, *51b*, 879−882.

[10] M. Semmelmann, D. Fenske, J. F. Corrigan, *J. Chem. Soc., Dalton Trans.* **1998**, 2541−2546.

[11] T. Langetepe, D. Fenske, *Z. Anorg. Allg. Chem.* **2001**, *627*, 820−826; D. Fenske, N. Zhu, T. Langetepe, *Angew. Chem.* **1998**, *110*, 2783−2787, *Angew. Chem. Int. Ed.* **1998**, *37*, 2640−2644.

[12] D. Fenske, T. Langetepe, M. M. Kappes, O. Hampe, P. Weis, *Angew. Chem.* **2000**, *112*, 1925, *Angew. Chem. Int. Ed.* **2000**, *39*, 1857−1860.

[13] S. Lebedkin, T. Langetepe, P. Sevillano, D. Fenske, M. M. Kappes, *J. Phys. Chem. B* **2002**, *106*, 9019−9026.

[14] P. Sevillano, T. Langetepe, D. Fenske, *Z Anorg. Allg. Chem.* **2003**, *629*, 207−214.

[15] V. W.-W. Yam, E. C.-C. Cheng, Z.-Y. Zhou, *Angew. Chem.* **2000**, *112*, 1749−1747, *Angew. Chem. Int. Ed.* **2000**, *39*, 1683−1685.

[16] V. W.-W. Yam, E. C.-C. Cheng, K.-K. Cheung, *Angew. Chem.* **1999**, *111*, 193−195, *Angew. Chem. Int. Ed.* **1999**, *38*, 197−199.

[17] S. Dehnen, A. Eichhöfer, D. Fenske, *Eur. J. Inorg. Chem.* **2002**, 279−317.

[18] X.-J. Wang, T. Langetepe, C. Persau, B.-S. Kang, G. M. Sheldrick, D. Fenske, *Angew. Chem.* **2002**, *114*, 3972−3977, *Angew. Chem. Int. Ed.* **2002**, *41*, 3818−3822.

[19] J. Gonzales, L. Roa, R. Fouret, P. Derllez, J. Lefebvre, Y. Gunet, *Phys. Stat. Sol.* **2001**, *225*, R12.-R14; S. Siebentritt, *Thin Solid Films* **2002**, *403*−*404*, 1−8; R. Caballero, C. Guillen, *Thin Solid Films* **2002**, *403*−*404*, 107−111.

 © 2004 Wiley-VCH Verlag GmbH & Co. KGaA, Weinheim

[20] A. Eichhöfer, D. Fenske, *J. Chem. Soc., Dalton Trans.* **2000**, 941−944.

[21] D. T. T. Tran, N. J. Taylor, J. F. Corrigan, *Angew. Chem.* **2000**, *112*, 965−967, *Angew. Chem. Int. Ed.* **2000**, *39*, 935−937.

[22] J. Olkowska−Oetzel, D. Fenske, P. Scheer, A. Eichhöfer, *Z. Anorg. Allg. Chem.* **2003**, *629*, 415−420.

[23] H. Schmidbaur, P. Bissinger, J. Lachmann, O. Steigelmann, *Z. Naturforsch., Teil B* **1992**, *47*, 1711−1716.

[24] P. G. Jones, C. Lensch, G. M. Sheldrick, *Z. Naturforsch., Teil B* **1982**, *37*, 141−143.

[25] P. Pyykkö, Y. Zhao, *Angew. Chem*. **1991**, *103*, 622−623, *Angew. Chem. Int. Ed. Engl.* **1991**, *30*, 604−605; J. Li, P. Pyykkö, *Chem. Phys. Lett.* **1992**, *197*, 586−590; P. Pyykkö, *Chem. Rev.* **1997**, *97*, 597−636.

[26] P. M. Van Calcar, M. M. Olmstead, A. L. Balch, *J. Chem. Soc., Chem. Commun.* **1995**, 1773−1774.

[27] W. J. Hunks, M. C. Jennings, R. J. Puddephatt, *Inorg. Chem.* **1999**, *38*, 5930−5931; D. B. Lenznoff, B.-Y. Xue, R. J. Batchelor, F. W. B. Einstein, B. O. Patrick, *Inorg. Chem.* **2001**, *40*, 6026−6034.

[28] S. Wang, J. P. Fackler, *Inorg. Chem.* **1990**, *29*, 4404−4407; J. Chen, T. Jiang, G. Wie, A. A. Mohamed, C. Homrighausen, J. A. Krause Bauer, A. E. Bruce, M. R. M. Bruce, *J. Am. Chem. Soc.* **1999**, *121*, 9225−9226.

[29] P. G. Jones, C. Thöne, *Chem. Ber.* **1991**, *124*, 2725−2729; S. Canales, O. Crespo, M. C. Gimeno, P. G. Jones, A. Laguna, F. Mendizabal, *Organometallics* **2000**, *19*, 4985−4994; S. Canales, O. Crespo, M. C. Gimeno, P. G. Jones, A. Laguna, F. Mendizabal, *Organometallics* **2001**, *20*, 4812−4818.

[30] P. Sevillano, A. Habtemariam, A. Castiñeiras, S. Parsons, M. E. García, P. J. Sadler, *J. Chem. Soc., Dalton Trans.* **1999**, 2861−2870.

[31] G. M. Sheldrick, *Acta Crystallogr., Sect. A* **1990**, *46*, 467−473; G. M. Sheldrick, *SHELXTL-97, Program for the Refinement of Crystal Structures*, University of Göttingen, **1997**.

Received October 23, 2003
Early View Article
Published Online February 5, 2004

 © 2004 Wiley-VCH Verlag GmbH & Co. KGaA, Weinheim

Tellurated Schiff Bases Formed from {2-[(4-Methoxyphenyl)telluro]ethyl}amine and Bis(2-aminoethyl) Telluride with *o*-Hydroxyacetophenone: Synthesis and Complexation Reactions with Hg^{II}, Pd^{II} and Ru^{II} − Crystal Structures of the Ligands, $[Ru(p\text{-cymene})Cl\{H_2NCH_2CH_2TeC_6H_4\text{-}4\text{-}OCH_3\}]Cl\cdot H_2O$ and $[RuCl\{4\text{-}MeOC_6H_4TeCH_2CH_2NHCH(CH_3)C_6H_4\text{-}2\text{-}O^-\}]$

Raghavendra Kumar P.,[a] Ajai K. Singh,*[a] R. J. Butcher,[b] P. Sharma,[a] and R. A. Toscano[c]

Keywords: Schiff bases / Ruthenium / Tellurium / X-ray diffraction / Synthetic methods

{2-[(4-Methoxyphenyl)telluro]ethyl}amine and bis(2-aminoethyl) telluride on treatment with *o*-hydroxyacetophenone gave the Schiff bases 4-$MeOC_6H_4TeCH_2CH_2N{=}C(CH_3)C_6H_4$-2-OH (**L¹**) and 2-$HOC_6H_4(CH_3)C{=}NCH_2CH_2TeCH_2CH_2N{=}C(CH_3)C_6H_4$-2-OH (**L³**), respectively. The reduction of **L¹** and **L³** with $NaBH_4$ resulted in 4-$MeOC_6H_4TeCH_2CH_2NHCH(CH_3)C_6H_4$-2-OH (**L²**) and 2-$HOC_6H_4(CH_3)CHNHCH_2CH_2TeCH_2CH_2NHCH(CH_3)C_6H_4$-2-OH (**L⁴**), respectively, which have 1 or 2 chiral centers. The ^1H and ^{13}C NMR spectra of **L¹** to **L⁴** were found to be characteristic. Treatment of **L¹** with $[Ru(p\text{-cymene})Cl_2]_2$ resulted in $[Ru(p\text{-cymene})(4\text{-}MeOC_6H_4TeCH_2CH_2NH_2)Cl]Cl\cdot H_2O$ (**1**) whereas in the reaction of **L²** with $[Ru(p\text{-cymene})Cl_2]_2$, the *p*-cymene ligand is lost resulting in [RuCl(**L²**-H)] (**4**). The reactions of **L¹**, **L³** and **L⁴** with $HgBr_2$ resulted in complexes of the type $[HgBr_2\cdot(\mathbf{L})_2]$ while Na_2PdCl_4 reacted with **L¹** to give [PdCl(**L¹**-H)]. The solid-state structures of **L¹**, **L³**, **1** and **4** were determined by single-crystal X-ray diffraction studies. The very swift formation of the tellurated amine from a tellurated Schiff base (**L¹**) by hydrolysis has been observed for the first time and has resulted in **1**. The Ru–N and Ru–Te bond lengths in **1** are 2.142(3) and 2.6371 (4) Å, respectively. The replacement of the *p*-cymene ligand with a hybrid organotellurium ligand (**L²**-H), resulting in **4**, is also a first example of its kind. The Ru center in **4** has a square-planar geometry, with the Ru–N, Ru–Te, Ru–O and Ru–Cl bond lengths being 2.041(6), 2.4983(8), 2.058(5) and 2.308(2) Å, respectively. In the crystals of **4** there are secondary intermolecular Te···Cl interactions and intermolecular N–H···O hydrogen bonds. This is the first example in which coordinated Te in a complex is engaged in two intermolecular secondary interactions.

(© Wiley-VCH Verlag GmbH & Co. KGaA, 69451 Weinheim, Germany, 2004)

Introduction

Schiff bases have been studied extensively as ligands but known tellurated Schiff bases are rare.[1] Some important tellurated Schiff bases reported so far are 1,6-bis[2-(butyltelluro)phenyl]-2,5-diazahexa-1,5-diene,[2] Schiff bases derived by treating bis(*o*-formylphenyl) telluride and *o*-(butyltelluro)-benzaldehyde with chiral amines (*R*)-(+)-[(1-phenylethyl)-amine] and (1*R*,2*S*)-(−)-norephedrine, respectively,[3] and macrocyclic Schiff bases.[4]

In all three instances the tellurated aldehydes were treated with amines to prepare Schiff bases. If a tellurated amine is treated with aldehydes or ketones then a wider range of Schiff-base ligands may be designed by varying the carbonyl group containing compound. We have designed $NH_2CH_2CH_2TeAr$[5] and $NH_2CH_2CH_2TeCH_2CH_2NH_2$,[6] which may be used for this purpose and it was therefore thought worthwhile to synthesize the series **L¹** to **L⁴**. Their metal complexes, in which a metal−tellurium bond is formed, are of interest and so the reactivity of these ligands with species containing Hg^{II}, Pd^{II} and Ru^{II} has been studied. Tellurium being a very "soft" donor does not coordinate with common species of the 3d transition metals. The reaction of **L¹** with $[Ru(p\text{-cymene})Cl_2]_2$ (*p*-cymene = 1-methyl-4-isopropylbenzene) resulted in $[RuCl_2(H_2NCH_2CH_2TeC_6H_4OCH_3)]Cl\cdot H_2O$ (**1**), in which the ligand seems to have been generated by hydrolysis of the Schiff base **L¹**. This is the first example of very easy hydrolysis of a tellurated Schiff base effected by traces of water present in organic solvents. The reaction of $[Ru(p\text{-cymene})Cl_2]_2$ with **L²** resulted in a complex [RuCl(**L²**-H)] (**4**) by loss of a *p*-cymene ligand. This is also the first example where *p*-cymene is replaced by a hybrid organotellurium ligand. **L¹**, **L²**, **1** and **4** have been characterized by single-crystal X-ray dif-

[a] Department of Chemistry, Indian Institute of Technology, New Delhi 110016, India
E-mail: aksingh@chemistry.iitd.ac.in
[b] Department of Chemistry, Howard University, Washington, DC 20059, USA
[c] Instituto de Quimica, UNAM, Circuito Exterior, Coyoacan, D. F. 04510, Mexico

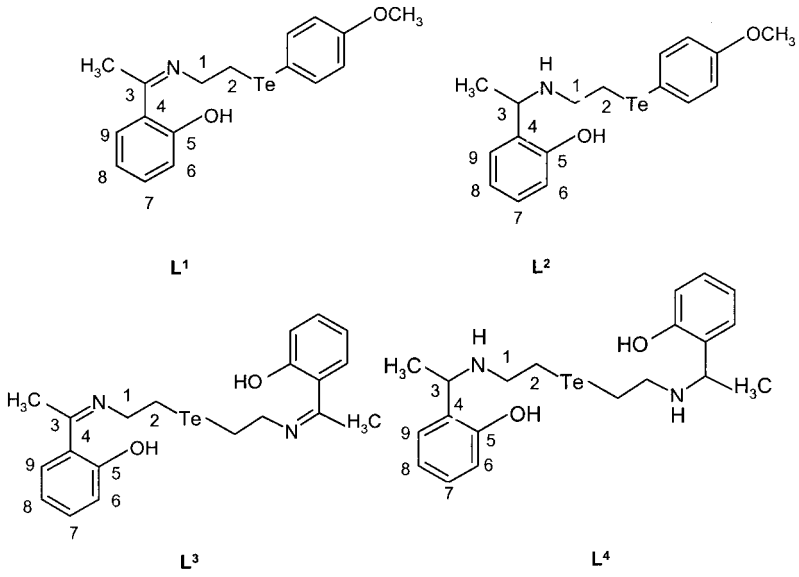

fraction studies. The results of these investigations are reported in this paper.

Results and Discussion

All the tellurated Schiff bases and their reduction products $\mathbf{L^1}$ to $\mathbf{L^4}$ are stable and can be stored under ambient conditions up to 6 months. They have good solubility in $CHCl_3$, CH_2Cl_2, CH_3CN, EtOH and acetone. In MeOH the solubility is moderate for $\mathbf{L^3}$ but good for the other three ligands. In hexane all four ligands either are partially soluble or insoluble. Complexes **1** and **4** are stable under ambient conditions and soluble in $CHCl_3$, CH_2Cl_2, CH_3CN, EtOH, MeOH and acetone but insoluble in hexane. Complex **2** and the mercury complexes of $\mathbf{L^1}$ and $\mathbf{L^3}$ are poorly soluble in $CHCl_3$ and CH_2Cl_2 and insoluble in hexane, acetone, and acetonitrile. $[HgBr_2{\cdot}(\mathbf{L^4})_2]$ is soluble in $CHCl_3$, CH_2Cl_2 and acetonitrile. All the mercury complexes, however, decompose in DMSO. All the ligands as well as **4** are non-electrolytes. The molecular weights were found to be consistent with the monomeric nature of $\mathbf{L^1}$ and $\mathbf{L^2}$. The molar conductivity of **1** was found to be lower than that of a 1:1 electrolyte probably due to association in the solution. **4** is a non-electrolyte but molecular weight measurement suggests intermolecular association in solution. The IR spectra of $\mathbf{L^1}$ and $\mathbf{L^3}$ are characteristic and show >C=N stretching vibrations at 1612 cm^{-1}, which are absent in the spectra of $\mathbf{L^2}$ and $\mathbf{L^4}$. The Te−C(alkyl) vibrations are observed in the IR spectra at 513 to 518 cm^{-1}, whereas Te−C(aryl) vibrations appear at 292 cm^{-1}. In all mercury complexes the potentially polydentate ligands appear to coordinate through the tellurium atom alone since the $-TeCH_2$ signal is deshielded ($\delta \approx 0.4-0.5$ ppm). The ν(Hg−Br) resonance appears in the IR spectra at 278 or 288 cm^{-1}. In complex **2**, the palladium atom appears to be coordinated to a monoanionic tridentate $\mathbf{L^1}$ since both $-TeCH_2$ and $-NCH_2$ are deshielded ($\delta \approx 0.36$ and 0.25 ppm, respectively) and the protons *ortho* and *para* to the oxygen atom are shielded ($\delta \approx 0.2$ ppm). This is corroborated by the $^{13}C\{^1H\}$ NMR spectrum of **2** and a red shift (ca. 17 cm^{-1}) in the >C=N− stretching frequency. Unfortunately, crystals of complexes **2**, **3**, **5** and **6** suitable for X-ray diffraction could not be obtained. In the course of the reaction of $\mathbf{L^1}$ with $[Ru(p\text{-cymene})Cl_2]_2$; the ligand is first hydrolyzed by traces of water present in the solvents resulting in $NH_2CH_2CH_2TeC_6H_4$-4-OMe, which generates complex **1**. This hydrolysis appears to be catalyzed by metallic species since in their absence it was not observed. This is the first example where a tellurated Schiff base is hydrolyzed by traces of water present in the solvent so rapidly and this is probably induced by the metal. Such metal-induced hydrolysis has also been reported earlier for common Schiff-base ligands.[7] The reaction of $\mathbf{L^2}$ with $[Ru(p\text{-cymene})Cl_2]_2$ resulted in the replacement of the *p*-cymene ring with the Te,N,O ligand. So far no hyrbrid organotellurium ligand has been able to displace this ring[1,8] and this is the first example of such behaviour. However, the replacement of the *p*-cymene ring in $[Ru(p\text{-cymene})Cl_2]_2$ has been reported earlier with some polydentate hybrid phosphanes.[9] The reactions of $\mathbf{L^3}$ and $\mathbf{L^4}$ with $[Ru(p\text{-cymene})Cl_2]_2$ and $[Ru(DMSO)_4Cl_2]$ gave intricate mixtures which are very difficult to separate.

Molecular Structures of $\mathbf{L^1}$ and $\mathbf{L^3}$

The structures of $\mathbf{L^1}$ and $\mathbf{L^3}$ are shown in Figures 1 and 2 with selected bond lengths and angles given in Table 1. In $\mathbf{L^1}$, Te−C(11) [2.111(3) Å] is shorter than Te−C(10) [2.142(3) Å]. For $\mathbf{L^3}$, Te−C(10A) and Te−C(10B) are 2.143(4) and 2.148(4) Å, respectively. These values are closer to that of Te−C(10) in $\mathbf{L^1}$ and consistent with the earlier reports that Te−C(aryl) bonds are shorter than Te−C(alkyl) bonds.[10] In $\mathbf{L^1}$ the angle C(11)−Te(1)−C(10) is 94.29(11)° which is consistent with the

 © 2004 Wiley-VCH Verlag GmbH & Co. KGaA, Weinheim

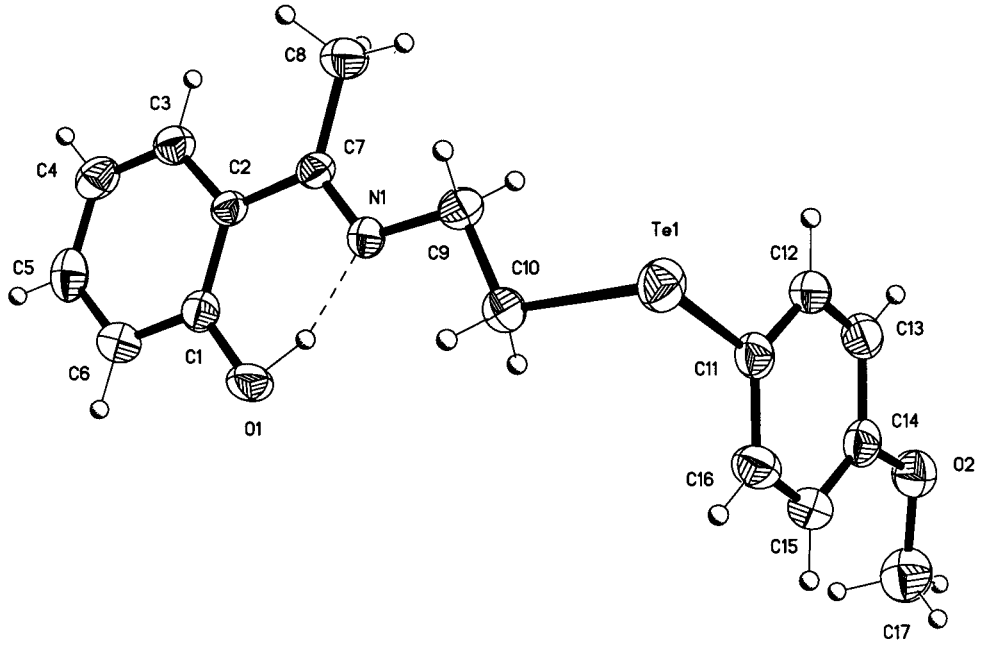

Figure 1. Molecular structure of **L**[1]

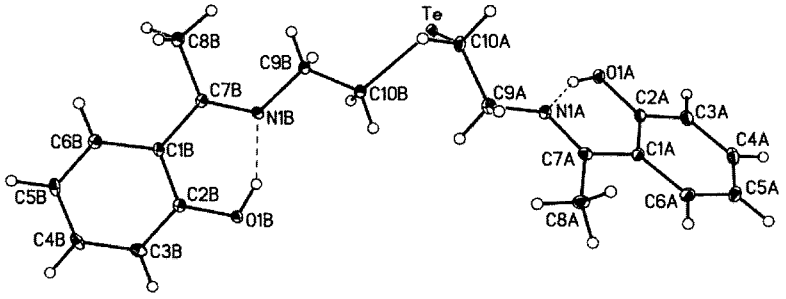

Figure 2. Molecular structure of **L**[3]

C(10A)−Te−C(10B) angle of 94.88(14)° in **L**[3] as well as other related values reported in the literature.[10] The molecules of both these ligands have intramolecular hydrogen bonding. The azomethine bond length is nearly the same in both ligands, N(1)−C(7) is 1.284(3) Å, with N(1B)−C(7B) and N(1A)−C(7A) both being 1.287(4) Å.

Molecular Structures of 1 and 4

The molecular structure of **1** is shown in Figure 3 and selected bond lengths and angles are given in Table 1. In the lattice of **1** there is one water molecule per molecule of the complex. The Ru−N bond length is 2.142(3) Å (sum of covalent radii ca. 1.95 Å) and consistent with literature reports of 2.056(6) Å in $[Ru(bipy)_3][PF_6]_2$,[11] 2.042(5)−2.154(6) Å in Ru^{II} complexes of 2-(arylazo)pyridines,[12] 1.990(3)−2.087(5) Å for Ru^{II} complexes of tetradentate ligands based on 2,6-bis(pyrazol-1-yl)pyridine,[13] 2.060(5) and 2.079(4) Å for [Ru(*p*-cymene)Cl{2,3-bis(2-pyridyl)pyrazine}]BF_4 [14] and 2.077(3)−2.113(3) for Ru^{II} complexes of oxazoline-based ligands. The Ru−Te bond length is 2.6371(4) Å which is consistent with earlier reports [2.619(8)−2.656(8) Å] of Ru^{II} complexes of hybrid organotellurium ligands.[15] The bond angles at the Ru center are normal. The bond angles at Te and the coordinating N atom are consistent with their nearly trigonal-pyramidal [92.28(11)−106.82(9)°] and tetrahedral [120.0(2)°] geometries, respectively.

The molecular structure of **4** is shown in Figure 4 and selected bond lengths and angles are given in Table 1. The Ru−N bond length is 2.041(6) Å which is shorter than that of **1** but consistent with the literature reports mentioned above. The Ru−Te bond length 2.4983(8) Å is significantly shorter than that of **1** and also shorter than the sum of covalent radii of 2.62 Å. The Ru−O bond length is 2.058(5) Å (sum of covalent radii ca. 1.91 Å) and agrees with the values of 2.034(5)−2.232(5) Å reported for complexes of Ru^{II} with a variety of ligands.[16] The Ru−Cl bond length of 2.308(2) Å (sum of covalent radii ca. 2.24 Å) is somewhat shorter than the reported range of 2.404(3)−2.434(1) Å for complexes of the [Ru(*p*-cymene)Cl_2] moiety with hybrid organotellurium ligands.[15] There are two interesting features of the structure of **4**. The first is the intermolecular second-

 © 2004 Wiley-VCH Verlag GmbH & Co. KGaA, Weinheim

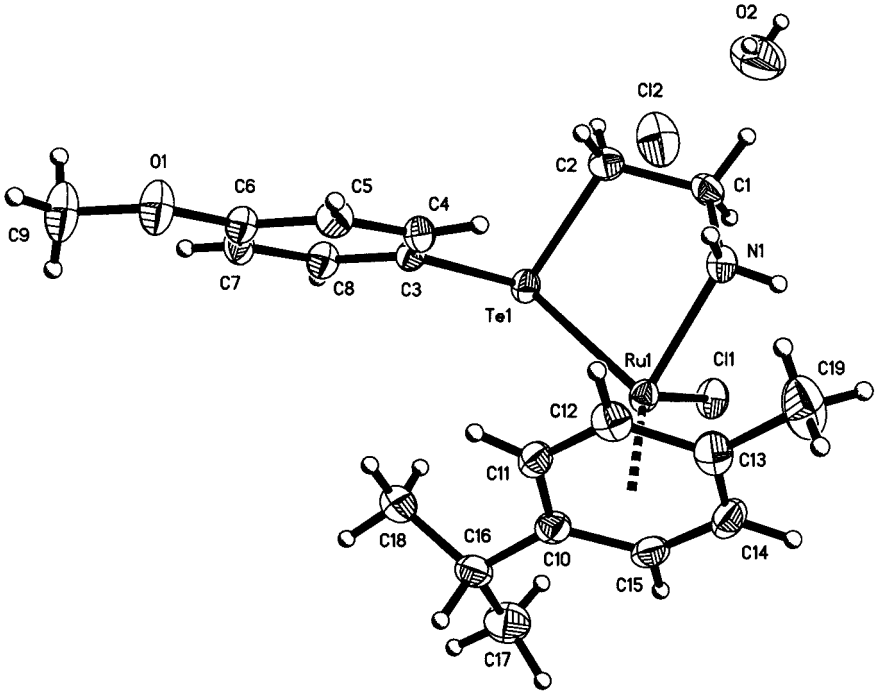

Figure 3. Molecular structure of [Ru(*p*-cymene)Cl($H_2NCH_2CH_2TeC_6H_4OCH_3$)]Cl·$H_2O$ (**1**)

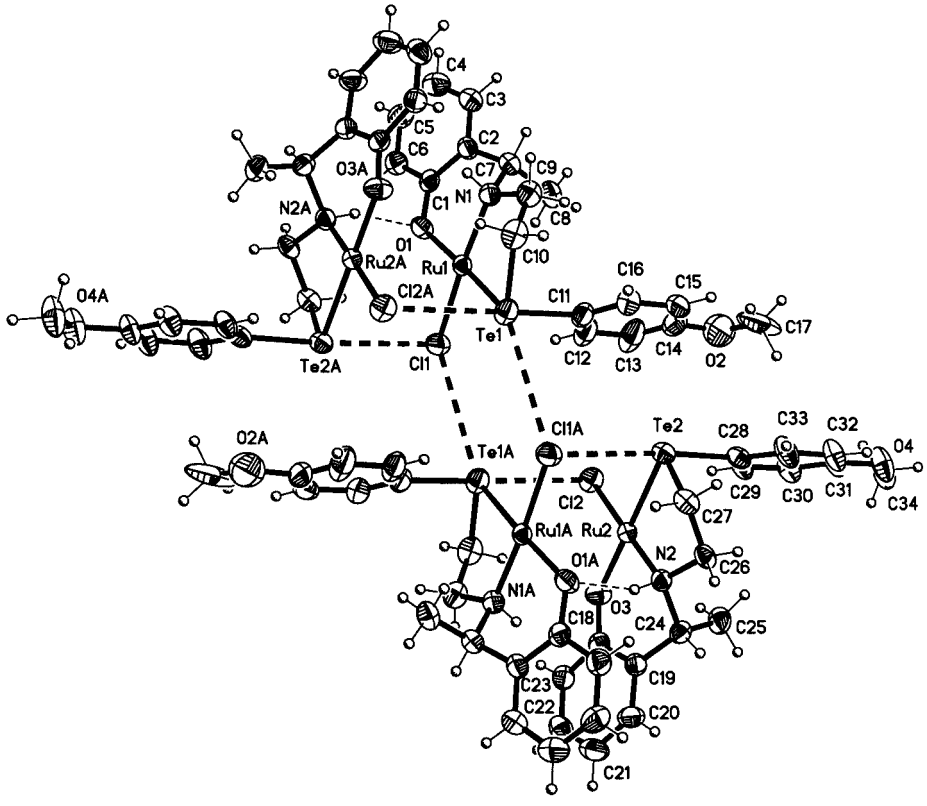

Figure 4. Molecular structure of **4**

ary interactions between each Te and two Cl atoms of neighboring molecules [Te···Cl distances of 3.322(2)−3.805(2) Å are less than the sum of van der Waals radii of 4.0 Å], which makes the geometry around the Te center distorted pseudo-octahedral. The second feature of interest is the intermolecular N−H···O hydrogen bond. The bond angles at Ru (Table 1) suggest that the N, O, Te and Cl centers are arranged around it in an almost square-planar

 © 2004 Wiley-VCH Verlag GmbH & Co. KGaA, Weinheim

Table 1. Selected bond lengths [Å] and angles[°]; symmetry transformation used to generate equivalent atoms: #1: $-x+1,-y+1,-z+1$

L^1			
Te(1)−C(11)	2.111(3)	C(11)−Te(1)−C(10)	94.29(11)
Te(1)−C(10)	2.142(3)	C(7)−N(1)−C(9)	122.6(2)
N(1)−C(7)	1.284(3)	N(1)−C(7)−C(8)	122.6(3)
N(1)−C(9)	1.470(3)	N(1)−C(9)−C(10)	108.2(2)
C(9)−C(10)	1.506(4)	N(1)−C(7)−C(2)	117.6(3)
O(1)−C(1)	1.330(3)	C(16)−C(11)−Te(1)	120.2(2)
O(1)−H(1)	0.91(3)	C(12)−C(11)−Te(1)	122.1(2)
H(1)···N(1)	1.64(3)	O(1)−H(1)···N(1)	155(3)
O(1)···N(1)	2.496(3)		
L^3			
Te−C(10A)	2.143(4)	C(10A)−Te−C(10B)	94.88(14)
Te−C(10B)	2.148(4)	C(7A)−N(1A)−C(9A)	120.6(3)
N(1B)−C(9B)	1.466(4)	C(7B)−N(1B)−C(9B)	121.9(3)
N(1B)−C(7B)	1.287(4)	N(1A)−C(7A)−C(1A)	116.5(3)
N(1A)−C(7A)	1.287(4)	N(1A)−C(7A)−C(8A)	124.4(3)
N(1A)−C(9A)	1.468(5)	N(1B)−C(7B)−C(1B)	117.2(3)
O(1B)−C(2B)	1.347(4)	N(1B)−C(7B)−C(8B)	123.8(3)
O(1A)−C(2A)	1.337(4)	N(1B)−C(9B)−C(10B)	109.1(3)
O(1A)−H(1A)	0.72(4)	N(1A)−C(9A)−C(10A)	110.5(3)
O(1B)−H(1B)	0.91(5)	C(9B)−C(10B)−Te	113.0(2)
C(9A)−C(10A)	1.512(5)	C(9A)−C(10A)−Te	115.5(2)
C(9B)−C(10B)	1.524(5)	O(1A)−H(1A)···N(1A)	144(5)
H(1A)···N(1A)	1.89(5)	O(1B)−H(1B)···N(1B)	152(4)
H(1B)···N(1B)	1.68(5)		
O(1A)···N(1A)	2.510(4)		
O(1B)···N(1B)	2.516(4)		
1			
Ru (1)−N(1)	2.142(3)	N(1)−Ru(1)−Te(1)	82.48(9)
Ru(1)−Te(1)	2.6371(4)	Cl(1)−Ru(1)−Te(1)	82.42(2)
Te(1)−C(3)	2.110(3)	N(1)−Ru(1)−Cl(1)	85.33(10)
Te(1)−C(2)	2.149(4)	C(2)−Te(1)−C(3)	97.40(15)
N(1)−C(1)	1.481(5)	C(3)−Te(1)−Ru(1)	106.82(9)
		C(2)−Te(1)−Ru(1)	92.28(11)
		C(1)−N(1)−Ru(1)	120.0(2)
4			
Ru(1)−N(1)	2.041(6)	Ru(2)−N(2)	2.048(6)
Ru(1)−O(1)	2.058(5)	Ru(2)−O(3)	2.041(5)
Ru(1)−Cl(1)	2.308(2)	Ru(2)−Cl(2)	2.3116(19)
Ru(1)−Te(1)	2.4983(8)	Ru(2)−Te(2)	2.5030(7)
Te(1)−C(11)	2.113(8)	Te(2)−C(28)	2.109(7)
Te(1)−C(10)	2.132(8)	Te(2)−C(27)	2.117(7)
Te(1)···Cl(2)#1	3.416(2)	Te(2)···Cl(1)#1	3.322(2)
Te(1)···Cl(1)#1	3.805(2)	O(3)−C(18)	1.328(8)
O(1)−C(1)	1.323(8)	O(4)−C(31)	1.351(9)
O(2)−C(17)	1.231(12)	O(4)−C(34)	1.411(9)
O(2)−C(14)	1.530(14)	N(2)−C(26)	1.501(8)
N(1)−C(9)	1.501(9)	N(2)−C(24)	1.513(9)
N(1)−C(7)	1.508(9)		
N(1)−Ru(1)−O(1)	89.5(2)	O(3)−Ru(2)−N(2)	92.1(2)
N(1)−Ru(1)−Cl(1)	175.66(18)	N(2)−Ru(2)−Cl(2)	178.89(18)
O(1)−Ru(1)−Cl(1)	91.66(14)	O(3)−Ru(2)−Cl(2)	88.99(14)
N(1)−Ru(1)−Te(1)	90.18(18)	N(2)−Ru(2)−Te(2)	88.84(17)
O(1)−Ru(1)−Te(1)	174.59(14)	O(3)−Ru(2)−Te(2)	178.94(14)
Cl(1)−Ru(1)−Te(1)	89.03(6)	Cl(2)−Ru(2)−Te(2)	90.05(6)
C(11)−Te(1)−C(10)	97.0(3)	C(28)−Te(2)−C(27)	93.4(3)
C(11)−Te(1)−Ru(1)	97.4(2)	C(28)−Te(2)−Ru(2)	96.07(19)
C(10)−Te(1)−Ru(1)	87.3(2)	C(27)−Te(2)−Ru(2)	89.46(18)
C(11)−Te(1)−Cl(1)#1	80.3(2)	C(28)−Te(2)−Cl(1)#1	171.4(2)
C(10)−Te(1)−Cl(1)#1	131.5(2)	C(27)−Te(2)−Cl(1)#1	78.1(2)
Ru(1)−Te(1)−Cl(1)#	141.28(4)	Ru(2)−Te(2)−Cl(1)#1	85.18(4)
Cl(2)#1−Te(1)−Cl(1)#1	97.06(5)	C(18)−O(3)−Ru(2)	125.7(4)
C(1)−O(1)−Ru(1)	126.8(5)	C (31)−O(4)−C(34)	117.4(7)
C(17)−O(2)−C(14)	103.9(13)	C(26)−N(2)−C(24)	110.0(5)
C(9)−N(1)−C(7)	111.3(6)	C(26)−N(2)−Ru(2)	117.6(4)
C(9)−N(1)−Ru(1)	117.6(5)	C(24)−N(2)−Ru(2)	111.9(4)
C(7)−N(1)−Ru(1)	110.4(4)		

geometry. The Te···Cl secondary interaction observed in **4** has not been reported so far for coordinated Te in any complex of Te ligands. The present one is the first example of its kind.

Conclusion

Tellurated Schiff bases have been synthesized from tellurated amines and characterized structurally. This route has been rarely used, however. The reactions of 4-$MeOC_6H_4$-$TeCH_2CH_2N{=}C(CH_3)C_6H_4$-2-OH (**$L^1$**) with [Ru(*p*-cymene)$Cl_2$]$_2$ first results in the hydrolysis of **L^1** which appears to be metal-promoted. Thereafter, the tellurated amine, (4-$MeOC_6H_4TeCH_2CH_2NH_2$) forms complexes with the Ru^{II} moiety. The reaction of 4-$MeOC_6H_4TeCH_2CH_2$-$NHCH(CH_3)C_6H_4$-2-OH (**L^2**) with [Ru(*p*-cymene)Cl_2]$_2$ resulted in loss of a *p*-cymene ring. So far, in the reaction of [Ru(*p*-cymene)Cl_2]$_2$ with Te ligands, this has never been reported and the present example is the first of its kind. The Te···Cl secondary interaction observed in **4** has not been reported so far for coordinated Te in any complex of Te-based ligands and the present one is the first example.

Experimental Section

General: C and H analyses were carried out with a Perkin−Elmer elemental analyzer 240 C. Tellurium contents were estimated by atomic absorption spectroscopy. The ^1H and $^{13}C\{^1H\}$ NMR spectra were recorded with a Bruker Spectrospin DPX-300 NMR spectrometer operating at 300.13 and 75.47 MHz, respectively. IR spectra in the range of 4000−250 cm^{-1} were recorded with a Nicolet Protége 460 FT-IR spectrometer as KBr or CsI pellets. The conductivity measurements were carried out in acetonitrile (concentration ca. 1 mM) using an ORION conductivity meter model 162. The molecular masses (concentration ca. 5 mM) in chloroform were determined with a Knauer vapor pressure osmometer model A0280. The melting points determined in open capillary are reported as such. {2-[(4-Methoxyphenyl)telluro]ethyl}amine[5] and bis(2-aminoethyl) telluride[6] were prepared by the reported methods.

X-ray Diffraction Analyses: X-ray diffraction data for **L^3**, **1** and **4** were collected with a Bruker Smart APEX CCD diffractometer, using graphite-monochromated Mo-K_α radiation (λ = 0.71073 Å) at 293(2) K. An analytical face-indexed absorption correction was applied. The structures where solved by direct methods. Refinement was carried out using full-matrix least-squares analyses with anisotropic thermal parameters for all non-hydrogen atoms. Hydrogen atoms were placed in calculated positions and refined using a riding model with fixed isotropic thermal parameters. Calculations were carried out with SMART software for data collection and data reduction and SHELXTL for solution and refinement.[17] A summary of relevant crystallographic results appears in Table 2. For **L^1**, the data were collected with a Bruker SMART 1K CCD diffractometer using X-rays of wavelength 0.71073 Å (Mo-K_α source). A semiempirical absorption correction was applied.[18] Cell refinement was done with the SMART and SAINT programs.[19] The structure was solved in a similar manner to those of **L^3**, **1** and **2** using SHELXTL.[20] CCDC-214420 (**1**), -214421 (**L^1**), -214422 (**4**) and -214423 (**L^3**) contain the supplementary crystallographic data for this paper. These data can be obtained free of charge at

 © 2004 Wiley-VCH Verlag GmbH & Co. KGaA, Weinheim

Table 2. Crystal data and structural refinements for L^1, L^3, **1** and **4**

	L^1	L^3	**1**	**4**
Empirical formula	$C_{17}H_{19}NO_2Te$	$C_{20}H_{24}N_2O_2Te$	$C_{19}H_{29}Cl_2NO_2RuTe$	$C_{17}H_{20}ClNO_2RuTe$
Formula mass	396.93	452.01	603.00	534.46
Color	yellow	yellow	orange	orange
Crystal size [mm]	0.262 × 0.076 × 0.066	0.02 × 0.02 × 0.66	0.126 × 0.126 × 0.114	0.218 × 0.214 × 0.194
Crystal system	monoclinic	monoclinic	monoclinic	monoclinic
Space group	$P2_1/c$	$P2_1/c$	$P2_1/c$	$P2_1/n$
Unit cell dimensions [Å, °]	a = 16.399(1)	a = 14.6456(12)	a = 10.2639(4)	a = 14.725(1)
	b = 7.5318(4)	b = 18.8812(15)	b = 19.459(1)	b = 13.276(1)
	c = 13.368(1)	c = 6.9923(5)	c = 10.964(1)	c = 20.562(2)
	β = 101.909(1)	β = 98.902(2)	β = 95.202(2)	β = 99.052(2)
Volume [Å^3]	1615.6(2)	1910.3(3)	2180.9(2)	3969.6(6)
Z	4	4	4	8
Density (calcd.) [Mg·m^{-3}]	1.632	1.572	1.837	1.789
Absorption coefficient [mm^{-1}]	1.845	1.572	2.288	2.372
F(000)	784	904	1184	2064
θ range [°]	2.54−25.01	2.16−24.73	1.99−24.99	1.83−25.03
Index ranges	$-19 \le h \le 19$	$-16 \le h \le 17$	$-12 \le h \le 12$	$-17 \le h \le 17$
	$-8 \le k \le 8$	$-22 \le k \le 21$	$-23 \le k \le 23$	$-15 \le k \le 15$
	$-15 \le l \le 15$	$-8 \le l \le 8 \le$	$-13 \le l \le 13$	$-24 \le l \le 24$
Reflections collected	12714	11272	17640	32038
Independent reflections	2832 [R(int) = 0.0441]	3255 [R(int) = 0.0513]	3825 [R(int) = 0.0440]	7012 [R(int) = 0.0570]
Completeness to maximum θ [%]	99.8	99.8	99.9	100.0
Max./min. transmission	0.8970/0.7222	0.928019/0.782123	0.8165/0.6977	0.6831/0.6116
Data/restraints/parameters	2832/0/195	3255/0/236	3825/0/351	7012/0/425
Goodness-of-fit on F^2	0.959	0.992	1.033	0.997
Final R indices [$I > 2\sigma(I)$]	$R1$ = 0.0283, $wR2$ = 0.0524	$R1$ = 0.0278, $wR2$ = 0.0574	$R1$ = 0.0265, $wR2$ = 0.0408	$R1$ = 0.0478, $wR2$ = 0.1067
R indices (all data)	$R1$ = 0.0415, $wR2$ = 0.0551	$R1$ = 0.0480, $wR2$ = 0.0636	$R1$ = 0.0342, $wR2$ = 0.0423	$R1$ = 0.0722, $wR2$ = 0.1159
Largest diff. peak/hole [e·Å^{-3}]	0.541/−0.243	0.610/−0.387.	0.473/−0.416	1.027 (0.83 Å from Ru2)/−0.572

www.ccdc.cam.ac.uk/conts/retrieving.html [or from the Cambridge Crystallographic Data Center, 12 Union Road, Cambridge CB2 1EZ, UK; Fax: (internat.) + 44-1223/336-033; E-mail: deposit@ccdc.cam.ac.uk].

Synthesis of L^1: {2-[(4-Methoxyphenyl)telluro]ethyl}amine (1.39 g, 5.0 mmol) was stirred in dry ethanol (20 mL) at room temperature for 0.5 h. *o*-Hydroxyacetophenone (0.68 g, 5.0 mmol), dissolved in dry ethanol (20 mL), was added to the above solution dropwise with stirring. The mixture was stirred at room temp. for a further 2 h. The solvent was evaporated in a rotary evaporator resulting in a yellow precipitate. The precipitate, on recrystallization from chloroform/hexane (1:1), afforded yellow single-crystals of L^1. Yield 1.61 g (85%); m.p. 82−83 °C. Λ_M = 0.9 cm^2·mol^{-1}·ohm^{-1}. $C_{17}H_{19}NO_2Te$ (396.9): calcd. C 51.44, H, 4.82, N 3.53, Te 32.15; found C 51.26, H 4.81, N 3.16, Te 31.86. Molecular mass: calcd. 396.6; found 399.0. ^{1}H NMR ($CDCl_3$, TMS, 25 °C): δ = 2.27 (s, 3 H, CH_3), 3.13 (t, 2 H, 2-H), 3.81 (s, 3 H, OCH_3), 3.92 (t, 2 H, 1-H), 6.76−6.82 (m, 3 H, ArH *m* to Te and 7-H), 6.945 (d, J = 8.4 Hz, 1 H, 9-H), 7.30−7.32, (m, 1 H, 8-H), 7.505 (d, J = 8.1 Hz, 1 H, 6-H), 7.745 (d, J = 8.4 Hz, 2 H, ArH *o* to Te), 16.00 (br. s, 1 H, OH) ppm. ^{13}C{1H} NMR ($CDCl_3$, 25 °C, TMS): δ = 8.32 (CH_3), 14.54 (C-2), 50.87 (C-1), 55.11 (OCH_3), 99.67 (ArCTe), 115.21 (ArC *m* to Te), 117.11 (C-6), 118.63 (C-8), 119.10 (C-4), 127.97 (C-9), 132.40 (C-7), 141.34 (ArC *o* to Te), 159.90 (Ar-$COCH_3$), 163.53 (C-5), 171.38 (C-3) ppm.

Synthesis of [Ru(*p*-cymene)Cl($H_2NCH_2CH_2TeC_6H_4$-4-OCH_3)]-Cl·H_2O (1): $[RuCl_2(p\text{-cymene})]_2$ (0.62 g, 1 mmol) was dissolved in dichloromethane (10 mL). A solution of L^1 (0.79 g, 2 mmol), prepared in dichloromethane (20 mL), was added with vigorous stirring. The mixture was stirred for a further 3 h. The solvent was removed in a rotary evaporator under reduced pressure. The resultant precipitate was recrystallized from chloroform/hexane (1:1). The dark-red crystals of **1** were washed immediately with dichloromethane and recrystallized again to give dark-orange single crystals. Yield ca. 0.85 g (ca. 60%); m.p. 160 °C (dec.). Λ_M = 43.0 cm^2·mol^{-1}·ohm^{-1}. Molecular mass: calcd. 603; found 648. $C_{19}H_{27}Cl_2NORuTe{\cdot}H_2O$ (603): calcd. C 39.01, H 4.65, N 2.39, Te 21.81; found C 38.97, H 4.83, N 2.56, Te, 21.22. ^{1}H NMR ($CDCl_3$, 25 °C, TMS): δ = 1.22 (d, J = 6.6 Hz, 3 H, CH_3 of *i*Pr), 1.315 (d, J = 6.6 Hz, 3 H, CH_3 of *i*Pr), 2.27 (s, 3 H, CH_3 *p* to *i*Pr), 2.69−2.74 (sept, 1 H, CH of *i*Pr), 2.69−2.72 (t, 2 H, $TeCH_2$), 3.53−3.56 (t, 2 H, NCH_2), 3.83 (s, 3 H, OCH_3), 5.13−5.96 (m, 4 H, ArH of *p*-cymene), 7.045 (d, J = 8.4 Hz, 2 H, ArH *m* to Te), 8.005 (d, J = 8.7 Hz, 2 H, ArH *o* to Te), 8.46 (br. s, 2 H, NH_2) ppm. ^{13}C{^{1}H} NMR ($CDCl_3$, 25 °C, TMS): δ = 17.28 ($TeCH_2$), 18.89 (*p*-cymene CH_3), 24.69 and 25.73 (CH_3 of *i*Pr of *p*-cymene), 30.75, 31.41 (CH of *i*Pr of *p*-cymene), 42.55 (NCH_2), 55.36 (OCH_3), 76.58−85.13 (ArC of *p*-cymene *m* and *o* to *i*Pr), 101.51 (ArCTe), 104.75 ($ArCCH_3$ of *p*-cymene), 105.88 (ArC-*i*Pr of *p*-cymene), 115.15−116.34 (ArC *m* to Te), 138.09 (ArC *o* to Te), 161.69 (Ar-$COCH_3$) ppm. IR (KBr): nu(tilde) = 361 ν(Ru−Cl), 440 ν(Ru−N) cm^{-1}.

Synthesis of [PdCl(L^1-H)] (2): $Na_2[PdCl_4]$ (0.294 g, 1 mmol) was dissolved in water (5 mL). A solution of L^1 (0.397 g, 1 mmol) prepared in acetone (10 mL) was added with vigorous stirring. An orange precipitate of **2** was immediately obtained which was filtered and dried. The orange solid was recrystallized from chloroform/methanol/hexane to give crystals of **2**. Yield ca. 0.37 g (ca.72%); m.p. 162 °C. $C_{17}H_{18}ClNO_2PdTe$ (533.8): calcd. C 37.97, H 3.37, N 2.60, Te 23.80; found C 39.48, H 3.47, N 2.43, Te 23.65. ^{1}H NMR ($CDCl_3$, 25 °C, TMS): δ = 2.39 (s, 3 H, CH_3), 3.49 (t, 2 H, 2-H), 3.82 (s, 3 H, OCH_3), 4.17 (t, 2 H, 1-H), 6.61−6.66 (m, 3 H,

 © 2004 Wiley-VCH Verlag GmbH & Co. KGaA, Weinheim

ArH *m* to Te and 7-H), 6.915 (d, J = 8.7 Hz, 1 H, 9-H), 7.12−7.14, (m, 1 H, 8-H), 7.335 (d, J = 9.0 Hz, 1 H, 6-H), 8.065 (d, J = 9.0 Hz, 2 H, ArH *o* to Te) ppm. $^{13}C\{1H\}$ NMR ($CDCl_3$, 25 °C, TMS): δ = 13.38 (CH_3), 19.29 (C-2), 62.76 (C-1), 55.01 (OCH_3), 102 (ArCTe), 115.38 (ArC *m* to Te), 115.71 (C-6), 120.86 (C-8), 125.01 (C-4), 127.68 (C-9), 130.86 (C-7), 138.58 (ArC *o* to Te), 159.90 ($ArCOCH_3$), 163.53 (C-5), 171.38 (C-3) ppm. IR (KBr): $\tilde{\nu}$ = 306 ν(Pd−Cl), 486 ν(Pd−N) cm^{-1}.

Synthesis of $[HgBr_2{\cdot}(L^1)_2]$ (3): $HgBr_2$ (0.720 g, 2 mmol) was dissolved in acetone (5 mL). A solution of $\mathbf{L^1}$ (1.588 g, 4 mmol), prepared in chloroform (10 mL), was added with stirring. The mixture was stirred for a further 0.5 h. A yellow solid separated out which was filtered, washed with acetone and dried. Yield 1.66 g (ca. 85%); m.p. 138 °C. $C_{34}H_{38}Br_2HgN_2O_2Te_2$ (1154): calcd. Te 22.8; found Te 21.6. ^1H NMR ($CDCl_3$, 25 °C, TMS): δ = 2.38 (s, 6 H, CH_3), 3.56 (t, 4 H, 2-H), 3.82 (s, 6 H, OCH_3), 4.04 (t, 4 H, 1-H), 6.80−6.83 (m, 3 H, ArH *m* to Te and 7-H), 6.925 (d, J = 9.0 Hz 1 H, 9-H), 7.505 (d, J = 7.8 Hz, 1 H, 6-H), 7.745 (d, J = 8.7 Hz, 2 H, ArH *o* to Te) ppm; signal due to 8-H merged with that of chloroform (δ = 7.26 ppm).

Synthesis of L^2: $\mathbf{L^1}$ (0.40 g, 1 mmol) and $NaBH_4$ (0.38 g, 10 mmol) were heated to reflux in dry ethanol (100 mL) for 24 h. The solution was cooled and the solvent was evaporated in vacuo. The ligand was extracted with dichloromethane and the extract dried with sodium sulfate. The solvent was removed in vacuo. $\mathbf{L^2}$ was obtained as highly viscous pale yellow oil. Yield 0.28 g (70%); Λ_M = 0.4 $cm^2{\cdot}mol^{-1}{\cdot}ohm^{-1}$. $C_{17}H_{21}NO_2Te$ (399): calcd. Te 31.98; found Te 31.31. ^1H NMR ($CDCl_3$, 25 °C, TMS): δ = 1.38 (d, J = 6.6 Hz, 3 H, CH_3), 1.87−1.97 (br. s, 1 H, NH), 2.83−2.98 (m, 4 H, 1-H + 2-H), 3.78 (s, 3 H, OCH_3), 3.83−3.88 (m, 1 H, CH), 6.71−6.79 (m, 4 H, ArH *m* to Te and 7-H + 9-H), 6.885 (d, J = 7.5 Hz, 1 H, 6-H), 7.09−7.14 (m, 1 H, 8-H), 7.655 (d, J = 8.7 Hz, 2 H, ArH *o* to Te), 11.40 (very br. s, OH) ppm. $^{13}C\{1H\}$ ($CDCl_3$, 25 °C, TMS): δ = 8.83 (C-1), 22.27 (CH_3), 47.65 (C-1), 55.09 (OCH_3), 58.19 (C-3) 99.67 (ArCTe), 115.29 116.67 (ArC *m* to Te), 118.95 (C-6), 120.20 (C-8), 126.50 (C-4), 127.90 (C-9), 128.26 (C-7), 140.23−141.07 (ArC *o* to Te), 157.12 ($ArCOCH_3$), 159.91 (C-5) ppm.

Synthesis of $[RuCl(L^2\text{-}H)]$ (4): $[RuCl_2(p\text{-cymene})]_2$ (0.62 g, 1 mmol) was dissolved in dichloromethane (10 mL). A solution of $\mathbf{L^2}$ (0.80 g, 2 mmol), prepared in dichloromethane (20 mL), was added with vigorous stirring. The mixture was stirred for a further 3 h. The solvent was removed in a rotary evaporator under reduced pressure. The dark orange single crystals of **4** were grown from chloroform/hexane (1:1). Yield 0.72 g (67%); m.p. 100 °C (dec.). Molecular mass: calcd. 535.41; found 1037. Λ_M = 0.9 $cm^2{\cdot}mol^{-1}{\cdot}ohm^{-1}$. $C_{17}H_{20}ClNO_2RuTe$ (534.4): calcd. C 38.21, H 3.77, N 2.62, Te 23.88; found C 39.01, H 4.20, N 2.22, Te 23.16. IR (KBr): $\tilde{\nu}$ = 361 ν(Ru−Cl), 450 ν(Ru−N) cm^{-1}.

Synthesis of L^3: Bis(2-aminoethyl) telluride (1.13 g, 2.5 mmol) was stirred at room temperature in dry ethanol (20 mL) for 0.5 h. 2-Hydroxyacetophenone (0.68 g, 5 mmol), dissolved in dry ethanol (20 mL), was added to the above solution dropwise with stirring. The mixture was stirred at room temp. for a further 6 h, was then kept at 0−5 °C for 24 h. $\mathbf{L^3}$ separated as a yellow precipitate. The precipitate was recrystallized at 0−5 °C from chloroform/hexane (1:1) to give yellow single crystals of $\mathbf{L^3}$. Yield 1.13 g (80%); m.p. 95−96 °C. Λ_M = 0.86 $cm^2{\cdot}mol^{-1}{\cdot}ohm^{-1}$. Molecular mass: calcd. 452; found 444.5. $C_{20}H_{24}N_2O_2Te$ (452): calcd. C 53.14, H, 5.35, N 6.20, Te 28.23; found C 52.52, H 5.42, N 6.74, Te 27.66. ^1H NMR ($CDCl_3$, 25 °C, TMS): δ = 2.32 (s, 6 H, CH_3), 3.02−3.07 (t, 4 H, $TeCH_2$), 3.94−3.99 (t, 4 H, 1-H), 6.75−6.80 (m, 2 H, 8-H), 6.915 (d, J = 8.1 Hz, 2 H, 9-H) 7.26−7.30 (t, 2 H, 7-H), 7.502 (d, J = 8.1 Hz, 2 H, 6-H), 15.93 (br. s, 1 H, OH) ppm. $^{13}C\{^1H\}$ NMR ($CDCl_3$, 25 °C, TMS): δ = 3.49 (C-2), 14.73 (CH_3), 51.64 (NCH_2), 117.27 (C-6), 118.57 (C-8), 119.36 (C-4), 128.06 (C-9), 132.43 (C-7), 163.32 (C-5), 171.60 (C-3) ppm.

Synthesis of $[HgBr_2(L^3)_2]$ (5): $HgBr_2$ (0.360 g, 1 mmol) was dissolved in acetone (5 mL). A solution of $\mathbf{L^3}$ (0.904 g, 2 mmol), prepared in chloroform (10 mL), was added with stirring. The mixture was stirred for a further 1 h. A yellow solid separated out which was filtered, washed with acetone and dried. Yield 1.01 g (80%); m.p. 142 °C. $C_{34}H_{38}Br_2HgN_2O_2Te_2$ (1264): calcd. Te 20.25; found Te 19.88. ^1H NMR ($CDCl_3$, 25 °C, TMS): δ = 2.29 (s, 12 H, CH_3), 3.49−3.53 (t, 8 H, 2-H), 4.07−4.11 (t, 8 H, 1-H), 6.75−6.80 (t, 4 H, 8-H), 6.873 (d, J = 8.1 Hz, 4 H, 9-H), 7.22−7.27 (m, 4 H, 7-H), 7.48 (d, J = 6.9 Hz, 4 H, 6-H), 15.13 (br. s, OH) ppm.

Synthesis of L^4: $\mathbf{L^3}$ (0.452 g, 1 mmol) and $NaBH_4$ (0.38 g, 10 mmol) were heated to reflux in dry ethanol (100 mL) for 24 h. The solution was cooled and the solvent was evaporated in vacuo. The ligand was extracted with dichloromethane and the extract dried with sodium sulfate. The solvent was removed in vacuo affording $\mathbf{L^4}$ as a highly viscous pale yellow oil. Yield 0.31 g (67%); Λ_M = 0.90 $ohm^{-1}{\cdot}cm^2{\cdot}mol^{-1}$. $C_{17}H_{21}NO_2Te$ (456): calcd. Te 25.52; found Te 24.93. ^1H NMR ($CDCl_3$, 25 °C, TMS): δ = 1.361, 1.365 (2 d, J = 6.6, 9.9 Hz, 6 H, CH_3), 2.54−2.75 (m, 8 H, 1-H + 2-H), 3.83−3.84 (m, 2 H, CH), 6.67−6.74 (m, 4 H, 7-H + 9-H), 6.86 (d, J = 7.2 Hz, 2 H, 6-H), 7.03−7.08 (m, 2 H, 8-H), 11.40 (very br. s, OH) ppm.

Synthesis of $[HgBr_2(L^4)_2]$ (6): $HgBr_2$ (0.360 g, 1 mmol) was dissolved in acetone (5 mL). A solution of $\mathbf{L^4}$ (0.904 g, 2 mmol), prepared in chloroform (10 mL), was added with stirring. The mixture was stirred for a further 1 h. A yellow solid separated out which was filtered, washed with acetone and dried. Yield 1.02 g (ca.80%); m.p. 105 °C. $C_{34}H_{38}Br_2HgN_2O_2Te_2$ (1272): calcd. Te 20.12; found Te 19.35. ^1H NMR ($CDCl_3$, 25 °C, TMS): δ = 2.16 (s, 12 H, CH_3), 2.81 (br. s, 8 H, 1-H), 3.10 (br. s, 8 H, 2-H), 3.99 (m, 2 H, CH), 6.77−6.79 (m, 4 H, 7-H + 9-H), 6.99 (d, J = 6 Hz, 2 H, 6-H), 7.09−7.11 (m, 2 H, 8-H) ppm.

Acknowledgments

R. K. P. thanks UGC (India) for a fellowship. A. K. S. thank CSIR (India) for the research project no. 1(1849)/03/EMR-II. P. S., on leave from Instituto de Quimica, UNAM, is thankful to DGAPA, UNAM for financing a sabbatical stay at IITD.

[1] [1a] A. K. Singh, V. Srivastava, *J. Coord. Chem.* **1992**, *27*, 237−253. [1b] A. K. Singh, S. Sharma, *Coord. Chem. Rev.* **2000**, *209*, 49−98.
[2] N. Al-Salim, T. A. Hamor, W. R. McWhinnie, *J. Chem. Soc., Chem. Commun.* **1986**, 453−455.
[3] S. C. Menon, A. Panda, H. B. Singh, R. J. Butcher, *Chem. Commun.* **2000**, 143−144.
[4] S. C. Menon, H. B. Singh, R. P. Patel, R. J. Butcher, *Organometallics* **1997**, *16*, 563−571.
[5] A. K. Singh, V. Srivastava, *Phosphorus, Sulfur Silicon Relat Elem.* **1990**, *47*, 471−475.
[6] V. Srivastava, R. Batheja, A. K. Singh, *J. Organomet. Chem.* **1994**, *484*, 93−96.
[7] G. L. Eichhorn, J. C. Bailar Jr., *J. Am. Chem. Soc.* **1953**, *75*, 2905−2907; I. Jardine, F. J. McQuillin, *Tetrahedron Lett.* **1972**, 459−461.
[8] A. K. Singh, *Proc. Indian Acad. Sci. (Chem. Sci.)* **2002**, *114*, 357−366.

 © 2004 Wiley-VCH Verlag GmbH & Co. KGaA, Weinheim

[9] P. Braunstein, F. Naud, A. Pfaltz, S. J. Rettig, *Organometallics* **2000**, *19*, 2676−2683.
[10] A. K. Singh, J. Sooriyakumar, M. Kadarkaraisamy, J. E. Drake, M. B. Hursthouse, M. E. Light, R. J. Butcher, *Polyhedron* **2002**, *21*, 667−674; A. K. Singh, J. Sooriyakumar, R. J. Butcher, *Inorg. Chim. Acta* **2001**, *312*, 163.
[11] D. P. Rillema, D. S. Jones, H. A. Levy, *Chem. Commun.* **1979**, 849−851.
[12] M. Shivakumar, K. Pramanik, P. Ghosh, A. Chakravorty, *Inorg. Chem.* **1998**, *37*, 5968−6969.
[13] C. A. Bessel, R. F. See, D. L. Jameson, M. R. Churchill, K. J. Takeuchi, *J. Chem. Soc., Dalton Trans.* **1993**, 1563−1576.
[14] A. Singh, N. Singh, D. S. Pandey, *J. Organomet. Chem.* **2002**, *642*, 48−57.
[15] A. K. Singh, M. Kadarkaraisamy, M. Mishra, J. Sooriyakumar, J. E. Drake, M. B. Hursthouse, M. E. Light, J. P. Jasinski, *Inorg. Chim. Acta* **2001**, *320*, 133−140; A. K. Singh, J. Sooriyakumar, J. E. Drake, M. B. Hursthouse, M. E. Light, *J. Organomet. Chem.* **2000**, *613*, 244−249; A. K. Singh, M. Kadarkaraisamy, G. S. Murthy, J. Srinivas, B. Varghese, R. J. Butcher, *J. Organomet. Chem.,* **2000**, *605*, 39−44.
[16] W. H. Leung, E. Y. Y. Chan, W. T. Wong, *Inorg. Chem.* **1999**, *38*, 136; S. Patra, B. Mondal, B. Sarkar, M. Nlemeyer, G. K. Lahiri, *Inorg. Chem.* **2003**, *42*, 1322−1327; M. Maji, S. Ghosh, S. K. Chattopadhyay, T. C. W. Mak, *Inorg. Chem.* **1997**, *36*, 2938−2943; T. Tanase, T. Aiko, Y. Yamamoto, *Chem. Commun.* **1996**, 2341−2342.
[17] Bruker, SMART System, Version 5.163; SHELXTL, Version 6.10, Bruker AXS Inc., Madison, Wisconsin, USA, **2000**.
[18] G. M. Sheldrick, SAINT, SADABS, Version 6.02, Bruker AXS Inc., Inc., Madison, Wisconsin, USA, **1999**.
[19] Bruker, SMART, Version 5.624; SAINT, Version 6.04, programs using the Windows NT system, Bruker AXS Inc., Madison, Wisconsin, USA, **2001**.
[20] G. M. Sheldrick, SHELXTL, Version 5.10, Bruker AXS Inc., Madison, Wisconsin, USA, **1997**.

Received July 5, 2003
Early View Article
Published Online February 5, 2004

 © 2004 Wiley-VCH Verlag GmbH & Co. KGaA, Weinheim

Sodium Hydro(isothiocyanato)borates: Synthesis and Structures[‡]

Heinrich Nöth*[a] and Marcus Warchhold[a]

Dedicated to Prof. Dr. B. Krebs on the occasion of his 65th birthday

Keywords: Crown compounds / Sodium / NMR spectroscopy / Borates

Sodium thiocyanate reacts in THF solution with 18-crown-6 to give the molecular compound Na(18-crown-6)(THF)NCS (**3**) with the N atom of the NCS anion oriented towards Na^+. The same reaction with 15-crown-5 yields the ion pair Na(15-crown-5)NCS (**4**). In contrast, $Na(NCS)(py)_4$, obtained by treating a solution of $Na(H_3BNCS)$ in THF with pyridine, yields $Na(py)_4(NCS)$ (**5**), which has a chain structure with hexacoordinate Na atoms coordinated to five N atoms and an S atom. Na(NCS) in THF adds 1 equiv. of BH_3 to give $Na(H_3BNCS)\cdot n$THF. Addition of 18-crown-6 to this solution yields crystals of the salt $[Na(18\text{-crown-6})(THF)_2][H_3BNCS]$ (**1**), as shown by X-ray crystallography. Both the cation and the anion show site disorder. However, when 15-crown-5 is used for complexation, the salt $[Na(15\text{-crown-5})(THF)][H_3BNCS]$ (**2**) can be isolated. Its anion shows an almost linear B–N–C–S unit. Only a mixture of (catecholato)-(isothiocyanato)borates results on treating Na(NCS) in THF with catecholborane. However, the borate $Na[catB(NCS)_2]$ is readily formed by adding Na(NCS) to *B*-(isothiocyanato)catecholborane. Single crystals of this compound were obtained as the salt $[Na(18\text{-crown-6})(THF)_2][catB(NCS)_2]$ (**6**). On the other hand, the reaction of Na(NCS) with 9-borabicyclo[3.3.1]nonane (9-BBN) in THF yields Na[(9-BBN)NCS)]·*n*THF, and, on addition of 18-crown-6, the complex $[Na(18\text{-crown-6})(THF)_2][(9\text{-BBN})NCS]$ was isolated. Suitable crystals for X-ray structure determination were, however, only obtained by crystallization from tetrahydropyran. This solvate has the rather unusual structure $[Na(18\text{-crown-6})(thp)_2][\{(9\text{-BBN})NCS\}_2Na(thp)_4]$ (**8**). The sodiate anion has an Na atom coordinated by two S and four O atoms. DFT calculations support these experimental results: The (isothiocyanato)borates are more stable than the thiocyanato isomers. For the latter a bent structure of the B–S–C–N unit with a B–S–C bond angle of 105.7° is predicted.
(© Wiley-VCH Verlag GmbH & Co. KGaA, 69451 Weinheim, Germany, 2004)

Introduction

It is well known that the reducing power of alkali metal tetrahydroborates can be influenced by introducing various substituents at the boron atom.[2] In general, there are two routes to these "mixed" hydroborates: (i) reactions of MBH_4 (M = Li, Na, K) with protic reagents HX (X = CN, RCOO, RO), or (ii) addition of the BH_3 component of $H_3B{\cdot}L$ (L = THF, Me_2S, NR_3) to a nucleophilic anion X^- (X = R, NR_2, OR, CN, NCS). The action of $BH_3{\cdot}$THF on MSCN was first reported by Aftandilian et al.[3] They concluded from IR data that the BH_3 unit is attached to the S atom of the thiocyanate anion to give $(H_3B{-}SCN)^-$. Klanberg et al.,[4] however, showed that $Li[B(NCS)_4]$ contains isothiocyanate substituents. About 18 years later, Hui analyzed the IR spectra again[5] and came to the conclusion that the adduct of BH_3 with NCS^- is better formulated as the isomer $(H_3B{-}NCS)^-$. Moreover, NMR spectroscopic data also favored the isothiocyanato structure.[6] In order to finally settle the question of isomerism we studied several borate complexes containing the NCS anion by X-ray crystallography.

Results

Crown Ether Complexes of Na(NCS) and Na($H_3B{-}NCS$)

The compound $Na(H_3B{-}NCS)$, was prepared as shown in Equation (1) and precipitated as the 18-crown-6 solvate **1** by adding the ligand to its THF solution. In previously reported reactions the salt $Na(H_3B{-}NCS)$ was precipitated as a dioxane solvate.[2,4]

$$NaSCN + BH_3{\cdot}THF \xrightarrow[THF]{\text{18-crown-6}} \underset{\mathbf{1}}{Na(H_3B\text{-}NCS){\cdot}THF{\cdot}18\text{-crown-6}} \quad (1)$$

Table 1 summarizes some information on the IR data of H_3BNCS^- salts, some of our experimental results as well as results obtained by DFT[7] calculations. In addition IR data for Na(SCN)(15-crown-5) and MeNCS[8] are included.

[‡] Metal Tetrahydoborates and Tetrahydroborato Metallates, 29. Part 28: Ref.[1]

[a] Department of Chemistry, University of Munich, Butenandtstr. 5–13, 80377 München, Germany
E-mail: H.Noeth@lrz.uni-muenchen.de

Table 1. IR bands [cm^{-1}] reported for $(H_3B-NCS)^-$ compared with Na(NCS)(15-crown-5), MeNCS and DFT calculation (for NCS^-)

	Ref.[2]	Ref.[5]	Ref.[5]	**1**	Na(NCS)(14-crown-4)[9]	MeNCS[8]	$(H_3BNCS)^-$, DFT calcd.
νBH	2380−2300	2380, 2330, 2290	2334, 2295, 2260	2365, 2325	–	–	2358, 2355, 2354
νNCS	2175, 2085	2180, 2080	2158, 2055	2172, 2050	2045	2129	2149

We found in most samples of **1** an IR band at 2050 cm^{-1} with different intensities (weak to medium), in addition to a strong band at 2172 cm^{-1}. The band at 2050 cm^{-1} is most likely due to the presence of NCS^-, as can be deduced from the band found at 2045 cm^{-1} observed in Na(NCS)(15-crown-5).[9] In order to make reliable assignments we performed DFT calculations at the B3LYP/6-311**G(d,p) level. There should be two IR-active B−H stretching frequencies at 2355 and 2358 cm^{-1}. Because the calculations were also performed for C_1 symmetry, the degeneracy for ν_{as} (2355 cm^{-1}) is removed, but the third vibration is close to the degenerate band and probably was not resolved experimentally. Moreover, the BH vibrations couple with the CN vibration, for which only one band is predicted at 2149 cm^{-1}, in acceptable agreement with experimental values. The IR data for **1** and MeNCS suggest that the H_3B group is *N*-coordinated to the NCS anion.

Another argument for the presence of a B−N bond in **1** comes from ^{14}N and ^{13}C NMR spectroscopic data. $\delta^{14}N$ for **1** is observed at $\delta = -244$ ppm; the ^{14}N resonance for MeNCS is found at $\delta = -290$ ppm.[10]

The ^{13}C NMR signal is split into a 1:1:1 triplet due to C−N coupling ($^1J_{^{13}C^{14}N} = 24$ Hz), which is also found for isocyanides.[11,12] In contrast, the ^{11}B NMR spectroscopic data for **1** ($\delta = -27$ ppm, $^1J_{^{11}B^1H} = 96$ Hz) do not allow a distinction between B−N or B−S bonding. For instance, the ^{11}B NMR signal of $(H_3BSH)^-$ is found at $\delta = -25$ ppm[13] and that of $(H_3BNC)^-$ at $\delta = -27$ ppm.[14]

Recrystallization of the 18-crown-6 solvate of $Na(H_3B-NCS)$ from THF always caused the formation of Na(NCS)(18-crown-6). This also happened when 15-crown-5 was used. All attempts to obtain single crystals of $Na(H_3B-NCS)$(18-crown-6) from THF solutions failed. When crystallization of $Na(H_3B-NCS)$ was performed in an excess of BH_3·THF in the presence of the 18-crown-6 ligand then suitable crystals for an X-ray structure determination were obtained. However, these showed site disorder for the anion and for THF molecules in the [Na(18-crown-6)$(THF)_2$] cation (see below). In contrast, when 15-crown-5 was used as a ligand then single crystals of compound **2** were obtained without disorder, due to the lower symmetry of the cation $[Na(15\text{-crown-5})(THF)]^+$ [Equation (2)].

$$\mathrm{Na[NCS] \xrightarrow{+BH_3\cdot THF} Na[H_3B\text{-}NCS]\cdot THF \xrightarrow{+\ 15\text{-crown-5}} \underset{\mathbf{2}}{Na[H_3B\text{-}NCS]\cdot 15\text{-crown-5}}} \quad (2)$$

In THF solution $Na(H_3B-NCS)$ shows a slight tendency to rearrange according to Equation (3). The solutions are fairly stable at room temperature. On heating a 0.1 M solution for 4 d under reflux only 40% of $Na(H_3B-NCS)$ decomposed.

$$2\ Na(H_3B-NCS) \rightarrow Na(BH_4) + Na[H_2B(NCS)_2] \quad (3)$$

In order to have a solid basis for comparing the IR spectra of the H_3B-NCS anion with the Na(NCS) complexes this salt was treated with 18-crown-6 and 15-crown-5 in THF solution; compounds **3** and **4** were isolated as single crystals. On the other hand, when $Na(H_3B-NCS)$ was treated in THF solution with an excess of pyridine, crystals of the compound Na(NCS)·4.5py (**5**) were obtained. Thus, pyridine removes the BH_3 group from $Na(H_3B-NCS)$ in THF solution.

Na(NCS)(18-crown-6)$(THF)_2$	Na(NCS)(15-crown-5)	$Na(NCS)\cdot(py)_{4.5}$
3	**4**	**5**

Structures

Compounds **3** and **4** are tight ion pairs, with Na coordinated to the N atom of the NCS groups (Figures 1 and 2) while **5** is a coordination polymer with a chain structure in which the Na ions are hexacoordinate, with four py molecules in equatorial positions and an N and S atom of two different NCS anions in *trans* positions (Figure 3). Compound **3** contains an octacoordinate Na ion which sits in the center of the crown ligand. The coordination sphere is completed by a THF molecule and an *N*-bonded NCS anion. In contrast, compound **4** contains a hexacoordinate Na ion, which is present in a distorted pentagonal-pyramidal environment. The Na−N bond lengths increase in the series **3** to **5**. Within the errors of standard deviations one can consider the N−C bond lengths as equal, and this holds also for the C−S bond lengths. The average Na−O distance in **3** is significantly longer than in **4**, while the Na−O distance to the THF molecule in **3** is about 0.3 Å shorter than the distances to the O atoms of the crown ether. Selected molecular parameters are summarized in Table 2, others are found in the captions to the figures.

The trihydro(isothiocyanato)borate **1** crystallizes in the triclinic space group $P\bar{1}$ with $Z = 1$. The compound is ionic with formula $[Na(18\text{-crown-6})(THF)_2]^+[H_3B-NCS]^-$ (see Figure 4). Because the Na ion occupies a crystallographic

 © 2004 Wiley-VCH Verlag GmbH & Co. KGaA, Weinheim

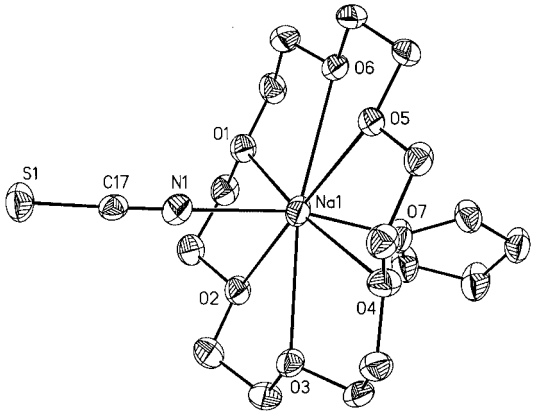

Figure 1. Molecular structure of Na(NCS)(18crown-6)$(THF)_2$ (**3**) (ORTEP); selected bond lengths [Å]: N1−C17 1.156(3), C17−S1 1.635(3), Na1−N1 2.375(3), Na1−O1 2.439(2), Na1−O2 2.756(2), Na1−O3 2.781(2), Na1−O4 2.760(2), Na1−O5 2.779(2), Na1−O6 2.814(2), Na1−O7 2.419(2); selected bond angles [°]: Na1−N1−C17 175.9(2), N1−C17−S1 178.2(2), O1−Na1−O2 62.71(6), O2−Na1−O3 60.45(6), O3−Na1−O4 59.76(5), O4−Na1−O5 59.47(6), O5−Na1−O6 58.99(6), O6−Na1−O1 61.53(6), O1−Na1−O7 90.15(8), O2−Na1−O7 81.80(6), O3−Na1−O7 85.25(7), O4−Na1−O7 82.71(7), O5−Na1−O7 97.16(6), O6−Na1−O7 83.91(7), N1−Na1−O1 87.36(7), N1−Na1−O2 85−07(7), N1−Na1−O3 84.81(8), N1−Na1−O4 100.34(9), N1−Na1−O5 85.87(8), N1−Na1−O6 106.61(7), N1−Na1−O7 166.27(8)

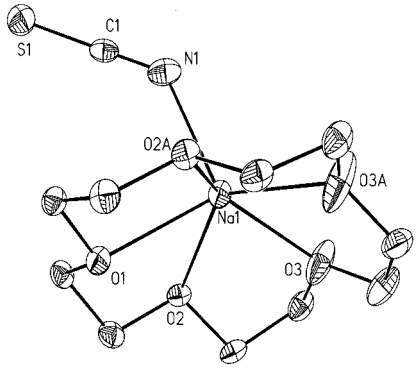

Figure 2. Molecular structure of Na(NCS)(15-crown-5) (**4**) (ORTEP); selected bond lengths [Å] (see also Table 1): Na1−O1 2.369(4), Na1−O2 2.461(3), Na1−O3 2.356(4), O1−C2 1.426(4), O2−C3 1.421(4), O2−C4 1.426(4), O3−C5 1.411(5), O3−C6 1.344(5); selected bond angles [°]: C1−N1−Na1 133.6(5), N1−Na1−O1 94.5 (2), N1−Na1−O3 121.3(2), N1−Na1−O2 97.13(9), O1−Na1−O3 127.3(2), O2−Na1−O3A 132.8(2), O2−Na1−O2A 136.5(1), O3−Na1−O2A 132.8(1)

inversion center the THF molecules are present in *trans* positions. The structure of this cation has been observed already in several $[Na(18\text{-crown-6})(THF)_2]^+$ complexes with various anions.[15−18] Moreover, the two orientations of the anion result from a crystallographic inversion center in the middle of the two N−C bonds (equal 1:1 occupancy). Therefore, there are large errors regarding the bond lengths of the linear B−N−C−S unit.

In contrast, no disorder problem was associated with compound **2**, which is also ionic. It crystallizes in the orthorhombic space group $P2_12_12_1$. Figure 5 shows the two ions. The cation closely resembles compound **4** whose NCS ligand has been replaced by a THF molecule. The

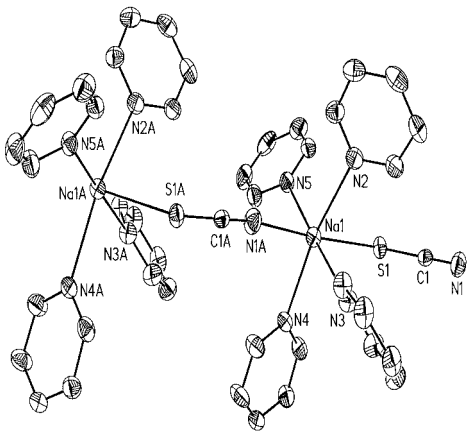

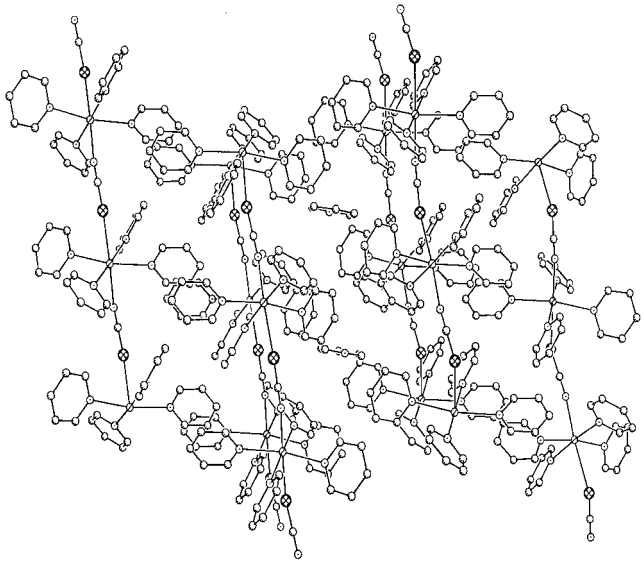

Figure 3. (top) Part of the chain structure of Na(NCS)·4py (ORTEP); solvent of crystallization has been omitted for clarity; selected bond lengths [Å]: Na1−N1A 2.417(3), Na1−S1 3.603(1), S1−C1 1.639(3), C1−N1 1.151(3), Na1−N2 2.519(2), Na1−N3 2.505(2), Na1−N4 2.521(2), Na1−N5 2.483(2), N2−C2 1.328(3), N2−C6 1.324(3), N3−C7 1.326(3), N3−C11 1.328(3), N4−C12 1.320(3), N4−C16 1.331(3), N5−C17 1.328(3), N5−C21 1.321(3); selected bond angles [°]: Na1−S1−C1 116.25(9), S1−C1−N1 178.4(2), N2−Na1−N3 84.69(8), N3−Na1−N4 87.03(7), N4−Na1−N5 91.69(7), N5−Na1−N2 96.13(8), N2−Na1−N4 170.20(8), N3−Na1−N5 175.21(8), N2−Na1−S1 88.45(6), N3−Na1−S1 94.92(7), N4−Na1−S1 87.03(6), N5−Na1−S1 80.40(6), S1−Na1−N1A 172.80(7), N1A−Na1−N4 92.67(8), C2−N2−C6 117.1(2), C7−N3−C11 116.6(2), C12−N4−C16 115.1(2), C17−N5−C21 116.3(2); (bottom) view down the *b* axis of the unit cell of **5**

Table 2. Selected bonding parameters of Na(NCS) solvates **3**−**5**

	3	**4**	**5**
Space group	$P2_1/c$	$Pmn2_1$	$I2/a$
Na1−N1	2.375(3)	2.393(5)	2.417(3)
N1−C1	1.156(3)	1.170(8)	1.151(3)
C1−S1	1.635(3)	1.633(7)	1.639(3)
Na1−N1−C1	175.9(2)	133.6(5)	173.6(2)
N1−C1−S1	178.2(2)	179.3(5)	178.4(2)
Na1−S1−C1	–	–	116.3(2)

 © 2004 Wiley-VCH Verlag GmbH & Co. KGaA, Weinheim

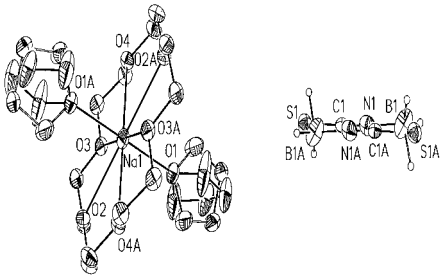

Figure 4. Molecular structure of [Na(18-crown-6)(THF)$_2$][H_3B-NCS] showing the two orientations of the anion; only the parameters for the cation are given; selected bond lengths [A]: Na1−O1 2.320(2), Na1−O2 2.818(2), Na1−O3 1.719 (1), Na1−O4 2.777(1); selected bond angles [°]: O1−Na1−O2 94.99(6), O1−Na1−O3 88.75(6), O1−Na1−O4 95.44(6), O2−Na1−O3 60.15(9), O2−Na1−O3 60.15(4), O3−Na1−O4 61.37(5), O2−Na1−O3A 119.85(4), O3−Na1−O4A 118.63(5); due to the inversion center at Na1 the THF molecules are site disordered (SOF = 0.5; both orientations are shown)

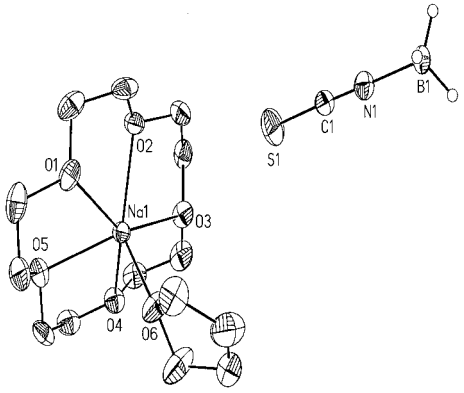

Figure 5. Molecular structure of [Na(15-crown-5)(THF)][H_3B-NCS] (**2**); selected bond lengths [A]: B1−N1 1.609(7), N1−C1 1.154(6), C1−S1 1.603(6), Na1−O1 2.384(4), Na1−O2 2.375(4), Na1−O3 2.371(4), Na1−O4 2.361(4), Na1−O5 2.366(4), Na1−O6 3.031 (7), O1−C2 1.437(8), O2−C4 1.396(7), O2−C3 1.412(7), O3−C5 1.435(7), O3−C6 1.430(8), O4−C7 1.455(8), O4−C8 1.423(9), O5−C9 1.449(7), O5−C10 1.412(8), O6−C12 1.417(8), O6−C15 1. 426(8), C−C(crown) 1.45(1) to 1.503(9); selected bond angles [°]: B1−N1−C1 179.1(6), N1−C1−S1 178.6(7), O1−Na1−O2 70.0(2), O1−Na1−O3 136.3(2), O1−Na−O5 71.0(2), O2−Na1−O3 70.7(2), O2−Na1−O4 140.5(2), O2−Na1−O5 124.7(2), O2−Na1−O6 95.9(2), O3−Na1−O4 70.4(2), O3−Na1−O5 119.1(2), O3−Na1−O6 96.92(2), O4−Na1−O5 70.5(2), O4−Na1−O6 95.6(2), O5−Na1−O6 131.6(2), C2−O1−C11 114.4(6), C3−O2−C4 115.8(5), C5−O3−C6 114.2(5), C7−O4−C8 115.8(5), C9−O5−C10 114.2(5), C12−O6−C15 105.3(6)

H_3B-NCS anion has an almost linear B−N−C−S skeleton [bond angles B−N−C = 178.7(4)° and N−C−S = 178.9(4)°]. The B−N bond is comparatively long [1.575(5) Å] for a tetrahedral boron atom bound to a two-coordinate N atom. On the other hand, the C−N bond is very short [1.150(5) Å], and corresponds to a C−N triple bond. However, the short C−S bond [1.613(4) Å] is indicative of a double bond. With these structure determinations it is proved that the reaction of borane·THF with Na(NCS) results exclusively in formation of the trihydro(isothiocyanato)borate anion. This seems logical considering the strengths of the B−N and B−S bonds.

Calculations

In order to support the experimental bonding parameters of the [H_3B-NCS]$^-$ ion we performed MO calculations on this anion at the B3LYP and MP2(fc) level of theory with the basis set 6-311++G(d,p). These calculations were started with C_1 symmetry for the anion as found experimentally (however, it should be noted that the determined B−H bond lengths have high e.s.d.s), but resulted in C_{3v} symmetry for both methods. Table 3 shows the calculated values; it also contains the experimental data.

Except for the C−S bond lengths all data are in good agreement with those found for compound **2**. Due to the disorder in the anion of compound **1** as well as of [Bu_4N][H_3B-NCS][6] these data are too inaccurate to use them for comparison.

In order to also obtain information on the structure of the isomeric trihydro(thiocyanato)borate and its stability we performed analogous calculations for [H_3B-SCN]$^-$ (see Table 4). One can see that the C−N bond length is practically the same whether the BH_3 group is *N*- or *S*-coordinated but the C−S bond is to be expected to be longer in the trihydro(thiocyanato)borate than in the trihydro(isothiocyanato)borate. More importantly, the B−S−C−N unit is not linear, and a B−S−C bond angle of about 104° is to be expected. In each case the trihydro(isothiocyanato)borate is more stable than its isomer by −27 kJ/mol or −57 kJ/mol, respectively, depending on the level of theory (Table 4). This is reflected also in the calculation of the reaction energies as shown in Equations (4)−(6).

$$BH_3{\cdot}THF + NCS^- \rightarrow H_3B-NCS^- + THF;\ \Delta E = -96\ kJ \quad (4)$$

$$BH_3{\cdot}THF + SCN^- \rightarrow H_3B-SCN^- + THF;\ \Delta E = -38\ kJ \quad (5)$$

$$2\ BH_3{\cdot}THF + NCS^- \rightarrow H_3B-NCS-BH_3^- + 2\ THF;\ \Delta E = -109\ kJ \quad (6)$$

All these reactions are exothermic. The trihydro(thiocyanato)borate is less favored. However, a thiocyanatobis(trihydroborate) [Equation (6)] should also be stable but we were unable to detect this anion, even in concentrated solutions.

Further (Isothiocyanato)borates

In principle, many more (isothiocyanato)borates may be accessible simply by addition of NCS^- as nucleophile to a sufficiently Lewis-acidic boron center. We have studied two of them. In the first case we allowed catecholborane, catBH, to react with Na(NCS), and in the second case we used 9-borabicyclo[3.3.1]nonane (9-BBN).

The ^{11}B NMR spectra recorded for the reaction mixture of catecholborane with Na(NCS) revealed that several borate anions are formed. Table 5 shows the product distribution. We could not separate the mixture by fractional crystallization or separate Na[cat$B(NCS)_2$] (**6**) by adding di-

 © 2004 Wiley-VCH Verlag GmbH & Co. KGaA, Weinheim

Table 3. Calculated and experimental bond lengths [Å] and bond angles [°] for H_3B-NCS^-

	MP2(fc)/6-311**G(d,p)	B3LYP/6-311**G(d,p)	**2**	**1**	$[Bu_4N][H_3B-NCS]$[6]
B−N	1.560	1.648	1.575(5)	1.54(2)	1.81(2)
N−C	1.185	1.168	1.150(5)	1.09(2)	1.143(4)
C−S	1.631	1.641	1.613(4)	1.66(3)	1.661(4)
S−C−N	180.0	180.0	178.9	178(1)	179.4(3)
C−N−B	180.0	180.0	178.7(4)	176(2)	179.1(8)

Table 4. Calculated bond lengths [Å]and bond angles [°]for H_3B-SCN^-

	MP2(fc)/6-311**G(d,p)	B3LYP/6-311**G(d,p)
B−S	1.992	2.044
N−C	1.187	1.167
C−S	1.679	1.687
S−C−N	177.4	177.2
C−S−B	103.0	105.7
ΔE (to H_3B-NCS^-)	+27 kJ/mol	+57 kJ/mol

Table 5. Product distribution resulting in the reaction of catecholborane with Na(NCS) in THF monitored by ^{11}B NMR spectroscopy

	$\delta^{11}B$ [ppm]; $^1J_{B,H}$ [Hz]	Amount
catBH	23.0 (d); 190	7%
$Na[B(cat)_2]$	12.3 (s)	58%
$Na[catB(NCS)_2]$	−0.1 (quint); 24 $^1J_{B,N}$	8%
$Na[H_2B(NCS)_2]$	−19.5 (t); 115	27%

oxane. There is, however, an unusual feature in the proton-decoupled ^{11}B NMR spectrum of the products formed in solution, because the quintuplet at $\delta = -0.1$ ppm does not vanish. Therefore, this signal excludes the presence of B−H bonds. Moreover, the chemical shift excludes a BH_4 anion ($\delta^{11}B = -41$ ppm).[19] This is also revealed by the fact that the intensity of the five signals is 1:2:3:2:1 while BH_4^- requires a 1:4:6:4:1 intensity. However, the observed coupling pattern corresponds to the coupling of the boron nucleus with two nuclei of spin $I = 1$. Therefore, the observed coupling is due to $^1J_{^{11}B^{14}N}$. Such a coupling has already been detected for ^{15}N-enriched (isothiocyanato)borates $B(NCS)_{4-n}X_n^-$ (X = F, Cl; n = 1, 2, 3)[20] which have, however, not been isolated as alkali metal salts. The observed coupling constant $^1J_{^{11}B^{14}N}$ corresponds to those found for these species (21−28 Hz). Usually it is difficult to observe $^1J_{^{11}B^{14}N}$ couplings because of rapid quadrupole relaxation as both nuclei have strong quadrupole moments which generally leads to broad unresolved signals. For instance, no such coupling is observed for diazido(catecholato)borate whose structure is very similar to that of **6**.[21]

The synthesis of pure sodium catecholatobis(isothiocyanato)borate can be readily achieved by the reaction sequence shown in Equation (7).

Compound **6** not only shows a well-resolved 1:2:3:2:1 quintuplet in the ^{11}B NMR spectrum but also a 1:1:1:1 quadruplet in the ^{14}N NMR spectrum. Moreover, in concentrated THF solutions of **6** the ^{13}C resonance for the isothiocyanato group can also be detected as a broad signal at $\delta = 131$ ppm.

Single crystals of **6** separated from the THF solution after addition of 18-crown-6. They have the composition $[Na(18\text{-crown-6})(THF)_2][catB(NCS)_2]$. The crystals are triclinic, space group $P\bar{1}$, $Z = 2$. Figure 6 shows the structures of the two ions. The anion has almost C_{2v} symmetry, which by calculation is shown to be an energy minimum.

Table 6 contains selected experimentally determined and calculated data for the $[catB(NCS)_2]$ anion. There is good agreement between both except that the experimentally determined B−N−C bond angle is 12.3° smaller than calculated. The N−B bonds are shorter than in (H_3B-NCS). Moreover, the C−S bond is shorter than in free NCS^- (0.04 Å) and shorter by 0.023 Å than in $(H_3B-NCS)^-$. The calculated vibrational frequencies fit well with experimental values if multiplied by a factor of 0.96.[22] Calculation predicts 2150 cm^{-1} for the A_1 vibration of the NCS group and 2112 cm^{-1} for the B_1 vibration. These were found in the IR spectrum at 2150 and 2115 cm^{-1} and in the Raman spectrum at 2144 and 2108 cm^{-1}, respectively.

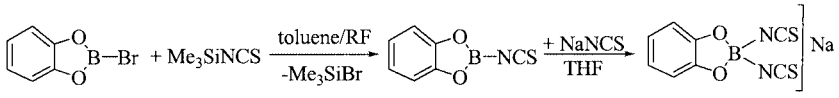

(7)

6

 © 2004 Wiley-VCH Verlag GmbH & Co. KGaA, Weinheim

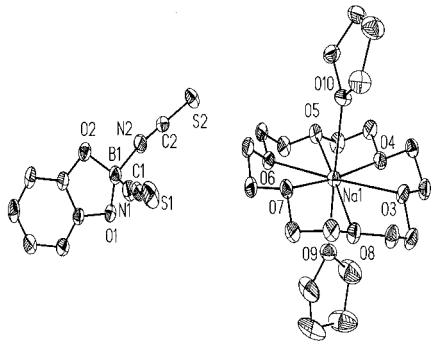

Figure 6. Structure of [Na(18-crown-6)(THF)$_2$][B(cat)(NCS)$_2$] (**6**); selected bond lengths [Å]: B1−O1 1.452(4), B1−O2 1.447(4), B1−N1 1.551(4), B1−N2 1.535(5), N1−C1 1.164(4), N2−C2 1.161(4), C1−S1 1.593(4), C2−S2 1.587(4), O2−C3 1.368(4), O2−C8 1.373(4), C3−C8 1.393(4), Na1−O3 2.697(2), Na1−O4 2.835(2), Na1−O5 2.906(2), Na1−O6 2.704(2), Na1−O7 2.703(2), Na−O8 2.672(2), Na1−O9 2.307(2), Na1−O10 2.305(2), O3−C9 1.410(4), O3−C20 1.432(3), O5−C12 1.420(4), O5−C13 1.412(4), O6−C14 1.418(4), O6−C15 1.420(3), O7−C16 1.420(4), O7−C17 1.432(3), O8−C18 1.424(3), O8−C19 1.424(4), O9−C10 1.484(4), O9−C21 1.409[(5), O10−C25 1.423(4), O10−C28 1.410(4); selected bond angles [°]: O3−Na1−O4 60.65(6), O4−Na1−O5 60.65(6), O5−Na1−O6 59.70(6), O6−Na1−O7 62.10(6), O7−Na1−O8 61.34(6), O8−Na1−O3 61.38(6), O3−Na1−O10 86.53(8), O4−Na1−O10 87.71(8), O5−Na1−O10 83.78(7), O6−Na1−O10 91.72(8), O7−Na1−O10 87.25(8), O8−Na1−O10 101.12(8), O9−Na1−O10 170.9(1), O1−B1−O2 107.9(3), N1−B1−N2 104.8(3), B1−N1−C1 163.0(3), B1−N2−C2 166.9(3)

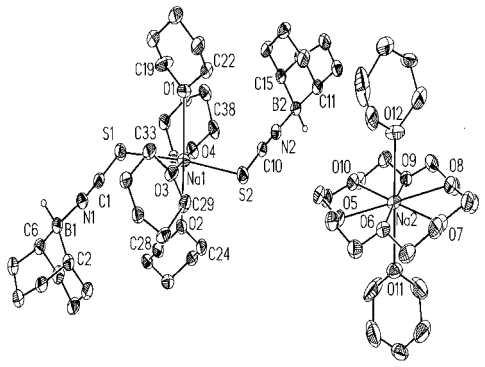

Figure 7. Structure of [Na(18-crown-6)(thp)$_2$][Na(thp)$_4${(9-BBN)NCS}$_2$] (**8**); selected bond lengths [A]: N1−C1 1.168(5), N2−C10 1.166(5), C1−S1 1.563(6), S2−C10 1.595(6), B1−N1 1.564(7), B2−N2 1.568(7), Na1−S1 3.254(2), Na1−S2 3.034(2), Na1−O1 2.377(3), Na1−O2 2.329(3), Na1−O3 2.302(3), Na1−O4 2.322(3), B1−C2 1.617(7), B1−C6 1.609(6), B2−C11 1.596(6), B2−C15 1.607(6); selected bond angles [°]: B1−N1−C1 174.7(4), N1−C1−S1 177.8(4), B2−N2−C10 175.1(4), N2−C10−S1 178.2(4), O1−Na1−O2 177.4(1), O1−Na1−O3 89.2(1), O1−Na1−O4 92.6(1), O2−Na1−O3 90.7(1), O2−Na1−O4 87.4(1), O3−Na1−O4 176.4(1), S1−Na1−O1 87.93(9), S1−Na1−O2 89.46(9), S1−Na1−O3 89.46(9), S1−Na1−O4 87.43(9), S2−Na1−O1 95.6(1), S2−Na1−O2 96.60(9), S2−Na1−O3 86.38(9), S2−Na1−O4 96.60(9), N1−B1−C2 111.8(4), N1−B1−C6 110.0(4), N2−B2−C11 109.2(4), N2−B2−C15 110.2(4), C2−B1−C6 105.7(4), C1−B2−C15 106.9(4); data for the cation [Na(18-crown-6)(thp)$_2$]; selected bond lengths [A]: Na2−O5 2.733(3), Na2−O6 2.690(4), Na2−O7 2.707(3), Na2−O8 2.819(3), Na2−O10 2.682(3), Na2−O11 2.342(4), Na2−O12 2.364(4); selected bond angles [°]: O5−Na2−O6 60.4(1), O6−Na2−O7 61.7(1), O7−Na2−O10 177.3, O11−Na2−O12 176.4(1), O6−Na2−O10 121.1(1)

Table 6. Experimental and calculated bond lengths [Å] and bond angles [°] of the anion [catB(NCS)$_2$]$^-$

	Experimental data	Calculated data[a]
B−O	1.465(4)	1.482
B−N	1.543(5)	1.527
N−C	1.163(4)	1.174
C−S	1.590(4)	1.614
O−B−O	107.9(3)	105.3
N−B−N	104.8(3)	107.8
B−N−C	163.0(3), 166.9(3)	177.3
N−C−S	177.8(3), 178.8(3)	178.6

[a] B3LYP/6-311*G(d) level of theory.

When Na(NCS) is treated with 9-borabicyclo[3.3.1]nonane (9-BBN) in THF, the solution shows a single doublet in the ^{11}B NMR spectrum at $\delta = -11.4$ ppm, $^1J_{^{11}B^1H} = 100$ Hz. This is compatible with the presence of an *N*-bonded NCS anion in Na[(9-BBN)NCS] (**7**).

Addition of 18-crown-6 to the solution of **7** precipitates the crown ether complex, which, after drying followed by dissolution in THF, leads to two ^{11}B NMR signals at $\delta = -6.3$ and 31.0 ppm. None of them shows any multiplicity due to B,H coupling. The signal at $\delta = 31.0$ ppm may be due to a 9-BBN(NCS)·THF solvate [9-BBN(NMe$_2$): $\delta^{11}_B = 47.7$ ppm;[23] Ph$_2$BBr·OEt$_2$: $\delta^{11}_B = 33.4$ ppm[24]] and the latter could be due to its dimer. But this interpretation is speculative.

The crown ether complex of **7** can be crystallized from THF solution. Its crystals have the composition Na(18-crown-6)(THF)$_2$[(9-BBN)NCS]. Although a good data set could be collected for the monoclinic crystals, the structure could not be resolved satisfactorily. However, crystallization of **7** from tetrahydropyran (thp) produced single crystals of [Na(18-crown-6)(thp)$_3$][(9-BBN)NCS] which proved to be [Na(18-crown-6)(thp)$_2$][Na(thp)$_4${(9-BBN)NCS}$_2$] (**8**) in the solid state. As shown in Figure 7 the cation is similar in structure to [Na(18-crown-6)(THF)$_2$]$^+$ [15−18] with two thp molecules in *trans* positions. In the anionic part of the compound the sodium cation is surrounded by four thp molecules and two sulfur atoms which are supplied by two (9-BBN)NCS anions. The S1−Na1−S2 bond angle is 174.47(6)°, and the O1−Na1−O2 and O3−Na1−O4 bond angles are 177.4(1) and 176.4(1)°, respectively. This results in an averaged S1−Na1−O bond angle of 88.5°, and an averaged S2−Na1−O bond angle of 91.5°. Interestingly, the two Na−S bond lengths are significantly different, with Na1−S1 3.254(2) and Na1−S2 3.045(2) Å. Also, the Na−O bonds differ, spanning a range from 2.302(3) to 2.377(3) Å. However, the bonding parameters for the two 9-BBN units are rather similar as shown, for instance, by the two B−N bond lengths, which are 1.564(5) and 1.568(5) Å.

 © 2004 Wiley-VCH Verlag GmbH & Co. KGaA, Weinheim

Discussion

It is now well established from previous results and those presented here that the NCS^- anion coordinates to the boron atom of BH_3 through its N atom. Although this was already deduced from spectroscopic data[3−5] this is now ascertained by X-ray structural results for the solid state. From a chemical point of view this seems logical because the B−N bond is much stronger than the B−S bond; therefore, (isothiocyanato)borates should be favored over (thiocyanato)borates, and this is supported by DFT calculations. This argument is valid also for borane derivatives.

In general, the addition of the NCS^- anion to a borane unit (BH_3, catecholborane, 9-BBN) is not necessarily the best preparative route, in particular not for BH_3 and catecholborane because the (isothiocyanato)borates formed can react with the borane by hydrogen exchange giving rise ultimately to the formation of tetrahydroborate. This kind of behavior is particularly noticeable for reactions of alkali metal alkoxides with BH_3 in THF,[7] but also for catecholborane, which, on addition of a nucleophile, gives an organyloxoborate in analogy to the BH_3/OR^- reaction. In the case of 9-BBN we did not observe this behavior: there was a straightforward reaction to the borate **7** without any by-products. Most likely this is due to the bulky R_2B group of the 9-borabicyclo[3.3.1]nonyl group.

The ligand distribution reaction can be retarded or even prevented when an (isothiocyanato)borane is treated with NCS^- as shown for (isothiocyanato)catecholborane, which leads to the bis(isothiocyanato)borate **6**.

Although a series of (isothiocyanato)borates $B(NCS)_{4-n}X_n^-$ is known,[19] no crystal structures of their salts have been reported. This is also the case for the (thiocyanato)hexaborate $B_6H_5(SCN)^{2-}$ where it is deduced from vibrational spectroscopy that the NCS group is *S*-bonded.[25] In $B_6H_5(SeCN)^{2-}$ the presence of the B−Se bond has been established.[26] Obviously the B_6H_5 unit acts as a soft acid.

On average, the B−N bonds of the (isothiocyanato)borates are longer [1.542(5)−1.575(5) Å] than in tetrakis(dihydropyridino)borate [1.546(2) Å].[27] One would have expected the opposite because the N atom of the isothiocyanate ion is sp-hybridized while in the (dihydropyridinato)borate the N atom resides in a planar environment and, therefore, is sp^2-hybridized. Obviously the B−N bond of the investigated (isothiocyanato)borates is weaker than in the aminoborate derivative.

While crown ether complexes of the alkali metal thiocyanates have been investigated in the early days of the polyether complexes[28] the only compound which is akin to **4** is the dicyclohexano-15-crown-5 complex of Na(NCS) whose bonding parameters resemble those of **4**.[29] As shown, the two crown ether complexes **3** and **4** have molecular structures. In the case of the 18-crown-6 complex the sodium ion is octacoordinate. The Na−N bond is shorter than the Na−O bond to the coordinated THF molecule while all bonds to the O atoms of the crown are more than 0.3 Å longer. On the other hand, in the crown ether compound **4** the Na−N bond is somewhat longer than in complex **3** in spite of the fact that the sodium ion is only hexacoordinate, and has the geometry of a distorted pentagonal pyramid; the Na−N bond in $[Na(15\text{-crown-5})(NCMe)]^+$ is even longer.[29] Moreover, the crown ether in this cation is less symmetrically bonded than in **4**, which has a mirror plane through the atoms S, C, N, Na and O1. In contrast, the hexacoordinate Na ion in the pyridine complex **5** approaches an octahedral geometry. Moreover, the Na−N bond in the acetonitrile adduct [2.960(7) Å] is longer than in **4**. This is not unusual. The Na−N bond of the NaNCMe unit is even longer than in **4** and only about 0.1 Å shorter than the Na−N bonds to the pyridine molecules. In this case the octahedral coordination site is filled by a sulfur atom, and this leads to a zig-zag arrangement of the building blocks. Na−S bonds are also present in the anion of **8**. In this case, the NCS anion behaves similarly to the pyridine complex of Na(SCN) except for the fact that in **5** each Na ion is *N*- and *S*-coordinated as a consequence of the *B*-bonded NCS group in **8**. From this point of view it is surprising that there is no Na−S coordination in compounds **1** and **2** nor in the 18-crown-6·THF complex of **6** where the S atom of the *B*-bonded NCS anion is not able to replace a THF molecule coordinated to Na.

In the anion of the catecholatoborate **6** both the O−B−O and the N−B−N bond angles are smaller than the ideal tetrahedral bond angle. However, in the bis(catecholato)borate anion the O−B−O bond angles are even more acute by 3°.[30] Moreover, the B−O bonds in **6** are shorter than those found for comparable (catecholato)boranes such as catecholborane−oxazolidine [B−O, 1.479(2), 1.481(2) Å],[31] bis(catechol)diborane−lutidine [B−O 1.489(2), 1.498(2) Å][32] as well as in the bis(catechol)borate anion [B−O 1.470−1.485(9) Å].[30] Also, the B−N bonds are shorter in **6** than in catecholborane−oxazolidine [1.541(2) and 1.548(2) Å] or the lutidine adduct [1.659(2) Å]. The structural parameters of **6**, therefore, show the inductive effect of the isothiocanate group.

Compound **8** has an unusual and unexpected structure. It is one of the rare examples of a complexed sodium sodiate. The cation, $[Na(18\text{-crown-6})(thp)_2]^+$, is rather similar to $[Na(18\text{-crown-6})(THF)_2]^+$. Obviously, the anion $[(9\text{-BBN})NCS]^-$ is a fairly good base as it coordinates twice to a sodium ion through Na−S bonds. Its coordination sphere is completed by the addition of four thp molecules. A relationship with the so-called "ate complexes" is noticeable.

It follows from the present study that the NCS^- ion coordinates to boron centers through its N atoms favoring (isothiocyanato)borate structures. The study of substituted hydroborates offers interesting insights into the coordination chemistry of their alkali metal salts. It seems that small effects of the ligands determine their structure. So, neither the sulfur atom nor the BH_3 hydrogen atoms of H_3B-NCS^- are able to replace a THF molecule from $[Na(18\text{-crown-6})(THF)_2]^+$ in contrast to the sulfur atom of $(9\text{-BBN})NCS^-$ in the presence of tetrahydropyran.

 © 2004 Wiley-VCH Verlag GmbH & Co. KGaA, Weinheim

Experimental Section

General: All experiments were conducted under anhydrous conditions (N_2 blanket or vacuum). Commercial grade chemicals were used, and solvents dried by conventional procedures. NMR spectroscopic data were recorded with a Jeol 400 instrument, and IR data were taken with a Nicolet FT 20 instrument. Raman spectra were recorded with a Perkin−Elmer 2000 NIR FT spectrometer operated with an Nd-YAG laser at 1064 nm. For X-ray structure determinations a Siemens P4 diffractometer equipped with a CCD detector and an LT 2 low-temperature device and Mo-K_α radiation was used. Microchemical analyses were performed at the departmental microanalytical laboratory.

Crown Ether Complexes of Na(NCS): Na(SCN) was dissolved in THF and an equimolar amount of the crown ether (18-crown-6, 15-crown-5) added. After partial removal of the solvent, the solution was kept in the refrigerator. The crystals which formed within a few days were isolated and used for X-ray structure determination. The yield was not determined and no analysis performed.

Sodium Trihydro(isothiocyanato)borates. a) A solution of BH_3 in THF (2.12 mmol, 50 mL) was added with vigorous stirring to a suspension of Na(NCS) (0.508 g, 6.27 mmol) in THF (50 mL). The suspension turned rapidly into a clear solution. ^{11}B NMR spectroscopy showed that more than 90% of the borane had been consumed. Then, a solution of 18-crown-6 (1.925 g, 7.28 mmol) in 10 mL of THF was added followed by the addition of methylcyclohexane. This produced a white precipitate which was isolated by filtration and, after drying in vacuo, was found to have the composition Na(18-crown-6)(H_3B-NCS). Yield: 1.7 g (74%). From the filtrate, which was kept at 8 °C, a few single crystals of [Na(18-crown-6)$(THF)_2$][H_3B-NCS] (**1**) separated after several days; m.p. 155 °C (dec.). $C_{13}H_{27}BNNaO_6S$ (359.15): calcd. C 43.37, H 7.58, N 3.90, S 8.92; found C 43.28, H 7.48, N 3.77, S 8.93. ^{11}B NMR (THF): δ = −27.3 (q, $^1J^1_H{}^{11}_B$ = 96 Hz) ppm. ^{13}C NMR: δ = 128.4 (t, $^1J^{13}_C{}^{14}_N$ = 24 Hz) ppm. ^{14}N NMR: δ = 128.4 ($^1J^{11}_B{}^{14}_N$ = 25 Hz) ppm. IR: $\tilde{\nu}$ = 2365 m, 2325 m, 2172 st, 1353 m, 1248 m, 1155 m, 1109 st, 969 st, 840 m cm^{-1}. Raman (crystals): $\tilde{\nu}$ = 2918 st, 2833 st, 2361 w, 2331 w, 2150 m, 1477 m, 1281 m, 1264 m, 1244 m, 863 st cm^{-1}. **b)** The complex [Na(15-crown-5)][H_3B-NCS] (**2**) was prepared in a similar manner. No precipitate formed after addition of methylcyclohexane. Single crystals separated from the solution at 8 °C. These were isolated by filtration. X-ray structure determination showed them to be [Na(15-crown-5)THF]-[H_3B-NCS]. The compound was isolated from the filtrate after partial evaporation of the solvents. After drying in vacuo, it was found to have the composition Na(15-crown-5)(H_3B-NCS). Yield: 676 mg (85%); m.p. 168 °C (dec.). $C_{16}H_{34}BNNaO_5S$ (375.13): calcd. C 41.60, H 7.25, N 3.73, S 8.54; found C 41.80, H 6.92, N 3.72, S 8.28. IR: $\tilde{\nu}$ = 2365 m, 2307 m, 2161 st, 1349 m, 1248 m, 1154 m, 1105 st, 963 st, 839 m cm^{-1}.

***B*-(Isothiocyanato)catecholborane:** Trimethylsilylisothiocyanate (2.0 mL, 1.80 g, 14.2 mmol) was added to a solution of *B*-bromocatecholborane (1.722 g, 8.699 mmol) in toluene (10 mL). After refluxing the solution for 24 h, the ^{11}B NMR spectrum showed a quantitative reaction. All volatile components were removed in vacuo (1 Torr). The residue (1.22 g of a brown oil) was heated to 100 °C in vacuo. From the gas phase a solid separated as a colorless powder which, on storing, turned slowly orange. The product quickly hydrolyzes in moist air. Yield: 1.16 g (75%); m.p. 146−148 °C (dec.). $C_7H_4BNO_2S$ (177.01): calcd. C 47.51, H 2.28, N 7.91, S 18.11; found C 48.89, H 2.63, N 7.97, S 17.31. ^{1}H NMR ($CDCl_3$): δ = 7.1−7.2 (m) ppm. ^{11}B NMR: δ = 18.1 ppm. ^{13}C NMR: δ = 112.8 (C-2/5), 123.7 (C-3/4), 147.4 (C-1/6), 143.1 (br., NCS) ppm. ^{14}N NMR: δ = −280 ppm. IR: $\tilde{\nu}$ = 2074 m, 1625 m, 1473 st, 1440 st, 1351 st, 1349 st, 1096 st, 808 st, 741 w cm^{-1}. Raman: $\tilde{\nu}$ = 3071 m, 2092 w, 1627 m, 1440 m, 1399 st, 1231 st, 1142 w, 1006 m, 810 m, 612 w cm^{-1}.

Sodium Catecholatobis(isothiocyanato)borate (6): A solution of Na(NCS) (0.194 g, 2.39 mmol) in THF (10 mL) was added with stirring to a solution of *B*-(isothiocyanato)catecholborane (0.429 g, 2.42 mmol) in THF (5 mL). Stirring was continued at 0 °C for 1 h, then 18-crown-6 (0.91 g, 3.4 mmol) was added. After addition of methylcyclohexane (10 mL), the clear solution turned turbid. Insoluble material was removed by filtration and the filtrate kept at −20 °C. Within 1 d [Na(18-crown-6)$(THF)_2$][catB$(NCS)_2$] separated as colorless prisms (used for X-ray structure determination) which, on drying in vacuo, lost THF and became opaque. Yield 1.04 g of [Na(18-crown-6)][catB$(NCS)_2$] (65%); m.p. 51−54 °C. $C_{20}H_{28}BN_2NaO_8S_2$ (522.13): calcd. C 45.99, H 5.40, N 5.36, S. 12.27; found C 46.88, H 5.64, N 4.76, S 11.80. ^{1}H NMR ([D$_8$]THF): δ = 6.4−5.5 (m) ppm. ^{11}B NMR: δ = −0.1 (quint, $^1J^{11}_B{}^{14}_N$ = 24 Hz) ppm. ^{13}C NMR: δ = 108.7 (C-2/5), 118.5 (C-3/4), 151.1 (C-1/6), 130.9 (br., NCS) ppm. ^{14}N NMR: δ = −248 (1:2:3:2:1 quint, $^1J^{13}_C{}^{14}_N$ = 24 Hz) ppm.

Sodium (Isothiocyanato)-9-boratabicyclo[3.3.1]nonane: A solution of Na(NCS) (0.530 g, 6.54 mmol) in THF (35 mL) was added at 0 °C with stirring to a solution of 9-BBN (0.803 g, 6.59 mmol) in THF (15 mL). After warming to ambient temperature, 18-crown-6 was added (2.00 g, 7.57 mmol) followed, after some time, by methylcyclohexane (10 mL). A precipitate formed which was isolated by filtration. After drying in vacuo, the product was practically free of THF. Cooling the filtrate to −20 °C afforded small amounts of clear needles which were highly intergrown. They were used for X-ray crystal structure determination. NMR spectroscopic data were obtained from a freshly prepared solution in THF (without adding the crown ether). Single crystals suitable for an X-ray structure determination were obtained by recrystallization of the crystals from tetrahydropyran. Yield (from THF): 2.84 g (71%); m.p. 98−102 °C (dec.). $C_{21}H_{39}BNNaO_6S$ (467.25): calcd. C 53.96, H 8.41, N 3.00, S 6.86; found C 49.88, H 8.21, N 2.97, S 6.75. ^{11}B NMR (THF): δ = −11.4 (d, $^1J^{11}_B{}^1_H$ = 100 Hz) ppm. ^{13}C NMR: δ = 26.1, 26.3 ($CH_2CH_2CH_2$), 31.2, 34.5 ($CHCH_2CH_2$), 125.8 (NCS) ppm. ^{14}N NMR: δ = −224 ($h_{1/2}$ = 75 Hz) ppm. IR (nujol): $\tilde{\nu}$ = 2301, 2271 w, 2231 w, 2138 st, 2069 st, BH, 1472 m, 1352 st, 1248 m, 1112 st, 1058 m, 967 st, 671 m cm^{-1}.

X-ray Structure Determinations: Suitable crystals were selected from the solution, in most cases at −20 °C, and covered with perfluoro ether oil. The selected crystal was mounted on a glass fiber and put rapidly on the goniometer head which was flushed with cold nitrogen gas. The size of the unit cell was determined from the data of five sets of 15 frames taken at different orientations, using the program SMART.[33] Data collection was performed with the program SMART[33] and data from 1250 frames were used for data reduction (program SAINT[33]). Structure solutions were performed by direct methods in SHELX 97.[34] Non-hydrogen atoms were refined anisotropically, hydrogen positions on C atoms were in most cases observed, but were put in calculated positions. The BH hydrogen atoms were found in the Fourier map and were freely refined using isotropic thermal parameters. Table 7 shows relevant crystallographic parameters and data related to structure solution and refinement. In Figures 1−7 the thermal ellipsoids are depicted at a 25% probability level. CCDC-217263 to -217269 contain the supplementary crystallographic data for this paper. These data can be obtained free of charge at www.ccdc.cam.ac.uk/conts/retriev-

 © 2004 Wiley-VCH Verlag GmbH & Co. KGaA, Weinheim

Table 7. Crystallographic data and data related to structure solution

Compound	**1**	**2**	**3**	**4**	**5**	**6**	**8**
Empirical formula	$C_{21}H_{43}BNNaO_8S$	$C_{15}H_1BNNaO6S$	$C_{17}H_{32}BNNaO_7S$	$C_{11}H_{20}NNaO_5S$	$C_{47}H_{45}N_{11}Na_2S_2$	$C_{28}H_{44}BN_2NaO_{10}S_2$	$C_{60}H_{11}B_2N_2Na_2O_{12}S_2$
Formula mass	503.42	387.27	417.49	301.33	437.02	666.57	1184.23
Crystal size [mm]	0.30 × 0.30 × 0.30	0.20 × 0.30 × 0.20	0.20 × 0.20 × 0.20	0.50 × 0.10 × 0.01	0.40 × 0.40 × 0.30	0.50 × 0.20 × 0.20	0.30 × 0.20 × 0.1
Crystal system	triclinic	orthorhombic	monoclinic	orthorhombic	monoclinic	triclinic	triclinic
Space group	$P\bar{1}$	$P2_12_12_1$	$P2_1/c$	$Pmn2_1$	$I2/a$	$P\bar{1}$	$P\bar{1}$
a [Å]	9.1572(8)	10.2715(9)	8.079(7)	12.087(1)	14.232(5)	9.3035(6)	11.793(2)
b [Å]	9.2664(8)	13.391(1)	16.947(2)	7.2845(9)	9.506(4)	13.472(1)	16.438(4)
c [Å]	9.3535(8)	15.754(1)	16.557(2)	8.343(1)	36.29(2)	14.672(1)	19.069(4)
α [°]	89.667(2)	90	90	90	90	78.2700(1)	67.538(4)
β [°]	86.394(2)	90	100.869(2)	90	99.156(9)	87.6120(1)	82.468(5)
γ [°]	62.840(1)	90	90	90	90	75.1770(1)	85.903(4)
V [Å^3]	704.5(1)	2166.9(3)	2226.2(3)	734.6(2)	4847(4)	1740.4(2)	3386(1)
Z	1	4	4	2	4	2	2
ρ(calcd.) [Mg/m^3]	1.187	1.187	1.246	1.362	1.198	1.272	1.162
μ [mm^{-1}]	0.171	0.196	0.200	0.264	0.172	0.218	0.148
F(000)	272	832	896	320	1832	708	1290
Index range	$-11 \le h \le 11$	$-11 \le h \le 11$	$-8 \le h \le 8$	$-15 \le h \le 11$	$-16 \le h \le 11$	$-12 \le h \le 9$	$-14 \le h \le 16$
	$-11 \le k \le 11$	$-14 \le k \le 14$	$-21 \le k \le 20$	$-9 \le k \le 9$	$-12 \le k \le 12$	$-16 \le k \le 16$	$-21 \le k \le 21$
	$-11 \le l \le 11$	$-17 \le l \le 17$	$-20 \le l \le 21$	$-10 \le l \le 10$	$-46 \le l \le 46$	$-18 \le l \le 18$	$-22 \le l \le 23$
2θ [°]	58.18	46.52	55.68	56.48	58.72	58.38	38.46
Temp. [K]	183(2)	193(2)	193(2)	193(2)	193(2)	193(2)	193(2)
Refl. collected	4157	9645	12313	4159	13877	10172	19970
Refl. unique	2170	3115	3416	1554	4792	5338	10513
Refl. observed (4σ)	1780	2655	2408	1293	2354	3588	4444
R (int.)	0.0164	0.0557	0.0458	0.0384	0.0515	0.0236	0.0443
No. variables	218	227	244	194	281	397	766
Wt. scheme	0.0674/0.2171	0.1083/0.8019	0.0795/0.3187	0.058/0.00	0.0585/0.00	0.0803/0.6382	0.1413/0.00
GOOF	1.054	1.029	1.025	1.035	0.892	1.071	0.900
Final *R*. (4σ)	0.0472	0.595	0.0500	0.0549	0.0439	0.0538	0.075
Final *wR2*[a]	0.1288	0.1639	0.1290	0.1170	0.938	0.1482	0.1930
Largest res. peak	0.237	0.493	0.206	0.419	0.258	0.442	0.504

[a] $w^{-1} = s^2F_o^2 + (xP)^2 + yP$; $P = (F_o^2 + 2F_c^2)/3$.

ing.html [or from the Cambridge Crystallographic Data Centre, 12 Union Road, Cambridge CB2 1EZ, UK; Fax: (internat.) + 44-1223-336-033; E-mail: deposit@ccdc.cam.ac.uk].

Acknowledgments

We thank Chemetall GmbH, Frankfurt, and the University of Munich for the support of this work and Mr. P. Mayer for recording many NMR spectra.

[1] M. Bremer, H. Nöth, M. Warchhold, *Eur. J. Inorg. Chem.* **2003**, 111−119.
[2] J. Seyden-Penne, *Reductions by the Alumino- and Borohydrides in Organic Synthesis*, 2nd ed., Wiley-VCH, New York, Chichester, Weinheim, Brisbane, Singapore, Toronto, **1997**.
[3] V. D. Aftandilian, H. C. Miller, E. L. Muetterties, *J. Am. Chem. Soc.* **1960**, *83*, 2471−2474.
[4] F. Klanberg, *Z. Anorg. Allg. Chem.* **1962**, *316*, 197−207.
[5] B. C. Hui, *Inorg. Chem.* **1980**, *19*, 3185−3186.
[6] M. Thomann, PhD Thesis, University of Munich, **1992**.
[7] M. Warchhold, PhD Tesis, University of Munich, **2001**.
[8] A. J. Costoulas, R. L. Werner, *Aust. J. Chem.* **1959**, *12*, 601−612.
[9] P. W. Schultz, D. L. Ward, A. I. Popov, G. E. Lwoi, *J. Phys. Chem.* **1996**, *100*, 18085−18087.
[10] G. J. Martin, M. L. Martin, *^{15}N NMR Spectroscopy*, Springer Publishers, Berlin, Heidelberg, New York, **1981**.
[11] I. Morishima, A. Miguno, T. Ymezawa, *J. Chem. Soc., Chem. Commun.* **1970**, 1321−1323.
[12] M.-X. Zhang, P. E. Eaton, R. Gilardi, *Angew. Chem.* **2000**, *112*, 434−426; *Angew. Chem. Int. Ed.* **2000**, *39*, 401−404.
[13] R. Spielvogel, *J. Chem. Soc., Chem. Commun.* **1966**, 765−766.
[14] P. C. Wad, K. E. Pureöö, E. A. Sullian, I. R. Berscheid, *Inorg. Chem.* **1970**, *9*, 2146−2150.
[15] L. M. Engelhardt, W. P. Leung, A. H. White, *J. Chem. Soc., Chem. Commun.* **1983**, 386−390.
[16] S. I. Bailey, L. M. Engelhardt, W.-P. Leung, C. L. Raston, L. M. Ritchie, A. H. White, *J. Chem. Soc., Dalton Trans.* **1985**, 1747.
[17] D. J. Darensbourg, C. G. Bauch, A. I. Rheingold, *Inorg. Chem.* **1987**, *26*, 977−980.
[18] J. van den Broeke, M. Lutz, U. Kooijman, A. L. Speck, B. J. Dealmann, G. van Koten, *Organometallics* **2001**, *20*, 2114−2117.
[19] A. Quassas, J. C. Duplan, B. Febet, B. Frange, *Magn. Res. Chem.* **1990**, *28*, 693−695.
[20] H. Nöth, B. Wrackmeyer, *Nuclear Magnetic Resonance Spectroscopy of Boron Compounds, NMR, Basic Principles and Progress* (Eds.: P. Diehl, E. Fluck, R. Kosfeld), Springer Publishers, Heidelberg, New York, **1978**, vol. 14, Table 82.
[21] W. Fraenk, Ph D Thesis, University of Munich, **2001**.
[22] J. B. Foresman, A. Frisch, *Exploring Chemistry with Electronic Structure Methods*, 2nd ed., Gaussian Inc., Pittsburg, **1993**.
[23] G. W. Kramer, H. C. Brown, *J. Organomet. Chem.* **1977**, *132*, 9−27.
[24] Ref.[20], Table 83.
[25] W. Preetz, S. Zander, C. Bruhn, *Z. Naturforsch., Teil B* **1998**, *53*, 816−818.
[26] H. Nöth, M. Warchhold, *Z. Naturforsch., Teil B* **2002**, *58*, 123−126.

 © 2004 Wiley-VCH Verlag GmbH & Co. KGaA, Weinheim

[27] C. J. Pedersen, *Angew. Chem.* **1988**, *100*, 1053−1059, *Angew. Chem. Int. Ed. Engl.* **1988**, *27*, 1053−1059.
[28] G. W. Buchanan, S. Mathias, C. Bensimon, J. P. Charland, *Can. J. Chem.* **1992**, *70*, 981−985.
[29] E. Rentschler, W. Massa, S. Vogler, K. Dehnicke, D. Fenske, G. Baum, *Z. Anorg. Allg. Chem.* **1991**, *592*, 59−72.
[30] M. Bandini, P. G. Gozzi, M. Monari, R. Perciaccante, S. Selva, A. Umani-Ronchi, *Chem. Commun.* **2001**, 1318−1319.
[31] P. Nguyen, Ch. Dai, N. J. Taylor, W. P. Power, T. B. Marder, N. L. Pickett, N. C. Norman, *Inorg. Chem.* **1995**, *34*, 4290−4291.
[32] W. Clegg, M. R. J. Elsegood, F. J. Lawlor, N. C. Norman, N. L. Pickett, E. G. Robeins, A. J. Scott, P. Nguyen, T. B. Marder, *Inorg. Chem.* **1998**, *37*, 5289−5294.
[33] *SMART*, *SAINT*, *SHELXTL*, Version 5, Siemens X-ray Analytical Instruments, Madison, **1994**.
[34] G. Sheldrick, *SHELXL-97*, University of Göttingen, **1997**.

Received August 19, 2003
Early View Article
Published Online February 5, 2004

 © 2004 Wiley-VCH Verlag GmbH & Co. KGaA, Weinheim

Nitrogen Trifluoride as a Bifunctional Lewis Base: Implications for the Adsorption of NF_3 on Solid Surfaces

Paola Antoniotti,[a] Stefano Borocci,[b] and Felice Grandinetti*[b]

Keywords: Ab initio calculations / Nitrogen trifluoride / Lewis bases / Isomeric structures

The structure, stability, and thermochemistry of isomeric adducts between NF_3 and the Lewis acids $BH_{3-n}F_n$ (n = 0–3) have been investigated at the coupled-cluster and at the Gaussian-3 (G3) level of theory. At the CCD/cc-pVDZ level both the nitrogen- and the fluorine-coordinated structures of all $BH_{3-n}F_n$–(NF_3) (n = 0–3) adducts were characterized as true minima on the potential energy surface, thus providing the first theoretical evidence for the behavior of NF_3 as a bifunctional Lewis base when interacting with neutral Lewis acids. At the G3 level, and 298.15 K, including the contribution of the entropy term, the H_3B–NF_3 adduct is predicted to be more stable than H_3B–F–NF_2 by 4.3 kcal mol^{-1}; this free energy difference is 3.7 kcal mol^{-1} at the CCSD(T)/cc-pVTZ//CCD/cc-pVDZ level of theory. Conversely, at the latter computational level, the fluorine-coordinated isomers of the BH_2F–(NF_3), BHF_2–(NF_3), and BF_3–(NF_3) adducts are practically degenerate with the nitrogen-coordinated ones. $BH_{3-n}F_n$–(NF_3) (n = 0–3) complexes feature typical bond dissociation energies of ca. 1–2 kcal mol^{-1}, and are predicted to be thermodynamically stable only at low temperatures. However, the appreciable influence of the basis set superposition error (BSSE) prevents a quantitative assessment of these small computed dissociation energies. Finally, we briefly discuss the implications of our calculations for the adsorption of NF_3 on solid surfaces.

(© Wiley-VCH Verlag GmbH & Co. KGaA, 69451 Weinheim, Germany, 2004)

Introduction

Nitrogen trifluoride, NF_3 (gas), is extensively used by the electronic industry in etching and cleaning processes,[1,2] e.g. to remove contaminant residues from chemical vapor deposition chambers and in plasma etching and reactive-ion etching of various materials.[3–8] Compared with more traditional fluorinated gases such as CF_4 and C_2F_6, NF_3 offers advantages of a shorter atmospheric lifetime and avoids carbon contamination residues, thereby boosting productivity by > 30% and decreasing effluent emissions by ca. 90%.[1,2] Thus, the recent industrial use of NF_3 has increased remarkably, stimulating considerable experimental and theoretical interest in the interaction of NF_3 and NF_3-based plasmas with material surfaces.[9–22] In particular, a complete understanding of the etching process requires details of the geometric and electronic structure of NF_3 adsorbed on a solid surface. When interacting with Si(001), NF_3 undergoes slow dissociative chemisorption, with spontaneous and competitive formation of Si–N and Si–F bonds.[11,20a,21] Similarly, the interaction of NF_3 with Ru(0001) leads, at least partially, to molecular decomposition on the surface, leaving F, NF or NF_2 fragments, and it has been suggested that all the NF_x moieties (x = 1–3) are oriented exclusively with their nitrogen end toward the metal.[3] Conversely, an investigation[17] on the thermal, electron, and photon-stimulated chemistries of NF_3 adsorbed on Pt(111) at low temperature revealed that adsorption and thermal desorption of NF_3 is molecular, with no evidence for dissociation. This suggests that NF_3 is very weakly held and behaves like a physisorbed species. Interestingly, the available experimental evidence points to different positions of NF_3 and orientations of its dipole moment with respect to the surface and the neighboring molecules. Thus, details of the possible orientation of NF_3 with respect to a metal surface still pose stimulating experimental and theoretical questions. From the fundamental point of view, a first step is to investigate the still unexplored behavior of NF_3 as a bifunctional Lewis base when interacting with a *neutral* Lewis acid. Experimental and theoretical investigations on the ligation of NF_3 to ionic Lewis acids such as H^+,[23,24] Li^+,[25,26] CH_3^+,[27,28] and NF_2^+ [29,30] clearly indicate that both the M–NF_3^+ and MF–NF_2^+ isomeric structures (M = H, Li, CH_3, and NF_2) can, in principle, exist as distinguishable species in the gas phase, and that the nature of the M^+ electrophile has a substantial effect on both the relative stability of the two isomers and on the their energy difference. Conversely, experimental and theor-

[a] Dipartimento di Chimica Generale ed Organica Applicata, Università degli Studi di Torino
C.so M. D'Azeglio 48, 10125 Torino, Italy
[b] Dipartimento di Scienze Ambientali and Istituto Nazionale di Fisica della Materia (INFM), Unità di Viterbo, Università della Tuscia,
L.go dell'Università, s.n.c., 01100 Viterbo, Italy
Fax: (internat.) + 39-0761-357179
E-mail: fgrandi@unitus.it

etical studies performed on complexes between NF_3 and neutral Lewis acids, such as BH_3,[31−34] BH_2F,[34] BHF_2,[34] BF_3,[31,33−36] BCl_3,[36] AlH_3,[37] $Ga(CH_3)_3$,[38] HF,[39] and ClF,[40] have invariably assumed that nitrogen trifluoride behaves exclusively as a nitrogen donor that can form adducts such as H_3B-NF_3, F_3B-NF_3, and H_3Al-NF_3. However, in keeping with the behavior of bifunctional base toward ionic Lewis acids, NF_3 could also interact with neutral Lewis acids as a fluorine base, forming adducts such as $H_3B-F-NF_2$, $F_3B-F-NF_2$, and $H_3Al-F-NF_2$. The structure and stability of such complexes appears to be unexplored. Therefore, stimulated by our continuing experimental and theoretical interest in the chemistry of nitrogen trifluoride and closely related neutral and ionic species,[24,26,28,30,41−51] we undertook a detailed theoretical investigation on the structure and stability of the isomeric adducts arising from the ligation of NF_3 to BH_3, BH_2F, BHF_2 and BF_3. The results discussed here confirm the expectation that, even with neutral Lewis acids, NF_3 can behave not only as a nitrogen but also as a fluorine base, forming isomeric structures of comparable stability. Concerning the interaction with solid surfaces, these findings support the suggestion that the molecular physisorption of NF_3 may occur by different orientations, and that this adsorption could be critically affected by the nature of the surface and the strength of the interaction.

Computational Details

Quantum chemical calculations have been performed using the Unix versions of the GAUSSIAN 98[52] and MOLPRO 2000.1[53] sets of programs installed on an Alphaserver 1200 and a DS20E Compaq machine.

Geometries of the investigated species have been optimised by analytical-gradient techniques at the coupled-cluster level of theory,[54,55] including the contribution from double substitutions (CCD), using the Dunning's correlation consistent double-zeta basis set (cc-pVDZ).[56] The located structures were unambiguously characterized as true minima on the surface by computing the corresponding CCD/cc-pVDZ harmonic frequencies, obtained by numerical differentiation of the analytical first derivatives of the CCD/cc-pVDZ total energies. The CCD/cc-pVDZ numerical force constants of the $BH_3-(NF_3)$ and the $BF_3-(NF_3)$ adducts were subsequently used to refine their geometries at the CCSD/cc-pVDZ level. For all investigated species, CCD/cc-pVDZ optimised geometries were used to perform single-point calculations at the coupled cluster level of theory, including the contribution from single and double substitutions and an estimate of connected triples, CCSD(T), using the cc-pVTZ basis set. The CCD/cc-pVDZ unscaled frequencies were used to calculate the zero-point vibrational energies (ZPE) of the investigated species and the vibrational contribution to their thermal correction (TC), obtained at 298.15 K by standard statistical mechanics formulas.[57] The overall TC term was finally obtained by adding the translational (1.5 *RT*) and rotational (*RT* or 1.5 *RT* for linear and non-linear species, respectively) contributions at this temperature. Total entropies at 298.15 K of the investigated species were obtained using the CCD/cc-pVDZ unscaled frequencies and moments of inertia. The influence of the basis set superposition error (BSSE) on the dissociation energies calculated at the CCSD(T)/cc-pVTZ//CCD/cc-pVDZ level was estimated using the full counterpoise method by Boys and Bernardi.[58]

Total energies of the $BH_3-(NF_3)$ complexes were also obtained using the G3 procedure of Pople and co-workers.[59] This composite method consists of a sequence of well-defined single-point calculations, at the MP2(fc), MP4(fc), and QCISD(T) levels of theory, used to calculate, according to an additivity scheme, the total energy of a species at its MP2(full)/6-31G(d) optimised geometry ("full" and "fc" denote the inclusion or not of the valence electrons for the calculation of the correlation energies). A small higher-level empirical term is also included, which depends on the number of valence electron pairs. The ZPE is calculated at the HF/6-31G(d) level and scaled by 0.8929, and the G3 energies at 0 K, G3(0 K), corrected at 298.15 K by adding the thermal contribution calculated using the scaled HF/6-31G(d) frequencies for the vibrations in the harmonic approximation and the classical approximation

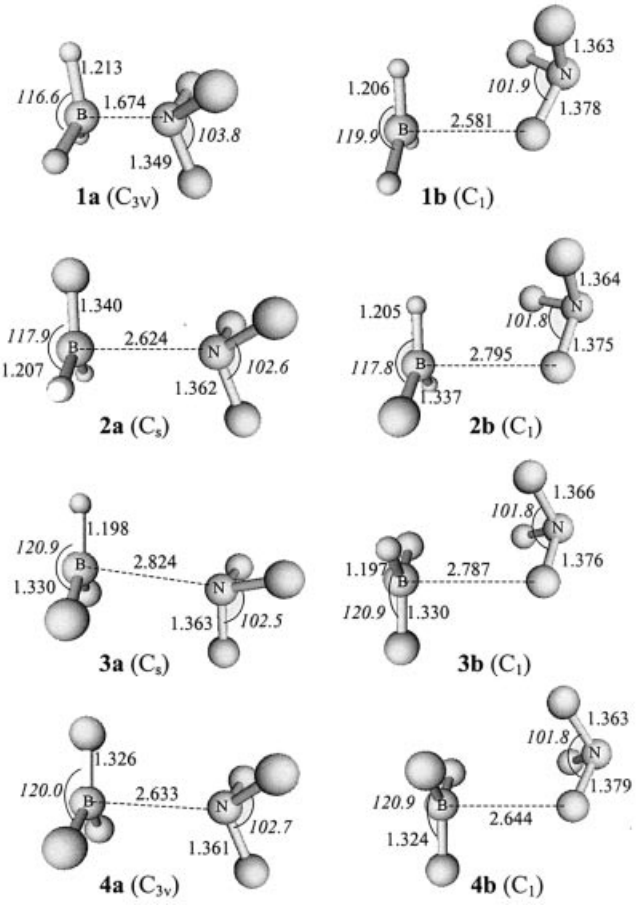

Figure 1. CCD/cc-pVDZ optimised geometries [Å and °] of the $BH_{3-n}F_n-(NF_3)$ ($n = 0-3$) isomeric structures (largest and smallest unlabeled circles are fluorine and hydrogen atoms, respectively)

 © 2004 Wiley-VCH Verlag GmbH & Co. KGaA, Weinheim

for translation (1.5 *RT*) and rotation (*RT* or 1.5 *RT* for linear and non-linear species, respectively). A further *RT* term is added to convert the G3(298.15 K) total energies into G3 enthalpies. The 6-31G(d), 6-31+G(d), and 6-31G(2df,p) basis sets standard in Gaussian 98 were used with six Cartesian d-functions, while the G3large basis set, downloaded from the website suggested in ref.[59], uses five "pure" d-functions. Both the 6-31G(2df,p) and the G3large basis sets use a set of "pure" seven f-functions.

Results and Discussion

Structure, Stability, and Thermochemistry of the $BH_{3-n}F_n-(NF_3)$ ($n = 0-3$) Isomeric Structures

To investigate the conceivable behavior of nitrogen trifluoride as a bifunctional Lewis base when interacting with neutral Lewis acids we searched for distinct isomeric structures arising from the ligation of $BH_{3-n}F_n$ ($n = 0-3$) to the N and the F atom(s) of NF_3. Starting from different initial geometries, we located the $BH_{3-n}F_n-NF_3$ and $BH_{3-n}F_n-F-NF_2$ complexes **1a** and **1b** ($n = 0$), **2a** and **2b** ($n = 1$), **3a** and **3b** ($n = 2$), and **4a** and **4b** ($n = 3$) as true energy minima on the CCD/cc-pVDZ potential energy surface. Their optimised structures (Figure 1) and absolute and relative energies, at the CCSD(T)/cc-pVTZ//CCD/cc-pVDZ level of theory, (Table 1) are given here. The energy, enthalpy and free energy changes of the reaction in Equation (1) for the various isomeric structures are reported in Table 2.

$$BH_{3-n}F_n-(NF_3) \rightarrow BH_{3-n}F_n + NF_3\ (n = 0\text{-}3) \quad (1)$$

For comparative purposes, the geometries of the complexes **1a**, **1b**, **4a**, and **4b** were refined at the CCSD/cc-pVDZ level, but we found only negligible differences with respect to the CCD/cc-pVDZ optimised structures. The geometries of **1a** and **1b** were also optimised at the CCD/aug-cc-pVDZ level of theory, but, with respect to the CCD/cc-pVDZ parameters, the largest variations were only about 0.5° in the bond angles and about 0.05 Å in the bond lengths.

Table 2. CCSD(T)/cc-pVTZ//CCD/cc-pVDZ dissociation energies (ΔE), enthalpies (ΔH), and free energies (ΔG) of $BH_{3-n}F_n-(NF_3)$ isomeric structures into $BH_{3-n}F_n$ and NF_3 ($n = 0-3$) [kcal mol^{-1}] (for connectivities of the species, see Figure 1)

Species	ΔE (0 K)[a][b]	ΔH (298.15 K)[a][b]	ΔG (298.15 K)[a][b]	BSSE
1a	8.7 (9.4)	9.9 (10.6)	−2.4 (−0.7)	3.5
1b	1.2 (1.2)	1.1 (0.9)	−6.0 (−5.0)	2.0
2a	1.0	0.6	−6.1	1.2
2b	1.2	0.7	−5.7	1.9
3a	1.2	0.5	−5.9	1.1
3b	1.5	0.8	−6.5	2.0
4a	1.8	1.1	−6.3	1.4
4b	2.0	1.3	−6.8	2.3

[a] Not including the BSSE. [b] G3 values given in parentheses.

As with all previous theoretical investigations on the geometric and electronic structure of the H_3B-NF_3 complex **1a**,[31−34] the CCD/cc-pVDZ optimised geometry points to an n-donor−p-acceptor complex, with partial electron transfer from the N atom of NF_3 to the B atom of BH_3. The N−F bond length of free NF_3, computed as 1.368 Å at the CCD/cc-pVDZ level of theory (experimental value is 1.365 Å[60]), reduces by 0.019 Å, whereas the B−H distance of free BH_3, computed as 1.207 Å at the CCD/cc-pVDZ level of theory, increases by 0.006 Å. In addition, the $-BH_3$ moiety of **1a** deviates slightly from planarity, and the F−*N*−F angle is larger than that of free NF_3 by 1.7°. At the CCSD(T)/cc-pVTZ//CCD/cc-pVDZ level, the energy changes obtained at 0 K and the enthalpy change at 298.15 K of the reaction according to Equation (1) are, for isomer **1a**, 8.7 and 9.9 kcal mol^{-1}, respectively. The inclusion of the appreciable contribution of the entropy term leads to a free-energy change at 298.15 K of −2.4 kcal mol^{-1}, and the still experimentally unobserved complex **1a**

Table 1. CCSD(T)/cc-pVTZ total energies [atomic units], thermal corrections [atomic units], and total entropies [cal mol^{-1} K^{-1}] of the $BH_{3-n}F_n-(NF_3)$ ($n = 0-3$) isomeric structures (for connectivities of the species, see Figure 1)

Species	CCSD(T)/cc-pVTZ[a]	ZPE[b]	*TC* (298.15 K)[b]	*S* (298.15 K)[c]	ΔE (0 K)[d]	ΔG (298.15 K)[d]
1a	−380.23837	0.04425	0.00527	70.2	0.0	0.0
1b	−380.22159	0.03934	0.00750	87.6	+7.5 (+8.2)	+3.7 (+4.3)
2a	−479.43833	0.03533	0.00795	94.9	0.0	0.0
2b	−479.43835	0.03495	0.00811	95.7	−0.3	−0.4
3a	−578.66098	0.02991	0.00865	101.1	0.0	0.0
3b	−578.66151	0.02994	0.00855	97.9	−0.3	+0.6
4a	−677.87454	0.02436	0.00899	102.3	0.0	0.0
4b	−677.87472	0.02426	0.00898	100.1	−0.2	+0.5
BH_3	−26.53739	0.02644	0.00288	47.3		
BH_2F	−125.75496	0.02286	0.00292	53.2		
BHF_2	−224.97804	0.01819	0.00312	58.5		
BF_3	−324.19061	0.01265	0.00347	63.0		
NF_3	−353.68018	0.01080	0.00349	64.2		

[a] At CCD/cc-pVDZ optimised geometries. [b] Based on CCD/cc-pVDZ harmonic frequencies. [c] Based on CCD/cc-pVDZ harmonic frequencies and moments of inertia. [d] G3 values given in parentheses.

 © 2004 Wiley-VCH Verlag GmbH & Co. KGaA, Weinheim

is predicted to dominate the mixture at equilibrium below ca. −33°C. The energy, enthalpy, and free-energy change of the reaction according to Equation (1) for isomer **1a** were also calculated using the G3 procedure. This method usually furnishes thermochemical data that are as accurate as ca. 2 kcal mol^{-1}.[59] However, the absence of compounds similar to those studied here in the G3 data-base suggests caution in assuming that this "standard" level of accuracy will be obtained here. However, the G3 data agree well with those obtained at the CCSD(T)/cc-pVTZ//CCD/cc-pVDZ level of theory (Table 2), and so we used only the latter approach to calculate the thermochemistry of the more complex $BH_{3-n}F_n-(NF_3)$ ($n = 1-3$) isomeric structures. We note also that, for isomer **1a**, both the CCSD(T)/cc-pVTZ//CCD/cc-pVDZ and the G3 values of ΔE at 0 K of the reaction according to Equation (1) are in good agreement with those previously obtained[33] at the MP2/6-31G(d) and at the B3LYP/6-31G(d) computational levels (8.9 and 9.9 kcal mol^{-1}, respectively).

The C_1-symmetry structure **1b** arises from the ligation of the boron atom of BH_3 with one of the fluorine atoms of NF_3 and its characterization as a true energy minimum on the CCD/cc-pVDZ potential energy surface provides the first theoretical evidence for the behavior of NF_3 as a bifunctional Lewis base when interacting with a *neutral* Lewis acid. Compared with the nitrogen-coordinated isomer **1a**, the optimised geometry of **1b** suggests a much weaker interaction between the two BH_3 and NF_3 building moieties. Thus, the B−F bond length results as large as 2.581 Å, and the other optimised parameters, are quite similar to those predicted for free BH_3 and NF_3. Consistently, from Table 2, the CCSD(T)/cc-pVTZ//CCD/cc-pVDZ energy change at 0 K and the enthalpy change at 298.15 K of the reaction according to Equation (1) are obtained for isomer **1b** as 1.2 and 1.1 kcal mol^{-1}, respectively, and the corresponding free energy change at 298.15 K results as −6.0 kcal mol^{-1}. Therefore, this complex is predicted to be dominant in the equilibrium mixture at temperatures lower than ca. −227 °C. At 0 K, isomer **1a** is predicted to be more stable than **1b** by 7.5 kcal mol^{-1} at the CCSD(T)/cc-pVTZ//CCD/cc-pVDZ level of theory and by 8.2 kcal mol^{-1} at the G3 level. However, consistent with the character of loosely bound species of **1b**, at 298.15 K the free energy difference with **1a** reduces to 3.7 kcal mol^{-1} at the CCSD(T)/cc-pVTZ//CCD/cc-pVDZ level of theory, and to 4.3 kcal mol^{-1} at the G3 level.

The nitrogen-coordinated isomers **2a**, **3a**, and **4a** and the fluorine-coordinated isomers **2b**, **3b**, and **4b** of the adducts between NF_3 and the fluorinated Lewis acids BH_2F, BHF_2, and BF_3 reveal minima on the CCD/cc-pVDZ potential energy surface, which is consistent with the results for $BH_3-(NF_3)$ complexes. This provides additional positive evidence for NF_3 having the character of a bifunctional Lewis base when interacting with neutral Lewis acids. In addition, Figure 1 and Tables 1 and 2 clearly indicate that, on passing from BH_3 to BH_2F, BHF_2, and BF_3, the structure and stability of the $BH_{3-n}F_n-(NF_3)$ ($n = 1-3$) complexes are appreciably affected. Thus, the nitrogen-coordinated structures **2a**, **3a**, and **4a** feature B−N distances that are remarkably longer than for **1a**, and the parameters of the BH_2F, BHF_2, BF_3, and NF_3 moieties are practically coincident with the geometries computed for the free molecules.[61] This is consistent with the weak interaction energies computed between the BH_2F, BHF_2, BF_3, and NF_3 building blocks. At the CCSD(T)/cc-pVTZ//CCD/cc-pVDZ level, ΔE at 0 K for the reaction according to Equation (1) is 1.0, 1.2 and 1.8 kcal mol^{-1} for complexes **2a**, **3a** and **4a**, respectively. The value for **4a** has been computed as 3.0 kcal mol^{-1} at the MP2/6-31G(d) level of theory[33,35] and 1.3 kcal mol^{-1} at the B3LYP/6-31G(d) level.[33] Therefore, passing from BH_3 to BH_2F, BHF_2, and BF_3, the stability of the nitrogen-coordinated isomers of $BH_{3-n}F_n-(NF_3)$ ($n = 0-3$) complexes is drastically reduced. Figure 1 and Table 2 indicate, however, that, on passing from $H_3B-F-NF_2$ isomer **1b** to the analogous fluorine-coordinated structures **2b**, **3b**, and **4b**, the B−F bond lengths are only slightly elongated, and the geometry of the $-NF_3$ moiety remains essentially unaltered. The stability of the four complexes is consistently quite similar and, in particular, at the CCSD(T)/cc-pVTZ//CCD/cc-pVDZ level of theory, ΔE at 0 K for the reaction according to Equation (1), computes as 1.2 kcal mol^{-1} for complexes **1b** and **2b**, 1.5 kcal mol^{-1} for **3b**, and 2.0 kcal mol^{-1} for **4b**. Therefore, whereas the nitrogen-coordinated isomer **1a** of the $BH_3-(NF_3)$ complex is appreciably more stable than the fluorine-coordinated isomer **1b**, the energy difference between the nitrogen- and the fluorine-coordinated isomers of the $BH_2F-(NF_3)$, $BHF_2-(NF_3)$, and $BF_3-(NF_3)$ adducts is considerably smaller. In particular (Table 1), the fluorine-coordinated structures **2b**, **3b**, and **4b** are predicted to be practically degenerate with the nitrogen-coordinated structures **2a**, **3a**, and **4a**. This conclusion is not essentially affected by inclusion of the thermal and entropy contributions at room temperature. Therefore, the present calculations indicate not only that NF_3 could behave as a bifunctional Lewis base when interacting with a neutral Lewis acid, but also that the fluorine-coordinated isomer could be degenerate or even thermodynamically more stable than the nitrogen-coordinated one.

Generally speaking, the interaction between NF_3 and the boranes is very weak and the computed energy changes of the reaction according to Equation (1) could be, in principle, significantly affected by the BSSE. Although the use of the counterpoise method is not undisputed,[62] we employed it to appreciate the influence of the BSSE on our CCSD(T)/cc-pVTZ//CCD/cc-pVDZ interaction energies. The obtained values (Table 2) amount to 3.5 kcal mol^{-1} for isomer **1a** and range around 1.5 kcal mol^{-1} for the other $BH_{3-n}F_n-(NF_3)$ adducts ($n = 0-3$). This confirms that, at least in percentage terms, the BSSE should significantly affect the computed interaction energies of our complexes. Nevertheless, it does not alter the essential conclusions from our calculations, although it suggests caution in the quantitative assessment of our computed interaction energies.

None of the presently investigated $BH_{3-n}F_n-(NF_3)$ adducts ($n = 1-3$) has been experimentally observed. From

 © 2004 Wiley-VCH Verlag GmbH & Co. KGaA, Weinheim

Table 2, the free energy change of the reaction according to Equation (1) for complexes **2a**−**4a** and **2b**−**4b** is invariably predicted to be around −6 kcal mol^{-1}, and all these species should dominate the equilibrium mixtures at well below −200 °C. Interestingly, it has been reported[36] that NF_3 and BF_3 undergo weak association below −125 °C, but the heat of dissociation was so small that a true equilibrium expression was unobtainable.

Nitrogen trifluoride is firmly established as a much weaker Lewis base than ammonia.[63] Comparison of our results on $BH_{3-n}F_n$−(NF_3) adducts (n = 0−3) with the previously investigated $BH_{3-n}F_n$−NH_3 complexes (n = 0−3)[32−34,64] fully confirms this expectation. We note in particular that, at the MP2/TZ2P level of theory,[64] the B−N distance of the F_3B−NH_3 complex is 1.678 Å, which is much shorter than the F_3B−NF_3 of complex **4a**, and the bond energy of F_3B−NH_3 amounts to more than 20 kcal mol^{-1}.

Implications for the Adsorption of NF_3 on Solid Surfaces

As noted in the Introduction, the present theoretical investigation on the conceivable behavior of NF_3 as a bifunctional Lewis base was stimulated by a study on the thermal, electron, and photon-stimulated chemistry of nitrogen trifluoride adsorbed on solid Pt(111).[17] All the peaks observed in the temperature-programmed desorption spectra of adsorbed NF_3 lie below 70 K − suggesting that this molecule is very weakly held and behaves like a physisorbed species. In addition, the available experimental evidence points to different positions of NF_3 and orientations of its dipole moment with respect to the surface and the neighboring molecules. Our calculations provide supporting, although indirect, evidence for conceivably different orientations of NF_3 ligated to a solid surface. Thus, when interacting with the neutral Lewis acids $BH_{3-n}F_n$ (n = 0−3), NF_3 may undergo not only ligation by nitrogen but also by fluorine, leading to isomeric structures that are practically degenerate, especially for the weakest Lewis acids, BH_2F, BHF_2, and BF_3. Although our investigated $BH_{3-n}F_n$−(NF_3) complexes (n = 0−3) are much too simple to be effective models to mimic the interaction of NF_3 with a solid surface, if one perceives the fixation of NF_3 to Pt(111) as an interaction as weak as that occurring in our investigated adducts, it is reasonable to assume that it occurs not only by the nitrogen but also by the fluorine atom(s). Of course, for solids other than platinum, the possible molecular adsorption of NF_3 by different orientations should be critically affected not only by the nature of the surface but also by the strength of the interaction. Due to the widespread industrial use of nitrogen trifluoride in the treatment of solid surfaces, a more detailed investigation of these aspects could be of experimental and theoretical interest.

Acknowledgments

The authors wish to thank the Italian Ministero dell'Istruzione, dell'Università e della Ricerca (MIUR) and Consiglio Nazionale delle Ricerche (CNR) for financial support.

[1] F. Ishii, Y. Kita, in: *Advanced Inorganic Fluorides* (Eds.: T. Nakajima, B. Žemva, A. Tressaud), Elsevier, Amsterdam, **2000**, chapter 19, p. 629.
[2] D. T. Meshri, in: *Advanced Inorganic Fluorides* (Eds.: T. Nakajima, B. Žemva, A. Tressaud), Elsevier, Amsterdam, **2000**, chapter 20, p. 673.
[3] V. M. Donnelly, D. L. Flamm, W. C. Dautremont-Smith, D. J. Werder, *J. Appl. Phys.* **1984**, *55*, 242.
[4] J. A. Barkanic, D. M. Reynolds, R. J. Jaccodine, H. Stenger, J. Parks, H. L. Vedage, *Solid State Technol.* **1989**, *32*, 109.
[5] J. Kikuchi, M. Iga, H. Ogawa, S. Fujimura, H. Yano, *Jpn. J. Appl. Phys.* **1994**, *33*, 2207.
[6] V. Yu. Fominski, O. I. Naoumenko, V. N. Nevolin, A. P. Alekhin, A. M. Markeev, L. A. Vyukov, *Appl. Phys. Lett.* **1996**, *68*, 2243.
[7] J. G. Langan, S. W. Rynders, B. S. Felker, S. E. Beck, *J. Vac. Sci. Technol. A* **1998**, *16*, 2108.
[8] B. E. E. Kastenmeier, G. S. Oehrlein, J. G. Langan, W. R. Entley, *J. Vac. Sci. Technol. A* **2000**, *18*, 2102.
[9] M. M. Walczak, A. L. Johnson, P. A. Thiel, T. E. Madey, *J. Vac. Sci. Technol. A* **1988**, *6*, 675.
[10] J. I. Steinfeld, *Chem. Rev.* **1989**, *89*, 1291.
[11] J. A. Shorter, J. G. Langan, J. I. Steinfeld, *Surf. Sci.* **1989**, *219*, L560.
[12] M. Konuma, E. Bauser, *J. Appl. Phys.* **1993**, *74*, 62.
[13] D. N. Kuvatsos, F. A. Stevie, R. J. Jaccodine, *J. Electrochem. Soc.* **1993**, *140*, 1160.
[14] [14a] A. Jenichen, *Surf. Sci.* **1995**, *331−333*, 1503. [14b] A. Jenichen, *J. Phys. Chem.* **1996**, *100*, 9820.
[15] [15a] E. Vileno, M. K. LeClair, S. L. Suib, M. B. Cutlip, F. S. Galasso, S. J. Hardwick, *Chem. Mater.* **1995**, *7*, 683. [15b] E. Vileno, M. K. LeClair, S. L. Suib, M. B. Cutlip, F. S. Galasso, S. J. Hardwick, *Chem. Mater.* **1996**, *8*, 1217.
[16] J. G. Langan, S. E. Beck, B. S. Felker, S. W. Rynders, *J. Appl. Phys.* **1996**, *79*, 3886.
[17] K. H. Junker, J. M. White, *Surf. Sci.* **1997**, *382*, 67.
[18] M. R. Baklanov, S. Vanhaelemeersch, W. Storm, W. Vandervost, K. Maex, *J. Vac. Sci. Technol. B* **1998**, *16*, 164.
[19] S. E. Kim, C. Steinbruchel, *Solid State Electr.* **1999**, *43*, 1019.
[20] [20a] T. W. Little, F. S. Ohuchi, *Mater. Res. Soc., Symp. Proc.* **1997**, *439*, 251. [20b] T. W. Little, F. S. Ohuchi, *Surf. Sci.* **2000**, *445*, 235. [20c] A. Endou, T. W. Little, A. Yamada, K. Teraishi, M. Kubo, S. S. C. Ammal, A. Miyamoto, M. Kitajima, F. S. Ohuchi, *Surf. Sci.* **2000**, *445*, 243.
[21] R. Miotto, A. C. Ferraz, G. P. Srivastava, *Surf. Sci.* **2000**, *454−456*, 152.
[22] P. Tegeder, E. Illenberger, *Chem. Phys. Lett.* **2001**, *341*, 401.
[23] J. J. Fisher, T. B. McMahon, *J. Am. Chem. Soc.* **1988**, *110*, 7599.
[24] F. Grandinetti, J. Hrušàk, D. Schröder, S. Karrass, H. Schwarz, *J. Am. Chem. Soc.* **1992**, *114*, 2806.
[25] V. V. Yakobson, D. G. Musaev, A. S. Zyubin, A. M. Mebel, O. P. Charkin, *Koord. Khim.* **1989**, *15*, 1478.
[26] F. Grandinetti, V. Vinciguerra, *J. Mol. Struct. (Theochem)* **2001**, *574*, 185.
[27] T. B. McMahon, T. Heinis, G. Nicol, J. K. Hovey, P. Kebarle, *J. Am. Chem. Soc.* **1988**, *110*, 7591.
[28] F. Grandinetti, P. Cecchi, V. Vinciguerra, *Chem. Phys. Lett.* **1997**, *281*, 431.
[29] K. Hiraoka, M. Nasu, S. Fujimaki, S. Yamabe, *J. Phys. Chem.* **1995**, *99*, 15822.
[30] F. Grandinetti, V. Vinciguerra, *Int. J. Mass Spectrom.* **2002**, *216*, 285.
[31] O. de la Luz Rojas, *J. Am. Chem. Soc.* **1977**, *99*, 2902.
[32] M. Sana, G. Leroy, C. Wilante, *Organometallics* **1992**, *11*, 781.
[33] A. Skancke, P. N. Skancke, *J. Phys. Chem.* **1996**, *100*, 15079.
[34] K. R. S. Chandrakumar, S. Pal, *J. Phys. Chem. A* **2002**, *106*, 11775.
[35] T. A. Ford, D. Steele, *J. Phys. Chem.* **1996**, *100*, 19336.
[36] A. D. Craig, *Inorg. Chem.* **1964**, *3*, 1629.

 © 2004 Wiley-VCH Verlag GmbH & Co. KGaA, Weinheim

[37] A. Boutalib, *J. Phys. Chem. A* **2003**, *107*, 2106.
[38] E. A. Piocos, B. S. Ault, *J. Phys. Chem.* **1992**, *96*, 7589.
[39] R. Lascola, R. Withnall, L. Andrews, *J. Phys. Chem.* **1988**, *92*, 2145.
[40] E. R. Waclawik, A. C. Legon, J. H. Holloway, *Chem. Phys. Lett.* **1998**, *295*, 289.
[41] F. Cacace, F. Grandinetti, F. Pepi, *Angew. Chem. Int. Ed. Engl.* **1994**, *33*, 123.
[42] M. Aschi, F. Cacace, F. Grandinetti, F. Pepi, *J. Phys. Chem.* **1994**, *98*, 2713.
[43] F. Cacace, F. Grandinetti, F. Pepi, *J. Phys. Chem.* **1994**, *98*, 8009.
[44] M. Aschi, F. Grandinetti, F. Pepi, *Int. J. Mass Spectrom. Ion Processes* **1994**, *130*, 117.
[45] F. Cacace, F. Grandinetti, F. Pepi, *J. Chem. Soc., Chem. Commun.* **1994**, 2173.
[46] F. Cacace, F. Grandinetti, F. Pepi, *Inorg. Chem.* **1995**, *34*, 1325.
[47] F. Grandinetti, F. Pepi, A. Ricci, *Chem. Eur. J.* **1996**, *2*, 495.
[48] F. Grandinetti, P. Cecchi, V. Vinciguerra, *Int. J. Mass Spectrom. Ion Processes* **1998**, *175*, 317.
[49] M. Aschi, F. Grandinetti, V. Vinciguerra, *Chem. Eur. J.* **1998**, *4*, 2366.
[50] M. Aschi, F. Grandinetti, *J. Mol. Struct. (Theochem)* **2000**, *497*, 205.
[51] P. Antoniotti, F. Grandinetti, *Chem. Phys. Lett.* **2002**, *366*, 676.
[52] M. J. Frisch, G. W. Trucks, H. B. Schlegel, G. E. Scuseria, M. A. Robb, J. R. Cheeseman, V. G. Zakrzevski, J. A. Montgomery, R. E. Stratman, J. C. Burant, S. Dapprich, J. M. Millam, A. D. Daniels, K. N. Kudin, M. C. Strain, O. Farkas, J. Tomasi, V. Barone, M. Cossi, R. Cammi, B. Mennucci, C. Pomelli, C. Adamo, S. Clifford, J. Ochterski, G. A. Petersson, P. Y. Ayala, Q. Cui, K. Morokuma, D. K. Malick, A. D. Rabuck, K. Raghavachari, J. B. Foresman, J. Cioslowski, J. V. Ortiz, A. G. Baboul, B. B. Stefanov, G. Liu, A. Liashenko, P. Piskorz, I. Komaromi, R. Gomperts, R. L. Martin, D. J. Fox, T. Keith, M. A. Al-Laham, C. Y. Peng, A. Nanayakkara, C. Gonzalez, M. Challacombe, P. M. W. Gill, B. G. Johnson, W. Chen, M. W. Wong, J. L. Andres, M. Head-Gordon, E. S. Replogle, J. A. Pople, *GAUSSIAN 98* (Revision A.7), Gaussian, Inc., Pittsburgh, PA, **1998**.
[53] MOLPRO is a package of ab initio programs written by H.-J. Werner and P. J. Knowles, with contributions from R. D. Amos, A. Bernhadsson, A. Berning, P. Celani, D. L. Cooper, M. J. O. Deegan, A. J. Dobbyn, F. Eckert, C. Hampel, G. Hetzer, T. Korona, R. Lindh, A. W. Lloyd, S. J. McNicholas, F. R. Manby, W. Meyer, M. E. Mura, A. Nicklass, P. Palmieri, R. Pitzer, G. Rauhut, M. Schatz, H. Stoll, A. J. Stone, R. Tarroni, and T. Thorsteinsson.
[54] K. Raghavachari, G. W. Trucks, J. A. Pople, M. Head-Gordon, *Chem. Phys. Lett.* **1989**, *157*, 479.
[55] C. Hampel, K. Peterson, H-J. Werner, *Chem. Phys. Lett.* **1992**, *190*, 1, and references cited therein.
[56] D. E. Woon, T. H. Dunning, Jr., *J. Chem. Phys.* **1993**, *98*, 1358.
[57] D. A. Mc Quarry, *Statistical Mechanics*, Harper and Row, New York, **1973**.
[58] S. Boys, F. Bernardi, *Mol. Phys.* **1970**, *19*, 553.
[59] L. A. Curtiss, K. Raghavachari, P. C. Redfern, V. Rassolov, J. A. Pople, *J. Chem. Phys.* **1998**, *109*, 7764.
[60] M. Otake, C. Matsumura, Y. Morino, *J. Mol. Spectrosc.* **1968**, *28*, 316.
[61] The CCD/cc-pVDZ optimised geometries of BH_2F, BHF_2 and BF_3 are: BH_2F: d_{B-H} = 1.207 Å, d_{B-F} = 1.336 Å, ∠ F−B−H = 117.2°; BHF_2: d_{B-H} = 1.199 Å, d_{B-F} = 1.329 Å, ∠ F−B−H = 120.9°; BF_3: d_{B-F} = 1.323 Å.
[62] [62a] U. E. Senff, P. G. Burton, *J. Phys. Chem.* **1985**, *89*, 797. [62b] M. J. Frish, J. E. DelBene, J. S. Binkley, H. F. Schaefer, *J. Chem. Phys.* **1986**, *84*, 2279. [62c] M. Gutowski, G. Chalasinski, *J. Chem. Phys.* **1993**, *98*, 5540.
[63] E. P. L. Hunter, S. G. Lias, *J. Phys. Chem. Ref. Data* **1998**, *27*, 413.
[64] [64a] V. Jonas, G. Frenking, M. T. Reetz, *J. Am. Chem. Soc.* **1994**, *116*, 8741. [64b] V. Jonas, G. Frenking, *J. Chem. Soc., Chem. Commun.* **1994**, 1489.

Received May 21, 2003
Early View Article
Published Online February 16, 2004

 © 2004 Wiley-VCH Verlag GmbH & Co. KGaA, Weinheim

EurJIC
European Journal of Inorganic Chemistry

Issue 6/2004

Pages 1131–1352

Papers available ahead of print in Early View at www.interscience.wiley.com

Earliest available Table of Contents:
Automatically, free of charge by e-mail through
www.interscience.wiley.com/alerts

COVER PICTURE

The cover picture shows the results of modelling the diffusion of phthalodinitrile through the zeolite pores. Once inside, phthalodinitrile reacts to form a large phthalocyanine guest that remains entrapped inside the zeolite cavity. The resulting zeolite–guest chemistry resembles at molecular level a ship in a bottle that is a typical souvenir in many harbour cities. The zeolite-encapsulated guest shows many promising applications as discussed in the Microreview by A. Corma and H. Garcia on p. 1143 ff.

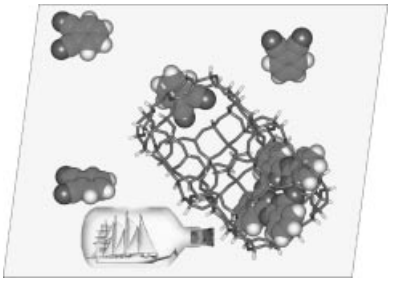

MICROREVIEW

Contents

1143 **A. Corma,* H. Garcia***

Supramolecular Host-Guest Systems in Zeolites Prepared by Ship-in-a-Bottle Synthesis

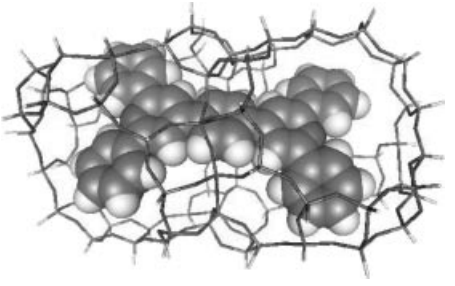

Keywords: Host-guest systems / Phthalocyanines / Ship-in-a-bottle synthesis / Supramolecular chemistry / Zeolites / Zeozymes

 © 2004 Wiley-VCH Verlag GmbH & Co. KGaA, Weinheim

EurJIC
European Journal of Inorganic Chemistry

Issue 6/2004

Pages 1131–1352

Papers available ahead of print in Early View at www.interscience.wiley.com

Earliest available Table of Contents:
Automatically, free of charge by e-mail through
www.interscience.wiley.com/alerts

COVER PICTURE

The cover picture shows the results of modelling the diffusion of phthalodinitrile through the zeolite pores. Once inside, phthalodinitrile reacts to form a large phthalocyanine guest that remains entrapped inside the zeolite cavity. The resulting zeolite–guest chemistry resembles at molecular level a ship in a bottle that is a typical souvenir in many harbour cities. The zeolite-encapsulated guest shows many promising applications as discussed in the Microreview by A. Corma and H. Garcia on p. 1143 ff.

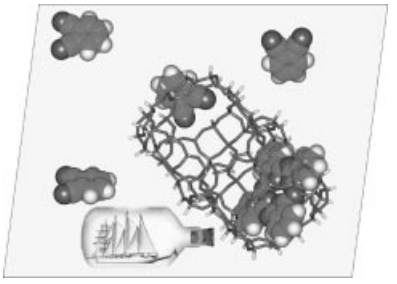

MICROREVIEW

Contents

1143 **A. Corma,* H. Garcia***

Supramolecular Host-Guest Systems in Zeolites Prepared by Ship-in-a-Bottle Synthesis

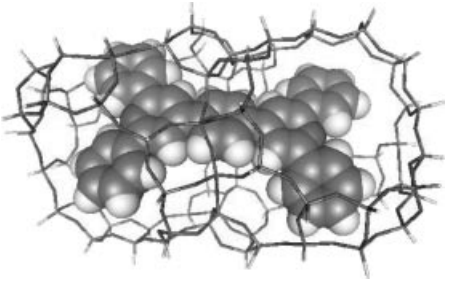

Keywords: Host-guest systems / Phthalocyanines / Ship-in-a-bottle synthesis / Supramolecular chemistry / Zeolites / Zeozymes

 © 2004 Wiley-VCH Verlag GmbH & Co. KGaA, Weinheim

SHORT COMMUNICATIONS

1165 **J. Wang, Q. Chen,* B. Hou, Z. Peng**

Synthesis and Magnetic Properties of Single-Crystals of $MnFe_2O_4$ Nanorods

Keywords: Iron / Magnetic properties / Nanorods / Nanowires / X-ray diffraction

1169 **Y. Hou, S. Gao,* T. Ohta, H. Kondoh**

Towards 3-D Spherical Self-Assembly by Ternary Surfactant Combinations: The Case of Magnetite Nanoparticles

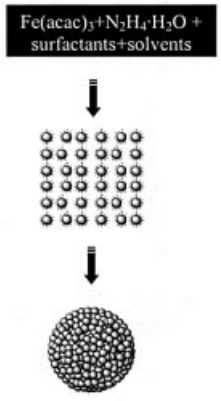

Keywords: Self-assembly / Magnetic properties / Magnetite / Nanoparticles / Super paramagnet

FULL PAPERS

1175 **M. Hogenbirk, G. Schat, O. S. Akkerman, F. Bickelhaupt,* J. Schottek, M. Albrecht, R. Fröhlich, G. Kehr, G. Erker,* H. Kooijman, A. L. Spek**

(μ-Methylene)bis(methylzirconocene): Preparation, Molecular Structure, and Thermal Disproportionation

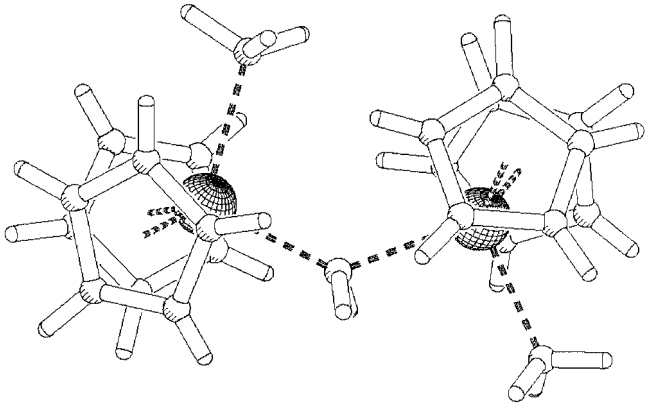

Keywords: Magnesium / Metallocenes / Zirconium / Configuration at carbon

1183 **S. Derakhshan, E. Dashjav, H. Kleinke***

The Predicted Structures of the New Pnictides HfMQ in Contrast to ZrMQ (M = Ti, V; Q = P, As)

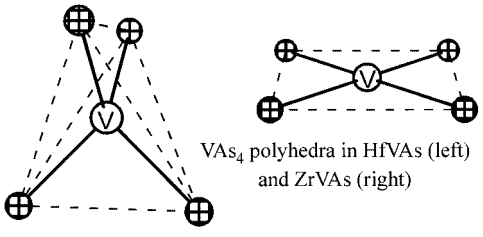

VAs_4 polyhedra in HfVAs (left) and ZrVAs (right)

Keywords: Structure map / X-ray diffraction / Electronic structure / Phosphides / Arsenides

 © 2004 Wiley-VCH Verlag GmbH & Co. KGaA, Weinheim

1190 **I. Billard,* S. Mekki, C. Gaillard, P. Hesemann, G. Moutiers, C. Mariet, A. Labet, J.-C. G. Bünzli**

Eu^{III} Luminescence in a Hygroscopic Ionic Liquid: Effect of Water and Evidence for a Complexation Process

Keywords: Ionic liquids / Lanthanides / Europium / Luminescence / Complexation

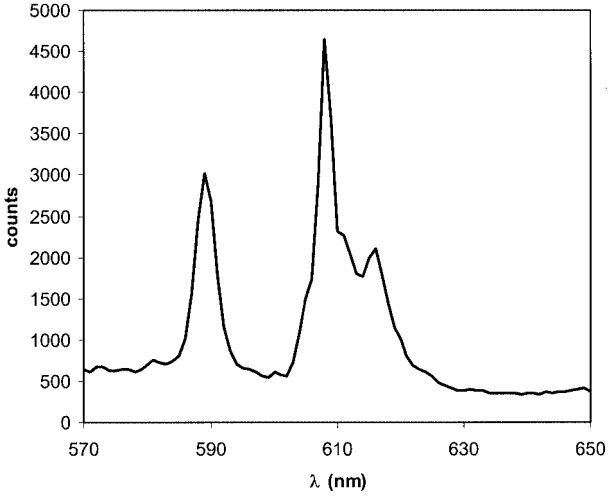

1198 **T. Sheng, H. Vahrenkamp***

Long Range Metal-Metal Interactions Along Fe−NC−Ru−CN−Fe Chains

Keywords: Chain structures / Cyanide complexes / Polynuclear complexes / Metal−metal interactions

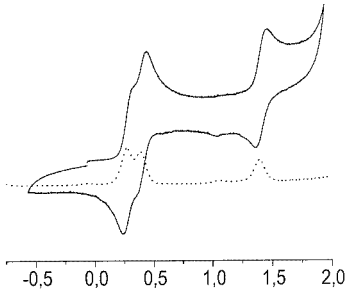

1204 **Q. Knijnenburg, D. Hetterscheid, T. M. Kooistra, P. H. M. Budzelaar***

The Electronic Structure of (Diiminopyridine)cobalt(I) Complexes

Keywords: Charge transfer / Cobalt / Density functional calculations / NMR spectroscopy / Radicals

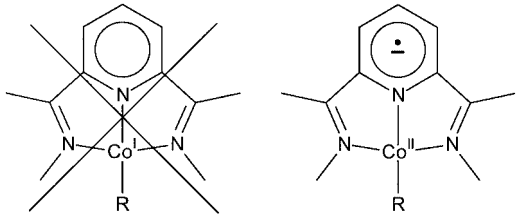

1212 **J. Saloni, S. Roszak,* K. Hilpert, M. Miller, J. Leszczynski**

Quantum Chemical Studies of Neutral and Ionized DyX, DyX_2, and DyX_3 Species (X = F, Cl, Br, I) and the Implications for the Mass Spectra of Gaseous DyX_3

Keywords: Halides / Lanthanides / Mass spectrometry / Quantum chemical calculations / Thermochemistry

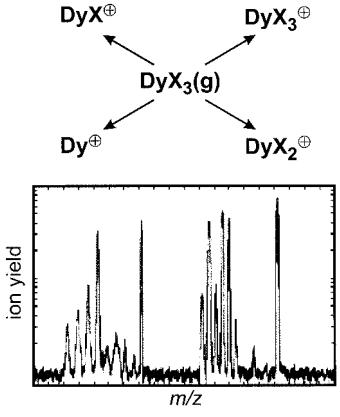

 © 2004 Wiley-VCH Verlag GmbH & Co. KGaA, Weinheim

1219 **U. Baisch, D. Belli Dell'Amico,* F. Calderazzo, L. Labella, F. Marchetti, A. Merigo**

N,*N*-Dialkylcarbamato Lanthanide Complexes, a Series of Isotypical Coordination Compounds

Keywords: Coordination modes / Lanthanides / Lanthanide contraction

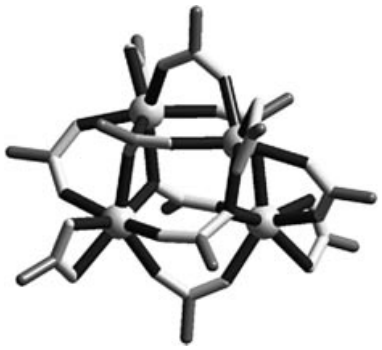

1225 **V. Balland, E. Anxolabéhère-Mallart,* F. Banse,* E. Rivière, S. Bourcier, M. Nierlich, J.-J. Girerd***

Synthesis, Structure and Characterizations in Solid State and Solution of Dinuclear Pentacoordinated Fe^{II} and Mn^{II} Complexes and of a Linear Tetranuclear Fe^{III} Complex Obtained with the Ligand *N*,*N*,*N*′,*N*′-Tetrakis[(6-methyl-2-pyridyl)methyl]propane-1,3-diamine

Keywords: N ligands / Iron / Manganese / Tetranuclear complexes / Bioinorganic chemistry

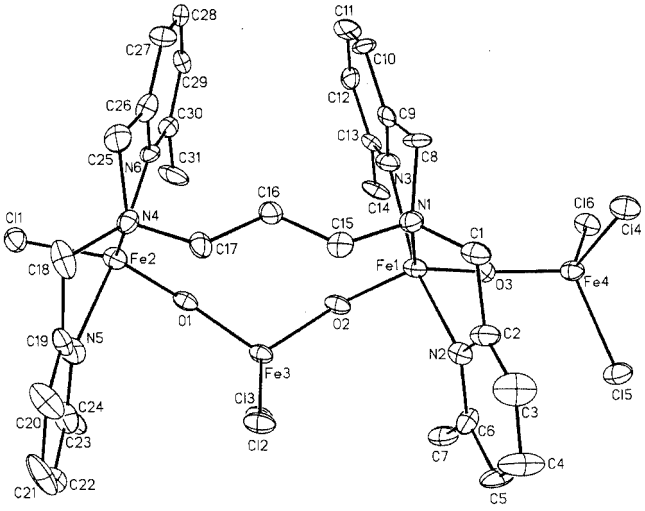

1234 **P. Mastrorilli, C. F. Nobile,* G. P. Suranna, F. P. Fanizzi, G. Ciccarella, U. Englert, Q. Li**

Synthesis and Carbonylation of Platinum(II) Organometallic Complexes with Bis(phosphanyl) Monosulfides − Crystal Structures of $[\kappa^2P,S\text{-}\{Ph_2CH_2P(S)Ph_2\}Pt(CH_3)(Cl)]$ and $[\kappa P,\mu\text{-}\kappa S\text{-}\{Ph_2CH_2CH_2P(S)Ph_2\}Pt\text{-}(CH_3)]_2[BF_4]_2$

Keywords: Platinum / P,S ligands / Carbonyl ligands / Bridging ligands / Mass spectrometry

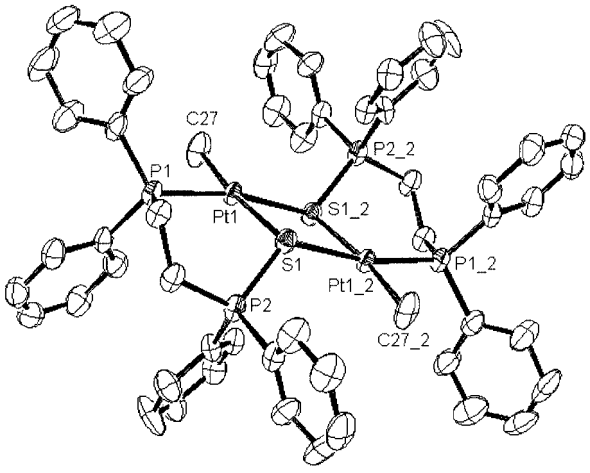

1243 **R. Fischer, H. Görls, D. Walther***

Polymetallated 4-*tert*-Butylcalix[4]arene Complexes of Sodium and Potassium Stabilized by Crown Ethers: Syntheses, Structures and Activation of Carbon Dioxide

Keywords: Alkali metals / Calixarenes / Carbon dioxide fixation / Carboxylation / Crown compounds

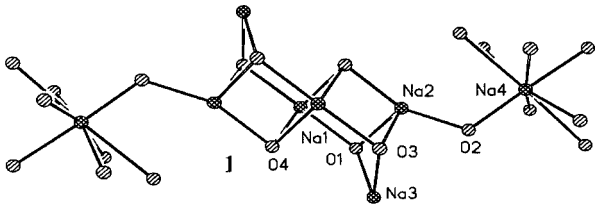

$$\text{Ph-CO- C(F)H-Me} \xrightarrow[\text{b) } Me_2SO_4]{\text{a) } \mathbf{1}/CO_2} \text{Ph-CO- C(F)Me- COOMe}$$

 © 2004 Wiley-VCH Verlag GmbH & Co. KGaA, Weinheim

1253 **Y. A. Pozdniakova, K. A. Lyssenko, A. A. Korlyukov, I. V. Blagodatskikh, N. Auner, D. Katsoulis, O. I. Shchegolikhina***

Alkali-Metal-Directed Hydrolytic Condensation of Trifunctional Phenylalkoxysilanes

Keywords: Hydrolytic condensation / Potassium / Self-assembly / Silanes / Sodium / Template synthesis

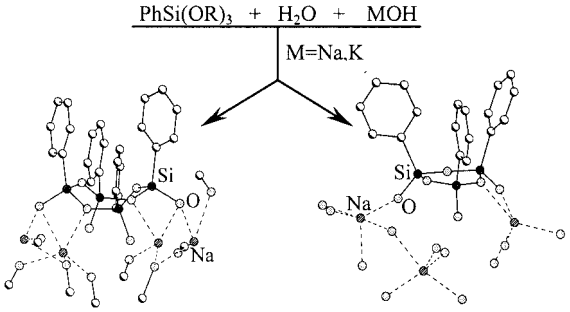

1262 **R. D. Hartnell, D. P. Arnold***

Peripherally Metallated Porphyrins: the First Examples of *meso*-η^1-Palladio(II) and -Platinio(II) Complexes with Chelating Diamine Ligands

Keywords: N ligands / Palladium / Platinum / Porphyrins

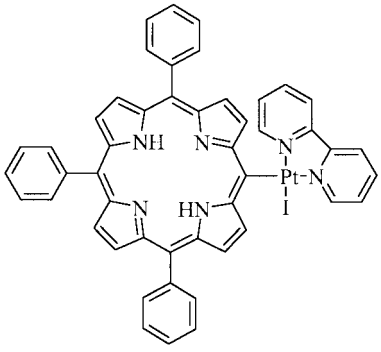

1270 **S.-M. Ying, J.-G. Mao***

Novel Layered Lead(II) Aminodiphosphonates with Carboxylate-Sulfonate and 1,3,5-Benzenetricarboxylate Ligands as Pendant Groups or Intercalated Species

Keywords: Hydrothermal synthesis / Layered compounds / Carboxylates / Sulfonates

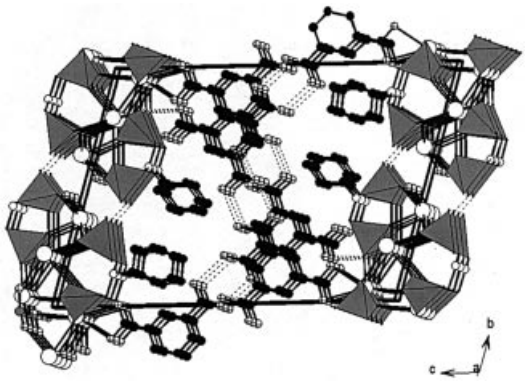

1277 **P. Bergamini,* V. Bertolasi, F. Milani**

The Construction of P−O/P−N Ligands on Platinum and Palladium

Keywords: Template synthesis / Ligand design / P ligands / Platinum / Palladium

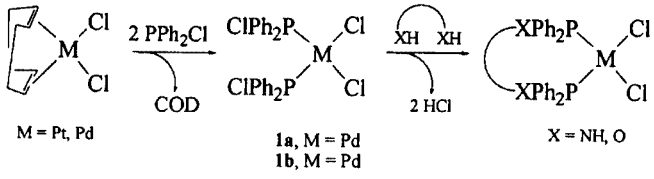

1285 **A. Mohamadou,* C. Jubert, N. Gruber, J.-P. Barbier**

Configuration of Octahedral Metal Compounds − Equilibrium, Crystal and Molecular Structure of Nickel(II) Complexes of Linear N_2O_4, N_4S_2 or N_6 Donors Set Atoms Ligands

Keywords: Configuration determination / N,O ligands / N,S ligands / Nickel / Potentiometry

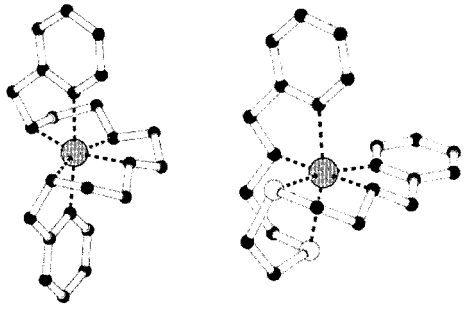

 © 2004 Wiley-VCH Verlag GmbH & Co. KGaA, Weinheim

1292 D. Pappalardo,* M. Mazzeo, P. Montefusco, C. Tedesco, C. Pellecchia

Neutral and Cationic Methylaluminium Complexes of 2-Anilinotropone Ligands: Synthesis, Characterization, and Reactivity toward Ethylene

Keywords: Aluminium / N,O ligands / Alkenes / Cations / Polymerizations

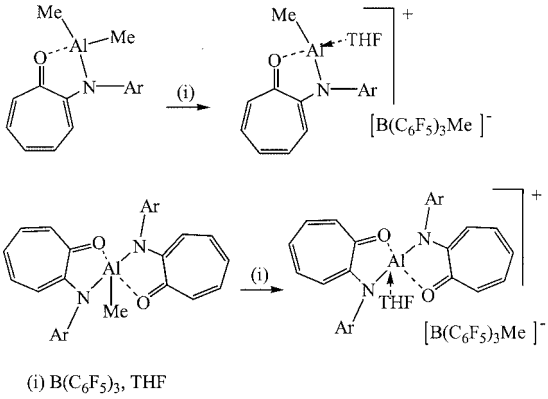

1299 A. Antiñolo, I. Dorado, M. Fajardo, A. Garcés, I. López-Solera, C. López-Mardomingo, M. M. Kubicki, A. Otero,* S. Prashar

Synthesis, Structural Characterisation and Reactivity of New Dinuclear Monocyclopentadienyl Imidoniobium and -tantalum Complexes − X-ray Crystal Structures of [{Nb(η^5-$C_5H_4SiMe_3$)Cl_2}$_2$(μ-1,4-NC_6H_4N)], [{Ta(η^5-C_5Me_5)Cl_2}$_2$(μ-1,4-NC_6H_4N)] and [{Ta(η^5-C_5Me_5)$(CH_2SiMe_3)_2$}$_2$(μ-1,4-NC_6H_4N)]

Keywords: Cyclopentadienyl ligands / Half-sandwich complexes / N ligands / Niobium / Tantalum

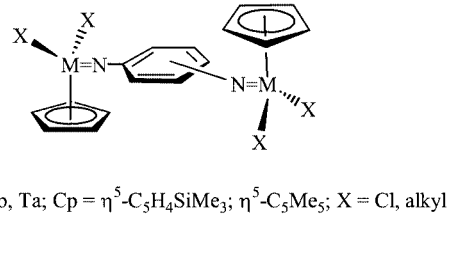

1311 S.-L. Ma, W.-X. Zhu,* S. Gao, Q.-L. Guo, M.-Q. Xu

Synthesis, Structure and Magnetic Properties of a μ-Carboxylato-Bridged Ferromagnetic Trinuclear Copper(II) Complex with Lariat Tetraazacrown Ether as Ligand

Keywords: Copper / Macrocyclic ligands / X-ray diffraction / Magnetic properties

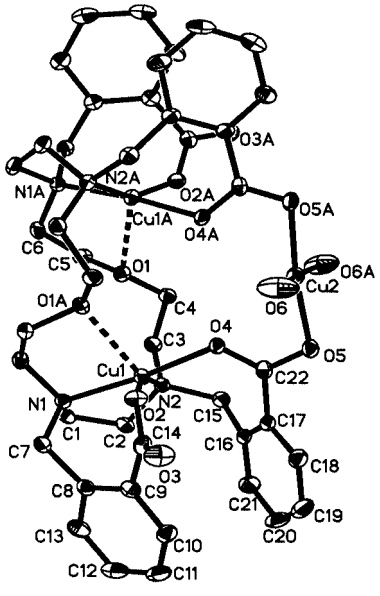

 © 2004 Wiley-VCH Verlag GmbH & Co. KGaA, Weinheim

1318 **H. Alves, D. Simão, I. Cordeiro Santos, V. Gama, R. Teives Henriques, H. Novais, M. Almeida***

A Series of Transition Metal Bis(dicyanobenzenedithiolate) Complexes [M(dcbdt)$_2$] (M = Fe, Co, Ni, Pd, Pt, Cu, Au and Zn)

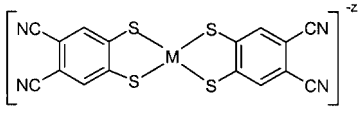

Keywords: Coordination chemistry / EPR spectroscopy / Magnetic properties / S ligands / Transition metals

1330 **A. Enzmann, M. Eckert, W. Ponikwar, K. Polborn, S. Schneiderbauer, M. Beller,* W. Beck***

Aminomethyl and Aminoacetyl Complexes of Palladium(II), Platinum(II), Iron(II) and Rhenium(I) with *N*-Phthaloyl as Amino Protecting Group and Mechanistic Studies on the Palladium-Catalyzed Amidocarbonylation

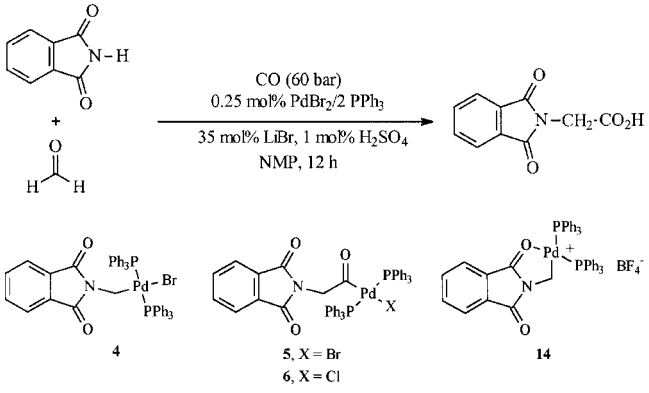

Keywords: Amidocarbonylation / Iron / Palladium / Platinum / Rhenium

1341 **G.-S. Fang, J.-S. Huang, N. Zhu, C.-M. Che***

(Nitrido)ruthenium(VI) and -osmium(VI) Complexes with Catecholate Auxiliaries: Synthesis, Structure, and Conversion into a (Phosphoraniminato)osmium(V) Complex

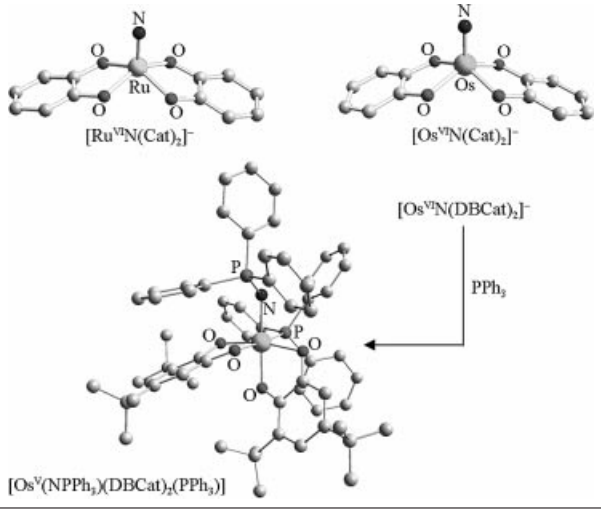

Keywords: Nitrides / O ligands / Ruthenium / Osmium / Structure elucidation

1349 **M. Ponikvar,* B. Sedej, J. F. Liebman**

The Solid-State Lanthanoid-Assisted Hydrolysis of the Solvolytically "Inert" $[AsF_6]^-$ Ion

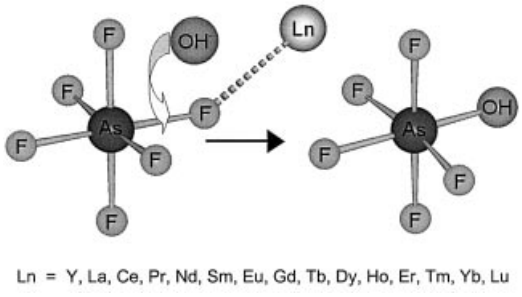

Keywords: Arsenic / Hydrolysis / $LnF_n(AsF_6)_{3-n}$ compounds / Rare-earth elements / Solid-state reactions

 © 2004 Wiley-VCH Verlag GmbH & Co. KGaA, Weinheim

Supramolecular Host-Guest Systems in Zeolites Prepared by Ship-in-a-Bottle Synthesis

Avelino Corma*[a] and Hermenegildo Garcia*[a]

Keywords: Host-guest systems / Phthalocyanines / Ship-in-a-bottle synthesis / Supramolecular chemistry / Zeolites / Zeozymes

Zeolites have a microporous system defining large cavities interconnected by smaller windows. These cages can accommodate large molecules whose size, however, can be too big to cross the windows. The most important examples of these tridirectional zeolites are faujasites X and Y, but examples of other suitable zeolites are Beta, EMT and MCM-22. The inclusion of large guests inside the cavities starts from smaller precursors that can diffuse through the zeolite pores and then react inside the cavities to form the target guest. This microreview discusses the special characterisation techniques necessary to study these systems, differentiating those that serve to assess the identity and purity of the guests from those that address the internal vs. external location of the guests with respect to the zeolite host. It is organized by grouping the examples of ship-in-a-bottle synthesis according to the potential application of the system as catalysts, photocatalysts, sensors, in molecular machines, etc. Although proper credit is given to the pioneering reports on ship-in-a-bottle synthesis, the emphasis is placed on the most recent examples of the literature covering up to mid 2003.
(© Wiley-VCH Verlag GmbH & Co. KGaA, 69451 Weinheim, Germany, 2004)

A. General Aspects

1. Introduction

Zeolites owe their importance to their use as catalysts in gas-phase, large-scale petrochemical processes such as catalytic cracking, Friedel−Crafts alkylation and alkylaromatic isomerisation or disproportionation.[1−6] Zeolites are easy to separate from the reaction products, thereby offering convenient reactor design and allowing continuous-flow operation. Because they are thermally stable and chemically robust, zeolites can be almost completely regenerated by calcination in air when they become deactivated by the presence of large organic products that remain adsorbed.

The promising results of gas-phase reactions in zeolites have triggered an intense research effort aimed at

[a] Instituto de Tecnología Química CSIC-UPV, Universidad Politécnica de Valencia,
Avda. de los Naranjos s/n, 46023 Valencia, Spain

Avelino Corma Canos was born in Moncófar, Spain. He was a postdoc in the Department of Chemical Engineering at Queen's University (Canada, 1977−1979). He is director of the Instituto de Tecnología Química (UPV-CSIC) at the Universidad Politécnica de Valencia since 1990. His current research field is structured nanomaterials and molecular sieves as catalysts, covering aspects of synthesis, characterisation and reactivity. Avelino Corma has written about 500 articles on these subjects in international journals, three books, and a number of reviews and book chapters. He is co-author of more than 80 patents, six of them being commercialised. He is the recipient of numerous awards, including the Dupont Award on New Materials (1995), the Ciapetta and Houdry Awards from the ACS, the F. Gault Award of the European Catalysis Society and the Spain National Award on Science and Technology.

Hermenegildo García (Herme) was born in Canals (Spain) in June of 1957 and studied chemistry at the Faculty of Science of the Universidad de Valencia (Spain) where he graduated in 1979 with Honors. He did his PhD on preparative organic photochemistry under the guidance of Prof. Miguel A. Miranda and this was awarded, also with Honors by the Universidad de Valencia in 1983. Then, he moved to the Technical University of Valencia where he initiated his career in 1983 first as Assistant Professor, becoming finally Full Professor in 1996. In 1991 he was appointed member of the Institute of Chemical Technology, a joint centre depending on the Spanish National Research Council (CSIC) and the Technical University of Valencia that was founded in that year. He stayed as a postdoc at the Chemistry Department of the University of Reading (U.K.) with Prof. Andrew Gilbert in 1987, and later took three periods of sabbatical leave in 1992−1993 (one year), 1995 (six months) and 2000 (three months) at the University of Ottawa joining the Laser Flash Photolysis group led by Prof. J. C. (Tito) Scaiano. He has co-authored over 200 papers most of them dealing with the application of zeolites as hosts of organic guests and as solid catalysts. He holds three international patents. His main current interests are in supramolecular photochemistry and photocatalysis, the development of photoactive nanoscopic materials and heterogeneous catalysis.

MICROREVIEWS: This feature introduces the readers to the authors' research through a concise overview of the selected topic. Reference to important work from others in the field is included.

developing the potential of zeolites as acid-base and redox catalysts for the production of chemicals and fine chemicals.[7,8] As a result of these studies, heterogeneous catalysis of organic reactions by zeolites can be considered a mature field, and the industrial applications of zeolites for membranes, adsorption-separation and in the production of fine and specialty chemicals are expected to grow in the near future.

In addition to the current importance of zeolites in heterogeneous catalysis, it is likely that these solids will also attract interest in materials science for the development of functional materials, and in nanotechnology.[9] For these applications, zeolites provide a rigid matrix in which some active component or components can be included. Enantioselective catalysis, sensors, solid lasers, intelligent switches, membranes, waveguides and solar cells are emerging fields in which zeolites can be applied. The main problem to be solved for the application in nanotechnology is the preparation of submillimeter films in which the pores are oriented with respect to the substrate. Progress on film preparation has been made by "in situ" crystallisation of gels or the covalent attachment of zeolite particles to the substrate.[10−13]

A system that has vast potential for application in catalysis as well as for nanotechnology is that in which a functional guest is incarcerated inside the zeolite supercages without the possibility of diffusing out of the particle. In the field of catalysis, there are a number of reviews summarising the use of encapsulated coordination complexes as oxidation catalysts[14,15] and the possible strategies for the preparation of zeolite ship-in-a-bottle complexes, including the use of flexible ligands and zeolite synthesis around the complexes.[16] The generation of organic carbocations entrapped within the zeolite during a chemical reaction in the liquid phase has also been reviewed.[17] Considering the zeolites as catalysts, these carbocations are generally undesired species that poison and block the catalytic site, but in other cases their preparation has been purposely achieved.[17−19] This microreview focuses on the preparation, characterisation and properties of such supramolecular guest-zeolite materials, with special emphasis on their applications. Firstly, we will comment briefly on the main characteristics of zeolites as hosts. Then, we will describe adsorption procedures and the ship-in-a-bottle synthesis. We will cover characterisation techniques of encapsulated guests and how to address the internal vs. external location of the guest. The main body of the microreview describes the examples reported of ship-in-a-bottle synthesis. We have classified them according to the potential application that these host-guest systems can have.

2. Zeolites: Composition and Chemical Structure

Zeolites are crystalline aluminosilicates whose structure is formed by an array of corner-sharing SiO_4^{4-} or AlO_4^{5-} tetrahedra.[20−22] These building blocks become arranged in a periodic way to form channels and cages on a nano- and subnanometer scale of strictly regular dimensions, named micropores. The pores of the zeolites are open to the exterior and to the surrounding medium, thus allowing diffusion of molecules from the exterior to the interior of the zeolite particle. The existence of these accessible micropores ranks zeolites at the top of the list of solids exhibiting large specific surface areas, typically above 300 $m^2 \cdot g^{-1}$ with an internal void volume above 0.1 $cm^3 \cdot g^{-1}$.

A zeolite framework containing exclusively oxygen-sharing SiO_4^{4-} tetrahedra is neutral. Al is a near neighbour of Si in the periodic table, both elements having similar ionic radii. When an Al atom replaces an Si atom isomorphically in the framework, this becomes negatively charged, one negative charge being introduced by each AlO_4^{5-} tetrahedron. The overall negative charge of these aluminosilicates requires the presence of organic or inorganic cations to maintain the electroneutrality of the solid.

Although there are natural zeolites, most of the over 100 zeolites known are synthetic. The first synthesis of zeolite Y by Barrer in the mid 1950s was an attempt to mimic the conditions under which natural zeolites were supposed to have formed on the Earth.[23−32] This synthesis has been widely recognized as one of the most important advances in the chemistry of the last century. Zeolites are obtained in the laboratory by crystallisation (either static or under continuous agitation) of gels containing alumina and silica in an aqueous medium at temperatures in the range of 100−190 °C and autogenous pressure, for several days or weeks.[33] Besides silica and alumina, the gel can be prepared from other sources of Al, Si and some other metals, and it may also contain quaternary ammonium cations to direct the crystallisation of a given crystal structure.

Zeolites are classified based on the symmetry of their unit cell, each structure being denoted by three capital letters.[34] An alternative classification that is more convenient here is according to the dimensions of the micropores (Scheme 1). In this regard the zeolites can be classified as having a small, medium or large pore size depending on whether the number of oxygen atoms and Si plus Al atoms is 8, 10 or 12, respectively.[35] The number of oxygen atoms defining the minimum ring of a pore determines roughly the dimension of the pores, which are approximately 3, 5 and 7 Å for the small-, medium- and large-pore zeolites, respectively. Recently, new structures containing pores of different dimensions have been reported.[36−39]

There has been an intense search for extra-large-pore zeolites (those having pores with more than 12-membered rings), but the success has been limited in the sense that, although some extra-large-pore zeolites or zeotypes have been synthesised, the resulting pores are not spherical and the minimum axis and structure are not much different from those of large-pore zeolites.[40,41]

Another aspect of importance regarding the micropore system of zeolites is the geometry of the pores. In this regard zeolites can be classified as uni-, bi- and tridirectional zeolites, depending on whether the channel system is arranged along one, two or the three Cartesian axes. The directionality of the zeolite pore system is relevant with respect to the ability of zeolites to include guests inside the micropores. Diffusion coefficients in unidirectional zeolites

 © 2004 Wiley-VCH Verlag GmbH & Co. KGaA, Weinheim

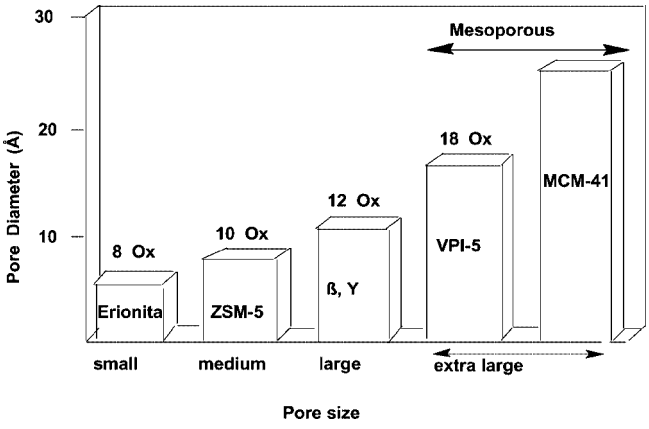

Scheme 1

are typically smaller than those of tridirectional zeolites, which contain a much more open pore system.[42]

The phenomenon of inclusion of a molecule inside the rigid pores defined by the zeolite framework is commonly denoted with terms like adsorption, incorporation, inclusion or encapsulation. The latter three terms are used when the residence time inside the pores is indefinitely long, while in catalysis in which the access of the reagents and substrates to the internal sites is a necessary step in the mechanism and the products have to migrate away from the sites, the terms adsorption and desorption are the preferred ones.

The ability of zeolites to include organic or inorganic guests in their interior gives rise to a supramolecular chemistry in which the properties of the guest-zeolite assembly differs from the molecular properties of the guest in solution.[43] The control of the molecular properties by the zeolite may arise basically by the combination of any of at least five main factors including: (i) restriction of the mobility and conformational flexibility of the guest; (ii) shape-selectivity effects in which the molecular size of the reactants, transition states and products relative to the dimensions of the pores play a decisive role; (iii) compartmentalisation of the reaction cavity favouring geminate recombination and disfavouring escape effects; (iv) polarity of the zeolite internal voids promoting and stabilizing charged species; and (v) the presence of cooperating active sites in close proximity to the encapsulated species. Here we will provide examples that illustrate how incorporation into a zeolite can alter the *intrinsic molecular properties* of the included guest.

Different terms have been coined to refer to the zeolite adsorption-encapsulation chemistry. For instance, zeolites were initially defined by Barrer as molecular sieves to denote that certain molecules can access the interior of the pores, while others are too large and are size-excluded from the interior, the zeolites behaving as sieves of molecular dimensions.[20] In fact, zeolites commercially available from Aldrich are still indicated in the catalogue as molecular sieves instead of the three-letter code applied by the International Zeolite Association to classify any zeolite. Kochi coined the term *molecular pocket* to describe the effective protection of reactive guests occurring by encapsulation inside the rigid matrix defined by zeolite inert crystal structure.[44] The most general descriptor, *reaction cavity*, refers to the importance of certain properties of the environment surrounding reacting molecules such as flexibility and deformability, dimensions, and polarity among others.[45]

3. Adsorption Procedures

Guests can gain access to the interior of the zeolite particles through the micropores following different adsorption protocols which depend on the Coulombic charge of the guest, its diffusion coefficient, its stability and persistence. The simplest adsorption procedure for neutral guests that can diffuse into the pores consists of dissolving them in an inert solvent, preferably apolar, and placing the solution in contact with thermally dehydrated zeolite samples. Adsorption can be carried out by stirring the solid in the solution at room temperature or by heating. Due to the activation energy for diffusion within the micropores, mild heating can have a very large effect facilitating the adsorption.

It has to be remarked that the pores of hydrophilic zeolites are filled by co-adsorbed water, and this water has to be desorbed before proceeding to the inclusion of any guest. Typically, co-adsorbed water can be evacuated by heating the zeolite at temperatures above 100 °C under reduced pressure or by heating at higher temperatures under atmospheric pressure. After dehydration, water can be regained partially or completely very quickly upon exposure to the ambient moisture.

For guest adsorption from solutions, the nature of the solvent has a large influence. This effect is generally rationalised in terms of competition between guest or solvent adsorption. If a solvent is strongly adsorbed within the zeolite then the co-adsorption of the guest is impeded. On the other hand, if the interaction of the solvent and the zeolite is weak then solute adsorption is favoured. The interaction of the zeolite with solvents and simple guests can be discussed quantitatively by means of calorimetry, measuring the specific heat of adsorption. In the case of polar zeolites, it can be said that, in general, apolar, aprotic solvents promote adsorption of larger amounts of the guests than protic solvents.

Incorporation of guests inside the zeolite micropores can also be accomplished in the gas phase in those cases where the vapour pressure of the guests is sufficiently high at room temperature or when the substrate to be adsorbed can be heated to appropriate temperatures. Chemical vapour deposition chambers can be used for this purpose. The absence of solvent in vapour-phase adsorption facilitates the inclusion of the guest and, in addition, the resulting samples are free of contamination from adventitious presence of residual solvent molecules.

For cationic compounds, incorporation of the cation requires the exchange with the charge-balancing cation. This is easily done when the counterbalance cation is an alkali or alkaline earth cation. The ion exchange is normally carried out in water as solvent. A single ion exchange normally leads to partial cation replacement, the percentage of ex-

 © 2004 Wiley-VCH Verlag GmbH & Co. KGaA, Weinheim

change depending on the initial solution concentration. The ion exchange is usually repeated two or three times increasing the initial solution concentration of the cationic guest to achieve a high level of ion exchange. Given that there are different positions where the charge-balancing cations can be located with respect to the zeolite framework, it can occur that, depending on the relative size of the cation being introduced with respect to the existing one, normally Na^+ or another alkali metal ion, not all the families of pre-existing cations can be exchanged. A prototypical case are faujasites in which the type-I and -II cations located inside the sodalite cages or hexagonal prisms are difficult to exchange.[20−22]

4. Ship-in-a-Bottle Synthesis

Besides incorporation of a guest from the exterior into the interior of the zeolite particle, a particular case is the in situ formation of species by adsorbing suitable precursors that will be transformed into the final guest. The zeolite may play an active role in the generation of the species by containing active sites that would interact with the guest precursor, promoting the transformation. Typically, the zeolite can have acidic or basic sites, but metallic centres can also be present. The type of transformations used to generate a trapped species can be elimination, substitution or a redox process. An example of the above reactions is the generation of organic radical cations by adsorbing the neutral precursor and abstracting a single electron. Another example is the generation of a carbocation by protonation and dehydration of an alcohol (Scheme 2).

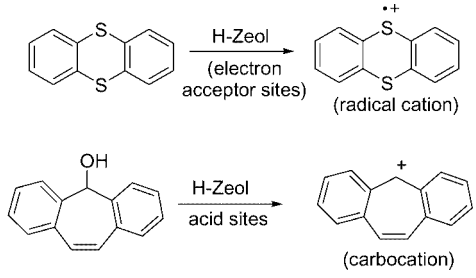

Scheme 2

In most cases in which an immediate precursor is adsorbed, this compound contains most of the bonds of the final species and there is not a large difference in the size of the precursor and the final species. However, in some cases the final species that is formed in the zeolite arises from the coupling of several precursors and there is a notable increase in the number of atoms and size of the final guest.

For this situation and using tridirectional zeolites as hosts a possibility can be envisioned in which, due to the large molecular size of the resulting guest, it remains imprisoned inside the zeolite structure after its synthesis with an impeded diffusion. The internal voids of tridirectional zeolites have a geometry encompassing large cavities interconnected only by smaller windows. The most frequent cases are faujasites X and Y, whose internal voids are formed by almost spherical cavities of 13 Å diameter, called supercages, tetrahedrally interconnected through 12-membered-ring windows of only 7.4 Å diameter. Also, zeolite Beta has oval cages (7.4 × 11 Å) defined by the crossing of two perpendicular 12-membered-ring channels (ca. 7.4 Å) whose axes are slightly shifted. For these topologies, a situation can occur in which a guest has a molecular size that, on one hand, allows it to be accommodated inside the cages but, on the other, is too big to cross the smaller cavity windows. These guests will remain immobilized by the rigid zeolite framework but they can still interact with small substrates able to diffuse through the micropores.

The term ship-in-a-bottle was most probably coined by Herron, whilst working at the R&D centre of Dupont at Wilmington, who reported the synthesis of several types of metallic complexes encapsulated within zeolites.[46] The term ship-in-a-bottle alludes to the similarity of the resulting complex imprisoned within the zeolite framework with the artistic bottles containing a ship larger than the bottle neck. However, even before this term was coined other researchers had most probably already used this methodology. Thus, as an example, Romanovskii, publishing in Russian[47−49] and Schulz-Ekloff[50,51] independently synthesised metallic phthalocyanines inside faujasite X by treating *o*-phthalodinitrile with a transition-metal-exchanged faujasite at temperatures above 200 °C, a reaction that is archetypical of a ship-in-a-bottle synthesis.

Normally, the reactions employed in a ship-in-a-bottle synthesis also work well in solution. In those cases in which a homogeneous catalyst is needed in solution, the ship-in-a-bottle synthesis requires the presence of active sites in the micropores of the zeolites. These sites can be acidic, basic or metal atoms. Reactions suitable for a ship-in-a-bottle synthesis should start from precursors of suitable size and should give high product yields, or the by-products should be small enough to be separated by solid-liquid extraction. In fact, the only purification treatment applicable to the ship-in-a-bottle synthesis is solid-liquid extraction as this treatment is based on the desorption of starting material and by-products.

An alternative and complementary procedure to the ship-in-a-bottle synthesis is to build the bottle around the ship. This consists in performing the crystallisation of the zeolite from a gel that contains the preformed guest. Two obvious limitations of this methodology is that the guest has to survive the relatively harsh conditions of the zeolite synthesis in terms of pH and temperatures for long periods, and the zeolite crystal structure should still be formed in the presence of the guest. The ease of crystallisation explains why the build-the-bottle-around-the-ship approach has been employed almost exclusively for faujasites X and Y.

An approach worthy of being explored more systematically would be exactly the reverse of a ship-in-a-bottle synthesis, the target being the synthesis of new zeolite structures by using large guests molecules that could act, in principle, as templates or structure-directing agents for the crystallisation of the aluminosilicate. A precedent of this is the

 © 2004 Wiley-VCH Verlag GmbH & Co. KGaA, Weinheim

synthesis of extra-large-pore UTD-10 using a Co^{II} complex of 1,8-bis(trimethylammonio)-3,6,10,13,16,19-hexaazabicyclo[6.6.6]icosane reported by Balkus, Jr.[16,52]

After a successful ship-in-a-bottle synthesis the main feature of the resulting zeolite containing a big organic guest inside the cavities is that the guest becomes immobilized and imprisoned inside the cages without the possibility of diffusing out of the particle. In the field of supramolecular chemistry of rotaxanes and catenanes, Stoddart has coined the term "mechanical immobilisation" to describe a situation in which one of the components of a supramolecular assembly cannot diffuse independently from the other and both of which are held in place by physical forces without the existence of a covalent bond between them.[53,54] According to this definition, the same term will apply to the system comprising a big guest encapsulated within a tridirectional zeolite since, despite the fact that there is no covalent bond connecting both entities, the guest remains entrapped, without the possibility of escape, due to physical (forbidden van der Waals atomic overlapping) forces.

Also useful when dealing with ship-in-a-bottle synthesis is Turro's "@" notation used to indicate that the guest is assumed to be located inside the particle and not exclusively or predominantly on the external surface.[55]

5. Characterisation Techniques

When performing a ship-in-a-bottle synthesis there are two crucial issues that need to be addressed independently. These two questions are the identity and purity of the encapsulated species and the location of the guests with respect to the zeolite particle.

The techniques to study the nature of the guest differ if we are dealing with a completely inorganic guest, such as metal clusters, or an organic species. In the case of purely inorganic guests X-ray diffraction, EXAFS, XANES and electron microscopy are the most important tools, together with some particular techniques such as diffuse reflectance UV/Vis, Raman and Mössbauer spectroscopy. The dispersion and size distribution of the clusters for heavy atoms can be determined by X-ray diffraction and can also be observed by electron-microscopic techniques. Even UV/Vis spectroscopy can be useful for this purpose since some typical inorganic clusters absorb visible light, the λ_{max} of the band being related to the average cluster size. IR and Raman spectroscopy on the other hand can also provide some information about the nature of the guest and, by means of probe molecules, can indirectly report on the ability of the clusters to interact with adsorbates. CO, NH_3 and pyridine are among the favourite probe molecules for Lewis-acid clusters.[56]

Spectroscopy,[57] including UV/Vis,[58] IR,[59−61] Raman[62] and multinuclear solid-state NMR,[63] is also one of the favourite techniques to determine the nature of metallic complexes or organic guests incorporated inside the zeolite pores.[64] It is worth noting that in these techniques either the zeolite framework does not give any signal or, in the worst case, at only certain spectral wavelengths. For instance, zeolites composed of silicon and not containing any other heteroatom are transparent in the UV/Vis spectrum at wavelengths longer than 220 nm. It has been reported that highly pure zeolites absorb exclusively in the vacuum UV region ($\lambda < 200$ nm). Since UV/Vis radiation penetrates deep inside the zeolite particle, it is possible to record the optical spectrum of a guest that is occluded inside the zeolite grain without interference of the zeolite framework, in a similar way as the optical spectra of organic guests are recorded in other matrices. Perhaps the major peculiarity is that diffuse reflectance techniques,[65] rather than the transmission techniques typically used for solutions, are used to record the UV/Vis spectrum.

Also, in IR spectroscopy zeolites are transparent at most IR wavelengths and, importantly, in the 3400−1300 cm^{-1} zone characteristic of the principal organic functional groups.[60] Zeolites possess a strong absorption due to the T−O bonds at around 1000 cm^{-1}, accompanied by weaker framework O−H stretching bands in the 3700−3500 cm^{-1} zone. Apart from these localised regions, the zeolite framework does not interfere in the IR absorption of the incorporated guests.

Solid-state ^{13}C NMR spectroscopy can also be used for identification purposes.[63] However, the low sensitivity of this technique makes it not very useful unless isotopically ^{13}C-labelled compounds are used or the guest loading is sufficiently high. Other nuclei such as ^{19}F, ^{29}Si, ^{31}P, etc. can be important in some particular cases.

One of the most useful approaches to determine the nature of the species resulting after the ship-in-a-bottle synthesis is to compare the reported spectroscopic properties of a species in solution with that recorded for the zeolite sample. Caution should be exercised when comparing the spectra, since some other species or by-products may have also similar properties. Particularly important as identity criteria are IR and Raman spectra taken as fingerprints due to the large number of peaks with various intensities appearing in these spectra. However, there are some cases in which the spectra of the species in other media are not available or the spectroscopic features are too general to be attributed unambiguously to a single species. One common reason for this is the instability of the species in other media. In these cases, or in general as a complementary strategy to the analysis of the spectroscopic data, one approach to determine the nature of the incorporated guest consists in dissolving the zeolite framework with concentrated hydrofluoric acid or with a mixture of HF and HNO_3 and extract the guest or the products derived from it that can thus be analysed. The limitation of this approach is the instability of the guest to this aggressive treatment. However, it is worth mentioning that some organic groups can survive HF treatment and, when this occurs, the method becomes useful. On the other hand, given the large amount of inorganic salts present in the liquor resulting after dissolving the zeolite, extraction of the guest from these solutions is problematic. High loading and low polarity of the guest facilitates the extraction.

A good practice when performing the ship-in-a-bottle synthesis is to analyse the extractable products. In principle,

 © 2004 Wiley-VCH Verlag GmbH & Co. KGaA, Weinheim

it is logical to assume that the products observed in solution, if bulky enough, will also be trapped inside the zeolite pores since it is expected that it will be formed equally outside and inside the zeolite grain. If, on the other hand, the recoverable products are not bulky enough to remain entrapped inside the zeolite, they can give a useful information on the operating reaction mechanism and their formation has to be compatible with the overall reaction scheme.

6. Evidence to Support the Internal Location of Encapsulated Guests

Once the nature of the species is known, a different question that requires specific techniques to be answered is the location (internal vs. external) of the guests. The fact that a synthesis has succeeded does not guarantee that the guest is located predominantly in the interior of the grains. In fact it would be reasonable to assume that during the synthesis a distribution of guests between the external surface and the internal pores occurs. Since the total surface area in a zeolite is predominantly internal (over one order of magnitude larger than the external surface), it is logical to consider that most of the guests are located internally, particularly when dealing with high loading samples.

However, ship-in-a-bottle syntheses conducted using amorphous silicas have demonstrated in some cases that the product can also be formed on these non-porous solids. Likewise, in the case of small- or medium-pore-size zeolites in which large guests cannot be accommodated within the interior of the micropores, the synthesis can also succeed. For these solids (either non-porous or small-pore-size zeolites) there is no doubt that the product formed has to be located exclusively on the external surface. Therefore, the formation of the product (as assessed by spectroscopic means) in a tridirectional zeolite can never be taken as evidence per se of its location.

Direct evidence of the internal location of guests can be obtained when the guests are heavy metal atoms by means of high-resolution X-ray diffraction, neutron scattering or high-resolution transmission electron microscopy. These techniques have been applied in fact to the study of zeolites devoid of any guest to address the crystallographic position of the charge-balancing cations. However, organic compounds do not normally give a clear signal or image with these techniques due to the low atomic weight of carbon. Nevertheless Baerlocher et al. have reported direct evidence of organic guest location by high-resolution X-ray diffraction.[66] Thus, the location of organic guests has to be addressed indirectly and generally by a combination of several techniques since each of them have serious limitations that can induce errors if no special precautions are taken.

It is frequently assumed that exhaustive solid-liquid extraction can be a proof of the internal location of bulky guests. Molecules small enough to diffuse through the internal pores should be recoverable by solid-liquid extraction even if they are adsorbed internally. However, this assumption has to be proved and supported by appropriate blank controls. Thus, known amounts of a compound can be adsorbed on a zeolite and then extracted to determine the efficiency of the extraction protocol. On the other hand, large guests supported on amorphous silicas can also be submitted to solid-liquid extraction to determine the efficiency of the recovery when these guests are deposited on the external surface. In any case, it can be stated that, although exhaustive solid-liquid extractions are a necessary workup in a ship-in-a-bottle synthesis, the fact that the zeolite still contains some guest after this treatment is only a weak indication of its internal location, particularly for low residual loading of the guest.

An indirect technique used to address the location of a guest in a zeolite is isothermal gas adsorption. Surface area and pore volume measurements should reflect a decrease in the specific values due to the presence of the guest occupying the internal void. However, in order to provide meaningful data isothermal gas adsorption requires prior evacuation of co-adsorbed water by thermal desorption under reduced pressure. Thermal treatment must be then carefully performed since mild desorption conditions could still leave some residual water adsorbed on strong sites and a more severe treatment may lead to the decomposition of the organic guest. Since most organic compounds start to degrade at temperatures above 300 °C, this is approximately the common limit for pre-treatment of these surface area measurements. For certain zeolites, particularly those having strongly acidic sites, 300 °C may not be sufficient to desorb all the adsorbed water completely and the porosity measurements will therefore be disguised. On the other hand, a labile organic guest may not resist prolonged heating at high temperature.

XPS provides an elemental analysis of a shallow layer (approx. 20 nm depth for soft X-rays) of the zeolite grain. XPS analysis can be quantitative by integrating the area of the peak corresponding to each element and calibrating the response of each atom using standards. A technique that is used in materials science to determine the depth of a metal corrosion is to combine XPS analysis and fast atom bombardment that produces the disappearance and ablation of the outermost layer exposed to the high-energy sputtering. The Ar^+ ion can be used for this purpose. If the combination of XPS and Ar^+ ion sputtering is applied to zeolites, a map of the elemental composition vs. the time of exposure to the Ar^+ beam is obtained. The time of the Ar^+ sputtering can be related to the depth of penetration from the external surface to the interior of the zeolite particle due to the destruction and evacuation of the exposed zeolite framework. Therefore, a plot of the percentage of a given element vs. penetration depth can be obtained. If the percentage of C atoms with respect to the total of other atoms (O + Si + Al) increases along the distance from the particle surface, this can indicate that the guest is located predominantly in the interior of the grains. Figure 1 shows a reported example of the use of XPS/sputtering for the purpose of mapping out the C composition along the particle radius.

The limitation of the XPS combined with fast atom sputtering technique may arise from the texture and mor-

 © 2004 Wiley-VCH Verlag GmbH & Co. KGaA, Weinheim

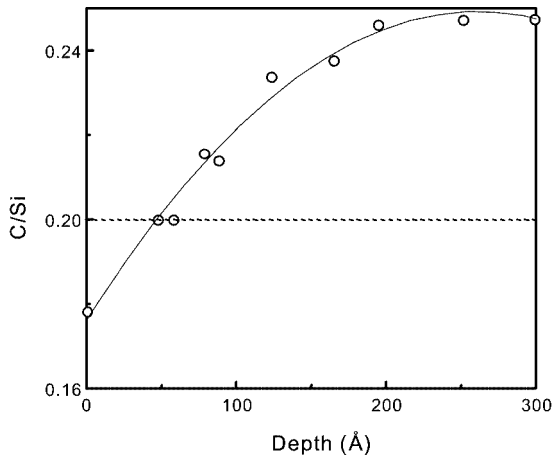

Figure 1. XPS analysis of the atomic C/Si ratio along the depth of penetration on a zeolite particle containing tris(4-methoxyphenyl)methyl cation (taken from ref.[67]; reprinted with permission; © 1996 American Chemical Society)

phology of the zeolite samples. While for continuous and flat surfaces, such as those of metals, the above technique really provides a map of the composition along the penetration in the material, when working with powders composed of individual particles of micrometer size the situation is more complicated. Depending on the sample preparation and how the powder is presented, the differences in the composition along the time of sputtering may not really reflect differences along the zeolite particle depth, but rather differences from particle to particle. Differences in the packing of the particles, sedimentation and other aspects related to the agglomeration of a multitude of particles, rather than penetration inside an individual zeolite particle, can also be responsible for differences in the XPS upon Ar^+ sputtering.

For many zeolites, the location of charge-balancing cations in as-synthesised, highly crystalline samples has been conclusively demonstrated by high-resolution X-ray diffraction and neutron scattering. If a guest is replacing a significant fraction of these structural cations, it can be assumed that they will occupy the initial positions of the original cations. Even if the crystallographic positions are not exactly the same for the initial cation and the replacing guest, it is reasonable to assume that the positions have to be as close as possible in order to minimize the electrostatic energy. Thus, if a large fraction of a cation located internally is replaced by a bulky guest, the guest has to be also within the micropores.

A related case is that of protonic zeolites having acidic hydroxy ≡Si−(OH)−Al≡ bridges. In IR spectroscopy, different framework hydroxy groups may exhibit different absorptions. In particular, for fully protonic HY zeolite there are distinctive IR hydroxy bands related to external silanols (3740 cm^{-1}), acidic bridged OH inside the sodalite cage (3670 cm^{-1}), OH in the supercage (3650 cm^{-1}), and OH in the sodalite hexagonal prisms (ca. 3550 cm^{-1}).[56] These peaks appear as sharp absorption bands in the spectra of dehydrated HY samples, and some other OH groups can also be present depending on the type of sample and the presence or not of non-framework Al. If as a result of a ship-in-a-bottle synthesis a bulky guest is located in the Y supercage replacing these protons totally or partially, then quantification of the peak corresponding to the vibration of this type of hydroxy groups in the IR spectra for exactly the same weight of the zeolite before and after the ship-in-a-bottle synthesis should reflect the decrease in the population of these acidic OH groups. Since the location of these groups is known, their replacement requires that the formed guest occupies a position close to the original OH.

However, also in this case there are some artifacts that can influence the intensity of the OH groups without being actually replaced. Since these OH groups are acidic, the presence of residual amounts of solvents, reactant, or by-products may broaden the acidic OH peak considerably, giving the impression that its intensity has decreased or making the peak integration inexact. In order for these measurements to be valid, the spectrum of the sample after the ship-in-a-bottle synthesis has to be recorded under conditions in which nothing alters the OH groups. Blank controls in which a zeolite sample is submitted to an analogous ship-in-a-bottle treatment but without a necessary reagent to form the entrapped guest is also a good practice to compare the IR spectra with and without guest.

B. Applications of Zeolite-Embedded Guest Systems Obtained by Ship-in-a-Bottle Synthesis

1. Ship-in-a-Bottle Systems as "Zeozymes"

There are some enzymes in which a metallic complex is embedded with the tridimensional structure of a protein. The metallic complex acts as the catalytic site while the access of the substrate to the site is controlled by the surrounding protein skeleton. Other properties such as solubility and the micropolarity of the environment site isolation are also determined by the protein. Inspired by the enzyme constitution, it is possible to imagine an analogous system comprising a catalytically active metallic complex but embedded within an inorganic matrix. The term "zeozyme" was constructed by the combination of the words *zeolite* and *enzyme* and refers to the latter possibility.[15,68,69] There is no doubt that this application of ship-in-a-bottle synthesis will attract a renewed interest in coming years motivated by the understanding of new enzymatic systems.

In this context, probably the first example of a synthesis termed as a ship-in-a-bottle synthesis was a Co^{II}−salen complex that was prepared by adsorbing the flexible salen ligand into a Co^{II}-ion-exchanged zeolite.[46]

Transition metal complexes of salen are widely used as catalysts in homogeneous solution for a large number of reactions such as epoxidation of alkenes, epoxide ring aperture, nucleophilic additions to carbonyl and imine groups, CO_2 fixation, etc.[70−74] The term *salen* for the ligand is the acronym standing for bis(salicylidene)ethylenediamine. These salen complexes are a particular case of Schiff-base

 © 2004 Wiley-VCH Verlag GmbH & Co. KGaA, Weinheim

complexes, since one of the coordination bonds between the metal atom and the ligand occurs through the imine group that is known in organic chemistry as the Schiff base.

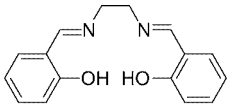

salen

In contrast to the flexibility of the salen ligand (particularly through the ethylene bridge), the resulting metal complex is rigid and becomes entrapped inside the zeolite cavities.[46] Encapsulated Co^{II}−salen complex shows affinity for O_2, forming a 1:1 adduct exhibiting a somewhat lower binding equilibrium than in solution, but an excellent resistance to undergo autooxidation even at elevated temperatures.[46] This system has a resemblance to that of hemoglobin, the Co^{II}−salen acting as a prosthetic group binding oxygen reversibly and the zeolite behaving as an "*inorganic*" protein. This example developed by *bioinspiration* is the origin of the word *zeozymes*.

Since Co^{II}−salen many other transition-metal−salen complexes, such as those of $V{=}O^{2+}$ [75] and iron,[76] have been reported. The influence of the preparation procedure and reaction temperature on the efficiency of the complex formation has been studied for Rh^{III}−salen encapsulated in zeolites X and Y.[77,78]

Jacobs has used a biomimetic approach to design encapsulated mono- and polynuclear iron catalysts with activity similar to *monooxygenase* metalloproteins that catalyse the incorporation of oxygen atoms from dioxygen into organic substrates.[79]

Metallophthalocyanines can also be entrapped inside faujasites X and Y by a ship-in-a-bottle synthesis starting from *o*-phthalodinitrile and the transition-metal-exchanged zeolite or by a build-the-bottle-around-the-ship strategy. Balkus, Jr. has made significant contributions in this area and has written several reviews on the preparation and catalytic activity of encapsulated metallophthalocyanines.[75,80] As mentioned earlier in the introductory sections, after the pioneer work of Romanovskii and Schulz-Ekloff, Herron coined the term ship-in-a-bottle synthesis and, as well as the first metallic complexes, he also prepared iron−phthalocyanine inside faujasites X and Y by thermal tetramerisation of *o*-phthalodinitrile templated by iron ions (Scheme 3).[81] His idea was to mimic the activity of cytochrome P 450, which is able to oxidize alkanes with molecular oxygen, but replacing the flexible, but labile protein surrounding the prosthetic iron centre by the rigid and robust zeolite framework.

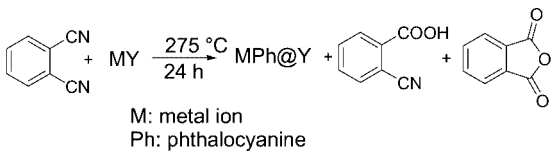

Scheme 3

The molecular size of the flat, relaxed geometry of the phthalocyanine macrocycle (about 14 Å of diameter) is too large to be accommodated inside the supercages of faujasites, whose free volume is also a function of the nature of the charge-balancing cations occupying site-III positions in the supercage. Since it is a fact that the ship-in-a-bottle synthesis of phthalocyanines is feasible, it has been proposed that the heteroaromatic macrocycle adopts a roof-like, rather than a flat, conformation to fit inside the cavities. Figure 2 shows a molecular modelling of Cu^{II}−phthalocyanine inside an ideal all-silica faujasite. Furthermore, in an interesting report, the synthesis of much bulkier iron−tetra-*tert*-butylphthalocyanine (estimated diameter of 19 Å) has been successfully accomplished starting from pre-encapsulated $[HFe_3(CO)_{11}]$ iron−carbonyl clusters and 4-*tert*-butyldicyanobenzene inside NaY.[82] Based on the characterisation by EXAFS, Mössbauer, FT-IR and diffuse-reflectance UV/Vis spectroscopy, the authors propose that the tetra-*tert*-butylphthalocyanine is located inside the zeolite supercage in a conformation far from planar.[82] Due to the steric compression compared to the parent iron−phthalocyanine, the tetra-*tert*-butyl derivative exhibits higher activity and selectivity toward terminal hydroxylation of *n*-hexane and *trans*-epoxidation of stilbenes with PhIO. This higher regioselectivity indicates a preferential attack of oxygen in the active Fe=O species on the terminal carbon atoms of the substrate. It would be of interest to gain a deeper understanding of the conformation, strain and location of this very large phthalocyanine complex.

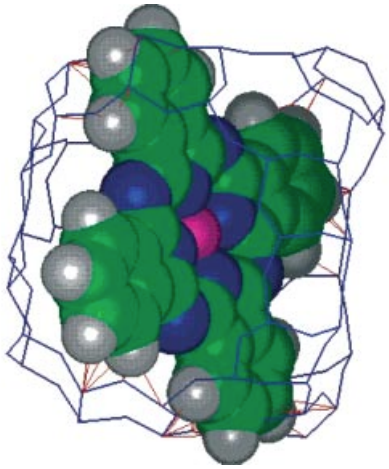

Figure 2. Molecular model showing copper−phthalocyanine encapsulated inside the supercage of zeolite Y (see also ref.[83])

An approach to avoid forcing the steric compression of phthalocyanine has been to use novel zeotypes with pore sizes larger than those of conventional faujasites. Co^{II}−phthalocyanine has been encapsulated in the large cavities of zeolite EMT at a loading of one complex for every six supercages.[84] The resulting Co−phthalocyanine@EMT exhibits a turnover number for the oxidation of ethylbenzene with molecular oxygen of about 22000. Likewise, Jacobs and co-workers have reported the

 © 2004 Wiley-VCH Verlag GmbH & Co. KGaA, Weinheim

encapsulation of iron−phthalocyanine inside large-pore-size VPI-5, which is a monodirectional aluminophosphate of extra-large pore size.[85−87] The VPI-5-occluded iron−phthalocyanine acts as a catalyst for alkane oxygenation using iodosobenzene. Jacobs has also reported an interesting further elaboration of the encapsulated phthalocyanine by preparing a composite in which the fibres of a partially crosslinked poly(dimethylsiloxane) polymer holds the zeolite containing the phthalocyanine complex.[88] This poly(dimethylsiloxane)/zeolite composite acts as a membrane at the interphase between aqueous hydrogen peroxide and hydrophobic cycloalkene and can promote the catalytic oxidation of alkenes, mimicking again the activity of cytochrome P 450.[88]

In an attempt to increase the stability and the turnover numbers of the encapsulated metallophthalocyanines, Balkus, Jr. described the synthesis of Ru^{II}−perchloro-[89] and -perfluorophthalocyanine[75,90−92] inside zeolite X. The methodology followed in this case was to build the bottle around the ship.[91] These perhalophthalocyanines show activity for the oxidation of cyclohexane with *tert*-butyl hydroperoxide and cyclohexene and stilbene with oxygen.[92] The perfluorinated phthalocyanine shows no signs of deactivation, in contrast to the nonfluorinated analogues.[91]

Related to encapsulated metallophthalocyanines are the attempts of ship-in-a-bottle synthesis of *meso*-tetrasubstituted porphyrins that formally possess the same aromatic macrocycle. This synthesis has been attempted by condensation of pyrrole with aldehydes (Scheme 4).[93] Although porphyrins are expected to be more flexible than phthalocyanines, and porphyrins are among the products observed in the solution during the ship-in-a-bottle synthesis, spectroscopic characterisation reveals that it is a precursor of the protoporphyrin type that is present inside the zeolite. It has been assumed that the lower thermodynamic stability of porphyrins as compared to phthalocyanines makes their ship-in-a-bottle synthesis unsuccessful, particularly the last oxidative aromatisation step that requires the achievement of planarity. In this context, and given the number of enzymes having metalloporphyrins and their interesting catalytic activity, it would be of interest for the development of the zeozyme concept to explore other zeolites with larger pores as hosts for porphyrins.

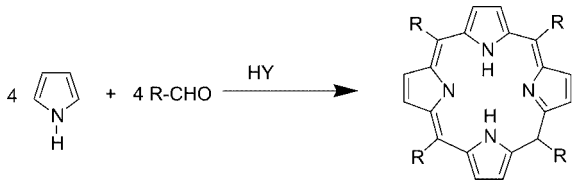

Scheme 4

There are metalloporphyrins, however, that can be encapsulated within faujasite by using the build-the-bottle-around-the-ship approach, crystallising the zeolite gel around the porphyrin. One example is the preparation of the metallotetrakis(*N*,*N*,*N*-trimethylanilinium)porphyrin cation entrapped in faujasite Y that was used as a catalyst for the oxidation of cyclohexene.[94] The latter strategy of crystallising the zeolite around the guest may work well for faujasites for which no structure-directing agent is required. In this case, the metallic complex has to be sufficiently robust to resist the hydrothermal zeolite crystallisation (typically above 100 °C and alkaline pH for at least a few hours) and has to have a relatively high solubility in water.

2. Ship-in-a-Bottle Systems as Catalysts

Moving further from the initial zeozyme concept to the broader use in catalysis, one general methodology to transform a successful homogeneous catalyst into a heterogeneous one consists in immobilizing it onto a large-surface-area support. Immobilisation of the homogeneous catalyst permits its recovery from the reaction mixture and its reuse in consecutive runs. Immobilisation also allows the design of continuous flow reactors in which the catalyst is in a different phase than the reactants and products. In this context, the ship-in-a-bottle methodology has been used since the early days to prepare efficient solid catalysts.

a. Hydrogenation

Carbonylmetal clusters have been synthesised in zeolites, and remain trapped in the cages, by the ship-in-a-bottle methodology.[95,96] Thus, neutral carbonyl clusters of Pd, Rh and Ir have been synthesised in the α cages of Y zeolite. The general procedure involves an ion-exchange process of amine complexes such as $[Pt(NH_3)_4]^{2+}$, $[Pd(NH_3)_4]^{2+}$, $[Rh(NH_3)_5Cl]^{2+}$, $[Ir(NH_3)_5Cl]^{2+}$, and even an $[Rh(H_2O)_6]^{3+}$ complex, with NaY zeolite, followed by calcination, reduction and CO treatment under different reaction conditions. In this way, the ship-in-a-bottle synthesis of $Pd_{13}(CO)_x$, $Rh_6(CO)_{16}$, and $Ir(CO)_3Cl$ has been successfully achieved.[97−100] When a more basic faujasite zeolite (NaX) is used, anionic carbonylmetal clusters of platinum $\{[Pt_{15}(CO)_{30}]^{2-}\}$, rhodium $\{[Rh_6(CO)_{15}]^{2-}\}$, and dimetallic Pt−Rh $\{[PtRh_5(CO)_{15}]^{-}\}$, and Fe−Rh $\{[Fe_2Rh_4(CO)_{16}]^{2-}\}$ can also be prepared inside the supercavities.[101−104]

Some mononuclear Ir species can migrate through the channels and cavities of the zeolites when heated. After CO treatment they give either neutral carbonyl clusters such as $[Ir_4(CO)_{12}]$ or $[Ir(CO)_{16}]$ when using zeolite NaY,[105−108] or anionic clusters when zeolite NaX is used.

Encapsulated metal−salen complexes have also been used as catalysts for reactions different from those catalysed by enzymes. Hölderich and co-workers have prepared Pd^{II}− and chiral Co^{II}−salen complexes encapsulated within zeolites and used them as carbonyl hydrogenation catalysts.[109] Encapsulated Pd^{II}−salen is able to promote the hydrogenation of methyl pyruvate with complete selectivity at conversions higher than 70% and that of methyl acetoacetate with a product selectivity of 92% at about 50% conversion, while bulkier substrates such as isopropyl and *tert*-butyl pyruvate gave less or no conversion.[109]

 © 2004 Wiley-VCH Verlag GmbH & Co. KGaA, Weinheim

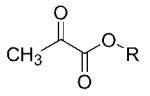
alkyl pyruvate

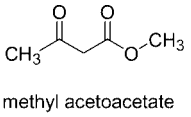
methyl acetoacetate

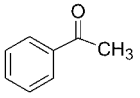
acetophenone

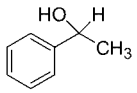
1-phenylethanol

In the case of the chiral Co^{II}–salen complex, although the selectivity for the conversion of acetophenone to 1-phenylethanol using the encapsulated Co complex was complete, the enantiomeric excesses at 25 °C were very low (8%) although higher than those of the homogeneous complex at lower temperatures (−10 °C). In agreement with the work on Mn^{III}–salen complexes, which will be mentioned shortly, the presence of large substituents on the ligand also precludes the ship-in-a-bottle synthesis of the Co complex and the resulting complex is located exclusively on the external surface, leading to enantiomeric excesses lower than those achieved with the same complex in homogeneous phase.[109]

Heterogeneous hydrogenation catalysts based on incarcerated metallic complexes other than salen have also been widely used. A complex of (cyclooctadiene)Rh^{I} and prolinamide or *N-tert*-butylprolinamide has been prepared inside zeolite, the resulting solids exhibiting a higher specific activity for the hydrogenation of alkenes than their homogeneous counterparts.[110] For the enantioselective hydrogenation of methyl (*Z*)-2-acetamido-3-phenylacrylate the enantiomeric excess was much higher with the heterogenized catalyst than with the homogeneous complex.

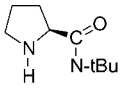
N-tert-butylprolinamide

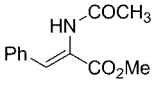
methyl (*Z*)-2-acetamido-3-phenylacrylate

b. Acid Catalysis

The heteropolyacid $H_3PW_{12}O_{40}$ is an almost spherical cluster of about 8 Å diameter. Its Keggin structure, with a central tetrahedral PO_4 core and internal tungsten atoms, makes this compound very rigid and undeformable preventing it from crossing the 7.4 Å windows of faujasites. One important property of phosphotungstic acid is its strong acidity, even higher than that exhibited by pure sulfuric acid due to the negative charge delocalisation through the outer oxygen layer of the structure. In spite of this superacidity, phosphotungstic acid has been synthesised inside the cavities of zeolite Y without destroying the crystal structure. ^{31}P MAS NMR spectroscopy shows a broad signal at $\delta = -14.4$ ppm that is assigned to the Keggin heteropolyacid interacting with the zeolite Al atoms. The encapsulated heteropolyacid exhibits high activity for *m*-xylene isomerisation and disproportionation.[111]

c. Oxidation Catalysis

Picolinic acid as a ligand for Fe^{III} was used successfully by Barton for the oxidation of cyclohexane by hydrogen peroxide.[112] Garcia and co-workers reported the encapsulation of iron picolinate inside a series of zeolites and found that the zeolites containing the encapsulated picolinate complex are efficient and reusable heterogeneous catalysts for the oxidation of cyclohexane to cyclohexyl hydroperoxide, cyclohexanol and cyclohexanone.[113] Mordenite was found to be the best host for this purpose.[113] Analogously, vanadyl picolinate encapsulated within NaY is also active for the oxidation of alkanes, alcohols and benzene with hydrogen peroxide.[114,115] Jacobs has also reported the ship-in-a-bottle synthesis of an iron complex of a tetradentate N_4 ligand derived from 2-pyridinecarboxamide that is able to effect the oxidation of cyclohexane to cyclohexyl hydroperoxide as well as cyclohexanol and cyclohexanone.[116] In most of these iron oxidations it is widely assumed that the catalytically active species is a high-valent $Fe^{IV}=O$ species.

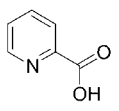
picolinic acid

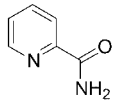
2-pyridinecarboxamide

Many related ligands can be easily derived from salen by modifying the ethylenediamine bridge or by introducing substituents in the salicylidene aromatic moiety and they can be easily obtained by the condensation of a primary diamine with salicylaldehyde. This reaction is normally carried out by stirring an ethanolic solution of the salicylaldehyde and the diamine at room temperature until the product has formed (Scheme 5).

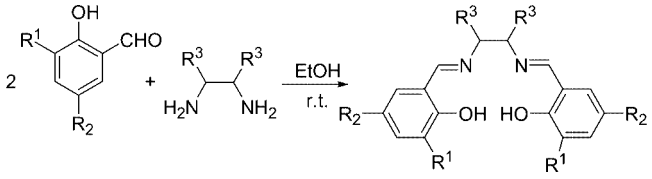

Scheme 5

Chiral salen ligands can be easily obtained if one uses a single enantiomer of a chiral diamine, as has been reported in solution. In fact the most important application of salen complexes is as asymmetric catalysts for the enantioselective epoxidation of alkenes using the manganese complex of bis(2,4-di-*tert*-butylsalicylidene)-1,2-cyclohexanediamine that is commonly known as the Katsuki–Jacobsen catalyst.[117,118]

In 1997, and almost simultaneously, two independent communications reported the ship-in-a-bottle synthesis of a chiral manganese Schiff-base complex inside faujasite and

 © 2004 Wiley-VCH Verlag GmbH & Co. KGaA, Weinheim

EMT zeolites and used them as enantioselective catalysts for the heterogeneous epoxidation of alkenes.[119] (*Z*)-Methylstyrene and indene are two favourite substrates for the study of the enantioselectivity of asymmetric epoxidation. The enantiomeric excesses obtained with these zeolite-bound Mn^{III}−salen complexes were only modest (about 60%), particularly compared to the enantiomeric excesses that can be achieved in solution for the bis(2,4-di-*tert*-butylsalicylidene) derivative. It has to be noted, however, that due to steric restrictions the actual chiral salen ligand encapsulated within the Y zeolite cages lack the bulky *tert*-butyl substituents. Molecular modelling predicts that the tetra-*tert*-butyl-substituted salen ligand is too large to be accommodated inside the zeolite Y supercage. Figure 3 shows a visualisation of the Mn^{III}−salen complex obtained by freezing the geometry of zeolite Y devoid of framework Al to the crystallographic positions and optimising the geometry of the complex at the semiempirical MNDO level. A recent report, however, has challenged this modelling by claiming the preparation of the tetra-*tert*-butylsalen derivative inside the supercages of zeolite Y.[120] The authors have claimed to be able to prepare the encapsulated complex by adsorbing the preformed bulky ligand into the zeolite pores, something that molecular modelling predicts should not be possible. Recently, chiral vanadyl−di-*tert*-butylsalen complexes have been grafted in the walls of MCM-41.[121]

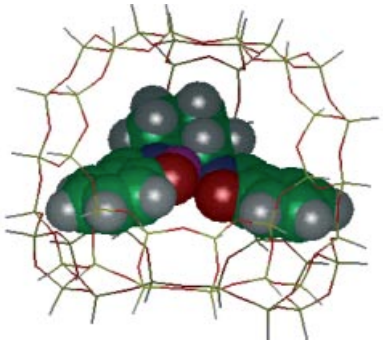

Figure 3. Molecular model of chiral Schiff-base Mn^{III}−bis(salicylidene)cyclohexanediamine lacking *tert*-butyl groups encapsulated within zeolite Y

The low enantiomeric excesses obtained using zeolite-encapsulated complexes can be rationalised considering that the asymmetric induction requires, as determined in solution, a precise "*side-on*" approach of the alkene to the oxomanganese epoxidation centre, the role of the bulky *tert*-butyl substituents being to impede the approach from other directions (Scheme 6). This process is completely disrupted when the complex is encapsulated in the zeolite, the geometry of the voids being the main factor dictating the possible approaches between the guest and the alkene. In addition, the presence of other Mn species in the solid, particularly as Mn^{II}, that can act as unselective epoxidation centres, has also been determined by EPR spectroscopy and electrochemistry.[122,123]

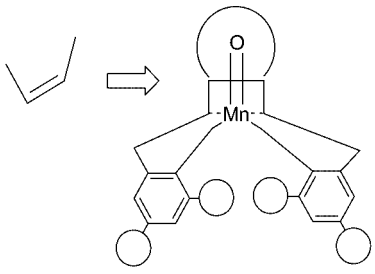

side-on approach of the alkene to the encumbered Mn=O bond

Scheme 6

A Co^{II}−Schiff-base complex derived from *N*,*N*′-bis(salicylidene)-1,2-diphenylethylenediamine has also been encapsulated within zeolite by the template method and studied as co-catalyst for the ruthenium-catalysed oxidation of benzylic alcohols.[124] The resulting zeolite-bound complex shows several distinctive facts with respect to the same complex in solution including: (i) higher reaction rates due to site isolation; (ii) no need for triphenylphosphane as axial ligand; and (iii) relative lack of influence of the solvent in which the reaction is carried out.[124]

3. Ship-in-a-Bottle Systems as Photocatalysts

Besides being catalysts for thermal reactions, zeolite-embedded guests prepared by ship-in-a-bottle synthesis have also been widely used as photocatalysts. In this latter case, the solid absorbs light and converts it into chemical energy by generating a highly reactive species. The photocatalytic generation of the $^{\cdot}OH$ radical from O_2, H_2O_2 or other sources is an emblematic example of conversion of light into chemical energy. Photocatalysis is obviously less developed than catalysis but is showing great promise for air and water purification.

In the following sections we will describe examples of ship-in-a-bottle-prepared systems whose use as a photocatalyst has been described.

a. Transition Metal Complexes

i) Tris(bipyridyl)ruthenium and Related Poly(pyridyl) Complexes

Tris(bipyridyl)ruthenium was one of the first large guests for which a ship-in-a-bottle synthesis was reported. The initial synthetic procedure by Lundsford et al.[125] was later improved by Dutta.[126] The method consists of the initial introduction of $[Ru(NH_3)_4]^{3+}$ followed by addition of an excess of 2,2′-bipyridine and prolonged heating at 220 °C. The excess of ligand is removed by continuous solid-liquid extraction. Calzaferri has shown that the purity of the encapsulated $[Ru(bpy)_3]^{2+}$ complex decreases upon increasing the loading of the complex due to diffusion problems.[127]

 © 2004 Wiley-VCH Verlag GmbH & Co. KGaA, Weinheim

Other species present as impurities have an $[Ru(bpy)_n(NH_3)_{6-2n}]^{2+}$ ($n < 3$) stoichiometry. However, essentially pure samples of included $[Ru(bpy)_3]^{2+}$ can be obtained for loadings lower than one complex for every two supercages.[127]

Tris(bipyridyl)ruthenium is a complex that exhibits a high phosphorescence quantum yield. Since this phosphorescence is quenched by oxygen, a sensor based on this ruthenium complex has been developed.[128] $[Ru(bpy)_3]^{2+}$ has also been a favourite probe molecule for studies dealing with photoinduced electron transfer as well as in basic studies on long charge storage.[125,126,129,130] These studies rely on the easy emission detection in opaque powders.

In an attempt to increase the efficiency of the charge separation, Dutta and co-workers reported the ship-in-a-bottle synthesis of tris(bipyridyl)ruthenium in nanometric zeolite X.[139] Caution has to be taken in this case to avoid acid formation during each step of the ship-in-a-bottle synthesis, since otherwise the crystallinity of the nanoscopic X zeolite is considerably reduced and the advantages of the use of nanocrystals disappear. Under conditions in which 90% of the crystallinity is preserved, it was observed that the photoinduced electron transfer between $[Ru(bpy)_3]^{2+}$ and methylviologen is about a factor of two more efficient in nanocrystals than in conventional micrometer-sized crystallites.[139]

Besides tris(bipyridyl)ruthenium(II) other metal−polypyridyl complexes such as $[Co(bpy)_3]^{2+}$,[140] $[V{=}O(bpy)_2]^{2+}$,[141] and $[Fe^{II}(bpy)_3]^{2+}$ [79,142] have also been synthesised. In the case of $[Fe^{II}(bpy)_3]^{2+}$, Bossmann, Braun and co-workers have studied the use of the resulting solid as a heterogeneous photo-Fenton catalyst.[142] In the Fenton reaction, aggressive ·OH radicals are formed by reaction of Fe^{II} with hydrogen peroxide [Equation (1)]. Then, this ·OH radical can initiate the oxidative degradation of the vast majority of organic molecules either by C−H hydrogen abstraction, nucleophilic addition to unsaturated multiple bonds or by single-electron oxidation. The Fenton reaction requires a stoichiometric amount of iron(II) with respect to the ·OH radical. A variant of this Fenton process that only requires catalytic amounts of Fe is the photo-Fenton reaction in which the Fe^{III} formed in Equation (1) is reduced back to Fe^{II} by light, with the additional generation of a second ·OH radical. One problem of this photochemical reaction is that the aquated iron ion has a low extinction coefficient in the visible region and therefore UV light is required. The advantage of the use of the $[Fe^{II}(bpy)_3]^{2+}$ complex is that it absorbs visible light with a high molar absorptivity, thus increasing the efficiency and practicality of Equation (2).

$$Fe^{2+} + H\text{-}OO\text{-}H \longrightarrow Fe(OH)^{2+} + {\bullet}OH \quad (1)$$

$$Fe^{3+} + H_2O \xrightarrow{h\nu} Fe^{2+} + H^+ + {\bullet}OH \quad (2)$$

In a further refinement, these authors have co-doped the encapsulated $[Fe^{II}(bpy)_3]^{2+}$ with TiO_2 clusters that have been prepared after the ship-in-a-bottle synthesis of $[Fe^{II}(bpy)_3]^{2+}$ by hydrolysis of $TiCl_3$.[142] Apparently, the presence of TiO_2 enhances the photocatalytic activity of the iron complex by acting as an electron relay from the donor to the iron(III) complex. The photocalytic activity of this $[Fe^{II}(bpy)_3]^{2+}$ system in acidic aqueous solutions has been studied in the presence and absence of H_2O_2 using 2,4-xylidine, a recalcitrant non-biodegradable pollutant, as model compound.

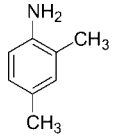

2,4-xylidine

Fundamental studies on electron transfer within the zeolite matrix have been done by using metal−polypyridyl complexes. For instance, Fukuzumi and co-workers have also synthesised $[Fe(bpy)_3]^{2+}$ encapsulated inside NaY at a loading of one molecule per 10 supercages and converted it into $[Fe(bpy)_3]^{3+}$ by chemical oxidation with chlorine.[143] Observation of an extremely slow reaction between ferrocene and encapsulated $[Fe(bpy)_3]^{3+}$ has led to the suggestion of the occurrence of a long-range electron transfer through the zeolite framework.[143] An analogous *through-framework* electron transfer between tris(bipyridyl)ruthenium and methylviologen has been demonstrated using ITQ-2 as zeolite (Scheme 7).[130] In this case, the zeolite defines a topology comprising external cups and internal 10-membered channels. The (polypyridyl)ruthenium complex is located in the open cups of the zeolite while viologen as electron acceptor is incorporated inside the 10-membered-ring channels of the zeolite. Upon photoexcitation of $[Ru(bpy)_3]^{2+}$, an electron transfer to encapsulated MV^{++} occurs.

b. Organic Cations

i) Pyrylium and Derivatives

The first ship-in-a-bottle syntheses in zeolites were used to prepare encapsulated metallic complexes. In most of these early cases, the key feature in the encapsulation was

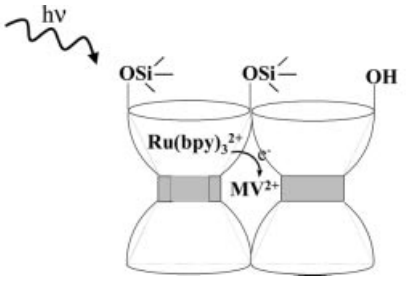

Scheme 7

 © 2004 Wiley-VCH Verlag GmbH & Co. KGaA, Weinheim

the formation of a coordinative bond between a metal ion and a heteroatom having lone electron pairs.

In contrast to this, the hallmark of organic synthesis is the formation of new C−C bonds by coupling of nucleophilic and electrophilic reagents in the absence of a metal. In this regard, one of the first ship-in-a-bottle *organic* (as opposed to coordination chemistry) synthesis was the encapsulation by Corma, Garcia and Miranda of the 2,4,6-triphenylpyrylium ion inside zeolite HY.[144] This pyrylium ion is obtained in solution by treating 2 equiv. of chalcone with acetophenone in the presence of strong liquid Brönsted acids, such as perchloric or tetrafluoroboric acid.[145] The reaction mechanism involves the aldol reaction of chalcone and acetophenone, followed by aromatisation by hydrogen transfer. By emulating this solution reaction successfully, but using the Brönsted acid sites of microporous HY zeolite instead of a liquid acid, it was possible to obtain the encapsulated 2,4,6-triphenylpyrylium (Scheme 8). Alternatively, the chalcone can be synthesised in situ catalysed by the same HY zeolite by allowing acetophenone and benzaldehyde to react.

The above procedure requires HY samples of sufficient acidity to promote the aldolic condensation. Recently, Miranda, Braun and Bossmann have reported[146] a more simple procedure to perform the ship-in-a-bottle synthesis of 2,4,6-triphenylpyrylium. This recent process has the advantage of starting from the commercial HSO_4^- salt of 2,4,6-triphenylpyrylium and commercial NaY in aqueous suspension to achieve the encapsulation of the dye. Formally, the whole process is a true ion exchange in aqueous solution of a bulky, size-excluded 2,4,6-triphenylpyrylium ion by internal Na^+. All the available information indicates that under these conditions the pyrylium ion undergoes a hydrolytic ring opening and the more flexible 1,3,5-triphenyl-2-pentene-1,5-dione migrates inside the zeolite supercage (Scheme 9). Once inside, dehydration by mild baking of the solid reforms the pyrylium heterocycle. Among the many advantages of this improved procedure, the major ones are the purity reproducibility of the encapsulated 2,4,6-triphenylpyrylium, the use of neutral, commercial NaY and the possibility to control the loading of the pyrylium cation in a reproducible way to achieve essentially a complete filling of one dye molecule per supercage. Concerning reproducibility, the crucial step is the baking of the zeolite to accomplish the complete cyclisation of the pentenedione.

2,4,6-Triphenylpyrylium salts such as those with BF_4^-, HSO_4^- and ClO_4^- are soluble in organic solvents such as CH_2Cl_2, CH_3CN and alcohols. These salts of 2,4,6-triphenylpyrylium are well-known electron-transfer photosensitizers in organic solvents.[147] Analogously, 2,4,6-triphenylpyrylium@Y is a solid photocatalyst that is able to promote photoinduced electron-transfer processes in organic solvents, such as one-way (*Z*)/(*E*) isomerisation of stilbene[148,149] and Diels−Alder cyclodimerisation of 1,4-cyclohexadiene.[150] Moreover, 2,4,6-triphenylpyrylium@Y can also be an effective photocatalyst in aqueous solution while, as mentioned above, simple salts of TP^+ cannot be used in water at neutral or basic pH due to the hydrolytic ring opening. Thus, one interesting feature of the encapsulation is that the occluded 2,4,6-triphenylpyrylium becomes persistent in water and can be used as a solid photocatalyst in water.[151] When encapsulated inside zeolites, 2,4,6-triphenylpyrylium has been found to be an efficient photocatalyst for the degradation and partial mineralisation of pesticides in water upon solar light irradiation. Some of the pesticides that can be degraded by the photocatalytic irradiation of encapsulated 2,4,6-triphenylpyrylium are phenol, aniline, 4-chlorophenoxyacetic acid,[152] methylparathion,[153] fenvalerate[154] and propoxur.[155] The case of 2,4,6-triphenylpyrylium@Y constitutes an example of the opportunities of encapsulated guests in photocatalysis.

Evidence supports the proposition that the photocatalytic mechanism involves the generation of ·OH radicals formed through photoinduced electron transfer from water

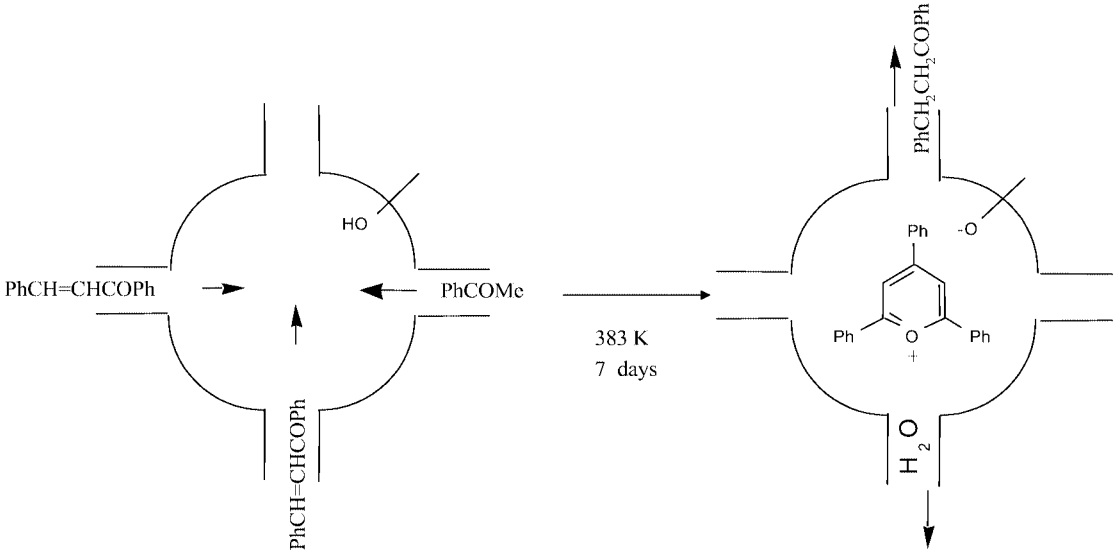

Scheme 8

 © 2004 Wiley-VCH Verlag GmbH & Co. KGaA, Weinheim

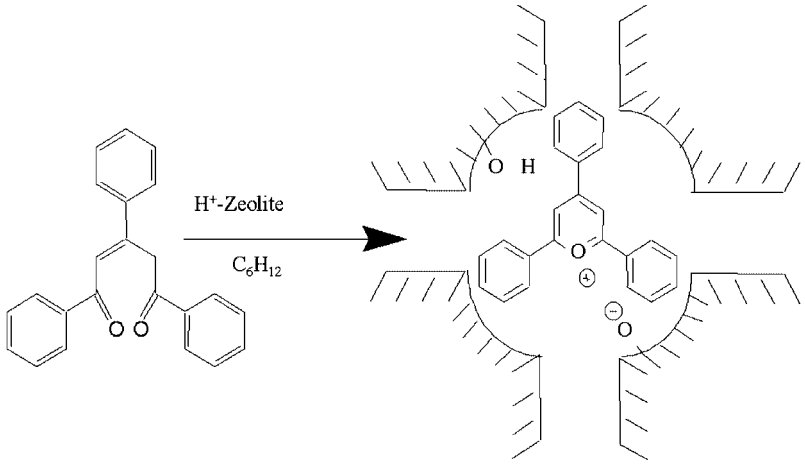

Scheme 9

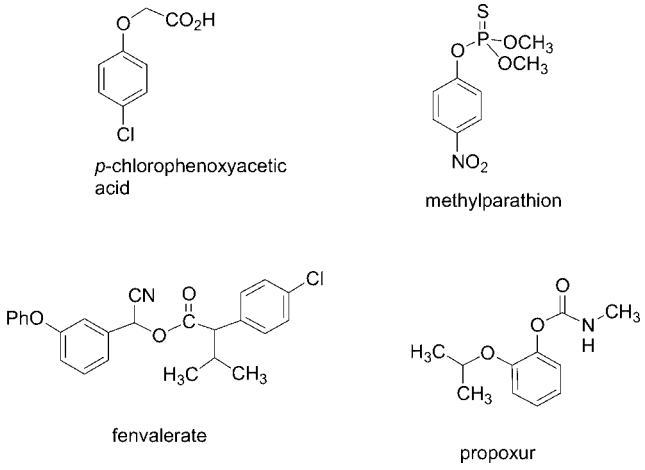

to the dye in its excited state.[151] Interestingly, encapsulation also protects the dye from self-degradation by ·OH. Even irradiation of a suspension of 2,4,6-triphenylpyrylium encapsulated within zeolites in distilled water produces the build-up of a 10^{-2} to 10^{-3} M concentration of H_2O_2.[151] This lack of self-degradation has been rationalised based on the molecular modelling that indicates that the zeolite framework binds the 2,4,6-triphenylpyrylium tightly and it does not allow the size increase required in the nucleophilic attack (Scheme 10).[151] Self-degradation is a common phenomenon that precludes the use of organic photosensitizers as photocatalysts. This conformational immobilisation of 2,4,6-triphenylpyrylium is also responsible for the observation of room-temperature phosphorescence.[156]

After the initial synthesis of 2,4,6-triphenylpyrylium and in an effort to improve its photocatalytic activity and stability, the ship-in-a-bottle synthesis of some derivatives was successfully accomplished. Thus, 2,4,6-triphenylthiapyrylium has been obtained encapsulated in zeolites Y and Beta by allowing acetophenone and benzaldehyde dissolved in cyclohexane to react in the presence of acid zeolites, wherein the solvent and zeolites have been previously saturated with H_2S (Scheme 11).[157] Compared to oxygen, the lower electronegativity of the S atom, similar to carbon, increases the aromaticity of the thiapyrylium ring and therefore its thermal stability. Also, the photocatalytic activity of 2,4,6-triphenylthiapyrylium is superior to that of the pyrylium analogue (Figure 4), 2,4,6-triphenylthiapyrylium encapsulated within zeolites Y and Beta exhibiting in addition a much higher photostability thus making possible its reuse.

Tetraphenylbipyrylium is a bulky molecule that requires not one but two neighbouring supercages for it to be accommodated, thus making its ship-in-a-bottle synthesis especially challenging. The preparation of this dication inside the pores of zeolite Y has been accomplished employing the same reaction type as that followed for the synthesis of triphenylpyrylium, but using terephthaldehyde instead of

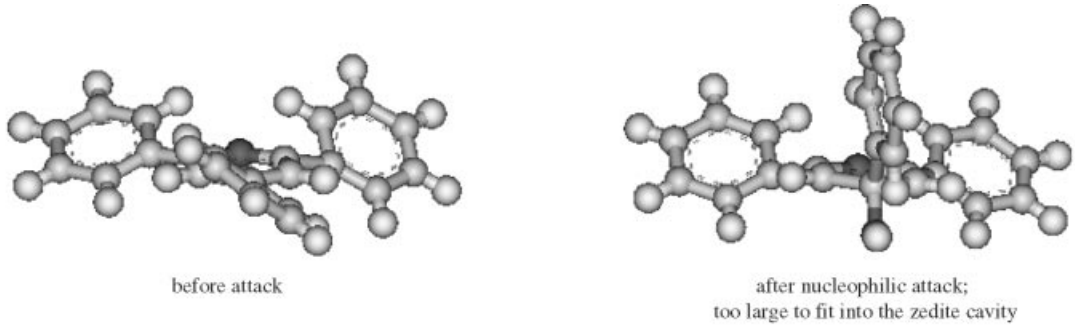

Scheme 10

 © 2004 Wiley-VCH Verlag GmbH & Co. KGaA, Weinheim

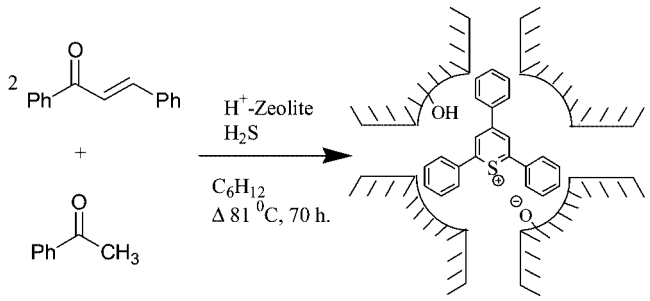

Scheme 11

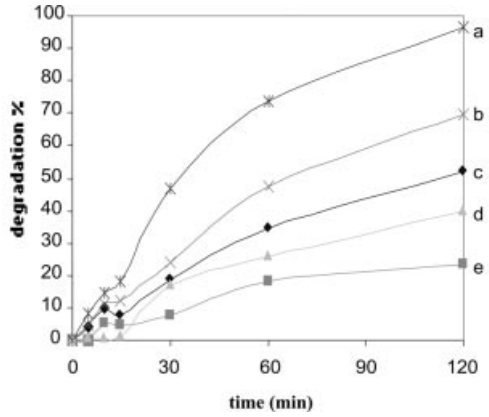

Figure 4. Plot of the phenol disappearance vs. time upon irradiation of an aqueous solution (20 mL) of phenol (δ = 40 ppm) in the presence of solid photocatalysts (30 mg) under identical conditions; a: 2,4,6-triphenylthiapyrylium@HBeta; b: 2,4,6-triphenylthiapyrylium@HY; c: P-25 TiO_2 standard; d: 2,4,6-triphenylpyrylium@HBeta; e: 2,4,6-triphenylpyrylium@HY

benzaldehyde.[158] Figure 5 provides a view of the model showing the tetraphenylbipyrylium occupying two zeolite Y supercages. However, although bipyrylium encapsulated within zeolite Y also exhibits the photocatalytic activity characteristic of 2,4,6-triphenylpyrylium, its efficiency is somewhat lower.

ii) Trityl Cations and Derivatives

Carbocations derived from the parent trityl cation are among the most stable in solution due to charge delocalisation through the aryl rings. Under appropriate conditions and in the absence of nucleophiles and moisture the parent trityl cation becomes indefinitely persistent in solution. Obviously, the presence of electron-donor substituents on the aryl rings stabilizes the carbocation further. One property of these trityl ions is the colour, which changes from the yellow of the unsubstituted trityl to orange, following the Woodward rules of additivity, according to the nature of the substituent. Some of these cations find application as dyes or pigments, malachite green and rose aniline being two examples among many others.[159]

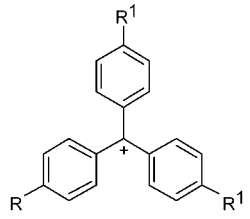

Trityl cations

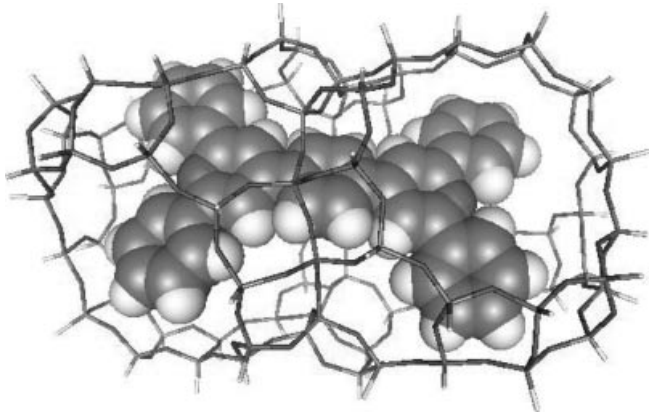

Figure 5. Model of tetraphenylbipyrylium showing the occupancy of two neighbour supercages (taken from ref.[158])

These trityl dyes have been prepared inside zeolite Y and Beta in their H^+ or La^{3+} forms by treating an aromatic aldehyde with electron-rich benzene derivatives such as anisole or *N*,*N*-dimethylaniline, as indicated in Scheme 12.[67,156] Evidence in support of the internal location of the dyes was obtained by the good fitting between the experimental high-resolution X-ray diffraction and the Rietveld refinement of a model in which the zeolite Y supercage contained the dye at one third of cage occupancy (Figure 6).[67] The resulting encapsulated dyes showed activity as heterogeneous photosensitizers to promote the radical-cation-mediated dimerisation of 1,3-cyclohexadiene.

Maciel and co-workers have followed a different strategy to form these encapsulated trityl cations consisting in the reaction of CCl_4 with benzene using the HY zeolite as catalyst. By using ^{13}C MAS NMR spectroscopy, isotopically labelled $^{13}CCl_4$ and studying the reaction of $Ph_3{}^{13}C^+$ with bulky nucleophiles, they reached the conclusion that the product was located predominantly in the internal cavities of the zeolites, in contrast to the simple adsorption of Ph_3CCl in HY that leads to the deposition of the bulky cation exclusively on the external surface of the particles.[160]

4. Ship-in-a-Bottle Systems as Electrocatalysts

Electrochemistry is a convenient tool to study the population of an electroactive guest located at the outermost supercages or subsurface zones since the electrochemical oxidation or reduction process has to be accompanied by the concomitant diffusion of a charge-balancing electrolyte. This diffusion limits the depth in which electrochemistry occurs in the particle.

One interesting application of zeolite-embedded guests is in electrocatalysis[161,162] and the development of selective electrodes.[163,164] In this case the electrode, normally a metallic conductor, is modified by depositing a film of a zeolite-

 © 2004 Wiley-VCH Verlag GmbH & Co. KGaA, Weinheim

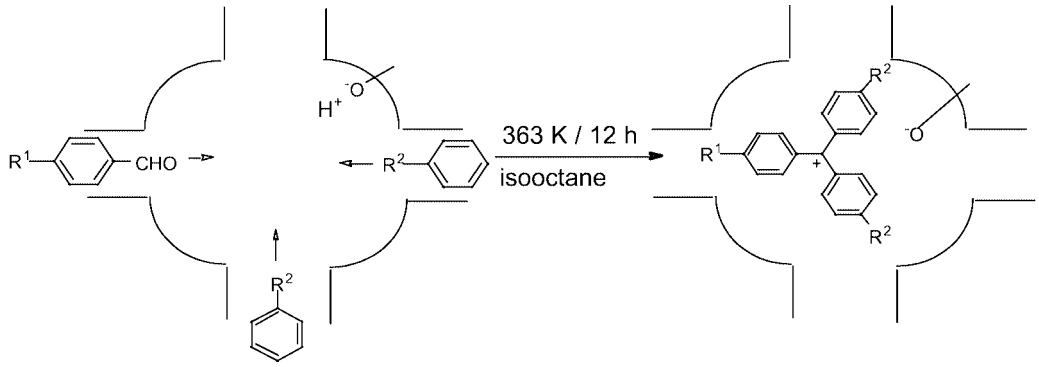

Scheme 12

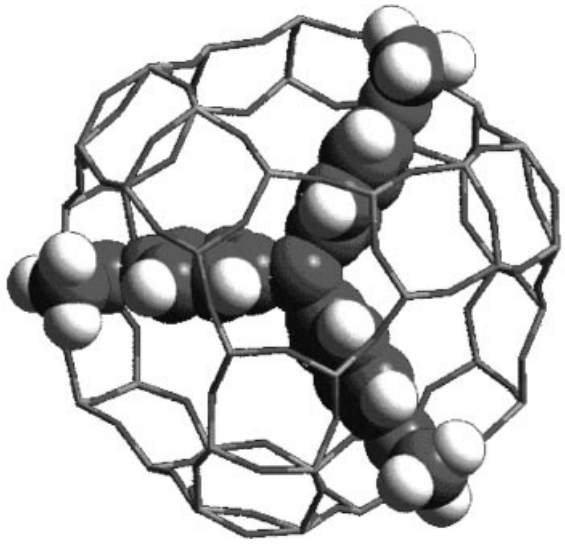

Figure 6. Molecular model of the tris(4-methoxyphenyl)methyl cation based on the Rietveld refinement of the high-resolution XRD pattern (taken from ref.[67]; reprinted with permission; © 1996 American Chemical Society)

encapsulated guest that increases the electrochemical response towards an analyte or promotes an electrochemical process.

Most of the transition metal complexes have a characteristic electrochemical response due to the changes in the metal oxidation number. By means of electrochemistry, Bedioui, Balkus and co-workers have provided experimental evidence of the site isolation arising from the encapsulation of a large guest in a single zeolite supercage. Thus, Rh^{III}−phthalocyanine@NaY exhibits a reversible reduction peak interpreted as the transition between Rh^{III}−phthalocyanine/Rh^{II}−phthalocyanine, while in solution this reversible reduction peak is not observed due to dimerisation/dismutation of the Rh^{II} species.[165]

Balkus, Jr. and Bedioui have prepared zeolite-encapsulated metal−salen compounds and studied their electrochemical response.[166] Apparently, the electrochemical behaviour of the encapsulated complexes is similar to that in solution and the redox potential peaks of the zeolite-encapsulated complexes appear at similar values as in homogeneous solution. In this context, an interesting controversy is how deep in the particle the electrochemical techniques can probe and if the electrochemical response is purely extrazeolitic, due to zeolite-bound complexes, or really intrazeolitic.[167−169]

Organic guests can also exhibit an electrochemical response.[123,170−172] 2,4,6-Triphenylpyrilium encapsulated inside zeolites has been shown to promote the electrochemical response of dopamine, norepinephrine and other catecholamine neurotransmitters by a factor of up to 20. This can serve to develop electrodes that allow the detection of smaller concentrations of analytes that exhibit a selective response for a substrate.

5. Ship-in-a-Bottle Systems as Sensors and Photochromic Systems

The large surface area, the porosity and even the shape-selective adsorption of zeolites are also very interesting for the development of solid sensors in which a zeolite-entrapped guest can report on the presence of certain analytes.

As mentioned earlier, metal−polypyridyl complexes such as $[Ru(bpy)_3]^{2+}$ are strongly photoluminescent either in solution or when encapsulated within zeolites. The actual emission decay kinetics is sensitive to the environment of the complex and to the presence of quencher molecules such as oxygen.

Rare-earth cations are also strongly luminescent, but in contrast to normal emission from organic lumophores, the atomic emission may consist of sharp atomic lines rather than broad emission bands. Luminescent rare-earth complexes have also been used as sensors.[173−176] However, atomic photoluminescence presents, in general, two problems. On one hand, the excitation of the atomic orbital of the cation is difficult since rare-earth cations do not absorb in the visible or even in the UV and light absorption is a prerequisite for the emission. On the other hand, the presence of water and other ligands containing O−H groups coordinating the rare-earth cation thwarts the emission by providing an efficient radiationless deactivation pathway consisting in the vibration of the O−H group in resonance with the decay of the excited atomic electronic state. Both problems can be overcome by complexation of the rare-earth cation. Formation of a suitable rare-earth complex prevents the quenching of water and at the same time it

 © 2004 Wiley-VCH Verlag GmbH & Co. KGaA, Weinheim

introduces new ligand-to-metal transition bands in the visible that allows easy excitation of the rare-earth cation. Encapsulation of these luminescent complexes within zeolites can serve to obtain a highly luminescent solid in which site isolation and compartmentalisation provided by the zeolite framework reduces the self-quenching and emission reabsorption that occurs in pure crystals of the complex. Photoluminescent Eu^{3+},[177] Nd^{3+} [178] and Tb^{3+} [179] complexes with trifluoroacetylacetophenone, bis(perfluoromethanesulfonyl)aminate or tetrarylporphyrinate have been prepared by ship-in-a-bottle synthesis within a series of zeolites.

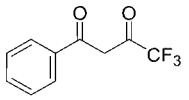

4,4,4-trifluoro-1-phenyl-butane-1,3-dione

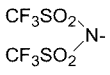

bis(trifluoromethyl-sulfon)amidate

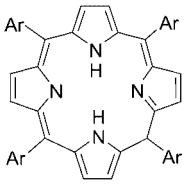

tetraarylporphyrin

9-(4-Methoxyphenyl)xanthylium has also been prepared by a ship-in-a-bottle synthesis inside the cavities of zeolites Y and Beta by electrophilic attack of preformed xanthylium cation[180] on electron-rich anisole (Scheme 13).[181] The resulting 9-arylxanthylium remains entrapped inside the zeolite supercages, molecular modelling indicating that the conformational rotation of the anisyl substituent over the xanthylium cores is impeded by the encapsulation (Figure 7). An interesting consequence of the conformational freezing in 9-(4-methoxyphenyl)xanthylium@HY is the observation of fluorescence. In solution these dyes do not emit at room temperature due to the efficient radiationless deactivation mechanism consisting in the flipping of the electron-rich anisyl group around the electron-poor xanthylium moiety, the observation of room-temperature emission for 9-(4-methoxyphenyl)xanthylium@HY is taken as an experimental confirmation of the molecular model of the 9-anisylxanthylium encapsulated within zeolite Y supercages. In a certain sense, encapsulation has the same effect as decreasing the temperature, both methodologies diminishing the conformational mobility. Photoluminescence from encapsulated 9-(4-anisyl)xanthylium is quenched by nucleophiles and this quenching can be the basis for the development of sensing systems.

Spiropyrans with a chromene substructure are typical photochromic compounds in solution.[182] Upon illumination of the colourless spiro form, ring opening with formation of the merocyanine isomer leads to the development of colour, depending on the actual substitution of the spiropyran (Scheme 14). Upon standing in the dark, the thermodynamically unstable open merocyanine isomer undergoes

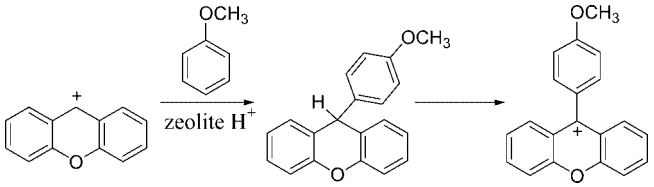

Scheme 13

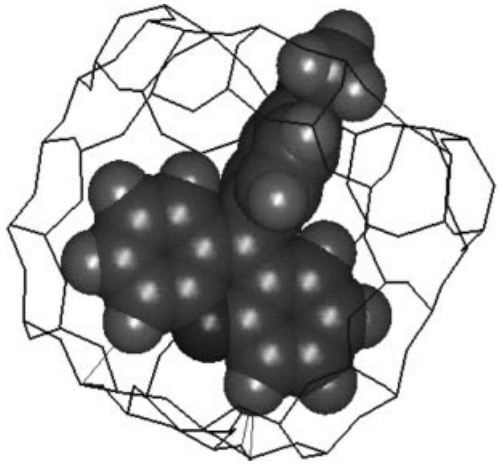

Figure 7. Molecular model of the 9-(4-methoxyphenyl)xanthylium cation encapsulated within an *all-silica* zeolite Y supercage (taken from ref.[181]; reprinted with permission; © 1996 American Chemical Society)

thermal ring-closure back to the spiropyran form (Scheme 14).

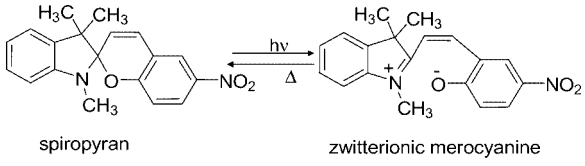

Scheme 14

For some applications as photochromic pigments it would be of interest to support spiropyrans on a solid. The molecular size and the conformational rigidity of the spiro form precludes adsorption of these chromotropic compounds inside the cavities of faujasite, and a ship-in-a-bottle synthesis is required. This has been accomplished by Garcia et al. by treating 1,3,3-trimethylindoline with 4-nitrosalicylaldehyde in the presence of zeolite NaY (Scheme 15).[183] In contrast, spiropyran can be adsorbed on mesoporous MCM-41[184] without requiring any synthesis.

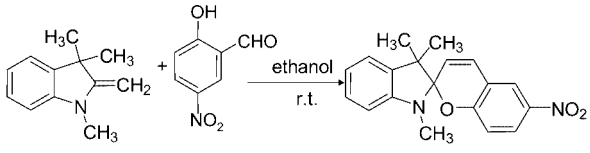

Scheme 15

 © 2004 Wiley-VCH Verlag GmbH & Co. KGaA, Weinheim

However, although in situ spectroscopic characterisation and product studies have demonstrated the formation of encapsulated spiropyran, it appears that the reversibility of the ring opening and closure is strongly modified by the polar environment of the zeolite supercage and/or the presence of weak acid sites as compared to ethanol solution. As a consequence, in a few irradiation/dark cycles the zeolite-containing spiropyran becomes strongly coloured and this colour does not disappear upon standing in the dark. These facts have been interpreted as indicating that in the zeolite the open merocyanine form tends to become stabilized, protonated and (*Z*)/(*E*)-isomerized, in contrast to the rapid and selective cyclisation observed in solution (Scheme 14).

Azo dyes such as methyl orange adsorbed in mesoporous Y zeolites have been prepared by coupling of *N*,*N*-dimethylaniline with diazonium cations.[185] Apparently, the dimensions of the transition states are too large to fit inside the supercages of regular dimensions and as result the azo dyes are not formed in the cages, but in the mesopores formed by defects in the crystal structure of the zeolite. Zeolite Y can be specially treated with citric acid and similar strongly complexing organic hydroxy acids to promote the formation of mesopores by damaging partially the crystal structure. The resulting azo dye incorporated inside the zeolite can act as a pigment and fluorescent solid.

6. Ship-in-a-Bottle Systems in Molecular Switches

As mentioned in the Introduction, one of the novel potential applications of zeolite-encapsulated guests is as functional materials in nanotechnology. One of the current strategies in nanotechnology is the "*bottom-up*" approach in which a molecule comprising several subunits is designed on purpose to produce a given effect upon external stimulus. These functional molecules are frequently termed as molecular devices since they perform certain actions at the molecular level that are characteristic of common mechanical devices. One type of such molecular devices are the so-called molecular machines in which one unit of the molecule is able to perform a cyclic movement emulating, at the simplest level, a machine.[53,186,187] While many of these molecular machines have been synthesised and the proof of principle at the molecular level has been sufficiently demonstrated, one general problem in this area is how to organize and assemble the individual molecular machines so that a coherent and co-operative response can be obtained from the assembly. In this regard, zeolites may provide a compartmentalized and organized space in which the molecular machines can be entrapped and held in place on the surface of a given support.

A preliminary step towards the direction of assembling molecular machines is their synthesis inside the zeolite micropores. One of the most common components in molecular machinery is the so-called "blue box", which is a bipyridinium macroring that acts as an electron-poor moiety forming charge-transfer complexes with electron-rich subunits in rotaxanes and catenanes.[188] Figure 8 shows a model of this blue-box encapsulated within zeolites.

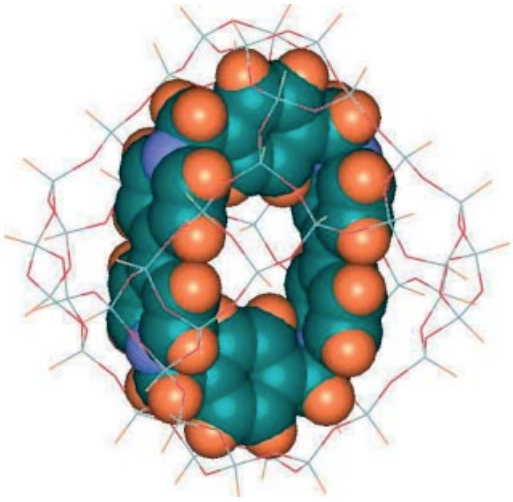

Figure 8. Molecular modelling of the bis(bipyridinium)cyclophane macrocycle inside the zeolite Y supercages

Besides spectroscopic characterisation, formation of the bipyridinium macrocycle was confirmed by dissolving the zeolite with HF and recovering the macrocycle from the solution.[188] The key factor in the success of the ship-in-a-bottle synthesis is the "*templating*" effect of the zeolite cavity approaching the distant pyridine N atoms in the open intermediate (Figure 9). The shape of the cage and the position of the positive charges in the same cage are responsible for the larger yield for cyclophane macrocycle formation inside zeolite Y than in solution, where the yield of cyclisation is only about 3%.

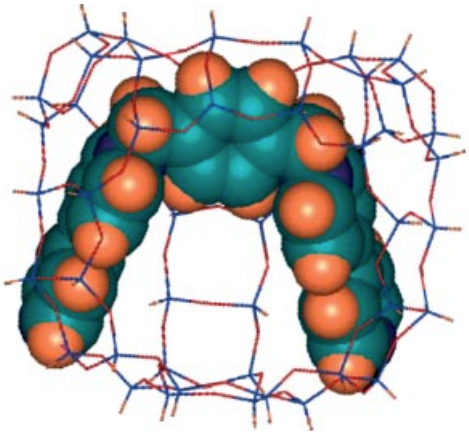

Figure 9. Molecular model of the open dicationic precursor of the blue box encapsulated within the supercage of zeolite Y; note the distance between the terminal N atoms (taken from ref.[188a]; reprinted with permission; © 2002 American Chemical Society)

A further development has been the ship-in-a-bottle synthesis of a [2]catenane comprising the *blue box* interlocked with a hydroquinolyl polyether macrocycle. The ship-in-a-bottle synthesis parallels the route followed in solution for

this [2]catenane, initiating the procedure by ion-exchanging the precursor in the zeolite (Scheme 16).

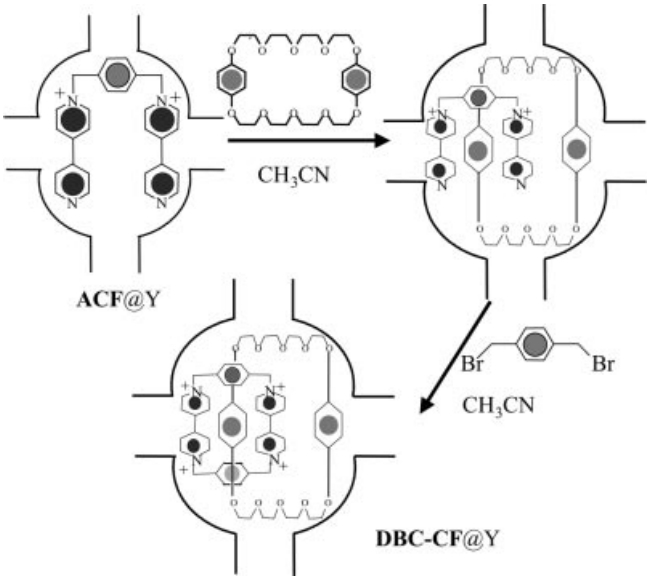

Scheme 16

Upon photochemical excitation at the charge-transfer band of the [2]catenane an electron transfer and a corresponding charge separation occur (Figure 10). The most important effect of the encapsulation of the catenane inside the zeolite has been the observation of a dramatic enhancement of the lifetime of the viologen radical cation. In solution the geminate radical ion pair generated instantaneously upon excitation of the charge-transfer complex lives in the picosecond time regime and this short lifetime makes the operation of any co-conformational[189] and atomic movement that could occur in the state of charge separation generated as a consequence of the photoinduced electron transfer impossible. Co-conformational changes would occur in the microsecond or longer timescale. In this regard, the above results have demonstrated that encapsulation of these molecular switches inside the zeolite would increase the lifetime of the radical cation sufficiently to allow movements of the interlocked rings, but the actual occurrence of these co-conformational changes is yet to be demonstrated.

7. Ship-in-a-Bottle Synthesis of Conducting Polymers

Conducting organic polymers such as polyacetylenes, polyanilines and polypyrrols have promising applications in the field of charge storage, as antistatic coatings and in electronics. A general problem associated with conducting polymers is their degradability upon exposure of the charged polymer to the atmosphere. A way to circumvent this decomposition is to encapsulate the polymers within the pores of zeolites that will protect them from the attack of external reagents. The field of encapsulated polymers has been subjected to periodic reviews.[190−193] Among the most recent contributions are the preparation of parent polyacetylene by polymerisation of acetylene in Ni-exchanged zeolites, essentially filling the void volume.[194,195] Electrochemical

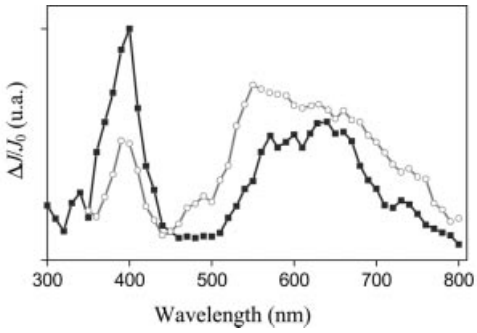

Figure 10. Diffuse reflectance UV/Vis transient spectra recorded for the catenane (circles) and for the bipyridinium cyclophane (squares) encapsulated within the supercages of zeolite Y (data taken from ref.[188b]; reproduced by permission of The Royal Society of Chemistry)

measurements indicate that the polymer can be charged, but the polymer becomes degraded in the first use.[196] The spontaneous formation of polarons has also been reported.[197] Spange has recently reviewed the cationic polymerisation of vinyl ether, furan and other polymers within MCM-41.[198−200]

C. Concluding Remarks

Since the initial, seminal work of Herron and Schulz-Ekloff on the ship-in-a-bottle synthesis of metal complexes, a considerable number of examples of this and other types of guests have been reported. These reports have continued to explore the application of zeolites containing encapsulated guests as catalysts and zeozymes, but other fields like photocatalysis, electrocatalysis, sensors and development of functional materials have also benefited from ship-in-a-bottle methodologies. In the near future, and given the current impetus in nanotechnology, it can be anticipated that the systems based on the ship-in-a-bottle synthesis will attract renewed interest in order to develop active components for photonics (laser cavities, harmonic generators, light switches, wave guides, etc.) and as intelligent devices such as activable membranes, chromotropic layers. Also, the ship-in-a-bottle synthesis could find applications in molecular machines as a way to assemble and modify the properties of supramolecular systems.

The special properties of zeolites as hosts in terms of site isolation, space compartmentalisation, polarity and the presence of acidic and other sites are very interesting and can contribute to the operation and design of these hybrid solids. This field will also benefit from the continuous advances in the characterisation techniques, some of which have become routine, allowing a safer and firmer determination of the encapsulated material as well as from the preparation of zeolite films on substrates.[201,202]

Acknowledgments

Financial support by the Spanish Ministry of Science and Technology (project MAT2003-01226) and Generalidad Valenciana (grupos 03-020) is gratefully acknowledged.

 © 2004 Wiley-VCH Verlag GmbH & Co. KGaA, Weinheim

[1] B. W. Wojciechowski, A. Corma, *Catalytic Cracking, Catalysts Kinetics and Mechanisms*, Marcel Dekker, New York, **1984**.
[2] J. M. Thomas, *Angew. Chem. Int. Ed. Engl.* **1988**, *27*, 1673−1691.
[3] J. M. Thomas, *Angew. Chem. Int. Ed. Engl.* **1995**, *106*, 913−937.
[4] J. M. Thomas, R. G. Bell, P. A. Wright, *Bull. Soc. Chim. Fr.* **1994**, *131*, 463−485.
[5] P. B. Venuto, *Adv. Catal.* **1968**, *18*, 259−371.
[6] P. B. Venuto, *Microporous Mater.* **1994**, *2*, 297−411.
[7] [7a] *Heterogeneous Catalysis and Fine Chemicals II* (Eds.: M. Guisnet, J. Barbier, J. Barrault, C. Bouchoule, D. Duprez, G. Pérot, C. Montassier), Elsevier, Amsterdam, **1991**. [7b] *Heterogeneous Catalysis and Fine Chemicals III* (Eds.: M. Guisnet, J. Barbier, J. Barrault, C. Bouchoule, D. Duprez, G. Pérot, C. Montassier), Elsevier, Amsterdam, **1993**.
[8] [8a] A. Corma, H. García, *Chem. Rev.* **2002**, *102*, 3837−3892. [8b] A. Corma, H. García, *Chem. Rev.* **2003**, *103*, 4307−4365.
[9] M. E. Davis, *Nature* **2002**, *417*, 813−821.
[10] N. B. Milestone, F. Mizukami, Y. Kiyozumi, K. Maeda, S. Niwa, *Proc. Int. Zeolite Conf., 12th, Baltimore, MD, United States, July 5−10, 1998* **1999**, *3*, 1833−1839.
[11] J. Hedlund, M. Noack, P. Kolsch, D. Creaser, J. Caro, J. Sterte, *J. Membrane Sci.* **1999**, *159*, 263−273.
[12] Y. H. Chiou, T. G. Tsai, S. L. Sung, H. C. Shih, C. N. Wu, K. J. Chao, *J. Chem. Soc., Faraday Trans.* **1996**, *92*, 1061−6.
[13] E. R. Geus, M. J. Den Exter, H. Van Bekkum, *J. Chem. Soc., Faraday Trans.* **1992**, *88*, 3101−9, 1 plate.
[14] S. J. Kulkarni, *Stud. Surf. Sci. Catal.* **1998**, *113*, 151−161.
[15] J. Weitkamp, U. Weiss, S. Ernst, *Stud. Surf. Sci. Catal.* **1995**, *94*, 363−80.
[16] K. J. Balkus Jr., A. G. Gabrielov, *J. Incl. Phenom. Mol. Recog.* **1995**, *21*, 159−84.
[17] A. Corma, H. Garcia, *Top. Catal.* **1998**, *6*, 127−140.
[18] J. A. Lercher, R. A. Van Santen, H. Vinek, *Catal. Lett.* **1994**, *27*, 91−96.
[19] A. Corma, H. García, *J. Chem. Soc., Dalton Trans.* **2000**, 1381−1394.
[20] R. M. Barrer, *Zeolites and Clay Minerals as Sorbents and Molecular Sieves*, Academic Press, London, **1978**.
[21] D. W. Breck, *Zeolite Molecular Sieves: Structure, Chemistry and Use*, John Wiley and Sons, New York, **1974**.
[22] *Introduction to Zeolite Science and Practice* (Eds.: H. van Bekkum, E. M. Flanigen, J. C. Jansen), Elsevier, Amsterdam, **1991**.
[23] R. M. Barrer, *Mol. Sieves Pap. Conf.* **1968**, 39−46.
[24] R. M. Barrer, W. M. Meier, *Trans. Faraday Soc.* **1958**, *54*, 1074−85.
[25] R. M. Barrer, W. M. Meier, *Helv. Phys. Acta* **1956**, *29*, 229−30.
[26] R. M. Barrer, *J. Chem. Soc.* **1948**, 2158−63.
[27] R. M. Barrer, *Annu. Rep. Prog. Chem.* **1945**, *41*, 31−46.
[28] R. M. Barrer, *J. Chem. Soc.* **1948**, 127−32.
[29] R. M. Barrer, *J. Soc. Chem. Ind.* **1945**, *64*, 130−1.
[30] R. M. Barrer, F. W. Bultitude, J. W. Sutherland, *Trans. Faraday Soc.* **1957**, *53*, 1111−23.
[31] R. M. Barrer, J. W. Sutherland, *Proc. R. Soc. London, Ser. A* **1956**, *237*, 439−63.
[32] R. M. Barrer, W. Buser, W. F. Grutter, *Helv. Chim. Acta* **1956**, *39*, 518−30.
[33] C. S. Cundy, P. A. Cox, *Chem. Rev.* **2003**, *103*, 663−701.
[34] W. M. Meier, D. H. Olson, C. Baerlocher, *Zeolites* **1996**, *17*, 1−229.
[35] M. E. Davis, *Acc. Chem. Res.* **1993**, *26*, 111−115.
[36] A. Corma, C. Corell, J. Perez-Pariente, *Zeolites* **1995**, *15*, 2−8.
[37] H. Kalipcilar, T. C. Bowen, R. D. Noble, J. L. Falconer, *Chem. Mater.* **2002**, *14*, 3458−3464.
[38] T. Boix, M. Puche, M. A. Camblor, A. Corma, US patent, **2002**, 6471941.
[39] R. Castaneda, A. Corma, V. Fornes, F. Rey, J. Rius, *J. Am. Chem. Soc.* **2003**, *125*, 7820−7821.
[40] M. E. Davis, *Chem. Eur. J.* **1997**, *3*, 1745−1750.
[41] R. L. Bedard, C. L. Boves, N. Coombs, A. J. Holmes, T. Jiang, S. J. Kirby, P. M. Macdonald, A. M. Malek, G. A. Ozin, S. Petrov, N. Plavac, R. A. Ramik, M. R. Steele, D. Young, *J. Am. Chem. Soc.* **1993**, *115*, 2300−2313.
[42] A. Corma, M. J. Diaz-Cabanas, J. Martinez-Triguero, F. Rey, J. Rius, *Nature* **2002**, *418*, 514−517.
[43] J. C. Scaiano, H. García, *Acc. Chem. Res.* **1999**, *32*, 783−793.
[44] K. B. Yoon, J. K. Kochi, *J. Am. Chem. Soc.* **1988**, *110*, 6586−6588.
[45] R. G. Weiss, V. Ramamurthy, G. S. Hammond, *Acc. Chem. Res.* **1993**, *26*, 530−536.
[46] N. Herron, *Inorg. Chem.* **1986**, *25*, 4714−17.
[47] V. Y. Zakharov, B. V. Romanovskii, *Vest. Moskov. Univ. 3, Khim.* **1977**, *18*, 348−50.
[48] V. Y. Zakharov, B. V. Romanovskii, *Vest. Moskov. Univ. 3, Khim.* **1977**, *18*, 143−5.
[49] V. Y. Zakharov, O. M. Zakharova, B. V. Romanovskii, R. E. Mardaleishvili, *React. Kin. Catal. Lett.* **1977**, *6*, 133−7.
[50] H. Diegruber, P. J. Plath, G. Schulz-Ekloff, *J. Mol. Catal.* **1984**, *24*, 115−26.
[51] G. Meyer, D. Woehrle, M. Mohl, G. Schulz-Ekloff, *Zeolites* **1984**, *4*, 30−4.
[52] K. J. Balkus Jr., S. J. Kim, A. M. Sargeson, *Mater. Res. Soc., Symp. Proc.* **1997**, *454*, 217−224.
[53] V. Balzani, A. Credi, F. M. Raymo, J. F. Stoddart, *Angew. Chem. Int. Ed.* **2000**, *39*, 3348−3391.
[54] F. M. Raymo, J. F. Stoddart, *Polym. Mater. Sci. Eng.* **1999**, *80*, 33−34.
[55] The symbol "@" has been introduced by N. J. Turro to indicate a guest incorporated inside a host.
[56] A. Corma, *Chem. Rev.* **1995**, *95*, 559−614.
[57] J. W. Niemantsverdriet, *Spectroscopy in Catalysis*, VCH, Weinheim, **1993**.
[58] A. Terenin, *Adv. Catal.* **1964**, *15*, 227−284.
[59] L. J. Bellamy, *The Infrared Spectra of Complex Molecules*, 3rd ed., **1980**, vol. 2.
[60] L. J. Bellamy, *The Infrared Spectra of Complex Molecules*. 3rd ed., **1975**.
[61] L. H. Little, *Infrared Spectra of Adsorbed Molecules*, Willmer Brothers Limited, New York, **1966**.
[62] B. Schrader, *Infrared and Raman Spectroscopy (Methods and Applications)*, VCH Publishers Inc., Weinheim, **1995**.
[63] G. Engelhardt, D. Michel, *High-Resolution Solid-State NMR of Silicates and Zeolites*, John Wiley & Sons, Norwich, U. K., **1987**.
[64] W. N. Delgass, G. L. Haller, R. Kellerman, J. H. Lunsford, *Spectroscopy in Heterogeneous Catalysis*, Academic Press, New York, **1979**.
[65] G. Kortum, *Reflectance Spectroscopy*, Springer, Berlin, **1969**.
[66] B. Hennessy, S. Megelski, C. Marcollu, V. Shklover, C. Bärlocher, G. Calzaferri, *J. Phys. Chem. B* **1999**, *103*, 3340−3351.
[67] M. L. Cano, A. Corma, V. Fornes, H. Garcia, M. A. Miranda, C. Baerlocher, C. Lengauer, *J. Am. Chem. Soc.* **1996**, *118*, 11006−11013.
[68] J. Weitkamp, *Proceedings of the 9th International Zeolite Conference*, Montreal, **1992**.
[69] *Zeolites and Related Microporous Materials: State of the Art 1994* (Eds.: J. Weitkamp, H. G. Karge, H. Pfeifer, W. Hölderich), Elsevier, Amsterdam, **1994**.
[70] E. N. Jacobsen, W. Zhang, A. R. Muci, J. R. Ecker, L. Deng, *J. Am. Chem. Soc.* **1991**, *113*, 7063.
[71] E. N. Jacobsen, J. L. Leighton, L. E. Martinez, US Patent, **1999**, 5929232.
[72] B. D. Brandes, E. N. Jacobsen, *Inorg. Chem.* **1994**, *33*, 67−72.
[73] E. N. Jacobsen, J. M. Cormick, M. Palucki, *Tetrahedron Lett.* **1995**, *36*, 5460.
[74] L. E. Martínez, J. L. Leighton, D. H. Carsten, E. N. Jacobsen, *J. Am. Chem. Soc.* **1997**, *117*, 5897−5898.

 © 2004 Wiley-VCH Verlag GmbH & Co. KGaA, Weinheim

[75] K. J. Balkus Jr., A. K. Khanmamedova, K. M. Dixon, F. Bedioui, *Appl. Catal. A* **1996**, *143*, 159−173.
[76] F. Bedioui, L. Roue, J. Devynck, K. J. Balkus Jr., *J. Electrochem. Soc.* **1994**, *141*, 3049−52.
[77] K. J. Balkus Jr., A. A. Welch, B. E. Gnade, *Zeolites* **1990**, *10*, 722−9.
[78] K. J. Balkus Jr., A. A. Welch, B. E. Gnade, *J. Incl. Phenom. Mol. Recog.* **1991**, *10*, 141−51.
[79] P. P. Knops-Gerrits, P. A. Jacobs, *NATO ASI Ser., Ser. 3* **1998**, *44*, 413−416.
[80] K. J. Balkus Jr., *Phthalocyanines* **1996**, *4*, 285−305.
[81] N. Herron, *J. Coord. Chem.* **1988**, *19*, 25−38.
[82] M. Ichikawa, T. Kimura, A. Fukuoka, *Stud. Surf. Sci. Catal.* **1991**, *60*, 335−42.
[83] E. Armengol, A. Corma, V. Fornés, H. García, J. Primo, *Appl. Catal. A* **1999**, *181*, 305−312.
[84] S. Ernst, Y. Traa, U. Deeg, *Stud. Surf. Sci. Catal.* **1994**, *84*, 925−32.
[85] R. F. Parton, F. Thibault-Starzyk, R. A. Reynders, P. J. Grobet, P. A. Jacobs, C. P. Bezoukhanova, W. Sun, Y. Wu, *J. Mol. Catal. A: Chem.* **1995**, *97*, 183−6.
[86] R. F. Parton, C. P. Bezoukhanova, F. Thibault-Starzyk, R. A. Reynders, P. J. Grobet, P. A. Jacobs, *Stud. Surf. Sci. Catal.* **1994**, *84*, 813−20.
[87] R. F. Parton, L. Uytterhoeven, P. A. Jacobs, *Stud. Surf. Sci. Catal.* **1991**, *59*, 395−403.
[88] F. R. Parton, I. F. J. Vankelecom, M. J. A. Casselman, C. P. Bezoukhanova, J. B. Uytterhoeven, P. A. Jacobs, *Nature* **1994**, *370*, 541.
[89] J. D. Hoefelmeyer, K. J. Balkus, Jr., *Book of Abstracts, 215th ACS National Meeting, Dallas, March 29−April 2* **1998**, CHED-435.
[90] K. J. Balkus Jr., M. Eissa, R. Lavado, *Chem. Ind.* **1997**, *69*, 363−378.
[91] K. J. Balkus Jr., A. Khanmamedova, M. Eissa, *Stud. Surf. Sci. Catal.* **1995**, *97*, 189−95.
[92] K. J. Balkus Jr., M. Eissa, R. Lavado, *Stud. Surf. Sci. Catal.* **1995**, *94*, 713−19.
[93] F. Algarra, M. A. Esteves, V. Fornes, H. Garcia, J. Primo, *New. J. Chem.* **1998**, *22*, 333−338.
[94] B.-Z. Zhan, X.-Y. Li, *Chem. Commun.* **1998**, 349−350.
[95] B. C. Gates, *J. Mol. Catal.* **1984**, *86*, 95.
[96] E. Cariati, D. Roberto, R. Ugo, *Chem. Rev.* **2003**, *103*, 3707.
[97] L. I. Sheu, H. Knözinger, W. M. H. Sachtler, *Catal. Lett.* **1989**, *2*, 129.
[98] E. Mantovani, N. Palladino, A. Zanobi, *J. Mol. Catal.* **1977**, *78*, 285.
[99] E. J. Rode, M. E. Davis, B. E. Hanson, *J. Catal.* **1985**, *96*, 574.
[100] L. F. Rao, A. Fukuoka, N. Kosugui, H. Kuroda, M. Ichikawa, *J. Phys. Chem.* **1990**, *94*, 5317.
[101] G. J. Li, T. Fujimoto, A. Fukuoka, M. Ichikawa, *Catal. Lett.* **1992**, *12*, 171.
[102] L. Brabec, *J. Mol. Catal. A* **2001**, *169*, 127.
[103] L. Brabeck, J. Nováková, *J. Mol. Catal. A* **2001**, *166*, 283.
[104] A. Kukuoka, L. F. Rao, N. Kozugi, H. Kuroda, M. Ichikawa, *Appl. Catal.* **1989**, *50*, 295.
[105] P. Gelin, F. Lefebure, B. Elleuch, C. Naccache, Y. Ben Taarit, *ACS Symp. Ser.* **1983**, *218*, 455.
[106] S. Kawi, B. C. Gates, *Catal. Lett.* **1991**, *10*, 263.
[107] G. Bergeret, P. Gallezot, L. Lefebvre, *Stud. Surf. Sci. Catal.* **1986**, *28*, 401.
[108] S. Kawi, B. C. Gates, *J. Chem. Soc., Chem. Commun.* **1991**, 994.
[109] W. Kahlen, A. Janssen, W. F. Holderich, *Stud. Surf. Sci. Catal.* **1997**, *108*, 469−476.
[110] A. Zsigmond, K. Bogar, F. Notheisz, *Catal. Lett.* **2002**, *83*, 55−58.
[111] B. Sulikowski, J. Haber, A. Kubacka, K. Pamin, Z. Olejniczak, J. Ptaszynski, *Catal. Lett.* **1996**, *39*, 27−31.
[112] D. H. R. Barton, D. Doller, *Acc. Chem. Res.* **1992**, *25*, 504−512.
[113] M. Alvaro, B. Ferrer, H. Garcia, A. Sanjuan, *Tetrahedron* **1999**, *55*, 11895−11902.
[114] A. Kozlov, K. Asakura, Y. Iwasawa, *Chem. Lett.* **1997**, 313−314.
[115] Z. Bai, M. Fang, S. Chen, *Cuihua Xuebao* **2002**, *23*, 29−32; cf. Chem. Abstr. **2002**, 144874.
[116] P. P. Knops-Gerrits, M. L′Abbe, W. H. Leung, A. M. Van Bavel, G. Langouche, I. Bruynseraede, P. A. Jacobs, *Stud. Surf. Sci. Catal.* **1996**, *101*, 811−820.
[117] N. Hosoya, A. Hatayama, R. Irie, H. Sasaki, T. Katsuki, *Tetrahedron* **1994**, *50*, 4311−4322.
[118] P. G. Potvin, S. Branchet, *J. Org. Chem.* **1992**, *57*, 629−6635.
[119][119a] T. Bein, S. B. Ogunwumi, *Book of Abstracts, 212th ACS National Meeting, Orlando, FL, August 25−29* **1996**, CATL-006. [119b] M. J. Sabater, A. Corma, A. Domenech, V. Fornes, H. Garcia, *Chem. Commun.* **1997**, 1285−1286.
[120] S. Ernst, H. Disteldorf, X. Yang, *Microp. Mesopor. Mater.* **1998**, *22*, 457.
[121] C. Baleizao, B. Gigante, D. Das, M. Alvaro, H. Garcia, A. Corma, *Chem. Commun.* **2003**, 1860−1861.
[122] A. Domenech, P. Formentin, H. Garcia, M. J. Sabater, *Eur. J. Inog. Chem.* **2000**, 1339−1344.
[123] A. Domenech, P. Formentin, H. Garcia, M. J. Sabater, *J. Phys. Chem. B* **2002**, *106*, 574−582.
[124] A. Zsigmond, F. Notheisz, Z. Frater, J. E. Backvall, *Stud. Surf. Sci. Catal.* **1997**, *108*, 453−459.
[125] W. De Wilde, G. Peeters, J. H. Lunsford, *J. Phys. Chem.* **1980**, *84*, 2306−2310.
[126] P. K. Dutta, J. A. Incavo, *J. Phys. Chem.* **1987**, *91*, 4443.
[127] P. Laine, M. Lanz, G. Calzaferri, *Inorg. Chem.* **1996**, *35*, 3514−3518.
[128] T. E. Brook, R. Narayanaswamy, *Sens. Actuators, B* **1998**, *51*, 77−83.
[129] N. Castagnola, P. K. Dutta, *Stud. Surf. Sci. Catal.* **2001**, *135*, 4508−4516.
[130] A. Corma, V. Fornes, M. S. Galletero, H. Garcia, J. C. Scaiano, *Chem. Commun.* **2002**, 334−335.
[131] J. R. Kincaid, K. Maruszewski, D. P. Strommen, K. Handrich, *Inorg. Chem.* **1991**, *30*, 4579−4582.
[132] J. R. Kincaid, K. Maruszewski, *Inorg. Chem.* **1995**, *34*, 2002−2006.
[133] J. S. Krueger, J. E. Mayer, T. E. Mallouk, *J. Am. Chem. Soc.* **1988**, *110*, 8232−4.
[134] H. Lee, P. K. Dutta, *J. Phys. Chem. B* **2002**, *106*, 11898−11904.
[135] M. K. Nazeeruddin, A. Kay, I. Rodicio, R. Humphry-Baker, E. Müller, P. Liska, N. Vlachopoulos, M. Grätzel, *J. Am. Chem. Soc.* **1993**, *115*, 6382.
[136] Y. S. Park, E. J. Lee, Y. S. Chun, Y. D. Yoon, K. B. Yoon, *J. Am. Chem. Soc.* **2002**, *124*, 7123−7135.
[137] M. Vitale, N. B. Castagnola, N. J. Ortins, J. A. Brooke, A. Vaidyalingam, P. K. Dutta, *J. Phys. Chem. B* **1999**, *103*, 2408−2416.
[138] H. Garcia, H. D. Roth, *Chem. Rev.* **2002**, *102*, 3947−4008.
[139] N. B. Castagnola, P. K. Dutta, *J. Phys. Chem. B* **1998**, *102*, 1696−1702.
[140] S. K. Tiwary, S. Vasudevan, *Chem. Phys. Let.* **1997**, *277*, 84−88.
[141] P. P. Knops-Gerrits, C. A. Trujillo, B. Z. Zhan, X. Y. Li, P. Rouxhet, P. A. Jacobs, *Top. Catal.* **1996**, *3*, 437−449.
[142] S. H. Bossmann, N. Shahin, H. Le Thanh, A. Bonfill, M. Worner, A. M. Braun, *ChemPhysChem* **2002**, *3*, 401−407.
[143] S. Fukuzumi, Y. Yoshida, T. Urano, T. Suenobu, H. Imahori, *J. Am. Chem. Soc.* **2001**, *123*, 11331−11332.
[144] A. Corma, V. Fornes, H. Garcia, M. A. Miranda, J. Primo, M.-J. Sabater, *J. Am. Chem. Soc.* **1994**, *116*, 2276−80.
[145] K. Dimroth, C. Reichardt, K. Vogel, *Org. Synth.* **1969**, *49*, 121−4.
[146] A. M. Amat, A. Arques, S. H. Bossmann, A. M. Braun, S. Gob, M. A. Miranda, *Angew. Chem. Int. Ed.* **2003**, *42*, 1653−1655.
[147] M. A. Miranda, H. García, *Chem. Rev.* **1994**, *94*, 1063.

 © 2004 Wiley-VCH Verlag GmbH & Co. KGaA, Weinheim

[148] A. Corma, V. Fornés, H. García, M. A. Miranda, J. Primo, M. J. Sabater, *J. Am. Chem. Soc.* **1994**, *116*, 2276.
[149] A. Corma, V. Fornés, H. García, M. A. Miranda, M. J. Sabater, *J. Am. Chem. Soc.* **1994**, *116*, 9767−9768.
[150] V. Fornés, H. García, M. A. Miranda, F. Mojarrad, M.-J. Sabater, N. N. E. Suliman, *Tetrahedron* **1996**, *52*, 7755−7760.
[151] A. Sanjuán, M. Alvaro, G. Aguirre, H. García, J. C. Scaiano, *J. Am. Chem. Soc.* **1998**, *120*, 7351−7352.
[152] A. Sanjuan, G. Aguirre, M. Alvaro, H. Garcia, *Appl. Catal. B* **1998**, *15*, 247−257.
[153] A. Sanjuán, A. Guillermo, M. Alvaro, H. García, *Water Res.* **2000**, *34*, 320.
[154] A. Sanjuan, G. Aguirre, M. Alvaro, H. Garcia, J. C. Scaiano, M. N. Chretien, K.-S. Focsaneanu, *Photochem. Photobiol. Sci.* **2002**, *1*, 955−959.
[155] A. Sanjuán, G. Aguirre, M. Alvaro, H. García, J. C. Scaiano, *Appl. Catal. B* **2000**, *25*, 257.
[156] M. L. Cano, F. L. Cozens, H. García, V. Martí, J. C. Scaiano, *J. Phys. Chem.* **1996**, *100*, 18152−19157.
[157] M. Alvaro, H. Garcia, M. Narayana Pillai, in *PCT Int. Appl.* **2003**, Wo 0311456.
[158] M. Alvaro, E. Carbonell, A. Domenech, V. Fornes, H. Garcia, M. Narayana, *ChemPhysChem* **2003**, *4*, 483−487.
[159] D. F. Duxbury, *Chem. Rev.* **1993**, *93*, 381−433.
[160] T. Tao, G. E. Maciel, *J. Am. Chem. Soc.* **1995**, *117*, 12889−90.
[161] D. R. Rolison, *Chem. Rev.* **1990**, *90*, 867−878.
[162] D. R. Rolison, C. A. Bessel, *Acc. Chem. Res.* **2000**, *33*, 737−744.
[163] C. Song, *Stud. Surf. Sci. Catal.* **1998**, *113*, 163−186.
[164] J. Devynck, F. Bedioui, *J. Phys. IV* **1994**, *4*, 131−46.
[165] F. Bedioui, L. Roue, E. Briot, J. Devynck, K. J. Balkus Jr., J. F. Diaz, *New. J. Chem.* **1996**, *20*, 1235−1241.
[166] K. J. Balkus, F. Bedioui, E. Deboysson, J. Devynck, *J. Chem. Soc., Faraday Trans.* **1991**, *87*, 3831−3834.
[167] K. J. Balkus, F. Bedioui, L. Roue, E. Briot, J. Devynck, S. L. Bell, *J. Electroanal. Chem.* **1994**, *373*, 19−29.
[168] D. B. Rolison, C. A. Bessel, M. D. Baker, C. Senaratne, J. Zhang, *J. Phys. Chem.* **1996**, *100*, 8610−8611.
[169] F. Bedioui, J. Devynck, K. J. Balkus Jr., *J. Phys. Chem.* **1996**, *100*, 8607−8609.
[170] A. Domenech, M. T. Domenech-Carbo, H. Garcia, M. S. Galletero, *Chem. Commun.* **1999**, 2173−2174.
[171] A. Domenech, H. Garcia, M. Alvaro, E. Carbonell, *J. Phys. Chem. B* **2003**, *107*, 3040−3050.
[172] A. Domenech, H. Garcia, M. T. Domenech-Carbo, M. S. Galletero, *Anal. Chem.* **2002**, *74*, 562−569.
[173] T. Yamada, S. Shinoda, H. Tsukube, *Chem. Commun.* **2002**, 1218−1219.
[174] A. Prasana de Silva, D. B. Fox, T. S. Moody, S. M. Weir, *Pure Appl. Chem.* **2001**, *73*, 503−511.
[175] A. Vogler, H. Kunkely, *Top. Cur. Chem.* **2001**, *213*, 143−182.
[176] D. Parker, *Coord. Chem. Rev.* **2000**, *205*, 109−130.
[177] M. Alvaro, V. Fornés, S. García, H. García, J. C. Scaiano, *J. Phys. Chem. B* **1998**, *102*, 8744−8750.
[178] M. Ryo, Y. Wada, T. Okubo, T. Nakazawa, Y. Hasegawa, S. Yanagida, *J. Mater. Chem.* **2002**, *12*, 1748−1753.
[179] Q. Xu, Z. Zhao, L. Li, G. Liu, H. Ding, J. Yu, R. Xu, *Stud. Surf. Sci. Catal.* **2001**, *135*, 3481−3487.
[180] F. L. Cozens, H. García, J. C. Scaiano, *Langmuir* **1994**, *10*, 2246−2249.
[181] M. L. Cano, F. L. Cozens, V. Fornes, H. Garcia, J. C. Scaiano, *J. Phys. Chem.* **1996**, *100*, 18145−18151.
[182] R. Guglielmetti, *Photochromism (Revis. Ed.)* **2003**, 855−878.
[183] I. Casades, S. Constantine, D. Cardin, H. Garcia, A. Gilbert, F. Marquez, *Tetrahedron* **2000**, *56*, 6951−6956.
[184] I. Casades, M. Alvaro, H. Garcia, M. Narayana Pillai, *Photochem. Photobiol. Sci.* **2002**, *1*, 219−223.
[185] C. Schomburg, D. Woehrle, *Zeolites* **1996**, *17*, 232−236.
[186] V. Balzani, F. Scandola, *Supramolecular Photochemistry*, Horwood, England, Chichester, **1991**.
[187] P. R. Ashton, R. Ballardini, V. Balzani, A. Credi, K. R. Dress, E. Ishow, C. J. Kleverlann, O. Kocian, J. A. Preece, N. Spencer, J. F. Stoddart, M. Venturi, S. Wenger, *Chem. Eur. J.* **2000**, *6*, 3558−3574.
[188][188a] M. Alvaro, B. Ferrer, V. Fornes, H. Garcia, J. C. Scaiano, *J. Phys. Chem. B* **2002**, *106*, 6815−6820. [188b] M. Alvaro, M. N. Chretien, B. Ferrer, V. Fornés, H. García, J. C. Scaciano, *Chem. Commun.* **2001**, 2106−2107.
[189] The term co-conformation in supramolecular assemblies refers to changes in the relative distance and position of the individual components of the catenane or rotaxane, rather than conformational motions within each element.
[190] D. J. Cardin, *Adv. Mater.* **2002**, *14*, 553−563.
[191] D. J. Maia, M.-A. De Paoli, O. L. Alves, A. J. G. Zarbin, S. Das Neves, *Quim. Nova* **2000**, *23*, 204−215.
[192] E. Ruiz-Hitzky, P. Aranda, *Anal. Quim., Int. Ed.* **1997**, *93*, 197−212.
[193] T. Bein, *Stud. Surf. Sci. Catal.* **1996**, *102*, 295−322.
[194] M. Alvaro, H. Garcia, A. Gilbert, D. Cardin in *PCT Int. Appl.* **2001**, Wo 2001005840.
[195] D. J. Cardin, S. P. Constantine, A. Gilbert, A. K. Lay, M. Alvaro, M. S. Galletero, H. Garcia, F. Marquez, *J. Am. Chem. Soc.* **2001**, *123*, 3141−3142.
[196] M. Alvaro, B. Ferrer, H. Garcia, A. Lay, F. Trinidad, J. Valenciano, *Chem. Phys. Lett.* **2002**, *356*, 577−584.
[197] M. S. Galletero, M. Alvaro, H. Garcia, C. J. Gomez-Garcia, A. K. Lay, *Phys. Chem. Chem. Phys.* **2002**, *4*, 115−120.
[198] S. Spange, *Angew. Chem. Int. Ed.* **2003**, *42*, 4430−4432.
[199] S. Spange, A. Graeser, H. Mueller, Y. Zimmermann, P. Rehak, C. Jaeger, H. Fuess, C. Baehtz, *Chem. Mater.* **2001**, *13*, 3698−3708.
[200] S. Spange, A. Graser, A. Huwe, F. Kremer, C. Tintemann, P. Behrens, *Chem. Eur. J.* **2001**, *7*, 3722−3728.
[201] M.-K. Jung, M.-H. Kim, S.-S. Hong, *Microporous Mesoporous Mater.* **1998**, *26*, 153−159.
[202] T. Sano, Y. Kiyozumi, K. Maeda, M. Toba, S. Niwa, F. Mizukami, *J. Mater. Chem.* **1992**, *2*, 141−142.

Received November 7, 2003

 © 2004 Wiley-VCH Verlag GmbH & Co. KGaA, Weinheim

Synthesis and Magnetic Properties of Single-Crystals of $MnFe_2O_4$ Nanorods

Jun Wang,[a] Qianwang Chen,*[a] Binyang Hou,[a] and Zhenmeng Peng[a]

Keywords: Iron / Magnetic properties / Nanorods / Nanowires / X-ray diffraction

Single-crystals of $MnFe_2O_4$ nanorods with an average diameter of 20 nm and length of 250 nm were synthesized by a hydrothermal process at 180 °C after 12 h. High-resolution transmission electron microscopy (HRTEM) and electron diffraction (ED) analysis revealed that the nanorods grow along the [110] axis, which is one of the easy magnetization axes of the material $MnFe_2O_4$. It was found that the nanorods exhibited a saturation magnetization (*Ms*) of 68.02 emu/g, which is much higher than that of quasi-spherical particles of $MnFe_2O_4$, prepared by other approaches such as solid-state reaction methods (*Ms* = 36.7 emu/g), and coprecipitation processes followed by annealing in vacuo at 400 °C (*Ms* = 24.4 emu/g). The oriented growth along the easy magnetization axis of $MnFe_2O_4$ was suggested to be responsible for the improvement of magnetic properties of $MnFe_2O_4$ nanorods.

(© Wiley-VCH Verlag GmbH & Co. KGaA, 69451 Weinheim, Germany, 2004)

Introduction

In the nanoscale regime, magnetic nanoparticles have been a subject of increasing interest from both fundamental and technological points of view.[1] It has been shown that the shape of magnetic particles strongly influences their magnetic properties.[2,3] Nanorods and nanowires not only exhibit unique magnetic properties but are also key components for ultrahigh-density magnetic recording media.[4] Many efforts have been made to synthesize nanorods and nanowires of magnetic materials.[5,6] For example, Chaudret et al.[7,8] prepared magnetic nanorods of cobalt by thermal decomposition. Iron nanorods were synthesized through controlled coalescence of spherical iron nanoparticles protected by trioctylphosphane oxide (TOPO).[9] Acicular iron particles were prepared by reduction of ferrous ions with sodium borohydride in tubular lecithin.[10]

The substance $MnFe_2O_4$, one of the most important magnetic materials, has been widely used in electronic applications[11,12] and contrast-enhancement agents in magnetic resonance imaging (MRI) technology,[13−16] in addition to recording media. Several techniques have been developed to synthesize $MnFe_2O_4$ nanoparticles, such as solid-phase reactions,[17] mechanical ball-milling,[18,19] thermal decomposition,[20] and coprecipitation methods.[13,14,21,22] However, the synthesis of $MnFe_2O_4$ nanorods has seldom been reported. The coprecipitation process can provide a quick and easy way to prepare $MnFe_2O_4$ nanoparticles; however, it usually yields nanoparticles with large size-distributions and less well-defined crystals. The rapid formation process is also very disadvantageous to synthesize single-crystal nanorods or nanowires as the product is formed far from equilibrium conditions. The hydrothermal process is one of the more successful ways to grow crystals of many different materials such as quartz and malachite. This technique has also been used to grow dislocation-free single-crystals; grains formed in this process could have a better crystallinity than those from other processes.

Our aim was to develop a low-temperature hydrothermal process for the preparation of $MnFe_2O_4$ nanorods that might find applications in perpendicular recording media.

Results and Discussion

X-ray diffraction (XRD) patterns for the samples obtained at different reaction conditions, which are compatible with cubic $MnFe_2O_4$ crystals (JCPDS card No. 73−1964), are shown in Figures 1 and 2. They revealed that the samples were pure $MnFe_2O_4$ crystals without impurity phases. From Figure 1, one can see that the reflection peaks become sharper and stronger on increasing the hydrothermal temperature and the time period, indicating that crystallinity tends to improve. For example, the crystallinity of the sample prepared at 180 °C (see A in Figure 1) was better after 6 h than after 3 h (see B in Figure 1). The dimensions and shapes of the particles were found to depend strongly on reaction conditions such as temperature, time, and the pH of the reaction system. Uniform $MnFe_2O_4$ nanorods were synthesized at 180 °C after 12 h. Lower temperatures and shorter time periods were favorable for the formation of quasi-spherical particles. For example, the products were dominated by quasi-spherical particles when the reaction was carried out at 140 °C (see A in Figure 3); when the

[a] Structure Research Laboratory and Department of Materials Science & Engineering, University of Science & Technology of China,
Hefei 230026, China
Fax: (internat.) + 86-551-3607292
E-mail: cqw@ustc.edu.cn

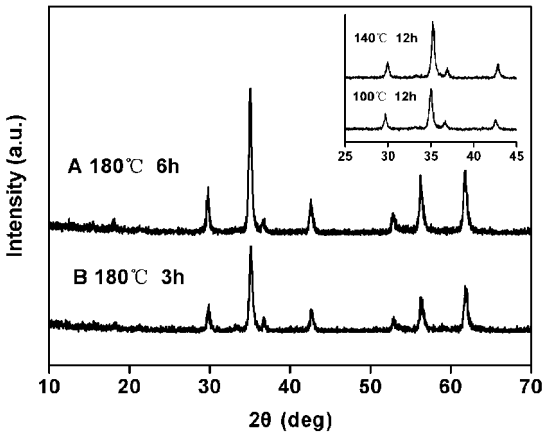

Figure 1. The XRD patterns of the samples prepared at 180 °C after 6 h (A) and 3 h (B); the inset shows XRD patterns of the samples formed at 140 °C and 100 °C after 12 h

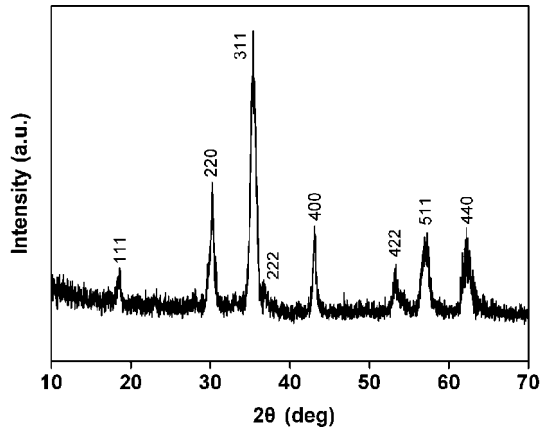

Figure 2. The XRD pattern of the sample prepared at 180 °C after 12 h

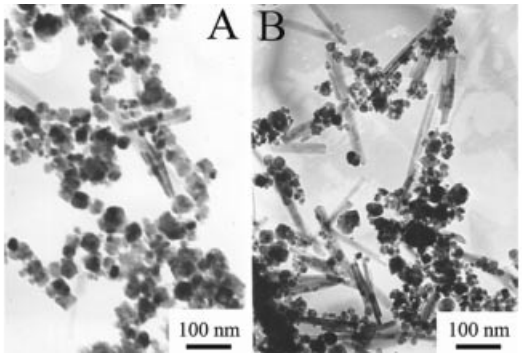

Figure 3. TEM images of the samples obtained at 140 °C after 12 h (A) and at 180 °C after 6 h (B)

temperature was increased to 180 °C, nanorods formed as the major product of the reaction (see A in Figure 4). At 180 °C, as the reaction time was reduced to 6 h, the product was also dominated by quasi-spherical particles (see B in Figure 3). It should be noted that the initial pH of the system had to be higher than 11, otherwise quasi-spherical particles were obtained.

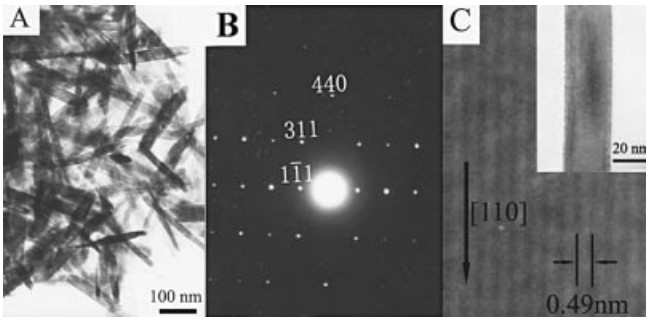

Figure 4. Representative TEM image of $MnFe_2O_4$ nanorods (A), ED pattern of a single-crystals of a nanorod (B) and HRTEM image of the nanorod in the inset (C); the inset in C is a magnified image of one individual $MnFe_2O_4$ nanorod shown in A; the sample was obtained after 12 h at 180 °C.

As shown in Figure 4 (see A), uniform nanorods with an average length of 250 nm and a width of 20 nm were produced at 180 °C after 12 h. From the XRD pattern of the sample shown in Figure 2, we found that the ratio between the intensities of the (220) and (311) diffraction peaks was higher than the conventional value (0.5 versus 0.28), indicating the oriented growth of the nanoparticles. Figure 4 (see B) shows the electron diffraction (ED) patterns obtained from one typical nanorod. The diffraction spots suggest that the nanorod was a single crystal. The high-resolution transmission electron microscopy (HRTEM) image further supports the existence of these $MnFe_2O_4$ nanorods as single crystals (see C in Figure 4). The lattice fringes (ca. 0.49 nm) observed in this image agree well with the separation between the [111] lattice planes. Combined with the result from ED, it was confirmed that the nanorods grew along the [110] plane, which is one of the easy magnetization axes of the $MnFe_2O_4$ nanorods.[23,24]

Indeed, single-crystals of nanorods and nanowires are formed because the relative growth rates of the various faces favor oriented growth along one crystal direction. The experimental conditions such as temperature, time, and pH influence the relative growth rates and can then be used to control the morphology and dimensions of the nanoparticles.

The magnetic properties of the Mn-ferrite samples obtained at 180 °C (see A in Figure 5) and 140 °C (see B in Figure 5) after 12 h were evaluated by a vibrating sample magnetometer. The hysteresis loops of the samples measured at room temperature (Figure 5) show ferromagnetic behavior with a saturation magnetization of 68.02 emu/g, which is slightly smaller than the corresponding bulk material (80 emu/g).[13,25] The reason may mainly depend on the nature of ultrafine particles: surface disorder, cation distribution, and defects etc. For example, a surface-disordered layer could serve as a nonmagnetic layer and decrease saturation magnetization. However, the saturation magnetization of the nanorods is much higher than that for $MnFe_2O_4$ quasi-spherical nanoparticles synthesized by other methods, such as solid-state reactions at 1200 °C (Ms = 36.7 emu/g),[26] coprecipitation followed by annealing in vacuo at 400 °C (Ms = 24.4 emu/g),[25] and is

 © 2004 Wiley-VCH Verlag GmbH & Co. KGaA, Weinheim

also higher than that of our sample (see B in Figure 5) that was hydrothermally prepared at 140 °C after 12 h (*Ms* = 55.8 emu/g), in which quasi-spherical particles are the major products. It is, therefore, reasonable to suggest that the growth along the easy magnetic axis could improve the magnetic properties of the nanorods. During the measurement process, the $MnFe_2O_4$ nanorods tend to align along the magnetic line of force, which makes the easy magnetization axis correspond to the magnetic line of force. Magnetization makes all the net magnetic moments of the $MnFe_2O_4$ nanorods orientate themselves along the magnetic line of force. As a result, the saturation magnetization can be improved. It is, therefore, reasonable to suggest that in addition to the nonmagnetic layer on the surface of the nanoparticles, the morphology could also be an important factor determining the magnetic properties; growth of nanorods along the easy magnetization axis is a way to improve the magnetic properties of nanosized materials.

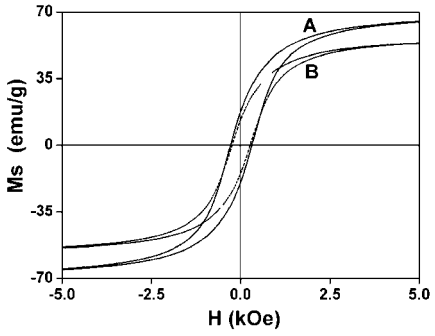

Figure 5. Magnetic hysteresis curves of $MnFe_2O_4$ samples hydrothermally obtained at 180 °C (A) and at 140 °C (B) after 12 h; the measurements were carried out at room temperature

Conclusions

Single crystals of $MnFe_2O_4$ nanorods were synthesized by a hydrothermal process at 180 °C after 12 h. The nanorods (average diameter of 20 nm and length of 250 nm) were found to grow along the easy magnetization axis [110] of the $MnFe_2O_4$ nanoparticles. The saturation magnetization of the nanorods (*Ms* = 68 emu/g) increases significantly to that of quasi-spherical particles prepared by other methods, which indicates that the controlled growth of nanorods along the easy magnetization axis of magnetic materials is a way to improve their magnetic properties. This process might be of general interest for the synthesis of nanorods and other ferrite materials in order to improve their magnetic properties.

Experimental Section

General: The chemical reagents used in this work were iron(III) chloride ($FeCl_3 \cdot 6\,H_2O$), manganese(II) chloride ($MnCl_2 \cdot 4H_2O$), and sodium hydroxide (NaOH). All chemicals were of analytical grade. The reaction is described by Equation (1):

$$MnCl_2 + 2\,FeCl_3 + 8\,NaOH \rightleftarrows MnFe_2O_4 + 4\,H_2O + 8\,NaCl \quad (1)$$

$MnCl_2 \cdot 4H_2O$ and $FeCl_3 \cdot 6\,H_2O$ were dissolved in water at concentrations of 0.05 M and 0.1 M, respectively, ($[Fe^{3+}]/[Mn^{2+}]$ = 2:1. 35 mL). The metal-ion solution mixture was put into a Teflon™-lined stainless autoclave. Sodium hydroxide (0.880 g) dissolved with 5.0 mL distilled water was slowly added dropwise into the Teflon-lined stainless autoclave. A brown precipitate formed immediately. The autoclave was placed into an oven and kept at 180 °C for 12 hours, then allowed to cool to room temperature. The product was washed several times with distilled water and absolute ethanol. The products were finally dried in oven at 60 °C for 12 hours.

X-ray diffraction was performed on a Rigaku X-ray diffractometer with high-strength Cu-K_α radiation. Transmission electron microscope (TEM) images were taken with a Hitachi model H-800 with an accelerating voltage of 200 kV. High-resolution transmission electron microscopy (HRTEM) images were recorded on JEOL-2010 with an accelerating voltage of 200 kV. Their magnetic properties were evaluated on a BHV-55 vibrating sample magnetometer (VSM).

Acknowledgments

This work was supported by the National Natural Science Foundation under the contract No. 20125103 and 90206034.

[1] J. L. Dormann, D. Fiorani, *Magnetic Properties of Fine Particles*, North-Holland, Amsterdam, **1992**.
[2] M. Ozaki, H. Suzuki, K. Takahashi, E. Matijevic, *J. Colloid Interface Sci.* **1986**, *113*, 76.
[3] M. Ozaki, T. Egami, N. Sugiyama, E. Matijevic, *J. Colloid Interface Sci.* **1988**, *126*, 212.
[4] Q. F. Zhan, Z. Y. Chen, D. S. Xue, F. S. Li, *Phys. Rev. B* **2002**, *66*, 134436.
[5] [5a] Y. N. Xia, P. D. Yang, Y. G. Sun, Y. Y. Wu, B. Mayers, B. Gates, Y. D. Yin, F. Kim, H. Q. Yan, *Adv. Mater.* **2003**, *15*, 353. [5b] C. J. Murphy, N. R. Jana, *Adv. Mater.* **2002**, *14*, 80. [5c] S. Valizadeh, L. Hultman, J. M. George, P. Leisner, *Adv. Funct. Mater.* **2002**, *12*, 766. [5d] F. S. Li, L. Y. Ren, *Phys. Status Solidi A* **2002**, *193*, 196.
[6] [6a] L. Vayssieres, N. Beermann, S. E. Lindquist, A. Hagfeldt, *Chem. Mater.* **2001**, *13*, 233. [6b] L. Vayssieres, L. Rabenberg, A. Manthiram, *Nano Letters* **2002**, *2*, 1393. [6c] N. Cordente, M. Respaud, F. Senocq, M. J. Casanove, C. Amiens, B. Chaudret, *Nano Letters* **2001**, *10*, 565.
[7] F. Dumestre, B. Chaudret, C. Amiens, M. C. Fromen, M. J. Casanove, P. Renaud, P. Zurcher, *Angew. Chem. Int. Ed.* **2002**, *41*, 4286.
[8] [8a] Z. A. Peng, X. Peng, *J. Am. Chem. Soc.* **2001**, *123*, 1389. [8b] J. M. Petrovski, Z. L. Wang, *J. Phys. Chem. B* **1998**, *102*, 3316.
[9] S. J. Park, S. Kim, S. Lee, Z. G. Khim, K. Char, T. Hyeon, *J. Am. Chem. Soc.* **2000**, *122*, 8581.
[10] [10a] J. L. Cain, D. E. Nikles, *IEEE Trans. Magn.* **1997**, *33*, 3718. [10b] J. L. Cain, D. E. Nikles, *J. Appl. Phys.* **1996**, *79*, 4860.
[11] B. Gillot, *Eur. Phys. J. Appl.* **1998**, *4*, 243.
[12] M. Sugimoto, *J. Am. Ceram. Soc.* **1999**, *82*, 269.
[13] Z. X. Tang, C. M. Sorensen, K. J. Klabunde, G. C. Hadjipanayis, *Phys. Rev. Lett.* **1991**, *67*, 3602.
[14] G. U. Kulkarni, K. R. Kannan, T. Arunarkavalli, C. N. R. Rao, *Phys. Rev. B* **1994**, *49*, 724.
[15] P. J. van der Zaag, V. A. M. Brabers, M. T. Johnson, A. Noordermeer, P. E. Bongers, *Phys. Rev. B* **1995**, *51*, 12009.

 © 2004 Wiley-VCH Verlag GmbH & Co. KGaA, Weinheim

[16] B. Gillot, M. Laarj, S. Kacim, *J. Mater. Chem.* **1997**, *7*, 827.
[17] M. D. Nasr-Allah, G. A. El-shobaky, *Thermochimica Acta* **2001**, *375*, 137.
[18] M. Muroi, R. Street, P. G. McCormick, J. Amighian, *Phys. Rev. B* **2001**, *63*, 184414.
[19] J. Ding, P. G. McCormick, R. Street, *J. Magn. Magn. Mater.* **1997**, *171*, 309.
[20] G. Balaji, N. S. Gajbhiye, G. Wilde, J. Weissmuller, *J. Magn. Magn. Mater.* **2002**, *242−245*, 617.
[21] Z. X. Tang, J. P. Chen, C. M. Sorensen, K. J. Klabunde, G. C. Hadjipanayis, *Phys. Rev. Lett.* **1992**, *68*, 3114.
[22] J. P. Chen, C. M. Sorensen, K. J. Klabunde, G. C. Hadjipanayis, E. Devlin, A. Kostikas, *Phys. Rev. B* **1996**, *54*, 9288.
[23] Y. L. Li, G. D. Li, *Physics of Ferrite*, Publishing House of Electronics Industry of Science, Beijing, **1978**, p. 381.
[24] D. F. Wan, X. L. Ma, *Magnetic Physics*, Publishing House of Electronics Industry, Beijing, **1999**, p. 169.
[25] M. Zheng, X. C. Wu, B. S. Zou, Y. J. Wang, *J. Magn. Magn. Mater.* **1998**, *183*, 152.
[26] J. F. Hu, H. W. Qin, Y. Z. Wang, S. G. Zhang, Z. X. Wang, *J. Mater. Sci. Lett.* **2001**, *20*, 1531.

Received August 10, 2003

 © 2004 Wiley-VCH Verlag GmbH & Co. KGaA, Weinheim

Towards 3-D Spherical Self-Assembly by Ternary Surfactant Combinations: The Case of Magnetite Nanoparticles

Yanglong Hou,[a,b] Song Gao,*[a] Toshiaki Ohta,[b] and Hiroshi Kondoh[b]

Keywords: Self-assembly / Magnetic properties / Magnetite / Nanoparticles / Super paramagnet

Here we report on a facile one-step route to assemble magnetite nanoparticles into 3D-spherical aggregates with an average diameter of 100 nm. The self-assembly approach was achieved in a solvothermal reduction reaction with a ternary surfactant combination comprising trioctylphosphane oxide (TOPO), polyvinylpyrrolidone (PVP), and oleic acid as the "mortar". Transmission electron microscopy (TEM) investigations indicated that the spherical aggregates were composed of magnetite nanoparticles. The mean size of the individual magnetite particles was estimated to be 6 nm, calculated by the Scherrer equation with the powder X-ray diffraction (XRD) data. The formation mechanism of magnetite spheres can be attributed to the cooperation of the ternary surfactants described above. Magnetic measurements performed by a Quantum Design SQUID magnetometer on the nanoparticles exhibited superparamagnetic behavior above liquid-nitrogen temperatures. Fourier-transform infrared spectroscopy (FTIR), inductively coupled plasma-atomic emission spectrometer (ICP-AE) and X-ray photoelectron spectroscopy (XPS) were also used in the characterization of the assembled magnetite spheres.
(© Wiley-VCH Verlag GmbH & Co. KGaA, 69451 Weinheim, Germany, 2004)

Introduction

In recent years, the assembled nanostructures have attracted much interest because of their potential for application in magnetic recording, molecular recognition, biological labeling, and electronic devices.[1−10] The development of simple routes for the fabrication of ordered nanostructures is indispensable for producing new nanodevices. A number of techniques have been exploited in assembly approaches to nanoparticles, such as aerosol-assisted, thiol-modified, DNA-directed, electrostatic-interaction-assisted, and recognition-mediated synthesis.[11−14] The construction of organized metal nanoparticles has recently been a major issue.[15−18] An efficient approach to build self-assembled structures is to harness the spontaneous control of noncovalent interactions between the building blocks, including van der Waals forces,[19,20] π−π interactions,[21] electrostatic forces,[22,23] and hydrogen bonding.[24−26] These molecular interactions are usually constructed through polymer functionalization of nanoscale materials, after which such polymer-functionalized nanoparticles are used as building blocks to fabricate an assembled structure system. For example, Rotello and co-workers reported that monolayer polymer-protected gold nanoparticles self-assembled into spherical aggregates through hydrogen-bonding interactions.[26] The self-assembly of 2-caroxyterthiophene (TTP-COOH) coated Fe_3O_4 aggregates was also achieved by π−π interactions.[21] However, the preparation of ordered nanostructures for applications has been more challenging.

Herein, we report an intriguing finding of self-assembly magnetic particles into spherical aggregates. Our strategy is to use a ternary surfactant combination such as trioctylphosphane oxide (TOPO), polyvinylpyrrolidone (PVP), and oleic acid for the assembly of magnetite nanoparticles. In the presence of these surfactants, the spherical aggregates of magnetite were obtained by a solvothermal reduction of iron(III) acetylacetonate with hydrazine in ethylene glycol. Note that the spherical aggregates of magnetite nanoparticles formed spontaneously without any external force.

Results and Discussion

Powder XRD and TEM measurements were employed to study the structure and the morphology of the obtained products. The XRD pattern of the sample (Figure 1) reveals the characteristic diffraction peaks of magnetite (JCPDS file, 19−629). The broad nature of the peaks results from nanosized magnetite aggregates. The average size of the individual magnetite particles is about 6 nm, calculated by the

[a] State Key Laboratory of Rare Earths Materials Chemistry and Applications, College of Chemistry and Molecular Engineering, Peking University,
Beijing 100871, P. R. China
Fax: (internat.) +86-10-6275-1708
E-mail: gaosong@pku.edu.cn
[b] Department of Chemistry, School of Science, The University of Tokyo,
Tokyo 113-0033, Japan
Supporting information for this article is available on the WWW under http://www.eurjic.org or from the author.

Scherrer equation.[27] In addition, far-IR and XPS spectra were applied to confirm the formation of magnetite rather than hematite. The far-FTIR spectrum of the sample is in good agreement with that of commercially available magnetite powder (Alfa catalog No 44120, see Supporting Information Figure S1), suggesting the formation of magnetite. Furthermore, as shown in the XPS spectra (Figure S2, see Supporting Information), the binding energy of Fe $2p_{3/2}$ is 711.4 eV, which is very close to that of magnetite. TEM images (Figure 2) show that the mean size of the spherical aggregates is about 100 nm. The selected-area electron diffraction (SAED) pattern of the sample indicates the crystalline characteristics of magnetite aggregates (see c in Figure 2). The formation process of assembled magnetite aggregates is illustrated in Scheme 1. It is well-known that the dipole−dipole interaction between magnetic nanoparticles strongly affects their shape and properties. However, this magnetic interaction scarcely contributes to the formation of spherical nanostructures of magnetite nanoparticles; similar behavior has also been observed in the TTP-COOH-coated Fe_3O_4 nanoparticle system.[21] In the present system, the key factor that directs the assembly of spheres is considered to be the combination of ternary surfactants on the surface of the magnetite nanoparticles, although the interaction between magnetite nanoparticles and surfactants is not fully understood. When only PVP was used in the reaction, iron nanoparticles (ca. 60 nm) without spherical aggregation were obtained,[28] whereas the similar systems with PVP and oleic acid produced magnetite nanoparticles where the size could be controlled.[29,30] It was supposed that the process to produce assembled spherical nanostructures was controlled by the diffusion growth,[31] that is, a number of nanoparticles aggregated around a single nanoparticle automatically forming spherical aggregates, which have the lowest surface energy. As the reaction progresses, magnetite nanoparticles coated with surfactants were initially produced. This is followed by the assembly of the individual surfactant-coated magnetite nanoparticles into spherical structures with the help of intermolecular interactions, which result from the cooperation of TOPO, oleic acid, and PVP.[31,32] The total content of the surfactants was 54.4 wt-%, estimated by ICP measurements. As shown in the FTIR pattern (Figure S3, see Supporting Information), the characteristic peak of PVP in the sample ($\tilde{\nu}$ = 3398 cm^{-1}) has a small blue-shift, relative to that of neat

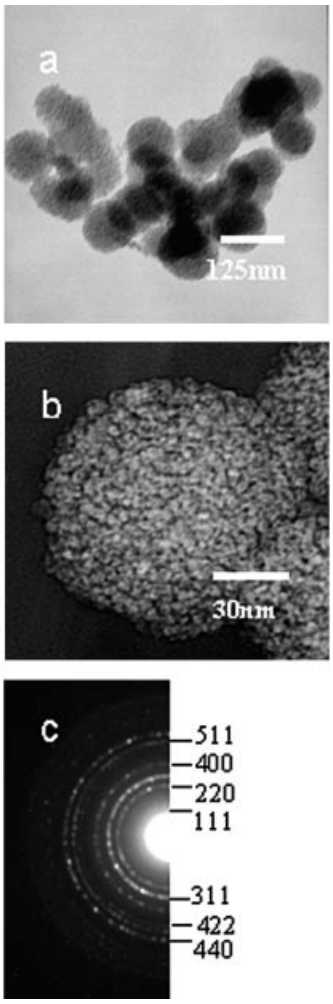

Figure 2. TEM images of (a) self-assembled spherical aggregates, (b) an enlarged image of a individual sphere, and (c) the selected-area electron diffraction pattern of the sample

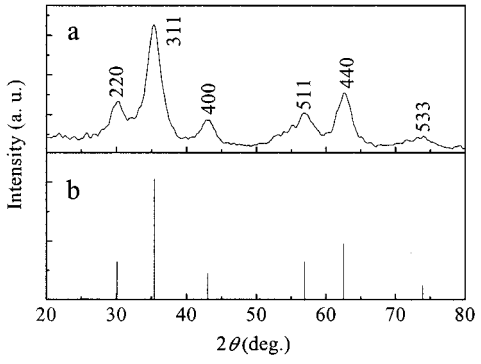

Figure 1. XRD patterns of the sample (a) and commercial magnetite powder (b) with JCPDS No. 19-629

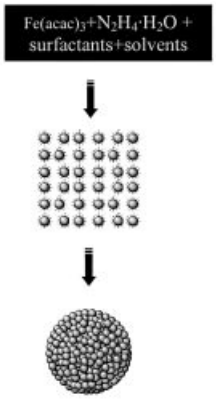

Scheme 1. Schematic pattern of self-assembly of 3D magnetic spheres

 © 2004 Wiley-VCH Verlag GmbH & Co. KGaA, Weinheim

PVP, while the peak intensities of TOPO and oleic acid are obviously weakened, which is most likely ascribed to the interaction of the surfactants with the nanoparticles. This result also confirms the above description on the formation process of nanoparticle aggregates. Further studies are required to characterize the structural features and the interaction between the nanoparticles and the surfactants in the assembled magnetite aggregates.

The magnetization curves were measured as a function of temperature with an applied field of 100 Oe between 5 and 300 K using field-cooling (FC) and zero-field-cooling (ZFC) procedures. When the sample is cooled to the zero magnetic field temperature, the total magnetization of the particles will be zero since the magnetic moments of individual particles are randomly oriented. An external magnetic field energetically favors the reorientation of the moments of the individual particles along the applied field at low temperatures. As the temperature increases, more and more particles reorient their magnetization with the external field and the total magnetization increases, and reaches the maximum at the blocking temperature (T_B = 70 K), shown in Figure 3. At this temperature, the thermal energy becomes similar to the energy gained by aligning the particle magnetic vectors in the weak field; the transition from ferromagnetic to superparamagnetic behavior is observed. At temperatures higher than T_B, one can see that the magnetization decreases and follows a Curie−Weiss law corresponding to the superparamagnetic behavior, also suggesting the absence of strong dipole−dipole interactions. Such behavior has been reported for several particle systems, in agreement with theoretical predictions.[33] In the case of field cooling, magnetization monotonously increases as the temperature decreases. Below T_B, the field-cooling curve splits from the zero-field-cooling curve.

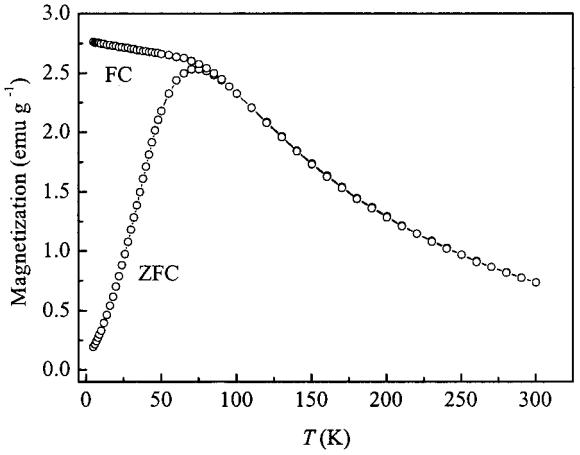

Figure 3. ZFC and FC curves of self-assembled magnetite spherical aggregates measured with a field of 100 Oe

The divergence of magnetization below T_B in ZFC-FC procedures is attributed to the existence of the magnetic anisotropy barriers. The derivative of the magnetization decay plot, $f(T)$ represents the distribution of anisotropy energy barriers.[34]

$$f(T) = \frac{d}{dT}\left(\frac{M_{ZFC}}{M_{FC}}\right) \quad (1)$$

This is represented by Equation (1) where M_{ZFC} denotes only the contribution of nanoparticles, for which the energy barriers are overcome by the thermal energy at the measurement; while M_{FC} represents the contribution of all the nanoparticles. The calculated magnetic anisotropy distribution of 6 nm spherical Fe_3O_4 aggregates is shown in Figure 4 and fitted by the Gauss function. The center and width values are 33.0 K and 40.7 K, respectively. The narrow distribution indicates that the nanoparticles have a uniform size. For superparamagnetic particles, $T_B = KV/25k$, where T_B is the blocking temperature, K denotes the magnetic anisotropy constant, k the Boltzmann's constant, and V the volume of the particles; below T_B the free movement ($\mu_p = Ms \cdot V$) is blocked by the anisotropy, where Ms represents the saturation magnetization. Above T_B, kT activates the magnetic moment so that the system appears to have the characteristics of a superparamagnet. The anisotropy constant can be estimated by referring to the experimental data of the blocking temperature. In the present system, the anisotropy constant of the assembled magnetite nanoparticle with a size of 6 nm is 2.14×10^6 erg·cm^{-3}.

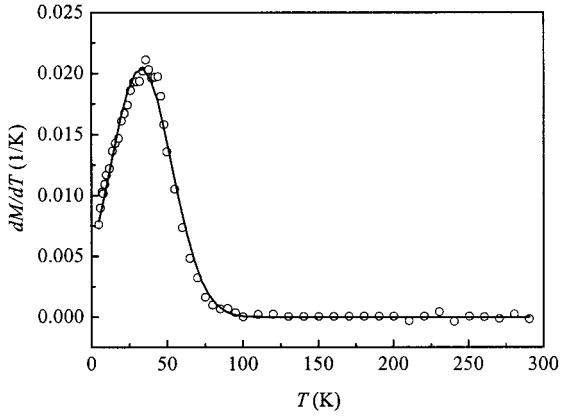

Figure 4. The energy barrier distribution of magnetic anisotropy in the self-assembled magnetite aggregates

A representative hysteresis loop of assembled Fe_3O_4 spheres is shown in Figure 5. At 300 K, the saturation magnetization of the assembled Fe_3O_4 particles is 83 emu/g at 30 kOe, while that of the commercial magnetic liquid is 123 emu/g(Fe).[35] The decrease of the saturation magnetization is most likely attributed to the existence of surfactants on the surface of the Fe_3O_4 nanoparticles. Some studies suggested that the noncollinear spin structure, which originated from pinning the surface spins and coated surfactants to the iron oxide interface, results in the reduction of the magnetic moment in such nanoparticles.[36] The coercive force of self-assembled spheres is 292 Oe at 5 K (as shown

 © 2004 Wiley-VCH Verlag GmbH & Co. KGaA, Weinheim

by the inset in Figure 5), while the coercivity at room temperature is almost negligible, which is a characteristic of superparamagnetic materials.[37,38]

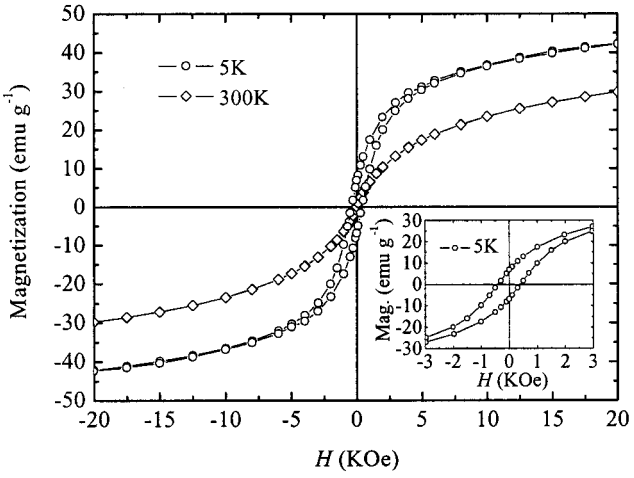

Figure 5. Magnetization of self-assembled magnetite aggregates as a function of the applied field measured at 5 K and 300 K. The inset is an enlarged magnetization curve of self-assembled Fe_3O_4 nanoparticles at 5 K

Conclusion

In this work, a facile and effective route has been developed to build 3D, spherical aggregates of nanoparticles with ternary surfactants as the "mortar". The results reveal that the self-assembly strategy is an efficient way to create novel nanostructured systems. The magnetic behavior of spherical magnetite aggregates shows superparamagnetic characteristics above liquid-nitrogen temperatures. The magnetic anisotropy distribution of the spherical magnetite aggregates has also been deduced from magnetic data.

Experimental Section

General: The synthesis and assembly of magnetite spheres was performed by a one-step procedure, in which $Fe(acac)_3$ (acac = acetylacetonate) was partially reduced by a mixture of hydrazine and ethylene glycol and spontaneously assembled into spherical nanostructures in the presence of a combination of surfactants including TOPO, PVP, and oleic acid. In a typical procedure, a solution of 70 mL was first prepared by dissolving $Fe(acac)_3$ (0.2 g), TOPO (99 %, 0.2 g), PVP (M_r = 55,000, 0.2 g), and oleic acid (0.1 mL) in ethylene glycol, after which 10 % $N_2H_4{\cdot}H_2O$ (2 mL) was added. The mixture was transferred into an autoclave and heated to 180 °C for 12 h and then allowed to cool to room temperature. The black products deposited onto the bottom of the autoclave indicated the formation of magnetite. The final product was collected and washed with methanol/$CHCl_3$ (1:1) and distilled water to remove possible excess surfactants, $N_2H_4{\cdot}H_2O$, and by-products. The black product was then dried in vacuo at 60 °C for 12 h. Powder XRD patterns of the sample were obtained on a Rigaku Dmax/2000 diffractometer with Cu-K_α radiation. TEM images to determine the size and morphology of the product were collected with a HITACHI H-800 electron microscope (200 kV). IR spectra (KBr pellets) were recorded on a NICOLET Magna-IR 750 spectrophotometer. X-ray photoelectron spectroscopy (XPS) data were collected on a ESCA-lab5. The content of magnetite in the product was determined on an inductively coupled plasma-atomic emission spectrometer (ICP). Magnetic studies were carried out by using a Quantum Design SQUID magnetometer.

Acknowledgments

Financial support from the National Science Fund for Distinguished Young Scholars (20125104), NFSC no.20221101, and the Chinese Postdoctoral Research Fund are gratefully acknowledged.

[1] M. Bruchez, M. Moronne, P. Gin, S. Weiss, A. P. Alivisatos, *Science* **1998**, *281*, 2013−2016.
[2] C. B. Murray, S. Sun, H. Doyle, T. Betley, *MRS. Bull.* **2001**, 985−989.
[3] J. Z. Zhang, Z. L. Wang, J. Jiu, S. Chen, G. Y. Liu. *Self-assembled Nanostructures*, Kluwer, New York, **2003**.
[4] S. Sun, C. B. Murray, D. Weller, L. Folks, A. Moser, *Science* **2000**, *287*, 1989−1992.
[5] M. Green, P. O'Brien, *Chem. Commun.* **2001**, 1912−1913.
[6] E. V. Shevchenko, D. Talapin, A. L. Rogach, A. Kornowski, M. Haase, H. Weller, *J. Am. Chem. Soc.* **2001**, *124*, 11480−11485.
[7] F. Dumestre, B. Chaudret, C. Amiens, M. C. Fromen, M. J. Casanove, P. Renaud, P. Zurcher, *Angew. Chem. Int. Ed.* **2002**, *41*, 4286−4289.
[8] H. Bönnemann, R. M. Richards, *Eur. J. Inorg. Chem.* **2001**, 2455−2480.
[9] G. Schmid, N. Beyer, *Eur. J. Inorg. Chem.* **2002**, 835−837.
[10] J. S. Bradley, B. Tesche, W. Busser, M. Maase, M. T. Reetz, *J. Am. Chem. Soc.* **2000**, *122*, 4631−4636.
[11] Y. Lu, H. Fan, A. Stump, T. L. Ward, T. Rieker, C. J. Brinker, *Nature* **1999**, *398*, 223−226.
[12] L. Motte, M. P. Pileni, *Appl. Surf. Sci.* **2000**, *164*, 60−67.
[13] R. C Mucic, J. J. Storhoff, C. A. Mirkin, R. L. Letsinger, *J. Am. Chem. Soc.* **1998**, *120*, 12674−12675.
[14] B. L. Frankamp, O. Uzun, F. Iihan, A. K. Boal, V. M. Rotello, *J. Am. Chem. Soc.* **2002**, *124*, 15146−15147.
[15] A. P. Alivisatos, K. P. Johnsson, X. Peng, T. E. Wilson, C. J. Loweth, M. P. Bruchez Jr., P. G. Schultz, *Nature* **1996**, *382*, 609−611.
[16] X. Peng, L. Manna, W. Yang, J. Wickham, E. Scher, A. Kadavanich, A. P. Alivisatos, *Nature* **2000**, *404*, 59−61.
[17] K. Naka, H. Itoh, Y. Chujo, *Langmuir* **2003**, *19*, 5496−5501.
[18] L. E. Euliss, S. G. Grancharov, S. O'Brien, T. J. Deming, G. D. Stucky, C. B. Murray, G. A. Held, *Nano Lett.* **2003**, *3*, 1489−1493.
[19] J.-M. Lehn, *Supramolecular chemistry*, VCH, Weinheim, **1995**.
[20] R. P. Andres, J. D. Bielefeld, J. I. Henderson, D. B. Janes, V. R. Kolagunta, C. P. Kubiak, W. J. Mahiney, R. G. Osifchin, *Science* **1996**, *273*, 1690−1694.
[21] J. Jin, T. Iyoda, C. Cao, Y. Song, L. Jiang, T. J. Li, D. B. Zhu, *Angew. Chem. Int. Ed.* **2001**, *40*, 2135−2138.
[22] M. C. T. Fyfe, J. F. Stoddart, *ACC. Chem. Res.* **1997**, *30*, 393−401.
[23] F. Caruso, R. Caruso, H. Mohwald, *Science* **1998**, *282*, 1111−1114.
[24] C. A. Mirkin, R. L. Letsinger, R. C. Mucic, J. J. Storhoff, *Nature* **1996**, *382*, 607−609.
[25] J. Rebek, *Acc. Chem. Res.* **1999**, *32*, 278−286.
[26] A. K. Boal, F. Ilhan, J. E. Derouchey, T. Thurn-Albercht, T. P. Russell, V. M. Rottello, *Nature* **2000**, *404*, 746−748.
[27] H. P. Klug, L. E. Alexander, *X-ray Diffraction Procedures for polycrystalline and Amorphous Materials*; John Wiley & Sons, New York, **1962**, pp. 491−538.

 © 2004 Wiley-VCH Verlag GmbH & Co. KGaA, Weinheim

[28] Y. L. Hou, S. Gao, *J. Alloy Com.* **2004**, *365*, 112−116.
[29] S. Sun, H. Zeng, *J. Am. Chem. Soc.* **2002**, *124*, 8204−8205.
[30] Y. Hou, J. Yu, S. Gao, *J. Mater. Chem.* **2003**, *13*, 1983−1987.
[31] D. V. Goia, E. Matijevi, *New J. Chem.* **1998**, 1203−1215.
[32] X. Peng, J. Wickham, A. P. Alivisatos, *J. Am. Chem. Soc.* **1998**, *120*, 5343−5344.
[33] E. del Barco, J. Asenjo, X. X. Zhang, R. Pieczynski, A. Julià, J. Tejada, R. F. Ziolo, *Chem. Mater.* **2001**, *13*, 1487−1490.
[34] A. J. Rondinone, A. C. S. Samia, Z. J. Zhang, *J. Phys. Chem. B* **1999**, *103*, 6876−6880.
[35] K. S. Suslick, M. Fang, T. Hyeon, *J. Am. Chem. Soc.* **1996**, *118*, 11960−11961.
[36] R. H. Kodama, A. E. Berkowitz, E. J. McNiff, S. Foner, *Phys. Rev. Lett.* **1996**, *77*, 394−397.
[37] I. Prigogine, S. A. Rice, *Advances in Chemical Physics*, John Wiley & Sons, New York, **1997**, vol. 98.
[38] *Nanoscale materials in Chemistry:* Kenneth J. Klabunde (Ed.), John Wiley & Sons, New York, **2001**, 205.

Received October 24, 2003

 © 2004 Wiley-VCH Verlag GmbH & Co. KGaA, Weinheim

(μ-Methylene)bis(methylzirconocene): Preparation, Molecular Structure, and Thermal Disproportionation

Marijke Hogenbirk,[a,b] Gerrit Schat,[a] Otto S. Akkerman,[a] Friedrich Bickelhaupt,*[a] Jörg Schottek,[c] Markus Albrecht,[c] Roland Fröhlich,[c][‡] Gerald Kehr,[c] Gerhard Erker,*[c] Huub Kooijman,[d] and Anthony L. Spek[d][‡]

Keywords: Magnesium / Metallocenes / Zirconium / Configuration at carbon

The title compound $[(\mu\text{-}CH_2)(ZrCp_2Me)_2]$ (**4**) was prepared by the reaction of $[Cp_2Zr(Cl)Me]$ (**6**) with $CH_2(MgBr)_2$ (**5**) or $(CH_2Mg)_n$ (**7**). It had been expected that the carbon atom bridging the two zirconium atoms of **4** might be a candidate for a planar tetracoordinate carbon atom, but the X-ray crystal structures of two different modifications (crystals 1 and 2) showed it to be non-planar; however, the widened Zr–C–Zr angle of 132.7(1) and 134.0(3)°, respectively, and an unsymmetrical coordination of the central μ-CH_2 group (average: Zr1–CH_2 2.225 Å, Zr2–CH_2 2.242 Å) indicates a tendency towards planarity. While **4** is relatively stable in THF solution, it disproportionates in toluene solution to give the 1,3-dizirconacyclobutane $(Cp_2ZrCH_2)_2$ (**8**) and $[Cp_2ZrMe_2]$ (**9**), especially in the presence of magnesium salts; a tentative mechanism is presented. Reaction of **4** with $B(C_6F_5)_3$ yielded the methyl-bridged cationic complex **17**, which, on treatment with trityl chloride, was transformed into the corresponding chloro complex **18**; the latter was characterized by an X-ray crystal structure determination. With THF and tetrahydrothiophene, **17** formed the unsymmetrical adducts **19a** and **19b**, respectively; NMR spectroscopic data revealed dynamic symmetrization due to methyl-group exchange at 280 and 213 K, respectively.

(© Wiley-VCH Verlag GmbH & Co. KGaA, 69451 Weinheim, Germany, 2004)

Introduction

Tetracoordinate carbon centers strongly prefer a tetrahedral geometry, as is common knowledge since the early work of van't Hoff and Le Bel.[1] Two strategies have been applied to stabilize the unfavorable planar geometry: one of them uses strain to force the carbon atom into planarity, the other stabilizes the planar carbon atom electronically by di- or polysubstitution with metal atoms.[2−5]

Thus, in the gas phase, the Al_4C^- ion (**1**; Scheme 1) has been shown by PES spectroscopy and by calculation to have a planar D_{4h} symmetry.[4] Erker et al. have been successful in preparing stable compounds involving a planar tetracoordinate carbon atom incorporated into a π- or an aromatic system such as **2**; the asterisk marks the planar carbon atom.[6] Another example of such a dimetallic compound is **3**. In this case the planarity around the carbon atom was not effected, but a widening of the Zr−CH−CH_2 angle approaching local C_{2v} symmetry, as indicated in Scheme 1, shows the incipient tendency of this carbon atom to become severely distorted as well.[7]

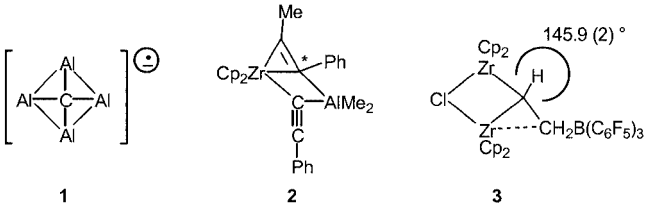

1 2 3

Scheme 1

It remains a challenge to try and prepare a stable planar tetracoordinate saturated carbon atom. In this context, we investigated the possibility that the methylene carbon atom in $[(\mu\text{-}CH_2)(Cp_2ZrMe)_2]$ (**4**) might be a candidate.

[a] Scheikundig Laboratorium, Vrije Universiteit,
De Boelelaan 1083, 1081 HV Amsterdam, The Netherlands
Fax: (internat.) + 31-20-444-7488
E-mail: bicklhpt@few.vu.nl
[b] Present address: AKZO Nobel, N. V. Organon,
Molenstraat 110, P. O. Box 20, 5340 BH Oss, The Netherlands
[c] Organisch-Chemisches Institut der Universität Münster,
Corrensstraße 40, 4400 Münster, Germany
Fax: (internat.) + 49-251-833-9772
[d] Bijvoet Center for Biomolecular Research, Crystal and Structural Chemistry, Utrecht University,
Padualaan 8, 3584 CH Utrecht, The Netherlands
[‡] Correspondence concerning the crystallography should be addressed to these authors.

Results and Discussion

Synthesis of [(μ-CH_2)($Cp_2ZrMe)_2$] (4)

The methylene di-Grignard reagent $CH_2(MgBr)_2$ (**5**)[9−11] seemed to be a promising starting material; reaction of **5** with 2 equiv. of chloro(methyl)zirconocene (**6**)[12] is expected to yield the desired **4** (Method I, Scheme 2). Methylenemagnesium $(CH_2Mg)_n$ (**7**)[9] is potentially an alternative synthon for this purpose (Method II); originally, it was considered less attractive because it is obtained via **5**, but at a later stage **7** turned out to offer certain advantages (vide infra).

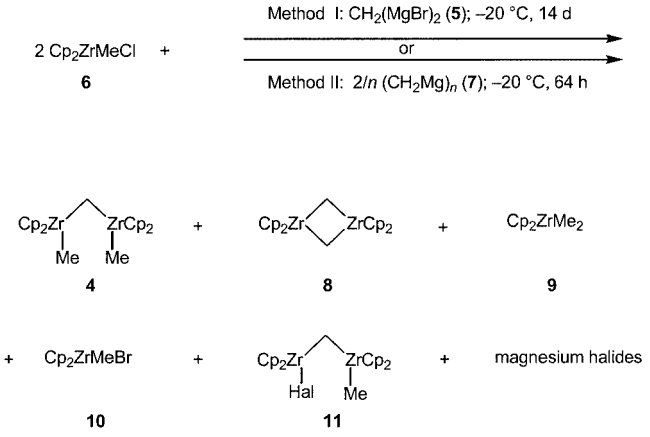

Scheme 2

According to Method I, **5** (in benzene/diethyl ether) and **6** (in toluene) were treated at low temperatures and during longer periods. After removal of the solvents, the residue was extracted with pentane and subsequently with benzene. Table 1 shows the relative amounts of the products **4**, **8**, **9**, **10**, and **11** in the pentane and the benzene extract, respectively. The compounds were identified by ^1H NMR spectroscopy, the signals of **8**[12] and **9**[13] being in agreement with literature data, and those of **10** showing a great similarity to those of **6**. Furthermore, the structure of **4** (containing a small amount of impurity, presumably **11**) was established by X-ray crystal structure determination (vide infra).

Table 1. Formation of **4** and of by-products from **6**[a]

Reactant	Extract	**4**	**8**	**9**	**6/10**	**11**
5	pentane	16	8	37	37[b]	2
5	benzene	68	7	6	10[b]	9
7	pentane	14	14	14	53[c]	5
7	benzene	66	4	4	21[c]	5

[a] Relative amounts (%). [b] **10** only. [c] **6** + **10**.

We assume that **8** and **9** are formed by disproportionation of **4**; this reaction will be discussed later. Compound **10** is formed from **6** by halogen exchange with the bromide ion derived from **5**, while **11** probably results from the reaction of **5** with **6** and Cp_2ZrCl_2 (Scheme 3), present as an impurity in the starting material **6** (about 10%). The structural assignment of **11** as a minor side-product is only tentative and this holds, in particular, for the halogen involved. An argument for the halogen being chlorine (**11′**) might be derived from the observation (vide infra) that when the bromine-deficient **7**, instead of **5**, was treated with **6**, the chlorine atom in the latter was not fully replaced to give **10**, whereas **11** remained unchanged. Furthermore, the crystal structure analysis of **4** (vide infra) indicates the presence of (some) bromine as an impurity at this position (**11"**).

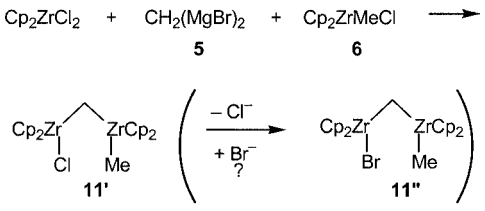

Scheme 3

From the composition of the extracts with benzene as compared to those with pentane, it is obvious that a certain degree of purification of **4** was accomplished by sequential extraction. Hydrolysis of the residues that were insoluble in both solvents, followed by titration (Mg^{2+} with EDTA and OH^- with HCl),[14] indicated that about 10% of the di-Grignard reagent **5** had not reacted. An exact determination of the yields is difficult and has not been attempted. However, from a preparative point of view, this route to **4** appears to be an attractive one, as was concluded from the results of the titration and, after evaporation of the solvent, from the visual observation that the pentane extract contained only a very small amount of material while the benzene extract, containing a substantial amount of material, consisted of nearly 70% of **4**.

The reaction of **5** with **6** was performed under a variety of conditions; a reaction temperature of −20 °C and a relatively long reaction time of 14 d appeared to provide the best results. The extraction with benzene had to be performed quickly and at 5 °C (around the melting point of benzene) because at room temperature the proportion of the side products **8** and **9** increased significantly. After the workup procedure (extraction with pentane and benzene), the extracts contained fewer magnesium salts than the original reaction mixture. This is presumably due to the low solubility of such salts in hydrocarbons, which is only slightly increased by the presence of diethyl ether; this diethyl ether is introduced with the solvent of **5** (vide supra) and successively depleted during the extraction. As disproportionation of **4** now occurred at a lower rate than before workup (**8** can be readily recognized by its red color), we speculated that magnesium halides might play a role in this disproportionation process.

To test this hypothesis, we investigated the formation of **4** from **6** and **7** (Method II), because in this case the amount of magnesium salts in the final product is strongly reduced. Unfortunately, it is not possible to obtain **7** completely bro-

 © 2004 Wiley-VCH Verlag GmbH & Co. KGaA, Weinheim

mide-free.[9] The amount of residual salts depends on the intensity of extraction of $MgBr_2$ from **7** with THF, two to four extractions being a compromise between purity and yield of **7**.[9] In our case, titration after hydrolysis of **7** showed that the Mg^{2+}/OH^- ratio was 1:1.6 (instead of 1:2 as required for pure **7**), indicating a formal **7**/$MgBr_2$ ratio of 80:20 (in reality this product consists of a mixture of various oligomeric combinations of the two formal constituents).[9] Nevertheless, it is obvious that the amount of magnesium halides present after formation of **4** should be reduced considerably. Now, as expected, short periods at temperatures higher than −20 °C did not immediately lead to formation of side products; after about 10 min at 5 °C, the red color of **5** was not observed. In the product mixture, some starting material **6** was identified (^{1}H NMR spectroscopy). As **7** contained much less (magnesium) bromide than **5**, complete halogen exchange transforming **6** to **10** did not occur; instead, a mixture of both **6** and **10** was formed.

The absolute yield of **4** from **7** was determined by ^{1}H NMR spectroscopy with cyclopentane as internal standard and found to be 56% (in a ratio of 53:3 for the benzene and the pentane extract, respectively). According to ^{1}H NMR spectroscopy, **4** obtained by this procedure was converted into **8** and **9** much more slowly, confirming our assumption that magnesium halides promote the disproportionation.

Another attractive aspect of Method II is that the reaction with **7** is much faster than with **5** (64 h versus 14 d, see Scheme 2).

Structural Characterization of 4

After several attempts, yellow-orange crystals of **4**, suitable for an X-ray crystal-structure determination, were isolated from a product mixture obtained from Method II by dissolving the material in toluene/heptane (5:1) and repeated crystallizations at −80 °C. At room temperature, the crystals were quickly transferred into Lindemann glass capillaries in a glovebox under nitrogen and afterwards kept at −20 °C. The structure (**4**, crystal 1) is shown in Figure 1; selected bond lengths and angles are presented in Table 2.

A second single crystal of **4** was obtained from the reaction of **5** with **6** that was carried out in toluene (0 °C to room temperature). After workup and removal of the magnesium halides, pentane was added. From the toluene/pentane (5:2) solution bright yellow crystals of **4** were obtained at −30 °C. A second X-ray crystal structure analysis was performed with these crystals, which turned out to be of a second polymorph of **4** (**4**, crystal 2). They contained a disordered impurity that is possibly **11**′′ [$(Cp_2ZrBr)CH_2(Cp_2ZrMe)$]. Aside from this crystallographic complication, the two independent structure determinations of **4** gave practically identical results as far as the molecular structure of **4** is concerned, even though the crystal packing is completely different, as is reflected by the space group symmetry: $P2_12_12_1$ (orthorhombic) for crystal 1 versus $P\bar{1}$ (triclinic) for crystal 2. Table 2 gives a comparison of selected structural parameters of **4** obtained by these two independent X-ray crystal-structure analyses.

Table 2. Selected bond lengths and angles for **4**

	Crystal 1[a]	Crystal 2[b]	Average
Zr1−C11	2.368(3)	2.334(6)	2.351
Zr2−C23	2.294(4)	2.332(7)	−
Zr1−C12	2.225(3)	2.225(6)	2.225
Zr2−C12	2.247(3)	2.236(5)	2.242
Zr1−C12−Zr2	132.7(1)	134.0(3)	133.4
C11−Zr1−C12	101.2(1)	101.3(2)	101.3
C12−Zr2−C23	93.8(1)	92.9(2)	93.4
C11−Zr1−C12−Zr2	−0.6(3)	1.6(5)	1.1
Zr1−C12−Zr2−C23	175.7(3)	−178.7(5)	−177.2

[a] Determined in Utrecht. [b] Determined in Münster.

In the solid state, **4** is unsymmetrical. It crystallizes in an "antiperiplanar" conformation in which the methyl groups are on opposite sides of the molecule with (averaged) dihedral angles C11−Zr1−C12−Zr2 = 1.1° and Zr1−C12−Zr2−C23 = −177.2°. This specific orientation may be steric in origin, although related μ-oxozirconocene complexes usually favor a bisected (i.e. perpendicular) allene-type conformational orientation. Thus, in $[(Cp_2ZrMe)_2O]$ (**12**)[15] and related systems,[16] the Zr−O−Zr angle is close to linear [**12**: 174.1(3)°] and the Me−Zr···Zr−Me dihedral angle is close to 90°. In contrast, complex **4** favors an almost coplanar arrangement of the Zr−C σ-vectors. In the analogous and sterically rather crowded methylene-bridged complex $[(Cp^*)(C_2B_9H_{11})Zr]_2(\mu\text{-}CH_2)$ (**13**),[17] the bulky dicarbollide ligands at the zirconium atom are *trans*-oriented, too.

Of special interest is the wide bond angle at the methylene carbon atom: Zr−C12−Zr (133.4°). While the geometry around C12 is clearly not planar, it shows a pro-

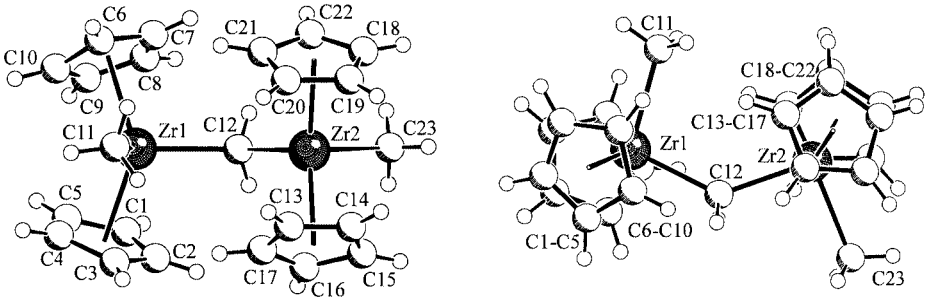

Figure 1. Two views of the molecular structure of **4** (crystal 1)

 © 2004 Wiley-VCH Verlag GmbH & Co. KGaA, Weinheim

nounced tendency of flattening in the direction of D_{2h} symmetry. This may be compared with several related structures. Compound **3**[7] has a much smaller Zr1−C1−Zr2 angle [101.86(10)°], but this is due to the fact that it is incorporated into a four-membered ring (involving a chlorine atom); in this case, it is the external angle Zr2−C1−C2 [145.9 (2)°] that is opened up. In **13**, the angles around the methylene carbon atom are rather normal [Zr−CH_2−Zr (119.14°) and H−C−H (108.74°)]; the Zr−CH_2 bond lengths [2.187(6) and 2.176(7) Å] are slightly shorter than those in **4** (2.225 and 2.242 Å). These shorter bonds may signal more s-character in the Zr−CH_2 bond of **13**, although a stabilizing bridging Zr···H−B interaction has also been considered.[17] The wider bond angles in **4** might also be considered as indicators for more s-contribution to the Zr−CH_2 bonds. Apparently, a number of different effects with a complicated interplay are involved. The Zr−CH_3 σ-bonds are in the expected range (see Table 2).[15,17] It must be noted, however, that the Zr1/2−C12 linkages are different from each other. While the Zr2−C12 bond (average 2.242 Å) is in the typical range for zirconium−carbon σ-bonds, the Zr1−C12 bond is shorter at (averaged) 2.225 Å. The latter value is close to the Zr−CH_2 bond lengths observed in the (μ-methylene)zirconocene system **13**.[17] The Zr−C(Cp) bond lengths of **4** lie in a range between 2.491 and 2.570 Å.

In general, the NMR spectroscopic data (Table 3) are in line with the crystal structure. A major difference is that, in solution, the structure is symmetrical, as the two methyl groups and the four cyclopentadienyl groups show only one signal each. Even at −100 °C, only one signal is observed for the methyl groups, which means that the conformational equilibrium in **4** has a very low barrier.

Table 3. NMR spectroscopic data for **4** (δ in ppm)

Group	δ(^{1}H)[a]	δ(^{1}H)[b]	δ(^{13}C)[a]	δ(^{13}C)[b]
Cp	5.73	6.11	109.1 (170.7)[c]	109.8 (171.5)[c]
CH_2	3.68	3.76	146.4 (107.2)[c]	145.8 (106.5)[c]
CH_3	−0.32	−0.46	22.5 (115.9)[c]	22.0 (117.6)[c]

[a] In [D_8]toluene. [b] In [D_8]THF. [c] $^1J_{C,H}$ [Hz] in parentheses.

The deshielded ^{13}C NMR chemical shift of δ= 146 ppm and the small $^1J_{C,H}$ coupling constant of 107 Hz are typical for a methylene group bridging between two metal atoms. Methylene groups in 1,3-dimetallacyclobutanes are even more deshielded,[10,18] as exemplified by the value of δ = 173 ppm for **8**. For methylene groups bridging between two transition metal atoms, such as manganese or rhodium, metal−metal bonding has been invoked,[18] but in **4**, the Zr−Zr distance of 4.10 Å clearly excludes such interactions, as the Zr−Zr distance in the metal is 3.2 Å.[19]

As discussed above, the large Zr−CH_2−Zr angle of 133.4° may be an indication of a relatively high s-character of these bonds, which facilitates the accommodation of electron density released from the metal atoms towards the carbon atom. As a consequence, less s-character is left for the C−H bonds, which explains the small $^1J_{C,H}$ value of 107 Hz (cf. $^1J_{C,H}$ = 117 Hz for the methyl groups) because in the latter, the carbon atom is bonded to only *one* metal atom.

Thermal Disproportionation of 4

In order to further investigate the disproportionation of **4** to **8** and **9**, as mentioned above, the benzene extract of a mixture obtained by Method I containing approximately 70% of **4** was subjected to a kinetic analysis. For this purpose, the solution was kept at 5 °C (cold room) while the solvent was removed by distillation under vacuum into a vessel cooled by liquid nitrogen, followed by high-vacuum pumping. A sample of the residue was dissolved in [D_8]toluene and transferred into an NMR tube, which was subsequently sealed. In the NMR spectrometer, the tube was warmed to 55 °C and the ^{1}H NMR spectrum was recorded. As determination of the absolute concentration of the components was not possible, their relative concentration was derived from the ratio between the intensity of their signals (per proton) and that of the solvent. The sum of the integrals of all cyclopentadienyl signals remained unchanged, which means that decomposition to insoluble products had not occurred. Taking into account the low initial concentrations of **8** and **9** formed during the synthesis of **4** (see Table 1), the two products were newly formed in a ratio of 1:2 as required by stoichiometry (Scheme 4).

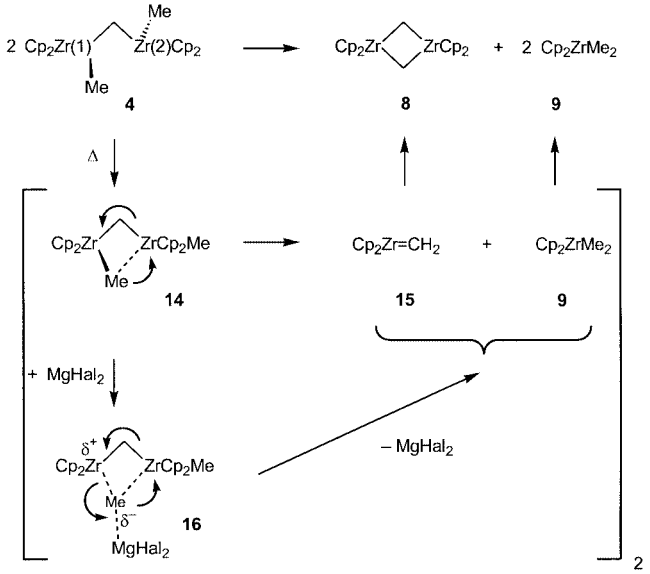

Scheme 4

The disproportionation of **4** follows roughly first-order kinetics with $k = 19 \times 10^{-5}$ s^{-1}. A conceivable mechanism is presented in Scheme 4. In the transition state, **14**, of the first and rate-determining step, a methyl group migrates from Zr1 to Zr2, while, simultaneously, the Zr2−CH_2 bond starts to cleave. This produces **9** and the carbene complex **15** which, being highly unstable, immediately dimerizes to form **8**. However, several observations suggest that this

 © 2004 Wiley-VCH Verlag GmbH & Co. KGaA, Weinheim

mechanism may be too simple. In the first place, it does not explain the strong influence of magnesium salts mentioned above. Secondly, when an identical sample of **4** obtained by Method I was dissolved in [D_8]THF instead of [D_8]toluene, the stability increased considerably: at 55 °C, only a small percentage of **4** had undergone disproportion after 64 h, and after 9.5 months at room temperature, the intensity of the signals of **4** had decreased by only 35%. This may be tentatively explained by the strong coordination of $MgHal_2$ by THF, which "inactivates" the salt.

This is supported by two other experiments with a sample of **4** that had been purified and made (practically) salt-free by repeated crystallization from toluene/heptane (5:1), followed by ^{1}H NMR spectroscopy in [D_8]toluene. After heating the solution at 60 °C, 50% of **4** had survived after one month; again, kinetic order (first order) and product formation (**8**/**9** = 1:2) were unchanged. However, when an excess of $MgBr_2$ was added to this salt-free toluene solution, disproportionation occurred within a few hours, although in this case product formation was less straightforward: initially, signals of **9** and **10** were observed while those of **8** appeared only later and in a ratio smaller than 1:2; in addition, unidentified products were formed (singlets at δ = 5.78, 5.76, 0.30, −0.10 ppm).

Thus, it is obvious that magnesium salts do play an important role. From the fact that the reaction is of first order, it follows that they act as catalysts; a tentative rationalization is shown in Scheme 4. One can imagine that in an apolar medium, $MgHal_2$ coordinates to **4**, presumably at the "external" methyl group at Zr1 (Figure 1) as shown in **16**. This will accelerate the cleavage of the Me−Zr2 bond and thus promote migration of the methyl group and the ensuing cleavage process.

Cation Formation

Dimethylzirconocene reacts with the strong Lewis acid $B(C_6F_5)_3$ and a variety of related reagents with abstraction of a methyl anion equivalent to form the respective methylzirconocene cation.[20] A similar reaction was observed when **4** was treated with $B(C_6F_5)_3$ in dichloromethane at low temperature: a methyl group was transferred from a zirconium to a boron atom to yield **17** (Scheme 5). The dimetallic cation of **17** is characterized by a single Cp resonance in the ^{1}H NMR spectrum at δ = 6.60 ppm, integrating for 20 protons (δ(^{13}C) = 114.5 ppm), in addition to ^{1}H NMR resonances of the CH_2 group at δ = 8.01 ppm (**4**: δ = 3.77 ppm) and of the bridging methyl group at δ = −1.05 ppm. The ^{13}C NMR methylene resonance is markedly different from that of its neutral precursor **4** [**17**: δ = 186.6 ppm ($^1J_{C,H}$ = 124 Hz); **4**: δ = 145.1 ppm ($^1J_{C,H}$ = 107 Hz)]. The ^{13}C NMR resonance of the bridging CH_3 group of **17** occurs at δ = 47.4 ppm [$^1J_{C,H}$ = 109 Hz; cf. δ = 22.7 ppm ($^1J_{C,H}$ = 118 Hz) for **4**].

Complex **17** is not stable in dichloromethane solution for a prolonged time at ambient temperature as it reacts with this solvent to yield the chloride-bridged complex **18**. On a preparative scale, it was synthesized by treatment of **17** with trityl chloride to cleanly furnish **18** [CH_2: δ(^{1}H) = 8.53 ppm; δ(^{13}C) = 193.7 ppm ($^1J_{C,H}$ = 124 Hz)] and 1,1,1-triphenylethane. Single crystals of **18** were obtained from a concentrated CD_2Cl_2 solution in an NMR tube. The X-ray crystal structure analysis (Figure 2) shows the formation of the four-membered metallacycle, although a 1:1 disorder of the μ-Cl and μ-CH_2 groups allows the calculation of average Zr−Cl/CH_2 bond lengths and angles only inside the framework of **18**.

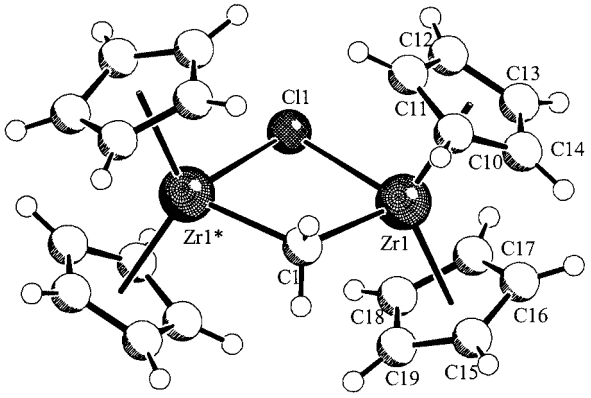

Figure 2. View of the molecular structure of **18** (the counterion has been omitted for clarity)

The addition of 1 equiv. of tetrahydrofuran to **17** opens the μ-CH_3 bridge with formation of the unsymmetrically substituted (μ-methylene)dizirconocene cation **19a** [μ-CH_2: δ(^{1}H) = 5.13 ppm; δ(^{13}C) = 163.4 ppm ($^1J_{C,H}$ = 106 Hz); Scheme 5]. The THF-stabilized cation shows dynamic NMR spectra. At room temperature and above it exhibits a single Cp resonance (in CD_2Cl_2, 600 MHz) which decoalesces below 280 K into an equal intensity pair of C_5H_5 singlets (δ = 6.38 and 6.17 ppm at 218 K). This probably indicates a process where THF is readily removed from the dinuclear complex to re-form the C_s-symmetric methyl-bridged cation **17**. Attack of THF can then occur at either side of the dimetallic complex, which leads to the observed

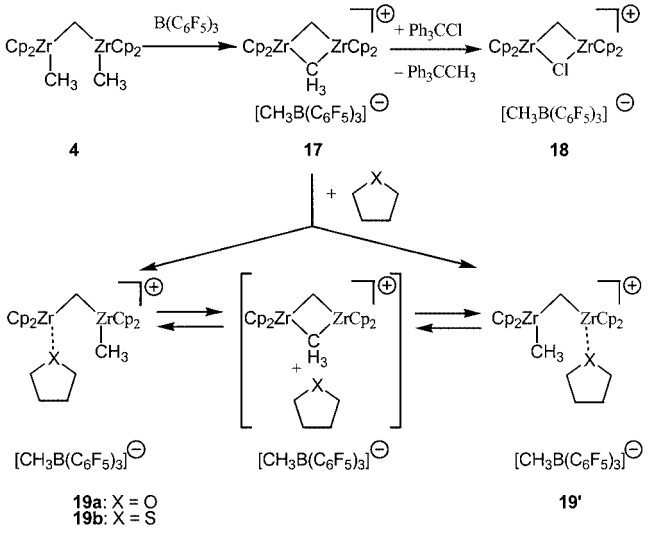

Scheme 5

 © 2004 Wiley-VCH Verlag GmbH & Co. KGaA, Weinheim

equilibration process (Scheme 5). From the dynamic ^1H NMR spectra of **19a**, a Gibbs activation energy of $\Delta G^{\neq}(280\ K) = 13.1 \pm 0.5$ kcal mol^{-1} was estimated.

Tetrahydrothiophene (THT) reacts similarly with **17** to form the unsymmetrical THT adduct **19b** (Scheme 5). It shows a pair of Cp ligand signals (1:1 intensity) at very low temperature in CD_2Cl_2 (193 K: $\delta(^1H)$ = 6.35, 6.17 ppm; $\delta(^{13}C)$ = 111.5, 110.5 ppm) in addition to a μ-CH_3 singlet at $\delta(^1H) = -0.53$ ppm ($\delta(^{13}C)$ = 10.2 ppm) and a μ-CH_2 resonance at $\delta(^1H)$ = 5.59 ppm and $\delta(^{13}C)$ = 169.2 ppm ($^1J_{C,H}$ = 107 Hz) in addition to the THT ligand and the $[CH_3B(C_6F_5)_3]^-$ anion resonances. Warming of the sample in the NMR spectrometer rapidly leads to coalescence of the Cp signals. From the dynamic ^1H NMR spectra a barrier of $\Delta G^{\neq}(213\ K) = 9.9 \pm 0.5$ kcal mol^{-1} was obtained for the dynamic equilibration process of **19b**.

Conclusion

The title compound [(μ-CH_2)($Cp_2ZrMe)_2$] (**4**) was obtained from [Cp_2Zr(Cl)Me] (**6**) and the two methylenedimagnesium reagents $CH_2(MgBr)_2$ (**5**) or $(CH_2Mg)_n$ (**7**). The X-ray crystal structure of **4** showed that the carbon atom of the central methylene group is non-planar, but a widened Zr−C−Zr angle of 133.4° indicates the tendency of this carbon atom to become planar. On first inspection, **4** may just be regarded as a methane derivative where the central methylene group bears two very bulky (Cp_2ZrMe) substituents. These have a tendency to become oriented far away from each other, thereby leading to an increased metal−CH_2−metal angle.

However, there are some noteworthy features of **4** which may be caused by factors other than simply by steric strain. Planarization of methane derivatives eventually would result in a transition from sp^3- to sp^2-hybridization of the central carbon atom.[2] By this type of re-hybridization, a doubly occupied p-orbital would develop which is oriented perpendicular to the plane of the σ-bonds. One must note that in complex **4** the electrophilic Cp_2ZrCH_3 substituents are both oriented such that their available acceptor orbitals[21] could, in principle, interact with this developing p-orbital at the bridging carbon atom and potentially stabilize it. In the observed unsymmetrical situation, it appears that the metallocene group at Zr1 (see Figure 1) could just have started to profit from such a developing electronic interaction. This might be the reason why the corresponding Zr1−C12 bond is slightly shorter than its adjacent Zr2−C12 neighbor. This is probably only a small energetic effect, but it seems that **4** represents a system where the bonding features of the central methylene carbon atom are just in the initial stage of being distorted from the common pseudo-tetrahedral coordination environment of tetracoordinate carbon toward its unusual planar-tetracoordinate isomer. This unusual structural feature may actually bear some relevance to its chemical behavior: **4** turned out to be relatively stable in THF solution, but it disproportionates in toluene solution to give the 1,3-dizirconacyclobutane [($Cp_2ZrCH_2)_2$] (**8**) and dimethylzirconocene [Cp_2ZrMe_2] (**9**). This reaction appears to be catalyzed by magnesium salts.

Reaction of **4** with $B(C_6F_5)_3$ yielded the methyl-bridged cationic complex **17** which, on treatment with trityl chloride, was transformed into the corresponding chloro complex **18**. The latter has been characterized by X-ray crystal structure determination. With THF and tetrahydrothiophene, **17** formed the adducts **19a** and **19b**, respectively, which are unsymmetrical in solution at low temperatures.

Experimental Section

General Remarks: Most of the experiments were performed using a high-vacuum sealed-glass apparatus,[11,14] in Schlenk-type glassware or in a glove box. Solvents were dried before use by distillation from liquid NaK alloy under argon. Magnesium was triply sublimed. For the determination of some NMR spectra, the solution obtained from a reaction was concentrated to dryness by distilling off the solvent under vacuum into a vessel cooled by liquid nitrogen, followed by pumping under high vacuum; subsequently, the sample was redissolved in a deuterated solvent in a high vacuum system and finally the NMR tube was sealed. NMR spectra were measured with a Bruker WH 90, AC 200, WM 250 or a Varian Unity Plus (^1H: 600 MHz) spectrometer. GCMS analysis was performed with a Hewlett Packard 5890 GC/5970 MS combination with a 50-m Chrompack CP Sil 5 column.

X-ray Crystal-Structure Determinations

4 (Crystal 1): Data collection by locally modified CAD4 software (*CAD-4 Software*, version 5, Enraf−Nonius, Delft, The Netherlands, **1989**); structure solution: SHELXS-86 (G. M. Sheldrick, *SHELXS-86, Program for Crystal Structure Solution*, University of Göttingen, Germany, **1986**); structure refinement: SHELX-76 (G. M. Sheldrick, *SHELX-76, Program for crystal structure solution and refinement*; University of Göttingen, Germany, **1976**); graphics PLATON (A. L. Spek, *PLATON, A multi-purpose crystallographic tool*, Utrecht University, The Netherlands, 2003, internet: http://www.cryst.chem.uu.nl/platon/).

4 (Crystal 2) and 18: Data sets were collected with an Enraf Nonius CAD4 diffractometer. Programs used: data collection EXPRESS (Nonius B.V., **1994**), data reduction MolEN (K. Fair, Enraf−Nonius B.V., **1990**), structure solution SHELXS-97 (G. M. Sheldrick, *Acta Crystallogr.* **1990**, *A46*, 467−473), structure refinement SHELXL-97 (G. M. Sheldrick, Universität Göttingen, **1997**), graphics SCHAKAL (E. Keller, Universität Freiburg, **1997**).

CCDC-221605 (**4**, crystal 1), -221381 (**4**, crystal 2) and -221380 (**18**) contain the supplementary crystallographic data for this paper. These data can be obtained free of charge at www.ccdc.cam.ac.uk/conts/retrieving.html [or from the Cambridge Crystallographic Data Centre, 12 Union Road, Cambridge CB2 1EZ, UK; Fax: (internat.) + 44-1223-336-033; E-mail: deposit@ccdc.cam.ac.uk].

(μ-Methylene)bis[dicyclopentadienyl(methyl)zirconium] (4)

Method I: At −20 °C, a solution of **6**[12] (185.2 mg, 0.68 mmol) in toluene (20 mL) was added to a solution of **5** (0.34 mmol) in diethyl ether/benzene (1:1; 12.4 mL). The reaction mixture was stirred at −20 °C for 14 d, after which time the mixture had become yellow-orange and homogeneous. The solution was kept at 5 °C (cold room) while the solvent was removed by distillation under vacuum

 © 2004 Wiley-VCH Verlag GmbH & Co. KGaA, Weinheim

into a vessel cooled by liquid nitrogen followed by high vacuum pumping, and the solid residue was extracted with pentane (10 mL, 5 times) and benzene (10 mL), and filtered. Hydrolysis and titration[11] of the residue in the reaction vessel showed that about 10% of **5** had not reacted (a small part may be lost during the workup procedure as well). Titration with EDTA revealed that some of the magnesium salts dissolved in the benzene extract. The yield of **4** was about 60% as determined by ^{1}H NMR spectroscopy with cyclopentane as internal standard. The ratios of products in the pentane and in the benzene extract are reported in Table 1. The NMR spectroscopic data for **4** are presented in Table 3. ^{1}H NMR spectroscopic data for by-products (200 MHz, [D_8]toluene, reference [D_7]toluene at δ = 2.03 ppm). **8:** δ = 6.27 (s, 4 H, CH_2), 6.09 (s, 20 H, Cp) ppm; the data are in agreement with those reported previously.[10] **9:** δ = 5.64 (s, 10 H, Cp), −0.25 (s, 6 H, Me) ppm; the data are similar to those reported previously.[13] **10:** δ = 5.68 (s, 10 H, Cp), 0.15 (s, 3 H, Me) ppm. **11:** δ = 5.89 (s, 10 H, Cp), 5.82 (s, 10 H, Cp), 4.37 (s, 2 H, CH_2), −0.15 (s, 3 H, Me) ppm.

Method II: At −20 °C, a solution of **6** (92.9 mg, 0.34 mmol) in toluene (10 mL) was added to a suspension of **7**[9,11] (0.17 mmol of **7**; see general text for the composition of the reagent) in THF (6.2 mL). The mixture was stirred at −20 °C for 64 h; this was followed by stirring at 5 °C for 2 h and at room temperature for 2 h while the solvents were removed by distillation under vacuum into a vessel cooled by liquid nitrogen followed by high vacuum pumping. The reaction vessel was evacuated at room temperature for 2 h. At room temperature, the residue was extracted with pentane (10 mL), filtered, and subsequently extracted with benzene (10 mL). Analysis by ^{1}H NMR spectroscopy with cyclopentane as internal standard showed that the total yield of **4** was 56% (53% in the benzene extract; 3% in the pentane extract). The composition of the extracts is reported in Table 1. Compound **4** was purified by crystallization from a toluene/heptane (5:1) solution at −80 °C. At room temperature, the crystals were quickly transferred into Lindemann capillaries in a glove box under nitrogen and afterwards kept at −20 °C.

X-ray Crystal Structure of 4 (Crystal 1): $C_{23}H_{28}Zr_2$, M_r = 486.91, orange crystal, 0.2 × 0.2 × 0.3 mm, orthorhombic, space group $P2_12_12_1$ (no. 19) with a = 10.0234(14), b = 13.8914(6), c = 14.3841(18) Å, V = 2002.8(4) Å^3, Z = 4, $\rho_{calcd.}$ = 1.615 g cm^{-3}, $F(000)$ = 984, $\mu_{Mo\text{-}K\alpha}$ = 1.03 mm^{-1}. 6884 reflections measured with an Enraf−Nonius CAD4-T diffractometer with a rotating anode ($\lambda_{Mo\text{-}K\alpha}$ = 0.71073 Å, T = 100 K, θ_{max} = 34.9°), 6358 unique (R_{int} = 0.027), 5063 observed [$I > 2.5\sigma(I)$]. Structure solved with SHELXS-86. 305 parameters refined with SHELX-76, R = 0.0355, R_w = 0.0358, S = 1.61, residual density in the range −1.00, 1.40 e$^-$/Å^3. Hydrogen atom coordinates, with exception of the methyl moieties, were refined. The low value of the displacement parameters of methyl group C11 in comparison with the other methyl group might be explained as substitutional disorder with Br. However, no satisfactory disorder model could be refined, suggesting that, if any, only a very small fraction of Br is present.

Method III: The single crystals used for the X-ray crystal structure analysis in Münster (Table 2, crystal 2) were obtained as follows: A solution of **6** (0.63 g, 2.32 mmol) in toluene (10 mL) was cooled to 0 °C. Then, a solution of **5** [diethyl ether/benzene (1:1), 50 mL, 0.025 M, 1.25 mmol of **5**) was added. The ice bath was removed and the mixture stirred at room temperature for 1 h. Dioxane (2.5 mL) was added and the mixture stirred for 15 min. The solvent was then removed in vacuo. The residue was suspended in toluene (15 mL), the magnesium halide precipitate was removed by filtration, and the clear solution concentrated to about 5 mL. Pentane (2 mL) was added and the solution cooled to −30 °C to yield bright yellow crystals of **4** (0.37 g, 65%).

X-ray Crystal-Structure Analysis of 4 (Crystal 2): $C_{23}H_{28}Zr_2{\cdot}1/2$ correctly represents composition of crystal ($C_{22.86}H_{27.58}Br_{0.14}Zr_2$), M = 734.88, yellow crystal 0.40 × 0.40 × 0.05 mm, a = 10.787(1), b = 13.028(1), c = 13.066(1) Å, α = 63.55(1), β = 69.77(1), γ = 80.83(1)°, V = 1542.6(2) Å^3, $\rho_{calcd.}$ = 1.582 g cm^{-3}, μ = 11.06 cm^{-1}, empirical absorption correction with ψ-scan data (0.666 ≤ T ≤ 0.947), Z = 2, triclinic, space group $P\bar{1}$ (no. 2), λ = 0.71073 Å, T = 223 K, ω/2θ scans, 6565 reflections collected (±h, +k, ±l), [(sinθ)/λ] = 0.62 Å^{-1}, 6275 independent (R_{int} = 0.031) and 4199 observed reflections [$I \geq 2\sigma(I)$], 356 refined parameters, R = 0.049, wR^2 = 0.129, max. residual electron density 0.68 (−1.20) e$^-$/Å^3, hydrogen atoms calculated and refined as riding atoms, in the second independent molecule 7% of the terminal CH_3 group is substituted by Br, in addition the bridging CH_2 group is split over two positions due to symmetry.

Synthesis of 17: Solid **4** (120 mg, 0.25 mmol) was mixed with solid $B(C_6F_5)_3$ (126 mg, 0.25 mmol). Toluene (10 mL) was then slowly added at −78 °C. The mixture was stirred at −78 °C for 20 min and then allowed to warm to room temperature. The toluene phase was decanted from the precipitated oil. The remaining product was washed twice with pentane to give **17** as a yellow powder (70 mg, 28%). $C_{41}H_{28}BF_{15}Zr_2$ (998.9): calcd. C 49.30, H 2.83; found C 48.72, H 3.04. ^{1}H NMR (CD_2Cl_2, 360 MHz, 213 K): δ = 8.01 (s, 2 H, CH_2), 6.60 (s, 20 H, Cp), 0.36 (br., 3 H, CH_3−[B]), −1.05 (s, 3 H, Zr−CH_3) ppm. ^{13}C NMR (CD_2Cl_2, 90.6 MHz, 213 K): δ = 186.6 (t, $^1J_{C,H}$ = 124 Hz, CH_2), 147.4 [d, $^1J_{C,F}$ = 236 Hz, *o*-$B(C_6F_5)_3$], 136.4 [d, $^1J_{C,F}$ = 246 Hz, *p*-$B(C_6F_5)_3$], 135.5 [d, $^1J_{C,F}$ = 243 Hz, *m*-$B(C_6F_5)_3$], 127.8 [s, *ipso*-$B(C_6F_5)_3$], 114.5 (d, $^1J_{C,H}$ = 174 Hz, Cp), 47.4 (q, $^1J_{C,H}$ = 109 Hz, μ-CH_3), 9.2 (br., CH_3−[B]) ppm.

Synthesis of 18

Method I: A solution of $B(C_6F_5)_3$ (0.14 g, 2.74 mmol) in CH_2Cl_2 (10 mL) was added dropwise to a solution of **4** (0.14 g, 2.90 mmol) in CH_2Cl_2 (15 mL) at −78 °C. The reaction mixture was stirred at −78 °C for 2 h and then at room temperature for 12 h. Pentane (5 mL) was then added. Cooling to −45 °C gave a red precipitate that was isolated and dried in vacuo to yield **18** (55 mg, 19%). ^{1}H NMR (CD_2Cl_2, 360 MHz, 300 K): δ = 8.53 (s, 2 H, CH_2), 6.69 (s, 20 H, Cp), 0.49 (br., 3 H, CH_3−[B]) ppm. ^{11}B NMR (CD_2Cl_2, 64.2 MHz, 300 K): δ = −15.1 ppm. ^{13}C NMR (CD_2Cl_2, 90.6 MHz, 300 K): δ = 193.5 (t, $^1J_{C,H}$ = 124 Hz, CH_2), 148.0 [d, $^1J_{C,F}$ = 233 Hz, *o*-$B(C_6F_5)_3$], 138.9 [d, $^1J_{C,F}$ = 246 Hz, *p*-$B(C_6F_5)_3$], 136.1 [d, $^1J_{C,F}$ = 242 Hz, *m*-$B(C_6F_5)_3$], 129.3 [s, *ipso*-$B(C_6F_5)_3$], 115.5 (d, $^1J_{C,H}$ = 175 Hz, Cp), 11.7 (br., CH_3−[B]) ppm. ^{19}F NMR (CD_2Cl_2, 282.2 MHz, 300 K): δ = −126.1, −162.9, −165.4 [*o*-, *p*-, *m*-$B(C_6F_5)_3$] ppm. Single crystals of **18** were obtained by slow evaporation of the solvent from a solution of the complex in CD_2Cl_2.

X-ray Crystal-Structure Analysis of 18: $C_{21}H_{22}ClZr_2{\cdot}CH_3B(C_6F_5)_3$, M = 1019.30, red crystal 0.40 × 0.25 × 0.15 mm, a = 10.768(1), b = 11.305(1), c = 16.283(1) Å, α = 71.93(1), β = 86.31(1), γ = 88.91(1)°, V = 1880.5(3) Å^3, ρ = 1.800 g cm^{-3}, μ = 7.31 cm^{-1}, empirical absorption correction with ψ-scan data (0.759 ≤ T ≤ 0.898), Z = 2, triclinic, space group $P\bar{1}$ (no. 2), λ = 0.71073 Å, T = 223 K, ω/2θ scans, 6979 reflections collected (±h, −k, ±l), [(sinθ)/λ] = 0.59 Å^{-1}, 6612 independent (R_{int} = 0.033) and 3880 observed reflections [$I \geq 2\sigma(I)$], 551 refined parameters, R = 0.038, wR^2 = 0.071, max. residual electron density 0.59 (−0.41) e$^-$/Å^3, hydrogen atoms calculated and refined as riding atoms, the bridg-

 © 2004 Wiley-VCH Verlag GmbH & Co. KGaA, Weinheim

ing CH_2 and Cl groups are split over two positions due to symmetry.

Method II: Complex **4** (50 mg, 0.10 mmol) was mixed with solid $B(C_6F_5)_3$ (53 mg, 0.10 mmol). Toluene (10 mL) was added slowly at −78 °C. The mixture was stirred at −78 °C for 20 min. A precooled solution (−78 °C) of trityl chloride (30 mg, 0.10 mmol) in toluene (10 mL) was then added. The mixture was warmed to room temperature and then stirred for another 10 min. The toluene phase was separated from the precipitated oil of the organometallic product **18** (see above) and washed twice with pentane. From the combined organic phases 1,1,1-triphenylethane[22] was recovered as a white powder (34 mg 35%). M.p. 95 °C.

Reaction of 17 with THF

Formation of 19a: Compound **4** (20 mg, 41 μmol) was dissolved in 0.5 mL of CD_2Cl_2. A solution of $B(C_6F_5)_3$ (21 mg, 41 μmol) in CD_2Cl_2 (0.5 mL) was added at −78 °C. After 10 min, THF (3 mg, 43 μmol) in $CD_2Cl_2$was added. The solution was flame-sealed in an NMR tube and the temperature-dependent NMR spectra of the resulting complex **19a** were recorded. ^{1}H NMR (600 MHz, CD_2Cl_2, 218 K): δ = 6.38 (s, 10 H, Cp), 6.17 (s, 10 H, Cp), 5.34 (s, 2 H, CH_2), 3.58 (m, THF), 1.61 (m, THF), 0.42 (br., 3 H, CH_3−[B]), −0.43 (s, 3 H, Zr−CH_3) ppm. ^{1}H NMR (600 MHz, CD_2Cl_2, 300 K): δ = 6.34 (s, 20 H, Cp), 5.13 (s, 2 H, CH_2), 3.58 (m, THF), 1.69 (m, THF), 0.62 (br., 3 H, CH_3−[B]), −0.22 (s, 3 H, Zr−CH_3) ppm. Coalescence of the Cp signals at 280 K, Δν (at the limiting low temperature) is 126 Hz, $\Delta G^{\neq}$ (280 K) = 13.1 ± 0.5 kcal mol^{-1}. ^{13}C NMR (150.6 MHz, [D$_8$]THF, 218 K): δ = 163.4 (t, $^1J_{C,H}$ = 106 Hz, CH_2), 150.4 [d, $^1J_{C,F}$ = 236 Hz, *o*-$B(C_6F_5)_3$], 138.4 [d, $^1J_{C,F}$ = 246 Hz, *p*-$B(C_6F_5)_3$], 136.8 [d, $^1J_{C,F}$ = 243 Hz, *m*-$B(C_6F_5)_3$], 130.8 [s, *ipso*-$B(C_6F_5)_3$], 117.5 (d, $^1J_{C,H}$ = 174 Hz, Cp), 114.5 (d, $^1J_{C,H}$ = 174 Hz, Cp), 43.5 (q, $^1J_{C,H}$ = 122 Hz, Zr-CH_3), 11.2 (br., CH_3−[B]) ppm.

Reaction of 17 with Tetrahydrothiophene (THT)

Formation of 19b: As described above, **4** (40 mg, 82 μmol) was treated in CD_2Cl_2 first with $B(C_6F_5)_3$ (42 mg, 82 μmol) and then with tetrahydrothiophene (7 mg, 85 μmol) at −78 °C to form **19b**. A sample of the solution was flame-sealed in an NMR tube for spectroscopic characterization. ^{1}H NMR (600 MHz, CD_2Cl_2, 183 K): δ = 6.35 (s, 10 H, Cp), 6.17 (s, 10 H, Cp), 5.59 (s, 2 H, CH_2), 3.08 (br., free THT), 2.82 (br., coordin. THT), 1.83 (br., coordin. THT), 1.68 (br., free THT), 0.40 (br., 3 H, CH_3−[B]), −0.53 (s, 3 H, Zr−CH_3) ppm. ^{1}H NMR (600 MHz, CD_2Cl_2, 300 K): δ = 6.29 (s, 20 H, Cp), 5.59 (s, 2 H, CH_2), 3.02 (m, THT), 1.87 (m, THT), 0.41 (br., 3 H, CH_3−[B]), −0.50 (s, 3 H, Zr−CH_3) ppm. Coalescence of the Cp signals at 213 K, Δν (lower limit) = 109 Hz, $\Delta G^{\neq}$ (213 K) = 9.9 ± 0.5 kcal mol^{-1}. ^{13}C NMR (150.6 MHz, CD_2Cl_2, 183 K): δ = 169.2 (t, $^1J_{C,H}$ = 107 Hz, CH_2), 147.5 [d, $^1J_{C,F}$ = 237 Hz, *o*-$B(C_6F_5)_3$], 137.5 [d, $^1J_{C,F}$ = 246 Hz, *p*-$B(C_6F_5)_3$], 135.5 [d, $^1J_{C,F}$ = 243 Hz, *m*-$B(C_6F_5)_3$], 127.8 [s, *ipso*-$B(C_6F_5)_3$], 111.5 (d, $^1J_{C,H}$ = 175 Hz, Cp), 110.5 (d, $^1J_{C,H}$ = 175 Hz, Cp), 42.5 (m, α-THT), 32.5 (m, β-THT), 26.5 (q, $^1J_{C,H}$ = 110 Hz, Zr−CH_3), 10.2 (br., CH_3−[B]) ppm.

Acknowledgments

Financial support from the Fonds der Chemischen Industrie and the Deutsche Forschungsgemeinschaft is gratefully acknowledged. This work was supported in part (A. L. S.) by the Council for Chemical Sciences of the Netherlands Organization for Scientific Research (CW-NWO).

[1] [1a] J. H. van t Hoff, *Arch. Neerl. Sci. Exactes Nat.* **1874**, 445. [1b] J. A. LeBel, *Bull. Soc. Chim. Fr.* **1874**, *22*, 337.
[2] [2a] R. Hoffmann, R. W. Alder, C. F. Wilcox, Jr., *J. Am. Chem. Soc.* **1970**, *92*, 4992. [2b] R. Hoffmann, *Pure Appl. Chem.* **1971**, *28*, 181.
[3] D. Röttger, G. Erker, *Angew. Chem.* **1997**, *109*, 840−856; *Angew. Chem. Int. Ed. Engl.* **1997**, *36*, 812−827.
[4] X. Li, L.-S. Wang, A. I. Boldyrev, J. Simons, *J. Am. Chem. Soc.* **1999**, *121*, 6033−6038.
[5] D. W. Stephan, *Angew. Chem.* **2000**, *112*, 511; *Angew. Chem. Int. Ed.* **2000**, *39*, 501, and references cited therein.
[6] G. Erker, M. Albrecht, C. Krüger, S. Werner, *Organometallics* **1991**, *10*, 3791−3793.
[7] J. Schottek, G. Erker, R. Fröhlich, *Angew. Chem.* **1997**, *109*, 2585−2588; *Angew. Chem. Int. Ed. Engl.* **1997**, *36*, 2475−2477.
[8] [8a] G. M. Smith, M. Sabat, T. J. Marks, *J. Am. Chem. Soc.* **1987**, *109*, 1854. [8b] P. Binger, F. Sandmeyer, C. Krüger, J. Kuhnigk, R. Goddard, G. Erker, *Angew. Chem.* **1994**, *106*, 213; *Angew. Chem. Int. Ed. Engl.* **1994**, *33*, 197. [8c] R. Gleiter, S. J. Silverio, P. Binger, F. Sandmeyer, G. Erker, *Chem. Ber.* **1995**, *128*, 775. [8d] T. Cuenca, M. Galakov, E. Royo, P. Royo, M. Bochmann, *J. Organomet. Chem.* **1997**, *543*, 209. [8e] Y. Sahin, M. Hartmann, G. Geiseler, D. Schweikart, C. Balzereit, G. Frenking, W. Massa, A. Berndt, *Angew. Chem.* **2001**, *113*, 2725; *Angew. Chem. Int. Ed.* **2001**, *40*, 2662. [8f] C. Präsang, M. Hoffmann, G. Geiseler, W. Massa, A. Berndt, *Angew. Chem.* **2002**, *114*, 1597; *Angew. Chem. Int. Ed.* **2002**, *41*, 1526. [8g] A. Maier, M. Hoffmann, H. Pritzkow, W. Siebert, *Angew. Chem.* **2002**, *114*, 1600; *Angew. Chem. Int. Ed.* **2002**, *41*, 1529.
[9] J. W. Bruin, G. Schat, O. S. Akkerman, F. Bickelhaupt, *J. Organomet. Chem.* **1985**, *288*, 13−25.
[10] B. J. J. van de Heisteeg, G. Schat, O. S. Akkerman, F. Bickelhaupt, *J. Organomet. Chem.* **1986**, *308*, 1−10.
[11] B. J. J. van de Heisteeg, G. Schat, O. S. Akkerman, F. Bickelhaupt in *Organometallic Syntheses* (Ed.: R. B. King, J. J. Eisch), Elsevier, Amsterdam, **1986**, vol. 4, p. 389−395.
[12] J. R. Surtees, *J. Chem. Soc., Chem. Commun.* **1965**, 567.
[13] P. C. Wailes, H. Weigold, A. P. Bell, *J. Organomet. Chem.* **1972**, *34*, 155−164.
[14] A. D. Vreugdenhil, C. Blomberg, *Recl. Trav. Chim. Pays-Bas* **1963**, *82*, 453−460.
[15] W. E. Hunter, D. C. Hrncir, R. Vann Bynum, R. A. Penttila, J. L. Atwood, *Organometallics* **1983**, *2*, 750−755.
[16] G. Erker, U. Dorf, C. Krüger, Y.-H. Tsay, *Organometallics* **1987**, *6*, 680.
[17] D. J. Crowther, N. C. Baenziger, R. F. Jordan, *J. Am. Chem. Soc.* **1991**, *113*, 1455−1457.
[18] W. A. Hermann, *J. Organomet. Chem.* **1983**, *250*, 319−343.
[19] A. F. Wells, *Structural Inorganic Chemistry*, 5th ed., Clarendon Press, Oxford, **1984**, p. 1288.
[20] [20a] X. Yang, C. L. Stern, T. J. Marks, *J. Am. Chem. Soc.* **1994**, *116*, 10015. [20b] Review: E. Y.-X. Chen, T. J. Marks, *Chem. Rev.* **2000**, *100*, 1391.
[21] [21a] H. H. Brinzinger, L. S. Bartell, *J. Am. Chem. Soc.* **1970**, *92*, 1105. [21b] J. W. Lauher, R. Hoffmann, *J. Am. Chem. Soc.* **1976**, *98*, 1729. [21c] J. C. Green, *Chem. Soc. Rev.* **1998**, *27*, 263.
[22] M. Kuntze-Fechner, *Ber. Dtsch. Chem. Ges.* **1903**, *36*, 472−475.

Received October 20, 2003
Early View Article
Published Online February 5, 2004

 © 2004 Wiley-VCH Verlag GmbH & Co. KGaA, Weinheim

The Predicted Structures of the New Pnictides HfMQ in Contrast to ZrMQ (M = Ti, V; Q = P, As)

Shahab Derakhshan,[a] Enkhtsetseg Dashjav,[a] and Holger Kleinke*[a]

Keywords: Structure map / X-ray diffraction / Electronic structure / Phosphides / Arsenides

The new pnictides HfTiP, HfTiAs and HfVAs have been prepared through arc-melting. These arsenides form the predicted structures with (distorted) $TiAs_4$ and VAs_4 tetrahedra, while the structures of both Zr analogs (ZrTiAs and ZrVAs) are comprised of $TiAs_4$ and VAs_4 square planes, respectively. These differences stem from significant differences in the metal atom substructures. On the other hand, HfTiP and ZrTiP are isostructural. These variations were predicted by utilizing a structure map for metal-rich pnictides and chalcogenides M_2Q (M = valence-electron poor transition metal, Q = pnicogen or chalcogen) presented in the year 2000. The HfMQ structure is stabilized by strong Hf–Q, M–Q and M–M bonds, and to a minor extent by Hf–Hf and Hf–M bonding interactions. All three new $Hf_{1-\delta}M_{1+\delta}Q$ phases exhibit significant phase ranges.

(© Wiley-VCH Verlag GmbH & Co. KGaA, 69451 Weinheim, Germany, 2004)

Introduction

The ternary equiatomic early transition-metal pnictides MM′Q (M, M′: element of groups 3−5; Q: P, As, Sb) typically occur in one of two common crystal structures. These structures differ in the metal−nonmetal coordination spheres (but with the same coordination numbers) as well as in the metal−metal bonding, while the nonmetal atoms are always surrounded by nine metal atoms in form of a tricapped trigonal prism, and the larger M atoms are situated in a square pyramid formed by five Q atoms. In the first variant, the Co_2Si type (ordered variant: TiNiSi[1]), the smaller M′ atoms are tetrahedrally coordinated by four Q atoms, whereas in the second variant, the La_2Sb type (ordered variant: CeScSi[2]), the $M'Q_4$ polyhedra are best described as square planes.

These differences may be understood to stem from different metal atom substructures, which contain stronger M−M and M−M′ bonds in case of the Co_2Si structures. As shown earlier,[3] the major structure determining factors for such metal-rich pnictides and chalcogenides are the valence-electron concentration of M, the relative extension of the d orbitals of M (reflected in the principal quantum number), the radius ratio r_M/r_Q, and the electron deficit of the Q atoms. As for the metal atoms, higher valence-electron concentration, larger d orbitals and larger atomic radii all facilitate stronger M−M bonding. On the other hand, larger atomic sizes and larger electron deficits of the Q atoms would lead to larger coordination numbers for the Q atoms. Given the fact that the known structure types all have comparable packing efficiencies, more M−M bonds occur with smaller coordination numbers of the Q atoms. Obviously these factors can cancel each other, one example being Zr_2S and Hf_2P that are isostructural.

All these factors were summarized empirically in the power product $\mathbf{f} = vec_M \times n_M^2 \times (r_M/r_Q)/(8 - e_Q)^2$, wherein vec_M equals the valence-electron concentration per M atom after (formally) reducing the Q atoms, n_M the main quantum number of the M atoms, (r_M/r_Q) the radius ratios based on the Slater radii,[4] and $(8 - e_Q)$ the electron deficit of the Q atoms in their neutral state − in analogy to the $(8 - N)$ rule. Plotting the averaged coordination number of the Q atoms <C.N.(Q)> of all M_2Q pnictides and chalcogenides, including the ternaries with two different M atoms as well as two different Q atoms, against **f** gave a structure map with distinct domains of the (then) eleven different structure types of this family.[3]

For all of the factors contributing to the power product **f** are readily available, **f** may be calculated for all hypothetical, still uncovered M_2Q binaries as well as $M_{1-\delta}M'_{1+\delta}Q$ and $M_2Q_{1-\delta}Q'_\delta$ ternaries. Then, the domain and thus the structure type can be predicted, unless the compound in question either does not exist or forms a new type. However, unlike well-known structure maps such as Pettifor's[5] or Villars',[6] this approach even suggests information about unknown types, namely the averaged coordination number of the Q atoms.

The (in part systematic) subsequent recovery of new members of this M_2Q family proved the usability of this structure map: the ternary arsenide, $Zr_{1-\delta}Ti_{1+\delta}As$, was postulated to form the La_2Sb type, which was subsequently proven to be correct.[7] $Zr_{1-\delta}V_{1+\delta}As$[8] is at the border be-

[a] Department of Chemistry, University of Waterloo
Waterloo, Ontario, Canada N2 L 3G1
Fax: (internat.) +1-519-746-0435
E-mail: kleinke@uwaterloo.ca

tween the Co_2Si and La_2Sb representatives of this family, depending on the exact Zr:V ratio, and always forms the La_2Sb structure. Harbrecht et al. uncovered with Zr_6STe_2 ($\equiv Zr_2S_{0.33}Te_{0.67}$)[9] the first example of a new compound in this family that occurs in a new type, and its <C.N.(Q)> value is indeed eight − thus a nice fit in the structure map. Furthermore, an extension to other stoichiometries is possible, as demonstrated by us for the M_5Q_3 compounds.[10,11]

This work deals with the new hafnium phosphides and arsenides $Hf_{1-\delta}Ti_{1+\delta}P$, $Hf_{1-\delta}Ti_{1+\delta}As$, and $Hf_{1-\delta}V_{1+\delta}As$. As illustrated in Table 1, the power product **f** clearly places these three new materials into the Co_2Si domain, together with ZrTiP,[12] ZrVP and HfVP,[13] ZrNbP and HfNbP,[14] and V_2P[15] and in contrast to ZrTiAs and ZrVAs (as well as La_2Sb[16] and Zr_2Sb[17]). Our investigations confirmed the Co_2Si type in all three new cases introduced.

Table 1. Overview of M_2Q compounds in the Co_2Si and La_2Sb types. Hypothetical compounds are in italic

Compound	f	Structure	Reference
HfNbP	15.1	Co_2Si	[14]
TaVP	13.6	Co_2Si	[12]
ZrNbP	12.5	Co_2Si	[14]
HfVP	12.1	Co_2Si	[13]
HfVAs	10.5	Co_2Si	this work
HfTiP	10.2	Co_2Si	this work
ZrVP	9.8	Co_2Si	[13]
HfTiAs	8.9	Co_2Si	this work
V_2P	8.4	Co_2Si	[15]
ZrTiP	8.3	Co_2Si	[12]
ZrVAs	8.5	La_2Sb	[8]
La_2Sb	8.1	La_2Sb	[16]
Zr_2Sb	7.4	La_2Sb	[17]
ZrTiAs	7.2	La_2Sb	[7]
HfTiSb	7.1	predicted La_2Sb	hypothetical
ZrTiSb	5.7	predicted La_2Sb	hypothetical

Results and Discussion

Structure Map

Several ternary phosphides, arsenides and antimonides of Zr and Hf form the Co_2Si type. Typically, the second metal is a late transition-metal atom, as in ZrMP (M = Fe, Co),[18,19] HfMP (M = Fe, Co, Ni),[20] ZrMAs and HfMAs (M = Fe, Co, Ni),[21] and ZrMSb and HfMSb (M = Fe, Ni).[22,23] With the exception of ZrNiP (Ni_2In type)[24] and HfNiP, these Zr and Hf compounds are always isostructural. Only few examples are known with Zr or Hf and a second early transition metal, namely the phosphides ZrTiP,[12] ZrVP and HfVP,[13] ZrNbP and HfNbP[14] (all Co_2Si type), while the arsenides known to date form the La_2Sb type (i.e. ZrTiAs and ZrVAs[7,8]). Furthermore, no such antimonides were uncovered to date.

Employing the structure map for M_2Q compounds, the hitherto unknown pnictides HfTiP, HfTiAs and HfVAs were predicted to form the Co_2Si type (cf. the overview in Table 1).[7,8] Our investigations presented here prove this to be correct. Knowledge of the structures of related pnictides published before could not be used for this prediction, as ZrTiAs and ZrVAs both occur only in the La_2Sb type, while ZrTiP crystallizes (like HfTiP) in the Co_2Si type.

In particular, one might have correctly assumed HfTiP to be isostructural with ZrTiP, but following this logic, HfTiAs should be isostructural with ZrTiAs, which is not the case. A thorough theoretical investigation of ternary phosphides MM′P, with M and M′ being an early transition-metal element,[25] was based on Extended Hückel calculations,[26,27] using the atomic parameters of Zr and Nb. This work analyzed four different possible structure types, namely Cu_2Sb, Co_2Si, Fe_2P and Ni_2In. For 14 valence-electrons, the Co_2Si type was calculated to be electronically preferred, which is the case for MNbP, MVP and MVAs with M = Zr, Hf. Similar compounds with 13 valence-electrons − explicitly mentioned was HfTiP in that article − were predicted to form the Cu_2Sb type, which exhibits a M atom substructure related to that of the La_2Sb type. To summarize, the latter method, which exclusively used valence-electron concentrations for rationalizing structural trends, correctly identified ZrVP, HfVP and HfVAs, but failed to foresee correctly ZrTiAs, ZrVAs, HfTiP and HfTiAs.

Crystal Structure

Since the Co_2Si type (*anti*-$PbCl_2$) is a well-known structure type, its description may be kept short here. We are therefore concentrating on the differences to the La_2Sb type, for ZrTiAs and ZrVAs adopt the latter, and HfTiAs and HfVAs the former type. In the following, we will discuss the differences between HfVAs and ZrVAs, whose structures are shown in Figure 1.

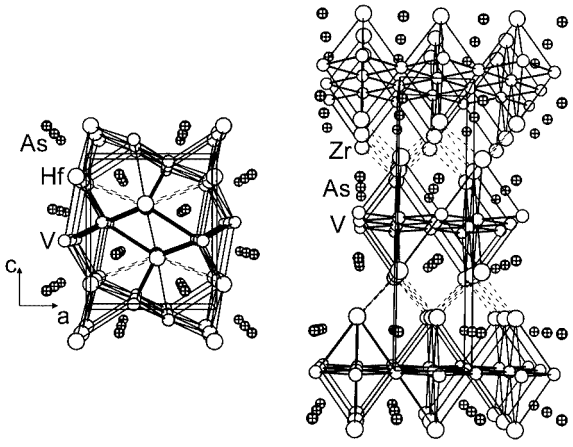

Figure 1. Crystal structures of HfVAs (left) and ZrVAs (right)

Both structures comprise three atomic positions, one As, one M(1) (mainly the group 4 element, i.e. Zr or Hf) and one M(2) (mainly V) site. Depending on the exact M:V ratio of $Zr_{1-\delta}V_{1+\delta}As$ and $Hf_{1-\delta}V_{1+\delta}As$, the M(1) site may exhibit up to 15% V in ZrVAs and 9% V in HfVAs, and the M(2) site up to 43% Zr in ZrVAs and 2% Hf in HfVAs. It is noted that in the case of MTiAs, the M(2) site cannot

 © 2004 Wiley-VCH Verlag GmbH & Co. KGaA, Weinheim

include any Zr of Hf contributions, but M(1) up to 42% Ti in ZrTiAs and 40% Ti in HfTiAs.

In both structures, ZrVAs and HfVAs, the As atom is surrounded by nine transition-metal atoms forming a (distorted) tri-capped trigonal prism (deltahedral tetrakaidecahedron), namely five M(1) and four M(2) atoms. Furthermore, the M(1) atoms are located in (distorted) As_5 square pyramids in both structures, but the V atom in a (distorted) As_4 tetrahedron in HfVAs and in an As_4 planar "square" (more precisely: rectangle) in ZrVAs. These coordination polyhedra are depicted in Figure 2.

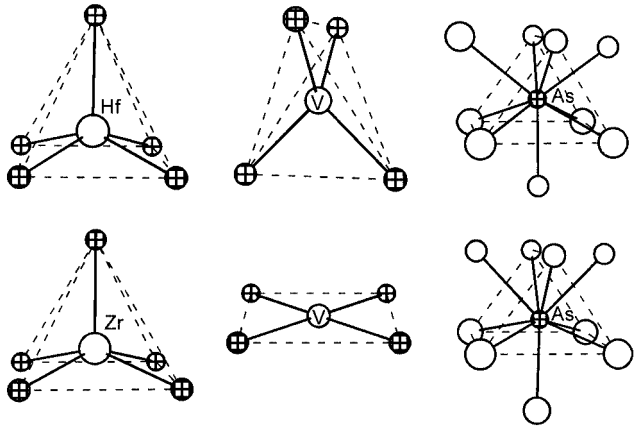

Figure 2. Coordination polyhedra of HfVAs (top) and ZrVAs (bottom)

The different coordination numbers of M(1) and M(2) reflect a likely reason why the smaller V atom prefers the M(2) site in both cases. As well, the coordination number of four inhibits an incorporation of the group 4 element to some extent; only in the case of ZrVAs may the M(2) site exhibit significant amounts of it.

Of particular interest are the differences in metal−metal bonding in these structures, for the only (yet obvious) difference between the formulas ZrVAs and HfVAs is the main quantum number of the group 4 metal atoms. Size and electronegativity of Zr and Hf atoms are virtually equivalent. ZrVAs comprises sheets of corner-sharing Zr_2V_4 octahedra (tetragonally elongated, i.e. of D_{4h} symmetry), wherein the apices are occupied by Zr atoms. Then, the V atoms form planar square nets, whose interatomic distances are much shorter than the Zr−V distances, namely 268 pm vs. 326 pm in $Zr_{0.85}V_{1.15}As$ (each 4 × per V atom). Additional M−M bonding occurs between the sheets of octahedra in form of Zr−Zr bonds of 341 pm.

More complex, and truly three-dimensional, is the bonding situation in HfVAs. V−V zigzag chains with short interatomic distances of 266 pm (in $Hf_{0.97}V_{1.03}As$) run along the *b* axis. While that bond length is similar to the V−V bonds in ZrVAs, the multitude is smaller, with two bonds per V atom in HfVAs, compared to four bonds per V atom in ZrVAs. Each V atom in HfVAs is additionally connected to Hf atoms at rather short distances of 2 × 298 pm and 2 × 308 pm, and longer ones of 321 pm and 334 pm. The Hf−Hf distances vary between 329 pm and 363 pm.

The four Hf−V distances between 298 pm and 308 pm and the six Hf−Hf between 329 and 363 pm stand against the four Zr−V at 326 pm and four Zr−Zr distances at 340 pm of ZrVAs. It is evident that the Hf atoms in HfVAs participate in more and shorter M−M bonds than the Zr atoms in ZrVAs. Remembering that the radii of the Zr and Hf atoms are virtually equivalent (e.g., Slater radii: 155 pm for both atoms, Pauling's single bond radii: 145 pm for Zr and 144 pm for Hf[28]), the reason behind this cannot be of steric nature. Since the relative extension of the *d* orbitals is higher in case of the *5d* elements, they principally tend to form more and stronger M−M bonds than the *4d* elements. This fact was used to explain the site preferences of the Ta atoms in ternary niobium tantalum sulfides,[29,30] as well as the differences between the structures of ZrNiP and HfNiP.[20] Similarly, the different main quantum numbers of Zr and Hf led to the different power factors **f** of ZrVAs and HfVAs, which ultimately results in the occurrence in different structure domains in our structure map, namely the La_2Sb and Co_2Si domains, respectively.

The differences in bond lengths (Table 2) between $Hf_{0.97}V_{1.03}As$ and $Hf_{0.92}V_{1.08}As$ stem from size differences between Hf and V (Slater radius of V: 135 pm). The same is true for $Hf_{0.84}Ti_{1.16}As$ and $Hf_{0.60}Ti_{1.40}As$. Although the latter two compounds are less Hf-rich, their unit cell volumes and bond lengths are larger than those of the V compounds, because of the larger size of Ti, compared to V (140 pm vs. 135 pm).

Table 2. Selected interatomic distances [pm]

Bond	No.	*d*[a]	*d*[b]	*d*[c]	*d*[d]
M(1)−As	2 ×	273.6(2)	272.0(1)	271.7(2)	269.9(1)
M(1)−As	2 ×	278.2(2)	277.5(1)	273.3(2)	271.3(1)
M(1)−As	1 ×	294.5(2)	292.4(2)	286.2(3)	284.9(1)
M(1)−M(1)	2 ×	335.3(2)	334.9(2)	329.2(2)	327.70(9)
M(1)−M(1)	2 ×	361.34(7)	360.41(8)	358.88(9)	357.06(6)
M(1)−M(1)	2 ×	369.6(2)	367.4(2)	362.7(2)	360.1(2)
M(1)−M(2)	2 ×	299.5(2)	297.8(2)	298.3(3)	296.2(2)
M(1)−M(2)	2 ×	315.2(3)	313.8(2)	308.1(3)	306.0(2)
M(1)−M(2)	1 ×	333.2(3)	331.9(2)	320.6(3)	318.5(2)
M(1)−M(2)	1 ×	336.9(3)	336.2(2)	333.8(3)	331.6(2)
M(2)−As	2 ×	257.3(3)	256.8(2)	252.0(3)	251.01(2)
M(2)−As	1 ×	263.0(4)	261.7(3)	259.6(4)	257.5(2)
M(2)−As	1 ×	267.0(4)	266.5(3)	258.4(4)	256.9(2)
M(2)−M(2)	2 ×	275.3(4)	274.4(4)	265.9(5)	265.1(3)

[a] $Hf_{0.84(1)}Ti_{1.16}As$. [b] $Hf_{0.602(5)}Ti_{1.40}As$. [c] $Hf_{0.97(2)}V_{1.03}As$. [d] $Hf_{0.916(6)}V_{1.084}As$.

Mixed Occupancies

All four structures analyzed here exhibit mixed occupancies on at least one metal atom site, that is, Hf/Ti and Hf/V mixtures. The same is true for $Zr_{0.58}Ti_{1.42}As$, $Zr_{1.43}V_{0.57}As$ and $Zr_{0.85}V_{1.15}As$, but not for ZrTiAs at the exact 1:1 ratio of Zr:Ti. The latter indicates a strong preference for ordering, for the two available atom sites as well as atom kinds are quite different. Hf/Ti mixed occupancies were observed in $(Hf,Ti)_7Sb_4$ [31] with almost no differences

 © 2004 Wiley-VCH Verlag GmbH & Co. KGaA, Weinheim

between the metal atom sites, and Zr/V and Zr/Ti mixed occupancies with intermediate ordering in $(Zr,V)_{13}Sb_{10}$,[32] $(Zr,V)_{11}Sb_8$,[33] and (Zr,Ti)Sb.[34] All of these observations may be explained with the various extents of the differences between the metal atom sites of the respective structures.

Electronic Structure

To further characterize HfMAs and to gain more insight into the differences between ZrMAs and HfMAs, we analyze the band structures of HfTiAs and HfVAs, as ZrVAs and ZrTiAs were investigated before. The Densities Of States (DOS) and selected Crystal Orbital Hamilton Populations (COHP)[35] curves, each cumulated over the whole unit cell, are shown in Figure 3 (HfTiAs) and Figure 4 (HfVAs). The facts, that the structures are isotypic and the constituent elements similar, are reflected in comparable, yet not equivalent, shapes of the DOS curves. As a consequence of the different valence-electron concentration, due to Ti being a 4th and V a 5th group element, the DOS of HfVAs is shifted up by more than 0.5 eV with respect to HfTiAs, with both Fermi levels fixed at 0 eV. In both cases, the energy windows shown exclude the As-*s* dominated peak, which occurs well below −7 eV. A pseudo gap (at −2.0 eV in the Ti and −2.7 eV in the V case) separates the As-*p* peak from the metal-centered states.

Hf, Ti and V contributions below −2.0 eV and −2.7 eV, respectively, are indicative of covalent M−As bonding character. As may be seen in the COHP curves on the right sides of the Figure 3 and 4, all M−As interactions are strong, and only bonding states are filled. Virtually no M−As states are found in the vicinity of the Fermi level. The same statements can be made in the cases of ZrTiAs and ZrVAs.

A second pseudo gap is located within the M-*d* peak, separating bonding M(2)−M(2) interactions from the antibonding ones. The Fermi level is found slightly below this local minimum in HfTiAs, and slightly above it in HfVAs. In both cases the Fermi level is located in the midst of the metal *d* states, emphasizing the importance of the *d* states for the bonding and thus crystal structure. The V−V bonds are optimized in HfVAs, that is, the transition from bonding to antibonding character takes place directly at the Fermi level. The Ti−Ti bonds in HfTiAs would gain bonding character by an increase of valence-electrons, because empty bonding states are found up to 1 eV above the Fermi level.

That Hf is the most electropositive element here, and thus the higher oxidized M atom, reflects itself in fewer filled Hf−Hf bonding states, compared to both Ti−Ti and V−V states. Therefore, the Hf−Hf interactions are less dominant,

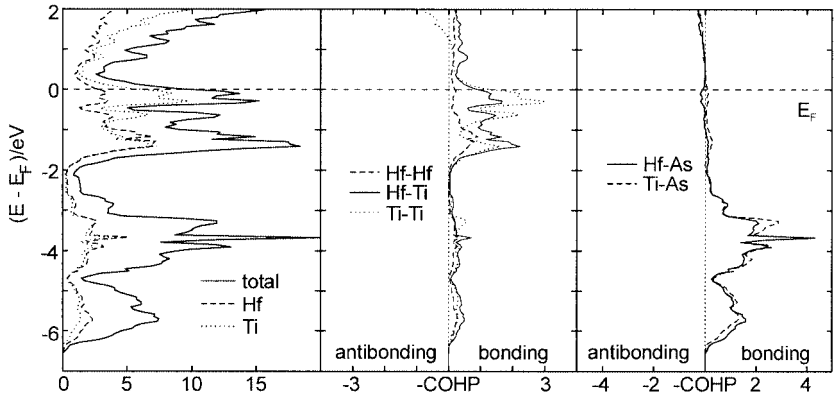

Figure 3. Densities of states (left) and selected cumulated COHP curves for HfTiAs

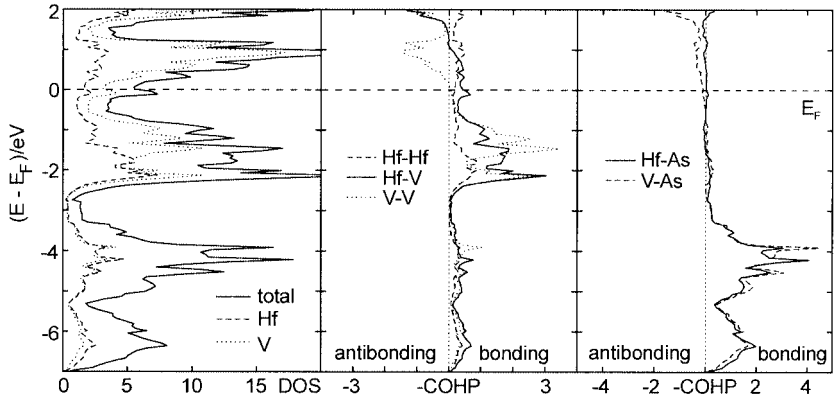

Figure 4. Densities of states (left) and selected cumulated COHP curves for HfVAs

 © 2004 Wiley-VCH Verlag GmbH & Co. KGaA, Weinheim

and they exhibit exclusively bonding states within the depicted energy window. The latter is also true for the Hf−Ti interactions in HfTiAs, but not for the Hf−V interactions in HfVAs. The latter turn into antibonding character about 1 eV above the Fermi level.

The most striking difference between the M−M COHP curves of the Zr and Hf arsenides under consideration is the relative importance of the Ti−Ti and V−V interactions, in relation to the other kinds. While they seem to be the strongest in all cases, they are less dominant in the Hf cases, particularly compared to the Hf−Ti and Hf−V bonds, respectively. In turn, the Hf−M′ bonds are thus more important in the HfM′As structures than the Zr−M′ bonds in ZrM′As. This observation is in tune with the assumption that Hf may form stronger metal−metal bonds than Zr because of the larger extension of its *5d* orbitals, as all the metal−metal interactions rely almost exclusively on the *d* states.

Conclusion

Three new compounds, all with significant phase ranges, have been introduced: $Hf_{1-\delta}Ti_{1+\delta}P$, $Hf_{1-\delta}Ti_{1+\delta}As$, and $Hf_{1-\delta}V_{1+\delta}As$, all crystallizing in the Co_2Si type. This completes the series of ternary Zr/Hf − Ti/V phosphides and arsenides that form either the Co_2Si or the La_2Sb type. Evidently all these compounds fit into the recently published M_2Q structure map based on the power product $\mathbf{f} = vec_M \times n_M^2 \times (r_M/r_Q)/(8 - e_Q)^2$ − higher **f** values are indicative of more M−M bonding. On the other hand, electron counting or basic analogy considerations failed to explain the respective crystal structures, as for both structure variants examples exist with 13 as well as 14 valence-electrons, and seemingly analogous compounds such as ZrTiAs and HfTiAs occur in different types, while ZrTiP and HfTiP are isostructural.

While all kinds of M−M bonding occur in both types, the Hf−Hf and Hf−Ti/V bonds of HfTiAs and HfVAs are shorter than the respective Zr-containing bonds in ZrTiAs and ZrVAs (the latter both La_2Sb type). That difference may be understood based on the different main quantum numbers n_{Zr} and n_{Hf}, considering that higher quantum numbers enable the metal atom to form stronger M−M bonds (cf. n_M in the power product **f**).

Experimental Section

Syntheses of HfMP and HfMAs

All experiments started from the elements as purchased in microcrystalline form from Aldrich, with purities above 99.5%. The first steps were the syntheses of the monopnictides HfP, HfAs, TiP, TiAs, and VAs as starting materials, which were necessary to minimize mass losses due to vaporization of phosphorus or arsenic during arc-melting and tube attacks during annealing in tantalum containers, respectively. The monoarsenides were prepared starting from the elements in the stoichiometric 1:1 ratios in evacuated fused silica tubes at 800 °C, and TiP was synthesized at 400 °C under addition of trace amounts of iodine. Then, more metal was added to reach the target ratio of metal/pnicogen of 2:1. These mixtures were thoroughly ground, pressed into pellets and then arc-melted twice under a flow of Argon. This procedure led to the synthesis of HfTiP, HfTiAs and HfVAs in yields of 80−90%, as estimated based on the powder diagrams obtained using an X-ray powder diffractometer with position-sensitive detector (Inel). Higher yields were obtained in the HfTiP system by annealing the mixtures in sealed tantalum containers at 1400 °C over a period of several days (without prior arc-melting).

Phase Ranges of $Hf_{1-\delta}Ti_{1+\delta}P$ and $Hf_{1-\delta}M_{1+\delta}As$

$Zr_{1-\delta}Ti_{1+\delta}As$ and $Zr_{1-\delta}V_{1+\delta}As$ (both La_2Sb type) exhibit significant phase ranges, with $0 \le \delta \le 0.42(1)$ and $-0.43(4) \le \delta \le 0.15(1)$, respectively.[7,8] $Zr_{1-\delta}V_{1+\delta}P$ and $Hf_{1-\delta}V_{1+\delta}P$ (both Co_2Si type) were reported to have significant phase widths as well ($0 \le \delta \le 0.40$ and $0 \le \delta \le 0.55$).[13] Therefore, we varied the Hf:M ratios to determine the phase ranges of $Hf_{1-\delta}Ti_{1+\delta}P$ and $Hf_{1-\delta}M_{1+\delta}As$. These investigations were started with arc-melting different mixtures in the arsenic system:

$HfAs + Ti \rightarrow Hf_{1-\delta}Ti_{1+\delta}As + Hf_3As + ?$ (**I**)

$0.75\ Hf + 0.25\ Ti + TiAs \rightarrow Hf_{1-\delta}Ti_{1+\delta}As + ?$ (**II**)

$0.5\ Hf + 0.5\ Ti + TiAs \rightarrow Hf_{1-\delta}Ti_{1+\delta}As + Ti_3As + ?$ (**III**)

$0.25\ Hf + HfAs + 0.75\ V \rightarrow Hf_{1-\delta}V_{1+\delta}As + Hf_3As + ?$ (**IV**)

$HfAs + V \rightarrow Hf_{1-\delta}V_{1+\delta}As + ?$(**V**)

$0.75\ Hf + 0.25\ V + VAs \rightarrow Hf_{1-\delta}V_{1+\delta}As + V_3As + ?$ (**VI**)

The products of the reactions (**I**) − (**VI**), as determined by X-ray powder diffraction, indicate different phase ranges for the Ti- and V-containing Hf arsenides, namely $0 < \delta < 0.5$ for $Hf_{1-\delta}Ti_{1+\delta}As$ and $-0.25 < \delta < 0.25$ for $Hf_{1-\delta}V_{1+\delta}As$. The symbol "?" implies the presence of unidentified compounds in small yields.

Analogous investigations in the Hf−Ti−P system were carried out at 1400 °C, for arc-melting proved to be more difficult, most likely due to phosphorus vaporization. Reactions aiming at $Hf_{1-\delta}Ti_{1+\delta}P$ were carried out with δ varying between −0.5 and +0.5, and $Hf_{1-\delta}Ti_{1+\delta}P$ was formed as the main product when $-0.2 \le \delta \le 0.5$. The lattice dimensions of the Co_2Si type phases were determined from their X-ray powder diagrams by least-square refinements (assuming orthorhombic symmetry). EDS analyses (LEO, 1530, with integrated EDAX Pegasus 1200) on several selected crystals of the Co_2Si phases did not reveal any incorporation of impurity elements, such as Si or oxygen stemming from the silica tube or Ta coming from the tantalum container, or iodine from the synthesis of TiP. According to the averaged values of these analyses (summarized in Table 3), $Hf_{1-\delta}Ti_{1+\delta}P$ exists between $Hf_{0.6}Ti_{1.4}P$ and $Hf_{1.2}Ti_{0.8}P$ (i.e. $-0.2 \le \delta \le 0.4$). An increasing Hf content is reflected in larger cell volumes, for Hf atoms are larger than Ti atoms (e.g., Slater radii: 155 pm vs. 140 pm).

Table 3. Lattice dimensions of powdered HfTiP samples and EDX results of selected crystals thereof

Target	EDX	*a*/pm	*b*/pm	*c*/pm	*V*/nm³
"$Hf_{0.5}Ti_{1.5}P$"	$Hf_{0.61}Ti_{1.39}P$	661.4(7)	350.8(3)	803.7(9)	0.1865(6)
"$Hf_{0.6}Ti_{1.4}P$"	$Hf_{0.58}Ti_{1.42}P$	662.9(4)	351.3(2)	805.8(6)	0.1877(4)
"$Hf_{0.7}Ti_{1.3}P$"	$Hf_{0.80}Ti_{1.20}P$	665.7(5)	352.3(2)	807.6(6)	0.1894(4)
"$Hf_{0.8}Ti_{1.2}P$"	$Hf_{0.80}Ti_{1.20}P$	668.0(5)	354.0(4)	809.4(8)	0.1914(6)
"$Hf_{0.9}Ti_{1.1}P$"	$Hf_{0.87}Ti_{1.13}P$	668.5(6)	354.6(4)	810.3(6)	0.1921(5)
"HfTiP"	$Hf_{1.03}Ti_{0.97}P$	670.5(5)	354.8(2)	812.4(6)	0.1933(4)
"$Hf_{1.1}Ti_{0.9}P$"	$Hf_{1.12}Ti_{0.88}P$	670.3(6)	355.0(2)	812.9(5)	0.1934(4)
"$Hf_{1.2}Ti_{0.8}P$"	$Hf_{1.23}Ti_{0.77}P$	673.4(6)	355.4(2)	815.9(8)	0.1953(5)

 © 2004 Wiley-VCH Verlag GmbH & Co. KGaA, Weinheim

Crystal Structure Studies of $Hf_{1-\delta}M_{1+\delta}As$

From each of the reactions (**I**), (**III**), (**IV**), and (**VI**), one single crystal was selected for structure refinements, to prove the formation of the Co_2Si type and to analyze the occupancy factors. Based on the powder data, the products were at the phase range borders; thus, determining their Hf/M ratios will give the phase width.

A Smart Apex CCD diffractometer (Bruker) using Mo-K_α radiation was employed for the data collections. In all four cases, 606 frames were collected with 0.3° scans in ω for exposure times of 60 seconds per frame. The data were corrected for Lorentz and Polarization effects. The unit cell dimensions and the systematic absences were consistent with the space group *Pnma* (and its noncentrosymmetric subgroup $Pn2_1a$), which is the space group of the Co_2Si type. This was subsequently confirmed by the successful structure refinements using SHELXL[36] yielding satisfying residual factors. Refining the structures in the noncentrosymmetric subgroup $Pn2_1a$ did not yield significant changes, but instead resulted in high correlations.

The Co_2Si type comprises three crystallographically independent atom sites (all on a mirror plane, Wyckoff notation 4*c*). The Si site was treated as the As site, and the two metal atom sites [denoted as M(1) and M(2)] were refined as being mixed occupied by Hf and M (Ti and V, respectively), with the sums of the occupancy factors fixed at 100%. M(1) is the Ti site in TiNiSi, and the Hf site in isostructural HfCoAs.[21]

In each case investigated here, the M(1) site was mainly occupied with Hf atoms, but exhibited always some Ti or V content. The M(2) site was either mixed occupied (with Hf as the minor component), or solely a Ti/V site, namely on the Hf-poor side of the phase range. Furthermore, the Hf contents of M(2) on the Hf-rich side [0.022(5) and 0.018(5)] may be regarded as insignificant. The refined formulas were $Hf_{0.84(1)}Ti_{1.16}As$, $Hf_{0.602(5)}Ti_{1.40}As$, $Hf_{0.97(2)}V_{1.03}As$, and $Hf_{0.916(6)}V_{1.084}As$, respectively. Crystallographic details are given in the Table 4. Atomic positions, occupancy factors, and displacement parameters are listed in Table 5. Further details of the crystal structure investigations can be obtained from the Fachinformationzentrum Karlsruhe, 76344 Eggenstein-Leopoldshafen, Germany, on quoting the depository numbers CSD-413262, -413263, -413264 and -413265.

Table 5. Atomic coordinates and equivalent displacement parameters [$pm^2 \times 10^{-1}$] of $Hf_{1-\delta}M_{1+\delta}As$

Atom[a]	*x*	*z*	$U_{eq.}$	Occupancy
M(1)[b]	0.4575(1)	0.6660(1)	4.7(3)	0.820(9) Hf, 0.180 Ti
M(1)[c]	0.4567(1)	0.6665(1)	6.3(3)	0.602(5) Hf, 0.398 Ti
M(1)[d]	0.4564(1)	0.6670(1)	6.6(3)	0.95(1) Hf, 0.05 V
M(1)[f]	0.45633(7)	0.66738(6)	5.1(2)	0.916(6) Hf, 0.084 V
M(2)[b]	0.3665(4)	0.0594(4)	4(1)	0.022(5) Hf, 0.978 Ti
M(2)[c]	0.3666(4)	0.0598(3)	5.2(6)	1 Ti
M(2)[d]	0.3720(5)	0.0578(4)	5(1)	0.018(5) Hf, 0.982 V
M(2)[e]	0.3714(3)	0.0581(2)	5.6(4)	1 V
As[b]	0.2438(3)	0.3589(2)	4.5(6)	1 As
As[c]	0.2456(2)	0.3593(2)	6.6(4)	1 As
As[d]	0.2428(3)	0.3607(3)	7.1(7)	1 As
As[e]	0.2432(2)	0.3600(1)	4.9(3)	1 As

[a] All atoms located on Wyckoff site 4*c*, with $y = 1/4$. [b] $Hf_{0.84(1)}Ti_{1.16}As$. [c] $Hf_{0.602(5)}Ti_{1.40}As$. [d] $Hf_{0.97(2)}V_{1.03}As$. [f] $Hf_{0.916(6)}V_{1.084}As$.

Electronic Structure Calculations

The band structures were calculated employing the self-consistent tight-binding *first principles* LMTO approximations (LMTO = linear muffin tin orbitals[37,38]). In the LMTO approach, the density functional theory is used with the local density approximation (LDA).[39] The integration in *k* space was performed by an improved tetrahedron method[40] on grids of 462 irreducible *k* points of the first Brillouin zone. Void space was filled with four so-called empty spheres. As structure models, we chose the structural parameters obtained from the refinements of $Hf_{0.84}Ti_{1.16}As$ and $Hf_{0.97}V_{1.03}As$ (using Hf parameters for M(1) and Ti and V parameters for M(2), respectively).

Table 4. Crystal data and structure refinements

Empirical formula	$Hf_{0.84}Ti_{1.16}As$	$Hf_{0.60}Ti_{1.40}As$	$Hf_{0.97}V_{1.03}As$	$Hf_{0.92}V_{1.08}As$
Molecular mass [g/mol]	280.74	249.34	300.52	293.83
Temperature [K]	293(2)	293(2)	293(2)	293(2)
Wavelength [pm]	71.073	71.073	71.073	71.073
Space group	*Pnma*	*Pnma*	*Pnma*	*Pnma*
Cell dimensions, *a* [pm]	684.3(2)	680.5(2)	674.1(2)	669.7(1)
b [pm]	361.34(7)	360.41(8)	358.88(9)	357.06(6)
c [pm]	832.2(2)	829.3(2)	807.3(2)	802.1(1)
V [nm^3]	0.20577(7)	0.20339(8)	0.19530(9)	0.19180(5)
No. of formula units per cell	4	4	4	4
Calculated density [mg/m^3]	9.06	8.14	10.22	10.18
Absorp. coeff. [mm^{-1}]	62.4	51.8	72.7	71.5
F(000)	477	428	506	496
Crystal size [μm]	50 × 45 × 20	42 × 39 × 14	44 × 42 × 20	49 × 45 × 14
Theta range	3.86−29.99°	3.87−33.13°	3.94−29.99°	3.96−35.01°
Reflections collected	796	949	733	791
Independent reflections (R_{int})	331 (0.032)	415 (0.078)	316 (0.034)	424 (0.022)
Absorption correction	sadabs	sadabs	sadabs	sadabs
Max. and min. transmission	1.00−0.60	1.00−0.61	1.00−0.69	1.00−0.74
Goodness-of-fit on F^2	1.213	0.901	1.358	1.129
$R(F)$, $R_w(F^2)$ (obsd. data)	0.043, 0.098	0.044, 0.083	0.047, 0.091	0.034, 0.075
$R(F)$, $R_w(F^2)$ (all data)	0.049, 0.100	0.061, 0.088	0.054, 0.093	0.038, 0.077
Extinction coefficient	0.0000(9)	0.0000(6)	0.0017(8)	0.0009(6)
Max. diff. peak, hole [e/$Å^3$]	6.09, −3.07	5.06, −2.86	3.43, −3.32	3.30, −3.25

 © 2004 Wiley-VCH Verlag GmbH & Co. KGaA, Weinheim

Acknowledgments

Financial support from NSERC, CFI, OIT (Ontario Distinguished Researcher Award for H. K.), the Province of Ontario (Premier's Research Excellence Award for H. K.) and the Canada Research Chair program (CRC for H. K.) is appreciated.

[1] C. B. Shoemaker, D. P. Shoemaker, *Acta Crystallogr.* **1965**, *18*, 900−905.
[2] I. R. Mokra, O. I. Bodak, *Dopov. Akad. Nauk Ukrain. RSR* **1979**, 312−315.
[3] H. Kleinke, B. Harbrecht, *Z. Anorg. Allg. Chem.* **2000**, *626*, 1851−1853.
[4] J. C. Slater, *J. Chem. Phys.* **1964**, *41*, 3199−3204.
[5] D. G. Pettifor, *Solid State Commun.* **1984**, *51*, 31−34.
[6] P. Villars, *J. Less-Commun. Met.* **1983**, *92*, 215−238.
[7] C.-S. Lee, E. Dashjav, H. Kleinke, *Chem. Mater.* **2001**, *13*, 4053−4057.
[8] E. Dashjav, C.-S. Lee, H. Kleinke, *J. Solid State Chem.* **2002**, *169*, 96−102.
[9] G. Örlygsson, M. Conrad, B. Harbrecht, *Z. Anorg. Allg. Chem.* **2001**, *627*, 1017−1022.
[10] C.-S. Lee, E. Dashjav, H. Kleinke, *J. Alloys Comp.* **2002**, *338*, 60−68.
[11] S. Derakhshan, E. Dashjav, H. Kleinke, *Mat. Res. Soc., Symp. Proc.* **2002**, *755*, 341−346.
[12] Y. F. Lomnytska, Y. B. Kuz′ma, *J. Alloys Comp.* **1998**, *269*, 133−137.
[13] Y. F. Lomnitskaya, M. S. Brilyak, Y. B. Kuz′ma, *Neorg. Mater.* **1992**, *28*, 373−377.
[14] G. A. Marking, H. F. Franzen, *J. Alloys Comp.* **1994**, *204*, L17−L20.
[15] R. Berger, L. E. Tergenius, *Acta Chem. Scand., Ser. A* **1976**, *30*, 387−389.
[16] Y. Wang, L. D. Calvert, J. B. Taylor, *Acta Crystallogr., Sect. B* **1980**, *36*, 220−221.
[17] E. Garcia, J. D. Corbett, *J. Solid State Chem.* **1988**, *73*, 440−451.
[18] S. Rundqvist, P. C. Nawapong, *Acta Chem. Scand.* **1966**, *20*, 2250−2254.
[19] N. Chaichit, P. Chalugune, S. Rukvichai, P. Choosang, V. Kaewchansilp, C.-A. Pontchour, P. Phavanantha, *Acta Chem. Scand., Ser. A* **1978**, *32*, 309−311.
[20] H. Kleinke, H. F. Franzen, *Z. Anorg. Allg. Chem.* **1996**, *622*, 1893−1900.
[21] H. Kleinke, H. F. Franzen, *Z. Anorg. Allg. Chem.* **1998**, *624*, 51−56.
[22] H. Kleinke, C. Felser, *J. Solid State Chem.* **1999**, *144*, 330−338.
[23] H. Kleinke, *Z. Anorg. Allg. Chem.* **1998**, *624*, 1272−1278.
[24] Y. B. Kuz′ma, J. Y. Pivan, *Russ. J. Inorg. Chem.* **1979**, *24*, 1421.
[25] G. J. Miller, J. Cheng, *Inorg. Chem.* **1995**, *34*, 2962−2968.
[26] R. Hoffmann, *J. Chem. Phys.* **1963**, *39*, 1397−1412.
[27] M.-H. Whangbo, R. Hoffmann, *J. Am. Chem. Soc.* **1978**, *100*, 6093−6098.
[28] L. Pauling, *The Nature of the Chemical Bond*; 3rd ed.; Cornell University Press: Ithaca, New York, **1948**.
[29] X. Yao, G. Marking, H. F. Franzen, *Ber. Bunsenges.* **1992**, *96*, 1552−1557.
[30] M. Köckerling, H. F. Franzen, *Croat. Chem. Acta* **1995**, *68*, 709−719.
[31] H. Kleinke, *Inorg. Chem.* **1999**, *38*, 2931−2935.
[32] H. Kleinke, *Chem. Commun. (Cambridge)* **1998**, 2219−2220.
[33] H. Kleinke, *J. Mater. Chem.* **1999**, *9*, 2703−2708.
[34] H. Kleinke, *J. Am. Chem. Soc.* **2000**, *122*, 853−860.
[35] R. Dronskowski, P. E. Blöchl, *J. Phys. Chem.* **1993**, *97*, 8617−8624.
[36] G. M. Sheldrick, *SHELXTL*; Version 5.12 ed.; Siemens Analytical X-ray Systems: Madison, WI, **1995**.
[37] O. K. Andersen, *Phys. Rev. B* **1975**, *12*, 3060−3083.
[38] H. L. Skriver, *The LMTO Method*; Springer: Berlin, **1984**.
[39] L. Hedin, B. I. Lundqvist, *J. Phys. C* **1971**, *4*, 2064−2083.
[40] P. E. Blöchl, O. Jepsen, O. K. Andersen, *Phys. Rev. B* **1994**, *49*, 16223−16233.

Received July 16, 2003
Early View Article
Published Online February 10, 2004

 © 2004 Wiley-VCH Verlag GmbH & Co. KGaA, Weinheim

Eu^{III} Luminescence in a Hygroscopic Ionic Liquid: Effect of Water and Evidence for a Complexation Process

Isabelle Billard,*[a] Soufiane Mekki,[a] Clotilde Gaillard,[a] Peter Hesemann,[b] Gilles Moutiers,[c] Clarisse Mariet,[c] Alexandre Labet,[c] and Jean-Claude G. Bünzli[d]

Keywords: Ionic liquids / Lanthanides / Europium / Luminescence / Complexation

The spectroscopic characteristics (excitation, emission and lifetime) of Eu^{III} dissolved in 1-methyl-3-butylimidazolium bis(trifluoromethanesulfon)imide (BumimTf_2N) are reported. In a first series of experiments, the effect of the presence of water in BumimTf_2N was examined. It appears that non-degassed solutions are most probably inhomogeneous, displaying large water clusters leading to an intense diffusion of the red light of an He:Ne laser. In these samples, the Eu emission spectrum is close to that observed in slightly acidic aqueous solutions. In contrast, when the samples were degassed the solution appeared homogeneous and water can be considered as a competitive ligand for the first coordination sphere of Eu. In a subsequent series of experiments, tetrabutylammonium chloride (TBACl) was added to the solution and the resultant species investigated. The ensuing enhancement in the metal-centered luminescence has been interpreted in terms of changes in the inner coordination sphere of the Eu^{III} ion and possible structures are discussed. (© Wiley-VCH Verlag GmbH & Co. KGaA, 69451 Weinheim, Germany, 2004)

Introduction

Room-temperature ionic liquids (RTIL) appear as "multi-purpose liquids" able to replace usual organic solvents in almost every field of chemistry (e.g. catalysis, synthesis, electrochemistry).[1] Both the cationic and the anionic components of these liquids can be easily varied, and they can therefore be tailored for particular applications or to have specific sets of properties. As a consequence, RTILs represent a green alternative to volatile organic solvents, offering environmentally safe processes.

In particular, in the field of nuclear waste reprocessing, there is still a need for improved routes for the actinide/lanthanide separation/extraction. In addition to promising studies on the use of ionic liquids for liquid/liquid extraction,[2] a recent study has shown that some ionic liquids display reasonable stability under α and γ irradiation,[3] thus reinforcing their potential interest for the nuclear fuel industry. However, despite the increasing number of publications devoted to ionic liquids, the solvation effects, the solute-solvent and solvent-solvent interactions as well as the general structural organization of these solvents are still hardly known. These fundamental aspects are of tremendous importance for understanding the solvating properties of these new solvents, thus limiting their applications for liquid/liquid extraction. In order to gain a better insight into these questions, we have undertaken a spectroscopic investigation on the solvation of Eu^{III} in 1-methyl-3-butylimidazolium bis(trifluoromethanesulfon)imide (BumimTf_2N, see Scheme 1). This ionic liquid has been chosen because it can be used, among others, for biphasic separations such as liquid extraction in view of its hydrophobic properties. Eu^{III} has been chosen as a representative lanthanide ion and as a good homologue of Am^{III}, an actinide of great interest in the nuclear fuel cycle. In this work, we take advantage of the specific properties of Eu^{III} to investigate its solvation in BuminTf_2N by means of luminescence measurements. Specific attention has been paid to the role

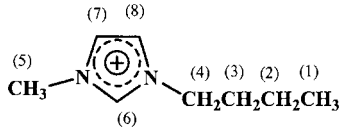

cation: Bumim

anion: $(CF_3SO_2)_2N^-$ (Tf_2N)

Scheme 1

[a] IReS, Chimie Nucléaire,
B. P. 28, 67037 Strasbourg Cedex 2, France
E-mail: isabelle.billard@ires.in2p3.fr
[b] CNRS UMR 5076, Hétérochimie Moléculaire et Macromoléculaire, Laboratoire de Chimie Organométallique,
8, rue de l'Ecole Normale, 34296 Montpellier Cedex 05, France
E-mail: hesemann@cit.enscm.fr
[c] CEA Saclay, INSTN/UECCC,
91191 Gif-sur-Yvette, France
E-mail: gilles.moutiers@cea.fr
[d] Swiss Federal Institute of Technology, Institute of Molecular and Biological Chemistry, Laboratory of Lanthanide Supramolecular Chemistry, BCH 1402,
1015 Lausanne, Switzerland
E-mail: jean-claude.bunzli@epfl.ch

 © 2004 Wiley-VCH Verlag GmbH & Co. KGaA, Weinheim **DOI: 10.1002/ejic.200300588**

of water (considered as a solute) in the luminescence properties of Eu^{III} and the effect of added tetrabutylammonium chloride has also been investigated.

Results and Discussion

Effect of Water on the Spectroscopic Characteristics of Eu^{III}

Results

Europium triflate (5×10^{-3} M) in $BumimTf_2N$ turns to a slight brownish color after degassing (procedure II, see Exp. Sect.) and a very weak absorption band located at 394 nm can be observed corresponding to the transition with the largest oscillator strength in the Eu^{III} spectrum namely the $^5L_6 \leftarrow {}^7F_{0,1}$ transition (Figure 1). The spectrum of a more concentrated and degassed solution (4×10^{-2} M) is displayed in Figure 2, from which a molar absorption coefficient of 0.8 $M^{-1}\cdot cm^{-1}$ (λ = 394 nm) could be estimated. This value is of the same order of magnitude as that reported for Eu^{III}(aq) i.e. 2.4 $M^{-1}\cdot cm^{-1}$.[4] In two previous studies,[5,6] various lanthanide triflates were dissolved in RTILs, particularly in $BumimPF_6$, at concentrations far below the maximum concentration obtained by us. This may be due in part to the use, in these studies, of anhydrous lanthanide salts.

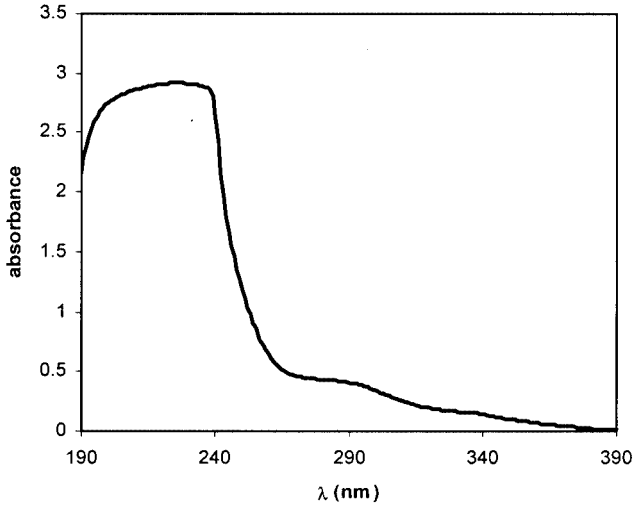

Figure 1. Absorption spectrum of the $BumimTf_2N$ batch used in this work (non-degassed)

RTILs are known to be hygroscopic[1,7,8] and previous studies have provided insight into the dependence of the kinetics of water absorption by RTILs upon experimental conditions.[7–9] In order to obtain a deeper understanding of the influence of water on europium luminescence in $BumimTf_2N$, a solution was submitted to cycles combining various degassing procedures and storage durations during which the solution was simply kept in the quartz cuvette with a Teflon cap. Table 1 summarizes these cycles and displays the decay behavior (either mono- or biexponential),

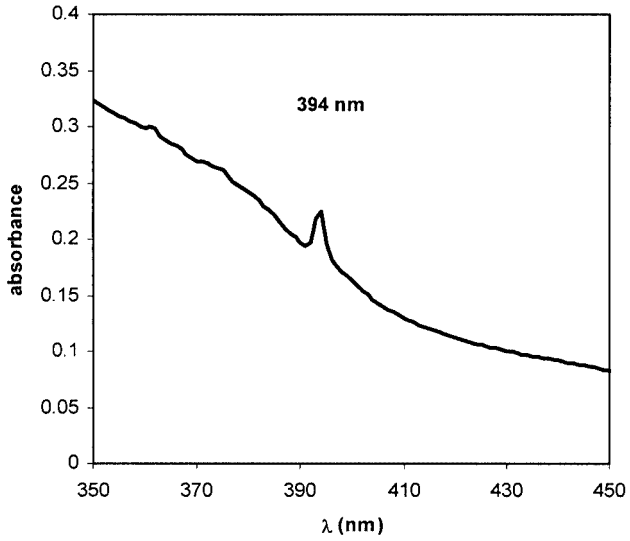

Figure 2. Absorption spectrum of the Eu^{III} triflate salt 4×10^{-2} M in $BumimTf_2N$

the corresponding lifetimes and relative intensities during the cycles. In this table, $t = 0$ corresponds to the end of the first degassing procedure and positive t values indicate the time elapsed since $t = 0$, when the data (decay profile and emission/excitation spectra) were recorded. By definition, the notation $t = -1$ means that the measurement was performed *before* this first degassing procedure when the ionic liquid water content was constant with time (see section "water contents"). Note that a lifetime decay could be obtained for the non-degassed (probably heterogeneous) sample, since no fluctuations of the luminescence intensity were observed. Figure 3 presents the excitation spectra obtained at times equal to −1, 0, and 13 d of the cycle, while emission spectra are displayed in two separate figures (Figure 4, a and b) in view of the large differences in emission intensities. For t = 25 d, the excitation and emission spectra are very similar to those for t = 13 d and are therefore not shown.

Table 1. Decay behavior, lifetime values (μs), relative intensities (%) and $R_{612/589}$ values for the Eu^{III} triflate salt in $BumimTf_2N$ along the degassing/storage cycle (see text)

t [d]	Procedure	Decay characteristics	$R_{612/589}$
−1	no degassing	monoexponential τ = 159 μs	< 1
0	degassing (I)	biexponential τ_1 = 643 μs (19%) τ_2 = 1596 μs (81%)	3.4
6	storage	monoexponential τ = 350 μs	n. d.
13	degassing (II)	biexponential τ_1 = 689 μs (85%) τ_2 = 2556 μs (15%)	3.4
20	storage	monoexponential τ = 681 μs	n. d.
25	storage	monoexponential τ = 545 μs	3.4

 © 2004 Wiley-VCH Verlag GmbH & Co. KGaA, Weinheim

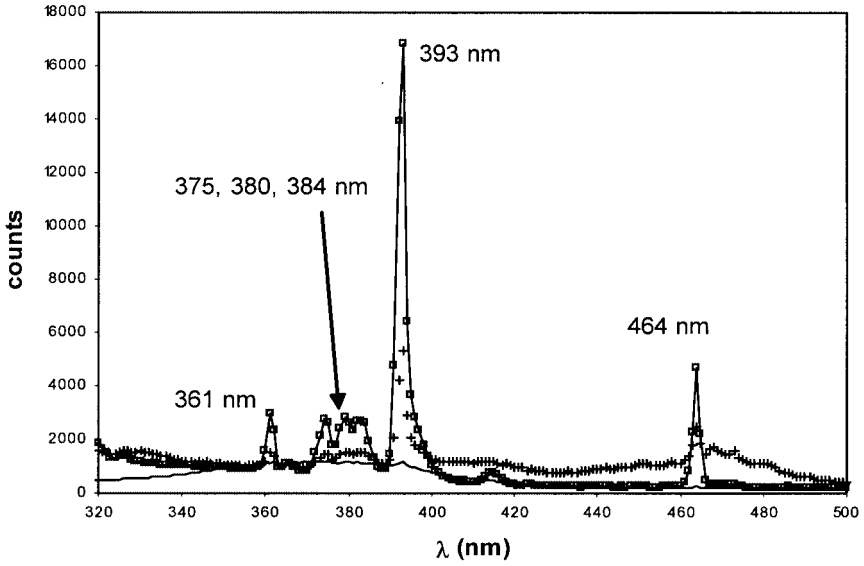

Figure 3. Excitation spectra of the Eu^{III} triflate salt 5×10^{-3} M in $BumimTf_2N$ during the degassing cycle; emission wavelength: $\lambda = 609$ nm; solid line: $t = -1$ d; open squares: $t = 0$ d (procedure I); +++: $t = 13$ d (procedure II)

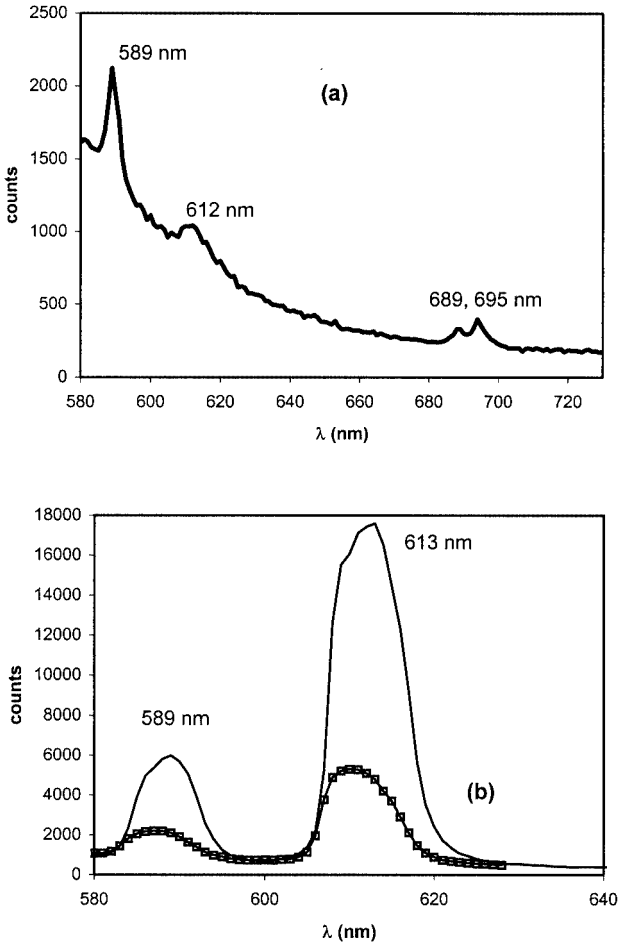

Figure 4. a: Emission of the Eu^{III} triflate salt 5×10^{-3} M in $BumimTf_2N$ at $t = -1$ d (see text and Table 1); excitation wavelength: $\lambda = 394$ nm; b: emission of the Eu^{III} triflate salt 5×10^{-3} M in $BumimTf_2N$ in function of the degassing procedure (see text and Table 1); excitation wavelength: $\lambda = 393$ nm; solid line: $t = 0$ d (procedure I); open squares: $t = 13$ d (procedure II)

For all samples the excitation spectra essentially display f-f transitions, indicating no antenna effect from the ionic liquid. The energies of these transitions do not vary which is in contrast to their intensities which substantially decrease over time after the first degassing procedure. Similar behavior was observed for the emission spectra and lifetimes. Using excitation at other wavelengths (data not shown), the emission was similar in shape and the intensity change reflects the relative intensities observed in the excitation spectra. The lifetimes exhibit peculiar behavior: a single exponential decay was measured for the non-degassed solution with a short lifetime of 0.159 ms, which became biexponential upon degassing, with much longer lifetimes of 0.64 and 1.6 ms. After 6 d of storage, the decay was again characterized by a single exponential but this again became biexponential after the second degassing. For the air- and water-tight solution, biexponential behavior was still observed more than 12 d after degassing and the lifetime values were perfectly stable.

Discussion

The intense diffusion of the He:Ne laser light by the non-degassed europium solution compared with almost zero diffusion for pure non-degassed $BumimTf_2N$ points to the presence of large aggregates (clusters) in the former. Hence the non-degassed europium solution, which contains approximately 80 H_2O molecules per Eu^{III} ion, should be better considered as being an emulsion. The emission spectrum of the non-degassed sample (Figure 4, a) is very similar to the one obtained for $Eu^{3+}{}_{aq}$ in slightly acidic aqueous solution,[4,10] although the corresponding lifetime is larger (0.159 ms compared with 0.111 ms for $Eu^{3+}{}_{aq}$, see Table 1). The presence of high-energy O−H oscillators in the inner coordination sphere of Eu^{III} is known to induce a severe quenching of the luminescence.[11] The short lifetime measured for the ionic liquid solution suggests that Eu^{III} is heav-

 © 2004 Wiley-VCH Verlag GmbH & Co. KGaA, Weinheim

ily hydrated, possibly to the same extent as in an aqueous solution. Indeed, triflate is only slightly more coordinating than perchlorate[12] and should not bind to the Eu^{III} ion in water. In contrast, no data are available on the coordinating strength of Tf_2N^- but since it is present in large excess in the solutions, inner-sphere coordination cannot be excluded. The longer lifetime measured in the RTIL could be due to the limited amount of water in $BumimTf_2N$ leading to a decreased inner-sphere hydration number n and/or a decreased outer sphere hydration number m in the $\{[Eu(A^-)_x(H_2O)_n]^{(3-x)+}(H_2O)_m(A^-)_{(3-x)}\}$ aggregates (A^- stands for an anion). In water, n is fractional (and x is essentially equal to zero), reflecting a fast equilibrium between 8- and 9-coordinate species,[13] while both nona- octa- and hexahydrated Ln^{III} ions have been evidenced in the solid state. The contribution of second-sphere oscillators to the luminescence decay is not well known, but in the case of Eu^{III} complexes with cyclen derivatives, it has been estimated to be 0.25 ms^{-1}.[14]

In contrast, the degassed sample at the beginning of the cycle ($t = 0$) exhibited completely different Eu^{III} spectroscopic properties, indicating a large loss of inner-sphere water molecules. This is illustrated by the increased intensity of the hypersensitive transition ($^5D_0 \rightarrow {}^7F_2$) at ca. 613 nm by a factor > 3 (see Figure 4, b). The relative broadness of the bands and their lack of crystal-field fine structure may indicate that Eu^{III} is imbedded into a medium with properties similar to those of a glass. The degassing procedure drastically decreases the total water amount but some water remains. A water content of 50 ppm still corresponds to one molecule of water per Eu^{III} ion.

No information can be gained on which form of water is better extracted in the degassing procedure[9] whether already accommodated in the solvent prior to solution preparation or introduced with the europium salt. As a matter of fact, the absence of laser light diffusion after degassing is evidence for a homogeneous solution and the changes in the emission spectra show that europium is now solvated in the RTIL and no longer in "water clusters". The biexponential behavior of the luminescence decay either in the air- and water-tight cuvette or at the beginning of the storage can be considered to reflect the presence of two different Eu^{III} species in solution. One explanation could be the formation of inner-sphere complexes with the counterions [Equations (1) and (2)].

$$\{[Eu(H_2O)_n]^{3+}(H_2O)_m\} \rightleftarrows [Eu(H_2O)_n]^{3+} + m\,H_2O \rightleftarrows [Eu(H_2O)_x]^{3+} + (m + n - x)\,H_2O \quad (1)$$

$$[Eu(H_2O)_x]^{3+} + y\,A^- \rightleftarrows [Eu(A)_y(H_2O)_{x-y}]^{3-y)+} + y\,H_2O \quad (2)$$

In Equation (2), A^- has been taken as being a monodentate anion, but the triflate could also be bidentate or even act as bridging moiety. The latter assumption is, however, not very probable in view of the relatively high dilution of the solutions. In water, phenomenological calibration curves have been reported which relate the number of inner-sphere water molecules to the lifetimes measured in water and deuterated water.[11,15] In the absence of structural information on the solvated species in RTILs, and because these phenomenological correlations cannot be easily transposed from one solvent to another, no such relationship is available and therefore an estimate of x is not within reach with the present lifetime data. We note, however, that 1.6 ms is a rather long lifetime [cf. 2.10 ms for $Eu(ClO_4)$ in anhydrous acetonitrile][16] and since the RTIL medium is not dielectrically too different from an organic solvent, the associated species probably contains, on average, less than one water molecule. The subsequent transformation of the decay into a single exponential curve, with a concomitant decrease in lifetime after few days of storage reflects a rehydration of the Eu^{III} ion, although not completely, since both the lifetime and the $R_{612/589}$ ratio remain substantially larger than in the non-degassed solution. We have interpreted this in terms of several different hydrated species being in equilibrium. When several water molecules are coordinated in the inner sphere, their lifetimes become comparable. This makes a mathematical resolution of the decays difficult. Moreover, fast water exchange reactions lead to an averaging of the species on the time scale of the luminescence experiment (ms).

After applying degassing procedure II (see Exp. Sect.), the solution again contained two Eu^{III} species, one having a relatively short lifetime (which corresponds to the short lifetime measured after procedure I was applied), while the other featured a much longer lifetime than the long lifetime of the previous sample. This clearly demonstrates that further dehydration has occurred. The value of this lifetime, 2.56 ms, probably implies that an anhydrous species has been formed but again, this assessment will need to be confirmed by determining the exact nature of the species in solution. When re-hydration occurred, the decay turned again into a single exponential curve with a lifetime intermediate between the ones obtained after the first and the second degassing procedures.

The results presented above are of great practical interest and show that, for luminescence measurements, caution should be paid to the degassing procedure and to the water intake by the sample. It should be stressed, however, that luminescence measurements can be performed with reasonable confidence (i.e. results are reproducible) because, as can be seen from Table 1, the absorption of water under our experimental conditions was slow. These slow kinetics compared with those observed by Seddon and co-workers[8] or by Tran and co-workers[9] are mainly due to the absence of vigorous stirring and to the use of a cap for the cuvettes in our case.

Spectroscopy in the Presence of Tetrabutylammonium Chloride (TBACl)

Results

The data presented in Figures 5−8 were recorded immediately after the end of the degassing procedure. Figures 5 and 6 display the excitation and emission spectra for

 © 2004 Wiley-VCH Verlag GmbH & Co. KGaA, Weinheim

ratios r = [TBACl]/[Eu] = 4.5, 6 and 9. Compared with Figures 3 and 4, the main difference is the strong band centered around 330 nm seen in the excitation spectra and the well-defined structure in the Eu emission spectra. For comparison, a solution containing only TBACl in $BumimTf_2N$ displays a single very broad band of very low intensity centered at 375 nm.

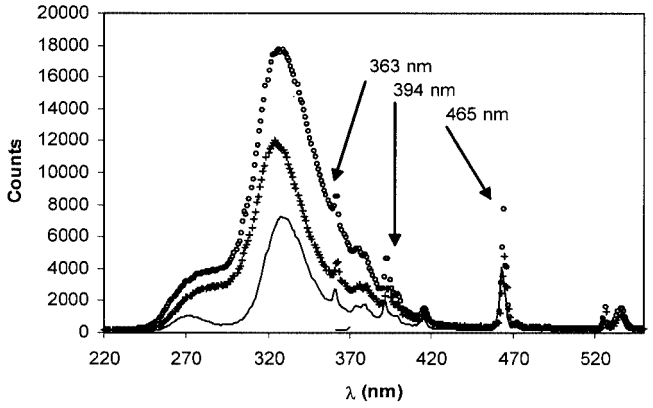

Figure 5. Excitation of the Eu^{III} triflate salt 5×10^{-3} M in $BumimTf_2N$ containing TBACl; emission at λ = 608 nm; solid line: r = 9; +++: r = 6; open circles: r = 4.5

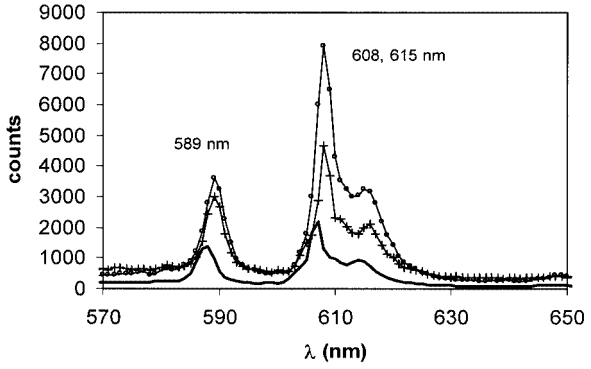

Figure 6. Emission of Eu^{III} triflate salt 5×10^{-3} M in $BumimTf_2N$ containing TBACl; excitation wavelength: λ = 464 nm; solid line: r = 9; +++: r = 6; open circles: r = 4.5

The total excitation intensity decreases as a function of r, as does the total emission intensity. For all the samples, in contrast to what was obtained without TBACl, the luminescence decays are single exponential curves, even after the degassing procedure. The Eu^{III} lifetime values as a function of the total TBACl amount are displayed in Table 2. Although incomplete dissolution occurs for $r < 4.5$, a lifetime value could be obtained.

Table 2. Lifetime values for the solutions of the Eu^{III} triflate salt containing added TBACl

r = [TBACl]/[Eu]	τ [μs]
3.5	2038
4.5	2060
6	2560
9	2760

The excitation and emission spectra of the Eu^{III}/TBA-triflate/$BumimTf_2N$ solution (r = 6) are displayed in Figures 7 and 8, together with the data for TBACl for the sake of comparison. Compared with the addition of chloride, the emission intensity was lower when the triflate was added and the bands were much broader.

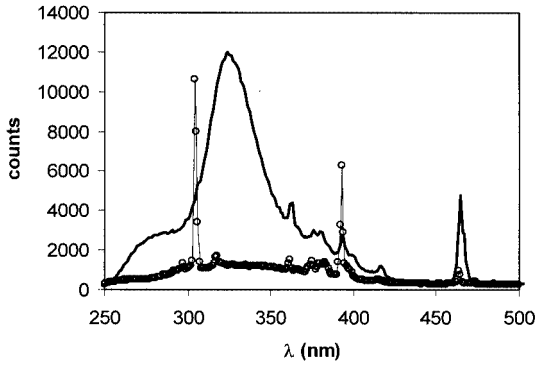

Figure 7. Excitation spectra of solutions of the Eu^{III} triflate salt 5×10^{-3} M in $BumimTf_2N$ (λ_{em} = 608 nm); solid line: with TBACl, r = 6; open circles: with TBA-triflate, r = 6; the sharp peak at 304 nm is due to the excitation light (608 nm is the second harmonic)

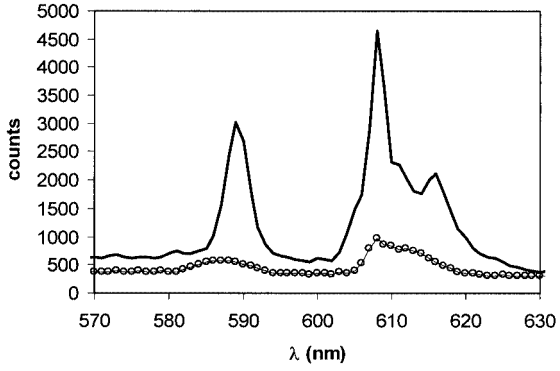

Figure 8. Emission spectra of solutions of the Eu^{III} triflate salt 5×10^{-3} M in $BumimTf_2N$ (λ_{ex} = 464 nm); solid line: with TBACl, r = 6; open circles: with TBA-triflate, r = 6

The effect of progressive water absorption by $BumimTf_2N$ as a function of time has also been studied. In the case of TBACl, and in contrast to the solutions to which no TBA salt was added, the increasing amount of water had no effect at all on the Eu^{III} lifetime and decay behavior for r = 9. Even after 22 d of storage, the lifetime changed by less than 10 μs. On the other hand, the lifetime of the solution to which TBA triflate had been added decreased as a function of time (from τ = 1180 μs after degassing to 492 μs after 3 d of storage).

 © 2004 Wiley-VCH Verlag GmbH & Co. KGaA, Weinheim

Discussion

There is no physical evidence for stating that the introduction of TBACl strongly modifies the course of the degassing procedure. Therefore, the single exponential behavior of the decays after the degassing procedure shows that the Eu^{III} coordination sphere is strongly modified compared with the solution without TBACl. This is also illustrated by the changes observed in the excitation and emission spectra as a function of *r*. In comparison with what is known about europium luminescence in other solvents,[16−18] these changes can be ascribed to a complexation process. Slight changes can be observed in the emission spectra at $r = 3$ and 9, especially in the value of $R_{612/589}$. This experimental fact, together with the reduced solubility observed for $r < 4.5$ would indicate that at least two different complexes are present in solution, depending on *r*. TBACl is a 1:1 electrolyte, but it is not clear from our experiments whether it is entirely dissociated in $BumimTf_2N$. Although a detailed symmetry analysis is not possible due to the relative broadness of the emission bands, we note that $^5D_0 \rightarrow {}^7F_1$ generates one symmetrical band while 2−3 components can be seen for the $^5D_0 \rightarrow {}^7F_2$ transition, indicating a relatively high symmetry around the Eu^{III} ion. Trivalent europium is known to form a stable hexachloride with an elpasolite structure and O_h symmetry.[19] In ethanol solution, this species either dissociates or reacts with the solvent to give a species with D_2 symmetry.[20] It is noteworthy that the $^5D_0 \rightarrow {}^7F_2$ spectrum reported for the latter species is very similar to the one reported in Figure 6 for $r = 6$ and so are the spectra for $[Cl^-]/[Eu] = 26$ (in ethanol)[20] and $r = 9$ (Figure 6). Therefore we may safely conclude that upon addition of TBACl, polychloro species are formed in RTIL solution.

The implications of single exponential behavior of the decays of the emission spectra and the lifetime values changing as a function of the ligand concentration (TBACl case) have been discussed long ago[21] and have been revisited recently.[22] Both papers agree that such experimental facts point to a photochemically induced complexation reaction occurring in the solution. It was also agreed that the excitation and emission data collected for $r = 9$ (lifetime plateau value, see Table 2) are those of the higher complex obtained with a lifetime of 2760 μs.

The luminescence enhancement observed could be explained in two ways: (i) the interaction of chloride ions in the inner coordination sphere results in a ligand-to-metal transfer state reflected in the excitation spectrum (Figure 7) and energy transfer takes place between this state and Eu^{III}. Such a state is observed around 33 000 cm^{-1} [23] for $[EuCl_6]^{3-}$ in the solid state and excitation in such states may result in metal-centered luminescence when they lie at relatively high energy, which is the case here. Moreover, the spectrum displayed in Figure 8 (top) matches perfectly well the one published earlier for $[EuCl_6]^{3-}$ in ethanol.[20] (ii) The inner-sphere chloride ions act as relays between the metal ion and the $Bumim^+$ or TBA^+ cations in the second solvation shell, allowing a through-bond energy transfer.

Finally, the quite different spectroscopic properties observed upon addition of TBA triflate, in particular the absence of luminescence enhancement, point to a much weaker interaction between the added anions and the metal ion so that competition with water molecules easily leads to hydrated species with quenched luminescence.

Conclusion

For the first time, a spectroscopic investigation of Eu^{III} dissolved in $BumimTf_2N$ has been conducted particularly with respect to the effect of water and added TBA chloride. The results pinpoint the importance of degassing procedures and storage conditions, in view of the highly hygroscopic nature of the solvent. A complexation process between Eu^{III} and the added TBA salts has been evidenced and some insight into the species in equilibrium and the composition of the inner coordination sphere of Eu^{III} has been obtained. A first conclusion is that the behavior of the Eu^{III} ion in degassed $BumimTf_2N$ displays trends similar to that exhibited in other organic hygroscopic solvents (e.g. acetonitrile or ethanol), with respect to both its coordination and spectroscopic properties. On the other hand, non-degassed solutions exhibit a highly inhomogeneous nature. In view of the evaluation of RTILs for use in future lanthanide/actinide extraction processes it is essential that basic data on the solvation of metal ions in these liquids be at hand. From this standpoint, the results presented here are very encouraging since they demonstrate that complexation processes analogous to those in common solvents take place in the investigated RTIL, and that they can be monitored by a highly sensitive technique such as time-resolved luminescence. However, some differences have also been unraveled and we are now concentrating our efforts on gathering structural data on these solutions in order to get a much deeper understanding of the nature of the solvated and complexed species in equilibrium.

Experimental Section

Synthesis of $BumimTf_2N$ and Experimental Methods: All chemicals were of the highest reagent grade (Aldrich) and were used without further purification. All aqueous solutions were prepared with deionized water (Millipore de-ionization system, $\omega = 18.3\ M\Omega\ cm^{-1}$). The synthesis of $BumimTf_2N$ was derived from the previously reported synthesis of $BumimPF_6$ [23] and was typically performed as described in the following.

First Step. Synthesis of BumimCl: A three-necked round-bottom flask under argon, equipped with a water refrigerant, was loaded with methylimidazole (1 mol, 82.11 g) and *n*-chlorobutane (1 mol, 92.57 g). The mixture was stirred under argon at 70 °C for 48 h until the appearance of a pale yellow viscous mixture. This was then transferred into a flask and stored at 3−5 °C under argon until quantitative precipitation (ca. 12 h). White crystals were obtained which were washed several times with ethyl acetate and filtered each time with a Büchner apparatus. The crystals were transferred to a dry box containing phosphorus pentoxide and placed

 © 2004 Wiley-VCH Verlag GmbH & Co. KGaA, Weinheim

under vacuum. A fine white powder of BumimCl was obtained. Yields were typically around 80%.

Second Step. Synthesis of BumimTf$_2$N: A solution of BumimCl (110 g) in water (150 mL) was added to a solution of LiTf$_2$N (200 g) in water (300 mL) and the resultant mixture was stirred at 70 °C for 16 h. Two phases were obtained and the upper layer (aqueous) was decanted. The lower phase (BumimTf$_2$N) was washed several times with de-ionized water (10 × 350 mL). BumimTf$_2$N, as a transparent and slightly viscous liquid, was transferred and stored in a dry box under vacuum containing phosphorus pentoxide. Typical yields: ca. 80%. The water content of the samples was determined by Karl Fischer titration, using standard procedures (Mettler DL18 titrator, hydranal composite 5 (Fluka) and analytical grade methanol). Absorption spectra in the range 190−900 nm were recorded with a Uvikon 930 (Kontron) spectrometer with 1-cm quartz cuvettes. In all cases, the reference was an empty quartz cuvette. No precaution was taken for the storage of the samples which were simply left in the quartz cuvettes (with Teflon cap), so that the water content may have changed with time (see the relevant study in the text). Emission and excitation spectra were recorded with a classical spectrofluorimeter (Photon Technology International) which does not allow for time-resolution but was corrected for gain efficiency of the detector. Data are also presented as $R_{612/589}$, the ratio of the intensity of the $^5D_0 \rightarrow {}^7F_2$ transition (around 612 nm) with that of the $^5D_0 \rightarrow {}^7F_1$ transition (around 589 nm) for an excitation at λ_{exc} = 394 nm. The uncertainty on the value of $R_{612/589}$ is in the range of ±10%. The time-resolved emission spectroscopy (TRES) apparatus has been described in detail elsewhere.[24,25] Briefly, for decay measurements, the excitation wavelength was set to 266 nm and the decays were recorded at λ = 612 or 589 nm, depending on the transition efficiency. As is usual for time-resolved experiments of this kind, the data analysis was performed by systematically excluding the first 10 μs of each decay, for which the intense short-lived luminescence of the pure BumimTf$_2$N dominates and thus precludes any detection of the long-lived europium species. Therefore, in the following, the discussion of the decay behavior only corresponds to lifetimes ascribable to Eu^{III}. The importance of the decay behavior (either mono- or multiexponential) has been stressed in other papers[22,26] and the quality of the fits was assessed both by the usual χ^2 test and the shape of the residuals (experimental minus calculated values). The error in the lifetime values was of the order of ±3%. Although the measurements of the luminescence spectra and decays are easy to perform under the experimental conditions of this work, they cannot be conducted under optimum conditions for europium assays. For most of the feasible excitation wavelengths, the absorption of the sample was way above the usual 0.05 limit, for which a linear relationship holds between concentration and emission intensity, because of solvent absorption. All experiments were performed at a controlled temperature of 294 K.

Purification and Characterization: The purification procedure previously used for BumimPF$_6$ [27] was also applied to BumimTf$_2$N. However, the absorption band in the range 250−300 nm observed for non-purified BumimPF$_6$,[27] was still present in the absorption spectrum of the purified BumimTf$_2$N (Figure 1). It is probable that some organic impurities still remain. To the best of our knowledge, the absorption spectrum of ultra-pure BumimTf$_2$N is not known, so that comparison with our batch is impossible. On the other hand, repeated measurements of the absorption spectrum showed that the BumimTf$_2$N batch used in this work was stable for more than four months. Due to the synthetic procedure, BumimTf$_2$N contains water even after purification on an alumina column. The presence of water is a common feature of room-temperature ionic liquids[1,7,28,29] and numerous works have pinpointed the large influence of water on various physico-chemical properties of RTILs.[8,30] This very important point will be addressed in this work.

Water Contents and Dissolution of Salts in BumimTf$_2$N: A previous study[8] focused on the effect of water on the properties of various RTILs, such as BumimBF$_4$ or BumimPF$_6$. In particular, it was shown that above a certain water content (around a molar fraction of 0.5), the viscosities and densities of the resultant mixtures became water-like, so that these samples have to be considered as aqueous solutions of RTILs and not as hydrated RTILs. Another study has shown that water absorption by BumimTf$_2$N may be rapid and important.[9] For the BumimTf$_2$N batch used in this work, the amount of water was equal to 5000 ± 50 ppm (i.e. 0.4 M or 0.5% w/w) after purification. This is a consequence of the numerous water washes at the end of the synthesis and the subsequent purification on the alumina column. This batch is thus not water-saturated when compared with values of up to 14000 ppm reported in the literature for BumimTf$_2$N,[1] but nevertheless contains a substantial amount of water. After several months of storage, the water content did not change much as shown by a new determination of the water content of 5100 ± 500 ppm. In order to control the water content of the samples, we degassed them according to two different methods. In procedure I, batches of 5 mL were pumped at room temperature for 18 h and, additionally, at 50 °C for 10 h (residual pressure: 1.8 mbar); the resultant water content was below 100 ppm (i.e. 8×10^{-3} M or 0.01% w/w). In a few cases (see below), samples were further degassed at 70 °C for 48 h (procedure II). Finally, a solution of europium triflate was degassed (procedure I) directly in a quartz cuvette connected to the degassing setup by a quartz-glass tube. In this case, by use of a tap, the solution in the cuvette was air- and water-tight but, due to the bulkiness of the setup, only lifetime measurements could be performed. Europium(III) triflate (Aldrich), tetrabutylammonium chloride (Aldrich) and triflate (Aldrich), and NaCl (Prolabo) were used as received. Hygroscopic salts were kept in a desiccator with P_4O_{10}. Unless otherwise specified, the europium concentration was 5×10^{-3} M. Possible changes in density from one sample to another due to different water contents were not considered in the determination of the concentration. A common value d = 1.43 for the density (non-degassed BumimTf$_2$N) has been assumed for all the BumimTf$_2$N samples in this work. Even though the europium triflate salt contains 4 water molecules per europium unit, the amount of water introduced with the salt is negligible compared with the water already present in the non-degassed solvent. Upon addition of europium triflate to BumimTf$_2$N, a slightly cloudy solution was obtained which indicates either an incomplete dissolution or, more probably, the formation of inhomogeneous clusters. In fact, these samples strongly diffuse the red light of an He:Ne laser. On the other hand, light diffusion was no more clearly observed even after degassing the samples using procedure I (solutions become clear) or II, so that these samples may be considered as being homogeneous (see also discussion). Various amounts of tetrabutylammonium chloride together with europium triflate (r = [TBACl]/[Eu^{III}] = 3−9) were introduced into BumimTf$_2$N. Due to the very slow rate of dissolution, a small amount of CH_3CN (on the order of 0.5 mL), which is totally miscible in BumimTf$_2$N, was also added to the BumimTf$_2$N solutions prior to degassing in order to speed up the process. Considering the vapor pressure, it can be safely assumed that all CH_3CN was removed at the end of the degassing procedure. Despite this modified dissolution procedure, not all the salts dissolve for r < 4.5, even after degassing (procedure I). No attempts were

 © 2004 Wiley-VCH Verlag GmbH & Co. KGaA, Weinheim

made to determine the exact composition of the undissolved residue. For $r > 4.5$, dissolution was fully achieved after degassing. Finally, a single solution of europium triflate with tetrabutylammonium triflate (TBA-triflate, $r = 6$) was prepared and degassed.

Acknowledgments

This work has been performed with the financial help of the French "Groupement de Recherches" PARIS. We thank Prof. K. R. Seddon for an interesting discussion about degassing procedures. The help of Dr. M. Roynette for the Karl Fischer measurements is greatly acknowledged. J.-C. G. B. is grateful to the Swiss National Science Foundation for financial support.

[1] P. Wasserscheid, T. Welton, *Ionic Liquids in Synthesis*, Wiley-VCH, Weinheim, **2003**.
[2] A. E. Visser, R. D. Rogers, *J. Solid State Chem.* **2003**, *171*, 109.
[3] D. Allen, G. Baston, A. E. Bradley, T. Gorman, A. Haile, I. Hamblett, J. E. Hatter, M. J. F. Healey, B. Hodgson, R. Lewin, K. V. Lovell, B. Newton, W. R. Pitner, D. W. Rooney, D. Sanders, K. R. Seddon, H. E. Sims, R. C. Thied, *Green Chem.* **2002**, *4*, 152.
[4] W. T. Carnall, in *Handbook on the Physics and Chemistry of Rare Earths: Non-metallic Compounds I*, North Holland, Amsterdam, **1979**, vol. 3, chapter 24.
[5] L. C. Branco, J. N. Rosa, J. J. Moura Ramos, C. A. M. Afonso, *Chem. Eur. J.* **2002**, *8*, 3671.
[6] S. G. Lee, J. H. Park, J. Kang, J. K. Lee, *Chem. Commun.* **2001**, 1698.
[7] J. L. Anthony, E. J. Maginn, J. F. Brennecke, *J. Phys. Chem. B* **2001**, *105*, 10942.
[8] K. R. Seddon, A. Stark, M. J. Torres, *Pure Appl. Chem.* **2000**, *72*, 2275.
[9] C. D. Tran, S. H. De Paoli Lacerda, D. Oliveira, *Appl. Spectrosc.* **2003**, *57*, 152.
[10] A. Nehlig, M. Elhabiri, I. Billard, A. M. Albrecht-Gary, K. Lützenkirchen, *Radiochim. Acta* **2002**, *91*, 37.
[11] Y. Haas, G. Stein, *J. Phys. Chem.* **1971**, *75*, 3677.
[12] J.-C. G. Bünzli, A. Milicic-Tang, in *Handbook on the Physics and Chemistry of Rare Earths*, Elsevier Science, Amsterdam, **1995**, vol. 21, chapter 145.
[13] E. N. Rizkalla, G. R. Choppin, in *Handbook on the Physics and Chemistry of Rare Earths*, Elsevier Science, Amsterdam, **1991**, vol. 15, chapter 103.
[14] A. Beeby, I. Clarkson, R. Dickins, S. Faulkner, D. Parker, L. Royle, A. de Sousa, J. Williams, M. Woods, *J. Chem. Soc., Perkin Trans. 2* **1999**, 493.
[15] R. M. Supkowski, W. deW. Horrocks Jr, *Inorg. Chim. Acta* **2002**, *340*, 44.
[16] G. R. Choppin, D. R. Peterman, *Coord. Chem. Rev.* **1998**, *174*, 283.
[17] D. Parker, J. Williams, *J. Chem. Soc., Dalton Trans.* **1996**, 3613.
[18] J.-C. G. Bünzli, G. R. Choppin, *Lanthanide Probes in Life, Chemical and Earth Sciences: Theory and Practice*, Elsevier, Amsterdam, **1989**.
[19] O. A. Serra, L. C. Thompson, *Inorg. Chem.* **1976**, *15*, 504.
[20] C. Görller-Walrand, N. De Moitié-Neyt, Y. Beyens, J.-C. G. Bünzli, *J. Chem. Phys.* **1982**, *77*, 2261.
[21] W. deW. Horrocks Jr, V. K. Arkle, F. J. Liotta, D. R. Sudnick, *J. Am. Chem. Soc.* **1983**, *105*, 3455.
[22] I. Billard, K. Lützenkirchen, *Radiochim. Acta* **2003**, *91*, 285.
[23] G. Blasse, *Struct. Bonding* **1976**, *26*, 43.
[24] M. Bouby, I. Billard, A. Bonnenfant, G. Klein, *Chem. Phys.* **1999**, *240*, 353.
[25] I. Billard, A. Rustenholtz, L. Sémon, K. Lützenkirchen, *Chem. Phys.* **2001**, *270*, 345.
[26] I. Billard, E. Ansoborlo, K. Apperson, S. Arpigny, A. E. Azehna, D. Birch, P. Bros, H. Burrows, G. R. Choppin, L. Couston, V. Dubois, T. Fanghänel, G. Geipel, S. Hubert, J. I. Kim, T. Kimura, R. Klenze, A. Kronenberg, M. Kumke, G. Lagarde, G. Lamarque, S. Lis, C. Madic, G. Meinrath, C. Moulin, R. Nagaishi, D. Parker, G. Plancque, F. Scherbaum, E. Simoni, S. Sinkov, C. Viallesoubranne, *Appl. Spectrosc.*, **2003**, *57*, 1027.
[27] I. Billard, G. Moutiers, A. Labet, A. El Azzi, C. Gaillard, C. Mariet, K. Lützenkirchen, *Inorg. Chem.* **2003**, *42*, 1726.
[28] K. R. Seddon, *J. Chem. Tech. Biotechnol.* **1997**, *68*, 351.
[29] D. S. H. Wong, J. P. Chen, J. M. Chang, C. H. Chou, *Fluid Phase Equilib.* **2002**, *194/197*, 1089.
[30] U. Schröder, J. D. Wadhawan, R. G. Compton, F. Marken, P. A. Z. Suarez, C. S. Consorti, R. F. de Souza, J. Dupont, *New J. Chem.* **2000**, *24*, 1009.

Received August 22, 2003
Early View Article
Published Online February 10, 2004

 © 2004 Wiley-VCH Verlag GmbH & Co. KGaA, Weinheim

Long Range Metal-Metal Interactions Along Fe−NC−Ru−CN−Fe Chains

Tianlu Sheng[a] and Heinrich Vahrenkamp*[a]

Keywords: Chain structures / Cyanide complexes / Polynuclear complexes / Metal−metal interactions

Trinuclear complexes with linear Fe^{II}–NC–Ru^{II}–CN–Fe^{II} arrays were obtained by attachment of FeCp(dppe) units to the cyanoruthenium complexes *trans*-[$Ru(CN)_2(Py)_4$] (Py = pyridine, 4-methylpyridine, 4-ethylpyridine) . From their cyclic voltammograms it can be concluded that there are long-range metal–metal interactions between their external iron centers. Partial oxidation led to the isolation of the corresponding mixed-valent Fe^{II}–NC–Ru^{II}–CN–Fe^{III} complexes. For these the long range metal–metal interactions are evident from a broad MMCT band in the NIR spectra. The MMCT properties were quantified by an analysis using the Hush formalism.
(© Wiley-VCH Verlag GmbH & Co. KGaA, 69451 Weinheim, Germany, 2004)

Introduction

Cyanide-linked coordination polymers have attractive optical, electrical and magnetic properties.[1−3] The basis of these are metal−metal interactions across the bridging cyanide ligands. For this reason numerous studies have been undertaken on cyanide-bridged low-molecular complexes, with the purpose of elucidating the molecular equivalents of the bulk properties in terms of electron transfer, metal−metal charge transfer and molecular magnetism.[4]

The simplest objects of study in this respect would be chain-like complexes with linear arrays of metals and bridging cyanide ligands. It turns out, however, that long chains of this kind are difficult to synthesize, and until today no such complex with more than three metal atoms has been unambiguously identified in solution or obtained analytically pure. Moreover, proof of long-range metal−metal interactions in trinuclear complexes with M−CN−M′−CN−M arrays, for instance by the typical splitting of the cyclovoltammetric redox waves, has been achieved in only a rather small number of cases.[5,6−8]

Our own investigations in the area of chain-like cyanide-bridged trinuclear complexes have virtually doubled the number of species for which evidence of remote metal−metal interactions exists.[9−14] For the first time we could also subject a group of such complexes to preparative one-electron oxidations and isolate mixed-valent trinuclear complexes with Fe^{II}-(μ-CN)-Pt^{II}-(μ-CN)-Fe^{III} arrays.[9] Yet, despite a wide variation of the building blocks, the supporting ligands, the oxidation states of the metals and the shape of the M−CN−M′−CN−M chains we have not yet found conclusive evidence as to which factors govern the occurrence and the extent of their remote metal−metal interactions.

The present study contributes one such piece of evidence. The complexes under investigation have *trans*-[$Ru^{II}(CN)_2Py_4$] units at the center and FeCp(dppe) units at the external positions which turned out to be favorable for redox reactions and spectroscopic measurements. $RuPy_4(CN)_2$-centered complexes with external $Ru(NH_3)_5$ [7] and $Ru(Py)_4Cl$ units[15] have already been described and subjected to electrochemical and spectroscopic measurements as well as a theoretical treatment of vibronic coupling in them.

Results and Discussion

Preparations and Structures

Previously we have investigated L_nM-(μ-CN)-$M'^{II}(Py)_4$-(μ-CN)-ML_n complexes with M'^{II} ions from the first row of the transition metals at the center.[16] Their octahedral $M'X_2Py_4$ cores are labile, and hence $M'(NC)_2Py_4$ arrangements in the trinuclear complexes could not be prevented, even when starting from $M'(CN)_2Py_4$ complexes (cyanide-isocyanide rearrangement). In contrast, octahedral Ru^{II} complexes are quite inert, and it could be anticipated that the *trans*-[$Ru(CN)_2Py_4$] array would be maintained after the attachment of two organometallic L_nM units. This was expected to be favorable in two respects: first, the attachment of the cyanide's carbon terminus (the π-acceptor orientation of CN^-) to ruthenium should raise the Ru^{II}/Ru^{III} redox potential, and second the attachment of the nitrogen terminus (the σ-donor orientation of CN^-) to the L_nM unit should lower the redox potential of the latter. Hence it would be likely that a partially oxidized (i.e. mixed-valent) species would have the oxidation state M^{II}−NC−Ru^{II}−CN−M^{III}, and that electronic communication between M^{II} and M^{III}

[a] Institut für Anorganische und Analytische Chemie der Universität Freiburg,
Albertstr. 21, 79104 Freiburg, Germany
Fax: (internat.) + 49-(0)761-203-6001
E-mail: vahrenka@uni-freiburg.de

 © 2004 Wiley-VCH Verlag GmbH & Co. KGaA, Weinheim **DOI: 10.1002/ejic.200300656**

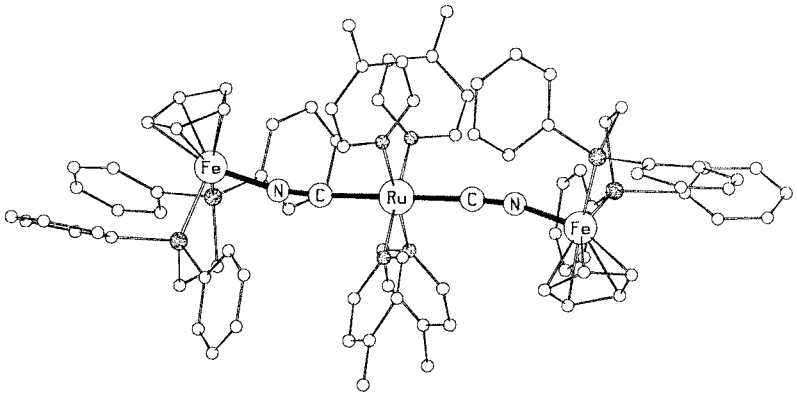

Figure 1. Molecular structure of the trinuclear cation of **2b**

would be facile[9] due to the *trans*-configuration of the central Ru^{II} ion.

The combination of $RuPy_4$ and FeCp(dppe) units confirmed this assumption. [$Ru(CN)_2Py_4$] complexes [Py = pyridine (**1a**), 4-methylpyridine (**1b**) or 4-ethylpyridine (**1c**)] were synthesized in which the variation of the pyridines provided a variation of the electron density at ruthenium. Their treatment with [FeCp(dppe)(CH_3CN)]Br yielded the trinuclear complexes [Cp(dppe)Fe−NC−$RuPy_4$−CN−Fe(dppe)Cp] $(PF_6)_2$ (**2a**−**c**) in a straightforward way. When crystallized with PF_6 counterions, **2a**−**c** are orange, air-stable, crystalline solids.

The identities of **2b** and **2c** were confirmed by crystal structure determinations. Figure 1 shows the structure of **2b** as a representative example. Table 1 lists the relevant bond lengths and angles.

Table 1. Relevant bond lengths (Å) and angles (°) in **2b** and **2c**

	2b	**2c**
Ru−N(Py)	2.086−2.120(7)	2.094−2.099(3)
Ru−C(CN)	2.061(9)	2.034(3)
C−N(CN)	1.16(1)	1.164(4)
Fe−N(CN)	1.911(7)	1.923−1.931(3)
Fe−P	2.185−2.195(3)	2.202−2.206(1)
N−Ru−N	89.2−90.3(3)	86.4−91.7(1)
C−Ru−N	88.0−90.8(3)	88.7−91.7(1)
C−Ru−C	178.3(5)	177.9(1)
Ru−C−N	175.2(7)	176.3−177.5(3)
Fe−N−C	166.6(7)	170.9−174.8(3)

The two structural units of complexes **1**, the $Ru(CN)_2Py_4$ unit and the Cp(dppe)Fe−NC unit, compare favorably with those in related complexes. Various $RuPy_4X_2$ complexes,[17] including $Ru(CN)_2Py_4$,[15] display the close to ideally octahedral coordination of ruthenium and the *trans* arrangement of the two ligands X. The isocyanide-ligated FeCp(dppe) unit is almost superimposable with that in dinuclear Cr−CN−Fe[18] and trinuclear Pt(CN-Fe)$_2$ complexes.[9] The electronic situation of complexes **2** is nicely reflected in the bond lengths and angles along the Ru−C−*N*−Fe arrays. The withdrawal of electron density from the cyanide ligand enhances the Ru→C π-backbonding, thereby making the Ru−C bonds rather short (cf. the Ru−N bonds). Likewise the lack of significant Fe→N π-backdonation results in Fe−N bond lengths that are significantly longer than the Fe−C bonds in related complexes with M−*N*−C−Fe arrays.[9,16,18] The various degrees of π-backdonation also explain a feature which is observed here like in most of our other M−C−*N*−M′ complexes: for the cyanide ligand the M−C−N angle (here Ru−C−N) is always close to 180°, while the M′−*N*−C angle (here Fe−*N*−C) shows significant bending, the average value of which in complexes **2** is 170°.

Redox Chemistry

The cyclic and square-wave voltammograms of **2a**−**c** show three waves in the oxidative range (see Figure 2 and Table 2). The first two of these are a closely spaced pair assignable to the FeCp(dppe) units.[9,18] The third one, at high voltage, belongs to the $RuPy_4$ unit. Characteristically the position of the Ru^{II}/Ru^{III} wave responds to the nature of the pyridine ligands, the more electron-rich of which in **2b** and **2c** facilitate the oxidation. The redox potentials for the FeCp(dppe) units are typically lower than that of Cp(dppe)Fe−CN (0.48 V), reflecting the more electron-rich state of iron due to the attachment of the cyanide's nitrogen.

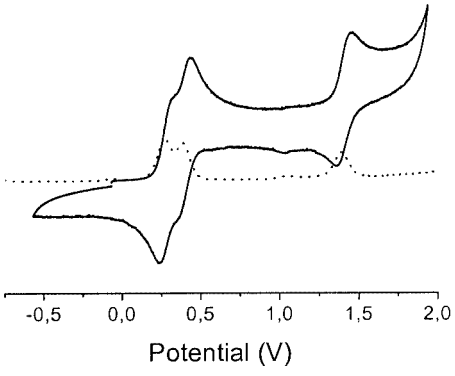

Figure 2. Cyclic (solid line) and square-wave voltammogram (dotted line) of **2b** (in CH_3CN, potentials vs. Ag/AgCl, scan rate 100 mV/s)

 © 2004 Wiley-VCH Verlag GmbH & Co. KGaA, Weinheim

Table 2. Cyclovoltammetric data of complexes **2**[a]

	$E_{1/2}$ (1)	$E_{1/2}$ (2)	$E_{1/2}$ (3)
2a	0.29	0.40	1.52
2b	0.28	0.39	1.40
2c	0.27	0.38	1.40

[a] In CH_3CN, potentials (V) against Ag/AgCl, scan rate 100 mV/s.

The occurrence of two redox steps for the Cp(dppe)Fe units is the indicator of electronic communication between them. The potential separation of 110 mV is in the usual range.[9,12,13] Thus, complexes **2** are the third group of complexes synthesized by us for which a low-spin central unit with unfilled e_g orbitals enables electronic interactions between the two terminal redox-active organometallic units.

The potential separation is large enough to enable partial chemical oxidation of the FeCp(dppe) units. After treating **2a−c** with one equivalent of ferrocinium hexafluorophosphate in dichloromethane, the mixed-valent trinuclear complexes
$[Cp(dppe)Fe-NC-RuPy_4-CN-Fe(dppe)Cp](PF_6)_3$
(**3a−c**) could be isolated in good yields. Complexes **3** are only the second group of trinuclear complexes that have been isolated in the mixed-valent state. Prior to our work[9] the mixed-valent species could only be observed spectroscopically as transient species during redox titrations.

The identity of complexes **3** is evident from their analytical composition and from the fact that their voltammograms are identical to those of the corresponding complexes **2**. As before,[9] we failed to obtain crystals of a complex **3** suitable for X-ray analysis. Thus, the structural consequences of mixed valence in this type of complexes are still unknown. However, the spectroscopic data of **3a−c** (see below) clearly identify them as such.

Spectroscopy

The ν(CN) bands of complexes **1−3** (Table 3) provide good evidence for their structure and for their electronic situation. As expected, the symmetrical *trans*-configuration of the $Ru(CN)_2Py_4$ units in **1** and **2** gives rise to only one cyanide band in the IR spectra. Complexes **3**, with two distinctively different FeCp(dppe) units, show two widely separated ν(CN) absorptions.

Table 3. ν(CN) bands (in KBr, cm^{-1}) in the IR spectra

	1	**2**	**3**
a	2060	2071	2020, 2089
b	2055	2070	2014, 2090
c	2058	2070	2007, 2088

The ν(CN) band positions in complexes **2** are slightly raised relative to those in complexes **1**. As discussed by us several times before[9−13,16,18] this indicates that the kinematic effect (impediment of CN vibration due to the attachment of the second metal) is almost completely outbalanced by the π* effect (enhanced π-backdonation from ruthenium due to electron withdrawal by iron).

Complexes **3** provide a rare case of an internal reference for the size of these effects. The ν(CN) band position for the $Ru-C-N-Fe^{III}$ fragment is dramatically lowered because the Fe^{III} center is a much stronger electron acceptor than the Fe^{II} center. This induces a stronger π-backdonation from the Ru^{II} center into the CN-π* orbitals, causing a serious weakening of the C−N bond. We have observed this phenomenon in di- and trinuclear complexes before,[9,18] the most pronounced cases being the $L_nM-C-N-FeCl_3$ complexes with a ν(CN) band shift of −60 to −80 cm^{-1}.[19] The other ν(CN) band of complexes **3**, originating from the $Ru-C-N-Fe^{II}$ fragment, is now at significantly higher wavenumbers than in **1** or **2**. This is consistent with the opposite shift of the first band: there is less π-backdonation available on this side of the ruthenium atom, resulting in a lesser weakening of the C−N bond and hence a more pronounced appearance of the kinematic effect. Thus the IR spectra of complexes **1−3** are a demonstration of the classical *trans* effect observed in the IR spectra of octahedral metal carbonyls.

The absorptions in the electronic spectra of complexes **1−3** are listed in Table 4. Complexes **1** are yellow due to the tailing off of their strong absorption band in the near UV region. Complexes **2** are orange due to a weak absorption in the early visible range which results from the FeCp(dppe) units. Complexes **3** have deeper orange or brown colors which mostly results from an intensification of the latter absorption. This, in turn, results from the fact that the FeCp(dppe) absorption sits on the high-energy tail of a very broad medium-intensity absorption in the NIR. Figure 3 displays this for **3a**.

Table 4. Absorption bands [λ (ε·10^{-3})] in the visible and NIR spectra[a]

	1	**2**	**3**
a	374 (22.5)	368 (11.4), 540 (sh)	351 (19.0), 520 (sh), 980 (2.6)
b	369 (18.3)	376 (19.3), 560 (sh)	344 (17.3), 475 (1.7), 990 (2.8)
c	376 (24.1)	368 (23.1), 560 (sh)	342 (21.6), 475 (1.9), 970 (3.6)

[a] Dichloromethane solutions, λ in nm, ε in $M^{-1}cm^{-1}$.

The NIR absorption is a typical MMCT band, and it classifies complexes **3** as class II mixed-valent species according to Robin and Day.[20] We assign it as a long-range $Fe^{II} \rightarrow Fe^{III}$ electron transfer across the *trans*-$Ru(CN)_2$ center, in analogy to such transfers for *trans*-PtL_2-[9] and Fe(Pc)-centered[12] complexes. Alternatively, it might be considered a $Ru^{II} \rightarrow Fe^{III}$ electron transfer across a single cyanide bridge, in analogy to our observations for related $Fe(bpy)_2$-centered complexes.[21] This, however, is unlikely based on the redox potentials observed for the Ru and Fe units (cf. Table 2) and on our observations for short-range MMCT in complexes with similar redox properties.[10,12]

The MMCT bands observed here occur at higher energies than the ones observed by us before for PtL_2-[9] and

 © 2004 Wiley-VCH Verlag GmbH & Co. KGaA, Weinheim

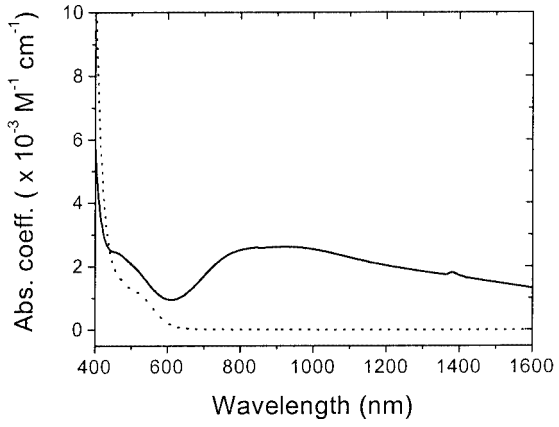

Figure 3. Electronic spectra of **2a** (dotted line) and **3a** (solid line) in dichloromethane

Fe(Pc)-centered[12] complexes with external FeCp(dppe) units. At first glance this might imply that the electronic interaction between the two iron centers is smaller than in the latter complexes. However, the quantitative treatment disproved this. It was done as before[9,12,18] by applying the Hush formalism for non-delocalized mixed-valent species according to Equation (1) and (2).[22]

$$H_{ab} = \tilde{\nu}_{max} a = 2.06 \cdot 10^{-2} (\tilde{\nu}_{max}/d)(\varepsilon_{max}\Delta\nu_{1/2}/\tilde{\nu}_{max})^{1/2} \quad (1)$$

$$a^2 = 4.24 \cdot 10^{-4} (\varepsilon_{max}\Delta\nu_{1/2}/\tilde{\nu}_{max} d^2) \quad (2)$$

For the computations $\tilde{\nu}_{max}$ was taken as 10000 cm^{-1} and $\Delta\nu_{1/2}$ as 6500 cm^{-1}, which is somewhat uncertain due to the large bandwidths of the MMCT bands. The value of d, the Fe−Fe distance, was taken from the structures of **2b** and **2c** as 10.2 Å. With these data the metal−metal interaction parameter, H_{ab}, is about 9000 cm^{-1} and the electron delocalization parameter a^2 about 0.8% for complexes **3**. Both these values are higher than the ones for the mixed-valent species with Fe^{II}−NC−Pt^{II}−CN−Fe^{III} backbones,[9] which indicates that the Fe···Ru···Fe system investigated here is a viable electronic conductor, as proposed in the introduction. In dinuclear species with M−CN−Fe(dppe)Cp arrays the electronic interaction between M and Fe, due to the 50% shorter distance, is naturally much stronger.[18,19]

Conclusions

This work has shown that Ru^{II} units with nitrogen ligands, which are famous as the external redox-active centers in classical mixed-valent dinuclear complexes,[23] are also favorable as the central units in trinuclear mixed-valent complexes. By a suitable choice of ligands on the three metal centers and by the suitable orientation of the bridging cyanide ligands it was ensured that a linear Fe−*N*−C−Ru−C−*N*−Fe array was obtained and that one-electron oxidations take place primarily at the iron centers. The basis for this is the inertness of octahedral Ru^{II}, which allows the unnatural orientation of the cyanide bridges (carbon attached to the electron-poor and nitrogen attached to the electron-rich metal) to persist.

These features have allowed, for the second time, the isolation of partially oxidized mixed-valent trinuclear complexes, i.e. the Fe^{II}−NC−Ru^{II}−CN−Fe^{III} species. Their spectroscopic investigation has identified their localized Fe^{II}/Fe^{III} nature and revealed a low-energy metal−metal charge transfer, which puts the complexes into class II of mixed-valent species according to the classification of Robin and Day. The electron delocalization parameter a^2 is of the order of 1%, which is considerably smaller than in related dinuclear complexes, but compares favorably with the values for other trinuclear complexes.

Among the trinuclear complexes of the type M-(μ-CN)-M′-(μ-CN)-M with organometallic units at the external positions only those with heavy and late transition metals at the center have allowed the detection of mixed valence by cyclic voltammetry and to investigate it by preparative redox chemistry, the prominent examples being those with Au^{I},[24] Pt^{II},[9] and Ru^{II} (this work). Their common feature is the low-spin electronic state with filled d_{xy}, d_{xz} and d_{yz} orbitals, i.e. those orbitals which provide π-interactions with the bridging cyanide ligands. This points to the π-bonding orbitals as the pathway for the metal−metal interactions. However, it is still too early to generalize this observation, and further studies, both preparative and theoretical, are necessary to gain a real understanding of these phenomena.

Experimental Section

For the general experimental and measuring techniques, see ref.[18] The starting materials $[RuCl_2(DMSO)_4]$,[25] $[Ru(CN)_2(pyridine)_4]$,[17] and $[FeCp(dppe)(CH_3CN)]Br$[26] were prepared as published.

1b: A mixture of $[RuCl_2(DMSO)_4]$ (300 mg, 0.62 mmol) and 10 mL of 4-methylpyridine was stirred at 100 °C for 30 min. After cooling to room temp. KCN (150 mg, 2.31 mmol) in 3 mL of water was added. After refluxing for 20 min all volatiles were removed in vacuo at 80 °C. The residue was extracted with 20 mL of dichloromethane. After filtration the extract was evaporated to dryness, leaving behind 230 mg (65%) of **1b** as a yellow powder, m.p. 280 °C (dec.). $C_{26}H_{28}N_6Ru \cdot 0.5CH_2Cl_2$ (525.62 + 42.46): calcd. C 56.03, H 5.15, N 14.79; found C 56.57, H 5.77, N 14.97.

1c: Prepared similarly to **1b** from $[RuCl_2(DMSO)_4]$ (300 mg, 0.62 mmol), 10 mL of 4-ethylpyridine and KCN (210 mg, 3.23 mmol). The dichloromethane extract was evaporated to 3 mL and chromatographed over a 10 × 1.5 cm silica gel column with CH_3CN/CH_2Cl_2 (1:4). A single yellow band was collected. Evaporation to dryness left behind 210 mg (51%) of **1c** as a yellow powder, m.p. 210 °C (dec.). $C_{30}H_{36}N_6Ru \cdot CH_2Cl_2$ (581.72 + 84.93): calcd. 55.85, H 5.75, N 12.61; found C 55.62, H 5.40, N 12.39.

2a: Complex **1a** (94 mg, 0.20 mmol) and $[FeCp(dppe)(CH_3CN)]Br$ (258 mg, 0.40 mmol) in 10 mL of dichloromethane were stirred for 8 h. NH_4PF_6 (68 mg, 0.42 mmol) was then added and the mixture stirred for a further 30 min. After filtration, slow diffusion of diethyl ether into the filtrate led, within one week, to the precipitation of 246 mg (63%) of **2a** as orange crystals, m.p. 180 °C (dec.).

 © 2004 Wiley-VCH Verlag GmbH & Co. KGaA, Weinheim

Table 5. Crystallographic details

	2b·$2CH_2Cl_2$	**2c**·CH_3OH
Empirical formula	$C_{90}H_{90}Cl_4F_{12}Fe_2N_6P_6Ru$	$C_{93}H_{98}F_{12}Fe_2N_6OP_6Ru$
Molecular mass	2024.07	1942.36
Crystal size [mm]	0.2 × 0.1 × 0.1	0.6 × 0.3 × 0.3
Space group	*C*2/*c*	$P2_1/n$
Z	4	4
a (Å)	18.959(3)	19.865(5)
b (Å)	23.469(3)	22.317(6)
c (Å)	22.118(3)	21.351(6)
α (°)	90	90
β (°)	112.926(2)	96.209(5)
γ (°)	90	90
V (Å^3)	9064(2)	9410(4)
d(calcd.) (gcm^{-3})	1.48	1.37
μ(Mo-K_α) (mm^{-1})	0.78	0.64
hkl range	*h*: −23 to 23	*h*: −26 to 25
	k: −23 to 30	*k*: −31 to 23
	l: −29 to 15	*l*: −29 to 16
Measured reflections	23013	62769
Independent reflections	10546	25936
Observed refl. [$I > 2\sigma(I)$]	1680	15018
Parameters	546	1162
Refined reflections	10546	25936
R_1 (obsd.refl.)	0.070	0.051
wR_2 (all refl.)	0.208	0.164
Residual electron density [e/Å^3]	+1.7/-2.1	+1.0/-0.7

$C_{84}H_{78}F_{12}Fe_2N_6P_6Ru{\cdot}2CH_2Cl_2$ (1798.16 + 169.86): calcd. C 52.49, H 4.20, N 4.27; found C 52.52, H 4.32, N 4.36.

2b: Complex **1b** (114 mg, 0.20 mmol) and [FeCp(dppe)(CH_3CN)]Br (258 mg, 0.40 mmol) in 10 mL of methanol were stirred for 3 days. Addition of NH_4PF_6 (91 mg, 0.56 mmol) produced a red precipitate. This was filtered off and extracted with 6 mL of dichloromethane. After filtration the filtrate was layered with 1 mL of petroleum ether (60−70 °C) and 10 mL of diethyl ether. Within one week 273 mg (67%) of **2b** had precipitated as orange crystals, m.p. 255 °C (dec.). $C_{88}H_{86}F_{12}Fe_2N_6P_6Ru{\cdot}2CH_2Cl_2$ (1854.27 + 169.86): calcd. C 53.40, H 4.48, N 4.15; found C 53.65, H 4.66, N 4.12.

2c: Prepared similarly to **2b** from **1c** (67 mg, 0.10 mmol), [Cp(dppe)-Fe(CH_3CN)]Br (129 mg, 0.20 mmol) and NH_4PF_6 (34 mg, 0.21 mmol). Yield 80 mg (38%) of **2c** as orange crystals, m.p. 230 °C (dec.). $C_{92}H_{94}F_{12}Fe_2N_6P_6Ru{\cdot}2CH_2Cl_2$ (1910.38 + 169.86): calcd. C 54.27, H 4.75, N 4.04; found C 54.31, H 5.04, N 4.07.

3a: [Cp_2Fe]PF_6 (6.6 mg, 0.02 mmol) was added to a solution of **2a** (39 mg, 0.02 mmol) in 6 mL of dichloromethane. After stirring for 1 h the mixture was filtered and the filtrate layered with 10 mL of petroleum ether (60−70 °C). After 3 days 20 mg (51%) of **3a** had separated as brown crystals, m.p. 155 °C (dec.). $C_{84}H_{78}F_{18}Fe_2N_6P_7Ru$ (1943.13): calcd. C 51.92, H 4.05, N 4.32; found C 52.36, H 4.49, N 4.32.

3b: Prepared similarly to **3a** from **2b** (41 mg, 0.20 mmol). Yield: 30 mg (75%) of **3b** as orange crystals, m.p. 250 °C (dec.). $C_{88}H_{86}F_{18}Fe_2N_6P_7Ru$ (1999.23): calcd. 52.87, H 4.34, N 4.20; found C 52.86, H 4.60, N 4.22.

3c: Prepared similarly to **3a** from (42 mg, 0.20 mmol) of **2c**. Yield: 24 mg (58%) of **3c** as orange crystals, m.p. 220 °C (dec.). $C_{92}H_{94}F_{18}Fe_2N_6P_7Ru$ (2055.34): calcd. C 53.76, H 4.61, N 4.09; found C 53.05, H 4.81, N 3.99.

Structure Determinations:[27] Crystals of **2b** were obtained by layering a solution of **2b** in dichloromethane with hexane/diethyl ether, and those of **2c** by slow diffusion of diethyl ether into a solution of **2c** in methanol/dichloromethane. Diffraction data were recorded at −30 °C on a Bruker Smart CCD diffractometer and subjected to empirical absorption corrections. The structures were solved and refined with the SHELX program suite.[28] All hydrogen atoms were included with fixed distances and isotropic temperature factors 1.2-times those of their attached atoms. Parameters were refined against F^2. The *R* values are defined as $R_1 = \Sigma|F_o - F_c|/\Sigma F_o$ and $wR_2 = [\Sigma\{w(F_o^2 - F_c^2)^2\}/\Sigma\{w(F_o^2)^2\}]^{1/2}$. Drawings were produced with SCHAKAL.[29] Table 5 lists the crystallographic data.

Acknowledgments

This work was supported by the Deutsche Forschungsgemeinschaft (GK 307). We are indebted to Drs. W. Deck and H. Brombacher for help with the structure determinations.

[1] V. Balzani, A. Juris, M. Venturi, C. Campagna, S. Serroni, *Chem. Rev.* **1996**, *96*, 759−833.
[2] K. R. Dunbar, R. A. Heintz, *Prog. Inorg. Chem.* **1997**, *45*, 283−391.
[3] C. A. Bignozzi, J. R. Schoonover, F. Scandola, *Prog. Inorg. Chem.* **1997**, *44*, 1−95.
[4] H. Vahrenkamp, A. Geiß, G. N. Richardson, *J. Chem. Soc., Dalton Trans.* **1997**, 3643−3651.
[5] For references prior to 1997, see ref.[4]
[6] N. G. Connelly, G. R. Lewis, M. T. Moreno, A. G. Orpen, *J. Chem. Soc., Dalton Trans.* **1998**, 1905−1911.
[7] A. V. Macatangay, J. F. Endicott, *Inorg. Chem.* **2000**, *39*, 437−446.
[8] S. M. Kuang, P. E. Fanwick, R. A. Walton, *Inorg. Chem.* **2002**, *41*, 147−151.
[9] G. N. Richardson, U. Brand, H. Vahrenkamp, *Inorg. Chem.* **1999**, *38*, 3070−3079.

 © 2004 Wiley-VCH Verlag GmbH & Co. KGaA, Weinheim

[10] A. Geiß, H. Vahrenkamp, *Eur. J. Inorg. Chem.* **1999**, 1793−1803.
[11] G. N. Richardson, H. Vahrenkamp, *J. Organomet. Chem.* **2000**, *593−594*, 44−48.
[12] A. Geiß, M. J. Kolm, C. Janiak, H. Vahrenkamp, *Inorg. Chem.* **2000**, *39*, 4037−4043.
[13] R. Appelt, H. Vahrenkamp, *Inorg. Chim. Acta* **2003**, *350*, 387−398.
[14] M.-L. Flay, H. Vahrenkamp, *Eur. J. Inorg. Chem.* **2003**, 1719−1726.
[15] B. J. Coe, T. J. Meyer, P. S. White, *Inorg. Chem.* **1995**, *34*, 3600−3609.
[16] T. Sheng, H. Vahrenkamp, *Inorg. Chim. Acta*, in print.
[17] B. J. Coe, T. J. Meyer, P. S. White, *Inorg. Chem.* **1995**, *34*, 593−602.
[18] N. Zhu, H. Vahrenkamp, *Chem. Ber./Recueil* **1997**, *130*, 1241−1252.
[19] T. Sheng, H. Vahrenkamp, *J. Argentine Chem. Soc.*, in print.
[20] M. B. Robin, P. Day, *Adv. Inorg. Chem. Radiochem.* **1967**, *10*, 247−422.
[21] N. Zhu, H. Vahrenkamp, *J. Organomet. Chem.* **1998**, *573*, 67−72.
[22] N. S. Hush, *Prog. Inorg. Chem.* **1967**, *8*, 391−444.
[23] C. Creutz, *Prog. Inorg. Chem.* **1983**, *30*, 1−73.
[24] N. C. Brown, G. B. Carpenter, N. G. Connelly, J. G. Crossley, A. Martin, A. G. Orpen, A. L. Rieger, P. H. Rieger, G. H. Worth, *J. Chem. Soc., Dalton Trans.* **1996**, 3977−3984.
[25] I. P. Evans, A. Spencer, G. Wilkinson, *J. Chem. Soc., Dalton Trans.* **1973**, 204−209.
[26] P. M. Treichel, D. C. Molzahn, *Synth. React. Inorg. Met.-Org. Chem.* **1979**, *9*, 21−29.
[27] CCDC-219798 (for **2b**) and -219799 (for **2c**) contain the supplementary crystallographic data for this paper. These data can be obtained free of charge at www.ccdc.cam.ac.uk/conts/retrieving.html [or from the Cambridge Crystallographic Data Center, 12, Union Road, Cambridge CB2 1EZ, UK; Fax: (internat.) +44-1223/336-033; E-mail: deposit@ccdc.cam.ac.uk].
[28] *SHELX* program package for the Bruker Smart CCD diffractometer, version 5.1, **2002**.
[29] E. Keller, *SCHAKAL for Windows*, Universität Freiburg, **2001**.
Received September 19, 2003
Early View Article
Published Online February 16, 2004

 © 2004 Wiley-VCH Verlag GmbH & Co. KGaA, Weinheim

The Electronic Structure of (Diiminopyridine)cobalt(I) Complexes

Quinten Knijnenburg,[a] Dennis Hetterscheid,[a] T. Martijn Kooistra,[a] and Peter H. M. Budzelaar*[a]

Keywords: Charge transfer / Cobalt / Density functional calculations / NMR spectroscopy / Radicals

DFT calculations show that square-planar $LCo^{I}R$ complexes of a diiminopyridine ligand are best regarded as containing low-spin Co^{II} antiferromagnetically coupled to a ligand radical anion. The lowest triplet state, corresponding to a $3d_{z^2} \rightarrow \pi^*$ excitation, is calculated to be only a few kcal/mol above the ground state, and is thermally accessible. The anomalous ^1H NMR chemical shifts of the LCoR complexes are suggested to be due to thermal population of the triplet state at room temperature.

(© Wiley-VCH Verlag GmbH & Co. KGaA, 69451 Weinheim, Germany, 2004)

Introduction

Diamagnetic square-planar d^8 complexes of Co^{I} are much rarer[1,2] than the corresponding Rh^{I} and Ir^{I} species. Apparently, such Co^{I} species easily "escape" to the high-spin state or to higher oxidation states like Co^{II} or Co^{III}. Nevertheless, this type of Co^{I} complex is of great interest because the resemblance to its heavier Rh^{I} congener might be accompanied by a rich catalytic chemistry similar to that of Rh. Therefore, the recent observation that the diiminopyridine ligand L is able to stabilize Co^{I} in a low-spin, square-planar state,[3] while still leaving a coordination site available for further chemistry, is significant.

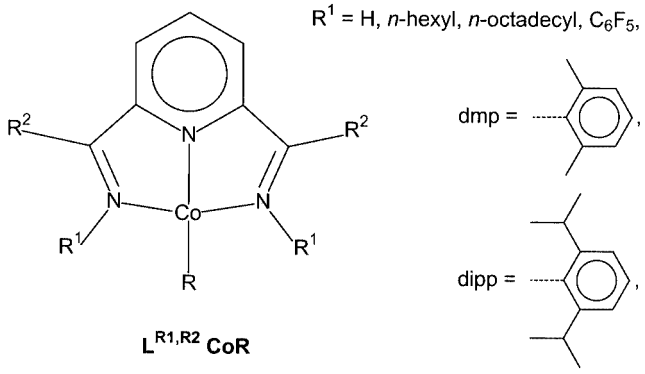

The complexes $LCo^{I}X$ (X = halide, alkyl) were reported to have unusual ^1H NMR chemical shifts for the pyridine Hγ and imine methyl groups,[3] when compared to the analogous Rh^{I} and Ir^{I} species.[4,5] The possibility that these unusual shifts might reflect an unusual electronic structure of the Co^{I} complexes prompted us to prepare a few additional Co and Rh complexes and to undertake a theoretical investigation of these species. In the present work, we report that the bonding in the Co^{I} species indeed shows several unexpected features. Diiminopyridine complexes of Co^{II} have been studied theoretically in the context of olefin polymerisation.[6] Experimental[7] and theoretical[8] studies of bis(diiminopyridine) complexes of the first-row transition metals Mn−Zn have revealed the non-innocent character of the ligand and the importance of biradical character in the metal-ligand interaction. The present work shows that biradical character can be even more pronounced in mono(ligand) complexes of cobalt.

Results and Discussion

Synthesis and Characterisation

2,6-Diacetylpyridine, anilines and amines are commercially available. 2,6-Dibenzoylpyridine is easily synthesised by Friedel−Crafts acylation of pyridine-2,6-dicarboxylic acid dichloride and benzene.[9] The diiminopyridine ligands were prepared from the condensation of two equivalents of the appropriate aniline or amine with diacylpyridine. The cobalt dichloride complexes can be synthesised in air. The reduction and subsequent alkylation of the cobalt dichloride complexes to monoalkyl complexes (e.g. $LCoCH_2SiMe_3$) can be achieved in one step using two equivalents of $LiCH_2SiMe_3$, or in two steps via a cobalt monochloride complex, as described earlier.[3] Alkyl complexes [$L^{dipp,Me}CoR$] having the bulky dipp group at R^1 react with hydrogen to form the hydride [$L^{dipp,Me}CoH$]. This complex is very reactive and could not be isolated in pure form, so it was only characterised by NMR spectroscopy. The complexes [LCoR], bearing smaller substituents at R^1 (dmp, alkyl), also react with hydrogen, but after reaction no reson-

[a] Metal-Organic Chemistry, University of Nijmegen, Toernooiveld 1, 6525 ED Nijmegen, The Netherlands
Fax: (internat.) +31-24-355-3450
E-mail: budz@sci.kun.nl

 © 2004 Wiley-VCH Verlag GmbH & Co. KGaA, Weinheim DOI: 10.1002/ejic.200300569

ances due to Co complexes could be recognized in the spectra. The chloride complexes [LCoCl] do not react with hydrogen. The rhodium complex [$L^{dipp,Me}$RhCl] can be easily converted into the desired alkyl complex by addition of alkyllithium. This demonstrates the importance of steric shielding of the metal: the analogous but more open complex [$L^{dmp,Me}$RhCl] could only be converted into the alkyl by an elaborate indirect route.[4]

Structures and Lowest-Energy States of [LCoR] Complexes

The Rh and Ir model complexes [$L^{H,Me}$MR] (M = Rh, Ir; R = H, Me, Cl) have normal closed-shell ground states stable to symmetry breaking. In contrast, for all cobalt complexes studied theoretically the restricted DFT (b3lyp) solution is unstable. The unrestricted $m_S = 0$ solution ("U_0") is 10−20 kcal/mol lower in energy, depending on the ligand. At the restricted DFT (RDFT) level, the optimised structures of the hydride and methyl complexes are non-planar, with the hydride or methyl group bent out of the coordination plane by a significant amount (typically around 20°). Re-optimisation at the unrestricted DFT (UDFT) level, however, results in planar or near-planar structures in all cases.[10]

In the optimised geometries, the Co−N (Table 1) and Co−Cl distances are systematically too large by about 0.04

Table 1. Calculated bond lengths (Å) and singlet-triplet separations (kcal/mol) for $L^{R1,R2}$MR complexes

M	R	R^1	R^2	State[a]	M−N_{py}	M−N_{im}	C−N_{im}	C_{py}−C_{im}	ΔE_{ST} [b]
Co	H	H	Me	s	1.881	1.894	1.328	1.452	7.3 (5.5)
				t	1.891	1.922	1.326	1.454	
	Me			s	1.884	1.898	1.328	1.452	8.5 (7.6)
				t	1.897	1.928	1.327	1.452	
	Cl			s	1.840	1.901	1.318	1.454	9.1 (8.7)
				t	1.857	1.923	1.321	1.452	
Rh	H	H	Me	s	2.001	2.035	1.313	1.470	9.9
				t	2.042	2.070	1.328	1.456	
	Me			s	1.990	2.040	1.314	1.467	12.6
				t	2.038	2.073	1.329	1.456	
	Cl			s	1.927	2.032	1.310	1.464	18.7
				t	1.973	2.060	1.324	1.452	
Ir	H	H	Me	s	2.005	2.027	1.322	1.462	17.2
				t	2.054	2.063	1.336	1.453	
	Me			s	1.990	2.029	1.324	1.459	21.0
				t	2.049	2.058	1.336	1.455	
	Cl			s	1.925	2.029	1.320	1.456	26.4
				t	1.979	2.059	1.332	1.449	
Co	H	*n*-C_6H_{13}	Me	s	1.867	1.931	1.328	1.455	5.7
				t	1.876	1.948	1.330	1.454	
	Me			s	1.878	1.960	1.328	1.452	6.3
				t	1.890	1.983	1.330	1.451	
	Cl			s	1.834	1.955	1.321	1.453	8.0
				t	1.850	1.967	1.326	1.451	
	H	dipp	Me	s	1.871	1.944	1.332	1.452	5.6
				t	1.882	1.966	1.333	1.451	
	Me			s	1.881	1.965	1.332	1.450	7.2
				t	1.892	1.990	1.333	1.449	
	Cl			s	1.836	1.972	1.323	1.451	8.4
				t	1.852	1.984	1.329	1.448	
	H	C_6F_5	Me	s	1.882	1.930	1.338	1.451	5.1
				t	1.884	1.951	1.338	1.450	
	Me			s	1.892	1.949	1.339	1.448	6.4
				t	1.896	1.977	1.338	1.447	
	H	dmp	Ph	s	1.876	1.930	1.339	1.459	4.6
				t	1.882	1.952	1.338	1.460	
	Me			s	1.890	1.961	1.338	1.456	6.1
				t	1.894	1.989	1.337	1.456	
	H	dmp	CF_3	s	1.882	1.914	1.337	1.455	6.4
				t	1.890	1.946	1.332	1.456	
	Me			s	1.898	1.945	1.336	1.451	8.3
				t	1.902	1.982	1.331	1.452	
Co (pyrazine!)	H	H	Me	s	1.870	1.907	1.324	1.454	6.9
				t	1.876	1.935	1.324	1.453	
(phosphinimine!)	H	H	(Me_2P)	s	1.947	1.953	1.607	1.803	5.1
				t	1.967	1.963	1.611	1.801	

[a] s = U_0 state for Co, RDFT singlet for Rh, Ir; t = $U_1(z^2)$ triplet. [b] In kcal/mol, estimated from U_0 and $U_1(xz)$ energies (see text); b3lyp/SV(P); for M = Co, R^1 = H, R^2 = Me: values calculated using the TZVPP basis set at the b3lyp/SV(P) geometries given in parentheses.

 © 2004 Wiley-VCH Verlag GmbH & Co. KGaA, Weinheim

Å, as is evident from a comparison with the X-ray structures shown in Figure 1. The calculated Co−C distance appears to be about right, but this agreement is fortuitous, since the experimental value is for a CH_2SiMe_3 group while the calculated value is for a Me group, which *should* have a shorter Co−C distance.[11] Thus, Co simply appears to be too large in the calculations. Distances *within* the ligand are reproduced satisfactorily.

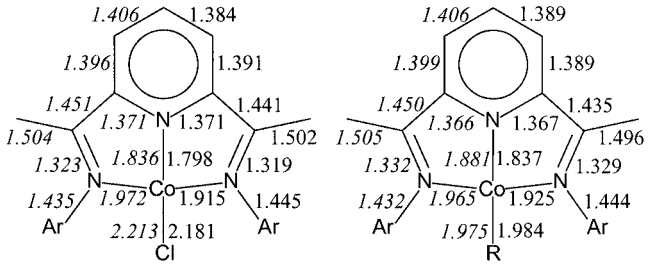

Figure 1. Observed and *calculated* bond lengths for [$L^{dipp,Me}$CoR] complexes: R = Cl[3a] (left) and CH_2SiMe_3 [3b] or *Me* (right)

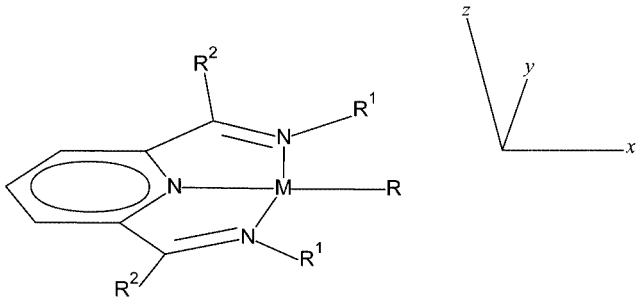

The U_0 wavefunctions have S^2 values of 0.80−1.05.[12a] They have one "pair" of occupied α and β orbitals, corresponding to bonding and antibonding combinations of the metal $3d_{xz}$ and ligand π* orbitals, respectively (Figure 2). The remaining orbitals are all fairly cleanly paired. This means that the U_0 "states" are nearly 50:50 mixtures of singlet and triplet states, where the relevant triplet state corresponds to the $3d_{xz}\rightarrow\pi^*$ excitation of a hypothetical true [$LCo^{I}R$] species. These triplets, indicated here by $U_1(xz)$, were also obtained separately from unrestricted $m_S = 1$ calculations, and they have S^2 values of 2.00−2.10, indicating little spin contamination. The true singlet energies were then estimated from the energies ε_0, ε_1 of the unrestricted solutions U_0, $U_1(xz)$ and their S^2 values by extrapolating the presumed linear relation between energy and S^2 to $S^2 = 0$ [Equation (1)]:[12b,13]

$$\varepsilon_S \approx \frac{S_1^2\varepsilon_0 - S_0^2\varepsilon_1}{S_1^2 - S_0^2} \quad (1)$$

The singlet-triplet separation calculated from this varies between 9 and 13 kcal/mol. These results show that the singlet ground state is best described as a square-planar, low-spin $Co^{II}R$ fragment ($3d_{xz}$ singly occupied) antiferromagnetically coupled to a ligand radical anion. In this respect, these complexes are more extreme than the L_2Co^+ complexes considered in earlier work,[8] where only about half of the 3d→π* transfer of electron density was in the form of unpaired electron density, the remainder being "classical" back-donation. Related to this, complexes [LMnR] have been shown to contain a ligand radical anion antiferromagnetically coupled to a *high-spin* Mn^{II} centre.[14] If the ligand is simply considered as a uni-negative ligand and its unpaired electron is ignored, complexes [LCoR] can be seen as relatives of the (also square-planar) low-spin Co^{II} amido complex [$CoBz\{N(SiMe_2CH_2PPh_2)_2\}$].[15] Thus, reduction of high-spin [$LCoCl_2$] to low-spin [LCoCl][3] actually occurs at the ligand rather than at the metal, but is accompanied by a spin flip at the metal, possibly induced by the higher ligand-field of the ligand radical anion. A related reduction-induced spin flip was observed in L_2Mn^{2+}.[7]

Interestingly, the $U_1(xz)$ triplet is not the lowest-lying triplet state. According to our calculations, the $U_1(z^2)$ ($3d_{z^2}\rightarrow\pi^*$) triplet is the lowest one; this always lies about 3−5 kcal/mol below the $U_1(xz)$ triplet and hence about 4.5−9 kcal/mol above the singlet ground state. The geometries calculated for U_0 and $U_1(z^2)$ are very similar, typically differing by less than 0.01 Å in bond lengths. The clearest exception is the $Co-N_{im}$ bond, which can be up to 0.03 Å longer in the triplet state.

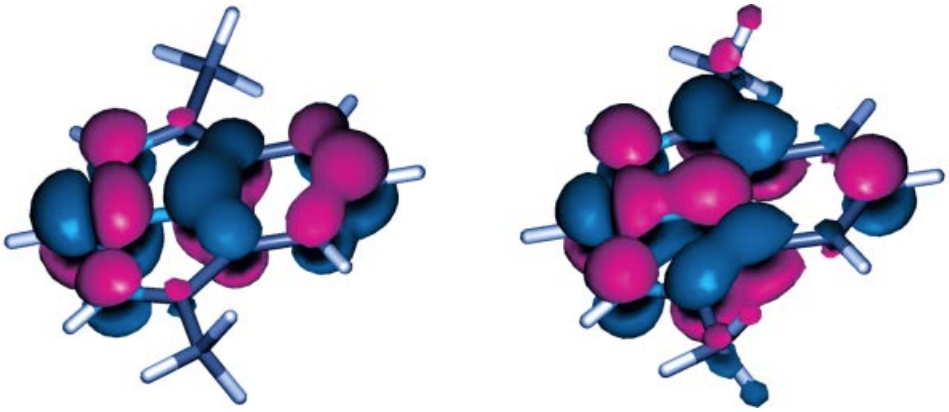

Figure 2. Singly occupied UDFT α- and β-orbitals of U_0 solution for [$L^{H,Me}$CoH]

 © 2004 Wiley-VCH Verlag GmbH & Co. KGaA, Weinheim

Substituent Effects on the Singlet-Triplet Separation in Co Complexes

In order to check whether the unusual bonding described above applies not only to simple models but also to "real" systems, we have studied a number of combinations of substituents. Table 1 shows the calculated geometries and singlet-triplet gaps for all systems studied. All values have been calculated at the b3lyp/SV(P) level. For the smallest model system $L^{H,Me}$, we have also calculated energies with the TZVPP basis set. This resulted in somewhat smaller gaps, especially for the hydride. It is likely that basis-set improvement would also lower the gaps for the other systems. However, such calculations are not feasible for the large systems studied here.

The most remarkable result is probably that the singlet-triplet gaps are so insensitive to changes in R, R^1 and R^2. Interpreting the small changes we do see is not so easy, given that they correspond to an excitation from a $3d_{xz}\rightarrow\pi^*$ *singlet* to a $3d_{z^2}\rightarrow\pi^*$ *triplet*. Since, however, we find that the energy difference between the $3d_{xz}\rightarrow\pi^*$ and $3d_{z^2}\rightarrow\pi^*$ triplets is fairly constant, we need only discuss the $3d_{xz}\rightarrow\pi^*$ singlet to $3d_{xz}\rightarrow\pi^*$ triplet gap. This gap, which in the wavefunction picture corresponds to an exchange integral, will be larger if the regions of high electron density of the relevant metal and ligand orbitals (mainly Co $3d_{xz}$ and N $2p_z$) overlap more. Changes in any of the groups R, R^1 and R^2 are therefore expected to affect the gap in two different ways. Steric hindrance at nitrogen will weaken the Co−imine coordination and hence decrease the gap. However, electronic factors that strengthen the pyridine and/or imine coordination will increase the gap.

We consistently see an increasing gap when changing R in the order H < Me < Cl, in steps of about 1 kcal/mol. This is presumably a direct electronic effect: in this order, the *trans* effect of the R group decreases and the $Co-N_{py}$ distance decreases (by 0.03−0.04 Å).

Introducing bulky groups at nitrogen (R^1 = *n*-hexyl or dipp, compared to R^1 = H) decreases the gap by about 2 kcal/mol. This is probably a mostly steric effect: the $Co-N_{im}$ distance is 0.04−0.05 Å longer for these *N*-substituted derivatives. Introducing instead the very electron-withdrawing C_6F_5 group at N has very little additional effect, decreasing the gap further by only 0.5 kcal/mol. Since the steric effects of C_6F_5 and dipp should be similar here, it is clear that the electronic effect is rather small. Replacing the backbone (R^2) methyl groups by phenyls has a somewhat larger effect (about 1 kcal/mol for $L^{dmp,Ph}$ relative to $L^{dipp,Me}$). This is most likely due to increased delocalisation of the ligand π*-orbital. The effect is modest because the phenyls cannot become coplanar with the ligand skeleton for steric reasons. Surprisingly, replacing the backbone methyls by CF_3 groups results in an *increase* of the gap by about 1 kcal/mol. At the same time, the Co−imine distance decreases by about 0.03 Å, indicating that the CF_3 substituents strengthen the Co−imine coordination,[16] which is consistent with the increased gap.

Finally, we have considered two more exotic systems: diiminopyrazine and bis(phosphinimino)pyridine. Complexes of the diiminopyrazine ligand show a singlet-triplet gap that is marginally smaller than that calculated for the diiminopyridine complexes. The Co-ring nitrogen distance is slightly smaller, and the Co−imine distances are slightly larger, due to the replacement of Cγ by the smaller nitrogen atom. It is remarkable that such a major change in the π-acceptor character of the ligand has so little effect on the gap. Perhaps the reason is that the diiminopyridine and diiminopyrazine complexes are all completely biradicals, so the variation in ligand π-acceptor strength does not influence the electronic structure.

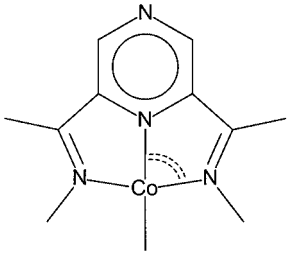

diiminepyrazine

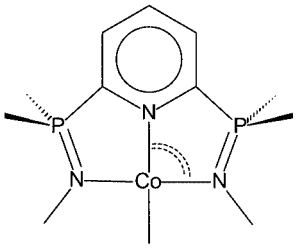

bis(phosphinimine)pyridine

The bis(phosphinimine)pyridine system,[17] too, is fully a biradical. For this ligand, we calculate a gap which is smaller by about 2 kcal/mol, i.e. as much as is attainable using substituent effects *within* the diiminopyridine system. The most likely explanation is that here the N−Co−N angles are closer to their ideal value of 90°. The exchange integral determining the gap is reduced because the N $2p_z$ orbitals are now closer to a nodal plane of the $3d_{xz}$ orbital. It looks like bis(phosphinimino)pyridines can be considered as a useful extension (in an electronic sense) of the diiminopyridine ligands.

Correlation with NMR Results

Table 2 contains the observed ^{1}H NMR chemical shifts for a number of LMR complexes, some of which were only generated in situ. We concentrate on the data for $L^{dipp,Me}$, although the other ligands behave similarly. NMR spectroscopic data for several Co^I complexes have already been reported.[3] The shifts for pyridine Hβ are fairly normal. However, for Co the Hγ resonance shows an abnormal low-field shift with increasing ligand field of the group R, from δ = 9.53 ppm for [$L^{dipp,Me}$CoCl] to δ = 10.80 ppm for [$L^{dipp,Me}$CoH]. Even the value for [$L^{dipp,Me}$CoCl] is already high, given that this resonance is found at δ = 7.97 ppm for the free ligand and at δ = 7.80 ppm for [$L^{dipp,Me}$RhCl]. Simultaneous with the low-field shift of the Hγ resonance, the imine methyl (R^2) group shifts from δ = 2.30 ppm (for free $L^{dipp,Me}$) via δ = 0.05 ppm (for [$L^{dipp,Me}$CoCl]) to δ = −1.65 ppm (for [$L^{dipp,Me}$CoH]), while for Rh it never goes below δ = +0.7 ppm. The magnitudes of these curious shifts are emphasised in Table 3, where for Hβ, Hγ and imine Me the values for Co are given relative to the corresponding Rh values.

 © 2004 Wiley-VCH Verlag GmbH & Co. KGaA, Weinheim

Table 2. NMR spectroscopic data for diiminopyridine complexes of Co^{I} and Rh^{I}[a]

Ligand R^1,R^2	Complex	Pyridine Hβ	Hγ	Imine CH_3	*N*-alkyl $C^{\alpha}H_2$	$C^{\beta}H_2$	$C^{\gamma}H_2$	$C^{\delta}H_2$
dipp,Me	free L	8.59	7.97	2.30				
	LCoCl	6.91	9.53	0.05				
	$LCoCH_2SiMe_3$	7.62	9.89	−0.85				
	LCoBz	7.68	10.27	−1.16				
	LCoMe	7.86	10.19	−1.15				
	LCoEt	7.99	10.25	−1.33				
	LCoH	7.60	10.80	−1.65				
	LRhCl	6.85	7.80	1.07				
	$LRhCH_2SiMe_3$	7.21	8.06	0.87				
	LRhMe	7.24	8.10	0.72				
	LRhBz	7.06	7.84	0.79				
dmp,Me	$LCoCH_2SiMe_3$	7.71	10.06	−1.28				
dmp,Ph	$LCoCH_2SiMe_3$		9.91	n/a				
n-C_6H_{13},Me	$LCoCH_2SiMe_3$	7.31	9.71	−0.16	5.19	2.22	1.55	1.23
n-$C_{18}H_{37}$,Me	$LCoCH_2SiMe_3$	7.31	9.71	−0.15	5.21	2.26	1.59	

[a] δ (ppm), in C_6D_6, 20 °C.

Table 3. Estimated "anomalous" shifts ($\Delta\delta = \delta_{LCoX} - \delta_{LRhX}$) of $L^{dipp,Me}$ complexes

Complex	Pyridine Hβ	Hγ	Imine CH_3
LCoCl	−0.06	+1.73	−1.02
$LCoCH_2SiMe_3$	+0.41	+1.83	−1.72
LCoBz	+0.62	+2.35	−2.12
LCoMe	+0.62	+2.09	−1.87
LCoH[a]	+0.36	+2.70	−2.37

[a] Using LRhMe as reference.

It is tempting to correlate these NMR shifts with the remarkable electronic structures of the LCoR complexes. The biradical character of singlet LCoR should not, by itself, result in anomalous NMR shifts. However, the calculated singlet-triplet gaps for the "real" systems are rather small (5−8 kcal/mol) and are expected to become smaller with larger basis sets: a decrease of 1.8 kcal/mol is calculated for the model system [$L^{H,Me}$CoH] on going from SV(P) to TZVPP (Table 1). Thus, the extrapolated gap for [$L^{dipp,Me}$CoH] at the b3lyp/TZVPP level is only 3.8 kcal/mol. Allowing for an error of only a few kcal/mol in the gaps we could already have a sizeable thermal population of the triplet state. Rapid spin-flip would then result in averaged shifts containing a contribution of the triplet-state paramagnetic shift. With an estimated Fermi contact term *a* of −1.5 G for Hγ[18] and an anomalous NMR shift of about 2 ppm, the fraction, *f*, of triplet population of [$L^{dipp,Me}$CoMe] calculated from Equation (2) should be about 2%, corresponding to a singlet-triplet gap of about 2 kcal/mol.

$$\Delta\delta \approx f\frac{a\gamma_e^2\eta}{4\gamma_H kT} \qquad (2)$$

At present, we have no way of verifying this hypothesis. At room temperature, no triplet EPR signal is observed, but this would not be expected anyway because of rapid relaxation. At 4 K, where a signal should normally be observable, the triplet population would be so small as to escape detection. Temperature-dependent ^{1}H NMR studies are hampered by solubility and (especially for the more interesting alkyls) stability problems.

The anomalous shifts increase with decreasing singlet-triplet gap, which agrees with the above hypothesis. However, the changes in observed shifts suggest that the triplet population changes only by a factor of about two over the whole range of Cl···H, corresponding to a gap change of about 0.3 kcal/mol, smaller than our calculated change of about 2 kcal/mol.

Conclusions

[$LCo^{I}X$] complexes have a diamagnetic ground state with a square-planar coordination geometry. In contrast to their heavier Rh^{I} and Ir^{I} analogues, they are best regarded as containing low-spin Co^{II} antiferromagnetically coupled to a ligand radical anion. The lowest-lying triplet state, corresponding to a $3d_{z^2}\rightarrow\pi^*$ excitation, lies only a few kcal/mol above the ground state. The singlet-triplet separation decreases with increasing ligand-field strength of the group X at Co. We suggest that the anomalous ^{1}H NMR shifts observed for these Co complexes, but not for their Rh and Ir analogues, are due to thermal population of the triplet state at room temperature. The triplet state is so low in energy that it can certainly be involved in chemical reactions. Obviously, the availability of both a singlet biradical and a triplet state multiplies the number of reaction paths accessible to the complex. Whether this is relevant to polymerisation catalysis of LCo complexes remains to be established.

Experimental Section

General Remarks: All manipulations were carried out under an atmosphere of argon using standard Schlenk techniques or in a con-

 © 2004 Wiley-VCH Verlag GmbH & Co. KGaA, Weinheim

ventional nitrogen-filled glove box. Solvents were refluxed over an appropriate drying agent and distilled under nitrogen prior to use. NMR spectra were recorded on Varian and Bruker spectrometers at ambient temperature. Commercially available chemicals were used as received. The starting material 2,6-dibenzoylpyridine,[9] the ligands $L^{dmp,Me}$ and $L^{dipp,Me}$ [19] and the complexes $[L^{dipp,Me}Rh^{I}Cl]$,[20] $[L^{dipp,Me}Co^{II}Cl_2]$, $[L^{dmp,Me}Co^{II}Cl_2]$,[19] $[L^{dipp,Me}Co^{I}Cl]$, $[L^{dipp,Me}Co^{I}CH_3]$, $[L^{dipp,Me}Co^{I}Bz]$ and $[L^{dipp,Me}Co^{I}CH_2SiMe_3]$[3] were synthesised according to literature procedures.

Methods: All calculations were carried out with the Turbomole program[21] coupled to the PQS Baker optimiser.[22] Geometries were fully optimised at the unrestricted ("singlet" or "triplet") b3-lyp level[23] level using the Turbomole SV(P) basis set on all atoms (pseudopotential basis on Co). For the smallest model system, improved final energies were then obtained from single-point calculations using a TZVPP basis and a fine ("m4") integration grid. Zero-point energy (ZPE) and thermal corrections were not included. Orbital plots were prepared using Molden.[24] For triplet states of a minimal model system ($R^1 = R^2 = H$, R = Cl, Me, H) Fermi contact terms were estimated using the Gaussian 98 package,[25] a LANL2DZ basis[26] for the metal atom, and the 6-31G* basis[27] for the ligand atoms.

$L^{dmp,Ph}$: 2,6-Dibenzoylpyridine (1.50 g, 5.23 mmol) and dimethylaniline (0.60 g, 4.96 mmol; 0.95 equiv.) were dissolved in benzene (50 mL). After the addition of a small amount of camphorsulfonic acid, the solution was refluxed overnight, using a Dean−Stark water trap. The solution was placed in the dark for a week over molecular sieves. Recrystallisation from hot methanol offered 0.30 g of yellow needles, which, according to GC analysis, consisted of 82% of the desired product together with 18% of the monocondensed product.

$L^{hex,Me}$: 2,6-Diacetylpyridine (1.00 g, 6.13 mmol) and *n*-hexylamine (1.245 g, 12.27 mmol, 2.0 equiv.) were dissolved in benzene (50 mL). After the addition of a small amount of camphorsulfonic acid, the solution was refluxed overnight, using a Dean−Stark water trap. The solvent was removed in vacuo, and 1.83 g (90.9%) of product was obtained as a yellow oil. ^{1}H NMR (200 MHz, $CDCl_3$): δ = 7.96 (d, $^3J_{H,H}$ = 7.7 Hz, 2 H, Py *H*β), 7.59 (t, $^3J_{H,H}$ = 7.7 Hz, 1 H, Py *H*γ), 3.42 (t, $^3J_{H,H}$ = 7.2 Hz, 4 H, hex *H*α), 2.29 (s, 6 H, N=C*Me*), 1.64 (quint, 4 H, $^3J_{H,H}$ = 7.2 Hz, hex *H*β), 1.26 (m, 12 H, hex *H*γδε), 0.80 (t, $^3J_{H,H}$ = 7.2 Hz, 6 H, hex *H*ζ) ppm. ^{13}C NMR (75 MHz, $CDCl_3$): δ = 166.33 (N=*C*), 156.26 (Py *C*α), 136.45 (Py *C*γ), 120.85 (Py *C*β), 52.57 (hex *C*α), 31.77, 30.81, 27.39, 22.65 (hex *C*β−ε), 14.05 (hex *C*ζ), 13.61 (N=C*Me*) ppm.

$L^{octadec,Me}$: 2,6-Diacetylpyridine (1.00 g, 6.13 mmol) and *n*-octadecylamine (3.30 g, 12.26 mmol, 2 equiv.) were dissolved in benzene (50 mL). After the addition of a small amount of acetic acid, the solution was refluxed overnight, using a Dean−Stark water trap. The solvent was removed in vacuo yielding a yellow oil, which solidified upon cooling with ice. The yield was 3.88 g (95%). ^{1}H NMR (200 MHz, $CDCl_3$): δ = 7.98 (d, $^3J_{H,H}$ = 7.7 Hz, 2 H, Py *H*β), 7.59 (t, $^3J_{H,H}$ = 7.7 Hz, 1 H, Py *H*γ), 3.43 (t, $^3J_{H,H}$ = 7.2 Hz, 4 H, octadec *H*α), 2.28 (s, 6 H, N=C*Me*), 1.66 (quint, 4 H, $^3J_{H,H}$ = 7.1 Hz, octadec *H*β), 1.25−0.90 (m, 60 H, octadec *H*γ-ρ), 0.80 (t, $^3J_{H,H}$ = 6.8 Hz, 6 H, octadec *H*ς) ppm. ^{13}C NMR (50 MHz, $CDCl_3$): δ = 167.0 (N=*C*), 156.9 (Py *C*α), 137.1 (Py *C*γ), 121.6 (Py *C*β), 53.3 (octadec *C*α), 32.6, 31.5, 30.4 (several), 30.1, 28.4, 23.3, 14.8 (octadec *C*β−ς), 14.3 (N=C*Me*) ppm.

$[L^{dmp,Ph}Co^{II}Cl_2]$: Part of the mixture of mono- and dicondensed dibenzoylpyridine (0.30 g containing 499 μmol of $L^{dmp,Ph}$) and $CoCl_2{\cdot}6H_2O$ (0.15 g, 630 mmol, 1.26 equiv.) were dissolved in 10 mL of THF. Almost immediately a colour change could be observed and a golden brown solid precipitated. After stirring for an additional hour at room temperature, this solid was filtered off, washed twice with THF (5 mL) and dried in vacuo. The yield was 0.195 g (63.8%). ^{1}H NMR (200 MHz, CD_2Cl_2): δ = 108.80 (2 H, Py *H*β), 37.45 (1 H, Py *H*γ), 6.04, 5.74, −1.37 (3 × 4 H, Ph $H_{o,m}$, dmp H_m), 3.20 (2 H, Ph H_p), −11.62 (2 H, dmp H_p), −26.99 (12 H, dmp *Me*) ppm.

$[L^{hex,Me}Co^{II}Cl_2]$: $L^{hex,Me}$ (2.16 g, 6.55 mmol) and $CoCl_2{\cdot}6H_2O$ (1.16 g, 4.87 mmol; 0.74 equiv.) were dissolved in 50 mL of THF and stirred for 15 min. The solvent was removed in vacuo, leaving 2.83 g (102%, presumably containing some residual THF) of the red-brown product. ^{1}H NMR (400 MHz, CD_2Cl_2): δ = 104.14 (2 H, Py *H*β), 71.35 (4 H, hex *H*α), 13.90 (1 H, Py *H*γ), −1.55 (6 H, hex *H*ζ), −3.25 (4 H, hex *H*ε), −5.12 (6 H, N=C*Me*), −7.12 (4 H, hex *H*δ), −12.88 (4 H, hex *H*γ), −39.74 (4 H, hex *H*β) ppm.

$[L^{octadec,Me}Co^{II}Cl_2]$: $L^{octadec,Me}$ (1.10 g, 1.65 mmol) and $CoCl_2{\cdot}6H_2O$ (0.39 g, 1.64 mmol, 1.0 equiv.) were dissolved in 20 mL of THF and stirred for an hour. The solvent was removed in vacuo, leaving 1.21 g (93%) of the red-brown product. ^{1}H NMR (200 MHz, CD_2Cl_2): δ = 106.0 (2 H, Py *H*β), 71.7 (4 H, octadec *H*α), 14.1 (1 H, Py *H*γ), −5.6 (6 H, N=C*Me*), 1.7, 1.4−0.8 (several), 0.5, 0.2, −1.6, −3.6, −7.1, −13.4, −41.1 (68 H, octadec, *H*β-ς) ppm.

$[L^{dipp,Me}Co^{I}H]$: This complex was generated in situ by addition of 2 mL of H_2 to an NMR sample of $[L^{dipp,Me}Co^{I}CH_2SiMe_3]$. ^{1}H NMR (300 MHz, C_6D_6): δ = 10.80 (t, $^3J_{H,H}$ = 7.8 Hz, 1 H, Py *H*γ), 7.60 (m, 4 H, Py *H*β, dipp H_p), 7.46 (d, $^3J_{H,H}$ = 7.8 Hz, 4 H, dipp H_m), 3.41 (sept, 4 H, $^3J_{H,H}$ = 6.9 Hz, C*H*Me$_2$), 1.31 and 0.29 (d, 12H each, $^3J_{H,H}$ = 6.9 Hz, CH*Me*$_2$), −1.65 (s, 6 H, N=C*Me*) ppm. ^{13}C NMR (100 MHz, C_6D_6): δ = 168.5 (N=*C*), 160.1 (dipp C_i), 156.5 (Py *C*α), 140.2 (dipp C_o), 126.3 (dipp C_p), 124.1 (dipp C_m), 123.6 (Py *C*β), 117.8 (Py *C*γ), 28.6 (*C*HMe$_2$), 25.4 (N=C*Me*), 23.3 and 22.5 (CH*Me*$_2$) ppm.

$[L^{dipp,Me}Co^{I}Et]$: This complex was generated in situ by addition of 2 mL of ethene to an NMR sample of $[L^{dipp,Me}Co^{I}H]$. ^{1}H NMR (300 MHz, C_6D_6): δ = 10.25 (t, $^3J_{H,H}$ = 7.5 Hz, 1 H, Py *H*γ), 7.99 (d, $^3J_{H,H}$ = 7.5 Hz, 2 H, Py *H*β), 7.52 (t, $^3J_{H,H}$ = 7.5 Hz, 2 H, dipp H_p), 7.39 (d, $^3J_{H,H}$ = 7.5 Hz, 4 H, dipp H_m), 3.13 (sept, 4 H, $^3J_{H,H}$ = 6.7 Hz, C*H*Me$_2$), 1.51 (q, 2 H, $^3J_{H,H}$ = 7.5 Hz, Co*CH*$_2$CH$_3$), 1.17 and 0.75 (d, 12H each, $^3J_{H,H}$ = 6.7 Hz, CH*Me*$_2$), −1.19 (t, $^3J_{H,H}$ = 7.5 Hz, 3 H, CoCH$_2$C*H*$_3$) −1.33 (s, 6 H, N=C*Me*) ppm. ^{13}C NMR (100 MHz, C_6D_6): δ = 165.3 (N=*C*), 157.9 (dipp C_i), 154.9 (Py *C*α), 140.9 (dipp C_o), 126.6 (dipp C_p), 124.1 (dipp C_m), 122.6 (Py *C*β), 117.6 (Py *C*γ), 28.3 (*C*HMe$_2$), 26.1 (N=C*Me*), 24.2 and 23.1 (CH*Me*$_2$) 12.8 CoCH$_2$*C*H$_3$ ppm. The signal for Co*C*H$_2$ was not observed.

$[L^{dmp,Me}Co^{I}CH_2SiMe_3]$: $[L^{dmp,Me}Co^{II}Cl_2]$ (0.276 g, 553 μmol) was added to a solution of $LiCH_2SiMe_3$ (0.115 g, 1.21 mmol; 2 equiv.) in 8 mL of hexane. The mixture was stirred for one hour, after which it was filtered. The filtrate was evaporated to dryness; the yield was not determined. ^{1}H NMR (200 MHz, C_6D_6): δ = 10.06 (t, $^3J_{H,H}$ = 7.8 Hz, 1 H, Py *H*γ), 7.71 (d, $^3J_{H,H}$ = 7.8 Hz, 2 H, Py *H*β), 7.34 (d, $^3J_{H,H}$ = 6.2 Hz, 2 H, dmp H_p), 7.26 (d, $^3J_{H,H}$ = 6.2 Hz, 4 H, dmp H_m), 0.80 (s, 2 H, Co*CH*$_2$), −0.63 (s, 9 H, Si*Me*$_3$), −1.28 (s, 6H N=C*Me*) ppm. The addition of H_2 to the NMR sample resulted in a colour change from deep red-purple to green and disappearance of all the complex-related ^{1}H NMR signals.

$[L^{dmp,Ph}Co^{I}CH_2SiMe_3]$: $[L^{dmp,Ph}Co^{II}Cl_2]$ (0.195 g, 313 μmol) was added to a solution of $LiCH_2SiMe_3$ (0.065 g, 684 μmol, 2.2 equiv.)

 © 2004 Wiley-VCH Verlag GmbH & Co. KGaA, Weinheim

in 5 mL of hexane. An immediate colour change to green was observed. After 2 h the mixture was filtered, and the filtrate was evaporated to dryness, yielding a green powder (yield not determined). ^{1}H NMR (200 MHz, C_6D_6): δ = 9.91 (t, $^3J_{H,H}$ = 8 Hz, 1 H, Py *H*γ) ppm. The rest of the peaks could not be unambiguously assigned. The addition of H_2 to the NMR sample resulted in disappearance of all the complex-related ^{1}H NMR signals.

[L^{hex,Me}Co^{I}CH$_2$SiMe$_3$]: A 1 M solution of $LiCH_2SiMe_3$ (1.6 mL, 1.60 mmol, 2.0 equiv.) in pentane and 8 mL of hexane were added to [L^{hex,Me}Co^{II}Cl$_2$] (0.45 g, 0.79 mmol). The mixture was stirred for one hour, after which it was filtered. The filtrate was evaporated to dryness, yielding 0.153 g of [L^{hex,Me}Co^{I}CH$_2$SiMe$_3$] (33.8%) as a thick dark-red oil. ^{1}H NMR (200 MHz, C_6D_6): δ = 9.72 (t, $^3J_{H,H}$ = 7.6 Hz, 1 H, Py *H*γ), 7.31 (d, $^3J_{H,H}$ = 7.6 Hz, 2 H, Py *H*β), 5.19 (t, $^3J_{H,H}$ = 7.6 Hz, 4 H, hex *H*α), 2.22 (quint, $^3J_{H,H}$ = 7.6 Hz, 4 H, hex *H*β), 1.54 (quint, $^3J_{H,H}$ = 7.6 Hz, 4 H, hex *H*γ), 1.22 (m, 8 H, hex *H*δ, ε), 0.82 (t, $^3J_{H,H}$ = 7.2 Hz, 6 H, hex *H*ζ), 0.02 (s, 2 H, CoC*H*$_2$), −0.14 (s, 9 H, Si*Me*$_3$), −0.18 (s, 6 H, N=C*Me*) ppm. ^{13}C NMR (75 MHz, C_6D_6): 162.42 (N=*C*), 152.18 (Py *C*α), 122.50 (Py *C*β), 114.01 (Py *C*γ), 59.35 (hex *C*α), 32.20 and 22.89 (hex *C*δ, ε), 29.08 and 27.36 (hex *C*β, γ), 20.39 (N=C*Me*), 14.21 (hex *C*ζ), 3.00 (Si*Me*$_3$) ppm. The signal for Co*C*H$_2$ was not found. The addition of H_2 to the ^{1}H NMR sample resulted in a colour change from dark red to green-brown and a loss of all the complex-related ^{1}H NMR signals.

[L^{octadec,Me}Co^{I}CH$_2$SiMe$_3$]: A 1 M solution of $LiCH_2SiMe_3$ (0.90 mL, 900 μmol, 2.45 equiv.) in pentane and 8 mL of hexane were added to [L^{octadec,Me}Co^{II}Cl$_2$] (0.292 g, 368 μmol). The mixture was stirred for two hours, after which it was filtered, and the solvent was removed in vacuo leaving a deep purple-red product. ^{1}H NMR (400 MHz, C_6D_6): δ = 9.71 (t, $^3J_{H,H}$ = 7.6 Hz, 1 H, Py *H*γ), 7.31 (d, $^3J_{H,H}$ = 7.6 Hz, 2 H, Py *H*β), 5.21 (t, $^3J_{H,H}$ = 7.6 Hz, 4 H, octadec *H*α), 2.26 (quint, $^3J_{H,H}$ = 7.6 Hz, 4 H, octadec *H*β), 1.59 (quint, $^3J_{H,H}$ = 7.2 Hz, 4 H, octadec *H*γ), 1.5−1.1 (m, 56 H, octadec *H*δ−ρ) ppm. octadec *H*ς is presumably obscured by the resonance of traces of hexane. The signals for Co*C*H$_2$, Si*Me*$_3$ and N=C*Me* could not be unambiguously assigned.

[L^{dipp,Me}Rh^{I}CH$_3$]: Toluene (2 mL) was added to a mixture of [L^{dipp,Me}Rh^{I}Cl] (100 mg, 0.16 mmol) and MeLi (7.1 mg, 0.32 mmol, 2 equiv.) and the reaction mixture was stirred for three days. The obtained product was filtered off and the filtrate was evaporated to dryness, yielding 91 mg of [L^{dipp,Me}Rh^{I}CH$_3$] (84%) as a dark green solid. ^{1}H NMR (300 MHz, C_6D_6): δ = 8.19 (t, $^3J_{H,H}$ = 7.9 Hz, 1 H, Py *H*γ), 7.34 (d, $^3J_{H,H}$ = 7.7 Hz, 2 H, Py *H*β), 7.22−7.10 (m, 6 H, dipp *H*$_{m,p}$), 3.19 (sept., 4 H, $^3J_{H,H}$ = 6.8 Hz, *CH*Me$_2$), 2.12 (d, $^2J_{RhH}$ = 1.1 Hz, 3 H, Rh*Me*), 0.99 (m, 24 H, CH*Me*$_2$), 0.73 (s, 6 H, N=C*Me*) ppm. ^{13}C NMR (75 MHz, C_6D_6): δ = 166.8 (N=*C*), 155.3 (d, $^2J_{RhC}$ = 2.7 Hz, Py *C*α), 148.3 (dipp *C*$_i$), 140.6 (Py *C*γ), 140.4 (dipp *C*$_o$), 123.6 (dipp *C*$_m$), 123.1 (Py *C*β), 28.2 (*C*HMe$_2$), 23.9 and 23.6 (CH*Me*$_2$), 18.9 (N=C*Me*), 1.2 (d, $^1J_{RhC}$ = 21.0 Hz, Rh*Me*) ppm. dipp *C*$_p$ is presumably obscured by the resonance of the C_6D_6 solvent.

[L^{dipp,Me}Rh^{I}Bz]: Toluene (2 mL) was added to a mixture of [L^{dipp,Me}Rh^{I}Cl] (100 mg, 0.27 mmol) and Bz_2Mg (41 mg, 0.27 mmol, 1 equiv.). The mixture was stirred for 24 h. The magnesium salts were separated from the reaction products by filtration and the filtrate was evaporated to dryness, yielding a purple powder. Hexane (5 mL) was added, the mixture was filtered and the filtrate was evaporated to dryness, yielding [L^{dipp,Me}Rh^{I}Bz] as a purple powder. ^{1}H NMR (C_6D_6, 200 MHz): δ = 7.97 (t, $^3J_{H,H}$ = 7.9 Hz, 1 H, Py *H*γ), 7.31−7.17 (m, 8 H, dipp *H*$_{m,p}$, Py *H*β), 7.21 (t, $^3J_{H,H}$ = 7.3 Hz, 2 H, Bz *H*$_m$), 6.65 (m, 1 H, Bz *H*$_p$), 5.59 (d, $^3J_{H,H}$ = 6.9 Hz, 2 H, Bz *H*$_o$), 3.69 (d, $^2J_{RhH}$ = 2.6 Hz, 2 H, RhC*H*$_2$), 3.17 (sept., 4 H, $^3J_{H,H}$ = 6.8 Hz, *CH*Me$_2$), 1.01−0.92 (m, 30 H, N=C*Me*, CH*Me*$_2$) ppm. ^{13}C NMR (C_6D_6 75 MHz): δ = 166.8 (d, $^2J_{RhC}$ = 2.3 Hz, N=*C*), 156.2 (d, $^2J_{RhC}$ = 2.9 Hz, Py *C*α), 151.9 (d, $^2J_{RhC}$ = 1.7 Hz, Bz *C*$_i$), 148.4 (dipp *C*$_i$), 141.0 (Py *C*γ), 140.6 (dipp *C*$_o$), 127.3 (Bz *C*$_o$), 127.0 (Bz *C*$_m$), 126.5 (dipp *C*$_p$), 124.2 (dipp *C*$_m$), 123.6 (Py *C*β), 119.6 (Bz *C*$_p$), 28.6 (*C*HMe$_2$), 24.0 and 23.8 (CH*Me*$_2$), 19.5 (d, $^3J_{RhC}$ = 1.7 Hz, N=C*Me*) ppm. The Rh*C*H$_2$ signal was not detected.

[L^{dipp,Me}Rh^{I}CH$_2$SiMe$_3$]: A 1.0 M solution of $LiCH_2SiMe_3$ in pentane (0.54 mL 0.54 mmol, 2 equiv.) and 4 mL of toluene were added to [L^{dipp,Me}Rh^{I}Cl] (170 mg, 0.27 mmol, 1 equiv.). The mixture was stirred for 24 h. The solvent was removed in vacuo, yielding a green-brown powder. Hexane (5 mL) was added, the mixture was filtered and the filtrate was evaporated to dryness, yielding [L^{dipp,Me}Rh^{I}CH$_2$SiMe$_3$] as a green powder. ^{1}H NMR (C_6D_6, 300 MHz): δ = 8.06 (t, $^3J_{H,H}$ = 7.9 Hz, 1 H, Py *H*γ), 7.24 (d, $^3J_{H,H}$ = 8.1 Hz, 2 H, Py *H*β), 7.15−7.03 (m, 6 H, dipp *H*$_{m,p}$), 3.26 (sept., $^3J_{H,H}$ = 6.8 Hz, 4 H, *CH*Me$_2$), 1.87 (d, $^2J_{Rh;H}$ = 2.2 Hz, 2 H, RhC*H*$_2$), 1.28 and 0.97 (2 × d, $^3J_{H,H}$ = 6.6 Hz, 12 H each, CH*Me*$_2$), 0.86 (s, 6 H, N=C*Me*), 0.29 (s, 9 H, Si*Me*$_3$) ppm. ^{13}C NMR (C_6D_6 75 MHz): δ = 165.8 (d, $^2J_{RhC}$ = 0.9 Hz, N=*C*), 156.3 (d, $^2J_{RhC}$ = 3.2 Hz, Py *C*α), 149.4 (dipp *C*$_i$), 141.1 (Py *C*γ), 140.6 (dipp *C*$_o$), 126.7 (dipp *C*$_p$), 124.3 (dipp *C*$_m$), 123.6 (Py *C*β), 28.2 (*C*HMe$_2$), 24.5 and 24.3 (CH*Me*$_2$), 19.9 (d, $^3J_{Rh,C}$ = 2.0 Hz, N=C*Me*), 6.7 (d, $^1J_{Rh,C}$ = 33.0 Hz, Rh*C*H$_2$), 4.0 (Si*Me*$_3$) ppm.

[1] Selected examples of square-planar Co^{I} complexes [all except ref.[1f] with tetradentate and fairly rigid ligands]. Bis(salicylideneiminato): [1a] F. Arena, C. Floriani, A. Chiesi-Villa, C. Guastini, *Inorg. Chem.* **1986**, *25*, 4589. [1b] S. Gambarotta, F. Arena, C. Floriani, P. F. Zanazzi, *J. Am. Chem. Soc.* **1982**, *104*, 5082. [1c] G. Fachinetti, C. Floriani, P. F. Zanazzi, A. R. Zanari, *Inorg. Chem.* **1979**, *18*, 3469. Porphyrinato: [1d] P. Doppelt, J. Fischer, R. Weiss, *Inorg. Chem.* **1984**, *23*, 2958. Phthalocyaninato: [1e] H. Huckstadt, H. Homborg, *Z. Anorg. Allg. Chem.* **1998**, *624*, 715. Bis(imino)succinonitrile: [1f] S.-M. Peng, D.-S. Liaw, Y. Wang, A. Simon, *Angew. Chem. Int. Ed. Engl.* **1985**, *24*, 210. Miscellaneous: [1g] Y.-S. You, G.-H. Lee, S.-M. Peng, *J. Chin. Chem. Soc. (Taipei)* **1996**, *43*, 261.

[2] Co^{I} is more often tetrahedral. Selected examples (without ligand constraints): L_4Co^+: [2a] N. Lu, N. C. Norman, A. G. Orpen, M. J. Quayle, P. L. Timms, G. R. Whittell, *J. Chem. Soc., Dalton Trans.* **2000**, 4032. [L_3CoCl]: [2b] R. A. Jones, A. L. Stuart, J. L. Atwood, W. E. Hunter, *J. Crystallogr. Spectrosc. Res.* **1983**, *13*, 273. One of the few examples with nitrogen donors is [(tpz)Co(CO)]: [2c] J. L. Detrich, R. Konecny, W. M. Vetter, D. Doren, A. L. Rheingold, K. H. Theopold, *J. Am. Chem. Soc.* **1996**, *118*, 1703.

[3] [3a] V. C. Gibson, M. Humphries, K. Tellmann, D. Wass, A. J. P. White, D. J. Williams, *Chem. Commun.* **2001**, 2252. [3b] T. M. Kooistra, Q. Knijnenburg, J. M. M. Smits, A. D. Horton, P. H. M. Budzelaar, A. W. Gal, *Angew. Chem. Int. Ed.* **2001**, *40*, 4719.

[4] S. Nuckel, P. Burger, *Organometallics* **2001**, *20*, 4345.

[5] E. L. Dias, M. Brookhart, P. S. White, *Organometallics* **2000**, *19*, 4995.

[6] P. Margl, L. Deng, T. Ziegler, *Organometallics* **1999**, *18*, 5701.

[7] B. de Bruin, E. Bill, E. Bothe, T. Weyhermuller, K. Wieghardt, *Inorg. Chem.* **2000**, *39*, 2936.

[8] P. H. M. Budzelaar, B. de Bruin, A. W. Gal, K. Wieghardt, J. H. Van Lenthe, *Inorg. Chem.* **2001**, *40*, 4649.

[9] N.-E. Andersson, T. O. Soine, *J. Am. Pharm. Ass.* **1950**, *39*, 463.

[10] Burger reported that non-planar structures also form easily for Rh and Ir and are sometimes even preferred.[4] However, in

 © 2004 Wiley-VCH Verlag GmbH & Co. KGaA, Weinheim

that case they do not become planar when allowed to go unrestricted, and indeed there is no unrestricted solution lower than the restricted one.

[11] Compare for example, $[(dmg)_2Co(CH_2SiMe_3)(py)]$, where Co−C = 2.031 Å: [11a] L. Randaccio, N. Bresciani-Pahor, P. J. Toscano, L. G. Marzilli, *J. Am. Chem. Soc.* **1981**, *103*, 6347; with $[(dmg)_2Co(Me)(im)]$, where Co−C = 1.986 Å: [11b] V. Pattabhi, M. Nethaji, E. J. Gabe, F. L. Lee, Y. le Page, *Acta Crystallogr., Sect. C* **1984**, *40*, 1155.

[12] [12a] Usually, unrestricted solutions with $S^2 = 1$ correspond to small singlet-triplet gaps.[13f] However, if the preference of the "pure" singlet for a biradical structure is strong enough, full mixing (leading to $S^2 \approx 1$) will occur also for larger singlet-triplet separations. Apparently, that is the case here. [12b] Noodleman uses Equation (1′), which is similar to Equation (1) but has $\hat{S}_1^2$ set to the ideal value of 2;[13a−13c] Bachler uses a similar expression.[13d,13e]

$$\varepsilon_S \approx \frac{2\varepsilon_0 - S_0^2\varepsilon_1}{2 - S_0^2} \qquad (1')$$

Spin contamination is always present in both the U_0 and U_1 solutions. Contamination of U_0 skews the result of Equation (1′) towards larger gaps. We prefer Equation (1) because it treats spin contamination in U_0 and U_1 on an equal basis. In any case, results obtained with Equation (1′) would differ only marginally from the ones we calculate with Equation (1).

[13] [13a] L. Noodleman, J. G. Norman, *J. Chem. Phys.* **1979**, *70*, 4903. [13b] L. Noodleman, *J. Chem. Phys.* **1981**, *74*, 5737. [13c] L. Noodleman, E. J. Baerends, *J. Am. Chem. Soc.* **1984**, *106*, 2316. [13d] V. Bachler, P. Chaudhuri, K. Wieghardt, *Chem. Eur. J.* **2001**, *7*, 404. [13e] V. Bachler, G. Olbrich, F. Neese, K. Wieghardt, *Inorg. Chem.* **2002**, *41*, 4179. [13f] T. Onishi, Y. Takano, Y. Kitagawa, T. Kawakami, Y. Yoshioka, K. Yamaguchi, *Polyhedron* **2001**, *20*, 1177.

[14] H. Sugiyama, G. Aharonian, S. Gambarotta, G. P. A. Yap, P. H. M. Budzelaar, *J. Am. Chem. Soc.* **2002**, *124*, 12268.

[15] M. D. Fryzuk, D. B. Leznoff, R. C. Thompson, S. J. Rettig, *J. Am. Chem. Soc.* **1998**, *120*, 10126.

[16] We tentatively explain this somewhat counterintuitive result as follows. Initially, the diiminopyridine ligand has two low-lying acceptor orbitals, which we here denote π^*_{xz} and π^*_{yz} for their association with the corresponding Co 3d orbitals. π^*_{yz} is slightly higher in energy, but its overlap with Co $3d_{yz}$ is larger. Back-donation to both orbitals is possible. The CF_3 groups stabilize π^*_{yz} because that orbital has a larger density on the imine groups. In the singlet state, this results in more back-donation to π^*_{yz} at the expense of π^*_{xz}. In the triplet state, however, one full electron has already been transferred into π^*_{xz}, so further back-donation into π^*_{yz} is difficult.

[17] S. Al-Benna, M. J. Sarsfield, M. Thornton-Pett, D. L. Ormsby, P. J. Maddox, P. Brès, M. Bochmann, *J. Chem. Soc., Dalton Trans.* **2000**, 4247.

[18] Calculated at the UB3LYP/6-31G* level, see refs.[25−27]

[19] [19a] B. L. Small, M. Brookhart, A. M. A. Bennett, *J. Am. Chem. Soc.* **1998**, *120*, 4049. [19b] G. J. P. Britovsek, V. C. Gibson, B. S. Kimberley, P. J. Maddox, S. J. McTavish, G. A. Solan, A. J. P. White, D. J. Williams, *Chem. Commun.* **1998**, 849. [19c] B. L. Small, M. Brookhart, *J. Am. Chem. Soc.* **1998**, *120*, 7143. [19d] G. J. P. Britovsek, M. Bruce, V. C. Gibson, B. S. Kimberley, P. J. Maddox, S. Mastroianni, S. J. McTavish, C. Redshaw, G. A. Solan, S. Strömberg, A. J. P. White, D. J. Williams, *J. Am. Chem. Soc.* **1999**, *121*, 8728.

[20] H. F. Haarman, J. M. Ernsting, M. Kranenburg, H. Kooijman, N. Veldman, A. L. Spek, P. W. N. M. van Leeuwen, K. Vrieze, *Organometallics* **1997**, *16*, 887.

[21] [21a] R. Ahlrichs, M. Bär, H.-P. Baron, R. Bauernschmitt, S. Böcker, M. Ehrig, K. Eichkorn, S. Elliott, F. Furche, F. Haase, M. Häser, C. Hättig, H. Horn, C. Huber, U. Huniar, M. Kattannek, A. Köhn, C. Kölmel, M. Kollwitz, K. May, C. Ochsenfeld, H. Öhm, A. Schäfer, U. Schneider, O. Treutler, K. Tsereteli, B. Unterreiner, M. Von Arnim, F. Weigend, P. Weis, H. Weiss, Turbomole Version 5, January **2002**. Theoretical Chemistry Group, University of Karlsruhe. [21b] O. Treutler, R. Ahlrichs, *J. Chem. Phys.* **1995**, *102*, 346.

[22] [22a] PQS version 2.4, 2001, Parallel Quantum Solutions, Fayetteville, Arkansas, USA (the Baker optimiser is available separately from PQS upon request). [22b] J. Baker, *J. Comput. Chem.* **1986**, *7*, 385.

[23] [23a] C. Lee, W. Yang, R. G. Parr, *Phys. Rev. B* **1988**, *37*, 785. [23b] A. D. Becke, *J. Chem. Phys.* **1993**, *98*, 1372. [23c] A. D. Becke, *J. Chem. Phys.* **1993**, *98*, 5648. [23d] All calculations were performed using the Turbomole functional "b3-lyp", which is not identical to the Gaussian "B3LYP" functional.

[24] G. Schaftenaar, J. H. Noordik, *J. Comput.-Aided Mol. Design* **2000**, *14*, 123.

[25] Gaussian 98, Revision A.9: M. J. Frisch, G. W. Trucks, H. B. Schlegel, G. E. Scuseria, M. A. Robb, J. R. Cheeseman, V. G. Zakrzewski, J. A. Montgomery Jr., R. E. Stratmann, J. C. Burant, S. Dapprich, J. M. Millam, A. D. Daniels, K. N. Kudin, M. C. Strain, O. Farkas, J. Tomasi, V. Barone, M. Cossi, R. Cammi, B. Mennucci, C. Pomelli, C. Adamo, S. Clifford, J. Ochterski, G. A. Petersson, P. Y. Ayala, Q. Cui, K. Morokuma, D. K. Malick, A. D. Rabuck, K. Raghavachari, J. B. Foresman, J. Cioslowski, J. V. Ortiz, A. G. Baboul, B. B. Stefanov, G. Liu, A. Liashenko, P. Piskorz, I. Komaromi, R. Gomperts, R. L. Martin, D. J. Fox, T. Keith, M. A. Al-Laham, C. Y. Peng, A. Nanayakkara, M. Challacombe, P. M. W. Gill, B. Johnson, W. Chen, M. W. Wong, J. L. Andres, C. Gonzalez, M. Head-Gordon, E. S. Replogle, J. A. Pople, Gaussian, Inc., Pittsburgh PA, **1998**.

[26] J. P. Hay, W. R. Wadt, *J. Chem. Phys.* **1985**, *82*, 2999.

[27] [27a] W. J. Hehre, R. Ditchfield, J. A. Pople, *J. Chem. Phys.* **1972**, *56*, 2257. [27b] P. C. Hariharan, J. A. Pople, *Chem. Phys. Lett.* **1972**, *16*, 217. [27c] P. C. Hariharan, J. A. Pople, *Theoret. Chim. Acta* **1973**, *28*, 213.

Received August 15, 2003
Early View Article
Published Online February 10, 2004

 © 2004 Wiley-VCH Verlag GmbH & Co. KGaA, Weinheim

Quantum Chemical Studies of Neutral and Ionized DyX, DyX_2, and DyX_3 Species (X = F, Cl, Br, I) and the Implications for the Mass Spectra of Gaseous DyX_3

Julia Saloni,[a,d] Szczepan Roszak,*[a] Klaus Hilpert,[b] Mirosław Miller,[c] and Jerzy Leszczynski[d]

Keywords: Halides / Lanthanides / Mass spectrometry / Quantum chemical calculations / Thermochemistry

The mass spectrum pattern of DyF_3(g) and the appearance potentials for identified ions were measured and compared with the respective data obtained previously for $DyCl_3$, $DyBr_3$, and DyI_3. The structural parameters, total energies, and vibrational frequencies of DyX_3, DyX_2, and DyX (X = F, Cl, Br, I) neutral and single ionized species were determined by quantum-chemical studies. The theoretical appearance potentials of different ions, calculated from energies of gaseous species, are in the good agreement with the experimental data. Fragmentation energies of the DyX_n^+ ion, where n = 1, 2, 3, were computed and compared with the mass spectra patterns of the respective vapour species. A theoretical electron population analysis indicates the involvement of the s and f valence electrons of Dy in the bond formation as well as in the ionization processes. The σ-back donation from halogen atoms to the dysprosium center partially compensates the electron density loss. The ionization strengthens the bonding in the DyX and DyX_2 molecules. The ionization of DyX_3 destroys the C_{3v} symmetrical structure due to the Jahn–Teller effect. Contrary to the other studied systems, the open shell character of DyX_3^+ arises not only from unpaired electrons of dysprosium but also from electron density on halogen atoms.

(© Wiley-VCH Verlag GmbH & Co. KGaA, 69451 Weinheim, Germany, 2004)

Introduction

Knudsen effusion mass spectrometric studies of metal halide vapors show evidence for the significant fragmentation of gaseous species due to the electron bombardment used for the ionization. The mechanism of the ionization and fragmentation processes leading to the formation of particular ions recorded in the mass spectra is poorly understood. The molecular structures and the bonding nature of the species taking part in such processes are not directly available experimentally, and supplementary theoretical data is usually scarce. The few combined experimental and theoretical studies (e.g. ref.[1]) that exist allow a discussion of the energetic considerations and a quantitative analysis of fragmentation data.[2,3] Unfortunately, experimental mass spectra for metal halides published in the literature depend, to some extent, on the construction of the ion source of the mass spectrometer and on the energy of the ionising electrons. In order to correlate the theoretical predictions of the mass spectrum patterns with experimental data, the "true" mass spectra, obtained by the integration of peak areas, not by recording their intensities, should be taken into account.[4] In spite of this, mass spectra of gaseous metal halides recorded by different authors show similar characteristic trends for the ion intensities. The highest thermodynamic stability is not necessarily the most important condition for that particular ion to be the most abundant in the mass spectrum. However, the structures, bonding, and the charge distribution of ions formed upon ionization/fragmentation processes should, to some extent, correlate with the mass spectrum. Moreover, as was shown previously,[1,3] the thermochemical stability of neutral species and ions can be used for the elucidation of the fragmentation behavior of gaseous species. The above considerations motivated the analysis of the structural and thermochemical properties of gaseous species obtained by experimental and theoretical approaches for metal halide systems presented in this work. The recent development of quantum chemical methods has resulted in the efficient sup-

[a] Institute of Physical and Theoretical Chemistry, Wroclaw University of Technology,
Wybrzeże Wyspiańskiego 27, 50-370 Wroclaw, Poland
Fax: (internat.) +48-71-320-3364
E-mail: roszak@mml.ch.pwr.wroc.pl
[b] Research Center Jülich, Institute for Materials and Processes in Energy Systems,
52425 Jülich, Germany
[c] Institute of Inorganic Chemistry and Metallurgy of Rare Elements, Wroclaw University of Technology,
Wybrzeże Wyspiańskiego 27, 50−370 Wroclaw, Poland
[d] Computational Center for Molecular Structure and Interactions, Jackson State University,
Jackson, MS 39217, USA

port of the theory of mass spectra in organic chemistry (e.g. ref.[5]). To the best of our knowledge, such studies for metal halide vapors are yet to be performed.

In the present study we report an experimental and quantum chemical analysis of neutral and ionic species detected upon studying the vaporization of DyX_3 by Knudsen effusion mass spectrometry. The vaporization of dysprosium halides has been investigated by different methods. Brunetti et al.[6] and Kapala et al.[7] have published a comparison of thermodynamic data reported in the literature. Recently, the vaporization thermodynamics of $DyCl_3$,[7,8] $DyBr_3$,[9] and DyI_3 [10] were investigated by means of Knudsen effusion mass spectrometry using different equipment and experimental conditions. The ion-molecule reactions in the $DyCl_3$ vapors were studied as well.[8] The mass spectrometric analysis of DyF_3 vapors performed in the present work complements our previous investigations.[7,9,10] The vapors of DyX_3 are predominantly monomeric, although mass spectrometric studies show evidence for dimeric,[7−10] trimeric,[8,10] or even tetrameric[8] species. In the past few years several quantum chemical studies have been carried out on gaseous lanthanide halides. The structures of monomeric[7,11−13] and dimeric[7,14] complexes of LnX_3 and other properties, including vibrational modes, have been presented. The results of the calculations were used for the interpretation of experimental infrared spectra of the gaseous phase[12] and for the estimation of the thermodynamic functions of gaseous species required for the third law treatment of equilibrium partial pressures.[7]

In the present work the theoretical structures and vibrational frequencies of DyX_3^+ molecular ions and their fragments (DyX_2^+, DyX^+) are reported. Their ionization potentials and appearance potentials were also calculated and compared with the values determined experimentally. The nature of the chemical bonding was studied applying Mulliken and natural bond orbital (NBO) electron population analysis. This information on structures, stabilities, and dissociation energies of gaseous ions is a significant step toward the better understanding of ionization and fragmentation processes in metal halide vapors and should thereby allow the prediction of their mass spectra.

Results

Mass Spectrometric Investigations

The mass spectrum of the DyF_3 vapors was recorded over a temperature range of 1208−1587 K. Table 1 shows the mass spectral data of gaseous DyF_3 interpolated for 1430 K. The data for gaseous DyX_3, where X = Cl, Br, I; obtained in previous studies are shown in Table 1 as well. The ionization of DyX_3 species by electron bombardment results, in addition to molecular ions, in the formation of DyX_n^+ fragments, where n = 0−2. Such fragmentation paths are generally characteristic for metal halide molecules (e.g. ref.[15]). The increasing fragmentation of gaseous DyX_3 on going from iodide to fluoride can easily be seen from the data in Table 1, despite the fact that they obtained with different spectrometers, at different temperatures, and with different energies of ionizing electrons. The same regularity can be seen for other metal halides.[15]

Table 1. Experimental mass spectra of the gaseous DyX_3 species

DyX_3	E_{el} (eV)	T (K)	DyX_3^+	DyX_2^+	DyX^+	Dy^+	Ref.
DyF_3	34	1430	0.50	100	20	19	this work
$DyCl_3$	50	1000	13.7	100	10.9	19.9	[7]
$DyCl_3$	25	1008	12.4	100	16.7	5.9	[8]
$DyBr_3$	15	1053	24.8	100	13.6	–	[9]
DyI_3	15	1053	69.9	100	–	–	[10]

Figure 1 shows the ionization efficiency curves (IEC) obtained for the different ions detected in DyF_3 vapors. Table 2 summarizes the appearance potentials obtained from the IEC curves for the ionic species of mass spectra recorded for different DyX_3 compounds. As expected, the ionization potentials of gaseous DyX_3 and the respective appearance potentials of the fragment ions increase on going from dysprosium iodide to dysprosium fluoride. However, the respective values for $DyCl_3$ and $DyBr_3$ are very similar in every case. The ionization and appearance potentials obtained experimentally should only be considered as an upper limit to the adiabatic values.[16]

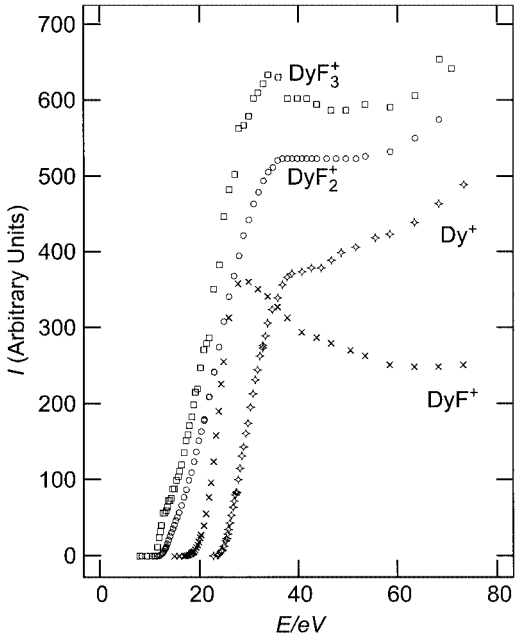

Figure 1. Ionization efficiency curves obtained for ions coming from DyF_3(g)

Theoretical Studies

The computed geometries, vibrational frequencies, and charge and spin densities on the Dy atom obtained for the neutral and ionized DyX (Table 3), DyX_2 (Table 4), and DyX_3 (Table 5) species are shown below. The bond length in DyX decreases significantly after the electron is removed (Table 3). The increased bond strength is indicated by a

 © 2004 Wiley-VCH Verlag GmbH & Co. KGaA, Weinheim

Table 2. Experimental and theoretical ionization potentials and appearance potentials (in eV) of ions detected in the mass spectra of the DyX_3 vapors

DyX_3	Ref.(exp.)	IP (DyX_3) exp.	IP (DyX_3) theor.	AP (DyX_2^+) exp.	AP (DyX_2^+) theor.	AP (DyX^+) exp.	AP (DyX^+) theor.	AP (Dy^+) exp.	AP (Dy^+) theor.
DyF_3	this work	11.1	12.68	12.5	13.05	19.3	16.62	24.9	22.36
$DyCl_3$	[8]	10.0	10.42	11.4	11.87	15.1	14.49	20.1	18.06
$DyBr_3$	[9]	10.4	9.68	11.2	11.22	14.8	14.52	20.1	16.31
DyI_3	[24]	9.6	8.87	10.4	10.41	12.9	11.96	16.0	14.32

blue-shift of the stretching vibrations in the cations relative to the parent molecules. Spin-density calculations for DyX indicate four f and one s unpaired electrons on Dy. The ionization removes the nonbonding s electron and leads to an increase in the Coulomb interactions in the cation. Only the single valence electron from the s shell is involved in the Dy−X bond; the ionization removes the second one (Table 6). The charge transfer of 0.703 electrons from Dy to the halogen atom is not affected by the ionization process, indicating that the bond strength is enhanced mostly due to the increase in the ionic contribution.

The bonding in DyX_2 moieties is similar to that observed in DyX; the bond lengths are again shorter in the cations. The increasing strength of the bonds is confirmed by the blue-shifted stretching vibrational modes (Table 4). The polarization of the electronic density of the chemical bonds is similar to that in DyX. The charge transfer in the DyX_2 molecule is approximately double that in DyX. The spin-density analysis in the molecule as well as in the cation indicates the almost exclusive localization of the open-shell electrons on Dy. The ionization removes an electron from the f orbital; however, the loss of electronic density at the metal is compensated by the σ-back-donation of electrons from the halogens to the d and p valence-orbitals of dysprosium. The total atomic charge on the Dy center in $DyCl_2^+$ amounts to only 1.939 electrons (Table 6). The value of the positive charge localized on the central atom is consistent with the first two ionization potentials of Dy (5.927 eV and 11.67 eV).[17] The direct ionization of the f electron would involve about 20 eV (the third ionization potential of Dy is 22.8 eV [17]). A rearrangement of the electronic density on Dy is observed instead, and the loss of valence electrons from the f orbital of Dy is accompanied by σ-back-donation from the halogens.

The DyX_3 molecules follow trends observed in smaller compounds. The structures with C_{3v} symmetry are almost planar (Table 5). The experimental bond lengths are well reproduced by the present calculations.[18−20] The available vibrational frequencies for $DyCl_3$ (58, 85, 328, 340 cm^{-1} [18]) are in excellent agreement with the calculated values (56, 82, 331, 344 cm^{-1}). The Mulliken spin densities indicate the localization of unpaired electrons exclusively on the Dy atom, and the electron transfer from Dy to the halogen atoms is only slightly lower than the values of charge transfers in the DyX and DyX_2 molecules. However, the orbital electronic distribution on Dy is similar to that on the DyX_2^+ cation but not to its neutral precursors DyX and

Table 3. Theoretical bond lengths (r_e), stretching frequencies ($\tilde{\nu}_1$), total atomic charges (q) and atomic spin densities on dysprosium atoms in neutral and ionized DyX species

DyX	Electronic state molecule	Electronic state cation	r_e (Å) molecule	r_e (Å) cation	q(Dy) (electrons) molecule	q(Dy) (electrons) cation	Spin density (Dy) molecule	Spin density (Dy) cation	$\tilde{\nu}_1$ (cm^{-1}) molecule	$\tilde{\nu}_1$ (cm^{-1}) cation
DyF	6	5	2.020	1.971	0.632	1.707	5.110	4.009	497.9	581.1
DyCl	6	5	2.565	2.437	0.702	1.683	5.094	4.006	272.7	338.9
DyBr	6	5	2.711	2.586	0.724	1.653	5.041	4.004	180.9	236.2
DyI	6	5	2.969	2.809	0.702	1.579	5.024	4.013	139.5	179.8

Table 4. Theoretical bond lengths (r_e), bond angle (X−Dy−X), vibrational frequencies ($\tilde{\nu}$), total atomic charges (q) and atomic spin densities on the dysprosium atom in neutral and positively charged DyX_2 moieties

DyX_2	Electronic state molecule	Electronic state cation	r_e (Å) molecule	r_e (Å) cation	X−Dy−X (°) molecule	X−Dy−X (°) cation	q(Dy) (electrons) molecule	q(Dy) (electrons) cation	Spin density (Dy) molecule	Spin density (Dy) cation	$\tilde{\nu}$ (cm^{-1}) molecule	$\tilde{\nu}$ (cm^{-1}) cation
DyF_2	5	6	2.047	1.916	123.9	113.3	1.437	2.108	3.922	4.935	487.2	668.1 (ν_1)
											147.4	71.1 (ν_2)
											504.1	626.7 (ν_3)
$DyCl_2$	5	6	2.549	2.360	131.3	123.3	1.525	1.938	4.006	4.897	274.3	386.3 (ν_1)
											69.7	55.3 (ν_2)
											287.8	392.1 (ν_3)
$DyBr_2$	5	6	2.711	2.506	138.1	116.3	1.495	1.901	4.011	4.914	174.9	250.7 (ν_1)
											35.5	40.6 (ν_2)
											206.9	294.4 (ν_3)
DyI_2	5	6	2.938	2.799	143.6	140.7	1.417	1.742	4.019	4.652	127.4	122.3 (ν_1)
											27.3	28.4 (ν_2)
											169.3	350.6 (ν_3)

 © 2004 Wiley-VCH Verlag GmbH & Co. KGaA, Weinheim

Table 5. Theoretical (r_e) and experimental (r_g) bond lengths, bond angle (X−Dy−X), total atomic charges (q) and atomic spin densities on the dysprosium atom in neutral and ionized DyX_3 species

DyX_3	Electronic state molecule	cation	R (Å) molecule[a]	cation[b]	X−Dy−X (°) molecule	cation[c]	q(Dy) (electrons) molecule	cation	Spin density (Dy) molecule	cation
DyF_3	6	5	2.012 2.09[d] 2.02[e]	1.918 (2.118)	119.9	121.2 (56.2)	2.000	2.057	4.973	3.045
$DyCl_3$	6	5	2.447 2.49[d] 2.47[e] 2.461[f]	2.335 (2.518)	118.9	113.3 (66.0)	1.810	1.785	4.983	4.982
$DyBr_3$	6	5	2.604 2.615[e] 2.609[f]	2.517 (2.673)	120.0	118.3 (69.2)	1.799	1.741	4.972	4.969
DyI_3	6	5	2.820 2.818[e]	2.758 (2.893)	120.0	122.5 (72.5)	1.644	1.600	4.941	4.886

[a] C_3v symmetry. [b] Cs symmetry. The distorted pyramid with halogen atoms at the base and one shorter and two longer (given in parentheses) bonds. [c] X_1-Dy-X_2 and X_2-Dy-X_2 (in parentheses) angles. [d] Ref.[18] [e] Ref.[19] [f] Ref.[20]

Table 6. The valence orbital populations on dysprosium from Mulliken and natural bond orbital (in parentheses) population analysis in $DyCl_n$ molecules and $DyCl_n^+$ cations ($n = 0-3$)

	s	p	d	f	Total charge on Dy atom
Dy	2.000 (0.000)	0.000 (0.000)	0.000 (0.000)	10.000 (10.000)	0.000 (0.000)
Dy^+	1.000 (1.000)	0.000 (0.000)	0.000 (0.000)	10.000 (10.000)	1.000 (1.000)
DyCl	1.108 (0.99)	0.040 (0.02)	0.140 (0.08)	10.009 (10.00)	0.703 (0.909)
$DyCl^+$	0.067 (0.05)	0.020 (0.01)	0.196 (0.13)	10.013 (10.00)	1.704 (1.816)
$DyCl_2$	0.160 (0.12)	0.090 (0.01)	0.240 (0.14)	9.984 (9.96)	1.525 (1.762)
$DyCl_2^+$	0.116 (0.07)	0.133 (0.01)	0.617 (0.411)	9.195 (9.15)	1.939 (2.360)
$DyCl_3$	0.197 (0.13)	0.230 (0.02)	0.623 (0.39)	9.139 (9.09)	1.811 (2.373)
$DyCl_3^+$	0.166 (0.09)	0.170 (0.01)	0.493 (0.31)	9.384 (9.34)	1.786 (2.240)

DyX_2. Two s and one f electrons of Dy are involved in the bond formation. The strong σ-back-donation to the d and p orbitals leads to a total charge of 1.811 electrons on Dy. Contrary to smaller systems the ionization of DyX_3 leads to dramatic changes. The unpaired electrons are no longer localized exclusively on the Dy center. The symmetry of the parent molecule (C_{3v}) is destroyed, and the cation undergoes a Jahn−Teller distortion, leading to C_s symmetry. The atomic charge localized on dysprosium is almost unchanged relative to the molecule, indicating a contribution of electronic density from the halogen atoms to the ionization process (Table 6). The consecutive ionization energies of dysprosium are 5.927, 11.67, and 22.8 eV. The active participation of halogen atoms in the ionization in the DyX_3 molecule is consistent with the increasing consecutive ionization potential of Dy. The third ionization potential (22.8 eV) is significantly higher than those (17.48, 13.01, 11.84, and 10.454 eV for F, Cl, Br, and I, respectively[21]) of the halogens.

For the reasons given in the previous section it was interesting to compare the experimental values of the ionization/fragmentation potentials with those obtained theoretically for adiabatic processes. The calculated ionization and appearance potentials are given in Table 2. The values generally agree with the respective potentials derived from the IEC taking into account the accuracy of experimental values of about ±0.5 eV. In most cases the theoretical values are somewhat smaller than the experimental ones. These differences become clearly larger for DyX^+ and Dy^+ ions in comparison to DyX_3^+ and DyX_2^+, probably due to the larger kinetic energy of two or three X fragments resulting in the fragmentation processes leading to these ions. More importantly, this agreement indicates the correct prediction of the structures of the studied species and validates the discussion concerning the nature of the bonding. In Figure 2 we display the ionization energies and energies of subsequent dissociations of the Dy−X bonds in the charged species obtained from the theoretical AP values in Table 2. The comparatively low dissociation energy of the first bond in the DyX_3^+ species could explain the highest intensity of the DyX_2^+ ions in all the mass spectra of dysprosium halides. The dissociation of subsequent halogen atoms from the ionic fragments becomes energetically less preferable. The tendency of increasing the dissociation energy of the Dy−X bond in going from the DyX_3^+ to the DyX^+ ionic species can be seen for all dysprosium halides with the exception of dysprosium bromide. At present we are not able to offer an explanation for this phenomenon.

Discussion and Conclusions

The mass spectrum patterns of the gaseous DyX_3 species consist of molecular ions and the DyX_2^+, DyX^+, and Dy^+ fragment ions, with DyX_2^+ being the most intense for all dysprosium halides. The ionization and appearance potentials obtained for these ions by quantum chemical methods

 © 2004 Wiley-VCH Verlag GmbH & Co. KGaA, Weinheim

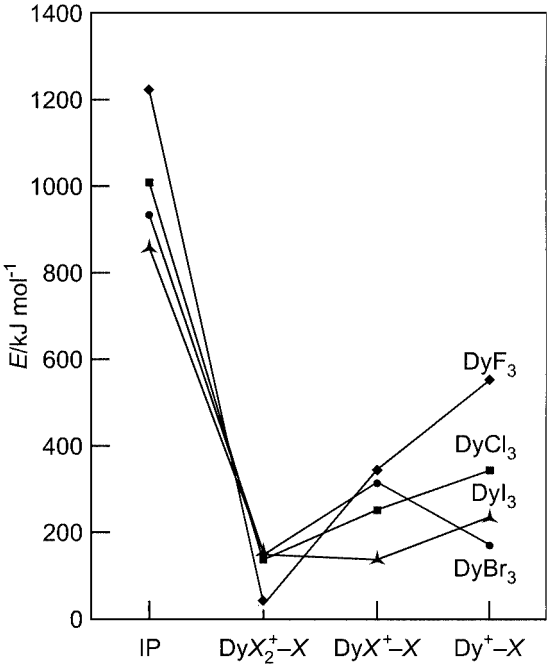

Figure 2. Ionization energies of DyX_3 and fragmentation energies for the DyX_n^+ ions ($n = 1-3$)

in the present study agree well with the experimental values. The thermodynamic meaning of the appearance potentials is the energy of dissociation of the metal−halide bonds in the neutral molecule. For instance, AP(DyF^+) correlates with the energy of the process

$$DyF_3(g) + e \rightarrow DyF^+ + 2F + 2e$$

Combinations of appearance potentials should yield the dissociation energies of the halogen−metal bond in ions. For instance the difference AP(DyF^+) − AP(DyF_2^+) should correlate with the energy of the dissociation process

$$DyF_2^+ \rightarrow DyF^+ + F$$

As already mentioned, the experimental appearance-potentials yield, in fact, upper limits of adiabatic values. Moreover, the accuracy of the AP values, usually reported, is no better than ±0.5 eV. Therefore the determination of the energies of the dissociation/fragmentation processes from experimental appearance potentials is limited.

The available experimental energetic data (ionization and appearance potentials) are reasonably reproduced by the calculated values. More importantly, the calculations reproduce the perturbations in the measured data that originate from the increasing importance of relativistic contributions in heavier halogens. The chemical bonds are formed due to the charge transfer of the electronic density from dysprosium to the halogen atoms. The atomic charge on Dy amounts to 0.702 (DyCl), 1.525 ($DyCl_2$), and 1.811 ($DyCl_3$) leading to a negative charge on chlorine of −0.702, −0.762, and −0.604 electrons, respectively. In the first-order approximation this electron transfer can be considered as an additive process. The increasing positive charge on the metal atom enhances the Coulomb interactions in the cations, leading to a shortening of the Dy−X distance. This charge transfer involves s electrons in DyX and DyX_2. In DyX_3, the f electrons also take part in the bonding (Table 6). The transfer of the f electron is compensated, however, by a similar amount of electronic density due to the σ-back-donation from halogen atoms to the d and p orbitals of Dy. The highest atomic charge in DyX_3 is close to two. This observation is consistent with the Dy values of the two lowest ionization potentials, which are smaller than those of the halogens. The open-shell electrons are localized almost exclusively on the dysprosium atom. The number of electrons confirms the involvement of one s, two s, and two s + one f electrons in the DyX, DyX_2, and DyX_3 bonding, respectively. The atomic charge on the metal atom in DyX_3 disagrees with the established model of the $Dy^{3+}X_3^-$ bonding scheme.[22] It is consistent, however, with the very high value of the third ionization potential of Dy. Due to the σ-back-donation of electrons from the halogens, a more appropriate model for the metallic center in DyX_3 is the Dy^{2+} cation in the excited electronic state, corresponding to an electron excitation from the f to the d orbital. The computations indicate the active participation of the f orbital in the bonding process in DyX_2^+ cations and DyX_3 molecules.

The ionization of DyCl removes the s electron, increasing the charge of Dy from 0.703 to 1.703 electrons. The ionization of $DyCl_2$ corresponds to the removal of the f electron. The charge on Dy increases from 1.525 to 1.939 electrons due to the compensation for electrons involved in the bonding by the σ-back-donation. The unpaired electrons are localized at the Dy center. The removal of the nonbonding f electron from the metal atom increases the Coulomb interactions. However, the ionization process does not affect the charge transfer. The increased contribution of the ionic interactions leads to shorter bonds. The effect of the increased bond strength is confirmed by a blue shift of the corresponding stretching vibrations. The ionization of DyX_3 is more complicated. Ionized $DyCl_3^+$ is subject to the Jahn−Teller effect, and the symmetrical C_{3v} molecules are distorted to the C_s geometry. The total spin-density indicates that open-shell electrons are also localized on the halogen atoms. The above observation agrees with the high values of the third IP of Dy and the preferred ionization of halogen atoms. Such a distribution of electronic density allows the value of the charge on the metallic center to be close to two electrons. The removal of the f electron is again compensated by the σ-back-donation. The bond formation and ionization processes in DyX, DyX^+, DyX_2, DyX_2^+, and DyX_3 lead to the electron loss from the Dy center involving less than two electrons. The primary process of the electron transfer from the metal (including the ionization process) is promptly compensated by the σ-back-donation from halogen atoms. The above processes are consistent with the two lowest IPs of Dy being lower than the first potentials of the halogens. An attempt to remove more electrons from Dy was not successful, and in the DyX_3^+ cation

 © 2004 Wiley-VCH Verlag GmbH & Co. KGaA, Weinheim

the halogen atoms also contribute to the electron-loss process.

Experimental Section

Mass Spectra of Gaseous DyX_3: The mass spectrum of DyF_3 vapors and the ionization efficiency curves for ions identified in the mass spectrum were recorded on a CH5 mass spectrometer (Finnigan MAT, Bremen, Germany)[23] in Julich. Knudsen cells made of Mo with an edged effusion orifice of 0.8 mm diameter were employed in every case. The energy of the ionising electrons, 34 eV, was calibrated with the ionization potentials of Hg, In, and Ag measured prior to the recording of the DyF_3 mass spectra. Mass spectra and appearance potentials for ions present in the mass spectra of $DyCl_3$,[7,8] $DyBr_3$,[9] and DyI_3 [10] were taken from our previous studies. The mass spectrum of $DyCl_3$ [8] and the appearance potentials for ions in the DyI_3 mass spectrum[24] were also taken from the literature.

Theoretical Methods: The quantum-chemical calculations were carried out using the density functional theory (DFT) approach, using Becke's three-parameter functional[25] with Vosko et al.'s local correlation part[26] and Lee et al.'s[27] non-local part (abbreviated as B3LYP). All the calculations were carried out using the relativistic effective core potentials (RECPs) developed by the Stuttgart/Dresden groups that retain the outer $4s^24p^64d^{10}5s^25p^64f^{10}6s^2$ shells of dysprosium and ns^2np^7 of halogen atoms.[28–30] The corresponding basis sets are characterized as the (12s, 11p, 9d,8f) collection contracted to [5s, 5p, 4d, 2f] for Dy and (4s, 4p) contracted to [2s, 3p] for halogen atoms. The basis sets of the halogens were additionally supplemented by two d polarization and a set of sp diffuse functions proposed as part of the SDB-aug-cc-PVTZ and aug-cc-PVTZ basis sets.[31,32] Because of the ionic nature of the chemical bonds in the studied complexes, the validity of the basis sets was checked by the computation of the ionization potential of Dy and electron affinities of halogen atoms. The agreement between the calculated ionization potential of Dy (6.02 eV) and its experimental value (5.927 eV [17]) indicates the reasonable treatment of high-spin electronic states in the Dy atom (sextet) as well as in the Dy^+ cation (quintet) within the applied density functional theory method. The theoretical values of electronic affinities for F (3.33 eV), Cl (3.72 eV), Br (3.51 eV), and I (3.35 eV) agree satisfactorily with the respective experimental data of 3.401, 3.61, 3.36, and 3.059 eV.[21] The availability of unpaired electrons on the f orbitals of dysprosium allows for the rich manifold of electronic states in the studied compounds. The calculations for the studied molecules and cations were performed for the different electronic states allowed by the electronic configurations of the participating atoms, to ensure the location of the proper electronic ground state. Spin-orbit contributions have been neglected in the present calculations. Previous calculations, which estimated such contributions for lanthanide trihalides,[33] indicated that although not negligible, spin-orbit effects constitute only a few percent of the studied properties and do not change the qualitative picture. All geometrical structures were optimized. The location of true minima was confirmed in calculations of vibrational frequencies. The electronic density distributions were studied applying the Mulliken population analysis and the natural bond orbital (NBO) analysis.[34] Because both approaches lead to a similar qualitative picture, the results of the Mulliken populations are discussed in detail in the text. Although differences in electronegativity between halogen atoms lead to some quantitative differences,[34] the qualitative picture of the electron-density distribution is similar and detailed results are illustrated for dysprosium chloride. The calculations were carried out using the Gaussian 98 package of programs.[35]

Acknowledgments

This work was facilitated in part by the Polish State Committee for Scientific Research under grant 3 T09A 020 19, NSF Grant No. 9805465 & 9706268, ONR Grant No. N00014−98-1-0592, and the Army High Performance Computing Research Center under the auspices of the Department of the Army, Army Research Laboratory cooperative agreement number DAAH04−95-2-0003/contract number DAAH04−95-C-0008. This work does not necessarily reflect the policy of the government, and no official endorsement should be inferred. We would like to thank the Mississippi Center for Supercomputing Research, Poznan and Wroclaw Supercomputing and Networking Centers, and the Interdisciplinary Center for Mathematical and Computational Modeling of Warsaw University for a generous allotment of computer time.

[1] D. Schroeder, J. Loos, H. Schwarz, R. Thissen, O. Dutuit, *Inorg. Chem.* **2001**, *40*, 3161.
[2] R. G. Cooks, P. S. H. Wong, *Acc. Chem. Res.* **1998**, *31*, 379.
[3] G. Wang, R. B. Cole, *J. Electr. Spectr. Rel. Phenomen.* **2000**, *108*, 153.
[4] L. N. Gorokhov, *Proc. II Int. Symp. on High Temperature Mass Spectrometry*, July 7−10, 2003, Plyos, Russia, p. 57.
[5] J. C. Lorquet, *Int. J. Mass Spectrom.* **2000**, *200*, 43.
[6] B. Brunetti, P. Vassallo, V. Piacente, P. Scardala, *J. Chem. Eng. Data* **1999**, *44*, 509.
[7] J. Kapała, S. Roszak, S. Nunziante Cesaro, M. Miller, *J. Alloys Comp.* **2002**, *345*, 90.
[8] Yu. Kuznetsov, M. F. Butman, L. S. Kudin, A. M. Pogrebnoi, G. G. Burdukovskaja, *Teplofiz. Vys. Temp.* **1997**, *35*, 731; *Chem. Abstr.* **1998**, *128*, 7741n.
[9] K. Hilpert, M. Miller, F. Ramondo, *J. Chem. Phys.* **1995**, *102*, 6194.
[10] K. Hilpert, M. Miller, F. Ramondo, *Thermochim. Acta*, in press.
[11] L. Joubert, G. Picard, J.-J. Legendre, *Inorg. Chem.* **1998**, *37*, 1984.
[12] A. Kovacs, R. J. M. Konings, *Vibr. Spectr.* **1997**, *15*, 131.
[13] V. G. Solomonik, O. Y. Marochko, *J. Struct. Chem.* **2000**, *41*, 725.
[14] A. Kovacs, *J. Mol. Struct.* **1999**, *482/483*, 403.
[15] J. W. Hastie, in *High Temperature Vapors, Materials Science and Technology Series*, Academic Press, New York, **1975**, p. 91.
[16] J. A. Morris, in *Mass spectrometry, Vol. 5, MTP International Review of Science, Physical Chemistry Series 1* (Ed.: A. Maccoll), Butterworths, London, **1972**.
[17] W. C. Martin, L. Hagan, J. Reader, J. Sugar, *J. Phys. Chem. Ref. Data* **1974**, *3*, 771.
[18] E. Myers, D. T. Graves, *J. Chem. Eng. Data* **1977**, *22*, 436.
[19] M. Hargittai, *Coord. Chem. Rev.* **1988**, *91*, 35.
[20] M. Hargittai, *Chem. Rev.* **2000**, *100*, 2233.
[21] *CRC Handbook of Chemistry and Physics, 83rd Edition* (Ed.: D. R. Lide), CRC Press, Boca Raton, **2002**.
[22] *Lanthanide and Actinide Chemistry and Spectroscopy, ACS Symp. Series 131* (Ed.: N. M. Edelstein), ACS, Washington D. C., **1980**.
[23] K. Hilpert, *J. Electrochem. Soc.* **1989**, *136*, 2099.
[24] O. Kaposi, L. Lelik, A. Balthazar, *High Temp. Sci.* **1983**, *16*, 299.
[25] D. Becke, *J. Chem. Phys.* **1993**, *98*, 5648.
[26] S. H. Vosko, L. Wilk, M. Nusiar, *Can. J. Phys.* **1980**, *58*, 1200.
[27] C. Lee, W. Yang, R. G. Parr, *Phys. Rev. B* **1988**, *37*, 785.
[28] M. Dolg, H. Stoll, H. Preuss, R. M. Pitzer, *J. Phys. Chem.* **1993**, *97*, 5852.

 © 2004 Wiley-VCH Verlag GmbH & Co. KGaA, Weinheim

[29] A. Bergner, M. Dolg, W. Kuechle, H. Stoll, H. Preuss, *Mol. Phys.* **1993**, *80*, 1431.
[30] W. Kuechle, M. Dolg, H. Stoll, H. Preuss, *Mol. Phys.* **1991**, *74*, 1245.
[31] E. Woon, T. H. Dunning Jr., *J. Chem. Phys.* **1995**, *103*, 4572.
[32] J. M. L. Martin, A. Sundermann, *J. Chem. Phys.* **2001**, *114*, 3408.
[33] E. Reed, L. A. Curtiss, F. Weinhold, *Chem. Rev.* **1988**, *88*, 899.
[34] C. Adamo, P. Maldivi, *J. Phys. Chem. A* **1998**, *102*, 6812.
[35] M. J. Frisch, G. W. Trucks, H. B. Schlegel, G. E. Scuseria, M. A. Robb, J. R. Cheeseman, V. G. Zakrzewski, J. A. Montgomery, Jr., R. E. Stratmann, J. C. Burant, S. Dapprich, J. M. Millam, A. D. Daniels, K. N. Kudin, M. C. Strain, O. Farkas, J. Tomasi, V. Barone, M. Cossi, R. Cammi, B. Mennucci, C. Pomelli, C. Adamo, S. Clifford, J. Ochterski, G. A. Petersson, P. Y. Ayala, Q. Cui, K. Morokuma, N. Rega, P. Salvador, J. J. Dannenberg, D. K. Malick, A. D. Rabuck, K. Raghavachari, J. B. Foresman, J. Cioslowski, J. V. Ortiz, A. G. Baboul, B. B. Stofanov, C. Liu, A. Liashenko, P. Piskorz, I. Komaromi, R. Gomperts, R. L. Martin, D. J. Fox, T. Keith, M. A. Al-Laham, C. Y. Peng, A. Nanayakkara, M. Challacombe, P. M. W. Gill, B. Johnson, W. Chen, M. W. Wong, J. L. Andres, C. Gonzalez, M. Head-Gordon, E. S. Replogle, J. A. Pople, *Gaussian 98, Revision A.11.3*, Gaussian, Inc., Pittsburgh PA, **2002**.

Received September 3, 2003
Early View Article
Published Online February 10, 2004

 © 2004 Wiley-VCH Verlag GmbH & Co. KGaA, Weinheim

N,*N*-Dialkylcarbamato Lanthanide Complexes, a Series of Isotypical Coordination Compounds

Ulrich Baisch,[a,b] Daniela Belli Dell'Amico,*[a] Fausto Calderazzo,[a] Luca Labella,[a] Fabio Marchetti,[a] and Alessandra Merigo[a,c]

Keywords: Coordination modes / Lanthanides / Lanthanide contraction

The preparations of the *N*,*N*-dialkylcarbamato complexes with analytical formulae $[Ln(O_2CNR_2)_3]$ (Ln = Pr, Nd, Eu, Gd, Ho, Er, Yb, Lu, R = *i*Pr; Ln = Nd, Eu, Gd, R = Bu; Ln = Nd, R = Et), using $[LnCl_3(ether)_x]$ (ether = THF or dimethoxyethane, DME), NHR_2, and CO_2 are reported. X-ray diffraction of the diisopropylcarbamato derivatives, including a reinvestigation of $[Yb_4(O_2CNiPr_2)_{12}]$, showed these complexes to be tetranuclear and isotypical over a range of 12 atomic numbers. The lanthanide contraction has been evaluated based on the lengths of four different types of Ln–O bond.
(© Wiley-VCH Verlag GmbH & Co. KGaA, 69451 Weinheim, Germany, 2004)

Introduction

The synthesis, characterization, and reactivity of *N*,*N*-dialkylcarbamato transition metal complexes have been extensively studied in these laboratories and elsewhere.[1−6] As far as lanthanide (Ln) derivatives are concerned, the structurally characterized examples have resulted from work carried out within this research group,[7,8] with the sole exception of the heteroleptic binuclear complex $[Sm_2(C_5Me_5)_4(THF)\{\mu\text{-}\eta^2\text{-}:\eta^1\text{-}NN(CO_2)Ph_2\}]$, prepared[9] by carbonation of the precursor $[Sm_2(C_5Me_5)_4\{\mu\text{-}\eta^2\text{-}:\eta^1\text{-}NNPh_2\}]$. Moreover, structurally defined homoleptic derivatives of lanthanides with oxygen donors are rather rare. A literature survey has in fact shown that, with these restrictions, even the well-established classes of the β-diketonato[10−12] and carboxylato[13,14,15] complexes are not extensively represented. However, it appears that when bulky coordinated ligands are present, isostructural behavior may be more easily observed. This is evidenced by the synthesis of the isopropoxy μ_5-oxo derivatives of general formula $[Ln_5(\mu_5\text{-}O)(OiPr)_{13}]$ which have been shown to crystallize in the $P2_1/n$ (no. 14) space group for Ln = Nd, Gd, Er, i.e. over a range of nine atomic numbers.[16]

Recently, a preliminary communication from these laboratories showed that the metrical data of the isotypical tetranuclear complexes $[Ln_4(O_2CNiPr_2)_{12}]$ allowed the lanthanide contraction in these complexes to be evaluated in the sequence from neodymium to ytterbium.[17] In this paper, the preparation of the derivatives $[Ln(O_2CNR_2)_3]$ (R = *i*Pr, Ln = Pr, Nd, Eu, Gd, Ho, Er, Lu; R = Et, Ln = Nd; R = Bu, Ln = Nd, Eu, Gd) and the full details of the crystal and molecular structures of the isotypical compounds $[Ln_4(O_2CNiPr_2)_{12}]$ (Ln = Nd, Eu, Gd, Ho, Er, Yb, Lu) are reported.

Results and Discussion

The carbamato complexes $[Ln(O_2CNR_2)_3]$ have been mainly prepared[7,8,17] starting from the derivatives $[LnCl_3(ether)_x]$ (ether = THF or dimethoxyethane, DME),[18] which have a low nuclearity and react promptly with NHR_2 and CO_2 according to Equation (1).

$$[LnCl_3(ether)_x] + 6\,NHR_2 + 3\,CO_2 \rightarrow [Ln(O_2CNR_2)_3] + 3\,[NH_2R_2]Cl + x\,ether \quad (1)$$

As previously reported, in the cases of erbium and ytterbium,[7,8,17] the unsolvated chlorides $LnCl_3$ have been found to be useful starting materials for the synthesis of the carbamato complexes. Consistent with the fact that erbium and ytterbium are late lanthanide elements, and in the hypothesis that the chemical properties of these compounds are mainly governed by the ionic radius of the central metal cation, the preparation of the carbamato derivative was also attempted with lutetium trichloride. This has now been found to react with the $NHiPr_2/CO_2$ system giving the corresponding carbamato derivative in good yield. Conversely, this synthetic route met with failure for the lighter lantha-

[a] Università di Pisa, Dipartimento di Chimica e Chimica Industriale,
Via Risorgimento 35, 56126 Pisa, Italy
E-mail: belli@dcci.unipi.it
[b] Present address: Department Chemie der Ludwig-Maximilians-Universität München,
Butenandtstrasse 5−13 (Haus D), 81377 München, Germany
[c] Present address: Lucchini C. R. S.,
Viale della Resistenza 2, 57025 Piombino, Livorno, Italy

nides. The extended structures of the anhydrous lanthanide chlorides could be responsible for their poor or even lack of reactivity. In this context, it is useful to point out that the anhydrous trichlorides have the structure of UCl_3 ($CN = 9$) from lanthanum to gadolinium, while from dysprosium to lutetium the structures are like that of YCl_3 ($CN = 6$).[19] The lower coordination number towards the end of the series, associated with the usual trend towards smaller ionic radii in the same direction, may be responsible for the higher reactivity of the heavier metal halides. In fact, it is reasonable that the primary stage of the reaction sequence towards the formation of the carbamato derivatives is amine association. This is presumably more likely to occur with ytterbium and lutetium with a reduced coordination number, thus initiating the chain of reactions towards the final product.

The yields of the *N*,*N*-dialkylcarbamato complexes (R = *i*Pr, Bu) varied from moderate to good. The workup was rather simple, requiring a preliminary filtration of the reaction mixture to eliminate the dialkylammonium chloride, followed by concentration of the filtrate containing the product.

The solubility of the products in non-polar solvents depends on the nature of the R group. For instance, the *N*,*N*-diethylcarbamato complex of neodymium $[Nd(O_2CNEt_2)_3]$, presumably possessing a polynuclear structure, is only sparingly soluble in hydrocarbons. For this reason it is more conveniently prepared by treatment of the soluble $[Nd(O_2CNBu_2)_3]$ in a hydrocarbon solution with $NHEt_2$ and CO_2 according to an $O_2CNR_2/O_2CNR'_2$ substitution reaction, originally reported for the titanium(III) complexes,[20] and more latterly extended to other metal cations.[5,21]

Table 1. IR spectra of the tetranuclear complexes $[Ln_4(O_2CN{i}Pr_2)_{12}]$ in the 1650−1350 cm^{-1} region

Ln	Medium	Wavenumber[a] (cm^{-1})			
Pr	PCTFE	1591	1527	1518	1353
Nd	Nujol	1593	1515	1479	1354
Eu	PCTFE	1597	1533	1488	1354
Gd	PCTFE	1598	1537	1485	1355
Ho	Nujol	1601	1538	1489	1354
Er	Nujol	1602	1540	1490	1355
Yb	Nujol	1604	1541	1491	1355
Lu	Nujol	1610	1530	1490	1354

[a] Bands at about 1460 and 1380 cm^{-1}, attributable to the CH_3 and CH_2 groups. Bending vibrations are not reported.

The IR spectra of these derivatives show intense and broad bands in the 1650−1350 cm^{-1} region due to the stretching vibrations of the O_2CN moieties (see Table 1, and the Exp. Sect.). As expected for complexes having analogous molecular structures, the spectra of $[Ln_4(O_2CN{i}Pr_2)_{12}]$ are almost identical, except for a shift of the highest frequency band towards higher wavenumbers along the series. Chisholm and Extine[3] studied the effect of isotopic substitution ($^{18}O_2CN$ and $O_2{}^{13}CN$) on the position of the highest frequency band for some dialkyl-carbamato complexes of zirconium, niobium and tantalum. They concluded that for a bidentate group the vibration is mostly NC in character, while for a monodentate arrangement there is a predominant OC contribution. According to this interpretation, the data in Table 1 would tend to suggest an increase of the NC bond order from Pr to Lu. The following data within this paper on the observed trend of Ln−O bond lengths (vide infra) are relevant to this specific point.

Magnetic susceptibility measurements have been carried out on $[Nd_4(O_2CN{i}Pr_2)_{12}]$, $[Eu_4(O_2CN{i}Pr_2)_{12}]$, and $[Gd(O_2CNBu_2)_3]$, see Table 2. The magnetic moments at room temperature agree with the experimental values usually encountered with these paramagnetic centers and, for neodymium and gadolinium, they correspond to the calculated values.[22,23] The europium (III) derivatives frequently show more complicated magnetic behavior as the first excited level is close to the ground state (about 250 cm^{-1} higher) so that it may become thermally populated. Variable temperature studies have been performed for the europium and gadolinium compounds. In the range 70−270 K, the magnetic susceptibility of the gadolinium derivative follows the Curie−Weiss law. On the contrary, the europium compound in the 70−170 K range shows, as expected, a temperature dependent μ value, the magnetic moment becoming independent of temperature above 170 K.

The diisopropyl derivatives can be easily recrystallized from heptane with formation of single crystals suitable for X-ray diffraction studies. They are isotypical and the complete structural determination was performed for the neodymium, europium, gadolinium, holmium, erbium and lu-

Table 2. Magnetic susceptibilities of the $[Ln(O_2CNR_2)_3]$ derivatives

Ln	R[a]	*T* /K	χ_{corr} /cgsu	Diam. Corr,[b]/cgsu	μ_{eff} /BM ($\mu_{calcd.}$)[c]	Ref.
Nd	*i*Pr	297	$5250\cdot10^{-6}$	$-302\cdot10^{-6}$	3.53 (3.62)	this work
Eu[d]	*i*Pr	295	$3210\cdot10^{-6}$	$-302\cdot10^{-6}$	2.76 (0)	this work
Gd[d]	Bu	270	$24400\cdot10^{-6}$	$-373\cdot10^{-6}$	7.28 (7.94)	this work
Er	*i*Pr	295	$35400\cdot10^{-6}$	$-302\cdot10^{-6}$	9.11 (9.58)	[8]
Yb	Et	295	$7645\cdot10^{-6}$	$-231\cdot10^{-6}$	4.23 (4.54)	[8]
Yb	*i*Pr	295	$7576\cdot10^{-6}$	$-302\cdot10^{-6}$	4.21 (4.54)	[8]

[a] The compounds are tetranuclear for R = *i*Pr; the nuclearity of the ethyl and butyl derivatives is unknown. [b] Pascal constants have been used for H, C, N, and O, the diamagnetic correction for Ln^{3+} being $-16\cdot10^{-6}$ cgsu. [c] $\mu_{calcd.} = g[J(J+1)]^{1/2}$; $g = 3/2 + [S(S+1) - L(L+1)]/2J(J+1)$. [d] See text for the variable−temperature measurements.

 © 2004 Wiley-VCH Verlag GmbH & Co. KGaA, Weinheim

tetium complexes.[24] Although the ytterbium compound had been previously studied, a new crystallographic determination was carried out in order to have more accurate bond parameters.

The molecules of $[Ln_4(O_2CN\mathit{i}Pr_2)_{12}]$ are slightly prolate spheroids with a maximum diameter of about 16.4 Å. The external shell of the molecules is composed of isopropyl groups, and this accounts for the solubility of these species in hydrocarbons. The crystal packing of these large molecules leaves relatively large cavities which can accommodate solvent molecules such as toluene, heptane, or isooctane. The different nature of the lattice solvent, however, does not affect either the space group or the molecular structure of the compounds, as shown by the smooth trend of the Ln−O distances vs. the number of *f* electrons (Figure 2).

The lanthanide carbamato molecules have C_2 symmetry, the carbamato ligands being situated around four metal atoms as shown in Figure 1. Two metal atoms are related to the other two by a two-fold axis, the quadruplet building a sort of elongated tetrahedron (ditrigon). Three different coordination modes are exhibited by the ligands, which chelate three, two, or one metal atom, labelled **[a]**, **[b]**, and **[c]**, respectively.

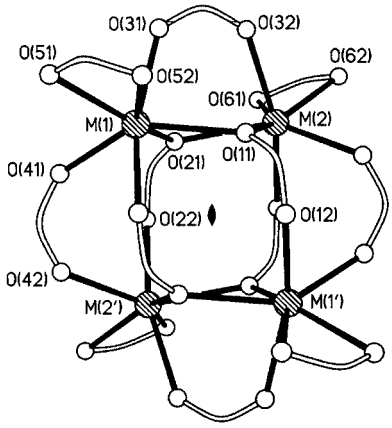

Figure 1. Schematic representation of the $[Ln_4(O_2CN\mathit{i}Pr_2)_{12}]$ core projected down the two-fold axis, showing the metal and oxygen labelling

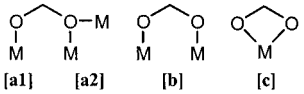

The ligands chelating three metal atoms have a tri-coordinated oxygen atom which shows the longest Ln−O distances and has been indicated as the **[a2]** type and a di-coordinated one, the **[a1]** type. Table 3 shows the Ln−O distances found in the known structures of $[Ln_4(O_2CN\mathit{i}Pr_2)_{12}]$ listed by metal and by ligation type. For each type the weighted means are also reported. The mean values and the standard deviations have been calculated using the expressions below.[25]

$$\bar{x} = \frac{\sum_i \left(\frac{x_i}{\sigma_i^2}\right)}{\sum_i \left(\frac{1}{\sigma_i^2}\right)}$$

$$\sigma(\bar{x}) = \sqrt{\frac{1}{\sum_i \left(\frac{1}{\sigma_i^2}\right)}}$$

The lanthanide is hepta-coordinated and the coordination polyhedra of M(1) and M(2) are almost superimposable. They may be considered as a heavy distortion of a pentagonal bipyramid (idealized symmetry D_{5h}), according to the catalogue of seven-vertex polyhedra proposed by Britton and Dunitz.[26]

Taking into account the mean values of the Ln−O distances of Table 3, the **a2** distance is the longest, being about 6% greater than the **a1** type (see Table 3 for the individual M−O distances). This lengthening is certainly due to the tri-coordination of the oxygen in the **a2** type. In contrast, the Ln−O distances of type **c** are stretched by about 4%, with a small O−Ln−O angle of about 56°. Finally, for each compound the Ln−O distances of types **a1** and **b** are rather similar, the differences being within 1%.

In order to show the trend of the Ln−O distances as a function of the nature of the lanthanide, the mean values of the distances for each bond type (**a1**, **a2**, **b**, and **c**) have been plotted against the number of *f* electrons of the metal cation. Figure 2 shows the result when the distances of each type were fitted with the quadratic function $d(\text{Ln}-\text{O}) = A_0 - A_1 \cdot n + A_2 \cdot n^2$, where *d* is the distance, *n* is the number of *f* electrons and A_0, A_1, and A_2 are the fitting parameters. The curves show rather similar slopes, suggesting that the metal radius contraction should mainly account for the trend. In the case of the Ln−O **a1** distances some adjacent couples, such as Yb/Lu or Ho/Er, do not show a significant contraction. However, the trend along the series is analogous to that found for the other bond types.

As has been underlined in a previous preliminary communication[17] from these laboratories, the trend of the Ln−O bond shortening is parabolic,[27] i.e. the early lanthanides contract their radii slightly more rapidly than the later ones (Figure 2). Since we now add the data for the Eu, Er and Lu derivatives and the more accurate data for the Yb derivative, we further confirm the general trend of the distances. The A_2 parameter of the fitting is $1.71 \cdot 10^{-4}$ for the Ln−O distances of the **b** type compared with a mean value of $4.87 \cdot 10^{-4}$ for the other types. The well−known lanthanide contraction was originally recognized[27b] on the basis of X-ray crystallographic determinations on the oxides and fluorides of the Ln^{3+} ions, which are not isostructural along the whole series. The contraction was evaluated to be 15% from cerium to lutetium, a correction being required for the decreased coordination number along the series. [27c,27d]

The **a1** bonds represent the maximum approach of the oxygen to the metal. The **a1** fitting corresponds to the equa-

 © 2004 Wiley-VCH Verlag GmbH & Co. KGaA, Weinheim

Table 3. M−O distances in isotypical diisopropylcarbamato derivatives of lanthanides. See text for the classification of bond types **[a1]**, **[a2]**, **[b]**, and **[c]**

		Nd	Eu	Gd	Ho	Er	Yb	Lu
O(12)−M(1′)[a]	**[a1]**	2.320(10)	2.273(4)	2.259(4)	2.223(5)	2.225(3)	2.198(4)	2.192(6)
O(22)−M(2′)	**[a1]**	2.336(10)	2.295(5)	2.288(4)	2.247(5)	2.229(4)	2.213(5)	2.218(6)
O**[a1]**−M (mean)		**2.328(7)**	**2.282(3)**	**2.274(3)**	**2.235(4)**	**2.226(2)**	**2.204(3)**	**2.205(4)**
O(11)−M(2)	**[a2]**	2.499(10)	2.453(4)	2.427(5)	2.398(5)	2.348(3)	2.361(4)	2.342(5)
O(21)−M(1)	**[a2]**	2.466(10)	2.429(4)	2.379(5)	2.371(5)	2.392(3)	2.345(4)	2.328(5)
O(11)−M(1)	**[a2]**	2.474(9)	2.420(4)	2.401(4)	2.364(5)	2.348(3)	2.329(4)	2.313(5)
O(21)−M(2)	**[a2]**	2.484(9)	2.416(4)	2.404(4)	2.367(5)	2.346(3)	2.326(4)	2.315(5)
O**[a2]**−M (mean)		**2.481(5)**	**2.430(2)**	**2.403(2)**	**2.375(3)**	**2.359(2)**	**2.340(2)**	**2.325(3)**
O(31)−M(1)	**[b]**	2.373(10)	2.306(5)	2.298(4)	2.264(5)	2.246(4)	2.221(5)	2.219(6)
O(32)−M(2)	**[b]**	2.362(10)	2.305(5)	2.295(4)	2.272(5)	2.273(4)	2.233(5)	2.227(6)
O(41)−M(1)	**[b]**	2.338(10)	2.296(5)	2.275(4)	2.239(6)	2.251(4)	2.217(5)	2.212(6)
O(42)−M(2′)	**[b]**	2.307(10)	2.304(6)	2.304(5)	2.262(5)	2.245(4)	2.231(5)	2.221(6)
O**[b]**−M (mean)		**2.345(5)**	**2.303(3)**	**2.292(2)**	**2.261(3)**	**2.254(2)**	**2.226(3)**	**2.220(3)**
O(51)−M(1)	**[c]**	2.407(10)	2.340(6)	2.324(5)	2.298(6)	2.298(4)	2.278(5)	2.269(7)
O(52)−M(1)	**[c]**	2.420(10)	2.382(6)	2.375(6)	2.342(6)	2.342(4)	2.320(5)	2.312(6)
O(61)−M(2)	**[c]**	2.434(10)	2.380(5)	2.373(5)	2.338(6)	2.329(4)	2.321(5)	2.309(6)
O(62)−M(2)	**[c]**	2.421(10)	2.375(5)	2.364(5)	2.321(6)	2.302(4)	2.290(5)	2.280(6)
O**[c]**−M (mean)		**2.421(5)**	**2.371(3)**	**2.358(3)**	**2.325(3)**	**2.318(2)**	**2.302(3)**	**2.294(3)**

[a] ′: $-x$, y, $3/2 - z$.

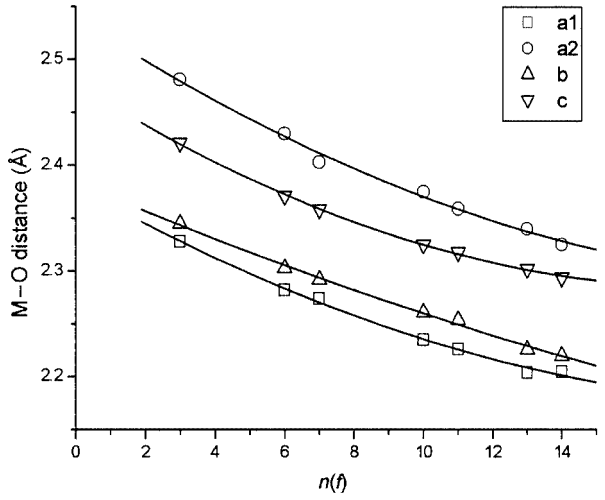

Figure 2. Polynomial fittings of different types of Ln−O distances in the isotypical $[Ln_4(O_2CNiPr_2)_{12}]$ vs. the 4*f* electronic configuration.

tion $d(\text{Ln}-\text{O}) = 2.381 - 0.0188 \cdot n + (4.24 \cdot 10^{-4}) \cdot n^2$. By extrapolation it can be anticipated that 2.381 Å should be shortest La−O distance of this type if the lanthanum carbamato derivative had the same structure as the compounds reported in this paper.

It is remarkable that the cerium(III) derivative $[Ce_4(O_2CNiPr_2)_{12}]$ also turned out to be a tetranuclear species.[28] It shows a less symmetrical molecular structure than the compounds described herein. In the molecule the coordination number is seven for three of the cerium atoms and eight for the fourth one. Because of the different structural arrangement, a comparison of the Ce−O distances with those found in the isotypical species herein described is in general difficult. On the other hand, the unique Ce−O distance of type **a1** involving hepta-coordinated cerium [Ce(3)−O(82)] in this complex is 2.368 Å corresponding to a length increase of 0.04 Å with respect to the neodymium complex.

Conclusions

A class of molecular compounds of the trivalent lanthanides, i.e. the *N*,*N*-dialkylcarbamato complexes, has been exhaustively defined as far as their preparation and characterization are concerned. The *N*,*N*-diisopropyl derivatives from Nd to Lu are isotypical species, consisting of tetranuclear molecules, $[Ln_4(O_2CNiPr_2)_{12}]$, where the metal center is hepta-coordinated. The structural determinations have allowed the lanthanide contraction over a range of 12 atomic numbers to be monitored.

The solubility of these complexes in hydrocarbons can be tuned by varying the nature of the alkyl group, thus allowing these compounds to be used as precursors to other derivatives in slightly polar, non-coordinating solvents.

Experimental Section

All preparations were carried out under a dry atmosphere (N_2 or CO_2). Solvents were freshly distilled from the usual drying agents under nitrogen. In the case of the lutetium derivative, commercially available anhydrous $LuCl_3$ was used as received (Aldrich). Elemental analyses (C,H,N) were carried out at the Laboratorio di Microanalisi della Facoltà di Farmacia, Università di Pisa, with a Carlo Erba mod. 1106 analyzer. IR spectra were measured with a FT-IR Perkin−Elmer mod. 1725X spectrophotometer. Magnetic measurements were performed with a magnetic balance (Faraday method) using $CuSO_4 \cdot 5H_2O$ for calibration. The lanthanide complexes $LnCl_3(ether)_x$ (ether = DME or THF) were prepared as previously reported.[17]

 © 2004 Wiley-VCH Verlag GmbH & Co. KGaA, Weinheim

Synthesis of $[Ln_4(O_2CNiPr_2)_{12}]$ (Ln = Pr, Nd, Eu, Gd, Ho, Er, Yb, Lu): The syntheses were carried out by treating the solvated chlorides $[LnCl_3(ether)_x]$ (ether = DME, x = 0.5, Ln = Nd; x = 1, Ln = Pr; x = 2, Ln = Eu, Gd, Ho, Yb; ether = THF, x = 1.5, Ln = Nd; x = 0, Ln = Lu) with $NHiPr_2$ and CO_2 in toluene. Analysis for $C_{21}H_{42}LnN_3O_6$, Ln = Pr, M = 573.49: calcd. Pr 24.6, CO_2 23.0%; found Pr 25.2; CO_2 23.3%. Ln = Nd, M = 576.83: calcd. Nd 25.0, CO_2 22.9%; found Nd 25.2, CO_2 21.5%. Ln = Eu, M = 584.55: calcd. Eu 26.0, CO_2 22.6%; found Eu 25.2, CO_2 22.5%. Ln = Gd, M = 589.84: calcd. Gd 26.7, CO_2 22.4%; found Gd 25.2, CO_2 21.2%. Ln = Ho, M = 597.52: calcd. Ho 27.6, CO_2 22.1%; found Ho 27.5, CO_2 21.7%. Ln = Er, M = 599.85: calcd. Er 27.9, CO_2 22.0%; found Er 27.5, CO_2 21.7%. Ln = Yb, M = 605.63: calcd. Yb 28.6, CO_2 21.8%; found Yb 28.8, CO_2 20.9%. Ln = Lu, M = 607.56: calcd. Lu 28.8, CO_2, 21.7%; found Lu 29.6; CO_2 21.3%.

Colors of the products are: green (Pr), violet (Nd), pale pink (Eu), colorless (Gd, Yb, Lu), yellow-pink (Ho), and pink (Er). The approximate solubility of the tetranuclear ytterbium compound is $6\cdot10^{-3}$ M in toluene. Analyses of the products, once dried in vacuo, were consistent with the formula $[Ln(O_2CNiPr_2)_3]_n$. When obtained as single crystals by recrystallization from hydrocarbons (C_nH_m = heptane, isooctane, or toluene), their compositions corresponded to $Ln_4(O_2CNiPr_2)_{12}\cdot2C_nH_m$ (Ln = Nd, n = 8, m = 18; Ln = Eu, Er, n = 7, m = 8; Ln = Gd, Ho, Yb, Lu, n = 7, m = 16).

Two typical experiments are described below.

a) Europium: A solution of $NHiPr_2$ (16.0 mL, 114.2 mmol) was stirred in a flask under CO_2 until gas absorption was complete. At this point, $[EuCl_3(DME)_2]$ (5.02 g; 11.45 mmol) was added, the suspension was stirred for 23 h and then filtered. The filtrate was evaporated to dryness and the pale-pink residue was treated with heptane (50 mL). The product was recovered by filtration and dried in vacuo (2.75 g, 41% yield).

b) Lutetium: A solution of $NHiPr_2$ (8.0 mL, 57.08 mmol) in toluene (200 mL) was stirred in a flask under CO_2 up to completion of the gas absorption. Anhydrous $LuCl_3$ (1.58 g, 5.62 mmol) was introduced and the suspension was stirred under CO_2 for 2 days. The mixture was filtered and the filtrate was evaporated to dryness in vacuo. The colorless residue was recrystallized from heptane (1.22 g, 36% yield).

Synthesis of $[Ln(O_2CNBu_2)_3]$ (Ln = Nd, Eu, Gd): The syntheses were carried out starting from $[LnCl_3(DME)_x]$ (x = 0.5, Ln = Nd; x = 2, Ln = Eu, Gd). The dimethoxyethane adduct $[LnCl_3(DME)_x]$ was treated with $NHBu_2$ and CO_2 in toluene. Analysis for $C_{27}H_{54}N_3LnO_6$. Ln = Nd, M = 660.99: calcd. C 49.1, H 8.2, N 6.4, Nd, 21.8, CO_2, 20.0%; found C 48.7, H 8.7, N 6.1, Nd, 22.1, CO_2, 20.0%. Ln = Eu, M = 668.71: calcd. Eu, 22.7, CO_2, 19.7%; found Eu, 20.8, CO_2, 17.4%. Ln = Gd, M = 674.00: calcd. Gd, 23.3, CO_2, 19.6%; found Gd, 21.7, CO_2, 18.0%.

A typical experiment is described: A solution of dibutylamine (5.0 mL, 29.67 mmol) in heptane (50 mL) was saturated with CO_2 and $[NdCl_3(DME)_{0.5}]$ (0.74 g, 2.50 mmol) was then added. After 12 h stirring the suspension was filtered and the violet product was obtained by evaporating the filtrate to dryness (1.23 g, 74% yield). IR (1700−1300 cm^{-1}, Nujol mull, cm^{-1}): 1528 s, 1490 s, 1430 s, 1325 s.

Synthesis of $[Nd(O_2CNEt_2)_3]$: $[Nd(O_2CNBu_2)_3]$ (6.77 g, 10.24 mmol) in heptane (100 mL) was treated with $NHEt_2$ (7.0 mL, 67.66 mmol) under CO_2. The violet product precipitated and after 1 h stirring the liquid phase had become colorless. The suspension was filtered and the solid was dried in vacuo (4.36 g, 86% yield). Analysis for $C_{15}H_{30}N_3NdO_6$. M = 492.66: calcd. Nd, 29.3, CO_2, 26.8%; found: Nd, 28.6, CO_2, 26.9%. IR (range 1700−1300 cm^{-1}, PCTFE mull, cm^{-1}): 1610 w, 1545 s, 1493 s, 1457 s, 1436 s, 1313 s.

X-ray Crystallography: Only the structure determination of $Yb_4(O_2CNiPr_2)_{12}\cdot2C_7H_{16}$ is presented in detail, the other determinations being performed in a similar manner. A summary of data collection is in Table 4. The X-ray measurements were carried out with a Bruker P4 diffractometer equipped with graphite-monochromated Mo-K_α radiation (λ = 0.71073 Å). The crystals, prepared as described before, are colorless prisms. One of them was sealed in a glass capillary under a nitrogen atmosphere saturated with heptane vapor and the unit cell parameters listed in Table 4 were derived from the setting angles of 34 intense reflections. Data were collected in the $\omega/2\theta$ scan mode, and three standard reflections were monitored every 97 measurements for checking crystal decay and equip-

Table 4. Crystal data and structure refinement of isotypical lanthanide carbamates $[Ln_4(O_2CNiPr_2)_{12}]$, monoclinic, $C2/c$ space group

Lanthanide	Eu[a]	Er[a]	Yb[b]	Lu[b]
Empirical formula	$C_{98}H_{184}Eu_4N_{12}O_{24}$	$C_{98}H_{184}Er_4N_{12}O_{24}$	$C_{98}H_{200}Yb_4N_{12}O_{24}$	$C_{98}H_{200}Lu_4N_{12}O_{24}$
Molecular mass	2522.5	2583.7	2622.9	2630.6
Temperature [K]	293(2)	293(2)	293(2)	293(2)
Wavelength [Å]	0.71073	0.71073	0.71073	0.71073
a [Å]	29.000(2)	28.369(5)	29.046(2)	29.023(5)
b [Å]	20.357(1)	20.091(3)	19.802(2)	19.749(2)
c [Å]	23.004(1)	22.874(3)	23.088(2)	23.065(2)
β [deg]	107.02(1)	106.368(9)	107.135(8)	107.13(1)
Volume [Å^3]	12985(5)	12509(3)	12690(2)	12634(3)
Z	4	4	4	4
$\rho_{calcd.}$ [Mg·m^{-3}]	1.290	1.372	1.373	1.383
μ [mm^{-1}]	1.967	2.720	2.984	3.162
Data/restr./param.	15257/0/567	19840/0/622	7969/0/592	8738/6/467
$R(F_o)$ [$I > 2\sigma(I)$][c]	0.0418	0.0447	0.0325	0.0406
Rw (F_o^2) [$I > 2\sigma(I)$][c]	0.1082	0.1267	0.0666	0.0888
Goodness-of-fit on F^2 [c]	0.997	1.020	1.045	1.019

[a] Clathrate solvent: toluene. [b] Clathrate solvent: heptane. [c] $R(F_o) = \Sigma||F_o| - |F_c||/\Sigma|F_o|$; $Rw(F_o^2) = [\Sigma[w(F_o^2 - F_c^2)^2]/\Sigma[w(F_o^2)^2]]^{1/2}$; $w = 1/[\sigma^2(F_o^2) + (AQ)^2 + BQ]$ where $Q = [\max(F_o^2,0) + 2F_c^2]/3$; GOF = $[\Sigma[w(F_o^2 - F_c^2)^2]/(N - P)]^{1/2}$, where N, P are the numbers of observations and parameters, respectively.

 © 2004 Wiley-VCH Verlag GmbH & Co. KGaA, Weinheim

ment stability. Data reduction was carried out using the XSCANS program.[29] A set of 7669 reflections was collected between θ = 2.3 and 25.0° and corrected for Lorentz and polarization effects and for absorption by the ψ−scan method. After merging the equivalent reflections $\{R_{int} = [\Sigma|F_o^2 - F_o^2(mean)|/\Sigma(F_o^2)] = 0.0251\}$, 5848 unique reflections satisfying the condition $I > 2\sigma(I)$ were retained for the following calculations. The systematic absences strongly suggested the space groups *Cc* or *C*2/*c*. The solution was found by direct methods in the centrosymmetric space group and completed through the subsequent difference Fourier maps. Calculations were carried out with the SHELX-97 and SHELXTL programs.[30,31] In the final refinement cycles, based on F^2, anisotropic thermal parameters were used for all non hydrogen atoms. The final reliability factors are listed in Table 4.

CCDC-211411 [for $Eu_4(O_2CN{i}Pr_2)_{12}$], -211412 [for $Er_4(O_2CN{i}Pr_2)_{12}$], -211413 [for $Yb_4(O_2CN{i}Pr_2)_{12}$], and -211414 [for $Lu_4(O_2CN{i}Pr_2)_{12}$] contain the supplementary crystallographic data for this paper. These data can be obtained free of charge at www.ccdc.cam.ac.uk/conts/retrieving.html [or from the Cambridge Crystallographic Data Center, 12, Union Road, Cambridge CB2 1EZ, UK; Fax: (internat.) +44-1223-336-033; E-mail: deposit@ccdc.cam.ac.uk].

Acknowledgments

The authors wish to thank the Ministero dell' Istruzione, dell' Università e della Ricerca (MIUR), Programmi di Ricerca Scientifica di Rilevante Interesse Nazionale, Cofinanziamento MURST 2000−2001, and the Consiglio Nazionale delle Ricerche (CNR, Roma), Programma Materiali Speciali per Tecnologie Avanzate II, for financial support of this work. The authors also wish to thank Prof. Joachim Strähle, Universität Tübingen, for suggestions and helpful comments. A generous gift of lanthanide oxides by Rhône-Poulenc is gratefully acknowledged.

[1] G. Chandra, A. D. Jenkins, M. F. Lappert, R. C. Srivastava, *J. Chem. Soc. (A)* **1970**, 2550−2558.
[2] M. H. Chisholm, M. W. Extine, *J. Am. Chem. Soc.* **1974**, *96*, 6214−6216.
[3] M. H. Chisholm, M. W. Extine, *J. Am. Chem. Soc.* **1977**, *99*, 782−792.
[4] F. Calderazzo, G. Dell' Amico, R. Netti, M. Pasquali, *Inorg. Chem.* **1978**, *17*, 471−473.
[5] D. Belli Dell'Amico, F. Calderazzo, L. Labella, F. Marchetti, G. Pampaloni, *Inorg. Chem. Commun.* **2002**, *5*, 733−745, and references cited therein.
[6] D. Belli Dell'Amico, F. Calderazzo, L. Labella, F. Marchetti, G. Pampaloni, *Chem. Rev.* **2003**, *103*, 3857−3897.
[7] D. Belli Dell'Amico, F. Calderazzo, F. Marchetti, G. Perego, *J. Chem. Soc., Chem. Commun.* **1979**, 1103−1105.
[8] D. Belli Dell'Amico, F. Calderazzo, F. Marchetti, G. Perego, *J. Chem. Soc., Dalton Trans.* **1983**, 483−487.
[9] W. J. Evans, C. A. Seibel, J. W. Ziller, *Inorg. Chem.* **1998**, *37*, 770−776.
[10] T A Zoan, N. P. Kuzmina, S. N. Frolovskaya, A. N. Rykov, N. D. Mitrofanova, S. I. Troyanov, A. P. Pisarevsky, L. I. Martynenko, Y. M. Korenev, *J. Alloys Compounds* **1995**, *225*, 396−399.
[11] N. P. Kuz'mina, A. T. Zoan, A. P. Pisarevskii, L. I. Martynenko, Y. T. Struchkov, *Koord. Khim.* **1994**, *20*, 707−711.
[12] A. S. Batsanov, Y. T. Struchkov, G. V. Trembovetskii, I. A. Murav'eva, L. I. Martynenko, V. I. Spitsyn, *Dokl. Akad. Nauk SSSR* **1988**, *280*, 903−906.
[13] Y. J. Kim, D.-Y. Jung, *Chem. Commun.* **2002**, 908−909.
[14] W. J. Evans, D. G. Giarikos, J. W. Ziller, *Organometallics* **2001**, *20*, 5751−5758.
[15] Q.-H. Jin, X. Li, Y.-Q. Zou, K.-B. Yu, *Acta Crystallogr., Sect. C* **2001**, *C57*, 676−677.
[16] M. Kritikos, M. Moustiakimov, M. Wijk, G. Westin, *J. Chem. Soc., Dalton Trans.* **2001**, 1931−1938.
[17] U. Abram, D. Belli Dell'Amico, F. Calderazzo, C. Della Porta, U. Englert, F. Marchetti, A. Merigo, *Chem. Commun.* **1999**, 2053−2054.
[18] D. Belli Dell'Amico, F. Calderazzo, C. Della Porta, A. Merigo, P. Biagini, G. Lugli, T. Wagner, *Inorg. Chim. Acta* **1995**, *240*, 1−3.
[19] A. F. Wells, *Structural Inorganic Chemistry*, 5th ed., Clarendon Press, Oxford, **1984**.
[20] D. Belli Dell'Amico, F. Calderazzo, U. Giurlani, G. Pelizzi, *Chem. Ber.* **1987**, *120*, 955−964.
[21] C. S. McCowan, T. L. Groy, M. T. Caudle, *Inorg. Chem.* **2002**, *41*, 1120−1127.
[22] N. N. Greenwood, E. Earnshaw, *Chemistry of the Elements*, Pergamon Press, Oxford, **1989**, p. 1443.
[23] A. Merigo, PhD Dissertation, Univ. of Pisa, **2000**.
[24] The samarium derivative $Sm_4(O_2CN{i}Pr_2)_{12}$ has been prepared by U. Baisch in the course of his doctoral thesis work at the Department für Chemie, Ludwigs-Maximilians-Universität München (U. Baisch, W. Schnick, *Z. Anorg. Allg. Chem.* **2003**, *629*, 2073−2078.
[25] W. C. Hamilton, *Statistics in Physical Science*, The Ronald Press Co., N. Y., **1964**, p. 43.
[26] D. Britton, J. D. Dunitz, *Acta Crystallogr., Sect. A* **1973**, *29*, 362−371.
[27] [27a] E. A. Quadrelli, *Inorg. Chem.* **2002**, *41*, 167−169. [27b] D. H. Templeton, C. H. Dauben, *J. Am. Chem. Soc.* **1954**, *76*, 5237. [27c] R. D. Shannon, C. T. Prewitt, *Acta Crystallogr., Sect. B* **1969**, *25*, 925. [27d] R. D. Shannon, *Acta Crystallogr., Sect. A* **1976**, *32*, 751.
[28] U. Baisch, D. Belli Dell'Amico, F. Calderazzo, L. Labella, F. Marchetti, D. Vitali, *J. Mol. Cat. A: Chemical* **2003**, *204−205*, 259−265.
[29] XSCANS, X-ray Single Crystal Analysis System, rel. 2.1, Siemens Analytical X-ray Instruments Inc., Madison, Wisconsin, USA, **1994**.
[30] G. M. Sheldrick, SHELXTL-Plus, rel. 5.1, Siemens Analytical X-ray Instruments Inc., Madison, Wisconsin, USA, **1997**.
[31] G. M. Sheldrick, *Programs for Crystal Structure Analysis* (rel. 97-2), Institut für Anorganische Chemie der Universität, Tammanstrasse 4, 3400 Göttingen, Germany, **1998**.

Received September 12, 2003
Early View Article
Published Online February 16, 2004

 © 2004 Wiley-VCH Verlag GmbH & Co. KGaA, Weinheim

Synthesis, Structure and Characterizations in Solid State and Solution of Dinuclear Pentacoordinated Fe^{II} and Mn^{II} Complexes and of a Linear Tetranuclear Fe^{III} Complex Obtained with the Ligand *N*,*N*,*N*′,*N*′-Tetrakis-[(6-methyl-2-pyridyl)methyl]propane-1,3-diamine

Véronique Balland,[a] Elodie Anxolabéhère-Mallart,*[a] Frédéric Banse,*[a] Eric Rivière,[a] Sophie Bourcier,[b] Martine Nierlich,[c] and Jean-Jacques Girerd*[a]

Keywords: N ligands / Iron / Manganese / Tetranuclear complexes / Bioinorganic chemistry

Two neutral complexes $[(L_6{}^3{}4M)Fe_2Cl_4]\cdot 2H_2O\cdot 2CHCl_3$ (**1**) and $[(L_6{}^3{}4M)Mn_2Cl_4]\cdot CH_3CN$ (**2**) have been synthesized {$L_6{}^3{}4M$ = *N*,*N*,*N*′,*N*′-tetrakis[(6-methyl-2-pyridyl)methyl]propane-1,3-diamine} and their molecular structures established by X-ray crystallography. Both structures are similar, with each metal center in a trigonal-bipyramidal environment. No magnetic coupling is observed between the metal centers. UV/Vis spectra and cyclic voltammograms were recorded in CH_2Cl_2 and CH_3CN solutions. Both complexes are stable in CH_2Cl_2, whereas only **2** is stable in CH_3CN. On the contrary, **1** is in equilibrium with another Fe^{II} species in CH_3CN. When this last solution is aerated, monocrystals of the neutral linear tetranuclear complex $[(L_6{}^3{}4M)Fe_4(\mu\text{-}O)_3Cl_6]\cdot 2CH_3CN$ (**3**) can be isolated. Its structure is unusual with two Fe^{III} ions pentacoordinate and the two others tetracoordinate with only chloro ligands and oxo bridges. The magnetic properties reveal that two consecutive metal centers are strongly antiferromagnetically coupled.
(© Wiley-VCH Verlag GmbH & Co. KGaA, 69451 Weinheim, Germany, 2004)

Introduction

Much of the interest in the coordination chemistry of iron and manganese ions has been driven by their involvement in a number of biological systems, and in particular in the active sites of catalytic systems. Dioxygen interaction with heme- or nonheme-iron enzymes is of fundamental importance in aerobic life processes[1], including metabolism.[2,3] Whatever the system considered, interaction between dioxygen and an Fe^{II} ion leads to a superoxo adduct to Fe^{III}. In dioxygen fixation, this reaction is reversible. For substrate oxidations, reduction of the superoxo group leads to a peroxo form which evolves toward a high-valent iron−oxo entity. Often, complexes synthesized with various amine/polypyridine-, amine/polyimidazole- or polypyrazole-based ligands can reproduce the reactivity and transient peroxo motifs observed in the catalytic cycles of natural systems.[4−6]

To synthesize iron complexes, which are functional or spectroscopic models of the transient species formed during the catalytic cycle of natural systems for alkane hydroxylation, we have used a series of amine/pyridine ligands with variable length and a number of functions.[7] We report here the synthesis and structure of a dinuclear Fe^{II} complex $[(L_6{}^3{}4M)Fe_2Cl_4]\cdot 2H_2O\cdot 2CHCl_3$ (**1**) with the new hexadentate ligand *N*,*N*,*N*′,*N*′-tetrakis[(6-methyl-2-pyridyl)methyl]-propane-1,3-diamine ($L_6{}^3{}4M$; Figure 1), which upon reaction with O_2 leads to a linear tetranuclear Fe^{III} complex $[(L_6{}^3{}4M)Fe_4(\mu\text{-}O)_3Cl_6]\cdot 2CH_3CN$, (**3**). Magnetic data in the solid state, and UV/Vis and electrochemical characterizations in solution are also reported.

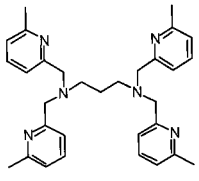

$L_6{}^3{}4M$

Figure 1. Structure of the ligand *N*,*N*,*N*′,*N*′-tetrakis[(6-methyl-2-pyridyl)methyl]propane-1,3-diamine ($L_6{}^3{}4M$)

Given the importance of Mn^{III} tetranuclear complexes in relation with the oxygen-evolving center[8,9] the previous

[a] Laboratoire de Chimie Inorganique, UMR CNRS 8613, Université Paris-Sud,
91405 Orsay, France
[b] Laboratoire des Mécanismes Réactionnels, UMR CNRS 7651, Ecole Polytechnique,
91128 Palaiseau, France
[c] DRECAM/SCM bat 125, CEA Saclay,
91191 Gif-sur-Yvette, France

result prompted us to prepare the analogous Mn complexes. Indeed, we have prepared $[(L_6{}^34M)Mn_2Cl_4]\cdot CH_3CN$ (**2**). Nevertheless, due to the higher oxidation potential for Mn^{III}/Mn^{II}, no reaction was observed with O_2. Electrochemical properties of **1** are presented and compared to those of **2**.

Results and Discussion

X-ray Crystal Structures

The structures of complexes **1** and **2** are analogous, as shown in Figures 2 and 3, respectively. The crystallographic data are reported in Table 4.

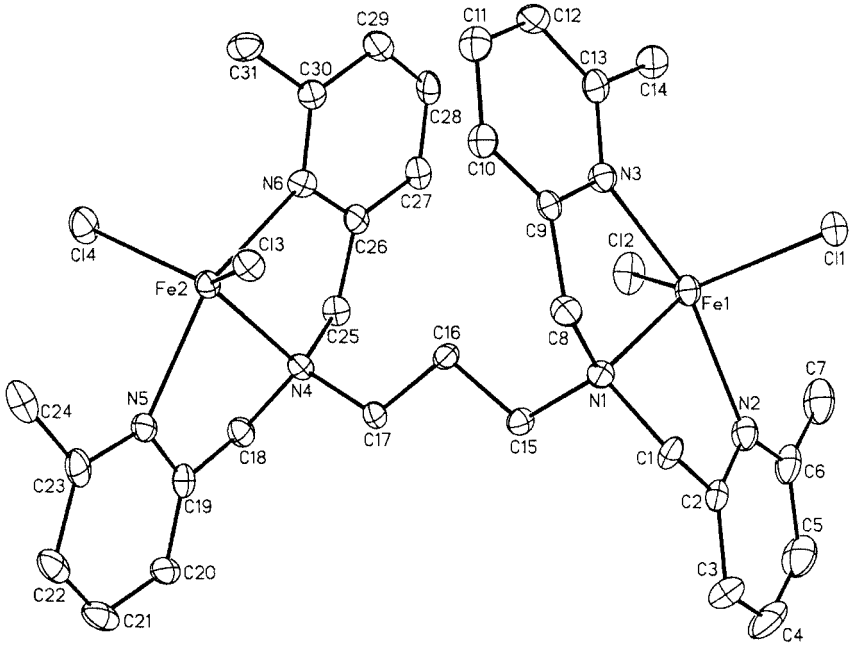

Figure 2. Crystal structure of **1** (2 H_2O and 2 $CHCl_3$ not shown)

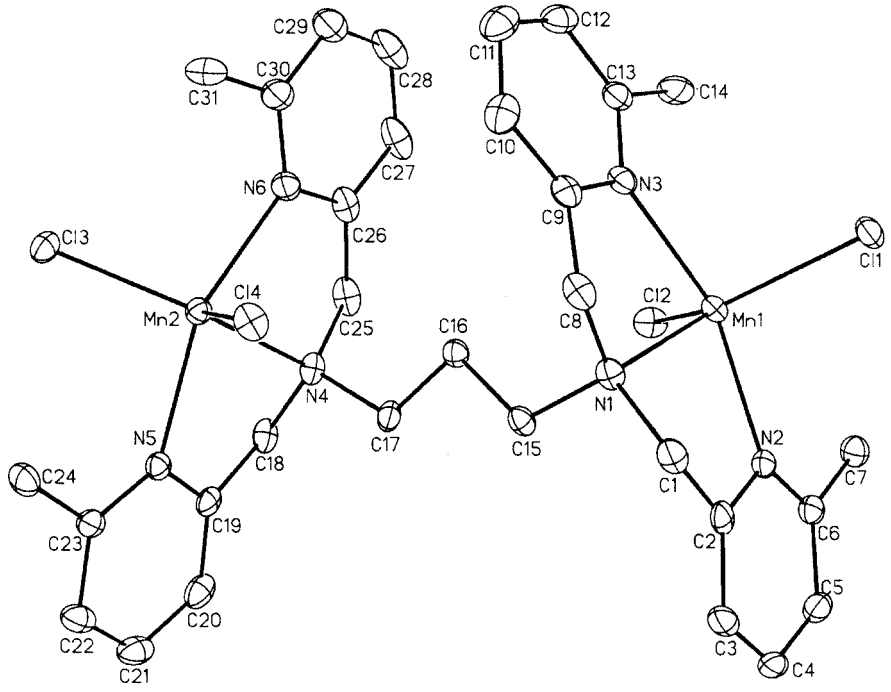

Figure 3. Crystal structure of **2** (CH_3CN not shown)

 © 2004 Wiley-VCH Verlag GmbH & Co. KGaA, Weinheim

The metal/ligand ratio is 2:1 for both complexes and they exhibit two similar coordination sites. Each metal ion is surrounded by three nitrogen atoms from the ligand and two chloride ions. The geometries at the metal centers can be described as distorted trigonal bipyramids with the amino nitrogen atom, the metal center and the two chloro ligands defining the equatorial plane. Complexes containing pentacoordinate Fe^{II} ions with a similar geometry have been recently reported by Britovsek et al. with imine/pyridine ligands.[10]

The bond lengths and angles for **1** and **2** are reported in Table 1. For both complexes, the two coordination sites present small variations of the bond lengths and angles. The metal−N distances, 2.2 Å for Fe^{II} and 2.3 Å for Mn^{II}, are indicative of a high-spin state for each metal.[11−13] For complex **2** the shortest Mn−N distance occurs with the pyridine nitrogen atom, as for complexes with similar aminopyridine ligands,[14,15] which accords with a better π-acceptor character of the pyridines. The correlation between the bond lengths and the π-acceptor character of the ligand indicates minimal steric congestion at the metal center. Coordination of the ligand is therefore governed by electronic interactions. Surprisingly, this effect is not observed with the Fe^{II} complex **1**. The $Fe-N_{amino}$ bonds (ca. 2.19 Å) are shorter than the $Fe-N_{pyridine}$ ones (between 2.21 and 2.26 Å). This can be related to an enhanced steric hindrance at the metal centers in **1**. Indeed, contraction of the metal ion from Mn^{II} to Fe^{II} shortens the metal−ligand distances. However, the steric hindrance provided by the methyl groups on the pyridines lengthens the Fe−pyridine bonds.

Table 1. Selected bond lengths [Å] and angles [°] for complexes **1** and **2**

	1	**2**
M1−Cl1	2.3197(11)	2.3784(14)
M1−Cl2	2.3145(11)	2.3899(14)
M2−Cl3	2.2962(10)	2.3817(16)
M2−Cl4	2.3243(12)	2.3788(15)
M1−N1	2.188(3)	2.302(4)
M1−N2	2.253(3)	2.267(4)
M1−N3	2.217(3)	2.280(4)
M2−N4	2.192(3)	2.320(4)
M2−N5	2.256(3)	2.297(4)
M2−N6	2.230(3)	2.278(4)
Cl1−M1−Cl2	126.10(4)	123.61(6)
Cl3−M2−Cl4	128.93(4)	120.93(6)

The same conclusion is suggested by the Cl−M−Cl angles. For **1**, these are 128.93 and 126.10°, which are very similar to those of complexes with related structures.[10] Compared with **1**, the diminution of the angles observed for the Mn complex **2** (123.61 and 120.93°) is accompanied by elongation of the M−Cl bond lengths, which minimizes the repulsion between both chloride ions. Those Mn^{II}−Cl distances (around 2.38 Å) are shorter than those usually found (around 2.42 Å) for hexacoordinate Mn^{II} complexes containing at least one chloride ion. For a pseudo-square-pyramidal high-spin Mn^{II} complex containing one chloride ion, Bucher et al.[13] observed an even shorter Mn−Cl distance (2.331 Å). Therefore, the diminution of the Mn−Cl distance can be related to both the diminution of the metal coordination number and the steric hindrance around the metal center. The structure of complex **3** is represented in Figure 4.

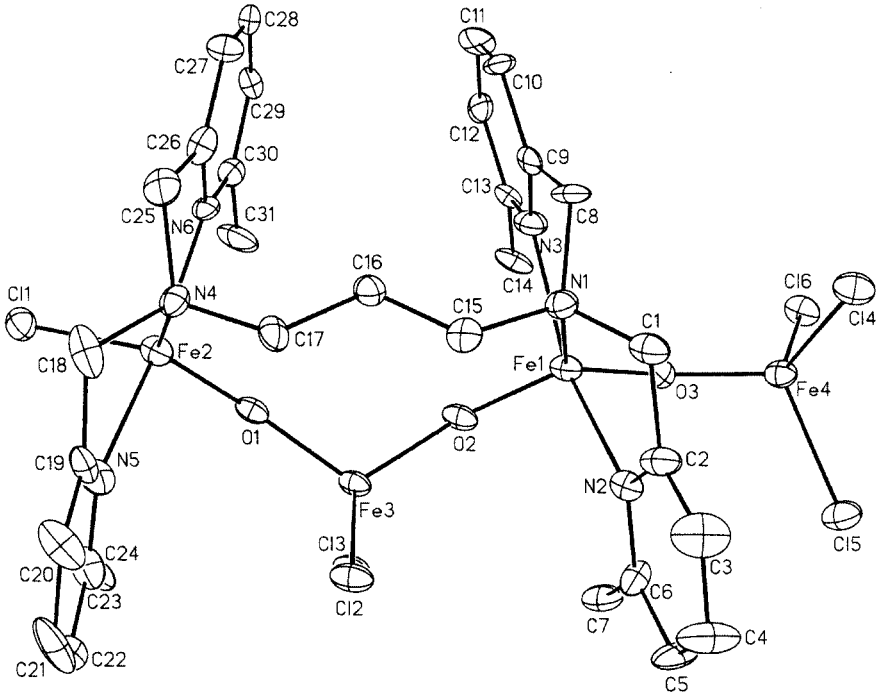

Figure 4. Crystal structure of **3** (2 CH_3CN not shown)

 © 2004 Wiley-VCH Verlag GmbH & Co. KGaA, Weinheim

Table 2. Selected bond lengths [Å] and angles [°] for complex **3**

Fe1−O2	1.765(9)	Fe1−N1	2.203(11)		
Fe1−O3	1.811(9)	Fe1−N2	2.195(11)		
		Fe1−N3	2.176(10)		
Fe2−O1	1.749(9)	Fe2−N4	2.150(11)	Fe2−Cl1	2.251(4)
		Fe2−N5	2.171(11)		
		Fe2−N6	2.159(10)		
Fe3−O2	1.788(9)			Fe3−Cl2	2.260(4)
Fe3−O1	1.812(9)			Fe3−Cl3	2.246(4)
Fe4−O3	1.736(9)			Fe4−Cl4	2.256(4)
				Fe4−Cl5	2.243(4)
				Fe4−Cl6	2.248(4)
Fe1−O2−Fe3	157.3(5)				
Fe1−O3−Fe4	144.7(6)				
Fe2−O1−Fe3	151.4(5)				

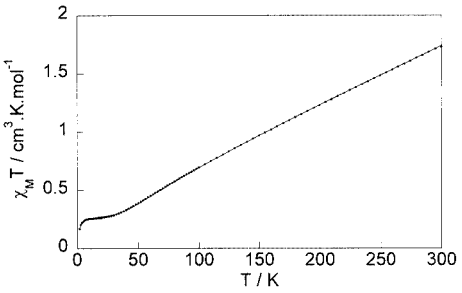

Figure 5. $\chi_M T$ vs. T for **3** (the solid line represents the best fit and the dots represent the experimental data)

The molecule is a neutral tetranuclear Fe^{III} complex, corresponding to the formula $[(L_6{}^3 4M)Fe_4(\mu\text{-}O)_3Cl_6]$. The Fe^{III} ions are in a linear configuration with three single oxo bridges. Selected bond lengths and angles are listed in Table 2.

Several reported tetranuclear Fe^{III} complexes with similar ligands[16−20] all exhibit closed structures with hexacoordinate Fe^{III} ions bridged by oxo and carboxylato groups. With the new ligand $L_6{}^3 4M$, the tetranuclear complex is linear and only two iron centers, Fe(1) and Fe(2), are coordinated to the ligand. As for **1** and **2**, the geometry at those metal centers can be considered as distorted trigonal-bipyramidal since Fe(1) and Fe(2) are surrounded by only three nitrogen atoms from the ligand and two exogeneous ligands: two oxo bridges for Fe(1) and one oxo bridge and one terminal chloride ion for Fe(2). Fe(3) and Fe(4) are not coordinated to the ligand and have tetrahedral geometries. Fe(3) is surrounded by two chloride ions and two bridging oxygen ligands, and Fe(4) by three chloride ions and one bridging oxygen ligand. The Fe(1)/Fe(4) fragment is reminiscent of unsymmetrical diiron(III) complexes.[21−25] As indicated in Table 2, all the Fe−O bond lengths are around 1.8 Å, which is typical of μ-oxo bridges for symmetrical as well as unsymmetrical units.[26] The Fe−O−Fe angles are around 150°, as observed for the other unsymmetrical (μ-oxo)diiron(III) complexes[21−24] with the exception of that reported recently by Raffard−Pons y Moll et al. (ca. 180°).[25]

An unsymmetrical structure, similar to the one of **3**, has been obtained for an $Fe^{III}-Ni^{II}$ complex with diphenylphosphate as bridging and terminal ligands.[27] Thus, the four inorganic centers are the Fe^{III}, the Ni^{II} and the P atoms. However, the structure given here for **3** is, as far as we know, the first reported tetranuclear unsymmetrical unit with only Fe^{III} ions.

Magnetic Properties

The temperature dependence of the magnetic susceptibility was measured for the three complexes in the range 300−5 K.

For complexes **1** and **2** $\chi_M T$ vs. T curves follow a Curie law, indicating no coupling between the metal ions, in agreement with the two independent coordination sites. At room temperature $\chi_M T$ is 6.7 $cm^3 \cdot K \cdot mol^{-1}$ for **1** and 8.9 $cm^3 \cdot K \cdot mol^{-1}$ for **2**. The value obtained for **1** is characteristic of two independent $S = 2$ Fe^{II} ions with $g = 2.11$. For **2**, the two Mn^{II} ions are high spin ($S = 5/2$) with a g of 2.02.

The magnetic susceptibility of the tetranuclear complex **3** as a crystalline powder material was recorded. Experimental data are represented as $\chi_M T$ vs. T in Figure 5, together with the fit.

The data were fitted to the Van Vleck formula,[28] assuming three identical oxo bridges, with full diagonalization of a $6^4 \times 6^4$ matrix. The $\chi_M T$ at 0 K differs from the zero expected and corresponds to a paramagnetic impurity, and the usual Curie−Weiss expression adapted to the high-spin Fe^{II} complex **1** was used to account for this low temperature data. The strong antiferromagnetic coupling obtained is $J = -241$ cm^{-1} and the amount of impurity is 2%. Attempts to fit the curve with three different J values have been made. The quality of the fits obtained was similar to the one reported here. Furthermore, the three J values obtained were of the same order and similar to that found when only one J was considered.

The high antiferromagnetic coupling is quite usual for single oxo-bridged unsymmetrical dinuclear Fe^{III},[21−25] and is reminiscent of the linear tetranuclear Mn^{IV} we obtained previously.[29] When the two central ions (b,c) are strongly antiferromagnetically coupled, the two terminal spins (a,d) appear to be coupled by an antiferromagnetic (AF) effective interaction. In this present case we found that if $IJ_{ab}/J_{bc}\, I << 1$ there is an effective $J_{eff} = 2.5J_{ab}{}^2/J_{bc}$. The lowest spin states are then predicted to be those of an $S_i = 5/2$ pair: $S = 0-5$. The constants obtained here led to first states of $S = 0$ ($E = 0$ cm^{-1}), $S = 1$ ($E = 114$ cm^{-1}), $S = 2$ ($E = 360$ cm^{-1}), $S = 3$ ($E = 760$ cm^{-1}). The next state is not $S = 4$ but $S = 1$ at 1014 cm^{-1}; $S = 4$ is found at $E = 1372$ cm^{-1}. The first states thus obey, qualitatively, the idea proposed, but the agreement is not quantitative since the individual J values do not obey the condition for the validity of the perturbation theory. Qualitatively, we can retain the idea that the two external spins are AF-coupled through an almost diamagnetic system, as explained by Philouze et al.[29]

 © 2004 Wiley-VCH Verlag GmbH & Co. KGaA, Weinheim

EPR

The EPR spectrum of complex **2** was recorded as a frozen solution in CH_2Cl_2 at 4 K in the range 500−8000 G (Figure 6). There are no hyperfine transitions, while the broad resonances seen are typical of low-symmetry mononuclear Mn^{II} complexes,[13,30] which is consistent with the independence of the two metal centers. The main derivative line at $g = 4.2$ indicates a rhombic symmetry with E/D close to 1/3. According to this attribution, the spectrum is similar to those obtained by simulation with D between 0.2 and 0.3 cm^{-1}.[31] As far as we know, **2** is the first trigonal-bipyramidal complex with both X-ray structure and EPR characterizations.

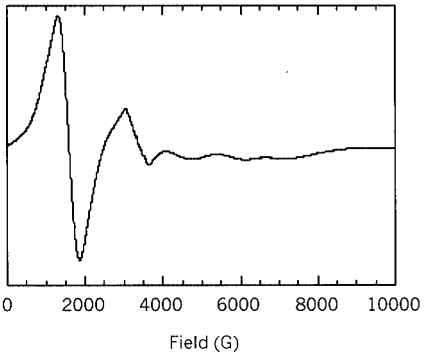

Figure 6. EPR spectra of **2** recorded in CH_2Cl_2 at 4 K at the frequency of 9.38667 GHz

No signal could be detected (at 4 K) for **3** dissolved CH_3CN. The neutral structure characterized for **3** in the solid state remains, therefore, intact in CH_3CN.

UV/Vis

UV/Vis spectra of both **1** and **2**, recorded in CH_2Cl_2, show an intense band at 268 nm that is attributed to pyridine π−π* transitions.

The Fe^{II} complex **1** shows two other bands, at 313 and 390 nm, corresponding to MLCT transitions from Fe^{II} to pyridine π* orbitals. The calculated ε values are 950 and 880 $M^{-1}\cdot cm^{-1}$, respectively. The intensity of those bands is usually around 1000 $M^{-1}\cdot cm^{-1}$ for high-spin Fe^{II} complexes.[32]

For complex **2**, no bands other than the 268 nm one are observed, except for a shoulder at 313 nm with an ε of 400 $M^{-1}\cdot cm^{-1}$.

The UV/Vis spectrum of **3** recorded in CH_3CN (Figure 7) presents three intense bands below 400 nm. The first at 262 nm is attributed to pyridine π−π* transitions with an ε of 29000 $M^{-1}\cdot cm^{-1}$. A large band with several components is observed around 335 nm (ε = 23000 $M^{-1}cm^{-1}$). In this 320−350 nm area, intense $Cl^-\rightarrow Fe^{III}$ charge-transfer bands are expected, as reported previously for dinuclear complexes with $-O-FeCl_3$ fragments,[23,25] and possibly amine-to-metal charge transfer as well.[33,34] The other intense band (381 nm, ε = 20000 $M^{-1}\cdot cm^{-1}$) may be attributed to an oxo→Fe^{III} charge-transfer transition.[35,36] The spectral features reported for μ-oxodiiron(III) complexes with aminopyridine and chloro ligands, which present an intense band around 320 nm and another at about 380 nm,[37,38] are also consistent with these assignments.

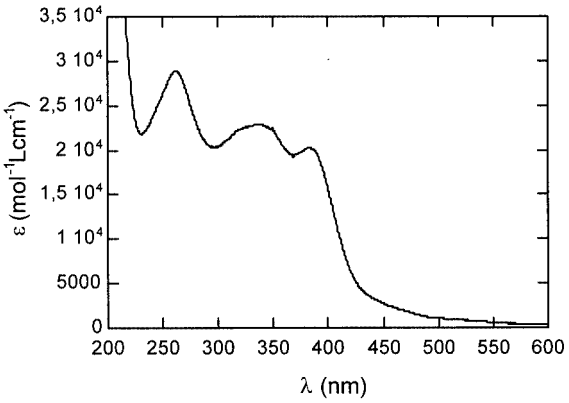

Figure 7. UV/Vis spectrum of the tetranuclear complex **3** in acetonitrile; the extinction coefficients are calculated per one molecule

Electrochemistry

The electrochemical behavior in CH_2Cl_2 of **1** (Figure 8) reveals an oxidation wave at $E_p = 0.63$ V. On the reverse scan, two waves are observed, at 0.53 and 0.04 V. Based on the peak height[39] the wave at 0.63 V is attributed to a two-electron oxidation corresponding to the simultaneous oxidation of the two Fe^{II} sites. The intensity of the cathodic wave at 0.5 V is smaller than the anodic one, thus indicating that the wave is not totally chemically reversible. Indeed, a second cathodic wave is seen on the reverse scan at a less positive potential ($E_p = 0.04$ V). The cyclic voltammogram of **1** can be compared with those reported for several complexes obtained with tetradentate aminopyridine ligand and two chloride ions. The electrochemical potentials for the Fe^{II}/Fe^{III} redox process are observed between 0 and 0.3 V.[12] The much higher potential observed here is related to the pentacoordinate geometry adopted by the iron center, which destabilizes the Fe^{III} species.

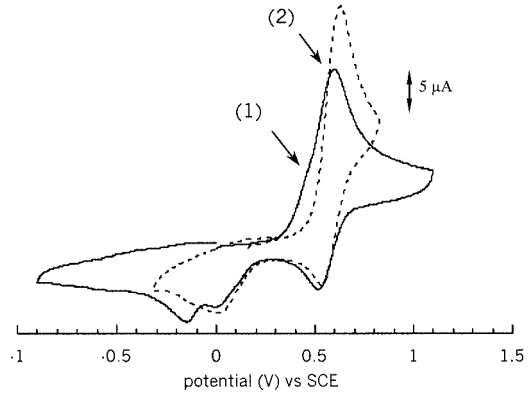

Figure 8. Cyclic voltammogram recorded in CH_2Cl_2 (- - -) and CH_3CN (———) under argon for **1**; concentration 1 mM, scan rate 100 mV s^{-1}, temperature 20 °C

 © 2004 Wiley-VCH Verlag GmbH & Co. KGaA, Weinheim

The cyclic voltammogram recorded at 100 mV·s^{-1} on a CH_2Cl_2 solution of **2** (Figure 9) shows two oxidation waves, at 1.15 and 1.65 V. Reversing the potential scanning at 1.35 V allows the reversibility of the first wave to be observed ($E_{1/2}$ = 1.1 V; ΔE_p = 100 mV). The intensity of the peak indicates a two-electron process, attributed to the oxidation of the two Mn^{II} ions. The characteristic oxidation peak of the free chloride ion at 1.3 V is, notably, not observed, indicating that the two chloride ions both remain coordinated to the Mn^{II} ion and to the generated Mn^{III} center. The second oxidation wave (1.65 V) is totally irreversible, even when the scan rate is increased to 5 V s^{-1}. This second oxidation is attributed to the generation of an Mn^{IV} species − a strong oxidant that readily reacts with any trace of nucleophilic impurity in the solvent − and, therefore, no reversibility of the oxidation wave is seen under the present experimental conditions. Electrochemical data reported for Mn complexes with chloro ligands are listed in Table 3.

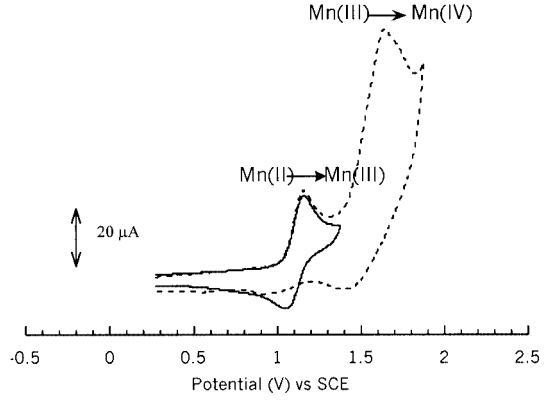

Figure 9. Cyclic voltammogram recorded in CH_2Cl_2 for **2**; concentration 1 mM, scan rate 100 mV s^{-1}, temperature 20°C

The electrochemical potential for the Mn^{II}/Mn^{III} process for **2** is much higher than those reported for mononuclear hexacoordinate Mn^{II} with two chloride ions.[40] However, it is similar to that obtained for a pentacoordinate monochloro−Mn^{II} complex for which $E_{1/2}$ = 1.14V.[13] It is surprising that the $E_{1/2}$ values are so close for both pentacoordinate complexes as the number of chloride ions coordinated is different.

In the electrogenerated $[2]^{2+}$ species the manganese ion is pentacoordinate with two chloride ions. This species was found to be more stable than the pentacoordinate monochloro−Mn^{III} complex obtained by Bucher.[13] Indeed, Bucher et al. observed a reorganization of the Mn^{III} species, leading to an hexacoordinate complex. Moreover, the pentacoordinate $[\mathbf{2}]^{2+}$ species is oxidized at a higher potential (1.65 V) than the hexacoordinate dichloro−Mn^{III} complex obtained by Hubin et al.[40] (1.33 V) and lies in the same range as the hexacoordinate monochloro−Mn^{III} complex reported by Brudenell et al. (1.56 V).[14] Complex **2** was also studied in CH_3CN. The cyclic voltammetry shows potentials identical to the one in CH_2Cl_2 solution.

Conversion of Complex 1 into Complex 3

Complex **1**, which is stable in aerated CH_2Cl_2, reacts upon O_2 exposure in CH_3CN to form complex **3**. To understand the chemical or structural modifications allowing this reactivity, complex **1** was studied in CH_3CN by cyclic voltammetry. Under argon, two anodic signals were observed, at 0.46 and 0.60 V (denoted 1 and 2 in Figure 8). The reverse scan showed three cathodic waves, at 0.5, 0 and −0.15 V. Increasing the scan rate led to the disappearance of wave 1 and the increase of wave 2 (not shown). The intensity of the resulting unique oxidation wave was identical to that observed in CH_2Cl_2 This behavior indicates that the two oxidation waves correspond to two Fe^{II} species in equilibrium. By analogy with the study in CH_2Cl_2, wave 2 is attributed to a two-electron oxidation of the neutral complex **1** and is therefore correlated to the two reduction peaks at 0.5 and 0 V. The first oxidation signal (0.46 V) is completely irreversibile. The relative intensity of waves 1 and 2 indicates that the amount of Fe^{II} species responsible for the anodic process at 0.46 V is very low in solution. Nevertheless, it is very likely that this Fe^{II} species, which forms only in CH_3CN, is responsible for the reactivity of **1** with O_2 in the same solvent. Similar behavior has been observed with a parent Fe^{II} complex,[7,25] for which the reactivity with O_2 was related to its slight instability in CH_3CN.

When the solution was open to air, the intensity of the wave at −0.15 V increased. This wave (−0.15 V) was also observed when the potential was scanned from 0.25 V towards reduction potential, thus indicating the air oxidation of the bulk solution. Concomitantly, UV/Vis spectra

Table 3. Cyclic voltammetry data for several Mn complexes; $E_{1/2}$ given vs. SCE; for irreversible waves E_P only is given

	II/III	III/IV	(II,II)/(III,III)	(III,III)/(IV,IV)	Ref.
($L_6^3$4M)Mn_2Cl_4 (**2**)			1.1	1.65 (E_P)	this work
$[Mn(L_1)Cl_2]PF_6$ [a]	0.34	1.1			[40]
$[Mn(L_2)Cl_2]PF_6$ [b]	0.16	0.93			[40]
[Mn(dmptacn)Cl]ClO_4 [c]	0.71	1.33			[14]
$[Mn_2(tmpdtnp)Cl_2](ClO_4)_2$ [d]			0.82	1.56 (E_P)	[14]
[(tmc)MnCl]BF_4 [e]	1.14	1.36			[13]

[a] L_1 = 4,11-dimethyl-1,4,8,11-tetraazabicyclo[6.6.2]hexadecane. [b] L_2 = 4,10-dimethyl-1,4,7,10-tetraazabicyclo[5.5.2]tetradecane. [c] dmptacn = 1,4-bis(2-pyridylmethyl)-1,4,7-triazacyclononane. [d] tmpdtnp = 1,3-bis[4,7-bis(2-pyridylmethyl)-1,4,7-triazacyclonon-1-yl]propane. [e] tmc = 1,4,8,11-tetramethyl-1,4,8,11-tetraazacyclotetradecanes.

 © 2004 Wiley-VCH Verlag GmbH & Co. KGaA, Weinheim

were recorded on the same CH_3CN solution of **1**. The spectrum did not show any change under argon. On the contrary, two large absorption bands at 335 and 360 nm appeared when the solution was exposed to air. These new bands are tentatively attributed to the formation in CH_3CN solution of a polynuclear Fe^{III} species with Cl^- ligands and oxo bridges.[23−25] Most likely, this species is responsible for the cathodic wave at −0.15 V.

In the mass spectrum of a CH_3CN solution of **1** under air the peak seen at m/z= 836 is attributed, according to the isotopic distribution, to the $[(L_6{}^34M)Fe_3(\mu\text{-}O)_2Cl_4]^+$ cation (Figure 10). A second peak, at m/z = 621.2, is attributed to the Fe^{II} complex $[(L_6{}^34MH)FeCl_2]^+$. It is attractive to propose that the UV/Vis spectrum with absorption bands at 335 and 360 nm as well as the −0.15 V reduction wave are related to the cation $[(L_6{}^34M)Fe_3(\mu\text{-}O)_2Cl_4]^+$. The ultimate entity isolated from this CH_3CN solution was the structurally characterized tetranuclear complex $[(L_6{}^34M)Fe_4(\mu\text{-}O)_3Cl_6]$, and therefore $[(L_6{}^34M)Fe_3(\mu\text{-}O)_2Cl_4]^+$ can be considered as a precursor of the tetranuclear complex. A possible structure for $[(L_6{}^34M)Fe_3(\mu\text{-}O)_2Cl_4]^+$ is presented in Figure 11.

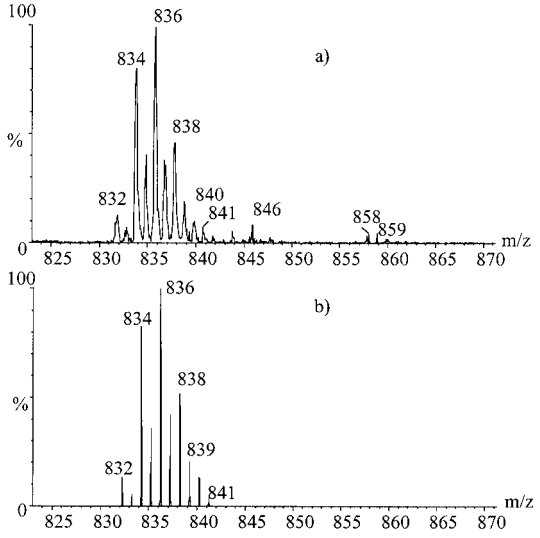

Figure 10. ESI-MS of $[(L_6{}^34M)Fe_3(\mu\text{-}O)_2Cl_4]^+$: (a) experimental spectrum; (b) calculated spectrum

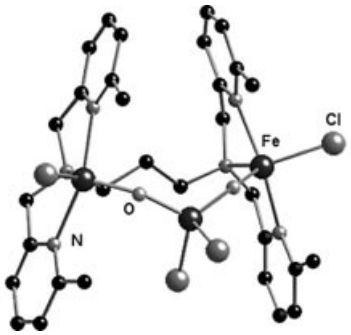

Figure 11. Possible structure for $[(L_6{}^34M)Fe_3(\mu\text{-}O)_2Cl_4]^+$

Conclusion

The neutral complexes **1** and **2** have been obtained and characterized. They present identical structures: each contains high-spin pentacoordinate metal centers in a trigonal-bipyramidal environment. The metal centers are involved in two different coordination sites and present no magnetic coupling. Both complexes are stable in CH_2Cl_2 solution and their neutral structure is retained. However, in CH_3CN, **2** is stable whereas **1** is unstable and transforms partially into a new complex species that equilibrates with **1**, as indicated by cyclic voltammogram. This latter complex is probably responsible for the reactivity of **1** with O_2 in CH_3CN, which leads to the formation of the linear tetradentate neutral complex **3**. The four metal centers are strongly antiferromagnetically coupled by single oxo bridges and exhibit different coordination sites: two are bound to the ligand and pentacoordinate whereas the two others are only tetracoordinate with chloro ligands and oxo bridges in their coordination sphere. This structure is uncommon and is, to the best of our knowledge, the first reported linear tetraferric complex.

Experimental Section

General Methods: All manipulations were carried out by using standard Schlenk techniques. Starting materials were purchased from Acros. Solvents were purchased from Merck and used without further purification.

Physical Methods: Electronic absorption spectra were recorded with a Varian Cary 5E spectrophotometer. FT-IR spectra were recorded with a Perkin−Elmer Spectrum1000 (s = sharp, i = intense, m = medium, w = weak, b = broad). Magnetic data were recorded with an MPMS5 magnetometer (Quantum Design Inc.). The calibration was made at 298 K using a palladium reference sample furnished by Quantum Design Inc. EPR spectra were recorded with an X-band Bruker ESP 300 E. Cyclic voltammograms were measured using an EGG PAR model M270 scanning potentiostat operating at a scan rate of 10−1000 mV s^{-1}. Studies were carried out under argon in acetonitrile or CH_2Cl_2 solutions using 0.2 M tetrabutylammonium perchlorate (puriss. grade, Fluka) as the supporting electrolyte, and 10^{-3} M of the complex. The working electrode was a glassy-carbon disk (0.32 cm^2) polished with 1 μm polishing powder. The reference electrode was $Ag/AgClO_4$ (+0.3 V vs. SCE), which was separated from the rest of the solution by a salt bridge containing the solvent/supporting electrolyte, with a Pt wire as an auxiliary electrode. All potentials are given vs. SCE electrode. The $E_{1/2}$ potentials are calculated as the mid-point between the anodic and the cathodic peak potentials. The mass spectra of ions formed by electrospray were acquired with a Quattro II (Micromass, Manchester, UK) triple quadrupole mass spectrometer. Typical optimized values for the source parameters were: capillary 2.5 kV, counter-electrode 0.49 kV source temperature of 80°C, RF lens 0.5 V, skimmer lens offset 0; cone voltage 20 V. Sample solutions were prepared in CH_3CN. All solutions were infused at a flow rate of 10 μL min^{-1} by a Harvard Apparatus (Southnatic, MA, USA) syringe pump. Crystallographic data were collected with a Nonius Kappa CCD area detector diffractometer[41] using graphite-monochromated Mo-K_α radiation. The lattice parameters were determined from ten images recorded with 2° -scans and later re-

 © 2004 Wiley-VCH Verlag GmbH & Co. KGaA, Weinheim

Table 4. Crystallographic data for complexes **1**−**3**

	1	**2**	**3**
Empirical formula	$C_{33}H_{44}Cl_{10}Fe_2N_6O_2$	$C_{33}H_{41}Cl_4Mn_2N_7$	$C_{35}H_{44}Cl_6Fe_4N_8O_3$
Formula mass	1022.94	787.41	1060.88
Crystal size [mm]	0.20 × 0.15 × 0.05	0.20 × 0.10 × 0.10	0.10 × 0.05 × 0.01
Temperature [K]	123	123	123
Crystal system	monoclinic	monoclinic	triclinic
Space group	$P2_1/c$	$P2_1/c$	$P\bar{1}$
a [Å]	19.811(4)	15.893(3)	10.130(2)
b [Å]	8.497(2)	15.408(3)	11.743(2)
c [Å]	26.687(5)	16.796(3)	19.080(4)
α [°]	90	90	87.21(3)
β [°]	103.94(3)	116.49(3)	83.50(3)
γ [°]	90	90	85.89(3)
V [Å^3]	4360(1)	3681(1)	2247.4(8)
Z	4	4	2
μ [mm^{-1}]	1.316	1.010	1.665
F(000)	2088	1624	1080
λ (Mo-K_α)	0.71073	0.71073	0.71073
2θ range [°]	2.52, 24.71	2.71, 24.71	2.58, 24.77
$h_{min.}/h_{max.}$	0, 23	0, 18	0, 11
$k_{min.}/k_{max.}$	0, 9	0, 15	−13, 13
$l_{min.}/l_{max.}$	−31, 30	−19, 17	−19, 19
No. of measured reflections	19700	22959	13975
No. of unique reflections	7199	5811	7078
No. of refined parameters	505	415	505
$R1$ [on F^2, $I > 2\sigma(I)$]	0.0708	0.0479	0.0970
$wR2$ (on F^2)	0.1674	0.1273	0.191

fined on all data. The data were recorded at 123 K. A 180° -range was scanned with 2° steps with a crystal−detector distance fixed at 30 mm. Data were corrected for Lorentz polarization. The structures were solved by direct methods with SHELXS[42] and refined by full-matrix least squares on F^2 with anisotropic thermal parameters for all non-H atoms with SHELXL-97.[43] In complex **1**, one solvent molecule ($CHCl_3$) was disordered on two sites with 0.5 occupancy. H atoms (except H atoms of solvent molecules, CH_3Cl and H_2O in **1**, CH_3CN in **2** and **3**) were introduced at calculated positions as riding atoms with isotropic displacement parameters of 1.2 (CH, and CH_2) or 1.5 (CH_3) times that of the parent atom. Molecular plots were drawn with SHELXTL.[44] All calculations were performed with a Silicon Graphics R10000 workstation. CCDC-199949 (**1**), -199950 (**3**), -199951 (**2**) contain the supplementary crystallographic data for this paper. These data can be obtained free of charge at www.ccdc.cam.ac.uk/conts/retrieving.html [or from the Cambridge Crystallographic Data Centre, 12 Union Road, Cambridge CB2 1EZ, UK; Fax: (internat.) + 44-1223/336-033; E-mail: deposit@ccdc.cam.ac.uk].

Synthesis of $L_6^3$4M: *N*,*N*,*N*′,*N*′-Tetrakis[(6-methyl-2-pyridyl)methyl]propane-1,3-diamine. The ligand was synthesized as *N*,*N*,*N*′,*N*′-tetrakis(2-pyridylmethyl)ethane-1,2-diamine[45] using 2-(chloromethyl)-6-methylpyridine hydrochloride (8 g) and propane-1,3-diamine (835 μL) as starting materials. The product was recrystallized from cyclohexane and obtained as a white powder (4.35 g).

Synthesis of $[(L_6^3$4M)$Fe_2Cl_4]\cdot 2H_2O\cdot 2CHCl_3$ (1): 1 equiv. of ligand (100 mg) in THF (2 mL) was added to a solution of 2 equiv. of $FeCl_2\cdot 2H_2O$ (66 mg) in THF (3 mL) under argon. The mixture was then stirred at room temperature for 30 min and concentrated. After removal of most of the solvent, a yellow solid precipitated, which was filtered off (80 mg, 53% yield). $C_{31}H_{38}Cl_4Fe_2N_6\cdot H_2O$ (766.21): calcd. C 48.60, H 5.26, N 10.97; found C 48.66, H, 5.22, N 10.33. FT-IR: $\tilde{\nu}$ = 1605 (s, i), 1577 (s, m), 1458 (s, i), 1043 (s, w), 1010 (s, m), 841 (s, w), 782 (s, m) cm^{-1}. Crystals of **1** were obtained by slow diffusion of *tert*-butyl methyl ether into a solution of the powder dissolved in $CHCl_3$.

Synthesis of $[(L_6^3$4M)$Mn_2Cl_4]\cdot 2CH_3CN$ (2): 1 equiv. of ligand (50 mg) in THF (2 mL) was added to a solution of 2 equiv. of $MnCl_2\cdot 4H_2O$ (40 mg) in THF (4 mL). The mixture was then stirred at room temperature for 30 min, and the resultant white precipitate was filtered off and collected (56 mg, 74% yield). $C_{31}H_{38}Cl_4Mn_2N_6$ (746.4): calcd. C 49.88, H 5.13, N 11.26; found C 49.19, H, 5.17, N 11.97. FT-IR: $\tilde{\nu}$ = 1607 (s, i), 1578 (s, i), 1454 (s, i), 1043 (s, w), 1010 (s, mi), 860 (s, m), 781 (b, m), 300 (b, m) cm^{-1}. The white powder was dissolved in CH_3CN and crystals of **2** were obtained by slow diffusion of *tert*-butyl methyl ether into the solution. All characterizations of complex **2** were performed with crystals.

Synthesis of $[(L_6^3$4M)$Fe_4(\mu\text{-}O)_3Cl_6]\cdot 2CH_3CN$ (3): Complex **3** was isolated after evolution of a solution of **1** in CH_3CN in air; X-ray quality crystals were obtained by slow evaporation of the solvent CH_3CN. In an alternative method a solution of **1** in CH_3CN was heated under air at 70°C for 24 h. Crystals of **3** were obtained after an additional 24 h, when the solution was allowed to cool to room temperature. $C_{31}H_{38}Cl_6Fe_4N_6O_3$ (978.8): calcd. C 38.04, H 3.91, N 8.58; found C 37.70, H 3.87, N 8.54. FT-IR: $\tilde{\nu}$ = 1610 (s, i), 1578 (s, m), 1469 (s, i), 1456 (s, i), 854 (s, i), 818 (b, i), 790 (s, i), 352 (s, i) cm^{-1}. The three bands around 800 cm^{-1} can be attributed to Fe−O modes, by comparison with other (μ-oxo)diiron(III) complexes.[26]

[1] S. J. Lippard, J. M. Berg, *Principles of Bioinorganic Chemistry*, University Sciences Books, Mill Valley, **1994**.
[2] M. Sono, M. P. Roach, E. D. Coulter, J. H. Dawson, *Chem. Rev.* **1996**, *96*, 2841.
[3] B. J. Wallar, J. D. Lipscomb, *Chem. Rev.* **1996**, *96*, 2625.

 © 2004 Wiley-VCH Verlag GmbH & Co. KGaA, Weinheim

[4] K. C. M. Costas, L. Que, K. Chen, L. Que, *Coord. Chem. Rev.* **2000**, *200−202*, 517.
[5] J. Dubois, T. J. Mizoguchi, S. J. Lippard, *Coord. Chem. Rev.* **2000**, *200−202*, 443.
[6] J.-J. Girerd, F. Banse, A. J. Simaan, *Struct. Bonding.* **2000**, *97*, 146.
[7] N. Raffard, V. Balland, J. Simaan, S. Létard, M. Nierlich, K. Miki, F. Banse, E. Anxolabéhère-Mallart, J.-J. Girerd, *C. R. Chim.* **2002**, *5*, 99.
[8] V. K. Yachandra, M. P. Klein, *Chem. Rev.* **1996**, *96*, 2927.
[9] W. Rüttinger, G. C. Dismukes, *Chem. Rev.* **1997**, *97*, 1.
[10] G. J. P. Britovsek, V. C. Gibson, B. S. Kimberley, S. Mastroianni, C. Redshaw, G. A Solan, A. J. P. White, D. J. Williams, *J. Chem. Soc., Dalton Trans.* **2001**, 1639.
[11] J. Bernal, I. M. Jensen, K. B. Jensen, C. J. Mckenzie, H. Toftlund, J-P. Tuchagues, *J. Chem. Soc., Dalton Trans.* **1995**, 3667.
[12] J. Simaan, J. Guilhem, S. Poussereau, G. Blondin, J-J. Girerd, D. Defaye, C. Philouze, J. Guilhem, L. Tchertanov, *Inorg. Chim. Acta* **2000**, *299*, 221.
[13] C. Bucher, E. Duval, J-M. Barbe, J-N. Verpeaux, C. Amatore, R. Guilard, L. Le Pape, J-M. Latour, S. Dahaoui, C. Lecomte, *Inorg. Chem.* **2001**, *40*, 5722.
[14] S. J. Brudenell, L. Spiccia, A. M. Bond, G. D. Fallon, D. C. R. Hockless, G. Lazarev, P. J. Mahon, E. R. T. Tiekink, *Inorg. Chem.* **2000**, *39*, 881.
[15] I. Romero, M-N. Collomb, A. Deronzier, A. Llobet, E. Perret, J. Pécaut, L. Lepape, J.-M. Latour, *Eur. J. Inorg. Chem.* **2001**, 69.
[16] H. Toftlund, K. S. Murray, P. R. Zwack, L. F. Taylor, O. P. Anderson, *J. Chem. Soc., Chem. Commun.* **1986**, 2673.
[17] J. L. Sessler, J. W. Sibert, V. Lynch, *Inorg. Chem.* **1990**, *29*, 4143.
[18] J. L. Sessler, J. W. Sibert, V. Lynch, J. T. Markert, C. L. Wooten, *Inorg. Chem.* **1993**, *32*, 621.
[19] N. Arulsamy, J. Glerup, D. J. Hodgson, *Inorg. Chem.* **1994**, *33*, 3043.
[20] A. K. Boudalis, N. Lalioti, G. A. Spyroulias, C. P. Raptopoulou, A. Terzis, V. Tangoulis, S. P. Perlepes, *J. Chem. Soc., Dalton Trans.* **2001**, 955.
[21] P. Gomez-Romero, G. C. Defotis, G. B. Jameson, *J. Am. Chem. Soc.* **1986**, *108*, 851.
[22] P. Gomez-Romero, E. H. Witten, W. M. Reiff, G. B. Jameson, *Inorg. Chem.* **1990**, *29*, 5211.
[23] P. Gómez-Romero, E. H. Witten, W. M. Reiff, G. Backes, J. Sanders-Loehr, G. B. Jameson, *J. Am. Chem. Soc.* **1989**, *111*, 9039.
[24] J. Wang, M. S. Mashuta, Z. Sun, J. F. Richardson, D. N. Hendrickson, R. M. Buchanan, *Inorg. Chem.* **1996**, *35*, 6642.
[25] N. Raffard-Pons Y Moll, F. Banse, K. Miki, M. Nierlich, J.-J. Girerd, *Eur. J. Inorg. Chem.* **2002**, 1941.
[26] D. M. Kurtz Jr., *Chem. Rev.* **1990**, *90*, 585.
[27] L. Yin, P. Cheng, S. P. Yan, X-Q. Fu, J. Li, D.-Z. Liao, Z.-H. Jiang, *J. Chem. Soc., Dalton Trans.* **2001**, 1398.
[28] O. Kahn, *Molecular Magnetism*, VCH Publishers, New York, Weinheim, Cambridge, **1993**.
[29] C. Philouze, G. Blondin, J.-J. Girerd, J. Guilhem, C. Pascard, D. Lexa, *J. Am. Chem. Soc.* **1994**, *116*, 8557.
[30] R. D. Dowsing, J. F. Gibson, M. Goodgame, P. J. Hayward, *J. Chem. Soc., A* **1970**, 1133.
[31] F. E. Mabbs, D. Collison, *Electron Paramagnetic Resonance of d Transition Metal Compounds*, Elsevier, Amsterdam, **1992**.
[32] P. Mialane, A. Novorojkine, G. Pratviel, L. Azéma, M. Slany, F. Godde, A. Simaan, F. Banse, T. Kargar-Grisel, G. Bouchoux, J. Sainton, O. Horner, J. Guilhem, L. Tchertanova, B. Meunier, J. J. Girerd, *Inorg. Chem.* **1999**, *38*, 1085.
[33] S. Poussereau, G. Blondin, M. Césario, J. Guilhem, G. Chottard, F. Gonnet, J.-J. Girerd, *Inorg. Chem.* **1998**, *37*, 3127.
[34] M. D. Snodin, L. Oud-Moussa, U. Wallmann, S. Lecomte, V. Bachler, E. Bill, H. Hummel, T. Weyermüller, P. Hildebrandt, K. Wiegardt, *Chem. Eur. J.* **1999**, *5*, 2554.
[35] C. A. Brown, G. J. Remar, R. L. Musselman, E. I. Solomon, *Inorg. Chem.* **1995**, *34*, 688.
[36] P. C. Junk, B. J. Mccool, B. Moubaraki, K. S. Murray, L. Spiccia, J. D. Cashion, J. W. Steed, *J. Chem. Soc., Dalton Trans.* **2002**, 1024.
[37] A. Hazell, K. B. Jensen, C. J. Mckenzie, H. Toftlund, *Inorg. Chem.* **1994**, *33*, 3127.
[38] A. Nivorozhkin, E. Anxolabéhère-Mallart, P. Mialane, R. Davydov, J. Guilhem, M. Cesario, J.-P. Audière, J.-J. Girerd, S. Styring, L. Schussler, J.-L. Seris, *Inorg. Chem.* **1997**, *36*, 846.
[39] The intensity of the oxidation wave was compared with that of a related Fe^{II} complex (ref.[7]), for which it was shown that the wave was a one-electron oxidation process.
[40] T. H. Hubin, J. M. Mccormick, N. W. Alcock, D. H. Bush, *Inorg. Chem.* **2001**, *40*, 435.
[41] N. B. V. Kappa-Ccd Software, Delft, The Netherlands, **1998**.
[42] G. M. Sheldrick, *Acta Chrystallogr., Sect. A* **1990**, 467.
[43] G. M. Sheldrick, *SHELXTL-97, Program for the refinement of crystal structures*, University of Göttingen, Germany, **1997**.
[44] G. M. Sheldrick, University of Göttingen, Germany, **1999**; distributed by Bruker AXS, Madison, Wisconsin, USA.
[45] H-R. Chang, J. K. McCuster, H. Toflund, S. R. Wilson, A. X. Trautwein, H. Winkler, D. N. Hendrickson, *J. Am. Chem. Soc.* **1990**, *112*, 6814.

Received June 18, 2003
Early View Article
Published Online February 16, 2004

 © 2004 Wiley-VCH Verlag GmbH & Co. KGaA, Weinheim

Synthesis and Carbonylation of Platinum(II) Organometallic Complexes with Bis(phosphanyl) Monosulfides − Crystal Structures of [κ^2*P*,*S*-{$Ph_2CH_2P(S)Ph_2$}Pt(CH_3)(Cl)] and [κ*P*,μ-κ*S*-{$Ph_2CH_2CH_2P(S)Ph_2$}Pt-(CH_3)]$_2$[BF_4]$_2$

Piero Mastrorilli,[a] Cosimo F. Nobile,*[a] Gian P. Suranna,[a] Francesco P. Fanizzi,[b,f] Giuseppe Ciccarella,[c] Ulli Englert,[d] and Qi Li[e]

Dedicated to Professor Adriano Sacco on the occasion of his 80th birthday

Keywords: Platinum / P,S ligands / Carbonyl ligands / Bridging ligands / Mass spectrometry

The neutral complexes of formula [κ^2*P*,*S*-(dppmS)Pt(CH_3)(Cl)] (**1**) and [κ^2*P*,*S*-(dppeS)Pt(CH_3)(Cl)] (**2**) [dppmS = $Ph_2PCH_2P(S)Ph_2$, dppeS = $Ph_2P(CH_2)_2P(S)Ph_2$] have been synthesised and characterised. Reaction of **1** and **2** with $AgBF_4$ carried out in CH_3CN or CH_3CN/CH_2Cl_2 affords the corresponding monomeric cationic complexes [κ^2*P*,*S*-(dppmS)Pt(CH_3CN)(CH_3)][BF_4] (**3**) and [κ^2*P*,*S*-(dppeS)Pt(CH_3CN)(CH_3)][BF_4] (**4**). Complexes **3** and **4** partially dissociate in CD_2Cl_2, giving, in the case of **3**, the asymmetric dimer {[κ^2*P*,*S*-(dppmS)](CH_3)Pt{κ*P*,μ-κ*S*-(dppmS)}Pt(CH_3)(CH_3CN)][BF_4]$_2$ (**5**), and, in the case of **4**, the symmetrical sulfur-bridged dimer [κ*P*,μ-κ*S*-(dppeS)Pt(CH_3)]$_2$[BF_4]$_2$ (**6**). Pure **6** can be obtained by heating **4** under vacuum. Exposing CD_2Cl_2 solutions of the cationic complexes **3** and **4** to CO at ambient conditions brings about the formation of the monomeric methyl carbonyl complexes [κ^2*P*,*S*-(dppmS)Pt(CO)(CH_3)][BF_4] (CO *trans* to P, **7a**) and [κ^2*P*,*S*-(dppeS)Pt(CO)(CH_3)][BF_4] (CO *trans* to P, **8a**), which slowly transform into their CO *cis* to P isomers **7b** and **8b**, respectively. The single-crystal X-ray diffraction studies of **1**·CD_2Cl_2 and **6**·2CD_2Cl_2 are reported. Mass spectrometric analyses with APCI and ESI interfaces were also performed for all new complexes.

(© Wiley-VCH Verlag GmbH & Co. KGaA, 69451 Weinheim, Germany, 2004)

Introduction

Heteroditopic ligands, those ligands that possess at least two types of chemical functionality capable of binding to a metal centre, have been receiving ever-growing attention in the field of coordination and organometallic chemistry. Such ligands, characterised by the stability advantages typical for chelates, may also confer interesting catalytic properties to their metal complexes owing to the generation of very different *trans* effects and, therefore, reactive sites within the same molecule.[1−3]

In this framework P,S bidentate ligands are appealing since the peculiar features of sulfur favour a strong coordination to soft metal centres.[4,5] In particular P,(P)S ligands exhibit a heteroditopic behaviour[6−12]that has been recently exploited in catalysis.[13,14]

Following our studies in the coordination chemistry of heteroditopic ligands,[15−17] we became interested in the synthesis and reactivity of neutral and cationic methyl complexes of platinum(II) with the heteroditopic ligands dppmS and dppeS.

Results and Discussion

The synthesis of the complexes [κ^2*P*,*S*-(dppmS)Pt(CH_3)Cl] (**1**) and [κ^2*P*,*S*-(dppeS)Pt(CH_3)Cl] (**2**) was carried out starting from [(cod)Pt(CH_3)(Cl)] (cod = 1,5-cyclooctadiene) and an equivalent of the appropriate bis(phosphanyl) monosulfide ligand.

[a] Dipartimento di Ingegneria delle Acque e di Chimica, Polytechnic of Bari and CNR Centre I.C.C.O.M., Via Orabona, 4, 70125 Bari, Italy
Fax: (internat.) + 39-080-5963611
E-mail: nobile@poliba.it
[b] Dipartimento di Scienze e Tecnologie Biologiche e Ambientali, University of Lecce, Via Monteroni, 73100, Lecce, Italy
[c] Dipartimento di Ingegneria dell'Innovazione, University of Lecce, Via Monteroni, 73100, Lecce, Italy
[d] Institut für Anorganische Chemie der RWTH, Prof. Pirlet Str. 1, 52074 Aachen, Germany
[e] Department of Chemistry, Beijing Normal University, Beijing 100875, P. R. China
[f] Consortium C.A.R.S.O., Cancer Research Center 70010, Valenzano-Bari, Italy

Subsequently, the coordinated chlorides of **1** and **2** were removed by reaction with silver tetrafluoroborate in acetonitrile or acetonitrile/dichloromethane. The absence of the IR bands of Pt−Cl stretching at 276 cm^{-1} for **1** and 273 cm^{-1} for **2** is evidence for the effective chloride abstraction.

The vacant coordination site was occupied by the acetonitrile, thus obtaining the cationic complexes [κ^2P,S-(dppmS)Pt(CH_3)(CH_3CN)][BF_4] (**3**) and [κ^2P,S-(dppeS)Pt(CH_3)(CH_3CN)][BF_4] (**4**) (Scheme 1). End-on coordination of the acetonitrile leads to two $\tilde{\nu}_{C\equiv N}$ bands in the IR spectra (at 2325 and 2297 cm^{-1} for **3**, and 2323 and 2295 cm^{-1} for **4**), both blue-shifted with respect to free CH_3CN.

The spectroscopic data both in solution (NMR) and in the solid state (IR) confirm a κ^2P,S coordination for complexes **1**−**4**. A first evidence in this respect is given by the 20−25 cm^{-1} red-shift of the phosphanyl sulfide stretching frequencies in the IR spectrum. The $\tilde{\nu}_{(P=S)}$ bands at 605 cm^{-1} (dppmS) and at 610 cm^{-1} (dppeS) of the free ligands are shifted in the neutral complexes **1** and **2** to 585 cm^{-1} and 591 cm^{-1}, respectively. In the case of cationic complexes **3** and **4** the $\tilde{\nu}_{(P=S)}$ bands are found at 580 cm^{-1} and 586 cm^{-1}, respectively.

Consistently, the $^{31}P\{^1H\}$ NMR signals ascribed to the sulfur-bound phosphorus in **1**−**4** are all flanked by ^{195}Pt satellites due to ^2J[P(S),Pt] (23 Hz for **1**, 58 Hz for **2**, 39 Hz for **3**, and 55 Hz for **4**).

The direct ^1J(P,Pt) values found for **1**−**4**, ranging from 4606 to 4695 Hz (Table 1), are in agreement with a relatively weak *trans* influence of the ligand positioned *trans* to coordinated P,[18] chloride for **1** and **2**, CH_3CN for **3** and **4**.

Moreover the values of the coupling constants for the ^1H and $^{13}C\{^1H\}$ NMR methyl signals of complexes **1**−**4** are entirely in agreement with a configuration in which the methyl group is *cis* with respect to the phosphorus atom directly coordinated to the platinum centre.[18−20] The observed ranges are: ^3J(H,P) = 3.4−4.6, ^2J(H,Pt) = 68−74, ^2J(C,P) = 5.8−8.3 Hz, and ^1J(C,Pt) = 605−650 Hz.

Table 1. $^{31}P\{1H\}$ and $^{195}Pt\{1H\}$ NMR spectroscopic data (δ, ppm, CD_2Cl_2, 298 K) (see Figure 3 for numbering of **5**)

	δ(P)	δ[P(S)]	δ(Pt)	J(P,P) Hz	^1J(P,Pt) Hz	^2J(P,Pt) Hz
1	15.4	50.8	−4354	29	4609	23
2	10.1	36.6	−4390	8	4606	58
3	14.1	52.7	−4532	24	4694	39
4	7.6	39.7	−4517	7	4695	55
5	12.8 (P^3)	52.0 (P^4)	−4512 (Pt^2)	20 (P^3,P^4)	4724(Pt^2,P^3)	[a]
	22.3 (P^1)	52.1 (P^2)	−4502 (Pt^1)	28 (P^1,P^2)	4469(Pt^1,P^1)	[a]
6	16.1	38.0	−3982	[a]	4331	[a]

[a] Signal not resolved.

Crystals of **1** suitable for XRD analysis were obtained by solvent evaporation from a CD_2Cl_2 solution. An ORTEP view of its molecular structure in the crystal is given in Figure 1. The crystals contain one molecule of clathrated CD_2Cl_2 per complex molecule.

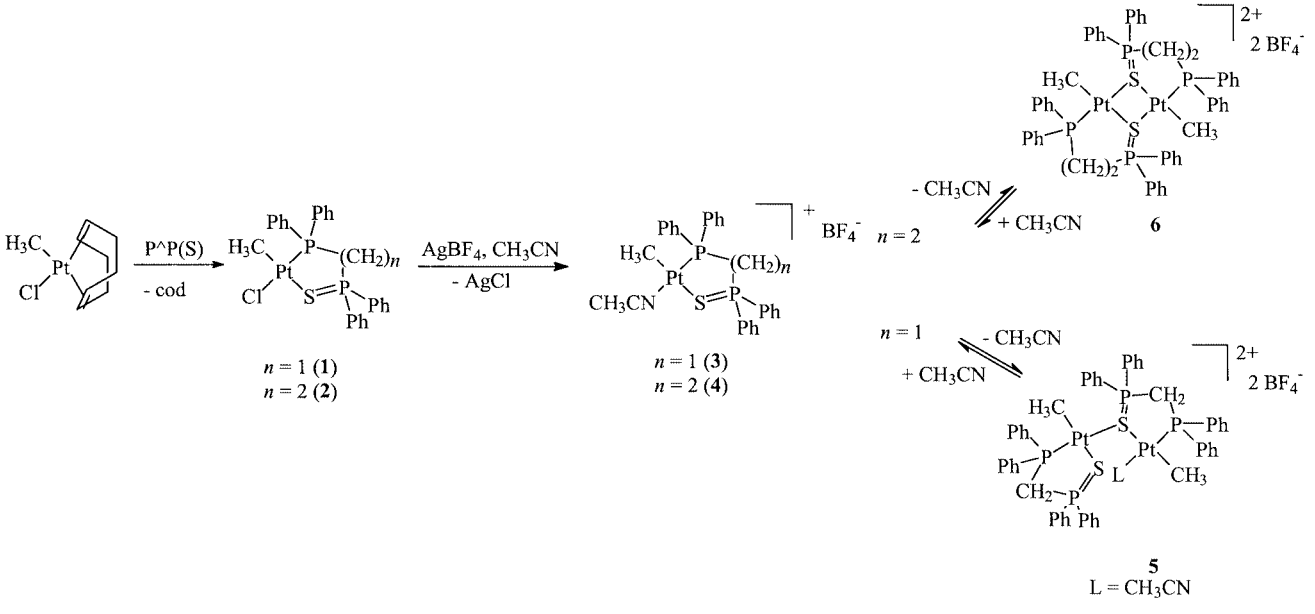

Scheme 1. Synthesis of neutral and cationic Pt^{II} complexes

 © 2004 Wiley-VCH Verlag GmbH & Co. KGaA, Weinheim

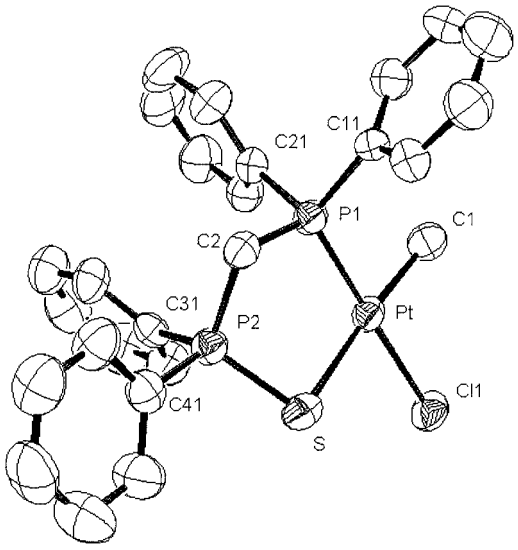

Figure 1. ORTEP drawing of **1**. The solvent molecule was omitted for clarity; displacement ellipsoids are scaled to 50% probability

Table 2. Selected bond lengths (Å) and angles (°) for **1**·CD_2Cl_2 and **6**·$2CD_2Cl_2$

1		**6**	
Pt−Cl(1)	2.3775(14)	Pt(1)−C(27)	2.069(10)
Pt−P(1)	2.1806(15)	Pt(1)−P(1)	2.220(3)
Pt−S	2.4243(18)	Pt(1)−S(1_2)	2.403(3)
Pt−C(1)	2.056(6)	Pt(1)−S(1)	2.427(3)
P(2)−S	1.993(2)	S(1)−P(2)	2.043(4)
Cl(1)−Pt−P(1)	177.71(7)	C(27)−Pt(1)−P(1)	89.3(4)
Cl(1)−Pt−S	87.74(6)	C(27)−Pt(1)−S(1_2)	95.1(4)
Cl(1)−Pt−C(1)	88.71(17)	P(1)−Pt(1)−S(1_2)	167.80(9)
P(1)−Pt−S	94.46(6)	C(27)−Pt(1)−S(1)	172.6(4)
P(1)−Pt−C(1)	89.12(17)	P(1)−Pt(1)−S(1)	96.33(9)
S−Pt−C(1)	175.87(18)	S(1_2)−Pt(1)−S(1)	80.41(9)
		P(2)−S(1)−Pt(1_2)	117.57(14)
		P(2)−S(1)−Pt(1)	103.27(13)
		Pt(1_2)−S(1)−Pt(1)	99.59(9)

Pt and its coordinating atoms P(1), S, C(1), and Cl(1) occur with an essentially square-planar geometry. The maximum deviation of a least-squares study occurs for C(1) and amounts to 0.032(6) Å. The platinum coordination is characterised by metal-centred angles between 89.12(17)° and 87.74(6)°. The sum of the four angles on platinum is 360.03(18)°. Interestingly, the different *trans* influence of phosphorus and sulfur can be evidenced by comparison of Pt−Cl and Pt−C bond lengths with similar compounds: for instance, the Pt−C(1) bond length [2.056 (6) Å] is considerably shortened due to the presence of the *trans* sulfur donor atom with respect to a complex in which the methyl group is *trans* to a P^{III} atom as in the bridging complex [$Pt_2Me_4(\mu$-dmpm$)_2$] [dmpm: bis(dimethylphosphanyl)methane] (Table 2).[22] As for the Pt−Cl(1) and Pt−P(1) bond lengths, they are similar to other platinum complexes embodying the *trans* P−Pt−Cl substructure such as complexes of formula {bis[bis(*o*-isopropylphenyl)phosphanyl]-methane}$PtCl_2$ [20] and (P^N)Pt(Me)Cl (P^N: chiral phosphanyl oxazoline).[23]

When the cationic species **3** and **4** are dissolved in CH_2Cl_2, a dissociation equilibrium of CH_3CN takes place as evidenced by the appearance in the IR, ^1H and ^{13}C NMR spectra (CD_2Cl_2 solutions) of free acetonitrile signals.

In the case of **4**, the $^{31}P\{^1H\}$ NMR spectrum in CD_2Cl_2 shows the appearance of ca. 25% of a new species **6**, which gives two broad singlets centred at δ = 16.1 and δ = 38.0 ppm. The signal at δ = 16.1 ppm, ascribable to a P atom directly bound to the platinum centre, is flanked by ^{195}Pt satellites from which a ^1J(P,Pt) of 4331 Hz could be extracted. The signal at δ = 38.0 ppm, ascribable to a P atom bound to a coordinated sulfur atom, only shows broadening at the base which could be due to unresolved ^{195}Pt satellites with a small ^2J(P,Pt) value.

In principle, acetonitrile dissociation which takes place by dissolving **4** in dichloromethane (or CD_2Cl_2) could result in *i*) BF_4^- coordination in the place of CH_3CN; *ii*) CH_2Cl_2 (or CD_2Cl_2) coordination [24] in the place of CH_3CN; *iii*) dimerisation of the coordinatively unsaturated platinum species to give sulfur bridged dimers.

The possible coordination of the tetrafluoroborate in the place of acetonitrile has been ruled out by recording $^{19}F\{^1H\}$ NMR spectra (282 MHz) of **4** in CD_2Cl_2. The only signals present were ascribable to ionic free BF_4^- [δ = −152.98 (s, $^{10}BF_4^-$), δ = −153.02 ppm(s, $^{11}BF_4^-$)].

On the other hand, substitution of dichloromethane for a nitrile group, as already reported in a similar system,[23] should result in a significant increase of the ^1J(P,Pt). In our case, on the contrary, a slight decrease of the ^1J(P,Pt) is observed (Table 1).

The remaining hypothesis *iii*), (formation of the dimers), could be supported by the aforementioned small ^2J(P,Pt) coupling constants which is consistent with a P atom bound to a bridging sulfur and suggests the dimer structure [κ*P*,μ-κ*S*-(dppeS)Pt$(CH_3)]_2[BF_4]_2$ (**6**) (Scheme 1).

The presence of the two sulfur atoms in the coordination sphere of each platinum results in the downfield shift observed in the ^{31}P NMR spectrum for the P atoms directly bound to the Pt centre when comparing **4** with **6**.

In order to shift the dissociation equilibrium between the acetonitrile monomeric complex **4** and **6** to the right, we have heated solid **4** under vacuum. The reaction led quantitatively to the synthesis of **6** that, after crystallisation from CD_2Cl_2, could be submitted for the single-crystal XRD analysis.

The structure of **6** represents the first structurally characterised sulfur bridged bis(phosphanyl) monosulfide dimeric complex. An ORTEP view of its molecular structure in the crystal is given in Figure 2. The crystals contain two molecules of clathrated CD_2Cl_2 per complex molecule.

The asymmetric unit of **6** consists of half a centrosymmetric divalent cation, one tetrafluoroborate anion, and one solvent molecule, CD_2Cl_2. The coordination around platinum is that of a distorted square with angles ranging from 80.4° to 96.3°. Two neighbouring coordination sites are occupied by the two bridging sulfur atoms of the chelat-

 © 2004 Wiley-VCH Verlag GmbH & Co. KGaA, Weinheim

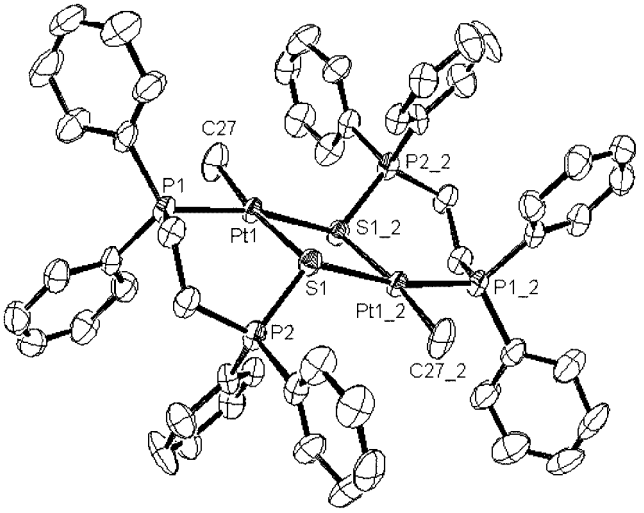

Figure 2. ORTEP drawing of **6**. Solvent molecules and counter anions were omitted for clarity; displacement ellipsoids are scaled to 40% probability

ing ligands; thus a four membered planar Pt_2S_2 ring around the crystallographic inversion centre is formed. The coordination sphere of each metal is completed by the methyl carbon and the donor phosphorus atom of the chelating ligand. The Pt−S bond lengths [2.402(3) and 2.427(3) Å] are similar to those [2.4094(17) Å and 2.4227(17) Å] observed for the related sulfur bridged complex $[Pt(C_6F_5)_2(\mu\text{-}SPPh_2C_5H_5)]_2$ [25] and are similar to that [2.4243(18) Å] observed for the parent complex **2** in which the sulfur atom is terminally bound.

The P−S distances of 2.043(4) Å are intermediate between the expected value for a P=S double bond and a P−S single bond, and the sulfur atoms are pyramidal, as indicated by the sum of the angles at the sulfur atom (320.4°).[25] Dihedral angles between the Pt_2S_2 plane and the phenyl rings range between 60.9(5)° and 76.7(5)°.

Owing to its bridging coordination mode, the P=S band in the IR spectrum was significantly red-shifted with respect to the monomeric cation **4** ($\tilde{\nu}_{(P=S)}$ changed from 586 cm^{-1} for **4** to 532 cm^{-1} for **6**).

In the case of **3**, the NMR spectra recorded in CD_2Cl_2 show the appearance of 45% of a new species different from the expected **6** homologue.

The $^{31}P\{^1H\}$ NMR spectrum of this new species consists of four signals with equal integrals: a doublet of doublets centred at δ = 22.3 and a doublet centred at δ = 52.1 ppm mutually coupled [^2J(P,P) 28 Hz], a doublet centred at δ = 12.8 and a doublet of doublets centred at δ = 52.0 ppm mutually coupled with a ^2J(P,P) 20 Hz. The further splitting observed in the signals at δ = 22.3 and δ = 52.0 corresponds to a mutual coupling of 4 Hz. The signals at δ = 22.3 and δ = 12.8 ppm, flanked by ^{195}Pt satellites from which ^1J(P,Pt) of 4469 Hz and 4724 Hz could be extracted are attributed to two chemically different Pt-bound P atoms. The partially overlapped signals at δ = 52.1 and δ = 52.0 ppm are ascribable to P atoms bound to coordinated sulfur. Both signals show broadening only at the base as unresolved ^{195}Pt satellites with a small ^2J(P,Pt) value. Moreover, the ^1H NMR spectrum shows, together with free CH_3CN (δ = 1.97 ppm) two peaks in the region of coordinated acetonitrile, one belonging to complex **3** at δ = 2.52 ppm and the other (δ = 2.54 ppm), having the same integration of the free CH_3CN, belonging to the new species.

All these spectroscopic features suggest that the species formed by partial CH_3CN dissociation on dissolving **3** in CD_2Cl_2, is the unsymmetrical dimer $[\{\kappa^2P,S\text{-}(dppmS)\}(CH_3)Pt\{\kappa P,\mu\text{-}\kappa S\text{-}(dppmS)\}Pt(CH_3)(CH_3CN)][BF_4]$ (**5**) depicted in Figure 3. The proposed structure is substantiated by ESI-MS analyses (vide infra) and by the observed ^3J(P,P) 4 Hz coupling constant between P^1 (bonded to Pt^1) and P^4 (bonded to the bridging sulfur).

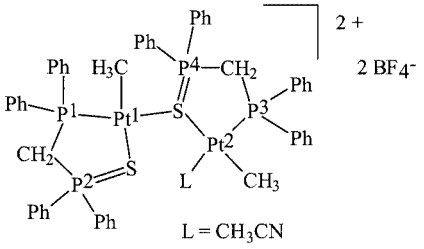

Figure 3. Alleged structure for complex **5**

The two methyl signals for **5** occurred in the ^1H NMR spectrum as doublets (with satellites) centred at δ = 0.74 ppm [^3J(H,P) = 3, ^2J(H,Pt) = 64 Hz, CH_3 *cis* to CH_3CN] and δ = 0.06 ppm [^3J(H,P) = 3.9, ^2J(H,Pt) = 66.9 Hz, CH_3 *cis* to bridging S]. Assignment of ^1H, ^{31}P, ^{13}C, ^{195}Pt NMR spectral features is reported in Table 1 and in the Exp. Sect.

The equilibrium between **3** and **5** or **4** and **6** (Scheme 1) completely shifts towards the acetonitrile species by adding CH_3CN to the $[D_2]$dichloromethane solutions.[26]

Heating solid **3** under vacuum for 8 h resulted in an enrichment of the equilibrium mixture in **5** (the dimer/monomer ratio passed from 0.82 to 3.0, based on total phosphorus, as assessed by ^{31}P NMR spectra in CD_2Cl_2). Attempts to shift the dissociation equilibrium between the acetonitrile monomeric complex **3** and **5** completely to the right, by prolonging the heating for 2.5 days, resulted in a complex mixture of products containing, according to ^{31}P integration data, ca. 43% of **5**.

It is interesting to note that the homologous cations $[\kappa^2P,S\text{-}(dppmS)Pd(CH_3CN)(CH_3)]^+$ and $[\kappa^2P,S\text{-}(dppeS)Pd(CH_3CN)(CH_3)]^+$, recently prepared by us,[17] are stable in CH_2Cl_2 solution as monomeric acetonitrile complexes.

The difference in behaviour between **3** and **4** observed in dichloromethane, i.e. the formation of the unsymmetrical or symmetrical dimers **5** or **6**, deserves a comment.

Theoretical calculations indicate that Pt_2S_2 rings adopt a planar conformation in Pt^{II} complexes of formulae *trans*-$[Pt_2(\mu\text{-}SR)_2L_2L'_2]$ or $[Pt_2(\mu\text{-}RS)_2L_4]$, and a hinged arrangement in Pt^{II} complexes of formula *cis*-$[Pt_2(\mu\text{-}RS)_2L_2L'_2]$.[27]

 © 2004 Wiley-VCH Verlag GmbH & Co. KGaA, Weinheim

Moreover, given that the sulfur atom usually adopts a pyramidal geometry in bridging ligands like thiolates[28,29] and phosphino sulfides [25] with a Pt−S−Pt angle close to 100°,[30] a bidentate S L ligand must possess some specific structural features in order to form stable Pt^{II} complexes of structure:

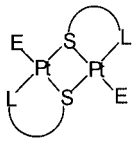

In our case, where E = CH_3 and S^L = $Ph_2P(CH_2)_nPPh_2(S)$, the length of the methylene chain might be discriminating for the stability of the symmetrical dimer complexes. It seems, from our experimental data, that in the case of dppmS, only one sulfur bridge can be borne, because closing the Pt_2S_2 core with the second sulfur would result in a hinge distortion unfavourable for these types of compounds.[27]

On the contrary, the more flexible six-membered platinacycles of the symmetric dimer **6** obtained with dppeS, better fit into the geometrical constraints imposed by the planar core structure and the pyramidality of the bridging sulfur atom.

Such a hypothesis seems to be confirmed by studies carried out by Dervisi on Ni^{II}, Pd^{II}, Pt^{II} complexes of the related ligand 1-(diphenylphosphanyl)butane-2-thiolate (PS^-). It was found, in fact, that, under suitable conditions Ni^{II} and Pd^{II} formed sulfur bridged dimeric complexes of formula $[Ni(PS)Cl]_2$ and $[Pd(PS)Cl]_2$, both containing two five-membered metallacycles [31] whereas, attempts to prepare the analogous Pt^{II} complex were unsuccessful, leading only to the $[Pt(PS)_2]$ monomeric species.[32]

When CD_2Cl_2 solutions of **3** and **4** were exposed to an atmospheric pressure of carbon monoxide at room temperature, a fast reaction took place leading to carbonyl complexes **7a** and **8a** (Scheme 2) as evidenced by the appearance, in the IR spectra, of strong $\tilde{\nu}_{CO}$ bands at 2113 and 2112 cm^{-1}, respectively. The corresponding carbonyl resonances of **7a** and **8a** in the $^{13}C\{^1H\}$ NMR spectrum appear as doublets of doublets due to couplings with inequivalent P atoms, and are centred at δ = 177.7 and δ = 176.2 ppm, respectively.

The multinuclear NMR spectra of the reaction solution of **3** under CO ($P_{atm.}$) recorded every 2 days for one week showed the progressive isomerisation of **7a** into **7b** (Scheme 2). In fact the decrease of $^{31}P\{^1H\}$ NMR signals at δ = 25.3 and δ = 59.3 ppm attributed to the coordinated P and P(S) atoms of **7a,** respectively, was observed. Simultaneously new signals at δ = 31.2 and δ = 67.9 ppm [*J*(P,P) 72 Hz] appeared and were attributed to **7b**. The relatively low value of the ^1J(P,Pt) found for **7b** (1556 Hz) strongly supports the structure with the methyl group *trans* to the P atom. Comparable ^1J(P,Pt) are found for coordinated P atoms *trans* to CH_3 groups in complexes of formula $[(P\ P)Pt(Me)CO]^+$ [P P = 1,3-(diphenylphosphanyl)propane, ^1J(P,Pt) = 1593 Hz,[33] P P = BINAP, ^1J(P,Pt) = 1735 Hz .[19]]

The $^{13}C\{^1H\}$ NMR spectra of **7b** and **8b** show the carbonyl resonances at δ = 168.6 and δ = 167.9 ppm, respectively.

Figure 4 shows the $^{13}C\{^1H\}$ and $^{195}Pt\{^1H\}$ spectra of the CD_2Cl_2 reaction solution after carbonylation of **3** at two different times demonstrating the progressive enrichment in **7b**.

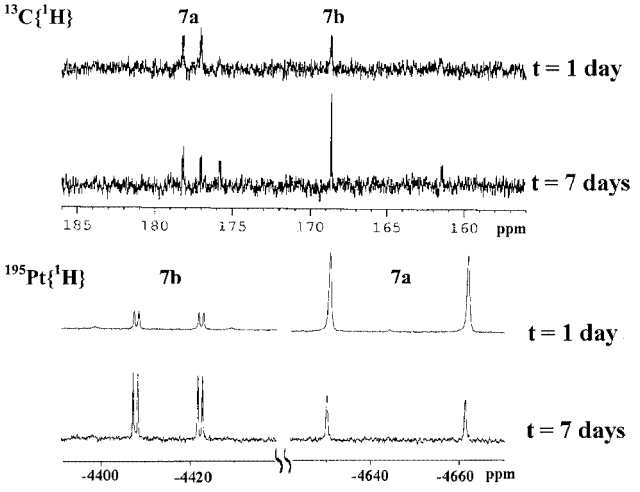

Figure 4. $^{13}C\{^1H\}$ (125 MHz) and $^{195}Pt\{^1H\}$ (107 MHz) NMR spectra (298 K, CD_2Cl_2) of the reaction solutions obtained by carbonylation of **3** recorded after 1 day (top traces) and after 7 days (lower traces)

An analogous behaviour was observed in the carbonylation of the cationic complex **4** which results in the immediate formation of **8a** that slowly isomerises into **8b** (Scheme 2). Table 3 summarises selected spectroscopic features of **7a**−**b** and **8a**−**b**.

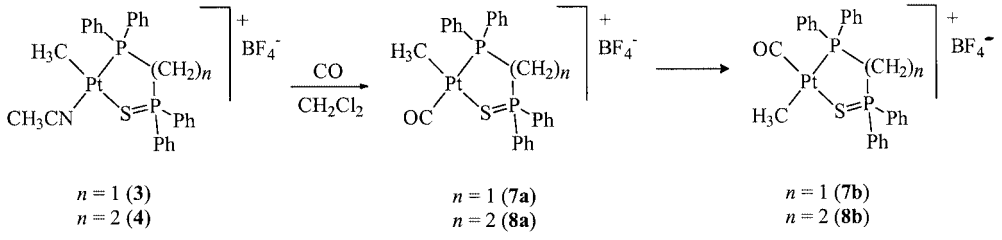

n = 1 (**3**)
n = 2 (**4**)

n = 1 (**7a**)
n = 2 (**8a**)

n = 1 (**7b**)
n = 2 (**8b**)

Scheme 2. Carbonylation of **3** and **4**

 © 2004 Wiley-VCH Verlag GmbH & Co. KGaA, Weinheim

Table 3. $^{31}P\{1H\}$ and $^{195}Pt\{1H\}$ NMR spectroscopic data (δ, ppm) of **7a**−**b** and **8a**−**b**

	δ(P)	δ[P(S)]	δ(Pt)	*J*(P,P) Hz	^1J(P,Pt) Hz	^2J(P,Pt) Hz
7a	25.3	59.3	−4646	33	3336	20
7b	31.2	67.9	−4415	72	1556	113
8a	13.8	43.1	−4560	[a]	3372	55
8b	3.6	40.8	−4328	31	1576	105

When acetonitrile solutions of **3** or **4** were exposed to CO at ambient conditions, the CH_3CN excess prevented the carbonylation reaction.

Conclusion

Methyl chloro platinum(II) complexes with the heteroditopic dppmS and dppeS ligands have been prepared and characterised. Chloride abstraction from the neutral complexes carried out in acetonitrile leads to the formation of the solvento species, which have been isolated in the pure state. Loss of acetonitrile, which leads to dimeric species, has been studied both in solution and in the solid state. In the case of the dppeS, the symmetric dimer **6** could be obtained by heating the corresponding acetonitrile complex under vacuum. This reaction represents an interesting example of clean solid state molecular rearrangement. The type of dimer formed in solution by loss of acetonitrile (mono bridged or dibridged) has been found to be strictly related to the number of the methylene groups in the ligand backbone. Carbonyl complexes obtained by substitution of acetonitrile with CO have also been synthesised and their isomerisation reactions, in solution, have been studied.

Experimental Section

General Remarks: All manipulations were carried out using standard Schlenk techniques under nitrogen as inert gas. Acetonitrile, dichloromethane, diethyl ether and *n*-hexane were dried and distilled under nitrogen; $AgBF_4$ and Celite™ were purchased from Fluka. NMR spectra in solution were recorded at 298 K on a Bruker AM 500 or a Bruker Avance DRX500 spectrometer (CARSO) or a Varian Mercury 300; frequencies are referenced to Me_4Si (^1H, ^{13}C), 85% H_3PO_4 (^{31}P), H_2PtCl_6 (^{195}Pt) and $CFCl_3$ (^{19}F). IR spectra were recorded with a Bruker Vector 22 FT instrument. C, H, N and S elemental analyses were carried out on a Eurovector CHNS-O Elemental Analyser. Cl elemental analyses were performed by potentiometric titration using a Metrohm DMS Titrino.

LC-MS analyses were performed with an Agilent HPLC system equipped with DAD, autosampler and MS systems (Agilent 1100 LC-MS SL series). All samples were dissolved in the same HPLC-grade solvent, which was used as eluent. The used interfaces were APCI or ESI for neutral complexes and ESI for cationic complexes. APCI conditions: negative ion mode, flow rate 0.5 mL/min, nitrogen as nebulizing and drying gas, nebulizer pressure 60 psi, vaporizer temperature 350 °C, corona current 25 μA, drying gas flow 5 L/min, drying gas temperature 300 °C (unless otherwise specified), capillary voltage 4000 V. ESI conditions: positive ion mode, flow rate 0.5 mL/min, nitrogen as nebulizing and drying gas, nebulizer pressure 30 psi, drying gas flow 13 L/min, capillary voltage 4000 V. The fragmentor voltage was varied from 0 to 400 V by 50 V increments in order to obtain clean and intense spectra. Other optimal conditions are specified below for each complex. Mass spectrometry data were acquired in the Scan mode (mass range m/z = 50−3000).

The ligands dppmS and dppeS have been prepared by the procedure described in ref.[17]

The complex [(cod)Pt(CH_3)Cl] was synthesised according to ref.[18]

Synthesis of [(P^P(S)Pt(CH_3)(Cl)] 1 and 2: A solution of bis(phosphanyl) monosulfide [hereafter denoted as P^P(S)] in CH_2Cl_2 was added to a CH_2Cl_2 solution containing an equimolar amount of [(cod)Pt(CH_3)Cl], kept under vigorous stirring at room temperature. After 3 h the solvent was evaporated to ca. one fifth of the volume and addition of *n*-hexane caused the precipitation of the desired complexes as white solids. Filtration followed by washings with 3 × 5 mL *n*-hexane and drying in vacuo afforded **1** and **2** in high yield. Scales and analytical data are given below.

Synthesis of [(P^P(S)Pt(CH_3)(CH_3CN)]BF_4 3 and 4: A solution of silver tetrafluoroborate in CH_3CN was added dropwise to a suspension containing an equimolar amount of [(P^P(S)Pt(CH_3)(Cl)] in CH_3CN kept under vigorous stirring at room temp. in the dark. The mixture was stirred for 10 minutes at room temp. and the suspension was then filtered through Celite™, obtaining a colourless solution which was evaporated to dryness in vacuo. The solid was washed with diethyl ether (2 × 10 mL) and dried in vacuo. Scales and analytical data are given below.

Synthesis of *af*-Dimethyl-*bd,ec*-bis{(diphenylphosphanylethyl-κ*P*)-diphenylphosphanyl Sulfide, μ-κ*S*)}diplatinum(II) Bis(tetrafluoroborate) [μ-(dppeS)Pt(CH_3)]$_2$[BF_4]$_2$ (6): Solid **4** (50 mg, 0.065 mmol) was heated under high vacuum in a Schlenk tube at 90 °C for 30 h obtaining a white solid (47 mg) consisting of pure dimer **6**. Crystallisation from slow evaporation of a CD_2Cl_2 solution gave colourless crystals suitable for XRD analysis. M.p. 169 °C (dec.). IR (KBr): $\tilde{\nu}$ = 3056 (w), 2962 (w), 2886 (w), 1482 (m), 1437 (s), 1261 (m), 1060 (vs, br., BF_4^-), 997 (s), 803 (m), 750 (m), 692 (s), 532 (s, P=S), 488 (w) cm^{-1}. LC-MS: exact mass calcd. for the dication $C_{54}H_{54}P_4Pt_2S_2$: 1280.2 amu. ESI; found 1315 $[M + Cl]^+$, 640 $[M/2]^+$. $C_{54}H_{54}B_2F_8P_4Pt_2S_2$: calcd. C 44.58, H 3.74, S 4.41; found C 44.80, H 3.81, S 4.38. ^1H NMR (500 MHz, CD_2Cl_2): δ = −0.13 [d, ^3J(H,P) = 3.2, ^2J(H,Pt) = 66.4 Hz, 6 H, 2 CH_3], 3.21 [m, 4 H, P(S)CH_2CH$_2$P], 2.95 [m, 4 H, P(S)CH$_2$CH_2P], 7.45−8.18 (m, 40 H, $H_{arom.}$) ppm. $^{13}C\{^1H\}$ NMR (125 MHz, CD_2Cl_2): δ = 1.9 [br. s, ^1J(C,Pt) = 624 Hz, CH_3], 21.1 [dd, ^1J(C,P) = 43, ^2J(C,P) = 6 Hz, P−CH_2CH$_2$−P(S)], 26.8 [br. d, ^1J(C,P) = 53 Hz, P−CH$_2$−CH_2−P(S)], 129.7 (s), 129.8 (s), 130.5 (s), 130.7 (s), 132.9 [d, ^2J(C,P) = 3 Hz], 133.4 [d, ^1J(C,P) = 11 Hz], 133.6 [d, ^2J(C,P) = 11 Hz], 135.7 [d, ^1J(C,P) = 3 Hz] ppm.

***a*-Chloro-*b*-methyl-*cd*-{(diphenylphosphanylmethyl)diphenylphosphanyl Sulfide-κ^2-*P*,*S*}platinum(II) (1):** Scale and yield: dppmS, (384 mg, 0.92 mmol) in 9 mL CH_2Cl_2; [(cod)Pt(CH_3)(Cl)], (326 mg, 0.92 mmol) in 3 mL CH_2Cl_2; yield: 570 mg (94%). M.p. 151 °C (dec). IR (KBr): $\tilde{\nu}$ = 3067 (m), 2966 (m), 2899 (m), 2798 (w), 1484 (m), 1434 (vs), 1100 (vs), 995 (m), 800 (s), 738 (vs), 725 (vs), 683 (vs) 585 (s, P=S str.), 536 (s), 503 (s), 494 (s), 276 (m, Pt-Cl) cm^{-1}. LC-MS: exact mass calcd. for $C_{26}H_{25}ClP_2PtS$: 661.05 amu; APCI;

 © 2004 Wiley-VCH Verlag GmbH & Co. KGaA, Weinheim

found 697 [M + Cl]$^-$; 661 [M]$^-$. $C_{26}H_{25}ClP_2PtS{\cdot}CH_2Cl_2$: calcd. C 43.4, H 3.64, S 4.3; found C 43.6, H 3.53, S 4.4. ^{1}H NMR (500 MHz, CD_2Cl_2): δ = 0.42 [d, ^3J(H,P) = 3.9, ^2J(H,Pt) = 73.3 Hz, 3 H, CH_3], 3.87 [pseudo-t, ^2J(H,P) = 10.3, ^3J(H,Pt) = 44.8 Hz, 2 H, CH_2], 7.31 (m, 4 H_{meta} of Ph_2P-Pt), 7.34−7.41 [m, 4 H_{meta} of $Ph_2P(S)-Pt$ overlapped with 2 H_{para} of Ph_2P-Pt], 7.48 [m, 2 H_{para} of $Ph_2P(S)-Pt$], 7.58 (m, 4 H_{ortho} of Ph_2P-Pt), 7.68 [m, 4 H_{ortho} of $Ph_2P(S)-Pt$] ppm. ^{13}C{^{1}H} NMR (125 MHz, CD_2Cl_2): δ = −5.7 [d, ^2J(C,P) = 8, ^1J(C,Pt) = 628 Hz, CH_3], 42.8 [dd, ^1J(C,P) = 56, ^1J(C,P), CH_2], 128.8 (s), 128.9 (s), 129.4 (s), 129.5 (s), 131.6 [d, ^2J(C,P) = 2 Hz], 132.1 [d, ^1J(C,P) = 11 Hz], 133.3 [d, ^2J(C,P) = 3 Hz], 133.8 [d, ^1J(C,P) = 12, ^2J(C,Pt) = 38 Hz] ppm.

***a*-Chloro-*b*-methyl-*cd*-{(diphenylphosphanylethyl)diphenylphosphanyl Sulfide-κ^{2}P,S}platinum(II) (2):** Scale and yield: dppeS, (511 mg, 1.20 mmol) in 10 mL CH_2Cl_2; [(cod)Pt(CH_3)(Cl)], (425 mg, 1.20 mmol) in 4 mL CH_2Cl_2; yield: 738 mg (91%). M.p. 173 °C (dec). IR (KBr): ṽ = 3051 (m), 2936 (m), 2885 (m), 1482 (m), 1438 (vs), 1102 (vs), 1001 (m), 818 (s), 726 (vs), 670 (vs), 591 (s, P=S str.), 532 (s), 518 (s), 488 (m), 273 (m, Pt-Cl) cm^{-1}. LC-MS: exact mass calcd. for $C_{27}H_{27}ClP_2PtS$: 675.06 amu; APCI; found 710 [M + Cl]$^-$; 695 [M + Cl − CH_3]$^-$. ESI; found 681 [M − Cl + CH_3CN]$^+$, 640 [M − Cl]$^-$. $C_{27}H_{27}ClP_2PtS$: calcd. C 48.0, H 4.03, Cl 5.24, S 4.7; found C 49.1, H 3.96, Cl 5.11, S 4.3. ^{1}H NMR (500 MHz, CD_2Cl_2): δ = 0.39 [d, ^3J(H,P) = 4.6, ^2J(H,Pt) = 74.2 Hz, 3 H, CH_3], 2.65−2.85 [m, 4 H, CH_2-CH_2], 7.35−7.90 [20 H, $H_{arom.}$] ppm. ^{13}C{^{1}H} NMR (125 MHz, CD_2Cl_2): δ = −3.55 [d, ^2J(C,P) = 7, ^1J(C,Pt) = 649 Hz, CH_3], 22.4 [dd, ^1J(C,P) = 40, ^2J(C,P) = 4 Hz, P−CH_2CH_2−P(S)], 25.6 [d, ^1J(C,P) = 54 Hz, P−CH_2CH_2−P(S)], 128.7 (s), 128.8 (s), 129.4 (s), 129.5 (s), 131.2 [d, ^2J(C,P) = 3 Hz], 131.7 [d, ^1J(C,P) = 10 Hz], 133.1 [d, ^2J(C,P) = 3 Hz], 133.6 [d, ^1J(C,P) = 10, ^2J(C,Pt) = 34 Hz] ppm.

***a*-Acetonitrile-*b*-methyl-*cd*-{(diphenylphosphanylmethyl)diphenylphosphanyl Sulfide-κ^2-*P,S*)}platinum(II) Tetrafluoroborate (3):** Scale and yield: [(dppmS)Pt(CH_3)(Cl)], (528 mg, 0.80 mmol) in 30 mL CH_3CN; $AgBF_4$, (156 mg, 0.80 mmol) in 25 mL CH_3CN; yield: 494 mg (92%). IR (KBr): ṽ = 3069 (m), 2952 (s), 2869 (s), 2324 (w, CN), 2304 (w, CN), 1486 (m), 1432 (s), 1062 (vs, br, BF_4^-), 789 (vs), 736 (vs), 682 (vs), 580 (m, P=S str.), 545 (s), 490 (s), 360 (m) cm^{-1}. M.p. 163 °C (dec). LC-MS: exact mass calcd. for the cation $C_{28}H_{28}NP_2PtS$: 667.11 amu. ESI; found 667 [M]$^+$; 626 [M − CH_3CN]$^+$. $C_{28}H_{28}BF_4NP_2PtS$: calcd. C 44.6, H 3.74, N 1.9, S 4.2; found C 44.9, H 3.87, N 1.0, S 4.7, Cl absent. The following spectroscopic features refer to the exchange product obtained in CD_3CN. ^{1}H NMR (500 MHz, CD_3CN): δ = 0.36 [d, ^3J(H,P) = 3.4, ^2J(H,Pt) = 70.3 Hz, 3 H, CH_3], 4.23 [psudo-t, ^2J(H,P) = 11.3, ^3J(H,Pt) = 46.3 Hz, 2 H, CH_2], 7.30−7.75 [m, 20 H, $H_{arom.}$] ppm. ^{13}C{^{1}H} NMR (125 MHz, CD_3CN): δ = −7.6 [d, ^2J(C,P) = 6, ^1J(C,Pt) = 606 Hz, CH_3], 40.0 [dd, ^1J(C,P) = 52, ^1J(C,P) = 33 Hz, CH_2], 129.8 (s), 129.9 (s), 130.1 (s), 130.2 (s), 132.6 [d, ^2J(C,P) = 11 Hz], 133.1 (br. S), 134.5 (2 C overlapped) ppm. ^{31}P{^{1}H} NMR (202 MHz, CD_3CN): δ = 14.9 [d, ^2J(P,P) = 21, ^1J(P,Pt) = 4639 Hz Ph_2P], 53.0 [d, ^2J(P,P) = 21, ^2J(P,Pt) = 37 Hz, $Ph_2P(S)$] ppm. ^{195}Pt{^{1}H} NMR (107 MHz, CD_3CN): δ = −4532 [br. d, ^1J(P,Pt) = 4639 Hz] ppm.

***a*-Acetonitrile-*b*-methyl-*cd*-{(diphenylphosphanylethyl)diphenylphosphanyl Sulfide-κ^{2}P,S}platinum(II) Tetrafluoroborate (4):** Scale and yield: [(dppeS)Pt(CH_3)(Cl)]: (690 mg, 1.04 mmol) in 35 mL CH_3CN; $AgBF_4$: (202 mg, 1.04 mmol) in 30 mL CH_3CN; yield: 719 mg of **4** (90%). IR (KBr): ṽ = 3063 (m), 2938 (m), 2894 (m), 2330 (w, CN), 2300 (w, CN), 1484 (m), 1436 (s), 1038 (vs, br, BF_4^-), 812 (m), 751 (s), 697 (vs), 586 (s, P=S str.), 538 (vs), 495 (s) cm^{-1}. M.p. 138 °C (dec). LC-MS: exact mass calcd. for the cation $C_{29}H_{30}NP_2PtS$: 681.12 amu. ESI; found 681 [M]$^+$; 640 [M − CH_3CN]$^+$. $C_{29}H_{30}BF_4NP_2PtS$: calcd. C 45.3, H 3.94, N 1.8, S 4.2; found C 44.8, H 3.86, N 1.5, S 3.5, Cl absent. The following spectroscopic features refer to the exchange product obtained in CD_3CN. ^{1}H NMR (500 MHz, CD_3CN): δ = 0.24 [dd, ^2J(H,Pt) = 72.0, ^3J(H,P) = 3.5, ^4J(H,P) = 1.5 Hz, 3 H, CH_3], 2.96 (m, 4 H, CH_2CH_2), 7.45−7.85 (m, 20 H, $H_{arom.}$) ppm. ^{13}C{^{1}H} NMR (125 MHz, CD_3CN): δ = −5.3 [d, ^2J(C,P) = 6, ^1J(C,Pt) = 627 Hz, CH_3], 21.9 [dd, ^1J(C,P) = 44, ^2J(C,P) = 4 Hz, P−CH_2CH_2−P(S)], 25.1 [d, ^1J(C,P) = 55 Hz, P−CH_2−CH_2−P(S)], 129.6 (s), 129.7 (s), 130.2 (s), 130.3 (s), 132.0 [d, ^2J(C,P) = 10 Hz], 132.5 [d, ^2J(C,P) = 3 Hz], 134.0 [d, ^1J(C,P) = 11, ^2J(C,Pt) = 36 Hz], 134.2 [d, ^2J(C,P) = 3 Hz] ppm. ^{31}P{^{1}H} NMR (202 MHz, CD_3CN): δ = 6.8 [s, ^1J(P,Pt) = 4620 Hz, Ph_2P], 41.2 [s, ^2J(P,Pt) = 46, ^2J(P,Pt) = 55 Hz, $Ph_2P(S)$] ppm. ^{195}Pt{^{1}H} NMR (107 MHz, CD_3CN): δ = −4505 [br. d, ^1J(P,Pt) = 4614 Hz] ppm.

Spectroscopic Features of 5: See Figure 3 for atom numbering. ^{1}H NMR (500 MHz, CD_2Cl_2): δ = 0.06 [d, ^3J(H,P) = 3.9, ^2J(H,Pt) = 66 Hz, CH_3 *cis* to bridging S], 0.74 [d, ^3J(H,P) = 3.0, ^2J(H,Pt) = 64 Hz, CH_3 *cis* to CH_3CN], 2.54 (s, coord. CH_3CN), 4.88 [ps t, ^2J(H,P) = 11 Hz, CH_2 of the bridging dppmS], 4.11 [ps t, ^2J(H,P) 11 Hz, CH_2 of the non-bridging dppmS], 7.22−7.89 [m, $H_{arom.}$] ppm. ^{13}C{^{1}H} NMR (125 MHz, CD_2Cl_2): δ = −4.8 [br. s, ^1J(C,Pt) = 598 Hz, Pt^2-CH_3], −2.9 [br. s, ^1J(C,Pt) = 588 Hz, Pt^1-CH_3], 36.6 [dd, ^1J(C,P) = 49, ^1J(C,P) = 32 Hz, $P^3CH_2P^4$, 39.7 [dd, ^1J(C,P) = 51, ^1J(C,P) = 31 Hz, $P^1CH_2P^2$], 125−135 [$C_{arom.}$] ppm. ^{31}P{^{1}H} NMR (202 MHz, CD_2Cl_2): δ = 12.8 [d, ^2J(P,P) = 20, ^1J(P,Pt) = 4724 Hz, P^3], 22.3 [dd, ^2J(P,P) = 28, ^3J(P^1-P^4) = 4, ^1J(P,Pt) = 4469 Hz, P^1], 52.0 [dd, ^2J(P,P) = 20, ^3J(P^1-P^4) = 4 Hz, P^4], 52.1 [d, ^2J(P,P) = 28 Hz, P^2] ppm. ^{195}Pt{^{1}H} NMR (107 MHz, CD_2Cl_2): δ = −4502 [br. d, ^1J(P,Pt) = 4469 Hz, Pt^1]. δ = −4512 [br. d, ^1J(P,Pt) = 4724 Hz, Pt^2] ppm.

Carbonylation of 3 and 4: The complexes **3** and **4** were dissolved in CD_2Cl_2 (≈ 10 mg in 0.6 mL) in an NMR tube connected with a CO/vacuum manifold. The solution, kept at room temp., was exposed to an atmospheric pressure of carbon monoxide and followed for two weeks by multinuclear NMR spectroscopy.

^{31}P{^{1}H} and ^{195}Pt{^{1}H} NMR features for **7a**−**b** and **8a**−**b** are collected in Table 4.

LC-MS for **7**: Exact mass calcd. for the cations $C_{27}H_{25}OP_2PtS$: 654.07 amu. ESI; found 654 [M]$^+$, 626 [M − CO]$^+$.

LC-MS for **8**: exact mass calcd. for the cations $C_{28}H_{27}OP_2PtS$: 668.09 amu. ESI; found 668 [M]$^+$, 640 [M − CO]$^+$.

***a*-Carbonyl-*b*-methyl-*cd*-{(diphenylphosphanylmethyl)diphenylphosphanyl Sulfide-*P,S*}platinum(II) Tetrafluoroborate (7a):** IR (CD_2Cl_2): ṽ= 2113 (CO) cm^{-1}. ^{1}H NMR (500 MHz, CD_2Cl_2): δ = 0.75 [d, ^2J(H,Pt) = 72.3, ^3J(H,P) = 6.4 Hz, 3 H, CH_3], 4.31 [m, 4 H, CH_2CH_2], 7.40−7.81 [m, 20 H, $H_{arom.}$] ppm. ^{13}C{^{1}H} NMR (125 MHz, CD_2Cl_2): δ = −10.1 [d, ^2J(C,P) = 5, ^1J(C,Pt) = 502 Hz, CH_3], 38.4 [dd, ^1J(C,P) = 52, ^2J(C,P) = 31 Hz, CH_2], 129.8 (2 C overlapped), 129.9 (2 C overlapped), 132.3 [d, ^2J(C,P) = 11 Hz], 133.2 [d, ^1J(C,P) = 3 Hz], 134.2 [d, ^2J(C,P) = 12, ^2J(C,Pt) = 28 Hz], 134.3 [d, ^1J(C,P) = 3 Hz,], 177.7 [dd, ^2J(C,P) = 145, ^3J(C,P) = 12, ^1J(C,Pt) = 1582 Hz, CO] ppm.

***a*-Carbonyl-*b*-methyl-*dc*-{(diphenylphosphanylmethyl)diphenylphosphanyl Sulfide-*P,S*}platinum(II) Tetrafluoroborate (7b):** IR (CD_2Cl_2): ṽ = 2090 (CO) cm^{-1}. ^{1}H NMR (500 MHz, CD_2Cl_2): δ = 1.34 [dd, ^2J(H,Pt) = 57.7, ^3J(H,P) = 6.4, ^4J(H,P) = 0.6 Hz, 3 H, CH_3], 4.50 [m, 4 H, CH_2CH_2], 7.42−7.86 [m, 20 H, $H_{arom.}$] ppm. ^{13}C{^{1}H} NMR (125 MHz, CD_2Cl_2): δ = −7.3 [dd, ^2J(C,P) = 73, ^3J(C,P) = 15 Hz,^1J(C,Pt) = 381 Hz, CH_3], 34.1 [dd, ^1J(C,P) =

 © 2004 Wiley-VCH Verlag GmbH & Co. KGaA, Weinheim

Table 4. Crystal data and structure refinement for **1**·CD_2Cl_2 and **6**·2CD_2Cl_2

	1·CD_2Cl_2	**6**·2CD_2Cl_2
Empirical formula	$C_{27}H_{25}D_2Cl_3P_2PtS$	$C_{56}H_{54}D_4B_2Cl_4F_8P_4Pt_2S_2$
Molecular mass	748.97	1628.28
Temperature	293(2) K	293(2) K
Wavelength	0.71073 Å	0.71073 Å
Crystal system	monoclinic	triclinic
Space group	$P2_1/c$	$P\bar{1}$
a (Å)	8.8991(5)	10.966(5)
b (Å)	16.6324(9)	11.919(5)
c (Å)	20.1000(11)	12.984(5)
α [°]	90	79.459(9)
β [°]	102.4610(10)	65.545(10)
γ [°]	90	87.527(10)
Volume	2905.0(3) Å^3	1517.6(11) Å^3
Z	4	1
Density (calculated)	1.708 g/cm^3	1.782 g/cm^3
Absorption coefficient	5.303 mm^{-1}	5.016 mm^{-1}
F(000)	1456	792
Crystal size	0.36 × 0.25 × 0.13 mm	0.26 × 0.19 × 0.06 mm
θ range for data collection	1.60° ≤ θ ≤ 28.35°	2.04° ≤ θ ≤ 28.43°
Index ranges	−11≤ h ≤ 9, −21≤ k ≤ 22, −26 ≤ l ≤ 26	−14≤ h ≤ 14, −15≤ k ≤ 15, −17 ≤ l ≤ 17
Reflections collected	23079	21037
Independent reflections	7220 [R(int) = 0.0605]	7570 [R(int) = 0.1033]
Data/parameters	7220/308	7570/352
Goodness-of-fit on F^2	0.989	1.068
Final R indices [$I > 2\sigma(I)$]	R_1 = 0.0468	R_1 = 0.0745
Final wR_2 indices (all data)	wR_2 = 0.0842	wR_2 = 0.1594
Largest diff. Peak and hole	1.395 and −0.783 eÅ^{-3}	2.721 and −2.857 e·Å^{-3} (close to Pt)

51, ^2J(C,P) = 25 Hz, CH_2], 129.9 (s), 130.0 (2 C overlapped), 130.1 (s), 132.3 [d, ^2J(C,P) = 11 Hz], 133.0 [d, ^1J(C,P) = 3 Hz], 133.4 [d, ^2J(C,P) = 13, ^2J(C,Pt) = 14 Hz], 134.7 [d, ^1J(C,P) = 3 Hz,] 168.6 [d, J(C,P) = 8, ^1J(C,Pt) = 1815 Hz, CO] ppm.

***a*-Carbonyl-*b*-methyl-*cd*-{(diphenylphosphanylethyl)diphenylphosphanyl Sulfide-*P,S*}platinum(II) Tetrafluoroborate (8a):** IR (CD_2Cl_2): ṽ= 2112 (CO) cm^{-1}. ^{1}H NMR (500 MHz, CD_2Cl_2): δ = 0.57 [dd, ^2J(H,Pt) = 74.3, ^3J(H,P) = 6.4, ^4J(H,P) = 1.0 Hz, 3 H, CH_3], 3.20 [m, 4 H, CH_2CH_2], 7.52−7.84 [m, 20 H, $H_{arom.}$] ppm. ^{13}C{^{1}H} NMR (125 MHz, CD_2Cl_2): δ = −8.0 [d, ^2J(C,P) = 5, ^1J(C,Pt) = 528 Hz, CH_3], 21.0 [dd, ^1J(C,P) = 40, ^2J(C,P) = 5 Hz, P−CH$_2$CH$_2$−P(S)], 25.1 [dd, ^2J(C,P) = 2 Hz ^1J(C,P) = 54 Hz, P−CH$_2$−CH$_2$−P(S)], 129.8 (s), 129.9 (s), 130.1 (s), 130.2 (s), 131.6 [d, ^2J(C,P) = 11 Hz], 133.0 [d, ^1J(C,P) = 3 Hz], 134.0 [d, ^2J(C,P) = 11, ^2J(C,Pt) = 25 Hz], 134.3 [d, ^1J(C,P) = 3 Hz,], 176.2 [dd, ^2J(C,P) = 148, ^3J(C,P) = 2 Hz; ^1J(C,Pt) = 1392 Hz, CO] ppm.

***a*-Carbonyl-*b*-methyl-*dc*-{(diphenylphosphanylethyl)diphenylphosphanyl Sulfide-P,S}platinum(II) Tetrafluoroborate (8b):** IR (CD_2Cl_2): ṽ = 2096 (CO) cm^{-1}. ^{1}H NMR (500 MHz, CD_2Cl_2): δ = 1.28 [d, ^2J(H,Pt) = 55.4, ^3J(H,P) = 6.5 Hz, 3 H, CH_3], 3.40 [m, 4 H, CH_2CH_2], 7.46−7.89 [m, 20 H, $H_{arom.}$] ppm. ^{13}C{^{1}H} NMR (125 MHz, CD_2Cl_2): δ = 2.5 [dd, ^2J(C,P) = 75, ^3J(C,P) = 7 Hz,,^1J(C,Pt) = 358 Hz, CH_3], 21.2 [dd, ^1J(C,P) = 31, ^2J(C,P) = 5 Hz, P−CH$_2$CH$_2$−P(S)], 25.2 [d, ^1J(C,P) = 50, ^3J(C,Pt) = 17 Hz, P−CH$_2$−CH$_2$−P(S)], 130.0 (s), 130.1 (s), 130.3 (s), 130.4 (s), 132.1 [d, ^2J(C,P) = 11 Hz], 132.7 [d, ^1J(C,P) = 3 Hz], 133.1 [d, ^2J(C,P) = 12, ^2J(C,Pt) = 13 Hz], 134.7 [d, ^1J(C,P) = 3 Hz,], 167.9 [d, J(C,P) = 7 Hz; ^1J(C,Pt) = 1859 Hz, CO] ppm.

MS Analyses: All complexes were submitted for LC-MS analyses by using APCI and API-ES sources and positive and negative ionisation modes at different fragmentor voltages. The negative APCI spectrum of **1** in dichloromethane gave a very intense base peak at m/z = 697 [M + Cl]$^-$ (fragmentor voltage: 0 V). Increasing the fragmentor voltage the intensity of the [M + Cl]$^-$ ion decreased with the concomitant appearance of the [M]$^-$ ion (m/z = 661). At 200 V the base peak is represented by [M]$^-$ ion and the [M + Cl]$^-$ ion disappeared. The negative APCI mass spectrum of a dichloromethane solution of **2** displayed the [M + Cl]$^-$ ion (m/z = 710) and [M + Cl − CH_3]$^-$ (m/z = 695) at a fragmentor voltage of 100 V. Using CH_3CN as solvent and the ESI interface (positive ions) at a fragmentor voltage of 120 V the [M − Cl + CH_3CN]$^+$ (m/z = 681) and [M − Cl]$^+$ ions (m/z = 640, 100% relative abundance) were detected.

Complex **3** was first dissolved and analysed in acetonitrile. ESI-MS spectra were acquired in positive ion mode at a drying gas temperature of 300 °C. At a fragmentor voltage of 0 V the spectrum is dominated by a peak at m/z = 667 which corresponds to the cationic part of the complex [M]$^+$$BF_4^-$. A base peak at m/z = 626 was observed at fragmentor 200 V corresponding to the [M − CH_3CN]$^+$ ion due to the loss of a coordinated acetonitrile molecule. The use of dichloromethane as solvent (and eluent) for **3** and a fragmentor voltage of 350 V confirmed the presence of [M]$^+$ and [M − CH_3CN]$^+$ ions and showed the appearance of a new peak at m/z = 1287 attributable to the dimeric cation [2M − 2CH_3CN + Cl]$^+$. The latter ion may arise from complex **5,** which is formed by dissolving **3** in CH_2Cl_2, after substitution of a chloride for the coordinated acetonitrile. The relative abundance of the peak at m/z = 1287 passed from 5.0% to 10.0% lowering the 300 °C drying gas temperature down to 100 °C.

The mass spectrometric behaviour of **4** was similar to that of its homologue **3**. The base peak of ESI-MS spectra of **4** in acetonitrile was the [M]$^+$ ion (m/z = 681) at fragmentor voltages in the range

 © 2004 Wiley-VCH Verlag GmbH & Co. KGaA, Weinheim

0−100 V. At 150 V the base peak was represented by the $[M - CH_3CN]^+$ ion (m/z = 640). The dichloromethane solution of **4** showed, in the 0−350V fragmentor voltage range, the m/z = 1315 ion corresponding to the cationic part of **6** (which is formed by dissolving **4** in CH_2Cl_2) plus a chloride ion.

The positive ESI-MS spectra of pure **6** were acquired in dichloromethane and were analyzed under the same conditions applied for **4**. The $[M + Cl]^+$ ion (m/z = 1315) was observed in the 0−350V fragmentor voltage range whereas the m/z = 640 peak, corresponding to the monocharged halfed dimer was the most intense peak in the fragmentor voltage range 0−100 V.

Chloride adduct formation is a consequence of the use of dichloromethane. No evidence of doubly charged ions was found: the strong tendency of the dicationic species to form single charged adducts in the presence of the above mentioned negative ions probably represents the optimal ionization pathway.

The positive ESI-MS spectra of dichloromethane solutions of carbonyl species **7** and **8** were acquired under the same conditions reported for **3** and showed intense $[M]^+$ ions (m/z = 654 for **7**, m/z = 668 for **8**) in the fragmentor voltage range 0−200 V. At 250 V the loss of the CO molecule gave the $[M - CO]^+$ ions (m/z = 626 for **7**, m/z = 640 for **8**) as base peaks.

X-ray Structure Determinations of 1·CD_2Cl_2 and 6·2CD_2Cl_2:[34] Single crystals were obtained by slowly evaporating solutions of the compounds in CD_2Cl_2. The stoichiometries of the resulting solvates were **1**·CD_2Cl_2 and **6**·2CD_2Cl_2. Data were collected at room temperature with a Bruker SMART D8 goniometer equipped with an APEX detector. The structures were solved by direct methods.[35] The final structure model with anisotropic displacement parameters for all non-hydrogen atoms and H atoms riding in idealized positions was refined on F^2.[36] Crystal data, parameters of data collection, and convergence results are compiled in Table 4. Table 2 summarises selected bond lengths and angles.

Acknowledgments

Italian MURST (PRIN 2002 project, prot. 031332) is gratefully acknowledged for financial support. We thank Dr. Vito Gallo, Dr. Antonino Rizzuti and Dr. Giuseppe Romanazzi for their help.

[1] A. Bader, E. Lindner, *Coord. Chem. Rev.* **1991**, *108*, 27−110.
[2] C. S. Slone, D. A. Weinberger, C. A. Mirkin, *Prog. Inorg. Chem.* **1999**, *48*, 233−350.
[3] P. Braunstein, F. Naud, *Angew. Chem. Int. Ed.* **2001**, *40*, 680−699.
[4] J. R. Dilworth, N. Wheatley, *Coord. Chem. Rev.* **2000**, *199*, 89−158.
[5] R. Romeo, L. Monsù Scolaro, M. R. Plutino, A. Romeo, F. Nicolò, A. Del Zotto, *Eur. J. Inorg. Chem.* **2002**, 629−638.
[6] S. O. Grim, J. D. Mitchell, *Inorg. Chem.* **1977**, *16*, 1762−1770.
[7] R. Colton, J. Ebner, B. F. Hoskins, *Inorg. Chem.* **1988**, *27*, 1993−1999.
[8] J. Browning, G. W. Bushnell, K. R. Dixon, R. W. Hilts, *J. Organomet. Chem.* **1993**, *452*, 205−218.
[9] T. C. Blagborough, R. Davis, P. Ivison, *J. Organomet. Chem.* **1994**, *467*, 85−94.
[10] S. M. Aucott, A. M. Z. Slawin, J. D. Woollins, *Eur. J. Inorg. Chem.* **2002**, 2408−2418.
[11] S. M. Aucott, A. M. Z. Slawin, J. D. Woollins, *Polyhedron* **2003**, *22*, 361−368.
[12] D. E. Berry, J. Browning, K. R. Dixon, R. W. Hilts, *Can. J. Chem.* **1988**, *66*, 1272−1282.
[13] M. J. Baker, M. F. Giles, A. Guy, M. J. Taylor, R. J. Watt, *J. Chem. Soc., Chem. Commun.* **1995**, 197−198.
[14] L. Gonsalvi, H. Adams, G. J. Sunley, E. Ditzel, A. Haynes, *J. Am. Chem. Soc.* **2002**, *124*, 13597−13612.
[15] I. Brassat, U. Englert, W. Keim, D. Keitel, S. Killat, G. P. Suranna, R. Wang, *Inorg. Chim. Acta* **1998**, *280*, 150−162.
[16] I. Brassat, W. Keim, S. Killat, M. Moethrath, P. Mastrorilli, C. F. Nobile, G. P. Suranna, *J. Mol. Catal. A* **2000**, *157*, 41−58.
[17] G. P. Suranna, P. Mastrorilli, C. F. Nobile, W. Keim, *Inorg. Chim. Acta* **2000**, *305*, 151−156.
[18] G. P. C. M. Dekker, A. Buijs, C. J. Elsevier, K. Vrieze, P. W. N. M. van Leeuwen, W. J. J. Smeets, A. L. Spek, Y. F. Wang, C. H. Stam, *Organometallics* **1992**, *11*, 1937−1948.
[19] A. Scrivanti, V. Beghetto, A. Bastianini, U. Matteoli, G. Menchi, *Organometallics* **1996**, *15* 4687−4694.
[20] S. J. Dossett, A. Gillon, A. G. Orpen, J. S. Fleming, P. G. Pringle, D. F. Wass, M. D. Jones, *Chem. Commun.* **2001**, 699−700.
[21] T. Y. H. Wong, S. J. Rettig, B. R. James, *Inorg. Chem.* **1999**, *38*, 2143−2149.
[22] S. S. M. Ling, R. J. Puddephatt, L. Manojlovic-Muir, K. Muir, *Inorg. Chim. Acta* **1983**, *77*, L95−L96 and refs. therein.
[23] A. J. Blacker, M. L. Clarke, M. S. Loft, M. F. Mahon, J. M. J. Williams, *Organometallics* **1999**, *18*, 2867−2873.
[24] The synthesis of monomeric dichloromethane Pt^{II} complexes by $AgBF_4$ induced chloride abstraction from [(L)Pt(R)Cl] is reported in: R. Sinigalia, R. A. Michelin, F. Pinna, G. Strukul, *Organometallics* **1987**, *6*, 728−734 (L = diphosphane, R = CF_3) and in ref.[23] of this paper (L = phosphanyloxazoline, R = CH_3).
[25] E. Delgado, E. Hernandez, E. Lalinde, H. Lang, N. Mansilla, M. T. Moreno, G. Rheinwald, F. Zamora, *Inorg. Chim. Acta* **2001**, *315*, 1−8.
[26] The NMR spectroscopic data reported in Table 1 for **3** and **4** were obtained from the spectra recorded in CD_2Cl_2 and therefore refer to the CH_3CN complexes, different from data reported in the Exp. Sect. that refer to the CD_3CN complexes quantitatively obtained in [D_3]acetonitrile.
[27] M. Capdevila, W. Clegg, P. Gonzales-Duarte, A. Jarid, A. Lledos, *Inorg. Chem.* **1996**, *35*, 490−497.
[28] An example with alkyl thiolate: E. W. Abel, D. G. Evans, J. R. Koe, M. B. Hursthouse, M. Mazid, M. F. Mahon, K. C. Molloy, *J. Chem. Soc., Dalton Trans.* **1990**, 1697−1704.
[29] A recent example with aryl thiolate: G. Rivera, S. Bernès, C. Rodriguez de Barbarin, H. Torrens, *Inorg. Chem.* **2001**, *40*, 5575−5580.
[30] The Pt−S−Pt′ angle observed in Pt^{II} complexes with thioether bridging ligands is of the same magnitude. In $Pt_2(CH_3)_4[(C_2H_5)_2S]_2$ the Pt−S−Pt′ angle is 100.1(1)°. See: D. P. Bancroft, F. A. Cotton, L. R. Falvello, W. Schwotzer, *Inorg. Chem.* **1986**, *25*, 763−770.
[31] A. Dervisi, R. L. Jenkins, K. M. A. Malik, M. B. Hursthouse, S. Coles, *Dalton Trans.* **2003**, 1133−1142.
[32] A. Dervisi, personal communication.
[33] T. Kégl, L. Kollàr, L. Radics, *Inorg. Chim. Acta* **1997**, *265*, 249−254.
[34] CCDC-194011 and -202636 contain the supplementary crystallographic data for this paper. These data can be obtained free of charge at www.ccdc.cam.ac.uk/conts/retrieving.html [or from the Cambridge Crystallographic Data Centre, 12 Union Road, Cambridge CB2 1EZ, UK; Fax: (internat.) + 44-1223/336-033; E-mail: deposit@ccdc.cam.ac.uk].
[35] G. M. Sheldrick, SHELXS 97, *Program for Crystal Structure Solution*, University of Göttingen, Germany, **1997**.
[36] G. M. Sheldrick, SHELXL 97, *Program for Crystal Structure Refinement*, University of Göttingen, Germany, **1997**.

Received July 3, 2003
Early View Article
Published Online February 10, 2004

 © 2004 Wiley-VCH Verlag GmbH & Co. KGaA, Weinheim

Polymetallated 4-*tert*-Butylcalix[4]arene Complexes of Sodium and Potassium Stabilized by Crown Ethers: Syntheses, Structures and Activation of Carbon Dioxide

Reinald Fischer,[a] Helmar Görls,[a] and Dirk Walther*[a]

Keywords: Alkali metals / Calixarenes / Carbon dioxide fixation / Carboxylation / Crown compounds

4-*tert*-Butylcalix[4]arene and 18-crown-6 react with NaH in THF to form the complex [(18-crown-6)(THF)Na_4(4-*tert*-butylcalix[4]arene-4H)]$_2$·3THF (**1**). Analogously, the reaction with 4-*tert*-butyltetrathiacalix[4]arene in DMF results in the formation of [(18-crown-6)Na(dmf)$_{1.5}$]$_2$[(4-*tert*-butyltetrathiacalix[4]arene-4H)$_2$$Na_6(dmf)_2$] (**2**) The X-ray analysis of **1** shows an Na_6O_6 skeleton consisting of two fused open heterocubanes. Two Na^+ ions are encapsulated in the cavities of the calix[4]arene units. Additionally, two peripheral Na^+ ions, each surrounded by a crown ether and one THF ligand, are connected to the central Na_6O_6 skeleton by one bridging oxygen of the calix[4]arene. In contrast, **2** contains the highly symmetrical anion [(4-*tert*-butyltetrathiacalix[4]arene-4H)$_2$$Na_6(dmf)_2$]$^{2-}$ and crown-ether-stabilized cations. While **1** shows a dynamic process in solution above 40 °C, the structure of the highly symmetrical compound **2** remains stable at higher temperatures. The solid-state structure of the potassium complex [(dibenzo-18-crown-6)K_4(4-*tert*-butylcalix[4]arene-4H)(THF)$_3$]$_2$·4THF (**4**) is similar to **1**; however, the calix[4]arene units in the open heterocubane structure of **4** are shifted less than half a diameter to one another than in the sodium complex **1**. According to the ^{1}H NMR spectra complex **3a**, containing 18-crown-6, has a very similar structure to the related complex **4**. Both **1** and **4** absorb carbon dioxide in THF and are active CO_2-transfer reagents towards 2-fluoropropiophenone; complex **2** is much less active. This clearly demonstrates the subtle influence of the structure of the alkali metal complexes on the CO_2 reactivity in these types of compounds.

(© Wiley-VCH Verlag GmbH & Co. KGaA, 69451 Weinheim, Germany, 2004)

Introduction

Calixarenes and their metal complexes have attracted great interest during the last 20 years due to a number of attractive aspects in different areas. A great number of derivatives have been synthesized, structurally characterized and used for application in supramolecular chemistry (especially host-guest complexes), for selective metal coordination, as models for simulating catalytic oxide surfaces, and as catalysts and sensors.[1−7]

Interactions with alkali metal ions have been intensively investigated mainly due to their importance for the separation of the alkali metals and as models for metal-ion transport.[8] The first complex of the monoanion of 4-*tert*-butylcalix[4]arene with Cs^+ was described 1991 by Harrowfield.[9] In 1993 Atwood isolated a monometallated sodium complex in which two oxygens of the calixarene unit chelate to the metal.[10] A number of other alkali metal complexes with monoanionic and dianionic calixarenes are also known.[11−13] Recently, Harrowfield described partially deprotonated thiacalixarene complexes of the Li−Cs series,[14] and in 1995 Bock et al. published the molecular structure of [Li_3(calix[4]arene-3H)(NH_3)]$_2$ the first alkali metal complex of a multiply deprotonated calix[4]arene.[15]

Surprisingly little is known about alkali metal complexes with fully deprotonated calix[4]arenes of the type [M_4(4-*tert*-butylcalix[4]arene-4H)(solv)$_x$]$_2$, which are useful building blocks for the preparation of transition metal complexes. The first complex of this type with Li as the metal center was described by Davidson.[16] Recently, Floriani,[17] and Fromm[18] prepared and structurally elucidated polymetallated alkali metal complexes with Li, Na and K using different synthetic procedures. Partial hydrolysis of the lithium derivative resulted in the formation of the doubly protonated Li complex.[18] Furthermore, the syntheses and structures of dialkylated alkali metal calix[4]arene complexes were recently described, and their reaction with crown ethers in solution investigated by NMR spectroscopy.[19]

It is well-known that alkali-metal phenolates react with carbon dioxide to form complexes of hitherto unknown structures which can undergo self-carboxylation to form salicylic acid or the *para*-hydroxybenzoic acid. Additionally, some alkali-metal phenolates are also able to carboxylate

[a] Institut für Anorganische und Analytische Chemie of the Friedrich-Schiller-Universität Jena,
August-Bebel-Str. 2, 07743 Jena, Germany
Fax: (internat.) +49-3641-948-102
E-mail: cdw@uni-jena.de

activated aliphatic C−H bonds in dipolar aprotic solvents to form aliphatic carboxylic acids upon hydrolysis.[20−24]

Generally, calixarene alkali metal complexes containing phenolate groups linked in the two *ortho* positions by methylene groups should be of great interest in CO_2 chemistry, especially for the design of metal complexes which could be active in both the fixation and the activation of carbon dioxide. To the best of our knowledge, this aspect of calixarene metal chemistry has been completely ignored so far.

Here we report on the synthesis and molecular structures of new polymetallated sodium and potassium calix[4]arene complexes in combination with crown ethers, which act as competitive ligands. Our aim was to construct soluble systems which would be active in both CO_2 fixation and in carboxylation reactions of activated aliphatic C−H bonds.

Results and Discussion

Scheme 1 displays the starting calix[4]arene **A** and its sulfur-bridged analogue **B**, as well as the three crown ethers used as co-ligands.

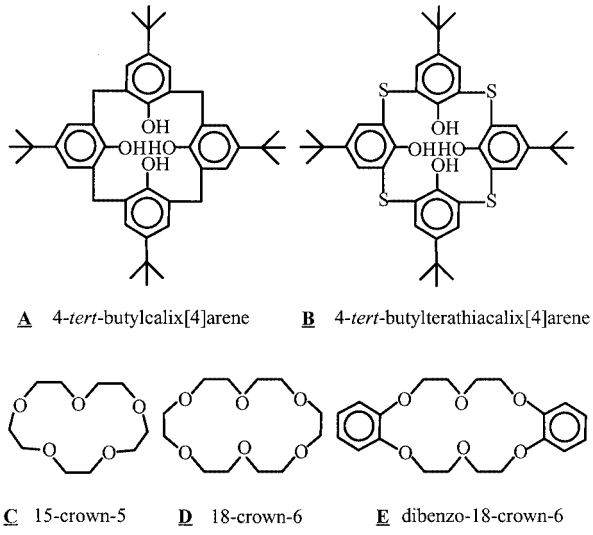

Scheme 1. The calix[4]arenes **A** and **B** and the crown ethers **C**−**E** used as ligands

Sodium Complexes with 4-*tert*-Butylcalix[4]arene (1 and 2)

In the absence of traces of water sodium hydride readily reacts with the calix[4]arene **A** in THF to form completely deprotonated products. In the presence of 15-crown-5 (**C**), which is tailor-made for Na^+, the resulting reaction product is insoluble even in polar solvents such as THF, DMF or DMSO. We assume, therefore, that the fully deprotonated calixarene-containing sodium complex consists either of separated ions, which cannot be solvated effectively in organic solvents, or forms a polymeric structure.

However, with 18-crown-6 (**D**) as co-ligand, a crown ether which does not "fit" effectively to Na^+,[25] complex **1** was obtained as a THF-soluble product. From this solution we isolated well-shaped single crystals containing three non-coordinated molecules of THF per dimeric unit [18-crown-6)(THF)Na_4(4-*tert*-butylcalix[4]arene-4H)]$_2$. THF is very easily eliminated from this complex at 0 °C or by bubbling a stream of inert gas through the solution. Complex **1** is formed in a very selective reaction in high yields. Even if an excess of 18-crown-6 was used as a competitor ligand for the calix[4]arene, only complex **1** was formed. This shows that the sodium strongly prefers the charged ligand to the neutral one. Single crystals were grown from THF solution and the structure of **1** was confirmed crystallographically with the molecular structure illustrated in Figure 1.

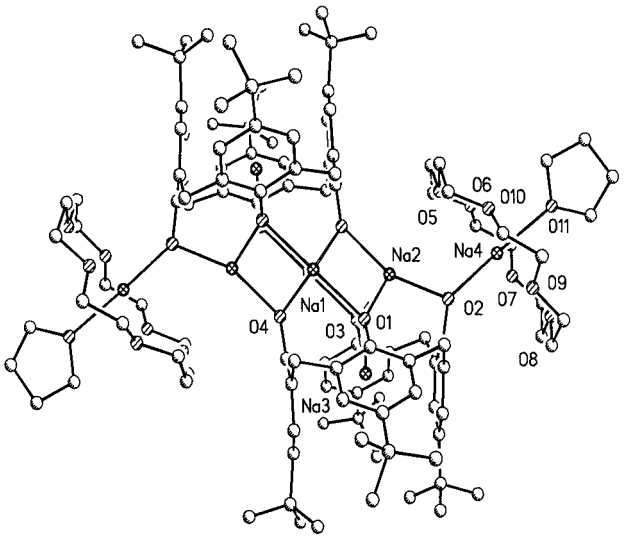

Figure 1. Molecular structure of [(18-crown-6)(THF)Na_4(4-*tert*-butylcalix[4]arene-4 H)]$_2$·3THF (**1**); non-coordinated THF and hydrogen atoms have been omitted for clarity; selected bond lengths (A): Na(1)−O(1) 2.275(3), Na(1)−O(3) 2.281(3), Na(1)−O(4) 2.292(3), Na(2)−O(1) 2.383(3), Na(2)−O(2) 2.199(3), Na(2)−O(3) 2.359(3), Na(2)−O(4A) 2.232(3), Na(3)−O(1) 2.327(3), Na(3)−O(3) 2.356(3), Na(4)−O(2) 2.216(3), Na(4)−O(5) 2.802(4), Na(4)−O(6) 2.805(4), Na(4)−O(7) 2.661(4), Na(4)−O(8) 2.714(4), Na(4)−O(9) 2.672(4), Na(4)−O(10) 2.820(4), Na(4)−O(11) 2.381(4), Na(1)···Na(1A) 2.931(3), Na(1)···Na(2) 3.152(2); selected bond angles (°): O(11)−Na(4)−O(5) 99.60(14), O(11)−Na(4)−O(6) 84.2(2), O(11)- Na(4)−O(7) 86.9(2), O(11)−Na(4)−O(8) 83.13(13), O(11)−Na(4)−O(9) 86.1(2), O(11)−Na(4)−O(10) 81.6(2), (11)−Na(4)−O(2) 177.7(2), O(1)−Na(1)−O(3A) 171.68(12), O(1)−Na(1)−O(4A) 93.73(11), O(1)−Na(1)−O(4) 90.77(10), O(2)−Na(2)−O(4A) 153.33(12), O(2)−Na(2)−O(1) 101.50(11), O(2)−Na(2)−O(3) 102.82(11), O(1)−Na(2)−O(3) 86.91(10), Na(1)−O(1)−Na(3) 118.7(3), Na(1A)−O(3)−Na(3) 117.3(3)

Figure 2 shows the Na_6O_6 skeleton of **1**, with the Na(1)−O(4)−Na(1A)−O(4A)−plane fusing two heterocubane units. Since there are no bonding interactions between Na(3) and O(4) or Na(3A) and O(4A), two "open" heterocubane units result.

Compound **1** can be considered as an intermediate between the fully lithiated compound (with the coordination number 4 for Li)[18] and the potassium compound (open heterocubane structure), reflecting also the intermediate size of the Na cation between Li and K.

Furthermore, in **1** the two calix[4]arene units are shifted by half a diameter with respect to one another. This is different to the reported pyridine-stabilized sodium complex

 © 2004 Wiley-VCH Verlag GmbH & Co. KGaA, Weinheim

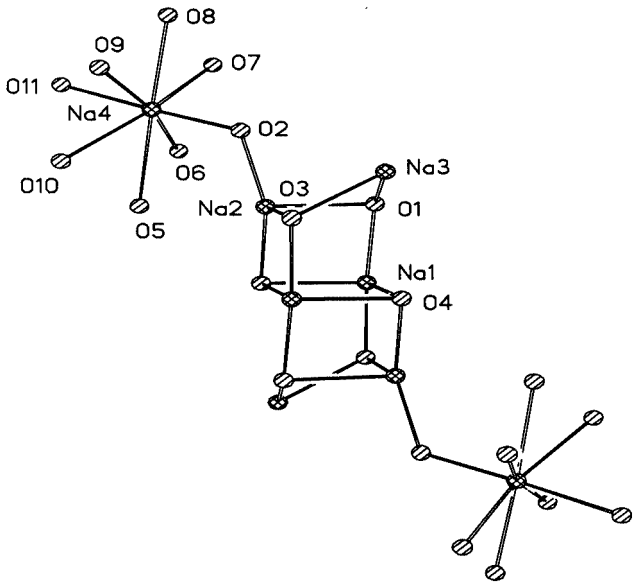

Figure 2. Na_8O_8 cluster core of **1** with the central Na_6O_6 skeleton

[(pyridine)$_4$Na$_4$(4-*tert*-butylcalix[4]arene-4H)]$_2$·THF in which this shift is very small.[10] Consequently, the sodium atoms in the plane fusing the two heterocubanes exhibit coordination numbers of four in **1**, in contrast to the above pyridine complex where these Na^+ ions have a coordination number of five.

In the central Na_6O_6 skeleton the oxygen atoms of the calix[4]arene are situated at the corners of a deformed rhomb, in contrast to their positions in the free calix[4] arene where these oxygens occupy the corners of a square.[26] Na(3) and Na(3A) are encapsulated in the cavities of the calix[4]arenes and are in contact with the aromatic π-systems of two calix[4]arene phenyl rings. These rings are almost parallel to each other and the Na−C bond lengths (between 2.931 and 3.500 Å) are similar to previously reported values.[18,19]

The peripheral Na(4) and Na(4A) atoms, with a coordination number of eight, each surrounded by the six oxygens of 18-crown-6 and one THF oxygen, are linked to the central Na_6O_6 skeleton by only one bridging calixarene phenolate. The six crown ether oxygens adopt almost coplanar positions with the sodium ion out of this plane (deviation from the least-squares plane: 0.15 Å, shifted in the direction of the coordinated phenolate). Furthermore, the coordinated THF and the oxygen of the phenolate group lie *trans* to each other, perpendicular to the plane formed by the crown ether. This type of coordination is, in principle, well-known for symmetric 18-crown-6 sodium complexes of the type [(18-crown-6)NaL$_2$]X (L = THF,[27−30] H_2O[31,32] with different anions; for a review see ref.[33]). Moreover, asymmetric types of the composition [(18-crown-6)Na(X)] (L = THF or 1,3-dioxolane; X = anionic ligand) have recently been found as well.[34−36]

The Na−O(crown) distances in **1** [between 2.661(4) and 2.805(4) Å] are considerably longer than the Na−O(THF) distance [2.381(4) Å]. These values lie in a typical range for the above type of asymmetric compounds. As expected, the Na−O(phenolate) distance [2.216(3) Å] is the shortest Na−O bond due to the anionic nature of the Na_6O_6 skeleton containing the calixarene units.

The ^{1}H NMR spectrum in [D$_8$]THF at room temperature suggests that the structure found in the solid state is also maintained in solution at ambient temperature (Figure 3). As expected for this structure three signals of *tert*-butyl groups in a 2:1:1 ratio (at δ = 0.76, 0.95 and 1.29 ppm), and four signals for the *meta*-protons of the phenolates at δ = 6.27, 6.54, 6.84 and 6.90 ppm are observed at 20 °C. Furthermore, four doublets belonging to the bridging methylene groups at δ = 2.71, 2.82, 3.77 and 4.73 ppm appear.

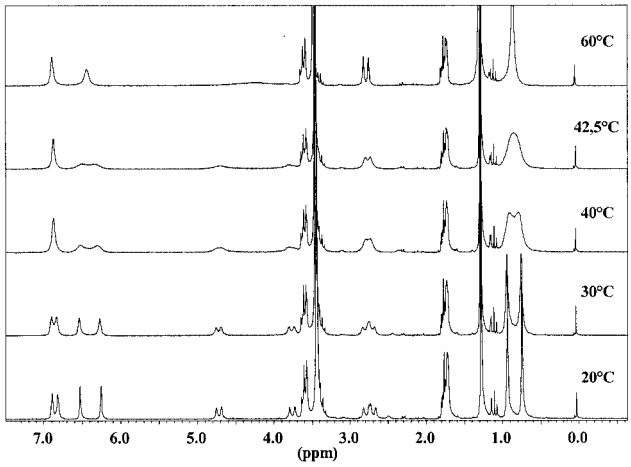

Figure 3. Temperature-dependent ^{1}H NMR spectra of **1** in [D$_8$]THF

Increasing the temperature results in a significant change of the NMR spectra. At 42.5 °C the two signals at higher field coalesce and at higher temperatures only two signals for the *tert*-butyl protons in a ratio of 2:2 (at δ = 0.82 and 1.25 ppm) appear. The signals of the *meta*-protons of the phenolates (at δ = 6.40 and 6.84 ppm) and of the bridging CH_2 (at δ = 2.74 and 4.19 ppm) show the same behavior, indicating that at higher temperature two pairs of equivalent phenolates exist in the molecule.

The reversible nature of the temperature-dependent ^{1}H NMR spectra implies a dynamic process, the activation energy of which (ΔH = 65.0 ± 0.5 kJ·mol^{-1}) can be calculated from the temperature of coalescence and the separation of the signals in the ^{1}H NMR spectra.

One possibility to explain this dynamic behavior would be the dissociation of **1** into the ions [Na(18-crown-6)]$^+$ and [(4-*tert*-calix[4]arene-4H)Na$_3$]$_2^-$. However, this process can be excluded because in this case three different species would exist in solution above 40 °C: the starting compound **1** and the ionic compounds [Na(18-crown-6)]$^+$ and [(4-*tert*-butylcalix[4]arene)Na$_3$]$_2^-$. This is not in agreement with the simple ^{1}H NMR pattern at high temperatures. However, a translation process involving the translation of one calix[4]-arene unit in the direction defined by the Na(2)−Na(2A)

 © 2004 Wiley-VCH Verlag GmbH & Co. KGaA, Weinheim

axis, and the translation of the other calix[4]arene in the opposite direction, could explain the NMR spectroscopic data. Simultaneously, the sodium ions Na(4) and Na(4A) would undergo a 1,3-shift. An alternative process would be the synchronized rotation of both calix[4]arene units in **1** around their central axis. The rhomb of Na(1)−Na(2)−Na(1A)−Na(2A) may be fixed during this process in which **1** would act in solution as a "temperature-dependent molecular slide clutch". A similar process, with an activation enthalpy, ΔH^{Θ}, of 45 kJ·mol^{-1} was recently found for a mononuclear Zn calixarene complex.[37] Although the NMR spectroscopic data do not allow us to distinguish between the translation and the rotation process in **1**, it is reasonable to favor the translation process, since a rotation would require more activation energy than a simple transition process.

The reaction of the sulfur-bridged calix[4]arene **B** with $NaN(SiMe_3)_2$ in the presence of 18-crown-6 in a molecular ratio of 1:4:1 in THF results in an insoluble product. Recrystallization from DMF gives well-shaped single crystals of the composition [(18-crown-6)Na(dmf)$_{1.5}$]$_2$[(4-*tert*-butyltetrathiacalix[4]arene-4H)$_2$Na$_6$(dmf)$_2$] (**2**). Complex **2** contains the same molecular ratio between calix[4]arene, sodium and 18-crown-6 as **1**; however the ^{1}H NMR spectrum of **2** exhibits only a simple pattern indicating a high symmetry of the molecule.

Unfortunately, due to the poor crystal quality only the structural motif could be determined by X-ray analysis. However, the complex is undoubtedly an ionic compound consisting of two [(dmf)$_n$Na$^+$(18-crown-6)]$^+$ (n = 1, 2) cations and the anion [(dmf)$_2$Na$_6$(4-*tert*-butyltetrathiacalix[4]arene$_2$]$^{2-}$. Figure 4 displays the structure motif of the anionic part.

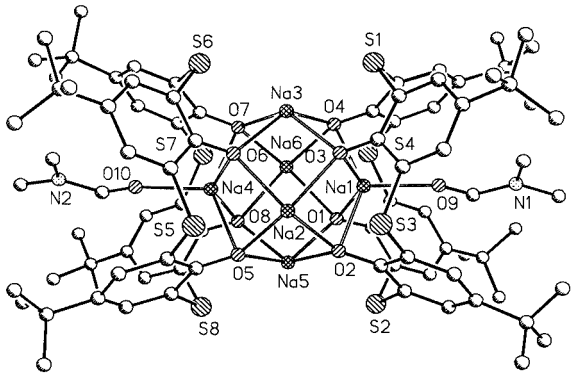

Figure 4. Structural motif of the [(4-*tert*-butyltetrathiacalix[4]arene-4H)$_2$Na$_6$(dmf)$_2$]$^{2-}$ anion of **2**; the counterions [(dmf)$_2$Na(18-crown-6)]$^+$, [(dmf)Na(18-crown-6)]$^+$ and the hydrogen atoms have been omitted for clarity

Complex **2** contains two perpendicular mirror planes, one of which consists of Na(2), Na(3), Na(5) and Na(6), and the other S(1), S(2), S(6) and S(8). The central unit of the structure is an octahedron with Na(1), Na(2), Na(3), Na(4), Na(5) and Na(6) at the corners. Every plane of the octahedron is capped by an oxygen of the phenolate rings. The sodium atoms Na(3), Na(2) Na(5), and Na(6) form square pyramids, with the Na ions at the apex and four oxygens in the base. In addition, the oxygen atoms of the calix[4]arene phenolates are located at the corners of a cube and the 4-*tert*-butyltetrathiacalix[4]arene moieties are in an eclipsed arrangement. There is no interaction of the Na$^+$ ions with the free electron-pairs of the sulfur atoms. In contrast to the sodium-calixarene complex **1**, where a sodium atom is found inside the cavities, the cavities of **2** contain a DMF molecule, which coordinates to Na(1) and Na(4).

The two counterions [(dmf)Na$^+$(18-crown-6)] and [(dmf)$_2$Na$^+$(18-crown-6)] have different coordination environments. In [(dmf)Na$^+$(18-crown-6)] the crown ether oxygens are arranged in a "boat form" with the sodium ion below the plane. The coordination of six oxygens of the crown ether and one DMF molecule results in a coordination number of seven for the sodium ion. This arrangement is similar to that in compound **5** and will be discussed in more detail below.

The structural motif of the other cation [(dmf)$_2$Na$^+$(18-crown-6)] is typical of the above-mentioned group of symmetrical [(18-crown-6)NaL$_2$]$^+$ complexes,[27−33] with a hexagonal-bipyramidal arrangement of the eight oxygen ligands surrounding the sodium ion. The sodium ion is situated in the center of the plane formed by the six oxygens of the crown ether compound. In addition, the two DMF ligands lie *trans* to each other.

The ^{1}H NMR spectrum in [D$_8$]THF is in agreement with this highly symmetrical structure found in the solid state: besides the DMF protons only one singlet for the protons of the *tert*-butyl groups (at δ = 1.14 ppm), one singlet for the *meta* CH groups of the aromatic rings (at δ = 7.42 ppm) and one singlet for the OCH$_2$ groups of the crown ether (at δ = 3.59 ppm), with the expected intensities, were observed. According to the ^{1}H NMR spectrum, this structure is maintained even at higher temperatures.

Potassium Complexes with 4-*tert*-Butylcalix[4]arene and Crown Ethers

The reaction of **A** with KN(SiMe$_3$)$_2$ and 18-crown-6 (**D**) in a molar ratio of 1:4:1 in THF afforded a mixture of the two compounds **3a** and **3b** even if the molecular ratio of **A**/18-crown-6 was varied from 1:1 to 1:2. Complex **3a** crystallized as large, colorless crystals of the composition [(18-crown-6)K$_4$(4-*tert*-butylcalix[4]arene-4H)(THF)$_n$], and **3b** crystallized as fine needles. Separation of **3a** from the reaction mixture was possible by repeated decanting of **3a** from the suspension followed by washing the crystals with THF at −78 °C. According to the ^{1}H NMR spectrum the purity of **3a** was greater than 95%. However, since **3a** could not be isolated as single crystals suitable for X-ray crystallography, we performed a similar reaction with the closely related dibenzo-18-crown-6 instead of 18-crown-6 to get better crystals of this type of compound.

Reaction of ligand **A** with KN(SiMe$_3$)$_2$ and dibenzo-18-crown-6 (**E**) in a molar ratio of 1:4:1 in THF did indeed yield the complex [(dibenzo-18-crown-6)K$_4$(4-*tert*-butylcalix[4]arene-4H)(THF)$_3$]$_2$·4THF (**4**) in a mixture with a second product of the composition [(dibenzo-18-crown-

 © 2004 Wiley-VCH Verlag GmbH & Co. KGaA, Weinheim

6)$_2$K$_4$(4-*tert*-butylcalix[4]arene-4H)] (according to the ^{1}H NMR spectrum of the reaction mixture). Single crystals of compound **4** grown from THF were suitable for X-ray analysis. Figure 5 shows the molecular structure and contains selected bond lengths and bond angles in the figure caption; Figure 6 shows the K_8O_8 core.

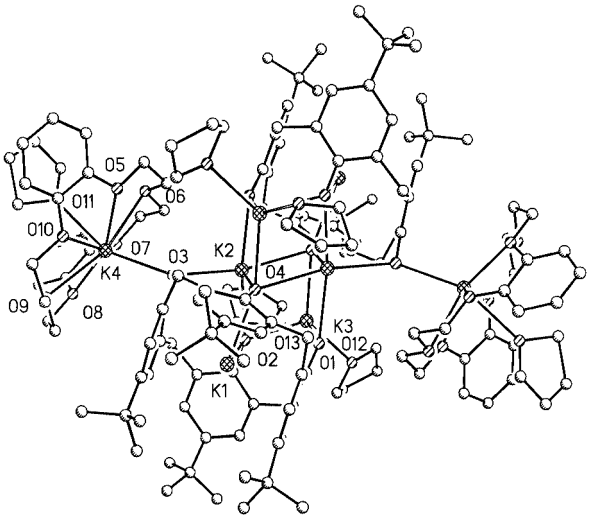

Figure 5. Molecular structure of **4**; non-coordinated THF and hydrogen atoms have been omitted for clarity; selected bond lengths (A): K(1)−O(2) 2.704(4), K(1)−O(4) 2.842(4), K(2)−O(2) 2.619(4), K(2)−O(3) 2.599(4), K(2)−O(4) 2.574(4), K(3)−O(1A) 2.702(4), K(2)−K(2A) 3.477(2), K(3)−O(1) 2.744(4), K(3)−O(2) 2.678(4), K(3)−O(12) 2.776(7), K(3)−O(13) 2.833(6), K(3)−K(2A) 2.6391(18Å, K(4)−O(3) 2.681(4), K(4)−O(5) 2.827(5), K(4)−O(6) 2.779(4), K(4)−O(7) 2.797(5) Å, K(4)−O(8) 2.848(5), K(4)−O(9) 2.812(5), K(4)−O(10) 2.841(5), K(4)−O(11) 2.758(8)

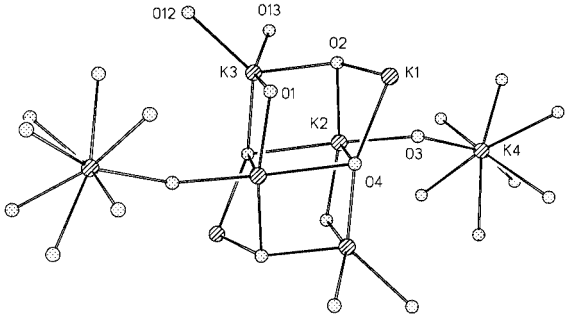

Figure 6. The K_8O_8 core in **4** with the central K_6O_6 skeleton and the two peripheral K^+ ions (each surrounded by the crown ether oxygens and one oxygen of THF) bridged by O(3) and O(3A), respectively

The molecular structure of **4** shows some similarities to the sodium compound **1**. In both complexes the central M_6O_6 moiety consists of two fused open heterocubanes where the corners are occupied alternately by alkali metal cations and oxygens of the calix[4]arenes. However, there are remarkable differences in the details of the structure. In contrast to **1**, the central heterocubane units in **4** are arranged nearly perpendicularly, and the peripheral [(THF)K(4)(dibenzo-18-crown-6)]$^+$ unit interacts with the phenolate oxygen bridge O(3) of the central skeleton and not with O(2) as found in **1**.

The calixarene oxygens coordinate to the central potassium rhomb containing K(2), K(3), K(2A) and K(3A). K(2) and K(2A) have coordination numbers of five, with a distorted square-pyramidal arrangement of the phenolate oxygen atoms. K(3) and K(3A) also have a coordination number of five due to three phenolate oxygen atoms and two coordinated THF molecules.

The two calix[4]arene units are shifted less than half a diameter with respect to one another, therefore the [(THF)K(dibenzo-18-crown-6)]$^+$ moieties are much closer to the central K_6O_6 skeleton.

The structure of **4** is very similar to the reported structures of the complexes [(THF)$_5$K$_4$(4-*tert*-butylcalix[4]arene-4 H)]$_2$·4THF[17] and [(THF)$_5$K$_4$(4-*tert*-butylcalix[4]arene-4 H)]$_2$·THF.[18] The most remarkable difference consists in the different coordination of the peripheral ions K(4) and K(4A), indicating the influence of the crown ether ligand: as they are surrounded by the crown ether oxygens and one THF, both K(4) and K(4A) are only coordinated to one calix[4]arene oxygen bridge, in contrast to the previously described THF-stabilized complexes, where two oxygen bridges link these K^+ ions.

K(1) and K(1A) inside the calix[4]arene cores are bonded to only two oxygen atoms of the phenolates, although they also interact with the π-electron systems of the two nearly parallel phenolates. The K(1)−C_{aromat} distances lie within reported ranges[18] [2.931(3)−3.435(4) Å for the first ring and 3.058(4)−3.152(3) Å for the second ring]. However, there are also contacts to the *ipso* carbon atoms of the other two phenyl rings [K(1)−C_{ipso} = 2.977(3) and 2.964(5) Å].

The structure of the crown ether part is very similar to that in the sodium compound **1**. The coordination number of the potassium ion is eight, and the crown ether oxygens are arranged in an almost coplanar arrangement. The potassium ion lies above this plane, with a deviation of 0.53 Å. This structural motif is known for 18-crown-6 complexes of both sodium and potassium.[38] The K−O(crown) distances in **4** vary between 2.779(4) and 2.848(5) Å. As expected for the coordination of an anionic oxygen ligand, the K−O distance to the bridging calix[4]arene moiety [K(1)−O(3) 2.681(4) Å] is significantly shorter than the other K−O distances.

The ^{1}H NMR spectrum of **4** is in agreement with the structure found in the solid state and is very similar to that of **3a**, which contains 18-crown-6 instead of dibenzo-18-crown-6. Therefore, we assume that **3a** has a similar nonionic cluster-like structure to that of complex **4**.

The temperature-dependent ^{1}H NMR spectra of complex **3a** give evidence for an interesting reversible reaction. At ambient temperature three chemically different *tert*-butyl protons in a molecular ratio 2:1:1 are observed at δ = 1.15, 1.11 and 1.08 ppm. Upon warming, the signals of the *tert*-butyl protons and the *meta* protons of the phenolate groups become more and more equal and, in a simultaneous process, the intensity of the original signals of **3a** disappears, while new signals of a highly symmetric compound appear without coalescence. At 55 °C the ^{1}H NMR spectrum contains only signals for chemically equivalent phenolate

 © 2004 Wiley-VCH Verlag GmbH & Co. KGaA, Weinheim

groups. Therefore, we assume that a reversible, temperature-dependent dissociation of compound **3a** may proceed according to Equation (1):

$$\mathbf{3a} \rightleftarrows 2\,[K(18\text{-crown-6})(THF)_2]^+ + [K_3(calix[4]arene\text{-}4H)]_2^{2-} \quad (1)$$

Due to the similarities with the ^1H NMR spectrum of the anion of **2** we suggest that the anion $[K_3(calix[4]arene\text{-}4H)]_2^{2-}$ could have a similar molecular structure.

One of the reasons for the different behavior between the sodium complex **1** and the potassium complex **3a** in solution at increasing temperatures may be the different coordinating ability of 18-crown-6 to Na^+ and K^+, which favors the formation of an ionic product for K^+.

Fixation of CO_2 by 1, 2 and 4 and CO_2-Transfer Reaction with 2-Fluoropropiophenone

Sodium phenolate reacts with carbon dioxide to give a product of unknown structure which is able to carboxylate activated aliphatic C−H bonds in dipolar aprotic solvents.[13−17] Therefore it may be expected that some of the above alkali metal calix[4]arene complexes containing four linked phenolate rings should, in principle, be capable of carboxylating activated C−H bonds.

Compound **1** reacts rapidly with CO_2 in THF. If water is not excluded very carefully the resulting products are $NaHCO_3$ and compound **5** [Equation (2)], which could be obtained as single crystals from THF.

$$\mathbf{1} + 3\,CO_2 + 3\,H_2O \rightarrow \underset{\mathbf{5}}{[Na(18\text{-crown-6})][(calix[4]arene\text{-}H)]} + 3\,NaHCO_3$$

The X-ray structure of **5** (Figure 7) shows that the compound contains a single deprotonated $[calix[4]arene\text{-}3H]^-$ anion that is connected to the counterion $[Na(18\text{-crown-6})]^+$ by a phenolate bridge of the calix[4]arene monoanion [Na−O(3) = 2.454(5) Å]. The other three oxygens of the calixarene unit do not coordinate [Na−O distances: Na···O(1) 4.869(5), Na···O(2) 3.507(6), Na···O(4) 3.984(4) Å]. The O···O distances between the calixarene oxygens of O(1)···O(2) [2.932(6) Å], O(1)···O(4) [2.669(6) Å], O(2)···O(3) [2.597(6) Å], and O(3)···O(4) [2.528(6) Å] are typical for intramolecular hydrogen bonds. The much shorter separations between the phenolate oxygen atom O(3) and its neighboring atoms O(2) and O(4) suggests rather strong intramolecular hydrogen bonds between these atoms. In contrast, the other O···O distances are significantly longer, although they are also in the range of hydrogen bonds. A more detailed discussion about the nature of the hydrogen-bond system is, however, not possible, because the hydrogen atoms were not found in the Fourier map. In this connection it is interesting to note that, in the known monometallated sodium compound of **A**,[10] containing methanol as co-ligand, and the tetrathia analogue **B**,[14] with water and THF as co-ligands, the calixarene units also form an intramolecular hydrogen-bond system. However, in these complexes the two calixarene oxygens act as bidentate chelating ligands, in contrast to **5**, where only one oxygen of the calixarene is coordinated. This reflects again the stronger ligand-effect of the crown ether compared with the other ligands in the above complexes. The coordinated 18-crown-6 is folded away from the calix[4]arene moiety, so there is no space for another THF molecule to coordinate to the sodium cation, which has a coordination number of seven. The structure of the crown ether part in **5** is very different from that in complex **1**, where the oxygens form a coplanar arrangement: the crown ether oxygens in **5** form a "distorted boat" with the plane formed by O(6), O(7), O(9), and O(10). The sodium ion lies below this plane, whereas the other two oxygens [O(5) and O(8)] are above the plane, with very different deviations from the least-square plane [1.86 Å for O(5) and 0.80 Å for O(8)]. According to a search of the Cambridge Crystallographic Database a few other 18-crown-6 complexes of sodium exist in which an analogous arrangement has been found.[39,44] It is, however, noteworthy that the six calixarene oxygens in similar sodium complexes can assume a chair form as well.[41,42]

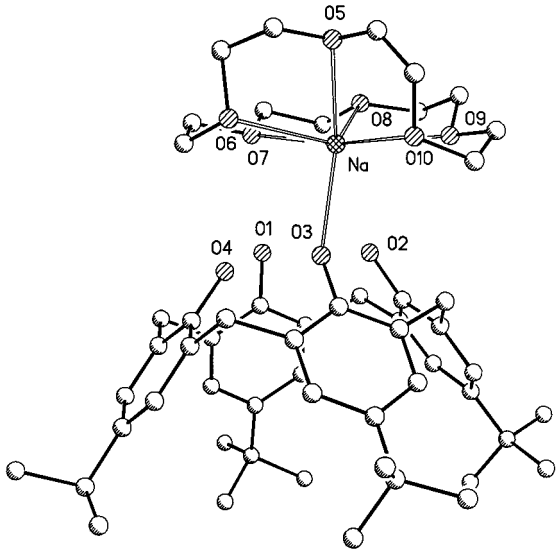

Figure 7. $[Na(18\text{-crown-6})(4\text{-}tert\text{-butylcalix[4]arene-H})]\cdot OEt_2$ (**5**); the non-coordinated ether and the hydrogen atoms have been omitted for clarity; selected bond lengths (Å): Na−O(3) 2.454(4), Na−O(5) 2.522(5), Na−O(6) 2.612(6), Na−O(7) 2.532(5), Na−O(8) 2.574(5), Na−O(9) 2.586(5), Na−O(10) 2.703(6); selected bond angles (°): O(3)−Na−O(5) 148.2(2), O(3)−Na−O(6) 94.8(2), O(3)−Na−O(7) 89.2(2), O(3)−Na−O(8) 113.4(2), O(3)−Na−O(9) 101.6(2), O(3)−Na−O(10) 97.4(2), Na(1)−O(1)−Na(3) 118.7(3)

Compound **5** displays a simple NMR spectrum. In the ^1H NMR spectrum only one singlet is observed for the *tert*-butyl groups (at δ = 1.17 ppm) and for the *meta* protons of the calix[4]arene unit (at δ = 6.87 ppm). The OH protons appear at δ = 13.39 ppm. Furthermore, two doublets of the calix[4]arene CH_2 protons were observed at δ = 3.07 and 5.52 ppm. The crown ether CH_2 protons give a signal at δ = 3.62 ppm. From these data we can conclude that, in solution, the $(18\text{-crown-6})Na^+$ moiety jumps from one phenol oxygen to another.

 © 2004 Wiley-VCH Verlag GmbH & Co. KGaA, Weinheim

In contrast to these results, the reaction of **1** with carbon dioxide, with strict exclusion of moisture, proceeds differently. When a solution of **1** in hot THF under an atmosphere of CO_2 is quickly cooled down in a dry ice bath, a clear solution is obtained, although the starting compound is only sparingly soluble in cold THF. This is the first evidence for the formation of a reaction product with CO_2. In the ^1H NMR spectrum the signals of **1** disappear upon uptake of carbon dioxide and a set of new signals appear at δ = 1.17 (s), 3.07 (d), 3.62 (s), 5.52 (d) and 6.87 ppm (br). The CO_2-containing complex could not be isolated because the weakly coordinated CO_2 is easily eliminated during work up. The final product is again the complex **1**. This clearly demonstrates that the CO_2 fixation is a reversible reaction. The same behavior was observed for **2**, meaning that both **1** and **2** are able to act as reversible CO_2 carriers.

To prove that the CO_2 products are capable of transferring their CO_2 to activated aliphatic C−H bonds we investigated the reactions of **1**, **2** and **4** in THF with 2-fluoropropiophenone under an atmosphere of carbon dioxide. After 24 h the reaction mixture was treated with dimethyl sulfate to yield the methyl ester of the unstable 3-ketocarboxylic acid. For comparison, the same reaction was carried out with sodium phenolate, which is known to act as a CO_2-transfer reagent.

Figure 8 shows that in all four reactions 2-benzoyl(2-fluoro)methylpropionate was formed, although in veryy different yields. Whereas sodium phenolate/CO_2 and **2**/CO_2 show very little activity (9% and 8% yield, respectively), the systems **1**/CO_2 and **4**/CO_2 are very efficient CO_2-transfer reagents that form the carboxylation product in a highly selective reaction (about 90%).

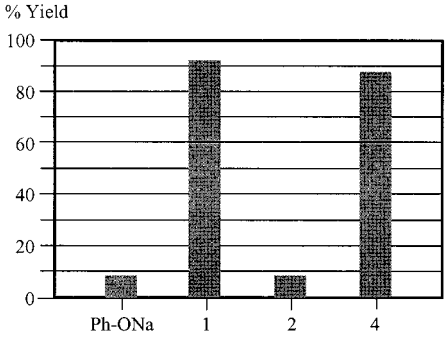

Figure 8. Carboxylation of 2-fluoropropiophenone by the complexes **1**/CO_2, **2**/CO_2, **4**/CO_2 and PhONa/CO_2 (for comparison) in THF at ambient temperature; reaction time: 24 h, molar ratio: 2-fluoropropiophenone/complex = 1:4; the yield was determined by ^{19}F NMR spectroscopy

Although the reasons for the remarkable difference in the carboxylation reactivity are hitherto unknown, the following points attract attention. Generally, CO_2-transfer reactions between NaOPh/CO_2 and substrates containing aliphatic activated C−H bonds such as acetone or acetophenone only proceed efficiently if dipolar aprotic solvents are used as solvent; the activity in THF is very low.[23] The reaction with 2-fluoropropiophenone confirms this (Figure 8). To explain this solvent-dependent activity, we assume that dipolar aprotic solvents (such as DMF, DMSO or *N*-methyl-ε-caprolactam) are stronger ligands than THF and can additionally split the Na−O bonds of the NaOPh oligomer in solution. This could result in more-reactive species which carboxylate activated C−H bonds much better than the "closed" heterocubane system found in complexes of the type (LNaOPh)[23,24] or polymeric NaOPh.[24] In contrast, **1** and **4** are complexes with "open" heterocubane structures in which the Na−O bonds should be more reactive in carboxylation reactions of activated aliphatic C−H bonds. The different structure of **2**, which exhibits a highly symmetrical anionic structure, could then explain why **2** is less active.

Conclusions

Sodium and potassium complexes of calix[4]arenes and crown ethers yield different types of stable molecular structures depending on the diameter of the alkali metal cations, the different size of the cavities of the calix[4]arenes and the different efficiency of the coordination by additional crown ether ligands. Even a relatively small difference of the size in the cavities of **A** (C−CH_2 = 1.516−1.581 Å) and **B** (C−S = 1.777 Å) results in a completely different structure type for complexes **1** and **2**, even though the ratio between 18-crown-6, Na^+ ions and calix[4] arene is the same. While **1** shows a dynamic process in solution above 40 °C, the structure of the highly symmetrical compound **2** remains stable at higher temperatures.

The structure of the potassium compound **4** is also different from the related sodium complex **1**. In **4** the calix[4]arene units are less shifted with respect to the plane fusing the two heterocubane units, and the coordination of the peripheral $[(THF)K(dibenzo\text{-}18\text{-}crown\text{-}6)]^+$ is also different. Temperature-dependent ^1H NMR spectra suggest, in this case, that a dissociation process proceeds resulting in the formation of ionic species.

Compounds **1** and **4**, containing the calix[4]arene **A**, are active CO_2-transfer reagents towards 2-fluoropropiophenone, in contrast to **2**, which contains the calix[4]arene **B**. This clearly demonstrates the subtle influence of the structure of the alkali-metal complexes on the CO_2 reactivity in these types of compounds.

Experimental Section

Due to the sensitivity of the substances to moisture and partly to air all manipulations were carried out under an atmosphere of argon. The solvents DMF and DMSO were dried with molecular sieves and THF with benzophenone/sodium, and freshly distilled before use.

4-*tert*-Butyltetrathiacalix[4]arene was prepared from 4-*tert*-butylphenol and sulfur in a solution of tetraethylene glycol dimethyl ether.[20] 4-*tert*-Butylcalix[4]arene, sodium hydride, $NaN(SiMe_3)_2$, $KN(SiMe_3)_2$, 4-*tert*-butylphenol, dibenzo-18-crown-6, 15-crown-5 and 18-crown-6 were purchased from Aldrich and tetraethylene glycol dimethyl ether from Merck-Schuchardt.

 © 2004 Wiley-VCH Verlag GmbH & Co. KGaA, Weinheim

Most of the synthesized complexes contain extremely weakly bound THF in the crystals which is extremely easily released when not in contact with the mother liquor. In addition, THF is very easily eliminated from complex **1** even at −78 °C in a stream of inert gas. The other complexes (except **2** and **5**) eliminate solvent when handled at 0 °C. This resulted in problems in obtaining microanalyses for **1**, **3a**, and **4** from the bulk material. Furthermore, only approximate yields (%) could be calculated on the basis of complex compositions due to loss of non-coordinated volatile solvents. These problems are well-known for alkali metal compounds of calixarenes containing volatile ligands.[12,14,18]

^{1}H and ^{13}C NMR spectra were recorded on a Bruker AC 200 F spectrometer. Mass spectra were recorded on a Finnigan MAT SSQ 710.

[(18-Crown-6)(THF)Na$_4$(4-*tert*-butylcalix[4]arene-4H)]$_2$·3THF (1): 18-Crown-6 (0.33 g, 1.25 mmol) and sodium hydride (0.13 g, 5.42 mmol) were added to a suspension of **A** (0.81 g, 1.25 mmol) in THF (50 mL). The reaction mixture was stirred and heated in a water bath to reflux. Hydrogen gas was liberated while the starting materials gradually dissolved. The hot solution was filtered through a Schlenk frit. Complex **1** crystallized from the filtrate. The colorless crystals lost non-coordinated THF and formed an amorphous powder. Yield: 1.3 g (ca. 95% based on the composition [(18-crown-6)(THF)Na$_4$(4-*tert*-butylcalix[4]arene-4H)]$_2$. ^{1}H NMR (200 MHz, [D$_8$]THF, 20 °C): δ = 0.76 (s, 9 H, *t*Bu), 0.95 (s, 9 H, *t*Bu), 1.29 (s, 18 H, *t*Bu), 2.71 (d, $^2J_{H,H}$ = 13.1 Hz, 2 H, CH$_2$), 2.82 (d, $^2J_{H,H}$ = 13.6 Hz, 2 H, CH$_2$), 3.45 (s, 24 H, CH$_2$O), 3.77 (d, $^2J_{H,H}$ = 13.6 Hz, 2 H, CH$_2$), 4.73 (d, $^2J_{H,H}$ = 13.3 Hz, 2 H, CH$_2$) 6.27 (s, 2 H, *m*-CH), 6.54 (s, 2 H, *m*-CH), 6.84 (s, 2 H, *m*-CH), 6.90 (s, 2 H, *m*-CH) ppm. ^{1}H NMR (200 MHz, [D$_8$]THF, 60 °C): δ = 0.86 (s, 18 H, *t*Bu), 1.25 (s, 18 H, *t*Bu), 2.74 (d, $^2J_{H,H}$ = 13.3 Hz, 4 H, CH$_2$), 3.38 (s, 24 H, OCH$_2$), 4.19 (br., 4 H, CH$_2$), 6.40 (s, 4 H, *m*-CH), 6.84 (s, 4 H, *m*-CH) ppm. ^{13}C{^{1}H} NMR (50.3 MHz, [D$_8$]THF, 60 °C): δ = 32.1, 32.6 (CH$_3$, *t*Bu), 33.9 (CH$_2$), 34.8 (C, *t*Bu), 70.5 (CH$_2$O), 123.6, 134.3 (br., *o*-C), 125.7, 132.1 (*m*-CH), 129.3, 163.7 (*ipso*-C). Well-shaped crystals suitable for the X-ray analysis crystallized from a solution in THF.

[(18-Crown-6)Na(dmf)$_{1.5}$]$_2$[(4-*tert*-butyltetrathiacalix[4]arene-4H)$_2$Na$_6$(dmf)$_2$] (2): 18-Crown-6 (0.33 g, 1.25 mmol) and sodium hydride (0.13 g, 5.42 mmol) were added to a suspension of **B** (0.90 g, 1.25 mmol) in THF (50 mL). The reaction mixture was stirred and heated in a water bath to reflux. Hydrogen gas was liberated during the reaction. The resulting white precipitate was separated from the reaction mixture by filtration through a Schlenk frit. Single crystals for X-ray analysis of **2** were obtained by recrystallization of the precipitate from a solution in DMF. Yield: 2.85 g (91%) of colorless needles of **2**. C$_{119}$H$_{171}$N$_5$Na$_8$O$_{25}$S$_8$: calcd. C 56.90, H 6.86, N 2.79, S 10.21; found C 56.07, H 6.81, N 3.21, S 9.44. ^{1}H NMR (200 MHz, [D$_7$]DMF, 30 °C): δ = 1.14 (s, 36 H, *t*Bu), 3.59 (s, 24 H, OCH$_2$), 7.43 (s, 8 H, *m*-CH) ppm. ^{13}C{^{1}H} NMR (50.3 MHz, [D$_7$]DMF, 30 °C): δ = 32.0 (CH$_3$, *t*Bu), 33.6 (C, *t*Bu), 70.5 (CH$_2$O), 126.3, 134.3, 132.3, 135.9, 171.1 (*ipso*-C) ppm.

[(18-Crown-6)K$_4$(4-*tert*-butylcalix[4]arene-4H)(THF)$_n$] (3a): A suspension of **1** (0.81 g, 1.25 mmol) in THF (50 mL) was reacted with 18-crown-6 (0.33 g, 1.25 mmol) and KN(SiMe$_3$)$_2$ (1.07 g, 5.38 mmol). Large colorless crystals of **3a** were decanted from a suspension of fine needles of **3b**. The crystals of **3a** were washed with THF at −78 °C in order to remove impurities of **3b** from the surface of the crystals. The colorless crystals very easily lost non-coordinated THF when not in contact with the mother liquor and formed an amorphous powder. Yield: 0.04 g of the amorphous product **3a** approximately 3% based on the composition [(18-crown-6)K$_4$(4-*tert*-butylcalix[4]arene-4H)]. According to the ^{1}H NMR spectrum the purity of the product was greater than 95%.
3a: ^{1}H NMR (200 MHz, [D$_8$]THF, 10 °C): δ = 1.08 (s, 9 H, *t*Bu), 1.11 (s, 9 H, *t*Bu), 1.15 (s, 18 H, *t*Bu), 2.67 (br., CH$_2$), 3.45 (s, 24 H, CH$_2$O), 4.44 (br., CH$_2$), 6.63 (s, 4 H, *m*-CH), 6.91 (s, 4 H, *m*-CH) ppm. ^{1}H NMR (200 MHz, [D$_8$]THF, 55 °C): δ = 1.12 (s, 36 H, *t*Bu), 2.67 (br., CH$_2$), 3.46 (s, 24 H, CH$_2$O), 4.44 (br., CH$_2$), 6.82 (s, 8 H, *m*-CH) ppm.
3b: ^{1}H NMR (200 MHz, [D$_8$]THF, 10 °C): δ = 1.11 (s, 36 H, *t*Bu), 2.70 (br., 4 H, CH$_2$), 3.46 (s, 48 H, CH$_2$O), 4.50 (br., 4 H, CH$_2$), 6.66 (s, 8 H, *m*-CH) ppm.

[(Dibenzo-18-crown-6)K$_4$(4-*tert*-butylcalix[4]arene-4 H)(THF)$_3$]$_2$·4THF (4): Dibenzo-18-crown-6 (0.45 g, 1.25 mmol) and KN(SiMe$_3$)$_2$ (1.07 g, 5.38 mmol) were added to a suspension of **1** (0.81 g, 1.25 mmol) in THF (50 mL). The reaction mixture was stirred and heated in a water bath to reflux while the starting materials gradually dissolved. The hot solution was filtered through a Schlenk frit. Compound **4** crystallized from the filtrate as a mixture with "K$_4$(4-*tert*-butylcalix[4]aren-4H)(dibenzo-18-crown-6)$_2$(THF)$_n$". The large colorless crystals of **4** were separated from the fine needles of the by-product by pouring off the suspension. The colorless crystals lost non-coordinated THF and formed an amorphous powder. Yield: 0.44 g of a white amorphous crude product. (ca. 25% based on the composition [(dibenzo-18-crown-6)K$_4$(4-*tert*-butylcalix[4]arene-4H)(THF)$_3$]$_2$. ^{1}H NMR (200 MHz, [D$_8$]THF, 10 °C): δ = 1.09 (s, 9 H, *t*Bu), 1.10 (s, 9 H, *t*Bu), 1.15 (s, 18 H, *t*Bu), 3.00 (d, $^2J_{H,H}$ = 11.7 Hz, 2 H, CH$_2$), 3.92 (br., 8 H, O-CH$_2$), 3.99 (br., 8 H, O-CH$_2$), 4.46 (br., 2 H, CH$_2$), 6.73 (br., 8 H, *m*-CH), 6.82 (br., 8 H, *o*-C$_6$H$_4$) ppm.

[(18-Crown-6)Na](4-*tert*-butylcalix[4]arene-H)·OEt$_2$ (5): Carbon dioxide gas and water (54 μL, 3.0 mmol) were added to a suspension of crude product of **1** (1.07 g, 1.0 mmol) in THF (50 mL). The reaction mixture was then stirred and heated in a water bath to reflux. The hot solution was filtered through a Schlenk frit. The complex **5·THF** crystallized from the clear filtrate. Single crystals of **5·OEt$_2$** suitable for X-ray analysis were obtained by recrystallization of **5·THF** from diethyl ether. Yield: 0.54 g (58%) of colorless **5·THF**. C$_{56}$H$_{79}$NaO$_{10}$: calcd. C 71.92, H 8.52; found C 71.46, H 8.98. ^{1}H NMR (200 MHz, [D$_8$]THF, 25 °C): δ = 1.17 (s, 36 H, *t*Bu), 3.07 (d, $^2J_{H,H}$ = 12.1 Hz, 4 H, CH$_2$), 3.62 (s, 24 H, O-CH$_2$), 5.52 (d, $^2J_{H,H}$ = 12.1 Hz, 4 H, CH$_2$), 6.87 (br., 8 H, *m*-CH), 13.39 (s, 3 H, OH) ppm. ^{13}C{^{1}H} NMR (50.3 MHz, [D$_8$]THF, 25 °C): δ = 32.1 (CH$_3$, *t*Bu), 34.1, 35.1, 70.8 (O-CH$_2$), 124.8, 131.2, 139.4, 154.2 (*ipso*-C) ppm.

Reaction of 1 with CO$_2$: A suspension of **1** (1.0 mmol) in THF (50 mL) under a carbon dioxide atmosphere was refluxed, resulting in a clear solution which was quickly cooled down in a dry ice bath. No precipitation was observed. ^{1}H NMR (200 MHz, [D$_8$]THF, 25 °C): δ = 1.17 (s, 36 H, *t*Bu), 3.07 (d, $^2J_{H,H}$ = 12.0 Hz, 4 H, CH$_2$), 3.62 (s, 24 H, O-CH$_2$), 5.52 (d, $^2J_{H,H}$ = 12.0 Hz, 4 H, CH$_2$), 6.87 (s, 8 H, *m*-CH) ppm. Carbon dioxide was liberated from this product during warming of the solution to reflux under an atmosphere of argon. The NMR spectroscopic data of the resulting precipitate were identical to those of the starting compound **1**.

Carboxylation of 2-Fluoropropiophenone: A suspension of **1** (1.0 mmol), **2** (1.0 mmol) or **4** (1.0 mmol) in THF (30 mL) was warmed to reflux under an atmosphere of carbon dioxide. The solution was then quickly put in a dry ice cooling bath. 2-Fluoropropiophenone (0.152 g, 1.0 mmol) was then added from a syringe. The reaction mixture was shaken for 24 h followed by addition of

 © 2004 Wiley-VCH Verlag GmbH & Co. KGaA, Weinheim

dimethyl sulfate (0.69 g, 5.5 mmol) and Na_2CO_3 (0.5 g). The mixture was then shaken for 24 h. Yield of 2-fluoro-2-benzoyl-methylpropionate (as determined by ^{19}F NMR spectroscopy): 92% for **1**/CO_2; 8% for **2**/CO_2; 89% for **4**/CO_2. ^1H NMR (200 MHz, $CDCl_3$, 25 °C): δ = 1.86 (d, $^3J_{H,F}$ = 22.6 Hz, 3 H, CH_3), 3.76 (s, 3 H, $COOCH_3$), 7.42−8.04 (m, 5 H, Ph) ppm. $^{13}C\{^1H\}$ NMR (50.3 MHz $CDCl_3$, 25 °C): δ = 20.9 (d, $^2J_{F,C}$ = 23.3 Hz, CH_3), 53.1 ($COOCH_3$), 97.0 (d, $^1J_{F,C}$ = 195.1 Hz, CF), 20.9 (d, $^2J_{F,C}$ = 23.3 Hz, CH_3), 128.5 (CH), 129.6 (d, $^4J_{F,C}$ = 5.6 Hz, *m*-CH), 130.0 (d, $^3J_{F,C}$ = 20.4 Hz, *i*pso-C), 133.8 (CH), 168.7 (d, $^2J_{F,C}$ = 25.6 Hz, $COOCH_3$), 191.6 (d, $^2J_{F,C}$ = 25.2 Hz, C=O) ppm. ^{19}F NMR (188.3 MHz, $CDCl_3$, $CFCl_3$, 25 °C): δ = −151.9 (q, $^3J_{H,F}$ = 22.6 Hz) ppm. MS (EI): *m*/*z* = 210 [M^+], 179 [$M^+ - OCH_3$], 151 [$M^+ - COOCH_3$], 105 [PhCO]. GC-IR: ν(C=O) = 1777 cm^{-1}, ν($COOCH_3$) = 1712 cm^{-1}.

Carboxylation with **2**/CO_2 yielded the product in very low yield. Upon reaction with dimethyl sulfate, white crystals of 4-*tert*-butyltetrathiacalix[4]arene tetramethyl ether[44] crystallized as the first product from the reaction mixture. ^1H NMR (200 MHz, $CDCl_3$, 25 °C): δ = 1.28 (s, 36 H, *t*Bu), 3.42 (s, 12 H, OCH_3), 7.42 (s, 8 H, *m*-CH) ppm.

Crystal Structure Determination: The intensity data for the compounds were collected on a Nonius KappaCCD diffractometer, using graphite-monochromated Mo-K_α radiation. Data were corrected for Lorentz and polarization effects, but not for absorption effects.[45,46] The structures were solved by direct methods (SHELXS[47]) and refined by full-matrix least-squares techniques against F_o^2 (SHELXL-97[48]). All hydrogen atoms were included at calculated positions with fixed thermal parameters. All non-hydrogen atoms were refined anisotropically.[48] The *R*1 values are relatively high, since the compounds are large systems that contain both slightly disordered coordinated and non-coordinated solvent molecules. In addition, *tert*-butyl groups cause high anisotropic displacement parameters. This is typical for a number of similar compounds.[14,18] Very recently the general reasons for the difficulties in obtaining low *R*1 values have been discussed in detail.[14]

Since the quality of the data of both modifications of compound **2** is too low, we will only publish the conformation of the molecule and the crystallographic data. We have not deposited the data with the Cambridge Crystallographic Data Center. Although the *R*1 value for **4** is also high, the estimated standard derivations (e.s.d.) for the bond lengths and angles are small (see Figure 5), therefore the structural data have been deposited. XP (SIEMENS Analytical X-ray Instruments, Inc.) was used for structure representations

Crystal Data for 1:[49] $C_{148}H_{224}Na_8O_{29}$, M_r = 1325.60 g·mol^{-1}, colorless prism, size 0.40 × 0.35 × 0.32 mm^3, triclinic, space group $P\bar{1}$, *a* = 16.6116(6), *b* = 17.3483(9), *c* = 17.9319(9) Å, α = 97.769(2)°, β = 105.557(2)°, γ = 115.616(2)°, *V* = 4297.3(3) $Å^3$, *T* = −90 °C, *Z* = 2, $\rho_{calcd.}$ = 1.024 g·cm^{-3}, μ(Mo-K_α) = 0.86 cm^{-1}, *F*(000) = 1432, 11345 reflections in *h*(0/17), *k*(−19/17), *l*(−19/18), measured in the range 4.93° ≤ Θ ≤ 23.31°, completeness Θ_{max} = 91.3%, 11345 independent reflections, 8317 reflections with $F_o > 4\sigma(F_o)$, 946 parameters, 0 restraints, $R1_{obs}$ = 0.087, $wR2_{obs}$ = 0.246, $R1_{all}$ = 0.118, $wR2_{all}$ = 0.2704, GOOF = 1.092, largest difference peak and hole: 0.523/−0.426 e·$Å^{-3}$.

Crystal Data for 2: $C_{108}H_{136}N_{20}Na_8O_5S_8$, M_r = 2234.77 g·mol^{-1}, colorless prism, size 0.04 × 0.03 × 0.03 mm^3, monoclinic, space group $P2_1/n$, *a* = 12.8900(1), *b* = 32.1789(5), *c* = 33.4040(4) Å, β = 94.988(8)°, *V* = 13803.0(3) $Å^3$, *T* = 20 °C, *Z* = 4, $\rho_{calcd.}$ = 1.075 g·cm^{-3}, μ(Mo-K_α) = 2.05 cm^{-1}, *F*(000) = 4720, 77462 reflections in *h*(−15/12), *k*(−38/41), *l*(−32/43), measured in the range 1.22° ≤ Θ ≤ 27.41°, completeness Θ_{max} = 87.3%, 27449 independent reflections.

Crystal Data for 4:[49] $C_{168}H_{232}K_8O_{30}$, M_r = 3044.34 g·mol^{-1}, colorless prism, size 0.32 × 0.28 × 0.20 mm^3, monoclinic, space group $P2_1/n$, *a* = 16.7197(2), *b* = 18.9198(5), *c* = 27.1965(6) Å, β = 97.489(1)°, *V* = 8529.8(3) $Å^3$, *T* = −90 °C, *Z* = 2, $\rho_{calcd.}$ = 1.185 g·cm^{-3}, μ(Mo-K_α) = 2.69 cm^{-1}, *F*(000) = 3264, 62897 reflections in *h*(−21/18), *k*(−24/19), *l*(−34/35), measured in the range 1.31° ≤ Θ ≤ 27.45°, completeness Θ_{max} = 97.5%, 19016 independent reflections, R_{int} = 0.096, 10537 reflections with $F_o > 4\sigma(F_o)$, 803 parameters, 4 restraints, $R1_{obs}$ = 0.132, $wR2_{obs}$ = 0.347, $R1_{all}$ = 0.214, $wR2_{all}$ = 0.395, GOOF = 1.280, largest difference peak and hole: 3.123/−1.179 e·$Å^{-3}$.

Crystal Data for 5:[49] $C_{56}H_{79}NaO_{10}·C_4H_{10}O$, M_r = 1009.30 g·mol^{-1}, colorless prism, size 0.32 × 0.30 × 0.28 mm^3, monoclinic, space group $P2_1$, *a* = 12.6427(5), *b* = 12.7316(3), *c* = 18.4929(6) Å, α = 90.00°, β = 94.233(1)°, γ = 90.00°, *V* = 2968.5(2) $Å^3$, *T* = −90 °C, *Z* = 2, $\rho_{calcd.}$ = 1.129 g·cm^{-3}, μ(Mo-K_α) = 0.82 cm^{-1}, *F*(000) = 1096, 4475 reflections in *h*(0/14), *k*(0/14), *l*(−20/20), measured in the range 2.21° ≤ Θ ≤ 23.26°, completeness Θ_{max} = 99.4%, 4475 independent reflections, 3732 reflections with $F_o > 4\sigma(F_o)$, 648 parameters, 7 restraints, $R1_{obs}$ = 0.068, $wR2_{obs}$ = 0.171, $R1_{all}$ = 0.100, $wR2_{all}$ = 0.201, GOOF = 1.129, Flack-parameter −0.1(9), largest difference peak and hole: 0.544/−0.319 e·$Å^{-3}$.

Acknowledgments

Financial support for this work from the Deutsche Forschungsgemeinschaft (SFB 436), and the Fonds der Chemischen Industrie is gratefully acknowledged.

[1] A. F. D. de Namor, R. M. Cleverley, L. Z. Zapata-Ormachea, *Chem. Rev.* **1998**, *98*, 2495−2525.
[2] A. Ikeda, S. Shinkai, *Chem. Rev.* **1997**, *97*, 1713−1734.
[3] A. F. D. de Narmor, R. M. Cleverley, L. Z. Ormachea, *Chem. Rev.* **1998**, *98*, 2495−2525.
[4] D. Roundhill, *Prog. Inorg. Chem.* **1995**, *43*, 533−592.
[5] C. Wieser, C. B. Dielemann, D. Matt, *Coord. Chem. Rev.* **1997**, *165*, 93−161.
[6] C. D. Gutsche, in *Calixarenes Revisited. Monographs in Supramolecular Chemistry, No 1* (Ed.: J. F. Stoddart), RSC, Cambridge **1998**.
[7] C. Floriani, R. Floriani-Moro, *Adv. Organomet. Chem.* **2001**, *47*, 167−233.
[8] V. Böhmer, *Angew. Chem.* **1995**, *107*, 785 −818.; *Angew. Chem. Int. Ed. Engl.* **1995**, *34*, 713−1734.
[9] J. M. Harrowfield, M. I. Ogden, W. R. Richmond, A. H. White, *J. Chem. Soc., Chem. Commun.* **1991**, 1159−1161.
[10] F. Hamada, K. D. Robinson, G. W. Orr, J. L. Atwood, *Supramol. Chem.* **1993**, *2*, 19.
[11] P. Thuery, Z. Asfari, J. Vicens, V. Lamare, J.-F. Dozol, *Polyhedron* **2002**, *21*, 2497−2503 and references cited therein.
[12] S. R. Dubberley, A. J. Blake, P. Mountford, *Chem. Commun.* **1997**, 1603 −1604.
[13] T. A. Hanna, L. Liu, L. N. Zakharov, A. L. Rheingold, W. H. Watson, C. D. Gutsche, *Tetrahedron* **2002**, *58*, 9751−9757.
[14] A. Bilyk, A. K. Hall, J. M. Harrowfield, M. W. Hosseini, B. W. Skeleton, A. H. White, *Inorg. Chem.* **2001**, *40*, 672−686.
[15] H. Bock, A. John, C. Näther, Z. Havlas, *J. Am. Chem. Soc.* **1995**, *117*, 9367−9368.
[16] M. G. Davidson, J. A. K. Howard, S. Lamb, C. W. Lehmann, *Chem. Commun.* **1997**, 1607−1608.
[17] G. Guillemot, E. Solari, C. Rizzoli, C. Floriani, *Chem. Eur. J.* **2002**, *8*, 2072 −2080.

 © 2004 Wiley-VCH Verlag GmbH & Co. KGaA, Weinheim

[18] E. D. Gueneau, K. M. Fromm, H. Goesmann, *Chem. Eur. J.* **2003**, *9*, 509−514.
[19] S. R. Dubberley, A. J. Blake, P. Mountford, *Dalton Trans.* **2003**, 2418−2427 and references cited therein.
[20] G. Bottachio, G. P. Chiosoli, *J. Chem. Soc., Chem. Commun.* **1966**, 618.
[21] G. Bottachio, G. P. Chiosoli, M. Felicioli, *Gazz. Chim. Ital.* **1973**, *103*, 105−116.
[22] G. Bottachio, M. Marchi, G. P. Chiosoli, *Gazz. Chim. Ital.* **1976**, *106*, 499−500.
[23] D. Walther, U. Ritter, S. Geßler, J. Sieler, M. Kunert, *Z. Anorg. Allg. Chem.* **1994**, *620*, 101−106 and references cited therein.
[24] M. Kunert, M. Nauck, J. Sieler, E. Dinjus, *Chem. Ber./Recueil* **1997**, *130*, 1461−1465 and references cited therein.
[25] R. M. Izatt, J. S. Bradshaw, S. A. Nielsen, J. D. Lamp, J. J. Christensen, D. Sen, *Chem. Rev.* **1985**, *85*, 271−339.
[26] G. D. Andreetti, R. Ungaro, A. Pochini, *J. Chem. Soc., Chem. Commun.* **1979**, 1005−1007.
[27] D. J. Darensbourg, C. G. Bauch, A. L. Rheingold, *Inorg. Chem.* **1987**, *26*, 977−980.
[28] W. Liaw, D. Ou, Y. Li, W. Lee, C. Chuang, Y. Lee, G. Lee, S. Peng, *Inorg. Chem.* **1995**, *34*, 3747− 3754.
[29] E. S. Schmidt, A. Jokisch, H. Schmidbauer, *J. Am. Chem. Soc.* **1999**, *121*, 9758−9759.
[30] S. Anfang, M. Karl, N. Faza, W. Massa, J. Magull, K. Dehnicke, *Z. Anorg. Allg. Chem.* **1997**, *623*, 1425−1432.
[31] H. Zhang, X. Wang, B. K. Teo, *J. Am. Chem. Soc.* **1996**, *118*, 11813−11821.
[32] M. A. Bush, M. R. Truter, *J. Chem. Soc. B* **1971**, 1440−1446.
[33] J. W. Steed, *Coord. Chem. Rev.* **2001**, *215*, 171−221.
[34] K. M. Fromm, E. D. Gueneau, J.-P. Rivera, G. Bernadelli, *Z. Anorg. Allg. Chem.* **2002**, *628*, 171−178.
[35] J. W. Steed, P. C. Punkt, *J. Chem. Soc., Dalton Trans.* **1999**, 2141−2146.
[36] T. Akutagawa, T. Hasegawa, T. Nakamura, S. Takeda, T. Inabe, K. Sugiura, Y. Sakata, A. E. Underhill, *Chem. Eur. J.* **2001**, 4902−4912.
[37] T. Kajiwara, S. Yokozawa, T. Ito, N. Iki, N. Morohashi, *Angew. Chem.* **2002**, *114*, 2180−2182; *Angew. Chem. Int. Ed.* **2002**, *41*, 2076−2078.
[38] G. G. Tanalova, N. S. A. Elkarim, V. S. Talanov, R. E. Hanes Jr., H.-S. Hwang, R. A. Bartsch, R. D. Rogers, *J. Am. Chem. Soc.* **1999**, *121*, 11281−11290.
[39] W. Uhl, F. Hannemann, *J. Organomet. Chem.* **1999**, *579*, 18−23.
[40] P. Doppelt, J. Fischer, L. Richard, R. Weiss, *New. J. Chem.* **1987**, *11*, 357−360.
[41] M. Tahiri, P. Doppelt, J. Fischer, R. Weiss, *Inorg. Chem.* **1988**, *27*, 2897−2899.
[42] M. Dobler, J. D. Dunitz, P. Seiler, *Acta Crystallogr., Sect. B* **1974**, *30*, 2741−2743.
[43] H. Kumagai, M. Hasegawa, S. Miyanari, Y. Sugawa, Y. Sato, T. Hori, S. Udea, H. Kamiyama, S. Miyano, *Tetrahedron Lett.* **1997**, *38*, 3971−3972.
[44] P. Lhotak, M. Himl, S. Pakhoverova, I. Stibor, *Tetrahedron Lett.* **1998**, *39*, 8915−8918.
[45] COLLECT, Data Collection Software, Nonius B. V., The Netherlands, **1998**.
[46] Z. Otwinowski, W. Minor, "Processing of X-ray Diffraction Data Collected in Oscillation Mode", in *Methods in Enzymology*, Vol. 276, Macromolecular Crystallography, Part A (Eds.: C. W. Carter, R. M. Sweet), Academic Press, **1997**, pp. 307−326.
[47] G. M. Sheldrick, *Acta Crystallogr., Sect. A* **1990**, *46*, 467−473.
[48] G. M. Sheldrick, SHELXL-97 (Release 97-2), University of Göttingen, Germany, **1997**.
[49] CCDC-216538 (**1**), -216539 (**4**), and -216540 (**5**) contain the supplementary crystallographic data for this paper. These data can be obtained free of charge via www.ccdc.cam.ac.uk/conts/retrieving.html (or from the Cambridge Crystallographic Data Centre, 12 Union Road, Cambridge CB2 1EZ, UK; Fax: (internat.) + 44-1223-336-033; or deposit@ccdc.cam.ac.uk).

Received August 8, 2003
Early View Article
Published Online February 10, 2004

 © 2004 Wiley-VCH Verlag GmbH & Co. KGaA, Weinheim

Alkali-Metal-Directed Hydrolytic Condensation of Trifunctional Phenylalkoxysilanes

Yulia A. Pozdniakova,[a] Konstantin A. Lyssenko,[a] Alexandr A. Korlyukov,[a] Inessa V. Blagodatskikh,[a] Norbert Auner,[b] Dimitris Katsoulis,[c] and Olga I. Shchegolikhina*[a]

Keywords: Hydrolytic condensation / Potassium / Self-assembly / Silanes / Sodium / Template synthesis

The alkali-metal-directed hydrolysis of phenyltrialkoxysilanes, $PhSi(OR)_3$ (R = Me, Et, *n*Bu), was performed under various reaction conditions. The alkali metal ions were used both as templating entities and as structural elements. The crystalline sodium and potassium phenylsiloxanolates (Na-PhS and K-PhS) were obtained in two different molecular compositions based on a *cis*-tetraphenylcyclotetrasiloxanolate, *cis*-$[PhSi(O)O^-]_4$, or on a *cis*-triphenylcyclotrisiloxanolate, *cis*-$[PhSi(O)O^-]_3$, anions assembled into a chain or double-layer supramolecular structure through coordination with alkali cations and hydrogen-bonding contacts. Conditions for selective preparation of crystalline Na-PhS or K-PhS of both structural types were identified. The molecular and crystal structures of $[(Na^+)_3\{PhSi(O)O^-\}_3]\cdot 8H_2O$ (**2**), $[(Na^+)_3\{PhSi(O)O^-\}_3]\cdot 4H_2O\cdot 1EtOH$ (**3**) and $[(K^+)_3\{PhSi(O)O^-\}_3]_2\cdot 7H_2O\cdot 3MeOH$ (**4**) were determined by single-crystal X-ray analysis.

(© Wiley-VCH Verlag GmbH & Co. KGaA, 69451 Weinheim, Germany, 2004)

Introduction

The hydrolytic condensation of trifunctional organosilanes [e.g. $RSiCl_3$ or $RSi(OR)_3$], generally used for the preparation of silsesquioxane materials, is a multistep and rather complicated process. Due to a statistical distribution of intermediate components the process is very sensitive to a combination of experimental factors and usually produces a wide range of products, from small oligomers and polyhedral silsesquioxanes to mixtures of resin materials and gels.[1] The purpose of our investigations is to direct a hydrolytic condensation process to the formation of only one desired compound, with a well-defined structure, using a template. The proposed method includes the assembling of silicon-containing species on the template through non-covalent bonding, thus bringing the functional groups attached at the silicon atom into close contact. Such a mutual arrangement will favor the cyclocondensation and, finally, the formation of well-organized architecture. Subsequent removal of the template will give an individual siloxane molecule with a well-defined structure.

[a] A. N. Nesmeyanov Institute of Organoelement Compounds, Russian Academy of Sciences,
Vavilova 28, 119991 Moscow, Russian Federation
E-mail: olga@ineos.ac.ru
[b] Chemistry Department, Goethe University of Frankfurt, Marie Curie Strasse 11, 60439 Frankfurt, Germany
[c] Dow Corning Corporation, Midland, MI 48686, USA

At present the template and self-assembly approach to the design of metal-based molecules and supramolecules from oligodentate ligands and appropriate metal ions is one of the most popular and fastest growing areas of experimental chemistry that offers an alternative to the classical organic route. The effectiveness of metal-mediated self-assembly for the construction of one-, two- and three-dimensional structures has been demonstrated in an enormous number of examples published in various articles, reviews and books.[2] As an alternative to the traditional approaches used in siloxane chemistry we have taken advantage of a metal-directed self-assembly strategy to selectively create metallasiloxane molecules with well-defined architectures by hydrolysis of various trifunctional alkoxysilanes in the presence of alkaline and/or transition and lanthanide metal ions.[3]

The focus of our present work is a study of the alkali-metal-directed hydrolytic condensation of phenyltrialkoxysilanes under a wide variety of different experimental conditions. The alkali metal ions were used both as templating entities and as structural elements.

Literature data on the synthesis and structure of alkali metal organosiloxanolates are presented in details in our previous publication[4] and references cited therein.

Results

Reactions of phenyltrialkoxysilanes $PhSi(OR)_3$ (R = *n*Bu, Et, Me) with NaOH or KOH [Si/Na(K) = 1:1] were

performed in the presence of water according to Scheme 1 and the description given in the Exp. Sect. The H_2O/Si ratio was varied within the range 1−12:1. Alcohols (*n*BuOH, EtOH, MeOH) or their mixtures with either aromatic solvents (xylene, toluene, benzene) or with hexane, were used as solvents.

$$PhSi(OR)_3 + MOH + x\,H_2O \xrightarrow{\text{solvent}} [PhSi(O)OM]_n{\cdot}L$$

R = Me, Et, *n*Bu; M = Na, K; x = 1–12, n = 3, 4; L = ROH, H_2O

Scheme 1

From some reaction solutions suitable single crystals were isolated and their molecular and crystal structures were determined by X-ray analysis. Trapping reactions of the bulk samples with Me_3SiCl were used in order to establish a correspondence between one element in the crystal structure (namely the size of the siloxanolate cycle) and the overall crystalline mass composition (Scheme 2). The corresponding trimethylsiloxy-substituted derivatives of alkali metal phenylsiloxanolates were analyzed by NMR spectroscopy and GPC.

$$[PhSi(O)OM]_n{\cdot}L + x\,Me_3SiCl \xrightarrow[-\,n\,MCl,\,-\,py{\cdot}HCl]{\text{solvent, py}} [PhSi(O)OSiMe_3]_n$$

M = Na, K; n = 3, 4

Scheme 2

The analytical data obtained from the above combination of physical methods proved unambiguously that crystalline sodium phenylsiloxanolates (Na-PhS) as well as potassium phenylsiloxanolates (K-PhS) are compounds that contain cyclic phenylsiloxanolate fragments, *cis*-$[PhSi(O)O^-]_n$, surrounded by sodium or potassium ions. Two different molecular structures can be generated based on either a *cis*-tetraphenylcyclotetrasiloxanolate (Figure 1) or on a *cis*-triphenylcyclotrisiloxanolate fragment (Figures 2−4); their specific formation depends on the reaction conditions (see below).

Sodium phenylsiloxanolates of both types crystallize in good yields over a wide range of different reaction conditions (Table 1). Crystalline sodium phenylsiloxanolate, based on a *cis*-tetraphenylcyclotetrasiloxanolate fragment (Na-PhS-4), was selectively produced from the reaction of $PhSi(OnBu)_3$ [4] with sodium hydroxide in *n*BuOH, in the presence of an equimolecular amount of water (molar ratio H_2O/Si = 1:1). Crystalline Na-PhS-4 was isolated in about 80% yield under similar conditions from the reaction of $PhSi(OEt)_3$ in ethanol. A single crystal of *cis*-$[(Na^+)_4\{PhSi(O)O^-\}_4]{\cdot}8n$BuOH (**1**; Figure 1), obtained from $PhSi(OnBu)_3$, was characterized by X-ray crystallography.[4] Treatment of both crystalline bulks with Me_3SiCl yielded *cis*-$[PhSi(O)OSiMe_3]_4$ exclusively.

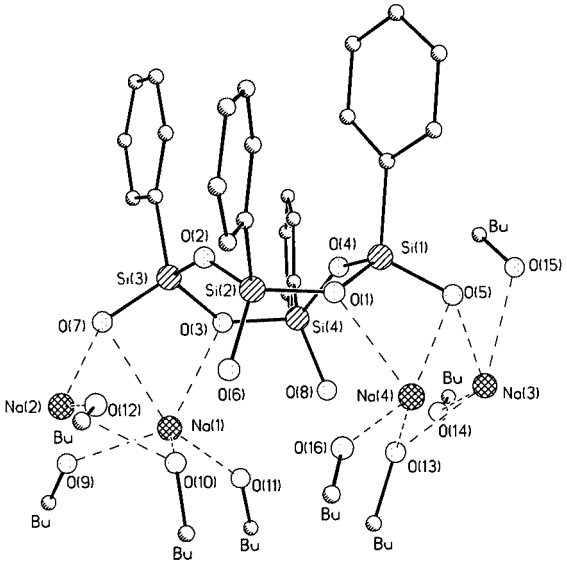

Figure 1. General view of the molecular structure of sodium phenylsiloxanolate **1**[4]

Crystalline sodium phenylsiloxanolate based on a *cis*-triphenylcyclotrisiloxanolate fragment (Na-Ph-3) was synthesized from $PhSi(OEt)_3$ under different reaction conditions. A summary of reactions performed with $PhSi(OEt)_3$ under different conditions is given in Table 1. The formation of the six-membered cycle was promoted by an increase of the H_2O/Si ratio and/or by the addition of a strongly hydrophobic solvent (hexane) to the reaction medium. Reactions performed in pure ethanol solution with a high excess of water (H_2O/Si = 4−12:1; Table 1, Entries 2 and 3) led to the selective formation of Na-PhS-3 as the only crystalline product in yields up to 63%. A single crystal (Table 1, Entry 3; H_2O/Si = 12:1) was characterized as *cis*-$[(Na^+)_3\{PhSi(O)O^-\}_3]{\cdot}8H_2O$ (**2**) by X-ray analysis (Figure 2). The use of an ethanol/hexane mixture as reaction

Table 1. Formation of Na-PhS-3 and/or Na-PhS-4 from $PhSi(OEt)_3$ under different experimental conditions

Entry	H_2O/Si ratio	Solvent	Yield of crystalline Na-PhS[a] (%)	Na-PhS-3/Na-PhS-4 ratio
1	1:1	ethanol	83	−:1
2	4:1	ethanol	42	1:−
3	12:1	ethanol	63	1:−
4	1:1	ethanol/hexane	95	1:1
5	2:1	ethanol/hexane	95	1:−

[a] Amorphous, powder-like by-products add to 100%; their trimethylsiloxy derivatives are the set of oligomers.

 © 2004 Wiley-VCH Verlag GmbH & Co. KGaA, Weinheim

medium resulted in the selective formation of Na-PhS-3 in yields up to 95% even at molar H_2O/Si ratios of about 2:1 (Table 1, Entry 5). Derivatization of the crystalline bulk materials (Table 1, Entries 2, 3 and 5) with Me_3SiCl afforded the quantitative formation of *cis*-$[PhSi(O)OSiMe_3]_3$ in all cases.

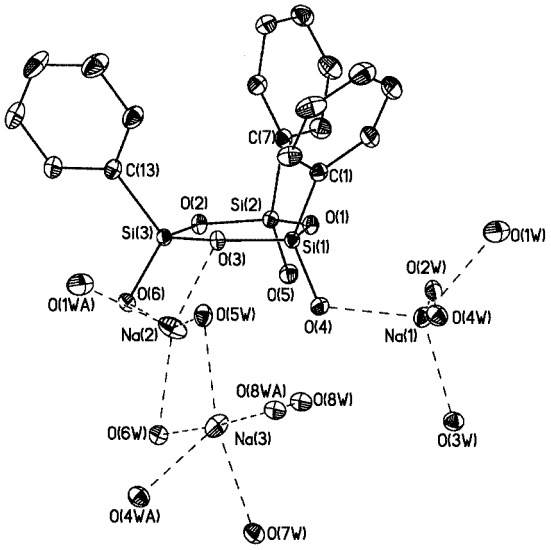

Figure 2. General view of **2** with thermal ellipsoids at 50% probability level

X-ray structure analysis of a single crystal isolated from the hydrolysis of $PhSi(OEt)_3$ in EtOH/hexane solution (molar ratio H_2O/Si = 1:1; Table 1, Entry 4) documents the formation of $[(Na^+)_3\{PhSi(O)O^-\}_3]\cdot 4H_2O\cdot 1EtOH$ (**3**; Figure 3). The molecular structure of **3** differs from that of compound **2** with respect to the coordination sphere of the sodium cations. In **3** one solvate molecule of ethanol replaces four water molecules in the molecular unit. Although the molecular structure of Na-PhS-3 is based on a trisiloxanolate cycle as the main fragment, the trapping reaction of the whole crystalline bulk with Me_3SiCl yielded a mixture of $[PhSi(O)OSiMe_3]_3$ and $[PhSi(O)OSiMe_3]_4$ in a molar ratio of 1:1. Thus, the formation of both structural types occurs under these reaction conditions.

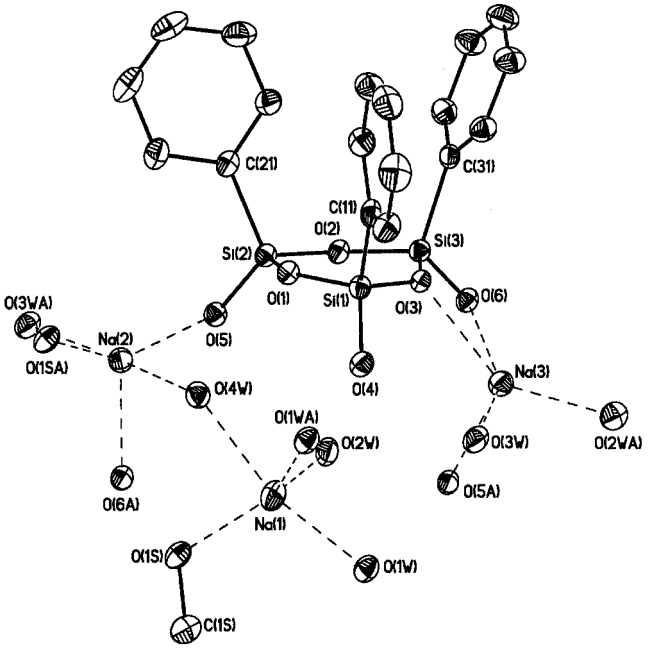

Figure 3. General view of **3** with thermal ellipsoids at 50% probability level

No crystalline products could be isolated from reactions of $PhSi(OMe)_3$ with NaOH in the presence of different amounts of water (H_2O/Si = 1−10:1) and in different solvents (MeOH, MeOH/benzene, MeOH/toluene, MeOH/hexane). The derivatization of the products obtained with Me_3SiCl gave a mixture of oligomers, as proven by GPC analytical methods.

Crystallization of potassium phenylsiloxanolate, unlike the corresponding sodium salt, occurs only under a narrow range of conditions, probably due to a higher solubility of the potassium siloxanolate intermediate compared to its sodium analogue. Thus, the use of a high dielectric constant medium (neat alcohol, excess of water) results in a low yield

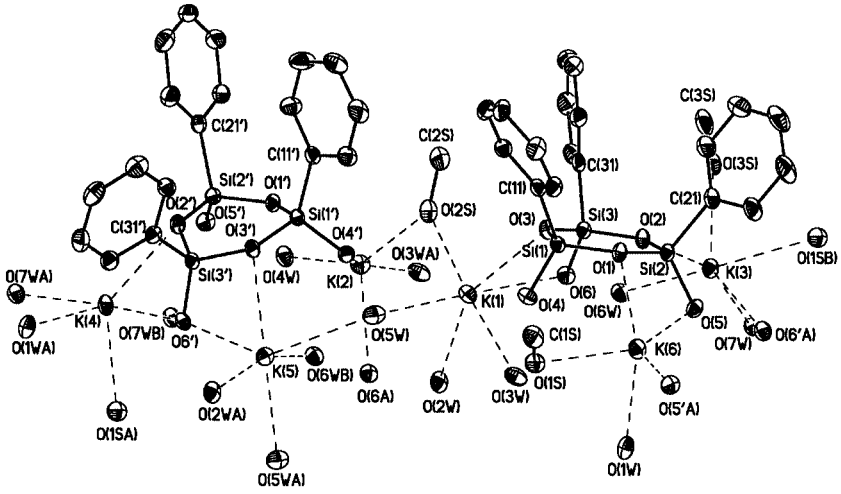

Figure 4. General view of **4** with thermal ellipsoids at 50% probability level

 © 2004 Wiley-VCH Verlag GmbH & Co. KGaA, Weinheim

of crystalline material or even prevents crystallization. A defined molar ratio of H_2O/Si from 1:1 to 1.5:1 is required for a successful crystallization.

The reaction of $PhSi(OMe)_3$ with KOH, even in an equimolar ratio of H_2O/Si in neat MeOH, did not yield any crystalline material. In contrast, reactions of $PhSi(OnBu)_3$ and of $PhSi(OEt)_3$ with KOH using an equimolar ratio of H_2O/Si in pure *n*BuOH or EtOH, respectively, gave crystalline potassium phenylsiloxanolate with a tetraphenylcyclotetrasiloxanolate fragment (K-PhS-4), but only in low yields ranging from 10 to 28%. Although we failed to grow suitable single crystals for X-ray analysis, reactions of the crystalline bulk with Me_3SiCl yielded $[PhSi(O)OSiMe_3]_4$ selectively, proving the formation of a potassium salt based on a tetrasiloxanolate cyclic fragment.

Decreasing the dielectric constant of the reaction medium by addition of non-polar solvent supports the bulk crystallization of potassium triphenylcyclotrisiloxanolate (K-PhS-3). Crystalline materials in high yields (up to 95%) were isolated from phenyltrialkoxysilanes $PhSi(OR)_3$ (R = Me, Et, *n*Bu) used for KOH treatment in mixtures of MeOH/benzene, EtOH/toluene, and of *n*BuOH/xylene. In all cases the derivatization of the crystalline bulk with Me_3SiCl gave exclusively $[PhSi(O)OSiMe_3]_3$. A single crystal suitable for X-ray analysis was obtained from the reaction of $PhSi(OMe)_3$. The molecular structure is shown in Figure 4 and proves the formation of $[(K^+)_3\{PhSi(O)O^-\}_3]_2 \cdot 7H_2O \cdot 3MeOH$ (**4**).

Molecular Structures of 2, 3, and 4

The single-crystal X-ray investigations revealed that the independent unit cells of compounds **2** and **3** contain one triphenylcyclotrisiloxanolate anion, three sodium cations and water (**2**) or water and alcohol molecules (**3**) (Figures 2 and 3, respectively). The peculiarity of the crystal structure of the potassium salt **4** is the presence of two independent siloxanolate anions and, consequently, of six potassium cations (see Table 2, Figure 4) in the unit cell. In all molecular structures the geometry of the siloxanolate anions is characterized by typical bond lengths and angles usually observed for this class of compounds (Tables 3 and 4).[5,6] Thus, the Si−C bonds of the Si−Ph groups are equal to 1.862(2) Å (average value), the cyclic Si−O bonds are significantly elongated [1.639(2)−1.661(1) Å] compared to terminal analogues [1.577(2)−1.596(1) Å]. The six-membered Si−O cycles exhibit an all-*cis* arrangement of the phenyl substituents. Their conformations vary from an approximately planar one in **2** and in **4** (in one of the two independent molecules) to an envelope conformation in **3** [deviation of Si(3) atom], and a distorted boat conformation [deviation of Si(3′) and O(1′) atoms] for the second independent molecule in **4**. This variation of the siloxanolate ring conformations is in line with the high flexibility of the siloxanolate rings.

The coordination sphere of the alkali cations is predominantly determined and formed by the negatively charged siloxanolates oxygen atoms and water (in **2**), and the sur-

Table 2. Crystallographic data and parameters of refinement for **2**−**4**

	2	**3**	**4**
Empirical formula	$C_{18}H_{31}Na_3O_{14}Si_3$	$C_{20}H_{29}Na_3O_{11}Si_3$	$C_{19.5}H_{28}K_3O_{11}Si_3$
Formula mass	624.67	598.67	1279.98
Crystal system	triclinic	monoclinic	triclinic
T [K]	110	110	110
Space group	$P\bar{1}$	$P2_1/c$	$P\bar{1}$
Radiation	Mo-K_α (λ = 0.71072 Å)		
Scan type	ω-scan with 0.3 step and 10 s exposure per frame		
Diffractometer	Smart 1000 K CCD		
a [Å]	9.2873(5)	16.803(4)	10.569(3)
b [Å]	9.3329(5)	9.761(2)	16.387(5)
c [Å]	17.7565(9)	17.177(4)	16.658(4)
α [°]	79.822(1)	90	101.352(6)
β [°]	83.524(1)	103.979(5)	97.692(6)
γ [°]	63.844(1)	90	92.636(6)
V [Å^3]	1358.7(1)	2734(1)	2795(1)
Z	2	4	4
μ [cm^{-1}]	2.88	2.76	6.70
$D_{calcd.}$ [g·cm^{-3}]	1.527	1.454	1.521
$2\theta_{max}$ [°]	60	54	60
Total number of reflections	10451	11641	23178
Independent reflections [*R*(int)]	74550 (0.0152)	5582 (0.0519)	15938 (0.0315)
*R*1 for refl.with $I > 2\sigma(I)$	0.0351 (for 6564 refl.)	0.0464 (for 3136 refl.)	0.0591 (for 10645 refl.)
*wR*2 for all reflections	0.0978 (for 7455 refl.)	0.0929 (for 5582 refl.)	0.1482 (for 15938 refl.)
GOF	1.052	0.96	1.065

 © 2004 Wiley-VCH Verlag GmbH & Co. KGaA, Weinheim

Table 3. Selected bond lengths [Å] and angles [°] in **2** and **3**

	2	**3**
Bond lengths:		
Si(1)−O(1)	1.652(1)	1.645(2)
Si(1)−O(3)	1.652(1)	1.659(2)
Si(1)−O(4)	1.584(1)	1.576(2)
Si(1)−C(11)	1.861(1)	1.864(3)
Si(2)−O(1)	1.6533(9)	1.648(2)
Si(2)−O(2)	1.643(1)	1.669(2)
Si(2)−O(5)	1.594(1)	1.576(2)
Si(2)−C(21)	1.864(1)	1.864(3)
Si(3)−O(2)	1.638(1)	1.660(2)
Si(3)−O(3)	1.6529(9)	1.650(2)
Si(3)−O(6)	1.596(1)	1.580(2)
Si(3)−C(31)	1.857(1)	1.864(3)
Bond angles:		
O(1)−Si(1)−O(3)	107.38(5)	105.5(1)
O(1)−Si(1)−O(4)	110.01(5)	111.2(1)
O(3)−Si(1)−O(4)	107.38(5)	109.2(1)
O(1)−Si(1)−C(11)	107.67(6)	107.1(1)
O(3)−Si(1)−C(11)	106.70(5)	109.3(1)
O(4)−Si(1)−C(11)	113.81(5)	114.0(1)
O(1)−Si(2)−O(2)	105.23(5)	105.2(1)
O(1)−Si(2)−O(5)	110.87(5)	111.3(1)
O(2)−Si(2)−O(5)	112.10(5)	112.2(1)
O(1)−Si(2)−C(21)	107.26(5)	107.3(1)
O(2)−Si(2)−C(21)	108.20(5)	107.1(1)
O(5)−Si(2)−C(21)	112.78(6)	113.1(1)
O(2)−Si(3)−O(3)	106.74(5)	106.7(1)
O(2)−Si(3)−O(6)	112.21(5)	112.6(1)
O(3)−Si(3)−O(6)	108.99(5)	109.2(1)
O(2)−Si(3)−C(31)	109.31(6)	108.1(1)
O(3)−Si(3)−C(31)	108.02(5)	108.0(1)
O(6)−Si(3)−C(31)	111.37(6)	112.0(1)
Si(1)−O(1)−Si(2)	133.31(6)	135.6(1)
Si(3)−O(2)−Si(2)	135.02(6)	131.9(1)
Si(3)−O(3)−Si(1)	131.67(6)	132.1(1)

Table 4. Selected bond lengths [Å] and angles [°] for two independent molecules in **4**

	4A	**4B**
Bond lengths:		
Si(1)−O(1)	1.638(2)	1.645(2)
Si(1)−O(3)	1.641(2)	1.648(2)
Si(1)−O(4)	1.590(2)	1.591(2)
Si(1)−C(11)	1.857(3)	1.859(3)
Si(2)−O(1)	1.652(2)	1.660(2)
Si(2)−O(2)	1.649(2)	1.642(2)
Si(2)−O(5)	1.579(2)	1.576(2)
Si(2)−C(21)	1.858(3)	1.861(3)
Si(3)−O(2)	1.653(2)	1.654(2)
Si(3)−O(3)	1.648(2)	1.649(2)
Si(3)−O(6)	1.591(2)	1.579(2)
Si(3)−C(31)	1.863(3)	1.860(3)
Bond angles:		
O(1)−Si(1)−O(3)	106.6(1)	106.2(1)
O(1)−Si(1)−O(4)	111.4(1)	111.2(1)
O(3)−Si(1)−O(4)	110.1(1)	110.0(1)
O(1)−Si(1)−C(11)	108.7(1)	109.8(1)
O(3)−Si(1)−C(11)	109.1(1)	108.7(1)
O(4)−Si(1)−C(11)	110.8(1)	110.9(1)
O(1)−Si(2)−O(2)	105.5(1)	111.4(1)
O(1)−Si(2)−O(5)	109.2(1)	112.5(1)
O(2)−Si(2)−O(5)	112.9(1)	105.5(1)
O(1)−Si(2)−C(21)	108.5(1)	107.3(1)
O(2)−Si(2)−C(21)	108.7(1)	109.7(1)
O(5)−Si(2)−C(21)	111.7(1)	110.3(1)
O(2)−Si(3)−O(3)	106.9(1)	106.5(1)
O(2)−Si(3)−O(6)	112.4(1)	111.3(1)
O(3)−Si(3)−O(6)	110.4(1)	112.0(1)
O(2)−Si(3)−C(31)	108.0(1)	106.4(1)
O(3)−Si(3)−C(31)	105.5(1)	106.4(1)
O(6)−Si(3)−C(31)	113.3(1)	113.8(1)
Si(1)−O(1)−Si(2)	134.4(1)	132.3(1)
Si(2)−O(2)−Si(3)	133.3(1)	132.4(1)
Si(1)−O(3)−Si(3)	132.5(1)	131.9(1)

rounding siloxanolate oxygen atoms, water and alcohol molecules (ethanol in **3**, and methanol in **4**, respectively). In spite of the differences in the number of solvate molecules in sodium salts **2** and **3**, both are characterized by some common features: only two of the cations are directly connected to the siloxanolate ring's oxygen atoms, while the coordination sphere of the third cation contains only the solvate molecules, and thus can consequently be described as a "bridging cation". An equivalent "bridging sodium" was previously detected in the corresponding salt **1**[4] and therefore is probably a general feature of such sodium salts. In contrast to compounds **1**−**3**, in salt **4** all potassium atoms are linked to the siloxanolate ring's oxygen atoms; this is probably due to the larger van der Waals radius of potassium cations. The number of oxygen atoms coordinated to the potassium or to the sodium cations in **2**−**4** varies between five and six and is dependent mainly on the type of coordinated oxygen atoms (in water or in alcohol molecules). The Na−O and K−O distances are 2.287(3)−2.599(2) Å, and 2.625(3)−3.053(3) Å, respectively, with the shortest contacts to the water molecules. The coordination polyhedra of the alkali metal atoms are distorted trigonal-bipyramidal or octahedral, depending on the coordination number.

The presence of a significant amount of solvate molecules (water and alcohol) leads to the formation of a complicated hydrogen-bonding network, with O···O distances varying from 2.568(1) to 3.037(2) Å. Analysis of the crystal structures of **2**−**4** revealed that, depending on the solvate contents and the nature of the cations, the hydrogen bonds are formed solely between the solvate and Si−O$^-$ (**3**) and/or only between the solvate molecules (**2**, **4**). In general, the hydrogen bonds between solvate and $^-$O−Si are characterized by slightly shorter O···O distances than those between solvate molecules. The maximum number of hydrogen bonds formed by the siloxanolate oxygen atoms is three, with a pseudo-tetrahedral arrangement around the oxygen atom. The number and strength of these hydrogen bonds is mainly dominated by the coordination of the corresponding Si−O$^-$ bond to the alkali metal atom, resulting in a systematic shortening of the hydrogen bond lengths of the centers weakly coordinated or uncoordinated by alkali.

In **2**−**4** the hydrogen-bonding pattern leads to an overall supramolecular architecture: the molecules are assembled into double layers (Figure 5), which have a hydrophilic "filling" (alkali, water and alcohol molecules) and a hydrophobic "coating" (Ph groups).

 © 2004 Wiley-VCH Verlag GmbH & Co. KGaA, Weinheim

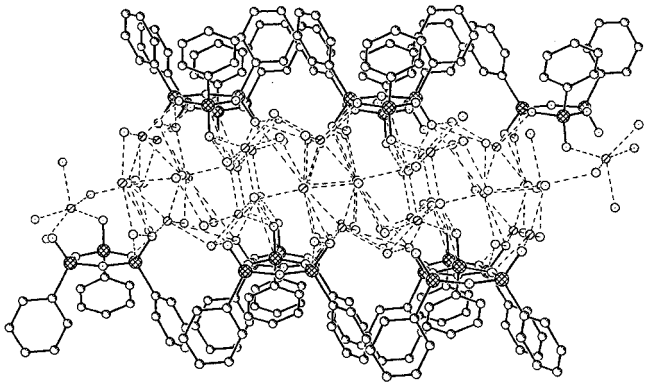

Figure 5. Double-layer structure in **2**−**4**

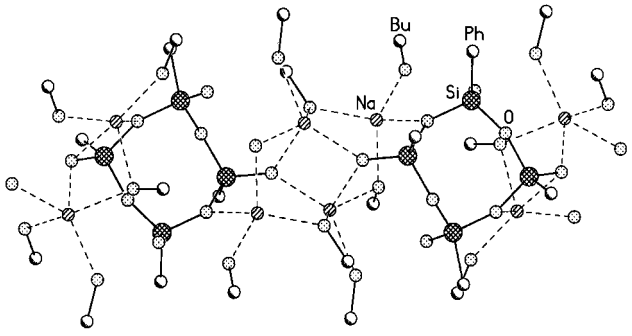

Figure 6. Cyclotetrasiloxanolate tetraanion/tetracation arrangement to form chains in **1**;[4] phenyl groups are omitted for clarity

The packing of the sodium phenylsiloxanolates **2** and **3**, based on trisiloxanolate cycles, is different from that of the sodium phenylsiloxanolate based on a tetrasiloxanolate cycle:[4] the molecules of the latter are assembled into a chain-like structure by coordination bonds. Each chain is surrounded by phenyl substituents and solvated alcohol molecules without bridging ions connecting neighboring chains (Figure 6).

Discussion

Several coupled equilibrium reactions must take place when the hydrolysis of trialkoxysilane is performed in an alcoholic medium in the presence of an equimolar amount of the base (e.g. NaOH; Scheme 3. As a result of these reactions, and a rapid proton-cation exchange,[7] the generation of a labile alkaline intermediate, suggested[4] to be [PhSi(OH)(OR)(O^-Na^+)] (A) (Scheme 3), is quite possible. Presumably, these alkaline intermediates, containing solvent-separated ion pairs,[8] tend to associate (equilibrium I),[9] forming complex aggregates (B) in which an ionic part (alkali metal ion, alcohol and water molecules) is surrounded by silicon species containing functional OH and OR groups. These groups can undergo a condensation process with both water and alcohol elimination resulting in the formation of either a mixture of oligomers or cyclic products, depending on the reaction parameters (Scheme 4). The equilibrium I is a function[10] of the charge density of M^+, the solvating ability of the solvent, the nucleophilicity of the anion, and the solvent/salt ratio. Such a complicated and multi-argument process leads to results that are relatively difficult to predict. In the course of our study we found an appropriate set of conditions whereby the condensation process can be selectively directed to the generation of cyclotri- or cyclotetrasiloxanolate anions as-

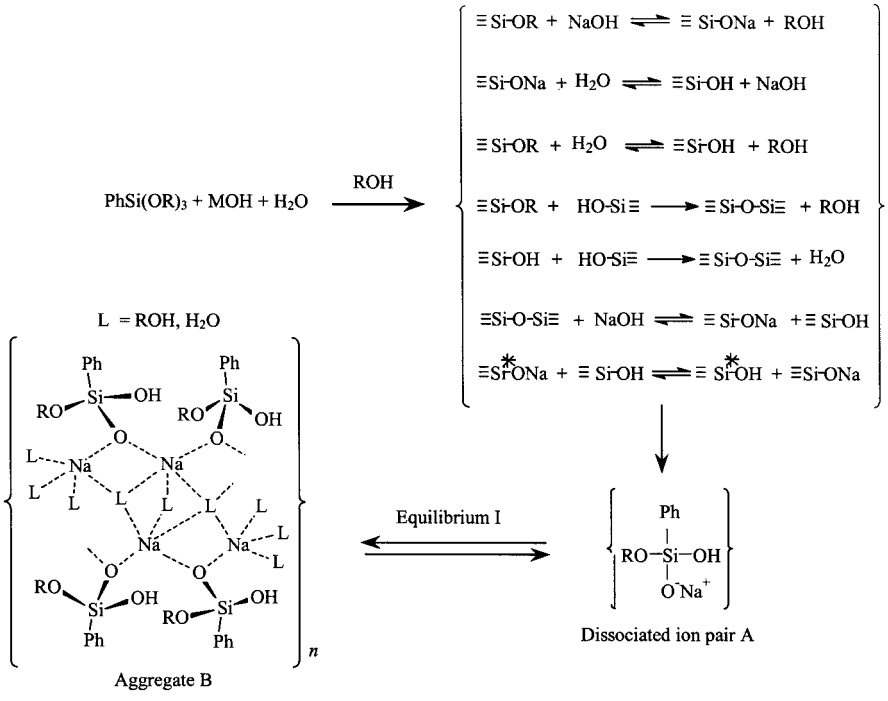

Scheme 3

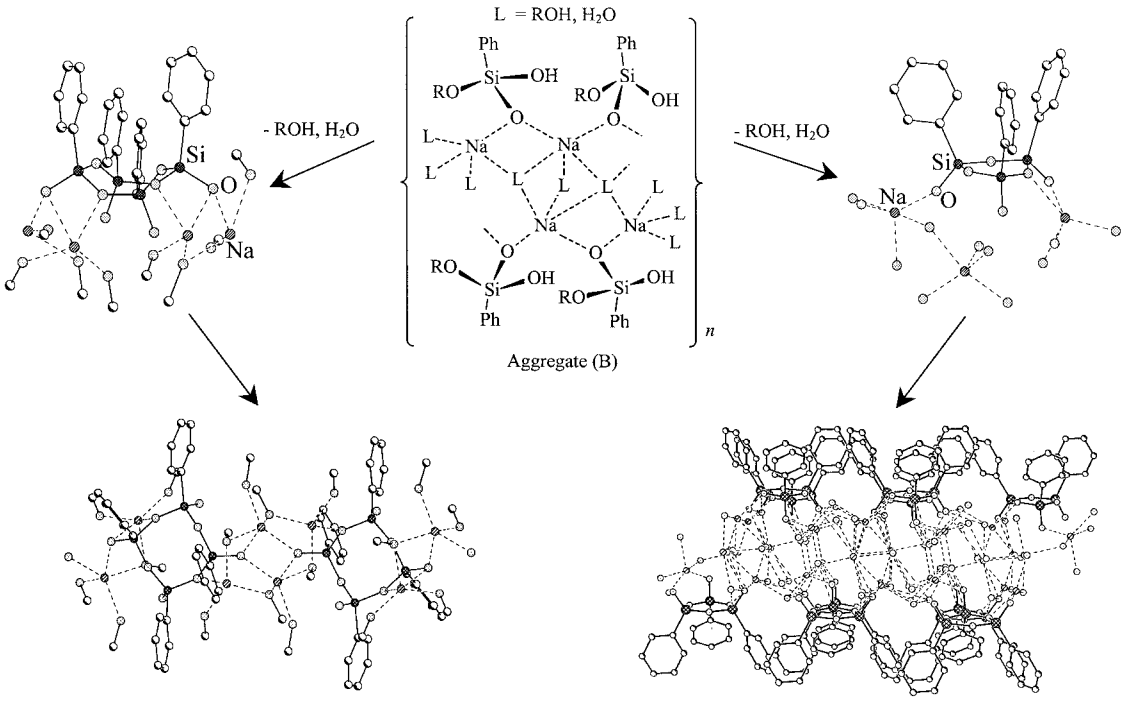

Scheme 4

sembled into supramolecular architectures (double layers or chains) through coordination with metal cations and hydrogen bonding.

The high-yield crystallization of sodium phenylsiloxanolate of different structural types in a wide range of conditions can be explained by the possible shift of equilibrium I to the formation of the complex aggregates (B).

In contrast, crystallization of potassium phenylsiloxanolate from an alcohol solution is quite rare. Moreover, an excess of water ($H_2O/Si > 1.5:1$) prevents crystallization. This could be caused by the tendency of potassium phenylsiloxanolate to exist as a solvent-separated ion pair (A). A decrease in the dielectric constant of the reaction medium should shift the equilibrium I to the opposite side and force the crystallization. This is in line with the experimental data — a high-yield crystallization of potassium phenylsiloxanolate was achieved only upon addition of non-polar aromatic solvents.

The *cis* configuration of sodium and potassium phenylsiloxanolates of both structural forms should be governed by the existence of aggregates B as micelles in the reaction solutions. The presence of these micelles was detected in our preliminary investigations of the reaction solutions by a light-scattering method. These results are now under further investigation and will be published elsewhere.

The removal of metal ions by treatment of the crystals obtained with Me_3SiCl gave the corresponding cyclosiloxanes without a change of their size or configuration. It has to be noted that the *cis*-tetraphenyl(trimethylsiloxy)cyclotetrasiloxane obtained exhibits properties of a plastically crystalline (3D) mesophase.[11] The analogous removal of metal ions from Na-PhS-4 by reaction with dilute HCl solution gives *cis*-$[PhSi(O)OH]_4$ in high yield.[3b]

Experimental Section

General: ^1H and ^{29}Si NMR spectra were recorded with a Bruker DRX-500 spectrometer (500 MHz for ^1H and 99 MHz for ^{29}Si) at 20 °C in C_6D_6 or $CDCl_3$ as solvents and with TMS as internal reference standard. GPC was performed with a Waters instrument with an M-600 pump and an M-484 UV detector (wavelength 254 nm) on U-Styragel 500, 1000 Å columns, using a Maxima information processing computer system. Structure-determined[12] crystals of $[PhSi(OSiMe_3)O]_{12}$ (retention time = 16.12 min), $[PhSi(OSiMe_3)O]_6$ (retention time = 16.95 min), $[PhSi(OSiMe_3)O]_4$ (retention time = 17.43 min) and $[PhSi(O)OSiMe_3]_3$ [13] (retention time = 17.79 min) were used as the standards. THF was used as an eluent. Calculations on KOH were made based on the content of KOH (85%, Aldrich). The H_2O/Si ratio in the synthesis with KOH was calculated taking into account the water content in KOH (15% according to Aldrich).

General Synthesis of Na-PhS: A mixture of phenyltrialkoxysilane, sodium hydroxide, water and solvents was stirred vigorously either at room temperature or under reflux conditions until the solution became completely transparent; for completion, the solution was stirred for an additional hour. Within a few hours or days (depending on the alkoxysilane and amount of water) crystals formed and precipitated from the solution. The crystalline bulk was separated by filtration through a Schott filter, washed with hexane and dried in vacuo (10 Torr/40 °C/1 h).

General Synthesis of K-PhS: A mixture of phenyltrialkoxysilane, potassium hydroxide, water and solvents was vigorously stirred at

 © 2004 Wiley-VCH Verlag GmbH & Co. KGaA, Weinheim

room temperature until a clear solution had formed. For completion, stirring was continued for an additional hour. Most of the solvents (ca. 75%) were removed in a rotary evaporator, and an equal amount of an aromatic solvent was added to the residue. White, tiny needle-like crystals precipitated within 20 h (usually after cooling of the reaction mixture to ca. 10 °C). The crystalline solid was filtered, washed with hexane and dried in vacuo (10 Torr/40 °C/1 h).

General Procedure for the Trimethylsilylation of Alkali Metal Phenylsiloxanolates: Na-PhS or K-PhS was added as a solid to a vigorously stirred mixture of dry hexane, Me_3SiCl and pyridine at room temperature. The mixture was refluxed for 1 h, then cooled to room temperature, filtered and washed with water until it was chloride-free. After drying with Na_2SO_4, the solvent was removed and the residue was dried under vacuum (10 Torr/40 °C/1.5 h). The remaining product was characterized by NMR spectroscopy and GPC.

Na-PhS Obtained from PhSi(O*n*Bu)$_3$ and Trimethylsilylation:[4] $PhSi(OnBu)_3$ (5 g, 15.4 mmol), NaOH (0.62 g, 15.4 mmol), and H_2O (0.28 g, 15.4 mmol) in *n*-butanol (15 mL). Yield of Na-PhS-4: 2.35 g (78%). $[C_6H_5Si(O)ONa]_4\cdot 3nBuOH = C_{36}H_{50}Na_4O_{11}Si_4$ (863): calcd. C 50.10, H 5.84, Na 10.66, Si 13.02; found C 50.43, H 6.14, Na 10.95, Si 12.98. The Na-PhS-4 obtained above (2.35 g, 2.7 mmol), Me_3SiCl (1.17 g, 10.8 mmol) and pyridine (0.64 g, 8.1 mmol) in benzene (40 mL) were allowed to react to give 2.3 g (96%) of a white solid product. GPC (THF): one peak corresponding to $[PhSi(OSiMe_3)O]_4$ (retention time: 17.43 min).

Na-PhS Obtained from PhSi(OEt)$_3$ in Ethanol and Trimethylsilylation: H_2O/Si = 1:1 (Table 1, Entry 1). $PhSi(OEt)_3$ (4.98 g, 20.7 mmol), NaOH (0.83 g, 20.7 mmol), and H_2O (0.37 g, 20.7 mmol) were allowed to react in ethanol (10.5 mL). Yield of Na-PhS-4: 3.18 g (83%). $[C_6H_5Si(O)ONa]_4\cdot 2EtOH = C_{28}H_{32}Na_4O_{10}Si_4$ (733): calcd. C 45.89, H 4.40, Na 12.55, Si 15.33; found C 45.51, H 4.27, Na 12.62, Si 15.13. Na-PhS-4 (3.18 g, 4.3 mmol), Me_3SiCl (5.65 g, 52.0 mmol), and pyridine (3.48 g, 44.0 mmol) were allowed to react in hexane (50 mL) according to the General Procedure. Yield of the white solid product: 2.49 g (74%). GPC (THF): one peak corresponding to $[PhSi(OSiMe_3)O]_4$ (retention time: 17.43 min).

Na-PhS Obtained from PhSi(OEt)$_3$ in Ethanol and Trimethylsilylation: H_2O/Si = 4:1 (Table 1, Entry 2). $PhSi(OEt)_3$ (4.98 g, 20.7 mmol), NaOH (0.83 g, 20.7 mmol), and H_2O (1.49 g, 82.8 mmol) were allowed to react in ethanol (35 mL). Yield of crystalline Na-PhS-3: 1.59 g (42%). $[C_6H_5Si(O)ONa]_3\cdot 3H_2O = C_{18}H_{21}Na_3O_9Si_3$ (535): calcd. C 40.44, H 3.96, Na 12.91, Si 15.76; found C 40.50, H 3.73, Na 12.80, Si 15.63. Na-PhS-3 (1.59 g, 3.0 mmol), Me_3SiCl (3.83 g, 35.2 mmol), and pyridine (1.85 g, 23.4 mmol) were allowed to react in benzene (40 mL). A colorless, transparent liquid was formed: 1.6 g (85%). GPC (THF): one peak corresponding to $[PhSi(OSiMe_3)O]_3$ (retention time 17.79 min).

Na-PhS Obtained from PhSi(OEt)$_3$ in Ethanol and Trimethylsilylation: H_2O/Si = 12:1 (Table 1, Entry 3). $PhSi(OEt)_3$ (4.98 g, 20.7 mmol), NaOH (0.83 g, 20.7 mmol) and H_2O (4.48 g, 248.4 mmol) were allowed to react in ethanol (15 mL). Yield of crystalline Na-PhS-3: 2.33 g (60%). A suitable single crystal was analyzed by X-ray crystallography to give the molecular composition $[(Na^+)_3\{PhSi(O)O^-\}_3]\cdot 8H_2O$ (**3**). $[C_6H_5Si(O)ONa]_3\cdot 4H_2O = C_{18}H_{23}Na_3O_{10}Si_3$ (553): calcd. C 40.54, H 5.04, Na 11.66, Si 16.17; found C 40.12, H 5.20, Na 11.49, Si 16.25. Na-PhS-3 (2.33 g, 4.2 mmol), Me_3SiCl (5.00 g, 46.0 mmol), and pyridine (2.64 g, 33.4 mmol) were allowed to react in benzene (80 mL). A colorless, transparent liquid product was formed: 1.58 g (63%). GPC (THF): one peak corresponding to $[PhSi(OSiMe_3)O]_3$ (retention time. 17.79 min).

Na-PhS Obtained from PhSi(OEt)$_3$ in Ethanol/Hexane and Trimethylsilylation: H_2O/Si = 1:1 (Table 1, Entry 4). $PhSi(OEt)_3$ (4.98 g, 20.7 mmol), NaOH (0.83 g, 20.7 mmol), and H_2O (0.38 g, 20.7 mmol) were allowed to react in a mixture of ethanol (7 mL) and hexane (10 mL) to give two fractions of crystals. Yield of the first fraction: 1.64 g (45%). $[C_6H_5Si(O)ONa]_4\cdot EtOH = C_{26}H_{26}Na_4O_9Si_4$ (687): calcd. C 45.47, H 3.82, Na 13.39, Si 16.36; found C 45.52, H 3.63, Na 12.98, Si 16.19. Yield of the second fraction: 1.82 g (50%). $[C_6H_5Si(O)ONa]_3\cdot 2H_2O = C_{18}H_{19}Na_3O_8Si_3$ (517): calcd. C 41.85, H 3.71, Na 13.36, Si 16.31; found C 41.70, H 4.05, Na 13.17, Si 17.08. A suitable single crystal from the second fraction was analyzed by single-crystal X-ray crystallography, giving the molecular composition $[(Na^+)_3\{PhSi(O)O^-\}_3]\cdot 4H_2O\cdot EtOH$ (**2**). The first fraction of the Na-PhS crystalline compound (1.64 g, 2.4 mmol), Me_3SiCl (2.78 g, 25.6 mmol), and pyridine (1.21 g, 15.3 mmol) were allowed to react in hexane (30 mL) to give 1.28 g (76%) of a white solid product. GPC (THF): one peak corresponding to $[PhSi(OSiMe_3)O]_4$ (retention time: 17.43 min). The second fraction of the Na-PhS crystalline product (1.82 g, 3.5 mmol), Me_3SiCl (2.66 g, 24.5 mmol), and pyridine (1.11 g, 14.0 mmol) were allowed to react in hexane (20 mL). A colorless liquid product was formed: 1.72 g (78%). GPC (THF): one peak corresponding to $[PhSi(OSiMe_3)O]_3$ (retention time: 17.79 min).

Na-PhS Obtained from PhSi(OEt)$_3$ in Ethanol/Hexane and Trimethylsilylation: H_2O/Si = 2:1 (Table 1, Entry 5). $PhSi(OEt)_3$ (4.98 g, 20.7 mmol), NaOH (0.83 g, 20.7 mmol), and H_2O (0.75 g, 41.4 mmol) were allowed to react in a mixture of ethanol (21 mL) and hexane (21 mL). Yield: 3.56 g (95%) of a crystalline solid. $[C_6H_5Si(O)ONa]_3\cdot 3H_2O = C_{18}H_{21}Na_3O_9Si_3$ (535): calcd. C 40.44, H 3.96, Na 12.91, Si 15.76; found C 40.71, H 4.28, Na 13.32, Si 16.01. Na-PhS (3.56 g, 6.6 mmol), Me_3SiCl (6.45 g, 59.3 mmol), and pyridine (3.13 g, 39.6 mmol) were allowed to react in hexane (35 mL). A colorless liquid product was formed: 2.92 g (70%). GPC (THF): one peak corresponding to $[PhSi(OSiMe_3)O]_3$ (retention time: 17.79 min).

K-PhS Obtained from PhSi(O*n*Bu)$_3$ in *n*BuOH (H_2O/Si = 1:1) and Trimethylsilylation: $PhSi(OnBu)_3$ (4.73 g, 14.6 mmol), KOH (0.96 g, 14.6 mmol), and H_2O (0.12 g, 6.6 mmol) in *n*BuOH (5 mL) were allowed to react. Yield: 0.85 g (28.6%) of needle-like crystals. $[C_6H_5Si(O)OK]_4\cdot nBuOH\cdot 2H_2O = C_{28}H_{34}K_4O_{11}Si_4$ (815): calcd. C 41.25, H 4.20, K 19.18, Si 13.78; found C 41.19, H 4.03, K 19.28, Si 13.53. K-PhS-4 (0.85 g, 1 mmol), Me_3SiCl (1.57 g, 14.4 mmol), and pyridine (0.76 g, 9.6 mmol) in hexane (10 mL) were allowed to react to give a white crystalline product: 0.69 g (82%). GPC (THF): one peak corresponding to $[PhSi(O)OSiMe_3]_4$ (retention time: 17.43 min).

K-PhS Obtained from PhSi(OEt)$_3$ in EtOH (H_2O/Si = 1:1) and Trimethylsilylation: $PhSi(OEt)_3$ (4.98 g, 20.7 mmol), KOH (1.37 g, 20.7 mmol), and H_2O (0.17 g, 9.3 mmol) in EtOH (5 mL) were allowed to react to give 0.4 g (10%) of small needle-like crystalline material. $[C_6H_5Si(O)OK]_4\cdot EtOH = C_{26}H_{26}K_4O_9Si_4$ (751): calcd. C 41.57, H 3.49, K 20.82, Si 14.95; found C 41.75, H 3.38, K 20.95, Si 15.07. K-PhS-4 (0.4 g, 0.5 mmol), Me_3SiCl (0.62 g, 5.7 mmol), and pyridine (0.27 g, 3.4 mmol) in hexane (10 mL) were allowed to react to yield a white crystalline product: 0.3 g (67%). GPC (THF): one peak corresponding to $[PhSi(O)OSiMe_3]_4$ (retention time: 17.43 min).

K-PhS Obtained from PhSi(O*n*Bu)$_3$ in *n*BuOH/*o*-Xylene (H_2O/Si = 1.5:1) and Trimethylsilylation: $PhSi(OnBu)_3$ (4.73 g, 14.6 mmol),

 © 2004 Wiley-VCH Verlag GmbH & Co. KGaA, Weinheim

KOH (0.96 g, 14.6 mmol), and H_2O (0.26 g, 14.6 mmol) were allowed to react in a mixture of butanol (7 mL) and *o*-xylene (28 mL). A crystalline solid product was formed: 2.43 g (72%). $[C_6H_5Si(O)OK]_3{\cdot}3H_2O{\cdot}n$BuOH = $C_{22}H_{31}K_3O_{10}Si_3$ (657): calcd. C 39.14, H 4.93, K 17.38, Si 12.48; found C 38.77, H 4.62, K 17.21, Si 12.83. K-PhS-3 (2.43 g, 3.7 mmol), Me_3SiCl (3.04 g, 28.0 mmol), and pyridine (1.33 g, 16.8 mmol) were allowed to react in hexane (30 mL). A colorless liquid product was formed. Yield 1.53 g (67%). GPC (THF): one peak corresponding to $[PhSi(OSiMe_3)O]_3$ (retention time: 17.79 min).

K-PhS Obtained from $PhSi(OEt)_3$ in EtOH/Toluene (H_2O/Si = 1.5:1) and Trimethylsilylation: $PhSi(OEt)_3$ (4.98 g, 20.7 mmol), KOH (1.37 g, 20.7 mmol), and H_2O (0.37 g, 20.7 mmol) were allowed to react in a mixture of ethanol (7 mL) and toluene (28 mL). Yield of solid K-PhS-3: 3.97 g (92%). $[C_6H_5Si(O)OK]_3{\cdot}5H_2O$ = $C_{18}H_{25}K_3O_{11}Si_3$ (619): calcd. C 35.68, H 4.46, K 17.64, Si 14.02; found C 35.93, H 4.07, K 17.52, Si 13.61. K-PhS-3 (3.97 g, 6.4 mmol), Me_3SiCl (6.12 g, 56.3 mmol), and pyridine (2.67 g, 33.8 mmol) were allowed to react in hexane (100 mL). A colorless liquid product was formed. Yield 3.29 g (81%). GPC (THF): one peak corresponding to $[PhSi(OSiMe_3)O]_3$ (retention time: 17.79 min).

K-PhS Obtained from $PhSi(OMe)_3$ in MeOH/Benzene (H_2O/Si = 1.5:1) and Trimethylsilylation: $PhSi(OMe)_3$ (5.31 g, 26.8 mmol), KOH (1.77 g, 26.8 mmol), and H_2O (0.48 g, 26.8 mmol) were allowed to react in a mixture of methanol (7 mL) and benzene (28 mL). Crystalline K-PhS-3 formed: 5.09 g (95%). $[C_6H_5Si(O)OK]_3{\cdot}MeOH{\cdot}2H_2O$ = $C_{19}H_{23}K_3O_9Si_3$ (597): calcd. C 38.23, H 3.88, K 19.65, Si 14.12; found C 38.01, H 3.69, K 19.61, Si 13.86. A single crystal was analyzed by X-ray crystallography. The molecular composition is $[(K^+)_3\{PhSi(O)O^-\}_3]_2{\cdot}7H_2O{\cdot}3MeOH$ (**4**). K-PhS-3 (5.06 g, 8.5 mmol), Me_3SiCl (7.85 g, 72.2 mmol), and pyridine (3.43 g, 43.4 mmol) were allowed to react in hexane (80 mL). A liquid, colorless product formed. Yield 4.47 g (83%). GPC (THF): one a peak corresponding to $[PhSi(OSiMe_3)O]_3$ (retention time: 17.79 min).

NMR Data for $[PhSi(OSiMe_3)O]_4$: ^{1}H NMR (500 MHz, C_6D_6, 20 °C): δ = 0.21 (s, 9 H, $SiMe_3$), 7.11 (t, ^3J = 7.4 Hz, 2 H, *m*-C_6H_5Si), 7.28 (t, ^3J = 7.4 Hz, 1 H, *p*-C_6H_5Si), 7.33 (d, ^3J = 7.4 Hz, 2 H, *o*-C_6H_5Si) ppm. $^{29}Si\{^1H\}$ NMR (99 MHz, C_6D_6, 20 °C): δ = 10.99 ($OSiMe_3$), −78.49 (O_3SiPh) ppm.

NMR Data for $[PhSi(OSiMe_3)O]_3$: ^{1}H NMR (500 MHz, $CDCl_3$, 20 °C): δ = 0.24 (s, 9 H, $SiMe_3$), 7.25 (t, ^3J = 7.4 Hz, 2 H, *m*-C_6H_5Si), 7.36 (t, ^3J = 7.4 Hz, 1 H, *p*-C_6H_5Si), 7.50 (d, ^3J = 7.4 Hz, 2 H, *o*-C_6H_5Si) ppm. $^{29}Si\{^1H\}$ NMR (99 MHz, C_6D_6, 20 °C): δ = 11.58 ($OSiMe_3$), −69.56 (O_3SiPh) ppm.

X-ray Crystal Structure Determination: Colorless single crystals of compounds **2**, **3**, and **4** were grown from solutions (see above). Details of crystal data, data collection and structure refinement parameters for siloxanolate salts **2**−**4** are given in Table 2. The structures were solved by direct methods and refined by a full-matrix least-squares technique against F^2, with anisotropic temperature factors for all non-hydrogen atoms. All hydrogen atoms in **2**−**4** were located from the Fourier synthesis of electron density and refined in the isotropic approximation. Data reduction and further calculations were performed using SAINT[14] and SHELXTL PLUS 5[15] on an IBM PC AT. CCDC-217730 to -217732 for crystal structures **2**−**4** contain the supplementary crystallographic data for this paper. These data can be obtained free of charge at www.ccdc.cam.ac.uk/conts/retrieving.html [or from the Cambridge Crystallographic Data Centre, 12 Union Road, Cambridge CB2 1EZ, UK; Fax: (internat.) + 44-1223-336-033; E-mail: deposit@ccdc.cam.ac.uk].

Acknowledgments

Financial support of this work by Dow Corning Corporation and Deutsche Forschungsgemeinschaft (DFG) is gratefully acknowledged.

[1] [1a] M. G. Voronkov, V. I. Lavrentyev, *Top. Curr. Chem.* **1982**, *102*, 199−236. [1b] R. H. Baney, M. Itoh, A. Sakakibara, T. Suzuki, *Chem. Rev.* **1995**, *95*, 1409−1430.

[2] [2a] J.-M. Lehn, *Supramolecular Chemistry*, VCH, Weinheim, **1995**. [2b] J. W. Steed, J. L. Atwood, *Supramolecular Chemistry*, John Wiley & Sons, Chichester, **2000**. [2c]S. Leininger, B. Olenyuk, P. J. Stang, *Chem. Rev.* **2000**, *100*, 853−908. [2d] C. Piguet, G. Bernardelli, G. Hopfgartner, *Chem. Rev.* **1997**, *97*, 2005−2062. [2e] M. Yoshizawa, T. Kusukawa, M. Fujita, S. Sakamoto, K. Yamaguchi, *J. Am. Chem. Soc.* **2001**, *123*, 10454−10459.

[3] [3a] Yu. A. Molodtsova, Yu. A. Pozdniakova, K. A. Lyssenko, I. V. Blagodatskikh, D. E. Katsoulis, O. I. Shchegolikhina, *J. Organomet. Chem.* **1998**, *571*, 31−36. [3b] O. I. Shchegolikhina, Yu. A. Pozdnyakova, Yu. A. Molodtsova, S. D. Korkin, S. S. Bukalov, L. A. Leites, K. A. Lyssenko, A. S. Peregudov, N. Auner, D. E. Katsoulis, *Inorg. Chem.* **2002**, *41*, 6892−6904.

[4] O. I. Shchegolikhina, Yu. A. Pozdniakova, M. Yu. Antipin, D. E. Katsoulis, N. Auner, B. Herrschaft, *Organometallics* **2000**, *19*, 1077−1082.

[5] Yu. T. Struchkov, S. V. Lindeman, *J. Organomet. Chem.* **1995**, *488*, 9−14.

[6] P. D. Lickiss, *Adv. Inorg. Chem.* **1995**, *42*, 147−262.

[7] K. A. Andrianov, A. I. Chernyshov, V. M. Kopylov, P. L. Prihod'ko, S. E. Esipov, *Zh. Obshch. Khim.* **1979**, *50*, 1044−1048.

[8] [8a] L. H. Sommer, *Stereochemistry*, McGraw-Hill, New York, **1965**. [8b] L. H. Sommer, *Stereochemistry and Reaction Mechanisms of Organosilicon Compounds*, Mir, Moscow, **1966**.

[9] [9a] M. Szwarc, *Carbanions, Living Polymers and Electron-Transfer Processes*, John Wiley & Sons, New York, London, Sydney, Toronto, **1968**. [9b] M. Szwarc, *Anion Polymerisation*, Mir, Moscow, **1971**.

[10] N. R. Poonia, A. V. Bajaj, *Chem. Rev.* **1979**, *79*, 389−445.

[11] E. Matukhina, O. Shchegolikhina, N. Makarova, Yu. Pozdniakova, D. Katsoulis, Yu. Godovsky, *Liq. Cryst.* **2001**, *28*, 869−879.

[12] I. V. Blagodaskikh, O. I. Shchegolikhina, Yu. A. Pozdniakova, Yu. A. Molodtsova, A. A. Zhdanov, *Izv. Akad. Nauk SSSR* **1994**, *6*, 1057−1062.

[13] Unpublished data.

[14] *SMART V5.051 and SAINT V5.00, Area detector control and integration software*, Bruker AXS, Inc., Madison, WI 53719, USA, **1998**.

[15] G. M. Sheldrick, *SHELXTL Version 5, Software Reference Manual*, Siemens Industrial Automation, Madison, WI 53719, USA, **1994**.

Received August 20, 2003
Early View Article
Published Online February 10, 2004

 © 2004 Wiley-VCH Verlag GmbH & Co. KGaA, Weinheim

Peripherally Metallated Porphyrins: the First Examples of *meso*-η¹-Palladio(II) and -Platinio(II) Complexes with Chelating Diamine Ligands

Regan D. Hartnell[a] and Dennis P. Arnold*[a]

Keywords: N ligands / Palladium / Platinum / Porphyrins

The oxidative addition of bis(dibenzylideneacetone)platinum(0) to *meso*-bromo-5,15-diarylporphyrins in the presence of PPh_3 has been shown to be an effective way of synthesising η¹-organoplatinum porphyrins in high yields. This methodology has been extended to synthesise various palladio- and platinioporphyrins that utilise bidentate nitrogen donor ligands [*N*,*N*,*N*′,*N*′-tetramethylethylenediamine (tmeda) and 2,2′-bipyridyl (bpy)] in order to enforce a *cis* configuration at the metal centre. The products were characterised by multinuclear NMR and UV-Vis spectroscopy as well as fast-atom bombardment and high-resolution electrospray ionisation mass spectroscopy.
(© Wiley-VCH Verlag GmbH & Co. KGaA, 69451 Weinheim, Germany, 2004)

Introduction

There has been considerable interest in the investigation of the synthesis and properties of various types of organometallic porphyrins. Traditionally the "organometallic" fragment of the molecule involves a metal−carbon bond between the metal bound in the central cavity of the porphyrin macrocycle and either an alkyl or aryl moiety that has either σ- or π-bonding character.[1] These investigations have often been directed towards the catalytic activation of small molecules, usually in a biomimetic sense. The recent discovery and investigation of porphyrinoid macrocycles with modified cavities, such as inverted or "N-confused" porphyrins[2] and azuliporphyrins,[3] has somewhat increased the number of examples in this area; however, the centrally coordinated metal is still intimately involved in the organometallic character of the molecule. There are also several examples of porphyrinoid compounds covalently bound to organometallic fragments such as metallocenes,[4] or with one of the porphyrin pyrrole rings participating in an η⁵-pyrrolyl−metal arrangement.[5]

Besides the examples discussed above, there is also a small group of peripherally metallated η¹-organometallic porphyrins. Examples in this area include mercurated porphyrins,[6] *meso*-tellurium trichloride appended porphyrins,[7] porphyrinyl boronates[8] and the recent Grignard-like metalloporphyrin of Therien.[9] Our publications have been the only reports of isolated η¹-organopalladio- and organoplatinioporphyrins[10−13] and these are the only examples with transition metals directly bonded to porphyrin carbons. Compounds of type **1** are involved in the catalytic reactions for the coupling of *meso*-haloporphyrins with simple terminal alkynes, alkynylstannanes or alkynylzincs and alkenylorganometallics.[14−17] The key initial step in these couplings is the oxidative addition of the *meso*-carbon−halogen bond to a zerovalent palladium species, usually a bis(phosphane) moiety. Several years ago, we serendipitously isolated the resulting *meso*-η¹-organopalladium(II) porphyrin from one of these reactions[12] and have recently embarked on a systematic study of this type of palladium compound and their more robust organoplatinum(II) analogues. One possible area of interest in *meso*-η¹-platinioporphyrins relates to the combination of the cytotoxicity of the *cis*-platinum centre and the tumour selectivity and photodynamic effect of the porphyrin.[18−20] In this paper we report our synthesis for the first time of *meso*-η¹-organometallic porphyrins of palladium(II) and platinum(II) with chelating nitrogen ligands, namely *N*,*N*,*N*′,*N*′-tetramethylethylenediamine (tmeda) and 2,2′-bipyridyl (bpy).

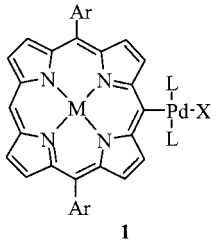

1

Results and Discussion

Syntheses of Palladio- and Platinioporphyrins

As part of our ongoing investigation of η¹-organometallic *meso*-platinio- and palladioporphyrins, we were very

[a] Synthesis and Molecular Recognition Program, School of Physical and Chemical Sciences, Queensland University of Technology,
G. P. O. Box 2434, Brisbane, 4001, Australia
Fax: (internat.) +61-7-3864-1804
E-mail: d.arnold@qut.edu.au

 © 2004 Wiley-VCH Verlag GmbH & Co. KGaA, Weinheim DOI: 10.1002/ejic.200300600

keen to synthesise platinioporphyrins with chelating ligands, in order to enforce a *cis* arrangement of the platinum fragment. This had been achieved for the palladioporphyrins by the use of various diphosphanes, for example, 1,2-bis(diphenylphosphanyl)ethane (dppe), 1,3-bis(diphenylphosphanyl)propane (dppp) and 1,1′-bis(diphenylphosphanyl)ferrocene (dppf).[13] These η^1-organometallic *meso*-palladioporphyrins were readily synthesised by the oxidative addition of a zerovalent palladium species into a 10-bromo-5,15-diarylporphyrin. The zerovalent palladium species is usually prepared in situ by the addition of the convenient palladium precursor, $Pd_2(dba)_3$ (dba = dibenzylideneacetone, 1,5-diphenylpenta-1,4-dien-3-one) to the bidentate phosphane in degassed toluene at 105 °C, to which the bromoporphyrin is later added. Under these conditions, the reaction is usually completed within 30 minutes. After removal of the solvent and recrystallisation, the desired η^1-organometallic *meso*-palladioporphyrin is obtained in high yields (> 80 %).

Having developed this efficient methodology for our palladioporphyrin analogues, we naturally sought to prepare the analogous platinioporphyrin species. After several attempts it was soon apparent that the intervening zerovalent platinum species that is formed in situ from $Pt(dba)_2$ and a diphosphane (dppe or dppp) is too stable to undergo the oxidative addition step with the haloporphyrin. This appears to be because the redistribution of ligands on Pt favours the apparently inert $18e^-$ species [e.g. $Pt(dppe)_2$]. The analogous reaction was also attempted several times with less stable, more sterically hindered zerovalent platinum species prepared from larger bidentate diphosphanes, namely 2,2′-bis(di-*p*-tolylphosphanyl)-1,1′-binaphthyl (tol-BINAP) and dppf. However, these also failed to undergo the oxidative addition step with a haloporphyrin to give the desired platinioporphyrin. In order to ensure that the $Pt(dba)_2$ substance that was being used throughout the investigations above was of high quality and not the cause of problematic side-reactions, we carried out a control reaction between monodentate triphenylphosphane, $Pt(dba)_2$ and a bromoporphyrin **2** (Table 1 shows the structures of compounds **2**−**14**). This reaction proceeded smoothly, as evident from TLC that the $Pt(dba)_2$ was consumed to form either $Pt(PPh_3)_3$ or $Pt(dba)(PPh_3)_2$ in situ and that **2** was being converted into a much more polar compound. Continual TLC analysis showed that the initial more polar compound was slowly being converted into a slightly more mobile product. This observation is in line with previous reports[10,11] that the initially formed product of the oxidative addition step is the *cis* isomer **3**, which with continued heating, isomerises slowly (ca. 6 hours) to the *trans* isomer **4**. This method has the distinct advantage over the previous method[10,11] that it avoids the use of air- and moisture-sensitive $Pt(PPh_3)_3$, which if not freshly prepared may be of doubtful quality.

With the viability of the dba-ligand method proven, as explained above, a different tactic was attempted in order to prepare the desired *cis*-orientated organoplatinum porphyrins. It is well-known that aromatic iodo groups undergo palladium(0)-catalysed coupling reactions at a much greater rate than those of bromo analogues.[21] This has also been shown to be true for 5-bromo-15-iodo-10,20-diarylporphyrins, which are found to undergo palladium(0)-catalysed coupling reactions at the iodo-substituted position preferentially over the bromo-substituted position.[17,22] With this in mind, the oxidative addition reactions of the platinum(0) diphosphane precursors were repeated with a range of iodoporphyrins; unfortunately, these also failed to give the desired η^1-organometallic porphyrins.

Table 1. Correspondence of compound numbers and structures

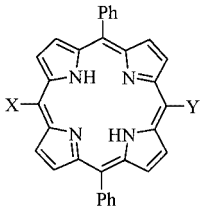

Compound	X	Y
2	H	Br
3	H	*cis*-$Pt(PPh_3)_2Br$
4	H	*trans*-$Pt(PPh_3)_2Br$
5	H	Pd(tmeda)Br
6	H	Pd(bpy)Br
7	Br	Br
8	Pd(tmeda)Br	Pd(tmeda)Br
9	Ph	I
10	H	H
11	Ph	H
12	Ph	Pt(tmeda)I
13	Ph	Pt(bpy)I
14	Ph	*trans*-$Pt(PPh_3)_2I$

After these disappointing results with bidentate diphosphanes, a new methodology that utilises bidentate nitrogen donor ligands was developed in order to approach the desired *cis*-orientated organoplatinum porphyrins. This reaction was initially attempted with palladium, since it is known to undergo oxidative addition reactions much more readily than platinum analogues. These reactions are well-known from the work of Canty and co-workers, who have used these N-ligands to make interesting Pd^{IV} complexes.[23] Thus, when $Pd_2(dba)_3$ was treated with an excess of tmeda and an equivalent of bromoporphyrin **2** in degassed toluene at 105 °C, it was soon evident that the starting material was being consumed and converted into a much more polar compound. The reaction was completed after approximately one hour and the solution was filtered to remove any palladium metal resulting from decomposition of the Pd^0 precursors. After two recrystallisations from $CHCl_3$/cyclohexane, product **5** was obtained in high yield as an air- and moisture-stable dark purple solid. This procedure was similarly carried out with 2,2′-bipyridine as the nitrogen donor ligand to produce a high yield of the similar η^1-organometallic porphyrin **6**. Unlike the porphyrinyl-palladium bidentate diphosphane analogues,[12,13] it

 © 2004 Wiley-VCH Verlag GmbH & Co. KGaA, Weinheim

was found that these compounds are relatively stable towards silica and thus may be purified by column chromatography if required; as long as efforts are taken to ensure that any solvents used during the purification process are thoroughly free from acid. The reaction was repeated with the dibromoporphyrin species (**7**), tmeda and $Pd_2(dba)_3$ in order to prepare the bis(palladated) species. TLC analysis suggested that the desired double oxidative addition had occurred analogously; however, the product precipitated from the hot toluene solution. The precipitate was collected but it was found to be extremely insoluble in all common organic solvents and thus was not amenable to further purification. Other attempts at producing a bis(palladated) porphyrin system using the more soluble 5,15-bis(3′,5′-di-*tert*-butylphenyl)porphyrin also gave insoluble products that were difficult to purify thoroughly. FAB mass spectra of **8** (see below) indicated that the desired bis(palladium) porphyrin was formed. Initial thoughts were that the bidentate tmeda fragment could be flexible enough to act as a bridging group between two η^1-palladioporphyrin macrocycles, thus forming an oligomeric or polymeric species. However, the same result was seen with the less flexible 2,2′-bipyridine ligand, which suggests that they are not forming oligomers and that these examples of bis(palladiated) porphyrin species with bidentate nitrogen ligands are inherently insoluble.

Attempts at preparing the analogous platinioporphyrin systems with bromoporphyrin **2** failed, so the reactions were repeated with an iodoporphyrin. The iodoporphyrin chosen was 5-iodo-10,15,20-triphenylporphyrin (H_2TrPP-I) (**9**). This porphyrin was chosen due to its ease of synthesis in high yields, from the readily available starting material diphenylporphyrin (H_2DPP) (**10**).[11,24] The one free *meso*-position of triphenylporphyrin (H_2TrPP) (**11**) lends itself ideally to selective iodination.[17,22] This method avoids the tedious chromatographic separation procedures required to remove other iodoporphyrins that would be present if **10** itself were iodinated by similar procedures. Thus, when the more reactive iodoporphyrin **9** was utilised, the desired platinioporphyrins with bidentate nitrogen ligands were formed in good yields. As expected the formation of platinioporphyrins **12** and **13** was somewhat slower than the analogous palladioporphyrins **5** and **6**. The latter were formed in high yields within one hour, whilst **12** and **13** required overnight heating in degassed toluene with an excess of the platinating agent, but were eventually formed in good yields (ca. 80 %). Platinioporphyrins **12** and **13** were purified by column chromatography on silica support in order to remove a trace of the starting iodoporphyrin **9** and no degradation was seen during this procedure. It is important to note that even though these oxidative addition reactions are carried out on the free-base porphyrins, no metallation of the central porphyrin cavity is seen in any of these reactions, even after prolonged heating at 105 °C in toluene. This has been a general observation in all our metallation reactions. Moreover, Pd-catalysed couplings on free base porphyrins are readily carried out, as has been shown by several groups.[15,16,25] Indeed, we have found from qualitative reactivity comparisons of Pt insertions, that the bromo free bases react faster than either Ni^{II} or Zn^{II} substrates.[26] For all of these free-base η^1-organometallic porphyrins, it was found that the addition of a small amount of base (1 % triethylamine) to the mobile phase used during any of the chromatographic procedures greatly improved the tractability of these species. If base was omitted, it was found that the porphyrin macrocycle tended to protonate very readily on the column due to the strong electron donating properties of the η^1-organometallic fragment,[10−13] further enhanced by the electron-donating properties of the bidentate nitrogen ligands.

With metalloporphyrins **12** and **13** in hand, we investigated the substitution of the bidentate nitrogen donor ligands by chelating diphosphane ligands whose coordination to the soft Pt^{II} centre is expected to be favoured.

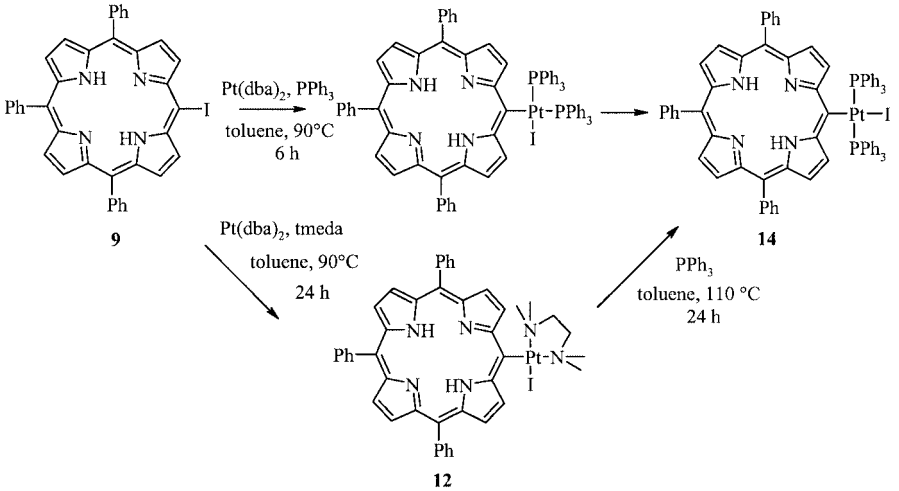

Scheme 1

 © 2004 Wiley-VCH Verlag GmbH & Co. KGaA, Weinheim

Unfortunately, both **12** and **13** failed to undergo any ligand exchange reactions with a variety of bis(phosphanyl) ligands (dppe, dppp and dppf). It was surprising that the ligand exchange did not occur at all even with excess phosphane ligand, elevated temperatures, and prolonged reaction times. In all cases, the bis(N-donor)-chelated species was quantitatively recovered with no noticeable decomposition detectable by ^{1}H NMR spectroscopy. However, it is encouraging to observe that these species are quite stable and unlikely to decompose under a variety of different solvents and reaction conditions, so their use for the construction of multiporphyrin arrays with Pt^{II} connectors should be possible. The ligand exchange did occur with the simple monophosphane, PPh_3 to yield **14** in approximately 50 % yield, implying that the problems may be steric in origin. However, it was observed that H_2TrPP (**11**) was also produced in an approximately equal amount. Clearly, the organometallic platinioporphyrin **14** is best prepared by using our original, direct oxidative addition of a zerovalent Pt bis(phosphane) species (see Scheme 1), as discussed above.[10−13]

NMR Spectra of Palladio- and Platinioporphyrins

There are several aspects of interest in the NMR spectra of these η^1-organometallic porphyrins. The first observation is the facial asymmetry of the porphyrin due to the favoured, approximately orthogonal disposition of the N−Metal−N plane of the organometallic fragment and the plane of the porphyrin macrocycle. This arrangement gives rise to two different signals for the *o*-hydrogens of the phenyl groups in the 5,15-positions of the porphyrin. The unequal faces of the porphyrin are also clearly evident in the case of **5** where different nonequivalent *m*-hydrogens on the 5,15-phenyl groups are also seen. This feature was less apparent in our previous compounds with bidentate aryl diphosphanes because of overlap of many aryl signals.[12,13] The porphyrin β-hydrogens appear as four doublets (^1J = 4.7 Hz), typical of substituted porphyrins of this symmetry and all peaks are shifted from those encountered in the corresponding parent haloporphyrins. The biggest shifts are understandably experienced by the peaks arising from the 3,7-β-hydrogens adjacent to the organometallic fragment, which are shifted downfield by approximately δ = 0.8 ppm. In the case of **5** and **6**, this peak appears to be shifted even more downfield than the 20-*meso*-proton which is observed as a sharp singlet at about δ = 9.8 ppm. In those species containing a 2,2′-bipyridyl ligand, namely **6** and **13**, the peaks arising from the bipyridine unit appear as a series of eight mutually coupled signals over a δ = 4 ppm range (see Figure 1). The signals from the protons that are above the porphyrin plane are somewhat shielded by the macrocycle and this is demonstrated by large upfield shifts of about δ = 1 ppm from corresponding signals in the free ligand. Interestingly, the signals arising from the 6′-proton of the bipyridine moiety in **6** and **13** are strongly shifted downfield to δ = 9.7 and 10.4 ppm, respectively, demonstrating the effect of the halogen as a neighbouring electronegative centre. In NOESY experiments on **6** and **13**, a strong cross-peak is seen that represents the NOE between the 3,7-β-hydrogens of the porphyrin and the 6′′-proton of the bipyridine fragment. All peaks in these spectra have been assigned by careful examination of the 1-D spectra and a series of DQF-COSY and NOESY 2-D NMR experiments (see Figure 2). Similar spectra are observed for **5** and **12**, with signals for the tmeda fragment appearing in the upfield region between δ = 1.6 and 3.2 ppm. It is clear that the metallo-substituent is rotating slowly on the NMR timescale, mostly orthogonal to the plane of the porphyrin to give two singlets for the methyl groups corresponding to those that are *cis* and those that are *trans* to the porphyrin. A dipolar coupling cross-peak from one of these methyl singlets to the 3,7-β-hydrogens of the porphyrin reveals that the more upfield peak around δ = 1.6 ppm arises from the methyl groups that are *cis* to the porphyrin.

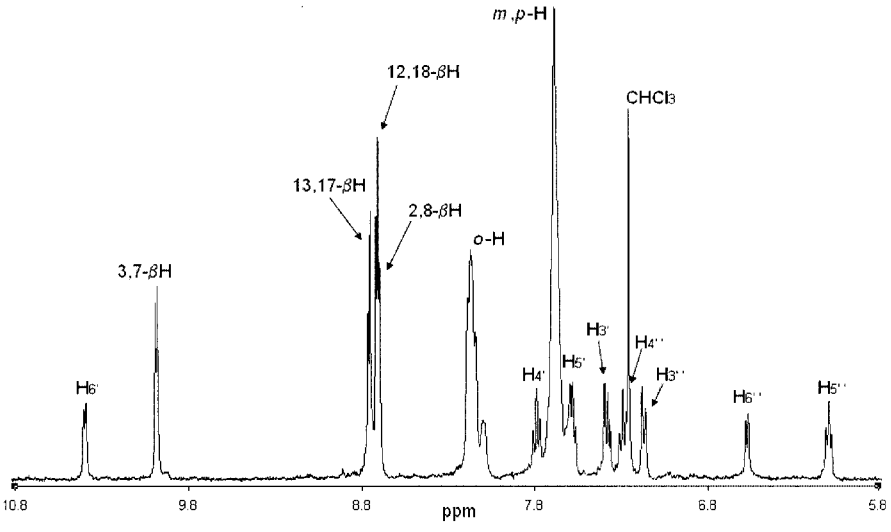

Figure 1. ^{1}H NMR spectrum of [PtI(H_2TrPP)(bpy)] (**13**) in $CDCl_3$ at 293 K

 © 2004 Wiley-VCH Verlag GmbH & Co. KGaA, Weinheim

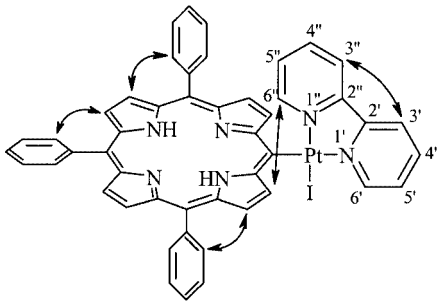

Figure 2. Numbering scheme for the bpy fragment and through-space correlations revealed by the NOESY spectrum of **13**

Mass and UV-Visible Absorption Spectra of Palladio- and Platinioporphyrins

All species gave mass spectra (ESI high-resolution for **5** and **6** and FAB for **12** and **13**) that displayed either the molecular ions of the respective complexes or their halide-exchanged analogues. For example, **6** did not give any molecular ion signal peaking at m/z = 805.0744 for the bromo complex, rather the most abundant peak in the spectrum corresponded extremely well with that for the iodo complex (calculated m/z = 851.0622; found m/z = 851.0722), which indicates that iodide from the NaI internal calibration standard had induced exchange. Also present in the spectra were the analogous chloro complexes from CH_2Cl_2 used in the introduction of the samples into the mass spectrometer. For platinioporphyrins **12** and **13**, the FAB mass spectra displayed the desired molecular ions for the appropriate parent compounds. In line with our observations that the halogen is less labile on the platinioporphyrins than on the palladioporphyrins, **13** displayed only a very small (< 10 %) cluster for the chloro-complex, whilst **12** did not display any analogous peak at all. In all mass spectra, fragmentation occurred and appropriate masses were recognised. These included fragments corresponding to the parent porphyrin macrocycle and fragments after loss of the halide. On the other hand, the MALDI-TOF spectra of all compounds displayed no parent molecular ions, but only clusters representing the porphyrin macrocycle, indicating that considerable fragmentation occurs during laser-induced ionisation. Bis(palladated)porphyrin **8** gave a strong parent molecular ion (calculated m/z = 1065.1; found m/z = 1065.2) as well as peaks corresponding to the loss of either one or both of the organometallic fragments. Peaks for the chloro analogues were also detected.

The UV-Visible spectra of these organometallic porphyrins are quite typical for di- and triphenylporphyrin derivatives. The wavelengths of the principal visible absorption bands for all complexes and the precursors are displayed in Table 2. Some trends can be distinguished, even with this limited number of examples. All groups other than H in the *meso* positions cause a red-shift, which is usual for these and related porphyrinic systems.[15] It can be seen that the *meso*-η^1-organometallic fragment exerts a similar effect on the electronic spectra to that of a simple halo substituent. There is a red-shift of the Soret band of approximately 10−15 nm and similar shifts for the Q bands relative to the base porphyrin macrocycles, after formation of the organometallic species. The nature of the nitrogen-donor ligands has very little effect on the electronic absorption spectrum for similar metallated species, for example, compare **5** and **6** or **12** and **13** to phosphane-ligated species like **14** and those previously reported.[10−13] They all have very similar electronic spectra although the phosphane-coordinated species displays slightly more red-shifted bands. The bis(palladated) species **8** continues the trend seen with mono-(palladated) **5**; the spectrum of **8** displays an even larger red-shift of all bands. This could be a sign of greater macrocycle distortion in order to cope best with the electronic and steric demands of the two organometallic fragments as well as the expected electron donating effect on the energy of the HOMO.

Table 2. Wavelengths for the principal UV-Visible absorption bands for the *meso*-metalloporphyrins and their precursors (in CH_2Cl_2)

Compound	λ_{max} (nm)				
Soret	IV	III	II	I	
2	420	510	545	587	642
5	417	518	551	588	642
6	418	516	550	589	640
8	427	529	567	607	665
9	421	519	554	595	651
10	405	502	535	575	630
11	411	508	542	583	637
12	426	527	564	599	655
13	426	526	563	597	653
14	434	528	567	601	659

Conclusion

The combination of $Pt(dba)_2$ and monodentate phosphane ligands with various haloporphyrins has been shown to be an effective way of synthesising η^1-organoplatinum porphyrins in high yields. An advantage of this method over previous methods is that it avoids the use of unstable Pt^0 phosphane complexes. This method has also been extended for the first time to synthesise various palladio- and platinioporphyrins that utilise bidentate nitrogen donor ligands in order to enforce a *cis* configuration of the metal centre. The availability of these stable *cis*-orientated organometallic porphyrins will allow for variation of architectures when incorporated with other suitable tectons in self-assembled supramolecular systems.

Experimental Section

General Remarks: Syntheses involving zerovalent metal precursors were carried out under high-purity argon using conventional Schlenk techniques. Porphyrin starting materials 10-bromo-5,15-diphenylporphyrin (**2**)[17] and 5,10,15-triphenylporphyrin (**11**)[11] were prepared by literature procedures and $Pt(dba)_2$ by the method of Cherwinski and co-workers.[27] All other reagents and ligands were

 © 2004 Wiley-VCH Verlag GmbH & Co. KGaA, Weinheim

used as received from Sigma−Aldrich. Toluene was AR grade, stored over sodium wire, and degassed by heating and purging with argon at 105 °C. All other solvents were AR grade, and dichloromethane and chloroform were stored over anhydrous sodium carbonate. Analytical TLC was performed using Merck silica gel 60 F_{254} plates and column chromatography was performed using Merck silica gel (230−400 mesh). NMR spectra were recorded on Bruker Avance 400 MHz or Varian Unity 300 MHz instruments in $CDCl_3$ solutions, using $CHCl_3$ as the internal reference at δ = 7.26 ppm for ^1H spectra, and external 85 % H_3PO_4 as the reference for proton-decoupled $^{31}P\{^1H\}$ spectra. UV-Vis spectra were recorded on a Cary 3 spectrometer in dichloromethane. High resolution ESI mass spectra were recorded on a Bruker BioApex 47e FTMS fitted with an Analytica Electrospray Source. The samples were dissolved in dichloromethane and diluted with either dichloromethane/methanol (1:1) or methanol, and solutions were introduced into the source by direct infusion (syringe pump) at 60 μL/h, with a capillary voltage of 80 V. The instrument was calibrated using internal NaI. Positive ion FAB mass spectra were recorded on a Kratos Concept instrument at the Central Science Laboratory, University of Tasmania. Samples were dissolved in dichloromethane, and dispersed in a 4-nitrobenzyl alcohol matrix. In the data below, masses given are for the strongest observed peak in the molecular ion spectrum. In all compounds, this *m*/*z* value agreed with the predicted molecular mass, although in most cases it represented a mixture of M and M + 1 due to partial protonation of the free base porphyrin. Elemental analyses were carried out by the Microanalytical Service, The University of Queensland.

***trans*-[PtBr(H_2DPP−)(PPh_3)$_2$] (4):** Toluene (25 mL) was added to a Schlenk flask and degassed by bubbling argon through the solution at 90 °C. Bromoporphyrin **2** (20 mg, 0.037 mmol) was added and stirred for 5 min. Pt(dba)$_2$ (29 mg, 0.044 mmol) and triphenylphosphane (35 mg, 0.132 mmol) were added and the solution stirred at 105 °C. TLC analysis (50 % $CHCl_3$/*n*-hexane/1 % Et_3N) of the reaction mixture clearly showed disappearance of the starting material after about 30 min and that the initially formed *cis* isomer was slowly being converted into the *trans* isomer. After about 6 h the isomerisation was considered complete and the reaction mixture was cooled to room temperature and the solvent removed in vacuo. The residue (now air stable) was purified on a SiO_2 column and eluted with 50 % $CHCl_3$/*n*-hexane/1 % Et_3N; the major purple fraction was collected and the solvent removed in vacuo. The residue was recrystallised from $CHCl_3$/*n*-hexane to give **4** as dark purple crystals in 94 % yield. The data (^1H and ^{31}P NMR spectroscopy) of this compound agreed well with those of a genuine sample prepared previously using Pt(PPh_3)$_3$.[13]

General Procedure for the Preparation of Compounds 5, 6 and 8: As an example of this method, tmeda (35 μL, 0.25 mmol) and $Pd_2(dba)_3$ (43 mg, 0.046 mmol) were added sequentially to a stirred solution of bromoporphyrin **2** (25 mg, 0.046 mmol) in dry toluene (15 mL) that had been degassed at 90 °C. The reaction was maintained at 90 °C under an argon atmosphere and monitored by TLC (50 % $CHCl_3$/*n*-hexane/1 % Et_3N). When the reaction was considered to be complete by the total disappearance of starting material; the solution (now air stable) was filtered through a fine glass frit and the solvent removed in vacuo. The residue was recrystallised twice from $CHCl_3$/cyclohexane to give a dark purple solid that was dried thoroughly under high vacuum.

[PdBr(H_2DPP−)(tmeda)] (5): The desired complex **5** (34 mg) was obtained in 93 % yield. ^1H NMR (400 MHz, $CDCl_3$, 25 °C): δ = −2.78 (br. s, 2 H, NH), 1.50 [s, 6 H, (CH_3)$_2$N], 2.37 (m, 2 H, NCH_2CH$_2$N), 2.43 (m, 2 H, NCH$_2$$CH_2$N), 2.70 [s, 6 H, ($CH_3$)$_2$N], 7.65−7.75 (m, 2 H, one pair *m*-H on 10,20-phenyl), 7.75−7.85 (overlapping m, 4 H, one pair *m*-H on 10,20-phenyl and *p*-H on 10,20-phenyl), 8.05−8.10 (m, 2 H, *o*-H on 10,20-phenyl), 8.25−8.35 (m, 2 H, *o*-H on 10,20-phenyl), 8.82, 8.90, 9.18, 10.04 (each d, $^3J_{H,H}$ = 4.7 Hz, 2 H, β-H), 9.92 (s, 1 H, *meso*-H) ppm. UV-Vis: λ_{max} (ε/10^3 M^{-1}·cm^{-1}) = 417 (356), 518 (16.9), 551 (13.0), 588 (8.6), 642 (11.5) nm. High-resolution ESI MS: $[M]^+$ accurate mass calculated for $C_{38}H_{38}BrN_6Pd(+1)$: 765.1375; found: 765.1385.

[PdBr(H_2DPP−)(bpy)] (6): The desired complex **6** (36 mg) was obtained in 91 % yield. ^1H NMR (400 MHz, $CDCl_3$, 25 °C): δ = −2.93 (br. s, 2 H, NH), 5.95 (t, $^3J_{H,H}$ = 6.5 Hz, 1 H, 5′′-H), 6.02 (d, $^3J_{H,H}$ = 6.5 Hz, 1 H, 6′′-H), 7.05 (t, $^3J_{H,H}$ = 6.5 Hz, 1 H, 4′′-H), 7.13 (d, $^3J_{H,H}$ = 6.5 Hz, 1 H, 3′′-H), 7.32 (d, $^3J_{H,H}$ = 6.5 Hz, 1 H, 3′-H), 7.48 (t, $^3J_{H,H}$ = 6.5 Hz, 1 H, 5′-H), 7.62 (t, $^3J_{H,H}$ = 6.5 Hz, 1 H, 4′-H), 7.65−7.75 (m, 6 H, *m*,*p*-H on 10,20-phenyl), 8.05−8.15 (m, 2 H, *o*-H on 10,20-phenyl), 8.20−8.25 (m, 2 H, *o*-H on 10,20-phenyl), 8.79, 8.92, 9.17, 10.25 (each d, $^3J_{H,H}$ = 4.7 Hz, 2 H, β-H), 9.70 (d, $^3J_{H,H}$ = 6.5 Hz, 1 H, 6′-H), 9.91 (s, 1 H, *meso*-H) ppm. UV-Vis: λ_{max} (ε/10^3 M^{-1}·cm^{-1}) = 418 (492), 516 (15.2), 550 (9.9), 589 (6.3), 640 (7.0) nm. High-resolution ESI MS: I/Br exchanged product $[M]^+$ accurate mass calculated for $C_{42}H_{30}IN_6Pd(+1)$: 851.0622; found: 851.0722.

Bis(palladio)porphyrin (8): This was prepared by a similar procedure as above, but using dibromoporphyrin (**7**) and the appropriate amounts of tmeda and $Pd_2(dba)_3$. The crude yield was quantitative, however, the product is not sufficiently soluble for further purification and ^1H NMR analysis. UV-Vis: λ_{max} (rel. int.) = 427 (37.8), 529 (3.3), 567 (5.6), 607 (1.0), 665 (4.9) nm. FAB MS: $[M]^+$ mass calculated for $C_{44}H_{52}Br_2N_8Pd_2(+1)$: 1065.2; found: 1065.2.

H_2TrPP-I (9): Pyridine (250 μL), iodine (24 mg, 0.1 mmol) and bis(trifluoroacetoxy)iodobenzene (40 mg, 0.1 mmol) were added to a solution of triphenylporphyrin (**13**) (50 mg, 0.093 mmol) dissolved in $CHCl_3$ (25 mL). The reaction vessel was protected from light and stirred at room temperature. Periodically, the progress of the reaction was checked by TLC (30 % CH_2Cl_2/*n*-hexane). After 36 h it was found that there was total consumption of the starting material and the presence of a faster-moving spot. The solvent was removed in vacuo and the residue purified by column chromatography on SiO_2 and eluted with 50 % CH_2Cl_2/*n*-hexane. The major fraction was collected and the solvent removed and the residue recrystallised from CH_2Cl_2/*n*-pentane. The desired haloporphyrin (**9**) was collected as bright purple crystals in a 97 % yield. ^1H NMR (400 MHz, $CDCl_3$, 25 °C): δ = −2.71 (br. s, 2 H, NH), 7.7−7.8 (m, 9 H, *m*,*p*-H on 10,15,20-phenyl), 8.1−8.2 (m, 6 H, *o*-H on 10,15,20-phenyl), 8.78, 8.80 (overlapping d), 8.87, 9.68 (each d, $^3J_{H,H}$ = 4.7 Hz, 2 H, β-H) ppm. UV-Vis: λ_{max} (ε/10^3 M^{-1}·cm^{-1}) = 421 (433), 519 (19.7), 554 (11.6), 595 (5.5), 651 (4.9) nm. High-resolution ESI MS: $[M + H]^+$ accurate mass calculated for $C_{38}H_{26}IN_4(+1)$: 665.1202; found: 665.1212. $C_{38}H_{25}IN_4$: calcd. C 68.68, H 3.79, N 8.43; found C 68.54, H 3.70, N 8.27.

General Procedure for the Preparation of Compounds 12 and 13: As an example of this method, tmeda (28 μL, 0.19 mmol) and Pt(dba)$_2$ (125 mg, 0.19 mmol) were added sequentially to a stirred solution of iodoporphyrin (**9**) (25 mg, 0.038 mmol) in dry toluene (15 mL) that had been degassed at 90 °C. The reaction was maintained at 90 °C under an argon atmosphere and monitored by TLC (50 % $CHCl_3$/*n*-hexane/1 % Et_3N). When the reaction was considered complete (after 24 h by the total disappearance of starting material), the solution (now air stable) was filtered through a fine glass frit and the solvent removed in vacuo. The residue was dissolved in $CHCl_3$, loaded onto a SiO_2 column, and eluted with $CHCl_3$/1 %

 © 2004 Wiley-VCH Verlag GmbH & Co. KGaA, Weinheim

Et_3N; the major purple/green band was collected. The solvent was removed in vacuo and the residue recrystallised from $CHCl_3$/cyclohexane to give a dark purple solid that was dried thoroughly under high vacuum.

[PtI(H_2TrPP−)(tmeda)] (12): The desired complex **12** (31 mg) was obtained in 83 % yield. ^{1}H NMR (400 MHz, $CDCl_3$, 25 °C): δ = −2.40 (br. s, 2 H, NH), 1.87 [s, 6 H, $(CH_3)_2$N], 3.27 (overlapping m, 4 H, NCH_2CH_2N), 3.27 [s, 6 H, $(CH_3)_2$N], 7.60−7.80 (m, 9 H, *m*,*p*-H on 10,15,20-phenyl), 8.00−8.10 (m, 3 H, *o*-H on 10,15,20-phenyl), 8.25−8.35 (m, 3 H, *o*-H on 10,15,20-phenyl), 8.67, 8.72, 8.78, 10.12 (each d, $^3J_{H,H}$ = 4.7 Hz, 2 H, β-H) ppm. UV-Vis: λ_{max} (ε/10^3 M^{-1}·cm^{-1}) = 426 (395), 527 (8.9), 564 (10.5), 599 (2.8), 655 (8.1) nm. FAB MS: $[M]^+$ mass calculated for $C_{44}H_{41}IN_6Pt(+1)$: 976.2; found: 976.0. $C_{44}H_{41}IN_6Pt$: calcd. C 54.16, H 4.23, N 8.61; found C 54.47, H 4.13, N 8.39.

[PtI(H_2TrPP−)(bpy)] (13): The desired complex **13** (30 mg) was obtained in 78 % yield. ^{1}H NMR (400 MHz, $CDCl_3$, 25 °C): δ = −2.39 (br. s, 2 H, NH), 6.10 (t, $^3J_{H,H}$ = 6.2 Hz, 1 H, 5′′-H), 6.58 (d, $^3J_{H,H}$ = 6.2 Hz, 1 H, 6′′-H), 7.19 (d, $^3J_{H,H}$ = 6.2 Hz, 1 H, 3′′-H), 7.30 (t, $^3J_{H,H}$ = 6.2 Hz, 1 H, 4′′-H), 7.41 (d, $^3J_{H,H}$ = 6.2 Hz, 1 H, 3′-H), 7.60 (t, $^3J_{H,H}$ = 6.2 Hz, 1 H, 5′-H), 7.60−7.75 (m, 9 H, *m*,*p*-H on 10,15,20-phenyl), 7.80 (t, $^3J_{H,H}$ = 6.2 Hz, 1 H, 4′-H), 8.10−8.25 (m, 6 H, *o*-H on 10,15,20-phenyl), 8.70, 8.75, 8.80, 10.00 (each d, $^3J_{H,H}$ = 4.7 Hz, 2 H, β-H), 10.40 (d, $^3J_{H,H}$ = 6.2 Hz, 1 H, 6′-H) ppm. UV-Vis: λ_{max} (ε/10^3 M^{-1}·cm^{-1}) = 426 (379), 526 (13.0), 563 (14.1), 597 (5.9), 653 (8.6) nm. FAB MS: $[M]^+$ mass calculated for $C_{48}H_{33}IN_6Pt(+1)$: 1016.2; found: 1016.1. $C_{48}H_{33}IN_6Pt$: calcd. C 56.76, H 3.27, N 8.27; found C 56.53, H 4.38, N 8.34.

***trans*-[PtI(H_2TrPP)(PPh_3)$_2$] (14)**

Method A: The phosphane PPh_3 (5.2 mg, 0.02 mmol) was added to a refluxing solution of complex **13** (10 mg, 0.01 mmol) in toluene. The solution was refluxed under argon for 24 h. The solvent was removed in vacuo and the residue purified by column chromatography on SiO_2, and eluted with 50 % $CHCl_3$/*n*-hexane/1 % Et_3N to remove the by-product (**11**). The solvent was removed and the residue recrystallised from toluene/*n*-pentane to give the desired complex **14** in a 52 % yield.

Method B: Toluene (50 mL) was added to a Schlenk flask and degassed by bubbling argon through the solvent at 90 °C. Iodoporphyrin **9** (50 mg, 0.075 mmol) was added and stirred for 5 min. $Pt(dba)_2$ (59 mg, 0.090 mmol) and triphenylphosphane (47 mg, 0.18 mmol) were added and the solution stirred at 90 °C. TLC analysis (50 % $CHCl_3$/*n*-hexane/1 % Et_3N) of the reaction mixture clearly showed disappearance of the starting material after about 30 min and that the initially formed *cis* isomer was slowly being converted into the *trans* isomer. After about 6 h the isomerisation was considered complete; the reaction mixture was cooled to room temperature and the solvent removed in vacuo. The residue (now air stable) was purified by column chromatography and eluted with 50 % $CHCl_3$/*n*-hexane/1 % Et_3N; the major purple fraction was collected and the solvent removed in vacuo. The residue was recrystallised from $CHCl_3$/*n*-pentane to give 90 mg of **14** as dark purple crystals in 87 % yield. Some I/Cl exchange was found to occur when left in chlorinated solvents for extended periods. ^{1}H NMR (400 MHz, $CDCl_3$, 25 °C): δ = −3.13 (br. s, 2 H, NH), 6.40−6.60 (m, 18 H, PPh_3), 7.20−7.30 (m, 12 H, PPh_3), 7.60−7.70 (m, 9 H, *m*,*p*-H on 10,15,20-phenyl), 8.05−8.15 (m, 4 H, *o*-H on 10,20-phenyl), 8.20−8.25 (m, 2 H, *o*-H on 15-phenyl), 8.26, 8.63, 8.65 (overlapping d), 9.65 (each d, $^3J_{H,H}$ = 4.7 Hz, 2 H, β-H) ppm. ^{31}P NMR: δ = 24.0 (s, $^1J_{Pt-P}$ = 2976 Hz), UV-Vis: λ_{max} (ε/10^3 M^{-1}·cm^{-1}) = 434 (299), 528 (11.0), 567 (13.8), 601 (7.2), 659 (12.4) nm. High-resolution ESI MS: $[M]^+$ accurate mass calculated for $C_{74}H_{55}IN_4P_2Pt(+1)$: 1385.2690; found: 1385.2690.

Acknowledgments

R. D. H. thanks the Faculty of Science, Queensland University of Technology for a Post-Graduate Scholarship.

[1] [1a] P. J. Brothers, *Adv. Organomet. Chem.* **2001**, *46*, 223−321. [1b] R. Guilard, A. Tabard, E. van Caemelbecke, K. M. Kadish, in *The Porphyrin Handbook, vol. 3* (Eds.: K. M. Kadish, K. M. Smith, R. Guilard), Academic Press, San Diego, **2000**, p. 295−345.

[2] [2a] I. Schmidt, P. J. Chmielewski, *Chem. Commun.* **2002**, 92−93. [2b] K. Araki, H. Winnischofer, H. E. Toma, H. Maeda, A. Osuka, H. Furuta, *Inorg. Chem.* **2001**, *40*, 2020−2025. [2c] H. Furuta, N. Kubo, H. Maeda, T. Ishizuka, A. Osuka, H. Nanami, T. Ogawa, *Inorg. Chem.* **2000**, *39*, 5424−5425. [2d] H. Furuta, T. Ogawa, Y. Uwatoko, K. Araki, *Inorg. Chem.* **1999**, *38*, 2676−2682. [2e] P. J. Chmielewski, L. Latos-Grazynski, I. Schmidt, *Inorg. Chem.* **2000**, *39*, 5475−5482. [2f] L. Latos-Grazynski, P. J. Chmielewski, *New J. Chem.* **1997**, *21*, 691−700.

[3] [3a] T. D. Lash, D. A. Colby, S. R. Graham, G. M. Ferrence, L. F. Szczepura, *Inorg. Chem.* **2003**, *42*, 7326−7338. [3b] S. R. Graham, G. M. Ferrence, T. D. Lash, *Chem. Commun.* **2002**, 894−895. [3c] M. A. Muckey, L. F. Szczepura, G. M. Ferrence, T. D. Lash, *Inorg. Chem.* **2002**, *41*, 4840−4842. [3d] A. Gosh, T. Wondimagegn, H. J. Nilsen, *J. Phys. Chem. B* **1998**, *102*, 10459−10467.

[4] [4a] S. W. Rhee, Y. H. Na, Y. Do, J. Kim, *Inorg. Chim. Acta* **2000**, *309*, 49−56. [4b] S. W. Rhee, B. B. Park, Y. Do, J. Kim, *Polyhedron* **2000**, *19*, 1961−1966. [4c] A. K. Burrell, W. Campbell, D. L. Officer, *Tetrahedron Lett.* **1997**, *38*, 1249−1252. [4d] R. W. Wagner, P. A. Brown, T. E. Johnson, J. S. Lindsey, *J. Chem. Soc., Chem. Commun.* **1991**, 1463−1466. [4e] H. J. H. Wang, L. Jaquinod, D. J. Nurco, M. G. H. Vicente, K. M. Smith, *Chem. Commun.* **2001**, 2646−2647.

[5] [5a] K. K. Dailey, T. B. Rauchfuss, *Polyhedron* **1997**, *16*, 3129−3136. [5b] K. K. Dailey, G. P. A. Yap, A. L. Rheingold, T. B. Rauchfuss, *Angew. Chem. Int. Ed. Engl.* **1996**, *35*, 1833−1837. [5c] E. Campazzi, E. Solari, R. Scopelliti, C. Floriani, *Inorg. Chem.* **1999**, *38*, 6240−6245. [5d] L. Bonomo, E. Solari, G. Martin, R. Scopelliti, C. Floriani, *Chem. Commun.* **1999**, 2319−2320.

[6] [6a] K. M. Smith, K. C. Langry, O. M. Minnetian, *J. Org. Chem.* **1984**, *49*, 4602−4609. [6b] I. K. Morris, K. M. Snow, N. W. Smith, K. M. Smith, *J. Org. Chem.* **1990**, *55*, 1231−1236. [6c] O. M. Minnetian, I. K. Morris, K. M. Snow, K. M. Smith, *J. Org. Chem.* **1989**, *54*, 5567−5574. [6d] J. W. Buchler, G. Herget, *Z. Naturforsch., B: Chem. Sci.* **1987**, *42*, 1003−1008.

[7] K.-I. Sugiura, T. Matsumoto, S. Ohkouchi, Y. Naitoh, T. Kawai, Y. Takai, K. Ushiroda, Y. Sakata, *Chem. Commun.* **1999**, 1957−1958.

[8] A. G. Hyslop, M. A. Kellett, P. M. Iovine, M. J. Therien, *J. Am. Chem. Soc.* **1998**, *120*, 12676−12677.

[9] M. J. Therien, International Patent, WO 02/104072 A2, United States of America, **2002**, p. 1−69.

[10] M. J. Hodgson, P. C. Healy, M. L. Williams, D. Arnold, *J. Chem. Soc., Dalton Trans.* **2002**, 4497−4504.

[11] R. D. Hartnell, A. J. Edwards, D. P. Arnold, *J. Porphyrins Phthalocyanines* **2002**, *6*, 695−707.

[12] D. P. Arnold, Y. Sakata, K.-I. Sugiura, E. I. Worthington, *Chem. Commun.* **1998**, 2331−2332.

[13] D. P. Arnold, P. C. Healy, M. J. Hodgson, M. L. Williams, *J. Organomet. Chem.* **2000**, *607*, 41−50.

[14] [14a] V. S.-Y. Lin, S. G. DiMagno, M. J. Therien, *Science* **1994**, *264*, 1105−1111. [14b] P. N. Taylor, J. Huuskonen, G. Rumbles, R. T. Aplin, E. Williams, H. L. Anderson, *Chem. Commun.*

 © 2004 Wiley-VCH Verlag GmbH & Co. KGaA, Weinheim

1998, 909−910. [14c] D. A. Shultz, K. P. Gwaltney, H. Lee, *J. Org. Chem.* **1998**, *63*, 4034−4038. [14d] K.-I. Sugiura, Y. Fujimoto, Y. Sakata, *Chem. Commun.* **2000**, 1105−1106.

[15] [15a] S. G. DiMagno, V. S. Y. Lin, M. J. Therien, *J. Org. Chem.* **1993**, *58*, 5983−5993. [15b] D. P. Arnold, R. C. Bott, H. Eldridge, F. M. Elms, G. Smith, M. Zojaji, *Aust. J. Chem.* **1997**, *50*, 495−503.

[16] S. G. DiMagno, V. S. Y. Lin, M. J. Therien, *J. Am. Chem. Soc.* **1993**, *115*, 2513−2515.

[17] S. Shanmugathasan, C. K. Johnson, C. Edwards, E. K. Matthews, D. Dolphin, R. W. Boyle, *J. Porphyrins Phthalocyanines* **2000**, *4*, 228−232.

[18] N. J. Wheate, J. G. Collins, *Coord. Chem. Rev.* **2003**, *241*, 133−145.

[19] [19a] R. Song, Y.-S. Kim, Y. S. Sohn, *J. Inorg. Biochem.* **2002**, 83−88. [19b] R. Song, Y.-S. Kim, C. O. Lee, Y. S. Sohn, *Tetrahedron Lett.* **2003**, *44*, 1537−1540. [19c] H. Brunner, K.-M. Schellerer, *Z. Naturforsch., B: Chem. Sci.* **2002**, 751−756.

[20] [20a] V. Chaleix, V. Sol, Y.-M. Huang, M. Guilloton, R. Granet, J. C. Blais, P. Krausz, *Eur. J. Org. Chem.* **2003**, 1486−1493. [20b] W. J. A. de Vree, M. C. Essers, J. F. Koster, W. Sluiter, *Cancer Res.* **1997**, *57*, 2555−2558. [20c] C. Sousa, C. Maziere, T. S. E. Melo, O. Vincent-Fiquet, J. C. Rogez, R. Santus, J. C. Maziere, *Cancer Letters* **1998**, *128*, 177−182.

[21] [21a] B. A. Markies, A. J. Canty, W. De Graaf, J. Boersma, M. D. Janssen, M. P. Hogerheide, W. A. A. Smeets, A. L. Spek, G. van Koten, *J. Organomet. Chem.* **1994**, *482*, 191−199. [21b] W. Tao, S. Nesbitt, R. F. Heck, *J. Org. Chem.* **1990**, *55*, 63−69.

[22] R. W. Boyle, C. K. Johnson, D. Dolphin, *J. Chem. Soc., Chem. Commun.* **1995**, 527−528.

[23] [23a] A. Bayler, A. J. Canty, P. G. Edwards, B. W. Skelton, A. H. White, *J. Chem. Soc., Dalton Trans.* **2000**, 3325−3330. [23b] A. Bayler, A. J. Canty, B. W. Skelton, A. H. White, *J. Organomet. Chem.* **2000**, *595*, 296−299. [23c] A. J. Canty, *Acc. Chem. Res.* **1992**, *25*, 83−90. [23d] N. J. Hovestad, J. L. Hoare, J. T. B. H. Jastrzebski, A. J. Canty, W. J. J. Smeets, A. L. Spek, G. van Koten, *Organometallics* **1999**, *18*, 2970−2980. [23e] D. Kruis, B. A. Markies, A. J. Canty, J. Boersma, G. van Koten, *J. Organomet. Chem.* **1997**, *532*, 235−242. [23f] B. A. Markies, A. J. Canty, W. de Graaf, J. Boersma, M. D. Janssen, M. P. Hogerheide, W. J. J. Smeets, A. L. Spek, G. van Koten, *J. Organomet. Chem.* **1994**, *482*, 191−199.

[24] [24a] M. O. Senge, W. W. Kalisch, I. Bischoff, *Chem. Eur. J.* **2000**, *6*, 2721−2738. [24b] M. O. Senge, X. Feng, *J. Chem. Soc., Perkin Trans. 1* **2000**, 3615−3621. [24c] X. Feng, I. Bischoff, M. O. Senge, *J. Org. Chem.* **2001**, *66*, 8693−8700. [24d] X. Feng, M. O. Senge, *J. Chem. Soc., Perkin 1* **2001**, 1030−1038.

[25] [25a] D. P. Arnold, L. J. Nitschinsk, *Tetrahedron Lett.* **1993**, *34*, 693−696. [25b] Y. Chen, X. P. Zhang, *J. Org. Chem.* **2003**, *68*, 4432−4438.

[26] R. D. Hartnell, D. P. Arnold, O. Locos, *unpublished results* **2003**.

[27] W. J. Cherwinski, B. F. G. Johnson, J. Lewis, *J. Chem. Soc., Dalton Trans.* **1974**, 1405−1409.

Received August 28, 2003
Early View Article
Published Online February 10, 2004

 © 2004 Wiley-VCH Verlag GmbH & Co. KGaA, Weinheim

Novel Layered Lead(II) Aminodiphosphonates with Carboxylate-Sulfonate and 1,3,5-Benzenetricarboxylate Ligands as Pendant Groups or Intercalated Species

Shao-Ming Ying[a] and Jiang-Gao Mao*[a]

Keywords: Hydrothermal synthesis / Layered compounds / Carboxylates / Sulfonates

The hydrothermal reaction of lead(II) carbonate with 3-sulfobenzoic acid, 3-HO_3S–C_6H_4–CO_2H, and isopropylimino-bis(methylenephosphonic acid), $(CH_3)_2CHN(CH_2PO_3H_2)_2$ (H_4L^1), gave a new layered lead(II) carboxylate-phosphonate, $Pb_7(3\text{-}O_3S\text{–}C_6H_4\text{–}CO_2)(L^1)_3(H_2O)_2\cdot 2H_2O$ (**1**), whereas the hydrothermal reaction of lead(II) carbonate with **1**, 3,5-benzenetricarboxylic acid (H_3BTC) and *N*-cyclohexylimino-bis(methylenephosphonic acid), $C_6H_{11}N(CH_2PO_3H_2)_2$ (H_4L^2), afforded a layered complex, $Pb_3(HL^2)(H_2L^2)(H_2BTC)(H_2O)\cdot H_3BTC\cdot H_2O$ (**2**). The structure of complex **1** contains <010> lead(II) carboxylate-phosphonate hybrid layers, with the sulfonate group of the carboxylate-sulfonate ligand as the pendant group. In complex **2**, the lead(II) ions are interconnected through bridging diphosphonate ligands, and results in the formation of a lead(II) diphosphonate slab, which are further interlinked via hydrogen bonds between non-coordinated phosphonate oxygen atoms to form a <001> layer. The doubly protonated H_2BTC anion is bidentately chelated to a lead(II) ion through a carboxylate group, whereas the neutral H_3BTC ligand is intercalated between two layers, forming hydrogen bonds with the non-coordinated carboxylate groups of the H_2BTC anion.
(© Wiley-VCH Verlag GmbH & Co. KGaA, 69451 Weinheim, Germany, 2004)

Introduction

Materials with open-framework and microporous structures are a class of very important compounds due to their traditional applications in catalysis, separations, sorbents, and ion exchange. Further, it is expected that these compounds could be used as hybrid composite materials in electro-optical and sensing applications.[1,2] Studies of metal phosphonates have shown that the use of bifunctional or multifunctional anionic units, such as diphosphonates, aminophosphonates or phosphonocarboxylates can lead to new materials with microporous or open-framework structures.[3–6] Recently, we have isolated a microporous Cd^{II} complex with the *N*,*N*′-bis(phosphonomethyl)-1,10-diaza-18-crown ether.[7] Several porous Zr^{IV} complexes with aza-crown ether functionalized phosphonic acids have been synthesized using phosphoric acid as the spacer.[8] The direct use of two types of ligands in the preparation, such as a phosphonic acid and a carboxylic acid, has been found to be another effective method for the exploration of hybrid open-frameworks; however, such reports are still rare.[2,9,10] A 3-D open-framework tin(II) phosphonopropionate oxalate and a layered tin(II) methylphosphonate oxalate have previously been reported by Cheetham and co-workers,[9] and a microporous zinc(II) complex of phosphonopropionic acid and 1,3,5-benzene-tricarboxylic acid (H_3BTC) has been isolated, in which the tricarboxylate moiety remains non-coordinated and is also severely disordered.[2] Recently, we reported two novel porous lead(II) carboxylate-phosphonates in which both types of ligands act as multidentate metal linkers.[10] We have initiated a research program in order to study the intercalation chemistry of the layered lead(II) diphosphonates with various types carboxylic acids and sulfonic acids. Such hybrids may have good proton conductivities, as well as ion-exchange properties, due to the presence of protons with greater acidity. The hydrothermal reaction of lead(II) carbonate with 3-sulfobenzoic acid, 3-$HO_3S-C_6H_4-CO_2H$, and isopropylimino-bis(methylenephosphonic acid), $(CH_3)_2CHN(CH_2PO_3H_2)_2$ (H_4L^1), gave a new layered lead(II) carboxylate-phosphonate, $Pb_7(3\text{-}O_3S-C_6H_4-CO_2)(L^1)_3(H_2O)_2\cdot 2H_2O$ (**1**), whereas the hydrothermal reaction of lead(II) carbonate with **1**, 3,5-benzenetricarboxylic acid (H_3BTC) and *N*-cyclohexylimino-bis(methylenephosphonic acid), $C_6H_{11}N(CH_2PO_3H_2)_2$ (H_4L^2), afforded a layered complex, $Pb_3(HL^2)(H_2L^2)(H_2BTC)(H_2O)\cdot H_3BTC\cdot H_2O$ (**2**). Herein, we report on the syntheses, characterizations and crystal structures of these compounds.

Results and Discussion

The hydrothermal reaction of lead(II) carbonate with 3-sulfobenzoic acid, 3-$HO_3S-C_6H_4-CO_2H$, and isopro-

[a] State Key Laboratory of Structural Chemistry, Fujian Institute of Research on the Structure of Matter, Chinese Academy of Sciences,
Fuzhou 350002, P. R. China
Fax: (internat.) +86-591-3714946
E-mail: mjg@ms.fjirsm.ac.cn

 © 2004 Wiley-VCH Verlag GmbH & Co. KGaA, Weinheim DOI: 10.1002/ejic.200300607

pylimino-bis(methylenephosphonic acid), $(CH_3)_2CHN(CH_2PO_3H_2)_2$ (H_4L^1), gave a new layered lead(II) carboxylatephosphonate, $Pb_7(3\text{-}O_3S{-}C_6H_4{-}CO_2)(L^1)_3(H_2O)_2{\cdot}2H_2O$ (**1**), whereas the hydrothermal reaction of lead(II) carbonate with **1**, 1,3,5-benzenetricarboxylic acid (H_3BTC) and *N*-cyclohexylimino-bis(methylenephosphonic acid), $C_6H_{11}N(CH_2PO_3H_2)_2$ (H_4L^2), afforded a layered complex, $Pb_3(HL^2)(H_2L^2)(H_2BTC)(H_2O){\cdot}H_3BTC{\cdot}H_2O$ (**2**). We believe that many more new inorganic-organic hybrid materials will be developed using the synthetic technique of mixing two different types of ligands.

$Pb_7(3\text{-}O_3S{-}C_6H_4{-}CO_2)(L^1)_3(H_2O)_2{\cdot}2H_2O$ (**1**) is the first structurally characterized metal phosphonate-sulfonate hybrid. It is composed of seven lead(II) ions, three fully deprotonated L^1 ligands, one $3\text{-}O_3S{-}C_6H_4{-}CO_2$ dianion, two aqua ligands and two lattice water molecules. As shown in Figure 1, Pb1 is six-coordinate and is bonded to a tridentate chelating L^1 anion (N3, O52 and O62), two phosphonate oxygen atoms from two other L^1 anions (O13 and O12), as well as to a carboxylate oxygen atom from a carboxylate-sulfonate ligand. Pb1 exhibits a distorted octahedral coordination geometry. Pb2 is four-coordinate and is bonded to three phosphonate oxygen atoms from three L^1 anions and one carboxylate oxygen atom from a sulfonate ligand. The coordination geometry around Pb2 can be described as a ψ-PbO_4 trigonal bipyramid, with the fifth coordination site occupied by the lone pair of electrons from the Pb^{II} ion. Pb3 is five-coordinate and is bonded to a tridentate chelating L^1 anion (N2, O32, O42) and two phosphonate oxygen atoms from two other L^1 anions; it exhibits a ψ-PbO_5 octahedral geometry, with the sixth coordination site occupied by the lone pair of electrons from the Pb^{II} ion. Pb4, Pb5 and Pb6 have a coordination geometry similar to that exhibited by Pb3; they are all five-coordinate and are bonded to a bidentate chelating L^1 ligand (O51 and O52 for Pb4; O31 and O43 for Pb5; O52 and O63 for Pb6) and three phosphonate oxygen atoms from three other L^1 anions. Pb7 is four-coordinate and is bonded to two phosphonate oxygen atoms from two L^1 anions and two aqua ligands, and exhibits a ψ-PbO_4 trigonal bipyramidal geometry with the fifth coordination site occupied by the lone pair of electrons

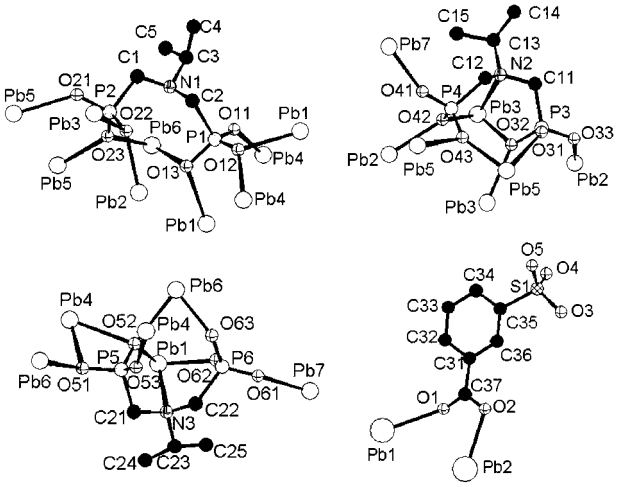

Figure 2. The coordination modes of L^2 and sulfo-carboxylate ligands in complex **1**

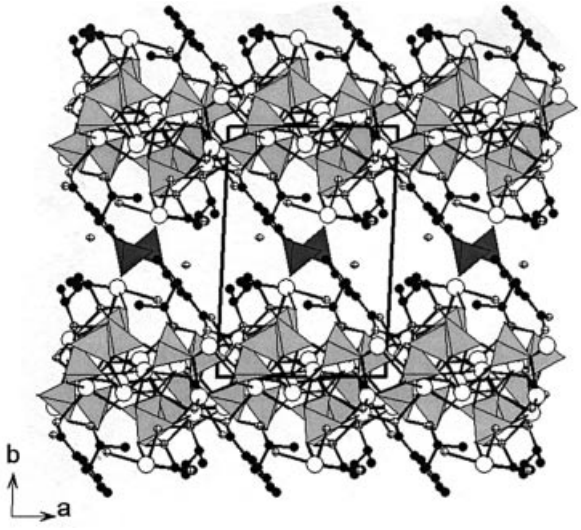

Figure 3. View of the structure of complex **1** down the c-axis. The $C{-}PO_3$ and $C{-}SO_3$ tetrahedra are shaded in light and dark gray, respectively. Pb, N, O and C atoms are represented by open, octanded, crossed and black circles, respectively.

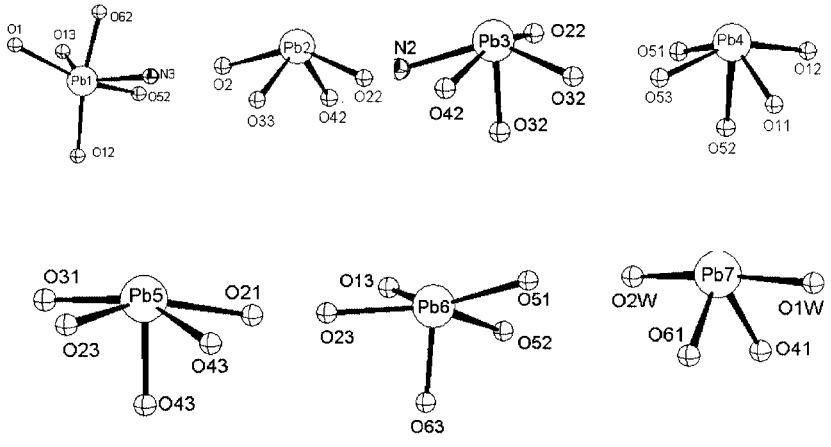

Figure 1. The coordination geometries around the lead(II) ions in complex **1**

 © 2004 Wiley-VCH Verlag GmbH & Co. KGaA, Weinheim

Table 1. Bond lengths [Å] and angles [°] for complex **1** (symmetry transformations used to generate equivalent atoms: #1 $-x+2, -y+2, -z$; #2 $-x+2, -y+2, -z+1$; #3 $-x+1, -y+2, -z$; #4 $x-1, y, z$; #5 $-x+1, -y+2, -z+1$; #6 $x, 1+y, z$)

Pb(1)−O(62)	2.39(2)	Pb(1)−O(52)	2.450(15)
Pb(1)−O(13)	2.495(15)	Pb(1)−O(12)#1	2.619(15)
Pb(1)−N(3)	2.643(19)	Pb(1)−O(1)	2.712(15)
Pb(2)−O(33)	2.372(16)	Pb(2)−O(22)	2.512(16)
Pb(2)−O(42)#2	2.556(16)	Pb(2)−O(2)	2.647(16)
Pb(3)−O(32)	2.339(15)	Pb(3)−O(42)	2.369(15)
Pb(3)−O(32)#2	2.577(15)	Pb(3)−N(2)	2.618(17)
Pb(3)−O(22)	2.651(14)	Pb(4)−O(53)#3	2.409(17)
Pb(4)−O(11)	2.427(16)	Pb(4)−O(12)#1	2.530(15)
Pb(4)−O(51)	2.574(18)	Pb(4)−O(52)	2.747(18)
Pb(5)−O(43)#4	2.391(16)	Pb(5)−O(23)	2.471(15)
Pb(5)−O(31)#4	2.537(15)	Pb(5)−O(21)#5	2.567(14)
Pb(5)−O(43)#2	2.664(15)	Pb(6)−O(63)	2.30(2)
Pb(6)−O(23)	2.621(16)	Pb(6)−O(13)	2.669(14)
Pb(6)−O(51)#3	2.680(17)	Pb(6)−O(52)	2.710(16)
Pb(7)−O(61)#2	2.287(18)	Pb(7)−O(41)	2.335(16)
Pb(7)−O(1 W)	2.56(2)	Pb(7)−O(2 W)	2.65(3)
Hydrogen bonds			
O(3 W)···O(1 W)	2.80(3)	O(4 W)···O(1 W)	2.85(5)
O(4 W)···O(4)#6	2.80(3)		
O(62)−Pb(1)−O(52)	92.5(7)	O(62)−Pb(1)−O(13)	76.1(7)
O(52)−Pb(1)−O(13)	74.0(5)	O(62)−Pb(1)−O(12)#1	165.2(7)
O(52)−Pb(1)−O(12)#1	73.0(5)	O(13)−Pb(1)−O(12)#1	96.2(5)
O(62)−Pb(1)−N(3)	72.4(6)	O(52)−Pb(1)−N(3)	70.8(6)
O(13)−Pb(1)−N(3)	130.8(5)	O(12)#1−Pb(1)−N(3)	104.9(6)
O(62)−Pb(1)−O(1)	74.8(6)	O(52)−Pb(1)−O(1)	157.2(5)
O(13)−Pb(1)−O(1)	84.4(5)	O(12)#1−Pb(1)−O(1)	117.5(5)
N(3)−Pb(1)−O(1)	121.1(5)	O(33)−Pb(2)−O(22)	80.1(5)
O(33)−Pb(2)−O(42)#2	103.8(5)	O(22)−Pb(2)−O(42)#2	84.7(5)
O(33)−Pb(2)−O(2)	78.9(6)	O(22)−Pb(2)−O(2)	146.9(5)
O(42)#2−Pb(2)−O(2)	75.9(6)	O(32)−Pb(3)−O(42)	79.1(6)
O(32)−Pb(3)−O(32)#2	80.4(5)	O(42)−Pb(3)−O(32)#2	77.9(5)
O(32)−Pb(3)−N(2)	71.2(5)	O(42)−Pb(3)−N(2)	72.9(5)
O(32)#2−Pb(3)−N(2)	142.3(5)	O(32)−Pb(3)−O(22)	74.3(5)
O(42)−Pb(3)−O(22)	151.6(5)	O(32)#2−Pb(3)−O(22)	106.9(4)
N(2)−Pb(3)−O(22)	89.0(5)	O(53)#3−Pb(4)−O(11)	81.8(7)
O(53)#3−Pb(4)−O(12)#1	150.8(6)	O(11)−Pb(4)−O(12)#1	83.5(6)
O(53)#3−Pb(4)−O(51)	83.0(6)	O(11)−Pb(4)−O(51)	130.5(6)
O(12)#1−Pb(4)−O(51)	87.6(6)	O(53)#3−Pb(4)−O(52)	82.4(6)
O(11)−Pb(4)−O(52)	76.1(5)	O(12)#1−Pb(4)−O(52)	69.7(5)
O(51)−Pb(4)−O(52)	55.2(5)	O(43)#4−Pb(5)−O(23)	87.2(5)
O(43)#4−Pb(5)−O(31)#4	82.9(5)	O(23)−Pb(5)−O(31)#4	76.5(5)
O(43)#4−Pb(5)−O(21)#5	76.8(5)	O(23)−Pb(5)−O(21)#5	148.7(5)
O(31)#4−Pb(5)−O(21)#5	126.7(5)	O(43)#4−Pb(5)−O(43)#2	79.9(5)
O(23)−Pb(5)−O(43)#2	76.7(5)	O(31)#4−Pb(5)−O(43)#2	148.7(4)
O(21)#5−Pb(5)−O(43)#2	74.2(5)	O(63)−Pb(6)−O(23)	82.7(7)
O(63)−Pb(6)−O(13)	95.0(7)	O(23)−Pb(6)−O(13)	77.3(5)
O(63)−Pb(6)−O(51)#3	109.3(8)	O(23)−Pb(6)−O(51)#3	139.4(6)
O(13)−Pb(6)−O(51)#3	136.6(5)	O(63)−Pb(6)−O(52)	78.1(7)
O(23)−Pb(6)−O(52)	137.5(5)	O(13)−Pb(6)−O(52)	67.1(5)
O(51)#3−Pb(6)−O(52)	83.0(5)	O(61)#2−Pb(7)−O(41)	80.2(6)
O(61)#2−Pb(7)−O(1 W)	83.1(7)	O(41)−Pb(7)−O(1 W)	84.5(7)
O(61)#2−Pb(7)−O(2 W)	99.4(10)	O(41)−Pb(7)−O(2 W)	83.8(9)
O(1 W)−Pb(7)−O(2 W)	167.4(10)		

from the Pb^{II} ion. The Pb−O distances are in the range 2.287(18) to 2.747(18) Å, and the Pb−N distances range from 2.618(17) to 2.643(19) Å; these distances are similar to those reported for other Pb^{II} aminodiphosphonates.[10−12] The three L^1 anions in complex **1** adopt three different types of coordination modes (see Figure 2). The L^1 anion that contains P1 and P2 chelates Pb6 in a bidentate fashion, and also forms bridges with eight other Pb^{II} ions. Its amine group remains non-coordinated and four phosphonate oxygen atoms act as μ_2 metal linkers. The diphosphonate anion that contains P3 and P4 chelates Pb3 in a tridentate manner (N2, O32 and O42), chelates Pb5 in a bidentate fashion (O31, O43), and forms bridges with five other lead(II) ions. The three phosphonate oxygen atoms are

 © 2004 Wiley-VCH Verlag GmbH & Co. KGaA, Weinheim

bidentate. The third L^1 anion is bonded to Pb1 in a tridentate fashion, chelates Pb4 and Pb6 bidentately and also forms bridges with three other lead(II) ions. O52 acts as a μ_3 metal linker, and only O51 is a μ_2 bridging group. This kind of coordination mode has not been reported before. The carboxylate-sulfonate anion is bidentate, forming bridges with two Pb^{II} ions through the carboxylate group. The sulfonate group remains non-coordinated. Based on the requirements of charge balance, both types of ligands have been completely deprotonated.

The interconnection of the above Pb^{II} polyhedra through the diphosphonate L^1 anions, as well as through the carboxylate-sulfonate ligands, results in a <010> hybrid layer. The interlayer distance is approximately 14.9 Å. The sulfonate group acts as a pendant group, hanging between two layers (Figure 3). The lattice water molecules are also located in the middle of the interlayer space, forming hydrogen bonds with the non-coordinated sulfonate groups, as well as with the aqua ligands (Table 1). The O(4 W)···O(4) (symmetry code: x, $1 + y$, z) contact distance is only 2.60(4) Å, indicating that the hydrogen bond between the lattice water molecule and the sulfonate group is very strong.

$Pb_3(HL^2)(H_2L^2)(H_2BTC)(H_2O)\cdot H_3BTC\cdot H_2O$ (**2**) also has a layered structure and contains 1,3,5-benzene-tricarboxylate ligands that behave both as a pendant group and as an intercalated species. As shown in Figure 4, Pb1 is four-coordinate and is bonded to four phosphonate oxygen atoms from three diphosphonate ligands (1 H_2L^2 and 2 HL^2). Its coordination geometry can be described as a ψ-PbO_4 square pyramid with the fifth coordination site occupied by the lone pair of electrons. Pb2 is five-coordinate and is bonded to a bidentate carboxylate group of the H_2BTC anion and three phosphonate oxygen atoms from three diphosphonate ligands (1 H_2L^2 and 2 HL^2). Its coordination geometry can be described as a ψ-PbO_5 octahedron with the sixth site occupied by the lone pair of electrons. The Pb(2)−O(6) bond of 2.766(10) Å is significantly longer than the Pb(2)−O(5) bond [2.584(13) Å]. Pb3 is five-coordinate and is bonded to four phosphonate oxygen atoms from three diphosphonate ligands (1 H_2L^2 and 2 HL^2) and an aqua ligand. It has a ψ-PbO_5 octahedral geometry that is similar to that of Pb2. The Pb−O distances range from 2.407(12) to 2.767(13) Å; these distances are similar to those in complex **1** and those observed in other lead(II) phosphonates,[10−12] as well as to those reported for the lead(II) complex with H_3BTC.[13]

The HL^2 anion that contains P2 and P3 is heptadentate; it chelates Pb1 in a bidentate manner (O21 and O32) and forms bridges with five other lead(II) ions. The O23 and O32 atoms are bidentate metal linkers. Both phosphonate groups are fully deprotonated, but the amine group remains protonated. The H_2L^2 anion containing P4 and P5 is tetradentate; it chelates Pb3 in a bidentate fashion (O41 and O53) and also connects with two other Pb^{II} ions. The O42 atom is a bidentate metal linker. The P4 and P5 phosphonate groups are tridentate and unidentate, respectively. Based on the P−O distance and the charge balance, the P5 phosphonate group should be 1H-protonated, so does the amine group, hence the doubly protonated diphosphonate anion carries two negative charges. The H_2BTC anion in complex **2** is bidentately chelated to Pb2 (O5 and O6) and the other two carboxylate groups remain non-coordinated, while all three carboxylate groups of the neutral H_3BTC ligand in complex **2** are non-coordinated (Figure 4). This is unlike the situation in porous lead(II) phosphonate-carboxylates in which all three carboxylate groups are involved in metal coordination.[10]

The interconnecting lead(II) ions, via bridging amino diphosphonate ligands, leads to the formation of a slab along the *a*-axis. Such slabs are further interlinked via strong hydrogen bonds between the non-coordinated phosphonate oxygen atoms to form a <001> layer (Figure 5). The O(33)···O(52) distance (symmetry code: $-x$, $y - 1$, $-z$) is 2.509(17) Å (Table 2). The non-coordinated dicarboxylate moiety of H_2BTC is orientated towards the interlayer space, and is able to form hydrogen bonds with the carboxylate groups of the neutral H_3BTC ligand (Table 2, Figure 6).

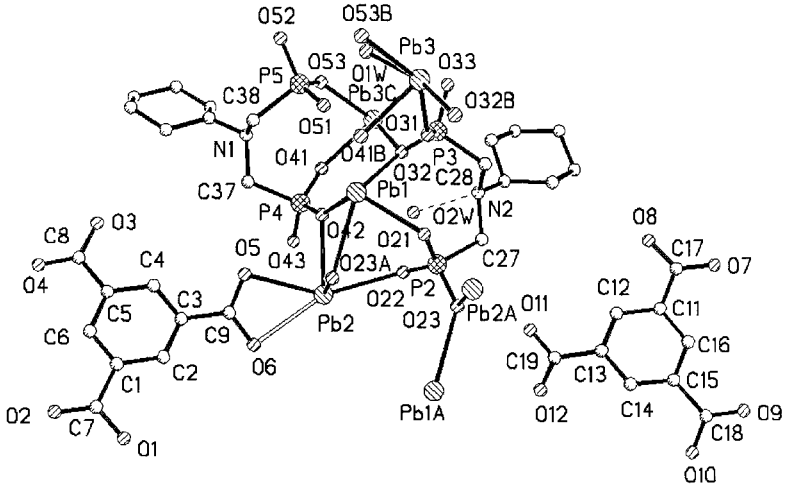

Figure 4. The asymmetric unit of complex **2**. The elongated Pb-O bond is represented by an open line; hydrogen bond is drawn as a dotted line; symmetry codes for the generated atoms: a) $-x$, $-y$, $-z$; b) $x + 1$, y, z; c) $-1 + x$, y, z

 © 2004 Wiley-VCH Verlag GmbH & Co. KGaA, Weinheim

Such hydrogen bonding creates a six-membered ring that consists of two carboxylate groups, one from H_3BTC and one from H_2BTC (Figure 6). The aqua ligands are located at the cavities within the 2-D layer, and form hydrogen bonds with the non-coordinated phosphonate oxygen atoms, as well as with the amine groups (Table 2). The interlayer space of about 21.4 Å is much larger than that of complex **1**, mainly due to the intercalation of the H_3BTC molecules.

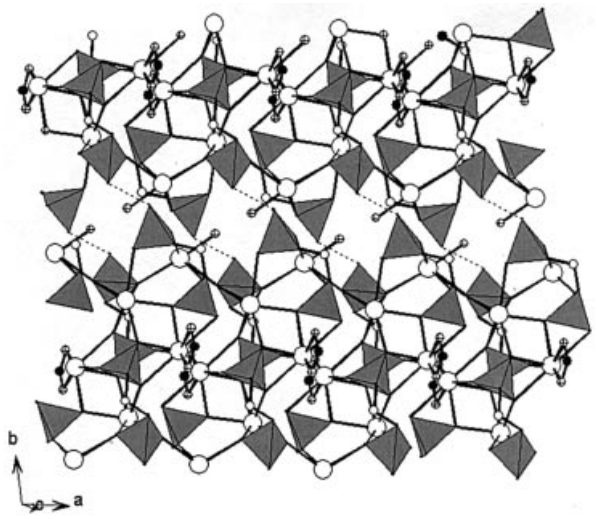

Figure 5. A <001> layer formed by the interconnection of lead(II) ion by bridging diphosphonate ligands in complex **2**; the pendant H_2BTC anions have been omitted for clarity; the $C-PO_3$ tetrahedra are shaded in gray, and Pb, N, O and C atoms are represented by open, octanded, crossed and black circles, respectively

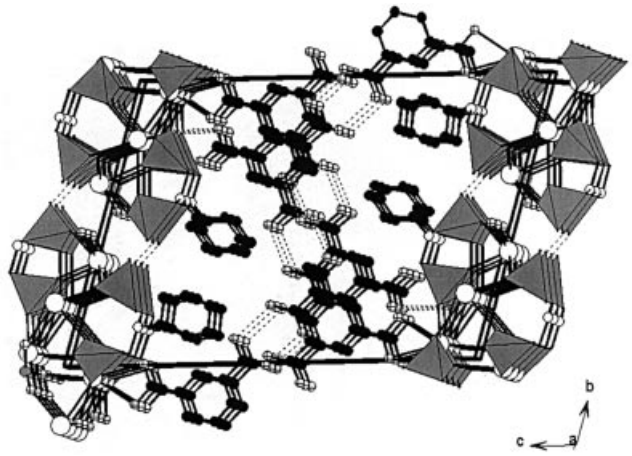

Figure 6. View of the structure of complex **2** down the *a*-axis; the $C-PO_3$ tetrahedra are shaded in gray, and Pb, N, O and C atoms are represented by open, octanded, crossed and black circles, respectively; hydrogen bonds are drawn as dotted lines.

The XRD powder patterns for complexes **1** and **2** were collected on a Philips X′Pert-MPD diffractometer using graphite-monochromated Cu-K_α radiation in the angular range $2\theta = 5-70°$. The powder patterns of **1** and **2** match those calculated from their single-crystal structure data, thus both compounds exist as a single phase.

The IR spectra of complexes **1** and **2** show the asymmetric and symmetric vibrations of the carboxyl group at 1531

Table 2. Bond lengths [Å] and angles [°] for complex **2** (symmetry transformations used to generate equivalent atoms: #1 $-x, -y, -z$; #2 $x+1, y, z$; #3 $x-1, -1-y, -z$; #4 $x-1, y, z$; #5 $x, y, z-1$; #6 $x-1, y-1, z-1$; #7 $-x-1, -y, -z$)

Pb(1)−O(21)	2.429(12)	Pb(1)−O(42)	2.495(13)
Pb(1)−O(32)	2.605(12)	Pb(1)−O(23)#1	2.688(11)
Pb(2)−O(23)#1	2.418(11)	Pb(2)−O(42)	2.517(13)
Pb(2)−O(5)	2.584(13)	Pb(2)−O(22)	2.628(12)
Pb(3)−O(41)#2	2.316(12)	Pb(3)−O(1 W)	2.345(13)
Pb(3)−O(53)#2	2.407(12)	Pb(3)−O(31)	2.687(11)
Pb(3)−O(32)#2	2.744(11)		
Hydrogen bonds			
O(1 W)···O(51)	2.601(22)	O(1 W)···O(33)#3	2.803(19)
O(33)···O(52)#3	2.509(17)	O(2 W)···N(2)	2.858(19)
O(2 W)···O(31)#4	2.735(17)	O(2 W)···O(22)	2.769(16)
O(1)···O(7)#5	2.695(18)	O(2)···O(8)#5	2.625(19)
O(3)···O(9)#6	2.613(18)	O(4)···O(10)#6	2.657(19)
O(11)···O(43)#7	2.613(19)		
O(21)−Pb(1)−O(42)	99.6(5)	O(21)−Pb(1)−O(32)	74.9(4)
O(42)−Pb(1)−O(32)	77.7(4)	O(21)−Pb(1)−O(23)#1	74.7(4)
O(42)−Pb(1)−O(23)#1	70.4(4)	O(32)−Pb(1)−O(23)#1	130.8(3)
O(23)#1−Pb(2)−O(42)	74.6(4)	O(23)#1−Pb(2)−O(5)	82.8(4)
O(42)−Pb(2)−O(5)	74.0(4)	O(23)#1−Pb(2)−O(22)	82.2(4)
O(42)−Pb(2)−O(22)	75.6(4)	O(5)−Pb(2)−O(22)	148.7(4)
O(41)#2−Pb(3)−O(1 W)	77.0(5)	O(41)#2−Pb(3)−O(53)#2	80.5(4)
O(1 W)−Pb(3)−O(53)#2	74.0(5)	O(41)#2−Pb(3)−O(31)	71.4(4)
O(1 W)−Pb(3)−O(31)	76.3(5)	O(53)#2−Pb(3)−O(31)	142.8(4)
O(41)#2−Pb(3)−O(32)#2	89.3(4)	O(1 W)−Pb(3)−O(32)#2	157.5(5)
O(53)#2−Pb(3)−O(32)#2	86.3(4)	O(31)−Pb(3)−O(32)#2	116.5(3)

 © 2004 Wiley-VCH Verlag GmbH & Co. KGaA, Weinheim

and 1419 cm^{-1} for complex **1**, and 1576 and 1454 cm^{-1} for complex **2**, respectively. The differences in $\nu_{as}(COO)$ and $\nu_s(COO)$ are much larger than 95 cm^{-1} in both complexes, indicating the bidentate coordination mode for the carboxylate groups.[14] Complex **2** also exhibits a strong absorption band at 1722 cm^{-1} assigned to the non-coordinating carboxylate groups (COOH). The vibrations of the phosphonic group groups can be seen in the region 900−1100 cm^{-1}.[7] The broad bands at 3406 cm^{-1} (for complex **1**) and 3428 cm^{-1} (for complex **2**) indicate the presence of the water molecules in both compounds. Those frequencies which are characteristic of the fundamental and split $\nu_{as}(S-O)$ stretching modes for complex **1** appear in the range 1200−1000 cm^{-1}.

The TGA curves of complex **1** exhibit two steps corresponding to weight losses. The first step indicates the loss of two lattice water molecules and two aqua ligands, which starts at 55 °C and ends at 210 °C. The observed weight loss of 2.8% is in good agreement with the theoretical weight loss (2.94%). The second weight loss step starts at 375 °C and continues up to 800 °C, and indicates the loss of the aminodiphosphonate and carboxylate-sulfonate ligands. The final products are $Pb_2P_2O_7$ and $PbSO_4$ (in a molar ratio of about 3:1), based on the X-ray power pattern. The total weight loss of 14.2% is similar to that calculated (15.65%). The TGA diagram for complex **2** reveals three main steps corresponding to weight losses. The first step involves the loss of the lattice water molecule and the aqua ligand, which starts at about 90 °C and ends at about 282 °C. The observed weight loss of 2.4% is in good agreement with the calculated value (2.2%). The second step, which covers a temperature range from 282 °C to 345 °C, corresponds to the loss of intercalated H_3BTC. The third step starts at 345 °C and ends at 710 °C, and involves two overlapping processes: the loss of one water molecule formed by the condensation of the hydrogen phosphonate groups, and the loss of the diphosphonate ligand and the H_2BTC anion. The final products are $Pb_2P_2O_7$ and $Pb(PO_3)_2$ (in a molar ratio of 1:1), based on the XRD powder pattern. The total weight loss is 41.3% is similar to that calculated (42.1%).

Conclusion

In summary, two novel layered lead(II) carboxylate-phosphonate hybrids were obtained by the hydrothermal reactions of lead(II) carbonate with amino-diphosphonic acid and 3-sulfobenzoic acid (or, 1,3,5-benzenetricarboxylic acid). In both compounds, the 2-D inorganic-organic layer is formed by the lead(II) ions that are interconnected through the diphosphonate ligands. The sulfonate group of the carboxylate-sulfonate ligand in complex **1** acts as a pendant group between the 2-D layers, whereas the 1,3,5-benzenetricarboxylate ligands in complex **2** act both as a pendant ligand and as the intercalated species between two metal-diphosphonate layers. It is believed that a wide range of novel open-frameworks and microporous materials can be developed using this ligand-hybrid technique.

Experimental Section

Materials and Methods: All chemicals were obtained from commercial sources and used without further purification. Elemental analyses were performed on a Vario EL III elemental analyzer. Thermogravimetric analyses were carried out with a TGA/SBTA851 unit at a heating rate of 15 °C/ min under a nitrogen atmosphere. IR spectra were recorded on a Magna 750 FT-IR spectrometer as KBr pellets in the 4000−400 cm^{-1} range. ^1H and ^{31}P NMR spectra were recorded on a Varian Unity 500 NMR in D_2O. H_3PO_4 (85%) was used as ^{31}P standard reference. The XRD powder patterns were collected on a Philips X′Pert-MPD diffractometer using graphite-monochromated Cu-K_α radiation in the angular range $2\theta = 5-70°$ with a step size of 0.02° and a counting time of 3 seconds per step.

Preparation of H_4L^1 and H_4L^2: H_4L^1 and H_4L^2 were prepared by a Mannich type reaction according to procedures described previously.[11]

Isopropylamine (100 mmol, 5.911 g) was mixed with hydrochloric acid (16.0 cm^3), deionized water (20 mL) and phosphorous acid (400 mmol, 32.8 g). The mixture was allowed to reflux at 120 °C for 1 h, paraformaldehyde (300 mmol, 9 g) was then added in small portions over a period of 1 h, and the mixture was refluxed for one additional hour. Removal of solvents afforded 16.8 g of a white powder of H_4L^1 (yield 68.1%). Its purity was confirmed by NMR spectroscopic measurements and elemental analysis. ^{31}P NMR spectroscopy shows a single peak at 9.50 ppm. ^1H NMR: $\delta = 1.37$ (CH_3, d, 6 H, $J_{H-H} = 5.5$ Hz), 3.57 ($N-CH_2-PO_3$, d, 4 H, $J_{H-P} = 12.5$ Hz), 4.16 (Me_2-CH-N, sept., 1 H) ppm. Elemental analysis for H_4L^1, $C_5H_{15}NO_6P_2$ (247.12): calcd. C 24.86, H 6.62, N 4.88; found C 24.29, H 6.07, N 5.67.

H_4L^2 was obtained in a yield of 77.5% by a Mannich type reaction using cyclohexylamine (100 mmol, 9.92 g), hydrochloric acid (16.0 cm^3), deionized water (20.0 mL), phosphorous acid (400 mmol, 32.8 g) and paraformaldehyde (300 mmol, 9.0 g), in a similar method to that of H_4L^1. ^{31}P NMR spectroscopy shows a single peak at 8.75 ppm. ^1H NMR: $\delta = 1.16$, 1.36, 1.67, 1.91 and 2.06 (for five CH_2- groups of cyclohexyl, d), 1.51 (CH- of cyclohexyl, t, 1 H), 3.51 ($N-CH_2-PO_3$, d, 4 H, $J_{H,P} = 13.0$ Hz) ppm. Elemental analysis for H_4L^2, $C_8H_{19}NO_6P_2$ (288.54): calcd. C 33.24, H 6.81, N 4.59; found C 33.45, H 6.62, N 5.33.

$Pb_7(3\text{-}O_3S-C_6H_4-CO_2)(L^1)_3(H_2O)_2\cdot 2H_2O$ (1) and $Pb_3(HL^2)(H_2L^2)(H_2BTC)(H_2O)\cdot H_3BTC\cdot H_2O$ (2): A mixture of $PbCO_3$ (1.0 mmol, 0.267 g), H_4L^1 (0.5 mmol, 0.124 g), 3-sulfobenzoic acid monosodium salt (0.5 mmol, 0.112 g) and deionized water (10 mL) was sealed into a bomb equipped with a Teflon liner (20 mL), and then heated at 180 °C for 5 days. Colorless prismatic crystals of complex **1** were recovered in ca. 71% yield based on Pb. Elemental analysis for **1**, $C_{22}H_{45}N_3O_{27}P_6Pb_7S$ (2451.82): calcd. C 10.67, H 1.38, N 1.82; found C 10.77, H 1.84, N 1.71%. IR data (KBr, cm^{-1}): $\tilde{\nu}$ = 3406 (s), 2962 (m), 2933 (m), 2875 (m), 2798 (m), 2407 (m), 1732 (m), 1651 (m), 1587 (m), 1531 (s), 1419 (s), 1383 (s), 1302 (m), 1200 (m), 1084 (vs), 1032 (vs), 966 (vs), 839 (m), 752 (m), 679 (m), 588 (s), 557 (s), 507 (m), 480 (m).

A mixture of $PbCO_3$ (1.0 mmol, 0.267 g), H_4L^2 (0.5 mmol, 0.144 g), 1,3,5-benzenetricarboxylic acid (0.5 mmol, 0.105 g) and deionized water (10 mL) was sealed into a bomb equipped with a Teflon liner (20 mL), and then heated at 180 °C for 5 days. Prismatic colorless crystals of complex **2** were recovered in ca. 60% yield based on Pb. Elemental analysis for **2**, $C_{34}H_{48}N_2O_{26}P_4Pb_3$

 © 2004 Wiley-VCH Verlag GmbH & Co. KGaA, Weinheim

(1646.19): calcd. C 23.93, H 2.42, N 1.62; found C 24.79, H 2.92, N 1.70%. IR data (KBr, cm^{-1}): $\tilde{\nu}$ = 3428 (s), 3021 (s), 2979 (s), 2940 (s), 2862 (s), 2648 (s), 2542 (s), 1878 (m), 1722 (vs), 1614 (s), 1576 (s), 1454 (s), 1381 (s), 1281 (vs), 1111 (vs), 1051 (vs), 987 (s), 933 (s), 777 (m), 744 (s), 692 (s), 621 (m), 526 (m), 442 (m).

Crystal Structure Determination: Single crystals of complexes **1** and **2** were mounted on a Siemens Smart CCD diffractometer equipped with a graphite-monochromated Mo-K_α radiation (λ = 0.71073 Å). Intensity data were collected by the narrow frame method at 293 K. The data sets were corrected for Lorentz polarization, as well as for absorption, by ψ scan technique. Both structures were solved by direct methods and refined by full-matrix least-squares fitting on F^2 by SHELX-97.[15] All non-hydrogen atoms, except for N(2), C(2), C(3), C(14), C(15), C(22) and C(23) in complex **1**, and C(23) in complex **2,** were refined with anisotropic thermal parameters. Those atoms refined with isotropic thermal parameters were non-positive if refined anisotropically; this was caused by the problem resulting from correcting the absorption due to the presence of very heavy Pb atoms. The final difference Fourier maps showed featureless residual peaks of 3.16 e·$Å^{-3}$ (for complex **1**, 0.91 Å from Pb(2) atom) and 3.56 e $Å^{-3}$ (for complex **2**, 1.02 Å from Pb(1) atom), respectively. All hydrogen atoms were located at geometrically calculated positions. The hydrogen atoms for the water molecules were not included in the refinements. The large standard deviations for the bond lengths in complex **1** are due to the poor quality of the single crystals, which is very common for metal phosphonates; efforts were made to isolate better quality crystals, however they were unsuccessful. Crystallographic data and structural refinements are summarized in Table 3. Important bond lengths and angles are listed in Tables 1 and 2 for complexes **1** and **2**, respectively.

Table 3. Crystal data and structure refinement for complexes **1** and **2**
($R1 = \Sigma||F_o| - |F_c||/\Sigma|F_o|$, $wR2 = \{\Sigma[w(F_o^2 - F_c^2)^2]/\Sigma[w(F_o^2)^2]\}^{1/2}$)

Compound	**1**	**2**
Empirical formula	$C_{22}H_{45}N_3O_{27}P_6Pb_7S$	$C_{34}H_{48}N_2O_{26}P_4Pb_3$
Molecular mass	2451.82	1646.19
Crystal system	triclinic	triclinic
Space group	$P\bar{1}$ (No.2)	$P\bar{1}$ (No. 2)
a (Å)	10.1796(4)	7.1392(1)
b (Å)	14.9014(6)	15.5844(1)
c (Å)	16.4192(6)	21.3980(1)
α/°	80.314(1)	105.658(1)
β/°	77.032(1)	90.757(1)
γ/°	85.037(1)	96.214(1)
V/Å^3	2389.43(16)	2276.65(4)
Z	2	2
D_c/g·cm^{-3}	3.408	2.401
μ(Mo-K_α)/mm^{-1}	24.902	11.301
F (000)	2188	1560
Reflections collected	12523	11815
Unique reflections	8397 (R_{int} = 0.081)	7925 (R_{int} = 0.0495)
Observed data [$I > 2\sigma(I)$]	6427	6850
No. of parameters refined	560	618
Goodness-of-fit on F^2	1.083	1.195
$R1$, $wR2$ [$I > 2\sigma(I)$]	0.0634, 0.1459	0.0627, 0.1532
$R1$, $wR2$ (all data)	0.0925, 0.1656	0.0746, 0.1600

CCDC-217199 and -217200 contain the supplementary crystallographic data for this paper. These data can be obtained free of charge at www.ccdc.cam.ac.uk/conts/retrieving.html [or from the Cambridge Crystallographic Data Centre, 12 Union Road, Cambridge CB2 1EZ, UK; Fax: (internat.) +44-1223-336-033; E-mail: deposit@ccdc.cam.ac.uk].

Acknowledgments

This work was supported by the National Natural Science Foundation of China (No. 20371047), the Introduction of Overseas Elitists Program by the Chinese Academy of Sciences and the Scientific Research Foundation for the Returned Overseas Chinese Scholars, State Education Ministry.

[1] A. K. Cheetham, G. Ferey, T. Loiseau, *Angew. Chem. Int. Ed.* **1999**, *38*, 3268−3292.
[2] J. Zhu, X. Bu, P. Feng, G. D. Stucky, *J. Am. Chem. Soc.* **2000**, *122*, 11563−11564.
[3] A. Distler, L. Lohse, S. C. Sevov, *J. Chem. Soc., Dalton Trans.* **1999**, 1805−1812; V. Soghomonian, Q. Chen, R. C. Haushalter, J. Zubieta, *Angew. Chem. Int. Ed. Engl.* **1995**, *34*, 223−226.
[4] S. Drumel, P. Janvier, D. Deniaud, B. Bujoli, *J. Chem. Soc., Chem. Commun.* **1995**, 1051−1052; U. Costantino, M. Nocchetti, R. Vivani, *J. Am. Chem. Soc.* **2002**, *124*, 8428−8434; S. O. H. Gutschke, D. J. Price, A. K. Powell, P. T. Wood, *Angew. Chem. Int. Ed.* **1999**, *38*, 1088−1090; E. Galdecka, Z. Galdecki, P. Gawryszewska, J. Legendziewicz, *New J. Chem.* **2000**, *24*, 387−391; L.-M. Zheng, P. Yin, X.-Q. Xin, *Inorg. Chem.* **2002**, *41*, 4084−4086.
[5] N. Stock, S. A. Frey, G. D. Stucky, A. K. Cheetham, *J. Chem. Soc., Dalton Trans.* **2000**, 4292−4296; S. Ayyappan, G. D. Delgado, A. K. Cheetham, G. Ferey, C. N. R. Rao, *J. Chem. Soc., Dalton Trans.* **1999**, 2905−2907; F. Fredoueil, M. Evain, D. Massiot, M. Bujoli-Doeuff, P. Janvier, A. Clearfield, B. Bujoli, *J. Chem. Soc., Dalton Trans.* **2002**, 1508−1512; S. Drumel, M. Bujolidoeuff, P. Janvier, B. Bujoli, *New J. Chem.* **1995**, *19*, 239−242.
[6] A. Distler, S. C. Sevov, *Chem. Commun.* **1998**, 959−960; S. J. Hartman, E. Todorov, C. Cruz, S. C. Sevov, *Chem. Commun.* **2000**, 1213−1214; J.-G. Mao, Z. Wang, A. Clearfield, *Inorg. Chem.* **2002**, *41*, 6106−6111; R. Vivani, U. Costantino, M. Nocchetti, *J. Mater. Chem.* **2002**, *12*, 3254−3260.
[7] J.-G. Mao, Z. Wang, A. Clearfield, *Inorg. Chem.* **2002**, *41*, 3713−3720.
[8] B. Zhang, A. Clearfield, *J. Am. Chem. Soc.* **1997**, *119*, 2751−2752; A. Clearfield, D. M. Poojary, B. Zhang, B. Zhao, A. Derecskei-Kovacs, *Chem. Mater.* **2000**, *12*, 2745−2752.
[9] N. Stock, G. D. Stucky, A. K. Cheetham, *Chem. Commun.* **2000**, 2277−2278; B. Adair, S. Natarajan, A. K. Cheetham, *J. Mater. Chem.* **1998**, *8*, 1477−1479.
[10] J.-L. Song, J.-G. Mao, Y.-Q. Sun, A. Clearfield, *Eur. J. Inorg. Chem.*, **2003**, 4218.
[11] J.-G. Mao, Z. Wang, A. Clearfield, *Inorg. Chem.* **2002**, *41*, 2334−2340; J.-G. Mao, Z. Wang, A. Clearfield, *J. Chem. Soc., Dalton Trans.* **2002**, 4541−4546.
[12] A. Cabeza, M. A. G. Aranda, S. Bruque, A. Clearfield, *J. Mater. Chem.* **1999**, *9*, 571−578; Z.-M. Sun, J.-G. Mao, Y.-Q. Sun, H.-Y. Zeng, A. Clearfield, *New J. Chem.* **2003**, *27*, 1326−1330.
[13] M. R. S. J. Foreman, T. Gelbrich, M. B. Hursthouse, M. J. Plater, *Inorg. Chem. Commun.* **2000**, *3*, 234−238.
[14] R. Cao, Q. Shi, D. Sun, M. Hong, W. Bi, Y. Zhao, *Inorg. Chem.* **2002**, *41*, 6161−6168.
[15] G. M. Sheldrick, *SHELXTL*, *Crystallographic Software Package*, version 5.1, Bruker-AXS, Madison, WI, **1998**.

Received August 29, 2003
Early View Article
Published Online February 16, 2004

 © 2004 Wiley-VCH Verlag GmbH & Co. KGaA, Weinheim

The Construction of P−O/P−N Ligands on Platinum and Palladium[‡]

Paola Bergamini,*[a] Valerio Bertolasi,[a] and Federico Milani[a]

Keywords: Template synthesis / Ligand design / P ligands / Platinum / Palladium

A variety of diphenyldiphosphinites have been prepared in a very stable form as Pt^{II} or Pd^{II} complexes by adding diols to a solution containing *cis*-[$MCl_2(PPh_2Cl)_2$] (M = Pt or Pd) preformed in situ from *cis*-[MCl_2(1,5-COD)] (M = Pt; M = Pd) and PPh_2Cl. This synthetic pathway can be used for diphosphinites derived from aliphatic 1,2 and 1,3 diols and also from the aromatic catechol. Besides the P–O bond, it is also shown here that the P–N bond can also be formed via nucleophilic attack of an amine group on coordinated PPh_2Cl in the presence of a base resulting in some AMPP and BAMP complexes of Pt^{II} and Pd^{II}. The X-ray crystal structures of the [*cis*-1,2-cyclohexanediyl bis(diphenylphosphinite)]platinum dichloride, of the AMPP palladium complex from (1*R*,2*S*)-(−)-norephedrine and of the BAMP palladium complex [*P*,*P*′-diphenyl-1,2-cyclohexanediylbis(imino)bisphosphane]-palladium dichloride have been determined. The chemical and optical stabilities of many complexes in solution have been monitored by ^{31}P NMR spectroscopy.
(© Wiley-VCH Verlag GmbH & Co. KGaA, 69451 Weinheim, Germany, 2004)

Introduction

P-donor chiral ligands are widely used in metal-based asymmetric catalysis, because of the intrinsic ability of phosphorus to favour the substrate coordination, to stabilise intermediates of various processes and to provide selectivity through steric effects.[2] So far the most significant success is still represented by the asymmetric hydrogenation of prochiral olefins using Rh^{I} complexes of chiral diphosphanes.[3]

Research in this field has been developed since the early seventies and a large variety of chiral diphosphanes have been prepared and tested. Although great success has been achieved in the enantioselective conversion of some substrates, a few problems still remain unsolved:

i) Rh or Ru/chiral diphosphane catalysts are very efficient but their activity is restricted to a narrow group of transformations because only highly functionalised substrates (e.g. amino acids precursors) undergo coordination, the primary step of the process.

ii) The synthesis of chiral diphosphanes is often expensive and time consuming and requires delicate and awkward reactants.[4]

For these reasons the design and preparation of new ligands for chiral catalysts is still a lively topic and groups of phosphorated compounds other than diphosphanes have been taken into consideration. In particular chiral diphosphinites,[5] AMPP ("aminophosphanes-phosphinites") and BAMP ["bis(amino)phosphanes"][6] have been recently considered particularly for their synthetic accessibility based on the reaction of chlorophosphanes with diols, amino-ols and diamines (Scheme 1).

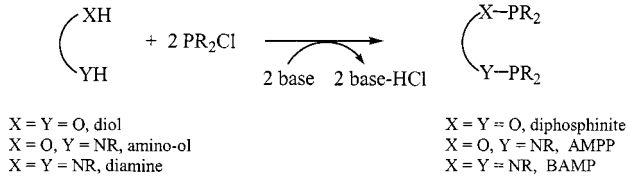

Scheme 1

The wide variety of asymmetric precursors belonging to these groups, especially from the natural chiral pool, enormously extends the number of easily accessible structural variations on the basic structure of these ligands.

Although the classical preparation of 1,2-(diphenyl)diphosphinites from diols and chlorodiphenylphosphane has been described in some papers as an easy clean process,[7] some problems have been raised[8] and in our hands this reaction gave poor and variable results because of the tendency of both the reagent chlorodiphenylphosphane and of the reaction products to undergo oxidative processes giving a variety of P^{V} species. On the other hand we noticed that 1,2-diphenylphosphinites are greatly stabilised by coordination to metal ions and therefore we have recently proposed an alternative synthetic pathway where a few examples of diphosphinite ligands were built up in the coordination sphere of Pt^{II} or Pd^{II} acting as templates.[1]

[‡] Part 2. Part 1: Ref.[1].

[a] Dipartimento di Chimica e Centro di Strutturistica Diffrattometrica dell'Università di Ferrara,
Via L. Borsari 46, 44100 Ferrara, Italy
Fax: (internat.) + 39-0532-240709
E-mail: bgp@unife.it

With the aim to demonstrate the generality of the above metal template method, in this paper we extend its application to the preparation of different kinds of coordinated diphosphinites, and also show that the P−N bond can be formed by nucleophilic substitution on coordinated chlorophosphane by an amine group leading to aminophosphane-phosphinites (AMPP) or bis(amino)phosphanes (BAMP).

Results and Discussion

i) Preparation of Coordinated Diphosphinites

In our previous paper we showed that 1,2- and 2,3-bis(diphenylphosphinito)butanediols and isopropyl bis(diphenylphosphinito)tartrate can be prepared as coordinated ligands on Pt and Pd by a two-step process, starting from $[MCl_2(1,5\text{-COD})]$ (M = Pt, Pd), whose reaction with chlorodiphenylphosphane gave the intermediate complexes *cis*-$[MCl_2(PPh_2Cl)_2]$ (**1a**, M = Pt; **1b,** M = Pd), characterised in situ by ^{31}P NMR spectroscopy and converted into the relative diphenylphosphinite complex by addition of the corresponding diols in the presence of a base (Scheme 2).[1]

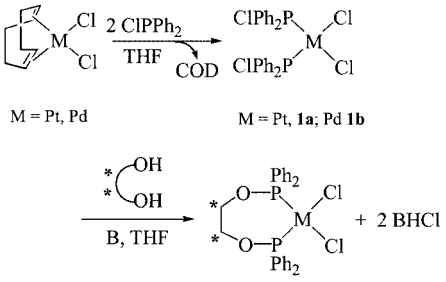

Scheme 2

In this paper we show that this template synthesis can be extended to other ligands: in particular we prepared the diphenylphosphinite from *cis*-1,2-cyclohexanediol in the platinum-coordinated form. This ligand is the optically inactive form derived from (1*R*,2*S*)-cyclohexanediol, and is the diastereomeric form of the optically active (1*R*,2*R*) or (1*S*,2*S*)-cyclohexane-1,2-diyl bis(diphenylphosphinite), which have already been tested in asymmetric catalysis.[9]

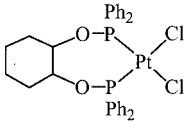

2a

Complex **2a** co-precipitated with py·HCl from the reaction mixture in THF and was purified by extraction with water and dichloromethane.

Due to the equivalence of the two phosphorus atoms, the ^{31}P NMR of **2a** shows a broad single signal at δ = 87.9 ppm, with satellites and $^1J_{Pt,P}$ = 3995 Hz, a typical value for a phosphorus atom *trans* to a chloride atom. The broadness of the signal is due to the fast equilibrium between two conformational forms where one P atom occupies the equatorial position while the other one is axial and vice versa.

A variable-temperature experiment showed, at low temperature (− 55 °C), two distinct signals with satellites (δ_{P_A} = 74.8 ppm, $^1J_{Pt,P_A}$ = 3834 Hz, δ_{P_B} = 98.7 ppm $^1J_{Pt,P_B}$ = 4149 Hz), which coalesce at 25 °C into the above described broad singlet, which becomes sharper at +55 °C.

Solutions of **2a** in pure chloroform or in a $CHCl_3$/acetone mixture, examined by ^{31}P NMR, did not show any sign of decomposition even in the presence of oxygen and/or water after five days.

A recrystallisation of **2a** at room temperature from dichloromethane and diethyl ether gave crystals for X-ray crystal structure determination.

In order to demonstrate also that aromatic bis(diphenylphosphinites) can be formed on Pt, complex **3a** derived from catechol was prepared. The functionalisation of catechol can be proposed as a simple model for more complicated and more relevant aromatic systems like calixarenes.[10]

The ^{31}P spectrum of **3a** in $CHCl_3$ is a sharp singlet with satellites at δ = 93.4 ppm ($^1J_{Pt,P}$ = 4043 Hz); when the solution was treated with an excess of soluble CN^-, the spectrum changed into a singlet at δ = 114.1 ppm, due to the free ligand **3**. The following addition of $[PdCl_2(1,5\text{-COD})]$ to this solution gave the Pd analogue **3b** in situ, showing a singlet shifted to δ = 122 ppm. This chemical shift trend, with the Pd complex downfield and the Pt complex upfield, relative to the free ligand, has been found in general for the diphosphinites we have considered here and for the previously reported analogues.[1]

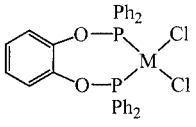

M = Pt, **3a**
M = Pd, **3b**

Using the optically active (*R*,*R*)-(−)-2,4-pentanediol, which gave the optically active Pt and Pd complexes **4a** and **4b**, we succeeded in demonstrating that it is possible to obtain eight-membered rings by this route.

The platinum complex **4a** has been obtained from $[PtMe_2(1,5\text{-COD}]$ by treatment with PPh_2Cl to give the dimethyl intermediate, which is then treated with (*R*,*R*)-(−)-2,4-pentanediol, giving the immediate precipitation of **4a**.

The reaction occurs via nucleophilic attack of both the OH groups on the phosphorus atoms. The outgoing HCl causes the protonolysis of the two Pt−Me groups giving rise to the final dichloro complex. The use of the dimethyl intermediate is very convenient because it avoids the use of the base and produces volatile CH_4 as the only side product.

 © 2004 Wiley-VCH Verlag GmbH & Co. KGaA, Weinheim

Because of the instability of the corresponding precursor [$PdMe_2$(1,5-COD)], the corresponding palladium complex **4b** was obtained from [$PdCl_2$(1,5-COD)].

The complete characterisation of **4a** and **4b** is reported in the Exp. Sect. It is worth noting that for **4a** the value of $^1J_{Pt,P}$ = 4176 Hz, is more than 100 Hz larger than the corresponding coupling constant in seven-membered ring complexes.

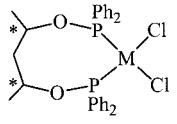

M = Pt, **4a**
M = Pd, **4b**

ii) Preparation of Coordinated AMPP

After the preparation of a series of bis(diphenylphosphinites) we reasoned that X−P bonds other than O−P could be conveniently built by nucleophilic substitution of chloride on the coordinated phosphorus centre.

Due to the interest in the catalysis of both aminophosphane-phosphinites (AMPP) and bis(amino)phosphanes (BAMP),[6] we tried to use amino groups (NH_2 or NHR) as nucleophiles in order to form N−P bonds.

By adding 1,2-amino-ols to a solution containing the preformed intermediates **1a** or **1b**, we succeeded in obtaining some examples of coordinated AMPP (Scheme 3).

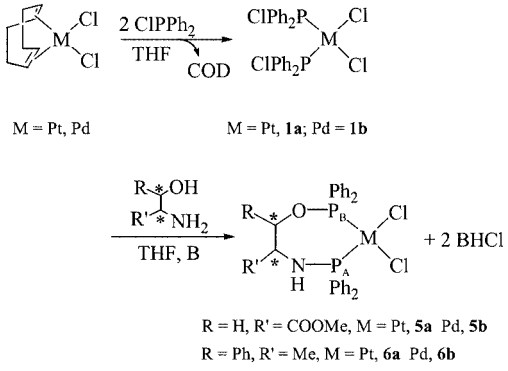

M = Pt, Pd M = Pt, **1a**; Pd = **1b**

R = H, R' = COOMe, M = Pt, **5a** Pd, **5b**
R = Ph, R' = Me, M = Pt, **6a** Pd, **6b**

Scheme 3

By following the reactions using ^{31}P NMR spectroscopy, we noticed that the formation of the O−P bond is the first step occurring in a few minutes, followed by the slow making of N−P, with ring closure.

In this case it is necessary to assist the reaction using NEt_3, which is a stronger base than the $-NH_2$ group, in order to avoid the protonation of the amine group, which will make it unreactive.

We chose the methyl ester of the natural occurring amino acid L-serine, bearing an OH group in the β position, for this reaction and we obtained the Pt complex **5a** and the Pd analogue **5b**.

The ^{31}P NMR spectrum of **5a** shows two doublets of doublets with satellites at δ = 43.5 ppm (P_A, $^1J_{Pt,P_A}$ = 3887 Hz; $^2J_{P_BP_A}$ = 12 Hz) and 94.7 ppm (P_B, $^1J_{Pt,P_B}$ = 4075 Hz; $^2J_{P_AP_B}$ = 12 Hz) in the ranges expected for aminophosphane and phosphinites respectively.

The palladium complex **5b** presents two doublets at δ = 67.8 ppm (P_A, $^2J_{P_BP_A}$ = 32 Hz) and 124.9 ppm (P_B, $^2J_{P_AP_B}$ = 32 Hz) both at lower fields with respect to the corresponding peaks in **5a**.

Another example of optically active AMPP complexes, **6a** and **6b**, have been obtained via template synthesis using the optically active amino alcohol (1*R*,2*S*)-(−)-norephedrine.

In ^{31}P NMR, **6a** is characterised by two doublets with satellites, due to the aminophosphinic moiety 45.9 ppm (P_A, $^1J_{Pt,P_A}$ = 3917 Hz and $^2J_{P_BP_A}$ = 11 Hz) and the phosphinitic group at 93.8 (P_B, $^1J_{Pt,P_B}$ = 4104 Hz and $^2J_{P_AP_B}$ = 11 Hz) ppm. ^{1}H NMR spectroscopy is very useful for checking the identity of the product and its purity (see Exp. Sect. for complete assignments): in particular at δ = 2.0 ppm a singlet is visible with satellites ($^3J_{PtH}$ = 55 Hz) belonging to the nitrogen bonded proton.

The palladium complex **6b**, obtained by treatment of **1b** with (1*R*,2*S*)-(−)-norephedrine and NEt_3 in benzene, shows two doublets at δ = 70.5 ppm (P_A, $^2J_{P_BP_A}$ = 35 Hz) and 123.6 ppm (P_B, $^2J_{P_AP_B}$ = 35 Hz). Its X-ray crystal structure has been determined (see further).

In these reactions the use of NEt_3 as a base affects the purity of the products, always contaminated by NEt_3HCl, which therefore require purification procedures.

In order to avoid salt contamination we reasoned that the use of a heterogeneous base could be convenient. With this aim, we tried to add solid $NaHCO_3$ to the reaction mixture in THF, together with a water sequestrating agent (e.g. anhydrous Na_2SO_4). Under these conditions, the reaction between **1b** and (1*R*,2*S*)-(−)-norephedrine gave complex **7b**, where the O−P bond is formed while the second-coordinated PPh_2Cl has been hydrolysed to PPh_2OH by the equivalent of water resulting from the reaction of $NaHCO_3$ with HCl. This indicates that the dehydrating agents (Na_2SO_4 or molecular sieves) that we tried, in order to avoid this hydrolytic process, are not efficient in comparison with the competing hydrolysis of the homogeneous coordinated PPh_2Cl.

Complex **7b** contains a coordinated monodentate aminophosphinite (AMP), a type of ligand mentioned previously for its ability to give P/N six-membered chelate rings of interest in catalysis.[6]

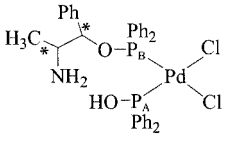

7b

The reaction of preformed **1a** with the aminoalcohol L-prolinol bearing a secondary amino group gave complex **8a**.

 © 2004 Wiley-VCH Verlag GmbH & Co. KGaA, Weinheim

The NMR spectroscopic data of **8a** are consistent with the data previously reported for the same complex obtained by the classical synthetic procedure from the preformed ligand.[11]

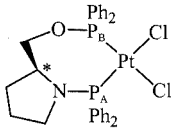

8a

iii) Preparation of Coordinated BAMP

Finally we have considered the possibility of extending the metal template method to the preparation of BAMP ligands.

The most interesting member of this group is the *N*,*N*′-bis(diphenylphosphanyl)-1,2-diaminocyclohexane ($DACHP_2$), whose palladium complex has recently been described as an efficient tool for the resolution of racemic amino acids.[12]

The platinum complex has been obtained from [$PtMe_2$(1,5-COD] by treatment with PPh_2Cl to give the dimethyl intermediate, which is then treated with (1*R*,2*R*)-*trans*-diaminocyclohexane, resulting in the immediate precipitation of **9a**. The corresponding palladium complex **9b** was obtained starting from [$PdCl_2$(1,5-COD)] (see Exp. Sect.). We determined the X-ray crystal structure of **9b**, recrystallised from dichloromethane and diethyl ether.

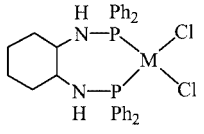

M = Pt, **9a**
M = Pd, **9b**

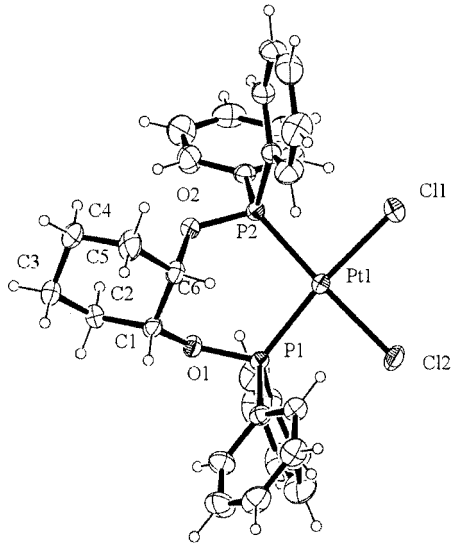

Figure 1. ORTEP view of compound **2a** showing the thermal ellipsoids at 30% level of probability

iv) X-ray Crystal Structures of 2a, 6b and 9b

By the slow diffusion of Et_2O into CH_2Cl_2 solutions, crystals suitable for structure diffractometric analysis were obtained for one member of each group: diphosphinites (**2a**), AMPP (**6b**) and BAMP (**9b**).

An ORTEP[13] view of each structure (**2a**, **6b** and **9b**) is given in Figure 1−3 and a selection of bond lengths and angles is reported in Table 1. All the complexes present a slightly distorted square-planar geometry with the metal centre bonded to two chloride and two phosphorus atoms belonging to the ligand. The seven-membered chelate rings resemble twisted half-chair conformations.

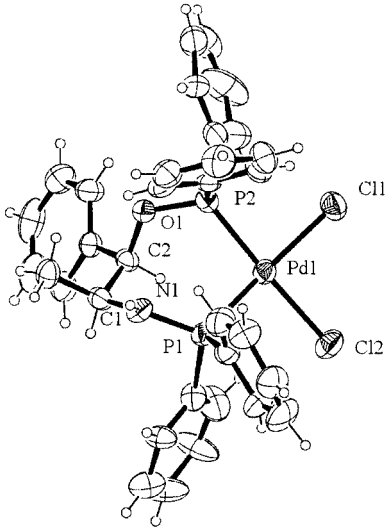

Figure 2. ORTEP view of compound **6b** showing the thermal ellipsoids at 30% level of probability

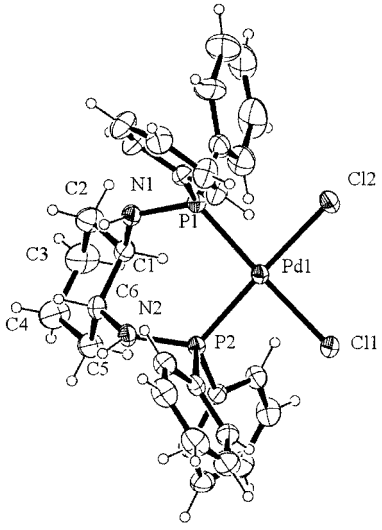

Figure 3. ORTEP view of compound **9b** showing the thermal ellipsoids at 30% level of probability

The molecules of complex **2a**, in the crystals, display C1 and C6 atoms in configurations (*R*) and (*S*), respectively. Since the solution does not show optical activity, it is evident that this compound crystallizes with separation of the

 © 2004 Wiley-VCH Verlag GmbH & Co. KGaA, Weinheim

Table 1. Selected bond lengths (Å) and angles (°) (* values of the four independent molecules of the asymmetric unit)

Compound	**2a**	**6b***	**9b**
Pt1/Pd1−Cl1	2.364(2)	2.358(3), 2.359(3), 2.358(3), 2.358(3)	2.383(1)
Pt1/Pd1−Cl2	2.359(1)	2.359(3), 2.345(2), 2.345(3), 2.357(3)	2.367(1)
Pt1/Pd1−P1	2.223(1)	2.286(2), 2.261(2), 2.248(5), 2.239(2)	2.238(1)
Pt1/Pd1−P2	2.218(1)	2.230(2), 2.252(2), 2.244(2), 2.222(2)	2.263(1)
P1−O1	1.605(3)		
P2−O2	1.597(4)		
P2−O1		1.609(6), 1.598(6), 1.595(7), 1.614(7)	
P1−N1		1.694(8), 1.663(8), 1.675(8), 1.670(8)	1.663(3)
P2−N2			1.656(3)
O1−C1	1.452(4)		
O1−C2		1.442(9), 1.463(9), 1.422(12), 1.440(10)	
O2−C6	1.456(5)		
N1−C1		1.463(12), 1.485(12), 1.499(13), 1.450(12)	1.462(6)
N2−C6			1.462(5)
C1−C2		1.521(12), 1.546(13), 1.531(17), 1.536(12)	
C1−C6	1.511(7)		1.521(6)
Cl1−Pt1/Pd1−Cl2	88.19(4)	91.0(1), 91.0(1), 91.4(1), 89.6(1)	91.13(3)
Cl1−Pt1/Pd1−P1	171.67(4)	169.6(1), 169.6(1), 169.6(1), 163.5(1)	174.34(3)
Cl1−Pt1/Pd1−P2	88.82(4)	86.9(1), 88.5(1), 89.1(1), 88.5(1)	86.24(3)
Cl2−Pt1/Pd1−P1	85.59(4)	88.1(1), 86.1(1), 85.2(1), 90.1(1)	86.35(4)
Cl2−Pt1/Pd1−P2	177.01(3)	176.4(1), 176.4(1), 175.2(1), 173.6(1)	176.87(3)
P1−Pt1/Pd1−P2	97.41(4)	93.5(1), 95.0(1), 95.1(1), 93.5(1)	96.12(3)
Pt1/Pd1−P1−O1	118.5(1)		
Pt1/Pd1−P2−O1		116.9(2), 114.6(2), 115.3(3), 119.5(3)	
Pt1/Pd1−P2−O2	118.1(1)		
Pt1/Pd1−P1−N1		116.9(3), 116.1(3), 115.7(3), 118.1(3)	120.0(1)
Pt1/Pd1−P2−N2			123.2(1)

enantiomers. The C1 and C2 atoms in complex **6b** are in configurations (*S*) and (*R*), respectively. In complex **9b** both C1 and C6 atoms display the (*R*) configuration. The molecules in the crystals are coupled by means of two N2−H···Cl1 and N1−H···Cl2 hydrogen bonds: N2···Cl1(x + 1, y, z) = 3.236(3) Å and N1···Cl2(x+ 1, y, z) = 3.348(3) Å.

Conclusions

The preparation of a variety of Pt^{II} and Pd^{II} complexes through the metal template procedure proves that this new method can be proposed as an easy and accessible general synthetic pathway to P−O and P−N containing ligands, which are obtained in a convenient metal-stabilized form.

Experimental Section

All reactions and manipulations were routinely performed under dry nitrogen by using standard Schlenk-tube techniques. Tetrahydrofuran was bi-distilled over $LiAlH_4$, while diethyl ether and benzene were purified by distillation over sodium/benzophenone. Pyridine and triethylamine were distilled and stored over KOH. $CDCl_3$, used as solvent for NMR spectra, was dried with molecular sieves (4 Å).

PPh_2Cl (d = 1.23 g·mL^{-1}) was purified by distillation under nitrogen, stored at −15 °C and checked by ^{31}P NMR spectroscopy before use. All the other solvents and chemicals were reagent grade and, unless otherwise stated, were used as received from commercial suppliers. ^1H and ^{31}P NMR spectra (always ^1H decoupled) were recorded with a Bruker AC200 spectrometer operating at 200.13 MHz (^1H) and 81.01 MHz (^{31}P). Peak positions are given in ppm relative to tetramethylsilane (^1H) and to external 85% H_3PO_4 (^{31}P). Elemental analyses (C,H,N) were performed using a Carlo Erba model 1106 elemental analyser. Optical rotations were obtained with a Perkin−Elmer 241 at 25 °C.

Literature methods were used for the preparation of [$PtCl_2$(1,5-COD)],[14] [$PtMe_2$(1,5-COD)][15] and [$PdCl_2$(1,5-COD)].[16]

Synthesis of 2a: PPh_2Cl (144 μL, 0.802 mmol) was added dropwise, whilst stirring at room temperature, to a suspension of [$PtCl_2$(1,5-COD)] (0.150 g, 0.401 mmol) in THF (25 mL) placed in a Schlenk flask. The immediate formation of the dichloro diphosphane complex **1a** was unambiguously confirmed by ^{31}P NMR spectroscopy (δ =73.4 ppm, $^1J_{Pt,P}$ = 4069 Hz [1]).
The addition of pyridine (65 μL, 0.802 mmol) and *cis*-1,2-cyclohexanediol (0.047 g, 0.401 mmol) gave a cloudy mixture, which persisted whilst stirring at room temperature for 18 h. The white precipitate, composed of **2a** and pyridinium chloride, was then filtered, re-dissolved in CH_2Cl_2 and the solution was washed with 10 mL of water three times, dried with Na_2SO_4 and then taken to dryness under vacuum to give pure **2a** as a white solid. Yield 0.170 g (56%). $C_{30}H_{30}Cl_2O_2P_2Pt$ (750.5): calcd. C 48.01, H 4.03; found C 47.95, H 4.31. ^1H NMR (200 MHz, $CDCl_3$, 25 °C): δ = 1.2−1.5 (m, 4 H, CH), 1.6−1.9 (m, 4 H, CH), 4.5 (m, 2 H, CH−O), 7.3−7.9 (m, 20 H, Ph) ppm. ^{31}P NMR (81.01 MHz, $CDCl_3$, 25 °C): δ = 87.9 ppm (br. s, $^1J_{Pt,P}$ = 3995 Hz). Recrystallisation of crude **2a** from dichloromethane/ethanol gave crystals suitable for diffractometric study.

Synthesis of 3a: Complex **3a** was prepared in the same way as above using catechol (0.044 g, 0.401 mmol). After 18 h a small amount of

 © 2004 Wiley-VCH Verlag GmbH & Co. KGaA, Weinheim

pyridinium chloride was filtered off, while the product remained in solution. The product was confirmed by ^{31}P NMR spectroscopic inspection. The solution was taken to dryness under vacuum and the oily residue was redissolved in CH_2Cl_2 (1 mL). Pure **3a**, as a white solid, was precipitated by addition of Et_2O (15 mL) and separated by filtration; yield 0.270 g (90%). $C_{30}H_{24}Cl_2O_2P_2Pt$ (744.4): calcd. C 48.40, H 3.25; found C 47.91, H 3.35. ^1H NMR (200 MHz, $CDCl_3$, 25 °C): δ = 6.1 (m, 2 H, CH), 6.85 (m, 2 H, CH), 7.4−8.1 (m, 20 H, Ph) ppm. ^{31}P NMR (81.01 MHz, $CDCl_3$, 25 °C): δ = 93.7 (s, $^1J_{Pt,P}$ = 4043 Hz) ppm.

Synthesis of 4a: [$PtMe_2$(1,5-COD)] (0.100 g, 0.300 mmol) was dissolved in bi-distilled THF (20 mL) and PPh_2Cl (108 μL, 0.600 mmol) was added. After checking the complete formation of the Pt containing intermediate [$PtMe_2(PPh_2Cl)_2$] by ^{31}P NMR spectroscopy (δ =100.3 ppm, $^1J_{Pt,P}$ = 1915 Hz), the solution was treated with (2*R*,4*R*)-(−)-pentanediol (0.031 g, 0.300 mmol). The initially clear solution was kept at room temperature for three days and during this time the progressive precipitation of a white solid was observed. Later the pure solid product was filtered away and dried under vacuum over P_2O_5. Yield 0.140 g (63%). $C_{29}H_{30}Cl_2O_2P_2Pt$ (738.5): calcd. C 47.17, H 4.09; found C 46.88, H 4.24. ^1H NMR (200 MHz, $CDCl_3$, 25 °C): δ = 0.8 (d, $^3J_{H,H}$ = 7.3 Hz, 6 H, CH_3), 1.8 (t, $^3J_{H,H}$ = 7.3 Hz, 2 H, CH_2), 4.35 (m, 2 H, CH), 7.3−8.1 (m, 20 H, Ph) ppm. ^{31}P NMR (81.01 MHz, $CDCl_3$, 25 °C): δ = 91.8 ppm (s, $^1J_{Pt,P}$ = 4176 Hz). $[\alpha]_D^{25}$ = −42.6 (*c* = 0.55, CH_2Cl_2).

Synthesis of 4b: PPh_2Cl (126 μL, 0.700 mmol) was added to [$PdCl_2$(1,5-COD)] (0.100 g, 0.350 mmol) suspended in 25 mL of dry THF: the solution turned yellow and the presence of **1b** was checked by ^{31}P NMR spectroscopy (δ =96 ppm, broad singlet) .[1] At this point pyridine (57 μL) and (2*R*,4*R*)-(−)-2,4-pentanediol (0.036 g, 0.350 mmol) were added to the solution which became cloudy. After stirring for 24 h the solid (**4b** and pyHCl) was filtered, redissolved in 1 mL of CH_2Cl_2 and extracted three times with water (10 mL). The organic phase was taken to dryness, resulting in **4b** as a yellow powder. Yield 0.100 g (44%). $C_{29}H_{30}Cl_2O_2P_2Pd$ (649.8): calcd. C 53.60, H 4.65; found C 53.80, H 4.73. ^1H NMR (200 MHz, $CDCl_3$, 25 °C): δ = 0.75 (d, $^3J_{H,H}$ = 7.3 Hz, 6 H, CH_3), 1.8 (t, $^3J_{H,H}$ = 7.3 Hz, 2 H, CH_2), 4.35 (m, 2 H, CH), 7.5−8.2 (m, 20 H, Ph) ppm. ^{31}P NMR (81.01 MHz, $CDCl_3$, 25 °C): δ = 121.8 (s) ppm. $[\alpha]_D^{25}$ = −61.4 (*c* = 0.5, CH_2Cl_2).

Synthesis of 5a: PPh_2Cl (96 μL, 0.535 mmol) was added dropwise whilst stirring at room temperature to a suspension of [$PtCl_2$(1,5-COD)] (0.100 g, 0.267 mmol) in THF (25 mL), resulting in **1a**. The addition of triethylamine (0.802 mmol) and L-serin methyl ester hydrochloride (0.042 g, 0.267 mmol) gave a cloudy mixture due to the formation of partially insoluble NEt_3 hydrochloride.
After 2 hours, another 50 mL of THF was added and the solution was stirred for a further two hours. The white precipitate was then filtered away and the solution, containing the impure product was taken to dryness. The residue was dissolved in CH_2Cl_2 and water was added in order to eliminate NEt_3HCl. The organic layer was finally dried with Na_2SO_4 and then taken to dryness under vacuum to give pure **5a** as a white solid. Yield 0.090 g (45%) $C_{28}H_{27}Cl_2NO_3P_2Pt$ (753.5): calcd. C 44.64, H 3.61, N 1.86; found C 44.60, H 3.80, N 1.89. ^1H NMR (200 MHz, $CDCl_3$, 25 °C): δ = 3.4 (br. s, $^3J_{PtH}$ = 45 Hz, 1 H, NH), 3.75 (s, 3 H, CH_3O), 4.0 (m, 1 H, CH−N), 4.4 (m, 2 H, C-CH_2O), 7.3−8.0 (m, 20 H, Ph) ppm. ^{31}P NMR (81.01 MHz, $CDCl_3$, 25 °C): δ = 43.6 (d, P_A, $^1J_{Pt,P_A}$ = 3885, $^2J_{P_BP_A}$ = 12 Hz), 94.9 (d, P_B, $^1J_{Pt,P_B}$ = 4074, $^2J_{P_AP_B}$ = 12 Hz) ppm. $[\alpha]_D^{25}$ = −20.8 (*c* = 0.58, CH_2Cl_2).

Synthesis of 6a: This complex was prepared in the same manner as **5a**, but by replacing L-serin methyl ester hydrochloride with (1*R*,2*S*)-(−)-di(norephedrine) (0.041 g, 0.267 mmol). The reaction gave **6a** as a white solid. Yield 0.096 g (46%). $C_{33}H_{31}Cl_2NOP_2Pt$ (785.5): calcd. C 50.46, H 3.98, N 1.78; found C 49.96, H 4.03, N 1.98. ^1H NMR (200 MHz, $CDCl_3$, 25 °C): δ = 0.95 (d, $^3J_{H,H}$ = 7.3 Hz, 3 H, CH_3), 2.0 (br. s, $^3J_{PtH}$ = 55 Hz, 1 H, NH), 4.0 (br. s, 1 H, CH−N), 5.35 (m, 1 H, CH−O), 6.8−8.2 (m, 25 H, CH arom.) ppm. ^{31}P NMR (81.01 MHz, $CDCl_3$, 25 °C): δ = 45.9 (d, P_A, $^1J_{Pt,P_A}$ = 3917, $^2J_{P_BP_A}$ = 11.3 Hz), 93.8 (d, P_B, $^1J_{Pt,P_B}$ = 4104, $^2J_{P_AP_B}$ = 11.5 Hz) ppm. $[\alpha]_D^{25}$ = −42.8 (*c* = 0.54, CH_2Cl_2).

Synthesis of 6b: [$PdCl_2$(1,5-COD)] (0.150 g, 0.525 mmol) was suspended in distilled benzene (25 mL) and PPh_2Cl (189 μL, 1.050 mmol) was added to give the immediate formation of the yellow soluble intermediate **1b**. Triethylamine (147 μL, 1.050 mmol) and (1*R*,2*S*)-(−)-norephedrine (0.080 g, 0.525 mmol) were added in sequence, followed by the precipitation of NEt_3HCl. After 18 hours of stirring, the solution containing **6b** was separated by filtration, and taken to dryness. The yellow-orange solid product was purified by recrystallisation from CH_2Cl_2 and diethyl ether Yield 0.215 g (59%). $C_{33}H_{31}Cl_2NOP_2Pd$ (696.9): calcd. C 56.88, H 4.48, N 2.01; found C 56.54, H 4.48, N 1.91. ^1H NMR (200 MHz, $CDCl_3$, 25 °C): δ = 0.95 (d, $^3J_{H,H}$ = 7.3 Hz, 3 H, CH_3), 2.0 (br. s, 1 H, NH), 3.9 (br. s, 1 H, CH−N), 5.2 (m, 1 H, CH−O), 6.8−8.2 (m, 25 H, Ph) ppm. ^{31}P NMR (81.01 MHz, $CDCl_3$, 25 °C): δ = 70.5 (d, P_A, $^2J_{P_BP_A}$ = 35 Hz), 123.6 (d, P_B, $^2J_{P_AP_B}$ = 35 Hz) ppm. $[\alpha]_D^{25}$ = −13.2 (*c* = 0.53, CH_2Cl_2). Recrystallisation of crude **6b** from dichloromethane/diethyl ether gave crystals suitable for a diffractometric study.

Synthesis of 7b: PPh_2Cl (189 μL, 1.050 mmol) was added to a suspension containing [$PdCl_2$(1,5-COD)] (0.150 g, 0.525 mmol) in 25 mL of bi-distilled THF: the mixture became clear and yellow and the complete formation of **1b** was checked by ^{31}P NMR spectroscopy. A large excess (0.500 g each) of $NaHCO_3$ and Na_2SO_4, previously dried at 120 °C for 10 h, was suspended in this solution, followed by the addition of (1*R*,2*S*)-(−)-norephedrine (0.079 g, 0.525 mmol). After stirring vigorously for 24 h, the salts were eliminated by filtration and the solution was taken to dryness, giving a solid residue of **7b**; yield 0.220 g (59%), which was recrystallised with CH_2Cl_2 and diethyl ether. $C_{33}H_{33}Cl_2NO_2P_2Pd$ (714.9): calcd. C 55.44, H 4.65, N 1.96; found C 55.72, H 4.90, N 2.01. ^1H NMR (200 MHz, $CDCl_3$, 25 °C): δ = 1.1 (d, $^3J_{H,H}$ = 7.3 Hz, 3 H, CH_3), 3.0 (m, 2 H, NH_2), 3.2 (br. s, 1 H, CH−N), 4.6 (m, $^3J_{H,H}$ = 8.2 Hz, 1 H, CH−O), 7.0−8.0 (m, 25 H, Ph) ppm. ^{31}P NMR (81.01 MHz, $CDCl_3$, 25 °C): δ = 63.2 (d, P_A, $^2J_{P_BP_A}$ = 15 Hz), 115.4 (d, P_B, $^2J_{P_AP_B}$ = 15 Hz) ppm.

Synthesis of 8a: PPh_2Cl (144 μL, 0.802 mmol) was added dropwise, whilst stirring at room temperature, to a suspension of [$PtCl_2$(1,5-COD)] (0.150 g, 0.401 mmol) in THF (25 mL), resulting in **1a**. The addition of triethylamine (112 μL, 0.802 mmol) and 40 μL of L-prolinol (0.401 mmol, *d* = 1.025 g·mL^{-1}) gave a cloudy mixture due to the formation of partially insoluble triethylamine hydrochloride. After stirring for 24 h at room temperature the salt was filtered away and the solution treated as above (see preparation of **5a**) to obtain **8a** as a white solid; yield 0.153 g (52%). $C_{29}H_{29}Cl_2NOP_2Pt$ (735.5): calcd. C 47.36, H 3.97, N 1.90; found C 46.96, H 4.12, N 1.89. ^1H NMR (200 MHz, $CDCl_3$, 25 °C): δ = 1.5−4.0 (m, 6 H, CH_2), 3.3−3.8 (m, 2 H, CH_2−O), 4.9 (br. s, 1 H, CH−N), 7.0−8.0 (m, 25 H, Ph) ppm. ^{31}P NMR (81.01 MHz, $CDCl_3$, 25 °C): δ = 51.3 (d, P_A, $^1J_{Pt,P_A}$ = 4030, $^2J_{P_BP_A}$ = 14 Hz), 80.7 (d, P_B, $^1J_{Pt,P_B}$ = 3941, $^2J_{P_AP_B}$ = 14 Hz) ppm. $[\alpha]_D^{25}$ = +17.8 (*c* = 0.53, CH_2Cl_2).

 © 2004 Wiley-VCH Verlag GmbH & Co. KGaA, Weinheim

Synthesis of 9a: The complex was prepared from [$PtMe_2$(1,5-COD)] (0.100 g, 0.300 mmol), following the same procedure described above for **4a**, replacing the diol with (1*R*,2*R*)-*trans*-diaminocyclohexane (0.034 g, 0.300 mmol). The precipitation of **9a** occurred within five minutes as a white solid, which was filtered and dried with P_2O_5; yield 0.170 g (77%). $C_{30}H_{32}Cl_2N_2P_2Pt$ (748.5): calcd. C 48.14, H 4.31, N 3.74; found C 47.88, H 4.38, N 3.67. ^{1}H NMR (200 MHz, CD_2Cl_2, 25 °C): δ = 0.6−1.0 (m, 4 H, CH), 1.5 (m, 2 H, CH), 1.7 (d, 2 H, CH), 2.4 (s, $^3J_{PtH}$ = 32 Hz, 2 H, NH), 3.3 (br. s, 2 H, CH−N), 7.3−8.0 (m, 20 H, Ph) ppm. ^{31}P NMR (81.01 MHz, CD_2Cl_2, 25 °C): δ = 40.6 (s, $^1J_{Pt,P}$ = 4003 Hz) ppm.

Synthesis of 9b: This palladium complex was prepared as described above for **6b**, using THF as solvent and replacing the amino-ol with (1*R*,2*R*)-*trans*-diaminocyclohexane (0.060 g, 0.525 mmol). The product co-precipitated with NEt_3HCl in two hours and after filtration was re-dissolved in CH_2Cl_2 and extracted three times with water. The organic phase, taken to dryness, gave pure **9b** as a yellow solid; yield 0.160 g (46%). $C_{30}H_{32}Cl_2N_2P_2Pd$ (659.9): calcd. C 54.61, H 4.89, N 4.25; found C 54.68, H 4.70, N 4.55. ^{1}H NMR (200 MHz, CD_2Cl_2, 25 °C): δ = 0.6−1.0 (m, 4 H, CH), 1.5 (m, 2 H, CH), 1.7 (d, 2 H, CH), 2.3 (s, 2 H, NH), 3.3 (br. s, 2 H, CH−N), 7.3−8.0 (m, 20 H, Ph) ppm. ^{31}P NMR (81.01 MHz, CD_2Cl_2, 25 °C): δ = 65.9 ppm (s). $[\alpha]_D^{25}$ = +32.8 (*c* = 0.54, CH_2Cl_2). Recrystallisation of crude **9b** from dichloromethane/diethyl ether gave crystals suitable for a diffractometric study.

Removal of Coordinated Ligands from Platinum and Their Transfer to Palladium: This experiment was performed with the platinum complexes **4a**, **5a**, **6a** and **8a**. In a typical experiment, an excess of tetrabutylammonium cyanide (5 equiv.) was added to a solution containing the Pt complex (0.010 g) in $CDCl_3$ (0.8 mL). The progress of the reaction was monitored by ^{31}P NMR spectroscopy. After 15 min the spectrum showed the signals of the free ligand:

4: δ = 105.8 ppm (s)

5: δ = 116.9 ppm (s)

6: δ = 112.8 ppm (s) (PO), 38.8 ppm (s) (PN)

8: δ = 114.1 ppm (s) (PO), 46.4 ppm (s) (PN).

At this point an excess (2 equiv.) of [$PdCl_2$(1,5-COD)] was added to the solution and after ten minutes the signals of the corresponding palladium dichloride complex were visible in the ^{31}P NMR spectrum.

In an analogous manner the treatment of the palladium complex **9b** with tetrabutylammonium cyanide in $CDCl_3$, followed by the addition of [$PtCl_2$(1,5-COD)], allowed the observation of the spectrum of ligand **9** (δ = 33.6 ppm, s) and then of **9a**, assigned by comparison with a genuine sample.

The palladium complex **7b**, containing the monodentate aminophosphinite ligand **7**, after addition of CN^-, also gave the free ligand [δ = 111.5 ppm (s), PO] together with another unidentified phosphorus containing product [δ = 62.7 ppm (s)].

Chemical Stability Tests: In a typical experiment, 10^{-2} M solutions of the complex in $CDCl_3$, CH_2Cl_2, THF and benzene were prepared without exclusion of air and the ^{31}P NMR spectrum monitored after 30 min, 5 h and after 3 days. No changes were observed. A few drops of water were then added to each solution and the spectrum checked after 3 min and then after 24 h. Under these conditions all of the spectra were also found to be unchanged.

Optical Stability Tests: The values of $[\alpha]_D^{25}$ were determined for solutions of complexes **4a**, **4b**, **5a**, **6a**, **6b**, **8a** and **9b** as reported above. The optical rotations were redetermined for the same solutions after 3 days and each value was found unchanged.

X-ray Crystal Structure Determinations: X-ray diffraction data for compounds **2a**, **6b** and **9b** were collected on a Nonius Kappa CCD diffractometer, at room temperature (*T* = 295 K), with graphite monochromated Mo-K_α radiation (λ = 0.7107 Å) and corrected for Lorentz polarization and absorption (SORTAV)[17] effects. The structures were solved by direct methods (SIR97)[18] and refined (SHELXL-97)[19] by full-matrix least-squares with anisotropic non-hydrogen and hydrogen atoms on calculated positions, riding on their carrier atoms.

Crystal Data. 2a: $C_{30}H_{30}Cl_2O_2P_2Pt{\cdot}CH_2Cl_2$; trigonal, space group $P3_2$, *a* = 9.8264(1), *c* = 29.2991(2) Å, *V* = 2450.04(4) Å^3, *Z* = 3, $D_{calcd.}$ = 1.699 g·cm^{-3}. Intensity data collected with θ ≤ 30°; 9447 independent reflections measured; 8644 reflections observed [$I > 2\sigma(I)$]. Final *R* (observed reflections) = 0.028 and *Rw* (all reflections) = 0.063, *S* = 1.026, Flack parameter [20] = −0.012(3).

6b: $C_{33}H_{31}Cl_2NOP_2Pd{\cdot}1/2CH_2Cl_2$; triclinic, space group *P*1, *a* = 11.6343(2), *b* = 14.3753(3), *c* = 20.3486(4) Å, α = 93.0527(7), β = 92.4847(7), γ = 91.6164(9)°, *V* = 3393.6(1) Å^3, *Z* = 4, $D_{calcd.}$ = 1.447 g·cm^{-3}. Intensity data collected with θ ≤ 27°; 26342 independent reflections measured; 20677 reflections observed [$I > 2\sigma(I)$]. Final *R* = 0.098 (observed reflections) and *Rw* = 0.281 (all reflections), *S* = 1.029, Flack parameter = 0.03(4). The asymmetric unit contains four independent molecules of the complex and two molecules of dichloromethane.

9b: $C_{30}H_{32}Cl_2N_2P_2Pd$; monoclinic, space group $P2_1$, *a* = 7.5164(1), *b* = 16.2585(3), *c* = 12.4538(2) Å, β = 96.4409(7)°, *V* = 1512.32(4) Å^3, *Z* = 2, $D_{calcd.}$ = 1.449 g·cm^{-3}. Intensity data collected with θ ≤ 30°, 7940 independent reflections measured; 7416 reflections observed [$I > 2\sigma(I)$]. Final *R* = 0.039 (observed reflections), *Rw* = 0.101 (all reflections), *S* = 1.043, Flack parameter = 0.00(2).

CCDC-219076, 219077 and CCDC-219078 contain the supplementary crystallographic data for this paper. These data can be obtained free of charge at www.ccdc.cam.ac.uk/conts/retrieving.html [or from the Cambridge Crystallographic Data Centre, 12 Union Road, Cambridge CB2 1EZ, UK; Fax: (internat.) +44-1223-336-033; E-mail: deposit@ccdc.cam.ac.uk].

[1] P. Bergamini, V. Bertolasi, M. Cattabriga, V. Ferretti, U. Loprieno, N. Mantovani, L. Marvelli, *Eur. J. Inorg. Chem.* **2003**, 918−925.

[2] S. J. Berners-Price, P. J. Sadler, *Structure and Bonding* **1988**, *70*, 26−102.

[3] W. S. Knowles, *Angew. Chem. Int. Ed.* **2002**, *41*, 1998−2007.

[4] M. Nógrádi, *Stereoselective Synthesis*, VCH, Weinheim, Germany, **1987**.

[5] [5a] T. V. RajanBabu, S. Shin, *Org. Lett.* **1999**, *1*, 1229−1232. [5b] N. Derrien, C. B. Dousson, S.M. Roberts, U. Berens, M. J. Burk, M. Ohff, *Tetrahedron: Asymmetry* **1999**, *10*, 3341−3352. [5c] W. Hu, M. Yan, C. Lau, S. M. Yang, A. S. C. Chan, *Tetrahedron Lett.* **1999**, *40*, 973−976.

[6] [6a] F. Agbossou, J. Carpentier, F. Hapiot, I. Suisse, A. Mortreux, *Coord. Chem. Reviews* **1998**, 178−180, 1615−1645. [6b] F. Agbossou-Niedercorn, I. Suisse, *Coord. Chem. Reviews* **2003**, *242*, 145−158.

[7] A. S. C. Chan, W. Hu, C. C. Pai, C. P. Lau, *J. Am. Chem. Soc.* **1997**, *119*, 9570.

[8] L. D. Quin, *A guide to Organophosphorus Chemistry*, John Wiley & Sons, New York, **2000**, p. 59.

[9] [9a] V. I. Tararov, R. Kadyrov, T. H. Reirmeier, J. Holz, A. Börner, *Tetrahedron: Asymmetry* **1999**, *10*, 4009−4015. [9b] V.

 © 2004 Wiley-VCH Verlag GmbH & Co. KGaA, Weinheim

I. Taranov, R. Kadyrov, T. H. Reirmeier, J. Holz, A. Börner, *Tetrahedron Lett.* **2000**, *41*, 2351−2355.
[10] [10a] M. Stolmàr, C. Floriani, A. Chiesi-Villa, C. Rizzoli, *Inorg. Chem.* **1997**, *36*, 1694−1701. [10b] C. Jeunesse, C. Dieleman, S. Steyer, D. Matt, *J. Chem. Soc., Dalton Trans.* **2001**, 881−892.
[11] S. Naïli, J. Carpentier, F. Agbossou, A. Montreux, *Organometallics* **1995**, *14*, 401−406.
[12] J. Bravo, C. Cativiela, J. E. Chaves, R. Navarro, E. P. Urriolabeitia, *Inorg. Chem.* **2003**, *42*, 1006−1013.
[13] M. N. Burnett, C. K. Johnson, ORTEPIII, Report ORNL-6895, Oak Ridge National Laboratory, Oak Ridge, TN, **1996**.
[14] J. X. Mc Dermott, J. F. White, G. M. Whitesides, *J. Am. Chem. Soc.* **1976**, *98*, 6521.
[15] R. Bassan, K. H. Bryars, L. Judd, A. G. Platt, P. G. Pringle, *Inorg. Chim. Acta* **1986**, L41−L42.
[16] D. Drew, J. R. Doyle, *Inorg. Synth.* **1972**, 13, 47.
[17] R. H. Blessing, *Acta Crystallogr., Sect. A* **1995**, *51*, 33−38.
[18] A. Altomare, M. C. Burla, M. Camalli, G. L. Cascarano, C. Giacovazzo, A. Guagliardi, A. G. G. Moliterni, G. Polidori, R. Spagna, *J. Appl. Crystallogr.* **1999**, *32*, 115−116.
[19] G. M. Sheldrick, SHELXL-97, *Program for Crystal Structures Refinement*, University of Göttingen, Germany, **1997**.
[20] H. D. Flack, *Acta Crystallogr., Sect. A* **1983**, *39*, 876−881.

Received September 11, 2003
Early View Article
Published Online February 16, 2004

 © 2004 Wiley-VCH Verlag GmbH & Co. KGaA, Weinheim

Configuration of Octahedral Metal Compounds − Equilibrium, Crystal and Molecular Structure of Nickel(II) Complexes of Linear N_2O_4, N_4S_2 or N_6 Donors Set Atoms Ligands

Aminou Mohamadou,*[a] Caroline Jubert,[a] Nathalie Gruber,[b] and Jean-Pierre Barbier[a]

Keywords: Configuration determination / N,O ligands / N,S ligands / Nickel / Potentiometry

Two new nickel(II) complexes of symmetric hexadentate mixed-ligand N,O [1,12-bis(2-pyridyl)-5,8-dioxa-2,11-diazadodecane (pydado)] and N,S [1,12-bis(2-pyridyl)-5,8-dithia-2,11-diazadodecane (pydadt)] donor atoms have been synthesised as perchlorate salts and characterised by X-ray crystallography and ligand-field spectroscopy. In both complexes the Ni^{2+} ion is hexacoordinate. The cation $[Ni(pydado)]^{2+}$ is pseudo-octahedral with the two pyridyl groups in *trans* position; all Ni–N and Ni–O bond lengths are practically equivalent. In $[Ni(pydadt)]^{2+}$ complex, however, the size of the thioether sulfur atoms imposes a C_{2v} symmetry; the pyridyl groups and the sulfur atoms are in *trans* positions and all Ni–N bond lengths are equivalent. The comparison of these structures with those of octahedral cobalt, copper and zinc complexes with the same ligands shows that their configurations depend not only on the nature of the two central donor atoms of the ligand, but also on the nature of the metallic ion. In aqueous solution, the stability constants of the Ni^{II} chelates with these two ligands, determined by potentiometry, show the formation of $[Ni(LH)]^{3+}$ and $[NiL]^{2+}$ species in all cases. The chelating power of the pydadt ligand is slightly greater than that of pydado.
(© Wiley-VCH Verlag GmbH & Co. KGaA, 69451 Weinheim, Germany, 2004)

Introduction

The bioinorganic chemistry of the transition metal complexes has become increasingly important since the discovery that metal ions are found at the active site of several very important classes of metalloenzymes.[1] The catalytic activity of these compounds depends on the nature of the donors atoms of the ligand[2] and the configuration of the complex.[3] In this case, considerable interest has developed in nickel complexes with mixed-donor ligands in order to elucidate the relationship between the donor atoms of the ligand and the geometry around the metal ion.[4]

Nickel(II) complexes of linear ether or thioether ligands with different numbers of oxygen or sulfur donor atoms and a heterocyclic nitrogen have attracted attention recently.[5] In order to elucidate the effects of the distinctive structural features of the ligands on the properties of the resulting complexes, we described earlier the coordination complexes of cobalt, copper and zinc with three linear hexadentate ligands [1,12-bis(2-pyridyl)-2,5,8,11-tetraazadodecane (pytrien), 1,12-bis(2-pyridyl)-5,8-dioxa-2,11-diazadodecane (pydado) and 1,12-bis(2-pyridyl)-5,8-dithia-2,11-diazadodecane (pydadt)].[6,7] These ligands contain ether oxygen or thioether donors as well as aliphatic and aromatic nitrogen donors in the their ligand framework (Scheme 1).

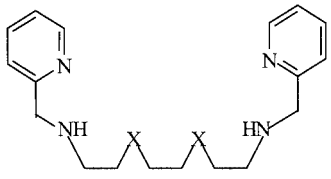

X = O (pydado)
X = S (pydadt)
X = NH (pytrien)

Scheme 1

As a continuation of our interest in the study of complexes that model the active sites in metalloproteins and to better understand the physicochemical properties of such complexes, especially the stereochemistry of the metallic centre, we present here the thermodynamic constants of the metal chelates formed by these ligands in aqueous solution as well as the syntheses of the nickel(II) complexes. Their configuration has been investigated by crystal structures and compared to those described earlier.[6−8]

[a] Université de Reims Champagne-Ardenne, GRECI, Faculté des Sciences,
BP 1039, 51687 Reims cedex 2, France
E-mail: aminou.mohamadou@univ-reims.fr
[b] Université Louis Pasteur de Strasbourg, Service Commun de Rayons X,
4, rue Blaise Pascal, 67070 Strasbourg cedex, France

Results and Discussion

Synthesis

The violet nickel(II) complex of pydado was synthesised by the treatment of an aqueous solution of the ligand hydrochloride salt with tetramethylammonium hydroxide and one equivalent of nickel(II) perchlorate hexahydrate. The pink nickel(II) compound of pydadt was obtained by treating an ethanolic suspension of the ligand hydrochloride salt and four equivalents of sodium acetate with nickel(II) perchlorate hexahydrate. The two complexes were obtained as perchlorate salts, as confirmed by the presence of a strong band at 1090 cm^{-1} in the IR spectra. The chromatography studies of each nickel(II) complexes indicate the presence of only one diastereoisomer. Crystals suitable for structure determination were obtained by recrystallisation from water (compound **1**) or from a water/ethanol (1:2, v/v) mixture (compound **2**) by slow evaporation of the solvent at room temperature.

Solution Equilibria: Metal Chelate Formation Constants

The ligand equilibrium constants of the ligands pytrien,[9] and pydado and pydadt were determined previously.[7] The thermodynamic constants for the two ligands studied are listed in Table 1.

Table 1. Protonation constants ($\log K^n_H$), stability constants ($\log\beta$) and deprotonation constants ($\log K$) for Ni^{2+} complexes of pydado and pydadt (I = 1 M KNO_3 and 20 °C)[a]

	Ligands[b]				Complexes		
	$\log K^1_H$	$\log K^2_H$	$\log K^3_H$	$\log K^4_H$	$\log\beta_{110}$	$\log\beta_{111}$	$\log K$
pydado	8.63(3)	7.76(4)	2.36(4)	1.5(6)	12.85(1)	15.38(7)	2.53
pydadt	8.32(5)	7.58(4)	2.40(6)	1.6(5)	13.88(2)	16.24(5)	2.36

[a] Values in parentheses represent 1σ standard deviation for the last significant digit. [b] From ref.[7]

Complexation of Ni^{2+} with pydado and pydadt occurs below pH 3. The NiL species with these two ligands are completely formed at pH 5.5 (pydado) and pH 4.5 (pydadt). The protonated metal chelate Ni(HL) is formed in small amounts: a maximum of 10% of the analytical Ni^{2+} concentration with pydadt at pH 2.6, and a third, along with Ni^{2+} and NiL species, with pydado at pH 3.1.

The stability constants $\beta = |MHL^{3+}|/|M^{2+}||L||H^+|$ for the equilibrium in Equation (1) for nickel(II) complexes of pydado and pydadt appear in Table 1. The stability constants of the complex with pydado are smaller than those with pydadt. These results are in good agreement with those described by Martell and co-workers[10] in the coordination of pyridyl ligands possessing ether (O) or thioether (S) donor atoms. A thioether donor coordinates more strongly to divalent transition metals than an ether donor. The preference of these metals to bind to the softer thioether may be also explained by the larger size of the sulfur atom, allowing it to approach the metal ion more closely, with less contraction of the ligand backbone.[11] The stability constants for the nickel(II) complex with pytrien are higher than those with pydado and pydadt; this is in agreement with the chelating power of nitrogen atom with regard to ether oxygen or thioether sulfur atoms.

$$M^{2+} + L + H^+ \rightleftarrows M(HL)^{3+} \quad (1)$$

The chelate protonation constants for the equilibrium in Equation (2), defined as $K = [MHL^{3+}]/[ML^{2+}][H^+]$, also appear in Table 1.

$$ML^{2+} + H^+ \rightleftarrows MHL^{3+} \quad (2)$$

The protonation constant of $[NiL]^{2+}$ (L = pydado and pydadt) is close to the protonation constant K^3_H. Therefor, the K values do not allow the determination of the protonated nitrogen atom.

X-ray Diffraction Studies

The structures of complexes $[Ni(pydado)](ClO_4)_2\cdot H_2O$ (**1**) and $[Ni(pydadt)](ClO_4)_2$ (**2**) were determined by single-crystal X-ray diffraction. Pertinent crystallographic and refinement details are reported in Table 2.

Table 2. X-ray experimental data for compounds **1** and **2**

	1	**2**
Formula	$C_{18}H_{28}Cl_2N_4NiO_{11}$	$C_{18}H_{26}Cl_2N_4NiO_8S_2$
M	606.06	620.17
Crystal system	triclinic	monoclinic
Space group	$P\bar{1}$	$P2_1/c$
a (Å)	9.3915(5)	11.6381(2)
b (Å)	11.444(5)	17.4104(4)
c (Å)	12.4039(5)	24.8793(5)
α (deg)	93.656(5)	90
β (deg)	98.551(5)	94.987(5)
γ (deg)	108.023(5)	90
V (Å^3)	1245.1(2)	5022.1(3)
T (K)	173	294
Z	2	8
μ(Mo-$K\alpha$) (mm^{-1})	1.058	1.203
F000	1288	628
Reflections measured	8140	11871
Unique reflections collected	3164	7083
$wR(F^2)$	0.074	0.066
$R1$ [$I > 3\sigma(I)$]	0.053	0.041
R_{int}	0.04	0.04

[Ni(pydado)][ClO_4]$_2\cdot H_2O$ (1)

The molecular structure of this complex consists of $[Ni(pydado)]^{2+}$ cations and ClO_4^- anions. The two perchlorate anions are both ordered, with Cl−O bond lengths (average, 1.399 Å) and O−Cl−O bond angles (average 110.9°) similar to those reported earlier.[6,7] A view of the cation with the labelling scheme is shown in Figure 1.

 © 2004 Wiley-VCH Verlag GmbH & Co. KGaA, Weinheim

Principal bond lengths and angles are listed in Table 3. The nickel(II) centre is coordinated by two aromatic nitrogens [N(1) and N(4)], two secondary amine nitrogens [(N2) and N(3)] and two ether oxygens [O(1) and O(2)]. Though several isomers can be obtained with a linear hexadentate ligand, the one observed here has the pyridine nitrogen atoms in the *trans* positions; the same isomer have been found for a zinc(II) complex.[7]

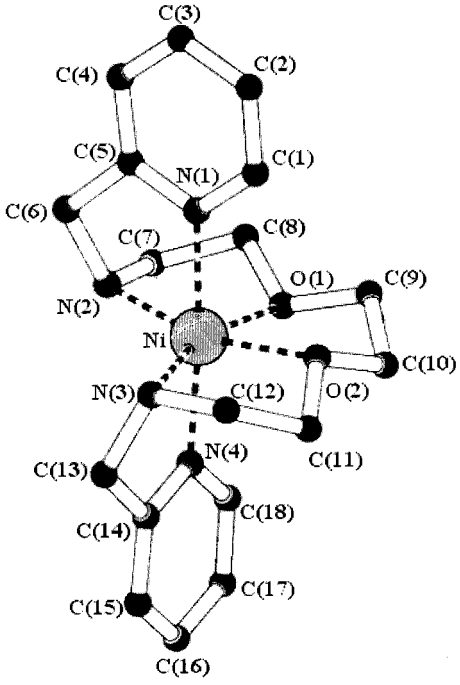

Figure 1. A PLUTON projection of the cation $[Ni(pydado)]^{2+}$ and the atom labelling-scheme; hydrogen atoms are omitted for clarity

The N(1)−Ni−N(4), N(2)−Ni−O(2) and N(3)−Ni−O(1) bond angles are 175.3(1)°, 159.8(1)° and 160.2(2)°, respectively. All nickel-donor atom bond lengths are slightly different [$Ni-N_{amine}$ (average 2.076 Å), $Ni-O_{ether}$ (average 2.084 Å) and $Ni-N_{pyridyl}$ (average 2.090 Å)]. Thus, the coordination geometry around the nickel atom is described as a slightly distorted octahedron, which is occupied by N(2), O(1), O(2) and N(3) at the equatorial sites and N(1) and N(4) at the axial sites. The two oxygen donor atoms are practically in the equatorial plane [N(1)−Ni−O(1): 92.8° and N(1)−Ni−O(2): 90.4°], whereas the two secondary amine nitrogen atoms are located below and above this plane, respectively [N(1)−Ni−N(2): 80.4° and N(1)−Ni−N(3): 96.9°].

Compared to the $[Zn(pydado)]^{2+}$ complex described earlier,[7] all metal-donor atom bond lengths in the nickel complex are smaller than those in the zinc complex, which is consistent with the larger radius of Zn^{II}. Conversely, the five chelate bond angles of 79.4(1)−83.3(2)° [average 81.4°] subtended by the ligand at the nickel atom are larger than their analogues of 74.1(1)−81.2(2)° [average 77.7°] in the zinc complex, in agreement with a smaller distortion in the nickel compound.

Table 3. Selected bond lengths (Å) and angles (°) for complexes **1** and **2**

Complex **1**			
Ni−N(1)	2.088 (4)	Ni−N(4)	2.092(4)
Ni−N(2)	2.078(4)	Ni−O(1)	2.085(3)
Ni−N(3)	2.074(4)	Ni−O(2)	2.083(3)
N(1)−Ni−N(2)	80.4(2)	N(2)−Ni−O(2)	159.8(1)
N(1)−Ni−N(3)	96.9(2)	N(3)−Ni−O(1)	160.2(2)
N(1)−Ni−N(4)	175.3(1)	N(3)−Ni−O(2)	83.3(2)
N(1)−Ni−O(1)	92.8(1)	N(3)−Ni−N(4)	80.7(2)
N(1)−Ni−O(2)	90.4(1)	O(1)−Ni−O(2)	79.4(1)
N(2)−Ni−N(3)	115.4(2)	N(4)−Ni−O(1)	90.7(1)
N(2)−Ni−N(4)	97.0(2)	N(4)−Ni−O(2)	93.3(1)
N(2)−Ni−O(1)	83.2(1)		
Complex 2			
Ni(1)−S(1)	2.469(1)	Ni (2)−S(3)	2.440(1)
Ni (1)−S(2)	2.470(1)	Ni (2)−S(4)	2.463(1)
Ni (1)−N(1)	2.087(3)	Ni (2)−N(5)	2.098(3)
Ni (1)−N(2)	2.083(3)	Ni (2)−N(6)	2.099(3)
Ni (1)−N(3)	2.079(3)	Ni (2)−N(7)	2.104(3)
Ni (1)−N(4)	2.091(3)	Ni (2)−N(8)	2.101(3)
N(1)−Ni(1)−N(2)	79.7(1)	N(5)−Ni(2)−N(6)	79.6(1)
N(1)−Ni(1)−N(3)	99.1(1)	N(5)−Ni(2)−N(7)	100.0(1)
N(1)−Ni(1)−N(4)	94.4(1)	N(5)−Ni(2)−N(8)	90.1(1)
N(1)−Ni(1)−S(1)	165.06(9)	N(5)−Ni(2)−S(3)	164.5(1)
N(1)−Ni(1)−S(2)	90.44(8)	N(5)−Ni(2)−S(4)	94.14(9)
N(2)−Ni(1)−N(3)	178.8(1)	N(6)−Ni(2)−N(7)	179.1(1)
N(2)−Ni(1)−N(4)	98.5(1)	N(6)−Ni(2)−N(8)	101.0(1)
N(2)−Ni(1)−S(1)	86.46(9)	N(6)−Ni(2)−S(3)	85.0(1)
N(2)−Ni(1)−S(2)	94.85(9)	N(6)−Ni(2)−S(4)	94.57(9)
N(3)−Ni(1)−N(4)	81.3(1)	N(7)−Ni(2)−N(8)	79.9(1)
N(3)−Ni(1)−S(1)	94.8(1)	N(7)−Ni(2)−S(3)	95.42(9)
N(3)−Ni(1)−S(2)	85.37(9)	N(7)−Ni(2)−S(4)	84.61(9)
N(4)−Ni(1)−S(1)	93.07(9)	N(8)−Ni(2)−S(3)	94.09(9)
N(4)−Ni(1)−S(2)	166.39(9)	N(8)−Ni(2)−S(4)	164.40(9)
S(1)− Ni(1)−S(2)	85.18(4)	S(3)−Ni(2)−S(4)	85.73(4)

The crystal structure of complex **1** shows two, three-centre bifurcated H-bonds[12] between each secondary amine hydrogen and two oxygen atoms of each perchlorate anion [H(01)···O(4): 2.558 Å, H(01)···O(6): 2.416 Å and H(02)···O(7): 3.501 Å, H(02) ··O(9): 2.125 Å]. In the lattice of this complex, the intermolecular distances between the oxygen atom of the water of crystallisation and two oxygen atoms of one of the two perchlorate anions [O(11)···O(3): 3.217 Å and O(11)···O(5): 3.372 Å] are less than the sum of their van der Waals radii. This suggests that these species are also involved in hydrogen bonding interactions.

$[Ni(pydadt)][ClO_4]_2$ (2)

Compound **2** crystallises in a triclinic system with eight molecules in the unit cell. In the crystal lattice, the two enantiomeric isomers of the $[Ni(pydadt)]^{2+}$ cations are present in equal parts, giving a racemate. Three of the four ClO_4^- anions are ordered, whereas the fourth, in which each oxygen atom occupies two sets of positions, is disordered. Each perchlorate anion forms a two-centre chelate H-bond[12] between one oxygen atom and each of two secondary amine hydrogens (O···HN, average 2.132 Å). A per-

 © 2004 Wiley-VCH Verlag GmbH & Co. KGaA, Weinheim

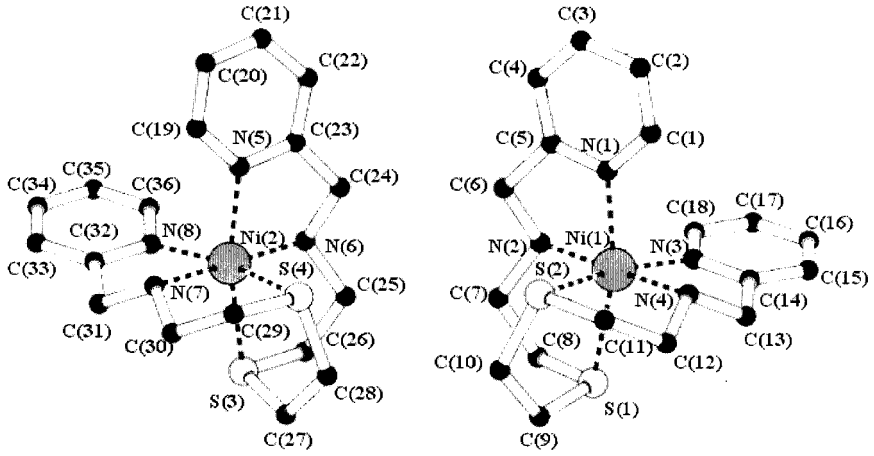

Figure 2. A PLUTON projection of the two enantiomeric cations of $[Ni(pydadt)]^{2+}$ and the atom labelling-scheme; hydrogen atoms are omitted for clarity

spective drawing of the two enantiomers cations with atom labelling is illustrated in Figure 2, relevant bond lengths and angles are given in Table 3.

The molecular structure of complex **2** shows that each $[Ni(pydadt)]^{2+}$ cation is hexacoordinate, with the two aromatic nitrogen atoms in the *cis* positions, whereas the two amino nitrogen atoms are in the *trans* positions. In each enantiomer, the bond lengths of the same donor atoms (N or S), while not always exact, are quite close [Ni(1)−N: average 2.085 Å; Ni(1)−S: 2.470 Å; Ni(2)−N: average, 2.101 Å], with the exception of the isomer labelled Ni(2), where the two Ni−S bond lengths are different [Ni(2)−S(3): 2.440 Å and Ni(2)−S(4): 2.463 Å]. In addition, the variation of the Ni−N and Ni−S bond lengths is opposite in the two enantiomers: the Ni(1)−N bond lengths are slightly shorter than Ni(2)−N (−0.016 Å), while the Ni(1)−S bonds are slightly longer than Ni(2)−S (average +0.018 Å). The $N_{py}-Ni-S$ (average 165°) and $N_{amino}-Ni-N_{amino}$ (average 179°) bond angles, which are practically the same in the two enantiomers, are not very close to those of an ideal octahedral geometry. According to the result obtained from ligand field spectroscopy (see below), complex **2** has C_{2v} symmetry.

Absorption Spectra

The electronic spectra of the two nickel(II) compounds (**1** and **2**) in the solid state are no different to those obtained in aqueous solution. The absorption spectra for these compounds exhibit essentially similar patterns in the 250−500 nm region, with two strong bands possibly due to intraligand[13] and charge-transfer transitions.

In the visible region, $[Ni(pydado)](ClO_4)_2$ (**1**) displays two bands at 890 nm and 560 nm. These two bands arise from $^3A_{2g}\rightarrow{}^3T_{2g}$ and $^3A_{2g}\rightarrow{}^3T_{1g}(^3F)$ transitions. The third band at higher energy is completely obscured by a metal-ligand charge transfer. These observations are consistent with an octahedral geometry around the Ni^{2+} ion. The ligand-field parameters were calculated using the energy levels given by Lever: 10 Dq = 11230 cm^{-1}, Racah parameter B = 860 cm^{-1}. These parameters, and those of the octahedral $[Ni(pytrien)](ClO_4)_2$ complex (10 Dq = 12360 cm^{-1}, B = 826 cm^{-1}),[8] are in agreement with NiN_4O_2 and NiN_6 chromophores, respectively.

The spectrum of $[Ni(pydadt)](ClO_4)_2$ (**2**) shows two more-intense absorption bands centred around 890 nm and 540 nm. Each band present shoulders, which indicates a lowering of the symmetry around the Ni^{2+} ion. These two absorption envelopes could be cleanly resolved into just three (10360 cm^{-1}, 11560 cm^{-1} and 12050 cm^{-1}) and two (16950 cm^{-1} and 18800 cm^{-1}) Gaussian components, respectively. The corresponding energy levels[14a] for these transitions are given in Figure 3; they are in agreement with those calculated for a C_{2v} symmetry,[14b] and described by Meredith and Palmer[15] for a $[Ni(histidine)_2(OH_2)_2]$ complex.

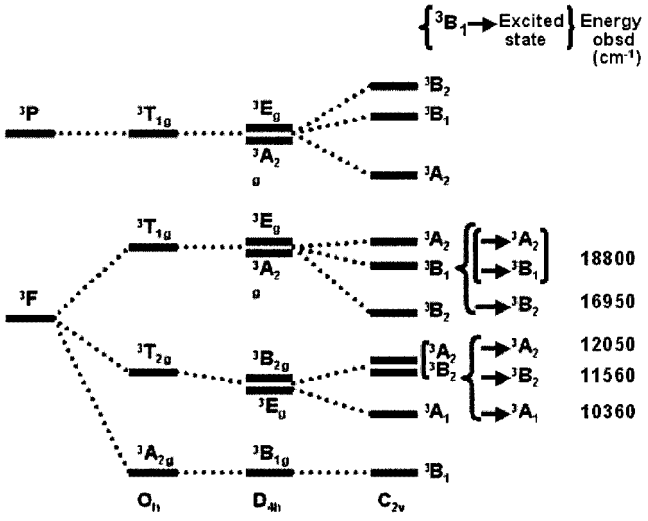

Figure 3. Observed energy levels[15] for $[Ni(pydadt)](ClO_4)_2$ with free ion and high symmetry

 © 2004 Wiley-VCH Verlag GmbH & Co. KGaA, Weinheim

Configuration of the Octahedral Complexes

We have studied the coordination of first-row transition metals (cobalt, nickel, copper and zinc) with the linear hexadentate ligands pytrien,[6] pydado[7] and pydadt,[7] which possess two central N, O and S donors, respectively. These ligands, with three different donor atoms, are of the type A B C C B A, in which A represents a pyridyl nitrogen atom, B a secondary amine nitrogen atom and C the central heteroatom (N, O or S). Disregarding isomerism due to the fact that the secondary amine nitrogen donor can became stereogenic, and the non-planarity of the chelate rings formed upon complexation, there are many possibilities of ligand arrangement, meaning that there are four pairs of enantiomers possible with these $A_2B_2C_2$ donor sets. Generally, only one pair of enantiomers, which were resolved, was observed, indicating a stereoselectivity introduced by the different ligating atoms.[16]

All possible diastereoisomers of our complexes with linear hexadentate ligands are shown in Scheme 2. When dealing with this kind of octahedral compound, the α (or β)-*cis* or *cis-trans-cis* types of nomenclature are not adequate to describe the geometry of the complex, as they do not differentiate between the wrapping of the ligand around the metal ion in all the isomers; for example, the two configurations I and III (Scheme 2) are both *cis-trans-cis*. Therefore the extension of the Saito method,[17] introduced by Hartshorn and House,[18] was used to describe the configuration of the octahedral complexes obtained with these three linear hexadentate ligands; for each sequence of three donor atoms, the descriptors m and f indicate meridional and facial ligand segments, respectively. Consequently, each isomer of octahedral complexes with a linear hexadentate ligand can be described with four characters, with pairs of enantiomers having the same labelling.

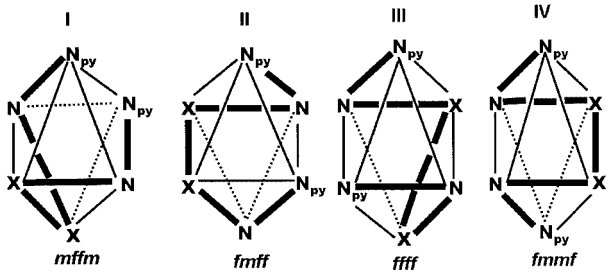

Scheme 2

The X-ray crystal structures of the cobalt, nickel, copper and zinc complexes with the three hexadentate ligands show that the four compounds isolated with each ligand crystallise in the same diastereoisomer as the four described above. $[M(pytrien)]^{n+}$ (n = 3 for Co and n = 2 for Ni, Cu and Zn), $[M(pydado)]^{2+}$ and $[M(pydadt)]^{2+}$ have the configuration II, IV and I, respectively (Figure 4). As the only difference between these ligands is the two central heteroatoms, the stereoselectivity of these complexes is introduced by the central ligating atoms. In the crystal lattice, $[Cu(pydado)]^{2+}$ or $[Ni(pydadt)]^{2+}$ are racemates, whereas the others complexes have only one of the two enantiomers for the corresponding configurations. With each ligand, disregarding the

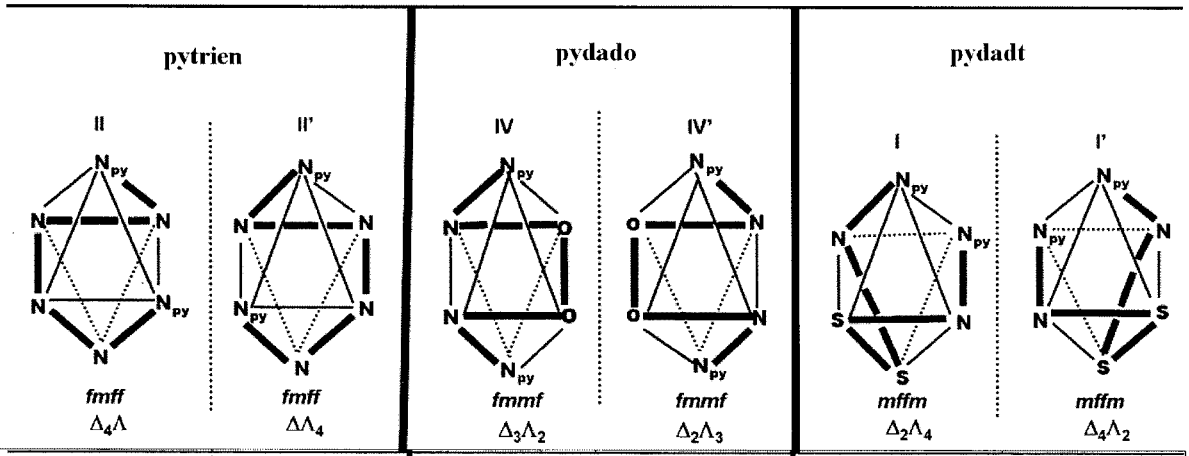

AC_NH [a]	*R R S S*	*S S R R*	*S S*	*R R*	*R R*	*S S*
Cobalt	$[Co(pytrien)]^{3+}$	-	-	$[Co(pydado)]^{2+}$ [b]	[b]$[Co(pydadt)]^{2+}$	-
Nickel	$[Ni(pytrien)]^{2+}$ [c]	-	$[Ni(pydado)]^{2+}$	-	$[Ni(pydadt)]^{2+}$	$[Ni(pydadt)]^{2+}$
Copper	$[Cu(pytrien)]^{2+}$	-	Racemic distorted tetrahedral		Powder form	
Zinc	-	$[Zn(pytrien)]^{2+}$	$[Zn(pydado)]^{2+}$	-	-	$[Zn(pydadt)]^{2+}$

[a] Absolute configuration of the secondary amine nitrogen atoms. [b] Ref.[8] [c] Ref.[24]

Figure 4. The configurations of cobalt, nickel, copper and zinc complexes with pytrien, pydado and pydadt ligands

 © 2004 Wiley-VCH Verlag GmbH & Co. KGaA, Weinheim

nature of the metal ion, the cobalt and zinc compounds are always enantiomers, while the nickel complexes have either the enantiomeric configuration of the cobalt or the zinc complex.

A comparison of all octahedral metal complexes of pytrien and pydado shows that the donor atoms 5 and 6 (Scheme 3) are reversed in the octahedron. The absolute configuration of the stereogenic amine nitrogen atom 2 is retained for the two cobalt (*R*) and the two zinc (*S*) complexes, whereas it is inverted in the nickel compounds.

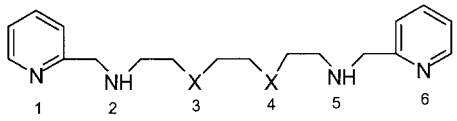

Scheme 3

The large size of the sulfur donor atoms of the pydadt ligand does not allow the facial coordination of the heteroatoms 1, 2 and 3 (Scheme 3) around the metal ion. Therefore, an mffm configuration is imposed for all $[M(pydadt)]^{2+}$ cations, so that the bulky pyridyl groups and the larger thioether sulfur atoms are in *trans* positions.

Conclusion

The equilibrium constants of the Ni^{II} chelates with pydado and pydadt determined by potentiometry show the formation of $[NiLH]^{3+}$ and $[NiL]^{2+}$ species in all cases; $[NiLH]^{3+}$species are present in small amounts around pH 3, while $[NiL]^{2+}$ are fully formed in neutral medium. The stability constants of the $[Ni(pydadt]^{2+}$ species are slightly greater than those of $[Ni(pydado]^{2+}$, in agreement with analogous ligands described by Martell and co-workers.[10,11] Comparison of the thermodynamic constants of these nickel(II) complexes and the other M^{II} complexes (M = cobalt, copper and zinc) of the same ligands,[7] shows that the values of the stability constants follow the Irving−Williams series.

X-ray crystallographic studies show that the Ni−N and Ni−O bond lengths in $[Ni(pydado]^{2+}$ cation are practically identical, and this is in good agreement with the electronic spectrum, which is easily interpreted in O_h symmetry. However, the presence of the thioether sulfur atoms in the $[Ni(pydadt]^{2+}$ complex, in which the Ni−S bond lengths are always longer than Ni−N (+0.376 Å), leads to a large distortion around the nickel ion, with the bulky pyridyl groups and sulfur donor atoms in *trans* positions. This distortion is corroborated with the nature of the electronic spectrum of $[Ni(pydadt]^{2+}$ complex, characteristic for C_{2v} symmetry.

The crystal structures of some octahedral first-row transition metal complexes with these kinds of symmetrical linear hexadentate ligands show clearly that the two central heteroatom donors introduce a stereoselectivity of the complexes obtained and therefore dictate their configuration. Conversely, the central metal ion imposes their conformation; for example, cobalt and zinc always have an inverse conformation.

Experimental Section

Chemicals and Starting Materials: All solvents were purified by conventional procedures[20] and distilled prior to use. Chemicals commercially available (Aldrich) were used as supplied without further purification. The ligands, 1,12-bis(2-pyridyl)-5,8-dioxa-2,11-diazadodecane (pydado) and 1,12-bis(2-pyridyl)-5,8-dithia-2,11-diazadodecane (pydadt) were obtained as tetrahydrochloride salts from the condensation of 2-pyridine carboxaldehyde and triethylene dioxa(or dithia)diamine, as described previously.[7]

CAUTION: *Although we have experienced no problems while handling any of the perchlorate substances described herein, readers are advised to handle these compounds as potentially explosive compounds.*

Elemental analyses (C, H and N) were carried out on a Perkin−Elmer 2400 C, H, N element analyser in our university. The metal analysis was performed on an ICP AES Liberty Series II Varian apparatus. Magnetic susceptibilities were determined at room temperature (20 °C) using $HgCo(SCN)_4$ as a calibrant; diamagnetic susceptibility corrections were calculated from Pascal's constants.[21]

Potentiometry: All chemicals used were of analytical grade. HNO_3 and KOH were purchased from Prolabo. KNO_3 and $Ni(NO_3)_2{\cdot}3H_2O$ were purchased from Fluka. The metal ion solutions were prepared (ca. 0.01 M) and standardised with $Na_2H_2edta{\cdot}2H_2O$. All measurements were performed in a thermoregulated cell at (20.0 ± 0.1) °C, under N_2 to prevent absorption of CO_2, as described previously.[7]

The measurement apparatus consist of a microprocessor burette (Metrohm Dosimat 665) and a pH meter (Metrohm 713) equipped with a combined pH glass electrode (Metrohm AG 9101) linked to a PC. The stability constants were calculated and refined with the computer program PROTAF.[22]

Spectroscopy: The UV/Vis. spectra were recorded on a Perkin−Elmer Lambda 6 spectrophotometer. Gaussian deconvolution of visible absorption spectra were performed using an application developed under "QUATTRO PRO" by J. Rimbault in our laboratory. IR spectra were obtained in KBr pellet.

$[Ni(pydado)](ClO_4)_2{\cdot}H_2O$ (1): A solution of tetramethylammonium hydroxide 0.5 M was added dropwise to an aqueous solution (30 mL) of pydado·4HCl (0.49 g, 1 mmol) and nickel(II) perchlorate hexahydrate (0.36 g, 1 mmol) to adjust the pH to around 8. Slow evaporation of the solvents at room temperature yielded violet crystals, suitable for X-ray diffraction studies, after two months. Yield: ca. 75%; m.p. 255 °C. $C_{18}H_{28}Cl_2N_4NiO_{11}$: calcd. C 35.7, H 4.6, N 9.2, Ni 9.7; found C 35.8, H 4.3, N 9.3, Ni 9.5. $\chi_M = 4310 \times 10^{-6}$ uem cgs, $\mu_{eff} = 3.18\ \mu_B$. UV/Vis (H_2O): λ_{max} (ε) = 890 nm (12 $mol^{-1}{\cdot}L{\cdot}cm^{-1}$), 560 (13).

$[Ni(pydadt)](ClO_4)_2$ (2): A mixture of sodium acetate trihydrate (0.54 g, 4 mmol) and the ligand pydadt·4HCl (0.54 g, 1 mmol) in absolute ethanol (30 mL) was stirred, whilst boiling, for 10 min in a water bath. The mixture was then cooled and the sodium chloride that precipitated was filtered. Nickel perchlorate hexahydrate

 © 2004 Wiley-VCH Verlag GmbH & Co. KGaA, Weinheim

(0.36 g, 1 mmol) in absolute ethanol (20 mL) was added dropwise to the filtrate and the solution was stirred for 2 h at room temperature. The mauve powder formed was filtered off and washed with ethanol. Recrystallisation from water/ethanol (1:5) gave pink crystals suitable for X-ray diffraction after three weeks. Yield: ca. 70%; m.p. 270 °C. $C_{18}H_{26}Cl_2N_4NiO_8S_2$: calcd. C 34.9, H 4.2, N 9.0, Ni 9.5; found C 34.7, H 3.9, N 8.9, Ni 9.1. $\chi_M = 4550 \times 10^{-6}$ uem cgs, $\mu_{eff} = 3.27\ \mu_B$. UV/Vis (H_2O): λ_{max} (ε) = 965 nm sh, 890 (40 $mol^{-1}\cdot L\cdot cm^{-1}$), 830 sh; 570 sh, 540 (23).

Crystal Structure Determinations: The crystal data were collected on a Kappa CCD diffractometer using monochromatic Mo-K_α radiation (λ = 0.71073Å). The structures were solved by direct methods. After refinement of the non-hydrogen atoms, Fourier difference maps revealed maxima of residual electron density close to positions expected for hydrogen atoms. Hydrogen atoms were introduced as fixed contributors at calculated positions [C−H = 0.95 Å; B(H) = 1.3 Beq]. Final difference maps revealed no significant maxima. All calculations were performed with the Nonius OpenMoleN package.[23] Neutral-atom scattering factor and anomalous dispersion coefficients were taken from a standard source.[24] Molecular drawings were produced with the PLUTON software package.[25]

CCDC-213876 [for Ni(pydado)]$(ClO_4)_2\cdot H_2O$] and -213877 [for Ni(pydadt)]$(ClO_4)_2$] contain the supplementary crystallographic data for this paper. These data can be obtained free of charge at www.ccdc.cam.ac.uk/conts/retrieving.html [or from the Cambridge Crystallographic Data Centre, 12 Union Road, Cambridge CB2 1EZ, UK; Fax: (internat.) +44-1223-336-033; E-mail: deposit@ccdc.cam.ac.uk].

Acknowledgments

We are grateful to Prof. J. G. Fischer and Dr. A. De Cian (Université Louis Pasteur, Strasbourg, France) for the single-crystal X-ray analyses. We thank Dr. R. M. Hartshorn, University of Canterbury, for his advice on the geometrical configurations. C. Jubert thanks la Region Champagne-Ardenne for the award of a fellowship.

[1] [1a] J. C. Noveronn, M. M. Olmstead, P. K. Mascharak, *J. Am. Chem. Soc.* **1999**, *121*, 3553. [1b] B. A. Brennan, G. Alms, M. J. Nelson, L. T. Durney, R. C. Scarrow, *J. Am. Chem. Soc.* **1996**, *118*, 9194. [1c] J. R. Lancaster Jr., *The Bioinorganic Chemistry of Nickel* (Ed.: J. R. Lancaster), VCH Publishers, New York, **1988**. [1d] R. Cammack, *The Bioinorganic Chemistry of Nickel* (Ed.: J. R. Lancaster), VCH Publishers, New York, **1989**; chapter 8. [1e] R. H. Holm, P. Kennepohl, E. I. Solomon, *Chem. Rev.* **1996**, *96*, 2239, and references cited therein.

[2] [2a] J. Xia, J. Dong, S. Wang, R. A. Scott, P. A. Lindahl, *J. Am. Chem. Soc.* **1995**, *117*, 7065. [2b] R. Cammack, C. Bagyanka, K. Kovacs, *Eur. J. Biochem.* **1989**, *182*, 357. [2c] S. L. Tan, J. A. Fox, N. Kojima, C. T. Walsh, W. H. Orme-Johnson, *J. Am. Chem. Soc.* **1984**, *106*, 3064.

[3] [3a] M. K. Eidsness, R. A. Scott, B. C. Prickril, D. V. DerVartanian, J. LeGall, I. Moura, J. J. G. Moura, H. D. Peck Jr., *Proc. Natl. Acad. Sci., U. S. A.* **1989**, *86*, 147. [3b] M. K. Eidsness, R. J. Sullivan, R. A. Scott, *The Bioinorganic Chemistry of Nickel* (Ed.: J. R. Lancaster), VCH Publishers, New York, **1989**; chapter 4.

[4] [4a] N. Goswami, D. Eichhorn, *Inorg. Chem.* **1999**, *38*, 4329. [4b] E. Pereira, L. Gomes, D. B. Castro, *J. Chem. Soc., Dalton Trans.* **1998**, 629. [4c] E. Bouwman, R. K. Henderson, A. K. Powell, J. Reedijk, *J. Chem. Soc., Dalton Trans.* **1998**, 3495. [4d] T. Pandiyan, C. Duran de Bazua, M. Soriano-Garcia, *Fresenius' J. Anal. Chem.* **1996**, *354*, 636. [4e] M. Palaniandavar, T. Pandiyan, M. Lakshiminarayanan, H. Manohar, *J. Chem. Soc., Dalton Trans.* **1995**, 445.

[5] [5a] C. P. Kulatilleke, S. N. Goldie, M. J. Hegg, L. A. Ochrymowycz, D. B. Rorabacher, *Inorg. Chem.* **2000**, *39*, 1444. [5b] C. R. Lucas, S. Liu, *J. Chem. Soc., Dalton Trans.* **1994**, 185. [5e] B. Adhikary, S. Liu, C. R. Lucas, *Inorg. Chem.* **1993**, *32*, 5957.

[6] C. Jubert, A. Mohamadou, E. Guillon, J. P. Barbier, *Polyhedron* **2000**, *19*, 1447.

[7] C. Jubert, A. Mohamadou, J. Marrot, J. P. Barbier, *J. Chem. Soc., Dalton Trans.* **2001**, 1230.

[8] C. Jubert, PhD Thesis, University of Reims, **2001**; p. 105.

[9] [9a] S. D. Kim, J. K. Kim, W. S. Jung, *Bull. Kor. Chem. Soc.* **1996**, *17*, 80. [9b] S. D. Kim, J. K. Kim, W. S. Jung, *Polyhedron* **1998**, *17*, 1223.

[10] [10a] S. A. Bedell, J. H. Timmons, A. E. Martell, I. Murase, *Inorg. Chem.* **1982**, *21*, 1525. [10b] W. R. Harris, I. Murase, J. H. Timmons, A. E. Martell, *Inorg. Chem.* **1978**, *17*, 889. [10c] J. H. Timmons, W. R. Harris, I. Murase, A. E. Martell, *Inorg. Chem.* **1978**, *17*, 2192.

[11] R. G. Lacoste, A. E. Martell, *Inorg. Chem.* **1964**, *3*, 881.

[12] H. R. Hoveyda, V. Karunaratne, C. J. Nichols, S. J. Rettig, A. K. W. Stephens, C. Orvig, *Can. J. Chem.* **1998**, *76*, 414.

[13] [13a] M. Ray, S. Mukherjee, R. N. Mukherjee, *J. Chem. Soc., Dalton Trans.* **1990**, 3635. [13b] M. Ray, R. N. Mukherjee, *Polyhedron* **1992**, *11*, 2929.

[14] [14a] A. B. P. Lever, *Inorganic Electronic Spectroscopy*, Elsevier, Amsterdam, Oxford, New York, Tokyo, 2nd ed., **1984**, p. 126. [14b] A. B. P. Lever, *Inorganic Electronic Spectroscopy*, Elsevier, Amsterdam, Oxford, New York, Tokyo, 2nd ed., **1984**, p. 517.

[15] P. L. Meredith, T. A. Palmer, *Inorg. Chem.* **1971**, *10*, 1049.

[16] J. C. Bailar Jr., *Coord. Chem. Rev.* **1990**, *100*, 1.

[17] Y. Saito, *Top. Stereochem.* **1978**, *10*, 95.

[18] R. M. Hartshorn, D. A. House, *J. Chem. Soc., Dalton Trans.* **1998**, 2577.

[19] N. Arulsamy, J. Glerup, A. Hazell, D. J. Hodgson, C. J. Mc Kenzie, H. Toftlund, *Inorg. Chem.* **1994**, *33*, 3023.

[20] D. Perrin, W. L. F. Armarego, R. D. Perrin, *Purification of Laboratory Chemicals*, Pergamon, Oxford, 3rd ed., **1988**.

[21] A. Earnshaw, *Introduction to Magnetochemistry*, Academic Press, London, **1968**, p. 5.

[22] [22a] R. Fournaise, C. Petitfaux, *Talanta* **1987**, *34*, 385. [22b] R. Fournaise, C. Petitfaux, *Analusis* **1990**, *18*, 242.

[23] *OpenMoleN, Interactive Structure Solutions*, Nonius B. V., Delft, The Netherlands, **1997**.

[24] D. T. Cromer and J. T. Waber, *International Tables for X-ray Crystallography*, **1974**, IV, The Kyonoch Press, Birmingham, Table 2.2b and Table 2.3.1.

[25] A. L. Spek, *WINPL98, Interactive Molecular Graphics and Calculations Program for Windows*, University of Utrecht, The Netherlands, **2000**.

Received September 12, 2003
Early View Article
Published Online February 16, 2004

 © 2004 Wiley-VCH Verlag GmbH & Co. KGaA, Weinheim

Neutral and Cationic Methylaluminium Complexes of 2-Anilinotropone Ligands: Synthesis, Characterization, and Reactivity toward Ethylene

Daniela Pappalardo,*[b] Mina Mazzeo,[a] Pasquale Montefusco,[a] Consiglia Tedesco,[a] and Claudio Pellecchia[a]

Keywords: Aluminium / N,O ligands / Alkenes / Cations / Polymerizations

Some new aluminium complexes bearing bidentate monoanionic 2-anilinotroponate ligands have been synthesized and characterized. Reaction of 2-(2,6-diisopropylanilino)tropone or 2-(perfluoroanilino)tropone with $AlMe_3$ (1 equiv.) gave, by methane elimination, compounds [2-(2,6-diisopropylanilino)tropone]$AlMe_2$ (**1**) and [2-(perfluoroanilino)-tropone]$AlMe_2$ (**2**), respectively, as yellow solids. Reaction of **1** with 1 equiv. of the ligand furnished, by protodealumination of a second Al–CH_3 bond, the [2-(2,6-diisopropylanilino)tropone]$_2$AlMe derivative **3**. The structure of **3** has been determined by single-crystal X-ray diffraction, showing a five-coordinate aluminium atom with a distorted trigonal-bipyramidal geometry. Compounds **1** and **3** underwent methyl abstraction reactions with $B(C_6F_5)_3$; the resulting cationic species was trapped in the presence of THF in dichloromethane solution. The reactivity of the synthesized compounds in ethylene polymerisation has also been explored.

(© Wiley-VCH Verlag GmbH & Co. KGaA, 69451 Weinheim, Germany, 2004)

Introduction

Organometallic aluminium complexes are widely employed in organic synthesis and in catalysis.[1] In particular, organoaluminium compounds are currently used in polymerisation chemistry, e.g. in cationic,[2,3] anionic,[4−6] and ring-opening polymerisation.[7] In addition, alkylaluminium complexes have long been known to catalyse olefin oligomerizations,[8] and are the preferred cocatalysts in various important industrial processes catalysed by transition metals, such as the Ziegler−Natta olefin polymerisation,[9] the Wilke alkene dimerization[10] and the Ziegler nickel effect.[11]

The disclosure by Coles and Jordan in 1997 that certain cationic methylaluminium amidinate compounds promote ethylene polymerisation, although with low activity,[12] has encouraged a growing interest in exploring the reactivity of various aluminium compounds. Dialkylaluminium compounds bearing monoanionic chelating ligands, such as the *N*,*N* bidentate aminotroponiminate,[13] the tridentate *N*,*N*,*N* pyridylaminoamide[14] or the tridentate *O*,*N*,*N* and *O*,*N*,*O* pendant arm Schiff-base ligands[15] showed, after activation with the ionising agents traditionally used in homogeneous Ziegler−Natta catalysis {i.e. $B(C_6F_5)_3$ or $[(C_6H_5)_3C][B(C_6F_5)_4]$}, some activity for ethylene polymerisation catalysis. In this regard, we reported recently the synthesis of alkylaluminium compounds bearing phenoxy-imine or *N*,*N* imino-amide ligands that undergo decomposition reactions after alkyl abstraction with $B(C_6F_5)_3$; the cationic species were instead obtained in the presence of THF. Toluene solutions of the aluminium salicylaldiminate compounds, if activated with $B(C_6F_5)_3$, polymerise ethylene to solid polyethylene with low activity.[16] Furthermore, the simple bis(dichloroaluminium)ethane[17] and alkylaluminium compounds themselves,[18] activated with ionising agents, can catalyse the polymerisation of ethylene, also with low activity.

Although cationic alkyl complexes have been isolated and characterized, it is still unclear if they are directly responsible for the catalytic activity. Monitoring the reaction of alkylaluminium aminotroponiminate cationic complex with [D_4]ethylene, Jordan excluded that intact cationic species are the active ethylene polymerisation catalysts, while their main reaction is a β-H transfer to generate the corresponding cationic aluminium hydride.[13b] In fact, according to recent theoretical studies on ethylene polymerisation at aluminium centres, mononuclear aluminium species are unlikely to produce polymers, because chain transfer is too easy relative to propagation.[19] Therefore, more complex structures for the active species have to be considered. Computational studies showed that dinuclear species could be involved and, recently,[19c] an aluminium bis(iminophosphorano)methanediide complex, based on a spirocyclic carbon centre subtended by two $AlMe_2$ units, was shown to polymerise ethylene with higher activity.[20]

[a] Dipartimento di Chimica, Università di Salerno,
84081 Baronissi, Salerno, Italy
Fax: (internat.) + 39-089-965296
E-mail: pappalardo@unisannio.it
[b] Permanent address: Dipartimento di Scienze Geologiche e Ambientali, Università del Sannio,
Via Port'Arsa 11, 82100 Benevento, Italy

 © 2004 Wiley-VCH Verlag GmbH & Co. KGaA, Weinheim **DOI: 10.1002/ejic.200300116**

We report here the synthesis and characterization of some new aluminium complexes carrying bidentate monoanionic anilinotropone ligands[21] (Scheme 1), along with their reactivity with ion-generating activators, and some preliminary data on their reactivity in ethylene polymerisation.

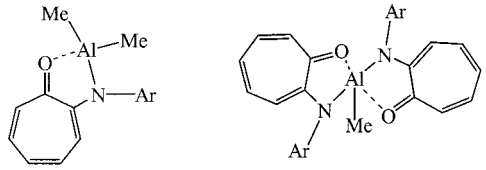

1 Ar = 2,6-(C_6H_3)*i*Pr_2
2 Ar = C_6F_5

3 Ar = 2,6-(C_6H_3)*i*Pr_2

Scheme 1

Results and Discussion

Synthesis of [2-(Anilino)tropone]$AlMe_2$ Derivatives

Recently, Brookhart has described neutral anilinotropone-based nickel(II) compounds[22] that can polymerise ethylene in the absence of an activator, with an activity higher than the analogous neutral nickel salicylaldiminate compounds reported by Grubbs.[23] We therefore synthesized the [2-(anilino)tropone]dimethylaluminium derivatives **1** and **2** to test their reactivity with olefins.

Treatment of 2-(2,6-diisopropylanilino)tropone[21] with $AlMe_3$ (1 equiv.) in toluene at 0 °C for 2 h produces [2-(2,6-diisopropylanilino)tropone]$AlMe_2$ (**1**) as a yellow solid. The reaction proceeds by protodealumination of the Al−CH_3 bond, with concomitant elimination of methane (Scheme 2), as evidenced by ^{1}H and ^{13}C NMR analysis. In the ^{1}H NMR spectrum ([D_6]benzene, room temperature) the N*H* singlet (δ = 8.86 ppm) of the ligand disappears, while a new singlet appears at high field [δ = −0.21 ppm (6 H)] accounting for the AlMe_2 protons. Similarly, in the ^{13}C NMR spectrum ([D_6]benzene, room temperature) a new signal at δ = −8.3 ppm is observed, which is attributable to AlMe_2 carbon atoms. The signal of the carbonyl carbon atom shifts from δ = 177.3 ppm in the free ligand to δ = 173.7 ppm in the aluminium compound **1**, indicating a change in electronic density after coordination to Al. The ^{1}H NMR spectrum has one signal for the AlMe_2 protons, one multiplet for C*H*Me_2 [δ = 3.09 ppm (2 H)] and two doublets for the methyl groups of CHMe_2 [δ = 1.21 ppm (6 H) and 0.89 ppm (6 H)]. The ^{13}C NMR spectrum confirms this picture: one signal for *C*HMe_2 (δ = 28.7 ppm), two signals for the methyl carbon atoms of CHMe_2 (δ = 25.9 and 24.5 ppm), one signal for the AlMe_2 groups. This pattern is compatible with a mirror symmetry passing through the tropone seven-membered ring, and perpendicular to the 2,6-disubstituted phenyl group; the AlMe_2 groups are equivalent, therefore they should lie symmetrically above and below the plane. Thus, the molecule belongs to the C_s symmetry group.

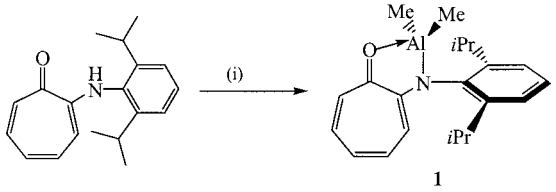

1

Scheme 2. Reaction conditions: (i): $AlMe_3$, toluene, 0 °C

The compound was further characterized by both FT-IR spectroscopy and EI mass spectrometry. The slight difference in the FT-IR spectrum between the stretching frequency of the carbonyl group in **1** (1598 cm^{-1}) and in the ligand (1601 cm^{-1}) could be explained by considering that in **1** the carbonyl group is reasonably coordinated to the metal atom while in the free ligand the C=O group is involved in hydrogen bonding with the NH group. The molecular ion peak in the EI mass spectrum is at m/z = 336.

The reaction of 2-(perfluoroanilino)tropone with $AlMe_3$ (1 equiv.) in toluene, at 0 °C, proceeds similarly (Scheme 3), affording [2-(perfluoroanilino)tropone]$AlMe_2$ (**2**) as a yellow solid, which has been characterized by ^{1}H and ^{13}C NMR analysis and EI mass spectrometry. The NMR spectroscopic data are compatible with a mirror symmetry passing through the seven-membered tropone ring and perpendicular to the perfluorophenyl group, as hypothesized for **1**.

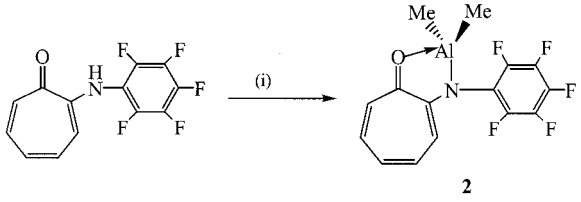

2

Scheme 3. Reaction conditions: (i): $AlMe_3$, toluene, 0 °C

Synthesis of [2-(2,6-Diisopropylanilino)tropone]$_2$AlMe (3)

The title compound was initially obtained as a secondary product in a preparation of **1**, upon accidentally using an excess of ligand, and was identified by NMR spectroscopy in [D_6]benzene solution. Compound **1** can be converted quantitatively into **3** by simply adding 1 equiv. of the ligand in toluene solution at room temperature (Scheme 4).

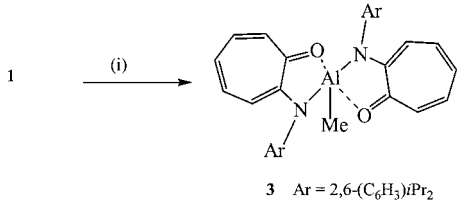

3 Ar = 2,6-(C_6H_3)*i*Pr_2

Scheme 4. Reaction conditions: (i): 2-(2,6-diisopropylanilino)tropone, toluene, room temperature

 © 2004 Wiley-VCH Verlag GmbH & Co. KGaA, Weinheim

Compound **3** has been fully characterised by ^1H and ^{13}C NMR spectroscopy, elemental analyses, EI MS, FT-IR spectroscopy, and single-crystal X-ray diffraction. Diagnostic signals in the ^1H NMR spectrum ([D_6]benzene, room temperature; Figure 1) are a singlet at $\delta = -0.06$ ppm (3 H), attributable to the Al*Me* protons, four doublets at $\delta = 0.99, 1.03, 1.06, 1.48$ ppm (6 H each) that are attributable to the CH*Me*$_2$ protons, and two multiplets for C*H*Me$_2$ at $\delta = 3.07$ (2 H) and 3.37 ppm (2 H). The ^{13}C NMR spectrum exhibits resonances for the corresponding carbon atoms: one signal at $\delta = -6.7$ ppm, attributable to Al*Me*, four signals for the methyl carbon atoms at $\delta = 23.9, 25.4, 25.5$ and 26.5 ppm, and two signals at $\delta = 28.8$ and 29.8 ppm for the *C*HMe$_2$ carbon atoms. This picture is consistent with a C_2 symmetry of the molecule in solution.

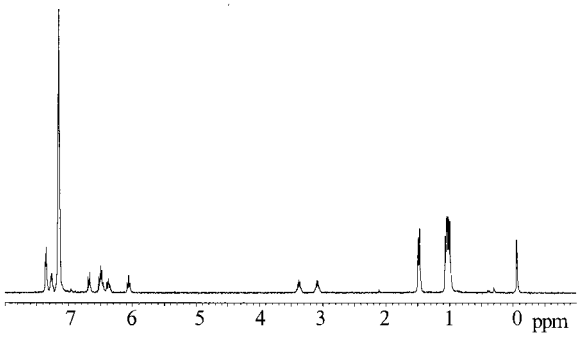

Figure 1. ^1H NMR spectrum of **3** (C_6D_6, room temperature)

The compound was further characterized by EI mass spectrometry, which shows the molecular ion peak at $m/z = 603$ $[M]^+$ and a peak at $m/z = 587$ $[M - CH_3]^+$. In the FT-IR spectrum, the stretching frequency of the carbonyl group appears at 1597 cm^{-1}.

Complex **3** crystallized as regular yellow prisms from toluene at −20 °C. The molecular structure of **3** (Figure 2) and the corresponding selected interatomic distances and angles (Table 1) are reported here. The X-ray structure determination shows that the space group is *C*2/*c*, with a crystallographic twofold axis parallel to the *b* axis and passing through the Al atom and methyl group C atom. Therefore the C_2 molecular axis, observed in solution, is preserved in the crystal. The unit cell contains four molecules of **3** and eight molecules of toluene disordered over a mirror plane; this feature affects the overall quality of the structural data.

The compound contains a five-coordinate Al atom with a highly distorted, approximate trigonal-bipyramidal geometry (tbp).[24] The O atoms occupy the apical positions, while the N atoms and the methyl group carbon atom lie in the equatorial plane; the C_2 molecular axis bisects the angle between the two N atoms.

The seven-membered tropone ring is almost planar with rmsd 0.024 Å; carbon atoms C1 and C7 deviate most from the seven-atoms least-squares plane by 0.039(4) and −0.034(4) Å, respectively. A comparison between the carbon−heteroatom bond lengths in compound **3** and in the free ligand[22] evidenced that the C1−O1 bond [1.292(5) Å] is longer than in the free ligand (1.252 Å), while C7−N1 [1.335(5) Å] is statistically almost the same as in the free ligand (1.355 Å). Some contribution from resonance form B in Scheme 5 cannot be excluded.

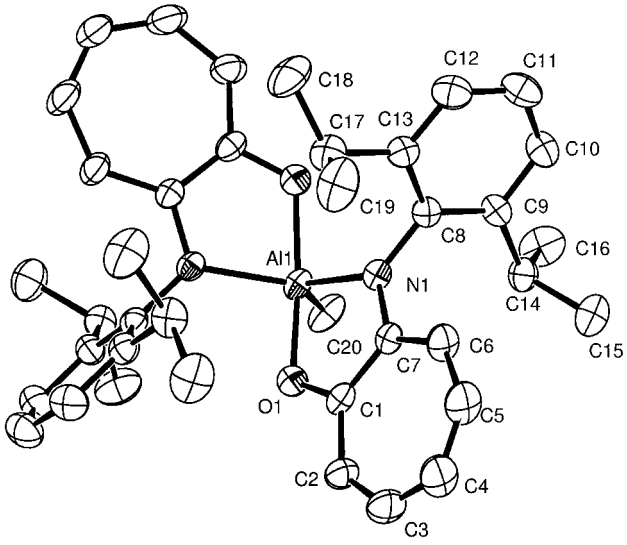

Figure 2. Molecular structure of **3**; thermal ellipsoids are drawn at 20% probability; H atoms omitted for clarity

Table 1. Selected bond lengths [Å] and angles [°]; symmetry-equivalent atoms indicated with the letter "e"

Al(1)−O(1)	1.865(3)	N(1)−Al(1)−O(1)	80.85(16)
Al(1)−N(1)	1.956(4)	N(1)−Al(1)−O(1e)	91.43(16)
Al(1)−C(20)	1.981(6)	O(1)−Al(1)−O(1e)	164.0(2)
O(1)−C(1)	1.292(5)	N(1)−Al(1)−N(1e)	122.3(2)
N(1)−C(7)	1.335(5)	N(1)−Al(1)−C(20)	118.84(12)
N(1)−C(8)	1.429(6)	O(1)−Al(1)−C(20)	97.99(11)
C(1)−C(2)	1.405(6)		
C(1)−C(7)	1.432(6)		
C(2)−C(3)	1.415(7)		
C(3)−C(4)	1.367(8)		
C(4)−C(5)	1.377(8)		
C(5)−C(6)	1.370(6)		
C(6)−C(7)	1.435(6)		

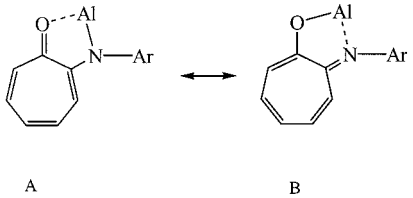

Scheme 5

The aniline six-membered ring is almost perfectly planar (rmsd 0.005 Å), with the N1, C14, and C17 atoms practically lying in the same plane. The aniline ring forms a dihedral angle of 58.6(1)° with the plane defined by the tropone seven-membered ring.

 © 2004 Wiley-VCH Verlag GmbH & Co. KGaA, Weinheim

Five-coordinate aluminium complexes play an important role as initiators for the controlled polymerisation of polar monomers. Complexes bearing tetradentate macrocyclic or chelating ligands (such as porphyrins,[25] salen-type ligands[26]), or bulky monoanionic bidentate ligands,[27] catalyse the living ring-opening polymerisation of propene oxide. The generation of highly electrophilic cationic species and their catalytic application has also been explored.[7b,28]

Generation of Cationic Species and Their Reactivity Toward Ethylene

For catalytic applications, cationic aluminium species are more attractive than neutral ones, because of their increased Lewis acidity. The stability of group-13 alkyl cations depends strongly on the ancillary ligand and the kind of counter anion. Bochmann has described the preparation of the bis(cyclopentadienyl)aluminium cation from the corresponding methyl compound after reaction with $B(C_6F_5)_3$;[3] however, simple alkylaluminium compounds, if treated with the activators commonly used in homogeneous olefin polymerisation catalysis {i.e. $B(C_6F_5)_3$ or $[(C_6H_5)_3C][B(C_6F_5)_4]$}, undergo degradation reaction with cleavage of a $B-C_6F_5$ bond.[29] The cationic alkylaluminium species was trapped in the presence of bases[7a] or using coordinating solvents, such as diethyl ether and THF.[30]

We have generated cationic complexes from the synthesized aluminium compounds by NMR tube reactions with $B(C_6F_5)_3$. When **1** and $B(C_6F_5)_3$ are mixed in C_6D_6 at room temperature, a brown oil precipitates, thus preventing NMR solution analysis. The reaction was consequently studied in CD_2Cl_2 solution. After in situ treatment of **1** with of $B(C_6F_5)_3$ (1 equiv.), the ^1H NMR spectrum shows a resonance at $\delta = +0.45$ ppm, which is attributable to the *free* anion $[MeB(C_6F_5)_3]^-$,[31] therefore indicating that the main reaction is methyl abstraction by $B(C_6F_5)_3$. The initially formed cationic species is degraded rapidly, generating a mixture of unidentified organometallic species. Ethylene was added to a freshly prepared solution of **1** and $B(C_6F_5)_3$ in CD_2Cl_2; monitoring the reaction at room temperature showed that ethylene was consumed and that a solid polymer was formed.

Attempts to isolate and better characterize the cationic species in the absence of bases were unsuccessful. Trapping of the cationic species was instead achieved in the presence of THF. When $B(C_6F_5)_3$ (1 equiv.) was added to a CD_2Cl_2 solution of **1** containing THF (1 equiv.), the THF-coordinated methyl cation of {[2-(2,6-diisopropylanilino)-tropone]AlMe(THF)}$^+$[MeB$(C_6F_5)_3]^-$ (**1a**) was formed (Scheme 6). Characteristic ^1H NMR resonances are the signals at $\delta = -0.27$ ppm for Al*Me*$^+$ (3 H) and at $\delta =$ 0.45 ppm for B*Me* (3 H). The pattern of signals in the ^1H NMR spectrum is consistent with the C_1 symmetry group (i.e. two signals for the C*H*Me$_2$ groups and four doublets for the methyl groups of CH*Me*$_2$). Accordingly, the THF methylenic hydrogen atoms in α-positions with respect to the oxygen atom are diastereotopic, and appear as two multiplets at $\delta = 4.40$ (2 H) and 4.26 ppm (2 H); the β-hydrogen atoms, instead, appear as a multiplet centred at $\delta =$ 2.25 ppm (4 H). After addition of a further equivalent of THF, the THF methylenic hydrogen atoms in α-positions with respect to the oxygen atom coalesce in a multiplet centered at $\delta = 4.20$ ppm, and the numbers and multiplicity of the signals are the same as in the neutral starting compound, i.e. one signal for the C*H*Me$_2$ and two doublets for the methyl groups of the CH*Me*$_2$. Such behaviour can, probably, be explained by assuming, in the presence of excess THF, there is a rapid exchange process between free and bound THF.

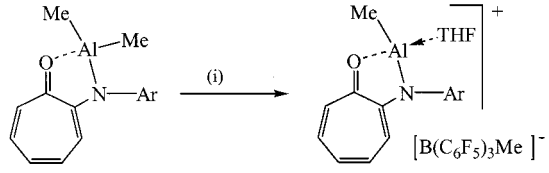

1 Ar = 2,6-(C_6H_3)*i*Pr$_2$ **1a** Ar = 2,6-(C_6H_3)*i*Pr$_2$

Scheme 6. Reaction conditions: (i): $B(C_6F_5)_3$, THF in CD_2Cl_2

Attempts to generate clean cationic species from the monomethylaluminium compound **3** with $B(C_6F_5)_3$ in the absence of coordinating agents were unsuccessful, leading always to a mixture of unidentified species. Addition of ethylene to a freshly prepared solution of **3** and $B(C_6F_5)_3$ did not result in monomer consumption or production of solid polymer, unlike the behaviour of **1** in the analogous experiment (see above). Since compounds **1** and **3** were prepared using the same reagents, but in different stoichiometric ratios, the implication of some metal impurity in the polymerization activity of the aluminium species **1** can be ruled out.[19] In fact, while the reaction of **1** with $B(C_6F_5)_3$ (1 equiv.) generates a cationic methylaluminium compound, abstraction of the methyl group from **3** generates a cationic species that lacks any Al−C bond suitable for chain growth by ethylene insertion.

The cationic species {[2-(2,6-diisopropilanylino)tropone]$_2$-Al(THF)}$^+$[MeB$(C_6F_5)_3]^-$ (**3a**) was cleanly generated by the reaction of **3** with of $B(C_6F_5)_3$ (1 equiv.) in the presence of THF (1 equiv.) in CD_2Cl_2 (Scheme 7). The product was characterized by ^1H and ^{13}C NMR spectroscopy at room temperature.

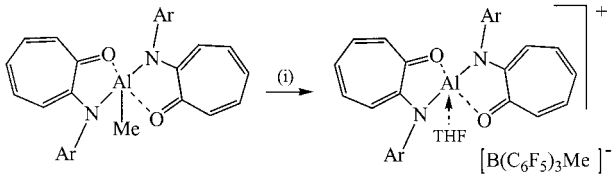

3 Ar = 2,6-(C_6H_3)*i*Pr$_2$ **3a** Ar = 2,6-(C_6H_3)*i*Pr$_2$

Scheme 7. Reaction conditions: (i): $B(C_6F_5)_3$, THF in CD_2Cl_2

In the ^1H NMR spectrum, the singlet of Al*Me* of the neutral starting compound **3** disappears, while a new signal appears at $\delta = 0.45$ ppm, which is attributable to the "free" anion $[MeB(C_6F_5)_3]^-$, indicating that alkyl abstraction has

 © 2004 Wiley-VCH Verlag GmbH & Co. KGaA, Weinheim

occurred. The numbers of signals (i.e. four doublets for the CH*Me*$_2$ protons, and two multiplets for C*H*Me$_2$ in the ^{1}H NMR spectrum; four signals for the methyl carbon atoms and two signals for the isopropylic *C*HMe$_2$ carbon atom in the ^{13}C NMR spectrum) indicate that the cation preserves the C_2 symmetry observed in solution in the neutral compound. Integration shows that the cation is supported by one molecule of coordinated THF. Interestingly, the THF methylenic hydrogen atoms in α-positions with respect to the oxygen atom, being diastereotopic, appear as two multiplets at δ = 4.38 (2 H) and 3.93 ppm (2 H); the β-hydrogen atoms, instead, appear as a multiplet centred at δ = 2.13 ppm (4 H) (Figure 3). This suggests that the THF molecule substitutes the methyl group of the corresponding neutral compound, and therefore is situated on the C_2 symmetry axis.

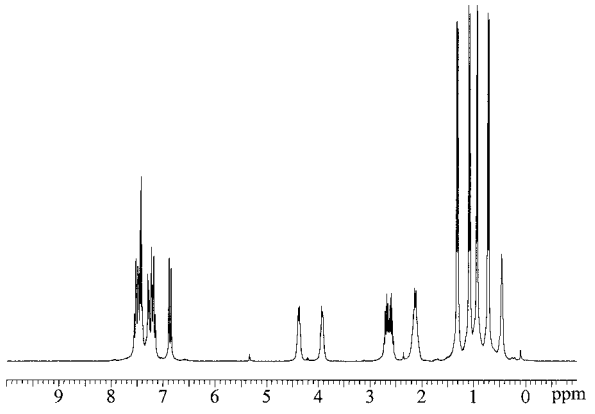

Figure 3. ^{1}H NMR spectrum of **3a** (CD_2Cl_2, room temperature)

Conclusions

Two new 4-coordinate aluminium complexes, namely [2-(2,6-diisopropylanilino)tropone]AlMe$_2$ (**1**) and [2-(perfluoroanilino)tropone]AlMe$_2$ (**2**), have been synthesized. A five-coordinate bis[2-(2,6-diisopropylanilino)tropone]AlMe derivative (**3**) has also been synthesized and characterized by single-crystal X-ray diffraction studies, which indicate a distorted trigonal-bipyramidal geometry around Al. Compounds **1** and **3** undergo methyl abstraction reactions with B(C_6F_5)$_3$; the resulting cationic species are stable in the presence of THF in dichloromethane solution. The reactivity of the synthesized compounds in ethylene polymerisation has also been explored. Interestingly, after reaction with B(C_6F_5)$_3$, compound **1** polymerizes ethylene to give a solid polymer, whereas compound **3** does not. This finding indicates that polymerization does not occur at a different metal contaminant.[19]

As Lewis acids, neutral, but especially cationic aluminium compounds, should be useful as catalysts to polymerize substrates containing a Lewis-basic atom. Experiments are in progress to ascertain if these compounds could be involved in the polymerization of polar monomers.

Experimental Section

General: Sensitive materials were manipulated under dry nitrogen using Schlenk or glove-box techniques. Toluene, heptane, and THF were heated under reflux in the presence of sodium and benzophenone and distilled under nitrogen prior to use. AlMe$_3$ was purchased from Aldrich and used as received. The 2-(2,6-diisopropylanilino)tropone and (perfluoroanilino)tropone ligands,[21] and B(C_6F_5)$_3$[30] were synthesized according to literature procedures. NMR spectra were recorded with a Bruker Avance 400 MHz spectrometer; chemical shifts were referenced to the residual protio impurity of the deuterated solvent. EI MS data were obtained with a Finnigan Thermoquest GCQ Plus 2000 spectrometer, using a direct exposure probe. Infrared spectra were recorded with a FT-IR Bruker Vector 22.

[2-(2,6-Diisopropylanilino)tropone]AlMe$_2$ (1): A toluene solution of 0.21 M AlMe$_3$ (4 mL, 0.85 mmol) was slowly added to a solution of 2-(2,6-diisopropylanilino)tropone (240 mg, 0.85 mmol) in toluene (15 mL) at 0 °C with stirring. The solution was then stirred for 2 h. Subsequently, the volatiles were removed under reduced pressure to give the product as an orange solid (yield 229 mg, 80%). ^{1}H NMR (400 MHz, C_6D_6): δ = 7.17 (d, 2 H, C*H*), 7.07 (d, 1 H, C*H*), 6.55 (m, 1 H, C*H*), 6.44 (d, 1 H, C*H*), 6.34 (m, 1 H, C*H*), 6.11 (t, 1 H, C*H*), 3.09 [m, 2 H, C*H*(CH$_3$)$_2$], 1.21 [d, 6 H, CH(C*H*$_3$)$_2$], 0.89 [d, 6 H, CH(C*H*$_3$)$_2$], −0.21 [s, 6 H, Al(C*H*$_3$)$_2$] ppm. ^{1}H NMR (400 MHz, CD_2Cl_2): δ = 7.38−7.28 (m, 3 H, C*H*), 7.28 (t, 2 H, C*H*), 6.87 (t, 2 H, C*H*), 6.57 (d, 1 H, C*H*), 2.93 [m, 2 H, C*H*(CH$_3$)$_2$], 1.20 [d, 6 H, CH(C*H*$_3$)$_2$], 0.99 [d, 6 H, CH(C*H*$_3$)$_2$], −0.74 [s, 6 H, Al(C*H*$_3$)$_2$] ppm. ^{13}C NMR (100 MHz, C_6D_6): δ = 173.7 (C=O), 167.4 (C−N), 144.4, 139.9 (*C*H), 138.4 (*C*H), 126 (*C*H), 125.7 (*C*H), 123.6 (*C*H), 122.3 (*C*H), 28.7 [*C*H(CH$_3$)$_2$], 25.9 [CH(*C*H$_3$)$_2$], 24.5 [CH(*C*H$_3$)$_2$], −8.3 [Al(*C*H$_3$)$_2$] ppm. EI MS (35 eV): *m*/*z* = 336 [M]$^+$, 324 [M − CH$_3$]$^+$. FT-IR: $\tilde{\nu}$ = 1598 (C=O) cm^{-1}. $C_{21}H_{28}AlNO$ (337.44): calcd. C 74.75, H 8.36, N 4.15; found C 74.54, H 8.56, N 4.29.

[2-(Perfluoroanilino)tropone]AlMe$_2$ (2): A solution of 2-(perfluoroanilino)tropone (300 mg, 1.04 mmol) in dry toluene (10 mL) was added dropwise to a toluene solution of 0.26 M AlMe$_3$ (10 mL, 1.14 mmol) at 0 °C. The solution was then stirred for 2 h and left to reach room temperature. The resulting solution was subsequently concentrated and cooled to −20 °C; compound then **2** precipitated as an orange powder; yield 150 mg (42%). ^{1}H NMR (400 MHz, C_6D_6): δ = 6.99 (d, 1 H, C*H*), 6.52 (t, 2 H, C*H*), 6.18 (t, 2 H, C*H*), −0.17 [s, 6 H, Al(C*H*$_3$)$_2$]. ^{13}C NMR (100 MHz, C_6D_6): δ = 175.1 (C-1), 165.8 (C-2), 139.7 (*C*H), 139.1 (*C*H), 126.2 (*C*H), 124.3 (*C*H), 118.9 (*C*H), −9.3 [Al(CH$_3$)$_2$] ppm. EI MS(35 eV): *m*/*z* = 346 [M]$^+$, 328 [M − CH$_3$]$^+$.

[2-(2,6-Diisopropylanilino)tropone]$_2$AlMe (3): [2-(2,6-Diisopropilanilino)tropone]AlMe$_2$ (82 mg, 0.24 mmol) was dissolved in dry toluene (10 mL). A solution of 2-(2,6-diisopropylanilino)tropone (68 mg, 0.24 mmol) in toluene (5 mL) was then added and the resulting solution stirred at room temperature for 2 h. The volatiles were then removed under reduced pressure to give the product as an orange solid in almost quantitative yield. ^{1}H NMR (400 MHz, C_6D_6): δ = 7.34 (d, 4 H, C*H*), 7.26 (m, 2 H, C*H*), 6.68 (d, 2 H, C*H*), 6.49 (m, 4 H, C*H*), 6.47 (t, 2 H, C*H*), 6.04 (t, 2 H, C*H*), 3.37 [m, 2 H, C*H*(CH$_3$)$_2$], 3.07 (m, 2 H, C*H*(CH$_3$)$_2$], 1.48 [d, 6 H, CH(C*H*$_3$)], 1.06 [d, 6 H, C*H*(C*H*$_3$)], 1.03 [d, 6 H, C*H*(C*H*$_3$)], 099 [d, 6 H, C*H*(C*H*$_3$)], −0.06 (s, 3 H, AlC*H*$_3$) ppm. ^{1}H NMR (400 MHz, CD_2Cl_2): δ = 7.32−7.03 (m, 10 H, C*H*), 6.70 (m, 4 H, C*H*), 6.46 (d, 2 H, C*H*), 3.05 [m, 2 H, C*H*(CH$_3$)$_2$], 2.77 [m, 2 H, C*H*(CH$_3$)$_2$],

 © 2004 Wiley-VCH Verlag GmbH & Co. KGaA, Weinheim

1.27 [d, 6 H, CH(CH_3)], 1.16 [d, 6 H, CH(CH_3)], 1.05 [d, 6 H, CH(CH_3)], 0.78 [d, 6 H, CH(CH_3)], −0.83 (s, 3 H, AlCH_3) ppm. ^{13}C NMR (100 MHz, C_6D_6): δ = 175.2 (C=O); 166.6 (C−N); 144.4, 143.8, 142.3, 138.4, 137.5, 127.0, 125.5, 124.4, 124.1, 122.5, 121.1; 29.8 and 28.8 [*C*H(CH$_3$)$_2$]; 26.5, 25.5, 25.4, and 23.9 [CH(*C*H$_3$)$_2$]; −6.7 (Al*C*H$_3$) ppm. EI MS(35 eV): *m*/*z* = 603 [M]$^+$, 587 [M − CH$_3$]$^+$. FT-IR: $\tilde{\nu}$ = 1597 (C=O) cm^{-1}. $C_{39}H_{47}N_2O_2Al$ (602.79): calcd. C 77.71, H 7.86, N 4.65; found C 77.23, H 8.16, N 4.34.

Generation of {[2-(2,6-Diisopropylanilino)tropone]AlMe(THF)}$^+$-[MeB(C$_6$F$_5$)$_3$]$^-$ (1a): Compound **1** (17 mg, 50 μmol) was dissolved in CD_2Cl_2 (0.5 mL). THF (4 μL, 50 μmol) and B(C$_6$F$_5$)$_3$ (26 mg, 50 μmol) were then added sequentially, and the so-obtained solution was analysed by NMR spectroscopy at room temperature. ^{1}H NMR (400 MHz, CD_2Cl_2): δ = 7.76 (m, 2 H, C*H*), 7.66 (m, 1 H, C*H*), 7.46−7.35 (m, 4 H, C*H*), 6.99 (d, 1 H, C*H*), 4.40 (m, 2 H, OCH_2), 4.26 (m, 2 H, O-CH_2), 2.66 (m, 1 H, C*H*(CH$_3$)$_2$], 2.57 (m, 1 H, C*H*(CH$_3$)$_2$], 2.25 (s, 4 H, CH_2), 1.21 (d, 6 H, CHCH_3), 1.01 (d, 3 H, CHCH_3), 0.92 (d, 3 H, CHCH_3), 0.45 (s, 3 H, BCH_3), −0.27 (s, 3 H, AlCH_3) ppm. ^{13}C NMR (100 MHz, CD_2Cl_2): δ = 169.4 (C=O), 168.0, 144.4, 143.8, 142.3, 141.3, 134.5, 133.2, 129.5, 128.0, 126.6, 125.8, 125.3, 76.2 (O*C*H$_2$), 29.2 (2 peaks overlapped, *C*H), 25.9 (*C*H$_2$CH$_2$O), 25.0, 24.8, 23.9 (CH*C*H$_3$), 10.0 (B*C*H$_3$) ppm. Successively, one further eqivalent of THF was added to the solution, and the sample analysed by NMR spectroscopy at room temperature. ^{1}H NMR (400 MHz, CD_2Cl_2): δ = 7.65 (m, 2 H, C*H*), 7.55 (m, 1 H, C*H*), 7.46−7.27 (m, 4 H, C*H*), 6.90 (d, 1 H, C*H*), 4.20 (s, 8 H, OCH_2), 2.60 [m, 2 H, C*H*(CH$_3$)$_2$], 2.11 (s, 8 H, CH_2), 1.20 (d, 6 H, CHCH_3), 1.00 (d, 6 H, CHCH_3), 0.46 (s, 3 H, BCH_3), −0.48 (s, 3 H, AlCH_3) ppm. ^{13}C NMR (100 MHz, CD_2Cl_2): δ = 169.4 (C=O), 167.9, 144.0, 143.2, 142.2, 133.0, 129.4, 127.8, 126.2, 125.3, 125.2; 76.0 (O*C*H$_2$), 29.2 (*C*H), 25.7 (*C*H$_2$CH$_2$O), 25.4, 23.7 (CH*C*H$_3$), 10.2 (B*C*H$_3$), −14.0 (Al*C*H$_3$) ppm.

Generation of {[2-(2,6-Diisopropylanilino)tropone]$_2$Al(THF)}$^+$-[MeB(C$_6$F$_5$)$_3$]$^-$ (3a): Compound **3** (15 mg, 25 μmol) was dissolved in CD_2Cl_2 (0.5 mL). Dry THF (2 μL, 25 μmol) and B(C$_6$F$_5$)$_3$ (13 mg, 25 μmol) were then added sequentially, and the resulting solution was analysed by NMR spectroscopy at room temperature. ^{1}H NMR (300 MHz, CD_2Cl_2): δ = 7.60−7.10 (m, 14 H) and 6.85 (d, 2 H) (phenyl and tropone *H*), 4.38 (m, 2 H, OCH_aH$_b$), 3.93 (m, 2 H, OCH$_a$*H*$_b$), 2.67 [m, 2 H, C*H*(CH$_3$)$_2$], 2.59 [m, 2 H, C*H*(CH$_3$)$_2$], 2.13 (m, 4 H, CH_2), 1.32 [d, 6 H, CH(CH_3)], 1.08 [d, 6 H, CH(CH_3)], 0.93 [d, 6 H, CH(CH_3)], 0.72 [d, 6 H, CH(CH_3)], 0.45 (s, 3 H, BCH_3) ppm. ^{13}C NMR (75 MHz, CD_2Cl_2): δ = 169.9 (*C*=O), 167.4, 143.8, 143.2 (quaternary carbon atoms), 140.8 (*C*H), 140.2 (*C*H), 138.5 (quaternary carbon atom), 130.3 (*C*H), 128.3 (*C*H), 125.4 (*C*H), 123.9 (*C*H), 75.7 (OCH$_2$CH$_2$), 29.7 [*C*H(CH$_3$)$_2$], 29.2 [*C*H(CH$_3$)$_2$], 25.9 (OCH$_2$*C*H$_2$), 24.9 [CH(*C*H$_3$)], 23.7 [CH(*C*H$_3$)] ppm.

X-ray Crystallography: A prismatic yellow crystal of **3** (0.56 × 0.48 × 0.40 mm) was selected and mounted in a Lindemann capillary under an inert gas. Diffraction data were then measured at room temperature with a Rigaku AFC7S diffractometer using graphite-monochromated Mo-K_α radiation (λ = 0.71069 Å). Data reduction was performed with the crystallographic package TEXSAN.[32] The ψ-scan method was used to correct data for absorption. Structures were solved by direct methods using the program SIR92[33] and refined by means of full-matrix least squares based on F^2 including all diffraction data using the program SHELXL-97.[34] The electron density map revealed a disordered toluene molecule. A rigid body refinement was performed for the solvent molecule, considering two distinct toluene molecules with half occupancy. The hydrogen atoms of the methyl groups were assumed to be disordered over two sites rotated 60° to each other. Anisotropic displacement parameters were used for all non-hydrogen atoms except those belonging to the solvent molecule. Hydrogen atoms were positioned geometrically and refined using a riding model. Finally, a total of 226 parameters were refined considering 4174 intensity data. Maximum and minimum residual densities were 0.35 and −0.34 e·Å^{-3}, respectively. Final disagreement indices were R_1 = 0.0829 for 1336 reflections with $F_o > 4\sigma(F_o)$, R_1 = 0.255 and wR_2 = 0.146 for all 4174 data. ORTEP drawings performed by means of the program ORTEP32.[35] Crystallographic data for **3**: Formula: $C_{39}H_{47}AlN_2O_2{\cdot}2C_7H_8$, M = 787.03, system: monoclinic, space group *C*2/*c*, Z = 4; a = 18.321(6), b = 10.145(3), c = 25.506(7) Å; β = 91.40(3)°, V = 4739(2) Å^3, D_x = 1.103 g·cm^{-3}, $\mu_{calcd.}$ = 0.08 mm^{-1}. Crystallographic data (excluding structure factors) have been deposited with the Cambridge Crystallographic Data Centre as supplementary publications no. CCDC-204539. Copies of the data may be obtained free of charge on application to CCDC, 12 Union Road, Cambridge CB2 EZ, UK [Fax: (internat.) + 44-1223-336-033; E-mail: deposit@ccdc.cam.ac.uk].

Acknowledgments

The authors are grateful to Professor A. Immirzi for valuable discussions, to Dr. A. Moresco (ICIS, CNR, Padova, Italy) for the elemental analyses and to Mr. R. Miranda for EI MS measurements. This work was supported by the Italian Ministry of University and Research (Progetto Giovani Ricercatori 2001 and PRIN 2002).

[1] J. J. Eish, "Aluminum" in: *Comprehensive Organometallic Chemistry II* (Eds.: E. W. Abel, F. G. A. Stone, G. Wilkinson), Elsevier, Oxford, UK, **1995**, chapter 10, pp. 431−502.
[2] *Cationic Polymerization: Mechanism, Synthesis and Applications* (Ed.: K. Matyjaszewski), Marcel Dekker, New York, **1996**.
[3] M. Bochmann, D. M. Dawson, *Angew. Chem. Int. Ed. Engl.* **1996**, *35*, 2226−2228.
[4] [4a] M. Kukoki, T. Aida, S. Inoue, *J. Am. Chem. Soc.* **1987**, *109*, 4737−4738. [4b] M. Kukoki, T. Watanabe, T. Aida, S. Inoue, *J. Am. Chem. Soc.* **1991**, *113*, 5903−5904.
[5] [5a] M. Dimonie, D. Mardare, S. Coca, V. Drăgutan, I. Ghivirigă, *Macromol. Rapid Commun.* **1992**, *13*, 37−44. [5b] D. Mardare, K. Matyjaszewski, *Macromol. Rapid Commun.* **1994**, *15*, 37−44.
[6] F. Coslèdan, P. B. Hitchcock, M. F. Lappert, *Chem. Commun.* **1999**, *13*, 705−706.
[7] [7a] J. A. Jeger, D. A. Atwood, *Inorg. Chem.* **1997**, *37*, 2034−2039. [7b] M. A. Munoz-Hernandez, M. L. McKee, T. S. Keizer, B. C. Yearwood, D. A. Atwood, *J. Chem. Soc., Dalton Trans.* **2002**, 410−414. [7c] S. Inoue, *J. Polym. Sci., Part A.: Polym. Chem.* **1998**, *21*, 3114 and refs therein. [7d] Z. Zhong, P. J. Dijkstra, J. Feijen, *Angew. Chem. Int. Ed.* **2002**, *41*, 4510−4513.
[8] K. Ziegler, H.-G. Gellert, K. Zosel, E. Holzkamp, J. Schneider, M. Söll, W.-R. Kroll, *Justus, Liebigs Ann. Chem.* **1960**, *629*, 121−166.
[9] J. Boor, Jr., *Ziegler−Natta Catalysts and Polymerizations*, Academic Press, New York, **1979**.
[10] U. Birkenstock, H. Bönneman, B. Bogdanovic, D. Walter, G. Wilke, in: *Advances in Chemistry Series*, American Chemical Society, Washington, DC, **1968**, vol. 70, p. 250.
[11] K. Fischer, K. Jonas, P. Misbach, R. Stabba, G. Wilke, *Angew. Chem.* **1973**, *85*, 1002; *Angew. Chem. Int. Ed. Engl.* **1973**, *12*, 943.
[12] [12a] M. P. Coles, R. F. Jordan, *J. Am. Chem. Soc.* **1997**, *119*,

 © 2004 Wiley-VCH Verlag GmbH & Co. KGaA, Weinheim

8125−8126. [12b] S. Dagorne, I. A. Guzei, M. P. Coles, R. F. Jordan, *J. Am. Chem. Soc.* **2000**, *122*, 274−289.
[13] [13a] E. Ihara, V. G. Young, Jr., R. F. Jordan, *J. Am. Chem. Soc.* **1998**, *120*, 8277−8278. [13b] A. V. Korolev, E. Ihara, I. A. Guzei, V. G. Young, Jr., R. F. Jordan, *J. Am. Chem. Soc.* **2001**, *123*, 8291−8309.
[14] M. Bruce, V. C. Gibson, C. Redshaw, G. A. Solan, A. J. P. White, D. J. Williams, *Chem. Commun.* **1998**, 2523−2524.
[15] P. A. Cameron, V. C. Gibson, C. Redshaw, J. A. Segal, M. D. Bruce, A. J. P. White, D. J. Williams, *Chem. Commun.* **1999**, 1883−1884.
[16] D. Pappalardo, C. Tedesco, C. Pellecchia, *Eur. J. Inorg. Chem.* **2002**, 621−628.
[17] H. Martin, H. Bretinger, *Makromol. Chem.* **1992**, *193*, 1283−1288.
[18] J. S. Kim, L. M Wojieinski II, S. Liu, J. C. Sworen, A. Sen, *J. Am. Chem. Soc.* **2000**, *122*, 5668−5669.
[19] [19a] G. Talarico, P. H. M. Budzelaar, *Organometallics* **2000**, *19*, 5691−5695. [19b] G. Talarico, V. Busico, P. H. M. Budzelaar, *Organometallics* **2001**, *20*, 4721−4726. [19c] G. Talarico, P. H. M. Budzelaar, *Organometallics* **2002**, *21*, 34−38.
[20] R. G. Cavell, K. Aparna, R. P. Kamalesh Babu, Q. Wang, *J. Mol. Cat. A: Chem.* **2002**, *189*, 137−143.
[21] F. A. Hicks, M. Brookhart, *Org. Lett.* **2000**, *2*, 219−221.
[22] [22a] F. A. Hicks, M. Brookhart, *Organometallics* **2001**, *20*, 3217−3219. [22b] F. A. Hicks, J. C. Jenkins, M. Brookhart, *Organometallics* **2003**, *22*, 3533−3545.
[23] T. R. Younkin, E. F. Connor, J. I. Henderson, S. K. Friedrich, R. H. Grubbs, D. A. Bansleben, *Science* **2000**, *287*, 460−462.
[24] The tbp geometry has been assessed, according to ref.[7b], using the geometric parameter $\tau = (\beta - \alpha)/60$, where β = O1−Al1−O1 angle and α = N1−Al1−N1 angle. A value of zero applies to a compound with a perfect square-pyramidal geometry and a value of 1 to a perfect trigonal-bipyramidal geometry. In this case $\tau = 0.70$.
[25] [25a] A. Le Borgne, N. Spassky, C. Lin Jun, A. Momtaz, *Makromol. Chem.* **1988**, *189*, 637−650.-. [25b] H. Sugimoto, C. Kawamura, M. Kuroki, T. Aida, S. Inoue, *Macromolecules* **1994**, *27*, 2013−2018.
[26] T. Aida, S. Inoue, *Macromolecules* **1981**, *14*, 1166−1169.
[27] B. Antelmann, M. H. Chisholm, S. S. Iyer, J. C. Huffman, D. Navarro-Llobet, M. Pagel, *Macromolecules* **2001**, *34*, 3159−3175.
[28] D. A. Atwood, J. A. Jegier, D. Rutherford, *J. Am. Chem. Soc.* **1995**, *117*, 6779−6780.
[29] [29a] The reaction between AlR_3 and $B(C_6F_5)_3$ has been described in a patent application as a convenient approach to the synthesis of $Al(C_6F_5)_3$: P. Biagini, G. Lugli, L. Abis, P. Andreussi (Enichem Elastomeri S. r. l.), Eur. Patent Appl. EP 0 694 548 A1 **1996**, p. 1−9. [29b]M. Bochmann, M. J. Sarfield, *Organometallics* **1998**, *17*, 5908−5912.
[30] G. Klosin, R. G. Roof, E. Y.-X. Chen, K. A Abboud, *Organometallics* **2000**, *19*, 4684−4686.
[31] X. Yang, C. L. Stern, T. J. Marks, *J. Am. Chem. Soc.* **1994**, *116*, 10015−10031.
[32] *TEXSAN*, Crystal Structure Analysis Package, Molecular Structure Corporation, **1985−1992**.
[33] A. Altomare, G. Cascarano, C. Giacovazzo, A. Guagliardi, M. C. Burla, G. Polidori, M. Camalli, *J. Appl. Crystallogr.* **1994**, *27*, 435.
[34] G. M. Sheldrick, *SHELXL-97, A Program For Refining Crystal Structures*, University of Göttingen, Germany, **1997**.
[35] L. J. Farrugia, *J. Appl. Crystallogr.* **1997**, *30*, 565.

Received February 27, 2003
Early View Article
Published Online February 10, 2004

 © 2004 Wiley-VCH Verlag GmbH & Co. KGaA, Weinheim

Synthesis, Structural Characterisation and Reactivity of New Dinuclear Monocyclopentadienyl Imidoniobium and -tantalum Complexes − X-ray Crystal Structures of [{Nb(η^5-$C_5H_4SiMe_3$)Cl_2}$_2$(μ-1,4-NC_6H_4N)], [{Ta(η^5-C_5Me_5)Cl_2}$_2$(μ-1,4-NC_6H_4N)] and [{Ta(η^5-C_5Me_5)(CH_2SiMe_3)$_2$}$_2$-(μ-1,4-NC_6H_4N)]

Antonio Antiñolo,[b] Iván Dorado,[a] Mariano Fajardo,[a] Andrés Garcés,[a] Isabel López-Solera,[a] Carmen López-Mardomingo,[c] Marek M. Kubicki,[d] Antonio Otero,*[b] and Sanjiv Prashar[a]

Keywords: Cyclopentadienyl ligands / Half-sandwich complexes / N ligands / Niobium / Tantalum

The preparation of a family of dinuclear monocyclopentadienyl imidoniobium and -tantalum complexes was achieved by two different synthetic routes. The diimido complexes [{M(Cp′)Cl_2}$_2$(μ-1,*i*-NC_6H_4N)] [Cp′ = η^5-$C_5H_4SiMe_3$, M = Nb, *i* = 4 (**1**); Cp′ = η^5-$C_5H_4SiMe_3$, M = Nb, *i* = 3 (**2**); Cp′ = η^5-$C_5H_4SiMe_3$, M = Nb, *i* = 2 (**3**); Cp′ = η^5-C_5Me_5, M = Nb, *i* = 4 (**4**); Cp′ = η^5-C_5Me_5, M = Nb, *i* = 3 (**5**); Cp′ = η^5-$C_5H_4SiMe_3$, M = Ta, *i* = 4 (**6**); Cp′ = η^5-$C_5H_4SiMe_3$, M = Ta, *i* = 3 (**7**)] were prepared by the reaction of one equivalent of the trichloro precursor [{MCl_3}$_2$(μ-1,*i*-NC_6H_4N)] (M = Nb, Ta, *i* = 4, 3 or 2) with two equivalents of either $C_5H_4(SiMe_3)_2$ or C_5Me_5-($SiMe_3$). Complexes **1**–**7** can also be prepared by the reaction of two equivalents of [MCp′Cl_4] (Cp′ = η^5-$C_5H_4SiMe_3$, M = Nb, Ta; Cp′ = η^5-C_5Me_5, M = Nb, Ta) with one equivalent of the corresponding aniline compound, *N*,*N*,*N*′,*N*′-tetrakis(trimethylsilyl)-1,4-, -1,3-, or -1,2-phenylenediamine, respectively. The synthesis of [{Ta(Cp′)Cl_2}$_2$(μ-1,*i*-NC_6H_4N)] [Cp′ = η^5-C_5Me_5, *i* = 4 (**8**); Cp′ = η^5-C_5Me_5, *i* = 3 (**9**)] was only successful with the second preparative method. The reaction of **1**, **2** and **8** with alkylating reagents gave the corresponding tetraalkyl derivatives, [{M(Cp′)R_2}$_2$(μ-1,*i*-NC_6H_4N)] [Cp′ = η^5-$C_5H_4SiMe_3$, M = Nb, R = Me, *i* = 4 (**10**); Cp′ = η^5-$C_5H_4SiMe_3$, M = Nb, R = CH_2SiMe_3, *i* = 4 (**11**); Cp′ = η^5-$C_5H_4SiMe_3$, M = Nb, R = CH_2Ph, *i* = 4 (**12**); Cp′ = η^5-$C_5H_4SiMe_3$, M = Nb, R = Me, *i* = 3 (**13**); Cp′ = η^5-$C_5H_4SiMe_3$, M = Nb, R = CH_2SiMe_3, *i* = 3 (**14**); Cp′ = η^5-$C_5H_4SiMe_3$, M = Nb, R = CH_2Ph, *i* = 3 (**15**); Cp′ = η^5-C_5Me_5, M = Ta, R = Me, *i* = 4 (**16**); Cp′ = η^5-C_5Me_5, M = Ta, R = CH_2SiMe_3, *i* = 4 (**17**); Cp′ = η^5-C_5Me_5, M = Ta, R = CH_2Ph, *i* = 4 (**18**)]. The alkylated complexes with other stoichiometries, [{M(Cp′)(Me)(X)}$_2$(μ-1,4-NC_6H_4N)] [Cp = η^5-$C_5H_4SiMe_3$, M = Nb, X = Cl (**19**); Cp = η^5-$C_5H_4SiMe_3$, M = Nb, X = NMe_2 (**20**); Cp = η^5-C_5Me_5, M = Ta, X = Cl (**21**)], were also prepared. The molecular structures of complexes **1**, **8** and **17** were determined by single-crystal X-ray diffraction studies.

(© Wiley-VCH Verlag GmbH & Co. KGaA, 69451 Weinheim, Germany, 2004)

Introduction

Imido derivatives of early transition metals have been widely studied and, in particular, a large number of well-established imido compounds of the d^0 metals niobium and tantalum are known.[1] For example, half-sandwich imido compounds of Nb and Ta of general formula M(η^5-C_5R_5')(NR)X_2 are well documented[2] and these are of considerable interest since an "isolobal" relationship between [M(η^5-C_5R_5')(NR)] (M = group 5 metal) and [M(η^5-C_5R_5')$_2$] (M = Group 4 metal) fragments has been established.[3] In fact, it has been claimed that monocyclopentadienyl imido group 5 metal complexes could behave in a similar manner to metallocenes of group 4 metals in olefin polymerisation catalytic processes.[2g] However, to date several species of this type have been used as catalysts without much success.[4] Two main preparative pathways have been employed in the synthesis of half-sandwich imido group 5 metal complexes. Firstly, reaction of the appropriate cyclopentadienide reagent with imido-containing [M(NR)Cl_3L_2] (M = Nb, Ta) precursors[5] has been employed and, sec-

[a] Departamento de Tecnología Química, Ambiental y de los Materiales, E.S.C.E.T., Universidad Rey Juan Carlos, 28933 Móstoles, Madrid, Spain
Fax: (internat.) + 34-91-488-7068
E-mail: S.Prashar@escet.urjc.es
[b] Departamento de Química Inorgánica, Orgánica y Bioquímica, Universidad de Castilla-La Mancha, Facultad de Químicas, Campus Universitario, 13071-Ciudad Real, Spain
Fax: (internat.) + 34-926-295-318
E-mail: Antonio.Otero@uclm.es
[c] Departamento de Química Orgánica, Campus Universitario, Universidad de Alcalá, 28871 Alcalá de Henares, Madrid, Spain
[d] Laboratoire de Synthèse et d'Electrosynthèse Organométalliques, CNRS UMR 5632, Faculté des Sciences Gabriel, Université de Bourgogne, 6 bd Gabriel, 21000 Dijon, France

ondly, the most general method involves the introduction of the imido group into precursors containing the cyclopentadienyl ligand.[6] On considering the different possible pathways to achieve this transformation, the one that is particularly noteworthy is that in which the imido group is incorporated by breaking the Si−N bond of a silylamine or -amide derivative.[7] The use of this last method, developed by our research group, gives rise to an interesting series of organo-diimido complexes [{Nb(L)$_2$Cl$_3$}$_2$(μ-1,*i*-NC$_6$H$_4$N)] (L = CH$_3$CN or *t*Bupy) by reaction of NbCl$_5$ with the appropriate aniline *N*,*N*,*N*′,*N*′-tetrakis(trimethylsilyl)-1,4-, -1,3-, or -1,2-phenylenediamine in the presence of CH$_3$CN or *t*Bupy.[8] As a continuation of our research in this field[9] we are currently interested in the preparation of half-sandwich diimidoniobium and -tantalum complexes in order to synthesise new types of dinuclear complexes in which the two metal centres are linked by conjugated π-systems. This class of diimido complex is rare, particularly with an aryl ligand.[10] The work described in this paper focuses on the synthesis and structural characterisation of half-sandwich imidoniobium and -tantalum complexes, and some aspects of their reactivity.

Results and Discussion

The preparation of derivatives [{M(Cp′)Cl$_2$}$_2$(μ-1,*i*-NC$_6$H$_4$N)] (Cp′ = η^5-C$_5$H$_4$SiMe$_3$, η^5-C$_5$Me$_5$; M = Nb, Ta; *i* = 3, 4) was initially undertaken by reaction of the appropriate complex [{M(L)$_2$Cl$_3$}$_2$(μ-1,*i*-NC$_6$H$_4$N)] (L = CH$_3$CN; M = Nb, Ta; *i* = 3, 4)[8] with different cyclopentadienide reagents, namely M(C$_5$H$_4$SiMe$_3$) (M = Li, Na, K) or K(C$_5$Me$_5$), in several solvents and under different experimental conditions. However, in all cases an intractable mixture of products was obtained. As an alternative method to prepare the aforementioned complexes, we decided to use milder cyclopentadienyl transfer reagents, such as the silylated compounds C$_5$H$_4$(SiMe$_3$)$_2$ and C$_5$Me$_5$(SiMe$_3$). This method has previously been used by Green et al.[11] to prepare cyclopentadienyl-imido complexes with constrained geometry and by Maatta et al.[12] for the preparation of imido-containing monocyclopentadienyl vanadium derivatives. However, the trichloro complexes [{M(L)$_2$Cl$_3$}$_2$(μ-1,*i*-NC$_6$H$_4$N)] (L = CH$_3$CN; M = Nb, Ta; *i* = 3, 4), do not react with the silylated cyclopentadienyl reagents. This lack of reactivity is probably due to the presence of two additional ligands (L) in the coordination sphere which diminishes the acidity of the metal centre making the elimination of the expected SiMe$_3$Cl by-product unfavourable. In order to increase the reactivity of the diimidoniobium and -tantalum precursors towards the cyclopentadienyl reagents, alternative compounds without donor ligands were employed, namely [{MCl$_3$}$_2$(μ-1,*i*-NC$_6$H$_4$N)] (M = Nb, Ta), which were prepared from the reaction of MCl$_5$ with the appropriate *N*,*N*,*N*′,*N*′-tetrakis(trimethylsilyl)phenylenediamine in CH$_2$Cl$_2$.[8] When these diimido complexes were reacted with the appropriate silylated cyclopentadienyl reagents in a 1:2 molar ratio in CH$_2$Cl$_2$ at 90 °C (see Exp. Sect.), the cyclopentadienyl-containing dinuclear species [{M(Cp′)Cl$_2$}$_2$(μ-1,*i*-NC$_6$H$_4$N)] [Cp′ = η^5-C$_5$H$_4$SiMe$_3$, M = Nb, *i* = 4 (**1**); Cp′ = η^5-C$_5$H$_4$SiMe$_3$, M = Nb, *i* = 3 (**2**); Cp′ = η^5-C$_5$H$_4$SiMe$_3$, M = Nb, *i* = 2 (**3**); Cp′ = η^5-C$_5$Me$_5$, M = Nb, *i* = 4 (**4**); Cp′ = η^5-C$_5$Me$_5$, M = Nb, *i* = 3 (**5**); Cp′ = η^5-C$_5$H$_4$SiMe$_3$, M = Ta, *i* = 4 (**6**); Cp′ = η^5-C$_5$H$_4$SiMe$_3$, M = Ta, *i* = 3 (**7**)] were isolated (Scheme 1).

A number of reactions did not, however, give the desired products. These involved tantalum derivatives formed from C$_5$Me$_5$(SiMe$_3$) and the derivatives [{MCl$_3$}$_2$(μ-1,2-NC$_6$H$_4$N)] (M = Nb, Ta) formed from the reagents C$_5$Me$_5$(SiMe$_3$) and C$_5$H$_4$(SiMe$_3$)$_2$. This procedure has provided a useful synthetic route to dinuclear monocyclopentadienyl imido species of these metals, particularly with the reagent C$_5$H$_4$(SiMe$_3$)$_2$, in high yields (about 80% for the tantalum

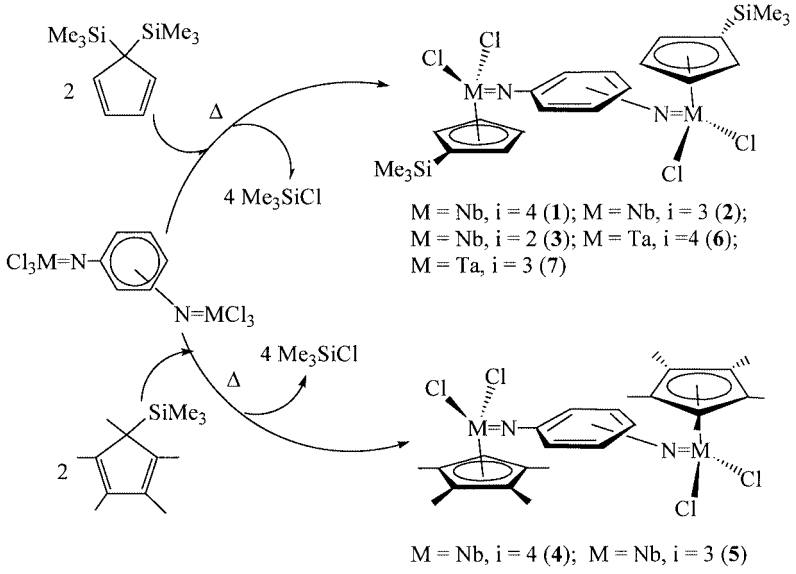

Scheme 1

 © 2004 Wiley-VCH Verlag GmbH & Co. KGaA, Weinheim

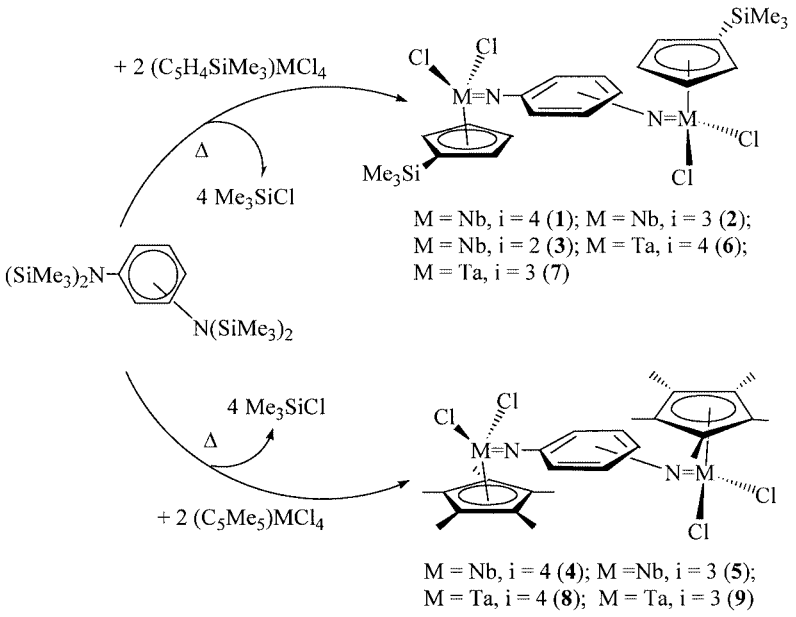

Scheme 2

complexes and quantitative yields for the niobium complexes). The overall reactions for the tantalum species require long reaction times of about one week. In order to improve this, an alternative method was considered to prepare the complexes. This method consisted of the reaction of the appropriate $MCp'Cl_4$ precursor (Cp′ = η^5-$C_5H_4SiMe_3$, η^5-C_5Me_5; M = Nb, Ta) with the corresponding *N*,*N*,*N*′,*N*′-tetrakis(trimethylsilyl)phenylenediamine derivative (Scheme 2).

This synthetic route, which is an adaptation of that previously described by Gibson et al.[3a] for the preparation of imido-containing niobium complexes, is an easy way to prepare cleanly (by elimination of $SiMe_3Cl$) the corresponding diimidoniobium and -tantalum complexes **1**−**7** as well as the new tantalum complexes [{Ta(η^5-C_5Me_5)Cl_2}$_2$(μ-1,*i*-NC_6H_4N)] [*i* = 4 (**8**), *i* = 3 (**9**)] in quantitative yields (see Exp. Sect.). On using this method the reaction times for the preparation of tantalum complexes are considerably shortened (to about 30 h). In wet solvents the materials evolve to the appropriate oxo-containing complexes with elimination of the corresponding diamine.[13] For example, solutions of **8** or **9** in wet CH_2Cl_2 give rise to the oxo complex [{Ta(η^5-C_5Me_5)Cl_3}$_2$(μ-O)].[14] Complexes **1**−**9**, as well as other complexes described in this work, were characterised by ^{1}H, ^{13}C NMR and IR spectroscopy (see Exp. Sect.). The ^{1}H and ^{13}C NMR spectra of **1**−**9** exhibit the characteristic signals for both the cyclopentadienyl and phenylene groups. This observation agrees with a structural situation where a diimidophenylene group bridges two metal atoms, which are, in turn, located in the plane formed by this ligand, in a three-legged piano-stool geometry around each metal centre (see Scheme 1). Free rotation around the N−C bond would be expected in solution and, for this reason, although a *trans*-disposition of both cyclopentadienyl ligands was considered in Scheme 1, alternative dispositions corresponding to other rotamers should also be considered.

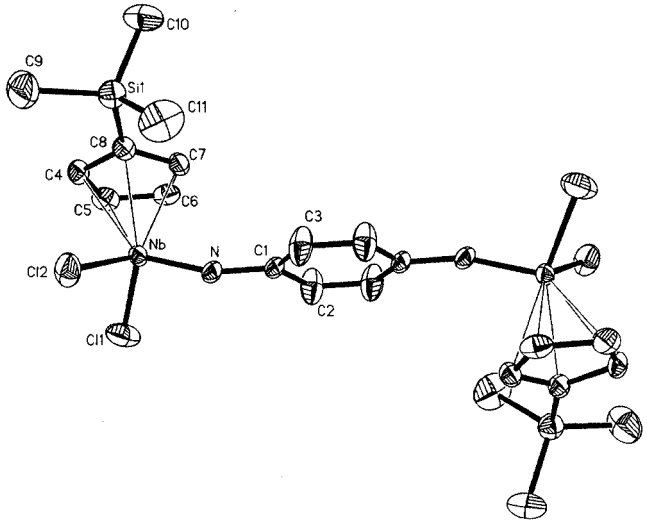

Figure 1. Molecular structure and atom-labelling scheme for [{Nb(η^5-$C_5H_4SiMe_3$)Cl_2}$_2$(μ-1,4-NC_6H_4N)] (**1**), with thermal ellipsoids at 30% probability

Complexes **1**−**9** were analysed by variable-temperature ^{1}H NMR spectroscopy in order to study this proposed dynamic behaviour. However, even at −90 °C there was no evidence of restricted rotation, probably due to the low energy value for the rotation barrier. The IR spectra of each complex contains a band between 1300−1370 cm^{-1}, which is characteristic of the terminal imido ligand.[3a] Several vibrational spectroscopic studies of group 5 imido complexes have been carried out.[15] In order to establish unequivocally the structural disposition of these complexes, an X-ray molecular analysis of compounds **1** and **8** was carried out. The molecular structures and atomic numbering schemes are shown in Figure 1 and 2, respectively. Selected bond lengths and angles for **1** and **8** are given in Table 1.

 © 2004 Wiley-VCH Verlag GmbH & Co. KGaA, Weinheim

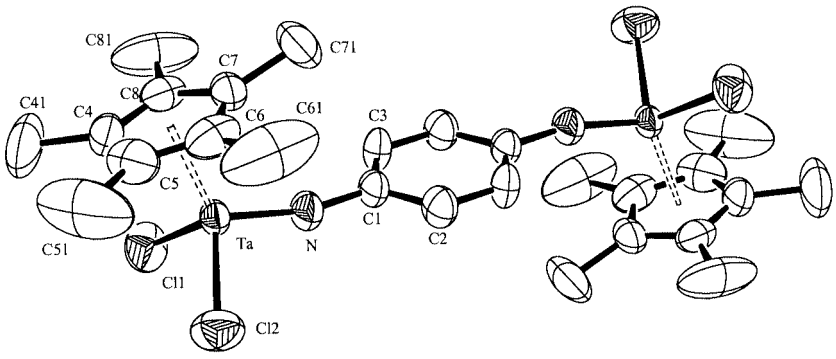

Figure 2. Molecular structure and atom-labelling scheme for [{Ta(η^5-C_5Me_5)Cl_2}$_2$(μ-1,4-NC_6H_4N)] (**8**), with thermal ellipsoids at 30% probability

Table 1. Selected bond lengths (Å) and angles (°) for **1** and **8**

	1	**8**
M−N	1.776(8)	1.783(5)
M−Cl1	2.343(3)	2.325(2)
M−Cl2	2.344(3)	2.339(2)
M−C4	2.468(9)	2.468(7)
M−C5	2.47(1)	2.478(7)
M−C6	2.39(1)	2.382(7)
M−C7	2.36(1)	2.365(6)
M−C8	2.42(1)	2.382(6)
N−C1	1.39(1)	1.377(7)
N−M−Cl1	101.7(3)	102.3(2)
N−M−Cl2	103.5(3)	104.3(2)
Cl1−M−Cl2	106.0(1)	105.4(1)
M−N−C1	161.0(7)	166.4(5)

The structures of **1** and **8** consist of dinuclear complexes of niobium and tantalum, respectively. The metal atoms are bound to the cyclopentadienyl ring in an η^5 mode, to two chlorine atoms and to the nitrogen from the imido group in a three-legged piano-stool conformation. The cyclopentadienyl rings are in a *trans* disposition with respect to each other. The metal atom is out of the plane defined by N, C1, C2 and C3 by 0.54(2) and 0.39(1) Å for complexes **1** and **8**, respectively.

The metal-nitrogen distances lie within the range expected for a triple bond[3a,16,17] [1.776(8) and 1.783(5) Å for **1** and **8**, respectively]. The M−N−C1 angles of 161.0(7)° for **1** and 166.4(5)° for **8** deviate slightly from linear. Such deviations are normally in the range 12−15° (see Table 2). In the case of [Nb(=NPh)(η^5-$C_5H_4SiMe_3$)$_2$Cl] extended-Hückel molecular-orbital calculations established that the imido bond angles for "linear imide" in this class of complex can vary up to 140° with little effect on the Nb−N bonding.[18] Therefore we propose that in **1** and **8** the nitrogen atom is sp hybridized.

The cyclopentadienyl group is in a typical[3a] eclipsed fashion with respect to the imido group for both complexes (see Figure 3a). The slight lengthening of the M−C4 [2.468(9) and 2.468(7) Å for **1** and **8**, respectively] and M−C5 [2.47(1) and 2.478(7) Å for **1** and **8**, respectively] distances with respect to other M−C ring distances may be due to the *trans* influence of the imido group.

The second part of this work involves the study of alkylation reactions of complexes **1**, **2** and **8**. The reaction of alkylating reagents, MeLi, Me_3SiCH_2MgCl or $Mg(CH_2C_6H_5)_2(THF)_2$, in a 1:4 molar ratio with **1**, **2** or **8** afforded the per-alkylated complexes, [{M(Cp′)R_2}$_2$(μ-1,*i*-NC_6H_4)] [Cp′ = η^5-$C_5H_4SiMe_3$, M = Nb, R = Me, *i* = 4 (**10**); Cp′ = η^5-$C_5H_4SiMe_3$, M = Nb, R = CH_2SiMe_3, *i* = 4 (**11**); Cp′ = η^5-$C_5H_4SiMe_3$, M = Nb, R = CH_2Ph, *i* = 4

Table 2. Selected structural data for imido complexes

	M−N (Å)	M−N−C (°)	Ref.
[{Nb(η^5-$C_5H_4SiMe_3$)Cl_2}$_2$(μ-1,4-NC_6H_4N)] (**1**)	1.776(8)	160.9(7)	This work
[{Ta(η^5-C_5Me_5)Cl_2}$_2$(μ-1,4-NC_6H_4N)] (**8**)	1.783(5)	166.4(5)	This work
[{Ta(η^5-C_5Me_5)(CH_2SiMe_3)$_2$}$_2$(μ-1,4-NC_6H_4N)] (**17**)	1.794(5)	167.4(5)	This work
[Nb(=NAr)(η^5-C_5H_5)(NH*t*Bu)Cl][a]	1.793	168.5	[17a]
[Nb(=NAr)(η^5-C_5H_5)Cl_2][a]	1.761	165.6	[3a]
[Nb(=NAr)(η^5-C_5H_5)Cl_2][b]	1.763	166.6	[17b]
[Nb(=NAr)(η^5-C_5H_5)(η^2-NH*t*Bu)(CH_2*t*Bu)H][a]	1.787	174.6	[17c]
[Ta(=NAr)(η^5-C_5Me_5)Cl_2][a]	1.780	171.3	[3a]
[Ta(=NAr)(η^5-C_5Me_5)Cl_2][b]	1.774	169.9	[16]
[Ta(=NAr)(η^5-C_5Me_5)(CO){Si($SiMe_3$)$_3$}H][a]	1.812	171.4	[17d]
[Ta(=NAr)(η^5-C_5H_5)(PMe_3)($SiMe_2Cl$)H][a]	1.821	171.8	[17e]

[a] Ar = C_6H_3*i*Pr_2-2,6. [b] Ar = $C_6H_3Me_2$-2,6.

 © 2004 Wiley-VCH Verlag GmbH & Co. KGaA, Weinheim

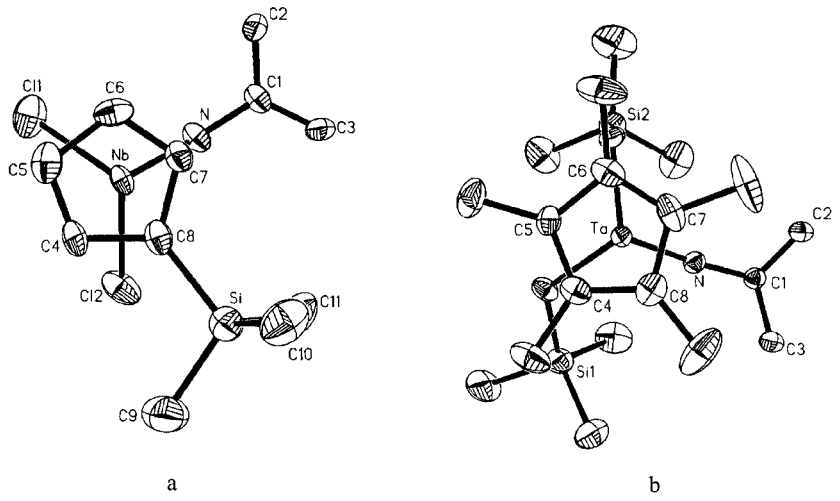

Figure 3. View along the ring centroid-metal vector (a) for compound **1**, and (b) for compound **17**

(**12**); Cp′ = η^5-$C_5H_4SiMe_3$, M = Nb, R = Me, *i* = 3 (**13**); Cp′ = η^5-$C_5H_4SiMe_3$, M = Nb, R = CH_2SiMe_3, *i* = 3 (**14**); Cp′ = η^5-$C_5H_4SiMe_3$, M = Nb, R = CH_2Ph, *i* = 3 (**15**); Cp′ = η^5-C_5Me_5, M = Ta, R = Me, *i* = 4 (**16**); Cp′ = η^5-C_5Me_5, M = Ta, R = CH_2SiMe_3, *i* = 4 (**17**); Cp′ = η^5-C_5Me_5, M = Ta, R = CH_2Ph, *i* = 4 (**18**)] (Scheme 3).

Finally, the reactions of **1** and **8** with the milder alkylating agent $ZnMe_2$, in a 1:2 molar ratio yielded the chloromethyl complexes [{M(Cp′)(Me)(Cl)}$_2$(μ-1,4-NC_6H_4N)] [Cp′ = η^5-$C_5H_4SiMe_3$, M = Nb (**19**); Cp′ = η^5-C_5Me_5, M = Ta (**21**)], while the reaction of **19** with $LiNMe_2$ in a 1:2 molar ratio (see Exp. Sect.) afforded the amido-containing

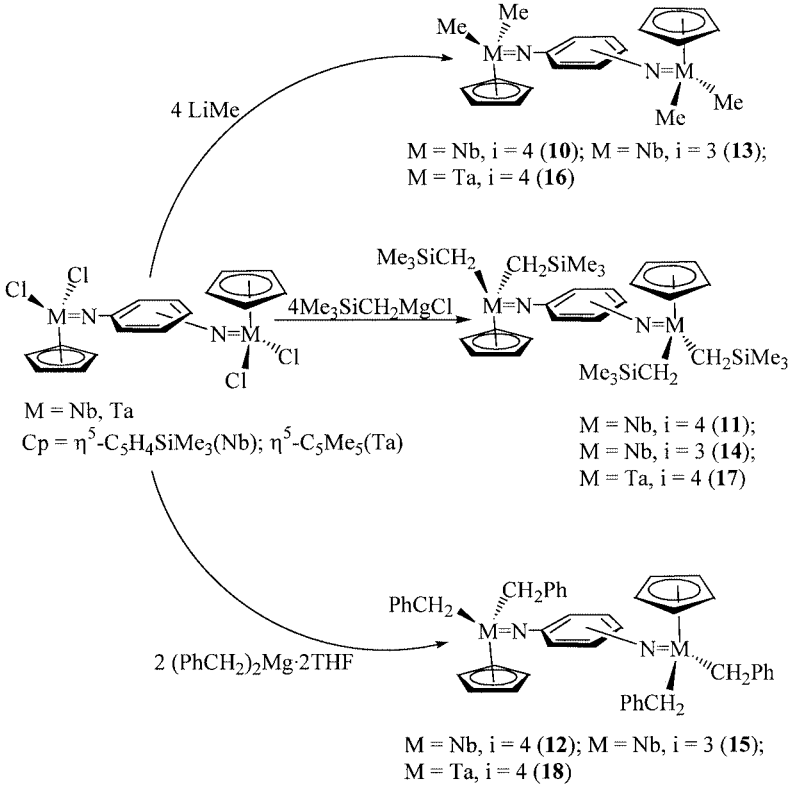

Scheme 3

 © 2004 Wiley-VCH Verlag GmbH & Co. KGaA, Weinheim

complex [{Nb(η^5-$C_5H_4SiMe_3$)(Me)(NMe_2)}$_2$(μ-1,4-NC_6H_4N)] (**20**).

The ^{1}H and ^{13}C NMR spectra for complexes **10**−**18** are similar to those found for the parent complexes with regards to both the cyclopentadienyl and phenylene groups (see Exp. Sect.). In addition, the spectra also contain the resonances due to the alkyl groups attached to the metal centre. In these complexes the four alkyl groups are both chemically and magnetically equivalent and only one set of signals for these groups is present. For example, one singlet corresponding to methyl groups for complexes **10**, **13** and **16** was observed in the ^{1}H NMR spectra. Furthermore, in all the complexes the metal atom is a pro-chiral centre and so the protons of the methylene groups (for CH_2SiMe_3 or CH_2Ph) for complexes **11**, **12**, **14**, **15**, **17** and **18** are diastereotopic and, therefore, give rise to two doublets of an AB spin-system in their ^{1}H NMR spectra (see Exp. Sect.). For **19**−**21** the two metal atoms of the binuclear moiety are chiral centres and the stereoisomer the *meso*-(*R*,*S*) and the enantiomers *rac*-(*R*,*R*) and -(*S*,*S*) are formed (see Scheme 4). The ^{1}H and ^{13}C NMR spectra of these complexes exhibit two sets of signals in a 1:1 ratio, corresponding to the presence of both diastereomers (*R*,*R*/*S*,*S*) and (*R*,*S*) (see Exp. Sect.).

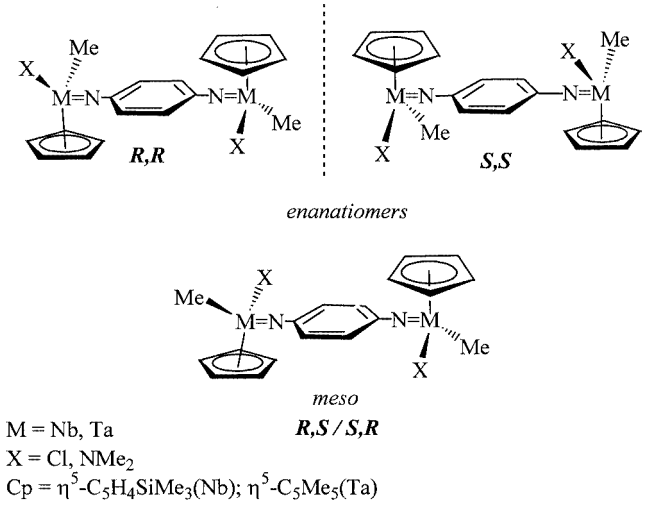

Scheme 4

The IR spectra of complexes **10**−**21** show a band at ca. 1300−1350 cm^{-1}, which is characteristic of the terminal imido ligand.[3a] In accordance with the different spectroscopic data described for alkyl-containing complexes, a structural disposition similar to that found for the chloro complexes can be expected (see Scheme 3). The X-ray crystal-structure determination for **17** confirmed this situation. The molecular structure and atomic numbering scheme are shown in Figure 4. Selected bond lengths and angles for **17** are given in Table 3.

Table 3. Selected bond lengths (Å) and angles (°) for **17**

M−N	1.794(5)
M−C4	2.473(7)
M−C5	2.533(6)
M−C6	2.492(7)
M−C7	2.397(7)
M−C8	2.428(7)
M−C9	2.149(6)
M−C10	2.193(7)
N−C1	1.377(8)
N−M−C9	104.7(3)
N−M−C10	100.9(3)
C9−M−C10	104.0(3)
M−N−C1	167.4(5)

The structure of **17** consists of a dinuclear complex where the metal atoms are bound to the cyclopentadienyl rings in an η^5 mode. In addition, the tantalum atoms are linked to two methylene groups from CH_2SiMe_3 and to the nitrogen atom from the imido group. Complex **17** adopts a three-legged piano-stool conformation about the metal centres. The cyclopentadienyl rings are in a *trans* disposition with respect to each other. The metal atom is out of the plane defined by N, C1, C2 and C3, by 0.36(1) Å. The metal-

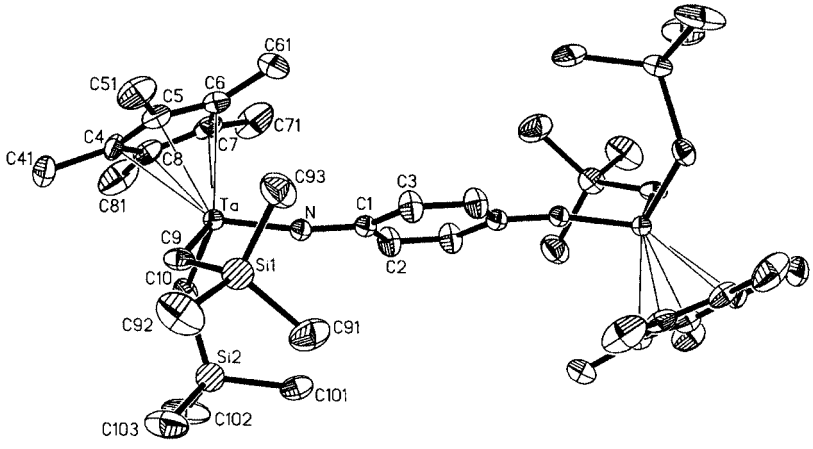

Figure 4. Molecular structure and atom-labelling scheme for [{Ta(η^5-C_5Me_5)(CH_2SiMe_3)$_2$}$_2$(μ-1,4-NC_6H_4N)] (**17**), with thermal ellipsoids at 30% probability

 © 2004 Wiley-VCH Verlag GmbH & Co. KGaA, Weinheim

nitrogen distance of 1.794(5) Å and the M−*N*−C1 angle of 167.4(5)° lie within the range expected for a triple bond (see Table 2).[3a,16,17]

The cyclopentadienyl group in **17** is in a staggered disposition with respect to the imido group (Figure 3b), in contrary to the eclipsed disposition observed in **1** and **8** (Figure 3a). The slight lengthening of the M−C4 [2.473(7) Å] and M−C5 [2.533(6) Å] distances is probably due to the *trans* influence of the imido group.

Conclusions

In this paper we report the synthesis of new dinuclear monocyclopentadienyl imidoniobium and -tantalum complexes and their reactivity towards different alkylating agents. The molecular structures of several of these complexes have been determined by single-crystal X-ray diffraction studies.

Experimental Section

General Remarks: All reactions were performed using standard Schlenk-tube techniques under an atmosphere of dry nitrogen. Solvents were distilled from appropriate drying agents and degassed before use. Literature methods were employed for the synthesis of the following compounds: *N*,*N*,*N*′,*N*′-tetrakis(trimethylsilyl)phenylenediamine,[19] $[Nb(\eta^5\text{-}C_5H_4SiMe_3)Cl_4]$,[20] $[\{NbCl_3\}_2(\mu\text{-}1,i\text{-}NC_6H_4N)]$ (*i* = 4, 3 or 2),[8a] $C_5H_4(SiMe_3)_2$,[21] $[Ta(\eta^5\text{-}C_5H_4SiMe_3)Cl_4]$,[22] $[\{TaCl_3\}_2(\mu\text{-}1,i\text{-}NC_6H_4N)]$ (*i* = 4 or 3),[8b] $[Ta(\eta^5\text{-}C_5Me_5)Cl_4]$,[23] $C_5Me_5(SiMe_3)$,[24] $[Nb(\eta^5\text{-}C_5Me_5)Cl_4]$,[25] and $[Mg(CH_2Ph)_2(THF)_2]$.[25] All commercial products were purchased from Aldrich and were used without further purification: LiMe, $Mg(CH_2SiMe_3)Cl$, $ZnMe_2$ and $LiNMe_2$. IR spectra were recorded on a Perkin−Elmer 883 and Perkin−Elmer IR-FT Spectrophotometer 2000. ^1H and ^{13}C NMR spectra were recorded on a Gemini-200 and/or UNITY-300 (Varian) spectrometer. Chemical shifts were measured relative to residual ^1H and ^{13}C resonances for $[D_1]$chloroform and $[D_6]$benzene as solvents. C, H and N analyses were carried out with a Perkin−Elmer 240−13, Perkin−Elmer 240 C and/or Heraeus-CHN−O-Rapid microanalyzer.

Preparation of $[\{Nb(\eta^5\text{-}C_5H_4SiMe_3)Cl_2\}_2(\mu\text{-}1,4\text{-}NC_6H_4N)]$ (1), $[\{Nb(\eta^5\text{-}C_5H_4SiMe_3)Cl_2\}_2(\mu\text{-}1,3\text{-}NC_6H_4N)]$ (2) and $[\{Nb(\eta^5\text{-}C_5H_4SiMe_3)Cl_2\}_2(\mu\text{-}1,2\text{-}NC_6H_4N)]$ (3). Method A: CH_2Cl_2 (70 mL) was added to a mixture of $[Nb(\eta^5\text{-}C_5H_4SiMe_3)Cl_4]$ and the corresponding *N*,*N*,*N*′,*N*′-tetrakis(trimethylsilyl)phenylenediamine in a Teflon valve ampoule. The ampoule was placed in an oil bath and heated at 65 °C for 24 h. The solvent was removed under vacuum and the solids obtained were identified as **1**, **2** and **3**, respectively.

Complex 1: From $[Nb(\eta^5\text{-}C_5H_4SiMe_3)Cl_4]$ (1.15 g, 3.09 mmol) and 1,4-$\{(Me_3Si)_2N\}_2C_6H_4$ (0.61 g, 1.54 mmol). 1.08 g of a red solid was obtained (Yield: 100%).

Complex 2: From $[Nb(\eta^5\text{-}C_5H_4SiMe_3)Cl_4]$ (1.05 g, 2.83 mmol) and 1,3-$\{(Me_3Si)_2N\}_2C_6H_4$ (0.56 g, 1.41 mmol). 1.0 g of a red solid was obtained (Yield: 100%).

Complex 3: From $[Nb(\eta^5\text{-}C_5H_4SiMe_3)Cl_4]$ (1.01 g, 2.72 mmol) and 1,2-$\{(Me_3Si)_2N\}_2C_6H_4$ (0.54 g, 1.36 mmol). 0.96 g of a dark brown solid was obtained (Yield: 100%).

Method B: CH_2Cl_2 (60 mL) was added to the corresponding complex $[\{NbCl_3\}_2(\mu\text{-}1,i\text{-}NC_6H_4N)]$ (*i* = 4, 3 or 2) in a Teflon valve ampoule. $C_5H_4(SiMe_3)_2$ was added to this green suspension and the ampoule was placed in an oil bath and heated at 90 °C for 24 h. The initial green suspension changed to a red solution. The solvent was removed under vacuum and the solids obtained were identified as **1**, **2** and **3**, respectively.

Complex 1: From $[\{NbCl_3\}_2(\mu\text{-}1,4\text{-}NC_6H_4N)]$ (0.80 g, 1.59 mmol) and $C_5H_4(SiMe_3)_2$ (0.74 mL, 3.18 mmol). 1.12 g of a red solid was obtained (Yield: 100%). ^1H NMR (300 MHz, $CDCl_3$, 25 °C): δ = 0.26 (s, 18 H, 2 × $C_5H_4Si\mathit{Me}_3$), 6.60 and 6.75 (2m, each 4 H, 2 × $C_5\mathit{H}_4$), 6.89 (s, 4 H, $C_6\mathit{H}_4$) ppm. $^{13}C\{^1H\}$ NMR (75 MHz, $CDCl_3$, 25 °C): δ = −0.5 ($C_5H_4Si\mathit{Me}_3$), 114.7, 122.0 and 125.9 (C^{ipso}; $\mathit{C}_5H_4SiMe_3$) 124.3 and 153.9 (C^{ipso}; C_6H_4) ppm. IR (CsI/Nujol): $\tilde{\nu}$ = 3090m, 1483s, 1395m, 1370s, 1311vs, 1253vs, 1172s, 1099m, 1074w, 1045s, 1004w, 990m, 903s, 840vs, 764m, 703w, 635w, 530w, 423m, 380s and 330m cm^{-1}. $C_{22}H_{30}Cl_4N_2Nb_2Si_2$ (706.3): calcd. C 37.41, H 4.28, N 3.97; found C 37.05, H 4.48, N 4.08.

Complex 2: From $[\{NbCl_3\}_2(\mu\text{-}1,3\text{-}NC_6H_4N)]$ (0.71 g, 1.41 mmol) and $C_5H_4(SiMe_3)_2$ (0.66 mL, 2.82 mmol). 1.0 g of a red solid was obtained (Yield: 100%). ^1H NMR (300 MHz, $CDCl_3$, 25 °C): δ = 0.29 (s, 18 H, 2 × $C_5H_4Si\mathit{Me}_3$), 6.62 and 6.76 (2m, each 4 H, 2 × $C_5\mathit{H}_4$), 6.62 (1 H), 6.72 (2 H) and 7.13 (1 H) (3m, $C_6\mathit{H}_4$) ppm. $^{13}C\{^1H\}$ NMR (50 MHz, $CDCl_3$, 25 °C): δ = −0.5 ($C_5H_4Si\mathit{Me}_3$), 114.4, 122.2 and 126.3 (C^{ipso}; $\mathit{C}_5H_4SiMe_3$), 118.9, 122.1, 128.3 and 155.6 (C^{ipso}; C_6H_4) ppm. IR (KBr): $\tilde{\nu}$ = 3093m, 2953m, 2598m, 1567s, 1462s, 1410m, 1370m, 1332m, 1306m, 1283m, 1250s, 1170s, 1047s, 1036s, 971w, 903s, 839vs, 780s, 757s, 694s, 680m, 630s, 419w and 374s cm^{-1}. $C_{22}H_{30}Cl_4N_2Nb_2Si_2$ (706.3): calcd. C 37.41, H 4.28, N 3.97; found C 37.40, H 4.55, N 3.68.

Complex 3: From $[\{NbCl_3\}_2(\mu\text{-}1,2\text{-}NC_6H_4N)]$ (0.77 g, 1.53 mmol) and $C_5H_4(SiMe_3)_2$ (0.72 mL, 3.06 mmol). 1.08 g of a red solid was obtained (Yield: 100%). ^1H NMR (300 MHz, $CDCl_3$, 25 °C): δ = 0.28 (s, 18 H, 2 × $C_5H_4Si\mathit{Me}_3$), 6.68 and 6.76 (2m, each 4 H, 2 × $C_5\mathit{H}_4$), 6.93 (m, 4 H, $C_6\mathit{H}_4$) ppm. $^{13}C\{^1H\}$ NMR (75 MHz, $CDCl_3$, 25 °C): δ = −0.6 ($C_5H_4Si\mathit{Me}_3$), 114.1, 124.2 and 125.9 (C^{ipso}; $\mathit{C}_5H_4SiMe_3$), 125.5, 126.1, and 150.1 (C^{ipso}; C_6H_4) ppm. IR (CsI/Nujol): $\tilde{\nu}$ = 3101w, 1577w, 1436m, 1395w, 1371m, 1328m, 1315m, 1253s, 1170m, 1115w, 1048m, 1039w, 987w, 966(md), 933w, 903s, 842vs, 754s, 748s, 632w, 398m, 379s and 336m cm^{-1}. $C_{22}H_{30}Cl_4N_2Nb_2Si_2$ (706.3): calcd. C 37.41, H 4.28, N 3.97; found C 36.62, H 4.06, N 4.06.

Preparation of $[\{Nb(\eta^5\text{-}C_5Me_5)Cl_2\}_2(\mu\text{-}1,4\text{-}NC_6H_4N)]$ (4). Method A: Dichloromethane (60 mL) was added to a mixture of $[\{NbCl_3\}_2(\mu\text{-}1,4\text{-}NC_6H_4N)]$ (0.62 g, 1.23 mmol) and $C_5Me_5(SiMe_3)$ (0.60 mL, 2.47 mmol) in a Teflon valve ampoule. The ampoule was placed in an oil bath and heated to 90 °C for 24 h. The resulting solution was allowed to cool down to room temperature, filtered and the solvent removed under vacuum to give 0.83 g of **4** as a purple, analytically pure, crystalline solid. (Yield: 100%).

Method B: A Teflon valve NMR tube was charged with a solution of $[Nb(\eta^5\text{-}C_5Me_5)Cl_4]$ (15 mg, 0.04 mmol) and [1,4-$\{(SiMe_3)_2N\}_2C_6H_4$] (8 mg, 0.02 mmol) in $CDCl_3$. The mixture was placed in an oil bath, heated to 65 °C and monitored by ^1H NMR spectroscopy. After 24 h the reaction was complete and gave **4** as the only product. ^1H NMR (300 MHz, $CDCl_3$, 25 °C): δ = 2.07 (s, 30 H, 2 × $C_5\mathit{Me}_5$), 6.79 (s, 4 H, $C_6\mathit{H}_4$) ppm. $^{13}C\{^1H\}$ NMR (75 MHz, $CDCl_3$, 25 °C): δ = 11.8 ($C_5\mathit{Me}_5$), 123.9 (C_5Me_5) 125.1 and 151.1 (C^{ipso}; C_6H_4) ppm. IR (CsI/Nujol): $\tilde{\nu}$ = 1476s, 1311s, 1262w, 1094w, 1022m, 1003w, 990w, 840m, 799w, 488w, 393m and

 © 2004 Wiley-VCH Verlag GmbH & Co. KGaA, Weinheim

366m cm^{-1}. $C_{26}H_{34}Cl_4N_2Nb_2$ (702.2): calcd. C 44.47, H 4.88, N 3.99; found C 44.04, H 4.92, N 4.22.

Preparation of [{Nb(η⁵-C_5Me_5)Cl_2}$_2$(μ-1,3-NC_6H_4N)] (5): The synthesis of **5** was carried out in an identical manner to **4**.

Method A: [{$NbCl_3$}$_2$(μ-1,3-NC_6H_4N)] (1.42 g, 2.82 mmol) and $C_5Me_5(SiMe_3)$ (1.38 mL, 5.63 mmol). 1.98 g of **5** was obtained as a pink solid (Yield: 100%).

Method B: [Nb(η⁵-C_5Me_5)Cl_4] (17 mg, 0.046 mmol) and [1,3-{$(SiMe_3)_2N$}$_2C_6H_4$] (9 mg, 0.023 mmol). (Yield: 100%). ^{1}H NMR (300 MHz, $CDCl_3$, 25 °C): δ = 2.09 (s, 30 H, 2 × C_5Me_5), 6.43 (1 H), 6.60 (2 H) and 7.08 (1 H) (3m, C_6H_4) ppm. $^{13}C\{^1H\}$ NMR (75 MHz, $CDCl_3$, 25 °C): δ = 11.9 (C_5Me_5), 124.0 (C_5Me_5) 120.2, 122.2, 128.2 and 153.6 (C^{ipso}; C_6H_4) ppm. IR (CsI/Nujol): ṽ = 1566s, 1415m, 1338m, 1284s, 1236s, 1149w, 1079w, 1026m, 971w, 897w, 865m, 847w, 791m, 687w, 485w, 469w, 402m and 362s cm^{-1}.$C_{26}H_{34}Cl_4N_2Nb_2$ (702.2): calcd. C 44.47, H 4.88, N 3.99; found C 44.21, H 5.06, N 4.07.

Preparation of [{Ta(η⁵-$C_5H_4SiMe_3$)Cl_2}$_2$(μ-1,4-NC_6H_4N)] (6) and [{Ta(η⁵-$C_5H_4SiMe_3$)Cl_2}$_2$(μ-1,3-NC_6H_4N)] (7). Method A: CH_2Cl_2 (40 mL) was added to a mixture of [Ta(η⁵-$C_5H_4SiMe_3$)Cl_4] and the corresponding *N*,*N*,*N*′,*N*′-tetrakis(trimethylsilyl)phenylenediamine in a Teflon valve ampoule. The ampoule was placed in an oil bath and heated at 70 °C for 16 h. The resulting deep-red solution was allowed to cool down to room temperature. The solution was filtered and the solvent removed under reduced pressure. The final products obtained were identified as **6** and **7**, respectively.

Complex 6: From [Ta(η⁵-$C_5H_4SiMe_3$)Cl_4] (0.81 g, 1.76 mmol) and 1,4-{$(Me_3Si)_2N$}$_2C_6H_4$ (0.35 g, 0.88 mmol). 0.78 g of a red solid was obtained (Yield: 100%).

Complex 7: From [Ta(η⁵-$C_5H_4SiMe_3$)Cl_4] (0.81 g, 1.76 mmol) and 1,3-{$(Me_3Si)_2N$}$_2C_6H_4$ (0.35 g, 0.88 mmol). 0.78 g of a yellow oil was obtained (Yield: 100%).

Method B: CH_2Cl_2 (40 mL) was added to the corresponding [{$TaCl_3$}$_2$(μ-1,*i*-NC_6H_4N)] (*i* = 4 or 3) in a Teflon valve ampoule. $C_5H_4(SiMe_3)_2$ was added to this red suspension and the ampoule was placed in an oil bath and heated at 90 °C for 72 h. The resulting red solution was filtered and the solvent was removed under vacuum. The final products were washed several times with hexane at −40 °C and identified as **6** and **7**, respectively.

Complex 6: From [($TaCl_3$)$_2$(μ-1,4-NC_6H_4N)] (1.71 g, 2.52 mmol) and $C_5H_4(SiMe_3)_2$ (1.30 mL, 5.02 mmol). 1.72 g of a red solid was obtained (Yield: 78%). ^{1}H NMR (300 MHz, $CDCl_3$, 25 °C): δ = 0.25 (s, 18 H, 2 × $C_5H_4SiMe_3$), 6.59 and 6.71 (2m, each 4 H, 2 × C_5H_4), 6.75 (s, 4 H, C_6H_4) ppm. $^{13}C\{^1H\}$ NMR (75 MHz, $CDCl_3$, 25 °C): δ = −0.4 ($C_5H_4SiMe_3$), 114.3, 120.6 and 123.1 (C^{ipso}; $C_5H_4SiMe_3$) 125.0 and 153.0 (C^{ipso}; C_6H_4) ppm. IR (CsI/Nujol): ṽ = 3090w, 1491s, 1333vs, 1254s, 1172m, 1043m, 905s, 841vs and 413m cm^{-1}. $C_{22}H_{30}Cl_4N_2Si_2Ta_2$ (882.4): calcd. C 29.95, H 3.43, N 3.17; found C 29.62, H 3.61, N 3.15.

Complex 7: From [($TaCl_3$)$_2$(μ-1,3-NC_6H_4N)] (1.71 g, 2.52 mmol) and $C_5H_4(SiMe_3)_2$ (1.30 mL, 5.02 mmol). 1.57 g of a yellow oil was obtained (Yield: 71%). ^{1}H NMR (300 MHz, $CDCl_3$, 25 °C): δ = 0.28 (s, 18 H, 2 × $C_5H_4SiMe_3$), 6.60 and 6.72 (2m, each 4 H, 2 × C_5H_4), 6.26 (1 H), 6.39 (2 H) and 7.17 (1 H) (3m, C_6H_4) ppm. $^{13}C\{^1H\}$ NMR (75 MHz, $CDCl_3$, 25 °C): δ = −0.4 ($C_5H_4SiMe_3$), 113.9, 120.8 and 123.6 (C^{ipso}; $C_5H_4SiMe_3$), 121.9, 122.7, 127.1 and 154.9 (C^{ipso}; C_6H_4) ppm. IR (CsI/Nujol): ṽ = 3098w, 1573vs, 1470vs, 1320vs, 1252vs, 1171s, 905s, 840vs and 417m cm^{-1}. $C_{22}H_{30}Cl_4N_2Si_2Ta_2$ (882.4): calcd. C 29.95, H 3.43, N 3.17; found C 29.76, H 3.65, N 3.31.

Preparation of [{Ta(η⁵-C_5Me_5)Cl_2}$_2$(μ-1,4-NC_6H_4N)] (8): Dichloromethane (40 mL) was added to a mixture of [Ta(η⁵-C_5Me_5)Cl_4] (1.72 g, 3.76 mmol) and [1,4-{$(SiMe_3)_2N$}$_2C_6H_4$] (0.75 g, 1.88 mmol) in a Teflon valve ampoule. The ampoule was placed in an oil bath and heated to 90 °C for 48 h. The resulting solution was allowed to cool down to room temperature, filtered and the solvent removed under vacuum to give 2.00 g of **8** as a red, analytically pure, crystalline solid. (Yield: 100%). An X-ray-quality sample was obtained from a saturated dichloromethane solution at −40 °C. ^{1}H NMR (300 MHz, $CDCl_3$, 25 °C): δ = 2.16 (s, 30 H, 2 × C_5Me_5), 6.65 (s, 4 H, C_6H_4) ppm. $^{13}C\{^1H\}$ NMR (75 MHz, $CDCl_3$, 25 °C): δ = 11.4 (C_5Me_5), 121.6 (C_5Me_5) 125.4 and 150.7 (C^{ipso}; C_6H_4) ppm. IR (CsI/Nujol): ṽ = 1485vs, 1338vs, 1091m, 1028s, 995m and 844s cm^{-1}. $C_{26}H_{34}Cl_4N_2Ta_2$ (878.3): calcd. C 35.56, H 3.90, N 3.19; found C 35.50, H 4.07, N 3.47.

Preparation of [{Ta(η⁵-C_5Me_5)Cl_2}$_2$(μ-1,3-NC_6H_4N)] (9): The synthesis of **9** was carried out in an identical manner to **8**, from [Ta(η⁵-C_5Me_5)Cl_4] (0.81 g, 1.75 mmol) and [1,3-{$(SiMe_3)_2N$}$_2C_6H_4$] (0.35 g, 0,88 mmol). 0.96 g of **9** was obtained as an orange solid (Yield: 100%). ^{1}H NMR (300 MHz, $CDCl_3$, 25 °C): δ = 2.18 (s, 30 H, 2 × C_5Me_5), 6.11 (1 H), 6.28 (2 H) and 7.10 (1 H) (3m, C_6H_4) ppm. $^{13}C\{^1H\}$ NMR (75 MHz, $CDCl_3$, 25 °C): δ = 11.5 (C_5Me_5), 121.8 (C_5Me_5) 122.4, 122.5, 127.0 and 153.7 (C^{ipso}; C_6H_4) ppm. IR (CsI/Nujol): ṽ = 1568vs, 1315vs, 1026s, 864m and 351s cm^{-1}. $C_{26}H_{34}Cl_4N_2Ta_2$ (878.3): calcd. C 35.56, H 3.90, N 3.19; found C 35.23, H 4.00, N 3.19.

Preparation of [{Nb(η⁵-$C_5H_4SiMe_3$)Me_2}$_2$(μ-1,4-NC_6H_4N)] (10) and [{Nb(η⁵-$C_5H_4SiMe_3$)Me_2}$_2$ (μ-1,3-NC_6H_4N)] (13): MeLi was added at −78 °C to a suspension of complex **1** or **2** in hexane (50 mL). The mixture was allowed to warm up to room temperature and was stirred for 5 h. The solution was filtered and the residue extracted with hexane (2 × 20 mL). The extracts and the solution were combined and the solvent was removed in vacuo to give a solid, which was identified as **10** or **13**, respectively.

Complex 10: From [{Nb(η⁵-$C_5H_4SiMe_3$)Cl_2}$_2$(μ-1,4-NC_6H_4N)] (0.85 g, 1.20 mmol) and MeLi (3.44 mL, 4.81 mmol). 0.70 g of a brown solid was obtained (Yield: 93%). ^{1}H NMR (300 MHz, C_6D_6, 25 °C): δ = 0.09 (s, 18 H, 2 × $C_5H_4SiMe_3$), 0.77 (s, 12 H, 4 × Nb-*Me*), 5.91 (m, 8 H, 2 × C_5H_4), 7.19 (s, 4 H, C_6H_4) ppm. $^{13}C\{^1H\}$ NMR (75 MHz, C_6D_6, 25 °C): δ = −0.1 ($C_5H_4SiMe_3$), 37.8 (Nb-*Me*), 113.0, 113.1 and 116.7 (C^{ipso}; $C_5H_4SiMe_3$) 125.4 and 153.7 (C^{ipso}; C_6H_4) ppm. IR (CsI/Nujol): ṽ = 1477m, 1407m, 1317m, 1251s, 1174m, 1091w, 1046m, 982w, 904m, 879w, 838vs, 807m, 756m, 695w, 631w, 493w and 422w cm^{-1}. $C_{26}H_{42}N_2Nb_2Si_2$ (624.6): calcd. C 50.00, H 6.78, N 4.48; found C 50.15, H 6.70, N 4.26.

Complex 13: From [{Nb(η⁵-$C_5H_4SiMe_3$)Cl_2}$_2$(μ-1,3-NC_6H_4N)] (1.66 g, 2.35 mmol) and MeLi (6.71 mL, 9.40 mmol). 1.35 g of a brown solid was obtained (Yield: 92%). ^{1}H NMR (300 MHz, C_6D_6, 25 °C): δ = 0.10 (s, 18 H, 2 × $C_5H_4SiMe_3$), 0.75 (s, 12 H, 4 × Nb-*Me*), 5.89 and 5.93 (2m, each 4 H, 2 × C_5H_4), 7.02 (3 H) and 7.30 (1 H) (2m, C_6H_4) ppm. $^{13}C\{^1H\}$ NMR (50 MHz, C_6D_6, 25 °C): δ = −0.2 ($C_5H_4SiMe_3$), 38.1 (Nb-*Me*), 112.6, 113.2 and 117.4 (C^{ipso}; $C_5H_4SiMe_3$), 121.1, 121.3, 128.0 and 157.4 (C^{ipso}; C_6H_4) ppm. IR (CsI/Nujol): ṽ = 1567s, 1409m, 1338m, 1303m, 1250s, 1174m, 1150m, 1045m, 956w, 904m, 838vs, 780m, 757m, 693w, 632w and 495w cm^{-1}. $C_{26}H_{42}N_2Nb_2Si_2$ (624.6): calcd. C 50.00, H 6.78, N 4.48; found C 50.04, H 7.10, N 4.09.

Preparation of [{Nb(η⁵-$C_5H_4SiMe_3$)(CH_2SiMe_3)$_2$}$_2$(μ-1,4-NC_6H_4N)] (11): A slight excess of [Mg(CH_2SiMe_3)Cl] (4.3 mL,

 © 2004 Wiley-VCH Verlag GmbH & Co. KGaA, Weinheim

4.3 mmol) was added, at −78 °C, to a suspension of complex **1** (0.68 g, 0.97 mmol) in hexane (50 mL). The mixture was allowed to warm up to room temperature and was stirred overnight. The solution was filtered and the residue extracted with hexane (2 × 20 mL). The extracts and the solution were combined. The resulting orange solution was concentrated to 25 mL. Cooling of this solution to −40 °C gave compound **11** (0.70 g, 0.77 mmol) as an orange crystalline solid. (Yield: 79%). ^{1}H NMR (300 MHz, C_6D_6, 25 °C): δ = 0.18 (s, 18 H, 2 × $C_5H_4Si\mathit{Me}_3$), 0.24 (s, 36 H, 4 × $CH_2Si\mathit{Me}_3$), 0.16 and 1.53 (2d, $^2J_{H,H}$ = 10.2 Hz, each 4 H, 4 × $C\mathit{H}_2SiMe_3$), 5.78 and 6.21 (2m, each 4 H, 2 × $C_5\mathit{H}_4$), 7.21 (s, 4 H, $C_6\mathit{H}_4$) ppm. ^{13}C{^{1}H} NMR (75 MHz, C_6D_6, 25 °C): δ = 0.0 ($C_5H_4Si\mathit{Me}_3$), 2.8 ($CH_2Si\mathit{Me}_3$), 55.0 ($\mathit{C}H_2SiMe_3$), 108.0, 115.8 and 119.6 (C^{ipso}; $\mathit{C}_5H_4SiMe_3$) 125.1 and 153.6 (C^{ipso}; C_6H_4) ppm. IR (CsI/Nujol): ṽ = 1478s, 1408w, 1314s, 1241s, 1174m, 1092w, 1048m, 1040m, 1003w, 988m, 938s, 901s, 831vs, 814s, 755m, 735m, 701m, 682m, 632w, 549w, 534w, 468m, 416w and 373w cm^{-1}. $C_{38}H_{74}N_2Nb_2Si_6$ (913.3): calcd. C 49.97, H 8.17, N 3.07; found C 50.05, H 8.26, N 3.30.

Preparation of [{Nb(η^5-$C_5H_4SiMe_3$)(CH_2SiMe_3)$_2$}$_2$(μ-1,3-NC_6H_4N)] (14): A slight excess of [$Mg(CH_2SiMe_3)Cl$] (5.2 mL, 5.2 mmol) was added, at −78 °C, to a suspension of complex **2** (0.83 g, 1.17 mmol) in hexane (50 mL). The mixture was allowed to warm up to room temperature and was stirred overnight. The solution was filtered and the residue extracted with hexane (2 × 20 mL). The extracts and the solution were combined. The solvent was removed and the resulting yellow oil was identified as **14** (0.95 g, 1.04 mmol) (Yield: 89%). ^{1}H NMR (300 MHz, C_6D_6, 25 °C): δ = 0.20 (s, 18 H, 2 × $C_5H_4Si\mathit{Me}_3$), 0.27 (s, 36 H, 4 × $CH_2Si\mathit{Me}_3$), 0.21 and 1.57 (2d, $^2J_{H,H}$ = 10.5 Hz, each 4 H, 4 × $C\mathit{H}_2SiMe_3$), 5.89 and 6.28 (2m, each 4 H, 2 × $C_5\mathit{H}_4$), 6.92 (2 H), 7.08 (1 H) and 7.16 (1 H) (3m, $C_6\mathit{H}_4$) ppm. ^{13}C{^{1}H} NMR (50 MHz, C_6D_6, 25 °C): δ = 0.0 ($C_5H_4Si\mathit{Me}_3$), 2.9 ($CH_2Si\mathit{Me}_3$), 55.2 ($\mathit{C}H_2SiMe_3$), 107.8, 115.9 and 120.2 (C^{ipso}; $\mathit{C}_5H_4SiMe_3$) 120.4, 120.6, 128.3 and 157.4 (C^{ipso}; C_6H_4) ppm. IR (CsI/Nujol): ṽ = 1566s, 1409m, 1336m, 1302s, 1280s, 1246s, 1175m, 1152w, 1045m, 931s, 905s, 838vs, 754s, 697s, 633w, 572w, 472w and 416w cm^{-1}. $C_{38}H_{74}N_2Nb_2Si_6$ (913.3): calcd. C 49.97, H 8.17, N 3.07; found C 49.41, H 8.18, N 3.24.

Preparation of [{Nb(η^5-$C_5H_4SiMe_3$)(CH_2Ph)$_2$}$_2$(μ-1,4-NC_6H_4N)] (12) and [{Nb(η^5-$C_5H_4SiMe_3$)(CH_2Ph)$_2$}$_2$(μ-1,3-NC_6H_4N)] (15): Diethyl ether (60 mL) was added at −78 °C to a mixture of complex **1** or **2** and [$Mg(CH_2Ph)_2(THF)_2$]. The mixture was allowed to warm up to room temperature and was stirred overnight. The solution was filtered and the residue was extracted with diethyl ether (2 × 20 mL). The extracts and the solution were combined. The solvent was removed to give a yellow and a pale yellow solid, respectively, and these were identified as the corresponding compounds **12** and **15**.

Complex 12: From **1** (0.75 g, 1.06 mmol) and [$Mg(CH_2Ph)_2(THF)_2$] (0.74 g, 2.12 mmol). 0.88 g was obtained (Yield: 90%). ^{1}H NMR (300 MHz, C_6D_6, 25 °C): δ = 0.11 (s, 18 H, 2 × $C_5H_4Si\mathit{Me}_3$), 1.55 and 2.13 (2d, $^2J_{H,H}$ = 8.1 Hz, each 4 H, 4 × $C\mathit{H}_2Ph$), 5.63 and 5.72 (2m, each 4 H, 2 × $C_5\mathit{H}_4$), 6.79 (s, 4 H, $C_6\mathit{H}_4$), 6.81−7.07 (m, 20 H, 4 × $CH_2\mathit{Ph}$) ppm. ^{13}C{^{1}H} NMR (75 MHz, C_6D_6, 25 °C): δ = 0.1 ($C_5H_4Si\mathit{Me}_3$), 43.4 ($\mathit{C}H_2Ph$), 111.6, 112.5 and 112.2 (C^{ipso}; $\mathit{C}_5H_4SiMe_3$) 124.9 and 153.5 (C^{ipso}; C_6H_4), 125.4, 129.0, 130.5 and 138.9 (C^{ipso}; $CH_2\mathit{Ph}$) ppm. IR (CsI/Nujol): ṽ = 1594m, 1477s, 1408m, 1314s, 1250s, 1205m, 1176s, 1093m, 1035s, 1004w, 995w, 985m, 920w, 902m, 885w, 835vs, 817vs, 760s, 750s, 696vs, 632w, 537w, 515w, 446w and 428w cm^{-1}. $C_{50}H_{58}N_2Nb_2Si_2$ (929.0): calcd. C 64.64, H 6.29, N 3.02; found C 65.33, H 6.94, N 2.74.

Complex 15: From **2** (0.75 g, 1.06 mmol) and [$Mg(CH_2Ph)_2(THF)_2$] (0.74 g, 2.12 mmol). 0.85 g was obtained (Yield: 86%). ^{1}H NMR (300 MHz, C_6D_6, 25 °C): δ = 0.15 (s, 18 H, 2 × $C_5H_4Si\mathit{Me}_3$), 1.70 and 2.11 (2d, $^2J_{H,H}$ = 8.1 Hz, each 4 H, 4 × $C\mathit{H}_2Ph$), 5.64 and 5.79 (2m, each 4 H, 2 × $C_5\mathit{H}_4$), 6.612 (2 H), 6.73 (1 H) and 7.16 (1 H) (3m, $C_6\mathit{H}_4$), 6.85−7.08 (m, 20 H, 4 × $CH_2\mathit{Ph}$) ppm. ^{13}C{^{1}H} NMR (75 MHz, C_6D_6, 25 °C): δ = 0.2 ($C_5H_4Si\mathit{Me}_3$), 43.6 ($\mathit{C}H_2Ph$), 111.9, 112.3 and 112.9 (C^{ipso}; $\mathit{C}_5H_4SiMe_3$) 119.8, 120.7, 128.0 and 157.3 (C^{ipso}; C_6H_4), 125.5, 129.1, 130.6 and 138.8 (C^{ipso}; $CH_2\mathit{Ph}$) ppm. IR (CsI/Nujol): ṽ = 1592s, 1565s, 1549m, 1513w, 1484s, 1409m, 1367m, 1343m, 1304s, 1290s, 1251s, 1234s, 1207m, 1177m, 1159w, 1123w, 1084w, 1043m, 1025m, 995w, 901m, 837vs, 820s, 805s, 784w, 758s, 695m, 686m, 633w, 541w, 516w, 499w, 443w and 430w cm^{-1}. $C_{50}H_{58}N_2Nb_2Si_2$ (929.0): calcd. C 64.64, H 6.29, N 3.02; found C 64.69, H 6.85, N 2.88.

Preparation of [{Ta(η^5-C_5Me_5)Me_2}$_2$(μ-1,4-NC_6H_4N)] (16): A solution of MeLi (2.28 mmol) diluted in Et_2O (10 mL) was added dropwise, at −78 °C, to a suspension of complex **8** (0.5 g, 0.57 mmol) in hexane (50 mL). The mixture was stirred overnight at room temperature. The resulting yellow solution was filtered and the residue extracted with hexane (2 × 25 mL). The solvent was removed in vacuo to give 0.36 g of a yellow solid, which was identified as complex **16** (Yield: 80%). ^{1}H NMR (300 MHz, $CDCl_3$, 25 °C): δ = 0.01 (s, 12 H, 4 × Ta-Me), 1.96 (s, 30 H, 2 × $C_5\mathit{Me}_5$), 6.68 (s, 4 H, $C_6\mathit{H}_4$) ppm. ^{13}C{^{1}H} NMR (75 MHz, $CDCl_3$, 25 °C): δ = 10.7 ($C_5\mathit{Me}_5$), 46.5 (Ta-Me), 115.9 (C_5Me_5) 125.0 and 151.9 (C^{ipso}; C_6H_4) ppm. IR (CsI/Nujol): ṽ = 1493s, 1332vs, 1086m, 1026m, 1007m, 835s, 804m and 500m cm^{-1}. $C_{30}H_{46}N_2Ta_2$ (796.6): calcd. C 45.23, H 5.82, N 3.52; found C 44.82, H 5.79, N 3.36.

Preparation of [{Ta(η^5-C_5Me_5)(CH_2SiMe_3)$_2$}$_2$(μ-1,4-NC_6H_4N)] (17): A solution of $Mg(CH_2SiMe_3)Cl$ (2.28 mmol) diluted in Et_2O (10 mL) was added dropwise, at −78 °C, to a suspension of complex **8** (0.5 g, 0.57 mmol) in hexane (50 mL). The mixture was stirred overnight at room temperature. The resulting yellow solution was filtered and the residue was extracted with hexane (2 × 25 mL). The solvent was removed in vacuo to give 0.53 g of a yellow solid, which was identified as complex **17** (Yield: 86%). ^{1}H NMR (300 MHz, $CDCl_3$, 25 °C): δ = 0.04 (s, 36 H, 4 × $CH_2Si\mathit{Me}_3$), −1.14 and 0.21 (2d, $^2J_{H,H}$ = 11.9 Hz, each 4 H, 4 × $C\mathit{H}_2SiMe_3$), 1.97 (s, 30 H, 2 × $C_5\mathit{Me}_5$), 6.63 (s, 4 H, $C_6\mathit{H}_4$) ppm. ^{13}C{^{1}H} NMR (75 MHz, $CDCl_3$, 25 °C): δ = 2.8 ($CH_2Si\mathit{Me}_3$), 11.1 ($C_5\mathit{Me}_5$), 58.5 ($\mathit{C}H_2SiMe_3$), 115.6 (C_5Me_5) 125.1 and 151.7 (C^{ipso}; C_6H_4) ppm. IR (CsI/Nujol): ṽ = 1489s, 1332vs, 1241s, 1089m, 1024m, 962m, 850vs and 465m cm^{-1}. $C_{42}H_{78}N_2Si_4Ta_2$ (1085.3): calcd. C 46.48, H 7.24, N 2.58; found C 46.46, H 7.28, N 2.96.

Preparation of [{Ta(η^5-C_5Me_5)(CH_2Ph)$_2$}$_2$(μ-1,4-NC_6H_4N)] (18): A solution of $Mg(CH_2Ph)_2(THF)_2$ (0.4 g, 1.14 mmol) diluted in Et_2O (20 mL) was added dropwise, at −78 °C, to a solution of complex **8** (0.5 g, 0.57 mmol) in Et_2O (30 mL). The mixture was stirred overnight at room temperature. The solvent was removed in vacuo and the resulting yellow residue was extracted with CH_2Cl_2 (2 × 15 mL). The filtrate was placed in a freezer at −40 °C to afford 0.44 g of **18**, after 16 h, as a yellow crystalline solid. The product contained ca. 0.25 equivalents of residual CH_2Cl_2 (by ^{1}H NMR spectroscopy and elemental analysis). Yield: 68%. ^{1}H NMR (300 MHz, $CDCl_3$, 25 °C): δ = 1.35 and 2.06 (2d, $^2J_{H,H}$ = 11.3 Hz, each 4 H, 4 × $C\mathit{H}_2Ph$), 1.94 (s, 30 H, 2 × $C_5\mathit{Me}_5$), 6.40 (s, 4 H, $C_6\mathit{H}_4$), 6.90−7.10 (m, 20 H, 4 × $CH_2\mathit{Ph}$) ppm. ^{13}C{^{1}H} NMR (75 MHz, $CDCl_3$, 25 °C): δ = 11.0 ($C_5\mathit{Me}_5$), 67.5 ($\mathit{C}H_2Ph$), 115.3 (C_5Me_5) 124.7 and 151.2 (C^{ipso}; C_6H_4), 123.2, 127.9, 129.7 and 144.6 (C^{ipso}; $CH_2\mathit{Ph}$) ppm. IR (CsI/Nujol): ṽ = 1593s, 1483vs, 1332vs, 1200m, 1024m, 835s, 742s and 452m cm^{-1}.

 © 2004 Wiley-VCH Verlag GmbH & Co. KGaA, Weinheim

$C_{54}H_{62}N_2Ta_2{\cdot}0.25CH_2Cl_2$ (1122.2): calcd. C 58.06, H 5.61, N 2.50; found C 57.84, H 5.73, N 2.88.

Preparation of [{Nb(η^5-$C_5H_4SiMe_3$)ClMe}$_2$(μ-1,4-NC_6H_4N)] (19): $ZnMe_2$ (1.13 mL, 2.26 mmol) was added at room temperature to a suspension a complex **1** (1.60 g, 2.26 mmol) in toluene (50 mL). The mixture was stirred for 12 h. The red solution was filtered and the residue extracted with toluene (3 × 20 mL). The extracts and the solution were combined. The solvent was removed to give a brown solid, which was identified as **19** (1.3 g; yield: 86%). ^{1}H NMR (300 MHz, C_6D_6, 25 °C, two isomers): δ = 0.16 (s, 36 H, 4 × $C_5H_4Si\mathit{Me}_3$), 1.34 and 1.35 (2s, each 6 H, 4 × Nb-*Me*), 5.69, 5.84, 5.85 and 6.17 (4m, each 4 H, 4 × $C_5\mathit{H}_4$), 6.93 (s, 8 H, 2 × $C_6\mathit{H}_4$) ppm. ^{13}C{^{1}H} NMR (75 MHz, C_6D_6, 25 °C, two isomers): δ = −0.4 ($C_5H_4Si\mathit{Me}_3$), 38.8 (Nb-*Me*), 110.5, 110.6, 113.5, 113.6, 115.6, 115.7, 116.7 (C^{ipso}) and 116.8 (C^{ipso}; $\mathit{C}_5H_4SiMe_3$), 124.7 and 154.1 (C^{ipso}; C_6H_4) ppm. IR (CsI/Nujol): $\tilde{\nu}$ = 1595w, 1512w, 1310s, 1250s, 1171m, 1093m, 1045m, 1004w, 986m, 903m, 837vs, 757s, 631m, 523w, 477w, 419m and 377w cm^{-1}. $C_{24}H_{36}Cl_2N_2Nb_2Si_2$ (665.5): calcd. C 43.32, H 5.45, N 4.21; found C 43.00, H 5.26, N 3.93.

Preparation of [{Nb(η^5-$C_5H_4SiMe_3$)(NMe_2)Me}$_2$(μ-1,4-NC_6H_4N)] (20): Diethyl ether (50 mL) was added at −78 °C to a mixture of complex **19** (1.15 g, 1.73 mmol) and an excess of $LiNMe_2$ (0.19 g, 3.80 mmol). The mixture was allowed to warm up to room temperature and was stirred for 12 h. The solution was filtered and the residue was extracted with diethyl ether (2 × 20 mL). The extracts and the solution were combined. The solvent was removed and the residue was extracted with pentane (2 × 30 mL). The resulting solution was concentrated to dryness to give a dark brown oil, which was identified as **7** (1.05 g, Yield: 89%). ^{1}H NMR (300 MHz, C_6D_6, 25 °C, two isomers): δ = 0.16 (s, 36 H, 4 × $C_5H_4Si\mathit{Me}_3$), 0.72 (s, 12 H, 4 × Nb-*Me*), 3.28 (br., 24 H, 4 × $N\mathit{Me}_2$), 5.86, 5.92, 5.97 and 6.07 (4m, each 4 H, 4 × $C_5\mathit{H}_4$), 6.97 (s, 8 H, 2 × $C_6\mathit{H}_4$) ppm. ^{13}C{^{1}H} NMR (50 MHz, C_6D_6, 25 °C, two isomers): δ = 0.2 ($C_5H_4Si\mathit{Me}_3$), 13.7 (Nb-*Me*), 53.3 ($N\mathit{Me}_2$), 113.2, 113.3, 113.4 113.5 and 113.6 (C^{ipso}; $\mathit{C}_5H_4SiMe_3$), 124.6 and 153.2 (C^{ipso}; C_6H_4) ppm. IR (CsI/Nujol): $\tilde{\nu}$ = 1485s, 1419w, 1315s, 1249m, 1178w, 1090w, 1040m, 987w, 962m, 904w, 837vs, 802m, 756w, 632w, 543w, 489w, and 383w cm^{-1}. $C_{28}H_{48}N_4Nb_2Si_2$ (682.7): calcd. C 49.26, H 7.09, N 8.21; found C 48.68, H 6.71, N 7.32.

Preparation of [{Ta(η^5-C_5Me_5)ClMe}$_2$(μ-1,4-NC_6H_4N)] (21): A solution of $ZnMe_2$ (1.26 mmol, 2 M in toluene) was added, at room temperature, to a suspension of complex **8** (0.55 g, 0.63 mmol) in toluene (50 mL). The mixture was stirred overnight at room temperature. The resulting yellow solution was filtered and the solvent was removed in vacuo to give 0.39 g of a yellow solid, which was identified as complex **21** (Yield: 75%). ^{1}H NMR (300 MHz, C_6D_6, 25 °C, two isomers): δ = 0.82 and 0.83 (2s, each 6 H, 4 × Ta-*Me*), 1.80 (s, 60 H, 4 × $C_5\mathit{Me}_5$), 6.91 (s, 8 H, 2 × $C_6\mathit{H}_4$) ppm. ^{13}C{^{1}H} NMR (75 MHz, C_6D_6,, 25 °C, two isomers): δ = 10.8 ($C_5\mathit{Me}_5$), 41.2 and 41.3 (Ta-*Me*), 118.1 (C_5Me_5) 125.6 and 152.1 (C^{ipso}; C_6H_4) ppm. IR (CsI/Nujol): $\tilde{\nu}$ = 1491s, 1335vs, 1088m, 1026m, 994m, 837s and 491m cm^{-1}. $C_{28}H_{40}Cl_2N_2Ta_2$ (837.4): calcd. C 40.16, H 4.81, N 3.35; found C 40.05, H 4.68, N 3.16.

X-ray Structure Determinations for [{M(Cp)Cl$_2$}$_2$(μ-1,4-NC_6H_4N)] [M = Nb, Cp = η^5-$C_5H_4SiMe_3$ (1); M = Ta, Cp = η^5-C_5Me_5 (8)] and [{M(Cp)(CH_2R)$_2$}$_2$(μ-1,4-NC_6H_4N)] [M = Ta, Cp = η^5-C_5Me_5, R = $SiMe_3$ (17)]: Intensity data for compounds **1** and **17** were collected on a Nonius-Mach3 diffractometer equipped with a graphite monochromator (Mo-K_α radiation, λ = 0.71073 Å) using an ω/2θ scan technique. In the case of **1** the specimen diffracted only weakly. The final unit-cell parameters were determined from 25 well-centred reflections and refined by the least-squares method. The space group was determined from the systematic absences and

Table 4. Crystal data and structure refinement for **1**, **8** and **17**

	1	**8**	**17**
Formula	$C_{22}H_{30}Cl_4N_2Nb_2Si_2$	$C_{26}H_{34}Cl_4N_2Ta_2$	$C_{42}H_{78}N_2Si_4Ta_2$
Mol. mass	706.28	878.25	1085.32
T (K)	293(2)	110(1)	250(2)
Cryst. syst.	orthorhombic	monoclinic	triclinic
Space group	*Pbca*	$P2_1/a$	$P\bar{1}$
a (Å)	13.331(1)	13.269(1)	9.617(1)
b (Å)	12.547(1)	8.5840(1)	10.547(1)
c (Å)	17.796(1)	13.802(1)	14.943(1)
			75.28(1)
β (deg)		100.33(1)	72.84(1)
			65.33(1)
V (Å^3)	2976.6(4)	1546.6(2)	1301.0(2)
Z	4	2	1
Dc (g cm^{-3})	1.576	1.886	1.385
μ (mm^{-1})	1.223	7.432	4.321
F(000)	1416	836	546
Crystal dimensions (mm)	0.3 × 0.2 × 0.2	0.40 × 0.18 × 0.15	0.3 × 0.3 × 0.4
θ range (deg)	2.29 to 27.95	3.08 to 27.53	2.15 to 28.00
hkl ranges	$-17 \le h \le 0$	$-13 \le h \le 17$	$-12 \le h \le 12$
	$0 \le k \le 16$	$-10 \le k \le 11$	$-13 \le k \le 13$
	$0 \le l \le 23$	$-17 \le l \le 17$	$0 \le l \le 19$
Data/parameters	3577/142	3454/154	6505/226
Goodness-of-fit on F^2	1.135	1.233	1.129
Final *R* indices [$I > 2\sigma(I)$][a]	R_1 = 0.0746	R_1 = 0.0345	R_1 = 0.0461
	wR_2 = 0.1800	wR_2 = 0.0792	wR_2 = 0.1508
Largest diff. peak (e·Å^{-3})	0.827/−0.650	0.850/−0.881	2.494/−2.221

[a] $R_1 = \Sigma(F_o - F_c)/\Sigma(F_o)$; $wR_2 = \{\Sigma[w(F_o^2 - F_c^2)^2]/\Sigma[w(F_o^2)^2]\}^{0.5}$

 © 2004 Wiley-VCH Verlag GmbH & Co. KGaA, Weinheim

this was vindicated by the success of the subsequent solutions and refinements. Empirical absorption correction was performed for compound **17**. Intensities for **8** were measured on a Nonius-KappaCCD diffractometer at low temperature and treated with Scalpack and DENZO routines.[27] The crystal data and details of data collection and structure analyses are summarised in Table 4.

All structures were solved by direct methods using the SHELXS computer program[28] and refined in F^2 by a full-matrix least-squares procedure (SHELXL-97).[29] All non-hydrogen atoms were refined with anisotropic thermal parameters for all compounds. The hydrogen atoms were included in calculated positions and were refined with an overall isotropic temperature factor using a riding model. Weights were optimised in the final cycles.

CCDC-205739 (for **1**), -205740 (for **8**) and -205742 (for **17**) contain the supplementary crystallographic data for this paper. These data can be obtained free of charge at www.ccdc.cam.ac.uk/conts/retrieving.html [or from the Cambridge Crystallographic Data Centre, 12 Union Road, Cambridge CB2 1EZ, UK; Fax: (internat.) + 44-1223/336-033; E-mail: deposit@ccdc.cam.ac.uk].

Acknowledgments

We gratefully acknowledge financial support from the Ministerio de Ciencia y Tecnología, Spain (Grant no. BQU2002-04638-C02-01), the Junta de Comunidades de Castilla-La Mancha (PAC-02-003), the Dirección General de Investigación de la Consejería de Educación de la Comunidad Autónoma de Madrid (Grant no. 07N-0036/98) and the Universidad Rey Juan Carlos (PIPR-02-09).

[1] D. E. Wigley, *Prog. Inorg. Chem.* **1994**, *42*, 239−482.

[2] See for example: [2a] V. C. Gibson, D. N. Williams, W. Clegg, D. C. R. Hockless, *Polyhedron* **1989**, *8*, 1819−1820. [2b] U. Siemeling, V. C. Gibson, *J. Organomet. Chem.* **1992**, *426*, C25−C27. [2c] V. C. Gibson, A. D. Poole, U. Siemeling, D. N. Williams, W. Clegg, D. C. R. Hockless, *J. Organomet. Chem.* **1993**, *462*, C12−C14. [2d] T. C. Baldwin, S. R. Huber, M. A. Bruck, D. E. Wigley, *Inorg. Chem.* **1993**, *32*, 5682−5686. [2e] A. D. Poole, V. C. Gibson, W. Clegg, *J. Chem. Soc., Chem. Commun.* **1992**, 237−239. [2f] J. K. Cockcroff, V. C. Gibson, J. A. K. Howard, A. D. Poole, U. Siemeling, C. Wilson, *J. Chem. Soc., Chem. Commun.* **1992**, 1668−1670. [2g] M. C. W. Chan, J. M. Cole, V. C. Gibson, J. A. K. Howard, C. Lehmann, A. D. Poole, U. Siemeling, *J. Chem. Soc., Dalton Trans.* **1998**, 103−112. [2h] M. L. H. Green, J. T. James, J. F. Saunders, J. Souter, *J. Chem. Soc., Dalton Trans.* **1997**, 1281−1288.

[3] See for example: [3a] D. N. Williams, J. P. Mitchell, A. D. Poole, U. Siemeling, W. Clegg, D. C. R. Hockless, P. A. O′Neil, V. C. Gibson, *J. Chem. Soc., Dalton Trans.* **1992**, 739−751. [3b] V. C. Gibson, *Angew. Chem.* **1994**, *106*, 1640−1648; *Angew. Chem. Int. Ed. Engl.* **1994**, *33*, 1565−1573. [3c] V. C. Gibson, *J. Chem. Soc., Dalton Trans.* **1994**, 1607−1618. [3d] V. C. Gibson, A. D. Poole, *J. Chem. Soc., Chem. Commun.* **1995**, 2261−2262.

[4] [4a] M. P. Coles, V. C. Gibson, *Polym. Bull.* **1994**, *33*, 529−533. [4b] S. Scheuer, J. Fischer, J. Kress, *Organometallics* **1995**, *14*, 2627−2629. [4c] D. M. Antonelli, A. Leins, J. M. Stryker, *Organometallics* **1997**, *16*, 2500−2502. [4d] M. C. W. Chan, K. C. Chew, C. I. Dalby, V. C. Gibson, A. Kohlmann, I. R. Little, W. Reed, *Chem. Commun.* **1998**, 1673−1674.

[5] See for example: [5a] S. Schmidt, J. Sundermeyer, *J. Organomet. Chem.* **1994**, *472*, 127−138. [5b] Y-W. Chao, P. A. Wexler, D. E. Wigley, *Inorg. Chem.* **1990**, *29*, 4592−4594. [5c] A. Antiñolo, M. Fajardo, C. Huertas, A. Otero, S. Prashar, A. M. Rodríguez, *J. Organomet. Chem.* **1999**, *585*, 154−161.

[6] See for example: [6a] M. L. H. Green, J. T. James, J. F. Saunders, *Chem. Commun.* **1996**, 1343−1344. [6b] M. I. Alcalde, P. Gómez-Sal, A. Martín, P. Royo, *Organometallics* **1999**, *18*, 1144−1150.

[7] See for example: [7a] A. Castro, M. V. Galakhov, M. Gómez, F. Sánchez, *J. Organomet. Chem.* **1999**, *580*, 161−168. [7b] T. I. Gountchev, T. D. Tilley, *J. Am. Chem. Soc.* **1997**, *119*, 12831−12841.

[8] [8a] I. Dorado, A. Garcés, C. López-Mardomingo, M. Fajardo, A. Rodríguez, A. Antiñolo, A. Otero, *J. Chem. Soc., Dalton Trans.* **2000**, 2375−2382. [8b] I. Dorado, A. Garcés, C. López-Mardomingo, M. Fajardo, M. Kubicki, A. Antiñolo, A. Otero, *Dalton Trans.* **2003**, 910−917.

[9] A. Antiñolo, M. Fajardo, A. Otero, S. Prashar, *Eur. J. Inorg. Chem.* **2003**, 17−28.

[10] See for example: [10a] E. A. Maatta, D. D. Devore, *Angew. Chem.* **1988**, *100*, 583−585; *Angew. Chem. Int. Ed. Engl.* **1988**, *27*, 569−571. [10b] E. A. Maatta, C. Kim, *Inorg. Chem.* **1989**, *28*, 623−624. [10c] R. K. Rosen, R. A. Andresen, N. M. Edelstein, *J. Am. Chem. Soc.* **1990**, *112*, 4588−4590. [10d] G. Hogarth, R. L. Mallors, T. Norman, *J. Chem. Soc., Chem. Commun.* **1993**, 1721−1723. [10e] W. Clegg, R. J. Errington, D. C. R. Hockless, J. M. Kirk, C. Redshaw, *Polyhedron* **1992**, *11*, 381−384. [10f] D. E. Wheeler, J.-F. Wu, E. A. Maatta, *Polyhedron* **1998**, *17*, 969−976. [10g] M. Liangand, E. A. Maatta, *Inorg. Chem.* **1992**, *31*, 953−956. [10h] G. Hogarth, D. E. Humphry, N. Kaltsoyanis, W.-F. Kim, M. Lee, T. Norman, S. P. Redmond, *J. Chem. Soc., Dalton Trans.* **1999**, 2705−2723.

[11] [11a] D. M. Antonelli, M. L. H. Green, P. Mountford, *J. Organomet. Chem.* **1992**, *438*, C4−C8. [11b] P. T. Gomes, M. L. H. Green, A. M. Martín, P. Mountford, *J. Organomet. Chem.* **1997**, *541*, 121−125.

[12] [12a] D. D. Devore, J. D. Lichtenhan, F. Takusayawa, E. A. Maatta, *J. Am. Chem. Soc.* **1987**, *109*, 7408−7416. [12b] E. A. Maatta, *Inorg. Chem.* **1984**, *23*, 2560−2561.

[13] A. Antiñolo, I. López-Solera, A. Otero, S. Prashar, *J. Organomet. Chem.* **2001**, *631*, 151−164.

[14] P. Jernakoff, C. M. Bellefon, G. L. Geoffroy, A. L. Rheingold, S. J. Geib, *Organometallics* **1987**, *6*, 1362−1364.

[15] [15a] A. V. Korolvev, A. L. Rheingold, D. S. William, *Inorg. Chem.* **1997**, *36*, 2647−2655. [15b] K. S. Heinselman, V. M. Miskowski, S. J. Geib, L. C. Wang, M. D. Hopkins, *Inorg. Chem.* **1997**, *36*, 5530−5538.

[16] M. V. Galakhov, M. Gómez, G. Jiménez, M. A. Pellinghelli, P. Royo, A. Tiripicchio, *Organometallics* **1994**, *13*, 1564−1566.

[17] [17a] M. J. Humphries, M. L. H. Green, M. A. Leech, V. C. Gibson, M. Jolly, D. N. Williams, M. R. J. Elsegood, W. Clegg, *J. Chem. Soc., Dalton Trans.* **2000**, 4044−4051. [17b] M. J. Humphries, M. L. H. Green, R. E. Douthwaite, L. H. Rees, *J. Chem. Soc., Dalton Trans.* **2000**, 4555−4562. [17c] A. D. Poole, D. N. Williams, A. M. Kenwright, V. C. Gibson, W. Clegg, D. C. R. Hockless, P. A. O′Neil, *Organometallics* **1993**, *12*, 2549−2555. [17d] U. Burckhardt, T. D. Tilley, *J. Am. Chem. Soc.* **1999**, *121*, 6328−6329. [17e] G. I. Nikonov, P. Mountford, J. C. Green, P. A. Cooke, M. A. Leech, A. J. Blake, J. A. K. Howard, D. A. Lemenovskii, *Eur. J. Inorg. Chem.* **2000**, 1917−1921.

[18] A. Antiñolo, P. Espinosa, M. Fajardo, P. Gómez-Sal, C. López-Mardomingo, A. Martin-Alonso, A. Otero, *J. Chem. Soc., Dalton Trans.* **1995**, 1007−1013.

[19] H. Bock, J. Meuret, C. Näther, U. Krynitz, *Chem. Ber.* **1994**, *127*, 55−65.

[20] A. M. Andreu, F. A. Jalón, A. Otero, P. Royo, A. M. M. Lanfranchi, A. Tiripicchio, *J. Chem. Soc., Dalton Trans.* **1987**, 953−956.

[21] E. W. Abel, M. O. Dunster, *J. Organomet. Chem.* **1971**, *33*, 161−167.

[22] M. J. Bunker, A. DeCian, M. L. H. Green, J. J. E. Moreau, N. Siganporia, *J. Chem. Soc., Dalton Trans.* **1980**, 2155−2161.

[23] R. D. Sanner, S. T. Carter, W. J. Bruton, *J. Organomet. Chem.* **1982**, *240*, 157−162.

[24] G. Hidalgo, M. Mena, F. Palacios, P. Royo, R. Serrano, *J. Organomet. Chem.* **1988**, *340*, 37−40.

 © 2004 Wiley-VCH Verlag GmbH & Co. KGaA, Weinheim

[25] [25a] H. Yasuda, T. Okamoto, A. Nakamura, in *Organometallic Syntheses* (Eds.: R. B. King, J. J. Eisch), Elsevier, Amsterdam, **1988**, vol. 4, p. 40. [25b] J. de la Mata, R. Fandos, M. Gómez, P. Gómez-Sal, S. Martinez-Carrera, P. Royo, *Organometallics* **1990**, *9*, 2846−2850.
[26] R. R. Schrock, *J. Organomet. Chem.* **1976**, *122*, 209−225.
[27] Z. Otwinowski, W. Minor, *Methods Enzymol.* **1997**, *276*, 307−326.
[28] G. M. Sheldrick, *Acta Crystallogr., Sect. A* **1990**, *46*, 467−473.
[29] G. M. Sheldrick, *Program for the Refinement of Crystal Structures from Diffraction Data*, University of Göttingen, Göttingen, Germany, **1997**.

Received July 31, 2003
Early View Article
Published Online February 10, 2004

 © 2004 Wiley-VCH Verlag GmbH & Co. KGaA, Weinheim

Synthesis, Structure and Magnetic Properties of a μ-Carboxylato-Bridged Ferromagnetic Trinuclear Copper(II) Complex with Lariat Tetraazacrown Ether as Ligand

Shu-Lan Ma,[a] Wen-Xiang Zhu,*[a] Song Gao,[b] Qian-Ling Guo,[a] and Miao-Qiong Xu[a]

Keywords: Copper / Macrocyclic ligands / X-ray diffraction / Magnetic properties

Four *o*-toluic acid pendant groups have been attached to a tetraaza crown ether to prepare the novel tetraazamacrocyclic ligand H_4L, 4,7,13,16-tetrakis(2-carboxybenzyl)-1,10-dioxa-4,7,13,16-tetraazacyclooctadecane. The trinuclear copper(II) complex of the ligand, $[Cu_3L{\cdot}2H_2O]^{2+}{\cdot}2NO_3^-{\cdot}2H_2O$, has been newly synthesized, and its subsequent structural characterization has revealed that it consists of three Cu^{II} cores with a isosceles triangular array and that there is a two-fold rotation axis that passes through the Cu2 center. The complex contains two symmetry-related CuN_2O_3 cores in a distorted square-pyramidal geometry and one CuO_4 core in a distorted square-plane geometry. The two μ-bidentate *syn-anti* carboxylate groups bridge Cu1 with Cu2, and Cu1A with Cu2. The trinuclear copper(II) complex units are connected in a one-dimensional zigzag chain via μ-H_2O–NO_3^--bridged hydrogen bonds. Variable-temperature susceptibility measurements (2–300 K) reveal a ferromagnetic coupling, J_a = 8.08 cm^{-1}, between the μ-carboxylato-bridged Cu1 and Cu2, or Cu1A and Cu2, and a weak antiferromagnetic interaction, J_b = –0.40 cm^{-1}, between Cu1 and Cu1A.
(© Wiley-VCH Verlag GmbH & Co. KGaA, 69451 Weinheim, Germany, 2004)

Introduction

Multimetallic complexes are of great interest due to the special chemical and physical properties that result from the mutual interaction of two or more metal centers.[1] Trinuclear transition metal complexes have received increasing attention recently, partly because of the lack of metallobiomolecules for which the trinuclear core can act as a synthetic analogue. Polynuclear copper(II) complexes possess potential applications as, for example, molecular magnets and as models of metal enzymes.[2] The recent discovery of a ferromagnetically coupled Cu^{II} triad in a subunit of methane mono-oxygenase,[3] and an X-ray structure analysis of ascorbate oxidase from zucchini, which revealed an angled trimeric Cu^{II} unit,[4] have all stimulated an increasing interest in trinuclear copper systems. To date, the magnetic properties of many trinuclear copper(II) compounds have been reported, most of which exhibit antiferromagnetic interactions,[5−12] except for a few examples with ferromagnetic exchange.[13−16]

The acetate ion can provide a strong superexchange path in copper compounds. This is illustrated by an early study on hydrated copper acetate.[17] The carboxylate groups can bridge the metal cores through monodentate, and *syn-syn*, *syn-anti* and *anti-anti* bidentate coordination modes. Both *syn-syn*[17−20] and *anti-anti* modes[21,22] may promote an antiferromagnetic interaction, but the *syn-anti* bridging mode may cause either ferromagnetic[18,22−25] or antiferromagnetic interaction.[26,27] Complexes with s*yn-syn*-bridged carboxylate groups are very common, but those with *syn-anti* modes are very few.

Many reported polyazamacrocyclic copper(II) complexes are mononuclear and the carboxylate groups nearly all have a monodentate coordination mode,[28−31] with only a few showing bidentate modes.[32] The synthesis of polynuclear complexes of polyazamacrocycles is more difficult and challenging primarily due to a lack of suitably characterized ligands. For $[Cu_2(OAc)_2L]_n(ClO_4)_{2n}$, where L is a hexaazamacrocyclic ligand, *syn-anti* acetate bridges result in a pseudodinuclear structure,[26] but the acetate ions are not attached to the macrocyclic crown ether. Surprisingly, we succeeded in preparing a tetraazamacrocyclic ligand, 4,7,13,16-tetrakis(2-carboxybenzyl)-1,10-dioxa-4,7,13,16-tetraazacyclooctadecane), and prepared its novel trinuclear complex, $[Cu_3L(H_2O)_2]^{2+}{\cdot}2NO_3^-{\cdot}2H_2O$. Here we report the crystal structure and magnetic property of the complex, which involves both *syn-anti* μ_2-*O*,*O′* bidentate and monodentate carboxylate groups and exhibits a ferromagnetic exchange interaction.

[a] Department of Chemistry, Beijing Normal University,
Beijing 100875, P. R. China
Fax: (internat.) + 86-10-62200567
E-mail: wx-zhu@263.net
[b] State Key Laboratory of Rare Earth Materials Chemistry and Application, College of Chemistry and Molecular Engineering, Peking University,
Beijing 100871, P. R. China

Results and Discussion

IR Spectrum

The band at 1121 cm^{-1}, assigned to ν_{C-O-C} for the free ligand, is shifted to 1086 cm^{-1} in the complex, indicating the complexation of the ether oxygen atoms to the Cu^{2+} ion. The complex exhibits strong bands corresponding to ν_{as}(COO) at 1595 and 1567cm^{-1}, and ν_s(COO) at 1426 and 1366 cm^{-1}. Since the carboxylate group can coordinate to the metal ion in either bidentate or monodentate fashion, the "$\Delta\nu$ criterion" [$\Delta\nu = \nu_{asymm}(COO) - \nu_{symm}(COO)$] was employed to determine the coordination mode of the carboxylate group. The $\Delta\nu$ value of 168 and 201 cm^{-1} in our complex are very similar to that reported for the copper(II) complexes with both bidentate μ_2-*O*,*O*′ and monodentate carboxylate groups,[33] thus indicating the carboxylate groups behave both as bridging bidentate ligands between Cu^{II} atoms,[14,15] and as monodentate ligands. In addition, the band at 1384 cm^{-1} reveals the free nitrate in the complex. A broad band centered at 3426 cm^{-1} for the complex can be assigned to the ν_{O-H} stretch of coordinated or uncoordinated water molecules.

Description of the Structure

The complex consists of a discrete $[Cu_3L(H_2O)_2]^{2+}$ cation, two lattice water molecules and two uncoordinated nitrate anions. The cation of the complex with the atomic labeling scheme (Figure 1) and selected bond lengths and bond angles (Table 1) are given here. The molecule has a twofold symmetry, and the twofold rotation axis passes through the Cu2 center. The complex contains two symmetry-related CuN_2O_3 cores in a distorted square-pyramidal geometry and one CuO_4 core in a distorted square-planar geometry. The two μ-bidentate *syn-anti* carboxylate groups, O4−C22−O5 and O4A−C22A−O5A, bridge Cu2 with the crystallographically equivalent Cu1 and Cu1A cores at 4.554 Å, forming an isosceles triangle. The Cu1 and Cu1A ions are placed on the triangle base, with a longer distance of 4.852 Å connected by the N−$(CH_2)_2$−O spacer. The overall result is a 16-membered ring Cu3 cluster (Figure 2).

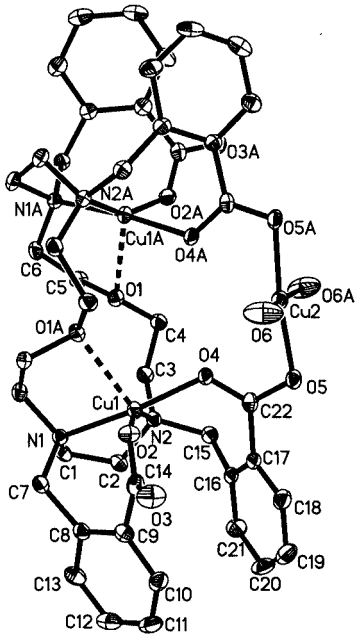

Figure 1. Thermal ellipsoids plot of the cation of $[Cu_3L{\cdot}2H_2O]^{2+}$ with labeling of selected atoms; ellipsoids shown at the 30% probability level

The distorted square-pyramidal Cu1 core consists of N1, N2, O2, O4, and O1A, in which N1, N2, O2 and O4 form the basal plane, and the apical positions are occupied by O1A. The distorted square-pyramidal Cu1A core consists of N1A, N2A, O2A, O4A and O1. The N1, N2, N1A, N2A, O1 and O1A atoms are all from the crown ether ring. O2 and O2A are from two carboxylate groups with a monodentate coordination mode, while O4 and O4A are from two other carboxylate groups with bidentate mode. Unlike Cu1 or Cu1A, the Cu2 ion is tetracoordinated to O5 and O5A, from the other oxygen atom of two μ_2-bidentate carboxylate groups, and O6 and O6A, from two water molecules. The deviations from the mean square-plane defined by Cu2, O5, O5A, O6 and O6A are −0.0951, 0.0225, 0.0225, 0.0251 and 0.0251 Å, respectively. Thus, the Cu2 ion is slightly above the basal square plane.

The complex obviously has a different structure from that of other reported macrocyclic polyazapolycarboxylato copper(II) complexes.[28−31] The nearly equal bond lengths of C22−O4 [1.263(4) Å] and C22−O5 [1.258(4) Å] show the bidentate coordination mode, while the significantly different lengths of C14−O2 [1.280(5) Å] and C14−O3 [1.241(5) Å] confirm its monodentate mode. The Cu−O bond lengths of the carboxylate group that bridges Cu1 and Cu2, 1.953(3) and 1.955(3) Å for Cu1−O4 and Cu2−O5, respectively, are nearly equal, but the Cu−O−C−O−Cu superexchange path is not symmetric. The crown ether ring is severely twisted to meet the requirement of the coordination geometry. The six donor atoms of crown ring, N 1, N2, N1A, N2A, O1 and O1A, are not coplanar and roughly adopt a boat conformation, which is in contrast with the chair conformation of the tetrakis(2-cyanobenzyl)-substituted tetraazacrown ether **2** in the solid state.[34] This may be due to steric hindrance from the four bulk pendant arms and the coordination requirement of the trinuclear complex.

Because of the limited cavity size of the parent macrocyclic free base (1,10-dioxa-4,7,13,16-tetraazacyclooctadecane) there are only two dinuclear complexes with its derivative ligand containing four (2-pyridyl)methyl pendant arms, from which the pyridyl nitrogen atoms are coordinated with the central metal atoms.[35,36] To our knowledge, the present complex is the first trinuclear complex of this tetraazamacrocyclic ligand.

There are intermolecular hydrogen bonds in the crystal of the complex. Oxygen atoms from the water molecule (O10) and the disordered nitrate anion (O7 and O9′) act as hydrogen-bond acceptors for the coordinated water mol-

 © 2004 Wiley-VCH Verlag GmbH & Co. KGaA, Weinheim

Table 1. Selected bond lengths [Å] and bond angles [°] for the complex

Cu(1)−O(2)[a]	1.964(3)	Cu(1)−O(4)	1.953(3)
Cu(1)−N(1)	2.021(3)	Cu(1)−N(2)	2.061(3)
Cu(1)−O(1)#1	2.503(3)	Cu(1)#1−O(1)	2.503(3)
Cu(2)−O(5)	1.955(3)	Cu(2)−O(5)#1	1.955(3)
Cu(2)−O(6)	1.896(3)	Cu(2)−O(6)#1	1.896(3)
C(14)−O(2)	1.280(5)	C(14)−O(3)	1.241(5)
C(22)−O(4)	1.263(4)	C(22)−O(5)	1.258(4)
O(2)−Cu(1)−O(4)	90.00(11)	O(2)−Cu(1)−N(1)	94.36(12)
O(4)−Cu(1)−N(1)	173.78(12)	O(2)−Cu(1)−N(2)	154.98(12)
O(4)−Cu(1)−N(2)	91.09(11)	O(5)−Cu(2)−O(5)#1	173.10(15)
O(5)−Cu(2)−O(6)	89.40(13)	O(5)−Cu(2)−O(6)#1	90.16(13)
O(5)#1−Cu(2)−O(6)	90.16(13)	O(5)#1−Cu(2)−O(6)#1	89.40(13)
O(6)−Cu(2)−O(6)#1	172.7(3)	C(14)−O(2)−Cu(1)	127.6(2)
C(22)−O(4)−Cu(1)	124.4(3)	C(22)−O(5)−Cu(2)	110.0(2)
O(2)−C(14)−O(3)	122.9(4)	O(4)−C(22)−O(5)	120.9(4)

[a] Symmetry transformations used to generate equivalent atoms: #1: $-x$, y, $-z + {}^1/_2$.

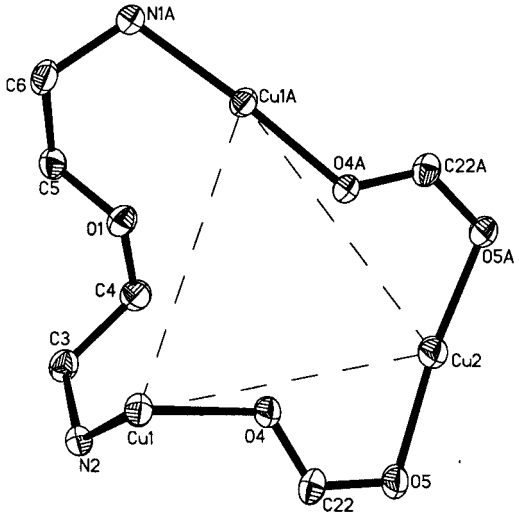

Figure 2. The 16-membered ring, showing the triangular Cu_3 skeleton and bridges

ecule involving O6. The water molecule involving O10, also as a hydrogen donor, is hydrogen-bonded to the uncoordinated oxygen atom (O3) of the carboxylate group, as well as to O8 and O8′ of its adjacent nitrate anion. Moreover, the nitrate anion is also hydrogen-bonded to the coordinated water molecule of the adjacent $[Cu_3L(H_2O)_2]^{2+}$ unit. Interatomic distances and bond angles are listed in Table 2. These hydrogen bonds form a μ-H_2O−NO_3^- "band" consisting of four water molecules and two nitrate ions to tie the molecules together, forming a one-dimensional zigzag chain in the unit cell (Figure 3). In addition, the adjacent chains are linked by a π-π stacking interaction between the phenyl rings C8−C13 and C8B−C13B (related by $-x + 1/2$, $-y + 1/2$, $-z + 1$). The interacting rings are strictly coplanar by symmetry and are separated by 3.356 Å, with their centroids being offset by 1.85 Å. The complex may thus be stabilized by both the hydrogen bonding and π-π stacking interaction.

Table 2. Hydrogen-bonding parameters

D−H···A[a]	H···A [Å]	D···A [Å]	D−H···A [°]
O6−H6C···O7(i)	1.768	2.582	172.5
O6−H6C···O9′(i)	2.171	2.738	126.5
O6−H6D···O10	1.817	2.615	163.7
O10−H10A···O8(i,i)	2.206	2.967	153.4
O10−H10A···O8′(i,i)	1.963	2.776	168.6
O10−H10B···O3	2.015	2.808	161.6

[a] Symmetry code: (i): $-x$, y, $-z + {}^1/_2$; (ii): x, $-y + 2$, $z + {}^1/_2$.

Magnetic Properties

The variable-temperature magnetic susceptibility χ_m per trinuclear Cu^{II} unit has been measured. At room temperature $\chi_m T$ is 1.27 $cm^3\ mol^{-1}$ K, which is slightly higher than the expected 1.12 $cm^3\ mol^{-1}$ K for three uncoupled spin-only Cu^{II} ions ($S = 1/2$, $g = 2$). $\chi_m T$ increases upon cooling, reaching 1.88 $cm^3\ mol^{-1}$ K at 2.14 K (Figure 4). A plot of ${\chi_m}^{-1}$ versus T is essentially linear, and least-squares fitting of the data to the Curie−Weiss law gave $C = 1.24$ $cm^3\ mol^{-1}$ K and $\theta = +1.16$ K. The increase of $\chi_m T$ upon cooling, and the small positive Weiss constant suggest a ferromagnetic interaction between Cu^{II} ions in the trimer.

To estimate the magnitude of the magnetic coupling in the trinuclear complex, an isotropic Heisenberg−Dirac−van Vleck (HDVV) Hamiltonian [Equation (1)] was used:

$$H = -2J_{12}(S_1 \cdot S_2) - 2J_{13}(S_1 \cdot S_3) - 2J_{23}(S_2 \cdot S_3) \quad (1)$$

where $J_{12,}$ J_{13} and J_{23} are the exchange coupling constants (negative for an antiferromagnetic AF interaction, positive for a ferromagnetic F interaction) and $S_1 = S_2 = S_3 = {}^1/_2$ for the three Cu^{II} centers. For the geometry of an isosceles triangle with C_{2c} symmetry, two coupling constant are in-

 © 2004 Wiley-VCH Verlag GmbH & Co. KGaA, Weinheim

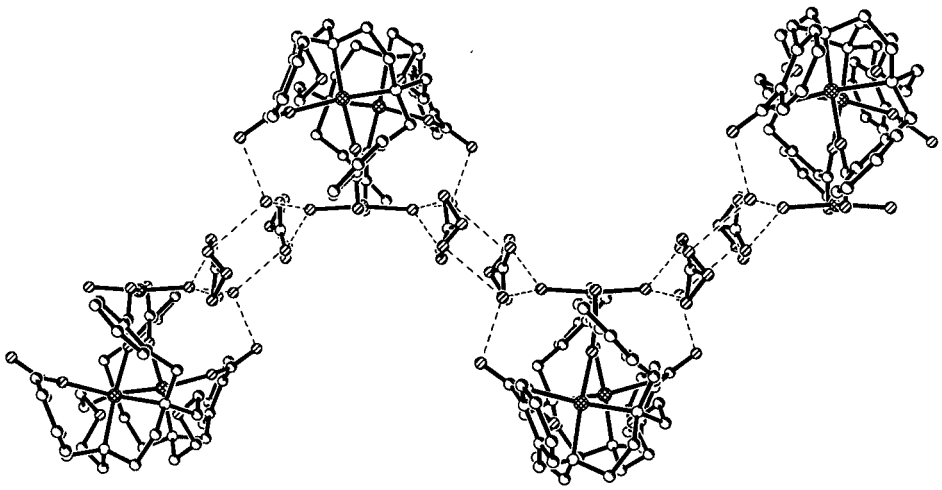

Figure 3. One-dimensional chain structure in the crystal linked by hydrogen bonding (viewed along the *a* axis, hydrogen atoms omitted for clarity)

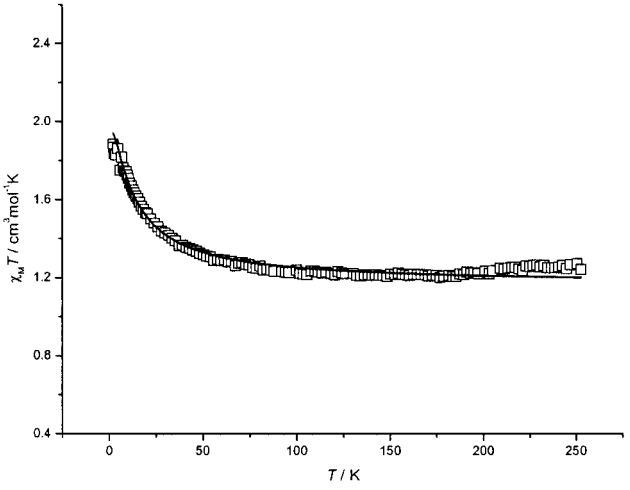

Figure 4. Temperature dependence of $\chi_m T$ of the complex, measured at 10 kOe; solid line corresponds to the best theoretical fitting (see text)

volved.[37] Thus, we employed Equation (2) to describe the low-lying electronic states:

$$H = -2J_a(S_1 \cdot S_2 + S_1 \cdot S_3) - 2J_b(S_2 \cdot S_3) \quad (2)$$

where $J_a = J_{12} = J_{13}$ is the coupling constant between bidentate carboxylato-bridged Cu2 and Cu1, or Cu2 and Cu1A, while $J_b = J_{23}$ is that between Cu1 and Cu1A, which are connected by the N−$(CH_2)_2$−O spacer (Figure 2). Application of van Vleck's susceptibility equation, and adding the Zeeman term to the preceding Hamiltonian (considering equal and isotropic *g* values for the three copper ions), gives Equation (3) for the molar susceptibility:

$$\chi_m = \frac{Ng^2\beta^2}{4kT} \frac{10\exp(J_a + 2J_b)/kT + \exp(-2J_a + 2J_b)/kT + 1}{2\exp(J_a + 2J_b)/kT + \exp(-2J_a + 2J_b)/kT + 1} \quad (3)$$

The best fit of the data through Equation (3) gives $g = 2.04$, $J_a = 8.08\ cm^{-1}$ and $J_b = -0.40\ cm^{-1}$. The reliability factor, defined as $R\ (\chi_m T) = (\chi_m T_{obs} - \chi_m T_{calcd.})^2/(\chi_m T_{obs})^2$, is 4.02×10^{-4}. The calculated data curve (solid line in Figure 4) matches the experimental magnetic data well. The positive J_a and the small negative J_b imply a ferromagnetic exchange interaction between the μ-carboxylato-bridged Cu2 and Cu1, or Cu2 and Cu1A, with a weak antiferromagnetic exchange interaction between Cu1 and Cu1A.

The magnetization measured at 1.84 K increases with the field, and reaches 3.25 Nβ per Cu_3 at 70 kOe, which is slightly higher than the expected saturation value of 3 Nβ for three spin-only Cu^{II} ions with $S = {}^1/_2$, $g = 2.0$ (Figure 5).

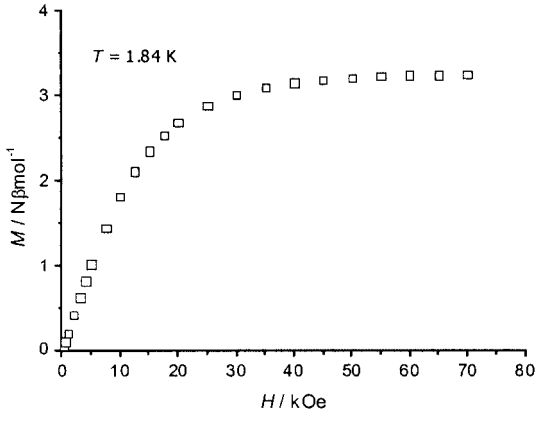

Figure 5. Magnetization versus field up to $H = 70$ kOe (at 1.84 K)

The exchange coupling in acetato- and related carboxylato-bridged complexes is largely determined by the conformation of the bridge and the interaction between the d orbitals of the metal ion and the bridge. In complexes where the metal ions are bridged in a *syn-syn* manner, the Cu−Cu distances are very small (e.g. 2.64 Å[38]) and the

 © 2004 Wiley-VCH Verlag GmbH & Co. KGaA, Weinheim

exchange coupling constants are very large, and nearly all with antiferromagnetic interaction. The dimeric complex $Cu_2(OAc)_4{\cdot}2H_2O$ ($2J = -286\ cm^{-1}$) is one example of such bridging.[39] As previously noted, the magnitude of the antiferromagnetic interaction depends on the overlap of the magnetic orbitals centered on nearest-neighbor copper ions. In such complexes, the acetato ligands interact directly with the d orbitals of the copper ions. However, in complexes containing *syn-anti* type bridges, the exchange coupling constants ($J \approx 4-7\ cm^{-1}$) are usually smaller and the exchange is ferromagnetic.[22−25] This might be because the *syn-anti* bridging carboxylate groups bind copper ions with a Cu−Cu distance that is too long to form a direct interaction (such as the Cu−Cu distance of 4.554 Å in the present complex). For the *syn-anti* conformation of the Cu−O−C−O′−Cu′ bridges, the 2p orbitals of O and O′ belonging to the magnetic orbitals centered on Cu and Cu′, respectively, are unfavorably oriented to give a strong overlap. This reduces the antiferromagnetic contribution, which would lead ultimately to an overall ferromagnetic behavior.[25]

Rodríguez-Fortea et al. have recently reported a theoretical study of the exchange coupling through *syn-anti* bridging carboxylate groups.[40] Their computational study showed that the calculated coupling constant in the *syn-anti* case is weakly ferromagnetic ($+10.2\ cm^{-1}$). Because of the rareness of the *syn-anti* case, the authors can only compare their results with the one available compound with a *syn-anti* coordination mode. The coupling constant of $+8.08\ cm^{-1}$ in our present compound agrees well with the result above, providing an important *syn-anti* case.

Conclusion

The novel tetraazamacrocyclic ligand containing four pendent *o*-toluic acid groups has been prepared by the hydrolysis of the cyano groups. Because of the strong coordinating ability of the carboxylate groups and the large steric hindrance from the four bulk *o*-toluic acid pendant arms, we obtained its trinuclear copper(II) complex. For the complex, the three Cu^{II} cores are in an isosceles triangular arrangement and adjacent copper ions are connected by μ_2-didentate *syn-anti* carboxylate groups and an $N-(CH_2)_2-O$ spacer. The trinuclear copper(II) complex units are connected into a one-dimensional zigzag hydrogen-bonding chain. Magnetic property studies revealed a ferromagnetic interaction, which corresponds with the magnetic coupling observed for other *syn-anti*-bridged complexes.

Experimental Section

General Remarks: All commercially available chemicals were of analytical grade and were used as received. C, H and N were determined using an Elementar vario EL elemental analyzer. The IR spectra were recorded with a Nicolet-AVATAR 360 FT-IR spectrometer using KBr pellets in the 4000−400 cm^{-1} regions. Variable-temperature magnetic susceptibility data for a crystalline sample of complex were obtained in an external field of 10.0 kG with an Oxford Maglab 2000 system magnetometer from 300 to 2 K. 1,10-Dioxa-4, 7,13,16-tetraazacyclooctadecane (**1**) was prepared according to a literature procedure.[41]

4,7,13,16-Tetrakis(2-cyanobenzyl)-1,10-dioxa-4,7,13,16-tetraazacyclooctadecane (2): To prepare compound **2** (Scheme 1) a mixture of azacrown ether **1** (0.26 g, 1 mmol) and anhydrous K_2CO_3 (1.10 g, 8 mmol) was heated under reflux in acetonitrile (15 mL) for 4 h, and then an acetonitrile solution (15 mL) of 2-(bromomethyl)benzonitrile (0.78 g, 4 mmol) was added. The resultant mixture was heated under reflux for a further 20 h. The so-obtained precipitate was then filtered off and the mother liquor was cooled slowly to room temperature. After 2 h, colorless plate crystals of **2** formed from the mother liquor. Mp 119−121°C. $C_{44}H_{48}N_8O_2$ (720.9): calcd. C 73.29, H 6.66, N 14.89; found C 73.10, H 6.39, N 14.79. ^1H NMR (500 MHz, $CDCl_3$): δ (ppm): = 2.79−2.83 (m, 16 H, NCH_2), 3.56−3.58 (t, $J_{H,H}$ = 5.5 Hz, 8 H, OCH_2), 3.80 (s, 8 H, CH_2), 7.31−7.34 (t, $J_{H,H}$ = 7.7 Hz, 4 H, ArH), 7.49−7.53 (m, 4 H, ArH), 7.59−7.61 (d, $J_{H,H}$ = 7.7 Hz, 8 H, ArH) ppm. IR (KBr pellet): $\tilde{\nu}$ = 2223 s, 1596 m, 1483 m, 1447 s, 1363 m, 1350 m, 1310 m, 1284 m, 1121 s, 1063 s, 1051 s, 937 m, 772 m, 561 w cm^{-1}.

4,7,13,16-Tetrakis(2-carboxybenzyl)-1,10-dioxa-4,7,13,16-tetraazacyclooctadecane Tetrahydrochloride ($H_4L{\cdot}4HCl$): A solution of azacrown ether **2** (0.72 g, 1.0 mmol) in 4 M aqueous HCl (30 mL) was heated under reflux overnight (see Scheme 1). The solvent was then removed by evaporation on a water bath. The resultant residue was dissolved in aqueous HCl (1:1, 10 mL) and heated at 70−80°C. After cooling, plate crystals were obtained as the tetrahydrochloride salt. $C_{44}H_{56}Cl_4N_4O_{10}$ (942.4): calcd. C 56.05, H 5.94, N 6.79;

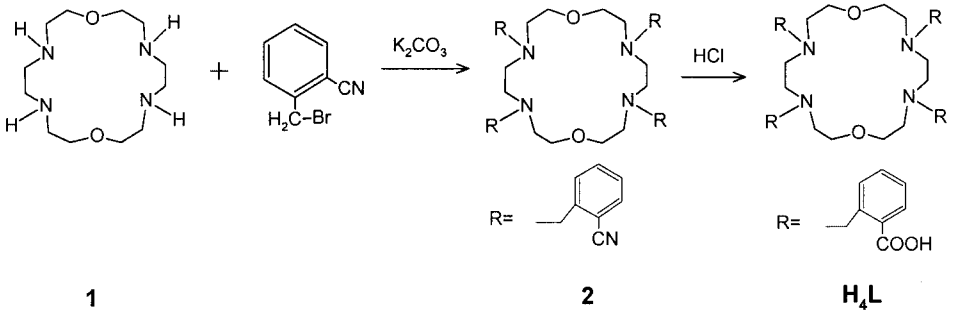

1 **2** **H_4L**

Scheme 1

 © 2004 Wiley-VCH Verlag GmbH & Co. KGaA, Weinheim

found C 55.87, H 6.13, N 6.41. IR (KBr pellet): $\tilde{\nu}$ = 3390 s, 1704 s, 1600 m, 1579 m, 1449 s, 1399 s, 1300 s, 1230 s, 1119 m, 1081 m, 971 w, 745 m, 650 m cm^{-1}.

$[Cu_3L{\cdot}2H_2O]^{2+}{\cdot}2NO_3^-{\cdot}2H_2O$: $Cu(NO_3)_2{\cdot}3H_2O$ (0.04 g, 0.15 mmol) was added to a water/methanol (1:4, 10 cm^3) solution of the ligand $H_4L{\cdot}4HCl$ (0.047 g, 0.05 mmol). The pH of the reaction solution was adjusted to 5 with triethylamine. Subsequent slow concentration at room temperature afforded blue crystals suitable for X-ray determination. $C_{44}H_{56}Cu_3N_6O_{20}$ (1179.57): calcd. C 44.76, H 4.75, N 7.12; found C 44.51, H 4.41, N 7.35. IR (KBr pellet): $\tilde{\nu}$ = 3429 m, 1608 m, 1594 s, 1567 s, 1457 m, 1426 s, 1384 s, 1365 s, 1336 s, 1285 w, 1086 m, 991 w, 745 m cm^{-1}.

X-ray Crystallographic Study: An X-ray diffraction analysis of a crystal (0.60 × 0.26 × 0.22 mm) was preformed with a Bruker SMART 1000 CCD diffractometer at 293 K with graphite-monochromatized Mo-K_α radiation (λ = 0.71073 Å). Semiempirical absorption corrections were applied using the SADABS program. The structure was solved by direct methods and refined by full-matrix least squares on F^2 using the SHELXS-97 and SHELXL-97 programs.[42] All non-hydrogen atoms were refined with anisotropic displacement parameters. The hydrogen atoms were generated geometrically and treated by a mixture of independent and constrained refinements. Disorder of the nitrate anion was found in the crystal. The site occupation factor for each nitrate anion was refined to 70.4 and 29.9%, respectively. Crystallographic data and details of the structure refinements are summarized in Table 3. CCDC-205577 contains the supplementary crystallographic data for this paper. These data can be obtained free of charge at www.ccdc.cam.ac.uk/conts/retrieving.html or from the Cambridge Crystallographic Data Centre, 12 Union Road, Cambridge, CB2 1EZ, UK [Fax: (internat.) + 44-1223-336-033; E-mail: deposit@ccdc.cam.ac.uk].

Table 3. Crystal data and structure refinement details for the complex

Empirical formula	$C_{44}H_{56}Cu_3N_6O_{20}$
Formula mass	1179.57
Temperature	293(2) K
Wavelength	0.71073 Å
Crystal system, space group	monoclinic, *C*2/*c*
Unit cell dimensions	*a* = 29.454(16) Å
	b = 9.756(6) Å
	c = 17.473(10) Å
	β = 110.157(9)°
Volume	4713(4) $Å^3$
Z, calculated density	4, 1.662 Mg/m^3
Absorption coefficient	1.430 mm^{-1}
F(000)	2436
Crystal size	0.60 × 0.26 × 0.22 mm
θ range for data collection	2.21−25.00°
Limiting indices	$-34 \le h \le 32$, $-11 \le k \le 11$, $-10 \le l \le 20$
Reflections collected/unique	9907/4119 [*R*(int) = 0.0464]
Completeness to θ = 25.00°	99.2%
Absorption correction	semiempirical from equivalents
Max. and min. transmission	1.000000 and 0.747142
Refinement method	full-matrix least squares on F^2
Data/restraints/parameters	4119/93/371
Goodness of fit on F^2	1.020
Final *R* indices [$I > 2\sigma(I)$]	*R*1 = 0.0417, *wR*2 = 0.0827
Extinction coefficient	0.00043(7)
Largest diff. peak/hole	0.432/−0.425 e·$Å^{-3}$

Acknowledgments

We are grateful to the Municipal Natural Science Foundation of Beijing (No. 2022011).

[1] O. Kahn, *Comments Inorg. Chem.* **1984**, *3*, 105−131.
[2] R. H. Holm, P. Kennepohl, E. I. Solomon, *Chem. Rev.* **1996**, *96*, 2239−2314.
[3] H. H. T. Nguyen, A. K. Shiemke, S. J. Jacobs, B. J. Hales, M. E. Linstrom, S. I. Chan, *J. Biol. Chem.* **1994**, *269*, 14995−15005.
[4] A. Messerschmidt, R. Huber, *Eur. J. Biochem.* **1990**, *187*, 341−352.
[5] J. Sanmartín, M. R. Bermejo, A. M. García-Deibe, O. R. Nascimento, L. Lezama, T. Rojo, *J. Chem. Soc., Dalton Trans.* **2002**, 1030−1035.
[6] P. A. Angaridis, P. Baran, R. Boca, F. Cervantes-Lee, W. Haase, G. Mezei, R. G. Raptis, R. Werner, *Inorg. Chem.* **2002**, *41*, 2219−2228.
[7] I. Castro, M. L. Calatayud, F. Lloret, J. Sletten, M. Julve, *J. Chem. Soc., Dalton Trans.* **2002**, 2397−2403.
[8] E.-Q. Gao, Q.-H. Zhao, J.-K. Tang, D.-Z. Liao, Z.-H. Jiang, S.-P. Yan, *J. Chem. Soc., Dalton Trans.* **2001**, 1537−1540.
[9] L. Zhao, L. K. Thompson, Z.-Q. Xu, D. O. Miller, D. R. Stirling, *J. Chem. Soc., Dalton Trans.* **2001**, 1706−1710.
[10] H. L. Sandoval, R. Contreras, A. Escuer, R. Vicente, S. Bernès, H. Nöth, G. J. Leigh, N. B. Behrens, *J. Chem. Soc., Dalton Trans.* **2002**, 2648−2653.
[11] S. Ferrer, F. Lloret, I. Bertomeu, G. Alzuet, J. Borrás, S. G. Granda, M. L. González, J. Haasnoot, *Inorg. Chem.* **2002**, *41*, 5821−5830.
[12] Q.-Y. Chen, Z.-Q. Pan, Q.-H. Luo, L.-M. Zhen, X.-L. Hu, Z.-L. Wang, Z.-Y. Zhou, C.-H. Yeung, *J. Chem. Soc., Dalton Trans.* **2002**, 1315−1318.
[13] J.-K. Tang, H.-M. Wang, P. Cheng, X. Liu, D.-Z. Liao, Z.-H. Jiang, S.-P. Yan, *Polyhedron* **2001**, *20*, 675−680.
[14] L. Gutierrez, G. Alzuet, J. A. Real, J. Cano, J. Borrás, A. Castiñeiras, *Eur. J. Inorg. Chem.* **2002**, 2094−2102.
[15] L. Gutierrez, G. Alzuet, J. A. Real, J. Cano, J. Borrás, A. Castiñeiras, *Inorg. Chem.* **2000**, *39*, 3608−3614.
[16] G. A. van Albada, I. Mutikainen, O. Roubeau, U. Turpeinen, J. Reedijk, *Inorg. Chim. Acta* **2002**, *331*, 208−215.
[17] B. N. Figgis, R. L. Martin, *J. Chem. Soc.* **1956**, *214*, 451−456.
[18] H.-J. Chen, Z.-W. Mao, S. Gao, X.-M. Chen, *Chem. Commun.* **2001**, 2320−2321.
[19] E. Ruiz, P. Alemany, S. Alvarez, J. Cano, *J. Am. Chem. Soc.* **1997**, *119*, 1297−1303.
[20] J. Li, F.-X. Zhang, Z.-X. Tang, Q.-Z. Shi, *Acta Chim. Sin.* **2001**, *59*, 1116−1120.
[21] R. L. Rardin, P. Poganiuch, A. Bino, D. P. Goldberg, W. B. Tolman, S.-C. Liu, S. J. Lippard, *J. Am. Chem. Soc.* **1992**, *114*, 5240−5249.
[22] M. Inoue, M. Kubo, *Inorg. Chem.* **1970**, *9*, 2310−2314.
[23] P. J. Corvan, W. E. Estes, R. R. Weller, W. E. Hatfield, *Inorg. Chem.* **1980**, *19*, 1297−1300.
[24] D. K. Towle, S. K. Hoffman, W. E. Hatfield, P. Singh, P. Chaudhuri, *Inorg. Chem.* **1988**, *27*, 394−399.
[25] E. Colacio, J.-P. Costes, R. Kivekas, J.-P. Laurent, J. Ruiz, *Inorg. Chem.* **1990**, *29*, 4240−4246.
[26] P. K. Coughlin, S. J. Lippard, *J. Am. Chem. Soc.* **1984**, *106*, 2328−2336.
[27] R. L. Carlin, K. Kopinga, O. Kahn, M. Verdaguer, *Inorg. Chem.* **1986**, *25*, 1786−1789.
[28] M. K. Moi, M. Yanuck, S. V. Deshpande, H. Hope, S. J. DeNardo, C. F. Meares, *Inorg. Chem.* **1987**, *26*, 3458−3463.
[29] J. Chapman, G. Ferguson, J. F. Gallagher, M. C. Jennings, D. Paker, *J. Chem. Soc., Dalton Trans.* **1992**, 345−353.

 © 2004 Wiley-VCH Verlag GmbH & Co. KGaA, Weinheim

[30] J. Costa, R. Delgado, M. G. B. Drew, V. Felix, *J. Chem. Soc., Dalton Trans.* **1998**, 1063−1071.
[31] K. Y. Choi, I. H. Suh, J. G. Kim, Y. S. Park, S. I. Jeong, I. K. Kim, C. P. Hong, S. N. Choi, *Polyhedron* **1999**, *18*, 3013−3018.
[32] A. Reisen, M. Zehnder, T. A. Kaden, *J. Chem. Soc., Chem. Commun.* **1985**, 1336−1338.
[33] Y.-Y. Wang, L.-J. Zhou, Q. Shi, Q.-Z. Shi, *Transition Met. Chem.* **2002**, *27*, 145−148.
[34] S.-L. Ma, W.-X. Zhu, S.-J. Dong, Q.-L. Guo, Y.-B. She, *Chin. J. Chem.*, in press.
[35] D. Tétard, A. Rabion, J.-B. Verlhac, J. Guilhem, *J. Chem. Soc., Chem. Commun.* **1995**, 531−532.
[36] J.-M. Vincent, S. B. Barbry, C. Pierre, J.-B. Verlhac, *J. Chem. Soc., Dalton Trans.* **1999**, 1913−1914.
[37] M.-X. Ren, Q.-J. Meng, *Chin. J. Inorg. Chem.* **2002**, *18*, 486−488.
[38] P. de Meester, S. A. Fletcher, A. C. Skapsky, *J. Chem. Soc., Dalton Trans.* **1973**, 2575−2578.
[39] J. Lewis, F. E. Mabbs, L. K. Royston, W. R. Smail, *J. Chem. Soc., A* **1969**, 291−296.
[40] A. R. Fortea, P. Alemany, S. Alvarez, E. Ruiz, *Chem. Eur. J.* **2001**, *7*, 627−637.
[41] J. F. Biernat, E. Luboch, *Tetrahedron* **1984**, *40*, 1927−1929.
[42] G. M. Sheldrick, *SHELXS-97* and *SHELXL-97*, University of Göttingen, Germany, **1997**.

Received May 8, 2003
Early View Article
Published Online February 16, 2004

 © 2004 Wiley-VCH Verlag GmbH & Co. KGaA, Weinheim

A Series of Transition Metal Bis(dicyanobenzenedithiolate) Complexes [M(dcbdt)$_2$] (M = Fe, Co, Ni, Pd, Pt, Cu, Au and Zn)

Helena Alves,[a] Dulce Simão,[b] Isabel Cordeiro Santos,[a] Vasco Gama,[a] Rui Teives Henriques,[a,b] Horácio Novais,[b] and Manuel Almeida*[a]

Keywords: Coordination chemistry / EPR spectroscopy / Magnetic properties / S ligands / Transition metals

A series of new M[(dcbdt)$_2$]$^{-z}$ complexes of the dicyanobenzodithiolate (dcbdt) ligand with a range of transition metals (M = Co, Pd, Pt, Cu, Au and Zn) in different oxidation states (z = 0.4, 1, 2) were prepared as their nBu$_4$N salts and characterised by X-ray diffraction, cyclic voltammetry, EPR and static magnetic susceptibility. Their properties are discussed in comparison with the Ni and Fe analogues described by us recently. The structures of these complexes belong to four distinct groups: i) the Zn^{II} compound **10** is triclinic $P\bar{1}$ with the metal in a tetrahedral coordination geometry; ii) other M^{II} complexes [M = Pt (**8**), Pd (**7**), Co (**3**) and Cu (**5**)] are monoclinic $C2/m$, and are isostructural with the Ni^{II} analogue, presenting a perfectly planar square geometry; iii) the Co^{III} compound **4** is triclinic $P\bar{1}$, and isostructural with the Fe and Ni analogues, with a strong dimerisation of the M(dcbdt)$_2$ units and the metal in a square-pyramidal coordination geometry; iv) the M^{III} salts with M = Au (**2**), Cu (**6**) and Pt (**9**) are monoclinic $P2_1/c$ and the complexes are arranged as pseudo-dimers. The EPR and static magnetic-susceptibility measurements show that the Co^{II} (**3**), Cu^{II} (**5**), Pt^{III} (**9**) and Co^{III} (**4**) complexes are paramagnetic corresponding to an S = 1/2 state, except for Co^{III}, which is in a high-spin S = 1 configuration. The solid state EPR spectra of the Co^{II} compound presents a hyperfine structure typical of the I = 7/2 ^{59}Co. The temperature dependence of the paramagnetic susceptibility of the Pt^{III} compound follows a singlet-triplet model with a dimer antiferromagnetic coupling, J, of 984 K.

(© Wiley-VCH Verlag GmbH & Co. KGaA, 69451 Weinheim, Germany, 2004)

Introduction

During the last few years there has been a renewed interest in the study of transition metal bis(dithiolene) complexes which, in their square-planar coordination geometry, can be used as building blocks for conducting and or magnetic molecular materials.[1] These complexes can be seen as the inorganic analogues of TTF-type donors, which so far have provided the largest number of known organic conductors and superconductors, where the central C=C bond is replaced by a transition metal. In fact these inorganic complexes have frontier orbitals that are isolobal with the corresponding TTF analogues. Depending on the metal and on the oxidation state, these complexes can present different magnetic moments. Furthermore, the choice of the transition metal provides access to a diversity of different ground states. These are important features for the study and design of molecular materials with specific magnetic properties.

[a] Instituto Tecnológico e Nuclear,
Estrada Nacional no. 10, 2686-953 Sacavém, Portugal
Fax: (internat.) + 351-21-994-1455
E-mail: malmeida@itn.mces.pt
[b] Instituto Superior Técnico
Av. Rovisco Pais, 1049-001 Lisboa, Portugal
Fax: (internat.) + 351-21-841-7862
E-mail: dulce@mail.ist.utl.pt

Bis(dithiolene) complexes based on extended and delocalised π-ligands are expected to be more promising for conducting materials due to the accessibility of a wider range of oxidation states and the possibility of larger solid-state interactions.[1−4] Although bis(dithiolene) complexes of metals from groups 10 and 11 tend to adopt a square-planar geometry, favourable for extended π-π interactions and electron delocalisation in stacked structures, in some cases, namely for Fe and Co, other structures and different metal coordination environments are possible. All known Fe^{III} bis(dithiolene) complexes are dimeric with a square-pyramidal coordination geometry.[5,6] For Co^{III}, further to this dimeric structure, examples of trimeric[7] or even polymeric structures are also known.[8]

Recently, after the synthesis of the new extended aromatic ligand 4,5-dicyanobenzene-1,2-dithiolate (dcbdt), we have reported a study of the nickel complexes [Ni(dcbdt)$_2$]$^{z-}$, which can exist in a variety of different, easily accessible oxidation states (z = 0.4, 1, 2).[9] The Ni^{III} complex with this ligand and z = 1 was found to present a strongly dimerised geometry, rare for Ni, and the salt (nBu$_4$N)$_2$[Ni(dcbdt)$_2$]$_5$, with segregated stacks of partially oxidised Ni complexes, is a semiconductor with relatively high electrical conductivity. As judged from preliminary data published on the gold analogue (nBu$_4$N)$_2$-[Au(dcbdt)$_2$]$_5$,[10,11] the partially oxidised state, [M(dcbdt)$_2$]^z

 © 2004 Wiley-VCH Verlag GmbH & Co. KGaA, Weinheim DOI: 10.1002/ejic.200300476

with $z = 0.4$, seems to be a general feature of complexes with this ligand.

More recently the iron complex $[Fe(dcbdt)_2]_2^{2-}$ was also described and it presents a similar dimerised structure, with magnetic properties similar to the Ni analogue.[12] Thus, both for fundamental reasons and also in order to evaluate their possible use as building blocks for conducting or magnetic materials, it appears of obvious interest to study similar complexes with different transition metals.

In this paper we report a comparative study of a diversity of $[M(dcbdt)_2]^z$ complexes with different transition metals: M = Fe, Co, Ni, Cu, Zn, Pd, Pt and Au.

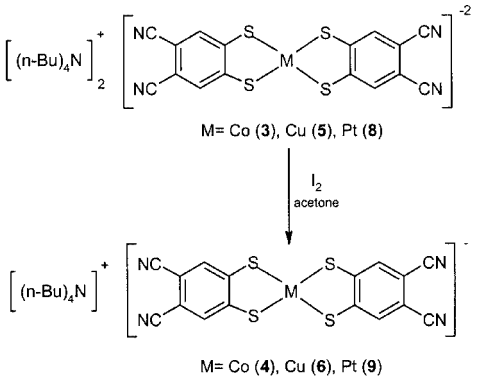

Scheme 2

Results and Discussion

Synthesis

The synthesis of the different metal complexes was performed following a general common procedure, similar to that previously described for nickel[9] and using the ligand 4,5-dicyanobenzene-1,2-dithiol (**1**) obtained from the aromatic dibenzyl sulfide 1,2-bis(benzylthio)benzene-4,5-dicarbonitrile. The benzothiol **1** was reacted, in a basic medium, with chloride salts of the different metals and the resulting metal complex precipitated as a tetrabutylammonium salt by addition of $(n\text{Bu})_4\text{Br}$ (Scheme 1).

The oxidation state of the resulting complex depends on the starting metal salt, the reaction conditions and the redox stability of the final product. The dianionic complexes were obtained from MCl_2 salts, with final yields in the range of 25−65% after recrystallisation from acetone, as deep-blue crystals for cobalt(II) (**3**), as orange crystals for palladium(II) (**7**) as red crystals for platinum(II) (**8**), as brown crystals for copper(II) (**5**) and as orange crystals for zinc(II) (**10**).

With exception of Pd and Zn, the monoanionic complexes could be obtained by oxidation of the corresponding dianions with iodine in acetone solution, as summarised in Scheme 2, leading to crystals of cobalt(III) (**4**), platinum(III) (**9**) and copper(III) (**6**) complexes, all of which are different shades of green. Attempts to oxidise the palladium(II) complex with iodine, or other oxidising agents, always led to decomposition.

The monoanionic complexes could be obtained directly after complexation for gold(III) (**2**), as green crystals, from the $KAuCl_4$ salt and also, as described previously, for iron(III) from $FeCl_3$.[12] For cobalt, the monoanionic complex $[Co(dcbdt)_2]^-$ (**4**) could also be obtained directly, starting from $CoCl_2$ and oxidation by prolonged exposure to air.

All complexes were characterised by elemental analysis (C, H, N, S) and by IR and UV/Visible spectroscopy. ^1H and ^{13}C NMR spectra were also recorded, giving rise to the expected peak-intensity ratios, according to the molecular structure and stoichiometry, for compounds **2**, **6**, **7**, **8** and **10**. For the paramagnetic compounds **4**, **5** and **9**, only the peaks of the tetrabutylammonium ion could be observed.

The cyclic voltammograms of $(n\text{Bu}_4\text{N})[M(dcbdt)_2]$ (M = Au, Co, Cu, Pt) and $(n\text{Bu}_4\text{N})_2[M(dcbdt)_2]$ (M = Pd, Zn) complexes were recorded in acetonitrile with reference to Ag/AgCl. The redox potentials observed are summarised in Table 1 together with those previously reported for the Ni and Fe compounds.

At lower potentials a redox process associated with the couple $[M(dcbdt)_2]^{2-}/[M(dcbdt)_2]^-$ is usually observed. This is reversible for M = Co ($E_{1/2} = -0.20$ V), Cu ($E_{1/2} = -0.07$ V) and Pd ($E_{1/2} = 0.36$ V), quasi-reversible for Pt ($E_{1/2} = 0.06$ V, with $\Delta E = 0.13$ V) and was not observed for Zn in the range of the experiment. An irreversible reduction wave of $[M(dcbdt)_2]^-$ to $[M(dcbdt)_2]^{2-}$ is observed for Au at −1.33 V and at −0.44 V for Fe. The difference in the oxidation potentials of the different complexes explains their chemical behaviour during the synthesis: the salts of Co, Pt, Cu, Pd, Zn are obtained in their dianionic form, $[n\text{Bu}_4\text{N}]_2[M(dcbdt)_2]$, while those of iron and gold, with

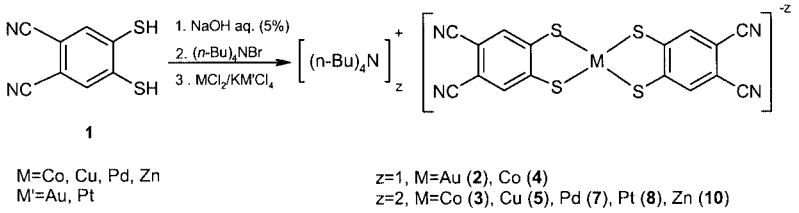

Scheme 1

 © 2004 Wiley-VCH Verlag GmbH & Co. KGaA, Weinheim

Table 1. Cyclic voltammetry data of $(n\mathrm{Bu_4N})[\mathrm{M(dcbdt)_2}]$ (M = Au, Co, Cu, Pt, Fe) and $(n\mathrm{Bu_4N})_2[\mathrm{M(dcbdt)_2}]$ (M = Pd, Zn) in acetonitrile (ref. $Ag/AgNO_3$)

M	$[M(dcbdt)_2]^{2-}/[M(dcbdt)_2]^{-}$ $E_{1/2}$ [V]	$[M(dcbdt)_2]^{-}/[M(dcbdt)_2]_5^{2-}$ E_1	E_2
Pt	0.06	0.80	1.14
Pd	0.36 qr	0.80	1.02
Cu	−0.07	0.99	1.11
Co	−0.21	0.91	0.99
Au	−1.33	0.81	1.20
Fe[12]	–	0.89	1.07
Ni[9]	0.08		
Zn	–	0.89	1.27

very negative potentials for the process $[M(dcbdt)_2]^{2-}/[M(dcbdt)_2]^{-}$, are obtained in the monoanionic form $(n\mathrm{Bu_4N})[M(dcbdt)_2]$. The synthesis of the monoanionic complexes $(n\mathrm{Bu_4N})[M(dcbdt)_2]$ [M = Co (**4**), Pt (**9**) and Cu (**6**)] requires an additional oxidation step. The high redox potential for this process in the palladium complex explains the difficulty to obtain to the Pd^{III} species employing common oxidising agents. The platinum complex is also difficult to oxidise, in comparison with the other salts, which is consistent with the slightly positive potential presented. As previously found for $[Ni(dcbdt)_2]$,[9] the redox potentials of these dcbdt complexes are significantly higher than the corresponding ones in complexes with the more simple bdt (1,2-benzenedithiolate) ligand. This feature is a consequence of the electron-withdrawing nature of the CN groups, which stabilises the dianionic state. As an example, we found a potential of −0.07 V for $[Cu(dcbdt)_2]^{2-}/[Cu(dcbdt)_2]^{-}$ versus Ag/AgCl, while the corresponding potential for $Cu(bdt)_2$ is −0.56 V.[13] A similar difference in redox potentials is found for other metals.

At higher positive potentials, a series of complex oxidation processes with larger current waves occur, showing, in general, two superimposed waves, which can be associated with a multielectron transfer process leading to the formation of $[M(dcbdt)_2]_5^{2-}$ (Scheme 3), similar to previous observations for M = Ni.[9]

$$5[M(dcbdt)_2]^{-} \rightleftharpoons [M(dcbdt)_2]_5^{2-} + 3e^{-}$$

Scheme 3

In fact, the compounds $(n\mathrm{Bu_4N})_2[M(dcbdt)_2]_5^{2-}$ (M = Au and Ni) have already been obtained by electrocrystallisation,[9,10] and a study of similar compounds, with different transition metals, will be reported in a subsequent publication.[14]

X-ray Diffraction Studies

The crystals obtained for compounds **3**, **4**, **7**, **8** and **10** enabled their crystal structure determination by X-ray diffraction. The refinement of the crystal structures of compounds **2**, **6** and **9** was limited by a small degree of disorder affecting only the cation. The reduced diffraction power of the crystals of compound **5** allowed only the determination of the lattice parameters, which are similar to those of Pt, Pd and Co. Crystallographic data of these compounds are listed in Table 2 and 3.

Table 2. Crystallographic data for compounds $(n\mathrm{Bu_4N})_2[\mathrm{M(dcbdt)_2}]$ (M = Co, Pd, Pt, Zn)

	Co (**3**)	Pd (**7**)	Pt (**8**)	Zn (**10**)
Crystal size (mm)	0.8 × 0.7 × 0.6	0.6 × 0.24 × 0.16	0.8 × 0.7 × 0.4	0. 7 × 0.3 × 0.2
Crystal Colour and shape	dark-blue prism	orange plate	red prism	orange prism
Empirical formula	$C_{48}H_{76}CoN_6S_4$	$C_{48}H_{76}N_6S_4Pd$	$C_{48}H_{76}N_6S_4Pt$	$C_{48}H_{76}N_6S_4Zn$
Molecular mass	924.32	971.79	1060.48	930.76
Crystal system	monoclinic	monoclinic	monoclinic	triclinic
Space group (no.)	*C*2/*m* (12)	*C*2/*m* (12)	*C*2/*m* (12)	$P\bar{1}$ (2)
a (Å)	19.6405(20)	19.6043(8)	19.6071(9)	12.9364(20)
b (Å)	13.4112(19)	13.4907(10)	13.4674(6)	14.9367(10)
c (Å)	9.7637(14)	9.7772(8)	9.7599(4)	15.8187(17)
α (°)				70.6391(94)
β (°)	94.005(10)	93.150(5)	93.300(4)	79.7745(83)
γ (°)				80.0083(92)
V (Å^3)	2565.5(2)	2581.9(3)	2572.9(2)	2715.8(6)
Z, $D_{calcd.}$ (Mg/m^3)	2, 1.197	2, 1.250	2, 1.369	2, 1.138
μ (mm^{-1})	4.419	0.558	2.926	0.641
F(000)	994	1032	1096	1000
Theta range (°)	4.51 to 72.62	1.83 to 26.06	1.84 to 27.99	1.67 to 25.98
Index range (*h*,*k*,*l*)	−23/23, 0/16, −11/0	−24/24, −16/0, 0/−12	−25/25, −17/0, −12/0	−15/15, −18/17, −19/0
Refl. collected	2414	2785	3315	10733
Refl. unique/R_{int}	2272/R_{int} = 0.0385	2626/R_{int} = 0.0283	3141/R_{int} = 0.0118	10340/R_{int} = 0.0215
T max./min.	0.9962/0.3368	0.9998/0.9693	0.9999/0.9023	0.9995/0.9400
No. of refined parameters	155	154	154	532
Goodness-of-fit on F^2	1.044	1.084	1.084	1.016
Final R_1, [$I > 2\sigma(I)$], wR_2	0.0581/0.1389	0.0519/0.0949	0.0353/ 0.0747	0.0626/0.1278

 © 2004 Wiley-VCH Verlag GmbH & Co. KGaA, Weinheim

Table 3. Crystallographic data for compounds (nBu$_4$N)[M(dcbdt)$_2$] (M = Au, Co, Cu, Pt)

	Au (**2**)	Co (**4**)	Cu (**6**)	Pt (**9**)
Crystal size [mm]	0.40 × 0.20 × 0.04	0.82 × 0.22 × 0.20	0.60 × 0.20 × 0.10	0.30 × 0.30 × 0.05
Crystal Colour/Shape	green plate	dark-green needle	dark-green needle	green plate
Empirical formula	$C_{32}H_{40}N_5S_4Au$	$C_{32}H_{40}N_5S_4Co$	$C_{32}H_{40}N_5S_4Cu$	$C_{32}H_{40}N_5S_4Pt$
Molecular mass	819.90	681.87	686.47	818.02
Crystal System	monoclinic	triclinic	monoclinic	monoclinic
Space group	$P2_1/c$	$P\bar{1}$	$P2_1/c$	$P2_1/c$
a (Å)	7.9094(6)	9.481(2)	7.8539(2)	7.9032(8)
b (Å)	20.918(3)	13.096(2)	20.9006(9)	20.837(2)
c (Å)	20.624(3)	15.917(3)	20.6126(6)	20.5885(16)
α (°)		66.642(10)		
β (°)	90.294(9)	86.285(16)	90.351(3)	90.147(7)
γ (°)		70.358(10)		
V (Å^3)	3412.0(7)	1703.7(5)	3383.5(2)	3390.5(6)
Z, $D_{calcd.}$ (Mg/m^3)	4, 1.596	1.329	4, 1.348	4, 1.603
μ (mm^{-1})	4.586	0.778	3.442	4.415
F(000)	1640	716	1440	1636
Theta range (°)	1.97 to 24.96	1.79 to 25.97	3.01 to 72.01	2.19 to 26.98
Index range (h,k,l)	−9/0, −24/0, −24/−24	−11/11, −16/15, −19/1	−1/9, −24/0, −24/24	−10/0, −26/0, −26/26
Refl. collected	6278	7389	7288	3393
Refl. unique/R_{int}	5827/R_{int} = 0.1111	6634/R_{int} = 0.0225	5914/R_{int} = 0.0396	7310/R_{int} = 0.0343
T max./min.	0.8967/0.4629	0.9990/0.8922	0.9999/0.6905	0.9991/0.4272
No of refined parameters	319	398	506	7310/16/369
Goodness-of-fit on F^2	1.000	1.037	1.036	1.033
Final R_1, [$I > 2\sigma(I)$], wR_2	0.0835/0.1776	0.0640/0.1548	0.0784/0.1965	0.0773/0.1696

The structures observed can be classified into the following four groups: *i*) the Zn^{II} compound is triclinic, $P\bar{1}$, with the metal in a tetrahedral coordination geometry; *ii*) the other M^{II} complexes (M = Pt, Pd, Co and Cu) are monoclinic, $C2/m$, and isostructural with the Ni^{II} analogue described previously,[9] presenting a perfectly square-planar geometry; *iii*) the Co^{III} compound is triclinic, $P\bar{1}$, and isostructural with the Fe[12] and Ni[9] analogues, with a strong dimerisation of the M(dcbdt)$_2$ units and the metal in a square-pyramidal coordination geometry; *iv*) the M^{III} complexes with M = Au, Cu and Pt are monoclinic, $P2_1/c$, and present the complexes as pseudo-dimers.

Among the M^{II} complexes, the crystal structures of the (nBu$_4$N)$_2$[M(dcbdt)$_2$] salts with M = Co (**3**), Pd (**7**), Pt (**8**), and Zn (**10**) were determined by X-ray diffraction and their crystallographic data are listed in Table 2. For M = Cu (**5**) only the unit-cell parameters could be obtained, monoclinic, $C2/m$, with a = 19.753 Å, b = 13.440 Å, c = 9.792 Å, β = 93.44°, indicating a structure similar to those of Pt, Pd and Co. These compounds are isostructural with (nBu$_4$N)$_2$-[Ni(dcbdt)$_2$], described previously.[9]

Figure 1 presents the ORTEP diagrams of the complex anions in compounds **3**, **4**, **6** and **10**, showing the atomic labelling scheme, which is the same in the analogous compounds **2**, **7**, **8**, **9** with different metals; selected bond lengths and angles for these compounds are presented in Table 4 and Table 5.

In compound **10**, the [Zn(dcbdt)$_2$]$^{2-}$ anion is located in a general position and the metal has a tetrahedral coordination geometry. The average Zn−S bond length (2.316 Å) is similar to those found in many other Zn^{II} bis(dithiolate) complexes.[15−17] The ligands preserve their planarity (rms atomic deviations are 0.008 and 0.011 Å) but they present a dihedral angle of 78.28°. The Zn atom is significantly deviated (0.337 Å) from the average plane of the ligand containing S1 and S2, while it is much less deviated (0.028 Å) from the average plane of the second ligand containing S3 and S4. This distortion is imposed by the crystal packing, in which the anionic complexes are well separated by the cations, as shown in Figure 2. There are several hydrogen bonds between cation and anion units but this alternating packing prevents any possible interaction between the anion units.

In compounds **3**, **7** and **8** the transition metal atom is located at an inversion centre and the [M(dcbdt)$_2$]$^{2-}$ dianion presents a perfectly planar geometry, since all atoms lie in a mirror plane. The crystal structure of these compounds is made up of [M(dcbdt)$_2$]$^{2-}$ layers containing mirror planes at y = 0 and y = 1/2. These layers are separated by cation layers, as shown in Figure 3 for M = Co, thus preventing any short anion-anion interactions.

In **4** the Co^{III} complex presents a strong dimerisation of the [Co(dcbdt)$_2$]$^-$ units that are related by an inversion centre (iv in Figure 1) located between the two cobalt atoms. In the [Co(dcbdt)$_2$]$_2^{2-}$ units, besides the equatorial Co−S bonds, with distances Co−S(1) 2.1780(13) Å, Co−S(2) 2.1902(13) Å, Co−S(3) 2.1823(12) Å and Co−S(4) 2.2000(13) Å, there are two apical Co−S(3)* bonds at 2.3638(13) Å with a Co−Co* distance of 3.1534(10) Å. This dimerisation is typical of many Co^{III} bisdithiolene complexes,[5,6,18−20] with the metal presenting a square-pyramidal coordination geometry, with a metal-over-sulfur overlap mode, equatorial Co−S distances typically in the range 2.16−2.19 Å and apical Co−S bond lengths varying

 © 2004 Wiley-VCH Verlag GmbH & Co. KGaA, Weinheim

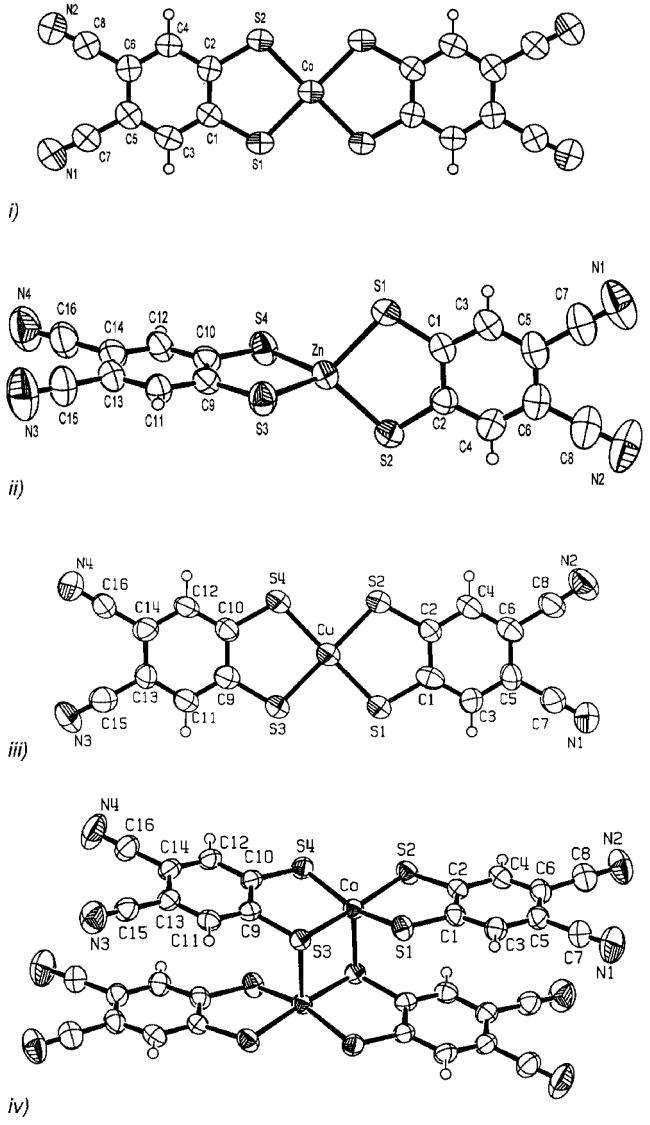

Figure 1. ORTEP diagrams: (i) $[Co(dcbdt)_2]^{2-}$ dianion in **3**, (ii) $[Zn(dcbdt)_2]^{2-}$ dianion in **10**, (iii) $[Cu(dcbdt)_2]^{-}$ monoanion in **6** and (iv) $[Co(dcbdt)_2]_2^{2-}$ in **4**; the diagrams are drawn with 50% probability thermal ellipsoids; the adopted numbering scheme is the same in isostructural compounds **2**, **7**, **8** and **9**

from 2.38 to 2.43 Å. As shown in Figure 4 (see a) the ligands are slightly distorted, repelling each other and making the distance between their mean planes larger than the central Co−S distance.

The crystal structure of **4** is identical to those of the Ni and Fe analogues previously described by us.[9,12] Along the *c* and *b* axes the dimerised anions and the cations are alternating, whereas along the *a* axis the $[Co(dcbdt)_2]_2^{2-}$ dimers are arranged in chains due to several weak interactions connecting two side-by-side $[Co(dcbdt)_2]^{-}$ units of adjacent dimers, namely the hydrogen bonds N(4)···H(4*) and N(4*)···H(4) at 2.609 Å and 156°, S(4)···H(12) at 3.248 Å and a short S(4)···S(4*) contact at 3.817 Å (see Figure 5).

In the other M^{III} complexes with M = Au (**2**), Cu (**6**) and Pt (**9**), the anions are located in a general position near the inversion centres and therefore form pseudo-dimers, as

Table 4. Selected bond lengths [Å] for $(nBu_4N)_2[M(dcbdt)_2]$ (M = Co, Pd, Pt, Zn)

	Co (**3**)	Pd (**7**)	Pt (**8**)	Zn (**10**)
M−S(1)	2.1754(11)	2.2930(13)	2.2710(10)	2.3240(11)
M−S(2)	2.1830(10)	2.2849(15)	2.2694(12)	2.3107(12)
M−S(3)				2.3273(11)
M−S(4)				2.3047(12)
S(1)−C(1)	1.746(4)	1.742(5)	1.742(4)	1.734(4)
S(2)−C(2)	1.744(4)	1.735(6)	1.732(5)	1.747(4)
S(3)−C(9)				1.747(4)
S(4)−C(10)				1.749(4)
C(1)−C(2)	1.389(6)	1.408(7)	1.403(6)	1.430(5)
C(1)−C(3)	1.400(6)	1.401(7)	1.401(6)	1.383(5)
C(4)−C(2)	1.412(5)	1.398(7)	1.405(7)	1.381(5)
C(4)−C(6)	1.381(6)	1.385(7)	1.385(7)	1.375(5)
C(5)−C(3)	1.378(6)	1.386(7)	1.388(7)	1.377(6)
C(5)−C(6)	1.413(6)	1.394(7)	1.394(7)	1.402(6)
C(5)−C(7)	1.433(6)	1.441(7)	1.438(7)	1.437(6)
C(6)−C(8)	1.440(6)	1.439(8)	1.444(7)	1.449(6)
C(7)−N(1)	1.141(6)	1.137(7)	1.142(7)	1.133(6)
C(8)−N(2)	1.137(6)	1.134(7)	1.148(6)	1.135(6)
C(9)−C(11)				1.395(5)
C(9)−C(10)				1.413(5)
C(10)−C(12)				1.372(5)
C(14)−C(12)				1.379(5)
C(11)−C(13)				1.382(5)
C(13)−C(14)				1.390(5)
C(13)−C(15)				1.419(5)
C(14)−C(16)				1.437(6)
C(15)−N(3)				1.145(5)
C(16)−N(4)				1.136(5)

shown in Figure 6 for **9**. The values of the M−S bond lengths in these complexes, presented in Table 5, are similar to the values published for other monoanionic bis(dithiolene) complexes. A remarkable common feature of these pseudo-dimers is that the complex units deviate only slightly from planarity in such a way that the ligands are closer than the central MS_4 atoms (Figure 4; see b for **6**, c for **2** and d for **9**). In fact, the distance between the average planes defined by the benzene rings of neighbouring complex units is about 3.43 Å, and almost the same for all three metal complexes, whereas the planes of the central MS_4 atoms within the dimer are further apart by 0.15 Å, 0.20 Å, and 0.23 Å for Cu, Pt, and Au, respectively (see Table 6). This is at variance with the strong Co, Fe and Ni dimers previously described, where there are two short M−S central bonds and a distortion of the ligands separating their extremities from each other (Figure 4, a).

The relatively short distance between the benzene rings clearly denotes the existence of a significant ligand−ligand interaction in the present complexes. In this respect it is worthwhile to mention that in **9** the overlap mode between the two closest $M(dcbdt)_2$ units is obtained by a small shift along the short axis of the complexes, leading to a more direct metal−metal interaction, while for **6** and **2** the overlap is obtained by shifts along both the long and short axes, leading to both metal−metal and metal−sulfur interactions.

It is also worthwhile to note that while along the *b* and *c* axes the dimers alternate with cations without any short

 © 2004 Wiley-VCH Verlag GmbH & Co. KGaA, Weinheim

Table 5. Selected bond lengths (Å) for (nBu$_4$N)[M(dcbdt)$_2$] (M = Au, Co, Cu, Pt)

	Au (**2**)	Co (**4**)	Cu (**6**)	Pt (**9**)
M−S(1)	2.311(4)	2.1780(13)	2.1843(19)	2.255(3)
M−S(2)	2.298(4)	2.1902(13)	2.1743(18)	2.261(3)
M−S(3)	2.312(4)	2.1823(12)	2.1786(18)	2.267(3)
M−S(4)	2.302(4)	2.2000(13)	2.176(2)	2.269(3)
M−S(3)#1[a]		2.3638(13)		
S(1)−C(1)	1.753(13)	1.723(4)	1.755(6)	1.725(12)
S(2)−C(2)	1.760(15)	1.726(4)	1.757(6)	1.732(11)
S(3)−C(9)	1.714(19)	1.749(4)	1.739(7)	1.744(13)
S(4)−C(10)	1.765(18)	1.721(4)	1.736(6)	1.728(11)
C(1)−C(2)	1.42(2)	1.422(6)	1.409(8)	1.385(15)
C(1)−C(3)	1.38(2)	1.387(6)	1.393(9)	1.396(16)
C(2)−C(4)	1.34(2)	1.394(6)	1.368(8)	1.406(15)
C(4)−C(6)	1.38(2)	1.373(7)	1.379(9)	1.365(16)
C(5)−C(3)	1.36(2)	1.373(6)	1.378(8)	1.370(16)
C(5)−C(7)	1.43(2)	1.445(7)	1.428(9)	1.443(17)
C(6)−C(5)	1.44(2)	1.409(7)	1.404(9)	1.413(16)
C(6)−C(8)	1.41(2)	1.432(7)	1.436(8)	1.447(16)
C(7)−N(1)	1.17(2)	1.117(7)	1.128(8)	1.123(16)
C(8)−N(2)	1.15(2)	1.152(6)	1.128(8)	1.129(16)
C(10)−C(12)	1.34(2)	1.408(6)	1.381(8)	1.430(15)
C(10)−C(9)	1.45(2)	1.409(6)	1.418(8)	1.385(17)
C(11)−C(9)	1.39(2)	1.384(6)	1.403(8)	1.390(16)
C(12)−C(14)	1.41(2)	1.369(6)	1.389(8)	1.372(16)
C(13)−C(11)	1.42(2)	1.375(6)	1.394(8)	1.381(16)
C(13)−C(15)	1.45(3)	1.429(7)	1.442(9)	1.440(17)
C(14)−C(13)	1.42(2)	1.416(6)	1.395(8)	1.421(16)
C(14)−C(16)	1.43(2)	1.445(7)	1.418(9)	1.440(17)
C(15)−N(3)	1.07(2)	1.121(6)	1.159(8)	1.135(16)
C(16)−N(4)	1.17(2)	1.121(7)	1.144(9)	1.140(16)

[a] #1 $-x, -y, -z + 1$.

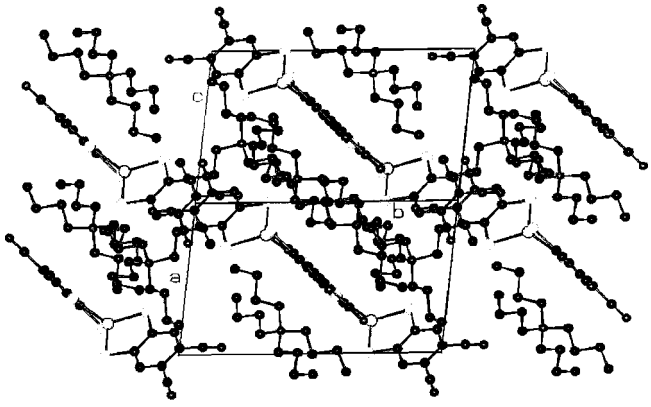

Figure 2. View of the crystal structure of (nBu$_4$N)$_2$[Zn(dcbdt)$_2$] (**10**) along the [101] direction

inter-dimer contacts in the *b*,*c* plane, along *a* they are connected in chains through short S2−S3* contacts at 3.692(4) Å and hydrogen bonds N2−H3* and N3−H12* at 2.628(11) Å and 2.554(11) Å, respectively, as shown in Figure 7 for **9**. The interplanar distances and the short inter- and intra-dimer distances observed for **2**, **4**, **6** and **9** are given in Table 6.

Magnetic Properties

The M^{II} complexes of Co (**3**) and Cu (**5**), as d^7 and d^9 species respectively, and the Pt^{III} (**9**) complex, as a d^7 system, are expected to be paramagnetic with one unpaired electron. The Ni^{III} and the Fe^{III} complexes were previously described as paramagnetic with $S = 1/2$.[9,12] The remaining complexes of this family presented in this paper are expected to be diamagnetic. These expectations were con-

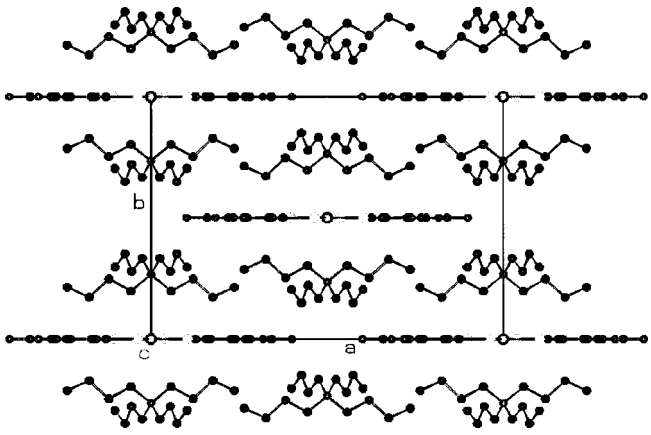

Figure 3. View of the crystal structure of (nBu$_4$N)$_2$[Co(dcbdt)$_2$] (**3**) along the *c* axis

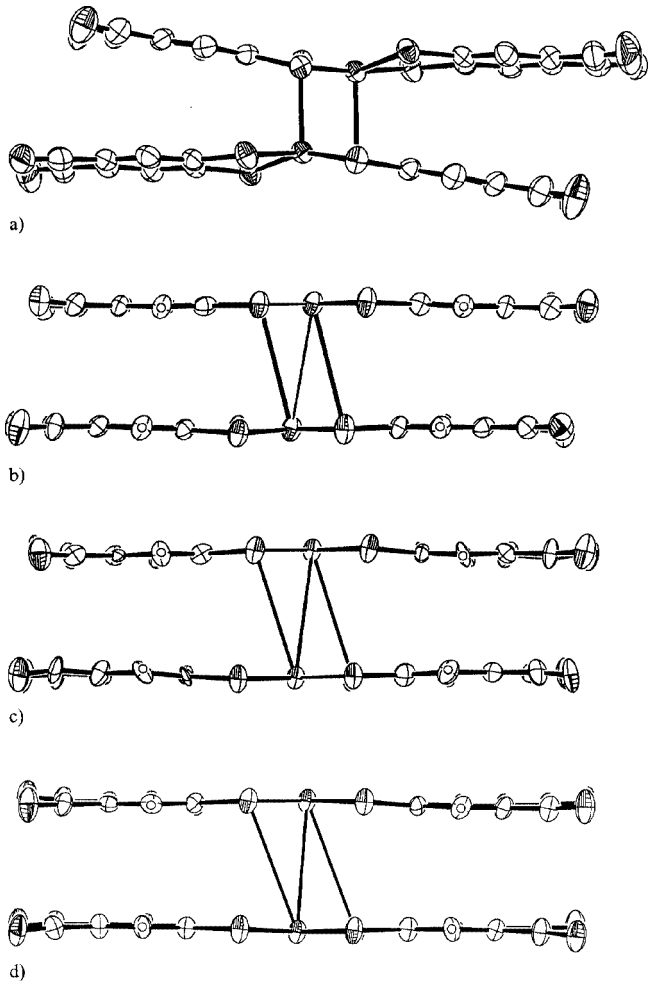

Figure 4. Side view of: a) the [Co(dcbdt)$_2$]$_2$ dimer in **4**, b) the [Cu(dcbdt)$_2$]$_2$ pseudo-dimer in **6**, c) the [Au(dcbdt)$_2$]$_2$ pseudo-dimer in **2** and d) the [Pt(dcbdt)$_2$]$_2$ pseudo-dimer in **9**

 © 2004 Wiley-VCH Verlag GmbH & Co. KGaA, Weinheim

Table 6. Distances (Å) between complex units in $(n\mathrm{Bu_4N})[\mathrm{M(dcbdt)_2}]$ compounds

M	Au(**2**)	Co(**4**)	Cu(**6**)	Pt(**9**)
Interplanar:				
MS_4-MS_4	3.67		3.60	3.63
Bz−Bz	3.43		3.45	3.42
Intradimer:				
M···M*	4.057(2)[a]	3.153(1)[b]	3.960(1)[a]	3.909(1)[a]
M···S*	3.822(6)[a]	2.364(1)[b]	3.648(2)[a]	3.915(4)[a]
Interdimer:	S2−S3[c] 3.626(5)	S4−S[d] 3.8117(2)	S1−S4[c] 3.772(2)	S2−S3[c] 3.692(4)
	N2−H3[c] 2.668(16)	N4−H4[d] 2.609(6)	N1−H4[c] 2.574(7)	N2−H3[c] 2.628(11)
	N3−H12[c] 2.578(17)		N4−H11[c] 2.524(7)	N3−H12[c] 2.554(11)

[a] $-x,1-y,1-z$. [b] $-x,-y,-z+1$. [c] $x\pm1,y,z$. [d] $1-x,-y,1-z$.

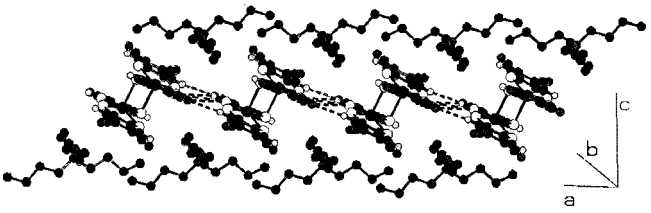

Figure 5. Crystal packing of $(n\mathrm{Bu_4N})_2[\mathrm{Co(dcbdt)_2}]_2$ (**4**), showing the side-by-side interactions between the $\mathrm{Co(dcbdt)_2}$ dimers along the *a* axis

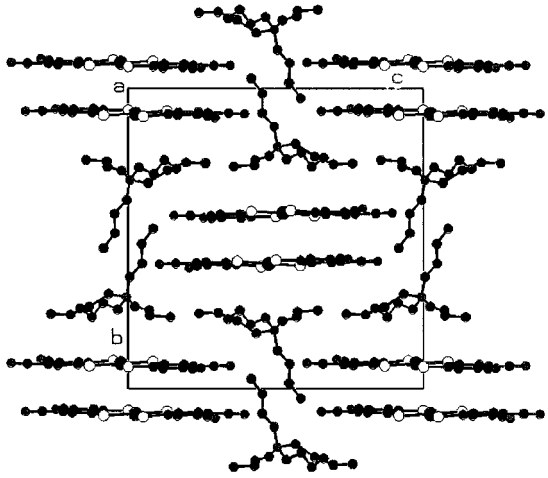

Figure 6. Crystal structure of $(n\mathrm{Bu_4N})_2[\mathrm{Pt(dcbdt)_2}]_2$ (**9**) viewed along the *a* axis

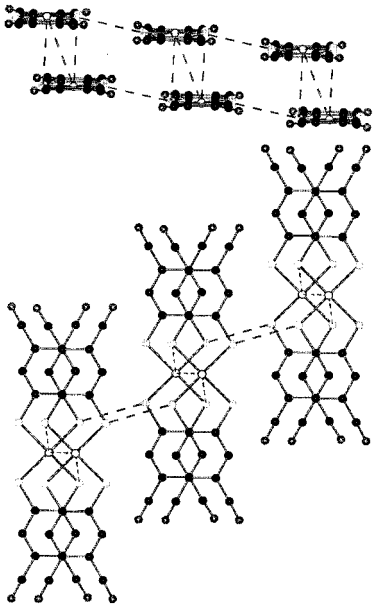

Figure 7. Side and top view of the chains, along the *a* axis, of $\mathrm{Pt(dcbdt)_2^-}$ pairs in compound **9**; the dashed lines emphasise the close interactions between the pairs and within a pair

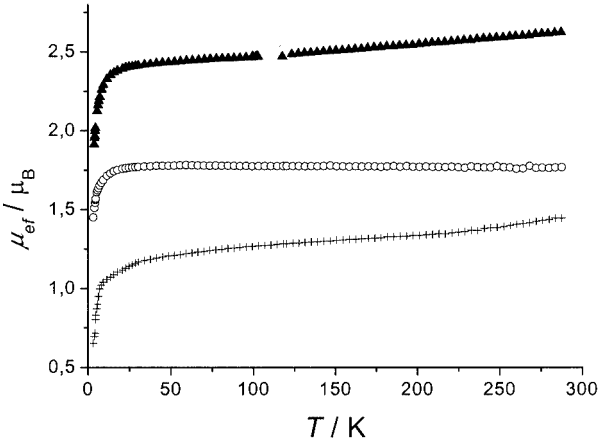

Figure 8. Effective magnetic moments as a function of temperature of $(n\mathrm{Bu_4N})_2[\mathrm{Cu(dcbdt)_2}]$ (**3**) (circles), $(n\mathrm{Bu_4N})_2[\mathrm{Co(dcbdt)_2}]$ (**4**) (triangles) and $(n\mathrm{Bu_4N})_2[\mathrm{Co(dcbdt)_2}]_2$ (**5**) (crosses)

firmed by EPR spectroscopic and static magnetic susceptibility measurements, with the exception of the $\mathrm{Co^{III}}$ complex which, as a d^6 system, seems to have a high-spin $S = 1$ configuration.

The EPR spectrum of an acetone solution of **5** at room temperature exhibits a quadruplet of lines, centred at $g = 2.045$ with an average hyperfine field constant of, a_o, of 80.8 G, due to the hyperfine interaction of the electron spin with the nuclear $I = 3/2$ spin of the copper nuclides. The powder EPR spectrum presents a pattern typical of a system with axial symmetry ($g_{\|} = 2.082$ and $g_{\perp} = 2.024$).

The static paramagnetic susceptibility, χ_P, of **5**, calculated from raw data assuming a diamagnetic contribution of -6.14×10^{-4} emu/mol, as estimated from tabulated Pascal constants, leads to an effective magnetic moment, $\mu_{eff.}$, of 1.77 μ_B. As shown in Figure 8, this value remains fairly constant above 20 K, (Figure 8) and is very close to the one

 © 2004 Wiley-VCH Verlag GmbH & Co. KGaA, Weinheim

expected for an $S = 1/2$ system with $g = 2$. Below 20 K there is a reduction of μ_{eff}, denoting the presence of minor antiferromagnetic interactions.

Single crystals of $(n\mathrm{Bu_4N})_2[\mathrm{Co(dcbdt)_2}]$ (**3**) at room temperature present a complex EPR signal of an octet of lines with variable separation, depending on the crystal orientation (Figure 9). This type of spectra is typical of the hyperfine structure due to the $I = 7/2$ spin of ^{59}Co.[21−23] However this hyperfine structure is observed only for particular orientations and the signal presents a strong g-factor anisotropy.

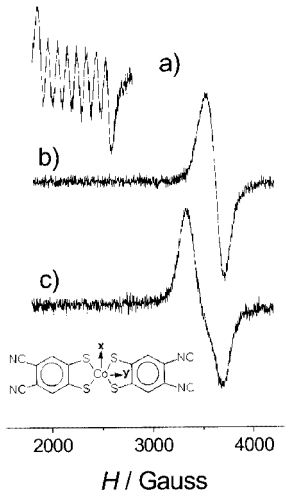

Figure 9. EPR spectra of a single crystal of $(n\mathrm{Bu_4N})_2[\mathrm{Co(dcbdt)_2}]$ (**4**) at 300 K, with the magnetic field in the b,c plane for two orientations 90° apart: a) along the long axis of the complex, b) along the short axis in the plane of the complex, c) perpendicular to the plane of the complex

A study of the EPR spectra with oriented single crystals allowed us to deduce an almost uniaxial rhombic anisotropy related to the symmetry axes of the complex as well as the anisotropy of the hyperfine tensor a_0. The principal axes of the a_0- and g-tensors are expected to coincide. As previously discussed in the crystallographic section, the Co^{II} complex is planar and lies parallel to the a,c plane, with the long axis making an angle of approximately 29° with a. The narrowest signal, with an apparent single EPR line with a peak-to-peak width of 14.6 mT, and the minimum g value at $g_x = 1.936$ is observed when the magnetic field is along the short axis in the plane of the complex (Figure 9, a). Along this direction the hyperfine coupling constant is negligible ($A_x < 2$ mT).

When the magnetic field is along the long axis in the plane of the complex, the maximum width is observed in the EPR signal that presents an octet extending over 73.4 mT and centred at $g_y = 3.156$ (Figure 9, a). Deviations of ±40° from this g_{max} orientation still present an octet with negligible extent variations of only ±1 mT. An octet is observed over all this angular range, corresponding to a hyperfine coupling constant, A_y, of 9.2 mT.

An intermediate situation is observed when the magnetic field is perpendicular to the plane of the complex (along the b axis). For this orientation an EPR signal with no resolved octet but well-separated maxima and minima, corresponding to a linewidth of 35.7 mT, is observed centred at $g_z = 1.994$. This suggests a small hyperfine component for this direction of $A_z = 4.5$ mT.

To the best of our knowledge this is the first example of a pure Co compound in which hyperfine structure is observed in the solid state. The hyperfine structure can be observed without the interference of significant dipolar interactions thanks to the large separation of the complexes in the structure, where the closest Co−Co distance is 9.76 Å along c, without any contact between the anions, and 12.4 Å between different layers separated by the cations. A detailed analysis of the observed anisotropy in the A and g-tensors in terms of the metal and ligand orbitals involved in the SOMO will be the subject of a subsequent publication.

The static paramagnetic susceptibility of **3** leads, in a similar way, to an effective magnetic moment, μ_{eff}, significantly larger than that of the Cu analogue (Figure 8). At room temperature μ_{eff} is about 2.55 μ_B, which decreases almost linearly with temperature upon cooling to 2.40 μ_B at 20 K. Below this temperature a more drastic reduction of μ_{eff} is observed. This larger magnetic moment is in fair agreement with the larger average g-value observed in the EPR spectrum, since for $g = 2.82$ and $S = 1/2$ a μ_{eff} value of 2.44 μ_B is expected. The small linear decrease of the effective moment observed between room temperature and 20 K most probably denotes the presence of a non-negligible temperature-independent paramagnetism.

Compound **9** is EPR silent at room temperature, as is also the case for the Ni and Fe analogues. Below 110 K a signal starts to appear, as shown in Figure 10 for a powder at 60 K. This signal can be described as coming from a doublet $S = 1/2$ state showing rhombic anisotropy with $g_x = 2.246$, $g_y = 2.054$ and $g_z = 1.785$. The more intense lines correspond to $I = 0$ platinum isotopes (66.2% natural

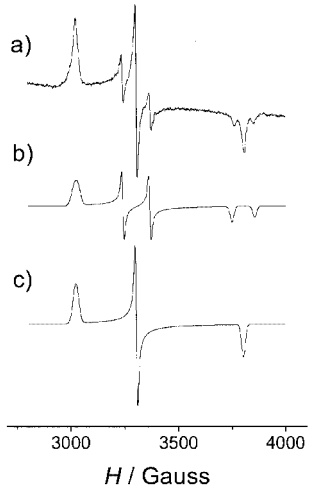

Figure 10. Experimental EPR spectra of $(n\mathrm{Bu_4N})[\mathrm{Pt(dcbdt)_2}]$ (**9**) as a polycrystalline sample at 60 K: (a) simulated spectra for 33.8% natural abundance of ^{195}Pt isotope with $I = 1/2$, and $A_x = 0$ mT, $A_y = 13$ mT and $A_z = 9.3$ mT (b), and 66.2% of Pt isotopes with $I = 0$ (c), both with $g_x = 2.246$, $g_y = 2.054$, $g_z = 1.785$

 © 2004 Wiley-VCH Verlag GmbH & Co. KGaA, Weinheim

abundance), and the satellites around the medium- and high-field components are due to the 33.8% natural abundance of the ^{195}Pt isotope with $I = 1/2$. The anisotropic hyperfine coupling tensor has $A_x < 4$ mT (the satellites are not resolved for this component), $A_y = 13$ mT and $A_z = 9.3$ mT. Assuming a situation similar to $Pt(mnt)_2^-$, and the same coordinate system,[24] x is the shortest axis in the plane of the complex, y the longest and z is normal to the plane of the complex.

As, in this compound, the magnetic susceptibility follows a single-triplet model due to the dimerisation of $[Pt(dcbdt)_2]^-$, we looked for a possible signature of the $S = 1$ state in the EPR spectrum. The half-field signal corresponding to the forbidden $\Delta M_S = 2$ transition, was only visible at 4.2 K as a weak signal. Other signals coming from the triplet $S = 1$ state, if existing, are obscured by the spectrum of the doublet state described above.

The observation of an EPR signal of the triplet state in metal complexes is, in general rare, and most dimerised complexes are EPR silent, as reported for $(n\mathrm{Bu_4N})[Ni(dcbdt)_2]$[9] and $(n\mathrm{Bu_4N})[Fe(dcbdt)_2]$;[12] the number of Pt^{III} complexes studied by EPR spectroscopy is small. The $[Pt(dmit)_2]^-$ species, which is isolated and undimerised, presents a smaller g anisotropy than the present compound, with a hyperfine coupling being detected.[25] $[Pt(mnt)_2]^-$, also an undimerised species, studied by Kirmse et al. as a diluted paramagnetic centre in a diamagnetic host, shows a large anisotropy of the hyperfine coupling tensor, with $A_x = 0$.[24] In the *cis*-diammineplatinum α-pyridone complex, a mixed-valence compound, there is dimer formation, with the Pt−Pt distance of 2.7745 Å, much shorter than in **9**. No hyperfine interactions were observed in the single-crystal spectrum.[26]

The paramagnetic susceptibility of **9**, calculated after a correction for diamagnetism estimated from tabulated Pascal's constants as -4.3×10^{-4} emu/mol, is quite similar to that of the Ni analogue (Figure 11). At room temperature the paramagnetic susceptibility is 3.6×10^{-4} emu/mol, and it decreases upon cooling to about 100 K, where it reaches a minimum. At lower temperatures the magnetic susceptibility becomes dominated by a Curie tail of impurities or defects and increases again. The EPR spectra suggest that these impurities are defects of undimerised $Pt(dcbdt)_2^-$ units. Taking into account the structure with dimers of paramagnetic $Pt(dcbdt)_2^-$ units, this behaviour can be described by a singlet-triplet model of antiferromagnetically coupled $S = 1/2$ dimers[27] and a low-temperature Curie tail, [Equation (1)], as previously done in the case of the Ni and Fe compounds.[9,12]

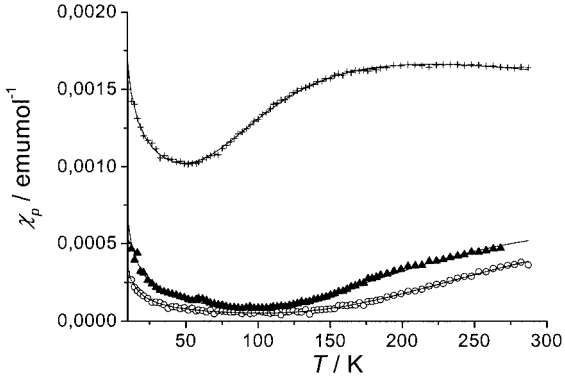

Figure 11. Magnetic susceptibility of $(n\mathrm{Bu_4N})[Pt(dcbdt)_2]$ (**9**) (circles), $(n\mathrm{Bu_4N})[Fe(dcbdt)_2]$ (squares)[12] and $(n\mathrm{Bu_4N})[Ni(dcbdt)_2]$ (triangles),[9] as a function of temperature; the line is a fit to Equation (1)

$$\chi_P = A + C/T + (Ng^2\mu_B^2/k_BT)[\exp(-2J/k_BT) + 3]^{-1} \quad (1)$$

A reasonable fit to Equation (1) was obtained with $J = 984$ K, $g = 2.9$, $A = 4 \times 10^{-5}$ emu/mol and a Curie tail corresponding to 1.5% of $S = 1/2$ spins. This g-value is certainly unrealistic because it is significantly larger than the highest g-value observed in the EPR spectra. This disagreement is probably due to the rather low temperature range of the experimental susceptibility data (when compared with the J value), which is inappropriate to obtain accurate fitting parameters.

Many Co^{III} bis(dithiolene) complexes are diamagnetic, but with some ligands, namely substituted benzodithiolates, high-spin $S = 1$ configurations are known.[13] The $[Co^{III}(dcbdt)_2]_2^{2-}$ compound (**5**) was found to be paramagnetic and its effective magnetic moment is also plotted in Figure 8 as a function of temperature. This paramagnetic behaviour demonstrates that the $[Co^{III}(dcbdt)_2]^-$ anions are in a high-spin $S = 1$ configuration. The effective magnetic moment observed is, however, significantly lower than the $S = 1$ value, demonstrating the presence of strong antiferromagnetic interactions. In spite of the crystal structure, with $[Co^{III}(dcbdt)_2]^-$ anions as dimers, packed side by side along a, the magnetisation data could not be fitted to any dimer or alternating-chain model.

Conclusion

In conclusion we have prepared and characterised several new members of the series of complexes $M(dcbdt)_2$ with different transition metals. These complexes are characterised by relatively low oxidation potentials, due to the extended nature of the ligands, and, as already described for M = Ni and Au, are expected to lead easily to partially oxidised, potentially electrically conducting. The Co^{II} complex is the first example of a pure Co compound in which hyperfine structure is observed in the solid state; the Co^{III} complex presents a high-spin configuration. The fuller use of these complexes in the preparation of conducting or magnetic molecular materials is presently under way.

Experimental Section

General: DMF, acetonitrile and dichloromethane were distilled from over phosphorus pentoxide and benzene was distilled from over sodium. Other chemicals were commercially obtained and

 © 2004 Wiley-VCH Verlag GmbH & Co. KGaA, Weinheim

used without any further purification. 4,5-Dicyanobenzene-1,2-dithiol (**1**) was synthesised as described previously.[9] Elemental analyses were performed by the analytical services of IST and ITN. ^{1}H and ^{13}C NMR: Varian (300 MHz), [D$_6$]DMSO as solvent, and TMS as internal standard. IR: Perkin-Elmer 1330 spectrophotometer. VIS-UV-NIR: Cary 5G Varian spectrophotometer. Cyclic voltammetry data were obtained using a CV-50 W BAS Voltammetric Analyser. The measurements were performed at room temperature in acetonitrile solutions containing nBu$_4$ClO$_4$ as supporting electrolyte, with a scan rate of 100 mV/s, platinum working- and counter- electrodes and using a Ag/AgCl reference electrode.

EPR spectra in the range 4−300 K were obtained with an X-Band Bruker ESP 300E spectrometer equipped with a microwave bridge ER041XK, a rectangular cavity operating in T102 mode, a Bruker variable-temperature unit, an Oxford ESR-900 cryostat and a field controller ER 032M system. The modulation amplitude was kept well below the linewidth and the microwave power well below saturation.

Magnetic susceptibility measurements in the range 2−300 K were performed using a longitudinal Faraday system (Oxford Instruments) with a 7 T superconducting magnet, under a magnetic field of 5 T and forward- and reverse-field gradients of 1 T/m. Polycrystalline samples (10−15 mg) were placed inside a previously calibrated thin wall Teflon bucket. The force was measured with a microbalance (Sartorius S3D-V). Under these conditions the magnetisation was found to be proportional to the applied magnetic field.

Tetrabutylammonium Salt of Gold(III) Bis(4,5-dicyanobenzene-1,2-dithiolate) (nBu$_4$N)[Au(dcbdt)$_2$] (2): Compound **1** (0.2 g, 1.04 mmol) was dissolved in 5 mL of aqueous NaOH (5%). A solution of nBu$_4$NBr (0.17 g, 0.52 mmol) in EtOH/H$_2$O (1:1; 5 mL) was added, followed by a solution of KAuCl$_4$ (0.22 g, 0.52 mmol) in the same solvent. The mixture was stirred and a green precipitate was formed almost immediately. The solution was filtered and the precipitate was washed with EtOH. The crude material was recrystallised from acetone/iBuOH to give **2** as light-green needles (0.1 g, 1.2 mmol, 25%). M.p. 249−250 °C. ^{1}H NMR (300 MHz, [D$_2$]DCM, 25 °C, TMS): δ = 1.00 (t, J = 8.4 Hz, 12 H, CH$_3$), 1.41 (m, 8 H, CH$_2$), 1.59 (m, 8 H, CH$_2$), 3.07 (t, J = 7.2 Hz, 8 H, CH$_2$), 7.50 (s, 4 H, Ar−H) ppm. ^{13}C NMR (300 MHz, [D$_2$]DCM, 25 °C, TMS): δ = 13.77, 20.09, 24.26, 59.57, 113.77, 116.80, 132.98, 143.24) ppm. IR (KBr pellet): $\tilde{\nu}$ = 3060 (w, Ar−H), 2960−2860 (m, C−H), 2220 (s, C≡N), 1550 (w, C=C), 350 (w, S−Au) cm^{-1}. UV/Vis (CH$_2$Cl$_2$): λ_{max} (ε) = 264.2 (8500), 304.3 (34800), 367.6 (3300 mol^{-1} dm^3 cm^{-1}). C$_{32}$H$_{40}$AuN$_5$S$_4$ (820.02): calcd. C 46.87, H 4.93, N 8.54, S 15.64; found C 47.09, H 4.86, N 8.33, S 15.56.

Tetrabutylammonium Salt of Cobalt(II) Bis(4,5-dicyanobenzene-1,2-dithiolate) (nBu$_4$N)$_2$[Co(dcbdt)$_2$] (3): Compound **1** (0.48 g, 2.50 mmol) was dissolved in 5 mL of aqueous NaOH (5%). A solution of nBu$_4$NBr (0.80 g, 2.50 mmol) in EtOH/H$_2$O (1:1; 5 mL) was added, followed by a solution of CoCl$_2$·6H$_2$O (0.30 g, 1.26 mmol) in the same solvent. The mixture was stirred and a dark-blue precipitate was formed almost immediately. The solution was filtered and the precipitate was washed with EtOH. The crude material was recrystallised from acetone/iBuOH to give **3** as dark-blue crystals (0.64 g, 0.693 mmol, 55%). M.p. 254−255 C. IR (KBr pellet): $\tilde{\nu}$ = 3060 (w, Ar−H), 2960−2860 (m, C−H), 2220 (s, C≡N), 1550 (w, C=C), 530 (w, S−Co) cm^{-1}. UV/Vis (CH$_2$Cl$_2$): λ_{max} (ε) = 293.1 (91300), 322.0 (72600), 364.3 (41700), 589.0 (6700), 645.1 nm (17800 mol^{-1} dm^3 cm^{-1}). C$_{48}$H$_{76}$CoN$_6$S$_4$ (924.34): calcd. C 62.37, H 8.28, N 9.09, S 13.87; found C 61.10, H 8.13, N 9.42, S 14.94.

Tetrabutylammonium Salt of Cobalt(III) Bis(4,5-dicyanobenzene-1,2-dithiolate) (nBu$_4$N)[Co(dcbdt)$_2$] (4): A solution of I$_2$ (47.7 mg, 0.18 mmol) in acetone was added to a solution of **3** (0.17 g, 0.18 mmol) in acetone (50 mL). The solution was stirred until a colour change to dark green was observed. Ethanol was added and the solution was slowly evaporated to give **4** as dark-green needles (54.5 mg, 0.08 mmol, 46%). This compound can be also prepared directly from the ligand and CoCl$_2$ in the presence of air as follows: Compound **1** (0.17 g, 0.89 mmol) was dissolved in 5 mL of aqueous NaOH (5%). A solution of nBu$_4$NBr (0.14 g, 0.44 mmol) in EtOH/H$_2$O (1:1) (5 mL) was added, followed by a solution of CoCl$_2$·6H$_2$O (0.11 g, 0.44 mmol) in the same solvent. The mixture was stirred for 2 hours while a dark green precipitate was formed. The solution was filtered and the precipitate was washed with EtOH. The crude material was recrystallised from EtOH to give **4** as black/green crystals (77.3 mg, 0.11 mmol, 26%). M.p. 288−289 °C. ^{1}H NMR (300 MHz, [D$_6$]DMSO, TMS): δ = 0.90 (s, 12 H, CH$_3$), 1.27 (m, 8 H, CH$_2$), 1.49 (m, 8 H, CH$_2$), 3.08 (s, 8 H, CH$_2$) ppm. ^{13}C NMR (300 MHz, [D$_6$]DMSO, TMS): δ = 18.52, 24.21, 28.03, 62.50) ppm. IR (KBr pellet): $\tilde{\nu}$ = 3060 (w, Ar−H), 2980−2880 (m, C−H), 2220 (s, C≡N), 1560 (w, C=C), 430 (w, S−Co) cm^{-1}. UV/Vis (CH$_2$Cl$_2$): λ (ε) = 285.3 nm (8100 mol^{-1} dm^3 cm^{-1}), 318.0 (7000), 364.0 (4300), 411.9 (2100), 645.0 (1500). C$_{32}$H$_{40}$CoN$_5$S$_4$ (681.87): calcd. C 56.35, H 5.93, N 10.28, S 18.83; found C 57.23, H 6.22, N 10.25, S 18.84.

Tetrabutylammonium Salt of Copper(II) Bis(4,5-dicyanobenzene-1,2-dithiolate) (nBu$_4$N)$_2$[Cu(dcbdt)$_2$] (5): Compound **1** (0.30 g, 1.56 mmol) was dissolved in 5 mL of aqueous NaOH (5%). A solution of nBu$_4$NBr (0.51 g, 1.56 mmol) in EtOH/H$_2$O (1:1; 5 mL) was added, followed by a solution of CuCl$_2$·2H$_2$O (0.13 g, 0.78 mmol) in the same solvent. The mixture was stirred and a brown precipitate was formed almost immediately. The solution was filtered and the precipitate was washed with EtOH. The crude material was recrystallised from acetone to give **5** as brown needles (0.19 g, 0.20 mmol, 26%). M.p. 243−245 °C. ^{1}H NMR (300 MHz, [D$_6$]DMSO, 25 °C, TMS): δ = 0.99 (s, 24 H, CH$_3$), 1.48 (m, 16 H, CH$_2$), 1.86 (m, 16 H, CH$_2$), 3.59 (m, 16 H, CH$_2$) ppm. ^{13}C NMR (300 MHz, [D$_6$]DMSO, 25 °C, TMS): δ = 15.32, 20.55, 24.55, 50.49 ppm. IR (KBr pellet): $\tilde{\nu}$ = 3060 (w, Ar−H), 2960−2860 (m, C−H), 2220 (s, C≡N), 1540 (w, C=C), 430 (w, S−Cu) cm^{-1}. UV/Vis (CH$_2$Cl$_2$): λ (ε) = 320.1 nm (72500 mol^{-1} dm^3 cm^{-1}), 386.5 (18800). C$_{48}$H$_{76}$CuN$_6$S$_4$ (928.95): calcd. C 62.05, H 8.26, N 9.05, S 13.81; found C 61.74, H 7.98, N 8.90, S 14.13.

Tetrabutylammonium Salt of Copper(III) Bis(4,5-dicyanobenzene-1,2-dithiolate) (nBu$_4$N)[Cu(dcbdt)$_2$] (6): A solution of I$_2$ (51.9 mg, 0.20 mmol) in acetone was added to a solution of **5** (0.17 g, 0.18 mmol) in acetone (50 mL). The solution was stirred until a colour change to green was observed. Ethanol was added and the solution was slowly evaporated to give **6** as dark-green needles (90.2 mg, 0.13 mmol, 64%). M.p. 233−234 °C. ^{1}H NMR (300 MHz, [D$_6$]acetone, 25 °C, TMS): δ = 0.98 (t, J = 7.2 Hz, 12 H, CH$_3$), 1.44 (m, 8 H, CH$_2$), 1.84 (m, 8 H, CH$_2$), 3.45 (t, J = 8.6 Hz, 8 H, CH$_2$), 7.51 (s, 4 H, Ar−H) ppm. ^{13}C NMR (300 MHz, [D$_6$]acetone, 25 °C, TMS): δ = 13.91, 20.41, 24.44, 59.39, 114.22, 126.73, 131.33, 143.73 ppm. IR (KBr pellet): $\tilde{\nu}$ = 3060 (w, Ar−H), 2980−2880 (m, C−H), 2220 (s, C≡N), 1510 (s, C=C), 420 (w, S−Cu) cm^{-1}. UV/Vis (CH$_2$Cl$_2$): λ (ε) = 300.1 nm (137600), 395.0 (58200 mol^{-1} dm^3 cm^{-1}). C$_{32}$H$_{40}$CuN$_5$S$_4$ (686.49): calcd. C 55.99, H 5.87, N 10.20, S 18.68; found C 55.03, H 6.47, N 9.91, S 19.19.

Tetrabutylammonium Salt of Palladium(II) Bis(4,5-dicyanobenzene-1,2-dithiolate) (nBu$_4$N)$_2$[Pd(dcbdt)$_2$] (7): Compound **1** (0.41 g, 2.13 mmol) was dissolved in 5 mL of aqueous NaOH (5%). A solu-

 © 2004 Wiley-VCH Verlag GmbH & Co. KGaA, Weinheim

tion of nBu$_4$NBr (0.70 g, 2.17 mmol) in EtOH/H$_2$O (1:1; 5 mL) was added, followed by a solution of K_2PdCl_4 (0.33 g, 1.01 mmol) in the same solvent. The mixture was stirred and an orange precipitate was formed almost immediately. The solution was filtered and the precipitate was washed with EtOH. The crude material was recrystallised from acetone/iBuOH to give **7** as red crystals (0.62 g, 0.64 mmol, 63%). M.p. 263−264 °C. ^{1}H NMR (300 MHz, [D$_6$]DMSO, 25 °C, TMS): δ = 0.93 (t, J = 7.2 Hz, 24 H, CH$_3$), 1.31 (m, 16 H, CH$_2$), 1.56 (m, 16 H, CH$_2$), 3.32 (t, J = 6.0 Hz, 16 H, CH$_2$), 7.28 (s, 4 H, Ar−H) ppm. ^{13}C NMR (300 MHz, [D$_6$]DMSO, 25 °C, TMS): δ = 14.17, 19.88, 23.74, 58.24, 96.41, 116.02, 131.49 ppm. IR (KBr pellet): ν̃ = 3060 (w, Ar−H), 2980−2840 (m, C−H), 2200 (s, C≡N), 1530 (m, C=C), 430 (w, S−Pd) cm^{-1}. UV/Vis (CH$_2$Cl$_2$): λ_{max} (ε) = 300.7 nm (53800), 345.0 (72300), 425.2 (13800 mol^{-1} dm^3 cm^{-1}). $C_{48}H_{76}N_6PdS_4$ (971.81): calcd. C 59.32, H 7.88, N 8.64, S 13.20; found C 58.51, H 8.11, N 8.86, S 13.05.

Tetrabutylammonium Salt of Platinum(II) Bis(4,5-dicyanobenzene-1,2-dithiolate) (nBu$_4$N)$_2$[Pt(dcbdt)$_2$] (8): Compound **1** (0.28 g, 1.46 mmol) was dissolved in 5 mL of aqueous NaOH (5%). A solution of nBu$_4$NBr (0.47 g, 1.46 mmol) in EtOH/H$_2$O (1:1; 5 mL) was added, followed by a solution of K_2PtCl_4 (0.52 g, 1.25 mmol) in the same solvent. The mixture was stirred and a red precipitate was formed almost immediately. The solution was filtered and the precipitate was washed with EtOH. The crude material was recrystallised from acetone/iBuOH to give **8** as red crystals (0.38 g, 0.36 mmol, 35%). M.p. 270−271 °C. ^{1}H NMR (300 MHz, [D$_2$]DCM, 25 °C, TMS): δ = 0.92 (t, J = 5.3 Hz, 24 H, CH$_3$), 1.28 (m, 16 H, CH$_2$), 1.53 (m, 16 H, CH$_2$), 3.15 (s, 16 H, CH$_2$), 7.36 (s, 4 H, Ar−H) ppm. ^{13}C NMR (300 MHz, [D$_2$]DCM, 25 °C, TMS): δ = 12.13, 17.85, 21.73, 56.17, 96.74, 111.48, 130.20, 143.11 ppm. IR (KBr pellet): ν̃ = 3060 (w, Ar−H), 2960−2860 (m, C−H), 2210 (s, C≡N), 1525 (m, C=C), 530 (m, S−Pt) cm^{-1}. UV/Vis (CH$_2$Cl$_2$): λ_{max} (ε) = 230.4 nm (42400), 279.0 (38300), 382.3 (31900), 449.8 (7800 mol^{-1} dm^3 cm^{-1}). $C_{48}H_{76}N_6PtS_4$ (1060.50): calcd. C 54.36, H 7.22, N 7.92, S 12.09; found C 55.73, H 7.61, N 8.12, S 12.74.

Tetrabutylammonium Salt of Platinum(III) Bis(4,5-dicyanobenzene-1,2-dithiolate) (nBu$_4$N)[Pt(dcbdt)$_2$] (9): A solution of I$_2$ (45.0 mg, 0.18 mmol) in acetone was added to a solution of **8** (0.38 g, 0.36 mmol) in acetone (100 mL). The solution was stirred until a colour change to green was observed. Ethanol was added and the solution was slowly evaporated to give **9** as dark-green needles (99.0 mg, 0.12 mmol, 33%). M.p. 250−251 °C. ^{1}H NMR (300 MHz, [D$_2$]DCM, 25 °C, TMS): δ = 0.94 (t, J = 7.1 Hz, 12 H, CH$_3$), 1.32 (m, 8 H, CH$_2$), 1.58 (m, 8 H, CH$_2$), 3.18 (s, 8 H, CH$_2$) ppm. ^{13}C NMR (300 MHz, [D$_2$]DCM, 25 °C, TMS): δ = 13.39, 18.89, 23.54, 53.79 ppm. IR (KBr pellet): ν̃ = 3060 (w, Ar−H), 2960−2860 (m, C−H), 2220 (s, C≡N), 1550 (w, C=C), 420 (w, S−Pt) cm^{-1}. UV/Vis (CH$_2$Cl$_2$): λ_{max} (ε) = 280.2 (80600), 347.1 nm (20400 mol^{-1} dm^3 cm^{-1}). $C_{32}H_{40}N_5PtS_4$ (818.03): calcd. C 46.98, H 4.94, N 8.56, S 15.68; found C 48.40, H 4.91, N 8.48, S 15.14.

Tetrabutylammonium Salt of Zinc(II) Bis(4,5-dicyanobenzene-1,2-dithiolate) (nBu$_4$N)$_2$[Zn(dcbdt)$_2$] (10): Compound **1** (0.14 g, 0.73 mmol) was dissolved in 5 mL of aqueous NaOH (10%). A solution of nBu$_4$NI (0.26 g, 0.73 mmol) in EtOH/H$_2$O (1:1; 5 mL) was added, followed by a solution of $ZnCl_2$ (0.05 g, 0.36 mmol) in the same solvent. The mixture was stirred and an orange precipitate was formed almost immediately. The solution was filtered and the precipitate was washed with EtOH. The crude material was recrystallised from acetonitrile/iBuOH to give **10** as orange crystals (0.22 g, 0.24 mmol, 65%). M.p. 205−206 °C. ^{1}H NMR (300 MHz, [D$_6$]acetone, 25 °C, TMS): δ = 0.96 (t, J = 7.4 Hz, 24 H, CH$_3$), 1.41 (m, 16 H, CH$_2$), 1.76 (m, 16 H, CH$_2$), 3.39 (m, 16 H, CH$_2$), 7.69 (s, 4 H, Ar−H) ppm. ^{13}C NMR (300 MHz, [D$_6$]acetone, 25 °C TMS): δ = 13.83, 20.31, 24.43, 59.36, 104.15, 114.02, 118.46, 132.88 ppm. IR (KBr pellet): ν̃ = 3040−3090 (w, Ar−H), 2960−2860 (m, C−H), 2240 (s, C≡N), 1540 (s, C=C), 420 (w, S−Zn) cm^{-1}. UV/Vis (CH$_2$Cl$_2$): λ_{max} (ε) = 310.3 (43400), 385.5 nm (20500 mol^{-1} dm^3 cm^{-1}). $C_{48}H_{76}N_6S_4Zn$ (930.79): calcd. C 61.94, H 8.23, N 9.03, S 13.78; found C 61.87, H 8.92, N 2.3, S 13.78.

X-ray Crystallographic Study: All diffraction measurements were made at room temperature with the crystals mounted in a glass capillary. An Enraf−Nonius TURBO CAD4 diffractometer equipped with graphite monochromated Cu-K_α radiation (λ = 1.5418 Å) was used for measurements of compounds **3** and **6**. All the other crystals were measured on an Enraf−Nonius CAD4 diffractometer using graphite-monochromated Mo-K_α radiation (λ = 0.71069 Å) in the ω-2θ scan mode. Lorentz, polarisation effects and empirical absorption correction based on psi-scan were applied to the collected intensities. The structures were solved by direct methods using SIR97[28] and refined by full-matrix least-squares methods using the program SHELXL-97[29] and the winGX software package.[30] All non-hydrogen atoms were refined anisotropically. Hydrogen atoms were placed in calculated positions. In the compound (nBu$_4$N)[Cu(dcbdt)$_2$] (**6**) the cation unit was found to be disordered and was refined over two positions with occupancy factors of 0.608 and 0.392, respectively. The cation disorder of compounds **2** and **9** could not be fitted by any model. Molecular graphics were prepared with ORTEP3[31] and SCHAKAL-97.[32] Crystal data and structure refinement details are summarised in Table 1 and Table 2.

CCDC-213103, -213104, -213105, -213106, -213107, -213108, -213109 and -213110 for compounds **2**, **4**, **6**, **9**, **3**, **7**, **8** and **10**, respectively, contain the supplementary crystallographic data for this paper. These data can be obtained free of charge at www.ccdc.cam.ac.uk/conts/retrieving.html [or from the Cambridge Crystallographic Data Centre, 12, Union Road, Cambridge CB2 1EZ, UK; Fax: (internat.) +44-1223/336-033; E-mail: deposit@ccdc.cam.ac.uk].

Acknowledgments

This work was partially supported by FCT (Portugal) under contract POCTI 35452/99. HA also acknowledges FCT for the doctoral grant. This work also benefited from COST action D14/0003/99.

[1] N. Robertson, L. Cronin, *Coord. Chem. Rev.* **2002**, *227*, 93−127.
[2] L. Alcácer, H. Novais, in: *Extended Linear Chain Compounds* (Ed.: J. S. Miller), Plenum Press, New York, **1983**, vol. 3, pp. 319−351.
[3] P. Cassoux, L. Valade, H. Kobayashi, A. Kobayashi, R. A. Clark, A. E. Underhill, *Coord. Chem. Rev.* **1991**, *110*, 115−160.
[4] P. I. Clemenson, *Coord. Chem. Rev.* **1990**, *106*, 171−203.
[5] D. Coucouvanis, *Prog. Inorg. Chem.* **1970**, *11*, 233−371.
[6] J. A. McCleverty, *Prog. Inorg. Chem.* **1968**, *10*, 49.
[7] V. Gama, R. T. Henriques, M. Almeida, L. Veiros, M. J. Calhorda, A. Meetsma, J. L. De Boer, *Inorg. Chem.* **1993**, *32*, 3705−3711.
[8] V. Gama, R. T. Henriques, G. Bonfait, M. Almeida, A. Meetsma, S. V. Smaalen, J. L. De Boer, *J. Am. Chem. Soc.* **1992**, *114*, 1986−1989.
[9] D. Simão, H. Alves, D. Belo, S. Rabaça, E. B. Lopes, I. C. Santos, V. Gama, M. T. Duarte, R. T. Henriques, H. Novais, M. Almeida, *Eur. J. Inorg. Chem.* **2001**, 3119−3126.

 © 2004 Wiley-VCH Verlag GmbH & Co. KGaA, Weinheim

[10] H. Alves, D. Simão, E. B. Lopes, D. Belo, V. Gama, M. T. Duarte, H. Novais, R. T. Henriques, M. Almeida, *Synth. Met.* **2001**, *120*, 1011−1012.
[11] H. Alves, I. C. Santos, E. B. Lopes, D. Belo, V. Gama, D. Simão, H. Novais, M. T. Duarte, R. T. Henriques, M. Almeida, *Synth. Met.* **2003**, *133−134*, 397−399.
[12] H. Alves, D. Simão, H. Novais, I. C. Santos, C. Giménez-Saiz, V. Gama, J. C. Waerenborgh, R. T. Henriques, M. Almeida, *Polyhedron* **2003**, *22*, 2481−2486.
[13] M. J. Baker−Hawkes, E. Billig, H. B. Grey, *J. Am. Chem. Soc.* **1966**, *88*, 4870−4875.
[14] H. Alves, E. B. Lopes, I. C. Santos, R. T. Henriques, M. Almeida, paper to be published.
[15] G. R. Lewis, I. Dance, *J. Chem. Soc., Dalton Trans.* **2000**, 3176.
[16] N. M. Comerlato, W. T. A. Harrison, R. A. Howie, J. N. Low, A. C. Silvino, J. L. Wardell, S. M. S. V. Wardell, *Acta Crystallogr., Sect. C* **2002**, *58*, 105.
[17] J. Stach, R. Kirmse, J. Sieler, U. Abram, W. Dietzsch, R. Bottcher, L. K. Hansen, H. Vergooossen, M. C. M. Gribnau, C. P. Keijzers, *Inorg. Chem.* **1986**, *25*, 1369.
[18] W. C. Hamilton, I. Bernal, *Inorg. Chem.* **1967**, *6*, 2003.
[19] A. L. Balch, I. G. Dance, R. H. Holm, *J. Am. Chem. Soc.* **1968**, *90*, 1139.
[20] J. V. Rodrigues, I. C. Santos, V. Gama, R. T. Henriques, J. C. Waerenborgh, M. T. Duarte, M. Almeida, *J. Chem. Soc., Dalton Trans.* **1994**, 2655−2660.
[21] J. A. Weil, J. R. Bolton, J. Wertz, *Electron Paramagnetic Resonance*, Wiley-Interscience Publication, New York, **1994**.
[22] F. A. Walker, J. Bowen, *J. Am. Chem. Soc.* **1985**, *107*, 7632−7635.
[23] B. M. Hoffman, D. L. Diemente, F. Basolo, *J. Am. Chem. Soc.* **1970**, *92*, 61−65.
[24] R. Kirmse, W. Dietzsch, B. V. Solovev, *J. Inorg. Nucl. Chem.* **1977**, *39*, 1157−1160.
[25] I. Kochurani, H. B. Singh, J. P. Jasinski, E. S. Paight, R. J. Butcher, *Polyhedron* **1997**, *16*, 3505−3510.
[26] J. K. Barton, D. J. Szalda, H. N. Rabinowitz, J. V. Waszczak, S. J. Lippard, *J. Am. Chem. Soc.* **1979**, *101*, 1434−1441.
[27] R. L. Carlin, *Magnetochemistry*, Springer-Verlag, Berlin, **1986**.
[28] A. Altomare, M. C. Burla, M. Camalli, G. Cascarano, G. Giacovazzo, A. Guagliardi, A. G. G. Moliterni, G. Polidori, R. Spagna, *J. Appl. Crystallogr.* **1999**, *32*, 115−119.
[29] G. M. Sheldrick, *SHELXL-97, A Program for Crystal Structure Refinement*, University of Göttingen, Göttingen, **1997**.
[30] L. J. Farrugia, *J. Appl. Crystallogr.* **1999**, *32*, 837−838.
[31] L. J. Farrugia, *J. Appl. Crystallogr.* **1997**, *30*, 565.
[32] E. Keller, *SCHAKAL-97, A Computer Program for the Representation of Molecular and Crystallographic Models*, Kristallographisches Institut der Universität Freiburg i. Br., Germany, Freiburg, **1997**.

Received July 18, 2003
Early View Article
Published Online February 10, 2004

 © 2004 Wiley-VCH Verlag GmbH & Co. KGaA, Weinheim

Aminomethyl and Aminoacetyl Complexes of Palladium(II), Platinum(II), Iron(II) and Rhenium(I) with *N*-Phthaloyl as Amino Protecting Group and Mechanistic Studies on the Palladium-Catalyzed Amidocarbonylation

Armin Enzmann,[a] Markus Eckert,[b] Walter Ponikwar,[a][‡] Kurt Polborn,[a][‡] Stefan Schneiderbauer,[a][‡] Matthias Beller,*[b] and Wolfgang Beck*[a]

Dedicated to Dr. Hachiro Wakamatsu

Keywords: Amidocarbonylation / Iron / Palladium / Platinum / Rhenium

New aminomethyl and aminoacetyl complexes with *N*-phthaloyl as the amino protecting group were synthesised by oxidative addition of *N*-phthaloylmethyl or -acetyl halide to carbonylmetallates or to $Pd(PPh_3)_4$ or $[Pt(C_2H_4)(PPh_3)_2]$ to give $[Re\{C(O)CH_2N\text{-phthaloyl}\}(CO)_5]$ (**1**), $[FeCp(CH_2N\text{-phthaloyl})(CO)_2]$ (**2**), $[FeCp\{C(O)CH_2N\text{-phthaloyl}\}(CO)_2]$ (**3**), *trans*-$[PdBr(CH_2N\text{-phthaloyl})(PPh_3)_2]$ (**4**) and *trans*-$[Pd\{C(O)CH_2N\text{-phthaloyl}\}(X)(PPh_3)_2]$ (X = Br, Cl; **5**, **6**). The bis(phosphane) complexes $[Pd(CH_2N\text{-phthaloyl})(X)(R_2PCH_2CH_2PR_2)]$ and $[Pd\{C(O)CH_2N\text{-phthaloyl}\}(X)(R_2PCH_2CH_2PR_2)]$ (X = Cl, Br; R = Ph, C_6H_{11}) **8**–**13** were obtained by ligand exchange from **4**, **5** or **6** with the corresponding bis(phosphanes). Halide abstraction from **4**, **5**, **6**, **10**, **11** or **12** gives the cationic complexes **14** and **15** with formation of a five-membered chelate ring which includes one carbonyl atom of the phthaloyl group. The reaction of **6** with the tridentate ligand $PhP(CH_2CH_2PPh_2)_2$ affords the five-coordinate complex **16** and from $[Pt(C_2H_4)(PPh_3)_2]$ and organic halides the platinum(II) complexes *trans*-$[Pt(CH_2N\text{-phthaloyl})(Cl)(PPh_3)_2]$ (**17**) and $[PtC(O)CH(CH_2Ph)N\text{-phthaloyl}(Cl)(PPh_3)_2]$ (**18**) were isolated. The structures of **2**, **11**, **14**, **15** and **16** were determined by single-crystal X-ray analysis. The mechanism of the palladium-catalysed amidocarbonylation was studied using phthalimide, formaldehyde and CO as a model system which gives *N*-phthaloylglycine in good yield. The proposed elementary steps in the palladium-catalysed amidocarbonylation could be verified by use of the possible intermediates phthaloyl-NCH_2OH and phthaloyl-NCH_2Br as substrates, by oxidative addition of phthaloylmethyl bromide to Pd^0, by insertion of CO into the palladium-carbon-bond of **4** and **8** with formation of **5** or **9**, respectively, and by use of the isolated possible intermediates **4**, **5** and **14** as catalysts. Thus, all crucial steps of the palladium-catalysed amidocarbonylation with the model system phthalimide/formaldehyde/CO have been verified for the first time.

(© Wiley-VCH Verlag GmbH & Co. KGaA, 69451 Weinheim, Germany, 2004)

Introduction

Aminomethyl and aminoacyl complexes are possible intermediates in the metal-catalysed amidocarbonylation, i.e. the formation of α-amino acids from aldehydes, amide and carbon monoxide. This three component reaction was discovered by Wakamatsu et al.[1] using octacarbonyldicobalt as a catalyst and was more recently developed into a highly efficient process with palladium catalysts.[2] Here we report on the synthesis of new aminomethyl and aminoacetyl metal complexes with *N*-phthaloyl as the *N*-protecting group,[3] on their role and use as catalysts in amidocarbonylation reactions and on experiments which support the mechanism of the palladium-catalysed amidocarbonylation.

Several η^1- and η^2- (side-on) coordinated aminomethyl complexes are formed from methylene immonium salts $[H_2C{=}NR_2]^+ X^-$ and organometallic compounds.[4] η^1-Aminomethyl complexes of cobaloxime result from the reduced form of bis(dimethylglyoximato)cobalt(II), formaldehyde and aniline.[5] An interesting formation of η^2-$(CHR\text{-}NH_2)$ metal complexes is the photochemical decarboxylation of α-aminocarboxylatocobalt(III) complexes.[6] The insertion of imines into the palladium−acyl bond gives *N*-acyl-aminomethyl chelate complexes, a reaction which may provide a route for the palladium-catalysed formation of polypeptides.[7] Metalated α-amino acid derivatives of

[a] Department Chemie der Ludwig-Maximilians-Universität München
Butenandtstr. 5−13, Haus D, 81377 München, Germany
Fax: (internat.) + 49-89-2180-7464
E-mail: wbe@cup.uni-muenchen.de
[b] Leibniz-Institut für Organische Katalyse (IfOK) an der Universität Rostock e.V.
Buchbinderstr. 5−6, 18055 Rostock, Germany
Fax: (internat.) + 49-381-466-9324
E-mail: matthias.beller@ifok.uni-rostock.de
[‡] X-ray analysis.

nickel,[8] palladium[7] and manganese[9] of the form L_nM-$C(O)CR_2$-N(*R*)-C(O)R have also been obtained by sequential insertion of carbon monoxide and imine into metal-carbon σ-bonds,[7−9] and recently an interesting palladium-catalysed synthesis of Münchnones (1,3-oxazolium 5-oxides, first isolated by Huisgen et al.[10]) and of α-amino acid derivatives from imines, CO and acyl chloride building blocks has been developed.[11] Its mechanism is similar to that of amidocarbonylation. Rhodium complexes with *N*-protected aminomethyl ligands have been prepared from $[RhCp(CH_2I)(I)(PMe_3)]$ and amides.[12] A general method for the preparation of η^1-aminomethyl and -aminoacetyl complexes with a protected amino group is the reaction of anionic organometallic compounds [Co(dimethylglyoximate)]$^-$ [13] or of metal carbonyls[14,15] with phthaloylmethyl halide, phthaloylglycyl chloride or with mixed anhydrides of *N*-protected α-amino acids.[16,17] The *N*-protected aminomethyl and aminoacetyl metal carbonyls can be interconverted by CO insertion[14,15] or decarbonylation,[14,15,17] respectively, and could be useful for the synthesis of peptides.[14]

Phthalimidomethyl and -acetyl Complexes of Iron and Rhenium Carbonyls

In continuation of our recent work,[14] new examples of metal carbonyls with *N*-protected η^1-aminomethyl and -aminoacetyl ligands (**1**−**3**) were obtained by reactions of the metal carbonyls $[FeCp(CO)_2]^-$ and $[Re(CO)_5]^-$ with phthaloylmethyl chloride and phthaloylacetyl chloride, respectively.

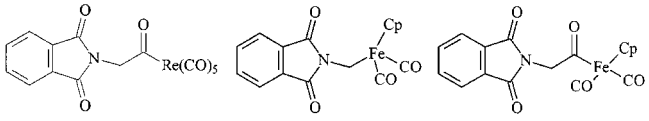

1 **2** **3**

Compounds **1**−**3** show the characteristic M(CO) and MeC=O absorptions in their IR spectra (see Exp. Sect.). The ^1H and ^{13}C NMR spectra of **1**−**3** exhibit the expected signals.

Crystals of **1** suitable for X-ray diffraction were obtained by layering a frozen solution of **2** in CH_2Cl_2 with *n*-pentane. The molecule of **2** (Figure 1) has the classic "piano stool" structure as, for example, in $[FeCp(COCH_3)(CO)(PPh_3)]$.[18] The Fe1−C8 distance [2.042(3) Å] is typical for an iron-carbon σ-bond and of similar length as in $[Co(CH_2$*N*-phthaloyl$)(CO)_4]$ from Marko and co-workers[15] and in $[FeCp(CH_3)(CO)\{Ph_2PN(CH_3)CH(CH_3)Ph\}]$.[19] In the crystal, the Cp rings of different molecules of **1** are arranged in a parallel fashion. Metzler-Nolte et al.[20] have reported the synthesis and structure of $[MoCp(CH_2CH_2$-*N*-phthaloyl$)(CO)_3]$ which is a homologue of the corresponding aminomethyl complex.[14]

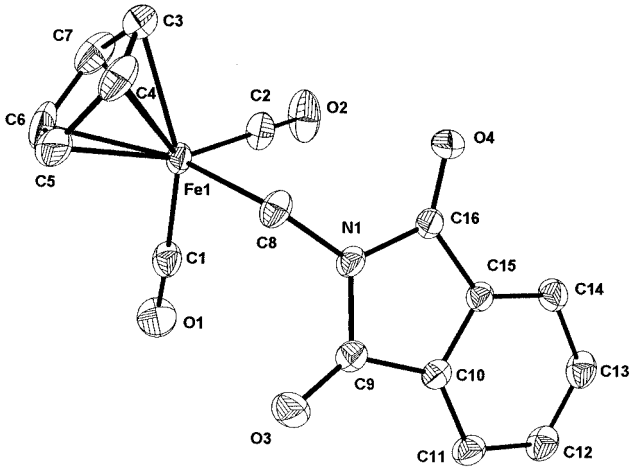

Figure 1. Molecular structure of **2** in the crystal; selected bond lengths (Å) and bond angles (°): Fe(1)−C(1) 1.755(3), O(3)−C(9) 1.204(3), Fe(1)−C(2) 1.750(3), O(4)−C(16) 1.208(3), Fe(1)−C(8) 2.042(3), N(1)−C(8) 1.450(3), O(1)−C(1) 1.144(3), N(1)−C(9) 1.395(3), O(2)−C(2) 1.140(3), N(1)−C(16) 1.391(3); C(2)−Fe(1)−C(1) 93.71(14), O(1)−C(1)−Fe(1) 176.0(3), C(1)−Fe(1)−C(8) 92.77(12), O(2)−C(2)−Fe(1) 177.3(3), C(2)−Fe(1)−C(8) 92.07(12), N(1)−C(8)−Fe(1) 119.7(2), C(16)−N(1)−C(9) 111.4(2), O(3)−C(9)−N(1) 124.9(2), C(16)−N(1)−C(8) 124.1(2), O(4)−C(16)−N(1) 124.6(2), C(9)−N(1)−C(8) 124.2(2)

Synthesis of Phthaloylmethyl and -acetyl Complexes of Palladium(II) and Platinum(II)

Palladium Complexes

The oxidative addition of organic halides to zero-valent palladium and platinum complexes is a general method for the synthesis of σ-bonded organometallic complexes.[21] This method was successfully applied for the synthesis of the *N*-phthaloylaminomethyl- and -acetylpalladium complexes **4**−**6**, which were prepared from $Pd(PPh_3)_4$ and *N*-phthaloylaminomethyl bromide, *N*-phthaloylaminoacetyl chloride or bromide, respectively. The formation of **4** takes several days (as expected, the methyl bromide is less reactive than the acetyl halides) and here the phosphonium salt **7** is formed as a by-product. A smaller quantity of $Pd(PPh)_4$ than stoichiometrically needed proved to be favourable for good yields of **4**. In a separate experiment it was shown that **7** does not react with $Pd(PPh_3)_4$.

Complexes **4**−**6** decompose slowly in solution. *N*-Phthaloylglycine is formed from **5** and **6** in the presence of moisture. It is interesting to note that complexes **4**−**6** react with the bis(phosphanes) $R_2P(CH_2)_2PR_2$ (R = Ph, C_6H_{11}) to give the complexes **8**−**13**. These reactions proceed by a *trans* → *cis* rearrangement.

In the IR spectra of **4**−**13** the phthaloyl absorptions at 1720 and 1770 cm^{-1} are characteristic. The acetyl carbonyl band of **5**, **6**, **9**, **10**, **12** and **13** is observed between 1660 and 1680 cm^{-1}. In the ^{31}P NMR spectra of **4**−**6** only one signal

 © 2004 Wiley-VCH Verlag GmbH & Co. KGaA, Weinheim

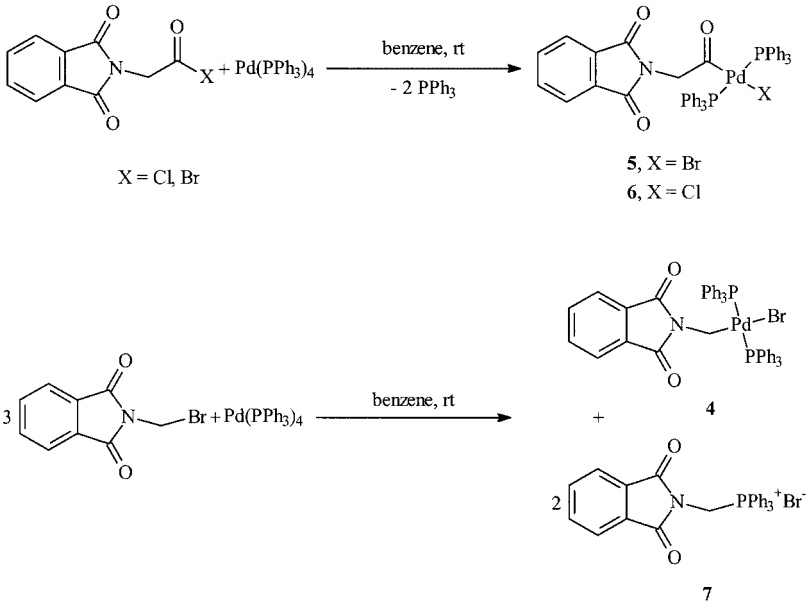

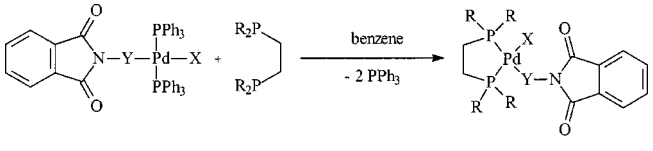

	8	9	10	11	12	13
Y	CH_2	$CH_2C(O)$	$CH_2C(O)$	CH_2	$CH_2C(O)$	$CH_2C(O)$
X	Br	Br	Cl	Br	Br	Cl
R	Ph	Ph	Ph	C_6H_{11}	C_6H_{11}	C_6H_{11}

is found, i.e. these complexes are formed as single *trans*-isomers. The X-ray structure determination of **11** (Figure 2) gave bonding parameters which lie in the usual range. Abstraction of halide ions from complexes **4**–**6** and **10**–**12** gives the cationic chelate complexes **14** and **15** in which coordination of one carbonyl oxygen atom of the phthaloyl group takes place.

Interestingly, complexes **14** and **15** are formed from the aminoacetyl complexes **5**, **6**, **11** and **12** by spontaneous decarbonylation, which is probably due to the stability of the formed five-membered chelate ring in **14** and **15** and which should involve alkyl migration.[22] In light of this, the reactions of **5** and **6** to **14** — the *trans* → *cis* isomerisation — can also be understood as being due to an alkyl migration.

The structures of **14** and **15** were confirmed by X-ray diffraction (Figure 3 and 4, respectively). The chelate ring in **14** and **15** has the same structural feature as in the palladium and platinum complexes obtained by oxidative addition of α-bromohippuric acid ester to Pd^0 or Pt^0 and subsequent reaction with $AgBF_4$.[23] An analogous chelate ring is also formed by insertion of imines into the metal–acetyl bond.[7–9] A similar chelate ring is formed from Ni^0 imine complexes and carbon dioxide.[24] The C–Pd–O bite angles in **14** and **15** (82–83°) are very similar to that of the above-mentioned complexes.[7,8,23] The Pd–C bonds in **14** and **15** (2.07–2.08 Å) are longer than that in [Pd{O=C(Ph)NHCHCO$_2$Me}(bipy)]$^+$ [23] which is due to the strong *trans*-influence of the phosphane ligand.

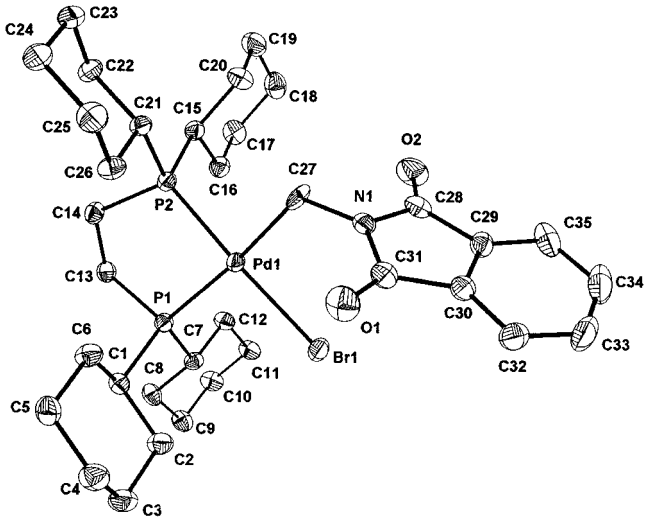

Figure 2. Molecular structure of **11** in the crystal; selected bond lengths (Å) and bond angles (°): Pd(1)–C(27) 2.160(5), N(1)–C(31) 1.402(6), Pd(1)–P(1) 2.3197(13) O(1)–C(31) 1.210(6), Pd(1)–P(2) 2.2324(13) O(2)–C(28) 1.207(6), Pd(1)–Br(1) 2.5068(6), C(28)–C(29) 1.500(7), N(1)–C(27) 1.402(5), C(29)–C(30) 1.365(7), N(1)–C(28) 1.379(6), C(30)–C(31) 1.490(7); C(27)–Pd(1)–P(2) 89.03(12), C(31)–N(1)–C(27) 127.9(5), P(2)–Pd(1)–P(1) 86.66(5), O(1)–C(31)–N(1) 124.8(5), C(27)–Pd(1)–Br(1) 94.32(11), N(1)–C(31)–C(30) 106.3(5), P(1)–Pd(1)–Br(1) 91.25(4), O(1)–C(31)–C(30) 128.9(5), N(1)–C(27)–Pd(1) 115.3(3), O(2)–C(28)–N(1) 124.9(5), C(28)–N(1)–C(27) 121.0(5), N(1)–C(28)–C(29) 106.7(5), C(28)–N(1)–C(31) 110.9(4), O(2)–C(28)–C(29) 128.4(6)

The reaction of **6** with the tridentate ligand $PhP(CH_2CH_2PPh_2)_2$ affords the five-coordinate, 18-electron aminoacetylpalladium complex **16**. The X-ray structure determination (Figure 5) shows the molecule of **16** as a dis-

 © 2004 Wiley-VCH Verlag GmbH & Co. KGaA, Weinheim

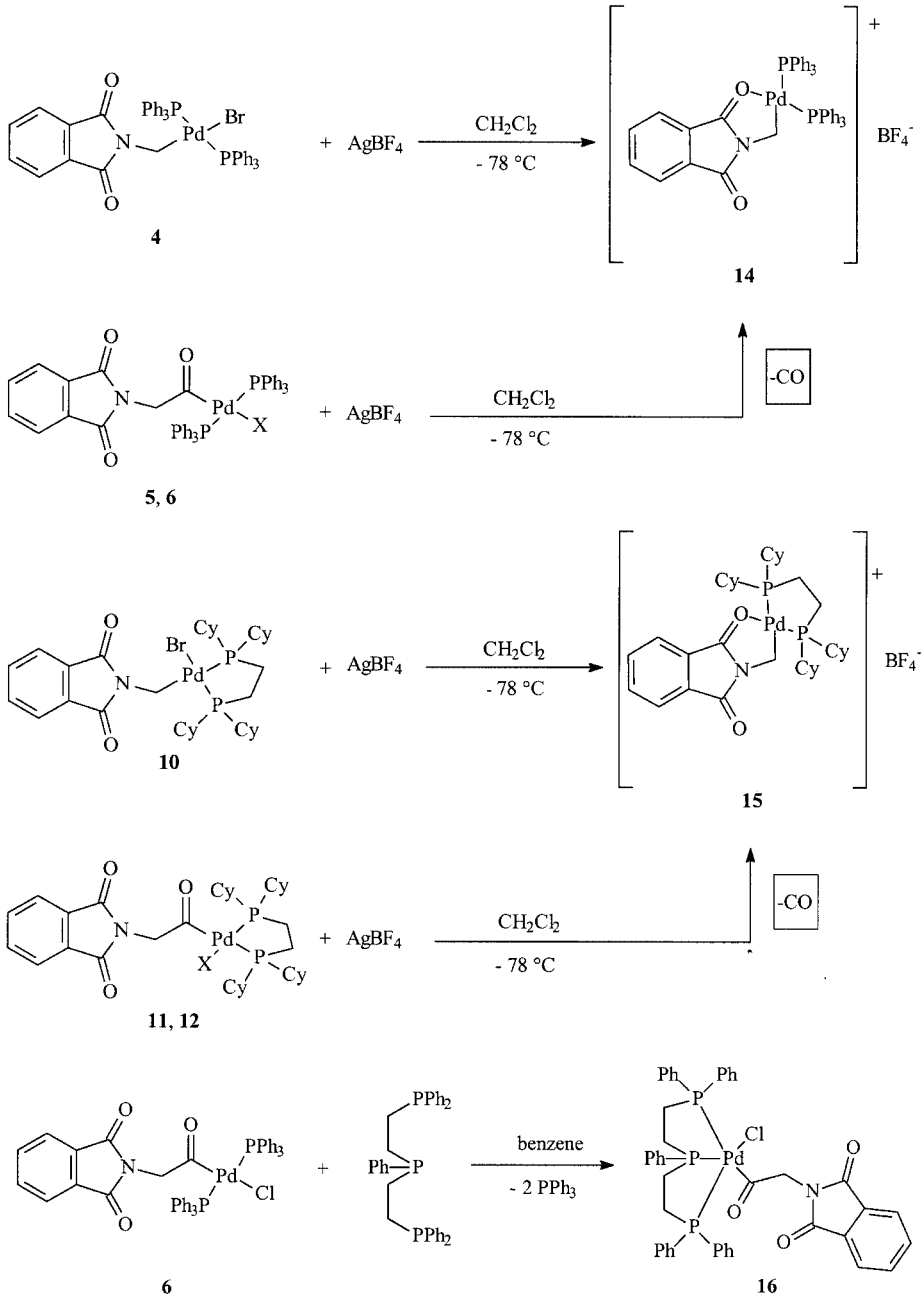

torted trigonal bipyramid with P(1) and P(3) in the axial positions. The P(1), P(3) and Cl(1) atoms lie in a plane (sum of angles 360°). The unusually long Pd−Cl(1) bond (2.69 Å) is remarkable. In the crystal of **16** there are large voids which are occupied by solvent molecules (dichloromethane and *n*-pentane).

Similar five-coordinate palladium and platinum complexes are intermediates in many catalytic reactions,[25] and a series of such complexes with chelate ligands has been isolated and structurally characterised.[25−27]

Platinum Complexes

The platinum complexes **17** and **18** were obtained by oxidative addition of *N*-phthaloylglycyl chloride or *N*-phthaloylphenylalanyl chloride to $[Pt(C_2H_4)(PPh_3)_2]$. The

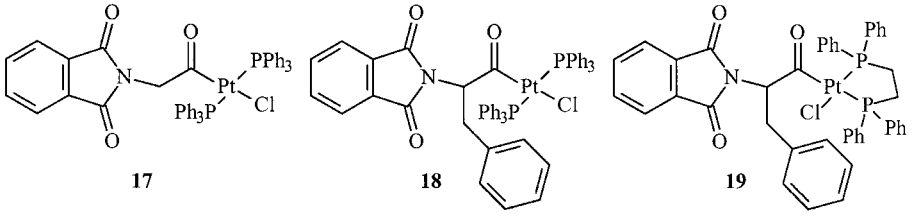

 © 2004 Wiley-VCH Verlag GmbH & Co. KGaA, Weinheim

bis(diphenylphosphanyl)ethane complex **19** was synthesised from **18** by ligand exchange.

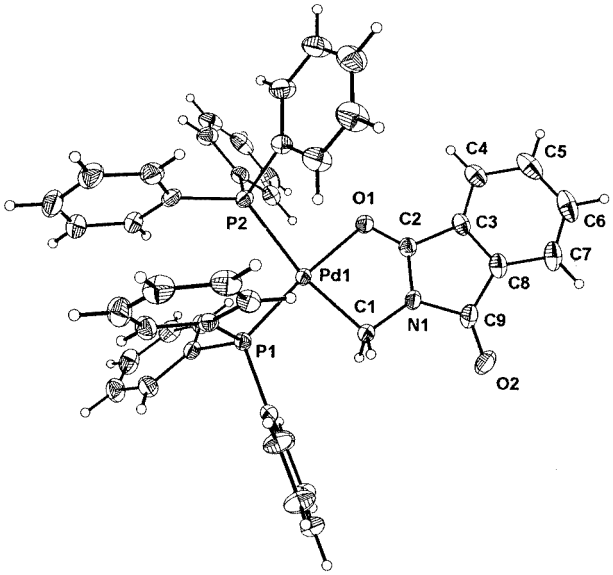

Figure 3. Molecular structure of **14** in the crystal; selected bond lengths (Å) and bond angles (°): Pd(1)−C(1) 2.066(4), N(1)−C(1) 1.454(6), O(2)−C(9) 1.194(6), Pd(1)−P(1) 2.2194(12), N(1)−C(2) 1.341(6), C(2)−C(3) 1.480(6), Pd(1)−P(2) 2.3882(12), N(1)−C(9) 1.429(6), C(8)−C(9) 1.474(8), Pd(1)−O(1) 2.125(3), O(1)−C(2) 1.232(5); C(1)−Pd(1)−O(1) 83.05(15), C(2)−O(1)−Pd(1) 108.0(3), N(1)−C(2)−C(3) 108.9(4), O(1)−Pd(1)−P(2) 87.12(9), C(2)−N(1)−C(9) 111.0(4), O(1)−C(2)−C(3) 127.7(4), C(1)−Pd(1)−P(1) 91.08(13), C(9)−N(1)−C(1) 127.7(4), O(2)−C(9)−C(8) 130.6(5), P(1)−Pd(1)−P(2) 98.50(4), C(2)−N(1)−C(1) 121.0(3), N(1)−C(9)−C(8) 105.0(4), N(1)−C(1)−Pd(1) 103.5(3), O(1)−C(2)−N(1) 123.4(4), O(2)−C(9)−N(1) 124.5(5)

Experiments on the Mechanism of the Palladium-Catalyzed Amidocarbonylation

The proposed mechanism of the palladium-catalysed amidocarbonylation with aldehydes, amides and CO is shown in Scheme 1.[3]

In order to study the elementary steps of the mechanism the palladium-catalysed formation of phthaloylglycine from phthalimide, formaldehyde and CO was chosen as a model system. In the absence of CO and Pd^{2+}, phthalimide reacts with formaldehyde to give *N*-(hydroxymethyl)phthalimide.[13] The chosen reactants seemed to be favourable because phthalimide cannot form an oxazolone ring as side-product and the aldehyde does not carry β-hydrogen atoms. Hence, β-hydride elimination is not possible and a satisfying yield of 55% of the glycine derivative was achieved at 120 °C and 60 bar CO using 0.25 mol % $PdBr_2$ and 0.5 mol % PPh_3 as catalyst in the presence of 35 mol % LiBr and 1 mol % H_2SO_4. The yield strongly decreases at lower temperature (Table 1).

The following results confirm the previously proposed mechanism:[2]

1) With (hydroxymethyl)phthalimide or (bromomethyl)phthalimide as substrate the same yield of phthaloylglycine (55%) is obtained as with phthalimide and paraformaldehyde (Table 1). In many experiments[2] the temperature of 120 °C proved to be favourable. Experiments 3 and 4 in Table 2 demonstrate the need for halide and acid as cocatalysts.

2) Oxidative addition of the organic halide to Pd^0 was verified by the isolation of complex **4** from the reaction of (bromomethyl)phthalimide and $Pd(PPh_3)_4$.

3) The insertion of carbon monoxide into the aminoalkyl−palladium bond (which may occur via alkyl

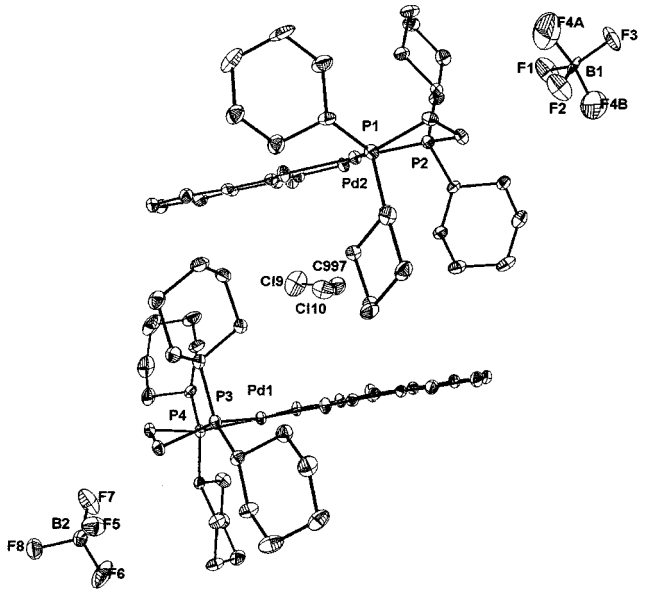

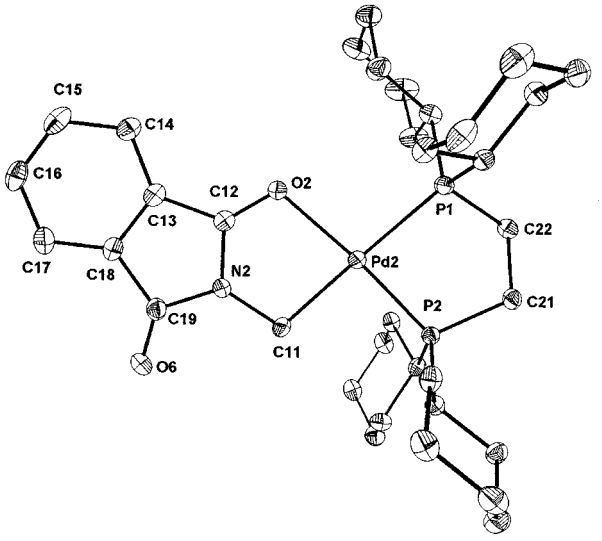

Figure 4. Molecular structure of **15** in the crystal; selected bond lengths (Å) and bond angles (°): Pd(2)−C(11) 2.083(4), N(2)−C(11) 1.464(5), O(6)−C(19) 1.202(5), Pd(2)−P(1) 2.3193(11) N(2)−C(12) 1.364(5), C(12)−C(13) 1.473(5), Pd(2)−P(2) 2.2203(10) N(2)−C(19) 1.403(5), C(18)−C(19) 1.488(6), Pd(2)−O(2) 2.148(3), O(2)−C(12) 1.238(5); C(11)−Pd(2)−O(2) 82.71(12), C(12)−O(2)−Pd(2) 109.4(3), N(2)−C(12)−C(13) 107.6(4), O(2)−Pd(2)−P(1) 98.49(7), C(12)−N(2)−C(19) 111.0(3), O(2)−C(12)−C(13) 129.7(4), C(11)−Pd(2)−P(2) 92.66(11), C(19)−N(2)−C(11) 127.7(3), O(6)−C(19)−C(18) 129.7(4), P(1)−Pd(2)−P(2) 86.12(4), C(12)−N(2)−C(11) 121.1(3), N(2)−C(19)−C(18) 105.9(4), N(2)−C(11)−Pd(2) 104.2(2), O(2)−C(12)−N(2) 122.6(4), O(6)−C(19)−N(2) 124.4(4)

 © 2004 Wiley-VCH Verlag GmbH & Co. KGaA, Weinheim

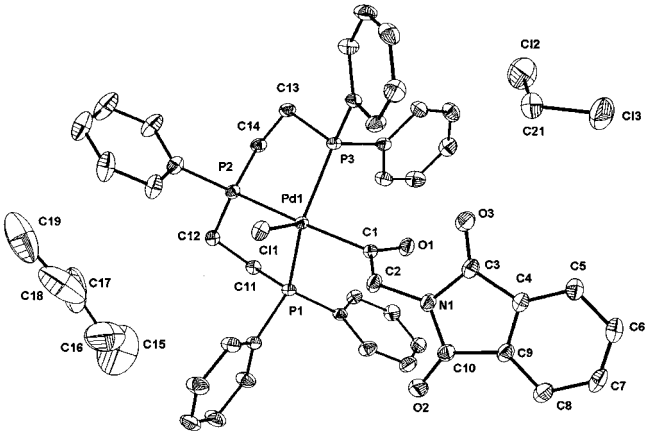

Figure 5. Molecular structure of **16** in the crystal; selected bond lengths (Å) and bond angles (°): Pd(1)−C(1) 2.035(2), Pd(1)−Cl(1) 2.6855(6), C(3)−N(1) 1.399(3), Pd(1)−P(1) 2.3133(6), C(1)−C(2) 1.540(3), N(1)−C(10) 1.379(3), Pd(1)−P(2) 2.3381(6), O(1)−C(1) 1.195(3), O(2)−C(10) 1.214(3), Pd(1)−P(3) 2.3297(6), C(2)−N(1) 1.454(3), O(3)−C(3) 1.195(3); P(1)−Pd(1)−P(2) 85.20(2), C(1)−Pd(1)−P(3) 91.67(6), C(2)−C(1)−Pd(1) 115.07(15) P(1)−Pd(1)−P(3) 137.67(2) P(1)−Pd(1)−Cl(1) 114.10(2) N(1)−C(2)−C(1) 112.64(19) P(3)−Pd(1)−P(2) 85.30(2), P(2)−Pd(1)−Cl(1) 97.626(19) C(10)−N(1)−C(2) 124.8(2), C(1)−Pd(1)−P(1) 89.82(7), P(3)−Pd(1)−Cl(1) 108.02 (2) C(10)−N(1)−C(3) 111.9(2), C(1)−Pd(1)−Cl(1) 93.61(7), O(1)−C(1)−Pd(1) 125.99(17) C(3)−N(1)−C(2) 122-.8(2) C(1)−Pd(1)−P(2) 168.76(7) O(1)−C(1)−C(2) 118.9(2)

Table 1. Palladium-catalysed amidocarbonylation with the model system phthalimide/formaldehyde

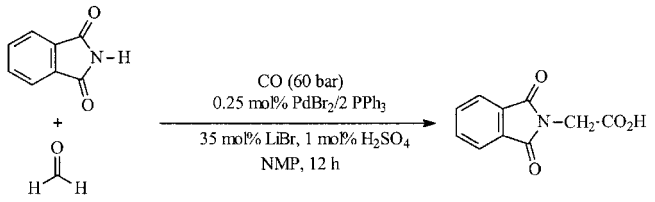

Exp.	Temperature (°C)	Yield (%)[a]
1	80	–
2	100	20
3	120	55

[a] Isolated yield.

migration[22]) has been realized with the alkyl complexes **4** and **8** in CD_2Cl_2 solutions. The reaction was followed by ^{31}P NMR spectroscopy in a high pressure NMR tube. With **4** at 60 °C and 50 bar CO after 180 min the signal (δ = 19.7 ppm) of the acetyl complex **6** was detected (besides

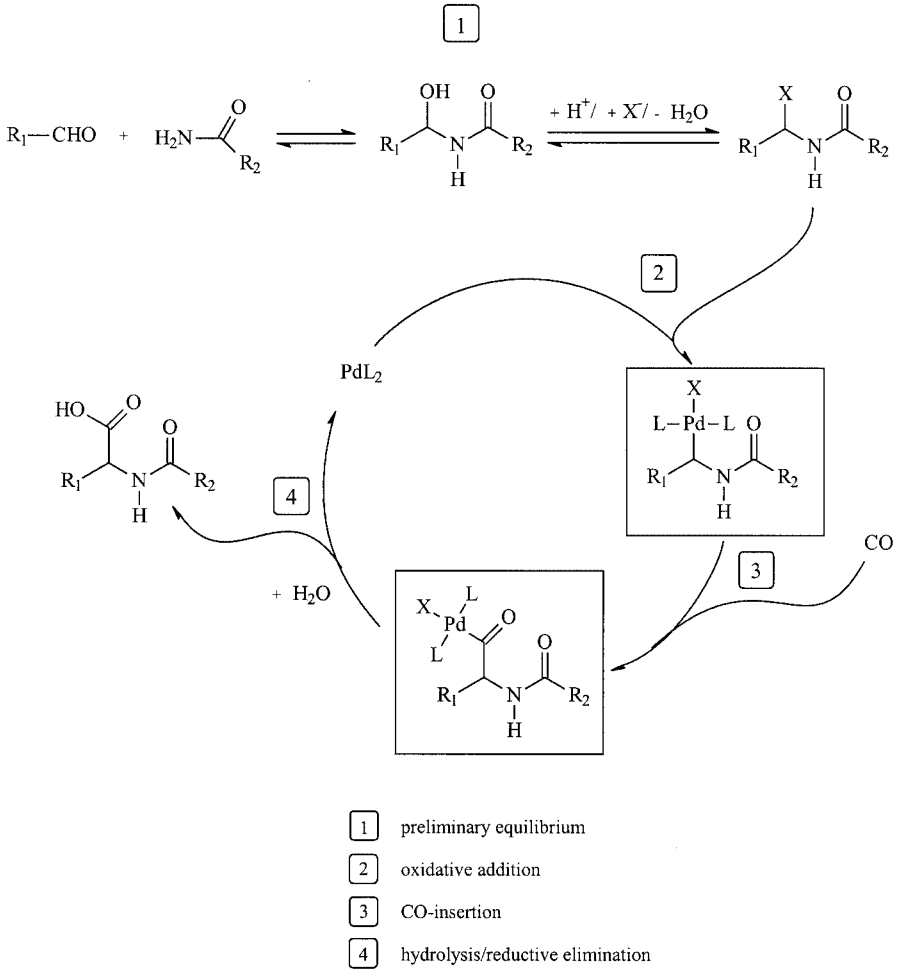

Scheme 1

 © 2004 Wiley-VCH Verlag GmbH & Co. KGaA, Weinheim

that of **7** at δ = 21.9 ppm). Similarly, with **8** at 50 bar CO and 130 °C after 1 h two ^{31}P NMR doublets were observed (with low intensity) which correspond to **9**. Obviously the CO insertion is more difficult with **8**, which has a bis(phosphane) chelate ligand.

The reverse decarbonylation reaction has been observed in CH_2Cl_2 solution of **12** where, after 1−2 days at 20 °C, the ^{31}P NMR signals of **11** appeared. Also, the spontaneous decarbonylation of **5**, **6**, **11** and **12** when treated with Ag^+ should be mentioned here.

4) The final step of the catalytic cycle — the hydrolysis of the acetylpalladium complex and formation of palladium(0) and phthaloylglycine — is supported by the observation that *N*-phthaloylglycine and palladium black are formed from solutions of **5** and **6** in CH_2Cl_2 in contact with air. It is remarkable that in entry 6 (Table 2) without addition of water phthaloylglycine was not formed from phthaloylmethyl bromide. Addition of methanol (entry 7, Table 2) gave *N*-phthaloylglycine (20%) and *N*-(methoxy)methylphthalimide (65%) as products.

Table 2. Use of intermediates in the model system phthalimide/formaldehyde

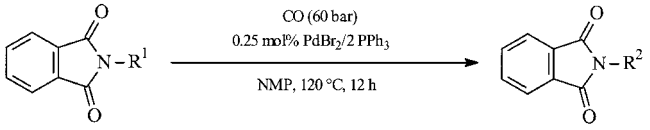

Exp.	R^1	Addition [equiv.]	H_2SO_4 [equiv.]	LiBr [equiv.]	Product yield [%][a] R^2	
1	H	CH_2O [1.0]	0.001	0.35	$-CH_2CO_2H$	55
2	$-CH_2OH$	−	0.01	0.35	$-CH_2CO_2H$	57
3	$-CH_2OH$	−	−	0.35	$-CH_2CO_2H$	10
4	$-CH_2OH$	−	0.01	−	−	
5	$-CH_2Br$	H_2O [1.0]	0.01	−	$-CH_2CO_2H$	48
6	$-CH_2Br$	−	0.01	−	−	
7	$-CH_2Br$	MeOH [1.0]	0.01	−	$-CH_2CO_2Me$ + $-CH_2OMe$	20 65
8	$-CH_2OMe$	−	0.01	−	−	
9	$-CH_2OMe$	−	0.01	0.35	−	

[a] Isolated yield.

5) Finally, the complexes **4**, **5** and **14**, which are possible intermediates in the amidocarbonylation, were used as catalysts for the reaction of phthalimide with paraformaldehyde. Under standard conditions (0.25 mol % complex, 120 °C, 60 bar CO, in NMP, 12 h) *N*-phthaloylglycine was obtained in yields of 48, 45 or 51% which corresponds to the activity of the normal catalyst $PdBr_2{\cdot}2PPh_3$.

In summary, all critical steps of the palladium-catalysed amidocarbonylation (Scheme 1) have been fully established for the model system phthalimide/formaldehyde/CO.

Experimental Section

The complexes $Pd(PPh_3)_4$,[28] $[Pt(C_2H_4)(PPh_3)_2]$[29] *N*-phthaloylglycyl chloride, *N*-phthaloylglycyl bromide[30] and *N*-phthaloylphenylalanyl chloride[31] were prepared according to the literature. The other starting materials were used as purchased.

Pentacarbonyl(*N*-phthaloylaminoacetyl)rhenium(I) (1): Dirheniumdecacarbonyl (700 mg, 1.1 mmol) was added to a mixture of 20.1 g of Na/Hg (6.63 mmol Na) and 25 mL of THF while stirring and cooling to −78 °C. After 1 h, the mixture was allowed to warm up to room temperature and was stirred for 2 h. The dark-red solution was removed with a syringe and added slowly to a solution of 380 mg of *N*-phthaloylglycyl chloride in 15 mL of THF at −78 °C. After 2 h of stirring at room temperature, the suspension was filtered and the filtrate was concentrated in vacuo. The resulting residue was washed several times with water, dried in vacuo and crystallised from CH_2Cl_2/*n*-pentane to give 735 mg of the colourless product (84% yield). ^1H NMR (270 MHz, 25 °C, $CDCl_3$): δ = 7.85−7.60 (m, 4 H, C_6H_4), 4.46 (s, 2 H, CH_2) ppm. $^{13}C\{^1H\}$ NMR (100.5 MHz, 25 °C, $CDCl_3$): δ = 246.3 [ReC(O)R], 181.9 [$Re(CO)_5$], 180.7 [$Re(CO)_5$], 167.9 (CON), 134.0, 132.3, 123.4 (C_6H_4), 69.4 (CH_2) ppm. IR (Nujol): $\tilde{\nu}$ = 2141 m, 2066 s, 2039, 2012 s, 1774 w, 1713 s, 1619 s cm^{-1}. $C_{15}H_6NO_8Re$ (514.4): calcd. C 35.02, H 1.18, N 2.72; found C 34.57, H 1.26, N 2.69.

Dicarbonyl(cyclopentadienyl)(*N*-phthaloylaminomethyl)iron(II) (2): Na/Hg (10.24 g, 3.3 mmol Na) was treated with a solution of bis(dicarbonylcyclopentadienyliron) (400 mg, 1.1 mmol) in 20 mL of THF at −78 °C. While stirring, the mixture was allowed to warm up to room temperature. After 3 h, the solution was removed with a syringe and added slowly to a solution of bromomethylphthalimide (456 mg, 1.9 mmol) in 15 mL of THF at −78 °C. The resulting dark red solution was stirred for 2 h at −78 °C and 3 h at room temperature. The colourless precipitate was separated by centrifugation. The dark red solution was concentrated in vacuo and the residue was crystallised from a CH_2Cl_2/*n*-pentane mixture. One of the resulting yellow crystals was selected for X-ray analysis. The rest of the product was dried in vacuo. Yield: 423 mg (66%). ^1H NMR (270 MHz, 25 °C, $CDCl_3$): δ = 7.80−7.20 (m, 4 H, C_6H_4), 4.94 (s, 5 H, C_5H_5), 3.99 (s, 2 H, CH_2) ppm. $^{13}C\{^1H\}$ NMR (100.5 MHz, 25 °C, $CDCl_3$): δ = 215.8 [$Fe(CO)_2$], 168.7 (CON), 133.7, 133.4, 122.7, (C_6H_4), 85.4 (C_5H_5), 11.2 ($FeCH_2$) ppm. IR (Nujol): $\tilde{\nu}$ = 2002 s, 1960 s, 1770 m, 1708 s cm^{-1}. $C_{16}H_{11}FeNO_4$ (337.1): calcd. C 57.01, H 3.29, N 4.15; found C 56.83, H 3.24, N 4.14.

Dicarbonyl(cyclopentadienyl)(*N*-phthaloylaminoacetyl)iron(II) (3): Na/Hg (3.66 g, 1.1 mmol Na) was treated with a solution of bis(dicarbonylcyclopentadienyliron) (140 mg, 0.4 mmol) in 15 mL of THF at −78 °C. While stirring, the mixture was allowed to warm up to room temperature. After 3 h, the solution was removed with a syringe and added slowly to a solution of *N*-phthaloylaminoacetyl chloride (180 mg, 0.8 mmol) in 15 mL of THF at −78 °C. The resulting dark solution was stirred for 1 h at −78 °C and 1 h at room temperature. The colourless precipitate was separated by centrifugation. The dark red solution was concentrated in vacuo and the residue was crystallised from a CH_2Cl_2/*n*-pentane mixture to afford 222 mg of yellow crystals (76% yield). ^1H NMR (270 MHz, 25 °C, $CDCl_3$): δ = 7.80−7.50 (m, 4 H, C_6H_4), 4.94 (s, 5 H, C_5H_5), 4.56 (s, 2 H, CH_2) ppm. IR (Nujol): $\tilde{\nu}$ = 2016 s, 1963 s, 1773 w, 1708 s, 1665 s cm^{-1}. $C_{17}H_{11}FeNO_5$ (365.1): calcd. C 55.92, H 3.04, N 3.84; found C 55.52, H 3.10, N 3.96.

***trans*-Bromo(*N*-phthaloylaminomethyl)bis(triphenylphosphane)-palladium(II) (4):** (Bromomethyl)phthalimide (200 mg, 0.83 mmol) was dissolved in 30 mL of benzene and $Pd(PPh_3)_4$ (960 mg, 0.83 mmol) was added at room temperature. After stirring for 2 days the resulting precipitate was separated by centrifugation, and

 © 2004 Wiley-VCH Verlag GmbH & Co. KGaA, Weinheim

washed with a small amount of benzene and pentane. The by-product **7** was extracted from the residue with methanol. The remaining solid was dissolved in CH_2Cl_2 and precipitated with pentane. The yellow product was washed with a small amount of benzene and dried in vacuo. Yield: 178 mg (73%). ^1H NMR (400 MHz, 25 °C, CD_2Cl_2): δ = 7.84−7.30 (m, 34 H, C_6H_4, PPh_3), 2.71 (br., 2 H, CH_2) ppm. $^{13}C\{^1H\}$ NMR (100.5 MHz, 25 °C, CD_2Cl_2): δ = 169.2 (CON), 135.0, 133.1, 131.3, 130.2, 128.3, 128.0, 121.9 (C_6H_4, PPh_3), 54.0 (CH_2) ppm. $^{31}P\{^1H\}$ NMR (109.4 MHz, 25 °C, CD_2Cl_2): δ = 26.8 (s) ppm. IR (KBr): $\tilde{\nu}$ = 3057 w, 1771 w, 1699 s, 1436 s cm^{-1}. $C_{45}H_{36}BrNO_2P_2Pd{\cdot}0.25CH_2Cl_2$ (892.3): calcd. C 60.94, H 4.12, N 1.57; found C 60.91, H 3.92, N 1.47.

***trans*-Bromo(*N*-phthaloylaminoacetyl)bis(triphenylphosphane)palladium(II) (5):** *N*-Phthaloylglycyl bromide (220 mg, 0.77 mmol) was dissolved in 30 mL of benzene and $Pd(PPh_3)_4$ (1202 mg, 0.77 mmol) was added at room temperature. After stirring for 1 h the resulting precipitate was separated by centrifugation, washed with benzene and diethyl ether and dried in vacuo to give 592 mg of the yellow product (76% yield). ^1H NMR (270 MHz, 25 °C, CD_2Cl_2): δ = 7.88−7.25 (m, 34 H, C_6H_4, PPh_3), 4.03 (s, 2 H, CH_2) ppm. $^{13}C\{^1H\}$ NMR (100.5 MHz, 25 °C, CD_2Cl_2): δ = 228.8 [PdC(O)R], 166.8 (CON), 135.1, 134.0, 131.8, 130.5, 128.3, 123.2 (C_6H_4, PPh_3), 39.8 (CH_2) ppm. $^{31}P\{^1H\}$ NMR (109.4 MHz, 25 °C, CD_2Cl_2): δ = 19.8 (s) ppm. IR (KBr): $\tilde{\nu}$ = 3054 w, 1772 w, 1719 s, 1684 s, 1436 s cm^{-1}. $C_{46}H_{36}BrNO_3P_2Pd$ (899.1): calcd. C 61.45, H 4.04, N 1.56; found C 61.57, H 4.15, N 1.56.

***trans*-Chloro(*N*-phthaloylaminoacetyl)bis(triphenylphosphane)palladium(II) (6):** *N*-Phthaloylglycyl chloride (132 mg, 0.57 mmol) was dissolved in 20 mL of benzene and $Pd(PPh_3)_4$ (890 mg, 0.57 mmol) was added at room temperature. After stirring for 1 h the resulting precipitate was separated by centrifugation, washed with benzene and diethyl ether and dried in vacuo. The colourless product was obtained in 81% yield (487 mg). ^1H NMR (270 MHz, 25 °C, CD_2Cl_2): δ = 7.72−7.36 (m, 34 H, C_6H_4, PPh_3), 3.96 (s, 2 H, CH_2) ppm. $^{13}C\{^1H\}$ NMR (100.5 MHz, 25 °C, CD_2Cl_2): δ = 210.4 [PdC(O)R], 166.6 (CON), 134.8, 133.8, 131.7, 131.0, 130.4, 128.2, 123.0 (C_6H_4, PPh_3), 21.9 (CH_2) ppm. $^{31}P\{^1H\}$ NMR (109.4 MHz, 25 °C, CD_2Cl_2): δ = 20.30 (s) ppm. IR (KBr): $\tilde{\nu}$ = 1770 w, 1716 s, 1660 s, 1437 s cm^{-1}. $C_{46}H_{36}ClNO_3P_2Pd$ (854.6): calcd. C 64.65, H 4.25, N 1.64; found C 64.69, H 4.30, N 1.65.

***N*-Phthaloylaminomethyltriphenylphosphonium Bromide (7):** This compound was obtained as by-product with **4**. Compound **7** was also prepared from bromomethylphthalimide and triphenylphosphane in benzene. ^1H NMR (400 MHz, 25 °C, CD_2Cl_2): δ = 7.72−7.36 (m, 34 H, C_6H_4, PPh_3), 3.96 (s, 2 H, CH_2) ppm. $^{13}C\{H\}$ NMR (100.5 MHz, 25 °C, CD_2Cl_2): δ = 166.5 (CON), 135.8 (d, $^4J_{P,C}$ = 3 Hz, PPh_3), 135.1 (C_6H_4), 134.5 (d, $^2J_{P,C}$ = 10.0 Hz, PPh_3), 131.0 (C_6H_4), 130.4 (d, $^3J_{P,C}$ = 12.5 Hz, PPh_3), 123.9 (C_6H_4), 116.3 (d, $^1J_{P,C}$ = 84.6 Hz, PPh_3), 35.9 (d, $^1J_{P,C}$ = 57.3 Hz, PCH_2) ppm. $^{31}P\{^1H\}$ NMR (109.4 MHz, 25 °C, CD_2Cl_2): δ = 20.3 (s) ppm. $C_{27}H_{21}BrNO_2P$ (502.3): calcd. C 63.72, H 4.40, N 2.79, Br 15.89; found C 64.56, H 4.21, N 2.67, Br 15.91. The found analyses are from the by-product of **4**.

***cis*-Bromo[1,2-bis(diphenylphosphanyl)ethane](*N*-phthaloylaminomethyl)palladium(II) (8):** *trans*-Bromo(*N*-phthaloylaminomethyl)bis(triphenylphosphane)palladium(II) (**4**; 500 mg, 0.57 mmol) and bis(diphenylphosphanyl)ethane (230 mg, 0.57 mmol) were stirred in 20 mL of benzene for 2 h. The precipitate was separated by centrifugation, washed with benzene and diethyl ether and dried in vacuo to give 318 mg of the yellow product (75% yield). ^1H NMR (400 MHz, 25 °C, CD_2Cl_2): δ = 7.85−7.25 (m, 24 H, C_6H_4, PPh_2), 3.36 (4t, $^3J_{P,H}$ = 6.8 Hz, 2 H, CH_2), 2.41 (m, 2 H, P-CH_2), 2.06 (m, 2 H, P-CH_2) ppm. $^{13}C\{^1H\}$ NMR (100.5 MHz, 25 °C, CD_2Cl_2): δ = 167.0 (CON), 135.1, 134.0, 131.6, 131.2, 130.6, 128.0, 122.8 (C_6H_4, PPh_2), 49.5 (CH_2); 21.1 (P-CH_2), 19.6 (P-CH_2) ppm. $^{31}P\{^1H\}$ NMR (109.4 MHz, 25 °C, CD_2Cl_2): δ = 58.80 (d, $^2J_{P,P}$ = 32 Hz, 1 P), 36.81 (d, $^2J_{P,P}$ = 32 Hz, 1 P) ppm. IR (KBr): $\tilde{\nu}$ = 3051 w, 2937 w, 1773 w, 1695 s, 1442 s cm^{-1}. $C_{35}H_{30}BrNO_2P_2Pd$ (744.9): calcd. C 56.44, H 4.06, N 1.88; found C 56.80, H 4.15, N 1.86.

***cis*-Bromo[1,2-bis(diphenylphosphanyl)ethane](*N*-phthaloylaminoacetyl)palladium(II) (9):** *trans*-Bromo(*N*-phthaloylaminoacetyl)bis(triphenylphosphane)palladium(II) (**5**; 180 mg, 0.23 mmol) and bis(diphenylphosphanyl)ethane (108 mg, 0.27 mmol) were stirred in 15 mL of benzene for 2 h at room temperature. The precipitate was separated by centrifugation, washed with benzene and diethyl ether and dried in vacuo to give 158 mg of the pale yellow product (89% yield). ^1H NMR (270 MHz, 25 °C, CD_2Cl_2): δ = 7.90−7.10 (m, 24 H, C_6H_4, PPh_2), 4.61 (s, CH_2), 2.42 (m, 2 H, CH_2CH_2), 2.19 (m, 2 H, CH_2CH_2) ppm. $^{31}P\{^1H\}$ NMR (109.5 MHz, 25 °C, CD_2Cl_2): δ = 42.47 (d, $^2J_{P,P}$ = 43 Hz, 1 P), 27.58 (d, $^2J_{P,P}$ = 43 Hz, 1 P). IR (Nujol): $\tilde{\nu}$ = 1771, 1715, 1672, 1435 cm^{-1}. $C_{36}H_{30}BrNO_3P_2Pd$ (772.9): calcd. C 55.94, H 3.91, N 1.88, Br, 10.34; found C 55.82, H 3.52, N 1.78, Br 10.18.

***cis*-Chloro[1,2-diphenylphosphanyl)ethane](*N*-phthaloylaminoacetyl)palladium(II) (10):** Complex **6** (163 mg, 0.19 mmol) and 1,2-bis(diphenylphosphanyl)ethane (80 mg, 0.20 mmol) in 25 mL of benzene were stirred at room temperature. After 30 min a clear solution was obtained and after 2 h a yellow precipitate appeared which was centrifuged off and washed several times with benzene and *n*-pentane. Pale yellow powder. Yield: 109 mg (79%). ^1H NMR (400 MHz, 25 °C, Cd_2Cl_2): δ = 7.87−7.20 (m, 24 H, PPh_2, C_6H_4), 4.64 (s, 2 H, CH_2), 2.47 (m, 2 H, CH_2CH_2), 2.18 (m, 2 H, CH_2CH_2) ppm. $^{31}P\{H\}$ NMR (109.4 MHz, 25 °C, CD_2Cl_2): δ = 44.88 (d, $^2J_{P,P}$ = 41 Hz, 1 P), 28.5 (d, $^2J_{P,P}$ = 41 Hz, 1 P) ppm. IR (Nujol): $\tilde{\nu}$ = 1770, 1716, 1670, 1437 cm^{-1}. $C_{36}H_{30}ClNO_3P_2Pd$ (728.5): calcd. C 59.36, H 4.15, N 1.92; found C 59.53, H 4.50, N 2.01.

***cis*-Bromo[1,2-bis(dicyclohexylphosphanyl)ethane](*N*-phthaloylaminomethyl)palladium(II) (11):** *trans*-Bromo(*N*-phthaloylaminomethyl)bis(triphenylphosphane)palladium(II) (**4**; 167 mg, 0.19 mmol) and bis(dicyclohexylphosphanyl)ethane (81 mg, 0.19 mmol) were stirred in 25 mL of benzene for 2 h at room temperature. The precipitate was separated by centrifugation, washed with benzene and diethyl ether and crystallised from CH_2Cl_2/pentane. One of the resulting yellow crystals was selected for X-ray analysis. The rest were dried in vacuo to afford 102 mg of product (70% yield). ^1H NMR (400 MHz, 25 °C, CD_2Cl_2): δ = 7.70−7.40 (m, 4 H, C_6H_4), 3.46 (pseudo-t, $^3J_{P,H}$ = 6.1 Hz, 2 H), 2.40−1.00 (m, 48 H, C_6H_{11}, CH_2CH_2) ppm. $^{13}C\{^1H\}$ NMR (100.5 MHz, 25 °C, CD_2Cl_2): δ = 168.7 (CON), 133.7, 132.5, 128.3, 121.8 (C_6H_4), ca. 53.7 (CH_2), 35.8−26.0 (C_6H_{11}), 25.3 (dd, $^1J_{P,C}$ = 27.6, $^2J_{P,C}$ = 21.5 Hz, CH_2), 20.2 (dd, $^1J_{P,C}$ = 19.8, $^2J_{P,C}$ = 19.4 Hz, CH_2) ppm. $^{31}P\{^1H\}$ NMR (109.4 MHz, 25 °C, CD_2Cl_2): δ = 74.02 (d, $^2J_{P,P}$ = 18 Hz, 1 P), 66.34 (d, $^2J_{P,P}$ = 18 Hz, 1 P) ppm. IR (Nujol): $\tilde{\nu}$ = 1770 w, 1701 s, 1417 s. $C_{35}H_{54}BrNO_2P_2Pd$ (769.1): calcd. C 54.66, H 7.08, N 1.82; found C 55.00, H 6.69, N 1.81.

***cis*-Bromo[1,2-bis(dicyclohexylphosphanyl)ethane](*N*-phthaloylaminoacetyl)palladium(II) (12):** *trans*-Bromo(*N*-phthaloylaminoacetyl)bis(triphenylphosphane)palladium(II) (**5**; 152 mg, 0.17 mmol) and bis(dicyclohexylphosphanyl)ethane (72 mg, 0.17 mmol) were stirred in 20 mL of benzene for 2 h at room temperature. The pre-

 © 2004 Wiley-VCH Verlag GmbH & Co. KGaA, Weinheim

cipitate was separated by centrifugation, washed with benzene and diethyl ether and dried in vacuo to give 103 mg of the yellow product (88% yield). ^{1}H NMR (270 MHz, 25 °C, CD_2Cl_2): δ = 7.83−7.65 (m, 4 H, C_6H_4), 4.99 (s, 2 H, CH_2), 2.20−1.20 (m, 48 H, C_6H_{11}, CH_2CH_2) ppm. ^{13}C NMR (100.5 MHz, 25 °C, CD_2Cl_2): δ = 206.4 [PdC(O)R], 167.7 (CON), 133.7, 132.5, 123.0 (C_6H_4), 35.0−26.0 (C_6H_{11}), 30.6 (CH_2), 24.5 (dd, $^1J_{P,C}$ = 21.5 Hz, $^2J_{P,C}$ = 27.6 Hz, CH_2CH_2), 19.4 (dd, $^1J_{P,C}$ = 10.4 Hz, $^2J_{P,C}$ = 14.8 Hz, CH_2CH_2) ppm. ^{31}P{^{1}H} NMR (109.4 MHz, 25 °C, CD_2Cl_2): δ = 67.05 (d, $^2J_{P,P}$ = 34 Hz, 1 P), 54.68 (d, $^3J_{P,P}$ = 34 Hz, 1 P) ppm. $C_{36}H_{54}BrNO_3P_2Pd$ (797.1): calcd. C 54.25, H 6.83, N 1.76, Br 10.02; found C 53.94, H 6.92, N 1.66, Br 9.87.

***cis*-Chloro[1,2-bis(diphenylphosphanyl)ethane](*N*-phthaloylaminoacetyl)palladium(II) (13):** Compound **6** (180 mg, 0.21 mmol) and bis(diphenylphosphanyl)ethane (90 mg, 0.21 mmol) were stirred in 30 mL of benzene. After 1 h a clear solution was obtained from which, after 2−3 h, a yellow precipitate appeared. The solid was centrifuged off and washed several times with benzene and *n*-pentane, and dried in vacuo. Yellow powder. Yield: 136 mg (86%). ^{1}H NMR (270 MHz, 25 °C, CD_2Cl_2): δ = 7.85−7.65 (m, 4 H, C_6H_4), 5.04 (s, 2 H, CH_2), 2.25−1.20 (m, 48 H, C_6H_{11}, CH_2CH_2) ppm. ^{31}P{H} NMR (109.4 MHz, 25 °C, CD_2Cl_2): δ = 69.43 (d, $^2J_{P,P}$ = 31 Hz, 1 P), 54.68 (d; $^3J_{P,P}$ = 31 Hz, 1 P). IR (Nujol): $\tilde{\nu}$ = 1767 w, 1714 s, 1677 m, 1436 m cm^{-1}. $C_{36}H_{54}ClNO_3P_2Pd{\cdot}0.25CH_2Cl_2$ (773.9): calcd. C 56.26, H 7.10, N 1.81; found C 56.63, H 7.04, N 1.43.

Complex 14: A solution of **6** (50 mg, 0.06 mmol) in 15 mL of dichloromethane was treated with $AgBF_4$ (12 mg, 0.06 mmol) at −78 °C. The mixture was allowed to warm up to room temperature and was stirred for 4 h. The colourless solid was separated by centrifugation and the yellow solution was concentrated and layered with *n*-pentane. Yellow crystals suitable for X-ray diffraction were obtained. Yield: 38 mg (72%). Complex **14** was also obtained from **4** or **5** using the same procedure. ^{1}H NMR (270 MHz, 25 °C, CD_2Cl_2): δ = 7.80−7.15 (m, 40 H, C_6H_4, PPh_3), 3.22 (pseudo-t, $^3J_{P,H}$ = 2 Hz, 2 H, CH_2) ppm. ^{31}P{H} NMR (109.4 MHz, 25 °C, CD_2Cl_2): δ = 36.42 (br., 1 P), 18.77 (br., 1 P) ppm. IR (Nujol): $\tilde{\nu}$ = 1777 w, 1711 m, 1635 s, 1439 s cm^{-1}. $C_{45}H_{36}BF_4NO_3Pd{\cdot}0.25CH_2Cl_2$ (899.2): calcd. C 60.44, H 4.06, N 1.56; found C 60.44, H 4.23, N 1.53.

Complex 15: A solution of **12** (127 mg, 0.18 mmol) in 20 mL of CH_2Cl_2 was cooled to −78 °C, treated with $AgBF_4$ (35 mg, 0.18 mmol) and stirred for 1 h. Then, the mixture was warmed up to room temperature and was stirred for another 1 h. The solid was separated by centrifugation, the yellow solution was concentrated and the oily residue was stirred in pentane for 12 h, whereby a pale yellow powder was formed, which was centrifuged off and dried in vacuo. The solid was dissolved in CH_2Cl_2 and filtered through celite. The clear, yellow solution was cooled with liquid nitrogen and layered with *n*-pentane. After 2 days pale yellow crystals were obtained which were suitable for X-ray crystallography. Pale yellow powder, 74 mg (53%). Complex **15** was also prepared from **11** or **13**, using the same procedure. ^{1}H NMR (270 MHz, 25 °C, CD_2Cl_2): δ = 7.90−7.70 (m, 4 H, C_6H_4), 3.43 (pseudo-t, $^3J_{P,H}$ = 6.4 Hz, 2 H, CH_3), 2.20−1.20 (m, 48 H, C_6H_{11}, CH_2CH_2) ppm. ^{31}P{^{1}H} NMR (109.4 MHz, 25 °C, CD_2Cl_2): δ = 83.37 (d, $^2J_{P,P}$ = 15 Hz, 1 P), 71.36 (d, $^2J_{P,P}$ = 15 Hz, 1 P) ppm. IR (Nujol): $\tilde{\nu}$ = 1775, 1725, 1636 cm^{-1}. $C_{36}H_{54}BF_4NO_3P_2Pd{\cdot}0.25CH_2Cl_2$ (797.2): calcd. C 53.11, H 6.89, N 1.76; found C 53.39, H 6.77, N 1.59.

[Bis(2-diphenylphosphanylethyl)phenylphosphane]chloro(*N*-phthaloylaminoacetyl)palladium(II) (16): Bis(diphenylphosphanylethyl)phenylphosphane (120 mg, 0.22 mmol) was added to a solution of **6** (130 mg, 0.15 mmol) in 25 mL of benzene and stirred for 3 h. The yellow precipitate was centrifuged off, washed several times with benzene and *n*-pentane and dried in vacuo. The pale yellow powder was dissolved in dichloromethane. The solution was filtered through celite and layered with *n*-pentane. After some days pale yellow crystals were formed which were suitable for X-ray diffraction. Yield 66%. ^{1}H NMR (270 MHz, 25 °C, CD_2Cl_2): δ = 8.00−7.00 (m, 29 H, C_6H_4, PPh_2, PPh), 4.34 (s, 2 H, CH_2), 3.50−2.10 (m, 8 H, $PCH_2CH_2PCH_2CH_2P$) ppm. ^{31}P{^{1}H} NMR (109.4 MHz, 25 °C, CD_2C_2): δ = 80.0 (t, $^2J_{P,P}$ = 36.8 Hz, 1 P, PPh), 35.5 (d, $^2J_{P,P}$ = 36.7 Hz, 2 P, -PPh_2) ppm. IR (Nujol): $\tilde{\nu}$ = 1769 w, 1714 s, 1699 w, 1663 m cm^{-1}. $C_{44}H_{39}ClNO_3P_3Pd$ (864.6): calcd. C 61.13, H 4.55, N 1.62; found C 61.31, H 5.29, N 1.14.

***trans*-Chloro(*N*-phthaloylaminoacetyl)bis(triphenylphosphane)platinum(II) (17):** (η^2-Ethene)bis(triphenylphosphane)platinum(0) (126 mg, 0.17 mmol) was dissolved in 20 mL of benzene and *N*-phthaloylglycyl chloride (67 mg, 0.30 mmol) was added to the yellow solution at room temperature. After stirring for 1 h the resulting precipitate was separated by centrifugation, washed with benzene and diethyl ether and dried in vacuo to give 175 mg of colourless product (93% yield). ^{1}H NMR (270 MHz, 25 °C, $CDCl_3$): δ = 7.50−6.80 (m, 34 H, C_6H_4, PPh_3), 3.30 (s, 2 H, CH_2) ppm. ^{13}C{^{1}H} NMR (100.5 MHz, 25 °C, CD_2Cl_2): δ = 210.2 [PtC(O)R], 166.9 (CON), 135.0, 133.4, 132.1, 130.5, 130.1, 128.2, 122.9 (C_6H_4, PPh_3), 59.0 (CH_2) ppm. ^{31}P{^{1}H} NMR (109.4 MHz, 25 °C, CD_2Cl_2): δ = 35.8 (sat), 20.6 (s), 5.3 (sat) ppm; $^1J_{P,Pt}$ = 3330 Hz. IR (KBr): $\tilde{\nu}$ = 1772 w, 1717 s, 1658 s, 1435 s cm^{-1}. $C_{46}H_{36}ClNO_3P_2Pt$ (959.7): calcd. C 58.60, H 3.85, N 1.49; found C 58.60, H 3.87, N 1.41.

***trans*-Chloro(*N*-phthaloylphenylalanyl)bis(triphenylphosphane)platinum(II) (18):** (η^2-Ethene)bis(triphenylphosphane)platinum(0) (340 mg, 0.5 mmol) was dissolved in 25 mL of benzene and *N*-phthaloylphenylalanyl chloride (67 mg, 0.30 mmol) was added to the yellow solution at room temperature. After stirring for 12 h the resulting precipitate was separated by centrifugation, washed with benzene and diethyl ether and dried in vacuo to afford 377 mg of an almost colourless product (73% yield). ^{1}H NMR (270 MHz, 25 °C, $CDCl_3$): δ = 7.90−7.05 (m, 34 H, C_6H_4, PPh_3), 6.87 (m, 3 H, *p*-C_6H_4), 6.50 (m, 2 H, C_6H_4), 3.84 (dd, $^3J_{H,H}$ = 4.1 Hz, $^2J_{H,H}$ = 12.3 Hz, 1 H, CH), 3.02 (dd, $^2J_{H,H}$ = 14.1 Hz, $^3J_{H,H}$ = 4.1 Hz, 1 H, CH_2), 2.74 (dd, $^2J_{H,H}$ = 14.3, $^3J_{H,H}$ = 12.1 Hz, 1 H, CH_2) ppm. ^{13}C{^{1}H} NMR (100.5 MHz, 25 °C, $CDCl_3$): δ = 213.6 [PtC(O)R], 171.4 (CON), 138.0, 135.3, 133.7, 131.6, 130.6, 128.6, 128.0, 126.0, 123.4, 123.1 (C_6H_4, Ph, PPh_3), 60.5 (CH), 41.1 (CH_2) ppm. ^{31}P{^{1}H} NMR (109.4 MHz, 25 °C, $CDCl_3$): δ = 37.4 (sat), 21.8 (s), 6.3 (sat, $^1J_{P,Pt}$ = 3399 Hz), 37.0 (sat), 21.6 (s), 6.1 (sat, $^1J_{P,Pt}$ = 3385 Hz) ppm. IR (KBr): $\tilde{\nu}$ = 1776 w, 1714 s, 1654 s, 1438 s cm^{-1}. $C_{53}H_{42}ClNO_3P_2Pt$ (1033.4): calcd. C 61.60, H 4.10, N 1.36; found C 61.21, H 4.06, N 1.23.

***cis*-Chlorobis[1,2(diphenylphosphanyl)ethane](*N*-phthaloylphenylalanyl)platinum(II) (19):** Complex **18** (220 mg, 0.21 mmol) and bis(diphenylphosphanylethane) (84 mg, 0.21 mmol) were stirred in 20 mL of benzene at room temperature. After 1 h a clear yellow solution was obtained. After 1 day stirring the solution was concentrated to 5 mL and diethyl ether was added. The resulting precipitate was centrifuged off, washed several times with diethyl ether and then with pentane and dried in vacuo. Colourless powder. Yield 131 mg (69%). ^{1}H NMR (270 MHz, 25 °C, $CDCl_3$): δ = 8.20−6.80 (m, 29 H, PPh_2, C_6H_5, C_6H_4), 5.07 (m, 1 H, CH), 3.91 (dd, $^2J_{H,H}$ = 14.1 Hz, $^3J_{H,H}$ = 3.3 Hz, CH_2), 2.94 (dd, $^2J_{H,H}$ = 14.1 Hz, $^3J_{H,H}$ = 13.0 Hz, CH_2), 2.30−1.80 (m, 4 H, CH_2CH_2)

 © 2004 Wiley-VCH Verlag GmbH & Co. KGaA, Weinheim

Table 3. Crystallographic data for **2**, **11**, **14**, **15** and **16**

	2	**11**	**14**	**15**	**16**
Formula	$C_{16}H_{11}FeNO_4$	$C_{35}H_{54}BrNO_2P_2Pd$	$C_{45}H_{36}BF_4NO_2P_2Pd$	$C_{71}H_{110}B_2Cl_2F_8N_2O_4P_4Pd_2$	$C_{50}H_{53}Cl_3NO_3P_3Pd$
M_r	337.11	769.04	877.90	1636.81	1021.59
Crystal system	monoclinic	monoclinic	triclinic	triclinic	monoclinic
Space group	$P2_1/c$	$P2_1/n$	$P\bar{1}$	$P\bar{1}$	$P2_1/n$
a (Å)	8.2954(8)	11.8160(10)	10.518(3)	11.4737(13)	17.3883(10)
b (Å)	9.7015(11)	19.938(4)	12.860(2)	16.723(2)	15.7147(9)
c (Å)	17.635(2)	15.5380(10)	15.348(4)	21.594(3)	18.4968(10)
α (°)	90	90	97.19	109.956(2)	90
β (°)	92.108(9)	107.64	92.90	93.573(2)	106.3910(1)
γ (°)	90	90	105.80	103.714(2)	90
V (Å^3)	1418.2(3)	3488.4(8)	1974.0(8)	3736.6(8)	4848.9(5)
Z	4	4	2	2	4
$\rho_{calcd.}$ (g·cm^{-3})	1.579	1.464	1.477	1.455	1.399
μ (mm^{-1}]	1.080	1.800	0.610	0.706	0.689
Crystal size (mm)	0.47 × 0.40 × 0.13	0.38 × 0.25 × 0.25	0.40 × 0.35 × 0.30	0.30 × 0.20 × 0.20	0.35 × 0.30 × 0.25
2θ range (°)	2.31−24.97	3.82−50.00	3.96−50.32	2.04−58.72	2.84−58.62
Index range	$0 \le h \le 9$	$-14 \le h \le 1$	$0 \le h \le 12$	$-15 \le h \le 11$	$-22 \le h \le 22$
	$-11 \le k \le 0$	$-23 \le k \le 1$	$-14 \le k \le 14$	$-20 \le k \le 20$	$-20 \le k \le 20$
	$-20 \le l \le 20$	$-17 \le l \le 18$	$-14 \le l \le 14$	$-26 \le l \le 26$	$-23 \le l \le 23$
Collected reflns.	2678	7505	6333	22301	27917
Independent reflns.	2493	61118	5963	11720	9343
R_{int} (%)	0.0075	0.0357	0.0193	0.0344	0.0243
Max./min. transmissions	0.9999/0.8133	1.000/0.825		1.0000/0.8232	1.0000/0.8991
Parameters	688	1592	892	1700	2104
$R1/wR2$ [$F > 4\sigma(F)$]	0.0402/0.0791	0.0463/0.0927	0.0446/0.1165	0.0386/0.0927	0.0295/0.0776
GoF	1.093	1.024	1.032	0.935	0.986
Largest diff. peak and hole [e·Å^{-3}]	0.259/−0.206	0.821/0.514	0.653/−0.783	0.556/−0.582	0.529/−0.469

ppm. $^{31}P\{^1H\}$ NMR (109.5 MHz, 25 °C, CD_2Cl_2): δ = 42.91 (d, sat), 35.89 (d, 1 P), 28.85 (d, sat), $^1J_{P,Pt}$ = 4233.9 Hz; 51.89 (d, sat), 32.54 (d, 1 P), 13.17 (d, sat) ppm; $^1J_{P,Pt}$ = 1539.0, $^2J_{P,P}$ = 5.9 Hz. $C_{43}H_{36}ClNO_3P_2Pt$ (907.2): calcd. C 56.93, H 4.00, N 1.54; found C 56.46, H 4.06, N 1.26.

X-ray Structure Determination: The data in Table 3 were collected on an Enraf Nonius CAD 4 diffractometer (**2**), a Siemens P4 diffractometer (for **11**, **14**) or a Siemens P4 diffractometer with a SMART area detector (for **15**, **16**). CCDC-153852 (**2**), -226832 (**11**), -226831 (**14**), -226833 (**15**) and -226834 (**16**) contain the supplementary crystallographic data for this paper. These data can be obtained free of charge at www.ccdc.cam.ac.uk/conts/retrieving.html [or from the Cambridge Crystallographic Data Centre, 12 Union Road, Cambridge CB2 1EZ, UK; Fax: (internat.) + 44-1223/336-033; E-mail: deposit@ccdc.cam.ac.uk].

Amidocarbonylation Experiments

The general procedure is described in ref.[2]

1. *N*-Phthaloylglycine: Phthalimide (3.68 g, 25 mmol), paraformaldehyde (0.76 g, 25 mmol), $PdBr_2$ (16.7 mg, 0.0625 mmol) and PPh_3 (33 mg, 0.125 mg, 0.5 mol %) in 25 mL of *N*-methylpyrrolidine were reacted at 120 °C under 60 bar CO in a 300 mL high-pressure reactor for 12 h. The product was recrystallised from water/2-propanol. Isolated yield: 2.82 g (55%); m.p. 193 °C. ^1H NMR (400 MHz, 25 °C, [D$_6$]DMSO): δ = 13.0 (br. s, 1 H, COO*H*), 7.85−7.97 (m, 4 H, *H*-aromat.), 4.32 (s, 2 H, *H*-2) ppm. $^{13}C\{^1H\}$ NMR (100 MHz, 25 °C, [D$_6$]DMSO): δ = 169.0 (*C*OOH), 167.4 (C-4), 134.9 (*C*-4′), 131.5 (*C*-6), 123.5 (*C*-5), 39.8 (*C*-2) ppm. IR (KBr): $\tilde{\nu}$ = 2985 m, 2936 w, 1773 s, 1724 s, 1416 s, 1247 s cm^{-1}. MS (CI, 70 eV): *m*/*z* = 206 [M + H$^+$], 188 [M + H$^+$ − H_2O], 160 [M$^+$ − CO_2H], 133, 103.

2. Reaction of *N*-(bromomethyl)phthalimide with Methanol and Carbon Monoxide: *N*-(Bromomethyl)phthalimide (1.48 g, 20 mmol), methanol (1 mL, 25 mmol) in 25 mL of NMP, $PdBr_2$ (13.5 mg, 0.05 mol, 0.25 mol %) and PPh_3 (27 mg, 0.1 mmol, 0.5 mol %) were reacted at 120 °C under 60 bar CO for 12 h. The volatile components were removed in vacuo and the residue was taken up in a saturated aqueous solution of $NaHCO_3$, which was then extracted twice with ethyl acetate. The combined organic phases were dried over $MgSO_4$ and the solvent was removed in vacuo. A sample of 1.0 g of the product (3.5 g) was purified by chromatography on silica (100 g, elution with hexane/ethyl acetate, 7:3).

Methyl *N*-Phthaloylglycinate: R_f = 0.28; isolated yield 0.25 g (20%). ^1H NMR (400 MHz, 25 °C, [D$_6$]DMSO): δ = 7.90−8.05 (m, 4 H, *H*-aromat.), 4.50 (s, 2 H, *H*-2), 3.72 (s, 3 H, OC*H*$_3$) ppm. $^{13}C\{1H\}$ NMR (100 MHz, 25 °C, [D$_6$]DMSO): δ = 168.1 (*C*OOH), 167.1 (*C*-4), 134.9 (*C*-4′), 131.4 (*C*-6), 123.5 (*C*-5), 52.5 (O*C*H$_3$), 38.8 (*C*-2) ppm. IR (KBr): $\tilde{\nu}$ = 3475 w, 2977 w, 1774 m, 1751 s, 1727 s, 1423 s, 1399 m, 1374 m, 1224 s cm^{-1}. MS (CI, 70 eV): *m*/*z* = 219 [M$^+$], 188 [M + H$^+$ − CH_3OH], 160 [M$^+$ − CO_2CH_3], 133, 104, 76.

***N*-(Methoxymethyl)phthalimide:** R_f = 0.5; isolated yield 0.70 g (65%). ^1H NMR (400 MHz, 25 °C, [D$_6$]DMSO): δ = 7.88−7.93 (m, 4 H, *H*-aromat.), 4.95 (s, 2 H, *H*-2), 3.28 (s, 3 H, OC*H*$_3$) ppm. $^{13}C\{1H\}$ NMR (100 MHz, 25 °C, [D$_6$]DMSO): δ = 167.8 (*C*-4), 134.9 (*C*-4′), 131.4 (*C*-6), 123.6 (*C*-5), 68.4 (*C*-2), 52.5 (O*C*H$_3$) ppm. MS (CI, 70 eV): *m*/*z* = 191 [M$^+$], 160, 133, 104, 76.

Acknowledgments

Support by the "Fonds der Chemischen Industrie" and by the "Deutsche Forschungsgemeinschaft" is gratefully acknowledged.

 © 2004 Wiley-VCH Verlag GmbH & Co. KGaA, Weinheim

[1] H. Wakamatsu, J. Uda, N. Yamakami, *J. Chem. Soc., Chem. Commun.* **1971**, *1540*; DEB **1971**, 2115 985 (*Chem. Abstr.* **1972**, *76*, 25 585); H. Wakamatsu, *Kagaku* **1989**, *44*, 448.

[2] M. Beller, M. Eckert, *Angew. Chem.* **2000**, *112*, 1026−1044; *Angew. Chem. Int. Ed.* **2000**, *39*, 1010−1027; M. Beller, M. Eckert, F. Vollmüller, S. Bogdanovic, H. Geissler, *Angew. Chem.* **1997**, *109*, 1534−1536; *Angew. Chem. Int. Ed. Engl.* **1997**, *36*, 1494−1496; M. Beller, M. Eckert, F. Vollmüller, *J. Mol. Cat.* **1998**, *135*, 23−33; D. Gördes, H. Neumann, A. Jacobi von Wangelis, C. Fischer, K. Drauz, H.-P. Krimmer, *Adv. Synth. Catal.* **2003**, *345*, 510−516; M. Beller, W. A. Moradi, M. Eckert, H. Neumann, *Tetrahedron Lett.* **1999**, *40*, 4523−4526.

[3] Ch. Easton, C. A. Hutton, *Synlett* **1998**, 457. It is of interest that H. Wakamatsu, the pioneer in organometallic amino acid chemistry, in his bachelor thesis used phthaloylamino acid for the synthezis of phthaloyl peptide esters: K. Yamashita, H. Wakamatsu, Y. Sahashi, *J. Agr. Chem. Soc., Jpn.* **1953**, *27*, 649−652.

[4] E. W. Abel, R. J. Rowley, *J. Chem. Soc., Dalton Trans.* **1975**, 1096−1099; C. W. Fong, G. Wilkinson, *J. Chem. Soc., Dalton Trans.* **1975**, 1100−1104; M. Matsumoto, K. Nakatsu, K. Tani, A. Nakamura, S. Otsuka, *J. Am. Chem. Soc.* **1974**, *96*, 6777−6778; S. S. Crawford, G. Firestein, H. D. Kaesz, *J. Organomet. Chem.* **1975**, *91*, C57−C60; D. J. Sepelak, C. G. Pierpont, E. K. Barefield, J. T. Budz, C. A. Poffenberger, *J. Am. Chem. Soc.* **1976**, *98*, 6178−6185.

[5] G. N. Schrauzer, R. J. Windgassen, *Nature* **1967**, *214*, 492; G. L. Blackmer, T. M. Vickrey, J. N. Marx, *J. Organomet. Chem.* **1974**, *72*, 261−267.

[6] A. L. Poznyak, V. I. Pavlovski, *Angew. Chem.* **1988**, *100*, 812−819; *Angew. Chem. Int. Ed. Engl.* **1988**, *27*, 789−795; *Z. Anorg. Allg. Chem.* **1982**, *485*, 225−233; A. L. Poznyak, V. I. Pavloski, E. B. Chuklanova, T. N. Polynova, M. A. Porai-Koshits, *Monatsheft Chem.* **1982**, *113*, 561−564; E. Natarajan, P. Natarajan, *Inorg. Chem.* **1992**, *31*, 1215−1220; R. M. Hartshorn, S. G. Telfer, *Dalton* **1999**, 3565−3571; R. M. Hartshorn, S. G. Telfer, *J. Chem. Soc., Dalton Trans.* **2000**, 2801−2808; S. Das, G. R. A. Johnson, N. B. Nazhat, R. Saadalla-Nazhat, *J. Chem. Soc., Faraday Trans. I* **1984**, *80*, 2759−2766; D. M. Tonei, L.-J. Baker, P. J. Brothers, G. R. Clark, D. C. Ware, *Chem. Commun.* **1998**, 2593−2594 and references cited therein.

[7] R. D. Dghaym, K. J. Yaccato, B. A. Arndtsen, *Organometallics* **1998**, *17*, 4−6; S. Kacker, J. S. Kim, A. Sen, *Angew. Chem.* **1998**, *110*, 1335−1337; *Angew. Chem. Int. Ed.* **1998**, *37*, 1251−1253; L. Cavallo, *J. Am. Chem. Soc.* **1999**, *121*, 4238−4241; R. D. Dghaym, R. Dhawan, B. A. Arndtsen, *Angew. Chem.* **2001**, *113*, 3328−3330; *Angew. Chem. Int. Ed.* **2001**, *40*, 3228−3230.

[8] J. L. Davis, B. A. Arndtsen, *Organometallics* **2000**, *19*, 4657−4659.

[9] D. Lafrance, J. L. Davis, R. Dhawan, B. A. Arndtsen, *Organometallics* **2001**, *20*, 1128−1136.

[10] R. Huisgen, H. Gotthardt, H. O. Bayer, F. C. Schaefer, *Angew. Chem.* **1964**, *76*, 185−186; *Angew. Chem. Int. Ed. Engl.* **1964**, *3*, 136−137; H. O. Bayer, R. Huisgen, R. Knorr, F. C. Schaefer, *Chem. Ber.* **1970**, *103*, 2581−2597; E. Funke, R. Huisgen, *Chem. Ber.* **1971**, *104*, 3222−3228.

[11] R. Dhawan, R. D. Dghaym, B. A. Arndtsen, *J. Am. Chem. Soc.* **2003**, *125*, 1474−1475.

[12] M. Steinmetz, H. Werner, *J. Organomet. Chem.* **1989**, *369*, 309−319.

[13] G. L. Blackmer, Ch.-W. Tsai, *J. Organomet. Chem.* **1978**, *155*, C17−C20.

[14] W. Beck, W. Petri, *J. Organomet. Chem.* **1977**, *127*, C40; W. Petri, W. Beck, *Chem. Ber.* **1984**, *117*, 3265−3269.

[15] I. Nagy-Gergely, G. Szalontai, F. Ungváry, L. Markó, M. Moret, A. Sironi, C. Zucchi, A. Sisak, C. M. Tschoerner, A. Martinelli, A. Sorkau, G. Pályi, *Organometallics* **1997**, *16*, 2740−2742.

[16] R. W. Hungate, F. Miller, M. S. Goodman, *Tetrahedron Lett.* **1988**, *29*, 4273−4276.

[17] C. Amiens, G. Balavoine, F. Guibé, *J. Organomet. Chem.* **1993**, *443*, 207−219.

[18] I. Bernal, H. Brunner, M. Muschiol, *Inorg. Chim. Acta* **1988**, *142*, 235−242; R. E. Marsh, *Inorg. Chim. Acta* **1989**, *157*, 1−2; H. Y. Liu, L. L. Koh, K. Eriks, W. P. Giering, A. Prock, *Acta Crystallogr. Sect.* **1990**, *C 46*, 51−54.

[19] H. Brunner, B. Hammer, I. Bernal, M. Draux, *Organometallics* **1983**, *2*, 1595−1603; s. auch: S. G. Davies, I. M. Dordor-Hedgecock, K. H. Sutton, M. Whittaker, *J. Am. Chem. Soc.* **1987**, *109*, 5711−5719.

[20] A. Hess, O. Brosch, T. Weyhermüller, N. Metzler-Nolte, *J. Organomet. Chem.* **1999**, *589*, 75−84.

[21] A. J. Canty, G. K. Anderson, in *Comprehensive Organometallic Chemistry II* (Eds.: R. W. Abel, F. G. A. Stone, G. Wilkinson), Pergamon Press. **1995**, *9*, 233, 433.

[22] F. Calderazzo, *Angew. Chem.* **1977**, *89*, 365−317; *Angew. Chem. Int. Ed. Engl.* **1977**, *16*, 299−310; B. A. Markies, D. Kruis, M. H. P. Prietveld, K. A. N. Verkerk, J. Boersma, H. Kooijam, M. T. Lakin, A. L. Spek, G. van Koten, *J. Am. Chem. Soc.* **1995**, *117*, 5263−5274 and references cited therein; K. Frankcombe, K. Cavell, R. Knott, B. Yates, *Chem. Commun.* **1996**, 781−782; A. J. Canty, in *Comprehensive Organometallic Chemistry II* (Eds.: E. W. Abel, F. G. A. Stone, G. Wilkinson), *Pergamon*, Pr*ess* **1995**, *9*, 255−256.

[23] B. Kayser, C. Missling, J. Knizek, H. Nöth, W. Beck, *Eur. J. Inorg. Chem.* **1998**, 375−379.

[24] D. Walther, *Z. Chem.* **1989**, *29*, 146.

[25] L. Maresca, G. Natile, *Comments Inorg. Chem.* **1993**, *14*, 349−366; M. E. Cucciolito, A. Panunzi, F. Ruffo, V. G. Albano, M. Monari, *Organometallics* **1999**, *18*, 3482−3489; V. G. Albano, G. Natile, A. Panunzi, *Coord. Chem. Rev.* **1994**, *133*, 67−114; V. G. Albano, M. Monari, I. Orabona, Panunzi, G. Roviello, F. Ruffo, *Organometallics* **2003**, *22*, 1223−1230.

[26] See, for example: R. Garrone, A. M. Romano, R. Santi, R. Millini, *Organometallics* **1998**, *17*, 4519−4522 and references cited therein.

[27] S. Aizawa, T. Iida, S. Funahashi, *Inorg. Chem.* **1996**, *35*, 5163−5167.

[28] D. R. Coulson, *Inorg. Synth. XIII*, 121.

[29] U. Nagel, *Chem. Ber.* **1982**, *115*, 1998−1999.

[30] S. Gabriel, *Ber. Dtsch. Chem. Ges.* **1907**, *40*, 2647−2650.

[31] R. Pfaehler, *Ber. Dtsch. Chem. Ges.* **1913**, *46*, 1700−1702.

Received August 30, 2003
Early View Article
Published Online February 17, 2004

 © 2004 Wiley-VCH Verlag GmbH & Co. KGaA, Weinheim

(Nitrido)ruthenium(VI) and -osmium(VI) Complexes with Catecholate Auxiliaries: Synthesis, Structure, and Conversion into a (Phosphoraniminato)osmium(V) Complex

Guo-Su Fang,[a,b] Jie-Sheng Huang,[b] Nianyong Zhu,[b] and Chi-Ming Che*[a,b]

Keywords: Nitrides / O ligands / Ruthenium / Osmium / Structure elucidation

Treatment of $[NnBu_4][M^{VI}NCl_4]$ (where M = Ru, Os) with catechol (H_2Cat) and 3,5-di-*tert*-butylcatechol (H_2DBCat) in the presence of 2,6-dimethylpyridine (2,6-Me_2Py) gave $[NnBu_4][M^{VI}N(Cat)_2]$ (where M = Ru **1a**, Os **1b**) and [2,6-Me_2PyH][$M^{VI}N(DBCat)_2$] (where M = Ru **2a**, Os **2b**), respectively, in 75–90 % yields. Reaction of **2b** with triphenylphosphane afforded the (phosphoraniminato)osmium(V) complex $[Os^{V}(NPPh_3)(DBCat)_2(PPh_3)]$ (**3**) in 90 % yield. X-ray crystal structure determinations on **1a**, **1b** and **3** reveal M≡N distances of 1.603(4) and 1.641(8) Å (for **1a** and **1b**, respectively) and an Os–N($NPPh_3$) distance of 2.077(3) Å (for **3**). The C–O distances in the three complexes range from 1.341(4) to 1.374(7) Å, indicating that the coordinated catecholate ligands adopt the catecholate(2–) state, rather than the semiquinonate(1–) or quinone states.

(© Wiley-VCH Verlag GmbH & Co. KGaA, 69451 Weinheim, Germany, 2004)

Introduction

(Nitrido)ruthenium and -osmium complexes are among the most extensively studied high-valent ruthenium and osmium compounds.[1] Stable mononuclear species with Ru≡N or Os≡N bonds have become accessible through many types of auxiliary ligands, including halides,[2] phosphanes/arsanes/stibanes[3−5] silyloxy,[6] alkyl,[6−8] thiocyanate,[7] thiolate or dithiolene,[7,9−11] ammine,[12,13] cyanide,[14] pyridine or polypyridine,[4,15−18] ureato,[19] cysteine(2−),[20] alkoxide,[21] diamine,[22] *N*-pyridinecarbonyl and/or *N*-hydroxybenzoyl diamide,[23] hydrotris(pyrazolyl)-borate,[24−27] trispyrazolylmethane,[28,29] imidodiphosphanylchalcogenido,[30,31] Schiff bases,[32] *meso*-octamethylporphrinogen,[33] porphyrin,[34,35] and aryl/alkyl acetylide.[36] The ruthenium and osmium ions in these nitrido complexes have exclusively a high oxidation state of +6 and therefore demonstrate the remarkable ability of the nitrido group to stabilize ruthenium(VI) and osmium(VI) species.

We have recently been interested in exploring the chemistry of (nitrido)ruthenium and -osmium complexes bearing catecholate ligands (the oxygen analogues of dithiolenes such as 1,2-benzenedithiolates), which is an important type of non-innocent ligands known to have three oxidation states, namely, catecholate(2−), semiquinonate(1−), and quinone, in complexes with metal ions.[37,38] We envisage that this new class of (nitrido)ruthenium and -osmium complexes may exhibit rich redox chemistry. The different oxidation states of the coordinated catecholate ligands, if achievable, would significantly regulate the reactivity of the Ru≡N and Os≡N functional groups. On the other hand, given the remarkable ability of the nitrido group to stabilize ruthenium(VI) and osmium(VI) species and the ambiguity in charge distribution in ruthenium and osmium catecholate complexes such as $[Os(Cat)_3]$ (H_2Cat = catechol), $[Ru(DBCat)_3]$ (H_2DBCat = 3,5-di-*tert*-butylcatechol), and $[Os(DBCat)_3]$,[39,40] a ruthenium(VI)/osmium(VI) catecholate complex with clear charge distribution might be obtained by introducing a nitrido group in the complex. The structure determination of the (nitrido)metal catecholates may provide a unique opportunity to examine the structural features of genuine Ru^{VI}- or Os^{VI}-catecholate(2−) bonds.

In the present work, we report on the synthesis of (nitrido)ruthenium(VI) and -osmium(VI) complexes $[M^{VI}N(L)_2]^-$ (where L = Cat, M = Ru **1a**, Os **1b**; L = DBCat, M = Ru **2a**, Os **2b**) and the crystal structures of $[NnBu_4][Ru^{VI}N(Cat)_2]$ (**1a**) and $[NnBu_4][Os^{VI}N(Cat)_2]$ (**1b**). These, to the best of our knowledge, are the first examples of isolated mononuclear (nitrido)metal complexes containing catecholate auxiliaries. Prior to this work, only dinuclear (μ-nitrido)metal complexes, such as the Fe(μ-N)Fe complexes prepared by Wieghardt and co-workers,[41,42] were known to contain catecholate ligands. Interestingly, the (nitrido)osmium complex $[Os^{VI}N(DBCat)_2]^-$ reacted with tri-

[a] Coordination Chemistry Institute and the State Key Laboratory of Coordination Chemistry, Nanjing University, Nanjing 210093, P. R. China
[b] Department of Chemistry and Open Laboratory of Chemical Biology of the Institute of Molecular Technology for Drug Discovery and Synthesis, The University of Hong Kong, Pokfulam Road, Hong Kong
Fax: (internat.) + 852-2857-1586
E-mail: cmche@hku.hk

phenylphosphane to afford an unprecedented (phosphoraniminato)osmium(v) complex, $[Os^{V}(NPPh_3)(DBCat)_2(PPh_3)]$ (**3**). This unusual reaction, along with the crystal structure of **3**, is also described here.

Results and Discussion

Synthesis and Characterization of $[M^{VI}N(Cat)_2]^-$ and $[M^{VI}N(DBCat)_2]^-$ (M = Ru, Os)

Treatment of $[NnBu_4][M^{VI}NCl_4]$ (M = Ru/Os) with two equivalents of catechol in methanol in the presence of 2,6-dimethylpyridine readily gave a solution containing mainly the (nitrido)ruthenium/osmium catecholate complex **1a/1b** (see Scheme 1), which was isolated in approximately 80 % yield upon workup. By employing 3,5-di-*tert*-butylcatechol instead of catechol, the same reactions afforded **2a/2b** as a precipitate (Scheme 1, note that **2a/2b** could have two geometrical isomers but only one of them is shown), which can be readily separated from the reaction mixtures by filtration. An NMR-pure product of **2a/b** was obtained in up to 90 % yield after washing with diethyl ether and drying. The counter-cation in **1** is tetrabutylammonium $[NnBu_4]^+$, as could be expected. However, we were surprised to find that **2** took $[2,6\text{-}Me_2PyH]^+$ (which was generated during the reaction) as a counter-cation, as revealed by ^1H NMR measurements (see below). This might result from a supramolecular interaction/recognition between $[M^{VI}N(DBCat)_2]^-$ and $[2,6\text{-}Me_2PyH]^+$ ions or from a low solubility of the $[2,6\text{-}Me_2PyH]^+$ salts of $[M^{VI}N(DBCat)_2]^-$ in methanol.

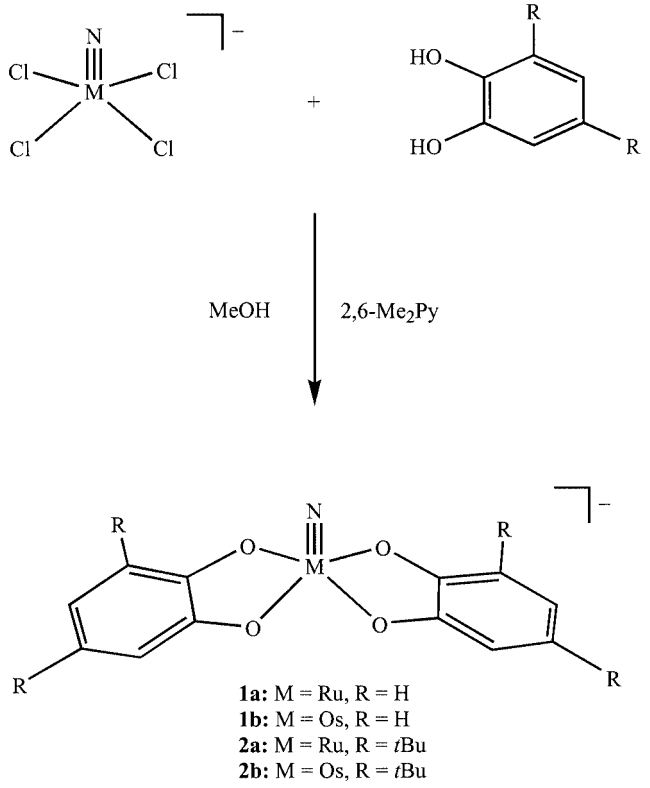

Scheme 1. Syntheses of **1** and **2**

Complexes **1a**, **1b**, **2a** and **2b** are diamagnetic, air-stable solids, having good solubility in common organic solvents, such as dichloromethane, acetonitrile, and tetrahydrofuran. In solution at room temperature, **1a** and **1b** are stable for months. The solutions of **2a** and **2b** can be stored at −20 °C for several weeks.

The ^1H NMR spectra of **1a** and **1b** both show two well-resolved multiplets with δ = 6.62, 6.89 ppm (for **1a**) and 6.71, 7.00 ppm (for **1b**), together with the normal signals of $[NnBu_4]^+$. The spectrum of **1a** is shown in Figure 1a as an example. There are no $[NnBu_4]^+$ signals in the ^1H NMR spectra of **2a** and **2b**. Instead, a set of signals at δ = 2.8, 7.5, and 8.2 ppm, assignable to $[2,6\text{-}Me_2PyH]^+$, was observed (see Figure 1b,c). Note that although **2a/2b** may have two geometric isomers (with C_s and C_2 symmetries, respectively), only a single set of the coordinated catecholate signals was located in the spectrum. Probably, only one of the isomers is present in solution, or the signals of the two isomers are not different enough to be clearly resolved.

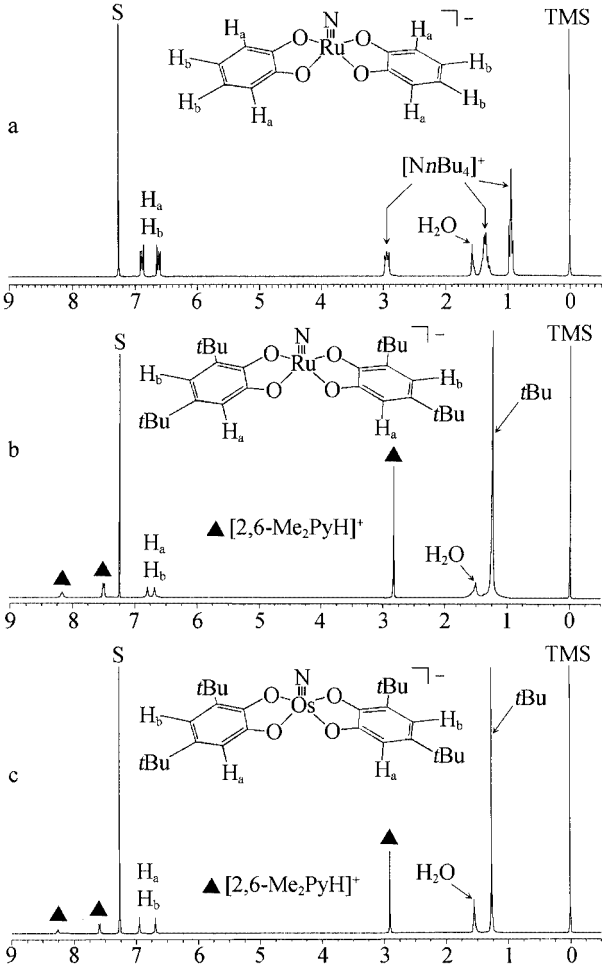

Figure 1. ^1H NMR spectra of a) **1a**, b) **2a**, and c) **2b** in $CDCl_3$; the water is mainly from the $CDCl_3$ solvent

Negative-ion FAB mass spectra of **1a**, **1b**, **2a** and **2b** show intense cluster peaks assignable to $[M^{VI}N(Cat)_2]^-$ or

 © 2004 Wiley-VCH Verlag GmbH & Co. KGaA, Weinheim

$[M^{VI}N(DBCat)_2]^-$; the observed and simulated isotope-distribution patterns are virtually identical.

In the IR spectra of **1a**, **1b**, **2a** and **2b**, sharp and intense bands, ascribable to $\nu_{Ru\equiv N}/\nu_{Os\equiv N}$ appear at 1049 (**1a**) and 1051 cm^{-1} (**2a**) for the ruthenium species and at 1093 (**1b**) and 1097 cm^{-1} (**2b**) for the osmium species. The $\nu_{M\equiv N}$ frequency of **1a**/**1b** is appreciably higher than the corresponding frequency of the sulfur analogues $[NnBu_4][M^{VI}N(S_2C_6H_4)_2]$ (M = Ru, Os; $S_2C_6H_4$ = 1,2-benzenedithiolate; $\nu_{Ru\equiv N}$ = 1024 cm^{-1}, $\nu_{Os\equiv N}$ = 1063 cm^{-1}) reported by Sellmann and co-workers.[10] The study of the effect of catecholate auxiliaries on the M≡N bond by comparing the $\nu_{M\equiv N}$ frequencies of **1a** and **2a**, or **1b** and **2b**, is complicated by the different counter-cations in the nitrido complexes.

Structures of $[NnBu_4][M^{VI}N(Cat)_2]$ (M = Ru, Os)

Complexes **1a** and **1b** are isostructural and they both crystallize in the monoclinic space group *C*2/*c*, with very similar unit-cell dimensions (see Table 1). This resembles their sulfur analogues $[NnBu_4][M^{VI}N(S_2C_6H_4)_2]$ (M = Ru, Os),[10] which are also isostructural and have similar unit-cell dimensions, except that the 1,2-benzenedithiolate complexes both crystallize in the orthorhombic space group $Pna2_1$. Figure 2 shows the ORTEP drawings of the $[M^{VI}N(Cat)_2]^-$ anions of **1a** and **1b** with atom-numbering schemes. Selected bond lengths and angles for the two (nitrido)metal catecholate complexes are given in Table 2.

As shown in Figure 2 and Table 2, the $[M^{VI}N(Cat)_2]^-$ anions of **1a** and **1b** feature a slightly distorted square-pyramidal coordination geometry with the nitrido group situated at the apical position (ca. 0.62 Å above the basal plane constituted by the four oxygen atoms of the catecholate ligands) as in their sulfur analogues $[M^{VI}N(S_2C_6H_4)_2]^-$ (M = Ru, Os; the nitrido groups are ca. 0.69 Å above the basal plane).[10] However, contrary to the lack of symmetry of $[Ru^{VI}N(S_2C_6H_4)_2]^-$ and $[Os^{VI}N(S_2C_6H_4)_2]^-$ in the corresponding crystal structures, the structures of **1a** and **1b** have a C_2 axis along the M≡N bond of $[M^{VI}N(Cat)_2]^-$. The

Table 1. Crystal data for **1a**, **1b** and **3**

	1a	**1b**	**3**
Formula	$C_{28}H_{44}N_2O_4Ru$	$C_{28}H_{44}N_2O_4Os$	$C_{64}H_{70}NO_4OsP_2$
Cryst. system	monoclinic	monoclinic	orthorhombic
Fw	573.72	662.85	1169.35
Space group	*C*2/*c*	*C*2/*c*	$Pna2_1$
a (Å)	10.357(2)	10.330(2)	18.771(4)
b (Å)	14.014(3)	14.039(3)	14.644(3)
c (Å)	20.748(4)	20.766(4)	20.851(4)
α (deg)	90	90	90
β (deg)	100.74(3)	100.55(3)	90
γ (deg)	90	90	90
V ($Å^3$)	2959(1)	2961(1)	5732(2)
Z	4	4	4
ρ_{calc} (g cm^{-3})	1.288	1.487	1.355
2θ range (deg)	51.02	50.66	50.92
GOF	0.99	0.98	0.98
*R*1	0.032	0.035	0.026
*wR*2	0.075	0.073	0.071

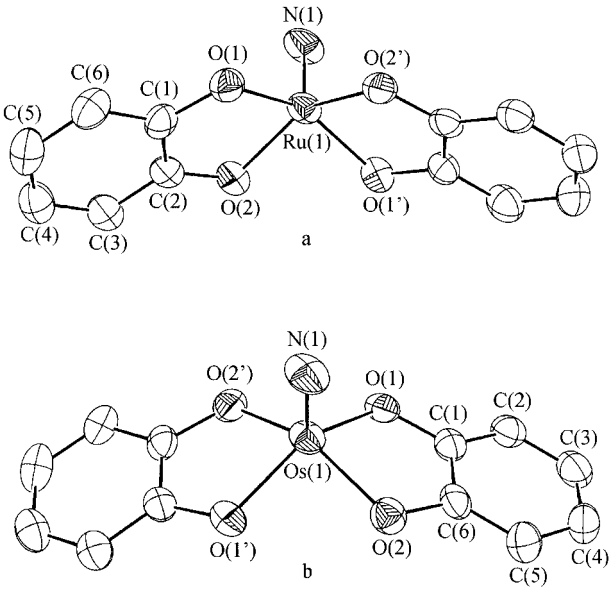

Figure 2. ORTEP drawings of a) **1a** and b) **1b** with omission of hydrogen atoms and counter-cations (thermal ellipsoid probability level: 30 %)

Table 2. Selected bond lengths (Å) and angles (deg) of **1a** and **1b**

	1a [M = Ru]	**1b** [M = Os]
M(1)−O(1)	1.954(3)	1.971(4)
M(1)−O(2)	1.962(2)	1.971(4)
M(1)−N(1)	1.603(4)	1.641(8)
C(1)−O(1)	1.366(4)	1.374(7)
C(2)−O(2)	1.352(4)	1.370(7)[a]
C(1)−C(2)	1.386(5)	1.373(9)
C(2)−C(3)	1.389(5)	1.374(9)
C(3)−C(4)	1.375(5)	1.379(10)
C(4)−C(5)	1.359(6)	1.387(10)
C(5)−C(6)	1.405(6)	1.360(9)
C(6)−C(1)	1.366(5)	1.386(8)
N(1)−M(1)−O(1)	107.08(8)	109.7(1)
N(1)−M(1)−O(2)	109.56(7)	107.6(1)
M(1)−O(1)−C(1)	111.6(2)	112.3(3)
M(1)−O(2)−C(2)	111.7(2)	112.4(4)[b]
O(1)−M(1)−O(2)	82.9(1)	82.2(2)
O(1)−M(1)−O(2′)	85.8(1)	86.1(2)
O(1)−M(1)−O(1′)	145.8(2)	140.7(2)
O(2)−M(1)−O(2′)	140.9(1)	144.9(3)

[a] C(6)−O(2). [b] Os(1)−O(2)−C(6).

Ru≡N distance in **1a** is 1.603(4) Å, slightly shorter than the Os≡N distance in **1b** [1.641(8) Å]. These Ru≡N/Os≡N distances are similar to those reported for $[NnBu_4][Ru^{VI}N(S_2C_6H_4)_2]$ [1.613(5) Å] and $[NnBu_4][Os^{VI}N(S_2C_6H_4)_2]$ [1.64(1) Å].[10] The average values of the N−M−O angles in **1a** and **1b** are 108.3 and 108.7°, respectively and are larger than the average N−M−S values in $[NnBu_4][Ru^{VI}N(S_2C_6H_4)_2]$ (107.6°) and $[NnBu_4][Os^{VI}N(S_2C_6H_4)_2]$ (107.2°), suggesting a greater repulsion between the π-electrons of the M≡N bond and the bonding electrons of the M−O bonds.[10]

The M−O distances in **1a** [1.954(3) and 1.962(2) Å] and **1b** [1.971(4) Å] fall in a narrower range than those in

 © 2004 Wiley-VCH Verlag GmbH & Co. KGaA, Weinheim

[Ru(DBCat)$_3$] [1.941(10)−1.997(10) Å] and [Os(DBCat)$_3$] [1.947(7)−1.984(7) Å], reported by Pierpont and co-workers.[40] The C−O distances of **1a** [1.352(4), 1.366(4) Å] and **1b** [1.370(7), 1.374(7) Å] are significantly longer than those in the [Ru(DBCat)$_3$] [1.299(5), 1.319(6) Å] and [Os(DBCat)$_3$] [1.32(1) Å] complexes.[40] Since metal catecholate complexes typically feature C−O distances of, for example, 1.281(3) and 1.334(13) Å when the coordinated catecholate ligands adopt the semiquinonate(1−) and catecholate(2−) states, respectively,[40] the long C−O distances in **1a** and **1b**, together with their short M−O distances, should reveal a clear charge distribution in the two nitrido complexes, that is, the coordinated catecholate ligands are all in the catecholate(2−) state and their ruthenium and osmium ions are both in an oxidation state of +6.

Note that high-valent ruthenium(VI)/osmium(VI) catecholate complexes are still sparse. Besides the Os^{VI} species [Os(Cat)$_3$] and [Os(DBCat)$_3$],[39,40] several (oxo)osmium(VI) complexes bearing catecholate auxiliaries have been prepared and characterized by Griffith and co-worker through spectroscopic means.[43] Complexes **1a** and **1b** reported in this work are, to the best of our knowledge, the only ruthenium(VI)/osmium(VI) complexes with catecholate ligands whose charge distribution has been confirmed by X-ray structure determination.

Reaction of $[Os^{VI}N(DBCat)_2]^-$ with Triphenylphosphane to Form $[Os^{V}(NPPh_3)(DBCat)_2(PPh_3)]$

The (nitrido)ruthenium/osmium complexes **1a**, **1b**, **2a** and **2b** are reactive toward PPh_3. Treatment of **2b** with PPh_3 in acetonitrile at room temperature for 0.5 h afforded the (phosphoraniminato)osmium(V) complex $[Os^{V}(NPPh_3)(DBCat)_2(PPh_3)]$ (**3**) in 90 % yield (see Scheme 2). However, the products of the reactions of **1a**, **1b** and **2a** with PPh_3 remain to be identified.

Complex **3** is a paramagnetic solid, stable toward moist air both in solid state and in solution. The ESR spectrum of **3** in solid state shows a single signal with a *g* value of 1.99, resembling the spectrum of a ruthenium(V) species (g = 2.11).[44] This indicates that the osmium(V) in **3** adopts a low-spin state, as is usual for heavy transition-metals.[44] The positive-ion FAB mass spectrum of **3** is dominated by an intense cluster peak at m/z = 1172, which can be attributed to the protonated parent ion ($[M + H]^+$).

The formation of a (phosphoraniminato)osmium(V) complex from the reaction of a (nitrido)osmium(VI) complex with phosphane is unusual. Previous reactions of (nitrido)osmium(VI) complexes, such as $[Os^{VI}NX_4]^-$ (X = Cl, Br),[3,4] $[Os^{VI}N(tpy)Cl_2]^+$ (tpy = 2,2′:6′,2′′-terpyridine),[45] $[Os^{VI}N(L)Cl]$ (L = salen and its derivatives),[32] and $[Os^{VI}N(L)Cl_2]$ (L = $[Co(\eta^5\text{-}C_5H_5)\{PO(OEt)_2\}_3]^-$)[31,46] all gave (phosphoraniminato)osmium(IV) and, much less frequently, (phosphoraniminato)osmium(III) complexes. Meyer and co-workers reported that electrochemical oxidation of *trans*-$[Os^{IV}(NPPh_3)(tpy)Cl_2]^+$ presumably gave *trans*-$[Os^{V}(NPPh_3)(tpy)Cl_2]^{2+}$ but this (phosphoraniminato)osmium(V) species was not isolated or characterized. The remarkable stability of complex **3** might arise from the unique binding behavior of the 3,5-di-*tert*-butylcatecholate ligands.

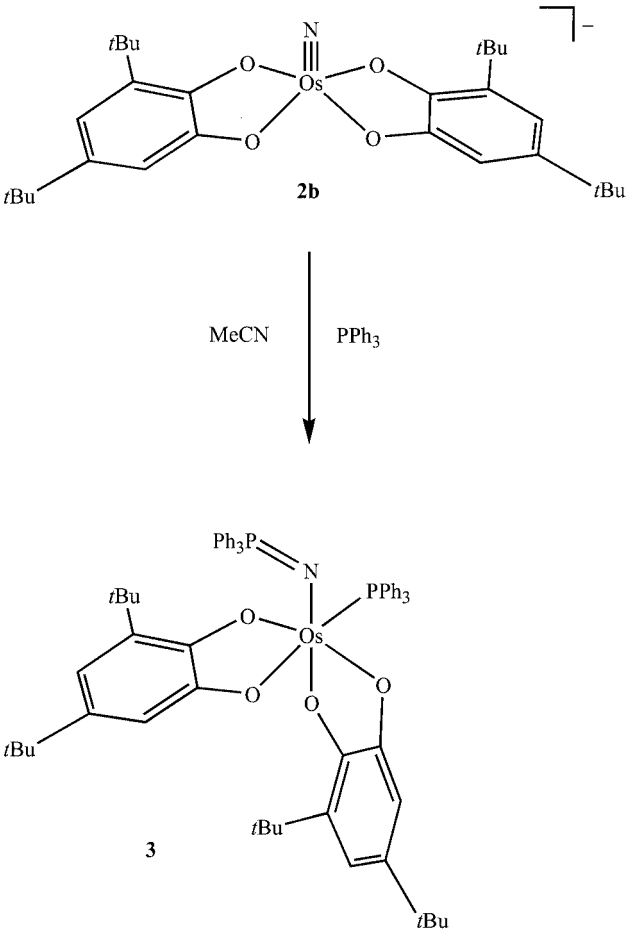

Scheme 2. Reaction of **2b** to form **3**

Stable osmium(V) complexes are not unprecedented in the literature.[1] We once isolated and structurally characterized several (oxo)osmium(V) complexes.[1] Recently, Meyer and co-workers prepared and characterized the (imido)osmium(V) complex $[Os^{V}(NH)(Tp)Cl_2]$ [Tp = hydrotris(pyrazol-1-yl)borate].[47] The coordination of phosphanes to high-valent osmium, as in the case of **3**, is much less common than that to low-valent osmium. A few (dioxo)osmium(VI) complexes, *trans*-$[Os^{VI}O_2X_2(PR_3)_2]$, were prepared by Walton and co-workers in early 1980s.[48]

Structure of $[Os^{V}(NPPh_3)(DBCat)_2(PPh_3)]$

Complex **3** crystallized in the orthorhombic space group $Pna2_1$. The ORTEP drawing of the complex is depicted in Figure 3. A surprising feature in this structure is the helical Os(DBCat)$_2$ arrangement, coupled with the *cis* arrangement of the $NPPh_3$ and PPh_3 groups. Such groups are expected to be *trans* to each other according to the structure of the nitrido precursor **2b** (which we were unable to determine by X-ray crystallography but should be similar to the structure of **1b**, shown in Figure 2). Probably, a *trans* arrangement of the $NPPh_3$ and PPh_3 groups would suffer

 © 2004 Wiley-VCH Verlag GmbH & Co. KGaA, Weinheim

Table 3. Selected bond lengths (Å) and angles (deg) of $[Os^{V}(NPPh_3)(DBCat)_2(PPh_3)]$ (**3**) compared with those of $[Os^{IV}(DBCat)_2(PPh_3)_2]$

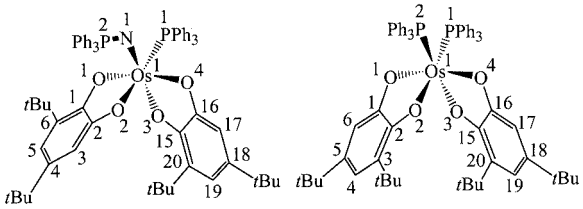

3 $[Os^{IV}(DBCat)_2(PPh_3)_2]$

Os(1)−O(1)	1.962(3) [1.982(4)][a]	Os(1)−O(2)	2.061(2) [2.042(4)]
Os(1)−O(3)	2.000(3) [2.048(5)]	Os(1)−O(4)	2.008(3) [2.001(4)]
Os(1)−N(1)	2.077(3) [2.350(2)][b]	Os(1)−P(1)	2.297(1) [2.357(2)]
N(1)−P(2)	1.616(3)	C(1)−O(1)	1.342(5) [1.341(8)]
C(2)−O(2)	1.343(4) [1.333(7)]	C(15)−O(3)	1.351(4) [1.321(7)]
C(16)−O(4)	1.341(4) [1.326(8)]	C(1)−C(2)	1.418(5) [1.422(9)]
C(2)−C(3)	1.373(6) [1.414(9)]	C(3)−C(4)	1.368(6) [1.394(9)]
C(4)−C(5)	1.407(6) [1.390(9)]	C(5)−C(6)	1.371(6) [1.380(10)]
C(6)−C(1)	1.419(5) [1.396(9)]	C(15)−C(16)	1.430(6) [1.407(8)]
C(16)−C(17)	1.375(6) [1.402(9)]	C(17)−C(18)	1.389(6) [1.378(11)]
C(18)−C(19)	1.400(6) [1.409(10)]	C(19)−C(20)	1.386(6) [1.365(9)]
C(20)−C(15)	1.386(5) [1.423(10)]		
O(1)−Os(1)−O(2)	81.2(1) [80.3(2)]	O(1)−Os(1)−O(4)	167.2(1) [166.5(2)]
O(3)−Os(1)−O(4)	80.3(1) [79.4(2)]	O(3)−Os(1)−O(2)	85.6(1) [83.5(2)]
O(1)−Os(1)−O(3)	87.6(1) [91.6(2)]	O(2)−Os(1)−O(4)	93.7(1) [88.6(2)]
P(1)−Os(1)−O(2)	175.96(8) [164.7(1)]	N(1)−Os(1)−O(1)	96.9(1) [101.0(1)]
N(1)−Os(1)−O(2)	88.2(1) [90.1(1)]	N(1)−Os(1)−O(3)	171.6(1) [164.6(1)]
N(1)−Os(1)−O(4)	94.6(1) [86.6(1)]	Os(1)−N(1)−P(2)	128.7(2)

[a] The values for $[Os^{IV}(DBCat)_2(PPh_3)_2]$ (from ref.[49]) are in square brackets. [b] Os(1)−P(2).

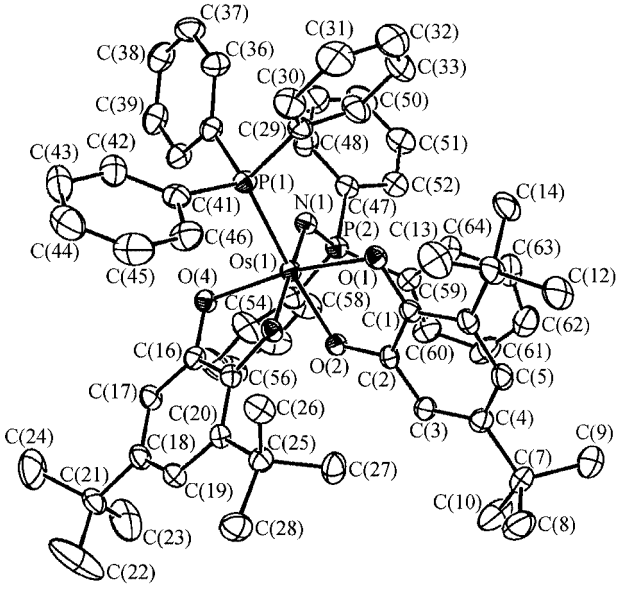

Figure 3. ORTEP drawing of **3** with omission of hydrogen atoms (thermal ellipsoid probability level: 30 %)

from significant steric interaction between the coordinated PPh_3 group and the *t*Bu groups of the bound catecholate ligands. Indeed, the structure of $[Os^{IV}(DBCat)_2(PPh_3)_2]$, reported by Pierpont and co-workers,[49] has also a helical $Os(DBCat)_2$ arrangement and *cis* PPh_3 ligands. Table 3 shows the selected bond lengths and angles for **3**; the corresponding geometric parameters of $[Os^{IV}(DBCat)_2(PPh_3)_2]$ are also given in the table for comparison.

It can be seen that both **3** and $[Os^{IV}(DBCat)_2(PPh_3)_2]$ have an $[Os(DBCat)_2(PPh_3)]$ moiety. However, the orientations of the coordinated catecholate ligands in the two complexes are different (see Table 3). A comparison between the geometrical parameters of **3** and $[Os^{IV}(DBCat)_2(PPh_3)_2]$ reveals additional differences in the $[Os(DBCat)_2(PPh_3)]$ moieties of the two structures. First, the Os−P(phosphane) distance in **3** is appreciably shorter than that in $[Os^{IV}(DBCat)_2(PPh_3)_2]$ [2.297(1) vs. 2.357(2) Å]. Second, the P(1)−Os(1)−O(2) moiety in $[Os^{IV}(DBCat)_2(PPh_3)_2]$ is more bent than that in **3** [164.7(1) vs. 175.96(8)°].

The OsO_4NP core in **3** can be best described as a distorted octahedron with the P(1) and O(2) atoms situated at the axial positions. The Os(1) atom and the four equatorial atoms O(1), O(3), O(4), and N(1) are basically co-planar, and the axial P(1)−Os(1)−O(2) moiety is almost linear [with an angle of 175.96(8)°]. One of the major distortions of the OsO_4NP core from a regular octahedron lies in a significant lengthening of the axial bond at the P(1) side [cf. Os(1)−P(1) 2.297(1) Å, Os(1)−O(2) 2.061(2) Å].

The Os−O distances in **3** range from 1.962(3) to 2.061(2) Å, which compare well with those in $[Os^{IV}(DBCat)_2(PPh_3)_2]$ [1.982(4)−2.048(5) Å], except that the average distance in **3** [2.008(3) Å] is slightly shorter than that in $[Os^{IV}(DBCat)_2(PPh_3)_2]$ [2.018(5) Å]. The C−O distances in **3** [1.341(4)−1.351(4) Å] are similar to, or even longer than,

 © 2004 Wiley-VCH Verlag GmbH & Co. KGaA, Weinheim

Table 4. Key bond lengths (Å) and angles (deg) of (phosphoraniminato)osmium complexes

Complex	Os−N	N−P	Os-*N*−P	ref.
trans-$[Os^{IV}(NPPh_3)(tpy)Cl_2]PF_6$	2.093(5)	1.618(5)	132.5(3)	[45]
cis-$[Os^{IV}(NPPh_2Me)(tpy)Cl_2]PF_6$	2.061(6)	1.619(6)	132.2(4)	[45]
$[Os^{IV}(NPPh_3)(salophen)Cl]$[a]	1.92(1)	1.56(1)	149.6(10)	[32]
$[Os^{IV}(NPPh_3)(L)Cl_2]$[b]	1.893(5)	1.575(5)	137.5(3)	[46]
$[Os^{V}(NPPh_3)(DBCat)_2(PPh_3)]$ (**3**)	2.077(3)	1.616(3)	128.7(2)	This work

[a] salophen = *N*,*N*′-bis(salicylidene)*o*-phenylenediamine dianion. [b] L = $[Co(\eta^5\text{-}C_5H_5)\{PO(OEt)_2\}_3]^-$

those in $[Os^{IV}(DBCat)_2(PPh_3)_2]$ [1.321(7)−1.341(8) Å], consistent with the $DBCat^{2-}$ state of the coordinated catecholate ligands in **3**.

Complex **3** has an Os(1)−N(1) distance of 2.077(3) Å and an N(1)−P(2) distance of 1.616(3) Å. These Os−N(phosphoraniminato) and N−P distances are similar to those in *trans*-$[Os^{IV}(NPPh_3)(tpy)Cl_2]PF_6$ and *cis*-$[Os^{IV}(NPPh_2Me)(tpy)Cl_2]PF_6$,[45] but considerably longer than those in $[Os^{IV}(NPPh_3)(salophen)Cl]$[32] and $[Os^{IV}(NPPh_3)(L)Cl_2]$[46] (see Table 4). The Os−*N*−PPh_3 angle in **3** is 128.7(2)°. As shown in Table 4, this is the smallest Os−*N*−PR_3 angle ever found in the crystal structures of (phosphoraniminato)osmium complexes.

Conclusion

We have prepared several (nitrido)ruthenium(VI) and -osmium(VI) complexes bearing catecholate auxiliaries, which constitute a new class of mononuclear (nitrido)metal complexes. X-ray structure determinations on $[NnBu_4][Ru^{VI}N(Cat)_2]$ and $[NnBu_4][Os^{VI}N(Cat)_2]$ confirm that the catecholate ligands in these (nitrido)ruthenium(VI) and -osmium(VI) complexes all adopt the catecholate(2−) state, rather than the semiquinonate(1−) or quinone states. The structure determinations on $[NnBu_4][Ru^{VI}N(Cat)_2]$ and $[NnBu_4][Os^{VI}N(Cat)_2]$, together with those on their 1,2-benzenedithiolate counterparts reported by Sellmann and co-workers,[10] allow for a direct comparison between the effects of oxygen and sulfur donors on the structures of (nitrido)metal complexes. Incorporation of 3,5-di-*tert*-butylcatecholate auxiliaries into a (nitrido)osmium species results in an unusual reactivity of the nitrido complex toward tertiary phosphane, affording an unprecedented (phosphoraniminato)osmium(V) complex.

Experimental Section

General Remarks: All solvents were purified by standard methods before use. Catechol, 3,5-di-*tert*-butylcatechol, 2,6-dimethylpyridine, and triphenylphosphane (Aldrich) were used as received. $[NnBu_4][M^{VI}NCl_4]$ (M = Ru, Os) were prepared according to the reported procedures.[2] ^{1}H NMR spectra were recorded on a Bruker DPX-300 or −400 FT-IR spectrometer (chemical shifts, δ, are relative to tetramethylsilane). Infrared spectra were recorded on a Bio-Rad FTS-165 spectrometer. Fast atom bombardment (FAB) mass spectra were obtained on a Finnigan Mat 95 mass spectrometer. The ESR spectrum was recorded on a Bruker EMX100 ESR spectrometer. Elemental analyses were performed by the Institute of Chemistry, the Chinese Academy of Sciences.

Preparation of $[NnBu_4][M^{VI}N(Cat)_2]$ (M = Ru 1a, Os 1b): Several drops of 2,6-dimethylpyridine were added under nitrogen to a solution of H_2Cat (22 mg, 0.2 mmol) in methanol (5 mL). After being stirred for 0.5 h, the mixture was treated with $[NnBu_4][M^{VI}NCl_4]$ (0.1 mmol) and further stirred for 0.5 h. Slow evaporation of the solvent led to precipitation of the desired product as a microcrystalline solid, which was collected by filtration, washed with diethyl ether, and dried in vacuo.

$[NnBu_4][Ru^{VI}N(Cat)_2]$ (1a): Yield: 48.8 mg (85 %). ^{1}H NMR (400 MHz, $CDCl_3$): δ = 0.95 (t, 12 H), 1.34 (m, 16 H), 2.92 (t, 8 H), 6.62 (m, 4 H), 6.89 (m, 4 H) ppm. IR (Nujol): 1049 cm^{-1} ($\nu_{Ru\equiv N}$). FAB MS: *m*/*z* = 332 $[Ru^{VI}N(Cat)_2]^-$. $C_{28}H_{44}N_2O_4Ru$ (573.7): calcd. C 58.62, H 7.73, N 4.88; found C 58.20, H 7.42, N 4.53.

$[NnBu_4][Os^{VI}N(Cat)_2]$ (1b): Yield: 49.7 mg (75 %). ^{1}H NMR (400 MHz, $CDCl_3$): δ = 1.00 (t, 12 H), 1.46 (m, 16 H), 3.15 (t, 8 H), 6.71 (m, 4 H), 7.00 (m, 4 H) ppm. IR (Nujol): 1093 cm^{-1} ($\nu_{Os\equiv N}$). FAB MS: *m*/*z* = 422 $[Os^{VI}N(Cat)_2]^-$. $C_{28}H_{44}N_2O_4Os{\cdot}H_2O$ (680.9): calcd. C 49.39, H 6.81, N 4.11; found C 49.79, H 6.50, N 3.91.

Preparation of $[2,6\text{-}Me_2PyH][M^{VI}N(DBCat)_2]$ (M = Ru 2a, Os 2b): Several drops of 2,6-dimethylpyridine were added under nitrogen to a solution of H_2DBCat (445 mg, 2 mmol) in methanol (20 mL). After being stirred for 0.5 h, the mixture was treated with $[NnBu_4][M^{VI}NCl_4]$ (1 mmol), which resulted in precipitation of the desired product immediately. The precipitate was collected by filtration, washed with diethyl ether, and dried in vacuo.

$[2,6\text{-}Me_2PyH][Ru^{VI}N(DBCat)_2]$ (2a): Yield: 598 mg (90 %). ^{1}H NMR (300 MHz, $CDCl_3$): δ = 1.25 (s, 36 H), 2.84 (s, 6 H), 6.69 (s, 2 H), 6.80 (s, 2 H), 7.51 (d, 2 H), 8.18 (t, 1 H) ppm. IR (Nujol): 1051 cm^{-1} ($\nu_{Ru\equiv N}$). FAB MS: *m*/*z* = 556 $[Ru^{VI}N(DBCat)_2]^-$. $C_{35}H_{50}N_2O_4Ru{\cdot}0.5CHCl_3$ (723.5; a sample recrystallized from chloroform/diethyl ether): calcd. C 58.93, H 7.03, N 3.87; found C 59.36, H 6.88, N 4.15.

$[2,6\text{-}Me_2PyH][Os^{VI}N(DBCat)_2]$ (2b): Yield: 602 mg (80 %). ^{1}H NMR (300 MHz, $CDCl_3$): δ = 1.26 (d, 36 H), 2.89 (s, 6 H), 6.69 (d, 2 H), 6.94 (d, 2 H), 7.58 (d, 2 H), 8.25 (t, 1 H) ppm. IR (Nujol): 1097 cm^{-1} ($\nu_{Os\equiv N}$). FAB MS: *m*/*z* = 646 $[Os^{VI}N(DBCat)_2]^-$. $C_{35}H_{50}N_2O_4Os{\cdot}H_2O$ (771.0): calcd. C 54.52, H 6.80, N 3.63; found C 54.55, H 6.44, N 3.80.

Reaction of $[2,6\text{-}Me_2PyH][Os^{VI}N(DBCat)_2]$ (2b) with Triphenylphosphane: A mixture of **2b** (180 mg, 0.2 mmol) and PPh_3 (130 mg, 0.5 mmol) in acetonitrile (10 mL) was stirred for 0.5 h and gave a purple-red solution. After removal of the solvent, the residue

 © 2004 Wiley-VCH Verlag GmbH & Co. KGaA, Weinheim

was transferred onto an alumina column with dichloromethane as an eluent. The purple-red band was collected and concentrated to dryness by rotary evaporation to give a purple-red solid, which was identified as $[Os^{V}(NPPh_3)(DBCat)_2(PPh_3)]$ (**3**).

$[Os^{V}(NPPh_3)(DBCat)_2(PPh_3)]$ (3): Yield: 210 mg (90 %). FAB MS: m/z = 1172 $[M + H]^+$. $C_{64}H_{70}NO_4OsP_2$ (1169.4): calcd. C 65.73, H 6.03, N 1.20; found C 65.77, H 5.92, N 1.05.

X-ray Crystallographic Study: Diffraction-quality crystals of **1a** and **1b** were obtained by slow evaporation of their methanol solutions at room temperature, whereas those of **3** were obtained by slow evaporation of its acetonitrile/diethyl ether (3:1, v/v) solution at −20 °C. Crystals of the dimensions of 0.6 × 0.2 × 0.1 (**1a**), 0.2 × 0.15 × 0.1 (**1b**), and 0.7 × 0.5 × 0.4 mm (**3**) mounted in glass capillaries were used for data collection at −20 °C on a MAR diffractometer with a 300 mm image plate detector using graphite-monochromatized Mo-K_α radiation (λ = 0.71073 Å). The data were collected with 2.5° (**1a**), 3° (**1b**), and 1.5° (**3**) oscillation steps of φ, 480 s (**1a** and **1b**) and 240 s (**3**) exposure time and 120 mm scanner distance. Eighty (**1a**), 50 (**1b**), and 123 (**3**) images were collected. The images were interpreted and intensities integrated using the DENZO[50] program. The structures were solved by direct methods by employing the SIR-97[51] program on PC. The ruthenium/osmium and many other non-hydrogen atoms were located according to the direct methods and the successive least-square Fourier cycles. The positions of the remaining non-hydrogen atoms were found after successful refinement by full-matrix least-squares using the SHELXL-97[52] program on PC. In the case of **1a**, one methyl group of the *n*Bu moiety was disordered into two positions.

CCDC-216402 (**1a**), CCDC-216401 (**1b**), CCDC-216403 (**3**) contain the supplementary crystallographic data for this paper. These data can be obtained free of charge at www.ccdc.cam.ac.uk/conts/retrieving.html [or from the Cambridge Crystallographic Data Centre, 12 Union Road, Cambridge CB2 1EZ, UK; Fax: (internat.) +44-1223/336-033; E-mail: deposit@ccdc.cam.ac.uk].

Acknowledgments

This work was supported by The University of Hong Kong, the Hong Kong University Foundation, Hong Kong Research Grants Council, and the University Grants Committee of the Hong Kong SAR of China (Area of Excellence Scheme, AoE/P-10/01).

[1] C.-M. Che, V. W.-W. Yam, *Adv. Inorg. Chem.* **1992**, *39*, 233.
[2] W. P. Griffith, D. Pawson, *J. Chem. Soc., Dalton Trans.* **1973**, 1315.
[3] W. P. Griffith, D. Pawson, *J. Chem. Soc., Chem. Commun.* **1973**, 418.
[4] D. Pawson, W. P. Griffith, *J. Chem. Soc., Dalton Trans.* **1975**, 417.
[5] H.-W. Lam, K.-F. Chin, C.-M. Che, R.-J. Wang, T. C. W. Mak, *Inorg. Chim. Acta* **1993**, *204*, 133.
[6] P. A. Shapley, H. S. Kim, S. R. Wilson, *Organometallics* **1988**, *7*, 928.
[7] N. Zhang, S. R. Wilson, P. A. Shapley, *Organometallics* **1988**, *7*, 1126.
[8] R. W. Marshman, P. A. Shapley, *J. Am. Chem. Soc.* **1990**, *112*, 8369.
[9] P. A. Shapley, W. A. Reinerth, *Organometallics* **1996**, *15*, 5090.
[10] D. Sellmann, M. W. Wemple, W. Donaubauer, F. W. Heinemann, *Inorg. Chem.* **1997**, *36*, 1397.
[11] W. A. Reinerth, P. A. Shapley, *Inorg. Chim. Acta* **1998**, *267*, 335.
[12] C.-M. Che, T.-C. Lau, H.-W. Lam, C.-K. Poon, *J. Chem. Soc., Chem. Commun.* **1989**, 114.
[13] H.-W. Lam, C.-M. Che, K.-Y. Wong, *J. Chem. Soc., Dalton Trans.* **1992**, 1411.
[14] C.-M. Che, M. H.-W. Lam, T. C. W. Mak, *J. Chem. Soc., Chem. Commun.* **1989**, 1529.
[15] D. W. Pipes, M. Bakir, S. E. Vitols, D. J. Hodgson, T. J. Meyer, *J. Am. Chem. Soc.* **1990**, *112*, 5507.
[16] D. C. Ware, H. Taube, *Inorg. Chem.* **1991**, *30*, 4598.
[17] D. C. Ware, H. Taube, *Inorg. Chem.* **1991**, *30*, 4605.
[18] K.-F. Chin, K.-K. Cheung, H.-K. Yip, T. C. W. Mak, C.-M. Che, *J. Chem. Soc., Dalton Trans.* **1995**, 657.
[19] W.-H. Leung, G. Wilkinson, B. Hussain-Bates, M. B. Hursthouse, *J. Chem. Soc., Dalton Trans.* **1991**, 2791.
[20] J. J. Schwab, E. C. Wilkinson, S. R. Wilson, P. A. Shapley, *J. Am. Chem. Soc.* **1991**, *113*, 6124.
[21] Z.-Y. Li, W.-Y. Yu, C.-M. Che, C.-K. Poon, R.-J. Wang, T. C. W. Mak, *J. Chem. Soc., Dalton Trans.* **1992**, 1657.
[22] C.-M. Che, K.-Y. Wong, H.-W. Lam, K.-F. Chin, Z.-Y. Zhou, T. C. W. Mak, *J. Chem. Soc., Dalton Trans.* **1993**, 857.
[23] P.-M. Chan, W.-Y. Yu, C.-M. Che, K.-K. Cheung, *J. Chem. Soc., Dalton Trans.* **1998**, 3183.
[24] T. J. Crevier, J. M. Mayer, *J. Am. Chem. Soc.* **1998**, *120*, 5595.
[25] T. J. Crevier, J. M. Mayer, *Angew. Chem.* **1998**, *110*, 1995; *Angew. Chem. Int. Ed.* **1998**, *37*, 1891.
[26] T. J. Crevier, B. K. Bennett, J. D. Soper, J. A. Bowman, A. Dehestani, D. A. Hrovat, S. Lovell, W. Kaminsky, J. M. Mayer, *J. Am. Chem. Soc.* **2001**, *123*, 1059.
[27] A. Dehestani, W. Kaminsky, J. M. Mayer, *Inorg. Chem.* **2003**, *42*, 605.
[28] K. D. Demadis, EI-S. EI-Samanody, G. M. Coia, T. J. Meyer, *J. Am. Chem. Soc.* **1999**, *121*, 535.
[29] EI-S. EI-Samanody, K. D. Demadis, T. J. Meyer, P. S. White, *Inorg. Chem.* **2001**, *40*, 3677.
[30] W.-H. Leung, J. L. C. Chim, I. D. Williams, W.-T. Wong, *Inorg. Chem.* **1999**, *38*, 3000.
[31] Q.-F. Zhang, K.-K. Lau, J. L. C. Chim, T. K. T. Wong, W.-T. Wong, I. D. Williams, W.-H. Leung, *J. Chem. Soc., Dalton Trans.* **2000**, 3027.
[32] T.-W. Wong, T. C. Lau, W.-T. Wong, *Inorg. Chem.* **1999**, *38*, 6181.
[33] L. Bonomo, E. Solari, R. Scopelliti, C. Floriani, *Angew. Chem.* **2001**, *113*, 2597; *Angew. Chem. Int. Ed.* **2001**, *40*, 2529.
[34] A. Antipas, J. W. Buchler, M. Gouterman, P. D. Smith, *J. Am. Chem. Soc.* **1980**, *102*, 198.
[35] S. K.-Y. Leung, J.-S. Huang, J.-L. Liang, C.-M. Che, Z.-Y. Zhou, *Angew. Chem.* **2003**, *115*, 354; *Angew. Chem. Int. Ed.* **2003**, *42*, 340.
[36] S.-W. Lai, T.-C. Lau, W. K.-M. Fung, N. Zhu, C.-M. Che, *Organometallics* **2003**, *22*, 315.
[37] C. G. Pierpont, R. M. Buchanan, *Coord. Chem. Rev.* **1981**, *38*, 45.
[38] C. G. Pierpont, *Coord. Chem. Rev.* **2001**, *219*, 415.
[39] M. B. Hursthouse, T. Fram, L. New, W. P. Griffith, A. J. Nielson, *Transition Met. Chem.* **1978**, *3*, 255.
[40] S. Bhattacharya, S. R. Boone, G. A. Fox, C. G. Pierpont, *J. Am. Chem. Soc.* **1990**, *112*, 1088.
[41] T. Jüstel, T. Weyhermüller, K. Wieghardt, E. Bill, M. Lengen, A. X. Trautwein, P. Hildebrandt, *Angew. Chem.* **1995**, *107*, 744; *Angew. Chem. Int. Ed. Engl.* **1995**, *34*, 669.
[42] T. Jüstel, M. Müller, T. Weyhermüller, C. Kressl, E. Bill, P. Hildebrandt, M. Lengen, M. Grodzicki, A. X. Trautwein, B. Nuber, K. Wieghardt, *Chem. Eur. J.* **1999**, *5*, 793.
[43] A. J. Nielson, W. P. Griffith, *J. Chem. Soc., Dalton Trans.* **1978**, 1501.

 © 2004 Wiley-VCH Verlag GmbH & Co. KGaA, Weinheim

[44] R. Neumann, C. Abu-Gnim, *J. Am. Chem. Soc.* **1990**, *112*, 6025.
[45] K. D. Demadis, M. Bakir, B. G. Klesczewski, D. S. Williams, P. S. White, T. J. Mayer, *Inorg. Chim. Acta* **1998**, *270*, 511.
[46] W.-H. Leung, E. Y. Y. Chan, T. C. Y. Lai, W.-T. Wong, *J. Chem. Soc., Dalton Trans.* **2000**, 51.
[47] M. H. V. Huynh, P. S. White, K. D. John, T. J. Meyer, *Angew. Chem.* **2001**, *113*, 4173; *Angew. Chem. Int. Ed.* **2001**, *40*, 4049.
[48] J. E. Armstrong, R. A. Walton, *Inorg. Chem.* **1983**, *22*, 1545.
[49] S. Bhattacharya, C. G. Pierpont, *Inorg. Chem.* **1991**, *30*, 2906.
[50] Z. Otwinowski, W. Minor, *Methods in Enzymology*, Vol. 276: Macromolecular Crystallography, Part A., (Eds: C. W. Carter, R. M. Sweet, Jr.), Academic Press, **1997**, 307.
[51] A. Altomare, M. C. Burla, M. Camalli, G. Cascarano, C. Giacovazzo, A. Guagliardi, A. G. G. Moliterni, G. Polidori, R. Spagna, *J. Appl. Crystallogr.* **1998**, *32*, 115.
[52] G. M. Sheldrick, SHELX97. Programs for Crystal Structure Analysis (Release 97−2). University of Göttingen, Germany, **1997**.

Received July 31, 2003
Early View Article
Published Online February 17, 2004

 © 2004 Wiley-VCH Verlag GmbH & Co. KGaA, Weinheim

The Solid-State Lanthanoid-Assisted Hydrolysis of the Solvolytically "Inert" $[AsF_6]^-$ Ion

Maja Ponikvar,*[a] Borka Sedej,[a] and Joel F. Liebman[b]

Keywords: Arsenic / Hydrolysis / $LnF_n(AsF_6)_{3-n}$ compounds / Rare-earth elements / Solid-state reactions

Results of elemental chemical analyses of the coordination compounds of the type $LnF_n(AsF_6)_{3-n}$ (Ln = Y, La, Ce, Pr, Nd, Sm, Eu, Gd, Tb, Dy, Ho, Er, Tm, Yb and Lu) indicated unexpectedly low stability of the generally highly hydrolytically stable $[AsF_6]^-$ ion. Experiments conducted on model compounds of the type $NdF_n(AsF_6)_{3-n}$ have shown that hydrolysis proceeded instantaneously during the reaction of the solid compound with water. The ligand substitution catalysis of the compounds is explained in terms of the distortion of the $[AsF_6]^-$ octahedra earlier shown by vibrational spectroscopy. The study contrasts formally related reactions on the solid–solvent interface as opposed to those in homogeneous solution. A new look at some long studied and well-known inorganic species is offered.
(© Wiley-VCH Verlag GmbH & Co. KGaA, 69451 Weinheim, Germany, 2004)

Introduction

The rare earth(III) fluoroarsenates(V) [$LnF_n(AsF_6)_{3-n}$ compounds] were isolated in the system LnF_3/AsF_5/aHF at room temperature and characterized by: (1) X-ray powder diffraction analysis; (2) spectroscopic methods (Infrared and Raman spectroscopy); (3) monitoring mass balances throughout the experiments; and (4) chemical analyses.[1] The results of elemental chemical analyses indicated the presumed composition of the obtained compounds.[1] Crystal structure data are still lacking for these compounds.

As reported in the literature, the $[AsF_6]^-$ ion is highly stable towards hydrolysis[2,3] and can be determined gravimetrically.[4,5] Klapötke confirmed the stability towards aqueous hydrolysis also for coordinated $[AsF_6]^-$ ions.[6] As part of their study, Clark and Jones[7] suggested that the $[AsF_6]^-$ ion partially hydrolyses through hard acid−hard base interactions. Ghorab and Winfield[8] studied ^{18}F exchange processes of this and other hexafluoropnictates in acetonitrile.

The results of chemical analyses of the $[AsF_6]^-$ ion in $LnF_n(AsF_6)_{3-n}$ compounds synthesized and characterized in our laboratories were low, irreproducible and in disagreement with the calculated amounts of the metal Ln^{III}, total fluoride $(F^-)_t$ and arsenic(V) (results of the determinations of $[AsF_6]^-$ were not reported or interpreted because of lack of the material for supporting experiments).

[a] Jožef Stefan Institute,
Jamova 39, SI-1000 Ljubljana, Slovenia
Fax: (internat.) +386-1-423-21-25
E-mail: maja.ponikvar@ijs.si
[b] Department of Chemistry and Biochemistry, University of Maryland, Baltimore County, Baltimore, MD 21250, USA
Fax: (internat.) +1-410-455-2608
E-mail: jliebman@umbc.edu

The aim of the current paper is to demonstrate the instantaneous process of hydrolysis of the generally highly hydrolytically stable $[AsF_6]^-$ ion in $NdF_n(AsF_6)_{3-n}$ compounds during suspension of these solid compounds in water and to offer a plausible interpretation of the obtained results.

Results and Discussion

The results of the determination of the $[AsF_6]^-$ ion in $LnF_n(AsF_6)_{3-n}$ compounds[1] were lower than theoretically calculated values and did not agree with the amount of determined Ln^{III} and $(F^-)_t$ ions [the following abbreviations are used within this paper: $(F^-)_t$ = total fluoride, $(F^-)_P$ = total fluoride in the precipitate, $(F^-)_F$ = free fluoride in the filtrate, $(F^-)_f$ = free fluoride in solution]. Moreover, repetition with several weights of the sample after suspension in water showed that the results were irreproducible. The amount of free fluoride $(F^-)_f$ [9] after suspending these solid compounds in water was also determined. The results of these analyses are presented in Table 1.

Judging by the results presented in Table 1, the differences between two independent parallel determinations of $[AsF_6]^-$ ions seem to increase with increasing fluoroacidity[1,10,11] of the rare-earth trifluorides along the series. The determined amounts of $(F^-)_f$ were abnormally high since binary compounds of the type LnF_3 do not release fluoride ions, as determined in aqueous suspension of the sample directly with a fluoride-ion-selective electrode. The amount of $(F^-)_f$ ions determined in these (binary) compounds was not higher than 0.1−0.2 % of the expected amount, that is, in the range of experimental error of the analytical procedure for fluoride ions.[12]

Table 1. Results of $[AsF_6]^-$ and $(F^-)_f$ analyses for in the coordination compounds of the type $LnF_n(AsF_6)_{3-n}$

Compound	$[AsF_6]^-$ [%] Calcd.	Found[a] 1	$(F^-)_f$ [%] 2	Found
$YF(AsF_6)_2$	77.78	67.9	68.3	5.1
$La(AsF_6)_3$	80.32	67.9	/	1.9
$CeF(AsF_6)_2$	70.37	68.6	68.6	0.5
$PrF(AsF_6)_2$	70.26	62.4	/	0.9
$PrF(AsF_6)_2$	70.26	68.1	68.0	0.5
$NdF(AsF_6)_2$	69.83	66.0	66.0	1.4
$SmF(AsF_6)_2$	69.05	63.3	63.1	1.0
$EuF(AsF_6)_2$	68.85	63.9	63.2	0.7
$GdF(AsF_6)_2$	68.19	58.6	59.2	/
$TbF(AsF_6)_2$	67.68	57.1	/	4.4
$DyF(AsF_6)_2$	67.55	55.3	56.6	6.7
$HoF(AsF_6)_2$	67.26	52.7	59.9	5.8
$ErF(AsF_6)_2$	66.98	59.2	60.2	4.8
ErF_2AsF_6	47.93	47.1	43.7	4.0
$TmF(AsF_6)_2$	66.78	62.2	65.1	2.5
$Tm_2F_3(AsF_6)_3$	58.94	53.5	49.8	5.5
$Yb_2F_3(AsF_6)_3$	58.44	51.5	50.9	4.5
$Lu_2F_3(AsF_6)_3$	58.21	52.8	51.2	3.9

[a] Amount of $[AsF_6]^-$ determined in two separate weights of the sample.

To explain the obtained results, ligand substitution catalysis through solution-phase hard acid−hard base interactions[7,8] was studied. Experiments conducted by using solid $KAsF_6$, solid lanthanide trifluorides or standard solutions of trivalent lanthanide salts revealed that addition of Ln^{III} or LnF_3 to acidic (HCl) aqueous solutions of $KAsF_6$ [with or without addition of solid NaF that represented a source of $(F^-)_f$] did not catalyze the fluoride exchange process in $[AsF_6]^-$ ions. The amounts of the $[AsF_6]^-$ ion determined (ranging from 82.2−82.6 %) in such samples agreed well with theoretically calculated amounts (82.85 %). The possibility of solution-phase catalysis was thus rejected.

The stability of the $[AsF_6]^-$ ion in coordination compounds of the type $LnF_n(AsF_6)_{3-n}$ in aqueous media was further studied in the neodymium model compounds $NdF(AsF_6)_2$ and $Nd(AsF_6)_3$ synthesized for this purpose in our laboratories. Elemental chemical analyses were conducted for both compounds. The results obtained are presented in Table 2.

The results revealed high precision of the obtained results for the determination of Nd^{III} and $(F^-)_t$ ions and high purity of the synthesized compounds, although the stoichiometry was not exact. However, for the purpose of our experiment, the stoichiometry of $NdF(AsF_6)_2$ and $Nd(AsF_6)_3$ was not important. The amount of $[AsF_6]^-$ ion was also determined (see Table 3). The results of these determinations were too low and irreproducible. It was obvious that during the process of suspending the solid compounds in water, the $[AsF_6]^-$ ion decomposed into the fluorohydroxyarsenic(v) species.

Table 3. Results of parallel determinations of $[AsF_6]^-$ in $NdF(AsF_6)_2$ and $Nd(AsF_6)_3$ including the results of determination of the amount of total fluoride in the precipitate $(F^-)_P$ and free fluoride in filtrate $(F^-)_F$

Compound	$[AsF_6]^-$ [%] Calcd.	Found	$(F^-)_P$ [%] Calcd.	Found	$(F^-)_F$ [%] Found
$NdF(AsF_6)_2$	69.83	61.2	19.93	19.6	9.3
		63.2		19.5	8.6
$Nd(AsF_6)_3$	79.71	66.3	19.93	19.5	9.5
		60.5		19.6	11.6
		62.2		19.6	10.6

As reported along with $[AsF_6]^-$, $[AsF_5OH]^-$ can also be determined gravimetrically by precipitation with tetraphenylarsonium chloride (TPAC).[5] Therefore, we investigated whether the precipitate formed was pure or whether $[AsF_5OH]^-$ coprecipitated with $[AsF_6]^-$. In this way, the amount of total fluoride ions in the precipitates $(F^-)_P$ and the amount of fluoride in the filtrates $(F^-)_F$ collected during the filtration of the precipitates were determined. The results are presented in Table 3.

These results indicated that the precipitates formed during the reaction of TPAC with $[AsF_6]^-$ ions in strongly acidic (HCl) media were pure and did not include any TPA-AsF_5OH. In Table 4, the sums of the amounts of fluoride present in the precipitates (calculated from the amount of determined $[AsF_6]$) and the filtrates in individual samples arecompared with the amount of $(F^-)_t$ determined.

As seen from the results, the differences between the sum of $(F^-)_P$ and $(F^-)_F$ and $(F^-)_t$ ranged from 0.8−2.2 %. Considering that precipitation is performed in hot (ca. 70−80 °C), strongly acidic (HCl) solution from which fluoride is lost in the form of relatively volatile HF, these differences are negligible. This indicates that during the initial stage of reaction of the sample with water, the strongly distorted AsF_6 unit partially decomposes. As a result, the fluorohydroxyarsenic(v) species are formed, which decom-

Table 2. The results of elemental chemical analysis of $NdF(AsF_6)_2$ and $Nd(AsF_6)_3$ compounds synthesized in our laboratories

Compound	Nd^{III} [%] Calcd.	Found	RSD[a] [%]	$(F^-)_t$ [%] Calcd.	Found	RSD [%]	As^V [%] Calcd.	Found	RSD [%]
$NdF(AsF_6)_2$	26.66	25.60	0.23	45.65	47.60	0.00	27.69	26.70	1.72
$Nd(AsF_6)_3$	20.29	20.60	0.28	48.10	50.30	0.11	31.61	27.30	1.48

[a] RSD = Relative Standard Deviation.

 © 2004 Wiley-VCH Verlag GmbH & Co. KGaA, Weinheim

Table 4. Sum of fluoride determined in the precipitate and in the filtrate compared to the amount of determined total fluoride

Compound	(F^-) in AsF_6^- [a] [%]	$(F^-)_F$ [%]	Sum [%]	Difference [%][b]
$NdF(AsF_6)_2$	36.9	9.3	46.2	−1.4
	38.1	8.6	46.7	−0.9
$Nd(AsF_6)_3$	40.0	9.5	49.5	−0.8
	36.5	11.6	48.1	−2.2
	37.8	10.6	48.4	−1.9

[a] The theoretical amount (%) of fluoride in $[AsF_6]^-$ is 60.34 %. [b] The amount of $(F^-)_t$ determined in $NdF(AsF_6)_2$ was 47.6 % and in $Nd(AsF_6)_3$ 50.3 % (see Table 1).

pose to a hydrated arsenic(V) species and fluoride and are subsequently determined in the filtrate according to the [Equation (1)].

$$[AsF_6]^- + 2\,nH_2O \rightarrow [AsF_{6-n}(OH)_n]^- + nF^- + nH_3O^+ \quad (1)$$

The amount of fluoride in the filtrates was determined in two ways: (1) after total decomposition with alkali hydroxide fusion; and (2) directly without prior decomposition. It is interesting to note that the amount of $(F^-)_F$ determined by the two ways was in agreement. This indicated that all the fluoride ions in the filtrate were present as free fluoride ions that can be determined by a fluoride-ion-selective electrode. Therefore, in a separate experiment with $Nd(AsF_6)_3$, we determined the amount of $(F^-)_f$ ions as a function of the pre-treatment conditions of an aliquot of the aqueous filtered suspension of the sample. Subsequently, the amount of $(F^-)_f$ was determined. The results are listed in Table 5.

Table 5. The amount of $(F^-)_f$ determined in $Nd(AsF_6)_3$ as a function of pre-treatment conditions of the sample

Pre-treatment conditions	$(F_f)^-$ [%]
Aqueous filtered suspension	1.6
An aliquot was heated to boiling	1.6
Conc. HCl (0.2 mL) was added to an aliquot	1.8
Conc. HCl (0.2 mL) was added to an aliquot and heated to boiling	9.2

The results indicated that the amount of $(F^-)_f$ determined in the filtered suspension of the sample increased in acidic (HCl) solution at higher temperatures. This observation is in agreement with previously conducted experiments. The covalently bonded fluorides in $LnF_n(AsF_6)_{3-n}$ compounds are therefore released into the solution under conditions of gravimetric determination of $[AsF_6]^-$.

Plausible Interpretation

In the vibrational spectra of rare earth(III) fluoroarsenates(V) more bands were observed than would be expected for a regular $[AsF_6]^-$ anion with O_h symmetry. Additionally, the strongest Raman (697−711 cm^{-1}) and the strongest infrared bands (765−768 cm^{-1}) are shifted to higher frequencies than that of the strongest band of the octahedral $[AsF_6]^-$ ion in $CsAsF_6$ [13] in which Raman-active symmetrical stretching, $\nu_1(A_{1g})$ appears at 685 cm^{-1} and infrared-degenerate stretching $\nu_3(F_{1u})$ at 699 cm^{-1}.[1]

The composition of rare earth(III) fluoroarsenates(V) and the fluorine acceptor abilities of AsF_5 suggests formation of a fluorine bridge between the Ln and As atoms (in agreement with the expected shifts in electron density according to "Gutmann's second rule" [14]). Consequently, the distorted octahedral $[AsF_6]^-$ ions of maximally C_{4v} symmetry are anticipated. The observed number of bands in vibrational spectra of rare earth(III) fluoroarsenates(V) support that assumption and indicate a covalent contribution to the bonding between LnF_3 and AsF_5 through fluorine bridges.[1]

Molecules undergo whatever distortion necessary to maximize the stability of the entire species (cations + anions). However, that the anion is distorted makes it easier for a positive, protic hydrogen to pull off a fluorine atom from the $[AsF_6]^-$ ion (presumably, at least one F has a longer Ln−F bond and so is enroute to dissociation) when suspending these solid compounds in water. Additionally, the arsenic atom has been made more vulnerable to attack by solvent H_2O or added $[OH]^-$ or other nucleophiles such as $[CO_3]^{2-}$, because the irregular octahedron provides more space around the As center, either because of stretched bonds or opened angles or both. Our suggested mechanism of the solid state F^-/OH^- exchange is schematically shown in Figure 1.

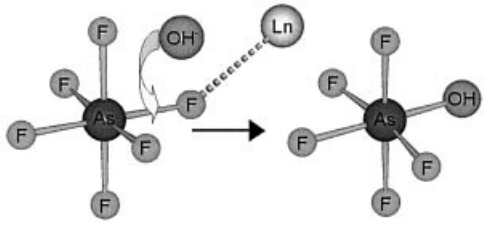

Figure 1. Schematic presentation of our suggested mechanism of the solid state F^-/OH^- exchange (Ln = Y, La, Ce, Pr, Nd, Sm, Eu, Gd, Tb, Dy, Ho, Er, Tm, Yb, Lu)

This reasoning that the distortion is stabilized by the rare-earth element is reminiscent of the generally accepted explanation for enzyme activity in terms of the enzyme stabilizing the transition state of the reaction.[15,16,17] The rare-earth ion stabilizes a distorted $[AsF_6]^-$ ion and so the energy of activation of hydrolysis is reduced relative to the

 © 2004 Wiley-VCH Verlag GmbH & Co. KGaA, Weinheim

free, undistorted anion. The Ln^{3+} cation may bind the F^- anion so strongly that the $[AsF_6]^-$ hydrolysis is not catalyzed; instead a complex was formed and the reaction is merely accelerated. This too, has counterparts in terms of some modes of enzyme inhibition.

In contrast to the observed process of hydrolysis of rare earth(III) fluoroarsenates(V) after suspension of the solid compounds in water, we noted no acceleration of the hydrolysis of the $[AsF_6]^-$ ion in a homogeneous aqueous solution to which a rare-earth trifluoride or a dissolved rare-earth ion had been added. This observation is explained by coordinative saturation of Ln^{III} (completely and strongly complexed or solvated) by either a F^- anion or a water molecule; the anion is thus protected from hydrolysis. The difference is analogous to inner- and outer-sphere electron transfer and the ease of redox reactions. We close by noting that solvation of the $[AsF_6]^-$ ion by neutral water as opposed to complexation with some cation will also kinetically stabilize this anion. Disappointingly, literature spectroscopic and structural data needed to further corroborate our understanding are lacking.

Experimental Section

General: All reagents were of analytical grade and all solutions were prepared using double-distilled water.

Sample Preparation: Coordination compounds of the general type $LnF_n(AsF_6)_{3-n}$ are sensitive to traces of moisture.[1] Therefore, test samples for determination of the total amount of each element, the $[AsF_6]^-$ ion, and free fluoride $(F^-)_f$ were prepared by weighing in a dry box, with a precision of ± 0.05 mg into air- and moisture-tight Teflon containers. The containers were cooled in liquid nitrogen in order to moderate subsequent reaction with water (20 mL) during suspension in a closed Erlenmeyer flask.

Analyses: Accurate and precise results of chemical analyses with an absolute error of less than 0.2−0.3 % for the determination of the Ln^{III} cation and the $[AsF_6]^-$ anion were obtained by the use of classical analytical methods;[18] a modified analytical technique with a fluoride-ion-selective electrode that enabled us to achieve an absolute error of analysis of less than 0.3 %[12] was applied to the determination of the fluoride anion. The amount of the $[AsF_6]^-$ anion was determined gravimetrically by precipitation with TPAC.[19] The amounts of $(F^-)_t$ and total fluoride in the precipitate $(F^-)_P$ were determined after total decomposition of the sample with alkali carbonate fusion using solid $KNaCO_3$. The amounts of $(F^-)_f$ and free fluoride $(F^-)_F$ in the filtrate after precipitation of the $[AsF_6]^-$ ions were estimated in aqueous suspension and acidic solution of the sample, respectively.[3,12] The analyses were performed by direct potentiometry with a fluoride-ion-selective electrode.[12] The amounts of rare earths(III) were determined by complexometric titrations with EDTA.[20,21,22] Solid $KAsF_6$ (Ozark Mahoning), solid LnF_3 (all from Alfa; the experiment with TmF_3 has not been conducted), standard solutions of Ln^{III} [C = 1000 mg/L, all from Merck, the Y^{III}, La^{III}, Ce^{III} and Tb^{III} standard solutions are declared as nitrates(V) in 2−3 % HNO_3 and the Ce^{III}, Pr^{III}, Nd^{III}, Sm^{III}, Eu^{III}, Gd^{III}, Dy^{III}, Ho^{III}, Er^{III}, Yb^{III} and Lu^{III} standard solutions are declared as the trivalent oxides in 2−3 % HNO_3], solid NaF (Merck), and $NdF(AsF_6)_2$ and $Nd(AsF_6)_3$ synthesized in our laboratories were used during the study of the stability of $[AsF_6]^-$ species.

Acknowledgments

J. F. L. thanks the American Chemical Society for funding for his European travel through its education division, international activities programs. We are grateful to Dr. David Berne (O.B.M.), Dr. Anna Berne, Prof. Boris Žemva, Prof. James S. Vincent and Prof. Ralph M. Pollack for their helpful comments related to this study and to Dr. Zoran Mazej for the preparation of the model compounds. We gratefully acknowledge the financial support of the Ministry of Education, Science and Sport of the Republic of Slovenia.

[1] M. Fele-Beuermann, K. Lutar, Z. Mazej, S. Milićev, B. Žemva, *J. Fluor. Chem.* **1998**, *89*, 83−89.
[2] M. Ponikvar, B. Pihlar, B. Žemva, *J. Fluor. Chem.* **2003**, *122*, 215−217.
[3] M. Ponikvar, B. Žemva, J. F. Liebman, *J. Fluor. Chem.* **2003**, *123*, 217−220.
[4] W. Lange, E. Müller, *Ber. Dtsch. Chem. Ges.* **1930**, *63*, 1058−1070.
[5] H. M. Dess, R. W. Parry, G. L. Vidale, *J. Am. Chem. Soc.* **1956**, *78*, 5730−5734.
[6] T. Klapötke, *Spectrosc. Lett.* **1989**, *22*, 183−190.
[7] H. R. Clark, M. M. Jones, *J. Am. Chem. Soc.* **1970**, *92*, 816−822.
[8] M. F. Ghorab, J. M. Winfield, *J. Fluor. Chem.* **1990**, *49*, 367−383.
[9] B. Sedej, *Talanta* **1976**, *23*, 335−336.
[10] M. Fele-Beuermann, S. Milićev, K. Lutar, B. Žemva, *Eur. J. Solid State, Inorg. Chem.* **1994**, *31*, 545−556.
[11] K. Lutar, H. Bormann, Z. Mazej, M. Tramšek, P. Benkič, B. Žemva, *J. Fluor. Chem.* **2000**, *101*, 155−160.
[12] M. Ponikvar, B. Sedej, B. Pihlar, B. Žemva, *Anal. Chim. Acta* **2000**, *418*, 113−118.
[13] G. M. Begun, A. C. Rutenberg, *Inorg. Chem.* **1967**, *6*, 2212−2216.
[14] V. Gutmann, *The Donor-acceptor approach to molecular interactions*, Plenum Press, New York, **1978**, p. 12−14.
[15] L. Pauling, *Am. Sci.* **1948**, *36*, 58.
[16] R. Wolfenden, *Acc. Chem. Res.* **1972**, *5*, 10−19.
[17] G. E. Lienhard, *Science* **1973**, *180*, 149−154.
[18] C. M. Beck II, *Anal. Chem.* **1991**, *63*, 993A−1003A.
[19] A. I. Vogel, *Vogel's textbook of quantitative inorganic analysis: Including elementary instrumental analysis*, Longman, London, 4th ed., **1978**, p. 482−483.
[20] J. S. Fritz, R. T. Oliver, D. J. Pietrzyk, *Anal. Chem.* **1958**, *30*, 111−114.
[21] G. Schwarzenbach, H. Flaschka, *Complexometric titrations*, Methuen, London, **1969**, p. 194−197.
[22] D. D. Perrin, *Masking and demasking of chemical reactions*, Wiley-Interscience, New York, **1970**, p. 56−57.

Received September 5, 2003
Early View Article
Published Online February 17, 2004

 © 2004 Wiley-VCH Verlag GmbH & Co. KGaA, Weinheim

EurJIC
European Journal of Inorganic Chemistry

Issue 7/2004

Pages 1353–1570

Papers available ahead of print in Early View at www.interscience.wiley.com

Earliest available Table of Contents:
Automatically, free of charge by e-mail through
www.interscience.wiley.com/alerts

COVER PICTURE

The cover picture shows how removal of interlayer water from a Zn–Al layered double hydroxide pillared by 1,1′-ferrocenedicarboxylate anions results in reorientation of the guest species and formation of a collapsed phase. Exposure of the collapsed phase to moist air leads to rapid recovery of the expanded phase. A material containing ferrocenecarboxylate anions has also been prepared and found to exhibit a basal spacing of 20.0 Å in the fully hydrated form, consistent with the presence of a bilayer of organometallic guest species. Details of the synthesis and characterization of these compounds are given in the article by M. Pillinger, I. S. Gonçalves et al. on p. 1389 ff.

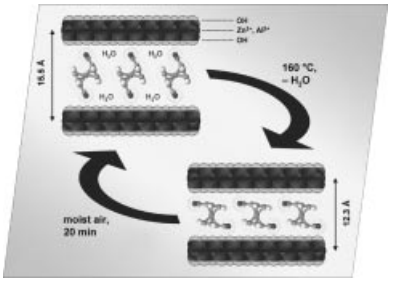

MICROREVIEW

Contents

1367 **J. Wachter**

Metal Telluride Clusters – From Small Molecules to Polyhedral Structures

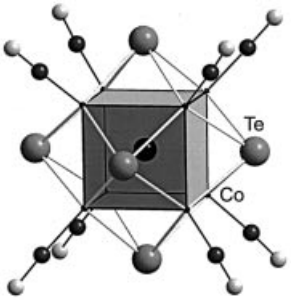

Keywords: Niobium / Tellurium / Polymetallic complexes / Clusters / Structures / Reactivity

 © 2004 Wiley-VCH Verlag GmbH & Co. KGaA, Weinheim

SHORT COMMUNICATIONS

1379 **I. V. Glukhov, M. Yu. Antipin, K. A. Lyssenko***

C−C Bond Variation in the 1-Phenyl-*o*-carborane: Steric versus Electronic Effects

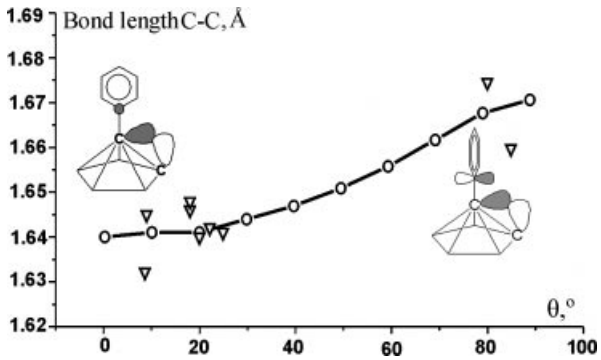

Keywords: Ab initio calculations / Atoms in molecules theory / C−C bond elongation / Carboranes / Electron density / Hydrogen bonds

1385 **D. Xiao, Y. Xu, Y. Hou, E. Wang,* S. Wang, Y. Li, L. Xu, C. Hu**

Synthesis and Structure of an Unprecedented Layered Vanadate Complex Containing Double-Helical Chains: $[\{Co^{III}(phen)_2\}_2V_8O_{23}]$

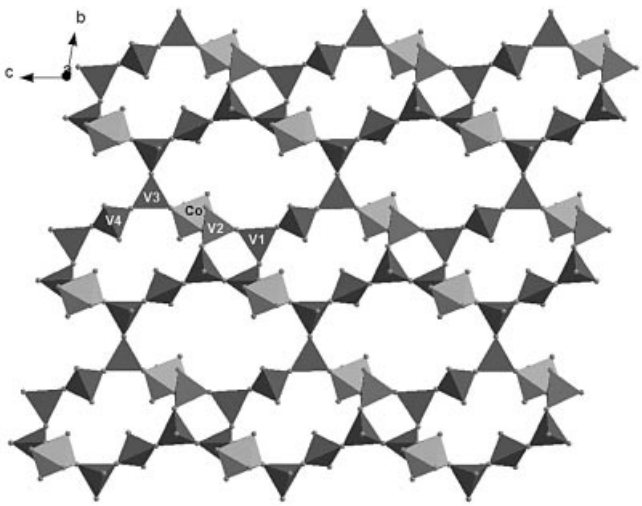

Keywords: Vanadium / Helical structures / Hydrothermal synthesis

FULL PAPERS

1389 **S. Gago, M. Pillinger,* T. M. Santos, J. Rocha, I. S. Gonçalves***

Synthesis and Properties of Zn−Al Layered Double Hydroxides Containing Ferrocenecarboxylate Anions

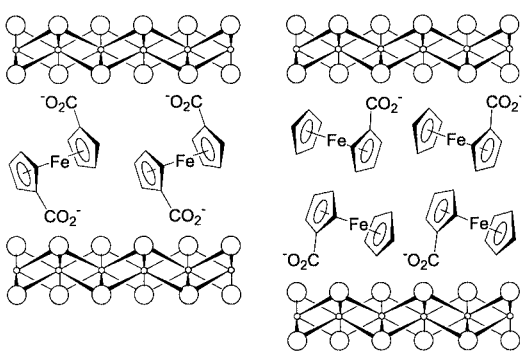

Keywords: Hydroxides / Layered compounds / Ferrocene / Host-guest systems / Organic-inorganic hybrid composites

 © 2004 Wiley-VCH Verlag GmbH & Co. KGaA, Weinheim

1396 **G. E. Herberich,* H. J. Eckenrath, T. Wagner, R. Wang**

Tetranuclear (Borole)rhodium Clusters with Hydrido and Methylthiolato Ligands − Structures of $[\{Rh(C_4H_4BMe)\}_4(\mu_3\text{-}H)(\mu_3\text{-}I)_3]$ and of $[\{Rh(C_4H_4BPh)\}_2(\mu\text{-}SMe)(\mu_3\text{-}SMe)]_2$ (2 *Rh*−*Rh*)

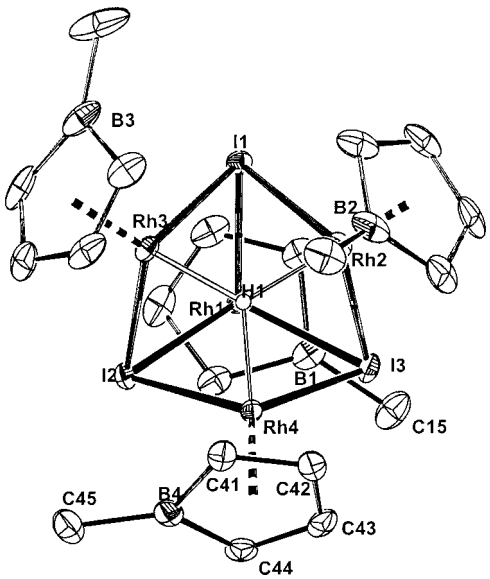

Keywords: Boron / Borole / Hydride ligands / Rhodium / S ligands

1402 **B. Grüner,* J. Bačkovský, R. Sillanpää, R. Kivekäs, I. Císařová, F. Teixidor, C. Viñas, B. Štíbr**

Amino-Substituted Ferra-bis(tricarbollides) − Metallatricarbaboranes Designed for Linear Molecular Constructions

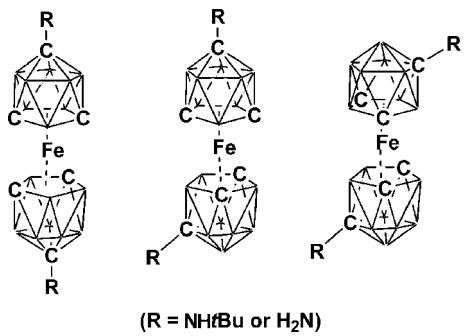

Keywords: Boranes / Carboranes / Metallacarboranes / Metallatricarbaboranes / Metallatricarbollides

1411 **A. M. Trzeciak,* B. Borak, Z. Ciunik, J. J. Ziółkowski, M. Fátima, C. Guedes da Silva, A. J. L. Pombeiro**

Structure, Electrochemistry and Hydroformylation Catalytic Activity of the Bis(pyrazolylborato)rhodium(I) Complexes [RhBp(CO)P] [P = $P(NC_4H_4)_3$, PPh_3, PCy_3, $P(C_6H_4OMe\text{-}4)_3$]

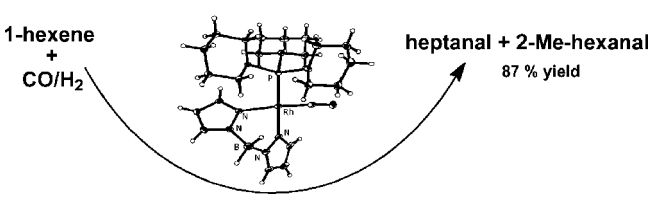

Keywords: Rhodium / N ligands / Electrochemistry / X-ray diffraction / Hydroformylation

 © 2004 Wiley-VCH Verlag GmbH & Co. KGaA, Weinheim

1420

P. C. Zachariadis, S. K. Hadjikakou,*
N. Hadjiliadis,* S. Skoulika,
A. Michaelides, J. Balzarini, E. De Clercq

Synthesis, Characterization and in Vitro Study of the Cytostatic and Antiviral Activity of New Polymeric Silver(I) Complexes with Ribbon Structures Derived from the Conjugated Heterocyclic Thioamide 2-Mercapto-3,4,5,6-tetrahydropyrimidine

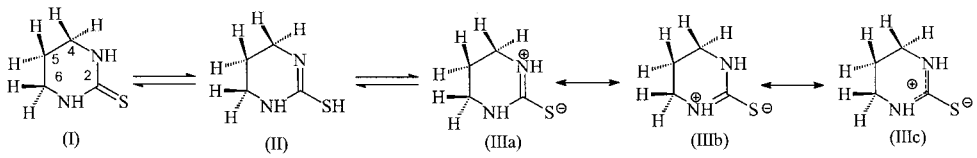

Keywords: Bioinorganic chemistry / Silver / X-ray diffraction / Cytostatic activity / Antiviral activity

1427

A. Myari, N. Hadjiliadis,* A. Garoufis*

Synthesis and Characterization of the Diastereomers Λ- and Δ-[Ru(bpy)$_2$(m-bpy-Gly-L-His-L-Lys)]Cl$_2$ – ^{1}H NMR Studies on their Interactions with the Deoxynucleotide Duplex d[(5′-CGCGAATTCGCG-3′)$_2$]

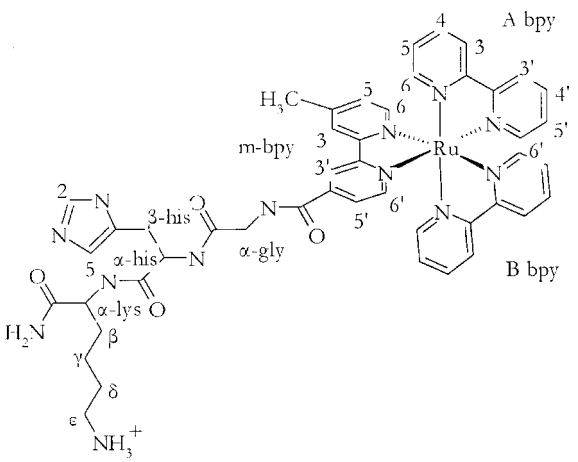

Keywords: Metallopeptides / Oligonucleotides / Ruthenium / Chemical nucleases / Groove

1440

P. A. N. Reddy, M. Nethaji,
A. R. Chakravarty*

Hydrolytic Cleavage of DNA by Ternary Amino Acid Schiff Base Copper(II) Complexes Having Planar Heterocyclic Ligands

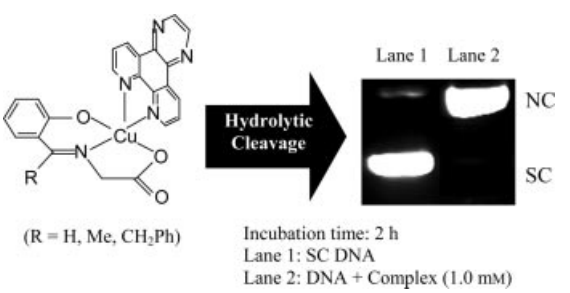

Keywords: Copper / Synthetic hydrolase / X-ray diffraction / Schiff bases / Phenanthroline bases

 © 2004 Wiley-VCH Verlag GmbH & Co. KGaA, Weinheim

1447 G. Calabrò, D. Drommi, C. Graiff, F. Faraone,* A. Tiripicchio

Rhodium(I), Palladium(II) and Platinum(II) Coordination Chemistry of the Short-Bite Chiral Ligands (S_c)-*N*,*N*-Bis(diphenylphosphanyl)-*sec*-butylamine, (R_a,R_a)-*N*,*N*-Bis(binaphthylphosphonito)phenylamine and (R_a,S_c)-*N*-(Diphenylphosphanyl)-*N*-(binaphthylphosphonito)-*sec*-butylamine

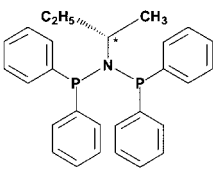

(S_c)-**1**

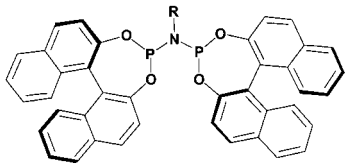

(R_a,R_a)-**2** R = Ph

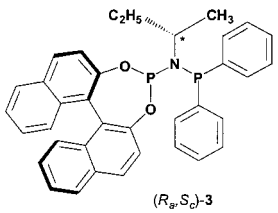

(R_a,S_c)-**3**

Keywords: Chiral ligands / Enantioselectivity / Hydroformylation / Palladium / Platinum / Rhodium

1454 D. Huang, W. Wang, X. Zhang, C. Chen, F. Chen, Q. Liu,* D. Liao, L. Li, L. Sun

Synthesis, Structural Characterizations and Magnetic Properties of a Series of Mono-, Di- and Polynuclear Manganese Pyridinecarboxylate Compounds

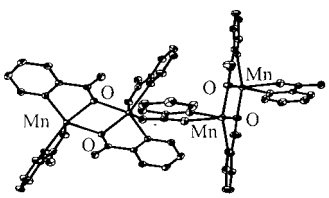

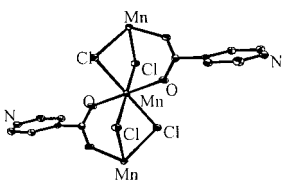

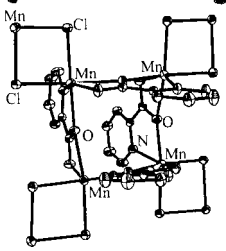

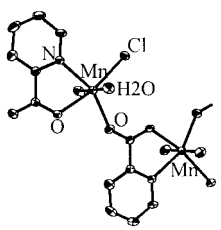

Keywords: Carboxylate ligands / Coordination polymers / Magnetic properties / Manganese / X-ray diffraction

1465 H.-F. Zhu, L.-Y. Kong, T. Okamura, J. Fan, W.-Y. Sun,* N. Ueyama

Syntheses, Crystal Structures and Electrospray Mass Spectra of Coordination Polymers of an *N*,*N*′-Bis(3-pyridylmethyl)-1,4-benzenebis(methylamine) Ligand and Silver(I) Salts

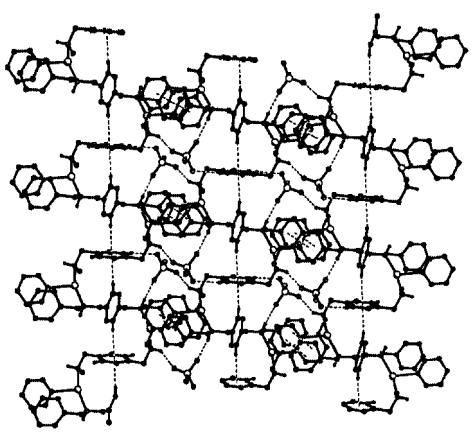

Keywords: Coordination polymers / Crystal engineering / Pi interactions / Silver / Supramolecular chemistry

 © 2004 Wiley-VCH Verlag GmbH & Co. KGaA, Weinheim

1474 **L. Yang, X. Shan, Q. Chen, Z. Wang, J. S. Ma***

The First Silver(I) Side-On η^2-Coordination Network Formed by Self-Assembly of Bis-(pyrrol-2-ylmethylene)hydrazine

Keywords: Coordination polymers / Hydrogen bonding / Schiff bases / Self-assembly / Silver

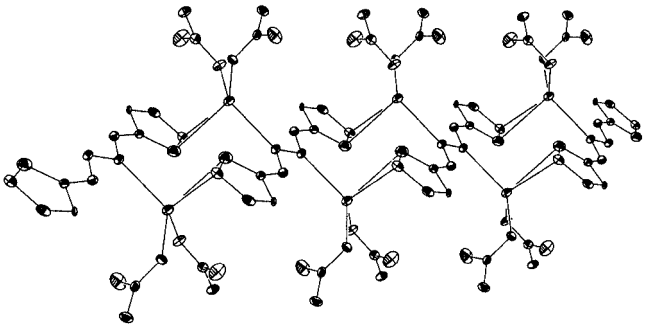

1478 **L. Yang, Q. Chen, Y. Li, S. Xiong, G. Li, J. S. Ma***

Self-Assembly of Bis(pyrrol-2-ylmethylene-amine) Ligands with Cu^{II} Controlled by Bridging [$-(CH_2)_n-$] Spacers and Weak Intermolecular C−H···Cu Hydrogen Bonding

Keywords: Copper / Helical structures / Hydrogen bonding / N ligands / Schiff bases / Self-assembly

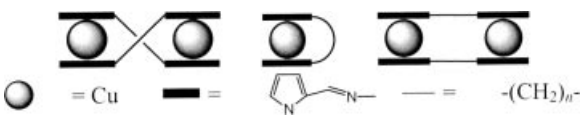

1488 **Y.-F. Hsu, J.-D. Chen***

Syntheses and Structural Characterization of Ag^I Complexes with the *N*,*N*′-Di(2-pyridyl)-oxamide Ligand

Keywords: Silver / Nitrogen heterocycles / Coordination polymers / Trinuclear complexes

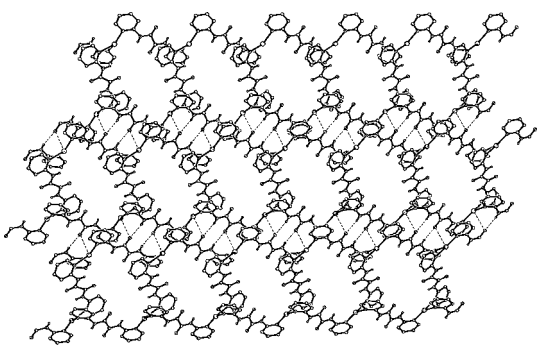

1494 **L. Busetto,* F. Marchetti, S. Zacchini, V. Zanotti**

Synthesis, Characterization and Reactivity of New (μ-Aminocarbyne)diruthenium Complexes Containing Alkynylimino Ligands

Keywords: Ruthenium / Dinuclear complexes / Carbynes / C−C coupling / Alkynylimino ligands

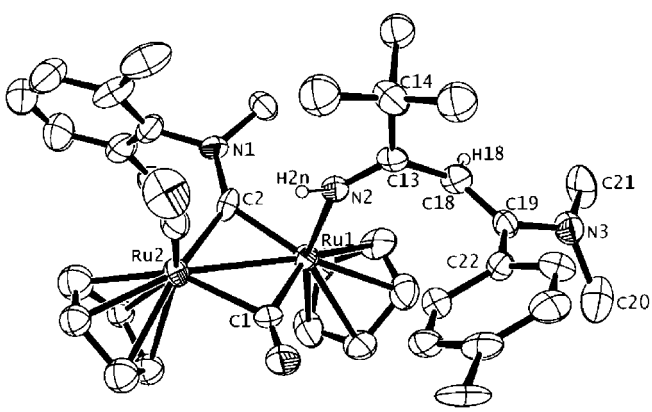

 © 2004 Wiley-VCH Verlag GmbH & Co. KGaA, Weinheim

1505 **A. Arrais, E. Diana, G. Gervasio,* R. Gobetto, D. Marabello, P. L. Stanghellini***

Synthesis, Structural and Spectroscopic Characterization of Four [(η^6-PAH)Cr(CO)$_3$] Complexes (PAH = Pyrene, Perylene, Chrysene, 1,2-Benzanthracene)

Keywords: Macrocyclic ligands / Chromium / X-ray diffraction / NMR spectroscopy / Vibrational spectroscopy / DFT calculations

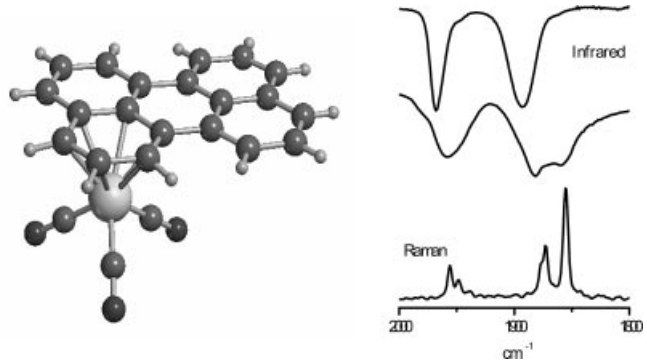

1514 **Y.-Q. Sun, M. Liang, W. Dong, G.-M. Yang,* D.-Z. Liao,* Z.-H. Jiang, S.-P. Yan, P. Cheng**

Hydrothermal Syntheses, Crystal Structures, Magnetism and Fluorescence Quenching of Oxamidato-Bridged Pentanuclear Cu$^{II}_4$Ln^{III} Complexes Containing Macrocyclic Ligands (Ln = Eu, Tb) and the Crystal Structure of a Hexanuclear Ni$^{II}_5$Sm^{III} Complex

Keywords: Hydrothermal synthesis / Macrocyclic ligands / Magnetic properties / Fluorescence

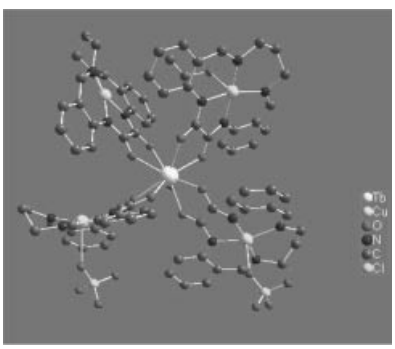

1522 **T. H. Kim, Y. C. Won, B. Y. Lee,* D. M. Shin, Y. K. Chung**

sp^3-C^1-Bridged 1,3-Me$_2$Cp/Amido Titanium and Zirconium Complexes and Their Reactivities towards Ethylene Polymerization

Keywords: Cyclopentadienyl / Zirconium / Titanium / Polymerization / Homogeneous catalysis

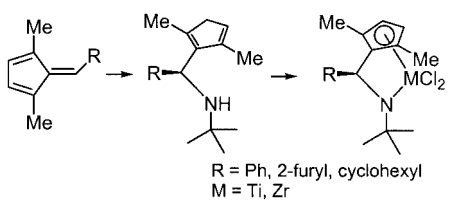

1530 **J.-P. Costes,* F. Dahan, G. Novitchi, V. Arion, S. Shova, J. Lipkowski**

Macrocyclic and Open-Chain Cu^{II}-4f (4f = Gd^{III}, Ce^{III}) Complexes with Planar Diamino Chains: Structures and Magnetic Properties

Keywords: Heterometallic complexes / Copper / Lanthanides / Macrocyclic ligands / Template synthesis / Magnetic properties

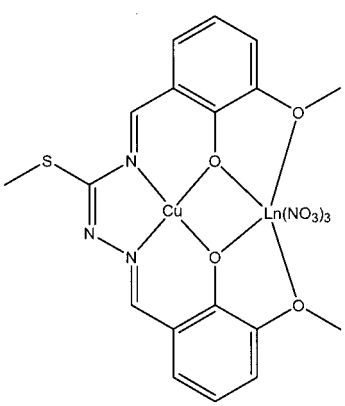

 © 2004 Wiley-VCH Verlag GmbH & Co. KGaA, Weinheim

1538 M. Mickoleit, K. Schmohl, M. Michalik, H. Oehme*

The Synthesis of Stable Intramolecularly Dialkylamino-Coordinated Silenes and Their Methyl Iodide Induced Isomerization into Cyclic Aminosilanes

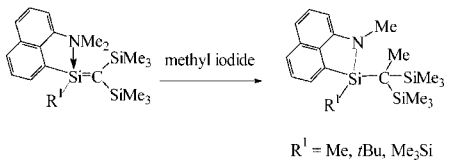

R^1 = Me, *t*Bu, Me_3Si

Keywords: Rearrangement / Silaethenes / Silanes / Silenes / Silicon

1545 O. Rotthaus, S. LeRoy, A. Tomas, K. M. Barkigia, I. Artaud*

A New Family of Low-Spin Co^{III} Bis(amidate) Complexes with Two *cis* or *trans* Cyanides

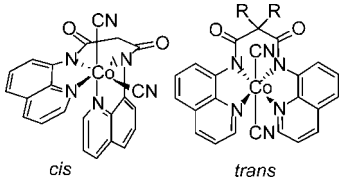

Keywords: Cobalt / Cyanides / N ligands

1552 G. Serratrice,* F. Biaso, F. Thomas, C. Béguin

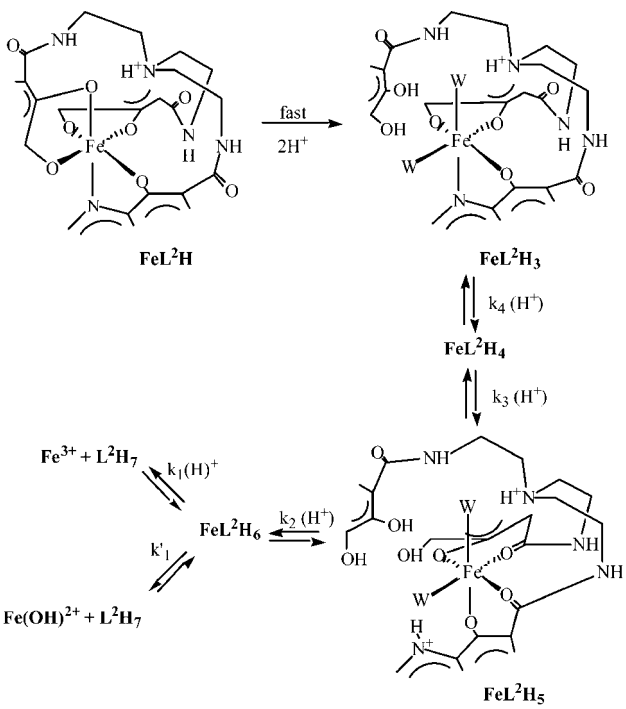

Mechanism of the Stepwise Dissociation of Fe^{III} Complexes with Tripodal Ligands as Siderophore Models

Keywords: Tripodal ligands / Iron / Kinetics and mechanisms / Dissociation / Catechol / 8-hydroxyquinoline

1566 X.-X. Hu, C.-L. Pan, J.-Q. Xu,* X.-B. Cui, G.-D. Yang, T.-G. Wang

One- and Three-Dimensional Coordination Polymers Containing Organic Ligands Produced Through in situ Hydrothermal Reactions

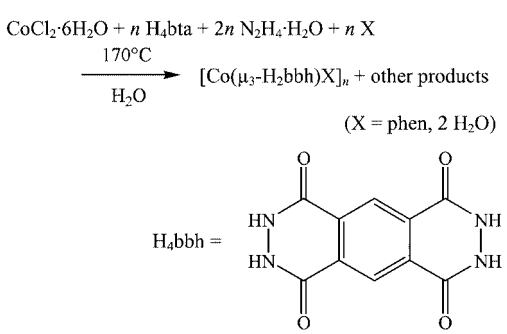

 © 2004 Wiley-VCH Verlag GmbH & Co. KGaA, Weinheim

Metal Telluride Clusters — From Small Molecules to Polyhedral Structures

Joachim Wachter[a]

Dedicated to Professor Dr. Henri Brunner on the occasion of his retirement

Keywords: Niobium / Tellurium / Polymetallic complexes / Clusters / Structures / Reactivity

Niobocene ditelluride complexes [(tBuC$_5$H$_4$)$_2$Nb(Te$_2$)H] (**1**) and [(C$_5$Me$_5$)$_2$Nb(Te$_2$H)] (**2**) are useful starting materials for the synthesis of heterometallic telluride complexes and clusters. The presence of free electron pairs, the propensity for Te–Te bond cleavage and the ability to eliminate Te ligands allow stepwise formation of polyhedral structures in reactions with binary transition metal carbonyl complexes or reactive organometallic fragments. Among the products are the first examples of organometallic derivatives of the elusive [MTe$_4$]$^{2-}$ ion. Ligand cross-transfer (CO versus Te) from one metal center to the other and subsequent charge separation lead to the formation of anionic metal telluride clusters and cationic carbonylniobocene species. The latter play a decisive role in tuning the electronic properties of the cluster units. Whereas the 17-electron fragment (tBuC$_5$H$_4$)$_2$Nb(CO) is directly anchored at the cluster cores by Te bridges, the 18-electron cation [Cp*$_2$Nb(CO)$_2$]$^+$ (Cp* = C$_5$Me$_5$) formed in situ is able to stabilize large and differently charged cluster anions. This is particularly the case in cobalt telluride cluster chemistry which is characterized by hexacapped cubic Co@Co$_8$ or heptacapped pentagonal-prismatic Co@Co$_{10}$ polyhedra. These compounds exhibit pronounced electron-sponge behavior, and crystallographic studies of differently charged clusters allow a correlation of different cluster charges and bond parameters important for understanding electronic structures.
(© Wiley-VCH Verlag GmbH & Co. KGaA, 69451 Weinheim, Germany, 2004)

Introduction

Metal telluride complexes are characterized by a wide and impressive structural variety[1] and recent developments focus on their ability for cluster aggregation.[2,3] Our interest in tellurium complex chemistry stems from the chemistry of chalcogen-rich organometallic complexes and the diversity of sulfur- and selenium-derived ligands.[4] During these studies we have found that bent dicyclopentadienylmetal fragments of the early transition metals are ideal organometallic substrates for the incorporation of chalcogenide ligands.[5] However, only a few comparative investigations have been carried out in which the coordination behavior of different chalcogens has been studied with the same transition metal,[6] although they reveal gradual but distinct changes when going from sulfur to tellurium.

It is a particular feature of the heavier group 5 metallocene fragments that they incorporate two chalcogenide ligands along with hydrogen in different coordination modes **A**–**C** (Scheme 1).[7,8] Obviously, the assembly of the main-group ligands not only depends on the nature of the chalcogen, but also on the substituents at the cyclopentadienyl ligand. Ligand rearrangements by breaking chalcogen–hydrogen and/or chalcogen–chalcogen bonds may lead to interconversion of one form into another. For example, [Cp*$_2$Nb(η-Se$_2$H)] (form **A**) may be easily converted by light into the corresponding forms **B** and **C**.[8b]

The presence of free electron pairs in metallocene dichalcogenides is an important prerequisite for the formation of

[a] Institut für Anorganische Chemie, Universität Regensburg, 93040 Regensburg, Germany

Joachim Wachter passed his Ph.D. in 1976 at the Universität Regensburg under the supervision of Prof. Dr. H. Brunner, after studying chemistry at the Universität München. In 1978/1979 he spent a year as a postdoctoral researcher with Prof. J. G. Riess in Nice. Since 1977 he has conducted research at the Universität Regensburg, which has led to more than 120 publications. His main scientific interests are the organometallic chemistry of the chalcogens, mixed ligands of the Group 15 and 16 elements, and the chemistry of metal telluride clusters.

MICROREVIEWS: This feature introduces the readers to the authors' research through a concise overview of the selected topic. Reference to important work from others in the field is included.

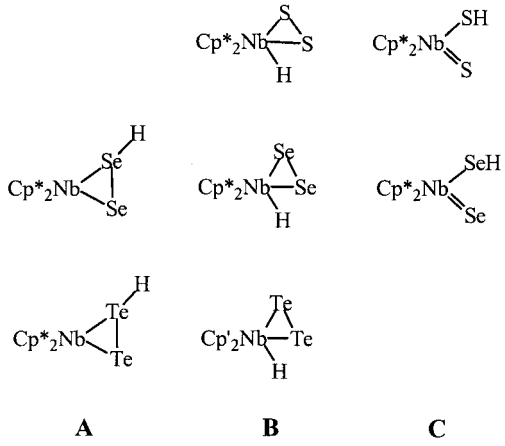

Scheme 1. Examples of the coordination modes of dichalcogenide ligands in $[Cp^*_2NbX_2H]$ complexes ($Cp^* = C_5Me_5$; X = S, Se, Te) and $[(t\text{BuC}_5H_4)_2Nb(Te_2)H]$

polymetallic compounds,[9] whereas the role of the different coordination modes of the hydrogen ligands is not yet fully understood. A specific feature, particularly in niobocene ditelluride chemistry, is the elimination of Te^0 or Te^{2-} building blocks and their transfer onto reactive organometallic compounds followed by the assembly of polyhedral clusters. The diversity of the obtained results is summarized in this microreview.

Activation of Elemental Tellurium in Hydridic Niobocene Derivatives

Convenient synthetic methods involve the use of hydride or boranate ligands containing alkyl-substituted niobocene derivatives. In both cases identical results are obtained. Thus, reaction of $[(t\text{BuC}_5H_4)_2NbH_3]$ or $[(t\text{BuC}_5H_4)_2NbBH_4]$ with elemental tellurium in THF forms $[(t\text{BuC}_5H_4)_2Nb(Te_2)H]$ (**1**) in good yields [Equation (1a)].[10] Replacement of the $t\text{BuC}_5H_4$ ligand by the more electron-rich peralkylated Cp* ligand in the analogous reactions gives $[Cp^*_2Nb(Te_2H)]$ (**2**) in excellent yields [Equation (1b)].[11] These results show that the formation of the structure types **A** or **B** for **1** and **2** depends more on the nature of the cyclopentadienyl ligands than on the nature of the hydride source.

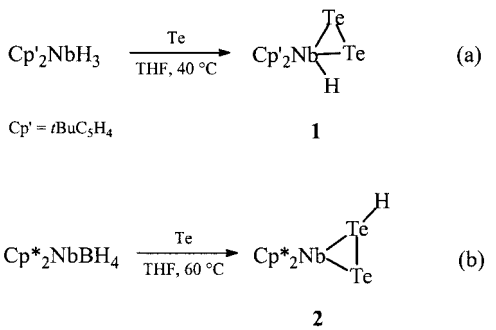

(1)

NMR spectroscopy alone is not suitable to assign complexes **1** and **2** to one of the structural types shown in Scheme 1. However, the presence of a Te_2 ligand along with a hydride ion in the dark orange $[(t\text{BuC}_5H_4)_2Nb(Te_2)H]$ (**1**) follows definitively from the crystal structure of $[(t\text{BuC}_5H_4)_2Nb(Te_2)H{\cdot}Cr(CO)_5]$ (**3**), which is the product of the addition of the Lewis acid fragment $Cr(CO)_5$ to **1** (Scheme 2a). Structural analogues of **1** are $[Cp^*_2Nb(S_2)H]$,[7] $[(t\text{BuC}_5H_4)_2Ta(S_2)H]$,[12] and $[Cp^*_2Ta(Te_2)H]$.[13]

The orange complex $[Cp^*_2Nb(Te_2H)]$ (**2**) exhibits in its ^{1}H NMR spectrum a hydride resonance at $\delta = -3.55$ ppm, whereas in the ^{125}Te NMR spectrum only one resonance ($\delta = -207.9$ ppm) is found, probably due to partially relaxed scalar ^{125}Te-^{93}Nb interactions.[11] The ^{1}H NMR spectrum of $[(C_5Me_4Et)_2Nb(Te_2H)]$ exhibits a symmetrical 14-line signal for the diastereotopic CH_2 protons of both ethyl groups, in agreement with a chiral center at one of the Te atoms.[14] A nearly identical pattern has been observed in $[(C_5Me_4Et)_2Nb(Se_2H)]$.[8b]

Polymetallic Telluride Complexes from $[(t\text{BuC}_5H_4)_2Nb(Te_2)H]$

As already noted, $[(t\text{BuC}_5H_4)_2Nb(Te_2)H]$ reacts with $[Cr(CO)_5THF]$ to give the dimetallic adduct $[(t\text{BuC}_5H_4)_2Nb(Te_2)H{\cdot}Cr(CO)_5]$ (**3**) in 90% yield. The crystal structure of **3** provides evidence for the presence of a $\mu,\eta^{1:2}$-Te_2 ligand and allows unambiguous localization of the hydride ion directly bonded to the Nb center (Figure 1).[10] Therefore, complex **3** is one of the few structurally characterized ditelluride complexes of the structural type **B**. The Te−Te distance of 2.695(1) Å is similar to those in other complexes containing side-on coordinated η^2-Te_2.[6b,6e,15]

A side-product in the synthesis of **1** is the homonuclear polymetallic complex $[(t\text{BuC}_5H_4)_6Nb_4Te_4O]$ (**4**), the formation of which depends on the residual concentration of air in the reaction mixture. Small amounts of **4** also form upon heating solutions of **1** (Scheme 2b).

The crystal structure of **4** shows two planar Nb_2Te_2 rings (Figure 2) connected by a linear oxygen bridge. Each of the "outer" Nb atoms [Nb(1), Nb(4)] is part of a niobocene fragment, whereas the coordination sphere of the "inner" Nb atoms [Nb(2), Nb(3)] is completed by only one ($t\text{BuC}_5H_4$) ligand. The linearity of the Nb−O−Nb bridge [angle (Nb−O−Nb) = 177.1(1)°] and the electron deficiency of the "inner" Nb atoms [Nb(2), Nb(3)] suggests the contribution of p_π oxygen orbitals. A similar structure has been found in $[(t\text{BuC}_5H_4)_6V_4S_4O]$.[16]

Formally, complex **4** contains four Nb^{IV} centers, but ^{1}H NMR spectroscopy indicates the diamagnetic nature of the molecule. This behavior seems to be characteristic for compounds with four-membered Nb_2Te_2 rings and may be explained by through-space Nb−Nb coupling (see below). In the case of **4** the Nb−Nb distances (3.43 Å) are only slightly longer than those in the related diamagnetic complex $[(C_5H_5)_2Nb(\mu\text{-}S)]_2$ [*d*(Nb−Nb) 3.2340(8) Å].[17]

 © 2004 Wiley-VCH Verlag GmbH & Co. KGaA, Weinheim

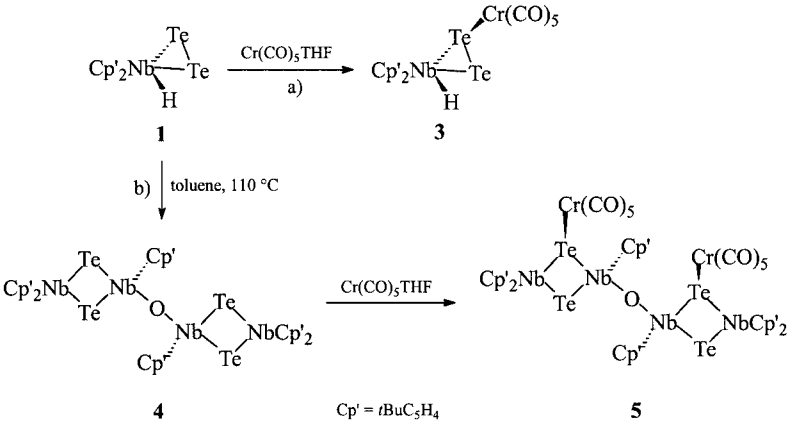

Scheme 2

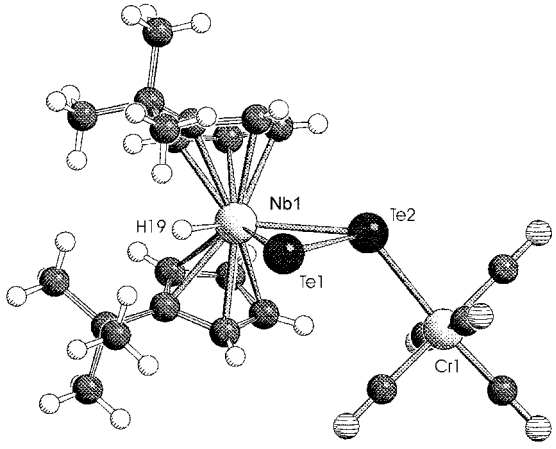

Figure 1. Molecular structure of $[(t\mathrm{BuC_5H_4})_2\mathrm{Nb(Te_2)H{\cdot}Cr(CO)_5}]$ (**3**)

The Te bridges of **4** are still accessible for the addition of two $Cr(CO)_5$ fragments although the steric situation of the bridges seems to be rather crowded (Scheme 2b). In the resulting complex $[(t\mathrm{BuC_5H_4})_6\mathrm{Nb_4Te_4O{\cdot}2Cr(CO)_5}]$ (**5**) the overall geometry of the starting complex has been preserved, but now the bulky $Cr(CO)_5$ groups are able to block the rotation around the Cp′−Nb bonds at room temperature, as follows from ^{1}H NMR spectroscopy.[10]

The reaction of $[(t\mathrm{BuC_5H_4})_2\mathrm{Nb(Te_2)H}]$ (**1**) with $[Fe_2(CO)_9]$ formally proceeds with insertion of an $Fe_2(CO)_6$ unit into the Te−Te bond of **1** (Scheme 3).[18] The resulting heterotrimetallic compound $[\{(t\mathrm{BuC_5H_4})_2\mathrm{NbH(Te)_2}\}\mathrm{Fe_2(CO)_6}]$ (**6**) forms the monoadduct $[\{(t\mathrm{BuC_5H_4})_2\mathrm{NbH(Te)_2Fe_2(CO)_6}\}{\cdot}\mathrm{Cr(CO)_5}]$ (**7**) with $[Cr(CO)_5THF]$ in nearly quantitative yield. ^{1}H NMR investigations reveal the presence of two isomers at room temperature in nearly equal amounts. Crystallization at −24 °C affords separation of the sterically more crowded *vic*-**7**. Its crystal structure (Figure 3) proves that the incoming $Cr(CO)_5$ fragment is

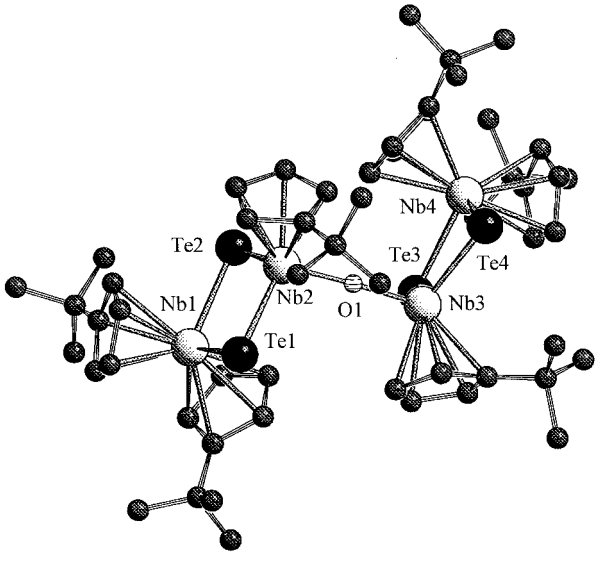

Figure 2. Molecular structure of $[(t\mathrm{BuC_5H_4})_6\mathrm{Nb_4Te_4O}]$ (**4**)

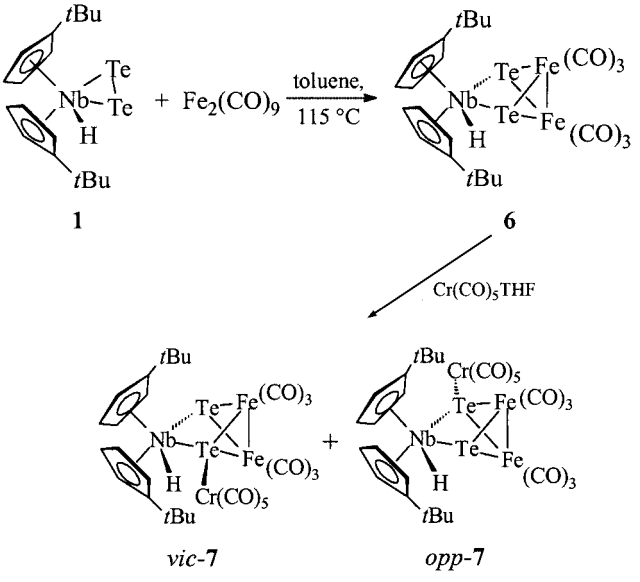

Scheme 3

 © 2004 Wiley-VCH Verlag GmbH & Co. KGaA, Weinheim

attached at the central Te atom and in the vicinity (*vic*) of the Nb−H moiety. Although the latter could not be localized directly, its presence follows from its stereochemical activity in the structure and from the ^{1}H NMR spectra.

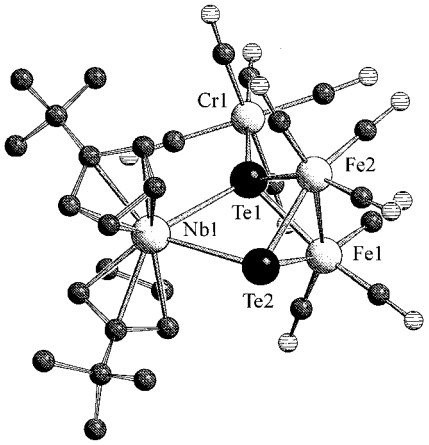

Figure 3. Molecular structure of *vic*-[{(tBuC$_5$H$_4$)$_2$-NbH(Te)$_2$Fe$_2$(CO)$_6$}·Cr(CO)$_5$] (*vic*-**7**); the hydrogen atom at Nb(1) may be located close to Te(1)[18]

Complexes **6** and **7** are some more examples of compounds with an Fe_2Te_2 core.[19] Generally, such derivatives are formal insertion products of a two-electron metal fragment into the Te−Te bond of [Fe$_2$(μ-Te$_2$)(CO)$_6$].[20]

The stability of the $NbTe_2Fe_2$ framework in **6** and **7** occurs for different reasons, because replacement of tBuC$_5$H$_4$ by the Cp* ligand results in a ligand (CO, Te) cross-transfer from one metal center to the other. A concomitant charge separation leads to the formation of distinct [Cp*$_2$Nb(CO)$_2$]$^+$ and [Fe$_3$H(μ$_3$-Te)(CO)$_9$]$^-$ ions [Equation (2)].[21] CO-containing intermediate products, which may be analogues of **6**, can be observed by IR spectroscopy, but they are not stable enough for isolation.

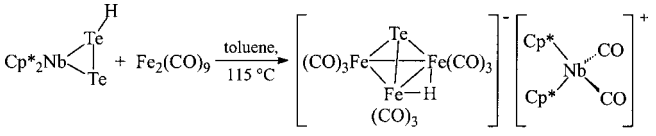

2 **8** (2)

Oxidative Elimination of Active Te^0 from [Cp*$_2$Nb(Te$_2$H)] (2)

Solutions of **2** are stable towards rearrangement into structural forms **B** and **C**. They are also stable with respect to spontaneous Te elimination, but with PPh_3 the corresponding phosphane oxide and elemental tellurium are formed, probably due to the presence of traces of air. No proof has been found for the existence of pseudo-tetrahedral [Cp*$_2$Nb(=Te)H], although the structurally related [Cp*$_2$Ta(=Te)H] is accessible in a similar reaction from [Cp*$_2$Ta(Te$_2$)H].[13]

In the presence of reactive transition metal fragments there is no precipitation of grey tellurium. Instead, depending on the reaction conditions a series of homo- and heterometallic telluride complexes or even clusters is formed which are the subject of the following sections.

A nice example of the elimination of Te^0 from [Cp*$_2$Nb(Te$_2$H)] is its reaction with an excess of [M(CO)$_5$(THF)] (M = Cr, W).[11] The resulting red-brown compounds *cyclo*-Te$_4$[M(CO)$_5$]$_4$ (**8**) are the first organometallic derivatives of a neutral molecular tellurium ring [Equation (3)].[12] The central feature of the structure of **8**-Cr is a Te$_4$ ring [d(Te−Te) = 2.854(3) Å mean], which is forced by the attached Cr(CO)$_5$ fragments into D_{2d} butterfly geometry (Figure 4). EHMO calculations carried out on the free hypothetical *cyclo*-Te$_4$ ring show that the square-planar (D_{4h}) structure is only 0.2 eV less favorable in total energies than the folded (D_{2d}) structure.[11]

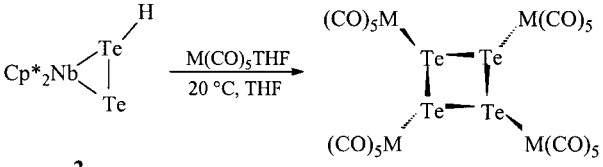

2 **8** (3)

M = Cr, W

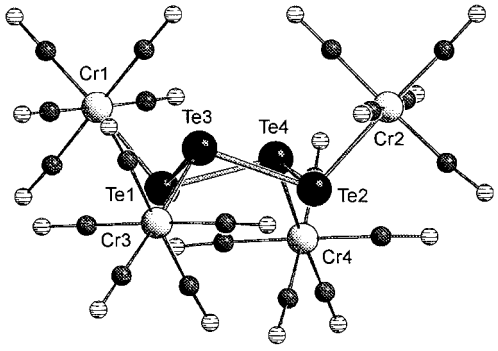

Figure 4. Side view of the structure of *cyclo*-Te$_4$[Cr(CO)$_5$]$_4$ (**8**-Cr)[11]

Another example of the incorporation of Te^0 from **2** into a Lewis acid metal fragment was observed in the reaction of **2** with [(C$_5$H$_5$)Mn(CO)$_2$(THF)], which gave [{(C$_5$H$_5$)Mn(CO)$_2$}$_3$(μ$_3$-Te)] in 80% yield.[25] This complex, which was first synthesized 1983 by Herberhold et al., possesses a trigonal-planar Te center.[26]

Interestingly, [Cp*$_2$Nb(Se$_2$H)], which is isostructural with **2**, gives a completely different result under identical reaction conditions: the carbonyl-free heterotrimetallic complex **9** is formed as the final product [Equation (4)],[23] which belongs to the class of *pseudo*-tetrahedral MX_4 compounds and which will be discussed shortly.[23,24] The observation of CO absorptions during the reaction by IR spectroscopy may be a hint for the addition of Cr(CO)$_5$ to one or more lone-pair electrons of the Nb(Se$_2$H) moiety [Equation (4)]. By contrast, the sterically less demanding tBuC$_5$H$_4$ ligand in **1** allows formation of a stable Cr(CO)$_5$ adduct

 © 2004 Wiley-VCH Verlag GmbH & Co. KGaA, Weinheim

(Scheme 2). The related complex $[(t\mathrm{BuC_5H_4})_2\mathrm{Ta(S_2)H}]$ can even add two $Cr(CO)_5$ fragments.[9]

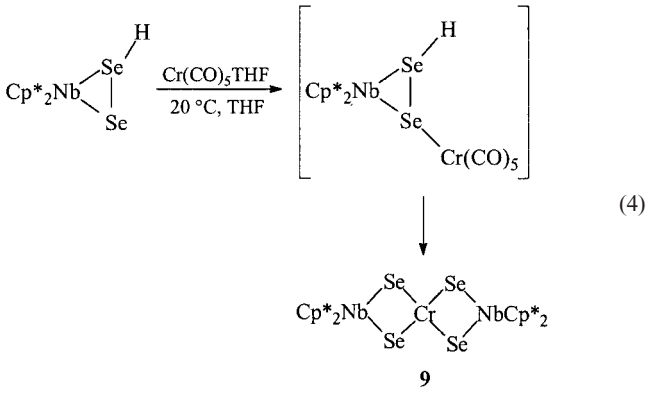

(4)

9

The Quest for Derivatives of the Tetratellurometalate Ion

Molecular polymetallic chalcogenido complexes containing a central *pseudo*-tetrahedral MX_4 (X = S, Se) unit show interesting electronic and optical properties.[27,28] Although it is known that replacement of sulfur by selenium increases nonlinear optical properties by a heavy metal effect,[29] the corresponding tetratellurometalates are still unknown. Examples of tellurometalates with coordination number four, in which the metal center is surrounded by polytelluride ligands, like in $[AuTe_7]^{3-}$, are known.[30]

Dimetallic tetrathio- and tetraselenometalates of the type $[(Cp^*_2Nb)_2MX_4]$ (M = Cr, Mo; X = S, Se) may be prepared from $[Cp^*_2Nb(\eta^2\text{-}X_2)H]$ derivatives and binary carbonyl transition metal complexes {e.g. $[M(CO)_6]$, $[Fe_2(CO)_9]$, $[Co_2(CO)_8]$} in boiling toluene.[23,24] An alternative route is the thermal decomposition of solutions of $[(t\mathrm{BuC_5H_4})_2\mathrm{Ta(S_2)H{\cdot}Cr(CO)_5}]$,[9] $[Cp^*_2\mathrm{Nb(S_2)H{\cdot}Cr(CO)_5}]$,[31] and the elusive $[Cp^*_2\mathrm{Nb(Se_2)H{\cdot}Cr(CO)_5}]$, respectively [Equation (4)].

Attempts to convert solutions of **3** in boiling toluene into $[(Cp^*_2Nb)_2CrTe_4]$ end up with green-black $[(t\mathrm{BuC_5H_4})_4\mathrm{Nb_2Te_2}]$ (**10**) along with small amounts of **4** [Equation (5)]. Complex **10** may be obtained in still better yield from the reaction of **1** with $[Cr(CO)_6]$ in boiling toluene.[31] The crystal structure of **10** contains a planar rhombohedral Nb_2Te_2 core to which four Cp′ ligands are coordinated. The conformation of the $(t\mathrm{BuC_5H_4})$ ligands is that of the achiral *meso* diastereomer (Figure 5). ^{1}H NMR spectroscopic investigations reveal a restricted rotation around the $(t\mathrm{BuC_5H_4})$–Nb bonds at −90 °C. Although a similar conformation has been found in the related complex $[(t\mathrm{BuC_5H_4})_4\mathrm{Zr_2Te_2}]$, there is no spectroscopic evidence for a restricted rotation around the $(t\mathrm{BuC_5H_4})$–Zr axis.[32]

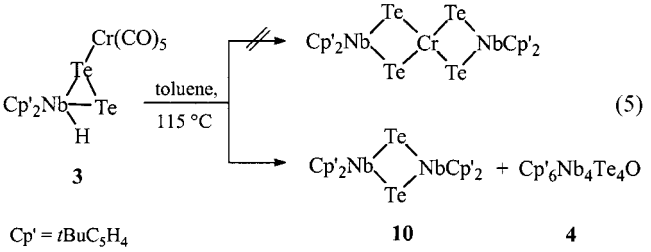

(5)

3 **10** **4**

Cp′ = $t\mathrm{BuC_5H_4}$

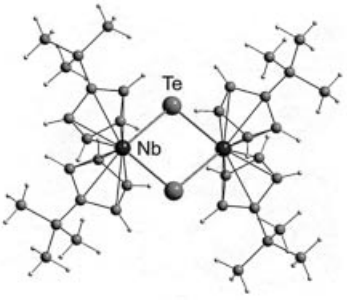

Figure 5. Molecular structure of $[(t\mathrm{BuC_5H_4})_4\mathrm{Nb_2Te_2}]$ (**10**)[31]

The bonding system within the four-membered Nb_2Te_2 ring in **10** is defined by a long transannular Te–Te distance [d = 4.262(1) Å] of nonbonding character and an Nb–Nb distance [3.647(1) Å], which is still longer than d(Nb–Nb) in **4**, but which is again consistent, according to DFT calculations,[10] with a through-space Nb–Nb coupling.

The μ_2-Te bridges in **10** exhibit nucleophilic character. Thus, reaction of **10** with MeI gives the violet salts $[(t\mathrm{BuC_5H_4})_4\mathrm{Nb_2Te(MeTe)}]\mathrm{I}$ or $[\mathrm{Cp'_4Nb_2(MeTe)_2}]\mathrm{I_2}$ according to the employed stoichiometry (1 or 2 equiv. of MeI).[10] Crystallographic studies of the cations reveal that addition of the electrophiles does not significantly affect the intraannular forces between opposite atoms in the Nb_2Te_2 ring.

Whereas reaction of **1** with $[Cr(CO)_6]$ in boiling toluene gives chromium-free **10** [Equation (6)], $[W(CO)_6]$ does not react under similar conditions. However, in decane at 140 °C the red tetrametallic complex $[\{(t\mathrm{BuC_5H_4})_4\mathrm{Nb_2WTe_4}\}\mathrm{W(CO)_4}]$ (**11**) is formed in 54% yield [Equation (6)].[31] According to X-ray crystallography, complex **11** contains a slightly distorted WTe_4 tetrahedron to which two niobocene fragments are coordinated (Figure 6). A $W(CO)_4$ fragment is inserted between two of the Te bridges of the central WTe_4 tetrahedron. Formally, complex **11** may be described as an organometallic derivative of the hitherto unknown $[WTe_4]^{2-}$ ion. This view is in agreement with W–Te bond lengths [average 2.574(2) Å] around W(1) in the range of W–Te double bonds and a *pseudo*-tetrahedral arrangement of the Te atoms around W(1).[33] Accordingly, the distances W(2)–Te(2) and W(2)–Te(3) are longer by 0.25 Å. The description of the entire metal–ligand bond system needs to take into account delocalization over the heavy atom skeleton, except for W(2).[31]

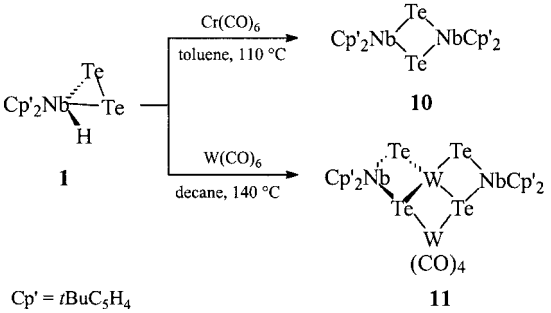

(6)

1 **10** **11**

Cp′ = $t\mathrm{BuC_5H_4}$

 © 2004 Wiley-VCH Verlag GmbH & Co. KGaA, Weinheim

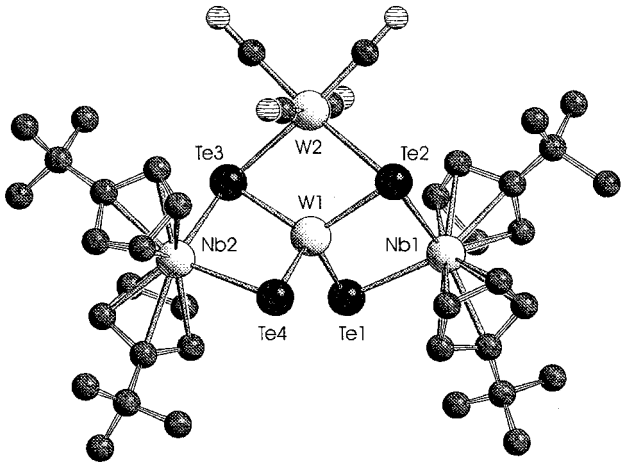

Figure 6. Molecular structure of $[\{(t\mathrm{BuC_5H_4})_4Nb_2WTe_4\}W(CO)_4]$ (**11**)[31]

A second example of a tetratellurometalate complex is $[(Cp^*_2Nb)_2NiTe_4]$ (**12**). The black-violet diamagnetic compound is accessible from the reaction of $[Ni(COD)_2]$ with $[Cp^*_2Nb(Te_2H)]$ in boiling toluene. The reaction with $[(t\mathrm{BuC_5H_4})_2Nb(Te_2)H]$ under analogous conditions does not give well-defined products.[34]

At first glance the molecular structure of **12** resembles those of the above-described bis(niobocene) tetrachalcogenidometalates. However, there is a remarkable distortion of the central $NiTe_4$ tetrahedron (Figure 7). This is expressed by Te−Ni−Te angles which split into three different groups between 78.2(1) and 139.2(1)° when compared to the WTe_4 core in **11**. The distortion is also expressed by interannular Te1···Te3 and Te2···Te4 distances of 3.100(7) and 3.122(7) Å, which may even be bonding interactions. In contrast, the transannular Te···Te distances within each of the $NiNbTe_2$ cycles are much longer (4.19 Å mean). Interestingly, complexes involving Ni_2Te_2 four-membered rings, like $[\{(\mathrm{triphos})Ni\}_2(\mu\text{-}Te)_2]$ [d(Te−Te) = 2.802(1) Å][35] and $[\{(C_5H\mathit{i}Pr_4)Ni\}_2(\mu\text{-}Te)_2]$ [d(Te−Te) = 3.052(5) Å] exhibit Te−Te distances that clearly have bonding character.[36]

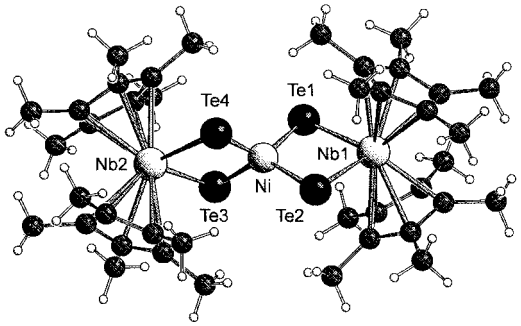

Figure 7. Molecular structure of $[(Cp^*_2Nb)_2NiTe_4]$ (**12**)[34]

Like $[(Cp^*_2Nb)_2CrSe_4]$ (**9**),[23] complex **12** is able to undergo two reversible oxidation steps and two reversible reduction steps in cyclic voltammetry.[37] The corresponding paramagnetic cation $[\mathbf{12}]^+$ has been obtained by oxidation of **12** with $[C_5H_5)_2Fe]^+$, but only in the presence of a chemically relatively inert anion, like $[BPh_4]^-$.

Formation of Metal Telluride Clusters

It has already been shown that insertion of an $Fe_2(CO)_6$ unit from $[Fe_2(CO)_9]$ into the Te−Te bond of **1** gives the heterotrimetallic complex **6** (Scheme 3). However, the $NbTe_2Fe_2$ framework seems to be destabilized by introduction of the Cp* ligand. Thus, reaction of **2** with $[Fe_2(CO)_9]$ finally results in a reductive elimination of Te^{2-}, which serves as a glue for the formation of the $[Fe_3H(\mu_3\text{-}Te)(CO)_9]^-$ cluster anion [Equation (2)].[19b,19g,38] The counterion is the rather stable $[Cp^*_2Nb(CO)_2]^+$ ion, which may have been formed by CO ligand transfer from enneacarbonyldiiron onto the niobocene fragment. In the following sections we will show that the in situ formation of this Nb^{III} cation exerts a considerable stabilization effect on anionic transition metal telluride clusters. It is striking that a corresponding $[(t\mathrm{BuC_5H_4})_2Nb(CO)_2]^+$ ion has not yet been observed thus far.

The reaction of **2** with $[Ru_3(CO)_{12}]$ in boiling toluene gives a rather heterogeneous mixture of neutral and salt-like carbonylruthenium clusters with tellurido and hydrido ligands (Scheme 4).[39] $[Ru_3(\mu_2\text{-}H)_2(\mu_3\text{-}Te)(CO)_9]$[40] (**13**; 11% yield) has been characterized indirectly by crystallography of $[Ru_3(\mu_2\text{-}H)_2(\mu_3\text{-}Te)(CO)_7(\mathrm{dppm})]$, which is a CO substitution product from the reaction of **13** with bis(diphenylphosphanyl)methane (dppm). Along with the already known cluster $[Ru_4(\mu_4\text{-}Te)_2(CO)_{11}]$ (**14**; 27%),[41] $[Cp^*_2Nb(CO)_2][Ru_5H(\mu_4\text{-}Te)(CO)_{14}]$ {$[Cp^*_2Nb(CO)_2]$[**15**]; 31%} and $[Cp^*_2Nb(CO)_2][Ru_6H(\mu_3\text{-}Te)_3(CO)_{15}]$ {$[Cp^*_2Nb(CO)_2]$[**16**]; 4%} have been isolated and characterized by X-ray crystallography. Cluster **14** exhibits inter-

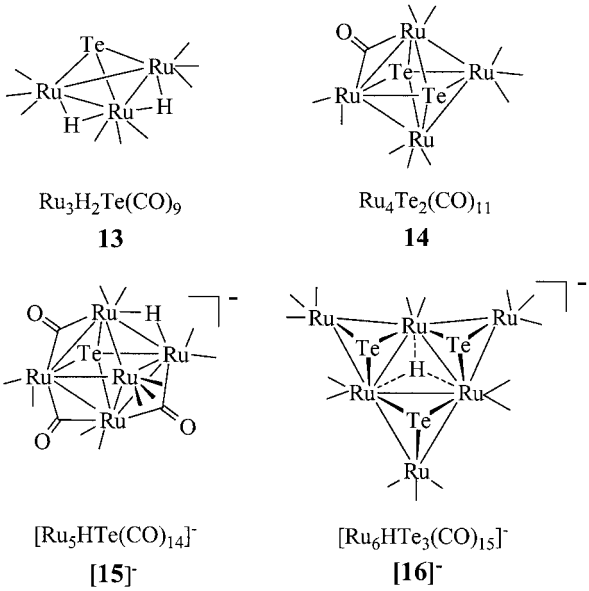

Scheme 4. Neutral and anionic clusters from the reaction of **2** with $[Ru_3(CO)_{12}]$ in boiling toluene; the corresponding cation in the case of $[\mathbf{15}]^-$ and $[\mathbf{16}]^-$ is $[Cp^*_2Nb(CO)_2]^+$

 © 2004 Wiley-VCH Verlag GmbH & Co. KGaA, Weinheim

esting redox properties: The reversible uptake of up to four electrons may be accompanied by structural rearrangements as suggested by theoretical studies.[39]

These structural motifs extend the knowledge of carbonylruthenium chalcogenide clusters.[42] The structure of the 74-electron anion $[\mathbf{15}]^-$ may be described by a slightly distorted Ru_5 square pyramid spanned by a μ_4-Te ligand. Thus, it belongs to the class of $[Ru_5X(CO)_{15}]$ clusters (X = S, Se, Te), of which only $[Ru_5S(CO)_{15}]$ has been synthesized thus far.[43] The triangular structure of $[\mathbf{16}]^-$ is mainly composed of three edge-linked Ru_3Te tetrahedra, in close analogy to the structure of $[Ru_6HS_3(CO)_{15}]^-$.[44]

It is striking that the CO/Ru ratio in all compounds is much higher than two, although attempts to increase the tellurium content by varying the stoichiometry and reaction conditions were not successful. The origin of the hydrido ligands in **13**, $[\mathbf{15}]^-$ and $[\mathbf{16}]^-$ may rather be ascribed to abstraction from the solvent[40,45] than hydrogen transfer from **2**. In this context it may be of interest that $[(t\mathrm{BuC_5H_4})_2\mathrm{Nb(Te_2)H}]$ does not give reasonable results under analogous reaction conditions.[46]

Another still more complex system concerns the reaction of $[\mathrm{Cp^*_2Nb(Te_2H)}]$ {or $[(\mathrm{C_5Me_4Et})_2\mathrm{Nb(Te_2H)}]$ for the purpose of better crystallization} with $[Co_2(CO)_8]$. This reaction is temperature-dependent and, contrary to other systems, it has been possible to isolate intermediate products, such as **17** and **18**, at 0 °C. These disappear at higher temperatures forming highly connected and symmetric molecular carbonylcobalt telluride cluster anions (Scheme 5).[47]

The bicapped trigonal-bipyramidal cobalt telluride cluster **17** consists of a triangular 47-electron $Co_3(CO)_6Te_2$ core [d(Co−Co) = 2.513(3) Å] to which a 17-electron $\mathrm{Cp^*_2Nb(CO)}$ fragment is attached by a covalent Te−Nb bridge (Figure 8). This structural motif is more current for niobocene derivatives comprising the $t\mathrm{BuC_5H_4}$ ligand, as will be shown later. Cluster **17** is the only example of an intermediate in which peralkylated niobocene telluride and carbonylcobalt building blocks are arranged together into a small covalent cluster. For this reason it may also be considered as the first step en route to polyhedral structures or even solid-state compounds.[48]

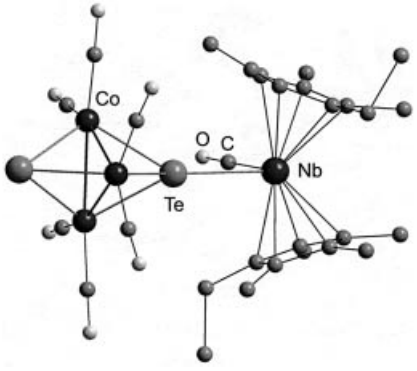

Figure 8. Molecular structure of $[(\mathrm{C_5Me_4Et})_2\mathrm{NbTe_2Co_3(CO)_7}]$ (**17**)[47]

The second product is the already known tetragonal-bipyramidal $[Co_4(\mu_4\text{-Te})_2(\mu_2\text{-CO})_2(CO)_8]$ (**18**),[49] which forms in remarkably good yield. However, at room temperature there is a considerable decrease of the yields of **17** and **18** and the ionic compounds **19**−**21**, the formation of which is completed by refluxing the mixture in toluene for 3 h, are formed instead (Scheme 5). From the fact that **18** does not react with **2** in an independent experiment one may conclude that as-yet-unidentified reactive niobocene telluride particles exist in solution and that these are responsible for the disappearance of **18** when raising the temperature.

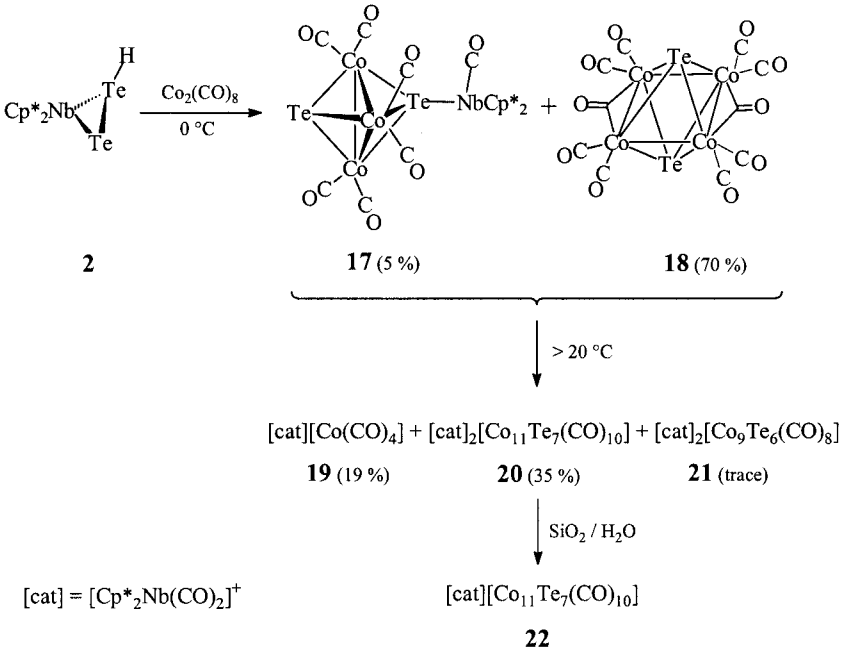

Scheme 5

 © 2004 Wiley-VCH Verlag GmbH & Co. KGaA, Weinheim

The mixture of **19**, **20** and **21** was separated by fractional crystallization and the resulting crystals were examined by X-ray crystallography. The structure of the yellow salt **19** consists of distinct $[Cp^*_2Nb(CO)_2]^+$ and $[Co(CO)_4]^-$ ions in a 1:1 ratio, whereas the cation/anion ratio is 2:1 in **20** and **21**. The structure of the dianion in **20** resembles that of the monoanion (see below). It may be described by a heptacapped pentagonal-prismatic Co_{10} polyhedron (Figure 9), while that in **21** is a hexacapped Co_8 cube (Figure 10). In addition, each of the two polyhedra contains an interstitial Co atom.[47]

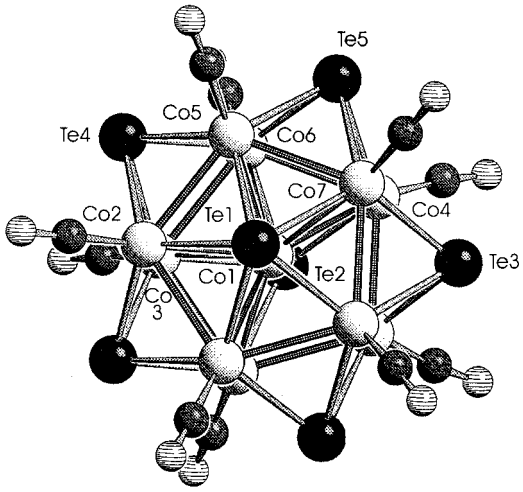

Figure 9. Structure of the $[Co_{11}Te_7(CO)_{10}]^-$ ion in **22**[47]

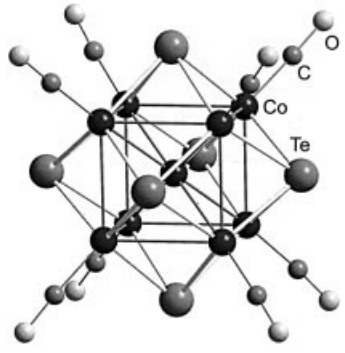

Figure 10. Structure of the $[Co_9Te_6(CO)_8]^{2-}$ ion in **21**[47]

The omnipresence of the $[Cp^*_2Nb(CO)_2]^+$ cation in the structures of compounds **19**−**22** is striking. The remarkably stable Nb^{III} derivative extends the series of dicarbonyl early transition metallocene complexes, for example $[Cp^*_2M(CO)_2]$ (M = Ti, Zr, Hf)[50] and $[(C_5H_5)_2V(CO)_2]^+$.[51] Furthermore, it takes the role of an organometallic template in the formation of cluster anions.

Although the cluster salt **21** is formed in only trace amounts its existence is important because it contains the first cobalt- and tellurium-containing representative in the class of metal-centered hexacapped $[M_9(\mu_4\text{-}E)_6L_8]$ clusters (M = Ni, Pd; E = GeEt, As, Te).[3a,52] According to various combinations of metals and ligands metal valence electron (MVE) counts of between 120 and 130 MVEs have been realized. No cluster has been described in different oxidation states thus far.[53] The anion in **21** contains 123 MVEs, but other electron counts have been realized by varying the cluster charges, as will be shown below.

Compound **20** contains the same dianion $[Co_{11}Te_7(CO)_{10}]^{2-}$ as has already been found in $[Ph_4P]_2$-$[Co_{11}Te_7(CO)_{10}]$. This compound was synthesized from $[Co_2(CO)_8]$, Na_2Te_2 and Ph_4PCl in methanol under solvothermal conditions.[54] Chromatography of **20** results in the formation of $[Cp^*_2Nb(CO)_2][Co_{11}Te_7(CO)_{10}]$ (**22**; Scheme 5). The loss of one $[Cp^*_2Nb(CO)_2]^+$ ion during the transfer **20** → **22** corresponds to a one-electron oxidation of $[Co_{11}Te_7(CO)_{10}]^{2-}$ by H^+. Electrochemical investigations confirm three reversible electron-transfer steps regardless of the charge of the anions (Scheme 6).[47] Concomitantly, the ν(CO) frequencies are a function of cluster charge *n* and decrease from 1961 (*n* = −1) to 1897 (*n* = −3) cm^{-1}, whereas the neutral species (*n* = 0) is too unstable in solution.

The redox behavior of the anions $[Co_{11}Te_7(CO)_{10}]^{1-,2-}$ is in agreement with considerable metallic interactions within the cluster core, which is also expressed by the small HOMO−LUMO gaps for both compounds.[47] According to DFT calculations the oxidized product (*n* = 0) should be less stable than the anions.

The structure of the $[Co_{11}Te_7(CO)_{10}]^-$ ion in **22** is that of a pentagonal prism formed by ten Co atoms in the center of which resides a further Co atom (Figure 9). All faces are capped by Te bridges. Alternatively, the $Co_{11}Te_7$ cage may be thought to be composed of five edge-sharing Co_5Te octahedra which are arranged around the fivefold Te(1)−Co(1)−Te(2) axis, with Co(1) as common vertex. These octahedra are nearly perfect, with Co−Te and Co−Co bond lengths of approximately equal order (between 2.50 and 2.61 Å).

Neutral clusters comprising the intact $Co_{11}Te_7$ cage are accessible by the reaction of phosphanes L with the salts **20** or **22** and subsequent chromatography on silica gel. In a very complex reaction the substituted clusters $[Co_{11}Te_7(CO)_{10-m}L_m]$ (*m* = 3, 4, 5) are formed, regardless of the charge of the initial cluster anion.[55] Electrochemical studies of the reaction of **22** with L = PMe_2Ph reveal that there is a stepwise substitution of CO groups, in which differently substituted cluster anions $[Co_{11}Te_7(CO)_{10-m}(PMe_2Ph)_m]^{n-}$ (*m* = 1−5, *n* = 1, 2) may be formed as intermediate products. Each of these intermediates exhibits at least three electron-transfer processes, leading to a total of 21 redox couples with 27 electroactive species. It is noteworthy that each replacement of a CO ligand by PMe_2Ph in $[\mathbf{1}]^-$ causes a shift of about 200 mV towards more negative potentials (Scheme 7).[55] As a consequence, reduction becomes more difficult and oxidation easier. Traces of oxygen or water (from SiO_2) are thought to be responsible for the oxidation.

The molecular structure of $[Co_{11}Te_7(CO)_5(PMe_2Ph)_5]$ contains the same cluster geometry as the precursor anion $[Co_{11}Te_7(CO)_{10}]^-$.[55] The replacement of five π-acceptor

 © 2004 Wiley-VCH Verlag GmbH & Co. KGaA, Weinheim

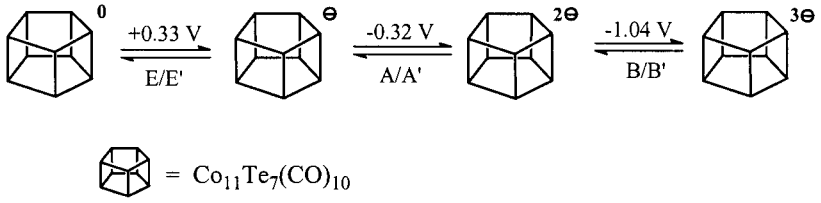

Scheme 6. Schematic representation of the electrochemistry of the $[Co_{11}Te_7(CO)_{10}]^{n-}$ anions ($n = 0-3$)

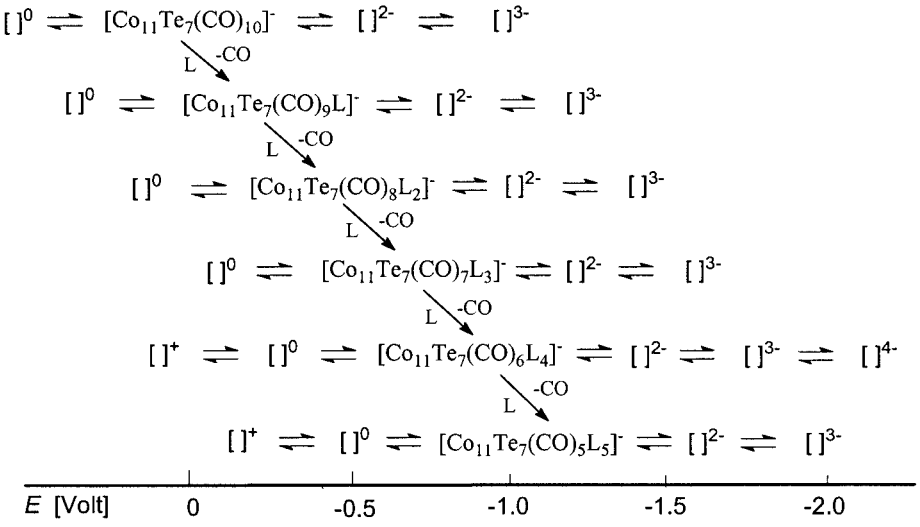

Scheme 7. Schematic summary of the electrochemical studies of the system $[Cp^*_2Nb(CO)_2][Co_{11}Te_7(CO)_{10}]/L$ (L = PMe_2Ph); compounds $[Co_{11}Te_7(CO)_{10-m}L_m]^0$ ($m = 3, 4, 5$) are accessible by synthetic means[55]

CO ligands by PMe_2Ph and the oxidation of the cluster core by one electron do not affect significantly the bond parameters in the $Co_{11}Te_7$ core when compared to the parent cluster anions. This is again in agreement with a *quasi-metallic* electron distribution within the cluster skeleton.

The rich redox chemistry of the $Co_{11}Te_7$ core resembles to some extent the electron-sink behavior of homoleptic carbonylmetal cluster anions.[56] A similar behavior may be expected for the cubic Co_9Te_6 core in **21** (Figure 10). This compound is not available in sufficient amounts (Scheme 5), but if $[(t\text{BuC}_5\text{H}_4)_2\text{Nb}(\text{Te}_2)\text{H}]$ (**1**) is used as starting material instead of **2** the neutral cluster $[\{(t\text{BuC}_5\text{H}_4)_2\text{Nb}(\text{CO})\}_3\text{Co}_9\text{Te}_6(\text{CO})_8]$ (**23**) forms in good yield (Scheme 8a).[57] This product contains a Co_9Te_6 core, to which three 17-electron $(t\text{BuC}_5\text{H}_4)_2\text{Nb}(\text{CO})$ fragments are attached by three of the six μ_4-Te ligands. No charge separation into distinct ionic building blocks, as described in Scheme 5, is observed. Interestingly, the reaction seems to proceed at 0 °C in an analogous manner to that of peralkylated **2** (Scheme 5). Accordingly, $[(t\text{BuC}_5\text{H}_4)_2\text{NbTe}_2\text{Co}_3(\text{CO})_7]$, an analogue of **17**, and $[Co_4Te_2(CO)_{10}]$ (**18**) are formed, although in low yields.[57][58]

For the purpose of crystallization it was necessary to treat **23** with $[Cr(CO)_5\text{THF}]$ (Scheme 8a). The central feature of the structure of the resulting cluster **24** is a $Co@Co_8$ cube. Its faces are bridged by six Te ligands to which three $(t\text{BuC}_5\text{H}_4)_2\text{Nb}(\text{CO})$ and three $Cr(CO)_5$ fragments are coordinated in a meridional manner with respect to the Te_6 octahedron (Figure 11).[57] The resulting outer octahedral shell of metal atoms has an average diameter of 11.6 Å, which means an expansion of the inner cubic shell by about 6.7 Å.

A somewhat different result is obtained when **1** is reduced with NaH. It is not yet clear if this reaction proceeds with hydride abstraction or with cleavage of the Te−Te bond. In the subsequent reaction of the obtained solution with $[Co_2(CO)_8]$ at 20 °C dark-brown $Na[Co_9Te_6(CO)_8]$ (**25**) is formed (Scheme 8b). Compound **25** crystallizes with THF as salt **26**, which is composed of $[Co_9Te_6(CO)_8]^-$ and $[Na(THF)_6]^+$ ions in a 1:1 ratio.[59] This means that **26** con-

 © 2004 Wiley-VCH Verlag GmbH & Co. KGaA, Weinheim

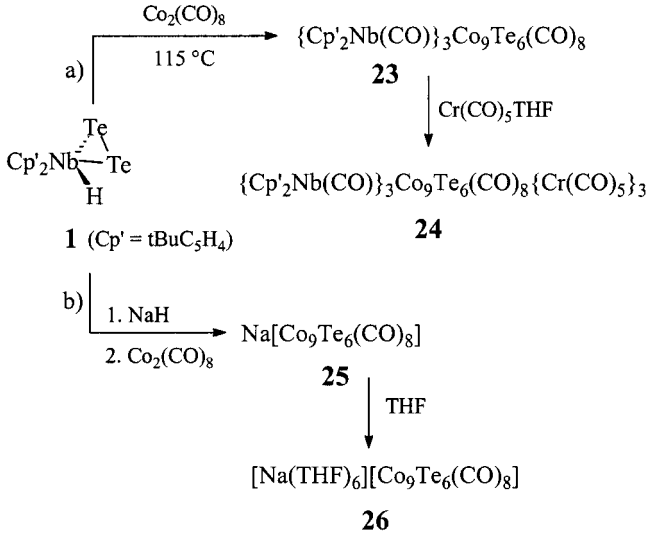

Scheme 8

Figure 11. Molecular structure of $[\{(t\mathrm{BuC_5H_4})_2\mathrm{Nb(CO)}\}_3\mathrm{Co_9Te_6(CO)_8}\{\mathrm{Cr(CO)_5}\}_3]$ (**24**); two of the $\mathrm{Cr(CO)_5}$ fragments, attached at the "free" μ_4-Te ligands, are omitted for the sake of clarity[57]

tains an oxidized form (122 MVEs) of the Co_9Te_6 cage with respect to that in **21** (123 MVEs). The metric parameters of both cubes and of the $Co@Co_8$ cage in **24** (124 MVEs) are very similar. This fact is currently under investigation from a theoretical point of view.

Conclusions

This microreview deals with synthesis and structure of niobocene ditelluride complexes and their application in cluster synthesis. The presence of free electron pairs, the propensity for Te−Te bond cleavage and the ability to eliminate Te^0 or Te^{2-} make them ideal molecular building blocks for the synthesis of polymetallic telluride complexes and clusters. Thus, in reactions with several binary carbonyl transition metal complexes a series of new homo- and heterometallic complexes and cluster compounds are formed, which range from simple adducts to polyhedral cluster frameworks (Scheme 9).

The stepwise build-up of telluride clusters may be facilitated by ligand (CO, Te) cross-transfer from one metal atom to the other. The carbonylniobocene species $[(t\mathrm{BuC_5H_4})_2\mathrm{Nb(CO)}]$ and $[\mathrm{Cp^*_2Nb(CO)_2}]^+$, the formation of which is directed by the organic substituents, play a decisive role in tuning the electronic properties of the cluster units: Whereas the 17-electron fragment may be directly anchored to the cluster core by Te bridges, the in situ formed 18-electron cation is able to stabilize large and differently charged cluster anions. An outstanding property of clusters derived from all-capped $Co@Co_8$ (type **VI**) and $Co@Co_{10}$ (type **VII**) polyhedra is their pronounced electron-sponge behavior. Crystal structure analyses allow correlation of cluster charge and bond parameters, and theoretical studies will provide insights into their electronic structures.

It has already been demonstrated that metal telluride complexes may be an important molecular basis for the preparation of binary solid-state phases such as β-CoTe[3b] and NiTe.[3a] Another area of interest may be the extension of polyhedral structures into supramolecular architectures. In this context it was suggested as early as 1985 to combine "discrete clusters into small aggregates" by means of covalent bridges that exist in the solid state.[60] This idea has been stimulated by the observation that the discrete cubic cluster $[Co_8S_6(SPh)_8]^{4-,5-}$ may be considered as a small solubilized fraction of the solid-state structure of pentlandite minerals, in which Co_8S_6 cubes are linked together by octahedral Co centers and sulfide bridges. Very recently it has been observed that octahedral $[Re_6(\mu_2\text{-}Se)_8]^{2+}$ core-containing clusters bearing ligands susceptible for self-organization of functional groups by hydrogen bonds arrange into zigzag chains of hydrogen-bonded cluster polymers.[61] A realization of these ideas with respect to our metal telluride clus-

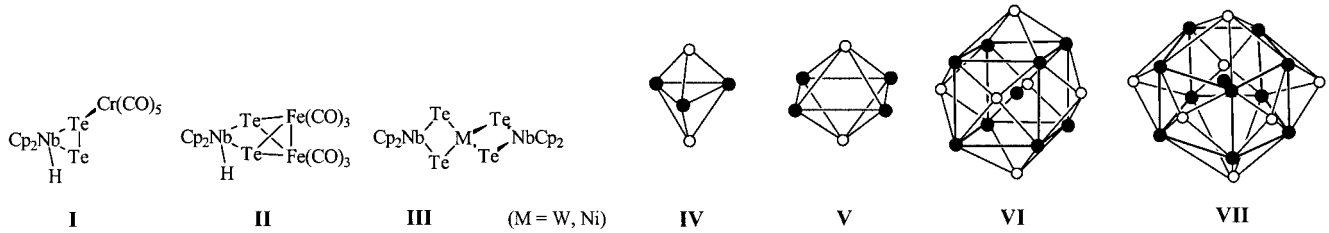

Scheme 9. Examples of heteropolymetallic telluride complexes (**I**−**III**) and cobalt telluride cluster frameworks (**IV**−**VII**; o = Te, • = Co)

 © 2004 Wiley-VCH Verlag GmbH & Co. KGaA, Weinheim

ters may envisage the facile CO substitution in the cluster anions in **20** and **22**. Thus, it should be possible to connect individual polyhedra by appropriate bifunctional donor ligands. On the other hand, reaction of the nucleophilic Te vertices with tellurophilic metal cations[2] may lead to the formation of inorganic networks.

Acknowledgments

I wish to thank my co-workers, who are cited in the literature section, for their numerous contributions and Prof. Yves Mugnier and his co-workers for their extremely valuable electrochemical studies. I am particularly indebted to Prof. Dr. H. Brunner for his continuous and generous support. I am also grateful to the Deutsche Forschungsgemeinschaft and the Deutscher Akademischer Auslandsdienst and the Ministère des Affaires Etrangères (program PROCOPE) for financial support.

[1] [1a] J. W. Kolis, *Coord. Chem. Rev.* **1990**, *105*, 195. [1b] L. C. Roof, J. W. Kolis, *Chem. Rev.* **1993**, *93*, 1037−1080.
[2] [2a] J. F. Corrigan, D. Fenske, *Chem. Commun.* **1996**, 943−944. [2b] J. F. Corrigan, D. Fenske, W. P. Power, *Angew. Chem. Int. Ed. Engl.* **1997**, *36*, 1176. [2c] J. F. Corrigan, D. Fenske, *Angew. Chem. Int. Ed. Engl.* **1997**, *36*, 1981−1983. [2d] J. F. Corrigan, D. Fenske, *Chem. Commun.* **1997**, 1836−1837. [2e] D. Fenske, J. F. Corrigan, in *Metal Clusters in Chemistry* (Eds.: P. Braunstein, L. A. Oro, P. R. Raithby), Wiley-VCH, Weinheim, **1999**, vol. 3, pp. 1303−1324. [2f]M. W. DeGroot, M. W. Cockburn, M. S. Workentin, J. F. Corrigan, *Inorg. Chem.* **2001**, *40*, 4678−4685.
[3] [3a] J. G. Brennan, T. Siegrist, S. M. Stuczinsky, M. L. Steigerwald, *J. Am. Chem. Soc.* **1989**, *111*, 9240−9241. [3b] M. L. Steigerwald, T. Siegrist, S. M. Stuczynski, *Inorg. Chem.* **1991**, *30*, 4940−4945. [3c] M. L. Steigerwald, T. Siegrist, E. M. Gyorgy, B. Hessen, Y.-U. Kwon, S. M. Tanzler, *Inorg. Chem.* **1994**, *33*, 3389−3395.
[4] [4a] M. Draganjac, T. B. Rauchfuss, *Angew. Chem. Int. Ed. Engl.* **1985**, *24*, 742−757. [4b] J. Wachter, *Angew. Chem. Int. Ed. Engl.* **1989**, *28*, 1613−1626.
[5] P. Royo, E. Ryan, in *Metallocenes* (Eds.: A. Togni, R. L. Halterman), Wiley-VCH, Weinheim, **1998**, vol. 1, pp. 378−401.
[6] [6a] G. Tainturier, M. Fahim, B. Gautheron, *J. Organomet. Chem.* **1989**, *373*, 193−202. [6b] W. Howard, G. Parkin, *J. Am. Chem. Soc.* **1994**, *116*, 606−615. [6c] W. A. Howard, G. Parkin, A. L. Rheingold, *Polyhedron* **1995**, *14*, 25−44. [6d] W. A. Howard, T. M. Truka, M. Waters, G. Parkin, *J. Organomet. Chem.* **1997**, *528*, 95−121. [6e] J. H. Shin, T. Hascall, G. Parkin, *Organometallics* **1999**, *18*, 6−9.
[7] H. Brunner, G. Gehart, W. Meier, B. Nuber, J. Wachter, *J. Organomet. Chem.* **1993**, *454*, 117−122.
[8] It should be noted that there are several examples of pseudotetrahedral $Cp^*_2M(=X)(H,Cl)$ (X = S, Se, Te) complexes which are, however, irrelevant with respect to the subject of this review: [8a] P. Royo, E. Ryan, in *Metallocenes* (Eds.: A. Togni, R. L. Halterman), Wiley-VCH, Weinheim, **1998**, vol. 1, pp. 319−414. [8b]H. Brunner, M. Kubicki, J.-C. Leblanc, W. Meier, C. Moise, A. Sadorge, B. Stubenhofer, J. Wachter, R. Wanninger, *Eur. J. Inorg. Chem.* **1999**, 843−848.
[9] H. Brunner, G. Gehart, J.-C. Leblanc, C. Moise, B. Nuber, B. Stubenhofer, F. Volpato, J. Wachter, *J. Organomet. Chem.* **1996**, *517*, 47−51.
[10] H. Brunner, H. Cattey, D. Evrard, M. Kubicki, Y. Mugnier, E. Vigier, J. Wachter, R. Wanninger, M. Zabel, *Eur. J. Inorg. Chem.* **2002**, 1315−1325.
[11] O. Blacque, H. Brunner, M. M. Kubicki, B. Nuber, B. Stubenhofer, J. Wachter, B. Wrackmeyer, *Angew. Chem. Int. Ed. Engl.* **1997**, *36*, 352−353.
[12] H.-J. Bach, H. Brunner, J. Wachter, M. M. Kubicki, J.-C. Leblanc, C. Moise, F. Volpato, B. Nuber, M. L. Ziegler, *Organometallics* **1992**, *11*, 1403−1407.
[13] J. H. Shin, G. Parkin, *Organometallics* **1994**, *13*, 2147−2149.
[14] In ref.[11] two quadruplets have been reported.
[15] [15a] J. M. Fischer, W. E. Piers, L. R. MacGillivray, M. J. Zaworotko, *Inorg. Chem.* **1994**, *34*, 2499−2500. [15b] D. Rabinovich, G. Parkin, *J. Am. Chem. Soc.* **1993**, *115*, 9822−9823. [15c] M. Di Vaira, M. Peruzzini, P. Stoppioni, *Angew. Chem. Int. Ed. Engl.* **1987**, *26*, 916−918.
[16] O. M. Kekia, A. L. Rheingold, *J. Organomet. Chem.* **1997**, *545*, 277−280.
[17] Yu. V. Skripkin, I. L. Eremenko, A. A. Pasynskii, Yu. T. Struchkov, V. E. Shklover, *J. Organomet. Chem.* **1984**, *267*, 285−292.
[18] M. Brandl, H. Brunner, J. Wachter, M. Zabel, *Organometallics* **2002**, *21*, 3069−3072.
[19] [19a] D. A. Lesch, T. B. Rauchfuss, *Organometallics* **1982**, *1*, 499−506. [19b] L. C. Roof, D. M. Smith, G. W. Drake, W. T. Pennington, J. W. Kolis, *Inorg. Chem.* **1995**, *34*, 337−345. [19c] P. Mathur, V. D. Reddy, R. Bohra, *J. Organomet. Chem.* **1991**, *401*, 339−346. [19d] L. C. Roof, W. T. Pennington, J. W. Kolis, *Angew. Chem. Int. Ed. Engl.* **1992**, *31*, 913−914. [19e] R. E. Bachmann, K. H. Whitmire, *Organometallics* **1993**, *12*, 1988−1992. [19f] M. Shieh, P.-F. Chen, S.-M. Peng, G.-H. Lee, *Inorg. Chem.* **1993**, *32*, 3389−3390. [19g] B. K. Das, M. G. Kanatzidis, *J. Organomet. Chem.* **1996**, *513*, 1−6.
[20] W. Hieber, J. Gruber, *Z. Anorg. Allg. Chem.* **1958**, *296*, 91−103.
[21] H. Brunner, J. Wachter, R. Wanninger, M. Zabel, *J. Organomet. Chem.* **2000**, *603*, 135−137.
[22] [22a] W. S. Sheldrick, M. Wachhold, *Angew. Chem. Int. Ed. Engl.* **1995**, *34*, 450. [22b] Y. V. Mironov, M. A. Pell, J. A. Ibers, *Angew. Chem. Int. Ed. Engl.* **1996**, *35*, 2854.
[23] O. Blacque, H. Brunner, M. M. Kubicki, D. Lucas, W. Meier, Y. Mugnier, B. Nuber, B. Stubenhofer, J. Wachter, *J. Organomet. Chem.* **1998**, *564*, 71−79.
[24] H. Brunner, G. Gehart, M. M. Kubicki, E. Lehrl, D. Lucas, W. Meier, Y. Mugnier, B. Nuber, B. Stubenhofer, J. Wachter, *J. Organomet. Chem.* **1996**, *510*, 291−295.
[25] B. Stubenhofer, PhD Thesis, Universität Regensburg, **1997**, pp. 61−66.
[26] M. Herberhold, D. Reiner, D. Neugebauer, *Angew. Chem. Int. Ed. Engl.* **1983**, *22*, 59−60.
[27] [27a] Q.-F. Zhang, M.-T. Bao, M.-C. Hong, R. Cao, Y.-L. Song, X.-Q. Xin, *J. Chem. Soc., Dalton Trans.* **2000**, 605−610. [27b] Q.-F. Zhang, W.-H. Leung, X.-Q. Xin, H.-K. Fun, *Inorg. Chem.* **2000**, *39*, 417−426.
[28] [28a] K. E. Howard, T. B. Rauchfuss, A. L. Rheingold, *J. Am. Chem. Soc.* **1986**, *108*, 297−299. [28b] P. A. Shapley, Z. Gebeyehu, N. Zhang, S. R. Wilson, *Inorg. Chem.* **1993**, *32*, 5646−5651. [28c] R. Schäfer, W. Kaim, J. Fiedler, *Inorg. Chem.* **1993**, *32*, 3199−3200. [28d] R. Schäfer, J. Fiedler, M. Moscherosch, W. Kaim, *J. Chem. Soc., Chem. Commun.* **1993**, 896−897. [28e] K. E. Howard, T. B. Rauchfuss, S. R. Wilson, *Inorg. Chem.* **1988**, *27*, 3561−3567.
[29] Q.-F. Zhang, Y. Song, W.-Y. Wong, W.-H. Leung, X. Xin, *J. Chem. Soc., Dalton Trans.* **2002**, 1963−1968.
[30] [30a] M. A. Ansari, J. C. Bollinger, J. A. Ibers, *J. Am. Chem. Soc.* **1993**, *115*, 3838−3839. [30b] M. A. Ansari, J. M. McConnachi, J. A. Ibers, *Acc. Chem. Res.* **1993**, *26*, 574−578.
[31] H. Brunner, J. Wachter, R. Wanninger, M. Zabel, *Eur. J. Inorg. Chem.* **2001**, 1151−1154.
[32] G. Erker, R. Nolte, G. Tainturier, A. Rheingold, *Organometallics* **1989**, *8*, 454−460.
[33] [33a] D. Rabinovich, G. Parkin, *Inorg. Chem.* **1995**, *34*, 6341−6361. [33b] D. R. Gardner, J. C. Fettinger, B. W. Eichhorn, *Angew. Chem. Int. Ed. Engl.* **1994**, *33*, 1859−1861.
[34] M. Brandl, H. Brunner, M. M. Kubicki, Y. Mugnier, E. Vigier, J. Wachter, M. Zabel, unpublished results.
[35] M. DiVaira, M. Peruzzini, P. Stoppioni, *J. Chem. Soc., Chem. Commun.* **1986**, 374−375.

 © 2004 Wiley-VCH Verlag GmbH & Co. KGaA, Weinheim

[36] H. Sitzmann, D. Saurenz, G. Wolmershäuser, A. Klein, R. Boese, *Organometallics* **2001**, *20*, 700−705.
[37] H. Cattey, Y. Mugnier, personal communication.
[38] J. W. van Hal, K. H. Whitmire, *Organometallics* **1998**, *17*, 5197−5201.
[39] M. Brandl, H. Brunner, H. Cattey, Y. Mugnier, J. Wachter, M. Zabel, *J. Organomet. Chem.* **2002**, *659*, 22−28.
[40] [40a] E. Sappa, O. Gambino, G. Cetini, *J. Organomet. Chem.* **1972**, *35*, 375−380. [40b] B. F. G. Johnson, J. Lewis, P. G. Lodge, P. R. Raithby, *J. Chem. Soc., Chem. Commun.* **1979**, 719−720.
[41] P. Mathur, B. H. S. Thimmappa, A. L. Rheingold, *Inorg. Chem.* **1990**, *23*, 4658−4665.
[42] C. Graiff, G. Predieri, A. Tiripicchio, *Eur. J. Inorg. Chem.* **2003**, 1659−1668.
[43] R. D. Adams, J. E. Babin, M. Tasi, *Organometallics* **1988**, *17*, 503−513.
[44] U. Bodensieck, H. Stoeckli-Evans, G. Süss-Fink, *Angew. Chem. Int. Ed. Engl.* **1991**, *30*, 1126.
[45] L. Garlaschelli, F. Greco, G. Peli, M. Manassero, M. Sansoni, R. Gobetto, L. Salassa, R. Della Pergola, *Eur. J. Inorg. Chem.* **2003**, 2108−2212.
[46] M. Brandl, PhD Thesis, Universität Regensburg, **2002**, p. 66.
[47] H. Brunner, D. Lucas, T. Monzon, Y. Mugnier, B. Nuber, B. Stubenhofer, A. C. Stückl, J. Wachter, R. Wanninger, M. Zabel, *Chem. Eur. J.* **2000**, *6*, 493−503.
[48] M. L. Steigerwald, T. Siegrist, S. M. Stuczynski, *Inorg. Chem.* **1991**, *30*, 2256−2257.
[49] R. C. Ryan, L. F. Dahl, *J. Am. Chem. Soc.* **1975**, *97*, 6904−6906.
[50] D. J. Sikora, M. D. Rausch, R. D. Rogers, J. L. Atwood, *J. Am. Chem. Soc.* **1981**, *103*, 1265−1267.
[51] F. Calderazzo, I. Ferri, G. Pampaloni, U. Englert, *Organometallics* **1999**, *18*, 2452−2458.
[52] [52a] D. Fenske, J. Ohmer, K. Merzweiler, *Angew. Chem. Int. Ed. Engl.* **1988**, *27*, 1512−1513. [52b] D. Fenske, H. Fleischer, C. Persau, *Angew. Chem. Int. Ed. Engl.* **1989**, *28*, 1665−1667. [52c] D. Fenske, C. Persau, *Z. Anorg. Allg. Chem.* **1991**, *593*, 61−68. [52d] J. P. Zebrowski, R. K. Hayaski, A. Bjarnason, L. F. Dahl, *J. Am. Chem. Soc.* **1992**, *114*, 3121−3125.
[53] [53a] E. Furet, A. LeBeuze, J.-F. Halet, J.-Y. Saillard, *J. Am. Chem. Soc.* **1995**, *117*, 4936−4944. [53b] R. Gautier, J.-F. Halet, J.-Y. Saillard, in *Metal Clusters in Chemistry* (Eds.: P. Braunstein, L. A. Oro, P. R. Raithby), Wiley-VCH, Weinheim, **1999**, vol. 3, pp. 1643−1663.
[54] R. Seidel, R. Kliss, S. Weissgräber, G. Henkel, *J. Chem. Soc., Chem. Commun.* **1994**, 2791−2792.
[55] H. Brunner, H. Cattey, W. Meier, Y. Mugnier, A. C. Stückl, J. Wachter, R. Wanninger, M. Zabel, *Chem. Eur. J.* **2003**, *9*, 3796−3802.
[56] [56a] G. Longoni, C. Femoni, M. C. Iapalucci, P. Zanello, in *Metal Clusters in Chemistry* (Eds.: P. Braunstein, L. A. Oro, P. R. Raithby), Wiley-VCH, Weinheim, **1999**, vol. 2, pp. 1137−1158, and references cited therein. [56b]F. Calderoni, F. Demartin, F. F. de Biani, C. Femoni, M. C. Iapalucci, G. Longoni, P. Zanello, *Eur. J. Inorg. Chem.* **1999**, 663−671.
[57] H. Brunner, A. C. Stückl, J. Wachter, R. Wanninger, M. Zabel, *Angew. Chem. Int. Ed.* **2001**, *40*, 2463−2465.
[58] R. Wanninger, PhD Thesis, Universität Regensburg, **2000**, pp. 88−89.
[59] A. Ebner, J. Wachter, M. Zabel, *J. Cluster Sci.*, in press.
[60] G. Christou, K. S. Hagen, J. K. Bashkin, R. H. Holm, *Inorg. Chem.* **1985**, *24*, 1010−1018.
[61] B. K. Roland, H. D. Selby, J. R. Cole, Z. Zheng, *Dalton Trans.* **2003**, 4307−4312.

Received December 15, 2003

 © 2004 Wiley-VCH Verlag GmbH & Co. KGaA, Weinheim

C−C Bond Variation in the 1-Phenyl-*o*-carborane: Steric versus Electronic Effects

Ivan V. Glukhov,[a] Mikhail Yu. Antipin,[a] and Konstantin A. Lyssenko*[a]

Keywords: Ab initio calculations / Atoms in molecules theory / C−C bond elongation / Carboranes / Electron density / Hydrogen bonds

Using the "Atoms in molecules" topological theory the nature of the C_{carb}–C_{carb} bond variation in 1-phenyl-*o*-carborane upon rotation of the phenyl ring was investigated within B3LYP/6-31G** calculations. Despite the low barrier to the rotation of the phenyl ring, the bond paths linking hydrogen atoms of the phenyl ring and the ones of the carborane cage were found for all conformations. The length of the C_{carb}–C_{carb} bond increases by 0.031 Å without large energetic inputs due to back-donation of the π-density of the phenyl ring to the antibonding C_{carb}–C_{carb} orbital.
(© Wiley-VCH Verlag GmbH & Co. KGaA, 69451 Weinheim, Germany, 2004)

Introduction

The C_{carb}−C_{carb} bond in icosahedral *o*-carboranes (i.e., that between two carbon atoms of the icosahedron) is characterized by several unusual features, among which its high "plasticity", which is reflected in significant variation of its length in organic and organometallic derivatives, can be especially emphasised.[1−3] In the case of metallacarboranes this can lead to the formation of pseudocloso structures[4] in which two carbon atoms of the cage are not chemically bonded. This is important not only from a theoretical point of view but also for understanding the isomerisation process that occurs between the *ortho*-, *meta*- and *para*-isomers of the carboranes. The plasticity of the C_{carb}−C_{carb} bond is in line with its low force constant[5] as well as with the intermediate type of interatomic interaction [positive value of the Laplacian of the electron density in the critical point (3,−1)] found for the homopolar C_{carb}−C_{carb} bond in the crystal of 8,9,10,12-tetrafluoro-*o*-carborane.[6]

Three factors are usually considered to be the main ones that influence the C_{carb}−C_{carb} distance in the *o*-carborane derivatives: steric repulsion between one or two substituents, an electronic effect due to electronegativity differences between the hydrogen atom and the substituent group and, finally, stereoelectronic effects as a result of charge transfer from the electron lone-pair or occupied orbital of a substituent to the antibonding orbital of the C_{carb}−C_{carb} bond.[3] The role of the latter can be dominant, as was demonstrated previously in the case of *o*-carborane dithia, diaryl- and dialkylphosphanyl derivatives.[3] In particular, in 1,2-$(SPh)_2$-*o*-carborane the charge transfer from the sulfur lone-pair to the antibonding orbital of the C_{carb}−C_{carb} bond leads to a C_{carb}−C_{carb} bond elongation of up to 1.798(3) Å.[3a] It should be noted that a similar C_{carb}−C_{carb} bond elongation (1.720 Å and 1.733 Å) was found in 1,2-diphenyl-*o*-carborane,[7] in which the possibility of charge transfer from the phenyl group to the C_{carb}−C_{carb} bond of the icosahedron is not so evident.

In order to study whether the bond elongation in diphenyl-*o*-carborane is the result of steric effects[1] or electronic ones, in this paper we have chosen 1-phenyl-*o*-carborane (**1**) as a model compound. Despite the fact that this compound is not sterically overcrowded with respect to the pure *o*-carborane we cannot exclude the influence of intramolecular H···H contacts on the molecular geometry. Such interactions are important in the formation of host-guest complexes of carboranes.[8] So, in addition to analysis of the phenyl interaction with the C_{carb}−C_{carb} bond, we paid great attention to the nature of the C_{ph}−H···H−B and C_{ph}−H···H-C_{carb} contacts.

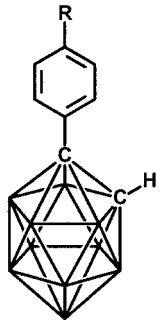

R = H (**1**), NH_2 (**2**), NO_2 (**3**)

[a] A. N. Nesmeyanov Institute of Organoelement Compounds, Russian Academy of Sciences,
119991 Moscow, Russian Federation
Fax: (internat.) +7-095/135-5085
E-mail: kostya@xray.ineos.ac.ru

According to the theoretical and experimental studies, the replacement of CH by a CPh group in the *o*-carborane has a small electronic influence on the cage, but results in significant steric changes in the molecule due to H···H contacts.[1] It was found that in the isolated molecule **1**, there is an optimum value of the torsion angle θ [C(2)−C(1)−C(13)−C(14)], equal to 25°,[9] defining the conformation of the ring with respect to the carborane cage (see Figure 1). Although the H···H contacts in all conformations are substantially shorter than the sum of the van der Waals radii the barrier to rotation of the phenyl ring according to the HF/6−31G* calculations is very small (2.1 kJ·mol^{-1}). This low barrier was also found in the gas phase by electron diffraction and in the solid state.[9] Compound **1** has two polymorphs with two and one independent molecules in the unit cells, respectively[9,10] (α and β forms). The molecules in these forms differ in the orientation of the phenyl ring, with θ values equal to 22.2° and 18.3° in the α and β forms, respectively. It should be noted that in the α form one of the independent molecules is disordered due to the superposition of different conformations.[9]

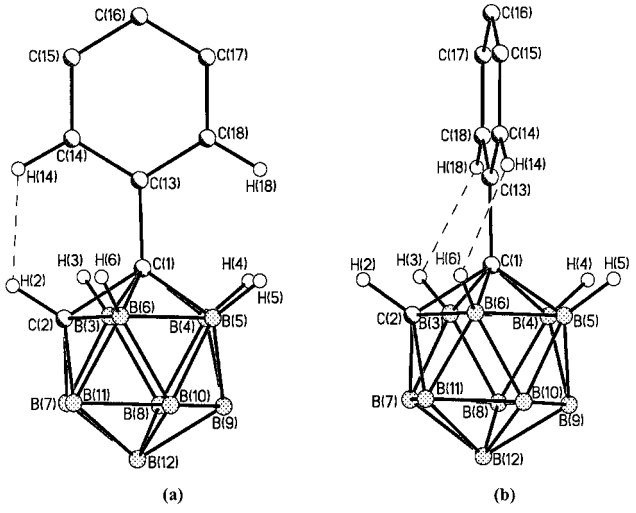

Figure 1. The general view and the numbering scheme of two limiting conformations of **1** with θ angles equal to 0° (a) and 90° (b); hydrogen atoms that do not participate in H···H contacts are omitted for clarity

Clearly, due to the low barrier of rotation, no significant back-donation from the phenyl group is expected, although we cannot exclude that this effect may be noticeable in the conformation with θ = 90° because, in this case, the π-density of the phenyl ring is positioned right above the $C_{carb}-C_{carb}$ bond, which makes charge transfer from the phenyl π-system to the antibonding orbital of the $C_{carb}-C_{carb}$ bond possible.

Results and Discussion

To investigate the nature of the $C_{carb}-C_{carb}$ bond elongation in mono- and diaryl-substituted *o*-carboranes we traced the changes in the icosahedron structure accompanying the phenyl ring rotation. We used a potential energy surface (PES) scan with the density functional B3LYP method at the 6−31G** level of theory along the coordinate corresponding to the above-mentioned torsion angle, changing from 0° to 90° in 10° steps with a full optimization of other geometric parameters at each step. The electron density distribution (EDD) properties and the most important bond lengths are summarized in Table 1.

The global minimum on the PES corresponds to the structure with θ = 30.2° which is close to the value obtained from the HF calculation (25°)[9] and is in good agreement with the experimental values (18° and 22°).[9,10] The geometry of the icosahedron obtained from the B3LYP calculation, in contrast to the HF one, is in excellent agreement with the X-ray diffraction data for the β form. In particular, the C(1)−C(2) bond length, according to HF and DFT calculations, and X-ray diffraction data, is equal to 1.626, 1.645 and 1.640 Å, respectively.

The estimated barrier to rotation of the phenyl ring is even lower (about 1.2 kJ·mol^{-1}) than reported earlier and the energy difference for the ideally eclipsed conformation (θ = 0°) and the conformation with θ = 90° becomes as low as 0.152 kJ·mol^{-1} (see Table 1).

To analyze the peculiarities and the nature of the intramolecular interactions in **1** we performed topological analysis of the EDD function $\rho(r)$ within Bader's "Atom in Molecules" theory (AIM).[11] Among the benefits of the AIM theory in analysis of the nature of the interactions is the availability of a clear definition of the chemical bonds and their properties in terms of the topological properties of the $\rho(r)$ function.

The characteristic set of critical points (CPs) contains CPs (3,−1) in the interatomic area of all expected chemical bonds, namely B−B, $C_{carb}-B$, $C_{carb}-C_{carb}$, $C_{ph}-C_{carb}$, $C_{ph}-H$, $C_{carb}-H$ and B−H. In addition, in line with the Poincaré−Hopf relationship[11] CPs (3,+1) were found for all triangular faces of the carborane icosahedron and in the center of the phenyl ring and, finally, CP (3,+3) was found in the center of the cage. Taking into account that in all bonds (with the exception of the $C_{carb}-B$ bonds, where the boron atom is bonded to one carbon atom), the Laplacian of the electron density $\nabla^2\rho(r)$ in CPs (3,−1) is negative, we may conclude that these bonds correspond to "shared-type" interatomic interactions. The other $C_{carb}-B$ bonds are characterized by the positive values of the $\nabla^2\rho(r)$ (0.1161−0.1511 a.u.)[12] in the CPs (3,−1). Taking into account the negative values of the electron energy density $h_e(r)$ [13] (−0.1022 to −0.1017a.u.) for these bonds, they may be considered as corresponding to the "intermediate type" of interatomic interactions.[11a] It should be noted that the values of the electron density in CPs (3,−1) for the $C_{carb}-B$ (0.1170−0.1214 a.u.) and B−B (0.1156−0.1235 a.u.) bonds are close to the corresponding values in CP (3,+1) (0.1099−0.1160 a.u.) for the triangular edges. For the $C_{carb}-C_{carb}$ bond the electron density is noticeably higher (0.1799 a.u.), as was found earlier for both small carboranes and icosahedral ones.[6,14,15] For comparison, the values of

 © 2004 Wiley-VCH Verlag GmbH & Co. KGaA, Weinheim

Table 1. The relative energies and important geometrical and topological parameters of **1** in CPs (3,−1) at different θ angles

θ	ΔE (kJ·mol^{-1})	C(1)−C(2) (Å)	C(1)−Ph (Å)	C(2)···B(3) (Å)	C(2)···B(6) (Å)	$\rho(r)$ [C(1)···C(2)] (a.u.)	$\nabla^2\rho(r)$ [C(1)···C(2)] (a.u.)
0	1.006	1.641	1.510	1.714	1.715	0.1816	−0.1819
10	0.620	1.642	1.511	1.713	1.716	0.1813	−0.1808
20	0.584	1.642	1.511	1.713	1.716	0.1812	−0.1801
30.2	0.000	1.645	1.512	1.712	1.717	0.1799	−0.1754
40	0.318	1.648	1.513	1.711	1.717	0.1789	−0.1710
50	0.860	1.652	1.514	1.711	1.717	0.1773	−0.1648
60	0.866	1.657	1.514	1.710	1.713	0.1754	−0.1568
70	1.162	1.663	1.514	1.708	1.711	0.1735	−0.1494
80	1.123	1.669	1.513	1.706	1.708	0.1713	−0.1408
90	1.158	1.672	1.513	1.705	1.706	0.1703	−0.1369

$\rho(r)$ (0.3082−0.3136 a.u.) in CPs (3,−1) for $C_{ph}-C_{ph}$ bonds are significantly higher than the corresponding values in CP (3,+1) (0.0202 a.u.) in the center of the phenyl ring.

At the same time, as a result of the forced H···H interactions between the hydrogen atoms of the phenyl ring and the carborane cage, some additional critical points appear. Starting from θ = 0° we found CP (3,−1) between the H(2) and H(14) atoms. Also, one CP (3,+1) appears as the result of the six-membered-ring formation. The distance between the hydrogen atoms is 2.007 Å. Although other H···H contacts H(4)···H(18) and H(5)···H(18) are about 0.4 Å longer (2.424 Å each) they do not correspond to attractive interactions. Rather small values of $\rho(r)$, positive values of $\nabla^2\rho(r)$ and positive values of $h_e(r)$ point to a "closed-shell" type of interaction for these two contacts.

The value of $\rho(r)$ in the CP (3,−1) for the H(2)···H(14) contact, equal to 0.0117 a.u., and other topological EDD parameters are close to those obtained for similar H···H interactions found in the biphenyl molecule [the $\rho(r)$ value is equal to 0.0136 a.u.][16a] and different polybenzoid compounds.[17] In spite of the fact that the validity of the analysis of $\rho(r)$ within AIM theory for weak interactions was at one point debatable,[16] later comparison of the $\rho(r)$ topology and potential energy density distribution function resolved this controversy:[11b] it was demonstrated by Bader that each bond path in the electron density is mirrored by the virial path, a line of maximum potential energy density, which, in turn, indicates that the presence of the bond path or critical point (3,−1) between the pair of atoms in question is the "universal indicator of bonding between atoms".[11b] Thus, H···H interactions observed both for the $\rho(r)$ and potential energy density functions lead to additional stabilization of the molecules (up to 46.9 kJ·mol^{-1} in chrysene).[17] The barrier to rotation of the ring in biphenyl is about 6.7 kJ·mol^{-1},[16a] which is only slightly higher than in **1**.

In this paper we have traced in detail the changes in the intramolecular contact network as a result of the phenyl ring rotation. For all conformations investigated intramolecular H···H distances that are significantly shorter than the sum of the van der Waals radii[18] were found. Surprisingly, the shortest H···H contact (2.007 Å) was observed for the $C_{carb}-H\cdots H-C_{ph}$ interaction at θ = 0°, while the minimum value for the H···H distance among all $C_{ph}-H\cdots H-B$ contacts is 2.023 Å at θ = 70° (see Table 2). At θ = 30° the $C_{carb}-H\cdots H-C_{ph}$ contact disappears and only $B-H\cdots H-C_{ph}$ contacts are present. The possibility of $B-H\cdots H-C_{ph}$ contact formation is more evident because the difference in the atomic charges of the hydrogen atoms in this case is higher than that for the $C_{carb}-H\cdots H-C_{ph}$ contact.

We also determined the contact interatomic separation (CIS) — the distance between two nuclei at which a "fold catastrophe" occurs.[16a] At the CIS distance the values of the electron density and its Laplacian become equal in the CPs (3,−1) and (3,+1), leading to loss of the interatomic

Table 2. Important geometrical and topological parameters in CPs (3,−1) of the intramolecular $C_{ph}-H\cdots H-C$ and $C_{ph}-H\cdots H-B$ contacts

θ	H(14)···H(X) (Å)	X[a]	$\rho(r)$ (a.u.)	$\nabla^2\rho(r)$ (a.u.)	H(18)···H(Y) (Å)	Y[a]	$\rho(r)$ (a.u.)	$\nabla^2\rho(r)$ (a.u.)
0	2.007	2	0.0117	0.0467				
10	2.030	2	0.0113	0.0460	2.264	4	0.0093	0.0363
20	2.086	2	0.0107	0.0452	2.166	4	0.0104	0.0389
30.2					2.106	4	0.0113	0.0412
40	2.232	6	0.0100	0.0391	2.092	4	0.0115	0.0419
50	2.110	6	0.0117	0.0440	2.122	4	0.0111	0.0412
60	2.041	6	0.0128	0.0466	2.206	4	0.0101	0.0386
70	2.023	6	0.0139	0.0472				
80	2.043	6	0.0127	0.0468	2.266	3	0.0100	0.0407
90	2.105	6	0.0119	0.0452	2.134	3	0.0115	0.0442

[a] X and Y are the number of hydorgen atoms, according to Figure 1.

 © 2004 Wiley-VCH Verlag GmbH & Co. KGaA, Weinheim

interaction line. Because of the large value of the increment used during the PES scan we could not determine precisely the CIS value for the B−H···H−C_{ph} interaction. Nevertheless, according to our estimations its value is about 2.27 Å, which is higher than the corresponding value obtained for the corresponding contact in biphenyl (2.179 Å).[16a,17] This can be explained by an increase of the electron density near the H atom of the B−H group in comparison to the C_{carb}−H one. This result confirms the supposition of other authors about the nontransferability of these values between different systems.[16a]

As concerns the X−H···H and H···H−C_{ph} bond angles of the X−H···H−C_{ph} (X = B or C_{carb}) interactions, they vary in the range 111.7−129.0° for the H···H−C angle and 99.8−118.8° for the X−H···H one. These values may be compared to those obtained for the intermolecular contacts of the B−H···H−N type for which the B−H···H angles are 95−115° and the N−H···H angles are equal to 150−170°.[19]

Despite almost unrestricted rotation of the phenyl ring and variation of the strength and number of the H···H contacts, we noticed some other changes in the carborane-cage geometry, accompanying the rotation of the phenyl group. The most dramatic change is the increase of the C(1)−C(2) bond length from 1.641 Å at θ = 0° to 1.672 Å at θ = 90°; the C(2)−B(3) and C(2)−B(6) distances decrease by only 0.009 Å each. Other bonds, including the C(1)−C(13) one, do not vary so significantly (only within 0.004 Å) and the C(14)−C(13)−C(18) *ipso* angle increases by 0.2°. Despite these geometric changes, the character of the chemical bonding for the C_{carb}−C_{carb} bond remains invariable [the value of $\nabla^2\rho(r)$ varies from 0.1816 to 0.1703 a.u.].

In contrast to these data, the C(2)−B(3) and C(2)−B(6) bonds are more sensitive to changes in the icosahedron. At a θ value close to 90°, the $\nabla^2\rho(r)$ values in CPs (3,−1) are close to zero (0.0016 and 0.0023 a.u.). This result suggests a change of the bonding nature from the shared type to an intermediate one, thus indicating that small variations of the C_{carb}−C_{carb} bond strength are sufficient for the change of the B−C_{carb} bonding type.

At the same time the C_{carb}−C_{carb} bond elongation causes not only an expected decrease of the $\rho(r)$ and the absolute $\nabla^2\rho(r)$ values but also a substantial increase of its ellipticity from 0.79 at θ = 0° to 0.96 at θ = 90°. The difference between the C_{carb}−C_{carb} bond path length and the corresponding interatomic distance is less than 0.001 Å at θ = 0° and does not increase at θ = 90°. The same difference for the C_{carb}−B_{carb} bonds is substantially bigger and, for instance, at θ = 90° it is equal to 0.114 Å. Thus, the C_{carb}−C_{carb} bond lengthening does not lead to a shift of the CP from the interatomic line; the high ellipticity value indicates either "banana bonding" or a substantial contribution of the π component.[20]

The minimum on the PES corresponding to the structure with θ = 30.2° is characterized by only one intramolecular B(4)−H(4)···H(18)−C(18) closed-shell interaction, with an interatomic separation equal to 2.106 Å. The phenyl ring is slightly inclined away from the contacting hydrogen atoms, with the B(4)−C(1)−C(13) angle equal to 118.2° The value of $\rho(r)$ at the CP (3,−1), equal to 0.0115 a.u., is slightly less than that in the biphenyl (0.0136 a.u.). At θ = 70° the corresponding interaction is even stronger, as is clear from the shorter distance between the hydrogen atoms (2.023 Å) and the maximum value of $\rho(r)$ (0.0139 a.u.). This conformation, however, does not correspond to the local minimum on the PES. Evidently, the total energy decrease related to this interaction is neutralized by energy inputs related to the lengthening of the C_{carb}−C_{carb} bond.

What is the reason for this C_{carb}−C_{carb} elongation? Starting with a θ value equal to 40°, at which the substantial growth of the C_{carb}−C_{carb} bond occurs (see Figure 2), the back-donation of the π-electron density of the phenyl ring to the anti-bonding C_{carb}−C_{carb} orbital becomes geometrically possible. It should be noted that the lengthening of the C_{carb}−C_{carb} bond is accompanied by an increase of its ellipticity, which can be explained by an increase of the π-bond contribution. At the same time the C_{carb}−C_{ph} distance and the *ipso* angle do not change, which allows us to conclude that the extent of such an interaction is rather small.

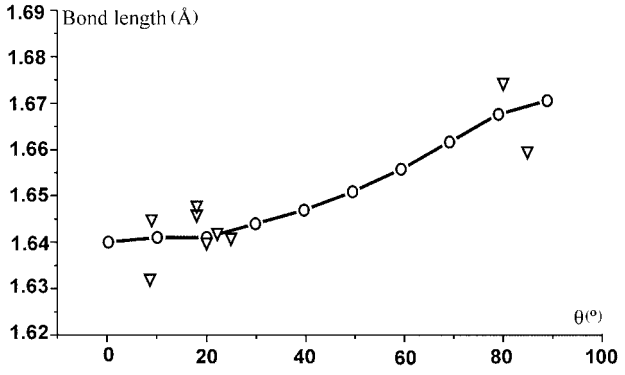

Figure 2. A plot of C_{carb}−C_{carb} bond length values vs. θ angles: the theoretical curve (circles) and the experimental data for phenyl-substituted *o*-carboranes (triangles)

To estimate if it is really observable we performed additional calculations on two derivatives of **1** with substituents in the phenyl ring in the *para* position with respect to the carborane cage. Two compounds were studied: with positive [NH_2 (**2**)] and negative [NO_2 (**3**)] mesomeric effects, their optimization was performed at the same level of theory using the same basis set for the conformation with a θ angle equal to 90°. The obtained data confirm the presence of the charge transfer from the phenyl ring to the antibonding orbital of the C−C bond. Thus, according to our calculations, at θ = 90° the C_{carb}−C_{carb} bond length in **2** is higher (1.680 Å), and in **3** is lower (1.669 Å) than in **1** (1.672 Å). It should be noted that the bond ellipticities for these derivatives also differ and are equal to 1.01 and 0.93 for **2** and **3,** respectively (in **1** at θ = 90° it is equal to 0.96). It should be noted that this effect cannot be explained by the alternation of the inductive effect of the substituted phenyl group that was checked for compounds **2** and **3** in the con-

 © 2004 Wiley-VCH Verlag GmbH & Co. KGaA, Weinheim

formation with θ = 0°. In this case, the value of the $C_{carb}-C_{carb}$ bond length coincides with that in **1**.

Using ellipticity values for the $C_{carb}-C_{carb}$ bond in **1** at different values of the θ angle and the same values in **2** and **3** at θ = 90° we found a linear correlation between the bond length and its ellipticity (see Figure 3). Such a correlation is characteristic of multiple bonds but not banana bonds, as in cyclopropane for example.[20] The observed ellipticity increase with the increase of the $C_{carb}-C_{carb}$ bond length is quite surprising and points to the unusual character of the bonding in *o*-carboranes.

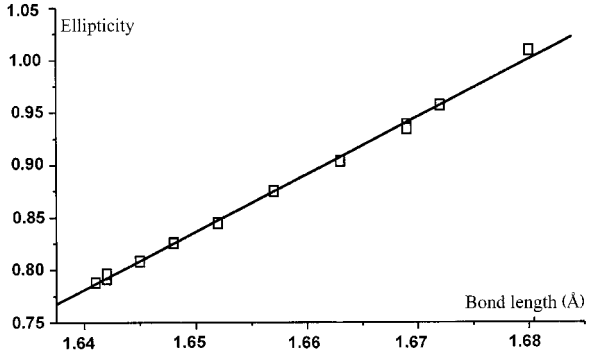

Figure 3. A plot of $C_{carb}-C_{carb}$ bond ellipticity vs. length; the dependence can be approximated by the linear function $y = 5.49105x - 8.22407$; the extrapolation to zero ellipticity gives a value of 1.50 Å for the bond length

Taking into account the low barrier to the rotation of the phenyl ring in **1** it is possible to suggest that the observed $C_{carb}-C_{carb}$ bond alternation accompanying rotation of the phenyl ring should also be observed in the crystal structures of different derivatives containing such a fragment.

To check our supposition we performed a search in the Cambridge Crystallographic Data Base[21] for ordered structures containing Ph-*o*-carborane fragment without other substituents in the carborane icosahedron, and with an *R* factor lower than 10% (five structures were found with REFCODEs FOSSIP,[22] NURLER,[23] TAVNAF,[24] ZUHTOL[10] and ZUHTOL1;[9] eight values were used). All analyzed values (bond lengths vs. θ angles) were found to be in good agreement with the theoretical curve, except for one value (not shown) in the crystal structure of FOSSIP, where the abnormally short $C_{carb}-C_{ph}$ bond length points to possible unresolved disorder of the phenyl ring. In Figure 2 the experimental and theoretical values are plotted against θ. It can be seen that a direct correlation exists between these values that allows one to predict the bond length value if the torsion angle, θ, is known.

Thus, both the theoretical and experimental data point to the fact that the dependence of the $C_{carb}-C_{carb}$ bond length on the torsion angle is caused by charge transfer from the phenyl ring to the antibonding orbital of this bond. A further question then arises: what can these results contribute to an explanation of the $C_{carb}-C_{carb}$ bong length elongation in 1,2-diphenyl-*o*-carborane (**4**)? Taking into account that the phenyl rings in **4** are almost perpendicular to the $C_{carb}-C_{carb}$ bond (θ values are equal to 81.5°/84° and 84°/89° for two independent molecules), and assuming that electron transfer has an additive effect, we obtain a value of 0.06 Å for the lengthening of this bond. Assuming also the inductive effect of the substituent replacement of the CH by the CPh group in the *o*-carborane according to B3LYP calculation,[25] which leads to an increase of the $C_{carb}-C_{carb}$ bond by approximately 0.02 Å at θ = 0°, we obtain a total value of 0.1 Å as the bond length difference between these compounds. Adding this value to the one for the $C_{carb}-C_{carb}$ distance in *o*-carborane (1.619 Å) leads to the bond length 1.720 Å, which is close to the experimental values for **4**.[7] At the same time, the difference in the $C_{carb}-C_{carb}$ bond in **4** [1.720(3) and 1.733(3) Å] can also be explained by the difference in the torsion angles: the shorter value is observed for the molecule with θ values deviating more from 90°.

Thus, the present study with the use of computational methods clearly shows that charge transfer from the phenyl ring to the carborane icosahedron exists and allows us to conclude that the $C_{carb}-C_{carb}$ bond in the *o*-carborane is characterized by a rather high π-component and that the bond length variation is caused not only by steric reasons but also electronic ones.

The presence of such an interaction is of interest from both theoretical and practical points of view. In particular, taking into account the high thermal stability of the carboranes, similar systems are of great interest for creation of new NLO materials.[26] Preliminary estimations show that the values of the first molecular hyperpolarizability for **2** is only slightly smaller than that in *p*-nitroaniline.[27] The study of 1,2-diaryl-*o*-carborane derivatives, like triazinyl-*o*-carboranes [the $C_{carb}-C_{carb}$ bond length is 1.712(3) Å],[28] in which the position of the aryl groups is constrained due to steric effects, might be promising for the design of NLO materials, and this will be the subject of our further investigations.

Computational Details

Ab initio calculations of **1**−**3** were performed with the Gaussian 98 program package[29] at the B3LYP level of theory. A potential-energy scan with C_1 symmetry of the molecules was carried out constraining one torsion angle and with full optimization of the other geometric parameters, with the 6−31G(d,p) basis set starting from the X-ray diffraction geometry. The torsion angle was changed in 10° steps starting from 0° up to 90°, except for 30°, because the value of 30.2° corresponds to the global minimum. As convergence criteria the normal threshold limits of 4.5×10^{-4} and 1.8×10^{-3} a.u. were applied for the maximum force and displacement, respectively. To enhance the B3LYP calculation accuracy the pruned (99,590) grid (keyword Grid=Ultrafine) was used. Topological analysis of the $\rho(r)$ function was performed using the MORPHY 98 program[30] based on the wavefunctions obtained from the B3LYP calculations.

 © 2004 Wiley-VCH Verlag GmbH & Co. KGaA, Weinheim

Acknowledgments

This work was supported by the Russian Foundation for Basic Research (grant no. 03-03-32214) and Support of Leading Schools of the President of the Russian Federation (YC-1209.2003.03).

[1] A. J. Welch, *Steric Effects in Metallacarboranes*, in *Metal Clusters in Chemistry* (Eds.: P. Braunstein, L. A. Oro and P. R. Raithby), Wiley-VCH, **1999**, 69−90.

[2] J. Llop, C. Viñas, F. Teixidor, L. Victori, R. Kivekäs, R. Sillanpää, *Organometallics* **2001**, *20*, 4024−4030.

[3] [3a] J. Llop, C. Viñas, J. M. Oliva, F. Teixidor, M. A. Flores, R. Kivekäs, R. Sillanpää, *J. Organomet. Chem.* **2002**, *657*, 232−238. [3b] R. Kivekäs, R. Sillanpää, F. Teixidor, C. Viñas, R. Nunez, *Acta Crystallogr., Sect. C* **1994**, *50*, 2025−2027. [3c] R. Kivekäs, R. Sillanpää, F. Teixidor, C. Viñas, R. Nuñez, M. Abad, *Acta Crystallogr., Sect. C* **1995**, *51*, 1864−1868.

[4] [4a] N. Carr, D. F. Mullica, E. L. Sappenfield, F. G. A. Stone, *Organometallics.* **1992**, *11*, 3697−3704. [4b] P. T. Brain, M. Bühl, J. Cowie, Z. G Lewis, A. J. Welch, *J. Chem. Soc., Dalton Trans.* **1996**, 231−237. [4c] J. Kim, M. Lamrani, J. Hwang, Y. Do, *Chem. Commun.* **1997**, 1761−1762. [4d] F. Teixidor, M. A. Flores, C. Vinas, R. Sillanpaa, R. Kivekas, *J. Am. Chem. Soc.* **2000**, *122*, 1963−1973.

[5] L. A. Leites, *Chem. Rev.* **1992**, *92*, 279−323.

[6] K. A. Lyssenko, M. Yu. Antipin, V. N. Lebedev, *Inorg. Chem.* **1998**, *37*, 5834−5843.

[7] Z. G. Lewis, A. J. Welch, *Acta Crystallogr., Sect. C* **1993**, *49*, 705−710.

[8] [8a] M. J. Hardie, C. L. Raston, *Eur. J. Inorg. Chem.* **1999**, 195−200. [8b] M. J. Hardie, C. L. Raston, B. Wells, *Chem. Eur. J.* **2000**, *6*, 3293−3298. [8c] P. C. Andrews, M. J. Hardie, C. L. Raston, *Coord. Chem. Rev.* **1999**, *189*, 169−198.

[9] P. T. Brain, J. Cowie, D. J. Donohoe, D. Hnyk, D. W. H. Rankin, D. Reed, B. D. Red, H. E. Robetson, A. J. Welch, M. Hofmann, P. Schleyer, *Inorg. Chem.* **1996**, *35*, 1701−1708.

[10] R. L. Thomas, G. M. Rosiar, A. J. Welch, *Acta Crystallogr., Sect. C* **1996**, *52*, 1024−1026.

[11] [11a] R. F. W. Bader, *Atoms In molecules. A Quantum Theory.* Clarendon Press, Oxford, **1990**. [11b]R. F. W. Bader, *J. Chem. Phys. A* **1998**, *102*, 7314−7323.

[12] Here and further on values are given for the conformation with $\theta = 30.2°$.

[13] According to the AIM theory, interatomic interactions fall into "shared" and "closed-shell" types. Shared interactions are characterized by negative $\nabla^2\rho(r)$ values and high $\rho(r)$ values in CP (3,−1), while in the case of closed-shell interactions (ionic bonds, some van der Waals complexes, etc.) the value of $\nabla^2\rho(r)$ is positive and the total $\rho(r)$ in CP (3,−1) is small. However, a positive $\nabla^2\rho(r)$ value is not a unique criteria of the closed-shell interaction. The necessary condition for realization of this type of interaction is a positive value of the energy density, which is related to $\nabla^2\rho(r)$ by the equation $h_e(r) = v(r) + g(r) = g(r) - 1/4\nabla^2\rho(r)$, where $v(r)$ and $g(r)$ are the potential and kinetic energy density, respectively. The value of $h_e(r)$ may still be negative if the potential energy density (a priori negative) exceeds the kinetic one in absolute value. Therefore, bonds that are characterized by a positive value of $\nabla^2\rho(r)$ and a negative value of $h_e(r)$ are referred to as an intermediate type of interatomic interaction.

[14] R. F. W. Bader, D. A. Legarre, *Can. J. Chem.* **1992**, *70*, 657−676.

[15] M. Yu. Antipin, R. Boese, D. Blaeser, A. Maulitz, *J. Am. Chem. Soc.* **1997**, *119*, 326−333.

[16] [16a] J. Cioslowski, S. T. Mixon, *J. Am. Chem. Soc.* **1992**, *114*, 4382−4387. [16b] J. Cioslowski, S. T. Mixon, W. D. Edwards, *J. Am. Chem. Soc.* **1991**, *113*, 1083−1085. [16c] J. Cioslowski, P. B. O'Connor, E. D. Fleischmann, *J. Am. Chem. Soc.* **1991**, *113*, 1086−1089. [16d] J. Cioslowski, L. Ediginton, B. B. Stefanov, *J. Am. Chem. Soc.* **1995**, *117*, 10381−10384.

[17] C. F. Matta, J. Hernández-Trujillo, T. Tang, R. Bader, *Chem. Eur. J.* **2003**, *9*, 1940−1951.

[18] R. S. Rowland, R. Taylor, *J. Phys. Chem.* **1996**, *100*, 7384−7391.

[19] W. T. Klooster, T. F. Koetzle, P. E. M. Siegbahn, T. B. Richardson, R. H. Crabtree, *J. Am. Chem. Soc.* **1999**, *121*, 6337−6343.

[20] E. Kraka, D. Kremer, in *Theoretical Models of Chemical Bonding. Part 2, The Concept of the Chemical Bond* (Ed.: Z. B. Maksic), Springer-Verlag, Berlin, **1990**, 453−487.

[21] Cambridge Crystallographic Data base, release **2003**.

[22] S. V. Lindeman, Yu. T. Struchkov, V. E. Shklover, I. A. Khotina, M. M. Teplyakov, V. V. Korshak, *Makromol. Chem.* **1987**, *188*, 1511−1519.

[23] E. S.Alekseyeva, J. A. K. Howard, J. A. H. MacBride, K. Wade, D. S. Yufit, *Private Communication*, **1998** contribution from Department of Chemistry, University of Durham, UK.

[24] W. Jiang, C. B. Knobler, M. F. Hawthorne, *Inorg. Chem.* **1996**, *35*, 3056−3058.

[25] P. Schleyer, K. Najafian, *Inorg. Chem.* **1998**, *37*, 3554−3470.

[26] K. Yu. Suponitsky T. V. Timofeeva, *Central Eur. J. Chem.* **1**, *1*, 1−9.

[27] I. V. Glukhov, M. Yu. Antipin, K. A. Lyssenko, K. Yu. Suponitsky, manuscript in preparation.

[28] O. N. Chupakhin, A. M. Prokhorov, D. N. Kozhevnikov, V. L. Rusinov, V. N. Kalinin, V. A. Olshevskaya, I. V. Glukhov, M. Yu. Antipin, *Mendeleev Commun.* **2003**, *4*, 165−167.

[29] M. J. Frisch, G. W. Trucks, H. B. Schlegel, G. E. Scuseria, M. A. Robb, J. R. Cheeseman, V. G. Zakrzewski, J. A. Montgomery, Jr., R. E. Stratmann, J. C. Burant, S. Dapprich, J. M. Millam, A. D. Daniels, K. N. Kudin, M. C. Strain, O. Farkas, J. Tomasi, V. Barone, M. Cossi, R. Cammi, B. Mennucci, C. Pomelli, C. Adamo, S. Clifford, J. Ochterski, G. A. Petersson, P. Y. Ayala, Q. Cui, K. Morokuma, D. K. Malick, A. D. Rabuck, K. Raghavachari, J. B. Foresman, J. Cioslowski, J. V. Ortiz, A. G. Baboul, B. B. Stefanov, G. Liu, A. Liashenko, P. Piskorz, I. Komaromi, R. Gomperts, R. L. Martin, D. J. Fox, T. Keith, M. A. Al-Laham, C. Y. Peng, A. Nanayakkara, M. Challacombe, P. M. W. Gill, B. Johnson, W. Chen, M. W. Wong, J. L. Andres, C. Gonzalez, M. Head-Gordon, E. S. Replogle, and J. A. Pople, *Gaussian 98, Revision A.7*, Gaussian, Inc., Pittsburgh (PA), **1998**.

[30] [30a] MORPHY98, a topological analysis program written by P. L. A Popelier with a contribution from R. G. A. Bone (UMIST, England). [30b] P. Popelier, *Chem. Phys. Lett.* **1994**, *228*, 160−164.

Received October 17, 2003

 © 2004 Wiley-VCH Verlag GmbH & Co. KGaA, Weinheim

Synthesis and Structure of an Unprecedented Layered Vanadate Complex Containing Double-Helical Chains: $[\{Co^{III}(phen)_2\}_2V_8O_{23}]$

Dongrong Xiao,[a] Yan Xu,[b] Yu Hou,[a] Enbo Wang,*[a] Shutao Wang,[a] Yangguang Li,[a] Lin Xu,[a] and Changwen Hu[a]

Keywords: Vanadium / Helical structures / Hydrothermal synthesis

A novel two-dimensional organic–inorganic hybrid vanadate complex $[\{Co^{III}(phen)_2\}_2V_8O_{23}]$ has been hydrothermally synthesized and characterized by elemental analyses, IR spectroscopy, XPS spectroscopy, TG analysis and single-crystal X-ray diffraction. The single-crystal X-ray diffraction analysis reveals that compound **1** contains an unprecedented neutral 2D framework constructed of 4,10,12-net sheets. To the best of our knowledge, compound **1** represents the first example of 2D layered vanadium oxide complex constructed of 4,10,12-net sheets. Furthermore, the title compound consists of left-handed and right-handed helical chains, which are further interconnected to form the double-helical chains. (© Wiley-VCH Verlag GmbH & Co. KGaA, 69451 Weinheim, Germany, 2003)

Introduction

A current focus on the chemistry of polyoxovanadates is the rational design and synthesis of organic−inorganic hybrid vanadium oxides in order to explore their potential applications in catalysis, medicine, biology, electron conductivity, magnetism and photochemistry.[1−4] Recently, the introduction of hydrothermal techniques and the use of organic−templating agents have led to the production of various organic−inorganic hybrid vanadium oxides with discrete clusters, one-dimensional (1D), two-dimensional (2D), and three-dimensional (3D) structures.[5−8] Typically, the organic substituents have been presented as charge-compensating cations and structural filling agents, such as organoammonium units. More recently, an important advance in this field is that the organic components directly coordinate to the inorganic vanadium oxide scaffoldings or to secondary metal centers.[3,4] The introduction of transition metal−ligand units will not only enrich the frameworks of vanadium oxides, but also improve their electronic and magnetic properties.[3−5] Based on this strategy, a large variety of organic−inorganic hybrid materials belonging to the $\{M_xL_yVO\}$ system (M = transition metal, L = organic ligand) have been isolated.[2−7]

Among the large amount of reported work, the design and synthesis of organic−inorganic materials with helical structures are of particular interest and great challenge.[9−12] It is well-known that vanadium exhibits a variety of coordination geometries, which can be used for the synthesis of double-helical structures.[12] We report the hydrothermal synthesis and crystal structure of an unprecedented layered solid-state vanadium oxide complex, $[\{Co^{III}(phen)_2\}_2V_8O_{23}]$ (**1**; phen = 1,10-phenanthroline), which consists of left-handed and right-handed helical chains. Furthermore, **1** represents the first example of a 2D layered vanadium oxide complex constructed of 4,10,12-net sheets.

Results and Discussion

The asymmetric unit of **1** (Figure 1) shows four crystallographically independent V atoms and one crystallographically independent Co atom. All vanadium sites exhibit distorted tetrahedral coordination geometries [V−O 1.589(5)−1.852(4) Å]. Each of the V(1), V(2) and V(3) atoms has a terminal vanadyl group (V=O), while V(4) has two terminal vanadyl groups. Moreover, V(2) and V(3) share oxygen atoms with one CoN_4O_2 octahedron and two VO_4 tetrahedra, while V(1) and V(4) only share oxygen atoms with VO_4 tetrahedra. The Co^{III} center adopts an octahedral geometry, being coordinated by four nitrogen donors [Co−N 1.929(4)−1.953(4) Å] of phen groups, and two oxygen atoms [Co−O 1.886(3)−1.898(4) Å] from the VO_4 units, which adopt *cis* orientation.

Single-crystal X-ray diffraction analysis reveals that compound **1** consists of an unprecedented neutral 2D frame-

[a] Institute of Polyoxometalate Chemistry, Department of Chemistry, Northeast Normal University, Changchun 130024, P. R. China
E-mail: wangenbo@public.cc.jl.cn
[b] Department of Chemical System Engineering, The University of Tokyo, 7-3-1 Hongo, Bunkyo-Ku, Tokyo 113-8656, Japan
Fax: (internat.) + 86-431-5684009
E-mail: wangenbo@public.cc.jl.cn

Supporting information for this article is available on the WWW under http://www.eurjic.org or from the author.

 DOI: 10.1002/ejic.200300534 © 2003 Wiley-VCH Verlag GmbH & Co. KGaA, Weinheim

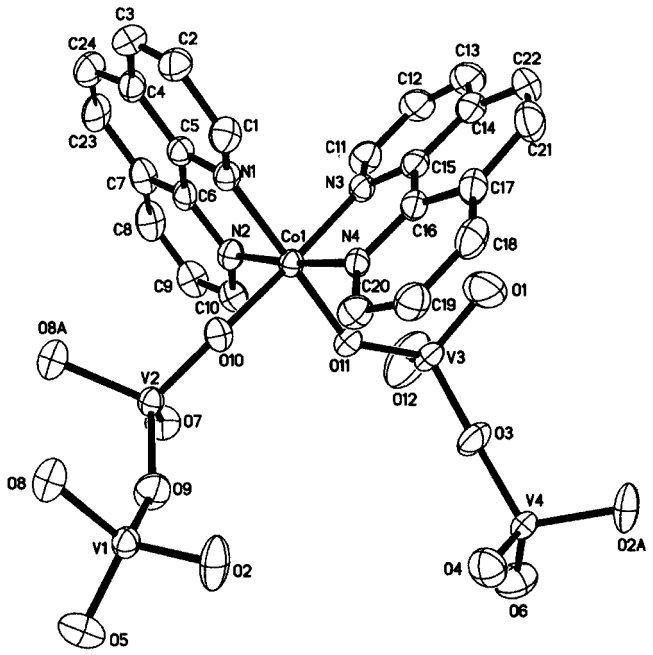

Figure 1. ORTEP drawing of compound **1** with thermal ellipsoids at 50 % probability; H atoms are omitted for clarity

work with $[Co^{III}(phen)_2]^{3+}$ coordination complex cations covalently linked to the vanadium oxide (V_8O_{23}) chains. Each V_8O_{23} chain is composed of alternating V_4O_{12} tetramer rings and V_4O_{13} units, which are linked by corner-sharing oxygen atoms. The V_4O_{12} tetramer rings and V_4O_{13} units of neighboring V_8O_{23} chains are further connected by $[Co^{III}(phen)_2]^{3+}$ fragments to form an extended 2D network with a unique 4,10,12-net structure (Figure 2 and Figure S1, see Supporting Information). To the best of our knowledge, compound **1** represents the first example of a 2D layered vanadium oxide complex that is constructed of 4,10,12-net sheets. The most interesting structural feature of compound **1** is that the CoN_4O_2 octahedra and VO_4 tetrahedra are connected to each other by corner-sharing oxygen atoms to form the right- and left-handed helical chains, which are further interconnected through oxygen atoms to produce the double-helical chains (Figure 3).

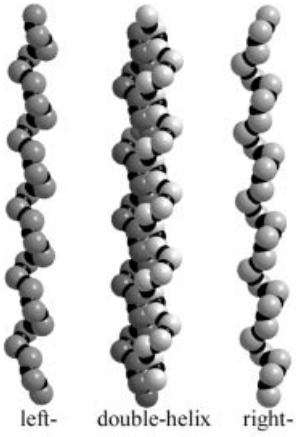

Figure 3. Space-filling view of the left-handed, right-handed, and double helices

It is striking that the adjacent layers are stably packed together, exhibiting an interesting three-dimensional supramolecular architecture through two types of supramolecular interactions. One interaction is the significant hydrogen bonding interaction between the hydrogen atoms of the phen groups and the unshared oxygen atoms of the inor-

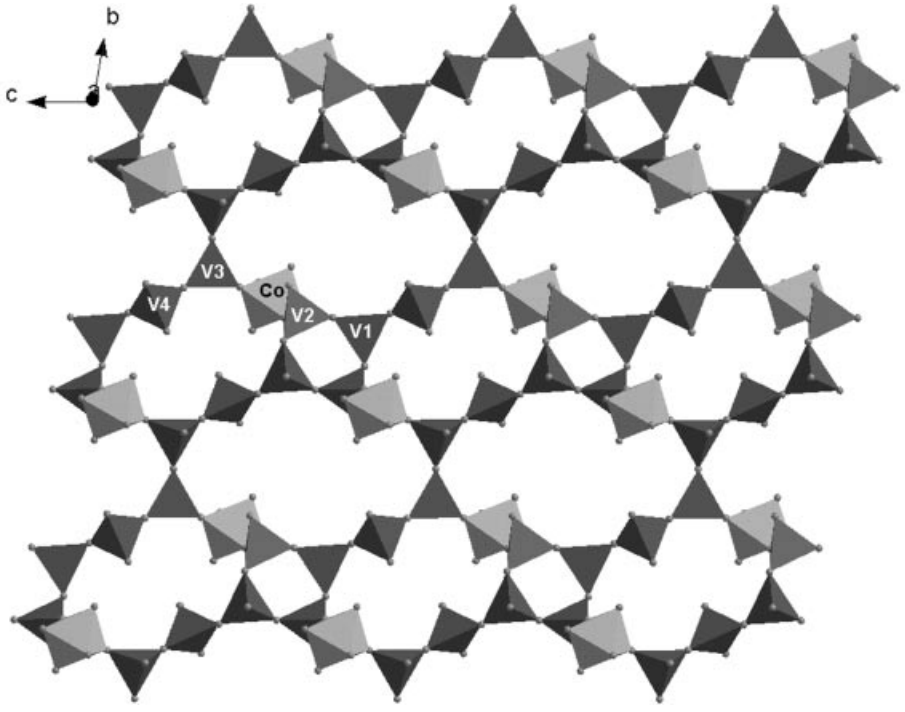

Figure 2. Polyhedral representation of compound **1** packed along the *a* axis; all C and H atoms are omitted for clarity

 © 2003 Wiley-VCH Verlag GmbH & Co. KGaA, Weinheim

ganic layers (Figure S3, see Supporting Information).The typical hydrogen bonds are C(1)−H(1)···O(5) 2.305 Å, C(3)−H(3)···O(6) 2.415 Å, and C(21)−H(21)···O(4) 2.562 Å (Table S1, see supporting information). The other interaction is the aromatic π−π stacking interactions of the phen groups between adjacent layers; the close-contact distance between adjacent phen rings is 3.40−3.43 Å (Figure S2, see Supporting Information).

The bond valence sum calculations[14a] indicate that all V metal centers are in the +5 oxidation state and the Co metal center is in the +3 oxidation state within compound **1**. No signal was found in the EPR spectrum, which confirms that all cobalt atoms in **1** are in the +3 oxidation state and all vanadium atoms are in the +5 oxidation state. The X-ray photoelectron spectrum (XPS) of compound **1** in the energy regions of V_{2p} shows one peak at 516.7 eV, attributable to V^{5+} (Figure S4, see Supporting Information).[14b] It is noteworthy that compound **1** is the first vanadate complex containing cobalt in the +3 oxidation state.

The TG curve of compound **1** (Figure S5, see Supporting Information) is divided into two stages. The first mass loss is equal to 6.12 % from 335 to 440 °C and the second mass loss is equal to 37.69 % from 445−630 °C. These two continuous mass loss regions are ascribed to loss of the phen groups. The total mass loss (43.81 %) is in agreement with the calculated value (44.66 %). The sample does not lose mass at temperatures higher than 630 °C.

The variable-temperature magnetic susceptibility of compound **1** was measured from 2 to 300 K at 5000 Oe and are displayed in Figure 4, plotted as the thermal variation of χ_M and $\chi_M T$. At 300 K, the $\chi_M T$ value is 3.527 emu·K·mol^{-1}, which is slightly higher than that of an isolated spin-only Co^{3+} ion (3.00 emu·K·mol^{-1}, S = 2, g = 2.0) with diamagnetic V^{5+} ions (S = 0). It gives g = 2.18 if we assume the Co^{3+} ions are uncoupled. As T is lowered, $\chi_M T$ decreases continuously to a value of 0.173 emu·K·mol^{-1} at 2 K. This behavior of the $\chi_M T$ curve indicates that antiferromagnetic interactions exist in **1**. The effective magnetic moment at 300 K, 5.35 μ_B, is in the range of experimentally observed values for Co^{3+} ions. The magnetism of a Co^{3+} ion in molecular compounds is fairly complex because of the combined effects of spin−orbit coupling and the distortion of the octahedral crystal field. The consequence is that $\chi_M T$ deviates from the Curie law for an isolated Co^{3+} ion as it decreases with temperature.[15]

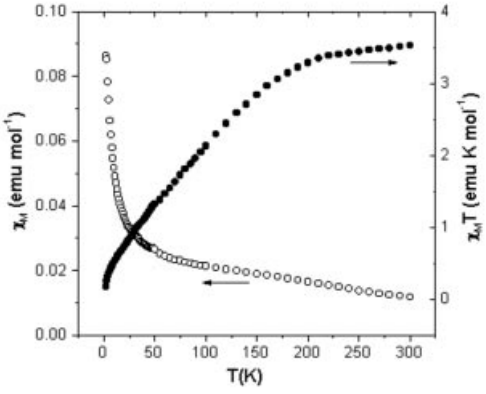

Figure 4. Thermal variation of χ_M and $\chi_M T$ for compound **1**

Conclusion

We have prepared the first vanadate complex with 4,10,12-net structure, in which the phen ligands coordinated to the cobalt−vanadate backbone. The title compound consists of left-handed and right-handed helical chains, which are further interconnected to form double-helical chains. The successful isolation of **1** confirms the observation that the transition-metal-complex moieties may profoundly influence the structure of the vanadium−oxide frameworks.

Experimental Section

Materials and General Methods: All chemicals were commercially purchased and used without further purification. Elemental analyses (C, H and N) were performed with a Perkin−Elmer 2400 CHN Elemental Analyzer. Co and V were determined by a PLASMASPEC(I) ICP atomic emission spectrometer. EPR spectrum was recorded with a Japanese JES-FE3AX spectrometer at 293 K. XPS analysis was performed with a VG ESCALABMKII spectrometer using an Mg-K_α (1253.6 eV) achromatic X-ray source. The vacuum inside the analysis chamber was maintained at 6.2×10^{-6} Pa during the analysis. IR spectrum was recorded in the range 400−4000 cm^{-1} with an Alpha Centaurt FT/IR Spectrophotometer using KBr pellets. TG analysis was performed with a Perkin−Elmer TGA7 instrument in a stream of N_2 with a heating rate of 10 °C·min^{-1}. X-ray powder diffraction (XRPD) patterns were recorded with a Siemens D5005 diffractometer with Cu-K_α (λ = 1.5418 Å) radiation. Variable-temperature magnetic susceptibility was measured (SQUID, Quantum Design) in the temperature range of 2−300 K at 5000 Oe.

Synthesis: In a typical synthesis procedure for **1**, a mixture of $Co(NO_3)_2{\cdot}6H_2O$ (0.25 mmol), V_2O_5 (0.65 mmol), H_2O_2 (30 %, 4 mL), phen (0.5 mmol) and H_2O (6 mL) was stirred in air for 30 min. The mixture was then sealed in an 18-mL Teflon-lined autoclave, which was heated to 170 °C for 120 h. After slow cooling to room temperature, the resulting purple block crystals **1** were filtered off, washed with distilled water, and dried at ambient temperature (yield: ca. 0.16 g, 80 % based on cobalt). Powder X-ray diffraction patterns of the bulk product are in good agreement with the calculated pattern base on the results from single-crystal X-ray diffraction (Figure S7, see Supporting Information). The use of NH_4VO_3 as an alternative vanadium source also leads to the same product (yield: ca. 0.13 g, 65 % based on cobalt). In the reaction, the role of H_2O_2 as oxidant is critical in the formation of compound **1**.[13] Elemental analyses results of the purple crystals are consistent with the stoichiometry of **1**. $C_{48}H_{32}Co_2N_8O_{23}V_8$ (1614.2): calcd. C 35.7, H 2.0, Co 7.3, N 6.9, V 25.2; found C 35.5, H 1.9, Co 7.5, N 7.0, V 25.0. FT/IR: $\tilde{\nu}$ = 3056 (w) cm^{-1}, 1605 (w), 1582 (w), 1518 (m), 1491 (w), 1460 (w), 1426 (m), 1343 (w), 1228 (w), 1148 (w), 1111 (w), 1038 (w), 982 (s), 961 (s), 926 (s), 866 (m), 853 (m), 793 (s), 750 (s), 703 (s), 526 (m), 445 (w).

X-ray Crystallography: The structure of compound **1** was determined by single-crystal X-ray diffraction. A purple single crystal of **1** with dimensions 0.581 × 0.498 × 0.418 mm was mounted onto a glass fiber. Data were collected with a Rigaku R-AXIS RAPID

 © 2003 Wiley-VCH Verlag GmbH & Co. KGaA, Weinheim

IP diffractometer using monochromated Mo-K_α (λ = 0.71073 Å) radiation at 293 K in the range of $1.59° < \theta < 27.48°$. Empirical absorption correction (ψ scan) was applied. The structure was solved by the direct method and refined by the full-matrix least-squares method on F^2 using the SHELXTL-97 software.[16] All non-hydrogen atoms were refined anisotropically. The hydrogen atoms were located from difference Fourier maps. A total of 8823 (5797 unique, R_{int} = 0.0526) reflections were measured. Structure solution and refinement based on 5797 independent reflections with $I > 2\sigma(I)$ and 403 parameters gave $R_1(wR_2) = 0.0560$ (0.1516) $\{R_1 = \Sigma||F_o| - |F_c||/\Sigma|F_o|$; $wR_2 = \Sigma[w(F_o^2 - F_c^2)^2]/\Sigma[w(F_o^2)^2]^{1/2}\}$. CCDC-215475 contains the supplementary crystallographic data for this paper. These data can be obtained free of charge at www.ccdc.cam.ac.uk/conts/retrieving.html [or from the Cambridge Crystallographic Data Centre, 12 Union Road, Cambridge CB2 1EZ, UK; Fax: (internat.) + 44-1223/336-033; E-mail: deposit@ccdc.cam.ac.uk].

Table 1. Crystal data and structure refinement for **1**

Empirical formula	$C_{48}H_{32}Co_2N_8O_{23}V_8$
M_r (gmol^{-1})	1614.20
λ (Å)	0.71073
Space group	$P\bar{1}$
a (Å)	8.940 (2)
b (Å)	11.950(2)
c (Å)	13.060(3)
α (°)	97.05(3)
β (°)	96.29(3)
γ (°)	103.01(3)
V (Å^3)	1335.5(5)
Z	1
D_c (gcm^{-3})	2.007
μ (mm^{-1})	2.029
Final R indices [$I > 2\sigma(I)$]	R_1[a] = 0.0560, wR_2[b] = 0.1516
R indices (all data)	R_1[a] = 0.0736, wR_2[b] = 0.1657

[a] $R_1 = \Sigma||F_o| - |F_c||/\Sigma|F_o|$. [b] $wR_2 = \Sigma[w(F_o^2 - F_c^2)^2]/\Sigma[w(F_o^2)^2]^{1/2}$.

Acknowledgments

This work was financially supported by the National Natural Science Foundation of China (20171010).

[1] [1a] L. C. W. Baker, D. C. Glick, *Chem. Rev.* **1998**, *98*, 3−49. [1b] P. Gouzerh, A. Proust, *Chem. Rev.* **1998**, *98*, 77−111. [1c] M. T. Pope, *Heteropoly and Isopoly Oxometalates*, Springer, Berlin, **1983**.

[2] [2a] D. W. Murphy, P. A. Christian, *Science* **1979**, *205*, 651−656. [2b] T. Chirayil, P. Y. Zavalij, M. S. Whittingham, *Chem. Mater.* **1998**, *10*, 2629−2640. [2c] M. T. Pope, A. Müller (Eds.), *Polyoxometalates: From Platonic Solids to Anti-Retroviral Activity*, Kluwer Academic Publishers, Dordrecht, Netherlands, **1994**.

[3] [3a] P. J. Hagrman, D. Hagrman, J. Zubieta, *Angew. Chem. Int. Ed.* **1999**, *38*, 2638−2684. [3b] P. J. Hagrman, R. C. Finn, J. Zubieta, *Solid State Sci.* **2001**, *3*, 745−774. [3c] U. Kortz, M. G. Savelieff, F. Y. Abou Ghali, L. M. Khalil, S. A. Maalouf, D. I. Sinno, *Angew. Chem. Int. Ed.* **2002**, *41*, 4070−4073. [3d] P. J. Hagrman, J. Zubieta, *Inorg. Chem.* **2001**, *40*, 2800−2809.

[4] [4a] Y. Xu, L.-H. An, L.-L. Koh, *Chem. Mater.* **1996,** 8, 814−818. [4b] P. J. Zapf, R. C. Haushalter, J. Zubieta, *Chem. Commun.* **1997**, 321−322. [4c] Y. Zhang, C. J. O'Connor, A. Clearfield, R. C. Haushalter, *Chem. Mater.* **1996**, *8*, 595−597. [4d] Y. Zhang, A. Clearfield, R. C. Haushalter, *Chem. Commun.* **1996**, 1055−1056. [4e] C.-M. Liu, Y.-L. Hou, J. Zhang, S. Gao, *Inorg. Chem.* **2002**, *41*, 140−143. [4f] C. W. Hu, Q. L. He, Y. H. Zhang, Y. Y. Liu, Y. F. Zhang, T. D. Tang, J. Y. Zhang, E. B. Wang, *Chem. Commun.* **1996**, 121−122.

[5] [5a] Y. P. Zhang, J. R. D. DeBord, C. J. O'Connor, R. C. Haushalter, A. Clearfield, J. Zubieta, *Angew. Chem. Int. Ed. Engl.* **1996**, *35*, 989−991. [5b] P. J. Hagrman, J. Zubieta, *Inorg. Chem.* **2000**, *39*, 3252−3260. [5c] R. L. LaDuuca Jr., R. S. Rarig Jr., J. Zubieta, *Inorg. Chem.* **2001**, *40*, 607−612. [5d] U. Kortz, J. Vaissermann, R. Thouvenot, P. Gouzerh, *Inorg. Chem.* **2003**, *42*, 1135−1139. [5e] U. Kortz, C. Marquer, R. Thouvenot, M. Nierlich, *Inorg. Chem.* **2003**, *42*, 1158−1162.

[6] [6a] X. M. Zhang, M. L. Tong, X. M. Chen, *Chem. Commun.* **2000**, 1817−1818. [6b] J. Tao, X. M. Zhang, M. L. Tong, X. M. Chen, *J. Chem. Soc., Dalton Trans.* **2001**, 770−771. [6c] L. R. Zhang, Z. Shi, G. Y. Yang, X. M. Chen, S. H. Feng, *J. Chem. Soc., Dalton Trans.* **2000**, 275−278.

[7] [7a] C.-M. Liu, S. Gao, H.-M. Hu, Z.-M. Wang, *Chem. Commun.* **2001**, 1636−1637. [7b] C.-M. Liu, S. Gao, H.-Z. Kou, *Chem. Commun.* **2001**, 1670−1671. [7c] C.-M. Liu, S. Gao, H.-M. Hu, X. L. Jin, H.-Z. Kou, *J. Chem. Soc., Dalton Trans.* **2002**, 598−601.

[8] [8a] Y. Lu, E. B. Wang, M. Yuan, G. Y. Luan, Y. G. Li, *J. Chem. Soc., Dalton Trans.* **2002**, 3029−3031. [8b] M. Yuan, Y. G. Li, E. B. Wang, Y. Lu, C. W. Hu, N. H. Hu, H. Q. Jia, *J. Chem. Soc., Dalton Trans.* **2002**, 2916−2920. [8c] Y. G. Li, E. B. Wang, H. Zhang, G. Y. Luan, C. W. Hu, *J. Solid State Chem.* **2002**, *163*, 10−16. [8d] G. Y. Luan, Y. G. Li, S. T. Wang, E. B. Wang, Z. B. Han, C. W. Hu, N. H. Hu, H. Q. Jia, *Dalton Trans.* **2003**, 233−235. [8e] Y. G. Li, G. J. H. De, M. Yuan, E. B. Wang, R. D. Huang, C. W. Hu, N. H. Hu, H. Q. Jia, *Dalton Trans.* **2003**, 331−334. [8f] Y. M. Chen, E. B. Wang, B. Z. Lin, S. T. Wang, *Dalton Trans.* **2003**, 519−520. [8g] M. H. Cao, C. W. Hu, G. Peng, Y. J. Qi, E. B. Wang, *J. Am. Chem. Soc.* **2003**, 125, 4982−4983. [8h] M. Yuan, Y. G. Li, E. B. Wang, C. G. Tian, L. Wang, C. W. Hu, N. H. Hu, H. Q. Jia, *Inorg. Chem.* **2003**, *42*, 3670−3676.

[9] C. Piguet, G. Bernardinelli, G. Hopfgartner, *Chem. Rev.* **1997**, *97*, 2005−2062.

[10] [10a] V. Amendola, L. Fabbrizzi, C. Mangano, P. Pallavivini, E. Roboli, M. Zema, *Inorg. Chem.* **2000**, *39*, 5803−5806. [10b] L. Carlucci, G. Ciani, D. W. v. Gudenberg, D. M. Proserpio, *Inorg. Chem.* **1997**, *36*, 3812−3813. [10c] K. A. Hirsch, S. R. Wilson, J. S. Moore, *Chem. Commun.* **1998**, 13−14. [10d] T. M. Garrett, *J. Chem. Soc., Chem. Commun.* **1990**, 557−558. [10e] J. -M. Lehn, A. Riganlt, *Angew. Chem. Int. Ed. Engl.* **1988**, *27*, 1095. [10f] O. Mamula, A. v. Zelewsky, T. Bark, G. Bernardinelli, *Angew. Chem. Int. Ed.* **1999**, *38*, 2945−2948.

[11] [11a] J. R. D. DeBord, Y. -J. Lu, C. J. Warren, R. C. Haushalter, J. Zubieta, *Chem. Commun.* **1997**, 1365−1366. [11b] C-Z. Lu, C.-D. Wu, S.-F. Lu, J.-C. Liu, Q.-J. Wu, H.-H. Zhuang, J.-S. Huang, *Chem. Commun.* **2002**, 152−153. [11c] J. Liang, Y. Wang, J. H. Yu, Y. Li, R. R. Xu, *Chem. Commun.* **2003**, 882−883.

[12] [12a] V. Soghomonian, Q. Chen, R. C. Haushalter, J. Zubieta, C. J. O'Connor, *Science* **1993**, *259*, 1596−1599. [12b] Z. Shi, S. H. Feng, S. Gao, L. Zhang, G. Yang, J. Hua, *Angew. Chem. Int. Ed.* **2000**, *39*, 2325−2327.

[13] [13a] D. W. Lee, P.-L. Hung, B. Spingler, S. J. Lippard, *Inorg. Chem.* **2002**, *41*, 521−531. [13b] W. G. Jackson, A. F. M. M. Rabman, D. C. Craig, *Inorg. Chem.* **2003**, *42*, 383−388.

[14] [14a] D. Brown, D. Altermatt, *Acta Crystallogr., Sect. B* **1985**, 244−247. [14b] R. Larsson, B. Folkesson, G. Schön, *Chem. Scr.* **1973**, *3*, 88−90.

[15] [15a] E. K. Brechin, O. Cador, A. Caneschi, C. Cadiou, S. G. Harris, S. Parsons, M. Vonci, R. E. P. Winpenny, *Chem. Commun.* **2002**, 1860−1861. [15b] O. Kahn, Molecular Magnetism, VCH, New York, **1993**.

[16] [16a] G. M. Sheldrick, *SHELXL 97*, *Program for Crystal Structure Refinement*, University of Göttingen, Germany, **1997**. [16b] G. M. Sheldrick, *SHELXL 97*, *Program for Crystal Structure Solution*, University of Göttingen, Germany, **1997**.

Received August 1, 2003

 © 2003 Wiley-VCH Verlag GmbH & Co. KGaA, Weinheim

Synthesis and Properties of Zn−Al Layered Double Hydroxides Containing Ferrocenecarboxylate Anions

Sandra Gago,[a] Martyn Pillinger,*[a] Teresa M. Santos,[a] João Rocha,[a] and Isabel S. Gonçalves*[a]

Keywords: Hydroxides / Layered compounds / Ferrocene / Host-guest systems / Organic-inorganic hybrid composites

Zn–Al layered double hydroxides (LDHs) intercalated by ferrocenecarboxylate (FcCOO) and 1,1′-ferrocenedicarboxylate [$Fc(COO)_2$] anions have been prepared by co-precipitation from aqueous solution. The Zn/Al ratio in the final materials was in the range of 1.8–1.9. Powder X-ray diffraction (XRD) indicates that the material Zn_2Al–$Fc(COO)_2$ contains a monolayer of guest anions resulting in a basal spacing of 15.5 Å. The material Zn_2Al–FcCOO exhibits a basal spacing of 20.0 Å, consistent with the formation of a bilayer of organometallic guest species. FTIR, FT Raman and ^{13}C MAS NMR spectroscopy confirm the presence of structurally intact ferrocenecarboxylate and 1,1′-ferrocenedicarboxylate anions. The nature of the Al centers in the samples was probed by 1- and 2-D (triple-quantum) ^{27}Al MAS NMR spectroscopy. Thermal properties were studied by thermogravimetric analysis and by measuring powder XRD patterns at increasing temperatures in the range of 25–450 °C. Up to 160 °C the materials lose interlayer water molecules. Dehydration of Zn_2Al–$Fc(COO)_2$ prompts reorientation of the ferrocene guest anions, resulting in the formation of a collapsed phase with an interlayer separation of 12.3 Å. The structural transformation is fully reversible upon hydration. Heat treatment of Zn_2Al–FcCOO only resulted in a gradual contraction of the interlayer separation and not the formation of a collapsed phase.

(© Wiley-VCH Verlag GmbH & Co. KGaA, 69451 Weinheim, Germany, 2004)

Introduction

Layered double hydroxides (LDHs), also known as anionic clays or hydrotalcite-like compounds, are an important class of ionic lamellar solids.[1] The structures of LDHs consist of positively charged mixed metal hydroxide layers separated by charge-balancing anions and water molecules. A broad range of compositions of the type $[M^{2+}_{1-x}M^{3+}_{x}(OH)_2](A^{m-})_{x/m}\cdot nH_2O$ (M^{2+} = Mg^{2+}, Zn^{2+}, Ni^{2+} etc., M^{3+} = Al^{3+}, Cr^{3+}, Ga^{3+} etc.) are possible, in which the M^{2+} and M^{3+} metal ions occupy octahedral positions in the hydroxide layers. The gallery anions A^{m-} are exchangeable, giving rise to a rich intercalation chemistry,[2] and the guest species may be organic or inorganic, simple or complex.[3] LDHs find uses as catalysts and catalyst supports,[4] adsorbents, anion scavengers, anion exchangers, polymer stabilizers, and antacids.[1] The synthesis of LDHs intercalated by metal coordination compounds and oxometalates was reviewed recently.[3b] Apart from cyano complexes, e.g. $Fe(CN)_6^{3-}$ and $Fe(CN)_6^{4-}$, there are few examples of LDHs intercalated by organometallic anions, especially those containing cyclopentadienyl (Cp = η^5-C_5H_5) and η^6-arene groups. Two exceptions are LDH intercalates containing ferrocenesulfonate[5] and ferrocenebutyrate anions,[6] and their use in clay-modified electrodes. These hybrid materials may also exhibit interesting photochemical or photophysical properties.[7] In the present work, Zn−Al LDHs intercalated by ferrocenecarboxylate and 1,1′-ferrocenedicarboxylate anions have been synthesized directly by co-precipitation from aqueous solution. The materials were characterized by powder X-ray diffraction, FTIR and Raman spectroscopy, magic-angle-spinning NMR (^{13}C, ^{27}Al) spectroscopy, and thermogravimetric analyses (TGA). As will be described, the interlayer arrangement of organometallic anions depends on a number of factors, including the presence of one or two carboxylate substituents in the guest molecules and the degree of hydration of the LDH. Such factors have previously been shown to be important for LDHs intercalated by organic carboxylic acids.[8,9] In this paper comparison will be made with these studies, in particular those concerning the aromatic guests terephthalate and benzoate.

Results and Discussion

Structural and Compositional Analysis

The structural formulae of the synthesized samples $Zn_2Al-Fc(COO)_2$ and $Zn_2Al-FcCOO$ conform to the de-

[a] Department of Chemistry, CICECO, University of Aveiro, 3810-193 Aveiro, Portugal
Fax: (internat.) +351-234-370084
E-mail: igoncalves@dq.ua.pt

Table 1. Chemical compositions and diffraction data for the LDH intercalates

Composition	x[a]	d(003) [Å]	c[b] [Å]	a (Å)	A_c[c] [Å^2/e]	t[d] [Å]
$Zn_{3.8}Al_2(OH)_{11.6}[Fc(COO)_2]\cdot 7H_2O$	0.345	15.5	46.35	3.04	23.2	115
$Zn_{3.5}Al_2(OH)_{11}[FcCOO]_2\cdot 8H_2O$	0.364	20.0	60.05	3.04	22.0	233

[a] Molar ratio $x = Al^{3+}/(Zn^{2+} + Al^{3+})$. [b] Lattice parameters a and c calculated from d(110) and d(003) planes, respectively. [c] Area per unit charge in the brucite-like layer, $A_c = (a^2\sin 60)/x$. [d] Average crystallite sizes calculated from the (003), (006), (009), (0012) and (0015) planes employing the Debye−Scherrer equation.

sired stoichiometric compositions except that the final Zn/Al atomic ratios are slightly lower than the value of 2.0 used in the starting solution (Table 1). This indicates an incomplete precipitation of the divalent cation, possibly due to the fact that the final pH used in the syntheses (7−8) is at the low end of the range appropriate for the synthesis of Zn−Al LDHs (7−9).[1]

The powder XRD patterns of $Zn_2Al-Fc(COO)_2$ and $Zn_2Al-FcCOO$, recorded at ambient temperature in the range of 3−70 °2θ, are typical of reasonably well-crystallized hydrotalcite-type compounds (Figure 1). Indexing was based on rhombohedral symmetry (polytype $3R_1$). The (00l) basal reflections can be easily identified as a series of symmetric, equally spaced peaks at angles below 30 °2θ. The high intensities combined with broad line-shapes indicate that the materials are of relatively high crystallinity but form as small crystallites. Furthermore, the alternation of the intensities of successive 00l reflections is indicative of a high concentration of electron density in the midplane of the interlayer region.[8a] The average crystallite sizes in the z direction were estimated from the (003), (006), (009), (0012) and (0015) planes using Scherrer's equation $L = 0.9\lambda/\beta_c\cos\theta$, where L is the crystallite size in Å along a line normal to the reflecting plane, λ is the wavelength of the radiation used, β_c is the instrument-corrected width of a reflection at half-height expressed in radians of 2θ, and θ is the Bragg diffraction angle. Values of 115 and 233 Å were found for $Zn_2Al-Fc(COO)_2$ and $Zn_2Al-FcCOO$, respectively (Table 1). The powder XRD patterns of the two LDHs also contain broad, asymmetric (*hkl*) reflections above ca. 2θ ≥ 30°, characteristic of turbostratic layered structures. Many organic-anion-pillared LDHs exhibit similar structural features.[10] The turbostratic effect is caused by a decrease in the ordering along the stacking axis due to the loss of van der Waals interactions between adjacent layers and the absence of a densely packed interlayer space formed by high charge density anions such as carbonate. On comparing the powder XRD patterns shown in Figure 1, it is evident that $Zn_2Al-FcCOO$ exhibits increased turbostratic disorder because the *hkl* reflections are broader and less intense, and in fact several are not observed. These differences are understandable when we consider the two types of guest species and the corresponding interlayer arrangements (see below).

The lattice parameter a, which corresponds to the average metal-metal distance in the layers, was calculated to be 3.04 Å for both samples ($a = 2d_{110}$). The parameter c was calculated as three times the spacing of the diffraction maximum

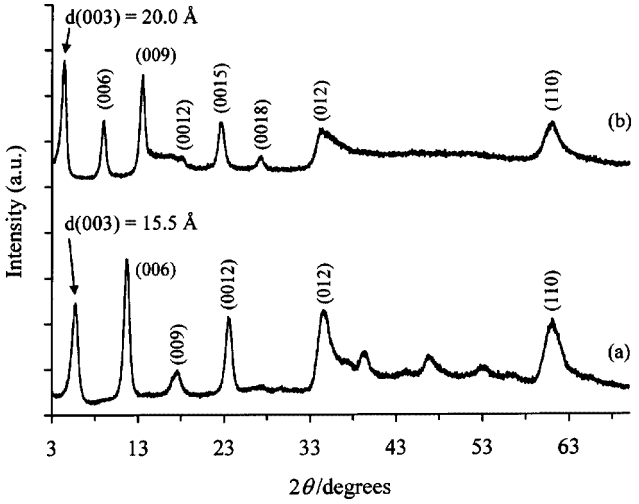

Figure 1. Powder XRD patterns at room temperature of (a) $Zn_2Al-Fc(COO)_2$ and (b) $Zn_2Al-FcCOO$

corresponding to planes (003), leading to values of 46.35 Å for $Zn_2Al-Fc(COO)_2$ and 60.05 Å for $Zn_2Al-FcCOO$. If the thickness of the brucite-like layer is taken as 4.77 Å, the gallery heights are 10.7 Å and 15.2 Å, respectively. In this work, the dimensions of the guest molecules have been estimated by using the structures of the heterobimetallic compounds $[LaL^1_3(CH_3OH)_4]_\infty$ (L^1 = 1,1′-ferrocenedicarboxylate) and $La_2L^2_6(CH_3OH)_2(H_2O)_5$ (L^2 = ferrocenecarboxylate), reported by Qing-jin and co-workers.[11] In $[LaL^1_3(CH_3OH)_4]_\infty$, two types of ferrocenedicarboxylato(2−) ligands exist, differing in their conformations. One of these is antiperiplanar with a torsion angle of 180°. The longest dimension of this molecule corresponds to one of the O···O distances and is equal to 7.48 Å. Taking into account the van der Waals radius of oxygen, this distance becomes 10.52 Å which is very similar to the observed gallery height. It is therefore reasonable to assume that the interlayer of $Zn_2Al-Fc(COO)_2$ consists of a monolayer of guest species with the longest dimension of each anion perpendicular to the brucite-like layers, as depicted in Figure 2. In this orientation, the area occupied by each molecule in the xy plane is equal to about 40 Å^2. The area per unit charge of the host lattice is given by $A_c = (a^2\sin 60)/x$, where a is the lattice parameter and x is the molar ratio of trivalent to total cations. For $Zn_2Al-Fc(COO)_2$, a = 3.04 Å and x = 0.345, and so A_c = 23.2 Å^2 (Table 1). Hence, the area available per divalent anion is approximately 46.4 Å^2. It follows that in a monolayer of 1,1′-ferrocenedicarboxyl-

 © 2004 Wiley-VCH Verlag GmbH & Co. KGaA, Weinheim

ate anions, the host layer charge can be balanced although relatively close packing of guest molecules is required.

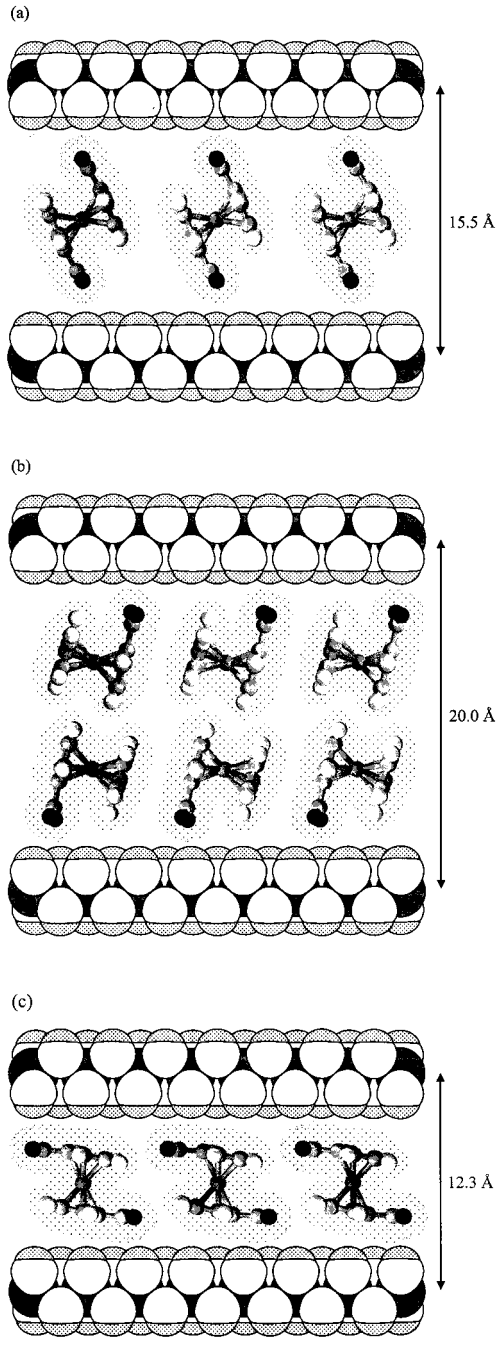

Figure 2. Models for the interlayer arrangement of guest species in (a) $Zn_2Al-Fc(COO)_2$ (fully hydrated sample = expanded phase), (b) $Zn_2Al-FcCOO$ (fully hydrated sample) and (c) $Zn_2Al-Fc(COO)_2$ (dehydrated sample = collapsed phase)

It is clear from the above calculations that the ferrocenecarboxylate anion would not be capable of spatially balancing the host layer charge of a Zn_2Al LDH, if arranged in a monolayer. The observed gallery height of $Zn_2Al-FcCOO$ is 15.2 Å, which suggests that a bilayer-like structure exists within the gallery. Figure 2(b) shows a possible arrangement of guest anions for which the calculated basal spacing exactly matches the observed value. Morlat-Thérias et al. reported Zn−Cr LDHs pillared by ferrocene mono- and disulfonate anions.[6] The basal spacings observed for their materials (20.0 and 15.0 Å, respectively) are very similar to those found in the present work for the corresponding carboxylate derivatives. It is worth noting that the interlayer arrangements for LDHs intercalated by mono- and disubstituted ferrocenes are similar to those usually reported for LDHs pillared by benzoate and terephthalate anions, respectively (with $M^{2+}/M^{3+} \approx 2$). Like 1,1′-ferrocenedicarboxylate, terephthalate anions tend to adopt a vertical orientation within the interlayer, at least under fully hydrated conditions.[3a,8,12] Benzoate anions form bilayer-like structures[8b] or monofilms of interdigitated species as found for methyl orange.[13] In all these LDH intercalates, the preferred orientation of the guest species permits a maximum interaction with the layers through hydrogen bonding with the layer hydroxyl groups, and at the same time the hydrophobic aromatic groups are located within the center of the galleries, as far apart as possible from the hydrophilic layer hydroxyls.

The organometallic-LDHs were further characterized by FTIR, Raman and MAS NMR spectroscopy. In the high frequency region (4000−2000 cm^{-1}), the IR spectra are dominated by broad bands at about 3410 cm^{-1}, attributable to the O−H stretches of weakly hydrogen-bonded water molecules and layer hydroxyl groups. A weak shoulder at about 3090 cm^{-1} (only observed for $Zn_2Al-FcCOO$) can be assigned to the C−H stretch of the cyclopentadienyl (Cp) rings of the guest. This band is stronger in the Raman spectra, and is located at 3108 cm^{-1} for $Zn_2Al-FcCOO$ and 3117 cm^{-1} for $Zn_2Al-Fc(COO)_2$. In the IR spectra, the C−C stretching vibration for the Cp rings appears at 1472 cm^{-1} for $Zn_2Al-FcCOO$ and 1487 cm^{-1} for $Zn_2Al-Fc(COO)_2$, weakly shifted compared with the corresponding bands for ferrocenecarboxylic acid (1475 cm^{-1}) and 1,1′-ferrocenedicarboxylic acid (1492 cm^{-1}). The two acids display strong bands in the solid state at about 1665 and 1300 cm^{-1}, due to C=O and C−O stretches. These bands are not observed in the spectra of the LDH intercalates, indicating that the guest species are deprotonated. This is confirmed by the presence of strong peaks at 1525 and 1391 cm^{-1} for $Zn_2Al-FcCOO$, and 1554 and 1401 cm^{-1} for $Zn_2Al-Fc(COO)_2$, assigned to $\nu_{as}(OCO)$ and $\nu_s(OCO)$, respectively. Below 750 cm^{-1}, the IR spectra of the two LDHs contain some bands due to the guest species (515 and 485 cm^{-1}) in addition to peaks arising from the host lattice. A broad band at about 630 cm^{-1} is due either to a vibrational mode of the hydroxyl groups and water or to a metal−oxygen vibration $\nu(M-O)$.[14] Two peaks at about 560 and 427 cm^{-1} can be attributed to $\nu(M-O)$ and $\delta(M-O-M)$, respectively. In the Raman spectra, the low frequency region is dominated by the intense ν_1 skeletal frequency at 324 cm^{-1} for $Zn_2Al-Fc(COO)_2$ and 314 cm^{-1} for $Zn_2Al-FcCOO$, both of which are weakly shifted compared with the corresponding bands for $Fc(COOH)_2$ and FcCOOH.

 © 2004 Wiley-VCH Verlag GmbH & Co. KGaA, Weinheim

Figure 3 shows the ^{13}C CP MAS NMR spectra of $Fc(COOH)_2$, FcCOOH and the corresponding organometallic-LDHs. Ferrocenecarboxylic acid gives rise to peaks at δ = 180.7 ppm due to the carboxyl carbon and δ = 70.8 ppm (with shoulders) due to the Cp carbons. A resolved shoulder at δ = 72.7 ppm can be attributed to the Cp carbon atom that is attached to the carboxylic acid group (*ipso* carbon). Similarly, 1,1′-ferrocenedicarboxylic acid gives rise to peaks at δ = 175.1 and 73.2 ppm, although in this case no resolved shoulder was observed for the *ipso* carbon. The main difference between these spectra and those of the organometallic-LDHs is that the peaks due to the *ipso* carbon atoms are shifted considerably to lower field, presumably due to deprotonation of the carboxylic acid groups. The ^{27}Al MAS NMR spectrum of $Zn_2Al-Fc(COO)_2$ contains a sharp peak at δ = 14 ppm with a broad low-frequency shoulder, assigned to octahedral aluminium (see a in Figure 4). Similar spectra have been reported in the literature for $Zn-Al-CO_3$ and $Mg-Al-CO_3$ LDHs.[15,16] The sheared triple-quantum ^{27}Al MAS NMR spectrum of this sample clearly shows the existence of two distinct Al sites (overlapping resonances S1 and S2, see b in Figure 4). The peak S1, at δ ca. 16 (F1) [δ ca. 14 (F2)], displays a distribution of isotropic chemical shifts. We speculate that this may be due to the presence of a range of slightly different local Al environments generated by the random insertion of Al in the layers.[16] The low-frequency F2 shoulder (S2) is essentially undistributed but it has an average quadrupole coupling constant larger than S1. Similar 1-D and 2-D spectra were obtained for $Zn_2Al-FcCOO$ (not shown).

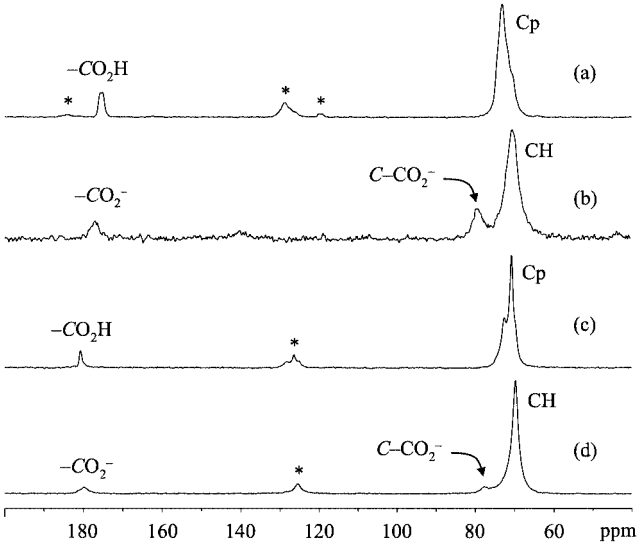

Figure 3. ^{13}C CP MAS NMR spectra of (a) $Fc(COOH)_2$, (b) $Zn_2Al-Fc(COO)_2$, (c) FcCOOH and (d) $Zn_2Al-FcCOO$; spinning side-bands are indicated with an asterisk

Thermal Properties

The TGA traces for $Zn_2Al-Fc(COO)_2$ and $Zn_2Al-FcCOO$ indicate three general regions of mass loss

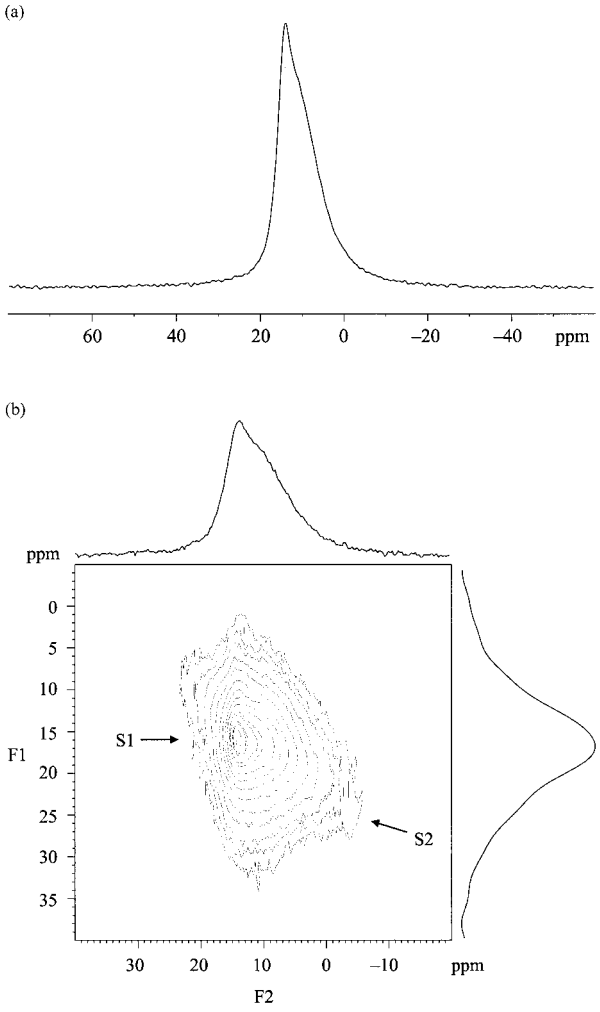

Figure 4. (a) ^{27}Al MAS NMR spectrum of $Zn_2Al-Fc(COO)_2$ and (b) sheared 3Q ^{27}Al MAS NMR spectrum of $Zn_2Al-Fc(COO)_2$

(Figure 5), the first two of which overlap to some extent. The first step, corresponding to removal of interlayer water, extends from room temperature to approximately 180 °C for $Zn_2Al-Fc(COO)_2$ (13.1% mass loss, DTG_{max} = 140 °C) and 160 °C for $Zn_2Al-FcCOO$ (10.6% mass loss, DTG_{max} = 80 °C). The second step, which takes place in the 180–240 °C range for $Zn_2Al-Fc(COO)_2$ (DTG_{max} = 214 °C) and 160–230 °C for $Zn_2Al-FcCOO$ (DTG_{max} = 196 °C), can be assigned to partial dehydroxylation of the double hydroxide layers.[17] The third step extends from about 280 °C to 520 °C and can be attributed to complete dehydroxylation and partial elimination/decomposition of the organometallic anions. The mass loss in this range is higher for $Zn_2Al-FcCOO$ (28.1%) than for $Zn_2Al-Fc(COO)_2$ (20.2%), consistent with the fact that the former has approximately double the number of intercalated ferrocenyl units due to the lower anion charge.

Powder XRD diagrams of $Zn_2Al-Fc(COO)_2$, recorded at increasing temperatures in the range of 25–450 °C, are shown in Figure 6. Only the basal reflections are displayed from which the interlayer spacing of the LDH may be deduced. As described above, the synthesized

 © 2004 Wiley-VCH Verlag GmbH & Co. KGaA, Weinheim

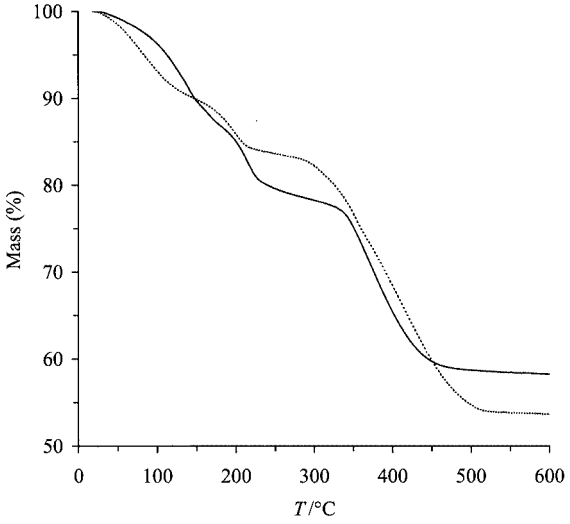

Figure 5. TGA curves for $Zn_2Al-Fc(COO)_2$ (——) and $Zn_2Al-FcCOO$ (− − −)

$Zn_2Al-Fc(COO)_2$ consists of a single expanded phase at room temperature characterized by a basal spacing of 15.5 Å. At 120 °C, the expanded phase can still be identified, although the basal reflections are reduced in intensity and shifted slightly to higher angles. In addition to this phase, a new "collapsed phase" is present characterized by a basal spacing of 12.3 Å. At this temperature, the water content was estimated to be 59% of the initial total. Further heating to 160 °C resulted in complete transformation of the expanded phase to the collapsed phase (water content = 19% of initial total). The basal spacing of 12.3 Å suggests a gallery height of 7.5 Å which fits very well with a model where the shortest dimension of the guest molecules is nearly perpendicular to the host layers (see c in Figure 2). We therefore conclude that removal of interlayer water is accompanied by a reorientation of the organometallic anions.[18] It can be assumed that the ferrocenyl units do not lie completely flat but are tilted slightly with respect to the host layers in order to maintain a hydrogen-bonding interaction between the carboxyl groups and hydroxide layers. The (003) reflection of the collapsed phase did not change much up to 300 °C, despite partial dehydroxylation of the layers. Transformation to an amorphous phase occurred above this temperature, i.e. during the third stage of weight loss observed by TGA. In a separate experiment, a sample of $Zn_2Al-Fc(COO)_2$ was heated to 160 °C and, after measuring the powder XRD pattern at this temperature, cooled to room temperature over ca. 15 min (under moist air), and the powder XRD pattern measured again (Figure 7). The results show complete recovery of the expanded phase, indicating that the structural transformation is fully reversible upon hydration. A TGA of the sample after measuring the powder XRD indicated that the total water content was equal to the initial value, within experimental error. The recovery of the expanded phase demonstrates that heat treatment (up to 160 °C) does not result in covalent grafting of the anions to the hydroxyl layers. These results are similar to those reported by Kooli et al. for a Mg_2Al-TA LDH (TA = terephthalate) prepared by co-precipitation at constant pH.[8b] Thus, it was found that the terephthalate anion initially adopts a vertical orientation between the layers, but above 150 °C the expanded structure collapses, with a shift in the position of the (003) reflection from 14.6 to 8.9 Å suggesting a horizontal arrangement for the anion. Cooling of the sample to room temperature under moist air led to complete recovery of the vertical arrangement.

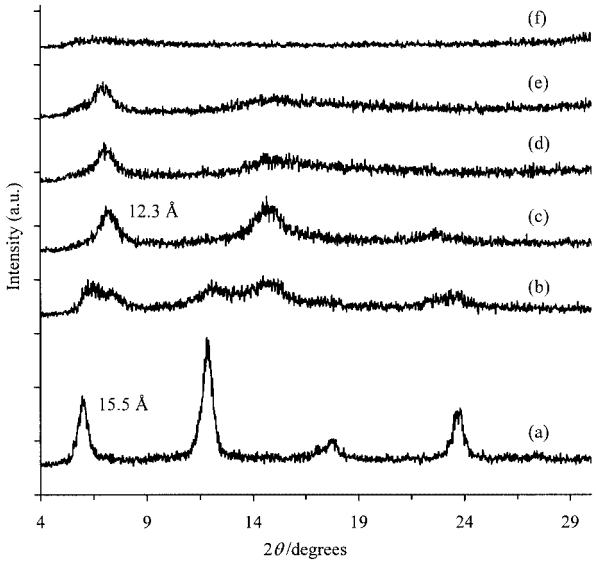

Figure 6. Powder XRD patterns of $Zn_2Al-Fc(COO)_2$ recorded at (a) room temperature, (b) 120 °C, (c) 160 °C, (d) 230 °C, (e) 300 °C and (f) 450 °C; the *d*(003) spacings for the expanded (15.5 Å) and collapsed (12.3 Å) phases are indicated

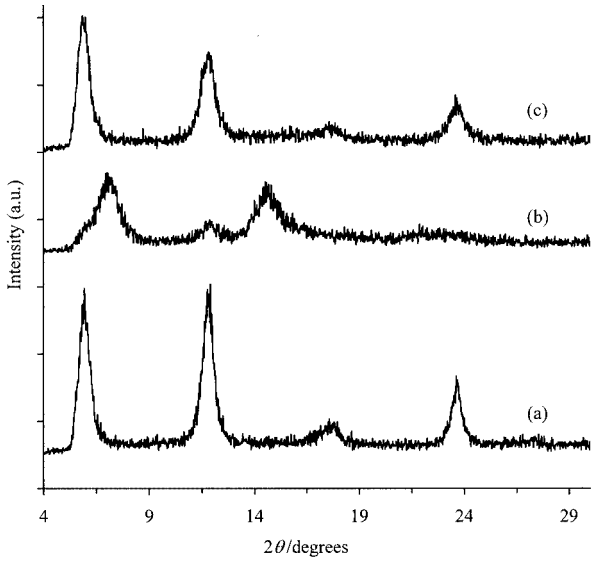

Figure 7. Powder XRD patterns of $Zn_2Al-Fc(COO)_2$ recorded at (a) room temperature, (b) 160 °C and (c) room temperature (after cooling the sample from 160 °C under moist air)

 © 2004 Wiley-VCH Verlag GmbH & Co. KGaA, Weinheim

Powder XRD diagrams of $Zn_2Al-FcCOO$, recorded at increasing temperatures in the range of 25−450 °C, did not indicate the formation of a new collapsed phase (Figure 8). Instead, there was a gradual contraction of the interlayer separation up to 160 °C, as evidenced by a slight shift of the basal reflections to higher 2θ values [the (003) peak was not clearly observed in these diffraction patterns, probably due to the nature of the sample holder]. At 230 °C, the (00*l*) reflections had disappeared and only a very broad weak feature was observed between 13 and 20 °2θ. The layered structure was therefore severely disrupted by the partial dehydroxylation which, as revealed by the TGA results, took place in the range 160−230 °C. Transformation to an amorphous phase was complete at 300 °C and no further change took place up to 450 °C.

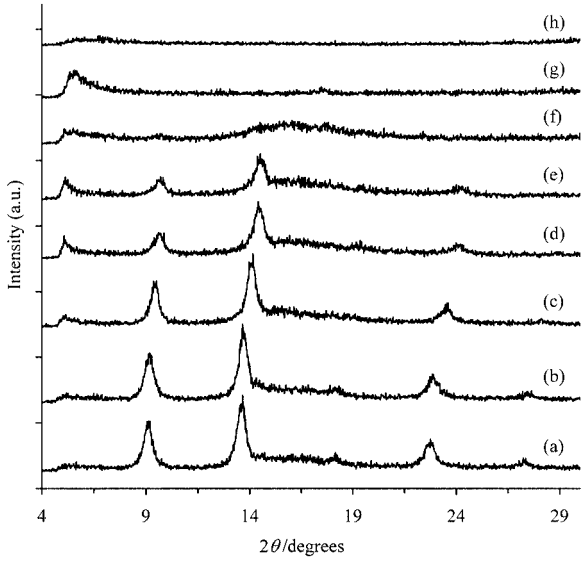

Figure 8. Powder XRD patterns of $Zn_2Al-FcCOO$ recorded at (a) room temperature, (b) 50 °C, (c) 80 °C, (d) 120 °C, (e) 160 °C, (f) 230 °C, (g) 300 °C and (h) 450 °C

Concluding Remarks

Zn−Al layered double hydroxides intercalated by ferrocene guests anions have successfully been prepared by co-precipitation from aqueous solution. In the case of 1,1-ferrocenedicarboxylate, the interlayer separation for the fully hydrated material indicates that the guest species adopt an antiperiplanar conformation and are arranged in a monolayer with the longest dimension perpendicular to the host layers. As observed for many organic-anion-pillared LDHs, water plays a critical role in stabilizing the expanded structure. Heat treatment results in a reorientation of the guest species such that the shortest dimension is nearly perpendicular to the host layers. The resultant collapsed phase is quite stable − the layered structure can still be identified by powder XRD after heat treatment at 300 °C. In the case of ferrocenecarboxylate guest anions, we conclude that bilayer structures are formed in the interlayer. The carboxyl groups are probably linked by hydrogen bonding to the hydroxide sheets with the aromatic groups located within the center of the gallery. Such an arrangement would result in a hydrophobic membrane-like region. This material may therefore have interesting adsorption properties, e.g. the ability to take up organic molecules (and swell in a direction perpendicular to the layers). The interlayer region may also provide a novel environment for photochemical reactions of photoactive molecules. These studies are currently under way in our laboratories in addition to efforts to prepare LDHs containing other types of organometallic anions.

Experimental Section

Materials and Methods: The reagents $Zn(NO_3)_2{\cdot}6H_2O$ (Riedel-de Haën), $Al(NO_3)_3{\cdot}9H_2O$ (Riedel-de Haën), 50% aqueous NaOH (Aldrich), 1,1′-ferrocenedicarboxylic acid [$Fc(COOH)_2$, Fluka] and ferrocenecarboxylic acid (FcCOOH, Fluka) were obtained from commercial sources and used as received.

Microanalyses for CHN were carried out at the Instituto de Tecnologia Química e Biológica, Oeiras, Portugal. Zn, Al and Fe were determined by ICP-OES at the Central Laboratory for Analysis, University of Aveiro (E. Soares). Room temperature powder XRD data were collected on a Philips X'pert diffractometer with a curved graphite monochromator (Cu-K_α radiation) in a Bragg−Brentano para-focusing optics configuration. Samples were step-scanned in 0.02 °2θ steps with a counting time of 1 s per step. The XRD measurements as a function of temperature were carried out in situ using the same diffractometer equipped with an Anton-Parr GmbH HTK16 high temperature chamber containing a Pt heating filament and a Pt−Pt/Rh (10%) thermocouple. The powdered sample was deposited on the filament which also acts as the sample holder. Heating rates of 10 °C min^{-1} were used. At a given temperature, samples were step-scanned in 0.02 °2θ steps with a counting time of 0.6 s per step. TGA studies were performed using a Shimadzu TGA-50 system at a heating rate of 5 °C min^{-1} under nitrogen.

IR spectra were obtained with KBr pellets using an FTIR Mattson-7000 infrared spectrophotometer. Raman spectra were recorded on a Bruker RFS100/S FT instrument (Nd:YAG laser, 1064 nm excitation, InGaAs detector). Solid-state NMR spectra were measured at 100.62 MHz for ^{13}C and 104.26 MHz for ^{27}Al with a (9.4 T) wide bore Bruker Avance 400 spectrometer. ^{13}C CP MAS NMR spectra were acquired with a 4 μs 90° proton pulse and 2 ms contact time with spinning rates of 7−8.5 kHz and 4 s recycle delays. Chemical shifts are quoted in ppm relative to TMS. Single-quantum ('conventional') ^{27}Al MAS NMR spectra were acquired using short and powerful radio-frequency pulses (0.6 μs, corresponding to π/12 pulses), a spinning rate of 14 kHz and a recycle delay of 1 s. Chemical shifts are quoted in ppm relative to $Al(H_2O)_6^{3+}$. The two-dimensional triple-quantum (3Q) ^{27}Al MAS NMR spectra were acquired using the three pulse z-filter sequence.[19,20] The lengths of the two hard pulses were 2.4 μs and 0.7 μs (radio-frequency magnetic field amplitude ν_1 = 150 kHz), and the length of the soft pulse was 11 μs (ν_1 = 7.5 kHz). The MAS rate was 14 kHz. 114 data points were acquired in the t_1 domain in increments of $(1/2\nu r)$ = 35.71 μs. The ppm scale of the sheared spectra was referenced to ν_0 frequency in the ν_2 domain and to $1.42\nu_0$ in the ν_1 domain (high-resolution dimension after shearing). The reference was $Al(H_2O)_6^{3+}$.

 © 2004 Wiley-VCH Verlag GmbH & Co. KGaA, Weinheim

Sample Preparation: The LDHs were prepared by a co-precipitation method similar to that described by Drezdon.[12] Reactions were carried out under nitrogen, using distilled deionized water which was freshly de-carbonated prior to use by vigorously boiling for 15 minutes. As an example, a solution of $Zn(NO_3)_2{\cdot}6H_2O$ (2.97 g, 10 mmol) and $Al(NO_3)_3{\cdot}9H_2O$ (1.88 g, 5 mmol) in decarbonated water (20 mL) was added dropwise to a solution of 1,1′-ferrocenedicarboxylic acid (1.37 g, 5 mmol) and 50% NaOH (3.25 g, 40 mmol) in decarbonated water (35 mL) with efficient mixing. Once addition was complete, the resultant light brown gel-like slurry was stirred for 48 h at 75 °C. The solid was isolated by filtration, washed several times with de-carbonated water and dried at room temperature under reduced pressure in a vacuum desiccator. This material is referred to as $Zn_2Al-Fc(COO)_2$. The same general method was used for the synthesis of $Zn_2Al-FcCOO$ (10 mmol ferrocenecarboxylic acid). In both cases, the pH at the end of the reaction was in the range of 7−8.

$Zn_2Al-Fc(COO)_2$: $Zn_{3.8}Al_2(OH)_{11.6}[Fc(COO)_2]{\cdot}7H_2O$ (897.87): calcd. Zn 27.68, Al 6.01, Fe 6.22, C 16.05; found Zn 27.60, Al 6.04, Fe 6.22, C 15.29. TGA up to 180 °C revealed a sample weight loss of 13.1% (calcd: for loss of $7H_2O$, 14.0%; for loss of $6H_2O$, 12.3%). IR (KBr): $\tilde{\nu}$ = 3420 cm^{-1} (br), 2370 (w), 1554 (s), 1487 (m), 1460 (m), 1401 (m), 1389 (m), 1364 (m), 1347 (sh), 1260 (sh), 1193 (w), 1053 (sh), 1026 (m), 821 (m), 798 (m), 625 (m), 564 (m), 518 (m), 485 (w), 427 (s). Raman (cm^{-1}): 3362, 3117, 1480, 1459, 1392, 1367, 1195, 1070, 1034, 922, 569, 504, 324. ^{13}C CP MAS NMR: δ = 70.7 (*C*H), 79.5 (*C*−CO_2^-), 177.0 (C−*C*O_2^-). ^{27}Al MAS NMR: δ = 14.1 ppm.

$Zn_2Al-FcCOO$: $Zn_{3.5}Al_2(OH)_{11}[FcCOO]_2{\cdot}8H_2O$ (1072.1): calcd. Zn 21.34, Al 5.03, Fe 10.42, C 24.65; found Zn 21.40, Al 4.97, Fe 10.80, C 25.79. TGA up to 150 °C revealed a sample weight loss of 10.6% (calcd: for loss of $8H_2O$, 13.4%; for loss of $6H_2O$, 10.4%). IR (KBr): $\tilde{\nu}$ = 3407 cm^{-1} (br), 3086 (sh), 2924 (sh), 2861 (sh), 2367 (w), 2342 (w), 1525 (s), 1472 (m), 1391 (m), 1361 (m), 1347 (sh), 1266 (sh), 1211 (sh), 1187 (w), 1105 (w), 1024 (m), 1005 (w), 918 (w), 841 (sh), 819 (m), 793 (m), 637 (m), 554 (m), 510 (m), 485 (m), 429 (s). Raman (cm^{-1}): 3390, 3108, 1473, 1411, 1392, 1361, 1188, 1107, 1060, 1032, 918, 560, 504, 382, 314. ^{13}C CP MAS NMR: δ = 69.8 (*C*H), 77.8 (*C*−CO_2^-), 179.9 (C−*C*O_2^-). ^{27}Al MAS NMR: δ = 14.6 ppm.

Acknowledgments

The authors are grateful to FCT, POCTI and FEDER for financial support (Project POCTI//QUI/37990/2001). SG thanks the University of Aveiro for a research grant. Paula Esculcas and Claudia Morais are acknowledged for assistance with the NMR experiments.

[1] *Layered Double Hydroxides: Present and Future* (Ed.: V. Rives), Nova Science Publishers, Inc., New York, **2001**.
[2] A. I. Khan, D. O'Hare, *J. Mater. Chem.* **2002**, *12*, 3191−3198.
[3] [3a] S. P. Newman, W. Jones, *New J. Chem.* **1998**, 105−115. [3b] V. Rives, M. A. Ulibarri, *Coord. Chem. Rev.* **1999**, *181*, 61−120.
[4] B. F. Sels, D. E. De Vos, P. A. Jacobs, *Catal. Rev. −Sci. Eng.* **2001**, *43*, 443−488.
[5] P. Wang, G. Zhu, *Electrochem. Commun.* **2002**, *4*, 36−40.
[6] [6a] S. Morlat-Thérias, C. Mousty, P. Palvadeau, P. Molinié, P. Léone, J. Rouxel, C. Taviot-Guého, A. Ennaqui, A. de Roy, J. P. Besse, *J. Solid State Chem.* **1999**, *144*, 143−151. [6b] S. Therias, B. Lacroix, B. Schöllhorn, C. Mousty, P. Palvadeau, *J. Electroanal. Chem.* **1998**, *454*, 91−97.
[7] M. Ogawa, K. Kuroda, *Chem. Rev.* **1995**, *95*, 399−438.
[8] [8a] M. Vucelic, G. D. Moggridge, W. Jones, *J. Phys. Chem.* **1995**, *99*, 8328−8337. [8b] F. Kooli, I. C. Chisem, M. Vucelic, W. Jones, *Chem. Mater.* **1996**, *8*, 1969−1977. [8c] S. P. Newman, S. J. Williams, P. V. Coveney, W. Jones, *J. Phys. Chem. B* **1998**, *102*, 6710−6719.
[9] N. Iyi, K. Kurashima, T. Fujita, *Chem. Mater.* **2002**, *14*, 583−589.
[10] V. Prevot, C. Forano, J. P. Besse, F. Abraham, *Inorg. Chem.* **1998**, *37*, 4293−4301.
[11] G. Dong, L. Yu-ting, D. Chun-ying, M. Hong, M. Qing-jin, *Inorg. Chem.* **2003**, *42*, 2519−2530.
[12] M. A. Drezdon, *Inorg. Chem.* **1988**, *27*, 4628−4632.
[13] U. Costantino, N. Coletti, M. Nocchetti, G. G. Aloisi, F. Elisei, *Langmuir* **1999**, *15*, 4454−4460.
[14] [14a] W. Kagunya, R. Baddour-Hadjean, F. Kooli, W. Jones, *Chem. Phys.* **1998**, *236*, 225−234. [14b] J. T. Kloprogge, R. L. Frost in *Layered Double Hydroxides: Present and Future* (Ed.: V. Rives), Nova Science Publishers, Inc., New York, **2001**, pp. 139−192.
[15] F. Thevenot, R. Szymanski, P. Chaumette, *Clays Clay Miner.* **1989**, *37*, 396−402.
[16] J. Rocha, M. del Arco, V. Rives, M. A. Ulibarri, *J. Mater. Chem.* **1999**, *9*, 2499−2503.
[17] [17a] F. Kooli, C. Depège, A. Ennaqadi, A. De Roy, J. P. Besse, *Clays Clay Miner.* **1997**, *45*, 92−98. [17b] I. Crespo, C. Barriga, M. A. Ulibarri, G. González-Bandera, P. Malet, V. Rives, *Chem. Mater.* **2001**, *13*, 1518−1527. [17c] F. Rey, V. Fornés, *J. Chem. Soc., Faraday Trans.* **1992**, *88*, 2233−2238.
[18] A referee suggested that the observed collapse of the interlayer distance for $Zn_2Al-Fc(COO)_2$ upon heating could be due to the removal of water molecules present between the carboxylate groups and the positive charges. Based on the agreement between calculated and experimental interlayer spacings, we firmly believe that the collapse is due to a reorientation of guest species (analogous to that reported in the literature for LDHs pillared by terephthalate anions).
[19] L. Frydman, J. S. Harwood, *J. Am. Chem. Soc.* **1995**, *117*, 5367−5368.
[20] J. P. Amoureux, C. Fernandez, S. Steuernagel, *J. Magn. Reson., Sect. A.* **1996**, *123*, 116−118.

Received September 11, 2003
Early View Article
Published Online February 16, 2004

 © 2004 Wiley-VCH Verlag GmbH & Co. KGaA, Weinheim

Tetranuclear (Borole)rhodium Clusters with Hydrido and Methylthiolato Ligands − Structures of $[\{Rh(C_4H_4BMe)\}_4(\mu_3\text{-}H)(\mu_3\text{-}I)_3]$ and of $[\{Rh(C_4H_4BPh)\}_2(\mu\text{-}SMe)(\mu_3\text{-}SMe)]_2$ (2 *Rh−Rh*)[‡]

Gerhard E. Herberich,*[a] Hartmut J. Eckenrath,[a,b] Trixie Wagner,[a,c] and Ruimin Wang[a]

Keywords: Boron / Borole / Hydride ligands / Rhodium / S ligands

The heterocubanes $[Rh(C_4H_4BR)(\mu_3\text{-}I)]_4$ (**1a**: R = Ph; **1b**: R = Me) can be hydrogenated in THF (suspension, 1 bar H_2, 20 °C) to give the μ_3-hydrido clusters $[\{Rh(C_4H_4BR)\}_4(\mu_3\text{-}H)(\mu_3\text{-}I)_3]$ (**2a**,**b**). The structure of **2b** consists of a $Rh_4(\mu_3\text{-}H)(\mu_3\text{-}I)_3$ core with idealized C_{3v} symmetry and four capping η^5-borole ligands. The Rh–Rh distances within the $Rh_3(\mu_3\text{-}H)$ cluster unit amount to 2.9448(6), 2.9647(6), and 2.9724(6) Å; the μ_3-H ligand is 0.064(5) Å above the Rh_3 plane with a mean Rh–H bond length of 1.83(5) Å. The tris(acetonitrile) salts $[Rh(C_4H_4BR)(NCMe)_3]BF_4$ (**4a**,**b**) react with NaSMe to give the methylthiolato complexes $[Rh(C_4H_4BR)(SMe)]_x$ (**3a**,**b**). In the crystal **3a** possesses a centrosymmetric stepped-ladder structure $[\{Rh(C_4H_4BPh)\}_2(\mu\text{-}SMe)(\mu_3\text{-}SMe)]_2$ (2*Rh–Rh*) (**3a**-Rh_4), with a Rh–Rh bond length of 2.9233(11) Å. In solution a dissociation equilibrium is observed with a predominating dinuclear complex $[Rh(C_4H_4BPh)(\mu\text{-}SMe)]_2$ (**3a**-Rh_2); in pyridine a closely related solvate $[Rh(py)(C_4H_4BPh)(\mu\text{-}SMe)]_2$ (**5**) with a static $Rh_2(\mu\text{-}SMe)_2$ core is formed.
(© Wiley-VCH Verlag GmbH & Co. KGaA, 69451 Weinheim, Germany, 2004)

Introduction

The recently described heterocubanes $[Rh(C_4H_4BR)(\mu_3\text{-}I)]_4$ (**1a**,**b**) are readily accessible[2a] and display a rich reaction chemistry.[2b] They possess a total of 72 valence electrons, with five electrons counted per μ_3-iodide ligand. Hence the Rh centers obey the 18-electron rule and therefore the complexes **1** are cage compounds. As they have no metal−metal bonds, they are not clusters in the sense of the widely accepted definition of a cluster given by Cotton.[3] The heterocubanes **1a** and **1b** undergo an exchange of (borole)rhodium vertices which is fast on the NMR timescale at ambient temperature,[2a] possibly via a dissociation−association equilibrium between tetra- and dinuclear species.

We have tried to vary the bridging ligand in these cage compounds in a number of ways,[4] and report here on two results. Homogeneous hydrogenation of the heterocubanes **1a**,**b** (R = Ph and Me, respectively) produces novel tetranuclear μ_3-hydrido clusters $[\{Rh(C_4H_4BR)\}_4(\mu_3\text{-}H)(\mu_3\text{-}I)_3]$ (**2a**,**b**), and treatment with NaSMe affords the methylthio complexes $[Rh(SMe)(C_4H_4BR)]_x$ (**3a**,**b**). In the case of **3b** a tetranuclear complex with a partially opened structure is found in the crystal and a dissociation−association equilibrium in solution.

Results and Discussion

Hydrogenation and Synthesis of Hydrido Clusters

The heterocubanes **1** readily react with dihydrogen in THF (1 bar, 20 °C, 3 h) to produce the μ_3-hydrido clusters **2** (Scheme 1) The basicity of the THF seems to be essential since no reaction is observed when dichloromethane is used as solvent. The products can be isolated as dark red crystals by cooling concentrated dichloromethane solutions. In solution they are slightly sensitive to air. They do not react with triethylamine or with iodomethane at ambient temperature and are decomposed by CF_3CO_2D in $CDCl_3$. We mention in passing that attempted hydrogenation of **1a**,**b** with $NaBHEt_3$ was unsuccessful and seemed to result in reductive decomposition.

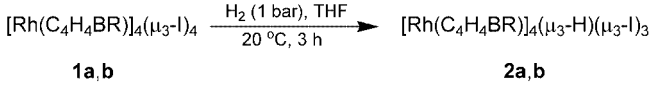

Scheme 1. Hydrogenation of the heterocubanes $[Rh(C_4H_4BR)(\mu_3\text{-}I)]_4$ (**1a**,**b**)

[‡] Borole Derivatives, 25. Part 24: Ref.[1]
[a] Institut für Anorganische Chemie, Technische Hochschule Aachen
52056 Aachen, Germany
Fax: (internat.) + 49-241-809-2288
E-mail: gerhard.herberich@ac.rwth-aachen.de
[b] Convertex Chemie GmbH, Chemie-Park Bitterfeld-Wolfen
06766 Wolfen, Germany
[c] Novartis Pharma AG, Central Technologies
4002 Basel, Switzerland

 © 2004 Wiley-VCH Verlag GmbH & Co. KGaA, Weinheim **DOI: 10.1002/ejic.200300630**

The ^{1}H NMR spectra of the product complexes **2a**,**b** display a quadruplet at high field [e.g. for **2a**: $\delta = -10.27$ ppm, $^1J_{Rh,H} = 21.5$ Hz] indicating the presence of a triply bridging hydrido ligand in a $Rh_3(\mu_3\text{-H})$ arrangement. The $Rh_3(\mu_3\text{-H})$ structural element was first found in the Fischer/Wawersik complex $[(RhCp)_3(\mu_3\text{-H})(\mu_3\text{-Cp})]$ [$\delta = -12.47$ ppm, $^1J_{Rh,H} = 26.5$ Hz],[5] and is known from a few other structurally characterized complexes,[6,7] including, for instance, the tetranuclear complex $[(RhCp^*)_4(\mu_3\text{-H})_4](BF_4)_2$[7b,7c] and the trimethylenemethane complex $[\{Rh(COD)\}_3(\mu_3\text{-H})\{\mu_3\text{-C}(CH_2)_3\}]$.[7a] We also see two types of borole ligands in a 3:1 ratio. In combination with the elemental analysis these observations define the formula and constitution of the clusters **2**.

Structure of the Hydrido Cluster 2b

Because of the novelty of these hydrido compounds we decided to characterize **2b** by an X-ray structure determination. Complex **2b** crystallizes in the monoclinic space group $P2_1/n$ with $Z = 4$ (Figure 1; produced with the Platon software package[8]). The central core of **2b** is a trigonal $Rh_4(\mu_3\text{-H})(\mu_3\text{-I})_3$ unit with idealized C_{3v} symmetry, and each Rh vertex is capped by a borole ligand. Note that the apical vertex (with Rh1) is similar to the vertices of **1b**, while the basal vertices belong to a true cluster unit $(\mu_3\text{-H})Rh_3$.

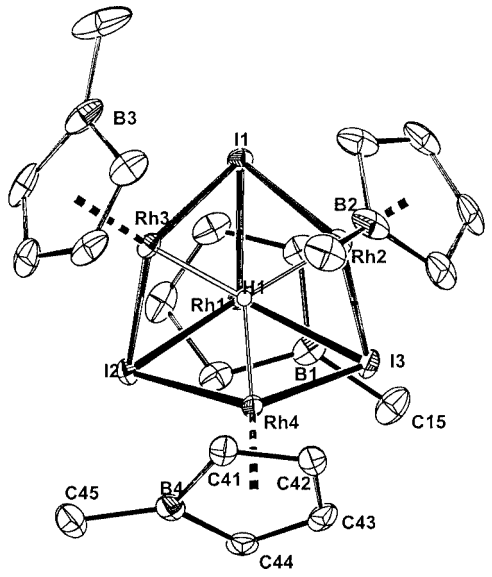

Figure 1. Molecular structure (PLATON plot,[8] at the 30% probability level) of **2b** in the crystal; see text for Rh−Rh interactions in the cluster; selected bond lengths (Å) and bond angles (°): I1−Rh1 2.7420(5), I1−Rh2 2.7181(6), I1−Rh3 2.7309(6), I2−Rh1 2.7272(6), I2−Rh3 2.7170(5), I2−Rh4 2.7285(6), I3−Rh1 2.7626(6), I3−Rh2 2.7398(6), I3−Rh4 2.7626(6), Rh1···Rh2 3.956(1), Rh1··Rh3 3.905(1), Rh1···Rh4 3.973(1), Rh2−Rh3 2.9647(6), Rh2−Rh4 2.9448(6), Rh3−Rh4 2.9724(6), Rh2−H1 1.82(5), Rh3−H1 1.82(5), Rh4−H1 1.83(5); I1−Rh1−I2 87.81(2), I1−Rh1−I3 85.87(2), I1−Rh2−I3 86.78(2), I1−Rh3−I2 88.24(2), I2−Rh1−I3 86.17(1), I2−Rh4−I3 86.14(1), Rh1−I1−Rh2 92.85(2), Rh1−I1−Rh3 91.06(2), Rh1−I2−Rh3 91.68(2), Rh1−I2−Rh4 93.47(2), Rh1−I3−Rh2 91.93(2), Rh1−I3−Rh4 91.95(1), Rh2−I1−Rh3 65.92(1), Rh2−I3−Rh4 64.71(2), Rh3−I2−Rh4 66.16(1)

The Rh−Rh distances between the apical Rh atom and the basal Rh centers amount to more than 3.90 Å and thus are nonbonding. The basal Rh atoms form a nearly regular triangle with Rh−Rh distances of 2.9448(6)−2.9724(6) Å. Known complexes with all-18e configurations and two center, two electron Rh−Rh bonds typically display Rh−Rh bond lengths of 2.72 Å,[5,6] while electron-deficient examples[7] tend to have longer bonds, with Rh−Rh distances up to about 3.0 Å.[9]

The Rh−I bond lengths average 2.737 Å [2.7170(5)−2.7626(6) Å] and are similar to those in **1a** and **1b** [2.7049(9)−2.777(1) Å],[3] while the Rh−(μ_2-I) distances [2.715−2.741 Å] seem to be marginally shorter.[10] The borole ligation to the metal is not detailed here. We only note that the Rh−B distances [2.307(6)−2.348(6) Å] are in the expected range (cf. the Rh−B bond lengths in the heterocubanes **1a**,**b**, which average to 2.325 Å[2a]).

The hydride ligand could be localized in the structure analysis and was refined isotropically. It lies 0.64(5) Å above the Rh_3 plane, and the Rh−H bond lengths observed average to 1.83(5) Å. This result is in reasonable agreement with the data for the cluster $[(RhCp^*)_4(\mu_3\text{-H})_4](BF_4)_2$ (as determined by neutron diffraction).[7b]

The hydrido clusters $[\{Rh(C_4H_4BR)\}_4(\mu_3\text{-H})(\mu_3\text{-I})_3]$ (**2a,b**) possess a total of 68 valence electrons, four less than the cage complexes **1**. Formally removing one iodo ligand from the cages **1** generates a $[\{Rh(C_4H_4BR)\}_4(\mu_3\text{-I})_3]^+$ fragment with three empty, metal-centered orbitals ready for σ-bonding. In C_{3v} symmetry these σ-orbitals combine to an a_1 and an e set of orbitals. Interaction with the 1s orbital of the hydrido ligand results in bonding of the hydrido ligand and metal-metal bonding, in other words, in a four center, two electron bond within the $(\mu_3\text{-H})Rh_3$ tetrahedron. The e set of MOs remains empty and accounts for the reduced electron count of **2a**,**b**.

Synthesis of Methylthiolato Complexes

The anionic ligand of the cage complexes **1** may be substituted in a two-step procedure, first removing the halide ligand by dehalogenation with silver salts such as $AgBF_4$ in acetonitrile, and then introducing a new ligand. Thus, the reaction of the tris(acetonitrile) salts **4a**,**b** with sodium methylthiolate in acetonitrile smoothly affords the robust, high-melting methylthiolato complexes **3a**,**b** (Scheme 2). The phenyl complex **3a** can be crystallized from hot toluene, while the methyl complex **3b** is scarcely soluble, even in toluene or CH_2Cl_2.

Structure of the Methylthiolato Complex 3a in the Crystal

The low-temperature NMR spectra of complex **3a** indicate that this compound is not of the heterocubane type.

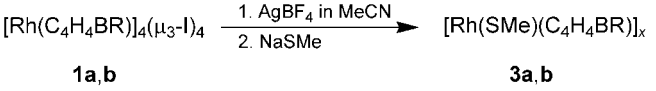

Scheme 2. Synthesis of the methylthiolato complexes $[Rh(SMe)(C_4H_4BR)]_x$ (**3a**,**b**)

 © 2004 Wiley-VCH Verlag GmbH & Co. KGaA, Weinheim

The X-ray single-crystal structure determination revealed that complex **3a** consists of tetranuclear [{Rh-(C_4H_4BR)}$_2$(μ-SMe)(μ$_3$-SMe)]$_2$ (2 *Rh*−*Rh*) (**3a**-Rh_4) molecules which display a crystallographic center of symmetry (Figure 2). The structure observed may formally be deduced from a cubanoid structure analogous to **1a**. Opening the heterocubane cage gives a stepped ladder, and coordinative unsaturation of the outer Rh centers is avoided by formation of dative Rh−Rh bonds [Rh1−Rh2 2.9233(11) Å]. Some additional stabilization by π-interactions with the sulfur lone-pairs may also be present. While the central rhombus is planar (as implied by the centrosymmetry of the molecule), the outer tetragons are folded along the line Rh1,Rh2 with a folding angle (between the plane Rh1,Rh2,S1 and Rh1,Rh2,S2) of 68.38(9)° in such a way that S2 is moved toward the central rhombus. Finally, we note that the molecule **3a**-Rh_4 may be viewed as a dimer of a dinuclear species **3a**-Rh_2. This view is supported by the fact that the connecting Rh2−S1′ and Rh2′−S1 bonds are markedly longer [2.461(2) Å] than the other Rh−S bonds in the same molecule [cf. Rh1−S1 2.326(2), Rh1−S2 2.303(3) Å and Rh2−S1 2.400(2), Rh2−S2 2.405(3) Å].

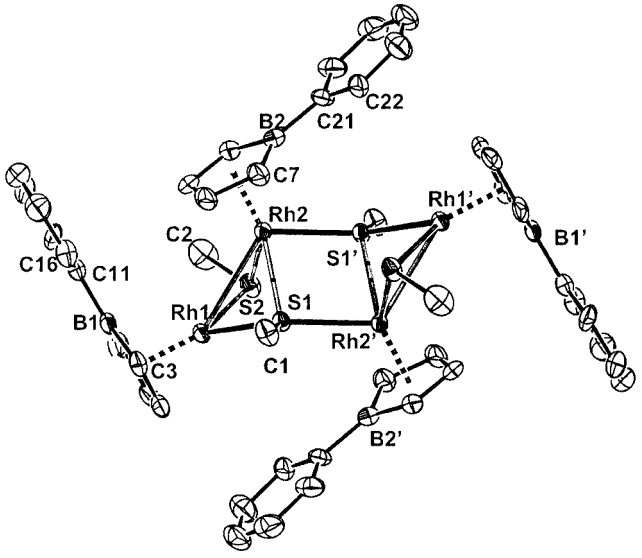

Figure 2. Molecular structure (PLATON plot,[8] at the 30% probability level) of **3a** in the crystal; selected bond lengths (Å) and bond angles (°):Rh1−Rh2 2.9233(11), Rh1−S1 2.326(2), Rh1−S2 2.303(2), Rh2−S1 2.400(2), Rh2−S2 2.405(3), Rh2−S1′ 2.461(2), S1−C1 1.818(8), S2−C2 1.826(10); Rh1−Rh2−S1 50.67(5), Rh1−Rh2−S2 50.06(6), Rh2−Rh1−S1 52.92(5), Rh2−Rh1−S2 53.21(7), S1−Rh1−S2 82.78(8), S1−Rh2−S2 79.14(8)

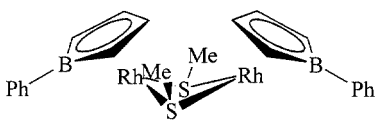

3a-Rh_2

Opening of heterocubane structures is also known from the family of complexes [$MX(PR_3)$]$_4$,[11] and small metal centers and bulky counter-ligands favor stepped-ladder structures. For instance, while the chloro complex [$CuCl(PPh_3)$]$_4$ is a heterocubane, the phenylthiolate adopts a [{$Cu(PPh_3)$}$_2$(μ-SPh)(μ$_3$-SPh)]$_2$ structure closely akin to that of **3a**. This structural difference is probably related to the bulkiness of the phenylthiolato ligands.

The Rh−S bond lengths in **3a** (2.32−2.46 Å) are shorter than the Rh−I bond lengths in **1a** (2.73−2.77 Å). The opening of the cubanoid structure to the stepped-ladder structure may again be caused by steric congestion. A detailed molecular modeling study would require a fully parametrized force-field to deal with the η^5-bonded phenylborole ligands. We therefore recurred to the following simplified approach for the generation of a hypothetical μ$_3$-SMe bridged heterocubane: Starting with the structure of **1a** the distances between the Rh centers and the heteroatoms were reduced to 2.35 Å (for pertinent reference data see ref.[10]), and the methyl groups were placed at an S−C distance of 1.8 Å in the radial direction. No conformational changes and no optimizations of the whole structure were performed. The resulting molecule exhibited prohibitively short C···H (1.9 Å), C···C (2.8 Å), and H···H (1.9 Å) interactions between the S−Me and B−Ph groups. On the basis of MM2 van der Waals parameters[12] an estimated destabilization of the cubanoid structure by approximately 100 kJ/mol was calculated.

Structure of the Methylthiolato Clusters 3a,b in Solution

The low-temperature ^{1}H NMR spectrum of **3a** (500 MHz, CD_2Cl_2, −80 °C) displays eight multiplets of equal intensity for the borole protons. This observation strongly suggests that the same structure that was found in the crystal is also present in the low-temperature solution. The stepped-ladder molecule **3a**-Rh_4 is a *meso* species with two chemically different borole ligands, both of which are in a chiral environment. Two sharp singlets are seen for the SMe groups, again in agreement with the assumption of a stepped-ladder structure in solution.

^{1}H NMR measurements at ambient temperature or above (in CD_2Cl_2, $CDCl_3$, or 1,1,2,2-$C_2D_2Cl_4$) produced spectra corresponding to effective C_{2v} symmetry. Using a 500 MHz spectrometer the signals were broad and blurred; on an 80 MHz machine the same solutions gave sharp, well-resolved signals with the characteristic hyperfine structure of the borole AA′BB′ four-spin system. Only one type of borole ligand and one type of SMe ligand were left. The chemical shifts are temperature dependent up to about 80 °C and then remain constant up to 120 °C (in 1,1,2,2-$C_2D_2Cl_4$), the highest temperature reached. These observations are readily explained by the assumption of a dissociation/association equilibrium between the tetranuclear species **3a**-Rh_4 and the dinuclear species **3a**-Rh_2, which was already mentioned above in the structural discussion (Scheme 3). We mention in passing that dinuclear species such as **3a**-Rh_2 could, in principle, form three stereoisomers, two *syn*-stereoisomers and one *anti*-stereoisomer, although only one species is seen in the NMR spectra. A comparison of the chemical shifts of the tetranuclear species from the spectrum measured at

 © 2004 Wiley-VCH Verlag GmbH & Co. KGaA, Weinheim

−80 °C and of the dinuclear species **3a**-Rh_2 exclusively present above 80 °C shows that at ambient temperatures **3a**-Rh_2 is already the predominant species. It is interesting to note here that the electronically related ruthenium complexes $[(RuCp^*)_2(\mu\text{-}SR)_2]$ are dinuclear, as confirmed by an X-ray structure determination of $[\{Ru(C_5Me_4Et)\}_2(\mu\text{-}SEt)_2]$.[13]

$[\{Rh(C_4H_4BPh)\}_2(\mu\text{-}SMe)(\mu_3\text{-}SMe)]_2 \rightleftharpoons 2\ [Rh(C_4H_4BPh)]_2(\mu\text{-}SMe)_2$

3a-Rh_4 **3a**-Rh_2

Sdheme 3. The dissociation equilibrium of the tetranuclear complex $[\{Rh(C_4H_4BR)\}_2(\mu\text{-}SMe)(\mu_3\text{-}SMe)]_2$ (2 *Rh*−*Rh*) (**3a**-Rh_4)

In the presence of pyridine complex **3a** shows a somewhat enhanced solubility, and in neat $[D_5]$pyridine it is moderately soluble. The ^1H NMR spectrum of this solution shows effective C_{2v} symmetry. The SMe groups appear as a sharp triplet not seen in the equilibrium mixture of Scheme 3. The triplet results from coupling with two Rh centers and indicates the formation of a new dinuclear species **5**, presumably of the formula $[\{Rh(py)(C_4H_4BPh)\}_2(\mu\text{-}SMe)_2]$. On attempted isolation complex **5** lost the pyridine completely, re-forming the cluster **3a**. The observation of the sharp triplet demonstrates that **3a**-Rh_2 cannot dissociate into a mononuclear species, not even in the presence of a good donor ligand. On the other hand, it also suggests that the tetranuclear species **3a**-Rh_4 is no longer present as it would, very likely, cause blurring of the hyperfine structure of the signal.

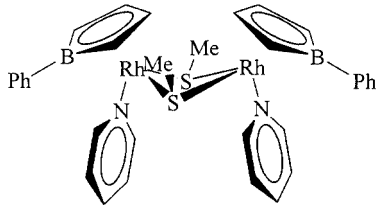

5

The analogous 1-methylborole complex **3b** poses the same structural problems. Because of the low solubility of this complex only ^1H NMR spectra could be measured and low-temperature measurements were not possible. Comparison of ^1H NMR measurements at 500 MHz and at 80 MHz revealed chemical-shift differences, suggesting that the methyl compound **3b** is also involved in a dissociation equilibrium in solution. An attempted X-ray structure determination showed the crystals to be polysynthetic twins, and no structure solution could be obtained. Thus the nuclearity of **3b** remains an open question.

Conclusion

The triple-decker complexes $[\{Rh(C_4H_4BR)\}_2(\mu\text{-}C_4H_4BR)]$ (R = Ph, Me) are among the most easily accessible borole complexes,[14] and therefore have been the starting point of a variety of studies.[1,2,15] In this paper we have described the first true cluster compounds with (borole)rhodium vertices. In preceding work we speculated that the fast exchange of (borole)rhodium vertices observed for the heterocubanes **1a**,**b** could occur via a dissociative formation of dinuclear intermediates.[2a] It was therefore particularly satisfying to find compelling evidence for the existence of the dinuclear species **3a**,**b**-Rh_2 in equilibrium with the tetranuclear clusters **3a**,**b**-Rh_4.

Experimental Section

General: Reactions were carried out under an atmosphere of dinitrogen by means of conventional Schlenk techniques. Hexane was distilled from potassium, CH_2Cl_2 from CaH_2, and THF and Et_2O from sodium benzophenone ketyl.

Secondary ion mass spectra (SIMS) were recorded on a Finnigan MAT-95 spectrometer. NMR spectra were recorded on a Varian Unity 500 spectrometer (^1H: 499.6 MHz; $^{13}C\{^1H\}$: 125.6 MHz; $^{11}B\{^1H\}$: 160.3 MHz). Chemical shifts are given in ppm; they were measured at ambient temperature and are relative to internal TMS for ^1H and ^{13}C and relative to $BF_3{\cdot}OEt_2$ as external reference for ^{11}B.

$[\{Rh(C_4H_4BPh)\}_4(\mu_3\text{-}H)(\mu_3\text{-}I)_3]$ (2a): The heterocubane $[Rh(C_4H_4BPh)(\mu_3\text{-}I)]_4$ (**1a**; 830 mg, 0.561 mmol) was suspended in THF (60 mL). A slow stream of hydrogen was passed through the flask with stirring for 3 h. Complex **1b** slowly dissolved as the reaction proceeded. The volatiles were then removed under vacuum. The residue was dissolved in CH_2Cl_2 (50 mL); the solution was filtered through a frit covered with kieselguhr, concentrated to a small volume (5 mL), and kept at −30 °C for 24 h. After removal of the mother liquor the crystals were washed with diethyl ether (2 × 5 mL) and dried under vacuum to give **2a** (560 mg, 74%) as dark red crystals, m.p. 212 °C (dec.); in solution somewhat sensitive to air, soluble in CH_2Cl_2, slightly soluble in benzene, insoluble in hexane, Et_2O and acetonitrile. $C_{40}H_{37}B_4I_3Rh_4$ (1353.3): calcd. C 35.50, H 2.76; found C 35.18, H 2.71. SIMS (NBA; negative ions): *m*/*z* (%) = 1110 (14) $[Rh_3I_3(C_4H_4BPh)_3]^-$, 497 (24) $[RhI_2(C_4H_4BPh)]^-$, 357 (27) $[RhI_2]^-$, 127 (100) $[I^-]$. ^1H NMR ($CDCl_3$): δ = −10.27 (q, $^1J_{Rh,H}$ = 21.5 Hz, μ_3-H), 3.84 (m, $N = {}^3J_{23} + {}^4J_{24}$ = 5.5 Hz, borole 2-/5-H), 4.49 (m, *N* = 5.5 Hz, 3 × borole 2′-/5′-H), 4.91 (m, *N* = 5.2 Hz, borole 3-/4-H), 5.11 (m, *N* = 5.2 Hz, 3 × borole 3′-/4′-H), 7.31−7.39 (m, $H_p + 3\ H_{p'} + 2\ H_m + 6\ H_{m'}$), 7.57 (m, 2 H_o), 7.62 (m, 6 $H_{o'}$) ppm. $^{13}C\{^1H\}$ NMR ($CDCl_3$): δ = 71.8 (br., borole C-2,5), 75.0 (br., borole C-2′,5′), 88.49 [d, $^1J_{Rh,C}$ = 9.3 Hz, borole C-3,4], 90.19 (d, $^1J_{Rh,C}$ = 8.3 Hz, borole C-3′,4′) 127.68 (C_m), 127.60 ($C_{m'}$), 129.09 ($C_{p'}$), 129.11 (C_p), 135.82 ($C_o + C_{o'}$), 136.7 (C_i), 137.08 ($C_{i'}$) ppm. $^{11}B\{^1H\}$ NMR ($CDCl_3$): δ = 20 ppm.

$[\{Rh(C_4H_4BMe)\}_4(\mu_3\text{-}H)(\mu_3\text{-}I)_3]$ (2b): The heterocubane $[Rh(C_4H_4BMe)(\mu_3\text{-}I)]_4$ (**1b**, 200 mg, 0.162 mmol) was dissolved in THF (20 mL) and hydrogenated as described above for **1a**. The raw product was dissolved in CH_2Cl_2 (10 mL); the solution was filtered through a frit covered with kieselguhr, concentrated to a small volume (1 mL), and kept at −30 °C for 24 h. After removal of the mother liquor the crystals were washed with hexane (2 × 5 mL) and dried under vacuum to give **2b** (148 mg, 82%) as dark red crystals, m.p. 155 °C (dec.); in solution somewhat sensitive to air, soluble in CH_2Cl_2, tetrahydrofuran and toluene, moderately soluble in Et_2O, insoluble in hexane. Crystals suitable for a single-crystal

 © 2004 Wiley-VCH Verlag GmbH & Co. KGaA, Weinheim

Table 1. Crystal data, data collection parameters, and convergence results for **2b** and **3a**

	2b	**3a**
Empirical formula	$C_{20}H_{29}B_4I_3Rh_4$	$C_{44}H_{48}B_4Rh_4S_4$
Molecular mass	1105.01	1159.94
Crystal system	monoclinic	orthorhombic
Space group	$P2_1/n$	*Pbca*
Radiation (λ[Å])	Mo-K_α (0.71073)	Cu-K_α (1.54184)
a (Å)	15.415(2)	8.408(4)
b (Å)	11.629(2)	22.058(7)
c (Å)	15.834(2)	23.915(7)
β (°)	104.769(10)	
V (Å^3)	2744.6(7)	4435(3)
Z	4	4
$d_{calcd.}$ [g/cm^3]	2.67	1.737
F(000)	2032	2304
μ [cm^{-1}]	5.746	13.819
Absorption correction	empirical	empirical
Max./min. transmission	0.9986/0.8981	0.9976/0.7565
Θ (°)	3−28	5−65
Temperature [K]	203	293
Scan mode	ω−2Θ	ω−Θ
Crystal size [mm]	0.36 × 0.28 × 0.20	0.35 × 0.15 × 0.06
Reflections collected	8687	3707
Reflections unique	6609[a]	3707
Reflections observed	5233	2460
Criterion for observation	$I > 2\sigma(I)$	$I > 2\sigma(I)$
Variables	288	255
R_1,[b] observed (all data)	0.0286 (0.0504)	0.0491 (0.0958)
wR_2,[c] observed (all data)	0.0567 (0.0598)	0.1228(0.1355)
GOF[d]	1.010	1.008
Max. residual density [e/Å^3]	0.89	1.495

[a] $R_{int} = 0.0236$. [b] $R_1 = \Sigma||F_o| - |F_c||/\Sigma|F_o|$. [c] $wR_2 = [\Sigma w(F_o^2 - F_c^2)2/\Sigma w(F_o^2)^2]^{1/2}$, where $w = 1/[\sigma^2(F_o^2) + (aP)^2]$ and $P = [\max(F_o^2,0) + 2F_c^2]/3$. [d] GOF $= [\Sigma w(F_o^2 - F_c^2)^2/\Sigma[(n - p)]^{1/2}$.

structure determination were obtained by very slowly concentrating a saturated solution of **2b** in diethyl ether. $C_{20}H_{29}B_4I_3Rh_4$ (1105.5): calcd. C 21.74, H, 2.65; found C 21.69, H 2.67. SIMS (NBA; positive ions): *m/z* (%) = 1106 (62) [M$^+$], 979 (18) [M$^+$ − I], 798 (100) [M$^+$ − I − Rh − C_4H_4BMe]; negative ions: *m/z* (%) = 435 (26) [$RhI_2(C_4H_4BMe)$]$^-$, 127 (100) [I$^-$]. ^{1}H NMR ($CDCl_3$): δ = −9.78 [q, $^1J_{Rh,H}$ = 21.4 Hz, μ_3-H), 0.40 (s, Me), 0.50 (s, 3 × Me′), 3.41 (m, *N* = 5.2 Hz, borole 2-/5-H), 4.15 (m, *N* = 5.2 Hz, 3 × borole 2′-/5′-H), 4.89 (m, *N* = 5.5 Hz, borole 3-/4-H), 5.42 (m, *N* = 5.5 Hz, 3 × borole 3′-/4′-H) ppm. ^{13}C{^{1}H} NMR ($CDCl_3$): δ = −2.31 (br., Me + Me′), 72.81 (br., borole C-2,5), 76.15 (br., borole C-2′,5′), 87.73 [d, $^1J_{Rh,C}$ = 9.3 Hz, borole C-3,4], 89.99 [d, $^1J_{Rh,C}$ = 8.7 Hz, borole C-3′,4′] ppm. ^{11}B{^{1}H} NMR ($CDCl_3$): δ = 25 ppm.

[{Rh(C_4H_4BPh)}$_2$(μ-SMe)(μ$_3$-SMe)]$_2$ (3a): Polymeric *catena*-[Rh(μ,η^5:η^6-C_4H_4BPh)BF_4][1] (650 mg, 1.971 mmol Rh) was dissolved in acetonitrile (10 mL) to give a solution of **4a**. This solution was added with stirring to a suspension of NaSMe (138 mg, 1.969 mmol) in acetonitrile (5 mL), and stirring was continued for 60 min. The solid raw product thus obtained was collected on a G4 frit covered with kieselguhr and washed with acetonitrile (5 × 10 mL). It was then eluted with CH_2Cl_2. The solvent was evaporated under vacuum, and the resulting solid was washed with acetone (2 × 5 mL) and dried under vacuum to afford **3a** (430 mg, 75%) as blackish red microcrystals, m.p. 238 °C, not air-sensitive, soluble in pyridine, slightly soluble in $CHCl_3$, CH_2Cl_2 and toluene, insoluble in diethyl ether, acetone, acetonitrile. Single crystals suitable for a single-crystal structure determination were obtained from a concentrated solution of **3a** in hot toluene by very slow cooling to ambient temperature. $C_{44}H_{48}B_4Rh_4S_4$ (1160.0) calcd. C 45.56, H 4.17; found C 45.93, H 4.16. ^{1}H NMR (80 MHz, $CDCl_3$, 25 °C): δ = 2.70 (s, Me), 3.96 (m, *N* = 5.8 Hz, borole 2-/5-H), 4.60 (m, *N* = 4.6 Hz, borole 3-/4-H), 7.24−7.43 (complex region, 2 H_p + 4 H_m), 7.73 (m, 4 H_o) ppm. ^{13}C{^{1}H} NMR (125.7 MHz, $CDCl_3$, 25 °C): δ = 23.84 (Me), 93.04 (br., borole C-3/4), 127.90 (C_m), 129.34 (C_p), 135.56 (C_o) ppm; signal for C-2/5 not observed. ^{11}B{^{1}H} NMR (160.4 MHz, $CDCl_3$, 25 °C): δ = 22 ppm.

Selected VT NMR Data for 3a: ^{1}H NMR (500 MHz, CD_2Cl_2, −80 °C): δ = 2.14 (s, μ_3-SMe), 2.47 (s, μ-SMe), 2.80 (m, 2 H, borole 2-H_2 or 5-H), 3.23 (m, 2 H, borole 2-H or 5-H), 3.53 (m, borole 2′-H or 5′-H), 3.75 (m, borole 2′-H or 5′-H), 3.92 (m, borole 3′-H or 4′-H), 4.35 (m, borole 3-H or 4-H), 4.52 (m, borole 3-H or 4-H), 5.46 (m, borole 3′-H or 4′-H), 7.36−7.40 (complex region, 2 H_p + 4 H_m), 7.47 (m, 4 $H_{m'}$), 7.53 (m, 2 $H_{p'}$), 7.65−7.70 (complex region, 4 H_o + 2 $H_{o'}$) ppm; assignments were made on the basis of (^{1}H,^{1}H)-COSY spectra. ^{1}H NMR (500 MHz, CD_2Cl_2, 25 °C): δ = 2.98 (br. s, 2 Me), 4.19 (br. s, 2 × borole 2-/5-H), 4.73 (br. s, 2 × borole 3-/4-H), 7.33 (m, 4 H_m), 7.42 (m, 2 H_p), 7.74 (m, 4 H_o) ppm. ^{1}H NMR (500 MHz, 1,1,2,2-$C_2D_2Cl_4$, 120 °C): δ = 3.13 (s, 2 Me), 4.28 (m, 2 × borole 2-/5-H), 4.82 (m, 2 × borole 3-/4-H), 7.28 (m, 4 H_m), 7.38 (m, 2 H_p), 7.71 (m, 4 H_o) ppm.

Data for 5: ^{1}H NMR (80 MHz, [D_5]pyridine, 25 °C): δ = 2.76 (t, $^3J_{Rh,H}$ = 1.4 Hz, 2 Me), borole 4.09 (m, *N* = 5.7 Hz, borole 2-/5-H), 5.26 (m, *N* = 5.0 Hz, borole 3-/4-H), 7.19−7.32 (complex region, 4 H_m + 2 H_p), 7.75 (m, 4 H_o) ppm.

 © 2004 Wiley-VCH Verlag GmbH & Co. KGaA, Weinheim

$[Rh(SMe)(C_4H_4BMe)]_x$ (3b): A solution of $AgBF_4$ (221 mg, 1.135 mmol) in acetonitrile (10 mL) was added with stirring to a suspension of **1b** (350 mg, 0.284 mmol) in acetonitrile (10 mL), and stirring was continued for 30 min. The resulting reaction mixture was filtered through a frit covered with kieselguhr into a flask containing a stirred suspension of NaSMe (79.5 mg, 1.134 mmol) in acetonitrile (5 mL). After stirring the reaction mixture for 60 min, the microcrystalline product was collected on a frit covered with kieselguhr and washed with acetonitrile (5 × 10 mL). It was then eluted with CH_2Cl_2. The solvent was evaporated under vacuum, and the resulting solid was washed with acetone (2 × 5 mL) and dried under vacuum to afford **3b** (180 mg, 70%) as blackish red microcrystals, m.p. 227 °C; not air-sensitive, slightly soluble in $CHCl_3$, CH_2Cl_2 and toluene, insoluble in diethyl ether, acetone, acetonitrile. ^{1}H NMR (80 MHz, $CDCl_3$, 25 °C): δ = 0.31 (s, B-Me), 2.83 (s, S-Me), 3.77 (m, N = 5.7 Hz, borole 2-/5-H), 5.24 (m, N = 5.8 Hz, borole 3-/4-H) ppm. ^{1}H NMR (500 MHz, $CDCl_3$, 25 °C): δ = 0.32 (s, Me), 2.71 (s, SMe), 3.69 (m, borole 2-/5-H), 5.22 (m, borole 3-/4-H) ppm.

X-ray Crystal Structure Determinations: The data collection was performed on an ENRAF-Nonius CAD4 diffractometer with Mo-K_α radiation for **2b** and Cu-K_α radiation for **3a** (where the crystals were small and the unit cell comparatively large) using a graphite monochromator. Crystal data, data collection parameters, and convergence results are given in Table 1. In the case of **3a** all residual electron density greater than 0.55 e/Å^3 was close to the two Rh atoms.

CCDC-216303 (for **2b**) and -216302 (for **3a**) contain the supplementary crystallographic data for this paper. These data can be obtained free of charge at www.ccdc.cam.ac.uk/conts/retrieving.html [or from the Cambridge Crystallographic Data Centre, 12 Union Road, Cambridge CB2 1EZ, UK; Fax: (internat.) + 44-1223-336-033; E-mail: deposit@ccdc.cam.ac.uk].

Acknowledgments

We thank Prof. Dr. U. Englert for helpful discussions. This work was generously supported by the Deutsche Forschungsgemeinschaft and the Fonds der Chemischen Industrie.

[1] G. E. Herberich, H. J. Eckenrath, U. Englert, *Organometallics* **1998**, *17*, 519−523.
[2] [2a] G. E. Herberich, H. J. Eckenrath, U. Englert, *Organometallics* **1997**, *16*, 4292−4298. [2b] G. E. Herberich, H. J. Eckenrath, U. Englert, *Organometallics* **1997**, *16*, 4800−4806.
[3] F. A. Cotton, *Quart. Rev. Chem. Soc.* **1966**, *20*, 389−401.
[4] H. J. Eckenrath, Doctoral Dissertation, Rheinisch-Westfälische Technische Hochschule Aachen, Aachen, Germany, **1997**.
[5] [5a] E. O. Fischer, H. Wawersik, *Chem. Ber.* **1968**, *101*, 150−155. [5b] O. S. Mills, E. F. Paulus, *J. Organomet. Chem.* **1968**, *11*, 587−594.
[6] [6a] T. Teppana, S. Jäärskeläinen, M. Ahlgrén, J. Pursiainen, T. A. Pakkanen, *J. Organomet. Chem.* **1995**, *486*, 217−228. [6b] S. Rossi, J. Pursiainen, M. Ahlgrén, T. A. Pakkanen, *J. Organomet. Chem.* **1990**, *391*, 403−414. [6c] J. Pursiainen, T. A. Pakkanen, S. Jäärskeläinen, *J. Organomet. Chem.* **1985**, *290*, 85−98.
[7] [7a] G. E. Herberich, U. Englert, L. Wesemann, P. Hofmann, *Angew. Chem.* **1991**, *103*, 329−331; *Angew. Chem. Int. Ed. Engl.* **1991**, *30*, 313−315. [7b] J. S. Ricci, T. F. Koetzle, R. J. Goodfellow, P. Espinet, P. M. Maitlis, *Inorg. Chem.* **1984**, *23*, 1828−1831. [7c] P. Espinet, P. M. Bailey, P. Piraino, P. M. Maitlis, *Inorg. Chem.* **1979**, *18*, 2706−2710. [7d] R. R. Burch, E. L. Muetterties, M. R. Thompson, V. W. Day, *Organometallics* **1982**, *2*, 474−478.
[8] PLATON: A. L. Spek, *Acta Crystallogr., Sect. A* **1990**, *46*, C34.
[9] Cf. data for $[(RhCp^*)_4(\mu_3\text{-}H)_4](BF_4)_2$: two short bonds of 2.655(1) Å and four long bonds of 2.829(1) Å;[7b,7c] and for the 44e cluster $[\{Rh(COD)\}_3(\mu_3\text{-}H)\{\mu_3\text{-}C(CH_2)_3\}]$: 2.977(1)−2.981(1) Å].[7a]
[10] A. G. Orpen, L. Brammer, F. H. Allen, O. Kennard, D. G. Watson, R. Taylor, *J. Chem. Soc., Dalton Trans.* **1989**, S1−S83.
[11] I. G. Dance, M. L. Scudder, L. J. Fitzpatrick, *Inorg. Chem.* **1985**, *24*, 2547−2550.
[12] N. L. Allinger, *J. Am. Chem. Soc.* **1977**, *99*, 8127−8134.
[13] U. Koelle, C. Rietmann, U. Englert, *J. Organomet. Chem.* **1992**, *423*, C20−C23.
[14] [14a] G. E. Herberich, B. Heßner, W. Boveleth, H. Lüthe, R. Saive, L. Zelenka, *Angew. Chem.* **1983**, *95*, 1024−1025; *Angew. Chem. Int. Ed. Engl.* **1983**, *22*, 966; *Angew. Chem. Suppl.* **1983**, 1503−1510. [14b] G. E. Herberich, U. Büschges, B. Heßner, H. Lüthe, *J. Organomet. Chem.* **1986**, *312*, 13−25.
[15] G. E. Herberich, U. Büschges, *Chem. Ber.* **1989**, *122*, 615−619.

Received September 3, 2003
Early View Article
Published Online February 26, 2004

 © 2004 Wiley-VCH Verlag GmbH & Co. KGaA, Weinheim

Amino-Substituted Ferra-bis(tricarbollides) − Metallatricarbaboranes Designed for Linear Molecular Constructions

Bohumír Grüner,*[a] Jaroslav Bačkovský,[a] Reijo Sillanpää,[b] Raikko Kivekäs,[c] Ivana Císařová,[d] Francesc Teixidor,[e] Clara Viñas,[e] and Bohumil Štíbr[a]

Keywords: Boranes / Carboranes / Metallacarboranes / Metallatricarbaboranes / Metallatricarbollides

Reactions between high purity $FeCl_2$ and the anion [*nido*-7-(*t*BuHN)-7,8,9-$C_3B_8H_{10}$)]$^-$ (**1**$^-$) have been used for efficient syntheses of the twelve-vertex double-cluster metallatricarbollide complexes of the *para*,*para* (*p*,*p*) type [*closo*-9,9′-$(RHN)_2$-*commo*-2,2′-Fe^{II}-1,7,9-($C_3B_8H_{10}$)-1′,7′,9′-($C_3B_8H_{10}$)] (**2**) (**2a**, R = *t*Bu and **2b**, R = H) (yields 42–45% for **2a**). Compound **2b**, which contains two reactive amino substituents conveniently attached to the tricarbollide subclusters in *p*-positions with respect to the metal center, was prepared via facile cleavage of the *t*Bu substituent in **2a** either by $AlCl_3$ or by thermal means. The structure of **2b** constitutes a good setting for the synthesis of building blocks for constructing linear metallatricarbollide rods of high stability. Two isomeric compounds of the *para*,*meta* (*p*,*m*) type **3**, [*closo*-9,10′-$(RHN)_2$-*commo*-2,2′-Fe-1,7,9-($C_3B_8H_{10}$)-1′,7′,10′-($C_3B_8H_{10}$)] (where R = *t*Bu **3a** and/or H **3b**), were isolated in smaller yields from reactions of high purity $FeCl_2$ with **1**$^-$ at higher temperatures. Also reported is the characterization of the *m*,*m*-type complex, [*closo*-10,10′-(*t*BuHN)$_2$-*commo*-2,2′-Fe^{II}-1,7,10-($C_3B_8H_{10}$)-1′,7′,10′-($C_3B_8H_{10}$)] (**4a**), and the two zwitterionic species of the new 7-L-7,8,10-$C_3B_8H_{10}$ type (**6**) [L = Me_3N **6a** and *t*Bu(Me)HN **6b**] isolated in moderate yields from the reaction of reagent grade $FeCl_2$ with **1**$^-$. The molecular structures of **2b**, **3a**, and **6b** were determined by single-crystal X-ray diffraction studies. Multinuclear (^1H and ^{11}B), two-dimensional [^{11}B-^{11}B]-COSY, and $^1H\{^{11}B$(selective)} magnetic resonance measurements enabled complete assignments of all resonances for all compounds and are in excellent agreement with the structures proposed.

(© Wiley-VCH Verlag GmbH & Co. KGaA, 69451 Weinheim, Germany, 2004)

Introduction

The first venture into the area of twelve-vertex metallatricarbollide chemistry was the synthesis of the mixed-sandwich cyclopentadienyl-ferratricarbollide analogues of ferrocene, the *closo* complexes [9-R-2-(η^5-C_5H_5)-2,1,7,9-$FeC_3B_8H_{10}$] [where R = H_2N, CH_3NH, $(CH_3)_2N$, *t*BuHN, and *t*BuCH$_3$N][1] and of the isomeric [10-R-2-(η^5-C_5H_5)-2,1,7,10-$FeC_3B_8H_{10}$] (where R = H_2N, CH_3NH, $(CH_3)_2N$, and *t*BuHN)[2] species. In contrast to double-cluster metal dicarbollide "full" sandwiches, which are quite common and easily available,[3] we have found that the corresponding metallatricarbollide counterparts cannot be prepared under comparable conditions. Finally it was recognized that such complexes could be synthesized only under forcing reaction conditions. In a preliminary communication[4] we reported a low-yield isolation of the first representatives of the double-cluster metallatricarbollide family, [*closo*-9,9′-(*t*BuHN)$_2$-*commo*-2,2′-M^{II}-1,7,9-($C_3B_8H_{10}$)-1′,7′,9′-($C_3B_8H_{10}$)], where M = Fe and Ru (yields 4% and 9%, respectively). In this paper we report full experimental details on substantially improved, simple and good yielding syntheses of the isomeric ferra-bis(tricarbollides) containing amine functionalities, (*t*BuHN or H_2N) in *m*- and *p*-positions with respect to the Fe center. Also reported are compounds of the still unknown 7-L-7,8,10-$C_3B_8H_{10}$ (L = amine) type which are formed by metal-promoted isomerization reactions. Structures are presented in a simplified manner: unmarked vertices in Schemes 1 and 2 stand for cluster BH units, while C denotes the CH vertex if no substituent is attached to it. General structures of individual types of compounds discussed in this work are in the Structures diagram.

[a] Institute of Inorganic Chemistry, Academy of Sciences of the Czech Republic (Research Center for New Inorganic Compounds and Advanced Materials, University of Pardubice)
25068 Řež, the Czech Republic
Fax: (internat.) +420-2-20940161
E-mail: gruner@iic.cas.cz
[b] Department of Chemistry, University of Jyväskylä,
40351 Jyväskylä, Finland
Fax: (internat.) +358-14-2602501
E-mail: resillan@jyu.fi
[c] Department of Chemistry, University of Helsinki,
P. O. Box 55, 00014, Finland
Fax: (internat.) +358-9-19150198
E-mail: raikkok@saunalahti.fi
[d] Faculty of Natural Sciences of Charles University,
Hlavova 2030, the Czech
12842, Prague 2, The Czech Republic
Fax: (internat.) +420-2-296084
E-mail: cisarova@natur.cuni.cz
[e] Institute of Material Sciences, Campus UAB
08193 Bellaterra, Spain
Fax: (internat.) +34-9-35 805 729
E-mail: teixidor@icmab.es

 © 2004 Wiley-VCH Verlag GmbH & Co. KGaA, Weinheim **DOI: 10.1002/ejic.200300686**

1

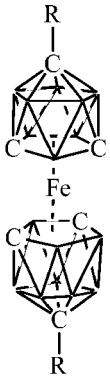

2 (R = NH*t*Bu, **2a**; H_2N, **2b**; NH*t*Bu and NH_2, **2c**)

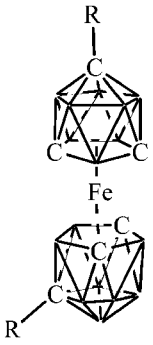

3 (R = NH*t*Bu, **3a**; H_2N, **3b**)

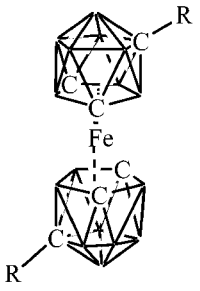

4 (R = NH*t*Bu, **4a**)

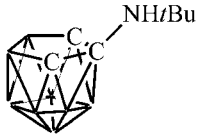

5$^-$

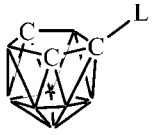

6 (L = Me_3N, **6a**; tBuMeHN, **6b**)

Results and Discussion

Syntheses

As shown in path i) of Scheme 1, the reaction between Tl[7-(*t*BuHN)-7,8,9-$C_3B_8H_{10}$] Tl(**1**$^-$) and an excess of highly pure $FeCl_2$ (99.99%) in a diglyme-mesitylene mixture led to formation of [*closo*-9,9′-(*t*BuHN)$_2$-*commo*-2,2′-Fe^{II}-1,7,9-($C_3B_8H_{10}$)-1′,7′,9′-($C_3B_8H_{10}$)] (**2a**). Complex **2a** was isolated as a single metallacarborane product in a significantly improved yield (43%, cf. a 4% yield in the previous method).[4]

Higher overall yields of the ferra bis(tricarbollides) (up to 62%) have been obtained when Na[7-(*t*BuH$_2$N)-7,8,9-$C_3B_8H_{10}$]$^-$ Na(**1**$^-$) was heated to reflux in diglyme in the presence of an excess of high-purity $FeCl_2$ (path ii) of Scheme 1). In this case, however, the main product **2a** (yield 45%) was always accompanied by the isomeric compound [9,10′-(*t*BuHN)$_2$-*commo*-2,2′-Fe-*closo*-1,7,9-($C_3B_8H_{10}$)-1′,7′,10′-($C_3B_8H_{10}$)] (**3a**) (yield 17%). The advantage of the Na(**1**$^-$) reaction is the good total yield of the sandwich compounds, but the presence of **3a** substantially complicates the isolation of **2a** since the mixture of **2a** and **3a** must be then separated by preparative liquid chromatography. Attempts at carrying out the reaction in a mesitylene-diglyme mixture or decreasing the reaction temperature led to similar isomeric mixtures and also to a substantial decrease in the total yield of **2a** and **3a** (ca. 25%). On the other hand, if the process was directed to obtain products with bare NH_2 groups (**2b** and **3b**), the pre-purified mixture of **2a** and **3a** could be first conveniently treated to remove the butoxide function (see text below), and the resultant products could be separated more easily.

Complex **3a** apparently originates from *dsd* isomerization on one of the tricarbollide ligands of **2a** in the reaction mixture as the concentration of **3a** increases with the reaction time. This observation is consistent with the similarly anomalous $p \rightarrow m$ isomerization path reported for the mixed-sandwich metallatricarbollide series.[2]

Consistent with the previously reported findings[2] are the isobutylene elimination reactions leading to H_2N derivatives in the series of bis(tricarbollide) iron sandwiches reported in this work. The reactions of both **2a** and **3a** with anhydrous $AlCl_3$ in hexane at reflux removes the *t*Bu substituent to give the complexes [*closo*-9,9′-(H_2N)$_2$-*commo*-2,2′-Fe^{II}-1,7,9-($C_3B_8H_{10}$)-1′,7′,9′-($C_3B_8H_{10}$)] (**2b**) and [*closo*-9,9′-(H_2N)$_2$-*commo*-2,2′-Fe^{II}-1,7,9-($C_3B_8H_{10}$)-1′,7′,10′-($C_3B_8H_{10}$)] (**3b**), respectively (yields of 82% and 80%, respectively, see paths iii) and ix) of Scheme 1). For the preparation of **3b**, it was convenient to apply the $AlCl_3$ reaction on a mixture of **2a** and **3a** obtained from the complexation of Na(**1**$^-$) as outlined above, which resulted typically in a total yield of 79% of the H_2N- derivatives **2b** and **3b**. The advantage of this approach is that the mixture of compounds **2b** and **3b** could be easily separated by conventional column chromatography. Alternatively, the isobutylene elimination, giving **2b**, could be achieved by briefly heating **2a** at 210 °C in vacuo (see path xi) of Scheme 1). This thermal cleavage is, however, accompanied by simultaneous formation of the isomeric [*closo*-9,10′-(H_2N)$_2$-*commo*-2,2′-Fe^{II}-1,7,9-($C_3B_8H_{10}$)-1′,7′,10′-($C_3B_8H_{10}$)] (**3b**) which, depending on reaction time, accompanies the main

 © 2004 Wiley-VCH Verlag GmbH & Co. KGaA, Weinheim

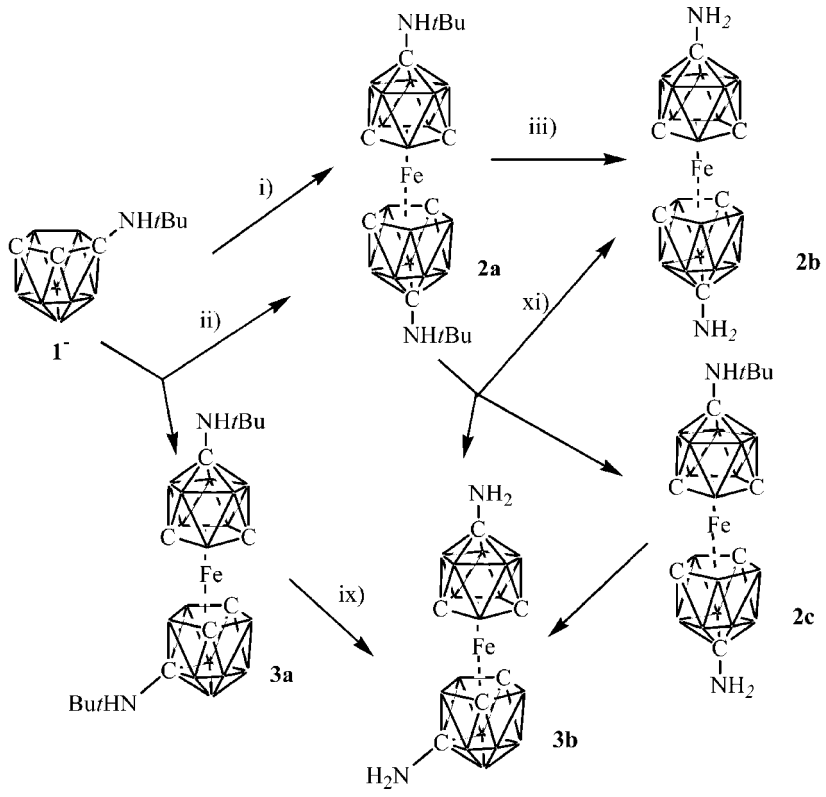

Scheme 1. Formation of ferratricarbollides, their thermal rearrangements and cleavage of their butyl groups. i) Tl(**1**$^-$), $FeCl_2$ (99.99%), diglyme/mesitylene (1:4), reflux. ii) Na(**1**$^-$), $FeCl_2$ (99.99%), diglyme, reflux. iii), ix) $AlCl_3$, hexane, reflux. xi) 210 °C, 15 min

product in small to moderate yields. Another by-product of this thermal cleavage is the linearly shaped [*closo*-9-(*t*BuHN),9′-(H_2N)-*commo*-2,2′-Fe^{II}-1,7,9-($C_3B_8H_{10}$)-1′,7′,10′-($C_3B_8H_{10}$)] (**2c**) (yield 20%). Complex **2c** evidently arises from one-side loss of a butyl group from **2a**. These side isobutylene-elimination reactions are the reason why **3a** cannot be obtained in good yields by thermal rearrangement of **2a**.

It should be noted that the iron complexation reactions outlined above are rather sensitive to the purity of the $FeCl_2$ employed since the reagent grade $FeCl_2$ used in the preliminary communication[4] provided completely different reaction products. This original reaction[4] has now been studied in more detail and has been found to be very complex. Based on multiple experiments, it was found that prolonged treatment of 7-(*t*BuH_2N)- *nido*-7,8,9-$C_3B_8H_{10}$ (**1**) with NaH and an excess of the reagent-grade $FeCl_2$ in diglyme at reflux (path i) of Scheme 2), followed by chromatographic separation, resulted in the isolation of complexes **2a** and **3a** in yields 4 and 6%, respectively. The reaction also gave trace amounts of the third *m*,*m*-substituted isomer, [*closo*-10,10′-(*t*BuHN)$_2$-*commo*-2,2′-Fe^{II}-(1,7,10-$C_3B_8H_{10}$)$_2$] (**4a**). Nevertheless, the formation of these three iron complexes represents only a side reaction mode (path ii) of Scheme 2). The main reaction mode (path iii) of Scheme 2) is, however, associated with the recently reported metal-promoted rearrangement of anion **1**$^-$ giving at lower temperatures (DME at reflux) the [8-*t*BuNH-*nido*-7,8,9-$C_3B_8H_{10}$]$^-$ (**5**$^-$) anion [and finally the neutral compound 8-*t*BuNH-*nido*-7,8,9-$C_3B_8H_{11}$ (**5**) upon protonation].[5] Under the reaction conditions now employed (diglyme at reflux) compound **5** was isolated in only trace amounts and the main reaction products were identified as 7-Me_3N-*nido*-7,8,10-$C_3B_8H_{10}$ (**6a**) and 7-*t*Bu(Me)HN-*nido*-7,8,10-$C_3B_8H_{10}$ (**6b**) (yields of 14 and 17%, respectively). These compounds are representatives of the zwitterionic 7-L-7,8,10-$C_3B_8H_{10}$ (**6**) family and it is reasonable to suppose that their formation is associated with further cage rearrangement of anion **5**$^-$, followed by in situ *N*-methylation by the solvent methyl groups (diglyme) (path ix) of Scheme 2). The rearrangement is evidently associated with the migration of the unsubstituted cage carbon C7 in **5**$^-$ into the C10 position. A similar rearrangement of the [7,8,9-$C_3B_8H_{11}$]$^-$ and 7-(CH_3)$_3$N-7,8,9-$C_3B_8H_{10}$ *nido*-tricarbollide compounds into their isomeric congeners, [7,8,10-$C_3B_8H_{11}$]$^-$ and 10-(CH_3)$_3$N-7,8,10-$C_3B_8H_{10}$, has already been subject of theoretical and experimental studies.[6,7]

X-ray Diffraction Studies

The structure of compound **2a** has already been determined by an X-ray diffraction study published in a preliminary communication.[4] The results of the X-ray diffraction analysis of the bis-tricarbollide complex [*closo*-9,9′-(H_2N)$_2$-*commo*-2,2′-Fe^{II}-1,7,9-($C_3B_8H_{10}$)-1′,7′,9′-$C_3B_8H_{10}$)] (**2b**) resulting from cleavage of the *t*Bu end groups is shown in Figure 1. As follows from the comparison of the crystallo-

 © 2004 Wiley-VCH Verlag GmbH & Co. KGaA, Weinheim

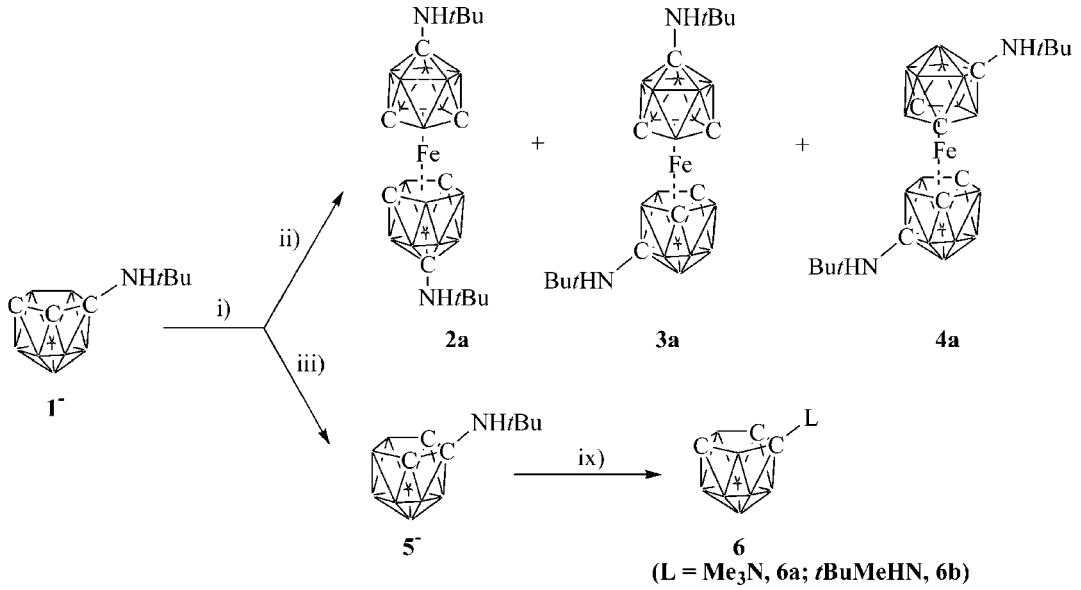

Scheme 2. Reactions with reagent grade $FeCl_2$ (metal-promoted rearrangements) i) Na(**1**$^-$), $FeCl_2$ (98%), diglyme, reflux. ii) side formation of ferratricabollides. iii) main reaction mode, the formation of zwitterions of the 7-L-7,8,10-$C_3B_8H_{10}$ type (**6**) (L = Me_3N **6a** and *t*Bu(Me)HN **6b**)

graphically determined structures of **2a**[4] and the structurally similar **2b**, a change in the *t*BuHN substituent for the unsubstituted H_2N group has no significant effect either on the N−C9 or C9−B distances. In contrast to **2a**, however, the molecules of **2b** are symmetrical, with two independent molecules in the unit cell. The iron atoms in both molecules are situated at the center of symmetry and the mutual configuration of the C_2B_3 pentagons is therefore exactly staggered. This means the C_2B_3 pentagonal planes flanking the metal center are parallel and the arrangement of the C9, Fe, and C9^i atoms is linear in both molecules. An interesting feature is that the two molecules form dimeric assemblies via a weak hydrogen bond N1−H1A−N2 with the N1−N2 distance being 3.378(2) Å and the N1−H1A−N2 angle being 172°.

The results of the X-ray diffraction analysis of the bis(tricarbollide) complex [*closo*-9,10′-(*t*BuHN)$_2$-*commo*-2,2′-Fe-1,7,9-($C_3B_8H_{10}$)-1′,7′,10′-($C_3B_8H_{10}$)] (**3a**) are shown in Figure 2. The tricarbollide subclusters in **3a** are different and Figure 2 shows *p*-substitution in one of the tricarbollide subunits and *m*-substitution in the second. However, no marked differences can be seen in the corresponding bond parameters between the cages. The mutual configuration of the C_2B_3 pentagons is staggered and the torsion angles are very close to the ideal value of 36° for a perfectly staggered conformation. As expected, the mean C_2B_3 pentagonal planes flanking the metal center in **3a** are very close to parallel, the dihedral angle between the planes being 2.25(1)°, and the C9−Fe2−B9′ jack-knife angle at 179.02(1)° is essentially linear. The disposition of the C9, Fe2, and C10′ atoms is reflected by the C9−M2−C10′ angle of 154.83(1)°.

The structure of 7-*t*Bu(Me)HN-*nido*-7,8,10-$C_3B_8H_{10}$ (**6b**), shown in Figure 3, confirms the 7,8,10 arrangement of the cage carbon atoms and the C7 substitution by the

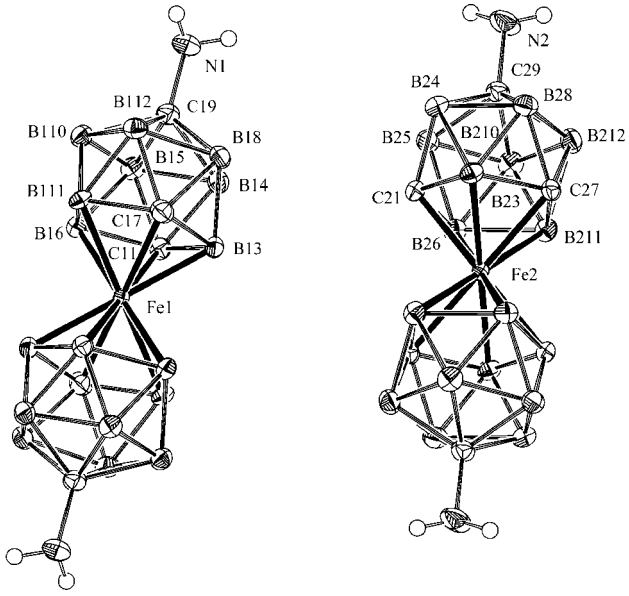

Figure 1. ORTEP representation of the molecular structure of **2b** with crystallographic numbering. Hydrogen positions omitted for clarity. Thermal ellipsoids are drawn at the 50% probability level. Both molecules are situated on a center of symmetry; selected bond lengths (Å): Fe1−C(11) 2.064(2), Fe1−C(17) 2.061(2), Fe2−C(21) 2.060(2), Fe2−C(27) 2.072(2), Fe1−B(13) 2.054(2), Fe1−B(16) 2.075(2), Fe1−B(111) 2.075(2), Fe2−B(23) 2.047(2), Fe2−B(26) 2.075(2), Fe2−B(211) 2.080(2), N1−C(19) 1.431(2), N2−C(29) 1.432(2)

*t*Bu(Me)HN group which causes the asymmetry of the molecule. However, upon comparing the bond parameters in **6b** with those found for the isomeric compound 7-*t*BuMeNH-*nido*-7,8,9-$C_3B_8H_{10}$ [6b] and the symmetrically substituted 10-Me_3N-*nido*-7,8,10-$C_3B_8H_{10}$,[6f] no significant conclusions could be drawn on the trends in the bond lengths

 © 2004 Wiley-VCH Verlag GmbH & Co. KGaA, Weinheim

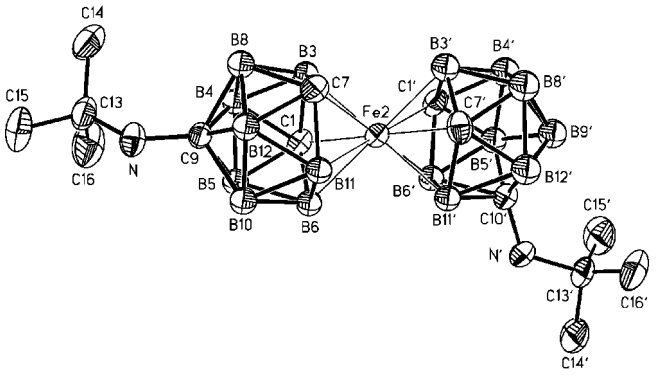

Figure 2. Molecular structure of **3a** with selected bond lengths (Å): Fe−C(1) 2.083(5), Fe−C(7) 2.067(5), Fe−C(1′) 2.078(4), Fe−C(7′) 2.064(5), Fe−B(3) 2.079(6), Fe−B(6) 2.084(6), Fe−B(11) 2.073(5), Fe−B(3′) 2.065(6), Fe−B(6′) 2.058(6), Fe−B(11′) 2.044(6), N−C(9) 1.433(5), N′−C(10) 1.424(6). Hydrogen positions omitted for clarity. Hydrogen atoms omitted for clarity. Thermal ellipsoids are drawn at the 50% probability level

associated with the upper C_3B_2 pentagon brought by the substituent. The largest differences can be seen for the longer inter-atomic distances B9−C10 [1.673(6) Å] and C10−B11 [1.609(6) Å] found in the structure of the symmetrically substituted derivative 10-Me_3N-*nido*-7,8,10-$C_3B_8H_{10}$. There is, however, some uncertainty due to the disorder in this structure.[6f]

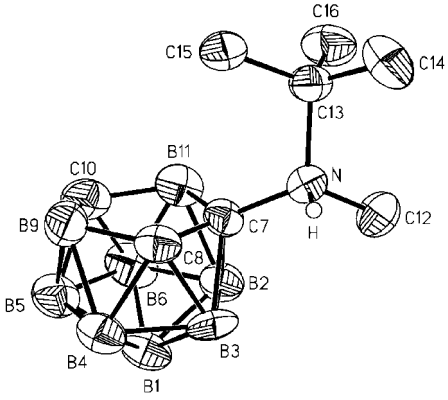

Figure 3. Molecular structure of **6b** with selected bond lengths (Å): N−C(7) 1.517(4), C(7)−C(8) 1.543(5), C(7)−B(11) 1.590(6), C(8)−B(9) 1.593(6), C(10)−B(9) 1.596(7), C(10)−B(11) 1.623(7). Hydrogen atoms omitted for clarity. Thermal ellipsoids are drawn at the 50% probability level

NMR Spectroscopy

Figure 4 shows simplified stick diagrams comparing the ^{11}B chemical shifts for selected complexes of types **2** and **3** with those of the structurally related mixed-sandwich *closo* compounds [9-*t*BuHN-2-(η^5-C_5H_5)-2,1,7,9-$FeC_3B_8H_{10}$][1] and [10-*t*BuHN-2-(η^5-C_5H_5)-2,1,7,10-$FeC_3B_8H_{10}$].[2] The NMR spectroscopic data are also consistent with the structures for the *p, p* substituted complexes of type **2** determined crystallographically. The ^{11}B NMR spectra of compounds **2a**[4] and **2b** show very similar 4:2:4:2:4 patterns of doublets with only slight differences. The same intensity patterns apply to the corresponding BH resonances in the ^1H NMR spectra, in which one singlet resonance of intensity 4, assigned to the magnetically equivalent CH cage units, was also clearly found. As seen in Figure 4, the ^{11}B NMR spectra are very similar to that of [9- *t*BuHN-2-(η^5-C_5H_5)-*closo*-2,1,7,9-$FeC_3B_8H_{10}$][1] which exhibits a general upfield shift of the all resonances in comparison with those of compounds of type **2**.

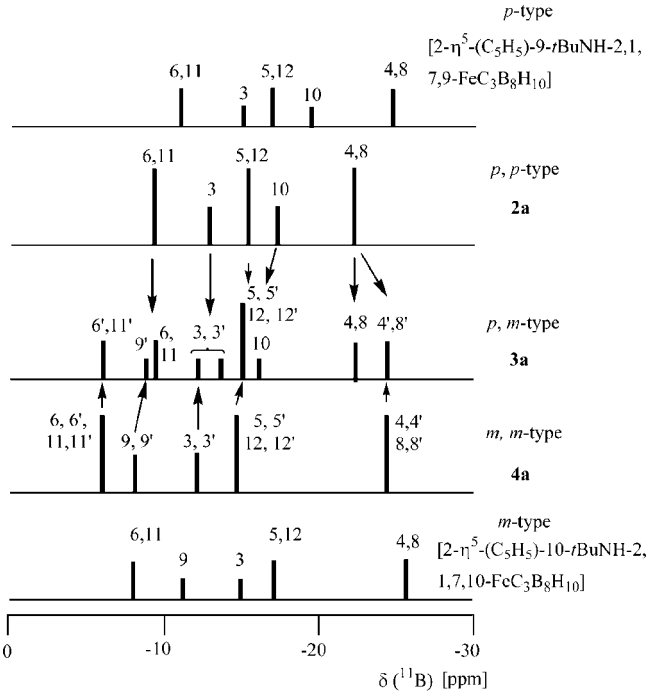

Figure 4. Stick representation and comparison of the ^{11}B NMR shifts for the *t*BuNH-substituted mixed sandwiches (data from ref.[1b,2]) and double-cluster ferratricarbollides **2a**, **3a**, and **4a**

Two sets of slightly shifted resonances with the same spectral patterns can be observed in the ^{11}B NMR spectrum of **2c**, those due to B10,10′ and B5,12,5′,12′ being coincidentally overlapping. The $^1H\{^{11}B\}$ NMR spectrum of **2c** contains two nonequivalent CH signals and also two related sets of resonances for each subcluster with coincidental overlaps for H6,11,6′,11′ and H3,3′. The ^{11}B NMR spectrum of **4a** (see Figure 4) with the *m,m* configuration of both ligands consists of 4:2:2:4:4 patterns of doublets as does the spectrum of the corresponding mixed-ligand complex [10-*t*BuHN-2-(η^5-C_5H_5)-*closo*-2,1,7,9-$FeC_3B_8H_{10}$].[2] The ^{11}B NMR spectra of the *p,m* type complexes **3a** and **3b** consist of two series of signals clearly attributable to those of the two nonequivalent tricarbollide ligands with *p*- and *m*- positioned substituents. The signals associated with the nonequivalent tricarbollide ligands can be clearly distinguished due to close similarities with the corresponding ^{11}B patterns found for **2b** and **4a**. The same similarities can be also found in the corresponding $^1H\{^{11}B\}$ NMR spectra of complexes **3a** and **3b**.

In accord with the absence of symmetry, the ^{11}B NMR spectra of the zwitterionic tricarbollide derivatives **6a** and **6b** consist of eight different signals with two coincidental overlaps found in the spectrum of **6b**. As shown in Figure 5,

 © 2004 Wiley-VCH Verlag GmbH & Co. KGaA, Weinheim

the ^{11}B NMR patterns show very close similarities with those of the structurally related anion [7-Me-*nido*-7,8,10-$C_3B_8H_{10}]^-$.[7] The ^{11}B NMR spectra of **6a** and **6b** themselves exhibit only slight differences in chemical shifts. Also eight singlets corresponding to BH signals were found in the $^1H\{^{11}B\}$ spectra of both compounds along with two different CH signals for each derivative. The respective ^1H NMR signals corresponding to Me_3N- and *t*Bu(Me)HN-substitution in **6a** and **6b** were clearly identified.

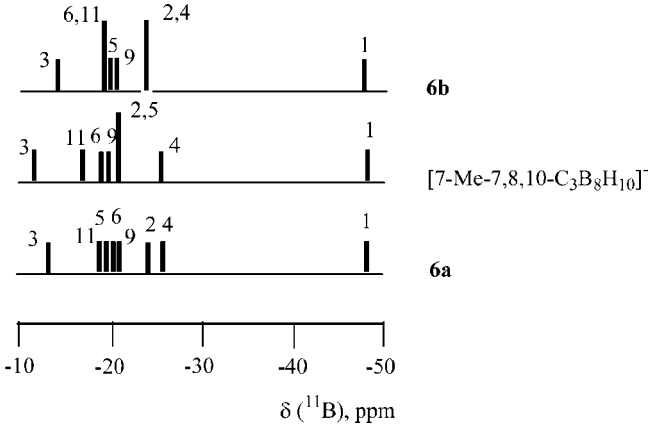

Figure 5. Stick representation and comparison of the ^{11}B NMR shifts for the zwitterions of the 7-L-7,8,10-$C_3B_8H_{10}$ type **6** (L = Me_3N **6a** and *t*Bu(Me)HN **6b**) with those for the [7-Me-*nido*-7,8,10-$C_3B_8H_{10}]^-$ anion (data from ref.[7])

Mass spectra of all the newly prepared compounds of types **2**, **3**, **4**, and **6** show theoretical cut-offs in their molecular-ion envelopes.

Conclusions

This work has opened up efficient preparative routes to the ferra bis(tricarbollides) of which compounds of type **2** with *p*,*p* orientation of the two reactive amino functionalities are the most important. These complexes are neutral and highly stable 26-cluster-electron *closo* complexes, perfect tricarbollide analogues of ferrocene. Optimization of the synthetic procedures has made these compounds generally feasible for their future synthetic use as metallacarborane building units for chemical constructions of linearly shaped oligomeric rod molecules. It was also demonstrated that cage isomerization of these compounds leads to *p*,*m* and *m*,*m* oriented shapes, which offers another modification in the area of structurally designed cluster chemistry. Moreover, it can be anticipated that the amine functions attached to the subclusters can be modified via analogous organic reactions, which should lead to other stable molecules with variable substituents. An important aspect of this work is that metal complexation reactions can be significantly affected by the purity of the metal reagent, which may significantly influence the nature of reaction products. This was documented by the metal-promoted isomerization reactions leading to new types of zwitterionic tricarbaborane compounds of type **6**. Aspects of this metallacarborane chemistry will be further developed and relevant experimental work in this area is in progress.

Experimental Section

General Procedures: All reactions were carried out with use of standard vacuum or inert-atmosphere techniques as described by Shriver[8] although some operations, such as preparative TLC, were carried out in air. The starting compound **1** was prepared according to the literature.[6g] Diethylene glycol dimethyl ether (diglyme) from Aldrich, 1,3,5-trimethylbenzene, benzene and hexane were dried with sodium wire and freshly distilled prior to use, the former being distilled at reduced pressure from sodium diphenylketyl. Dichloromethane was dried with CaH_2 and distilled before use. Aldrich anhydrous $FeCl_2$ of the three different purity grades 99.998% (H_2O < 10 ppm), 99.99% (H_2O < 100 ppm) and 98% was used. High-surface dry 96% NaH (prepared in this laboratory) was used. Other chemicals were reagent or analytical grade and were used as purchased. Preparative liquid chromatography was carried out using Aldrich silica gel (60−230 mesh) as the stationary phase under nitrogen. The mixtures of the isomeric derivatives **2a** and **3a** were separated by semi-preparative low-pressure chromatography on a pre-packed Merck Lobar® column LiChroprep® Si 60 (40−63μm), using hexane/CH_2Cl_2 (3:1, v/v) as the mobile phase, flow rate 7 mL/min, detection visual (the red bands) and by UV at 295 nm.

The purities of individual chromatographic fractions were checked by analytical TLC on Macherey−Nagel plates with UV indicator (silica gel on aluminium foil; detection by UV 254 nm followed by 2% aqueous $AgNO_3$ spray) and for the compounds of types **2** and **3** also by HPLC (see below). Melting points were measured in sealed capillaries and are uncorrected. Analyses were performed in the I.I.C. analytical laboratories using standard procedures. Low-resolution mass spectra were obtained using a Finnigan MAT MAGNUM ion trap quadrupole mass spectrometer equipped with a heated inlet option, as developed by Spectronex AG, Basle, Switzerland (70 eV, EI ionisation). Proton (^1H) and boron (^{11}B) NMR spectroscopy were performed at 11.75 Tesla with a Varian UNITY-500 instrument. The [^{11}B-^{11}B]-COSY[9] and $^1H\{^{11}B$(selective)$\}$[10] NMR experiments were essentially as described in other related papers from our laboratories.[11] Chemical shifts are given in ppm to high-frequency (low field) of Ξ = 160 MHz (nominally $F_3B{\cdot}OEt_2$ in $CDCl_3$) for ^{11}B (quoted ± 0.5 ppm) and Ξ = 500 MHz ($SiMe_4$) for ^1H (quoted ± 0.05 ppm), Ξ being defined as in ref.[12] Residual solvent ^1H resonances were used as internal secondary standards. Coupling constants $^1J_{BH}$ are taken from resolution-enhanced ^{11}B spectra with a digital resolution of ± 1 Hz. Analytical HPLC was used for monitoring the ratio of **2a** and **3a** or **2b** and **3b**. The system consisted of a Merck−Hitachi 6200 Intelligent pump, D-6000 Interface, Rheodyne 7125 injection valve with a 20-μL sample loop and a L 7450 Diode Array detector with 7000 Manager Software 2.1. Chromatographic conditions: analytical separation on a 4 × 250 mm I.D. steel column (LiChrosorb SI 60 (10 μm), Merck Darmstadt, packed by Labio Ltd., Prague), detection by Diode Array 200−300 nm, sensitivity range 0−2.0 A.U.F.S. Chromatographic data for the separation of **2a** and **3a**: hexane/CH_2Cl_2 (75:25, v/v) as the mobile phase, flow rate 1.0 mL/min, capacity factors (k'), selectivity (α) and resolution (*Rs*) for analytical separations were: **2a:** k_2' = 3.09 **3a**: $k_{3'}$ = 4.25, α = 1.38, *Rs* = 3.72; chromatographic conditions for the separation of **2b** and **3b**: CH_2Cl_2/CH_3CN (97:3, v/v) as the mobile phase, flow rate 1.0 mL/min, capacity factors (k') k_7' = 5.65 $k_{8'}$ = 10.4, α = 1.85, *Rs* = 5.3.

 © 2004 Wiley-VCH Verlag GmbH & Co. KGaA, Weinheim

[*closo*-9,9′-(*t*BuHN)$_2$-*commo*-2,2′-Fe^{II}-1,7,9-($C_3B_8H_{10}$)-1′,7′,9′-($C_3B_8H_{10}$)] (2a) and [*closo*-9,10′-(*t*BuHN)$_2$-*commo*-2,2′-Fe^{II}-1,7,9-($C_3B_8H_{10}$)-1′,7′,10′-($C_3B_8H_{10}$)] (3a): a) The starting salt $Tl^+\mathbf{1}^-$ [1b] (2.50 g, 6.11 mmol) was stirred in a mesitylene/diglyme solvent mixture (40 mL, 25:75, v/v), $FeCl_2$ (99.99%, 1.60 g, 12.7 mmol) was then added and the mixture heated and stirred under gentle reflux for 8 h. After cooling to room temperature, water (2 mL) was added dropwise and the solvents were removed by rotary evaporation. The dark residue was digested with Et_2O (20 mL) and 1 M HCl (10 mL). The organic layer was then separated and the aqueous phase extracted with two additional portions of diethyl ether (20 mL). The combined organic extracts were evaporated and the reddish solid was treated with three portions of hexane (15 mL), filtered, and the combined red hexane extracts were evaporated. Crude complex **2a** (680 mg, 49% yield) was then isolated by repeated extraction of the solid residue with hexane, filtration of the combined extracts, and evaporation of the solvent. The compound was purified by flash chromatography on a silica gel column (2.5 × 35 cm) by elution with hexane/benzene (65:35, v.v.) to isolate 602 mg (43%) of **2a** as a red, semi-crystalline material. An analytical sample was crystallized from a concentrated petroleum ether solution at ca. 5 °C (red needles) and identified by NMR spectroscopy as reported earlier.[4] b) Compound **1** (1.01 g, 4.91 mmol) was stirred in diglyme (15 mL), dry NaH (0.22 g, 9.17 mmol) was added, and the slurry was stirred at room temperature for 1 h and then heated at 80 °C (bath temperature) for 30 min. After cooling, $FeCl_2$ (99.99%, 1.33 g, 10.49 mmol) was added and the reaction mixture heated under gentle reflux for 3 h with stirring. The mixture was then worked-up as in the preceding experiment giving a mixture of compounds **2a** and **3a**. This was separated by semi-preparative liquid chromatography on a pre-packed Merck Lobar® column (see above) to separate two red bands of R_f = 0.25 and 0.20 (TLC in 25% CH_2Cl_2 in hexane), from which compounds **2a** and **3a** were obtained in respective yields of 514 mg (45%) and 194 mg (17%) after evaporation. Compound **3a** was crystallized from a warm pentane solution by cooling to 5 °C. **3a:** R_f = 0.20 (CH_2Cl_2/hexane, 25: 75, v/v); m.p. 152−155 °C. ^{11}B NMR (160.4 MHz, 25 °C, $CDCl_3$): δ = −6.6 [d, ^1J(B,H) = 174 Hz, 2 B, B6′,11′], −8.3 (d, 1 B, B9′), −9.2 [d, ^1J(B,H) = 153 Hz, 2 B, B6,11], −12.3 [d, ^1J(B,H) = 170 Hz, 1 B, B3′], −13.4 [d, ^1J(B,H) = 168 Hz, 1 B, B3], −15.2 [d, ^1J(B,H) = 174 Hz, 4 B, B5,12,5′,12′] −16.9 [d, ^1J(B,H) = 177 Hz, 1 B, B10], −22.4 [d, ^1J(B,H) = 177 Hz, 2 B, B4,8], −24.05 [d, ^1J(B,H) = 161 Hz, 2 B, B4′,8′] ppm, all theoretical [^{11}B-^{11}B] cross-peaks observed. ^{1}H{^{11}B} NMR (500 MHz, 25 °C, $CDCl_3$): δ = 3.78 (s, 1 H, H 3′), 3.66 (s, 1 H, H3), 3.32 (s, 2 H, H6′,11′), 3.05 (s, 1 H, H9′) 2.98 (s, 2 H, H6,11], 2.49 (s, 4 H, H5,12,5′,12′), 2.35 (s, 2 H, H4,8), 2.30 (m, 1 H, N*H*-*t*Bu), 2.12 (s, 1 H, H10), 2.07 (s, 4 H, cage C*H*), 1.52 (s, 2 H, H4′,8′), 1.22 and 1.19 (s, 18 H, *t*Bu) ppm. IR (KBr): $\tilde{\nu}$ = 2534 (B−H) cm^{-1}. MS (70 eV, EI): *m*/*z* (%) = 468 (4) [M$^+$], 465 (100) [M$^+$ − 3H]. $C_{14}H_{30}B_{16}FeN_2$ (465.30): calcd. B 37.17, N 6.01; found B 36.86, N 5.94.

[*closo*-9,9′-(H_2N)$_2$-*commo*-2,2′-Fe^{II}-1,7,9-($C_3B_8H_{10}$)-1′,7′,9′-($C_3B_8H_{10}$)] (2b) and [*closo*-9,10′-(H_2N)$_2$-*commo*-2,2′-Fe^{II}-1,7,9-($C_3B_8H_{10}$)-1′,7′,10′-($C_3B_8H_{10}$)] (3b): Compound **2a** or **3a** (200 mg, 0.57 mmol) was dissolved in hexane (20 mL) and $AlCl_3$ (800 mg, 6.0 mmol) was then added in one portion. The reaction slurry was stirred under gentle reflux for 2 h. After cooling, the reaction slurry was treated with water (10 mL) and the solvents were evaporated. The solid residue was treated with 10% aqueous KOH (15 mL), extracted with CH_2Cl_2 (2 × 15 mL), the organic portion was separated, and the solvent evaporated to give 124 mg (82%) of **2b** or 121 mg (80%) of **3b**. For the preparation of **3b**, it is convenient to apply the $AlCl_3$ reaction on a mixture of **2a** and **3a** obtained in the preceding experiment, which results typically in a total yield of 79% of the H_2N- derivatives **2b** and **3b**. The isomers were then separated by chromatography on a silica gel column (1.5 × 25 cm), using a CH_2Cl_2/MeCN mixture (95:5, v/v) as the mobile phase.

2b: R_f = 0.24 (CH_2Cl_2); m.p. >360 °C. ^{11}B NMR (160.4 MHz, 25 °C, $CDCl_3$): δ = −8.6 [d, ^1J(B,H) = 154 Hz, 2 B, B6,11], −12.6 [d, ^1J(B,H) = 169 Hz, 1 B, B3], −15.6 [d, ^1J(B,H) = 170 Hz, 2 B, B5,12], −17.3 [d, ^1J(B,H) = 165 Hz, 1 B, B10], −22.7 [d, ^1J(B,H) = 177 Hz, 2 B, B4,8] ppm, all theoretical [^{11}B-^{11}B] cross-peaks observed. ^{1}H{^{11}B} NMR (500 MHz, 25 °C, $CDCl_3$): δ = 4.09 (s, 1 H, H3), 2.92 (s, 2 H, H6,11), 2.44 (br. s, 1 H, N*H*), 2.33 (s, 2 H, H5,12), 2.26 (s, 2 H, H4,8), 1.97 (s, 1 H, H10), 1.86 (s, 2 H, cage C*H*) ppm. IR (KBr): $\tilde{\nu}$ = 2572 (B−H) cm^{-1}. MS (70 eV, EI): *m*/*z* (%) = 356 (15) [M$^+$], 353 (100) [M$^+$ − 3H]. $C_6H_{24}B_{16}FeN_2$ (353.08): calcd. B 48.99; found B 48.71.

3b: R_f = 0.14 (CH_2Cl_2); m.p. 282 °C. ^{11}B NMR (160.4 MHz, 25 °C, $CDCl_3$): δ = −6.6 [d, ^1J(B,H) = 167 Hz, 2 B, B6′,11′], −8.0 (d, 1 B, B9′), −8.7 [d, ^1J(B,H) = 156 Hz, 2 B, B6,11], −13.2 (d, 2 B, B3,3′], −14.9 [d, ^1J(B,H) = 179 Hz, 4 B, B5,12,5′,12′], −17.0 (d, 1 B, B10), −22.7 [d, ^1J(B,H) = 174 Hz, 2 B, B4,8], −23.4 [d, ^1J(B,H) = 156 Hz, 2 B, B4′,8′] ppm, all theoretical [^{11}B-^{11}B] cross-peaks observed. ^{1}H{^{11}B} NMR (500 MHz, 25 °C, $CDCl_3$): δ = 3.58 and 3.79 (s, 2 H, H3,3′), 3.17 (s, 2 H, H6′,11′), 2.95 (H9′), 3.04 (s, 2 H, H6,11), 2. 49 (br. s, 1 H, N*H*), 2.49 and 2.47 (s, 4 H, H (5,12,5′,12′)], 2.31 (s, 2 H, H4,8), 2.02 (s, 1 H, H10), 2.24 and 2.165 (4 H, cage CH), 1.56 (s, 2 H, H4′,8′) ppm. IR (KBr): $\tilde{\nu}$ = 2575 (B−H) cm^{-1}. MS (70 eV, EI): *m*/*z* (%) = 356 (13) [M$^+$], 354 (100) [M$^+$ −2H]. $C_6H_{24}B_{16}FeN_2$ (353.08): calcd. B 48.99; found B 48.30.

Thermal Decomposition of [*closo*-9,9′-(*t*Bu HN)$_2$-*commo*-2,2′-Fe^{II}-1,7,9-($C_3B_8H_{10}$)-1′,7′,9′-($C_3B_8H_{10}$)] (2a): Complex **2a** (100 mg, 0. 21 mmol) was sealed in a glass ampoule under vacuum and heated in a furnace for 15 min at 210 °C. The ampoule was then carefully opened, the residue dissolved in CH_2Cl_2 (3 mL) and mounted onto the top of a silica gel column (20 × 1.5 cm). Elution with a hexane/CH_2Cl_2 mixture (1: 1, v/v), followed by gradually increasing the content of CH_2Cl_2 to 100%, recovered a small amount of the starting compound (8 mg) and provided red compounds **2c** (18 mg, 20%) and **2b** (39 mg,51%). Subsequent elution with CH_2Cl_2/acetonitrile (9:1, v/v) eluted **3b** (10 mg, 13%), which was characterized as described above.

2c: R_f = 0.48 (CH_2Cl_2); m.p. 228−232 °C (dec. to **7** + **8**). ^{11}B NMR (160.4 MHz, 25 °C, $CDCl_3$): δ = −8.6 (d, 2 B, B6,11 or 6′,11′), −9.0 (d, 2 B, B6,11 or 6′,11′), −12.6 (d, 1 B, B3 or B3′), −13.0 (d, 1 B, B3 or B3′), −15.7 (d, 4 B, B5,12,5′,12′), −17.3 (d, 2 B, B10,10′), −22.7 (d, 2 B, B4,8 or 4′,8′), −22.8 (d, 2 B, B4,8 or 4′,8′) ppm. ^{1}H{^{11}B} NMR (500 MHz, 25 °C, $CDCl_3$): δ = 4,08 (s, 1 H, H3 or H3′), 4.05 (s, 1 H, H3 or H3′), 2.92 (s, 2 H, H6,11 or H6′,11′), 2.87 (s, 2 H, H6,11 or H6′,11′), 2.43 (br. s, 2 H, NH_2), 2.17 (br. s., 1 H, N*H*-*t*Bu), 2.372 (s, 2 H, H5,12 or H5′,12′), 2.32 (s, 2 H, H5,12 or H5′,12′), 2.09 (s, 1 H, H10 or H10′), 1.87 (s, 1 H, H10 or H10′), 2.31 (s, 2 H, H4,8 or H4′8′), 2.25 (s, 2 H, H4,8 or H4′8′), 1.87 (s, 2 H, cage C*H*), 1.73 (s, 2 H, cage C*H*), 1.19 (s, 9 H, *t*Bu) ppm. IR (KBr): $\tilde{\nu}$ = 2534 (B−H) cm^{-1}. MS (70 eV, EI): *m*/*z* (%) = 357 (1.4) [M$^+$], 354 (100) [M$^+$ − 3H].

[*closo*-10,10′-(*t*BuHN)$_2$-*commo*-2,2′-Fe^{II}-1,7,10-($C_3B_8H_{10}$)-1′,7′,10′-($C_3B_8H_{10}$)] (4a), 7-Me_3N-7,8,9-*nido*-$C_3B_8H_{10}$ (6a), and 7-*t*Bu(Me)HN-7,8,10-*nido*-$C_3B_8H_{10}$ (6b): To a stirred slurry of compound **1** (500 mg, 2.43 mmol) in diglyme (15 mL) was added dry NaH (120 mg, 5 mmol), the mixture was stirred at room temperature for 1 h, and then heated at 80 °C (bath) for 30 min. After

 © 2004 Wiley-VCH Verlag GmbH & Co. KGaA, Weinheim

Table 1. Crystal data and structure refinement for compounds **2b**, **3a**, and **6b**

Empirical formula	$C_6H_{24}B_{16}FeN_2$	$C_{14}H_{40}B_{16}FeN_2$	$C_8H_{23}B_8N$
Habit and size, mm	prism, 0.3 × 0.3 × 0.25	plate, 0.3 × 0.26 × 0.24	prism, 0.2 × 0.12 × 0.12
Crystal system	triclinic	orthorhombic	monoclinic
Space group	$P\bar{1}$ (No, 2)	$P2_12_12_1$	$P2_1/n$ (No. 14)
a, Å	7.0260(1)	11.425(2)	8.534(4)
b, Å	11.6020(2)	33.2485(11)	12.820(4)
c, Å	11.7410(2)	6.7392(11)	12.932(5)
α, deg	65.5910(9)	90	90
β, deg	81.8160(9)	90	99.58(3)
γ, deg	87.4050(9)	90	90
Z	2	4	4
μ, mm^{-1}	0.862	0.597	0.051
Wavelength, Å	0.71073	0.71069	0.71069
θ range in deg, % completeness	1−27.5, 99.4	1.9−25.0, 99.8	2.2−22.5, 99.9
No. of reflections measured	13158	2609	1965
No. of unique reflections; $R_{int.}$ [a]	3944; 0.022	2609	1824, 0.0615
No. of observed ref. [$I > 2\sigma(I)$]	3545	2235	721
No. of parameters	229	230	192
GOF[b] all data	1.078	1.074	0.816
Final R[c] indices [$I > 2\sigma(I)$]	$R1$ = 0.029, $wR2$ = 0.080	$R1$ = 0.0441, $wR2$ = 0.1063	$R1$ = 0.0609, $wR2$= 0.1030
R[c] indices (all data)	$R1$ = 0.032, $wR2$ = 0.083	$R1$ = 0.0619, $wR2$ = 0.1141	$R1$ = 0.2244, $wR2$ = 0.1218
w_1/w_2 [d]	0.0366/0.588	0.0494/1.8452	0.0356 /0.0000
max./min. Δρ, e·$Å^{-3}$	0.435/−0.381	0.259/−0.347	0.144/−0.142

[a] $R_{int} = \Sigma|F_o^2 - F_o^2(\text{mean})|/\Sigma F_o^2$ (summation is carried out only where more than one symmetry equivalent is averaged). [b] GOF = $[\Sigma[w(F_o^2 - F_c^2)^2]/(N_{reflns.} - N_{param.})]^{1/2}$. [c] $R(F) = \Sigma||F_o| - ||F_c||/\Sigma|F_o|$, $wR2 = [\Sigma[w(F_o^2 - F_c^2)^2]/\Sigma[w(F_o^2)^2]]^{1/2}$. [d] Weighting scheme $w = [\sigma^2(F_o^2) + (w_1P) + w_2P]^{-1}$, $P = [\max(F_o^2,0) + 2F_c^2]/3$.

cooling, reagent grade $FeCl_2$ (98%, 1580 mg, 12.5 mmol) was added and the mixture gently heated to reflux for 24 h with stirring. After cooling to room temperature, water (5 mL) was added dropwise and the diglyme removed by rotary evaporation. The dark residue was digested with Et_2O (50 mL) and 1 M HCl (40 mL). The organic layer was separated and the aqueous phase extracted with two additional 20 mL portions of Et_2O. The combined organic extracts were evaporated, the reddish solid was treated with three 20 mL portions of hexane and the solution thus obtained was filtered and the solvents evaporated to give a mixture of compounds **2a** and **3a**. The mixture was separated by preparative liquid chromatography on a silica gel column (25 × 1.5 cm), using 25% CH_2Cl_2 in hexane as the mobile phase to separate the red bands of R_f (anal., 25% CH_2Cl_2 in hexane) 0.25, 0.20, and 0.15. The first fractions contained trace quantities of compound **5**, which was identified from its NMR spectra.[5] Complexes **2a** (22 mg, 4%), **3a** (26 mg, 5%), and **4a** (12 mg 2%) were then isolated from individual fractions and purified by crystallization from concentrated petroleum ether at ca. 0 °C. The pale brown solid residue after hexane extraction was dissolved in 5% MeCN in CH_2Cl_2 and chromatographed on a silica gel column (25 × 1.5 cm), using CH_2Cl_2 and finally a CH_2Cl_2/MeCN (4:1, v/v) mixture (TLC monitoring). Evaporation of the two last fractions resulted in the isolation of compounds **6a** (66 mg, 14%) and **6b** (92 mg, 17%), which were recrystallized from hot CH_2Cl_2.

4a: R_f (CH_2Cl_2/hexane, 25:75, v/v) 0.16. ^{11}B NMR (160.4 MHz, 25 °C, $CDCl_3$): δ = −6.5 [d, ^1J(B,H) = 153, 4 B, B6,11,6′,11′], −8.1 (d, 2 B, B9,9′), −12.2 [d, ^1J(B,H) = 165, 2 B, B3,3′], −14.7 [d, ^1J(B,H) = 174, 4 B, B5,12,5′,12′], −23.7 [d, ^1J(B,H) = 165, 4 B, B4,8,4′,8′] ppm, all theoretical [^{11}B-^{11}B] cross-peaks observed. $^1H\{^{11}B\}$ NMR (500 MHz, 25 °C, $CDCl_3$): δ = 3.56 (s, 2 H, H3,3′), 3.42 (s, 4 H, H6,11,6′,11′), 3.13 (s, 2 H, H9,9′), 2.61 (s, 2 H, N*H*), 2.59 (s, 4 H, H5,12,5′,12′), 2.27 (s, 4 H, cage C*H*), 1.57 s (s, 4 H, H4,8,4′,8′), 1.25 (s, 18 H, *t*Bu) ppm. MS (70 eV, EI): *m*/*z* (%) = 468 (18) [M^+], 466 (100) [$M^+ - 2H$].

6a: R_f (CH_2Cl_2) 0.25; m.p. 298−300 °C. ^{11}B NMR (160.4 MHz, 25 °C, CD_3CN): δ = −12.8 [d, ^1J(B,H) = 159 Hz, 1 B, B3], −17.9 (d, 1 B, B11), −18.5 (d, 1 B, B5), −19.3 (d, 1 B, B6), −20.0 [d, ^1J(B,H) = 137 Hz, 1 B, B9], −23.4 [d, ^1J(B,H) = 153 Hz, 1 B, B2], −25.7 [d, ^1J(B,H) = 150 Hz, 1 B, B4], −48.0 [d, ^1J(B,H) = 143 Hz, 1 B, B1] ppm, all theoretical [^{11}B-^{11}B] cross-peaks observed, except uncertain B5−B9, B6−B11. $^1H\{^{11}B\}$ NMR (500 MHz, 25 °C, CD_3CN): δ = 3.08 (m, 9 H, Me), 2.31 (s, 1 H, H3), 2.15 (s, 1 H, cage C*H*), 1.68 (s, 1 H, H11), 1.67 (s, 1 H, cage C*H*), 1.36 (s, 1 H, H5), 1.36 (s, 1 H, H6), 1.89 (s, 1 H, H9), 1.58 (s, 1 H, H2), 1.12 (s, 1 H, H4), 0.01 (s, 1 H, H1) ppm. IR (KBr): $\tilde{\nu}$ = 2556 (B−H) cm^{-1}. MS (70 eV, EI): *m*/*z* (%) = 193 (8) [M^+], 192 (18) [$M^+ - H$]. $C_6H_{19}B_8N$ (191.78): calcd. B 45.14; found B 44.25.

6b: R_f (CH_2Cl_2) 0.12; m.p. 194−196 °C. ^{11}B NMR (160.4 MHz, 25 °C, CD_3CN): δ = −13.8 [d, ^1J(B,H) = 156 Hz, 1 B, B3], −18.2 (d, 2 B, B6,11), −19.9 (d, 1 B, B5), −20.5 [d, ^1J(B,H) = 134 Hz, 1 B, B9], −23.7 [d, ^1J(B,H) 145 Hz, 2 B, B2,4] −48.0 [d, ^1J(B,H) = 137 Hz, 1 B, B1] ppm, all theoretical [^{11}B-^{11}B] cross-peaks observed. $^1H\{^{11}B\}$ NMR (500 MHz, 25 °C, CD_3CN): δ = 6.19 (br. s, 1 H, N*H*), 2.15 (m, 3 H, Me), 2.01 (s, 1 H, H3), 1.95 (s, 1 H, H9), 1.19 (s, 1 H, H2 or H4), 1.70 (s, 1 H, cage C*H*), 1.66 (s, 1 H, H6 or H11), 1.35 (s, 1 H, H6 or H11), 1.55 (s, 9 H, *t*Bu), 1.27 (s, 1 H, H5), 0.87 (s, 1 H, cage CH), 0.06 (s, 1 H, H1) ppm. IR (KBr): $\tilde{\nu}$ = 2534 (B−H) cm^{-1}. MS (70 eV, EI): *m*/*z* (%) = 221 (52) [M^+], 220 (100) [$M^+ - H$]. $C_8H_{23}B_8N$ (219.76): calcd. B 39.35; found B 37.99.

X-ray Crystallography

Crystallographic Data for 2b: A red crystal of **2b** of dimensions 0.3 × 0.3 × 0.25 mm was mounted on a glass fiber with epoxy cement and placed on a four-circle Nonius−KappaCCD diffractometer equipped with a CCD area detector at 150(2)K with Mo-K_α radiation. The crystallographic details are summarized in Table 1. The structure was solved by the direct methods (SIR97)[13] and refined by a full-matrix least-squares procedure based on F^2 (SHELXL-

 © 2004 Wiley-VCH Verlag GmbH & Co. KGaA, Weinheim

97).[14] The hydrogen atoms were found on a difference Fourier map, but some of them behaved erroneously during refinement and were therefore fixed in idealized positions (riding model) and assigned temperature factors $H_{iso}(H) = 1.2U_{eq}$ (pivot atom). The final difference map displayed no peaks of chemical significance.

Crystallographic Data for 3a and 6b: A pale red crystal of **3a** and a colorless crystal of **6b** were analyzed at 294 K with a Rigaku AFC5S diffractometer with Mo-K_α radiation. The crystallographic details are summarized in Table 1. The structures were solved by the direct method and refined on F^2 with the SHELXL-97 program.[14] For **3a**, boron atoms were refined isotropically but the rest of the non-hydrogen atoms were refined with anisotropic thermal displacement parameters. Hydrogen atoms were placed in calculated positions and were treated as riding atoms using the SHELX97[14] default parameters. For **6b**, the reflection power of the crystal steeply dropped at high reflection angles and therefore the data collection was limited to $2\theta_{max.} = 45°$. The non-hydrogen atoms were refined with anisotropic thermal displacement parameters. Hydrogen atoms of the carborane cage were found from a difference Fourier map and refined with fixed *U*. The hydrogen atoms of the methyl groups were placed in calculated positions and treated as riding atoms. The final difference maps of **3a** and **6b** displayed no peaks of chemical significance.

CCDC-215766, -215767 and -215768 contain the supplementary crystallographic data of the compounds **3a**, **6b** and **2a** for this paper. These data can be obtained free of charge at wwww.ccdc.cam.ac.uk/conts/retrieving.hmtl [or from Cambridge Crystallographic Data Center, 12 Union Road, Cambridge CB2 1EZ, UK [Fax: (internat.) + 44-1223-336-033; E-mail: deposit@ccdc.cam.ac.uk].

Acknowledgments

We thank Drs. Z. Plzák and J. Fusek for MS and NMR measurements, respectively. Support from the Grant Agency of the Czech Republic (Grant No. 203/00/1042) and the Ministry of Education Youth and Sport of the Czech Republic (Project LN00A0028) are appreciated. Early stages of this work were also supported by the Spanish project AMB1999-1810-Ce and Generalitat de Catalunya (grant no 1996-SGR-00038 to B. G.).

[1] J. Holub, B. Grüner, I. Císařová, F. Teixidor, C. Viñas, B. Štíbr, *Inorg. Chem.* **1999**, *38*, 2775−2780.
[2] B. Grüner, A. Lehtonen, R. Kivekäs, R. Sillanpää, J. Holub, F. Teixidor, C. Viñas, B. Štíbr, *Inorg. Chem.* **2000**, *39*, 2577−2580.
[3] For review see, for example: [3a] G. B. Dunks, M. F. Hawthorne, in *Boron Hydride Chemistry* (Ed.: E. L. Muetterties), Academic Press, New York, **1975**; chapter 11, pp. 383−430. [3b] R. N. Grimes, in *Comprehensive Organometallic Chemistry* (Eds.: G. Wilkinson, F. G. A. Stone, E. Abel), Pergamon, **1982**, part I, chapter 5.5, pp. 459−542.
[4] B. Grüner, B. Štíbr, J. Holub, F. Teixidor, C. Viñas, R. Kivekäs, R. Sillanpää, *J. Chem. Soc., Dalton Trans.* **1999**, 3337−3338.
[5] B. Grüner, J. Holub, I. Císařová, B. Štíbr, *Eur. J. Inorg. Chem.* **2003**, 1533−1539.
[6] [6a] B. Štíbr, J. Holub, F. Teixidor, C. Viñas, *J. Chem. Soc., Chem. Commun.* **1995**, 795−796. [6b] B. Štíbr, J. Holub, I. Císařová, F. Teixidor, C. Viñas, J. Fusek, Z. Plzák, *Inorg. Chem.* **1996**, *35*, 3635−3642. [6c] B. Štíbr, J. Holub, I. Císařová, F. Teixidor, C. Viñas, *Inorg. Chim. Acta* **1996**, *245*, 129−131. [6d] R. Rousseau, S. Lee, E. Canadell, F. Teixidor, C. Viñas, B. Štíbr, *New J. Chem.* **1996**, *20*, 277−281. [6e] B. Štíbr, J. Holub, F. Teixidor, in *Advances in Boron Chemistry* (Ed.: W. Siebert), Royal Society of Chemistry, London, **1997**, pp. 333−340. [6f] J. Holub, B. Štíbr, D. Hnyk, J. Fusek, I. Císařová, F. Teixidor, C. Viñas, Z. Plzák, P. v. R. Schleyer, *J. Am. Chem. Soc.* **1997**, *119*, 7750−7759. [6g] B. Štíbr, J. Holub, J. Plešek, T. Jelínek, B. Grüner, F. Teixidor, C. Viñas, *J. Organomet. Chem.* **1999**, *582*, 282−285.
[7] A. M. Shedlow, P. J. Carroll, L. G. Sneddon, *Organometallics* **1995**, *14*, 4046−4047.
[8] D. F. Shriver, M. A. Drezdon, *Manipulation of Air Sensitive Compounds*, 2nd ed., John Wiley & Sons, New York, **1986**.
[9] See, for example: [9a] J. D. Kennedy, in *Multinuclear N. M. R.* (Ed.: J. Mason), Plenum Press, New York, **1987**, p. 221. [9b] W. C. Hutton, T. L. Venable, R. N. Grimes, *J. Am. Chem. Soc.* **1984**, *106*, 29. [9c] J. Schraml, J. M. Bellama, *Two-Dimensional NMR Spectroscopy*, John Wiley & Sons, New York, **1982**, and references cited therein.
[10] X. L. R. Fontaine, J. D. Kennedy, *J. Chem. Soc., Dalton Trans.* **1987**, 1573−1575.
[11] J. Plešek, B. Štíbr, X. L. R. Fontaine, J. D. Kennedy, S. Heřmánek, T. Jelínek, *Collect. Czech. Chem. Commun.* **1991**, *56*, 1618−1635.
[12] W. McFarlane, *Proc. R. Soc., London, Ser. A* **1968**, *306*, 185.
[13] A. Altomore, M. C. Burla, M. Camalli, G. Cascarano, C. Giacovazzo, A. Guagliardi, A. G. G. Molinerni, G. Polidori, R. Spagna, *J. Appl. Crystallogr.* **1999**, *32*, 115−119.
[14] G. M. Sheldrick, SHELX97, *Program for Crystal Structure Refinement from Diffraction Data*, University of Göttingen (Germany), **1997**.

Received September 30, 2003
Early View Article
Published Online February 26, 2004

 © 2004 Wiley-VCH Verlag GmbH & Co. KGaA, Weinheim

Structure, Electrochemistry and Hydroformylation Catalytic Activity of the Bis(pyrazolylborato)rhodium(I) Complexes [RhBp(CO)P] [P = $P(NC_4H_4)_3$, PPh_3, PCy_3, $P(C_6H_4OMe\text{-}4)_3$]

Anna M. Trzeciak,*[a] Beata Borak,[a] Zbigniew Ciunik,[a] Józef J. Ziółkowski,[a] M. Fátima C. Guedes da Silva,[b,c] and Armando J. L. Pombeiro[b]

Keywords: Rhodium / N ligands / Electrochemistry / X-ray diffraction / Hydroformylation

Rhodium complexes of formula [RhBp(CO)P] [Bp = bis(pyrazolylborate), P = $P(NC_4H_4)_3$ **1**, PPh_3 **2**, PCy_3 **3**, $P(C_6H_4OMe\text{-}4)_3$ **4**] have been prepared by exchange of the acetylacetonate ($acac^-$) ligand in [Rh(acac)(CO)P] complexes. The spectroscopic and electrochemical properties as well as X-ray data of [Rh(acac)(CO)P] and [RhBp(CO)P] complexes have been compared with the aim to estimate the relative donor properties of both anionic ligands ($acac^-$ and Bp^-). The cyclic voltammetric results indicate that the Bp^- ligand behaves as a much stronger electron donor than $acac^-$ and a value of the Lever E_L ligand parameter identical to that of the pyrazolate ligand (–0.24 V vs. NHE for each coordinating arm) is proposed for the bis- and tris(pyrazolyl)borate ligands, whereas $P(C_6H_4OMe\text{-}4)_3$ is also shown to have an identical E_L value (0.69 V) to that of $P(NC_4H_4)_3$. An improved linear relationship between the oxidation potential and the sum of the ligand E_L values for square-planar Rh^I complexes is also obtained and adjusted values for the Lever S_M and I_M parameters for the Rh^I/Rh^{II} redox couple are given. The *trans* influence of phosphanes was not observed in crystals of complexes **2** and **3**, in contrast to analogous acetylacetonato complexes in which the Rh–O bonds differ by ca. 0.04–0.06 Å. Complexes **1**–**4** are very attractive precursors for hydroformylation catalysts and yields of aldehydes of 80–87% have been obtained with all complexes without extra phosphane as co-catalyst. During the hydroformylation reaction, however, small amounts of a catalytically inactive $[RhBp(CO)_2]$ complex were formed.

(© Wiley-VCH Verlag GmbH & Co. KGaA, 69451 Weinheim, Germany, 2004)

Introduction

The exceptionally high catalytic activity of rhodium complexes in the hydroformylation of unsaturated compounds is well known.[1] Among the large number of rhodium catalyst precursors, the acetylacetonato complexes $[Rh(acac)(CO)_2]$, [Rh(acac)(CO)P] or $[Rh(acac)P_2]$ (acac: acetylacetonato, P: phosphorus ligands) are used very often, both in the laboratory and in industrial processes.[2−4] Many studies have shown that the acetylacetonato ligand is easily removed from the coordination sphere of rhodium in the presence of CO and H_2, facilitating the formation of active hydrido-carbonyl complexes.[5,6] In contrast to rhodium complexes with anionic oxygen-containing ligands, there are very few data reporting the application of rhodium complexes containing nitrogen ligands as catalyst precursors. The few known examples, including the active rhodium pyrazolylborate complexes in the high pressure hydroformylation of propylene (60−80 atm of H_2/CO) and 1-hexene (30−50 atm of H_2/CO), have been patented.[7]

Tris(pyrazolylborato) ligands are very often compared with cyclopentadienyl ligands in view of their similar electronic structure and steric properties.[8,9]

In this paper we report the results of structural as well as catalytic studies of rhodium bis(pyrazolylborate) complexes of the type [RhBp(CO)P] [Figure 1; Bp: bis(pyrazolylborate), P: $P(NC_4H_4)_3$ **1**, PPh_3 **2**, PCy_3 **3**, $P(C_6H_4OMe\text{-}4)_3$ **4**].

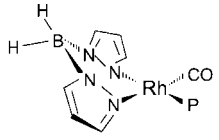

Figure 1. Structure of [RhBp(CO)P] complexes

We were also interested in comparing the properties of these complexes with those of a known family of square-

[a] Faculty of Chemistry, University of Wrocław,
14 F. Joliot-Curie St., 50-383 Wrocław, Poland
Fax: (internat.) + 48-71-375-7356
E-mail: jjz@wchuwr.chem.uni.wroc.pl
[b] Centro de Química Estrutural, Complexo I, Instituto Superior Técnico,
Av. Rovisco Pais, 1049-001 Lisboa, Portugal
E-mail: pombeiro@ist.utl.pt
[c] Universidade Lusófona de Humanidades e Tecnologias,
Av. Campo Grande 376, 1749-024 Lisboa, Portugal
E-mail: fatima.guedes@ist.utl.pt

planar rhodium complexes of formula [Rh(acac)(CO)P] (P: phosphorus ligand). In both types of complexes the rhodium(I) ion is coordinated by the chelating ligand through two nitrogen or oxygen atoms, forming a six-membered ring. Rhodium(I) complexes with β-diketonate ligands are known as model groups of rhodium complexes for which the *trans* effect, the effect of the steric and electronic properties of the phosphorus ligands, as well as the electrochemical, thermochemical and kinetic properties, have been discussed.[10−14] However, rhodium(I) complexes with bis(pyrazolylborato) ligands, although known for a long time, have not received any special attention.

Results and Discussion

Strategy of Synthesis

Complexes **1** and **4** were prepared and characterized for the first time in this paper (details in Exp. Sect.). Complex **2** was obtained earlier by reaction of $[RhCl(CO)_2]_2$ with KBp.[15,16] We adapted the other method of synthesis of [RhBp(CO)P] complexes, reported recently for $[RhTp^{Ph,Me}(CO)_2]$ and $[RhTp^{Ph,Me}(CO)(PPh_3)]$, based on the replacement of an $acac^-$ ligand by a bis(pyrazolylborate).[17] The reactions were performed with isolated [Rh(acac)(CO)P] complexes, at room temperature, and were complete in ca. 30 min, giving satisfactory yields of pure products.

Alternatively, the complexes [Rh(acac)(CO)P] were prepared "in situ" from $[Rh(acac)(CO)_2]$ and the appropriate amount of the phosphorus ligand P and further used for the substitution of anionic ligands ($acac^-$ for Bp^-; Scheme 1).

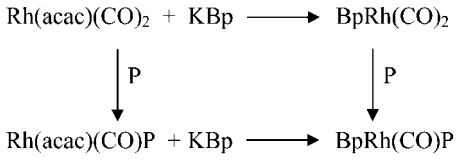

Scheme 1. Synthesis of [RhBp(CO)P] complexes

The third method of synthesis of the complexes consisted of the reaction of $[Rh(acac)(CO)_2]$ with KBp to give $[RhBp(CO)_2]$, followed by replacement of CO by the phosphane P. Independent of the reaction pathway, the [RhBp(CO)P] complexes were isolated as final products with yields of 70−90%.

IR and ^{31}P NMR Spectra

The ν(CO) frequencies in the IR spectra of [RhBp(CO)P] complexes are summarized in Table 1, where the IR data of analogous [Rh(acac)(CO)P] complexes are also presented for comparison. The ν(CO) frequencies in the bis(pyrazolylborato) complexes decrease with an increase of the σ/π-donor properties of the P ligands in the order $P(NC_4H_4)_3 > PPh_3 > P(C_6H_4OMe\text{-}4)_3 > PCy_3$. Similar changes of ν(CO) frequencies were observed in the IR spectra of [Rh(acac)(CO)P] and [Rh{$CF_3C(O)CHC(NH)Me$}(CO)P] complexes.[18] The highest ν(CO) frequencies were found for complexes with the Bp^- ligand, if rhodium compounds with the same phosphane ligand were compared. The positions of the IR bands suggest a weaker σ/π-donor character of the *N*,*N*-Bp^- ligand in comparison with *O*,*O*-$acac^-$ and *N*,*O*-bonded ones (β-ketoiminate). However, a more detailed analysis of the $J_{Rh,P}$ coupling constants in the ^{31}P NMR spectra leads to another conclusion. The $J_{Rh,P}$ coupling constants determined for [RhBp(CO)P] complexes are similar to those for β-ketoiminato complexes but lower than the corresponding $J_{Rh,P}$ values for acetylacetonato complexes (Table 1). Usually, $J_{Rh,P}$ decreases when the ligand σ/π-donor character increases. Therefore, according to this criterion, the *N*,*N*-Bp^- ligand should be a more effective donor than the *O*,*O*-acetylacetonato ligand, which is in agreement with the electrochemical results discussed below.

Following Tolman's rule for complexes in which the electronic effect dominates, the $J_{Rh,P}$ values decrease with a decrease of ν(CO) frequencies.[19] Such a dependence has been observed previously for both [Rh(acac)(CO)P] and [RhBp(CO)P] complexes (Figure 2). However, the plot of the experimental data fits not one curve but two almost parallel ones.

^1H NMR Spectra

The ^1H NMR spectra of complexes **1**−**4** contain six signals due to the inequivalent protons of the pyrazolyl rings. All resonances are located in the δ = 5.7−7.6 ppm range, similar to what was observed for other bis(pyrazolylborato) rhodium complexes (Table 2). The two signals of the 4-H protons are shifted upfield with respect to the remaining signals and are observed at ca. δ = 6 ppm. In all spectra

Table 1. IR and ^{31}P NMR spectroscopic data of [Rh(acac)(CO)P],[5,39] [RhBp(CO)P] and [Rh(N,O)(CO)P][18]

P	Rh(acac)(CO)P ν(CO) (cm^{-1})	Rh(acac)(CO)P δ (ppm) ($J_{Rh,P}$, Hz)	[RhBp(CO)P] ν(CO) (cm^{-1})	[RhBp(CO)P] δ (ppm) ($J_{Rh,P}$, Hz)	[Rh(N,O)(CO)P] (P *trans* to N) ν(CO) (cm^{-1})	[Rh(N,O)(CO)P] (P *trans* to N) δ (ppm) ($J_{Rh,P}$, Hz)	[Rh(N,O)(CO)P] (P *trans* to O) δ (ppm) ($J_{Rh,P}$, Hz)
$P(NC_4H_4)_3$	2008	102 (251.8)	2018	104 (224)	2001	104.3 (217.4)	107.5 (247.7)
PPh_3	1983	46 (177.4)	1987	44 (156)	1973	45.6 (150.7)	60.5 (175.3)
$P(C_6H_4\text{-}4\text{-}OMe)_3$	1964	41 (173)	1983	36 (154)			
PCy_3	1945	58 (170)	1966	51 (147)	1946	55.8 (143.7)	

 © 2004 Wiley-VCH Verlag GmbH & Co. KGaA, Weinheim

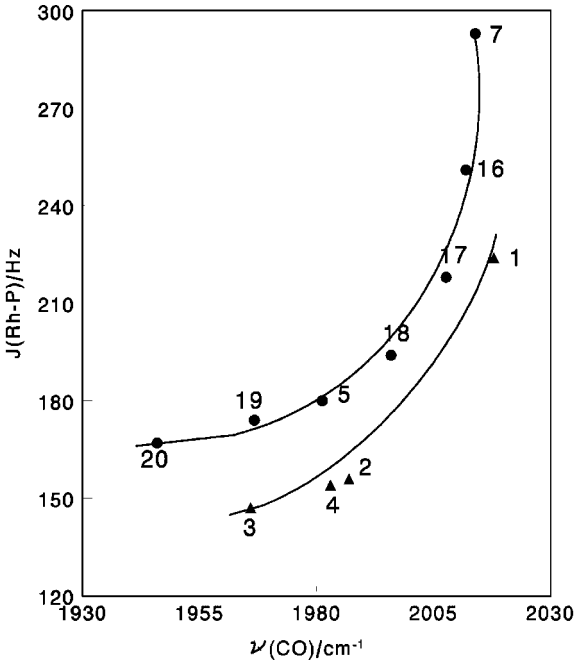

Figure 2. Plot of J(Rh-P) (^{31}P NMR) versus ν(CO) (IR) for RhBp(CO)(P) and Rh(acac)(CO)(P) complexes; RhBp(CO)(P): P = $P(NC_4H_4)_3$ **1**, PPh_3 **2**, PCy_3 **3**, $P(C_6H_4OMe\text{-}4)_3$ **4**; Rh(acac)(CO)(P): P = PPh_3 **5**, $P(OPh)_3$ **7**, $P(NC_4H_4)_3$ **16**, $PPh(NC_4H_4)_2$ **17**, $PPh_2(NC_4H_4)$ **18**, $P(C_6H_4OMe\text{-}4)_3$ **19**, PCy_3 **20**

Table 2. ^{1}H NMR spectroscopic data of bis(pyrazolylborato) ligands in complexes [RhBp(CO)P] (**1**−**4**) measured in $CDCl_3$

Complex	4-H	4′-H	3- or 5-H	3- or 5-H	3′- or 5′-H	3′- or 5′-H
1	5.95	6.27	6.78	7.57	7.63	7.67
2	5.69	6.19	6.29	7.41	7.42	7.56
3	6.06	6.13	7.36	7.46	7.49	7.52
4	5.70	6.18	6.32	6.91	6.94	7.42

(of complexes **1**−**4**) the signals arising from one pyrazolyl ring are better resolved than those in the second ring because of the higher values of the $J_{H,H}$ coupling constants (ca. 2.3 Hz).

The resonances of the 3-H and 5-H protons are observed at δ = 7.3−7.6 ppm, except in the spectra of **2** and **4**, in which one doublet (3-H or 5-H) is present at δ = 6.29 or 6.32 ppm, respectively. In Figure 3 the effect of temperature (in the temperature range from 20 to −60 °C) on the ^{1}H NMR spectra of **2** is presented.

The signals of the 4-H and 4′-H protons (δ = 5.69 and 6.19 ppm) do not change their positions when the temperature is lowered. In contrast, the resonance at δ = 6.29 ppm (3-H or 5-H) is shifted upfield and that at δ = 7.5 ppm (3′-H or 5′-H) is shifted downfield. The dynamics observed can be related only to small changes in the conformation of the pyrazolylborato ligand, because in bis(pyrazolylborato) complexes a change of coordination mode is not expected. The fluxional behaviour of tris(pyrazolylborato) complexes is well documented and is interpreted in terms of a $\kappa^2 \rightarrow \kappa^3$ equilibrium[9,20,21] (N,N-Tp$^-$ or N,N,N-Tp$^-$, respectively).

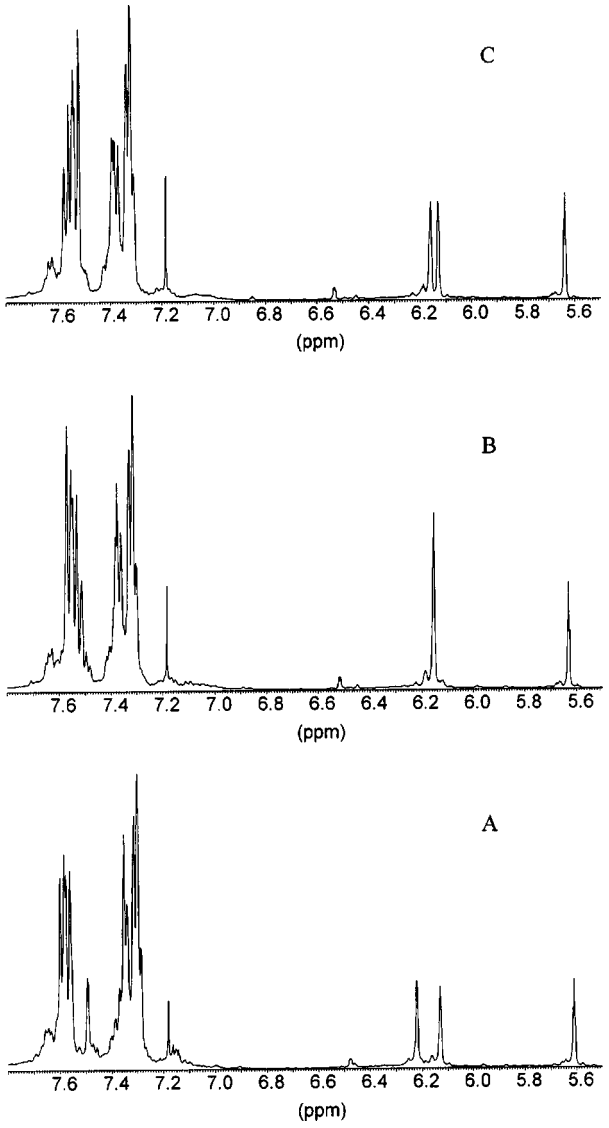

Figure 3. ^{1}H NMR spectra of complex **2** at 20 °C (A), −40 °C (B) and −60 °C (C)

Electrochemical Behaviour of the Rhodium(I) Complexes [RhBp(CO)P]

The cyclic voltammograms of the rhodium(I) complexes [RhBp(CO)P] were run in 0.2 M $[NBu_4][BF_4]/CH_2Cl_2$ (or NCMe), at a Pt- or C-disc electrode. They exhibit, at 200 mV s^{-1} (Table 3), an irreversible oxidation wave (I) at $^{I}E^{ox}_{p/2}$ in the range 0.63−0.95 V vs. NHE, which is followed, at a higher potential ($^{II}E^{ox}_{p/2}$ in the 1.0−1.6 V range), by a second irreversible wave (wave II), with a higher peak-current intensity (Figure 4, for complex **3**). In one case (compound **2**) the shape of the cyclic voltammogram changed rapidly with time, as shown by the alteration of the relative intensities of waves I and II, which is indicative of the instability of the complex in solution.

The oxidation potential of wave I is always substantially lower than that of the free bis(pyrazolylborate) (1.20 V for the KBp salt) and its electrode process is expected[11] to

 © 2004 Wiley-VCH Verlag GmbH & Co. KGaA, Weinheim

Table 3. Cyclic voltammetric data for the rhodium(I) complexes [RhBp(CO)P][a]

Complex	P	NCMe		CH_2Cl_2	
		$^{I}E_{p/2}^{ox}$	$^{II}E_{p/2}^{ox}$	$^{I}E_{p/2}^{ox}$	$^{II}E_{p/2}^{ox}$
1	$P(NC_4H_4)_3$	0.95	1.57	1.25	1.69
2	PPh_3	0.80	1.07[b]	0.74	1.27
3	PCy_3	0.63[c]	1.03	0.84[d]	1.20
4	$P(C_6H_4OMe\text{-}4)_3$	0.95[e]	1.44	0.93	1.67
	$[H_2Bp]H$[f]	1.14	–		
	$[H_2Bp]K$[g]	1.20	1.56		

[a] Potentials ($E_{p/2}$ = half-peak potential) in V ± 0.02 vs. NHE measured at a scan rate of 0.2 V s^{-1}, in 0.2 M $[NBu_4][BF_4]$/NCMe or CH_2Cl_2 at a Pt or C electrode. [b] Upon anodic scan, an irreversible cathodic wave is detected at 0.09 V vs. NHE. Relative peak currents of waves I and II change rapidly with time. By CPE (with strong passivation) a total of 4 faraday/mol was obtained (initial step approx. 1.5e). [c] CPE at a potential slightly above that of wave I led to the consumption of only 0.23 faraday/mol, with the disappearance of both waves I and II and the appearance of another wave at E_p^{ox} = 1.57 V. [d] For scan rates higher than 0.6 V/s the wave shows some reversibility. [e] For scan rates higher than 10 V/s the wave shows some reversibility. At 350 V/s it is the only wave detected. [f] Cathodic wave at E_p^{red} = −0.48 V due to H^+ reduction. [g] Cathodic wave at E_p^{red} = −1.53 V which, upon scan reversal, leads to an oxidation wave at 0.26 V.

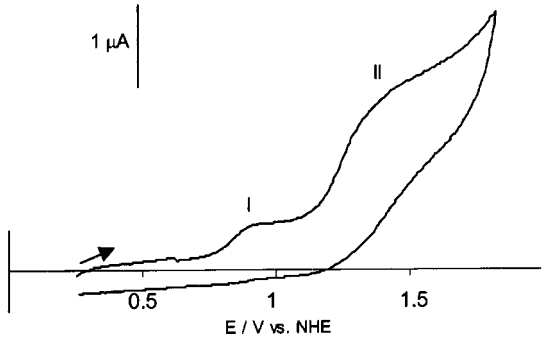

Figure 4. Cyclic voltammogram of complex **3** (2.4 mmol dm^{-3} in CH_2Cl_2 with 0.2 mol dm^{-3} $[NBu_4][BF_4]$) at a carbon disc (d = 0.5 mm) working electrode and at a scan rate of 0.2 V s^{-1}

involve, as the first step, the metal-centered, single-electron $Rh^I \rightarrow Rh^{II}$ oxidation. However, the overall number of electrons involved in each oxidation wave could not be measured due to the strong electrode passivation associated with the electrode processes.

Such an oxidation potential is also much lower (by ca. 0.5−0.7 V) than that exhibited[11] by the corresponding acetylacetonato complexes [Rh(acac)(CO)P], indicating a much stronger electron-donor character of the bis(pyrazolyl)borate ligand than that of acetylacetonate. In fact, the first oxidation potential should reflect the relative electron donor/acceptor abilities of the ligands as measured by the electrochemical E_L ligand parameter proposed by Lever, for which the empirical linear correlation [Equation (1)] has been shown to be applicable to many redox couples.[22,23] The redox potential of the complex (E) is expressed in V vs. NHE, ΣE_L is the sum of the E_L values (V vs. NHE) for all the ligands (additive effects), whereas S_M and I_M (V vs. NHE) depend upon the metal and redox couple, the spin state and the stereochemistry.

$$E = S_M \times (\Sigma E_L) + I_M \quad (1)$$

The E_L value for the bis(pyrazolylborate) ligand (for each of its 2e-donor *N*-coordinating arms) was assumed to be identical to those of the pyrazolate ligand (−0.24 V[22,23]) and of the related hydrotris(pyrazolyl)borate ligand (Tp′; −0.23 V for each of its 2e-donor *N*-coordinating arms) estimated in this study by taking into consideration the oxidation potential data reported[25] for the tetracoordinate Rh^I compounds [Rh(κ²-Tp′)(CO)(P)] [Tp′ = HBR_3 (R = 3,5-dimethylpyrazolyl); P = PPh_3, PCy_3, $P(NMe)_3$, $P(C_6H_4Me\text{-}4)_3$ or $P(C_6H_4Me\text{-}3)_3$] as well as Lever's previously established[11] linear relationship expressed by Equation (1), in which S_M = 1.93 and I_M = −1.29 V.[24] The E_L value thus estimated for Tp′ (−0.23 V for each N-ligating arm) is identical to that of pyrazolate (E_L = −0.24),[22,23] indicating that the pyrazolylborate group has a negligible influence on the σ/π-donor/acceptor properties of the pyrazolate ligand.

This E_L value (−0.24 or −0.23 V for each *N*-coordinating arm) is much lower than that reported for the acetylacetonate ligand (−0.08 V for each *O*-coordinating arm),[22] showing that pyrazolate, and bis- and tris(pyrazolylborate) ligands are much stronger electron-donor ligands than $acac^-$, in agreement with the above-mentioned conclusion based on the much lower oxidation potentials of the Bp^- complexes in this study in comparison with the analogous $acac^-$ complexes.

The order of the measured first oxidation potential values of the complexes (**3** < **2** < **1**, **4**) follows the expected reverse order of the electron-donor ability of the phosphane, i.e. $PCy_3 > PPh_3 > P(C_6H_4OMe\text{-}4)_3$, $P(NC_4H_4)_3$. Since complexes **1** and **4** have an identical oxidation potential, the tris(4-methoxyphenyl)phosphane ligand is pro-

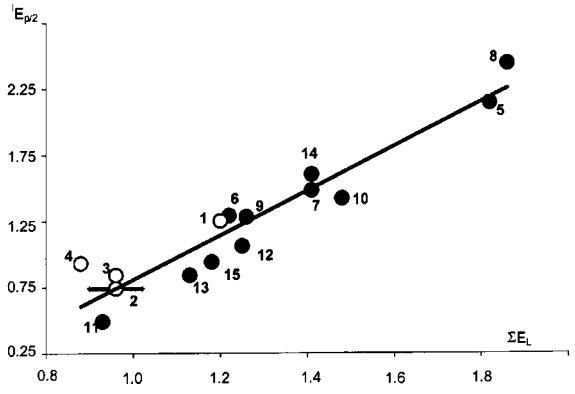

Figure 5. Plot of $^{I}Ep/2^{ox}$ (V versus NHE, measured in CH_2Cl_2) versus ΣE_L (V versus NHE) for [RhBp(CO)(P)] [P = $P(NC_4H_4)_3$ **1**, PPh_3 **2**, PCy_3 **3**, $P(C_6H_4OMe\text{-}4)_3$ **4**] (o) and for other tetracoordinate Rh^I complexes published elsewhere (see text) (•);[11,24] the E_L(L) value of CO taken from the literature (0.99 V) and that of Bp considered (see text) as that of pyrazolate (−0.24 V);[22,23] for $P(C_6H_4OMe\text{-}4)_3$ (complex **4**) the E_L value for tritolylphosphane was considered (0.37 V);[22,23] for PPh_3 an error bar comprising the E_L value taken from the literature (0.39 V)[22,23] and the one estimated from previous data (0.51 V)[11] is presented

 © 2004 Wiley-VCH Verlag GmbH & Co. KGaA, Weinheim

posed to exhibit an E_L value identical to that (0.69 V) we have obtained previously[11] for the *N*-pyrrolylphosphane $P(NC_4H_4)_3$.

The rhodium complexes of this study with ligands with known E_L values [**1**, **2** and **3**; for **4** the E_L value of tri(tolyl)-phosphane was taken for $P(C_6H_4OMe\text{-}4)_3$] fit the roughly linear plot of ${}^{I}E^{ox}_{p/2}$ vs. ΣE_L (Figure 5), which also contains the data reported by us[11] for the Rh^I complexes [Rh(O∩O)(CO)L] [O∩O = acac, L = CO **5**, PPh_3 **6**, $P(OPh)_3$ **7**; O∩O = PhC(O)CHC(O)Me (bac), L = CO **8**, PPh_3 **9**; O∩O = PhC(O)CHC(O)CF_3 (bta), L = PPh_3 **10**], as well as those reported by Werner et al. for [RhCl(L)[P*i*Pr_3)$_2$] [L = CPh_2 **11**, C=CPh_2 **12**, C=C=CPh_2 **13**, CO **14** and C_2H_4 **15**].[24]

The novel relationship expressed by Equation (2) (r = 0.95), considering also the complexes in the present study (Figure 6), allows the adjustment of S_M and I_M for the square-planar Rh^I/Rh^{II} redox couples: S_M = 1.68 and I_M = −0.87 V. Values of S_M = 1.93 and I_M = −1.29 V vs. NHE have been proposed previously[24] on the basis of the then available data.

$$E^{ox}_{p/2} = 1.68 \times \Sigma E_L - 0.87 \quad (2)$$

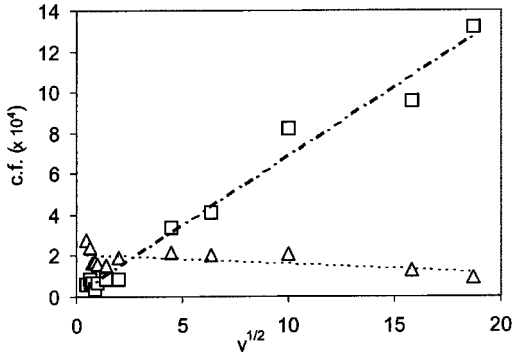

Figure 6. Plot of the current-function $i_p \cdot C^{-1} \cdot v^{-1/2}$ ($A \cdot M^{-1} \cdot V^{-1/2} s^{1/2}$) versus the square root of the scan rate ($V\ s^{-1}$), for waves I (□) and II (Δ) of complex **4** (Scheme 2)

In spite of the above-mentioned strong electrode passivation that normally precluded the controlled-potential electrolysis, in one of the cases (compound **3**) this could be achieved at the anodic wave I, leading to the total disappearance of both oxidation waves of the complex with the consumption of much less than 1 F/mol (ca. 0.2 F/mol). In addition, the reversibility of wave I in compound **4** and its current-function $i_p \cdot C^{-1} \cdot v^{-1/2}$ (i_p = peak current intensity, C = concentration, v = scan rate) increases with the scan rate, with concomitant disappearance of wave II (Figure 6). These observations suggest that wave II may result from the oxidation of a species generated in situ upon oxidation, at wave I, of the starting complex according to an Electron-Transfer-Chain-Catalysis (ETCC)-type process,[34,35] in which $E^0[(Rh')^{ox}/(Rh')^{red}] > E^0[Rh^{ox}/Rh]$, as shown in Scheme 2.

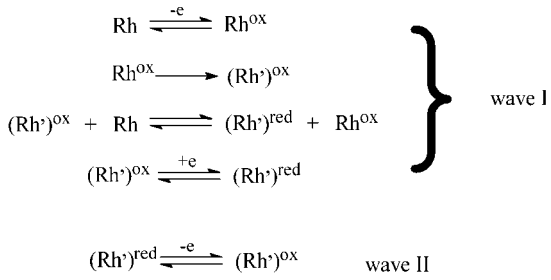

Scheme 2

X-ray Crystal Structures of 2, 3 and [Rh(acac)(CO)PCy_3] (20)

The molecular structures of the complexes [RhBp(CO)PPh_3] (**2**) and [RhBp(CO)PCy_3] (**3**) are shown in Figure 7 and 8, respectively, and selected bond lengths and angles are listed in Tables 4 and 5, respectively. The geometry about the rhodium atoms in both complexes is square planar, as expected for four-coordinate d^8 species, and the two nitrogen atoms of the bis(pyrazolylborato) anion, the carbonyl ligand and the P atom (from phosphane

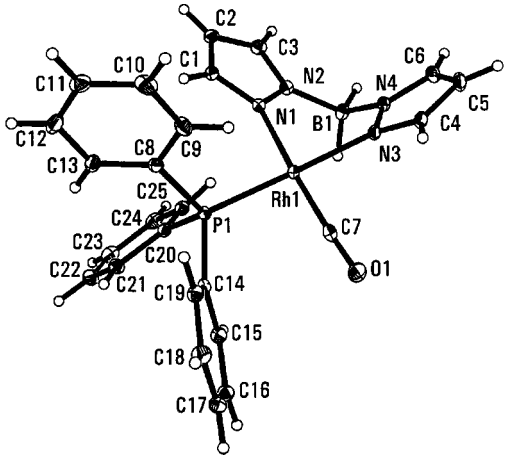

Figure 7. Molecular structure of RhBp(CO)PPh_3 (**2**)

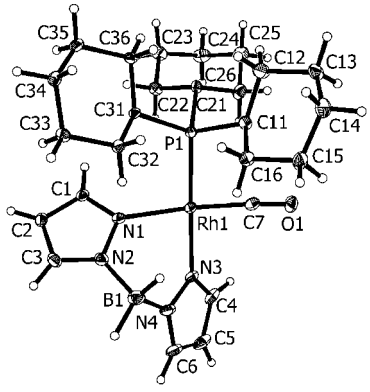

Figure 8. Molecular structure of RhBp(CO)PCy_3 (**3**)

 © 2004 Wiley-VCH Verlag GmbH & Co. KGaA, Weinheim

Table 4. Selected bond lengths (Å)

	[RhBp(CO)PPh$_3$] **2**	[RhBp(CO)PCy$_3$] **3**		[Rh(acac)(CO)PPh$_3$][28]	[Rh(acac)(CO)PCy$_3$] **20**		[Rh(N,O)(CO)PPh$_3$] (P *trans* to N)[a]	[Rh(N,O)(CO)PCy$_3$] (P *trans* to N)[b]
Rh−N1	2.0963(16)	2.087(3)	Rh−O1	2.029(5)	2.052(2)	Rh−O	2.040	2.045
Rh−N3	2.0891(15)	2.099(3)	Rh−O2	2.087(4)	2.096(2)	Rh−N	2.054	2.055
Rh−P	2.2614(5)	2.2808(12)	Rh−P	2.244(2)	2.2613(10)	Rh−P	2.279	2.286
Rh−C7	1.815(2)	1.807(5)	Rh−C6	1.801(8)	1.804(4)	Rh−C	1.803	1.788
C7−O	1.144(2)	1.151(5)	C6−O3	1.153(11)	1.160(4)	C−O	1.150	1.156

[a] Average values for complexes [Rh{CF$_3$C(O)CHN(H)Me}(CO)PPh$_3$] and [Rh{CF$_3$C(O)CHN(H)CMe$_3$}(CO)PPh$_3$].[18] [b] Average values for complexes [Rh{CF$_3$C(O)CHN(H)Me}(CO)PCy$_3$] and [Rh{CF$_3$C(O)CHN(H)CMe$_3$}(CO)PCy$_3$].[18]

Table 5. Selected bond angles (°)

Angle	[RhBp(CO)PPh$_3$] (**2**)	[RhBp(CO)PCy$_3$] (**3**)	Angle	[Rh(acac)(CO)PCy$_3$] (**20**)
N1−Rh−N3	87.26(6)	84.83(13)	O1−Rh−O2	87.50(9)
N1−Rh−P	93.05(4)	95.81(10)	O1−Rh−P	88.95(6)
N1−Rh−C7	176.09(7)	174.53(16)	O1−Rh−C6	177.54(12)
N3−Rh−P	176.93(4)	174.99(9)	O2−Rh−P	176.29(7)
N3−Rh−C7	89.54(7)	89.80(16)	O2−Rh−C6	94.60(12)
C7−Rh−P	90.27(6)	89.63(14)	C6−Rh−P	88.93(10)

ligand) are located approximately in the same plane. The Rh−N distances are equal [2.0963(16), 2.0891(15) Å in **2** and 2.087(3), 2.099(3) Å in **3**] within the experimental error (4σ). The Rh−N bonds lengths are similar to those in other complexes with Bp ligands {[RhBp$^{3,5\text{-Me}}{}_2$(C$_2$H$_4$)$_2$] 2.108(5), 2.106(6) Å[26] and [RhBp(PPh$_3$)$_2$] 2.130(2), 2.102(2) Å[26]} and in complexes with κ^2-Tp ligands {[RhTp^{Ph,Me}(CO)PPh$_3$] 2.099(2), 2.120(2) Å[25] and [RhTp^{Me,Me}(CO)PMe$_3$] 2.113(3), 2.101(3) Å[21]}. In β-ketoiminato complexes the Rh−N bonds are significantly shorter (Table 4).

The N1−Rh−N3 angles are slightly different [87.26(6) and 84.83(13)° in **2** and **3**, respectively], which can be explained by the bulkiness of PCy$_3$, represented by a cone angle (Θ) of 170° versus 145° for PPh$_3$.[19]

It is interesting to note that the *trans* effect of the phosphane is not observed, in contrast to [Rh(acac)(CO)PPh$_3$] and **20** (Figure 9) in which the two Rh−O bonds differ by ca. 0.06 Å[27] and 0.04 Å, respectively.

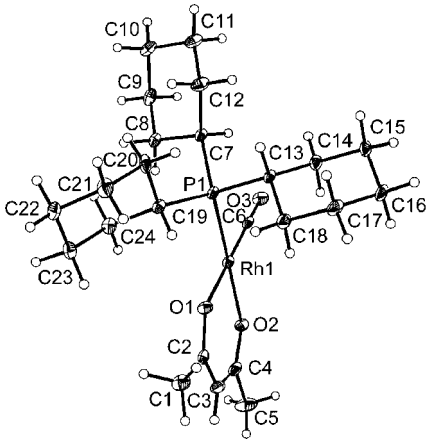

Figure 9. Molecular structure of Rh(acac)(CO)PCy$_3$ (**20**)

The Rh−P bond is longer in complex **3** [2.280(1) Å] than in complex **2** [2.2614(5) Å], as is common for rhodium complexes with PPh$_3$ and PCy$_3$ ligands. The Rh−PPh$_3$ bond in complex **2** [2.2614(5) Å] is longer than those in the related complexes [RhBp(PPh$_3$)$_2$] [2.2261(9) and 2.2503(10) Å][26] and [Rh(acac)(CO)PPh$_3$] [2.244(2) Å],[27] but shorter than that in [RhTp′(CO)PPh$_3$] [2.272(2) Å].[28] The Rh−PCy$_3$ bond in **3** [2.2613(10) Å] is relatively short when compared with the Rh−PCy$_3$ bonds in [RhBp(CO)PCy$_3$] [2.2808(12) Å], [RhTp′(CO)PCy$_3$] [2.292(1) Å],[28] [HRh(CO)(PCy$_3$)$_2$] [2.290(1), 2.297(1) Å][29] and in other acetylacetonatorhodium complexes: [Rh(acac){(*E*)-CH=CHCy}(PCy$_3$)$_2$]BF$_4$ [2.336(3), 2.357(3) Å][30] and [Rh(acac){CH=C=CPh$_2$}(PCy$_3$)$_2$]BF$_4$ [2.285(2) Å].[31] Such a short Rh−PCy$_3$ bond has, until now, only been reported for [Rh(acac)(PCy$_3$)$_2$] [2.252(1), 2.260(1) Å].[30]

A very interesting feature observed in complex **3** is that the angle formed by the rhodium, phosphorus and a carbon atom of one of the cyclohexyl rings [Rh−P−C7 117.53(10)°] differs distinctly from the two remaining angles [Rh−P−C13 110.72(11)° and Rh−P−C19 108.98(12)°]. The same effect has been observed in rhodium complexes with the β-ketoiminate ligand [Rh{CF$_3$C(O)CHC(NH)Me}(CO)PCy$_3$] and [Rh{CF$_3$C(O)CHC(NH)CMe$_3$}(CO)PCy$_3$],[18] and was explained as the result of an interaction between the cyclohexyl ring and the carbonyl ligand. In rhodium-triphenylphosphane complexes, the Rh−P−C(Ph) angles are less differentiated, and in [Rh(acac)(CO)PPh$_3$] they are equivalent.[27] One of the angles between a phosphorus atom and two carbons of one of the cyclohexyl rings in the Rh−PCy$_3$ complexes is also noticeably greater: in **3** the C7−P−C13 and C13−P−C19 angles are ca.104°, whereas the C7−P−C19 angle is ca. 111°. Similar values for the corresponding angles were found for [RhBp(CO)PCy$_3$] and for two complexes with β-

 © 2004 Wiley-VCH Verlag GmbH & Co. KGaA, Weinheim

ketoiminate ligands: [Rh{$CF_3C(O)CHC(NH)Me$}(CO)-PCy_3] and [Rh{$CF_3C(O)CHC(NH)CMe_3$}(CO)PCy_3].[18] In analogous complexes with PPh_3 all (Ph)C−P−C(Ph) angles are of similar magnitude.[18]

Catalytic Activity

Complexes **1**−**4** were tested as catalysts in 1-hexene hydroformylation under standardized reaction conditions (80 °C, 10 atm $H_2/CO = 1$) and at different catalyst concentrations and reaction times depending on the catalyst activity observed. The results presented in Table 6 demonstrate the generally high catalytic activity of all complexes, which produce ca. 80% of aldehydes and ca. 20% of 2-hexene when used without any additional free phosphane (the hydroformylation reaction yield increases in the presence of a phosphane co-catalyst[1]). To obtain the best results it is necessary to use a relatively high concentration of catalyst, expressed by a 1-hexene:Rh ratio of 280. However, with complex **3** a 1-hexene:Rh ratio of 800 gave the aldehyde in 78% yield. In reactions with catalysts **1**, **2** and **4** the yield of aldehydes increases with an increase of catalyst concentration. The increase of hydroformylation reaction yield with decrease of the 1-hexene:Rh ratio may be explained as an effect of the competition of the olefin and CO for access to rhodium: at higher concentrations of 1-hexene isomerization is dominant and the main reaction product is 2-hexene. It is interesting to note that the ratio of normal to branched aldehydes (*n*/*iso*) is only slightly dependent on the kind of phosphane coordinated to rhodium — it differs from 1.3 for **3** to 2.8 for **4**. The low *n*/*iso* ratio for **3** could be expected because of the rather strongly basic properties of PCy_3.[19] However, by comparison with results obtained for [Rh(acac)(CO){$P(NC_4H_4)_3$}],[5] one could expect a much higher *n*/*iso* ratio for **1**.

Table 6. Products of 1-hexene hydroformylation catalyzed by complexes **1**−**4**[a]

Catalyst	[1-hexene]/[Rh]	*t* (h)	Aldehydes (%)	2-Hexene (%)	*n*/*iso*
1	800	5	28	70	2.1
	400	3	73	27	2.0
	280	3	86	13	2.3
2	800	5	11	78	2.4
	400	3	37	19	2.6
	280	5	80	20	2.5
3	800	3	78	12	1.3
	280	2	87	11	1.3
4	800	5	44	32	2.8
	400	3	79	21	2.7

[a] Reaction conditions: 80 °C, 10 atm $CO/H_2 = 1$.

The second interesting feature of bis(pyrazolylborato)rhodium catalysts is the relatively high stability of the Rh−N bond under these reaction conditions. This is demonstrated by the presence of [$RhBp(CO)_2$] in all the post-reaction mixtures, as confirmed by the IR spectra, in which two strong ν(CO) bands are observed at 2019 and 2078 cm^{-1}, identical to [$RhBp(CO)_2$] prepared separately.[15] In contrast to [Rh(acac)$(CO)_2$], which reacts easily with CO/H_2 to produce [$Rh_4(CO)_{12}$] and [$Rh_6(CO)_{16}$], [$RhBp(CO)_2$] is not changed when heated at 80 °C under 10 atm CO/H_2 for 5 h. Both dicarbonyl complexes also exhibit different reactivity towards 1-hexene under hydroformylation reaction conditions: [Rh(acac)$(CO)_2$] produces ca. 90% of 2-hexene, and unchanged 1-hexene was found after the reaction with [$RhBp(CO)_2$].

We did not succeed in the isolation of catalytically active forms of rhodium complexes, however at this moment we cannot exclude that rhodium complexes with coordinated pyrazolylborate participate in the catalytic cycle.

Experimental Section

[Rh(acac)$(CO)_2$] was synthesized according to the method described previously.[32] [Rh(acac)(CO)PPh_3] and [Rh(acac)-(CO)PCy_3] (**20**) were obtained from the reaction of [Rh(acac)$(CO)_2$] with an equimolar amount of phosphane in hexane. Crystals of **20** suitable for X-ray analysis were obtained by recrystallization of the complex from toluene/hexane solution. 1-Hexene (Fluka) and toluene were distilled before use.

The electrochemical experiments were performed on an EG & G PAR 273 potentiostat/galvanostat connected to a PC computer through a GPIB interface (National Instruments PC-2A) or on an EG & G PAR 173 potentiostat/galvanostat and an EG & G PARC 175 Universal programmer. Cyclic voltammetry was performed in a two-compartment, three-electrode cell, at a platinum- or carbon-disc working electrode ($d = 0.5$ mm), probed by a Luggin capillary connected to a silver-wire pseudo-reference electrode; a platinum auxiliary electrode was employed. Controlled potential electrolysis was carried out in a two-compartment, three-electrode cell with platinum gauze working and counter electrodes in compartments separated by a glass frit; a Luggin capillary, probing the working electrode, was connected to a silver-wire pseudo-reference electrode. The experiments were performed under an inert atmosphere (N_2) at room temperature, the potentials were measured in 0.2 M $[NBu_4][BF_4]/CH_2Cl_2$ (or NCMe) in the presence of ferrocene as the internal standard, and the redox potential values are quoted relative to the normal hydrogen electrode (NHE) by using the $[Fe(\eta^5\text{-}C_5H_5)_2]^{0/+}$ couple with $E^{ox}_{1/2} = 0.77$ or 0.66 V vs. NHE in 0.2 M $[NBu_4][BF_4]/CH_2Cl_2$ or NCMe, respectively (values obtained relative to NHE by adding +0.24 V[33] to those we measured relative to the SCE). The controlled-potential electrolysis experiments were monitored regularly by cyclic voltammetry, thus assuring that no significant potential drift occurred along the electrolyses. Due to the strong working electrode passivation, the electrolyses had to be interrupted frequently for cleaning of this electrode.

FT-IR spectra were recorded on a Nicolet Impact 400 spectrometer and ^1H NMR spectra on a Bruker 300 MHz, or a Bruker 500 MHz spectrometer. Chemical shifts are referenced to TMS. GC-MS was performed on a Hewlett−Packard 8452A spectrometer.

Synthesis of [RhBp(CO)$P(NC_4H_4)_3$] (1): A mixture of [Rh(acac)$(CO)_2$] (0.11 g, 4.2×10^{-4} mol) and KBp (0.17 g, $9.1 \cdot 10^{-3}$ mol) in benzene (6 mL) was stirred for ca. 1 h. The precipitate of Kacac was separated by filtration, $P(NC_4H_4)_3$ (0.121 g, 5.3×10^{-4}) was added to the filtrate and the solution was stirred for 1 h. The solvent was removed under vacuum and the pale yellow

 © 2004 Wiley-VCH Verlag GmbH & Co. KGaA, Weinheim

product was obtained with 89% yield. $C_{19}H_{20}N_7BOPRh$ (507.10): calcd. C 47.94, H 4.20, N 20.16.; found C 47.64, H 4.47, N 19.74. IR (KBr): ν_{CO} 1987 vs; ν_{BH} 2411 m, 2362 m, 2326 w, 2272 w cm^{-1}.

Synthesis of [RhBp(CO)PPh$_3$] (2): KBp (0.06 g, 3.26×10^{-4} mol) was added to a solution of [Rh(acac)(CO)PPh$_3$] (0.107 g, 2.18×10^{-4} mol) in CH_3CN (3 mL). After stirring the mixture for ca. 15 min, the white precipitate of Kacac was removed by filtration. The clear filtrate was evaporated in vacuo giving the orange product in 76% yield. Crystals of **2** were obtained by slow evaporation of the solvents from a toluene/hexane solution. $C_{25}H_{23}N_4BOPRh$ (540.16): calcd. C 55.56, H 4.26, N 10.47; found C 55.71, H 4.30, N 11.00. IR (KBr): ν_{CO} 1987 vs; ν_{BH} 2411 m, 2362 m, 2326 w, 2272 w cm^{-1}. UV/Vis (CH_2Cl_2): λ (ε) = 266 (8500 $M^{-1}\cdot cm^{-1}$), 306 (4100), 360 (2000) nm; (toluene): 308 (4800 $M^{-1}\cdot cm^{-1}$), 360 (2400), 412 (1300) nm.

Synthesis of [RhBp(CO)PCy$_3$] (3): KBp (0.05 g, 2.98×10^{-4} mol) was added to a solution of [Rh(acac)(CO)PCy$_3$] (0.148 g, 2.98×10^{-4} mol) in CH_2Cl_2 (3 mL). After stirring the mixture for ca. 15 min, the white precipitate of Kacac was removed by filtration. The clear filtrate was evaporated in vacuo giving the yellow product in 68% yield. Crystals of **3** were obtained by slow evaporation of the solvents from a benzene/hexane solution. $C_{25}H_{41}N_4BOPRh$ (558.32): calcd. C 53.76, H 7.35, N 10.04; found C 54.09, H 7.53, N 9.69. IR (KBr): ν_{CO} 1966 vs; ν_{BH} 2411 m, 2368 m, 2328 w, 2268 w cm^{-1}. UV/Vis (CH_2Cl_2): λ = 270, 316, 362 nm.

Synthesis of [RhBp(CO){P(C$_6$H$_4$OMe-4)$_3$}] (4): A mixture of [Rh(acac)(CO)$_2$] (0.11 g, 4.2×10^{-4} mol) and KBp (0.17 g, 9.1×10^{-3} mol) in benzene (6 mL) was stirred for ca. 1 h. The precipitate of Kacac was separated by filtration, P(C$_6$H$_4$OMe-4)$_3$ (0.26 g, 7.4×10^{-4} mol) was added to the filtrate and the solution was stirred for 1 h. The solvent was removed under vacuum and the pale yellow product was obtained in 75% yield. $C_{28}H_{29}N_4BO_4PRh$ (630.25): calcd. C 53.38, H 4.60, N 8.89; found C 53.25, H 5.07, N 8.42. IR (KBr): ν_{CO} 1983 vs; ν_{BH} 2421 m, 2418 m cm^{-1}.

Hydroformylation of 1-Hexene: Hydroformylation was carried out at 80 °C in a steel autoclave (50 mL) containing a mixture of 1-hexene and toluene (1.5 mL each). The appropriate amount of catalyst was weighed in a small Teflon vessel and introduced into the autoclave under a nitrogen atmosphere. After introduction of the reagents, the autoclave was closed and filled with an equimolar H_2/CO mixture. The mixture was stirred magnetically and after 2−5 h the autoclave was cooled down. The organic products were separated by vacuum transfer and analysed by GC-MS.

X-ray Studies: Crystal data are given in Table 7, together with refinement details. X-ray data were collected at low temperature using an Oxford Cryosystem device on a Kuma KM4CCD κ-axis diffractometer with graphite-monochromated Mo-K_α radiation (λ = 0.71073 Å). Crystals were positioned at 65 mm from the CCD camera. 612 Frames were measured at 0.75° intervals with a counting time of 20 sec. Accurate cell parameters were determined and refined by a least-squares fit of 1900−2700 of the strongest reflections. The data were corrected for Lorentz and polarization effects. No absorption correction was applied. Data reduction and analysis were carried out with the Oxford Diffraction (Poland) Sp. z o.o (formerly Kuma Diffraction Wrocław, Poland) programs. Structures were solved by direct methods (program SHELXS-97[36]) and refined by the full-matrix least-squares method on all F^2 data using the SHELXL-97[37] programs. Non-hydrogen atoms were refined with anisotropic displacement parameters; hydrogen atoms were included from geometry of molecules and Δρ maps. During refinement they were fixed.

CCDC-215750 (for **20**), -215751 (for **2**) and -215752 (for **3**) contain the supplementary crystallographic data for this paper. These data can be obtained free of charge at www.ccdc.cam.ac.uk/conts/retrieving.html [or from the Cambridge Crystallographic Data Centre, 12 Union Road, Cambridge CB2 1EZ, UK; Fax: (internat.) +44-1223/336-033; E-mail: deposit@ccdc.cam.ac.uk].

Table 7. Crystal data and structure refinement for Rh(acac)(CO)PCy$_3$ (**20**), RhBp(CO)PPh$_3$ (**2**) and RhBp(CO)PCy$_3$ (**3**)

	2	**3**	**20**
Empirical formula	$C_{25}H_{23}BN_4OPRh$	$C_{25}H_{41}BN_4OPRh$	$C_{24}H_{40}O_3PRh$
Molecular mass	540.16	558.32	510.44
T (K)	120(2)	100(2)	100(2)
λ (Å)	0.71073	0.71073	0.71073
Crystal system	monoclinic	monoclinic	monoclinic
Space group	$C2/c$	$C2/c$	$P2_1/n$
a (Å)	20.1610(10)	31.121(6)	10.404(2)
b (Å)	15.2640(10)	8.939(2)	13.091(3)
c (Å)	17.0650(10)	23.893(5)	17.981(4)
β (°)	115.740(10)	127.67(3)	90.00(3)
V (Å^3)	4730.4(5)	5261.2(19)	2449.0(9)
Z	8	8	4
D_c (Mg·m^{-3})	1.517	1.402	1.384
μ (mm^{-1})	0.815	0.734	0.784
F(000)	2192	2312	1072
Crystal size (mm)	0.15 × 0.12 × 0.12	0.15 × 0.15 × 0.07	0.30 × 0.30 × 0.30
θ range for data collection (°)	3.52−28.78	3.43−24.99	3.31−28.71
Ranges of h,k,l	−26→27, −20→20, −15→22	−36→36, −10→8, −28→28	−13→13, −16→17, −21→23
Reflections collected	16508	14851	16678
Independent reflections (R_{int})	5632 (0.0195)	4609 (0.0463)	5763 (0.0651)
Data/parameters	5632/390	4609/298	5763/399
GOF(F^2)	1.138	1.136	1.045
Final R_1/wR_2 indices [$I > 2\sigma(I)$]	0.0276/0.0590	0.0483/0.0864	0.0515/0.0662
Largest diff. peak/hole (e·Å^{-3})	0.605/−0.617	0.934/−0.357	0.810/−0.672

 © 2004 Wiley-VCH Verlag GmbH & Co. KGaA, Weinheim

Acknowledgments

This work was supported by the State Committee for Scientific Research KBN (Poland) with the Grant PBZ KBN 15/T09/99/01D. The authors are indebted to Dr. E. Mieczyńska and I. Pryjomska for performing the catalytic tests.

[1] *Applied Homogeneous Catalysis with Organometallic Compounds. A Comprehensive Handbook in Two Volumes* (Eds.: B. Cornils, W. A. Herrmann), VCH, Weinheim, New York, **1996**.
[2] M. P. Magee, W. Luo, W. H. Hersh, *Organometallics* **2002**, *21*, 362.
[3] A. M. Trzeciak, J. J. Ziółkowski, *Coord. Chem. Rev.* **1999**, *190−192*, 883.
[4] A. J. Sandee, J. N. H. Reek, P. C. J. Kamer, P. W. N. M. van Leeuwen, *J. Am. Chem. Soc.* **2001**, *123*, 8468.
[5] A. M. Trzeciak, T. Głowiak, R. Grzybek, J. J. Ziółkowski, *J. Chem. Soc., Dalton Trans.* **1997**, 1831.
[6] A. M. Trzeciak, J. J. Ziółkowski, *Trans. Met. Chem.* **1987**, *12*, 405.
[7] Patent n° P 2058814, **1969**.
[8] D. M. Tellers, S. J. Skoog, R. G. Bergman, T. B. Gunnoe, W. D. Harman, *Organometallics* **2000**, *19*, 2428.
[9] S. Trofimenko, *J. Am. Chem. Soc.* **1967**, *21*, 3120.
[10] S. Serron, J. Huang, S. P. Nolan, *Organometallics* **1998**, *17*, 534.
[11] M. F. C. Guedes da Silva, A. M. Trzeciak, J. J. Ziółkowski, A. J. L. Pombeiro, *J. Organomet. Chem.* **2001**, *620*, 174.
[12] D. E. Graham, G. J. Lamprecht, I. M. Potgieter, A. Roodt, J. G. Leipold, *Trans. Met. Chem.* **1991**, *16*, 193.
[13] A. M. Trzeciak, J. J. Ziółkowski, *Inorg. Chim. Acta* **1995**, *96*, 15.
[14] G. J. J. Steyn, A. Roodt, I. Poletaeva, Yu. S. Varshavsky, *J. Organomet. Chem.* **1997**, *536*, 197.
[15] R. B. King, A. Bond, *J. Organomet. Chem.* **1974**, *73*, 115.
[16] F. Bonati, G. Minghetti, G. Banditelli, *J. Organomet. Chem.* **1975**, *87*, 365.
[17] M. Moszner, S. Wołowiec, A. Trösch, H. Vahrenkamp, *J. Organomet. Chem.* **2000**, *595*, 178.
[18] Yu. S. Varshavsky, M. R. Galding, T. G. Cherkasova, I. S. Podkorytov, A. B. Nikolskii, A. M. Trzeciak, Z. Olejnik, T. Lis, J. J. Ziółkowski, *J. Organomet. Chem.* **2001**, *628*, 195.
[19] C. A. Tolman, *Chem. Rev.* **1977**, *77*, 313.
[20] N. G. Connelly, D. J. H. Emslie, B. Metz, A. G. Orpen, M. J. Quayle, *Chem. Commun.* **1996**, 2289.
[21] K. Chauby, C. Serra Le Berre, Ph. Kalck, J.-C. Daran, G. Commenges, *Inorg. Chem.* **1996**, *35*, 6354.
[22] A. B. P. Lever, *Inorg. Chem.* **1990**, *29*, 1271.
[23] A. B. P. Lever, *Inorg. Chem.* **1991**, *30*, 1980.
[24] I. Kovacik, O. Gevert, H. Werner, M. Schmittel, R. Sollner, *Inorg. Chim. Acta* **1998**, *275−276*, 435.
[25] N. G. Connelly, D. J. H. Emslie, W. E. Geiger, O. D. Hayward, E. B. Linehan, A. G. Orpen, M. J. Quayle, P. H. Rieger, *J. Chem. Soc., Dalton Trans.* **2001**, 670.
[26] M. J. Baena, M. L. Reyes, L. Rey, E. Carmona, M. C. Nicasio, P. J. Perez, E. Gutierrez, A. Monge, *Inorg. Chim. Acta* **1998**, *273*, 244.
[27] J. G. Leipoldt, S. S. Basson, L. D. C. Bok, T. I. A. Gerber, *Inorg. Chim. Acta* **1978**, *26*, L35.
[28] N. G. Connelly, D. J. H. Emslie, W. E. Geiger, O. D. Hayward, E. B. Linehan, A. G. Orpen, M. J. Quayle, P. H. Rieger, *J. Chem. Soc., Dalton Trans.* **2001**, 670.
[29] M. A. Freeman, D. A. Young, *Inorg. Chem.* **1986**, *25*, 1556.
[30] J. G. Leipoldt, G. J. Lamprecht, G. J. van Zyl, *Inorg. Chim. Acta* **1985**, *96*, L31.
[31] M. A. Esteruelas, F. J. Lahoz, M. Martin, E. Onate, L. A. Oro, *Organometallics* **1997**, *16*, 4572.
[32] Yu. S. Varshavsky, T. G. Tcherkasova, *Zh. Neorg. Khim.* **1967**, *12*, 1709.
[33] A. J. Bard, L. R. Faulkner, *Electrochemical Methods*, John Wiley & Sons, New York, **1980**.
[34] M. F. C. Guedes da Silva, C. M. P. Ferreira, J. J. R. Fraústo da Silva, A. J. L. Pombeiro, *J. Chem. Soc., Dalton Trans.* **1998**, 4139.
[35] D. Astruc, *Electron Transfer and Radical Processes in Transition Metal Chemistry*, VCH, Weinheim, 1995, chapter 6.
[36] D. Astruc, *Angew. Chem. Int. Ed. Engl.* **1988**, *27*, 643 and references cited therein.
[37] G. M. Sheldrick, *Acta Crystallogr., Sect. A* **1990**, *46*, 467−473.
[38] G. M. Sheldrick, SHELXL-97, *Program for Crystal Structure Refinement*, University of Göttingen, **1997**.
[39] W. Simanko, K. Mereiter, R. Schmid, K. Kirchner, A. M. Trzeciak, J. J. Ziółkowski, *J. Organomet. Chem.* **2000**, *602*, 59.

Received July 28, 2003
Early View Article
Published Online February 17, 2004

 © 2004 Wiley-VCH Verlag GmbH & Co. KGaA, Weinheim

Synthesis, Characterization and in Vitro Study of the Cytostatic and Antiviral Activity of New Polymeric Silver(I) Complexes with Ribbon Structures Derived from the Conjugated Heterocyclic Thioamide 2-Mercapto-3,4,5,6-tetrahydropyrimidine

Panagiotis C. Zachariadis,[a] Sotiris K. Hadjikakou,*[a] Nick Hadjiliadis,*[a] Stavroula Skoulika,[b] Adonis Michaelides,[b] Jan Balzarini,[c] and Erik De Clercq[c]

Keywords: Bioinorganic chemistry / Silver / X-ray diffraction / Cytostatic activity / Antiviral activity

Silver(I) bromide reacts with 2-mercapto-3,4,5,6-tetrahydropyrimidine (StpmH$_2$, $C_4H_8N_2S$) in DMSO with an excess of triethylamine to give a water-insoluble complex of formula $[Ag_6(\mu_2\text{-}Br)_6(\mu_2\text{-}StpmH_2)_4(\mu_3\text{-}StpmH_2)_2]_n$ (**1**), while the reaction of silver(I) nitrate with StpmH$_2$ under the same conditions gives a water-insoluble complex of formula $[\{Ag_4(\mu_2\text{-}StpmH_2)_6\}(NO_3)_4]_n$ (**2**). The products were characterized by elemental analyses, and FT-IR far-IR, UV/Vis, ^{1}H and ^{13}C NMR spectroscopy. Crystal structures of complexes **1** and **2** were determined by X-ray diffraction. Complex **1**, $C_{24}H_{48}Ag_6N_{12}S_6$, crystallizes in the triclinic system space group $P\bar{1}$, a = 8.041(1) Å, b = 12.838(4) Å, c = 13.281(2) Å, α = 68.40(1)°, β = 72.97(1)°, γ = 87.80(2), Z = 2, forming a one-dimensional infinite ribbon structure by strong interatomic interactions of two μ_2-Br bonds with Ag(1). Complex **2**, $C_{24}H_{48}Ag_4N_{16}O_{12}S_6$, crystallizes in the orthorhombic system, space group $Cmc2_1$, and a = 32.148(3) Å, b = 9.461(2) Å, c = 7.234(1) Å, $\alpha = \beta = \gamma$ = 90°, Z = 8, forming infinite Ag–S–Ag chains which are bridged to each other by a sulfur atom of μ_2-StpmH$_2$ ligands. Complexes **1** and **2** were studied for their cytostatic activity against murine leukemia (L1210) and human T-lymphocyte (Molt4/C8 and CEM) cells and for their antiviral activity against a wide variety of viruses. They are markedly cytostatic at 50% inhibitory concentration (IC_{50}) values ranging from 3 to 17 μg/mL. None of the compounds showed appreciable antiviral activity at subtoxic concentrations.

(© Wiley-VCH Verlag GmbH & Co. KGaA, 69451 Weinheim, Germany, 2004)

Introduction

Research towards the design of infinite molecular components with specific chains and networks is a matter of great current interest.[1] This self-assembly process between metal ions and ligands is known to depend on the steric and interactive information stored in the ligand and also by the metal ions through their coordination geometry demands.[1b,1c] From this point of view, the ability of silver(I) thiolate or thionate complexes to adopt geometries with variable nuclearities and structural diversity makes the study of silver(I) chemistry very attractive.[2,3] Silver(I) complexes with sulfur-containing ligands exhibit a wide range of applications in medicine, in analytical chemistry or in the polymer industry.[2,3] The biomedical applications and uses of silver(I) complexes are related to their antibacterial action,[4] which appears to involve interaction with DNA.[5] The molecular design and structural characterization of silver(I) complexes is therefore an intriguing aspect of bioinorganic chemistry and metal-based drugs.[6]

A great deal of work has also been devoted to the study of thioamides because of their tendency to bridge metal centers forming oligo- and polynuclear species with potential usage as functional solid materials.[7] Furthermore, 2-mercapto-3,4,5,6-tetrahydropyrimidine can coordinate up to three metal centers at short distances, offering the possibility of studying the metal-metal interaction of d^{10} systems which have attracted considerable attention.[8] Such metal-metal interactions have been observed for silver(I) complexes containing aromatic heterocyclic thioamides like 2-mercaptopyridine,[1a,7] 2-mercaptonicotinic acid,[6b,9] 3-(*tert*-butyldimethylsilyl)pyridine-2-thione and 3,6-bis(*tert*-butyldimethylsilyl)pyridine-2-thione,[10a] 2-(triorganosilyl)-thiophenols and 2,6-bis(triorganosilyl)thiophenols,[10b] and 2-(triorganosilyl)methanethione[10c] and -thiophenol.[11] It is noteworthy that in all cases of complexes with a short sil-

[a] Section of Inorganic and Analytical Chemistry, Department of Chemistry, University of Ioannina,
45110 Ioannina, Greece
Fax: (internat.) +30-26510-44831
E-mail: shadjika@cc.uoi.gr
nhadjil@cc.uoi.gr
[b] Section of Physical Chemistry, Department of Chemistry, University of Ioannina,
45110 Ioannina, Greece
[c] Katholieke Universiteit Leuven, Rega Institute for Medical Research,
Minderbroedersstraat 10, 3000 Leuven, Belgium

 © 2004 Wiley-VCH Verlag GmbH & Co. KGaA, Weinheim **DOI: 10.1002/ejic.200300672**

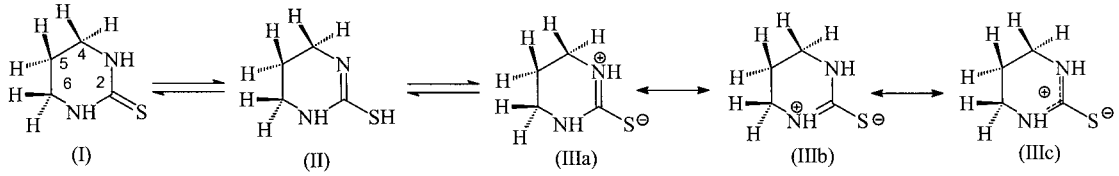

Figure 1. Tautomeric forms of 2-mercapto-3,4,5,6-tetrahydropyrimidine (thione I, thiol II and zwitterionic salt III)

ver(I)-silver(I) distance [shorter than twice the van der Waals radius for silver (3.44 Å)[6b]] there is no halogen atom in the coordination sphere of the metal center.

In this paper, we report the structural and spectroscopic characterization of two new silver complexes with the heterocyclic thioamide 2-mercapto-3,4,5,6-tetrahydropyrimidine (Figure 1) of formulae $[Ag_6(\mu_2\text{-}Br)_6(\mu_2\text{-}StpmH_2)_4(\mu_3\text{-}StpmH_2)_2]_n$ (**1**) and $[\{Ag_4(\mu_2\text{-}StpmH_2)_6\}(NO_3)_4]_n$ (**2**). The cytostatic activity of complexes **1** and **2** against murine leukemia (L1210) and human T-lymphocyte (Molt4/C8 and CEM) cells, and their antiviral properties, have also been studied.

Results and Discussion

General Aspects

The synthesis of complexes **1** and **2** was carried out in DMSO with an excess of triethylamine according to the reactions shown in Equation (1) and (2).

$$6n\ AgBr + 6n\ StpmtH_2 \xrightarrow[DMSO]{Et_3N} \{[Ag_6(\mu_2\text{-}Br)_6(\mu_2\text{-}StpmtH_2)_4(\mu_3\text{-}StpmtH_2)_2]_n\} \quad (1)$$

$$4n\ AgNO_3 + 6n\ StpmtH_2 \xrightarrow[DMSO]{Et_3N} \{[Ag_4(\mu_2\text{-}StpmtH_2)_6](NO_3)_4\}_n \quad (2)$$

No deprotonation of the thioamide ligand was observed, even though an excess of triethylamine was used. When 2-mercaptonicotinic acid was allowed to react with silver(I) chloride under the same reaction conditions, a hexanuclear, water-soluble aggregate of formula $[\{Ag_6(\mu_3\text{-}Hmna)_4(\mu_3\text{-}mna)_2\}^{2-}\cdot\{(Et_3NH)^+\}_2\cdot(DMSO)_2\cdot(H_2O)]$ was formed.[9] Complexes **1** and **2** have infinite ribbon structures (vide infra) which consist of Ag_3S_3 six-membered rings bridged by Br atoms in the case of **1** and two infinite Ag−S−Ag chains bridged by S atoms in the case of **2**. It is noteworthy that the geometry around the silver(I) ions in **1** is tetrahedral while for **2** the geometry around the silver(I) ions is trigonal.

The formulae of molecules **1** and **2** were first deduced from elemental analysis and spectroscopic data. Complexes **1** and **2** are soluble in DMSO and DMF. Crystals of the complexes are stable in air but were stored in darkness. The infinite-ribbon structures of complexes **1** and **2** seem to persist in DMSO solution, since the specific conductivity for complex **1** is $k = 16.15$ μs/cm at 22 °C and does not change up to 38 °C (see also ^{13}C NMR spectra). Complex **2**, on the other hand, has a specific conductivity of 162.45 μs/cm at 22 °C, increasing to 218.8 μs/cm at 38 °C due to the free NO_3^- counteranions.

With 3-(*tert*-butyldimethylsilyl)pyridine-2-thione, 3,6-bis-(*tert*-butyldimethylsilyl)pyridine-2-thione,[10a] 2-(triorganosilyl)thiophenols, 2,6-bis(triorganosilyl)thiophenols,[10b] or 2-(triorganosilyl)methanethione[10c] as ligands towards silver(I) ions, Zubieta et al.[10] have established that the extent of the association of silver(I) ions in their clusters depends intimately on the nature of thioamide. Thus, silver(I) with unbranched linear thiolate ligands are highly polymeric as silver(I) is unprotected from the approach of additional bridging thiolate groups, while bulky ligands such as substituted thiolates increase the aggregation degree of $[Ag(LS)]_n$ compounds.[10] In accordance with the above findings an aggregate of formula $[\{Ag_6(\mu_3\text{-}Hmna)_4(\mu_3\text{-}mna)_2\}^{2-}\cdot\{(Et_3NH)^+\}_2\cdot(DMSO)_2\cdot(H_2O)]$[9] was recently synthesized with the branched substituted 2-mercaptonicotinic acid. When the unbranched, non-aromatic 2-mercapto-3,4,5,6-tetrahydropyrimidine was used for the synthesis of complexes **1** and **2**, highly polymeric structures were obtained.

Infrared Spectroscopy

The infrared spectra of complexes **1** and **2** show distinct vibrational bands at 1559, 1214 cm^{-1} and 1564, 1221 cm^{-1}, respectively, which were assigned as the vibrations of the C−N bond (thioamide I and II bands) and at 1063, 619 cm^{-1} and at 1038, 627 cm^{-1}, respectively, which were attributed to the C−S bond vibrations (thioamide III and IV bands). The corresponding thioamide bands of the free 2-mercapto-3,4,5,6-tetrahydropyrimidine ligand are found at 1557, 1206, 1067 and 644 cm^{-1}, respectively. The new bands at 133 and 139 cm^{-1} in the far-IR spectra of complexes **1** and **2** were assigned to the vibrations of the Ag−S bond,[12] while bands also appear at 178, 137 cm^{-1} in the far-IR spectrum of **1** that can be attributed to the vibration of the Ag−Br bonds.

NMR Spectroscopy

The ^1H NMR spectrum of the free ligand $StpmH_2$ in $[D_6]$DMSO solution shows resonance signals at δ = 7.86 ppm for the amide proton and at δ = 3.20 and 1.75 ppm for the -CH_2- a and b protons. The signal of the amide protons is shifted to δ = 8.50 and 8.76 ppm, respectively, in the ^1H NMR spectra of complexes **1** and **2** in $[D_6]$DMSO solution, confirming the N/S-metal coordination.

The ^{13}C NMR peak assignments of complexes **1** and **2** were based on those of the free ligand, which shows signals

 © 2004 Wiley-VCH Verlag GmbH & Co. KGaA, Weinheim

at δ = 175.7 ppm for C(=S) (C^2, Figure 1), δ = 40.1 ppm for the two CH_2(-N) equivalent carbon atoms (C^4 and C^6, Figure 1) and at δ = 19.5 ppm for CH_2(-CH_2) (C^5, Figure 1). Complex **1** shows signals at δ = 169.9 ppm for C^2(=S), at δ = 40.7 and 40.3 ppm for C^4(-N) and C^6(-N), respectively, and at δ = 19.5 ppm for C^5. The corresponding signals for complex **2** are at δ = 169.4 ppm for C^2(=S), at δ = 41.4 and 41.0 ppm for C^4(-N) and C^6(-N), respectively, and at δ = 19.1 ppm for C^5. The presence of two signals for C^4 and C^6 of the ligand in both complexes, in contrast to the one in the case of the free ligand, indicates two different coordination modes in the complexes, in accordance with the structures determined by X-ray crystallography (see also conductivity measurements), and suggests that the infinite ribbon structures are persistent in DMSO solutions.

Crystal and Molecular Structures of Complexes $[Ag_6(\mu_2\text{-}Br)_6(\mu_2\text{-}StpmH_2)_4(\mu_3\text{-}StpmH_2)_2]_n$ (1) and $[\{Ag_4(\mu_2\text{-}StpmH_2)_6\}(NO_3)_4]_n$ (2)

Schakal diagrams of complexes **1** and **2** are shown in Figure 2 and 3, respectively, while selected bond lengths and angles are given in Table 1 and 2.

In complex **1**, three sulfur atoms bridge three silver(I) ions, forming a six-membered ring. Strong μ-S and μ-Br intramolecular interactions bridge two six-membered rings (R^1, R^2) through two silver(I) ions while this unit is also bridged by a third six-membered ring (R^3) through the remaining silver(I) ion, two strong μ-Br interactions and so on. Thus, a one-dimensional infinite ribbon structure is formed with strong interatomic interactions (Figure 4).

The Ag−S bond lengths are Ag(1)−S(2) = 2.504(2), Ag(1)−S(1) = 2.522(2), Ag(2)−S(2) = 2.562(2), Ag(2)−S(3) = 2.666(2), Ag(3)−S(1)^b = 2.4832(2), Ag(3)−S(3)^b = 2.554(2) and Ag(3)−S(3) = 2.949(2) Å (^{b}: $-x + 1, -y + 1, -z$). These values are similar to those measured in complexes with infinite ribbon structures, such as $[Ag_6(\mu_3\text{-}pyS)_4(\mu_4\text{-}pyS)_2]_n$ [1a] [pySH = 2-mercaptopyridine, Ag−S = 2.456(5)−2.959(5) Å], $[Ag_5(pyS)_4(pySH)BF_4]_n$ [7] (pySH = 2-mercaptopyridine, Ag−S = 2.45−2.90 Å),

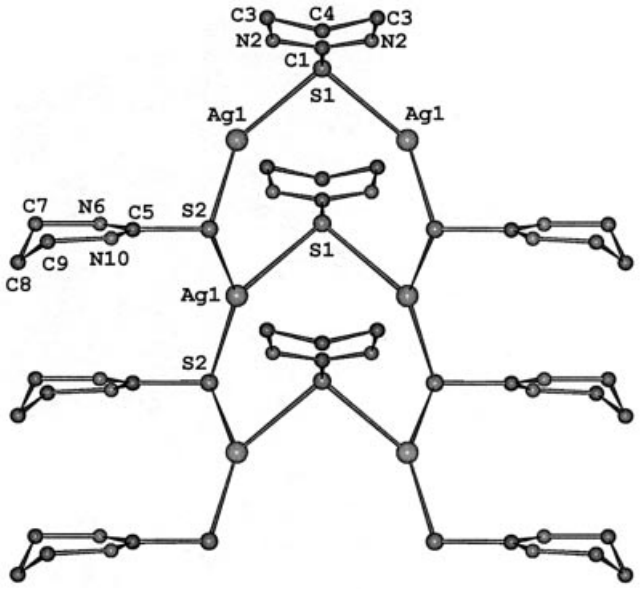

Figure 3. Schakal diagram of the crystal structure of complex **2**; the NO_3^- counterions are omitted for clarity

$[\{Ag_6(SPh)_8\}(Me_4N)_2]$[11] [Ag−S = 2.431(3)−2.878(2) Å], and in $[Ag(\mu_2\text{-}pyS)]_n$ [1a] [pySH = 2-mercaptopyridine, Ag−S = 2.587(4) and Ag−S(a) = 2.502 Å].

The Ag···Ag distances in **1** are Ag(2)−Ag(3) = 3.063(1) and Ag(3)−Ag(3)^b = 2.963(2) and are shorter than twice the van der Waals radius for silver (3.44 Å),[6b] indicating a strong Ag···Ag interaction. Other compounds with strong Ag···Ag interactions include $[Ag_6(\mu_3\text{-}pyS)_4(\mu_4\text{-}pyS)_2]_n$,[1] (pySH = 2-mercaptopyridine) with Ag···Ag = 2.959(2) Å, the neutral cluster $[Ag_6(\mu_3\text{-}Hmna)_6\cdot 8DMSO]$ (H_2mna = 2-mercaptonicotinic acid),[6b] with Ag···Ag = 2.911(1) Å, $[Ag_5(pyS)_4(pySH)BF_4]_n$ (pySH = 2-mercaptopyridine),[7] with Ag···Ag = 2.995 Å, $[\{Ag_6(\mu_3\text{-}Hmna)_4(\mu_3\text{-}mna)_2\}^{2-}\cdot\{(Et_3NH)^+\}_2\cdot(DMSO)_2\cdot(H_2O)]$,[9] with Ag···Ag = 2.916 Å, and $[\{Ag_6(SPh)_8\}\cdot(Me_4N)_2\}]$,[11] with Ag···Ag = 2.959(1) Å. It is noteworthy that in all these complexes with

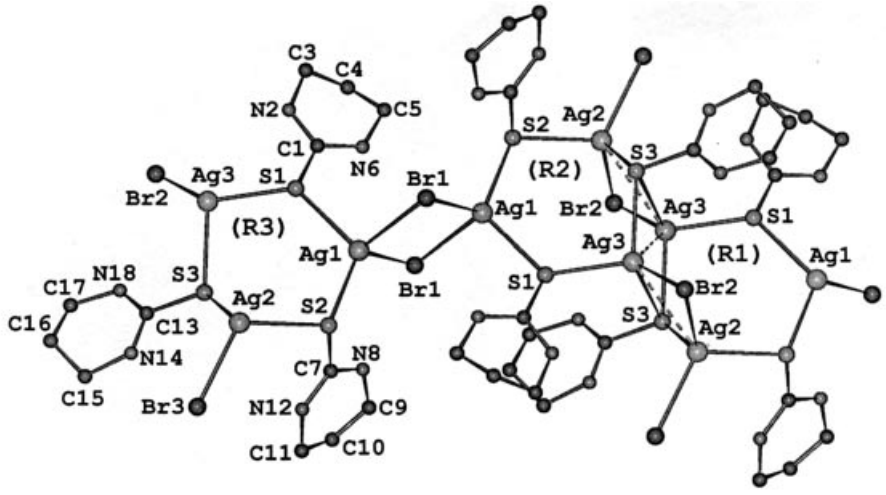

Figure 2. Schakal diagram of the crystal structure of complex **1**; the dashed lines represent short Ag···Ag contacts

 © 2004 Wiley-VCH Verlag GmbH & Co. KGaA, Weinheim

Table 1. Selected bond lengths (Å) and angles (°) for compound **1**, with esd's in parentheses

Ag(1)−S(2)	2.504(2)	Ag(1)−S(1)	2.522(2)
Ag(1)−Br(1)	2.724(1)	Ag(1)−Br(1)[a]	2.742(1)
Ag(2)−S(2)	2.562(2)	Ag(2)−Br(3)	2.637(1)
Ag(2)−S(3)	2.666(2)	Ag(2)−Br(2)	2.668(1)
Ag(2)−Ag(3)	3.063(1)	Ag(3)−S(1)[b]	2.482(2)
Ag(3)−S(3)b	2.554(2)	Ag(3)−Br(2)	2.600(1)
Ag(3)−S(3)	2.949(2)	Ag(3)−Ag(3)[b]	2.963(2)
S(1)−C(1)	1.707(8)	S(2)−C(7)	1.734(8)
S(3)−C(13)	1.732(7)	C(1)−N(6)	1.312(10)
C(1)−N(2)	1.320(10)	N(2)−C(3)[b]	1.456(11)
C(5)−N(6)	1.452(13)	C(7)−N(8)	1.305(11)
C(7)−N(12)	1.329(10)	N(8)−C(9)	1.479(14)
C(11)−N(12)	1.470(11)	C(13)−N(14)	1.313(9)
C(13)−N(18)	1.322(10)	N(14)−C(15)[c]	1.452(11)
C(17)−N(18)[d]	1.479(10)		
S(2)−Ag(1)−S(1)	115.84(7)	S(2)−Ag(1)−Br(1)	115.11(6)
S(1)−Ag(1)−Br(1)	107.97(6)	S(2)−Ag(1)−Br(1)[a]	116.70(6)
S(1)−Ag(1)−Br(1)[a]	103.49(6)	Br(1)−Ag(1)−Br(1)[a]	95.31(3)
Ag(1)−Br(1)−Ag(1)[a]	84.69(3)	S(2)−Ag(2)−Br(3)	116.04(6)
S(2)−Ag(2)−S(3)	97.16(7)	Br(3)−Ag(2)−S(3)	105.17(5)
Br(2)−Ag(2)−Ag(3)	53.42(3)	S(1)[b]−Ag(3)−S(3)[b]	99.07(7)
S(1)[b]−Ag(3)−Br(2)	127.07(6)	S(3)[b]−Ag(3)−Br(2)	112.74(6)
S(1)[b]−Ag(3)−S(3)	94.74(7)	S(3)[b]−Ag(3)−S(3)	115.35(5)
Br(2)−Ag(3)−S(3)	107.16(5)	S(1)[b]−Ag(3)−Ag(3)[b]	102.60(6)
S(3)[b]−Ag(3)−Ag(3)[b]	64.14(5)	Br(2)−Ag(3)−Ag(3)[b]	128.85(5)
S(3)−Ag(3)−Ag(3)[b]	51.21(5)	S(1)[b]−Ag(3)−Ag(2)	116.92(6)
S(3)[b]−Ag(3)−Ag(2)	141.78(5)	Br(2)−Ag(3)−Ag(2)	55.49(3)
S(3)−Ag(3)−Ag(2)	52.59(5)	Ag(3)[b]−Ag(3)−Ag(2)	94.17(4)
Ag(3)−Br(2)−Ag(2)	71.09(4)	Ag(3)[b]−S(1)−Ag(1)	127.89(9)
Ag(1)−S(2)−Ag(2)	114.65(8)	Ag(3)[b]−S(3)−Ag(2)	115.42(7)
Ag(3)[b]−S(3)−Ag(3)	64.65(5)	Ag(2)−S(3)−Ag(3)	65.91(5)

[a] $-x+1, -y, -z$. [b] $-x+1, -y+1, -z$. [c] $x-1, y, z$. [d] $-x, -y+1, -z$.

Table 2. Selected bond lengths (Å) and angles (°) for compound **2**, with esd's in parentheses

Ag(1)−S(2)	2.499(5)	Ag(1)−S(2)[a]	2.554(4)
Ag(1)−S(1)	2.669(5)	S(1)−C(1)	1.76(2)
S(2)−C(5)	1.769(14)	C(1)−N(2)	1.314(14)
N(2)−C(3)	1.468(17)	C(3)−C(4)	1.512(18)
C(5)−N(6)	1.307(19)	C(5)−N(10)	1.30(2)
N(6)−C(7)	1.50(2)	C(9)−N(10)	1.48(2)
S(2)−Ag(1)−S(2)[a]	145.96(16)	S(2)−Ag(1)−S(1)	124.58(16)
S(2)[a]−Ag(1)−S(1)	89.05(17)	Ag(1)[b]−S(1)−Ag(1)	95.6(2)
Ag(1)−S(2)−Ag(1)[b]	93.00(13)		

[a] $x, -y, z+1/2$. [b] $x, -y, z-1/2$.

a short silver(I)−silver(I) distance there is no halogen atom in the coordination sphere of the metal center. Complex **1** is therefore the first example of a silver(I) cluster containing a bromide ion in the coordination sphere of the metal center with an Ag···Ag interaction.

The C−S bond lengths found in complex **1** are S(1)−C(1) = 1.707(8), S(2)−C(7) = 1.734(8) and S(3)−C(13) = 1.732(7) Å, with a partial double-bond character, while the C−N bond lengths are C(1)−N(6) = 1.312(10), C(1)−N(2) = 1.320(10), C(7)−N(8) = 1.305(11), C(7)−N(12) = 1.328(10), C(13)−N(14) = 1.313(9) and C(13)−N(18) = 1.318(9) Å. These bond lengths, as well as the C−*N*−C and N−C−S bond angles, which are around 123° and 120°, respectively, indicate that the ligand coordinates to the silver(I) ion through its zwitterionic form IIIc (Figure 1).

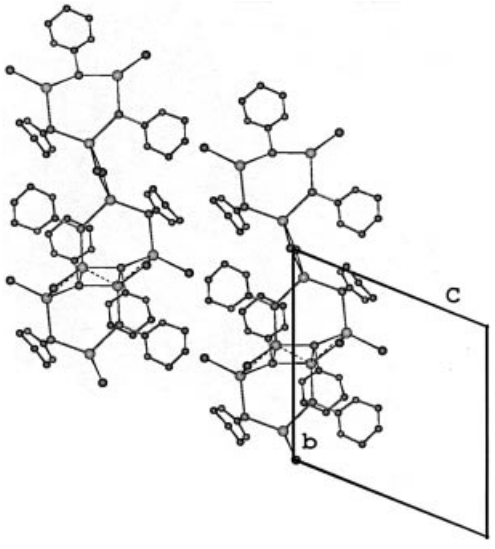

Figure 4. *bc* Projection of the crystal structure of complex **1**; part of the 1-D ribbon structure is presented

Complex **2** consists of two infinite Ag−S−Ag chains, parallel to the *c* axis, which are bridged to each other by a

 © 2004 Wiley-VCH Verlag GmbH & Co. KGaA, Weinheim

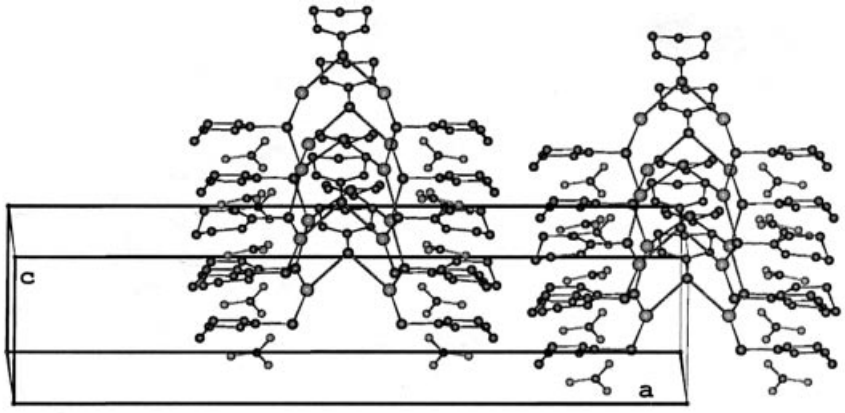

Figure 5. *ac* projection of the crystal structure of complex **2**; the NO_3^- counterions are shown

sulfur atom of the μ_2-StpmH$_2$ ligands. In this way, a one dimensional structure is obtained (Figure 5). A mirror plane parallel to the *bc* plane of the unit cell passes through atoms S(1), C(1) and C(4). The silver(I) ions are three-coordinate while the charge of the Ag^I ion is counterbalanced by a nitrate counterion.

The Ag−S bond lengths are Ag(1)−S(2) = 2.499(5), Ag(1)−S(2)^a = 2.554(4) and Ag(1)−S(1) = 2.669(5) Å (^{a}: x, $-y$, $-z + {}^1/_2$). The Ag−S bond lengths are similar to those found in **1**. No Ag···Ag interaction is observed in **2** [Ag(1)−Ag(1b) = 3.666 and Ag(1)−Ag(1c) = 3.954 Å, both of which are longer than the sum of the Van der Waals radii of two silver atoms]. The C−S bond lengths found in complex **2** are S(1)−C(1) = 1.76(2) and S(2)−C(5) = 1.769(14) Å, which correspond to a C−S single bond, while the C−N bond lengths are C(1)−N(2) = 1.314(14), C(5)−N(6) = 1.307(19) and C(5)−N(10) = 1.30(2) Å. Thus, both ligands have two equivalent short C−N bonds and a C−S single bond, forming the zwitterion IIIc (Figure 1) upon coordination to the silver(I) ion. This is further supported by the values of the C−*N*−C and N−C−S angles, which are around 123° and 120°, respectively. Therefore, a second coordination mode of the ligand is observed in complex **2** from the partial thionic form which is found in complex **1**. Moreover, although a tautomeric zwitterionic form is known to exist in the case of aromatic thioamide ligands,[1a,7,13] complex **2**, with a 2-mercapto-3,4,5,6-tetrahydropyrimidine ligand, is the first example of a coordination mode of S^-−Ag^+ and HN^+ counterbalanced by NO_3^- ions, i.e. with the ligand in its zwitterionic form. A possible charge distribution on the atoms of the unit cell in complex **2** is shown in Figure 6.

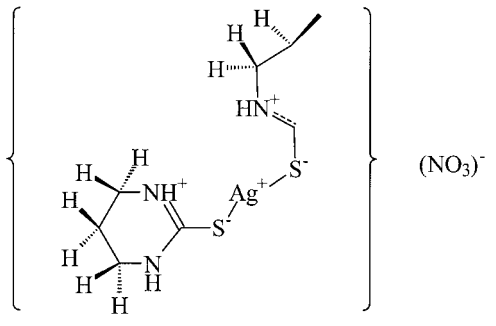

Figure 6. A possible charge distribution on the atoms in complex **2**

Biological Tests

Complexes **1** and **2** were evaluated for their inhibitory activity against the proliferation of murine leukemia (L1210) and human T-lymphocyte (Molt4/C8 and CEM) cells. Table 3 presents the antiproliferative effects of complexes **1** and **2**, as well as the activity of the ligand, as 50% inhibitory concentration (IC_{50}) values:

Table 3. Cytostatic activity of complexes **1** and **2** as 50% inhibitory concentration (IC_{50}) values against murine leukemia (L1210) and human T-lymphocyte (Molt4/C8 and CEM) cells

Compound	IC_{50} (μg/mL)		
	L1210	Molt4/C8	CEM
StpmH$_2$	>200	>200	>200
1	3.4 ± 0.1	3.6 ± 0.3	14 ± 5
2	3.5 ± 0.1	4.1 ± 1.1	17 ± 0

These findings indicate that complexes **1** and **2** show a pronounced cytostatic activity against the tumor cell-lines studied. None of the compounds show a pronounced activity against a wide spectrum of viruses (see Exp. Sect.) at subtoxic concentrations (3.2 μg/mL for **1** and 0.64−3.2 μg/mL for **2** in HEL and Vero cell cultures; data not shown).

Experimental Section

Materials and Instruments: All solvents used were of reagent grade. Silver(I) halides were freshly prepared by mixing aqueous solutions of $AgNO_3$ (Riedel) with the appropriate amount of NaBr (Merck or Aldrich). The precipitate was filtered off, washed with diethyl ether and dried in vacuo. 2-Mercapto-3,4,5,6-tetrahydropyrimidine (Aldrich) was used with no further purification. Elemental analyses for C, H, N, and S were carried out with a Carlo Erba EA model 1108 elemental analyzer. Melting points were measured in open tubes with a Stuart scientific apparatus and are uncorrected. Con-

 © 2004 Wiley-VCH Verlag GmbH & Co. KGaA, Weinheim

ductivity measurements were performed on a CONSORT C 831 conductometer, in DMSO solutions. IR spectra in the region of 4000−370 cm^{-1} were obtained from KBr discs, while far-IR spectra in the region of 400−30 cm^{-1} were obtained from polyethylene discs, with a Perkin−Elmer Spectrum GX FT-IR spectrophotometer. A Jasco UV/Vis/NIR V 570 series spectrophotometer was used to obtain the electronic absorption spectra. The ^1H and ^{13}C NMR spectra were recorded on a Bruker AC250 MHFT NMR instrument in [D_6]DMSO solutions. Chemical shifts are given in ppm referenced to internal TMS.

Synthesis and Crystallization of $[Ag_6(\mu_2\text{-}Br)_6(\mu_2\text{-}StpmH_2)_4(\mu_3\text{-}StpmH_2)_2]_n$ (1) and $[\{Ag_4(\mu_2\text{-}StpmH_2)_6\}(NO_3)_4]_n$ (2): Silver(I) bromide (1 mmol, 0.188 g) or silver(I) nitrate (0.170 g) were added to a clear solution of 2-mercapto-3,4,5,6-tetrahydropyrimidine (2 mmol, 0.2324 g) in 7 mL of DMSO. After stirring for 30 min, triethylamine (3.6 mmol, 0.5 mL) was added to the clear solution. The solution was then filtered and the filtrates were kept in darkness at room temp. After a few days colorless crystals of complex **1** or **2** suitable for crystallographic single crystal analysis were obtained.

1: Yield: 0.067 g (25%); m.p. 176−178 °C. $C_{24}H_{48}Ag_6Br_6N_{12}S_6$ (1823.7): calcd. C 15.81, H 2.65, N 9.22, S 10.55; found C 16.13, H 2.52, N 9.92, S 10.36. IR: $\tilde{\nu}$ = 3258 vs cm^{-1}, 2966 m, 1559 vs, 1432 m, 1362 vs, 1317 vs, 1215 vs, 1199 vs, 1072 m, 808 s, 694 s, 598 s, 566 s; far-IR: 178 m cm^{-1}, 133 m, 118 m, 111 m, 104 m. UV/Vis (DMSO): λ_{max} (log ε) = 263.5 nm (4.19). ^1H NMR (DMSO): δ = 8.572 (s, NH), 3.219 [t, $^3J_{HH}$ = 7.40 Hz, CH_2, -C(4)], 1.812−1.770 [q, $^3J_{HH}$ = 6.0 Hz, CH_2, -C(5)] ppm.

2: Yield: 0.034 g (10%); m.p. 209−211 °C. $C_{24}H_{48}Ag_4N_{16}O_{12}S_6$ (1376.5): calcd. C 20.94, H 3.51, N 16.28, S 13.97; found C 21.51, H 3.64, N 16.73, S 13.60. IR: $\tilde{\nu}$ = 3381 s cm^{-1}, 3229 s, 2965 m, 1564 vs, 1383 vs, 1309 s, 1221 s, 1196 s, 1073 m, 1038 m, 970 m, 815 m, 751 m, 627 m, 566 m, 519 m; far-IR: 286 m cm^{-1}, 282 m, 276 m, 273 m, 253 m, 246 m, 228 m, 222 m, 207 s, 199 m, 193 m, 175 m, 170 s, 158 m, 155 m, 147 m, 139 m, 128 s, 117 s, 112 m. UV/Vis (DMSO): λ_{max} (log ε) 257.5 nm (4.69). ^1H NMR (DMSO): δ = 8.76 (s), 3.25 (m), και 1.80 (m) ppm.

Cytostatic Activity Assays: To each well of a 96-well microtiter plate was added 5 × 10^4 L1210 or 7.5 × 10^4 Molt4/C8 or CEM cells and a given amount of the test compound dissolved in DMSO. The cells were allowed to proliferate for 48 hours (L1210) or 72 hours (Molt4/C8 or CEM) in a humidified, CO_2-controlled atmosphere. At the end of the incubation period, the cells were counted with a Coulter Counter. The IC_{50} (50% inhibitory concentration) is defined as the concentration of compound that reduced the number of living cells by 50%.

Inhibition of HIV-Induced Cytopathicity in CEM Cells: Human CEM (approx. 3 × 10^5 cells·mL^{-1}) cells were infected with 100 $CCID_{50}$ (1 $CCID_{50}$ being the viral dose required to infect 50% of the cell cultures) of HIV-1 (III_B) or HIV-2 (ROD) per milliliter and seeded in 200-μL wells of 96-well microtiter plates, containing appropriate dilutions of the test compounds. After 4 days of incubation at 37 °C, CEM giant-cell formation was examined microscopically.

Antiviral Activity Assays: The antiviral, other than *anti*-HIV, assays were based on inhibition of virus-induced cytopathicity in either human embryonic lung (HEL) [HSV-1, HSV-2, vaccinia virus, vesicular stomatitis virus (VSV), varicella-zoster virus, cytomegalovirus], human cervix carcinoma (HeLa) (VSV, Coxsackie virus B4, respiratory syncytial virus) or simian kidney (Vero) (parainfluenza-3 virus, reovirus-1, Sindbis virus, Coxsackie B4 virus and Punta Toro virus) cell cultures. Confluent cell cultures in microtiter 96-well plates were inoculated with 100 $CCID_{50}$ of virus [for CMV 100 plaque-forming units (PFU) and for VZV 20 PFU were used]. After a one to two hour virus-adsorption period, residual virus was removed, and the cell cultures were incubated in the presence of varying concentrations (400, 200, 100, ... μg/mL) of the test compounds. Viral cytopathicity was recorded as soon as it reached completion in the control virus-infected cell cultures that were not treated with the test compounds.

X-ray Structure Determination: Data were collected at room temperature on a Bruker P4 diffractometer, with graphite-monochromated Mo-K_α radiation (λ = 0.71073 Å), in the θ−2θ scan mode (1.93° < 2θ < 25.03° for **1** and 2.24° < 2θ < 24.98° for **2**). The structures were solved with SHELXS-97 and refined with SHELXL-97.[14] All non-hydrogen atoms were refined anisotropically. Hydrogen atoms were located by difference maps and refined isotropically. Relevant crystallographic data together with data collection and structure refinement details for both complexes are listed in Table 4.

CCDC-222599 (**1**) and -222600 (**2**) contain the supplementary crystallographic data for this paper. These data can be obtained free of charge at www.ccdc.cam.ac.uk/conts/retrieving.html [or from the Cambridge Crystallographic Data Centre, 12, Union Road, Cambridge CB2 1EZ, UK; Fax: (internat.) +44-1223/336-033; E-mail: deposit@ccdc.cam.ac.uk].

Table 4. Crystal data and the structure refinement details for compounds **1** and **2**

	1	**2**
Empirical formula	$C_{24}H_{48}Ag_6Br_6N_{12}S_6$	$C_{24}H_{48}Ag_4N_{16}O_{12}S_6$
Fw	1823.78	1376.64
Crystal system	triclinic	orthorhombic
Space group	$P\bar{1}$	$Cmc2_1$
a (Å)	8.041(1)	32.148(3)
b (Å)	12.838(4)	9.461(2)
c (Å)	13.281(2)	7.234(1)
α (°)	68.40(1)	
β (°)	72.97(1)	
γ (°)	87.80(2)	
V (Å^3)	1215.1(4)	2200.2(6)
Z	2	8
$\rho_{calcd.}$ (g cm^{-3})	2.492	2.078
μ (mm^{-1})	7.595	2.113
Reflections collected	4494	1451
Unique reflections	4168 (R_{int} = 0.0228)	1237 (R_{int} = 0.0514)
R[a] $wR2$[b] [$I > 2\sigma(I)$]	0.0426, 0.1071	0.0553, 0.1069
GOF	0.977	0.982

[a] $R = \Sigma||F_o| - |F_c||/\Sigma|F_o|$. [b] $wR2 = [\Sigma w(F_o^2 - F_c^2)^2/\Sigma w(F_o^2)^2]^{1/2}$.

Acknowledgments

This work was carried out in partial fulfillment of the requirements for an MSc thesis of Mr. P. C. Z. within the graduate program EPEAEK in Bioinorganic Chemistry financed by the Ministry of Education of Greece and coordinated by Professor N. Hadjiliadis. The study was also supported by the "Geconcerteerde Onderzoeksacties" (GOA-00/12), the René Descartes Prize-2001 of the European Commission (HPAW-2002−90001), and FORTIS/ISEP.

[1] [1a] M. Hong, W. Su, R. Cao, W. Zhang, J. Lu, *Inorg. Chem.* **1999**, *38*, 600−602. [1b] J.-M. Lehn, *Supramolecular Chemistry:*

 © 2004 Wiley-VCH Verlag GmbH & Co. KGaA, Weinheim

Concepts and Perspectives, VCH, Weinheim, **1995**. [1c]M. Hong, W. Su, R. Cao, M. Fujita, J. Lu, *Chem. Eur. J.* **2000**, *6*, 427−431.
[2] [2a] B. Krebs, G. Hengel, *Angew. Chem. Int. Ed. Engl.* **1991**, *30*, 769−788. [2b] P. G. Blower, J. R. Dilworth, *Coord. Chem. Rev.* **1987**, *76*, 121−185.
[3] [3a] E. S. Raper, *Coord. Chem.* **1985**, *61*, 115−184. [3b] E. S. Raper, *Coord. Chem. Rev.* **1994**, *129*, 91−156. [3c] E. S. Raper, *Coord. Chem. Rev.* **1996**, *153*, 199−255.
[4] [4a] Martidale *The Extra Pharmacopoeia*, 28th edition, The pharmaceutical press, London, **1982**. [4b] M. Wruble, *J. Am. Pharm. Assoc. Sci. Ed.* **1943**, *32*, 80−88.
[5] H. S. Rosenkranz, S. Rosenkranz, *Antimicrob. Agents Chemother.* **1972**, *2*, 373−379.
[6] [6a] K. Nomiya, Y. Kondoh, H. Nagano, M. Oda, *J. Chem. Soc., Chem. Commun.* **1995**, 1679−1680. [6b] K. Nomiya, S. Takahashi, R. Noguchi, *J. Chem. Soc., Dalton Trans.* **2000**, 2091−2097.
[7] W. Su, M. Hong, J. Weng, R. Cao, S. Lu, *Angew. Chem. Int. Ed.* **2000**, *39*, 2911−2914.
[8] [8a] J. Vicente, M. T. Chicote, C. Rubio, *Chem. Ber.* **1996**, *129*, 327−330. [8b] J. Vicente, M. T. Chicote, M. C. Lagunas, *Inorg. Chem.* **1993**, *32*, 3748−3754. [8c] O. Steigelmann, P. Bissinger, H. Schmidbaur, *Angew. Chem. Int. Ed. Engl.* **1990**, *29*, 1399−1400; *Angew. Chem.* **1990**, *102*, 1473−1474.
[9] P. C. Zachariadis, S. K. Hadjikakou, N. Hadjiliadis, A. Michaelides, S. Skoulika, Y. Ming, Y. Xiaolin, *Inorg. Chim. Acta* **2003**, *343*, 361−365.
[10] [10a] A. A. Perez-Lourido, J. A. Garcia-Vazquez, J. Romero, M. S. Louro, A. Sousa, Q. Chen, Y. Chang, J. Zubieta, *J. Chem. Soc., Dalton Trans.* **1996**, 2047−2054. [10b] E. Block, M. Gernon, H. Kang, G. Ofori-Okai, J. Zubieta, *Inorg. Chem.* **1989**, *28*, 1263−1271. [10c] K. Tang, M. Aslam, E. Block, T. Nicholson, J. Zubieta, *Inorg. Chem.* **1987**, *26*, 1488−1497.
[11] I. G. Dance, *Inorg. Chem.* **1981**, *20*, 1487−1492.
[12] [12a] G. A. Bowmaker, Effendy, J. V. Hanna, P. C. Healy, B. W. Skelton, A. H. White, *J. Chem. Soc., Dalton Trans.* **1993**, 1387−1397. [12b] P. Aslanidis, S. K. Hadjikakou, P. Karagiannidis, B. Kojic-Prodic, M. Luic, *Polyhedron* **1994**, *13*, 3119−3125.
[13] [13a] S. C. Davies, M. C. Durrant, D. L. Hughes, K. Leidenberger, C. Stapper, R. L. Richards, *J. Chem. Soc., Dalton Trans.* **1997**, 2409−2418. [13b] A. Paulo, A. Domingos, I. Santos, *J. Chem. Soc., Dalton Trans.* **1999**, 3735−3740. [13c] A. J. Lough, S. Park, R. Ramachandran, R. H. Morris, *J. Am. Chem. Soc.* **1994**, *116*, 8356−8357. [13d] S. Park, R. Ramachandran, A. J. Lough, R. H. Morris, *J. Chem. Soc., Chem. Commun.* **1994**, 2201−2002. [13e] M. Schlaf, A. J. Lough, R. H. Morris, *Organometallics* **1993**, *12*, 3808−3809.
[14] G. M. Sheldrick, *Programs for Crystal Structure Analysis* (Release 97-2). Institut fur Anorganische Chemie der Universität, Tammanstrasse 4, 3400 Göttingen, Germany, **1998**.

Received September 26, 2003
Early View Article
Published Online February 26, 2004

 © 2004 Wiley-VCH Verlag GmbH & Co. KGaA, Weinheim

Synthesis and Characterization of the Diastereomers Λ- and Δ-[Ru(bpy)$_2$-(m-bpy-Gly-L-His-L-Lys)]Cl$_2$ − ^{1}H NMR Studies on Their Interactions with the Deoxynucleotide Duplex d[(5′-CGCGAATTCGCG-3′)$_2$]

Alexandra Myari,[a] Nick Hadjiliadis,*[a] and Achilleas Garoufis*[a]

Keywords: Metallopeptides / Oligonucleotides / Ruthenium / Chemical nucleases / Groove

The synthesis and characterization of the diastereomeric complexes Λ- and Δ-[Ru(bpy)$_2$(m-bpy-GHK)]Cl$_2$, (GHK = glycine-L-histidine-L-lysine, m-bpy = 4|-methyl-2,2|-bipyridine) as well as their binding properties to the deoxynucleotide duplex d(5′-CGCGAATTCGCG-3′)$_2$ studied by means of NMR, ESI-MS and CD spectroscopy, are reported. The ROESY spectrum of Λ-[Ru(bpy)$_2$(m-bpy-GHK)]Cl$_2$ shows intramolecular cross peaks between the bpy H3 or H3′ protons and the aromatic H2 and H5 of the histidine imidazole ring, indicating that the peptide adopts an orientation with the imidazole ring close to the bpy ligand, possibly interacting by π-stacking. The absence of intramolecular cross peaks between the peptide and the bipyridine ligands in the ROESY spectrum of Δ-[Ru(bpy)$_2$(m-bpy-GHK)]Cl$_2$ on the other hand, shows that in this case the peptide is far from the two bpy ligands, having a different orientation from the Λ isomer. The isomers interact with the oligonucleotide duplex differently. Δ-[Ru(bpy)$_2$(m-bpy-GHK)]Cl$_2$ binds in the oligonucleotide major groove close to the central part of the sequence. Λ-[Ru(bpy)$_2$(m-bpy-GHK)]Cl$_2$ binds, probably non selectively, approaching the helix from the minor groove. It can be concluded that the peptide (GHK) binding leads the rest of the isomer to interact with the oligonucleotide in the case of the Δ isomer.
(© Wiley-VCH Verlag GmbH & Co. KGaA, 69451 Weinheim, Germany, 2004)

1. Introduction

The idea that low-molecular mass organic compounds (e.g., DNA targeting drugs) may bind selectively to DNA was raised several years ago.[1] There is evidence for ligands exhibiting antiviral activity and antineoplastic properties[2] or catalyzing the hydrolysis of DNA phosphodiesteric bonds (chemical nucleases).[3] The ways that such molecules bind to DNA are known and include covalent and noncovalent binding (intercalation, groove binding and electrostatic interactions). Some of them bind in specific domains of the DNA (sequence selectivity) or selectively from the major or minor groove depending on the relation of ligand−DNA recognition. Consequently, the structure of the incoming molecule is important due to different dimensions of the two DNA grooves when it approaches the bases. From the point of view of inorganic chemistry it is interesting to study the binding properties of the metal complexes of such ligands that may potentially combine the properties of the metal and the ligand. For instance the complex [Pt(net)$_2$(NH$_3$)$_2$]$^{2+}$ preserves the selective binding of netropsin (net) and binds in the AT rich region from the minor groove but induces DNA-cleavage near the binding sites upon X-ray irradiation.[4] On the other hand, the complex of the peptide GGKGGG with Cu^{2+} conjugated to netropsin binds to DNA in the same manner as the antibiotic alone, i.e. from the minor groove, assisted by the complex−peptide moiety through electrostatic and van der Waals interactions.[5,6] This compound generates oxygen active species upon activation by a mild oxidizer and induces cleavage in a specific DNA sequence region. Using photophysical techniques, Barton and co-workers have shown DNA sequence recognition by the metal peptide complex [Rh(phi)$_2$(phen′)]$^{3+}$ (phen′ = 1,10 phenanthroline conjugated with a 14/peptide and phi = phenanthrenequinonediamine) which binds at the 5′-ACAA-3′ region.[7] It is worth mentioning that the complex of Cu^{2+} with bis(salicylideneethylenediamine) (salen) conjugated with distamycine (DNA minor groove binder in AT rich regions) binds rather selectively to DNA. Upon activation, however, the cleavage is nonspecific.[8]

Ruthenium polypyridine complexes are undoubtedly the main class of molecules which may bind to DNA through intercalation, inducing cleavage of the DNA backbone through photoxidation.[9] The sequence specificity of these complexes has been investigated with known sequence oligonucleotides, mainly by means of NMR techniques, but no general rules about such selectivity have been

[a] Laboratory of Inorganic and General Chemistry, Department of Chemistry, University of Ioannnina,
Ioannina 45110, Greece
Fax: (internat.) +30-26510-44831
E-mail: nhadjis@cc.uoi.gr
agaroufi@cc.uoi.gr

suggested.[10−15] Our efforts are focused on the design and synthesis of ruthenium polypyridyl complexes able to recognize and bind to a specific DNA sequence. Peptides are important biological ligands having the functional groups essential for the formation of sequence specific contacts such as hydrogen bonds and van der Waals contacts. Hence, the incorporation of a peptide sequence may be an asset in the design of sequence specific binders. Our design of such complexes involves a Ru^{II} ion surrounded by polypyridine ligands, one of which is conjugated to the peptide sequence (Figure 1).

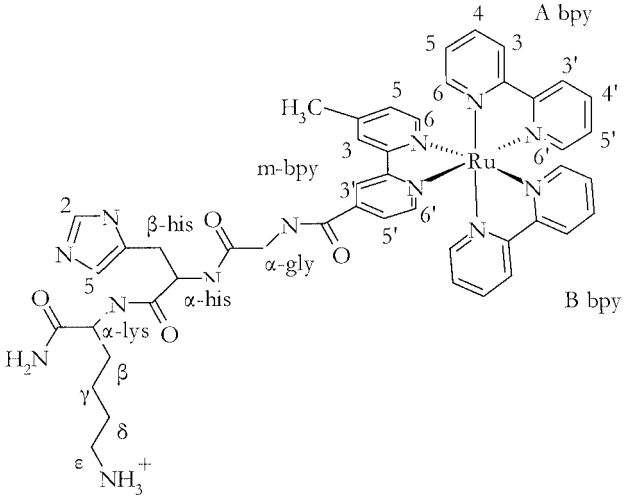

Figure 1. Structure of the complex Δ-$[Ru(bpy)_2(m\text{-}bpy\text{-}GHK)]^{2+}$ with atom numbering

Recently, we have focused our attention on the tripeptide Gly-His-Lys (GHK) related to GGH. Its Cu^{2+} complex conjugated with netropsin contributes to the binding reaction with the DNA from the minor groove in AT rich domains.[5,6] The DNA binding properties of the complex we designed were tested on the spectroscopically and crystallographically characterized Dickerson−Drew dodecamer, d(5′-CGCGAATTCGCG-3′)$_2$ which forms a self-complementary duplex the structure of which is known.[16,17] This paper describes the synthesis and characterization of the diastereomeric complexes Λ- and Δ-$[Ru(bpy)_2(m\text{-}bpy\text{-}GHK)]Cl_2$, derived from the compounds Λ- and Δ- *cis*-$[Ru(bpy)_2(py)_2]A$ (where A = *O*,*O*′-dibenzoyltartaric acid)[18,19] by a substitution of the two py molecules with the chelate ligand m-bpy-COOH followed by a solid-phase peptide synthesis. This was also our first attempt to investigate, by means of NMR, ESI-MS and CD spectroscopic techniques, their binding properties with the deoxynucleotide duplex d(5′-CGCGAATTCGCG-3′)$_2$. The possible selective cleavage of the oligonucleotide by these complexes is under investigation and the results will appear in a later publication.

2. Results and Discussion

2.1. Synthesis and Characterization of the $[Ru(bpy)_2(m\text{-}bpy\text{-}GHK)]Cl_2$ Isomers

2.1.1. Synthesis

The synthesis of the diastereomers Λ- and Δ-$[Ru(bpy)_2(m\text{-}bpy\text{-}GHK)]Cl_2$ was based on the enantiomerically pure complexes Λ- and Δ-*cis*-$[Ru(bpy)_2(py)_2]^{2+}$ as building blocks. These complexes were used as precursors for the synthesis of the tris(chelates) Λ- and Δ-$[Ru(bpy)_2(m\text{-}bpy\text{-}COOH)]^{2+}$.[20,21] Both pyridine molecules in the complex *cis*-$[Ru(bpy)_2(py)_2]^{2+}$ were substituted by the chelate ligand m-bpy-COOH (m-bpy-COOH = 4′-methyl-2,2′-bipyridine-4-carboxylic acid), the optical purity being retained in the resultant compounds. The carboxyl group of the ligand (m-bpy-COOH) remained free due to the higher propensity of the phenanthroline nitrogen donor atoms over the oxygen atoms for coordination to the Ru^{II} ion[24] assisted by the formation of a very stable five-membered chelate ring. These enantiomers were isolated as their $[PF_6]^-$ salts by the addition of HPF_6 (pH = 1) thus keeping the carboxyl group protonated. The tripeptide (GHK) was then conjugated to the m-bpy-COOH molecule through the solid state method SPPS, using the 2-chlorotrityl-H-Fmoc-resin by activation of the carboxyl group with succinic acid and DCC.[25] The isomers were isolated as TFA salts and then converted in to their water-soluble chlorides with LiCl in acetone.[15] The total procedure is detailed in Scheme 1.

2.1.2. Electrospray Ionization Mass Spectrometry

Positive electrospray spectra for both Λ- and Δ-$[Ru(bpy)_2(m\text{-}bpy\text{-}GHK)]Cl_2$ in aqueous media were recorded using the time-of-flight method to register all ions simultaneously without scanning.[26] Both spectra were generally the same, showing mainly two peaks of high intensity at 474.58 and 316.74 *m*/*z* arising from $[RuC_{46}H_{49}N_{13}O_4]^+$ (948.30 *m*/*z*) at doubly and triply charged states correspondingly. The very weak intensity of the peak at *m*/*z* = 948.30 indicates that the abundance of the peptide which is deprotonated both to the lysine terminal amino group and probably to any peptidic NH group or to the terminal amide group $[Ru(bpy)_2(m\text{-}bpy\text{-}CO\text{-}Gly\text{-}His\text{-}LysCONH_2)H^+]^+$ is very low. Indeed, a relatively high intensity peak that was observed at 474.58 *m*/*z* may be assigned to the doubly charged cation $[Ru(bpy)_2(m\text{-}bpy\text{-}CO\text{-}Gly\text{-}His\text{-}LysCONH_2)]^{2+}$ with all the peptidic NH groups being protonated. Finally the main peak of the spectrum at *m*/*z* = 316.74 can be assigned to the triply charged cation $[Ru(bpy)_2(m\text{-}bpy\text{-}CO\text{-}Gly\text{-}His\text{-}LysCONH_2)]^{3+}$ where the lysine terminal amino group (p*K*a = 10.4) [27] is protonated (Figure 2).

2.1.3. Circular Dichroism Spectroscopy

The CD spectra of the Δ- and Λ-diastereomers are not mirror images of each other as expected (Figure 3) since the presence of another chiral center in the peptide moiety

 © 2004 Wiley-VCH Verlag GmbH & Co. KGaA, Weinheim

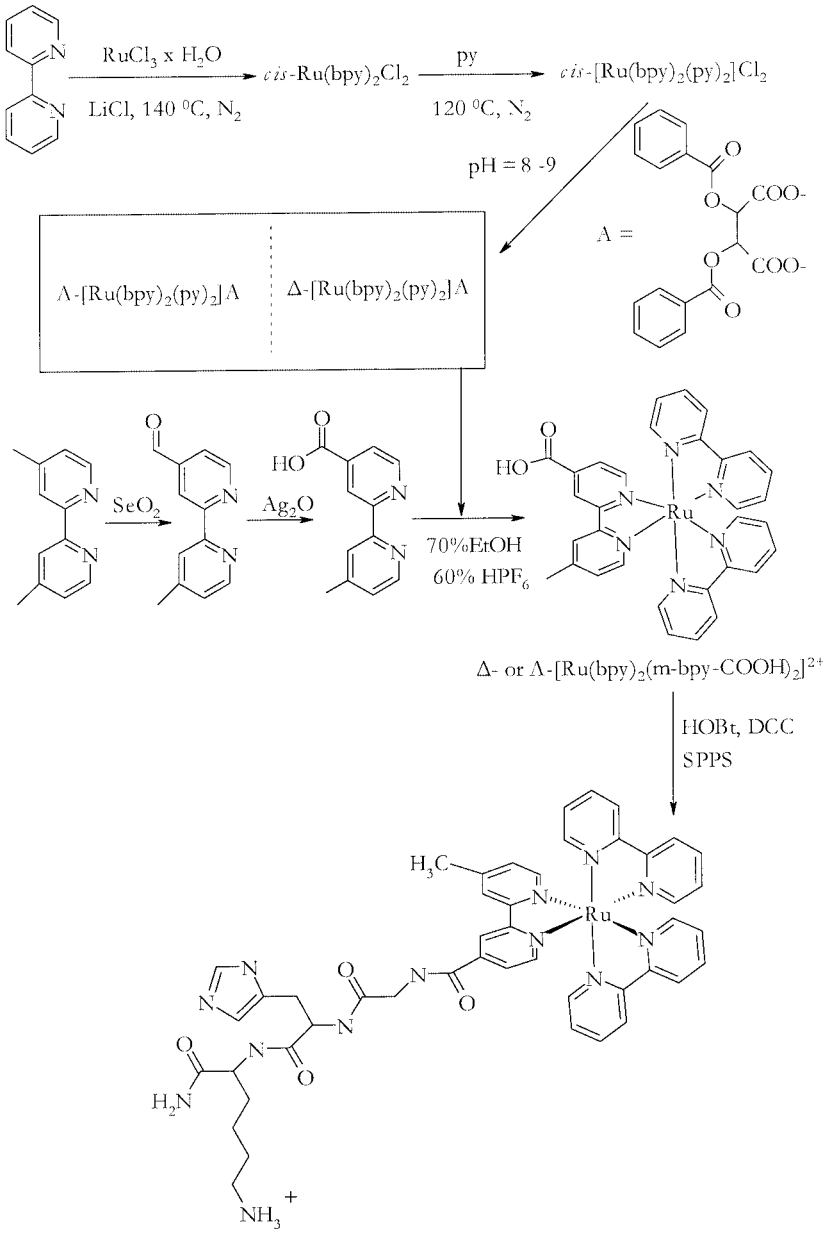

Scheme 1

besides the metal results in diastereomers. Assignments were made by comparison with similar complexes of known configuration.[20,28] The spectra of the isomers exhibit $\lambda_{max.}$ (nm) with $\Delta\varepsilon$ ($M^{-1}cm^{-1}$) at 479 nm (+6.7), 422 (−9.6), 295 nm (+90.1), 278 (−36.9) 226 nm (−13.5), 205 nm (+11.7), 195 nm (−14.8) for the Λ isomer and at 479 nm (− 4.6) 421.5 nm (+6.4), 295 nm (−60.8), 278 nm (+22.6), 225 nm (+5.2), 204 nm (−18.6), 190 nm (−11.5) for the Δ isomer.

2.1.4. NMR Spectroscopy

^{1}H NMR resonances of the diastereomers Λ- and Δ-[Ru(bpy)$_2$(m-bpy-GHK)]Cl$_2$ were assigned based on homo and heteronuclear 2-D COSY and TOCSY experiments. In the spectra of both isomers only one set of proton signals for the two bpy ligands were observed. The influence of the third non-symmetric ligand m-bpy-GHK on the bpy proton signals is insignificant and the differences in their magnetic environments are non-detectable. Similar behavior was also observed in the complexes [Ru(bpy)$_2$(HPIP)]$^{2+}$ [15] and [Ru(bpy)$_2$(pqx)]$^{2+}$,[29] where HPIP {HPIP is 2-(2-hydroxyphenyl)imidazo[4,5-*f*][1,10] phenanthroline} and pqx [pqx is 2-(2′-pyridyl)quinoxaline] are non-symmetric chelate ligands. On the other hand, the ligand m-bpy-GHK exhibits one set of proton resonances for each pyridine ring which differ significantly from each other. The pyridine ring, which is substituted by a methyl group at the 4th position, exhibits similar chemical shifts with the pyridine residues of the other two bpy ligands with the protons at the neighbor-

 © 2004 Wiley-VCH Verlag GmbH & Co. KGaA, Weinheim

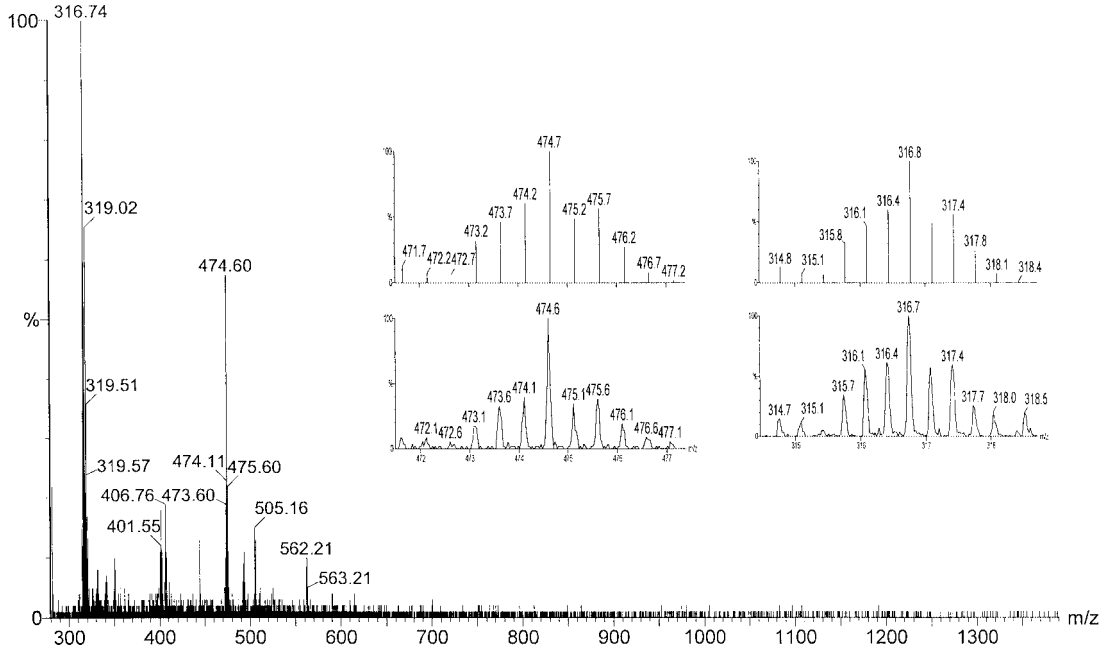

Figure 2. A typical electrospray mass scan of Λ-[Ru(bpy)$_2$(m-bpy-GHK)]Cl$_2$ in the positive mode. Insets, the calculated spectrum in comparison with the observed peaks for the cations Λ-[Ru(bpy)$_2$(m-bpy-GHK + H$^+$)]$^{3+}$ (*m*/*z* 316.74) and Λ-[Ru(bpy)$_2$(m-bpy-GHK)]$^{2+}$ (*m*/*z* 474.58)

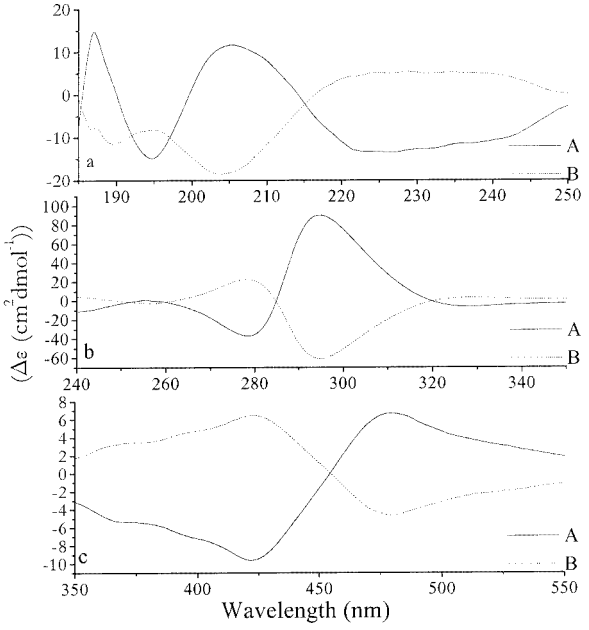

Figure 3. The CD spectra of A = Λ-[Ru(bpy)$_2$(m-bpy-GHK)]Cl$_2$ and B = Δ-[Ru(bpy)$_2$(m-bpy-GHK)]Cl$_2$ in the region (a) (190−250 nm), (b) (240−350 nm) and (c) (350−550 nm)

ing 3rd and 5th positions shifted upfield only by δ = −0.06 and −0.04 ppm respectively. In contrast, the protons H3′ and H5′ of the other pyridine ring of the m-bpy group are shifted downfield by about δ = +0.29 ppm (H3′) and δ = +0.78 ppm (H5′), indicating that the CO-GHK substitution at the 4th position provides a deshielding effect on these protons reducing the electron density of this pyridine ring.[30]

The chemical shifts of the peptide protons are similar for the diastereomers Λ- and Δ-[Ru(bpy)$_2$ (m-bpy-GHK)]Cl$_2$, differing only slightly (about ±0.01 ppm). The one exception being H2 of the histidine imidazole ring of the Λ- isomer which is shifted upfield by δ = −0.16 ppm compared with the shift of the equivalent resonance in the Δ isomer. This effect probably arises from a different configuration of the peptide in the isomers, with the histidine's imidazole ring being closer to the aromatic pyridine moieties in the case of the Λ isomer (Figure 4). A qualitative approach to the observed shielding by −0.16 ppm based on a method proposed by Cheney results in a distance of about 4 to 5 Å between the plane of one of the pyridine rings and H2 of the imidazole.[31] The ROE spectra of both isomers are similar as the cross peaks in the ROE map indicate. These can be assigned to dipolar interactions between the pyridine ring protons of rings on the same or adjacent metal bipyridine units. Additionally, two new cross peaks were observed in the spectrum of the Λ isomer (Figure 4), which we have assigned to the interaction of the bpy H3 or H3′ protons with both the aromatic protons H2 and H5 of the histidine imidazole ring. This indicates that it has a different orientation in the two diastereomers. Such a geometry will direct the imidazole ring in the case of Λ-[Ru(bpy)$_2$(m-bpy-GHK)]Cl$_2$ close to the bpy ligand possibly resulting in a π-stacking interaction. This would not be the case in the Δ isomer (Figure 4).

 © 2004 Wiley-VCH Verlag GmbH & Co. KGaA, Weinheim

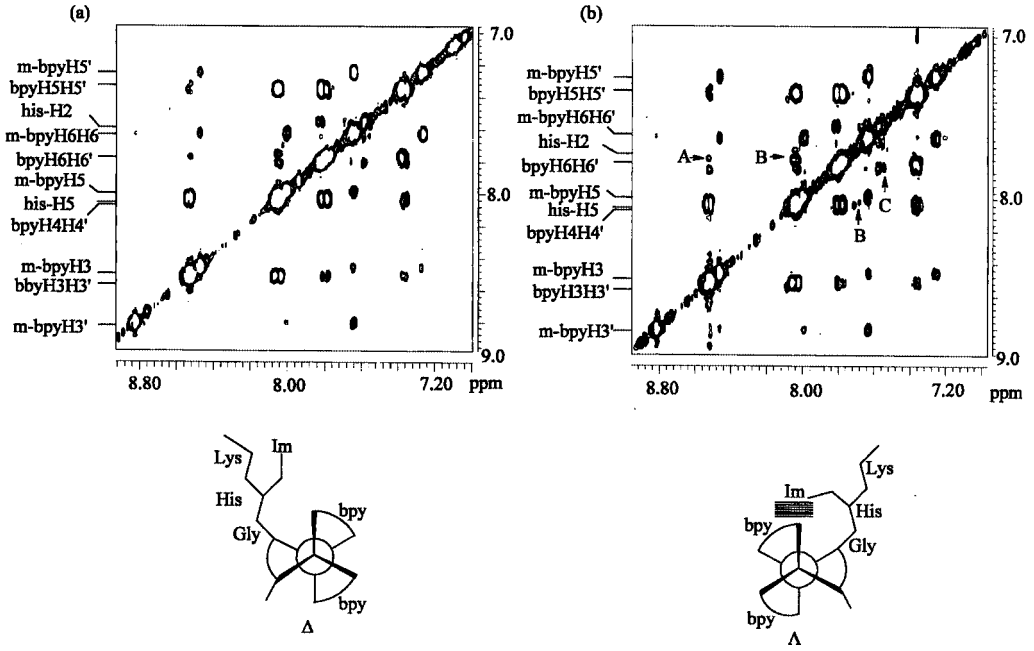

Figure 4. (a) Part of the ROESY spectrum (τ_m = 100 ms) of Δ-[Ru(bpy)$_2$(m-bpy-GHK)]Cl$_2$, following a qualitative model of the peptide orientation. (b) The same part of the ROESY spectrum under the same conditions for Λ-[Ru(bpy)$_2$(m-bpy-GHK)]Cl$_2$, following a qualitative model of the peptide orientation. The labeled cross peaks correspond to ROE contacts assigned to the protons: (A) hisH2-bpyH3H3′, (B) hisH2-bpyH4H4′, (C) hisH5-bpyH6H6′

2.2. Interactions of the Diastereomers [Ru(bpy)$_2$(m-bpy-GHK)]Cl$_2$ with the DNA Dodecamer Duplex [d(5′-CGCGAATTCGCG-3′)$_2$]

2.2.1 Assignments of the Proton Resonances of [d(5′-CGCGAATTCGCG-3′)$_2$]

1-D-NOE (Nuclear Overhauser Effect) experiments in 90% H_2O/10% D_2O were used to assign the amino and the imino resonances of the duplex. Five signals in the imino region (δ = 14 ppm) of the NMR spectrum of the dodecanucleotide were observed, indicating that only the terminal C···G bases do not form stable Watson−Crick hydrogen bonding. The two most downfield shifted resonances were identified as T7N3-H and T8N3-H in the A···T pairs and the other three as G2N1-H, G10N1-H and G4N1-H in the G···C pairs, typical for B-type DNA structures in aqueous solution.[32] In addition, the signals of the hydrogen-bonded exocyclic amino groups of the purines and pyrimidines were observed in the region of δ = −9.5 ppm, in contrast to the resonances of the non hydrogen-bonded amino groups C1-NH_2 and G12-NH_2 located at a higher field (δ ≈ 6 ppm).

Assignments of all non-exchangeable protons of the oligonucleotide were achieved by using the standard DQF COSY technique[33] and two-dimensional NOE spectroscopy.[34] Small differences in the proton assignments of the dodecamer exist between our findings and those reported in literature,[35] probably due to the slightly different conditions and the high field ^{1}H NMR (500 MHz) instrument used. In the NOESY map of [d(5′-CGCGAATTCGCG-3′)$_2$] the sequential assignments for the *n*H6/H8 → *n*H1′ => (*n* + 1)H6/H8 → (*n* + 1)H1′ (where the different arrows → and => denote *intra* and *inter* nucleotide distances-cross peaks, respectively) system

Table 1 ^{1}H NMR chemical shift data[a] for the diastereomers Λ- and Δ-[Ru(bpy)$_2$(m-bpy-GHK)]Cl$_2$ in the presence of the oligonucleotide [*d*(CGCGAATTCGCG)$_2$] at a molar ratio of 1:1

Proton[a]	Δ Isomer	Δ(δ)	Λ Isomer	Δ(δ)
bpy H3	8.34	−0.20	8.48	−0.06
bpy H3′	8.44	−0.10	8.48	−0.06
bpy H4	7.88	−0.17	8.01	−0.04
bpy H4′	7.97	−0.08	8.01	−0.04
bpy H5	7.33	−0.04	7.34	−0.04
bpy H5′	7.33	−0.04	7.34	−0.04
bpy H6	7.71	−0.09	7.75	−0.05
bpy H6′	7.71	−0.09	7.75	−0.05
m-bpy H6	7.59	−0.06	7.61	−0.04
m-bpy H6′	7.59	−0.06	7.61	−0.04
m-bpy H5	7.92	−0.08	7.94	−0.06
m-bpy H5′	7.22	−0.05	7.24	−0.03
m-bpy CH_3	2.49	−0.06	2.50	−0.04
m-bpy H3	8.76	−0.07	8.78	−0.05
m-bpy H3′	8.39	−0.09	8.42	−0.05
α-Gly	4.17	−0.00	4.16	−0.01
α-His	4.63	−0.04	4.65	−0.03
β-His	3.13	−0.02	3.15	−0.02
His H5	7.53	−0.04	7.54	−0.03
His H2	7.79	−0.04	7.80	+0.12
α-Lys	4.23	−0.02	4.25	−0.01
β-Lys	1.81	+0.01	1.82	+0.03
γ-Lys	1.37	+0.02	1.38	+0.04
δ-Lys	1.68	+0.01	1.66	−0.01
ε-Lys	2.88	−0.09	2.90	−0.07

[a] Concentration 10 mM, D_2O, 100 mM phosphate buffer (pH = 7.01), *T* = 303 K.

 © 2004 Wiley-VCH Verlag GmbH & Co. KGaA, Weinheim

Table 2. ^{1}H NMR chemical shifts in ppm of free d(CGCGAATTCGCG)$_2$ and the chemical shift differences induced by the addition of Λ- or Δ-[Ru(bpy)$_2$(m-bpy-GHK)]Cl$_2$ at a molar ratio of 1:1 in 100 mM phosphate buffer (pH = 7.01)

	H8/H6	Λ Isomer	Δ Isomer	H2/H5	Λ Isomer	Δ Isomer	H1′	Λ Isomer	Δ Isomer	H2′′	Λ Isomer	Δ Isomer	H2′	Λ Isomer	Δ Isomer
C1	7.60	−0.01	+0.01	5.88	−0.02	−0.03	5.72	−0.02	−0.01	2.39	−0.01	−0.02	1.94	−	−
G2	7.93	+0.02	+0.02				5.88	−0.02	−0.03	2.68	0.00	0.00	2.62	0.00	0.00
C3	7.25	0.00	−0.01	5.35	−0.06	−0.07	5.56	+0.02	+0.03	2.26	+0.01	+0.01	1.83	0.00	+0.01
G4	7.83	0.00	0.00				5.42	−0.01	−0.01	2.75	−	−	2.63	0.00	−
A5	8.09	0.00	0.00	7.21	+0.05	−0.02	6.13	−0.05	−0.06	2.90	−0.11	+0.05	2.68	0.00	0.00
A6	8.09	0.00	0.00	7.60	−0.01	0.00	5.97	−0.02	−0.03	2.90	−0.11	+0.05	2.49	+0.01	+0.02
T7	7.09	+0.02	0.00				5.88	−0.02	−0.03	2.53	−0.01	−0.01	1.94	−	−
T8	7.35	+0.05	−0.02				6.12	−0.04	−0.01	2.53	−0.01	−0.01	2.14	0.00	+0.03
C9	7.44	+0.01	0.00	5.60	+0.01	+0.01	5.64	0.00	−0.02	2.43	−	+0.01	2.04	−0.01	−0.01
G10	7.89	+0.00	−0.01				5.83	+0.02	+0.01	2.68	+0.02	0.00	2.62	0.00	0.00
C11	7.31	−0.01	0.00	5.42	−0.01	−0.01	5.72	−0.02	−0.01	2.31	−0.01	−0.03	1.87	−0.01	−0.02
G12	7.92	+0.01	0.00				6.13	−0.05	−0.06	2.62	−0.01	0.00	2.36	−0.01	−0.01

were observed for all the bases of the sequence.[36,37] Moreover, NOE cross peaks from each H8/H6 to its own H2′ and H2′′ are consistent, as expected, with a B-type right-handed DNA duplex.[37]

2.2.2 1-D ^{1}H NMR Spectroscopy

Table 1 and 2 show the ^{1}H NMR chemical shift data of the free oligonucleotide, the complexes Δ- and Λ-[Ru(bpy)$_2$(m-bpy-GHK)]Cl$_2$ and the changes induced by addition of the isomers to the oligonucleotide.

The ^{1}H NMR spectra of the samples containing the oligonucleotide and the Δ or the Λ isomer in molar ratios of 1:0.5 and 1:1 show only one set of resonances in all cases. This behavior indicates fast exchange (on the NMR time scale at ambient temperature) between the bound form(s), the free oligonucleotide, and the metal complex.

Upon decreasing the temperature to 283 K, a slight broadening of the signals was observed indicating that the fast exchange changes slowly to intermediate. Moreover, decreasing the temperature close to the solvent's freezing point did not yield separate resonances (coalescence point). Under these conditions only average NMR results of the bound form(s) could be observed. This clearly means that the NMR observations do not necessarily belong to only one single species but may be the average of different bound forms in a non-specific binding of the diastereomers to the oligonucleotide. Each NMR signal in the fast exchange kinetics represents a statistical average for all species present and the extracting of specific information is difficult. However, the achievement of slow exchange conditions is rather scarce even for highly specific compounds such as distamycine.[38] In such cases, the NMR results can only be considered as a qualitative analysis of the binding. The majority of Ru^{II} polypyridine complexes bind to DNA with fast to intermediate kinetics and conformational predictions have been given using additional methods such as molecular mechanics (MM) and molecular dynamics (MD) calculations, coupled with some of the NOE results as distance constraints.[11−15,39,40]

Upfield changes in the bpy proton signals of both diastereomers were observed which were largest in the case of the Δ isomer. In particular, the protons located at the end of the one pyridine ring of bpy namely H3′ and H4′ were shifted by δ = − 0.19 and − 0.17 ppm respectively. These values, followed by smaller but significant changes in chemical shifts of all other bpy protons, indicate that the ligand clearly binds to the oligonucleotide without intercalating between the bases. Intercalation would cause large upfield changes in the resonances of the ligand protons (δ = 0.3−1.0 ppm) and significant broadening of the signals due to intermediate exchange.[11] The observed electronic shielding of the H3′ and H4′ bpy protons from the DNA bases is close to the lower limit for binding by intercalation, showing that the vertical distance between these protons and the base planes is not very high.[41] According to Pullman and co-workers, the induced shielding effect for a five or a six membered aromatic ring from the DNA bases is a function of distance.[41,42] The observed 0.2 ppm upfield shift corresponds to a vertical distance between the base planes and H3′/ H4′ of the bpy aromatic ring system of about 5 Å which is not enough to cause intercalation. These slight changes in the chemical shifts of the complex protons are more consistent with other modes of binding, such us groove binding. In general, molecules which bind in the DNA grooves interact with the edges of the bases causing zero or insignificant shielding of the molecule's protons.[43] Complexes with ligands similar to bpy, as in the case of [Ru(Me$_2$bpy)$_2$}$_2$(μ-bpm)]$^{4+}$ (μ-bpm = 2,2′-bipyrimidine), associate in the minor groove of the DNA and induce very small changes in the ligand proton resonances (less than 0.1 ppm).[14] Small changes were observed in the pyridyl and aliphatic proton chemical shifts for the complex Δ-*cis*-α-[Ru{*R*,*R*)-picchxnMe$_2$}(phen)]$^{2+}$ (< 0.2 ppm) which binds selectively at the minor groove of the oligonucleotide [d(CGCGATCGCG)$_2$] and the [d(ATATCGATAT)$_2$] duplex.[39] This type of DNA−metal complex interaction is also known for the complex [Ru(bpy)$_3$]$^{2+}$ which binds to the DNA without intercalation.[44] In the case of Λ-[Ru(bpy)$_2$(m-bpy-GHK)]Cl$_2$ the changes observed were in the range of δ = −0.06 to −0.03 ppm for the bpy protons, sug-

 © 2004 Wiley-VCH Verlag GmbH & Co. KGaA, Weinheim

gesting a weak association with the oligonucleotide or a non-specific binding. The diffusion of shielding or deshielding effects induced by the interaction of the metal complex with DNA, for all proton signals of the Λ-[Ru(bpy)$_2$(m-bpy-GHK)] with approximately similar shifts, could be explained as being due to a non specific binding of this isomer.

The aromatic protons of the m-bpy-GHK ligand show small upfield shifts (less than 0.1 ppm) for both isomers. In addition, the peptide protons were shifted upfield except the lysine side chain protons Hα (shifted upfield in both isomers), Hβ (shifted downfield in both isomers) and Hγ (shifted downfield in both isomers). The Hδ proton, which is very close to the terminal amino group, was shifted slightly downfield and upfield in the Δ and Λ isomers, respectively, indicating that it probably interacts either with the charged phosphate groups of the DNA or with the aromatic π system of the bpy ligands. Similar results were observed in the case of the binding of the tripeptide Lys-Tyr-Lys to the tetranucleotide [d(5′-GCGC-3′)]$_2$, where the positively charged amino group of the lysine side chain interacts electrostatically with the phosphodiester backbone of the DNA.[45] Furthermore, the binding of Lys-Trp-Lys with the DNA involves electrostatic interactions between the lysine residues and the DNA backbone.[46]

The influence of the binding of the Δ isomer on the oligonucleotide proton resonances is focused on the protons located at the major groove, namely H2′ and H2′′ of the sugar moieties which are shifted more than the minor groove proton H1′. The highest shifts were observed for A5 H2′′ and A6 H2′′ and for C3 H5. The base C3 is located opposite G10 and probably H5 is affected by a complex binding close to the T8C9 base sequence. Thus, the most affected part of the oligonucleotide is the region from A5 to G10 in the major groove.

In an attempt to further investigate the binding modes of the peptide moiety of the complexes to the synthetic DNA fragment, all spectra were recorded in 90% H_2O /10% D_2O in order to observe the exchangeable amino and imino protons. The assignments in Table 3 were aided by the use of

Table 3. ^{1}H NMR chemical shifts of the exchangeable protons of free d(CGCGAATTCGCG)$_2$, Λ- or Δ-[Ru(bpy)$_2$(m-bpy-GHK)]Cl$_2$ and their adducts at a 1:1 molar ratio in 100 mM phosphate buffer (pH = 7.01), in H_2O/D_2O, 9:1

	GNH1/TNH$_3$	CNH$_4$ [a]	CNH$_4$ [b]	Peptide NH	Lys-CONH$_2$
A5-T8					
Δ Free	13.78				
Δδ Δ isomer	0.05				
Δδ Λ isomer	0.03				
A6-T7					
Δ Free	13.65				
Δδ Δ isomer	0.04				
ΔΔ Λ isomer	0.01				
G2-C11					
Δ Free	13.02	6.55	8.37		
Δδ Δ isomer	0.02	0.11	0.02		
Δδ Λ isomer	0.00	0.10	0.02		
G10-C3					
Δ Free	12.88	6.42	8.41		
Δδ Δ isomer	0.01	0.07	0.03		
Δδ Λ isomer	0.00	0.09	0.02		
G4-C9					
Δ Free	12.68	6.80	8.40		
Δδ Δ isomer	0.01	0.08	0.03		
Δδ Λ isomer	−0.02	0.08	0.02		
Gly-NH					
Δ isomer					
Δ Free/Δδ bonded Λ isomer				8.19/0.00	
Δ Free/Δδ bonded				8.16/−0.01	
Lys-NH					
Δ isomer					
Δ Free/Δδ bonded Λ isomer				8.10/0.02	
Δ Free/Δδ bonded				8.21/0.04	
His-NH					
Δ isomer					
Δ Free/Δδ bonded Λ isomer				8.24/−0.13	
Δ Free/Δδ bonded				8.25/−0.13	
Lys-CONH$_2$					
Δ isomer					
Δ Free/Δδ bonded Λ isomer					7.16/0.04
Δ Free/Δδ bonded					7.17/−0.01

[a] Hydrogen bonded. [b] Not hydrogen-bonded.

 © 2004 Wiley-VCH Verlag GmbH & Co. KGaA, Weinheim

NOE spectroscopy and by data available in the literature.[47−49]

The H8 proton (neighboring N7) of the guanine or the adenine residues of the oligonucleotide do not shift significantly in the presence of the diastereomers thus excluding any possibility of participation of this nitrogen in hydrogen bonding with the peptide complexes. O6 of guanine is also a good candidate but such interactions would affect the GO6···H4NC proton signal, which is not the case ($\Delta\delta$ = 0.02 to 0.03 ppm for both isomers). The other non-hydrogen bonded protons of the exocyclic amino group of C3, C9 and C11, (CN4-H) are shifted by about 0.1 ppm due to their interactions with both isomers (Figure 5). This downfield shift is significant but clearly not large enough to conclude that these protons participate in hydrogen bonding. This observation could, however, be due to hydrogen bonds which are bifurcated and longer than normal or indeed van der Waals interactions between the peptide residue of the complexes and the CN4-H protons of C3, C9 and C11.[50] A similar example is the interaction of the same DNA sequence with the drug *Distamycin A*, where small downfield shifts were observed for both protons of the adenine ring

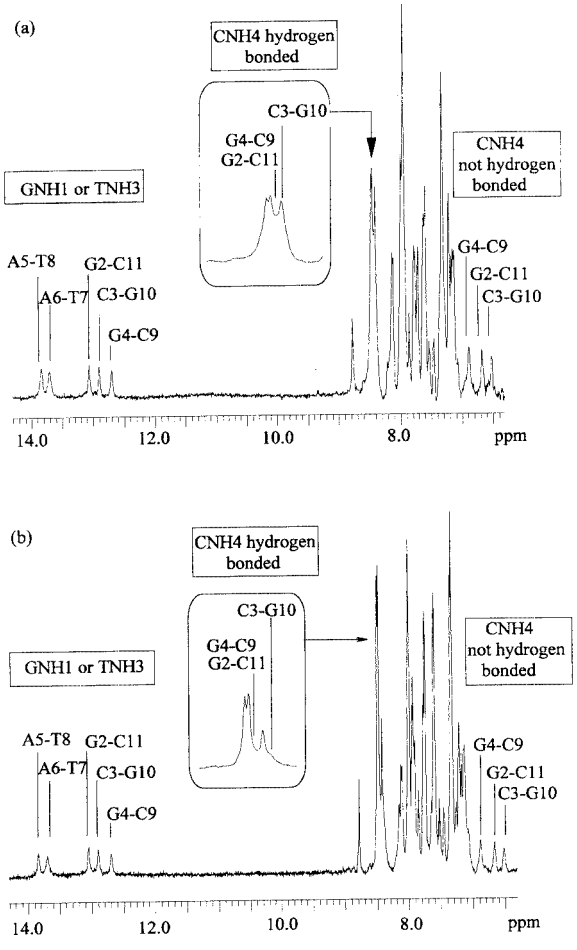

Figure 5. Part of the ^{1}H NMR spectra of the diastereoisomers showing the influence of (a) Δ-[Ru(bpy)$_2$(m-bpy-GHK)]Cl$_2$ and (b) Λ-[Ru(bpy)$_2$(m-bpy-GHK)]Cl$_2$ to the hydrogen bonds of GNH1, TNH3 and CNH4 in the base pairs CG and AT of the oligonucleotide duplex

and the NH of the drug's pyrrole groups[50] suggesting a groove interaction. The hydrogen-bonded proton of the AT base pair *A*N6-H···O4*T* does not seem to be affected by the binding because the neighboring proton signals of the thymine methyl group do not shift upfield. This excludes the possibility of interaction of these sites with the peptide. The A5H2 that shifts downfield by about 0.05 ppm reflects a possible association of the peptide with the A5N3 position.

Of the exchangeable peptide protons only the NH proton of the His group was shifted upfield by about −0.13 ppm in both diastereomers, suggesting that this site or the neighboring carbonyl (>C=O) participates in the binding of the complex to DNA.

2.2.3 2-D ^{1}H NMR Spectroscopy

Table 4 shows selected NOESY cross peaks observed between the isomers Λ- and Δ-[Ru(bpy)$_2$(m-bpy-GHK)]Cl$_2$ and [d(5′-CGCGAATTCGCG-3′)$_2$].

Table 4. Selective NOE cross peaks observed between the protons of the diastereomers Λ- and Δ-[Ru(bpy)$_2$(m-bpy-GHK)]Cl$_2$ and [d(5′-CGCGAATTCGCG-3′)$_2$] at a metal complex/duplex ratio of 1:1 in 100 mM phosphate buffer (pH = 7.01) at 303 K

Δ-[Ru(bpy)$_2$(m-bpy-GHK)]Cl$_2$	Λ-[Ru(bpy)$_2$(m-bpy-GHK)]Cl$_2$
(m-bpy-GHK)H3 → C9H2′′(W)	
(m-bpy-GHK)H3′ → C9H2′′ (S)	
(m-bpy-GHK)H5′ → C9H2′′ (S)	(m-bpy-GHK)H3′ → A6H1′(M)
	(m-bpy-GHK)H5′ → C9H1′ (W)
(bpy)H3′ → C9H2′′ (S)	
(bpy)H6H6′ → C1H2′ (M)	
(His)HA → A5H1′(W)	
	(Gly)NH → T8H1′(W)
(Lys)NH → A5A6H2′′ (M)	
(His)NH → T7T8H2′′ (M) → MeT8 (M)	

The NOE contacts, originating from the duplex conformation (B-form), are intact but the cross peak intensities of some of them are decreased indicating small perturbations of the helix conformation.[51] This observation allowed us to consider a "fix" B-DNA structure for the binding models. In addition, we observed a number of cross peaks between the ligand protons of the diastereomers. Intermolecular NOE effects were also observed between the diastereomeric complex protons and the dodecanucleotide (see Figure 6 and 7).

In the case of Δ-[Ru(bpy)$_2$(m-bpy-GHK)]Cl$_2$, distances of less than 5Å were observed between the aromatic protons of the ligands m-bpy and bpy with the H2′′ proton of C9 and T8 facing the major groove of the helix. The exchangeable NH protons of the peptide backbone, which extend from the 4th position of the ligand m-bpy, show cross peaks with protons that are also accessible from the major groove such as H2′′ of T7 and T8 and the thymine T8 methyl group. A few very weak intensity intermolecular NOE effects were observed between the lysine aliphatic side chain and the oligonucleotide protons indicating that this part of the peptide is located across the major groove of the helix.

 © 2004 Wiley-VCH Verlag GmbH & Co. KGaA, Weinheim

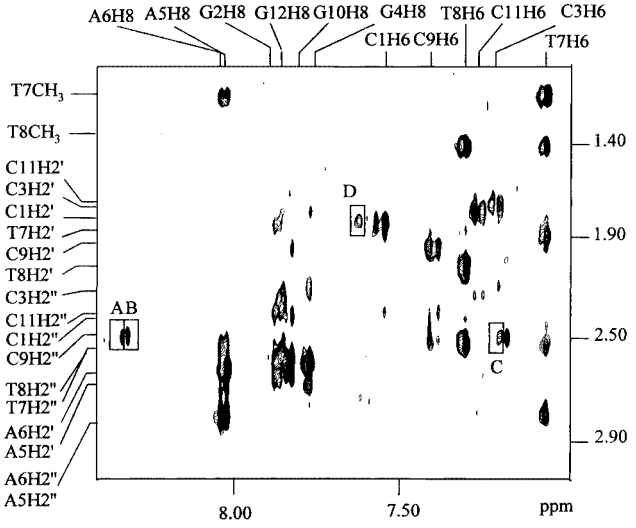

Figure 6. Part of the ^{1}H NOESY spectrum (τ_m = 400 ms) of the Δ-[Ru(bpy)$_2$(m-bpy-GHK)]Cl$_2$−[d(CGCGAATTCGCG)$_2$] adduct at a 1:1 molar ratio at 303 K with the oligonucleotide assignments of the base's aromatic protons (F2) and the major groove sugar protons H2′ and H2′′ for the bases adenine, thymine and cytosine (F1). The labeled cross peaks correspond to NOE contacts between the protons: (A) m-bpyH3′-C9H2′′, (B) bpyH3−C9H2′′, (C) m-bpyH5′-C9H2′′ (D) bpyH6H6′-C1H2′

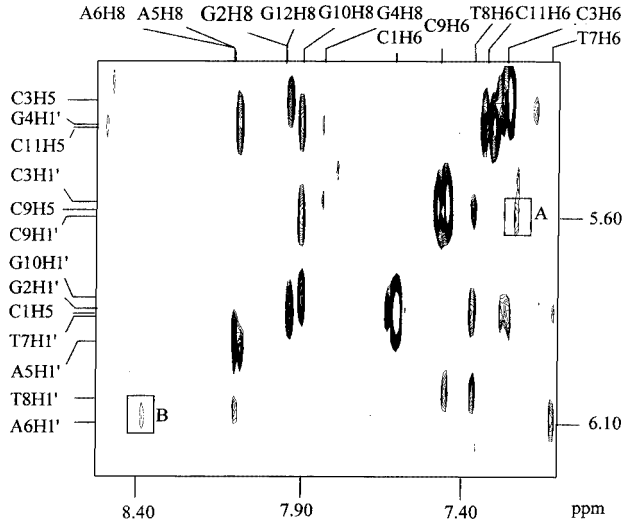

Figure 7. Part of the ^{1}H NOESY spectrum (τ_m = 400 ms) of the Λ-[Ru(bpy)$_2$(m-bpy-GHK)]Cl$_2$−[d(CGCGAATTCGCG)$_2$] adduct at a 1:1 molar ratio at 303 K with the oligonucleotide assignments of the base's aromatic protons (F2) and the minor groove sugar proton H1′ (F1). The labeled cross peaks correspond to NOEs between the protons: (A) m-bpyH5′-C9H1′, (B) m-bpyH3′-A6H1′

On the other hand, the intermolecular NOE contacts between Λ-[Ru(bpy)$_2$(m-bpy-GHK)]Cl$_2$ and the oligonucleotide are significantly less than in the case of the Δ isomer, suggesting a looser or non-specific binding of the isomer. A few of these take place between the ligand m-bpy protons H5′and H3′ with C9H1′ and the peptide backbone Gly-NH with the sugar proton H1′ of the base T8, all located in the helix minor groove. In contrast to the Δ isomer, no cross peak was observed between the other two bpy ligand protons of the complex and the oligonucleotide indicating that only the m-bpy-GHK moiety of the complex is close to [d(5′-CGCGAATTCGCG-3′)$_2$].

2.2.4 Binding Models

It is not possible to develop quantitative 3-D models of the way the diastereomers bind to the oligonucleotide duplex in the Ru^{II}complex/d[(CGCGAATTCGCG)$_2$] due to the fast exchange kinetics of the system, which does not allow taking all NOE results as distance constraints. Taking in to account (i) that there is no significant perturbation to the DNA helix (according to NOE's and the *inter* and *intra*-strand connectivity of the oligonucleotide protons), (ii) that the geometry around the Ru^{II} coordination sphere is fixed and (iii) that using selective NOE's that are not geometrically in disagreement, we have constructed simple binding models that are consistent with the observations from 1-D and 2-D NMR spectroscopy (Figure 8 and 9). The complexes manually docked at distances are consistent with the inter-proton NOE in many different combinations and the geometries of the complexes were optimized with respect to the "freeze" geometry of the Ru^{II} coordination sphere (angles and bond lengths) and the DNA structure. The structures which are more consistent with the NMR observations are presented in Figure 8 and 9.

The molecular model of the Δ-[Ru(bpy)$_2$(m-bpy-GHK)]$^{2+}$/d[CGCGAATTCGCG)$_2$] system shows the two bpy ligands of the complex close to the DNA bases, in agreement with the observed ≈0.2 ppm upfield shift changes of H3′ and H4′ in the 1-D NMR spectra. The location of the complex is also consistent with the small changes in the aromatic proton chemical shifts of the m-bpy-GHK ligand, oriented out of the helix groove and with the observed upfield shifts of the protons A5A6H2′, A5A6H2′′ and C3H5 (opposite G10), since the complex is located close to this part of the oligonucleotide. In the model of the Λ isomer (Figure 9), the bpy ligands are far from the DNA bases and the terminal positive amino group of the lysine is close to DNA phosphates, as has already been suggested based on the 1-D NMR spectra. The resultant model located Λ-[Ru(bpy)$_2$(m-bpy-GHK)]$^{2+}$ at the helix minor groove.

It is known that ruthenium tris-chelates involving 2,2′-bipyridine or 1,10-phenanthroline ligands bind at the DNA grooves. For example [Ru(phen)$_3$]$^{2+}$ [10] binds in the minor groove and [Ru(bpy)$_2$(phen)]$^{2+}$ shows a similar binding geometry.[52] In all cases, however, where the Ru^{II} complex comprises an intercalative ligand [e.g. dipyridophenazine (dppz)] together with two bpy or phen ligands, the complex binds to DNA through intercalation of this ligand between the bases and leads the other two ligands into the oligonucleotide minor groove (e.g. Δ-[Ru(phen)$_2$(dpq)]$^{2+}$,[12] Δ-[Ru(Me$_2$phen)$_2$(dppz)]$^{2+}$ [13] and [{Ru(Me$_2$bpy)$_2$}(μ-bpy)]$^{4+}$ [14]). Sometimes the "leader" ligand intercalates from the major groove as in the case of Δ-[Ru(phen)$_2$(dppz)]$^{2+}$ leading the phenanthroline molecules to be located next to the major groove.[11] The questions which thus arises are, what makes an octahedral Ru^{II} com-

 © 2004 Wiley-VCH Verlag GmbH & Co. KGaA, Weinheim

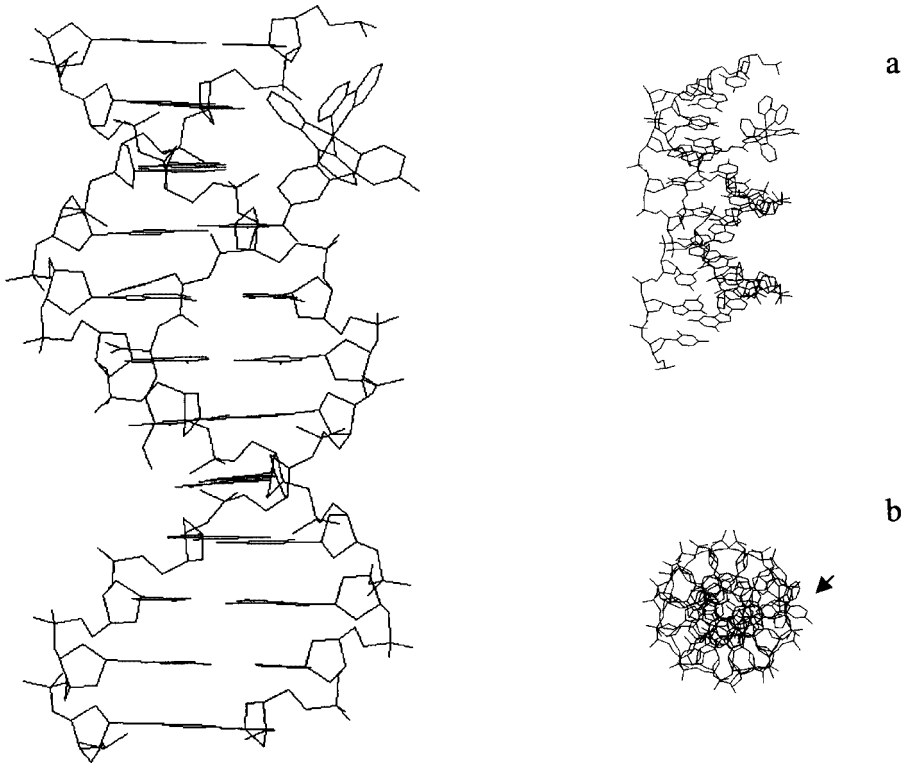

Figure 8. A molecular model of the interactions between Δ-[Ru(bpy)$_2$(m-bpy-GHK)]Cl$_2$ and [d(CGCGAATTCGCG)$_2$] reflects the average binding of the complex to the oligonucleotide. In the insets (a) a view across the major groove showing the complex orientation with the peptide back bone into the helix groove (b) top view along the *z*-axis showing a complex orientation where the peptide is bound to the oligonucleotide

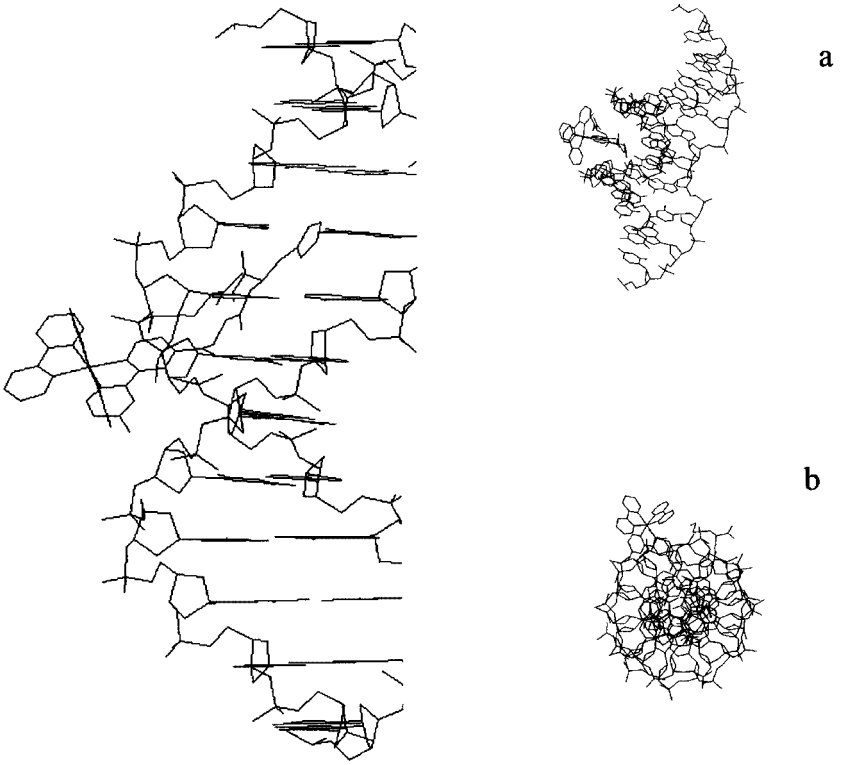

Figure 9. A molecular model of the interactions between Λ-[Ru(bpy)$_2$(m-bpy-GHK)]Cl$_2$ and the [d(CGCGAATTCGCG)$_2$] reflects the average binding of the complex to the oligonucleotide. In the insets (a) a view across the minor groove showing the complex orientation in the minor groove (b) top view along the *z*-axis showing the complex oriented with the m-bpy ligand towards to the helix

 © 2004 Wiley-VCH Verlag GmbH & Co. KGaA, Weinheim

plex approach from the minor or the major groove of the DNA helix? Is the intercalative ligand responsible for this?

In the case of Δ-[Ru(bpy)$_2$(m-bpy-GHK)]Cl$_2$ a non-intercalative and flexible ligand (m-bpy-GHK) which binds to the DNA major groove has been used, showing that it is probably the peptide which leads the other two bpy ligands of the isomer to interact with the major groove. In other words, the peptide affinity for the major groove is higher than that of Δ-[Ru(bpy)$_2$] for the minor. In contrast, the same ligand does not follow the same way of binding in the case of the Λ isomer. For this complex, the different orientation of the peptide (see Figure 4) from that in the Δ isomer gives the main role to the bpy ligands that lead the complex into the minor groove. In particular, in this context, the major groove binding of Δ-[Ru(bpy)$_2$(m-bpy-GHK)]Cl$_2$ is consistent with (i) the relative dimensions of the complex and the oligonucleotide major groove (estimated dimensions of the complex are 22 Å long and 11 Å wide, while the size of the major groove is 11.6 Å × 8.5 Å and the minor is 6.0 Å × 8.2 Å [53]), (ii) the formation of hydrogen bonds between the peptide backbone and the non-hydrogen bonded protons of the cytidine exocyclic NH_2 group, which was deduced from the 1-D NMR spectra, can be explained by an approach of the oligonucleotide by the complexes from the major groove, (iii) the fact that the major groove is rich in negatively charged phosphates and for this reason it prefers the positively charged cationic complex and the lysine's terminal NH_3^+ group as well. It seems that the peptide determines the way that the complex binds to the oligonucleotide followed by a possible binding of the other ligands.

In the case of the Λ isomer, weak intensity cross-peaks were observed only between the glycine NH with the H1′ of T8 and H3′/H5′, located on the one pyridine ring of the m-bpy ligand, with the A6 and C9H1′, indicating that only the m-bpy ligand of the complex interacts with the oligonucleotide probably from the minor groove.

3. Conclusion

In summary, it is concluded from the 1-D and 2-D NMR spectroscopic data that (i) the diastereomers bind to the oligonucleotide differently. The Δ isomer binds from the helix major groove, close to the central part of the sequence while the peptide moiety extends across the major groove from the base T8 to C11. The Λ isomer probably binds non-selectively, approaching the helix from the minor groove. (ii) The peptide binding, it would appear, leads the rest of the Δ isomer to interact with the oligonucleotide and thus may explain why the two bpy ligands were found to be located in the major groove in the case of the Δ isomer. The detection of sequence selectivity binding requires further studies with different DNA sequences. This work together with photo cleavage experiments of the oligonucleotides by such complexes is in progress.

4. Experimental Section

4.1. Starting Materials: All chemicals and solvents were of reagent grade and were used without further purification. The deoxynucleotide [d(5′-CGCGAATTCGCG-3′)] was purchased from OSWEL DNA (University of Southampton U.K.) and purified by chromatography on a 120 × 2.5 cm Sephadex G-25 superfine column, using distilled water as the eluent and lyophilized to dryness. The complexes *cis*-[Ru(bpy)$_2$Cl$_2$][18] Λ- and Δ-[Ru(bpy)$_2$(py)$_2$]A (where A = *O*,*O*′-dibenzoyltartaric acid) ,[19,20] and the ligand 4′-methyl-2,2′-bipyridine-4-carboxylic acid (m-bpy-COOH) were synthesized according to literature.[21]

4.2. Synthesis of the Peptide Conjugated Ru^{II} Complexes

Λ-, Δ-[Ru(bpy)$_2$(m-bpy-COOH)](PF$_6$)$_2$: Solid Λ- or Δ-[Ru(bpy)$_2$(py)$_2$]A (0.38 g) and m-bpy-COOH (0.105 g) were suspended in 70% ethanol in water (10 mL) and the mixture was heated to reflux overnight. The reaction mixture was cooled to room temperature and the solvent was reduced with a rotary evaporator to approximately 3 mL. After standing overnight, the mixture was filtered and the remaining solid was washed with water. The filtrate was acidified to pH = 1 by dropwise addition of aqueous 60% HPF_6 with vigorous stirring. The solid was collected on a fine-porosity glass filter, washed with water (2 × 5 mL), diethyl ether (2 × 5 mL) and oven dried at 110 °C overnight to provide pure Λ- or Δ-[Ru(bpy)$_2$(m-bpy-COOH)](PF$_6$)$_2$ as a red solid. Yield 0.30 g (82%). **Δ-[Ru(bpy)$_2$(m-bpy-COOH)](PF$_6$)$_2$:** $C_{32}H_{26}F_{12}N_6O_2P_2Ru$: calcd. C 41.9, H 2.9, N 9.2; found C 41.2, H 2.9, N 9.3. **Λ-[Ru(bpy)$_2$(m-bpy-COOH)](PF$_6$)$_2$:** $C_{32}H_{26}F_{12}N_6O_2P_2Ru$: calcd. C 41.9, H 2.9, N 9.2; found C 41.1, H 2.9, N 9.2.

Λ-, Δ-[Ru(bpy)$_2$(m-bpy-GHK)]Cl$_2$: Solid-phase peptide synthesis was used for peptide conjugation. The Fmoc strategy was followed using 2-chlorotrityl-H-Linker-Fmoc resin as the solid support. Piperidine was used as a deprotection reagent. DCC and HOBt were used as coupling reagents. The cleavage from the resin and the final deprotection of peptide side chain protecting groups were performed in one step by shaking with a 90% TFA solution in DMF. Anisol was used as a scavenger. The final products Λ- or Δ-[Ru(bpy)$_2$m-GHL]$^{2+}$ were isolated as trifuoroacetate salts which are insoluble in water. The trifluoroacetate anion was replaced by a chloride anion by mixing an acetone solution of the ruthenium peptide derivative with an excess of LiCl. [Ru(bpy)$_2$(m-bpy-GHK)]Cl$_2$ precipitated as an orange water soluble solid. The product was purified by reverse-phase HPLC using a DIONEX chromatograph and a Waters C18 column. Chromatography solvents were HPLC grade acetonitrile and water both containing 0.1% TFA. Yield approximately 30%. **Δ-[Ru(bpy)$_2$(m-bpy-GHK)]Cl$_2$:** ^{1}H NMR (500 MHz, D_2O, 10 mM, in 100 mM phosphate buffer, pH = 7.01, 303 K): δ = 8.83 (s, 1 H, m-bpy H3′), 8.54 (d, $^3J_{H,H}$ = 8.1 Hz, 4 H, bpy H3H3′), 8.48 (s, 1 H, m-bpy H3), 8.05 (t, $^3J_{H,H}$ = 7.5 Hz, 4 H, bpy H4H4′), 8.00 (d, $^3J_{H,H}$ = 5.8 Hz, 1 H, m-bpy H5), 7.79 (s, 1 H, His H2), 7.80 (d, $^3J_{H,H}$ = 5.7 Hz, 4 H, bpy H6H6′), 7.37 (t, $^3J_{H,H}$ = 6.3 Hz, 4 H, bpy H5H5′), 7.65 (d, $^3J_{H,H}$ = 5.8 Hz, 2 H, m-bpy H6H6′), 7.53 (s, 1 H, His H5), 7.27 (d, $^3J_{H,H}$ = 5.8 Hz, 1 H, m-bpy H5′), 4.63 (d, $^3J_{H,H}$ = 4.1 Hz, 1 H, His *a*-CH), 4.25 (d, $^3J_{H,H}$ = 4.2 Hz, 1 H, Lys *a*-CH), 4.17 (d, $^3J_{H,H}$ = 4.2 Hz, 1 H, Gly *a*-CH), 2.88 (t, $^3J_{H,H}$ = 7.5 Hz, 2 H, Lys ε-CH), 3.15 (m, $^3J_{H,H}$ = 7.5 Hz, 2 H, His β-CH), 2.49 (s, 3 H, m-bpy CH_3), 1.80 (m, 2 H, Lys β-CH), 1.67 (t, $^3J_{H,H}$ = 6.3 Hz, 2 H, Lys δ-CH), 1.37 (m, 2 H, Lys γ-CH), ppm. **Λ-[Ru(bpy)$_2$(m-bpy-GHK)]Cl$_2$:** ^{1}H NMR (500 MHz, D_2O, 10 mM, in 100 mM phosphate buffer, pH = 7.01, 303 K): δ = 8.83 (s, 1 H, m-bpy H3′), 8.54 (d, $^3J_{H,H}$ = 8.6 Hz, 4 H, bpy H3H3′),

 © 2004 Wiley-VCH Verlag GmbH & Co. KGaA, Weinheim

8.47 (s, 1 H, m-bpy H3), 8.05 (t, $^3J_{H,H}$ = 7.5 Hz, 4 H, bpy H4H4′), 8.00 (d, $^3J_{H,H}$ = 5.8 Hz, 1 H, m-bpy H5), 7.80 (d, $^3J_{H,H}$ = 5.7 Hz, 4 H, bpy H6H6′), 7.80 (s, 1 H, His H2), 7.65 (d, $^3J_{H,H}$ = 5.8 Hz, 2 H, m-bpy H6H6′), 7.54 (s, 1 H, His H5), 7.38 (t, $^3J_{H,H}$ = 6.3 Hz, 4 H, bpy H5H5′), 7.27 (d, $^3J_{H,H}$ = 5.8 Hz, 1 H, m-bpy H5′), 4.65 (d, $^3J_{H,H}$ = 5.0 Hz, 1 H, His *a*-CH), 4.26 (d, $^3J_{H,H}$ = 4.2 Hz, 1 H, Lys *a*-CH), 4.17 (d, $^3J_{H,H}$ = 4.6 Hz, 1 H, Gly *a*-CH), 3.17 (m, $^3J_{H,H}$ = 7.6 Hz, 2 H, His β-CH), 2.90 (t, $^3J_{H,H}$ = 7.5 Hz, 2 H, Lys ε-CH), 2.54 (s, 3 H, m-bpy CH_3), 1.82 (m, 2 H, Lys β-CH), 1.67 (t, $^3J_{H,H}$ = 6.3 Hz, 2 H, Lys δ-CH), 1.38 (m, 2 H, Lys γ-CH) ppm. **Δ-[Ru(bpy)$_2$(m-bpy-GHK)]Cl$_2$:** $C_{45}H_{49}F_{12}N_{13}O_4P_2Ru$: calcd. C 48.8, H 4.4, N 16.4; found C 49.0, H 4.5, N 16.4. **Λ-[Ru(bpy)$_2$(m-bpy-GHK)]Cl$_2$:** $C_{45}H_{49}F_{12}N_{13}O_4P_2Ru$: calcd. C 48.8, H 4.4, N 16.4; found C 48.7, H 4.6, N 16.3.

4.3. Physical Measurements

4.3.1 NMR Spectroscopy

Measurements were made with a Varian Unity-500 MHz instrument. 1-D ^{1}H NMR spectra were recorded at 303 K into 4096 data points, with a 6024 Hz spectral width after 128 transients. The water resonance was suppressed with a time-shared Redfield "2-1-4"-pulse. ^{1}H NOESY spectra were recorded in phase sensitive mode with a total 2048 × 256 points for a mixing time of 200 to 400ms, while ^{1}H ROESY spectra had mixing times (τ_m) of 60−120 ms. ^{1}H DQFCOSY spectra were collected using the TPPI method with a spectral width of 3125 Hz with a total of 2048 × 256 points and a relaxation delay of 1.5 s.

The amounts of the oligonucleotide were estimated by weighing, and the concentration of the sample was determined using its absorption at 260 nm .[22] In all NMR experiments carried out, a 100 mM Na_2HPO_4/NaH_2PO_4 (pH = 7.00) buffer was used. The lyophilized samples were dissolved in D_2O (99.96) and lyophilized again to dryness. These samples were finally dissolved in D_2O (99.996, 0.4 mL) and transferred to 5 mm NMR tubes.

The 1-D ^{1}H NMR spectra were recorded with sample concentration ≈ 100 OD_{260} units while 2-D NOE experiments were carried out in more concentrated samples (≈ 300 OD_{260}). ^{1}H NMR spectra of the labile oligonucleotide protons were recorded in 90% H_2O 10% D_2O (field-frequency lock). No internal chemical shift reference was added to the samples.

4.3.2 Electrospray Mass Spectrometry

ESI mass spectra were acquired with a Micromass Q-Tof quadrupole MS instrument. All spectra were recorded in TOF (time of flight) mode with a source temperature of 80 °C, and low cone voltage (ΔCS = 100−120V) to obtain gentle interface conditions.

4.3.3 CD spectroscopy

CD spectra were recorded with a Jasco J-720 spectropolarimeter. A 0.1-cm path length cuvette was used for the 190−250 nm region while a 2-cm path length cuvette was used for the 250−540 nm region. The blank was subtracted from the CD spectrum of the sample. Smoothing of the curves was performed using the Adjacent Averaging method from Microcal Origin 6.0.

4.4. Molecular Modeling

The 3-D binding models were constructed using the HyperChem. v. 6.0 molecular modeling software. The model of the oligonucleotide [d(CGCGAATTCGCG)$_2$] duplex was based on a standard B-type structure with a C2′ *endo* sugar conformation using the database of the program. The Ru^{II} complex was constructed in two steps. Firstly, the coordination sphere of the ruthenium was constructed using crystal structure data of similar complexes [23] and secondly, the peptide was conjugated at the 4th position of the ligand m-bpy. The complex was then manually docked close to the oligonucleotide duplex with respect to the observed NOE contacts, which were inserted as distance restraints. The NOE cross peaks were classified into three categories: weak (5 Å), medium (4 Å) and strong (3 Å) relative to the volume integral of the cytosine CH5/CH6 cross peak. Selective NOEs from the nine observations (Table 4) for Δ-[Ru(bpy)$_2$(m-bpy-GHK)]Cl$_2$ were inserted as distance restraints and the complexes were selectively and briefly energy minimized in the presence of the oligonucleotide using the AMBER force field. Several structures from different combinations of the intermolecular NOEs were observed and the most consistent one with the NMR spectroscopic data was presented as a possible binding model of the complex to the oligonucleotide duplex. In the case of Λ-[Ru(bpy)$_2$(m-bpy-GHK)]Cl$_2$, a similar procedure was followed and a structure that was more consistent with the NMR observations was maintained. Graphical outputs were obtained from the selected structures with the RasMol v. 2.6 software.

Acknowledgments

This work was supported by a PENED 2001 grant of the General Secretary of Research and Technology of the Greek Ministry of Industry.

[1] [1a] M. J. Waring, *Annu. Rev. Biochem.* **1981**, *50*, 159−192. [1b] L. H. Hurley, *J. Med. Chem.* **1989**, *32*, 2027−2033.
[2] H. Umezawa, K. Maeda, T. Takeuchi, Y. Okami, *J. Antibiot.* **1996**, *19A*, 200−209.
[3] D. S. Sigman, A. Mazumder, D. M. Perrin, *Chem. Rev.* **1993**, *93*, 2295−2316.
[4] S. L. Gronovski, V. A. Zubarev, *Nucleic Acid Res.* **1991**, *19*, 257−264.
[5] C. Bailly, J. S. Sun, P. Colson, C. Houssier, C. Helene, M. J. Waring, J. P. Henichart, *Bioconjugate Chem.* **1992**, *3*, 100−103.
[6] S. L. Gronovski, V. A. Nikolaev, V. A. Zubarev, A. N. Suroyava, A. L. Zhuze, B. K. Chernov, N. Y. Sidorova, A. S. Zasedatelev, G. V. Gurskii, *Mol. Biol.* **1993**, *6*, 839−849.
[7] N. J. Sardesai, J. K. Barton, *J. Biol. Inorg. Chem.* **1997**, *2*, 762−765.
[8] S. Rutier, J. L. Bernier, J. P. Catteau, C. Bailly, *Bioorg. Med. Chem. Lett.* **1977**, *7*, 1729−1730.
[9] I. Ortmans, C. Moucheron, A. Kirsch-De Mesmaeker, *Coord. Chem. Rev.* **1998**, *168*, 233−271.
[10] M. Eriksson, M. Leijon, C. Hiort, B. Norden, A. Graslund, *J. Am. Chem. Soc.* **1992**, *114*, 4933−4934.
[11] C. M. Dupureur, J. K. Barton, *Inorg. Chem.* **1997**, *36*, 33−38.
[12] J. G. Collins, A. D. Sleeman, J. R. Aldrich-Wright, I. Greguric, T. W. Hampley, *Inorg. Chem.* **1998**, *37*, 3133−3141.
[13] A. Greguric, I. D. Greguric, T. W. Hampley, J. R. Aldrich-Wright, J. G. Collins, *J. Chem. Soc., Dalton Trans.* **2002**, 849−855.
[14] F. M. Foley, F. R. Keene, J. G. Collins, *J. Chem. Soc., Dalton Trans.* **2001**, 2968−2974.
[15] A. Garoufis, J. G. Liu, L. N. Ji, N. Hadjiliadis, *J. Inorg. Biochem.* **2003**, *93*, 221−234.
[16] H. Drew, R. E. Dickerson, *J. Mol. Biol.* **1981**, *151*, 5353−5356.
[17] W. Nerdal, D. R. Hare, B. R. Reid, *Biochemistry* **1989**, *28*, 10008−10021.
[18] B. P. Sullivan, D. J. Salmon, T. J. Meyer, *Inorg. Chem.* **1978**, *17*, 3334−3341.
[19] O. Morgan, S. Wang, S. A. Bac, R. J. Morgen, R. D. Baker, T. C. Strekas, R. Engel, *J. Chem. Soc., Dalton Trans.* **1977**, 3773−3776.
[20] J. G. Liu, B. H. Ye, Q. L. Zhang, X. H. Zou, Q. X. Zhen, X. Tian, L. N. Ji, *J. Biol. Inorg. Chem.* **2000**, *5*, 119−128.

 © 2004 Wiley-VCH Verlag GmbH & Co. KGaA, Weinheim

[21] B. M. Peek, G. T. Ross, S. W. Edwards, G. J. Meyer, T. J. Meyer, B. W. Erickson, *Int. J. Peptide Protein Res.* **1991**, *38*, 114−123.
[22] P. N. Borer, in *Handbook of Biochemistry and Molecular Biology* (Ed.: G. D. Fasman), CRC, Cleveland, **1975**, p. 589−590.
[23] B. Kolp, H. Viebrock, A. von Zelewsky, D. Abeln, *Inorg. Chem.* **2001**, *40*, 1196−1198.
[24] P. Liska, N. Vlachopoulos, M. K. Nazeeruddin, P. Comte, M. Gratzel, *J. Am. Chem. Soc.* **1988**, *110*, 3686−3687.
[25] K. Barlos, O. Chatzi, D. Gatos, G. Stavropoulos, *Int. J. Peptide Protein Res.* **1991**, *37*, 513−520.
[26] I. V. Chernushevich, W. Ens, K. G. Standing, in *Electrospray Ionization Mass Spectrometry* (Ed.: R. B. Cole), John Wiley & Sons, Inc., **1997**, p. 203−234.
[27] http://www.imb-jena.de
[28] T. J. Rutherford, O. V. Gijte, A. Kirsch-De Mesmaeker, F. R. Keene, *Inorg. Chem.* **1997**, *36*, 4465−4474.
[29] A. Garoufis, A. Koutsodimou, N. Katsaros, C. A. Mitsopoulou, N. Hadjiliadis, *Polyhedron* **1999**, *18*, 361−369.
[30] G. Orellana, C. A. Ibarra, J. Santoro, *Inorg. Chem.* **1988**, *27*, 1025−1030.
[31] B. V. Cheney, *J. Am. Chem. Soc.* **1968**, *90*, 5386−5390.
[32] W. Saenger, *Principles of Nucleic Acid Structures*, Springer Verlag, **1984**.
[33] M. Rance, O. W. Sorensen, G. Bodenhousen, G. Wagner, R. R. Ernst, K. Wuthrich, *Biochem. Biophys. Res. Commun.* **1983**, 479−485.
[34] D. J. Patel, L. Shapiro, D. Hare, *J. Biol. Chem.* **1986**, *261*, 1233−1240.
[35] D. R. Hare, D. E. Wemmer, S. H. Chou, J. Drobny, *J. Mol. Biol.* **1983**, *169*, 319−336.
[36] R. M. Scheek, N. Russo, R. Boelens, R. Kaptein, J. H. van Boom, *J. Am. Chem. Soc.* **1983**, *105*, 2914−2916.
[37] R. M. Scheek, R. Boelens, N. Russo, J. H. van Boom, R. Kaptein, *Biochemistry* **1984**, *23*, 1371−1376.
[38] J. G. Pelton, D. E. Wemmer, *Biochemitry* **1988**, *22*, 8088−8096.
[39] E. M. Proudfoot, J. P. Mackay, P. Karuso, *Biochemistry* **2001**, *40*, 4867−4878.
[40] E. M. Proudfoot, J. P. Mackay, R. S. Vagg, K. A. Vickery, P. A. Williams, P. Karuso, *Chem. Commun.* **1997**, 1623−1628.
[41] C. Giessner-Prettre, B. Pulman, *Acad. Sci. Paris Ser. D* **1976**, *283*, 675−676.
[42] C. Giessner-Prettre, B. Pulman, P. N. Borer, L. S. Kan, P. O. P. Ts'o, *Biopolymers* **1976**, *15*, 2277−2286.
[43] W. D. Wilson, Y. Li., J. M. Veal, in *Advances in DNA Sequence Specific Agents* (Ed.: L. H. Hurley), JAI Pres Inc., Greenwich, Connecticut, **1992**, vol. 1, p. 89−165.
[44] C. V. Kumar, J. K. Barton, N. J. Turro, *J. Am. Chem. Soc.* **1985**, *107*, 5518−5523.
[45] R. Barthwal, A. Mujeeb, S. Kukreti, A. Gupta, G. Govil, *J. Mol. Recogn.* **1991**, *4*, 45−52.
[46] F. Brun, J. J. Toulme, C. Helene, *Biochemistry* **1975**, *14*, 558−563.
[47] J. G. Moe, I. M. Russu, *Nucleic Acids Res.* **1990**, *18*, 821−827.
[48] E. Liepinh, G. Otting, K. Wuthrich, *Nucleic Acids Res.* **1992**, *24*, 6549−6553.
[49] N. A. Froystein, E. Sletten, *J. Am. Chem. Soc.* **1994**, *116*, 3240−3250.
[50] R. E. Klevit, D. E. Wemmer, B. R. Reid, *Biochemistry* **1986**, *25*, 3296−3303.
[51] E. Moldreim, M. J. Hannon, I. Meisterman, A. Rodger, E. Sletten, *J. Inorg. Biol. Chem.* **2002**, *7*, 770−780.
[52] P. Lincoln, B. Norden, *J. Phys. Chem. B* **1998**, *102*, 9583−9594.
[53] S. Neidle, *DNA Structure and Recognition*, IRL Press, Oxford, **1994**, p. 33−34.

Received October 10, 2003
Early View Article
Published Online February 26, 2004

 © 2004 Wiley-VCH Verlag GmbH & Co. KGaA, Weinheim

Hydrolytic Cleavage of DNA by Ternary Amino Acid Schiff Base Copper(II) Complexes Having Planar Heterocyclic Ligands

Pattubala A. N. Reddy,[a] Munirathinam Nethaji,[a] and Akhil R. Chakravarty*[a]

Keywords: Copper / Synthetic hydrolase / X-ray diffraction / Schiff bases / Phenanthroline bases

The ternary copper(II) complexes [Cu(salgly)L] (L = phen, **1**; dpq, **2**), [Cu(salala)L] (L = phen, **3**; dpq, **4**) and [Cu(salphe)L] (L = phen, **5**; dpq, **6**), where salgly, salala and salphe are tridentate Schiff-base ligands derived from the condensation of salicylaldehyde with glycine, L-alanine and L-phenylalanine, respectively, are prepared and their nuclease activity studied (phen, 1,10-phenanthroline; dpq, dipyridoquinoxaline). The crystal structure of **3** displays a distorted square-pyramidal (4+1) coordination geometry in which the ONO-donor Schiff base is bonded to the metal atom in the basal plane. The chelating phen ligand displays an axial–equatorial mode of bonding. The complexes exhibit a d–d band near 670 nm and a charge transfer band near 370 nm in methanol. The one-electron paramagnetic complexes display axial EPR spectra in DMF glass at 77 K, indicating a $\{d_{x^2-y^2}\}^1$ ground state. The complexes are redox-active and exhibit a quasi-reversible Cu^{II}/Cu^{I} couple in DMF at approximately –0.6 V vs. SCE. They show catalytic activity in the oxidation of ascorbic acid by molecular oxygen. The ability of the complexes to bind calf thymus (CT) DNA follows the order: **2** ≈ **4** ≈ **6** > **1** ≈ **3** ≈ **5**. Complexes **1**–**6** show oxidative DNA cleavage activity in the presence of mercaptopropionic acid as a reducing agent. All the complexes show hydrolytic cleavage activity in the absence of light or any reducing agent. The oxidative and hydrolytic DNA cleavage efficiencies follow the order: **2** ≈ **4** ≈ **6** > **1** ≈ **3** ≈ **5**. The dpq complexes, which have a greater DNA binding ability, display enhanced nuclease activity than their phen analogues. The hydrolytic DNA cleavage rate of 1.8 h^{-1}, observed for **2**, is significantly high relative to most of the known copper-based synthetic hydrolases. Mechanistic pathways involved in the nuclease activity of the complexes are discussed.

(© Wiley-VCH Verlag GmbH & Co. KGaA, 69451 Weinheim, Germany, 2004)

Introduction

Designing metal complexes suitable for cleaving DNA under hydrolytic conditions is of considerable importance considering the advantages of a process that produces fragments similar to those formed by the restriction enzymes, relative to other nucleolytic processes, viz. oxidative cleavage of DNA in the presence of additives or photo-induced DNA cleavage.[1–10] While photo-cleavers require the presence of a photo-sensitizer that can be activated on irradiation with UV or visible light, the redox-active "chemical nucleases" are effective cleavers of DNA in the presence of a reducing agent or H_2O_2 as an additive.[11–21] The mechanistic pathways in the oxidative process generally involve abstraction of sugar hydrogen, electron transfer, or guanine base oxidation, depending on the reaction conditions. The oxidative processes form cleaved products that are not readily amenable to further enzymatic manipulations, and thus have limited use in molecular biology. The synthetic metallohydrolases, on the other hand, follow a mechanistic pathway targeted at the phosphodiester bonds linking the nucleosides, and involves metal-promoted acid/base catalysis which leads to the formation of fragments that can be used for further enzymatic religation. Among several types of transition metal complexes used as synthetic hydrolases, copper(II) and zinc(II) complexes are better suited for the hydrolysis of DNA due to the strong Lewis acid properties of these metal ions.

The present work stems from our interest to design ternary copper(II) complexes with amino acid based Schiff-base ligands and planar NN-donor heterocyclic ligands. While 1,10-phenanthroline (phen) and dipyridoquinoxaline (dpq) are used for binding to DNA, the Schiff bases containing different α-amino acids are designed to participate in the acid/base activity through their potentially labile carboxylate and/or phenolate oxygen atom binding site(s). We have synthesized a series of new ternary complexes, viz. [Cu(salgly)(L)] (L = phen, **1**; dpq, **2**), [Cu(salala)(L)] (L = phen, **3**; dpq, **4**) and [Cu(salphe)L] (L = phen, **5**; dpq, **6**), where salgly, salala and salphe are tridentate Schiff-base ligands derived from the condensation of salicylaldehyde with glycine, L-alanine and L-phenylalanine, respectively (Scheme 1). Complex **3** has been structurally characterized by X-ray crystallography. An important observation from

[a] Department of Inorganic and Physical Chemistry, Indian Institute of Science,
Bangalore 560012, India
Fax: (internat.) + 91-80-23600683
E-mail: arc@ipc.iisc.ernet.in

Supporting information for this article is available on the WWW under http://www.eurjic.org or from the author.

 © 2004 Wiley-VCH Verlag GmbH & Co. KGaA, Weinheim **DOI: 10.1002/ejic.200300514**

this study is the efficient hydrolytic DNA cleavage activities of the dpq complexes, with complex **2** showing a hydrolysis rate that is significantly higher than those generally observed for copper(II)-based synthetic hydrolases.[4,7]

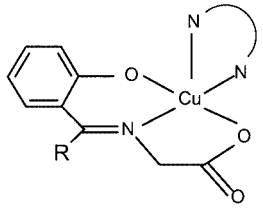

[Cu(salgly)(phen)] (R=H, **1**)
[Cu(salgly)(dpq)] (R=H, **2**)
[Cu(salala)(phen)] (R=Me, **3**)
[Cu(salala)(dpq)] (R=Me, **4**)
[Cu(salphe)(phen)] (R=CH_2Ph, **5**)
[Cu(salphe)(dpq)] (R=CH_2Ph, **6**)

Scheme 1

Results and Discussion

Synthesis and General Aspects

Complexes **1** and **2** have been prepared in high yields by the reactions of [Cu(salgly)(H_2O)]·0.5H_2O with 1,10-phenanthroline (phen) and dipyridoquinoxaline (dpq), respectively. Complexes **3**−**6** have been synthesized by the reactions of copper(II) acetate hydrate with the Schiff base H_2salala or H_2salphe in the presence of phen or dpq. The ternary complexes are stable in the solid state and moderately stable in solution. They have been characterized by elemental analysis, and from spectral and magnetic data (Table 1).

The non-electrolytic and one-electron paramagnetic ($\mu_{eff} \approx 1.8\ \mu_B$ at 25 °C) complexes show infrared spectral features that are characteristic of the Schiff base and the heterocyclic ligand. The carboxyl C=O stretch of the Schiff base is observed in the range 1620−1650 cm^{-1}. The electronic spectra of the complexes in methanol display a d-d band near 670 nm. In addition, the complexes exhibit a charge transfer (CT) transition at ca. 370 nm. They present an axial EPR spectrum in DMF-glass at 77 K, with a $g_{\|}$ value of ca. 2.22 ($A_{\|} \approx 170 \times 10^{-4}\ cm^{-1}$) and a $g_{\perp}$ value of 1.98, suggesting a $\{d_{x^2-y^2}\}^1$ ground state and a tetragonally distorted geometry for the complexes.[22] The Schiff bases H_2salala and H_2salphe are optically active. Complexes **3** and **4**, containing the dianionic salala ligand, are found to be optically active. In contrast, complexes **5** and **6** with the salphe ligand do not show any optical rotation; racemization could possibly have taken place as a result of complexation with the metal ion. A similar process has been reported earlier for phenylalanine-based Schiff-base complexes.[23,24]

Crystal Structure

Complex **3** has been characterized by single-crystal X-ray diffraction. The ORTEP view of the complex is shown in Figure 1. Selected bond lengths and angles are given in Table 2. The complex crystallizes in the monoclinic space group C_2 with two complexes and ten water molecules in the crystallographic asymmetric unit. The α-carbon atom of the amino acid Schiff base has an (*S*) configuration in both molecules. Based on the structural data, the complex has been formulated as [Cu{sal-(*S*)-ala}(phen)]·5H_2O. The crystal structure of the complex reveals the presence of a ternary structure consisting of a tridentate ONO-donor Schiff base, a bidentate N,N-donor heterocyclic base and a copper(II) center in the discrete monomeric species.[24] In the five-coordinate structure, the Schiff base is situated in the basal plane. The phen ligand displays axial-equatorial coordination. The distortion from the square-pyramidal geometry can be estimated from the τ values, 0.23 and 0.2, for two independent molecules in the asymmetric unit.[25] Significant hydrogen-bonding interactions involving the water molecules are observed. The complex displays intermolecular π-π stacking interactions of the phenolate phenyl moieties.

Redox and Catalytic Properties

The electron transfer behavior of complexes **1**−**6** was studied by cyclic and differential pulse voltammetric techniques using a glassy carbon working electrode in dimethylformamide (DMF); 0.1 M TBAP was used as the electrolyte. The electrochemical data are given in Table 1. The complexes exhibit a quasi-reversible cyclic voltammetric response near −0.6 V vs. SCE in DMF, with large ΔE_p values at a scan rate of 50 $mV \cdot s^{-1}$. The redox process is assigned to the Cu^{II}/Cu^{I} couple. The reduced species is unstable in the voltammetric time scale as can be seen from the i_{pa}/i_{pc} ratio which is less than 1 (i_{pa} and i_{pc} are the anodic and cathodic peak currents, respectively).

Table 1. Physico-chemical data for the ternary complexes **1**−**6**

Entry	Complex	IR[a] [cm^{-1}]		λ [nm] (ε [$dm^3\ M^{-1} \cdot cm^{-1}$])[b]		EPR[c]		Cyclic voltammetry[d]
		ν(C=O)	ν(C=N)	d-d band	CT band	g ($10^4 \times A$ [cm^{-1}])	$g_{\perp}$	$E_{1/2}$ [V] (ΔE_p [mV])
1	[Cu(salgly)(phen)] (**1**)	1642	1595	672 (103)	368 (3600)	2.21 (155)	1.99	−0.33 (440)
2	[Cu(salgly)(dpq)] (**2**)	1642	1605	660 (190)	369 (4300)	2.23 (175)	1.89	−0.26 (290)
3	[Cu(salala)(phen)] (**3**)	1635	1596	671 (98)	369 (4100)	2.19 (150)	1.98	−0.57 (600)
4	[Cu(salala)(dpq)] (**4**)	1605	1575	668 (229)	368 (4420)	2.22 (165)	2.00	−0.44 (255)
5	[Cu(salphe)(phen)] (**5**)	1625	1595	665 (195)	369 (3400)	2.25 (169)	2.05	−0.76 (160)
6	[Cu(salphe)(dpq)] (**6**)	1636	1599	663 (210)	369 (4150)	2.25 (175)	1.99	−0.65 (210)

[a] KBr disc. [b] In MeOH. [c] In DMF glass at 77 K. [d] CV data for the Cu^{II}/Cu^{I} couple in DMF/0.1 M TBAP. $E_{1/2} = 0.5(E_{pa} + E_{pc})$, $\Delta E_p = E_{pa} - E_{pc}$, where E_{pa} and E_{pc} are anodic and cathodic peak potentials, respectively. Scan rate, 50 mV s^{-1}.

 © 2004 Wiley-VCH Verlag GmbH & Co. KGaA, Weinheim

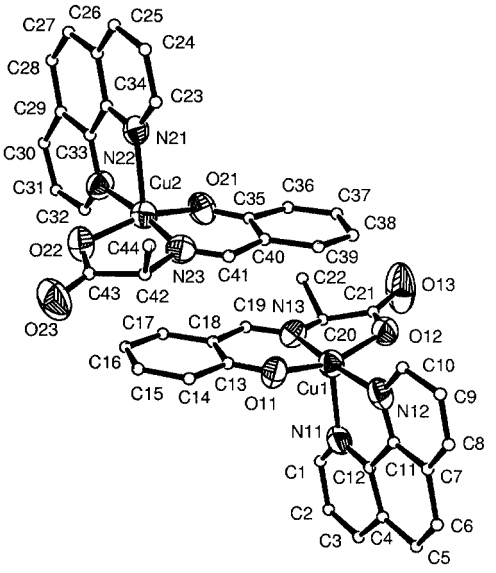

Figure 1. ORTEP diagram for two independent complexes of $[Cu(salala)(phen)]\cdot 5H_2O$ (**3**·$5H_2O$) with atom labeling scheme and thermal ellipsoids at the 50% probability level

Table 2. Selected bond lengths [Å] and bond angles [°] data for two independent molecules of $[Cu(salala)(phen)]\cdot 5H_2O$ (**3**·$5H_2O$) with e.s.d.s in the parenthesis

Molecule 1		Molecule 2	
Cu(1)−O(11)	1.918(7)	Cu(2)−O(21)	1.947(7)
Cu(1)−O(12)	1.982(7)	Cu(2)−O(22)	1.973(7)
Cu(1)−N(11)	2.280(9)	Cu(2)−N(21)	2.268(9)
Cu(1)−N(12)	1.994(9)	Cu(2)−N(22)	2.028(11)
Cu(1)−N(13)	1.899(10)	Cu(2)−N(23)	1.944(9)
O(11)−Cu(1)−O(12)	162.0(4)	O(21)−Cu(2)−O(22)	159.3(4)
O(11)−Cu(1)−N(11)	98.9(3)	O(21)−Cu(2)−N(21)	101.7(3)
O(11)−Cu(1)−N(12)	91.8(4)	O(21)−Cu(2)−N(22)	92.3(4)
O(11)−Cu(1)−N(13)	94.4(4)	O(21)−Cu(2)−N(23)	94.5(3)
O(12)−Cu(1)−N(11)	99.0(3)	O(22)−Cu(2)−N(21)	98.9(3)
O(12)−Cu(1)−N(12)	90.0(4)	O(22)−Cu(2)−N(22)	91.1(4)
O(12)−Cu(1)−N(13)	82.7(4)	O(22)−Cu(2)−N(23)	82.4(4)
N(11)−Cu(1)−N(12)	78.4(4)	N(21)−Cu(2)−N(22)	78.0(4)
N(11)−Cu(1)−N(13)	105.0(3)	N(21)−Cu(2)−N(23)	101.1(3)
N(12)−Cu(1)−N(13)	172.3(4)	N(22)−Cu(2)−N(23)	173.2(4)

Complexes **1**−**6** react readily with ascorbic acid (H_2A) in aqueous methanol to form an unstable brown copper(I) species, which readily converts to the parent copper(II) complex. The complexes retain the structure during the catalytic reaction with a H_2A/complex molar ratio of ca 30:1. Excess addition of H_2A leads to the formation of an inactive oxalato species, analyzed as [CuL(ox)] (ox = oxalate dianion). Oxalic acid is formed from the oxidation of the dehydroascorbate species (A).[26] The reduced copper(I) complex converts to the moderately stable bis(phen)- or bis(dpq)copper(I) species under an inert gas.

Oxidative Cleavage of DNA

The ability of the complexes **1**−**6** in inducing DNA cleavage has been studied by gel electrophoresis using supercoiled pUC19 DNA in 50 mM Tris-HCl/50 mM NaCl buffer (pH = 7.2). On reaction with SC DNA in the presence of mercaptopropionic acid (MPA), complexes **1**−**6** show nuclease activity (Figure 2). Control experiments using only complex **2** or MPA do not show any apparent DNA cleavage under similar experimental conditions. Complexes such as $[Cu(salgly)(H_2O)]$[27] and $[Cu(salgly)(bpy)]$[24] also do not cleave DNA in the presence of MPA. This indicates the necessity of planar heterocyclic bases such as phen or dpq for oxidative DNA cleavage. The DNA cleavage efficiencies of the complexes follow the order: **2** ≈ **4** ≈ **6** > **1** ≈ **3** ≈ **5**. The % DNA cleaved observed for the dpq complexes in the presence of MPA is similar to that observed for the bis(phen)copper(II) complex which is used as a standard (Table 3).[28] A 40 μM concentration of the dpq complex **2** showed complete conversion of the initial SC form to the NC form, while for the phen analogue, only 38% conversion of the SC form was seen. The similar values for the % DNA cleaved by the three dpq complexes suggests only a minor effect of the organic moieties, such as the methyl or benzyl group of the amino acid based Schiff bases, on the cleavage efficiency. Mechanistic studies involving the addition of the minor groove binder distamycin showed complete inhibition of the cleavage process, suggesting the minor groove binding preference of the complexes.[29] Fluorescence spectral studies using ethidium bromide as a probe shows a greater DNA binding ability of the dpq complexes than their phen analogues. The binding ability of the dpq complexes is similar to that observed for the bis(phen)copper(II) complex under similar experimental conditions. The hydroxyl radical scavenger DMSO completely inhibits the cleavage reaction. This indicates the possible involvement of the hydroxyl radical and/or the reactive copper−oxo species in the cleavage pathway. A similar pathway was pro-

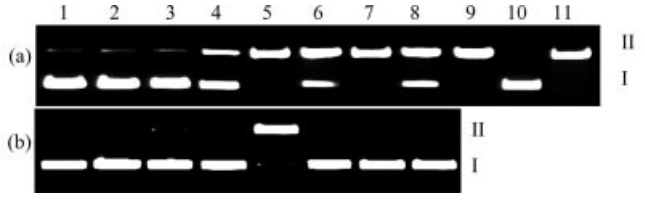

Figure 2. (a) Gel diagram showing the oxidative cleavage of supercoiled pUC19 DNA (0.5 μg) by complexes **1**−**6** and $[Cu(phen)_2(H_2O)](ClO_4)_2$ in the presence of 3-mercaptopropionic acid (MPA, 5 mM) and in the dark in 50 mM Tris-HCl/NaCl buffer containing DMF (10%): lane 1, DNA control; lane 2, DNA + MPA; lane 3, DNA + **2**; lane 4, DNA + MPA + **1**; lane 5, DNA + MPA + **2**; lane 6, DNA + MPA + **3**; lane 7, DNA + MPA + **4**; lane 8, DNA + MPA + **5**; lane 9, DNA + MPA + **6**; lane 10, DNA + MPA + $[Cu(salgly)(H_2O)]$; lane 11, DNA + MPA + $[Cu(phen)_2(H_2O)]^{2+}$; the complex concentration was 40 μM; forms I and II are supercoiled and nicked circular forms of DNA, respectively; (b) gel electrophoresis diagram for the cleavage of pUC19 DNA with complex **2** (40 μM) and MPA in the presence of different inhibiting reagents and in the dark in 50 mM Tris-HCl/NaCl buffer at 37 °C containing DMF (10%): lane 1, DNA control; lane 2, DNA + DMSO; lane 3, DNA + mannitol; lane 4, DNA + distamycin; lane 5, DNA + **2** + MPA; lane 6, DNA + DMSO + **2** + MPA; lane 7, DNA + mannitol + **2** + MPA; lane 8, DNA + distamycin + **2** + MPA; in the inhibition reactions, the reagent has been added to the DNA prior to the addition of the complex and MPA

 © 2004 Wiley-VCH Verlag GmbH & Co. KGaA, Weinheim

Table 3. DNA (SC pUC19, 0.5 μg) cleavage data of **1**−**6** and bis(phen)Cu^{II} complex in the dark, and in the presence of mercaptopropionic acid (MPA, 5 mM) and in the presence of different reagents in Tris-HCl buffer

Sl no.	Reaction conditions[a]	Form I [%] (SC)	Form II [%] (NC)
1	DNA control	98	2
2	DNA + MPA	97	3
3	DNA +**2**	97	3
4	DNA + MPA + **1**	62	38
5	DNA + MPA + **2**	2	98
6	DNA + MPA + **3**	40	60
7	DNA + MPA + **4**	1	99
8	DNA + MPA + **5**	34	66
9	DNA + MPA + **6**	1	99
10	DNA + MPA + [Cu(salgly)(H_2O)]	98	2
11	DNA + MPA + [Cu(phen)$_2$(H_2O)]$^{2+}$	1	99
12	DNA + MPA + DMSO + **2**	98	2
13	DNA + MPA + mannitol + **2**	99	1
14	DNA + MPA + distamycin + **2**	98	2

[a] Complex concentration is 40 μM. Incubation period: 1 h

posed by Sigman and co-workers for the oxidative cleavage reaction of the bis(phen)copper complex.[15]

Hydrolytic Cleavage of DNA

In the absence of any reducing agent or light, the complexes are found to cleave DNA hydrolytically (Table 4). At a concentration of 1.0 mM and an incubation time of 2 h, complex **1** which contains the ligand phen cleaves 55% of SC DNA, while complete cleavage is observed for the dpq complex **2** (Figure 3, a). Complexes [Cu(salgly)(H_2O)] and [Cu(salgly)(bpy)], which do not bind DNA, do not show any hydrolytic cleavage activity under similar conditions. The cleavage efficiency follows the order: **2** ≈ **4** ≈ **6** > **1** ≈ **3** ≈ **5**. To ascertain the hydrolytic nature of the DNA cleavage process, reactions were performed in the presence of DMSO and in the absence of oxygen in dark [Figure 3 (a), lanes 9 and 10]. The cleavage efficiency does not change in the presence of DMSO. This rules out the involvement of any radical hydroxyl species in the strand cleavage. The absence of smear in the gels for an incubation time of up to 6 h also precludes any radical cleavage. Once again, the extent of DNA cleavage is found to be the same under argon, suggesting the oxygen-independent cleavage pathway. This indicates the non-oxidative nature of the DNA cleavage. The cleavage reactions have also been studied using different complex concentrations and incubation times. The % DNA cleavage for complex **2** is 52, 91 and 100% after 1.5, 6 and 10 h incubation time, respectively, at a concentration of 500 μM. The data reveal the essential role of the α-amino acid Schiff bases in promoting the Lewis acid/base activity for the enhancement of the hydrolytic cleavage, while the primary role of the heterocyclic base is to bind DNA in the minor groove.[30]

The plot showing the extent of DNA cleavage by [Cu(salgly)(dpq)] (**2**) with reaction time is displayed in Figure 4. The decrease in form I (SC) and the formation of form II (NC) of DNA with time show the expected exponential nature of the curves. The plot of log (% SC-DNA) with time gave a linear fit from which the hydrolytic pseudo-first-order rate constant ($k_{obsd.}$) is obtained (5.0×10^{-4}·s^{-1} or 1.8 h^{-1}), using a complex concentration of 1 mM (Figure 4, inset). Ito and co-workers have reported a copper(II) complex

Table 4. Hydrolytic cleavage of DNA (SC pUC19, 0.5 μg) by complexes **1**−**6** in the absence of any reducing agent or light

Sl no.	Reaction conditions	Complex concentration [mM]	Incubation time [h]	Form I [%]	Form II [%]
1	DNA control	−	10	95	5
2	DNA + **1**	1.0	2	45	55
3	DNA + **2**	1.0	2	2	98
4	DNA + **3**	1.0	2	43	57
5	DNA + **4**	1.0	2	2	98
6	DNA + **5**	1.0	2	42	58
7	DNA + **6**	1.0	2	1	99
8	DNA + [Cu(salgly)(H_2O)]	1.0	2	97	3
9	DNA + **2**	0.25	10	59	41
10	DNA + **2**	0.5	1.5	48	52
11	DNA + **2**	0.5	6	9	91
12	DNA + **2**	0.5	10	0	100
13	DNA + DMSO + **2**	1.0	2	2	98
14	DNA + **2** (under argon)	1.0	2	1	99

 © 2004 Wiley-VCH Verlag GmbH & Co. KGaA, Weinheim

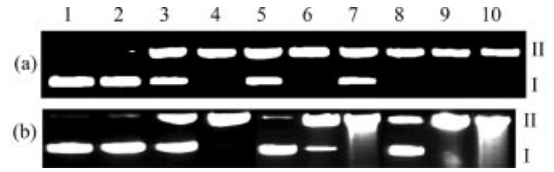

Figure 3. (a) Gel electrophoresis diagram showing the hydrolytic cleavage of supercoiled pUC19 DNA (0.5 μg) by complexes **1**−**6** (1 mM) under aerobic conditions in the dark and with an incubation time of 2 h in 50 mM Tris-HCl/NaCl buffer containing DMF (10%): lane 1, DNA control; lane 2, DNA + [Cu(salgly)(H_2O)]; lane 3, DNA + **1**; lane 4, DNA + **2**; lane 5, DNA + **3**; lane 6, DNA + **4**; lane 7, DNA + **5**; lane 8, DNA + **6**; lane 9, DNA + **2** (1 mM, under argon); lane 10, DNA + DMSO + **2** (1 mM); (b) effect of complex concentration and the incubation time on the % cleavage of supercoiled pUC19 DNA (0.5 μg) by **2** in the dark in 50 mM Tris-HCl/NaCl buffer containing DMF (10%); incubation times are 1.5 h for lanes 1−4, 6 h for lanes 5−7, and 10 h for lanes 8−10; lane 1, DNA control; lane 2, DNA + **2** (250 μM); lane 3, DNA + **2** (500 μM); lane 4, DNA + **2** (1.0 mM); lane 5, DNA + **2** (250 μM); lane 6, DNA + **2** (500 μM); lane 7, DNA + **2** (1.0 mM); lane 8, DNA + **2** (250 μM); lane 9, DNA + **2** (500 μM); lane 10, DNA + **2** (1.0 mM)

(0.095 mM) of *cis,cis*-1,3,5-triaminocyclohexane that has been shown to cleave DNA hydrolytically with a rate constant of 4.3 h^{-1}.[31] The rate of DNA hydrolysis by complex **2** is lower than this complex, but significantly higher than other copper(II) amine complexes, which have rate constants in the range 0.04−0.25 h^{-1}.[32−37] These studies were carried out under excess catalyst (pseudo-Michaelis−Menten) conditions and do not represent multiple turnover activity. The copper(II)−L-histidine complex is known to cleave DNA hydrolytically, however, at a rate of 0.76 h^{-1} with a complex concentration of 1.0 mM.[38] We have studied the saturation kinetics by varying the concentrations of both SC DNA (40−125 μM) and the complex (0.1−4.0 mM). Under Michaelis−Menten conditions, a 1.0 mM concentration of **2** is found to show saturation with a DNA concentration of 66.6 μM (Figure 5). The $k_{cat.}$ value obtained from the plot is 1.71 h^{-1} (2.85 × 10^{-2} min^{-1}).

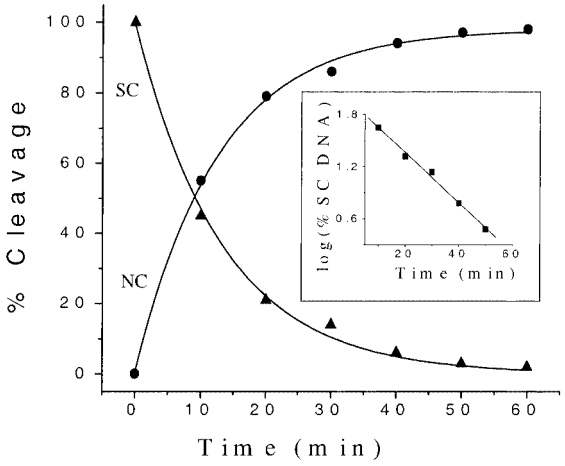

Figure 4. Hydrolytic cleavage of SC pUC19DNA (ca. 0.5 μg) showing the decrease in form I (SC DNA) and the formation of form II (NC DNA) with the incubation time (in the dark) using 1.0 mM concentration of **2**; inset shows the plot of log (% SC DNA) vs. time for complex **2** (1.0 mM) at 37 °C at pH = 7.2 for an incubation period of 10−60 min

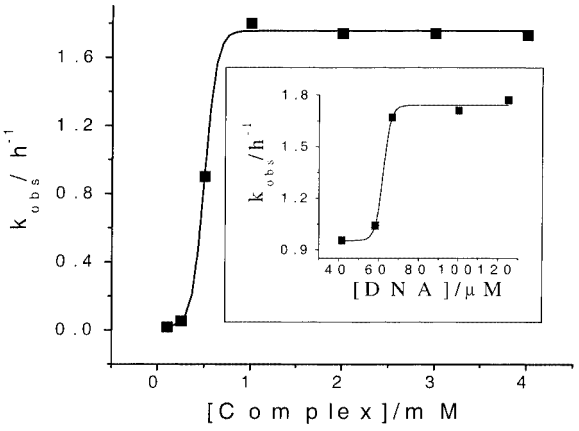

Figure 5. Saturation kinetics for the cleavage of SC pUC19 DNA (ca. 0.5 μg) by **2** at pH = 7.2 and 37 °C; inset displays the variation of the observed rate constant with SC DNA concentration (concentration of complex **2** is 1.0 mM)

Conclusion

Ternary copper(II) complexes having tridentate ONO-donor α-amino acid salicylaldimine Schiff bases and planar NN-donor heterocyclic bases are prepared and characterized. The crystal structure of **3** shows a CuN_3O_2 square-pyramidal (4+1) coordination. The complexes show efficient oxidative and hydrolytic cleavage activities. The dpq complexes, with higher DNA-binding abilities, exhibit efficient hydrolytic cleavage activities in the absence of any reducing agent and light. Mechanistic studies reveal the minor groove binding of the complexes and the involvement of the hydroxyl radical in the oxidative cleavage reactions. Hydrolytic cleavage occurs in the presence of DMSO and in the absence of oxygen. The role of heterocyclic base in complexes **1**−**6** is primarily to bind DNA at the minor groove. The amino acid Schiff bases with labile carboxylate and/or phenolato oxygen sites could be responsible for promoting the hydrolytic cleavage of DNA by utilizing the strong Lewis acid properties of copper in the +2 oxidation state. The observed DNA hydrolysis rate (1.8 h^{-1}) for **2** provides further scope for designing analogous amino acid or peptide-based copper(II) complexes or their hybrids to increase cleavage activity by enhancing the Lewis acid property of the metal ion, as well as for cellular use.

Experimental Section

Materials and Physical Measurements: All chemicals and reagents were purchased from commercial sources and were used without further purification. Glycine, L-alanine, L-phenylalanine, L-ascorbic acid and 2,2′-bipyridine were obtained from SD Fine Chemicals, Mumbai. Copper(II) acetate hydrate was bought from BDH (India). The solvents were purified by standard procedures.[39] The precursor complex [Cu(salgly)(H_2O)]·0.5H_2O, where salgly is the *N*-salicylideneglycinato dianion, was prepared by a literature method.[27] The other Schiff bases, viz. *N*-salicylidene-L-alanine

 © 2004 Wiley-VCH Verlag GmbH & Co. KGaA, Weinheim

(H_2salala) and *N*-salicylidene-L-phenylalanine (H_2salphe), were prepared by the condensation of salicylaldehyde with the respective L-amino acid in the presence of LiOH according to a reported procedure.[40] The dipyrido[3,2-*d*:2′,3′-*f*]quinoxaline (dpq) ligand, [Cu(salgly)(bpy)] and $[Cu(phen)_2(H_2O)](ClO_4)_2$ were prepared according to literature methods.[24,41,42] Calf thymus (CT) DNA and super-coiled (SC) pUC19 DNA were purchased from Bangalore Genie (India). Agarose (molecular biology grade) and ethidium bromide were from Sigma (USA). All solvents were purified before use as per standard procedures. The Tris-HCl buffer solution was prepared using deionized, sonicated triple distilled water.

Syntheses

Preparation of [Cu(salgly)(phen)] (1) and [Cu(salgly)(dpq)] (2): An aqueous methanolic solution (30 mL, 1:5 v/v) of $[Cu(salgly)(H_2O)]\cdot 0.5H_2O$ (0.39 g, 1.1 mmol) was treated with the heterocyclic base (0.22 g phen or 0.26 g dpq, 1.1 mmol) whilst stirring at 25 °C for 1 h. The product was isolated as a dark green solid in ca. 80% yield on evaporation of the solvent. The complex was crystallized by slow concentration of an aqueous methanolic solution at 5 °C. **1:** $C_{21}H_{15}CuN_3O_3$ (420.5): calcd. C 59.93, H 3.57, N 9.99; found C 59.67, H 3.88, N 9.86. IR (KBr phase): $\tilde{\nu}$ = 3417 br, 1642 s, 1595 s, 1359 m, 1199 m, 1122 m, 849 w, 719 m cm^{-1}. **2:** $C_{23}H_{15}CuN_5O_3$ (472.5): calcd. C 58.41, H 3.17, N 14.81; found C 58.18, H 3.09, N 14.75. IR (KBr disc): $\tilde{\nu}$ = 3427 br, 1642 s, 1605 s, 1528 s, 1455 m, 1342 m, 1122 m, 1086 m, 736 w, 436 w cm^{-1}.

Preparation of [Cu(salala)(phen)] (3), [Cu(salala)(dpq)](4), [Cu(salphe)(phen)] (5) and [Cu(salphe)(dpq)] (6): The complexes were prepared by a general method. An aqueous methanolic solution (20 mL, 1:4 v/v), containing copper(II) acetate hydrate (0.2 g, 1.0 mmol) and the heterocyclic base (0.22 g phen or 0.26 g dpq, 1.1 mmol), was treated with a methanolic solution (5 mL) of the Schiff base (0.19 g H_2salala or 0.27 g H_2salphe, 1.0 mmol) whilst stirring at 25 °C for 1 h. The color of the solution turned to dark green. Slow evaporation of the solvent at 5 °C gave the analytically pure product in ca. 70% yield; dark green crystalline blocks were obtained. The solid was isolated, washed with hexane and dried in vacuo over P_4O_{10}. **3:** $C_{22}H_{17}CuN_3O_3$ (434.5): calcd. C 60.76, H 3.91, N 9.67; found C 60.55, H 4.08, N 9.95. Polarimetric data: $[\alpha]_{589}$ = +26 (*c* = 10 mg/ml, MeOH). IR (KBr phase): $\tilde{\nu}$ = 3417 br, 1635 s, 1596 s, 1449 s, 1393 m, 1109 m, 1022 m, 915 m, 768 w cm^{-1}. **4:** $C_{24}H_{19}CuN_5O_3$ (488.5): calcd. C 58.96, H 3.89, N 14.33; found C 59.13, H 4.04, N 14.39. Polarimetric data: $[\alpha]_{589}$ = +29 (*c* = 10 mg/ml, MeOH). IR (KBr phase): $\tilde{\nu}$ = 3387 br, 1605 s, 1575 s, 1472 s, 1389 s, 1086 m, 822 m, 766 w, 736 w, 443 w cm^{-1}. **5:** $C_{28}H_{20}CuN_3O_3$ (509.5): calcd. C 65.95, H 3.93, N 8.24; found C 66.17, H 4.16, N 7.99. IR (KBr phase): $\tilde{\nu}$ = 3390 br, 1625 s, 1595 s, 1445 s, 1349 s, 1199 m, 1152 m, 849 m, 766 w, 499 w cm^{-1}. **6:** $C_{30}H_{20}CuN_5O_3$ (561.5): calcd. C 64.11, H 3.56, N 12.47; found C 64.30, H 3.92, N 12.27. IR (KBr phase): $\tilde{\nu}$ = 3430 br, 1636 s, 1599 s, 1450 s, 1383 s, 1129 m, 1022 m, 915 w, 768 w cm^{-1}.

DNA Binding and Cleavage Experiments: The concentration of the CT DNA, used for the binding experiments studied by spectroscopic methods, was determined by recording the absorption intensity at 260 nm with a known molar extinction coefficient of 6600 $dm^3\ mol^{-1}\ cm^{-1}$.[43] In order to compare the relative binding of complexes **1**−**6** to DNA with respect to the analogous phen complex, an ethidium bromide bound CT DNA solution in Tris-HCl / NaCl buffer (pH = 7.2) was treated with an increasing amount of the complex solution. The fluorescence intensities at 601 nm (510 nm excitation) of ethidium bromide (EB) in the bound form were plotted against the complex concentration. Competitive binding studies were done using an EB-bound DNA which show an enhanced emission intensity relative to free EB.[44,45] Binding of the complex resulted in the displacement of DNA-bound EB molecules, with a reduction of emission intensity due to fluorescence quenching of free EB by the solvent molecules.[46] The extent of complex binding to DNA was estimated from the relative decrease of the emission intensity of EB on addition of the complex. Bis(phen)copper(II) complex was used as a standard in the binding studies. The cleavage of DNA was monitored using agarose gel electrophoresis. Supercoiled pUC19 DNA (6μL, ca. 500 ng) in Tris-HCl buffer (50 mM) with 50 mM NaCl (pH = 7.2) was treated with the metal complex (40 μM in DMF) and 3-mercaptopropionic acid (2 μL, 100 μM), followed by dilution with the Tris-HCl buffer to a total volume of 20 μL. The samples were incubated at 37 °C for 1 h. A loading buffer containing 25% bromophenol blue, 0.25% xylene cyanol and 30% glycerol (3 μL) was added. Electrophoresis was performed at 60 V for 2 h in TAE buffer using 0.8% agarose gel containing 1.0 μg/mL ethidium bromide. Bands were viewed by UV light and photographed. The cleavage efficiency was measured by determining the ability of the complex to convert the supercoiled (SC) DNA to nicked circular form (NC). After electrophoresis, the proportion of DNA in each fraction was estimated quantitatively from the intensities of the bands using the UVITEC Gel Documentation System. The fraction of the original supercoiled DNA that was converted into the NC form at the end of the reaction was calculated after correcting for the low level of NC present in the original sample and the low affinity of ethidium bromide for SC relative to NC and linear forms of DNA.[47] For hydrolytic cleavage, DNA and complex were added in the dark and incubated for longer than required. Inhibition reactions were carried out by adding different reagents such as distamycin (200 μM) and DMSO (4 μL) prior to the addition of the complex.

X-ray Crystallography: Complex **3** was crystallized on slow concentration of an aqueous methanolic solution at room temperature. A crystal of approximate size 0.54 × 0.38 × 0.28 mm was mounted on a glass fiber with epoxy cement. All geometric and intensity data were collected using an automated Enraf−Nonius CAD4 diffractometer equipped with Mo-K_α radiation (λ = 0.71073 Å). The intensity data, collected using the ω-scan technique for 4550 reflections in the range $1.4° < \theta < 25°$, were corrected for Lorentz polarization effects and for absorption.[48] Structure determination was carried out using 3511 data with $I > 2\sigma(I)$ and 608 parameters using the SHELX system of programs[49] by a combination of Patterson and Fourier techniques and refined by full-matrix least squares on F^2. All non-hydrogen atoms were refined anisotropically. The hydrogen atoms were fixed in their calculated positions and were refined using a riding model. The perspective view of the molecule was obtained using ORTEP.[50] Selected crystal data are given in Table 5. CCDC-214929 contains the supplementary crystallographic data for this paper. These data can be obtained free of charge at www.ccdc.cam.ac.uk/conts/retrieving.html [or from the Cambridge Crystallographic Data Centre, 12 Union Road, Cambridge CB2 1EZ, UK; Fax: (internat.) + 44-1223/336-033; E-mail: deposit@ccdc.cam.ac.uk].

Supporting Information: Supporting information for this article is available (see footnote on the first page of this article). Figure S1 shows the relative binding of the complexes **1** and **2** to calf thymus DNA. Figures S2 and S3 display the gel electrophoresis diagrams pertaining to the saturation kinetic studies.

 © 2004 Wiley-VCH Verlag GmbH & Co. KGaA, Weinheim

Table 5. Selected crystal data for [Cu(salala)(phen)]·5H_2O (**3**·5H_2O)

Empirical formula	$C_{22}H_{27}CuN_3O_8$
Molecular mass	525.01
Temperature [K]	293
λ(Mo-K_α) [Å]	0.71073
Crystal system	monoclinic
Space group (no.)	*C*2 (5)
a [Å]	20.746(7)
b [Å]	21.592(6)
c [Å]	13.787(3)
β [°]	127.91(2)
V [Å^3]	4873(2)
Z	8
$D_{calcd.}$ [g cm^{-3}]	1.431
μ(Mo-K_α) [cm^{-1}]	9.47
F(000)	2184
Independent reflections [*R*(int)]	4403 (0.016)
Index ranges	$0 < h < 24$, $0 < k < 25$, $-16 < l < 12$
Absorption correction	ψ-scan
Goodness-of-fit on F^2	1.076
R (R_w) indices [$I > 2\sigma(I)$]	0.0694 (0.1925)
R (R_w) [all data]	0.0868 (0.2123)
Largest differential peak/hole	0.999/−0.760
Max./min. transmission	0.8275/0.7608
Weight factor: $w = [\sigma^2(F_o)^2 + (0.1598P)^2 + 1.9296P]^{-1}$; $P = (F_o^2 + 2F_c^2)/3$	

Acknowledgments

We thank the Council of Scientific and Industrial Research, New Delhi, for financial support. We also thank the Alexander von Humboldt Foundation, Germany, for donation of an electroanalytical system and the Convener, the Bioinformatics Center of IISc, for the database search. PANR thanks the CSIR for a scholarship.

[1] F. H. Westheimer, *Science* **1987**, *235*, 1173−1178.
[2] J. A. Cowan, *Chem. Rev.* **1998**, *98*, 1067−1087.
[3] D. E. Wilcox, *Chem. Rev.* **1996**, *96*, 2435−2458.
[4] A. Sreedhara, J. A. Cowan, *J. Biol. Inorg. Chem.* **2001**, *6*, 337−347.
[5] M. Komiyama, J. Sumaoka, *Curr. Opin. Chem. Biol.* **1998**, *2*, 751−757.
[6] J. K. Bashkin, *Curr. Opin. Chem. Biol.* **1999**, *3*, 752−758.
[7] E. L. Hegg, J. N. Burstyn, *Coord. Chem. Rev.* **1998**, *173*, 133−165.
[8] R. R. Breaker, *Chem. Rev.* **1997**, *97*, 371−390.
[9] R. Hettich, H.-J Schneider, *J. Am. Chem. Soc.* **1997**, *119*, 5638−5647.
[10] M. P. Fitzsimmons, J. K. Barton, *J. Am. Chem. Soc.* **1997**, *119*, 3379−3380.
[11] G. Pratviel, J. Bernadou, B. Meunier, *Angew. Chem. Int. Ed. Engl.* **1995**, *34*, 746−769.
[12] B. Meunier, *Chem. Rev.* **1992**, *92*, 1411−1456.
[13] D. S. Sigman, *Biochemistry* **1990**, *29*, 9097−9105.
[14] C. J. Burrows, J. G. Muller, *Chem. Rev.* **1998**, *98*, 1109−1152.
[15] D. S. Sigman, *Acc. Chem. Res.* **1986**, *19*, 180−186.
[16] D. S. Sigman, A. Mazumder, D. M. Perrin, *Chem. Rev.* **1993**, *93*, 2295−2316.
[17] W. K. Pogozelski, T. D. Tullius, *Chem. Rev.* **1998**, *98*, 1089−1107.
[18] B. Armitage, *Chem. Rev.* **1998**, *98*, 1171−1200.
[19] J. M. Veal, K. Merchant, R. L. Rill, *Nucleic Acids Res.* **1991**, *19*, 3383−3388.
[20] O. Zelenko, J. Gallagher, D. S. Sigman, *Angew. Chem. Int. Ed. Engl.* **1997**, *36*, 2776−2778.
[21] G. Pratviel, J. Bernadou, B. Meunier, *Adv. Inorg. Chem.* **1998**, *45*, 251−312.
[22] C. L. Foster, X. Liu, C. A. Kilner, M. T. Pett, M. A. Halcrow, *J. Chem. Soc., Dalton. Trans.* **2000**, 4563−4568.
[23] R. D. Gillard, R. Wootton, *J. Chem. Soc. B* **1970**, 364−371.
[24] P. A. N. Reddy, M. Nethaji, A. R. Chakravarty, *Inorg. Chim. Acta* **2002**, *337*, 450−458.
[25] A. W. Addison, T. N. Rao, J. Reedijk, J. V. Rijn, G. C. Verschoor, *J. Chem. Soc., Dalton Trans.* **1984**, 1349−1356.
[26] S. Lewin, *Vitamin C: Its Molecular Biology and Medical Potential*, Academic Press, London, **1976**.
[27] M. Kishita, A. Nakahara, M. Kubo, *Aust. J. Chem.* **1964**, *17*, 810−813.
[28] T. B. Thederahn, M. D. Kuwabara, T. A. Larsen, D. S. Sigman, *J. Am. Chem. Soc.* **1989**, *111*, 4941−4946.
[29] K. E. Erkkila, D. T. Odom, J. K. Barton, *Chem. Rev.* **1999**, *99*, 2777−2795.
[30] T. Gajda, Y. Düpre, I. Török, J. Harmer, A. Schweiger, J. Sander, D. Kuppert, K. Hegetschweiler, *Inorg. Chem.* **2001**, *40*, 4918−4927.
[31] U. Itoh, H. Hisada, T. Sumiya, M. Hosono, Y. Usui, Y. Fujii, *Chem. Commun.* **1997**, 677−678.
[32] J. Rammo, R. Hettich, A. Roigk, H.-J. Schneider, *Chem. Commun.* **1996**, 105−107.
[33] E. L. Hegg, J. N. Burstyn, *Inorg. Chem.* **1996**, *35*, 7474−7481.
[34] N. E. Dixon, R. J. Geue, J. N. Lambert, S. Moghaddas, D. A. Pearce, A. M. Sargesan, *Chem. Commun.* **1996**, 1287−1288.
[35] J. N. Burstyn, K. A. Deal, *Inorg. Chem.* **1993**, *32*, 3585−3586.
[36] K. A. Deal, A. C. Hengge, J. N. Burstyn, *J. Am. Chem. Soc.* **1996**, *118*, 1713−1718.
[37] K. A. Deal, J. N. Burstyn, *Inorg. Chem.* **1996**, *35*, 2792−2798.
[38] R. Ren, P. Yang, W. Zheng, Z. Hua, *Inorg. Chem.* **2000**, *39*, 5454−5463.
[39] D. D. Perrin, W. L. F. Armarego, D. R. Perrin, *Purification of Laboratory Chemicals*, Pergamon Press, Oxford, **1980**.
[40] A. S. Ceccato, A. Neves, M. A. de Brito, S. M. Drechsel, A. S. Mangrich, R. Werner, W. Haase, A. J. Bortoluzzi, *J. Chem. Soc., Dalton Trans.* **2000**, 1573−1577.
[41] J. G. Collins, A. D. Sleeman, J. R. Aldrich-Wright, I. Greguric, T. W. Hambley, *Inorg. Chem.* **1998**, *37*, 3133−3141.
[42] J. Foley, D. Kennefick, D. Phelan, S. Tyagi, B. Hathaway, *J. Chem. Soc., Dalton Trans.* **1983**, 2333−2338.
[43] M. E. Reichmann, S. A. Rice, C. A. Thomas, P. Doty, *J. Am. Chem. Soc.* **1954**, *76*, 3047−3053.
[44] M. J. Waring, *J. Mol. Biol.* **1965**, *13*, 269−282.
[45] J.-B. Le Pecq, C. Paoletti, *J. Mol. Biol.* **1967**, *27*, 87−106.
[46] L. C. Zheng, W. Jigui, W. Liufang, R. Min, J. Naiyong, G. Jie, *J. Inorg. Biochem.* **1999**, *73*, 195−202.
[47] J. Bernadou, G. Pratviel, F. Bennis, M. Girardet, B. Meunier, *Biochemistry* **1989**, *28*, 7268−7275.
[48] A. C. T. North, D. C. Phillips, F. S. Mathews, *Acta Crystallogr., Sect. A* **1968**, *24*, 351−359.
[49] G. M. Sheldrick, *SHELX-97, Programs for Crystal Structure Solution and Refinement*, University of Göttingen, Germany, **1997**.
[50] C. K. Johnson, *ORTEP, Report ORNL-5138*, Oak Ridge National Laboratory, Oak Ridge, TN, **1976**.

Received July 25, 2003
Early View Article
Published Online February 17, 2004

 © 2004 Wiley-VCH Verlag GmbH & Co. KGaA, Weinheim

Rhodium(I), Palladium(II) and Platinum(II) Coordination Chemistry of the Short-Bite Chiral Ligands (S_c)-*N*,*N*-Bis(diphenylphosphanyl)-*sec*-butylamine, (R_a,R_a)-*N*,*N*-Bis(binaphthylphosphonito)phenylamine and (R_a,S_c)-*N*-(Diphenylphosphanyl)-*N*-(binaphthylphosphonito)-*sec*-butylamine

Gianpiero Calabrò,[a] Dario Drommi,[a] Claudia Graiff,[b] Felice Faraone,*[a] and Antonio Tiripicchio[b]

Keywords: Chiral ligands / Enantioselectivity / Hydroformylation / Palladium / Platinum / Rhodium

The new short-bite chiral ligands (S_c)-*N*,*N*-bis(diphenylphosphanyl)-*sec*-butylamine [(S_c)-**1**], (R_a,R_a)-*N*,*N*-bis(binaphthylphosphonito)phenylamine [(R_a,R_a)-**2**] and (R_a,S_c)-*N*-(diphenylphosphanyl)-*N*-(binaphthylphosphonito)-*sec*-butylamine [(R_a,S_c)-**3**] have been treated with rhodium(I), palladium(II) and platinum(II) substrates. The (S_c)-**1** ligand reacts with [Pd(C_6H_5CN)$_2$Cl$_2$], [Pt(COD)Cl$_2$] and [Rh(COD)(THF)$_2$]PF$_6$ to afford the products [Pd(S_c-**1**)Cl$_2$] (**4**), [Pt(S_c-**1**)Cl$_2$] (**5**) and [Rh(COD)(S_c-**1**)]PF$_6$ (**6**), respectively, in high yields. By bubbling CO to a CH_2Cl_2 solution of **6**, we formed the dicarbonyl species [Rh(CO)$_2$(S_c-**1**)]PF$_6$ (**7**), which is stable only in solution under CO. Compounds **4** and **5** were characterized additionally by X-ray diffraction studies. The ligand (R_a,R_a)-**2** reacts with [Pd(C_6H_5CN)$_2$Cl$_2$] and [Pt(COD)I$_2$] to give [Pd(R_a,R_a-**2**)Cl$_2$] (**8**) and [Pt(R_a,R_a-**2**)I$_2$] (**9**), respectively; the reaction with [Rh(CO)$_2$Cl]$_2$ or [Rh(COD)(THF)$_2$]PF$_6$ affords a mixture of mono- and binuclear compounds, in which the ligand is oxidized to the corresponding phosphonate or is partially hydrolysed. The compounds [Pd(R_a,S_c-**3**)Cl$_2$] (**10**) and [Pt(R_a,S_c-**3**)I$_2$] (**11**) were obtained in the analogous reactions using the asymmetric (R_a,S_c)-**3** ligand. This ligand reacted with [Rh(CO)$_2$Cl]$_2$ in a 2:1 molar ratio in hexane to give a mixture of products in almost equal amounts. The $^{31}P\{^1H\}$ NMR spectrum recorded in $CDCl_3$ allowed us to identify the chelate [Rh(R_a,S_c-**3**)(CO)Cl] (**12**); the nature of the accompanying dinuclear species **13** is not clear. The catalytic systems formed by [Rh(acac)(CO)$_2$] and the ligands (R_a,R_a)-**2** and (R_a,S_c)-**3**, at ligand/metal ratios of 1:1 and 1:2, were unstable under the experimental conditions used (CO/H_2 pressure of 50 atm and temperature of 40 °C) for the hydroformylation of styrene; instead, metallic rhodium was afforded together with unidentified decomposition products.
(© Wiley-VCH Verlag GmbH & Co. KGaA, 69451 Weinheim, Germany, 2004)

Introduction

The design and synthesis of new chiral ligands remains a significant research subject for the development of transition metal-catalysed asymmetric syntheses. Satisfactory enantioselectivities have been obtained when many families of ligands, with very different features, have been prepared and applied in asymmetric catalytic reactions.[1] Among these ligands, the widest range of applications have been found for those containing atropisomeric C_2-symmetric moieties.[2]

Recently, we began[3] synthesising chiral short-bite ligands that resemble the well-known bis(diphenylphosphanyl)methane (dppm), phenylpyrophosphite, and phenylaminobis(diphenylphosphane) (dpppa), but contain atropisomeric C_2-symmetric binaphthyl moieties bonded to the phosphorus donor atoms rather than the phenyl groups. We have also reported[3] the application of these ligands in palladium−allyl-catalysed reaction of 1,3-diphenylallyl acetate with dimethylmalonate. Owing to their favourable structural features, short-bite ligands have been widely used in organometallic chemistry.[4] These bidentate ligands have their donor-atoms separated by one spacer atom; their coordination to a metal centre can produce either chelated mononuclear or bridged dinuclear complexes. In the mononuclear complexes, the short-bite ligand forms a strained four-membered ring with a very narrow bite angle; in the dinuclear complexes, two metal centres are held in close proximity by the features of the bridging short-bite ligand and can cooperate to activate a substrate. This property of the dinuclear complexes has been found to operate during homogeneous catalysis.[5]

When using short-bite chiral ligands, both coordination modes (chelated mononuclear or bridged dinuclear complexes) can, in principle, produce beneficial effects during

[a] Dipartimento di Chimica Inorganica, Chimica Analitica e Chimica Fisica, Università di Messina,
Salita Sperone, 31 Vill. S. Agata, 98166 Messina, Italy
Fax: (internat.) +39-090-393756
E-mail: faraone@chem.unime.it
[b] Dipartimento di Chimica Generale ed Inorganica, Chimica Analitica, Chimica Fisica, Università di Parma,
Parco Area delle Scienze 17A, 43100 Parma, Italy

catalytic enantioselective processes. In fact, the reduced number and rigidity of the conformational isomers formed by a strained four-membered metallacycle can induce a minor number of processes having different activation energies. For the bridged dinuclear complexes, novel modes of reactivity can be achieved for the activation of a substrate as a consequence of cooperative interactions between the metal centres.

As far as we know, only a few chiral, optically pure, short-bite ligands have been reported; of these ligands, only the diphosphane MiniPHOS has been explored as a catalyst precursor in asymmetric synthesis and it affords excellent enantioselectivities in representative carbon−carbon bond-formation reactions.[6]

Prior to studying catalytic systems formed from a metal substrate and a chiral P−N−P short-bite ligand in conventional metal-catalysed asymmetric carbon−carbon bond formation, we explored the coordinating properties of the synthesized (S_c)-*N*,*N*-bis(diphenylphosphanyl)-*sec*-butylamine, (R_a,R_a)-*N*,*N*-bis(binaphthylphosphonito)phenylamine and (R_a,S_c)-*N*-(diphenylphosphanyl)-*N*-(binaphthylphosphonito)-*sec*-butylamine.

Results and Discussion

Ligands

Scheme 1 presents the new short-bite chiral P−N−P ligands used in the reactions with rhodium(I), palladium(II) and platinum(II) substrates.

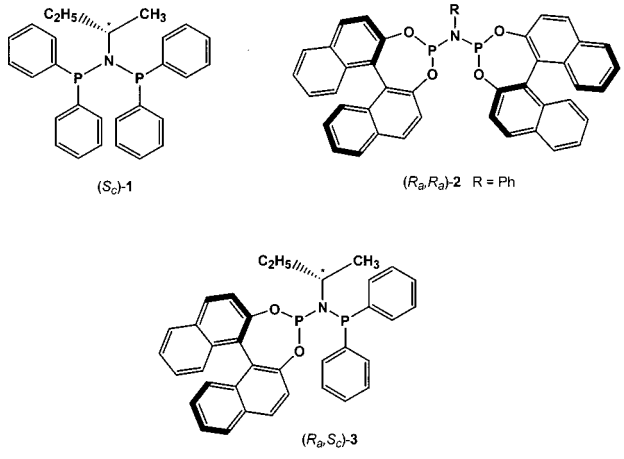

Scheme 1

These ligands were designed so that we could verify the effects that the position, nature, absolute configuration and number of stereogenic centres have on the enantioselective catalysis. The ligands were synthesized[3] by reacting the corresponding primary amine RNH_2 [R = Ph, (S_c)-(+)-*sec*-$C_2H_5CHCH_3$] with the chlorodiphenylphosphane or the phosphorochloridite derived from (R_a)-binaphthol in a 1:2 molar ratio in toluene at 0 °C in the presence of an excess of NEt_3. Ligands similar to (S_c)-**1** have been reported previously,[7] but their coordination chemistry has not been explored extensively. The ligands (S_c)-**1**, (R_a,R_a)-**2** and (R_a,S_c)-**3** should behave, in principle, either as chelating, originating, four-membered metallacycles or as bridging ligands giving dimetalllic species. Literature reports indicate that the presence of an alkyl or aryl group on the nitrogen atom favours the formation of a four-membered strained ring when the ligand coordinates to a metal centre.[8]

Reactions with Rhodium(I), Palladium(II) and Platinum(II) Substrates

The reaction of $[Pd(C_6H_5CN)_2Cl_2]$ with (S_c)-**1** in a 1:1 molar ratio in CH_2Cl_2 afforded $[Pd(S_c\text{-}\mathbf{1})Cl_2]$ (**4**) in high yield as a yellow orange solid that is stable to air and moisture for a long period of time. This complex was characterized by elemental analysis and ^1H and $^{31}P\{^1H\}$ NMR spectra; an X-ray diffractometric study established its nature as a mononuclear complex, with (S_c)-**1** chelating to the palladium(II) centre. The $^{31}P\{^1H\}$ NMR spectrum of **4** in $CDCl_3$ displays a singlet at δ = 29.6 ppm; in the ^1H NMR spectrum, the chiral moiety provides the signals at δ = 0.43 (t, $^3J_{H,H}$ = 7 Hz, CH_3), 0.79 (d, $^3J_{H,H}$ = 7 Hz, CH_3), 1.29 and 0.95 (m, diastereotopic CH_2) and 3.28 (m, CH) ppm.

Similarly to $[Pd(C_6H_5CN)_2Cl_2]$, $[Pt(COD)Cl_2]$ reacted with an equimolar amount of (S_c)-**1** in toluene to give $[Pt(S_c\text{-}\mathbf{1})Cl_2]$ (**5**) as a white microcrystalline solid that is stable to air for a long time in the solid state and in solution. An X-ray diffractometric study indicated that **5** is isostructural with **4**. In its $^{31}P\{^1H\}$ NMR spectrum in $CDCl_3$, the phosphorus atom resonance of **5** appears as a singlet at δ = 15.5 ppm having ^{195}Pt satellites ($^1J_{Pt,P}$ 3285 Hz); in the ^1H NMR spectrum, the pattern of the chiral moiety CHMeEt is the same as that obtained for **4**, except that it shows additional peaks due to ^{195}Pt satellites.

The addition of a THF solution of (S_c)-**1** to an equimolar solution of $[Rh(COD)(THF)_2]PF_6$, obtained in situ from $[Rh(COD)Cl]_2$ and NH_4PF_6, in THF, readily gave $[Rh(COD)(S_c\text{-}\mathbf{1})]PF_6$ (**6**) as an orange solid. Analytical and conductivity data, together with CO reactivity and NMR spectroscopic data, support this formulation. In fact, the $^{31}P\{^1H\}$ NMR spectrum in $CDCl_3$ displays a doublet at δ = 50.1 ppm ($^1J_{RhP}$ = 134 Hz). Upon bubbling CO into a CH_2Cl_2 solution of **6**, displacement of COD occurs readily with formation of the dicarbonyl species $[Rh(CO)_2(S_c\text{-}\mathbf{1})]PF_6$ (**7**) [$\tilde{\nu}_{CO}$ (CH_2Cl_2) = 2059 and 2098 cm^{-1}] together with small amount of another carbonyl compound, which is very likely to be the five-coordinate species $[Rh(CO)_3(S_c\text{-}\mathbf{1})]PF_6$; compound **7** requires a CO atmosphere and can be handled only in solution.

The ligand (R_a,R_a)-**2** reacts in solution with $[Pd(C_6H_5CN)_2Cl_2]$ and $[Pt(COD)I_2]$ to give $[Pd(R_a,R_a\text{-}\mathbf{2})Cl_2]$ (**8**) and $[Pt(R_a,R_a\text{-}\mathbf{2})I_2]$ (**9**), respectively, as yellow-orange solids (Scheme 2).

 © 2004 Wiley-VCH Verlag GmbH & Co. KGaA, Weinheim

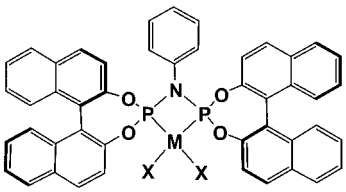

Scheme 2

These formulations are based on analytical and NMR spectroscopic data. The resonances of the phosphorus atoms appear in the $^{31}P\{^1H\}$ NMR spectra, recorded in $CDCl_3$, as singlets at higher fields than the free ligand, at δ = 82.1 and 94.5 ppm ($^1J_{Pt,P}$ = 5296 Hz) for **8** and **9**, respectively. Both **8** and **9** are moderately stable to air and moisture.

The reaction of (R_a,R_a)-**2** with $[Rh(CO)_2Cl]_2$ or $[Rh(COD)(THF)_2]PF_6$ leads to the formation of a mixture of compounds in which the ligand is oxidized to the corresponding phosphonate or is partially hydrolysed. We were not able to obtain fully characterized products from these mixtures.

The asymmetric (R_a,S_c)-**3** ligand reacts in CH_2Cl_2 with $[Pd(C_6H_5CN)_2Cl_2]$ in a 1:1 molar ratio to afford [Pd(R_a,S_c-**3**)Cl_2] (**10**) together with small trace amounts of **4**. The formation of **4** by $N-P_{Phosphonite}$ bond cleavage of **10** in the presence of trace amounts of H_2O[9] is very unlikely; most probably the formation of **4** is due to the presence of trace amounts of (S_c)-**1** as an impurity in the sample of the (R_a,S_c)-**3** ligand we used. Compound **10** is a yellow solid that is moderately stable in the presence of air or moisture; it was isolated in low yield after column chromatography. Its formulation is supported by the presence of two doublets in the $^{31}P\{^1H\}$ NMR spectrum recorded in $CDCl_3$ at δ = 81.8 and 39.9 ppm, with $^2J_{P,P}$ = 17 Hz, which correspond to the phosphonito and phosphino phosphorus atoms, respectively.

Similarly to $[Pd(C_6H_5CN)_2Cl_2]$, $[Pt(COD)I_2]$ reacted with (R_a,S_c)-**3** in a 1:1 molar ratio in toluene to give the product [Pt(R_a,S_c-**3**)I_2] (**11**) as a white microcrystalline solid that is moderately stable to air in the solid state and in solution. Its formulation is supported by the presence of resonances in the $^{31}P\{^1H\}$ NMR spectrum, recorded in $CDCl_3$, that correspond to phosphonito and phosphino phosphorus atoms, together with peaks due to ^{195}Pt satellites.

The reaction of (R_a,S_c)-**3** with $[Rh(CO)_2Cl]_2$ in a 2:1 molar ratio in hexane led to a mixture of products in almost equal amounts. The $^{31}P\{^1H\}$ NMR spectrum of the crude product, recorded in $CDCl_3$ (see a in Figure 1), allows us to identify the chelate [Rh(R_a,S_c-**3**)(CO)Cl] (**12**) and a dinuclear species **13**, the nature of which we are not able to fully explain.

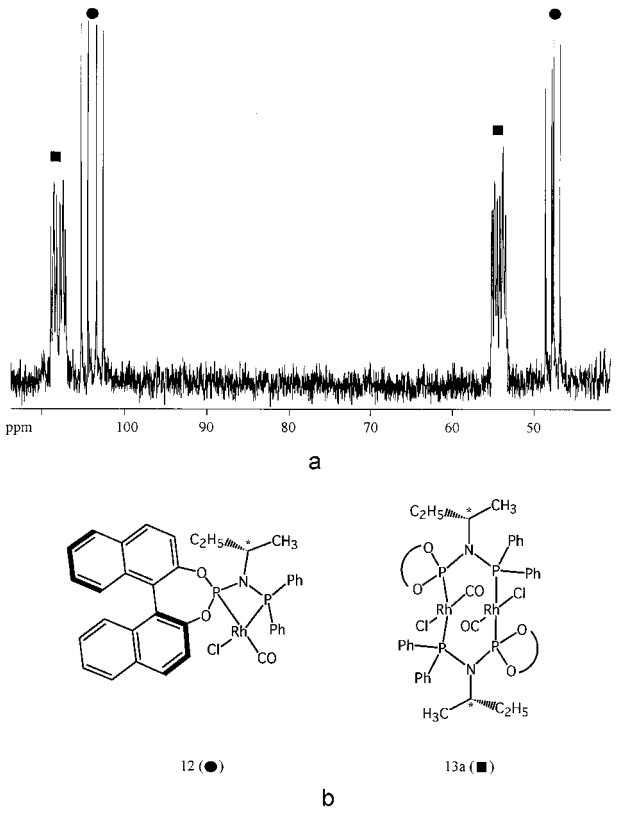

Figure 1. $^{31}P\{^1H\}$ NMR spectrum in $CDCl_3$ at 298 K: filled black square: compound **13**, filled black circle: compound **12**

The formulation of compound **12** as a chelated mononuclear species is supported by the pattern of the phosphorous atom resonances in the $^{31}P\{^1H\}$ NMR spectrum and the $^1J_{RhP}$ values. As expected for the proposed structure, compound **12** exhibits two doublets of doublets in the $^{31}P\{^1H\}$ NMR spectrum, recorded in $CDCl_3$, centred at δ = 103.9 ppm (dd, $^1J_{RhP}$ = 222, $^2J_{P,P}$ = 98 Hz) and at δ = 47.7 ppm (dd, $^1J_{RhP}$ = 122, $^2J_{P,P}$ = 98 Hz) for the phosphonito and phosphino phoshorus atoms, respectively; the value of $\tilde{\nu}_{CO}$ at 1990 cm^{-1} (nujol mull) in the IR spectrum supports a structure in which the carbonyl unit is in a trans position to the higher-trans-influence phosphonito group. As shown in Figure 1 (a), the NMR spectrum of the crude product also indicates, in the region of the phosphonito and phosphanyl phoshorus atom resonances, well-resolved signals at δ = 108.0 (ddd, $^1J_{RhP}$ = 133, $^2J_{P,P}$ = 46, $^2J_{P,P}$ = 35 Hz) and 54.4 ppm (ddd, $^1J_{RhP}$ = 124, $^2J_{P,P}$ = 46, $^2J_{P,P}$ = 35 Hz) arising from AA′BB′XX′ systems. These spectroscopic data allow us to assign a dinuclear structure to **13**, but they are not sufficient to fully characterize it. On the basis the $^{31}P\{^1H\}$ NMR spectroscopic data, we tentatively propose for **13** the dinuclear head-to-tail structure, **13a** (see b in Figure 1).[10] The large decrease in the value of $^1J_{RhP}$ on proceeding from **12** to **13** can also suggest an oxidation process from Rh^I to Rh^{II} and propose an $Rh^{II}-Rh^{II}$ undefined dimer formulation.[11,12] We have ascertained that **12** and **13** do not interconvert; the bulkiness of the binaphthyl

 © 2004 Wiley-VCH Verlag GmbH & Co. KGaA, Weinheim

moiety probably prevents the exchange reaction between **12** and **13**.

Crystal and Molecular Structure of [Pd(S_c-**1**)Cl_2] (**4**) and [Pt(S_c-**1**)Cl_2] (**5**)

Compounds **4** and **5** are isostructural. In the crystals of **4** (and of **5**), two crystallographically independent, but very similar, complexes of [Pd(S_c-**1**)Cl_2] (and of [Pt(S_c-**1**)Cl_2]) are present. ORTEP views of one of the two molecules of the complexes **4** and **5** are shown in Figure 2 and 3, respectively.

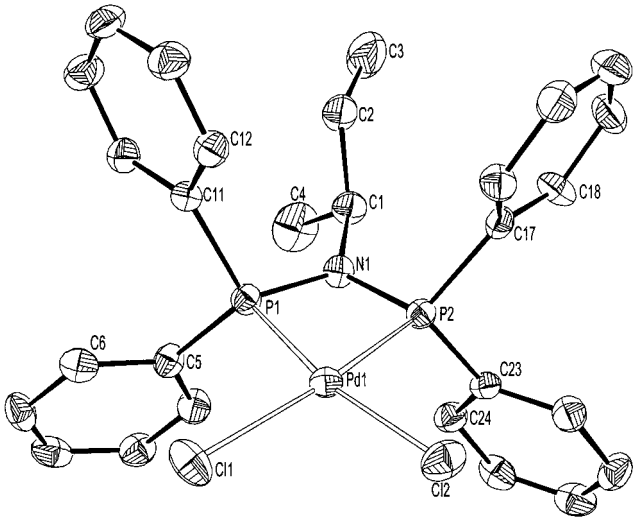

Figure 2. View of one of the two independent molecules of **4**, together with the atomic numbering system. Thermal ellipsoids are drawn at the 30% probability level

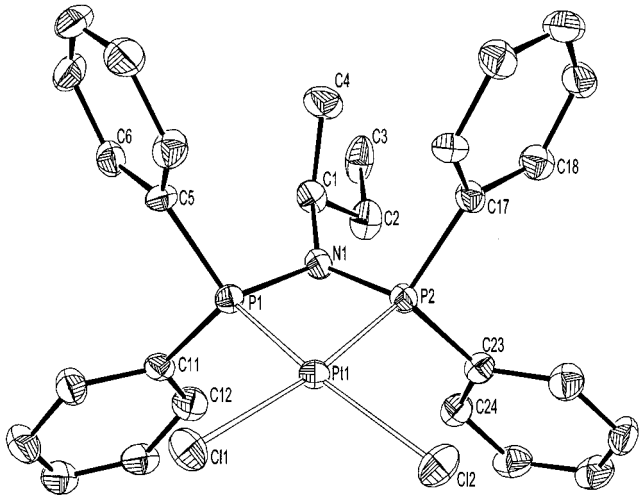

Figure 3. View of one of the two independent molecules of **5**, together with the atomic numbering system. Thermal ellipsoids are drawn at the 30% probability level

Lists of selected bond lengths and angles of **4** and **5** are given in Table 1 and 2, respectively.

Table 1. Selected bond lengths [Å] and angles [deg] for Molecule A in **4**

Pd(1A)−P(2A) 2.217(3)	Pd(1B)−P(1B) 2.212(3)
Pd(1A)−P(1A) 2.210(3)	Pd(1B)−P(2B) 2.225(3)
Pd(1A)−Cl(1A) 2.365(3)	Pd(1B)−Cl(2B) 2.351(3)
Pd(1A)−Cl(2A) 2.353(3)	Pd(1B)−Cl(1B) 2.348(3)
P(1A)−N(1A) 1.712(7)	P(1B)−N(1B) 1.727(8)
P(1A)−C(5A) 1.818(9)	P(1B)−C(5B) 1.794(11)
P(1A)−C(11A) 1.811(9)	P(1B)−C(11B) 1.801(10)
P(1A)−P(2A) 2.596(4)	P(1B)−P(2B) 2.598(3)
P(2A)−N(1A) 1.695(7)	P(2B)−N(1B) 1.682(8)
P(2A)−C(23A) 1.802(11)	P(2B)−C(17B) 1.812(9)
P(2A)−C(17A) 1.800(10)	P(2B)−C(23B) 1.809(10)
N(1A)−C(1A) 1.498(9)	N(1B)−C(1B) 1.498(8)
C(1A)−C(2A) 1.508(11)	C(1B)−C(4B) 1.480(12)
C(1A)−C(4A) 1.543(13)	C(1B)−C(2B) 1.566(14)
C(2A)−C(3A) 1.562(9)	C(2B)−C(3B) 1.447(10)
P(2A)−Pd(1A)−P(1A) 71.78(9)	P(1B)−Pd(1B)−P(2B) 71.70(9)
P(2A)−Pd(1A)−Cl(1A) 169.25(10)	P(1B)−Pd(1B)−Cl(2B) 169.49(11)
P(1A)−Pd(1A)−Cl(1A) 97.98(10)	P(2B)−Pd(1B)−Cl(2B) 98.71(11)
P(2A)−Pd(1A)−Cl(2A) 95.57(10)	P(1B)−Pd(1B)−Cl(1B) 95.86(11)
P(1A)−Pd(1A)−Cl(2A) 165.45(10)	P(2B)−Pd(1B)−Cl(1B) 165.18(11)
Cl(1A)−Pd(1A)−Cl(2A) 94.99(10)	Cl(2B)−Pd(1B)−Cl(1B) 94.23(11)
N(1A)−P(1A)−Pd(1A) 94.1(3)	N(1B)−P(1B)−Pd(1B) 93.9(3)
N(1A)−P(2A)−Pd(1A) 94.3(2)	N(1B)−P(2B)−Pd(1B) 94.7(3)
C(1A)−N(1A)−P(2A) 132.2(6)	C(1B)−N(1B)−P(2B) 126.8(7)
C(1A)−N(1A)−P(1A) 124.2(6)	C(1B)−N(1B)−P(1B) 131.0(7)
P(2A)−N(1A)−P(1A) 99.3(3)	P(2B)−N(1B)−P(1B) 99.3(3)
N(1A)−C(1A)−C(2A) 111.0(7)	N(1B)−C(1B)−C(4B) 113.0(8)
N(1A)−C(1A)−C(4A) 113.1(7)	N(1B)−C(1B)−C(2B) 109.0(7)
C(2A)−C(1A)−C(4A) 115.0(7)	C(4B)−C(1B)−C(2B) 115.6(8)
C(1A)−C(2A)−C(3A) 111.4(8)	C(3B)−C(2B)−C(1B) 110.4(9)

The metal center is in a slightly distorted square-planar environment, being coordinated by two chlorine atoms and two phosphorous atoms of the chelating (S_c)-**1** ligand. The chelating ligand forms a four-membered ring with the N1 atom deviating by ca. 0.15 Å from the plane formed by the P1, P2 and Pd1 (or Pt1) atoms. The P1−Pd1−P2 and P1−Pt−P2 bite angles are 71.7 and 72.0° in **4** and **5**, respectively. The absolute configuration of the chiral carbon atom C1 is confirmed to be *S*.

Catalysis

We used the catalytic systems formed by [Rh(acac)$(CO)_2$] and ligands (R_a,R_a)-**2** and (R_a,S_c)-**3**, at ligand-to-metal ratios of 1:1 and 1:2, in the hydroformylation of styrene. The catalytic runs were carried out in benzene solutions using an equimolar mixture of hydrogen and carbon monoxide gases. The catalytic systems so formed were unstable under the experimental conditions (using a CO/H_2 pressure of 50 atm and a temperature of 40 °C) and afforded metallic rhodium together with unidentified decomposition products. Thus, the ligands (R_a,R_a)-**2** and (R_a,S_c)-**3** are unsuitable for the enantioselective rhodium-catalysed hydroformylation of styrene.

 © 2004 Wiley-VCH Verlag GmbH & Co. KGaA, Weinheim

Table 2. Selected bond lengths [Å] and angles [deg] for molecule A in **5**

Pt(1A)−P(1A)	2.200(2)	Pt(1B)−P(1B)	2.201(2)
Pt(1A)−P(2A)	2.2014(19)	Pt(1B)−P(2B)	2.207(2)
Pt(1A)−Cl(2A)	2.357(2)	Pt(1B)−Cl(2B)	2.346(2)
Pt(1A)−Cl(1A)	2.360(2)	Pt(1B)−Cl(1B)	2.355(2)
P(1A)−N(1A)	1.702(6)	P(1B)−N(1B)	1.722(6)
P(1A)−C(5A)	1.795(8)	P(1B)−C(5B)	1.787(8)
P(1A)−C(11A)	1.807(8)	P(1B)−C(11B)	1.810(8)
P(1A)−P(2A)	2.590(3)	P(1B)−P(2B)	2.590(3)
P(2A)−N(1A)	1.689(6)	P(2B)−N(1B)	1.683(6)
P(2A)−C(23A)	1.795(9)	P(2B)−C(17B)	1.811(8)
P(2A)−C(17A)	1.816(8)	P(2B)−C(23B)	1.819(8)
N(1A)−C(1A)	1.503(8)	N(1B)−C(1B)	1.487(8)
C(1A)−C(2A)	1.512(10)	C(1B)−C(4B)	1.542(11)
C(1A)−C(4A)	1.523(10)	C(1B)−C(2B)	1.546(12)
C(2A)−C(3A)	1.522(10)	C(2B)−C(3B)	1.451(11)
P(1A)−Pt(1A)−P(2A)	72.11(8)	P(1B)−Pt(1B)−P(2B)	71.97(7)
P(1A)−Pt(1A)−Cl(2A)	167.57(8)	P(1B)−Pt(1B)−Cl(2B)	171.23(8)
P(2A)−Pt(1A)−Cl(2A)	97.15(8)	P(2B)−Pt(1B)−Cl(2B)	99.77(9)
P(1A)−Pt(1A)−Cl(1A)	99.35(8)	P(1B)−Pt(1B)−Cl(1B)	97.22(9)
P(2A)−Pt(1A)−Cl(1A)	171.28(8)	P(2B)−Pt(1B)−Cl(1B)	167.01(9)
Cl(2A)−Pt(1A)−Cl(1A)	91.53(8)	Cl(2B)−Pt(1B)−Cl(1B)	91.34(10)
N(1A)−P(1A)−Pt(1A)	93.7(2)	N(1B)−P(1B)−Pt(1B)	93.8(2)
N(1A)−P(2A)−Pt(1A)	94.0(2)	N(1B)−P(2B)−Pt(1B)	94.7(2)
C(1A)−N(1A)−P(2A)	133.0(5)	C(1B)−N(1B)−P(2B)	125.3(5)
C(1A)−N(1A)−P(1A)	123.4(5)	C(1B)−N(1B)−P(1B)	131.9(6)
P(2A)−N(1A)−P(1A)	99.6(3)	P(2B)−N(1B)−P(1B)	99.0(3)
N(1A)−C(1A)−C(2A)	111.8(6)	N(1B)−C(1B)−C(4B)	109.8(7)
N(1A)−C(1A)−C(4A)	112.3(6)	N(1B)−C(1B)−C(2B)	112.4(6)
C(2A)−C(1A)−C(4A)	113.8(7)	C(4B)−C(1B)−C(2B)	113.2(7)
C(1A)−C(2A)−C(3A)	113.6(7)	C(3B)−C(2B)−C(1B)	113.4(9)

Experimental Section

The ligands (S_c)-**1**, (R_a,R_a)-**2** and (R_a,S_c)-**3** were prepared as reported in the literature.[3] All other reagents were purchased from Sigma−Aldrich and Strem and used as supplied. All reactions were performed under dry nitrogen in a vacuum system or in Schlenk apparatus. All solvents were purified by conventional procedures and freshly distilled prior to use. For column chromatography, we used silica gel 60 (220−440 mesh) purchased from Fluka. IR spectra were obtained from Nujol mulls on KBr plates using a Perkin−Elmer FTIR 1720 spectrometer. ^{1}H and ^{31}P{^{1}H} NMR spectra were recorded with a Bruker AMX R300 instrument. ^{1}H NMR spectra were referenced to internal tetramethylsilane and ^{31}P{^{1}H} spectra to external 85% H_3PO_4; positive chemical shifts for all nuclei are at relatively higher frequencies. Elemental analyses were performed by Redox s.n.c., Monza, Milano.

[Pd(S_c-1)Cl$_2$] (4): Solid (S_c)-**1** (0.46 g, 1.04 mmol) was added to a solution of [Pd(PhCN)$_2$Cl$_2$] (0.40 g, 1.04 mmol) in CH_2Cl_2 (30 mL).The mixture was stirred at room temperature for about 30 min. During this time, the solution became turbid and its colour switched from dark- to bright-orange. After filtration, evaporation of the solvent under reduced pressure yielded a solid that was washed twice with hexane and crystallized from CH_2Cl_2/petroleum ether (3:1, 15 mL) to obtain an orange-yellow crystalline solid. Yield: 73% (0.470 g, 0.76 mmol). ^{1}H NMR ($CDCl_3$): δ = 8.02−7.55 (m, 20 H, Ar−H), 3.28 (m, 1 H, CH), 1.29 (m, 1 H, CH_2), 0.95 (m, 1 H, CH_2), 0.79 (d, ^3J = 7 Hz, 3 H, CH_3), 0.43 (t, ^3J = 7 Hz, 3 H, CH_3) ppm. ^{31}P{^{1}H} NMR ($CDCl_3$): δ = 29.6 (s) ppm. $C_{28}H_{29}Cl_2NP_2Pd$ (618.80): calcd. C 54.35, H 4.72, Cl 11.46, N 2.26; found C 54.26, H 4.68, Cl 11.70, N 2.14.

[Pt(S_c-1)Cl$_2$] (5): Following the same procedure used for the synthesis of **4**, compound **5** was obtained as a white crystalline solid by reacting [Pt(COD)Cl$_2$] (0.50 g, 1.33 mmol) and (S_c)-**1** (0.59 g, 1.33 mmol). Yield: 82% (0.777 g, 1.09 mmol). ^{1}H NMR ($CDCl_3$): δ = 8.00 (m, 10 H, Ar−H), δ = 7.50 (m, 10 H, Ar−H), 3.20 (m, 1 H, C*H), 1.02 (m, 1 H, CH_2), 0.87 (m, 1 H, CH_2), 0.77 (d, ^3J = 7 Hz, 3 H, CH_3), 0.41 (t, ^3J = 7 Hz, 3 H, CH_3) ppm. ^{31}P{^{1}H} NMR ($CDCl_3$): δ = 15.5 (t, $^1J_{Pt,P}$ = 3285 Hz) ppm. $C_{28}H_{29}Cl_2NP_2Pt$ (707.49): calcd. C 47.54, H 4.13, Cl 10.02, N 1.98; found C 47.50, H 3.98, Cl 9.94, N 1.89.

[Rh(COD)(S_c-1)]PF$_6$ (6): NH_4PF_6 (0.260 g, 1.6 mmol) was added to a solution of [Rh(COD)Cl]$_2$ (0.400 g, 0.8 mmol) in THF (25 mL). The bright-yellow solution was stirred at room temperature for 30 min. Upon adding the solid ligand (S_c)-**1** (0.706 g, 1.6 mmol), an instantaneous change of colour occurred from yellow to orange, together with formation of an orange precipitate. The solvent was evaporated under reduced pressure and the residual solid was washed three times with hexane to afford the pure title complex **6** as an orange powder. Yield: 65% (0.830 g, 1.04 mmol). ^{1}H NMR ($CDCl_3$): δ = 7.80−7.40 (m, 32 H, Ar−H), 3.06 (m, 1 H, C*H), 0.82 (m, 1 H, CH_2), 0.71 (m, 1 H, CH_2), 0.64 (d, ^3J = 7 Hz, 3 H, CH_3), 0.34 (t, ^3J = 6.8 Hz, 3 H, CH_3) ppm. ^{31}P{^{1}H} NMR ($CDCl_3$): δ = 50.1 (d, $^1J_{RhP}$ = 134 Hz), −143.9 (PF_6) ppm. $C_{36}H_{41}F_6NP_3Rh$ (797.55): calcd. C 54.22, H 5.18, F 14.29, N 1.76; found C 53.92, H 5.22, F 14.15, N 1.73.

[Pd(R_a,R_a-2)Cl$_2$] (8): A solution of (R_a,R_a)-**2** (0.563 g, 0.78 mmol) in toluene (10 mL) was added dropwise to a solution of [Pd(PhCN)$_2$Cl$_2$] (0.300 g, 0.78 mmol) in the same solvent (20 mL) that was cooled in an ice bath. The reaction mixture was stirred for 30 min; during this time, precipitation of an orange solid occurred. The solid was separated by filtration, washed a few times with petroleum ether and then dried under reduced pressure to give the product **8** as an orange solid. Yield: 74% (0.519 g, 0.58 mmol). ^{1}H NMR ($CDCl_3$): δ = 8.33−7.28 (m, 29 H, Ar−H) ppm. ^{31}P{^{1}H} NMR ($CDCl_3$): δ = 82.1 (s) ppm. $C_{46}H_{29}Cl_2NO_4P_2Pd$ (899.0): calcd. C 61.46, H 3.25, Cl 7.89, N 1.56; found C 61.36, H 3.15, Cl 8.02, N 1.50.

[Pt(R_a,R_a-2)I$_2$] (9): A solution of ligand (R_a,R_a)-**2** (0.130 g, 0.18 mmol) in toluene (10 mL) was added dropwise at room temperature to a solution of [Pt(COD)I$_2$] (0.100 g, 0.18 mmol) in the same solvent (20 mL). After 1 h, the bright-yellow solution was concentrated under reduced pressure until the volume was ca. 5 mL; after the addition of pentane (30 mL), a deep-yellow solid precipitated. This solid was crystallized from CH_2Cl_2/pentane (3:1, 10 mL) to obtain the pure complex **9** as a yellow powder. Yield: 79% (0.166 g, 0.14 mmol). ^{1}H NMR ($CDCl_3$): δ = 8.49 (m, 6 H, Ar−H), 8.04−7.95 (m, 11 H, Ar−H), 7.51−7.31 (m, 4 H, Ar−H), 6.89 (m, 4 H, Ar−H), 6.80−6.75 (m, 4 H, Ar−H) ppm. ^{31}P{^{1}H} NMR ($CDCl_3$): δ = 94.5 ($^1J_{Pt,P}$ = 5296 Hz) ppm. $C_{46}H_{29}I_2NO_4P_2Pt$ (1170.59): calcd. C 47.20, H 2.50, I 21.68, N 1.20; found C 46.98, H 2.58, I 21.48, N 1.26.

[Pd(R_a,S_c-3)Cl$_2$] (10): A solution of ligand (R_a,S_c)-**3** (0.108 g, 0.189 mmol) in CH_2Cl_2 (10 mL) was added to a solution of [Pd(PhCN)$_2$Cl$_2$] (0.073 g, 0.189 mmol) in the same solvent (25 mL). The reaction mixture was stirred for 30 min at room temperature. The solution was concentrated under reduced pressure until the volume was ca. 5 mL; after the addition of pentane (30 mL), a yellow solid precipitated. This solid was crystallized from CH_2Cl_2/pentane (3:1, 10 mL), washed twice with petroleum ether and then dried under vacuum to give compound **10**. Yield: 68% (0.101 g, 0.13 mmol). ^{1}H NMR ($CDCl_3$): δ = 8.04−7.95 (m, 22 H, Ar−H),

 © 2004 Wiley-VCH Verlag GmbH & Co. KGaA, Weinheim

Table 3. Crystal data and structural refinement for compounds **4** and **5** ($R_1 = \Sigma||F_o| - |F_c||/\Sigma|F_o|$, $wR_2 = \{\Sigma[w(F_c^2 - F_o^2)^2]/\Sigma[w(F_o^2)^2]\}^{1/2}$)

Compound	**4**	**5**
Formula	$C_{28}H_{29}Cl_2NP_2Pd$	$C_{28}H_{29}Cl_2NP_2Pt$
Formula mass	618.76	707.45
Wavelength (Å)	0.71073 (Mo-*Kα*)	0.71073 (Mo-*Kα*)
Crystal system	orthorhombic	orthorhombic
Space group	$P\ 2_12_12_1$	$P\ 2_12_12_1$
Unit cell dimensions (Å)	$a = 14.931(3)$	$a = 14.951(3)$
$b = 16.891(3)$	$b = 16.966(3)$	
$c = 21.089(5)$	$c = 21.053(5)$	
V (Å^3)	5319(2)	5340(2)
Z, density (calcd.) (Mg/m^3)	8, 1.545	8, 1.760
Abs. coefficient (cm^{-1})	10.37	55.93
F(000)	2512	2768
Crystal size (mm)	0.18 × 0.32 × 0.37	0.22 × 0.21 × 0.22
θ range (°)	1.54−28.22	1.54−27.98
Reflection collected, independent reflections	31872, 11746 [$R_{(int)} = 0.0788$]	31436, 11395 [$R_{(int)} = 0.0590$]
Obsd. reflections [$I > 2\sigma(I)$]	5209	8705
Data/restraints/parameters	11746/0/621	11395/0/621
Final R indices [$I > 2\sigma(I)$]	$R_1 = 0.0433$, $wR_2 = 0.0467$	$R_1 = 0.0406$, $wR_2 = 0.0916$
R indices (all data)	$R_1 = 0.1310$, $wR_2 = 0.0602$	$R_1 = 0.0608$, $wR_2 = 0.0991$

3.15 (m, 1 H, CH), 1.18 (m, 1 H, CH_2), 0.82 (m, 1 H, CH_2), 0.73 (d, ^3J = 7 Hz, 3 H, CH_3), 0.41 (t, ^3J = 7 Hz, 3 H, CH_3) ppm. $^{31}P\{^1H\}$ NMR ($CDCl_3$): δ = 81.8 (d, $^2J_{P,P}$ = 17 Hz), 39.9 (d, $^2J_{P,P}$ = 17 Hz) ppm. $C_{36}H_{31}Cl_2NO_2P_2Pd$ (784.91): calcd. C 57.74, H 4.17, Cl 9.47, N 1.87; found C 57.84, H 4.21, Cl 9.62, N 1.77.

[Pt(R_a,S_c-3)I$_2$] (11): Following the same procedure used for the synthesis of **10**, compound **11** was obtained as a white solid after reacting [Pt(COD)I_2] (0.094 g, 0.168 mmol) and solid (R_a,S_c)-**3** (0.096 g, 0.168 mmol) in CH_2Cl_2. Yield: 67% (0.115 g, 0.11 mmol). ^1H NMR ($CDCl_3$): δ = 8.04−7.95 (m, 22 H, Ar−H), 3.08 (m, 1 H, CH), 1.14 (m, 1 H, CH_2), 0.75 (m, 1 H, CH_2), 0.61 (d, ^3J = 7 Hz, 3 H, CH_3), 0.35 (t, ^3J = 7 Hz, 3 H, CH_3) ppm. $^{31}P\{^1H\}$ NMR ($CDCl_3$): δ = 98.3 (d, $^2J_{P,P}$ = 19, $^1J_{Pt,P}$ 4876 Hz), 45.8 (d, $^2J_{P,P}$ = 19, $^1J_{Pt,P}$ 3218 Hz) ppm. $C_{36}H_{31}Cl_2NO_2P_2Pt$ (1020.50): calcd. C 42.37, H 3.06, I 24.87, N 1.37; found C 42.34, H 3.01, I 24.69, N 1.31.

Reaction of [RhCO)$_2$Cl]$_2$ with (R_a,S_c)-3: Solid (R_a,S_c)-**3** (0.320 g, 0.56 mmol) was added at room temperature to a stirred solution of [Rh(CO)$_2$Cl]$_2$ (0.112 g, 0.288 mmol) in hexane (30 mL). After the addition, precipitation of a yellow compound was observed. The mixture was stirred for 30 min at room temperature, and then the solvent was evaporated under reduced pressure. The solid was washed with hexane (3 × 10 mL) until the filtered solution was colourless, i.e., indicating that the excess of [Rh(CO)$_2$Cl]$_2$ had been separated. The $^{31}P\{^1H\}$ NMR spectrum of the crude product (Figure 1), recorded in $CDCl_3$, indicated the presence of both [Rh(R_a,S_c-**3**)(CO)Cl] (**12**) and [Rh(μ-R_a,S_c-**3**)(CO)Cl]$_2$ (**13**) together with other species at very low concentrations. We failed to obtain compounds **12** and **13** as analytically pure solids, either by using column chromatographic methods or differences in their solubilities. The reaction of [RhCO)$_2$Cl]$_2$ with (R_a,S_c)-**3** in a 1:2 molar ratio also afforded a mixture of **12** and **13**. **Compound [Rh(R_a,S_c-3)(CO)Cl] (12):** IR (KBr, Nujol): $\tilde{\nu}_{CO}$ = 1990 cm^{-1}. ^1H NMR ($CDCl_3$): δ = 8.04−6.95 (m, 22 H, Ar−H), 2.66 (m, 1 H, CH), 1.23 (m, 1 H, CH_2), 0.81 (m, 1 H, CH_2), 0.49 (d, ^3J = 6 Hz, 1 H, CH_3), 0.23 (t, ^3J = 7 Hz, 3 H, CH_3) ppm. $^{31}P\{^1H\}$ NMR ($CDCl_3$): δ = 103.9 (dd, $^1J_{RhP}$ = 222, $^2J_{P,P}$ = 98 Hz), 47.7 (dd, $^1J_{RhP}$ = 122, $^2J_{P,P}$ = 98 Hz) ppm. **Compound [Rh(μ-R_a,S_c-3)(CO)Cl]$_2$ (13):** ^1H NMR ($CDCl_3$): δ = 8.04−6.95 (m, 44 H, Ar−H), 2.90 (m, 2 H, CH), 1.18 (m, 2 H, CH_2), 0.72 (m, 2 H, CH_2), 0.78 (d, ^3J = 7 Hz, 6 H, CH_3), 0.43 (d, ^3J = 7 Hz, 6 H, CH_3) ppm. $^{31}P\{^1H\}$ NMR ($CDCl_3$): δ = 108.0 (ddd, $^1J_{RhP}$ = 133, $^2J_{P,P}$ = 46, $^2J_{P,P}$ = 35 Hz), 54.4 (ddd, $^1J_{RhP}$ = 124, $^2J_{P,P}$ = 46, $^2J_{P,P}$ = 35 Hz) ppm.

X-ray Data Collection, Structural Solution and Refinement for Compounds 4 and 5: The intensity data of compound **4** and **5** were collected at room temperature on a Bruker Smart 1000 single-crystal diffractometer. Crystallographic and experimental details for the structures are summarized in Table 3.

The structures were solved by Patterson and Fourier methods and refined by full-matrix least-squares procedures (based on F_o^2)[13] with anisotropic thermal parameters used in the last cycles of refinement for all the non-hydrogen atoms.

The hydrogen atoms were introduced into geometrically calculated positions and refined riding on the corresponding parent atoms. In the final cycles of refinement, we used a weighting scheme: $w = 1/[\sigma^2F_o^2 + (0.0069\ P)^2]$ (**4**, **Pd**), $w = 1/[\sigma^2F_o^2 + (0.0454\ P)^2]$ (**5**, **Pt**), where $P = (F_o^2 + 2\ F_c^2)/3$.

CCDC-215879 (for **4**) and -215878 (for **5 Pt**) contain the supplementary crystallographic data for this paper. These data can be obtained free of charge at www.ccdc.cam.ac.uk/conts/retrieving.html [or from the Cambridge Crystallographic Data Centre, 12 Union Road, Cambridge CB2 1EZ, UK; Fax: (internat.) + 44-1223-336-033; E-mail: deposit@ccdc.cam.ac.uk].

[1] For the most versatile classes of ligands, see the following reviews. Bisoxazolines: [1a] A. Pfaltz, *Acc. Chem. Res.* **1993**, *26*, 339. [1b] A. K. Ghosh, P. Mathivanan, J. Cappiello, *Tetrahedron: Asymmetry* **1998**, *9*, 1. [1c] J. S. Johnson, D. A. Evans, *Acc. Chem. Res.* **2000**, *33*, 325. Phosphinooxazolines: [1d] G. Helmchen, A. Pfaltz, *Acc. Chem. Res.* **2000**, *33*, 336. [1e] A. Pfaltz, *Acta Chem. Scand., Ser. B* **1996**, *50*, 189. Phosphoramidites: [1f] B. L. Feringa, *Acc. Chem. Res.* **2000**, *33*, 346. Wide-bite-angle ligands: [1g] P. C. J. Kamer, P. W. N. M. van Leeuwen, J. N. H. Reek, *Acc. Chem. Res.* **2001**, *34*, 895. [1h] P. W. N. M. van Leeuwen, P. C. J. Kamer, J. N. H Reek, P. Dierkes, *Chem. Rev.* **2000**, *100*, 2741. Ligands derived from the quinoline back-

 © 2004 Wiley-VCH Verlag GmbH & Co. KGaA, Weinheim

bone: [1i] G. Franciò, C. G. Arena, F. Faraone, C. Graiff, M. Lanfranchi, A. Tiripicchio, *Eur. J. Inorg. Chem.* **1999**, 1219. [1j] G. Franciò, F. Faraone, W. Leitner, *Angew. Chem. Int. Ed.* **2000**, *39*, 1428.

[2] [2a] J. K. Whitesell, *Chem. Rev.* **1989**, *89*, 1581. [2b] L. Pu, *Chem. Rev.* **1998**, *98*, 2405. [2c] C. Rosini, L. Franzini, A. Raffaelli, P. Salvadori, *Synthesis* **1992**, 503. [2d] T. Ohkuma, M. Koizumi, H. Doucet, T. Pham, M. Kozawa, K. Murata, E. Katayama, T. Yokozawa, T. Ikariya, R. Noyori, *J. Am. Chem. Soc.* **1998**, *120*, 13529 and references cited therein. [2e] K. Mikami, S. Matsukawa, *Nature* **1997**, *385*, 613 and references cited therein.

[3] G. Calabrò, D. Drommi, G. Bruno, F. Faraone, *Dalton Trans.* **2004**, 81.

[4] [4a] A. L. Balch, in *Homogeneous Catalysis Using Metal Phosphine Complexes* (Ed.: L. H. Pignolet), Plenum Press, New York, **1983**, p. 167. [4b] G. R. Newkome, *Chem. Rev.* **1993**, *93*, 2067. [4c] R. Puddephatt, *J. Chem. Soc. Rev.* **1983**, *12*, 99. [4d] B. Chaudret, B. Delavaux, R. Poilblanc, *Coord. Chem. Rev.* **1988**, *86*, 191. [4e] M. S. Balakrishna, S. V. Reddy, S. S. Krishamurthy, J. F. Nixon, J. Burckett, St. Laurent, *Coord. Chem. Rev.* **1994**, *129*, 1. [4f] B. R. Sutherland, M. Cowie, *Organometallics* **1985**, *4*, 1801. [4g] J. T. Mague, *Organometallics* **1986**, *5*, 918. [4h] S. Lo Schiavo, G. Bruno, F. Nicolò, P. Piraino, F. Faraone, *Organometallics* **1985**, *4*, 2091. [4i] C. Arena, F. Faraone, M. Lanfranchi, E. Rotondo, A. Tiripicchio, *Inorg. Chem.* **1992**, *31*, 4797. [4j] M. Cowie, G. Vasapollo, B. R. Sutherland, J. P. Ennett, *Inorg. Chem.* **1986**, *25*, 2648. [4k] M. Cowie, T. G. Southern, *Inorg. Chem.* **1982**, *21*, 246. [4l] B. A. Vaartstra, K. N. O'Brien, R. Eisenberg, M. Cowie, *Inorg. Chem.* **1988**, *27*, 3668. [4m] D. J. Anderson, K. W. Kramarz, R. Eisenberg, *Inorg. Chem.* **1996**, *35*, 2688. [4n] J. R. Torkelson, F. H. Antwi-Nsiah, R. McDonald, M. Cowie, J. G. Pruis, K. J. Jalkanen, R. L. DeKock, *J. Am. Chem. Soc.* **1999**, *121*, 3666.

[5] [5a] E. Drend, D. Arnoldy, P. H. M. Budzelaar, *J. Organomet. Chem.* **1993**, *455*, 247. [5b] Y. Gao, J. K. Kuncheria, H. A. Jenkins, R. J. Puddephatt, G. P. A. Yap, *J. Chem. Soc., Dalton Trans.* **2000**, 3212. [5c] A. Scrivanti, V. Beghetto, E. Campagna, M. Zenato, U. Matteoli, *Organometallics* **1998**, *17*, 630. [5d] M. E. Broussard, B. Juma, S. G. Train, W. Peng, S. A. Laneman, G. G. Stanley, *Science* **1993**, *260*, 1784. [5e] G. Franciò, R. Scopelliti, C. G. Arena, G. Bruno, D. Drommi, F. Faraone, *Organometallics* **1998**, *17*, 338. [5f] S. J. Dossett, A. Gillon, G. Orpen, J. S. Fleming, P. G. Pringle, D. F. Wass, M. D. Jones, *Chem. Commun.* **2001**, 699.

[6] [6a] Y. Yamanoi, T. Imamoto, *J. Org. Chem.* **1999**, *64*, 2988. [6b] I. D. Gridnev, Y. Yamanoi, N. Higashi, H. Tsuruta, M. Yasutake, T. Imamoto, *Adv. Synth. Catal.* **2001**, *343*, 118. [6c] A. Marinetti, C. Le Menn, L. Ricard, *Organometallics* **1995**, *14*, 4983. [6d] R. P. Kamalesh Babu, S. S. Krishnamurthy, M. Nethaji, *Tetrahedron: Asymmetry* **1995**, *6*, 427.

[7] [7a] P. W. Lednor, W. Beck, H. G. Fick, H. Zippel, *Chem. Ber.* **1978**, *111*, 615. [7b] N. C. Payne, D. W. Stephan, *J. Organomet. Chem.* **1981**, *221*, 203.

[8] E. J. Sekabunga, M. L. Smith, T. R. Webb, W. E. Hill, *Inorg. Chem.* **2002**, *41*, 1205.

[9] S. Priya, M. S. Balakrishna, J. T. Mague, S. M. Mobin, *Inorg. Chem.* **2003**, *42*, 1272 and references cited therein.

[10] [10a] J. P. Farr, F. E. Wood, A. L. Balch, *Inorg. Chem.* **1983**, *22*, 3387. [10b] A. Maisonnat, J. P. Farr, A. L. Balch, *Inorg. Chim. Acta* **1981**, *53*, L217. [10c] J. P. Farr, M. M. Olmstead, A. L. Balch, *J. Am. Chem. Soc.* **1980**, *102*, 6654.

[11] We thank a referee for suggesting this possible dimer $Rh^{II}-Rh^{II}$ structure.

[12] P. H. M. Budzelaar, J. H. G. Frijns, A. G. Orpen, *Organometallics* **1990**, *9*, 1222.

[13] G. M. Sheldrick, *SHELXTL v5.1: Program for the Refinement of Crystal Structures* 97−2, University of Göttingen, Göttingen, Germany, **1998**.

Received August 4, 2003
Early View Article
Published Online February 26, 2004

 © 2004 Wiley-VCH Verlag GmbH & Co. KGaA, Weinheim

Synthesis, Structural Characterizations and Magnetic Properties of a Series of Mono-, Di- and Polynuclear Manganese Pyridinecarboxylate Compounds

Deguang Huang,[a] Wenguo Wang,[a] Xiaofeng Zhang,[a] Changneng Chen,[a] Feng Chen,[a] Qiutian Liu,*[a] Daizheng Liao,[b] Licun Li,[b] and Licheng Sun[c]

Keywords: Carboxylate ligands / Coordination polymers / Magnetic properties / Manganese / X-ray diffraction

Seven new manganese(II, III, IV) pyridinecarboxylate compounds $(Et_4N)[MnCl_2(pic)_2]$ (**1**, Hpic = picolinic acid) $[MnCl(pic)_2(H_2O)]\cdot H_2O$ (**2**), $[MnCl(pic)(H_2O)_2]_n$ (**3**), $[Mn(pic)_2]_n$ (**4**), $[MnCl(pic)]_n$ (**5**), $[MnCl_2(4\text{-}C_5H_4NHCOO)]_n$ (**6**) and $[Mn_2O_2(pic)_4]$ (**7**) were synthesized and structurally characterized. The picolinate ligand coordinates to the Mn ion forming a chelating five-membered ring which constructs diverse architectures by various bridging modes, such as μ-Cl, $\mu_{1,1}$- and $\mu_{1,3}$-carboxylate bridges (*syn-syn* and *syn-anti* modes). The interaction between the pyridyl rings is discussed, displaying a face-to-face π-π stacking for complex **6** and a T-shaped C–H···π attraction for complex **4**. Complex **3** has an infinite zigzag chain structure in which two neighboring Mn ions are linked by a carboxylate bridge in a *syn-anti* mode. In complex **4**, the $Mn(pic)_2$ fragments are joined to each other by double $\mu_{1,1}$-carboxylate bridges, forming a 2D layer structure. Complex **5** contains Mn_4O_4 square subunits which are connected by double μ-Cl bridges to form a grid-like 2D structure. The isonicotinate complex **6** has a zigzag chain structure containing mixed double μ-Cl and $\mu_{1,3}$-carboxylate bridges in a *syn-syn* mode. Protonation at the pyridyl-N position was found and identified by the IR and magnetic properties of **6**. The participation of an oxidizing agent like MnO_4^- leads to complexes containing higher valent manganese (**1**, **2** and **7**). The IR spectra of these complexes are discussed and found to be consistent with the structural features. The magnetic properties of complexes **4**, **5** and **6** have been investigated. Antiferromagnetic coupling interactions were observed and satisfactory fitting results were obtained with *J* values ranging from –0.63 cm^{-1} to –2.35 cm^{-1}. The magnetic parameters of these complexes, together with the parameters of other Mn complexes with comparable structures, are compared and discussed based on the bridging modes.
(© Wiley-VCH Verlag GmbH & Co. KGaA, 69451 Weinheim, Germany, 2004)

Introduction

Metal-ligand coordination polymers are attracting increasing attention owing to their potential applications as novel functional materials in catalysis, magnetism, molecular recognition and other fields.[1] Meanwhile, the increasing interest in the coordination chemistry of manganese also stems from the involvement of manganese in several biological redox-active systems,[2,3] especially in the oxygen-evolving complex[4] (OEC) of photosystem II (PS II), which is believed to be a tetranuclear $Mn^{II,III,IV}$ aggregate[5] with O- and N-donors from a carboxylate group and a histidine, respectively.[6] The binding[7] of water to the Mn site and the presence[8] of chloride anion are important structural features of the OEC.

Three isomers of pyridinecarboxylic acid, which contains both O- and N-donors, exhibit remarkable coordination modes to metal ions. Picolinic acid is the most commonly used to obtain metal complexes — its different coordination modes are shown in Scheme 1 — in which a chelating five-membered ring is always found. A number of Mn picolinate complexes with nuclearity[9–12] from 1 to 10 or with a polymeric structure[13] have been reported in the past two decades. However, only a few of these Mn complexes possess a polymeric structure[13] or contain a chloride ligand.[11]

Compared to the coordination modes of the picolinate, there is an obvious difference for 3-, and 4-pyridinecarboxylates, which do not form a chelate ring when they coordinate to metals. Mn complexes[14,15] of these ligands with a polymeric structure are also rare. In order to develop the diversity of the architectures in Mn pyridinecarboxylate chemistry, especially picolinate chemistry, we are interested in the preparation of Mn/pyridinecarboxylate complexes containing a chloride anion, to see what fascinating network topologies are obtained. In this work several Mn com-

[a] State Key Laboratory of Structural Chemistry, Fujian Institute of Research on the Structure of Matter, Chinese Academy of Sciences,
Fuzhou 350002, China
Fax: (internat.) + 86-591-371-4946
E-mail: lqt@ms.fjirsm.ac.cn
[b] Department of Chemistry, Nankai University,
Tianjing 300071, China
[c] State Key Laboratory of Fine Chemicals, Dalian University of Technology,
Dalian, China

 © 2004 Wiley-VCH Verlag GmbH & Co. KGaA, Weinheim **DOI: 10.1002/ejic.200300586**

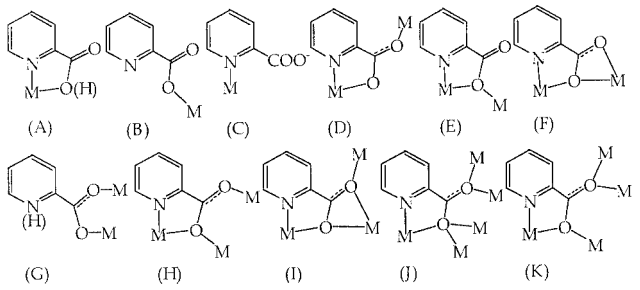

Scheme 1. Possible coordination modes of picolinate to metal ions; modes **A**, **D**, **E**, **H** and **I** have been found in Mn picolinate complexes

plexes with the Mn oxidation states from II to IV are reported, of which four complexes possess a chain-like structure and five contain Mn−Cl ligation.

Results and Discussion

Synthesis

Hundreds of manganese complexes containing Mn−Cl bonds have been reported, of which more than one hundred contain both O- and N-donors from a Schiff base and a nitrogen-containing heterocycle. In this work pyridinecarboxylic acid and $MnCl_2{\cdot}4H_2O$ were used to provide the O- and N-donors and the Cl, respectively. Complexes **1**−**7** were obtained by both conventional solution synthesis and solvothermal methods. Complex **5**, containing an Mn−Cl bond, was obtained in DMF by a solvothermal method, while with a similar molar ratio of reagents and the same reaction temperature to those used for preparing **5** (see Exp. Sect.), complex **4** was synthesized and was found not to contain an Mn−Cl component. This difference is considered to arise from the polarity of the solvents adopted for the syntheses of **4** and **5**. Depending on the polarity of the solvent, DMF or H_2O gives rise to the dissociation of the Mn−Cl bond, leading to the disappearance of the Cl component in complex **4**, while solvents with lower polarity favor the retention of the Mn−Cl bond in **5**. The participation of an oxidizing agent (MnO_4^-) results in the formation of complexes with higher valent manganese. Compounds **1**, **2** and **7** containing Mn^{III} and Mn^{IV} were obtained in the presence of the oxidizing agent or after a prolonged exposure to air. The dinuclear Mn^{IV} compound **7** has been obtained in other laboratories by different methods[10,16] with a difficulty in crystallizability. We have improved the synthesis by reducing the $KMnO_4$:$Mn(OAc)_2$ ratio to avoid the large amount of insoluble precipitates. A co-product, $Mn(pic)_3$, was obtained and isolated, leading to an improved crystallization of complex **7**.

Structure

The structures of mononuclear **1** and **2** are shown in Figure 1 and 2, respectively. Their structures contain an Mn unit together with a counterion for **1** or a solvate molecule for **2**. The Mn atom in both the compounds has a distorted octahedral coordination geometry, whilst Mn1 in complex **1** lies on a crystallographically imposed inversion centre. Both the chelating five-membered rings lie in the equatorial plane, with largest deviations of 0.1067 Å and 0.1447 Å for the constituent atoms of **1** and **2**, respectively. Two terminal *trans*-ligands coordinate to the Mn ion forming linear Cl−Mn−ClA (180° for **1**) and Cl−Mn−O5 [177.60(11)° for **2**] arrays. The Mn−Cl [2.504(1)−2.525(1) Å] and the $Mn-O_{H_2O}$ [2.324(4) Å] bond lengths are obviously lengthened, indicating a Jahn−Teller elongation of high spin d^4 Mn^{III} along the axial direction for the two Mn^{III} complexes. Consequently the $Mn^{III}-Cl$ and $Mn^{III}-O_{H_2O}$ bonds are longer than those found in the Mn^{II} complexes **3**−**6** (Table 1). This Jahn−Teller elongation has previously been observed in other Mn^{III} complexes, in which $Mn^{III}-Cl$ bond lengths of 2.510−2.541 Å were observed.[17] There was still some doubt as to whether the ligand is picolinic acid rather than picolinate. A bond valence sum (BVS) analysis[18] was therefore performed to calculate the oxi-

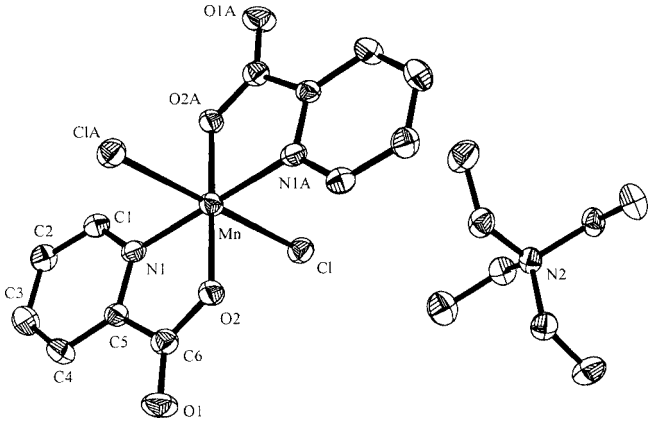

Figure 1. ORTEP representation of compound **1** showing 30% probability displacement ellipsoids and the atom numbering

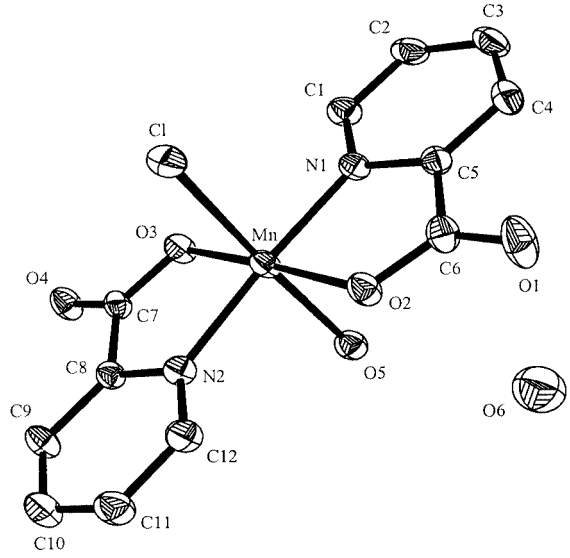

Figure 2. ORTEP representation of compound **2** showing 30% probability displacement ellipsoids and the atom numbering

 © 2004 Wiley-VCH Verlag GmbH & Co. KGaA, Weinheim

Table 1. Selected bond lengths (Å) and angles (°) for **1**−**7**

	1	**2**	**3**	**4**	**5**	**6**	**7**
Mn−O	1.903(3)	1.897(4) 1.901(4)	2.173(2) 2.205(2)	2.122(2)−2.232(2)	2.190(2)−2.342(2)	2.1260(18)	1.940(2) 1.918(1)
Mn−N	2.017(3)	2.010(5) 2.015(5)	2.272(3)	2.277(2) 2.297(3)	2.227(2)		2.009(2) 2.050(2)
Mn−Cl	2.525(1)	2.504(1)	2.4914(9)		2.501(1) 2.500(1)	2.570(1) 2.595(1)	
$Mn-O_{H_2O}$		2.324(4)	2.175(3) 2.181(3)				
$Mn-O_{oxo}$							1.809(1) 1.804(1)
Mn···Mn				3.507	4.425 3.637	3.621	2.701(1)
N−Mn−N	180	175.52(14)		115.63(10)			166.91(9) 94.26(9)
Cl−Mn−Cl	180				87.63(2)	180 82.77(3)−97.23(3)	
O−Mn−O	180	87.12(13)−87.49(13) 174.56(14)	81.44(7)−90.72(9) 178.51(8)	74.00(8)−113.17(8) 160.00(9)	57.33(5)−88.21(8)	180	83.08(9)−96.23(7) 164.82(9)−171.97(6)
O−Mn−N	82.55(13) 97.45(13)	82.54(13)−97.63(14)	72.99(7)−89.61(8) 154.43(8)	71.63(8)−97.55(9) 145.34(8)−155.06(9)	74.41(6)−100.44(6) 151.53(7)		80.61(6)−97.23(7) 173.56(6)
O−Mn−Cl	90.17(9) 89.83(9)	92.42(10)−93.00(10) 177.15(10)	89.46(6)−111.25(6) 167.30(5)		90.87(4)−104.91(5) 161.65(4)−172.24(4)	87.83(5)−92.17(5)	
N−Mn−Cl	86.98(10) 93.02(10)	90.96(11)−93.50(11)	94.32(6)		98.20(5)−97.87(5)		
Mn−Cl−Mn					91.59(2)	89.03(3)	
Mn−O−Mn				106.00(8)	155.00(7)		96.77(7)

dation state of the metal centre. The bond valences (s) were calculated according to Equation (1), where r is the observed bond length and r_0 and B are empirically determined parameters.[18]

$$s = exp[(r_0 - r)/B] \quad (1)$$

This BVS analysis did not support an Mn^{2+} oxidation state. X-band EPR spectra were recorded on a Bruker-ER420 spectrometer for complexes **1** and **2** as solid samples. No signals were observed, which could be an indication of the Mn^{III} ion since the EPR signal is very difficult to observe with traditional perpendicular polarization EPR spectroscopy at X-band for the spin $S = 2$ Mn^{III} ion. An obvious difference between **1** and **2** is that the terminal water ligand gives rise to extended hydrogen bonding interactions between neighboring molecules of **2**, such as O5···Cl [3.272(5) Å] and $O5\cdots O_{carboxyl}$ [2.736(5) and 2.873(6) Å], giving a one-dimensional chain structure. In contrast, the structure of complex **1**, with two chloride ligands, contains only the discrete ions.

Compound **3** has an infinite zigzag chain structure in which the Mn ions are linked to each other by $\mu_{1,3}$-OCO bridges in a *syn-anti* mode, as shown in Figure 3. The Mn ion is located at the center of a distorted octahedron and the picolinate chelate ring forms the equatorial plane together with Cl and the symmetrically related O1A atoms. All the bond lengths [2.170(2), 2.171(2), 2.176(2) and 2.209(2) Å for Mn−O; 2.275(2) Å for Mn−N; 2.492(1) Å for Mn−Cl] were used for the BVS analysis.[18] The BVS of Mn was calculated to be 2.097 by summing the values of *s*, which supports the oxidation state of the Mn^{II} ion. Interestingly, except for the O3 and O4 atoms, which lie in the axial direction, all the other atoms are coplanar, with the largest deviation from the least-squares plane being 0.0197 Å. Consequently, the zigzag chain contains all the atoms in the common plane except for the axial atoms. The O3−Mn−O4 axis [178.51(8)°] is perpendicular to the plane, with bond angles (O3−Mn−X and O4−Mn−X, X = N, O, Cl) ranging from 89.21(7)° to 90.49(11)°. Figure 4 shows a packing diagram of the compound, in which hydrogen bonding interactions of the type $O_{carboxylate}\cdots H-O_{aqua}$ [2.830(3) and 2.821(3) Å] and $Cl\cdots H-O_{aqua}$ [3.144(2) and 3.153(2) Å] link the neighboring parallel zigzag chains, constructing a two-dimensional double-layer network. Rectangular channels are observed in the polymeric structure, with dimensions of 3.22 × 4.16 Å. However, these channel dimensions are measured between atom centers. In a space-filling plot (Figure 4B) taking into account the van der Waals radii, there is only a small channel left. It should also be pointed out that no π-π stacking is observed between the pyridyl rings since their separation is too large (> 3.8 Å)[19] for a van der Waals interaction; the pyridyl rings are found in a parallel and face-to-face alignment.

The structure of compound **4** is shown in Figure 5. The BVS of the central Mn ion is calculated[18] to be 2.028, indicating an Mn^{II} oxidation state and the ligand to be a picolinate anion. In the $Mn(pic)_2$ fragment, the two chelating five-membered rings are nearly perpendicular to each other,

 © 2004 Wiley-VCH Verlag GmbH & Co. KGaA, Weinheim

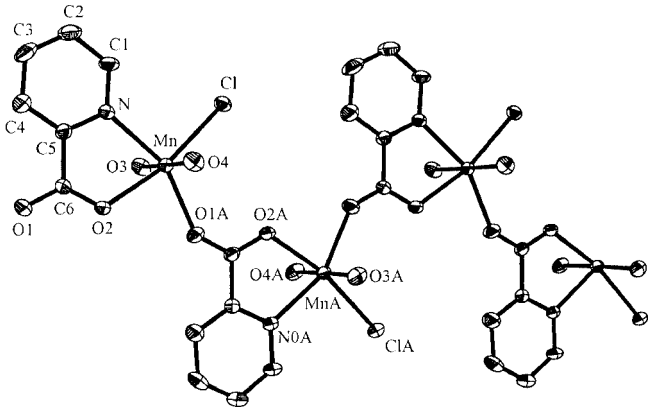

Figure 3. ORTEP representation of compound **3** showing 30% probability displacement ellipsoids and the atom numbering

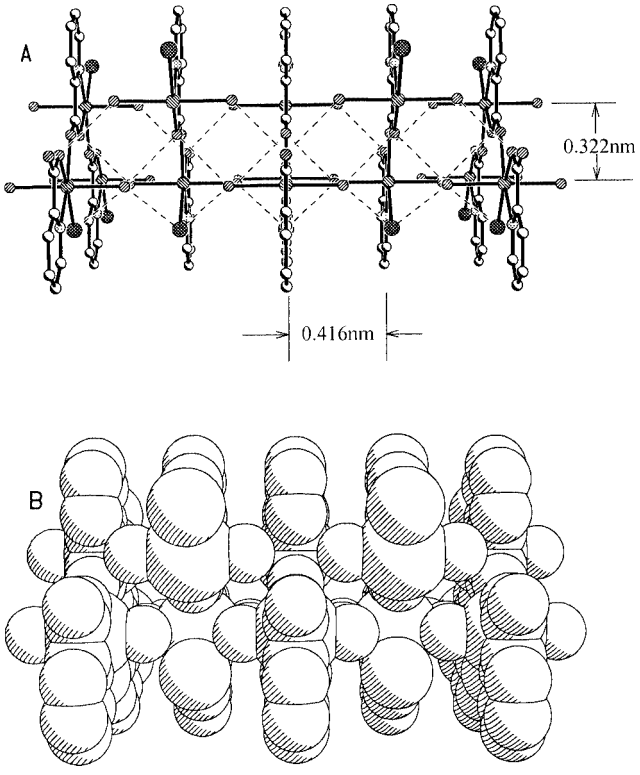

Figure 4. Packing diagram (A) of **3** showing the rectangular channels; hydrogen bonding interactions are shown by dotted lines; (B) space-filling plot to show the small channel space

with a dihedral angle of 85.2°. These fragments are linked pairwise by double μ-$O_{carboxylate}$ bridges to form [Mn_2(pic)$_4$] subunits, with an Mn···Mn distance of 3.507 Å. All the bond angles around the Mn ion range from 145.34(8)° to 160.00(9)° for *trans* angles and from 71.63(8)° to 115.63(10)° for the others, indicating a seriously distorted octahedral geometry. The picolinate anions link the Mn^{II} ions through a $\mu_{1,3}$-OCO bridge in a *syn-anti* mode together with an η^1-monodentate mode to construct a two-dimensional layer structure, as shown in Figure 6, in which π-π stacking has not been observed owing to the large separation between the parallel displaced pyridyl rings. However, a point-to-face (T-shape) interaction — a C−H···π attraction[19] — appears to exist between the pyridyl rings that are perpendicular to each other with a separation of 3.7 Å (Figure 6). An isostructural 2-pyrazinecarboxylate Mn^{II} complex[20] has been reported to have almost the same crystallographic data to that of **4**.

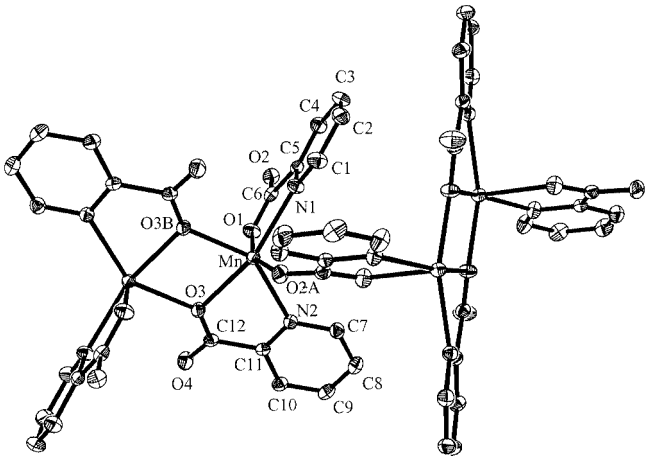

Figure 5. ORTEP representation of compound **4** showing 30% probability displacement ellipsoids and the atom numbering.

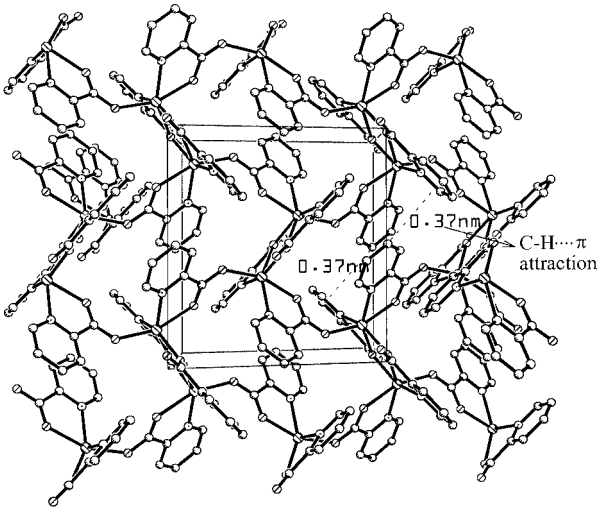

Figure 6. The 2D layer structure of compound **4** along the *a* axis

Complex **5** contains the simplest unit [Mn(pic)Cl], where the picolinate coordinates to the Mn center according to the coordination mode F (Scheme 1) to link two neighboring Mn atoms in the space group $P4_2/n$. The fragments combine, leading to a tetra-manganese [Mn_4(pic)$_4$] subunit, which has an alternating [Mn−O]$_4$ eight-membered ring that looks like a distorted square, as shown in Figure 7, with an Mn···Mn separation of 4.425 Å for each Mn···Mn edge and an O−Mn−O angle of 88.3°. The Mn−O [2.190(2), 2.342(2) and 2.232(2) Å], Mn−N [2.227(2) Å] and Mn−Cl [2.500(1), 2.501(1) Å] bond lengths were used for the BVS calculation[18] and the sum of the values of *s* is 1.98, indicating the Mn^{II} oxidation state. Two kinds of carboxylate bridges of the picolinate anion — a $\mu_{1,1}$-OCO

 © 2004 Wiley-VCH Verlag GmbH & Co. KGaA, Weinheim

bridge and a $\mu_{1,3}$-OCO bridge in a *syn-anti* mode — link simultaneously the Mn ions to form five- and four-membered chelating rings by O,N- and O,O-donors. A small dihedral angle of 4.0° for the two chelating rings indicates an approximate coplanarity of the picolinate ligand and the two Mn ions, as shown in Figure 7. Around the $[Mn-O]_4$ square, the neighbouring picolinates are perpendicular to each other with a dihedral angle of 89.0°, while the opposite ones are approximately parallel, with a dihedral angle of 11.9°.

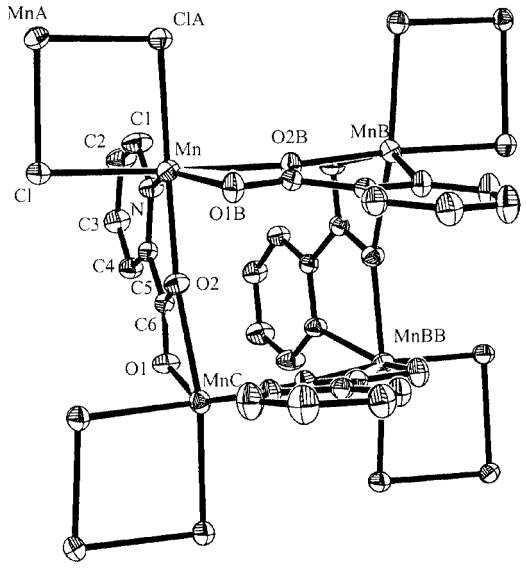

Figure 7. The unit structure of compound **5** showing 30% probability displacement ellipsoids and the atom numbering; a tetramanganese subunit $[Mn(pic)]_4$ is presented

The above $[Mn-O]_4$ squares are connected by double μ-Cl bridges forming the second type of $[Mn(\mu_2\text{-}Cl)_2Mn]$ square-like units, with an Mn−Cl distance of 2.501 Å and angles of 87.6−91.6°. An isostructural Cu analogue $[CuCl(pic)]_n$ has been reported to have similar metal-ligand square-like units.[21] The two types of squares are alternately linked by sharing the Mn ions to form a 2-D Mn_nCl_n quasi-planar grid-like sheet (Figure 8), while the picolinate planes protrude perpendicularly on both sides of the sheet. From the packing diagram (Figure 9), it can clearly be noticed that these salients interpenetrate to give a tightly packed structure without any hydrogen-bonding interactions.

The structure of the isonicotinate complex **6** is composed of a one-dimensional $[Mn(\mu\text{-}C_5H_4NHCOO)(\mu\text{-}Cl)_2]_n$ chain; the $Mn(C_5H_4NHCOO)Cl_2$ unit is shown in Figure 10. A carboxylate bridge in a *syn-syn* mode and double μ-Cl bridges exist between neighboring Mn ions. This is a novel coordination mode for Mn isonicotinate complexes. This is also the first example of a metal complex that contains mixed double Cl and single $\mu_{1,3}$-OCO bridges, the only similar bridging mode was found in $\{Hg_3(L)Cl_6\}_n$ [22] [L = 2,5-bis(pyridino)adipate] containing mixed single Cl and single $\mu_{1,3}$-OCO bridges. In addition, protonation at the pyridyl-N atom was found and was identified by IR spectroscopy (vide infra). A similar proton shift has been observed in a

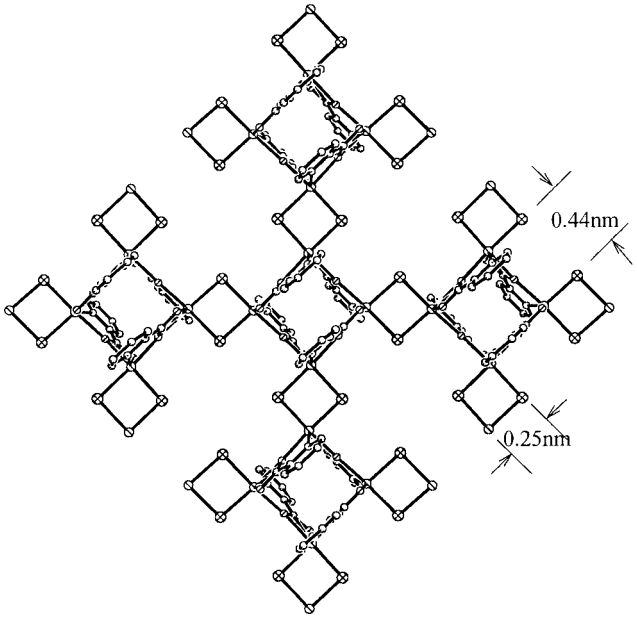

Figure 8. The 2D layer structure of **5** along the *c* axis

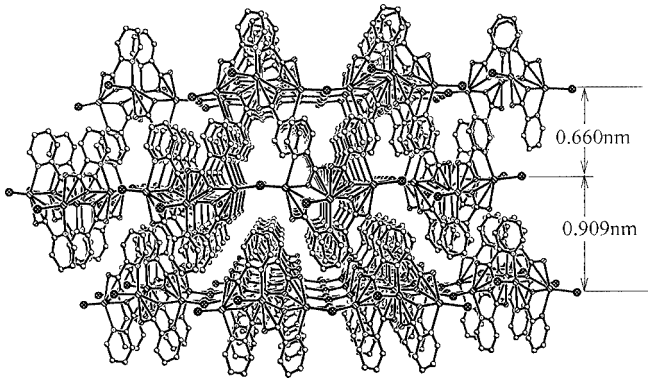

Figure 9. Packing diagram of **5** along the *a* axis showing the inlaid layer structure

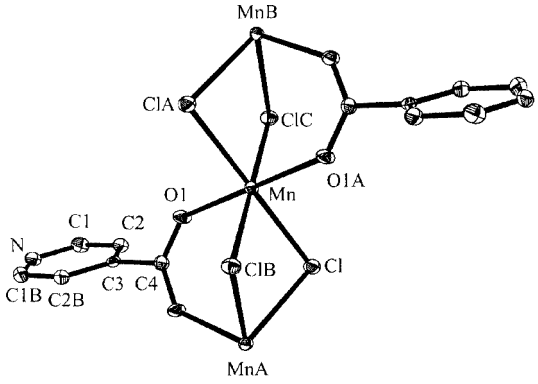

Figure 10. ORTEP representation of compound **6** showing 30% probability displacement ellipsoids and the atom numbering

few metal isonicotinate complexes.[23] The ESR spectra of **6** were recorded on a Bruker-ER420 spectrometer at X-band at room temperature and at 77 K as solid samples, showing strong signals at $g = 2$ and implying the existence of Mn^{II}

 © 2004 Wiley-VCH Verlag GmbH & Co. KGaA, Weinheim

species with spin $S = 5/2$. A BVS calculation[18] for the Mn ion gives the sum of the *s* values to be 1.99, confirming the Mn^{II} oxidation state. The Mn^{II} ion lies at a centre of symmetry, forming a slightly distorted octahedron with O−Mn−Cl angles ranging from 87.83(5)° to 92.17(5)°. Parallel pyridine rings are alternately insert between the neighboring zigzag chains (Figure 11) with a ring separation of 3.621 Å that is slightly larger than the sum of the van der Waals contact radii (3.4 Å) for two C atoms, showing a face-to-face π-π stacking interaction. Owing to the restriction by this arrangement, the pyridine rings cannot be coplanar with the carboxylic group, and the dihedral angle was observed to be 67.2° between the carboxylate group and the pyridyl ring. Hydrogen-bonding interactions (N−H···Cl) exist between the neighboring chains to construct a 2D layer structure.

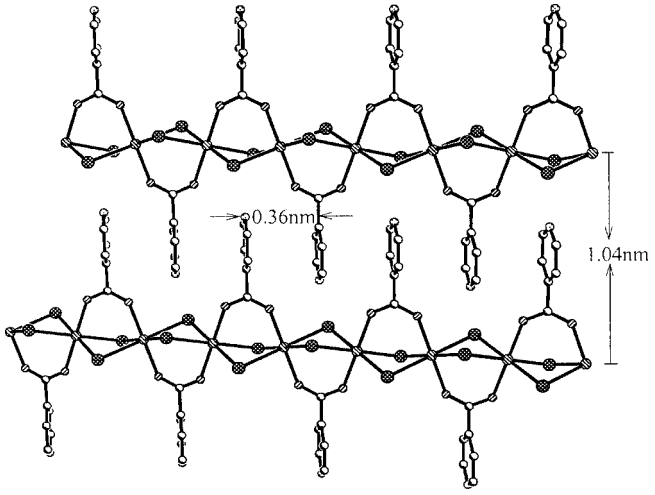

Figure 11. The 1D zigzag chain of complex **6**

Compound **7** contains Mn ions and double oxo-bridges as well as the picolinate ligands. It should be pointed out that the first such complex $[Mn_2O_2(pic)_4]\cdot CH_3CN$ was reported by Christou.[10] Similar structural parameters to those of $[Mn_2O_2(pic)_4]\cdot CH_3CN$, and the BVS of 4.1,[18] indicate that the Mn atom is definitely tetravalent in **7**. An interesting difference between both structures is the lower symmetry of **7** than that of $[Mn_2O_2(pic)_4]\cdot CH_3CN$. The structure of **7** is shown in Figure 12. A twofold axis passes through the Mn1 and Mn2 ions with an Mn−Mn bond length of 2.701(1) Å. Both the octahedral Mn ions coordinate differently to the picolinate ligands. Two nitrogen atoms are located in the *trans*-positions for the Mn1 ion, with an N1−Mn1−N1′ angle of 166.91(9)°, while they are in the *cis*-positions for Mn2, with an N2−Mn2−N2′ angle of 94.26(9)°. A similar situation is also observed for the carboxylate oxygen atoms: O1−Mn1−O1′ of 92.37(10)° and O4−Mn2−O4′ of 164.82(9)°. This is an important difference between **7** and $[Mn_2O_2(pic)_4]\cdot CH_3CN$, as in the latter both N atoms are axially arranged in the octahedron of any Mn ion.

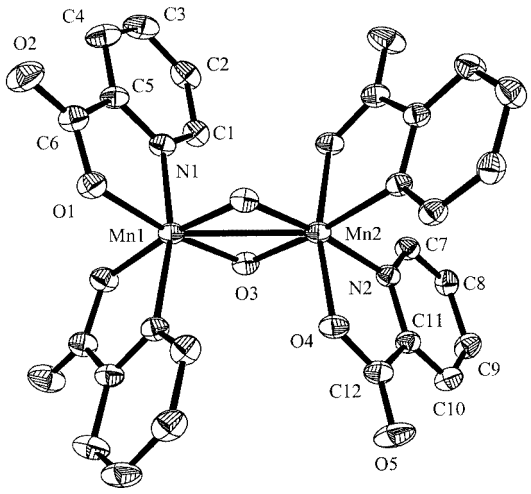

Figure 12. ORTEP representation of **7** showing 30% probability displacement ellipsoids and the atom numbering; Mn···Mn distance 2.701 Å

IR Spectroscopy

In agreement with previously published data,[9,10] the IR spectra of the Mn picolinate complexes (**1**−**5** and **7**) in the 400−4000 cm^{-1} region only exhibit signals related to the picolinate ligand, for example 1649, 1309, 1049 and 764 cm^{-1} for **1**; similar signals are found for the other complexes. The signals in the range from 1610 cm^{-1} to 1682 cm^{-1} can be assigned to the asymmetric stretching vibrations for the COO^- groups, and the signals between 1446 and 1497 cm^{-1} correspond to the symmetric stretching vibrations $\nu_s(COO^-)$. The isonicotinate signals for complex **6** are also similar to those reported previously.[15] The carboxylate in **6** exhibits similar asymmetric and symmetric stretching vibrations to those of other picolinate complexes. The N−H stretching frequency is observed at 3217 cm^{-1}, suggesting[24] protonation at the nitrogen atom of the pyridyl. Complexes **1** and **7** contain the carboxylate groups in unidentate coordination mode, and the separation (Δ) between $\nu_{as}(COO^-)$ and $\nu_s(COO^-)$ is 209 cm^{-1}, which is consistent with the generally accepted value[25] ($\Delta > 200$ cm^{-1}) for a unidentate-coordinated carboxylate, while complexes **5** and **6** give a separation value of less than 200 cm^{-1}, which is considered to correlate to a chelating carboxylate in **5** ($\Delta = 135-164$ cm^{-1}) or a bridging bidentate ligand in a *syn-syn* configuration in **6** ($\Delta = 174-197$ cm^{-1}). The strong and broad band centered at 3385 cm^{-1} for **3** is assigned to the H−O−H stretching vibration of the water ligand on the basis of the known structure. Medium-intensity absorptions are observed in the range from 3080 to 3120 cm^{-1} and can be attributed to the δ(CH) of the pyridyl.

Magnetic Properties

The magnetic properties of Mn complexes are often important. Complexes **1** and **2**, however, are mononuclear, and complex **3** has an Mn···Mn separation too large to permit magnetic exchange, while the magnetic properties have already been reported for $[Mn_2O_2(pic)_4]\cdot CH_3CN$.[10] There-

 © 2004 Wiley-VCH Verlag GmbH & Co. KGaA, Weinheim

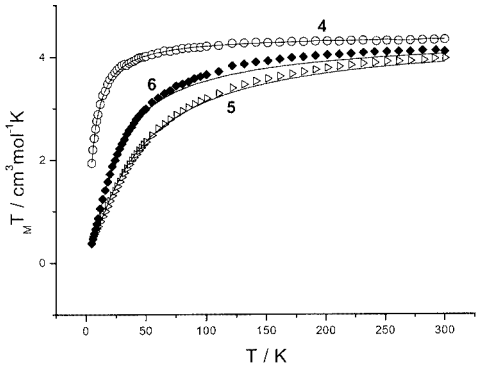

Figure 13. Thermal variations of the $\chi_M T$ product for **4** (circle), **5** (triangle) and **6** (square); the solid lines represent the best-fit curves

fore we report here the magnetic behavior of complexes **4**, **5** and **6**. Figure 13 shows the temperature dependence of the product ($\chi_M T$) of molar susceptibility and the temperature for the three complexes. For **4**, the value of μ_{eff} at 300 K amounts to 5.88 μ_B, close to the spin-only value of 5.92 μ_B for $S = 5/2$. For **5**, the value of μ_{eff} at 300 K amounts to 5.63 μ_B which is slightly lower than the spin-only value for $S = 5/2$. The effective magnetic moment smoothly decreases with a decrease of the temperature, indicating an antiferromagnetic interaction between neighboring magnetic species for both the complexes. Figure 6 and 8 show the 2D layer structures of **4** and **5**, which contain the [$Mn_2(\mu\text{-}O_{carboxylate})_2$] and [Mn2($\mu_{1,3}$-OCO)] moieties for **4**, and the [$Mn_2(\mu\text{-}Cl)_2$] and $Mn-O_{carboxylate}-Mn$ moieties for **5**. These moieties are arranged alternately to construct alternating chains along two directions, therefore an alternating chain with a classical spin S_{eff} is suggested as a model to analyze the magnetic data for both complexes (Scheme 2). The susceptibilities of the chains are obtained from Equation (2), which was deduced by Rojo[26] and is suitable for the fitting of an alternating chain model.

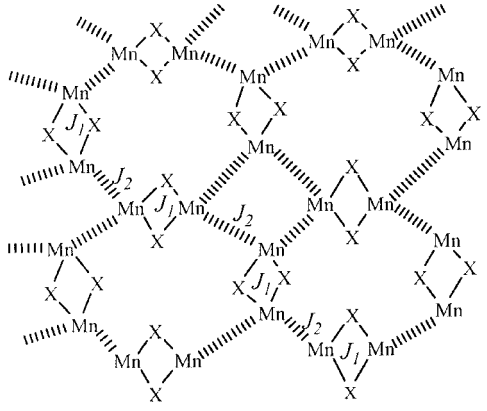

4: X = $O_{carboxylate}$ ⫶⫶⫶⫶⫶ = $\mu_{1,3}$–OCO

5: X = Cl ⫶⫶⫶⫶⫶ = μ–$O_{carboxylate}$

Scheme 2. An alternating chain ($J_1 - J_2$) with a classical spin S_{eff} is shown; the interactions between the S_{eff} chains are treated further according to a uniform chain

$$\chi_{chain} = \frac{Ng'^2\beta^2}{3kT}\left(\frac{1+u_1+u_2+u_1u_2}{1-u_1u_2}\right)$$

$$\text{where} \quad u_1 = Coth\left(\frac{J_1}{kT}\right) \qquad u_2 = Coth\left(\frac{J_2}{kT}\right) - \frac{kT}{J_2} \tag{2}$$

$$J_1 = J_1 S(S+1) \qquad g' = g[S(S+1)]^{1/2}$$

The magnetic interactions between the chains are treated based on the assumption that the alternating chain can be seen as an entity with classical spin S_{eff}. The S_{eff} should obey the Curie expressions [Equation (3)].

$$S_{eff}(S_{eff}+1) = 3k(\chi_{chain}T)/Ng^2\beta^2 \tag{3}$$

These S_{eff} entities are connected by $\mu_{1,3}$- or $\mu_{1,1}$-carboxylate bridges and can be treated as a uniform chain. Consequently, the magnetic susceptibilities of the systems can be calculated by Equation (4) for a classical chain.[27]

$$\chi_M = [Ng^2\beta^2 S_{eff}(S_{eff}+1)/3kT](1+u)/(1-u)$$

$$\text{where} \quad u = Coth[J_2 S_{eff}(S_{eff}+1)/kT] - kT/J_2 S_{eff}(S_{eff}+1) \tag{4}$$

The least-squares fitting results of the experimental data are: $g = 2.02$, $J_1 = -0.63$ cm^{-1}, $J_2 = -0.14$ cm^{-1} and $R = 4.63 \times 10^{-5}$ for **4**, and $g = 2.00$, $J_1 = -0.6$ cm^{-1}, $J_2 = -2.7$ cm^{-1} and $R = 4.92 \times 10^{-4}$ for **5**, where $R = \Sigma[(\chi_M)^{cal} - (\chi_M)^{obs}]^2/[(\chi_M)^{obs}]^2$.

The μ_{eff} value at 300 K for **6** amounts to 5.72 μ_B, close to the spin-only value of 5.92 μ_B for Mn^{II} with $S = 5/2$, supporting the protonation of the nitrogen atom in $C_5H_4N^+HCOO^-$. A uniform Mn chain model [Mn(μ-Cl)$_2$($\mu_{1,3}$-OCO)]$_n$ was used to fit the magnetic data of **6** and the magnetic susceptibility was calculated by Equation (5) for a uniform chain:[28]

$$\chi_M = \left(\frac{Ng^2\beta^2}{kT}\right)[A + Bx^2][1 + Cx + Dx^3]^{-1} \tag{5}$$

where $x = |J|/kT$, $A = 2.9167$, $B = 208.04$, $C = 15.543$ and $D = 2707.2$. These coefficients for magnetic susceptibility expressions for Heisenberg chains with $S = 5/2$ have beenused previously.[28] The least-squares fitting leads to $g = 2.00$, $J = -1.1$ cm^{-1} and $R = 2.4 \times 10^{-5}$.

Table 2 lists the magnetic parameters for the three complexes together with the parameters of other Mn complexes with similar structures. Complex **7**, containing the $Mn_2(\mu\text{-}O_{oxo})_2$ unit, shows the largest $|J|$ value among all the complexes in Table 2, which is believed to be correlated to the strong $Mn^{IV}-Mn^{IV}$ bonding interaction. Magnetically active chloride-bridged systems have been reported previously. Complexes containing an $Mn_2(\mu\text{-}Cl)_2$ unit reveal the exchange interactions via double μ-Cl bridges in the range $|J| = 0.2-16$ cm^{-1}, as shown in Table 2. The angular de-

 © 2004 Wiley-VCH Verlag GmbH & Co. KGaA, Weinheim

Table 2. Magnetic parameters for Mn complexes with μ-Cl, μ-O and $\mu_{1,3}$-OCO bridges

Complex	*g*	$Mn(\mu\text{-}Cl)_2Mn$				Mn−O−Mn				Ref.
		Mn···Mn (Å)	Mn−Cl−Mn (°)	$J_{Cl,OCO}$[a] (cm^{-1})	J_{Cl}[b] (cm^{-1})	Mn···Mn (Å)	Mn−O−Mn (°)	J_O (cm^{-1})	J_{OCO}[c] (cm^{-1})	
4	2.02					3.507	106.00(8)	−0.63	−0.14	[d]
5	2.00	3.585	91.59(2)		−1.81	4.425	155.00(7)	−2.35		[d]
6	2.00	3.637	89.03(3)	−1.1						[d]
A[e]	1.936					3.503	106.75	−0.48	−0.15	[20]
B[e]	2.02	3.515	90.2		−4.8					[29]
C[e]	2.05	3.344	86.37(2) 88.13(2)		−15.6					[30]
D[e]	2	4.05	98.6(1) 99.5 (1)		0.2					[31]
E[e]	2.02	3.664	93.36(2)		0.42					[32]
F[e]	2.00					4.41	151.0(1)	−1.42		[33]
7·MeCN	1.83					2.747(2)	98.1(2)	−86.5		[10]

[a] Magnetic exchange interaction through μ-Cl and $\mu_{1,3}$-OCO mixed bridges. [b] Magnetic exchange interaction through single atom μ-Cl or μ-O bridge. [c] Magnetic exchange interaction through $\mu_{1,3}$-OCO bridge. [d] This work. [e] **A**: $[Mn(pyz)_2]n$, pyz = 2-pyrazinecarboxylate. **B**: $[MnCl(MeCp)(PEt_3)]_2$. **C**: $[ppn]_2[Mn_2Cl_6]$. **D**: $[Mn(H_2dapd)C1_2]n$, H_2dapd = 2,6-diacetylpyridine dioxime. **E**: $[MnCl(pyz)(H_2O)]n$, **F**: $[\{Mn(bic)(H_2O)\}_2{\cdot}2Br]n$ (bic = bicinate).

pendence of the strength and nature of the magnetic coupling in M(μ-X)M systems has been studied in detail for Cu^{II}_2 and Cr^{III}_2 systems.[34] The Mn−Cl−Mn angle obviously plays an important role in determining the nature and strength of the chloride-mediated coupling. Complexes **5**, **6** and $[MnCl(MeCp)(PEt_3)]_2$ (**B**) have Mn−Cl−Mn angles very close to 90° in their $Mn_2(\mu\text{-}Cl)_2$ units and exhibit an antiferromagnetic coupling, while complexes **D** and **E** have angles larger than 90° and have weak ferromagnetic interactions. It seems that a smaller separation of the Mn^{II} ions (and/or smaller Mn−Cl−Mn angle) results in a larger $|J|$ value, implying that greater overlap between the magnetic orbitals in the $Mn_2(\mu\text{-}Cl)_2$ unit favors the antiferromagnetic exchange of the paramagnetic sites. Complexes **4** and $[Mn(pyz)_2]_n$ (**A**, pyz = 2-pyrazinecarboxylate), which are isostructural, both have an $Mn_2(\mu\text{-}O_{carboxylate})_2$ unit in their structures and exhibit a weak antiferromagnetic coupling. It should also be noted that magnetic coupling through a $\mu_{1,3}$-carboxylate bridge is dependent on the coordination mode of the carboxylate to the paramagnetic centers. There is an efficient overlap between the 3d magnetic orbital of the Mn^{2+} center and the 2p magnetic orbital of the carboxylate group in the order *syn-syn* > *anti-anti* > *syn-anti*.[35] Complexes **4** and **A** have the $\mu_{1,3}$-carboxylate bridges in a *syn-anti* mode, and are therefore less capable of transmitting magnetic interactions ($J_{\mu\text{-}OCO}$ = −0.14 cm^{-1}) than complex **6**, with the carboxylate in a *syn-syn* mode and double Cl bridges. In our work, the transfer pathway via a single-atom (O or Cl) bridge seems to be better than via a $\mu_{1,3}$-carboxylate bridge, $|J_{\mu\text{-}O}|$ or $|J_{\mu\text{-}Cl}| > |J_{\mu\text{-}OCO}|$. However, this is not general since exceptions have been reported by Nagata.[36] A larger $|J_{\mu\text{-}O}|$ value (−2.35 cm^{-1}) was observed for complex **5**, in spite of the larger Mn···Mn separation (4.425 Å). The only comparable complex is $[\{Mn(bic)(H_2O)\}_2{\cdot}2Br]_n$ [bic = bicinate = *N,N*-bis(2-hydroxyethyl)glycinate],[33] in which an Mn···Mn separation of 4.41 Å and Mn−O−Mn angle of 151° were found. It is thought that a linear Mn−O−Mn array may lead to an efficient overlap of the magnetic orbitals between the 3d magnetic orbitals of the Mn^{2+} and the 2p magnetic orbitals of the carboxylic oxygen atom. Consequently, complex **5** has a $|J_{\mu\text{-}O}|$ value larger than that of **4**. However, additional examples are required before such arguments can be considered valid.

Conclusion

Six new manganese picolinate or isonicotinate complexes were synthesized and structurally characterized. The chelating five-membered rings of the Mn picolinate construct diverse architectures, such as the zigzag chain of **3**, the 2D layer structure of **4** or the grid-like 2D structure of **5**, by $\mu_{1,3}$-OCO bridges in a *syn-anti* mode, and $\mu_{1,1}$-carboxylate or μ-Cl bridges, respectively. The isonicotinate complex **6** contains $MnCl_2(4\text{-}C_5H_4NHCOO)$ units which form an infinite zigzag chain by double μ-Cl and $\mu_{1,3}$-OCO bridges in a *syn-syn* mode.

In the syntheses of these complexes, the participation of an oxidizing agent leads to complexes with higher-valent manganese (III or IV for **1**, **2** and **7**). The removability of the chloride anion depends on the polarity of the solvent. Strongly polar DMF or H_2O allow the dissociation of the Mn−Cl bond, while other solvents favor the retention of the Mn−Cl bond in the products. This removability may be related to the doubts over whether the Cl^- ion is a ligand of the Mn site in OEC. We have assumed that the Cl^- ion is removable outside or inside the coordination sphere of the Mn ions.[37]

The IR spectra were discussed and various separations [$\Delta = \nu_{as}(COO) - \nu_s(COO)$] were obtained for these complexes, indicating unidentate, bidentate bridging or chelating coordination modes for the carboxylate groups. This is consistent with the structural features of the complexes. The

 © 2004 Wiley-VCH Verlag GmbH & Co. KGaA, Weinheim

N−H stretching frequency at 3217 cm^{-1} supports the structural analysis for complex **6**, with protonation at the nitrogen atom of the pyridyl unit.

Complexes **4**, **5** and **6** exhibit antiferromagnetic coupling interactions with J values ranging from -0.63 cm^{-1} to -2.35 cm^{-1}. Comparison of the magnetic parameters with those of other Mn complexes with comparable structures indicates the angular dependence of the strength and the nature of the magnetic coupling in M(μ-Cl)M systems: a smaller Mn−Cl−Mn angle results in a larger $|J|$ value.

Experimental Section

General: All manipulations were performed under aerobic conditions, and all commercially available reagents were used as received, except for the complex Et_4NMnO_4 which was prepared according to a literature procedure.[38] IR spectra were recorded on a Magna-75 FT-IR spectrophotometer as KBr pellets. The variable-temperature susceptibility was measured on a model CF-1 superconducting magnetometer with crystalline sample kept in a capsule at 5−300 K. Diamagnetic corrections were made with Pascal's constants for all the constituent atoms of the complexes determined. Elemental analyses were performed with an Elemental Analyzer Vario EL III.

$(Et_4N)[MnCl_2(pic)_2]$ (1): Tetraethylammonium hydroxide (25% in methanol; 0.5 mL) was added to a solution of picolinic acid (0.123 g, 1 mmol) in 10 mL of CH_2Cl_2/MeCN (1:1, v/v). The solution was stirred for 15 minutes and then $MnCl_2{\cdot}4H_2O$ (0.198 g, 1 mmol) was added. The reaction solution was refluxed for 18 h. After filtration, the filtrate was allowed to stand for one month at room temperature to deposit light-red crystals, which were collected, affording 0.068 g of complex **1**. Yield: 27% based on Hpic. $C_{20}H_{28}Cl_2MnN_3O_4$ (500.29): calcd. C 48.02, H 5.64, N 8.40, Mn 10.98; found C 48.48, H 5.72, N 8.73, Mn 11.05. IR (KBr): $\tilde{\nu}$ = 3080 (w) cm^{-1}, 2987 (w), 2922 (w), 1682 (vs), 1645 (m), 1606 (s), 1497 (m), 1473 (m), 1309 (s), 1275 (s), 1257 (s), 1236 (m), 1142 (s), 1049 (m), 764 (s).

$[MnCl(pic)_2(H_2O)]{\cdot}H_2O$ (2): $MnCl_2{\cdot}4H_2O$ (0.198 g, 1 mmol) was added to a solution of picolinic acid (0.123 g, 1 mmol) in 25 mL of CH_3OH and the solution was stirred for 30 minutes. Then, Et_4NMnO_4 (0.062 g, 0.25 mmol) was added in small portions to the reaction solution to give a dark-red solution. The mixture was filtered and the filtrate was evaporated at room temperature to yield green crystals, which were collected to afford 0.019 g of complex **2** with a yield of 10% based on Hpic. $C_{12}H_{12}ClMnN_2O_6$ (370.63): calcd. C 38.89, H 3.26, N 7.56, Mn 14.82; found C 39.97, H 3.31, N 7.66, Mn 14.90.

$[MnCl(pic)(H_2O)_2]_n$ (3): $MnCl_2{\cdot}4H_2O$ (0.594 g, 3 mmol) was added to a solution of picolinic acid (0.185 g, 1.5 mmol) in 40 mL of CH_3OH/CH_2Cl_2/MeCN (1:1:2, v/v/v) and the solution was refluxed for 24 h. After filtration light red crystals deposited from the filtrate at room temperature. The crystals were collected, affording 0.075 g of complex **3** with a yield of 20% based on Hpic. $C_6H_8ClMnNO_4$ (248.52): calcd. C 29.00, H 3.24, N 5.64, Mn 22.11; found C 29.28, H 3.27, N 5.77, Mn 22.24. IR (KBr): $\tilde{\nu}$ = 3385 (s) cm^{-1}, 3086 (w), 1610 (s), 1587 (s), 1566 (s), 1475 (m), 1446 (m), 1394 (s), 752 (s).

$[Mn(pic)_2]_n$ (4): A slurry composed of $MnCl_2{\cdot}4H_2O$ (0.198 g, 1.00 mmol) and picolinic acid (0.123 g, 1 mmol) in 12 mL of DMF (or CH_3OH/H_2O) was sealed into a 25-mL stainless steel reactor with a Teflon liner and heated at 145 °C for 72 h under autogenous pressure. After cooling the reactor, brown-red crystals were collected to afford 0.085 g of complex **4** with a yield of 57% based on Hpic. $C_{12}H_8MnN_2O_4$ (299.14): calcd. C 48.18, H 2.70, N 9.37, Mn 18.37; found C 48.33, H 2.76, N 9.48, Mn 18.46. IR (KBr): $\tilde{\nu}$ = 3089 (w) cm^{-1}, 3064 (w), 3020 (w), 1659 (s), 1624 (s), 1570 (m), 1408 (m), 1350 (s), 781 (m).

$[MnCl(pic)]_n$ (5): A slurry composed of $MnCl_2{\cdot}4H_2O$ (0.198 g, 1.00 mmol) and picolinic acid (0.123 g, 1 mmol) in 19 mL of MeCN (or EtOH) was sealed into a 25-mL stainless steel reactor with a Teflon liner and heated at 145 °C for 72 h under autogenous

Table 3. Crystal data, data collection and structure refinement for complexes **1**−**7**

Complex	**1**	**2**	**3**	**4**	**5**	**6**	**7**
Empirical formula	$C_{20}H_{28}N_3O_4Cl_2Mn$	$C_{12}H_{12}N_2O_6ClMn$	$C_6H_8NO_4ClMn$	$C_{12}H_8N_2O_4Mn$	$C_6H_4NO_2ClMn$	$C_6H_5Cl_2MnNO_2$	$C_{24}H_{16}N_4O_{10}Mn_2$
M	500.29	370.63	248.52	299.14	212.49	248.95	630.29
Crystal system	monoclinic	triclinic	monoclinic	monoclinic	tetragonal	monoclinic	monoclinic
Space group	$C2/c$	$P\bar{1}$	$P2_1/c$	$P2_1/c$	P4(2)/n	$C2/c$	$C2/c$
a (Å)	22.491(3)	6.7956(6)	11.8104(13)	10.4712(3)	9.7274(3)	11.956(4)	15.317(3)
b (Å)	7.4953(9)	10.6757(10)	9.9576(10)	10.9983(4)	9.7274(3)	10.403(4)	20.438(4)
c (Å)	15.837(2)	11.1699(9)	8.3149(9)	10.4124(2)	15.6894(8)	7.242(3)	9.6681(19)
α (°)	90.00	71.461(2)	90.00	90.00	90.00	90.00	90.00
β (°)	120.806(2)	83.0210(10)	100.213(2)	107.962(2)	90.00	103.463(5)	124.34(3)
γ (°)	90.00	71.960(2)	90.00	90.00	90.00	90.00	90.00
V (Å^3)	2293.1(5)	730.29(11)	962.37(18)	1140.70(6)	1484.57(10)	876.0(5)	2499.1(9)
Z	4	2	4	4	4	4	4
μ (mm^{-1})	0.839	1.117	1.630	1.168	2.077	2.070	1.077
T (K)	293(2)	293(2)	293(2)	293(2)	293(2)	293(2)	293(2)
Unique data	2010	2554	1688	1985	1309	777	2871
Observed data	1239	1648(9)	1383	1752	1038	718	2289
Refined parameters	138	199	118	172	100	61	182
R_1 [$I > 2\sigma(I)$]	0.0544	0.0534	0.0316	0.0358	0.0246	0.0254	0.0330
wR	0.1056	0.1173	0.0786	0.0924	0.0622	0.0933	0.0904

 © 2004 Wiley-VCH Verlag GmbH & Co. KGaA, Weinheim

pressure. Brown crystals formed after cooling the reactor and were collected, affording 0.140 g of complex **5** with a yield of 66% based on Mn. $C_6H_4ClMnNO_2$ (212.49): calcd. C 33.92, H 1.90, N 6.59, Mn 25.85; found C 34.10, H 1.95, N 6.68, Mn 25.99. IR (KBr): $\tilde{\nu}$ = 3120 (w) cm^{-1}, 3080 (w), 1610 (s), 1587 (s), 1566 (s), 1475 (m), 1446 (m), 1396 (s), 1296 (m), 752 (s).

$[MnCl_2(4\text{-}C_5H_4NHCOO)]_n$ (6): A solution of $MnCl_2{\cdot}4H_2O$ (0.198 g, 1 mmol) in 10 mL of CH_3OH was added to a solution of isonocotinic acid (0.246 g, 2 mmol) in 20 mL of H_2O and the solution was refluxed for 14 h. After filtration the filtrate was allowed to stand for three weeks at room temperature to deposit light red crystals, which were collected, affording 0.039 g (yield 16%) of complex 7. $C_6H_5Cl_2MnNO_2$ (248.95): calcd. C 28.92, H 2.01, N 5.62, Mn 22.09; found C 30.01, H 2.36, N 5.28, Mn 21.46. IR (KBr): $\tilde{\nu}$ = 3217 (s) cm^{-1}, 1614 (vs), 1591 (s), 1495 (m), 1417 (s), 1188 (m), 764 (s), 673 (s), 428 (s).

$[Mn_2O_2(pic)_4]$ (7): Glacial acetic acid (4 mL) and picolinic acid (0.492 g, 4 mmol) were added to a solution of $Mn(CH_3COO)_2{\cdot}4H_2O$ (0.490 g, 2 mmol) in 25 mL of CH_3OH/H_2O (4:1, v/v) to give a light brown solution. After 5 minutes, $KMnO_4$ (0.087 g, 0.55 mmol) in 10 mL of water was slowly added dropwise to the solution, which was then filtered. The solvents were evaporated from the filtrate at room temperature to yield red crystals, which were separated by filtration and identified to be $Mn(pic)_3$, a known compound. The filtrate was allowed to stand to deposit black crystals, which were collected to afford 0.158 g of complex **7** with a yield of 25% based on total available Mn. $C_{24}H_{16}Mn_2N_4O_{10}$ (630.29): calcd. C 45.74, H 2.56, N 8.89, Mn 17.43; found C 45.90, H 2.62, N 8.94, Mn 17.55. This complex has been prepared by other workers.[17] Similar IR data were observed to those[10] of a complex $[Mn_2O_2(pic)_4]{\cdot}CH_3CN$ with different crystallographic data.

X-ray Crystallography: Single crystals of complexes **1**−**7** were coated with epoxy resin and mounted on a glass fiber for X-ray diffraction. Refraction data were collected on Siemens Smart CCD diffractometer with Mo-K_α radiation (λ = 0.71073 Å) at 293 K using the ω-2θ scan mode for all the complexes except for **7**, which was scanned on a Weissenberg IP diffractometer. Metal ions together with the chloride ions were first located and other non-hydrogen atoms were found in subsequent difference Fourier syntheses. Hydrogen atoms were located by geometric calculations, except those in water ligands, but their positions and thermal parameters were fixed during the structure refinement. Further crystallographic details are given in Table 3. Selected bond lengths and angles are listed in Table 1. Structure solution and refinement were carried out by standard methods using the SHELXTL-97 program package[39] on a DELL™ personal computer.

CCDC-210998 to -211004 (for **1**−**7**) contain the supplementary crystallographic data for this paper. These data can be obtained free of charge at www.ccdc.cam.ac.uk/conts/retrieving.html [or from the Cambridge Crystallographic Data Centre, 12 Union Road, Cambridge CB2 1EZ, UK; Fax: (internat.) + 44-1223-336-033; E-mail: deposit@ccdc.cam.ac.uk].

Acknowledgments

This work was supported by The State Key Basic Research and Development Plan (G1998010100), NNSFC (No. 39970177, 20273084) and the Expert Project of Key Basic Research from the Ministry of Science & Technology.

[1] O. Kahn, C. Martinez, *Science* **1998**, *279*, 44−48; O. M. Yaghi, G. M. Li, H. L. Li, *Nature* **1995**, *378*, 703−706; M. Fujita, Y. Kwon, S. Washizu, K. Ogura, *J. Am. Chem. Soc.* **1994**, *116*, 1151−1152; T. Sawaki, T. Dewa, Y. Aoyama, *J. Am. Chem. Soc.* **1998**, *120*, 8539−8540; H. A. Brison, T. P. Pollagi, T. C. Stoner, S. J. Geib, M. D. Hopkins, *Chem. Commun.* **1997**, 1263−1264; J. S. Miller, A. J. Spstein, *Chem. Commun.* **1998**, 1319−1320; C. M. Drain, F. Nafiatis, A. Vasenko, J. D. Batteas, *Angew. Chem. Int. Ed.* **1998**, *37*, 2344−2347; S. Subramanian, M. J. Zaworotko, *Angew. Chem. Int. Ed. Engl.* **1995**, *34*, 2127−2129; M. S. E. Fallah, E. Rentschler, A. Caneschi, R. Sessoli, D. Gatteschi, *Angew. Chem. Int. Ed. Engl.* **1996**, *35*, 1947−1949; C. Janiak, *Dalton Trans.* **2003**, 2781−2804.

[2] K. Wieghardt, *Angew. Chem. Int. Ed. Engl.* **1989**, *28*, 1153−1172.

[3] W. F. Beyer, I. Fridovich, *Biochemistry* **1985**, *24*, 6460−6467.

[4] W. F. Beck, G. W. Brudvig, *J. Am. Chem. Soc.* **1988**, *110*, 1517−1523.

[5] A. Zouni, H. T. Witt, J. Kern, P. Fromme, N. Krauß, W. Saenger, P. Orth, *Nature* **2001**, *409*, 739−743; J. Amesz, *Biochim. Biophys. Acta* **1983**, *726*, 1−12.

[6] V. K. Yachandra, K. Sauer, M. P. Klein, *Chem. Rev.* **1996**, *96*, 2927−2950; H. Schiller, J. Dittmer, L. Iuzzolino, W. Dörner, W. Meyer-Klaucke, V. A. Solé, H.-F. Nolting, H. Dau, *Biochem.* **1998**, *37*, 7340−7350; X.-S. Tang, B. A. Diner, B. S. Larsen, M. L. Gilchrist, G. A. Lorigan, R. D. Britt, *Proc. Natl. Acad. Sci. USA* **1994**, *91*, 704−708; A. Magnuson, L.-E. Andréasson, *Biochem.* **1997**, *36*, 3254−3261; M. L. Ghirardi, C. Preston,, M. Seibert, *Biochem.* **1998**, *37*, 17112−17119.

[7] C. W. Hoganson, G. T. Babcock, *Science* **1997**, *277*, 1953−1956; J. M. Peloquin K. A., Campbell, D. W. Randall, M. A. Evanchik, V. L. Pecoraro, W. H. Armstrong, R. D. Britt, *J. Am. Chem. Soc.* **2000**, *122*, 10926−10942; C.-X. Zhang, J. Pan, L.-B. Li, T.-Y. Kuang, *Chin. Sci. Bull.* **1999**, *44*, 2209−2215.

[8] H. Wincencjusz, H. J. Van Gorkom, C. F. Yocum, Biochem. 1997, 36, 3663−3670.

[9] M. G. Barandika, Z. E. Serna, M. K. Urtiaga, J. I. R. de Larramendi, M. I. Arriortua, R. Cortes, *Polyhedron* **1999**, *18*, 1311−1316; P. Knuuttila, *Acta Chem. Scand. Ser. A* **1982**, *36*, 767−772; Y.-Z. Li, M. Wang, L.-F. Wang, C.-G. Xia, *Acta Crystallogr.* **2000**, *C56*, e445−e446; B. N. Figgis, C. L. Raston, R. P. Sharma, A. H. White, *Aust. J. Chem.* **1978**, *31*, 2545−2548; N. Okabe, M. Koizumi, *Acta Crystallogr., Sect. C* **1998**, *54*, 288−290.

[10] E. Libby, R. J. Webb, W. E. Streib, K. Folting, J. C. Huffman, D. N. Hendrickson, G. Christou, *Inorg. Chem.* **1989**, *28*, 4037−4040.

[11] M. A. S. Goher, M. A. M. Abu-Youssef, F. A. Mautner, A. Popitsch, *Polyhedron* **1993**, *12*, 1751−1756.

[12] E. Libby, K. Folting, C. J. Huffman, J. C. Huffman, G. Christou, *Inorg. Chem.* **1993**, *32*, 2549−2556; E. Libby, K. Folting, J. C. Huffman, G. Christou, *J. Am. Chem. Soc.* **1990**, *112*, 5354−5356; E. Libby, J. K. McCusker, E. A. Schmitt, K. Folting, D. N. Hendrickson, G. Christou, *Inorg. Chem.* **1991**, *30*, 3486−3495; H. J. Eppley, S. M. J. Aubin, W. E. Streib, J. C. Bollinger, D. N. Hendrickson, G. Christou, *Inorg. Chem.* **1997**, *36*, 109−115.

[13] X. S. Tan, Z. S. Ma, N. C. Shi, D. G. Fu, J. Chen, W. X. Tang, *J. Chem. Soc., Dalton Trans.* **1996**, 2735−2739; M. A. S. Goher, M. A. M. Abu-Youssef, F. A. Mautner, A. Popitsch, *Polyhedron* **1992**, *11*, 2137−2141.

[14] X. Hao, Y.-G. Wei, Q. Liu, S.-W. Zhang, *Acta Crystallogr., Sect. C* **2000**, *56*, 296−298; H.-J. Chen, Z.-W. Mao, S. Gao, X.-M. Chen, *Chem. Commun.* **2001**, 2320−2321; W. Lin, M. E. Chapman, Z. Wang, G. T. Lee, *Inorg. Chem.* **2000**, *39*, 4169−4173; M. A. S. Goher, N. A. Al-Salem, F. A. Mautner, *J. Coord. Chem.* **1998**, *44*, 119−131; M. A. M. Abu-Youssef, A. Escuer, M. A. S. Goher, F. A. Mautner, G. J. Reiss, R. Vicente, *Angew. Chem. Int. Ed.* **2000**, *39*, 1624−1626.

 © 2004 Wiley-VCH Verlag GmbH & Co. KGaA, Weinheim

[15] W. Lin, O. R. Evans, G. T. Yee, *J. Solid State Chem.* **2000**, *152*, 152−158; R. Hauptmann, M. Kondo, S. Kitagawa, *Z. Kristallogr.-New Cryst. Struct.* **2000**, *215*, 171−172; D. Xu, C. Zhang, Y. Xu, X. Huang, *Polyhedron* **1997**, *16*, 71−73.
[16] T. Matsushita, L. Spencer, D. T. Sawyer, *Inorg. Chem.* **1988**, *27*, 1167−1173.
[17] E. Larson, M. S. Lah, X. Li, J. A. Bonadies, V. L. Pecoraro, *Inorg. Chem.* **1992**, *31*, 373−378; S. P. Perlepes, A. G. Blackman, J. C. Huffman, G. Christou, *Inorg. Chem.* **1991**, *30*, 1665−1668.
[18] H. H. Thorp, *Inorg. Chem.* **1992**, *31*, 1585−1588; I. D. Brown, D. Altermatt, *Acta Crystallogr.* **1985**, *B41*, 244−247.
[19] C. Janiak, *J. Chem. Soc., Dalton Trans.* **2000**, 3885−3896.
[20] Y. C. Liang, M. C. Hong, J. C. Liu, R. Cao, *Inorg. Chim. Acta* **2002**, *328*, 152−158.
[21] B. Żurowska, J. Mroziński, *Inorg. Chim. Acta* **2003**, *342*, 23−28; M. A. S. Goher, A. K. Hafez, M. A. M. Abu-Youssef, A. Popitsch, H. P. Fritzer, F. A. Mautner, *Monatsh. Chem.* **1994**, *125*, 833−840.
[22] D.-D. Wu, T. C. W. Mak, *Inorg. Chim. Acta* **1995**, *237*, 163−167.
[23] D. F. Mullica, D. E. Pennington, J. E. Bradshaw, E. L. Sappenfield, *Inorg. Chim. Acta* **1992**, *191*, 3−6; J. Y. Lu, J. Macias, *CrystEngComm* **2002**, *4*, 17−19; Z. Wang, S. R. Wilson, B. M. Foxman, W. Lin, *Cryst. Eng.* **1999**, *2*, 91−100.
[24] N. S. Gill, R. H. Nuttall, D. E. Scaife, D. W. A. Sharp, *J. Inorg. Nucl. Chem.* **1961**, *18*, 79−87.
[25] G. B. Deacon, R. J. Phillips, *Coord. Chem. Rev.* **1980**, *33*, 227−250.
[26] R. Cortés, M. Drillon, X. Solans, L. Lezama, T. Rojo, *Inorg. Chem.* **1997**, *36*, 677−683.
[27] M. E. Fisher, *Am. J. Phys.* **1964**, *32*, 343−346.
[28] W. Hiller, J. Strähle, A. Datz, M. Hanack, W. E. Hatfield, L. W. ter Haar, P. Gütlich, *J. Am. Chem. Soc.* **1984**, *106*, 329−335.
[29] F. H. Kohler, N. Hebendanz, G. Muller, U. Thewalt, B. Kanellakopulos, R. Klenze, *Organometallics* **1987**, *6*, 115−125.
[30] J.-S. Sun, H. Zhao, X. Ouyang, R. Clerac, J. A. Smith, J. M. Clemente-Juan, C. Gomex-Garcia, E. Coronado, K. R. Dunbar, *Inorg. Chem.* **1999**, *38*, 5841−5855.
[31] B. C. Unni Nair, J. E. Sheats, R. Ponteciello, D. Van Engen, V. Petrouleas, G. C. Dismukes, *Inorg. Chem.* **1989**, *28*, 1582−1587.
[32] D. Huang, X. Zhang, C. Chen, F. Chen, Q. Liu, D. Liao, L. Li, L. Sun, *Inorg. Chim. Acta* **2003**, *353*, 284−291.
[33] Z. Sun, P. K. Gantzel, D. N. Hendrickson, *Polyhedron* **1998**, *17*, 1511−1516.
[34] O. Kahn, *Molecular Magnetism*, VCH, Weinheim, **1993**.
[35] E. Colacio, J. M. Dominguez-vera, M. Ghazi, R. Kivekäs, M. Klinga, J. M. Moreno, *Eur. J. Inorg. Chem.* **1999**, 441−445.
[36] H. Iikura, T. Nagata, *Inorg. Chem.* **1998**, *37*, 4702−4711.
[37] C. Chen, H. Zhu, D. Huang, Q. Liu, *Acta Botanica Sin.* **2000**, *42*, 1249−1252.
[38] T. Sala, M. V. Sargent, *J. Chem. Soc., Chem. Commun.* **1978**, 253−254.
[39] G. M. Sheldrick, *SHELXTL-97*, University of Göttingen, Germany, **1997**.

Received August 21, 2003
Early View Article
Published Online February 26, 2004

 © 2004 Wiley-VCH Verlag GmbH & Co. KGaA, Weinheim

Syntheses, Crystal Structures and Electrospray Mass Spectra of Coordination Polymers of an *N*,*N*′-Bis(3-pyridylmethyl)-1,4-benzenebis(methylamine) Ligand and Silver(I) Salts

Hui-Fang Zhu,[a] Ling-Yan Kong,[a] Taka-aki Okamura,[b] Jian Fan,[a] Wei-Yin Sun,*[a] and Norikazu Ueyama[b]

Keywords: Coordination polymers / Crystal engineering / Pi interactions / Silver / Supramolecular chemistry

Four new coordination frameworks $\{[Ag_2(L1)](NO_3)_2{\cdot}2H_2O\}_n$ (**1**), $\{[Ag(L1)](CF_3COO){\cdot}2.5H_2O\}_n$ (**2**), $\{[Ag_2(L1)_2][1,4\text{-}C_6H_4(COO)_2]{\cdot}7H_2O\}_n$ (**3**) and $\{[Ag(L1)]ClO_4\}_n$ (**4**) were obtained by the reaction of *N*,*N*′-bis(3-pyridylmethyl)-1,4-benzenebis(methylamine) (L1) with the corresponding silver(I) salts. X-ray diffraction analyses reveal that complex **1** has an infinite 1D chain structure, in which L1 acts as a tetradentate ligand. Complexes **2**, **3** and **4** have 2D network structures, and the L1 ligands in these complexes adopt two different coordination modes: one kind of ligand coordinates four silver(I) atoms using its four N atoms, and the other kind of ligand connects only two silver(I) atoms with the two N atoms of the benzenebis(methylamine) unit, while the pyridine units remain free of coordination. Complex $\{[Ag(L2)]ClO_4\}_n$ (**5**) was synthesized by reaction of *N*,*N*′-bis(3-pyridylmethyl)-1,4-benzenebis(methyleneamine) (L2) with silver(I) perchlorate. It has a novel 1D chain structure, which is different from that of **4** due to the different flexibility of the ligands L1 and L2. All of these complexes form 2D or 3D structures stabilized by hydrogen bonding, C–H···π and π-π interactions. The results revealed that the nature of the counteranions and the flexibility of the ligand have an impact on the structure of the supramolecular architectures. The complexes were also characterized by electrospray mass spectrometry.
(© Wiley-VCH Verlag GmbH & Co. KGaA, 69451 Weinheim, Germany, 2004)

Introduction

The crystal engineering of coordination polymeric networks based on multidentate ligands is a growing area of coordination and supramolecular chemistry. Many efforts have been devoted to the use of flexible ligands to achieve supramolecular arrays, due to the unpredictable nature of such systems.[1] A variety of networks can be expected since the flexible ligands can adopt different conformations according to the different geometry requirements of the metal ions.[2] It has been reported that chain-like bidentate ligands have the ability to form unique interwoven extended structural motifs such as polycatenanes, polyrotaxanes and helices.[3] Compared with bidentate ligands, long chain-like multidentate ligands are less documented. The silver(I) ion exhibits a diverse coordination geometry due to its variable coordination number. When flexible ligands react with silver(I) salts, interesting and unusual structures are often generated, such as helices, boxes, and brick walls.[4]

In our laboratory, we focus our attentions on the reactions of silver(I) salts with flexible multidentate ligands based on (pyridylmethyl)amine or (pyridylmethylene)amine groups linked by an ethylene spacer (e.g. L3−L6 in Scheme 1), and have obtained various frameworks with interesting structures.[5] For example, 1,2-bis(4′-pyridylmethyleneamino)ethane (L5) reacts with AgOTf or $AgNO_3$ to give a double-stranded helix chain and a 2D network, respectively.[5a] In order to further study the influence of multidentate organic ligands on the formation of the resultant structures, we use two multidentate ligands *N*,*N*′-bis(3-pyridylmethyl)-1,4-benzenebis(methylamine) (L1) and *N*,*N*′-bis(3-pyridylmethyl)-1,4-benzenebis(methylene)amine (L2) (Scheme 1) in this study. In these two ligands, a 1,4-benzenedimethyl or 1,4-benzenedimethylene group was employed, instead of the ethylene group of L3−L6, to examine the influence of the size and flexibility of the spacer group on the structure of the frameworks. Five non-interpenetrated complexes, $\{[Ag_2(L1)](NO_3)_2{\cdot}2H_2O\}_n$ (**1**), $\{[Ag(L1)](CF_3COO){\cdot}2.5H_2O\}_n$ (**2**), $\{[Ag_2(L1)_2][1,4\text{-}C_6H_4(COO)_2]{\cdot}7H_2O\}_n$ (**3**), $\{[Ag(L1)]ClO_4\}_n$ (**4**) and $\{[Ag(L2)]ClO_4\}_n$ (**5**) were synthesized by reactions of L1 and L2 with the corresponding silver(I) salts. The complexes

[a] Coordination Chemistry Institute, State Key Laboratory of Coordination Chemistry, Nanjing University,
Nanjing 210093, China
Fax: (internat.) +86-25-331-4502
E-mail: sunwy@nju.edu.cn
[b] Department of Macromolecular Science, Graduate School of Science, Osaka University,
Toyonaka, Osaka 560-0043, Japan
Supporting information for this article is available on the WWW under http://www.eurjic.org or from the author.

were also characterized by crystal structure and electrospray mass spectrometry.

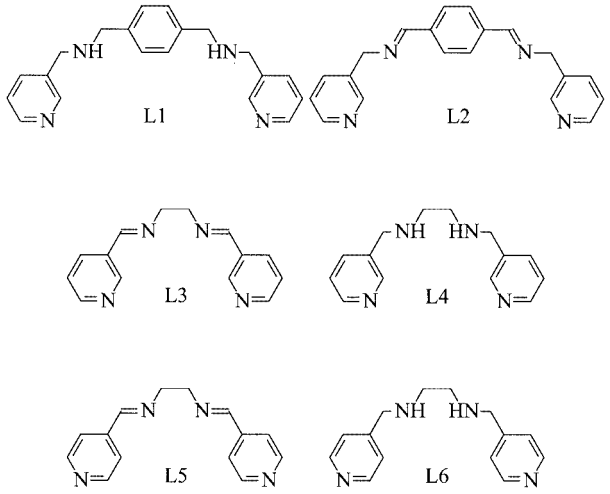

Scheme 1. Schematic drawing of pyridine-containing ligands L1−L6

Results and Discussion

Preparation of Compounds

The title complexes were readily prepared by reaction of L1 or L2 with silver(I) salts in the dark by layering (**1** and **3**), slow evaporation (**2** and **4**) and diffusion (**5**) methods at room temperature. The elemental analyses and X-ray crystal structure analyses confirmed the chemical formulation of these complexes. The complexes of L1 with different anions were found to show remarkable differences in solubility. Complex **2**, with the CF_3COO^- anion, is soluble in organic solvents such as methanol, ethanol, acetonitrile and has moderate solubility in water, while **1**, **3** and **4** are almost insoluble in water and have low solubility in organic solvents. Complex **5**, with L2, has almost no solubility in water and methanol but reasonable solubility in acetonitrile.

Crystal Structure Description

{[Ag$_2$(L1)](NO$_3$)$_2$·2H$_2$O}$_n$ (1)

When the flexible ligand L1 reacts with silver(I) nitrate, a new coordination polymer **1** is obtained and its structure was determined by X-ray crystallography. As shown in Figure 1a, the asymmetric unit of **1** consists of half a molecule of $[Ag_2(L1)](NO_3)_2]\cdot 2H_2O$. Each silver(I) atom is coordinated by two N atoms with an almost linear coordination geometry [N−Ag−N bond angle is 156.97(9)°, Table 1], one of which is from the benzenedimethylamine unit and the other one is from the pyridine unit of another L1 ligand. Each L1 ligand, in turn, coordinates four silver(I) atoms to generate an infinite 1D chain structure. It is noteworthy that C−H···π interactions[6] associate the 1D chains into a 2D network structure as illustrated in Figure 1b. Such an interaction occurs between the hydrogen atom (H5) bound to C10 (methylene directly attached to the benzene ring) and the pyridine group of a neighboring chain. The C10−H5−X (X refers to the centroid of the pyridine group) angle is 117° and the H···X distance is 2.88 Å. From the crystal-packing diagram of **1** (Figure S1 in the Supporting Information), it can be seen that the nitrate anions are connecting 2D cationic sheets through four C−H···O hydrogen bonds to form a 3D framework. The solvated water molecules are located in the 3D structure by forming one N−H···O(water) hydrogen bond with a cationic chain and three (water)O−H···O(nitrate anion) hydrogen bonds. The hydrogen bonding data are summarized in Table 2.

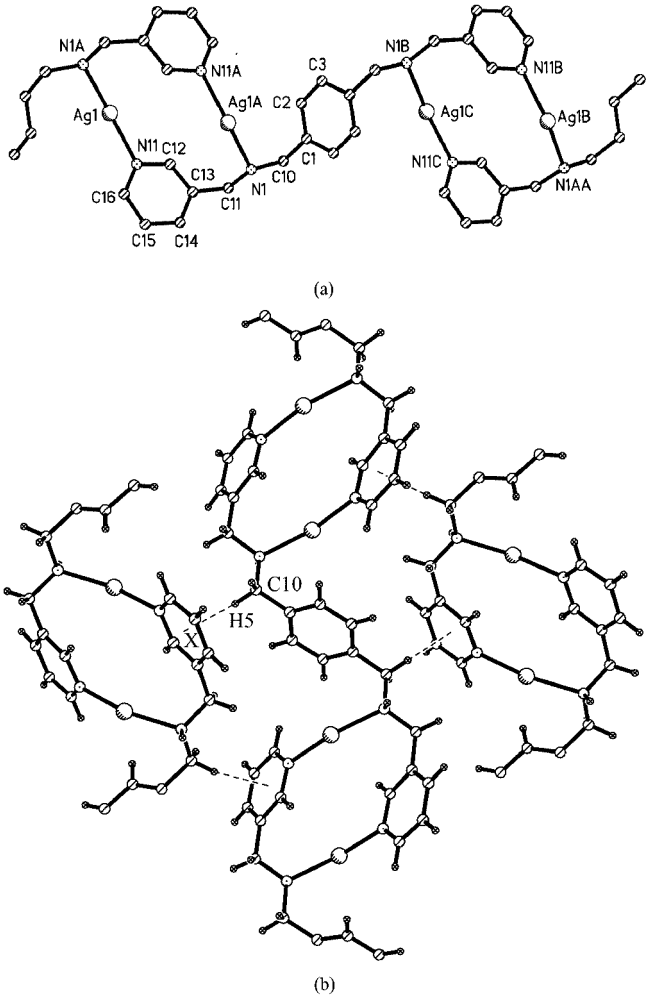

Figure 1. (a) One-dimensional chain structure of complex **1**; water molecules, hydrogen atoms and anions are omitted for clarity; (b) view of 2D cationic sheet of **1** with the C−H···π interactions indicated by dashed lines

In **1** two N atoms of each benzenebis(methylamine) unit in the L1 ligand coordinate to two Ag^I atoms, respectively, while in the reported metal complexes with ligands L3−L6 (Scheme 1) the two N atoms of each ethylenediamine or ethylenediimine unit coordinate to one metal atom in a chelate fashion.[5] This is due to the bulky and rigid 1,4-benzenedimethyl spacer in L1.

 © 2004 Wiley-VCH Verlag GmbH & Co. KGaA, Weinheim

Table 1. Selected bond lengths (Å) and angles (°) for complexes **1**–**5**[a]

$\{[Ag_2(L1)](NO_3)_2{\cdot}2H_2O\}_n$ (**1**)			
Ag1–N11	2.201(3)	Ag1–N1#1	2.211(3)
N11–Ag1–N1#1	156.97(9)		
$\{[Ag(L1)](CF_3COO){\cdot}2.5H_2O\}_n$ (**2**)			
Ag1–N11	2.218(3)	Ag1–N1	2.281(3)
Ag1–N101	2.314(3)		
N11–Ag1–N1	134.30(10)	N11–Ag1–N101	122.88(9)
N1–Ag1–N101	102.81(9)		
$\{[Ag_2(L1)_2][1,4\text{-}C_6H_4(COO)_2]{\cdot}7H_2O\}_n$ (**3**)			
Ag1–N111	2.222(2)	Ag1–N101	2.290(2)
Ag1–N1	2.322(2)		
N111–Ag1–N101	137.67(9)	N111–Ag1–N1	122.00(9)
N101–Ag1–N1	100.33(9)		
$\{[Ag(L1)]ClO_4\}_n$ (**4**)			
Ag1–N2	2.222(2)	Ag1–N1	2.258(2)
Ag1–N11	2.436(2)		
N2–Ag1–N1	157.98(7)	N2–Ag1–N11	109.65(8)
N1–Ag1–N11	89.69(8)		
$\{[Ag(L2)]ClO_4\}_n$ (**5**)			
Ag1–N11	2.272(3)	Ag1–N2#2	2.295(3)
Ag1–N21#3	2.320(2)		
N11–Ag1–N2#2	120.34(9)	N11–Ag1–N21#3	115.84(9)
N2#2–Ag1–N21#3	116.90(9)		

[a] Symmetry transformations used to generate equivalent atoms: #1: 1 − *x*, −*y*, 1 − *z*; #2: *x*, 1 + *y*, *z*; #3: −*x*, −1 − *y*, 1 − *z*.

Table 2. Hydrogen bonding data for complexes **1**–**5**

D–H···A[a]	Distance of D···A (Å)	Angle of D–H–A (°)
$\{[Ag_2(L1)](NO_3)_2{\cdot}2H_2O\}_n$ (**1**)		
N1–H1···O4#1	3.030(4)	158
O4–H12···O1#2	3.108(4)	161
O4–H12···O3#2	3.015(4)	138
O4–H13···O2	2.969(4)	154
C3–H3···O3#3	3.422(5)	167
C11–H6···O1#4	3.560(5)	169
C11–H7···O3#5	3.330(5)	161
C12–H8···O2#6	3.358(4)	140
$\{[Ag(L1)](CF_3COO){\cdot}2.5H_2O\}_n$ (**2**)		
N1–H1···O3	3.036(4)	173
N101–H2···O1#7	3.096(4)	168
O3–H24···O2#5	2.851(8)	145
C14–H10···F1#8	3.349(6)	142
$\{[Ag_2(L1)_2][1,4\text{-}C_6H_4(COO)_2]{\cdot}7H_2O\}_n$ (**3**)		
N1–H1···O12#9	3.141(5)	173
N101–H2···O1	3.104(5)	174
C11–H7···O2#9	3.332(6)	145
C11–H8···O2	3.438(6)	147
C110–H15···O3#7	3.245(9)	126
C110–H16···O12#9	3.349(6)	141
C111–H17···O2#7	3.377(6)	172
$\{[Ag(L1)]ClO_4\}_n$ (**4**)		
N1–H1···O2#10	2.987(9)	133
N2–H2···O3	3.122(12)	174
C3–H4···O1#11	3.386(4)	152
$\{[Ag(L2)]ClO_4\}_n$ (**5**)		
C5–H3···O2	3.359(4)	159
C6–H4···O3	3.241(4)	125
C11–H7···O4#12	3.418(4)	156
C14–H9···O1#12	3.341(4)	140
C15–H10···O4#6	3.512(4)	173

[a] Equivalent atoms generated by #1: 3/2 − *x*, −1/2 + *y*, 3/2 − *z*; #2: 2 − *x*, −*y*, 1 − *z*; #3: −1/2 + *x*, −1/2 − *y*, −1/2 + *z*; #4: −1/2 + *x*, −1/2 − *y*, 1/2 + *z*; #5: −1 + *x*, *y*, *z*; #6: 1 − *x*, −*y*, 1 − *z*; #7: 1 − *x*, −*y*, 2 − *z*; #8: 1 − *x*, 1 − *y*, 1 − *z*; #9: −*x*, −*y*, 2 − *z*; #10: −*x*, −*y*, 1 − *z*; #11: 1 + *x*, *y*, *z*; #12: 1/2 + *x*, −1/2 − *y*, 1/2 + *z*.

{[Ag(L1)](CF₃COO)·2.5H₂O}ₙ (2) and {[Ag₂(L1)₂][1,4-C₆H₄(COO)₂]·7H₂O}ₙ (3)

The same space group and the similar cell parameters (see Exp. Sect.) indicate that complexes **2** and **3** are isomorphous and isostructural. As a typical example, the structure of complex **2** is described here in detail. In complex **2**, the amount of disordered water molecules was confirmed by elemental analysis and thermogravimetric analysis. The TGA data of **2** show an initial weight loss of 7.6% (calcd. 7.7%) from 20 to 80 °C, representing the loss of uncoordinated water molecules; no further weight loss was observed over the temperature range 80–170 °C. The crystal structure of complex **2** (cationic part) is shown in Figure 2a with the atom numbering scheme. Each silver(I) atom is coordinated by two N atoms of the benzenebis(methylamine) units from two different L1 ligands, and one N atom of the pyridine unit of the third L1 ligand. The coordination environment of the silver(I) atom can be described as a triangle, with the N–Ag–N coordination angles varying from 102.81(9)° to 134.30(10)° (Table 1). The average Ag–N bond length of 2.271(3) Å in **2** is similar to those of reported silver(I) complexes with the same AgN_3 binding site, for example $[Ag_3(py\text{-}hep)_2](ClO_4)_3{\cdot}0.5CH_3CN$ [py-hep = 1,6-bis(4′-pyridyl)-2,5-diazahexane] exhibits an average Ag–N bond length of 2.297(5) and 2.314(5) Å for the two crystallographically independent silver atoms.[7] The remarkable structural feature of **2** is that the flexible ligand L1 adopts two different coordination modes at the Ag^I atoms: one kind of ligand coordinates four silver(I) atoms as a tetradentate ligand, and the other kind coordinates only two silver(I) atoms with the N atom of the benzenebis(methylamine) unit as a bidentate ligand, while the pyridine units remain free of coordination. In the reported metal complexes with L4 and L6 the ligands are all tetradentate and each ligand coordinates three different metal atoms.[5b,5d–5f] The whole structure of **2** can be described as the silver(I) atoms being bridged by the tetradentate L1

 © 2004 Wiley-VCH Verlag GmbH & Co. KGaA, Weinheim

ligands to form 1D chains, which are further linked by the bidentate L1 ligands to generate a wavelike 2D network structure (Figure 2b). In each 2D sheet, there are two kinds of macrometallacyclic rings: the smaller, 12-membered one contains two Ag^I atoms and two L1 ligands and the larger, 44-membered one is made up of two bidentate L1 ligands, two tetradentate L1 ligands and four three-coordinate silver(I) atoms. In addition, the large ring adopts a "chair" conformation to make the uncoordinated pyridine groups point inside of the ring; the large void space of the 44-membered ring is filled by uncoordinated pyridine groups, which may prevent the occurrence of interpenetration. Furthermore, these uncoordinated pyridine groups are stabilized in the large ring by C−H···π interactions.[8] For example as exhibited in Figure 2b, the C12−H9−X (X refers to the centroid of the uncoordinated pyridine group) angle is 142° and the H···X distance is 2.88 Å. The wavelike 2D networks are held together by hydrogen bonds to form a 3D structure (Figure S2). The trifluoroacetate anions and water molecules are sandwiched between the cationic 2D layers and are held there by two N−H···O, one O−H···O and one C−H···F hydrogen bonds (Table 2).

Similar C−H···π interactions (the C112−H19-centroid angle is 137° and the H···centroid distance is 2.88 Å) and crystal packing were found for complex **3**. The uncoordinated 1,4-benzenedicarboxylate anions and water molecules are also located in the voids between the 2D cationic layers and 3D structure is formed by two N−H···O and five C−H···O hydrogen bonds (Figure S3, Table 2).

{[Ag(L1)]ClO$_4$}$_n$ (4) and {[Ag(L2)]ClO$_4$}$_n$ (5)

As described above, the complex with a nitrate anion has a 1D chain structure while those with trifluoroacetate or 1,4-benzenedicarboxylate anions show a 2D network structure. To further investigate the influence of the anion on the structure of Ag^I complexes of L1, the reaction of silver(I) perchlorate with ligand L1 was carried out and complex **4** was isolated and characterized by X-ray crystallography. As shown in Figure 3a, the asymmetric unit of **4** consists of one molecule of [Ag(L1)]ClO_4. Each silver(I) atom is coordinated by two N atoms from the benzenebis(methylamine) units of two different L1 ligands, with an N−Ag−N angle of 157.98(7)°. In addition, an Ag−N distance of 2.436(2) Å indicates the occurrence of a weak interaction between the silver(I) atom and the N atom of the pyridine unit. Thus, the coordination environment of the silver(I) atom in **4** can be regarded as a T-shaped coordination mode, while the Ag^I atoms in **2** and **3** have a triangular coordination geometry. Similar T-shaped silver(I) atoms have been observed in Ag^I complexes with flexible bis(thioether) ligands.[4e] The L1 ligand in **4** adopts the same kind as in **2** and **3**, and in the 2D network structure of complex **4**, 12- and 44-membered macrometallacyclic rings similar to those observed in complexes **2** and **3** were also found. However, there is an obvious difference between the structures of **4** and **2** (**3**): the perchlorate anions are located in the voids of the 44-membered rings and held there through N−H···O and C−H···O hydrogen bonds (Table 2), while in the case of

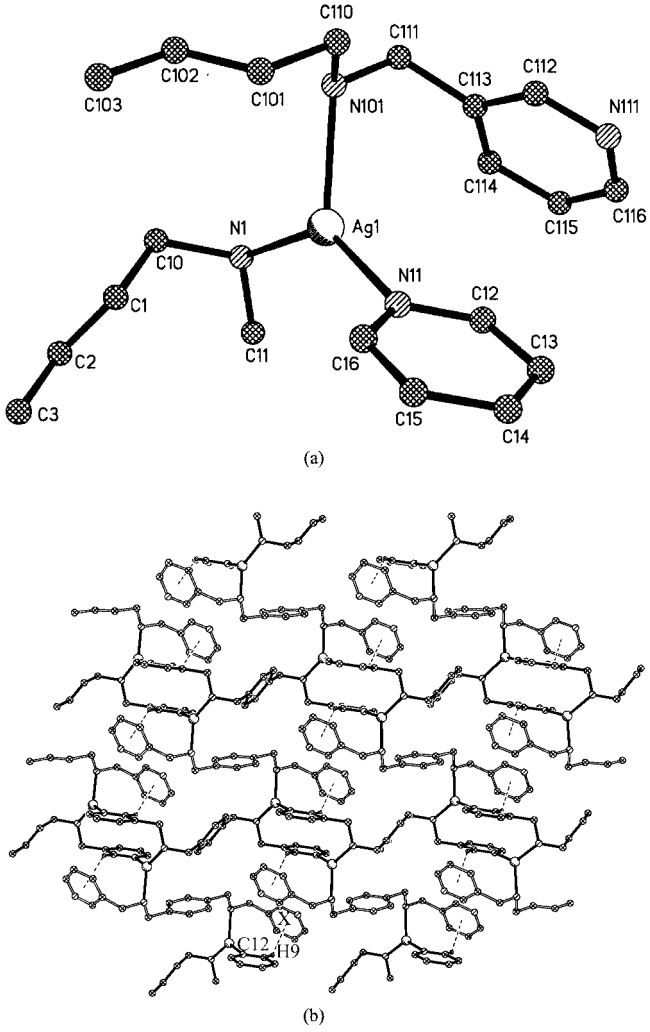

Figure 2. (a) Molecular structure of the asymmetric unit of complex **2**; (b) 2D cationic network structure of complex **2** with the C−H···π interactions indicated by dashed lines; the 1D chain substructure of complex **2** is indicated by solid lines, and the bidentate L1 ligands connecting the 1D chains are indicated by open lines.

complexes **2** and **3**, the anions occupy the void between the 2D cationic layers. This difference in the location of the anions in **4** and **2** (**3**) is caused by the different size of the anions. $CF_3CO_2^-$ and 1,4-$C_6H_4(COO)_2^{2-}$ in **2** and **3** are too large to fit in the void of the 44-membered ring, while the smaller perchlorate anion in **4** can. In addition, C−H···π interactions[9] in **4** occur between the benzene ring groups, rather than the pyridine groups observed in **2** and **3**. For example, the distance between the hydrogen atom (H5) bound to C5 (located at the benzene group of the bidentate ligand) and the centroid of the benzene group of the adjacent tetradentate ligand is 2.55 Å and the C5−H5−centroid angle is 155°. The uncoordinated pyridine rings of the bidentate ligand are parallel to each other and located above and below the 12-membered ring of the 2D network (Figure 3, b and c). The centroid-centroid separation of 3.66 Å between the uncoordinated and adjacent coordinated pyridine groups indicates the presence of π-π interactions.

 © 2004 Wiley-VCH Verlag GmbH & Co. KGaA, Weinheim

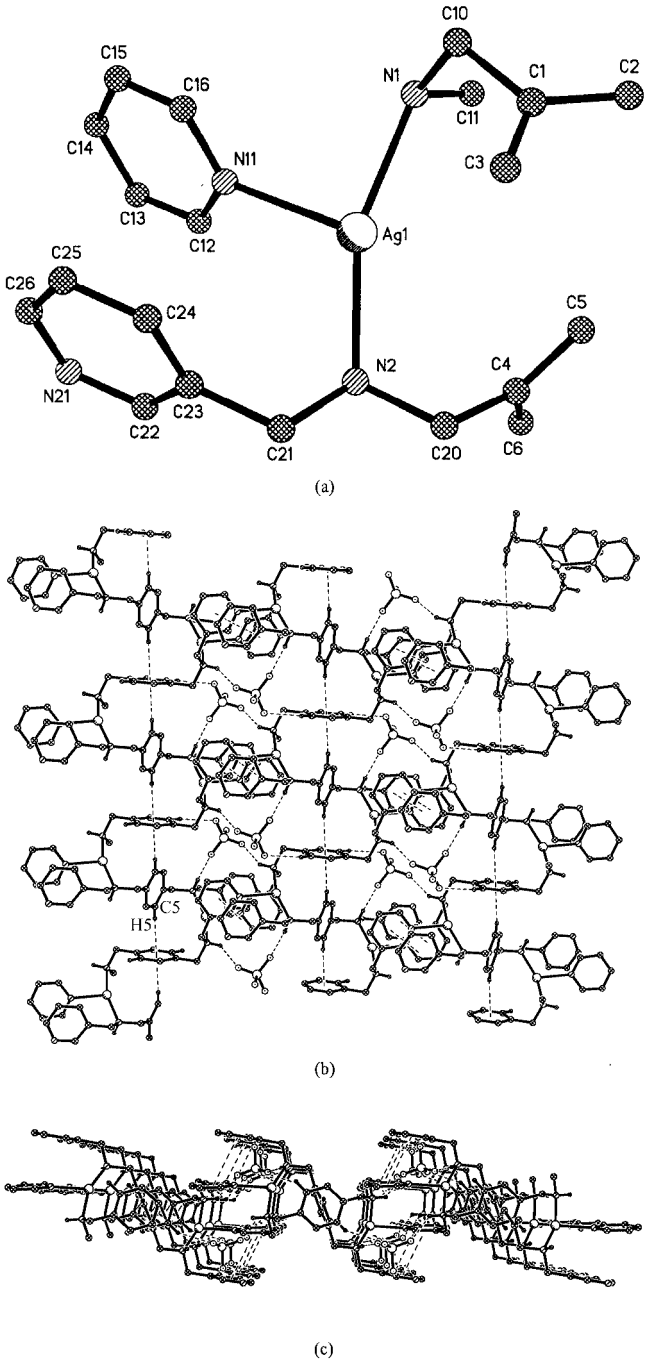

Figure 3. (a) Molecular structure of the asymmetric unit of complex **4**; (b) top and (c) side views of the 2D structure of **4** with the hydrogen bonds, π···π and C−H···π interactions indicated by dashed lines

In order to investigate the effect of the nature of the organic ligand on the structure of the complex, we prepared a Schiff-base ligand L2 by reducing the flexibility of the ligand L1. Reaction of L2 with silver(I) perchlorate gave an unexpected coordination polymer $\{[Ag(L2)]ClO_4\}_n$ (**5**) with a 1D chain structure. The coordination environment of the silver(I) atom is shown in Figure 4a with the atom numbering scheme. Each silver(I) atom in complex **5** is threefold coordinated by two pyridine N atoms from two different L2 ligands and one imine N atom of the other ligand, with Ag···N distances ranging from 2.272(3) to 2.320(2) Å and N−Ag−N bond angles in the range 115.84(9)−120.34(9)° (Table 1). There is only one kind of coordination mode for the L2 ligand in **5** as opposed to the two kinds of coordination modes for the L1 ligand in **2**, **3** and **4** as mentioned above. In addition to the 12-membered macrometallacyclic rings in **5**, which are the same as those in complexes **2**−**4**, there are also 34-membered rings formed by two L2 ligands bridging two silver(I) atoms, with an intra-ring Ag···Ag distance of 16.74 Å. These large 34-membered rings are linked by two Ag−N coordination bonds (N atom of imine group of other rings) to give the 12-membered ring and form a cationic 1D chain. It is interesting to note that three of the four N atoms of each L2 ligand participate in the coordination with three Ag^I atoms; the remaining imine N atom remains uncoordinated. In the reported metal complexes of L3 and L5, each ligand coordinates to two or three different metal atoms as bidentate, tridentate or tetradentate ligands, and the two imine N atoms in one ligand either both participate in coordination or both remain uncoordinated.[5a,5c,5e] For example, each L5 ligand in $[Cu(L5)(CH_3CN)]NO_3$ connects two Cu^I atoms using its two imine N and one pyridine N atoms, another pyridine

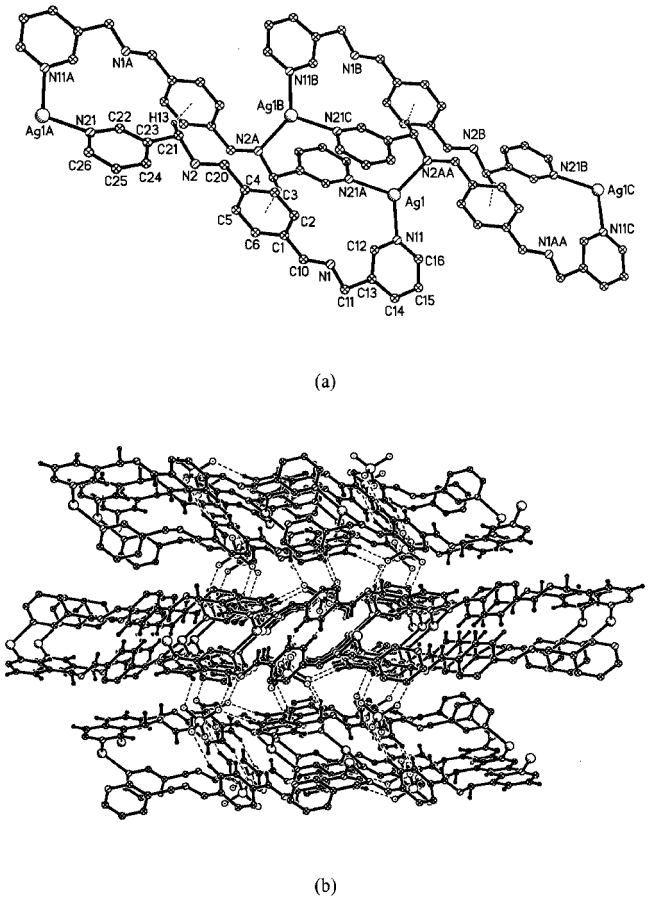

Figure 4. (a) 1D chain structure of complex **5** in which the C−H···π interactions are indicated by dashed lines; (b) crystal packing diagram of **5** with the hydrogen bonds indicated by dashed lines

 © 2004 Wiley-VCH Verlag GmbH & Co. KGaA, Weinheim

N atom of L5, rather than one of the imine N like for L2 in **5**, remains uncoordinated.[5e] As reported previously, the imine groups (i.e. -C=N-) in L2 ligand may conjugate with the central benzene ring group thereby decreasing the electron density around the imine N atoms. As a result the electron-donating ability of the imine group is reduced and the N atom of imine group is thus difficult to coordinate to a metal atom.[10] In the case of complex **5**, the imine group containing the N1 atom almost conjugates with the central benzene ring group, since the N1−C10−C1−C2 torsion angle is 0.6(4)°, and therefore the N1 atom does not coordinate to the silver(I) atom, whereas the N2−C20−C4−C5 torsion angle is 16.6(4)°, which means that the imine group containing the N2 atom does not strictly conjugate with the central benzene ring, and, consequently, the N2 atom coordinates to the silver(I) atom. Such a difference between the N1 and N2 imine groups may be caused by the π-π and C−H···π interactions since such interactions are related with the pyridylmethyl group on the N2 side; no such interactions were detected for the pyridylmethyl group on the N1 side. The centroid-centroid distance of 4.17 Å between the two pyridine groups within the 12-membered ring implies the existence of weak π-π interactions. In addition, there are C−H···π interactions[11] in the 34-membered ring, for example between the hydrogen atom (H13) bound to C21 (the methylene directly connecting pyridine group) and the benzene group of another ligand within the same ring (Figure 4, a). The H···centroid distance is 2.96 Å and the C−H−centroid angle is 150°. The Ag−N (N atom of the coordinated imine group) bond length is 2.295(3) Å (Table 1), which is shorter than those observed in the complexes $[Ag_2(L5)_2](CF_3SO_3)_2·H_2O$ and $[Ag_3(L5)_2](NO_3)_3·H_2O$ with the corresponding Ag−N bond lengths ranging from 2.328(2) to 2.405(2) Å and from 2.331(4) to 2.407(3) Å, respectively.[5a]

From the crystal-packing diagram of complex **5** shown in Figure 4 (see b) it can be seen that the cationic 1D chains and uncoordinated perchlorate anions are held together by five C−H···O hydrogen bonds (Table 2).

Electrospray (ES) Mass Spectra

Complexes **1**−**5** were further characterized by ES mass spectrometry and the spectroscopic data are summarized in Table 3. As revealed by X-ray analysis, complexes **1**−**4** are composed of the same ligand and metal atom, and each Ag^I atom is coordinated by at least two L1 ligands. Hence it is reasonable that the same three peaks at *m*/*z* = 319.2, 425.3, 744.8, corresponding to $[HL1]^+$, $[AgL1]^+$ and $[Ag(L1)_2]^+$ species, respectively, appear in the ES mass spectra of these complexes. In addition, there are peaks at *m*/*z* = 913.9, 964.7 and 950.8 corresponding to $[Ag_2(L1)_2(NO_3)]^+$, $[Ag_2(L1)_2(CF_3CO_2)]^+$ and $[Ag_2(L1)_2(ClO_4)]^+$ species in the ES mass spectra of **1**, **2** and **4**, respectively. As an example, the ES mass spectrum of complex **2** is shown in Figure 5. All the assignments are ensured by good agreement between the observed and calculated isotopic distributions. Figure 5 (see b) shows a typical example of a comparison between the experimental and calculated isotopic distributions for the peak at *m*/*z* = 964.7. The observation of mono- and dinuclear cationic species in the ES-MS spectra of complexes **1**−**5** (Table 3) confirms the coordination of the ligand to the Ag^I atom and suggests the presence of polymeric species in solution under the ES mass experimental conditions.

Conclusion

The present study shows that the reactions of the multidentate ligand L1 with various silver(I) salts can afford a variety of polymeric frameworks and that C−H···π interactions play an important role in the crystal structures. Furthermore, the results of the present study show that the nature of the counteranions has a great impact in determining the structure of the coordination polymers in this system.[12] Complex **1** contains two-coordinate silver(I) and a tetradentate L1 ligand, which may be responsible for the formation of the 1D chain structure. The 2D structures of complexes **2**, **3** and **4** all contain 12- and 44-membered macrometalla-

Table 3. ES mass spectroscopic data for complexes **1**−**5**

1		**2**		**3**	
m/*z*	Assignment	*m*/*z*	Assignment	*m*/*z*	Assignment
319.2	$[HL1]^+$	319.2	$[HL1]^+$	319.2	$[HL1]^+$
425.3	$[AgL1]^+$	425.3	$[AgL1]^+$	425.3	$[AgL1]^+$
744.8	$[Ag(L1)_2]^+$	744.8	$[Ag(L1)_2]^+$	744.8	$[Ag(L1)_2]^+$
913.9	$[Ag_2(L1)_2(NO_3)]^+$	964.7	$[Ag_2(L1)_2(CF_3CO_2)]^+$		
4		**5**			
m/*z*	Assignment	*m*/*z*	Assignment		
319.2	$[HL1]^+$	315.3	$[HL2]^+$		
425.3	$[AgL1]^+$	421.2	$[AgL2]^+$		
744.8	$[Ag(L1)_2]^+$	579.8	$[Ag_2(L2)_3]^{2+}$		
950.8	$[Ag_2(L1)_2(ClO_4)]^+$	736.7	$[Ag(L2)_2]^+$		
		1050.6	$[Ag(L2)_3]^+$		

 © 2004 Wiley-VCH Verlag GmbH & Co. KGaA, Weinheim

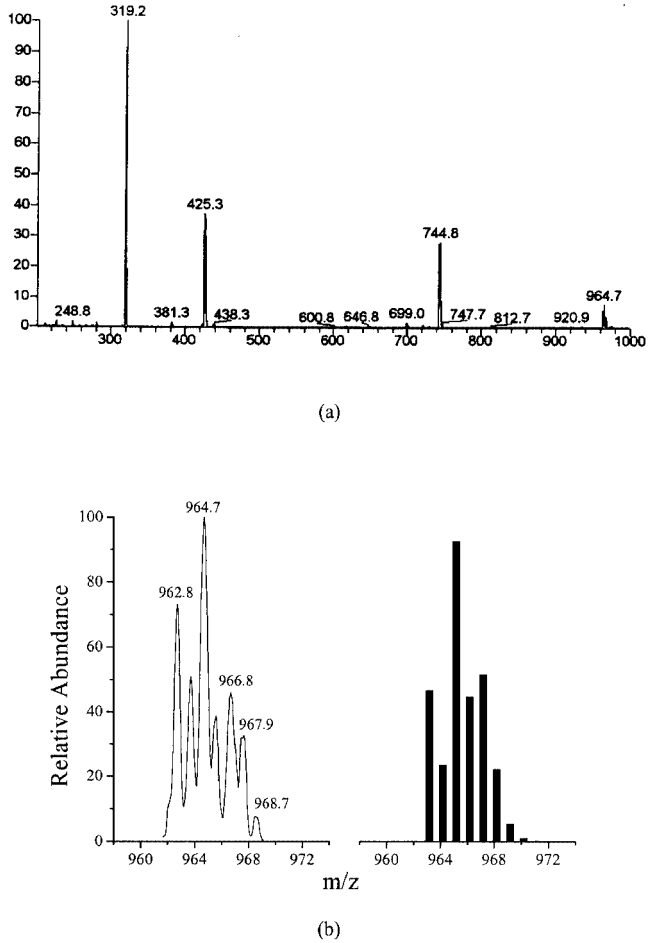

Figure 5. (a) The ES mass spectrum of complex **2**; (b) the observed (traces) and calculated (bars) isotopic distributions for the peak at m/z = 964.7

cyclic rings, although the structure of complex **4** is different from that of complex **2** or **3**. In **2** and **3**, the anions [$CF_3CO_2^-$ in **2** and 1,4-$C_6H_4(COO)_2^{2-}$ in **3**] are too large to fill the void of the 44-membered macrometallacyclic rings, whereas in **4**, the size of the perchlorate anion allows it to be accommodated in the void of the 44-membered ring by forming N−H···O and C−H···O hydrogen bonds. These results show that the size of the counteranions plays a key role in the construction of such coordination polymers. In complex **5**, due to the presence of the −C=N− imine group in the L2 ligand, a 1D chain structure is formed rather than a 2D network like **4**. The results show that the nature of ligand has a remarkable impact on the structure of the frameworks in this system.

Experimental Section

General: All commercially available chemicals were of reagent grade and used as received without further purification. Elemental analyses for C, H and N were carried out on a Perkin−Elmer 240C elemental analyzer at the Analysis Center of Nanjing University. Thermogravimetric and differential thermal analyses were taken on a simultaneous SDT 2960 thermal analyzer under N_2 with a heating rate of 10 °C/min. The electrospray mass spectral (ES-MS) measurements of the complexes were carried out on an LCQ System (Finnegan MAT, USA) using a mixing solution of methanol and water (1:1) as mobile phase. The samples for ES-MS measurements were prepared by redissolving the final isolated compounds in methanol (**1**−**4**) or in methanol and acetonitrile (1:1; for **5**). Ligands L1 and L2 were prepared by procedures reported previously.[10] All procedures for the synthesis and measurement of the silver(I) complexes were carried out in the dark.

Caution: *Perchlorate salts of metal complexes with organic ligands are potentially explosive and should be handled with care.*

Synthesis of $\{[Ag_2(L1)](NO_3)_2\cdot 2H_2O\}_n$ (1): Complex **1** was synthesized by the layering method. A solution of L1 (31.8 mg, 0.1 mmol) in ethanol (5 mL) was carefully layered over a solution of $AgNO_3$ (17.0 mg, 0.1 mmol) in water (10 mL). Colorless crystals were isolated in 61% yield by filtration after two weeks at room temperature. $C_{20}H_{26}Ag_2N_6O_8$: calcd. C 34.60, H 3.78, N 12.11; found C 34.63, H 3.76, N 11.94.

Synthesis of $\{[Ag(L1)](CF_3COO)\cdot 2.5H_2O\}_n$ (2): An aqueous (5 mL) solution of L1 (31.8 mg, 0.1 mmol) and a solution of CF_3COOAg (22.1 mg, 0.1 mmol) in water (5 mL) were mixed and allowed to stand in air at room temperature for about fifteen days. Light-brown crystals were obtained in 76% yield. $C_{22}H_{27}AgF_3N_4O_{4.5}$: calcd. C 45.22, H 4.66, N 9.59; found C 45.35, H 4.65, N 9.50.

Synthesis of $\{[Ag_2(L1)_2][1,4\text{-}C_6H_4(COO)_2]\cdot 7H_2O\}_n$ (3): A solution of L1 (31.8 mg, 0.1 mmol) in methanol (5 mL) was carefully layered over an aqueous solution of freshly prepared $[Ag(Py)_2]_2[1,4\text{-}C_6H_4(COO)_2]$ (Py = pyridine; 0.025 mmol mL^{-1}, 2 mL). Colorless crystals appeared within two weeks at room temperature in 43% yield. $C_{48}H_{62}Ag_2N_8O_{11}$: calcd. C 50.45, H 5.47, N 9.81; found C 50.48, H 5.51, N 9.73.

Synthesis of $\{[Ag(L1)]ClO_4\}_n$ (4): A methanol (5 mL) solution of L1 (31.8 mg, 0.1 mmol) and an acetonitrile (5 mL) solution of $AgClO_4\cdot H_2O$ (22.5 mg, 0.1 mmol) were mixed and allowed to stand at room temperature for ten days. Light-brown crystals were obtained in 63% yield. $C_{20}H_{22}AgClN_4O_4$: calcd. C 45.69, H 4.22, N 10.66; found C 45.60, H 4.30, N 10.58.

Synthesis of $\{[Ag(L2)]ClO_4\}_n$ (5): An aqueous (3 mL) solution of $AgClO_4\cdot H_2O$ (22.5 mg, 0.1 mmol) was added dropwise to a solution of L2 (31.4 mg, 0.1 mmol) in CH_3OH (6 mL) with stirring. The resulting precipitate was isolated and then dissolved in CH_3CN (8 mL) to give a clear solution. Crystals were obtained in 46% yield by slow diffusion of diethyl ether into the clear solution at room temperature for about two days. $C_{20}H_{18}AgClN_4O_4$: calcd. C 46.04, H 3.48, N 10.74; found C 46.24, H 3.68, N 10.75.

X-ray Crystal Structure Determination: The intensity data for complexes **1**−**5** (Table 4) were collected on a Rigaku RAXIS-RAPID Imaging Plate diffractometer at 200 K, using graphite-monochromated Mo-K_α radiation (λ = 0.7107 Å). The structures were solved by direct methods with SIR92,[13] and expanded using Fourier techniques.[14] All non-hydrogen atoms were refined anisotropically by the full-matrix least-squares method on F^2. The hydrogen atoms, except those from water molecules, were generated geometrically. The F1, F2 and F3 atoms in **2** have two positions with site occupation factors of 0.815(8) and 0.185(8), respectively. The O4, O5 and O6 atoms in **2** have site occupation factors of 0.429(13), 0.571(13) and 0.571(13), and the O2, O3 and O4 atoms in **4** are disordered over two positions with site occupation factors of

 © 2004 Wiley-VCH Verlag GmbH & Co. KGaA, Weinheim

Table 4. Crystallographic data for complexes **1**−**5**

Complex	**1**	**2**	**3**	**4**	**5**
Empirical formula	$C_{20}H_{26}Ag_2N_6O_8$	$C_{22}H_{27}AgF_3N_4O_{4.5}$	$C_{48}H_{62}Ag_2N_8O_{11}$	$C_{20}H_{22}AgClN_4O_4$	$C_{20}H_{18}AgClN_4O_4$
Molecular mass	694.21	584.35	1142.80	525.74	521.70
Crystal system	monoclinic	triclinic	triclinic	monoclinic	monoclinic
Space group	$P2_1/n$	$P\bar{1}$	$P\bar{1}$	$P2_1/n$	$P2_1/n$
a (Å)	8.625(8)	9.6191(15)	9.662(3)	9.503(4)	11.032(9)
b (Å)	12.192(12)	11.3789(15)	11.431(4)	19.101(8)	11.262(8)
c (Å)	11.590(11)	12.1015(14)	12.719(4)	11.675(4)	16.086(12)
α (°)		72.260(5)	64.93(2)		
β (°)	94.69(9)	83.813(7)	84.17(2)	100.66(3)	93.63(6)
γ (°)		71.706(9)	72.58(3)		
V (Å^3)	1215(2)	1197.7(3)	1213.7(7)	2082.5(14)	1995(3)
Z	2	2	1	4	4
$D_{calcd.}$ (g·cm^{-3})	1.898	1.620	1.564	1.677	1.737
μ [mm^{-1}]	1.670	0.903	0.875	1.131	1.181
Reflections collected	11227	11089	11868	20335	19762
Independent reflections	2709	5402	5477	4753	4569
R_{int}	0.0544	0.0385	0.0372	0.0780	0.0673
Obsd. reflections [$I > 2\sigma(I)$]	2008	4267	4410	3120	2955
Parameters refined	163	354	334	299	271
R (obsd. data)	0.0289	0.0412	0.0361	0.0322	0.0307
wR (obsd. data)	0.0486[a]	0.0928[b]	0.0814[c]	0.0455[d]	0.0522[e]
Goodness of fit	0.896	1.041	1.003	0.848	0.819
Residuals [e·Å^{-3}]	0.430; −0.400	0.726; −0.697	0.682; −0.574	0.570; −0.552	0.676; −0.455

[a] $w = 1/[\sigma^2(F_o)^2 + (0.0198P)^2]$, where $P = (F_o^2 + 2F_c^2)/3$. [b] $w = 1/[\sigma^2(F_o)^2 + (0.0550P)^2 + 0.0824P]$, where $P = (F_o^2 + 2F_c^2)/3$. [c] $w = 1/[\sigma^2(F_o)^2 + (0.0450P)^2]$, where $P = (F_o^2 + 2F_c^2)/3$. [d] $w = 1/\sigma^2(F_o)^2$. [e] $w = 1/[\sigma^2(F_o)^2 + (0.0214P)^2]$, where $P = (F_o^2 + 2F_c^2)/3$.

0.523(7) and 0.477(7), respectively. All calculations were carried out on an SGI workstation using the teXsan crystallographic software package of Molecular Structure Corporation.[15]

CCDC-218881 (**1**), -218882 (**2**), -218883 (**3**), -218884 (**4**) and -218885 (**5**) contain the supplementary crystallographic data for this paper. These data can be obtained free of charge at www.ccdc.cam.ac.uk/conts/retrieving.html [or from the Cambridge Crystallographic Data Centre, 12, Union Road, Cambridge CB2 1EZ, UK; Fax: (internat.) +44-1223/336-033; E-mail: deposit@ccdc.cam.ac.uk].

Acknowledgments

The authors are grateful to the National Natural Science Foundation of China (Grant No. 20231020) for financial support of this work.

[1] [1a] T. L. Hennigar, D. C. MacQuarrie, P. Losier, R. D. Rogers, M. J. Zaworotko, *Angew. Chem. Int. Ed. Engl.* **1997**, *36*, 972−973. [1b] M. Munakata, L. P. Wu, T. Kuroda-Sowa, *Adv. Inorg. Chem.* **1999**, *46*, 173−303. [1c] J. R. Black, N. R. Champness, W. Levason, G. Reid, *Inorg. Chem.* **1996**, *35*, 4432−4438. [1d] A. J. Blake, N. R. Brooks, N. R. Champness, M. Crew, A. Deveson, D. Fenske, D. H. Gregory, L. R. Hanton, P. Hubberstey, M. Schröder, *Chem. Commun.* **2001**, 1432−1433. [1e] D. M. L. Goodgame, D. A. Grachvogel, I. Hussain, A. J. P. White, D. J. Williams, *Inorg. Chem.* **1999**, *38*, 2057−2063.

[2] [2a] P. L. Caradoc-Davies, L. R. Hanton, W. Henderson, *J. Chem. Soc., Dalton Trans.* **2001**, 2749−2755. [2b] S. Muthu, J. H. K. Yip, J. J. Vittal, *J. Chem. Soc., Dalton Trans.* **2001**, 3577−3584.

[3] [3a] B. F. Hoskins, R. Robson, D. A. Slizys, *J. Am. Chem. Soc.* **1997**, *119*, 2952−2953. [3b] A. N. Khlobystov, A. J. Blake, N. R. Champness, D. A. Lemenovskii, A. G. Majouga, N. V. Zyk, M. Schroder, *Coord. Chem. Rev.* **2001**, *222*, 155−192. [3c] L. Carlucci, G. Ciani, P. Macchi, D. M. Proserpio, S. Rizzato, *Chem. Eur. J.* **1999**, *5*, 237−243. [3d] B. Schmaltz, A. Jouaiti, M. W. Hosseini, A. De Cian, *Chem. Commun.* **2001**, 1242−1243. [3e] L. Carlucci, G. Ciani, D. W. vonGudenberg, D. M. Proserpio, *Inorg. Chem.* **1997**, *36*, 3812−3813.

[4] [4a] M. J. Hannon, C. L. Painting, N. W. Alcock, *Chem. Commun.* **1999**, 2023−2024. [4b] C. M. Hartshorn, P. J. Steel, *Inorg. Chem.* **1996**, *35*, 6902−6903. [4c] X.-H. Bu, W. Chen, W.-F. Hou, M. Du, R.-H. Zhang, F. Brisse, *Inorg. Chem.* **2002**, *41*, 3477−3482. [4d] X.-H. Bu, W.-F. Hou, M. Du, W. Chen, R.-H. Zhang, *Cryst. Growth Des.* **2002**, *2*, 303−307. [4e] X.-H. Bu, W. Chen, M. Du, K. Biradha, W.-Z. Wang, R.-H. Zhang, *Inorg. Chem.* **2002**, *41*, 437−439.

[5] [5a] X.-M. Ouyang, B.-L. Fei, T.-a Okamura, H.-W. Bu, W.-Y. Sun, W.-X. Tang, N. Ueyama, *Eur. J. Inorg. Chem.* **2003**, 618−627. [5b] Y. Wang, X.-M. Ouyang, T.-a Okamura, W.-Y. Sun, N. Ueyama, *Inorg. Chim. Acta* **2003**, *353*, 68−74. [5c] X. M. Ouyang, Y. Wang, Y. Z. Li, Y. J. Liu, W. Y. Sun, W. X. Tang, *Chem. J. Chin. Univ.* **2002**, *23*, 2234−2236. [5d] B.-L. Fei, W.-Y. Sun, Y.-A. Zhang, K.-B. Yu, W.-X. Tang, *Inorg. Chim. Acta* **2000**, *306*, 106−111. [5e] W.-Y. Sun, B.-L. Fei, T.-A. Okamura, W.-X. Tang, N. Ueyama, *Eur. J. Inorg. Chem.* **2001**, 1855−1861. [5f] B.-L. Fei, W.-Y. Sun, K.-B. Yu, W.-X. Tang, *J. Chem. Soc., Dalton Trans.* **2002**, 805−811.

[6] [6a] P. L. Caradoc-Davies, D. H. Gregory, L. R. Hanton, J. M. Turnbull, *J. Chem. Soc., Dalton Trans.* **2002**, 15741580. [6b] K. Jitsukawa, K. Iwai, H. Masuda, H. Ogoshi, H. Einaga, *J. Chem. Soc., Dalton Trans.* **1997**, 3691−3698.

[7] B.-L. Fei, W.-Y. Sun, T.-a Okamura, W.-X. Tang, N. Ueyama, *New J. Chem.* **2001**, *25*, 210−212.

[8] [8a] P. L. Caradoc-Davies, L. R. Hanton, J. M. Hodgkiss, M. D. Spicer, *J. Chem. Soc., Dalton Trans.* **2002**, 1581−1585. [8b] C. Janiak, *J. Chem. Soc., Dalton Trans.* **2000**, 3885−3896. [8c] Y. Umezawa, S. Tsuboyama, K. Honda, J. Uzawa, M. Nishio, *Bull. Chem. Soc. Jpn.* **1998**, *71*, 1207−1213.

[9] [9a] Z. Dominguez, H. Dang, M. J. Strouse, M. A. Garcia-Gari-

 © 2004 Wiley-VCH Verlag GmbH & Co. KGaA, Weinheim

bay, *J. Am. Chem. Soc.* **2002**, *124*, 7719−7727. [9b] H. Suezawa, T. Yoshida, M. Hirota, H. Takahashi, Y. Umezawa, K. Honda, S. Tsuboyama, M. Nishio, *J. Chem. Soc., Perkin Trans. 2* **2001**, 2053−2058. [9c] H. Takahashi, S. Tsuboyama, Y. Umezawa, K. Honda, M. Nishio, *Tetrahedron* **2000**, *56*, 6185−6191.

[10] [10a] H.-F. Zhu, L. Li, T.-a Okamura, W. Zhao, W.-Y. Sun, N. Ueyama, *Bull. Chem. Soc. Jpn.* **2003**, *76*, 761−767. [10b] H.-F. Zhu, L. Li, J. Fan, W. Zhao, W.-Y. Sun, *Chin. J. Inorg. Chem.* **2003**, *19*, 25−28.

[11] [11a] P. R. Ashton, R. Ballardini, V. Balzani, I. Baxter, A. Credi, M. C. T. Fyfe, M. T. Gandolfi, M. Gómez-López, M.-V. Martínez-Díaz, A. Piersanti, N. Spencer, J. F. Stoddart, M. Venturi, A. J. P. White, D. J. Williams, *J. Am. Chem. Soc.* **1998**, *120*, 11932−11992. [11b] D. B. Amabilino, P. R. Ashton, C. L. Brown, E. Córdova, L. A. Godínez, T. T. Goodnow, A. E. Kaifer, S. P. Newton, M. Pietraszkiewicz, D. Philp, F. M. Raymo, A. S. Reder, M. T. Rutland, A. M. Z. Slawin, N. Spencer, J. F. Stoddart, D. J. Williams, *J. Am. Chem. Soc.* **1995**, *117*, 1271−1293.

[12] [12a] M. J. Hannon, C. L. Painting, E. A. Plummer, L. J. Childs, N. W. Aclock, *Chem. Eur. J.* **2002**, *8*, 2225−2238. [12b] O.-S. Jung, Y. J. Kim, Y.-A. Lee, J. K. Park, H. K. Chae, *J. Am. Chem. Soc.* **2000**, *122*, 9921−9925. [12c] M. A. Withersby, A. J. Blake, N. R. Champness, P. Hubberstey, W.-S. Li, M. Schröder, *Angew. Chem. Int. Ed. Engl.* **1997**, *36*, 2327−2329. [12d] C. He, B.-G. Zhang, C.-Y. Duan, J.-H. Li, Q.-J. Meng, *Eur. J. Inorg. Chem.* **2000**, 2549−2554. [12e] R. Vilar, *Angew. Chem. Int. Ed.* **2003**, *42*, 1460−1477. [12f] L. Carlucci, G. Ciani, D. M. Proserpio, A. Sironi, *Inorg. Chem.* **1998**, *37*, 5941−5943.

[13] SIR92: A. Altomare, M. C. Burla, M. Camalli, M. Cascarano, C. Giacovazzo, A. Guagliardi, G. Polidori, *J. Appl. Cryst.* **1994**, *27*, 435.

[14] DIRDIF94: P. T. Beurskens, G. Admiraal, G. Beurskens, W. P. Bosman, R. de Gelder, R. Israel and J. M. M. Smits, **1994**. The DIRDIF94 program system, Technical Report of the Crystallography Laboratory, University of Nijmegen, The Netherlands.

[15] teXsan: Crystal Structure Analysis Package, Molecular Structure Corporation, **1999**.

Received September 4, 2003
Early View Article
Published Online February 26, 2004

 © 2004 Wiley-VCH Verlag GmbH & Co. KGaA, Weinheim

The First Silver(I) Side-On η^2-Coordination Network Formed by Self-Assembly of Bis(pyrrol-2-ylmethylene)hydrazine

Lanying Yang,[a] Xufeng Shan,[b] Qingqi Chen,[c] Zhengping Wang,[b] and Jin Shi Ma*[a]

Keywords: Coordination polymers / Hydrogen bonding / Schiff bases / Self-assembly / Silver

This paper reports the first silver(I) network polymer formed by the self-assembly of bis(pyrrol-2-ylmethylene)hydrazine with silver nitrate, in which the silver centers are bonded to the C–N bonds of the pyrrole rings in an η^2-fashion. An X-ray crystal structure analysis revealed that the self-assembly of the bis(pyrrol-2-ylmethylene)hydrazine ligand with Ag^I gives a 2D sheet, which is further assembled to form a 3D network through weak intermolecular hydrogen bonding between the protons of the pyrrole rings and the oxygen atoms of the nitrate ions.
(© Wiley-VCH Verlag GmbH & Co. KGaA, 69451 Weinheim, Germany, 2004)

Introduction

The design and synthesis of supramolecular coordination polymers has attracted increasing attention during the last decade due to their potential applications as functional materials.[1,2] Multidimensional networks based on ligands with a rigid bridging spacer[3] or a flexible bridging spacer[4] have been reported. Coordination networks containing π-sandwiched silver(I) complexes with polycyclic aromatic compounds,[5] cyclopentadienyl rings,[6] and phenyl rings,[7] have been described. Small π-sandwiched silver(I) complexes have been reported recently[8] in which the silver centers are doubly sandwiched. In this paper we report a novel three-dimensional silver(I) coordination network formed by self-assembly of bis(pyrrol-2-ylmethylene)hydrazine with silver nitrate, in which the silver center, unlike its more common sandwich coordination, is side-on η^2-coordinated to the pyrrole ring. To the best of our knowledge, this is the first example of a silver(I) side-on η^2-complex with pyrrole.

Our group is currently exploring the use of pyrrole-based Schiff bases, such as the (pyrrol-2-ylmethylene)amine ligands **I**, as building blocks for supramolecular architectures. By varying the length and geometric arrangement of the bridging spacer, the bis(pyrrol-2-ylmethylene)hydrazines could form dinuclear double-stranded helicates,[9] trimeric triangles, or tetrameric squares.[10] To further explore the application of the (pyrrol-2-ylmethylene)amine ligand **I** in supramolecular self-assembly, we are interested in investigating the self-assembly of bis(pyrrol-2-ylmethylene)hydrazine (**L**), in which two (pyrrol-2-ylmethylene)amine units are directly linked between two imine N atoms. Bis(pyrrol-2-ylmethylene)hydrazine was synthesized by a simple condensation of 2-formylpyrrole with hydrazine, as shown in Scheme 1. Among the many metal ions attempted, Ag^I was found to form complex **1** with ligand **L**, which was stable enough to allow successful isolation and crystallization.

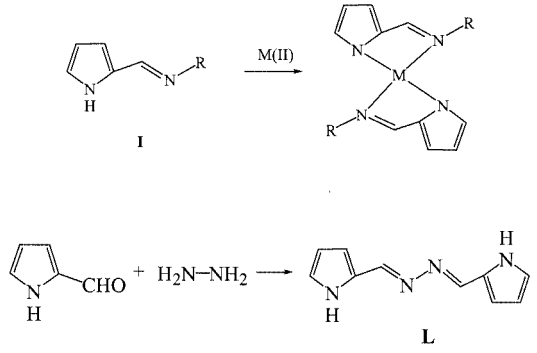

Scheme 1

Results and Discussion

Complex Analysis

The polymer **1**, prepared by simply treating ligand **L** with silver nitrate, has a melting point of 140 °C (dec.), and is insoluble in most common solvents, such as $CHCl_3$, CH_2Cl_2, THF, acetone, ethyl acetate and CH_3OH. The IR analysis confirms the formation of complex **1**, in which the

[a] CAS Key Laboratory of Photochemistry, Institute of Chemistry, Chinese Academy of Sciences,
Beijing 100080, China
Fax: (internat.) + 86-10/8261-7315
E-mail: jsma@iccas.ac.cn
[b] Department of Chemical Engineering, Harbin Engineering University,
Harbin 150001, China
[c] BioMarin Pharmaceutical, Inc.,
46 Galli Drive, Novato, CA 94949, USA

 © 2004 Wiley-VCH Verlag GmbH & Co. KGaA, Weinheim **DOI: 10.1002/ejic.200300638**

peak for nitrate is at 1382 cm^{-1} and is more intense than in **L**, the peak for ν_{N-H} is slightly shifted to a higher frequency (3222 cm^{-1}) with less intensity, while the peak for $\nu_{C=N}$ is not shifted (1631 cm^{-1}) but becomes much weaker than in the free ligand **L**. Attempts to analyze the polymer **1** by ^1H NMR spectroscopy in [D_6]DMSO or [D_5]pyridine failed since **1** decomposed.

X-ray Crystallographic Characterization

Complex **1** has the chemical formula $[Ag_2\mathbf{L}(NO_3)_2]_n$, indicating that two N−H protons remain in the ligand **L**, which is unique and surprising because the protons of pyrrolic NH groups in the (pyrrol-2-ylmethylene)amine ligands are usually removed upon coordinating to metal ions such as Zn^{II}, Ni^{II}, Cu^{II}, Co^{III}, Hg^{II}, Mn^{II} and Mn^{II}.[9−12]

The crystallographic study revealed that each ligand interacts symmetrically above and below the ligand plane in a di-η^2-fashion with two Ag^I ions, which coordinate to two imine-N atoms of two nearby ligands, resulting in an infinite one-dimensional (1D) stair-like polymeric structure as shown in Figure 1 (bottom). Due to an interaction between Ag^I and the five-membered rings in an η^2-fashion, the C5−N3 bond is found to be longer (1.413 Å) than the other four bonds (1.327−1.395 Å) in the pyrrole ring. The Ag1−N3 and Ag1−C5 (2.631 and 2.690 Å, respectively) bond lengths are within the normal range found in silver(I) sandwich complexes (2.47−2.92 Å),[5−8] indicating a moderate interaction between Ag^I and the pyrrole ring.

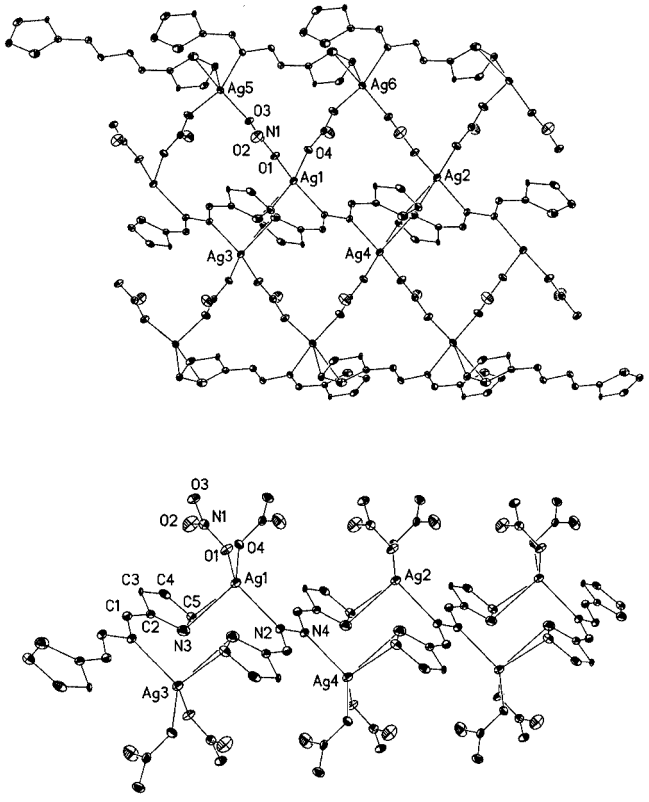

Figure 1. Perspective view of the 2D silver(I) polymer sheet of **1** (top), and the stair-like structure, with emphasis on the side-on η^2-coordination (bottom); hydrogen atoms are omitted for clarity

The adjacent 1D structures are assembled into a two-dimensional (2D) polymeric structure through the linkage of two silver atoms bridged by one nitrate group, with an Ag···Ag separation of 5.639 Å (Figure 1, top). In the 2D polymer sheet of **1**, the bis(pyrrol-2-ylmethylene)hydrazine ligands are arranged in rows in two directions, and the dihedral angle defined by the planes of the ligands in the two adjacent rows is 37.6°.

Each Ag^I center is four-coordinate to a nitrogen donor from the imine group of ligand **L**, a pyrrole ring of another ligand **L** in a side-on η^2-fashion, specifically with the C5−N3 bond (see Figure 1, bottom), and two oxygen atoms of two distinct nitrate ions. In turn, each nitrate ion is bound to two distinct Ag^I centers, while each ligand links four distinct Ag^I centers. This forms a unique stair-like Ag^I coordination polymer, in which the ligand **L** remains neutral, similar to the situation in silver(I) complexes with polycyclic aromatic compounds.[5]

The two (pyrrol-2-ylmethylene)amine units in ligand **L** adopt a *trans* arrangement about the N2−N4 bond, and are coplanar (σ = 0.019 Å). Ag1 and Ag4, bonded to two imine-N atoms of the ligand, are coplanar with ligand **L**. The Ag^I ions in **2** are also arranged into rows with a separation of 6.946 Å for the same row (e.g. Ag1−Ag2), and 4.828 Å for the adjacent separation (e.g. Ag1−Ag3).

The 2D sheets are further assembled to form a three-dimensional (3D) network through weak hydrogen bonding between the H atoms in the C3 and C4 positions of the pyrrole ring and the oxygen atoms of the nitrate ions in the two adjacent sheets (Figure 2). The C(pyrrole)−H···O(nitrate) angles are 154.2 and 142.1°, with an H···O separation (*d*) of 2.379 and 2.108 Å, respectively. These data fall in the range associated with weak hydrogen bonding.[13]

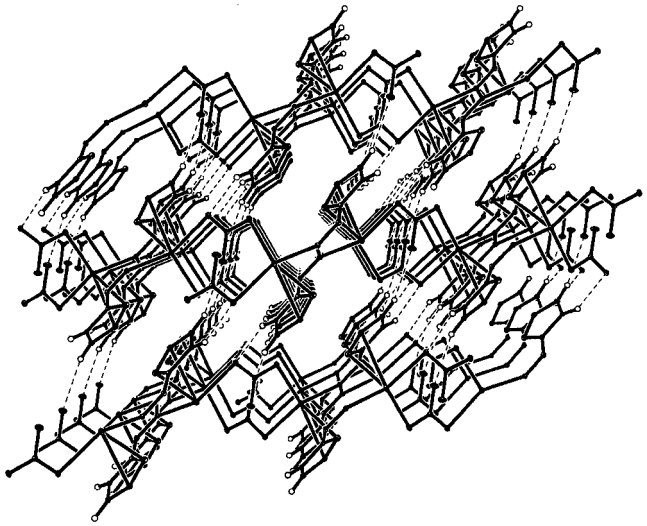

Figure 2. Perspective view of the three-dimensional network of **1** formed by weak intermolecular hydrogen bonding, viewed along the crystallographic *b* axis

In conclusion, a 2D polymer sheet of **2** is formed through self-assembly of bis(pyrrol-2-ylmethylene)hydrazine with silver nitrate. This is the first example of a 2D network

 © 2004 Wiley-VCH Verlag GmbH & Co. KGaA, Weinheim

polymer where the Ag^I center is side-on coordinated with a pyrrole ring in an η^2-fashion. The 2D sheet polymer is further assembled to form a 3D network through weak intermolecular hydrogen bonding of the type C(pyrrole)−H···O(nitrate).

Experimental Section

General Methods: Pyrrole-2-carbaldehyde was synthesized according to a literature method.[14] All reagents for syntheses and analyses were of analytical grade and used as received. Melting points were determined with a Yanaco MP-500 micro-melting point apparatus and are uncorrected. IR spectra were recorded with a Tensor 27 spectrometer. Raman spectra were recorded with an RFS100 spectrometer. ^{1}H NMR spectra were recorded with a Bruker Avance dpx 400 MHz instrument using TMS as internal standard. Elemental analyses were performed with Carlo Erba-120 elemental analyzer.

Preparation of Bis(pyrrol-2-ylmethylene)hydrazine (L): Pyrrole-2-carbaldehyde (0.95 g, 10 mmol) and hydrazine hydrate (0.25 g, 5 mmol) were dissolved in ethanol (15 mL). The mixture was stirred while a few drops of glacial acetic acid were added. After a few seconds, a yellow precipitate was observed. The suspension was stirred at room temperature for 1 h. The yellow solid was collected by suction filtration, washed with cold ethanol and dried under vacuum to give the expected product. An analytical sample was purified by recrystallization from ethanol. Yield: 0.56 g (60%). Mp. 186−187 °C. Selected FT-IR peaks (KBr pellets): $\tilde{\nu}$ = 3217s cm^{-1} (NH), 3105w (=CH), 3066w (=CH), 1632s (C=N), 1541w (ring), 1409s (ring), 1132m (ring CH), 1029m (ring CH). Raman: $\tilde{\nu}$ = 1584s cm^{-1} (C=N), 1532m (C=N), 1422m (ring), 1347m (ring), 1017s (ring). ^{1}H NMR (400 MHz, $CDCl_3$, 25 °C, TMS): δ = 6.30 (s, 2 H, pyrrole-H), 6.62 (s, 2 H, pyrrole-H), 6.98 (s, 2 H, pyrrole-H), 8.37 (s, 2 H, imine-H), 9.33 (br., 2 H, NH) ppm. UV/Vis (DMSO): λ = 357 nm (ε = 46500). $C_{10}H_{10}N_4$ (186.09): calcd. C 64.50, H 5.41, N 30.09; found C 64.72, H 5.55, N 30.47.

Preparation of $[Ag_2L(NO_3)_2]_n$ (1): Crystals of **1** were prepared by slow diffusion of a solution of $AgNO_3$ (34 mg, 0.2 mmol) in CH_3OH (6 mL) into a solution of **L** (18.6 mg, 0.1 mmol) in $CHCl_3$ (10 mL) in a sealed tube. After one week, light-yellow crystals of **1** suitable for X-ray analysis were obtained. Yield: 29 mg (55%). M.p. > 140 °C (decomp.). Selected FT-IR peaks (KBr pellet): $\tilde{\nu}$ = 3221m cm^{-1} (NH), 3138w (=CH), 3108w (=CH), 1630s (C=N), 1541w (ring), 1410sh (ring), 1382vs (NO_3^-), 1361s (ring), 1129m (ring CH), 1032m (ring CH). Raman: $\tilde{\nu}$ = 1576s cm^{-1} (C=N), 1441w (ring), 1362w (ring), 1012w (ring). $C_{10}H_{10}Ag_2N_6O_6$ (525.98): calcd. C 22.84, H 1.92, N 15.98; found C 22.75, H 1.87, N 15.68.

X-ray Data Collection and Structure Solution and Refinements: Single-crystal X-ray diffraction measurements were carried out with a Rigaku R-axis RAPID IP diffractometer. Determination of the unit-cell parameters and data collection were performed with Mo-K_α radiation (λ = 0.71073 Å) and unit-cell dimensions were obtained by least-squares refinement. The structure was solved by direct methods and empirical absorption corrections were applied using the ψ-scan method. The final refinement was carried out by full-matrix least-squares methods with anisotropic thermal parameters for non-hydrogen atoms on F^2. The hydrogen positions were calculated and refined as riding on the concerned atoms with fixed thermal factors. A total of 2754 reflections were measured in the range 2.52° ≤ θ ≤ 27.48° (*hkl* range indices: −12 ≤ *h* ≤ 12, −8 ≤ *k* ≤ 8, −14 ≤ *l* ≤ 14) with 1638 unique reflections [*R*(int) = 0.0303]. The structure was solved with SHELX-97[15] and refined with SHELX-97.[16] The details for structure analysis are summarized in Table 1. Selected bond lengths and angles are given in Table 2. CCDC-208538 contains the supplementary crystallographic data for this paper. These data can be obtained free of charge at at www.ccdc.cam.ac.uk/conts/retrieving.html. [or from the Cambridge Crystallographic Data Centre, 12 Union Road,-Cambridge CB2 1EZ, UK; Fax: (internat.) + 44-1223/336-033; E-mail: deposit@ccdc.cam.ac.uk].

Table 1. Crystallographic data for complex **1**

Empirical formula	$C_{10}H_{10}Ag_2N_6O_6$
Formula mass	525.98
Cryst color, habit	light yellow, needle
Crystal size [mm]	0.55 × 0.30 × 0.16
Crystal system	monoclinic
Space group	$P2_1/n$
T [K]	293(2)
a [Å]	9.8332(12)
b [Å]	6.9461(7)
c [Å]	10.8710(8)
β [°]	103.486(6)
V [Å^3]	722.04(13)
$D_{calcd.}$ [Mg/m^3]	2.419
Z	4
λ(Mo-K_α) [Å]	0.71073
μ(Mo-K_α) [mm^{-1}]	2.757
F(000)	508
R_1 [a]	0.0325
wR_2 [b]	0.0761
GOF	0.940

[a] $R_1 = \Sigma||F_o| - |F_c||/\Sigma|F_o||$. [b] $wR_2 = \Sigma||F_o| - |F_c||w^{1/2}/\Sigma|F_o|w^{1/2}$.

Table 2. Selected bond lengths [Å] and bond angles for the Ag^I network polymer **1**; symmetry transformations used to generate equivalent atoms: [i] $-x + 1/2, y - 1/2, -z + 3/2$; [ii] $-x + 1, -y, -z + 1$; see Figure 2 (bottom) for atom labeling

Bond lengths			
Ag1−N3	2.631(4)	Ag1−C5	2.690(4)
Ag1−N2	2.338(3)	Ag1−O4	2.494(3)
Ag1−O1	2.398(3)		
Bond angles			
N2−Ag1−O1	112.23(11)	N2−Ag1−O4	116.89(11)
O4−Ag1−O1	113.65(10)	N2−Ag1−N3	92.36(12)
O1^{i}−Ag1−N3^{ii}	111.06(12)	O4−Ag1−N3^{ii}	108.55(12)
N2−Ag1−C5^{ii}	97.66(12)	O1^{i}−Ag1−C5^{ii}	134.04(13)
O4−Ag1−C5^{ii}	79.22(11)	N3^{ii}−Ag1−C5^{ii}	30.78(13)

Acknowledgments

This was supported by the Major State Basic Research Development Program (G2000078100), NSFC (20172055) and CAS (CMS CX-200205). We thank Ms. S.-H. Zhou (Institute of Biophysics) for the NMR spectra and Ms. Y. Li (Institute of Chemistry) for X-ray analysis.

 © 2004 Wiley-VCH Verlag GmbH & Co. KGaA, Weinheim

[1] For reviews, see: [1a] J. M. Lehn, *Supramolecular Chemistry*, VCH, Weinham, **1995**. [1b] *Transition Metals in Supramolecular Chemistry* (Eds.: L. Fabbrizza, A. Poggi), Kluwer Academic, The Netherlands, **1994**. [1c] *Comprehensive Supramolecular Chemistry* (Ed.: J. M. Lehn), Pergamon Press, Oxford, **1995**. [1d] K. Biradha, M. Fujita, *Adv. Supramol. Chem.* **2000**, *6*, 1.

[2] For example: [2a] M. L. Tong, X. M. Chen, B. H. Ye, L. N. Ji, *Angew. Chem. Int. Ed.* **1999**, *38*, 2237−2240. [2b] S. S. Y. Chui, S. M. F. Lo, J. P. H. Charmant, A. G. Orpen, I. D. Williams, *Science* **1999**, *283*, 1148−1150. [2c] M. J. Zaworotko, *Angew. Chem. Int. Ed.* **2000**, *39*, 3052−3054, and references cited therein.

[3] For example: [3a] A. J. Blake, N. R. Champness, P. Hubberstey, W. S. Li, M. A. Withersby, M. Schroder, *Coord. Chem. Rev.* **1999**, *183*, 117−138. [3b] C. V. K. Sharma, G. A. Broker, J. G. Huddleston, J. W. Baldwin, R. M. Metzger, R. D. Rogers, *J. Am. Chem. Soc.* **1999**, *121*, 1137−1144. [3c] K. Biradha, C. Seward, M. J. Zaworotko, *Angew. Chem. Int. Ed.* **1999**, *38*, 492−495. [3d] S. Leininger, B. Olenyuk, P. J. Stang, *Chem. Rev.* **2000**, *100*, 853−908. [3e] T. K. Maji, S. Konar, G. Mostafa, E. Zangrando, T. H. Lu, R. Chaudhur, *Dalton Trans.* **2003**, 171−175.

[4] For example: [4a] D. M. L. Goodgame, D. A. Grachvogel, I. Hussain, A. J. P. White, D. J. Williams, *Inorg. Chem.* **1999**, *38*, 2057−2063. [4b] X. H. Bu, W. Chen, S. L. Lu, R. H. Zhang, D. Z. Liao, W. M. Bu, M. Shionoya, F. Brisse, J. Ribas, *Angew. Chem. Int. Ed.* **2001**, *40*, 3201−3203. [4c] X. H. Bu, W. Chen, W. F. Hou, M. Du, R. H. Zhang, F. Brisse, *Inorg. Chem.* **2002**, *41*, 3477−3482.

[5] [5a] M. Munakata, L. P. Wu, T. Kuorda-Sowa, M. Maekawa, Y. Suenaga, K. Sugimoto, *Inorg. Chem.* **1997**, *31*, 4903−4905. [5b] M. Munakata, L. P. Wu, G. L. Ning, T. Kuorda-Sowa, M. Maekawa, Y. Suenaga, N. Maeno, *J. Am. Chem. Soc.* **1999**, *121*, 4968−4976. [5c] M. Munakata, L. P. Wu, G. L. Ning, *Coord. Chem. Rev.* **2000**, *198*, 171−203. [5d] M. Munakata, J. C. Zhong, T. Kuorda-Sowa, M. Maekawa, Y. Suenaga, M. Kasahara, H. Konaka, *Inorg. Chem.* **2001**, *40*, 7087−7090. [5e] M. Munakata, L. P. Wu, T. Kuorda-Sowa, M. Maekawa, Y. Suenaga, T. Ohta, H. Konaka, *Inorg. Chem.* **2003**, *42*, 2553−2558.

[6] O. Crespo, C. Gimeno, P. G. Jones, A. Laguna, C. Sarroca, *Chem. Commun.* **1998**, 1481−1482.

[7] [7a] E. Bosch, C. Barnes, *Inorg. Chem.* **2001**, *40*, 3234−3236. [7b] E. Bosch, C. Barnes, *Inorg. Chem.* **2002**, *41*, 2543−2547.

[8] [8a] Y. Kuwatani, T. Yoshida, K. Hara, M. Yoshida, H. Matsuyama, M. Iyoda, *Org. Lett.* **2000**, *2*, 4017−4020. [8b] S. Hiraoka, T. Yi, M. Shiro, M. Shionoya, *J. Am. Chem. Soc.* **2002**, *124*, 14510−14511.

[9] L. Yang, Q. Chen, J. S. Ma, *Tetrahedron*, **2003**, *59*, 10037−10041.

[10] Z. Wu, Q. Chen, S. Xiong, B. Xin, Z. Zhao, L. Jiang, J. S. Ma, *Angew. Chem. Int. Ed.* **2003**, *42*, 3271−3274.

[11] [11a] J. H. Weber, *Inorg. Chim. Acta* **1967**, *6*, 258−262. [11b] C. J. Jones, J. A. McCleverty, *J. Chem. Soc. A* **1971**, 1052−1060. [11c] G. C. Van Stein, G. Van Koten, H. Passengier, O. Steinebach, K. Vrieze, *Inorg. Chim. Acta* **1984**, *89*, 79−87. [11d] A. Mohamadou, J. P. Barbier, *Inorg. Chim. Acta* **1990**, *169*, 17−18. [11e] S. Srivastava, R. Mishra, *J. Indian Chem. Soc.* **1995**, *72*, 719−720.

[12] [12a] S. Brooker, B. M. Carterr, *Acta Crystallogr., Sect. C* **1995**, *51*, 1522−1524. [12b] N. A. Bailey, A. Barrass, D. E. Fenton, M. S. Leal Gonzales, R. Moody, C. O. Rodriguez de Barbarin, *J. Chem. Soc., Dalton Trans.* **1984**, 2741−2746. [12c] S. I. Rooker, C. I. Simionescu, *Rev. Roum. Chim.* **1997**, *42*, 993−998. [12d] N. Yoshida, K. Ichikawa, *Chem. Commun.* **1997**, 1091−1092. [12e] N. Yoshida, K. Ichikawa, M. Shiro, *J. Chem. Soc., Perkin Trans. 2* **2000**, 17−26. [12f] F. Franceschi, G. Guillemot, E. Solari, C. Floriani, N. Re, H. Birkedal, P. Pattison, *Chem. Eur. J.* **2001**, *7*, 1468. [12g] M. Vazquez, M. Bermejo, M. Fondo, A. Garcia-Deibe, A. M. Gonzalez, R. Pedrido, *Eur. J. Inorg. Chem.* **2002**, 465−472.

[13] G. R. Desiraju, T. Steiner, *The Weak Hydrogen Bond in Structural Chemistry and Biology*, Oxford University Press, Oxford, **1999**.

[14] R. M. Silverstein, E. E. Ryskiewicz, C. Willard, *Org. Synth.* **1963**, *36*, 74−77.

[15] G. M. Sheldrick, *SHELX-97, Crystal Structure Solution*, University of Göttingen, Germany, **1997**.

[16] G. M. Sheldrick, *SHELX-97, Crystal Structure Refinement*, University of Göttingen, Germany, **1997**.

Received September 10, 2003
Early View Article
Published Online February 5, 2004

 © 2004 Wiley-VCH Verlag GmbH & Co. KGaA, Weinheim

Self-Assembly of Bis(pyrrol-2-ylmethyleneamine) Ligands with Cu^{II} Controlled by Bridging [−$(CH_2)_n$−] Spacers and Weak Intermolecular C−H···Cu Hydrogen Bonding

Lanying Yang,[a] Qingqi Chen,[b] Yan Li,[a] Shaoxiang Xiong,[a] Genpei Li,[c] and Jin Shi Ma*[a]

Keywords: Copper / Helical structures / Hydrogen bonding / N ligands / Schiff bases / Self-assembly

Bis(pyrrol-2-ylmetyhleneamine) ligands linked by alkyl spacers between the imine nitrogens are shown to give dinuclear dimers or mononuclear monomers, depending on the length of the alkyl linker, upon coordination with Cu^{II}. Ligands containing ethylene or hexylene linkers –$(CH_2)_n$– (n = 2, 6) give dinuclear dimers **5** and **8**, while propylene and butylene chains (n = 3, 4) give mononuclear monomers **6** and **7**. X-ray crystal structural analysis reveals that **5** exists as two very similar isomers **5a** and **5b**, in which the two ligands are bound to two Cu^{II} centers to form a distorted helical conformation. In the unit cells of **8**, two entirely different isomers **8a** and **8b** are found. In **8a** two ligands are side-by-side bound to two Cu^{II} centers to form a rectangular macrocycle, while in **8b** they are bonded to two Cu^{II} centers to form a distorted double-stranded helix. Moreover, X-ray structural analysis reveals that complexes **5**–**8** are further assembled into one-dimensional polymers through weak, intermolecular C–H···Cu hydrogen bonding, which plays a crucial role in stabilizing the crystal lattice.

(© Wiley-VCH Verlag GmbH & Co. KGaA, 69451 Weinheim, Germany, 2004)

Introduction

Metal-ion-assisted self-assembly is one of most powerful approaches to supramolecular architectures.[1] This strategy typically utilizes metal-ligand interactions to organize small molecules into large assemblies. Obviously the ligands are the key to such research. The dipyrrin ligands **I**, which are important synthetic precursors for porphyrins, bile pigments, and linear and cyclic polypyrroles,[2] were recently used for metal-ion-assisted self-assembly.[3,4] One of the advantages of using dipyrrins as a building block for self-assembly is their ability to form neutral complexes, meaning that counterions are not required, which makes it particularly convenient to purify the complexes by column chromatography since the complexes are not charged and are generally the least-polar component in the reaction mixtures.[3,4] This may also avoid the disordering problem in the solid state caused by counterions.

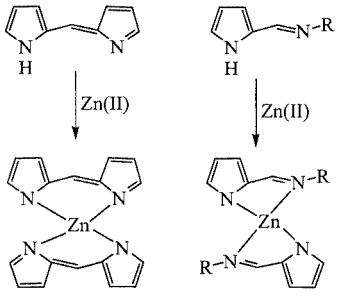

I Dipyrrin **II** Schiff-base Ligand

However, the use of dipyrrin for constructing supramolecular architectures by self-assembly is also limited by their availability and solubility in organic solvents. Spacer-bridged linear bis- or tris-dipyrrins are usually difficult to synthesize.[2,5] Moreover, linear poly(dipyrrin)s, such as tetradipyrrins, hexadipyrrins, have been reported to have limited solubility in common solvents.[5]

Having examined the chemical structure of dipyrrin **I**, we assumed that its simpler analogues **II** may possess similar coordinating properties to **I**, and may therefore be an ideal building block for supramolecular architectures. Ligands **II**, a pyrrol-2-yl Schiff base or pyrrol-2-ylmethyleneamine, could easily be prepared by condensation of 2-formylpyrrole with a primary amine. Complexes formed by **II** and

[a] Center for Molecular Science, Institute of Chemistry, Chinese Academy of Sciences,
Beijing 100080, China
Fax: (internat.) +86-10-8261-7315
E-mail: jsma@iccas.ac.cn
[b] BioMarin Pharmaceutical, Inc.,
46 Galli Drive, Novato, CA 94949, USA
[c] College of Chemistry and Molecular Engineering
Peking University, Beijing 100871, China

 © 2004 Wiley-VCH Verlag GmbH & Co. KGaA, Weinheim **DOI: 10.1002/ejic.200300639**

metal ions have been known for a long time,[6] and macrocycles containing pyrrol-2-ylmethyleneamine units, such as texaphyrins and expanded porphyrins,[7] have been extensively investigated. Linear spaced bis(pyrrol-2-ylmethyleneamine) and their complexes with metal ions have been reported,[8] which shows that both the preparation of ligands and the complexes are highly efficient, and that the metal complexes formed by pyrrol-2-ylmethyleneamines possess good solubility in common solvents. Attracted by those properties, our group recently investigated the use of pyrrol-2-ylmethyleneamine ligands for self-assembly.[9−11] By varying the spacers between two pyrrol-2-ylmethyleneamine units, a two-dimensional network polymer,[9] dinuclear dimeric helicates,[10,11] trinuclear trimeric triangle[11] and tetranuclear tetrameric square[11] complexes were generated, which demonstrated that pyrrol-2-ylmethyleneamine ligands are ideal building blocks for self-assembly. Relative to its close analogues — pyridine-imine ligands[12] — the pyrrole-Schiff-base ligand can form neutral complexes, which allows a simpler purification and characterization. In this paper we report the self-assembly of bis(pyrrol-2-ylmethyleneamine) ligands controlled by the length of the bridging spacers and an "unconventional" weak intermolecular C−H···Cu hydrogen bonding, which is found in all the four copper complex crystals. This weak hydrogen bonding plays a crucial role in the architecture of the chain or 1D network polymers.

Results and Discussions

Structural Characterization

The bis(pyrrol-2-ylmethyleneamine) ligands **1**−**4** were synthesized in high yields by condensation of alkyl diamines with 2-formyl-1*H*-pyrroles in ethanol (Scheme 1). They are symmetrical in chemical structure, possess two Schiff-base units, and have good solubility in common solvents. Their structures were fully characterized by ^{1}H and ^{13}C NMR spectroscopy, and mass spectrometry.

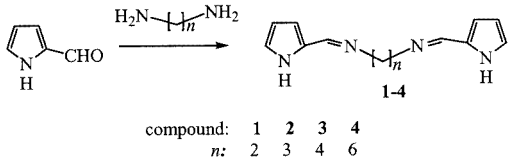

Scheme 1

The Cu^{II} complexes **5**−**8** were prepared in yields of 55−75% by reaction of each of ligands **1**−**4** with Cu^{II} (Scheme 2). Complexes **5**−**7** possess good solubility in common solvents such as dichloromethane, chloroform, THF, and DMF, but are less soluble in methanol, ethanol, acetone, hexane, benzene, toluene and water. Complex **8** is insoluble in most solvents. Crystals of compounds **5**−**8** are

Table 1. Crystallographic data and structure refinement summary for complexes **5**−**8**

	5	**6**	**7**	**8v**
Formula	$C_{24}H_{24}Cu_2N_8$	$C_{13}H_{14}CuN_4$	$C_{14}H_{16}CuN_4$	$C_{32}H_{40}Cu_2N_8$
Molecular mass	551.59	289.82	303.85	666.82
Crystal system	triclinic	orthorhombic	monoclinic	triclinic
Space group	$P\bar{1}$	Pbca	$P2_1/c$	$P1$
a (Å)	41.183(11)	10.293(4)	10.1934(10)	11.8053(12)
b (Å)	20.154(6)	13.981(5)	13.0476(18)	12.5048(11)
c (Å)	8.689(3)	17.615(7)	11.2974(14)	12.5727(8)
α (°)	90	90	90	106.186(5)
β (°)	90	90	113.525(5)	104.138(3)
γ (°)	90	90	90	110.336(2)
$D_{calcd.}$ (g cm^{-3})	1.524	1.519	1.465	1.425
Volume (Å^3)	7212(4)	2535.0(17)	1377.7(3)	1546.8(2)
Z	12	8	4	2
Absorption coefficient (mm^{-1})	1.798	1.709	1.576	1.411
F(000)	3384	1192	628	692
Crystal size (mm^3)	0.30 × 0.10 × 0.06	0.24 × 0.20 × 0.08	0.52 × 0.18 × 0.11	0.62 × 0.16 × 0.12
h	−49/49	−12/7	−13/13	−15/15
k	−23/20	−12/16	−16/16	−16/16
l	−10/8	−18/20	−14/14	−17/17
Theta range (°)	1.98/25.03	2.31/25.00	2.68/27.48	1.99/27.48
Total reflections	28087	8186	5807	10375
Independent reflections	6332	2201	3132	10375
parameters	460	164	172	759
R[a]	0.0708	0.0664	0.0360	0.0483
wR [b]	0.1173	0.1043	0.0666	0.1005
Goodness of fit	1.010	0.975	0.634	0.813
Largest diff. Peak and hole (e·Å^{-3})	0.514/−0.465	0.532/−0.421	0.275/−0.501	0.714/−0.616

[a] $R = \Sigma(||F_o| - |F_c||)/\Sigma F_o$. [b] $wR = [\Sigma(|F_o|^2 - |F_c|^2)^2/\Sigma(F_o^2)]^{1/2}$.

 © 2004 Wiley-VCH Verlag GmbH & Co. KGaA, Weinheim

stable for several months under cold and dark conditions. Their solutions in dichloromethane or chloroform were found to slowly decompose upon exposure to light and air.

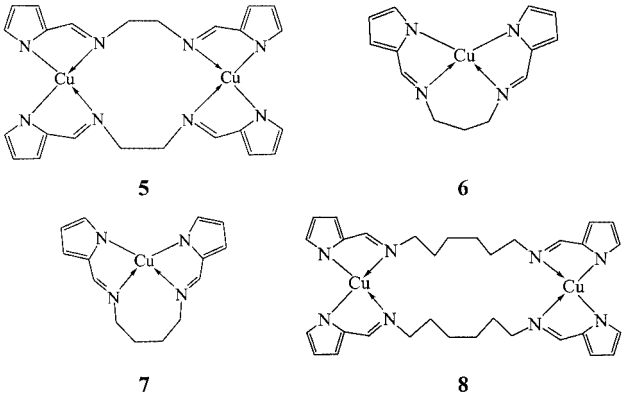

5 **6** **7** **8**

Scheme 2

Mass spectrometry was found to be especially informative in identifying the above reaction products. Analysis of the complexes, primarily by MALDI-TOF mass spectrometry, revealed that the molecular ions (*m*/*z*) observed in the mass spectra of **5** and **8** are 628 [M^+ + Cu] and 663 [M^+ + H], respectively, which were therefore assigned as dimeric complexes with a ligand:metal ratio of 2:2, while those of **6** and **7** are 289 [M^+] and 303 [M^+], respectively, which were assigned to the corresponding mononuclear monomeric complexes.

Crystal Structures

Crystals of **5**−**7** suitable for X-ray analysis were obtained by recrystallization from CH_2Cl_2/MeOH, whereas single crystals of **8** were prepared by layering a solution of $Cu(OAc)_2$ in CH_3OH upon a solution of **4** in $CHCl_3$ in a sealed tube with very careful diffusion. A summary of the crystal data of complexes **5**−**8** is given in Table 1.

By varying the length of the bridging −$(CH)_n$− spacer between the pyrrol-2-ylmethyleneamine units, self-assembly of bis(pyrrol-2-ylmethyleneamine) alkane ligands with Cu^{II} could offer mononuclear monomeric or dinuclear dimeric complexes. When n = 2, the self-assembly products are two very similar dinuclear dimeric complexes **5a** and **5b**, while in the case of n = 3 and 4, the products are the mononuclear monomeric complexes **6** and **7**, respectively, due to the greater flexibility of the spacer between the pyrrol-2-ylmethyleneamine units, which allows ligands **2** or **3** to coordinate to the same metal center. The tension of the shorter chain in ligand **1** makes it more likely to form a dinuclear dimeric complex. When n = 6, the complexation gives two

Table 2. Selected bond lengths for complex **5**−**8**

	Covalent bond lengths (Å)		Dative bond lengths (Å)	
5a	Cu(1)−N(1)	1.960(6)	Cu(1)−N(2)	2.006(6)
	Cu(1)−N(3)	1.947(6)	Cu(1)−N(4)	1.978(6)
	Cu(2)−N(5)	1.924(6)	Cu(2)−N(6)	1.983(6)
	Cu(2)−N(7)	1.947(7)	Cu(2)−N(8)	1.997(6)
5b	Cu(3)−N(9)	1.931(6)	Cu(3)−N(10)	1.973(6)
	Cu(3)−N(11)	1.963(6)	Cu(3)−N(12)	2.003(6)
6	Cu(1)−N(1)	1.944(7)	Cu(1)−N(2)	1.976(6)
	Cu(1)−N(4)	1.951(6)	Cu(1)−N(3)	1.984(6)
7	Cu−N(1)	1.959(3)	Cu−N(2)	2.005(2)
	Cu−N(4)	1.954(3)	Cu−N(3)	2.025(3)
8a	Cu(1)−N(1)	1.943(9)	Cu(1)−N(2)	2.028(9)
	Cu(1)−N(8)	1.981(9)	Cu(1)−N(7)	2.003(8)
	Cu(2)−N(4)	1.910(10)	Cu(2)−N(3)	1.934(10)
	Cu(2)−N(5)	1.940(12)	Cu(2)−N(6)	1.966(11)
8b	Cu(3)−N(9)	1.967(11)	Cu(3)−N(15)	1.979(6)
	Cu(3)−N(16)	1.945(8)	Cu(3)−N(10)	2.083(7)
	Cu(4)−N(12)	1.945(8)	Cu(4)−N(11)	2.045(6)
	Cu(4)−N(13)	1.980(8)	Cu(4)−N(14)	1.968(6)

Table 3. Selected bond angles (°) for **5**−**8**

5a			
N(3)−Cu(1)−N(1)	154.2(3)	N(5)−Cu(2)−N(7)	155.5(2)
N(3)−Cu(1)−N(4)	83.7(3)	N(5)−Cu(2)−N(6)	83.6(3)
N(1)−Cu(1)−N(4)	100.2(3)	N(7)−Cu(2)−N(6)	101.1(3)
N(3)−Cu(1)−N(2)	101.6(3)	N(5)−Cu(2)−N(8)	101.8(3)
N(1)−Cu(1)−N(2)	82.7(3)	N(7)−Cu(2)−N(8)	82.8(3)
N(4)−Cu(1)−N(2)	161.8(3)	N(6)−Cu(2)−N(8)	158.3(2)
5b			
N(9)−Cu(3)−N(11)	152.4(2)	N(9)−Cu(3)−N(12)	102.3(3)
N(9)−Cu(3)−N(10)	83.4(3)	N(11)−Cu(3)−N(12)	82.9(3)
N(11)−Cu(3)−N(10)	100.6(3)	N(10)−Cu(3)−N(12)	160.9(3)
6			
N(1)−Cu(1)−N(4)	101.9(3)	N(1)−Cu(1)−N(3)	166.9(2)
N(1)−Cu(1)−N(2)	82.6(3)	N(4)−Cu(1)−N(3)	82.5(3)
N(4)−Cu(1)−N(2)	175.3(3)	N(2)−Cu(1)−N(3)	92.7(3)
7			
N(4)−Cu−N(1)	100.45(11)	N(4)−Cu−N(3)	82.96(11)
N(4)−Cu−N(2)	160.71(10)	N(1)−Cu−N(3)	170.46(11)
N(1)−Cu−N(2)	83.19(11)	N(2)−Cu−N(3)	96.55(11)
8a			
N(1)−Cu(1)−N(8)	155.6(3)	N(4)−Cu(2)−N(3)	83.7(5)
N(1)−Cu(1)−N(7)	100.1(3)	N(4)−Cu(2)−N(5)	154.5(4)
N(8)−Cu(1)−N(7)	83.0(3)	N(3)−Cu(2)−N(5)	99.4(5)
N(8)−Cu(1)−N(2)	103.8(3)	N(4)−Cu(2)−N(6)	103.8(5)
N(8)−Cu(1)−N(2)	103.8(3)	N(3)−Cu(2)−N(6)	157.3(4)
N(7)−Cu(1)−N(2)	156.3(3)	N(5)−Cu(2)−N(6)	83.1(5)
8b			
N(16)−Cu(3)−N(9)	166.0(4)	N(12)−Cu(4)−N(13)	162.8(3)
N(16)−Cu(3)−N(15)	85.0(3)	N(12)−Cu(4)−N(14)	103.5(3)
N(9)−Cu(3)−N(15)	98.4(3)	N(13)−Cu(4)−N(14)	84.4(2)
N(16)−Cu(3)−N(10)	98.2(3)	N(12)−Cu(4)−N(11)	80.2(3)
N(9)−Cu(3)−N(10)	81.8(3)	N(13)−Cu(4)−N(11)	97.5(2)
N(15)−Cu(3)−N(10)	166.2(2)	N(14)−Cu(4)−N(11)	160.7(2)

 © 2004 Wiley-VCH Verlag GmbH & Co. KGaA, Weinheim

Table 4. The dihedral angles between two Cu−N−N terminal planes

	5a	5b	6	7	8a	8b
Dihedral angles (°)	33.8 (Cu1) 35.1 (Cu2)	36.9 (Cu3) 36.9 (Cu4)	12.3	22.6	37.4 (Cu1) 35.3 (Cu2)	20.6 (Cu3) 27.3 (Cu4)

dinuclear dimeric isomers — a side-by-side conformer (**8a**) and helical conformer (**8b**) — thus avoiding the steric crowding of six CH_2 groups constrained in a relatively small space which would be the case for a mononuclear monomer conformation. The crystallographic data show that the tetrahedral sp^3 angles in the spacers of all complexes are close to 109.5°, which also suggests that the dinuclear dimeric complexes **5** and **8** and mononuclear monomeric complexes **6** and **7** are stable species.

The Cu^{II} centers have a distorted square-planar geometry for complexes **5**−**8**. Each Cu^{II} center is tetracoordinate to four N atoms from two pyrrol-2-ylmethyleneamine units. The covalent Cu−N distance is in the range of 1.910−1.981 Å, while the dative Cu−N separation is between 1.940 and 2.083 Å. These distances are similar to the length range of Cu−N bonds found in the literature.[13] Selected bond lengths and angles for complexes **5**−**8** are shown in Table 2 and Table 3, respectively.

The dihedral angles, which are defined by the intersection of two pyrrol-2-ylmethyleneamine planes at the copper center, are in the range of 12.3−37.4°, indicating that the copper centers of complex **6** have the smallest deviation from the square-planar coordination geometry (see Table 4).

In the crystal of complex **5**, it was found that the unit cell contains two different isomers, **5a** and **5b**, both of which adopt a double-stranded helical conformation[13a,14] (Figure 1). However, **5b** has D_2 symmetry while **5a** has C_2 sym-

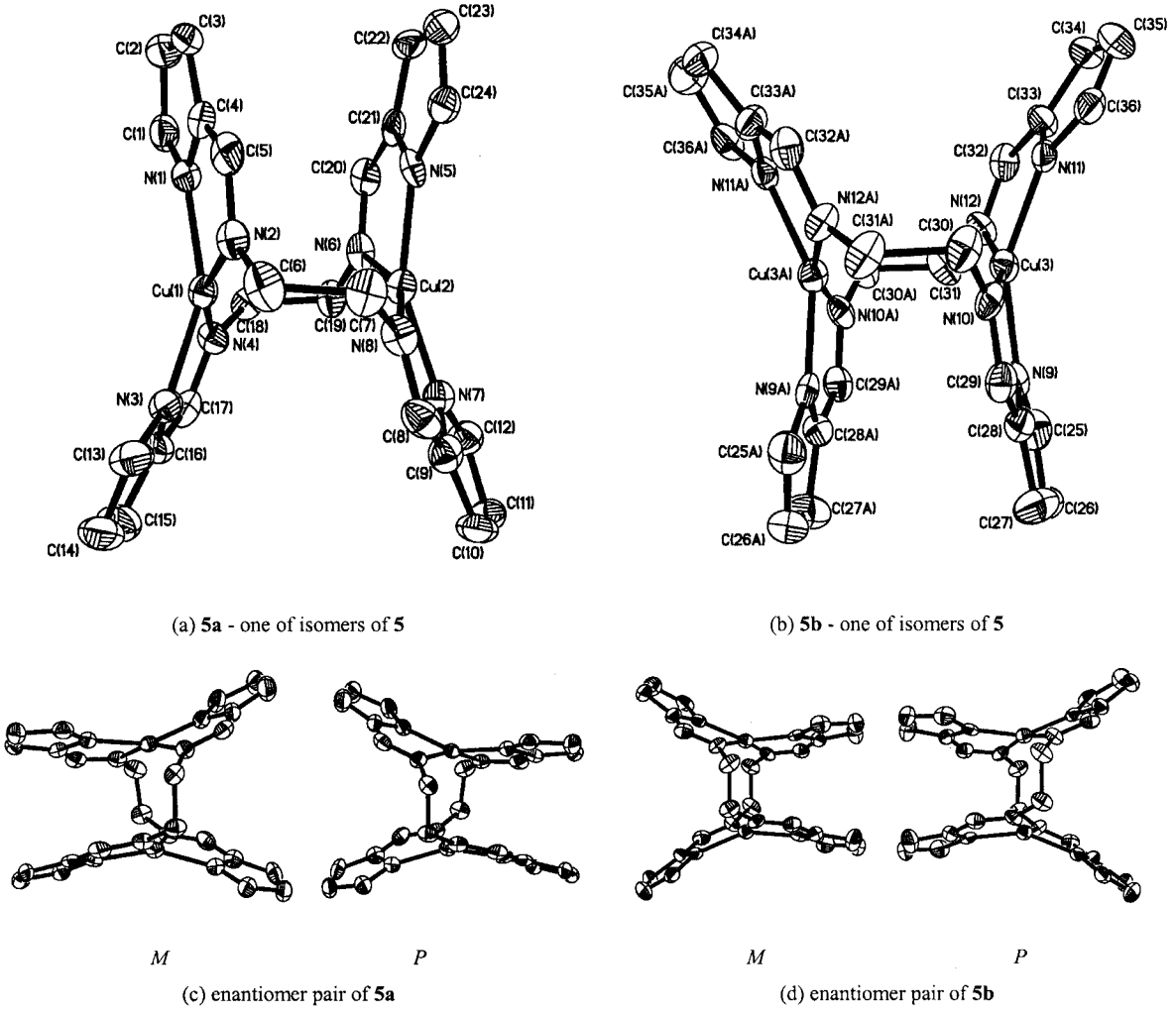

(a) **5a** - one of isomers of **5**

(b) **5b** - one of isomers of **5**

(c) enantiomer pair of **5a**

(d) enantiomer pair of **5b**

Figure 1. ORTEP views of complex **5** (30% thermal probability ellipsoids) with atom numbering; protons are omitted for clarity: (a) **5a**; (b) **5b**; (c) *M* and *P* helical enantiomers of **5a**; (d) *M* and *P* helical enantiomers of **5b**

 © 2004 Wiley-VCH Verlag GmbH & Co. KGaA, Weinheim

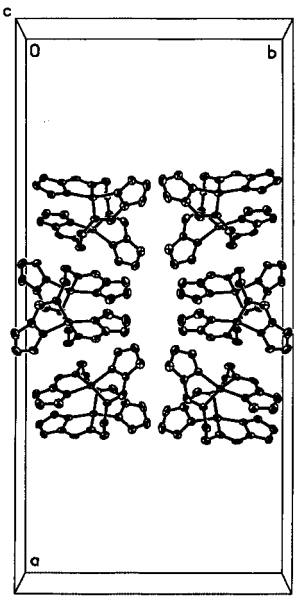

Figure 2. The enantiomer pairs of **5a** and **5b** arranged in the crystal; protons are omitted for clarity

metry. In addition, the torsion angles of the N(imine)−CH_2−CH_2−N(imine) groups in **5a** is −58.4° (N4−C18−C19−N6) and −56.8° (N2−C6−C7−N8) while the corresponding angle in **5b** is −61.8°.

In both **5a** and **5b**, two pyrrol-2-ylmethyleneamine units of the same ligand are found to adopt a *cis* arrangement, which is different from the *trans* arrangement of the Zn^{II} analogue and other bis(pyrrol-2-ylmethyleneamine)zinc(II) complexes.[9−11] This may be due to the geometry requirement of the different metal centers. The Cu···Cu distances are 3.242 Å and 3.257 Å for **5a** and **5b**, respectively. Interestingly, the *M* and *P* helical enantiomers of **5a** and **5b** are found in the crystal (see c and d in Figure 1) and they are arranged alternately (Figure 2).

Unlike complex **5**, complexes **6** and **7** are mononuclear complexes and each ligand uses all its N atoms to bind to the same metal center. The structures of complex **6** and **7** are very similar. However, the dihedral angles between the two Cu−N−N terminal planes are 12.3° and 22.6° for **6** and **7**, respectively, indicating that the Cu center in complex **6** is closer to an ideal square-planar geometry (Figure 3 and 4). Like complex **5**, *M* and *P* helical enantiomers are found for complexes **6** and **7** (Figure 3 and 4).

Interestingly, two different molecules (**8a**, **8b**) were found in the unit cell of complex **8**, which is similar to Dietrich-Buchecker's observations[15b] in solution. In **8a**, two pyrrol-2-ylmethyleneamine units in the same ligand adopt a *cis* arrangement along the hexylene chain (Figure 5). Two ligands are bound parallel to two copper centers to form an 18-membered rectangular macrocycle with cavity dimensions of approximately 7.7 × 3.9 Å. In **8b**, two pyrrol-2-ylmethyleneamine groups in the same ligand adopt a *trans* arrangement along the hexylene bridging chain, forming a distorted double-stranded helical configuration. As a result, this pattern of self-assembly also gives an 18-membered, distorted square-shaped macrocycle with cavity dimensions of approximately 6.4 × 6.1 Å.

The Cu···Cu distances are 8.405 Å for **8a** and 7.744 Å for **8b**, which are much longer than the corresponding distances

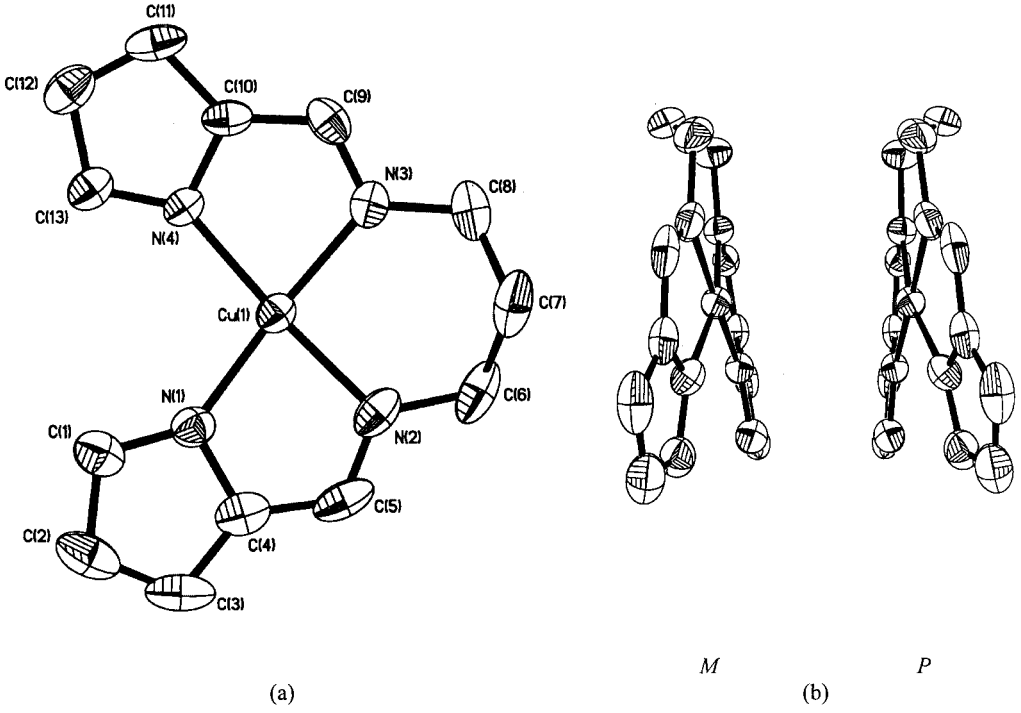

Figure 3. ORTEP views (30% thermal probability; protons are omitted for clarity) of: (a) complex **6**; (b) *M* and *P* helical enantiomers of **6**

 © 2004 Wiley-VCH Verlag GmbH & Co. KGaA, Weinheim

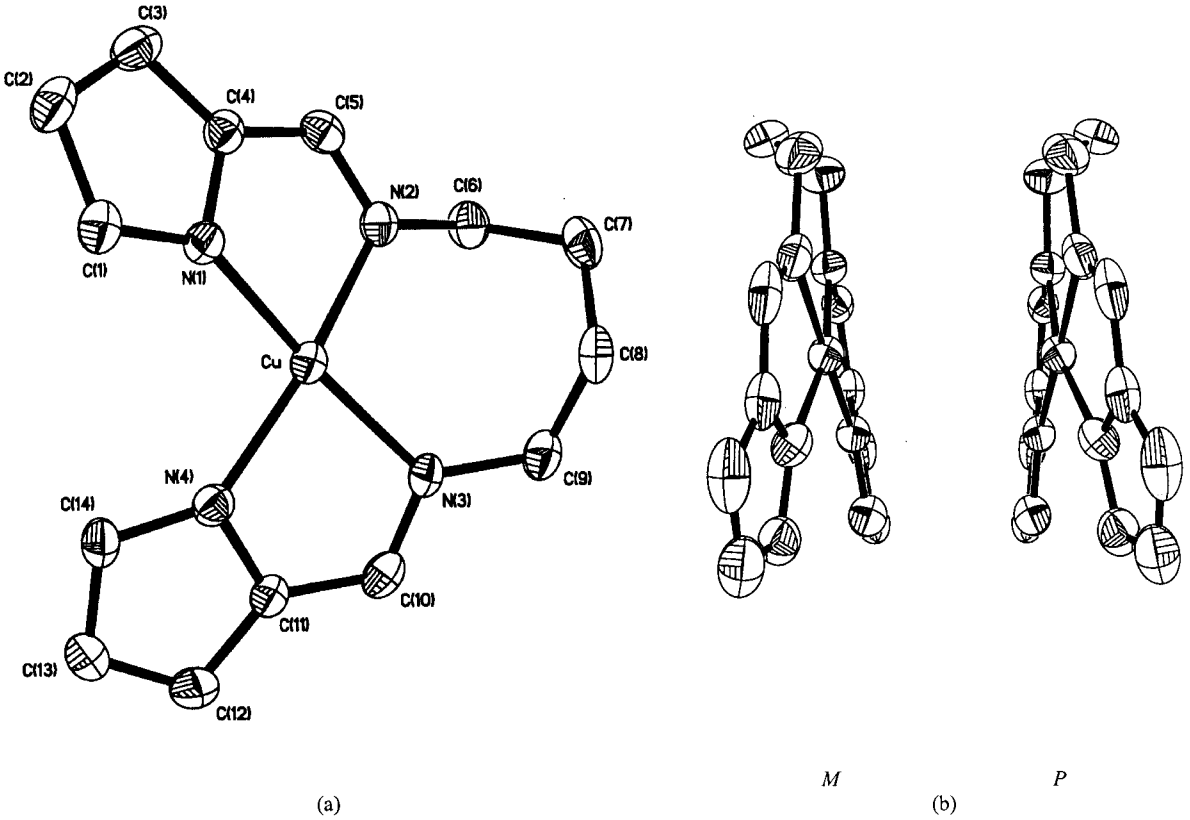

Figure 4. ORTEP view (30% thermal probability; protons are omitted for clarity) of: (a) complex **7**; (b) *M* and *P* helical enantiomers of **7**

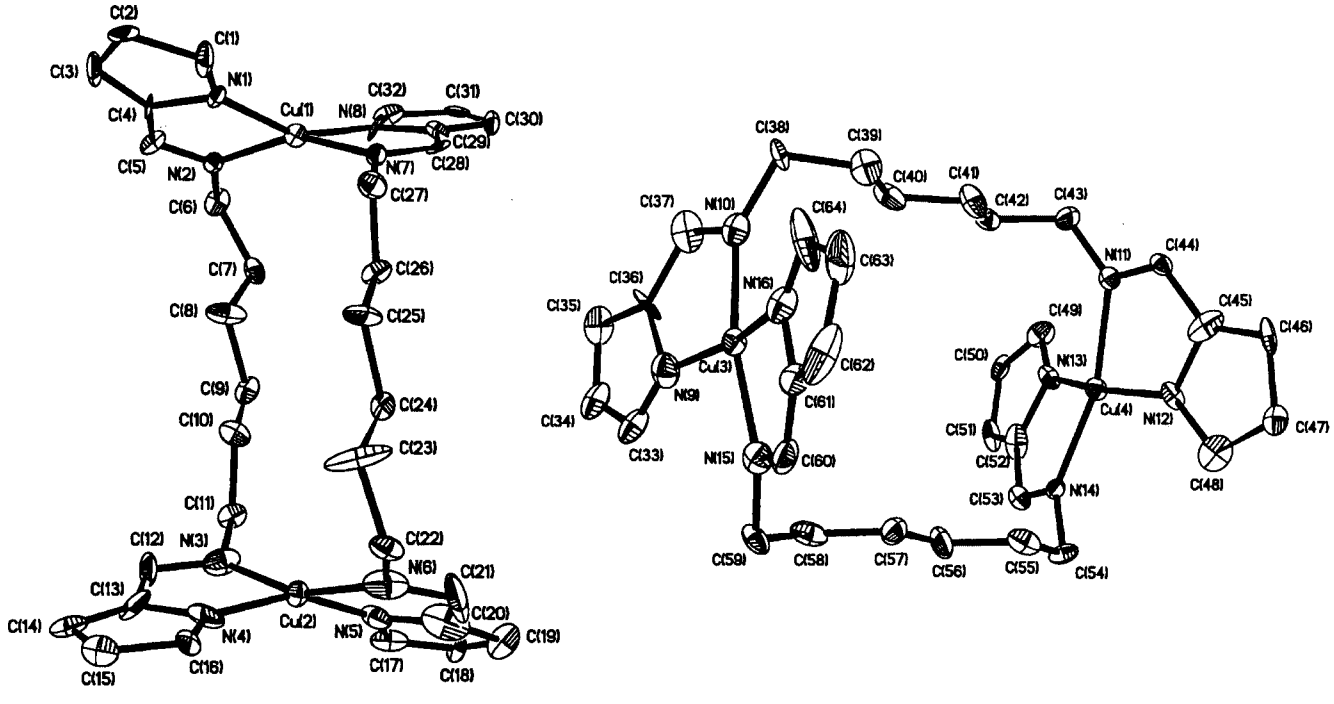

Figure 5. ORTEP view of complex **8** (30% thermal probability, protons are omitted for clarity) of: (a) **8a** (the C_{2h}-side-by-side conformer) and (b) **8b** (the *D_2-helical conformer)*

 © 2004 Wiley-VCH Verlag GmbH & Co. KGaA, Weinheim

in complex **5** due to the longer spacer of the ligand in complex **8**. In **8a**, the dihedral angles at the Cu centers are 37.4° [Cu(1)] and 35.3° [Cu(2)], which are very close to the value for complex **5**, but larger than that in **8b** (Table 4). Unlike complexes **5**−**7**, there is no enantiomer pair found in the crystal of complex **8**.

Weak Hydrogen Bonding

Weak hydrogen bonding has been known to play a crucial role in chemical and biological systems.[15] Interestingly, the crystallographic characterization suggests that the Cu^{II} centers in complexes **5**−**8** participate in weak hydrogen bonding, which plays a crucial role in the formation of chain-type polymers or 1D networks. Although regular weak hydrogen bonding is very common,[16] weak hydrogen bonding with Cu^{II} is rare.[16b] However, copper is an electron-rich metal atom with filled *d*-orbitals that is capable of forming hydrogen bonds with a suitable donor to form a three-center, four-electron interaction (3*c*-4*e*).[16b,16c,16f] In complexes **5**−**8**, the H···Cu separation (d) is in the range of 2.804−3.018 Å, the C−H···Cu separation (D) is in the range of 3.637−3.921 Å and the C−H···Cu angle (θ) is between 84.9 and 168.0° (Table 5), which are similar to the values for weak hydrogen bonding found in the literature.

In complex **5**, a hydrogen atom from the CH_2 group in one molecule is bound to the Cu^{II} center of the second molecule (Figure 6, a). As a result, a triple-row 1D network is formed though weak C−H···Cu interactions with a row of **5a** on each side and **5b** in the middle (see b and c in Figure 6).

Unlike complex **5**, in complexes **6** and **7** the hydrogen atom at the 3-position of the pyrrole ring in one molecule is bound to the Cu^{II} center of the second molecule to form 1D extended chains (Figure 7). Interestingly, in the packing diagram of **6**, the *M* and *P* isomers are arranged in alternating rows when viewed along the *c* axis (Figure 7, a). However, in the packing diagram of **7** the *M* and *P* enantiomers are arranged alternately in the same chain (Figure 7, b). The Cu···H distances (d), C−H···Cu distance (D) and C−H···Cu angles (θ) are 3.018 Å, 3.637 Å and 84.9°, respectively, for **6**, and 2.842 Å, 3.637 Å and 144.1°, respectively, for **7**, indicating a stronger interaction in **7** than in **6**.

Table 5. Parameters for C−H···Cu intermolecular hydrogen bonding in complexes **5**−**8**

	d (Å)	*D* (Å)	θ(C−H···Cu) (°)
5	2.993[a]	3.671[a]	133.7[a]
	2.804[b]	3.758[b]	168.0[b]
6	3.018	3.637	84.9
7	2.842	3.637	144.1
8	2.998[c]	3.921[c]	159.4[c]
	2.941[d]	3.739[d]	140.3[d]

[a] For C(6A)−H(6A)···Cu(3A). [b] For C(30B)−H(30B)···Cu(1B). [c] For C(43A)−H(43A)···Cu(1A). [d] For C(58B)−H(58B)···Cu(2B).

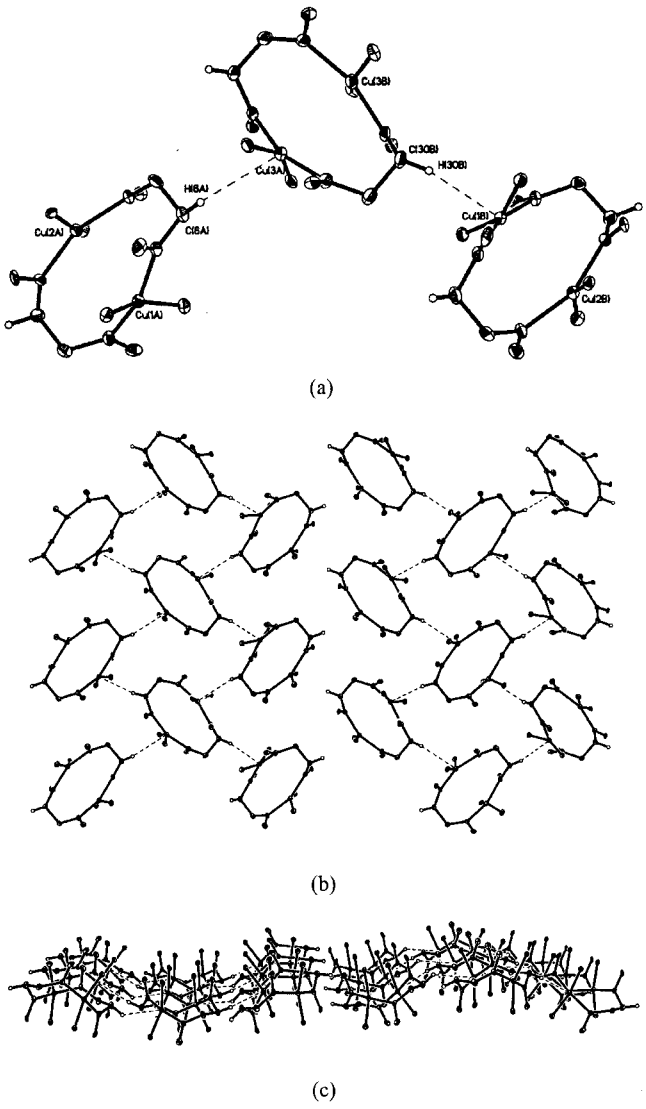

Figure 6. Weak hydrogen bonding in complex **5**; carbon atoms of the pyrrole ring are omitted for clarity: (a) weak C−H···Cu hydrogen bonding between **5a**−**5b**−**5a**; (b) view of triple-row 1D network along the *b* axis; (c) view of the triple-row 1D network along the *c* axis

Like complex **5**, one H atom of the CH_2 group in the bridge of each ligand is weakly bound to the Cu^{II} center from another molecule to form a 1D chain for complex **8**. However, unlike the interaction pattern in **5**, in which each molecule offers a hydrogen donor and a Cu^{II} acceptor to form the 1D networks, and also unlike the interaction pattern in **6** and **7**, in which each molecule acts as both acceptor and donor to form 1D chains, in complex **8** each helical conformer (**8b**) offers two hydrogen atoms from two different ligands and binds to two Cu^{II} centers of two side-by-side conformers (**8a**; Figure 8). In other words, **8b** acts only as a donor and **8a** acts only as an acceptor.

In conclusion, the self-assembly of bis(pyrrol-2-ylmethyleneamine) ligands with Cu^{II} gives mononuclear monomeric complexes or dinuclear dimeric complexes depending on the bridging spacer between the two pyrrol-2-ylmethyleneamine units. In all cases, the metal centers are four-coordinate with

 © 2004 Wiley-VCH Verlag GmbH & Co. KGaA, Weinheim

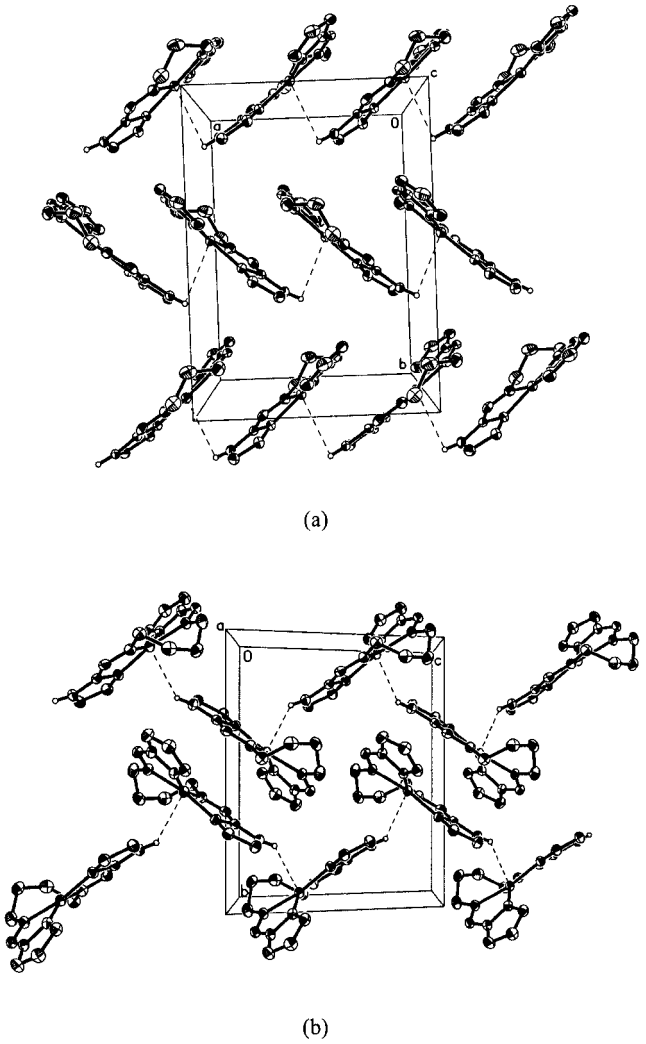

Figure 7. 1D chains formed through weak hydrogen bonding in complexes **6** and **7**: (a) one enantiomer of complex **6** in each row is ordered parallel through weak C−H···Cu hydrogen bonding, and the rows are arranged in a zigzag pattern; (b) 1D chains constructed through weak C−H···Cu hydrogen bonding in **7**

a distorted planar conformation. Moreover, the bis(pyrrol-2-ylmethyleneamine) ligands are doubly deprotonated, which allows the formation of neutral complexes in high yields. By varying the length of the bridging $-(CH)_n-$ spacer between the pyrrol-2-ylmethyleneamine units, self-assembly of bis(pyrrol-2-ylmethyleneamine)alkane ligands with Cu^{II} could offer mononuclear monomeric or dinuclear dimeric complexes. The self-assembly, which changes with the bridging spacers, reflects the steric requirement of the complexation. Intermolecular weak C−H···Cu hydrogen bonding is found in all complexes **5**−**8** and plays a major role in constructing 1D chains or network polymers.

In light of the high yields of the neutral complexes, their excellent solubility, the easy synthesis of the ligands and their great flexibility to generate supramolecules with interesting geometric structures, pyrrol-2-ylmethyleneamine has been demonstrated to be an ideal building block for supramolecular architectures through self-assembly. Our future work will be focused on the design, synthesis and self-assembly of ligands containing multiple pyrrol-2-ylmethyleneamine units.

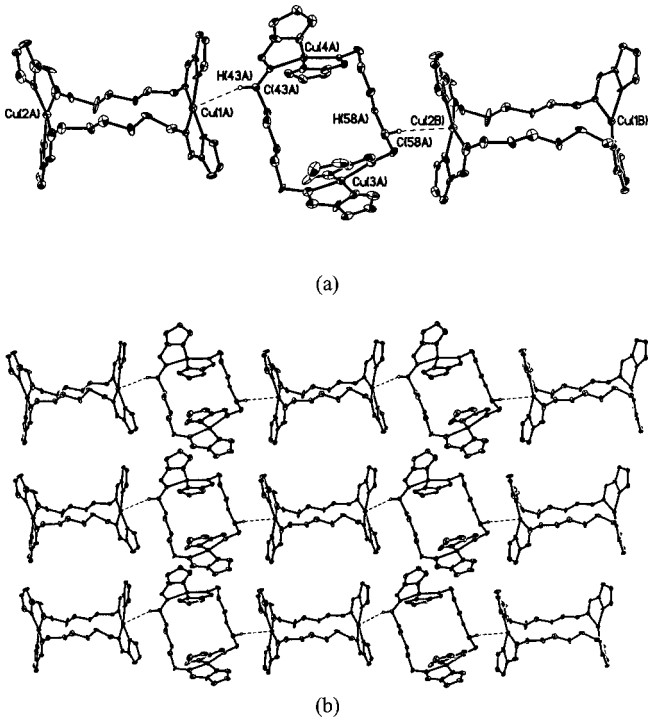

Figure 8. (a) 1D chain constructed by weak intermolecular hydrogen bonding in **8**; isomers **8a** and **8b** are arranged alternately; (b) the packing diagram of **8** showing the 1D chains

Experimental Section

All reagents for syntheses and analyses were of analytical grade and used as received. Melting points were determined on a Yanaco MP-500 micro-melting point apparatus. NMR spectra were recorded on a Bruker Avance dpx 400 MHz instrument using TMS as internal standard. Mass spectra were obtained on Bruker APEX II and KYKY-ZHP-5 spectrometers. IR spectra were recorded on a BIO-RAD FT-165 IR spectrometer. Elemental analyses were performed on a Carlo Erba-120 elemental analyzer.

General Procedure for the Synthesis of Ligands 1−4: Pyrrol-2-carbaldehyde (1.9 g, 20 mmol) and the linear diaminoalkane (10 mmol) were dissolved in ethanol (20 mL). The mixture was stirred for a while and then a few drops of glacial acetic acid were added. After a few seconds a white precipitate was observed. The suspension was stirred at room temperature for 2 h. The white solid was collected by suction filtration, washed with cold ethanol and dried under vacuum to give the expected product. The analytic sample was purified by re-crystallization from ethanol.

1,2-Bis(pyrrol-2-ylmethyleneamine)ethane (1): Yield: 1.61 g, 75%; m.p. 178−181 °C. ^{1}H NMR (400 MHz, $CDCl_3$, 25 °C, TMS): δ = 3.78 (s, 4 H, CH_2), 6.23 (dd, J = 3.5, 3.5 Hz, 2 H, pyrrole-H), 6.47 (dd, J = 3.5, 1.3 Hz, 2 H, pyrrole-H), 6.89 (m, 2 H, pyrrole-H), 8.04 (s, 2 H, imine-H) ppm. ^{13}C NMR (100 Hz, $CDCl_3$): δ = 61.4, 109.8, 114.5, 122.0, 130.1, 152.8 ppm. FAB-MS: *m*/*z* (%) =215 (30) [M^+ + H]. FT-IR (KBr pellet): $\tilde{\nu}$ = 3178, 3088, 2974, 2943, 2870, 1641, 1424, 1317, 1130, 1048, 1014, 828, 736 cm^{-1}.

 © 2004 Wiley-VCH Verlag GmbH & Co. KGaA, Weinheim

1,3-Bis(pyrrol-2-ylmethyleneamine)propane (2): Yield: 1.44 g, 65%; m.p. 119−120 °C. ^{1}H NMR (400 MHz, $CDCl_3$, 25 °C, TMS): δ = 1.96 (t, *J* = 7.0 Hz, 2 H, CH_2), 3.58 (t, *J* = 7.0 Hz, 4 H, CH_2), 6.21 (t, *J* = 3.2 Hz, 2 H, pyrrole-H), 6.45 (d, *J* = 3.2 Hz, 2 H, pyrrole-H), 6.86 (m, 2 H, pyrrole-H), 8.01 (s, 2 H, imine-H) ppm. ^{13}C NMR (100 Hz, $CDCl_3$): δ = 32.7, 58.3, 109.7, 114.2, 121.9, 130.4, 152.1 ppm. FAB-MS: *m*/*z* (%) = 229 (30) [M^+ + H]. FT-IR (KBr pellet): ν̃ = 3117, 3062, 2966, 2943, 2850, 1637, 1445, 1420, 1314, 1131, 1097, 1033, 989, 750 cm^{-1}.

1,4-Bis(pyrrol-2-ylmethyleneamine)butane (3): Yield: 1.89 g, 78%; m.p. 178−179 °C. ^{1}H NMR (400 MHz, $CDCl_3$, 25 °C, TMS): δ = 1.73 (m, 4 H, CH_2), 3.55 (t, *J* = 3.8 Hz, 4 H, CH_2), 6.25 (dd, *J* = 3.4, 3.2 Hz, 2 H, pyrrole-H), 6.52 (dd, *J* = 3.4, 1.0 Hz, 2 H, pyrrole-H), 6.94 (m, 2 H, pyrrole-H), 7.99 (s, 2 H, imine-H) ppm. ^{13}C NMR (100 Hz, $CDCl_3$): δ = 28.7, 59.8, 110.2, 115.3, 122.9, 129.7, 151.6 ppm. FAB-MS: *m*/*z* (%) = 243 (70) [M^+ + H]. FT-IR (KBr pellet): ν̃ = 3164, 2970, 2928, 2897, 2848, 1644, 1424, 1360, 1136, 1099, 1035, 995, 829, 728 cm^{-1}.

1,6-Bis(pyrrol-2-ylmethyleneamine)hexane (4): Yield: 2.16 g, 80%; m.p. 131−132 °C. ^{1}H NMR (400 MHz, $CDCl_3$, 25 °C, TMS): δ = 1.36 (m, 4 H, CH_2), 1.61 (m, 4 H, CH_2), 3.50 (t, *J* = 6.7 Hz, 4 H, CH_2), 6.22 (t, *J* = 2.9 Hz, 2 H, pyrrole-H), 6.47 (dd, *J* = 2.9, 1.3 Hz, 2 H, pyrrole-H), 6.86 (m, 2 H, pyrrole-H), 8.03 (s, 2 H, imine-H) ppm. ^{13}C NMR (100 Hz, $CDCl_3$): δ = 27.1, 31.3, 60.7, 109.5, 114.2, 122.0, 130.4, 152.1 ppm. FAB-MS: *m*/*z* (%) = 271 (30) [M^+ + H]. FT-IR (KBr pellet): ν̃ = 3166, 3096, 2972, 2932, 2899, 2851, 1646, 1424, 1367, 1319, 1362, 1098, 1019, 959, 830, 728, 605cm^{-1}.

General Procedure for the Synthesis of 5−7: A solution of $Cu(OAc)_2{\cdot}H_2O$ (0.2 g, 1 mmol) in methanol (20 mL) was added to a solution of ligand (**1**−**3**, 1 mmol) in methanol (10 mL). A yellow-green precipitate appeared quickly. After 1.5 h the precipitates were collected by suction filtration and washed with methanol. Crystals suitable for X-ray analysis were obtained by recrystallization from CH_2Cl_2/CH_3OH with a yield of 65−75%.

Cu^{II} Complex of 1,2-Bis(pyrrol-2-ylmethyleneamine)ethane (5): Yield: 193 mg, 70%; m.p. > 210 °C (decomp.). IR (KBr pellet): ν̃ = 3442, 3093, 2905, 1587, 1443, 1391, 1345, 1309, 1035, 738 cm^{-1}. MALDI-TOF-MS: 628 *m*/*z* = [M^+ + Cu]. $C_{24}H_{24}Cu_2N_8$ (551.59): calcd. C 52.26, H 4.39, N 20.31; found C 52.36, H 4.41, N 19.99.

Cu^{II} Complex of 1,3-Bis(pyrrol-2-ylmethyleneamine)propane (6): Yield: 188 mg, 65%; m.p. > 185 °C (decomp.). IR (KBr pellet): ν̃ = 3444, 3089, 2900, 2838, 1600, 1514, 1439, 1395, 1033, 735 cm^{-1}. MALDI-TOF-MS: *m*/*z* = 289 [M^+]. $C_{13}H_{14}CuN_4$ (289.82): calcd. C 53.87, H 4.87, N 19.33; found C 53.65, H 4.85, N 19.08.

Cu^{II} Complex of 1,4-Bis(pyrrol-2-ylmethyleneamine)butane (7): Yield: 227 mg, 75%; m.p. 160−161 °C. IR (KBr pellet): ν̃ = 3430, 3090, 2928, 2854, 1601, 1513, 1440, 1393, 1363, 1089, 1033, 744 cm^{-1}. MALDI-TOF-MS: *m*/*z* = 303 [M^+]. $C_{14}H_{16}CuN_4$ (303.85): calcd. C 55.34, H 5.31, N 18.44; found C 55.07, H 5.29, N 18.19.

Synthesis of Cu^{II} Complex of 1,6-Bis(pyrrol-2-ylmethyleneamine)-hexane (8): This complex was prepared by laying a solution of $Cu(OAc)_2{\cdot}H_2O$ (39 mg, 0.2 mmol) in CH_3OH (6 mL) on top of a solution of **4** (54 mg, 0.2 mmol) in $CHCl_3$ (8 mL) in a sealed tube. After several days, crystals of **8** suitable for X-ray analysis were obtained. Yield: 182 mg, 55%. m.p. > 250 °C (decomp.). FT-IR (KBr pellet): ν̃ = 3443, 3093, 2929, 2853, 1593, 1515, 1441, 1391, 1341, 1313, 1034, 740 cm^{-1}. MALDI-TOF-MS: *m*/*z* = 663 [M^+ + H]. $C_{32}H_{40}Cu_2N_8$ (663.81): calcd. C 57.90, H 6.07, N 16.88; found C 58.14, H 6.15, N 16.92.

X-ray Crystallography: Crystals suitable for X-ray diffraction studies were obtained as described above. Accurate unit cell parameters were determined by a least-squares fit of 2θ values, measured for 200 strong reflections, and intensity data sets were measured on a Bruker Smart 1000 CCD or Rigarku Raxis Rapid IP diffractometer with Mo-K_α radiation (λ = 0.71073 Å) at room temperature. The intensities were corrected for Lorentz and polarization effects, but no corrections for extinction were made. All structures were solved by direct methods. The non-hydrogen atoms were located in successive difference Fourier synthesis. The final refinement was performed by full-matrix least-squares methods with anisotropic thermal parameters for non-hydrogen atoms on F^2. The hydrogen atoms were added theoretically and treated as riding on the concerned atoms. Crystallographic data and experimental details for structure analyses are summarized in Table 1.

CCDC-209047 ... -209050 (for **5**−**8**, respectively) contain the supplementary crystallographic data for this paper. These data can be obtained free of charge at www.ccdc.cam.ac.uk/conts/retrieving.html. [or from the Cambridge Crystallographic Data Centre, 12, Union Road, Cambridge CB2 1EZ, UK; Fax: (internat.) + 44-1223/336-033; E-mail: deposit@ccdc.cam.ac.uk].

Acknowledgments

This work was supported by the Major State Basic Research Development Program (G2000078100), NSFC (20172055) and CAS (CMS CX-200205). We thank Ms. S.-H. Zhou (Institute of Biophysics) for the NMR spectra and Dr. H. Liu for helpful discussions on crystal-structure analysis.

[1] For reviews see: [1a] J.-M. Lehn, *Supramolecular Chemistry Concepts and Perspectives*, VCH, Weinheim, Germany, **1995**. [1b] P. N. W. Baxter, *Comprehensive Supramolecular Chemistry*, Pergamon, Oxford, **1996**, chapter 6. [1c] M. Fujita, *Comprehensive Supramolecular Chemistry*, Pergamon, Oxford, **1996**, chapter 7. [1d]C. Kaes, A. Katz, M. W. Hosseini, *Chem. Rev.* **2000**, *100*, 3553−3590.

[2] For reviews see: [2a] H. Falk, *The Chemistry of Linear Oligopyrroles and Bile Pigments*, Springer-Verlag, Wien, 1989. [2b] *The Porphyrins* (Ed.: D. Dolphin), Academic Press, New York, **1979**; vols. I−VII. [2c] K. M. Kadish, K. M. Smith, R. Guilard, *The Porphyrin Handbook*, Academic Press, San Diego, **2000**.

[3] [3a] Y. Zhang, A. Thompson, S. J. Rettig, D. Dolphin, *J. Am. Chem. Soc.* **1998**, *120*, 13537−13538. [3b] A. Thompson, S. J. Rettig, D. Dolphin, *Chem. Commun.* **1999**, 631−632. [3c] A. Thompson, D. Dolphin, *Org. Lett.* **2000**, *2*, 1315−1318. [3d] A. Thompson, D. Dolphin, *J. Org. Chem.* **2000**, *65*, 7870−7877. [3e] Q. Chen, Y. Zhang, D. Dolphin, *Tetrahedron Lett.* **2002**, *43*, 8413−8416.

[4] [4a] Y. Zhang, Z. Wang, C. Yan, G. Li, J. S. Ma, *Tetrahedron Lett.* **2000**, *41*, 7717−7721. [4b] Y. Zhang, J. S. Ma, *Org. Prep. Proceed. Int.* **2001**, *33*, 81−86. [4c] L. Yang, Y. Zhang, Q. Chen, J. S. Ma, *Monatsh. Chem.*, in press. [4d] L. Yang, Y. Zhang, Q. Chen, G. Yang, J. S. Ma, *Dyes Pigments*, in press.

[5] [5a] G. B. Maravin, A. Y. Tauber, A. F. Mironov, *Synlett* **1993**, 355−359. [5b] K. M. Valasinas, B. Frydman, *Tetrahedron Lett.* **1996**, *37*, 763−766. [5c] P. Morosini, M. Scherer, S. Meyer, L. Vynch, S. J. Lessler, *J. Org. Chem.* **1997**, *62*, 8848−8853. [5d] M. J. Kogan, *J. Heterocycl. Chem.* **1998**, *35*, 907−909. [5e] K. Okada, H. Takakura, K. Nomura, K. Saburi, *Tetrahedron Lett.* **2000**, *41*, 2915−2918. [5f] Q. Chen, D. Dolphin, *Can. J. Chem.* **2002**, *80*, 1668−1675.

 © 2004 Wiley-VCH Verlag GmbH & Co. KGaA, Weinheim

[6] [6a] A. Chakravorty, R. H. Holm, *Inorg. Chem.* **1964**, *3*, 1521−1524. [6b] J. H. Weber, *Inorg. Chem.* **1967**, *6*, 258−262. [6c] N. A. H. Male, M. Thornton-Pett, M. Bochmann, *J. Chem. Soc., Dalton Trans.* **1997**, 2487−2494.
[7] For reviews see: [7a] J. L. Sessler, S. J. Weghorn, *Expanded, Contracted, and Isomeric Porphyrins*, Pergamon Press, Oxford, **1997**. [7b]A. Jasat, D. Dolphin, *Chem. Rev.* **1997**, *97*, 2267−2340.
[8] [8a] N. A. Bailey, A. Barras, D. E. Fenton, M. S. Gonzales, R. Moody, C. O. R. D. Barbarin, *J. Chem. Soc., Dalton Trans.* **1984**, 2741−2746. [8b] S. Brooker, B. M. Carter, *Acta Crystallogr., Sect. C* **1995**, *51*, 1522−1524. [8c] M. Grigora, G. Stoica, I. Cianghe, C. I. Simionescu, *Rev. Roum. Chim.* **1997**, *42*, 993−998. [8d] F. Franceschi, G. Guillemot, E. Solari, C. Floriani, N. Re, H. Birkedal, P. Pattison, *Chem. Eur. J.* **2001**, *7*, 1468−1478. [8e] M. Vazquez, M. Bermejo, M. Fondo, A. Garcia-Deibe, A. M. Gonzalez, R. Pedrido, *Eur. J. Inorg. Chem.* **2002**, 465−472.
[9] L. Yang, X. Shan, Q. Chen, Z Wang, J. S. Ma, *Eur. J. Inorg. Chem.*, in press.
[10] L. Yang, Q. Chen, Q. Yang, J. S. Ma, *Tetrahedron* **2003**, *59*, 10037−10040.
[11] Z. Wu, Q. Chen, S. Xiong, B. Xin, Z. Zhao, L. Jiang, J. S. Ma, *Angew. Chem. Int. Ed.* **2003**, *42*, 3271−3274.
[12] [12a] A. G. J. Ligtenbarg, A. L. Spek, R. Hage, B. L. Feringa, *J. Chem. Soc., Dalton Trans.* **1999**, 659−661. [12b] S. Pal, S. Pal, *J. Chem. Soc., Dalton Trans.* **2002**, 2102−2108. [12c] T. M. Cameron, J. C. Gordon, R. Michalczyk, B. L. Scott, *Chem. Commun.* **2003**, 2282−2283. [12d] R. M. Ceder, G. Muller, M. Ordinas, M. Font-Bardia, X. Solans, *Dalton Trans.* **2003**, 3052−3059.
[13] [13a] C. Piguet, G. Bernardinelli, G. Hopfgartner, *Chem. Rev.* **1997**, *97*, 2005−2062 and references cited therein. [13b] M. Du, X.-H. Bu, Z. Huang, S.-T. Chen, Y.-M. Guo, *Inorg. Chem.* **2003**, *42*, 552−557. [13c] L. H. Patrick, B. T. William, *J. Am. Chem. Soc.* **1999**, *121*, 7270−7271. [13d] P. Malllayan, J. B. Raymond, W. A. Anthony, *Inorg. Chem.* **1996**, *35*, 467−471.
[14] M. Albrecht, *Chem. Rev.* **2001**, *101*, 3457−3497.
[15] [15a] C. O. Dietrich-Buchecker, J.-P. Sauvage, J.-P. Kintzinger, P. Maltese, C. Pascard, J. Guilhem, *New J. Chem.* **1992**, *16*, 931−934. [15b] C. O. Dietrich-Buchecker, J.-F. Nierengarten, J.-P. Sauvage, N. Armaroli, V. Balzani, L. De Cola, *J. Am. Chem. Soc.* **1993**, *115*, 11237−11244.
[16] [16a] G. R. Desiraju, T. Steiner, *The Weak Hydrogen Bond in Structural Chemistry and Biology*, Oxford University Press, Oxford, **1999**. [16b] D. Braga, F. Grepioni, E. Tegesco, K. Biradha, G. R. Desiraju, *Organometallics* **1997**, *16*, 1846−1856. [16c] D. Braga, F. Grepioni, G. R. Desiraju, *Chem. Rev.* **1998**, *98*, 1375−1405. [16d] L. Brammer, M. C. McCann, R. M. Bullock, R. K. McMullan, P. Sherwood, *Organometallics* **1992**, *11*, 2339−2341. [16e] E. O. Alyea, G. Ferguson, S. Kannan, *Chem. Commun.* **1998**, 345−346. [16f] M. Brookhart, M. L. H. Green, *J. Organomet. Chem.* **1983**, 395−408.

Received September 10, 2003
Early View Article
Published Online February 26, 2004

 © 2004 Wiley-VCH Verlag GmbH & Co. KGaA, Weinheim

Syntheses and Structural Characterization of Ag^{I} Complexes with the *N*,*N*′-Di(2-pyridyl)oxamide Ligand

Yi-Fen Hsu[a] and Jhy-Der Chen*[a]

Keywords: Silver / Nitrogen heterocycles / Coordination polymers / Trinuclear complexes

A series of the silver(I) complexes $\{[Ag(\mathbf{L})][NO_3]\}_\infty$ (**1**), $\{[Ag(\mathbf{L})(CH_3CN)][ClO_4]\}_\infty$ (**2**), $\{[Ag_2(\mathbf{L})_3(CH_3CN)_2][PF_6]_2\}_\infty$ (**3**), and $[Ag_3(\mathbf{L})_4(CH_3CN)_4][BF_4]_3$ (**4**) [where **L** = *N*,*N*′-di(2-pyridyl)oxamide] have been prepared by the reactions of AgX (X = NO_3^-, ClO_4^-, PF_6^- and BF_4^-) with **L**. All the complexes have been structurally characterized by X-ray crystallography, confirming that **1**–**3** are coordination polymers whereas **4** is a trinuclear complex. Complex **1** forms helical chains which are interlinked through a series of Ag···O interactions and C–H···O hydrogen bonds. In complexes **2** and **3**, a new set of interactions involving two Ag···O interactions and self-complementary double N–H···O hydrogen bonds were found to link the linear chains and ladder structures into polymer pairs (for **2**) and molecular sheets (for **3**). In complex **4**, the molecules are interlinked by extensive Ag···N interactions and π–π stacking interactions to form molecular bands.
(© Wiley-VCH Verlag GmbH & Co. KGaA, 69451 Weinheim, Germany, 2004)

Introduction

Recently, a great deal of effort has been devoted to the self-assembly of organic and inorganic molecules in the solid state, because it extends the range of new solids which can be designed to have particular physical and chemical properties.[1] Among the various types of interactions employed to create larger molecular arrays, covalent and hydrogen bonds are the most widely used.[2] The use of metal ions to link organic molecules is an alternative method for the design of inorganic supramolecules. The range and variety of self-assembling inorganic structures that can be constructed relies on the presence of suitable metal−ligand interactions and hydrogen bonds. We have recently reported the self-assembly of molecules through N−H···Cl[3a] and N−H···Br[3a] interactions.

Many topologically promising Ag^{I}-containing architectures have been constructed with nitrogen-containing bidentate building blocks.[4] These polymers include 1-D, 2-D and 3-D network structures.[4b] Despite some recent progress, the ability to predict and control the supramolecular assembly of molecules remains elusive, and much more work is required to understand the inter- and intramolecular forces that determine the patterns of molecular structure and crystal packing in the solid state. During our study on the reactions of Ag^{I} ion with the bidentate ligand *N*,*N*′-di(2-pyridyl)oxamide (**L**), (which contains both amide and pyridyl groups) we found that it can form coordination polymers capable of self-assembling into 2-D molecular structures through a series of interactions involving Ag···O weak covalent bonds and self-complementary double N−H···O hydrogen bonds.[5] It was also found that changing the counterion of Ag^{I} had a drastic effect on the structures of the Ag^{I} coordination polymer. The syntheses and structural characterization of Ag^{I} complexes of the types $\{[Ag(\mathbf{L})][NO_3]\}_\infty$, $\{[Ag(\mathbf{L})(CH_3CN)][ClO_4]\}_\infty$, $\{[Ag_2(\mathbf{L})_3(CH_3CN)_2][PF_6]_2\}_\infty$ and $[Ag_3(\mathbf{L})_4(CH_3CN)_4][BF_4]_3$ form the subject of this report.

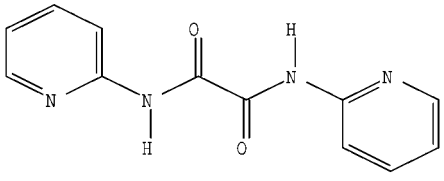

L

Results and Discussion

Syntheses

The ligand *N*, *N*′-di(2-pyridyl)oxamide (**L**) was prepared by reaction of 2-aminopyridine and oxalyl chloride in CH_2Cl_2, in accordance with a literature procedure.[6] The reactions of **L** with AgX (X = NO_3^-, ClO_4^-, PF_6^- and BF_4^-) in refluxing CH_3CN afforded the complexes $\{[Ag(\mathbf{L})][NO_3]\}_\infty$ (**1**), $\{[Ag(\mathbf{L})(CH_3CN)][ClO_4]\}_\infty$ (**2**), $\{[Ag_2(\mathbf{L})_3(CH_3CN)_2][PF_6]_2\}_\infty$ (**3**) and $[Ag_3(\mathbf{L})_4(CH_3CN)_4][BF_4]_3$ (**4**), respectively. All these complexes were structurally characterized by X-ray crystallography. Complexes **1**−**4** were insoluble in most organic solvents; crystals suitable for X-ray diffraction studies were obtained by layering their CH_3CN solutions with diethyl ether.

[a] Department of Chemistry, Chung-Yuan Christian University, Chung-Li, Taiwan, R. O. C.

 © 2004 Wiley-VCH Verlag GmbH & Co. KGaA, Weinheim **DOI: 10.1002/ejic.200300647**

Structure of the Ligand L

The crystal structure of the ligand belongs to the space group $P4bar2_1/c$ with eight molecules in each unit cell. Figure 1 shows the packing of these molecules. It can be seen that the ligand forms one dimensional chains in the solid state, and the molecules are held together by a series of donor-acceptor-donor-acceptor (DADA) quadruple hydrogen bonds and donor-acceptor (DA) double hydrogen bonds. The one dimensional chains interact with each other through extensive C−H···O interactions (H···O: 2.576 Å; ∠ C−H···O: 149.9°). The centrosymmetric DADA:ADAD self-complementary interaction involves two strong N−H···N and two weak C−H···O hydrogen bonds. The H···N distance in the N−H···N interaction is 2.220 Å, with an N−H···N angle of 153.2°, whereas the H···O distance in the C−H···O interaction is 2.451 Å, with a C−H···O angle of 121.3°. The centrosymmetric DA:AD double hydrogen bonds involve two N−H···N interactions; the H···N distance and N−H···N angle are 2.203 Å and 161.5°, respectively. Noticeably, this DADA:ADAD system involves two N−N, two N−C, and two N−C secondary interactions,[5c] which are all repulsive. This system is in marked contrast to the DADA:ADAD system (which has two strong N−H···N and two strong O−H···O interactions) found for 6-methyl-2-butylureidopyrimidone, in which four N−N and two N−O repulsive secondary interactions were observed.[7]

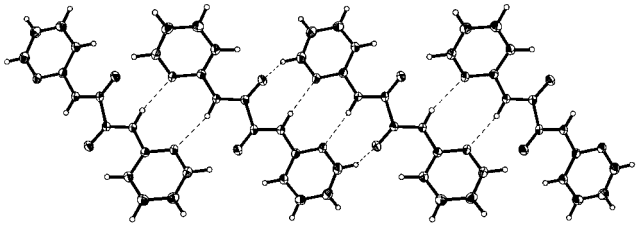

Figure 1. An ORTEP diagram of **L** showing the interactions among the ligands

Structure of 1

The single-crystal X-ray structure of complex **1** shows that the silver atom is bound to the nitrogen atoms of two symmetry-related **L** ligands [Ag−N(2): 2.183 (4), Ag−N(5A): 2.198 (3) Å] in a distinctly non-linear geometry [N(2)−Ag−N(5A): 154.95(13)°]. Selected bond lengths and angles are listed in Table 1. As illustrated in Figure 2 (a), the asymmetric unit of **1** consists of one [Ag(**L**)][NO_3] subunit, which under an appropriate symmetry operation produces the polymeric structure, Figure 2 (b). It is interesting to note that the bidentate ligand **L** in each cation is not flat, but twisted around the C−N bond, with a dihedral angle of 47.0° between the planes of the two pyridine rings, resulting in a series of single-twist helicates. Each single-twist helix contains two Ag^I−**L** units, as shown in Figure 2 (b). The helical chains are interlinked through a series of Ag···O−C (Ag···O: 3.567 Å) interactions and C−H···O (H···O = 2.555 Å, ∠ C−H−O: 144.2°) hydrogen bonds. The nitrate ions form bridges between adjacent chains through all three oxygen atoms [Figure 2 (c)] and link the cations through a series of Ag···O interactions (Ag···O: 2.695−3.336 Å) and N−H···O (H···O: 2.280 and 2.296 Å, ∠ N−H···O: 140.3 and 162.1°, respectively) hydrogen bonds. In addition to the weak interactions mentioned above, the **L** ligands in each helix experience π−π interactions, with interplanar distances of 3.905 Å between the pyridine rings.

Table 1. Selected bond lengths (Å) and angles (°) for complexes **1**−**4**

Complex **1**			
Ag−N(2)	2.183(4)	Ag−N(5A)	2.198(3)
N(2)−Ag−N(5A)	154.95(13)		
Complex **2**			
Ag(1)−N(3)	2.168(4)	Ag(1)−N(2)	2.188(4)
Ag(2)−N(7)	2.300(4)	Ag(2)−N(6)	2.305(4)
Ag(2)−N(9)	2.360(5)	Ag(2)−N(10)	2.372(5)
N(3)−Ag(1)−N(2)	164.29(14)	N(7)−Ag(2)−N(6)	145.13(14)
N(7)−Ag(2)−N(9)	97.30(17)	N(6)−Ag(2)−N(9)	103.24(16)
N(7)−Ag(2)−N(10)	103.68(17)	N(6)−Ag(2)−N(10)	98.77(17)
N(9)−Ag(2)−N(10)	103.1(2)		
Complex **3**			
Ag−N(3)	2.268(2)	Ag−N(1)	2.279(2)
Ag−N(5)	2.504(2)	Ag−N(7)	2.550(3)
N(3)−Ag−N(1)	150.12(8)	N(3)−Ag−N(5)	111.59(8)
N(1)−Ag−N(5)	92.36(8)	N(3)−Ag−N(7)	95.51(9)
N(1)−Ag−N(7)	102.01(9)	N(5)−Ag−N(7)	90.75(10)
Complex **4**			
Ag(1)−N(1)	2.257(5)	Ag(1)−N(9)	2.428(7)
Ag(2)−N(10)	2.220(6)	Ag(2)−N(5)	2.296(4)
Ag(2)−N(4)	2.298(5)		
N(1A)−Ag(1)−N(1)	125.4(2)	N(1A)−Ag(1)−N(9)	121.35(19)
N(1)−Ag(1)−N(9)	99.32(19)	N(1A)−Ag(1)−N(9A)	99.32(19)
N(1)−Ag(1)−N(9A)	121.35(19)	N(9)−Ag(1)−N(9A)	83.8(3)
N(10)−Ag(2)−N(5)	109.57(18)	N(10)−Ag(2)−N(4)	83.8(3)
N(5)−Ag(2)−N(4)	116.57(18)		

Structure of 2

The asymmetric unit and infinite molecular structure of **2** are depicted in Figure 3 (a and b), respectively. Selected bond lengths and angles are listed in Table 1. Figure 3 (b) shows that **2** is a coordination polymer of [Ag(**L**)(CH_3CN)][ClO_4]. The Ag metal centres possess two types of geometries. One has a distorted tetrahedral geometry in which two CH_3CN ligands and two **L** ligands coordinate to the metal centre, whereas the other has an approximately linear geometry [N(3)−Ag(1)−N(2): 164.29(14)°] in which the metal is coordinated by two **L** ligands. The largest N(7)−Ag(2)−N(6) angle is 145.13(14)°, whereas the remaining five angles are in the range 97.30(17) to 103.68 (17)°. The bidentate **L** ligand in each cation is not

 © 2004 Wiley-VCH Verlag GmbH & Co. KGaA, Weinheim

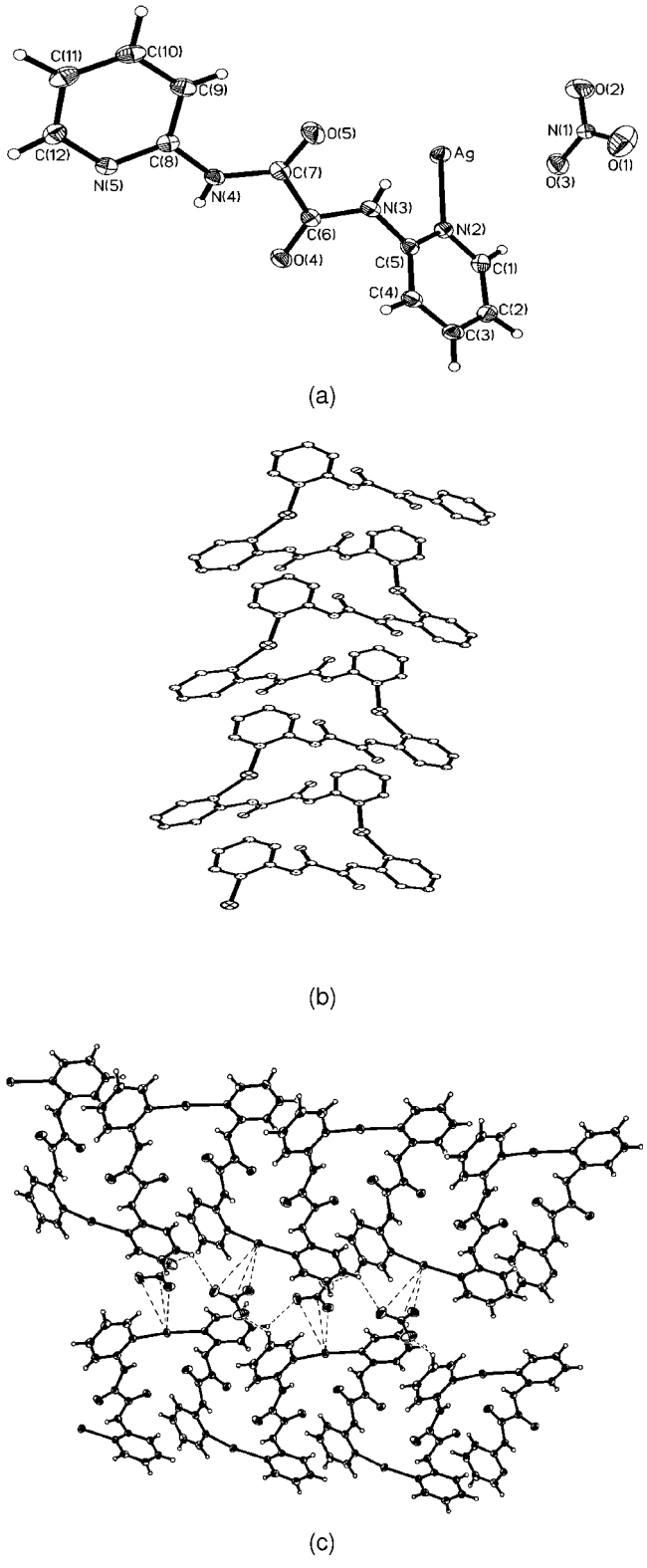

Figure 2. (a) The asymmetric unit of **1**; (b) an ORTEP diagram showing the helical structure of **1**; the hydrogen atoms are omitted for clarity; (c) the interactions between the anions and the cations

flat, but twisted around the C−N bonds, with a dihedral angle of 31.7° between the planes of the two pyridine rings. Most interestingly, each polymer chain is linked to the other through a series of self-complementary double hydrogen bonds and Ag···O interactions (Ag···O: 3.194 and 3.047 Å) to form polymer pairs. The DA:AD self-complementary interaction involves two strong N−H···O hydrogen bonds. The H···N distances are 2.474 and 2.422 Å and the corresponding angles are 132.6 and 141.4°, respectively. One of the ClO_4^- anions interacts with the methyl hydrogen of the CH_3CN ligand through two C−H···O hydrogen bonds (H···O: 2.302 and 2.544 Å and ∠ C−H−O: 139.5 and 133.3°, respectively); the other ClO_4^- anion interacts with the metal centre through a Ag···O interaction (Ag···O: 2.739 Å). The molecules are further linked through intermolecular π−π interactions, with interplanar distances of 3.859 Å between the pyridine rings.

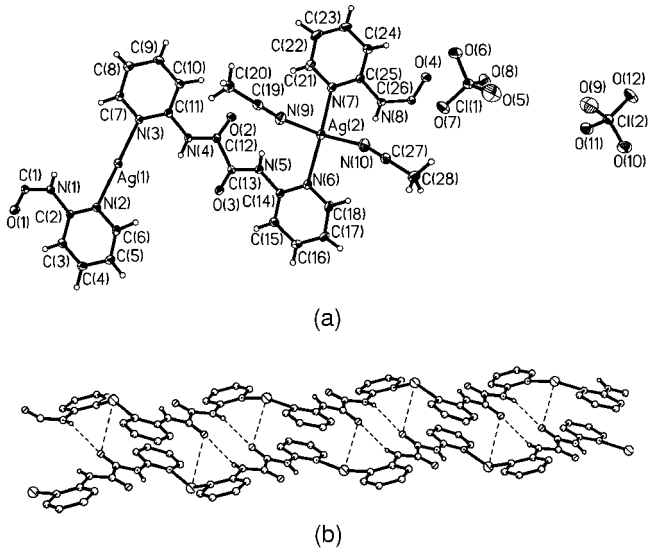

Figure 3. (a) The asymmetric unit of **2**; (b) the interactions between the cations; the pyridine hydrogen atoms are omitted for clarity

Structure of 3

The asymmetric unit of **3** is depicted in Figure 4 (a), and selected bond lengths and angles are listed in Table 1. The single-crystal X-ray structure of **3** shows that it is a coordination polymer consisting of $Ag_4(\mathbf{L})_4(CH_3CN)_2$ metallacycles, and forming a ladder-type structure [Figure 4 (b)]. The distorted tetrahedral coordination geometry of the Ag^I metal centre involves one CH_3CN ligand and three **L** ligands. The ladders are interlinked to each other through a series of self-complementary double N−H···O hydrogen bonds and Ag···O interactions (Ag···O: 3.085 Å) to form molecular sheets. The H···O distance in the strong N−H···O interaction is 2.290 Å, with an N−H−O angle of 161.6°. The PF_6^- anions interact with the pyridyl hydrogen atoms of the **L** ligands through C−H···F hydrogen bonds (H···F: 2.542 and 2.508 Å, with angles 143.4 and 152.7°, respectively). In marked contrast to the twisted conformations in complexes **1** and **2**, the bidentate **L** ligand in each cation of complex **3** is flat, with a dihedral angle of 0° between the planes of the two pyridine rings.

 © 2004 Wiley-VCH Verlag GmbH & Co. KGaA, Weinheim

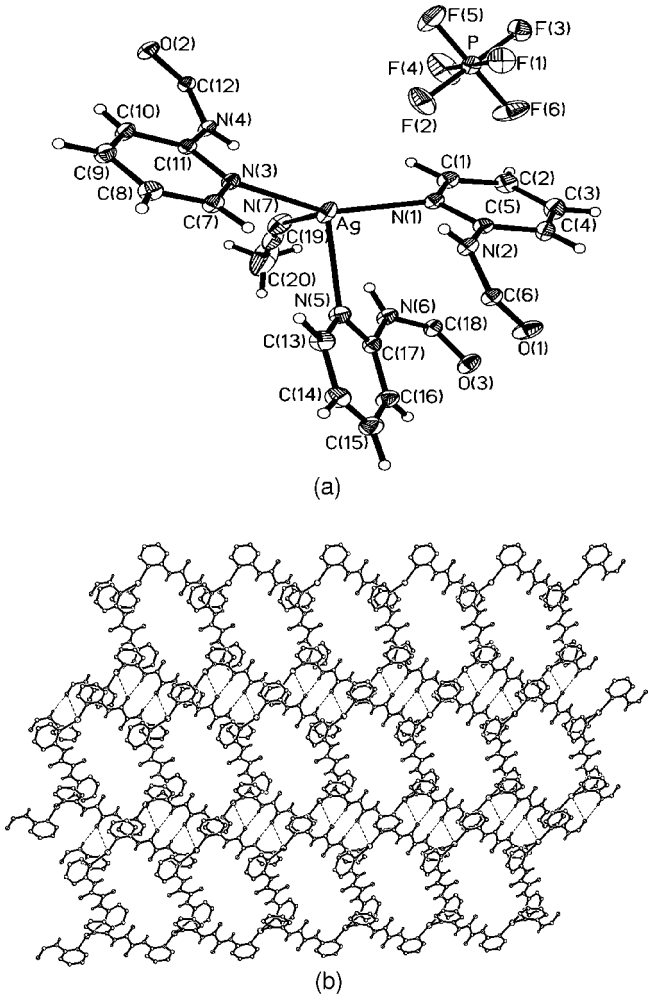

Figure 4. (a) The asymmetric unit of **3**; (b) an ORTEP diagram showing the ladder type structure of **3**; the CH_3CN molecules and the pyridyl hydrogen atoms are omitted for clarity

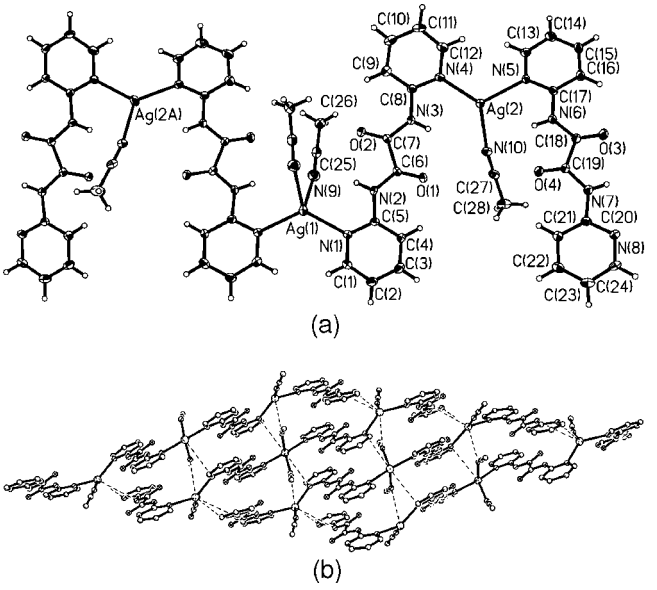

Figure 5. (a) An ORTEP diagram of **4**; (b) an ORTEP diagram showing the interactions among the molecules of **4**; the hydrogen atoms are omitted for clarity

In the structures of complexes **2** and **3**, a new set of interactions involving a pair of Ag···O interactions and self-complementary double N−H···O hydrogen bonds was found to self-assemble the coordination polymers into 2-D networks. By way of comparison, the complementary amide hydrogen bonds in the complexes $\{[AgL']X\}_\infty$ [L′ = *N*,*N*′-bis(3-pyridinecarboxamido)-1,2-ethane; X = ClO_4^-, $CF_3SO_3^-$ or NO_3^-][8] show H···O distances in the range 2.833 to 2.970 Å, which are significantly longer that those found for complexes **2** and **3** (2.290 to 2.474 Å).

Structure of 4

The ORTEP diagram of the trinuclear complex **4** and its packing diagram are depicted (see a and b in Figure 5), respectively. Selected bond lengths and angles are listed in Table 1. The single-crystal X-ray structure of **4** shows that the complex consists of a trinuclear cation $[Ag_3(\mathbf{L})_4(CH_3CN)_4]^{3+}$ and three BF_4^- anions. Two types of coordination geometries are observed for the metal centres. The Ag[I] ion, which is coordinated by two **L** ligands and one CH_3CN ligand, has a distorted triangular planar geometry, whereas the other, coordinated by two **L** and two CH_3CN ligands, has a distorted tetrahedral geometry. The dihedral angles between the planes of the two pyridine rings are 2.0 and 5.2°. The molecule is chiral with a C_2 axis bisecting the N(9)−Ag(1)−N(9A) angle. The trinuclear complexes are interlinked to each other through extensive Ag···N (Ag···N: 3.487 and 3.654 Å) and π−π stacking interactions to form molecular bands. These are interlinked by the BF_4^- anions through extensive C−H···F hydrogen bonds. The interplanar distances between the pyridine rings forming the π−π stacking interactions are 3.875, 3.619 and 3.783 Å, respectively.

In the four complexes mentioned above, the silver atoms of complexes **2**, **3** and **4** have distorted tetrahedral geometries, presumably due to the ligand constraints. Complex **3** has the greatest distortions, with the angles in the range 90.75(10) to 150.12(8)°. In complexes **2** and **4**, the tetrahedral silver atoms show a smaller degree of distortion, with angles in the range 97.30(17) to 145.13(14)° for **2** and 83.8(3) to 125.4(2)° for **4**.

Concluding Remarks

In this study, the coordination chemistry of AgX (X = NO_3^-, ClO_4^-, PF_6^- and BF_4^-) with *N*,*N*′-di(2-pyridyl)oxamide was investigated. Complex **1** is a coordination polymer which forms helical chains whereas complex **4** is a discrete trinuclear complex. In complexes **2** and **3**, a new set of interactions involving two Ag···O interactions and self-complementary double N−H···O hydrogen bonds was found, which link the linear chains and ladder structures of **2** and **3** into polymer pairs and molecular sheets, respec-

 © 2004 Wiley-VCH Verlag GmbH & Co. KGaA, Weinheim

tively. Obviously, the *N*,*N*′-di(2-pyridyl)oxamide ligand is sufficiently flexible to adjust to the stereochemical requirements for the formation of complexes **1**−**4** by twisting about the C−N bonds. It is also shown that the self-assembly frameworks of these Ag^I coordination polymers can be altered by changing their counterions. These frameworks are also highly influenced by coordination of CH_3CN solvent molecules to the Ag^I centres.

Experimental Section

General Procedures: All manipulations were carried out under dry, oxygen-free nitrogen by using Schlenk techniques, unless otherwise noted. Solvents were dried and deoxygenated by refluxing over the appropriate reagents before use. *n*-Hexane and diethyl ether were purified by distillation from sodium/benzophenone, dichloromethane from P_2O_5, and acetonitrile from CaH_2. The visible absorption spectra were recorded on a Hitachi U-2000 spectrophotometer. IR spectra were obtained from a Jasco FT/IR-460 plus spectrometer. Elemental analyses were obtained from a PE 2400 series II CHNS/O analyzer or a HERAEUS VaruoEL analyzer.

Materials: The reagents AgX (X = NO_3^-, ClO_4^-, BF_4^- and PF_6^-) were purchased from Aldrich Chemical Co. The ligand *N*, *N*′-di(2-pyridyl)oxamide was prepared according to a literature procedure.[6]

Syntheses: The complexes were synthesized by reaction of AgX (X = NO_3^-, ClO_4^-, PF_6^- and BF_4^-) with *N*, *N*′-di(2-pyridyl)oxamide in CH_3CN.

$[Ag(L)(NO_3)]_\infty$ (1): $AgNO_3$ (0.050 g, 0.294 mmol) and *N*,*N*′-di(2-pyridyl)oxamide (0.142 g, 0.587 mmol) were added successively to a flask containing 15 mL of CH_3CN. The mixture was then refluxed for 24 h to yield a yellow solution, and diethyl ether added to induce precipitation. The precipitate was filtered and washed with diethyl ether and then dried under reduced pressure to give the light yellow product. Yield: 0.087 g (72%). UV/Vis (CH_3CN): λ = 299 nm. IR (KBr disk): ν̃ = 3168 (br), 1686 (s), 1592 (m), 1574 (m), 1497 (m), 1432 (s), 1384 (m), 1302 (m), 1152 (w), 777 (w), 553 (w) cm^{-1}. $C_{12}H_{10}AgN_5O_5$ (412.12): calcd. C 34.97, H 2.44, N 16.99; found C 35.01, H 2.20, N 17.01.

$[Ag(L)(CH_3CN)(ClO_4)]_\infty$ (2): Prepared as described for **1**. Yield: 65%. UV/Vis (CH_3CN): λ = 282 nm. IR (KBr disk): ν̃ = 3164 (br), 1686 (s), 1592 (m), 1575 (m), 1497 (m), 1433 (s), 1302 (m), 1087 (m), 778(w), 625(w), 552(w), 483(w), 418(w) cm^{-1}. $C_{28}H_{26}Ag_2Cl_2N_{10}O_{12}$ (981.23): calcd. C 34.27, H 2.67, N 14.27; found C 34.67, H 2.28, N 14.28.

$[Ag_2(L)_3(CH_3CN)_2(PF_6)_2]_\infty$ (3): Prepared as described for **1**. Yield: 58%. UV/Vis (CH_3CN): λ = 314 nm. IR (KBr disk): ν̃ = 3167 (br), 1685 (s), 1574 (m), 1497 (m), 1433 (s), 1302 (m), 1151 (w), 842 (m), 779 (w), and 559 (w) cm^{-1}. $C_{44}H_{46}Ag_2F_{12}N_{14}O_7P_2$ (1388.60): calcd. C 38.06, H 3.34, N 14.12; found C 38.05, H 3.10, N 14.16.

Preparation of $[Ag_3(L)_4(CH_3CN)_4][BF_4]_3$ (4): Prepared as described for **1**. Yield: 89%. UV/Vis (CH_3CN): λ = 306 nm. IR (KBr disk): ν̃ = 3164 (br), 1686 (s), 1592 (m), 1575 (m), 1497 (m), 1433 (s), 1302 (m), 1051(m), 779 (m), 552 (w) cm^{-1}. $C_{56}H_{52}Ag_3B_3F_{12}N_{20}O_8$ (1717.22): calcd. C 39.17, H 3.05, N 16.31; found C 39.55, H 3.08, N 16.35.

X-ray Crystallography: The diffraction data of **1** was collected with a Bruker AXS diffractometer, which was equipped with graphite-monochromated Mo-K_α (0.71073 Å) radiation. Data reduction was carried by standard methods with use of well-established computational procedures.[9] Basic information pertaining to crystal parameters and structure refinement is summarized in Table 2. The structure factors were obtained after Lorentz and polarization cor-

Table 2. Crystal data for the ligand **L** and compounds **1**−**4**

Compound	**L**	**1**	**2**	**3**	**4**
Empirical formula	$C_{12}H_{10}N_4O_2$	$C_{12}H_{10}AgN_5O_5$	$C_{28}H_{26}Ag_2Cl_2N_{10}O_{12}$	$C_{22}H_{23}AgF_6N_7O_{3.5}P$	$C_{56}H_{52}Ag_3B_3F_{12}N_{20}O_8$
Formula mass	242.24	412.12	981.23	694.31	1717.22
Crystal system	tetragonal	monoclinic	triclinic	triclinic	monoclinic
Space group	$P4bar2_1/c$	$P2_1/n$	$P\bar{1}$	$P\bar{1}$	$C2/c$
a, Å	13.355(2)	10.578(1)	8.354(2)	9.121(1)	32.198(8)
b, Å	13.355(2)	9.237(1)	13.583(3)	12.456(2)	13.949(2)
c, Å	13.160(1)	14.705(1)	15.951(6)	13.443(2)	16.092(3)
α,°	90	90	104.49(3)	108.012(10)	90
β,°	90	104.915(5)	95.21(3)	103.289(9)	115.681(13)
γ,°	90	90	95.96(2)	105.532(12)	90
V, Å^3	2347.2(5)	1388.5(2)	1730.1(9)	1315.4(3)	6514(2)
Z	8	4	2	2	4
$D_{calcd.}$, g/cm^3	1.371	1.971	1.884	1.753	1.751
Crystal size, mm	0.2 × 0.4 × 0.2	0.1 × 0.8 × 0.1	0.1 × 0.4 × 0.1	0.4 × 0.4 × 0.4	0.1 × 0.8 × 0.2
μ(Mo-K_α), mm^{-1}	0.098	1.488	1.364	0.912	0.998
T, °C	25	25	25	25	25
Data/restraints/parameters	1428/0/204	2450/0/248	5986/0/567	4466/0/437	5727/3/477
Quality-of-fit indicator[a]	1.000	1.062	1.035	1.063	1.014
Final *R* indices [$I > 2\sigma(I)$][b] [c]	R_1 = 0.0418	*R*1 = 0.0381	*R*1 = 0.0408	*R*1 = 0.0308	*R*1 = 0.0591
	wR_2 = 0.0801	*wR*2 = 0.0918	*wR*2 = 0.1111	*wR*2 = 0.0787	*wR*2 = 0.1323
R indices (all data)	R_1 = 0.082	*R*1 = 0.0526	*R*1 = 0.0508	*R*1 = 0.0350	*R*1 = 0.1114
	wR_2 = 0.0943	*wR*2 = 0.0997	*wR*2 = 0.1207	*wR*2 = 0.0823	*wR*2 = 0.1610

[a] Quality-of-fit = $[\Sigma w(F_o^2 - F_c^2)^2/N_{observed} - N_{parameters})]^{1/2}$. [b] $R1 = \Sigma F_o - F_c/\Sigma F_o$. [c] $wR2 = [\Sigma w(F_o^2 - F_c^2)^2/\Sigma w(F_o^2)^2]^{1/2}$. $w = 1/[\sigma^2(F_o^2) + (ap)^2 + (bp)]$, $p = [\max.(F_o^2 \text{ or } 0) + 2(F_c^2)]/3$. **L**: $a = 0.0401$, $b = 0.000$; **1**: $a = 0.0499$, $b = 1.3564$; **2**: $a = 0.0651$, $b = 3.3187$; **3**: $a = 0.0362$, $b = 1.2567$; **4**: $a = 0.0624$, $b = 24.1437$

 © 2004 Wiley-VCH Verlag GmbH & Co. KGaA, Weinheim

rections. The positions of the heavy atoms, including the silver atoms, were located by the direct method. The remaining atoms were found in a series of alternating difference Fourier maps and least-square refinements.[10] The final residuals were $R_1 = 0.0381$, $wR2 = 0.0918$. The crystallographic procedures for **2**−**4** were similar to those for **1**. Basic information pertaining to crystal parameters and structure refinement is summarized in Table 2.

CCDC-219402 to -219406 contain the supplementary crystallographic data for this paper. These data can be obtained free of charge at www.ccdc.cam.ac.uk/conts/retrieving.html [or from the Cambridge Crystallographic Data Centre, 12 Union Road, Cambridge CB2 1EZ, UK; Fax: (internat.) + 44-1223/336-033; E-mail: deposit@ccdc.cam.ac.uk].

Acknowledgments

We are grateful to the National Science Council of the Republic of China for support.

[1] [1a] G. R. Desiraju, *Angew. Chem. Int. Ed. Engl.* **1995**, *34*, 2311−2327. [1b] G. R. Desiraju, *Chem. Commun.* **1997**, 1475−1482. [1c] J. M. Lehn, *Supramolecular Chemistry*, Wiley-VCH, Weinheim, **1995**.

[2] [2a] R. Robson, B. E. Abrahams, S. R. Batten, R. W. Gable, B. F. Hoskins, J. Lieu, *Supramolecular Architecture*, ACS publications, Washington, DC, **1992**. [2b] S. R. Batten, R. Robson, *Angew. Chem. Int. Ed.* **1998**, *37*, 1460−1494. [2c] O. M. Yaghi, H. Li, C. Davis, D. Richardson, T. L. Groy, *Acc. Chem. Res.* **1998**, *31*, 474−484. [2d] H. Gudbjartson, K. Biradha, K. M. Poirier, M. J. Zaworotko, *J. Am. Chem. Soc.* **1999**, *121*, 2599−2600. [2e] C. B. Aakeröy, K. R. Seddon, *Chem. Soc. Rev.* **1993**, 397−407. [2f] M. Fujita, K. Ogura, *Coord. Chem. Rev.* **1996**, *148*, 249−264. [2g] S.-I. Noro, R. Kitauta, M. Kondo, S. Kitagawa, T. Ishii, H. Matauzaka, M. Yamashita, *J. Am. Chem. Soc.* **2002**, *124*, 2568−2583. [2h] S. Kitagawa, M. Kondo, *Bull. Chem. Soc. Jpn.* **1998**, *71*, 1739−1753.

[3] [3a] C.-W. Su, C.-P. Wu, J.-D. Chen, L.-S. Liou, J.-C. Wang, *Inorg. Chem. Commun.* **2002**, *5*, 215−219. [3b] S.-H. Liu, J.-D. Chen, L.-S. Liou, J.-C. Wang, *Inorg. Chem.* **2001**, *40*, 6499−6501.

[4] [4a] A. J. Blake, N. R. Champness, P. Hubberstey, W.-S. Li, M. A. Withersby, M. Schröder, *Coord. Chem. Rev.* **1999**, *183*, 117−138. [4b] S. Muthu, J. H. K. Yip, J. J. Vittal, *J. Chem. Soc., Dalton Trans.* **2002**, 4561−4568, and references cited therein.

[5] [5a] R. P. Sijbesma, E. W. Meijer, *Curr. Opin. Colloid Interface Sci.* **1999**, *4*, 24−32. [5b] S. C. Zimmerman, P. S. Corbin, *Struct. Bonding* **2000**, *96*, 63−94. [5c] D. C. Sherrington, K. A. Taskinen, *Chem. Soc. Rev.* **2001**, *30*, 83−93. [5d] D. S. Lawrence, T. Jiang, M. Levett, *Chem. Rev.* **1995**, *95*, 2229−2260.

[6] M. C. Seidel, G. C. V. Tuyle, W. D. Weir, *J. Org. Chem.* **1970**, *35*, 1662−1664.

[7] F. H. Beijer, R. P. Sijbesma, H. Kooijman, A. L. Spek, E. W. Meijer, *J. Am. Chem. Soc.* **1998**, *120*, 6761−6769.

[8] S. Muthu, J. H. K. Yip, J. J. Vittal, *J. Chem. Soc., Dalton Trans.* **2001**, 3577−3584.

[9] *XSCANS, Release, 2.1*, Siemens Energy & Automation, Inc, Madison, Wisconsin, USA, **1995**.

[10] *SHELXTL 5.10*, Bruker Analytical X-ray Instruments Inc., Karlsruhe, Germany, **1997**.

Received September 12, 2003
Early View Article
Published Online February 26, 2004

 © 2004 Wiley-VCH Verlag GmbH & Co. KGaA, Weinheim

Synthesis, Characterization and Reactivity of New (μ-Aminocarbyne)diruthenium Complexes Containing Alkynylimino Ligands

Luigi Busetto,*[a] Fabio Marchetti,[a] Stefano Zacchini,[a] and Valerio Zanotti[a]

Keywords: Ruthenium / Dinuclear complexes / Carbynes / C−C coupling / Alkynylimino ligands

Addition of acetylides R′C≡CLi [R′ = Tol, Ph, Me_3Si, *n*Bu, C(Me)=CH_2] to the diruthenium complexes [Ru_2{μ-CN(Me)(R)}(μ-CO)(CO)($NCCMe_3$)$(Cp)_2$]$^+$ (R = Xy, **2a**; Bz, **2b**; Me, **2c**) results in the formation of [Ru_2{μ-CN(Me)(R)}(μ-CO)(CO){N(H)=C(CMe_3)(C≡CR′)}$(Cp)_2$]$^+$ (R = Xy, R′ = Tol, **3a**; R = Bz, R′ = Tol, **3b**; R = Me, R′ = Tol, **3c**; R = Xy, R′ = Ph, **4a**; R = Bz, R′ = Ph, **4b**; R = Me, R′ = Ph, **4c**; R = Bz R′ = H, **5**; R = Xy, R′ = *n*Bu, **6**; R = Xy, R′ = [C(Me)=CH_2], **7**), which contain an alkynylimino ligand, formed from addition of the acetylide to the Me_3CCN ligand. Structural and spectroscopic studies show that all these complexes contain the two Cp ligands in a relative *cis* arrangement, whereas two isomers arise from the different orientation of the substituents on the bridging aminocarbyne μ-CN(Me)(R) when R ≠ Me. Addition of secondary amines to **3**–**7** results in a stereo- and regioselective *cis* amination of the C–C triple bond to give the new complexes [Ru_2{μ-CN(Me)(R)}(μ-CO)(CO){N(H)=C(CMe_3)C(H)=C(NMe_2)(Tol)}$(Cp)_2$]$^+$ (R = Xy, **8a**; Bz, **8b**; Me, **8c**), [Ru_2{μ-CN(Me)(Xy)}(μ-CO)(CO){N(H)=C(CMe_3)C(H)=C(NC_5H_{10})(Tol)}$(Cp)_2$]$^+$(**9**) and [Ru_2{μ-CN(Me)(Xy)}(μ-CO)(CO){N(H)=C(CMe_3)C(H)=C(NMe_2)C(Me)=CH_2)}$(Cp)_2$]$^+$ (**10**) containing the hitherto unknown new imino-2-en-3-amine ligand. The solid-state structures of these products have been analyzed by X-ray analysis and, in solution, by NOE spectroscopic studies.

(© Wiley-VCH Verlag GmbH & Co. KGaA, 69451 Weinheim, Germany, 2004)

Introduction

Transition metal complexes containing η^1-coordinated imines represent an important field in classical coordination chemistry and organometallic chemistry.[1−3] Several synthetic routes for their synthesis have been developed in the last decade, including displacement of a labile ligand by free imine and modification of coordinated ligands.[4] Among the latter, some interesting examples are: a) oxidation of coordinated amines;[5] b) condensation of coordinated amines with free aldehydes and ketones;[6] c) reduction of coordinated nitriles.[7,8] Only in a limited number of cases the imino ligands have been obtained via addition of a carbon nucleophile to coordinated nitriles.[8,9] We have recently reported a particular case of the latter procedure employing acetylides as carbon nucleophiles.[10] Thus, addition of TolC≡CLi (Tol = *p*-MeC_6H_4) to [Fe_2{μ-CN(Me)(Xy)}(μ-CO)(CO)($NCCMe_3$)$(Cp)_2$]$^+$ (Xy = 2,6-$Me_2C_6H_3$), followed by protonation, in THF at low temperature, resulted in the formation of the complex [Fe_2{μ-CN(Me)(Xy)}(μ-CO)(CO){N(H)=C(CMe_3)(C≡CTol)}$(Cp)_2$]$^+$, which contains the new alkynylimino ligand HN=C(CMe_3)(C≡CTol). Unfortunately, the reported reaction occurs only in the case described, and, depending on the experimental conditions, other products can be formed. Thus, we have decided to investigate analogous reactions of diruthenium complexes. As will be shown in this paper, the reaction for the synthesis of alkynylimino complexes of ruthenium is very general: aromatic, aliphatic and functionalized acetylides can be used, as well as different groups on the aminocarbyne. Moreover, the high unsaturation of the alkynylimino ligand offers the possibility to exploit it for further modification, and some studies on nucleophilic additions are reported here.

[a] Dipartimento di Chimica Fisica ed Inorganica, Università di Bologna,
Viale Risorgimento 4, 40136, Bologna, Italy
Fax: (internat.) +39-0512093690
E-mail: busetto@ms.fci.unibo.it

Results and Discussion

Synthesis and Characterization of the Nitrile Complexes [Ru_2{μ-CN(Me)(R)}(μ-CO)(CO)($NCCMe_3$)$(Cp)_2$]$^+$ (R = Xy, 2a; Bz, 2b; Me, 2c)

One CO ligand in the diruthenium aminocarbyne complexes [Ru_2{μ-CN(Me)(R)}(μ-CO)$(CO)_2(Cp)_2$]$^+$ [R = Xy, **1a**; CH_2Ph (Bz), **1b**; Me, **1c**] [11] can be easily replaced by Me_3CCN after treatment with Me_3NO in THF and a slight excess of the nitrile compound (Scheme 1). The resulting complexes [Ru_2{μ-CN(Me)(R)}(μ-CO)(CO)($NCCMe_3$)$(Cp)_2$]$^+$ (R = Xy, **2a**; Bz, **2b**; Me, **2c**), obtained in good yields (85−88%), have been spectroscopically characterized. The IR spectra of **2a**−**c** show the presence of a terminal and a bridging CO, whereas the ^{1}H and ^{13}C spectra show

 © 2004 Wiley-VCH Verlag GmbH & Co. KGaA, Weinheim DOI: 10.1002/ejic.200300772

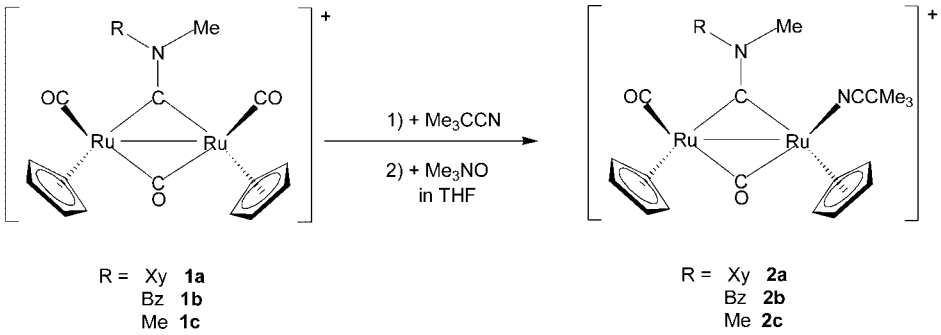

R = Xy **1a**, Bz **1b**, Me **1c**

R = Xy **2a**, Bz **2b**, Me **2c**

Scheme 1

resonances due to two inequivalent Cp ligands. Moreover, resonances typical of the Me_3CCN ligand are present in both the ^1H and ^{13}C NMR spectra, confirming coordination of the nitrile group in complexes **2a**−**c**.

It is worth noting that in the case of **2a,b,** where the bridging aminocarbyne ligand is non-symmetrically substituted, two isomers are present in solution (see Scheme 2, where the two isomers have been labeled α and β; α/β = 1.5), as a consequence of the different orientation of the substituents in the μ-CN(Me)(R) ligand and hindered rotation around the C−N bond.

Another explanation deriving from a possible *cis*−*trans* isomerisation of the two Cp ligands with respect to the Ru_2C_2 plane, is ruled out by the observation of only one isomer in the case of **2c** (R = Me). It is worth noting that the starting compounds **1a**−**c** adopt a *cis*-arrangement,[11] and this is the preferred geometry for the analogous (aminocarbyne)diruthenium and -diiron complexes.[12−14] The fact that the two isomers are due to the orientation of the μ-CN(Me)(R) ligand has been further supported in the case of **2a** by NOE spectroscopic measurements. Some important results arise from these studies: 1) in both isomers, the NOE is mutually generated between the two Cp ligands, as expected for a *cis* geometry. 2) NOE is generated in the major isomer (but not in the minor) between the NMe group and the Me_3CCN ligand. Thus, it is possible to assign the α structure to the major isomer. 3) In perfect agreement with this, NOE is observed in the minor isomer between the protons of the Xy group and the Me_3CCN ligand (β structure). 4) In both the α and β isomers, the Cp resonating at lower frequencies (< 5 ppm) is the one on the same side of the Xy group. It is noteworthy that in **2b,c** both Cp ligands resonate above 5 ppm in the ^1H NMR spectra, suggesting that the shift at lower frequencies of one Cp in **2a** is due to the presence of Xy.

Synthesis and Characterization of the Alkynylimino Complexes $[Ru_2\{\mu\text{-}CN(Me)(R)\}(\mu\text{-}CO)(CO)\{N(H)=C(CMe_3)(C{\equiv}CR')\}(Cp)_2]^+$ (R = Xy, R′ = Tol, 3a; R = Bz, R′ = Tol, 3b; R = Me, R′ = Tol, 3c; R = Xy, R′ = Ph, 4a; R = Bz, R′ = Ph, 4b; R = Me, R′ = Ph, 4c; R = Bz, R′ = H, 5; R = Xy, R′ = *n*Bu, 6; R = Xy, R′ = [C(Me) = CH_2], 7)

The nitrile complexes **2a**−**c** react, in THF at low temperature, with different acetylides R′C≡CLi (R′ = Tol, Ph, Me_3Si, *n*Bu, C(Me)=CH_2) affording, in good yields (56−75%), the new $[Ru_2(\mu\text{-}CN(Me)(R)\}(\mu\text{-}CO)(CO)\{N(H)=C(CMe_3)(C{\equiv}CR')\}(Cp)_2]^+$ (R = Xy, R′ = Tol, **3a**; R = Bz, R′ = Tol, **3b**; R = Me, R′ = Tol, **3c**; R = Xy, R′ = Ph, **4a**; R = Bz, R′ = Ph, **4b**; R = Me, R′ = Ph, **4c**; R = Bz R′ = H, **5**; R = Xy, R′ = *n*Bu, **6**; R = Xy, R′ = [C(Me)=CH_2], **7**) which contain an alkynylimino ligand, formed from addition of the acetylide to the Me_3CCN ligand (Scheme 3). The hydrogen of the NH group probably arises from the CH_2Cl_2 used to solubilize the residue obtained after evaporation of the THF during the work-up of the reaction (see next section). Interestingly, when $Me_3SiC{\equiv}CLi$ is used, cleavage of the Si−C(sp) bond occurs and, thus, the final product contains a proton instead of $SiMe_3$. Unexpectedly, this is the only way to obtain **5**, since addition of HC≡CNa to **2b** results in decomposition products.

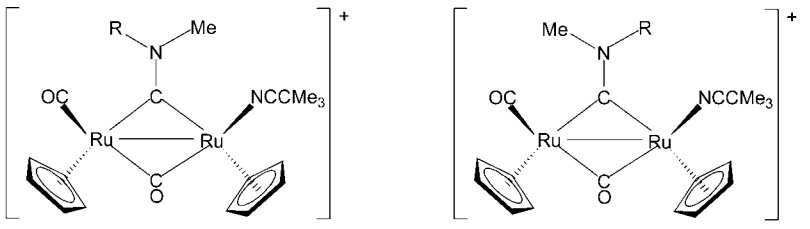

Isomer α Isomer β

Scheme 2

 © 2004 Wiley-VCH Verlag GmbH & Co. KGaA, Weinheim

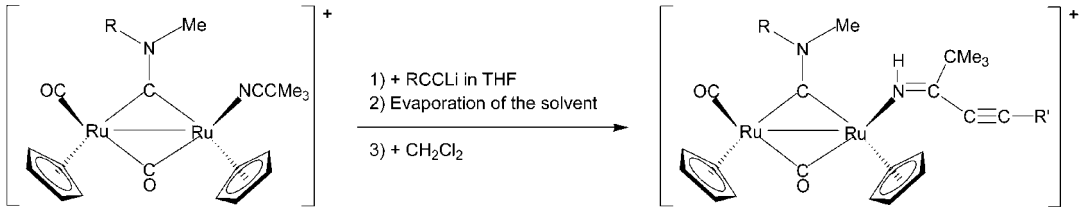

R = Xy **2a**
Bz **2b**
Me **2c**

R=	Xy	Bz	Me	Xy	Bz	Me	Bz	Xy	Xy
R'=	Tol	Tol	Tol	Ph	Ph	Ph	H	Bu	C(Me)=CH$_2$
	3a	**3b**	**3c**	**4a**	**4b**	**4c**	**5**	**6**	**7**

Scheme 3

Complexes **3**−**7** have been fully characterized by IR, ^{1}H and ^{13}C NMR spectroscopy; **3a** has also been characterized by X-ray crystallography, and **3b, 4b** and **5** by ESI MS. The mass spectra confirm the ionic nature of these complexes: a positive ion corresponding to the cation and a negative ion at *m*/*z* = 149, corresponding to $CF_3SO_3^-$ are, in fact, present. The IR spectra of **3**−**7** in CH_2Cl_2 show ν(CO) at ca. 1968 and 1810 cm^{-1} and bands at ca. 2200 cm^{-1} attributable to ν(C≡C); a broad signal at ca. 3320 cm^{-1} (in KBr) is a clear indication of the presence of the NH group. It is worth noting that in the ^{1}H NMR spectra of **3a, 4a, 6** and **7** (R = Xy), one Cp resonates below and one above δ = 5 ppm, whereas in the remaining alkynylimino compounds (R = Bz or Me) both resonances are above δ = 5 ppm, confirming the peculiar shielding effect of the Xy group on the closer Cp ligand. The ^{13}C NMR spectra show four high frequency resonances at δ ca. 310, 236, 202 and 184 ppm, in the typical regions for bridging aminocarbyne, bridging and terminal CO and imine carbon atoms, respectively.

As in **2c**, the NMR spectra of **3c** and **4c** show the presence in solution of only one species, whereas two isomers exist for all the complexes with R ≠ Me (see Scheme 4). The ratio of these isomeric forms is ca. 2:1 for complexes **3b**, **4b** and **5** (R = Bz), and increases up to 10−20:1 for **3a**, **4a**, **6** and **7** (R = Xy), in agreement with the different steric properties of the aminocarbyne substituents: thus, one isomer strongly predominates when the bulkier Xy group is present. Moreover, in all these cases, it can be assumed that the major species is the α-isomer, in which the bulky alkynylimino ligand is on the same side of the less bulky Me group.

The possible presence of *cis*-*trans* forms of the $Cp_2Ru_2(\mu\text{-}C)_2$ core, or of isomers deriving from the C=N iminic double bond, cannot be excluded, but they are less convincing since they would also entail the presence of isomers in the case of complexes with symmetrically substituted aminocarbyne. NOE measurements further support our hypothesis. For example, irradiation of the Cp resonance (δ = 5.46 ppm) of the major isomer of **3a** resulted in the enhancement of the resonances due to the other Cp ligand, the NMe group and some protons of the HN=C(CMe$_3$)(C≡CTol) ligand, in agreement with the proposed *cis*-α structure. Conversely, irradiation of the Cp resonating at lower frequency (δ = 4.95 ppm) affected only the resonance due to the other Cp (δ = 5.46 ppm) and the Xy group. Moreover, in the case of **3b**, because of the higher concentration of the minor isomer than in the case of **3a**, it has been possible to determine the relative orientation of the substituents in both the isomers via NOE measurements. The major isomer shows results similar to the ones reported for the major isomer of **3a**, indicating its *cis*-α structure. Conversely, in the minor isomer of **3b** it has been possible to detect an appreciable NOE between the two Cp ligands, between one Cp and the NMe group, and between the other Cp, the NBz and the alkynylimino ligand confirming a *cis*-β structure.

Further support is given to our stereochemical assignments from the X-ray structure of **3a**, which is reported in Figure 1, whereas relevant bond lengths and angles are reported in Table 1.

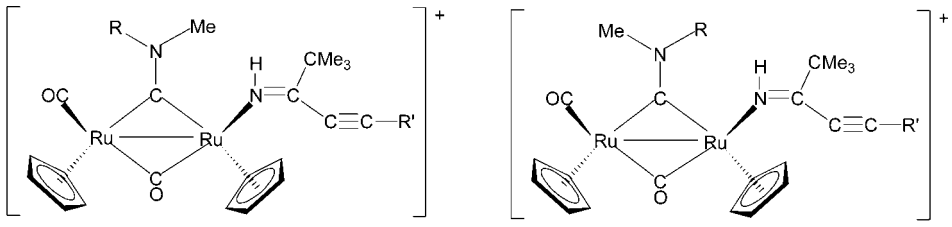

Isomer α Isomer β

Scheme 4

 © 2004 Wiley-VCH Verlag GmbH & Co. KGaA, Weinheim

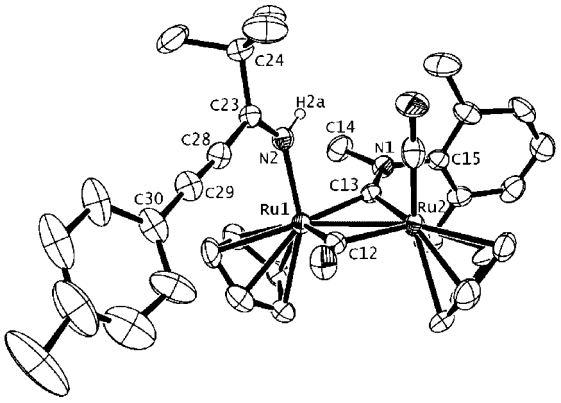

Figure 1. Molecular structure of **3a**, with key atoms labeled (all H atoms, apart from H2a have been omitted). Displacement ellipsoids are at 30% probability level

Table 1. Selected bond lengths (Å) and angles (°) for complex **3a**

Ru(1)−Ru(2)	2.7105(9)	C(23)−C(24)	1.518(11)
Ru(1)−C(12)	1.985(9)	C(23)−C(28)	1.438(11)
Ru(2)−C(12)	2.113(8)	C(28)−C(29)	1.218(13)
Ru(1)−C(13)	1.963(8)	C(29)−C(30)	1.405(14)
Ru(2)−C(13)	1.973(8)	C(13)−N(1)	1.328(11)
Ru(1)−N(2)	2.090(7)	N(1)−C(14)	1.502(12)
N(2)−C(23)	1.268(11)	N(1)−C(15)	1.432(11)
C(13)−N(1)−C(14)	121.1(7)	N(2)−C(23)−C(28)	119.1(8)
C(13)−N(1)−C(15)	121.4(7)	C(24)−C(23)−C(28)	117.0(7)
C(14)−N(1)−C(15)	117.2(7)	C(23)−C(28)−C(29)	175.0(10)
N(2)−C(23)−C(24)	123.9(7)	C(28)−C(29)−C(30)	176.9(11)

The molecular structure of **3a** is almost identical to the one previously reported for the analogous diiron complex $[Fe_2\{\mu\text{-}CN(Me)(Xy)\}(\mu\text{-}CO)(CO)\{N(H)=C(CMe_3)(C\equiv CTol)\}(Cp)_2]^+$,[10] and it can be better described as composed of two moieties, i.e. the $[Ru_2\{\mu\text{-}CN(Me)(Xy)\}(\mu\text{-}CO)(CO)(Cp_2)]$ unit and the alkynylimino ligand $HN=C(CMe_3)(C\equiv CTol)$. The Ru−Ru distance [2.7105(9) Å] is typical for a Ru−Ru single bond.[15−17] The C(13)−N(1) distance [1.328(11) Å] gives evidence of partial double bond character in the μ-CN(Me)(Xy) ligand, which could be alternatively described as a bridging iminium. The two Cp ligands lie on the same side of the mean plane determined by the inner Ru_2C_2 core in a mutual *cis*-position. Moreover, the bulky xylyl group on the bridging aminocarbyne ligand lies on the opposite side of the alkynylimino ligand. Thus, **3a** adopts, in the solid-state, a *cis*-α structure, which is also the predominant isomer revealed in solution by the NOE studies.

Reactions of $[Ru_2\{\mu\text{-}CN(Me)(R)\}(\mu\text{-}CO)(CO)\{N(H)=C(CMe_3)(C\equiv CR')\}(Cp)_2]^+$

Complexes **3a**−**c** react at room temperature in THF with an excess of Me_2NH or piperidine ($C_5H_{10}NH$) giving good yields (60−70%) of new products which show, from the ESI MS analyses, that the secondary amine has been added to **3a**−**c** without loss of the imino ligand. The ν(CO) and the disappearance of ν(C≡C) in the IR spectra suggests that addition has occurred on the C≡C bond; hence, the new products can be formulated as $[Ru_2\{\mu\text{-}CN(Me)(R)\}(\mu\text{-}CO)(CO)\{N(H)=C(CMe_3)C(H)=C(NMe_2)(Tol)\}(Cp)_2]^+$ (R = Xy, **8a**; Bz, **8b**; Me, **8c**) and $[Ru_2\{\mu\text{-}CN(Me)(Xy)\}(\mu\text{-}CO)(CO)\{N(H)=C(CMe_3)C(H)=C(NC_5H_{10})(Tol)\}(Cp)_2]^+$ (**9**) (Scheme 5).

Amination of alkynes is a widely used reaction in organic chemistry, and is promoted by a large variety of transition metals.[18] In our case, the reaction can be better viewed as the amination of an α,β-unsaturated imine η^1-coordinated to ruthenium. The reaction seems to be completely stereo- and regioselective. Amination of **3c**, which exists in solution as a single isomer, results in the formation of only a single species, whereas, amination of the complexes **3a,b**, which

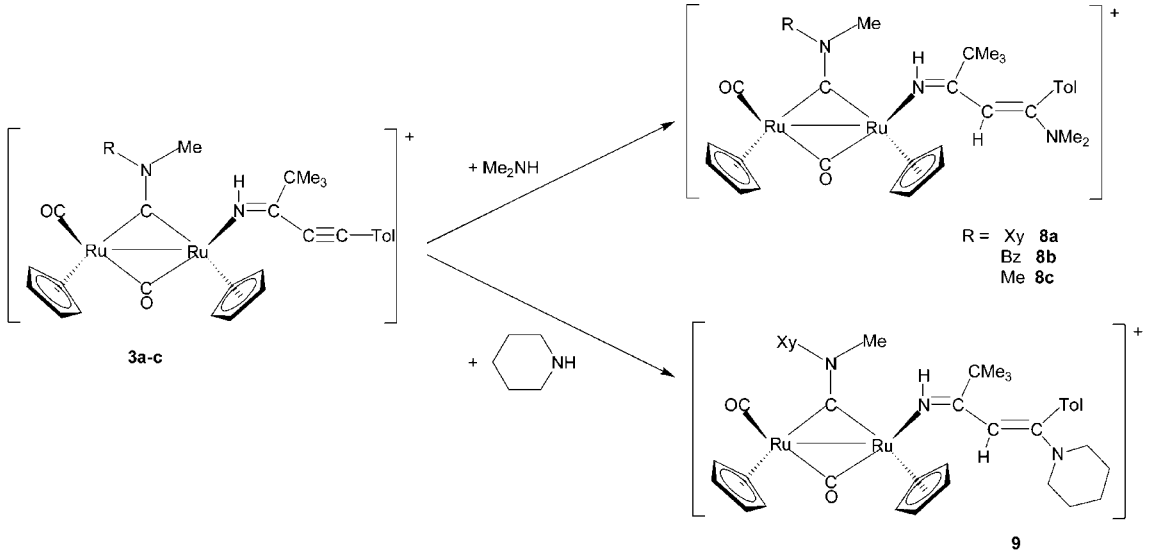

Scheme 5

 © 2004 Wiley-VCH Verlag GmbH & Co. KGaA, Weinheim

exist as two isomers (α and β) results in the formation of two products in the same ratio of the starting compounds (in the case of **8a** the concentration of the minor isomer is too low to be fully characterized).

In order to understand better the stereo- and regiochemistry of the addition, an X-ray study has been carried out on **8a**. The molecular structure of **8a** is reported in Figure 2, whereas the relevant bond lengths and angles are reported in Table 2. The molecule is chiral, but the racemic mixture is present within the crystal; two independent molecules are present in the asymmetric unit, with similar relative arrangement of the atoms, similar bond lengths and bond angles but opposite absolute structure. Differences are mainly attributable to packing effects and, in all cases, the parameters describing the bonds in the two molecules fall in the same ranges expected for a similar hybridization of the atoms and bond order. As in the case of **3a**, the structure of **8a** can be discussed in terms of two moieties, i.e. the $Ru_2\{\mu\text{-}CN(Me)(Xy)\}(\mu\text{-}CO)(CO)(Cp_2)$ unit and the new $HN{=}C(CMe_3)CH{=}C(NMe_2)(Tol)$ ligand. The former resembles the analogous unit in **3a** and does not need any further comments; it is, however, worth noting the fact that in this case the molecule also adopts a *cis*-α structure considering the relative position of the two Cp ligands and the orientation of the N(Me)(Xy) group on the aminocarbyne.

The new $HN{=}C(CMe_3)CH{=}C(NMe_2)(Tol)$ ligand is an imino-2-en-3-amine η^1-coordinated to one ruthenium atom via the imino nitrogen [Ru(1)−N(2) 2.077(13) and Ru(3)−N(5) 2.133(13) Å]. In agreement with this, the N(2)−C(13) [1.282(13) Å], N(5)−C(63) [1.248(13) Å], C(18)−C(19) [1.34(2) Å] and C(68)−C(69) [1.35(2) Å] distances are typical double bonds (compare 1.28 Å in free imines and oximes and 1.32 Å in ethylene for typical C=N and C=C, respectively),[19] whereas the C(13)−C(18) [1.493(14) Å] and C(63)−C(68) [1.502(15) Å] interactions are essentially single bonds {compare C(13)−C(14) [1.56(2) Å] and C(63)−C(64) [1.55(2) Å]}, suggesting the absence of conjugation between the imine and enamine. In fact, their two π-systems are nearly orthogonal [dihedral angles N(2)−C(13)−C(18)−C(19) −99.0(19)° and N(5)−C(63)−C(68)−C(69) 101(2)°]. The atoms of the enamine in the two molecules are nearly in the same plane [mean deviations 0.0510 and 0.0467 Å from the least-squares planes C(13)−C(18)−C(19)−N(3)−C(22) and C(63)−C(68)−C(69)−N(6)−C(72), respectively], and they all have sp^2 hybridization. These planes form relatively small angles with the planes of the NMe_2 units [i.e. 22.58(0.97) and 27.74(1.03)° for the two molecules], whereas the Tol groups lie considerably out of the enamine planes, with angles of 49.83(0.42) and 50.19(0.46)° for the two molecules, respectively.

On the basis of the X-ray analysis it is possible to conclude that the amination of the coordinated alkynylimine occurs in a *cis* fashion with the nucleophile adding regioselectively to the β-carbon. The nature of compound **8** and **9** has been further confirmed by IR and NMR spectroscopy. The IR spectra of **8** and **9** in CH_2Cl_2 show two ν(CO) at ca. 1965 and 1808 cm^{-1}, due to the terminal and bridging carbonyl, respectively, whereas a band at ca. 3325 cm^{-1} in the spectra in KBr is attributable to the NH stretching. The NMR spectra of **8** and **9** have been fully assigned using DEPT, gs-HSQC and gs-HMBC experiments.[20] The main features of the ^1H spectra are the presence of two inequiva-

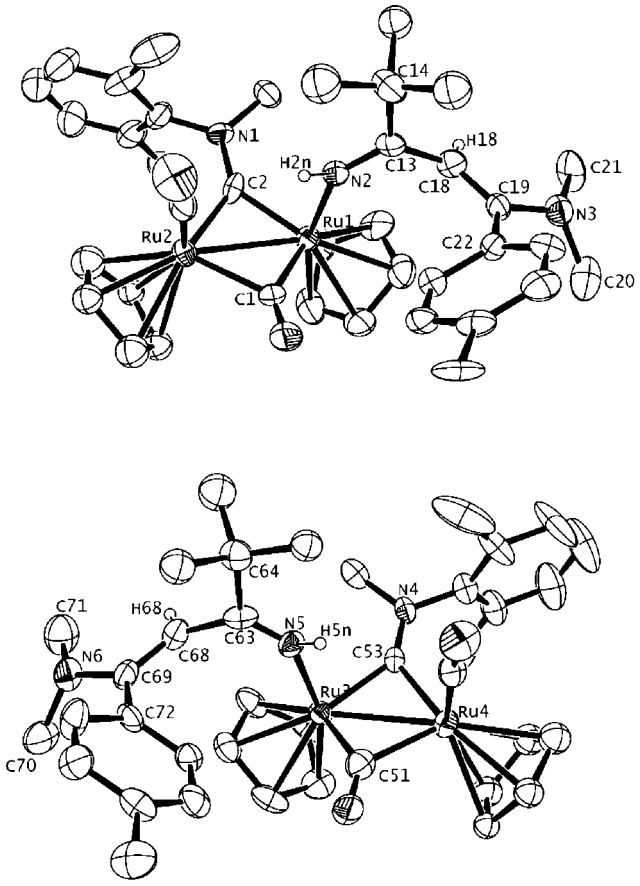

Figure 2. Molecular structure of the two independent molecules of **8a**, with key atoms labeled (all H atoms, apart from H2a, H18, H5n and H68 have been omitted). Displacement ellipsoids are at 30% probability level.

Table 2. Selected bond lengths (Å) and angles (°) for complex **8a**

Ru(1)−Ru(2)	2.7036(16)	Ru(3)−Ru(4)	2.7075(17)
Ru(1)−C(1)	1.965(17)	Ru(3)−C(51)	1.981(17)
Ru(2)−C(1)	2.096(16)	Ru(4)−C(51)	2.071(18)
Ru(1)−C(2)	1.922(13)	Ru(3)−C(53)	1.930(12)
Ru(2)−C(2)	1.967(14)	Ru(4)−C(53)	1.986(12)
Ru(1)−N(2)	2.077(13)	Ru(3)−N(5)	2.133(13)
N(1)−C(2)	1.335(13)	N(4)−C(53)	1.312(13)
N(2)−C(13)	1.282(13)	N(5)−C(63)	1.248(13)
C(13)−C(18)	1.493(14)	C(63)−C(68)	1.502(15)
C(13)−C(14)	1.56(2)	C(63)−C(64)	1.55(2)
C(18)−C(19)	1.34(2)	C(68)−C(69)	1.35(2)
C(19)−N(3)	1.402(18)	C(69)−N(6)	1.393(19)
C(19)−C(22)	1.493(15)	C(69)−C(72)	1.443(17)
N(2)−C(13)−C(18)	118.1(13)	N(5)−C(63)−C(68)	120.2(12)
C(13)−C(18)−C(19)	127.4(13)	C(63)−C(68)−C(69)	128.6(15)
C(18)−C(19)−N(3)	121.6(13)	C(68)−C(69)−N(6)	119.8(14)
C(18)−C(19)−C(22)	122.4(13)	C(68)−C(69)−C(72)	121.1(14)
N(3)−C(19)−C(22)	115.3(12)	N(6)−C(69)−C(72)	119.1(13)

 © 2004 Wiley-VCH Verlag GmbH & Co. KGaA, Weinheim

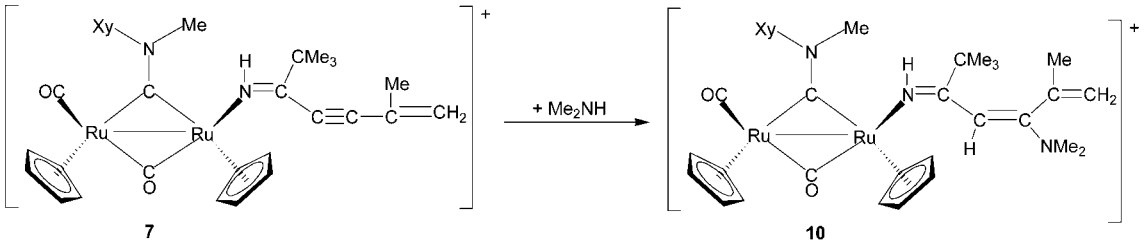

Scheme 6

lent Cp ligands, a broad resonance at δ ca. 6.5 ppm due to the iminic NH and a singlet at δ ca. 5 ppm due to the olefinic α-CH proton. Four different resonances at high frequency are present in the ^{13}C NMR spectra due to the bridging carbyne (ca. 310 ppm), the bridging CO (δ ca. 236 ppm), the terminal CO and the carbon of the imine (both at δ ca. 200 ppm). The α-CH olefinic carbon resonates at ca. 100 ppm, whereas the quaternary β-carbon resonates at δ = 155−156 ppm.

The NMR spectra of **8c** show the presence in solution of a single isomer, whereas two isomers are present in the case of **8a,b** and **9**, with ratios which perfectly correspond to the isomer ratios in the starting compounds **3a,b**. Therefore, it is possible to conclude that, in these cases, the two isomers present in solution are also the α and β isomers arising from the different orientation of the R- and Me groups on the aminocarbyne. The stereochemistry of all the addition products has been further confirmed by NOE experiments. For example, irradiation of the olefinic α-CH proton (δ = 5.20 ppm) of the major isomer of **9** resulted in the enhancement of the resonances due to the α-protons of the piperidine (δ = 3.11 ppm) and the Cp at higher frequency (δ = 5.38 ppm). In the same way, NOE was generated on the olefinic α-CH resonance, on the Cp resonating at δ = 4.98 ppm and in the aminocarbyne NMe resonance by irradiation of the Cp resonance at δ = 5.38 ppm. These data confirm that in this case the amination has occurred with a *cis* geometry and that the imino ligand in the major isomer is on the same side as the Me group of the aminocarbyne ligand (α isomer). Moreover, it is noteworthy that in this case the Cp resonating at lower frequency (δ = 4.98 ppm) is the one on the same side of the Xy group. The NOE observed on one Cp ligand when the other is irradiated agrees with a *cis* arrangement of the $Ru_2\{\mu\text{-}CN(Me)(Xy)\}(\mu\text{-}CO)(CO)(Cp)_2$ core.

Finally, the amination of **7**, which contains an iminoalkynyl ligand conjugated with an olefinic end group, i.e. $HN{=}C(CMe_3)C{\equiv}CC(Me){=}CH_2$, occurs regioselectively onto the C≡C bond affording the complex $[Ru_2\{\mu\text{-}CN(Me)(Xy)\}(\mu\text{-}CO)(CO)\{N(H){=}C(CMe_3)C(H){=}C(NMe_2)C(Me){=}CH_2\}(Cp)_2]^+$ (**10**) which contains the new 1-imino-2,4-dien-3-amine ligand $HN{=}C(CMe_3)CH{=}C(NMe_2)C(Me){=}CH_2$, in a 52% yield. In this case, the reaction is stereoselective, resulting only in the formation of the *cis* addition product (Scheme 6), as shown by NOE experiments.

Strong nucleophiles such as $NaBH_4$ or super-hydride ($LiBHEt_3$) react with **3**−**7** replacing the alkynylimino li-

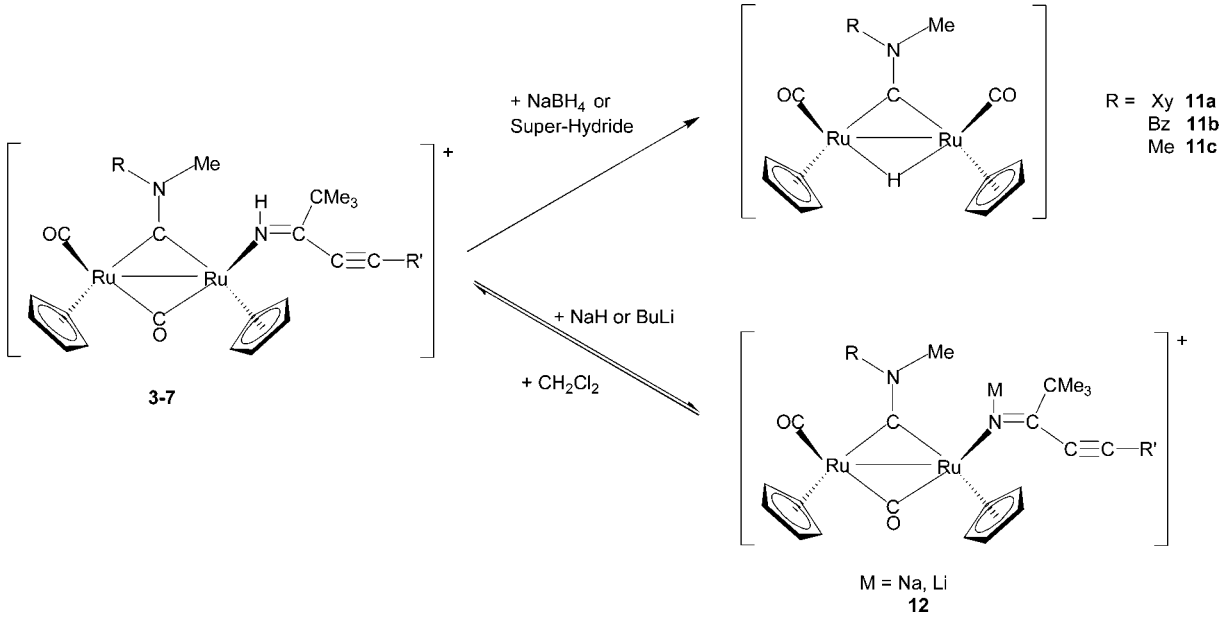

Scheme 7

 © 2004 Wiley-VCH Verlag GmbH & Co. KGaA, Weinheim

gand to give the hydrido complexes $[Ru_2\{\mu\text{-}CN(Me)(R)\}(\mu\text{-}H)(CO)_2Cp_2]$ (R = Xy, **11a**, Bz, **11b**; Me, **11c**),[21] whereas the reaction with nucleophiles having strong basic character such as NaH and *n*BuLi results in the almost quantitative formation of a new species, tentatively formulated as **12** (Scheme 7). Because of their instability, the latter compounds have not been isolated, but only characterised by IR spectroscopy. Compounds **12** show one terminal and one bridging ν(CO) absorption at wavenumbers similar to those of the cationic derivatives **3**−**7:** 1958 vs and 1803 s for the product obtained from **3a** and *n*BuLi, which should be compared with the IR spectrum of **3a** in THF (1961 vs, 1811 s). The reaction can easily be reversed by evaporation of the solvent in vacuo followed by dissolution of the residue in CH_2Cl_2. A simple explanation could be that metalation of the nitrogen of the imino ligand occurs and, thus, the new products can be formulated as $[Ru_2\{\mu\text{-}CN(Me)(R)\}(\mu\text{-}CO)(CO)\{N(M)=C(CMe_3)(C\equiv CR')\}(Cp_2)]^+$ (M = Li, Na, **12**). An alternative could be deprotonation of the NH instead of metalation, but this would afford a neutral azavinylidene species, in contrast with the IR data. It is noticeable that deprotonation of coordinated imines to give azavinylidene is quite well documented in the literature, whereas metalation is more rare.[4,22,23] Complexes of type **12** are also the product directly formed in THF during the reaction of **2a**−**c** with R′C≡CLi; the alkynylimino products **3**−**7** are, in fact, formed only after evaporation of THF and dissolution of the residue in CH_2Cl_2 (see above).

Conclusion

Nitriles are reported to be labile ligands and, therefore, very often used as intermediates for substitution reactions in organometallic chemistry. Nonetheless, addition of nucleophiles such as amines, alcohols and water have been extensively used for the synthesis of a large variety of metal complexes containing ligands such as azavinylidenes, amides, imidic esters and aminidines.[24,25] Addition of carbon nucleophiles is also known, although less common.[8,26] Despite our recent findings which demonstrated that the addition of acetylides to the nitrile ligand in (aminocarbyne)diiron complexes occurs only in one specific case,[10] we show here that the corresponding reaction is quite general for ruthenium: different substituents on the aminocarbyne have been used (i.e. Xy, Bz, Me) as well as aromatic and aliphatic acetylides. The alkynylimino complexes **3**−**7** are the only products formed in all the cases studied. Therefore, it seems that in the case of ruthenium there is no tendency at all for coupling between the imino and the aminocarbyne ligand, as found in the iron complex. Moreover, in the case of ruthenium it is not necessary to add strong acids, since the acidity of CH_2Cl_2 is sufficient for protonating the nitrogen, whereas the iron analogue requires the addition of strong acids. This suggests an enhanced basicity of the nitrogen in the case of ruthenium compared to iron, which could explain the different output of the two reactions.

The new alkynylimino ligand shows electrophilic properties. Nonetheless, it is not possible to use nucleophiles with a strong basic character, since they metalate the iminic nitrogen rather than adding to the triple bond. Conversely, strong nucleophiles such as $NaBH_4$ gives substitution and not addition. Thus, addition to the alkynylimino ligand can be achieved only using nucleophiles which are not too strong and not too basic, and here the case of secondary amines has been described. The reaction is completely regio- and stereoselective, resulting only in the addition to the β carbon of the ligand and protonation of the α carbon in a *cis* fashion. The resulting ligand can be described as an imino-2-en-3-amine ligand, which, as far as we know, has not been reported before. The procedure elaborated in this paper seems to be an interesting method of synthesizing new bimetallic complexes containing highly unsaturated ligands with heteroatoms.

Experimental Section

All reactions were carried out routinely under nitrogen using standard Schlenk techniques. Solvents were distilled immediately before use under nitrogen from appropriate drying agents. Infrared spectra were recorded with a Perkin−Elmer Spectrum 2000 FT-IR spectrophotometer and elemental analyses were performed on a ThermoQuest Flash 1112 Series EA Instrument. ESI MS spectra were recorded with a Waters Micromass ZQ 4000 with samples dissolved in CH_3CN. All NMR measurements were performed with Varian Gemini 300, Mercury 400 and Inova 600 instruments. The chemical shifts for ^1H and ^{13}C NMR spectra were referenced to internal TMS. The spectra were fully assigned via DEPT experiments and ^1H,^{13}C NMR spectra correlation through gs-HSQC and gs-HMBC experiments.[20] In some cases it has not been possible to assign all the resonances to the minor isomer, especially when it was present in very low concentration. NOE measurements were recorded using the DPFGSE-NOE sequence.[27] All chemicals were used as received from Aldrich Co., except $[Ru_2\{\mu\text{-}CN(Me)(R)\}(\mu\text{-}CO)(CO)_2(Cp)_2][CF_3SO_3]$ (R = Xy, **1a**; Bz, **1b**; Me, **1c**) which were prepared by published methods.[11] The acetylides R′C≡CLi [R′ = Tol, Ph, Me_3Si, *n*Bu, $C(Me)=CH_2$] were prepared just before use from the reaction of the appropriate alkyne R′C≡CH in THF at −50 °C with *n*BuLi (alkyne/*n*BuLi, 1.2).

$[Ru_2\{\mu\text{-}CN(Me)(R)\}(\mu\text{-}CO)(CO)(NCCMe_3)(Cp)_2][CF_3SO_3]$ (R = Xy, 2a; Bz, 2b; Me, 2c). General Procedure: Me_3NO (30.0 mg, 0.400 mmol) was added to a solution containing $[Ru_2\{\mu\text{-}CN(Me)(R)\}(\mu\text{-}CO)(CO)_2(Cp)_2][CF_3SO_3]$ (0.200 mmol) and Me_3CCN (0.1 mL, 0.905 mmol) in THF (5 mL). The resulting suspension was stirred at room temperature for 3 h and, then, the solid removed by filtration through a Celite pad. The solvent was removed under reduced pressure and the residue washed with petroleum ether (2 × 5 mL) and Et_2O (2 × 5 mL) affording the final product as a yellow-orange powder.

2a: $C_{28}H_{31}F_3N_2O_5Ru_2S$ (766.77): calcd. C 43.86, H 4.08, N 3.65; found C 44.02, H 3.99, N 3.54. Yield: 135.0 mg, 88%. ^1H NMR (300.04 MHz, $CDCl_3$, 25 °C) α-Isomer: δ = 1.26 (s, 9 H, CMe_3), 2.23, 2.42 (s, 6 H, $Me_2C_6H_3$), 4.30 (s, 3 H, N*Me*), 4.98, 5.38 (s, 10 H, *Cp*), 7.10−7.36 (m, 3 H, $Me_2C_6H_3$) ppm; β-Isomer: δ = 1.22 (s, 9 H, CMe_3), 2.19, 2.42 (s, 6 H, $Me_2C_6H_3$), 4.22 (s, 3 H, N*Me*), 4.71, 5.58 (s, 10 H, *Cp*), 7.10−7.36 (m, 3 H, $Me_2C_6H_3$) ppm. α/β =

 © 2004 Wiley-VCH Verlag GmbH & Co. KGaA, Weinheim

1.5. ^{13}C NMR (75.457 MHz, $CDCl_3$, 25 °C) α-Isomer: δ = 17.2, 18.2 (*Me*$_2$C$_6$H$_3$), 27.3 (C*Me*$_3$), 30.3 (*C*Me$_3$), 53.0 (N*Me*), 88.1, 89.7 (*Cp*), 128.6, 128.7, 129.4 (*C*H Me$_2$C$_6$H$_3$), 128.8, 131.7 (*C*Me Me$_2$C$_6$H$_3$), 134.3 (Me$_3$C*C*N), 147.6 (*C-ipso* Me$_2$C$_6$H$_3$), 200.4 (*C*O), 236.5 (μ-*C*O), 310.6 (μ-*C*) ppm; β-Isomer: δ = 17.6, 18.3 (*Me*$_2$C$_6$H$_3$), 27.4 (C*Me*$_3$), 30.4 (*C*Me$_3$), 54.6 (N*Me*), 87.2, 90.6 (*Cp*), 128.6, 128.7, 129.4 (*C*H Me$_2$C$_6$H$_3$), 128.8, 131.7 (*C*Me Me$_2$C$_6$H$_3$), 133.9 (Me$_3$C*C*N), 147.5 (*C-ipso* Me$_2$C$_6$H$_3$), 200.0 (*C*O), 235.2 (μ-*C*O), 310.2 (μ-*C*) ppm. IR (CH_2Cl_2, 25 °C): $\tilde{\nu}$ = 1982 vs (CO), 1819 s (μ-CO), 1529 m (C=N) cm^{-1}.

2b: $C_{27}H_{29}F_3N_2O_5Ru_2S$ (752.74): calcd. C 43.08, H 3.88, N 3.72; found C 42.92, H 3.97, N 3.52. Yield: 128.0 mg, 85%. ^{1}H NMR (300.04 MHz, $CDCl_3$, 25 °C) α-Isomer: δ = 1.18 (s, 9 H, C*Me*$_3$), 3.90 (s, 3 H, N*Me*), 5.30, 5.48 (s, 10 H, *Cp*), 5.63, 5.64 (d, AB, $^2J_{H,H}$ = 14.3 Hz, 2 H, C*H*$_2$Ph), 7.26−7.48 (m, 3 H, Me$_2$C$_6$*H*$_3$) ppm; β-Isomer: δ = 1.20 (s, 9 H, C*Me*$_3$), 3.82 (s, 3 H, N*Me*), 5.26, 5.51 (s, 10 H, *Cp*), 5.67, 5.78 (d, AB, $^2J_{H,H}$ = 14.8 Hz, 2 H, C*H*$_2$Ph), 7.26−7.48 (m, 3 H, Me$_2$C$_6$*H*$_3$) ppm. α/β = 1.5. ^{13}C NMR (75.457 MHz, $CDCl_3$, 25 °C) α-Isomer: δ = 27.6 (C*Me*$_3$), 30.5 (*C*Me$_3$), 49.1 (N*Me*), 70.6 (*C*H$_2$Ph), 88.0, 90.3 (*Cp*), 127.4−134.2 (Ph + Me$_3$C*C*N), 200.8 (*C*O), 237.0 (μ-*C*O), 304.6 (μ-*C*) ppm; β-Isomer: δ = 27.7 (C*Me*$_3$), 30.6 (*C*Me$_3$), 50.4 (N*Me*), 70.2 (*C*H$_2$Ph), 87.8, 90.5 (*Cp*), 127.4−134.2 (Ph + Me$_3$C*C*N), 200.0 (*C*O), 237.8 (μ-*C*O), 304.3 (μ-*C*) ppm. IR (CH_2Cl_2, 25 °C): $\tilde{\nu}$ = 1980 vs (CO), 1817 s (μ-CO), 1588 w, 1573.7 m, 1550 w (C=N) cm^{-1}.

2c: $C_{21}H_{25}F_3N_2O_5Ru_2S$ (676.64): calcd. C 37.28, H 3.72, N 4.14; found C 37.09, H 3.84, N 4.01. Yield: 117.7 mg, 87%. ^{1}H NMR (300.04 MHz, $CDCl_3$, 25 °C): δ = 1.14 (s, 9 H, C*Me*$_3$), 3.98, 4.06 (s, 6 H, N*Me*$_2$), 5.19, 5.39 (s, 10 H, Cp) ppm. ^{13}C NMR (75.457 MHz, $CDCl_3$, 25 °C): δ = 27.6 (C*Me*$_3$), 30.5 (*C*Me$_3$), 52.2, 53.4 (N*Me*$_2$), 89.9, 90.1 (Cp), 133.5 (Me$_3$C*C*N), 200.0 (*C*O), 237.8 (μ-*C*O), 302.6 (μ-*C*) ppm. IR (CH_2Cl_2, 25 °C): $\tilde{\nu}$ = 1978 vs (CO), 1815 s (μ-CO), 1599 m (C=N) cm^{-1}.

[Ru$_2${μ-CN(Me)(R)}(μ-CO)(CO){N(H)=C(CMe$_3$)(C≡CR′)}(Cp$_2$)]$^+$ (R = Xy, R′ = Tol, 3a; R = Bz, R′ = Tol, 3b; R = Me, R′ = Tol, 3c; R = Xy, R′ = Ph, 4a; R = Bz, R′ = Ph, 4b; R = Me, R′ = Ph, 4c; R = Bz, R′ = H, 5; R = Xy, R′ = *n*Bu, 6; R = Xy, R′ = [C(Me)=CH$_2$], 7). General Procedure: A solution of the appropriate acetylide R′C≡CLi (0.225 mmol) in THF (3 mL) was added dropwise to a solution of **2a−c** (0.150 mmol) in THF (6 mL) at −50 °C and the resulting red solution stirred at room temperature for 30 minutes. Then, the solvent was removed in vacuo and the residue dissolved in CH_2Cl_2 (5 mL) and chromatographed through an Al_2O_3 column. The final product was obtained as an orange fraction using CH_3CN as eluent.

3a: $C_{37}H_{39}F_3N_2O_5Ru_2S$ (882.93): calcd. C 50.33, H 4.45, N 3.17; found C 50.52, H 4.27, N 3.09. Yield: 86.1 mg, 65%. ^{1}H NMR (599.738 MHz, $CDCl_3$, 25 °C) α-Isomer: δ = 1.15 (s, 9 H, C*Me*$_3$), 2.21, 2.44 (s, 6 H, *Me*$_2$C$_6$H$_3$), 2.43 (s, 3 H, *p-Me*C$_6$H$_4$), 4.41 (s, 3 H, N*Me*), 4.95, 5.46 (s, 10 H, *Cp*), 7.10−7.65 (m, 7 H, Me$_2$C$_6$*H*$_3$ + *p*-MeC$_6$*H*$_4$) 7.45 (br., 1 H, N*H*) ppm; β-Isomer: δ = 1.09 (s, 9 H, C*Me*$_3$), 2.11, 2.48 (s, 6 H, *Me*$_2$C$_6$H$_3$), 2.40 (s, 3 H, *p-Me*C$_6$H$_4$), 4.24 (s, 3 H, N*Me*), 4.87, 5.62 (s, 10 H, *Cp*), 7.10−7.65 (m, 8 H, Me$_2$C$_6$*H*$_3$ + *p*-MeC$_6$*H*$_4$ + N*H*) ppm. α/β = 10. ^{13}C NMR (75.457 MHz, $CDCl_3$, 25 °C) α-Isomer: δ = 17.5, 18.4 (*Me*$_2$C$_6$H$_3$), 21.8 (*p-Me*C$_6$H$_4$), 26.8 (C*Me*$_3$), 42.2 (*C*Me$_3$), 53.2 (N*Me*), 89.0, 89.8 (*Cp*), 105.8, 117.0 (*C*≡*C*), 128.1−148.2 (Me$_2$*C*$_6$H$_3$ + *p*-Me*C*$_6$H$_4$), 184.3 (*C*=N), 201.7 (*C*O), 236.0 (μ-*C*O), 311.7 (μ-*C*) ppm; β-Isomer: δ = 17.8, 18.6 (*Me*$_2$C$_6$H$_3$), 21.7 (*p-Me*C$_6$H$_4$), 27.2 (C*Me*$_3$), 41.4 (*C*Me$_3$), 55.4 (N*Me*), 88.1, 91.2 (*Cp*), 105.8, 116.7 (*C*≡*C*), 128.1−148.2 (Me$_2$*C*$_6$H$_3$ + *p*-Me*C*$_6$H$_4$), 183.3 (*C*=N), 202.0 (*C*O), 236.0 (μ-*C*O), 312.7 (μ-*C*) ppm. IR (CH_2Cl_2, 25 °C): $\tilde{\nu}$ = 2200 m (C≡C), 1968 vs (CO), 1811 s (μ-CO), 1560 w, 1508 m (C=N) cm^{-1}. IR (KBr, 25 °C): $\tilde{\nu}$ = 3314 ms (NH) cm^{-1}.

3b: $C_{36}H_{37}F_3N_2O_5Ru_2S$ (868.91): calcd. C 49.76, H 4.29, N 3.22; found C 49.21, H 4.59, N 3.79. Yield: 86.0 mg, 66%. ^{1}H NMR (300.04 MHz, $CDCl_3$, 25 °C) α-Isomer: δ = 1.07 (s, 9 H, C*Me*$_3$), 2.33 (s, 3 H, *p-Me*C$_6$H$_4$), 3.95 (s, 3 H, N*Me*), 5.40, 5.50 (s, 10 H, *Cp*), 5.56, 5.67 (d, AB, $^2J_{H,H}$ = 14.1 Hz, 2 H, C*H*$_2$Ph), 7.04−7.56 (m, 10 H, C$_6$*H*$_5$ + *p*-MeC$_6$*H*$_4$ + N*H*) ppm; β-Isomer: δ = 1.04 (s, 9 H, C*Me*$_3$), 2.35 (s, 3 H, *p-Me*C$_6$H$_4$), 3.89 (s, 3 H, N*Me*), 5.34, 5.52 (s, 10 H, *Cp*), 5.79, 5.90 (d, AB, $^2J_{H,H}$ = 15.1 Hz, 2 H, C*H*$_2$Ph), 7.04−7.56 (m, 10 H, C$_6$*H*$_5$ + *p*-MeC$_6$*H*$_4$ + N*H*) ppm. α/β = 1.6. ^{13}C NMR (75.457 MHz, $CDCl_3$, 25 °C) α-Isomer: δ = 21.4 (*p-Me*C$_6$H$_4$), 26.9 (C*Me*$_3$), 43.7 (*C*Me$_3$), 48.9 (N*Me*), 70.8 (*C*H$_2$Ph), 88.5, 90.5 (*Cp*), 105.6, 116.7 (*C*≡*C*), 127.0−132.5 (CH *C*$_6$H$_5$ + *p*-Me*C*$_6$H$_4$), 134.2, 138.2, 142.0 (*C-ipso* Ph + *C-ipso* Tol + *C*−Me Tol), 183.6 (*C*=N), 202.4 (*C*O), 238.4 (μ-*C*O), 305.7 (μ-*C*) ppm; β-Isomer: δ = 21.8 (*p-Me*C$_6$H$_4$), 27.1 (C*Me*$_3$), 43.7 (*C*Me$_3$), 51.0 (N*Me*), 69.6 (*C*H$_2$Ph), 88.5, 90.6 (*Cp*), 105.5, 118.5 (*C*≡*C*), 127.0−132.5 (CH *C*$_6$H$_5$ + *p*-Me*C*$_6$H$_4$), 134.6, 138.2, 141.9 (*C-ipso* Ph + *C-ipso* Tol + *C*−Me Tol), 183.6 (*C*=N), 201.3 (*C*O), 239.2 (μ-*C*O), 305.8 (μ-*C*) ppm. IR (CH_2Cl_2, 25 °C): $\tilde{\nu}$ = 2201 m (C≡C), 1968 vs (CO), 1810 s (μ-CO), 1606 w, 1568 m, 1548 w, 1509 m (C=N) cm^{-1}. IR (KBr, 25 °C): $\tilde{\nu}$ = 3315 s (NH) cm^{-1}. MS (ESI): ES+ *m*/*z* = 721, ES− *m*/*z* = 149.

3c: $C_{30}H_{33}F_3N_2O_5Ru_2S$ (793.82): calcd. C 45.39, H 4.19, N 3.53; found C 45.28, H 4.23, N 3.42. Yield: 89.3 mg, 75%. ^{1}H NMR (300.04 MHz, $CDCl_3$, 25 °C): δ = 1.07 (s, 9 H, C*Me*$_3$), 2.44 (s, 3 H, *p-Me*C$_6$H$_4$), 4.05, 4.18 (s, 6 H, N*Me*$_2$), 5.34, 5.46 (s, 10 H, *Cp*), 7.03 (br., 1 H, N*H*), 7.08−7.58 (m, 4 H, *p*-MeC$_6$*H*$_4$) ppm. ^{13}C NMR (75.457 MHz, $CDCl_3$, 25 °C): δ = 21.4 (*p-Me*C$_6$H$_4$), 27.0 (C*Me*$_3$), 43.6 (*C*Me$_3$), 52.0, 53.8 (N*Me*$_2$), 88.2, 90.2 (*Cp*), 105.3, 116.8 (*C*≡*C*), 128.8, 129.7, 131.4, 132.0 (CH *p*-Me*C*$_6$H$_4$), 138.1, 141.8 (*C-ipso* + *C*−Me *p*-Me*C*$_6$H$_4$), 183.4 (*C*=N), 201.2 (*C*O), 238.7 (μ-*C*O), 303.6 (μ-*C*) ppm. IR (CH_2Cl_2, 25 °C): $\tilde{\nu}$ = 2201 m (C≡C), 1968 vs (CO), 1809 s (μ-CO), 1588 w, 1509 m (C=N) cm^{-1}. IR (KBr, 25 °C): $\tilde{\nu}$ = 3322 m (NH) cm^{-1}.

4a: $C_{36}H_{37}F_3N_2O_5Ru_2S$ (868.91): calcd. C 49.76, H 4.29, N 3.22; found C 49.22, H 4.01, N 3.58. Yield: 89.9 mg, 65%. ^{1}H NMR (300.04 MHz, $CDCl_3$, 25 °C) α-Isomer: δ = 1.15 (s, 9 H, C*Me*$_3$), 2.24, 2.44 (s, 6 H, *Me*$_2$C$_6$H$_3$), 4.41 (s, 3 H, N*Me*), 4.95, 5.45 (s, 10 H, *Cp*), 7.04 (br., 1 H, N*H*), 7.06−7.76 (m, 8 H, Me$_2$C$_6$*H*$_3$ + C$_6$*H*$_5$) ppm; β-Isomer: concentration too low to be characterized (α/β > 20:1). ^{13}C NMR (75.457 MHz, $CDCl_3$, 25 °C) α-Isomer: δ = 17.6, 18.5 (*Me*$_2$C$_6$H$_3$), 26.8 (C*Me*$_3$), 44.0 (*C*Me$_3$), 53.2 (N*Me*), 89.0, 89.9 (Cp), 105.0 120.1, (*C*≡*C*), 128.1−148.2 (Me$_2$*C*$_6$H$_3$ + *C*$_6$H$_5$), 184.2 (*C*=N), 201.5 (*C*O), 235.8 (μ-*C*O), 311.4 (μ-*C*) ppm. IR (CH_2Cl_2, 25 °C): $\tilde{\nu}$ = 2206 m (C≡C), 1969 vs (CO), 1814 s (μ-CO), 1568 w, 1525 m (C=N) cm^{-1}.

4b: $C_{35}H_{35}F_3N_2O_5Ru_2S$ (854.88): calcd. C 49.17, H 4.13, N 3.28; found C 49.55, H 4.01, N 3.60. Yield: 76.9 mg, 60%. ^{1}H NMR (300.04 MHz, $CDCl_3$, 25 °C) α-Isomer: δ = 1.08 (s, 9 H, C*Me*$_3$), 3.96 (s, 3 H, N*Me*), 5.40, 5.51 (s, 10 H, *Cp*), 5.58, 5.66 (d, AB, $^2J_{H,H}$ = 14.0 Hz, 2 H, C*H*$_2$Ph), 7.12−7.69 (m, 11 H, C$_6$*H*$_5$ + CH$_2$C$_6$*H*$_5$ + N*H*); β-Isomer: δ = 1.04 (s, 9 H, C*Me*$_3$), 3.90 (s, 3 H, N*Me*), 5.35, 5.53 (s, 10 H, *Cp*), 5.82, 5.91 (d, AB, $^2J_{H,H}$ = 14.0 Hz, 2 H, C*H*$_2$Ph), 7.12−7.69 (m, 11 H, C$_6$*H*$_5$ + CH$_2$C$_6$*H*$_5$ + N*H*) ppm. α/β = 1.9. ^{13}C NMR (75.457 MHz, $CDCl_3$, 25 °C) α-Isomer: δ = 27.0 (C*Me*$_3$), 43.8 (*C*Me$_3$), 49.0 (N*Me*), 70.9 (*C*H$_2$Ph), 88.5, 90.6 (*Cp*), 105.1, 119.8 (*C*≡*C*), 127.1−134.6 (*C*$_6$H$_5$ + CH$_2$*C*$_6$H$_5$), 183.6 (*C*=N), 202.4 (*C*O), 238.5 (μ-*C*O), 305.6 (μ-*C*); β-Isomer: δ = 26.9

 © 2004 Wiley-VCH Verlag GmbH & Co. KGaA, Weinheim

(C*Me*$_3$), 43.8 (*C*Me$_3$), 51.1 (N*Me*), 69.7 (*C*H$_2$Ph), 88.5, 90.6 (*Cp*), 104.6, 119.0 (*C*≡*C*), 127.1−134.6 (C_6H_5 + $CH_2C_6H_5$), 183.6 (*C*=N), 201.3 (*C*O), 239.3 (μ-*C*O), 305.6 (μ-*C*) ppm. IR (CH_2Cl_2, 25 °C): $\tilde{\nu}$ = 2206 m (C≡C), 1966 vs (CO), 1810 s (μ-CO), 1584 w, 1570 m, 1545 w (C=N) cm^{-1}. MS (ESI): ES+ *m*/*z* = 707, ES− *m*/*z* = 149.

4c: $C_{29}H_{31}F_3N_2O_5Ru_2S$ (778.78): calcd. C 44.73, H 4.01, N 3.60; found C 44.59, H 4.13, N 3.49. Yield: 84.1 mg, 72%. ^{1}H NMR (300.04 MHz, $CDCl_3$, 25 °C): δ = 1.04 (s, 9 H, C*Me*$_3$), 4.02, 4.15 (s, 6 H, N*Me*$_2$), 5.30, 5.42 (s, 10 H, *Cp*), 7.08 (br., 1 H, N*H*), 7.44−7.68 (m, 5 H, C_6H_5) ppm. ^{13}C NMR (75.457 MHz, $CDCl_3$, 25 °C): δ = 27.0 (C*Me*$_3$), 43.7 (*C*Me$_3$), 52.1, 53.8 (N*Me*$_2$), 88.2, 90.3 (*Cp*), 104.7, 120.0 (*C*≡*C*), 129.0, 131.0, 132.1 (C_6H_5), 183. 5 (*C*=N), 201.1 (*C*O), 238.6 (μ-*C*O), 303.7 (μ-*C*) ppm. IR (CH_2Cl_2, 25 °C): $\tilde{\nu}$ = 2206 m (C≡C), 1966 vs (CO), 1807 s (μ-CO), 1591 w (C=N) cm^{-1}. IR (KBr, 25 °C): $\tilde{\nu}$ = 3317 m (NH) cm^{-1}.

5: $C_{29}H_{31}F_3N_2O_5Ru_2S$ (778.78): calcd. C 44.73, H 4.01, N 3.60; found C 4.97, H 4.11, N 3.45. Yield: 65.4 mg, 56%. ^{1}H NMR (300.04 MHz, $CDCl_3$, 25 °C) α-Isomer: δ = 0.97 (s, 9 H, C*Me*$_3$), 2.14 (s, 1 H, *H*C≡C), 3.89 (s, 3 H, N*Me*), 5.33, 5.46 (s, 10 H, *Cp*), 5.49, 5.58 (d, AB, $^2J_{H,H}$ = 14.3 Hz, 2 H, C*H*$_2$Ph), 7.16−7.38 (m, 6 H, $CH_2C_6H_5$ + N*H*) ppm; β-Isomer: δ = 0.94 (s, 9 H, C*Me*$_3$), 2.13 (s, 1 H, *H*C≡C), 3.83 (s, 3 H, N*Me*), 5.28, 5.48 (s, 10 H, *Cp*), 5.44, 5.56 (d, AB, $^2J_{H,H}$ = 13.5 Hz, 2 H, C*H*$_2$Ph), 7.16−7.38 (m, 6 H, $CH_2C_6H_5$ + N*H*) ppm. α/β = 2.1. ^{13}C NMR (75.457 MHz, $CDCl_3$, 25 °C) α-Isomer: δ = 26.6 (C*Me*$_3$), 43.8 (*C*Me$_3$), 49.3 (N*Me*), 70.9 (*C*H$_2$Ph), 88.6, 90.6 (*Cp*), 93.9 (C≡*C*H), 118.8 (*C*≡CH), 127.0−129.3 (CH $CH_2C_6H_5$), 134.1 (*C-ipso* $CH_2C_6H_5$), 183.3 (*C*=N), 202.4 (*C*O), 238.5 (μ-*C*O), 305.0 (μ-*C*) ppm; β-Isomer: δ = 26.7 (C*Me*$_3$), 44.7 (*C*Me$_3$), 51.1 (N*Me*), 70.6 (*C*H$_2$Ph), 88.6, 90.6 (*Cp*), 93.7 (C≡*C*H), 118.8 (*C*≡CH), 127.0−129.3 (CH $CH_2C_6H_5$), 134.5 (*C-ipso* $CH_2C_6H_5$), 183.3 (*C*=N), 201.4 (*C*O), 238.9 (μ-*C*O), 306.6 (μ-*C*) ppm. IR (CH_2Cl_2, 25 °C): $\tilde{\nu}$ = 1967 vs (CO), 1809 s (μ-CO), 1587 w, 1570 m, 1545 w (C=N) cm^{-1}. MS (ESI): ES+ *m*/*z* = 631, ES− *m*/*z* = 149.

6: $C_{34}H_{41}F_3N_2O_5Ru_2S$ (852.60): calcd. C 47.90, H 4.85, N 3.29; found C 48.02, H 4.71, N 3.18. Yield: 88.2 mg, 69%. ^{1}H NMR (300.04 MHz, $CDCl_3$, 25 °C) α-Isomer: δ = 0.93 (t, $^3J_{H,H}$ = 7.3 Hz, 3 H, $CH_2CH_2CH_2CH_3$), 0.98 (s, 9 H, C*Me*$_3$), 1.45, 1.66 (m, 4 H, $CH_2CH_2CH_2CH_3$), 2.09, 2.36 (s, 6 H, *Me*$_2$C$_6$H$_3$), 2.61 (t, $^3J_{H,H}$ = 7.1 Hz, 2 H, $CH_2CH_2CH_2CH_3$), 4.29 (s, 3 H, N*Me*), 4.87, 5.34 (s, 10 H, *Cp*), 7.13−7.24 (m, 4 H, $Me_2C_6H_3$ + N*H*) ppm. β-Isomer: concentration too low to be characterized (α/β > 20:1). ^{13}C NMR (75.457 MHz, $CDCl_3$, 25 °C) α-Isomer: δ = 13.6 ($CH_2CH_2CH_2CH_3$), 17.5, 18.5 (*Me*$_2$C$_6$H$_3$), 26.8 (C*Me*$_3$), 19.7, 22.3, 29.8 ($CH_2CH_2CH_2CH_3$), 43.9 (*C*Me$_3$), 53.1 (N*Me*), 88.9, 89.9 (*Cp*), 109.2, 118.7, (*C*≡*C*), 128.8, 128.9, 129.6 (CH $Me_2C_6H_3$), 131.6, 133.0 (*C*Me $Me_2C_6H_3$), 148.1 (*C-ipso* $Me_2C_6H_3$), 184.4 (*C*=N), 201.8 (*C*O), 235.7 (μ-*C*O), 311.3 (μ-*C*) ppm. IR (CH_2Cl_2, 25 °C): $\tilde{\nu}$ = 2215 m (C≡C), 1967 vs (CO), 1812 s (μ-CO), 1558 w, 1519 m, 1507 m (C=N) cm^{-1}.

7: $C_{33}H_{37}F_3N_2O_5Ru_2S$ (832.87): calcd. C 47.59, H 4.48, N 3.36; found C 47.71, H 4.37, N 3.21. Yield: 86.7 mg, 67%. ^{1}H NMR (300.04 MHz, $CDCl_3$, 25 °C) α-Isomer: δ = 1.04 (s, 9 H, C*Me*$_3$), 2.08 (s, 3 H, *Me*C=CH$_2$), 2.16, 2.39 (s, 6 H, *Me*$_2$C$_6$H$_3$), 4.35 (s, 3 H, N*Me*), 4.90, 5.39 (s, 10 H, *Cp*), 5.65, 5.75 (br., 2 H, MeC=C*H*$_2$), 7.17−7.28 (m, 3 H, $Me_2C_6H_3$), 7.44 (br., 1 H, N*H*) ppm; β-Isomer: δ = 0.99 (s, 9 H, C*Me*$_3$), 2.00 (s, 3 H, *Me*C=CH$_2$), 2.15, 2.42 (s, 6 H, *Me*$_2$C$_6$H$_3$), 4.19 (s, 3 H, N*Me*), 4.78, 5.57 (s, 10 H, *Cp*) ppm. α/β = 20. ^{13}C NMR (75.457 MHz, $CDCl_3$, 25 °C) α-Isomer: δ = 17.6, 18.5 (*Me*$_2$C$_6$H$_3$), 22.5 (*Me*C=CH$_2$), 26.8 (C*Me*$_3$), 44.0 (*C*Me$_3$), 53.2 (N*Me*), 88.9, 89.9 (*Cp*), 105.9, 124.9 (*C*≡*C*), 127.7 (MeC=*C*H$_2$), 128.8, 128.9, 129.6 (*C*−H $Me_2C_6H_3$), 132.5 (Me*C*=CH$_2$), 131.6, 132.9 (*C*−Me $Me_2C_6H_3$), 148.1 (*C-ipso* $Me_2C_6H_3$), 184.1 (*C*=N), 201.6 (*C*O), 235.5 (μ-*C*O), 311.5 (μ-*C*) ppm; β-Isomer: δ = 17.8, 18.9 (*Me*$_2$C$_6$H$_3$), 27.1 (C*Me*$_3$), 56.9 (N*Me*), 88.0, 91.1 (*Cp*) ppm. IR (CH_2Cl_2, 25 °C): $\tilde{\nu}$ = 2193 m (C≡C), 1969 vs (CO), 1814 s (μ-CO), 1566 w, 1525 m (C=N) cm^{-1}.

[Ru$_2${μ-CN(Me)(R)}(μ-CO)(CO){N(H)=C(CMe$_3$)C(H)=C(NMe$_2$)-(Tol)}(Cp)$_2$]$^+$ (R = Xy, 8a; Bz, 8b; Me, 8c). General Procedure: Me_2NH (3 mL, 2 M in THF, 6 mmol) was added to a solution of **3a**−**c** (0.1 mmol) in THF (5 mL) and stirred at room temperature for 1 hour. The solvent was removed in vacuo and the residue dissolved in CH_2Cl_2 (4 mL) and chromatographed through Al_2O_3. The final product was obtained as an orange-yellow fraction using CH_3CN as eluent.

8a: $C_{39}H_{46}F_3N_3O_5Ru_2S$ (928.02): calcd. C 50.48, H 5.00, N 4.53; found C 50.26, H 5.14, N 4.89. Yield: 56.6 mg, 61%. ^{1}H NMR (300.04 MHz, $CDCl_3$, 25 °C) α-Isomer: δ = 0.68 (s, 9 H, C*Me*$_3$), 2.22, 2.45 (s, 6 H, *Me*$_2$C$_6$H$_3$), 2.38 (s, 3 H, *p*-*Me*C$_6$H$_4$), 2.89 (s, 6 H, N*Me*$_2$), 4.31 (s, 3 H, N*Me*), 5.08 (s, 1 H, *H*C=C), 4.97, 5.36 (s, 10 H, *Cp*), 6.69 (br., 1 H, N*H*), 7.12−7.32 (m, 7 H, $Me_2C_6H_3$ + *p*-MeC_6H_4) ppm. β-Isomer: concentration too low to be characterized (α/β > 20:1). ^{13}C NMR (75.457 MHz, $CDCl_3$, 25 °C) α-Isomer: δ = 17.8, 18.5 (*Me*$_2$C$_6$H$_3$), 21.3 (*p*-*Me*C$_6$H$_4$), 29.1 (C*Me*$_3$), 41.5 (N*Me*$_2$), 42.2 (*C*Me$_3$), 58.8 (N*Me*), 88.7, 89.8 (*Cp*), 100.5 (H*C*=C), 128.8, 128.9, 129.4, 129.6, 129.7 (*C*−H $Me_2C_6H_3$ + *p*-MeC_6H_4), 131.6, 133.2, 134.1 (*C*−Me $Me_2C_6H_3$ + *p*-MeC_6H_4), 140.1, 147.8 (*C-ipso* $Me_2C_6H_3$ + *p*-MeC_6H_4), 155.4 (HC=*C*), 201.0 (*C*=N), 202.9 (*C*O), 235.8 (μ-*C*O), 311.7 (μ-*C*) ppm. IR (CH_2Cl_2, 25 °C): $\tilde{\nu}$ = 1966 vs (CO), 1809 s (μ-CO), 1600 br, 1512 m (C=N) cm^{-1}. IR (KBr, 25 °C): $\tilde{\nu}$ = 3326 br. (NH) cm^{-1}. MS (ESI): ES+ *m*/*z* = 780, ES− *m*/*z* = 149.

8b: $C_{38}H_{44}F_3N_3O_5Ru_2S$ (913.99): calcd. C 49.94, H 4.85, N 4.60; found C 49.78, H 5.12, N 4.35. Yield: 54.8 mg, 60%. ^{1}H NMR (300.04 MHz, $CDCl_3$, 25 °C) α-Isomer: δ = 0.54 (s, 9 H, C*Me*$_3$), 2.32 (s, 3 H, *p*-*Me*C$_6$H$_4$), 2.82 (s, 6 H, N*Me*$_2$), 3.84 (s, 3 H, N*Me*), 4.88 (s, 1 H, *H*C=C), 5.21, 5.48 (s, 10 H, *Cp*), 5.55, 5.64 (d, AB, $^2J_{H,H}$ = 14.2 Hz, 2 H, C*H*$_2$Ph), 6.38 (br., 1 H, N*H*), 6.99−7.33 (m, 9 H, C_6H_5 + *p*-MeC_6H_4) ppm; β-Isomer: δ = 0.50 (s, 9 H, C*Me*$_3$), 2.28 (s, 3 H, *p*-*Me*C$_6$H$_4$), 2.80 (s, 6 H, N*Me*$_2$), 3.88 (s, 3 H, N*Me*), 4.92 (s, 1 H, *H*C=C), 5.23, 5.51 (s, 10 H, *Cp*), 5.75, 5.78 (d, AB, $^2J_{H,H}$ = 16.0 Hz, 2 H, C*H*$_2$Ph), 6.42 (br., 1 H, N*H*), 6.99−7.33 (m, 9 H, C_6H_5 + *p*-MeC_6H_4) ppm. α/β = 1.8. ^{13}C NMR (75.457 MHz, $CDCl_3$, 25 °C) α-Isomer: δ = 21.3 (*p*-*Me*C$_6$H$_4$), 29.0 (C*Me*$_3$), 41.5 (N*Me*$_2$), 43.6 (*C*Me$_3$), 48.6 (N*Me*), 70.7 (*C*H$_2$Ph), 88.3, 90.4 (*Cp*), 100.2 (H*C*=C), 127.4−129.6 (CH C_6H_5 + *p*-MeC_6H_4), 134.1, 134.5, 140.1 (*C-ipso* Ph + *C-ipso* Tol + *C*−Me Tol), 155.5 (HC=*C*), 200.1 (*C*=N), 203.4 (*C*O), 237.7 (μ-*C*O), 306.4 (μ-*C*) ppm; β-Isomer: δ = 21.5 (*p*-*Me*C$_6$H$_4$), 29.1 (C*Me*$_3$), 41.5 (N*Me*$_2$), 43.7 (*C*Me$_3$), 50.9 (N*Me*), 69.6 (*C*H$_2$Ph), 88.1, 90.6 (*Cp*), 101.4 (H*C*=C), 127.4−129.6 (CH C_6H_5 + *p*-MeC_6H_4), 134.0, 134.2, 140.1 (*C-ipso* Ph + *C-ipso* Tol + *C*−Me Tol), 155.2 (HC=*C*), 200.4 (*C*=N), 202.6 (*C*O), 239.3 (μ-*C*O), 306.43 (μ-*C*) ppm. IR (CH_2Cl_2, 25 °C): $\tilde{\nu}$ = 1962 vs (CO), 1806 s (μ-CO), 1589 w, 1569 w, 1570 m, 1542 m, 1504 m (C=N) cm^{-1}. IR (KBr, 25 °C): $\tilde{\nu}$ = 3324 br. (NH) cm^{-1}.

8c: $C_{32}H_{40}F_3N_3O_5Ru_2S$ (837.89): calcd. C 45.87, H 4.81, N 5.01; found C 46.13, H 4.65, N 5.33. Yield: 58.7 mg, 70%. ^{1}H NMR (300.04 MHz, $CDCl_3$, 25 °C): δ = 0.62 (s, 9 H, C*Me*$_3$), 2.37 (s, 3 H, *p*-*Me*C$_6$H$_4$), 2.85 (s, 6 H, N*Me*$_2$), 4.03, 4.09 (s, 6 H, μ-CN*Me*$_2$), 4.89 (s, 1 H, *H*C=C), 5.17, 5.46 (s, 10 H, *Cp*), 6.45 (br., 1 H, N*H*), 7.08−7.32 (m, 4 H, *p*-MeC_6H_4) ppm. ^{13}C NMR (75.457 MHz,

 © 2004 Wiley-VCH Verlag GmbH & Co. KGaA, Weinheim

$CDCl_3$, 25 °C): δ = 21.2 (*p*-*Me*C_6H_4), 28.9 (C*Me*$_3$), 41.3 (N*Me*$_2$), 43.5 (*C*Me$_3$), 51.6, 53.5 (μ-CN*Me*$_2$), 87.8, 90.0 (*Cp*), 99.9 (H*C*=C), 129.2, 129.5 (CH *p*-Me*C*$_6H_4$), 133.8 (*C*−Me *p*-Me*C*$_6H_4$), 140.0 (*C*-*ipso* *p*-Me*C*$_6H_4$), 155.2 (HC=*C*), 200.0 (*C*=N), 202.4 (*C*O), 238.1 (μ-*C*O), 304.8 (μ-*C*) ppm. IR (CH_2Cl_2, 25 °C): $\tilde{\nu}$ = 1964 vs (CO), 1806 s (μ-CO), 1588 w, 1559 m, 1510 m (C=N) cm^{-1}. IR (KBr, 25 °C): $\tilde{\nu}$ = 3326 br. (NH) cm^{-1}.

[Ru$_2${μ-CN(Me)(Xy)}(μ-CO)(CO){N(H)=C(CMe$_3$)C(H)=C-(NC$_5$H$_{10}$)(Tol)}(Cp)$_2$]$^+$ (9): $C_5H_{10}NH$ (0.6 mL, 5.1 mmol) was added to a solution of **3a** (88.5 mg, 0.1 mmol) in THF (5 mL) and stirred at room temperature for 1 h. The solvent was removed in vacuo and the residue dissolved in CH_2Cl_2 (4 mL) and chromatographed through Al_2O_3. The final product was obtained as an orange-yellow fraction using CH_3CN as eluent.

$C_{42}H_{50}F_3N_3O_5Ru_2S$ (968.08): calcd. C 52.11, H 5.21, N 4.34; found C 52.35, H 5.23, N 4.68. Yield: 67.8 mg, 70%. ^{1}H NMR (300.04 MHz, $CDCl_3$, 25 °C) α-Isomer: δ = 0.67 (s, 9 H, C*Me*$_3$), 1.69 (m, 6 H, β- + γ-C*H*$_2$ C_5H_{10}), 2.22, 2.44 (s, 6 H, *Me*$_2$C$_6$H$_3$), 2.38 (s, 3 H, *p*-*Me*C$_6$H$_4$), 3.11 (br., 4 H, α-C*H*$_2$ C_5H_{10}), 4.29 (s, 3 H, N*Me*), 5.20 (s, 1 H, *H*C=C), 4.98, 5.38 (s, 10 H, *Cp*), 6.67 (br., 1 H, N*H*), 7.08−7.32 (m, 7 H, Me$_2$C$_6$*H*$_3$ + *p*-MeC$_6$*H*$_4$) ppm; β-Isomer: δ = 0.56 (s, 9 H, C*Me*$_3$), 4.27 (s, 3 H, N*Me*), 4.75, 5.64 (s, 10 H, *Cp*) ppm. α/β = 20. ^{13}C NMR (75.457 MHz, $CDCl_3$, 25 °C) α-Isomer: δ = 17.8, 18.5 (*Me*$_2$C$_6$H$_3$), 21.4 (*p*-*Me*C$_6$H$_4$), 24.8 (γ-*C*H$_2$ C_5H_{10}), 26.6 (β-*C*H$_2$ C_5H_{10}), 29.0 (C*Me*$_3$), 44.2 (*C*Me$_3$), 50.8 (α-*C*H$_2$ C_5H_{10}), 52.9 (N*Me*), 88.6, 89.8 (*Cp*), 101.8 (H*C*=C), 128.8−130.1 (*C*−H Me$_2$C$_6$H$_3$ + *p*-MeC$_6$H$_4$), 133.2, 136.7, 137.8, (*C*−Me Me$_2$C$_6$H$_3$ + *p*-Me*C*$_6$H$_4$), 140.1, 147.8 (*C*-*ipso* Me$_2$*C*$_6$H$_3$ + *p*-Me*C*$_6$H$_4$), 156.0 (HC=*C*), 201.5 (*C*=N), 202.9 (*C*O), 235.9 (μ-*C*O), 311.7 (μ-*C*) ppm; β-Isomer: δ = 28.7 (C*Me*$_3$), 87.4, 91.0 (*Cp*) ppm. IR (CH_2Cl_2, 25 °C): $\tilde{\nu}$ = 1965 vs (CO), 1810 s (μ-CO), 1593 w, 1514 m (C=N) cm^{-1}. IR (KBr, 25 °C): $\tilde{\nu}$ = 3326 br. (NH) cm^{-1}. MS (ESI): ES+ *m*/*z* = 820, ES− *m*/*z* = 149.

[Ru$_2${μ-CN(Me)(Xy)}(μ-CO)(CO){N(H)=C(CMe$_3$)C(H)=C-(NMe$_2$)[C(Me)=CH$_2$)}(Cp)$_2$]$^+$ (10): Me_2NH (3 mL, 2 M in THF, 6 mmol) was added to a solution of **7** (100.0 mg, 0.120 mmol) in THF (6 mL) and stirred at room temperature for 1 hour. The solvent was removed in vacuo and the residue dissolved in CH_2Cl_2 (4 mL) and chromatographed through Al_2O_3. The final product was obtained as an orange-yellow fraction using CH_3CN as eluent.

$C_{35}H_{44}F_3N_3O_5Ru_2S$ (877.96): calcd. C 47.88, H 5.05, N 4.79; found C 47.56, H 5.41, N 4.52. Yield: 36.7 mg, 52%. ^{1}H NMR (300.04 MHz, $CDCl_3$, 25 °C) α-Isomer: δ = 0.96 (s, 9 H, C*Me*$_3$), 1.19 (s, 3 H, *Me*C=), 2.23, 2.43 (s, 6 H, *Me*$_2$C$_6$H$_3$), 2.85 (s, 6 H, N*Me*$_2$), 4.26 (s, 3 H, N*Me*), 4.92 (s, 1 H, *H*C=C), 4.96, 5.34 (s, 10 H, *Cp*), 5.19, 5.22 (br., 2 H, =C*H*$_2$), 6.53 (br., 1 H, N*H*), 7.21−7.30 (m, 3 H, Me$_2$C$_6$*H*$_3$ + *p*-MeC$_6$*H*$_4$) ppm; β-Isomer: concentration too low to be characterized (α/β > 20:1). ^{13}C NMR (75.457 MHz, $CDCl_3$, 25 °C) α-Isomer: δ = 17.7, 18.4 (*Me*$_2$C$_6$H$_3$), 21.5 (*Me*C=), 29.5 (C*Me*$_3$), 40.9 (N*Me*$_2$), 44.2 (*C*Me$_3$), 52.8 (N*Me*), 88.5, 89.8 (*Cp*), 100.2 (H*C*=C), 122.2 (=*C*H$_2$), 128.9, 129.0, 129.6 (*C*−H Me$_2$C$_6$H$_3$), 131.5, 133.2 (*C*−Me Me$_2$C$_6$H$_3$), 142.3 (Me*C*=CH$_2$), 147.8 (*C*-*ipso* Me$_2$*C*$_6$H$_3$), 156.6 (HC=*C*), 201.2 (*C*=N), 202.9 (*C*O), 236.1 (μ-*C*O), 312.2 (μ-*C*) ppm. IR (CH_2Cl_2, 25 °C): $\tilde{\nu}$ = 1967 vs (CO), 1810 s (μ-CO), 1593 w, 1516 m (C=N) cm^{-1}.

X-ray Crystallographic Study: Compounds **3a[CF$_3$SO$_3$]** and **8a[CF$_3$SO$_3$]** were crystallized from CH_2Cl_2/Et_2O. Crystal data were collected at room temperature on a Bruker AXS SMART 2000 CCD diffractometer using Mo-K_α radiation. Intensity data were measured over full diffraction spheres using 0.3° wide ω scans, crystal-to-detector distance 5.2 cm. Cell dimensions and orientation

Table 3. Crystal data and experimental details for **3a[CF$_3$SO$_3$]** and **10a[CF$_3$SO$_3$]**

Complex	**3a[CF$_3$SO$_3$]**	**8a[CF$_3$SO$_3$]**
Empirical formula	$C_{37}H_{39}F_3N_2O_5Ru_2S$	$C_{39}H_{46}F_3N_3O_5Ru_2S$
Formula mass	882.90	927.99
T, K	293(2)	293(2)
λ, Å	0.71073	0.71073
Crystal system	orthorhombic	monoclinic
Space group	$P2_12_12_1$	Cc
a, Å	12.245(2)	12.925(3)
b, Å	14.179(3)	24.789(5)
c, Å	22.219(4)	26.031(5)
α, °	90	90
β, °	90	96.43(3)
γ, °	90	90
Cell volume, Å^3	3857.7(13)	8288(3)
Z	4	8
$D_{calcd.}$, g·cm^{-3}	1.520	1.487
μ, mm^{-1}	0.894	0.836
F(000)	1784	3776
Crystal size, mm	0.35 × 0.25 × 0.19	0.28 × 0.22 × 0.15
θ limits, °	1.70−25.03	1.57−25.03
Reflections collected	34166	36307
Independent reflections	6830 [*R*(int) = 0.0617]	14605 [*R*(int) = 0.1155]
Data/restraints/parameters	6830/ 211/417	14605/554/778
Goodness on fit on F^2	1.075	0.934
*R*1 [$I > 2\sigma(I)$]	0.0661	0.0725
*wR*2 (all data)	0.1756	0.1940
Largest diff. peak and hole, e·Å^{-3}	3.835/−0.837	1.094/−1.154

 © 2004 Wiley-VCH Verlag GmbH & Co. KGaA, Weinheim

matrices were initially determined from least-squares refinements on reflections measured in 3 sets of 20 exposures collected in three different ω regions and eventually refined against all reflections. The software SMART [28] was used for collecting frames of data, indexing reflections and determination of lattice parameters. The collected frames were then processed for integration by the software SAINT and empirical absorption corrections were applied with SADABS.[29] Structures were solved by direct methods and structures refined by full-matrix least-squares based on all data using F^2.[30] Crystal data are listed in Table 3. Non-H atoms were refined anisotropically, unless otherwise stated. The hydrogen atoms were added in idealized positions except the ones attached to nitrogen atoms in **8a[CF_3SO_3]** which were located in the Fourier map and refined isotropically with isotropic thermal parameters defined as $U(H) = 1.2U_{eq}(N)$. The crystals of both **3a[CF_3SO_3]** and **8a[CF_3SO_3]** appeared to be racemically twinned with a refined Flack parameter of 0.47(7) and 0.41(7), respectively.[31] They were, therefore, refined using the TWIN refinement routine of SHELXTL. Some residual electron density peaks up to 3.835 e·Å^{-3} remain after refinement of **3a[CF_3SO_3]**, probably because of partial non-merohedral twinning. Different crystals of **3a[CF_3SO_3]** have been examined, and we have also tried to recrystallize them, without obtaining better results. Nonetheless, the data are fully consistent with the ones previously reported for the analogous complex [Fe_2{μ-CN(Me)(Xy)}(μ-CO)(CO){N(H)=C(CMe_3)(C≡CTol)}-$(Cp)_2$][CF_3SO_3].[10] One Cp ligand and the CMe_3 group in the unique molecule of **8a[CF_3SO_3]** are both disordered. Disordered atomic positions were split and refined isotropically using similar distance and similar U restraints and one occupancy parameter per disordered group.

CCDC-222309 and -222310 contain the supplementary crystallographic data for this paper. These data can be obtained free of charge at www.ccdc.cam.ac.uk/conts/retrieving.html [or from the Cambridge Crystallographic Data Centre, 12 Union Road, Cambridge CB2 1EZ, UK; Fax: (internat.) + 44-1223-336-033; E-mail: deposit@ccdc.cam.ac.uk].

Acknowledgments

We thank the Ministero dell'Università e della Ricerca Scientifica e Tecnologica (MIUR) (project: "New strategies for the control of reactions: interactions of molecular fragments with metallic sites in unconventional species") and the University of Bologna ("Funds for Selected Research Topics") for financial support.

[1] D. A. Knight, M. A. Dewey, G. A. Stark, B. K. Bennet, A. M. Arifand, J. A. Gladysz, *Organometallics* **1993**, *12*, 4523−4534.
[2] R. Castarlenas, M. A. Esteruelas, E. Oñate, *Organometallics* **2000**, *19*, 5454−5463.
[3] M. A. Jiménez-Tenorio, M. Jiménez-Tenorio, M. C. Puerta, P. Valerga, *Inorg. Chim. Acta* **2000**, *300−302*, 869−874.
[4] L. A. Francisco, P. S: White, J. L. Templeton, *Organometallics* **1996**, *15*, 5127−5136.
[5] T. B. Gunnoe, P. S. White, J. L. Templeton, *J. Am. Chem. Soc.* **1996**, *118*, 6916−6923.
[6] G. A. Stark, J. A. Gladysz, *Inorg. Chem.* **1996**, *35*, 5509−5513.
[7] L. F. Rhodes, L. M. Venanzi, *Inorg. Chem.* **1987**, *26*, 2692−2695.
[8] S. G. Feng, J. L. Templeton, *Organometallics* **1992**, *11*, 1295−1303.
[9] W. Y. Yeh, C. S. Ting, S. M. Peng, G. H. Lee, *Organometallics* **1995**, *14*, 1417−1422.
[10] V. G. Albano, S. Bordoni, L. Busetto, F. Marchetti, M. Monari, V. Zanotti, *J. Organomet. Chem.* **2003**, *684*, 37−43.
[11] V. G. Albano, L. Busetto, C. Camiletti, M. Monari, V. Zanotti, *J. Organomet. Chem.* **1998**, *563*, 153−159.
[12] V. G. Albano, L. Busetto, C. Camiletti, C. Castellari, M. Monari, V. Zanotti, *J. Chem. Soc., Dalton Trans.* **1997**, 4671−4676.
[13] V. G. Albano, S. Bordoni, L. Busetto, C. Camiletti, M. Monari, A. Palazzi, F. Prestopino, V. Zanotti, *J. Chem. Soc., Dalton Trans.* **1997**, 4665−4670.
[14] L. Busetto, L. Carlucci, V. Zanotti, V. G. Albano, M. Monari, *J. Organomet. Chem.* **1993**, *447*, 271−275.
[15] J. T. Mague, *Acta Crystallogr., Sect. C* **1995**, *51*, 831−833.
[16] D. L. Davies, S. A. R. Knox, K. A. Mead, M. J. Morris, P. Woodward, *J. Chem. Soc., Dalton Trans.* **1984**, 2293−2299.
[17] A. F. Wells, *Structural Inorganic Chemistry*, Claredon Press, Oxford, **1984**, p. 1288.
[18] F. Pohlki, S. Doye, *Chem. Soc. Rev.* **2003**, *32*, 104−114.
[19] M. B. Smith, J. March, *March's Advanced Organic Chemistry*, John Wiley & Sons, New York, **2001**, p. 20.
[20] W. Wilker, D. Leibfritz, R. Kerssebaum, W. Beimel, *Magn. Reson. Chem.* **1993**, *31*, 287−292.
[21] V. G. Albano, L. Busetto, M. Monari, V. Zanotti, *J. Organomet. Chem.* **2000**, *606*, 163−168.
[22] T. Daniel, M. Muller, H. Weiner, *Inorg. Chem.* **1991**, *30*, 3118−3120.
[23] R. Castarlenas, M. A: Esteruelas, E. G. Puebla, E. Oñate, *Organometallics* **2001**, *20*, 1545−1554.
[24] R. A. Michelin, M. Mozzon, R. Bertani, *Coord. Chem. Rev.* **1996**, *147*, 299−338.
[25] V. Y. Kukushkin, A. J. L. Pombeiro, *Chem. Rev.* **2002**, *102*, 1771−1802.
[26] M. E. Cucciolito, V. De Felice, F. Giordano, I. Orabona, F. Ruffo, *Eur. J. Inorg. Chem.* **2001**, 3095−3100.
[27] K. Stott, J. Stonehouse, J. Keeler, T. L. Hwang, A. J. Shaka, *J. Am. Chem. Soc.* **1995**, *117*, 4199−4200.
[28] *SMART & SAINT* Software Reference Manuals, Version 5.051, Bruker Analytical X-ray Instruments Inc., Madison, WI, **1998**.
[29] G. M. Sheldrick, *SADABS, Program for empirical absorption correction*, University of Göttingen, Germany, **1996**.
[30] G. M. Sheldrick, *SHELX97, Program for crystal structure determination*, University of Göttingen, Germany, **1997**.
[31] H. D. Flack, *Acta Crystallogr., Sect. A* **1983**, *39*, 876−881.

Received October 23, 2003
Early View Article
Published Online February 26, 2004

 © 2004 Wiley-VCH Verlag GmbH & Co. KGaA, Weinheim

Synthesis, Structural and Spectroscopic Characterization of Four [(η^6-PAH)Cr(CO)$_3$] Complexes (PAH = Pyrene, Perylene, Chrysene, 1,2-Benzanthracene)

Aldo Arrais,[a] Eliano Diana,[b] Giuliana Gervasio,*[b] Roberto Gobetto,[b] Domenica Marabello,[b] and Pier Luigi Stanghellini*[a]

Keywords: Macrocyclic ligands / Chromium / X-ray diffraction / NMR spectroscopy / Vibrational spectroscopy / DFT calculations

The thermal reaction of hexacarbonylchromium with the polycyclic aromatic hydrocarbons (PAHs) pyrene, perylene, chrysene and 1,2-benzanthracene has afforded four organometallic complexes of the type [(η^6-PAH)Cr(CO)$_3$], whose unprecedented structures were obtained by single-crystal X-ray analysis. The topology of the coordination of the Cr(CO)$_3$ fragment and its asymmetry with respect to the coordinating ring may depend on the opportunity to maintain the maximum aromaticity of the complexed ligand. DFT calculations, ^{1}H NMR, FT-IR and Raman spectroscopy have been used to elucidate the type of interaction between the PAH ligand and the carbonylmetal moiety, giving insight into the ligand-to-metal donor capacity and the intra- and intermolecular interactions.
(© Wiley-VCH Verlag GmbH & Co. KGaA, 69451 Weinheim, Germany, 2004)

Introduction

Polycyclic aromatic hydrocarbons (PAHs) have long been investigated in diverse fields of research, ranging from astrophysics[1] to molecular biology.[2] [(PAH)Cr(CO)$_3$] complexes are efficient organometallic precursors for the organic synthesis of PAH derivatives by selective nucleophilic attack on the metallated ring.[3] Some can also exhibit chirality, which is useful in stereochemical reactions for drug design as, in vivo, PAHs have multiple well-documented carcinogenic effects.[4]

In the solid state, PAHs often assume a layered architecture;[5] which suggests that they have potential as synthons in crystal engineering and in preparing advanced molecular solids.[6] Actually, the large delocalization of π-electron density allows the formation of complexes where intermolecular coupling ranges from weak interactions to the formation of charge-transfer complexes.[7] Alongside the well-known adducts of PAHs with classical electron-transfer organic counterparts, such as tetracyanoethylene (TCNE),[8] tetracyanoquinodimethane (TCNQ)[9] and 2,3-dichloro-5,6-dicyano-*p*-benzoquinone (DDQ),[10] more recently a few organometallic complexes have appeared, such as the ferrocene−pyrene system.[11] Two promising examples of [(η^6-arene)Cr(CO)$_3$]- and [(η^6-PAH)Cr(CO)$_3$]-type structures have been reported, i.e. the non-centrosymmetrical complex (benzene)Cr(CO)$_3$/thiourea[12] and the complex (phenanthrene)Cr(CO)$_3$/1,3,5-trinitrobenzene.[13] Interest in the latter derivatives is strengthened by the presence of the metal atom, which can tune the electronic properties of the adducts and allow the isolation of materials displaying useful magnetic and optical properties.[14,15]

Carbonyl(PAH)chromium derivatives also tend to maintain, in the solid state, a face-to-face packing of the aromatic rings, and they can provide carbonyl groups that can interact through weak intermolecular interactions such as the C−H···O hydrogen bond, which is crucial in the design of suitable molecular building blocks in crystal engineering.[16]

From these perspectives, we attempted to synthesise [(η^6-PAH)Cr(CO)$_3$] complexes, including large polycyclic aromatic compounds, focusing upon four important PAH frameworks: pyrene, perylene, chrysene and 1,2-benzanthracene. There are few reports of such large complexed ligands,[17] the main published derivatives concerning instead the homologues of [(η^6-benzene)Cr(CO)$_3$].[18−22] In fact, only four examples of [(η^6-PAH)Cr(CO)$_3$] complexes, where PAHs are unsubstituted naphthalene,[23] an-

[a] Dipartimento di Scienze e Tecnologie avanzate, Università del Piemonte Orientale,
Corso T. Borsalino 54, 13100 Alessandria, Italy
Fax: (internat.) + 39-0131-287416
E-mail: pierluigi.stanghellini@unito.it
pierluigi.stanghellini@unipmn.it
[b] Dipartimento di Chimica I. F. M., Università di Torino,
Via P. Giuria 7, 10125 Torino, Italy
Fax: (internat.) + 39-011-6707855
E-mail: giuliana.gervasio@unito.it
Supporting information for this article is available on the WWW under http://www.eurjic.org or from the author.

thracene,[24] phenanthrene[25] and triphenylene,[26] have been structurally determined.[27] For the former large PAH structures, however, a few metal coordination studies have been reported, with Ru,[28−31] Fe,[32,33] Mo[33,34] and Ti[35] as the η^6-bonded metal atoms. The PAH ligands used in the present work are illustrated in Scheme 1.

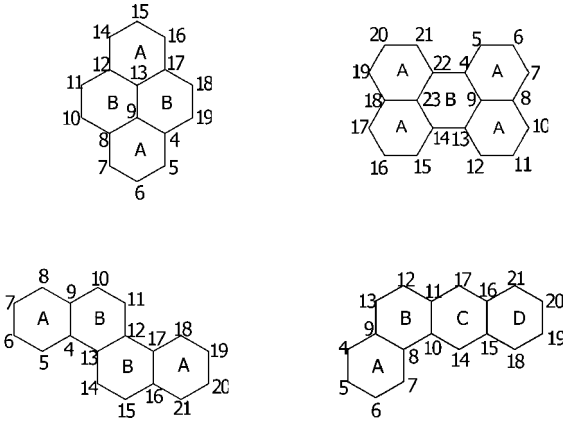

Scheme 1. Structure of the polycyclic aromatic hydrocarbon ligands pyrene, perylene, chrysene and 1,2-benzanthracene (the C atom numbering starts from C-4, as C-1, C-2 and C-3 always refer to carbonyl carbon atoms

Results and Discussion

Structure of the Complexes

(Pyrene)-, (perylene)-, (chrysene)- and (1,2-benzanthracene)tricarbonylchromium complexes (Figures 1−4) all coordinate the $Cr(CO)_3$ group on the face of a peripheral ring, with the metal atom ca. 1.74 Å from the ring centroid. The carbon atoms of the four ligands lie in a plane with a mean deviation from planarity of 0.021 (**1**), 0.028 (**2**), 0.029 (**3**) and 0.034 Å (**4**). The carbonyl groups lie between a staggered and an eclipsed orientation with respect to the carbon atoms of the coordinated ring. The plane formed by the three oxygen atoms is parallel to the plane of the coordinated ring; however, the chromium atom is not symmetrically linked to the six atoms of the aromatic ring, as occurs,

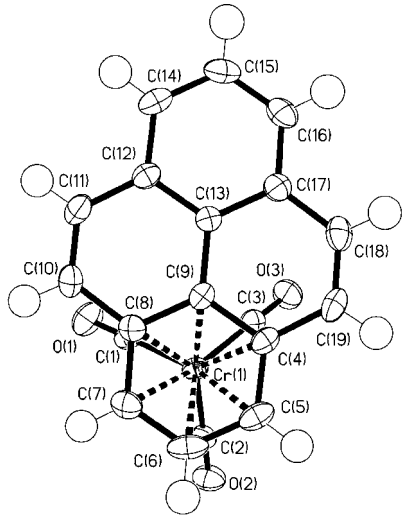

Figure 1. ORTEP plot of the complex [(η^6-pyrene)$Cr(CO)_3$] (**1**) (30% probability for the thermal ellipsoids) with the atom labeling

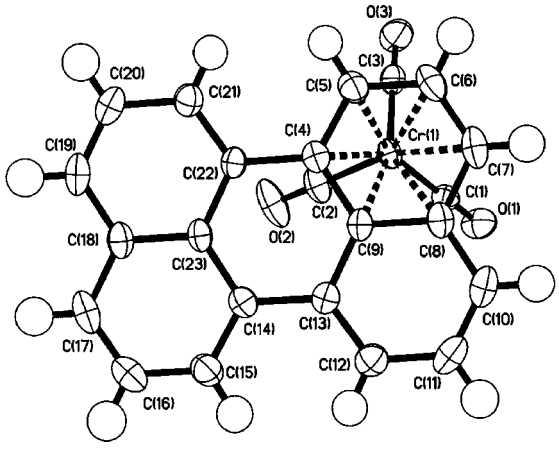

Figure 2. ORTEP plot of [(η^6-perylene)$Cr(CO)_3$] (**2**) (30% probability for the thermal ellipsoids) with the atom labeling

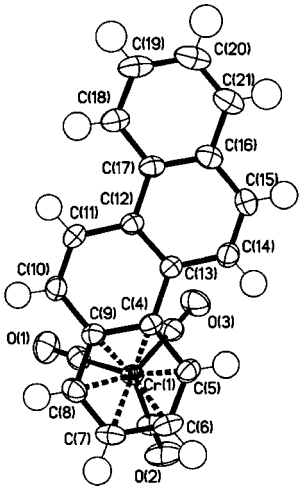

Figure 3. ORTEP plot of [(η^6-chrysene)$Cr(CO)_3$] (**3**) (30% probability for the thermal ellipsoids) with the atom labeling

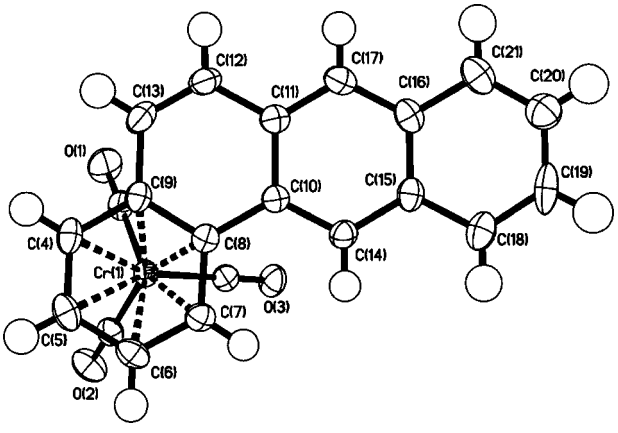

Figure 4. ORTEP plot of complex [(η^6-benzanthracene)$Cr(CO)_3$] (**4**) (30% probability for the thermal ellipsoids) with the atom labeling

 © 2004 Wiley-VCH Verlag GmbH & Co. KGaA, Weinheim

Table 1. Selected bond lengths [Å] and angles [°] for complexes **1**−**4**

Complex	**1**	**2**	**3**	**4**
Cr(1)−C(1)	1.831(3)	1.828(3)	1.833(3)	1.831(2)
Cr(1)−C(2)	1.812(3)	1.821(3)	1.822(3)	1.834(3)
Cr(1)−C(3)	1.830(3)	1.832(3)	1.836(3)	1.834(2)
Cr(1)−C(4)	2.268(3)	2.241(2)	2.273(3)	2.210(2)
Cr(1)−C(5)	2.219(3)	2.210(3)	2.217(3)	2.209(2)
Cr(1)−C(6)	2.192(3)	2.200(3)	2.224(3)	2.206(2)
Cr(1)−C(7)	2.214(3)	2.221(3)	2.217(3)	2.204(2)
Cr(1)−C(8)	2.272(3)	2.294(3)	2.212(3)	2.271(2)
Cr(1)−C(9)	2.282(3)	2.288(2)	2.280(3)	2.265(2)
C(1)−O(1)	1.142(3)	1.156(3)	1.163(3)	1.154(2)
C(2)−O(2)	1.154(3)	1.157(3)	1.147(3)	1.152(3)
C(3)−O(3)	1.148(3)	1.150(3)	1.143(3)	1.150(2)
C(4)−C(5)	1.403(3)	1.396(3)	1.436(3)	1.377(3)
C(4)−C(9)	1.431(3)	1.437(3)	1.415(3)	1.428(3)
C(5)−C(6)	1.393(4)	1.391(4)	1.387(3)	1.407(3)
C(6)−C(7)	1.375(3)	1.374(4)	1.400(4)	1.384(3)
C(7)−C(8)	1.419(3)	1.422(4)	1.381(4)	1.425(3)
C(8)−C(9)	1.413(3)	1.429(3)	1.419(3)	1.421(3)
Other C−C bonds	1.324−1.439(3)	1.343−1.471(3)	1.332−1.446(3)	1.338−1.458(3)
C(1)−Cr(1)−C(2)	89.54(11)	89.44(12)	89.67(13)	88.45(10)
C(1)−Cr(1)−C(3)	89.20(11)	88.97(12)	88.76(13)	89.43(10)
C(2)−Cr(1)−C(3)	88.87(12)	89.30(13)	88.12(13)	89.15(10)
O(1)−C(1)−Cr(1)	178.5(3)	179.5(3)	178.4(2)	179.0(2)
O(2)−C(2)−Cr(1)	179.3(3)	177.6(3)	178.1(3)	178.8(2)
O(3)−C(3)−Cr(1)	179.0(3)	178.4(3)	179.5(3)	179.7(2)

for example, in [{$C_6(CH_3)_6$}Cr(CO)$_3$].[36] The chromium atom is significantly farther from the carbon atoms connected to the condensed rings than the remaining Cr−C_{ring} distances (Table 1).

Coordination of a metal atom to an aromatic ring sometimes modifies the structure of the ring, typically by expansion of the ring, the loss of planarity of the ring and alternation of long and short C−C bonds.[37] In our case, the ligands are planar. Regular alternating of short/long C−C bonds of the coordinated ring may be observed in complexes **3** and **4** only where the coordinated ring is condensed to another ring.[38−41] In all complexes, however, the bonds adjacent to the coordinated rings are significantly long and therefore have a minor double-bond character. Further, C(10)−C(11) [1.327(3) Å] and C(18)−C(19) [1.324(3) Å] bonds in **1**, C(10)−C(11) [1.343(4) Å] and C(12)−C(13) [1.364(3) Å] bonds in **2**, C(10)−C(11) [1.332(3) Å] bond in **3** and C(12)−C(13) [1.326(3) Å] bond in **4** all show values corresponding to a double bond. Also, a set of short C−C bonds is located in the ligand on the opposite side with respect to the metal atom. We are confident of the accuracy of these values, even though the structural data of the complexes were collected at room temperature: in fact the estimated standard deviations (e.s.d.) of the C−C bond lengths are 0.003−0.004 Å.[42]

Considering the structural data, as expected there is no more than a negligible change in the PAH structures, owing to the very hard deformability of the fused rings. Variations of some structural parameters concerning the metal fragment and the relationship between the PAH and this fragment are expected to be more significant, such as (i) the average Cr−C_{CO} distance in the coordinated Cr(CO)$_3$ fragment and (ii) the distance between the chromium atom and the arene centroid. Table 2 collects these data, together with those of some other selected complexes with either greatly electron-releasing (diethylaminobenzene and hexamethylbenzene)[43] or electron-withdrawing (hexachlorobenzene)[44] arenes. Also included are some well-known [(PAH)Cr(CO)$_3$] complexes, together with [Cr(CO)$_6$] because of the exceptional electronic withdrawal of the (CO)$_3$ unit. The clear variation shown in Cr−C_{CO} is typical of an L−M−CO unit and of the well-known relationship between charge transfer and bond length. Thus, electron transfer from arene to Cr causes a significant shortening of the Cr−CO bond and vice versa a charge demand elongates this bond length. Accordingly, diethylaminobenzene shows the shortest distance[43] and hexachlorobenzene[44] {and, of course, [Cr(CO)$_6$]} the longest.[45] ν(CO) is another indirect, but sensible, parameter by which to measure this charge transfer.[46] Accordingly, the hexamethylbenzene complex shows the lowest and the hexachlorobenzene the highest value. The PAH ligands lie in between, showing a medium donating character; among them, pyrene is the best donating ligand, whereas perylene is the worst. The Cr−centroid distances [point (ii) above] are less significant in classifying charge-transfer effects, because arenes with substantial differences in donor−acceptor properties sometimes exhibit similar M−arene distances. Nevertheless, a long Cr−CO distance roughly corresponds to a short Cr−ring distance.

Bonding

The topology of the coordination of the Cr(CO)$_3$ fragment on the PAH ring is significant. Even if a statistical effect could be invoked for perylene, for all the other ligands

 © 2004 Wiley-VCH Verlag GmbH & Co. KGaA, Weinheim

Table 2. Structural and spectroscopic parameters of selected [(η^6-arene)$Cr(CO)_3$] complexes

Ligand	$Cr-C_{arene}$ [Å][a]	$Cr-C_{CO}$ [Å]	$Cr-C_{ring\ centroid}$ [Å]	ν_{CO} (A_1) [cm^{-1}] [60]	Ref.
$(CO)_3$		1.915(2) 74K		1987	[61]
Hexachlorobenzene	2.200(5)	1.879(5) av.	1.680(5)	2009	[62]
Benzene	2.220−2.240(2) (78 K, neutr.)	1.842(2) av.	1.726(2)	1974	[43]
Naphthalene	2.20	1.82 av.		1977	[21]
(triclinic form)	2.32				
Anthracene	2.218(9)	1.82(1) av.	1.76(1)	1978	[22]
	2.332(8)				
Phenanthrene	2.210(5)	1.834(6) av.		1980	[24]
(monoclinic form)	2.283(5)				
Phenanthrene	2.209(4)	1.828−1.857(5)	1.733(5)	1980	[23]
(orthorhombic form)	2.289(4)				
Pyrene (**1**)	2.208(3)	1.812−1.831(3)	1.746(3)	1959	this work
	2.274(3)				
Perylene (**2**)	2.220(3)	1.821−1.832(3)	1.745(3)	1968	this work
	2.274(3)				
Chrysene (**3**)	2.217(3)	1.822−1.836(3)	1.740(3)	1965	this work
	2.277(3)				
Benzanthracene (**4**)	2.207(2)	1.832(3) av.	1.727(2)	1966	this work
	2.268(2)				
Triphenylene	2.204(3)	1.833(3) av.	1.720(3)	1990 (KBr)	[25]
	2.258(3)				
Hexamethylbenzene	2.241(3)	1.836(3) av.	1.730(3)	1948	[36]
1,2,3-Trimethoxybenzene	2.224(2)	1.830−1.845(2)	1.755(2)	1963	[63]
	2.281(2)				
Diethylaminobenzene	2.185(2)−2.369(2)	1.813(2)av.	1.750(2)	1954	[63]

[a] The first value is the average Cr−C(ring-unsusbstituted) bond length, the second one is the average Cr−C(ring-junction) bond length.

the probability of the coordinating ring to bond the metal fragment is identical to that of any other ring types. The observed regioisomerism of the coordination could be explained by the different aromaticity between the free and the bonded PAH, which can be simply represented by the number of possible Kekulé covalent structures (KS).[47] In all cases KS decreases as a consequence of coordination. The real structure is that which, compared to the other possibilities, maintains the maximum aromaticity of the bonded ligand (Table 3). This simple approach agrees with the observed localized short and long C−C bond lengths found in the structures and also satisfactorily explains one of the most interesting stereochemical features of these complexes, that is the slipping of the $Cr(CO)_3$ fragment towards the unsubstituted carbon atoms of the arene ring and away from the ring junction carbon atoms.

Table 3. Number of the possible Kekulè structures (KS) of free and coordinated PAH ligands

Complex	**1**	**2**	**3**	**4**
Coordinating ring[a]	A B	A B	A B	A B C D
Number of KS	4 2	6 4	6 4	6 4 4 4
Number of KS of the free ligand	6	9	8	7
A[b]	1.5	1.5	1.3	1.2

[a] See Scheme 1. [b] Aromatic loss, i.e. the ratio between no. of KS of the free ligand with respect to the stable form of the coordinated ligand.

From another point of view, this agrees with the suggestion that, for non-symmetric aromatic rings, the metal atom should bind to the more electron-rich double bond.[48−49] The external C−C bonds have an overall double-bond character greater than that of the ring-junction C−C bond. Moreover, another effect can be present, which is a repulsion between the π-electron charge delocalized on the adjacent non-bonded rings and the negative charge induced on the Cr atom by the donation of the bonded ring. A closely related phenomenon has been evidenced in a series of [(substituted arene)$Cr(CO)_3$] complexes, where the electron repulsion tilts the arene substituents away from Cr.[21] If in the PAH ligand the adjacent ring can be viewed as a substituent of the bonded ring, as the overall structure is hardly deformable, it is the $Cr(CO)_3$ group that shifts towards the peripheral carbon atoms.[50]

To substantiate the previous simplified approach, a quantum mechanical calculation of the total energy has been performed.[51] The chosen model was complex **4**, which displays the highest number of possible regioisomers, named as the A, B, C and D complexes, according to the coordinating ring (Scheme 1). We made a single-point calculation on an idealized structure with the Cr atom perpendicular to the centre of the coordinating ring and the carbonyl groups in the staggered position with respect to the carbon atoms. For complex A, a calculation has also been carried out on the real structure: the difference is irrelevant. The B3LYP DFT method was used with a pseudopotential LANL2DZ basis set for the chromium atom and the 6-

 © 2004 Wiley-VCH Verlag GmbH & Co. KGaA, Weinheim

31G(d, p) basis for the other atoms. Figure 5 shows both the total energy and of the Mulliken charge on the Cr atom. Complex A is clearly the most stable conformation, as predicted by simple KS counting. The charge on the Cr atom can be related to the DFT-Mulliken mean charge density in the rings of the free 1,2-benzanthracene, which is D (−0.194) < A (−0.0368) < B (0.0254) < C (0.0327). As the main contribution to the PAH−Cr bond is the electron donation PAH→Cr, the most stable configuration should be given by the Cr coordination to the ring with the highest electron density. The A ring is preferred to the D ring, probably because of the maintenance of the maximum aromatic stabilisation energy.

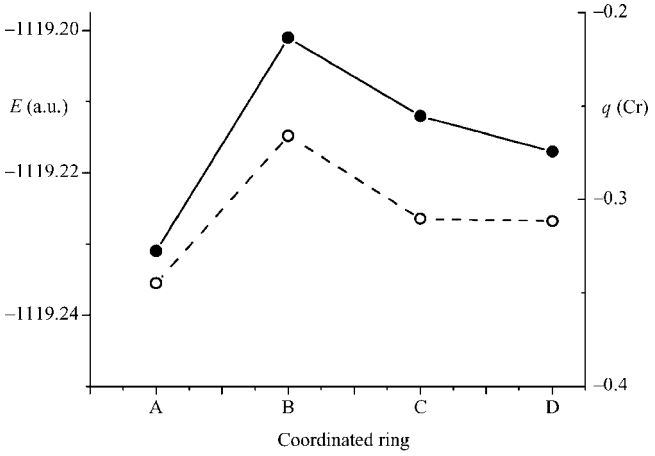

Figure 5. Total energy of the regioisomers of complex **4** (closed circles); Mulliken charge on the Cr atom (open circles)

Finally, the theoretical approach can be related to simple chemical properties of the complexes. For example, the linear PAHs, 1,2-benzanthracene in particular, whose aromaticity loss in the coordination is lower, are more stable and are obtained in better yield than the condensed PAHs.

Vibrational Analysis

The vibrational pattern of the [(PAH)Cr(CO)$_3$] complexes can be roughly divided into three types of modes, those of the PAH ligand, those of the Cr(CO)$_3$ unit and those derived by the interaction between the two fragments. In a first approximation the coupling between these sets of modes is negligible;[52] thus, a close comparison with the spectra of the free ligand is of significant help in the assignment. As an example, Figures 6 and 7 show the infrared and the Raman spectra of complex **1**, together with those of the ligand. The modes of the Cr(CO)$_3$ unit are immediately evident, as a very strong band in the 2000−1800 cm^{-1} region [ν(CO)] and in the 700−400 cm^{-1} region [δ(Cr−CO) and ν(Cr−CO)]. More doubtful is the assignment of the PAH−Cr modes, which lie below 300 cm^{-1} and are mixed with the ring deformation modes. Usually, only the PAH−Cr stretching can be assigned with some confidence to a medium-strong Raman band around 290 cm^{-1}. The remaining band pattern concerns the vibrations of the coordinated PAH ligand.

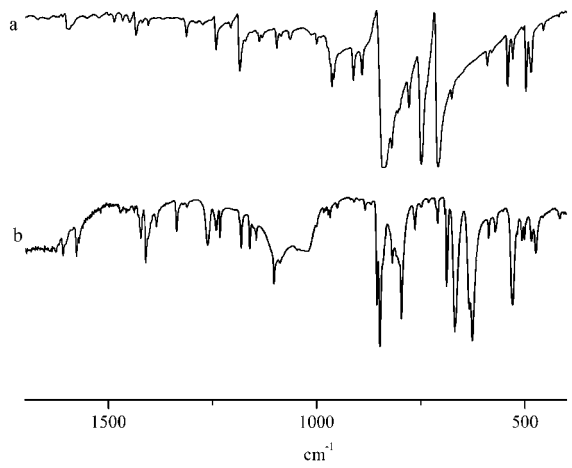

Figure 6. Solid-state infrared spectra in the 1600−400 cm^{-1} region of pyrene (a), complex **1** (b)

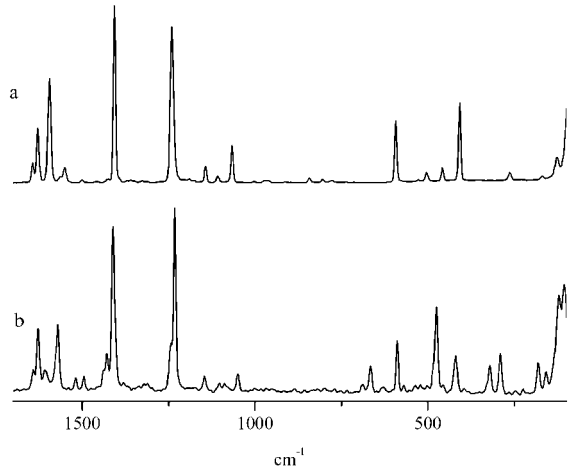

Figure 7. Solid-state Raman spectra in the 1600−200 cm^{-1} region of pyrene (a) complex **1** (b)

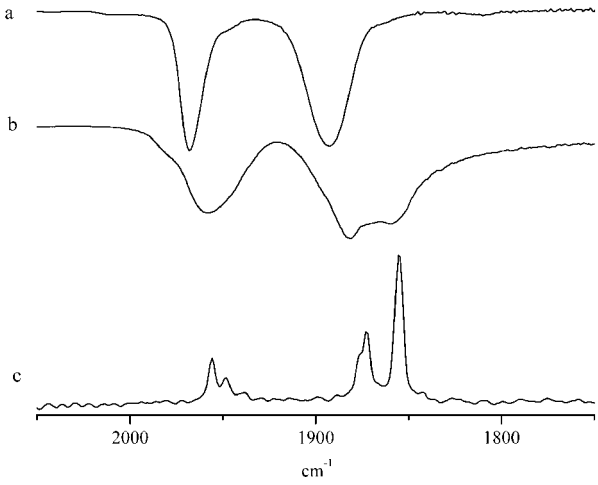

Figure 8. Spectra of complex **2** in the ν_{CO} region; (a): solution (toluene) infrared, (b): solid state infrared, (c): solid-state Raman

 © 2004 Wiley-VCH Verlag GmbH & Co. KGaA, Weinheim

The infrared ν(CO) spectrum in aliphatic and aromatic hydrocarbon solutions shows the usual behavior of an $M(CO)_3$ group with a local C_{3v} symmetry: a medium-strong high-frequency band (A_1) and a strong, broad (sometimes split) band at lower frequency (E). Both the IR and Raman spectral patterns in the solid state are more complex, because of the site and/or factor group effects, and are shifted to lower frequencies by 15−25 cm^{-1}, with respect to those in solution (Figure 8). This is clear spectroscopic evidence of what has been observed in the crystal packing, i.e. many C−H···O interactions.

The modes of the coordinated and uncoordinated aromatic ligand lie in typical fingerprint regions,[53] corresponding to C−H stretching (3200−3000 cm^{-1}), in-plane C−C stretching and C−H bending (1600−900 cm^{-1}), to out-of-plane C−H bending (900−700 cm^{-1}) and to out-of-plane C−C bending (below 500 cm^{-1}). Significant changes are evident in the ν(CH) region: the modes of the coordinated PAH move up with respect to those of the free PAH. The Raman spectra, which give rise to medium-strong bands, are clear in this respect (Figure 9). Separation of the CH vibrations of the bonded ring from those of the non-bonded ring is inapplicable. As DFT calculations on the free PAH show that the CH vibrators are strongly coupled, the pattern has to be considered as a whole.

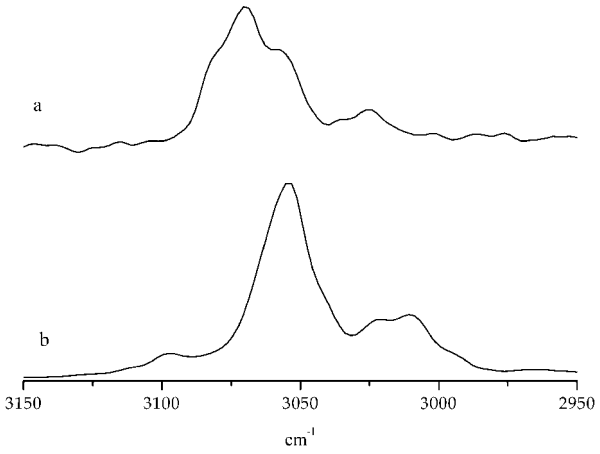

Figure 9. Solid-state Raman spectra of complex **1** (a), pyrene (b)

Even more interesting is the behavior of the γ(CH) modes, which are the most evident infrared fingerprint bands of the aromatic hydrocarbons, and are sensitive to the effect of metal coordination, usually reflected in an increase in the frequency.[52,54−56] For example, the IR spectrum of free pyrene shows two very strong bands at 838 and 748 cm^{-1}, easily assigned to the γ(CH) modes, which are clearly shifted to 855 and 796 cm^{-1} in complex **1**. The average shift (ca. 40 cm^{-1}) is similar to that found for perylene and complex **2** (ca. 30 cm^{-1}), but is definitely smaller than for the couple benzene/(benzene)$Cr(CO)_3$ ($\Delta\tilde{\nu} \approx 120$ cm^{-1}).[56] The γ(CH) modes have been separated into small sub-sets, corresponding to the vibrations of groups of adjacent H atoms (quadruplet, triplet, doublet and hydrogen solo).[53] Here too, DFT calculations show that this distinction is too rough and unacceptable, as the vibration of the CH units are all coupled. So the contribution to a γ(CH) mode is given by the vibration of all the CH units, belonging both to coordinated and to uncoordinated rings, and it is reasonable to expect that the last ones can attenuate the coordination effect. It could be relevant that with the linear PAH (chrysene and 1,2-benzanthracene) the attenuating effect of the uncoordinated part of the ligand is significant, because $\Delta\tilde{\nu}$ is very small (3 and 2 cm^{-1}, respectively).[57]

Usually, both ν(CH) and γ(CH) frequencies increase as a consequence of metal coordination, an explanation for which must include the extended framework of hydrogen bonds. This is an important factor in the rise of γ(CH), as a bending vibration that pulls the H atoms away from the equilibrium position is rendered more difficult by C−H···O interactions. The comparison between the spectra in the solid state and in solution is clear: in the last case rather small increases occur.[58] Presumably, the metal−ring interaction could also contribute to the shift − similar to the contributions observed in metallocene complexes.[52]

Conversely, the hydrogen interaction is expected to decrease ν(CH), so that the observed increase may be due to a simultaneous phenomenon that reinforces the C−H bond, thereby increasing the frequency. The π-donation from ring to metal atom might stabilize the σ frame, and so increase the C−C and C−H bond strengths. Owing to the small mass of hydrogen, ν(CH) values are particularly susceptible to small modifications of the C−H bond.

The vibrational pattern may also give some insight into the donor−acceptor properties of the PAH ligands. Theoretical and experimental infrared spectra have been reported to show significant differences in the intensity of the spectral regions between PAH molecules and the corresponding $[PAH]^+$ ions.[53][59] In particular, the latter exhibit an enhanced intensity in the ν(CC) and δ(CH) regions and a decreased intensity in the ν(CH) and γ(CH) regions with respect to the corresponding neutral molecule. On this basis an estimate of the intensity ratio $IR = \{I[\nu(CC) + \delta(CH)]/I[\nu(CH) + \gamma(CH)]\}$ for both free and complexed PAH could give information on the variation of the charge on the PAH as a consequence of coordination. Indeed, *IR* increases significantly from free to coordinated PAH for both pyrene (0.73 to 1.63) and chrysene (0.48 to 1.20), suggesting that these ligands are good donors, where the other two PAHs, which show the opposite trend (perylene: from 1.10 to 0.68; 1,2-benzanthracene: from 1.1 to 0.37), are bad donors.

NMR Analysis

VT ^1H NMR spectra can allow the assignment of the aromatic protons of the four complexes on the basis of simple chemical shift/scalar coupling considerations, double resonance measurements and 2D ^1H-^1H results.

In all cases, the coordination induces typical high-field shifts and a decrease of the scalar $^3J_{H,H}$ couplings. This upfield shift can be a combination of different effects such as partial sp rehybridization of the ring carbon atom, an increase in electron density on the aromatic ring, quenching of the ring current, or magnetic anisotropy of the

 © 2004 Wiley-VCH Verlag GmbH & Co. KGaA, Weinheim

chromium−ligand bond, as previously discussed.[60−63] The maximum up-field shift due to interaction with the $Cr(CO)_3$ fragment ($\Delta\delta$) occurs for the inner protons belonging to the peripheral ring, which supports metal coordination ($\Delta\delta$ = 3.06, 2.27, 2.71 and 2.70 ppm for **1**−**4**, respectively). The other protons belonging to the coordinated ring show $\Delta\delta \approx$ 2 ppm, whereas the chemical shifts of the protons of the uncoordinated rings are very close to those corresponding to the free ligand ($\Delta\delta \approx 0.2-0.6$ ppm). Detailed data are reported in Table 1SI of the Supporting Information (see also the footnote on the first page of this article).

We also attempted to evaluate the possible migration of the $Cr(CO)_3$ fragment on the different aromatic rings. Thermally induced rearrangements have been previously detected in many π complexes, e.g. in monosubstituted [(naphthalene)$Cr(CO)_3$][64−66] and monosubstituted [(biphenyl)$Cr(CO)_3$][67] derivatives. Haptotropic rearrangements reportedly require substantial activation energies, except in the presence of a coordinating solvent.[68,69] We thus performed a ^{1}H NMR study of complexes **1**−**4**. However, under our experimental conditions (from −100 to +80 °C, deuterated toluene solutions, presence of the free ligand), no line broadening of the ^{1}H resonances was observed, ruling out a fast degenerate haptotropic shift. This is not so surprising if the large energy differences of the possible regioisomers are considered, as has been evaluated for complex **4** by DFT calculations. Spin saturation transfer experiments[70] were also performed with complex **2**, which shows no energy differences between the possible regioisomers. No decrease in the intensity of the aromatic resonances were observed at +80 °C under saturation of the protons 5, 6 and 7, ruling out any haptotropic motion.

Experimental Section

Reactants and Solvents: Pyrene, perylene, chrysene and 1,2-benzanthracene (Aldrich), hexacarbonylchromium (Fluka) were commercial products and were used without further purification. SilicaGel60 was purchased from Merck. The solvents, *n*-heptane, petroleum benzin and toluene (Riedel), were dried with sodium and kept under N_2.

Warning: *Chrysene and 1,2-benzanthracene are active carcinogenic agents. They must be handled using all possible safety precautions, avoiding any contact or exposure.*

Synthesis of the Complexes: The synthetic methods used for the four complexes are very similar. We report as an example the detailed synthesis of the pyrene complex; for the other complexes, basic data are given.

(a) [(Pyrene)Cr(CO)$_3$] (1): Pyrene (250 mg, 1.24 mmol) was dissolved in petroleum benzin (boiling range 100−140 °C; 40 mL) in a flask (250 mL) equipped with an inlet inert gas bubbler and a reflux condenser. An Hg outlet bubbler was used to prevent air entering during the reaction. A gentle flow of N_2 was maintained for a few minutes to purge air from the flask. Hexacarbonylchromium (1.25 g, 5.68 mmol) was then added and the mixture was heated to reflux under vigorous stirring. A slight flow of N_2 was used periodically to remove CO and to maintain the presence of an inert gas in the reaction flask. The initial pale yellow solution turned bright red, and the conversion was measured by checking the characteristic infrared ν(CO) stretching bands of the starting [$Cr(CO)_6$] and of the reaction product. The reaction reached a maximum product concentration after ca. 2 d, when some decomposition began to appear. Heating was then stopped, and the solvent was evaporated under vacuum in a warm bath (45−50 °C, 2500 Pa). The resultant residue was dissolved in toluene (a few mL) and the solution was chromatographed on a 25-cm column, with SilicaGel60 as stationary phase and toluene as eluent. The excess [$Cr(CO)_6$] rapidly eluted, whilst a pale yellow band due to the remaining pyrene partially overlapped the deep red band of complex **1**. This fraction was collected and reduced to ca. 5 mL under a gentle flow of N_2. Crystallization under N_2 at 0 °C gave rise to bright red needles of pure complex **1** in a yield of ca. 45% (with respect to the starting pyrene). The crystals are stable in air for weeks and quite stable in solution, provided they are kept under anaerobic conditions.

(b) [(Perylene)Cr(CO)$_3$] (2): Reactants: perylene (200 mg, 0.79 mmol) and hexacarbonylchromium (1.25 g, 5.68 mmol); reaction conditions: as before; product: bulky dark purple crystals in ca. 35% yield after 4−5 d standing at −30 °C. **2** is air-stable in the solid state for several days, rather stable in anaerobic hydrocarbon solutions, and very unstable when dissolved in halogenated solvents (CH_2Cl_2, CCl_4), even under the strictest anaerobic conditions.

(c) [(Chrysene)Cr(CO)$_3$] (3): Reactants: chrysene (200 mg, 0.88 mmol) and [$Cr(CO)_6$] (1 g, 4.54 mmol); reaction conditions: as before; product: bright bulky red crystals (yield ca. 55%), obtained after 3−4 d standing at −30 °C; the complex is very stable on air, and quite stable in anaerobic solutions. Because **3** co-crystallizes with toluene, to avoid crystal efflorescence the crystals must be stored in the presence of toluene vapor at low temperatures.

(d) [(1,2-Benzanthracene)Cr(CO)$_3$] (4): Reactants: 1,2-benzanthracene (150 mg, 0.66 mmol) and $Cr(CO)_6$ (1 g, 4.54 mmol); reaction conditions: as before; product: bright red needles (yield ca. 65%), obtained after dissolution of **4** in benzene and 15 d of standing at 7 °C. The complex is stable in air in the solid state, and quite stable in solution under anaerobic conditions.

X-ray Structure Analysis: X-ray data for complexes **1**−**4** were collected at room temperature, with a Siemens P4 diffractometer, equipped with an APEX CCD detector 6 cm from the crystal. Graphite-monochromatized Mo-K_α radiation was used with a generator working at 50 kV and 40 mA for **1** and **2** and 35 mA for **3** and **4**. To avoid the loss of solvent (toluene), the crystal of **3** was mounted in a Lindemann glass capillary, with a drop of mother solution inside. Unit cell parameters were obtained by least-squares refinement of 46 (**1**), 31 (**2**), 60 (**3**) and 60 (**4**) reflections in the 2θ range 10−45°. For data collection and refinement, the package of Bruker AXS programs (SMART, SAINT, SADABS, SHELXTL)[71] was used. Owing to the small dimensions and low diffraction power of some crystals, the exposure time of the frames for data collections was 30 (**1** and **2**), 20 (**3**) and 10 s (**4**). The reflections were collected using the ω-scan technique ($\Delta\omega$ = 0.3°) and the intensities were corrected for absorption with the multi-scan method (SADABS) for **1**, **3** and **4**, while for **2** the numerical crystal faces method was applied (XPREP). In complex **3** a disordered molecule of toluene, lying on the inversion centre, was located. The non-hydrogen atoms were anisotropically refined. High thermal parameters were found for the four complexes. Hydrogen atoms in calculated positions were refined riding on the corresponding carbon atom. Crystal data and refinement parameters are

 © 2004 Wiley-VCH Verlag GmbH & Co. KGaA, Weinheim

Table 4. Crystal and structure refinement data for complexes **1**−**4**

Compound	**1**	**2**	**3**	**4**
Empirical formula	$C_{19}H_{10}CrO_3$	$C_{23}H_{12}CrO_3$	$C_{24.5}H_{15.5}CrO_3$	$C_{21}H_{12}CrO_3$
Formula mass	338.27	388.33	409.87	264.31
Temperature [K]	294(2)	293(2)	294(2)	298(2)
Wavelength [Å]	0.71073	0.71073	0.71073	0.71073
Crystal system, space group	monoclinic, $P2_1/n$	monoclinic, $C2/c$	triclinic, $P\bar{1}$	orthorhombic, *Pbca*
a [Å]	12.8686(17)	17.818(2)	9.990(9)	12.8320(10)
b [Å]	7.2639(9)	12.955(1)	10.172(9)	12.1077(10)
c [Å]	15.0804(18)	14.632(2)	10.391(8)	20.2644(16)
α [°]	90	90	94.033(15).	90
β [°]	95.837	101.073(2)	104.864(14)	90
γ [°]	90	90	108.807(14)	90
Volume [$Å^{-3}$]	1402.3(3)	3314.5(6)	952.5(14)	3148.4(4)
Z, calcd. density [g/cm^{-3}]	4, 1.602	8, 1.556	2, 1.429	8, 1.537
μ [mm^{-1}]	0.828	0.712 mm^{-1}	0.623	0.744
F(000)	688	1584	421	1488
Crystal size [mm]	0.040 × 0.08 × 0.28	0.02 × 0.16 × 0.38	0.30 × 0.32 × 0.44	0.18 × 0.34 × 0.36
Color, shape	dark red, prism	black, prism	red, prism	red, lamina
θ range for data collected [°]	2.72 to 28.31	1.96 to 28.31	2.06 to 28.37	2.01 to 28.35
Limiting indices	$-14 \le h \le 16$ $-9 \le k \le 8$ $-20 \le l \le 20$	$-23 \le h \le 23$ $-14 \le k \le 17$, $-19 \le l \le 19$	$-12 \le h \le 13$ $-13 \le k \le 12$ $-13 \le l \le 13$	$-16 \le h \le 17$ $-16 \le k \le 15$ $-26 \le l \le 25$
Reflections collected/unique	9792/3361 [*R*(int) = 0.0471]	11753/3879 [*R*(int) = 0.0474]	6914/4360 [*R*(int) = 0.0284]	21032/3761 [*R*(int) = 0.0371]
Refinement method	Full-matrix least squares on F^2	Full-matrix least squares on F^2	Full-matrix least squares on F^2	Full-matrix least squares on F^2
Data/restraints/parameters	3361/0/208	3879/0/244	4360/1/262	3761/0/221
Goodness-of-fit on F^2	0.644	0.734	0.828	0.880
Final *R* indices[a] [$I > 2\sigma(I)$]	*R*1 = 0.0361, *wR*2 = 0.0578	*R*1 = 0.0402, *wR*2 = 0.0828	*R*1 = 0.0445, *wR*2 = 0.0940	*R*1 = 0.0375, *wR*2 = 0.0907
R indices (all data)	*R*1 = 0.0975, *wR*2 = 0.0622	*R*1 = 0.0812, *wR*2 = 0.0870	*R*1 = 0.0698, *wR*2 = 0.0992 $eÅ^{-3}$	*R*1 = 0.0643, *wR*2 = 0.0951
Largest diff. peak/hole [$e·Å^{-3}$]	0.368/−0.215	0.426/−0.232	0.305/−0.233	0.488/−0.380

[a] $R1 = \Sigma||F_o| - |F_c||/\Sigma|F_o|$ for "observed" reflections having $F_o^2 > 2\sigma(F_o^2)$. $wR2 = [\Sigma(wF_o^2 - F_c^2)^2/\Sigma w(F_o^2)^2]^{1/2}$. Goodness-of-fit = $[\Sigma w(F_o^2 - F_c^2)^2/(\text{no. of unique reflections} - \text{no. of parameters})]^{1/2}$.

reported in Table 4. CCDC-211599 to·-211602 contain the supplementary crystallographic data for this paper. These data can be obtained free of charge at www.ccdc.cam.ac.uk/conts/retrieving.html [or from the Cambridge Crystallographic Data Centre, 12 Union Road, Cambridge CB2 1EZ, UK; Fax: (internat.) + 44-1223/336-033; E-mail: deposit@ccdc.cam.ac.uk].

Vibrational Analysis: Infrared spectroscopy measurements were recorded in solutions of dried *n*-heptane and toluene or in KBr pellets with a Bruker FTIR Equinox 55 spectrophotometer (resolution 2 cm^{-1}). Raman measurements were performed on crystal samples, sealed in a glass capillary under Ar, with a Bruker RFS 100 spectrophotometer (resolution 4 cm^{-1}) equipped with a 1.064 nm Nd:YAG laser, irradiating the samples with an average power set in the range 30−45 mW. Ab initio calculations of the free PAH were performed by employing the DFT B3LYP method with the Gaussian 98[72] package on a personal computer. We used a 6-31G** basis set and the vibrational frequencies and intensities and normal coordinates were calculated at the respective optimised structure. For the 1700−100 cm^{-1} region we employed a scaling factor of 0.9614. Normal coordinates were visualized with the Moldraw package.[73] The accordance between the scaled DFT and experimental frequencies was very good, and the intensity vibrational pattern was well fitted.

NMR Spectra: All NMR data were acquired with a Jeol EX 400 operating at 399.6 MHz. One-dimensional ^1H spectra were recorded in deuterated benzene and toluene solutions, with 32 K data points and a sweep width of 5827 Hz giving a digital resolution of 0.35 Hz; 64 accumulations were acquired with an acquisition time of 2.8 s. Two-dimensional ^1H-^1H spectra were acquired with a spectral width of 5500 Hz, 512 t_1 points, 2 K data points in t_2 and 32 transients for each t_2 points. Chemical shifts were referenced to tetramethylsilane (TMS).

Acknowledgments

We are indebted to the Italian MIUR (Ministero dell'Istruzione, dell'Università e della Ricerca) for their support (FIRB) of this research.

[1] J. Szczepanski, M. Vala, *Astrophys. J.* **1993**, *414*, 646−655.
[2] T. Watube, T. Ishizuka, M. Isobe, N. Ozawa, *Science.* **1982**, *215*, 403−405.
[3] J. A. Morley, N. F. Woolsey, *J. Org. Chem.* **1992**, *57*, 6487−6495.
[4] R. G. Harvey, *Polyciclic Hydrocarbons and Carcinogenesis*, American Chemical Society, Washington, DC, **1985**, pp. 406.
[5] A. I. Kitaigorodsky, *Molecular crystals and molecules*, Academic Press, New York, **1973**, pp. 38−48.
[6] V. Balzani, S. Campagna, G. Denti, A. Juris, S. Serroni, A. Venturi, *Acc. Chem. Res.* **1998**, *31*, 26−34.
[7] F. Casellato, C. Vecchi, A. Girelli, P. G. Farrell, *Thermochim. Acta* **1975**, *13*, 37−45.
[8] I. Ikemoto, H. Kuroda, *Acta Crystallogr., Sect. B* **1968**, *24*, 383−387.
[9] P. J. Munnoch, J. D. Wright, *J. Chem. Soc., Perkin Trans. 2* **1974**, 1397−1400.
[10] J. S. Lee, K. C. Huang, W. J. Wang, J. L. Wang, *Synth. Met.* **1995**, *70*, 1227−1228.
[11] R. Atencio, K. V. Domasevitch, M. J. Zaworotko, *Crystal Engineer.* **2000**, *3*, 63−69.

 © 2004 Wiley-VCH Verlag GmbH & Co. KGaA, Weinheim

[12] D. E. Eaton, A. G. Anderson, J. C. Calabrese, W. Tam, Y. Wang, *J. Am. Chem. Soc.* **1987**, *109*, 1886−1888.
[13] R. L. De, J. Von Seyerl, L. Zsolnai, G. Huttner, *J. Organomet. Chem.* **1979**, *175*, 185−191.
[14] D. Braga, F. Grepioni, K. Biradha, V. R. Pedireddi, G. R. Desiraju, *J. Am. Chem. Soc.* **1995**, *117*, 3156−3166.
[15] N. J. Long, *Angew. Chem. Int. Ed. Engl.* **1995**, *34*, 21−38.
[16] D. Braga, F. Grepioni, G. R. Desiraju, *Chem. Rev.* **1998**, *98*, 1375−1405.
[17] B. Deubzer, E. O. Fischer, H. P. Fritz, C. G. Kreiter, N. Kriebitzsch, H. D. Simmons, B. R. Willeford, Jr., *Chem. Ber.* **1967**, *100*, 3084−3096.
[18] E. O. Fischer, K. Oefele, *Chem. Ber.* **1957**, *90*, 2532−2535.
[19] G. Natta, R. Ercoli, F. Calderazzo, *Chem. Ind. (Milan)* **1958**, *40*, 287−289.
[20] G. Natta, R. Ercoli, F. Calderazzo, *Chem. Ind. (Milan)* **1958**, *40*, 1003−1007.
[21] A. D. Hunter, L. Shilliday, W. S. Furey, M. J. Zaworotko, *Organometallics* **1992**, *11*, 1550−1560.
[22] [22a] A. Solladié-Cavallo, *Polyhedron* **1985**, *4*, 901−927. [22b] W. E. Silverthorn, *Adv. Organomet. Chem.* **1975**, *13*, 47−137. [22c] C. V. Senoff, *Coord. Chem. Rev.* **1980**, *32*, 11−191.
[23] V. Kunz, W. Novacki, *Helv. Chim. Acta* **1967**, *50*, 1052−1059.
[24] F. Hanic, O. S. Mills, *J. Organomet. Chem.* **1968**, *11*, 151−158.
[25] [25a] K. W. Muir, G. Ferguson, G. A. Sim, *J. Chem. Soc., B.* **1968**, 467−471. [25b] J. M. Guss, R. Mason, *J. Chem. Soc., Dalton Trans.* **1973**, 1834−1838.
[26] R. D. Rogers, J. L. Atwood, T. A. Albright, W. A. Lee, M. D. Rausch, *Organometallics* **1984**, *3*, 263−270.
[27] Cambridge Structural Database (CSD), Cambridge, UK, **2002**.
[28] I. Chavez, A. Cisternas, M. Otero, E. Roman, U. Muller, *Z. Naturforsch., Teil B* **1990**, *45*, 658−666.
[29] L. C. Porter, J. R. Polam, J. Mahmoud, *Organometallics* **1994**, *13*, 2092−2096.
[30] L. C. Porter, J. R. Polam, S. Bodige, *Inorg. Chem.* **1995**, *34*, 998−1001.
[31] M. Crocker, M. Green, J. A. K. Howard, N. C. Norman, D. M. Thomas, *J. Chem. Soc., Dalton Trans.* **1990**, 2299−2301.
[32] R. G. Swisher, E. Sinn, R. N. Grimes, *Organometallics* **1985**, *4*, 896−901.
[33] H. Kubo, M. Hirano, S. Komiya, *J. Organomet. Chem.* **1998**, *556*, 89−100.
[34] N. P. Do Thi, S. Spichiger, P. Paglia, G. Bernardinelli, E. P. Kündig, P. L. Timms, *Helv. Chim. Acta* **1992**, *75*, 2593−2607.
[35] J. K. Seaburg, P. J. Fischer, V. G. Young, J. E. Ellis, *Angew. Chem. Int. Ed.* **1998**, *37*, 155−158.
[36] B. P. Byers, M. B. Hall, *Inorg. Chem.* **1987**, *26*, 2186−2188.
[37] S. M. Hubig, S. V. Lindeman, J. K. Kochi, *Coord. Chem. Rev.* **2000**, *200−202*, 831−873.
[38] M. Sodeoka, H. Yamada, M. Shibasaki, *J. Am. Chem. Soc.* **1990**, *112*, 4906−4911.
[39] R. H. Mitchell, Y. Chen, *Tetrahedron Lett.* **1996**, *37*, 6665−6668.
[40] R. H. Mitchell, Y. Chen, N. Khalifa, P. Zhou, *J. Am. Chem. Soc.* **1998**, *120*, 1785−1794.
[41] R. H. Mitchell, Z. Brkic, D. J. Berg, T. M. Barclay, *J. Am. Chem. Soc.* **2002**, *124*, 11983−11988.
[42] For example e.s.d.s of 0.002−0.003 Å were obtained by neutron data at 78 K on [$C_6H_6Cr(CO)_3$]: B. Rees, P. Coppens, *Acta Crystallogr., Sect. B* **1973**, *29*, 2516−2528.
[43] J. Y. Sailard, D. Grandjean, P. LeMaux, G. Jaouen, *New J. Chem.* **1981**, *5*, 153−160.
[44] P. G. Gassman, P. A. Deck, *Organometallics* **1994**, *13*, 1934−1939.
[45] B. Rees, A. Mitschler, *J. Am. Chem. Soc.* **1976**, *98*, 7918−7924.
[46] A. D. Hunter, V. Mozol, S. D. Tsai, *Organometallics* **1992**, *11*, 2251−2262.
[47] M. Randić, *Chem. Rev.* **2003**, *103*, 3449−3605.
[48] A. Stanger, R. Boese, N. Askenazi, P. Stellberg, *J. Organomet. Chem.* **1997**, *542*, 19−24.
[49] M. Nambu, D. L. Mohler, K. Hardcastle, K. K. Baldridge, J. S. Siegelpp, *J. Am. Chem. Soc.* **1993**, *115*, 6138−6142.
[50] E. L. Muetterties, J. R. Bleeke, E. J. Wucherer, T. A. Albright, *Chem. Rev.* **1982**, *82*, 499−525.
[51] T. A. Albright, P. Hofmann, R. Hoffmann, C. P. Lillya, P. A. Dobosh, *J. Am. Chem. Soc.* **1983**, *10*, 3396−3411.
[52] E. Diana, R. Rossetti, P. L. Stanghellini, S. F. A. Kettle, *Inorg. Chem.* **1997**, *36*, 382−391.
[53] S. R. Langhoff, *J. Phys. Chem.* **1996**, *100*, 2819−2841.
[54] A. Berces, T. Ziegler, *J. Phys. Chem.* **1994**, *98*, 13233−13242.
[55] J. Muller, T. Akhnoukh, P. E. Gaede, A. Guo, P. Moran, K. Qiao, *J. Organomet. Chem.* **1997**, *541*, 207−217.
[56] L. Schäfer, J. Southern, S. J. Cyvin, *Spectrochim. Acta* **1971**, *27A*, 1083−1090.
[57] Table 2SI of the Supporting Information lists the most important infrared and Raman bands of the complexes and the proposed assignment.
[58] For example, for complex **1**, $\Delta\gamma$(CH) is 18 cm^{-1} in solid-state spectra and ca. 0 cm^{-1} in CS_2 solution.
[59] D. M. Hudgins, L. J. Allamandola, *J. Phys. Chem. A* **1997**, *101*, 3472−3477.
[60] J. Price, T. S. Sorensen, *Can. J. Chem.* **1968**, *468*, 515−522.
[61] R. V. Emanuel, E. W. Randail, *J. Chem. Soc., A* **1969**, 3002−3006.
[62] M. J. McGlinchey, S. T. Tan, *Can. J. Chem.* **1974**, *52*, 2439−2443.
[63] M. J. McGlinchey, J. L. Fletcher, *Can. J. Chem.* **1975**, *53*, 1525−1529.
[64] E. P. Kündig, V. Desorby, C. Griver, B. Rudolf, S. Spichiger, *Organometallics* **1987**, *6*, 1173−1180.
[65] Y. F. Oprunenko, S. G. Malugina, Y. A. Ustynyuk, N. A. Ustynyuk, D. N. Kravtsov, *J. Organomet. Chem.* **1988**, *338*, 357−368.
[66] S. D. Cunningham, K. Oefele, B. R. Willeford, *J. Am. Chem. Soc.* **1983**, *105*, 3724−3725.
[67] Y. F. Oprunenko, N. G. Akhmedov, D. N. Laikov, S. G. Malyugina, V. I. Mstislavsky, A. R. Vitaly, Y. A. Ustynyuk, N. A. Ustynyuk, *J. Organomet. Chem.* **1999**, *583*, 136−145.
[68] B. Deubzer, H. P. Fritz, C. G. Kreiter, K. Öfele, *J. Organomet Chem.* **1967**, *7*, 289−299.
[69] K. M. Nicholas, R. C. Kerber, E. I. Stiefel, *Inorg. Chem.* **1971**, *10*, 1519−1521.
[70] P. Bergamini, E. Costa, S. Sostero, A. G. Orpen, P. G. Pringle, *Organometallics* **1991**, *10*, 2989−2990.
[71] Bruker AXS, Inc., Madison, Wisconsin, **2003**.
[72] M. J. Frisch, G. W. Trucks, H. B. Schlegel, G. E. Scuseria, M. A. Robb, J. R. Cheeseman, V. G. Zakrzewski, J. A. Montgomery, Jr., R. E. Stratmann, J. C. Burant, S. Dapprich, J. M. Millam, A. D. Daniels, K. N. Kudin, M. C. Strain, O. Farkas, J. Tomasi, V. Barone, M. Cossi, R. Cammi, B. Mennucci, C. Pomelli, C. Adamo, S. Clifford, J. Ochterski, G. A. Petersson, P. Y. Ayala, Q. Cui, K. Morokuma, D. K. Malick, A. D. Rabuck, K. Raghavachari, J. B. Foresman, J. Cioslowski, J. V. Ortiz, A. G. Baboul, B. B. Stefanov, G. Liu, A. Liashenko, P. Piskorz, I. Komaromi, R. Gomperts, R. L. Martin, D. J. Fox, T. Keith, M. A. Al-Laham, C. Y. Peng, A. Nanayakkara, M. Challacombe, P. M. W. Gill, B. Johnson, W. Chen, M. W. Wong, J. L. Andres, C. Gonzalez, M. Head-Gordon, E. S. Replogle, J. A. Pople, *Gaussian 98, Revision A.9*, Gaussian, Inc., Pittsburgh PA, **1998**.
[73] P. Ugliengo, D. Viterbo, G. Chiari, *Z. Kristallogr.* **1993**, *207*, 9−23.

Received June 14, 2003
Early View Article
Published Online February 17, 2004

 © 2004 Wiley-VCH Verlag GmbH & Co. KGaA, Weinheim

Hydrothermal Syntheses, Crystal Structures, Magnetism and Fluorescence Quenching of Oxamidato-Bridged Pentanuclear $Cu^{II}_4Ln^{III}$ Complexes Containing Macrocyclic Ligands (Ln = Eu, Tb) and the Crystal Structure of a Hexanuclear $Ni^{II}_5Sm^{III}$ Complex

Ya-Qiu Sun,[a,d] Mao Liang,[a] Wen Dong,[a] Guang-Ming Yang,*[a] Dai-Zheng Liao,*[a] Zong-Hui Jiang,[a,b] Shi-Ping Yan,[a,c] and Peng Cheng[a]

Keywords: Hydrothermal synthesis / Macrocyclic ligands / Magnetic properties / Fluorescence

Three novel oxamidato-bridged complexes incorporating a macrocyclic oxamide of formula $[(CuL)_3\{CuL(C_2H_5OH)\}Eu(H_2O)](ClO_4)_3\cdot 1.5H_2O$ (**1**), $[(CuL)_3\{CuL(C_2H_5OH)\}Tb(H_2O)](ClO_4)_3\cdot 2H_2O$ (**2**) and $[(NiL)_5Sm](ClO_4)_3\cdot 2H_2O$ (**3**) (CuL and NiL, H_2L = 2,3-dioxo-5,6,14,15-dibenzo-1,4,8,12-tetraazacyclopentadeca-7,13-dien), have been hydrothermally synthesized and structurally characterized. In these complexes, the central Ln^{III} and external copper (or nickel) ions are bridged by macrocyclic oxamide groups. The Eu^{III} (or Tb^{III}) ion of **1** (or **2**) resides in a distorted tricapped trigonal prismatic environment surrounded by eight oxygen atoms from four oxamide groups and one oxygen atom from a water molecule, whereas the Sm^{III} ion of **3** resides in a distorted bicapped square antiprismatic environment surrounded by ten oxygen atoms from five oxamide groups. Furthermore, there are hydrogen bonding interactions in **1** and **2** between perchlorate, ethanol and water moieties. Especially for **1** and **2**, O–H···O and weak coordination of ClO_4^- groups link the pentanuclear fragments and perchlorate ions to form a 1-D supramolecular architecture. The fluorescence of Eu^{III} and Tb^{III} are almost completely quenched in **1** and **2**. The magnetic properties of **1** and **2** have been characterized. (© Wiley-VCH Verlag GmbH & Co. KGaA, 69451 Weinheim, Germany, 2003)

Introduction

Molecular magnetism and macrocyclic compounds are two active fields of research encompassing chemistry, physics, biology, and material science.[1,2] The field of molecular-based magnetic materials has shown spectacular advances in the last two decades, especially for metal complex-based magnetic compounds.[2] Assembly of metal complexes which may act as light switchable magnets and single molecule magnets has attracted special attention in the latest decade.[3−5] The mechanisms responsible for the magnetic interactions between d ions are reasonably well understood, and efficient models have been proposed to rationalize the various types of magnetic behavior.[2,6] As far as magnetic coupling between f ions and d ions is concerned, the situation is much less advanced because the behavior of the Ln^{III} ion with a first-order orbital momentum is much more complicated. Indeed, the 4f configuration of a Ln^{III} ion is split into $^{2S+1}L_J$ states by the inter-electronic repulsion and the spin-orbit coupling. Each of these states is further split into Stark components due to the crystal field perturbation. It follows that it is in principle very difficult to determine not only the magnitude of the $Ln^{III}-Cu^{III}$ interactions but even their nature. It is therefore essential for further development of 3d-4f magnetochemistry in order to obtain accurate information on the 3d-4f magnetic interactions and a synthetic design without 3d-3d and 4f-4f magnetic interactions.[7,8] Since Gatteschi and co-workers discovered a ferromagnetic coupling between Cu^{II} and Gd^{III} ions in 1985,[9] the design and properties of molecular complexes simultaneously comprising lanthanide and transition metal ions[9−15] have been of considerable interest. However, most of the studies have been focused on the $Gd^{III}-Cu^{II}$ couple[9−15] which has been found to be directly ferromagnetic in most cases. In comparison, polynuclear complexes containing other $Ln^{III}-Cu^{II}$ couples have been poorly investigated.[12,16−18] In addition, the majority of the mixed metal complexes are bridged by polydentate Schiff bases, pyridonates, carboxylate or oxamide ligands.[12,13,19−21] In particular, the oxamide group has been noted as an efficient

[a] Department of Chemistry, Nankai University, Tianjin 300071, P. R. China
Fax: (internat.) +86-22-23502779
E-mail: coord@nankai.edu.cn
[b] State Key Laboratory of Coordination Chemistry, Nanjing University, Nanjing 210093, P. R. China
[c] State Key Laboratory of Earth Materials Chemistry and Applications, Peking University, Beijing 100871, P. R. China
[d] Department of Chemistry, Tianjin Normal University, Tianjin 300074, P. R. China

 © 2004 Wiley-VCH Verlag GmbH & Co. KGaA, Weinheim **DOI: 10.1002/ejic.200300464**

mediator of magnetic exchange between 3d-3d centers. However, heterometallic complexes of the macrocyclic oxamide, especially of those containing 3d-4f metals, have been rarely prepared,[22] although metal complexes of macrocyclic ligands have been of great interest to coordination chemists for their special structures, properties, and/or functionalities.[1][8a,23]

On the other hand, investigations of the effect of metal complexes upon the fluorescence of rare earth ions will give basic and useful information for the development of fluorescent materials, since the metal complexes reported so far are beyond enumeration and show a great variety of characteristic colors. Recently, many complexes containing rare earth ions have been prepared, and their fluorescent proprieties have been studied,[24−27] but heterometallic complexes of this kind, especially those containing 3d-4f metals have been rarely investigated.[12,27]

With these facts in mind and in continuation of our work on polynuclear macrocyclic complexes,[20−22] the macrocyclic oxamido-copper (II) and oxamido-nickel(II) complexes were used as ligands to synthesize new complexes. The result is that two novel pentanuclear $Cu^{II}_4Ln^{III}$ complexes (Ln = Eu, Tb) and one hexanuclear $Ni^{II}_5Sm^{III}$ complex have been isolated and structurally characterized, the magnetic and fluorescent properties of **1** and **2** have also been subjected to a preliminarily investigation.

Results and Discussion

Synthesis

The hydrothermal technique not only provides a pathway to stable structures utilizing inorganic molecular units of a desired geometry or composition but also allows the introduction of a variety of inorganic cations to act as templates in directing the organization of the complexes. In those reactions the Ln(III) ions were used as templating reagents. Under appropriate conditions, large single crystals were obtained in high yield.

Structures

Description of the Structure of 1

Complex **1** consists of pentanuclear $[(CuL)_3\{CuL(C_2H_5OH)\}Eu(H_2O)]^{3+}$ cations, monovalent ClO_4^- anions, and water. A perspective view of the pentanuclear cation is depicted in Figure 1, and selected bond lengths and angles are listed in Table 1. The central europium and external copper ions are bridged by macrocyclic oxamide groups. The external Cu1 ion is coordinated by four nitrogen atoms from the macrocyclic organic ligand, with the $[Cu1N_4]$ chromophore exhibiting near planarity. The Cu1 ion is displaced from the least-square plane by +0.1130Å. The coordination environment of Cu2 is similar to that of Cu1. Cu3 is located in a slightly distorted square-based pyramidal environment with the basal plane composed of atoms N9, N10, N11 and N12 from the macrocyclic oxamide groups, the axial position is occupied by an ethanol molecule. The deviations of the four donor atoms (N9, N10, N11 and N12) from their mean plane are −0.1756, +0.1023, −0.1645 and +0.1607 Å, respectively, and Cu3 is located +0.1521Å out of the plane. Cu4 is also located in a slightly distorted square pyramidal environment with the basal plane composed of atoms N13, N14, N15 and N16 from the macrocyclic oxamide groups, the axial position is occupied by perchlorate weakly coordinated with Cu4, and the Cu4···O14 distance is 2.460 Å. The central europium atom resides in a distorted tricapped trigonal prismatic environment surrounded by eight oxygen atoms from four oxamide groups and the O1w atom of the water molecule. The O1w, O3 and O8 atoms are located on the respective caps. The trigonal prism is composed of O1, O2, O4, O5, O6 and O7, with one basal plane constructed from O4, O5, O6 and the other basal plane constructed from O7, O1 and O2. The flank of the trigonal prism is slightly distorted square-planar because the deviations of the four oxygen atoms (O6, O2, O4, O7 of one flank) are −0.0980, −0.1101, +0.1046 and +0.1035 Å, respectively, and the deviations of atoms from another flank (O1, O2, O4, O5) are −0.1284, +0.1397, −0.1228 and +0.1115 Å, respectively. Thus, the coordination geometry around the europium ion can be described as distorted tricapped trigonal prismatic. As depicted in Figure 2, the cations are alternately bridged by perchlorates to give infinite chains in which O−H···O interactions between coordinated ethanol and perchlorate ($d_{O\cdots O}$ = 2.855 Å), and ClO_4^-→Cu weak coordination pull the cations together ($d_{O\cdots Cu}$ = 2.558 Å). Furthermore, there are other O−H···O interactions between coordinated water and free water and free perchlorate, the O···O distances are 2.850 and 2.972 Å, respectively. In addition, there are π-π interactions between benzene rings of the CuL units of different cations in the cell which are parallel to each other

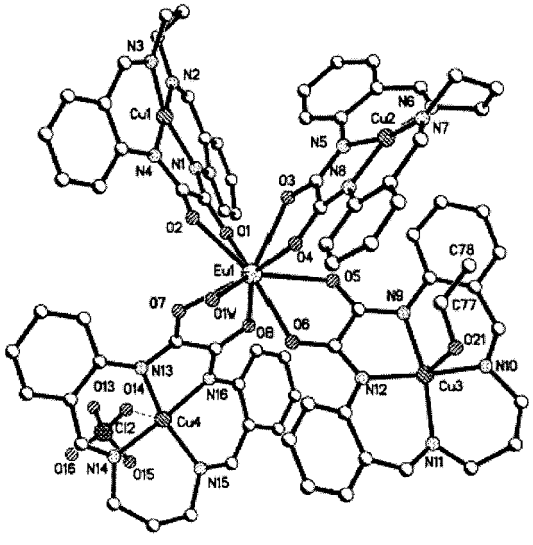

Figure 1. Perspective view of the pentanuclear complex cation of **1**

 © 2004 Wiley-VCH Verlag GmbH & Co. KGaA, Weinheim

Table 1. Selected Bond lengths (Å) and Angles (deg) for **1**

Eu(1)−O(6)	2.433(5)	Cu(1)−N(4)	1.944(6)
Eu(1)−O(2)	2.448(5)	Cu(1)−N(2)	1.947(7)
Eu(1)−O(1)	2.459(5)	Cu(1)−N(1)	2.012(5)
Eu(1)−O(7)	2.468(5)	Cu(1)−N(3)	2.047(7)
Eu(1)−O(4)	2.478(5)	Cu(3)−N(12)	1.993(6)
Eu(1)−O(5)	2.487(5)	Cu(3)−N(10)	2.002(7)
Eu(1)−O(1 W)	2.494(6)	Cu(3)−N(9)	2.016(6)
Eu(1)−O(3)	2.497(5)	Cu(3)−N(11)	2.031(6)
Eu(1)−O(8)	2.498(5)	Cu(3)−O(21)	2.423(6)
O(6)−Eu(1)−O(2)	144.32(17)	O(2)−Eu(1)−O(1 W)	72.87(18)
O(6)−Eu(1)−O(1)	146.84(16)	O(1)−Eu(1)−O(1 W)	132.74(17)
O(6)−Eu(1)−O(7)	95.64(18)	O(7)−Eu(1)−O(1 W)	65.40(19)
O(6)−Eu(1)−O(4)	77.06(18)	O(4)−Eu(1)−O(1 W)	69.29(18)
O(6)−Eu(1)−O(5)	64.42(16)	O(5)−Eu(1)−O(1 W)	128.73(17)
O(6)−Eu(1)−O(1 W)	71.60(18)	O(1 W)−Eu(1)−O(3)	121.80(18)
O(6)−Eu(1)−O(3)	124.78(17)	O(1 W)−Eu(1)−O(8)	117.01(17)
O(6)−Eu(1)−O(8)	76.95(17)	N(4)−Cu(1)−N(2)	176.1(3)
N(10)−Cu(3)−N(9)	92.3(3)	N(4)−Cu(1)−N(1)	84.3(2)
N(12)−Cu(3)−N(11)	90.5(3)	N(2)−Cu(1)−N(1)	93.6(3)
N(10)−Cu(3)−N(11)	94.1(3)	N(4)−Cu(1)−N(3)	89.6(3)
N(9)−Cu(3)−N(11)	162.5(3)	N(2)−Cu(1)−N(3)	93.5(3)
N(12)−Cu(3)−O(21)	89.4(2)	N(1)−Cu(1)−N(3)	160.1(3)
N(10)−Cu(3)−O(21)	90.6(3)	N(9)−Cu(3)−O(21)	95.2(2)

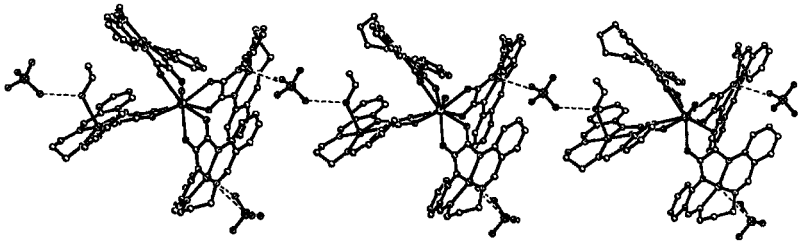

Figure 2. View of the self-assembled 1-D supramolecular architecture through O−H···O and weak coordination interactions of ClO_4^- for **1** and **2**

and the distance between carbon atoms is approximately 3.416 Å.

Description of the Structure of 2

X-ray structural analysis shows that the structure of the pentanuclear $[(CuL)_3\{CuL(C_2H_5OH)\}Tb(H_2O)]^{3+}$ cation is similar to that in **1** (Figure 3). There is an oxamide bridge between the Tb(III) and each Cu(II) ion. The coordination environments of the Cu1 and Cu2 ions are similar and slightly distorted square-planar with the basal planes composed of four nitrogen atoms from the macrocyclic oxamide groups with the axial positions occupied by perchlorates weakly coordinated to Cu1 and Cu2. The Cu3 ion is coordinated by four nitrogen atoms of the macrocyclic organic ligand with the $[Cu1N_4]$ chromophore exhibiting near planarity. Cu4 is located in a slightly distorted square pyramidal environment with the basal plane composed of atoms N13, N14, N15 and N16 from the macrocyclic oxamide groups, with the axial position being occupied by an ethanol molecule. The central terbium ion resides in a distorted tricapped trigonal prismatic environment surrounded by eight oxygen atoms from four oxamide groups and the O9 atom of a water molecule. The O9, O5 and O8 atoms are located on the respective caps, while the trigonal prism is composed of O1, O2, O3, O4, O6 and O7 with one basal plane constructed from O4, O2, O6 and the other basal plane constructed from O7, O1 and O3. As depicted in Figure 2, the cations are alternately bridged by perchlorates giving infinite chains in which the O−H···O interactions between coordinated ethanol and perchlorate groups ($d_{O\cdots O}$ = 2.825 Å), and $ClO_4^-\rightarrow$Cu weak coordination ($d_{O\cdots Cu}$ = 2.528 Å) pull the cations together. Furthermore, there are other O−H···O interactions between coordinated water and free water and free perchlorate and the O···O distances are 2.821 and 2.943 Å, respectively. In addition, there are π-π interactions between benzene rings of the CuL moieties of different cations in the cell which are parallel to each other and the distance between carbon atoms is approximately 3.400 Å (Table 2).

Description of the Structure of 3

Complex **3** consists of hexanuclear $[(NiL)_5Sm]^{3+}$ cations, monovalent ClO_4^- anions, and water. A perspective view of the hexanuclear cation is depicted in Figure 4, and selected bond lengths and angles are listed in Table 3. The central samarium and external nickel ions are bridged by

 © 2004 Wiley-VCH Verlag GmbH & Co. KGaA, Weinheim

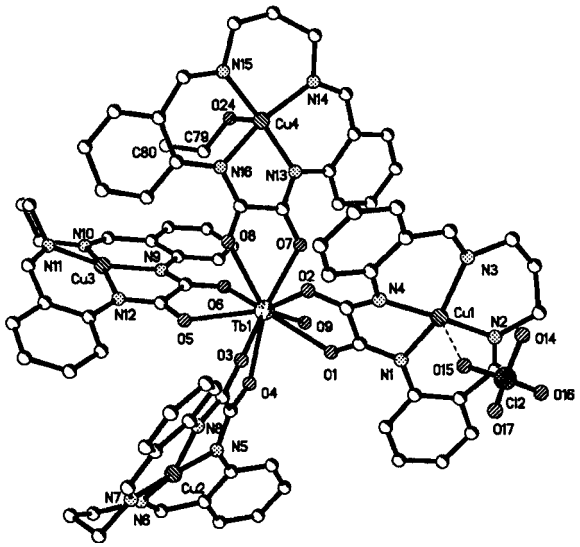

Figure 3. Perspective view of the pentanuclear complex cation of **2**

Table 2. Selected bond lengths (Å) and angles (deg) for **2**

Tb(1)−O(7)	2.377(5)	Cu(1)−N(4)	1.962(6)
Tb(1)−O(4)	2.401(5)	Cu(1)−N(2)	1.966(8)
Tb(1)−O(1)	2.405(5)	Cu(1)−N(1)	1.979(6)
Tb(1)−O(3)	2.424(5)	Cu(1)−N(3)	2.029(8)
Tb(1)−O(6)	2.434(5)	Cu(4)−N(13)	1.973(6)
Tb(1)−O(8)	2.447(5)	Cu(4)−N(15)	1.975(7)
Tb(1)−O(2)	2.452(5)	Cu(4)−N(16)	2.003(6)
Tb(1)−O(5)	2.454(5)	Cu(4)−N(14)	2.021(7)
Tb(1)−O(9)	2.491(6)	Cu(4)−O(24)	2.394(6)
O(7)−Tb(1)−O(4)	143.60(17)	O(4)−Tb(1)−O(9)	72.94(18)
O(7)−Tb(1)−O(1)	94.55(17)	O(1)−Tb(1)−O(9)	64.99(18)
O(7)−Tb(1)−O(3)	146.67(16)	O(3)−Tb(1)−O(9)	132.88(17)
O(7)−Tb(1)−O(6)	77.18(18)	O(6)−Tb(1)−O(9)	69.15(18)
O(7)−Tb(1)−O(8)	65.29(16)	O(8)−Tb(1)−O(9)	128.78(18)
O(7)−Tb(1)−O(2)	76.82(17)	O(2)−Tb(1)−O(9)	117.14(17)
O(7)−Tb(1)−O(5)	125.40(17)	O(5)−Tb(1)−O(9)	22.02(18)
O(7)−Tb(1)−O(9)	70.80(18)	N(4)−Cu(1)−N(2)	174.3(3)
N(13)−Cu(4)−O(24)	89.6(2)	N(4)−Cu(1)−N(1)	82.5(2)
N(15)−Cu(4)−O(24)	90.9(3)	N(2)−Cu(1)−N(1)	92.1(3)
N(16)−Cu(4)−O(24)	95.3(2)	N(4)−Cu(1)−N(3)	89.4(3)
N(14)−Cu(4)−O(24)	100.5(3)	N(2)−Cu(1)−N(3)	95.1(3)

macrocyclic oxamide groups. The external nickel ions are coordinated by four nitrogen atoms from the macrocyclic organic ligand, with the $[NiN_4]$ chromophore exhibiting a distorted planar arrangement. The deviations of the four donor atoms (N1, N2, N3 and N4) from their mean plane are −0.2695, +0.2713, −0.2627 and +0.2699 Å, respectively, and Ni1 is located −0.0089 Å out of the plane. The central samarium ion resides in a distorted bicapped square antiprismatic environment surrounded by ten oxygen atoms from five oxamide groups. O6 and O9 are located on the respective caps. The square antiprism is composed of O1, O2, O3, O4, O5, O7, O8 and O10, with one basal plane constructed from O1, O3, O7 and O10 and the other basal plane constructed from O2, O4, O5 and O8. The deviations of the atoms of one basal plane (O1, O3, O7, O10) are −0.1697, +0.1269, −0.1097 and +0.1525 Å, respectively. Thus, the coordination geometry around the samarium ion can be described as distorted bicapped square antiprismatic. In addition, there are π-π interactions between benzene rings of the NiL units of different cations in the cell which are parallel to each other and the distance between carbon atoms is approximately 3.301 Å.

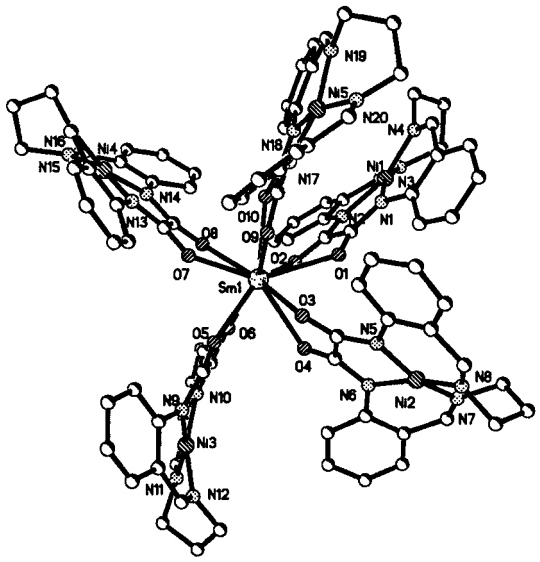

Figure 4. Perspective view of the hexanuclear complex cation of **3**

Table 3. Selected bond lengths (Å) and angles (deg) for **3**

Sm(1)−O(7)	2.428(6)	Sm(1)−O(9)	2.562(6)
Sm(1)−O(5)	2.461(6)	Sm(1)−O(8)	2.576(6)
Sm(1)−O(2)	2.482(5)	Sm(1)−O(4)	2.620(6)
Sm(1)−O(3)	2.505(5)	Ni(1)−N(4)	1.862(9)
Sm(1)−O(6)	2.530(6)	Ni(1)−N(3)	1.875(7)
Sm(1)−O(10)	2.530(6)	Ni(1)−N(2)	1.899(7)
Sm(1)−O(1)	2.552(6)	Ni(1)−N(1)	1.903(7)
O(7)−Sm(1)−O(5)	67.5(2)	O(10)−Sm(1)−O(9)	62.3(2)
O(7)−Sm(1)−O(2)	134.28(19)	O(1)−Sm(1)−O(9)	72.6(2)
O(5)−Sm(1)−O(2)	135.4(2)	O(7)−Sm(1)−O(8)	63.0(7)
O(7)−Sm(1)−O(3)	104.63(19)	O(5)−Sm(1)−O(8)	99.57(19)
O(5)−Sm(1)−O(3)	71.97(18)	O(2)−Sm(1)−O(8)	73.16(19)
O(2)−Sm(1)−O(3)	119.47(18)	O(3)−Sm(1)−O(8)	167.36(18)
O(7)−Sm(1)−O(6)	98.7(2)	O(6)−Sm(1)−O(8)	65.39(19)
O(5)−Sm(1)−O(6)	64.71(19)	O(10)−Sm(1)−O(8)	65.6(2)
O(2)−Sm(1)−O(6)	72.8(2)	O(1)−Sm(1)−O(8)	124.03(19)
O(3)−Sm(1)−O(6)	116.89(19)	O(9)−Sm(1)−O(8)	110.4(2)
O(7)−Sm(1)−O(10)	79.6(2)	O(7)−Sm(1)−O(4)	142.4(2)
O(5)−Sm(1)−O(10)	146.99(19)	O(5)−Sm(1)−O(4)	74.88(18)
O(2)−Sm(1)−O(10)	70.9(2)	O(2)−Sm(1)−O(4)	74.83(18)
O(3)−Sm(1)−O(10)	116.36(19)	O(3)−Sm(1)−O(4)	62.39(18)
O(6)−Sm(1)−O(10)	125.21(19)	O(6)−Sm(1)−O(4)	63.53(19)
O(7)−Sm(1)−O(1)	135.3(2)	O(10)−Sm(1)−O(4)	138.04(19)
O(5)−Sm(1)−O(1)	135.94(18)	O(1)−Sm(1)−O(4)	74.7(2)
O(2)−Sm(1)−O(1)	62.73(19)	O(9)−Sm(1)−O(4)	124.12(19)
O(3)−Sm(1)−O(1)	65.94(18)	O(8)−Sm(1)−O(4)	125.46(19)
O(6)−Sm(1)−O(1)	125.06(18)	N(4)−Ni(1)−N(3)	90.7(4)
O(10)−Sm(1)−O(1)	68.5(2)	N(4)−Ni(1)−N(2)	162.8(3)
O(7)−Sm(1)−O(9)	65.0(2)	N(3)−Ni(1)−N(2)	93.8(4)
O(5)−Sm(1)−O(9)	99.9(2)	N(4)−Ni(1)−N(1)	93.0(4)
O(2)−Sm(1)−O(9)	124.1(2)	N(3)−Ni(1)−N(1)	164.3(3)
O(3)−Sm(1)−O(9)	63.26(19)	N(2)−Ni(1)−N(1)	87.1(3)
O(6)−Sm(1)−O(9)	161.73(19)		

 © 2004 Wiley-VCH Verlag GmbH & Co. KGaA, Weinheim

IR and Electronic Spectra

The IR spectra of **1, 2** and **3** show three strong bands at around 1639, 1610 and 1448 cm^{-1} which can be attributed to the υ(N−C−O) stretching bands and are characteristic of the bridging oxamide group.[28] The broad bands of **1, 2** and **3** around 1090 cm^{-1} in each case can be attributed to the ClO_4^- group.[29]

The electronic absorption spectra of the **1** and **2** were measured in DMF solution. In complexes **1** and **2**, a broad strong band centered at 613 nm can be attributed to the d-d transitions of five or six coordinate copper atoms,[30] the latter geometry being due to the fact that DMF is axially bound to the distorted square planar Cu(II) sites. All complexes exhibit intense bands below 550 nm, assignable to charge-transfer transitions in the [CuL] chromophores and/or intraligand π-π* interactions.[28] The hypersensitive transition bands of the rare earth metal ions were not observed.[31]

Fluorescence Properties

The fluorescence spectra of the $Cu^{II}_4Ln^{III}$ complexes (Ln = Eu, Tb) are given in Figure 5. The fluorescence spectra of $Ln(ClO_4)_3{\cdot}6H_2O$, which are included in Figure 5 were also measured for comparison. $Eu(ClO_4)_3{\cdot}6H_2O$ and $Tb(ClO_4)_3{\cdot}6H_2O$ exhibit fluorescence bands attributable to $^5D_0 \rightarrow {}^7F_1$ transitions in the 580−700 nm region and $^5D_4 \rightarrow {}^7F_1$ transitions in the 440−600 nm region, respectively. These fluorescence bands disappear almost completely in both complexes. According to the most probable quenching mechanism, we presume that the energy transfer occurs from the excited Ln(III) to the Cu(II) center through the oxamidic oxygen bridges.[24−27]

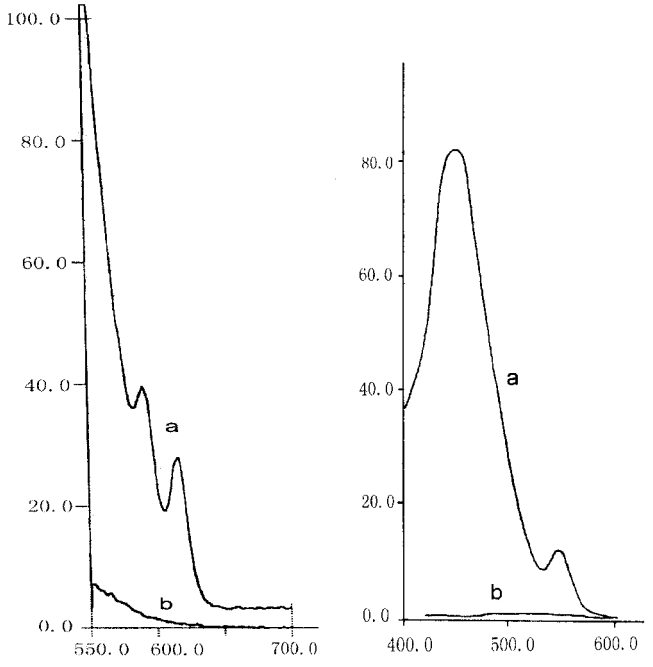

Figure 5. left: The fluorescence spectra of $Eu(ClO_4)_3{\cdot}6H_2O$ (a) and **1** (b), in DMF solution; the exciting wavelength is 394 nm; slim widths (excitation and emission sides) are 3 and 3 nm; ordinate scales are × 7 for (a) and for (b). right: The fluorescence spectra of $Tb(ClO_4)_3{\cdot}6H_2O$ (a) and **2** (b), in DMF solution; the exciting wavelength is 355 nm; slim widths (excitation and emission sides) are 2 and 2 nm; ordinate scales are × 8 for (a) and for (b)

Magnetic Properties

The magnetic susceptibilities (χ_M) of **1** was measured in the temperature range 2−300 K (Figure 6). The μ_{eff} value of 4.95 B.M. at room temperature continuously decreased with temperature to a value of 3.59 B.M. at 2 K. The μ_{eff} value is 3.59 B.M. at 2 K which is very close to the four copper(II)-only value(3.46 B.M.). This may be due to the thermal depopulation of excited levels ($J = 1-6$) of Eu(III), leading to the four copper(II)-only value since the $^7F_0$ ground state of Eu(III) is diamagnetic. As a first approach to simulating experimental magnetic behavior, the magnetic susceptibility of **1** was treated as sum of the contributions of one Eu(III) and four Cu(II) ions [Equation (1)].

$$\chi = 4\chi_{Cu} + \chi_{Eu} \tag{1}$$

where the first term $4\chi_{Cu}$ is the magnetic susceptibility for four Cu(II) ions [Equation (2)].

$$\chi_{Cu} = \frac{Ng^2\beta^2}{3KT}\frac{1}{2}\left(\frac{1}{2}+1\right) \tag{2}$$

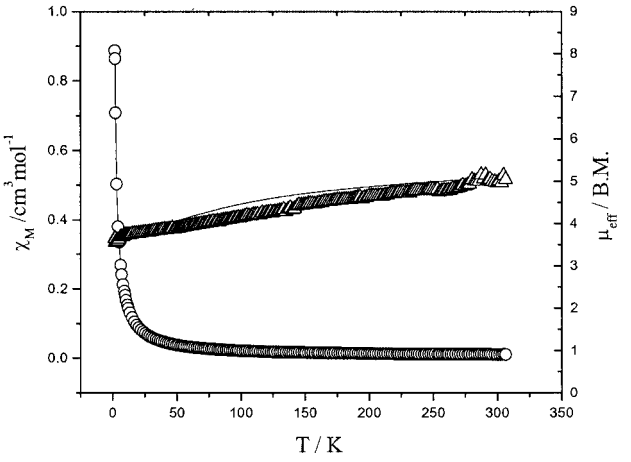

Figure 6. χ_M (circles) versus T and $\mu(T)$ (triangles) versus plots for the pentanuclear species **1**

The second term χ_{Eu} is the magnetic susceptibility for the Eu(III) ion. For the latter, the ^7F ground term is split by spin-orbit coupling into seven states, ^7F_J, with J taking integral values from 0 to 6. If the energy of the $^7F_0$ ground state is taken as the origin, the magnetic susceptibility may be expressed as in [Equation (3)].[32]

$$\chi_{Eu} = \frac{N\beta^2}{3KT}\frac{\left\{\begin{array}{l}144/x+(27/2-9/x)\exp(-x/6)+(135/2-15/x)\exp(-x/2)+\\(189-21/x)\exp(-2x)+(405-27/x)\exp(-10x/3)+(1485/2-\\33/x)\exp(-5x)+(2457/2-39/x)\exp(-7x)\end{array}\right\}}{\begin{array}{l}1+3\exp(-x/6)+5\exp(-x/2)+7\exp(-2x)+\\9\exp(-10x/3)+11\exp(-5x)+13\exp(-7x)\end{array}} \tag{3}$$

 © 2004 Wiley-VCH Verlag GmbH & Co. KGaA, Weinheim

Where $x = \zeta/KT$, ζ is the spin-orbit coupling constant for Eu(III). Taking into account the interaction between Cu(II) and Eu(III) ions, a correction for a molecular field can be made [Equation (4)].

$$\chi_M = \frac{\chi}{1-(2ZJ'/Ng^2\beta^2)\chi} \quad (4)$$

The least-squares fit of Equation (4) to the data yielded the parameters $g = 2.13$, $\zeta = 1358$, $ZJ' = -0.12$, where the agreement factor defined as:

$$R = \Sigma[(\chi_M)^{Cal} - (\chi_M)^{obsd}]^2 / \Sigma[(\chi_M)^{obsd}]^2$$

is 8.40×10^{-3}.

The value of ZJ' reveals weak antiferromagnetic interaction between the Cu(II) ions and the Eu(III) ion.

The magnetic susceptibilities (χ_M) of **2** were measured in the temperature range 4−300 K (Figure 7). The observed μ_{eff} value for **2** was 10.54 B.M. at room temperature. This value is slightly higher than that expected if the metal centers are not interacting (for, **2**, 10.32 B.M., assuming $g_{Cu} = 2.0$, $g_{Tb} = 3/2$). For **2**, this values declines gradually between 300 and 8 K, where at the latter temperature the μ_{eff} value is 9.41 B.M. Below 8 K, it falls sharply reaching 8.84 B.M. at 4 K. In contrast to the Cu_4Eu case, a similar treatment of **2** does not give reasonable results. To gain some information concerning the interaction between Tb and Cu, Kahn and Costes et al. have developed an experimental approach. For this, it appeared necessary to synthesize an isostructural Ln^{III} complex with a diamagnetic surrounding.[7d,33] Unfortunately, for **2**, we have been unable to crystallized an isostructural series. However, we synthesized a hexanuclear Ni_5Ln (Ln = Sm) complex using $Ni^{II}L$ as a ligand. Thus, to get insight into the strength of these interactions, accurate models involving both the orbital contribution and the ligand field effect have to be developed.

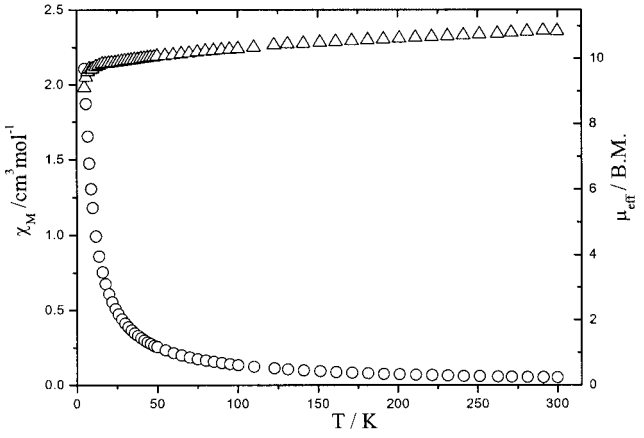

Figure 7. χ_M (circles) versus T and $\mu(T)$ (triangles) versus plots for the pentanuclear species **2**

Conclusion

Two novel oxamidato-bridged $Cu^{II}_4Ln^{III}$ pentanuclear complexes of formula $[(CuL)_3\{CuL(C_2H_5OH)\}Eu(H_2O)](ClO_4)_3\cdot1.5H_2O$, $[(CuL)_3\{CuL(C_2H_5OH)\}Tb(H_2O)](ClO_4)_3\cdot2H_2O$ and $[(NiL)_5Sm](ClO_4)_3\cdot2H_2O$ incorporating a macrocyclic oxamide have been hydrothermally synthesized and structurally characterized. The hydrogen bonds play an important role in the 1-D supramolecular architectures of **1** and **2**. The magnetic and fluorescent properties of **1** and **2** have also been characterized.

Experimental Section

Caution ! *Perchlorate salts of metal complexes with organic ligands are potentially explosive and should be handled very carefully and in small quantities.*

General Remarks: All the starting reagents were of A. R. grade and were used as purchased. The complex ligand CuL was prepared as described according to the literature.[34] The complex ligand NiL was prepared in the same way as CuL.

$[(CuL)_3\{CuL(C_2H_5OH)\}Eu(H_2O)](ClO_4)_3\cdot1.5H_2O$ (1): The complex was prepared by a hydrothermal reaction. A mixture of CuL, $Eu(ClO_4)_3\cdot6H_2O$, CH_3CH_2OH and H_2O in a molar ratio of 4.0:1.0:40:300 was sealed in an 18 cm^3 capacity Teflon-lined reactor which was kept at 160 °C for 72 h. Deep brown-green crystals of the compound were isolated (yield 89.5 % base on Eu) by filtering and washing with water. $C_{78}H_{75}Cl_3Cu_4EuN_{16}O_{23.5}$ (2125.0): calcd. C 44.09, H 3.56, N 10.55; found C 44.10, H 3.45, N 10.48. Main IR bands (KBr, cm^{-1}): $\tilde{\nu}$ = 3414 s (br), 1640 vs, 1610 vs, 1445 m, 1088 vs (br), 776 w, 620 w.

$[(CuL)_3\{CuL(C_2H_5OH)\}Tb(H_2O)](ClO_4)_3\cdot2.0H_2O$ (2): The complex was prepared in the same way as **1**, using terbium perchlorate instead of europium perchlorate. Deep brown-green crystals were obtained (yield 87 % based on Tb). $C_{78}H_{76}Cl_3Cu_4N_{16}O_{24}Tb$ (2141.0): calcd. C 43.76, H 3.58, N 10.47; found C 46.18, H 3.51, N 11.35. Main IR bands (KBr, cm^{-1}): $\tilde{\nu}$ = 3417 s (br), 1639 vs, 1615 vs, 1448 m, 1090 vs (br), 777 w, 623 w.

$[(NiL)_5Sm](ClO_4)_3\cdot2H_2O$ (3): The complex was prepared by a hydrothermal reaction. A mixture of NiL, $Sm(ClO_4)_3\cdot6H_2O$, CH_3CH_2OH and H_2O in a molar ratio of 4.0:1.0:40:300 was sealed in an 18 cm^3 capacity Teflon-lined reactor which was kept at 165 °C for 72 h. Deep brown-red crystals of the compound were isolated (yield 80.5 % base on Sm) by filtering and washing with water. $C_{95}H_{84}Cl_3N_{20}Ni_5O_{24}Sm$ (2440.1): calcd. C 46.76, H 3.47, N 11.48; found C 46.78, H 3.41, N 11.45. Main IR bands (KBr, cm^{-1}): $\tilde{\nu}$ = 3415 s(br), 1636 vs, 1611 vs, 1445 m, 1090 vs (br), 778 w, 621 w.

Physical Measurements: C, H and N analyses were determined on a Perkin−Elmer 240 Elemental analyzer. IR spectra were recorded in KBr discs on a Shimadzu IR-408 infrared spectrophotometer in the 4000−600cm^{-1} range. Electronic spectra in DMF were recorded on a Shimadzu UV-2101 PC scanning spectrophotometer. Variable-temperature magnetic susceptibilities were measured on an MPMS-7 SQUID magnetometer. Diamagnetic corrections were made with Pascal's constants for all the constituent atoms.[35]

X-ray Diffraction Data Collection and Structure Refinement − Crystallographic Studies: All data were collected on a Bruker Smart-1000-CCD area detector using graphite monochromated

 © 2004 Wiley-VCH Verlag GmbH & Co. KGaA, Weinheim

Table 4. Summary of crystallographic data for complexes **1, 2** and **3**

	1	**2**	**3**
Empirical formula	$C_{78}H_{75}O_{23.5}N_{16}Cl_3Cu_4Eu$	$C_{78}H_{76}O_{24}N_{16}Cl_3Cu_4Tb$	$C_{95}H_{84}O_{24}N_{20}Cl_3Ni_5Sm$
M	2125.01	2140.96	2440.07
System	triclinic	triclinic	monoclinic
Space group	$P\bar{1}$	$P\bar{1}$	$P2_1/n$
a (Å)	15.024(8)	14.901(4)	17.810(5)
b (Å)	16.994(8)	16.833(5)	24.023(7)
c (Å)	17.991(9)	17.778(5)	23.569(7)
α/°	74.806(8)	74.953(5)	90
β/°	82.516(8)	82.697(6)	102.984(6)
γ/°	70.220(7)	70.099(5)	90
V/Å^3	4167(3)	4045(2)	9826(5)
Z	2	2	4
ρ_{caled} g.cm^{-3}	1.694	1.758	1.649
μ(Mo-K_α) mm^{-1}	0.71073	0.71073	0.71073
Crystalsize mm	0.50 × 0.40 × 0.20	0.30 × 0.25 × 0.20	0.30 × 0.25 × 0.20
θ range/°	1.17−24.69	1.19−25.03	1.83 to 25.03
F(000)	2146	2040	4956
R1[a] [$I > 2\sigma(I)$]	0.0587	0.0520	0.0708
wR2[b] [$I > 2\sigma(I)$]	0.1291	0.1139	0.0919
GOF	0.992	1.029	0.912

Mo-K_α radiation (= 0.71073 Å). The structures were solved by direct method and subsequent Fourier difference techniques and refined using a full-matrix least-squares procedure on F^2 with anisotropic thermal parameters for all non-hydrogen atoms (SHELXS-97 and SHELXL-97).[36] Hydrogen atoms were added geometrically and refined with riding model positional parameters and fixed isotropic thermal parameters. Crystal data collection and refinement parameters are given in Table 4. CCDC 208850 (for **1**), 214752 (for **2**) and -218203 (for **3**) contain the supplementary crystallographic data for this paper. These data can be obtained free of charge at www.ccdc.cam.ac.uk/conts/retrieving.html [or from the Cambridge Crystallographic Data Center, 12 Union Road, Cambridge CB2 1EZ, UK; Fax: (internat.) + 44-1223/336-033; E-mail: deposit@ccdc.cam.ac.uk].

Acknowledgments

This work was supported by the National Natural Science Foundation of China (No.20071019, No.50172021 and No.90101028) and the National Natural Science Foundation of Tianjin (No. 013603711).

[1] *Coordination Chemistry of Macrocyclic Compounds* (Ed. G. A. Melson) Plenum, New York, **1979**.
[2] O. Kahn, *Molecular Magnetism,* VCH Publishers, New York, **1993**.
[3] [3a] J. S. Miller, J. C. Calabrese, H. Rommelmann, S. R. Chittipeddi, J. H. Zhang, W. M. Reiff, A. J. Epstein, *J. Am. Chem. Soc.* **1987**, *109*, 769. [3b] O. Kahn, Y. Pei, M. Verdaguer, J. P. Sletten, *J. Am. Chem. Soc.* **1988**, *110*, 782. [3c] H. Miyasaka, N. Matsumoto, H. Okawa, N. Re, E. Gallo, C. Floriani, *J. Am. Chem. Soc.* **1996**, *118*, 981. [3d] Z. J. Zhong, H. Seino, Y. Mizobe, M. Hidai, A. Fujishima, S. Ohkoshi, K. Hashimoto, *J. Am. Chem. Soc.* **2000**, *122*, 2952.
[4] [4a] P. Gütlich, Y. Garcia, T. Woike, *Coord. Chem. Rev.* **2001**, *219−221*, 839. [4b] S. Ohkoshi, K. Hashimoto, *J. Am. Chem. Soc.* **1999**, *121*, 10591. [4c] O. Sato, T. Iyoda, A. Fujishima, K. Hashimoto, *Science* **1996**, *272*, 704. [4d] S. Hayami, Z. Gu, M. Shiro, A. Einaga, A. Fujishima, O. Sato, *J. Am. Chem. Soc.* **2000**, *122*, 7126.
[5] [5a] R. Sessoli, D. Gatteschi, A. Caneschi, M. A. Novak, *Nature* **1993**, *365*, 141. [5b] D. Gatteschi, A. Caneschi, L. Pardi, R. Sessoli, *Science* **1994**, *265*, 1054. [5c] C. Cadiou, M. Murrie, C. Paulsen, V. Villar, W. Wernsdorfer, R. E. P. Winpenny, *Chem. Commun.* **2001**, 2666. [5d] M. P. Shores, J. J. Sokol, J. R. Long, *J. Am. Chem. Soc.* **2002**, *124*, 2279. [5e] C. Boskovic, E. K. Brechin, W. E. Streib, K. Folting, J. C. Bollinger, D. N. Hendrickson, G. Christou, *J. Am. Chem. Soc.* **2002**, *124*, 3725.
[6] O. Kahn, *Angew. Chem. Int. Ed. Engl.* **1995**, *24*, 834.
[7] [7a] J. P. Costes, F. Dahan, A. Dupuis, J. P. Laurent, *Inorg. Chem.* **1996**, *35*, 2400. [7b] I. Ramade, O. Kahn, Y. Jeannin, F. Robert, *Inorg. Chem.* **1997**, *36*, 930. [7c] M. L. Kahn, T. M. J. Y. Rajendirran, C. Mathoniere, O. Kahn, *C. R. Acad. Sci., Ser. IIc* **2000**, *3*, 131. [7d] J. P. Costes, F. Dahan, A. Dupuis, J. P. Laurent, *Chem. Eur. J.* **1998**, *4*, 1616. [7e] J. P. Costes, F. Dahan, A. Dupuis, J. P. Laurent, *Inorg. Chem.* **2000**, *39*, 169. [7f] J. P. Costes, F. Dahan, A. Dupuis, *Inorg. Chem.* **2000**, *39*, 165.
[8] [8a] A. Bencini, C. Benelli, A. Caneschi, A. Dei, D. Gatteschi, *Inorg. Chem.* **1986**, *25*, 5, 572. [8b] M. Andruh, I. Ramade, E. Codjovi, O. Guillou, O. Kahn, J. C. Trombe, *J. Am. Chem. Soc.* **1993**, *115*, 1822. [8c] C. Benelli, A. J. Blake, P. E. Y. Milne, J. M. Rawson, R. E. P. Winpenny, *Chem. Eur. J.* **1995**, *1*, 614.
[9] A. Bencini, C. Benelli, A. Caneschi, R. L. Carlin, A. Dei, D. Gatteschi, *J. Am. Chem. Soc.* **1985**, *107*, 8128.
[10] J. S. Miller, A. Epsttein, *Angew. Chem. Int. Ed. Engl.* **1994**, *33*, 385.
[11] M. Richter, *J. Phys. D: Appl. Phys.* **1998**, *31*, 1071. [11b] B. Cristiano, G. Dante, *J. Am. Chem. Soc.* **2002**, *6*, 2369.
[12] [12a] R. E. P. Winpenny, *Chem. Soc. Rev.* **1998**, *27*, 447. [12b] M. L. Kahn, C. Mathonière, O. Kahn, *Inorg. Chem.* **1999**, *38*, 3692. [12c] M. L. Kahn, M. Verelst, P. Lecante, C. Mathonière, O. Kahn, *Eur. J. Inorg. Chem.* **1999**, 527. [12d] O. Guillou, O. Kahn, R. L. Oushoorn, K. Boubekeur, P. Batail, *Inorg. Chim. Acta* **1992**, *198−200*, 119.
[13] [13a] F. Avecilla, C. Platas-Iglesias, R. Rodríguez-Cortiñas, G. Guillemot, J. C. G. Bünzli, C. D. Brondino, C. F. G. C. Geraldes, A. de Blas, T. Rodríguez-Blas, *J. Chem. Soc., Dalton Trans.* **2002**, 4658. [13b] C. Edder, C. Piguet, J. C. G. Bünzli, G. Hopfgartner, *Chem. Eur. J.* **2001**, *14*, 3014. [13c] C. Edder, C. Piguet, G. Bernardinelli, J. Mareda, C. G. Bochet, J. C. G. Bünzli, G. Hopfgartner, *Inorg. Chem.* **2000**, *39*, 5059. [13d] R. Rodrýguez-Cortinas, F. Avecilla, C. Platas-Iglesias, D. Imbert,

 © 2004 Wiley-VCH Verlag GmbH & Co. KGaA, Weinheim

J. C. G. Bünzli, A. Blas, T. Rodrýguez-Blas, *Inorg. Chem.* **2002**, *41*, 5336. [13e] M. Cantuel, G. Bernardinelli, D. Imbert, J. C. G. Bünzli, G. Hopfgartner, C. Piguet, *J. Chem. Soc., Dalton Trans.* **2002**, 1929.

[14] [14a] J. L. Sanz, R. Ruiz, A. Gleizes, F. Lloret, J. Faus, M. Julve, J. J. Borrás-Almenar, Y. Journaux, *Inorg. Chem.* **1996**, *35*, 7384. [14b] X. M. Chen, Y. L. Wu, Y. Y. Yang, S. M. J. Aubin, D. N. Hendrickson, *Inorg. Chem.* **1998**, *37*, 6186. [14c] J. P. Costes, F. Dahan, A. Dupuis, *Inorg. Chem.* **2000**, *39*, 5994. [14d] R. Baggio, M. T. Garland, Y. Moreno, O. Pena, M. Perec, E. Spodine, *J. Chem. Soc., Dalton Trans.* **2000**, 2061.

[15] [15a] A. J. Blake, R. O. Gould, C. M. Grant, P. E. Y. Milne, S. Parsons, R. E. P. Winpenny, *J. Chem. Soc., Dalton Trans.* **1997**, 485. [15b] S. Wang, S. J. Trepanier, M. J. Wagner, *Inorg. Chem.* **1993**, *32*, 833. [15c] Y. C. Liang, R. Cao, W. P. Su, M. C. Hong, W. J. Zhang, *Angew. Chem. Int. Ed.* **2000**, *39*, 3304. [15d] C. Brewer, G. Brewer, W. R. Scheidt, M. Shang, E. E. Carpenter, *Inorg. Chem. Acta* **2001**, *313*, 65.

[16] [16a] L. F. Lindoy, H. C. Lip, H. W. Louie, M. G. B. Drew, M. J. Hudson, *J. Chem. Soc., Chem. Commun.* **1977**, 778. [16b] J. M. Boncella, R. A. Anderson, *J. Chem. Soc., Chem. Commun.* **1984**, 809. [16c] W. J. Evans, L. Bloom, J. W. Grate, L. A. Hughes, W. E. Hunter, J. L. Atwood, *Inorg. Chem.* **1985**, *24*, 4620.

[17] [17a] S. Wang, Z. Pang, M. J. Wagner, *Inorg. Chem.* **1992**, *31*, 5381. [17b] S. Wang, Z. Pang, K. D. L. Smith, *Inorg. Chem.* **1993**, *32*, 4992. [17c] J. P. White, H. Deng, E. P. Boyd, J. Galluci, S. G. Shore, *Inorg. Chem.* **1994**, *33*, 1685. [17d] L. Chen, S. R. Breeze, R. J. Rousseau, S. Wagn, L. K. Thompson, *Inorg. Chem.* **1995**, *34*, 454.

[18] [18a] D. M. L. Goodgame, S. Menzer, A. T. Ross, D. J. Williams, *J. Chem. Soc., Chem. Commun.* **1994**, 2605. [18b] D. Deng, X. Zheng, C. Qian, J. Sun, A. Dormond, D. Baudry, M. Visseaux, *J. Chem. Soc., Dalton Trans.* **1994**, 1665. [18c] Y. J. Zhang, B. Q. Ma, S. Gao, J. R. Li, Q. D. Liu, G. H. Wen, X. X. Zhang, *J. Chem. Soc., Dalton Trans.* **2000**, 2249. [18d] Q. Y. Chen, Q. Y. Luo, Z. L. Wang, J. T. Chen, *Chem. Commun.* **2000**, 1033.

[19] G. Brewer, P. Kamaras, S. Prytkov, M. Shang, W. R. Scheidt, *J. Chem. Soc., Dalton Trans.* **1999**, 4511.

[20] E. Q. Gao, J. K. Tang, D. Z. Liao, Z. H. Jiang, S. P. Yan, G. L. Wang, *Helv. Chim. Acta* **2001**, *84*, 908.

[21] E. Q. Gao, W. M. Bu, G. M. Yang, D. Z. Liao, Z. H. Jiang, S. P. Yan, G. L. Wang, *J. Chem. Soc., Dalton Trans.* **2000**, 1431.

[22] [22a] J. K. Tang, Y. Z. Li, Q. L. Wang, E. Q. Gao, D. Z. Liao, Z. H. Jiang, *Inorg. Chem.* **2002**, *41*, 2188. [22b] J. K. Tang, L. Y. Wang, L. Zhang, E. Q. Gao, D. Z. Liao, Z. H. Jiang, S. P. Yan, P. Cheng, *J. Chem. Soc., Dalton Trans.* **2002**, *8*, 1607. [22c] E. Q. Gao, W. M. Bu, G. M. Yang, D. Z. Liao, Z. H. Jiang, S. P. Yan, G. L. Wang, *J. Chem. Soc., Dalton Trans.* **2002**, *7*, 1432. [22d] E. Q. Gao, J. K. Tang, D. Z. Liao, Z. H. Jiang, S. P. Yan, G. L. Wang, *Helv. Chim. Acta* **2001**, *84*, 908. [22e] J. K. Tang, Q. L. Wang, E. Q. Gao, J. T. Chen, D. Z. Liao, Z. H. Jiang, *Helv. Chim. Acta* **2002**, *85*, 175.

[23] [23a] C. T. Chen, K. S. Suslick, *Coord. Chem. Rev.* **1993**, *128*, 293. [23b] P. A. Vigato, S. Tamburini, D. E. Fenton, *Coord. Chem. Rev.* **1990**, *106*, 25.

[24] V. G. Berner, D. W. Darnall, E. R. Birnbaum, *Biochem. Biophys. Rea. Commun.* **1975**, *66*, 763.

[25] N. Higashiyama, G. Adachi, *Chem. Lett.* **1990**, 2029.

[26] M. Sakamoto, M. Hashimura, K. Marsuki, A. Matsumoto, H. Okawa, *Chem. Lett.* **1991**, 1007.

[27] M. Saksmoto, M. Hashimura, Y. Nakayama, A. Matsumoto, H. Okawa, *Bull. Chem. Soc. Jpn.* **1992**, *65*, 1162.

[28] F. Lloret, Y. Journaux, M. Julve, *Inorg. Chem.* **1990**, *29*, 3967.

[29] K. Nakamoto, *Infrared and Raman Spectra of Inorganic and Coordination Compounds*, Part B, 5th ed.; John Wiley & Sons, New York, **1997**.

[30] [30a] P. Labine, C. H. Jr Brubaker, *J. Inorg. Nucl. Chem.* **1971**, *31*, 3383. [30b] R. Barbucci, G. Cialdi, G. Ponticelli, P. Paoletti, *J. Am. Chem. Soc.* **1969**, ##, 1775.***((Author: volume number missing))***

[31] A. T. Baker, A. M. Hamer, S. E. Livingstore, *Transition Met. Chem.* **1984**, *9*, 423.

[32] R. M. Golding, *Applied Wave Mechanics*, D. Van Nostrand Inc., New York, **1969**, 253−254.

[33] M. L. Kahn, J. P. Sutter, S. Golhen, P. Guionneau, L. Ouahab, Q. Kahn, D. Chasseau, *J. Am. Chem. Soc.* **2000**, *122*, 3413.

[34] D. S. C. Black, H. Corrie, *Inorg. Nucl. Chem. Lett.* **1976**, *12*, 657.

[35] P. W. Selwood, *Magnetochemistry*, Interscience, New York, **1956**, p. 78.

[36] G. M. Sheldrick, *SHELXS-97* and *SHELXL-97, Software for Crystal Structure, Analysis*, Siemens Analytical X-ray Instruments Inc., Madision, WI, **1997**.

Received July 15, 2003
Early View Article
Published Online February 17, 2004

 © 2004 Wiley-VCH Verlag GmbH & Co. KGaA, Weinheim

sp^3-C^1-Bridged 1,3-Me_2Cp/Amido Titanium and Zirconium Complexes and Their Reactivities towards Ethylene Polymerization

Tae Ho Kim,[a] Young Chul Won,[a] Bun Yeoul Lee,*[a] Dong Mok Shin,[b] and Young Keun Chung[b]

Keywords: Cyclopentadienyl / Zirconium / Titanium / Polymerization / Homogeneous catalysis

sp^3-C^1-Bridged Cp/amido titanium and zirconium complexes are synthesized by using novel fulvenes that have substituents in the 1-, 4-, and 6-positions only. Thus, the nucleophilic attack of lithium *tert*-butylamide on 1,4-dimethyl-6-phenylfulvene, 6-(2-furyl)-1,4-dimethylfulvene and 6-cyclohexyl-1,4-dimethylfulvene, and subsequent aqueous workup, yields *t*BuN(H)–CHR–$C_5H_3Me_2$ (R = phenyl, **6**; R = 2-furyl, **7**; R = cyclohexyl, **8**) in 80, 88, and 60% yields, respectively. The reactions of the ligands with $M(NMe_2)_4$ (M = Ti or Zr) afford the desired bis(dimethylamido) complexes, which can be transformed by treatment with Me_2SiCl_2 to the dichloride complexes, (1,3-$Me_2C_5H_2$–CHR–N*t*Bu–κ*N*)MCl_2 (M = Ti, R = phenyl, **10**; M = Zr, R = phenyl, **11**; M = Ti, R = 2-furyl, **13**; M = Zr, R = 2-furyl, **14**; M = Zr, R = cyclohexyl, **15**). Complex **10** is very sensitive towards water, such that an oxo-bridged dimer, (1,3-$Me_2C_5H_2$–CHPh–NH*t*Bu)$ZrCl_2$–μO–$ZrCl_2$(1,3-$Me_2C_5H_2$–CHPh–NH*t*Bu) (**12**), is easily formed by the abstraction of water from the solvents. The solid structures of (1,3-$Me_2C_5H_2$–CHPh–N*t*Bu–κ*N*)$Zr(NMe_2)_2$, **10**, **11**, and **12** have been determined by X-ray crystallography. The complexes are active towards the polymerization of ethylene when activated with MAO. The activities are rather low and the molecular weight distributions are broad (M_w/M_n = 10–36).
(© Wiley-VCH Verlag GmbH & Co. KGaA, 69451 Weinheim, Germany, 2004)

Introduction

Various group 4 *ansa*-metallocene complexes, which have drawn attention as homogeneous Ziegler catalysts, can be synthesized from fulvenes. The C^1-bridged Cp/fluorenyl and C^1-bridged Cp/indenyl complexes are typical examples.[1] Some C^1-bridged Cp/Cp,[2] C^2-bridged Cp/Cp,[3] and C^3-bridged Cp/Cp complexes[4] are also obtained from fulvenes. Recently, Erker et al. reported on the syntheses of sp^3-C^1-bridged Cp/amido titanium and zirconium complexes using 6-*tert*-butylfulvene and 1,2,3,4-tetramethylfulvene.[5] Fulvenes are conventionally synthesized by the base-mediated coupling of cyclopentadiene with aldehydes or ketones.[6] If mono-substituted or 1,3-disubstituted cyclopentadienes are used, the substituents are located mainly in the 2-position or the 1,3-positions in the resulting fulvenes due to steric reasons. Recently, we reported on a synthetic route for the preparation of 1,4-dimethyl-6-phenylfulvene, which is a novel product as it has substituents in the 1-, 4-, and 6-positions only, and we demonstrated the synthesis of a C^1-bridged 1,3-Me_2Cp/fluorenyl zirconium complex using the fulvene.[7] Herein, we report on the syntheses and characterizations of C^1-bridged 1,3-Me_2Cp/amido zirconium and titanium complexes using fulvenes that have substituents in the 1-, 4- and 6-positions only. The complexes are characteristic since the methyl substituents on the cyclopentadienyl ligand are located next to the bridge.[8] In these complexes, the steric congestion at the reaction site is minimized, while an electronic effect is imposed by the substituents.[9]

Results and Discussion

Syntheses and Characterizations

6-(2-Furyl)-1,4-dimethylfulvene (**4**) and 6-cyclohexyl-1,4-dimethylfulvene (**5**) were synthesized by a similar method using the same conditions as that developed for the syn-

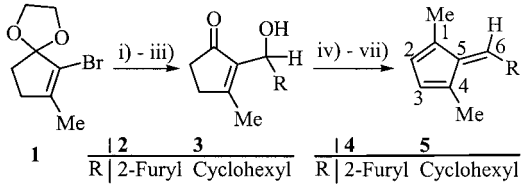

Scheme 1. i) *n*BuLi; ii) RC(O)H; iii) HCl; iv) dihydropyran, *p*-TsOH; v) MeLi; vi) HCl; vii) NaOMe

[a] Department of Molecular Science and Technology, Ajou University, Suwon,
442-749, Korea
Fax: (internat.) + 82-31-219-1844
E-mail: bunyeoul@ajou.ac.kr
[b] School of Chemistry and Center for Molecular Catalysis, Seoul National University,
Seoul 151-747, Korea

 © 2004 Wiley-VCH Verlag GmbH & Co. KGaA, Weinheim **DOI: 10.1002/ejic.200300703**

thesis of 1,4-dimethy-6-phenylfulvene (Scheme 1). The overall yields from the starting material **1** were 31% and 42% for **4** and **5**, respectively. The ^{1}H NMR spectra, ^{13}C NMR spectra, and the elemental analyses are in agreement with the fulvene structures of **4** and **5**.

The nucleophilic attack of lithium *tert*-butylamide on the fulvenes in THF, followed by aqueous workup, afforded the desired ligands **6**, **7**, and **8** in 80, 88, and 60% yields, respectively (Scheme 2). Substituted cyclopentadienes are frequently obtained as a set of isomers due to the rapid 1,5-sigmatropic rearrangement.[10] However, compounds **6**, **7**, and **8** were obtained as single isomers, as a result of the symmetry of the substituents, and were characterized unambiguously by ^{1}H and ^{13}C NMR spectroscopy. Comparison of the ^{13}C NMR spectra of the three compounds assists in the assignment of the signals. The signal at 125 ppm is assigned to Cp−*C*H and the signals for Cp−*C*(CH$_3$) are observed at 140−144 ppm. The signals assigned to Cp−*C*(bridgehead) and Cp−*C*H$_2$ are observed at 136−138 ppm and 44 ppm, respectively.

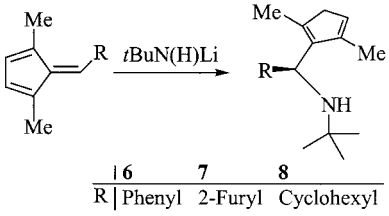

Scheme 2

The reaction of **6** with Zr(NMe$_2$)$_4$ at 100 °C for 2 days afforded the desired C^1-bridged 1,3-Me$_2$Cp/amido zirconium complex **9** (Scheme 3).[11] The dimethylamine formed was removed by a stream of nitrogen gas. When the reaction was carried out by heating without the stream of nitrogen, the reaction stops with the formation of unbridged tris(dimethylamido)Cp complex. The ^{1}H and ^{13}C NMR spectra support the structure shown in Scheme 3. Signals for the Cp protons are observed as a pair of doublets (J = 2.8 ppm) at 5.88 ppm and 5.48 ppm in the ^{1}H NMR spectrum (C$_6$D$_6$), and the methyl signals of the dimethylamido group are observed as a pair of singlets at 3.09 and 2.89 ppm. The signal for the bridgehead carbon on the Cp moiety is observed at 105.76 ppm in the ^{13}C NMR spectrum. Complex **9** is a solid, and single crystals suitable for X-ray crystallography were obtained by recrystallization in pentane at −30 °C. The X-ray crystallographic studies confirm the structure shown in Scheme 3. The thermal ellipsoid plot is shown in Figure 1.

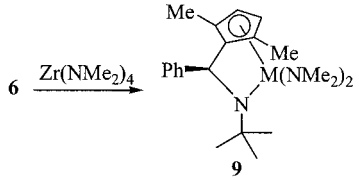

Scheme 3

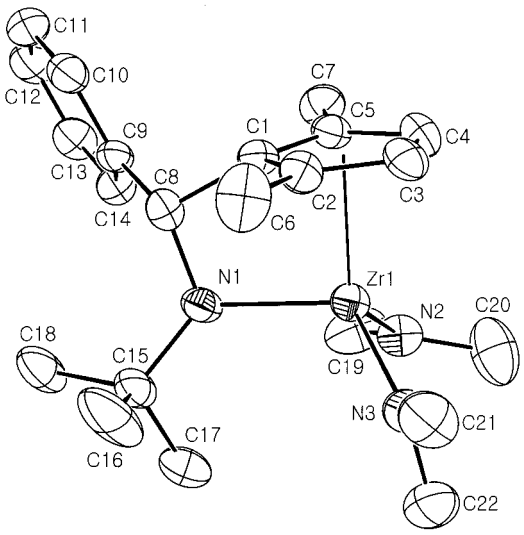

Figure 1. Thermal ellipsoid plot (30% probability level) of the structure of **9**

Similar reactions of **7** and **8** with Zr(NMe$_2$)$_4$, and reactions of **6** and **7** with Ti(NMe$_2$)$_4$, afforded the corresponding bis(dimethylamido) complexes. The reaction of **8** with Ti(NM$_2$)$_4$ was sluggish under identical conditions. The bis(dimethylamido) complexes are oily and therefore could not be purified by recrystallization; however, the ^{1}H and ^{13}C NMR spectra strongly support their formation. The crude products have been used for the proceeding chlorination reactions without further purification. The synthetic method described here is complementary to that developed by Erker, who obtained the Cp and tetramethylcyclopentadienyl analogues by treating the corresponding dilithium salts with TiCl$_2$(NMe$_2$) or ZrCl$_2$(NEt$_2$)$_2$(THF)$_2$.[5]

Erker attempted to convert (Me$_4$Cp−CH$_2$−N*t*Bu)Zr(NEt$_2$)$_2$ to (Me$_4$Cp−CH$_2$−N*t*Bu)ZrCl$_2$ by treatment with excess unpurified Me$_3$SiCl.[5] He unexpectedly obtained an μ-oxo complex, (Me$_4$Cp−CH$_2$−N*t*Bu)ZrCl$_2$−μO−ZrCl$_2$(Me$_4$Cp−CH$_2$−N*t*Bu). The yield of the μ-oxo complex was relatively low (40%), and a complicated mixture of unidentified products was observed in the ^{1}H NMR spectrum. When the reaction of two equivalents of carefully dried Me$_3$SiCl with the bis(dimethylamido) titanium complex of **6** in C$_6$D$_6$ was followed by ^{1}H NMR spectroscopy, it was seen that only one dimethylamido ligand was replaced by the chloride ligand giving (1,3-Me$_2$C$_5$H$_2$−CHPh−N*t*Bu−κ*N*)TiCl(NMe$_2$). Complete chlorination is achieved using Me$_2$SiCl$_2$.[12] Addition of four equivalents of Me$_2$SiCl$_2$ in C$_6$D$_6$ resulted in the formation of the desired dichloride complex **10** (Scheme 4). The ^{1}H and ^{13}C NMR spectra are in agreement with the structure of the dichloride complex. Single crystals of **10** suitable for X-ray crystallography were obtained in toluene at −30 °C and X-ray crystallographic studies confirm the dichloride structure (Figure 2).

Addition of two equivalents of Me$_2$SiCl$_2$ to the bis(dimethylamido)zirconium complex **9** in benzene and overnight stirring, resulted in the precipitation of a white solid. The ^{1}H and ^{13}C NMR spectra of the precipitate strongly sup-

 © 2004 Wiley-VCH Verlag GmbH & Co. KGaA, Weinheim

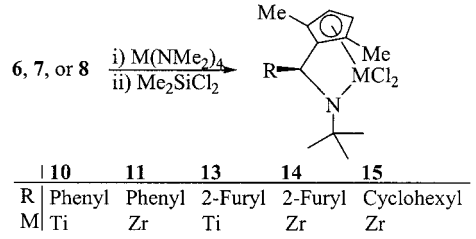

Scheme 4

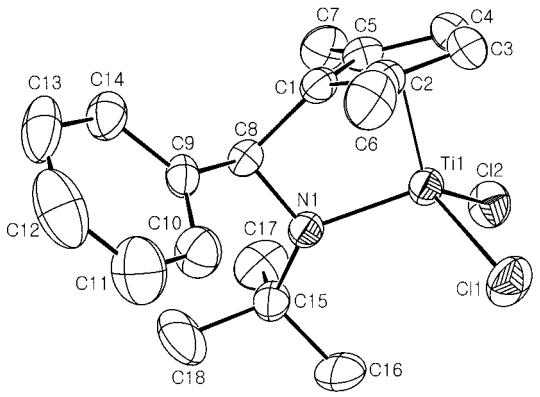

Figure 2. Thermal ellipsoid plot (30% probability level) of the structure of **10**

port the formation of the desired dichloride complex **11** (Scheme 4). The main features of the NMR spectra are almost identical to those observed for titanium complex **10**. However, X-ray crystallographic studies of a single crystal, which was obtained by dissolving the precipitate in benzene and by the slow addition of pentane vapor at room temperature, reveal the structure of an unexpected dinuclear μ-oxo complex, **12** (Figure 3). A similar dinuclear μ-oxo complex was observed by Erker when (Me_4Cp-CH_2-NtBu)$Zr(NEt_2)_2$ was treated with excess unpurified Me_3SiCl.[5]

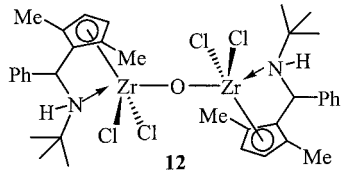

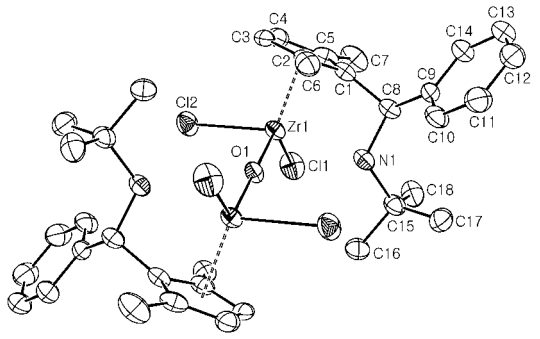

Figure 3. Thermal ellipsoid plot (30% probability level) of the structure of **12**

Since the ^1H and ^{13}C NMR spectra of the precipitate strongly support the structure of the desired mononuclear complex **11**, the formation of **12** may be attributed to the presence of water as an impurity in the recrystallization solvents. Single crystals suitable for X-ray crystallography were directly deposited when **9** and Me_2SiCl_2 were mixed in benzene and reacted without stirring for several days at room temperature. X-ray crystallographic studies of a single crystal obtained by this procedure reveal the desired structure of the mononuclear complex **11** (Figure 4). Complexes **13**–**15** were synthesized in a similar manner, by the reactions of two or three equivalents of Me_2SiCl_2 with the crude bis(dimethylamido) complexes, which are obtained by the reaction of **7** with $Ti(NMe_2)_4$ and reactions of **7** and **8** with $Zr(NMe_2)_4$ (Scheme 4).

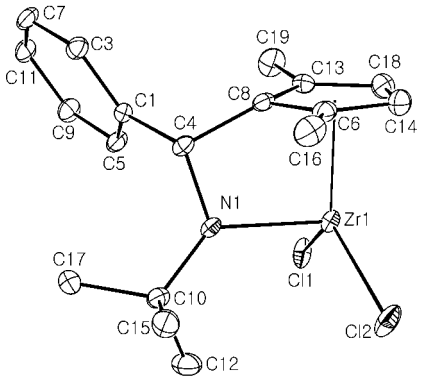

Figure 4. Thermal ellipsoid plot (30% probability level) of the structure of **11**

Crystal Structures of 9, 10, 11, and 12

The thermal ellipsoid plots of **9**, **10**, and **11** are shown in Figures 1, 2, and 4, respectively, and the selected bond lengths and angles are tabulated in Table 1. The crystal structures show the tetrahedral coordination geometry of the central zirconium or titanium atoms. The cyclopentadienyl ligands are η^5-coordinated, with a systematic increase in the Zr–C bond lengths on moving from the bridgehead carbon atom to the peripheral carbon atoms. The M–C distances observed for the titanium complex **10** are shorter than the corresponding distances observed for the zirconium complexes **9** and **11**, and the M–C distances observed for the bis(dimethylamido) complex **9** are longer than those observed for the dichloride complex **11**. A similar trend is observed for the M–N*t*Bu distances of **9**, **10**, and **11**. The Cl–M–Cl angle observed for the zirconium complex **11** [123.27(5)°] is greater than that observed for the titanium complex **10** [104.11(7)°], as well as for the N–Zr–N angle observed for **9** [104.56(16)°]. The bridge carbon atoms are out of the Cp planes, and consequently the $Cp^{centroid}-C^{bridgehead}-C^{bridge}$ bond angles deviate from the ideal value of 180°. The $Cp^{centroid}-C^{bridgehead}-C^{bridge}$ angle observed for the titanium complex **10** (152.1°) is smaller than those observed for the zirconium complexes **9** and **11** (156.2 and 155.8°, respectively), indicating that the bridge carbon atom is further out of the Cp plane in the

 © 2004 Wiley-VCH Verlag GmbH & Co. KGaA, Weinheim

Table 1. Selected bond lengths (Å) and angles (°)

	9	**10**	**11**	**12**
M−Cl(or N)[a]	2.033(4)	2.2801(15)	2.5292(18)	2.4688(13)
M−Cl(or N)	2.061(4)	2.2653(16)	2.4310(15)	2.4265(14)
M−NC^{bridge}	2.106(3)	1.924(4)	2.076(3)	2.536(4)[b]
M−$C^{bridgehead}$	2.420(4)	2.256(4)	2.390(4)	2.444(4)
M−$C^{cp}(CH_3)$[a]	2.466(4)	2.338(5)	2.484(4)	2.521(5)
M−$C^{cp}(CH_3)$	2.557(4)	2.315(5)	2.462(4)	2.483(4)
M-$C^{cp}H^a$	2.525(4)	2.360(5)	2.508(4)	2.549(5)
M−$C^{cp}H$	2.587(4)	2.373(5)	2.503(4)	2.514(4)
M−$Cp^{centroid}$	2.206	1.992	2.156	2.199
$C^{bridgehead}$−C^{bridge}	1.543(5)	1.543(6)	1.529(5)	1.513(6)
C^{bridge}−N	1.470(5)	1.469(5)	1.469(4)	1.485(5)
$Cp^{centroid}$−M−NC^{bridge}	90.7	97.1	91.0	
$Cp^{centroid}$-$C^{bridgehead}$-C^{bridge}	156.2	152.1	155.8	164.8
Cl(or N)−M−Cl (or N)	104.56(16)	104.11(7)	123.27(5)	87.04(5)
$C^{bridgehead}$−C^{bridge}−N	100.9(3)	97.3(3)	99.3(3)	103.3(3)
C^{bridge}−*N*−M	106.7(2)	107.1(3)	107.5(2)	98.1(3)
C^{bridge}−*N*−CMe_3	118.2(3)	120.4(3)	119.4(3)	117.9(4)
M−*N*−CMe_3	127.9(3)	129.5(3)	131.0(2)	129.8(3)

[a] Bond length with respect to the side to which the phenyl group is located. [b] Zr−O distance, 1.9526(5) Å.

titanium complex **10**. The $C^{bridgehead}$−C^{bridge}−N angles (100.9(3), 97(3) and 99.3(3) ° for **9**, **10**, and **11**, respectively) deviate from the ideal sp^3-tetrahedral angle (109.5°). The $Cp^{centroid}$−M−NC^{bridge} angles observed for **9**, **10**, and **11** are smaller than that observed for the related complex $(Me_4CpSiN)Zr(NR_2)_2$ (100.2°).[13] The $Cp^{centroid}$−M−NC^{bridge} angles observed for the zirconium complexes **9** and **11** (90.7 and 91.0°, respectively) are smaller than that observed for the titanium complex **10** (97.1°), reflecting that the constraint imposed by the Cp−C^{bridge}−N−M frame is larger in the zirconium complexes than in the titanium complex. The nitrogen atoms on the dimethylamido ligand in **10** form a perfect trigonal planar structure (sum of the bond angles are 359.1° and 359.9°). The nitrogen atoms bonded to the *tert*-butyl group in the dichloride complexes **10** and **11** also almost form a trigonal planar structure (sum of bonding angles, 357.0° and 357.9°, respectively), however, the corresponding nitrogen atoms in the bis(dimethylamido) complex **9** deviate from the trigonal planar structure (sum of the bond angles is 352.8°).

The thermal ellipsoid plot of **12** is shown in Figure 3 and the selected bond lengths and angles are tabulated in Table 1. The metrical parameters observed for **12** are very similar to those observed for $[Me_4Cp-CH_2-N(H)tBu]ZrCl_2-O-ZrCl_2[Me_4Cp-CH_2-N(H)tBu]$, with the exception of the Zr−O−Zr angle. A strictly linear Zr−O−Zr arrangement (180°) is observed for complex **12**, while a somewhat bent structure is observed for $[Me_4Cp-CH_2-N(H)tBu]ZrCl_2-O-ZrCl_2[Me_4Cp-CH_2-N(H)tBu]$ (the Zr−O−Zr angle is 168.2°).

Ethylene Polymerization Studies

The dichloride complexes **10**, **11**, and **13**−**15** are active towards the polymerization of ethylene when activated with MAO (Table 2). The activities are low compared with that of Cp_2ZrCl_2, but are similar to those of the cyclopentadienyl or tetramethylcyclopentadienyl analogues previously prepared by Erker.[5] The titanium complexes show higher activities relative to the zirconium complexes (entry 1 and 3 versus entry 2 and 4). The activity depends strongly on the substituent attached to the bridge carbon atom. The complexes that have the 2-furyl group show the highest activity (entry 3 and 4), and the activity of the zirconium complex that has the 2-furyl substituent is 10 times higher than the complex that has a phenyl substituent (entry 2 and 4). The complex *rac*-(EBI)$Zr(NMe_2)_2$ was reported to be less active than the corresponding dichloride complex when activated with MAO.[14] However, in this case, the bis(dimethylamido) complex **9** shows a higher activity than the corresponding dichloride complex **11** (entry 2 and 6). The titanium complex **13**, which shows the highest activity, produces a polymer with the highest molecular weight (M_w, 610,000). The molecular weight distributions are very broad (M_w/M_n = 10−36), indicating that there are several types of active species in the polymerization solution.

Table 2. Ethylene polymerization results

Entry	Compound[a]	Time (min)	Activity (kg/mol·h)	M_w[c]	M_w/M_n[c]
1	**10**[b]	30	92	34000	14
2	**11**	30	16	361000	36
3	**13**	10	318	610000	32
4	**14**	20	150	198000	29
5	**15**	30	71	348000	10
6	**9**	30	122	150000	24

[a] Polymerization conditions: 30 mL toluene, 60 °C, 10 μmol catalyst, Al/Zr or Ti = 500, 100 psig ethylene. [b] 5.0 μmol catalyst, Al/Zr or Ti = 1000. [c] Determined by GPC in 1,2,4-trichlorobenzene at 140 °C against polystyrene standards.

 © 2004 Wiley-VCH Verlag GmbH & Co. KGaA, Weinheim

Conclusion

sp^3-C^1−bridged Cp/amido CGC complexes (1,3-$Me_2C_5H_2$−CHR−N*t*Bu−κ*N*)MCl_2 (M = Ti, Zr; R = phenyl, 2-furyl, cyclohexyl) have been synthesized using novel fulvenes that have substituents in the 1-, 4-, and 6-positions only. The bis(dimethylamido) complexes, which have been prepared by the reaction of $M(NMe_2)_4$ with *t*BuN(H)−CHR−$C_5H_3Me_2$, can be transformed to the dichloride complexes by treatment with Me_2SiCl_2. The complexes are active towards the polymerization of ethylene when activated with MAO. The titanium complexes show higher activities relative to the zirconium complexes, and the titanium complex that has a 2-furyl group on the bridge carbon atom shows the highest activity. The molecular weight distributions are broad (M_w/M_n, 10−36).

Experimental Section

General Remarks: All manipulations were performed under an inert atmosphere using standard glove box and Schlenk techniques. Toluene, pentane, THF, diethyl ether, and benzene were distilled from benzophenone ketyl. Toluene used for the polymerization reaction was purchased from Aldrich (anhydrous grade) and purified further over Na/K alloy. Dichlorodimethylsilane was dried over CaH_2. Ethylene was purchased from Conley Gas (99.9%) and purified by contactwith molecular sieves and copper overnight under a pressure of 150 psig. Methylaluminoxane (MAO) was purchased as a solution in toluene from Akzo (7.6 weight% of Al, MMAO type 4). The NMR spectra were recorded on a Varian Mercury plus 400 spectrometer. Elemental analyses were carried out at the Inter-University Center Natural Science Facilities, Seoul National University. Gel permeation chromatograms (GPC) were obtained at 140 °C in trichlorobenzene using a Waters Model 150-C+ GPC, and the data were analyzed using a polystyrene analyzing curve.

Compound 2: *n*BuLi (3.82 g, 2.5 M in hexane, 13.8 mmol) at −78 °C was added dropwise to a Schlenk flask containing **1** (3.00 g, 13.8 mmol) in THF (5 mL), and the solution was stirred for 1 hour at −78 °C. Furfural (1.32 g, 13.8 mmol) was added and the solution was stirred for 2 hours at −78 °C. The solution was poured into a separating funnel containing water (20 mL), and the product was extracted with ethyl acetate (10 mL × 5). The combined organic layer was shaken with aqueous HCl (1 N, 20 mL) for about 30 seconds, in which step the ketal group was deprotected to give a carbonyl compound. The organic layer was washed with concentrated aqueous $NaHCO_3$ solution (20 mL). The organic layer was collected and dried over anhydrous $MgSO_4$. The solvent was removed to give a residue, which was purified by column chromatography on silica gel eluting with hexane and ethyl acetate (v/v, 2:1) (white solid, 1.44 g, 54%). M.p. 74 °C. ^{1}H NMR (400 MHz, $CDCl_3$, 25 °C): δ = 2.10 (s, 3 H, CH_3), 2.44−2.48 (m, 2 H, CH_2), 2.58−2.63 (m, 2 H, CH_2), 4.64 (d, $^3J_{H,H}$ = 8.8 Hz, 1 H, OH), 5.60 (d, $^3J_{H,H}$ = 8.8 Hz, 1 H, OCH), 6.22 [dd, $^3J_{H,H}$ = 3.2, $^3J_{H,H}$ = 0.8 Hz, 1 H, furyl-C(4)−H], 6.31 [dd, $^3J_{H,H}$ = 3.2, $^4J_{H,H}$ = 2.0 Hz, 1 H, furyl-C(5)−H], 7.34 [dd, $^4J_{H,H}$ = 2.0, $^3J_{H,H}$ = 0.8 Hz, 1 H, furyl-C(3)−H] ppm. $^{13}C\{^1H\}$ NMR (100 MHz, $CDCl_3$, 25 °C): δ = 17.41 (CH_3), 32.18 (CH_2), 34.65 (CH_2), 64.28 (COH), 106.26 [furyl-C(3 or 4)], 110.23 [furyl-C(3 or 4)], 137.27 (C=C), 142.04 [furyl-C(5)], 154.57 [furyl-C(2)], 173.18 (C=C), 210.05 (carbonyl) ppm. IR (neat): ṽ = 1635 and 1673 (C=C−C=O), 3315 (br., OH) cm^{-1}. $C_{11}H_{12}O_3$ (192.21): calcd. C 68.7, H 6.31; found C 68.8, H 6.50.

Compound 3: This compound was synthesized according to a procedure similar to that of **2**. It was purified by column chromatography on silica gel eluting with hexane and ethyl acetate (v/v, 2:1) (oil, 82%). ^{1}H NMR (400 MHz, $CDCl_3$, 25 °C): δ = 0.19 (td, $J_{H,H}$ = 12.0, $J_{H,H}$ = 3.2 Hz, 1 H, Cy-H), 1.00 (td, $J_{H,H}$ = 12.0, $J_{H,H}$ = 3.2 Hz, 1 H, Cy-H), 1.08−1.84 (m, 9 H, Cy-H), 2.05 (s, 3 H, CH_3), 2.38−2.43 (m, 2 H, CH_2), 2.52−2.62 (m, 2 H, CH_2), 3.66 (d, $^3J_{H,H}$ = 10.0 Hz, 1 H, OH), 4.10 (dd, $^3J_{H,H}$ = 10.0, $^3J_{H,H}$ = 8.4 Hz, 1 H, OCH) ppm. $^{13}C\{^1H\}$ NMR (100 MHz, $CDCl_3$, 25 °C): δ = 17.72 (CH_3), 25.93 (Cy-CH_2), 26.10 (Cy-CH_2), 26.46 (Cy-CH_2), 29.30 (Cy-CH_2), 29.46 (Cy-CH_2), 31.94 (CH_2), 34.64 (CH_2), 43.79 (Cy-CH), 73.14 (COH), 139.49 (C=C), 171.91 (C=C), 210.88 (carbonyl) ppm. IR (neat): ṽ = 2850 and 2923 (C=C−C=O), 3446 (br., OH) cm^{-1}. $C_{13}H_{20}O_2$ (208.30): calcd. C 75.0, H 9.70; found C 75.3, H 9.52.

6-(2-Furyl)-1,4-dimethylfulvene (4): Compound **2** (1.44 g, 7.50 mmol) was dissolved in CH_2Cl_2 (10 mL). Dihydropyran (0.95 g, 11 mmol) and pyridinium *p*-toluenesulfonate (PPTS) (0.19 g, 0.75 mmol) were then added at room temperature. The solution was stirred for 4 hours and then diluted with diethyl ether (50 mL). The solution was washed with saturated aqueous NaCl solution. The organic phase was collected and dried over anhydrous $MgSO_4$. Removal of the solvent using a rotary evaporator gave a residue that was purified by column chromatography on silica gel eluting with hexane and ethyl acetate (v/v, 2:1). Signals of two diastereomers are observed in the ^{1}H NMR spectrum. The yield was 1.77 g (yield, 85%). The compound was dissolved in diethyl ether (5 mL), and MeLi (6.4 mL, 1.5 M in diethyl ether, 9.6 mmol) was added dropwise at −78 °C. The solution was allowed to warm to room temperature and stirred overnight. Water (10 mL) was then added. The diethyl ether was removed using a rotary evaporator. Ethyl acetate (30 mL) was added to the residue and the mixture was poured into a separating funnel. The aqueous layer was removed and aqueous HCl (2 N, 30 mL) was added. The mixture was shaken vigorously for 2.5 minutes. The aqueous layer was removed and the organic layer was washed with saturated aqueous $NaHCO_3$ solution (30 mL). The organic layer was collected and dried over anhydrous $MgSO_4$. The solvent was removed using a rotary evaporator, thus giving a residue. NaH (0.23 g, 9.6 mmol) and anhydrous THF (10 mL) was added to the residue under a nitrogen atmosphere. Methanol (1.0 mL) was added using a syringe, upon which hydrogen gas was evolved and the solution became red. The solution was stirred for 20 minutes at room temperature under nitrogen. The solution was poured into a separating funnel containing water (20 mL), and the red compound was extracted with ethyl acetate (50 mL). The organic layer was dried over anhydrous $MgSO_4$. Removal of the solvent gave a red residue that was purified by column chromatography on silica gel eluting with hexane and ethyl acetate (v/v, 20:1). The yield was 0.750 g (overall yield from **2**, 58%). ^{1}H NMR (400 MHz, $CDCl_3$, 25 °C): δ = 2.09 (s, 3 H, CH_3), 2.31 (s, 3 H, CH_3), 5.97 [s, 1 H, fulvene-C(2 or 3)-H], 6.11 [quadruplet, $^4J_{H,H}$ = 1.2 Hz, 1 H, fulvene-C(2 or 3)−H)], 6.51 [dd, $^3J_{H,H}$ = 3.2, $^3J_{H,H}$ = 1.6 Hz, 1 H, furyl-C(4)−H], 6.73 [d, $^3J_{H,H}$ = 3.2 Hz, 1 H, furyl-C(3)−H], 6.80 [(s, 1 H, fulvene-C(6)−H)], 7.56 [dd, $^3J_{H,H}$ = 1.6, $^4J_{H,H}$ = 0.4 Hz, 1 H, furyl-C(5)−H)] ppm. $^{13}C\{^1H\}$ NMR (100 MHz, $CDCl_3$, 25 °C): δ = 13.09 (CH_3), 17.42 (CH_3), 112.22 (furyl-CH), 116.84 (furyl-CH), 119.38 (furyl-CH), 126.29 [fulvene-C(2 or 3)], 129.38 [fulvene-C(1 or 4)], 131.68 [fulvene-C(2 or 3)], 134.05 [fulvene-C(1 or 4)], 141.77 [fulvene-C(5)], 144.49 [fulvene-C(6)], 151.28 [furyl-C(2)] ppm. $C_{12}H_{12}O_1$ (172.22): calcd. C 83.7, H 7.04; found C 83.6, H 7.00.

 © 2004 Wiley-VCH Verlag GmbH & Co. KGaA, Weinheim

6-Cyclohexyl-1,4-dimethylfulvene (5): This compound was synthesized according to a procedure similar to that for **4**. It was purified by column chromatography on silica gel eluting with hexane and ethyl acetate (v/v, 50:1). A yellow oily compound was obtained in a 51% overall yield from **3**. ^{1}H NMR (400 MHz, $CDCl_3$, 25 °C): δ = 1.12−1.44 (m, 5 H, Cy-CH_2), 1.68−1.90 (m, 5 H, Cy-CH_2), 2.01 (s, 3 H, CH_3), 2.22 (s, 3 H, CH_3), 2.93 (qt, $^3J_{H,H}$ = 10.4, $^3J_{H,H}$ = 3.2 Hz, 1 H, Cy-CH), 5.92 [s, 1 H, fulvene-C(2 or 3)−H], 6.03 [quadruplet, $^4J_{H,H}$ = 1.2 Hz, 1 H, fulvene-C(2 or 3)−H], 6.11 [d, $^3J_{H,H}$ = 10.4 Hz, 1 H, fulvene-C(6)−H] ppm. $^{13}C\{^1H\}$ NMR (100 MHz, $CDCl_3$, 25 °C): δ = 12.68 (CH_3), 16.95 (CH_3), 25.79 (Cy-CH_2), 25.98 (Cy-CH_2), 33.12 (Cy-CH_2), 37.55 (Cy-CH), 125.34 [fulvene-C(2 or 3)], 130.03 [fulvene-C(1 or 4)], 130.28 [fulvene-C(2 or 3)], 133.43 [fulvene-C(1 or 4)], 142.65 [fulvene-C(5)], 144.10 [fulvene-C(6)] ppm. $C_{14}H_{20}$ (188.31): calcd. C 89.3, H 10.7; found C 89.0, H 10.5.

Substituted Cyclopentadiene (6): 1,4-Dimethyl-6-phenylfulvene (0.95 g, 5.21 mmol) was dissolved in cold THF (−30 °C, 40 mL) and lithium *tert*-butylamide (0.41 g, 5.21 mmol) was added. The solution was stirred overnight at room temperature. Water (20 mL) was added and the product was extracted with hexane (50 mL). It was purified by column chromatography on silica gel eluting with hexane and ethyl acetate (v/v, 10:1). The yield was 80% (1.06 g). ^{1}H NMR (400 MHz, $CDCl_3$, 25 °C): δ = 1.13 (s, 9 H, *t*Bu-H), 1.82 (quadruplet, $J_{H,H}$ = 2.0 Hz, 3 H, CH_3), 2.14 (s, 3 H, CH_3), 2.80 (quintet, $J_{H,H}$ = 2.0 Hz, 2 H, CH_2), 4.98 (s, 1 H, bridge-CH), 5.78 (d, $J_{H,H}$ = 2.0 Hz, 1 H, Cp-CH), 7.14 [t, $^3J_{H,H}$ = 8 Hz, 1 H, Ph-C(*para*)−H], 7.25 [t, $^3J_{H,H}$ = 8 Hz, 2 H, Ph-C(*meta*)−H], 7.46 [d, $^3J_{H,H}$ = 8 Hz, 2 H, Ph-C(*ortho*)−H] ppm. $^{13}C\{^1H\}$ NMR (100 MHz, $CDCl_3$, 25 °C): δ = 14.65 (CH_3), 15.92 (CH_3), 30.12 [C(*C*H_3)$_3$], 44.12 (CH_2), 51.41 [N*C*(CH_3)$_3$], 52.98 (NCH), 125.09 (Cp-CH), 125.69 [Ph-C(*para*)], 127.07 [Ph-C(*ortho* or *meta*)], 127.63 [Ph-C(*ortho* or *meta*)], 137.05 [Cp-C(bridgehead)], 143.02 [Cp-C(CH_3)], 143.11 [Cp-C(CH_3)], 145.66 [Ph-C(*ipso*)] ppm. $C_{18}H_{25}N_1$ (255.40): calcd. C 84.7, H 9.89, N 5.48; found C 84.6, H 10.1, N 5.15.

Substituted Cyclopentadiene 7: This compound was synthesized according to a procedure similar to that for **6**. It was purified by column chromatography on silica gel eluting with hexane and ethyl acetate (v/v, 50:1). The yield was 88%. ^{1}H NMR (400 MHz, $CDCl_3$, 25 °C): δ = 1.14 (s, 9 H, *t*Bu-H), 1.99 (quadruplet, $J_{H,H}$ = 2.0 Hz, 3 H, CH_3), 2.10 (s, 3 H, CH_3), 2.82 (quintet, $J_{H,H}$ = 2.0 Hz, 2 H, CH_2), 4.99 (s, 1 H, NCH), 5.83 (d, $J_{H,H}$ = 1.6 Hz, 1 H, Cp-CH), 6.10 [d, $^3J_{H,H}$ = 3.2 Hz, 1 H, furyl-C(3)−H], 6.28 [dd, $^3J_{H,H}$ = 3.2, $^3J_{H,H}$ = 2.0 Hz, 1 H, furyl-C(4)−H], 7.32 [d, $^3J_{H,H}$ = 2.0 Hz, 1 H, furyl-C(5)−H] ppm. $^{13}C\{^1H\}$ NMR (100 MHz, $CDCl_3$, 25 °C): δ = 14.32 (CH_3), 15.56 (CH_3), 29.87 [C(*C*H_3)$_3$], 44.15 (CH_2), 48.48 (NCH), 51.30 [N*C*(CH_3)$_3$], 105.49 [furyl-C(3 or 4)], 109.95 [furyl-C(3 or 4)], 124.79 (Cp-*C*H), 138.36 [Cp-C(bridgehead)], 140.49 [Cp-C(CH_3)], 140.75 [furyl-C(5)], 143.03 [Cp-C(CH_3)], 157.78 [furyl-C(2)] ppm. $C_{16}H_{23}O_1N_1$ (245.36): calcd. C 78.3, H 9.47, N 5.71; found C 78.2, H 9.50, N 5.83.

Substituted Cyclopentadiene 8: This compound was synthesized according to a procedure similar to that for **6**. It was purified by column chromatography on silica gel eluting with hexane and ethyl acetate (v/v, 30:1). The yield was 60%. ^{1}H NMR (400 MHz, $CDCl_3$, 25 °C): δ = 0.7−2.2 (m, 11 H, Cy-H), 1.00 (s, 9 H, *t*Bu-H), 1.94 (s, 3 H, CH_3), 2.10 (s, 3 H, CH_3), 2.65−2.82 (m, 2 H, Cp-CH_2), 3.34 (d, $J_{H,H}$ = 9.6 Hz, 1 H, NCH), 5.78 (s, 1 H, Cp-CH) ppm. $^{13}C\{^1H\}$ NMR (100 MHz, $CDCl_3$, 25 °C): δ = 14.33 (CH_3), 16.71 (CH_3), 26.66, 26.71, 26.83, 30.21 [C(*C*H_3)$_3$], 30.40, 32.11, 42.80, 43.62, 50.78, 55.89, 124.79 (Cp-CH), 136.70 [Cp-C(bridgehead)], 142.73 [Cp-C(CH_3)], 143.73 [Cp-C(CH_3)] ppm. $C_{18}H_{31}N_1$ (261.45): calcd. C 82.7, H 12.0, N 5.35; found C 82.9, H 12.1, N 5.40.

(1,3-$Me_2C_5H_2$-CHPh−N*t*Bu−κ*N*)Zr(NMe_2)$_2$ (9): Compound **6** (0.511 g, 2.00 mmol) and Zr(NMe_2)$_4$ (0.535 g, 2.00 mmol) were weighed in a flask and toluene (30 mL) was added. The solution was stirred for 2 days at 100 °C under a weak stream of nitrogen gas. The volatiles were removed to give a white oil, which was quite pure (analyzed by ^{1}H and ^{13}C NMR spectroscopy) (crude yield, 97%). Analytically pure single crystals suitable for X-ray crystallography were obtained in pentane at −30 °C. M.p. 135 °C. ^{1}H NMR (400 MHz, C_6D_6, 25 °C): δ = 1.24 (s, 9 H, *t*Bu-H), 1.54 (s, 3 H, CH_3), 2.19 (s, 3 H, CH_3), 2.89 (s, 6 H, NCH_3), 3.09 (s, 6 H, NCH_3), 5.48 (d, $^3J_{H,H}$ = 2.8 Hz, 1 H, Cp-H), 5.85 (s, 1 H, bridge-CH), 5.88 (d, $^3J_{H,H}$ = 2.8 Hz, 1 H, Cp-H), 7.13 [t, $^3J_{H,H}$ = 7.6 Hz, 1 H, Ph-C(*para*)−H], 7.25 [t, $^3J_{H,H}$ = 7.6 Hz, 2 H, Ph-C(*meta*)−H], 7.61 [d, $^3J_{H,H}$ = 7.6 Hz, 2 H, Ph-C(*ortho*)−H] ppm. $^{13}C\{^1H\}$ NMR (100 MHz, C_6D_6, 25 °C): δ = 13.52 (CH_3), 14.79 (CH_3), 32.24 [C(*C*H_3)$_3$], 43.58 [N(CH_3)$_2$], 47.37 [N(CH_3)$_2$], 56.20 [N*C*(CH_3)$_3$], 59.33 (bridge-CH), 105.76 [Cp-C(bridgehead)], 107.74 (Cp-CH), 112.60 (Cp-CH), 123.77 [Cp-C(CH_3)], 125.43 [Cp-C(CH_3)], 126.45 (Ph-C), 127.64 (Ph-C), 128.45 (Ph-C), 147.10 [Ph-C(*ipso*)] ppm. $C_{22}H_{35}N_3Zr$ (432.76): calcd. C 61.1, H 8.15, N 9.71; found C 61.3, H 8.23, N 9.65.

(1,3-$Me_2C_5H_2$−CHPh−N*t*Bu−κ*N*)$TiCl_2$ (10): The bis(dimethylamido) complex was synthesized according to a procedure similar to that of **9**, however, **6** (0.511 g, 2.00 mmol) and Ti(NMe_2)$_4$ (0.450 g, 2.00 mmol) were used. A deep red oil was obtained, which was quite pure (analyzed by ^{1}H and ^{13}C NMR spectroscopy). ^{1}H NMR (400 MHz, C_6D_6, 25 °C): δ = 1.28 (s, 9 H, *t*Bu-H), 1.44 (s, 3 H, CH_3), 2.13 (s, 3 H, CH_3), 3.01 (s, 6 H, NCH_3), 3.27 (s, 6 H, NCH_3), 5.44 (d, $^3J_{H,H}$ = 2.8 Hz, 1 H, Cp-H), 5.80 (s, 1 H, bridge-CH), 5.94 (d, $^3J_{H,H}$ = 2.8 Hz, 1 H, Cp-H), 7.12 [t, $^3J_{H,H}$ = 7.6 Hz, 1 H, Ph-C(*para*)−H], 7.24 [t, $^3J_{H,H}$ = 7.6 Hz, 2 H, Ph-C(*meta*)−H], 7.55 [d, $^3J_{H,H}$ = 7.6 Hz, 2 H, Ph-C(*ortho*)−H] ppm. $^{13}C\{^1H\}$ NMR (100 MHz, C_6D_6, 25 °C): δ = 13.76 (CH_3), 14.59 (CH_3), 32.11 [C(*C*H_3)$_3$], 48.42 [N(CH_3)$_2$], 52.65 [N(CH_3)$_2$], 59.95 [N*C*(CH_3)$_3$], 60.98 (bridge-CH), 103.29 [Cp-C(bridgehead)], 109.85 (Cp-CH), 115.62 (Cp-CH), 123.25 [Cp-C(CH_3)], 126.37 (Ph-C), 128.35 (Ph-C), 146.95 [Ph-C(*ipso*)] ppm. The crude residue was dissolved in toluene (12 mL) and dichlorodimethylsilane (1.03 g, 8.00 mmol) was added. The solution was stirred overnight. The volatiles were removed under a vacuum. The complex was dissolved in toluene and stored in a freezer (−30 °C) overnight to give red crystals which were suitable for X-ray crystallography (0.234 g, 37%). The major constituent of the mother liquor was the desired complex, but further isolation of the clean complex from the mother liquor was not achieved. M.p. 163 °C. ^{1}H NMR (400 MHz, C_6D_6, 25 °C): δ = 1.37 (s, 9 H, *t*Bu-H), 1.52 (s, 3 H, CH_3), 1.88 (s, 3 H, CH_3), 6.06 (d, $^3J_{H,H}$ = 3.6 Hz, 1 H, Cp-H), 6.08 (s, 1 H, bridge-CH), 6.20 (d, $^3J_{H,H}$ = 3.6 Hz, 1 H, Cp-H), 7.00−7.15 (m, 5 H, Ph-H) ppm. $^{13}C\{^1H\}$ NMR (100 MHz, C_6D_6, 25 °C): δ = 15.12 (CH_3), 17.88 (CH_3), 30.83 [C(*C*H_3)$_3$], 62.45 (bridge-CH), 63.76 [N*C*(CH_3)$_3$], 102.13 [Cp-C(bridgehead)], 122.14 (Cp-CH), 122.78 (Cp-CH), 127.76 (Ph-C), 127.92 (Ph-C), 128.44 (Ph-C), 138.47 [Cp-C(CH_3)], 138.79 [Cp-C(CH_3)], 141.43 [Ph-C(*ipso*)] ppm. $C_{18}H_{23}Cl_2NTi$ (372.15): calcd. C 58.1, H 6.24, N 3.76; found C 57.8, H 6.25, N 3.93.

(1,3-$Me_2C_5H_2$−CHPh−N*t*Bu−κ*N*)$ZrCl_2$ (11): Compound **9** (0.530 g, 1.22 mmol) was dissolved in toluene (20 mL) and dichlorodimethylsilane (0.315 g, 2.44 mmol) was added. The solution was stirred overnight, upon which a white solid precipitated. The solid was filtered and dried under vacuum. The yield was 44% (0.222 g).

 © 2004 Wiley-VCH Verlag GmbH & Co. KGaA, Weinheim

The major constituent of the filtrate was the desired complex. The reaction for 4 days without stirring gave single crystals suitable for X-ray crystallography. M.p. 194 °C. ^{1}H NMR (400 MHz, C_6D_6, 25 °C): δ = 1.27 (s, 9 H, *t*Bu-H), 1.60 (s, 3 H, CH_3), 1.99 (s, 3 H, CH_3), 5.77 (d, $^3J_{H,H}$ = 3.2 Hz, 1 H, Cp-H), 5.91 (s, 1 H, bridge-CH), 5.95 (d, $^3J_{H,H}$ = 3.2 Hz, 1 H, Cp-H), 7.00−7.10 [m, 3 H, Ph-C(*meta* or *para*)−H], 7.10−7.22 [m, 2 H, Ph-C(*ortho*)−H] ppm. ^{13}C{^{1}H} NMR (100 MHz, C_6D_6, 25 °C): δ = 14.00 (CH_3), 16.58 (CH_3), 30.70 [C(*C*H$_3$)$_3$], 57.84 [N*C*(CH$_3$)$_3$], 59.65 (bridge-CH), 104.27 [Cp-C(bridgehead)], 116.17 (Cp-CH), 116.40 (Cp-CH), 127.56 (Ph-C), 128.29 (Ph-C), 128.49 (Ph-C), 132.17 [Cp-C(CH_3)], 132.25 [Cp-C(CH_3)], 142.21 [Ph-C(*ipso*)] ppm. $C_{18}H_{23}Cl_2NZr$ (415.51): calcd. C 52.0, H 5.59, N 3.37; found C 51.7, H 6.00, N 3.34.

[1,3-Me$_2$C$_5$H$_2$−CH(C$_4$H$_3$O)−N*t*Bu−κ*N*]TiCl$_2$ (13): The bis(dimethylamido) complex was synthesized according to a procedure similar to that for **9**. The reaction time was 4 days. A deep red oil was obtained. ^{1}H NMR (400 MHz, C_6D_6, 25 °C): δ = 1.26 (s, 9 H, *t*Bu-H), 1.75 (s, 3 H, CH_3), 2.07 (s, 3 H, CH_3), 3.04 (s, 6 H, NCH_3), 3.22 (s, 6 H, NCH_3), 5.50 (d, $^3J_{H,H}$ = 2.8 Hz, 1 H, Cp-H), 5.91 (s, 1 H, bridge-CH), 5.94 (d, $^3J_{H,H}$ = 2.8 Hz, 1 H, Cp-H), 6.15−6.20 [m, 2 H, furyl-C(3 and 4)−H], 7.17 [dd, $^3J_{H,H}$ = 1.6, $^4J_{H,H}$ = 0.8 Hz, 1 H, furyl-C(5)−H] ppm. ^{13}C{^{1}H} NMR (100 MHz, C_6D_6, 25 °C): δ = 13.50 (CH_3), 14.49 (CH_3), 31.27 [C(*C*H$_3$)$_3$], 48.35 [N(CH_3)$_2$], 52.40 [N(CH_3)$_2$], 54.94 (bridge-CH), 59.62 [N*C*(CH$_3$)$_3$], 102.26 [Cp-C(bridgehead)], 106.94 [furyl-C(3 or 4)], 109.31 (Cp-CH), 110.75 [furyl-C(3 or 4)], 115.68 (Cp-CH), 123.23 [Cp-C(CH_3)], 126.06 [Cp-C(CH_3)], 139.91 [furyl-C(5)], 158.57 [furyl-C(2)] ppm. Chlorination was accomplished using the method and conditions developed for **10**. A crude red oil, which is quite pure (analyzed by NMR spectroscopy), was obtained by evaporation of all the volatiles, in a 86% yield. An analytically pure compound was obtained by recrystallization in pentane at −30 °C. M.p. 117 °C. ^{1}H NMR (400 MHz, C_6D_6, 25 °C): δ = 1.33 (s, 9 H, *t*Bu-H), 1.82 (s, 3 H, CH_3), 2.01 (s, 3 H, CH_3), 5.97 [d, $^3J_{H,H}$ = 3.6 Hz, 1 H, furyl-C(3)−H], 6.00 [dd, $^3J_{H,H}$ = 3.6, $^3J_{H,H}$ = 1.6 Hz, 1 H, furyl-C(4)−H], 6.14 (s, 1 H, bridge-CH), 6.16 (d, $^3J_{H,H}$ = 3.6 Hz, 1 H, Cp-H), 6.17 (d, $^3J_{H,H}$ = 3.6 Hz, 1 H, Cp-H), 6.92 [dd, $^3J_{H,H}$ = 1.6, $^4J_{H,H}$ = 0.8 Hz, 1 H, furyl-C(5)−H] ppm. ^{13}C{^{1}H} NMR (100 MHz, C_6D_6, 25 °C): δ = 15.08 (CH_3), 18.12 (CH_3), 29.29 [C(*C*H$_3$)$_3$], 55.88 (bridge-*C*H), 63.09 [N*C*(CH$_3$)$_3$], 102.95 [Cp-C(bridgehead)], 109.36 [furyl-C(3 or 4), 110.95 [furyl-C(3 or 4)], 121.52 (Cp-CH), 122.68 (Cp-CH), 137.46 [Cp-C(CH_3)], 138.83 [Cp-C(CH_3)], 141.31 [furyl-C(5)], 152.64 [furyl-C(2)] ppm. $C_{16}H_{21}Cl_2NOTi$ (362.12): calcd. C 53.1, H 5.85, N 3.86; found C 52.8 (52.6), H 6.32 (6.30), N 3.80 (3.75).

[1,3-Me$_2$C$_5$H$_2$−CH(C$_4$H$_3$O)−N*t*Bu−κ*N*]ZrCl$_2$ (14): The bis(dimethylamido) complex was synthesized according to a procedure similar to that for **9**. The reaction time was 4 days. A white oil was obtained. ^{1}H NMR (400 MHz, C_6D_6, 25 °C): δ = 1.21 (s, 9 H, *t*Bu-H), 1.92 (s, 3 H, CH_3), 2.13 (s, 3 H, CH_3), 2.91 (s, 6 H, NCH_3), 3.04 (s, 6 H, NCH_3), 5.56 (d, $^3J_{H,H}$ = 2.8 Hz, 1 H, Cp-H), 5.87 (d, $^3J_{H,H}$ = 2.8 Hz, 1 H, Cp-H), 5.93 (s, 1 H, bridge-CH), 6.18−6.22 [m, 2 H, furyl-C(3 and 4)−H], 7.18 [dd, $^3J_{H,H}$ = 2.8, $^4J_{H,H}$ = 0.8 Hz, 1 H, furyl-C(5)−H] ppm. ^{13}C{^{1}H} NMR (100 MHz, C_6D_6, 25 °C): δ = 13.22 (CH_3), 14.01 (CH_3), 31.21 [C(*C*H$_3$)$_3$], 43.52 [N(CH_3)$_2$], 47.14 [N(CH_3)$_2$], 53.45 (bridge-CH), 55.86 [N*C*(CH$_3$)$_3$], 105.55 [Cp-C(bridgehead)], 107.12 (Cp-CH), 107.71 [furyl-C(3 or 4)], 110.72 [furyl-C(3 or 4)], 112.55 (Cp-CH), 123.91 [Cp-C(CH_3)], 125.29 [Cp-C(CH_3)], 140.00 [furyl-C(5)], 158.71 [furyl-C(2)] ppm. Chlorination was accomplished by stirring the crude bis(dimethylamido) complex with 3.0 equivalents of dichlorodimethylsilane in pentane overnight. The precipitated white solid was filtered and dried under vacuum. The yield was 47%. M.p. 128 °C. ^{1}H NMR (400 MHz, C_6D_6, 25 °C): δ = 1.23 (s, 9 H, *t*Bu-H), 1.96 (s, 3 H, CH_3), 2.15 (s, 3 H, CH_3), 5.92 (d, $^3J_{H,H}$ = 2.8 Hz, 1 H, Cp-H), 5.94 (d, $^3J_{H,H}$ = 2.8 Hz, 1 H, Cp-H), 5.98 (s, 1 H, bridge-CH), 6.01 [d, $^3J_{H,H}$ = 3.2 Hz, 1 H, furyl-C(3)−H], 6.04 [dd, $^3J_{H,H}$ = 3.2, $^3J_{H,H}$ = 1.6 Hz, 1 H, furyl-C(4)−H], 6.99 [d, $^3J_{H,H}$ = 1.6 Hz, 1 H, furyl-C(5)−H] ppm. ^{13}C{^{1}H} NMR (100 MHz, C_6D_6, 25 °C): δ = 14.08 (CH_3), 16.77 (CH_3), 29.11 [C(*C*H$_3$)$_3$], 53.30 (bridge-CH), 57.53 [N*C*(CH$_3$)$_3$], 105.13 [Cp-C(bridgehead)], 108.93 [furyl-C(3 or 4)], 110.88 [furyl-C(3 or 4)], 115.55 (Cp-CH), 116.43 (Cp-CH), 131.91 [Cp-C(CH_3)], 132.27 [Cp-C(CH_3)], 141.17 [furyl-C(5)], 153.82 [furyl-C(2)] ppm. $C_{16}H_{21}Cl_2NOZr$ (405.47): calcd. C 47.4, H 5.23, N 3.46; found C 47.1, H 5.68, N 3.54.

[1,3-Me$_2$C$_5$H$_2$−CH(C$_6$H$_{11}$)−N*t*Bu−κ*N*]ZrCl$_2$ (15): The bis(dimethylamido) complex was synthesized according to a procedure similar to that for **9**. The reaction time was 4 days. A white oil was obtained. ^{1}H NMR (400 MHz, C_6D_6, 25 °C): δ = 0.9−2.5 (m, 11 H, Cy-H), 1.38 (s, 9 H, *t*Bu-H), 2.04 (s, 3 H, CH_3), 2.11 (s, 3 H, CH_3), 2.87 (s, 6 H, NCH_3), 3.01 (s, 6 H, NCH_3), 4.55 (d, $J_{H,H}$ = 8.0 Hz, 1 H, bridge-CH), 5.65 (d, $^3J_{H,H}$ = 2.8 Hz, 1 H, Cp-H), 5.92 (d, $^3J_{H,H}$ = 2.8 Hz, 1 H, Cp-H) ppm. ^{13}C{^{1}H} NMR (100 MHz, C_6D_6, 25 °C): δ = 13.31 (CH_3), 16.64 (CH_3), 27.23, 27.48, 27.83, 31.35 [C(*C*H$_3$)$_3$], 35.45, 44.00 [N(CH_3)$_2$], 44.31, 45.48, 46.94, 55.39, 62.80 (bridge-CH), 108.08 (Cp-CH), 109.03 [Cp-C(bridgehead)], 111.57 (Cp-CH), 123.54 [Cp-C(CH_3)], 124.03 [Cp-C(CH_3)] ppm. Chlorination was accomplished by stirring the crude bis(dimethylamido) complex with 3.0 equivalent dichlorodimethylsilane in pentane overnight. The precipitated white solid was filtered and dried under vacuum. The yield was 83%. ^{1}H NMR (400 MHz, C_6D_6, 25 °C): δ = 0.7−2.2 (m, 11 H, Cy-H), 1.39 (s, 9 H, *t*Bu-H), 1.87 (s, 3 H, CH_3), 1.94 (s, 3 H, CH_3), 4.89 (d, $^3J_{H,H}$ = 8.4 Hz, 1 H, bridge-C*H*), 5.96 (s, 2 H, Cp-H) ppm. ^{13}C{^{1}H} NMR (100 MHz, C_6D_6, 25 °C): δ = 13.82 (CH_3), 16.93 (CH_3), 26.32, 26.82, 27.04, 29.02 [C(*C*H$_3$)$_3$], 30.00, 35.68, 41.97, 56.69 [N*C*(CH$_3$)$_3$], 63.20 (bridge-CH), 107.54 [Cp-C(bridgehead)], 114.97 (Cp-CH), 116.39 (Cp-CH), 130.26 [Cp-C(CH_3)], 130.84 [Cp-C(CH_3)] ppm. $C_{18}H_{29}Cl_2NZr$ (421.56): calcd. C 51.3, H 6.95, N 3.32; found C 51.6, H 7.32, N 3.25.

Ethylene Polymerization: In a dry box, toluene (30 mL) was added to a dried 70 mL glass reactor. The activated complex, prepared by mixing the complex (10 μmol) and MAO (Al/Zr or Ti = 500), was added to the reactor. The reactor was assembled and removed from the dry box. The reactor was immersed in an oil bath whose temperature had been set to 60 °C, and stirred for 15 minutes, at which time the solution temperature reached that of the bath. Ethylene was fed under the pressure of 100 psig. After the polymerization reaction was performed for the given time, it was quenched by venting ethylene gas and pouring the mixture into acetone. The white precipitates were collected by filtration and dried under vacuum. Table 2 summarizes the polymerization results.

X-ray Crystallographic Study: Crystals of **9**, **10**, and **12** were coated with grease (Apiezon N) and mounted inside a thin glass tube with epoxy glue and placed on an Enraf−Nonius CCD single-crystal X-ray diffractometer using graphite-monochromated Mo-K_α radiation (λ = 0.71073 Å). The crystal of **11** was mounted onto a thin glass fiber with paratone and immediately placed in a cold nitrogen stream at 150 K on a MXC3 diffractometer (Mac Science) The structures were solved by direct methods (SHELXS-97)[15] and refined against all F^2 data (SHELXS-97). All non-hydrogen atoms were refined with anisotropic thermal parameters. The hydrogen atoms were treated as idealized contributions. The crystal data and

 © 2004 Wiley-VCH Verlag GmbH & Co. KGaA, Weinheim

Table 3. Crystallographic parameters of **9**, **10**, **11**, and **12**

	9	**10**	**11**	**12**
Empirical formula	$C_{22}H_{35}N_3Zr$	$C_{18}H_{23}Cl_2NTi$	$C_{18}H_{23}Cl_2NZr$	$C_{21}H_{27}Cl_2NO_{0.50}Zr$
Formula mass	432.75	372.17	415.49	463.56
Temperature [K]	293	293	150	293
a (Å)	11.5090(10)	19.7430(10)	8.982(5)	10.6331(6)
b (Å)	13.3210(10)	14.5910(10)	9.246(4)	12.3576(7)
c (Å)	15.3180(10)	16.3030(10)	11.639(7)	16.3256(10)
α [°]	90	90	83.84(4)	90
β [°]	101.808(2)	126.436(2)	70.32(4)	103.888(3)
γ [°]	90	90	84.76(4)	90
Volume [Å^3]	2298.7(3)	3778.4(4)	903.2(8)	2082.5(2)
Crystal system, space group	Monoclinic, $P2_1/n$	Monoclinic, $C2/c$	Triclinic, $P\bar{1}$	Monoclinic, $P2_1/c$
d (calcd.) [g/cm^3]	1.250	1.309	1.528	1.479
Z	4	8	2	4
Absorption coefficient [mm^{-1}]	0.488	0.732	0.901	0.791
F(000)	912	1552	424	952
Crystal size [mm]	0.2 × 0.15 × 0.15	0.3 × 0.2 × 0.15	0.3 × 0.2 × 0.2	0.3 × 0.2 × 0.2
θ range [°]	3.12 to 27.45	2.79 to 25.72	1.86 to 25.00	2.84 to 27.07
Limiting indices	$-14 \le h \le 14$	$-23 \le h \le 24$	$-10 \le h \le 10$	$-13 \le h \le 13$
	$-15 \le k \le 16$	$-15 \le k \le 17$	$0 \le k \le 10$	$-14 \le k \le 15$
	$-18 \le l \le 18$	$-19 \le l \le 19$	$-13 \le l \le 13$	$-20 \le l \le 20$
Reflections collected/unique	7542/4567 [R(int) = 0.0921]	6099/3501 [R(int) = 0.0655]	3237/3032 [R(int) = 0.0308]	8034/4536 [R(int) = 0.0726]
Data/restraints/parameters	4567/0/244	3501/0/205	3032/0/204	4536/0/241
Final R indices [$I > 2\sigma(I)$]	$R1$ = 0.0443, ω$R2$ = 0.0674	$R1$ = 0.0523, ω$R2$ = 0.1320	$R1$ = 0.0342, ω$R2$ = 0.0858	$R1$ = 0.0493, ω$R2$ = 0.0984
R indices (all data)	$R1$ = 0.1830, ω$R2$ = 0.0811	$R1$ = 0.1408, ω$R2$ = 0.1506	$R1$ = 0.0411, ω$R2$ = 0.0887	$R1$ = 0.1413, ω$R2$ = 0.1152
Largest diff. peak and hole [e·Å^3]	0.326 and −0.283	0.428 and −0.479	0.435 and −0.592	0.468 and −0.371
Goodness-of-fit on F^2	0.759	0.815	1.066	0.882

refinement results are summarized in Table 3. Selected bond lengths and angles are listed in Table 1.

CCDC-221028 (for **9**), -221029 (for **10**), -221030 (for **11**), and -221031 (for **12**) contain the supplementary crystallographic data for this paper. These data can be obtained free of charge at www.ccdc.cam.ac.uk/conts/retrieving.html [or from the Cambridge Crystallographic Data Centre, 12 Union Road, Cambridge CB2 1EZ, UK; Fax: (internat.) + 44-1223-336-033; E-mail: deposit@ccdc.cam.ac.uk].

[1] [1a] S. A. Miller, J. E. Bercaw, *Organometallics* **2002**, *21*, 934−945. [1b] W. Kaminsky, R. Engehausen, J. Kopf, *Angew. Chem.* **1995**, *107*, 2469−2470; *Angew. Chem. Int. Ed. Engl.* **1995**, *34*, 2273−2275. [1c] H. Alt, R. Zenk, *J. Organomet. Chem.* **1996**, *518*, 7−15. [1d] H. G. Alt, M. Jung, *J. Organomet. Chem.* **1998**, *568*, 87−112. [1e] C. A. Willoughby, W. M. Davis, S. L. Buchwald, *J. Organomet. Chem.* **1995**, *497*, 11−15.

[2] [2a] T. Koch, S. Blaurock, F. B. Somoza, A. Voigt, R. Kirmse, E. Hey-Hawkins, *Organometallics* **2000**, *19*, 2556−2563. [2b] D. T. Mallin, M. D. Rausch, Y. G. Lin, *J. Am. Chem. Soc.* **1990**, *112*, 2030−2031. [2c] R. Fierro, M. D. Rausch, G. S. Herrman, H. G. Alt, *J. Organomet. Chem.* **1995**, *485*, 11−17.

[3] [3a] J. J. Eisch, X. Shi, F. A. Owuor, *Organometallics* **1998**, *17*, 5219−5221. [3b] P.-J. Sinnema, P. J. Shapiro, B. Hohn, T. E. Bitterwolf, B. Twamley, *Organometallics* **2001**, *20*, 2883−2888. [3c] S. Fox, J. P. Dunne, M. Tacke, D. Schmitz, R. Dronskowski, *Eur. J. Inorg. Chem.* **2002**, 3039−3046.

[4] [4a] S.-D. Bai, X.-H. Wei, J.-P. Guo, D.-S. Liu, Z.-Y. Zhou, *Angew. Chem.* **1999**, *111*, 2051−2053; *Angew. Chem. Int. Ed.* **1999**, *38*, 1926−1928. [4b] S. Venne-Dunker, G. Kehr, R. Fröhlich, G. Erker, *Organometallics* **2003**, *22*, 948−958.

[5] [5a] K. Kunz, G. Erker, S. Doring, R. Fröhlich, G. Kehr, *J. Am. Chem. Soc.* **2001**, *123*, 6181−6182. [5b] K. Kunz, G. Erker, S. Doring, S. Bredeau, G. Kehr, R. Fröhlich, *Organometallics* **2002**, *21*, 1031−1041.

[6] [6a] K. J. Stone, R. D. Little, *J. Org. Chem.* **1984**, *49*, 1849−1853. [6b] I. Erden, F.-P. Xu, A. Sadoun, W. Smith, G. Sheff, M. Ossun, *J. Org. Chem.* **1995**, *60*, 813−820.

[7] Y. C. Won, H. Y. Kwon, B. Y. Lee, Y.-W. Park, *J. Organemet. Chem.* **2003**, *677*, 133−139.

[8] B. Y. Lee, Y. H. Kim, Y. C. Won, J. W. Han, W. H. Suh, I. S. Lee, Y. K. Chung, K. H. Song, *Organometallics* **2002**, *21*, 1500−1503.

[9] [9a] U. Wieser, F. Schaper, H.-H. Brintzinger, N. I. Makela, H. R. Knuuttila, M. Leskela, *Organometallics* **2002**, *21*, 541−545. [9b] U. Wieser, D. Babushkin, H.-H. Brintzinger, *Organometallics* **2002**, *21*, 920−923.

[10] P. Jutzi, *Chem. Rev.* **1986**, *86*, 983−996.

[11] [11a] G. M. Diamond, R. F. Jordan, J. L. Petersen, *J. Am. Chem. Soc.* **1996**, *118*, 8024−8033. [11b] J. N. Christopher, R. F. Jordan, J. L. Petersen, V. G. Jr. Young, *Organometallics* **1997**, *16*, 3044−3050. [11c] J. N. Christopher, G. M. Diamond, R. F. Jordan, J. L. Petersen, *Organometallics* **1996**, *15*, 4038−4044.

[12] B. Y. Lee, J. W. Han, I. S. Lee, Y. K. Chung, *J. Organomet. Chem.* **2001**, *627*, 233−238.

[13] D. W. Carpenetti, L. Kloppenburg, J. T. Kupec, J. L. Petersen, *Organometallics* **1996**, *15*, 1572−1581.

[14] I. Kim, R. F. Jordan, *Macromolecules* **1996**, *29*, 489−491.

[15] G. M. Sheldrick, *SHELXL*-97, University of Göttingen, Germany, **1997**.

Received October 7, 2003
Early View Article
Published Online February 26, 2004

 © 2004 Wiley-VCH Verlag GmbH & Co. KGaA, Weinheim

Macrocyclic and Open-Chain Cu^{II}-4f (4f = Gd^{III}, Ce^{III}) Complexes with Planar Diamino Chains: Structures and Magnetic Properties

Jean-Pierre Costes,*[a] Françoise Dahan,[a] Ghenadie Novitchi,[a,b] Vladimir Arion,[c] Sergiu Shova,[d] and Janusz Lipkowski[e]

Keywords: Heterometallic complexes / Copper / Lanthanides / Macrocyclic ligands / Template synthesis / Magnetic properties

Until now, the known structures of heterodinuclear Cu–Ln complexes involve compartmental Schiff-base ligands with saturated diamino chains. We report here two Cu–Ln complexes (Ln = Gd or Ce) which are the first structurally characterized Cu–Ln entities involving *S*-methylisothiosemicarbazide as the diamino bridge, with open chain and macrocyclic ligands. The macrocyclic Cu–Gd entity is a well isolated dinuclear complex whereas two hydrogen bonds join together a pair of binuclear Cu–Ce complexes to give tetranuclear {Cu–Ce···Ce–Cu} entities. The Cu–Gd complexes [H = -J($S_{Cu}S_{Gd}$)] exhibit ferromagnetic interactions between 5 and 5.5 cm^{-1}. Since the Cu–Ce complexes do not follow the Curie law due to the presence of orbital degeneracy, an analysis based on a simple spin-only Hamiltonian is not possible. Nevertheless, the EPR spectra of the Cu–Ce complexes do confirm the existence of magnetic interactions.
(© Wiley-VCH Verlag GmbH & Co. KGaA, 69451 Weinheim, Germany, 2004)

1. Introduction

Heteronuclear lanthanide (4f) and 3d metal coordination complexes are mainly studied for their interesting magnetic properties.[1−9] These bimetallic complexes are important for studying the nature of the magnetic exchange interactions between lanthanide and transition metal atoms, and they can potentially be used as magnetic materials[1−4] and high temperature superconductors.[10] Studies aimed at understanding the coupling mechanism in paramagnetic rare earth metal complexes with other spin carriers are mainly restricted to gadolinium(III) (S = 7/2) derivatives and S = 1/2 species such as copper(II)[5,6,11−24] or vanadyl(II)[25] metal centers. Consistently, in the great majority of Cu−Gd, VO−Gd, or radical−Gd species studied so far, the intramolecular interaction between the gadolinium ion and the 1/2 spin has been found to be ferromagnetic, but a few examples of complexes showing antiferromagnetic behavior do exist.[6,24−27] The most frequently used ligands are polydentate Schiff bases involving saturated diamino chains. In order to extend the number of known examples, we have considered simple Cu−Ln heterodinuclear complexes involving Schiff-base ligands with *S*-methylisothiosemicarbazide as the diamino chain. Indeed, the use of an unsaturated diamino chain introduces planarity into the five-membered metallacycle that can induce geometric modifications in the Cu−Ln bridge and, consequently, change the magnitude and/or the nature of the magnetic interaction. Keeping this in mind, we have also synthesized a macrocyclic Cu−Gd complex which should be more constrained. It should be stressed that these examples are the first structurally characterized Cu−Ln entities involving *S*-methylisothiosemicarbazide as the diamino bridge.

[a] Laboratoire de chimie de coordination du CNRS,
205 route de Narbonne, 31077 Toulouse Cedex, France
E-mail: costes@lcc-toulouse.fr
[b] Department of Chemistry Moldova State University,
A. Mateevici str. 60, 2009 Chisinau, Moldova
[c] Institut für Anorganische Chemie der Universität Wien,
Währingerstr. 42, 1090 Vienna, Austria
[d] Institute of Applied Physics, Academy of Sciences of Moldova,
Academiei str. 3, 2028 Chisinau, Moldova
[e] Institute of Physical Chemistry, Polish Academy of Sciences
Kasprzaka 44/52, 01 224 Warszawa, Poland

2. Results and Discussion

2.1 Synthesis of the Complexes

The reaction of 3-methoxysalicylaldehyde or 3-ethoxysalicylaldehyde with *S*-methylisothiosemicarbazide hydroiodide in a 2:1 molar ratio in methanol, followed by treatment with $AgNO_3$, removal of AgI and addition of $CuOAc_2·H_2O$ afforded red crystals of the **$CuL_A·(H_2O)$** and **$CuL_B·(H_2O)$** complexes, respectively (Scheme 1). The corresponding **H_2L_A** and **H_2L_B** ligands are represented in Scheme 2. **$CuL_C·2H_2O$** was obtained from $L_CCuBa(CF_3SO_3)_2$ by reaction with guanidinium sulfate in $CHCl_3/H_2O$ (1:1).[28]

 © 2004 Wiley-VCH Verlag GmbH & Co. KGaA, Weinheim **DOI: 10.1002/ejic.200300486**

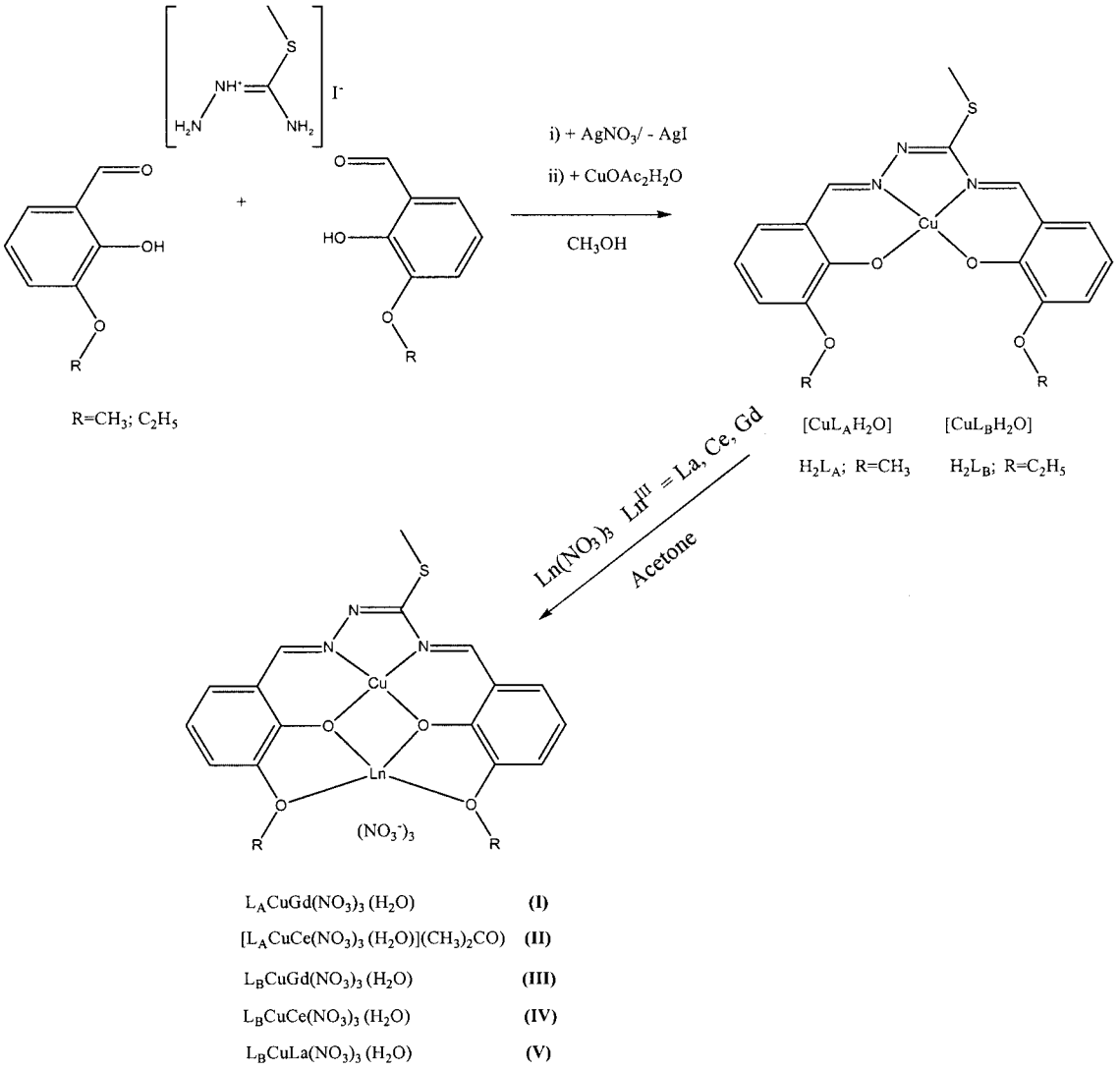

$L_ACuGd(NO_3)_3(H_2O)$ **(I)**

$[L_ACuCe(NO_3)_3(H_2O)](CH_3)_2CO$ **(II)**

$L_BCuGd(NO_3)_3(H_2O)$ **(III)**

$L_BCuCe(NO_3)_3(H_2O)$ **(IV)**

$L_BCuLa(NO_3)_3(H_2O)$ **(V)**

Scheme 1

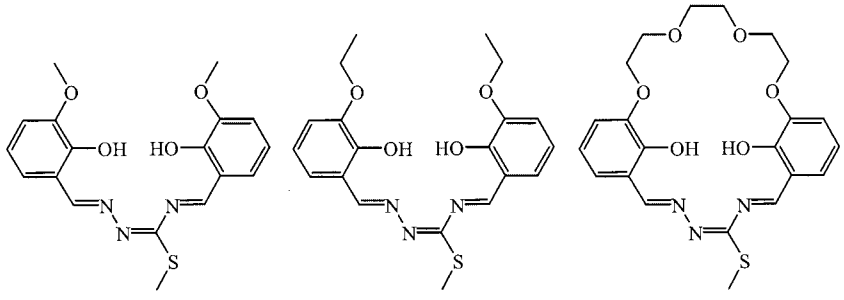

Scheme 2

The heterometallic complexes **I**−**V** were synthesized by reaction of the related copper complexes with $La(NO_3)_3{\cdot}6H_2O$, $Ce(NO_3)_3{\cdot}6H_2O$, or $Gd(NO_3)_3{\cdot}6H_2O$ in acetone, while **VI** was obtained by utilizing the same reaction in a mixture of dichloromethane and methanol.

2.2 Structures of the Complexes

2.2.1 $[L_ACuCe(NO_3)_3(H_2O)](CH_3)_2CO$ (II)

An X-ray crystallographic study of **II** shows that the unit cell contains two neutral dinuclear $[L_ACuCe(NO_3)_3(H_2O)]$

 © 2004 Wiley-VCH Verlag GmbH & Co. KGaA, Weinheim

species and two acetone molecules which are not coordinated to the copper or cerium ions but involved in hydrogen bonding with the cerium-coordinated water molecule. A perspective drawing of the asymmetric unit appears in Figure 1. The molecular structure of **II** is very similar to those of analogous 3d−4f Schiff-base complexes studied earlier.[12−14] The Ce^{III} and Cu^{II} ions are connected by two bridging phenoxo oxygen atoms, with a Cu···Ce distance of 3.457(1) Å. The Ce^{III} ion is eleven-coordinate, bound to oxygen atoms from the two bridging phenoxo groups, two methoxy groups, three nitrate anions acting as η^2 chelating ligands and one aqua ligand. The Ce−O bond lengths range from 2.503(4) to 2.900(4) Å. As usual, the shortest bonds involve the bridging O(1) and O(2) oxygen atoms, the longest ones corresponding to the methoxy groups, are 2.900(4) and 2.787(4) Å. This can be easily explained because the cerium ion is displaced from the mean O_4 ligand coordination plane by 0.962(5) Å. The Ce−O nitrato bond lengths are within 2.540(4)−2.604(4) Å, except for Ce−O(9) which is longer [2.756(4) Å]. The short intramolecular O(9)···Cu(1) contact [2.706(4) Å] is probably responsible for this lengthening. The Cu^{II} ion is located in the inner N_2O_2 cavity of the Schiff-base ligand and has a square-pyramidal (4+1) geometry, with the nitrogen and oxygen atoms of the ligand in the basal plane and the nitrato oxygen atom in the apical position. The *S*-methylisothiosemicarbazide fragment was found to be disordered over two positions with occupancy factors of 0.57 and 0.43 for the S(1) and S(1*) atoms respectively (Figure 1). This feature is characteristic of the *S*-methylisothiosemicarbazone moiety and has already been observed in a large number of complexes.[29,30] The five-membered ring formed by the *S*-methylisothiosemicarbazone moiety coordinated to the copper ion is perfectly planar and induces planarity in the whole ligand, which implies a better electronic delocalization. As a consequence, the Cu−N and Cu−O bond lengths are practically equal [1.890(3)−1.909(4) Å range] and slightly shorter than in the previous structurally characterized Cu−Ce complex.[31]

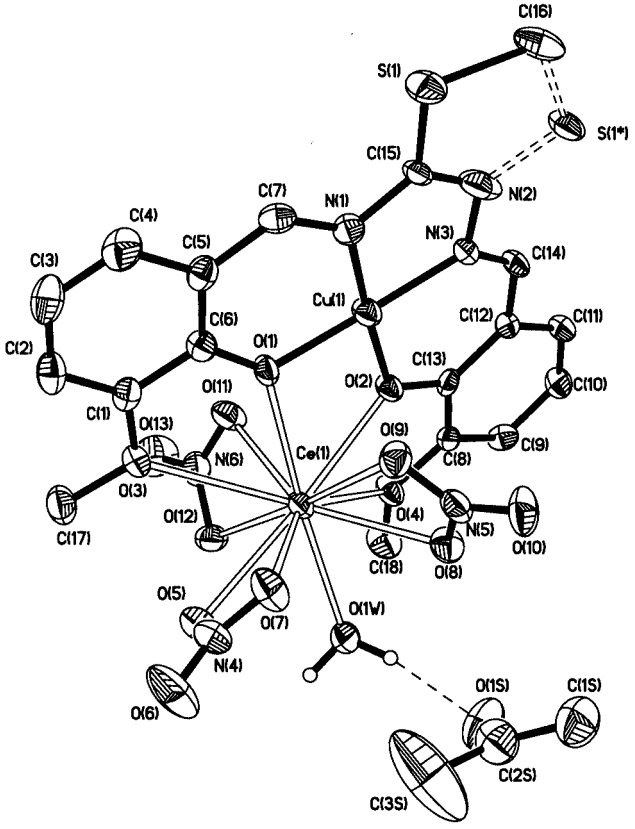

Figure 1. View of $[L_ACuCe(NO_3)_3(H_2O)](CH_3)_2CO$ (**II**); the thermal ellipsoids are drawn at the 50% probability level

A significant intermolecular interaction O(1*w*)−H···O(12)^i (*i*: 1 − *x*, −*y*, −*z*) between the coordinated water molecule O(1*w*) and the nitrato oxygen O(12) of the neighboring molecule with O(1*w*)−H: 0.86(1) Å, O(1*w*)−H···O(12): 1.99(2) Å, O(1*w*)···O(12)′: 2.831(6) Å and ∠O(1*w*)−H···O(12)′: 167(8)° should be mentioned. Two of the above mentioned H-bonds join together a pair

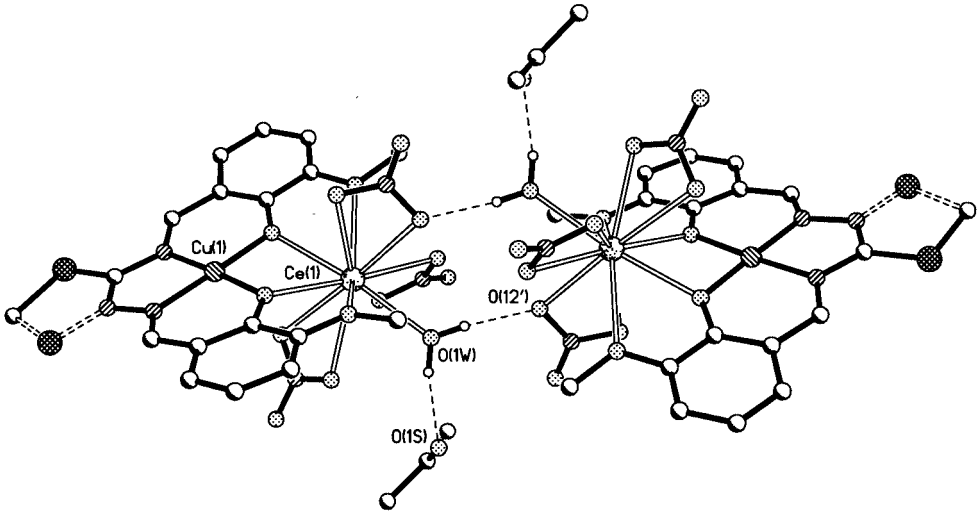

Figure 2. Structure of the tetranuclear entity $\{[L_ACuCe(NO_3)_3(H_2O)](CH_3)_2CO\}_2$

 © 2004 Wiley-VCH Verlag GmbH & Co. KGaA, Weinheim

of binuclear complexes **II** to give tetranuclear Cu−Ce···Ce−Cu units. The coordinated water molecules are also hydrogen-bonded to the oxygen atom of an acetone molecule [O(1*w*)−H: 0.87(1) Å, O(1*w*)−H···O(1S): 1.90(1) Å, O(1*w*)···O(1S): 2.757(6) Å and ∠O(1*w*)−H···O(1S): 173(6)°]. The resultant tetranuclear entity, formulated as $\{[L_ACuCe(NO_3)_3(H_2O)](CH_3)_2CO\}_2$, is depicted in Figure 2. Furthermore, the centrosymmetrically related tetranuclear $\{[L_ACuCe(NO_3)_3(H_2O)](CH_3)_2CO\}_2$ species are linked through π−π interactions, giving two-dimensional layers oriented parallel to the *ac* plane of the crystal. The distances between the mean planes of neighboring overlapping aromatic rings vary from 3.45 to 3.52 Å.

2.2.2 $L_CCuGd(NO_3)_3$ (VI)

The asymmetric unit of the macrocyclic complex **VI** is shown in Figure 3. In contrast to **II**, the copper ion in **VI** has a square-planar geometry and only two nitrate ions act as η^2 chelating ligands, the third one being mono-coordinated to the gadolinium ion. The bridging network Cu(O,O)Ln is not planar. The dihedral angle between the planes O(1)−Cu−O(2) and O(1)−Ln−O(2) is larger in **II** [24.3(2)°] than in **VI** [18.9(1)°].

Interestingly, the gadolinium ion is eleven-coordinate, bound to five oxygen atoms from nitrate ions and six oxygen atoms from the macrocyclic ligand. As in **II**, the distances of the gadolinium ion to the oxygen atoms of the alkoxy groups are the longest. The shortest Gd−O bond [2.330(4) Å] involves the mono-coordinated nitrate ion. The bonds involving the bridging phenoxo oxygen atoms [2.465(3) and 2.477(3) Å] are larger than in other Cu−Gd complexes.[5,6,13,14] The *S*-methylisothiosemicarbazide fragment was again found to be disordered over two positions.

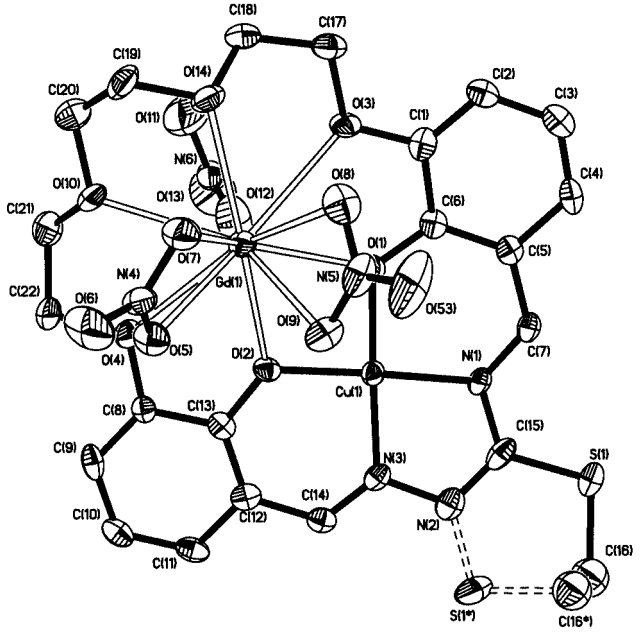

Figure 3. Molecular structure of $L_CCuGd(NO_3)_3$ (**VI**)

2.3. Magnetic Properties

Almost identical magnetic behavior is observed for compounds **I**, **III**, and **VI**. As an example, the data for **I** are quoted in Figure 4 in the form of the thermal variation of the $\chi_M T$ product, χ_M being the molar susceptibility corrected for diamagnetism. At 300 K, $\chi_M T$ for **I** is equal to 8.20 $cm^3mol^{-1}K$, which corresponds to the value expected for two uncoupled metal ions. Lowering the temperature causes $\chi_M T$ to increase to 9.89 $cm^3mol^{-1}K$ at 7 K. This value compares well with that (10.0 $cm^3mol^{-1}K$) expected for an $S = 4$ spin state resulting from ferromagnetic coupling between Cu^{II} ($S = 1/2$) and Gd^{III} ($S = 7/2$) and assuming $g_{Cu} = g_{Gd} = 2$. A quantitative analysis has been performed on the basis of an expression derived from the spin-only Hamiltonian $H = -J_{Cu\text{-}Gd}S_{Cu}S_{Gd}$. Taking into consideration the g values associated with the low lying levels $E(4) = 0$ [$g_4 = (7g_{Gd} + g_{Cu})/8$] and $E(3) = 4J$ [$g_3 = (9g_{Gd} - g_{Cu})/8$],[32] the following expression can be obtained [Equation (1)].

$$\chi T = N\alpha + \frac{4N\beta^2 T}{\kappa(T-\theta)} \cdot \frac{15g_4^2 + 7g_3^2 \cdot \exp(-\frac{4J}{kT})}{9 + 7 \cdot \exp(-\frac{4J}{kT})} \quad (1)$$

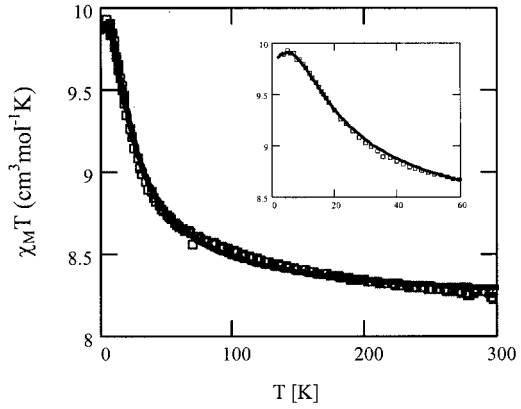

Figure 4. Thermal dependence of $\chi_M T$ for **I** at 0.1 T; the full line corresponds to the best data fit

Least-squares fitting of the experimental data led to the following set of parameters: $g_{Gd} = 1.99$, $g_{Cu} = 2.02$, $\theta = -0.02$ K, $J = 5.2$ cm^{-1} for **I**. The other two complexes give the following values: $g_{Gd} = 1.99$, $g_{Cu} = 2.01$, $\theta = -0.09$ K, $J = 5.5$ cm^{-1} for **III** and $g_{Gd} = 1.98$, $g_{Cu} = 2.02$, $\theta = -0.06$ K, $J = 4.98$ cm^{-1} for **VI**. The agreement factors $\Sigma(\chi T_{calc} - \chi T_{obs})^2/\Sigma(\chi T_{obs})^2$ are then respectively equal to $1\cdot10^{-5}$, $4\cdot10^{-5}$, and $2\cdot10^{-5}$. The small θ values suggest that second-order effects, such as intermolecular interactions or partial saturation at low temperature are, at best, very weak. The positive J value indicates a ferromagnetic coupling between Cu^{II} and Gd^{III}. This is further supported by the experimental values of the magnetization for **I** measured at 2.0 K which are correctly fitted by the Brillouin function

 © 2004 Wiley-VCH Verlag GmbH & Co. KGaA, Weinheim

for an $S = 4$ spin state, which confirms the ferromagnetic nature of the Cu−Gd interaction. The magnitude of the Cu−Gd interaction does not differ widely from one compound to the others.

It has been reported that the J_{CuGd} values and Cu···Gd distances could be correlated using an exponential function.[33] More recently, from the magnetic properties of several Cu−Gd complexes, we have found a satisfying correlation between the absolute value of the ferromagnetic coupling constant J_{CuGd} and the dihedral angle α defined by the two OCuO and OGdO planes of the bridging network.[5] The value obtained for **VI** is in good agreement with our previously published values. This relation implies that the dihedral angle must be lower than 18.9(1)° in **I** and **III** for the J values associated with them are larger. Unfortunately, the structural parameters for these complexes are not available. However we know the dihedral angle [24.2(2)°] for the Cu−Ce complex **II**. Since there is a decrease in the ionic radius on going from Ce^{III} to Gd^{III}, a decrease of α from 24.2(2)° to a value slightly lower than 18.9(1)° may be reasonably expected.

The magnetic behavior of the Cu−Ce compound **II** is more complex since the cerium ion does possess an orbital contribution, so that the observed $\chi_M T$ decrease in Figure 5 may be due to two concomitant factors namely depopulation of the Stark levels as T decreases and a possible Cu−Ce antiferromagnetic interaction.[18,33,34] A semi-qualitative analysis would necessitate the synthesis of the equivalent Ni−Ce complex with the nickel ion in a low spin state in order to evaluate the contribution of the Stark effect.[33] Unfortunately we did not succeed in preparing this complex. To complete our study we have considered the EPR spectra of complexes **IV** and **V**. For **IV** we observed a strong feature at $g = 2.04$ and a four component hyperfine structure centered at $g = 2.19$, these features being attributable to isolated copper ions (Figure 6, a). The spectrum of **V** consists of a single signal at $g = 2.07$ (Figure 6, b). It is tempting to attribute the difference to the presence of a (Cu−Ce) exchange interaction in **IV** which has no counterpart in **V** due to the diamagnetism of the lanthanum ions. To support this hypothesis we refer to the early work of Bleaney[35] devoted to the systems made up from two ions with very different relaxation rates. A recent review focuses on this question and gives the relaxation times for monomeric systems involving copper (10^{-8}, 10^{-9} s) and cerium

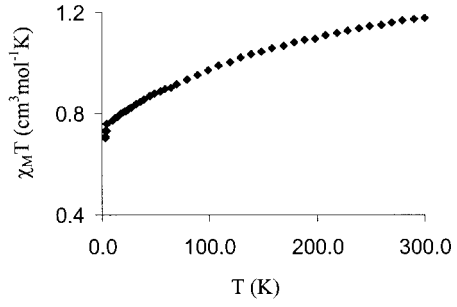

Figure 5. Thermal dependence of $\chi_M T$ for **$[L_A CuCe(NO_3)_3(H_2O)](CH_3)_2CO$ (II)**

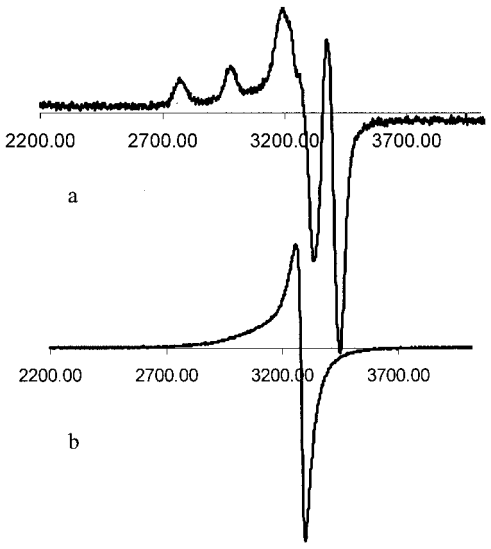

Figure 6. The solid state EPR spectra of (a) **$L_B CuCe(NO_3)_3(H_2O)$ (IV)** and (b) **$L_B CuLa(NO_3)_3(H_2O)$ (V)** at 90 K

ions (10^{-13} s).[36] In the case of complex **IV** the cerium resonance was not observed because the signals are strongly enlarged due to an abnormally low value of the spin lattice relaxation time. Contrary to the cerium ions, the copper ions have normal relaxation times that lead to an observable and even well-resolved spectrum. The absence or at least the lowering of the signal broadening would be due to a supplementary relaxation mechanism of the copper ions through the (Cu−Ce) exchange interaction. Due to the complexity of the relaxation mechanisms,[36] a more complete description of that behavior would necessitate further experimental data. Eventually this experimental evidence for a (Cu−Ce) exchange interaction gave no information concerning the sign of the interaction and we have to keep in mind that these interactions are very weak. Nevertheless, from the variation of the χT product at very low temperature for **II** (Figure 5) and from previous examples in literature,[31,34] it seems more likely that the Cu−Ce interaction is antiferromagnetic. Such an interaction is also present in **II**, but the π−π stacking present in this complex is responsible for the lower intensity of the parallel part of the spectrum.

3. Conclusion

The complexes considered in this work exhibit ferromagnetic $J_{Cu\text{-}Gd}$ interactions, as in the majority of previously published Cu−Gd complexes. Although the variation of the $J_{Cu\text{-}Gd}$ interactions is relatively limited, from 1.0 to 10.1 cm^{-1}, it appears that the decrease of the interaction parameter J can be related to an increase in the dihedral angle α defined by the two OCuO and OGdO planes of the bridging network.[5] The compounds described in this work fit in with the previous results. The best J values have been obtained with the most planar Cu−$(O)_2$−Gd cores corresponding to α angles near 0°. From a synthetic point of view, these complexes with *S*-methylisothiosemicarbazide as

 © 2004 Wiley-VCH Verlag GmbH & Co. KGaA, Weinheim

diamino chains are the first examples of structurally characterized Cu−Ln heterodinuclear complexes with planar and unsaturated diamino chains. Thus, it was tempting to investigate if the use of more planar ligands could increase this *J* value. Unfortunately, other constraints coming from the macrocyclic structure or a greater rigidity of the ligand did not allow us to obtain higher *J* values. Furthermore, the EPR spectra of the Cu−Ce complexes have given a satisfying confirmation for the existence of magnetic interactions in these complexes that do not follow the Curie law due to the presence of orbital degeneracy.

4. Experimental Section

All starting materials and solvents were purchased from Aldrich and were used without further purification. *S*-methylisothiosemicarbazide hydroiodide was obtained by the reaction of thiosemicarbazide with methyl iodide in dry ethanol.[37] Elemental analyses (C, H, N) were carried out by the Service de Microanalyse du Laboratoire de Chimie de Coordination, Toulouse. Magnetic susceptibility data were collected on powdered samples of a SQUID-based sample magnetometer on Quantum Design model MPMS instrument. All data were corrected for the diamagnetism of the ligands estimated from Pascal's constants.[38] The Nα parameter, which is very weak, was omitted in our calculations.

$CuL_A \cdot H_2O$: To a methanolic solution (50 mL) of 3-methoxysalicylaldehyde (0.3 g 2.0 mmol) was added dropwise a solution of *S*-methylisothiosemicarbazide hydroiodide (0.23 g, 1.0 mmol) in CH_3OH (15 mL). The obtained mixture was carefully stirred at 50 °C for 2 h. The resultant pale-yellow solution was heated to reflux for a further 20 min. After cooling to room temperature, a solution of $AgNO_3$ (0.26 g, 1.0 mmol) in CH_3OH/H_2O (1:2, 15 mL) was added. The AgI was removed by filtration and a solution of $Cu(CH_3COO)_2 \cdot H_2O$ (0.2 g, 1.0 mmol) in CH_3OH (15 mL) was added in one portion to the filtrate. The red product which crystallized overnight was filtered and washed with a small amount of cold methanol. Yield 0.32 g (70%). $C_{18}H_{19}CuN_3O_5S$: calcd. C 47.73, H 4.23, N 9.28; found C 48.65, H 4.53, N, 9.32%.

The complex **$CuL_B \cdot H_2O$** was prepared using an analogous experimental procedure. Yield 0.25 g (55%). $C_{20}H_{23}CuN_3O_5S$: calcd. C 49.94, H 4.82, N 8.74; found C 50.03, H 4.83, N 8.90%.

$CuL_C \cdot 2H_2O$ was prepared as described elsewhere.[30]

$L_ACuGd(NO_3)_3 \cdot H_2O$ (I): $CuL_A \cdot H_2O$ (0.22 g 0.5 mmol) dissolved in acetone (50 mL) was slowly added to an acetone solution (20 mL) of $Gd(NO_3)_3 \cdot 5H_2O$ (0.23 g 0.5 mmol) with vigorous stirring. After partial evaporation of the solvent bright brown crystals were formed, separated by filtration, washed with cold acetone and air dried. Yield 0.28 g (70%). $C_{18}H_{19}CuGdN_6O_{14}S$: calcd. C 27.15, H 2.41, N 10.55; found C 27.44, H 2.46, N 2.52%.

$[L_ACuCe(NO_3)_3(H_2O)](CH_3)_2CO$ (II), **$L_BCuGd(NO_3)_3(H_2O)$ (III)**, and **$L_BCuCe(NO_3)_3(H_2O)$ (IV)** were prepared similarly. Single crystals of **II** suitable for X-ray diffraction study were obtained by slow evaporation of an acetone solution of **$CuL_A \cdot H_2O$** and $Ce(NO_3)_3 \cdot 6H_2O$.

$[L_ACuCe(NO_3)_3(H_2O)](CH_3)_2CO$ (II): Yield 0.20 g (50%). $C_{21}H_{25}CeCuN_6O_{15}S$: calcd. C 30.13, H 3.01, N 10.04; found C 30.70, H 3.25, N 9.98%.

$L_BCuGd(NO_3)_3(H_2O)$ (III): Yield 0.25 g (45%). $C_{20}H_{23}CuGdN_6O_{14}S$: calcd. C 29.14, H 2.81, N 10.20; found C 28.92, H 2.83, N 9.94%.

$L_BCuCe(NO_3)_3(H_2O)$ (IV): 0.32 g (75%). $C_{20}H_{23}CeCuN_6O_{14}S$: calcd. C 29.76, H 2.87, N 10.41; found C 30.42, H 2.93, N 10.35%.

$L_BCuLa(NO_3)_3(H_2O)$ (V): 0.35 g (80%). $C_{20}H_{23}CuLaN_6O_{14}S$: calcd. C 29.80, H 2.88, N 10.43; found C 29.42, H 2.81, N 10.25%.

$L_CCuGd(NO_3)_3$ (VI): To **$CuL_C \cdot 2H_2O$** (0.27 g, 0.5 mmol) in a dichloromethane/methanol mixture (3:2 ratio) (50 mL) was added $Gd(NO_3)_3 \cdot 6H_2O$ (0.29 g, 0.6 mmol) in methanol (20 mL). The solution was heated to reflux for 15 min until the crystallization of the product had begun. The solvent was evaporated to 15 mL and methanol (20 mL) was added. The dark-red product was filtered, washed with methanol and dichloromethane and dried in vacuo. Yield 0.34 g (40%). $C_{22}H_{23}CuGdN_6O_{15}S$: calcd. C 30.57, H 2.68, N 9.72; found C 30.46, H 2.85, N 9.57%.

X-ray Crystallographic Studies of $[L_ACuCe(NO_3)_3(H_2O)](CH_3)_2CO$ (II): Crystallographic measurements for **II** were carried out on a Nonius Kappa CCD diffractometer equipped with a graphite-monochromated Mo-K_α radiation source. Intensity data were collected at 150 K using θ rotations with 2degree scan and a detector-to-crystal distance of 35 mm. The unit cell determination and data integration were carried out using the program DENZO-SMN.[39] Data sets were corrected for Lorentz and polarization effects. The absorption correction was introduced by a semi-empirical method from symmetry equivalent reflections.[40] The structure was solved by direct methods with the program SHELXS-97.[41] Refinement was performed using full-matrix least-squares on F^2, with anisotropic displacement parameters for the non-hydrogen atoms using the program SHELXL-97.[42] The hydrogen atoms of the polydentate ligand and solvent molecule (acetone) were placed in calculated positions and given isotropic displacement parameters equal to $1.2 \times U_{eq}$ of the relevant carbon atom. Positional parameters of the H atoms of water molecules were obtained from difference Fourier syntheses and were verified by the geometric parameters of corresponding hydrogen bonds.

X-ray Crystallographic Studies of $L_cCuGd(NO_3)_3$ (VI): The selected crystal of **VI** (orange-red plate) was mounted on a Stoe Imaging Plate Diffractometer System (IPDS) equipped with an Oxford Cryosystems cooler device at 160 K using a graphite monochromator (λ = 0.71073 Å). The crystal-to-detector distance was 80 mm. Data were collected[43] with a φ rotation movement (φ = 0.0−249.6°, Δφ = 1.3°). Numerical absorption[44] corrections were applied. Maximum and minimum transmission factors were respectively 0.7576 and 0.3294. The structure was solved by direct methods using SHELXS-97[41] and refined by full-matrix least-squares on F_o^2 with SHELXL-97[42] with anisotropic displacement parameters for all non-hydrogen atoms. H atoms were introduced by calculations using the riding model with isotropic thermal parameters 1.1 times higher than those of the riding atom. Scattering factors were taken from ref.[45] The molecular plot was obtained using the ZORTEP program.[46]

Crystallographic data (excluding structure factors) for the structures reported in this paper have been deposited with the Cambridge Crystallographic Data Center. Copies of the data (CCDC-215450 for **II** and CCDC-215647 for **VI**) can be obtained free of charge on application to CCDC, 12 Union Road, Cambridge CB2 1EZ, UK [Fax: (internat.) +44-1223/336-033, E-mail: deposit@ccdc.cam.ac.uk].

 © 2004 Wiley-VCH Verlag GmbH & Co. KGaA, Weinheim

Table 1. Summary of crystal data for **II** and **VI**

Compound	**II**	**VI**
Empirical formula	$C_{21}H_{25}CeCuN_6O_{15}S$	$C_{22}H_{23}CuGdN_6O_{15}S$
M	837.19	846.31
Temperature [K]	150	160
Wavelength [Å]	0.71073	0.71073
Space group	$P\bar{1}$	$P2_1/n$
a [Å]	9.8460(4)	9.103(1)
b [Å]	12.4470(5)	11.395(1)
c [Å]	13.8610(6)	26.997(3)
α [deg]	84.937(2)	90
β [deg]	71.745(2)	99.32(1)
γ [deg]	67.371(1)	90
V [Å^3]	1488.0(1)	2763.5(5)
Z	2	4
$\rho_{(calcd.)}$ [Mg·m^{-3}]	1.869	2.077
μ_{Mo} [mm^{-1}]	2.376	3.312
F(000)	832	1704
Crystal size [mm]	0.2 × 0.1 × 0.1	0.3 × 0.1 × 0.03
θ range [deg]	2.35 to 26.00	1.94 to 24.10
Index ranges	$-12 \le h \le 12$, $-15 \le k \le 15$, $-17 \le l \le 17$	$-10 \le h \le 10$, $-13 \le k \le 13$, $-30 \le l \le 30$
Number of reflections:		
Measured	10884	20916
Unique	5821 [$R_{(int)}$ = 0.0831]	4235 [$R_{(int)}$ = 0.0692]
Number of refined parameters	418	424
Max. and min. transmission	0.7971 and 0.6480	0.7576 and 0.3294
GOOF for F^2	1.107	0.903
[a]R [$I > 2\sigma(I)$]	0.0693	0.0284
[b]wR	0.0842	0.0499
$\Delta\rho_{max}$ and $\Delta\rho_{min}$ [e·Å^3]	1.605 and −0.921	1.164 and −0.706

[a] $R = \|\|F_o\| - |F_c\|\|/|F_o|$. [b] $wR = [w(|F_o^2| - |F_c^2|)^2 / w|F_o^2|^2]^{1/2}$.

Table 2. Selected bond lengths [Å] and angles [deg.] for **II** and **VI**

Bond	Compound		Bond	Compound	
	II[a]	**VI**[b]		**II**[a]	**VI**[b]
Ln(1)−O(2)	2.503(4)	2.465(3)	Ln(1)−O(1*w*)	2.512(3)	−
Ln(1)−O(3)	2.900(4)	2.774(3)	Ln(1)−O(7)	2.540(4)	2.590(3)
Ln(1)−O(1)	2.525(3)	2.477(3)	Ln(1)−O(5)	2.591(4)	2.481(3)
Ln(1)−O(12)	2.565(4)	2.330(4)	Ln(1)−O(11)	2.604(4)	−
Ln(1)−O(8)	2.592(4)	2.564(3)	Ln(1)−O(4)	2.787(4)	2.893(3)
Ln(1)−O(9)	2.756(4)	2.475(3)	Ln(1)−O(14)	−	2.594(3)
Ln(1)−O(15)	−	2.677(3)	Cu(1)−O(2)	1.890(3)	1.890(3)
Cu(1)−O(1)	1.891(4)	1.885(3)	Cu(1)−N(3)	1.909(4)	1.900(4)
Cu(1)−N(1)	1.900(4)	1.913(4)			
O(1)−Cu(1)−O(2)	86.7(2)	86.1(1)	O(1)−Cu(1)−N(1)	96.0(2)	95.5(2)
O(2)−Cu(1)−N(1)	177.0(2)	176.4(1)	O(1)−Cu(1)−N(3)	178.5(2)	178.2(2)
O(2)−Cu(1)−N(3)	94.7(2)	95.7(2)	N(1)−Cu(1)−N(3)	82.6(2)	82.7(2)
Cu(1)−O(2)−Ln(1)	102.7(2)	103.7(1)	Cu(1)−O(1)−Ln(1)	101.9(1)	103.4(1)

[a] Ln = Ce. [b] Ln = Gd.

The crystallographic data together with the refinement details for **II** and **VI** are summarized in Table 1, selected bonds lengths and angles are listed in Table 2.

Acknowledgments

Gh. Novitchi is grateful to NATO for financial support. S. Shova acknowledges INTAS for financial support, Projects 2000−00565.

[1] C. Benelli, D. Gatteschi, *Chem. Rev.* **2002**, *102*, 2369.
[2] Rudra, C. Raghu, S. Ramasesha, *Phys. Rev. B.* **2002**, *65*, 224411.
[3] M. Sakamoto, K. Manseki, H. Okawa, *Coord. Chem. Rev.* **2001**, *219−221*, 379.
[4] C. Piguet, C. Edder, S. Rigaut, G. Bernardinelli, J.-C. G. Bunzli, G. Hopfgarther, *J. Chem. Soc., Dalton Trans.* **2000**, 3999.

 © 2004 Wiley-VCH Verlag GmbH & Co. KGaA, Weinheim

[5] J.-P. Costes, F. Dahan, A. Dupuis, *Inorg. Chem.* **2000**, *39*, 165.
[6] J.-P. Costes, F. Dahan, A. Dupuis, J.-P. Laurent, *Inorg. Chem.* **2000**, *39*, 169.
[7] C. Piguet, J.-C. G. Bunzli, *Chem. Soc. Rev.* **1999**, *28*, 347.
[8] H. Okawa, H. Furutachi, D. E. Fenton, *Coord. Chem. Rev.* **1998**, *174*, 51.
[9] R. E. P. Winpenny, *Chem. Soc. Rev.* **1998**, *27*, 447.
[10] D. L. Nelson, M. S. Willingham, T. F. George, (Eds.), *Chemistry of High-Temperature Superconductors, ACS Symposium Series*, vol. 351. American Chemical Society, Washington D. C., **1987**.
[11] T. Kido, Y. Ikuta, Y. Sunatsuki, Y. Ogawa, N. Matsumoto, *Inorg. Chem.* **2003**, *42*, 398.
[12] J.-P. Costes, F. Dahan, A. Dupuis, J.-P. Laurent, *New. J. Chem.* **1998**, 1525.
[13] J.-P. Costes, F. Dahan, A. Dupuis, J.-P. Laurent, *Inorg. Chem.* **1996**, *35*, 2400.
[14] J.-P. Costes, F. Dahan, A. Dupuis, J.-P. Laurent, *Inorg. Chem.* **1997**, *36*, 3429.
[15] Bencini, C. Benelli, A. Caneschi, A. Dei, D. Gatteschi, *Inorg. Chem.* **1986**, *25*, 272.
[16] Benelli, A. Caneschi, D. Gatteschi, O. Guillou, L. Pardi, *Inorg. Chem.* **1990**, *29*, 1750.
[17] Bencini, C. Benelli, A. Caneschi, R. L. Carlin, A. Dei, D. Gatteschi, *J. Am. Chem. Soc.* **1985**, *107*, 8128.
[18] M. L. Kahn, T. M. Rajendiran, Y. Jeannin, C. Mathoniere, O. Kahn, *C. R. Acad. Sci. Paris, Serie IIc Chimie* **2000**, *3*, 131.
[19] M. Andruh, I. Ramade, E. Codjovi, O. Guillou, O. Kahn, J. C. Trombe, *J. Am. Chem. Soc.* **1993**, *115*, 1822.
[20] M. Sasaki, K. Manseki, H. Yjriuchi, M. Kumahai, M. Sakamoto, H. Sakiyama, Y. Nishida, M. Sakai, Y. Sadaoka, M. Ohba, H. Okawa, *J. Chem. Soc., Dalton Trans.* **2000**, 259.
[21] Ramade, O. Kahn, Y. Jeannin, F. Robert, *Inorg. Chem.* **1997**, *36*, 930.
[22] S. Mohanta, H.-H. Lin, C.-J. Lee, H.-H. Wei, *Inorg. Chem. Commun.* **2002**, *5*, 585.
[23] F. Avecilla, C. Platas-Iglesias, R. Rodriguez-Cortinas, G. Guillemot, J.-C. G. Bunzli, C. D. Brondino, C. F. G. C. Geraldes, A. de Blas, T. Rodriguez-Blas, *J. Chem. Soc., Dalton Trans.* **2002**, 4658.
[24] J. P. Costes, F. Dahan, A. Dupuis, J. P. Laurent, *Inorg. Chem.* **2000**, *39*, 5994.
[25] J. P. Costes, F. Dahan, B. Donnadieu, J. Garcia-Tojal, J. P. Laurent, *Eur. J. Inorg. Chem.* **2001**, 363.
[26] Lescop, D. Luneau, E. Belorisky, P. Fries, M. Guillot, P. Rey, *Inorg. Chem.* **1999**, *38*, 5472.
[27] Caneschi, A. Dei, D. Gatteschi, L. Sorace, K. Vostrikova, *Angew. Chem. Int. Ed.* **2000**, *39*, 246.
[28] V. B. Arion, E. Bill, M. Reetz, R. Goddard, D. Stöckigt, M. Maßau, V. Levitsky, *Inorg. Chim. Acta* **1998**, *282*, 61.
[29] V. B. Arion, V. C. Kravtsov, J. I. Gradinaru, Yu. A. Simonov, N. V. Gerbeleu, J. Lipkowski, J.-P. Wignacourt, H. Vezin, O. Mentre, *Inorg. Chim. Acta* **2002**, *328*, 123.
[30] V. B. Arion, V. C. Kravtsov, R. Goddard, E. Bill, J. I. Gradinaru, N. V. Gerbeleu, V. Levitschi, H. Vezin, Y. A. Simonov, J. Lipkowski, V. K. Bel'skii, *Inorg. Chim. Acta* **2001**, *317*, 33.
[31] J. P. Costes, F. Dahan, A. Dupuis, J. P. Laurent, *Chem. Eur. J.* **1998**, *4*, 1616.
[32] Bencini, D. Gatteschi, *EPR of Exchange Coupled Systems*; Springer-Verlag: Berlin, **1990**.
[33] Benelli, A. J. Blake, P. E. Y. Milne, J. M. Rawson, R. E. P. Winpenny, *Chem. Eur. J.* **1995**, *1*, 614.
[34] M. L. Kahn, C. Mathoniere, O. Kahn, *Inorg. Chem.* **1999**, *38*, 3692.
[35] B. Bleaney, R. J. Elliot, H. E. D. Scovil, *Proc. Phys. Soc.* **1951**, *A64*, 933.
[36] V. Clementi, C. Luchinat, *Acc. Chem. Res.* **1998**, *31*, 351.
[37] M. Freund, T. Paradies, *Ber. Dtsch. Chem. Ges.* **1901**, *34*, 3110.
[38] P. Pascal, *Ann. Chim. Phys.* **1910**, *19*, 5.
[39] Z. Otwinowski, W. Minor, in: *Methods in Enzymology* (Eds.: C. W. Carter, R. M. Sweet), Academic Press, London, **1996**, *vol. 276*, p. 307.
[40] XEMP ver. 4.2. Siemens Analytical X-ray Inst. Inc. **1990**.
[41] G. M. Sheldrick, *SHELXS-97. Program for Crystal Structure Solution*; University of Göttingen: Göttingen, Germany, **1990**.
[42] G. M. Sheldrick, *SHELXL-97. Program for the Refinement of Crystal Structures from Diffraction Data*; University of Göttingen: Göttingen, Germany, **1997**.
[43] *STOE*, IPDS Manual. Version 2.93. Stoe & Cie, Darmstadt, Germany, **1997**.
[44] Stoe, *X-SHAPE.* Crystal Optimization for Numerical Absorption Corrections, Revision 1.01. Stoe & Cie, Darmstadt, Germany, **1996**.
[45] *International Tables for Crystallography*; Kluwer Academic Publishers, Dordrecht, The Netherlands, **1992**; Vol. C.
[46] L. Zsolnai, H. Pritzkow, G. Huttner, *ZORTEP.* Ortep for PC, Program for Molecular Graphics, University of Heidelberg, Heidelberg, Germany, **1996**.

Received July 21, 2003
Early View Article
Published Online March 5, 2004

 © 2004 Wiley-VCH Verlag GmbH & Co. KGaA, Weinheim

The Synthesis of Stable Intramolecularly Dialkylamino-Coordinated Silenes and Their Methyl Iodide Induced Isomerization into Cyclic Aminosilanes[‡]

Martin Mickoleit,[a] Kathleen Schmohl,[a] Manfred Michalik,[b] and Hartmut Oehme*[a]

Keywords: Rearrangement / Silaethenes / Silanes / Silenes / Silicon

The reaction of the (dichloromethyl)oligosilanes $R(Me_3Si)_2SiCHCl_2$ **4a–d** (**4a**: R = Me; **4b**: R = *t*Bu; **4c**: R = Ph; **4d**: R = $SiMe_3$) with 8-(dimethylamino)-1-naphthyllithium leads to the intramolecularly donor-stabilized silenes **1a–d**. Whereas **1a**,**b**, and **d** were isolated as thermally stable yellow crystalline compounds, **1c** could not be separated in a pure form but was characterized by NMR spectroscopy and mass spectroscopy as well as by its chemical reactivity with a variety of substrates. Dynamic ^1H NMR spectroscopic studies of **1a** and **1d** revealed coalescence of the signals of the two $CSiMe_3$ groups. In agreement with theoretical calculations, this effect was interpreted as the result of internal rotations about the silene double bond. These findings and the known relatively long Si=C distances for **1d**, **2** and **3** help establish the ylide-like nature of the silenes prepared. Treatment of **1a–d** with water produced the silanols **9a–d**. Treatment of **1a**,**b**, and **d** with methyl iodide caused a rearrangement of the silenes, one methyl substituent formally migrating from the coordinated dimethylamino group to the silene carbon atom producing the respective cyclic aminosilanes **11a**,**b**, and **d**. As the outcome of the reaction of **1d** with benzaldehyde, 2,2-bis(trimethylsilyl)vinylbenzene (**14**) and a mixture of the two isomers of the cyclodisiloxane **13** were obtained.

(© Wiley-VCH Verlag GmbH & Co. KGaA, 69451 Weinheim, Germany, 2004)

Introduction

Silenes, silicon derivatives with a Si=C double bond, are known as extremely reactive compounds, which in absence of scavenger reagents rapidly undergo dimerization or polymerization. Only very few kinetically stabilized silenes have been isolated and structurally characterized.[1] Coordination of amines, THF or fluoride ions to the electrophilic silene silicon atom leads to an effective stabilization of the compounds;[2a] Wiberg et al. have succeeded in the isolation of an amine adduct of a silene, which is unstable in the absence of a donor molecule.[2b] Recently we presented the synthesis, by a new pathway, isolation and structural characterization of the first intramolecularly donor-stabilized silenes **1d**, **2**, and **3**.[3] The compounds proved to be thermally stable up to 140 °C and, compared with uncomplexed silenes, their reactivity was also dramatically reduced.

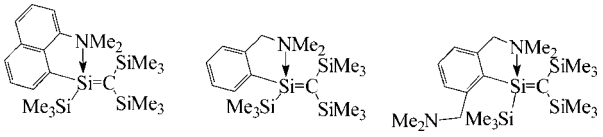

1d **2** **3**

In this paper we report on the general applicability of the newly developed synthetic route, describe some further stable silenes, and discuss the results of recent studies characterizing their chemical behavior. Dynamic NMR studies in combination with quantum mechanical calculations give an insight into rotational processes about the Si=C bonds of these compounds. Furthermore, we describe an unexpected methyl iodide induced isomerization of intramolecularly amine-coordinated silenes into cyclic aminosilanes.

Results and Discussion

Synthesis of Intramolecularly Donor-Stabilized Silenes

As described previously, the silenes **1d**, **2**, and **3** are easily accessible in a one-pot reaction by treatment of (dichloromethyl)tris(trimethylsilyl)silane (**4d**, $R^1 = SiMe_3$) with two equivalents of 8-(dimethylamino)-1-naphthyllithium, 2-(dimethylaminomethyl)phenyllithium or 2,6-bis(dimethylami-

[‡] Intramolecularly Donor-Stabilized Silenes, 4. Part 3: Ref.[3c]

[a] Fachbereich Chemie der Universität Rostock
18051 Rostock
Fax: (internat.) + 49-(0)381-4986382
E-mail: hartmut.oehme@chemie.uni-rostock.de
[b] Leibniz-Institut für Organische Katalyse
18055 Rostock

 © 2004 Wiley-VCH Verlag GmbH & Co. KGaA, Weinheim DOI: 10.1002/ejic.200300626

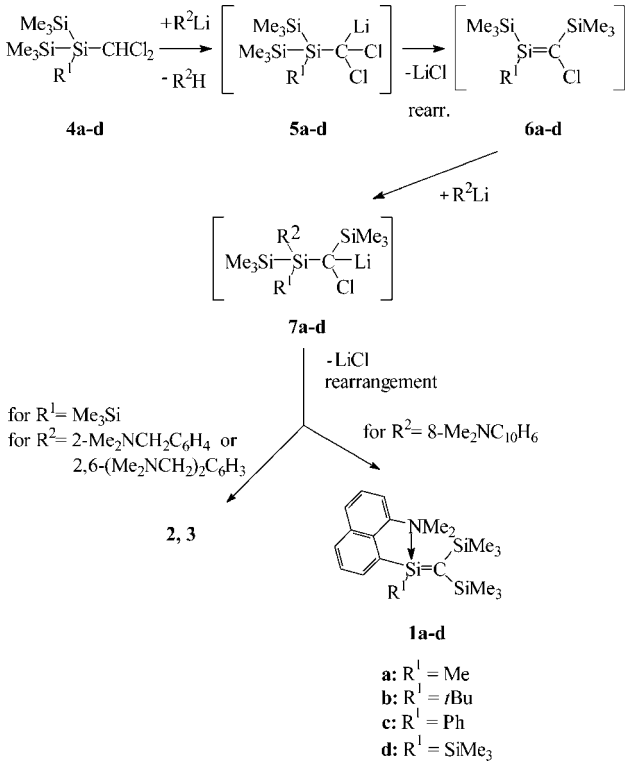

Scheme 1. The formation of the intramolecularly donor-stabilized silenes **1a**−**d**, **2**, and **3** by the reaction of the (dichloromethyl)oligosilanes **4a**−**d** with 8-(dimethylamino)-1-naphthyllithium, 2-(dimethylaminomethyl)phenyllithium and 2,6-bis(dimethylaminomethyl)phenyllithium, respectively (molar ratio 1:2)

nomethyl)phenyllithium, respectively, following the route outlined in Scheme 1.[3] The reaction path, which we have already discussed in detail,[3,4] involves the deprotonation of **4d**, lithium chloride elimination from **5d** and migration of one trimethylsilyl group from the central silicon atom to the neighboring carbon atom producing the transient silene **6d**. Subsequent addition of a second equivalent of the organolithium derivative across the Si=C double bond of **6d**, repeated elimination of LiCl, and a second trimethylsilyl migration leads to the formation of the silenes **1d**, **2**, and **3**. Whereas uncomplexed silenes, generated according to the same pattern by the reaction of **4d** with ordinary organolithium compounds (R^2Li = MeLi, PhLi, *n*BuLi, MesLi) immediately add excess R^2Li finally producing after hydrolysis the silanes $R^1R^2{}_2Si-CH(SiMe_3)_2$,[4] **1d**, **2**, and **3** proved to be stable with respect to the attack of an excess of the aryllithium compounds applied, could be isolated and structurally characterized. X-ray structural analyses were also performed. The high stability of these compounds can no doubt be attributed to the strong interaction between the amino groups and the silene silicon atoms, which dramatically reduces the electrophilic properties of the Si=C moieties of **1d**, **2**, and **3**.

The reaction path outlined involves the migration of two trimethylsilyl groups from the central silicon atom in **4d** (R^1 = $SiMe_3$) to the neighboring carbon atom replacing the two chlorine substituents and forming the $C(SiMe_3)_2$ unit in **1d**, **2**, and **3**. Consequently, one trimethylsilyl group of the original (dichloromethyl)tris(trimethylsilyl)silane (**4d**) can be replaced by any alkyl or aryl group, and treatment of these related (dichloromethyl)oligosilanes with dialkylaminoaryllithium compounds should produce stabilized silenes with a further carbon substituent at the silene silicon atom. We chose (dichloromethyl)methylbis(trimethylsilyl)silane (**4a**), *tert*-butyl(dichloromethyl)bis(trimethylsilyl)silane (**4b**), and (dichloromethyl)phenylbis(trimethylsilyl)silane (**4c**) and studied their reactions with 8-(dimethylamino)-1-naphthyllithium (molar ratio 1:2). The first experiments were unsuccessful, the main problem being the complete separation of the 1-(dimethylamino)naphthalene formed in the first step of the reaction by protonation of the aryllithium compound through the dichloromethylsilanes **4a**−**c**. As subsequently discovered, however, the high thermal stability of the products allowed the application of more aggressive purification methods. Thus, silene **1a** was generated by the reaction of **4a** with 8-(dimethylamino)-1-naphthyllithium (1:2) following the general procedure described for the synthesis of **1d**, **2**, and **3**;[3] to our surprise, this compound could be purified by distillation in vacuo (150 °C/0.0005 mbar) to give a yellow solid. Similarly, **1b** was obtained from **4b** and 8-(dimethylamino)-1-naphthyllithium (1:2). 1-(Dimethylamino)naphthaline was distilled from the product mixture (100 °C/0.01 mbar) and **1b** was obtained as an orange-yellow oil, which gradually solidified. Unfortunately, the crystal quality of **1a** was insufficient for an X-ray structural analysis, but extended NMR, IR, and MS spectroscopic studies as well as chemical reactions of **1a** and **1b** unambiguously confirmed the proposed structures. Particularly the ^{29}Si and ^{13}C chemical shifts of the silicon and carbon atoms of the Si=C groups in **1a** and **1b**, which are in good agreement with those of **1d**, **2**, and **3**,[3] characterize the compounds as intramolecularly donor-stabilized silenes (see Exp. Sect.).

Silene **1c**, the expected product of the reaction of **4c** with 8-(dimethylamino)-1-naphthyllithium (1:2) could not be obtained in a pure form. Aqueous workup of the reaction mixture, however, gave the silanol **9c** in a yield of approximately 80%. Similarly, treatment of the reaction mixture with methanol produced (8-dimethylamino-1-naphthyl)(methoxy)phenyl[bis(trimethylsilyl)methyl]silane **10** (78%). Both results indicate that silene **1c** was indeed formed and is indefinitely stable.

As expected for the magnetically non-equivalent $CSiMe_3$ groups of **1a**−**d**, two separate signals were observed in the ^1H NMR spectra at room temperature. For **1a** and **1d** dynamic ^1H NMR studies were performed, which revealed that at elevated temperatures coalescence of the signals of the two trimethylsilyl groups at the silene carbon atoms occurred. The data obtained were used for calculations of the rotational barriers about the Si=C bond in **1a** and **1d** (Table 1).

The assignment of the above-mentioned coalescence phenomena to rotation about the Si=C double bond is supported by theoretical calculations performed on **2** and a related silene bearing a methyl group at the silene Si instead of a Me_3Si group. These computations led to calculated

 © 2004 Wiley-VCH Verlag GmbH & Co. KGaA, Weinheim

Table 1. Coalescence temperatures (T_c) and signal separations ($\Delta\nu_c$) of the $CSiMe_3$ groups and rotational barriers ($\Delta G_o^{\neq}$) about the Si=C bond in **1a** and **1d**

	T_c (K)	$\Delta\nu_c$ (Hz)	$\Delta G_c^{\neq}$[a] (kJ·mol^{-1})
1a	317	95	63.3
1d	353	98	71.0

[a] The free energies of activation $\Delta G_c^{\neq}$ at the coalescence temperature were calculated from the Eyring equation.[5] The error limits were estimated to be $T_c = \pm 2$ K, $\Delta\nu_c = \pm 5\%$, and $\Delta G_c^{\neq} = \pm 1.0$ kJ·mol^{-1}.

values of the rotational barriers of the same order of magnitude as those found experimentally for **1a** and **1d**. These results will be communicated separately.[6]

The magnitude of the rotational barrier to isomer interconversion in uncomplexed silenes was found to be about 160 kJ·mol^{-1}.[1a] As expected, this figure is considerably lower than the height of the barrier to *cis*/*trans* isomerization in alkenes, which amounts to approximately 250 kJ·mol^{-1}.[7] The reported rotational barriers for the silene donor adducts THF·Me_2Si=$C(SiMe_3)SiMetBu_2$ and Me_3N·Me_2Si=$C(SiMe_3)SiMetBu_2$ of 50 kJ·mol^{-1} and 65 kJ·mol^{-1}, respectively,[8] are very close to those found for **1a** and **1d**. That means that the interaction of silenes with donor molecules leads to a weakening of the Si−C π-interaction, and **1a**−**d** as well as **2** and **3** may equally be described as ylidic compounds [Equation (1)].

The Reactions of the Silenes 1a, 1b, and 1d with Water, Methyl Iodide and Benzaldehyde

The established pyramidalization at the silene silicon atoms of **1a**, **2**, and **3** in the solid state[3] and the relatively low rotational barriers of the Si=C bonds in **1a** and **1d** point to a pronounced ylid-like character of the compounds [Equation (1)]. Consequently, compared with uncomplexed silenes, enhanced nucleophilic properties of the silene carbon atoms of the intramolecularly donor-stabilized silenes would be expected. This was confirmed by studies of the behavior of **1a**, **1b**, and **1d** towards methyl iodide. The reactions of the newly synthesized silenes with water and benzaldehyde were also investigated as a further method of characterization.

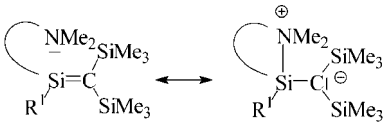

1a-d, 2, 3 (1)

The addition of water or alcohols across the Si=C double bonds with formation of silanols or alkoxysilanes, respectively, is typical of silenes and is frequently used for their chemical characterization.[1] Compounds **1a**−**c**, after treatment with water or methanol, also gave the expected products. **1a** proved to be extraordinarily moisture sensitive. Wet solvents immediately decolorize the yellow solutions of the silene to give a mixture of the two diastereomeric forms of the disiloxane **8** (Scheme 2). Compounds **1b** and **1c** are less reactive, but with excess water **1b**,**c** as well as **1a** are converted into the silanols **9b**, **9c**, and **9a**, respectively. The conversion of **1d** into the silanol **9d** has been previously described.[3b] The formation of **8** can be understood as the result of the addition of silanol **9a** to the Si=C unit of **1a**. As expected, thermolysis of **9a** (heating to 120 °C) also formed the disiloxane **8**. As mentioned above, methoxysilane **10** was prepared by addition of methanol to the impure silene for the characterization of **1c**.

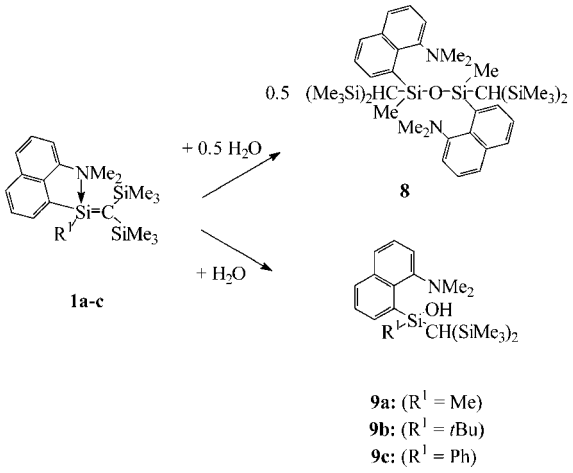

Scheme 2. The reaction of the intramolecularly donor-stabilized silenes **1a**−**c** with water.

The reaction of the stable amine-coordinated silenes with methyl iodide was expected to lead, after methylation of the nucleophilic $C(SiMe_3)_2$ group with H_3CI, to the intramolecularly donor-stabilized silylium iodides $[(Me_2NC_{10}H_6)R^1Si-CMe(SiMe_3)_2]^+ I^-$ or, alternatively, to the respective iodosilanes $(Me_2NC_{10}H_6)R^1SiI-CMe(SiMe_3)_2$. Hydrolysis of both products should then give the silanols $(Me_2NC_{10}H_6)R^1Si(OH)-CMe(SiMe_3)_2$. In fact, studies of the reaction of **1a**, **1b**, and **1d** with methyl iodide revealed an unforeseen rearrangement of the silenes finally producing the azasilaacenaphthenes **11a**, **11b**, and **11d**, respectively (Scheme 3). Formally, one methyl substituent migrates from the nitrogen atom to the silene carbon atom with simultaneous formation of a cyclic aminosilane. The rearrangement can be interpreted as an expected nucleophilic methylation of the silene carbon atoms by methyl iodide, but the resultant silylium salts are unstable, the iodide anion attacks one *N*-methyl group regenerating methyl iodide and forming an aminosilane function. The strong N→Si donor-acceptor interaction in **1a**, **1b**, and **1d** as well as in the intermediate silylium ions makes the nitrogen atom a good leaving group and the *N*-methyl substituent easily susceptible to a nucleophilic attack by the iodide anion. For

 © 2004 Wiley-VCH Verlag GmbH & Co. KGaA, Weinheim

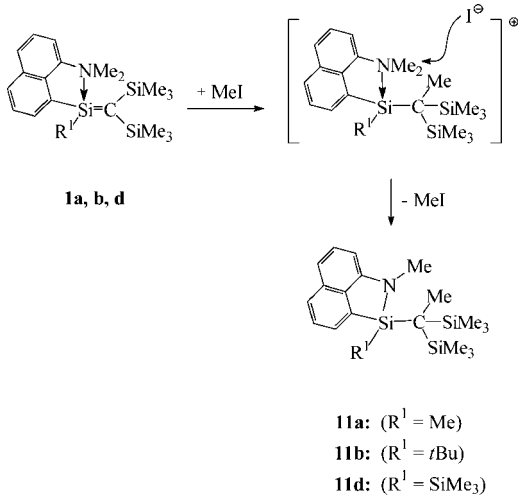

Scheme 3. The methyl iodide induced isomerization of the intramolecularly donor-stabilized silenes **1a**, **1b**, and **1d** into the cyclic aminosilanes **11a**, **11b**, and **11d**.

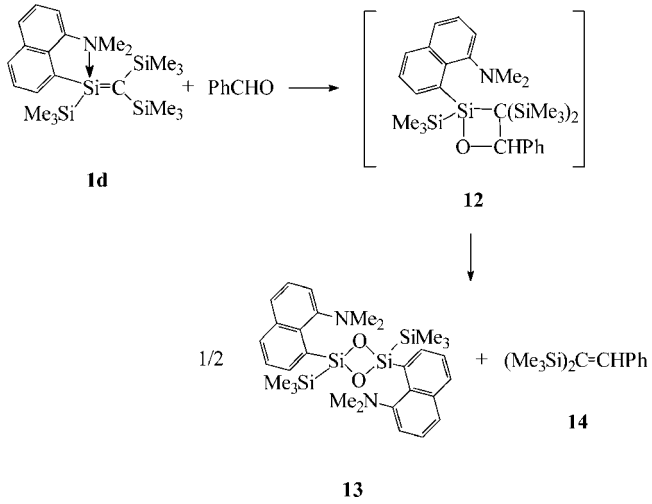

Scheme 4. The reaction of silene **1d** with benzaldehyde

a complete conversion of **1a**, **1b**, and **1d** into **11a**, **11b**, and **11d**, respectively, only catalytic quantities of methyl iodide were necessary. Indeed, the results of the experiments are independent of the molar ratio of silene to methyl iodide. In order to attempt to ethylate or allylate the silene carbon atom, **1d** was treated with ethyl iodide or allyl iodide, respectively. Surprisingly, however, even with excesses of these reagents only **11d**, the methylated derivative, could be isolated in high yield. The ethyl or allyl analogues of **11d** could not be detected. This indicates that the nucleophilic reaction of the silene with the liberated methyl iodide proceeds considerably faster than with ethyl iodide or allyl iodide.

The structures of **11a**, **11b**, and **11d** were elucidated on the basis of NMR and MS spectroscopic studies (see Exp. Sect.). The compounds proved to be stable towards water and solutions of **11a**, **11b**, and **11d** in THF/water remained unchanged.

Silenes normally react with carbonyl compounds to give an olefin and silanone oligomers.[1] In some cases 2-oxasiletanes and [2 +2] cycloadducts were isolated and, in particular, when aromatic ketones were used, [4 +2] cycloadducts and a variety of their isomerization products were also isolated.[1] Uncomplexed, kinetically stabilized 2,2-bis(trimethylsilyl)silenes, recently synthesized by the reaction of **4c** or **4d**, respectively, when treated with 2,4,6-triisopropylphenyllithium (1:2) afforded, after subsequent treatment with benzaldehyde, stable substituted 2-oxasiletanes.[4] Treatment of intramolecularly amine-coordinated silenes of the type described in this paper with carbonyl compounds are of particular interest, since this could be a promising route to intramolecularly donor-stabilized silanones.

Unfortunately, the reactivity of the intramolecularly donor-stabilized silenes towards carbonyl compounds proved to be rather low. In THF solution **1d** and **2**, which were chosen for these studies, did not react with benzaldehyde. The reaction of **1d** with benzaldehyde in heptane at room temperature required three days to proceed to completion; at 80 °C 5−6 h were needed. In both cases a colorless solid was obtained, which was identified as a mixture of the two isomeric forms of the cyclodisiloxane **13** (Scheme 4). Furthermore, 2,2-bis(trimethylsilyl)styrene (**14**) was isolated in an almost quantitative yield.

The suggested reaction path is outlined in Scheme 4 and is consistent with the standard course of the reaction of silenes with simple aromatic aldehydes.[1] The silene carbon atom attacks the carbonyl carbon atom and subsequent Si−O interaction leads to the formation of the oxasiletane **12**. The long reaction times are due to the strong nitrogen−silicon interaction in **1d** reducing the electrophilic properties of the silene silicon atom. Clearly, **12** is unstable and decomposes spontaneously producing the olefin **14** and a mixture of the two diastereomers of the cyclodisiloxane **13**, which may be considered as a dimer of an originally formed transient silanone. The two isomers of **13** could not be separated, but ^{1}H and ^{13}C NMR spectroscopic data as well as MS data of the mixture unambiguously confirmed the proposed structures. A comparable cyclodisiloxane was recently obtained by Belzner et al. as the result of an oxygen transfer from isocyanates to bis[2-(dimethylaminomethyl)-phenyl]silylene and was presumed to be the cyclodimer of an initially generated silanone.[9] The analytical data obtained for **14** proved to be identical to those reported for 2,2-bis(trimethylsilyl)styrene in the literature.[10] The reaction of **2** with benzaldehyde under comparable conditions similarly led to **14** but the respective disiloxane could not be identified.

Experimental Section

General: All reactions involving organometallic reagents were carried out under purified argon. NMR: Bruker AC 250 or Bruker ARX 300 instruments were used, temperature 30 °C, tetramethylsilane as internal standard. IR: Nicolet 205 FT-IR instrument. MS: Intectra AMD 402 spectrometer (EI with 70 eV or chemical ionization with isobutane). (Dichloromethyl)methylbis(trimethylsilyl)silane (**4a**),[4] *tert*-butyl(dichloromethyl)bis(trimethylsi-

 © 2004 Wiley-VCH Verlag GmbH & Co. KGaA, Weinheim

lyl)silane (**4b**),[11] and (dichloromethyl)phenylbis(trimethylsilyl)silane (**4c**)[4] as well as 1-[8-(dimethylamino)-1-naphthyl)-1,2,2-tris(trimethylsilyl)silene (**1d**),[3a] and 1-(2-dimethylaminophenyl)-1,2,2-tris(trimethylsilyl)silene (**2**)[3b] were prepared as described previously. 8-(dimethylaminomethyl)-1-naphthyllithium was prepared following the procedure given by Corriu et al.,[12] but was isolated as a brown amorphous powder. All yields given refer to amounts obtained after chromatographic separation and purification or recrystallization. The results of the elemental analyses of the compounds prepared were unsatisfactory in some cases (SiC formation). Therefore, high resolution mass spectra were recorded.

1-[8-(Dimethylamino)-1-naphthyl]-1-methyl-2,2-bis(trimethylsilyl)-silene (1a): At −78 °C, **4a** (1.50 g, 5.4 mmol) was added gradually to a suspension of 8-(dimethylamino)-1-naphthyllithium−diethyl ether (3.00 g, 11.7 mmol) in diethyl ether (30 mL). After warming to room temperature and stirring overnight, the solvent was removed in vacuo. Pentane was added and LiCl separated by filtration. The orange-yellow filtrate was concentrated and 1-(dimethylamino)naphthalene was removed by distillation in vacuo (80 °C/$5\cdot10^{-4}$ mbar). The residue was purified by kugelrohr distillation (150 °C/$5\cdot10^{-4}$ mbar). Care has to be taken not to exceed a temperature of 155 °C, otherwise decomposition reactions take place. Silene **1a** was obtained as a glassy oil. Crystallization from pentane gave yellow crystals. Yield 1.83 g (52%); m.p. 140−142 °C. ^{1}H NMR ([D$_6$]benzene): δ = 0.23 and 0.57 [2 broad s, 2 × 9 H, Si(CH$_3$)$_3$], 0.34 (s, 3 H, SiCH$_3$), 2.27 and 2.52 (2s, 2 × 3 H, NCH$_3$), 6.63−7.82 (m, 6 H, aryl-H) ppm. ^{13}C NMR ([D$_6$]benzene): δ = 5.0 (C=Si*C*H$_3$), 7.6 and 8.0 (Si=CSi*C*H$_3$, broad), 14.5 (Si=C), 45.6 and 52.8 (NCH$_3$), 115.5, 125.8, 127.6, 127.7, 128.4 and 132.5 (arom. CH), 132.3, 132.9, 138.1 and 147.4 (quat. arom. C) ppm. ^{29}Si NMR ([D$_6$]benzene): δ = −16.1 and −7.0 (SiMe$_3$), 36.0 (Si=C) ppm. UV/Vis (*n*-heptane): λ_{max} (ε) = 304 nm (14800). MS (70 eV): *m*/*z* (%) = 372 (100) [MH]$^+$, 357 (14) [MH − CH$_3$]$^+$. C$_{20}$H$_{33}$NSi$_3$ (371.8): calcd. C 64.62, H 8.95, N 3.77; found C 64.18, H 8.92, N 3.74.

1-*tert*-Butyl-1-[8-(dimethylamino)-1-naphthyl]-2,2-bis(trimethylsilyl)silene (1b): As described for **1a**. Compound **4b** (1.63 g, 5.17 mmol) and 8-(dimethylamino)-1-naphthyllithium−diethyl ether (2.60 g, 10.33 mmol) afforded, after separation of 1-(dimethylamino)naphthalene, 0.85 g (41%) of oily **1b**, which gradually solidified. ^{1}H NMR ([D$_6$]benzene): δ = 0.34 and 0.68 (2s, 2 × 9 H, SiCH$_3$), 0.84 (s, 9 H, CCH$_3$), 2.48 and 2.52 (2s, 2 × 3 H, NCH$_3$), 6.50−7.94 (m, 6 H, aryl-H) ppm. ^{13}C NMR ([D$_6$]benzene): δ = 9.24 and 9.19 ppm (SiCH$_3$), 24.6 (*C*CH$_3$), 28.7 (Si=C), 29.4 (C*C*H$_3$), 43.8 and 56.2 (NCH$_3$), 109.2, 113.9, 125.3, 127.5, 127.8 and 132.5 (arom. CH), 133.7, 134.8, 136.3 and 148.4 (quat. arom. C) ppm. ^{29}Si NMR ([D$_6$]benzene): δ = −10.2 and −7.8 (SiMe$_3$), 43.6 (Si=C) ppm. UV/Vis (*n*-heptane): λ_{max} (ε) = 308 nm (40660). MS (70 eV): *m*/*z* (%) = 413 (8) [M]$^+$, 398 (26) [M − CH$_3$]$^+$, 356 (100) [M − C(CH$_3$)$_3$]. HRMS calcd. for C$_{23}$H$_{39}$NSi$_3$ 413.23904; found 413.23850.

1,3-Bis[8-(dimethylamino)-1-naphthyl]-1,3-dimethyl-1,3-bis[bis(trimethylsilyl)methyl]disiloxane (8): Wet diethyl ether was added to a yellow ethereal solution of **1a** (2.0 g, 4.66 mmol) until the color had completely disappeared. After evaporation, the residue was recrystallized from acetone to give a mixture of two diastereomeric forms of **8** (ratio of 40:60). Yield 1.66 g (81%), m.p. 214−217 °C. The separation of the two diastereomers failed, but the NMR spectra of the mixture allowed the assignment of the signals of both forms. **Diastereomer 1:** ^{1}H NMR ([D$_6$]benzene): δ = −0.31, 0.48 [2s, 2 × 9 H, Si(CH$_3$)$_3$], 0.38 (s, 1 H, CH), 1.17 (s, 3 H, OSiCH$_3$), 2.15 and 2.60 (2s, 2 × 3 H, NCH$_3$), 7.05−8.75 (m,, 5 H aryl-H) ppm. ^{13}C NMR ([D$_6$]benzene): δ = 3.6 and 5.1 (SiMe$_3$), 4.3 (Si$_3$C), 9.1 (OSiCH$_3$),43.3 and 51.4 (NCH$_3$), 117.0, 125.3, 125.57, 125.63, 130.5 and 138.1 (arom. CH), 135.1, 136.3, 137.7 and 153.5 (quat. arom. C) ppm. ^{29}Si NMR ([D$_6$]benzene): δ = −5.5 (SiOSi), −1.0 and 0.8 (SiMe$_3$) ppm. **Diastereomer 2:** ^{1}H NMR ([D$_6$]benzene): δ = −0.07, 0.38 [2s, 2 × 9 H, Si(CH$_3$)$_3$], 0.44 (s, 1 H, CH), 0.75 (s, 3 H, OSiCH3], 2.32 and 2.46 (2s, 2 × 3 H, NCH$_3$), 7.05−8.75 (m, 5 H), aryl-Hppm. ^{13}C NMR ([D$_6$]benzene): δ = 3.9 and 5.4 (SiMe$_3$), 4.3 (Si$_3$C), 9.2 (OSiCH$_3$), 45.8 and 48.8 (NCH$_3$), 116.6, 124.9, 125.3, 126.0, 130.3 and 138.5 (arom. CH), 134.9, 136.1, 138.1 and 153.3 (quat. arom. C) ppm. ^{29}Si NMR ([D$_6$]benzene): δ = −5.3 (SiOSi), −0.6 and 0.8 (SiMe$_3$). **For the Mixture:** MS (70 eV): *m*/*z* (%) = 760 (38) [M]$^+$, 745 (5) [M − CH$_3$], 590 (16) [M − C$_{10}$H$_6$]$^+$, 372 (100) [(Me$_2$NC$_{10}$H$_6$)MeSiCH(SiMe$_3$)$_2$]$^+$. HRMS calcd. for C$_{40}$H$_{68}$N$_2$OSi$_6$ 760.39471; found 760.39430.

[8-(Dimethylamino)-1-naphthyl]methyl[bis(trimethylsilyl)methyl]-silanol (9a): An ethereal solution of **1a** (2.0 g, 4.66 mmol) was added to a mixture of THF/water (1:1). After a few minutes, the organic layer was separated and the solvents evaporated. The residue was purified by kugelrohr distillation (130 °C/$2\cdot10^{-2}$ mbar). Colorless oil, yield 1.04 g (57%). ^{1}H NMR ([D$_6$]benzene): δ = −0.14 (s, 1 H, CH), 0.00 and 0.27 [2s, 2 × 9 H, Si(CH$_3$)$_3$], 0.74 (s, 3 H, OSiCH$_3$), 2.28 and 2.39 (2s, 2 × 3 H, NCH$_3$), 6.32 (br.s, 1 H, OH), 6.92−7.91 (m, aryl-H) ppm. ^{13}C NMR ([D$_6$]benzene): δ = 3.2, 3.5, 6.1 and 7.74 (SiCH and SiCH$_3$), 44.6 and 48.3 (NCH$_3$), 116.9, 125.0, 125.4, 127.0, 130.4 and 136.0 (arom. CH), 134.1, 136.7, 139.8 and 151.5 (quat. arom. C) ppm. ^{29}Si NMR ([D$_6$]benzene): δ = −0.3 and 0.2 (SiMe$_3$), 3.0 (SiOH) ppm. IR (cap.): $\tilde{\nu}$ = 3439 cm^{-1} (br., OH$_{ass.}$). MS (70 eV): *m*/*z* (%) = 389 (100) [M]$^+$, 374 (23) [M − CH$_3$]$^+$, 230 (68) [M − CH(SiMe$_3$)$_2$]$^+$. C$_{22}$H$_{41}$NOSi$_4$ (389.8): calcd. C 61.63, H 9.05, N 3.59; found C 61.69, H 9.04, N 3.57.

***tert*-Butyl[8-(dimethylamino)-1-naphthyl][bis(trimethylsilyl)methyl]-silanol (9b):** As described for **1a**. Compound **4b** (1.1 g, 3.49 mmol) was treated with 8-(dimethylamino)-1-naphthyllithium−diethyl ether (1.75 g, 6.97 mmol), but silene **1b** was not isolated. Instead, after separation of LiCl, water was added to the pentane solution. Separation of the organic layer, evaporation of the solvent and kugelrohr distillation of the residue (140 °C/$2\cdot10^{-2}$ mbar) gave 0.80 g (53.1%) of **9b** in the form of a viscous oil. ^{1}H NMR ([D$_6$]benzene): δ = 0.06 and 0.45 (2s, 2 × 9 H, SiCH$_3$), 0.08 (s, 1 H, CH), 1.13 (s, 9 H, *t*Bu), 2.37 and 2.43 (2s, 2 × 3 H, NCH$_3$), 7.0−7.96 (m, 6 H, aryl-H), 10.0 (s, 1 H, SiOH) ppm. ^{13}C NMR ([D$_6$]benzene): δ = 4.7 and 5.2 (SiCH$_3$), 4.3 (CH), 22.1 (*C*CH$_3$), 28.7 (C*C*H$_3$), 46.9 and 47.4 (NCH$_3$), 119.4, 124.0, 125.3, 128.3, 128.8 and 131.0 (arom. CH), 136.6, 138.4, 151.6 and 154.2 (quat. arom. C) ppm. ^{29}Si NMR ([D$_6$]benzene): δ = −0.4 and 0.0 (SiMe$_3$), 5.4 (SiOH) ppm. MS (70 eV): *m*/*z* (%) = 431 (5) [M]$^+$, 416 (10) [M − CH$_3$]$^+$, 374 (100) [M − CMe$_3$]$^+$, 358 (4) [M − SiMe$_3$]$^+$. HRMS calcd. for C$_{23}$H$_{41}$NOSi$_3$ 431.24958; found 431.24913.

[8-(Dimethylamino)-1-naphthyl]phenyl[bis(trimethylsilyl)methyl]-silanol (9c): As described for **1a**. Compound **4c** (1.23 g, 3.6 mmol) was gradually added to a suspension of 8-(dimethylamino)-1-naphthyllithium−diethyl ether (2.00 g) in diethyl ether (60 mL) at −78 °C. After warming to room temperature and stirring overnight water (5 mL) was added. The organic layer was separated, evaporated and the residue was recrystallized from acetonitrile. Colorless crystals, m.p. 125−126 °C, yield 1.12 g (69%). ^{1}H NMR ([D$_6$]benzene): δ = 0.00 and 0.17 [2s, 2 × 9 H, Si(CH$_3$)$_3$], 0.11 (s, 1 H, CH), 1.74 and 2.35 (2s, 2 × 3 H, NCH$_3$), 6.83− 8.11 (11 H, aryl-H) ppm. ^{13}C NMR ([D$_6$]benzene): δ = 3.1 and 3.3 (SiCH$_3$), 7.5 (CH), 43.9 and 49.2 (NCH$_3$), 117.4, 124.6, 125.5, 127.3, 127.7, 129.0, 130.9, 134.9 and 137.0 (arom. CH), 134.2, 136.4, 137.3, 142.4 and

 © 2004 Wiley-VCH Verlag GmbH & Co. KGaA, Weinheim

151.2 (quat. arom. C) ppm. ^{29}Si NMR ([D$_6$]benzene): δ = −5.2 (SiOH), 0.2 and 0.3 ($SiMe_3$) ppm. MS (70 eV): *m/z* (%) = 451 (54) $[M]^+$, 292 (100) $[M - CH(SiMe_3)_2]^+$. $C_{25}H_{37}NOSi_3$ (451.2): calcd. C 66.46, H 8.25, N 3.10; found C 65.63, H 8.25, N 3.10. HRMS calcd. for $C_{25}H_{37}NOSi_3$ 451.21829; found 451.21910.

[8-(Dimethylamino)-1-naphthyl](methoxy)phenyl[bis(trimethylsilyl)-methyl]silane (10): At −78 °C **4c** (1.3 g, 3.8 mmol) was added to a suspension of 8-(dimethylamino)-1-naphthyllithium−diethyl ether (2.1 g, 1.05 mmol) in diethyl ether (60 mL). After warming to room temperature and stirring overnight the solvent was replaced by pentane and lithium chloride was filtered off. Addition of methanol (2 mL) to this solution and evaporation gave a viscous oil which was purified by kugelrohr distillation (170−180 °C/4 × 10^{-2} mbar). Yield 1.4 g (83%). ^{1}H NMR ([D$_6$]benzene): δ = 0.04 and 0.08 ppm (2s, 2 × 9 H, $SiCH_3$), 0.70 (s, 1 H, CH), 1.99 and 2.30 (2s, 2 × 3 H, NCH_3), 3.51 (s, 3 H, OCH_3), 7.03−8.19 (m, 12 H, aryl-H) ppm. ^{13}C NMR ([D$_6$]benzene): δ = 3.1 (Si_3C), 3.9 and 4.2 ($SiCH_3$), 46.8 and 47.8 (NCH_3), 51.9 (OCH_3), 117.8, 125.1, 125.8, 126.2, 127.3, 128.6, 131.0, 135.4 and 138.5 (arom. CH), 132.9, 136.0, 136.1, 139.7 and 153.6 (quat. arom. C) ppm. ^{29}Si NMR ([D$_6$]benzene): δ = −5.6 (SiOMe), −1.2 and 0.4 ($SiMe_3$) ppm. IR (cap.): $\tilde{\nu}$ = 1101 cm^{-1} ($SiOCH_3$). MS (70 eV): *m/z* (%) = 465 (53) $[M]^+$, 450 (13) $[M - CH_3]^+$,388 (18) $[M - Ph]^+$, 306 (100) $[M - CH(SiMe_3)_2]^+$. HRMS calcd. for $C_{26}H_{39}NOSi_3$ 465.23395; found 465.22990.

1,2-Dimethyl-2-[1,1-bis(trimethylsilyl)ethyl]-1-aza-2-silaacenaphthene (11a): To a solution of **4a** (1.75 g, 4.70 mmol) in dichloromethane (20 mL) was added methyl iodide (1 mL, 1.53 g, 10.8 mmol) and the solution was stirred for 48 h at room temperature. Evaporation of the solution and purification of the residue by column chromatography (silica gel, heptane) gave a yellow oil, yield 0.7 g (40%). ^{1}H NMR ([D$_6$]benzene): δ = −0.13 ppm and 0.13 [2s, 2 × 9 H, $Si(CH_3)_3$], 0.35 (s, 3 H, $SiCH_3$), 1.22 (s, 3 H), $CCH_3$2.78 (s, 3 H, NCH_3), 6.34−7.74 (m, 6 H, arom. CH) ppm. ^{13}C NMR ([D$_6$]benzene): δ = −1.0, 0.5, 1.3 and 3.4 (SiC), 13.7 (CCH_3), 31.6 (NCH_3), 101.8, 115.2, 126.5, 128.5, 128.6 and 129.9 (arom. CH), 132.5, 134.4 and 152.3 (one signal hidden, quat. arom. C) ppm. ^{29}Si NMR ([D$_6$]benzene): δ = 2.6 and 3.9 ($CSiMe_3$), 10.4 (ring-Si) ppm. MS (70 eV): *m/z* (%) = 371 (100) $[M]^+$, 356 (28) $[M - CH_3]^+$, 298 (14) $[M - SiMe_3]^+$. HRMS calcd. for $C_{20}H_{33}NSi_3$ 371.19203; found 371.18654.

2-*tert*-Butyl-1-methy-2-[1,1-bis(trimethylsilyl)ethyl]-1-aza-2-silaacenaphthene (11b): 11b can be obtained from **1b** and methyl iodide as described for **11a**. It can be prepared more easily, however, by treatment of the crude product mixture obtained after treatment of **4b** with 8-(dimethylamino)-1-naphthyllithium. A typical procedure follows: **4b** (0.93 g, 2.94 mmol) was added at −78 °C to a suspension of 8-(dimethylamino)-1-naphthyllithium−diethyl ether (1.48 g, 5.89 mmol) in diethyl ether (30 mL). The mixture was warmed to room temperature and was stirred for 12 h. After replacement of the solvent by *n*-pentane, LiCl was separated, the yellow solution evaporated and 1-(dimethylamino)naphthalene was removed by distillation at 100 °C/10^{-2} mbar. The residue was dissolved in dichloromethane (20 mL), methyl iodide (2.0 g, 14 mmol) was added and the solution was stirred for 24 h. Evaporation and recrystallization from acetonitrile gave 0.75 g (62%) pale greenish crystals of **11b**, m.p. 129−132 °C. ^{1}H NMR ([D$_6$]benzene): δ = −0.02 ppm and 0.08 (2s, 2 × 9 H, $SiCH_3$), 0.96 [s, 9 H, $C(CH_3)_3$], 1.44 (s, 3 H, CCH_3), 2.90 (s, 3 H, NCH_3), 6.33−7.71 (6 H, aryl-H) ppm. ^{13}C NMR ([D$_6$]benzene): δ = 1.8 and 2.1 ($SiCH_3$), 4.3 (*C*Me), 13.9 (CCH_3), 25.1 (CMe_4), 28.2 (*t*Bu CH_3), 32.4 (NCH_3), 101.3, 115.1, 126.5, 128.3, 128.5 and 129.8 (arom. CH), 132.5, 134.3, 135.0 and 154.3 (quat. arom. C) ppm. ^{29}Si NMR ([D$_6$]benzene): δ = 3.4 and 4.1 ($SiMe_3$), 10.5 (ring-Si) ppm. MS (70 eV): *m/z* (%) = 413 (15) $[M]^+$, 398 (14) $[M - CH_3]^+$, 356 (100) $[M - CMe_3]^+$. HRMS calcd. for $C_{23}H_{39}NSi_3$ 413.23904; found 413.23692.

1-Methyl-2-trimethylsilyl-2-[1,1-bis(trimethylsilyl)ethyl]-1-aza-2-silaacenaphthene (11d): As described for **11a**. Compound **1d**[3a,3b] (2.0 g, 4.66 mmol) and methyl iodide (1 mL, 1.53 g, 10.8 mmol) were stirred in dichloromethane (20 mL) for 48 h at room temperature. After evaporation a solid was obtained, which was recrystallized from acetonitrile. Pale yellow crystals, yield 1.28 g (64%), m.p. 165 °C. ^{1}H NMR ([D$_6$]benzene): δ = −0.07, 0.02 and 0.12 (3s, 3 × 9 H, $SiCH_3$), 1.36 (s, 3 H, CCH_3), 2.84 (s, 3 H, NCH_3), 6.30−7.70 (m, 6 H, aryl-H) ppm. ^{13}C NMR ([D$_6$]benzene): δ = −0.2, 0.7 and 1.2 ($SiCH_3$), 4.8 (Si_3C), 14.2 (CCH_3), 33.0 (NCH_3), 101.4, 114.7, 126.7 128.6 and 129.6 (arom. CH, one signal hidden), 133.0, 135.6, 135.7 and 153.5 (quat. arom. C) ppm. ^{29}Si NMR ([D$_6$]benzene): δ = −17.2 ($SiSiMe_3$), 3.0, 4.1 and 4.4 ($CSiMe_3$ and ring-Si) ppm. MS (70 eV): *m/z* (%) = 429 (15) $[M]^+$, 414 (6) $[M - CH_3]^+$, 356 (100) $[M - SiMe_3]^+$. $C_{22}H_{39}NSi_4$ (429.9): calcd. C 61.47, H 9.14, N 3.26; found C 61.02, H 9.16, N 3.27.

The Reaction of 1d with Benzaldehyde: Benzaldehyde (1.18 g, 11.6 mmol) was added to a solution of **1d** (5.00 g, 11.6 mmol) in *n*-heptane (120 mL) and the mixture was stirred for 6 h at 80 °C. After cooling to room temperature 1,3-bis[8-(dimethylamino)-1-naphthyl]-1,3-bis(trimethylsilyl)cyclodisiloxan (**13**) in the form of the mixture of the two diastereomers crystallized from the solution and was separated by filtration (2.04 g, 61%). The filtrate was evaporated and the residue purified by column chromatography (silica gel, heptane) to give 2.77 g (96%) of 2,2-bis(trimethylsilyl)vinylbenzene (**14**).[10]

Attempts to separate the two diastereomers of **14** failed, but ^{1}H and ^{13}C NMR studies of the mixture (80:20) allowed the assignment of the signals to both forms. **Diastereomer 1:** ^{1}H NMR ([D$_6$]benzene): δ = −0.07 ppm [s, 9 H, $Si(CH_3)_3$], 2.75 and 2.92 (2s, 2 × 3 H, NCH_3) ppm. ^{13}C NMR ([D$_6$]benzene): δ = −0.3 ($SiMe_3$), 43.3 and 54.0 (NCH_3), 114.2, 125.5, 125.6, 125.8, 128.2, 128.7, 134.0, 135.9, 137.6 and 141.4 (arom. C) ppm. **Diastereomer 2:** ^{1}H NMR ([D$_6$]benzene): δ = 0.01 [s, 9 H, $Si(CH_3)_3$], 2.69 and 2.76 (2s, 2 × 3 H, NCH_3) ppm. ^{13}C NMR ([D$_6$]benzene): δ = 0.0 ($SiMe_3$), 43.4 and 53.2 (NCH_3), 114.3, 125.6, 125.8, 129.3, 134.8, 135.1, 136.5, 137.1 and 151.7 (one signal hidden, arom. C) ppm. **For the Mixture:** ^{1}H NMR ([D$_6$]benzene): δ = 6.91−8.86 (m, 6 H, arom. CH) ppm. ^{29}Si NMR ([D$_6$]benzene): δ = −35.9 and −35.4 (OSiO), −22.1 and −18.7 ($SiMe_3$). MS (CI, isobutane): *m/z* (%) = 575 (50) $[M + H]^+$, 559 (15) $[M - CH_3]^+$, 501 (100) $[M - SiMe_3]^+$. $C_{30}H_{42}N_2O_2Si_4$ (575.0): calcd. C 62.66, H 7.36, N 4.87; found C 62.31, H 7.21, N 4.53.

Acknowledgments

We gratefully acknowledge the support of our work by the Deutsche Forschungsgemeinschaft and the Fonds der Chemischen Industrie. We thank Dr. W. Baumann and Prof. N. Stoll for recording NMR and mass spectra.

[1] Reviews: [1a] A. G. Brook, M. A. Brook, *Adv. Organomet. Chem.* **1996**, *39*, 71−158. [1b] T. Müller, W. Ziche, N. Auner in *The Chemistry of Organic Silicon Compounds, Vol. 2* (Eds.: Z. Rappoport, Y. Apeloig), John Wiley & Sons, New York, **1998**, p. 857−1062.

[2] [2a] N. Wiberg, H. Köpf, *J. Organomet. Chem.* **1986**, *315*, 9−18; N. Wiberg, G. Wagner, G. Reber, J. Riede, G. Müller, *Or-*

 © 2004 Wiley-VCH Verlag GmbH & Co. KGaA, Weinheim

ganometallics **1987**, *6*, 35−41. [2b] N. Wiberg, K.-S. Joo, K. Polborn, *Chem. Ber.* **1993**, *126*, 67−69.
[3] [3a] M. Mickoleit, K. Schmohl, R. Kempe, H. Oehme, *Angew. Chem.* **2000**, *112*, 1679− 1681; *Angew. Chem. Int. Ed.* **2000**, *39*, 1610−1612. [3b] M. Mickoleit, R. Kempe, H. Oehme, *Chem. Eur. J.* **2001**, *7*, 987−993. [3c] M. Pötter, U. Bäumer, M. Mickoleit, R. Kempe, H. Oehme, *J. Organomet. Chem.* **2001**, *621*, 261−266.
[4] K. Schmohl, H. Reinke, H. Oehme, *Eur. J. Inorg. Chem.* **2001**, 481−489.
[5] H. Kessler, *Angew. Chem.* **1970**, *82*, 237− 253; *Angew. Chem. Int. Ed. Engl.* **1970**, *9*, 219−235.
[6] D. Wandschneider, H. Oehme, A. Heintz, unpublished results, manuscript in preparation.
[7] H. Beyer, W. Walter, *Lehrbuch der Organischen Chemie*, Hirzel, Leipzig, **1998**.
[8] N. Wiberg, H.-S. Hwang-Park, H.-W. Lerner, S. Dick, *Chem. Ber.* **1996**, *129*, 471−478.
[9] J. Belzner, H. Ihmels, B. O. Kneisel, R. Herbst-Irmer, *Chem. Ber.* **1996**, *129*, 125−130.
[10] B.-Th. Gröbel, D. Seebach, *Chem. Ber.* **1977**, *110*, 852−859.
[11] K. Schmohl, H. Reinke, H. Oehme, *Z. Anorg. Allg. Chem.* **2001**, *627*, 2619−2624.
[12] R. Corriu, G. Lanneau, C. Priou, *Angew. Chem.* **1991**, *103*, 1153−1155; *Angew. Chem. Int. Ed. Engl.* **1991**, *30*, 1130−1132.

Received September 4, 2003
Early View Article
Published Online March 5, 2004

 © 2004 Wiley-VCH Verlag GmbH & Co. KGaA, Weinheim

A New Family of Low-Spin Co^{III} Bis(amidate) Complexes with Two *cis* or *trans* Cyanides

Olaf Rotthaus,[a] Sophie LeRoy,[a] Alain Tomas,[b] Kathleen M. Barkigia,[c] and Isabelle Artaud*[a]

Keywords: Cobalt / Cyanides / N ligands

Four low-spin dicyanodicarboxamidocobalt(III) complexes have been prepared from *N*,*N*′-bis(8-quinolyl)malonamide derivatives, the malonyl fragment of which was either unsubstituted $(Et_4N)[Co(BQM)(CN)_2]$ (**3a**), monosubstituted by a benzyl group $(Et_4N)[Co(mono\text{-}BenzBQM)(CN)_2]$ (**3b**), or disubstituted by two benzyl or two phenylethyl groups, $(Et_4N)[Co(di\text{-}BenzBQM)(CN)_2]$ (**3c**) and $(Et_4N)[Co(di\text{-}PhEtBQM)(CN)_2]$ (**3d**), respectively. The X-ray crystal structures of **3a** and **3c** reveal that the tetradentate ligand adopts a helical or a planar configuration around the cobalt centre of **3a** and **3c**, respectively. Complexes **3a**–**3d** were characterised in solution by ^1H NMR spectroscopy by 1D and 2D COSY H-H techniques. The solid-state structures of **3a** and **3c** are retained in solution, and complexes **3b** and **3d** adopt structures similar to **3a** and **3c**, respectively, showing that the level of the malonic substitution determines the configuration of the tetradentate ligand around the cobalt centre and forces the cyanide ligands to adopt either *cis* or *trans* orientations.

(© Wiley-VCH Verlag GmbH & Co. KGaA, 69451 Weinheim, Germany, 2004)

Introduction

Prompted by the work of Collins' group showing the capacity of deprotonated amides to be strong metal donors and to stabilize high oxidation states,[1] this area of chemistry has received increased attention with the recent findings that amides from a peptide backbone could also be nitrogen donors to the metal centre of metalloproteins, such as the nitrogenase P-cluster[2] or the nitrile hydratase family.[3] Our group[4] and others[5,6] have synthesised iron and cobalt mimics of the nitrile hydratase active site. Our choice of N_2S_2 tetradentate ligands has illustrated the new properties of this series of complexes.[4] We are now aiming to develop nitrogen-containing ligands to prepare new mononuclear complexes that could be used as catalysts for oxidation reactions.

It is well-known that introducing one or more carboxamido nitrogens in the metal environment increases the stability of Fe^{III} or Co^{III} complexes[1,7] and provides catalysts with significant catalytic activity for the oxidation of olefins or hydrocarbons with *t*BuOOH or H_2O_2.[7,8] Tetradentate ligands containing two amides usually derive from picolinic acid and afford six-coordinate complexes with four nitrogens that occupy the equatorial plane and two exogenous ligands in the axial positions.[9] We report here the synthesis and characterisation of a new family of dicyano Co^{III} complexes of *N*,*N*′-bis(8-quinolyl)malonamide derivatives. We show that different substitutions of the malonic fragment control the coordination geometry of the four nitrogen donors to the metal centre. The tetradentate chelate adopts a planar or a helical configuration around the metal cation, providing two types of complexes with two *cis* or *trans* cyanides.

[a] Laboratoire de Chimie et Biochimie Pharmacologiques et Toxicologiques, UMR 8601, Université René Descartes
45 rue des Sts Pères, 75270 Paris cedex 06, France
Fax: (internat.) +33-1-42868387
E-mail: isabelle.artaud@biomedicale.univ-paris5.fr
[b] Laboratoire de Cristallographie et de RMN biologiques, UMR 8015, Faculté de Pharmacie,
4 rue de l'Observatoire, 75270 Paris cedex 06, France
[c] Materials Science Department, Brookhaven National Laboratory,
Upton, New York, 11973, USA

Results and Discussion

Synthesis of Co^{III} Complexes

We have prepared a series of *N*,*N*′-bis(8-quinolyl)malonamide (BQM) derivatives, shown in Scheme 1, containing a malonyl fragment that is either unsubstituted (**1a**), monosubstituted by a benzyl group (**1b**), or disubstituted by two benzyl (**1c**), or two 2-phenylethyl (**1d**) groups. These ligands were easily synthesised by condensing 8-aminoquinoline with malonyl dichloride derivatives, as previously reported for the disubstituted malonamide compounds.[10] Cobalt(II) was reacted with the ligands as $CoCl_2$ in the presence of triethylamine as a soft base. Depending on the ligand sub-

stitution, two different procedures were applied, as outlined in Scheme 1. For the unsubstituted or monosubstituted compounds **1a** and **1b**, the Co^{II} insertion was carried out in a mixture of CH_2Cl_2 and MeOH and led to the precipitation of the Co^{II} complex **2a** and **2b**, respectively. Complex **2a** precipitated readily from the solution, and **2b** precipitated after concentration in vacuo. Once isolated, the Co^{II} complexes are sparingly soluble in any solvent and were oxidized suspended in aerated CH_2Cl_2 after addition of two equivalents of tetraethylammonium cyanide to stabilize the Co^{III} complexes (Scheme 1, route A). Orange precipitates of the Co^{III} complexes **3a** and **3b** were obtained after partial removal of the solvent and addition of diethyl ether. The Co^{II} complexes of the disubstituted compounds **1c** and **1d** are highly soluble in CH_2Cl_2/MeOH and, consequently, more difficult to isolate. The one-pot synthesis of the dicyano Co^{III} complexes in DMF was therefore preferred. After preparing the Co^{II} complexes in solution, the cyanide ligands were added as Et_4NCN at −30 °C and the oxidation was performed with the one-electron oxidizing agent 4-fluorobenzenediazonium hexafluorophosphate[10] (Scheme 1, route B). After removing the solvent, the crude products were redissolved in CH_2Cl_2 and complexes **3c** and **3d** were precipitated by addition of diethyl ether and isolated as orange powders in good yields.

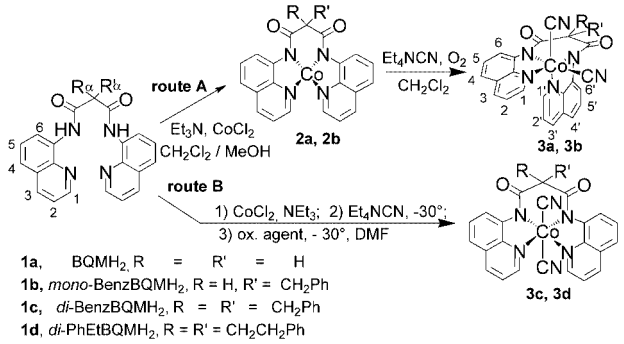

Scheme 1. Reaction pathways for the synthesis of the Co^{III} dicyano complexes

Characterisation of [Co^{II}(BQM)] (2a)

Co^{II} complexes were formed as intermediates during the synthesis of Co^{III} derivatives and, with the exception of **2a**, are not very stable under aerobic conditions, even as solids. Consequently, we characterised only **2a** to obtain some insight into the cobalt coordination. Its elemental analysis is in agreement with the formulation [Co^{II}(BQM)]. The IR spectrum of the ligand **1a** shows $\nu_{(N-H)}$ and $\nu_{(C=O)}$ vibrations at 3279 and 1646 cm^{-1}, respectively. The absence of the $\nu_{(N-H)}$ band and the shift of the $\nu_{(C=O)}$ band to a lower energy of 1605 cm^{-1} in the metal complex confirm that the amide nitrogens are coordinated to the Co in their deprotonated form. The X-band powder EPR spectrum at 4 K shows a single resonance at $g = 1.99$ characteristic of a low-spin Co^{II} state. This complex is four-coordinate and is probably square planar, as previously proposed for the Co^{II} complex of *N*,*N*′-bis(pyridin-2-ylmethylene)benzene-1,2-diamine, Co(bpb).[11] Co^{III} complexes with carboxamido nitrogen donors are typically six coordinate.[9] Thus, the oxidation was performed in the presence of cyanides to introduce two strong exogenous ligands to complete the cobalt coordination sphere and to stabilize the Co^{III} state.

X-ray Crystal Structure of (Et_4N)[Co(BQM)$(CN)_2$] (3a) and (Et_4N)[Co(di-BenzBQM)$(CN)_2$] (3c)

Crystals suitable for X-ray analysis were grown from CH_2Cl_2/hexane for **3a** and from acetonitrile/diethyl ether for **3c**. Views of the anions of **3a** and **3c** are presented in Figure 1 and 2. Selected bond angles and distances are listed in Table 1. In both structures the cobalt is six-coordinate in an octahedral environment to two deprotonated amide and two pyridyl nitrogens of the ligand and two exogenous cyanides. However, while the four nitrogen donors N1−N4 in **3c** (Figure 2) lie in the equatorial plane, with the two cyanides situated axially *trans* to each other, in **3a** (Figure 1) only three nitrogens (N1, N2 and N3) lie in the equatorial plane, with the fourth (N4) in an apical position and with the two cyanides occupying *cis* sites, one equatorial (C22−N5) and the other axial (C23−N6). Whereas in the *trans* configuration C11 deviates from the mean plane defined by N1N2C10C12N3N4 by 0.3 Å, the distortions are more important in the *cis* configuration. The angle between the planes N1N2N3 and N2C10C12N3 is 22° and the angle between C10C11C12 and N2C10C12N3 is 44°. Consequently the CH_2 fragment is in close proximity to the axial cyanide (C23N6).The distance between C11 of the CH_2 and C23 of the CN is 3.02 Å. This explains why a disubstituted derivative cannot adopt a *cis* configuration.

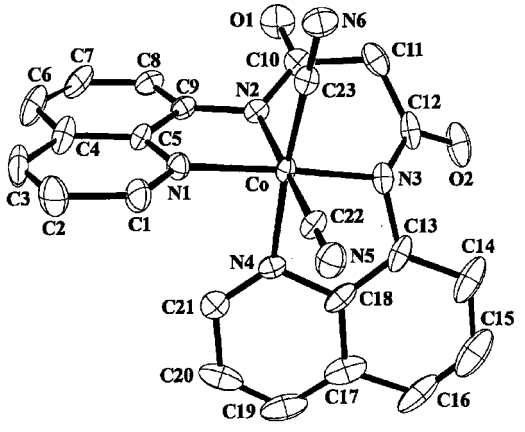

Figure 1. Thermal ellipsoid plot (50% probability level) of the anion of **3a**; H atoms are omitted for clarity

An unexpected aspect of the structure of **3a**, which crystallises with two water molecules per metal complex, is that the water molecules form an extended hydrogen-bonded network that links three chelates through the N5 nitrogens of the cyano group to the oxygens O1 and O2 of two additional ligands, as shown in Figure 3. The distance between the oxygen of a water and the cyano group (N5−O:

 © 2004 Wiley-VCH Verlag GmbH & Co. KGaA, Weinheim

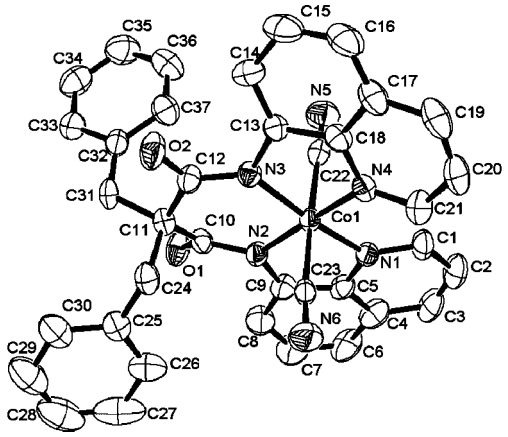

Figure 2. Thermal ellipsoid plot (50% probability level) of the anion of **3c**; H atoms are omitted for clarity

Table 1. Selected bond angles (°) and distances (Å) for complexes $[Co(BQM)(CN)_2]Et_4N$ (**3a**) and $[Co(di\text{-}BenzBQM)(CN)_2]Et_4N$ (**3c**)

	3a	**3c**
Co−N1	1.934(3)	1.957(4)
Co−N2	1.945(3)	1.933(4)
Co−N3	1.930(3)	1.931(4)
Co−N4	1.995(3)	1.959(4)
Co−C22	1.889(4)	1.932(6)
Co−C23	1.875(4)	1.922(6)
C22−N5	1.156(6)	1.132(7)
C23−N6	1.148(5)	1.151(7)
N2−Co−N4	98.06(12)	174.27(18)
N1−Co−N4	91.33(14)	99.22(16)
C23−Co−C22	83.7(2)	177.01(18)
C22−Co−N2	174.18(14)	92.4(2)
C23−Co−N4	170.6(2)	86.24(19)

2.89 Å) is clearly indicative of hydrogen bonding, as are the O2−O4 water molecule and O1−O3 water molecule distances of 2.73 and 2.82 Å, respectively. The water (O3)−water (O4) distance is 2.78 Å.

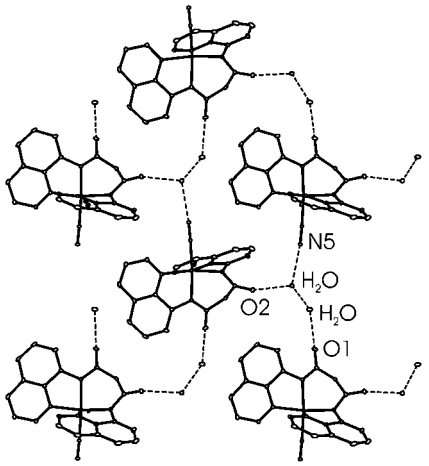

Figure 3. Hydrogen-bond network between water and **3a** molecules

Solution Structure of $(Et_4N)[Co(BQM)(CN)_2]$ (3a) and $(Et_4N)[Co(di\text{-}BenzBQM)(CN)_2]$ (3c)

With the strong cyanide ligands, these complexes exist in a low-spin Co^{III} state. Their structures can be readily analysed by ^1H NMR spectroscopy. NMR assignments were based on 1D and 2D COSY H-H experiments. The spectrum of **3c**, shown in Figure 4, indicates a solution structure with a C_2 symmetry, as in the solid state (Figure 2). Both quinolyl rings are equivalent and the pyridyl proton spin system (H^1, H^2, H^3) appears as a set of three well-resolved resonances between δ = 7.7 and 9.0 ppm. The proton labelling is indicated in Scheme 1. The same NMR spectrum was obtained when compound **3c** was prepared according to the procedure following route A (Scheme 1), or when the NMR sample was heated up to 360 K. In contrast, the spectrum of **3a**, shown in Figure 4, exhibits a more complicated pattern indicative of the lack of any symmetry, as in the crystal structure (Figure 1). The quinolyl resonances are split into two spin systems H^1, H^2, H^3, H^4, H^5, H^6 and $H^{1'}$, $H^{2'}$, $H^{3'}$, $H^{4'}$, $H^{5'}$, $H^{6'}$. Correlations were made by a 2D COSY experiment. For the assignments, the protons of the quinolyl ring in the equatorial plane were assumed to appear at chemical shifts very close to those found in the *trans* complex **3c**. The two pyridyl systems are very different. The *ortho* and *meta* pyridyl protons in the axial position are shifted upfield relative to those in the equatorial plane ($H^{1'}$: δ = 6.17 ppm; H^1: δ = 9.07 ppm; $H^{2'}$: δ = 7.28 ppm; H^2: δ = 7.87 ppm). Finally, the two malonyl protons are inequivalent; their signals appeared at two chemical shifts (δ = 2.97 and 5.02 ppm) located apart from the value of the unique CH_2 resonance (δ = 3.87 ppm) found for the free ligand. These results show that the unexpected solid-state structure of **3a** is retained in solution.

Solution Structure of $(Et_4N)[Co(mono\text{-}BenzBQM)(CN)_2]$ (3b) and $(Et_4N)[Co(di\text{-}PhEtBQM)(CN)_2]$ (3d)

Since NMR spectroscopy proved suitable for the analysis of the two structurally related complexes **3a** and **3c**, we also used this technique to determine whether the cyanides in complexes **3b** and **3d** were orientated in a *cis* or a *trans* fashion. The aim was to determine the influence of the malonyl substitution level on the coordination geometry and, for the disubstituted derivatives, the effect of lengthening the chain by one C−C bond. The NMR spectra of **3d** (Figure 4) and **3c** are very similar, supporting a planar configuration of the tetradentate chelate and a *trans* coordination of the cyanides to the cobalt cation. In contrast, the NMR spectrum of the monobenzylated derivative **3b** (Figure 4) displays, as for **3a**, two quinolyl proton spin-systems. The $H^{1'}$ and H^1 resonances are located in the upfield and downfield regions at δ = 6.11 ppm and 9.06 ppm, respectively. The H^α malonyl proton signal appears at δ = 5.55 ppm, a value similar to that of the low-field resonance found for one of the two malonyl protons H^α and $H^{\alpha'}$ in **3a**. The benzylic resonance appears at δ = 3.18 ppm, showing that the benzylic protons in **3b** are slightly shielded relative to those in the *trans* complex **3c**. Thus, the monobenzylated

 © 2004 Wiley-VCH Verlag GmbH & Co. KGaA, Weinheim

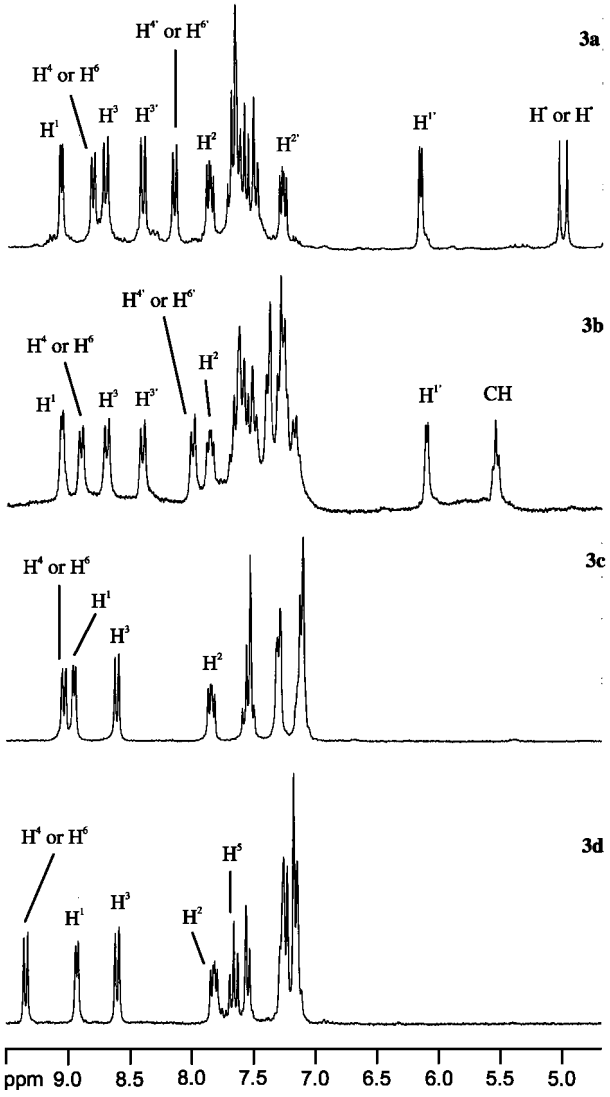

Figure 4. ^{1}H NMR spectra of the *cis*-**3a** and -**3b** and the *trans*-**3c** and -**3d** complexes at 250 MHz in [D_6]DMSO

and the unsubstituted complex, **3b** and **3a**, adopt the same helical arrangement of the N4 ligand and the same *cis* configuration of the cyanides.

It is noteworthy that while the NMR spectra of the two types of complexes are very different, their IR spectra do not reveal significant differences. They show a unique ν_{CN} stretching band at 2120 cm^{-1} suggesting that the two cyanides have the same surroundings. A similar observation has been reported for other *cis*-dicyano complexes such as *cis*-dicyanobis(1,10-phenanthroline)iron(II)[12] or bis(2,2′-bipyridine)-*cis*-dicyanoiron(III) perchlorate.[13]

Conclusion

In conclusion, we have prepared four new six-coordinate low-spin Co^{III} dicyano complexes that contain an *N*,*N*′-bis(8-quinolyl)malonamide ligand. Interestingly, the substitution level of the malonyl fragment determines whether the two cyanides are oriented *cis* or *trans* to the cobalt centre. The crystal structures of two representative complexes of this series have been solved. When unsubstituted or monosubstituted, the stable configuration is twisted with three nitrogens and one cyanide in the equatorial plane, and the fourth nitrogen and the second cyanide in apical positions. When disubstituted by two benzyl or two phenylethyl groups, the steric interaction of the malonyl substituent with the axial cyanide ligand destabilizes the *cis* configuration and forces the ligand to adopt a planar arrangement with two *trans* cyanides. Consequently, without changing the nature of the nitrogen donors, a disubstitution at the periphery of the ligand framework modulates the *cis* or *trans* coordination of the two exogenous ligands. Cyanides were introduced to facilitate the characterisation of the dicyano Co^{III} complexes, and therefore we next intend to introduce more labile exogenous ligands to compare the chemical reactivity of these complexes with the same nitrogen donor set and two *cis* or *trans* labile sites.

Experimental Section

Chemicals: All solvents and chemicals were purchased in analytical grade from SDS, Fluka or Aldrich. Sephadex LH-20 resin was purchased from Amersham Biosciences. Solvents were dried by standard procedures.

Spectroscopic Measurements: UV/Visible spectra were recorded at room temperature on a Safas UV *mc*^{2} spectrophotometer. X-band EPR spectra were recorded on a Bruker ESP300 spectrometer operating at a 9.5 GHz microwave frequency, with a 100 kHz modulation frequency and a 1 G modulation amplitude. ^{1}H NMR spectra were recorded at 300 K on a Bruker ARX-250 spectrometer. Chemical shifts are reported in ppm downfield from TMS. Infrared spectra were obtained with a Perkin−Elmer Spectrum One FT-IR spectrometer equipped either with a sample holder for KBr pellets or with a MIRacle™ single reflection horizontal ATR unit which allowed spectra of solid compounds to be recorded directly (marked as "neat"). Mass spectrometry (ESI^- and ESI^+) was performed on a Thermo Finnigan LCD Advantage spectrometer. Elemental analyses were carried out by the microanalysis service of Paris VI University.

***N*,*N*′-Bis(8-quinolyl)malonamide ($BQMH_2$) (1a):** Malonic acid chloride (972 μL, 9.5 mmol) was added under argon to a CH_2Cl_2 solution (100 mL) of 8-aminoquinoline (3.17 g, 22 mmol) and triethylamine (Et_3N, 3.0 mL, 20 mmoL). Then the mixture was stirred for 12 h at room temperature. After dissolution of all the precipitated condensation product by further addition of CH_2Cl_2 the solution was washed three times with water, then with saturated aqueous $NaHCO_3$ (30 mL each) and dried over $MgSO_4$. Removal of the solvent and recrystallisation of the product from CH_2Cl_2 afforded ligand **1a** as a white solid (1.32 g, 39%). $C_{21}H_{16}N_4O_2$ (356.13): calcd. C 70.78, H 4.49, N 15.73; found C 70.60, H 4.66, N 15.68. UV/Vis (CH_2Cl_2) λ_{max} (ε) = 243 (80000 $M^{-1}\cdot cm^{-1}$), 319 (13000) nm. IR (neat): $\tilde{\nu}$ = 3279 w (ν_{NH}) and 1646 s (ν_{CO}) cm^{-1}. ^{1}H NMR (250 MHz, $CDCl_3$): δ = 10.78 (s, 2 H, NH), 8.89 (dd, ^3J = 4.4, ^4J = 1.6 Hz, 2 H, H^1), 8.83 (dd, ^3J = 3.6, ^3J = 5.6 Hz, 2 H, H^5), 8.16 (dd, ^3J = 8.4, ^4J = 1.6 Hz, 2 H, H^3), 7.54 (d, ^3J = 3.6, 2 H, H^4 or H^6), 7.55 (d, ^3J = 5.6 Hz, 2 H, H^4 or H^6), 7.46 (dd, ^3J = 4.4, ^3J = 8.4 Hz, 2 H, H^2), 3.87 (s, 2 H, CH_2) ppm.

 © 2004 Wiley-VCH Verlag GmbH & Co. KGaA, Weinheim

2-Benzyl(ethyl malonate): NaH (0.96 g, 40 mmol) and then benzyl bromide (4.7 mL, 40 mmol) were slowly added to a dried THF solution (80 mL) of diethyl malonate (6 mL, 40 mmol). The reaction mixture was refluxed for 24 h. Then, diethyl ether was added (120 mL) and the solution was washed three times with water (3 × 80 mL) and dried over $MgSO_4$. After evaporation of the solvent, the slightly yellow residue was distilled off as a clear oil (bp, 133−135 °C, P 0.6 Torr, 6.3 g, 63%). ^1H NMR (250 MHz, $CDCl_3$): δ = 7.30−7.15 (m, 5 H, H-Ph), 4.14 (q, ^3J = 7.1 Hz, 4 H, CH_2(OEt)), 3.63 (t, ^3J = 7.8 Hz, 1 H, CH), 3.20 (d, ^3J = 7.8 Hz, 2 H, CH_2), 1.19 [t, ^3J = 7.1 Hz, 6 H, CH_3(OEt)] ppm.

2-Benzylmalonic Acid: 2-Benzyl(ethyl malonate) (5.2 g, 21 mmol) was poured onto pulverized KOH (4.7 g, 94 mmol) in an ice/water bath. The mixture rapidly became highly viscous and ethanol (2 mL) and water (1.3 mL) were added to allow stirring. After 6 h of stirring at 90 °C, the suspension was dissolved in H_2O (30 mL) and twice washed with CH_2Cl_2 (3 × 10 mL) before concentrated HCl was added to reach pH 1. The reaction product was collected by washing with CH_2Cl_2 (5 × 20 mL). The solution was dried over $MgSO_4$, and evaporation of the solvent afforded 2-benzylmalonic acid (1.7 g, 41%). ^1H NMR (250 MHz, [D_4]MeOH): δ = 7.30−7.10 (m, 5 H, H-Ph), 3.62 (t, ^3J = 7.7 Hz, 1 H, CH), 3.15 (d, ^3J = 7.7 Hz, 2 H, CH_2) ppm.

2-Benzyl-*N*,*N*′-bis(8-quinolyl)malonamide (mono-BenzBQMH$_2$) (1b): Under argon, 2-benzylmalonic acid (0.25 g, 1.3 mmol) was dissolved in 4 mL of $SOCl_2$ and the mixture was stirred for 4 h at 60 °C. After removal of the excess thionyl chloride in vacuo, 2-benzyldiethylmalonic acid chloride was obtained as a yellow oil, which was directly converted into **1b**. Two equiv. of 8-aminoquinoline (0.37 g, 2.6 mmol) were added to the acid chloride dissolved in dry toluene (5 mL). The orange suspension was stirred for 1 h at room temperature, then Et_3N (0.33 mL, 2.5 mmol) was added and the mixture stirred overnight at 60 °C. Then, CH_2Cl_2 (20 mL) was added, the solution was washed with H_2O (4 × 10 mL) and the organic layer was dried over $MgSO_4$. After recrystallization from CH_2Cl_2 **1b** was obtained as a white solid (0.37 g, 63%). UV/Vis (CH_2Cl_2) λ_{max} (ε) = 248 (18800 $M^{-1}\cdot cm^{-1}$), 307 (11700) nm. IR (neat): $\tilde{\nu}$ = 3271 w (ν_{NH}) and 1666 s (ν_{CO}) cm^{-1}. ^1H NMR (250 MHz, $CDCl_3$): δ = 10.60 (s, 2 H, NH), 8.85−7.76 (m, 4 H, H^1 + H^5), 8.12 (d, ^3J = 8.2 Hz, 2 H, H^3), 7.55−7.48 (m, 4 H, H^4 + H^6), 7.43 (dd, ^3J = 8.2, ^3J = 4.2 Hz, 2 H, H^2), 7.38−7.05 (m, H-Ph, 5 H), 3.91 (t, ^3J = 7.6 Hz, 1 H, CH), 3.59 (d, ^3J = 7.6 Hz, 2 H, CH_2) ppm. MS: *m*/*z* (%) = 447 (100) $[M + H]^+$).

2,2′-Dibenzyl-*N*,*N*′-bis(8-quinolyl)malonamide (di-BenzBQMH$_2$; 1c) and 2,2′-Bis(2-phenylethyl)-*N*,*N*′-bis(8-quinolyl)malonamide (di-PhEtBQMH$_2$; 1d): The disubstituted ligands **1c** and **1d** were synthesised according to Hirose et al,[14] but the saponification of the malonic esters was carried out as reported by Maslak et al.[15]

[Co(BQM)] (2a): Et_3N (0.56 mL, 4.2 mmol) was added under argon to a solution of the $BQMH_2$ ligand (**1a**; 0.3 g, 0.84 mmol) in a CH_2Cl_2/MeOH mixture (30 mL/20 mL). Upon addition of a methanolic solution (10 mL) of $CoCl_2$ (0.12 g, 0.92 mmol) the mixture turned orange and within five minutes [Co^{II}(BQM)] precipitated as a completely insoluble orange solid that was washed with CH_2Cl_2, MeOH and diethyl ether (20 mL each) (0.3 g, 73%). $C_{21}H_{16}CoN_4O_2\cdot 1.5H_2O$ (440.06): calcd. C 55.89, H 3.65, N 12.40; found C 57.28, H 3.89, N 12.72. IR (KBr): $\tilde{\nu}$ = 1605 s (ν_{CO}) cm^{-1}. EPR (powder, 4 K) *g* = 1.99.

(Et$_4$N)[Co(BQM)(CN)$_2$] (3a): Complex **2a** (0.1 g, 0.24 mmol) was suspended in CH_2Cl_2 (2 mL). Addition of a CH_2Cl_2 solution (5 mL) of tetraethylammonium cyanide (Et_4NCN, 75 mg, 0.48 mmol) resulted in the dissolution of the complex. Exposure of the solution to air caused oxidation of the cobalt. Stirring was continued for 2 h, then half of the solvent was evaporated and the product was precipitated by addition of diethyl ether. Purification over LH-20 (30 g) with CH_2Cl_2/MeOH (8:2) as eluent, and precipitation from CH_2Cl_2/pentane afforded (Et_4N)[Co(BQM)$(CN)_2$] as an orange powder (70 mg, 50%). $C_{31}H_{34}CoN_7O_2\cdot H_2O\cdot CH_2Cl_2$ (697.17): calcd. C 55.02, H 5.48, N 14.04; found C 54.89, H 5.46, N 13.99. UV/Vis (MeOH) λ (ε) = 257 (29900 $M^{-1}cm^{-1}$), 380 (6040) nm. IR (KBr): $\tilde{\nu}$ = 2126w (ν_{CN}) and 1601s (ν_{CO}) cm^{-1}. ^1H NMR (250 MHz, [D_6]DMSO): δ = 9.07 (d, ^3J = 5.0 Hz, 1 H, H^1), 8.81 (d, ^3J = 7.1 Hz, 1 H, H^4 or H^6), 8.71 (d, ^3J = 8.2 Hz, 1 H, H^3), 8.41 (d, ^3J = 8.1 Hz, 1 H, $H^{3'}$), 8.15 (d, ^3J = 7.2 Hz, 1 H, $H^{4'}$ or $H^{6'}$), 7.87 (dd, ^3J = 8.2, ^3J = 5.0 Hz, 1 H, H^2), 7.75−7.40 (m, 4 H, H^5 + $H^{5'}$, H^4 or $H^{4'}$ and H^6 or $H^{6'}$), 7.28 (dd, ^3J = 8.1, ^3J = 4.9 Hz, 1 H, $H^{2'}$), 6.17 (d, ^3J = 4.9 Hz, 1 H, $H^{1'}$), 5.02 (d, ^2J = 15.1 Hz, 1 H, H^α or $H^{\alpha'}$), 2.97 (d, ^2J = 15.1 Hz, 1 H, H^α or $H^{\alpha'}$) ppm. MS: *m*/*z* (%) = 465 (100) $[Co(BQM)(CN)_2]^-$.

(Et$_4$N)[Co(mono-BenzBQM)(CN)$_2$] (3b): Under argon, the monosubstituted ligand mono-$BenzBQMH_2$ (**1b**) (0.1 g, 0.22 mmol) was dissolved in CH_2Cl_2 (30 mL) and Et_3N (0.15 mL, 1.1 mmol) was added, followed by a solution of $CoCl_2$ (32 mg, 0.24 mmol) in MeOH (5 mL). After removal of three quarters of the solvent [Co^{II}-(mono-BenzBQM)] (**2b**) precipitated as a yellow powder and was collected by filtration, then washed with CH_2Cl_2, MeOH and diethyl ether (50 mg, 45%). Like **2a**, it is insoluble. The oxidation procedure described for **2a** was applied to **2b** (20 mg, 0.04 mmol) with Et_4NCN (12.5 mg, 0.08 mmol). (Et_4N)[Co(mono-BenzBQM)$(CN)_2$] (**3b**) was obtained as an orange powder (18 mg, 65%). $C_{38}H_{40}CoN_7O_2$ (685.26): calcd. C 66.56, H 5.88, N 14.30; found C 66.06, H 5.85, N 14.20. UV/Vis (MeOH): λ_{max} (ε) = 259 (31300 $M^{-1}cm^{-1}$) and 387 (6230) nm. IR (KBr): $\tilde{\nu}$ = 2125 w (ν_{CN}) and 1618 s (ν_{CO}) cm^{-1}. ^1H NMR (250 MHz, [D_6]DMSO): δ = 9.06 (d, ^3J = 5.2 Hz, H^1, 1 H), 8.90 (dd, ^3J = 7.3, ^4J = 1.2 Hz, 1 H, H^4 or H^6), 8.69 (d, ^3J = 8.1 Hz, 1 H, H^3), 8.40 (d, ^3J = 8.0 Hz, 1 H, $H^{3'}$), 8.00 (d, ^3J = 7.1 Hz, 1 H, $H^{4'}$ or $H^{6'}$), 7.86 (dd, ^3J = 8.1, ^3J = 5.2 Hz, 1 H, H^2), 7.75−7.45 (m, 4 H, H^5 +$H^{5'}$, H^4 or $H^{4'}$ and H^6 or $H^{6'}$), 7.45−7.00 (m, 6 H, $H^{2'}$ and H-Ph,), 6.11 (d, ^3J = 4.6 Hz, 1 H, $H^{1'}$), 5.55 (t, ^3J = 6.5 Hz, 1 H, CH), 3.18 (d, ^3J = 6.5 Hz, 2 H, CH_2) ppm. MS: *m*/*z* (%) = 555 (100) [Co(mono-BenzBQM)$(CN)_2]^-$.

(Et$_4$N)[Co(di-BenzBQM)(CN)$_2$] (3c) and (Et$_4$N)[Co(di-PhEtBQM)-(CN)$_2$] (3d): A mixture of $CoCl_2$ (27 mg, 0.21 mmol) and the ligand di-$BenzBQMH_2$ (**1c**; 0.11 g, 0.21 mmol) or di-$PhEtBQMH_2$ (**1d**; 0.12 g, 0.21 mmol), respectively, was dissolved in dry DMF (10 mL) under argon. After addition of Et_3N (0.11 mL, 0.84 mmol) the solution turned orange. Stirring at room temperature was continued for 30 min before the solution was cooled to −30 °C. Et_4NCN (0.2 g, 1.3 mmol) in DMF (5 mL) was then added, and the solution was stirred for a further 30 min at this temperature. Oxidation to Co^{III} was performed by addition of the oxidizing agent $C_6H_4FN_2PF_6$[10] (1.5 equiv.), dissolved in DMF (2 mL). The reaction mixture was allowed to warm to room temperature and DMF was removed in vacuo. The brown/orange solid was dissolved in acetonitrile (20 mL), the remaining white residue — unconverted ligand — was filtered off. An orange product was obtained after evaporation of the solvent. The product was further purified over LH-20 (30 g) with MeOH and finally precipitated with diethyl ether as an orange powder (3c: 0.13 g, 79%; 3d: 59 mg, 35%).

3c: $C_{45}H_{46}CoN_7O_2\cdot 3H_2O\cdot 3MeOH\cdot 1.5MeCN$ (945.93): calcd. C 62.18, H 6.98, N, 11.10; found C 61.94, H 6.96, N 11.07. UV/Vis (MeOH): λ_{max} (ε) = 268 (26500 $M^{-1}\cdot cm^{-1}$) and 400 (6090) nm. IR

 © 2004 Wiley-VCH Verlag GmbH & Co. KGaA, Weinheim

Table 2. Experimental crystallographic details for $[Co(BQM)(CN)_2]Et_4N$ (**3a**) and $[Co(di\text{-}BenzBQM)(CN)_2]Et_4N$ (**3c**)

Formula	$C_{31}H_{34}CoN_7O_2{\cdot}2H_2O$	$C_{37}H_{26}CoN_6O_2{\cdot}C_8H_{20}N{\cdot}C_2H_3N$
Crystallized from	dichloromethane/hexane	acetonitrile/diethyl ether
Mol. mass	631.61	816.87
Space group	*C*2/*c*	$Pbc2_1$
Z	8	4
T (K)	150	293
a (Å)	33.789 (4)	11.170 (2)
b (Å)	13.707 (2)	19.199 (3)
c (Å)	14.358 (2)	19.375 (3)
α (°)	90	90
β (°)	92.43(1)	90
V (Å^3)	6643 (9)	4155.0 (1)
Crystal colour	orange	orange
Crystal shape	irregular wedge	parallelepiped
Density calcd.	1.263	1.306
Dimensions (mm)	0.14 × 0.12 × 0.10	0.5 × 0.3 × 0.2
μ (mm^{-1})	0.561	0.462
λ (Å)	0.9037	0.71069
2θ range (°)	2.04−30.48	3.50−24.71
Absorption correction	none	MULABS[21]
reflections total/independent	43991/4614	20155/5343
Reflections with $I > 2\sigma(I)$	4306	4406
No of parameters refined	390	528
*R*1; *wR*2 [$I > 2\sigma(I)$]	0.072; 0.196[19]	0.0514; 0.1138
*R*1; *wR*2 (all data)	0.079; 0.209	0.0631; 0.1214
GOF	1.129	1.057

(KBr): $\tilde{\nu}$ = 2120 w (ν_{CN}) and 1601 s (ν_{CO}) cm^{-1}. ^{1}H NMR (250 MHz, [D$_6$]DMSO): δ = 9.03 (dd, ^3J = 7.3, ^4J = 1.9 Hz, 2 H, H^4 or H^6), 8.95 (d, ^3J = 5.3 Hz, 2 H, H^1), 8.60 (d, ^3J = 8.1 Hz, 2 H, H^3), 7.84 (dd, ^3J = 8.1, ^3J = 5.3 Hz, 2 H, H^2), 7.60−7.45 (m, 4 H, H^5 and H^4 or H^6), 7.35−7.00 (m, 10 H, H-Ph), 3.6−3.5 (m, 4 H, CH_2) ppm. MS: *m*/*z* (%) = 645 (100) $[Co(di\text{-}BenzBQM)(CN)_2]^-$.

3d: $C_{47}H_{50}CoN_7O_2{\cdot}2/3DMF{\cdot}1/3H_2O$ (858.04): calcd. C 68.54, H 6.50, N 12.51; found C 68.02, H 6.48, N 12.55. UV/Vis (MeOH): λ_{max} (ε) = 266 (28900 M$^{-1}{\cdot}$cm^{-1}) and 394 (7180) nm. IR (KBr): $\tilde{\nu}$ = 2117 w (ν_{CN}) and 1603 s (ν_{CO}) cm^{-1}. ^{1}H NMR (250 MHz, [D$_4$]MeOH): δ = 9.31 (d, ^3J = 7.8 Hz, 2 H, H^4 or H^6), 8.94 (d, ^3J = 5.3 Hz, 2 H, H^1), 8.52 (d, ^3J = 8.1 Hz, 2 H, H^3), 7.76 (dd, ^3J = 8.1, ^3J = 5.3 Hz, 2 H, H^2), 7.69 (t, ^3J = 7.8 Hz, 2 H, H^5), 7.57 (d, ^3J = 7.8 Hz, 2 H, H^4 or H^6), 7.3−7.0 (m, 10 H, H-Ph), 2.95−2.80 (m, 4 H, CH_2), 2.6−2.4 (m, 4 H, CH_2) ppm. MS: *m*/*z* (%) = 673 (100) $[Co(di\text{-}PhEtBQM)(CN)_2]^-$.

X-ray Crystallography: Crystal data for **3a** and **3c** are presented in Table 2. Data for **3a** were collected at beamline X7B (λ = 0.9376 Å) at the Brookhaven National Synchrotron Light Source with a MAR 345 image-plate detector and data for **3c** with an Excalibur system equipped with a CCD area detector. The structures were solved by use of isomorphous replacement for **3a**[16] and SHELXS 97[17] for **3c**. Refinement, based on F^2, was carried out by full-matrix least-squares with SHELXL-93[18] (**3a**) and SHELXL-97[19] (**3c**). Non-hydrogen atoms were refined anisotropically. The hydrogen atoms were positioned geometrically and refined riding on their carrier atom with isotropic thermal displacement parameters fixed at 1.2-times those of their parent atoms. The lattice of **3a** contains an extremely disordered molecule of solvation, which was unmodelable. The program SQUEEZE in the PLATON[20] suite of programs was used to treat this problem. The structure-factor calculation including SQUEEZE contribution for the final FCF file gave the following results: *R*1= 0.078 for 4366 reflections with $I > 2\sigma(I)$ and *wR*2 = 0.216 for 4614 reflections. ORTEP[21] diagrams of **3a** and **3c** are given in Figures 1 and 2.

CCDC-214648 (**3a**) and -211026 (**3c**) contain the supplementary crystallographic data for this paper. These data can be obtained free of charge at www.ccdc.cam.ac.uk/conts/retrieving.html [or from the Cambridge Crystallographic Data Centre, 12, Union Road, Cambridge CB2 1EZ, UK; Fax: (internat.) +44-1223/336-033; E-mail: deposit@ccdc.cam.ac.uk].

Acknowledgments

This work was supported by the European Commission, TMR-NOHEMIP research network No. ERBFMRXCT98−0174 and by the Division of Chemical Sciences, US Department of Energy, under contract DE-AC02-98CH10886 (at BNL). We thank the the EC for providing O. R. with a postdoctoral fellowship and Jack Fajer for helpful discussions.

[1] T. J. Collins, *Acc. Chem. Res.* **1994**, *27*, 279−285.
[2] J. W. Peters, M. H. B. Stowell, S. M. Soltis, M. G. Finnegan, M. K. Johnson, D. C. Rees, *Biochemistry* **1997**, *36*, 1181−1187.
[3] [3a] S. Nagashima, M. Nakasako, N. Dhomae, M. Tsujimura, K. Takio, M. Odaka, M. Yohda, N. Kamiya, I. Endo, *Nature Struct. Biol.* **1998**, *5*, 347−351. [3b] A. Miyanaga, S. Fushinobu, K. Ito, T. Wakagi, *Biochem. Biophys. Res. Commun.* **2001**, *288*, 1169−1174.
[4] [4a] M. Rat, R. Alves de Susa, A. Tomas, Y. Frapart, J. P. Tuchagues, I. Artaud, *Eur. J. Inorg. Chem.* **2003**, 759−765. [4b] S. Chatel, A. S. Chauvin, J. P. Tuchagues, E. Bill, J. C. Chottard, D. Mansuy, I. Artaud, *Inorg. Chim. Acta* **2002**, *336*, 19−28. [4c] M. Rat, R. Alves de Sousa, J. Vaissermann, P. Leduc, D. Mansuy, I. Artaud, *J. Inorg. Biochem.* **2001**, *24*, 207−213. [4d] S. Chatel, M. Rat, S. Dijols, P. Leduc, J. P. Tuchagues, D. Mansuy, I. Artaud, *J. Inorg. Biochem.* **2000**, *80*, 239−246.
[5] P. K. Mascharak, *Coord. Chem. Rev.* **2002**, *225*, 201−214 and references cited therein.

 © 2004 Wiley-VCH Verlag GmbH & Co. KGaA, Weinheim

[6] [6a] L. Heinrich, Y. Li, J. Vaissermann, J. C. Chottard, *Eur. J. Inorg. Chem.* **2001**, 1407−1409. [6b] L. Heinrich, A. Mary-Verla, Y. Li, J. Vaissermann, J. C. Chottard, *Eur. J. Inorg. Chem.* **2001**, 2203−2206. [6c] L. Heinrich, L. Yun, J. Vaissermann, G. Chottard, J. C. Chottard, *Angew. Chem.* **1999**, *38*, 3526−3528; *Angew. Chem. Int. Ed.* **1999**, *38*, 0000−0000.

[7] [7a] D. S. Marlin, P. K. Mascharak, *Chem. Soc. Rev.* **2000**, *29*, 69−74. [7b] F. A. Chavez, P. K. Mascharak, *Acc. Chem. Res.* **2000**, *33*, 539−545. [7c] J. M. Rowland, M. Olmstead, P. K. Mascharak, *Inorg. Chem.* **2001**, *40*, 2810−2817.

[8] C. P. Horwitz, D. R. Fooksman, L. D. Vuocolo, S. W. Gordon-Wylie, N. J. Cox, T. J. Collins, *J. Am. Chem. Soc.* **1998**, *120*, 4867−4868. [8b] S. S. Gupta, M. Stadler, C. A. Noser, A. Ghosh, B. Steinhoff, D. Lenoir, C. P. Horwitz, K. Schramm, T. J. Collins, *Science* **2002**, *296*, 326−328.

[9] [9a] M. Amisnar, K. J. Schenk, S. Meghdadi, *Inorg. Chim. Acta* **2002**, *33*, 19−26. [9b] S. K. Dutta, U. Beckmann, E. Bill, T. Weyhermüller, K. Wieghardt, *Inorg. Chem.* **2000**, *39*, 3355−3364. [9c] A. K. Patra, M. Ray, R. Mukherjee, *Inorg. Chem.* **2000**, *39*, 652−657. [9d] A. K. Patra, R. Mukherjee, *Polyhedron* **1999**, *18*, 1317−1322. [9e] M. Ray, R. Mukherjee, J. P. Richardson, R. M. Buchanan, *J. Chem. Soc., Dalton Trans.* **1993**, 2451−2456. [9f] M. Ray, R. N. Mukherjee, *Polyhedron* **1992**, *11*, 2927−2937.

[10] N. G. Connelly, W. E. Geiger, *Chem. Rev.* **1996**, *96*, 877−910.

[11] R. L. Chapman, R. S. Wagg, *Inorg. Chim. Acta* **1979**, *33*, 227−234.

[12] S. Zhan, Q. Meng, X. You, *Polyhedron* **1996**, 2655−2658.

[13] T. L. Lu, H. Y. Kao, D. I. Wu, K. C. Kong, C. H. Cheng, *Acta Crystallogr., Sect. C* **1988**, *44*, 1184−1186.

[14] T. Hirose, K. Hiratani, K. Kasuga, K. Saito, T. Koike, E. Kimura, Y. Nagawa, H. Nakanishi, *J. Chem. Soc., Dalton Trans.* **1992**, 2679−2683.

[15] P. Maslak, S. Varadarajan, J. D. Burkey, *J. Org. Chem.* **1999**, *64*, 8201.

[16] Coordinates were taken from the isomorphous Fe compound (submitted for publication).

[17] G. M. Sheldrick, *SHELXS-97, Program for Crystal Structure Solution*, University of Göttingen, Germany, **1997**.

[18] G. M. Sheldrick, *SHELXTL*. Version 5.0. Siemens *Analytical X-ray Instruments Inc. Madison*, WI, USA, **1995**.

[19] A. L Spek, *Acta Crystallogr., Sect. A* **1990**, *46*, C34. R. L. Chapman, R. S. Wagg, *Inorg. Chim. Acta* **1979**, *33*, 227−234.

[20] C. K. Johnson, ORTEP, *A Thermal Ellipsoid Plotting Program*, Oak Ridge National, Laboratories: Oak Ridge, TN **1976**.

[21] R. H. Blessing, *Acta Crystallogr., Sect. A* **1995**, *51*, 33−38.

Received September 11, 2003
Early View Article
Published Online March 5, 2004

 © 2004 Wiley-VCH Verlag GmbH & Co. KGaA, Weinheim

Mechanism of the Stepwise Dissociation of Fe^{III} Complexes with Tripodal Ligands as Siderophore Models

Guy Serratrice,*[a] Frédéric Biaso,[a] Fabrice Thomas,[a] and Claude Béguin[a]

Keywords: Tripodal ligands / Iron / Kinetics and mechanisms / Dissociation / Catechol / 8-hydroxyquinoline

The acid hydrolysis and formation kinetics of 1:1 ferric complexes with several tripodal hexadentate ligands were investigated over the $[H^+]$ range of 0.02–1.0 M at 25 °C and at an ionic strength of 2.0 M ($NaClO_4/HClO_4$). These ligands are based on a tris(2-aminoethyl)amine (TREN) spacer connected through a tris(amide) moiety to identical pendant bidentate chelating group arms such as catecholate (TRENCAMS, **L^3**), 8-hydroxyquinolinate (O-TRENSOX, **L^0**) or pyridinophenolate (TRENPYPOLS, **L^5**). Mixed ligands with chelating arms such as catecholate and 8-hydroxyquinolinate (TRENSOX2CAMS, **L^1** and TRENSOXCAMS2, **L^2**) were also investigated. An analogue of **L^0** (C-SOX, **L^4**) with a C-pivot scaffold instead of TREN was studied for comparison. The acid hydrolysis reaction was found to proceed in four kinetically distinguishable stages. A common mechanism in the series was followed when the ligand structure was varied. The first stage is very fast and can be attributed to the dissociation of one arm of the tripodal ligand. The second and third stages involve protonation of the complex which induces a change of coordination giving the corresponding tetracoordinated bis(salicylate) complex (coordination with carbonyl and *o*-hydroxy oxygen atoms). The final dissociation of the ligand proceeds in the fourth stage by one or two kinetically detectable steps. For the last step an important structural effect may be observed from 1.2×10^{-5} to 2.2×10^{-2} s^{-1} for the proton-independent step and from 1.2×10^{-6} to 0.18 $M^{-1}s^{-1}$ for the proton-dependent step. Differences in the rates and mechanism between the different tripodal ligands are discussed in terms of the global electrostatic charge of the ligand and the donor ability of the chelating subunit. The C–N bond rotation of the amide moiety and the importance, depending on the charge, of the H-bond network in the partially uncoordinated complexes have also been considered. The role of electrostatics in complex formation is discussed in relation to the Eigen-Wilkins mechanism.

(© Wiley-VCH Verlag GmbH & Co. KGaA, 69451 Weinheim, Germany, 2004)

Introduction

Microbial iron bio-availability is largely determined by the coordination chemistry of Fe^{III} with siderophores, a class of organic compounds having a high and specific chelating affinity for this cation.[1−3] Natural (siderophores) or synthetic Fe^{III} chelating agents can be used for therapeutic or agrochemical applications.[4,5] To gain a better understanding of the mechanism of Fe^{III} chelation and transport in biological systems, quantitative evaluations have been reported through measurements of the kinetics of the Fe^{III} uptake and release (through acid hydrolysis) in aqueous solution.[1] A better knowledge of the cleavage of the iron−oxygen bonds in iron chelates can help with the design of new biologically useful ligands, more precisely by improving iron exchange from ligands to proteins. Studying the sensitivity of the iron−oxygen bond to acid hydrolysis is also interesting since it is well known that, in some compartments of the cell (lysozomes for example), lower pH levels are present. There have been extensive kinetic studies of (hydroxamato)Fe^{III} complexes in relation to the predominance of the hydroxamate binding sites in siderophores.[6−13] The most studied, hexadentate desferrioxamine B (DFB, desferal), has three bidentate hydroxamate groups.[8,9] Fe^{III} complexes of dihydroxamate siderophores and siderophore models have been also investigated[7,10,11] but there are a few kinetic data available for the dechelation processes of complexes with other types of ligands.

In particular, numerous ligands having the tripodal structure have been synthesized and the thermodynamic data of their Fe^{III} complexes have been determined. The tripodal structure mimics the backbone of the tris(catecholate) siderophore enterobactin. It is based on tris(2-aminoethyl)amine (TREN) as a spacer. This central organizing unit is connected through a tris(amide) moiety to pendant arms each containing a bidentate chelating group such as catecholate (TRENCAM,[14] TRENCAMS[15]), hydroxamate (TRENDROX[16]), 8-hydroxyquinolinate (O-TRENSOX[17]), pyridinophenolate (TRENPYPOLS[18]) or hydroxypyridonate.[19] These ligands all exhibit strong complexing behavior towards Fe^{III}. Recently, we synthesized mixed tripodal li-

[a] Institut de Chimie Moléculaire de Grenoble, Laboratoire de Chimie Biomimétique, LEDSS, UMR CNRS 5616, Université Joseph Fourier,
B. P. 53, 38041 Grenoble Cedex 9, France
E-mail: guy.serratrice@ujf-grenoble.fr

Supporting information for this article is available on the WWW under http://www.eurjic.org or from the author.

 © 2004 Wiley-VCH Verlag GmbH & Co. KGaA, Weinheim **DOI: 10.1002/ejic.200300396**

gands involving both catecholate and hydroxyquinolinate chelating subunits (TRENSOX2CAMS and TRENSOX-CAMS2[20]). They have been shown to be more effective at pH = 7.4 than the parent homopodal ligands TREN-CAMS and O-TRENSOX. Another series of tripodal ligands bearing a C-pivot scaffold with either 8-hydroxyquinoline (C-SOX,[21] COX[22]) or catechol subunits (Cac-CAM[23]) has also been developed in our laboratory. A C-pivot allows the grafting of any desired substituent, e.g. a polyoxyethylene chain, in order to modulate the hydrophile-lipophile balance or the fluorescent group used for labeling.

We previously investigated the dissociation, by acid hydrolysis, of the Fe^{III}-TRENCAMS[15] and Fe^{III}-O-TRENSOX[17b] complexes. Acid hydrolysis has been described by a stepwise mechanism producing the tetracoordinate bis(salicylate) complex and subsequently leading to its complete dissociation. In contrast to the 8-hydroxyquinoline groups, the catecholate groups have been found to be very labile. In this paper, we report an extensive kinetic study on the acid hydrolysis and formation kinetics of 1:1 ferric complexes with the ligands TRENSOX2CAMS (**L^1**), TRENSOX-CAMS2 (**L^2**), CSOX (**L^4**), and TRENPYPOLS (**L^5**). The structures of the ligands together with those of O-TRENSOX (**L^0**) and TRENCAMS (**L^3**) are depicted in Figure 1. The interesting feature of these ligands is the possibility of two modes of coordination for each arm of the ligand depending on the pH: a lowering of the pH leads to a switch from the coordination with the bidentate unit (8-hydroxyquinolinate or catecholate) to the so called salicylate-like mode in which protonation of the pyridine nitrogen atoms or *meta*-phenolic oxygen atoms induce their replacement by the amide carbonyl oxygen atoms (see for 8-hydroxyquinoline as example in Figure 2). Such a switch is proposed for the mechanism of iron release from enterobactin making reduction easier.[24] There are significant structural differences (bidentate subunit, spacer) between these tripodal ligands which therefore make a comparative study particularly interesting in order to elucidate electrostatic and structural factors affecting the dissociation and the formation of complexes. Furthermore, this kinetic investigation provides data necessary to formulate mechanisms by which the complexes are formed and dissociated.

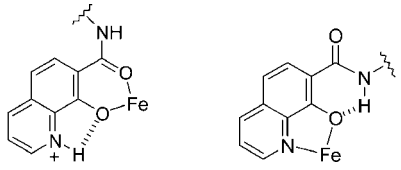

Figure 2. Salicylate (a) and 8-hydroxyquinolinate (b) mode of coordination of **L** with Fe^{III}

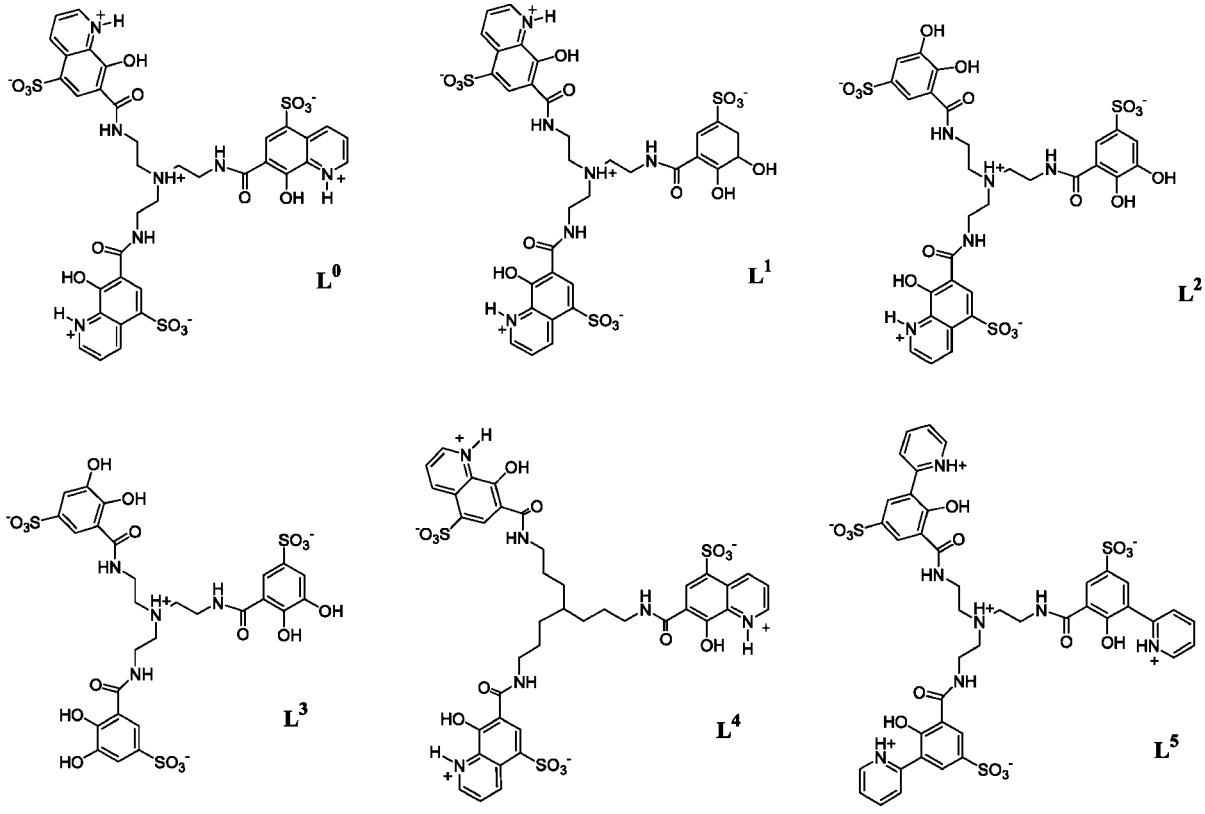

Figure 1. Chemical formulae of the tripodal ligands

 © 2004 Wiley-VCH Verlag GmbH & Co. KGaA, Weinheim

Results

Acid Hydrolysis Kinetics

General Observations

All the studied Fe**L**^{n} complexes (n = 0−5 as shown in Figure 1) have been previously characterized by UV/Vis spectrophotometry which showed protonated [Fe**L**^{n}H$_m$] species as the pH was lowered with acidic media.[15,17b,18,20] The acid hydrolysis kinetics of the complexes were investigated in aqueous solution (ionic strength I = 2 M, 25 °C) by the pH jump method under pseudo-first-order conditions with an excess of [H$^+$] (varying generally over the range 0.02−1.0 M) for solutions containing Fe^{III} and the tripodal ligand in a 1:1 molar ratio at an initial pH = 5. The k_{obs} rate constants were determined from the absorbance data versus time at the λ_{max} of the [Fe**L**^{n}] complex. The absorption spectra were also monitored (λ range 300−700 nm) using a diode array device in order to provide additional information on the intermediate species. As the pH was lowered, the spectral changes observed were the result of the change of the number ligands at the iron center and their mode of coordination due to protonation of the coordination sites. The structures of the protonated complexes which were formed during the acid hydrolysis were supported by their absorption spectra.[15,17b,18,20] The acid hydrolysis reaction was found to proceed in three or four kinetically distinguishable stages depending on the ligand. All reaction steps in the first stage were found to occur rapidly and exhibited a loss of absorbance at all the wavelengths (20% of the initial absorbance amplitude for all of the spectrum). This process (denoted stage 1) was too fast to be monitored by stopped-flow measurements and it can been attributed to the dissociation of one arm of the tripodal ligand. The second and the third stages caused a striking change in the spectrum. They involve protonation of the di-coordinated arms which induces a change of coordination to a salicylate mode giving the bis(salicylate) (tetra-coordinated) complex which has been clearly identified from our previous spectrophotometric studies.[15,17b,18,20] Finally, the dissociation of the ligand occurs in the fourth stage in one or two kinetically detectable steps. The successive rate constants are noted k_i where i = 4 and 3 for stages two and three, respectively, i = 2 and 1 for the two steps of the fourth stage (1 is for the last step of the dissociation).

Fe^{III}-TRENSOXCAMS2 (FeL^2)

Four first-order kinetic processes were observed in the [H$^+$] range of 0.001−1 M (Figure 3). The spectrum recorded after the dead time is similar to that of the complex [Fe**L**^{2}H$_3$] with a hydroxyquinolinate and catecholate coordination (λ_{max} = 540 nm) indicating rapid dissociation of a catechol arm and protonation of the tertiary nitrogen atom (Figure , a) since the value of its pK_a = 3.4.[20] A first-order absorbance decay was then measured in the time range of seconds (stage 2). The corresponding pseudo-first-order constant k_4^{obs} was found to vary linearly with [H$^+$] as shown in Figure S1 of the Supporting Information which suggests the rate law (3). The UV/Vis spectra were recorded as a function of the time and the spectrum at the end of stage 2 (Figure 4, b) was found to be similar to the spectrum of the [Fe**L**^{2}H$_4$] species (λ_{max} = 570 nm) having a hydroxyquinolinate coordination and a salicylate coordination with one catecholate arm (through carbonyl and hydroxy oxygen atoms).[20]

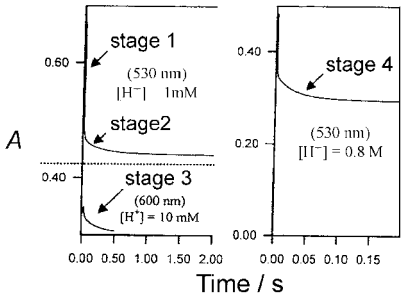

Figure 3. Acid hydrolysis kinetics of the Fe^{III}**L**^{2} complex: absorbance decay at λ = 530 or 600 nm; [Fe^{III}**L**^{2}] = 0.05 mM; [H$^+$] = 1 mM for stages 1 and 2, [H$^+$] = 10 mM for stage 3, [H$^+$] = 0.8 M for stage 4; solvent: water, I = 2 M (NaClO$_4$, HClO$_4$), 25 °C

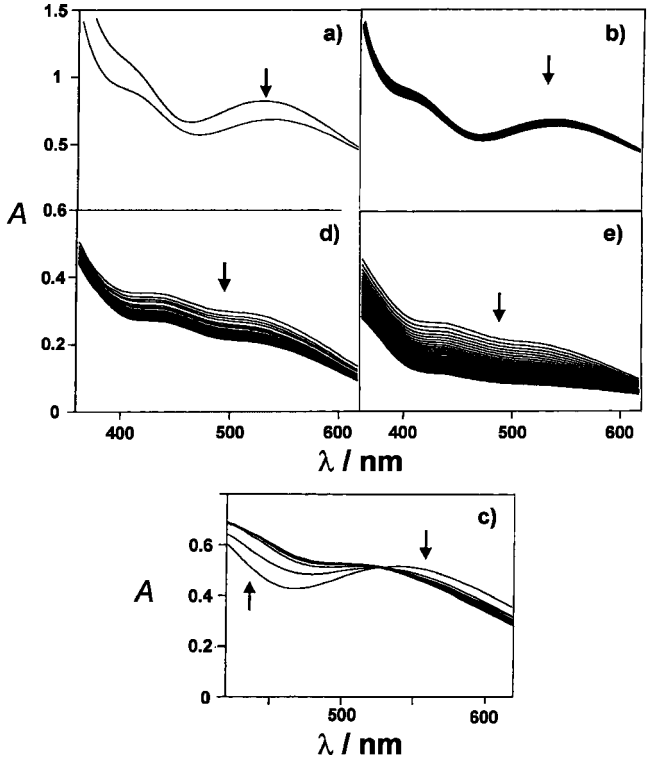

Figure 4. UV/Vis spectra recorded as a function of the time for the acid hydrolysis kinetics of the Fe^{III}**L**^{2} complex: (a) stage 1, 0−3 ms (b) stage 2, 0−1 s (c) stage 3, 0−500 ms (d) stage 4, step 1 0−0.5 s, (e) stage 4, step 2, 0.5−100 s; experimental conditions: see Figure 3; the arrow indicates the direction of change as the reaction proceeds

This is consistent with the following reactions (charges of the complexes and the ligand omitted) from which the

 © 2004 Wiley-VCH Verlag GmbH & Co. KGaA, Weinheim

values $k_4 = 4440 \pm 180$ M^{-1} s^{-1} and $k_{-4} \approx 0$ s^{-1} could be deduced [Equations (1)−(3)].

$$Fe\mathbf{L^2} + 3\,H^+ \rightleftarrows Fe\mathbf{L^2}H_3 \text{ (fast)} \quad (1)$$

$$Fe\mathbf{L^2}H_3 + H^+ \rightleftarrows Fe\mathbf{L^2}H_4\ (k_4, k_{-4}) \quad (2)$$

$$k_4^{obs} = k_4\,[H^+] + k_{-4} \quad (3)$$

The third stage exhibited a single-exponential absorbance decay measured at $\lambda = 600$ nm and was monitored over the $[H^+]$ range 0.01−0.07 M. The spectra collected during this stage exhibited an isosbestic point at 525 nm and a decrease of λ_{max} (Figure 4, c) characteristic of the formation of the $Fe\mathbf{L^2}H_5$ species having a bis(salicylate) coordination.[20] The rate constant k_3^{obs} did not show a variation with $[H^+]$ (mean value ≈ 60 s^{-1}, see Figure S2 in the Supporting Information). By analyzing the absorbance data at the end of this stage as a function of $[H^+]^n$ in the form of a Hill plot, a linear plot was obtained for $n = 1$ (Figure S3 in the Supporting Information). These data suggest a saturation behavior with a fast acid-basic pre-equilibrium preceding the rate determining step as given by Equations (4)−(6).

$$Fe\mathbf{L^2}H_4 + H^+ \rightleftarrows Fe\mathbf{L^2}H_5{}^*\ (K_3') \quad (4)$$

$$Fe\mathbf{L^2}H_5{}^* \rightleftarrows Fe\mathbf{L^2}H_5\ (k_3, k_{-3}) \quad (5)$$

$$k_3^{obs} = k_3\,K_3'\,[H^+]/(1 + K_3'\,[H^+]) + k_{-3} \quad (6)$$

Our results imply that $K_3'\,[H^+] >> 1$, so that $k_3^{obs} \approx k_3 + k_{-3}$. Since $[H^+]$ spans the range 0.01−0.07 M, the lower limit for K_3' can be evaluated as ≈10^3 M^{-1}. Since the pK_a value of the equilibrium $Fe\mathbf{L^2}H_5/Fe\mathbf{L^2}H_4$ has been reported as 2.2,[20] it can be inferred that $k_3/k_{-3} < \approx 10^{-0.8}$ ($1/K_a = K_3'k_3/k_{-3}$) allowing evaluation of an upper limit for k_3 as ≈ 10 s^{-1} and k_{-3} as ≈ 50 s^{-1}. The chemical identity of $Fe\mathbf{L^2}H_5{}^*$ will be discussed later.

The spectral change observed during stage 4 showed an absorbance decrease in two steps at all wavelengths (Figure 4, d and e) in two time ranges which is consistent with complete dissociation of the ligand. Two well separated single-exponential absorbance decays (measured at 500 nm) were monitored in the time range of 0.5 s and 100 s over the $[H^+]$ range of 0.2 to 0.65 M. The rate constants k_2^{obs} and k_1^{obs} exhibited linear variations with $[H^+]$ (Figure S4). This result can be interpreted by the successive dissociation reactions. The faster involves dissociation of one arm of the tripodal ligand (charge omitted for $[Fe\mathbf{L^2}H_n]$) [Equations (7) and (8)] with $k_2 = 33.1 \pm 1.9$ M^{-1} s^{-1} and $k_{-2} = 11.2 \pm 1.4$ s^{-1} and the slower involves dissociation of the ligand via two parallel acid-dependent and acid-independent pathways to give free iron(III) in agreement with the dissociation pathways proposed for ferric complexes with the hydroxamate ligand [Equations (9)−(11)[24]][6] {$[FeOH]^{2+}$ for $[Fe(OH)(OH_2)_5]^{2+}$, Fe^{3+} for $[Fe(OH_2)_6]^{3+}$}.

$$Fe\mathbf{L^2}H_5 + H^+ \rightleftarrows Fe\mathbf{L^2}H_6\ (k_2, k_{-2}, K_2) \quad (7)$$

$$k_2^{obs} = k_2\,[H^+] + k_{-2} \quad (8)$$

$$Fe\mathbf{L^2}H_6 + H^+ \rightleftarrows Fe^{3+} + \mathbf{L^2}H_7\ (k_1, k_{-1}, K_1) \quad (9)$$

$$Fe\mathbf{L^2}H_6 + H_2O \rightleftarrows FeOH^{2+} + \mathbf{L^2}H_7\ (k_1', k_{-1}', K_1') \quad (10)$$

$$Fe^{3+} + H_2O \rightleftarrows FeOH^{2+} + H^+\ (K_{Fe} = 0.0015\text{ M}) \quad (11)$$

By assuming relaxation conditions for the reverse reactions, the experimental rate law can be expressed as Equation (12).

$$k_1^{obs} = k_1[H^+] + k_1' + (k_{-1} + k_{-1}'\,K_{Fe}/(K_{Fe} + [H^+])([Fe^{III}]_e + [\mathbf{L^2}H_7]_e) \quad (12)$$

$[Fe^{III}]_e$ and $[\mathbf{L^2}H_7{}^+]_e$ are the total equilibrium concentrations of ligand and metal under our experimental conditions (calculated from absorbances at equilibrium). The term in parentheses calculated using the value of k_{-1}' (2200 M^{-1} s^{-1}) determined from formation kinetics study (vide infra) was found to be negligible (assuming k_{-1} also to be negligible). The fitted values are $k_1 = 0.0137 \pm 0.0005$ M^{-1} s^{-1} and $k_1' = 0.00237 \pm 0.00025$ s^{-1}.

It was found that $K_1\,K_2 = K_1'\,K_2/K_{Fe} = 10^{-2.68}$ is in reasonable agreement with the value $10^{-2.27}$ determined from measurements at equilibrium and at an ionic strength of 0.1 M.[20]

Fe^{III}−TRENSOX2CAMS (FeL^1)

Three distinct first-order kinetic processes could be detected (Figure S5). The spectrum recorded after the dead time suggests a bis-8-hydroxyquinolinate coordination (Figure S6a in the Supporting Information)[20] indicating rapid dissociation of a catechol arm and the formation of the $[Fe\mathbf{L^1}H_3]$ species taking account of the protonation of the tertiary nitrogen. The spectral change observed during stage 2 reflects the change of coordination to a bis(salicylate) mode with the two hydroxyquinoline arms (Figure S6b) in the $[Fe\mathbf{L^1}H_5]$ species. This is clearly supported by its absorbance spectrum.[20] Contrary to the $Fe\mathbf{L^2}$ complex, only one absorbance increase was monitored at 435 nm, in the time range of deciseconds, over the $[H^+]$ range of 0.03 to 0.9 M (Figure S5). It was supposed that formation of the $[Fe\mathbf{L^1}H_4]$ species, corresponding to the change of coordination to a salicylate mode for one 8-hydroxyquinoline arm, was not detectable under our experimental conditions. The absorbance increase allowed determination the rate constant k_3^{obs}. The variation of k_3^{obs} with $[H^+]$ (Figure S7) is linear for $[H^+] > 0.4$ M and exhibits an inverse proton dependence for $[H^+] < 0.4$ M. This behavior can best be

 © 2004 Wiley-VCH Verlag GmbH & Co. KGaA, Weinheim

explained by Equations (13)−(15), by analogy with Equations (9)−(11), yielding the rate expression according to Equation (16).

$$Fe\mathbf{L^1}H_4 + H^+ \rightleftarrows Fe\mathbf{L^1}H_5\ (k_3, k_{-3}) \quad (13)$$

$$Fe\mathbf{L^1}H_4 \rightleftarrows Fe\mathbf{L^1}H_4^*\ (k_3', k_{-3}') \quad (14)$$

$$Fe\mathbf{L^1}H_4^* + H^+ \rightleftarrows Fe\mathbf{L^1}H_5\ (K_3'', \text{fast}) \quad (15)$$

$$k_3^{obs} = k_3[H^+] + k_3' + (k_{-3}K_3''[H^+]) + k_{-3}')/(1 + K_3''[H^+]) \quad (16)$$

The non-linear fit of these data give the values $k_3 = 17.9 \pm 1.3$ M^{-1} s^{-1}, $k_{-3}' = 635 \pm 149$ s^{-1}, $K_3'' = 158 \pm 43$ M^{-1} (k_3' and k_{-3} could not be adjusted from the fit). The chemical identity of $Fe\mathbf{L^1}H_4$* and $Fe\mathbf{L^1}H_5$* will be discussed later.

The spectral change observed during stage 3 showed an absorbance decrease at all wavelengths (Figure S6c) and is consistent with dissociation of the ligand from the $Fe\mathbf{L^1}H_5$ species. A mono-exponential absorbance decay (measured at 435 nm) was monitored on a 1000 s time scale over the $[H^+]$ range of 0.2 to 1 M. The variation of k_1^{obs} vs. $[H^+]$ is shown in Figure 5. This can be interpreted by Equations (7) and (9)−(11) (replacing $\mathbf{L^2}$ for $\mathbf{L^1}$) and Equation (12) modified to give Equation (17) by considering Equation (7) as a fast pre-equilibrium.

$$k_1^{obs} = (k_1[H^+] + k_1')K_2[H^+]/(1 + K_2[H^+]) + [k_{-1} + k_{-1}' K_{Fe}/(K_{Fe} + [H^+])]([Fe^{III}]_e + [\mathbf{L^1}H_7]_e) \quad (17)$$

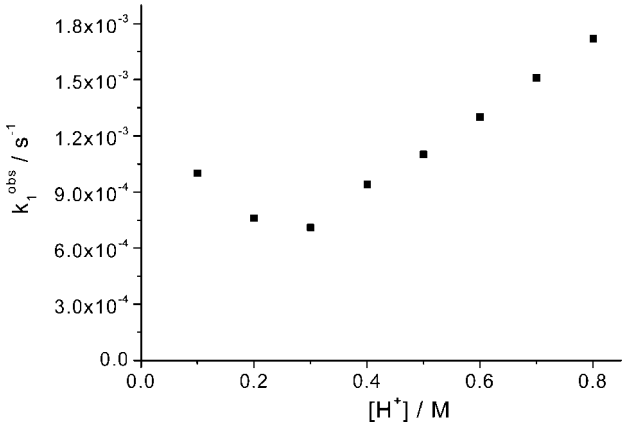

Figure 5. k_1^{obs} [s^{-1}] as a function of $[H^+]$ [M] in the acid hydrolysis kinetics of $Fe\mathbf{L^1}$; $[Fe\mathbf{L^1}] = 0.07$ mM; solvent: water, $I = 2$ M ($NaClO_4$, $HClO_4$), 25 °C

The term in parentheses was calculated using the value of k_{-1}' (1320 M^{-1} s^{-1}) determined from the formation kinetics study (vide infra) and assuming k_{-1} to be negligible. The fitted values are $k_1 = 0.0032 \pm 0.0004$ M^{-1} s^{-1} $k_1' \approx 0$ s^{-1} $K_2 = 1.70 \pm 0.55$ M^{-1}.

It was found that $K_1 K_2 \leq K_1' K_2/K_{Fe} = 10^{-3.55}$ (taking $k_1' \leq k_1/10$) which is in reasonable agreement with the value of $10^{-3.21}$ determined from measurements at equilibrium.[20]

Fe^{III}−CSOX (FeL^4)

Four distinct stages could be detected by measuring the absorbance decay at 600 nm (Figures S8 and S9). After the dead time, a bi-exponential decay of the absorbance was observed on a 10 s time scale with $[H^+]$ in the range of 0.02−0.1 M (stages 2 and 3). This decay could be fitted with a sum of two exponentials [Equation (18)].

$$A = A + A_1\exp(-k_4^{obs}\, t) + A_2\exp(-k_3^{obs}\, t) \quad (18)$$

The rate constants k_4^{obs} and k_3^{obs} vary apparently with $[H^+]$ with a non-zero intercept (Figure S10). This suggests two reversible elementary steps [Equations (19) and (20)].

$$Fe\mathbf{L^4}H_2 + H^+ \rightleftarrows Fe\mathbf{L^4}H_3\ (k_4, k_{-4}) \quad (19)$$

$$Fe\mathbf{L^4}H_3 + H^+ \rightleftarrows Fe\mathbf{L^4}H_4\ (k_3, k_{-3}) \quad (20)$$

The matrix formulation of the rate equations allows determination of analytical expressions for the observed rate constants. The following expressions can thus be deduced [Equations (21) and (22).

$$k_4^{obs} + k_3^{obs} = (k_4 + k_3)[H^+] + k_{-4} + k_{-3} \quad (21)$$

$$(k_4^{obs} - k_3^{obs})^2 = (k_4[H^+] + k_{-4})^2 + (k_3[H^+] + k_{-3})^2 + 2k_{-4}(k_3[H^+] - k_{-3}) - 2k_4(k_3[H^+] + k_{-3}) \quad (22)$$

The four microscopic constants were extracted from a non-linear least-squares refinement of the data according to Equations (21) and (22): $k_4 = 189 \pm 9$ M^{-1} s^{-1}, $k_{-4} = 10.0 \pm 0.4$ s^{-1}, $k_3 = 18.1 \pm 0.9$ M^{-1} s^{-1}, $k_{-3} = 1.20 \pm 0.05$ s^{-1}.

The spectral change observed during stage 4 showed an absorbance decrease at all wavelengths (Figure S9) and is consistent with dissociation of the ligand. A mono-ex-

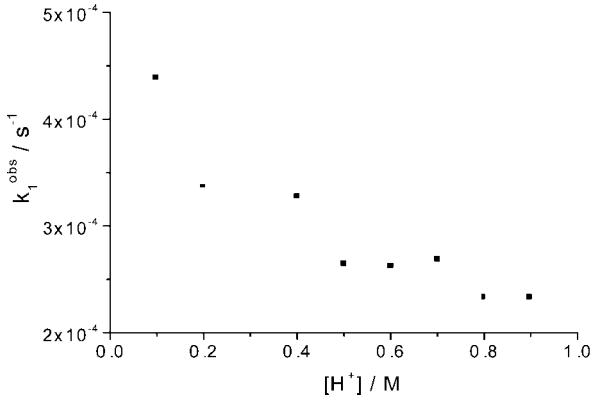

Figure 6. k_1^{obs} [s^{-1}] as a function of $[H^+]$ [M] in the acid hydrolysis kinetics of $Fe\mathbf{L^4}$; $[Fe\mathbf{L^4}] = 0.1$ mM; solvent: water, $I = 2$ M ($NaClO_4$, $HClO_4$), 25 °C

 © 2004 Wiley-VCH Verlag GmbH & Co. KGaA, Weinheim

ponential absorbance decay (measured at 435 nm) was monitored on a 10000 s time scale over the $[H^+]$ range of 0.1−1 M. The variation of k_1^{obs} vs. $[H^+]$ is shown in Figure 6.

This can be interpreted by Equations (9)−(11) and Equation (12) (by replacing FeL^2H_5 for FeL^1H_6 and L^2H_7 for L^1H_6). The term in parentheses was calculated using the value of k_{-1}' (1750 M^{-1} s^{-1}) determined from the formation kinetics study (vide infra) and assuming k_{-1} to be negligible. The fitted values are: $k_1' = (2.0 \pm 0.2) \times 10^{-4}$ s^{-1} and $k_1 \approx 0$ M^{-1} s^{-1}.

Fe^{III}−O−TRENSOX (FeL^0)

The acid hydrolysis kinetics have been previously published.[17b] Only the last step of the dissociation was not described. As for **Fe^{III}−CSOX**, release of the ligand is very slow (20000 s time scale) even at high H^+ concentrations. It was observed at 435 nm as a mono-exponential absorbance decay. The variation of k_1^{obs} vs. $[H^+]$ is shown in Figure 7. The fitted values from Equation (13) are $k_1' = 1.0 \times 10^{-5} \pm 1.0 \times 10^{-6}$ s^{-1} and $k_1 \approx 0$ M^{-1} s^{-1} [the term in parentheses in Equation (12) was calculated using the value of 789 M^{-1} s^{-1} for k_{-1}' [17b] and assuming k_{-1} to be negligible].

Fe^{III}−TRENPYPOLS (FeL^5)

The absorbance change was measured at 470 nm. Three stages were observed in the $[H^+]$ range of 0.001−1 M (Figure S11). The spectrum change after the dead time resulted in a decrease of λ_{max} from 495 to 469 nm (Figure S12a) and was attributed to the formation of a tetra-coordinated complex with one arm of the tripodal ligand in the pyridinophenolate coordination mode and the other in the salicylate coordination mode.[18] This very fast process was followed by a slight increase in the absorbance at 470 nm (stage 2) in the time range of 200 ms. The UV/Vis spectra recorded as a function of the time (Figure S12b) exhibited an isosbestic point at 540 nm and the spectrum at the end of this stage is similar to that of the bis(salicylate) complex $[FeL^5H_5]$.[18] The corresponding pseudo first-order constant k_3^{obs} was found to vary linearly with $[H^+]$ (Figure S13).

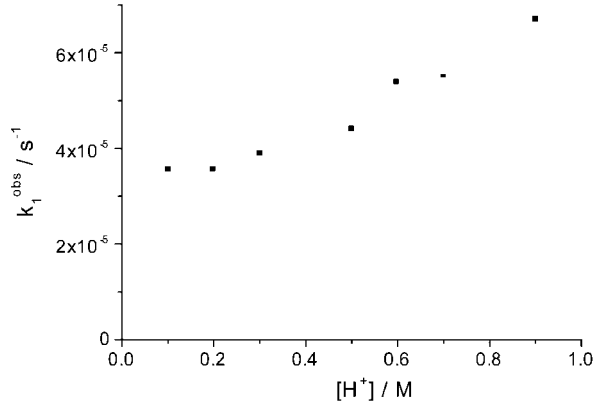

Figure 7. k_1^{obs} $[s^{-1}]$ as a function of $[H^+]$ [M] in the acid hydrolysis kinetics of FeL^0; $[FeL^0]$ = 0.07 mM; solvent: water, I = 2 M ($NaClO_4$, $HClO_4$), 25 °C

This is consistent with the reaction according to Equation (23) and and the rate law according to Equation (24) yielding the values $k_3 = 36 \pm 3$ M^{-1} s^{-1} and $k_{-3} = 18 \pm 1$ s^{-1}, respectively.

$$FeL^5H_4 + H^+ \rightleftarrows FeL^5H_5 \; (k_3, k_{-3}, K_3) \quad (23)$$

$$k_3^{obs} = k_3 [H^+] + k_{-3} \quad (24)$$

The spectral change observed during stage 3 showed an absorbance decrease at all wavelengths (Figures S12c and S12d) and resembles the spectra recorded for the formation reaction study. This is consistent with complete dissociation of the ligand. Two well-separated single-exponential absorbance decays (measured at 470 nm) were monitored in the time range of 5 s and 100 s over the $[H^+]$ range of 0.1−1 M. The rate constants k_2^{obs} exhibited linear variations with $[H^+]$ (Figure S14). The rate constants k_1^{obs} exhibited a linear proton dependence for $[H^+] > 0.2$ M and an inverse proton dependence for $[H^+] < 0.1$ (Figure 8). These successive dissociation reactions are consistent with reactions and rate laws according to Equations (7)−(12) (by replacing FeL^2H_5 with FeL^5H_5 and L^2H_7 with L^5H_7). The rate constants for Equation (7) have been determined as $k_2 = 4.9 \pm 0.2$ M^{-1} s^{-1}; $k_{-2} = 2.1 \pm 0.1$ s^{-1} and for Equations (9) and (10) the following could be evaluated from a non-linear least-squares fit of Equation (11) by taking for k_{-1}' the value of 514 M^{-1} s^{-1} determined from the formation kinetic studies (vide infra) and assuming k_{-1} to be negligible: $k_1 = (7.9 \pm 1.0) \times 10^{-3}$ M^{-1} s^{-1}; $k_1' = (9.6 \pm 5.7) \times 10^{-4}$ s^{-1}.

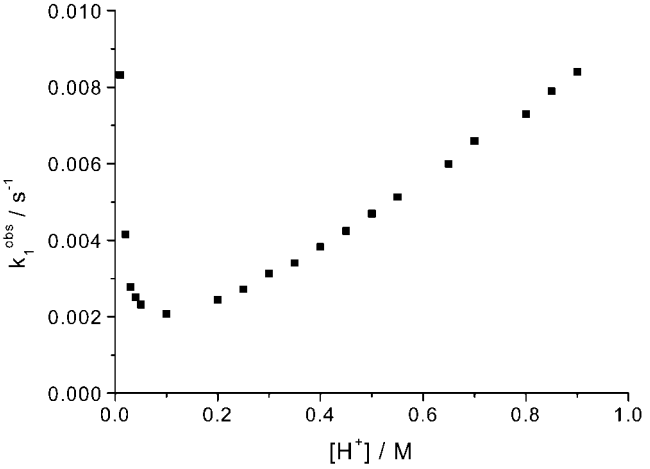

Figure 8. k_1^{obs} $[s^{-1}]$ as a function of $[H^+]$ [M] in the acid hydrolysis kinetics of FeL^5; $[FeL^5]$ = 0.2 mM; solvent: water, I = 2 M ($NaClO_4$, $HClO_4$), 25 °C

It was found that $K_1 K_2 = K_1' K_2 / K_{Fe} = 10^{-2.54}$ which is in reasonable agreement with the value of $10^{-1.79}$ determined from measurements at equilibrium.[18] The values of k_1, k_1', k_2, and k_{-2} for all the complexes are collected in Table 1.

 © 2004 Wiley-VCH Verlag GmbH & Co. KGaA, Weinheim

Table 1. Microscopic rate constants for the dissociation of the Fe$\mathbf{L}^{n}H_5$ (except for $\mathbf{L^4}$, Fe$\mathbf{L^4}H_4$) complexes

k_i [M^{-1} s^{-1}] (k_{-i} [s^{-1}])	Fe$\mathbf{L^0}$	Fe$\mathbf{L^1}$	Fe$\mathbf{L^2}$ [a]	Fe$\mathbf{L^3}$ [b]	Fe$\mathbf{L^4}$	Fe$\mathbf{L^5}$
k_2 (k_{-2})	–	–	33.1 (11.2)	fast	–	4.9 (2.1)
$10^3 \times k_1$	< 0.0012	3.2	13.7	184	< 0.02	7.9
$10^3 \times k'_1$ [s^{-1}]	0.012	< 0.32	2.37	22	0.20	0.96
$10^{-3} \times k'_{-1}$ [M^{-1} s^{-1}]	0.789	1.32	2.24	2.7	1.75	0.51

[a] Ref.[17b] [b] Ref.[15]

Formation Kinetics

The kinetics of formation of the ferric complex with ligands $\mathbf{L^1}$, $\mathbf{L^2}$, $\mathbf{L^4}$ and $\mathbf{L^5}$ were investigated by a stopped-flow spectrophotometric method under pseudo-first-order conditions: [Fe^{III}] and [H$^+$] >> [$\mathbf{L}^n$] and at an ionic strength I = 2 M at 25 °C. The absorbance change vs. time at λ = 435 nm showed a single exponential curve indicating that the complex formation reaction proceeds through a single rate-limiting step. It should be noted that the spectra recorded with time using a diode array device were identical to those recorded for the final step of acid hydrolysis. It has been found that the pseudo-first-order rate constants k^{obs} at a given acidity level ([H$^+$] varied from 0.03 to 1 M) show a linear variation as a function of [Fe^{III}]$_{tot}$ with a zero intercept, and at a given concentration of Fe^{III} have a linear variation as a function of 1/[H$^+$] (Figure 9, a as an example). This suggests that the main reaction is the formation of the complex [Fe$\mathbf{L}^{n}H_6$] through the hydrolyzed ferric ion FeOH^{2+} {for [Fe(OH)(OH$_2$)$_5$]$^{2+}$} according to Equation (10) (formation is the reverse reaction). This leads to the observed pseudo-first-order rate constant given by Equation (25), where [Fe^{3+}] = [Fe^{3+}]$_{tot}$ – [FeOH]$^{2+}$ – 2 [Fe$_2$(OH)$_2$]$^{4+}$ and [H$^+$] takes into account the protons involved in formation of FeOH^{2+} [Equation (11)] and the dimer Fe$_2$(OH)$_2^{4+}$ {for [Fe$_2$(OH)$_2$(OH$_2$)$_8$]$^{4+}$} [Equation (26)].[25]

$$k_{obs} = k_{-1}' K_{Fe} [Fe^{3+}]/[H^+] + k_1' \quad (25)$$

$$2\ Fe^{3+} \rightleftarrows Fe_2(OH)_2^{4+} + 2\ H^+ \ (K_{DFe} = 0.0024\ M) \quad (26)$$

A linear variation of k_{obs} versus [Fe^{3+}]/[H$^+$] was observed (Figure 9, b for $\mathbf{L^1}$, Figure S15 for $\mathbf{L^2}$, Figure S16 for $\mathbf{L^4}$ and Figure S17 for $\mathbf{L^5}$). Least-squares fits of the data yielded the values of k_{-1}' 1320 ± 60, 2240 ± 120, 1750 ± 40 and 514 ± 8 M^{-1} s^{-1} for $\mathbf{L^1}$, $\mathbf{L^2}$, $\mathbf{L^4}$ and $\mathbf{L^5}$, respectively ($k_1' \approx 0$ s^{-1} for all cases). The values of k_{-1}' are collected in Table 1 together with the values previously determined for the formation of Fe$\mathbf{L^0}$ and Fe$\mathbf{L^3}$.

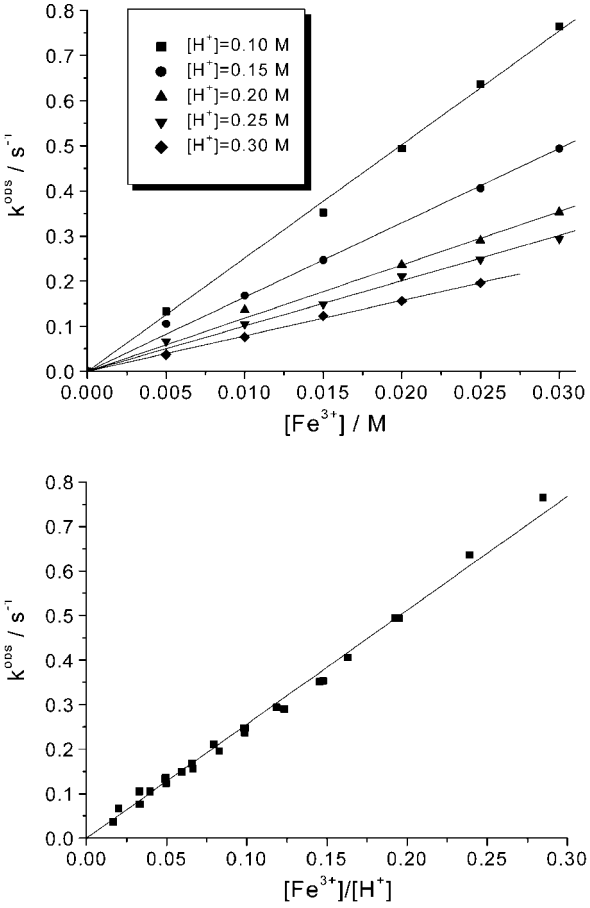

Figure 9. Complex formation kinetics of $\mathbf{L^1}$ with Fe^{III}: (a) k_{obs} [s^{-1}] as a function of [Fe^{3+}]$_{tot}$ [M] at various [H$^+$] [M]; [$\mathbf{L^1}$] = 0.1 mM; (b) k_{obs} [s^{-1}] as a function of [Fe^{3+}]/[H$^+$] according to Equation (25); solvent: water, I = 2 M (NaClO$_4$, HClO$_4$), 25 °C

Discussion

Dissociation Kinetics

Rate constant data for the stepwise acid dissociation of the Fe$^{III}\mathbf{L}^{n}$ complexes are summarized in Tables 1 and 2, including data already published for O–TRENSOX[17b] ($\mathbf{L^0}$) and O–TRENCAMS[15] ($\mathbf{L^3}$). For easy comparison of the kinetic data of stages 1–3, we have reported in Table 2 the state of protonation of the tertiary nitrogen atom (for $\mathbf{L^0}$, $\mathbf{L^1}$, $\mathbf{L^2}$, $\mathbf{L^3}$ and $\mathbf{L^5}$) and the mode of coordination of Fe^{III} in the different species according to the state of protonation, the number of arms coordinated to the metallic cation and the bidentate coordination (8-hydroxyquinolinate or -catecholate or -salicylate). The following discussion suggests elementary reaction pathways as depicted in Figure 10 for Fe$\mathbf{L^2}$, Figure S18 for Fe$\mathbf{L^1}$ and Figure 14 of ref.[17b] for Fe$\mathbf{L^0}$, as examples.

 © 2004 Wiley-VCH Verlag GmbH & Co. KGaA, Weinheim

Table 2. Recapitulative table of the measured hydrolysis rate constants for Fe**L″** → Fe**L″**H_5 including modes of protonation and coordination for each stage (charges are omitted)

Ligand	Species[a]	k_n [$M^{-1}s^{-1}$]	k_{-n} [s^{-1}]	Tertiary N[b]	Mode of coordination[c]
L^0	Fe**L^0**H			NH	NO/NO/NO
Ref.[17b]		fast			
	Fe**L^0**H_3			NH	NO/NO/free
	k_4	643	15		
	Fe**L^0**H_4			NH	NO/OOsal(ox)/free
	k_3	5.7	1.3		
	Fe**L^0**H_5			NH	OOsal(ox)/OOsal(ox)/free
L^1	Fe**L^1**			N	NO/NO/OO
		fast			
	Fe**L^1**H_2			N	NO/NO/free
	Fast	−			
	Fe**L^1**H_3			NH	NO/NO/free
	k_4	−	−		
	Fe**L^1**H_4			NH	NO/OOsal(ox)/free
	k_3	17.9			
	Fe**L^1**H_5			NH	OOsal(ox)/OOsal(ox)/free
	$K_3'' = 158$	−			
	Fe**L^1**H_4*			N	OOsal(ox)/OOsal(ox)/free
L^2	Fe**L^2**H			NH	NO/OO/OO
	Fe**L^2**H_3			NH	NO/OO/free
	k_4	4440	< 1		
	Fe**L^2**H_4			NH	NO/OOsal(cat)/free
	$K'_3 > 1000$	fast			
	Fe**L^2**H_5*			NH	O(ox)/OOsal(cat)/free
	k_3	< 10 s^{-1}	ca. 50		
	Fe**L^2**H_5			NH	OOsal(ox)/OOsal(cat)/free
L^3	Fe**L^3**H			NH	OO/OO/OO
Ref.[15]		fast			
	Fe**L^3**H_3			NH	OO/OO/free
		fast			
	Fe**L^3**H_5			NH	OOsal(cat)/OOsal(cat)/free
L^4	Fe**L^4**			C	NO/NO/NO
		fast			
	Fe**L^4**H_2			C	NO/NO/free
	k_4	189	10.0		
	Fe**L^4**H_3			C	NO/OOsal(ox)/free
	k_3	18.1	1.2		
	Fe**L^4**H_4			C	OOsal(ox)/OOsal(ox)/free
L^5	Fe**L^5**H			NH	NO*/NO*/NO*
		fast	−		
	Fe**L^5**H_3			NH	NO*/NO*/free
	k_4	fast	−		
	Fe**L^5**H_4			NH	NO*/OO*sal/free
	k_3	36	18		
	Fe**L^5**H_5			NH	OO*sal/OO*sal/free

[a] The different states of protonation during the pH jump (see text). [b] State of protonation of the anchor. [c] The coordination atoms of the three arms, separated by /, in the reverse order of the complete removal of the *n*th arm with Fe^{III}: "free" indicates an arm without a coordination bond to the iron atom, NO (NO*) refers to 8-hydroxyquinolinate (pyridinophenolate) bidentate coordination to Fe^{III}, OO refers to catecholate bidentate coordination to Fe^{III}, OOsal(ox) indicates salicylate bidentate coordination of a hydroxyquinoline arm to Fe^{III}, OOsal(cat) refers to salicylate bidentate coordination of a catechol arm to Fe^{III}, OO*sal represents salicylate bidentate coordination of a pyridinophenol arm to Fe^{III}.

Stage 1

On the basis of the spectral change, the reaction steps in this stage have been attributed to the dissociation of one arm of the ligand. This process is very fast whatever the type of chelating group. This suggests that the steric strain release in the complex may increase the rate of Fe−O and (or) Fe−N_{pyr} cleavage. We can also invoke, for the high kinetic lability of the hexacoordinate complex, the solvent rearrangement resulting from dissociation of the first bidentate group, as already supported for hydroxamate dissociation.[6] It can be suggested that the dissociated arm is maintained in proximity to the first coordination sphere of Fe^{III} through hydrogen bonds between the water molecules coordinated to Fe^{III} and the free arm. This results in a small motion of the arm as it dissociates from the Fe^{III} center

 © 2004 Wiley-VCH Verlag GmbH & Co. KGaA, Weinheim

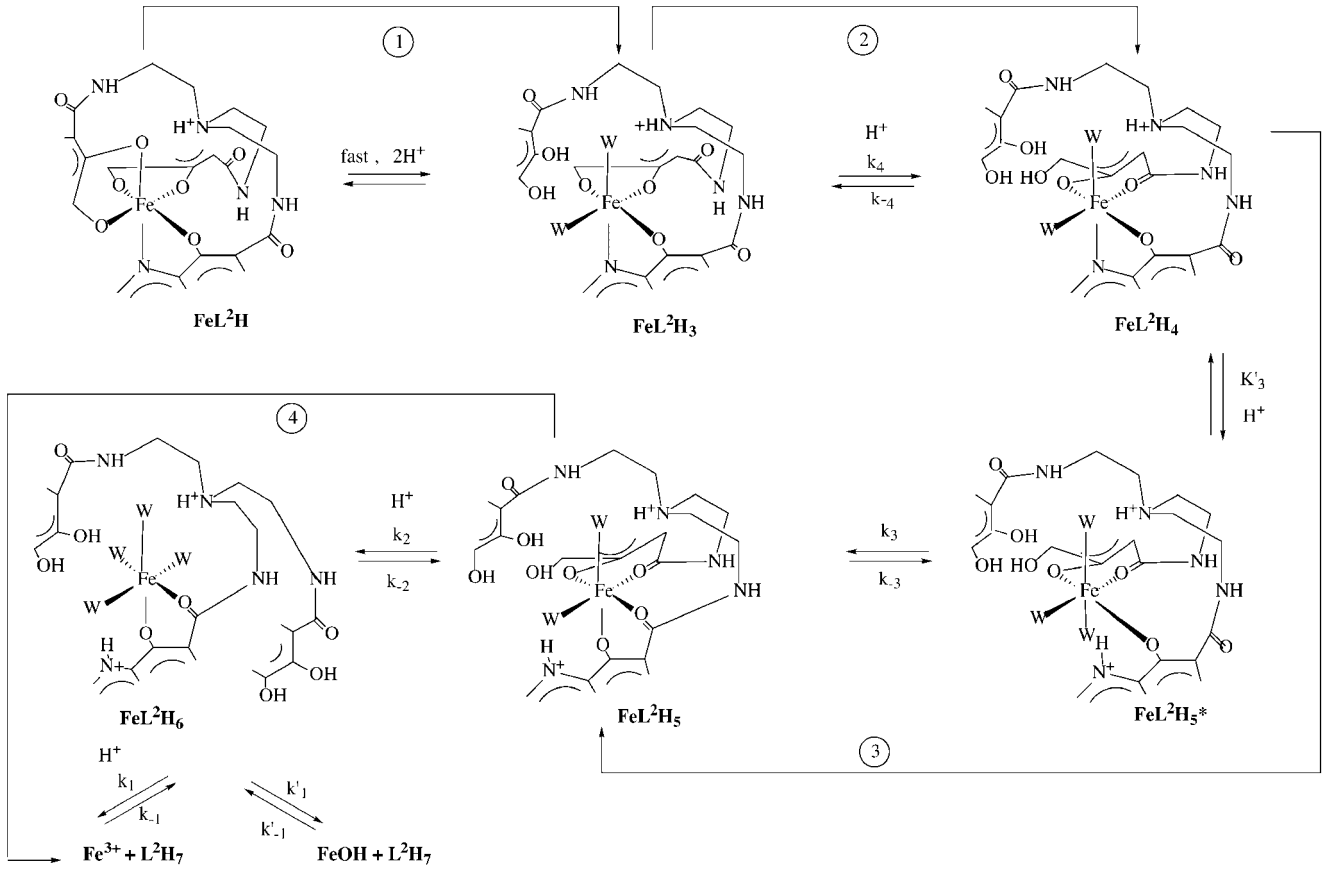

Figure 10. Proposed mechanism for the acid hydrolysis of the Fe$\mathbf{L^2}$H complex

and a slight solvent rearrangement. The reaction from the hexadentate to the tetradentate complex may therefore be a facile process.

Stages 2 and 3

Overall Scheme

These stages result in the formation of a bis(salicylate)-coordinated complex Fe$\mathbf{L}^n$H$_5$ (except Fe$\mathbf{L^4}$H$_4$) as clearly indicated by the spectra recorded at the end of stage 3 in agreement with the equilibrium studies previously published. Each stage is related to one arm of the ligand. It may involve the Fe−N$_{pyr}$ or Fe−O (depending on the type of bidentate group in $\mathbf{L}^n$) bond cleavage with protonation of N or O leading to an open-ring structure with the bidentate moiety, followed by the Fe−O(=C) bond closing the salicylate ring. It should be noted that this change of coordination requires conformational reorganization of the arm by rotation about the C−N amide bond in order to allow the carbonyl group to be in a suitable position favorable for salicylate coordination. Indeed, it has been shown that the carbonyl group is turned outside the Fe^{III} coordination sphere owing to hydrogen bond between the amide hydrogen atom and the *ortho*-oxygen atom (quinolinol or catechol or phenol) when Fe^{III} is coordinated with the bidentate group of each arm, as clearly evidenced.[22,26] We were able to obtain information on several elementary steps corresponding to stages 2 and 3 and rate constants k_4 and k_3, depending on the structure of the tripodal ligand, homopodand or heteropodand, and on the nature of the chelating subunit (catecholate, 8-hydroxyquinolinate, pyridinophenolate). Interesting correlations of the rate constants for same type of process with the chemical structures can be made.

Stages 2 and 3 for the Homopodate Fe$\mathbf{L}^n$H$_3$ Complexes (n = 0, 3, 4, 5)

The values of k_4 and k_3 clearly indicate the more labile character of the catechol arms (fast for the two arms in Fe$\mathbf{L^3}$H$_3$) compared with the pyridinophenol arms (first arm: fast, second arm: 36 M^{-1} s^{-1} in Fe$\mathbf{L^5}$H$_3$) and the 8-hydroxyquinoline arms (first arm: 643 and 189 M^{-1} s^{-1}, second arm: 5.7 M^{-1} s^{-1} and 18.1 M^{-1} s^{-1} in Fe$\mathbf{L^0}$H$_3$ and Fe$\mathbf{L^4}$H$_2$, respectively). This reflects (i) the higher donor strength of catecholate vs. pyridinophenolate and 8-hydroxyquinolinate which increases the electron density of the metal so that the bonds with the coordinated donor atoms are weakened; (ii) the chelate bulkiness which influences the rate of rotation about the C−N amide bond (pyridinophenol vs. catechol); (iii) the easier rotation of the am-

 © 2004 Wiley-VCH Verlag GmbH & Co. KGaA, Weinheim

ide bond in the catechol arm compared with in the 8-hydroxyquinoline arm that can be related to the electron-withdrawing effect of the 8-hydroxyquinoline group as clearly shown from the pK_a values of the carboxylic groups in the 2,3-dihydroxybenzoic acid (2.7) and in the 7-carboxy-8-hydroxyquinoline (1.9).[27]

Stages 2 and 3 for the Heteropodate FeL^nH_3 Complexes (n = 1, 2)

The reaction scheme developed from the analysis of the kinetic data is slightly different than for the homopodate complexes. For $\mathbf{L^1}$, only the stage $Fe\mathbf{L^1}H_4/Fe\mathbf{L^1}H_5$ was detected and can be described by Equations (13)−(15). This scheme, developed from an analysis of the kinetic data, has been proposed since the pK_a values of the tertiary amine nitrogen atom (1.9) and of the two hydroxyquinoline nitrogen atoms (2.4) are close.[20] We assumed a complicated kinetic pattern involving an acid-basic micro-equilibrium. A pictorial view of the proposed scheme is shown in Figure S18 (see also Table 2 for the state of protonation). The equilibrium between $Fe\mathbf{L^1}H_4$ and $Fe\mathbf{L^1}H_4$* [Equation (14)] involves proton transfer between the tertiary nitrogen atom and the quinoline nitrogen atom coordinated to the iron center, leading to the change of coordination of the 8-hydroxyquinoline moiety. The reaction according to Equation (15) involves the protonation of the tertiary amine nitrogen atom. The k_3 value (17.9 M^{-1} s^{-1}) is similar to the corresponding values determined for $Fe\mathbf{L^0}H_4$ (5.7 M^{-1} s^{-1}) and $Fe\mathbf{L^4}H_3$ (18.1 M^{-1} s^{-1}). The value of K_3'' (158 M^{-1}) is in agreement with the pK_a value (1.9) determined from static measurements at a 0.1 M ionic strength. The k_{-3}' value (635 s^{-1}) has no equivalent in the kinetic treatment to be related to the previously described micro-equilibrium. For $Fe\mathbf{L^2}H_3$ the value of k_4 (4440 M^{-1} s^{-1}) is consistent with the high lability of the catechol arm. For stage 3, we suggest that the pre-equilibrium [Equation (4)] is related to the Fe−N bond breaking of the 8-hydroxyquinoline arm leading to $Fe\mathbf{L^2}H_5$* (Figure 10) and that the last step [Equation (5)] is the change to the bidentate salicylate coordination of this arm ($Fe\mathbf{L^2}H_5$). The upper limit of 10 s^{-1} for k_3 is reasonable by comparison with the rate of rotation about the amide bond in hydroxamate ligands.[6]

Stage 4

In the last stage, leading from the tetradentate bis(salicylate) to the free ligand, at least two steps occur, corresponding to the Fe−O bond breakings of each salicylate arm. The rate constants for the leaving of the penultimate salicylate arms, k_2, could be measured only for $\mathbf{L^2}$ (33 s^{-1} M^{-1}) and $\mathbf{L^5}$ (4.9 s^{-1} M^{-1}). The smaller value for $Fe\mathbf{L^5}$ can be related to the bulkier access for the proton to the tetradentate complex with the pyridinophenol subunits in relation to the easy bond rotation between the pyridine and phenol moieties. The rate constants for the leaving of the last salicylate arm, k_1 (proton-dependent) and k'_1 (proton-independent) are well documented for all terms of the series (Table 2). About three orders of magnitude were observed, when measured, between k_2 and k_1 (or k'_1) for the release of two identical (salicylate) arms as already observed in related systems.[1]

Dependence of k_1 and k'_1 as a Function of Structure (Electrostatic Charge)

The important feature is that the rate constants k_1 and k_1' span over a range of several orders of magnitude: five orders for k_1 (184 to 0.0012×10^{-3} M^{-1} s^{-1}) and three and a half orders for k_1' (22 to 0.012×10^{-3} s^{-1}). Several trends in relation to the structure of the complex should be pointed out. The decrease of the rate constants k_1 and k_1' (except for $[Fe\mathbf{L^5}H_6]^{4+}$) in the series (Table 1) seems to be related mainly to the increase of the positive charges on the complexes evaluated without taking account of the sulfonate substituents, as in +3, +4, +5 and +6 for the iron(III) complexes with $\mathbf{L^3}$, $\mathbf{L^2}$, both $\mathbf{L^1}$ and $\mathbf{L^4}$ and $\mathbf{L^0}$, respectively. For the proton-dependent pathway (k_1) this is partly due to repulsion of the incoming H^+ by positive charges, suggesting that the dissociated 8-hydroxyquinoline arms of the ligand are maintained in proximity to the first coordination sphere of Fe^{III} probably through H-bonding between pyridinium nitrogen atoms and coordinated water molecules. It should be pointed out that k_1 for the complexes with the tris(8-hydroxyquinoline) ligands ($\mathbf{L^0}$ and $\mathbf{L^4}$) is 2 to 3 orders of magnitude slower than for the other complexes. This is probably due to enhanced repulsion for H^+ by positive charges suggesting a closer proximity for the dissociated arms than for the other ligands in $[Fe\mathbf{L^0}H_6]$ and $[Fe\mathbf{L^4}H_6]$. Indeed, pyridinium nitrogen atoms have been found to establish H-bonds with oxygen atoms coordinated to Fe^{III} in the structure of the tris(salicylate) complex with $\mathbf{L^0}$ forming a tight coordination sphere around the Fe^{III} center.[28] The value of 0.0079 M^{-1} s^{-1} for $[Fe\mathbf{L^5}H_6]^{4+}$ is high when compared with these highly charged complexes. This suggests a lower repulsion of the incoming H^+ by positive charges that are assumed to be far from the coordination sphere due to a free rotation of the pyridine ring relative to the phenol ring, thus disfavoring the formation of hydrogen bonds. For the proton-independent pathway, the decrease of k_1' parallels that of k_1.

Relationship between the Acid-Dependent and Acid-Independent Steps

The rate constants of these dissociations having acid-dependent and acid-independent steps vary in the same manner as a function of structure. We believe that this similarity is related to the structures of the transition states differing only by the presence of a proton. As the starting species is the same for these two steps, the transition state theory suggests a linear correlation between ln k_1 and ln k_1' [Equations (27) and (28)] as already discussed.[29,30]

$$\ln k_1 = \ln k_1' + \ln K_t \quad (27)$$

$$-\ln K_t = \Delta G_t^{\#}/RT \quad (28)$$

 © 2004 Wiley-VCH Verlag GmbH & Co. KGaA, Weinheim

$\Delta G_t^{\#}$ is the free energy difference between the deprotonated and the protonated transition states, K_t may be considered as the protonation constant for the transition state and pK_{At} (= log k_1 − log k'_1) may be considered as a pseudo-pK_A of the transition state. A good correlation with a slope of 0.96 and an intercept $\ln K_t = 1.83$ ($pK_{At} = 0.80$) was obtained for the complexes with **L**[1], **L**[2], **L**[3] and **L**[5] (Figure 11). The correlation was not attempted for **L**[0] and **L**[4] since, for these ligands, k_1 values were only obtained as superior limits.

This correlation indicates that all the complexes follow the same dissociation mechanism from salicylate coordination. The protonation of the transition state is reasonably constant for this series. This implies that the hydroxy group is not implied in the transition state since its pK_a varies over a large range (5.6−9.23) in the free ligand. The Fe−O=C bond cleavage can therefore be suggested as the rate-limiting step for dissociation after a fast opening of the chelate ring as shown in Figure 12.

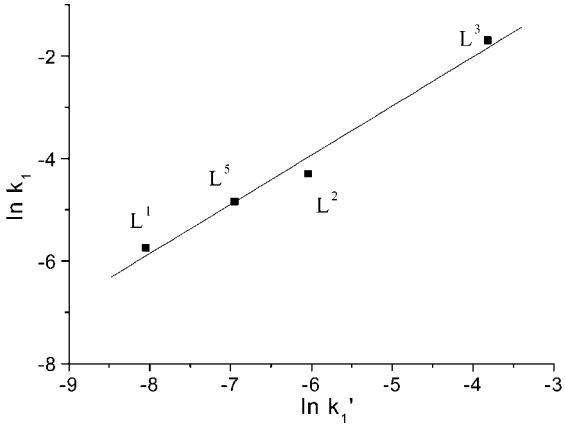

Figure 11. $\ln k_1$ vs. $\ln k_{-1}'$ for the final step dissociation of Fe**L**^{n} complexes; data were measured in aqueous 2.0 M $NaClO_4/HClO_4$ at 25 °C

Such a relationship has been observed for the dissociation of a large series of Fe^{III}-mono(hydroxamato) complexes yielding a slope of 0.9(1) in agreement with the theoretical value of 1, and an intercept $\ln K_1 = -0.6$ ($pK_{At} = -0.26$).[7] The correlation shows also that the transition state acidity of Fe^{III} (**L**[1] or **L**[2] or **L**[3] or **L**[5]) is lower than that of Fe^{III}(hydroxamic acid), i.e. that H^+ is more tightly bound in our series.

Linear Free Energy Relationships between k_1' and K_1'

The strong structural effect for the dissociation rate constants and the small dependence for the formation rate constants suggests a linear free energy relationships between $\ln k_1'$ and $\ln K_1'$ (K_1' has been calculated from k_1'/k_{-1}') [Equation (29)], where k_{-1}' (k_{-1}) is the formation rate constant when the active iron species is $FeOH^{2+}$ (Fe^{3+}). The theoretical basis for this correlation has been presented by Caudle and Crumbliss.[6]

$$\ln k_1' = \ln K_1' + \ln k_{-1}' \quad (29)$$

The plot $\ln k_1'$ vs. $\ln K_1'$ shown in Figure 13 (a) indicates a reasonably linear relation for the five complexes studied with a slope of 1.1 in agreement with the theoretical value of 1. This high degree of correlation suggests a similar mechanism in the final step of the dissociation. This implies a late transition state where the cleavage of the metal−ligand bonds are largely moved forward. The plot

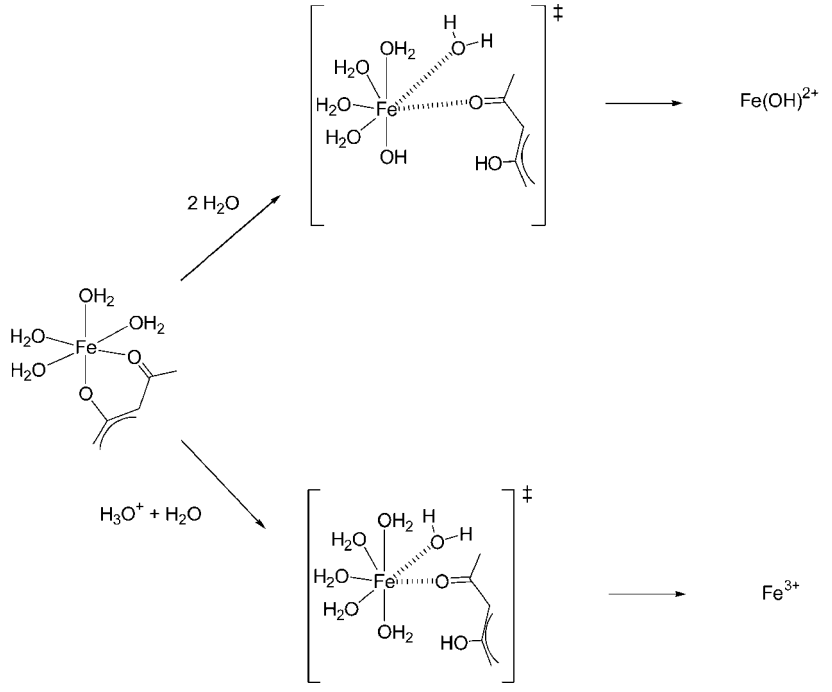

Figure 12. Transition states for proton-dependent and proton-independent dissociation of bidentate Fe−**L**^{n} complexes

 © 2004 Wiley-VCH Verlag GmbH & Co. KGaA, Weinheim

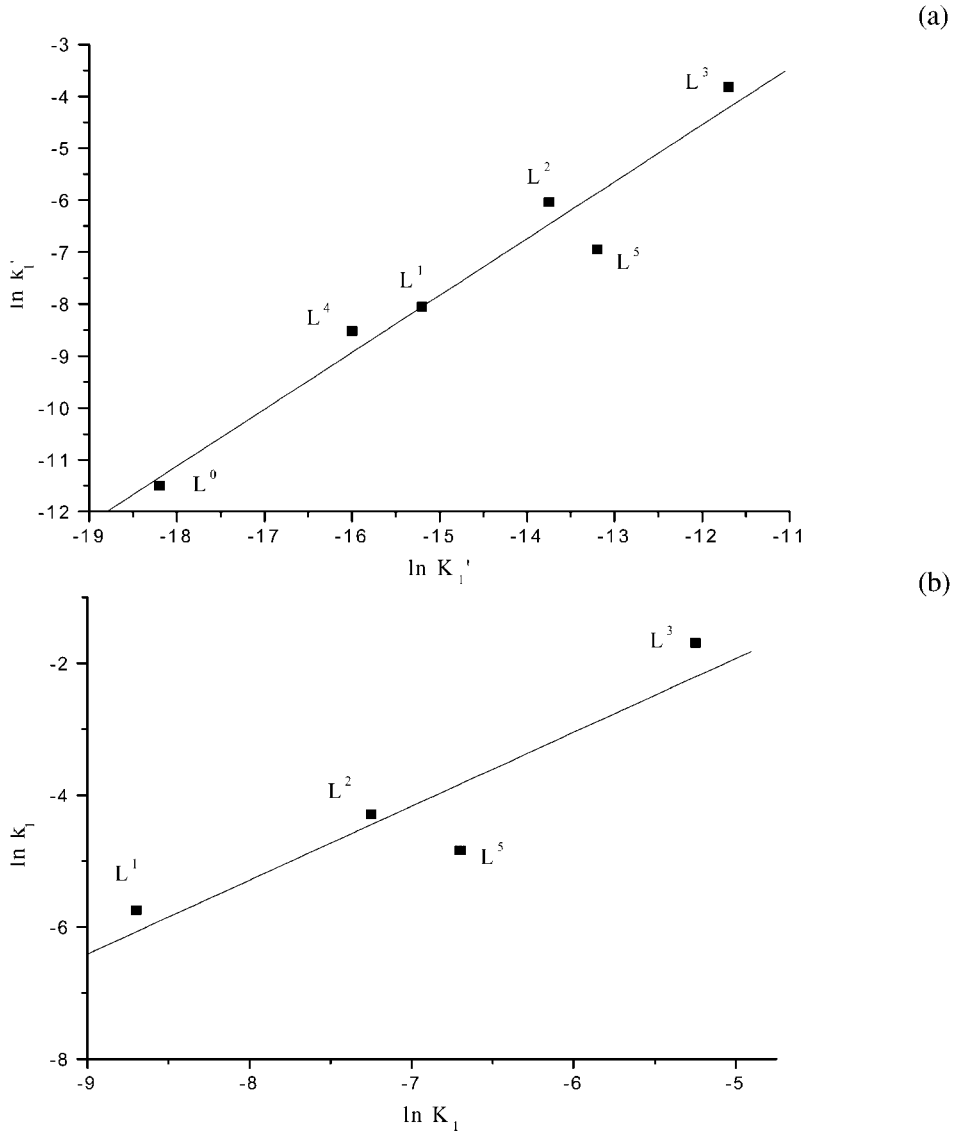

Figure 13. (a) ln k_1' vs. ln K_1' for proton-independent dissociation of bidentate Fe−**L**^{n} complexes; (b) ln k_1 vs. ln K_1 for proton-dependent dissociation of bidentate Fe−**L**^{n} complexes; data were measured in aqueous 2.0 M $NaClO_4/HClO_4$ at 25 °C

ln k_1 vs. ln K_1 (K'_1 calculated from K_1/K_{Fe}) also exhibits a reasonable correlation between data points for **L**^{1}, **L**^{2}, **L**^{3}, **L**^{5} with a slope of 1.1 (Figure 13, b) (a better correlation was obtained for the series **L**^{1}, **L**^{2}, **L**^{3}), as the correlation related to Equation (29) occurs. The proposed transition states are described in Figure 12.

Formation Kinetics

The rate-determining step is the coordination of Fe^{III} with one arm of the ligand through the salicylate coordination followed by a rapid coordination with a second arm of the ligand leading to the $[Fe\mathbf{L}H_5]^{n+}$ species. The spectra recorded during the formation of the complex using diode array device clearly show that coordination occurs through the 8-hydroxyquinoline arm for the mixed ligands **L**^{1} and **L**^{2}.

Ligand-substitution reactions at an iron center have been assumed to be controlled by water exchange from the inner coordination shell. The rate constants may be described according to the Eigen-Wilkins mechanism[31] with the fast formation step of an outer-sphere complex (K_{os}) followed by a rate-limiting step involving the water substitution of the monohydroxylated Fe^{III} species (k_{ex}) [Equation (30)], where S is a statistical factor to correct for the composition of the outer solvation shell.[6]

$$k_{-1}' = S\,K_{os}\,k_{ex} \tag{30}$$

The rate constant k_{-1}' was found to vary by a factor of about 5 for the six tripodal ligands studied. This result suggests charge effects of the ligand since increasing values for k_{-1}' were observed on going from $\mathbf{L^5}H_7^{4+}$, $\mathbf{L^0}H_7^{4+}$ to $\mathbf{L^1}H_7^{3+}$, $\mathbf{L^4}H_7^{3+}$, $\mathbf{L^2}H_7^{2+}$ and $\mathbf{L^3}H_7^{+}$ corresponding to a decreasing number of positive charges located on the N anchor and pyridine nitrogen atoms. The role of electro-

 © 2004 Wiley-VCH Verlag GmbH & Co. KGaA, Weinheim

statics in charge effect concerning complexation reactions with hydroxamate ligands has been largely discussed by Crumbliss and al.[6,32] with discussion involving the Fuoss equation and the Debye-Hückel interionic potential involving a', the distance between the center of the positive charge of the metallic cation and the center of the charge (positive or negative) on the ligand.[33−36] (see Supporting Information, S19). The calculated K_{os} values are, from these considerations, 0.024 M^{-1} for **L^0** and **L^5** (+2, +4), 0.039 M^{-1} for **L^1** and **L^4** (+2, +3), 0.062 M^{-1} for **L^2** (+2, +2) and 0.100 M^{-1} for **L^3** (+2, +1) and were found to exhibit a good correlation with the k_{-1}' rate constants determined for ligands with an 8-hydroxyquinoline group (for $\mathbf{L^0}H_7^{4+}$, $\mathbf{L^1}H_7^{3+}$, $\mathbf{L^2}H_7^{2+}$, $k_{-1}' = 789$, 1320, 2240 M^{-1} s^{-1}, respectively) (Figure S20). This indicates that the complex formation follows the Eigen-Wilkins model. By taking a water exchange rate constant of 1.2×10^5 s^{-1} [37,38] in Equation (30), an S value of 2/7 can be deduced for $\mathbf{L^0}H_7^{4+}$, $\mathbf{L^1}H_7^{3+}$ and $\mathbf{L^2}H_7^{2+}$ which is a reasonable statistical correction for solvent shell composition for this series of ligands with similar structures.[1,32]

Some comments for the other terms of the series can be made. For $\mathbf{L^3}H_7^{+}$, complex data point of the correlation that k_{-1}'/K_{os} falls slightly below the line defined by the $\mathbf{L^0}H_7^{4+}$, $\mathbf{L^1}H_7^{3+}$ and $\mathbf{L^2}H_7^{2+}$ complexes suggesting that K_{os} has probably been overestimated. A lower a' value is reasonable owing to the smaller catechol ring size in comparison with an 8-hydroxyquinoline ring. For $\mathbf{L^4}H_7^{3+}$ (C anchor) the k_{-1}' rate constant (1750 M^{-1} s^{-1}) is intermediate between those for $\mathbf{L^1}H_7^{3+}$ and $\mathbf{L^2}H_7^{2+}$. This may be due to a larger bulkiness of $\mathbf{L^4}H_7^{3+}$ leading to a higher value for a' and hence a higher value for K_{os} in comparison with $\mathbf{L^1}H_7^{3+}$. The tripodal anchor contains one additional CH_2 and does not allow hydrogen bonding with the carbonyl oxygen atoms similar to ligands with a Tren anchor, thus increasing the bulkiness of $\mathbf{L^4}H_7^{3+}$ with respect to $\mathbf{L^1}H_7^{3+}$. For $\mathbf{L^5}H_7^{4+}$ the k_{-1}' rate constant (514 M^{-1} s^{-1}) is lower than that for $\mathbf{L^0}H_7^{4+}$ (789 M^{-1} s^{-1}). A possible explanation could be that the entry of this ligand in the second coordination sphere of Fe^{III} is less favored owing to the flexibility of the binding cavity that allows rotation of the pyridine ring relative to the phenol ring and leads consequently to a smaller S value.

Conclusion

This work is the first report on the acid dissociation (and formation) kinetics of iron(III) complexes with a series of tripodal ligands, four homopodates [with two types of anchor (*tren* or C-anchor)], three types of arm (catechol or 8-hydroxyquinoline or pyridinophenol) and two heteropodates (mixing catechol or 8-hydroxyquinoline).

Analysis of kinetic data shows that there is a common mechanism in all the series when the ligand structure is varied. The mechanism of the dissociation is more complex than the successive departure of the three arms around the iron(III) as observed in the literature for linear ligands[1] (three successive bidentate moieties). The dissociation of the first arm (from a hexadentate to a tetradentate complex) is in all cases observed but too fast to be measured. The dissociation then follows a process going from the tetradentate complex with the originally di-coordination of the two concerned arms to the tetradentate bis(salicylate) complex. During this process, bond cleavage of Fe−N_{pyr} or Fe−O with protonation of N or O, followed by proton-independent Fe−O(=C) bond formation to close the salicylate ring could be characterized in most cases. The comparison of these reaction rate constants reflects the influence of chelate donor strength (catechol or pyridinophenol vs. 8-hydroxyquinoline) and the rate of rotation of the amide bond between the anchor and the arm in question. The rate constants for the leaving of the ultimate salicylate arm indicate a proton-dependent (k_1) and a proton-independent (k'_1) reaction. The rate constants k_1 and k_1' span over a range of several order of magnitude: five orders for k_1 (184 to 0.0012 $\times 10^{-3}$ M^{-1} s^{-1}) and three and a half orders for k'_1 (22 to 0.012 $\times 10^{-3}$ s^{-1}). The role of electrostatics in control of the dissociation rate of the last step is evidenced for the 8-hydroxyquinoline moieties. Interesting correlations could be obtained which yielded information on the transition states for the two mechanisms.

From thermodynamic and kinetic studies on aqueous solutions of such Fe^{III} complexes, we believe that analysis of rates of Fe−N or Fe−O bond cleavage of the species and the proposed structures for the transition states will help in the designing of new ligands for appropriate exchange of Fe^{III} in biological systems.

Experimental Section

Materials: All commercial reagents were of the highest purity grade and were used without further purification. Iron(III) stock solutions were prepared by dissolving the appropriate amount of ferric perchlorate hydrate (Aldrich) in standardized $HClO_4$ solution. The solutions were standardized for ferric ion concentration spectrophotometrically by using a molar extinction coefficient of 4160 M^{-1}·cm^{-1} at 240 nm.[39] The ligands were synthesized according to procedures previously described (**L^0**,[17a] **L^1**,[20] **L^2**,[20] **L^3**,[15] **L^4**,[40] **L^5**[18]).

Kinetics Studies: Kinetic measurements were performed with a KINSPEC UV (BIO-LOGIC Company, Claix, France) stopped-flow spectrophotometer equipped with a diode array detector (J & M) and connected to a microcomputer. The reported rate constants are the average of about 6 repeat determinations (standard deviation in the range 1−2%). The kinetic data were treated on-line with the commercial BIO-KINE program (BIO-LOGIC Company, Claix, France). The ionic strength was fixed at $I = 2$ M ($NaClO_4$, $HClO_4$) due to the H^+ concentrations which were up to 1 M. This allowed comparisons with literature data. Formation kinetics were carried out under pseudo-first-order conditions at 25 °C with Fe^{III} in excess with respect to the ligand. The Fe^{III} concentration spanned the range 5×10^{-3} to 3×10^{-3} M for each H^+ concentration which was over the range 0.03 to 0.1 M. A solution containing Fe^{III} and H^+ and a solution containing the ligand (1×10^{-4} M) at the same ionic strength were mixed on the stopped-flow apparatus. In each case, first order kinetics were observed. The acid

 © 2004 Wiley-VCH Verlag GmbH & Co. KGaA, Weinheim

hydrolysis kinetics of the $Fe^{III}-\mathbf{L}^{n}$ complexes were studied under pseudo-first-order conditions in the presence an of excess protons ($[H^+]$ range 0.01 to 1 M) at 25 °C. The initial pH of the $Fe^{III}-\mathbf{L}^{n}$ solution (ca. 1×10^{-4} M) was ca. 5.

Acknowledgments

The authors thank Professor J.-L. Pierre (LEDSS) for his interest in these studies and Professor P. Baret for managing the syntheses of the ligands $\mathbf{L}^{n}$.

[1] A.-M. Albrecht-Gary, A. L. Crumbliss, *Met. Ions Biol. Syst.* **1998**, *35*, 243−327.
[2] B. F. Matzanke, G. Müller-Matzanke and K. N. Raymond in *Physical Bioinorganic Chemistry Series: Iron Carriers and Iron Proteins* (Ed.: T. M. Loehr), VCH, New York, **1989**, p.1.
[3] J. R. Telford, K. N. Raymond in *Comprehensive Supramolecular Chemistry* (Eds.: J. M. Lehn, G. W. Gokel), Pergamon Press, London, **1996**, p. 245.
[4] R. R. Crichton in *Inorganic Biochemistry of Iron Metabolism*, John Wiley & Sons, Chichester, **2001**.
[5] [5a] J.-F. Briat, S. Lobréaux in *Metals Ions in Biological Systems* (Eds.: A. Sigel, H. Sigel), Marcel Dekker, Inc., New York, **1998**, vol. 35, chapter 14, p. 563; [5b] R. R. Crichton, R. J. Ward, chapter 16, p. 633; [5c] G. S. Tilbrook, R. C. Hider, chapter 18, p. 691.
[6] M. T. Caudle, A. L. Crumbliss, *Inorg. Chem.* **1994**, *33*, 4077−4085.
[7] M. T. Caudle, L. P. Cogswell, A. L. Crumbliss, *Inorg. Chem.* **1994**, *33*, 4759−4773.
[8] B. Monzyk, A. L. Crumbliss, *J. Am. Chem. Soc.* **1982**, *104*, 4921−4929.
[9] M. Birus, Z. Bradic, G. Krznaric, N. Kujundzic, M. Pribanic, P. C. Wilkins, R. G. Wilkins, *Inorg. Chem.* **1987**, *26*, 1000−1005.
[10] H. Boukhalfa, A. L. Crumbliss, *Inorg. Chem.* **2000**, *39*, 4318−4331.
[11] H. Boukhalfa, T. J. Brickman, S. K. Armstrong, A. L. Crumbliss, *Inorg. Chem.* **2000**, *39*, 5591−5602.
[12] Y. Hara, L. Shen, A. Tsubouchi, M. Akiyama, *Inorg. Chem.* **2000**, *39*, 5074−5082.
[13] Y. Hara, M. Akiyama, *J. Am. Chem. Soc.* **2001**, *39*, 7247−7256.
[14] S. J. Rodgers, C. W. Lee, C. Y. Ng, K. N. Raymond, *Inorg. Chem.* **1987**, *26*, 1622−1625.
[15] F. Thomas, C. Béguin, J.-L. Pierre, G. Serratrice, *Inorg. Chim. Acta* **1999**, *291*, 148−157.
[16] C. Y. Ng, S. J. Rodgers, K. N. Raymond, *Inorg. Chem.* **1989**, *28*, 2062−2066.
[17] [17a] P. Baret, C. Béguin, H. Boukhalfa, C. Caris, J.-P. Laulhère, J.-L. Pierre, G. Serratrice, *J. Am. Chem. Soc.* **1995**, *117*, 9760−9761. [17b] G. Serratrice, H. Boukhalfa, C. Béguin, P. Baret, C. Caris, J.-L. Pierre, *Inorg. Chem.* **1997**, *36*, 3898−3910.
[18] P. Baret, C. Béguin, G. Gellon, J.-L. Pierre, G. Serratrice, F. Thomas, J.-P. Laulhère, E. Saint-Aman, *Eur. J. Inorg. Chem.* **2000**, 1219−1227.
[19] M. Meyer, J. R. Telford, S. M. Cohen, D. J. White, J. Xu, K. N. Raymond, *J. Am. Chem. Soc.* **1997**, *119*, 10093−10103; S. M. Cohen, B. O'Sullivan, K. N. Raymond, *Inorg Chem.* **2000**, *96*, 4339−4346.
[20] A.-M. Albrecht, S. Blanc, F. Biaso, F. Thomas, P. Baret, G. Gellon, J.-L. Pierre, G. Serratrice, *Eur. J. Inorg. Chem.* **2003**, 2596−2605.
[21] F. Biaso, Thesis, Université Joseph Fourier, Grenoble, **2002**.
[22] D. Imbert, P. Baret, D. Gaude, I. Gautier-Luneau, G. Gellon, F. Thomas, G. Serratrice, J.-L. Pierre, *Chem. Eur. J.* **2002**, *8*, 1091−1100.
[23] D. Imbert, F. Thomas, P. Baret, G. Serratrice, D. Gaude, J.-L. Pierre, J.-P. Laulhère, *New J. Chem.* **2000**, *24*, 281−288.
[24] C.-W. Lee, D. J. Ecker, K. N. Raymond, *J. Am. Chem. Soc.* **1985**, *107*, 6920−6923.
[25] R. M. Milburn, W. C. Vosburgh, *J. Am. Chem. Soc.* **1955**, *77*, 1352−1355.
[26] A. Shanzer, S. Libman, S. Lifson, *Pure Appl. Chem.* **1992**, *64*, 1421−1428.
[27] D. Chapon, G. Serratrice, unpublished results.
[28] G. Serratrice, P. Baret, H. Boukhalfa, I. Gautier-Luneau, D. Luneau, J.-L. Pierre, *Inorg. Chem.* **1999**, *38*, 840−841.
[29] A. L. Crumbliss, in *CRC Handbook of Microbial Iron Chelates* (Ed.: G. Winkelman), CRC Press, Boca Raton, Fl, **1991**, chapter 7.
[30] L. E. Asher, E. Deutsch, *Inorg. Chem.* **1973**, *12*, 1774−1778.
[31] M. Eigen, R. G Wilkins, "Mechanism of Inorganic Reactions", *Adv. Chem. Ser.* **1965**, *55*.
[32] J. I. Wirgau, I. Spasojevic, H. Boukhalfa, I. Batinic-Haberle, A. C. Crumbliss, *Inorg. Chem.* **2002**, *41*, 1464−1473.
[33] R. M. Fuoss, *J. Am. Chem. Soc.* **1958**, *80*, 5059−5061.
[34] M. Z. Eigen, *Phys. Chem.* **1954**, *1*, 176−185.
[35] C.-T. Lin, D. B. Rorabacher, *Inorg. Chem.* **1973**, *12*, 2402−2410.
[36] N. J. Hair, J. K. Beattie, *Inorg. Chem.* **1977**, *16*, 245−250.
[37] M. Grant, R. B. Jordan, *Inorg. Chem.* **1981**, *20*, 55−60.
[38] T. W. Swaddle, A. E. Merbach, *Inorg. Chem.* **1981**, *20*, 4212−4216.
[39] R. Bastian, R. Weberling, F. Palilla, *Anal. Chem.* **1956**, *28*, 459−462.
[40] D. Imbert, Thesis, Université Joseph Fourier, Grenoble, **2000**.

Received June 25, 2004
Early View Article
Published Online March 5, 2004

 © 2004 Wiley-VCH Verlag GmbH & Co. KGaA, Weinheim

One- and Three-Dimensional Coordination Polymers Containing Organic Ligands Produced Through in situ Hydrothermal Reactions

Xi-Xue Hu,[a] Cheng-Ling Pan,[a] Ji-Qing Xu,*[a] Xiao-Bing Cui,[a] Guang-Di Yang,[b] and Tie-Gang Wang[a]

Keywords: Acylation / Coordination polymers / Hydrothermal synthesis / Cobalt

Two novel coordination polymers of cobalt(II), $[Co(\mu_3\text{-}H_2bbh)(phen)]_n$ (**1**) and $[Co(\mu_4\text{-}H_2bbh)(H_2O)_2]_n$ (**2**) (phen = 1,10-phenanthroline; H_4bbh = benzene-1,2,4,5-tetracarbo-1,2:4,5-dihydrazide), in which H_2bbh ligands are in situ generated by an acylation reaction of H_4bta (H_4bta = benzene-1,2,4,5-tetracarboxylic acid) with hydrazine hydrate under hydrothermal conditions have been synthesized and structurally characterized.
(© Wiley-VCH Verlag GmbH & Co. KGaA, 69451 Weinheim, Germany, 2004)

Introduction

The construction of metal-organic coordination polymers based on complexes of transition metals and multifunctional bridging ligands has proven to be an interesting field due to the intriguing network topologies and potential functions of this new class of materials.[1] Bridging ligands containing N-, and/or O-donors, for example multidentate aromatic polycarboxyl systems, including benzene-1,3-dicarboxylate,[2] -1,4-dicarboxylate,[1a,3] -1,2,3-tricarboxylate,[4] -1,2,4-tricarboxylate,[5] -1,3,5-tricarboxylate,[6] and especially benzene-1,2,4,5-tetracarboxylate,[7] have been widely used for hydrothermal syntheses of coordination polymers of metals,[8] and the syntheses occur mainly through direct interaction between the metal ion and the carboxylate group to construct one-, two- and three-dimensional networks in a variety of coordination modes. The hydro(solvo)thermal method has proved to be a promising technique in the preparation of highly stable, infinite metal−ligand frameworks[9] and the modification of organic ligands. So far, five types of organic ligand reactions under hydrothermal conditions have been uncovered, namely hydrolysis of ester or cyano groups into carboxylate groups,[8a,8c,9] substitution of a carboxylate group by a sulfonate group,[10] oxidative coupling of *o*-phenanthroline to generate a 2,2-biphenanthroline,[11] hydroxylation of aromatic rings[8b,12] and cycloaddition between the cyano group and the azide groups.[13] These reactions represent promising new routes for constructing novel coordination polymers under hydro(solvo)thermal condition.

We wanted to synthesize novel coordination polymers containing new ligands produced through an in situ reaction between the reactants under hydrothermal condition. Based on known reactions, it may be expected that generation of the target products could be achieved by utilizing an acylation reaction between benzene-1,2,4,5-tetracarboxylate and hydrazine hydrate.

Fortunately, we obtained two novel Co^{II} coordination polymers, $[Co(\mu_3\text{-}H_2bbh)(phen)]_n$ (**1**) and $[Co(\mu_4\text{-}H_2bbh)(H_2O)_2]_n$ (**2**). To the best of our knowledge, these are the first two examples in which new organic ligands have been generated by acylation and coordinated by transition metal ions to form novel polymers. Scheme 1 depicts equations representing the formation of the two compounds.

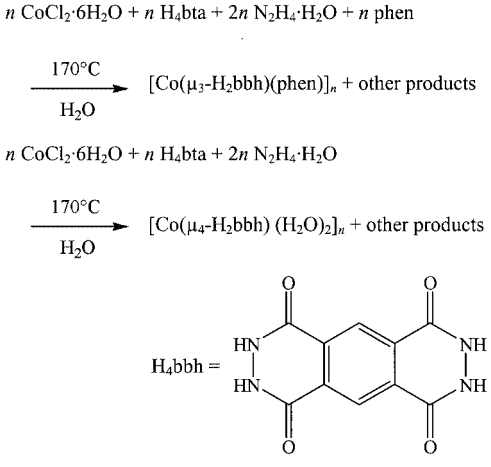

Scheme 1

[a] College of Chemistry and State Key Laboratory of Inorganic Synthesis and Preparative Chemistry, Jilin University, Changchun 130023, P. R. China
Fax: (internat.) + 86-431-8923907
E-mail: xjq@mail.jlu.edu.cn
[b] Key Lab of Supramolecular Structure and Spectroscopy, Jilin University, Changchun 130021, P. R. China

 © 2004 Wiley-VCH Verlag GmbH & Co. KGaA, Weinheim **DOI: 10.1002/ejic.200300436**

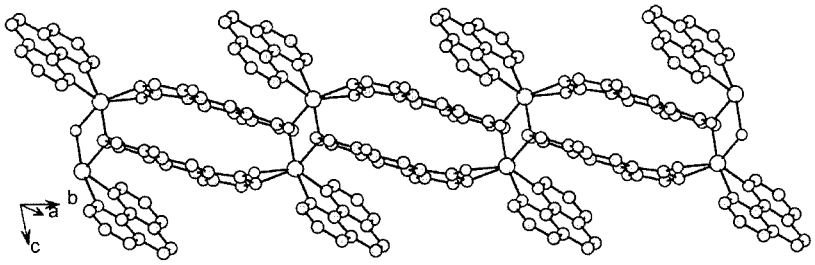

Figure 1. View of the double-chain structure of compound **1**

Results and Discussion

A single-crystal X-ray diffraction study revealed that compound **1** possesses a one-dimensional double-chain structure, as shown in Figure 1.

As shown in Figure 2, the coordination sphere of the Co^{II} site is defined by three acyl oxygen atoms O(2), O(3) and O(3A), one acylamino nitrogen atom N(5) and two nitrogen atoms N(1) and N(2) from phen, leading to a distorted octahedral geometry. In the coordination environment, N(5) and O(2), and N(1) and N(2) chelate the cobalt atom, while O(3) and O(3A) adopt a bidentate bridging mode connecting two cobalt atoms. The H_2bbh ligand shows a μ_3-coordination mode. No hydrogen atoms were found at N(3A) and N(5) by single-crystal X-ray analysis but the hydrogen atoms attached to C, N(4A) and N(6) were accurately located. The neighboring cobalt atoms are held together by the bridging acyl oxygen atoms with Co−Co(A) distances of 3.296(4) Å. It is very interesting that the Co_2O_2 cores including Co, Co(A), O(3) and O(3A) in adopting a parallelogram geometry are interconnected by H_2bbh bridging ligands to generate a centipede-like double-chain structure propagated along the *b* axis direction. In the double-chain, the planes of two H_2bbh ligands between each two Co_2O_2 cores are parallel to each other and perpendicular to the *bc* plane. The phen rings as auxiliary ligands on the same side of the chain are also parallel to each other.

As shown in Figure 3, the Co^{II} atom environment in **2** can be described as octahedral (Figure 3) with two acyl oxygen atoms [O(2) and O(2A)] from $[H_2bbh]^{2-}$ and two H_2O groups that comprise the equatorial plane, with the axial positions being occupied by two nitrogen atoms [N(1) and N(1A)] from $[H_2bbh]^{2-}$. The H_2bbh ligand displays a μ_4-coordination mode through an acyl oxygen atom and an acylamino nitrogen atom linking with four Co^{II} atoms.

Figure 4 shows the 3-D structure of compound **2** and Figure 5 shows a schematic representation revealing the 4-connected topology of the 3-D network of **2**. From these figures it can be seen that the Co atoms and H_2bbh ligands are alternately interconnected into 2-D sheets and these sheets are again interlinked to form the 3-D structure. Specifically, both the Co centers and the H_2bbh ligands can be divided into two classes. Each of the first type of Co atoms is connected to four H_2bbh ligands in the same layer, and each of the second type is connected to two H_2bbh ligands in the same layer and two H_2bbh groups in neighboring layers. Similarly, each of the first class of H_2bbh ligands is linked to four Co centers in the same layer, and each of the second type is linked to two Co centers in the

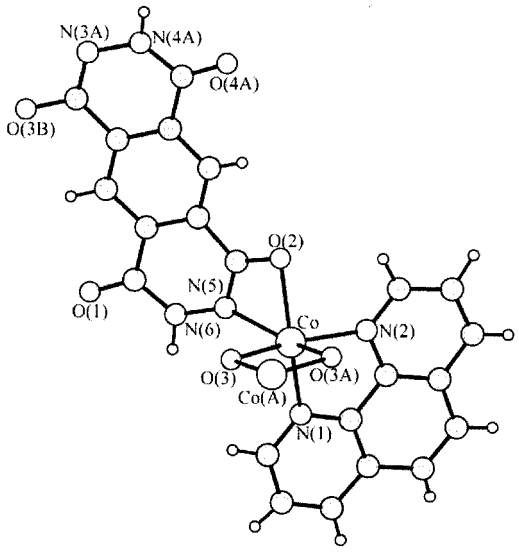

Figure 2. Coordination environment of the cobalt atom in compound **1**; selected interatomic distances [Å]: Co−O(3) 2.070(2), Co−O(3A) 2.099 (2), Co−O(2) 2.125(2), Co−N(1) 2.149(2), Co−N(2) 2.150(3), Co−N(5) 2.260(2), Co···Co 3.296(4); symmetry code A: $-x$, $-y + 1$, $-z + 2$

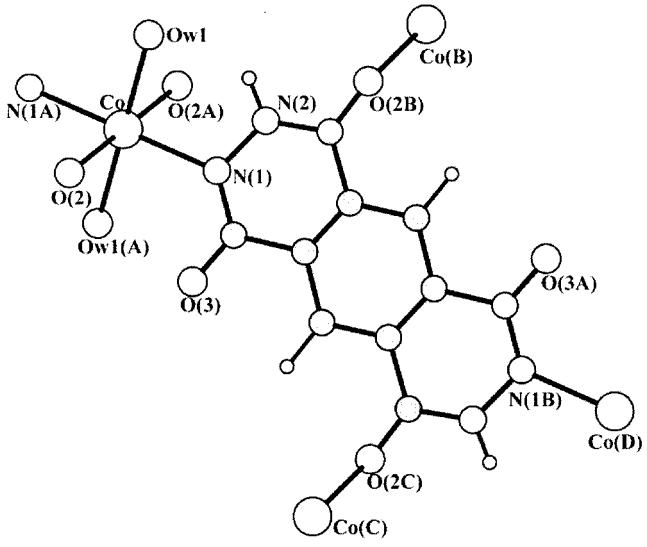

Figure 3. Coordination environment of the cobalt atom in compound **2**; selected interatomic distances [Å]: Co−O(2) 2.089(2), Co−N(1) 2.128(3), Co−O(w1) 2.145(2); symmetry code A: $-x$, $-y$, $-z$

 © 2004 Wiley-VCH Verlag GmbH & Co. KGaA, Weinheim

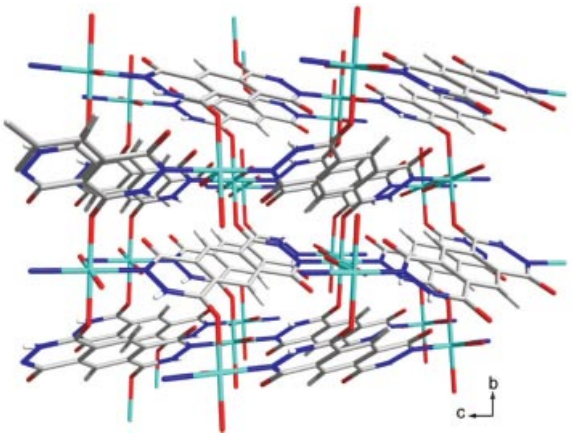

Figure 4. Packing diagram along the [100] direction for compound **2**

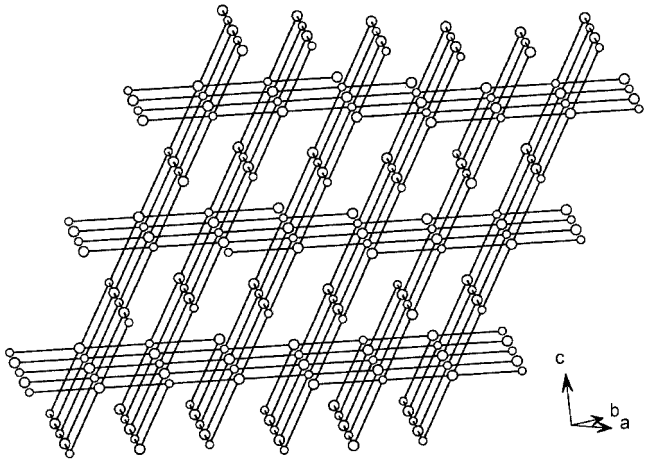

Figure 5. Representation showing the topology of the 3-D network for **2**; the H_2bbh ligands are shown as filled large circles and the cobalt atoms as open small cycles

same layer and two Co centers in neighboring layers. Through the second type of Co atoms and H_2bbh ligands, the layers are intergrated into the 3-D framework. Figure 4 indicates that in the solid state of **2**, there exist channels constructed of 22-membered rings consisting of three Co atoms and three H_2bbh ligands. In fact, the channels are intertwined in the 3-D network (Figure 5).

Compounds **1** and **2** were synthesized under similar conditions except for the use of phen in the preparation of **1** but not of **2**. However, **1** and **2** are of different structural types. The former is a chain while **2** displays a 3-D open framework. It is possible that the coordination ability and steric effect of the phen group are much larger than those of H_2O, resulting in th occurrence of this situation. This result clearly shows that auxiliary ligands, as well as bridging ligands, also play an important role in regulating the structures of synthesized compounds.

Preliminary magnetic studies of **1** and **2** show that the values of the effective magnetic moments μ_{eff} at room temperature are 4.50 μ_B and 4.53 μ_B per Co formula unit, respectively, while the spin-only magnetic moments are 3.87 μ_B with $S = 3/2$ and $g = 2.0$ $\{\mu_{eff} = g[s(s+1)]^{1/2}\mu_B\}$. The differences are due to additional orbital momentum. When the temperature was lowered, μ_{eff} gradually decreased from 4.50 μ_B and 4.53 μ_B at 300 K to 1.24 μ_B and 2.27 μ_B at 2.0 K for **1** and **2**, respectively. Both plots of $1/\chi_m$ vs. T obey the Curie−Weiss law $[\chi_m = C/(T - \theta)]$ at 5000 Oe with Weiss constants, $\theta_1 = -17.74$ K and $\theta_2 = -13.13$ K, and Curie constants, $C_1 = 2.668$ emu·mol^{-1}·K and $C_2 = 2.653$ emu·mol^{-1}·K for **1** and **2**, respectively, which indicates the occurrence of antiferromagnetic coupling between the Co^{II} atoms in **1** and **2**.

In conclusion, the reactivity of organic ligands under hydrothermal condition shows some differences from that under usual conditions, thus indicating that modification of organic ligands under hydrothermal conditions is very promising for the synthesis of useful new ligands. The work described herein once again provides strong evidence that a wide variety of new coordination polymers can be produced by hydrothermal generation of new bridging ligands in the presence of appropriate metal ions, although it remains a great challenge to develop this technique to a stage where a desired structure or crystal symmetry can be ensured.

Experimental Section

Syntheses of 1 and 2: Dark brown block crystals of **1** were synthesized hydrothermally from a mixture of $CoCl_2·6H_2O$, H_4bta, $N_2H_4·H_2O$, phen and H_2O (molar ratio 14:21:13: 8:1500) in a 30-mL Teflon-lined stainless steel autoclave (25 mL, capacity) under autogenous pressure heated to 170 °C for 4 d and cooled to room temperature. The crystalline product was filtered, washed with distilled water, and dried at ambient temperature to give 0.42 g of the compound (yield 41% based on cobalt). Orange block crystals of **2** (yield 46% based on cobalt) were obtained under the same reaction conditions and experimental procedures as those for **1** using a molar ratio of $CoCl_2·6H_2O/H_4$bta/$N_2H_4·H_2O/H_2O$ = 2.6:5:4.5:625.

1: $[C_{22}H_{12}CoN_6O_4]_n$ (483.31): calcd. C 54.67, H 2.50, N 17.39; found C 54.81, H 2.79, N 17.01. IR (KBr disk, cm^{-1}): $\tilde{\nu}$ = 1647.17 s, 1557.09 w, 1496.79 s, 1431.94 m, 1362.77 s, 1290.06 s, 1179.25 s, 1143.39 m, 1058.96 m, 945.70 m, 868.80 m, 841.09 s, 809.94 s, 724.79 s, 701.48 m, 674.65 m, 656.46 m, 550.63 m, 511.67 w, 429.38 s.

2: $[C_{10}H_8CoN_4O_6]_n$ (339.13): calcd. C 35.42, H 2.38, N 16.52; found C 35.11, H 2.16, N 16.91. IR (KBr disk, cm^{-1}): $\tilde{\nu}$ = 3298.82 s, 1605.70 s, 1504.72 s, 1384.57 s, 1326.70 w, 1305.67 s, 1181.43 s, 1149.88 s, 1060.12 s, 932.23 m, 902.57 s, 828.06 s, 761.35 s, 694.96 w, 679.55 m, 622.99 m, 562.08 s, 434.98 s, 421.50 w.

X-ray Crystallographic Studies

Compound 1: Dark brown block crystals, triclinic, space group $P\bar{1}$, a = 9.762(4), b = 10.169(4), c = 11.143 (4) Å, α = 80.96(3), β = 64.49(3), γ = 71.88(3)°, V = 948.4(7) Å^3, Z = 2, $D_{calcd.}$ = 1.692 g cm^{-3}, μ = 0.953 mm^{-1}. Data collections (4.06° ≤ 2θ ≤ 51.96°) were performed at 293(2) K with a Siemens P4 diffractometer (Mo-K_α, λ = 0.71073 Å). The structure was solved with direct methods and refined with full-matrix least squares (SHELXTL-97),[14] giving a final R_1 value of 0.0402 for 346 parameters and 3703 unique reflections with $I \geq 2\sigma(I)$ and wR_2 of 0.1040 for all 4533 reflections.

 © 2004 Wiley-VCH Verlag GmbH & Co. KGaA, Weinheim

Compound 2: Orange block crystals, monoclinic, space group $P2_1/c$, a = 6.8687(5), b = 7.5943(6), c = 10.0401(6), β = 95.250(4)°, V = 521.52(6) Å^3, Z = 2, D_c = 2.160 g cm^{-3}, μ = 1.689 mm^{-1}. Data collections (5.96° ≤ 2θ ≤ 46.44°) were performed at 293(2) K with a Bruker-AXS Smart CCD diffractometer (Mo-K_α, λ = 0.71073 Å). The structure was solved with direct methods and refined with full-matrix least squares (SHELXTL-97), giving a final R_1 value of 0.0277 for 105 parameters and 751 unique reflections with $I \geq 2\sigma(I)$ and wR_2 of 0.0799 for all 2395 reflections.

CCDC-208867 (**1**) and -208868 (**2**) contain the supplementary crystallographic data for this paper. These data can be obtained free of charge at www.ccdc.cam.ac.uk/conts/retrieving.html [or from the Cambridge Crystallographic Data Center, 12 Union Road, Cambridge CB2 1EZ, UK; Fax: (internat.) + 44-1223/336-033; E-mail: deposit@ccdc.cam.ac.uk].

Acknowledgments

This work was supported by the National Natural Science Foundation of China (no. 20271021 and no. 20333070).

[1] [1a] O. M. Yaghi, H. Li, C. David, D. Richardson, T. L. Groy, *Acc. Chem. Res.* **1998**, *31*, 474−484. [1b] S. R. Batten, R. Robson, *Angew. Chem. Int. Ed.* **1998**, *37*, 1460−1494. [1c] P. J. Hagrman, D. Hagrman, J. Zubieta, *Angew. Chem. Int. Ed.* **1999**, *38*, 2638−2684.
[2] K. Barthete, D. Riou, G. Férey, *Chem. Commun.* **2002**, 1492−1493.
[3] K. Barthelet, J. Marrot, D. Riou, G. Férey, *Angew. Chem. Int. Ed.* **2002**, *41*, 281−284.
[4] S. O. H. Gutschke, D. J. Price, A. K. Powell, P. T. Wood, *Angew. Chem. Int. Ed.* **2001**, *113*, 1974−1977.
[5] M. J. Plater, M. R. St. J. Foreman, R. A. Howie, J. M. S. Skakle, A. M. I. Slawin, *Inorg. Chim. Acta* **2001**, *315*, 126−132.
[6] S. M. F. Lo, S. S. Y. Chui, L. Y. Shek, Z. Y. Lin, X. X. Zhang, G. H. Wen, I. D. Williams, *J. Am. Chem. Soc.* **2000**, *122*, 6293−6294.
[7] L. J. Zhang, J. Q. Xu, Z. Shi, W. Xu, T. G. Wang, *J. Chem. Soc., Dalton Trans.* **2003**, 1148−1152.
[8] [8a] O. R. Evans, R. G. Xiong, Z. Y. Wang, G. K. Wong, W. B. Lin, *Angew. Chem. Int. Ed.* **1999**, *38*, 536−538. [8b] J. Tao, Y. Zhang, M. L. Tong, X. M. Chen, T. Yuen, C. L. Lin, X. Y. Huang, J. Li, *Chem. Commun.* **2002**, 1342−1343. [8c] W. B. Lin, Z. Y. Wang, L. Ma, *J. Am. Chem. Soc.* **1999**, *121*, 11249−11250.
[9] M. L. Tong, L. J. Li, K. Mochizuki, H. C. Chang, X. M. Chen, Y. Li, S. Kitagawa, *Chem. Commun.* **2003**, 428−429.
[10] R. G. Xiong, J. Zhang, Z.F. Chen, X. Z. You, C. M. Che, H. K. Fun, *J. Chem. Soc., Dalton Trans.* **2001**, 780−782.
[11] C. M. Liu, S. Gao, H. Z. Kou, *Chem. Commun.* **2001**, 1670−1671.
[12] X. M. Zhang, M. L. Tong, X. M. Chen, *Angew. Chem. Int. Ed.* **2002**, *41*, 1029−1031.
[13] R. G. Xiong, X. Xue, H. Zhao, X. Z. You, B. F. Abrahams, Z. L. Xue, *Angew. Chem. Int. Ed.* **2002**, *41*, 3800−3803.
[14] SHELXTL, version 5.1; Siemens, Industrial Automation, **1997**.

Received July 7, 2003
Early View Article
Published Online March 5, 2004

 © 2004 Wiley-VCH Verlag GmbH & Co. KGaA, Weinheim

EurJIC
European Journal of Inorganic Chemistry

Issue 8/2004

Pages 1571–1770

Papers available ahead of print in Early View at www.interscience.wiley.com

Earliest available Table of Contents:
Automatically, free of charge by e-mail through
www.interscience.wiley.com/alerts

COVER PICTURE

The cover picture shows a general cartoon of heterogeneous catalytic processes performed on Suzuki-type cross-coupling reactions. The submerged gear represents the hub in the system, holding the active sites of the catalysts which are triazatriolefinic palladium(0) complexes. The catalysts are anchored through oxidative electropolymerization of the pyrrole groups contained in their structures, and can be monitored through the electroactivity of additional ferrocene entities also present. Details are discussed in the article by A. Llobet, A. Roglans et al. on p. 1601 ff.

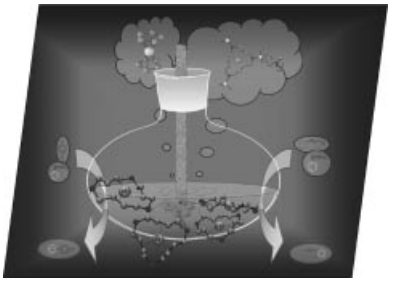

MICROREVIEW

Contents

1583 **F. Arnesano, L. Banci, I. Bertini,* S. Ciofi-Baffoni**

Perspectives in Inorganic Structural Genomics: A Trafficking Route for Copper

Keywords: Structural genomics / Copper / Metalloproteins / Chaperone proteins

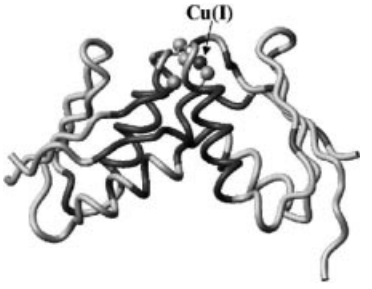

 © 2004 Wiley-VCH Verlag GmbH & Co. KGaA, Weinheim

SHORT COMMUNICATIONS

1595 **R. Wang, L. Xu, X. Li, Y. Li, Q. Shi, Z. Zhou, M. Hong,* A. S. C. Chan***

New Types of Homochiral Helical Coordination Polymers Constructed by *exo*-Bidentate Binaphthol Derivatives

Keywords: Helical structures / Chirality / N ligands / Silver

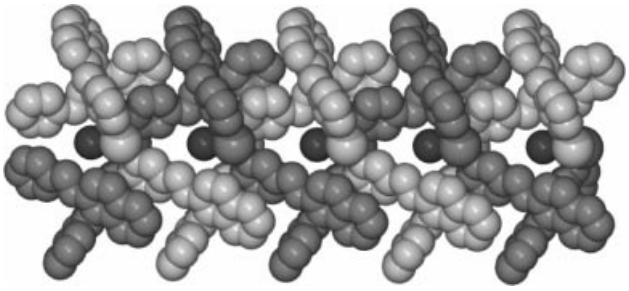

FULL PAPERS

1601 **A. Llobet,* E. Masllorens, M. Rodríguez, A. Roglans,* J. Benet-Buchholz**

Syntheses, Structures and Redox Properties of New Macrocyclic Triazatriolefinic Pd^0 Complexes and Their Polypyrrole Modified Electrodes − Application to Heterogeneous Catalytic Suzuki Cross-Coupling Reactions

Keywords: Heterogeneous catalysis / Macrocyclic ligands / Palladium / Pyrroles / Modified electrodes / Electrochemistry

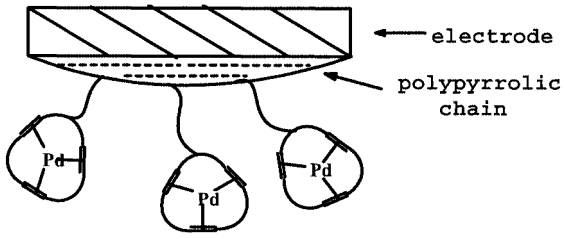

1611 **B. Modec,* J. V. Brenčič, J. Koller**

A Series of Molybdenum(V) Complexes with the Oxalato Ligand Engaged in Different Binding Roles − An Unusual Staggered Conformation of the μ_4-Oxalate in $[\{Mo_2O_4(\eta^2\text{-}C_2O_4)_2\}_2(\mu_4\text{-}C_2O_4)]^{6-}$

Keywords: Coordination modes / Molybdenum / Oxo ligands / Oxalate / Polyoxometalates

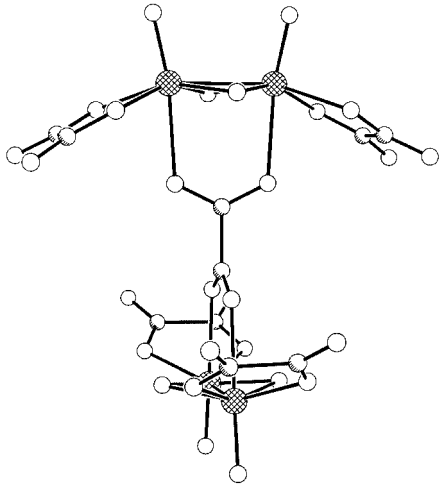

1621 **H. Ogata, T. Fukuda, K. Nakai, Y. Fujimura, S. Neya, P. A. Stuzhin, N. Kobayashi***

Absorption, Magnetic Circular Dichroism, IR Spectra, Electrochemistry, and Molecular Orbital Calculations of Monoaza- and Opposite Diazaporphyrins

Keywords: Cyclic voltammetry / Density functional calculations / Magnetic circular dichroism / Porphyrinoids / UV/Vis spectroscopy

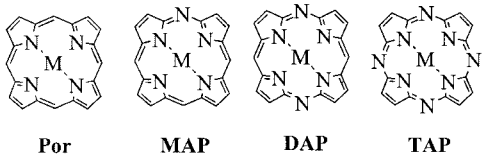

1630 **Y. Nie, S. Schwiegk, H. Pritzkow, W. Siebert***

One-Pot Synthesis of 1,6-Diiodo-2,3,4,5-tetracarba-*nido*-hexaboranes(6) and Mechanistic Studies on the Reaction System Alkynes/BI_3/$NaK_{2.8}$

Keywords: Boron / Boranes / Carboranes / Heterocycles / Iodine bridges

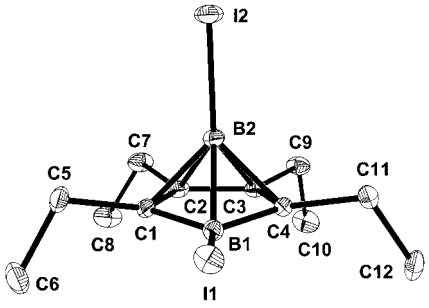

1639 **Z. Janas, L. B. Jerzykiewicz, K. Przybylak, P. Sobota,* K. Szczegot**

Titanium Complexes Stabilized by a Sulfur-Bridged Chelating Bis(aryloxo) Ligand as Active Catalysts for Olefin Polymerization

Keywords: Titanium / O ligands / S ligands / Polymerization / X-ray diffraction / Aluminum

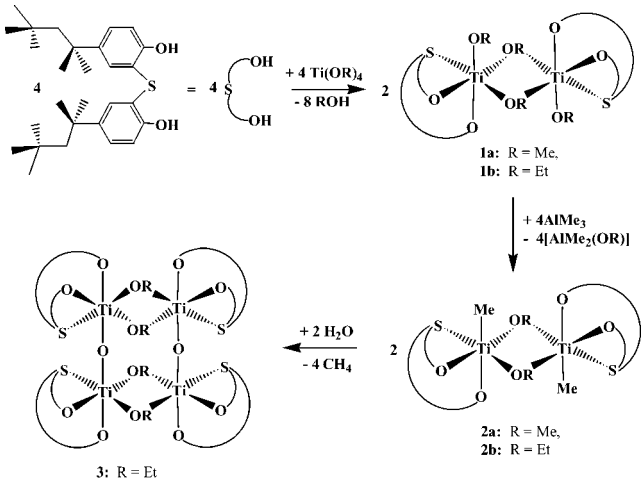

1646 **J. C. Röder, F. Meyer,* E. Kaifer, H. Pritzkow**

Pyrazolate-Based Dinucleating Ligands in L_2M_2 Scaffolds: Effects of Bulky Substituents and Co-ligands on Structures and M···H−C Interactions

Keywords: Nickel / Palladium / Dinuclear complexes / N-ligands / Pyrazole ligands

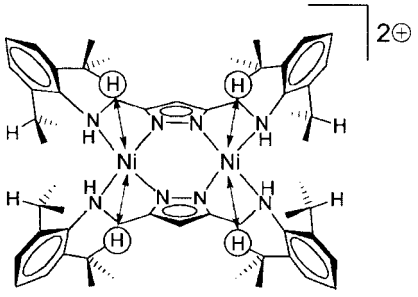

1661 **S. Pruvost, C. Hérold,* A. Hérold, P. Lagrange**

Structural Study of Novel Graphite−Lithium−Calcium Intercalation Compounds

Keywords: Calcium / Electron microscopy / Graphite / Intercalations / Lithium / X-ray diffraction

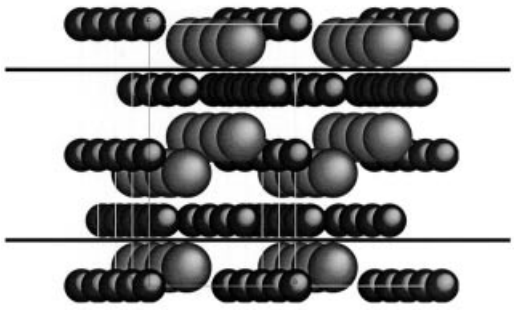

 © 2004 Wiley-VCH Verlag GmbH & Co. KGaA, Weinheim

1668 **T.-F. Wang,* T.-C. Wang, Y.-S. Wen**

Selective Reaction of Aminorhenium Complexes and the Formation of Cp-N-P Tridentate Complexes

Keywords: Rhenium / Cyclopentadienes / N ligands / P ligands / Tridentate ligands

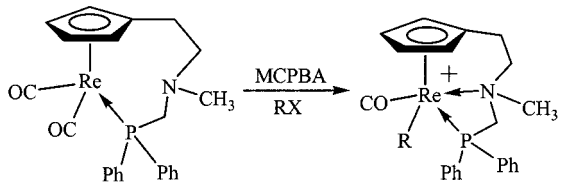

1675 **B. C. de Pater, H.-W. Frühauf, K. Vrieze, R. de Gelder, E. J. Baerends, D. McCormack, M. Lutz, A. L. Spek, F. Hartl***

Strongly Nucleophilic Rh^{I} Centre in Square-Planar Complexes with Terdentate (κ^3) 2,2′:6′,2″-Terpyridine Ligands: Crystallographic, Electrochemical and Density Functional Theoretical Studies

Keywords: Rhodium / Tridentate ligands / X-ray diffraction / Cyclic voltammetry / Density functional calculations

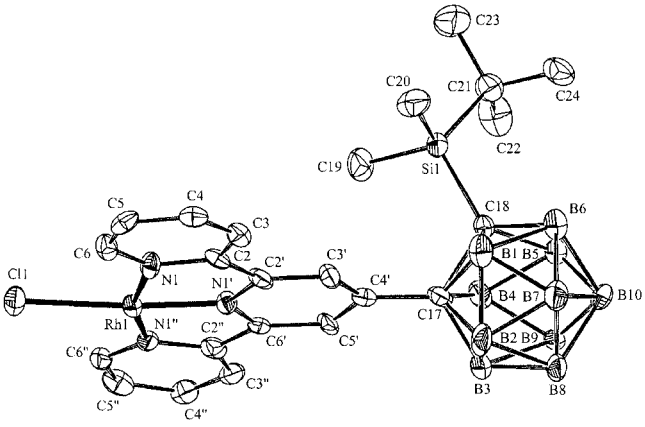

1687 **M. Le Hénanf, C. Le Roy, K. W. Muir, F. Y. Pétillon, P. Schollhammer, J. Talarmin***

Electrochemical Studies of Complexes with Oxo- or Hydroxo-Bridged $\{Mo_2(\mu\text{-}SMe)_3\}^+$ Centers: Cleavage of the Oxygen Bridge and Generation of Substrate-Binding Sites

Keywords: Dinuclear complexes / Molybdenum / Electrochemical reduction / Oxo, hydroxo bridges / Protonations / Aqua ligands

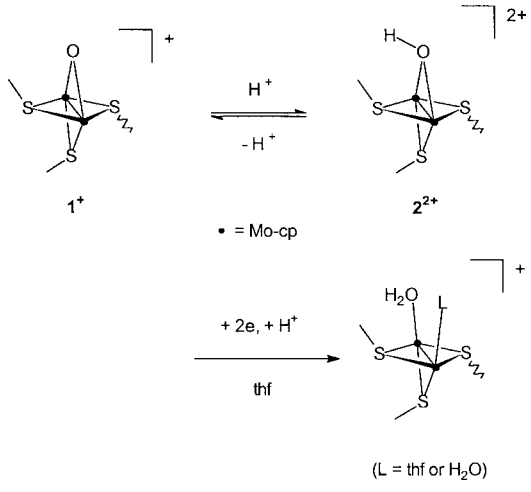

1701 **J.-R. Li, X.-H. Bu,* R.-H. Zhang**

The First (Trisulfoxide)metal Complexes: Synthesis and Crystal Structures of the 1D Lanthanide Coordination Polymers $[Ln(L)(MeOH)(NO_3)_3]_n$ and $\{[La(L)(DMF)_5](ClO_4)_3\}_n$ [L = 1,3,5-Tris(ethylsulfinyl)-2,4,6-trimethylbenzene, Ln = La^{III} and Nd^{III}]

Keywords: Coordination polymers / Helical structures / Lanthanides / Sulfoxide

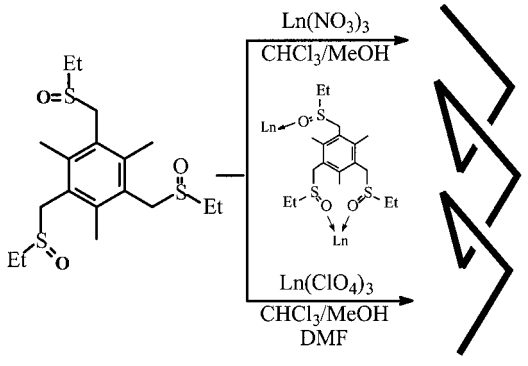

 © 2004 Wiley-VCH Verlag GmbH & Co. KGaA, Weinheim

1705 **F. P. Fanizzi,* N. Margiotta, M. Lanfranchi, A. Tiripicchio, G. Pacchioni, G. Natile***

A Molecular Tool for Measuring the Electron-Acceptor Ability of Ligands from Crystallographic Data

Keywords: Ab initio calculations / NMR spectroscopy / Pi ligands / Platinum / X-ray diffraction

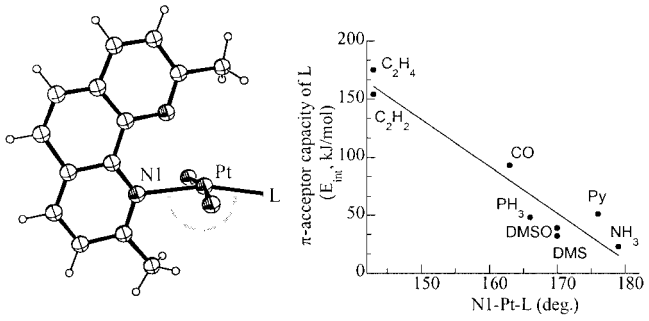

1714 **V. Passarelli,* F. Benetollo, P. Zanella**

The Ligating Ability of Functionalised Diaminodimethylsilanes towards Zirconium(IV)

Keywords: Chelates / NMR spectroscopy / N,O ligands / Silanes / Zirconium

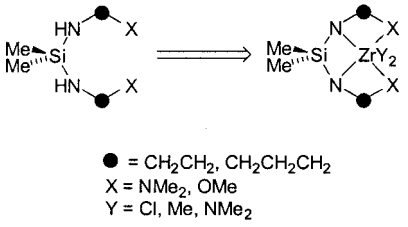

1724 **I. Luobeznova, L. Simkhovich, I. Goldberg,* Z. Gross***

Electronic Structures and Reactivities of Corrole−Copper Complexes

Keywords: Copper / Cyclic voltammetry / Electronic structure / Porphyrinoids / Structure elucidation

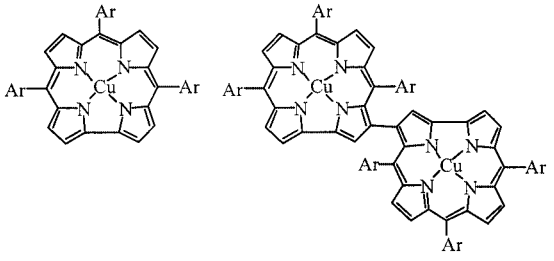

1733 **D. Udayakumar, M. Dan, C. N. R. Rao***

The First Amine-Templated Layered Metal Selenates

Keywords: Open-framework / Selenium / Hydrothermal chemistry / Amines / Template synthesis

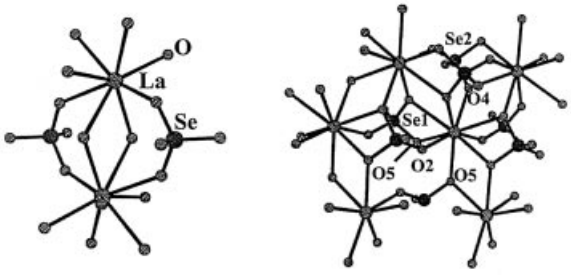

1740 **A. Krajete, G. Steiner, H. Kopacka, K.-H. Ongania, K. Wurst, M. O. Kristen, P. Preishuber-Pflügl, B. Bildstein***

Iminohydroxamato Early and Late Transition Metal Halide Complexes − New Precatalysts for Aluminoxane-Cocatalyzed Olefin Insertion Polymerization

Keywords: N,O ligands / N ligands / Chelates / Transition metals / Polymerization

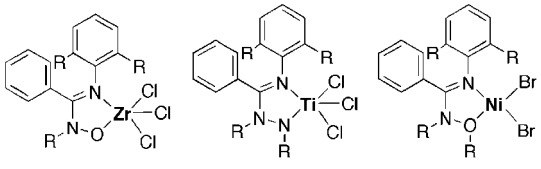

 © 2004 Wiley-VCH Verlag GmbH & Co. KGaA, Weinheim

1753 **A. Ghule, S.-H. Tzing, J.-Y. Chang, K. Ghule, H. Chang, Y. C. Ling***

Synthesis and Monitoring of α-$Bi_2Mo_3O_{12}$ Catalyst Formation using Thermo-Raman Spectroscopy

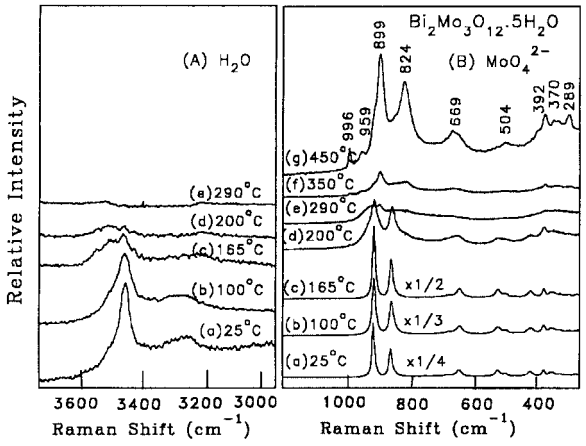

Keywords: Thermo-Raman spectroscopy / Thermochemistry / Dehydration / Phase transformations / Bismuth / α-$Bi_2Mo_3O_{12}$ catalyst

1763 **S. Vaduvescu, P. G. Potvin***

Linear Multinuclear Ru^{II} Photosensitizers

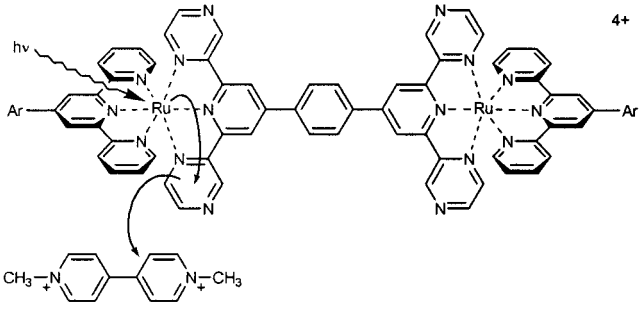

Keywords: Ruthenium / Tridentate ligands / Bridging ligands / Electron transfer / Photochemistry

 © 2004 Wiley-VCH Verlag GmbH & Co. KGaA, Weinheim

Perspectives in Inorganic Structural Genomics: A Trafficking Route for Copper

Fabio Arnesano,[a] Lucia Banci,[a] Ivano Bertini,*[a] and Simone Ciofi-Baffoni[a]

Keywords: Structural genomics / Copper / Metalloproteins / Chaperone proteins

Metal ions are essential for living organisms because they are involved in many fundamental biological processes. Increasing evidence indicates that there are no free copper ions in the cell; however, a recently discovered category of proteins (metallochaperones) is responsible for copper ion trafficking and delivery to either specific target enzymes or to membrane ATPases for metal translocation. A search in the available genomes for copper chaperones and soluble domains of the ATPases reveals a large variety of systems. In this Microreview, the example of copper transfer from outside a yeast cell into the Golgi organelle is considered, as well as related processes in other eukaryotes and in prokaryotes. The investigation of the structure and metal-binding properties of these proteins is crucial for understanding the process of copper trafficking at the molecular level and how coordination chemistry may contribute to the interpretation of the energetics of the metal environment.
(© Wiley-VCH Verlag GmbH & Co. KGaA, 69451 Weinheim, Germany, 2004)

Introduction

Life developed in an inorganic matrix, i.e. the Earth's crust. Living organisms have since learned how to acquire the correct amounts of essential inorganic elements and how to defend themselves from unnecessary or poisonous ones. Metal ions need a number of proteins both in order to be acquired/excreted, and in order to be transported from the outside of the cell to the final target, which is a metalloprotein.[1] Such processes are performed by soluble proteins[2−4] and membrane proteins, such as pumps[5−7] and permeases.[8] Such proteins are encoded in genomes or plasmids, but it is not obvious from a genome analysis which proteins are involved in the above processes. What can be done, however, is to search in the gene bank proteins similar to those already known to bind metal ions.[9,10] The identification of a metal-binding motif (i.e. a pattern of conserved amino acids acting as ligands) can be exploited in the search.[11] Another tool for the identification of proteins

[a] Magnetic Resonance Center CERM and Department of Chemistry, University of Florence,
Via Luigi Sacconi 6, 50019, Sesto Fiorentino, Florence, Italy
Fax: (internat.) + 39-055-4574271
E-mail: bertini@cerm.unifi.it

Fabio Arnesano (far right) was born in Lecce, Italy in 1973. He studied Chemistry at the University of Florence where he received his laurea degree in 1997 and his Ph.D. in 2000. He is currently a postdoctoral fellow at the Magnetic Resonance Center of the University of Florence. His research is devoted to NMR spectroscopy and biophysical characterization of metalloproteins and protein complexes involved in electron transfer and metal-trafficking processes, with a focus on heme and copper proteins.

Lucia Banci (center left) is Professor of Chemistry at the University of Florence, Italy. Her research interests are devoted to structural characterization of biological molecules through NMR spectroscopy, the methodological aspects of its application to proteins containing paramagnetic metal ions, computational simulations of protein structure and dynamics, and genome browsing and functional genomics.

Ivano Bertini (center right) was born in 1940, obtained the Italian degree of Doctor in Chemistry at the University of Florence in 1964 and then the Libera Docenza in 1969. He became full professor in General and Inorganic Chemistry in 1975 at the University of Florence, where he is now. He received the Laurea Honoris Causa from the University of Stockholm in 1998, from the University of Ioannina in 2002 and from the University of Siena in 2003. He is a member of the Academia Europaea and of the Italian Accademia dei Lincei. Following his initial studies on theoretical/physical inorganic chemistry, he has, since 1975, been studying the structure-function relationships of metalloproteins. In 1994, he transformed his laboratory into an NMR laboratory for studying the structural biology of metalloproteins. He has pursued the advancements of technology for determination of solution structures (particularly of paramagnetic metalloproteins), and he has developed a molecular biology department for protein expression and purification.

Simone Ciofi-Baffoni (far left) was born in Florence, Italy in 1971. He obtained his Ph.D. degree from the University of Florence in 2000. He is now a postdoctoral fellow at the same university. His research interest is focused on the structural and dynamic characterization of metalloproteins through NMR spectroscopy. His current research is particularly devoted to copper trafficking proteins to elucidate molecular mechanisms of copper homeostasis.

MICROREVIEWS: This feature introduces the readers to the author's research through a concise overview of the selected topic. Reference to important work from others in the field is included.

involved in processing metal ions is that of looking at bacterial genomes — often proteins that interact with each other are close in these genomes or they are part of a segment of DNA — called an operon — which encodes a number of interacting proteins, plus their regulator(s) and promoter(s).[12,13]

An example of this is provided by the *cop* operon of *Enterococcus hirae*,[14] responsible for copper uptake, availability, and export in the bacterium by encoding a repressor (CopY), a copper chaperone (CopZ), and an import and an export copper ATPase (CopA and CopB, respectively).[14] Understanding of the mechanisms of metal transport and regulation at the molecular level is crucial in order to shed light on a number of biological processes, including the functional defects of genes. In so doing, a lot can be learned about this area of biological inorganic chemistry, which represents a window for the expansion of the field of inorganic chemistry. The most successfully studied system is that regarding copper — as a case study, this review will be devoted to one of its trafficking pathways.

Copper can adopt two distinct oxidation states, either oxidized (Cu^{II}) or reduced (Cu^{I}). Copper proteins are involved in vital processes such as respiration, iron transport, oxidative stress protection, blood clotting and pigmentation.[15] However, because of its redox activity, free copper would be highly toxic, even at low concentrations. Therefore, free intracellular copper is absent, and its concentrations need to be regulated within very narrow limits.[16] Disruption of copper homeostasis has recently been implicated in disease states and pathophysiological conditions.[17–19]

Results and Discussion

Copper in Yeast: From the Outside to the Multicopper Oxidase Fet3

Genetic experiments with baker's yeast *Saccharomyces cerevisiae* resulted in the cloning of the first gene encoding a cellular membrane protein associated with high-affinity Cu transport (Ctr), denoted Ctr1.[20] Indeed, yeast cells lacking a functional Ctr1 gene are unable to load Cu onto cytochrome *c* oxidase.[21] Copper uptake through Ctr1 is preceded by reduction of Cu^{II} to Cu^{I}, a process mediated by the cell surface metalloreductase Fre1[22] (Figure 1).

All members of the Ctr1 family of Cu transporters have three potential transmembrane domains, a hydrophilic amino terminus typically rich in methionine residues, and a number of other conserved residues of as yet unknown functional importance.[8] The amino-terminal region (located outside the cell) of baker's yeast Ctr1 harbors eight repeats of the putative Cu-binding motif MXMXXM (M = methionine, X = generic amino acid). The carboxy-terminal region (located inside the cell, in the cytosol) of Ctr1 is rich in charged amino acids and contains quite well conserved cysteines.[8] Thus far, studies reveal that both the yeast and human Ctr1 proteins are present as homo-multimeric proteins, with high affinity for Cu.[23,24]

Several proteins are, on the other hand, implicated in low-affinity trans-membrane copper uptake in baker's yeast, including Fet4 and Ctr2. Fet4 has no significant homology to the Ctr family of high affinity copper transporters. However, biochemical and genetic evidence suggests that Fet4 is able to transport both iron and copper.[25] Ctr2, which bears homology to Ctr1, may be localized in the membrane of organelles present inside the cell, and may play a role in the mobilization of copper ions[26] between different locations inside the cells.[27] O'Halloran et al. have demonstrated that there is no free copper in a cell,[16] and therefore copper, just like other metal ions, needs to be accompanied to different cell compartments or to its final destination by proteins called chaperones, responsible for copper distribution inside the cytoplasm.[2,3] The carboxy terminus of Ctr1 contains two CXC motifs which are proposed to bind Cu^{I} and exchange it with metallochaperones.[28] In support of this, it has been recently observed that a C-ter-

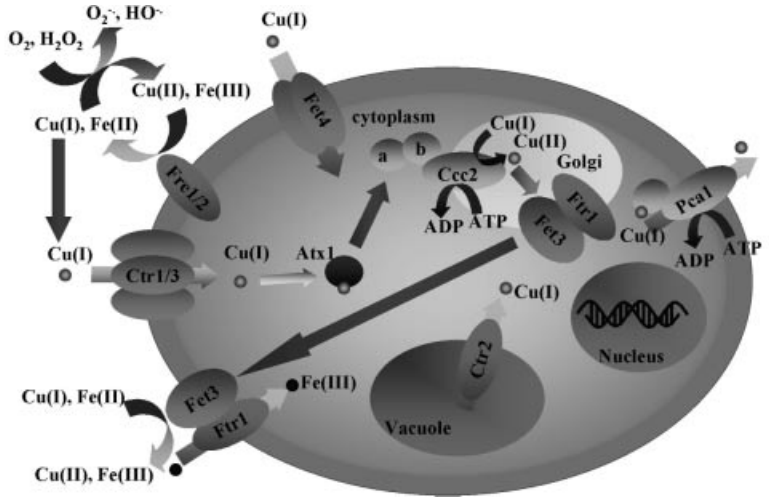

Figure 1. Some copper trafficking pathways in the yeast cell; depending on the extracellular copper concentration, copper can be transported inside the cell by two high-affinity copper transporters Ctr1 and Ctr3, or by a low-affinity Cu/Fe-transporter Fet4; Ctr2 could be involved in copper efflux from the vacuole; delivery of copper involves the metallochaperone Atx1 that shuttles copper to Ccc2, a P-type ATPase located in the trans-Golgi network, and is responsible for copper translocation; once copper is in the lumen of the secretory pathway, it is loaded onto Fet3, a multicopper-ferroxidase essential for high affinity iron uptake that partners with the Ftr1 protein

 © 2004 Wiley-VCH Verlag GmbH & Co. KGaA, Weinheim

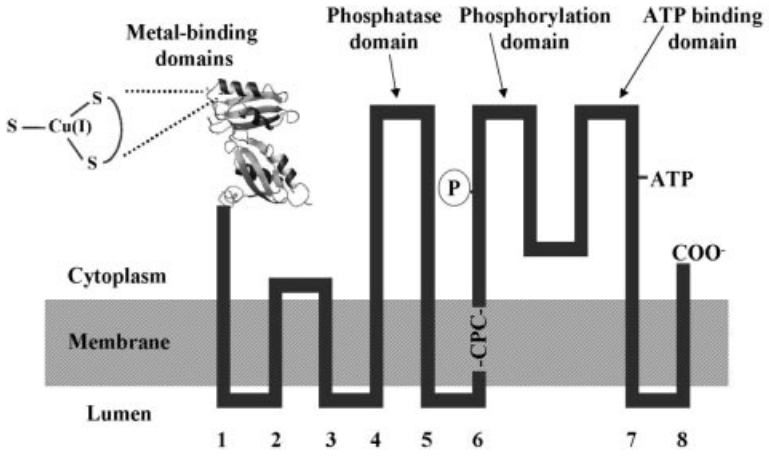

Figure 2. Schematic model of the copper-transporting ATPase Ccc2 from *S. cerevisiae*; the predicted transmembrane segments and the cytosolic domains are shown; "P" indicates a phosphate group; the copper binding motifs CXXC and CPC are also indicated; a similar structural organization is shared by all heavy metal P-type ATPases, but the number of N-terminal metal-binding domains is variable

minal domain of yeast Ctr1 exchanges Cu^{I} rapidly with the copper chaperone Atx1.[28] Atx1 delivers copper to the soluble copper domains of Ccc2, a P-type ATPase located in the Golgi membrane [29,30] (see Figure 1), which transfers copper to enzymes inside the Golgi organelle.[31] On the contrary, a different ATPase (Pca1), located on the cell membrane, appears to be involved in copper export from yeast.[32]

Ccc2 and Pca1 belong to the family of cation-transporting P-type ATPases (see Figure 2), which contain eight transmembrane segments, an ATP binding/phosphorylation domain (between transmembrane segments 6 and 7) and a phosphatase (or actuator) domain (between transmembrane segments 4 and 5).[5−7] Copper ATPases possess a variable number of N-terminal soluble metal-binding domains and a conserved CPx [C = cysteine, P = proline, x = C (cysteine) or H (histidine)] motif in transmembrane segment 6. Ccc2 has two soluble domains of about 70 amino acids, each containing a Cu^{I} binding CXXC motif. Pca1 contains only one domain preceded by a Cys-rich region of about 400 amino acids.[32]

Once Cu^{I} is bound to one or two soluble domains of Ccc2, it is transferred inside the Golgi organelle. It has been suggested that, during this transfer, Cu^{I} is oxidized to Cu^{II}, consistent with the more oxidizing environment of the Golgi organelle.[33] Copper is then loaded onto Fet3, a multicopper-ferroxidase essential for high-affinity iron uptake. When loaded with copper, Fet3 makes a complex with the iron transporter Ftr1[34] and, together, they move towards the cell membrane,[35] where Fet3 catalyzes the oxidation of Fe^{II} to Fe^{III}, which is then bound by Ftr1. Ftr1 and Fet3 are primarily expressed in oxygenated cultures, whereas anaerobic conditions induce the low affinity copper/iron transporter, Fet4.[36] Very recently, it has been observed that Fet3 also has a cuprous oxidase activity at the cell membrane, thus buffering the Cu^{I}/Cu^{II} ratio through an interplay with the cupric reductase Fre1.[37] By removing the Atx1 gene, iron uptake does not occur any more, as a consequence of failure to provide the metal cofactor to Fet3. These data, as well as other experimental evidence, point out at the tight interplay between copper and iron metabolisms. Figure 1 shows the mechanism by which Cu^{I} is acquired by Ctr1, taken by Atx1, released to the membrane protein Ccc2 and transferred to Fet3.

The structures of reduced apo- and Cu^{I}-loaded Atx1 were solved by NMR spectroscopy in Florence in collaboration with the Northwestern University[38] (Figure 3, top).

The solution structure of *S. cerevisiae* Cu^{I}-Atx1 exhibits a βαββαβ-fold with the Cu^{I} ion coordinated by two cysteine residues, Cys 15 (in loop 1) and Cys 18 (in helix α1), of a conserved CXXC motif. This fold is the same as that found by X-ray diffraction of the Hg^{II} derivative.[39] Atx1 shares significant sequence similarity (30 % residue identity) with a periplasmic mercury resistance protein, MerP.[40] Both the MerP solution structure[41] and the Hg^{II}-Atx1 crystal structure[39] show an Hg^{II} ion coordinated by the sulfur atoms of the two cysteines of the CXXC motif with a linear coordination geometry. In contrast, the solution structure of Cu^{I}-Atx1 has an average S−Cu−S angle of 120±40°, suggesting that Cu^{I} prefers a coordination number higher than two. EXAFS analyses of Cu^{I}-Atx1[42] and of its homologous protein, CopZ, from *Bacillus subtilis*[43] and *Enterococcus hirae*[44] showed that a third sulfur atom completes the coordination sphere of Cu^{I}, indicating its preference for a three-coordinate environment. A conserved Met residue, two residues upstream of the CxxC consensus motif, is a candidate for this third ligand. However, in the structures of Cu^{I}-Atx1 and Cu^{I}-CopZ from *B. subtilis*, the average positions of the Met sulfur atoms are 7.0±1 Å and 6.2±1 Å from copper, respectively, which rule their involvement in copper coordination.[38,45] Even in the Hg^{II}-Atx1 crystal structure[39] the Met sulfur is too far from copper (8.1 Å), suggesting it is not involved in metal coordination. The exposed location of the metal site suggests that the third ligand may be provided by an external thiol group.

These proteins are prepared by incubation of the apoprotein with a Cu^{I} complex in the presence of a thiol reductant, dithiothreitol (DTT).[29] In vivo, DTT is likely to be

 © 2004 Wiley-VCH Verlag GmbH & Co. KGaA, Weinheim

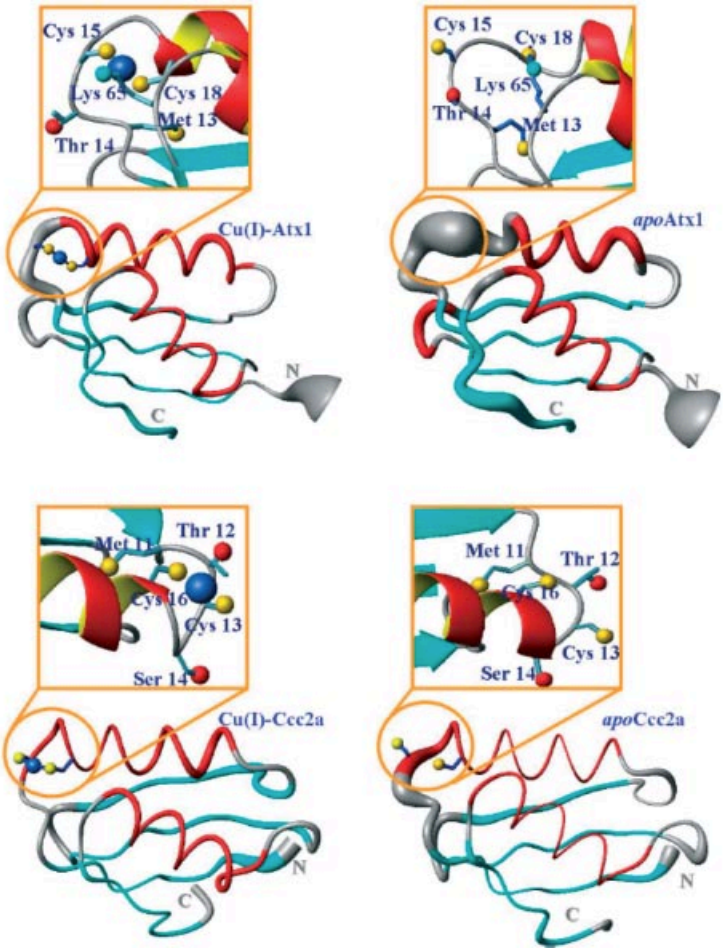

Figure 3. Solution structures of Cu^I- and apo-loaded Atx1 (top left and top right, respectively) and Cu^I- and apo-loaded Ccc2a (bottom left and bottom right, respectively); the structures are represented as a tube whose radius is proportional to the structural resolution; helices are colored in red and β-strands are colored in cyan; the insets show the copper binding site where copper is represented as a blue sphere; copper-binding cysteines and other neighbouring residues are also indicated

replaced by glutathione, which is present at high concentration (about 5 mM) inside the cell. When copper reduction is carried out with ascorbate, the EXAFS spectra of Cu^I-CopZ indicate that one oxygen atom of ascorbate is present in the first coordination sphere of copper, together with the two sulfur atoms of the Cys residues.[43] The three-coordinate environment of copper, with one ligand being exogenous and easily detectable, has a crucial role in the metal transfer process (see later).

The overall folding of apoAtx1 is essentially identical to that observed for the copper-bound form of the protein, with the exception of helix α1, which is shorter by one helical turn at the N-terminus.[38] Comparison of the Cu^I- and apo-conformations of the protein also reveals that the Cu^I-binding cysteines move from a buried site in the metal-bound form to a solvent-exposed conformation on the surface of the protein, after copper release (see Figure 3, top). Slight structural changes, involving both the charged and hydrophobic residues close to the metal-binding site,[38] may signal to the partner whether the metallochaperone is in the demetalated or in the copper-loaded form, and may trigger binding of Atx1 to Ccc2.

The structure of the first domain of Ccc2 (Ccc2a) was solved by NMR spectroscopy, and exhibits a βαββαβ, ferredoxin-like fold similar to that of its partner Atx1[46] (Figure 3, bottom). The overall fold of Ccc2a remains essentially unchanged upon copper loading. Unlike Atx1, only few conformational changes are observed in Ccc2a upon copper release, and the metal-binding region (including the conformation of the metal-binding cysteines), is well defined in both apo and holo forms, suggesting that the metal site in apoCcc2a is pre-organized to some extent to receive the copper ion.[46] Again, the structure indicates the copper environment is three-coordinate (S−Cu−S average angle 120±30°).

Modeling of the whole N-terminal region of Ccc2, encompassing the two soluble domains, was performed on the available structure of the homologous protein from *B. subtilis*,[47] and suggests that the two copper binding sites are far apart and cannot interact with each other. However,

 © 2004 Wiley-VCH Verlag GmbH & Co. KGaA, Weinheim

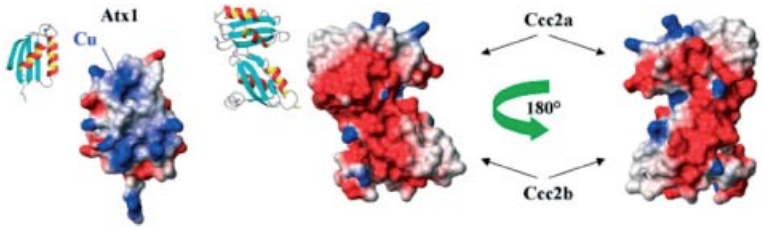

Figure 4. Electrostatic surface potential of Cu^{I}-Atx1 from *S. cerevisiae* and of a structural model of the two soluble domains of Ccc2 from *S. cerevisiae* based on the structure of CopAab from *B. subtilis*; the ribbon representations show the orientation of the two proteins; the copper binding cysteines of the CXXC motifs of Atx1 and Ccc2 domains are indicated in yellow; copper is shown as a blue sphere

they can interact with Atx1. Indeed, the surface of Atx1 is positively charged, whereas those of the Ccc2 domains are negative (Figure 4).[48] The electrostatic interaction is the long-distance driving force which brings the two partner proteins together.

The protein surface interacting with the partner can be monitored by NMR spectroscopy, through the mapping of $^{1}H/^{15}N$ chemical shift changes occurring in both proteins when titrated with the partner [Figure 5(A)].[48,49] These residues are located in loops 1 and 5, helix α1, and the C-terminal part of helix α2 in both proteins. Besides the metal-binding cysteines and the charged amino acids, some polar and hydrophobic residues are involved in interactions at the interface. As mentioned above, the hydrophobic patches at the protein interface are different between the apo and the copper-loaded forms of Atx1, whereas Ccc2a maintains a similar conformation and pattern of hydrophobic contacts around the metal-binding site, regardless the metalation state. Comparison with the structures of homologous proteins confirms that in most of the cases metal binding affects a hydrophobic patch around the metal site in metallochaperones, possibly for tuning and optimizing the hydrophobic interactions with the ATPase domains.[50]

Thermodynamic and kinetic considerations suggest that the copper chaperones are designed to increase significantly the rate of copper transfer between physiological partners and then to overcome the extraordinary copper chelation capacity of the eukaryotic cytoplasm. In this sense, metallochaperones work like enzymes, lowering the energetic barriers along a specific reaction pathway. The thermodynamic gradient for metal transfer between Atx1 and Ccc2 is shallow (K_{eq} = 1.5), establishing that transfer of copper from Atx1 to Ccc2 is not based on a higher copper affinity of the target domain.[51] Instead, Atx1 allows rapid metal transfer to the ATPase ($k_{ex} > 10^{3}\ s^{-1}$),[48] which, in turn, transfers copper across the membrane, thus driving the thermodynamic overall equilibrium. A low activation barrier for transfer between partners results from complementary electrostatic forces that orient the metal-binding loops of Atx1 and Ccc2 for formation of copper-bridged intermediates.[30,51]

As mentioned above, the exposed location of the metal-binding site allows copper to expand its coordination sphere, thus becoming three-coordinate. During the copper transfer process, the third labile copper ligand in Cu^{I}-Atx1 would be displaced by the first Cys of the CXXC motif on the partner molecule, to form a three-coordinate intermedi-

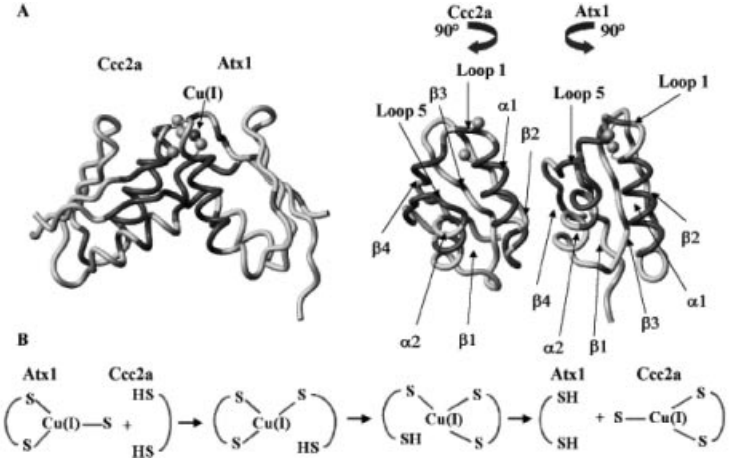

Figure 5. (A) The Ccc2a:Atx1 adduct model calculated using NMR chemical shift mapping; the view on the right-hand side shows the molecules rotated by 90° to expose the interaction surfaces; residues involved in the interaction are in dark grey; residues not involved in the interaction or not observed are in light grey; the copper ion is in dark grey and the sulfur atoms of the copper-binding cysteines are in light grey; secondary structure elements are indicated; (B) the proposed mechanism for copper transfer between Atx1 and a domain of the Ccc2 protein

 © 2004 Wiley-VCH Verlag GmbH & Co. KGaA, Weinheim

ate. When the second Cys of Ccc2 binds copper, one Cys of Atx1 is detached, thus weakening the interaction of copper with Atx1. In the final step, the second Cys of Atx1 is detached, (probably) replaced by an exogenous ligand, and the metallochaperone leaves in its apo form (see B in Figure 5). These structural changes are accompanied by an increase in mobility of residues at the interface, which may favor complex dissociation after copper release.[48]

What Determines Metal Selectivity?

The βαββαβ structure containing a CXXC metal-binding motif has been adopted in nature to carry a variety of metal ions (Cu, Hg, Zn, Cd, Pb) with selective affinity.[52−54] Atx1 shares significant structure similarity with a periplasmic mercury resistance protein (MerP), which interacts with a membrane protein of the detoxification operon.[40] The solution structure of MerP[41] shows an Hg^{II} ion coordinated by the two cysteines of the CXXC motif, with a linear coordination geometry. It has also been shown that MerP is capable of binding to other divalent metal ions with lower affinities.[54,55] Similarly, the copper chaperone CopZ from *E. hirae* forms specific metal complexes with copper, mercury, cadmium and cobalt with the following order of affinity: $Cu^{I} > Hg^{II} > Cd^{II} >> Co^{II}$.[56] In addition, soluble domains of bacterial zinc-transporting[57] and cadmium-transporting ATPases,[58] either experimentally found[59] or predicted to have the βαββαβ fold, possess the CXXC binding motif. Therefore, it can be inferred that the metal-binding selectivity does not reside in the overall fold but in sequence variations close to the metal site.

For zinc ATPases, sequence analysis leads to the earlier suggestion that an Asp residue, which is found just before the N-terminal cysteine of the CXXC consensus motif, may modulate metal-binding affinity.[9] EXAFS data on the N-terminal domain of the zinc ATPase ZntA from *E. coli* indicate that Zn is coordinated by two sulfur atoms and two N/O atoms.[59] The structure of ZntA has been recently solved[59] and suggests that the conserved Asp residue can indeed coordinate zinc. The presence of three negative charges (one aspartate and two cysteines) ought to provide a more favourable electrostatic contribution for the binding of a Zn^{II} ion with respect to a Cu^{I} ion. Moreover, in terms of hard/soft acid-base theory, the Asp oxygen will stabilize binding of the harder (or less polarizable) Zn^{II} ion more than the highly polarizable Cu^{I} ion. In copper chaperone sequences, the position immediately preceding the N-terminal Cys in the metal-binding loop is often occupied by a Thr residue, which provides a second-shell interaction for copper.[60−62] These data suggest that the amino acid at this position plays a role in metal ion selectivity.

Other factors could determine metal selectivity of the CXXC metal-binding motif in a βαββαβ structure, such as the size of the binding pocket (which can be controlled by the tightness of the turn of the binding loop), or by electrostatics. The nature of the residues in the turn of the metal-binding loop affects their interactions with the solvent and with other protein residues, and can contribute to the turn tightness and/or to electrostatic properties.

Comparison of Homologous Proteins

The genome-sequencing projects developed in the last few years have made available the primary sequence of an enormous number of new genes. The draft sequence of the human genome[63] is now available, together with the complete genomes of many other organisms (see http://www.ncbi.nlm.nih.gov). Functional associations of neighboring genes can be detected by bioinformatic tools and can be used to identify potential protein partners.[12,13] This huge amount of incoming information has stimulated the development of Structural Genomics projects (http://www.spineurope.org/, http://www.nigms.nih.gov/psi/ and http://www.rsgi.riken.go.jp/), with the aim of elucidating the function of proteins through the determination of their three-dimensional structure. The idea can be translated in the motto: "*From sequence to function through structure*". Moreover, genome sequencing allows us to compare homologous sequences in different species, in an "orthologue" approach, and to model them when sequence identity with at least one protein of known structure is higher than 30 %.[64] Structure similarities allow the function of one family of proteins to be predicted from that of the other. In the case of metalloproteins, conserved residues forming the consensus motifs for metal binding can be used as selection criteria in a genome-wide search, together with sequence identity thresholds.[11] An orthologue search shows that proteins homologous to yeast Atx1 and Ccc2 are found in all the eukaryotes and in many bacteria.[9] Structural models can be calculated using the high-resolution solution structures of yeast proteins as templates, and structural modelling allows us to identify common structural features, such as the hydrophobic core, electrostatic potential surfaces and metal-binding site residues.

Searches have shown that bacteria are very diverse, and may develop alternative routes for copper homeostasis.[9] *B. subtilis* has a CopZ which acts as chaperone[45] as well as a CopA which is an ATPase containing two soluble metal-binding domains.[60] In this organism it has been shown that the CopZ-CopA interaction mechanism is used for copper excretion.[65] It is peculiar that CopZ has opposite overall charge with respect to its eukaryotic homolog Atx1 and, of course, opposite charges are displayed by the two metal-binding domains of the ATPase.[66] In *B. subtilis*, the first domain of CopA is not well folded in vitro, but a point mutation at position 46 is sufficient to fold the protein properly.[67] It is possible that the first domain is not folded in vivo or not used at all. Copper ATPases of other bacteria have indeed only one soluble domain. In *E. hirae* the homologous proteins are thought to function in copper uptake.[68] The *cop* operon of *E. hirae*, in addition to the CopA ATPase and the copper chaperone CopZ, consists of two more genes, one encoding a repressor (CopY), which, upon receiving copper from CopZ, breaks its interaction with DNA.[44,69] The other is a second P-type copper ATPase

 © 2004 Wiley-VCH Verlag GmbH & Co. KGaA, Weinheim

(CopB), which is involved in the extrusion of copper when it reaches toxic levels[68] (Figure 6, top).

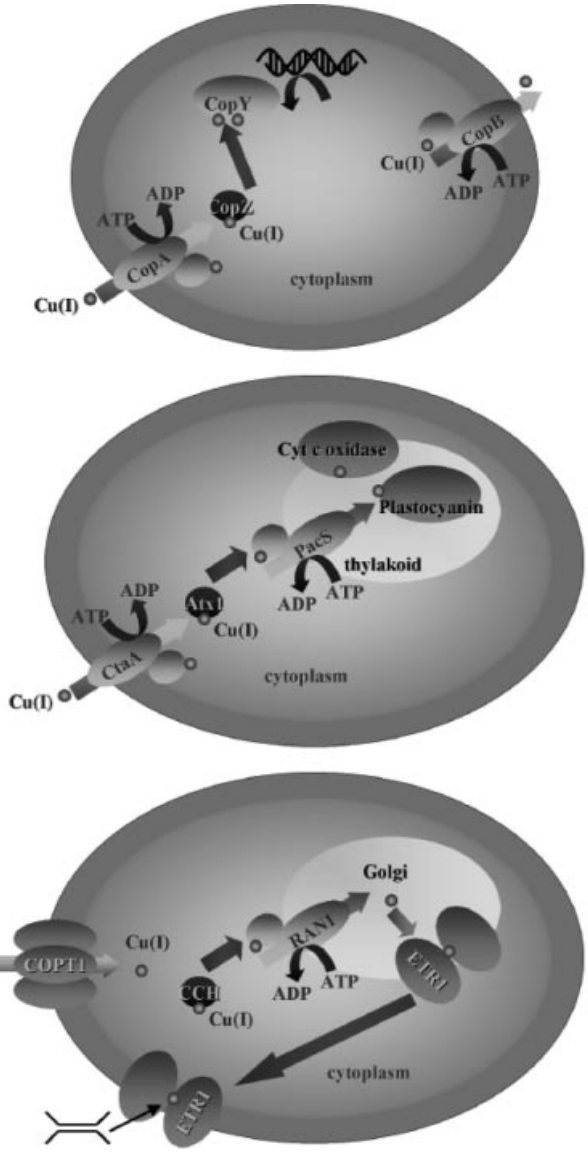

Figure 6. Copper-trafficking pathways in the bacterium *Enterococcus hirae* (top), in the cyanobacterium *Synechocystis* PCC 6803 (center) and in the plant *Arabidopsis thaliana* (bottom)

Some cyanobacteria have a peculiar cellular organization which involves organelles called thylakoids. These contain cytochrome *c* oxidase and plastocyanin, and both proteins require copper to function. In these bacteria, two copper-transporting ATPases are present, namely CtaA and PacS.[70] The former is located on the external cellular membrane and is involved in copper uptake, whereas the latter is on the thylakoid membrane and transports copper inside this organelle for its delivery to copper-requiring proteins.[71] Copper is shuttled between these two ATPases by a soluble small protein, which is able to interact with the soluble copper-binding domains of both ATPases.[70] Interestingly, this copper chaperone possesses a His residue on loop 5 in the position corresponding to Lys 65 in Atx1 from *S. cerevisiae*. The imidazole ring of the latter His is predicted to protrude from loop 5 of the cyanobacterial protein, providing a putative third copper ligand. This residue is proposed to influence the direction of metal transfer in the interaction of the chaperone with the amino-terminal domains of the two ATPases PacS and CtaA [72] (Figure 6, center).

Plants also need copper for a variety of functions. One of these functions is unique to this kingdom of life and involves binding of ethylene, an important endogenous plant hormone affecting many aspects of growth and development. Ethylene binding occurs through five copper-dependent ethylene receptors (ETR1, ERS1, ETR2, EIN4 and ERS2).[73] In *Arabidopsis thaliana*, one of the two plants for which the complete genome is available, a copper pathway similar to that of *S. cerevisiae* has been identified.[74] Using the yeast system as a guide, it has been postulated that copper enters the cell through COPT1, the homologue of yeast CTR2. Copper is shuttled by a soluble protein (CCH), the homologue of Atx1, to a copper ATPase (RAN1), which resides in the Golgi, like Ccc2.[74] Here, the ATPase delivers one copper ion to the ethylene receptors (ETR1 family), which thus become functional and move to the external cell membrane to sense ethylene concentrations.[74] Ethylene interacts with Cu^{I} in an electron-rich hydrophobic pocket formed by membrane-spanning helices of the ETR1 dimer[75] (Figure 6, bottom).

In humans, two P-type ATPases, Menkes (MNK)[76−78] and Wilson (WND)[79,80] proteins, and a copper chaperone (Hah1[81]), homologous to yeast Ccc2 and Atx1 respectively, are present. The key role of MNK and WND in the cellular copper trafficking is strongly determined by the intracellular localization mechanism by which these proteins manage to deliver copper to the recently synthesized copper proteins.[33,82] At low copper concentrations, both proteins are localized in the Golgi, where MNK transfers copper to lysyl oxidase, which is responsible for cross-linking collagen and elastin. At high copper concentrations, MNK moves to the external cell membrane and pumps out of the cell the excess of copper. When the intracellular copper levels are reduced, the protein returns to the Golgi membrane.[33] WND, also located in the Golgi membrane, incorporates copper (at low concentrations) into ceruloplasmin, a multicopper oxidase similar to Fet3. At high copper concentrations, WND moves from the Golgi membrane to a vesicular compartment where it releases copper. The copper-loaded vesicles are then discharged into the bile.[82]

Both proteins have six soluble metal-binding domains at the N-terminal region, in addition to an intramembrane potential metal-binding site containing a CPC motif. The soluble metal-binding domains were suggested to be involved in the copper-dependent regulation of WND. Indeed, the copper-bound N-terminal WND domains (1−6) interact with the ATP-binding domain less tightly than their apo forms, thus increasing the affinity of the domain for ATP.[83]

However, only binding of copper to the intramembrane CPC binding site is essential for the copper-dependent cata-

 © 2004 Wiley-VCH Verlag GmbH & Co. KGaA, Weinheim

lytic activity of the ATPase. This dependence is supported by the fact that mutations in the CPC motif destroy the activity,[84] whereas mutations in any or all of the six soluble domains do not.[85] It has been recently shown that affinity of the intramembrane copper-binding site is regulated by binding of copper to the 5th and 6th domains of WND, while the first four domains of WND are not involved in this process.[86] The need for six domains is not certain. Bacterial and yeast homologues have only one or two domains, suggesting that most of the metal-binding domains are not essential for the copper transport function.[9] A unique feature of mammalian copper-ATPases is their ability to undergo copper-dependent vesicular trafficking. Therefore, metal-binding domains 1−4 can be involved in the copper-dependent regulation of the ATPase subcellular localization, i.e. when copper concentration is increasing and all six metal-binding sites become occupied with the metal, the conformation of the N-terminal region changes,[87] thus inducing the translocation of the protein from the Golgi to the external cell membrane[88] or to a vesicular compartment.[89] Here, the copper ATPases act like their bacterial homologues, pumping excess copper out of the cytoplasm, thus detoxifying the cell.

The six metal-binding domains of MNK and WND are connected by linkers of different length. The longest flexible linker separates metal-binding domains 1−4 from domains 5 and 6.[9,90] Interestingly, it has been observed experimentally that the copper chaperone Hah1 interacts preferentially with domains 1−4 of WND.[53] It has been therefore proposed that domains 5 and 6 may receive copper from domains 1−4.[90] When Cu^{I}-Hah1 is added in large excess, copper is transferred to all six domains of WND, but Hah1 can also function as a regulator, by removing copper from N-terminal domains.[91] Although a slight excess of apo-Hah1 is sufficient to remove the first four copper atoms, removal of the other two copper atoms cannot be completed even using a large excess of apoHah1. It has been suggested that copper that is strongly bound to N-terminal domains of WND is essential for enzymatic activity, whereas exchangeable copper is bound to regulatory sites.[91]

The structures of a number of single metal-binding domains of MNK are available.[61,92] The other domains of MNK and WND have been modeled.[9] All the domains share a βαββαβ fold but display different surface charges. Interestingly, MNK possesses a seventh predicted βαββαβ domain between the first and the second metal-binding domains, but lacks a CXXC motif. In WND, only a short linker separates domains 1 and 2.[9] The arrangement of the last two soluble domains of MNK and WND, (i.e. those closest to the membrane) is thought to be similar to that of CopA from *B. subtilis* and Ccc2 (see above).[47]

Mutations and Illnesses

The advances in knowledge of the function of MNK and WND have been catalyzed by the fact that they are involved in two human disorders of copper transport.[93] Mutations of MNK in humans cause a copper deficiency disorder (Menkes' disease), and mutations of WND result in a Cu toxicity condition (Wilson's disease). The reason for different diseases caused by mutations in proteins of similar structure is related to the involvement of the two proteins in different patterns of cellular trafficking and their distinct pattern of tissue expression.[88,89] The Menkes gene is expressed in most tissues; the Wilson gene is expressed mainly in the liver, where it is responsible for biliary excretion of copper.

Different types of mutations have been identified which alter the copper metabolism in the Golgi (http://archive.uwcm.ac.uk/uwcm/mg/hgmd0.html). These mutations are mainly located in the transmembrane portion of the ATPases, with a few present in the soluble metal-binding and ATP-binding domains. One of the most common disease mutations, a H1069Q substitution, causes intracellular mislocalization of WND.[94] His 1069 is located in the ATP-binding domain of WND and is conserved in all copper-transporting ATPases from bacteria to mammals; experiments indicate that His 1069 is responsible for proper orientation of ATP in the catalytic site of WND prior to ATP hydrolysis.[95]

Several mutations found in Wilson's disease patients were shown to disrupt the ability of WND to interact with the soluble copper chaperone Hah1, which is homologous to yeast Atx1. Three disease-associated mutations (G85V, L492S, and G591D mutations) in the soluble metal-binding domains of WND, determine a marked reduction in interaction with Hah1, suggesting that the inability of Hah1 to deliver copper to WND constitutes the molecular basis of Wilson's disease in those patients harbouring these mutations.[96]

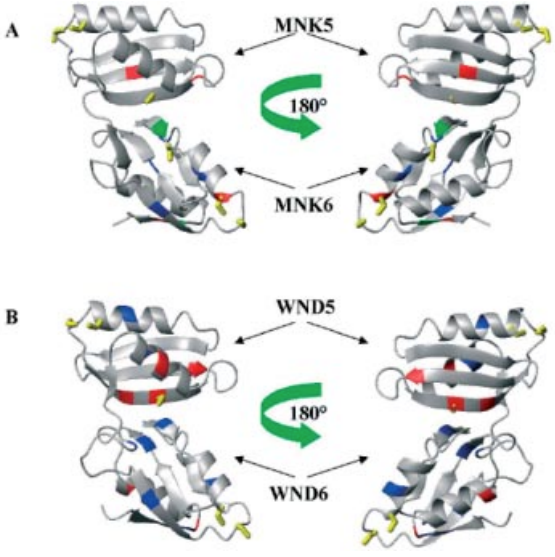

Figure 7. Structural models of the two linked soluble domains closest to the membrane (5 and 6) of the human Menkes (MNK) (A) and Wilson (WND) (B) proteins based on the structure of CopAab from *B. subtilis*; cysteine residues are indicated in yellow; mutations are coloured as follows: red = nucleotide substitutions (missense/nonsense), blue = small deletions, green = small insertions

 © 2004 Wiley-VCH Verlag GmbH & Co. KGaA, Weinheim

The two domains closer to the membrane (5 and 6), have been shown to be essential for the functional activity of both MNK[97] and WND.[86,98] A structural model of these two domains can be obtained using the structure of CopAab from *B. subtilis*[47] as template. Significantly, although the length of the short linker between these two domains is not exactly the same for MNK/WND and CopAab,[9] residues at the interface between the two CopA domains are conserved in the last two soluble domains of both MNK and WND,[47] thus supporting a similar quaternary arrangement for this pair of domains. Mapping disease mutations on the models of these domains shows that some of them are farther from the two metal-binding sites, but they can affect the interaction between these two domains (Figure 7).

Concluding Remarks and Perspectives

The biochemistry of metal ions is becoming increasingly important, because of its tremendous implications in medicine and biology, as witnessed by the large number of proteins, emerging from genome sequencing and genetic studies, that are involved in diseases linked to metal ion homeostasis. Several copper-trafficking pathways involving metallochaperone-like proteins and P-type ATPases modulate copper ion homeostasis and delivery in bacteria and eukaryotes. These systems are at the boundary between inorganic chemistry and genomics, which has raised our interest as chemists working in the field of *inorganic structural biology*. Taking advantage of the large amount of structural information on yeast Atx1 chaperone and Ccc2 transporters and their interactions with metals, the field is moving towards a deeper understanding of homologous systems, with particular interest in the Menkes and Wilson ATPases involved in neurodegenerative disorders in humans. In these systems, it will be very useful to study the influence of the metal sites on the three-dimensional structures of proteins and multiple domain organization, in order to envisage the possible causes of degeneration and diseases. Finally, the mechanism of copper translocation across membranes needs to be fully elucidated.

[1] L. A. Finney, T. V. O'Halloran, *Science* **2003**, *300*, 931−936.
[2] T. V. O'Halloran, V. C. Culotta, *J. Biol. Chem.* **2000**, *275*, 25057−25060.
[3] A. C. Rosenzweig, *Acc. Chem. Res.* **2001**, *34*, 119−128.
[4] H. S. Carr, D. R. Winge, *Acc. Chem. Res.* **2003**, *36*, 309−316.
[5] M. Solioz, C. D. Vulpe, *Trends Biochem. Sci.* **1996**, *21*, 237−241.
[6] C. Rensing, M. Ghosh, B. P. Rosen, *J. Bacteriol.* **1999**, *181*, 5891−5897.
[7] J. Camakaris, I. Voskoboinik, J. F. Mercer, *Biochem. Biophys. Res. Commun.* **1999**, *261*, 225−232.
[8] S. Puig, D. J. Thiele, *Curr. Opin. Chem. Biol.* **2002**, *6*, 171−180.
[9] F. Arnesano, L. Banci, I. Bertini, S. Ciofi-Baffoni, E. Molteni, D. L. Huffman, T. V. O'Halloran, *Genome Res.* **2002**, *12*, 255−271.
[10] L. Banci, A. Rosato, *Acc. Chem. Res.* **2003**, *36*, 215−221.
[11] Z. Zhang, A. A. Schaffer, W. Miller, T. L. Madden, D. J. Lipman, E. V. Koonin, S. F. Altschul, *Nucleic Acids Res.* **1998**, *26*, 3986−3990.
[12] C. von Mering, M. Huynen, D. Jaeggi, S. Schmidt, P. Bork, B. Snel, *Nucleic Acids Res.* **2003**, *31*, 258−261.
[13] M. Y. Galperin, E. V. Koonin, *Nat. Biotechnol.* **2000**, *18*, 609−613.
[14] A. Odermatt, H. Suter, R. Krapf, M. Solioz, *Ann. N. Y. Acad. Sci.* **1992**, *671*, 484−486.
[15] M. C. Linder, *Biochemistry of Copper*, Plenum Press, New York, **1991**, p. 1−13.
[16] T. Rae, P. J. Schmidt, R. A. Pufahl, V. C. Culotta, T. V. O'Halloran, *Science* **1999**, *284*, 805−808.
[17] L. M. Sayre, G. Perry, M. A. Smith, *Curr. Opin. Chem. Biol.* **1999**, *3*, 220−225.
[18] A. I. Bush, *Curr. Opin. Chem. Biol.* **2000**, 184−191.
[19] D. Strausak, J. F. Mercer, H. D. Hermann, W. Stremmel, G. Multhaup, *Brain Res. Bull.* **2001**, *55*, 175−185.
[20] A. Dancis, D. S. Yuan, D. Haile, C. Askwith, D. Elde, C. Moehle, J. Kaplan, R. D. Klausner, *Cell* **1994**, *76*, 393−402.
[21] J. Lee, J. R. Prohaska, D. J. Thiele, *Proc. Natl. Acad. Sci. USA* **2001**, *98*, 6842−6847.
[22] R. Hassett, D. J. Kosman, *J. Biol. Chem.* **1995**, *270*, 128−134.
[23] J. Lee, M. M. Pena, Y. Nose, D. J. Thiele, *J. Biol. Chem.* **2002**, *277*, 4380−4387.
[24] S. Puig, J. Lee, M. Lau, D. J. Thiele, *J. Biol. Chem.* **2002**, *277*, 26021−26030.
[25] R. Hassett, D. R. Dix, D. J. Eide, D. J. Kosman, *Biochem. J.* **2000**, *351*, 477−484.
[26] K. Kampfenkel, S. Kushnir, E. Babiychuck, D. Inze, M. Van Montagu, *J. Biol. Chem.* **1995**, *270*, 28479−28486.
[27] M. E. Portnoy, P. J. Schmidt, R. S. Rogers, V. C. Culotta, *Mol. Genet. Genomics* **2001**, *265*, 873−882.
[28] Z. Xiao, A. G. Wedd, *Chem. Commun.* **2002**, *6*, 588−589.
[29] S. J. Lin, R. Pufahl, A. Dancis, T. V. O'Halloran, V. C. Culotta, *J. Biol. Chem.* **1997**, *272*, 9215−9220.
[30] R. A. Pufahl, C. P. Singer, K. L. Peariso, S.-J. Lin, P. J. Schmidt, C. J. Fahrni, V. Cizewski Culotta, J. E. Penner-Hahn, T. V. O'Halloran, *Science* **1997**, *278*, 853−856.
[31] D. S. Yuan, A. Dancis, R. D. Klausner, *J. Biol. Chem.* **1997**, *272*, 25787−25793.
[32] M. R. Rad, L. Kirchrath, C. P. Hollenberg, *Yeast* **1994**, *10*, 1217−1225.
[33] I. Voskoboinik, J. Camakaris, *J. Bioenerg. Biomembr.* **2002**, *34*, 363−371.
[34] C. Askwith, D. Eide, A. Van Ho, P. S. Bernard, L. Li, S. Davis-Kaplan, D. M. Sipe, J. Kaplan, *Cell* **1994**, *76*, 403−410.
[35] R. Stearman, D. Yuan, Y. Yamaguchi-Iwan, R. D. Klausner, A. Dancis, *Science* **1996**, *271*, 1552−1557.
[36] L. T. Jensen, V. C. Culotta, *J. Mol. Biol.* **2002**, *318*, 251−260.
[37] X. Shi, C. Stoj, A. Romeo, D. J. Kosman, Z. Zhu, *J. Biol. Chem.*, **2003**, *278*, 50309−50315.
[38] F. Arnesano, L. Banci, I. Bertini, D. L. Huffman, T. V. O'Halloran, *Biochemistry* **2001**, *40*, 1528−1539.
[39] A. C. Rosenzweig, D. L. Huffman, M. Y. Hou, A. K. Wernimont, R. A. Pufahl, T. V. O'Halloran, *Structure Fold Des.* **1999**, *7*, 605−617.
[40] C. A. Liebert, A. L. Watson, A. O. Summers, *J. Mol. Evol.* **2000**, *51*, 607−622.
[41] R. A. Steele, S. J. Opella, *Biochemistry* **1997**, *36*, 6885−6895.
[42] R. Pufahl, C. P. Singer, K. L. Peariso, S.-J. Lin, P. J. Schmidt, C. J. Fahrni, V. Cizewski Culotta, J. E. Penner-Hahn, T. V. O'Halloran, *Science* **1997**, *278*, 853−856.
[43] L. Banci, I. Bertini, R. Del Conte, S. Mangani, W. Meyer-Klaucke, *Biochemistry* **2003**, *8*, 2467−2474.
[44] P. A. Cobine, G. N. George, C. E. Jones, W. A. Wickramasinghe, M. Solioz, C. T. Dameron, *Biochemistry* **2002**, *41*, 5822−5829.
[45] L. Banci, I. Bertini, R. Del Conte, J. Markey, F. J. Ruiz-Dueñas, *Biochemistry* **2001**, *40*, 15660−15668.
[46] L. Banci, I. Bertini, S. Ciofi-Baffoni, D. L. Huffman, T. V. O'Halloran, *J. Biol. Chem.* **2001**, *276*, 8415−8426.

 © 2004 Wiley-VCH Verlag GmbH & Co. KGaA, Weinheim

[47] L. Banci, I. Bertini, S. Ciofi-Baffoni, L. Gonnelli, X. C. Su, *J. Biol. Chem.* **2003**, *278*, 50506−50513.
[48] F. Arnesano, L. Banci, I. Bertini, F. Cantini, S. Ciofi-Baffoni, D. L. Huffman, T. V. O'Halloran, *J. Biol. Chem.* **2001**, *276*, 41365−41376.
[49] F. Arnesano, L. Banci, I. Bertini, A. M. J. J. Bonvin, *Structure*, in press.
[50] L. Banci, I. Bertini, R. Del Conte, *Biochemistry* **2003**, *42*, 13422−13428.
[51] D. L. Huffman, T. V. O'Halloran, *J. Biol. Chem.* **2000**, *275*, 18611−18614.
[52] S. Lutsenko, K. Petrukhin, M. J. Cooper, C. T. Gilliam, J. H. Kaplan, *J. Biol. Chem.* **1997**, *272*, 18939−18944.
[53] D. Larin, C. Mekios, K. Das, B. Ross, A. S. Yang, C. T. Gilliam, *J. Biol. Chem.* **1999**, *274*, 28497−28504.
[54] G. Veglia, F. Porcelli, T. DeSilva, A. Prantner, S. J. Opella, *J. Am. Chem. Soc.* **2000**, *122*, 2389−2390.
[55] T. M. DeSilva, G. Veglia, F. Porcelli, A. M. Prantner, S. J. Opella, *Biopolymers* **2002**, *64*, 189−197.
[56] A. Urvoas, B. Amekraz, C. Moulin, L. Le Clainche, R. Stocklin, M. Moutiez, *Rapid Commun. Mass Spectrom.* **2003**, *17*, 1889−1896.
[57] C. Rensing, B. Mitra, B. P. Rosen, *Proc. Natl. Acad. Sci. USA* **1997**, *94*, 14326−14331.
[58] G. Nucifora, L. Chu, T. K. Misra, S. Silver, *Proc. Natl. Acad. Sci. USA* **1989**, *86*, 3544−3548.
[59] L. Banci, I. Bertini, S. Ciofi-Baffoni, L. A. Finney, C. E. Outten, T. V. O'Halloran, *J. Mol. Biol.* **2002**, *323*, 883−897.
[60] L. Banci, I. Bertini, S. Ciofi-Baffoni, M. D'Onofrio, L. Gonnelli, F. C. Marhuenda-Egea, F. J. Ruiz-Dueñas, *J. Mol. Biol.* **2002**, *317*, 415−429.
[61] J. Gitschier, B. Moffat, D. Reilly, W. I. Wood, W. J. Fairbrother, *Nature Struct. Biol.* **1998**, *5*, 47−54.
[62] D. E. McRee, *Nat. Struct. Biol.* **1998**, *5*, 8−10.
[63] J. C. Venter, M. D. Adams, E. W. Myers, P. W. Li, R. J. Mural, G. G. Sutton, H. O. Smith, M. Yandell, C. A. Evans, R. A. Holt, J. D. Gocayne, P. Amanatides, R. M. Ballew, D. H. Huson, J. R. Wortman, Q. Zhang, C. D. Kodira, X. H. Zheng, L. Chen, M. Skupski, G. Subramanian, P. D. Thomas, J. Zhang, G. L. Gabor Miklos, C. Nelson, S. Broder, A. G. Clark, J. Nadeau, V. A. McKusick, N. Zinder, A. J. Levine, R. J. Roberts, M. Simon, C. Slayman, M. Hunkapiller, R. Bolanos, A. Delcher, I. Dew, D. Fasulo, M. Flanigan, L. Florea, A. Halpern, S. Hannenhalli, S. Kravitz, S. Levy, C. Mobarry, K. Reinert, K. Remington, J. Abu-Threideh, E. Beasley, K. Biddick, V. Bonazzi, R. Brandon, M. Cargill, I. Chandramouliswaran, R. Charlab, K. Chaturvedi, Z. Deng, V. Di Francesco, P. Dunn, K. Eilbeck, C. Evangelista, A. E. Gabrielian, W. Gan, W. Ge, F. Gong, Z. Gu, P. Guan, T. J. Heiman, M. E. Higgins, R.-R. Ji, Z. Ke, K. A. Ketchum, Z. Lai, Y. Lei, Z. Li, J. Li, Y. Liang, X. Lin, F. Lu, G. V. Merkulov, N. Milshina, H. M. Moore, A. K. Naik, V. A. Narayan, B. Neelam, D. Nusskern, D. B. Rusch, S. Salzberg, W. Shao, B. Shue, J. Sun, Z. Y. Wang, A. Wang, X. Wang, J. Wang, M.-H. Wei, R. Wides, C. Xiao, C. Yan, A. Yao, J. Ye, M. Zhan, W. Zhang, H. Zhang, Q. Zhao, L. Zheng, F. Zhong, W. Zhong, S. C. Zhu, S. Zhao, D. Gilbert, S. Baumhueter, G. Spier, C. Carter, A. Cravchik, T. Woodage, F. Ali, H. An, A. Awe, D. Baldwin, H. Baden, M. Barnstead, I. Barrow, K. Beeson, D. Busam, A. Carver, A. Center, M. L. Cheng, L. Curry, S. Danaher, L. Davenport, R. Desilets, S. Dietz, K. Dodson, L. Doup, S. Ferriera, N. Garg, A. Gluecksmann, B. Hart, J. Haynes, C. Haynes, C. Heiner, S. Hladun, D. Hostin, J. Houck, T. Howland, C. Ibegwam, J. Johnson, F. Kalush, L. Kline, S. Koduru, A. Love, F. Mann, D. May, S. McCawley, T. McIntosh, I. McMullen, M. Moy, L. Moy, B. Murphy, K. Nelson, C. Pfannkoch, E. Pratts, V. Puri, H. Qureshi, M. Reardon, R. Rodriguez, Y.-H. Rogers, D. Romblad, B. Ruhfel, R. Scott, C. Sitter, M. Smallwood, E. Stewart, R. Strong, E. Suh, R. Thomas, N. N. Tint, S. Tse, C. Vech, G. Wang, J. Wetter, S. Williams, M. Williams, S. Windsor, E. Winn-Deen, K. Wolfe, J. Zaveri, K. Zaveri, J. F. Abril, R. Guigó, M. J. Campbell, K. V. Sjolander, B. Karlak, A. Kejariwal, H. Mi, B. Lazareva, T. Hatton, A. Narechania, K. Diemer, A. Muruganujan, N. Guo, S. Sato, V. Bafna, S. Istrail, R. Lippert, R. Schwartz, B. Walenz, S. Yooseph, D. Allen, A. Basu, J. Baxendale, L. Blick, M. Caminha, J. Carnes-Stine, P. Caulk, Y.-H. Chiang, M. Coyne, C. Dahlke, A. D. Mays, M. Dombroski, M. Donnelly, D. Ely, S. Esparham, C. Fosler, H. Gire, S. Glanowski, K. Glasser, A. Glodek, M. Gorokhov, K. Graham, B. Gropman, M. Harris, J. Heil, S. Henderson, J. Hoover, D. Jennings, C. Jordan, J. Jordan, J. Kasha, L. Kagan, C. Kraft, A. Levitsky, M. Lewis, X. Liu, J. Lopez, D. Ma, W. Majoros, J. McDaniel, S. Murphy, M. Newman, T. Nguyen, N. Nguyen, M. Nodell, S. Pan, J. Peck, M. Peterson, W. Rowe, R. Sanders, J. Scott, M. Simpson, T. Smith, A. Sprague, T. Stockwell, R. Turner, E. Venter, M. Wang, M. Wen, D. Wu, M. Wu, A. Xia, A. Zandieh, X. Zhu, *Science* **2001**, *291*, 1304−1351.
[64] A. Sali, *Curr. Opin. Biotech.* **1995**, *6*, 437−451.
[65] D. S. Radford, M. A. Kihlken, G. P. M. Borrelly, C. R. Horwood, N. E. Le Brun, J. S. Cavet, *FEMS Microbiol. Lett.* **2003**, *220*, 105−112.
[66] L. Banci, I. Bertini, S. Ciofi-Baffoni, R. Del Conte, L. Gonnelli, *Biochemistry* **2003**, *42*, 1939−1949.
[67] L. Banci, I. Bertini, S. Ciofi-Baffoni, L. Gonnelli, X. C. Su, *J. Mol. Biol.* **2003**, *331*, 473−484.
[68] M. Solioz, J. V. Stoyanov, *FEMS Microbiol. Rev.* **2003**, *27*, 183−195.
[69] P. Cobine, W. A. Wickramasinghe, M. D. Harrison, T. Weber, M. Solioz, C. T. Dameron, *FEBS Lett.* **1999**, *445*, 27−30.
[70] S. Tottey, S. A. Rondet, G. P. Borrelly, P. J. Robinson, P. R. Rich, N. J. Robinson, *J. Biol. Chem.* **2002**, *277*, 5490−5497.
[71] S. Tottey, P. R. Rich, S. A. M. Rondet, N. J. Robinson, *J. Biol. Chem.* **2001**, *276*, 19999−20004.
[72] J. S. Cavet, G. P. Borrelly, N. J. Robinson, *FEMS Microbiol. Rev.* **2003**, *27*, 165−181.
[73] T. Hirayama, J. M. Alonso, *Plant Cell Physiol.* **2000**, *41*, 548−555.
[74] E. Himelblau, R. M. Amasino, *Curr. Opin. Plant Biol.* **2000**, *3*, 205−210.
[75] F. I. Rodriguez, J. J. Esch, A. E. Hall, B. M. Binder, G. E. Schaller, A. B. Bleecker, *Science* **1999**, *283*, 996−998.
[76] J. Chelly, Z. Tumer, T. Tonnesen, A. Petterson, Y. Ishikawa-Brush, N. Tommerup, A. P. Monaco, N. Horn, *Nat. Genet.* **1993**, *3*, 14−19.
[77] J. F. Mercer, J. Livingstone, B. Hall, J. A. Paynter, C. Begy, S. Chandrasekharappa, P. Lockhart, A. Grimes, M. Bhave, D. Siemieniak, T. W. Glover, *Nat. Genet.* **1993**, *3*, 20−25.
[78] C. D. Vulpe, B. Levinson, S. Whitney, S. Packman, J. Gitschier, *Nat. Genet.* **1993**, *3*, 7−13.
[79] P. C. Bull, G. R. Thomas, J. M. Rommens, J. R. Forbes, D. W. Cox, *Nat. Genet.* **1993**, *5*, 327−337.
[80] K. Petrukhin, S. G. Fischer, M. Pirastu, R. E. Tanzi, I. Chernov, M. Devoto, L. M. Brzustowicz, E. Cavanis, E. Vitale, J. J. Russo, *Nat. Genet.* **1993**, *5*, 338−343.
[81] L. W. Klomp, S. J. Lin, D. Yuan, R. D. Klausner, V. C. Culotta, J. D. Gitlin, *J. Biol. Chem.* **1997**, *272*, 9221−9226.
[82] S. Lutsenko, R. G. Efremov, R. Tsivkovskii, J. M. Walker, *J. Bioenerg. Biomembr.* **2002**, *34*, 351−362.
[83] R. Tsivkovskii, B. C. MacArthur, S. Lutsenko, *J. Biol. Chem.* **2001**, *276*, 2234−2242.
[84] J. R. Forbes, D. W. Cox, *Am. J. Hum. Genet.* **1998**, *63*, 1663−1674.
[85] I. Voskoboinik, J. Mar, D. Strausak, J. Camakaris, *J. Biol. Chem.* **2001**, *276*, 28620−28627.
[86] D. Huster, S. Lutsenko, *J. Biol. Chem.* **2003**, *2789*, 32212−32218.
[87] M. DiDonato, H. F. Hsu, S. Narindrasorasak, L. J. Que, B. Sarkar, *Biochemistry* **2000**, *39*, 1890−1896.
[88] M. J. Petris, J. F. Mercer, J. G. Culvenor, P. Lockhart, J. Camakaris, *EMBO J.* **1996**, *15*, 6084−6095.
[89] M. Schaefer, R. G. Hopkins, M. L. Failla, J. D. Gitlin, *Am. J. Physiol.* **1999**, *276*, G639−G646.

 © 2004 Wiley-VCH Verlag GmbH & Co. KGaA, Weinheim

[90] D. L. Huffman, T. V. O'Halloran, *Annu. Rev. Biochem.* **2001**, *70*, 677−701.
[91] J. M. Walker, R. Tsivkovskii, S. Lutsenko, *J. Biol. Chem.* **2002**, *277*, 27953−27959.
[92] S. J. Opella, T. DeSilva, G. Veglia, *Curr. Opin. Struct. Biol.* **2002**, *6*, 217−223.
[93] J. F. Mercer, *Trends Mol. Med.* **2001**, *7*, 64−69.
[94] A. S. Payne, E. J. Kelly, J. D. Gitlin, *Proc. Natl. Acad. Sci. USA* **1998**, *95*, 10854−10859.
[95] R. Tsivkovskii, R. G. Efremov, S. Lutsenko, *J. Biol. Chem.* **2003**, *278*, 13302−13308.
[96] I. Hamza, M. Schafer, L. W. Klomp, J. D. Gitlin, *Proc. Natl. Acad. Sci. USA* **1999**, *96*, 13363−13368.
[97] D. Strausak, S. La Fontaine, J. Hill, S. D. Firth, P. J. Lockhart, J. F. Mercer, *J. Biol. Chem.* **1999**, *274*, 11170−11177.
[98] J. R. Forbes, G. Hsi, D. W. Cox, *J. Biol. Chem.* **1999**, *274*, 12408−12413.

Received November 12, 2003

 © 2004 Wiley-VCH Verlag GmbH & Co. KGaA, Weinheim

New Types of Homochiral Helical Coordination Polymers Constructed by *exo*-Bidentate Binaphthol Derivatives

Ruihu Wang,[a,b] Lijin Xu,[a] Xingshu Li,[a] Yueming Li,[a] Qian Shi,[a,b] Zhongyuan Zhou,[a] Maochun Hong,*[b] and Albert S. C. Chan*[a]

Keywords: Helical structures / Chirality / N ligands / Silver

Assembly of axially chiral (*S*)-2,2′-bis(3-pyridylmethyleneoxy)-1,1′-binaphthalene [(*S*)-L_1] and (*S*)-2,2′-bis(4-pyridylmethyleneoxy)-1,1′-binaphthalene [(*S*)-L_2] with $AgNO_3$ resulted in a double-stranded helical coordination polymer encapsulating guest water molecules and a helix-like complex with inter-immersion clefts, respectively, in which helical chirality is due to axial chirality of the 1,1′-bi-2-naphthol scaffold.
(© Wiley-VCH Verlag GmbH & Co. KGaA, 69451 Weinheim, Germany, 2004)

Introduction

The designed construction of supramolecular frameworks with helical morphology has made tremendous progress because of their practical application in functional materials and in the understanding of molecular self-assembly procedures.[1−6] The well-documented single-, double-, triple- and quadruple-stranded as well as circular and cylindrical helical complexes have been prepared from organic ligands and cleverly selected metal ions using metal-directed programmed self-assembly.[1−5] Recently, the stereoselective synthesis of homochiral helical complexes from enantiopure ligands has become an area of interest owing to their potential application in molecular recognition, asymmetric catalysis, optical materials and biomimetic chemistry.[3−5] In general, the metallo-helicated chirality in these complexes may be defined either by the chirality of at least one optically active carbon center[3d,3e] or by terminal axially chiral scaffolds in which transformation of chiral information on the helix can take place at a distance of up to 2 nm.[4] Thus, the axially chiral ligands may be used as starting materials for the design of new chiral ligands. Several helical frameworks have been constructed by introducing oligopyridine chelating groups into the axially chiral scaffolds,[4,5] but monopyridine-donor groups have been seldom employed.[6]

Optically active 1,1′-bi-2-naphthol (BINOL) has been widely used as a starting material and auxiliary in asymmetric synthesis[7] and chiral recognition[8] owing to its axial chirality and configurational stability. Based on chiral BINOL-derived ligands, Lin and co-workers have recently prepared a series of novel homochiral metallo-supramolecular complexes.[9] Several helical metal complexes based on binaphthyl chiral twisting have been also constructed by introducing the oligopyridine group into the 3,3′-[5a] and 6,6′-positions[5b] of BINOL, but helical metal-organic complexes from 2,2′-positions substituted BINOL derivatives have seldom been reported despite the fact that BINOL may form infinite helical chains through intermolecular O−H···O hydrogen bonds.[10] As an extension of our previous work[11] and with the aim of introducing valuable functional chiral spacers into pyridine-donor ligands, we have designed optically active *exo*-bidentate ligands (*S*)-2,2′-bis(3-pyridylmethyleneoxy)-1,1′-binaphthalene [(*S*)-L_1] and (*S*)-2,2′-bis(4-pyridylmethyleneoxy)-1,1′-binaphthalene [(*S*)-L_2]. Herein, we wish to report the syntheses and characterization of a double-stranded helical coordination polymer encapsulating guest water molecules $[Ag\{(S)\text{-}L_1\}(NO_3)\cdot H_2O]_n$ (**1**) and a helix-like complex with in-

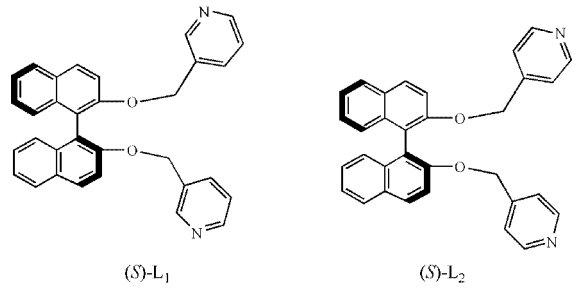

Scheme 1

[a] Open Laboratory of Chirotechnology of the Institute of Molecular Technology for Drug Discovery and Synthesis and Department of Applied Biology and Chemical Technology, The Hong Kong Polytechnic University,
Hong Hum, Hong Kong, China
E-mail: bcachan@polyu.edu.hk
[b] State Key Laboratory of Structural Chemistry, Fujian Institute of the Research on the Structure of Matter, Chinese Academy of Sciences,
Fuzhou, Fujian, 350002, China
E-mail: hmc@ms.fjirsm.ac.cn

terimmersion clefts $[Ag\{(S)\text{-}L_2\}(NO_3)]_n$ (**2**), assembled from (*S*)-L_1 and (*S*)-L_2 with $AgNO_3$, respectively (Scheme 1).

Results and Discussion

The chiral ligands (*S*)-L_1 or (*S*)-L_2 are readily prepared from commercially available (*S*)-BINOL and 3-picolyl chloride hydrochloride or 4-picolyl chloride hydrochloride in the presence of NaOH. (*S*)-L_1 and (*S*)-L_2 have five interesting characteristics as a result of incorporating the axially chiral 1,1′-binaphthol spacer into the pyridine-donor group: 1) the chirality of the ligands permits the formation of homochiral compounds; 2) the chiral twist of the binaphthyl group can be used to control the helical chirality; 3) the conformational rigidity of the binaphthyl group restricts its free rotation; 4) the divergency of the *exo*-bidentate pyridyl group prevents mononucleation of this ligand which is inclined to form a multinuclear complex or polymer; 5) the flexible rotation of the methylenepyridine unit may meet the requirement of the coordination environment of metal ions. Therefore, the linkage of the pyridyl group and the optically active BINOL scaffold affords the possibility of forming homochiral helical complexes.

(*S*)-L_1 and (*S*)-L_2 are soluble in most organic solvents; treating (*S*)-L_1 and (*S*)-L_2 with $AgNO_3$ in $MeCN/H_2O$ at 60 °C afforded colorless plate crystals of complexes **1** and **2**, respectively, in nearly quantitative yield. Complexes **1** and **2** are stable in air, and are insoluble in water and common solvents.

Single-crystal X-ray diffraction analysis reveals that complex **1** crystallizes in an orthorhombic space group $P2_12_12$ and has a double-helical structure with *M* (left-handed) configuration. As shown in Figure 1, each Ag^I center is coordinated by two nitrogen atoms from different (*S*)-L_1 ligands in a distorted linear geometry with the N(1)−Ag−N(2A) bond angle of 164.9(3)°. Bond lengths of Ag−N are 2.130(1) and 2.164(7) Å, which are typical values for Ag^I-N_{py} coordination distances.[11,12] Each (*S*)-L_1 ligand behaves in an *exo*-bidentate mode bridging a pair of adjacent Ag^I centers. The naphthyl rings are twisted with correspondingly linked pyridyl rings with dihedral angles between them of 8.6° and 33.4°. A dramatic twisting is observed between two naphthyl rings with a dihedral angle between them of 85.7°, which places the rings almost perpendicular to each other. The combination of these twistings results in the formation of the helical framework. The pyridyl and adjacent naphthyl rings from the other helical chain are approximately parallel with a dihedral angle between them of 7.5° and a distance between their centroids of 3.84 Å, indicating significant π−π interaction.[13] The intermolecular π−π interaction stabilizes the helical framework and produces a double-helical structure with an adjacent Ag···Ag separation of 4.29 Å between different helical chains. It is interesting to note that water molecules are encapsulated into the double helix as guest molecules (Figure 2). To the best of our knowledge, such a homochiral double-helical structure encapsulating guest water molecules is unprecedented.

Complex **2** crystallizes in the monoclinic space group C_2 and is a helix-like structure with *M* configuration. Similar to complex **1**, each Ag^I center is coordinated by two nitrogen atoms from different (*S*)-L_2 groups [Ag−N 2.195(4),

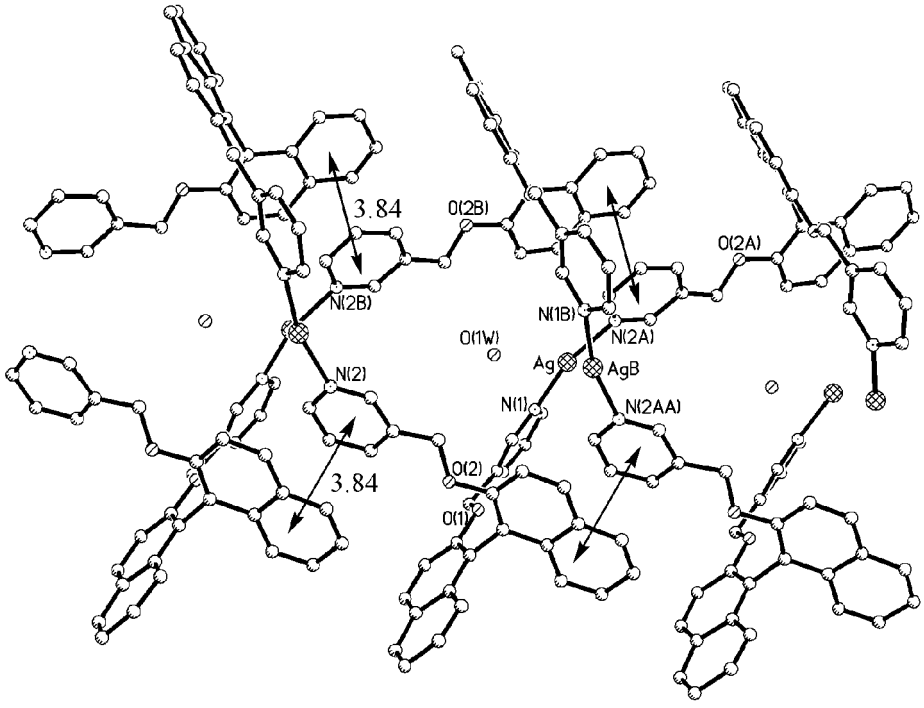

Figure 1. View of the double-helical chains encapsulating water molecules with counter anions, periphery water molecules and hydrogen atoms are omitted for clarity

 © 2004 Wiley-VCH Verlag GmbH & Co. KGaA, Weinheim

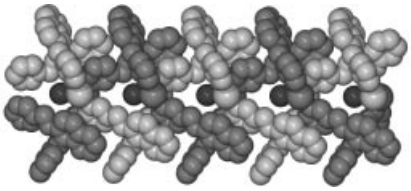

Figure 2. Space-filling diagram of the double-helical chains of **1** with counter anions, periphery water molecules and hydrogen atoms omitted for clarity

Ag−N 2.184(4) Å] in a distorted linear fashion with the N−Ag−N bond angle of 165.3(2)°. Three oxygen atoms from different $[NO_3]^-$ anions have weak interactions with the Ag^I center [Ag−O(12) 2.625(8), Ag−O(12 from complex A) 2.644(10), Ag−O(13 from complex B) = 2.859(9) Å]. Thus, the coordination environment of two N and 3 O atoms around the Ag^I centers can be best described as a slightly distorted triangular bipyramid. Two naphthyl rings with a twisting angle of 69.3° in *S*-L_2 have a smaller distortion than that in complex **1**, but the naphthyl rings and correspondingly linking pyridyl rings produce more twisting with dihedral angles between them of 42.3 and 85.4°, respectively, indicating that the metal coordination site at the 3-position of the pyridyl ring has more effect on the BINOL spacer than that at the 4-position. The interconnection of the *exo*-bidentate (*S*)-L_2 ligand and the Ag^I centers forms an infinite left-handed helix-like framework. The separations between two Ag^I centers bridged by the (*S*)-L_2 ligand and by the $[NO_3]^-$ anion (AgA−AgB) are

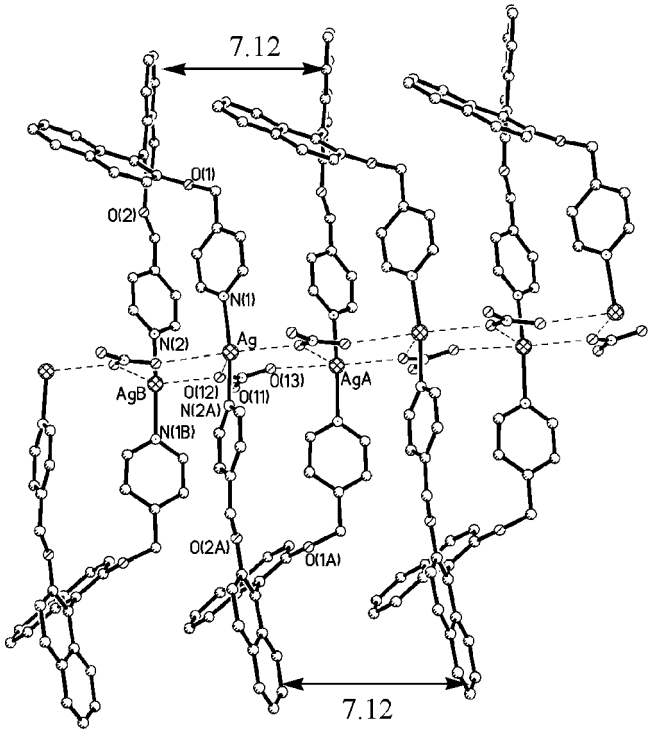

Figure 3. View of the helix-like chain of **2** with hydrogen atoms omitted for clarity

4.484 and 7.258 Å, respectively. It is worth noting that two adjacent ligands on the same side produce a cleft with a mean dimension of 7.12 Å (Figure 3). The (*S*)-L_2 moieties of adjacent helical chains are interimmersed into clefts of each other in an alternate fashion which effectively fills in the cleft void (Figure 4).[12]

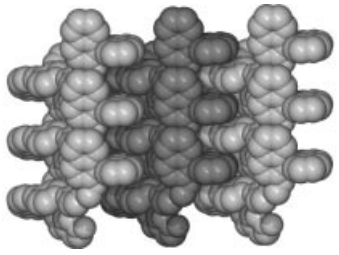

Figure 4. View of the pack diagram exhibiting interimmerse of clefts in **2**

It should be emphasized that the metal ions are not the center of chirality in complexes **1** and **2**. The chirality of the helical polymers is controlled by the inherently chiral twisting in the terminal BINOL spacer. Thus, the assembly of (*S*)-L_1 and (*S*)-L_2 with coordinatively flexible Ag^I centers results in the formation of the left-handed double-helical coordination polymer and the helix-like complex, respectively.

In conclusion, assembly of optically active (*S*)-L_1 and (*S*)-L_2 units with $AgNO_3$ produces a double-stranded helical coordination polymer encapsulating guest water molecules and a helix-like complex with interimmersion clefts, respectively, in which helical chirality is due to axial chirality of the BINOL scaffold. This research demonstrates that new types of homochiral helical complexes can be constructed through monopyridine-donor groups linking the 2,2′-positions of the terminal BINOL chiral scaffold. Moreover, the different orientation of the coordination sites in the pyridyl rings of such ligands can result in different structural motifs. Further investigations are in progress.

Experimental Section

General: (*S*)-1,1′-bi-2-naphthol, 3-picolyl chloride hydrochloride and 4-picolyl chloride hydrochloride were purchased from Acros. The other chemicals were commercially available and were used as purchased without further purification. The NMR spectra were recorded on a Varian Inova-500 spectrophotometer at room temperature and the chemical shifts were quoted in δ (ppm) relative to the deuterated solvent used. The optical rotation was measured with a Polarimeter 341. The mass spectra data were measured by the mass spectrometry laboratory at the Department of Applied Biology and Chemical Technology of The Hong Kong Polytechnic University and were recorded on a Fisons VG platform. The IR spectra were recorded as KBr disks on a Magna 750 FT-IR spectrophotometer. Elemental analyses were determined on an Elementar Vario ELIII elemental analyzer.

Synthesis of (*S*)-L_1: A mixture of (*S*)-1,1′-bi-2-naphthol (2.86 g, 10 mmol), 3-picolyl chloride hydrochloride (3.61 g, 22 mmol), and NaOH (1.76 g, 44 mmol) in acetone (50 mL) was stirred at reflux

 © 2004 Wiley-VCH Verlag GmbH & Co. KGaA, Weinheim

under nitrogen for 3 days. After cooling to room temperature, the inorganic salt was removed by filtration and washed several times with acetone. From the combined solution, the solvents were evaporated under reduced pressure, and the red oily residue was dissolved in ethyl acetate, washed twice with water, and once with brine. The organic layer was dried over anhydrous Na_2SO_4 and filtered. After the removal of the solvent under reduced pressure, the residue was purified by chromatography on silica gel to afford a light yellow oil-like substance. Yield: 4.12 g (88 % based on BINOL). ^{1}H NMR (500 MHz, $CDCl_3$): δ = 8.35 (dd, *J* = 1.5, 4.5 Hz, 2 H, py), 8.20 (d, *J* = 2.0 Hz, 2 H, py), 8.07 (dd, *J* = 9.0 Hz, 2 H, bi), 7.96 (d, *J* = 7.5 Hz, 2 H, bi), 7.67 (d, *J* = 9.0 Hz, 2 H, bi), 7.36 (td, *J* = 1.5, 6.5 Hz, 15 Hz, 2 H, bi), 7.29−7.32 (m, 2 H, bi), 7.24−7.27 (m, 2 H, bi), 7.12 (dd, *J* = 4.5, 7.5 Hz, 2 H, py), 7.00 (d, *J* = 8.0 Hz, 2 H, py), 5.19 (s, 4 H, -CH_2-) ppm. ^{13}C NMR ($CDCl_3$, 125 MHz): δ = 153.3, 148.4, 147.9, 135.0, 134.8, 133.4, 132.9, 129.5, 129.0, 128.1, 126.5, 124.6, 123.6, 119.4, 115.5, 67.7 ppm. $[\alpha]_D^{20}$ = −99.2 (*c* = 1, DMSO). Calcd. for $C_{32}H_{25}N_2O_2$ (469.19): calcd. C 81.91, H 5.33, N 5.97; found C 81.96, H 5.35, N 5.94. ES-MS: *m*/*z* = 469 (M^+ + 1). HRMS: calcd. $C_{32}H_{25}N_2O_2$ (M^+ + 1): *m*/*z* = 469.1916; found: 469.1938.

Synthesis of (*S*)-L_2: The procedure was similar to the synthesis of (*S*)-L_1 except that 4-picolyl chloride hydrochloride was used instead of 3-picolyl chloride hydrochloride. Yield: 3.75 g (80 % based on BINOL). ^{1}H NMR (500 MHz, $CDCl_3$): δ = 8.28 (dd, *J* = 1.5, 4.5 Hz, 4 H, py), 8.07 (d, *J* = 8.5 Hz, 2 H, bi), 7.97 (d, *J* = 8.5 Hz, 2 H, bi), 7.59 (d, *J* = 9.0 Hz, 2 H, bi), 7.35−7.38 (m, 2 H, bi), 7.26−7.29 (m, 2 H, bi), 7.03 (d, *J* = 8.5 Hz, 2 H, bi), 6.94 (d, *J* = 6.0 Hz, 4 H, py), 5.24 (s, 4 H, -CH_2-) ppm. ^{13}C NMR ($CDCl_3$, 125 MHz): δ = 153.7, 149.6, 146.9, 134.3, 130.0, 129.8, 128.3, 127.0, 125.6, 124.5, 121.3, 120.7, 115.5, 69.6 ppm. $[\alpha]_D^{20}$ = −82.8 (*c* = 1, DMSO). $C_{32}H_{25}N_2O_2$ (469.19): calcd. C 81.91, H 5.33, N 5.97; found C 81.97, H 5.38, N 5.92. ES-MS: *m*/*z* = 469 (M^+ + 1). HRMS: calcd. $C_{32}H_{25}N_2O_2$ (M^+ + 1): *m*/*z* = 469.1916; found 469.1925.

Preparation of {Ag[(*S*)-L_1](NO$_3$)·H_2O}$_n$ (1): A solution of $AgNO_3$ (0.017 g, 0.1 mmol) in H_2O (5 mL) was added to a stirred solution of (*S*)-L_1 (0.047 g, 0.1 mmol) in MeCN (10 mL). The reaction mixture was stirred for 5 h at 60 °C, and the colorless solution was then filtered. Colorless crystals of complex **1** were obtained by allowing the filtrate to evaporate slowly in air for two weeks. Yield: 0.059 g (90 %). $C_{32}H_{26}AgN_3O_6$ (656.43): calcd. C 58.50, H 3.95, N 6.40; found C 58.39, H 3.98, N 6.37. IR (KBr pellet): $\tilde{\nu}$ = 3048 (m, C−H), 2962 (m, CH_2), 1742 (w), 1619 (s, C−C), 1587 (s, C−C), 1506 (s, C−C), 1458 (m, C−C), 1434 (m, C−C), 1360 (w), 1385 (s, N−O), 1232 (m, C−O), 1151 (w, C−H), 1090 (m, C−H), 1016 (m, C−H), 965 (w), 916 (w), 864 (w), 808 (m), 751 (m), 700 (m), 654 (w), 573 (w), 430 (w), 405 (w).

Preparation of [Ag{(*S*)-L_2}(NO$_3$)]$_n$ (2): The procedure was similar to the synthesis of complex **1** except that (*S*)-L_2 was used instead of (*S*)-L_1. Yield: 0.060 g (94 %). $C_{32}H_{24}AgN_3O_5$ (638.4): calcd. C 60.15, H 3.76, N 6.58; found C 60.16, H 3.78, N 6.61. IR (KBr pellet): $\tilde{\nu}$ = 3058 (m, C−H), 2925 (m, −CH_2−), 1619 (s, C−C), 1588 (s, C−C), 1561 (w, C−C), 1501 (s, C−C), 1505 (s, C−C), 1469 (w, C−C), 1446 (m, C−C), 1424 (m, C−C), 1385 (s), 1362 (w), 1266 (m, C−O), 1148 (m, C−H), 1095 (m, C−H), 1047 (m, C−H), 1019 (m, C−H), 959 (w), 911 (w), 858 (w), 804 (m), 743 (m), 670 (w), 619 (w), 527 (w), 485 (w).

X-ray Crystallography: The crystal data and structural determination summary for **1** and **2** are listed in Table 1. Intensity data for **1** and **2** were measured on a Siemens Smart CCD diffractometer with graphite-monochromated Mo-K_α radiation (λ = 0.71073 Å) at 298 K. Empirical absorption corrections were applied by using the SADABS program.[14] The structures were solved by direct methods and all calculations were performed using the SHELXL PC program.[15] The positions of the H atoms were generated geometrically (C−H bond fixed at 0.96 Å), assigned isotropic thermal parameters, and allowed to ride on their parent carbon atoms before the final cycle of refinement. The structure was refined by full-matrix least-squares minimization of $\Sigma(F_o-F_c)^2$ with anisotropic thermal parameters for all atoms except the H atoms. CCDC-205478 and -205479 contain the supplementary crystallographic data for this paper. These data can be obtained free of charge at www.ccdc.cam.ac.uk/conts/retrieving.html [or from the Cambridge Crystallographic Data Centre, 12 Union Road, Cambridge CB2 1EZ, UK; Fax: (internat.) + 44-1223-336-033; E-mail: deposit@ccdc.cam.ac.uk].

Table 1. Crystallographic data for compounds **1** and **2**

	1	**2**
Empirical formula	$C_{32}H_{26}AgN_3O_6$	$C_{32}H_{24}AgN_3O_5$
M_r [g·mol^{-1}]	656.43	638.41
Crystal system	orthorhombic	monoclinic
Space group	$P2_12_12$	C_2
a [Å]	11.371(1)	25.225(5)
b [Å]	30.770(4)	7.258(1)
c [Å]	9.061(1)	16.881(3)
β [°]		105.781(3)
V [Å^3]	3170.3(7)	2973.9(9)
Z	4	4
T [K]	294(2)	294(2)
D_c [g·cm^{-3}]	1.375	1.426
μ [mm^{-1}]	0.681	0.722
λ [Mo-K_α, Å]	0.71073	0.71073
Reflections collected	21664	10102
Unique reflections	7280	6063
R_{int}	0.0493	0.0383
Parameters	380	370
S on F^2	1.021	1.005
R_1 [$I > 2\sigma(I)$][a]	0.0774	0.0552
wR_2 [all data][b]	0.2296	0.1574
Largest diff. peak and hole [e·Å^{-3}]	0.920 and −0.428	0.696 and −0.334

[a] $R = R_1 = \Sigma||F_o| - |F_c||/\Sigma|F_o|$. [b] $wR_2 = [\Sigma w(F_o^2 - F_c^2)^2/\Sigma w(F_o^2)^2]^{1/2}$.

Acknowledgments

We thank the Hong Kong Research Grants Council (Project No. PolyU5306/01P), The University Grants Committee Area of Excellence Scheme in Hong Kong (AoE P/10−0), and the Hong Kong Polytechnic University Area of Strategic Development Fund for financial support of this study.

[1] J. M. Lehn, *Supramolecular Chemistry, Concepts and Perspectives*, VCH Publishers, New York, **1995**.
[2] [2a] M. Albrecht, *Chem. Rev.* **2001**, *101*, 3457−3497. [2b] C. Piguet, G. Bernardinelli, G. Hopfgartner, *Chem. Rev.* **1997**, *97*, 2005−2062. [2c] O. S. Jung, Y. J. Kim, Y. A. Lee, J. K. Park, H. K. Chae, *J. Am. Chem. Soc.* **2000**, *122*, 9921−9925.
[3] [3a] I. Ojima, *Catalytic Asymmetric synthesis*, VCH: Weinheim, **2000**. [3b] J. Hamblin, L. J. Childs, N. W. Alcock, M. J. Hannon, *J. Chem. Soc., Dalton Trans.* **2002**, 164−169 and references cited therein. [3c] J. M. Vincent, C. Philouze, I. Pianet, J. B.

 © 2004 Wiley-VCH Verlag GmbH & Co. KGaA, Weinheim

Verlhac, *Chem. Eur. J.* **2000**, *6*, 3595−3599. [3d] T. Suzuki, H. Kotsuki, K. Isobe, N. Moriya, Y. Nakagawa, M. Ochi, *Inorg. Chem.* **1995**, *34*, 530−531. [3e] J. Schneider, M. Köckerling, R. Kopitzky, G. Henkel, *Eur. J. Inorg. Chem.* **2003**, 1727−1734.

[4] [4a] U. Knof, A. von Zelewsky, *Angew. Chem. Int. Ed.* **1999**, *38*, 302−322. [4b] C. R. Woods, M. Benaglia, F. Cozzi, J. S. Siegel, *Angew. Chem. Int. Ed. Engl.* **1996**, *35*, 1830−1834.

[5] [5a] A. Lützen, M. Hapke, J. Griep-Raming, D. Haase, W. Saak, *Angew. Chem. Int. Ed.* **2002**, *41*, 2086−2089. [5b] M. Kimura, M. Sano, T. Muto, K. Hanabusa, H. Shirai, *Macromolecules* **1999**, *32*, 7951−7953.

[6] Y. Cui, H. L. Ng, W. Lin, *Chem. Commun.* **2003**, 1388−1389.

[7] [7a] L. Pu, *Chem. Rev.* **1998**, *98*, 2405−2494. [7b] R. Noyori, *Angew. Chem. Int. Ed.* **2002**, *41*, 2008−2022.

[8] [8a] E. P. Kyba, G. W. Gokel, F. D. Jong, K. Koga, L. R. Sousa, M. G. Siegel, L. Kaplan, G. D. Y. Sogah, D. G. Cram, *J. Org. Chem.* **1977**, *42*, 4173−4184. [8b] M. Asakakawa, H. M. Janssen, E. W. Meijer, D. Pasini, J. F. Stoddart, *Eur. J. Org. Chem.* **1998**, 983−986.

[9] [9a] Y. Cui, S. J. Lee, Y. W. Lin, *J. Am. Chem. Soc.* **2003**, *125*, 6014−6015. [9b] Y. Cui, H. L. Ngo, P. S. White, W. Lin, *Inorg. Chem.* **2003**, *42*, 652−654. [9c] Y. Cui, H. L. Ngo, P. S. White, W. Lin, *Chem. Commun.* **2003**, 994−995. [9d] H. L. Ngo, W. Lin, *J. Am. Chem. Soc.* **2002**, *124*, 14298−14299. [9e] Y. Cui, H. L. Ngo, P. S. White, W. Lin, *Chem. Commun.* **2002**, 1666−1667. [9f] Y. Cui, O. R. Evans, H. L. Ngo, P. S. White, W. Lin, *Angew. Chem. Int. Ed.* **2002**, *41*, 1159−1162.

[10] [10a] F. Toda, K. Tanaka, H. Miyamoto, H. Koshima, I. Miyahara, K. Hirotsu, *J. Chem. Soc., Perkin Trans.* **1997**, *2*, 1877−1886. [10b] K. Mori, Y. Masuda, S. Kashino, *Acta Crystallogr., Sect. C* **1993**, *49*, 1224−1226.

[11] [11a] M. C. Hong, Y. J. Zhao, W. P. Su, R. Cao, M. Fujita, Z. Y. Zhou, A. S. C. Chan, *J. Am. Chem. Soc.* **2000**, *122*, 4819−4820. [11b] M. C. Hong, Y. J. Zhao, W. P. Su, R. Cao, M. Fujita, Z. Y. Zhou, A. S. C. Chan, *Angew. Chem. Int. Ed.* **2000**, *39*, 2468−2470. [11c] M. C. Hong, W. P. Su, R. Cao, M. Fujita, J. X. Lu, *Chem. Eur. J.* **2000**, *6*, 427−431.

[12] D. A. McMorran, P. J. Steel, *Chem. Commun.* **2002**, 2120−2121.

[13] C. Janiak, *J. Chem. Soc., Dalton Trans.* **2000**, 3885−3896.

[14] G. M. Sheldrick, *SADABS, Program for Empirical Absorption Correction of Area Detector Data*, University of Göttingen, Göttingen, **1996**.

[15] G. M. Sheldrick, *SHELXS97, Program for Crystal Structure Solution*, University of Göttingen, Göttingen, **1997**.

Received December 9, 2003

 © 2004 Wiley-VCH Verlag GmbH & Co. KGaA, Weinheim

Syntheses, Structures and Redox Properties of New Macrocyclic Triazatriolefinic Pd^0 Complexes and Their Polypyrrole Modified Electrodes − Application to Heterogeneous Catalytic Suzuki Cross-Coupling Reactions

Antoni Llobet,*[a] Ester Masllorens,[a] Montserrat Rodríguez,[a] Anna Roglans,*[a] and Jordi Benet-Buchholz[b]

Keywords: Heterogeneous catalysis / Macrocyclic ligands / Palladium / Pyrroles / Modified electrodes / Electrochemistry

New triolefinic macrocyclic ligands of the type (*E,E,E*)-1,6,11-tris(arenesulfonyl)-1,6,11-triazacyclopentadeca-3,8,13-triene (aryl: **a** = ferrocenyl, **b** = 4-pyrrol-1-ylphenyl, **c** = 4-methylphenyl) and their Pd^0 complexes (**1aab**, **1abb** and **1bcc**) have been prepared and characterized. Further structural characterization in the solid state has also been performed by means of X-ray diffraction analysis for the complex **1bcc**. The redox properties of both the ligands and their Pd complexes have been studied using cyclic voltammetric and coulombimetric techniques. In particular, complexes and ligands containing the pyrrole group do polymerize upon exposure to sufficiently positive potentials, on glassy carbon electrodes, generating highly stable modified electrodes. The new modified electrodes are efficient and selective heterogeneous catalysts for Suzuki cross-couplings, benefiting from simple removal of the catalyst from the reaction vessel. As an example, more than $2 \cdot 10^5$ metal cycles are achieved at 65 °C in the coupling of phenylboronic acid and cinnamyl bromide. Iodoarenes and phenylboronic acid are also converted into biphenyls with relatively good conversions.
(© Wiley-VCH Verlag GmbH & Co. KGaA, 69451 Weinheim, Germany, 2004)

Introduction

Homogeneous catalysis using transition metal (TM) complexes is a topic of current interest from a basic organic synthetic perspective and also from an industrial point of view.[1] Highly efficient homogeneous catalytic systems have been described even though their potential industrial applications have been hampered by the cost and difficulty in recovering the TM catalyst and also because of the presence of trace amounts of the TM in the final product.

One of the main strategies designed to overcome the above mentioned drawbacks consists of making TM catalysts heterogeneous by incorporating them into solid materials. In this context, the development of highly efficient catalysts to compensate for TM complex cost and the fabrication of robust heterogeneous systems with negligible leaching, is essential in order to consider them as potential candidates for the scale up process at an industrial plant.

Different approaches for making TM catalysts heterogeneous have been recently reviewed.[1b,2] Very elegant strategies based on biphasic systems (aqueous-organic[2b,3] or fluorous-organic[4] systems) have been developed in the last decade. Organic[1b,5] and inorganic[1b,6] polymer matrices have also been extensively used to immobilize TM catalysts. Among them, pyrrole electropolymerization is an attractive and convenient method given the synthetic versatility of the monomers and the stability of the resultant polypyrrole films.[7] In general, these films attached to the electrode surface via an electropolymerization process are much more stable than those obtained by simple deposition on materials such as polystyrene,[8] Nafion[9] or carbon paste.[10] The stability of the film is an important factor since it minimizes potential leaching processes from the solid surface. Furthermore the high electrical conductivity of the polypyrrole films allows the use of the conveniently designed electroactive ancillary groups, which do not participate in the catalytic transformation, but allow important aspects of the process to be monitored and thus act as built in chemical sensors.

Given the many positive aspects of the polypyrrole films just described, it is striking that they have been scarcely used with carbon−carbon bond formation catalysts in order to introduce heterogeneity. In this context it is worth mentioning the work of Jugé et al.[11] in which they initially functionalized the polypyrrole backbone with phosphane ligands. Subsequently the catalyst was generated in situ upon adding an appropriate Pd^0 complex.

[a] Departament de Química, Universitat de Girona,
Campus Montilivi S/N, 17071 Girona, Spain
Fax: (internat.) +34-972418150
E-mail: antoni.llobet@udg.es
anna.roglans@udg.es
[b] BIS-SUA-SPA X-ray Laboratory, Geb. Q18; Raum 490,
Bayer AG,
51368 Leverkusen, Germany

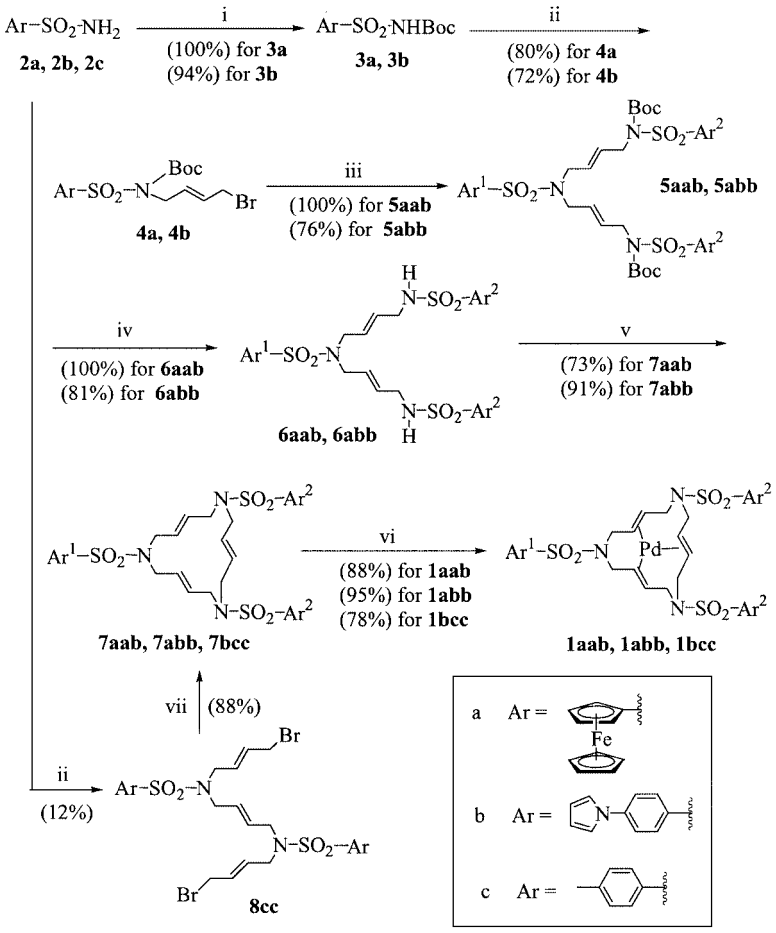

Scheme 1. Synthetic strategy; (i) $(t\text{BuOCO})_2O$, Et_3N, DMAP, CH_2Cl_2, 3.5 h.; (ii) 4 equiv. (*E*)-1,4-dibromo-2-butene, K_2CO_3, CH_3CN, reflux, 15 h (for **4a**), 7 h (for **4b**), 23 h (for **8cc**); (iii) to give **5aab**: 0.5 equiv. (4-pyrrol-1-ylphenyl)sulfonamide **2b**, K_2CO_3, CH_3CN, reflux, 16 h; to give **5abb**: 0.5 equiv. ferrocenesulfonamide **2a**, K_2CO_3, CH_3CN, reflux, 10 h; (iv) $HCl_{(aq)}$, EtOAc, room temp., 2 h for **7aab**; $HCl_{(g)}$, CH_2Cl_2, room temp., 2 h for **7abb**; (v) 1 equiv. (*E*)-1,4-dibromo-2-butene, K_2CO_3, CH_3CN, reflux, 16 h (for **7aab**) and 20 h (for **7abb**); (vi) 1.2 equiv. $Pd(dba)_2$, THF, reflux, 1 h; (vii) 1 equiv. **2b**, K_2CO_3, CH_3CN, reflux, 24 h

During the last two years, synthetic procedures for novel types of Pd^0-triazatriolefinic macrocyclic complexes such as (*E*,*E*,*E*)-1,6,11-tris(arenesulfonyl)-1,6,11-triazacyclopentadeca-3,8,13-trienepalladium(0), **1**, (see Scheme 1) have been reported.[12] These phosphane-free palladium(0) complexes are active and efficient catalysts for Suzuki cross-couplings,[13] butadiene telomerization,[14] and alkyne hydroarylation in ionic liquids.[15] They have also been anchored in polystyrene matrices allowing the catalyst to be separated from reaction products by simple filtration for subsequent re-use.[13]

We have recently reported[16] the preparation of related 15-membered macrocycles functionalized with ferrocenyl units at the sulfonamide groups, and their palladium(0) complexes. We have also reported[17] high activity and quantitative recovery of palladium(0) complexes, **1**, for the Heck reaction of diazonium salts with acrylates and styrene in a homogeneous phase.

Herein we present the synthesis, spectroscopic and electrochemical properties of new 15-membered triolefinic ligands containing pyrrole and/or ferrocene groups together with their corresponding Pd^0 complexes **1aab**, **1abb**, and **1bcc** (Scheme 1). Their redox properties as well as their chemical and electrochemical polymerization processes are also described. Finally the capacity of the corresponding modified electrodes to catalyze Suzuki cross-coupling reactions has been analyzed using two different substrates.

Results and Discussion

Synthesis and Structures

The preparation of the triaza olefinic ligands and their unsaturated 16-electron Pd^0 complexes, **1aab**, **1abb** and **1bcc**, is outlined in Scheme 1, according to the general method for the synthesis of related compounds.[12,16] Pd^0 complexes **1aab** and **1abb** were obtained in overall yields of 51% and 36%, respectively. The low yield for complex **1abb** was due to the poor solubility of several intermediates conferred by the two pyrrole groups. Complex **1bcc** was obtained in 8% overall yield by a different and more straightforward synthetic pathway (see Scheme 1). The main problem of this synthesis was that the bis(sulfonamide) **8cc** was obtained as the minor product, the major one (46% yield)

 © 2004 Wiley-VCH Verlag GmbH & Co. KGaA, Weinheim

being the monosulfonamide, *N*,*N*-bis[(*E*)-4-bromo-2-butenyl](4-methylphenyl)sulfonamide. Optimization of this step was not successful.[12a]

This versatile synthetic route allowed the aromatic groups to be easily changed. Thus, these aromatic groups can be used as auxiliary substituents to perform specific functions without modifying the intrinsic coordinating properties of the ligand. In the present case, ferrocene was chosen since it acts as a quantitative electrochemical sensor. On the other hand, an *N*-bonded pyrrole group was also selected since it converts the Pd complex into a monomer which can be easily polymerized. At sufficiently positive anodic potentials the pyrrole group polymerizes, ejecting its α-hydrogen atoms,[7] while forming a relatively stable and insoluble conducting polypyrrole material. This material strongly adheres to the electrode surface to which the Pd-triolefinic complex has been covalently attached.

The crystal structure of complex **1bcc·CH_2Cl_2** was solved by means of a single-crystal X-ray diffraction analysis. Figure 1 presents the ORTEP diagram of the molecule including selected bond lengths and angles with the corresponding labeling scheme.

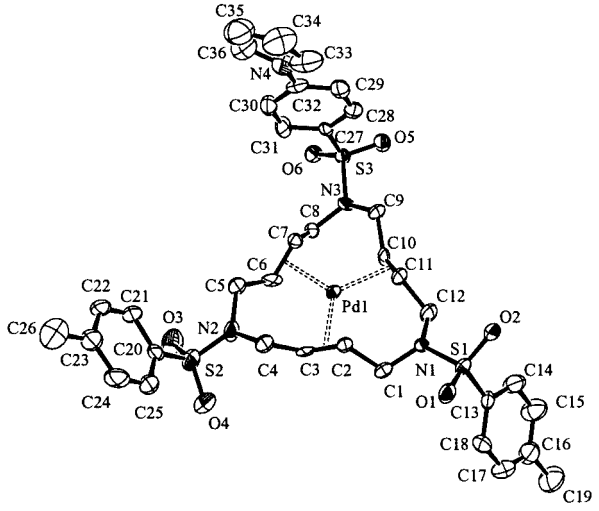

Figure 1. ORTEP plot (50 %) of complex **1bcc**, hydrogen atoms are omitted to fully appreciate the geometry of the complex; selected distances [Å] and angles [°]: Pd1−C2 2.196(6), Pd1−C3 2.216(7), Pd1−C6 2.164(17), Pd1−C7 2.214(9), Pd1−C10 2.186(7), Pd1−C11 2.187(7); C10−Pd1−C11 36.7(3), C10−Pd1−C6 115.9(4), C11−Pd1−C6 151.7(4), C10−Pd1−C2 121.9(3), C11−Pd1−C2 86.7(3), C6−Pd1−C2 121.6(4), C10−Pd1−C3 152.4(3), C11−Pd1−C3 122.5(3), C6−Pd1−C3 85.5(5), C2−Pd1−C3 37.0(2), C10−Pd1−C7 85.5(3), C11−Pd1−C7 117.9(3), C6−Pd1−C7 34.9(4), C2−Pd1−C7 151.6(3), C3−Pd1−C7 119.4(3), C3−C2−Pd1 72.3(4), C1−C2−Pd1 112.4(5), C2−C3−Pd1 70.7(4), C4−C3−Pd1 111.7(5), C5−C6−Pd1 114.4(10), C7−C6−Pd1 74.6(8), C8−C7−Pd1 111.3(7), C6−C7−Pd1 70.5(8), C11−C10−Pd1 71.7(4), C9−C10−Pd1 115.0(5), C10−C11−Pd1 71.6(4), C12−C11−Pd1 115.2(5)

The molecular structure of **1bcc** shows the macrocyclic ligand, **7bcc**, with all the olefinic *trans* double bonds coordinated to the palladium. The central point of the olefins and the palladium are all nearly situated in the same plane and thus the coordination of the palladium is slightly distorted trigonal planar. Bond lengths and angles are within the expected ranges for this type of complex.[12b] The three nitrogen atoms of the sulfonamides (N1, N2, N3) and the palladium center are also situated very close to a plane which will from now on be referred to as the main plane. The Pd−C bonds form a triangle with each olefinic group generating a three paddle helix centered at the palladium metal atom. It is also worth mentioning that the Pd complex suffers a slight disorder that is manifested in the chain of four carbon atoms (C5 to C8 with an occupancy factor of 80% and C5′ to C8′ with 20%) that links the amine atoms N2 and N3. For the molecular conformation with 80% occupancy, two of the paddles are oriented up (Pd1−C6−C7, Pd1−C10−C11) and one down (Pd1−C2−C3) if the helix is observed in a clockwise manner (following increasing values of the atom labeling scheme) with the helix parallel to the main plane, manifesting the asymmetry of the helix with regard to a hypothetical pseudo C_3 rotation axis perpendicular to the mentioned main plane. This relative orientation of the paddles is directly related to the conformation of the three six-membered rings fused to them containing N1 (Pd1, C11, C12, N1, C1, C2), N2 (Pd1, C3, C4, N2, C5, C6) and N3 (Pd1, C7, C8, N3, C9, C10), respectively. Thus when two neighboring paddles have different orientations, both a chair or a boat conformation are possible for the six member ring fused to them but when they have the same orientation then only a distorted chair or a distorted boat is possible. Indeed, two chair conformations were obtained for the six-membered rings containing the N1 and N2 atoms, respectively, whereas opposite orientations and a distorted boat was found for N3. The disordered atoms contained in the molecule with a 20% occupancy generate a paddle that has the opposite orientation with respect to that of the molecule with the 80% occupancy. The sulfonamides are oriented in such a way that the aromatic substituents are situated at 121.9° (C13−C18), 128.5° (C20−C25) and 97.3° (C27−C32) with regard to the main plane, with two of them directed over the plane, one up (S1, S3), and one down (S2). In the S3 case the *N*-pyrrolic substituent bonded to the phenyl ring is significantly rotated [C36−N4−C32−C30 torsion angle of −27.1°] to avoid steric interactions with its neighboring hydrogen atoms.

Redox Properties and Catalyst Immobilization

The redox properties of complexes **1aab**, **1abb** and **1bcc** were investigated by means of cyclic voltammetric and coulombimetric techniques. Figure 2 (A) shows the cyclic voltammograms of **1aab** in CH_2Cl_2+0.1 M nBu_4NPF_6 at a glassy carbon disk electrode using Ag/10 mM Ag^+ as the reference electrode in the dry box. By scanning anodically starting at 0.0 V a first wave was observed associated with the Fe^{III}/Fe^{II} couple at $E_{1/2}$ = 0.561 V ($E_{p,a}$ = 0.680 V, $E_{p,c}$ = 0.442 V, ΔE = 232 mV). The occurrence of a relatively high value of ΔE is a common phenomenon found in similar transition metal complex polymerization sys-

 © 2004 Wiley-VCH Verlag GmbH & Co. KGaA, Weinheim

tems,[18a] and is related to the intrinsic nature of the immobilized species as well as to the multiple processes which are taking place simultaneously.[7]

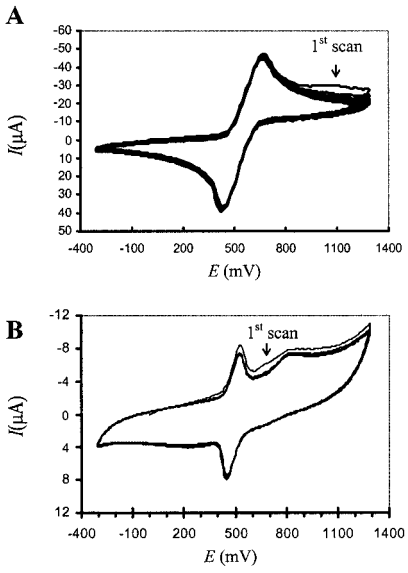

Figure 2. Top: Growth of a **C-glassy/poly-1aab** during the first 20 consecutive cyclic voltammetric scans on a glassy carbon disk electrode (3 mm diameter) in a 1 m M solution of **1** in CH_2Cl_2+0.1 M TBAP (υ = 0.1 V/s); bottom: cyclic voltammetric scan of **C-glassy/poly-1aab** ($\Gamma = 3.10 \times 10^{-10}$ mol cm^{-2}) upon transferring it to a blank electrolyte solution CH_2Cl_2+0.1 M TBAP (υ = 0.1 V/s); first and four consecutive scans

A second small and broad wave was also observed in the first scan with $E_{p,a}$ = 1.05 V which can be assigned to the irreversible oxidation of the pyrrole group with concomitant polymerization (the observation of this wave only in the first scan is typical for this kind of system and is related to the changes experienced on the electrode surface after the deposition of the first polypyrrole layer[7b,7c]). Modified electrodes, with units of the **1aab** monomer covalently bonded to the polypyrrole chain, can be obtained by scanning the potential region repeatedly from 0.0 V up to 1.30 V. This is depicted in Figure 2 (A) where, upon scanning 20 times over the indicated potential domain, a small but consistent increase of the intensity wave for the Fe^{III}/Fe^{II} couple was observed thus indicating the growth of the **C-glassy/poly-1aab** film on the electrode surface. Figure 2 (B) shows the cyclic voltammetric response of the film when transferred to a blank electrolyte solution. As in the previous case, a first wave due to the Fe^{III}/Fe^{II} couple can be observed ($E_{1/2}$ = 0.490 V, $E_{p,a}$ = 0.538, $E_{p,c}$ = 0.442, ΔE = 96 mV), as well as a second one, with $E_{p,a}$ = 0.83 V, that can be assigned to the electrochemically irreversible oxidation of palladium. The corresponding Pd^{II} reduction takes place through a broad wave found between 0 and 0.4 V. The electrochemical response of the Pd metal center can be determined from comparison of this system with the behavior shown in homogeneous phase by a family of related Pd complexes that we have described recently.[16] Also, the polymerization performed on the corresponding macrocyclic ligand **7aab** under equivalent conditions, does not show any significant wave around 0.8 V. This, together with the catalytic activity of the polymerized free ligands and complexes (vide infra), gives compelling evidence that the Pd metal remains coordinated to the triolefinic ligands in the generated modified electrodes containing the polypyrrolic films.

The films described here are highly stable. Upon scanning more than 40 times over the −2.0 to +2.0 V potential region in a fresh electrolyte solution, the decrease in charge under the Fe^{III}/Fe^{II} wave is insignificant. There is also some evidence for the preservation of the coordination environment of the Pd metal center in the complex structure, since the intensity of the anodic peak, corresponding to the $Pd^0 \rightarrow Pd^{II}$ transition, also maintains its intensity.

Similar films can also be built up by maintaining the electrode in the potential range 0.6−0.8 V with a potentiostat. As an example a film grown by maintaining E_{app} = 0.80 V, until a total charge of 7.22×10^{-3} C had passed, yielded a thin film with an apparent surface coverage of $\Gamma = 1.53 \times 10^{-9}$ mol/cm^2.

It is important to point out here that the whole process can be performed outside the dry box with carefully dried solvents under N_2 or Ar, but the Pd wave was only observed under rigorously anhydrous conditions in the dry box.

The polymerization process was also carried out for **1aab** utilizing carbon felt electrodes (1.0 × 0.5 × 0.5 cm), using the same protocols as with the glassy carbon electrodes previously described thus generating the corresponding **C-felt/poly-1aab**. Under these conditions, and using the voltamperometric methodology, different electrodes were generated with different amounts of deposited complex that, after proper cleaning, were used as catalysts. Their performance is described in the following section.

The redox properties of **1abb** parallel those of **1aab** except that the ferrocene waves have half the intensity observed in the previous case, as expected. For the complex **1bcc**, the absence of ferrocene substituents prevents the use of electrochemical monitoring since the polypyrrole backbone wave was not observed in our case, but they could also be used for catalytic purposes. The free ligands **7aab** and **7abb** can also be polymerized in the same manner as described for the Pd complex **1aab** generating very similar voltammograms except for the obvious absence of the wave due to the irreversible oxidation of Pd.

Catalytic Activity

To examine the catalytic efficiency and recovery of the **C-felt/poly-1aab** materials, two model Suzuki-type cross-coupling reactions were tested, namely the reaction of cinnamyl bromide, **9**, with phenylboronic acid, **10**, to afford *trans*-1,3-diphenylpropene, **11**,[19] together with minor amounts of regioisomer **12**,[20] and that of phenylboronic acid **10** with the iodoarenes **13a**−**b**, leading to the biphenyls **14a**−**b**[21] (see Scheme 2 and Table 1)

 © 2004 Wiley-VCH Verlag GmbH & Co. KGaA, Weinheim

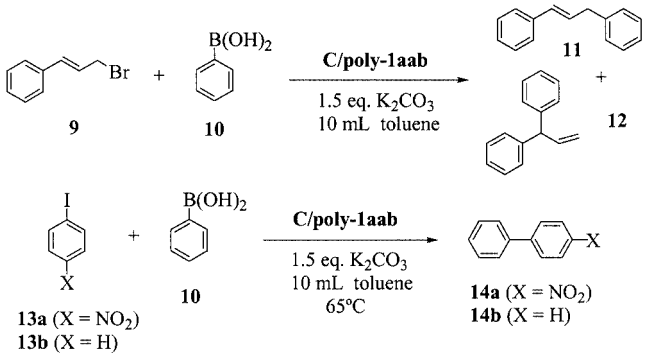

Scheme 2. Suzuki-type cross-coupling reactions tested

Typically, the reaction was carried out by stirring a reaction mixture containing cinnamyl bromide, phenylboronic acid, potassium carbonate, and the catalyst immobilized onto the electrode surface in an anhydrous, degassed toluene solution under nitrogen. The electrode was recovered by removing it from the solution vessel, and washing with toluene before using it again in a new reaction.

Entry 1 in Table 1 shows that at 27 °C after a reaction time of 48 hours, up to 10 mL total volume of the system "**C-felt/poly-1aab**, 16.8·nmols/**9**, 15.0 mM; **10,** 22.5 mM/K_2CO_3, 22.5 mM/toluene", is capable of generating 10.50 mM *trans*-1,3-diphenylpropene, **11**, and 1.65 mM of its isomeric product 3,3-diphenylpropene, **12**. This implies a substrate conversion of 81% with a TON of 7200 cycles and a TOF of 150 cycles per hour at 48 h. When the catalytic material had been reused in a fresh system, a sharp decrease in its activity (entry 2) was observed due to partial deactivation of the supported catalyst by undesired side reactions. It is interesting to point out here that at this temperature the isomeric ratio (**11**:**12**) remains relatively constant in the range 5.0−7.0.

Entries 3−5 in Table 1 show a spectacular increase of the catalyst performance when the temperature and the Substrate/Cat ratio are increased from 27 to 65 °C and from 8930 up to 13800 respectively leaving the rest of the system parameters unchanged. In particular, entry 3 shows a substrate conversion of 96% in 24 h with an isomeric ratio of 15.0. This result clearly shows that upon increasing the temperature and the Substrate/Cat ratio, the pathways that lead

Table 1. Suzuki coupling between cinnamyl bromide, **9**, and the iodoarenes, **13a**−**b**, with phenylboronic acid **10**.

Entry	*T*, °C	Substrate, mM	Cat%[a] (nmols)	Substrate/Cat[b] ($\times 10^3$)	Time, hours	Product, mM	Conversion, %[a]	TON (10^3)
1	27	**9** (15.0)	$1.12\cdot10^{-2}$ (16.80)	8.93	48	**11** (10.50) **12** (1.65)	81	7.2
2	27	**9** (15.0)	$1.12\cdot10^{-2}$ (16.80)[c]	8.93	48	**11** (2.85) **12** (0.45)	22	1.9
3	65	**9** (15.0)	$7.27\cdot10^{-3}$ (10.91)	13.8	24	**11** (13.50) **12** (0.90)	96	12.5
4	65	**9** (15.0)	$7.27\cdot10^{-3}$ (10.91)[c]	13.8	24	**11** (12.90) **12** (0.45)	89	12.2
5	65	**9** (15.0)	$7.27\cdot10^{-3}$ (10.91)[d]	13.8	24	**11** (7.20) **12** (0.45)	51	7.0
6	65	**9** (80.0)	$9.30\cdot10^{-4}$ (1.40)	107.5	24	**11** (67.20) **12** (4.00)	89	95.3
7	65	**9** (80.0)	$9.30\cdot10^{-4}$ (1.40)[c]	107.5	24	**11** (52.80) **12** (4.00)	71	79.8
8	65	**9** (80.0)	$9.30\cdot10^{-4}$ (1.40)[d]	107.5	24	**11** (32.80) **12** (2.40)	44	48.0
9	65	**13a** (78.7)	$1.51\cdot10^{-3}$ (11.88)	66.2	24	**14a** (23.61)	30	19.8
10	65	**13a** (78.7)	$1.51\cdot10^{-3}$ (11.88)[c]	66.2	24	**14a** (25.97)	33	21.8
11	65	**13a** (78.7)	$1.51\cdot10^{-3}$ (11.88)[d]	66.2	24	**14a** (13.77)	17.5	11.6
12	65	**13a** (78.7)	$1.51\cdot10^{-3}$ (11.88)[e]	66.2	24	**14a** (3.15)	4	2.4
13	65	**13b** (87.4)	$1.56\cdot10^{-3}$ (13.63)	64.1	24	**14b** (18.35)	21	13.5
14	65	**13b** (87.4)	$1.56\cdot10^{-3}$ (13.63)[c]	64.1	24	**14b** (17.04)	19.5	12.5
15	65	**13b** (87.4)	$1.56\cdot10^{-3}$ (13.63)[d]	64.1	24	**14b** (8.74)	10	6.6
16	65	**13b** (87.4)	$1.56\cdot10^{-3}$ (13.63)[e]	64.1	24	**14b** (3.50)	4	2.7

[a] Cat. is **C-felt/poly-1aab**.% indicates the molar percentage of the Pd complex in the **C-felt/poly-1aab** polymer with respect to the substrate. The total amount of the Pd complex in the **C-felt/poly-1aab** material in nanomoles is indicated in parentheses. [b] Molar ratio. [c] First reutilization. [d] Second reutilization. [e] Third reutilization.

 © 2004 Wiley-VCH Verlag GmbH & Co. KGaA, Weinheim

to **11** are kinetically favored with regard to those that lead to **12**. Entries 4 and 5 show the effect of reusing the catalyst after cleaning and soaking in a fresh solution with a slight decrease of the activity. Several experiments were performed in which the Substrate/Cat ratio was increased but the temperature was maintained at 65 °C. A 100% conversion and 100% isomeric purity was obtained although the deactivation became more severe upon reuse. Finally in entries 6−8 the Substrate/Cat ratio was strongly increased up to 107500. This decreased conversion to 89% and isomer selectivity to 16.8 but reduced the deactivation process on reuse (entries 7, 8) and generated an impressive overall TON of 223000. This is about an order of magnitude higher than had been described previously by anchoring similar Pd complexes but using polystyrene as a solid matrix.[13]

The results described above clearly show how, for the present system, the temperature and Substrate/Cat ratio are key parameters that strongly influence the catalytic performance. In particular the Substrate/Cat ratio can modulate: a) substrate conversion, b) isomer selectivity, c) reuse capacity and d) the TOF as well as the TON.

Iodoarene substrates were also tested for coupling reactions with phenyl boronic acid. Entries 9−16 in Table 1 show the results when **10** was treated with 4-iodonitrobenzene, **13a**, and iodobenzene, **13b**, respectively, using the similar catalytic system parameters as in the previous case i.e. at 65 °C and with a reaction time of 24 hours. In these cases conversions were lower (entries 9, 13), but the catalyst could be reused once without any significant loss of activity (entries 10, 14). In the second reuse (entries 11, 15) the catalyst activity was reduced to 50% of its initial performance and in the third (entries 12, 16) the activity was reduced dramatically until only 4% substrate conversion was observed.

To evaluate the degree of leaching during the catalytic experiments in the Suzuki cross-coupling reactions, a quantitative Pd analysis was carried out using Atomic Absorption Spectroscopy (AAS). It was shown that about 5% of the initial Pd had dissolved in the reaction solution during the first 24 h of the reaction. Nevertheless, this "leached Pd" does not significantly catalyze the Suzuki cross-coupling reaction, as verified by removing the **C-felt/poly-1aab** from a solution after a reaction time of 12 h and allowing the process to continue under the same conditions for a further 24 hours (see entry 9, Table 1). This experiment is thus evidence that the catalytic process proceeds in a true heterogeneous manner.[22]

Control experiments were carried out in the absence of the Pd complex. Suzuki coupling between cinnamyl bromide, **9**, and phenylboronic acid, **10**, under the same conditions as in entry 3 (Table 1) but without **C-felt/poly-1aab** ("**9**, 15.0 mM; **10**, 22.5 mM/K_2CO_3, 22.5 mM/toluene" up to 10 mL total volume at 65 °C for 24 h), afforded 4.65 m M of **11** and 0.3 m M of **12** (33% of conversion). The conversion between 4-iodonitrobenzene, **13a**, and phenylboronic acid, **10**, under similar conditions as in entry 9 ("**13a**, 78.7 mM; **10**, 118 mM/K_2CO_3, 118 mM/toluene" up to 10 mL total volume at 65 °C for 24 h) and without **C-felt/poly-1aab** is negligible.

Conclusion

New Pd^0 triolefinic complexes containing ancillary pyrrole and/or ferrocene groups have been prepared and characterized. These groups have been attached with the purpose of carrying out specific functions namely, electrochemical monitoring and anchoring via anodic electropolymerization, respectively. The new polypyrrole modified electrodes prepared in this way represent the first examples reported in the literature of a successful phosphane-free system, capable of efficiently catalyzing Suzuki cross-coupling reactions. The different parameters that govern system reactivity have been established putting forward the strong appeal of these new materials with regard to their high thermal and air stability as well as excellent solvent resistance.

Experimental Section

General Remarks: ^1H NMR (^{13}C NMR) spectra were recorded at 250 MHz (62.5 MHz) or at 200 MHz (50 MHz) using Me_4Si as internal standard. Chemical shifts are given in δ units. ESI mass spectra were acquired using a Navigator quadrupole instrument. The instrument was operated in the positive ion mode (ES+) at a probe tip voltage of 3 kV. HRMS and ICP analyses were obtained at "SCAI Unidad de Espectrometría de Masas de la Universidad de Córdoba", using a Micromass VG Mass Spectrometer and a Perkin−Elmer AA spectrophotometer respectively. Elemental analyses were determined at "Servei d'Anàlisi de la Universitat de Girona".

Cyclic voltammetric experiments and controlled-potential coulometry were carried out in a PAR 263A EG&G potentiostat using a three electrode cell. Glassy carbon disk electrodes (3 mm diameter) from BAS and carbon felt electrodes (0.5 × 0.5 × 0.5 cm) from SOFACEL were used as the working electrodes, platinum wires as auxiliary and Ag/10 mM Ag^+ as reference electrodes. Glassy carbon disk electrodes were routinely polished with 1 μm diamond paste. Cyclic voltammograms were performed in the dry box or outside with carefully dried solvents under N_2 or Ar, and at a potential scan rate of 100 mV/s. All electrochemical experiments were conducted in CH_2Cl_2 containing 0.1 M (nBu_4N)(PF_6) (TBAP) as the supporting electrolyte. All $E_{1/2}$ values reported were estimated from cyclic voltammetry as the average of the oxidative and reductive peak potentials ($E_{p,a}+E_{p,c}$)/2. Unless explicitly mentioned the concentration of the complexes was approximately 1 mM.

The protocol used for the preparation of the modified electrodes consisted of performing 20 repetitive CV scans at 100 mV/s from E_i = 0.0 V to E_{cl} = 1.3 V. Catalyst coverage for the modified electrodes was evaluated from the corresponding Fe^{III}/Fe^{II} wave charge.

Coupling product evolution was followed on a Hewlett−Packard 5890 gas chromatograph using naphthalene as an internal standard.

 © 2004 Wiley-VCH Verlag GmbH & Co. KGaA, Weinheim

Palladium(0) complexes **1aab**, **1abb** and **1bcc** were prepared according to a previously reported method described for macrocycles containing different arene units.[12a,16] Physical properties and spectroscopic data for all new compounds are described below.

(4-Pyrrol-1-ylphenyl)sulfonamide (2b): Compound was prepared by heating to reflux sulfanilamide (2.01 g, 11.4 mmol) and 2,5-dimethoxytetrahydrofuran (1.52 mL, 11.4 mmol) in glacial acetic acid according to a method for aniline derivatives[23] (yield 1.95 g, 8.8 mmol, 75%). M.p. 246−247 °C. IR (KBr): $\tilde{\nu}$ = 3349, 3260, 1600, 1513, 1334, 1296, 1165 cm^{-1}. ^1H NMR (200 MHz, [D$_6$]DMSO): δ = 6.12 (t, *J* = 2.2 Hz, 2 H), 7.17 (s, 2 H), 7.29 (t, *J* = 2.2 Hz, 2 H), 7.67 (AA′ part of a AA′BB′ system, *J* = 8.8 Hz, 2 H), 7.58 (BB′ part of a AA′BB′ system, *J* = 8.8 Hz, 2 H). ^{13}C NMR (50 MHz, [D$_6$]DMSO): δ = 111.9, 119.4, 119.6, 127.9, 140.8, 142.5.

***N*-(*tert*-Butyloxycarbonyl)ferrocenylsulfonamide (3a):** Starting from **2a** (0.80 g, 3.0 mmol); orange solid (yield 1.10 g, 3.0 mmol, 100%). M.p. 149−151 °C.[16] IR (KBr): $\tilde{\nu}$ = 3247, 3103, 2977, 1730, 1435, 1339, 1243, 1133 cm^{-1}. ^1H NMR (200 MHz, $CDCl_3$): δ = 1.42 (s, 9 H), 4.39 (s, 5 H), 4.42−4.45 (m, 2 H), 4.80−4.82 (m, 2 H), 7.05 (broad s, 1 H). ^{13}C NMR (50 MHz, $CDCl_3$): δ = 27.9, 69.8, 70.9, 83.5, 85.8, 149.5. ESI-MS (*m*/*z*): 383 $[M + NH_4]^+$, 365 $[M]^+$. $C_{15}H_{19}FeNO_4S$ (365.23): calcd. C 49.33, H 5.24, N 3.83; found C 49.39, H 5.28, N 3.66.

***N*-(*tert*-Butyloxycarbonyl)(4-pyrrol-1-ylphenyl)sulfonamide (3b):** Starting from **2b** (0.50 g, 2.3 mmol); colorless solid (yield 0.68 g, 2.1 mmol, 94%). M.p. 162−163 °C. IR (KBr): $\tilde{\nu}$ = 3312, 1741, 1594, 1511, 1415, 1340, 1151 cm^{-1}. ^1H NMR (200 MHz, $CDCl_3$): δ = 1.42 (s, 9 H), 6.41 (t, *J* = 2.3 Hz, 2 H), 7.17 (t, *J* = 2.3 Hz, 2 H), 7.53 (AA′ part of the AA′BB′ system, *J* = 8.8 Hz, 2 H), 8.08 (BB′ part of the AA′BB′ system, *J* = 8.8 Hz, 2 H). ^{13}C NMR (50 MHz, [D$_6$]DMSO): δ = 27.5, 82.2, 111.7, 118.8, 119.1, 129.2, 135.3, 143.2, 149.8. ESI-MS (*m*/*z*): 340 $[M + NH_4]^+$, 323 $[M + H]^+$. $C_{15}H_{18}N_2O_4S$ (322.38): calcd. C 55.88, H 5.63, N 8.69; found C 55.52, H 5.60, N 8.49.

***N*-[(*E*)-4-Bromo-2-butenyl]-*N*-(*tert*-butyloxycarbonyl)ferrocenylsulfonamide (4a):** Starting from **3a** (1.05 g, 2.8 mmol); orange solid (yield 1.15 g, 2.3 mmol, 80%). M.p. 122−124 °C.[24] IR (KBr): $\tilde{\nu}$ = 2978, 2930, 1721, 1336, 1140 cm^{-1}. ^1H NMR (200 MHz, $CDCl_3$): δ = 1.44 (s, 9 H), 3.93 (d, *J* = 6.4 Hz, 2 H), 4.29 (d, *J* = 5.0 Hz, 2 H), 4.42 (s, 5 H), 4.40−4.43 (m, 2 H), 4.79 (apparent t, *J* = 1.9 Hz, 2 H), 5.67−5.93 (m, 2 H). ^{13}C NMR (50 MHz, $CDCl_3$): δ = 28.0, 31.7, 47.5, 70.2, 70.6, 71.0, 84.0, 87.0, 129.1, 130.3, 150.9. ESI-MS (*m*/*z*): 561 $[M + Na + CH_3CN]^+$, 515 $[M + NH_4]^+$, 497 $[M]^+$. $C_{19}H_{24}BrFeNO_4S$ (498.21): calcd. C 45.80, H 4.86, N 2.81; found C 45.83, H 4.78, N 2.89.

***N*-[(*E*)-4-Bromo-2-butenyl]-*N*-(*tert*-butyloxycarbonyl)(4-pyrrol-1-ylphenyl)sulfonamide (4b):** Starting from **3b** (1.33 g, 4.3 mmol); colorless solid (yield 1.36 g, 3.0 mmol, 72%). M.p. 109−110 °C. IR (KBr): $\tilde{\nu}$ = 2973, 2926, 1723, 1593, 1514, 1333, 1157 cm^{-1}. ^1H NMR (200 MHz, $CDCl_3$): δ = 1.39 (s, 9 H), 3.98 (d, *J* = 7.2 Hz, 2 H), 4.47 (d, *J* = 5.5 Hz, 2 H), 5.79−6.08 (m, 2 H), 6.40 (t, *J* = 2.2 Hz, 2 H), 7.17 (t, *J* = 2.2 Hz, 2 H), 7.50 (AA′ part of the system AA′BB′, *J* = 9.0 Hz, 2 H), 7.99 (BB′ part of the system AA′BB′, *J* = 9.0 Hz, 2 H). ^{13}C NMR (50 MHz, $CDCl_3$): δ = 27.9, 31.6, 47.3, 84.8, 112.1, 119.0, 119.2, 129.9, 130.2, 130.3, 135.9, 144.2, 150.5. ESI-MS (*m*/*z*): 493−495 $[M + K]^+$, 472−474 $[M + NH_4]^+$, 455−457 $[M + H]^+$. $C_{19}H_{23}BrN_2O_4S$ (455.37): calcd. C 50.11, H 5.09, N 6.15; found C 49.68, H 5.00, N 6.00.

(*E*,*E*)-1,11-Bis(*tert*-butyloxycarbonyl)-1,11-bis(ferrocenylsulfonyl)-6-[(4-pyrrol-1-ylphenyl)sulfonyl]-1,6,11-triazaundeca-3,8-diene (5aab): Starting from **4a** (1.14 g, 2.3 mmol) and **2b** (0.25 g, 1.1 mmol); orange solid (yield 1.20 g, 1.1 mmol, 100%). M.p. 98−99 °C. IR (KBr): $\tilde{\nu}$ = 2977, 2929, 1725, 1596, 1509, 1361, 1132 cm^{-1}. ^1H NMR (200 MHz, $CDCl_3$): δ = 1.40 (s, 18 H), 3.78 (d, *J* = 5.5 Hz, 4 H), 4.23 (d, *J* = 5.5 Hz, 4 H), 4.39−4.44 (m, 14 H), 4.75 (apparent t, *J* = 2.2 Hz, 4 H), 5.39−5.65 (m, 4 H), 6.39 (t, *J* = 2.2 Hz, 2 H), 7.19 (t, *J* = 2.2 Hz, 2 H), 7.50 (AA′ part of the system AA′BB′, *J* = 8.8 Hz, 2 H), 7.83 (BB′ part of the AA′BB′ system, *J* = 8.8 Hz, 2 H). ^{13}C NMR (50 MHz, $CDCl_3$): δ = 28.0, 47.6, 47.7, 70.1, 70.6, 71.0, 83.8, 87.2, 111.7, 119.1, 120.0, 126.7, 128.9, 130.5, 136.9, 143.5, 151.0. ESI-MS (*m*/*z*): 1079 $[M + Na]^+$, 1074 $[M + NH_4]^+$. $C_{48}H_{56}Fe_2N_4O_{10}S_3$ (1056.87): calcd. C 54.55, H 5.34, N 5.30; found C 54.56, H 5.49, N 4.92.

(*E*,*E*)-1,11-Bis(*tert*-butyloxycarbonyl)-1,11-bis[(4-pyrrol-1-ylphenyl)sulfonyl]-6-(ferrocenylsulfonyl)-1,6,11-triazaundeca-3,8-diene (5abb): Starting from **4b** (1.30 g, 2.9 mmol) and **2a** (0.38 g, 1.4 mmol); yellow solid (yield 1.10 g, 1.1 mmol, 76%). M.p. 113−114 °C. IR (KBr): $\tilde{\nu}$ = 2979, 2930, 1729, 1596, 1510, 1356, 1335, 1168 cm^{-1}. ^1H NMR (200 MHz, $CDCl_3$): δ = 1.35 (s, 18 H), 3.73 (d, *J* = 5.0 Hz, 4 H), 4.37−4.39 (m, 11 H), 4.60 (apparent t, *J* = 2.0 Hz, 2 H), 5.51−5.79 (m, 4 H), 6.39 (t, *J* = 2.3 Hz, 4 H), 7.18 (t, *J* = 2.3 Hz, 4 H), 7.52 (AA′ part of the system AA′BB′, *J* = 8.7 Hz, 4 H), 7.95 (BB′ part of the system AA′BB′, *J* = 8.7 Hz, 4 H). ^{13}C NMR (50 MHz, $CDCl_3$): δ = 27.9, 47.6, 48.1, 68.6, 70.6, 70.7, 84.5, 87.5, 112.0, 119.0, 119.2, 128.7, 129.2, 130.0, 136.1, 144.0, 150.5. ESI-MS (*m*/*z*): 1036 $[M + Na]^+$, 1014 $[M + H]^+$. $C_{48}H_{55}FeN_5O_{10}S_3$ (1014.02): calcd. C 56.85, H 5.47, N 6.91; found C 56.74, H 5.52, N 6.88.

(*E*,*E*)-1,11-Bis(ferrocenylsulfonyl)-6-[(4-pyrrol-1-ylphenyl)sulfonyl]-1,6,11-triazaundeca-3,8-diene (6aab): Starting from **5aab** (0.96 g, 0.9 mmol); orange solid (yield 0.76 g, 0.9 mmol, 100%). M.p. 95−96 °C. IR (KBr): $\tilde{\nu}$ = 3274, 2922, 1595, 1508, 1328, 1135 cm^{-1}. ^1H NMR (200 MHz, $CDCl_3$): δ = 3.49 (d, *J* = 4.8 Hz, 4 H), 3.68 (d, *J* = 4.8 Hz, 4 H), 4.38−4.40 (m, 14 H), 4.54−4.64 (m, 6 H), 5.39−5.60 (m, 4 H), 6.40 (t, *J* = 2.2 Hz, 2 H), 7.17 (t, *J* = 2.2 Hz, 2 H), 7.50 (AA′ part of the system AA′BB′, *J* = 9.0 Hz, 2 H), 7.81 (BB′ part of the system AA′BB′, *J* = 9.0 Hz, 2 H). ^{13}C NMR (50 MHz, $CDCl_3$): δ = 44.3, 48.7, 68.5, 70.5, 70.7, 87.5, 111.9, 119.0, 119.8, 127.4, 128.9, 130.2, 136.2, 143.6. ESI-MS (*m*/*z*): 879 $[M + Na]^+$, 857 $[M + H]^+$. HRMS (*m*/*z* calcd. for [M +1]): 857.0888; found 857.0880.

(*E*,*E*)-1,11-Bis[(4-pyrrol-1-ylphenyl)sulfonyl]-6-[ferrocenylsulfonyl]-1,6,11-triazaundeca-3,8-diene (6abb): Starting from **5abb** (0.53 g, 0.5 mmol); yellow solid (yield 0.34 g, 0.4 mmol, 81%). M.p. 177−178 °C. IR (KBr): $\tilde{\nu}$ = 3277, 2923, 1597, 1509, 1333, 1159 cm^{-1}. ^1H NMR (200 MHz, $CDCl_3$): δ = 3.52−3.54 (m, 8 H), 4.36−4.38 (m, 7 H), 4.54 (apparent t, *J* = 2.0 Hz, 2 H), 5.00 (broad s, 2 H), 5.50−5.52 (m, 4 H), 6.39 (t, *J* = 2.2 Hz, 4 H), 7.15 (t, *J* = 2.2 Hz, 4 H), 7.49 (AA′ part of the system AA′BB′, *J* = 9.0 Hz, 4 H), 7.90 (BB′ part of the system AA′BB′, *J* = 9.0 Hz, 4 H). ^{13}C NMR (50 MHz, $CDCl_3$): δ = 44.4, 49.2, 68.6, 70.6, 70.8, 86.8, 111.9, 119.0, 119.9, 128.6, 128.9, 129.0, 136.2, 143.8. ESI-MS (*m*/*z*): 852 $[M + K]^+$, 836 $[M + Na]^+$, 814 $[M + H]^+$. $C_{38}H_{39}FeN_5O_6S_3$ (813.79): calcd. C 56.09, H 4.83, N 8.61; found C 56.44, H, 5.00, N 8.32.

(*E*,*E*,*E*)-1,6-Bis(ferrocenylsulfonyl)-11-[(4-pyrrol-1-ylphenyl)sulfonyl]-1,6,11-triazacyclopentadeca-3,8,13-triene (7aab): Starting from **6aab** (0.76 g, 0.9 mmol); orange solid (yield 0.60 g, 0.7 mmol, 73%). M.p. 150−151 °C. IR (KBr): $\tilde{\nu}$ = 2922, 1596, 1508, 1336, 1136 cm^{-1}. ^1H NMR (200 MHz, $CDCl_3$): δ = 3.55 (broad abs., 8 H), 3.70 (broad abs., 4 H), 4.38−4.40 (m, 14 H), 4.55 (apparent t,

 © 2004 Wiley-VCH Verlag GmbH & Co. KGaA, Weinheim

J = 1.9 Hz, 4 H), 5.50−5.52 (m, 6 H), 6.40 (t, J = 2.2 Hz, 2 H), 7.17 (t, J = 2.2 Hz, 2 H), 7.51 (AA′ part of the system AA′BB′, J = 8.8 Hz, 2 H), 7.82 (BB′ part of the system AA′BB′, J = 8.8 Hz, 2 H). ^{13}C NMR (50 MHz, $CDCl_3$): δ = 50.6, 50.7, 68.6, 70.6, 70.8, 86.2, 111.9, 119.0, 120.0, 128.5, 128.9, 129.3, 130.0, 135.7, 143.7. ESI-MS (*m*/*z*): 931 $[M + Na]^+$, 908 $[M]^+$. $C_{42}H_{44}Fe_2N_4O_6S_3 \cdot H_2O$ (926.73): calcd. C 54.43, H 5.00, N 6.05; found C 54.13, H, 4.98, N 5.81.

(*E*,*E*,*E*)-1,6-Bis[(4-pyrrol-1-ylphenyl)sulfonyl]-11-(ferrocenylsulfonyl)-1,6,11-triazacyclopentadeca-3,8,13-triene (7abb): Starting from **6abb** (0.86 g, 1.1 mmol); yellow solid (yield 0.83 g, 1.0 mmol, 91%). M.p. 139−140 °C. IR (KBr): $\tilde{\nu}$ = 2920, 1731, 1596, 1507, 1334, 1160, 1133 cm^{-1}. ^{1}H NMR (200 MHz, $CDCl_3$): δ = 3.56−3.71 (m, 12 H), 4.37−4.39 (m, 7 H), 4.54−4.56 (m, 2 H), 5.50−5.60 (m, 6 H), 6.41 (t, J = 2.2 Hz, 4 H), 7.16 (t, J = 2.2 Hz, 4 H), 7.50 (AA′ part of the system AA′BB′, J = 8.8 Hz, 4 H), 7.81 (BB′ part of the system AA′BB′, J = 8.8 Hz, 4 H). ^{13}C NMR (50 MHz, $CDCl_3$): δ = 50.1, 50.7, 68.5, 70.6, 70.7, 86.0, 111.9, 119.0, 119.8, 119.9, 128.6, 128.9, 129.3, 130.1, 135.5, 143.7. ESI-MS (*m*/*z*): 888 $[M + Na]^+$, 883 $[M + NH_4]^+$, 866 $[M + H]^+$. HRMS (*m*/*z* calcd. for [M +1]): 866.1804; found 866.1810.

(*E*,*E*,*E*)-1,14-Dibromo-*N*,*N*-bis[(4-methylphenyl)sulfonyl)-5,10-diazatetradeca-2,7,12-triene (8cc):[22] Yield 0.58 g, 0.9 mmol, 12%, starting from **2c** (2.51 g, 10.0 mmol).

(*E*,*E*,*E*)-1,6-Bis[(4-methylphenyl)sulfonyl)-11-[(4-pyrrol-1-ylphenyl)-sulfonyl]-1,6,11-triazacyclopentadeca-3,8,13-triene (7bcc): Starting from **8cc** (0.15 g, 0.23 mmol) and **2b** (0.05 g, 0.23 mmol); colorless solid (yield 0.14 g, 0.2 mmol, 88%). M.p. 127−128 °C. IR (KBr): $\tilde{\nu}$ = 2921, 1597, 1508, 1334, 1159, 1090 cm^{-1}. ^{1}H NMR (200 MHz, $CDCl_3$): δ = 2.43 (s, 6 H), 3.66−3.75 (m, 12 H), 5.51−5.60 (m, 6 H), 6.40 (t, J = 2.1 Hz, 2 H), 7.16 (t, J = 2.1 Hz, 2 H), 7.30 (AA′ part of the system AA′BB′, J = 8.2 Hz, 4 H), 7.52 (AA′ part of the system AA′BB′, J = 8.6 Hz, 2 H), 7.65 (BB′ part of the system AA′BB′, J = 8.2 Hz, 4 H), 7.83 (BB′ part of the system AA′BB′, J = 8.6 Hz, 2 H). ^{13}C NMR (50 MHz, $CDCl_3$): δ = 21.5, 50.5, 50.7, 50.8, 111.9, 119.1, 120.0, 123.9, 127.2, 128.9, 129.0, 129.6, 129.8, 135.7, 136.0, 143.6, 143.8. ESI-MS (*m*/*z*): 738 $[M + NH_4]^+$, 721 $[M + H]^+$. $C_{36}H_{40}N_4O_6S_3$ (720.92): calcd. C 59.98, H 5.59, N 7.77; found C 59.68, H 5.69, N 7.41.

(*E*,*E*,*E*)-1,6-Bis(ferrocenylsulfonyl)-11-[(4-pyrrol-1-ylphenyl)-sulfonyl]-1,6,11-triazacyclopentadeca-3,8,13-trienepalladium(0) (1aab): Starting from **7aab** (0.25 g, 0.3 mmol); yellow solid (yield 0.27 g, 0.3 mmol, 88%). M.p. 211−212 °C. IR (KBr): $\tilde{\nu}$ = 2917, 1596, 1508, 1333, 1137, 904 cm^{-1}. ^{1}H NMR (200 MHz, $CDCl_3$): δ = 1.51−1.65 (m, 4 H), 2.75 (t, J = 11.2 Hz, 2 H), 2.85−3.15 (m, 2 H), 3.65−3.72 (m, 2 H), 3.80−4.05 (m, 2 H), 4.32−4.81 (m, 14 H), 4.40 (s, 10 H), 6.38 (t, J = 2.4 Hz, 2 H), 7.10 (t, J = 2.4 Hz, 2 H), 7.45 (AA′ part of the system AA′BB′, J = 8.7 Hz, 2 H), 7.81 (BB′ part of the system AA′BB′, J = 8.7 Hz, 2 H). ^{13}C NMR (50 MHz, $CDCl_3$): δ = 45.1, 45.2, 48.1, 48.2, 49.3, 49.4, 49.5, 68.4, 68.5, 70.6, 70.8, 77.8, 78.1, 78.4, 78.6, 78.7, 78.9, 82.2, 82.9, 83.1, 85.4, 85.5, 85.9, 112.0, 118.9, 119.9, 128.7, 128.9, 134.9, 135.4, 143.7. ESI-MS (*m*/*z*): 1014 $[M]^+$. $C_{42}H_{44}Fe_2N_4O_6PdS_3 \cdot 1/2CH_2Cl_2$ (1057.59): calcd. C 48.27, H 4.29, N 5.30; found C 48.33, H 4.32, N 5.34.

(*E*,*E*,*E*)-1,6-Bis[(4-pyrrol-1-ylphenyl)sulfonyl]-11-(ferrocenylsulfonyl)-1,6,11-triazacyclopentadeca-3,8,13-trienepalladium(0) (1abb): Starting from **7abb** (0.40 g, 0.5 mmol); pale yellow solid (yield 0.43 g, 0.4 mmol, 95%). M.p. 162−163 °C. IR (KBr): $\tilde{\nu}$ = 2923, 1596, 1508, 1334, 1160 cm^{-1}. ^{1}H NMR (200 MHz, $CDCl_3$): δ = 1.50−1.66 (m, 4 H), 2.50−3.20 (m, 4 H), 3.70−3.80 (m, 2 H), 3.90−4.11 (m, 2 H), 4.23−4.77 (m, 10 H), 4.41 (s, 5 H), 6.38 (br. abs., 4 H), 7.10 (br. abs., 4 H), 7.40−7.50 (m, 4 H), 7.78−7.90 (m, 4 H). ESI-MS (*m*/*z*): 972 $[M + H]^+$. $C_{42}H_{43}FeN_5O_6PdS_3 \cdot C_6H_{14}$ (1058.46): calcd. C 54.47, H 5.43, N 6.62; found C 54.33, H 5.08, N 6.67.

(*E*,*E*,*E*)-1,6-Bis[(4-methylphenyl)sulfonyl)-11-[(4-pyrrol-1-ylphenyl)-sulfonyl]-1,6,11-triazacyclopentadeca-3,8,13-trienepalladium(0) (1bcc): Starting from **7bcc** (0.20 g, 0.3 mmol); colorless solid (yield 0.18 g, 0.2 mmol, 78%). M.p. 172−173 °C. IR (KBr): $\tilde{\nu}$ = 2922, 1596, 1507, 1336, 1161, 1094 cm^{-1}. ^{1}H NMR (200 MHz, $CDCl_3$): δ = 1.65−1.74 (m, 4 H), 2.38 (s, 6 H), 2.81 (t, J = 12.6 Hz, 2 H), 3.00−3.12 (m, 2 H), 3.70−3.80 (m, 2 H), 4.00−4.10 (m, 2 H), 4.60−4.70 (m, 4 H), 4.79 (d, J = 14.4 Hz, 2 H), 6.39 (broad abs., 2 H), 7.11 (broad abs., 2 H), 7.24−7.29 (m, 4 H), 7.45−7.54 (m, 2 H), 7.60−7.73 (m, 4 H), 7.80−7.90 (m, 2 H). ^{13}C NMR (100 MHz, $CDCl_3$): 21.4, 45.0, 45.2, 48.2, 49.4, 78.1, 78.3, 78.5, 78.6, 78.7, 78.8, 82.4, 82.9, 83.0, 111.9, 118.8, 118.9, 119.8, 119.9, 126.9, 127.1, 128.7, 128.9, 129.8, 129.9, 134.7, 135.0, 135.1, 135.2, 135.9, 143.4, 143.6, 143.7. ESI-MS (*m*/*z*): 827 $[M + H]^+$. $C_{36}H_{40}N_4O_6PdS_3 \cdot CH_2Cl_2$ (912.28): calcd. C 48.71, H 4.64, N 6.14; found C 48.60, H 4.72, N 5.89.

Preparation of Modified Electrodes

C-felt/poly-1aab: Electrode coating was performed through cycling the potential as described previously using a carbon felt electrode (0.5 × 0.5 × 0.5 cm) used as the working electrode in a 1 mM solution of **1aab** in CH_2Cl_2 0.1 M TBAP. After electropolymerization, the modified electrode was transferred to a blank electrolyte solution and five more potential cycles were performed. The electrode was then soaked overnight in anhydrous toluene before using it as a heterogeneous catalyst.

Catalysis

1,3-Diphenylpropene, under Catalysis by C-felt/poly-1aab (11): To a degassed mixture of cinnamyl bromide **9** (0.030 g, 0.150 mmol), phenylboronic acid **10** (0.028 g, 0.225 mmol), anhydrous potassium carbonate (0.031 g, 0.225 mmol), and the electrode containing the immobilized Pd^0-catalyst, **C-felt/poly-1aab** (see Table 1 for Pd nmols) anhydrous toluene (10 mL) was added under N_2. The mixture was stirred at 65 °C for 24 hours. Product yield was calculated by GC using naphthalene as internal standard. 1,3-Diphenylpropene **11** has the same retention time as authentic material and the correct mass by GC/MS. ^{1}H NMR (200 MHz, $CDCl_3$): δ = 3.52 (d, J = 5.9 Hz, 2 H), 6.32−6.50 (m, 2 H), 7.15−7.37 (m, 10 H). 3,3-Diphenyl-1-propene **12**[24] has been identified by GC/MS analysis and by ^{1}H NMR spectrum. ^{1}H NMR (200 MHz, $CDCl_3$): δ = 4.70 (d, J = 7.2 Hz, 1 H), 4.98 (b d, J = 17.0 Hz, 1 H), 5.20 (b d, J = 9.2 Hz, 1 H), 6.30 (b abs, 1 H), 7.20−7.30 (m, 10 H). The heterogeneous catalyst was removed from the reaction vessel, washed by stirring it in toluene and reused.

4-Nitrobiphenyl, under Catalysis by C-felt/poly-1aab (14a), General Method: To a degassed mixture of 4-iodonitrobenzene **13a** (0.20 g, 0.79 mmol), phenylboronic acid **10** (0.15 g, 1.18 mmol), anhydrous potassium carbonate (0.17 g, 1.18 mmol), and the modified electrode, **C-felt/poly-1aab** (0.0015% molar) anhydrous toluene (10 mL) was added under N_2. The mixture was stirred at 65 °C for 24 hours. The product yield was calculated by GC using naphthalene as internal standard. 4-Nitrobiphenyl **14a** has the same retention time as authentic material and the correct mass by GC/MS. The elec-

 © 2004 Wiley-VCH Verlag GmbH & Co. KGaA, Weinheim

trode with the polymeric catalyst was removed from the reaction vessel, washed by stirring in toluene and reused.

X-ray Crystallographic Study

X-ray Structure Determination of 1bcc: Very small colorless and mostly twinned crystals of **1bcc·CH_2Cl_2** were grown by slow evaporation of a dichloromethane solution at room temperature. After different trials, a data set of moderate quality was acquired from a small crystal needle with the dimensions 44 × 14 × 6 μm. Molecular formula $C_{37}H_{42}Cl_2N_4O_6Pd_1S_3$, M = 912.23, triclinic, a = 11.1889(12), b = 14.1440(14), c = 14.4425(14) Å, α = 117.683(4)°, β = 100.507(4)°, γ = 90.266(3)°, V = 1979.5(3) Å^3, space group $P\bar{1}$, Z = 2, μ = 0.812 mm^{-1}, $d_{calcd.}$ = 1.530 g/cm^3. The measurements were made on a Siemens P4 diffractometer equipped with a SMART-CCD-1000 area detector, a MACScience Co. rotating anode with Mo-K_α radiation, a graphite monochromator and a Siemens low temperature device LT2 (T = −120 °C). The measurements were made in the range 1.63 to 27.50°. 24003 reflections were collected of which 8939 were unique (R_{int} = 0.1292) and 3783 observed [$F_o > 4\sigma(F_o)$]. Full sphere data collection was carried out using ω and scans. Programs used: Data collection Smart V. 5.060 (Bruker AXS, 1999), data reduction Saint + Version 6.02 (Bruker AXS 1999) and absorption correction SADABS (max./min. transmission: 1.000000/0.709584, Bruker AXS 1999). Structure solution and refinement using SHELXTL Version 5.10 (Sheldrick, University of Göttingen, Germany, 1998). The structure was solved by direct methods and refined by full-matrix least-squares against F^2. All calculated hydrogen positions were refined and constrained. Final R_1 [$I > 2\sigma(I)$] = 0.0698 and $wR(F^2)$ [$I > 2\sigma(I)$] = 0.1459. The number of refined parameters was 503.

CCDC-216129 contains the supplementary crystallographic data for this paper. These data can be obtained free of charge at www.ccdc.cam.ac.uk/conts/retrieving.html [or from the Cambridge Crystallographic Data Center, 12, Union Road, Cambridge CB2 1EZ, UK; Fax: (internat.) +44-1223-336-033; E-mail: deposit@ccdc.cam.ac.uk].

Acknowledgments

We thank Dr. Moreno-Mañas for helpful discussions and for useful suggestions. This research has been financed by MECYT of Spain (Project Nos. BQU2002−04002-C02 and BQU2000−0458 and predoctoral grant to E.M.) and by CIRIT "Generalitat de Catalunya" (Project No. SGR2001−00291). A.L. is also grateful to CIRIT for the Distinction award and to Johnson and Matthey for a precious metals loan.

[1] [1a] *Comprehensive Organometallic Chemistry II* (Eds.: E. W. Abel, F. G. A. Stone, and G. Wilkinson), Pergamon Press, New York, **1995**, vol. 12. [1b] *Applied Homogeneous Catalysis with Organometallic Compounds* (Eds.: B. Cornils, W. A. Herrmann), Wiley-VCH, Weinheim, **2002**, vols. 1, 2, and 3. [1c] *Transition Metals for Organic Synthesis. Building Blocks and Fine Chemicals* (Eds.: M. Beller, C. Bolm), Wiley-VCH, Weinheim, **1998**, vols. 1 and 2. [1d] J. Tsuji, *Transition Metal Reagents and Catalysts. Innovations in Organic Synthesis*, John Wiley & Sons, Chichester, **2000**. [1e] *Handbook of Organopalladium Chemistry for Organic Synthesis* (Ed.: E. Negishi), John Wiley & Sons, New York, **2002**.

[2] [2a] W. A. Herrmann, B. Cornils, *Angew. Chem.* **1997**, *109*, 1074−1095; *Angew. Chem. Int. Ed. Engl.* **1997**, *36*, 1049−1067. [2b] *Aqueous-Phase Organometallic Catalysis* (Eds.: B. Cornils, W. A. Herrmann), Wiley-VCH, Weinheim, **1998**.

[3] [3a] W. A. Herrmann, C. W. Kohlpaintner, *Angew. Chem.* **1993**, *105*, 1588−1609; *Angew. Chem. Int. Ed. Engl.* **1993**, *32*, 1524−1544. [3b] B. Cornils, W. A. Herrmann, *Homogeneous Catalysts and Their Heterogenization or Immobilization* in *Applied Homogeneous Catalysis with Organometallic Compounds* (Eds.: B. Cornils, W. A. Herrmann), Wiley-VCH, Weinheim, **2002.** vol. 2, chapter 3.1.1, pages 601−603. [3c] F. Joó, A. Kathó, *J. Mol. Catal. (A)* **1997**, *116*, 3−26. [3d] B. Cornils, W. A. Herrmann, R. W. Eckl, *J. Mol. Catal. (A)* **1997**, *116*, 27−33.

[4] For reviews see: [4a] I. T. Horváth, *Immobilization by Other Liquids. Fluorous Phases* in *Applied Homogeneous Catalysis with Organometallic Compounds* (Eds.: B. Cornils, W. A. Herrmann), Wiley-VCH, Weinheim, **2002**, volume 2, chapter 3.1.1.2, pages 634−639. [4b]B. Cornils, *Angew. Chem.* **1997**, *109*, 2147−2149; *Angew. Chem. Int. Ed. Engl.* **1997**, *36*, 2057−2059. [4c] I. T. Horváth, *Acc. Chem. Res.* **1998**, *31*, 641−650.

[5] For general reviews see: [5a] P. Panster, S. Wieland, *Immobilization* in *Applied Homogeneous Catalysis with Organometallic Compounds* (Eds.: B. Cornils, W. A. Herrmann), Wiley-VCH, Weinheim, **2002**, volume 2, chapter 3.1.1.3, pages 646−663. [5b] P. Kalck, M. Dessoudeix, *Ligands or Complexes Containing Ancillary Functionalities* in *Aqueous-Phase Organometallic Catalysis* (Eds.: B. Cornils, W. A. Herrmann), Wiley-VCH, Weinheim, **1998**, chapter 3.2.3, pages 105−122. [5c] C. A. McNamara, M. J. Dixon, M. Bradley, *Chem. Rev.* **2002**, *102*, 3275−3299.

[6] For reviews on the use of immobilized metallic catalysts in inorganic solids see: [6a] J. H. Clark, D. J. Macquarrie, *Chem. Commun.* **1998**, 853−860. [6b] D. E. De Vos, M. Dams, B. F. Sels, P. A. Jacobs, *Chem. Rev.* **2002**, *102*, 3615−3640.

[7] [7a] D. Curran, J. Grimshaw, S. D. Perera, *Chem. Soc. Rev.* **1991**, *20*, 391−404. [7b] A. Deronzier, J. C. Moutet, *Coord. Chem. Rev.* **1996**, *147*, 339−371. [7c] A. Deronzier, J. C. Moutet, *Acc. Chem. Res.* **1989**, *22*, 249−255.

[8] W. J. Vining, T. J. Meyer, *Inorg. Chem.* **1986**, *25*, 2023−2033.

[9] R. Ramaraj, A. Kira, M. Kaneko, *Polym. Adv. Technol.* **1995**, *6*, 131−140.

[10] W. Kutner, *J. Electroanal. Chem.* **1989**, *259*, 99−111.

[11] [11a] O. Stéphan, N. Riegel, S. Jugé, *J. Electroanal. Chem.* **1997**, *421*, 5−8. [11b] N. Riegel, C. Darcel, O. Stéphan, S. Jugé, *J. Organomet. Chem.* **1998**, *567*, 219−233.

[12] [12a] S. Cerezo, J. Cortès, D. Galvan, E. Lago, C. Marchi, E. Molins, M. Moreno-Mañas, R. Pleixats, J. Torrejón, A. Vallribera, *Eur. J. Org. Chem.* **2001**, 329−337. [12b] S. Cerezo, J. Cortès, E. Lago, E. Molins, M. Moreno-Mañas, T. Parella, R. Pleixats, J. Torrejón, A. Vallribera, *Eur. J. Inorg. Chem.* **2001**, 1999−2006.

[13] J Cortès, M. Moreno-Mañas, R. Pleixats, *Eur. J. Org. Chem.* **2000**, 239−243.

[14] [14a] B. Estrine, B. Blanco, S. Bouquillon, F. Hénin, M. Moreno-Mañas, J. Muzart, C. Pena, R. Pleixats, *Tetrahedron Lett.* **2001**, *42*, 7055−7057. [14b] M. Moreno-Mañas, R. Pleixats, J. Spengler, C. Chevrin, B. Estrine, S. Bouquillon, F. Hénin, J. Muzart, A. Pla-Quintana, A. Roglans, *Eur. J. Org. Chem.* **2003**, 274−283.

[15] S. Cacchi, G. Fabrizi, A. Goggiamani, M. Moreno-Mañas, A. Vallribera, *Tetrahedron Lett.* **2002**, *43*, 5537−5540.

[16] A. Llobet, E. Masllorens, M. Moreno-Mañas, A. Pla-Quintana, M. Rodríguez, A. Roglans, *Tetrahedron Lett.* **2002**, *43*, 1425−1428.

[17] J. Masllorens, M. Moreno-Mañas, A. Pla-Quintana, A. Roglans, *Org. Lett.* **2003**, *5*, 1559−1561.

[18] [18a] M. Rodríguez, I. Romero, C. Sens, A. Llobet, A. Deronzier, *Electrochim. Acta* **2003**, *48*, 1047−1054. [18b] W. F. De Giovani, A. Deronzier, *J. Electroanal. Chem.* **1992**, *337*, 285−298.

 © 2004 Wiley-VCH Verlag GmbH & Co. KGaA, Weinheim

[18c] M. N. Collomb-Dunand-Sauthier, A. Deronzier, H. Le Bozec, M. Navarro, *J. Electroanal. Chem.* **1996**, *410*, 21−29.
[19] M. Moreno-Mañas, F. Pajuelo, R. Pleixats, *J. Org. Chem.* **1995**, *60*, 2396−2397.
[20] One possible mechanistic hypothesis for the formation of the two regioisomers, **11** and **12**, is that Pd^0 displace the bromide leaving group to form a π-allylpalladium complex intermediate. Reductive elimination after transmetallation takes place mainly at the less hindered site of the π-allyl intermediate yielding compound **11**. However, the reductive process at the most hindered site also occurs, affording small quantities of regioisomer **12**. For cross-coupling of allyl acetates with arylboronic derivatives, see: [20a] D. Bouyssi, V. Gerusz, G. Balme, *Eur. J. Org. Chem.* **2002**, 2445−2448. [20b] G. Ortar, *Tetrahedron Lett.* **2003**, *44*, 4311−4314.
[21] [21a] N. Miyaura, T. Yanagi, A. Suzuki, *Synth. Commun.* **1981**, *11*, 513−517. [21b] N. Miyaura, A. Suzuki, *Chem. Rev.* **1995**, *95*, 2457−2483. [21c] A. Suzuki, *J. Organomet. Chem.* **1999**, *576*, 147−168.
[22] R. A. Sheldon, M. Wallau, I. W. C. E. Arends, U. Schuchardt, *Acc. Chem. Res.* **1998**, *31*, 485−493.
[23] [23a] N. Clauson-Kaas, Z. Tyle, *Acta Chem. Scand.* **1952**, *6*, 667−670. [23b] N. Elming, N. Clauson-Kaas, *Acta Chem. Scand.* **1952**, *6*, 867−874.
[24] S. Araki, T. Shimizu, P. S. Johar, S.-J. Jin, Y. Butsugan, *J. Org. Chem.* **1991**, *56*, 2538−2542.

Received October 10, 2003
Early View Article
Published Online March 22, 2004

 © 2004 Wiley-VCH Verlag GmbH & Co. KGaA, Weinheim

A Series of Molybdenum(V) Complexes with the Oxalato Ligand Engaged in Different Binding Roles − An Unusual Staggered Conformation of the μ_4-Oxalate in $[\{Mo_2O_4(\eta^2\text{-}C_2O_4)_2\}_2(\mu_4\text{-}C_2O_4)]^{6-}$

Barbara Modec,*[a] Jurij V. Brenčič,[a] and Jože Koller[a]

Keywords: Coordination modes / Molybdenum / Oxo ligands / Oxalate / Polyoxometalates

Solvothermal reactions between mononuclear halooxomolybdates(V) and oxalic acid afforded smaller oligonuclear complexes with the oxalate ion engaged in different binding modes. The oxalate ion coordinates as a bidentate terminal ligand to each metal centre of the $\{Mo_2O_4\}^{2+}$ unit to form the anion of $(MeNC_5H_5)_2[Mo_2O_4(\eta^2\text{-}C_2O_4)_2py_2]$ (**1**; py = pyridine; $MeNC_5H_5^+$ = *N*-methylpyridinium cation). $(MeNC_5H_5)_6[\{Mo_2O_4(\eta^2\text{-}C_2O_4)_2\}_2(\mu_4\text{-}C_2O_4)]$ (**2**) with a tetradentate oxalate ion connecting two dinuclear subunits is a very rare example of a coordination compound with the oxalato ligand in a completely staggered conformation: the two CO_2 entities of the μ_4-oxalate ion are rotated by 90° with respect to each other. Ab initio MO calculations on $[\{Mo_2O_4(\eta^2\text{-}C_2O_4)_2\}_2(\mu_4\text{-}C_2O_4)]^{6-}$ revealed the isomer with the staggered conformation of the μ_4-oxalate ion to be of the lowest energy. The cyclic octanuclear anion of $(MeNC_5H_5)_2[Mo_8O_{16}(OMe)_8(\mu_8\text{-}C_2O_4)]$ (**3**) consists of four dinuclear subunits arranged around the central oxalate ion and additionally linked by pairs of methoxide bridges. Each oxygen atom of the oxalate ion bridges a pair of metal centres not connected by a metal–metal bond. The anionic part of $[MeNC_5H_2(Me)_3]_2[HNC_5H_2(Me)_3]_2[Mo_2O_3(\eta^2\text{-}C_2O_4)_4]$ (**4**) [$MeNC_5H_2(Me)_3^+$ = *N*-methylcollidinium cation; $HNC_5H_2(Me)_3^+$ = protonated 2,4,6-collidine] possesses an *anti*-$\{Mo_2O_3\}^{4+}$ structural fragment with a pair of bidentate oxalate ions coordinated to each molybdenum atom. The compounds were fully characterized by X-ray structural analysis and infrared spectroscopy.
(© Wiley-VCH Verlag GmbH & Co. KGaA, 69451 Weinheim, Germany, 2004)

Introduction

The continuous interest in polyoxometalates, in particular those with incorporated organic groups, is driven by their structural analogy to metal oxide surfaces, their use as models for the catalytic reactions taking place at these surfaces and also by the search for novel materials, distinguished by special structural and magnetic properties.[1] The mechanism of their formation is still not well understood. Mostly it is described as the self-assembly of known species. The basic building unit in the chemistry of molybdenum in the +5 oxidation state is a particularly stable dinuclear fragment, shown in Scheme 1 and henceforth symbolised by $\{Mo_2O_4\}^{2+}$. Its two d^1 metal centres are bridged by a pair of oxygen atoms. A single metal−metal bond with the usual length in the 2.5−2.6 Å range participates in the cohesion of the unit.[2] A set number of available coordination sites allows coordination of numerous ligands, while in their absence further aggregation takes place and larger, more stable assemblies are formed. The X-ray structure analyses of many $\{Mo_2O_4\}^{2+}$ compounds have shown that the structural integrity of the dinuclear unit remains intact irrespective of the nature of ligands completing the immediate environment of the metal atom.[2] Among the very diverse ligands which fulfil molybdenum's coordination demands, multidentate oxygen donor ligands have been used with the aim of assisting in the linkage of dinuclear blocks into polymeric materials. With only a few exceptions, the self-assembly process of dinuclear fragments prevailed, leading to discrete cluster species with the multidentate ligands incorporated into the metal oxide cores. As shown with some examples from the recent literature, various typical patterns of assembly can be recognized. For instance, the hexanuclear motif in $[(Mo_2O_4)_3(\mu_6\text{-}AsO_3)(\mu_2\text{-}SO_4)_3(\mu_2\text{-}OH)_3]^{6-}$,[3] $[(Mo_2O_4)_3(\mu_6\text{-}CO_3)(\mu_2\text{-}CO_3)_3(\mu_2\text{-}OH)_3]^{5-}$,[4] and $[(Mo_2O_4)_3(\mu_6\text{-}SO_3)(\mu_2\text{-}SO_3)_3(\mu_2\text{-}O)_3]^{8-}$,[5] is the same as first observed among the phosphomolybdates(V):[6] three $\{Mo_2O_4\}^{2+}$ building blocks are arranged around the central μ_6-bridging ligand [arsenate(III),[3] carbonate,[4] sulfate(IV)[5] or phosphate[6]] to form a planar hexanuclear moiety with three μ_2-bridging ligands [sulfate,[3] carbonate,[4] sulfate(IV)[5] or phosphate[6]] on its periphery. These hexanuclear moieties tend to aggregate even further: in

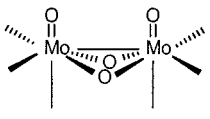

Scheme 1. $\{Mo_2O_4\}^{2+}$ structural unit

[a] Faculty of Chemistry and Chemical Technology, University of Ljubljana,
Askerčeva 5, 1000 Ljubljana, Slovenia
Fax: (internat.) + 386-1/2419-220
E-mail: barbara.modec@guest.arnes.si

$\{Mn^{II}[P_4Mo_6O_{28}(OH)_3]_2\}^{16-}$ and $\{Co^{II}[P_4Mo_6O_{28}(OH)_3]_2\}^{16-}$,[7] two recent examples of the basic hexanuclear motif with bridging phosphate ions, the transition metal cation is sandwiched between two hexanuclear moieties to form a "dimer". These "dimers" are linked further through strong ionic interactions into polymeric materials. However, the mixed-valent $[(Mo_2O_4)_3(Mo^{VI}O_4)(O_3PCH_2PO_3)_3]^{8-}$ reveals a new pattern of assembly.[8] Rather than sharing edges as in the above-described examples, three pairs of octahedra arranged around the central molybdate(VI) share corners. Apparently, the larger size of the μ_6-bridging ligand, molybdate(VI) vs. phosphate, arsenate(III) etc., induces the change in the connectivity between the $\{Mo_2O_4\}^{2+}$ blocks. The sulfate(IV) ion has also been seen to connect six $\{Mo_2O_4\}^{2+}$ units into a bulky $[(Mo_2O_4)_6(\mu_2\text{-}SO_3)_{12}(\mu_3\text{-}SO_3)_4]^{20-}$ core.[5] Its structure resembles that of an ε-Keggin derivative.[9] Another example, $[(Mo_2O_4)_{10}(P_2O_7)_{10}(CH_3COO)_8(H_2O)_4]^{28-}$, with coordinated pyrophosphate and acetate ions features an even larger assembly of dinuclear blocks.[10] These are arranged into two groups, one of six and the other of four dinuclear blocks to form two non-equivalent interconnected rings.

In only three cases does the interaction between the $\{Mo_2O_4\}^{2+}$ unit and the multidentate ligand result in a true polymeric material: (i) $[Mo_2O_4(PO_4)(HPO_4)]_n^{3n-}$ with $\{Mo_2O_4\}^{2+}$ units linked in a complicated manner by bridging phosphate ions into a two-dimensional array;[11] (ii) $[Mo_2O_4(C_2O_4)_2(H_2PO_4)]_n^{3n-}$ where μ_2-phosphate ions link dinuclear units into polymeric chains;[12] and (iii) $[Mo_2O_4(\mu_2\text{-}C_2O_4)Cl_2]_n^{2n-}$, prepared in our laboratory, which has infinite chains containing alternating $\{Mo_2O_4\}^{2+}$ units and bis(bidentate) oxalate ions.[13] Our choice of the oxalate ion among many oxygen donor ligands was governed by its ability to adopt several coordination modes. The binding mode the ligand eventually adopts depends, to a certain extent, upon the ratio between the ligand and the central atom. Studies of the interaction between the oxalate ion and the molybdenum(V) starting material resulted, apart from the polymeric $[Mo_2O_4(\mu_2\text{-}C_2O_4)Cl_2]_n^{2n-}$, in a series of smaller $\{Mo_2O_4\}^{2+}$ assemblies. We report herein on the syntheses and the characterization of $(MeNC_5H_5)_2[Mo_2O_4(\eta^2\text{-}C_2O_4)_2py_2]$ (**1**), $(MeNC_5H_5)_6[\{Mo_2O_4(\eta^2\text{-}C_2O_4)_2\}_2(\mu_4\text{-}C_2O_4)]$ (**2**), $(MeNC_5H_5)_2[Mo_8O_{16}(OMe)_8(\mu_8\text{-}C_2O_4)]$ (**3**) and $[MeNC_5H_2(Me)_3]_2[HNC_5H_2(Me)_3]_2[Mo_2O_3(\eta^2\text{-}C_2O_4)_4]$ (**4**).

Results and Discussion

Structural Studies

Crystal Structure of $(MeNC_5H_5)_2[Mo_2O_4(\eta^2\text{-}C_2O_4)_2py_2]$ (1)

The crystal structure of **1** consists of $[Mo_2O_4(\eta^2\text{-}C_2O_4)_2py_2]^{2-}$ anions (Figure 1) and *N*-methylpyridinium cations. Selected bond lengths are given in Table 1. Two molybdenum atoms are bridged by a pair of oxygen atoms to form the $\{Mo_2O_4\}^{2+}$ structural moiety. Its geometry follows a well-established pattern.[2] The distance between

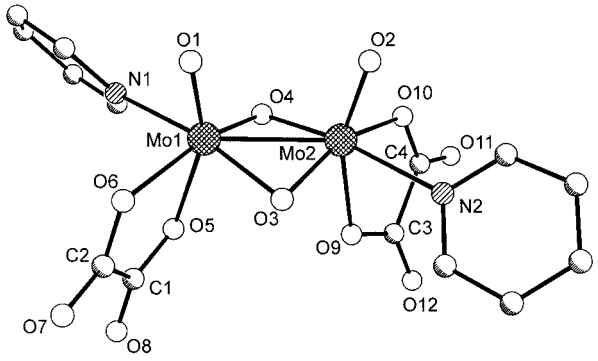

Figure 1. Drawing of $[Mo_2O_4(\eta^2\text{-}C_2O_4)_2py_2]^{2-}$, the anionic part of **1**, showing the atom labelling scheme; molybdenum atoms are cross-hatched; nitrogen atoms are lined bottom left to top right, oxygen atoms are unshaded and carbon atoms shaded, small-sized spheres; the same drawing scheme applies to all figures

Table 1. Selected bond lengths [Å] for **1**

Mo(1)−O(1)	1.690(2)	Mo(2)−O(2)	1.690(2)
Mo(1)−O(3)	1.944(2)	Mo(2)−O(3)	1.927(2)
Mo(1)−O(4)	1.932(2)	Mo(2)−O(4)	1.944(2)
Mo(1)−O(5)	2.179(2)	Mo(2)−O(9)	2.157(2)
Mo(1)−O(6)	2.120(2)	Mo(2)−O(10)	2.135(3)
Mo(1)−N(1)	2.260(3)	Mo(2)−N(2)	2.268(3)
Mo(1)−Mo(2)	2.5468(4)		

Table 2. Selected geometric parameters [Å, °] of the $\{Mo_2O_4\}^{2+}$ unit in some compounds

	Mo−Mo	Fold angle	O_b−Mo−O_b [a]	Mo−O_b−Mo
1	2.5468(4)	149.62(6)	94.02(10), 94.18(10)	82.16(9), 82.29(9)
2	2.5655(4)	160.21(5)	95.73(7)	82.73(7)
3	2.5770(4), 2.5786(4)	156.43(14), 156.83(18)	93.89(9)−94.47(9)	83.30(8)−83.94(8)
$[Mo_2O_4Cl_2(4\text{-}EtPy)_4]$[14] [b]	2.5489(5)	144.51(14)	92.3(1), 92.5(1)	82.29(9), 82.7(1)
$(PyH)_2[Mo_4O_8(OEt)_2(HOEt)_2Br_4]$[15] [c]	2.6060(4)	152.22(12)	93.61(8), 93.71(9)	82.09(8), 84.39(8)
$(Et_3NH)[Mo_6O_{12}(OMe)_4(acac)_3]$[16] [d]	2.595(1)−2.608(1)	152.6[e]	94−95[e]	80−85[e]
$(MeNC_5H_5)_{2n}[Mo_2O_4(C_2O_4)Cl_2]_n$ [13]	2.5607(7)	150.21(8)	93.31(10)	83.10(9)
$(3\text{-}MePyH)_{2n}[Mo_2O_4(C_2O_4)Cl_2]_n$ [13]	2.5832(4)	148.77(6)	92.84(7)	83.20(6)

[a] O_b denotes bridging oxygen atoms in the $\{Mo_2O_4\}^{2+}$ unit. [b] A neutral dinuclear compound. [c] Contains a tetranuclear anion built up from two $\{Mo_2O_4\}^{2+}$ units. [d] acac = acetylacetonate. Contains a hexanuclear anion with three $\{Mo_2O_4\}^{2+}$ units arranged around the central methoxide unit. [e] The angles were calculated from data of the CCDC.[17]

 © 2004 Wiley-VCH Verlag GmbH & Co. KGaA, Weinheim

molybdenum atoms, 2.5468(4) Å, is shorter than those observed in larger $\{Mo_2O_4\}^{2+}$ assemblies (see Table 2). The $Mo(O_b)_2Mo$ ring is not planar, instead it is folded about the line connecting the bridging oxygen atoms (O_b). The dihedral angle between two $Mo(O_b)_2$ planes, commonly denoted as the fold angle,[2] is 149.62(6)°. The six-coordination of each molybdenum atom is completed with a bidentate oxalate ion and a pyridine ligand.

Dinuclear oxalato complexes of molybdenum(v) have been studied before.[18] Their dinuclear nature, initially formulated on the basis of spectroscopic data and diamagnetism, was first confirmed by the X-ray structure analysis of $Ba[Mo_2O_4(\eta^2\text{-}C_2O_4)_2(H_2O)_2]\cdot 3H_2O$,[19] which was also the first crystal structure of an $\{Mo_2O_4\}^{2+}$-containing compound. The literature also mentions the $[Mo_2O_4(C_2O_4)_2py_2]^{2-}$ species, although no X-ray structural data were given to support its formulation.[20] In $Ba[Mo_2O_4(\eta^2\text{-}C_2O_4)_2(H_2O)_2]\cdot 3H_2O$,[19] in contrast to the well-documented and uniform tendency of Mo=O bonds to weaken bonds *trans* to themselves, no significant *trans* influence was observed. The molybdenum-to-oxalato-oxygen bond length *trans* to the oxo ligand is 2.14(4) Å compared to 2.11(3) Å for the same bond in the *cis* position. The earlier belief that the oxalato ligand has a low *trans* susceptibility compared to other ligands[21] was ruled out by the later structural determinations of a series of compounds containing the $[Mo_2O_4(\eta^2\text{-}C_2O_4)_2(H_2O)_2]^{2-}$ anion, which clearly indicated the existence of a *trans* influence.[22] However, the effect was not equally conspicuous in all these compounds. In the anion of **1**, two sets of non-equivalent bond lengths are observed, Mo(1)−O(5) = 2.179(2) Å vs. Mo(1)−O(6) = 2.120(2) Å and Mo(2)−O(9) = 2.157(2) Å vs. Mo(2)−O(10) = 2.135(3) Å. Again, the differences are smaller than those observed in various compounds with an operating *trans* influence. For example, in $[\{Mo_2O_4(C_2O_4)_2(H_2O)_2\}_2\{[Ln(H_2O)_4]_2(C_2O_4)\}]\cdot 7H_2O$ (Ln = La^{3+}, Ce^{3+})[23] the bis(bidentate) oxalate ions link two Mo^V_2 entities and two rare earth cations with two distinctly different bond lengths, 2.244(7)−2.251(3) Å vs. 2.143(3)−2.159(7) Å. These observations imply that there are other factors that influence the molybdenum-to-oxalato bond lengths.

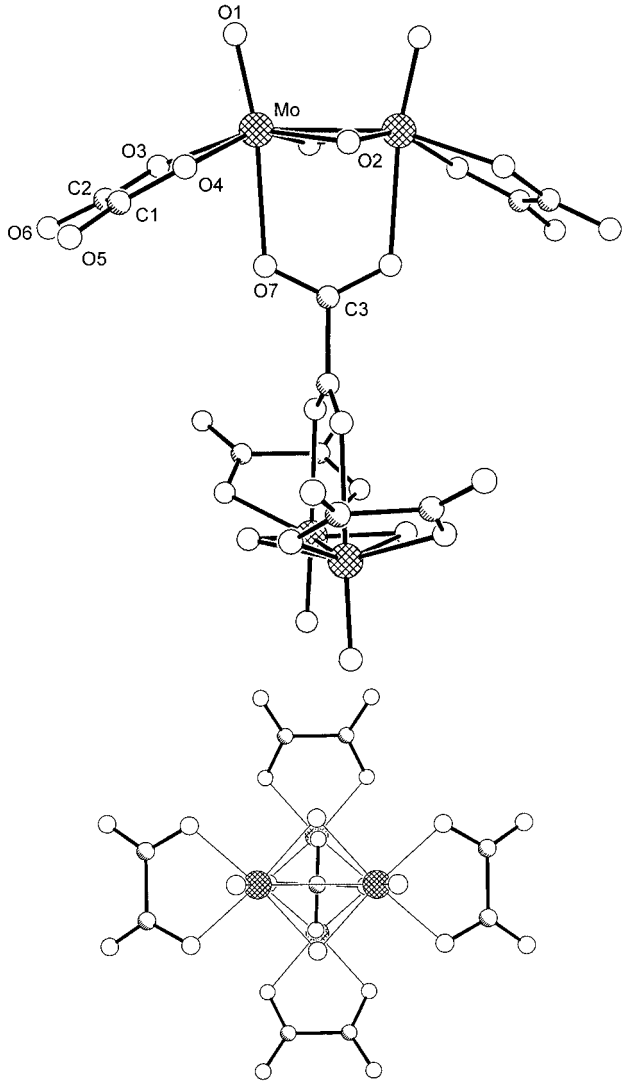

Figure 2. (a) (top) $[\{Mo_2O_4(\eta^2\text{-}C_2O_4)_2\}_2(\mu_4\text{-}C_2O_4)]^{6-}$, the anionic part of **2**, with the μ_4-oxalate ion in a staggered conformation; selected bond lengths [Å]: Mo−O(1) 1.678(2), Mo−O(2) 1.9397(18), Mo−O(2)[a] 1.9423(17), Mo−O(3) 2.0920(18), Mo−O(4) 2.0846(16), Mo−O(7) 2.3678(16), Mo−Mo[a] 2.5655(4), C(3)−O(7) 1.2548(19), C(3)−C(3)[b] 1.532(6); symmetry operations: [a] $-x, -y - 0.5, z$; [b] $-y - 0.25, x - 0.25, -z + 0.25$; (b) (bottom) the tetranuclear anion viewed along the improper fourfold axis

Crystal Structure of $(MeNC_5H_5)_6[\{Mo_2O_4(\eta^2\text{-}C_2O_4)_2\}_2(\mu_4\text{-}C_2O_4)]$ (2)

The crystal structure of **2** consists of tetranuclear $[\{Mo_2O_4(\eta^2\text{-}C_2O_4)_2\}_2(\mu_4\text{-}C_2O_4)]^{6-}$ anions (Figure 2) and *N*-methylpyridinium cations. The anion may be viewed as two $\{Mo_2O_4\}^{2+}$ subunits linked to each other through a μ_4-bridging oxalate ion. The Mo−Mo separation in the $\{Mo_2O_4\}^{2+}$ subunits, 2.5655(4) Å, is in agreement with the value expected for a single metal−metal bond. Each metal centre is attached to a bidentate oxalate ion, the corresponding molybdenum−oxygen distances are 2.0846(16) and 2.0920(18) Å. The terminal oxalate ions are tilted in an umbrella-like manner towards the other half of the anion, as if to shield the bridging oxalate ion. The relatively short distances, 2.7169(22) and 2.7359(23) Å, between a pair of coordinated oxygen atoms of the terminal oxalate ions to the oxygen atom of the μ_4-oxalate ion add support to this observation. This structural feature is readily apparent in Figure 2a. The four molybdenum atoms are related by an improper fourfold rotation axis, which passes through the C−C vector of the μ_4-oxalate ion and the centres of both $Mo(O_b)_2Mo$ rhombic units (Figure 2b). Consequently, the two metal−metal bond vectors are perpendicular to each other. Each oxygen atom of the bridging oxalate ion is coordinated to a different metal centre at a relatively long distance of 2.3678(16) Å. The lengthening of this bond when compared to the molybdenum-to-terminal-oxalate bond lengths may be explained in terms of the *trans* influence of

 © 2004 Wiley-VCH Verlag GmbH & Co. KGaA, Weinheim

Table 3. Selected geometric parameters [Å] of $\{Mo_2O_4\}^{2+}$ units with a third bridging ligand L[a]

	Mo−Mo	L	Mo−L
2	2.5655(4)	oxalate	2.3678(16)
3	2.5786(4), 2.5770(4)	oxalate	2.355(2)−2.395(2)
$[Mo^{II}_2Mo^{V}_2O_4(OH)_4(\mu_4\text{-}CO_3)(CO)_2(PMe_3)_6]$[24]	2.5522(9)	carbonate	2.419(3)
$[(Mo_2O_4)_3(\mu_6\text{-}CO_3)(\mu_2\text{-}CO_3)_3(\mu_2\text{-}OH)_3]^{5-}$ [4] [b]	2.5884(6)	carbonate	2.355(3)
$\{Na[(Mo_2O_4)_3(\mu_6\text{-}SO_3)(\mu_2\text{-}SO_3)_3(\mu_2\text{-}O)_3]_2\}^{15-}$ [5] [c]	2.597(5)	sulfate(IV)	2.36(2)
$[Mo_2O_4(\mu_2\text{-}SO_3)(SO_3)_4]^{8-}$ [5]	2.5872(18)	sulfate(IV)	2.27(1)
$[\{Mo_2O_4(\eta^2\text{-mal})_2\}_2(\mu_4\text{-mal})]^{6-}$ [25] [d]	2.555	malonate	2.321

[a] A multidentate oxygen donor ligand L coordinates to the dinuclear unit in all cited examples through two of its oxygen atoms, and to each metal centre with one. With the exception $[Mo_2O_4(\mu_2\text{-}SO_3)(SO_3)_4]^{8-}$, it binds in this manner to two or three $\{Mo_2O_4\}^{2+}$ units. [b] A μ_6-carbonate unit links three dinuclear units. [c] A μ_6-sulfate(IV) unit links three dinuclear units. [d] mal = $CH_2(COO)_2^{2-}$. A μ_4-malonate unit links two dinuclear units.

the terminal oxo group. A comparison with other $\{Mo_2O_4\}^{2+}$ compounds where multidentate oxygen donor ligands also coordinate to a pair of molybdenum atoms through two oxygen donor atoms in *trans* positions to the terminal oxo groups shows that the distances in **2** are within the normal range (Table 3).

The bridging oxalate ion is in a completely staggered conformation. The C−O distances of the μ_4-oxalate ion are equal, at 1.2548(19) Å, suggesting a bond character between a single and a double bond. For comparison, two sets of C−O distances are displayed within the bidentate oxalate ions, short ones, 1.216(3) and 1.219(3) Å, typical of localized double bonds, and longer ones, 1.291(3) and 1.294(3) Å. Hexaanions with two dinuclear subunits linked through a tetradentate oxalate ion have been observed before. Thio derivatives of the dinuclear unit, $\{Mo_2O_2(\mu_2\text{-}O)(\mu_2\text{-}S)\}^{2+}$ and $\{Mo_2O_2(\mu_2\text{-}S)_2\}^{2+}$, assemble in almost the same fashion as shown by $[\{Mo_2O_3S(\eta^2\text{-}C_2O_4)_2\}_2(\mu_4\text{-}C_2O_4)]^{6-}$ and $[\{Mo_2O_2S_2(\eta^2\text{-}C_2O_4)_2\}_2(\mu_4\text{-}C_2O_4)]^{6-}$, respectively.[26−28] The same structural type also occurs among very rare oxotungsten(V) compounds, such as $[\{W_2O_2S_2(\eta^2\text{-}C_2O_4)_2\}_2(\mu_4\text{-}C_2O_4)]^{6-}$.[28] Another example, $[Mo_4O_4S_2X_2(C_2O_4)_5]^{6-}$ (X = O or S), consists of one $\{Mo_2O_2(\mu_2\text{-}S)_2\}^{2+}$ unit, while the other displays a disorder in the double bridge.[29] The bridging atoms are partially oxygen and partially sulfur atoms. In contrast to a completely staggered configuration of the oxalate ion in **2**, the μ_4-oxalate ions in all the cited examples are planar. Ab initio MO calculations on the $[\{Mo_2O_4(\eta^2\text{-}C_2O_4)_2\}_2(\mu_4\text{-}C_2O_4)]^{6-}$ anion revealed the isomer with the staggered conformation of the oxalate ion to be the energetically more favoured one (Figure 3). The difference between the calculated energy of the anion with a staggered oxalate ion and that with a planar oxalate ion is 18 kcal/mol. AM1 and ab initio calculations on the oxalate dianion itself also indicated a slight preference for a completely staggered D_{2d} structure over a planar D_{2h} structure.[30] Bearing in mind that the bond lengths between the molybdenum atom and the oxalate oxygen atom in **2** are relatively long, this agreement is not surprising. The calculated barrier to rotation about the C−C bond in the oxalate dianion is smaller than in our case, ca. 5 kcal/mol. An oxalate ion coordinated to different metal ions usually adopts a planar or near-planar

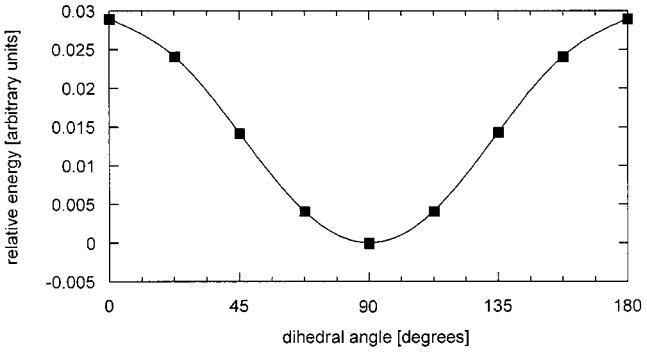

Figure 3. Relative energy of $[\{Mo_2O_4(\eta^2\text{-}C_2O_4)_2\}_2(\mu_4\text{-}C_2O_4)]^{6-}$ as a function of the dihedral angle in the μ_4-oxalate ion; 0.01 units correspond to 6.27 kcal/mol

form. Only a few deviations from planarity have been reported so far. In $[Ni(L1)(C_2O_4)]_n{\cdot}nH_2O$ (L1 represents a tetraaza macrocyclic ligand)[31] and $[Cu(C_2O_4)(H_2O)(4\text{-apy})_2]_n$ (4-apy = 4-aminopyridine)[32] the twist angles of the 1,1′-bis(monodentate) oxalate ion are 103° and 28°, respectively. In both these compounds the nonbonded oxalate oxygen atoms participate in significant hydrogen bonding interactions suggesting that these have an important influence over the ligand's conformation. In a recent study of the anhydrous alkali oxalates, in combination with K^+, Rb^+ and Cs^+ cations, both planar and staggered oxalate conformations were observed, showing that the conformation is determined mainly by packing effects.[33] On the other hand, the electronic structure calculations for the model compounds $[(HCOO)_3M_2(\mu_4\text{-}C_2O_4)M_2(HCOO)_3]$ ($HCOO^-$ stands for formate; and M_2 stands for pairs of Mo^{II} or W^{II} atoms linked by quadruple metal−metal bonds) employing density functional theory predicted the structure with the planar oxalate ion to be energetically more favoured than the one with the completely staggered oxalate ion by ca. 8 kcal/mol. This latter result is in line with the concept that the electronic coupling of M_2 units is maximized when the oxalate ion is in a planar conformation.[34]

Two other multidentate oxygen donor ligands, the malonate and sulfate ions, also form similar tetranuclear hexaanions in combination with the Mo^{V}_2 unit — $[\{Mo_2O_4(\eta^2\text{-}$

 © 2004 Wiley-VCH Verlag GmbH & Co. KGaA, Weinheim

mal)$_2$}$_2$(μ_4-mal)]$^{6-}$,[25] and [{$Mo_2O_2S_2(\eta^2$-$SO_4)_2$}$_2$(μ_4-SO_4)]$^{6-}$.[35] The latter is the closest structural relative to the anion in **2**. The inherent improper fourfold rotation symmetry of the μ_4-SO_4^{2-} ligand leads to the perpendicular orientation of the two {$Mo_2O_2(\mu_2$-$S)_2$}$^{2+}$ subunits. The elongated Mo_4 tetrahedron has two short (approx. 2.8 Å) and four long (approx. 6.8 Å) Mo−Mo distances. The corresponding distances within the Mo_4 tetrahedron in **2** are 2.5655(4) Å and 7.5913(4) Å.[36]

The fold angle in **2**, 160.21(5)°, is larger than in other {Mo_2O_4}$^{2+}$ compounds (see Table 2). Keeping the metal−metal bond length within the normal range, the less folded bridging moiety, where the value of the fold angle is larger, induces changes in the angles within the $Mo_2(O_b)_2$ rhombus, especially in the O_b−Mo−O_b angles, which become larger. In some of the selected examples in Table 2, the {Mo_2O_4}$^{2+}$ units are fused together by sharing bridging oxygen atoms. It is pertinent to note that such an assembly also induces stress upon the internal dimensions of the constituent dinuclear blocks.

Crystal Structure of ($MeNC_5H_5$)$_2$[Mo_8O_{16}(OMe)$_8$(μ_8-C_2O_4)] (3)

This compound consists of cyclic octanuclear [$Mo_8O_{16}(OMe)_8(\mu_8$-$C_2O_4)$]$^{2-}$ anions and *N*-methylpyridinium cations. As the centre of the ring lies on an inversion centre, the asymmetric unit consists of one half of the anion. Four {Mo_2O_4}$^{2+}$ blocks are connected by pairs of methoxide ligands, forming a ring around the oxalate anion (Figure 4a). The methoxide ions fold out from the ring, whereas the oxo groups fold into the ring. Short metal−metal distances [2.5770(4) Å and 2.5786(4) Å] within the dinuclear blocks alternate with longer non-bonding Mo···Mo contacts [3.2577(4) and 3.2655(4) Å] between the neighbouring dinuclear blocks. Each of the molybdenum centres displays a pseudo-octahedral coordination sphere consisting of six oxygen atoms. The terminal oxygen atoms lie at 1.683(2)−1.688(2) Å, bridging oxygen atoms at 1.926(2)−1.946(2) Å, and bridging methoxide ligands at 2.084(2)−2.122(2) Å. An oxygen atom of the central oxalate ion occupies the position *trans* to the molybdenyl group at a significantly longer distance, 2.355(2)−2.395(2) Å. It also functions as a third bridge between a pair of molybdenum atoms linked by methoxide ligands. The fold angles of the {Mo_2O_4}$^{2+}$ units are 156.43(14)° and 156.83(18)°. All metal atoms, terminal oxo groups and the oxalate ion lie in the plane. One half of the bridging methoxide ions and the bridging oxo groups lie above, and the other half below this plane (Figure 4b). The central oxalate ion is disordered over two positions. The C−O distances of the oxalate ion are in the 1.287(6)−1.317(7) Å range.

The planar configuration of the ring in **3** contrasts with the puckered arrangement observed in [$Mo_8O_{16}(OMe)_8$(R-py)$_4$], with a vacant central cavity.[37] However, the Mo−Mo bond lengths and the Mo···Mo non-bonding contacts in the two are basically the same. The pair illustrates how the oxalate or pyridine ligands influence the conformation of the ring obtained upon the assembly of four {Mo_2O_4}$^{2+}$ building blocks.

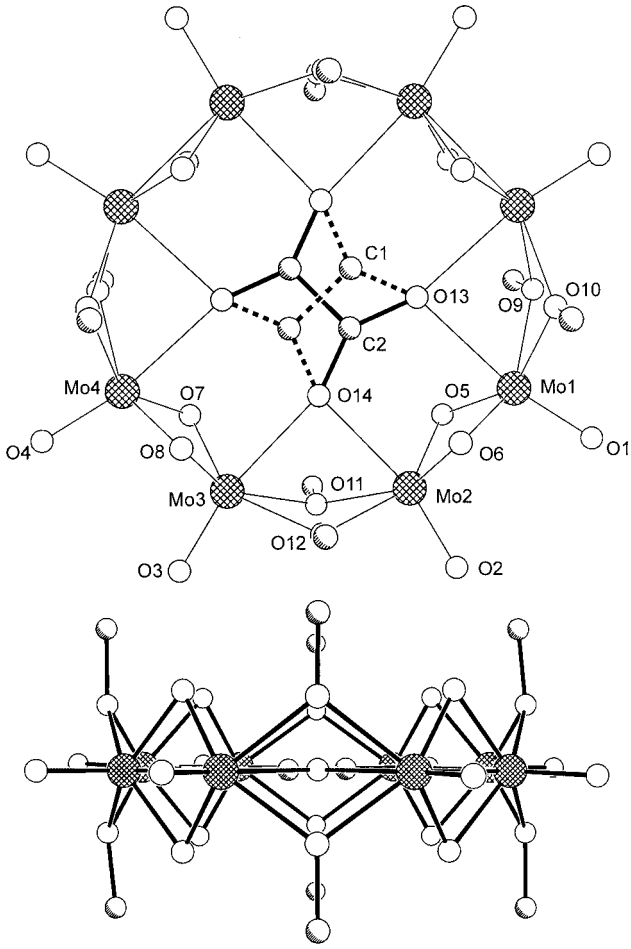

Figure 4. (a) (top) [$Mo_8O_{16}(OMe)_8(\mu_8$-$C_2O_4)$]$^{2-}$, the anionic part in **3**, with the oxalate ion disordered over two positions; selected bond lengths [Å]: Mo(1)−Mo(2) 2.5786(4), Mo(3)−Mo(4) 2.5770(4), Mo(1)−O(13) 2.386(2), Mo(2)−O(14) 2.355(2), Mo(3)−O(14) 2.373(2), Mo(4)−O(13)[a] 2.395(2); symmetry operation: [a] 2 − *x*, 1 − *y*, 2 − *z*; (b) (bottom) side view of the octanuclear anion showing the planar conformation of the ring

The anion [$Mo_8O_{16}(OMe)_8(\mu_8$-$C_2O_4)$]$^{2-}$ has been obtained before by the reaction of α-[(n-$C_4H_9)_4N]_4$[Mo_8O_{26}] with rhodizonic acid.[38] Its formation was explained in terms of a carbonyl insertion reaction coupled with ligand dissociation and redox processes. The same authors also reported the crystal structure of an ethoxide-bridged derivative, [$Mo_8O_{16}(OEt)_8(\mu_8$-$C_2O_4)$]$^{2-}$.[39] The same structural motif — four dinuclear building blocks forming a cycle — is also produced upon the linkage of {$Mo_2O_2(\mu_2$-$S)_2$}$^{2+}$ units through pairs of hydroxide bridges. The neutral cycle with the [$Mo_8S_8O_8(OH)_8$] composition can encapsulate various ligands, such as oxalate,[28,40a] molybdate(VI)[40b] or tungstate(VI) ions.[40c] The {$Mo_2O_2(\mu_2$-$S)_2$}$^{2+}$ unit forms in the presence of hydroxide ions even larger neutral cycles, which incorporate oxygen-donor guests with direct covalent interactions between the oxygen and molybdenum atoms. The inorganic backbone adapts its size and geometry to that of the guest anion. In the case of glutarate, a decanuclear ring

 © 2004 Wiley-VCH Verlag GmbH & Co. KGaA, Weinheim

was obtained, while with larger anions such as pimelate and trimesate, dodecanuclear rings were formed.[40]

Crystal Structure of $[MeNC_5H_2(Me)_3]_2[HNC_5H_2(Me)_3]_2[Mo_2O_3(\eta^2\text{-}C_2O_4)_4]$ (4)

The dinuclear complex $[Mo_2O_3(\eta^2\text{-}C_2O_4)_4]^{4-}$ (**4**; Figure 5) displays a centrosymmetric structure consisting of an *anti*-$\{Mo_2O_2(\mu_2\text{-}O)\}^{4+}$ core (Scheme 2). *N*-methylated collidine and protonated collidine molecules serve as countercations. Two molybdenum atoms are connected by a single oxygen atom, O(2), lying on the inversion centre. Consequently, the Mo−O−Mo bridge is linear with symmetrical Mo−O(2) bond lengths of 1.8534(2) Å. The two terminal oxygen atoms are *trans* to each other. Insofar as the dimensions of the *anti*-$\{Mo_2O_2(\mu_2\text{-}O)\}^{4+}$ unit are concerned, these are similar to other compounds containing this fragment.[41] Two bidentate oxalate ligands complete a distorted octahedral environment of each metal atom. The coordinated oxygen atoms of one oxalate ion, with bond lengths to the molybdenum atom of 2.032(2) and 2.081(2) Å, are *cis* to the Mo=O group. The corresponding bite angle is 78.37(9)°. The other oxalate ion binds with two distinctly different bond lengths, 2.0869(19) and 2.217(2) Å. The longer one is, as expected, *trans* to the terminal oxo group. The oxalate bite angle is smaller, 73.87(7)°. The oxalate bite angles are largely determined by the metal−oxygen distances: when these are longer than 2.1 Å, the oxygen−metal−oxygen angles become smaller than 80°.[42]

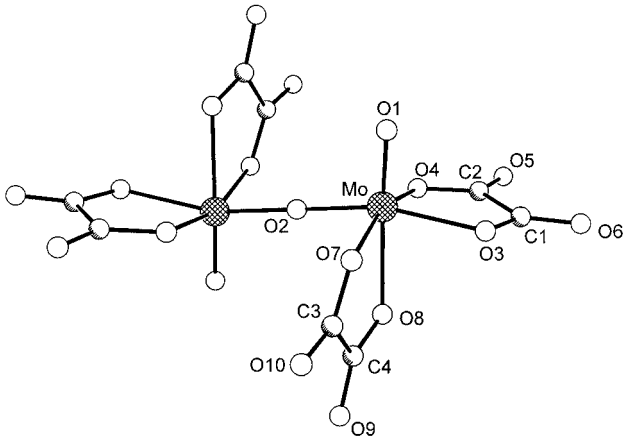

Figure 5. $[Mo_2O_3(\eta^2\text{-}C_2O_4)_4]^{4-}$ ion in **4**; selected bond lengths [Å]: Mo−O(1) 1.668(3), Mo−O(2) 1.8534(2), Mo−O(3) 2.081(2), Mo−O(4) 2.032(2), Mo−O(7) 2.0869(19), Mo−O(8) 2.217(2)

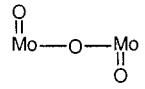

Scheme 2. *anti*-$\{Mo_2O_3\}^{4+}$ structural unit

Vibrational Spectroscopy

Although the oxalate absorption bands in the infrared spectra reflect its binding modes,[43] the overlap of some with pyridine absorptions prevents straightforward assignations. Among three sets of the characteristic oxalate bands, ν_{as}(OCO), ν_s(OCO) and δ(OCO), the carbon−oxygen asymmetric and symmetric stretching frequencies show the highest sensitivity to the metal coordination and thus to the binding mode employed. In addition, the metal−oxygen bond lengths also affect the number of bands.[44] The influence of the asymmetric binding on the infrared bands is clearly observed in the infrared spectra of $(MeNC_5H_5)_{2n}[Mo_2O_4(C_2O_4)Cl_2]_n$ and $(3\text{-}MePyH)_{2n}[Mo_2O_4(C_2O_4)Cl_2]_n$ where the bis(bidentate) oxalate ion bridges two metal centres in a highly asymmetric fashion, 2.172(2) vs. 2.312(2) and 2.1684(15) vs. 2.3183(16) Å, respectively.[13] Two sets of ν_{as}(OCO) [at 1671 and 1633 cm^{-1} for the $MeNC_5H_5^+$ compound, and at 1671 and 1633 cm^{-1} for the $3\text{-}MePyH^+$ compound] and ν_s(OCO) bands [at 1354, 1306 and 1288 cm^{-1} for the $MeNC_5H_5^+$ compound, and at 1353, 1302 and 1264 cm^{-1} for the $3\text{-}MePyH^+$ compound] are observed.

In **3**, with one type of oxalate ligand, each of the oxalate oxygen atoms bridges two molybdenum atoms with metal−oxygen distances of approximately the same length. The bands at 1659, 1635 [ν_{as}(OCO)], 1336, 1290 [ν_s(OCO)] and 813 cm^{-1} [δ(OCO)] are in accordance with expectations.[43] The terminal, bidentate binding mode in **1** gives rise to bands at 1705, 1667, 1633 [ν_{as}(OCO)], 1372, 1287 [ν_s(OCO)] and at 780 cm^{-1} [δ(OCO)]. Their frequencies agree very well with those reported for $Ba[Mo_2O_4(C_2O_4)_2(H_2O)_2]\cdot 3H_2O$ {1710, 1680, 1653 [ν_{as}(OCO)]; 1430, 1289 [ν_s(OCO)]; 793 cm^{-1} [δ(OCO)]}[19] and other compounds containing a bidentate oxalate ion.[45] The occurrence of a bidentate oxalate ion is also evident in the spectrum of **4** where the bands occur at 1709, 1682, 1633 [ν_{as}(OCO)], 1337, 1259 ν_s[(OCO)] and 799 cm^{-1} [δ(OCO)]. A multitude of bands {1705, 1681, 1657, 1633, 1574 [ν_{as}(OCO)]; 1360, 1322, 1288 [ν_s(OCO)]; 828, 800 cm^{-1} [δ(OCO)]} in the spectrum of **2** indicates both the bidentate and tetradentate binding modes of the oxalate ion. These are similar to those observed in $[H_3N(CH_2)_3NH_3]_3[Mo_4S_4O_4(C_2O_4)_5]\cdot 4.5H_2O$ [bands at 1716, 1688, 1600, 1506 in the ν_{as}(OCO) region; 1391, 1321, 1242 in the ν_s(OCO) region and 830, 794 cm^{-1} in the δ(OCO) region].[28]

Bands in the 1000−900 cm^{-1} region are associated with the Mo=O stretching vibrations. These are seen as strong bands at 949, 939 and 927 cm^{-1} for **1**, 958, 942 and 903 cm^{-1} for **2**, and for **3** and **4** as a single band at 962 and 960 cm^{-1}, respectively.

General Considerations

As observed before,[13−15,46] methanol and pyridines provide a medium where the formation of the $\{Mo_2O_4\}^{2+}$ fragment from the mononuclear halooxomolybdate(v) is a fast and reproducible process. The dinuclear unit with three coordination sites per metal atom and the oxalate ion is a system where the variation of the amount of one with respect to the other can produce discrete clusters when the amounts of the oxalate ion are large, or a polymeric material when the amounts of the oxalate ion are small. In the

 © 2004 Wiley-VCH Verlag GmbH & Co. KGaA, Weinheim

former case, $[Mo_2O_4(\eta^2\text{-}C_2O_4)_2py_2]^{2-}$ (**1**) and $[\{Mo_2O_4(\eta^2\text{-}C_2O_4)_2\}_2(\mu_4\text{-}C_2O_4)]^{6-}$ (**2**) were obtained. In **1** the oxalate ion occupies two out of three coordination sites of each metal atom in a bidentate fashion. One of the coordinated oxalate oxygen atoms is *cis* to the Mo=O group, and the other is in a less favourable *trans* position. Pyridine ligates to the remaining, third site. Considering both metal centres, two distinct geometries are possible. In **1**, the two pyridine ligands are on the opposite sides of the plane defined by a pair of Mo=O groups (*trans* to each other). The two pyridine ligands can also lie on the same side of the plane (*cis* to each other). The reaction conditions employed in the preparation of **1** apparently favour the *trans* isomer. Employing a huge excess of the oxalate ion afforded $[\{Mo_2O_4(\eta^2\text{-}C_2O_4)_2\}_2(\mu_4\text{-}C_2O_4)]^{6-}$ (**2**), where all three coordination sites of each metal centre are occupied with oxygen-donor ligands. Two belong to the bidentate oxalate ion and the third one to the bridging oxalate ion. Although the reaction medium for the preparation of **2** is mostly pyridine, pyridine does not coordinate. Reducing the ratio of oxalate vs. molybdate produces either a polymeric $[Mo_2O_4(C_2O_4)Cl_2]_n^{2n-}$, with one oxalate ion per dinuclear unit,[13] or a discrete octanuclear $[Mo_8O_{16}(OMe)_8(\mu_8\text{-}C_2O_4)]^{2-}$ (**3**) with one oxalate ion for every four dinuclear units, the major difference between the two synthetic procedures being the presence of pyridine. While the polymeric species is obtained in pyridine, the reaction mixture used in the case of **3** does not contain any. Methanol not only provides the reaction medium in the preparation of **3**, it is also a source of methoxide ions, which coordinate to the molybdenum atom and serve as bridges in the linkage of $\{Mo_2O_4\}^{2+}$ units. The role that methanol plays in the reaction mixtures merits additional comment as it is also consumed in the in situ formation of *N*-methylpyridinium cations. Their formation at elevated temperature requires apart from methanol, also pyridine and oxalic acid. *N*-Alkylation takes place when other pyridines are used as substrates as well, for example 2,4,6-collidine in the formation of **4**. The exact nature of this process is currently under investigation.[47] When no methanol is used, the only product isolated so far was $(PyH)_2[Mo_2O_4(\eta^2\text{-}C_2O_4)_2py_2]$, provided that a sufficient amount of the oxalate ion was present.

It is pertinent to mention briefly a series of structurally related species, dinuclear *cis*-$[Mo_2O_2(\mu_2\text{-}S)_2(\eta^2\text{-}C_2O_4)_2(H_2O)_2]^{2-}$, tetranuclear $[\{Mo_2O_2(\mu_2\text{-}S)_2(\eta^2\text{-}C_2O_4)_2\}_2(\mu_4\text{-}C_2O_4)]^{6-}$ and octanuclear $[Mo_8O_8S_8(OH)_8(\mu_8\text{-}C_2O_4)]^{2-}$, which are formed in the reactions between the thio-bridged dimer $\{Mo_2O_2(\mu_2\text{-}S)_2\}^{2+}$ and oxalate ions in aqueous media.[28,40e,40f] It was observed that the reaction products depend more upon the pH of the reaction medium than the stoichiometry. At pH ≈ 1.5, the dinuclear species is obtained, in less acidic medium, at pH ≈ 4, the tetranuclear one and at pH > 5, the octanuclear one. The binding modes of the oxalate ion were described as the competition between the chelating and the templating role of the ligand. The analogy between the thio-bridged species and the anions of **1**, **2** and **3** is unfortunately limited to their structures only. The same pattern of assembly of basic dinuclear units to form larger oligonuclear species can be recognized within the two series.

The preparation of **4** opens new perspectives. Similar amounts of the reagents were used as for the preparations of **1** or **2** with 2,4,6-collidine instead of pyridine. Given the low coordinating ability of 2,4,6-collidine due to methyl substituents in the *ortho* positions, the oxalate ion, as the only other ligand present in the reaction mixture, was forced to occupy more than two coordination sites in each metal atom environment. A singly oxo-bridged dimer, $\{Mo_2O_3\}^{4+}$, was formed. The four coordination sites of each metal atom are occupied by a pair of bidentate oxalate ions. It remains open for further studies to investigate how this system would respond to a reduced amount of oxalate ions, whether the oxalate ion would adopt the bis(bidentate) binding mode and as such connect dinuclear units, $\{Mo_2O_3\}^{4+}$ fragments in this case, into polymeric structures. It also seems feasible that the use of non-coordinating solvents could enable the coordination of the oxalate ion in less common binding modes and thus the synthesis of more complex architectures.

Conclusion

A series of discrete oxalato complexes of molybdenum(v) was accessed by solvothermal reactions of mononuclear halooxomolybdates(v) with oxalic acid. The oxalate ion binds to the dinuclear units, $\{Mo_2O_4\}^{2+}$ or $\{Mo_2O_3\}^{4+}$, as a terminal bidentate ligand as observed in $[Mo_2O_4(\eta^2\text{-}C_2O_4)_2py_2]^{2-}$ (**1**) and $[Mo_2O_3(\eta^2\text{-}C_2O_4)_4]^{4-}$ (**4**) or bridges two or four $\{Mo_2O_4\}^{2+}$ units as observed in $[\{Mo_2O_4(\eta^2\text{-}C_2O_4)_2\}_2(\mu_4\text{-}C_2O_4)]^{6-}$ (**2**) and $[Mo_8O_{16}(OMe)_8(\mu_8\text{-}C_2O_4)]^{2-}$ (**3**), respectively.

Experimental Section

General Remarks: Reactions were carried out in sealed glass tubes under autogenous pressure. Reagents were purchased from Aldrich and used without further purification. $(PyH)_2[MoOCl_5]$ and $(PyH)[MoOBr_4]$ were prepared by minor modification of a published procedure.[48] The IR and far-IR spectra were measured on solid samples as Nujol or poly(chlorotrifluoroethylene) mulls using a Perkin−Elmer 2000 series FT-IR spectrometer. Elemental analyses were performed by the Chemistry Department service at the University of Ljubljana.

$(MeNC_5H_5)_2[Mo_2O_4(\eta^2\text{-}C_2O_4)_2py_2]$ (1): A mixture of $(PyH)_2[MoOCl_5]$ (100 mg, 0.223 mmol), $H_2C_2O_4{\cdot}2H_2O$ (100 mg, 0.793 mmol), pyridine (4 mL), methanol (0.5 mL) and acetonitrile (0.5 mL) was placed in a glass tube which was sealed and subsequently heated in an electric oven maintained at 115 °C for 120 h. After cooling to room temperature, orange crystals of compound **1** were isolated in 40% yield (35 mg). IR: $\tilde{\nu}$ = 3047 (w), 2915 (w), 2851 (w), 1705 (vs), 1667 (vs), 1633 (vs), 1603 (vs), 1584 (s), 1494 (s), 1450 (s), 1372 (s), 1287 (m), 1254 (m), 1241 (m), 1216 (m), 1192 (m), 1163 (m), 1073 (m), 1015 (m), 949 (s), 939 (s), 927 (s), 897 (s), 780 (vs), 758 (vs), 734 (vs), 685 (vs), 649 (m), 639 (m), 524 (m), 482 (s), 451 (w), 435 (w), 348 (w), 320 (vs), 257 (s) cm^{-1}.

 © 2004 Wiley-VCH Verlag GmbH & Co. KGaA, Weinheim

$C_{26}H_{26}Mo_2N_4O_{12}$ (778.39): calcd. C 40.12, H 3.37, N 7.20; found C 40.25, H 3.48, N 7.08.

$(MeNC_5H_5)_6[\{Mo_2O_4(\eta^2\text{-}C_2O_4)_2\}_2(\mu_4\text{-}C_2O_4)]$ (2): A mixture of $(PyH)_2[MoOCl_5]$ (50 mg, 0.111 mmol), $H_2C_2O_4{\cdot}2H_2O$ (150 mg, 1.19 mmol), pyridine (4 mL), methanol (0.5 mL) and acetonitrile (0.5 mL) was placed in a glass tube which was sealed and subsequently heated for in an electric oven maintained at 115 °C 120 h. After cooling to room temperature, the reaction mixture consisted of a dark solution and a black oil. Orange-red crystals formed after a period of two weeks. Yield 43% (18 mg). IR: $\tilde{\nu}$ = 3390 (m), 3136 (w), 3040 (m), 1705 (vs), 1681 (vs), 1657 (vs), 1633 (vs), 1574 (vs), 1494 (vs), 1449 (w), 1360 (vs), 1322 (vs), 1288 (vs), 1229 (vs), 1188 (vs), 1059 (w), 1026 (w), 958 (vs), 942 (vs), 903 (s), 879 (m), 828 (m), 800 (vs), 770 (vs), 737 (vs), 682 (vs), 649 (m), 528 (vs), 467 (m), 449 (m), 411 (w), 395 (w), 359 (m), 326 (w), 311 (vs), 235 (w) cm^{-1}. $C_{46}H_{48}Mo_4N_6O_{28}$ (1516.7): calcd. C 36.43, H 3.19, N 5.54; found C 36.25, H 3.28, N 5.41.

$(MeNC_5H_5)_2[Mo_8O_{16}(OMe)_8(\mu_8\text{-}C_2O_4)]$ (3): A mixture of $(PyH)_2[MoOCl_5]$ (100 mg, 0.223 mmol), $H_2C_2O_4{\cdot}2H_2O$ (22 mg, 0.175 mmol), methanol (4.5 mL) and acetonitrile (0.5 mL) was placed in a glass tube which was sealed and subsequently heated in an electric oven maintained at 115 °C for 120 h. After cooling to room temperature, large orange crystals of compound **3** were separated manually from the orange microcrystalline phase. The yield based on **3** was 14% (6 mg). IR: $\tilde{\nu}$ = 3143 (w), 3092 (w), 1659 (vs), 1635 (vs), 1585 (m), 1492 (m), 1336 (m), 1290 (m), 1224 (w), 1190 (m), 1162 (w), 1015 (vs), 962 (vs), 813 (vs), 755 (vs), 724 (s), 680 (s), 528 (vs), 466 (vs), 437 (m), 412 (m), 380 (s), 288 (w), 275 (s), 217 (m), 151 (w) cm^{-1}. $C_{22}H_{40}Mo_8N_2O_{28}$ (1548.1): calcd. C 17.07, H 2.60, N 1.81; found C 16.95, H 2.51, N 1.92.

$[MeNC_5H_2(Me)_3]_2[HNC_5H_2(Me)_3]_2[Mo_2O_3(\eta^2\text{-}C_2O_4)_4]$ (4): A mixture of $(PyH)[MoOBr_4]$ (120 mg, 0.235 mmol), $H_2C_2O_4{\cdot}2H_2O$ (100 mg, 0.793 mmol), 2,4,6-collidine (4 mL), methanol (0.5 mL) and acetonitrile (0.5 mL) was placed in a glass tube which was sealed and subsequently heated in an electric oven maintained at 115 °C for 120 h. After cooling to room temperature, large black crystals of compound **4** were isolated in 47% yield (61 mg). IR: $\tilde{\nu}$ = 2920 (vs), 2849 (vs), 2671 (m), 2580 (m), 1912 (w), 1709 (vs), 1682 (vs), 1633 (vs), 1337 (m), 1274 (w), 1259 (m), 1224 (w), 1199 (m), 1171 (w), 1152 (w), 1039 (m), 997 (w), 960 (vs), 892 (m), 863 (w), 799 (vs), 786 (m), 721 (w), 535 (s), 517 (s), 477 (m), 445 (m), 366 (m), 350 (m), 312 (s), 264 (m), 220 (m), 193 (m). $C_{42}H_{52}Mo_2N_4O_{19}$ (1108.76): calcd. C 45.50, H 4.73, N 5.05; found C 45.68, H 4.59, N 4.97.

X-ray Crystallographic Study: The crystals were mounted on the tip of a glass fibre with a small amount of silicon grease and transferred to a goniometer head. Data were collected with a Nonius Kappa CCD diffractometer. For all compounds, data reduction and integration were performed with the software package DENZO-SMN.[49] Averaging of the symmetry-equivalent reflections largely compensated for the absorption effects. The coordinates of some or all of the non-hydrogen atoms were found by direct methods using the structure solution program SHELXS.[50] The positions of the remaining non-hydrogen atoms were located by use of a combination of least-squares refinement and difference Fourier maps with the SHELXL-97[50] program. Non-hydrogen atoms were refined with anisotropic displacement parameters. The hydrogen atoms were included in the structure factor calculations at idealized positions. The oxalate ion in **3** is disordered over two positions. The carbon atoms C(1) and C(2) of the disordered oxalate ion were refined anisotropically with the occupancy factors 0.51(1) and 0.49(1), respectively. Cell parameters and refinement results for compounds **1**−**4** are summarized in Table 4. CCDC-211525 (**1**), -211526 (**2**), -211527 (**3**) and -211528 (**4**) contain the supplementary crystallographic data for this paper. These data can be obtained free of charge at www.ccdc.cam.ac.uk/conts/retrieving.html [or from the Cambridge Crystallographic Data Centre, 12 Union Road, Cambridge CB2 1EZ, UK; Fax: (internat.) + 44-1223/336-033; E-mail: deposit@ccdc.cam.ac.uk].

Computational Details: Ab initio MO calculations on the $[\{Mo_2O_4(\eta^2\text{-}C_2O_4)_2\}_2(\mu_4\text{-}C_2O_4)]^{6-}$ ion at the HF/3-21G* level were performed in order to determine its energy as a function of the dihedral angle in the μ_4-oxalate ion. The Gaussian 98 suite of programs was used.[51] No geometry optimization was applied. The

Table 4. Crystallographic data for compounds **1**−**4**

	1	**2**	**3**	**4**
Empirical formula	$C_{26}H_{26}Mo_2N_4O_{12}$	$C_{46}H_{48}Mo_4N_6O_{28}$	$C_{22}H_{40}Mo_8N_2O_{28}$	$C_{42}H_{52}Mo_2N_4O_{19}$
Formula mass	778.39	1516.66	1548.08	1108.76
Crystal system	triclinic	tetragonal	triclinic	triclinic
Space group	$P\bar{1}$	$I4_1/acd$	$P\bar{1}$	$P\bar{1}$
T [K]	150(2)	200(2)	150(2)	293
a [Å]	9.7696(2)	16.5235(2)	7.4875(2)	9.2687(2)
b [Å]	11.5733(2)	16.5235(2)	10.9441(2)	11.3919(2)
c [Å]	14.0069(4)	40.6033(5)	14.3626(4)	12.3534(3)
α [°]	75.4096(10)	90	105.1707(10)	78.2266(8)
β [°]	86.8787(9)	90	103.5065(10)	69.0781(8)
γ [°]	69.0585(13)	90	105.5552(10)	86.8045(9)
V [Å^3]	1430.29(6)	11085.8(2)	1034.27(4)	1192.53(4)
Z	2	8	1	1
λ [Å]	0.71073	0.71073	0.71073	0.71073
μ [mm^{-1}]	0.949	0.980	2.439	0.605
Collected reflections	7850	10297	8539	7994
Unique reflections, R_{int}	4901, 0.0174	3164, 0.0206	4709, 0.0226	4159, 0.0129
Observed reflections	4405	2791	4092	3806
$R1$ [$I > 2\sigma(I)$]	0.0319	0.0299	0.0262	0.0334
$wR2$ [all data]	0.0822	0.0695	0.0605	0.1013

 © 2004 Wiley-VCH Verlag GmbH & Co. KGaA, Weinheim

atomic coordinates were taken as obtained from the X-ray diffraction study.

Acknowledgments

We are grateful to the Slovenian Ministry of Education, Science and Sport for supporting this work through research grant PS-0508-0103. We also thank the same agency for funds to purchase the Nonius Kappa CCD diffractometer.

[1] [1a] *Polyoxometalates: From Platonic Solids to Anti-Retroviral Activity* (Eds.: M. T. Pope, A. Müller), Kluwer Academic Publishers, Dordrecht, **1994**. [1b] C. L. Hill (Guest editor), *Chem. Rev.* **1998**, *98*, 1−390.
[2] H. K. Chae, W. G. Klemperer, T. A. Marquart, *Coord. Chem. Rev.* **1993**, *128*, 209−224.
[3] C. Livage, E. Dumas, C. Marchal-Roch, G. Herve, *C. R. Acad. Sci. Paris, Ser. IIc* **2000**, *3*, 95−100.
[4] M. J. Manos, A. D. Keramidas, J. D. Woollins, A. M. Z. Slawin, T. A. Kabanos, *J. Chem. Soc., Dalton Trans.* **2001**, 3419−3420.
[5] M. J. Manos, J. D. Woollins, A. M. Z. Slawin, T. A. Kabanos, *Angew. Chem. Int. Ed.* **2002**, *41*, 2801−2805.
[6] [6a] R. C. Haushalter, F. W. Lai, *Inorg. Chem.* **1989**, *28*, 2904−2905. [6b] R. C. Haushalter, F. W. Lai, *Angew. Chem. Int. Ed. Engl.* **1989**, *28*, 743−746.
[7] C. du Peloux, P. Mialane, A. Dolbecq, J. Marrot, E. Riviere, F. Secheresse, *J. Mater. Chem.* **2001**, *11*, 3392−3396.
[8] E. Dumas, C. Sassoye, K. D. Smith, S. C. Sevov, *Inorg. Chem.* **2002**, *41*, 4029−4032.
[9] [9a] A. Müller, S. Dillinger, E. Krickemeyer, H. Bögge, W. Plass, A. Stammler, R. C. Haushalter, *Z. Naturforsch., Teil B* **1997**, *52*, 1301−1306. [9b] M. I. Khan, A. Müller, S. Dillinger, H. Bögge, Q. Chen, J. Zubieta, *Angew. Chem. Int. Ed. Engl.* **1993**, *32*, 1780−1782. [9c] M. I. Khan, Q. Chen, J. Salta, C. J. O'Connor, J. Zubieta, *Inorg. Chem.* **1996**, *35*, 1880−1901. [9d] A. Müller, C. Beugholt, P. Kögerler, H. Bögge, S. Bud′ko, M. Luban, *Inorg. Chem.* **2000**, *39*, 5176−5177. [9e] P. Mialane, A. Dolbecq, L. Lisnard, A. Mallard, J. Marrot, F. Secheresse, *Angew. Chem. Int. Ed.* **2002**, *41*, 2398−2401.
[10] C. du Peloux, P. Mialane, A. Dolbecq, J. Marrot, F. Secheresse, *Angew. Chem. Int. Ed.* **2002**, *41*, 2808−2810.
[11] L. A. Mundi, R. C. Haushalter, *Inorg. Chem.* **1990**, *29*, 2879−2881.
[12] M.-Y. Lee, S.-L. Wang, *Chem. Mater.* **1999**, *11*, 3588−3594.
[13] B. Modec, J. V. Brenčič, D. Dolenc, J. Zubieta, *J. Chem. Soc., Dalton Trans.* **2002**, 4582−4586.
[14] B. Modec, J. V. Brenčič, *J. Cluster Sci.* **2002**, *13*, 279−302.
[15] B. Modec, J. V. Brenčič, J. Zubieta, *J. Chem. Soc., Dalton Trans.* **2002**, 1500−1507.
[16] M. Cindrič, G. Pavlovič, V. Vrdoljak, B. Kamenar, *Polyhedron* **2000**, *19*, 1471−1478.
[17] F. H. Allen, O. Kennard, R. Taylor, *Acc. Chem. Res.* **1983**, *16*, 146−153.
[18] P. C. H. Mitchell, *J. Inorg. Nucl. Chem.* **1964**, *26*, 1967−1976 and references cited therein.
[19] F. A. Cotton, S. M. Morehouse, *Inorg. Chem.* **1965**, *4*, 1377−1381.
[20] P. C. H. Mitchell, *J. Chem. Soc. A* **1969**, 146−152.
[21] W. S. McDonald, *Acta Crystallogr., Sect. B* **1978**, *34*, 2850−2853.
[22] [22a] B. Kamenar, B. Kaitner, N. Strukan, *Croat. Chem. Acta* **1991**, *64*, 329−341. [22b] N. Strukan, M. Cindrič, B. Kamenar, *Acta Crystallogr., Sect. C* **2000**, *56*, 639−641.
[23] P. Mialane, A. Dolbecq, G. Costaz, L. Lisnard, J. Marrot, F. Secheresse, *Inorg. Chem. Commun.* **2002**, *5*, 702−705.
[24] [24a] E. Carmona, F. Gonzales, M. L. Poveda, J. M. Marin, J. L. Atwood, R. D. Rogers, *J. Am. Chem. Soc.* **1983**, *105*, 3365−3366. [24b] R. Alvarez, J. L. Atwood, E. Carmona, P. J. Perez, M. L. Poveda, R. D. Rogers, *Inorg. Chem.* **1991**, *30*, 1493−1499.
[25] T. Shibahara, H. Kuroya, K. Matsumoto, S. Ooi, *Inorg. Chim. Acta* **1981**, *54*, L75−L76.
[26] T. Shibahara, S. Ooi, H. Kuroya, *Bull. Chem. Soc. Jpn.* **1982**, *55*, 3742−3746.
[27] K. Mannemann, R. Mattes, *J. Chem. Res.* **1979**, *100*, 1343.
[28] A. Dolbecq, B. Salignac, E. Cadot, F. Secheresse, *Bull. Pol. Acad. Sci.* **1998**, *46*, 237−271.
[29] B. Kamenar, B. Kaitner, N. Strukan, *Vestn. Slov. Kem. Drus.* **1992**, *39*, 357−366.
[30] M. J. S. Dewar, Y. J. Zhang, *THEOCHEM* **1990**, *68*, 157−162.
[31] J. Chang Kim, J. Cho, A. J. Lough, *Inorg. Chim. Acta* **2001**, *317*, 252−258.
[32] O. Castillo, A. Luque, J. Sertucha, P. Roman, F. Lloret, *Inorg. Chem.* **2000**, *39*, 6142−6144.
[33] R. E. Dinnebier, S. Vensky, M. Panthöfer, M. Jensen, *Inorg. Chem.* **2003**, *42*, 1499−1507.
[34] B. E. Bursten, M. H. Chisholm, R. J. H. Clark, S. Firth, C. M. Hadad, A. M. MacIntosh, P. J. Wilson, P. W. Woodward, J. M. Zaleski, *J. Am. Chem. Soc.* **2002**, *124*, 3050−3063.
[35] C. G. Kim, D. Coucouvanis, *Inorg. Chem.* **1993**, *32*, 2232−2233.
[36] The distance 7.5913(4) Å is longer than the shortest Mo···Mo contact (approx. 6.5 Å) between adjacent anions.
[37] B. Modec, J. V. Brenčič, L. Golič, *Polyhedron* **2000**, *19*, 1219−1225.
[38] Q. Chen, S. Liu, J. Zubieta, *Angew. Chem. Int. Ed. Engl.* **1988**, *27*, 1724−1725.
[39] Q. Chen, S. Liu, J. Zubieta, *Inorg. Chem.* **1989**, *28*, 4433−4434.
[40] [40a] B. Salignac, S. Riedel, A. Dolbecq, F. Secheresse, E. Cadot, *J. Am. Chem. Soc.* **2000**, *122*, 10381−10389. [40b] A. Dolbecq, E. Cadot, F. Secheresse, *Chem. Commun.* **1998**, 2293−2294. [40c] A. Dolbecq, C. du Peloux, A.-L. Auberty, S. A. Mason, P. Barboux, J. Marrot, E. Cadot, F. Secheresse, *Chem. Eur. J.* **2002**, *8*, 349−356. [40d] A. Dolbecq, E. Cadot, F. Secheresse, *C. R. Acad. Sci. Paris, Ser. IIc* **2000**, *3*, 193−197. [40e] F. Secheresse, E. Cadot, A. Dolbecq, *J. Solid State Chem.* **2000**, *152*, 78−86. [40f] E. Cadot, F. Secheresse, *Chem. Commun.* **2002**, 2189−2197.
[41] [41a] R. L. Thompson, S. Lee, S. J. Geib, N. J. Cooper, *Inorg. Chem.* **1993**, *32*, 6067−6075. [41b] J. E. Drake, A. G. Mislankar, R. Ratnani, *Inorg. Chem.* **1996**, *35*, 2665−2673. [41c] L. Stelzig, S. Kötte, B. Krebs, *J. Chem. Soc., Dalton Trans.* **1998**, 2921−2926. [41d] C. J. Doonan, D. A. Slizys, C. G. Young, *J. Am. Chem. Soc.* **1999**, *121*, 6430−6436.
[42] N. F. Curtis, I. Ross, N. McCormick, T. N. Waters, *J. Chem. Soc., Dalton Trans.* **1973**, 1537−1548.
[43] N. F. Curtis, *J. Chem. Soc. A* **1968**, 1584−1587.
[44] I. Castro, J. Faus, M. Julve, A. Gleizes, *J. Chem. Soc., Dalton Trans.* **1991**, 1937−1944.
[45] P. Roman, A. Luque, C. Guzman-Miralles, J. I. Beitia, *Polyhedron* **1995**, *14*, 2863−2869.
[46] The ready formation of the $\{Mo_2O_4\}^{2+}$ fragment in the alcohol/pyridine medium is followed by the aggregation of two, three, four or six dimers into tetra-, penta-, hexa-, deca- or dodecanuclear polyoxoalkoxymolybdenum(V) compounds. See also: [46a] B. Modec, J. V. Brenčič, I. Leban, *Inorg. Chem. Commun.* **1998**, *1*, 161−163. [46b] B. Modec, J. V. Brenčič, R. Rotar, L. Golič, K. Prout, *Acta Crystallogr., Sect. C* **1998**, *54*, 1573−1575. [46c] B. Modec, J. V. Brenčič, L. Golič, L. M. Daniels, *Polyhedron* **2000**, *19*, 1407−1414. [46d] B. Modec, J. V. Brenčič, L. Golič, G. Giester, *Inorg. Chim. Acta* **2000**, *307*, 32−40. [46e] B. Modec, J. V. Brenčič, J. Zubieta, P. J. Hagrman, *Inorg. Chem. Commun.* **2001**, *4*, 537−540. [46f] B. Modec, J. V. Brenčič, R. C. Finn, R. S. Rarig, J. Zubieta, *Inorg. Chim. Acta* **2001**, *322*, 113−119.
[47] It is known that *N*-methylpyridinium salts result from a nucleophilic attack of pyridine on methyl halide formed from methanol and hydrogen halide. This reaction takes place only in a strongly acidic medium. Moreover, the halogenation of alcohols proceeds more readily with tertiary and secondary al-

 © 2004 Wiley-VCH Verlag GmbH & Co. KGaA, Weinheim

cohols, but not with methanol. The reaction medium in our case is not acidic, as it contains mostly pyridine.
[48] G. R. Hanson, A. A. Brunette, A. C. McDonell, K. S. Murray, A. G. Wedd, *J. Am. Chem. Soc.* **1981**, *103*, 1953−1959.
[49] Z. Otwinowski, W. Minor, *Methods Enzymol.* **1997**, *276*, 307−326.
[50] G. M. Sheldrick, *SHELXS-97* and *SHELXL-97*, Universität Göttingen, **1997**.
[51] M. J. Frisch, G. W. Trucks, H. B. Schlegel, G. E. Scuseria, M. A. Robb, J. R. Cheeseman, V. G. Zakrzevski, J. A. Montgomery, Jr., J. E. Stratmann, J. C. Burant, S. Dapprich, J. M. Millam, A. D. Daniels, K. N. Kudin, M. C. Strain, O. Farkas, J. Tomasi, V. Barone, M. Cossi, R. Cammi, B. Menucci, C. Pomelli, C. Adamo, S. Clifford, J. Ochterski, G. A. Petersson, P. Y. Ayala, Q. Cui, K. Morokuma, D. K. Malick, A. D. Rabuck, K. Raghavachari, J. B. Foresman, J. Ciolslovski, J. V. Ortiz, B. B. Stefanov, G. Liu, A. Liashenko, P. Piskorz, I. Komaromi, R. Gomperts, R. L. Martin, D. J. Fox, T. Keith, M. A. Al-Laham, C. Y. Peng, A. Nanayakkara, C. Gonzales, M. Challacombe, P. M. W. Gill, B. Johnson, W. Chen, M. W. Wong, J. L. Andres, C. Gonzales, M. Head-Gordon, E. S. Replogle, J. A. Pople, *Gaussian 98*, Revision A.5, Gaussian, Inc., Pittsburgh PA, **1998**.

Received October 16, 2003
Early View Article
Published Online March 9, 2004

 © 2004 Wiley-VCH Verlag GmbH & Co. KGaA, Weinheim

Absorption, Magnetic Circular Dichroism, IR Spectra, Electrochemistry, and Molecular Orbital Calculations of Monoaza- and Opposite Diazaporphyrins

Hiroshi Ogata,[a] Takamitsu Fukuda,[a] Katsunori Nakai,[a] Yuichi Fujimura,[a] Saburo Neya,[b] Pavel A. Stuzhin,[c] and Nagao Kobayashi*[a]

Keywords: Cyclic voltammetry / Density functional calculations / Magnetic circular dichroism / Porphyrinoids / UV/Vis spectroscopy

Electronic absorption, magnetic circular dichroism (MCD), IR spectra, and cyclic and differential pulse voltammograms of metal-free and copper monoaza- and opposite diazaporphyrins are reported, together with molecular orbital (MO) calculations using the density functional theory (DFT) method. Introduction of nitrogen atoms at the *meso* position of porphyrins caused a blue-shift of the B band and a red-shift of the Q band, with a concomitant decrease and increase of the apparent absorption coefficient, respectively. On going from monoaza to diaza species, the apparent bandwidth at half-height of the B band and the splitting of the Q band do not change significantly for metal-free species, but increase for the copper species. The MCD peaks and troughs correspond closely to the peaks of the absorption spectra, so that these are interpreted as the superimposition of Faraday *B* terms. The MCD sign pattern (minus-to-plus on going from longer to shorter wavelengths) substantiates experimentally that the splitting between the HOMO and HOMO–1 orbital is larger than that between the LUMO and LUMO+1. Of the copper complexes of octaethylporphyrin (OEP), monoaza- (MAP), diaza- (DAP) and tetraazaporphyrins (TAP), CuTAP is the easiest to reduce and hardest to oxidize. The potential differences between the first oxidation and reduction couples were about 2.1–2.4 V. MO calculations using DFT succeeded in reproducing some of the above spectroscopic and electrochemical characteristics. In addition, some of the IR bands were assigned on the basis of the DFT calculations.

(© Wiley-VCH Verlag GmbH & Co. KGaA, 69451 Weinheim, Germany, 2004)

Introduction

Azaporphyrins (APs) are porphyrins whose *meso*-carbon atoms have been replaced by nitrogen atoms to a varying degree. Monoaza- (MAP)[1−3] and diaza-porphyrins (DAP)[4] were first synthesized in the second half of the 1930s, and since then their improved synthesis,[5−13] and electronic absorption,[14−18] fluorescence,[19−21] IR,[6,16] NMR,[6,9,14−16,22] and EPR[15,16,23] spectra have been reported. While the spectroscopic changes due to the introduction of nitrogen atom(s) have often attracted the attention of physical chemists, to date no-one has applied magnetic circular dichroism (MCD) to these species. MCD spectroscopy[24] provides ground- and excited-state degeneracy information, which is needed to fully understand the electronic structure of high symmetry molecules. We, therefore, have applied this spectroscopy to various phthalocyanine (Pc)[25] and low symmetry Pc derivatives[26] and confirmed its utility in analyzing the electronic structure of these large aromatic metallocomplexes. In addition, no-one has attempted to interpret the IR spectra of these low-symmetry compounds by quantum mechanical calculations either. Electrochemical data on APs have also been rarely reported; the first oxidation potentials of a few MAPs in butyronitrile[16] and the first reduction potentials of MAP- and DAP-reconstituted hemoproteins[27] were recorded in a tris-buffer solution. Accordingly, no oxidation and reduction potentials have been reported for single AP derivatives. We therefore report here the electronic absorption, MCD and IR spectra, and electrochemistry of metal-free and copper MAP and DAP, together with results of quantum mechanical calculations.

[a] Department of Chemistry, Graduate School of Science, Tohoku University,
Sendai 980−8578, Japan
Fax: (internat.) +81-22-217-7719
E-mail: nagaok@mail.tains.tohoku.ac.jp
[b] Department of Physical Chemistry, Graduate School of Pharmaceutical Science, Chiba University,
Inage-Yayoi, Chiba 263−8522, Japan
[c] Ivanovo State Academy for Chemistry and Technology
pr. F. Engel'sa 7, 153460, Russia

Results and Discussion

Electronic Absorption and MCD Spectroscopy

Figure 1 denotes the structures of the monoaza and diaza species used in this study. Figure 2 and 3 the show absorp-

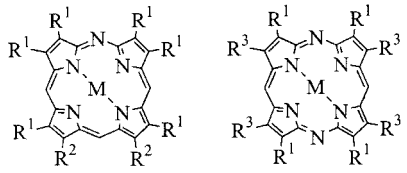

MAP DAP

H_2MAP M = H_2 $R^1 = CH_3$ $R^2 = CH_2CH_2CO_2CH_3$

CuMAP M = Cu $R^1 = CH_3$ $R^2 = CH_2CH_2CO_2CH_3$

H_2DAP M = H_2 $R^1 = CH_3$ $R^3 = C_4H_9$

CuDAP M = Cu $R^1 = CH_3$ $R^3 = C_4H_9$

Figure 1. Structures and abbreviations of the monoaza- (MAP) and diazaporphyrins (DAP) used in this study

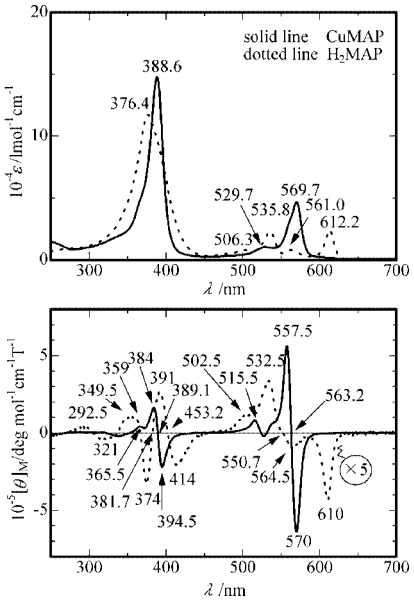

Figure 2. Electronic absorption (top) and MCD (bottom) spectra of CuMAP (solid lines) and H_2MAP (dotted lines) in chloroform; note the encircled magnification factor for the MCD of H_2MAP

tion and MCD spectra of the monoaza and diaza species, respectively.

Metal-Free Species

In the case of H_2MAP (Figure 2), the Q_{x00} and Q_{y00} bands appear at 612 and 536 nm, respectively. The wavelength of the former band is shorter than that of octaethylporphyrin (OEP)[28] by about 10 nm, while that of the latter is slightly longer by several nanometers. The splitting energy between the Q_{x00} and Q_{y00} bands is about 2320 cm^{-1}. The B band appears at 376 nm, which is shorter than that of OEP by more than 20 nm, while its shape is not symmetrical and the bandwidth is apparently larger than that of OEP. In H_2DAP, the two Q bands are red-shifted by about 11 nm, with a splitting energy of 2280 cm^{-1}, and are slightly more intense than in H_2MAP. The B band is only slightly blue-shifted, and the apparent absorption coefficient decreases.

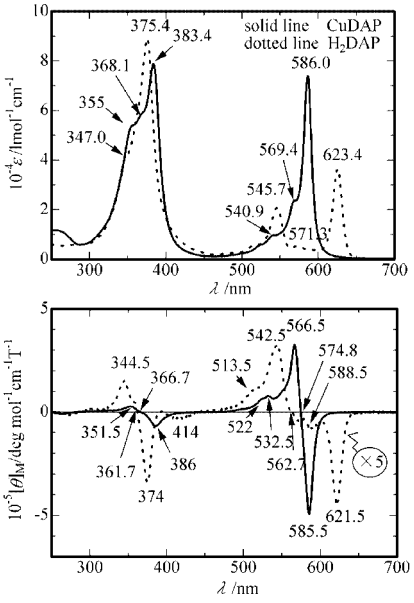

Figure 3. Electronic absorption (top) and MCD (bottom) spectra of CuDAP (solid lines) and H_2DAP (dotted lines) in chloroform; note the encircled magnification factor for the MCD of H_2DAP

The MCD peaks and troughs are observed roughly in the same positions as the absorption peaks and shoulders (Faraday *B* terms). In the Q-band region, the first and third peaks from the lower-energy side correspond to the Q_{x00} and Q_{y00} band for both H_2MAP and H_2DAP, since they show opposite signs. In the B region of H_2MAP, two dispersion curves appear, corresponding to the broad absorption spectra. These are considered to be due to pseudo-Faraday *A* terms produced by superimposition of at least four closely lying Faraday *B* terms.[30] In the B MCD of H_2DAP, the complexity of the spectra on the longer-wavelength side observed for H_2MAP decreases, and the most intense MCD trough and peak in this region appear to correspond to the absorption peak and shoulder, respectively.

Copper Species

The most intense Q- and B-band peaks of CuMAP appear at 570 and 389 nm, respectively. Since the corresponding bands of CuOEP occur at 560 and 399 nm, respectively,[28] the Q- and B-bands are shifted by about 10 nm to the red and blue, respectively, on introduction of one *meso*-nitrogen atom. In the case of CuDAP, the Q-band shifts further, to 586 nm, with an increase in intensity, while the B-band shifts to the blue, to 383 nm, with a loss of intensity. The apparent ratio of the absorption coefficient of the B-band to that of the Q-band [ε(B)/ε(Q)] decreases from about 12. 4 for CuOEP[28] to about 3.2 for CuMAP and further to about 1.1 for CuDAP, indicating that the Q-band becomes more intense with an increasing number of *meso*-nitrogen atoms.[29] In addition, the B-band is significantly broader than with CuMAP.

CuMAP shows dispersion-type MCD curves corresponding to the most intense Q- and B-band peaks. However,

 © 2004 Wiley-VCH Verlag GmbH & Co. KGaA, Weinheim

these are considered to be pseudo-Faraday *A* terms produced by two *B* terms of opposite sign.[30] The MCD trough at 570 nm coincides with the absorption maximum, while the MCD peak at 558 nm corresponds to an absorption shoulder seen at the shorter-wavelength side of the absorption peak at 570 nm. The wavelength of the inflection point of the B MCD matches the absorption peak wavelength. These apparent *A* terms are produced, since the degeneracy of the LUMO is not lifted markedly by introduction of one *meso*-nitrogen atom. The Q MCD of CuDAP also has a dispersion-type curve. However, these are also Faraday *B* terms, since the Q MCD trough at 586 nm and the peak at 567 nm correspond closely to the absorption peaks at 586 and 569 nm, respectively. This feature is more clearly seen in the B MCD curve, which is weaker than that of CuMAP. The MCD trough and peak at 386 and 352 nm closely correspond to absorption peaks at 383 and 355 nm, respectively, and the shape of the inflection point is not as clear as for the Q band, indicating a significant splitting of the Soret band. Since both CuMAP and CuDAP display a negative-to-positive MCD pattern, it is experimentally suggested that the splitting of the LUMO is smaller than that between the HOMO and HOMO−1.[31]

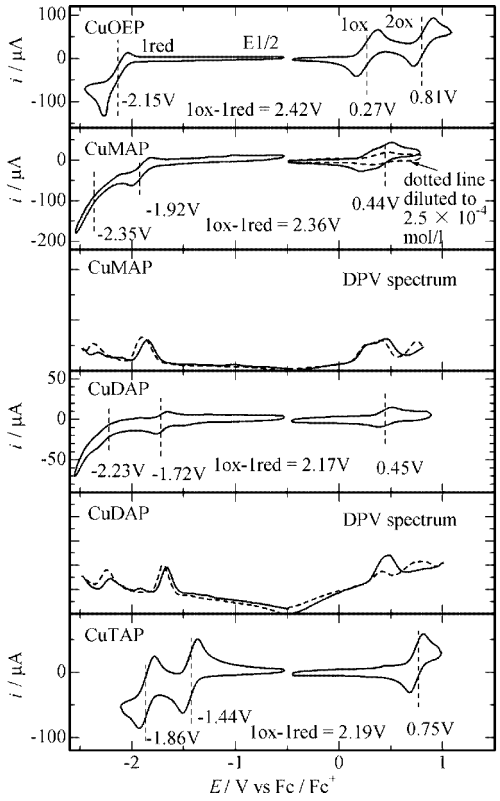

Figure 4. Cyclic and differential pulse voltammograms of CuOEP, CuMAP, CuDAP (opposite type), and CuTAP (from top to bottom) in *o*-DCB containing 0.1 mol/L TBAP

Electrochemistry

As described in the introductory portion, electrochemical data on MAP and DAP are still very rare, and even the first oxidation and reduction potentials of a single azaporphyrin derivative are not known. We therefore recorded the cyclic and differential pulse voltammograms of CuTAP and CuDAP, together with the CV curves of CuOEP and CuTAP in *o*-dichlorobenzene (*o*-DCB) (Figure 4). In the order OEP, MAP, DAP, and tetraazaporphyrin (TAP) — with increasing number of *meso*-nitrogen atoms — the first oxidation potential becomes more positive, since *meso*-nitrogen atoms withdraw electrons from the core of the skeleton, as follows: 0.27, 0.44, 0.45, 0.75 V, respectively. Similarly the first reduction potential varies as −2.15, −1.92, −1.72, −1.44 V, respectively, while the second reduction potential varies as (unmeasureable), −2.35, −2.23, −1.86 V, respectively. The potential difference between the first oxidation and reduction potentials of OEP derivatives is known to be 2.25 ± 0.15 V.[32] These values for CuMAP, CuDAP, and CuTAP are 2.36, 2.17, and 2.19 V, respectively, indicating that the introduction of *meso*-nitrogen atoms does not significantly affect the values. The slightly smaller value for CuDAP (2.17 V) is related to the appearance of the Q-band at longer wavelength due to its D_{2h} symmetry. The potential differences between the first and second reduction potentials for these species are 0.43, 0.51, and 0.42 V, respectively, in the above order, versus 0.42 ± 0.05 V reported for OEP derivatives.[32] These properties can be reproduced by MO calculations, as described in the next section.

MO Calculations

Orbital Energy

Molecular orbital calculations on a series of compounds between normal porphyrins and *meso*-azaporphyrins using CNDO/S Hamiltonian have been reported by Solovyov et al.[19,33] Important differences were found in the energies of the HOMOs between our results and those of Solovyov et al. Diamagnetic zinc was employed instead of paramagnetic copper as the central metal. As shown in Figure 5, the HOMO energy stabilizes moderately in contrast to almost no change reported by Solovyov et al., although the HOMO−1 orbital stabilizes significantly with increasing number of *meso*-nitrogen atoms, since this orbital has a large coefficient at the *meso* positions, as a_{2u} orbitals in D_{4h}-symmetric porphyrins and Pcs.

The LUMO also generally stabilizes with increasing number of *meso*-nitrogen atoms. Accordingly, these trends are in agreement with the observation (Figure 4) that both the first oxidation and reduction potentials become more positive with the introduction of *meso*-nitrogen atoms. As a result, the calculated energy differences between the HOMO and LUMO decrease in the order of OEP (3.027), MAP (2.939), DAP (2.690), and TAP (2.681 V), illustrating a good relationship with the experimental energy difference

 © 2004 Wiley-VCH Verlag GmbH & Co. KGaA, Weinheim

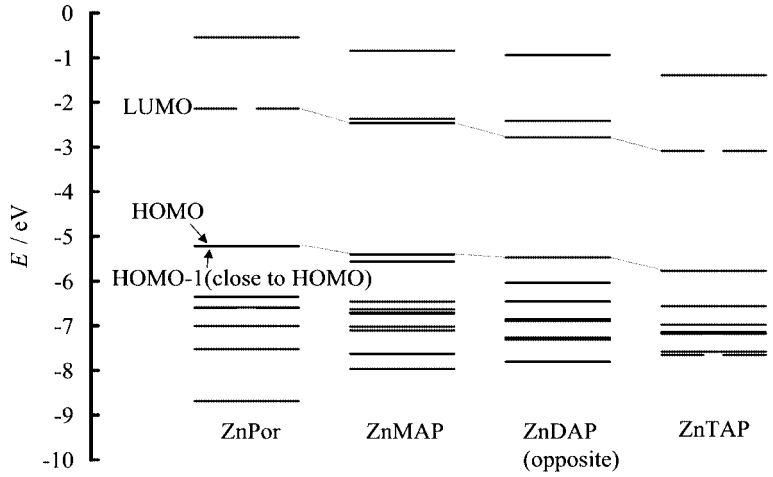

Figure 5. Partial energy diagram for ZnOEP, ZnMAP, ZnDAP (opposite type), and ZnTAP (left to right)

Table 1. Calculated transition energies, oscillator strength (*f*), and configurations for zinc monoaza- and opposite diazaporphyrins[a]

Energy (eV)	Wavelength (nm)	*f*	Configurations (coefficients of the wave function for each excitation)	Angles (°)[b]
ZnMAP				
2.430	510.3	0.0044	95→97 (0.5121) 94→96 (0.5025)	0
2.449	506.2	0.0215	95→96 (0.5343) 94→97 (−0.4661)	90
3.490	355.3	0.6457	95→97 (0.3444) 94→96 (−0.3334) 92→97 (0.2477) 88→96 (−0.1783) 91→97 (−0.1667)	0
3.498	354.5	0.0525	92→96 (0.5947) 90→97 (0.2365) 91→96 (0.1715) 94→97 (0.1240)	90
3.520	352.2	0.6269	94→97 (0.3565) 95→96 (0.3012) 92→96 (−0.2421) 91→96 (0.2392) 88→97 (0.1646)	90
3.583	346.0	0.0607	90→96 (0.5124) 92→97 (0.3765) 91→97 (0.1891) 94→96 (0.1086)	180
3.647	340.0	0.1571	91→96 (0.5952) 94→97 (−0.2086) 92→96 (−0.1242) 95→96 (−0.1216) 90→97 (0.1071)	90
3.736	331.9	0.1477	92→97 (0.4178) 91→97 (−0.4145) 90→96 (−0.2449) 94→96 (0.1613) 95→97 (−0.1175)	180
4.089	303.3	0.2050	88→96 (0.6634)	0
4.197	295.4	0.1484	88→97 (0.5224) 95→98 (−0.3885) 87→96 (0.1661)	90
ZnDAP				
2.457	504.7	0.1190	95→96(0.5741) 94→97(0.3740)	0
2.479	500.2	0.0119	95→97(0.5291) 94→96(−0.4899)	90
3.422	362.3	0.0430	92→96(0.6666) 94→97(0.1017)	180
3.594	344.9	0.5989	94→96(0.3587) 95→97(0.3190) 88→96(0.3047) 92→97(0.1938)	90
3.763	329.5	0.7029	94→97(0.5144) 95→96(−0.2055) 92→96(−0.1561) 88→97(0.1405)	180
3.833	323.5	0.1535	92→97(0.6255) 94→96(−0.1765) 95→97(−0.1123)	90
3.972	312.1	0.3136	88→96(0.6100) 92→97(−0.2068) 94→96(−0.1405) 95→97(−0.1251)	90
4.304	288.1	0.1821	88→97(0.6713) 94→97(−0.1052)	0
5.360	231.3	0.0697	91→98(0.6890)	0
5.387	230.1	0.0530	90→98(0.6896)	90

[a] MO number 95 is the HOMO. Excited states with energy less than ca. 5.4 eV and *f* greater than 0.04 are shown (first and second transitions are included, although some *f* values are smaller than 0.04). [b] Angles between dipole moments of the first and higher electronic transitions (°).

 © 2004 Wiley-VCH Verlag GmbH & Co. KGaA, Weinheim

between the first oxidation and reduction potentials (2.36, 2.17, and 2.19 V for CuMAP, CuDAP, and CuTAP, respectively). In addition, as suggested experimentally by a negative-to-positive MCD pattern for CuMAP and CuDAP, the calculated splitting between the HOMO and HOMO−1 is larger than that between the LUMO and LUMO+1 in these molecules. Thus, the calculated MO energies reproduce well the redox properties and one aspect of the MCD spectra.

Calculated Spectra

Table 1 summarizes the calculated absorption data of ZnMAP and ZnDAP. Not all the spectroscopic properties have been satisfactorily reproduced. However, the following results do reproduce the experimental trends. 1) The Q-band splitting is very small (less than 5 nm, ca. 150−180 cm^{-1}), as is discernible from the MCD of CuMAP and CuDAP (Figure 2 and 3). 2) The Q-band intensity is larger for the DAP species than for MAP. 3) Of the split Q-band, the one at longer wavelength is much stronger than that at shorter wavelength for the DAP species, as seen for CuDAP. 4) The purity of the Q-band increases with increasing number of *meso*-nitrogen atoms, since the energy difference between the HOMO and HOMO−1 increases. 5) The positions of the split Soret bands of DAP appear at shorter wavelength while their splitting is larger than for the MAP species. Judging from their configuration and intensity, the bands at 355 and 352 nm are the split Soret bands of ZnMAP, while the Soret bands of ZnDAP were estimated at 345 and 330 nm. On the other hand, the calculated features that do not agree with the experiments are as follows. 1) The Q-bands of the MAP species were calculated at slightly longer wavelength (510 and 506 nm) than those of the DAP species (505 and 500 nm). 2) Of the Q-bands of the MAP species, the band at longer wavelength is weaker than that at shorter wavelength. Thus, the calculations are able to roughly reproduce many of the experimental trends.

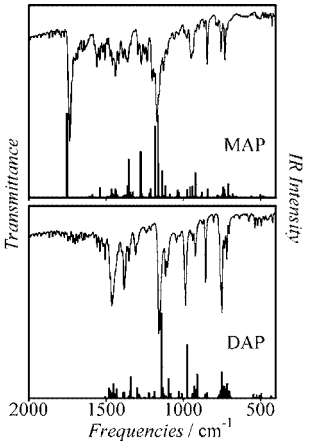

Figure 6. Experimental and calculated (bars) IR spectra of CuMAP (top) and CuDAP (bottom); in the calculation, Cu atoms were replaced by Zn

Structural Modelling and IR Spectra

Although the vibrational structures of tetraazaporphyrins (TAPs) and porphyrins (Pors) are expected to be similar because of the close resemblance of their skeletons, some differences were still detected between the experimental IR spectra of MAP and DAP, as depicted in Figure 6. One of the reasons for this obviously arises from the different substituents at the β-positions of the pyrroles. In order to eliminate the substituent effects and allow comparison of the IR spectra of MAP and DAP, quantum chemical calculations may be helpful. Accordingly, DFT calculations of IR spectra of MAP and DAP using the B3LYP[34] functional in combination with the 6−31G(d) basis set were performed, since this combination has been previously demonstrated to satisfactorily reproduce the experimental IR spectra of low symmetrical tetraaza-chlorin, bacteriochlorin, and isobacteriochlorin derivatives.[35,36] For simplicity of calculations, diamagnetic zinc was employed instead of paramagnetic copper as the central metal.

Table 2. Comparison of selected geometric parameters between ZnMAP and ZnDAP

ZnMAP		ZnDAP	
N5−C9	1.331	N5−C9	1.331
N5−C10	1.331	N5−C10	1.331
		N6−C1	1.331
		N6−C18	1.331
C5−C6	1.388	C5−C6	1.399
C5−C4	1.405	C5−C4	1.399
C14−C13	1.388	C14−C13	1.399
C14−C15	1.405	C14−C15	1.399
C19−C1	1.397		
C19−C18	1.397		
C2−C3	1.376	C2−C3	1.372
C7−C8	1.368	C7−C8	1.372
C11−C12	1.368	C11−C12	1.372
C16−C17	1.376	C16−C17	1.372
N1−N2	2.874	N1−N2	2.860
N2−N3	2.806	N2−N3	2.809
N3−N4	2.874	N3−N4	2.860
N4−N1	2.889	N4−N1	2.809
C9−N5−C10	123.4	C9−N5−C10	124.0
		C1−N6−C18	124.0
C4−C5−C6	126.9	C4−C5−C6	127.1
C13−C14−C15	127.0	C13−C14−C15	127.1
C18−C19C1	127.5		

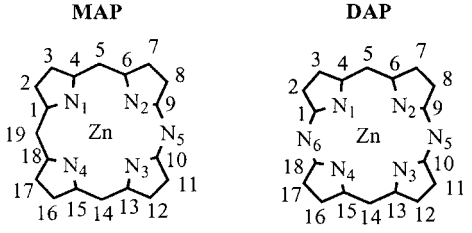

Figure 7. Positions of atoms used in calculating frequencies, ZnMAP (left) and ZnDAP (right)

 © 2004 Wiley-VCH Verlag GmbH & Co. KGaA, Weinheim

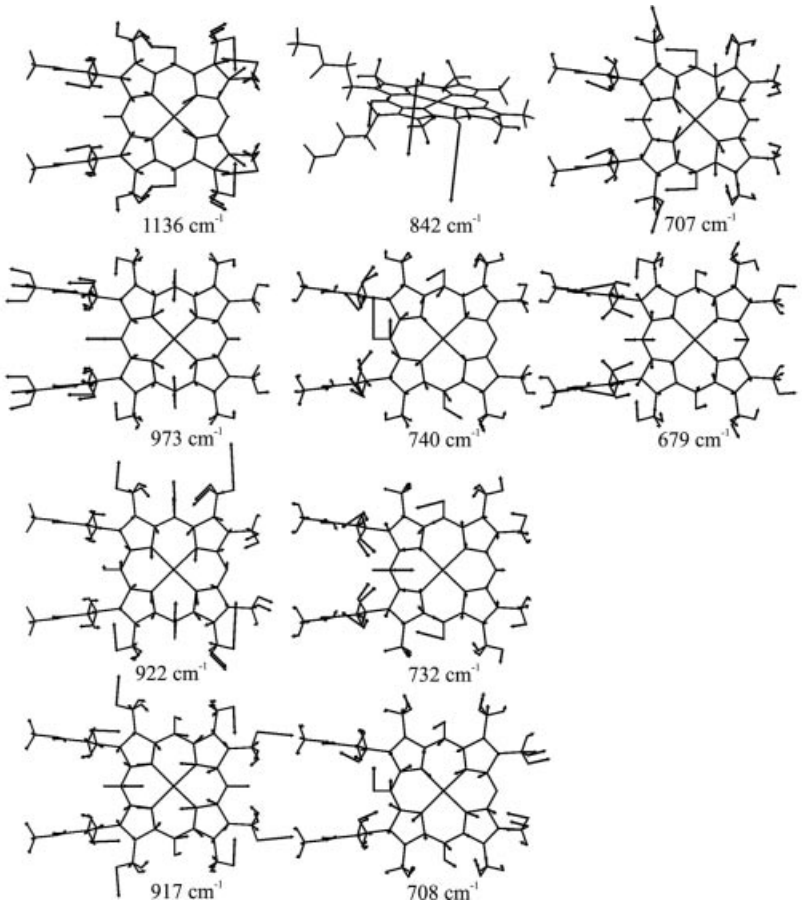

Figure 8. Atomic movements at the selected predicted frequencies of ZnMAP

MAP and DAP have planar skeletal structures with C_{2v} and D_{2h} symmetry, respectively. Table 2 presents selected bond lengths and angles obtained from the calculations (see also Figure 7). The lengths of the C−C and C−N bonds are 1.368−1.405 and 1.331 Å, respectively, which are within the typical values of aromatic compounds, implying a lack of strain in the molecules. The C−C−C and C−*N*−C angles are also normal. The $N_{pyrrole}-N_{pyrrole}$ distances across the azamethine group (i.e. N2−N3 for MAP and N2−N3 and N4−N1 for DAP) are shorter than the other $N_{pyrrole}-N_{pyrrole}$ distances (across the $C-H_{meso}$ group). This is simply because of the larger $C-C_{meso}-C$ bond angles than for the $C-N_{meso}-C$, and the central metal is, therefore, surrounded by the C_{2v}- and D_{2h}-type ligands, respectively.

The calculated harmonic vibrational frequencies (bars) are also listed in Figure 6. The calculated modes were assigned to experimental bands on the basis of both the frequency and intensity data. Some assignable vibrational modes are illustrated in Figure 8 and 9 using vector models. As shown, the correspondence between the experimental and calculated values is good, in particular in the energy region below 1200 cm^{-1}. An intense band at 1753 cm^{-1} for MAP obviously originates from the C=O stretching of the substituted esters. The other skeletal vibrations appear below about 1500 cm^{-1}. The out-of-plane motion of the hydrogens appears in the energy region below about 1000 cm^{-1}. In particular, the out-of-plane motion of the $C-H_{meso}$ groups was assigned to the peaks at 842 and 846 cm^{-1} for MAP and DAP, respectively, which demonstrates an independence of this type of vibration of the molecular structures. Although the intense bands at 1180 and 1163 cm^{-1} (MAP) and 1140 cm^{-1} (DAP) are energetically close, the former two bands originate from vibrations localized on the substituents, and the latter from inner skeletal vibrational modes. The effect of substituents was characterized by relatively intense bands. The in-plane motions of the skeleton are located at 1136, 973, 922, 917, 740, and 732 cm^{-1} for MAP and at 1340, 1132, 1094, 973, 928, 917, 910, 749, and 734 cm^{-1} for DAP. The above results illustrate that the DFT calculations are able to satisfactorily reproduce the experimental IR spectra.

Conclusion

Electronic absorption, MCD, and IR spectra, and redox potentials of metal-free and copper monoaza- and opposite diazaporphyrins have been reported, together with their molecular orbital (MO) and vibrational frequencies on the

 © 2004 Wiley-VCH Verlag GmbH & Co. KGaA, Weinheim

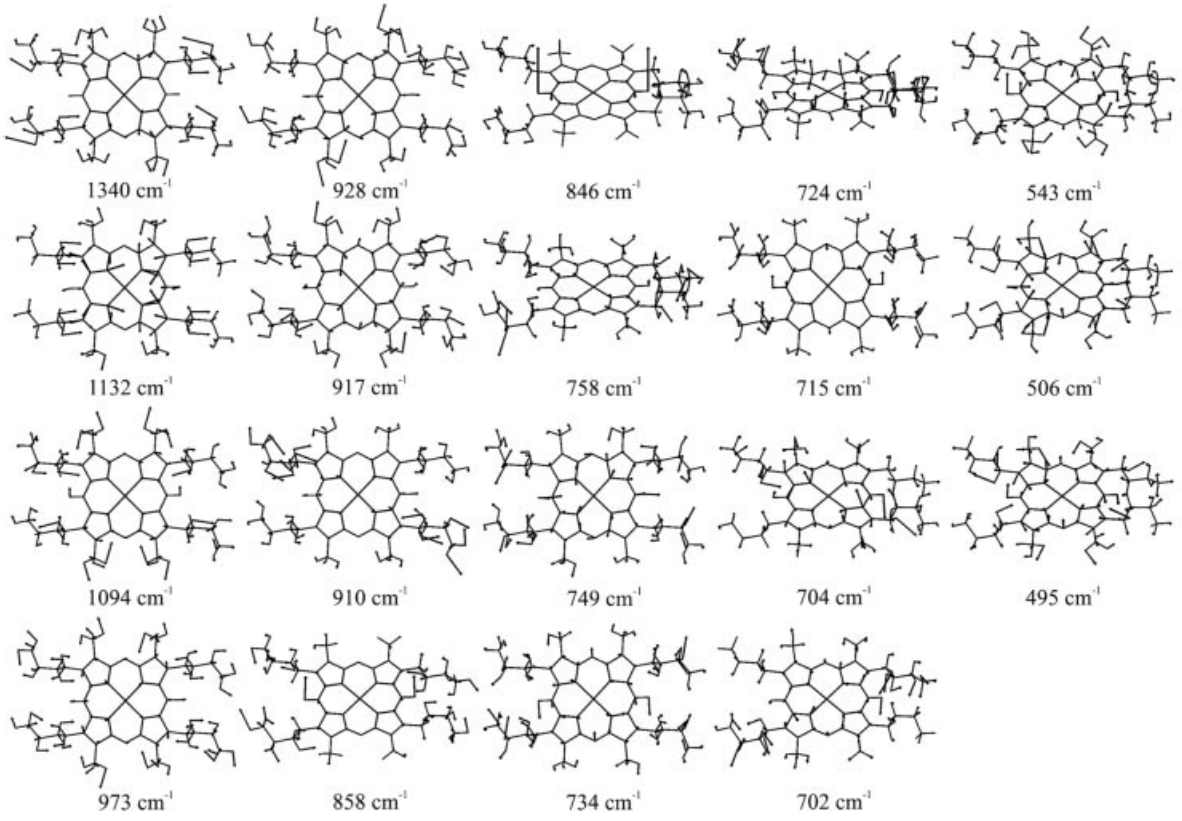

Figure 9. Atomic movements at the selected predicted frequencies of ZnDAP

basis of DFT calculations. The introduction of nitrogen atoms at the *meso* position of the porphyrins causes a blue-shift of the B-band and a red-shift of the Q-band with concomitant decrease and increase, respectively, of the apparent absorption coefficient. However, the bandwidth of the B-band and the splitting of the Q-band do not change systematically with the number of *meso*-nitrogen atoms. On going from monoaza to diaza species, the apparent bandwidth at half-height of the B-band and the splitting of the Q-band do not change significantly for metal-free species, although they increase for the copper species. All MCD curves are interpreted as the superimposition of Faraday *B* terms, since there is no orbital degeneracy in the excited states. The MCD sign pattern (minus-to-plus on going from longer to shorter wavelengths) substantiates experimentally that the splitting between the HOMO and HOMO−1 orbital is larger than that between the LUMO and LUMO+1. Of the copper complexes of octaethylporphyrin (OEP), monoaza- (MAP), diaza- (DAP) and tetraazaporphyrins (TAP), the first oxidation becomes more difficult, while the first reduction becomes easier with increasing number of *meso* nitrogen atoms. The potential differences between the first oxidation and reduction couples are about 2.1−2.4 V. MO calculations using DFT succeeded in reproducing some of the above spectroscopic and electrochemical characteristics. In addition, the good correspondence between the DFT calculations and experimental data enabled some IR bands to be assigned.

Experimental Section

Measurements: Mass spectra were obtained using a Micromass LCT Spectrometer (ESI-TOF mass). Electronic absorption spectra were recorded with a Hitachi U-3410 spectrophotometer using chloroform as solvent. Magnetic circular dichroism (MCD) measurements were made with a JASCO J-725 spectrophotometer equipped with a JASCO electromagnet that produces magnetic fields of up to 1.09 T. Its magnitude was expressed in terms of molar ellipticity per tesla, $[\theta]_M$/deg·mol^{-1}·dm^3·cm^{-1}·T^{-1}. IR spectra were recorded on a Shimadzu FTIR-8100M spectrometer using KBr disks. Cyclic voltammetry (CV) and differential pulse voltammetry (DPV) experiments were carried out with conventional three-electrode cells, in which a platinum wire auxiliary electrode, a glassy carbon working electrode (0.07 cm^2), and an Ag/AgCl wire reference electrode were employed. The solvent for electrochemical measurements, *o*-dichlorobenzene (*o*-DCB, Nacalai Tesque, specially prepared for HPLC) was used as supplied. Tetrabutylammonium perchlorate (TBAP) was used as an electrolyte. The ferrocenium/ferrocene (Fc^+/Fc) couple was used as an internal standard. In DCB containing 0.1 M TBAP, the Fc^+/Fc couple was observed at approximately +510 ± 20 mV vs. AgCl/Ag. All electrochemical work was carried out under an atmosphere of dry nitrogen. CV data were collected with a Hokuto Denko HA-501 potentiostat/galvanostat connected to a Hokuto Denko HB-104 function generator and a Graphtec WX1200 XY recorder. DPV data were collected with a Yanaco P-1100 polarographic analyzer connected to a Graphtec WX2400 XY recorder.

Materials: H_2DAP,[13] CuDAP,[12] and CuTAP[37] were synthesized as reported in our previous papers. CuMAP and CuOEP were ob-

 © 2004 Wiley-VCH Verlag GmbH & Co. KGaA, Weinheim

tained by reacting H_2MAP[38] or commercially available H_2OEP and $Cu(OAc)_2 \cdot H_2O$ in ethanol/dichloroethane (1:1 v/v) at 80 °C for 18 h, and subsequent purification using an alumina column and chloroform as eluent.

CuOEP: ESI-TOF: calcd. for $C_{36}H_{44}CuN_4$ 596.31; found 595.40. $C_{36}H_{44}CuN_4$ (596.31): calcd. C 72.51, H 7.44, N 9.40, found C 71.24, H 7.52, N 9.17.

CuMAP: ESI-TOF: calcd. for $C_{33}H_{35}N_5O_4Cu$ 629.21; found 629.24. $C_{33}H_{35}N_5CuO_4$ (629.21): calcd. C 62.99, H 5.61, N 11.13, found C 62.26, H 5.63, N 10.78.

Computational Methods: The Gaussian 98 program[39] running on an NEC TX7/AzusA computing system operated by Tohoku University Supercomputing System Information Synergy Center was used to perform DFT calculations of MOs (electron transitions) and frequencies. Since copper is paramagnetic, the central metal was taken to be zinc. B3LYP[34] with the 6−31G(d) basis set was used for all geometry optimization, MOs and frequency calculations. The transition energies and intensities of the lowest 30 singlet-singlet electronic transitions were determined by time-dependent DFT. An optimum scaling factor of 0.9613 was applied to the calculated frequencies in order to compare with the experimental data.[40]

Acknowledgments

This research was partially supported by the Ministry of Education, Science, Sports and Culture, with a Grant-in-Aid for the COE project "Giant Molecules and Complex Systems, 2004".

[1] H. Fischer, W. Friedrich, *Justus Liebigs Ann. Chem.* **1936**, *523*, 154−164.
[2] F. Endermann, H. Fischer, *Justus Liebigs Ann. Chem.* **1939**, *538*, 172−194.
[3] H. Fischer, H. Orth, *Die Chemie des Pyrroles*, Akad. Verlag, Leipzig, **1940**, Vol. II-ii, pp. 408−11.
[4] H. Fischer, H. Harberland, A. Muller, *Justus Liebigs Ann. Chem.* **1935**, *521*, 122−128.
[5] R. L. N. Harris, A. W. Johnson, I. T. Kay, *J. Chem. Soc., C* **1966**, 22−29.
[6] J. Engel, A. Gossauer, A. W. Johnson, *J. Chem. Soc., Perkin Trans. 1* **1978**, 871−875.
[7] A. M. Abeysekera, R. Grigg, J. F. Malone, J. T. King, J. O. Morley, *J. Chem. Soc., Perkin Trans. 2* **1985**, 395−402.
[8] R. K. Pandey, H. Zhou, K. Gerzevske, K. M. Smith, *J. Chem. Soc., Chem. Commun.* **1992**, 183−185.
[9] J. P. Singh, L. Y. Xie, D. Dolphin, *Tetrahedron Lett.* **1995**, *36*, 1567−1570.
[10] W. Metzger, H. Fischer, *Justus Liebigs Ann. Chem.* **1937**, *527*, 1−37.
[11] H. Fischer, A. Muller, *Justus Liebigs Ann. Chem.* **1937**, *528*, 1−8.
[12] O. G. Khelevina, N. V. Chizhova, P. A. Stuzhin, A. S. Semeikin, B. D. Berezin, *Russ. J. Coord. Chem. (Engl. Transl)* **1996**, *22*, 811−814.
[13] O. G. Khelevina, N. V. Chizhova, P. A. Stuzhin, A. S. Semeikin, B. D. Berezin, *Russ. J. Phys. Chem. (Engl. Transl)* **1997**, *71*, 74−78.
[14] S. Saito, H. A. Itano, *J. Chem. Soc., Perkin Trans. 1* **1986**, 1−7.
[15] A. L. Balch, M. M. Olmstead, N. Safari, *Inorg. Chem.* **1993**, *32*, 291−296.
[16] J. H. Fuhrhop, P. Kruger, W. S. Sheldrick, *Justus Liebigs Ann. Chem.* **1977**, 339−359.
[17] R. Grigg, R. J. Hamilton, M. L. Jozefowicz, C. H. Rochester, R. J. Terrell, H. Wickwar, *J. Chem. Soc., Perkin Trans. 2* **1973**, 407−413.
[18] J. A. Clarke, P. J. Dawson, R. Grigg, C. H. Rochester, *J. Chem. Soc., Perkin Trans. 2* **1973**, 414−416.
[19] S. S. Dvornikov, V. N. Knyukshto, V. A. Kuzmitsky, A. M. Shluga, K. N. Solovyov, *J. Lumin.* **1981**, *23*, 373−392.
[20] G. P. Gurinovich, G. N. Sinyakov, A. M. Shulga, *Izv. Akad. Nauk. SSSR. Ser. Fiz.* **1970**, *34*, 620−624.
[21] V. A. Mashenkov, K. N. Solov'ev, A. E. Turkova, N. A. Yushkevich, *Zh. Prikl. Specktrosk.* **1974**, *21*, 73−81.
[22] F. P. Monforts, B. Gerlach, *Tetrahedron Lett.* **1992**, *33*, 1985−1988.
[23] S. Neya, T. Kaku, N. Funasaki, Y. Shiro, T. Iizuka, K. Imai, H. Hori, *J. Biol. Chem.* **1995**, *270*, 13118−13123.
[24] M. J. Stillman, T. Nyokong, in *Phthalocyanines — Properties and Applications* (Ed.: C. C. Leznoff, A. B. P. Lever), VCH, New York, **1989**, Vol.1, Chapter 3, pp 133−289.
[25] [25a] N. Kobayashi, F. Furuya, G. -C. Yug, H. Wakita, M. Yokomizo, N. Ishikawa, *Chem. Eur. J.* **2002**, *8*, 1474−1484. [25b] N. Kobayashi, *Bull. Chem. Soc. Jpn.* **2002**, *75*, 1−19. [25c] Y. -H. TSE, N. Kobayashi, A. B. P. Lever, *Collect. Czech. Chem. Commun.* **2001**, *66*, 338−354. [25d] N. Kobayashi, A. Muranaka, *Chem. Commun.* **2000**, 1855−1856. [25e] N. Kobayashi, A. Muranaka, K. Ishii, *Inorg. Chem.* **2000**, *39*, 2256−2257. [25f] N. Kobayashi, T. Fukuda, D. Lelievre, *Inorg. Chem.* **2000**, *39*, 3632−3637. [25g] N. Kobayashi, R. Higashi, B. C. Titeca, F. Lamote, A. Ceulemans, *J. Am. Chem. Soc.* **1999**, *121*, 12018−12028. [25h] N. Kobayashi, *Chem. Commun.* **1998**, 487−488. [25i] N. Kobayashi, H. Lam, W. A. Nevin, P. Janda, C. C. Leznoff, T. Koyama, A. Monden, H. Shirai, *J. Am. Chem. Soc.* **1994**, *116*, 879−890. [25j] N. Kobayashi, Y. Kobayashi, T. Osa, *J. Am. Chem. Soc.* **1993**, *115*, 10994−10995.
[26] [26a] N. Kobayashi, J. Mack, K. Ishii, M. J. Stillman, *Inorg. Chem.* **2002**, *41*. 5350−5363. [26b] N. Kobayashi, T. Fukuda, *J. Am. Chem. Soc.* **2002**, *124*, 8021−8034. [26c] N. Kobayashi, H. Miwa, V. N. Nemykin,, *J. Am. Chem. Soc.* **2002**, *124*, 8007−8020. [26d] T. Fukuda, J. R. Stork, R. J. Potucek, M. M. Olmstead, B. C. Noll, N. Kobayashi, W. S. Durfee, *Angew. Chem. Int. Ed.* **2002**, *41*, 2565−2568. [26e] H. Miwa, E. A. Makarova, K. Ishii, E. A. Luk'yanets, N. Kobayashi, *Chem. Eur. J.* **2002**, *8*, 1082−1090. [26f] N. Kobayashi, S. Inagaki, V. N. Nemykin, T. Nonomura, *Angew. Chem. Int. Ed.* **2001**, *40*, 2710−2712. [26g] N. Kobayashi, T. Nonomura, K. Nakai, *Angew. Chem. Int. Ed.* **2001**, *40*, 1300−1303. [26h] N. Kobayashi, A. Muranaka, V. N. Nemykin, *Tetrahedron Lett.* **2001**, *42*, 913−915. [26i] V. N. Nemykin, N. Kobayashi, *Chem. Commun.* **2001**, 165−166. [26j] T. Nyokong, F. Furuya, N. Kobayashi, D. Du, W. Liu, J. Jiang, *Inorg. Chem.* **2000**, *39*, 128−135. [26k] J. Mack, N. Kobayashi, C. C. Lezonoff, M. J. Stillman, *Inorg. Chem.* **1997**, *36*, 5624−5634. [26l] N. Kobayashi, M. Togashi, T. Osa, K. Ishii, S. Yamauchi, H. Hino, *J. Am. Chem. Soc.* **1996**, *118*, 1073−1085.
[27] Y. Mie, K. Sonoda, S. Neya, N. Funasaki, I. Taniguchi, *Bioelectrochem. Bionerg.* **1998**, *46*, 175−184.
[28] K. M. Smith, *Porphyrins and Metalloporphyrins*, Elsevier, Holland, **1976**.
[29] CuTAP shows the Soret and Q_{00} band at 339 and 586 nm, respectively, in the same solvent, and this value becomes about 0.6.[37]
[30] [30a] A. Kaito, T. Nozawa, T. Yamamoto, M. Hatano, Y. Orii, *Chem. Phys. Lett.* **1977**, *52*, 154−160. [30b] A. Tajiri, J. Z. Winkler, *Naturforsch.* **1983**, *38a*, 1263−1269.
[31] [31a] J. Michl, *J. Am. Chem. Soc.* **1978**, *100*, 6801−6811. [31b] J. Michl, *J. Am. Chem. Soc.* **1978**, *100*, 6812−6818. [31c] J. D. Keegan, A. M. Stolzenberg, Y. Lu, R. E. Linder, G. Barth, A. Moscowitz, E. Bunnenberg, C. Djerassi, *J. Am. Chem. Soc.* **1982**, *104*, 4305−4317.
[32] J. H. Fuhrhop, K. M. Kadish, D. G. Davis, *J. Am. Chem. Soc.* **1973**, *95*, 5140−5147.
[33] A conceptual explanation on how the LUMO energy changes depending on the number and position of the *meso*-nitrogen atoms has already been reported: K. N. Solovyov, V. A. Mashenkov, T. F. Kachura, *Opt. Spect.* **1969**, *27*, 24−29.

 © 2004 Wiley-VCH Verlag GmbH & Co. KGaA, Weinheim

[34] [34a] A. D. Becke, *J. Chem. Phys.* **1993**, *98*, 5648−5652. [34b] C. Lee, W. Yang, R. G. Parr, *Phys. Rev. B* **1988**, *37*, 785−789.

[35] T. Fukuda, E. M. Makarova, E. A. Luk'yanets, N. Kobayashi, *Chem. Eur. J.* **2004**, *10*, 117−133.

[36] E. M. Makarova, T. Fukuda, E. A. Luk'yanets, N. Kobayashi, *submitted*.

[37] N. Kobayashi, H. Miwa, H. Isago, T. Tomura, *Inorg. Chem.* **1999**, *38*. 479−485.

[38] R. K. Pandey, K. R. Gerzevske, H. Zhou, K. M. Smith, *J. Chem. Soc., Perkin. Trans. 1* **1994**, 971−977.

[39] M. J. Frisch, G. W. Trucks, H. B. Schlegel, G. E. Scuseria, M. A. Robb, J. R. Cheeseman, V. G. Zakrzewski, J. A. Montgomery. Jr, R. E. Stratmann, J. C. Burant, S. Dapprich, J. M. Millam, A. D. Daniels, K. N. Kudin, M. C. Strain, O. Farkas, J. Tomasi, V. Barone, M. Cossi, R. Cammi, B. Mennucci, C. Pomelli, C. Adamo, S. Clifford, J. Ochterski, G. A. Petersson, P. Y. Ayala, Q. Cui, K. Morokuma, N. Rega, P. Salvador, D. D. Dannenberg, D. K. Malick, A. D. Rabuck, K. Raghavachari, J. B. Foresman, J. Cioslowski, J. V. Ortiz, A. G. Baboul, B. B. Stefanov, G. Liu, A. Liashenko, P. Piskorz, I. Komaromi, R. Gomperts, R. L. Martin, D. J. Fox, T. Keith, M. A. Al-Laham, C. Y. Peng, A. Nanayakkara, M. Challacombe, P. M. W. Gill, B. Johnson, W. Chen, M. W. Wong, J. L. Andres, C. Gonzalez, M. Head-Gordon, E. S. Replogle, J. A. Pople, *Gaussian 98, Revision A.11.3*, Gaussian, Inc., Pittsburgh, PA, 2002.

[40] M. W. Wong, *Chem. Phys. Lett.* **1996**, *256*, 391−399.

Received November 8, 2003
Early View Article
Published Online March 9, 2004

 © 2004 Wiley-VCH Verlag GmbH & Co. KGaA, Weinheim

One-Pot Synthesis of 1,6-Diiodo-2,3,4,5-tetracarba-*nido*-hexaboranes(6) and Mechanistic Studies on the Reaction System Alkynes/BI_3/$NaK_{2.8}$

Yong Nie,[a] Stefan Schwiegk,[a] Hans Pritzkow,[a] and Walter Siebert*[a]

Dedicated to Professor José Vicente on the occasion of his 60th birthday

Keywords: Boron / Boranes / Carboranes / Heterocycles / Iodine bridges

Attempts to prepare the tetracarba-*nido*-octaborane(8) derivative $(EtC)_4(BI)_4$ (**4**) by treatment of 3-hexyne with BI_3 (2 equiv.) and $NaK_{2.8}$ led to 2,3,4,5-tetraethyl-1,6-diiodo-2,3,4,5-tetracarba-*nido*-hexaborane(6) (**2a**) as the predominant product with trace quantities of **4** as well as 2,3-diethyl-1,4,5,6,7-pentaiodo-2,3-dicarba-*closo*-heptaborane(7) (**5**). Starting at –78 °C, reactions of 3-hexyne, 2-butyne or diphenylacetylene, respectively, with BI_3 (1 equiv.) and $NaK_{2.8}$ afforded the corresponding 1,6-diiodo-2,3,4,5-tetracarba-*nido*-hexaboranes(6) **2a**–**c** as the single carborane products. In the cases of 3-hexyne and diphenylacetylene, the formation of hexaorganylbenzene derivatives was also detected. To confirm the formation of **4** and **5**, the independent dehalogenation of *cis*-3,4-bis(diiodoboryl)-3-hexene (**3**) with $NaK_{2.8}$ has been studied, which indeed affords **4** and **5**, with the former being the predominant product. A mechanism for the formation of **2a** has been proposed, which involves iodoboration of the alkyne to give the borylalkene **1a**. This is followed by deiodination, presumably yielding the iodoborirene derivative **7**, which easily dimerizes to form the 1,4-diboracyclo-2,5-hexadiene derivative **8**. Subsequent rearrangement leads to the final C_4B_2-*nido*-carborane **2a**. To determine the stereochemistry of **1a**, its pyridine adduct **9** (and the isomer **9′**) and catechol derivative **10** (and the isomer **10′**), and the diisopropylamino derivative **11** have also been prepared. The new compounds have been characterized by MS and NMR spectroscopy, and the structures of **2a**, **3**, **9** and **9′** were confirmed by single-crystal X-ray analyses.
(© Wiley-VCH Verlag GmbH & Co. KGaA, 69451 Weinheim, Germany, 2004)

Introduction

The $(HC)_4(BR)_2$ organoborane/carborane system (**A**, **B**) has attracted considerable interest because the structures observed depend on the substituents (R) which attached to the boron atoms. Apart from the classical 1,4-diboracyclo-2,5-hexadienes **A**,[1] and non-classical 2,3,4,5-tetracarba-*nido*-hexaboranes(6) **B**,[2] the compounds **C**,[3a] **D**,[3b] **E**[3c] in between these two limits have also been reported. Peralkylated 2,3,4,5-tetracarba-*nido*-hexaboranes(6), known since the mid-1960s, are more stable than the parent compound $C_4B_2H_6$ [4] but their reactivities have only recently been studied.[5,6]

In order to investigate substitution reactions of **B**, functional groups (R) other than alkyl groups are needed at the boron atom(s). In 1994 we reported the formation of a 1,6-dichloro-2,3,4,5-tetracarba-*nido*-hexaborane(6)[7] derivative by photochemical transformation of 1,4-dichloro-2,3,5,6-tetrakis(isopropylidene)-1,4-diboracyclohexane. The low yield of the $(alkylC)_4(BCl)_2$ carborane did not allow further reactivity studies to be carried out. Wrackmeyer et al. were

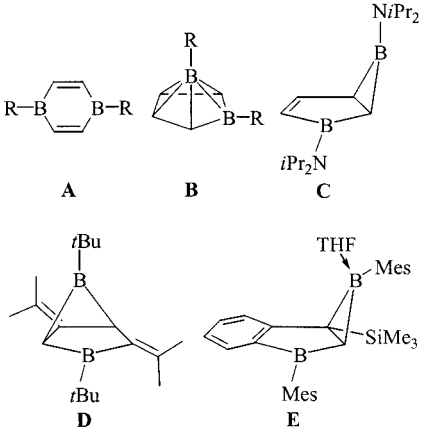

able to obtain 1,6-dibromo-2,3,4,5-tetracarba-*nido*-hexaboranes(6)[5a] in high yield by treating 1,4,6,9-tetraalkyl-3,8-diethyl-2,7-bis(diethylboryl)-5-stannaspiro[4.4]nona-1,3,6,8-tetraenes with BBr_3. They also studied the reactions between the peralkylated 2,3,4,5-tetracarba-*nido*-hexaboranes(6) and an excess of BBr_3 (and BI_3), whereby the corresponding B6-halo substituted carboranes were formed.[5b] Nucleophilic substitution reactions of such B-halo carboranes were found to replace the basal B6-halogen atom to give the corresponding carboranes with organyl,[5c] stan-

[a] Anorganisch-Chemisches Institut der Universität Heidelberg, Im Neuenheimer Feld 270, 69120 Heidelberg, Germany
Fax: (internat.) +49-(0)6221-545-609
E-mail: walter.siebert@urz.uni-heidelberg.de

 © 2004 Wiley-VCH Verlag GmbH & Co. KGaA, Weinheim **DOI: 10.1002/ejic.200300704**

nyl[5d] and diphenylphosphanyl[5e] groups as well as, in the 1,6-dibromo case, an *N*-bonded $[Fe_2(CO)_6(\mu\text{-}SN)]$ substituent in the 6-position.[5f] Currently there is no easy pathway to such B-functionalized C_4B_2-*nido*-carboranes.

In our efforts to prepare the iodo analog of the tetracarba-*nido*-octaborane(8) $(EtC)_4(BCl)_4$ [8] we have developed a one-pot route to 1,6-diiodo-2,3,4,5-tetracarba-*nido*-hexaboranes(6) involving alkynes, BI_3 and $NaK_{2.8}$ alloy. In this paper we report the synthesis and characterization of the resultant C_4B_2-*nido*-carboranes, and a possible mechanism for their formation is proposed.

Results and Discussion

Synthesis of 1,6-Diiodo-2,3,4,5-tetracarba-*nido*-hexaboranes(6)

The reaction between 3-hexyne, BI_3 (2 equiv.) and $NaK_{2.8}$ alloy at room temperature, in a one-pot manner (Scheme 1), gave a mixture of products. Its ^{11}B NMR spectrum shows two dominant signals at $\delta = 5.5$ and -52.7 ppm in a 1:1 ratio, typical of C_4B_2-*nido*-carboranes[2] (type **B**). The EI-MS spectrum exhibits the molecular ion pattern with the correct isotopic distribution for the formula $(EtC)_4(BI)_2$ (**2a**). The other peaks can be assigned to *nido*-$(EtC)_4(BI)_4$ (**4**) and the novel species *closo*-$(EtC)_2(BI)_5$ (**5**), respectively, both exhibiting the expected isotopic patterns. Compounds **4** and **5** were formed only in trace amounts.

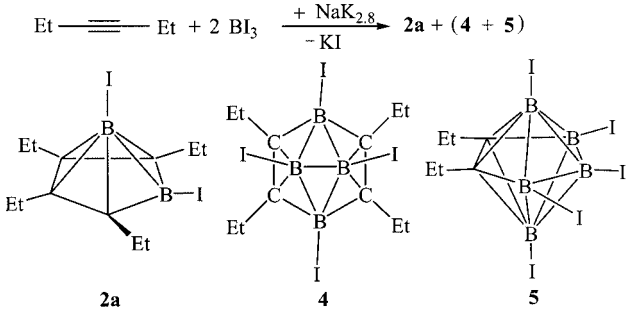

Scheme 1

Starting at low temperature (−78 °C) the same reaction gave **2a** as the single product in 51% yield as a yellow, sensitive and viscous oil. The yield can be increased to 66% when a 1:1 ratio of 3-hexyne and BI_3 was used (Scheme 2). In the latter case a very small amount of hexaethylbenzene could also be detected. The ^{11}B NMR spectrum of **2a** exhibits two signals at $\delta = 5.5$ and -52.5 ppm. The ^1H NMR spectrum shows an ABX_3 spin pattern for the methylene protons of the ethyl groups, and the ^{13}C NMR spectrum exhibits the corresponding four signals for the two different ethyl groups. The signals responsible for the skeletal carbon atoms non-adjacent to the basal boron were observed, while the signals for the other two skeletal carbon atoms (expected at ca. 105 ppm[5a]) were not observed. It should be noted that the formation of **2a** was first reported by Wrackmeyer et al.,[5a] (see Introduction) when they carried out reactions on a small scale for NMR spectroscopic studies. On standing at room temperature, yellow crystals of **2a** (vide infra) were obtained whereas the bromo compounds are oils.[5a,5b]

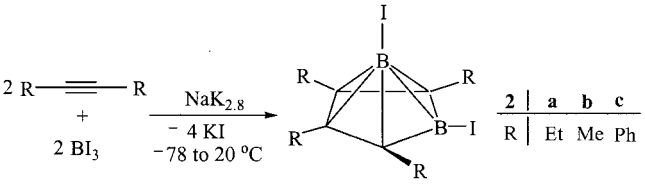

Scheme 2

The analogous reaction with 2-butyne proceeded smoothly but the yellowish *nido*-$(MeC)_4(BI)_2$ (**2b**) was obtained only in low yield. The ^{11}B NMR spectrum exhibits two signals at $\delta = 5.7$, -48.6 ppm and the ^1H NMR spectrum shows two singlets for the two different methyl groups. The ^{13}C NMR spectrum gives the corresponding signals for the methyl and the skeletal carbon atoms non-adjacent to the basal boron, while the signal for the other two skeletal carbon atoms was not observed. In the mass spectrum the molecular ion peak with the expected isotopic pattern was found.

Whereas calculations[10] suggest that such *nido*-carboranes bearing halogen substituents at the boron atom(s) would prefer a classical type **A** structure, we have found that **2a** and **2b** are perfectly stable like the bromo analogs.[5a,5b] The reaction of diphenylacetylene with $BI_3/NaK_{2.8}$ also proceeds but the orange-yellow *nido*-$(PhC)_4(BI)_2$ (**2c**) was also obtained in low yield. It was characterized by ^{11}B NMR spectroscopy ($\delta = 7.9$, -50.1 ppm), and the high-resolution mass spectrum exhibits the molecular ion peak having the correct isotopic distribution. Unfortunately, the formation of a significant amount of hexaphenylbenzene hampered the successful isolation and the recording of satisfactory NMR spectra. Moreover, it was found to be unstable at room temperature even when stored under nitrogen, as indicated by its color which turned from orange-yellow to pale yellow. This instability is different from the cases of **2a** and **2b**, and reminiscent of the instability of the iodoboration product of diphenylacetylene with BI_3, which leads to a 9,10-dihydro-9-boraanthracene derivative.[9]

In order to verify the formation of compounds **4** and **5**, the independent dehalogenation of **3**[11a] (Scheme 3) was carried out. Attempts to obtain **3** through a redox reaction of 3-hexyne and two equivalents of BI_3 were not successful.[11b] However, the halogen exchange reaction of **6**[12] with BI_3 led to **3**, a yellow crystalline solid, which is extremely sensitive to air and moisture. In solution it exhibited a ^{11}B NMR signal at $\delta = 11.8$ ppm. No change in the chemical shift was observed upon cooling the sample to −30 °C but only broadening of the signal. The significant shift to high field compared with that of **6** ($\delta = 53.9$ ppm) indicates some additional intra- or intermolecular interaction. An X-ray structural determination revealed that **3** forms an intramolecular B−I−B bridge to yield **3′**. In solu-

 © 2004 Wiley-VCH Verlag GmbH & Co. KGaA, Weinheim

tion a fast equilibrium is present as shown in Scheme 4, which explains the single ^{11}B NMR signal.

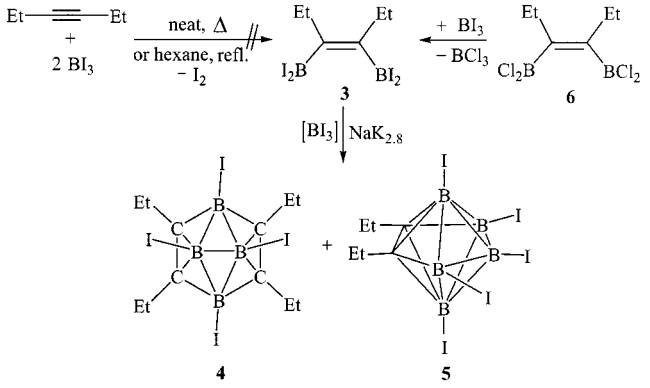

Scheme 3

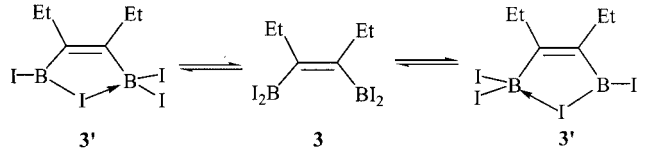

Scheme 4

The dehalogenation of **3** starting at −65 °C gave compound **4** in 29% yield. When the same reaction was carried out at room temperature, the yield was lower. Compound **4** exhibits two ^{11}B NMR signals at δ = −10.5 and −13.4 ppm, which are shifted to lower frequencies in comparison with *nido*-$(EtC)_4(BCl)_4$ [8] (δ = −1.5 and −5.5 ppm). In the mass spectrum, the molecular ion at *m*/*z* = 716 is the base peak and has the correct isotopic distribution, while the formation of **5** was only detected by a cutoff peak at *m*/*z* = 771 [M^+] of very low intensity.

To further study the scope and limitations of this approach, a series of other alkynes has been studied using the same or similar procedures. In the cases of 5-decyne, di-*tert*-butylacetylene, bis(trimethylsilyl)acetylene, and di-*p*-tolylacetylene, all the reactions led to decomposition products. The debromination reaction of 3-hexyne and BBr_3 (1 equiv.) afforded the known *nido*-$(EtC)_4(BBr)_2$ [5a] in 49% yield, together with a small amount of hexaethylbenzene, while the analogous reaction using BCl_3 gave a mixture of unidentified boron-containing species, and a significant amount of hexaethylbenzene. Surprisingly, the reaction system of diphenylacetylene-/BBr_3/$NaK_{2.8}$ led only to decomposition irrespective of whether the one-step or stepwise procedures were used. Efforts to produce the corresponding *nido*-C_4B_2 carboranes with CH cluster atoms, starting from ethyne or phenylacetylene, and BI_3 (or BBr_3), respectively, were not successful.

Mechanistic Considerations

There have been two similar dehalogenation reactions reported. One is the early study of the diphenylacetylene/$PhBBr_2$/K system by Lappert et al.,[13] in which they claimed to have obtained a perphenylated 1,4-diboracyclohexadiene derivative or an unknown carborane species. These results, however, could not be reproduced by Eisch et al.[14] The other system involves the alkynes/$MeBBr_2$/C_8K reaction reported by van der Kerk et al.,[15] who claimed to have obtained stable peralkylated 1,4-diboracyclohexadiene derivatives as the main products through a borylene mechanism, while Wrackmeyer et al.[16] (in the cases of 3-hexyne and 5-decyne) obtained the corresponding C_4B_2-*nido*-carboranes. No 1,4-diboracyclohexadiene derivatives could be detected.

In order to get an insight into the formation of **2**, we selected **2a** as our target compound. A possible pathway to **2a** is shown in Scheme 5. Iodoboration of 3-hexyne with BI_3 afforded **1a**, its dehalogenation presumably yielded the iodoborirene intermediate **7**, which might dimerize[1d,17] to give 1,4-diboracyclohexadiene **8** or the bicyclic analog of type C (see Introduction) with iodine at boron and ethyl at carbon atoms as intermediates to rearrange to the carborane **2a**.

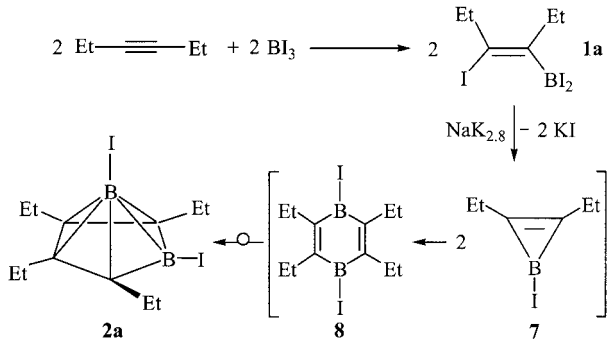

Scheme 5

The first step is the iodoboration of 3-hexyne to yield **1a**. In a study involving this step for the preparation of the 2,5-dihydro-1,2,5-thiadiborol,[9,18] the iodoboration product was reported to be a *cis*/*trans* mixture (ca. 2:3 *cis*/*trans* ratio) based on acetolysis which is an established method[19] for determining the stereochemistry of haloboration products (we repeated the acetolysis reaction and a ratio of 1:1 was obtained). The problem is that at room temperature the ^1H NMR spectrum shows two sets of ethyl signals and the ^{13}C NMR spectrum exhibits only six signals, whereas a *cis*/*trans* mixture should give more signals. Moreover, the ^{11}B NMR spectrum exhibits only one signal at δ = 40 ppm. As a result of this[20] some reactions were carried out with $[Fe_2(CO)_9]$ and Me_2S but unfortunately neither complexation nor adduct formation was observed. Later, the very similar reaction of 3-hexyne and BBr_3 was studied by Wrackmeyer.[21] Their results revealed that it is a stereoselective *cis*-addition, while the fast *cis*−*trans* isomerization led to a mixture. This allowed the assignment of both isomers by NMR spectroscopic methods. We tried to determine the stereochemistry of the present iodoboration products using a method more direct than acetolysis. It turned

 © 2004 Wiley-VCH Verlag GmbH & Co. KGaA, Weinheim

out, in agreement with Wrackmeyer's findings, that the reaction of 3-hexyne and BI_3 gave the *cis* isomer **1a** (Scheme 6), which underwent a slow isomerization to the thermodynamically more stable *trans* isomer **1a′**, thus allowing the characterization and even separation of both isomers. The pyridine adduct **9** and the catechol derivative **10** showed much faster *cis*−*trans* isomerizations than the parent **1a**, while the amino derivative **11** did not isomerize at room temperature even over a timescale of weeks. The X-ray structural analyses of **9** (*cis*) and **9′** (*trans*) unequivocally confirmed the stereochemical assignments.

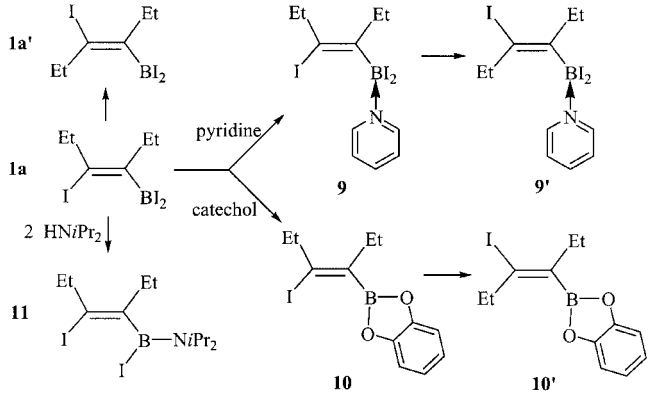

Scheme 6

The second step in the formation of **2a** is the dehalogenation of **1a**. Apart form the one-pot reactions, the stepwise reaction (see Exp. Sect.) also afforded **2a** in a somewhat lower yield (43%). Although we do not have direct evidence for the formation of the borirene intermediate **7**, we found ^{11}B NMR signals for the reaction mixtures which may be assigned to the corresponding 1,4-diboracyclohexadiene **8** (broad signals at ca. 68 and 67 ppm in the formation of **2a** and **2b**, respectively), near to the expected region for 1,4-diboracyclohexadienes (55−65 ppm).[22]

The redox reaction of **3** with 3-hexyne shown in Scheme 7 (analogous to the preparation of the corresponding 1,3-diiodo-2,3-dihydro-1,3-diborol derivatives[23] and the 1,4-diiodo-1,4-diboracyclohexene compounds[24]) indeed afforded the expected carborane **2a**. The reaction mixture showed a broad ^{11}B NMR signal at $\delta = 66$ ppm. As suggested by Schleyer et al.[17] the straightforward intramolecular rearrangement of 1,4-diboracyclohexa-2,5-dienes into carboranes is forbidden by symmetry and our attempts to separate **8** by distillation led gradually to **2a**, as evidenced by ^{11}B NMR spectroscopy and EI-MS (see Exp. Sect.). Although this redox reaction (Scheme 7) represents a new route to the corresponding 1,4-diboracyclohexadienes/C_4B_2-*nido*-carboranes, the difficult access to the *cis*-1,2-diborylalkene **3** prevents its practical application.

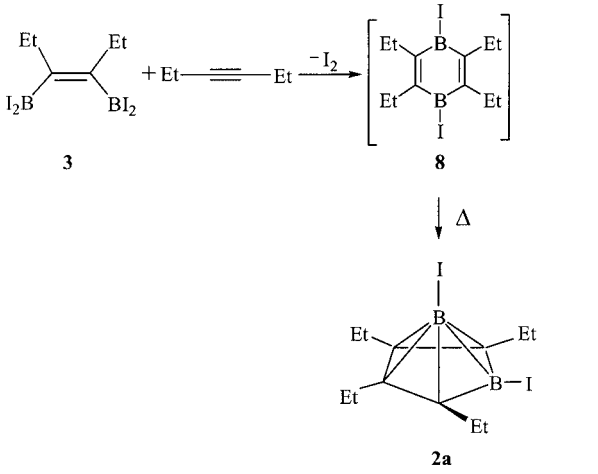

Scheme 7

X-ray Structural Analyses of 2a, 3, 9 and 9′

The structures of the C_4B_2-*nido*-carboranes were previously examined by electron diffraction studies of the hexamethyl derivative $(MeC)_4(BMe)_2$,[25] and by microwave spectroscopy[26] of the parent derivative $(HC)_4(BH)_2$.[4] The structures were confirmed by X-ray diffraction analyses.[3c,5f] In 1992, Berndt et al.,[3c] reported the structure of a benzo-annelated derivative, and in 1996 Herberhold, Wrackmeyer et al.[5f] published the structure of the first example of an "undisturbed" pentamethyl-*nido*-C_4B_2 carborane with an *N*-bonded $[Fe_2(CO)_6(\mu\text{-NS})]$ complex fragment in the 6-position. Derivatives of a benzo compound[3c] with transition metal complex fragments coordinated to the benzene ring have also been synthesized.[6b]

The molecular structure of **2a** is shown in Figure 1. Its C_4B_2 skeleton adopts the expected *nido* structure (C_s symmetry) with an apical six-coordinate boron atom. The B−B bond length of 1.821 Å is similar to, but slightly shorter

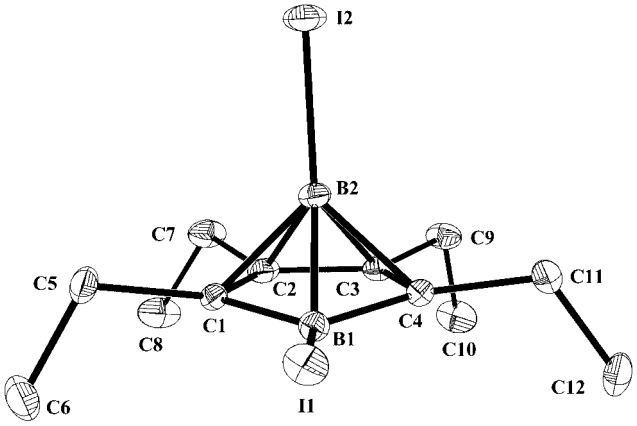

Figure 1. Molecular structure of **2a**, hydrogen atoms omitted for clarity, thermal ellipsoids are shown at the 40% probability level; selected bond lengths [A] and angles [°]: I1−B1 2.155(3), I2−B2 2.126(3), C1−C2 1.457(4), C2−C3 1.437(4), C3−C4 1.459(3), C1−B1 1.522(3), C4−B1 1.526(4), C1−B2 1.705(4), C2−B2 1.713(4), C3−B2 1.713(4), C4−B2 1.708(4), B1−B2 1.821(4); C2−C1−B1 108.3(2), C1−B1−C4 104.1(2), B1−C4−C3 107.9(2), C4−C3− C2 109.6(2), C3−C2−C1 109.2(2), B2−B1−I1 130.0(2), B1−B2−I2 140.1(2)

 © 2004 Wiley-VCH Verlag GmbH & Co. KGaA, Weinheim

than, the corresponding distances in the above-mentioned $(MeC)_4(BMe)[B(\mu\text{-}NS)Fe_2(CO)_6]$[5f] (1.836 Å), in the benzo-annelated structure[3c] (1.870 Å) and in the parent derivative $(HC)_4(BH)_2$ [26] (1.886 Å). The B2−C distances vary within a narrow range (1.705−1.713 Å), and are also slightly shorter than the values in the examples mentioned[5f,3c] (1.720−1.743 and 1.673−1.865 Å, respectively), which can be attributed to the different steric environments around the skeleton. The skeletal C−C distances were found to be almost identical (av. 1.451 Å), and are also similar to the average of 1.438 Å in $(MeC)_4(BMe)[B(\mu\text{-}SN)Fe_2(CO)_6$. The four skeletal carbon atoms are in one plane, and the four *exo*-polyhedral carbon atoms C5, C7, C9, C11 are bent out of the C_4 plane towards B2 by an average of 0.24 Å. The five-membered C_4B open face is not planar, with B1 lying ca. 0.15 Å below the C_4 plane. The dihedral angle between the C_4 plane and the C_2B1 plane is ca. 9°. The B−I bond lengths are 2.126 and 2.155 Å, respectively, and are similar to the reported values in some other B-iodinated polyhedral borane and carborane clusters, for example 2.133 Å (av.) in $HNB_{11}Cl_5I_6$,[27a] 2.09−2.17 Å in polyiodinated *p*-carboranes,[27b] and also similar to that of 2.10(4) Å in BI_3.[28]

The molecular structure of **3** is shown in Figure 2. The two BI_2 groups are in a *cis* arrangement, and the I1 atom is intramolecularly coordinated to B1, forming a unique B−I−B bridge. The boron atom B2 is tri-coordinate and the B2−I4 bond length of 2.107 Å is typical of an I−B(sp^2) distance. B1 is four-coordinate, however, and the B1−I2 and B1−I3 distances are 2.231 and 2.201 Å, respectively, and are very similar to the reported values for I−B(sp^3) bonds, e.g. 2.21(1) Å (av.) in $[Ph_2PBI_2]_2$ [29a] and 2.229 Å (av.) in $(vi_3P)BI_3$ [29b] (where vi is vinyl). The B−I bond lengths involving the bridging I1 atom are 2.160 and 2.383 Å, respectively, and the latter is longer than the sum of the covalent radii of the two atoms, indicating that the interaction between B1 and I1 is weak.

Figure 3 (a and b) show the structures of **9** (*cis*) and **9′** (*trans*), respectively. In both structures the boron atom is four-coordinate, adopting a slightly distorted tetrahedral geometry. The bond lengths and angles in both structures are very similar. The B−I bond lengths are 2.269 and 2.306 Å in **9**, and 2.275(3) and 2.294(3) Å in **9′**, respectively, similar to the corresponding values in compound **3**. The corresponding B−N distances of 1.587 Å in **9** and 1.596 Å in **9′**, respectively, are similar to, but slightly shorter than, those found in other pyridine adducts.[30]

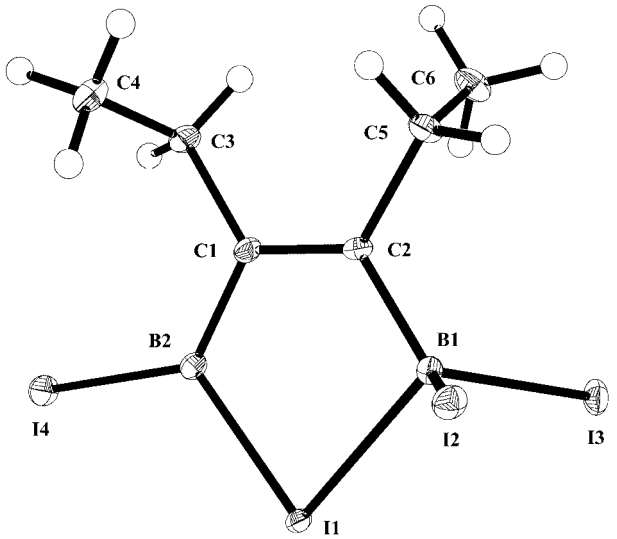

Figure 2. Molecular structure of **3**, thermal ellipsoids are shown at the 40% probability level; selected bond lengths [Å] and angles [°]: I1−B2 2.160(4), I1−B1 2.383(4), I2−B1 2.231(4), I3−B1 2.201(4), I4−B2 2.107(4), B1−C2 1.571(6), B2−C1 1.510(5), C1−C2 1.371(5), B2−I1−B1 81.1(2), C2−B1−I3 117.0(3), C2−B1−I2 111.0(3), I3−B1−I2 112.25(18), C2−B1−I1 102.8(2), I3−B1−I1 105.9(2), I2−B1−I1 106.8(2), C1−B2−I4 127.7(3), C1−B2−I1 113.8(3), I4−B2−I1 118.5(2), C2−C1−B2 118.5(3), C1−C2−B1 123.5(3)

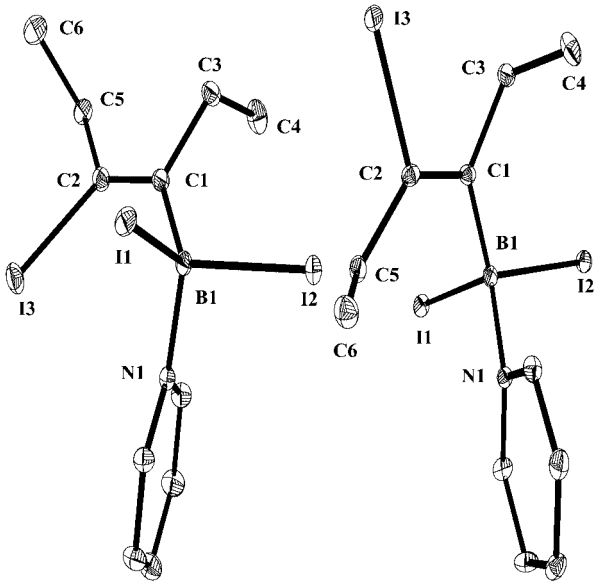

Figure 3. a) (left) Molecular structure of **9**, hydrogen atoms omitted for clarity, thermal ellipsoids are shown at the 40% probability level; selected bond lengths [Å] and angles [°]: I1−B1 2.269(3), I2−B1 2.306(3), I3−C2 2.141(3), N1−B1 1.587(4), B1−C1 1.600(4), C1−C2 1.343(4), N1−B1−C1 114.4(2), N1−B1−I1 111.8(2), C1−B1−I1 109.2(2), N1−B1−I2 101.4(2), C1−B1−I2 113.6(2), I1−B1−I2 106.1(1). b) (right) Molecular structure of **9′**, hydrogen atoms omitted for clarity, thermal ellipsoids are shown at the 40% probability level; selected bond lengths [Å] and angles [°]: I1−B1 2.275(3), I2−B1 2.294(3), I3−C2 2.160(3), N1−B1 1.596(4), B1−C1 1.607(4), C1−C2 1.342(4), N1−B1−C1 114.8(2), N1−B1−I1 111.3(2), C1−B1−I1 109.7(2), N1−B1−I2 100.8(2), C1−B1−I2 114.0(2), I1−B1−I2 105.7(1).

Conclusion

We have developed a one-pot synthesis of 1,6-diiodo-2,3,4,5-tetracarba-*nido*-hexaborane(6) derivatives involving disubstituted alkynes, BI_3 and $NaK_{2.8}$. Considering the ready availability of the starting materials and the product **2a**, it has been convenient to study the reactivities of such B−I functionalized carboranes and dehalogenation is a practical method for the preparation of carboranes. The formation of **4** from the dehalogenation of **3** confirms that bis(boryl-

 © 2004 Wiley-VCH Verlag GmbH & Co. KGaA, Weinheim

alkenes) are the precusors of *nido*-C_4B_4 carboranes. Such dehalogenation reactions at room temperature are more complex and give lower yields than at lower temperatures. A possible mechanism of the formation of C_4B_2-*nido*-hexaboranes(6) has been proposed and studied using **2a** as a representative example. The stereochemistry of the iodoboration product of the alkyne has been clarified as *cis*, using a more direct method than acetolysis, and the *cis*-*trans* isomerization exists in the addition product **1a** and some of the derivatives.

Experimental Section

All reactions and manipulations were performed in dry glassware under argon or nitrogen using standard Schlenk techniques. Solvents were dried, distilled, and saturated with nitrogen. NMR: Bruker DRX 200 spectrometer; $Et_2O{\cdot}BF_3$ was used as the external standard for ^{11}B NMR spectroscopy; as internal references for ^1H and ^{13}C NMR spectroscopy, the signals of the deuterated solvent ($CDCl_3$) were used and calculated relative to TMS. MS: ZAB-2F VH Micromass CTD spectrometer, and a JEOL MS Station JMS 700 spectrometer both using the EI ionization technique. Melting points (uncorrected) were measured with a Büchi apparatus, using capillaries which were filled under nitrogen and sealed.

2,3,4,5-Tetraethyl-1,6-diiodo-2,3,4,5-tetracarba-*nido*-hexaborane(6) (2a). Formation from 3-Hexyne, BI_3 (1 equiv.) and $NaK_{2.8}$

a) One-Pot Procedure: To a solution of BI_3 (872 mg, 2.23 mmol) in hexane (40 mL) at −78 °C was added 3-hexyne (190 mg, 2.3 mmol) dropwise, and $NaK_{2.8}$ (0.9 mL, excess) was then added with a syringe. The mixture was stirred for ca. 15 min, and the cooling bath was then removed. The reaction mixture was warmed to ambient temperature, stirred overnight, and then filtered (G4 frit) and the residue washed with hexane (2 × 15 mL). The solvent of the yellow filtrate was removed in vacuo, leaving a yellow viscous oil. Distillation at 80 °C/ 2×10^{-3} Torr gave **2a** (326 mg, 66%) as a yellow, air-sensitive oil, which slowly solidified. For reactions with up to 28 mmol of BI_3, longer reaction times (1 week) were needed (av. yield > 60%, m.p. 52 °C). ^1H NMR ($CDCl_3$, 200 MHz): δ = 1.20 (t, $^3J_{H,H}$ = 7.6 Hz, 6 H, CH_3), 1.26 (t, $^3J_{H,H}$ = 7.6 Hz, 6 H, CH_3), 1.87− 2.04 (m), 2.11− 2.38 (m, 8 H, CH_2) ppm. ^{11}B NMR ($CDCl_3$, 64 MHz): δ = 5.5 (s, B_{basal}, 1 B), −52.5 (s, B_{apical}, 1 B) ppm. ^{11}B NMR (C_6D_6, 64 MHz): δ = 5.9 (s, B_{basal}, 1 B), −52.4 (s, B_{apical}, 1 B) ppm. ^{13}C NMR ($CDCl_3$, 50 MHz): δ = 13.5, 14.2 (CH_3), 18.9, 20.4 (CH_2), 114.2 ppm (skeletal carbon atoms non-adjacent to the basal boron), the signals for the other basal carbon atoms not observed. EI-MS: *m*/*z* (%) = 440 (100) [M^+], 313 (20.3) [$M^+ - I$]. HR-MS (EI): *m*/*z* = 439.9842 [M^+]. Calcd. For $^{12}C_{12}{}^1H_{20}{}^{11}B_2{}^{127}I_2$ 439.9840 (Δ*m* = 0.2 mmu).

b) Stepwise Procedure: To a solution of BI_3 (2.165 g, 5.53 mmol) in hexane (50 mL) was added dropwise 3-hexyne (470 mg, 5.7 mmol) at −50 °C, and the resultant solution was warmed to ambient temperature. The resultant red solution (^{11}B NMR: δ = 40.5 ppm) was cooled to −60 °C again and $NaK_{2.8}$ (2 mL) was added with a syringe. The workup procedure which followed was similar to that of the one-pot procedure and yielded **2a** (520 mg, 43%).

Reactions of 3-Hexyne with BI_3 (2 equiv.) and $NaK_{2.8}$ at Different Temperatures

a): A solution of BI_3 (858 mg, 2.19 mmol) in hexane (35 mL) was added dropwise to a mixture of 3-hexyne (90 mg, 1.1 mmol) and $NaK_{2.8}$ (0.9 mL) at room temp. The reaction mixture became gray in ca. 20 min, and was stirred for 1 day, then filtered (G4 frit). The residue was washed with hexane (2 × 15 mL), and the slightly pink filtrate was dried in vacuo, leaving a red-brown oil (238 mg), which was a mixture of **2a**, **4** and **5**. EI-MS: *m*/*z* (%) = 440 (100) (**2a**), 716 (3.35) (**4**), and 771 (44.83) (**5**). HR-MS (EI): *m*/*z* = 439.9847 (**2a**); calcd. for $^{12}C_{12}{}^1H_{20}{}^{11}B_2{}^{127}I_2$ 439.9840 (Δ*m* = 0.6 mmu), *m*/*z* = 715.8150 (**4**); calcd. for $^{12}C_{12}{}^1H_{20}{}^{11}B_4{}^{127}I_4$ 715.8116 (Δ*m* = 3.4 mmu), *m*/*z* = 715.6464 (**5**); calcd. for $^{12}C_6{}^1H_{10}{}^{11}B_5{}^{127}I_5$ 715.6472 (Δ*m* = −0.8 mmu).

b): To a solution of BI_3 (3.126 g, 7.98 mmol) in hexane (30 mL) at −78 °C was added 3-hexyne (332 mg, 4.04 mmol) dropwise. The mixture immediately became yellow-brown, and $NaK_{2.8}$ (2 mL) was then added with a syringe. The reaction mixture was stirred at −78 °C for ca. 10 min, the cooling bath was removed, and the mixture was warmed to ambient temperature and stirred for 1 day. The mixture was then filtered (G4 frit), and the residue washed with hexane (2 × 15 mL). The yellow filtrate was dried in vacuo, leaving a yellow viscous oil, which was distilled to give **2a** (455 mg, 51%) as the single carborane product. In this case, no hexaethylbenzene was detected.

Formation of 2a from the Redox Reaction of 3-Hexyne and 3: 3-Hexyne (196 mg, 2.3 mmol) was added dropwise to a solution of **3** (1.357 g, 2.22 mmol) in hexane (25 mL) at −60 °C. The mixture was warmed to ambient temperature during which time it became deep brown indicating the formation of I_2. The ^{11}B NMR spectrum showed a signal at δ = 66 ppm. All the volatiles were removed in vacuo and the resultant red oil was distilled at 71 °C/ 8×10^{-2} Torr to give a yellowish oil (533 mg, 55%), which gradually became deep red. The ^{11}B NMR (C_6D_6, 64 MHz) data of the original distillate: δ = 57.6 (s), 45.7, 5.9, −9.0 (BI_3), −52.4 ppm; after three days, the corresponding signals were: δ = 57 (s), 32, 5.9, −52.4 ppm; after three weeks, there were only two ^{11}B NMR signals: δ = 5.9, −52.4 ppm (**2a**). The EI-MS spectrum was identical to that of authentic **2a**.

1,6-Diiodo-2,3,4,5-tetramethyl-2,3,4,5-tetracarba-*nido*-hexaborane(6) (2b): Same procedures as described for **2a**. 2-Butyne (426 mg, 7.9 mmol), BI_3 (3.09 g, 7.9 mmol), $NaK_{2.8}$ (2 mL). The final yellow viscous oil was distilled at 95 °C/ 3×10^{-2} Torr to give **2b** (225 mg, 15%) as a yellowish solid; m.p. 92−94 °C. ^1H NMR ($CDCl_3$, 200 MHz): δ = 1.72 (s, 6 H, CH_3), 1.87 (s, 6 H, CH_3) ppm. ^{11}B NMR ($CDCl_3$, 64 MHz): δ = 5.7 (s, B_{basal}), −48.6 (s, B_{apical}) ppm. ^{13}C NMR ($CDCl_3$, 50 MHz): δ = 11.29, 12.55 (CH_3), 110.7 ppm (skeletal carbon atoms non-adjacent to basal boron), the signals for the other basal carbon atoms not observed. EI-MS: *m*/*z* (%) = 384 (94) [M^+], 257 (100) [$M^+ - I$]. HR-MS (EI): *m*/*z* = 383.9218 [M^+]; calcd. for $^{12}C_8{}^1H_{12}{}^{11}B_2{}^{127}I_2$ 383.9215 (Δ*m* = 0.3 mmu).

1,6-Diiodo-2,3,4,5-tetraphenyl-2,3,4,5-tetracarba-*nido*-hexaborane(6) (2c): Same procedures as described for **2a**. Diphenylacetylene (1.38 g, 7.7 mmol), BI_3 (3.03 g, 7.7 mmol), $NaK_{2.8}$ (1.6 mL). The yellow filtrate was cooled, and some yellow solid (mainly hexaphenylbenzene) was filtered, and the yellow filtrate was dried in vacuo to give **2c** (147 mg, ca. 5%) and a small amount of hexaphenylbenzene as an orange yellow solid. ^{11}B NMR (CD_2Cl_2, 64 MHz): δ = 7.9 (s, B_{basal}), −50.1 (s, B_{apical}), (δ = 8.2 and −49.6 ppm in $CDCl_3$) ppm. EI-MS: *m*/*z* (%) = 632 (100) [M^+], 505 (69.6) [$M^+ - I$]. HR-MS (EI): *m*/*z* = 631.9855 [M^+]; calcd. for $^{12}C_{28}{}^1H_{20}{}^{11}B_2{}^{127}I_2$ 631.9841 (Δ*m* = 1.4 mmu).

***cis*-3,4-Bis(diiodoboryl)-3-hexene (3):**[11a] A portion of 3,4-bis(dichloroboryl)-3-hexene (**6**) (2.13 g, 8.7 mmol) was added to BI_3

 © 2004 Wiley-VCH Verlag GmbH & Co. KGaA, Weinheim

(4.653 g, 11.9 mmol) at room temperature. The resultant dark brown solution was stirred at room temperature for ca. 2.5 h. The reaction flask was connected to a condensation apparatus, the trap cooled to −78 °C, and the system was kept at ca. 60 mbar overnight. All volatiles were then removed under high vacuum, and the resultant dark brown residue was recrystallized five times from hexane (ca. 20 mL), four times at −84 °C, and the last time at −28 °C. Compound **3** (2.53 g, 47.5%) was obtained as a yellow crystalline solid, which can be kept at −28 °C for a long period of time, m.p. 70−72 °C. ^{1}H NMR (C_6D_6, 200 MHz): δ = 1.02 (t, $^3J_{H,H}$ = 7.5 Hz, 6 H, CH_3), 2.29 (q, $^3J_{H,H}$ = 7.5 Hz, 4 H, CH_2) ppm. ^{11}B NMR (C_6D_6, 64 MHz): δ = 11.8 ppm. ^{13}C NMR (C_6D_6, 50 MHz): δ = 14.8 (CH_3), 26.2 (CH_2), 178.4 (C=C) ppm. EI-MS: *m*/*z* (%) = 485 (100) [M^+ − I]. HR-MS (EI): *m*/*z* = 484.8128 [M^+ − I]; calcd. For $^{12}C_6{}^1H_{10}{}^{11}B_2{}^{127}I_3$ 484.8103 (Δ*m* = 2.5 mmu). $C_6H_{10}B_2I_4$(611.4): calcd. C 11.79, H 1.65; found C 12.23, H 1.61.

Tetraethyltetraiodotetracarba-*nido*-octaborane(8) (4): To a solution of **3** (2.3 g, 3.76 mmol) in hexane (40 mL) at −65 °C was added $NaK_{2.8}$ (1.5 mL, excess) dropwise with a syringe. After ca. 1 h the cooling bath was removed, and the reaction mixture was warmed to room temperature and stirred for 3 days. The reaction mixture was filtered (G4 frit) and the residue washed with hexane (2 × 15 mL), the light yellow filtrate dried in vacuo, leaving a yellow viscous oil which slowly solidified, containing **4** (385 mg, 28.6%) and a trace amount of **5**. ^{11}B NMR ($CDCl_3$, 64 MHz): δ = −10.5 (s, 2 B), −13.4 (s, 2 B) ppm. EI-MS: *m*/*z* (%) = 716 (100) [M^+] (**4**), 589 (91.7) [M_1^+ − I]. 771(4.3) [M^+] (**5**). HR-MS (EI): *m*/*z* = 715.8112 [M_1^+]; calcd. For $^{12}C_{12}{}^1H_{20}{}^{11}B_4{}^{127}I_4$ 715.8117 (Δ*m* = −0.5 mmu). *m*/*z* = 771.6440 [M_2^+]; Calcd. For $^{12}C_6{}^1H_{10}{}^{11}B_5{}^{127}I_5$ 771.6471 (Δ*m* = −3.1 mmu).

***cis*-3-Diiodoboryl-4-iodo-3-hexene (1a):**[9,18] The procedure in the literature was slightly modified. To a solution of BI_3 (3.245 g, 8.3 mmol) in pentane (50 mL) was added 3-hexyne (681 mg, 8.3 mmol) dropwise at −25 °C. The red mixture was warmed to ambient temperature and the deep pink solution was transferred to another flask, leaving a little black solid on the wall of the original flask. The solution was dried in vacuo to give analytically pure **1a** almost quantitatively as a deep red liquid. ^{1}H NMR ($CDCl_3$, 200 MHz): δ = 1.08 (t, $^3J_{H,H}$ = 7.4 Hz, 3 H, CH_3), 1.22 (t, $^3J_{H,H}$ = 7.6 Hz, 3 H, CH_3), 2.15 (q, $^3J_{H,H}$ = 7.6 Hz, 2 H, CH_2), 2.62 (q, $^3J_{H,H}$ = 7.4 Hz, 2 H, CH_2) ppm. ^{11}B NMR ($CDCl_3$, 64 MHz): δ = 40.0 ppm. ^{13}C NMR ($CDCl_3$, 50 MHz): δ = 14.2, 15.0 (CH_3), 24.7, 33.3 (CH_2), 106.4 (=C-I), 157.6 (br., =C−B) ppm.

***trans*-3-Diiodoboryl-4-iodo-3-hexene (1a′):** Slow isomerization of **1a** (*cis*) at room temperature afforded **1a′** (not complete within 5 weeks as indicated by NMR in a $CDCl_3$ solution, with partial decompostion). ^{1}H NMR ($CDCl_3$, 200 MHz): δ = 1.08 (t, $^3J_{H,H}$ = 7.2 Hz, 3 H, CH_3), 1.15 (t, $^3J_{H,H}$ = 6.7 Hz, 3 H, CH_3), 2.2 (q, $^3J_{H,H}$ = 7.2 Hz, 2 H, CH_2), 2.61 (q, $^3J_{H,H}$ = 6.7 Hz, 2 H, CH_2) ppm. ^{11}B NMR ($CDCl_3$, 64 MHz): δ = 43.5 ppm. ^{13}C NMR ($CDCl_3$, 50 MHz): δ = 12.8, 14.0 (CH_3), 33.6, 39.1 (CH_2), 114.6 (=C−I), 158.1 (br., =C−B) ppm.

***cis*-3-Diiodoboryl-4-iodo-3-hexene−Pyridine Adduct (9):** Pyridine (223 mg, 2.8 mmol) was added dropwise to a solution of **1a** (1.33 g, 2.8 mmol) in hexane (25 mL) at −25 °C. The color immediately turned to deep red and a yellow precipitate then appeared. The mixture was warmed to room temperature, the solvent removed in vacuo, and an orange-yellow powder **9** was obtained quantitatively. The X-ray quality crystals were grown from a toluene solution at −28 °C. M.p. 30 °C. ^{1}H NMR ($CDCl_3$, 200 MHz): δ = 1.05 (t, $^3J_{H,H}$ = 7.4 Hz, 3 H, CH_3), 1.29 (t, $^3J_{H,H}$ = 7.4 Hz, 3 H, CH_3), 2.77 (q, $^3J_{H,H}$ = 7.4 Hz, 2 H, CH_2), 2.86 (q, $^3J_{H,H}$ = 7.4 Hz, 2 H, CH_2), 7.70 (m), 8.19(m), 9.39 (m) (py-H) ppm. ^{11}B NMR ($CDCl_3$, 64 MHz): δ = −13.9 ppm. ^{13}C NMR ($CDCl_3$, 50 MHz): δ = 14.4, 14.9 (CH_3), 32.4, 39.5 (CH_2), 115.2 (=C−I), 126.6, 142.4, 147.6 ppm (py-C), the signal of the boron-bound carbon was not observed.

***trans*-3-Diiodoboryl-4-iodo-3-hexene−Pyridine Adduct (9′):** Slow isomerization of **9** (*cis*) at room temperature afforded **9′** within one week as yellow crystals from a CH_2Cl_2 solution. M.p. 108−110 °C, dec. ^{1}H NMR ($CDCl_3$, 200 MHz): δ = 0.74 (t, $^3J_{H,H}$ = 7.4 Hz, 3 H, CH_3), 1.25 (t, $^3J_{H,H}$ = 7.4 Hz, 3 H, CH_3), 1.94 (q, $^3J_{H,H}$ = 7.2 Hz, 2 H, CH_2), 2.98 (q, $^3J_{H,H}$ = 7.4 Hz, 2 H, CH_2), 7.76 (m), 8.26(m), 9.47 (m) (py-H) ppm. ^{11}B NMR ($CDCl_3$, 64 MHz): δ = −20.8 ppm. ^{13}C{^{11}B} NMR ($CDCl_3$, 50 MHz): δ = 12.9, 13.7 (CH_3), 38.8, 45.3 (CH_2), 120.0 (=C−I), 126.4, 142.9, 146.9 (py-C), 147.9 (C=C−B) ppm. The EI-MS failed to give definite information.

***cis*-3-(1,3,2-Benzodioxaborol-2-yl)-4-iodo-3-hexene (10):** A solution of **1a** (730 mg, 1.54 mmol) in CH_2Cl_2 (10 mL) was added dropwise to a solution of catechol (169 mg, 1.54 mmol) in CH_2Cl_2 (15 mL) at −45 °C. The reaction mixture was warmed to ambient temperature and the solvent removed in vacuo to give 455 mg (90%) of **10** as a deep red liquid. ^{1}H NMR ($CDCl_3$, 200 MHz): δ = 1.10 (t, $^3J_{H,H}$ = 7.6 Hz, 3 H, CH_3), 1.17 (t, $^3J_{H,H}$ = 7.4 Hz, 3 H, CH_3), 2.43 (q, $^3J_{H,H}$ = 7.6 Hz, 2 H, CH_2), 2.73 (q, $^3J_{H,H}$ = 7.4 Hz, 2 H, CH_2), 7.10- 7.33 (m, 4 H, C_6H_4) ppm. ^{11}B NMR ($CDCl_3$, 64 MHz): δ = 31.1 ppm. ^{13}C NMR ($CDCl_3$, 50 MHz): δ = 12.9, 14.4 (CH_3), 26.7, 35.7 (CH_2), 110.1 (=C−I), 112.7, 122.8, 147.9 ppm (C_6H_4), the boron-bound carbon n.o ppm. EI-MS: *m*/*z* (%) = 328 (50.6) [M^+], 246 (100) [M^+ − C_6H_{10}], 201 (99.8) [M^+ − I]. HR-MS (EI): *m*/*z* = 328.0116 [M^+]; calcd. For $^{12}C_{12}{}^1H_{14}{}^{11}B{}^{127}I{}^{16}O_2$ 328.0131 (Δ*m* = −1.5 mmu).

***trans*-3-(1,3,2-Benzodioxaborol-2-yl)-4-iodo-3-hexene (10′):** The isomerization of **10** (*cis*) at room temperature afforded **10′** within ca. 3 weeks (as indicated by NMR in a $CDCl_3$ solution). ^{1}H NMR ($CDCl_3$, 200 MHz): δ = 1.12 (t, $^3J_{H,H}$ = 7.6 Hz, 3 H, CH_3), 1.27 (t, $^3J_{H,H}$ = 7.4 Hz, 3 H, CH_3), 2.60 (q, $^3J_{H,H}$ = 7.4 Hz, 2 H, CH_2), 3.22 (q, $^3J_{H,H}$ = 7.6 Hz, 2 H, CH_2), 7.12- 7.33 (m, 4 H, C_6H_4) ppm. ^{11}B NMR ($CDCl_3$, 64 MHz): δ = 29.1 ppm. ^{13}C NMR ($CDCl_3$, 50 MHz): δ = 13.3, 15.6 (CH_3), 36.6, 39.9 (CH_2), 112.2 (=C−I), 112.6, 122.9, 147.9 ppm (C_6H_4), the boron-bound carbon n.o.

***cis*-3-(Diisopropylamino)iodoboryl-4-iodo-3-hexene (11):** Diisopropylamine (1.07 g, 10.6 mmol) was added dropwise to a solution of **1a** (2.45 g, 5.2 mmol) in hexane (50 mL) at −40 °C. The mixture was warmed to ambient temperature and filtered, the light yellow filtrate was dried in vacuo to give a red oil, which was distilled at 82 °C/ 5.9 × 10^{-2} Torr to give yellow **11** (1.8 g, 76%). ^{1}H NMR ($CDCl_3$, 200 MHz): δ = 1.04 (t, $^3J_{H,H}$ = 7.3 Hz, 3 H, Et CH_3), 1.14 (t, $^3J_{H,H}$ = 7.6 Hz, 3 H, Et CH_3), 1. 24 (d, $^3J_{H,H}$ = 6.7 Hz, 3 H, *i*Pr CH_3), 1.30 (d, $^3J_{H,H}$ = 6.7 Hz, 3 H, *i*Pr CH_3), 1.49 (d, $^3J_{H,H}$ = 7.2 Hz, 3 H, *i*Pr CH_3), 1.54 (d, $^3J_{H,H}$ = 7.2 Hz, 3 H, *i*Pr CH_3), 2.10 (m, 1 H, Et CH_2), 2.31 (m, 1 H, Et CH_2), 2.53 (q, $^3J_{H,H}$ = 7.4 Hz, 2 H, Et CH_2), 3.53 (sept, 1 H, *i*Pr CH), 3.95 (sept, 1 H, *i*Pr CH) ppm. ^{11}B NMR ($CDCl_3$, 64 MHz): δ = 28.1 ppm. ^{13}C NMR ($CDCl_3$, 50 MHz): δ = 14.2, 14.3, (Et CH_3), 21.0, 22.1, 23.0, 24.0 (*i*Pr CH_3), 25.5, 34.2 (Et CH_2), 47.8, 53.9 (*i*Pr CH), 110.1 ppm (=C−I), the boron-bound carbon n.o. EI-MS: *m*/*z* (%) = 447 (2.4) [M^+], 320 (100) [M^+ − I], 238 (39.8) [M^+ − I −$2C_3H_5$]. HR-MS (EI): *m*/*z* = 447.0079 [M^+]; calcd. for $^{12}C_{12}{}^1H_{24}N{}^{11}B{}^{127}I_2$ 447.0091 (Δ*m* = −1.2 mmu).

X-ray Structural Determinations: Crystal data and details of the structural determinations are listed in Table 1. The intensity data

 © 2004 Wiley-VCH Verlag GmbH & Co. KGaA, Weinheim

Table 1. Crystal data and structure refinement for **2a**, **3**, **9** and **9′**

	2a	**3**	**9**	**9′**
Empirical formula	$C_{12}H_{20}B_2I_2$	$C_6H_{10}B_2I_4$	$C_{11}H_{15}BI_3N$	$C_{11}H_{15}BI_3N$
Molecular weight	439.70	611.36	552.75	552.75
Crystal system	orthorhombic	monoclinic	monoclinic	orthorhombic
Space group	$Pna2_1$	$P2_1/n$	$P2_1/n$	Pbca
a (Å)	12.1078(7)	11.9871(7)	11.0923(9)	8.6602(4)
b (Å)	14.3226(8)	7.7401(4)	12.0214(10)	14.2028(7)
c (Å)	9.2587(5)	14.8450(9)	11.8779(10)	24.8358(13)
α [°]	90	90	90	90
β [°]	90	102.841(1)	92.848(2)	90
γ [°]	90	90	90	90
V (Å^3)	1605.6(2)	1342.9(2)	1581.9(2)	3054.8(3)
Z	4	4	4	8
$d_{calcd.}$ [g cm^{-3}]	1.819	3.024	2.321	2.404
μ (Mo-K_α) [mm^{-1}]	3.89	9.236	5.905	6.116
F(000)	832	1072	1008	2016
Crystal size [mm]	0.45 × 0.15 × 0.08	0.37 × 0.25 × 0.16	0.45 × 0.36 × 0.25	0.25 × 0.15 × 0.12
$\Theta_{max.}$ [°]	32.0	32.0	32.0	32.0
Index ranges *h*, *k*, *l*	0/17, 0/21, −13/13	−17/17, 0/11, 0/21	−16/16, 0/17, 0/17	0/12, 0/21, 0/36
Reflections collected	14404	412363	14891	29275
Independent (*R*int)	5198 (0.0274)	4559(0.0279)	5345(0.0270)	5281(0.0374)
No. of parameters	226	145	205	205
GooF	1.050	1.106	1.117	1.095
$R1(I > 2\sigma I)$	0.0219	0.0289	0.0273	0.0245
*wR*2 (all reflections)	0.0526	0.0734	0.0714	0.0592
Resid. electron density [e·Å^{-3}]	1.240/ −0.518	2.265/−2.149	1.476/ −2.388	1.695/−0.694

for **2a**, **3**, **9, 9′** were collected with a Bruker AXS Smart CCD diffractometer at 103(2) K (graphite-monochromated Mo-K_α radiation, λ = 0.71073 Å, , ω-scans). Data were corrected for Lorenz polarization and absorption effects (semiempirical, SADABS[31]). The structures were solved by direct methods (SHELXS-86)[32] and refined by least-squares methods based on F^2 with all measured reflections (SHELXL-97).[32] All non-hydrogen atoms were refined anisotropically. CCDC-219079 (for **2a**), -219080 (for **3**), -219081 (for **9**) and -219082 (for **9′**) contain the supplementary crystallographic data for this paper. These data can be obtained free of charge at www.ccdc.cam.ac.uk/conts/retrieving.html [or from the Cambridge Crystallographic Data Center, 12 Union Road, Cambridge CB2 1EZ, UK; Fax: (internat.) + 44-1223-336-033; E-mail: deposit@ccdc.cam.ac.uk].

Acknowledgments

We thank the Deutsche Forschungsgemeinschaft (DFG, Schwerpunktprogramm Polyeder) and the Fonds der Chemischen Industrie for financial support of this work.

[1] [1a] P. L. Timms, *Acc. Chem. Res.* **1973**, 118−123. and refs. therein. [1b] G. E. Herberich, B. Hessner, *J. Organomet. Chem.* **1978**, *161*, C36−C40. [1c] G. E. Herberich, B. Hessner, *Chem. Ber.* **1982**, *115*, 3115−3127. [1d] B. Wrackmeyer, G. Kehr, *Polyhedron* **1991**, *10*, 1497−1506 and refs. therein.

[2] [2a] P. Binger, *Tetrahedron Lett.* **1966**, 2675−2680. [2b] P. Binger, *Angew. Chem.* **1968**, *80*, 288−289; *Angew. Chem. Int. Ed. Engl.* **1968**, *7*, 286. [2c] R. Köster, M. A. Grassberger, *Angew. Chem.* **1967**, *79*, 197; *Angew. Chem. Int. Ed. Engl.* **1967**, *6*, 218. [2d] L. Killian, B. Wrackmeyer, *J. Organomet. Chem.* **1977**, *132*, 213−221. [2e] H. O. Berger, H. Nöth, B. Wrackmeyer, *Chem. Ber.* **1979**, *112*, 2884−2893.

[3] [3a] G. Herberlich, H. Ohst, H. Mayer, *Angew. Chem.* **1984**, *96*, 975−980; *Angew. Chem. Int. Ed. Engl.* **1984**, *23*, 969. [3b] M. Enders, H. Pritzkow, W. Siebert, *Angew. Chem.* **1992**, *104*, 628−629; *Angew. Chem. Int. Ed. Engl.* **1992**, *31*, 606−607. [3c] H. Michel, D. Steiner, S. Wocadlo, J. Allwohn, N. Stamatis, W. Massa, A. Berndt, *Angew. Chem.* **1992**, *104*, 629−632; *Angew. Chem. Int. Ed. Engl.* **1992**, *31*, 607.

[4] [4a] T. P. Onak, G. T. F. Wong, *J. Am. Chem. Soc.* **1970**, *92*, 5226−5226. [4b] V. R. Miller, R. N. Grimes, *Inorg. Chem.* **1972**, *11*, 862−865.

[5] [5a] B. Wrackmeyer, G. Kehr, *J. Organomet. Chem.* **1995**, *501*, 87−93. [5b] B. Wrackmeyer, A. Glöckle, *Z. Naturforsch., Teil B* **1996**, *51*, 859−864. [5c] B. Wrackmeyer, G. Kehr, unpublished results, cited in ref.[5b] [5d] B. Wrackmeyer, A. Glöckle, *Main Group Metal Chem.* **1997**, *20*, 181−189. [5e] B. Wrackmeyer, G. Kehr, A. Gloeckle, *Phosphorus, Sulfur, and Silicon* **1997**, *131*, 25−35. [5f] M. Herberhold, U. Bertholdt, W. Milius, A. Glöckle, B. Wrackmeyer, *Chem. Commun.* **1996**, 1219−1220.

[6] [6a] C. Balzereit, H. J. Winkler, W. Massa, A. Berndt, *Angew. Chem.* **1994**, *106*, 2394−2396; *Angew. Chem. Int. Ed. Engl.* **1994**, *33*, 2306. [6b] B. Deobald, J. Hauss, H. Pritzkow, D. Steiner, A. Berndt, W. Siebert, *J. Organomet. Chem.* **1994**, *481*, 205−210.

[7] J. Hauss, A. Krämer, H. Pritzkow, W. Siebert, *Z. Naturforsch., Teil B* **1994**, *49*, 1677−1683.

[8] [8a] M. Hildenbrand, *PhD Thesis*, University of Heidelberg, **1986**. [8b] A. Maier, *PhD Thesis*, University of Heidelberg, **2002**.

[9] R. Full, *PhD Thesis*, University of Würzburg, **1976**.

[10] T. Onak, M. Diaz, M. Barfield, *J. Am. Chem. Soc.* **1995**, *117*, 1403−1410.

[11] [11a] S. Schwiegk, *Master Degree Thesis*, University of Heidelberg, **1988**. [11b] Houben-Weyl, Methoden der Organischen Chemie, Band 13/3a; R. Köster, W. Siebert (Eds.), **1982**, p. 468. Information regarding the formation of *cis*-3,4-Bis(diiodoboryl)-3-hexene is not correct. The redox reaction only works when Et_2C_2 is treated with $RHC(BI_2)_2$ to give the corresponding 4,5-diethyl-1,3-diiodo-2,3-dihydro-1,3-diborols (p. 401). See also ref.[23] in this paper.

 © 2004 Wiley-VCH Verlag GmbH & Co. KGaA, Weinheim

[12] W. Siebert, M. Hildenbrand, P. Hornbach, G. Karger, H. Pritzkow, *Z. Naturforsch., Teil B* **1989**, *44*, 1179−1186.
[13] F. Joy, M. F. Lappert, B. Prokai, *J. Organomet. Chem.* **1966**, *5*, 506−519.
[14] J. J. Eisch, H. P. Becker, *J. Organomet. Chem.* **1979**, *171*, 141−153.
[15] [15a] S. M. Van der Kerk, A. C. M. Van Eekeren, G. J. M. Van der Kerk, *J. Organomet. Chem.* **1980**, *190*, C8−C10. [15b] S. M. Van der Kerk, P. H. M. Budzelaar, A. C. M. Van Eekeren, G. J. M. Van der Kerk, *Polyhedron* **1984**, *3*, 271−280.
[16] R. Schlögl, B. Wrackmeyer, *Polyhedron* **1985**, *4*, 885−892.
[17] P. H. M. Budzelaar, S. M. Van der Kerk, K. Krogh-Jespersen, P. v. R. Schleyer, *J. Am. Chem. Soc.* **1986**, *108*, 3960−3967.
[18] W. Siebert, R. Full, J. Edwin, K. Kinberger, *Chem. Ber.* **1978**, *111*, 823−831.
[19] [19a] H. C. Brown, *Hydroboration*, **1962**, Benjamin, New York. [19b] M. F. Lappert, B. Prokai, *J. Organomet. Chem.* **1964**, *1*, 384−400. [19c] J. R. Blackborow, *J. Chem. Soc., Perkin Trans. 2* **1973**, 1989−1993. [19d] J. R. Blackborow, *J. Organomet. Chem.* **1977**, *128*, 161−166.
[20] K. Kinberger, *PhD Thesis*, University of Würzburg, **1976**.
[21] B. Wrackmeyer, *Polyhedron* **1986**, *5*, 1709−1721.
[22] B. Wrackmeyer, R. Köster, Houben-Weyl, *Methoden der Organischen Chemie*, Vol. 13/3c, pp. 373−611, Thieme Verlag, Stuttgart, **1984**.
[23] W. Siebert, U. Ender, W. Herter, *Z. Naturforsch., Teil B* **1985**, *40*, 326−330.
[24] J.-K. Uhm, H. Roemich, H. Wadepohl, W. Siebert, *Z. Naturforsch., Teil B* **1988**, *43*, 306−308.
[25] J. Haase, *Z. Naturforsch., Teil A* **1973**, *28*, 785−788.
[26] J. P. Pasinski, R. A. Beaudet, *J. Chem. Soc., Chem. Commun.* **1973**, 928−929.
[27] [27a] H.-J. Yao, C.-H. Hu, P. Paetzold, *Z. Anorg. Allg. Chem.* **2001**, *627*, 2477−2480. [27b] W. Jiang, C. B. Knobler, C. E. Curtis, M. D. Mortimer, F. Hawthorne, *Inorg. Chem.* **1995**, *34*, 3491−3498.
[28] M. A. Ring, J. D. H. Donnay, W. S. Koski, *Inorg. Chem.* **1962**, *1*, 109−111.
[29] [29a] G. J. Bullen, P. R. Mallinson, *J. Chem. Soc., Dalton Trans.* **1972**, 1143−1148. [29b] U. Monkowius, S. Nogai, H. Schmidbaur, *Dalton Trans.* **2003**, 987−991.
[30] [30a] A. Maderna, H. Pritzkow, W. Siebert, T. Sommerfeld, L. S. Cederbaum, *Z. Naturforsch., Teil B* **1997**, *52*, 1315−1320. [30b] M. Bayer, H. Pritzkow, W. Siebert, *Z. Naturforsch., Teil B* **2002**, *57*, 295−300.
[31] G. M. Sheldrick, SADABS, University of Göttingen, **1999**.
[32] G. M. Sheldrick, SHELXS-86, University of Göttingen, **1986**, G. M. Sheldrick, SHELXL-97, University of Göttingen, **1997**.

Received October 6, 2003
Early View Article
Published Online March 9, 2004

 © 2004 Wiley-VCH Verlag GmbH & Co. KGaA, Weinheim

Titanium Complexes Stabilized by a Sulfur-Bridged Chelating Bis(aryloxo) Ligand as Active Catalysts for Olefin Polymerization

Zofia Janas,[a] Lucjan B. Jerzykiewicz,[a] Katarzyna Przybylak,[a] Piotr Sobota,*[a] and Krzysztof Szczegot[b]

Keywords: Titanium / O,S,O ligands / Polymerization / X-ray diffraction / Aluminum

The mixed-ligand complexes $[Ti_2(\mu\text{-}OR)_2(OR)_2(\kappa^3\text{-}tbop)_2]$ (**1a**) for R = Me and (**1b**) R = Et were prepared by the reaction of $Ti(OR)_4$ and H_2tbop {H_2tbop = 2,2′-thiobis[4-(1,1,3,3-tetramethylbutyl)phenol]} in methanol. Treatment of **1a** and **1b** with $AlMe_3$ led to the substitution of terminal alkoxy groups to create the organometallic compounds $[Ti_2(\mu\text{-}OR)_2(\kappa^3\text{-}tbop)_2(Me)_2]$ (**2a**) for R = Me and (**2b**) for R = Et. Controlled hydrolysis of **2b** causes the evolution of methane and the formation of the titanoxane compounds $[\{Ti_2(\mu\text{-}OEt)_2(\kappa^3\text{-}tbop)_2\}_2(\mu\text{-}O)_2]\cdot 2CH_2Cl_2$ (**3**). Structures of **1a**, **1b**, **2a**, **2b**, and **3** were confirmed by NMR spectroscopy; **1b** and **3** were further investigated with X-ray crystallography. Compounds **1a**, **1b**, **2a**, and **2b** were supported on $MgCl_2$ and when activated with aluminum alkyls, found to effectively polymerize ethylene.

(© Wiley-VCH Verlag GmbH & Co. KGaA, 69451 Weinheim, Germany, 2004)

Introduction

Titanium complexes with the formula $[Ti(tbmp)X_2]$ which is derived from the sulfide-linked bis(phenol) H_2tbmp [tbmp = 2,2′-thiobis(6-*tert*-butyl-4-methylphenolato); X = Cl, O*i*Pr] and activated with methylaluminoxane (MAO), were first reported by Kakugo et al. to be highly active in the polymerization of ethylene, propylene, styrene, and dienes, as well as the copolymerization of ethylene with styrene.[1−3] These titanium complexes were found to be more active than the methylene-bridged chelating aryloxide complexes of the type $[Ti(mbmp)X_2]$ [mbmp = 2,2′-methylenebis(6-*tert*-butyl-4-methylphenolato)].[4] This is in qualitative agreement with theoretical studies that showed S-bridged chelating alkoxides to have lower insertion barriers than their methylene-bridged or directly bridged analogues.[5−7] Although the Ti−S interaction in $[Ti(tbmp)X_2]$ is weak, it is likely to be of importance in stabilizing the active cationic species, facilitating its formation from $[Ti(tbmp)X_2]$ and MAO, making the coordination of the counterion more flexible.[8] Titanium bis(phenolato) and bis(naphtholato) complexes are well characterized either structurally or spectroscopically in addition to the kinetics and thermodynamics of the intra- and intermolecular rearrangement in bis(naphtholates) which are also described.[9−10] It is worth noting that molybdenum derivatives containing these ligands have also been intensively investigated and employed for asymmetric olefin metathesis[11] as well as for various ring-closing reactions.[12] However, structural data on thio analogues, especially of their ligand modifications, are still limited.[5,13]

Our work is primarily concerned with the synthesis and structural characterization of titanium compounds with the tridentate (OSO-function) thiobis(phenolato) ligand: 2,2′-thiobis[4-(1,1,3,3-tetramethylbutyl)phenolato] (tbop; Scheme 1). Except for the S-bridge, the tbop ligand appeared to have an extra attractive feature, that is, the long sterically hindered auxiliary group 4-(1,1,3,3-tetramethylbutyl) on the thiobis(phenolato) ligand. This substituent sufficiently increases solubility of the catalyst in hydrocarbons. It was interesting for us to see whether these features of the tbop ligand would help create highly active catalytic systems in the heterogeneous ethylene polymerization process.

Results and Discussion

The thiobis(phenol) H_2tbop reacts smoothly with $Ti(OR)_4$ (R = Me, Et) in an appropriate alcohol producing **1a** and **1b**, which are sparingly soluble in alcohols, but readily soluble in common organic solvents (such as toluene, hexane, CH_2Cl_2 and tetrahydrofuran) to give yellow crystals of the complexes $[Ti_2(\mu\text{-}OR)_2(OR)_2(\kappa^3\text{-}tbop)_2]$ (**1a**) for R = Me, (**1b**) for R = Et (Scheme 1).

Compounds **1a** and **1b** are very stable and can be stored for a long time in air. The ^{1}H NMR spectra are invariant over a wide temperature range and show two singlets of OCH_3 (δ = 4.61, 4.29 ppm) for **1a** and two sets of CH_3

[a] Faculty of Chemistry, University of Wrocław,
14 F. Joliot-Curie Street, 50-383 Wrocław, Poland
Fax: (internat.) + 48-71-3282348
E-mail: plas@wchuwr.chem.uni.wroc.pl
[b] Institute of Chemistry, University of Opole,
48 Oleska Street, 45-052 Opole, Poland

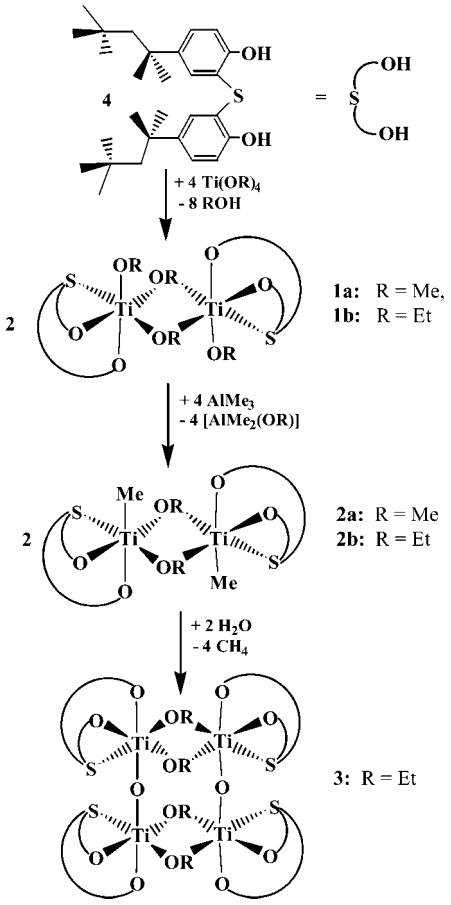

Scheme 1

(t, δ = 1.49; 1.37 ppm) and CH_2 (q, δ = 4.88; 4.78 ppm) resonances of OCH_2CH_3 for **1b** of terminal- and bridging-coordinated alkoxy groups , respectively, suggesting dimeric structures of these complexes exist in solution. A single-crystal X-ray diffraction study for **1b** in the solid state confirmed the structure deduced from ^{1}H NMR spectroscopy (Figure 1).

The crystal structure of **1b** comprises a centrosymmetric dimer with a planar Ti_2O_2 core. The coordination sphere around the titanium center can be described as octahedral with the oxygen atoms of the tbop ligand [O(11), O(21)] and of two bridging OEt groups [O(1), O(1)$^{(i)}$] forming the equatorial plane, while the O(2) oxygen atom of the terminal OEt ligand and the sulfur link of the tbop group occupy the apical sites. The two Ti−O(aryloxide) distances of 1.896(2) and 1.916(2) Å are in the expected range for Ti^{IV} complexes with nonbridging aryloxide ligands.[4] The Ti−O(ethoxide) distances of 1.762(2) and 2.009(2) Å are different according to their terminal and bridging nature, respectively, and are typical of $Ti_2(\mu\text{-}OR)_2(OR)$ moieties.[14] The Ti−S bond length of 2.800(1) Å is one of the longest so far reported in the literature;[15] this is substantially longer than Ti−S single bonds (typically 2.3−2.4 Å).[16] Shorter Ti−S bond lengths were reported in the following complexes: for example, $[Ti_2(\mu\text{-}O\textit{i}Pr)_2(O\textit{i}Pr)_2(\kappa^3\text{-tbmp})_2]$, where tbmp = 2,2′-thiobis(6-*tert*-butyl-4-methylphenolato) 2.719(1) Å, $[Ti(\kappa^3\text{-tbmp})\{\kappa^2\text{-}C_6H_4(CH_2NMe_2)_2\}Cl]$ 2.704(1) Å, and $[Ti(\kappa^3\text{-tbmp})Cl(O\textit{i}Pr)(HO\textit{i}Pr)]$ 2.693(1) Å.[5,13] The geometry of the Ti−S interaction in **1b** is characterized by the angle of 0.7° between the normal of the plane defined by S, C(12), C(22); the Ti−S direction is somewhat smaller than that found in $[Ti_2(\mu\text{-}O\textit{i}Pr)_2(O\textit{i}Pr)_2(\kappa^3\text{-tbmp})_2]$ (4°),[5] and is due to the interaction of one of the sulfur lone pairs with the electrophilic Ti atom. However, if the Ti−S interaction is disregarded the coordination can be described as a distorted square-based pyramid with an eight membered ring which has boat-boat conformation.

Reaction of complexes **1a** and **1b** with an excess of $AlMe_3$ in toluene produces light-yellow crystals of the thermally stable organometallic compounds $[Ti_2(\mu\text{-}OR)_2(\kappa^3\text{-tbop})_2(Me)_2]$ (**2a** for R = Me and **2b** for R = Et). Unfortunately, the poor quality of the X-ray data for **2b** prevents us from discussing the bond lengths and angles in detail.[17] Nonetheless, the central core of **2b** is clearly visible as a dimer similar to compound **1b** where the terminal ethoxides are substituted by methyl groups (Scheme 1). The $[Ti_2(\mu\text{-}OMe)_2(Me)_2]$ unit has been observed in the $[Ti_2(\mu\text{-}OMe)_2(tritox)_2(Me)_4]$ (tritox = tBu$_3$CO$^-$) complex obtained by controlled interaction of O_2 with the [Ti(tritox)$(Me)_3$] complex.[18] The presence of the Ti−C bonds was confirmed by the ^{1}H NMR spectra at room temperature as a singlet (δ = 2.22 ppm for **2a**; δ = 2.23 ppm for **2b**). For comparison, two singlets (δ = 1.38 and 1.36 ppm) of Ti−CH_3 for $[Ti(\kappa^2\text{-mbp})(CH_3)_2]$ [mbp = 2,2′-methylenebis(6-*tert*-butyl-4-methylphenolato)][4a] and one singlet (δ = 1.22 ppm) for $[Ti(CH_3)_4]\cdot Et_2O$ were detected.[19] Additional evidence for the formation of the Ti−C bond was achieved during controlled hydrolysis of **2b**. Treatment of **2b** with an excess of water in toluene resulted in the evolution of methane detected by GC-MS method and the changing color of the reaction mixture from yellow to orange-red. After workup of the post-reaction mixture, red crystals of $[\{Ti_2(\mu\text{-}OEt)_2(\kappa^3\text{-tbop})_2\}_2(\mu\text{-}O)_2]\cdot 2CH_2Cl_2$ (**3**) were isolated. The solid-state structure of **3** is shown in Figure 2.

Crystals of **3** consist of two $[Ti_2(\mu\text{-}OEt)_2(\kappa^3\text{-tbop})_2]$ units linked by two μ-O(oxo) atoms coordinated to the titanium atoms with two CH_2Cl_2 solvent molecules of crystallization. The four titanium atoms in **3** have equivalent distorted octahedral geometry. Also the individual Ti−μ-O(oxo) bond lengths are broadly similar and are in the range observed for titanoxanes; for example $[Ti_2(\mu\text{-}O)Cl_2(guaiacolato)_4]$,[20] $[Ti_4(\mu\text{-}O)_4(guaiacolato)_8]$,[20] and $[Ti_4(\mu\text{-}O)_4Cl_8(MeCN)_6]$[21] are formed in situ by controlled hydrolysis of the titanium species. The formation of compound **3** upon hydrolysis of **2b** with an excess of H_2O confirms particular stability of the μ-OR bridges. In contrast, upon deliberate hydrolysis of the monomeric compound [Ti(mbmp)$(O\textit{i}Pr)_2$] [mbmp = 2,2′-methylenebis(6-*tert*-butyl-4-methylphenolato)] with one equivalent of water, the formation of $[Ti(mbmp)_2]$ as a main product was observed and crystallographically confirmed.[4c]

 © 2004 Wiley-VCH Verlag GmbH & Co. KGaA, Weinheim

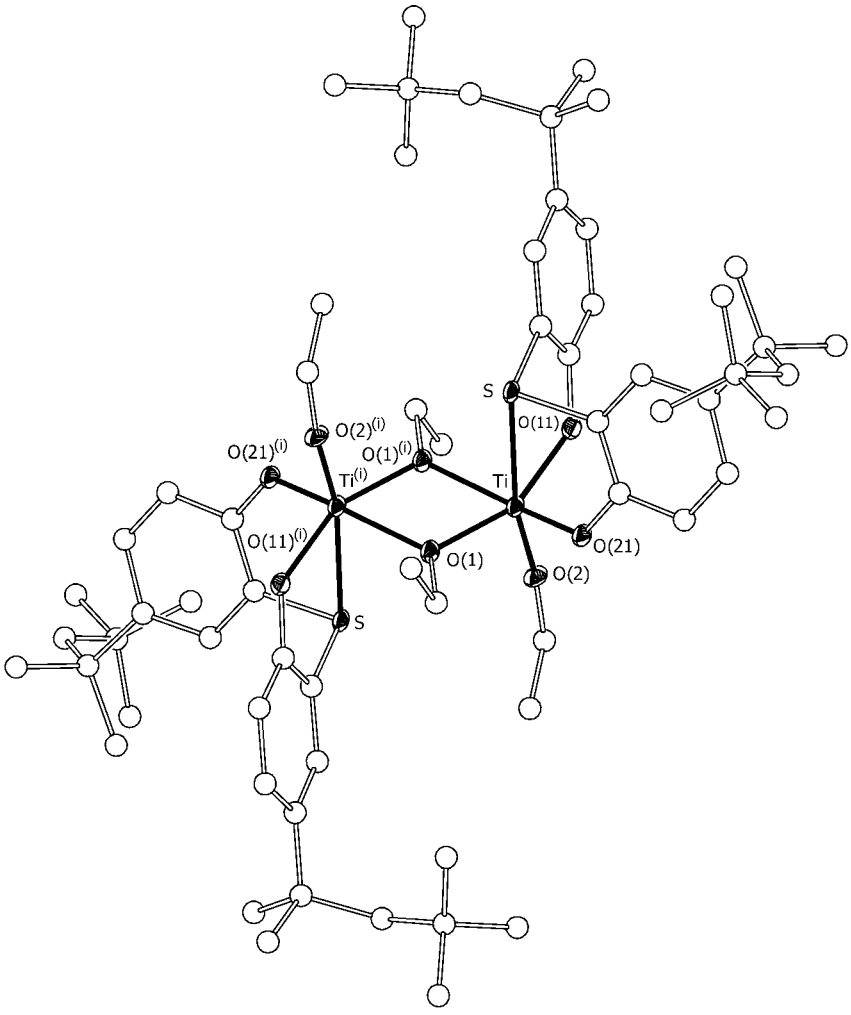

Figure 1. The molecular structure of **1b**; hydrogen atoms and second positions of disordered carbon atoms are omitted for clarity; the displacement ellipsoids are drawn at the 50% probability level; C atoms are represented by open circles of an arbitrary radii. Ti−Ti$^{(i)}$ 3.232(2), Ti−S 2.800(1), Ti−O(1) 2.009(2), Ti−O(2) 1.762(2), Ti−O(11) 1.896(2), Ti−O(21) 1.916(2); O(2)−Ti−O(11) 98.8(1), O(2)−Ti−O(21) 99.1(1), O(11)−Ti−O(21) 99.2(1), O(2)−Ti−O(1) 101.5(1), O(11)−Ti−O(1) 155.8(1), O(21)−Ti−O(1) 90.5(1), O(2)−Ti−O(1)$^{(i)}$ 102.4(1), O(11)−Ti−O(1)$^{(i)}$ 89.6(1), O(21)−Ti−O(1)$^{(i)}$ 155.2(1), O(1)−Ti−O(1)$^{(i)}$ 73.3(1), O(2)−Ti−S 169.5(1), O(11)−Ti−S 74.9(1), O(21)−Ti−S 74.1(1), O(1)−Ti−S 86.8(1), O(1)$^{(i)}$−Ti−S 86.1(1); symmetry transformations used to generate equivalent atoms: $^{(i)}$ $-x + 1, -y + 2, -z$

Catalysts based on complexes **1a**, **1b**, **2a**, and **2b** are highly active systems for the polymerization of ethylene. They were prepared in *n*-hexane by milling (see Exp. Sect.) a slurry of $MgCl_2(THF)_2$ with one equivalent of the titanium compound and $AlEt_2Cl$ or $AlEt_2Cl/AlEt_3$ (1:1) as the cocatalysts. Ethylene polymerization results; the polymer characterization data are summarized in Table 1.

For comparison of catalyst activities, titanocene dichloride ($[Cp_2TiCl_2]$) was used as a reference under the same conditions (Table 1, Entry 9). It turned out that the catalyst based on the complex **2b** (Entry 7) exhibited the highest catalytic activity (204,760 g·PE·mmol^{-1}·h^{-1}) for ethylene polymerization. This is about fourfold more than with catalysts based on $[Ti_2(\mu\text{-}OEt)_2(OEt)_4(\kappa^2\text{-maltolato})_2]$ (54,630 g·PE·mmol^{-1}·h^{-1}, 50 °C, 0.5 MPa, catalyst 0.01 mmol, $AlEt_2Cl/AlEt_3$ 5 mmol, in *n*-hexane)[20] and the species formulated as $[Ti(tbmp)X_2]$ (47,620 g·PE·mmol^{-1}·h^{-1}; 20 °C, 3 MPa, catalyst 0.2 mmol, MAO 25 mmol, in toluene),[2b] but is less than for $[Ti(tbmp)X_2]$/MAO (390,476 g·PE·mmol^{-1}·h^{-1} for X = Cl and 356,315 g·PE·mmol^{-1}·h^{-1} for X = O*i*Pr; 20 °C, 3 MPa, catalyst 0.001 mmol, MAO 5.17 mmol, toluene) originally reported by Kakugo.[1b,1c] Molecular weights of the polymers produced employing complexes **1a**, **1b**, **2a**, and **2b** under these conditions range from 637,000 to 1,010,000. Polydispersities M_w/M_n for **1a**, **1b**, **2a**, and **2b** (see Table 1) are much narrower than those reported for ethylene polymerization with catalysts based on $[Ti_2(\mu\text{-}OEt)_2(OEt)_4(\kappa^2\text{-maltolato})_2]$ (6.11)[20] and $[Ti(tbmp)X_2]$ (11.9).[2b] It would appear that for polymerization of ethylene, activation at least those systems with $M_w/M_n < 3$ (Entries 3, 4, 7) does afford a single well-defined active species. This indicates that the cocatalyst does not abstract the tbop ligand from the titanium center. In fact, this was confirmed by the results of the interaction of **1a** and **1b** with $AlMe_3$ that showed only the migration of the terminal OR groups to aluminium atoms (Scheme 1). The

 © 2004 Wiley-VCH Verlag GmbH & Co. KGaA, Weinheim

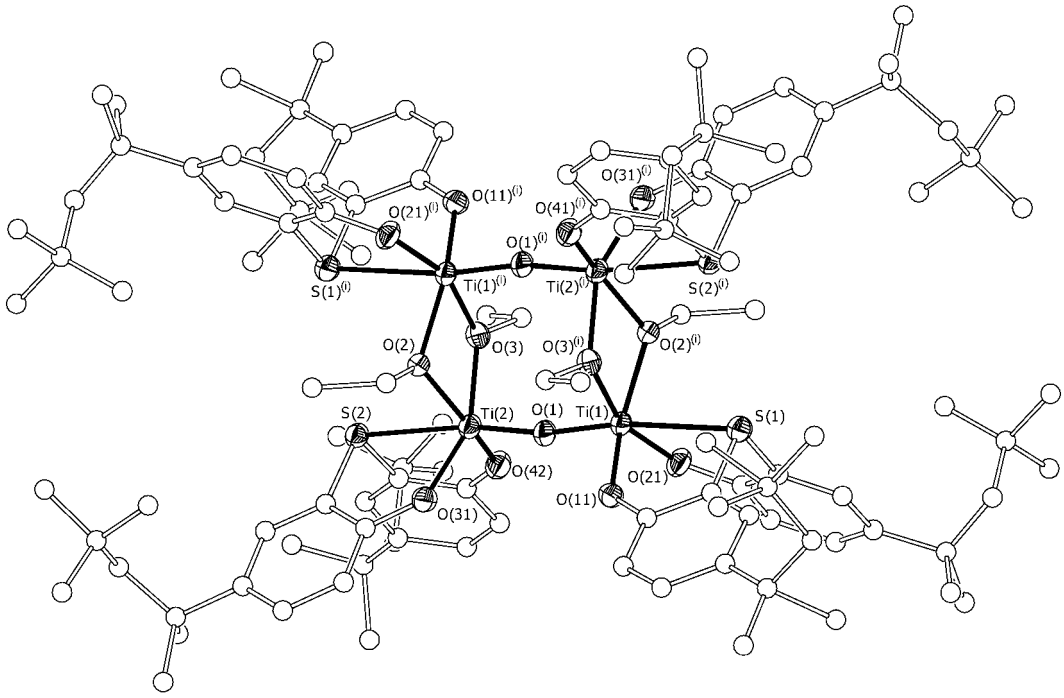

Figure 2. The molecular structure of **3** without solvent molecules with atom numbering scheme; the displacement ellipsoids are drawn at the 50% probability level; H atoms are excluded for clarity; C atoms are represented by circles of an arbitrary radii; selected bond lengths (A): Ti(1)−Ti(2)$^{(i)}$ 3.204(2), Ti(1)−S(1) 2.762(2), Ti(1)−O(1) 1.816(3), Ti(1)−O(2)$^{(i)}$ 2.000(3), Ti(1)−O(3)$^{(i)}$ 2.011(3), Ti(1)−O(11) 1.878(4), Ti(1)−O(21) 1.866(3), Ti(2)−S(2) 2.770(2), Ti(2)−O(1) 1.795(3), Ti(2)−O(2) 2.017(3), Ti(2)−O(3) 2.004(3), Ti(2)−O(31) 1.878(4), Ti(2)−O(41) 1.870(4); O(1)−Ti(1)−O(21) 99.1(2), O(1)−Ti(1)−O(11) 98.4(2), O(21)−Ti(1)−O(11) 98.7(2), O(1)−Ti(1)−O(2)$^{(i)}$ 101.6(2), O(21)−Ti(1)−O(2)$^{(i)}$ 92.5(2), O(11)−Ti(1)−O(2)$^{(i)}$ 155.2(2), O(1)−Ti(1)−O(3)$^{(i)}$ 99.1(2), O(21)−Ti(1)−O(3)$^{(i)}$ 158.5(2), O(11)−Ti(1)−O(3)$^{(i)}$ 89.9(2), O(2)$^{(i)}$−Ti(1)−O(3)$^{(i)}$ 72.7(2), O(1)−Ti(1)−S(1) 171.4(2), O(21)−Ti(1)−S(1) 75.6(2), O(11)−Ti(1)−S(1) 76.0(2), O(2)$^{(i)}$−Ti(1)−S(1) 85.6(1), O(3)$^{(i)}$ −Ti(1)−S(1) 87.5(1); symmetry transformations used to generate equivalent atoms: (i) $-x + 1, -y + 1, -z$

Table 1. Ethylene polymerization

Entry	Complex[a]	Cocatalyst	Activity[b]	M_w/M_n	D(g·cm^3)
1	**1a**	$AlEt_2Cl$	116,660	4.35	0.963
2	**1a**	$AlEt_2Cl/AlEt_3$ [c]	132,220	4.06	0.967
3	**1b**	$AlEt_2Cl$	120,590	2.94	0.960
4	**1b**	$AlEt_2Cl/AlEt_3$ [c]	150,590	2.77	0.957
5	**2a**	$AlEt_2Cl$	110,160	3.09	0.962
6	**2a**	$AlEt_2Cl/AlEt_3$ [c]	77,540	3.38	0.965
7	**2b**	$AlEt_2Cl$	204760	2.65	0.964
8	**2b**	$AlEt_2Cl/AlEt_3$ [c]	111,900	4.43	0.963
9	Cp_2TiCl_2	$AlEt_2Cl$	30,000	2.44	0.965

[a] Polymerization conditions: $[Ti]_0 = 0.005$ mmol·dm^{-3}, [Al] = 5 mmol·dm^{-3}, Mg/Ti = 10. [b] Units of activity are g·PE·mmol^{-1}·h^{-1}. [c] $AlEt_3Cl/AlEt_3$, 1:1.

preliminary polymerization results on our Ziegler−Natta-like systems are promising on account of the production of a polymer with sufficiently narrow particle-size distributions. To obtain polymers with satisfactory polydispersity properties and high bulk densities we are now investigating the properties of the new catalysts based on modified titanium complexes described here.

Conclusions

The reaction of $Ti(OR)_4$ with H_2tbop in 1:1 molar ratio results in the formation of dimeric mixed-ligand complexes **1a** and **1b**. Treatment of **1a** and **1b** with an excess of $AlMe_3$ leads to the substitution of only terminal alkoxides by methyl groups to form organometallic compounds **2a** and **2b**. The Ti−C bond in **2a** and **2b** is thermally stable but very sensitive to moisture. The reaction of **2b** with water affords the titanoxane species **3**. In fact, the μ-OR bridges in **2a** and **2b** are very stable and do not undergo substitution either by $-CH_3$ groups or alkoxy oxygen atoms. Compounds **1a**, **1b**, **2a**, and **2b** supported on $MgCl_2$ and activated with $AlEt_2Cl$ or $AlEt_2Cl/AlEt_3$ show very high activity in ethylene polymerization. Narrow molecular weight distribution for these systems indicates that the operation of heterogeneous single-site catalysts occurs.

Experimental Section

General Remarks: All operations were carried out under dry nitrogen, using standard Schlenk techniques. All the solvents were distilled under nitrogen from the appropriate drying agents prior to use. The compounds $Ti(OMe)_4$, $Ti(OEt)_4$, $AlMe_3$, $AlEt_2Cl$, and 2,2′-

 © 2004 Wiley-VCH Verlag GmbH & Co. KGaA, Weinheim

thiobis{4-(1,1,3,3-tetramethylbutyl)phenol} (H_2tbop) were obtained from the Aldrich Chemical Co. and used without further purification unless stated otherwise. Infrared spectra were recorded with a Perkin−Elmer 180 spectrophotometer as Nujol mulls. NMR spectra were performed with a Bruker ARX 300 spectrometer. Microanalysis were conducted with a ASA-1 (GDR, Karl- Zeiss-Jena) instrument (in-house).

Synthesis of $[Ti_2(\mu\text{-}OMe)_2(OMe)_2(\kappa^3\text{-}tbop)_2]$ (1a): $Ti(OMe)_4$ (1.40 g, 8.1 mmol) was added to a solution of H_2tbop (3.60 g, 8.1 mmol) in methanol (50 mL); the mixture was stirred at room temperature for 12 h . A yellow microcrystalline solid was filtered off, washed with methanol, and dried under vacuum. Yield 4.25 g (95 %). $C_{60}H_{92}O_8S_2Ti_2$: calcd. C 65.44, H 8.42, S 5.82; found C 65.12, H 8.25, S 6.12. IR (Nujol mulls, cm^{-1}): $\tilde{\nu}$ = 440 (w), 454 (w), 546 (vs), 576 (vs), 629 (s), 672 (s), 730 (s), 758 (s), 825 (vs), 866 (s), 880 (s), 888 (s), 1028 (s), 1070−1098 (br., s), 1122 (vs), 1208 (w), 1280 (w), 1249 (s), 1280 (vs), 1298 (vs), 1323 (w), 1362 (s), 1344 (w), 1396 (m), 1594 (w). ^{1}H NMR (300 MHz, C_6D_6, 25 °C): δ = 7.76−6.60 (12 H, C_6H_3), 4.61 (s, 6 H, μ-OCH_3), 4.29 (s, 6 H, OCH_3), 1.68 [s, 8 H, $C(CH_3)_2CH_2C(CH_3)_3$], 1.35 [s, 24 H, $C(CH_3)_2CH_2C(CH_3)_3$], 0.82 [s, 36 H, $C(CH_3)_2CH_2C(CH_3)_3$] ppm. ^{13}C NMR (300 MHz, C_6D_6, 25 °C): δ = 165.9, 142.2, 131.9, 129.8, 127.2, 115.9 (C_6H_3), 68.2, 63.0 (OCH_3), 57.1, 38.2, 32.5, 32.0, 31.8 [$C(CH_3)_2CH_2C(CH_3)_3$] ppm.

$[Ti_2(\mu\text{-}OEt)_2(OEt)_2(\kappa^3\text{-}tbop)_2]$ (1b): This compound was obtained in 90 % yield as a yellow crystalline solid from appropriate quantities of $Ti(OEt)_4$ and H_2tbop by a method similar to that of **1a**. Crystals suitable for the structure determination were obtained from the post-reaction mixture after standing for one day at room temperature. $C_{64}H_{100}O_8S_2Ti_2$: calcd. C 66.42, H 8.71, S 5.54; found C 66.93, H 8.98, S 6.12%. IR (Nujol mulls, cm^{-1}): $\tilde{\nu}$ = 310 (vw), 440 (w), 496 (s), 546 (vs), 580 (s), 622 (s), 680 (s), 740 (s), 764 (s), 834 (vs), 896 (vs), 930 (s), 976 (w), 1028 (s), 1070 (vs), 1122 (vs), 1208 (w), 1248 (s), 1282(vs), 1302 (vs), 1334 (s), 1544 (w), 1596 (m), 1652 (vw). ^{1}H NMR (300 MHz, C_6D_6, 25 °C): δ = 7.76−6.60 (12 H, C_6H_3), 4.98 (q, 4 H, μ-OCH_2CH$_3$), 4.71 (q, 4 H, OCH_2CH$_3$), 1.70 [s, 8 H, $C(CH_3)_2CH_2C(CH_3)_3$], 1.58 (t, 6 H, μ-OCH$_2$CH_3), 1.32 [m, 6 H, μ-OCH$_2$CH_3 and 24 H, $C(CH_3)_2CH_2C(CH_3)_3$], 0.82 [s, 36 H, $C(CH_3)_2CH_2C(CH_3)_3$] ppm. ^{13}C NMR (300 MHz, C_6D_6, 25 °C): δ = 166.3, 142.0, 131.9, 129.8, 127.3, 116.0 (C_6H_3), 76.8, 71.4 (OCH_2CH$_3$), 57.1, 38.1, 32.4, 31.9, 31.7 [$C(CH_3)_2CH_2C(CH_3)_3$], 18.9, 18.4 (OCH$_2$CH_3) ppm.

$[Ti_2(\mu\text{-}OMe)_2(Me)_2(\kappa^3\text{-}tbop)_2]$ (2a): $AlMe_3$ (0.26 g, 3.6 mmol) was added to an orange solution of **1a** (2.00 g, 1.8 mmol) in toluene (50 mL). The brown mixture was stirred for 24 h. The solvent was evaporated off to give an oily residue, after which addition of *n*-hexane (30 mL) and stirring gave a light yellow solid. This was filtered off, washed with *n*-hexane (3 × 5 mL) and dried in vacuo. Yield 1.43 g (74%). $C_{60}H_{92}O_6S_2Ti_2$: calcd. C 67.39, H 8.67, S 6.00; found C 67.12, H 8.62, S 5.89. IR (Nujol mulls, cm^{-1}): $\tilde{\nu}$ = 443 (w), 452 (w), 548 (vs), 572 (vs), 630 (s), 730 (s), 828 (vs), 867 (s), 882 (s), 1030 (s), 1073−1101(br., s), 1126 (vs), 1206 (w), 1282 (w), 1250 (s), 1278 (vs), 1294 (vs), 1320 (w), 1363 (s), 1340 (w), 1398 (m), 1594 (w). ^{1}H NMR (300 MHz, C_6D_6, 25 °C): δ = 7.88−6.69 (12 H, C_6H_3), 4.52 (s, 6 H, μ-OCH_3), 2.23 (s, 6 H, Ti−CH_3), 1.67 [s, 8 H, $C(CH_3)_2CH_2C(CH_3)_3$], 1.37 [s, 24 H, $C(CH_3)_2CH_2C(CH_3)_3$], 0.84 [s, 36 H, $C(CH_3)_2CH_2C(CH_3)_3$] ppm. ^{13}C NMR (300 MHz, C_6D_6, 25 °C): δ = 165.9, 142.2, 132.0, 130.0, 116.0 (C_6H_3), 68.4, (OCH_3), 57.1, 38.1, 32.4, 32.0, 31.8 [$C(CH_3)_2CH_2C(CH_3)_3$], 30.0 (T−CH_3) ppm.

$[Ti_2(\mu\text{-}OEt)_2(Me)_2(\kappa^3\text{-}tbop)_2]$ (2b): This compound was obtained in 59 % yield as a light yellow solid from appropriate quantities of **1b** and $AlMe_3$ by a similar method to that used to prepare **2a**. Crystals were obtained from the concentrated reaction mixture after standing for 3 days at room temperature. $C_{62}H_{96}O_6S_2Ti_2$: calcd. C 67.86, H 8.82, S 5.84; found C 67.25, H 8.68, S 5.28. IR (Nujol mulls, cm^{-1}): $\tilde{\nu}$ = 496 (m), 536 (s), 584 (s), 614 (m), 680 (m), 742 (m), 764 (m), 834 (s), 880 (s), 924 (w), 1024 (m), 1060 (m), 1116 (m), 1208 (w), 1250 (m), 1282 (s), 1302 (s), 1544 (vw), 1594 (w). ^{1}H NMR (300 MHz, C_6D_6, 25 °C): δ = 7.77−6.61 (12 H, C_6H_3), 4.78 (q, 4 H, μ-OCH_2CH$_3$), 2.23 (s, Ti−CH_3), 1.57 [s, 8 H, $C(CH_3)_2CH_2C(CH_3)_3$], 1.37 (t, 6 H, μ-OCH$_2$CH_3), 1.26 [s, 24 H, $C(CH_3)_2CH_2C(CH_3)_3$], 0.84 [s, 36 H, $C(CH_3)_2CH_2C(CH_3)_3$] ppm. ^{13}C NMR (300 MHz, C_6D_6, 25 °C): δ = 165.7, 142.6, 132.9, 129.5, 127.3, 115.8 (C_6H_3), 77.0 (OCH_2CH$_3$), 57.0, 38.1, 32.5, 32.0, 31.7 [$C(CH_3)_2CH_2C(CH_3)_3$], 30.5 (Ti−CH_3), 19.1 (OCH$_2$CH_3) ppm.

$[\{Ti_2(\mu\text{-}OEt)_2(\kappa^3\text{-}tbop)_2\}_2(\mu\text{-}O)_2]\cdot 2CH_2Cl_2$ (3): To a solution of **2b** (1.10 g, 0.8 mmol) in toluene (30 mL), 0.03 mL (1.7 mmol) of H_2O was added in one portion. The evolution of a gas was identified as methane by the GC-MS method. The reaction mixture was stirred for 2 h and then all volatiles were evaporated under vacuum. The residue was dissolved in CH_2Cl_2 (10 mL), CH_3CN (5 mL) was added and the mixture was left in a refrigerator. After 2 days, orange-red crystals suitable for X-ray study were isolated. Yield 0.56 g (54%). $C_{122}H_{184}Cl_4O_{14}S_4Ti_4$: calcd. C 62.72, H 7.94, Cl 6.07, S 5.49; found C 63.58, H 8.29, Cl 7.12, S 5.94%. IR (Nujol mulls, cm^{-1}): $\tilde{\nu}$ = 302 (vw), 448 (w), 500 (w), 538 (s), 580 (s), 622 (w), 640 (vw), 680 (m), 736 (s), 758 (s), 808 (vs), 828 (vs), 844 (s), 882 (m), 966 (vw), 1028 (m), 1084 (w), 1148 (vw), 1208 (vw), 1252 (m), 1280(s), 1298 (s), 1324 (w), 1544 (vw), 1594 (vw), 1652 (vw). ^{1}H NMR (300 MHz, C_6D_6, 25 °C): δ = 7.63−6.88 (24 H, C_6H_3), 5.96 (s, 4 H, CH_2Cl_2), 4.89 (q, 8 H, μ-OCH_2CH$_3$), 1.57 [s, 16 H, $C(CH_3)_2CH_2C(CH_3)_3$], 1.49 (t, 12 H, μ-OCH$_2$CH_3), 1.26 [s, 48 H, $C(CH_3)_2CH_2C(CH_3)_3$], 0.72 [s, 72 H, $C(CH_3)_2CH_2C(CH_3)_3$] ppm. ^{13}C NMR (300 MHz, C_6D_6, 25 °C): δ = 165.8, 142.5, 133.0, 129.8, 127.3, 115.7 (C_6H_3), 76.5 (μ-OCH_2CH$_3$), 57.2, 37.9, 32.1, 32.1, 31.8 [$C(CH_3)_2CH_2C(CH_3)_3$], 19.3 (μ-OCH$_2$CH_3).

Polymerization Test: A slurry of $MgCl_2(THF)_2$ (30 mmol) in *n*-hexane was milled under argon in a glass mill (capacity 250 mL, with 20 balls of diameter 5−15 mm) at room temperature for 6 h. Then the titanium compound (5 mmol) and *n*-hexane (50 mL) were added, and the mixture was milled for a further 24 h. The sample of pro-catalyst suspension (containing 0.01 % titanium) was activated with $AlEt_2Cl$ or $AlEt_2Cl/AlEt_3$ (1:1 molar ratio; 20 mmol) for 15 min at 323 K under argon to form a highly active catalyst. The polymerization of ethylene was carried out in *n*-hexane at 323 K in a stainless steel reactor (1 L), equipped with a stirrer, at 0.5 MPa ethylene pressure. The polymerization was quenched with a 5 % solution of HCl in methanol and dried under vacuum.

X-ray Crystallographic Study for 1b and 3: Crystal data collection and refinement are summarized in Table 2. Preliminary examination and intensity-data collections were carried out on a KUMA KM-4 κ-axis diffractometer with graphite-monochromated Mo-K_α and with a scintillation counter (**1b**) or a CCD camera (**3**). All data were corrected for Lorentz and polarization effects. Data reduction and analysis were carried out with the Kuma Diffraction programs.[22−23] The structures were solved by direct methods,[24] and refined by the full-matrix least-squares method on all F^2 data using the SHELXL-97 software.[25] Carbon bonded hydrogen atoms were included in calculated positions and refined in the riding mode using SHELXL-97 default parameters. All non-hydrogen atoms were refined with anisotropic displacement parameters. In the structure of **1b** one carbon atom of an ethanol molecule is disordered between two sites — occupancy factors for these two positions were set as 0.65 and 0.35,

 © 2004 Wiley-VCH Verlag GmbH & Co. KGaA, Weinheim

Table 2. Crystal data and structure refinement

	1b	**3**
Empirical formula	$C_{64}H_{100}O_8S_2Ti_2$	$(C_{120}H_{180}O_{14}S_4Ti_4)\cdot 2CH_2Cl_2$
Molecular mass	1157.32	2332.3
Habit	block	prism
Space group	$P\bar{1}$	$P\bar{1}$
Crystal system	triclinic	triclinic
Unit cell dimensions		
a (Å)	10.401(2)	13.898(5)
b (Å)	11.778(2)	16.122(4)
c (Å)	14.709(3)	17.841(6)
α (°)	91.00(3)	111.22(3)
β (°)	107.00(3)	92.94(3)
γ (°)	111.00(3)	108.18(3)
V (Å^3)	1593.6(5)	3479.0(19)
Z	1	1
T (K)	100.0(5)	100.0(5)
$D_{calcd.}$ (Mg/m^3)	1.206	1.113
μ (mm^{-1})	0.367	0.410
Crystal size (mm)	0.4 × 0.4 × 0.2	0.3 × 0.2 × 0.1
Absorption correction	none	none
Type of diffractometer	Kuma KM4	Kuma CCD-KM4
Diffraction geometry	ω-2θ scan	ω scan
θ (°)	2.21 to 25.11	3.7 to 28.45
Number of reflections collected	4397	24156
Number of unique reflections	4245	15306
$R_{(int)}$	0.0425	0.0570
Number of observed reflections	3393 [$I > 2\sigma(I)$]	6793 [$I > 2\sigma(I)$]
Refinement method	least-squares on F^2	least-squares on F^2
Number of parameters	361	689
Final R indices [$I > 2\sigma(I)$]	$R_1 = 0.0367$, $wR = 0.1000$	$R_1 = 0.0884$, $wR = 0.2188$
GooF = S	1.074	0.950
Largest diff. peak and hole eA^{-3}	0.554 and −0.496	0.751 and −0.571

$R_1 = \Sigma||F_o| - |F_c|| / \Sigma F_o|$; $wR_2 = \{\Sigma[w(F_o^2-F_c^2)^2] / \Sigma[w(F_o^2)^2]\}^{1/2}$; $S = \{\Sigma [w(F_o^2-F_c^2)^2] / (n-p) \}^{1/2}$

respectively. In the structure of **3** high temperature factors of some carbon atoms suggest their disorder, which could not be resolved. CCDC-198192 (for **1b**) and -198193 (for **3**) contain the supplementary crystallographic data for this paper. These data can be obtained free of charge at www.ccdc.cam.ac.uk/conts/retrieving.html [or from the Cambridge Crystallographic Data Centre, 12 Union Road, Cambridge CB2 1EZ, UK; Fax: (internat.) + 44-1223-336-033; E-mail: deposit@ccdc.cam.ac.uk].

Acknowledgments

The authors thank the State Committee for Scientific Research (Poland) for financial support of this work (grant no. 4 T09A 137 24).

[1] [1a] M. Kakugo, T. Miyatake, K. Mizunuma, *Chem. Express* **1987**, *2*, 445. [1b] T. Miyatake, K. Mizunuma, Y. Seki, M. Kakugo, *Makromol. Chem. Rapid Commun.* **1989**, *10*, 349. [1c] T. Miyatake, K. Mizunuma, M. Kakugo, *Macromol. Symp.* **1993**, *66*, 203.

[2] [2a] C. J. Schaverien, A. J. van der Linden, A. G. Orpen, *Polym. Prepr. (Am. Chem. Polym. Div.)* **1994**, *35*, 672. [2b] A. J. van der Linden, C. J. Schaverien, N. Meijboom, C. Ganter, A. G. Orpen, *J. Am. Chem. Soc.* **1995**, *117*, 3008.

[3] Patent, Mitsui Toatsu Chem. Inc. JP 05230133-A, **1992**.

[4] [4a] C. Floriani, F. Corazza, W. Lesueur, A. Chiesi-Villa, C. Guastini, *Angew. Chem. Int. Engl.* **1989**, *101*, 93. [4b] F. Corazza, C. Floriani, A. Chiesi-Villa, C. Guastini, *Inorg. Chem.* **1991**, *30*, 146. [4c] J. Okuda, S. Fokken, H-C. Kang, W. Massa, *Chem. Ber.* **1995**, *128*, 221.

[5] L. Porri, A. Ripa, P. Colombo, E. Miano, S. Capelli, S. V. Meille, *J. Organomet. Chem.* **1996**, *514*, 213.

[6] R. D. J. Froese, D. G. Musaev, T. Matsubara, K. Morokuma, *J. Am. Chem. Soc.* **1997**, *119*, 7190.

[7] R. D. J. Froese, D. G. Musaev, T. Matsubara, K. Morokuma, *Organometallics* **1999**, *18*, 373.

[8] E. Y.-X. Chen, T. J. Marks, *Chem. Rev.* **2000**, *100*, 1391.

[9] [9a] M. Mazzanti, C. Floriani, A. Chesi-Villa, C. Guastini, *J. Chem. Soc., Dalton Trans.* **1989**, 1793. [9b] P. J. Toscano, E. J. Schermerhorn, C. Dettelbacher, D. Macherone, J. Zubieta, *J. Chem. Soc., Chem. Commun.* **1991**, 933.

[10] T. J. Boyle, D. L. Barnes, J. A. Heppert, L. Morales, F. Takusagawa, J. W. Connolly, *Organometallics* **1992**, *11*, 1112.

[11] R. R. Schrock, J. Y. Jamieson, S. J. Dolman, S. A. Miller, P. J. Bonitatebus Jr., A. H. Hoveyda, *Organometallics* **2002**, *21*, 409 and references cited therein.

[12] S. L. Aeilts, D. R. Cefalo, P. J. Bonitatebus Jr., J. H. Houser, A. H. Hoveyda, R. R. Schrock, *Angew. Chem. Int. Ed.* **2001**, *40*, 1452.

[13] [13a] S. Fokken, T. P. Spaniol, H-Ch. Kang, W. Massa, J. Okuda, *Organometallics* **1996**, *15*, 5069. [13b] H-J. Krüger, *Angew. Chem. Int. Ed.* **1999**, *38*, 627. [13c] Y. Nakayama, H. Saito, N. Ueyama, A. Nakamura, *Organometallics* **1999**, *18*, 3149. [13d] P. L. Arnold,

 © 2004 Wiley-VCH Verlag GmbH & Co. KGaA, Weinheim

L. S. Natrajan, J. J. Hall, S. J. Bird, C. Wilson, *J. Organomet. Chem.* **2002**, *647*, 205.
[14] [14a] K. Watenpaugh, C. N. Caughlan, *Inorg. Chem.* **1966**, *5*, 1782. [14b] H. Haase, H. H. Hoppe, *Acta Crystallogr., Sect. B* **1968**, *24*, 281. [14c] A. Koshino, Y. Shuto, Y. Iitaka, *Acta Crystallogr., Sect. B* **1970**, *26*, 544.
[15] [15a] M. M. Olmstead, R. M. Kessler, H. Hope, M. D. Yanuck, W. K. Musker, *Acta Crystallogr., Sect. C* **1987**, *47*, 1890. [15b] T. T. Nadasdi, Y. Huang, D. W. Stephan, *Inorg. Chem.* **1993**, *32*, 347.
[16] *International Tables of Crystallography*, vol. C, Kluwer Academic, Dordrecht, **1992**.
[17] Space group $P\bar{1}$, a = 7.126(5) Å, b = 14.779(6) Å, c = 18.783(6) Å, α = 91.6(3)°, β = 97.9(4)°, γ = 93.9(2)°.
[18] T. V. Labben, P. Wolczanski, *J. Am. Chem. Soc.* **1987**, *109*, 424.
[19] S. Kleinhenz, K. Seppelt, *Chem. Eur. J.* **1999**, *5*, 3573.
[20] P. Sobota, K. Przybylak, J. Utko, L. B. Jerzykiewicz, A. J. L. Pombeiro, M. F. C. Guedes da Silva, K. Szczegot, *Chem. Eur. J.* **2001**, *7*, 951.
[21] G. R. Wille, J. Palin, M. G. B. Drew, *J. Chem. Soc., Dalton Trans.* **1994**, 1799 and references therein.
[22] Kuma Diffraction. KM-4 User's Guide, Version 10.1. Kuma Diffraction, Wrocław, Poland, **1996**.
[23] Kuma Diffraction. KM-4 CCD Software: version 1.161. KUMA Diffraction Instruments GmbH, Poland, **1995−1999**.
[24] G. M. Sheldrick, *Acta Crystallogr., Sect. A* **1990**, *46*, 467.
[25] G. M. Sheldrick, SHELXL-97: Program for the Refinement of Crystal Structures, University of Göttingen, Germany, **1997**.

Received October 22, 2003
Early View Article
Published Online March 9, 2004

 © 2004 Wiley-VCH Verlag GmbH & Co. KGaA, Weinheim

Pyrazolate-Based Dinucleating Ligands in L_2M_2 Scaffolds: Effects of Bulky Substituents and Coligands on Structures and M···H−C Interactions

Jens C. Röder,[b][‡] Franc Meyer,*[a] Elisabeth Kaifer,[b] and Hans Pritzkow[b]

Keywords: Nickel / Palladium / Dinuclear complexes / N-ligands / Pyrazole ligands

A series of nickel(II) and palladium(II) complexes $[L_2M_2]^{2+}$ have been prepared and structurally characterized, where L is a pyrazolate ligand with bulky 2,6-dimethyl- or 2,6-di(isopropyl)anilinomethyl side arms. Coordinating counter anions such as chloride can bind to axial sites of the dinickel species in a solvent-dependent process, giving rise to five-coordinate high-spin metal ions. In the case of weakly coordinating anions, the metal ions are found in roughly square-planar environments, and the structures are governed by the tendency of the bulky aryl groups to avoid each other, which forces the methyl or isopropyl substituents in the aryl 2- and 6-positions to approach the metal ions from the axial directions. This leads to drastic low-field shifts of the respective ^{1}H NMR signals, e.g. δ = 7.86 ppm for the isopropyl –CH which comes in close proximity to the low-spin nickel(II) center. The relevance of such low-field NMR resonances of protons close to the axial sites of d^8 metal ions for possible three-center four-electron M···H–C hydrogen bonds involving the filled d_z^2 orbital of the metal ion is discussed. In the present case, attractive M···H interactions are assumed to be of no major significance. This was corroborated by the structure of a further $[L_2Ni_2]^{2+}$ type complex where the anilinomethyl side arms bear only a single 2-isopropyl group, which was found rotated away from the metal. Additional spectroscopic and electrochemical properties of the various complexes are reported.

(© Wiley-VCH Verlag GmbH & Co. KGaA, 69451 Weinheim, Germany, 2004)

Introduction

At present, research on di- and oligonuclear transition metal complexes is a flourishing field with major interests focussed on biological mimicry and cooperative phenomena in catalysis and magnetism.[1–4] Among the diverse ligand frameworks that have been designed and employed in order to hold two metal centers in close proximity and to induce the sought-after cooperativity, pyrazole derived species appear particularly suited due to their well-known ability to span adjacent metal ions at a favorable distance of 2.4−4.6 Å.[5,6] Further control of the metal−metal separation, as well as of the steric and electronic properties of the individual metal ions, can be achieved by appropriate chelating side arms attached to the 3- and 5-positions of the heterocycle,[7,8] usually giving rise to either bis(μ-pyrazolato) bridged species L_2M_2 (**A**, Scheme 1)[9–15] or LM_2X complexes featuring secondary bridges within the dimetallic pocket (**B**).[16–24]

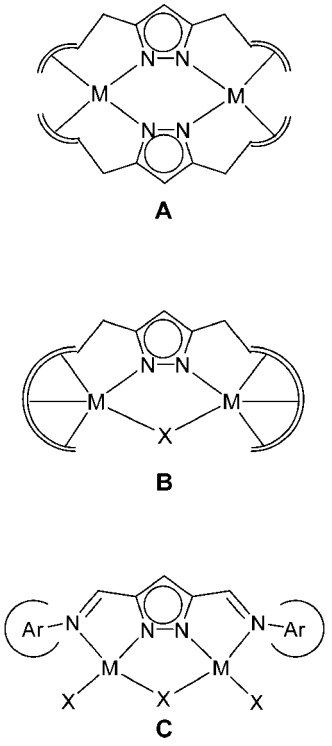

Scheme 1. Different types of dinuclear complexes with multifunctional pyrazolate-based ligands

[a] Institut für Anorganische Chemie der Georg-August-Universität Göttingen
Tammannstraße 4, 37077 Göttingen, Germany
Fax: (internat.) + 49-(0)551-393063
E-mail: franc.meyer@chemie.uni-goettingen.de
[b] Anorganisch-Chemisches Institut der Universität Heidelberg
Im Neuenheimer Feld 270, 69120 Heidelberg, Germany
[‡] New address: Crompton GmbH,
Ernst-Schering-Straße 14, 59192 Bergkamen, Germany

 © 2004 Wiley-VCH Verlag GmbH & Co. KGaA, Weinheim **DOI: 10.1002/ejic.200300778**

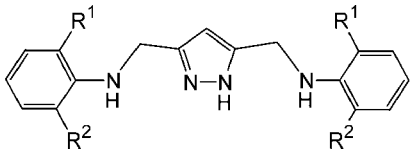

Scheme 2. Ligands used in this study[27]

In this contribution we report on the effects that coordinating versus non-coordinating co-ligands as well as bulky substituents at the chelating side arm donor atoms of L_2M_2 type compounds have on the solid-state structures, and we will particularly focus on unusual metal-ligand interactions that arise from the steric crowding in such systems. Nickel(II) and palladium(II) complexes of ligands $[L^1]^-$, $[L^2]^-$ and $[L^3]^-$ (Scheme 2) were initially prepared with the aim of providing diamine analogues of the bis(α-diimine) type dinuclear compounds **C**.[25,26] However, with $[L^1]^-$, $[L^2]^-$ and $[L^3]^-$, complexes of the type L_2M_2 (**A**) were favored in all cases, irrespective of the M:L ratio employed.

Results and Discussion

Syntheses of all complexes were readily achieved by deprotonation of the respective ligand precursor (HL^1, HL^2, or HL^3)[27] with one equivalent of KO*t*Bu in THF and subsequent addition of the respective metal salt.

Complexes of $[L^1]^-$: Solid-State Structures and Magnetic Properties

From the reaction between HL^1 and $NiCl_2{\cdot}6H_2O$, two structurally isomeric complexes $[L^1_2Ni_2Cl_2]$ (**1**) and $[L^1_2Ni_2]Cl_2$ (**2**) were obtained from acetone and CH_2Cl_2 solutions, respectively. The molecular structures of **1** and **2** are depicted in Figure 1 and 2 together with selected interatomic distances and bond angles.

In the green compound **1**, both nickel ions exist in roughly square-pyramidal coordination environments (τ = 0.11 and 0.18 for Ni1 and Ni2, respectively)[28] with the Cl ligands in axial positions. The metal ions are displaced slightly out of the planes of the basal N-donor atoms towards the axial ligands, which are located on opposite sides of the bimetallic framework defined by the two $\{N_4\}$ chelate ligands. As expected, the distances between the nickel and the coordinating amine N atoms are around 10% longer than the Ni−N(pyrazolate) distances [2.158(3) −2.224(3)Å versus 1.956(3) −1.978(3) Å]. The ligand side arm aryl substituents in **1** are oriented almost perpendicular to the plane of the pyrazolate, and hence perpendicular to the plane of the coordination framework. Due to the space required by the axial co-ligand, the adjacent aryl rings are pushed away from the chloride towards the back side of the dimetallic array. This situation has to balance two competing steric interactions: either some *ortho* methyl groups of the aryl substituents come quite close to the Cl atom [e.g. *d*(C21···Cl2) = 3.718 Å, *d*(C42···Cl1) = 3.942 Å], or the other *ortho* methyl groups are forced to approach the nickel ion from the reverse [C11, C41, C20, C32; *d*(Ni···C_{CH3}) = 3.482−3.783 Å]. In order to avoid an energetically unfavorable full eclipse of the opposing pairs of aryl rings, the respective five-membered chelate rings adopt different conformations (Scheme 3). For each nickel, one chelate ion is almost planar (at N3 and N4), while the second ring adopts an envelope conformation with the aryl groups in either an axial (N8) or an equatorial position (N7).

In the red compound **2**, the chloride ions are detached from their metal atoms, but they still remain associated with the complex via NH···Cl hydrogen bonds [*d*(N3···Cl5) =

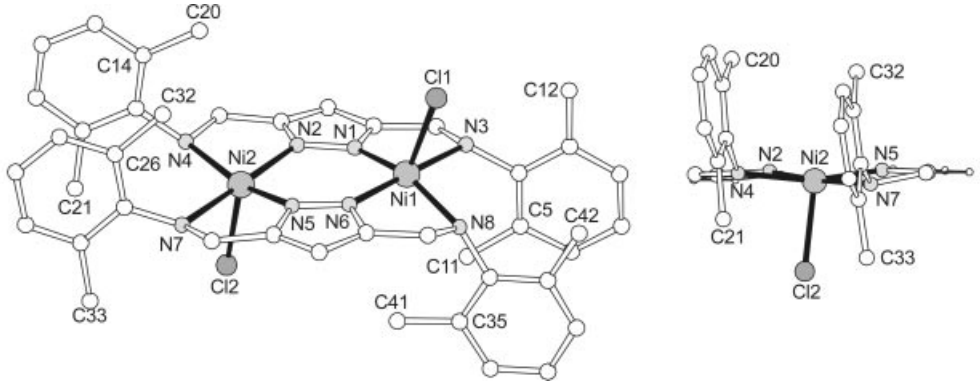

Figure 1. Molecular structure of **1**; in the interests of clarity all hydrogen atoms have been omitted; selected interatomic distances (Å) and bond angles (°): Ni1−N6 1.964(3), Ni1−N1 1.978(3), Ni1−N3 2.183(3), Ni1−N8 2.224(3), Ni1−Cl1 2.339(1), Ni1···Ni2 3.960, Ni2−N2 1.956(3), Ni2−N5 1.977(3), Ni2−N7 2.158(3), Ni2−N4 2.199(3), Ni2−Cl2 2.331(1); C5−C11−Ni1 82.2, C35−C41−Ni1 85.7, C14−C20−Ni2 82.3, C26−C32−Ni2 86.9

 © 2004 Wiley-VCH Verlag GmbH & Co. KGaA, Weinheim

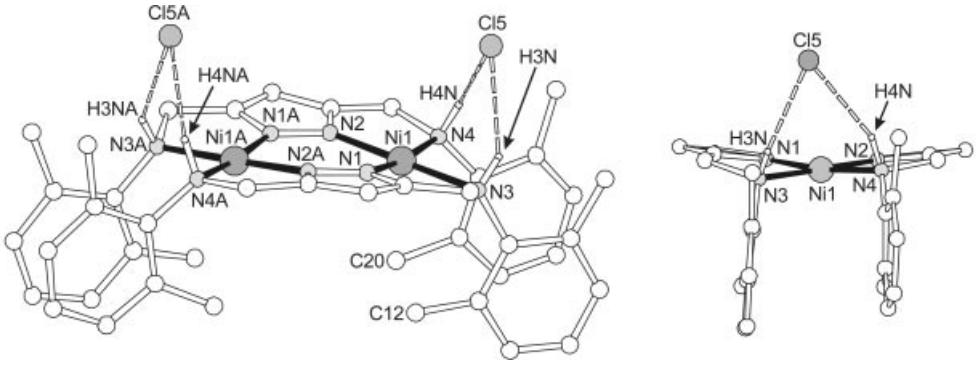

Figure 2. Molecular structure of **2**; in the interests of clarity all but the *N*-bound hydrogen atoms have been omitted; selected interatomic distances (Å) and bond angles (°): Ni1−N2 1.839(2), Ni1−N1 1.843(2), Ni1−N3 1.979(2), N1−N4 1.999(2), Ni1···Ni1A 3.830(8), Ni1···Cl5 3.214(2), N3−Cl5 3.160, N4−Cl5 3.229; N2−Ni1−N3 178.27(8), N1−Ni1−N4 172.48(9)

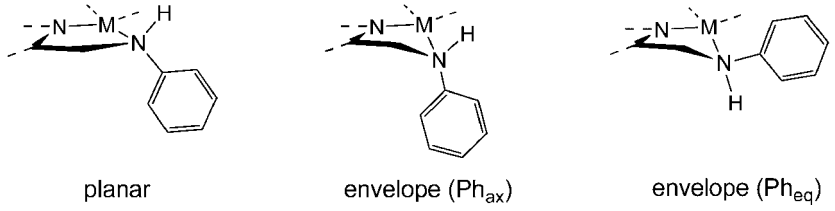

Scheme 3. Conformations of five-membered chelate rings

3.160 Å, *d*(N4···Cl5) = 3.229 Å]. The Ni···Cl distance is 3.214 Å [versus 2.339(1)/2.331(1) Å in **1**], i.e. clearly out of the bonding range, which leaves the metal ions in an approximately square-planar {N_4} environment and slightly decreases the Ni···Ni separation compared with **1** [3.830(1) Å versus 3.960(1) Å]. Due to the H-bonding pattern of the chloride ions, which are both located on one side of the bimetallic array, all aryl rings are directed downwards to the opposite side. Again, this forces two *ortho* methyl groups in close proximity to the metal ions [*d*(Ni···C12) = 3.417 Å, *d*(Ni···C20) = 3.284 Å]. Similar to the situation in **1**, the five-membered chelate rings feature different conformations in order to avoid a fully eclipsed stacking of the aryl groups. All Ni−N bond lengths are significantly shorter than in **1**, in accordance with the lower coordination number and the different spin state, i.e. a high-spin d^8 configuration in **1** compared with a low-spin configuration in **2**. It remains unclear, why the Cl^- ions in **2** are located on the same side of the bimetallic platform, while the Cl ligands in **1** are found on opposite sides.

The aryl rings facing each other in complexes **1** and **2** do not adopt an exact face-to-face alignment, but something of a slipped facial arrangement. To characterize the π-π stacking, one usually considers parameters such as the distance between, and the relative tilting of the planes of opposite aryl rings as well as the centroid−centroid distance (CC), and the angle between the centroid-centroid vector and the ring normal to one of the aryl planes.[29] In **1**, the planes are tilted by 4.3/5.1°, the CC distance is 3.81/4.15 Å, and the offset of the centroids is 1.41−2.13 Å, hence the distance between the centroid and the plane of the opposite aryl ring amounts to 3.49−3.57 Å. These latter values are in the typical range for interplanar distances of π-π stacked aromatic groups (3.3−3.8 Å).[29] In **2**, tilting of the aryl planes relative to each other is similar (6.2°), but the CC distance is somewhat shorter (3.55 Å) and the two rings are less displaced (offset 1.05/1.17 Å). Again, the interplanar separation of the aromatic groups (3.35/3.39 Å) is in the usual range.

The paramagnetic nature of **1** and the diamagnetic nature of **2** were confirmed by magnetic measurements. Temperature dependent data for the molar magnetic susceptibility and the effective magnetic moment of **1** are shown in Figure 3.

From ca. 4.7 B.M. at 300 K, the magnetic moment gradually decreases upon lowering the temperature, while the susceptibility curve exhibits a sharp maximum at around 60 K which is indicative of significant antiferromagnetic coupling between the two nickel(II) centers. Modeling the experimental data by the standard expression for the isotropic spin-Hamiltonian $H = -2J \cdot S_1 \cdot S_2$ (with $S_1 = S_2 = 1$) including a molar fraction p of uncoupled paramagnetic impurity [Equation (1)][4,30,31] yielded $J = -23.2\ cm^{-1}$, $g = 2.39$ and $p = 1.9\%$.

$$\chi = \chi_{dim}(1 - p) + 2\chi_{mono}p + 2N_{\alpha'} \quad (1)$$

The intra−dimer exchange term J proved to be the dominant contribution because a good quality fit was obtained despite the neglect of both a zero-field splitting parameter D as well as an inter−dimer interaction $z'J'$.[32] Relatively few bis(μ-pyrazolato)-bridged high-spin dinickel(II) complexes have been previously structurally charac-

 © 2004 Wiley-VCH Verlag GmbH & Co. KGaA, Weinheim

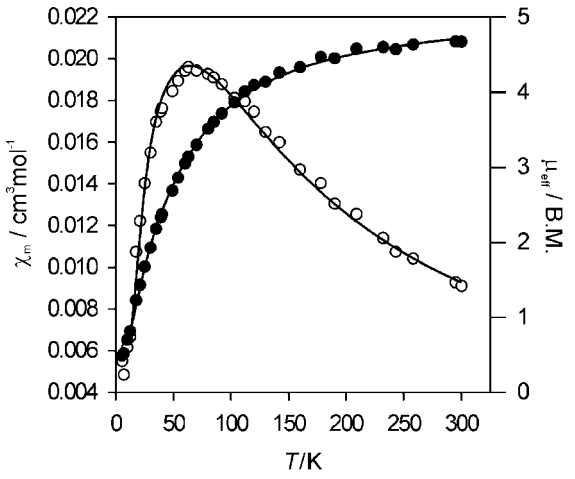

Figure 3. Temperature dependence of the molar magnetic susceptibility (open circles) and magnetic moment (solid circles) for **1**; the solid line represents the calculated fit (see text)

terized,[22,33,34] and even fewer have been studied with respect to their magnetic properties,[35] which precludes any definite magneto-structural correlations at the present stage. However, the rather large magnetic coupling in **1** is certainly due to the high degree of planarity of the $Ni(NN)_2Ni$ scaffold, in accordance with the magneto-structural trends observed in bis(μ-pyrazolato) dicopper(II) chemistry.[36,13]

The controlled synthesis of a complex with low-spin square-planar metal ions was achieved by treatment of $[L^1]^-$ with $[Ni(H_2O)_6](ClO_4)_2$. The molecular structure of the resultant compound **3**, obtained in crystalline form from acetonitrile/diethyl ether, is depicted in Figure 4.

The first coordination sphere of the nickel ions in **3** is quite similar to that in **2**, but less distorted with both metal centers nested within the plane of an overall planar framework. All five-membered chelate rings are roughly planar in this case. In the absence of any steric requirements of chloride counter-anions or co-ligands, the two aryl rings on both ends of **3** do not face each other, but one of them is pointing above and the other below the coordination plane. This gives rise to the sterically more favorable isomer **E** with approximate (non-crystallographic) C_{2h} symmetry (Scheme 4), in contrast to the C_{2v} isomer **D** that is imposed by the four NH···Cl bonds in **2** and the C_{2h} isomer **F** found for **1**. Note that the chiral D_2 isomer **G**, which should be quite similar to the C_{2h} isomer **E** in terms of steric effects, was not observed (neither were any isomers of lower symmetry). The C_{2h} isomer can be described as a *meso* form with an (*R*,*S*)(*S*,*R*) configuration of the four stereogenic N atoms, while the D_2 system represents a pair of enantiomers with (*R*,*R*)(*R*,*R*) or (*S*,*S*)(*S*,*S*) configurations. Interestingly, the *ortho* methyl groups in **3** are even closer to the nickel ions than in **2**, approaching from both axial directions [*d*(Ni···C11) = 3.033 Å, *d*(Ni···C32) = 3.110 Å].

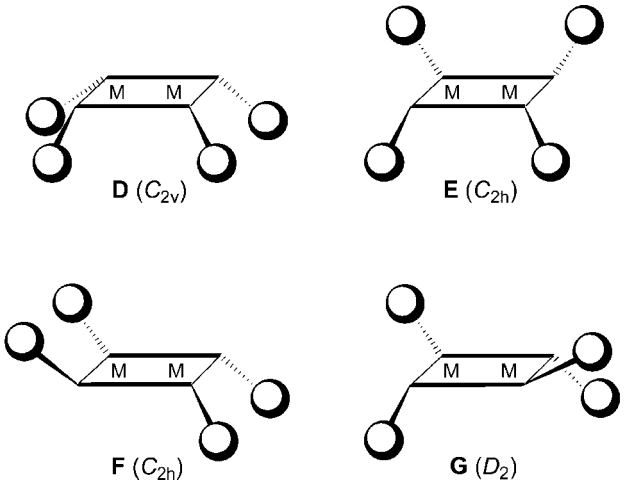

Scheme 4. Different stereoisomers of the $[L_2M_2]^{2+}$ platform (M = Ni, Pd); the balls represent the bulky aryl substituents

The set of dinickel complexes **1**–**3** exemplifies the influence of co-ligands (in this case Cl^-) within the first or second coordination shell on the structural features of the bimetallic scaffold. The sequence given in Figure 5 may

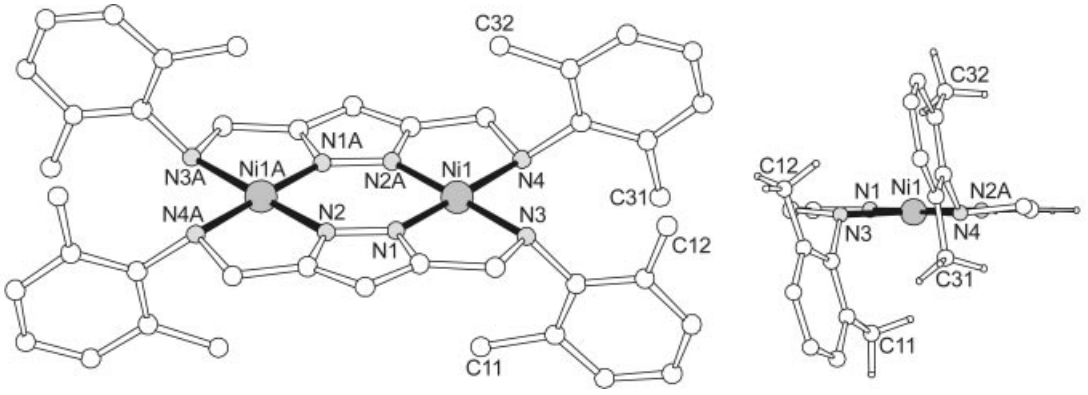

Figure 4. Molecular structure of the cation of **3**; in the interests of clarity only the hydrogen atoms of the methyl groups are shown in the right part; selected interatomic distances (Å) and bond angles (°): Ni1–N2A 1.834(2), Ni1–N1 1.843(2), Ni1–N3 1.957(1), Ni1–N4 1.972(2), Ni1···Ni1A 3.841, C11···Ni1 3.033, C32···Ni1 3.110; N2A–Ni1–N3 179.17(7), N1–Ni1–N4 179.08(7)

 © 2004 Wiley-VCH Verlag GmbH & Co. KGaA, Weinheim

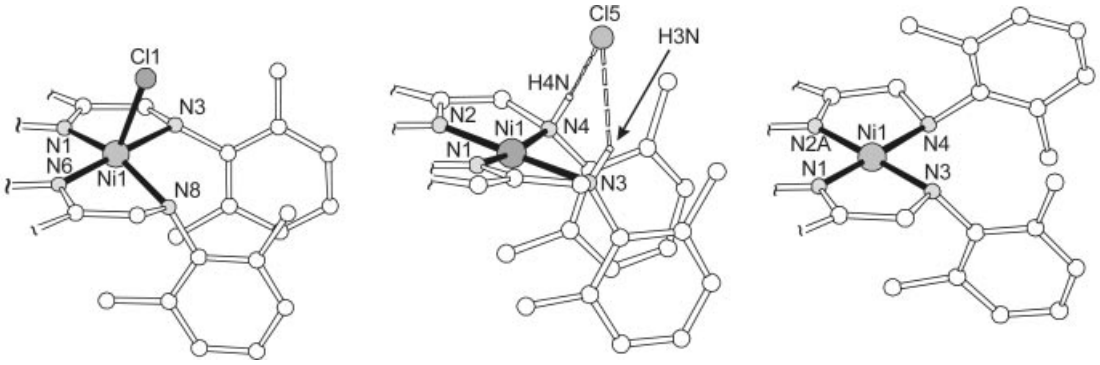

Figure 5. Comparative view of the Ni coordination in **1**, **2** and **3** with the chloride in the inner coordination sphere (**1**), outer coordination sphere (**2**), and without chloride (**3**)

then be viewed as a set of snapshots of the chloride dissociation process. The accompanying spectroscopic characteristics and solution properties of **1**−**3** are discussed below.

For comparison, a dipalladium complex **4** was prepared from $[L^1]^-$and $[Pd(NCMe)_4](BF_4)_2$ and crystallized (in low yield) from dichloromethane/light petroleum. The molecular structure of its cation is basically analogous to that of **3**. However, closer inspection reveals subtle differences which are revealed in Figure 6. In **4**, all chelate rings are more distorted towards an envelope conformation, which brings the adjacent aryl rings to partly stand opposite to each other and to move into the coordination plane. We believe two effects to be responsible for this. Firstly, the larger ionic radius of palladium(II) compared with nickel(II) (0.86 versus 0.72 Å) induces a larger separation between the aryl rings, allowing them to relax towards a more eclipsed stacking. Secondly, the larger palladium ion interferes more strongly with the *ortho* methyl groups, thus enforcing somewhat longer Pd···C distances (3.428 and 3.486 Å) in the axial positions of the metal center and pushing away the substituents. The parallel-displaced arrangement of the aromatic groups in these complexes (as well as in complexes **5**−**7**, see below) means that the interaction is more of the C−H···π type and driven by the known π-σ attraction, while π-π stacking is not favored.[29]

Complexes of $[L^1]^-$ in Solution

A solution of **1** (or, **2**) appears green in CH_2Cl_2 but red in MeCN, and dilution of a THF solution also causes a gradual change from green to red. This change in color is consistent with the crystallographic findings. In non-polar solvents and in concentrated solutions, the position of the equilibrium between **1** and **2** is shifted towards the neutral species $[L^1_2Ni_2Cl_2]$ and the more ionic $[L^1_2Ni_2]Cl_2$ is the less soluble compound that crystallizes from the solution. On the other hand, polar solvents such as MeCN or acetone favor the ionic form $[L^1_2Ni_2]Cl_2$, and the neutral **1** now becomes less soluble and precipitates first.

In order to obtain some further insight into these equilibria, a solution of the Cl-devoid complex **3** in CH_2Cl_2/MeCN (1:1) was titrated with $[(n\text{-hex})_4N]Cl$ and the mixture was analyzed by UV/Vis spectroscopy. Even in the presence of an excess of chloride, **3** was not fully converted into **1** in that solvent mixture. The absence of clear isosbestic points indicates the presence of more complex equilibria presumably involving, inter alia, species such as $[L^1Ni_2Cl]^+$.

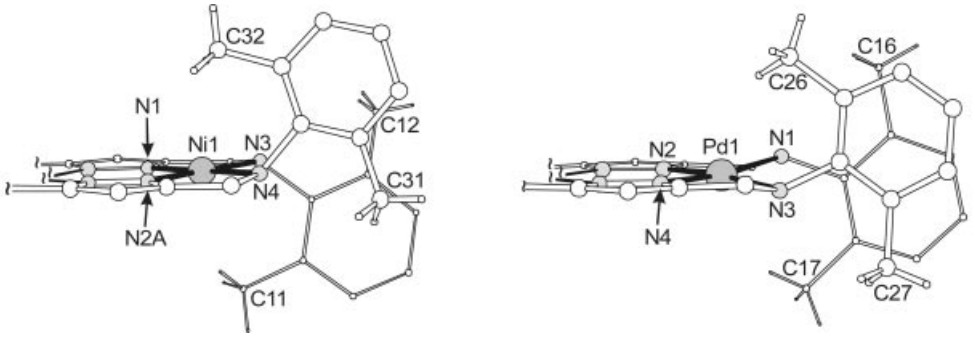

Figure 6. Comparative view of fragments of the molecular structures of **3** and **4**; in the interests of clarity only those hydrogen atoms bound to the methyl groups are shown; selected interatomic distances (Å) and bond angles for **4** are (°): Pd1−N2 1.969(2), Pd1−N4 1.970(2), Pd1−N1 2.110(2), Pd1−N3 2.123(2), Pd1···Pd1A 3.954, Pd1···C17 3.486, Pd1···C26 3.428; N4−Pd1−N1 173.49(8), N2−Pd1−N3 173.95(8)

 © 2004 Wiley-VCH Verlag GmbH & Co. KGaA, Weinheim

Solid state UV/Vis/NIR spectra of **1**−**3** were recorded for comparison and are depicted in Figure 7. As expected for five-coordinate high-spin nickel(II) ions, **1** shows a series of absorptions, including the broad band at around 1980 nm, that should correspond to the $^3B_1 \rightarrow {}^3E$ transition in idealized C_{4v} symmetry. The two distinct bands at 328 and 502 nm for **3** can be assigned to the $^1A_{1g} \rightarrow {}^1B_{1g}$ and $^1A_{1g} \rightarrow {}^1A_{2g}$ transitions of low-spin nickel(II) in an idealized D_{4h} environment, where the latter gives a reasonable value of the ligand field splitting, $\Delta \approx 20000\ cm^{-1}$.[37] The similarity of the band positions for **1** and **3** in the range 300−1000 nm with those observed in solution confirms that the overall structures elucidated by X-ray crystallography are essentially retained in solution.

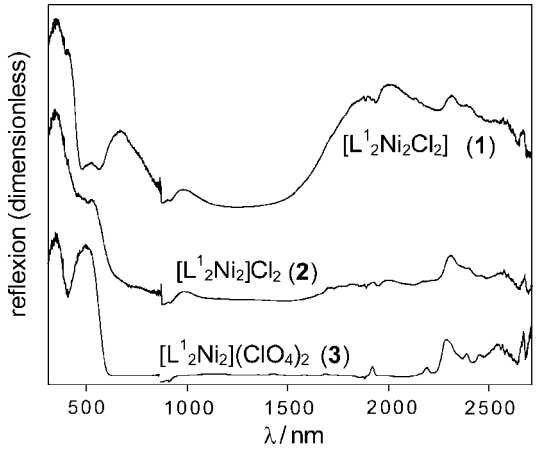

Figure 7. Solid state UV/Vis spectra of the dinickel complexes **1**, **2** and **3**

^1H NMR spectroscopy of diamagnetic **3** revealed unusual chemical shifts for the *ortho* methyl groups of the aryl rings (Figure 8; all signals have been unambiguously assigned by a series of 2D NMR experiments). While the CH_3 resonance appears at δ = 2.29 ppm in HL[1], the spectrum of **3** shows one signal shifted to higher field at δ = 1.08 ppm and two signals (of different intensities) at very low field, i.e. at δ = 4.17 and 4.20 ppm. These features can be rationalized by considering the positions of the methyl groups and, as is clearly seen in Figure 4, the high-field shifts of H12A−C and H31A−C are due to their location within the field of the ring current of the opposing aryl rings, while the deshielding of H11A−C and H32A−C results from their proximity to the filled d_z^2 orbital of the nickel(II) ion. The occurrence of two closely spaced resonances for the latter protons has been tentatively attributed to the presence of different isomers in solution, such as the C_{2h} and D_2 forms sketched in Scheme 4. These effects are even more pronounced in the case of complexes of $[L^2]^-$ and are discussed in more detail below. The diastereotopic nature of the CH_2 protons of the five-membered chelate rings is reflected by two well-separated sets of signals centered at δ = 3.43 and 4.15 ppm.

^1H NMR spectra of the palladium complex **4** in CD_2Cl_2 only show very broad resonances over a wide temperature range, presumably indicating a variety of dynamic and dissociative processes.

Complexes of $[L^2]^-$: Solid-State Structures and Spectroscopy

Similar to the preparation of **3** and **4**, the dinickel and dipalladium complexes $[L^2_2Ni_2](ClO_4)_2$ (**5**) and $[L^2_2Pd_2](BF_4)_2$ (**6**) were obtained by treatment of $[L^2]^-$ with $[Ni(H_2O)_6](ClO_4)_2$ or $[Pd(NCMe)_4](BF_4)_2$, respectively. Single crystals were grown from acetone/ethanol/light petroleum (**4**) or dichloromethane/light petroleum (**5**) and analyzed by X-ray crystallography. Both **5** and **6** crystallize in the triclinic space group $P\bar{1}$, and molecular structures of their cations are shown in Figure 9.

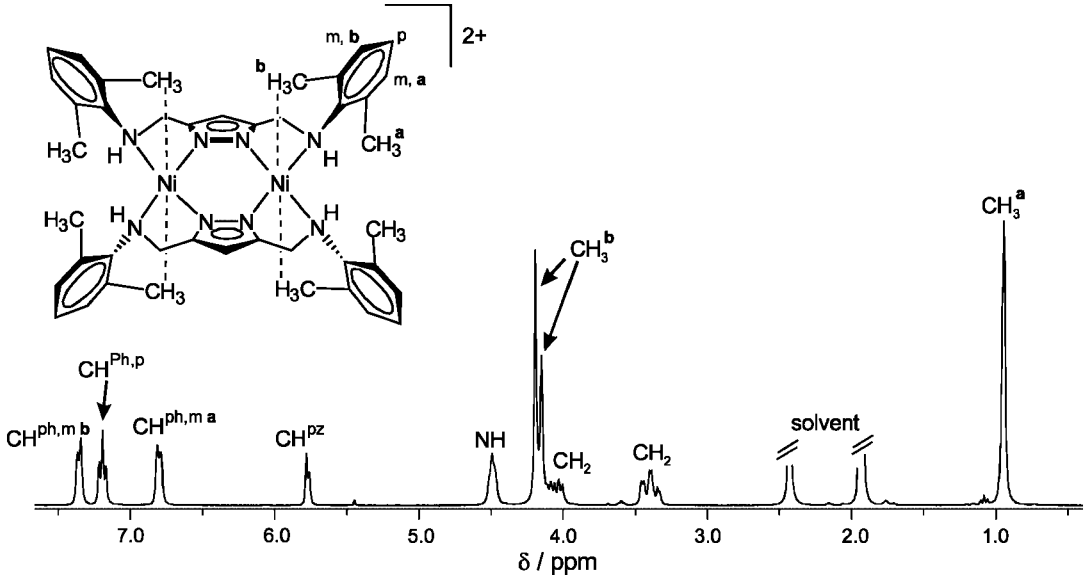

Figure 8. ^1H NMR spectrum of complex **3** in CD_3CN at 300 MHz and 293 K; the dashed lines in the graphical representation of **3** are not meant to indicate bonds

 © 2004 Wiley-VCH Verlag GmbH & Co. KGaA, Weinheim

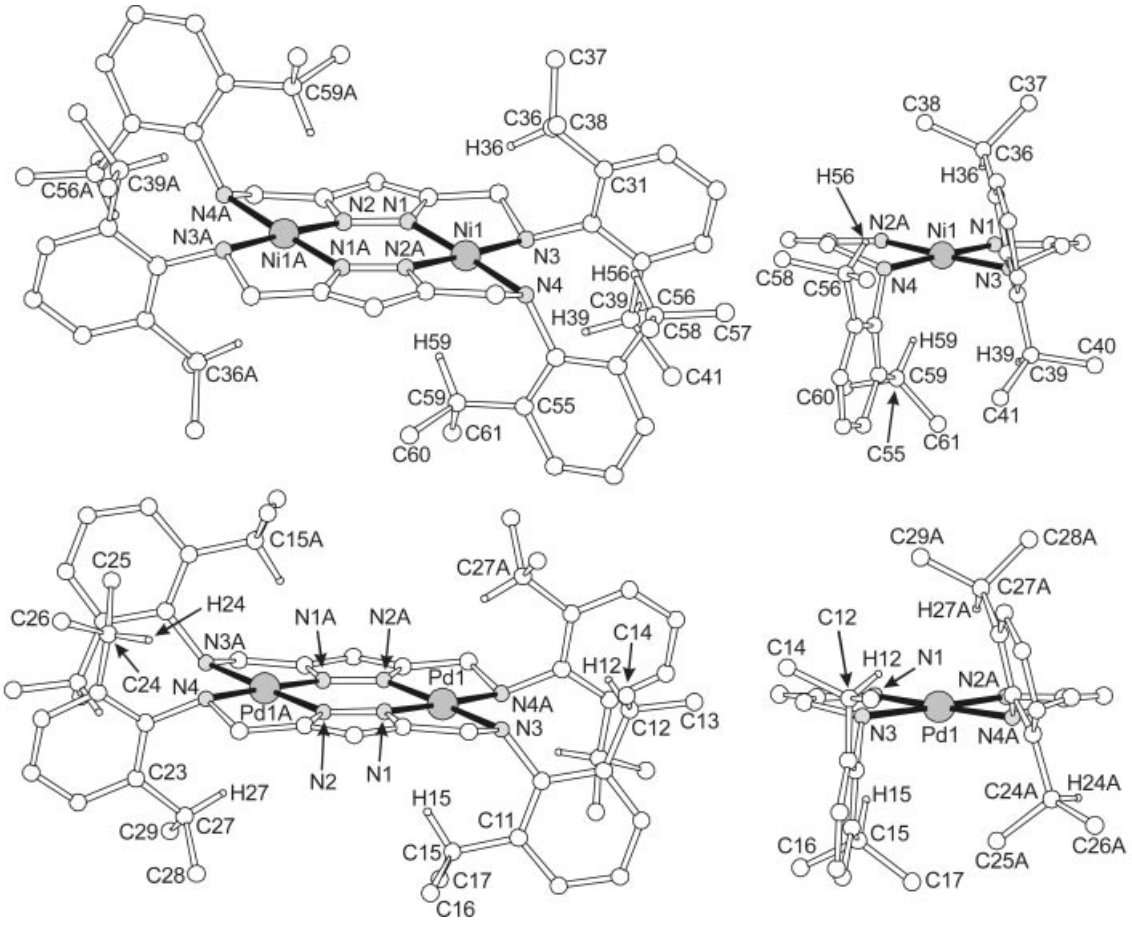

Figure 9. Molecular structures of the cations of **5** (top) and **6** (bottom); in the interests of clarity only a few hydrogen atoms are shown; selected interatomic distances (Å) and bond angles (°) for **5**: Ni1−N1 1.835(3), Ni1−N2A 1.848 (3), Ni1−N3 1.967(3), Ni1−N4 1.974(3), Ni1···Ni1A 3.842, C36···Ni1 3.269 C59···Ni1 3.114; N2A−Ni1−N3 177.25(11), N1−Ni1−N4 178.00(12); selected interatomic distances (Å) and bond angles (°) for **6**: Pd1−N1 1.968(3), Pd1−N2A 1.971(3), Pd1−N3 2.114(3), Pd1−N4A 2.123(3), Pd1···Pd1A 3.997, C15···Pd1 3.454, C27A···Pd1 3.377; N2A−Pd1−N3 176.09(12), N1−Pd1−N4A 176.19(12)

All metal ions are found in roughly SP-4 coordination environments. Due to the steric pressure exerted by the bulky 2,6-diisopropylphenyl substituents, however, the coordination planes of the metal ions are tilted by ca. 10° (**5**) or 8° (**6**) with respect to the planes of the pyrazolate heterocycles. The chelate rings adopt an envelope conformation with one aryl substituent in an axial position and one in an equatorial position for each half of the molecule (cf. Scheme 3). These structural features cause the methine proton of one isopropyl group of every aryl substituent to approach considerably close to the proximate metal ion from the axial direction [*d*(C36···Ni) = 3.269 Å and *d*(C59···Ni) = 3.114 Å in **5**, *d*(C15···Pd) = 3.454 Å and *d*(C27···Pd) = 3.377 Å in **6**]. The consequences for the ^{1}H NMR chemical shifts of these particular protons should be more pronounced than in **3**, since rotation is hindered for the isopropyl groups in **5**, while rotation of the methyl groups causes an averaging of the effect in **3**. The expected four CH_3 resonances for the non-equivalent isopropyl groups in **5** were seen in the low temperature (193 K) ^{1}H NMR spectrum in CD_2Cl_2 (Figure 10). Signals have been assigned based on a series of 2D NMR experiments ({^{1}H^{13}C}HSQC and {^{1}H^{13}C}HMBC), and the methine resonances of the isopropyl groups were found either at extremely low field (δ = 7.86 ppm; CH^B close to the nickel ion) or at very high field (δ = 1.86 ppm; CH^A opposing the proximate aryl ring) compared with the free ligand HL^2 (δ = 3.33 ppm at room temp.). At 193 K, the CH_2 protons at δ = 3.40 and 4.13 ppm showed a geminal coupling of ^2J = 10 Hz, in accordance with a fixed conformation of the five-membered chelate rings. At higher temperatures, a second set of resonances gradually developed, which were most clearly observed for the isopropyl-CH_3 groups and were also evident from the splitting of the signal at around 5.9 ppm for the pyrazolate H^4 proton (CH^{pz}). At 293 K, a 1:1 ratio of the two isomers was obtained. These different isomers have been tentatively assigned to the C_{2h} and D_2 forms of the bimetallic framework, where the two aryl substituents of each ligand are either on the same (C_{2h}) or on opposing sides (D_2). Interconversion was apparently rapid and may proceed either via a short-lived dissociation of the Ni−N bonds and inversion of the intermediate free amine, or via a sequence of deprotonation and inverse protonation of the *N*-bound protons.

In CD_3CN at higher temperatures all ^{1}H NMR signals of **5** became broad, except for the *para* protons of the aryl

 © 2004 Wiley-VCH Verlag GmbH & Co. KGaA, Weinheim

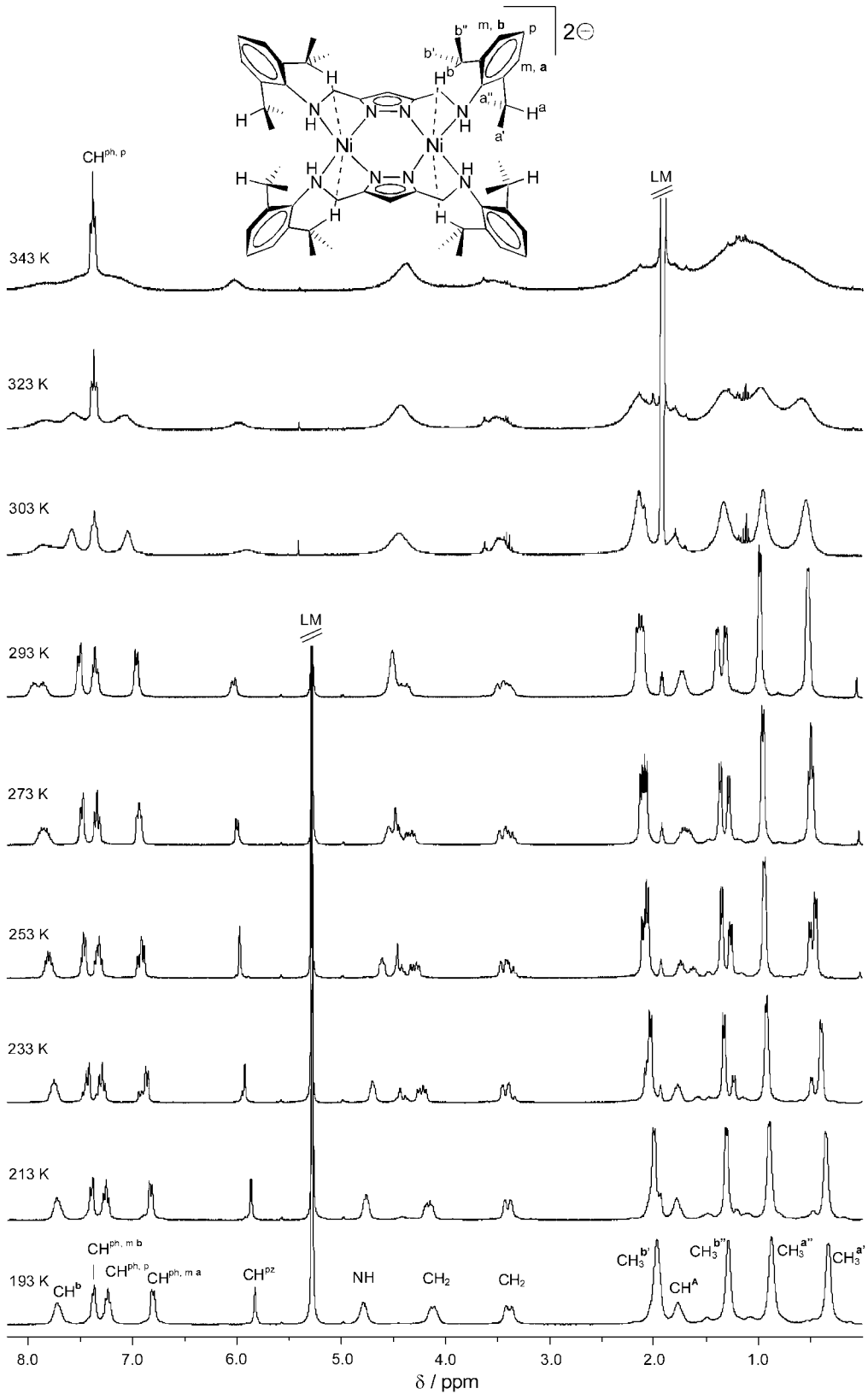

Figure 10. Temperature dependent ^{1}H NMR spectra of complex **5** in CD_3CN (303−343 K) and CD_2Cl_2 (193−293 K) at 300 MHz; the dashed lines in the graphical representation of **5** do not indicate bonds

groups. We assume dissociative processes according to Scheme 5 to be responsible for this phenomenon, which may also support the former explanation for the stereoisomer interconversion discussed above. Similar characteristics were observed for the ^{1}H NMR spectrum of **6**, but with a somewhat less pronounced deshielding of its CH^B protons.

 © 2004 Wiley-VCH Verlag GmbH & Co. KGaA, Weinheim

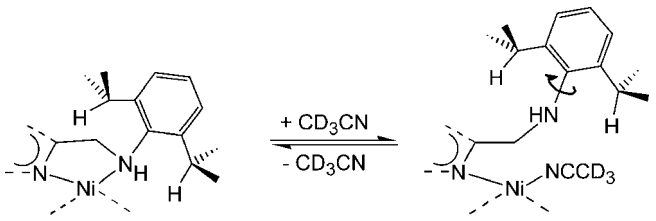

Scheme 5. Possible solvent-assisted side arm dissociation

When **5** was treated with two equivalents of HL^1, formation of **3** and the heteroleptic complex $[L^1L^2Ni_2]$ $(ClO_4)_2$ (**7**) was observed within minutes. However, ligand exchange did not proceed to completeness, and equilibrium was reached at ca. 70% exchange. The mixed-ligand species **7** could be prepared directly by treatment of a 1:1 mixture of $[L^1]^-$ and $[L^2]^-$ with two equivalents of $[Ni(H_2O)_6](ClO_4)_2$. Single crystals were obtained from a MeCN/diethyl ether solution and were analyzed by X-ray crystallography. The molecular structure of the cation of **7** is depicted in Figure 11 together with selected atom distances and bond angles.

In **7**, the two nickel ions were found in subtly different environments. While the coordination sphere of Ni2 is almost square-planar, Ni1 shows a slight tetrahedral distortion. Five-membered chelate rings of all possible conformations (planar, λ-twist, δ-twist) are present in **7**. The two pyrazolate heterocycles are tilted by 12.1° with respect to each other.

While the steric strain in **7** is somewhat relieved compared with **5**, the distances of the isopropyl CH atoms to the nickel ions are rather similar [*d*(Ni2···C48) = 3.230 Å and *d*(Ni···C32) = 3.200 Å versus 3.114 and 3.269 Å in **5**]. Also, the distances between the nickel atoms and the methyl groups of $[L^1]^-$ are similar to those in the homoleptic compound **3** (3.082 and 3.119 Å in **7** versus 3.033 and 3.110 Å in **3**).

The ^{1}H NMR spectrum of **7** is reminiscent of an overlay of the individual spectra of **3** and **5**. Chemical shifts of all signals assigned to the $[L^1]^-$ and $[L^2]^-$ ligand protons are quite similar to those in the homoleptic analogues. Deshielding of the isopropyl CH protons is only slightly less pronounced than in **5** (7.20 and 7.40 ppm versus 7.86 ppm; again, the two separate resonances are presumably due to the presence of different isomers in solution).

A ^{1}H NMR spectrum of the bulk crystalline material obtained from acetonitrile/diethyl ether by the synthetic procedure described above shows a $[L^1]^-$:$[L^2]^-$ ratio of approximately 2:1. We assume that **3**, **5** and **7** are initially formed in a statistical 1:1:2 mixture. Upon crystallization, however, both the less soluble **3** and **7** precipitate, while **5** remains in solution. As a consequence, the isolated crystalline material represents a 1:2 mixture of **3** and **7**, which gives rise to the observed 2:1 ratio of $[L^1]^-$:$[L^2]^-$ in the NMR spectroscopic analysis.

Comparative Discussion of Unusual ^{1}H NMR Shifts and Synthesis of a Complex of $[L^3]^-$

Close contacts between d^8 metal ions Pd^{II} and Pt^{II} in square-planar complexes and N−H or O−H bonds located above or below the coordination plane have been observed in several cases and investigated in detail.[38–41] Similar contacts with C−H bonds are less recognized and usually involve sp or sp^2 carbon atoms.[38,42–50] For some systems, these contacts have been interpreted in terms of three-center four-electron M···H−N and M···H−C hydrogen bonds involving the filled d_{z^2} orbital of the metal ion (Scheme 6), in contrast to three-center two-electron agostic interactions.

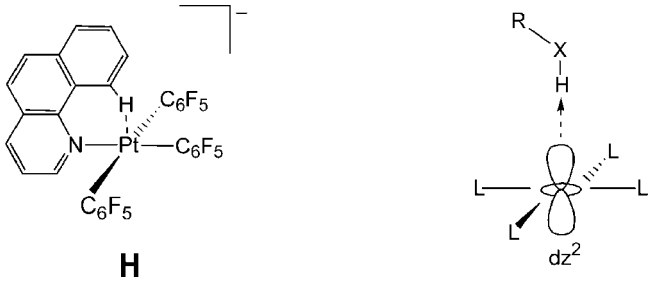

Scheme 6. Three-center four-electron M···H−X hydrogen bonds[50]

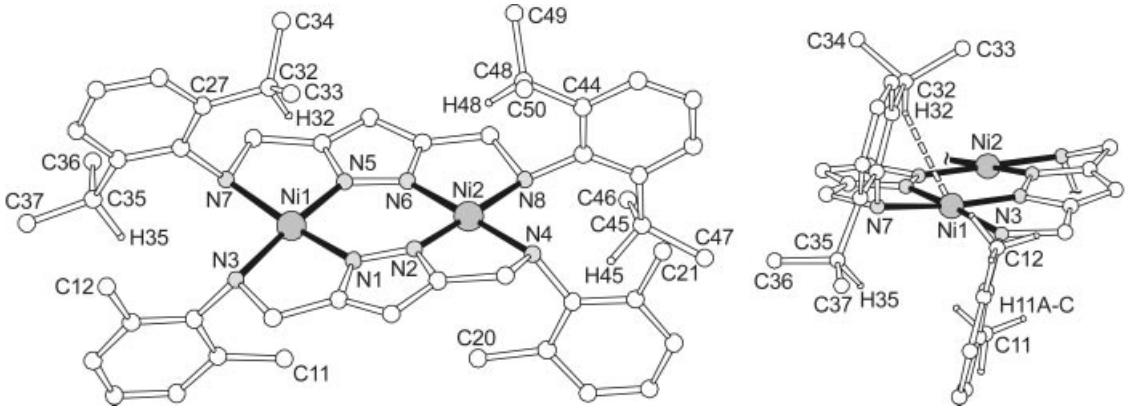

Figure 11. Molecular structure of the cation of **7**; in the interests of clarity only a few hydrogen atoms are shown; selected interatomic distances (Å) and range of selected bond angles (°): Ni1−N1 1.846(4), Ni1−N5 1.852(4), Ni1−N7 1.973(4), Ni1−N3 1.980(4), Ni2−N6 1.844(4), Ni2−N2 1.849(4), Ni2−N4 1.956(4), Ni2−N8 1.984(4), Ni1···Ni2 3.848, C32···Ni1 3.200, C11···Ni1 3.082, C20···Ni2 3.119; C48···Ni2 3.230; N1−Ni1−N7 173.5(2), N5−Ni1−N3 174.7(2), N6−Ni2−N4 178.6(2), N2−Ni2−N8 178.4(2)

 © 2004 Wiley-VCH Verlag GmbH & Co. KGaA, Weinheim

While a significant downfield ^{1}H NMR shift for an H atom in the vicinity of the metal is characteristic for such contacts (agostic interactions are typified by a large upfield shift), it does not provide conclusive evidence for the presence of an attractive M···H interaction. ^{195}Pt−^{1}H coupling constants are a much better indicator, and large values for $^1J_{Pt,H}$ have been observed, e.g. $^1J_{Pt,H}$ = 69 Hz in **H**.[49] Unfortunately no stable, well-defined platinum(II) complexes $[L_2Pt_2]^{2+}$ could be isolated with $[L^1]^-$ and $[L^2]^-$.

Even in the possible presence of weak attractive M···H components, however, these hydrogen bonds have to be in balance with significant repulsive forces, and X-ray crystal structures for many of the systems reported in the literature reveal strained ligand geometries, often in order to relieve the interactions. A detailed molecular mechanics study has supported the view that the axial M···H interactions are mainly repulsive in nature.[51] While we cannot rule out a minor attractive contribution to the M···H−C interaction for the present pyrazolate-based dinuclear nickel(II) and palladium(II) complexes, we believe that the Ni···H and Pd···H interactions are basically repulsive and that the H atoms are forced to lie close to the metal ions simply because of geometric constraints due to the bulky ligand substituents. This has been further corroborated by the structure of the dinickel complex of $[L^3]^-$ described below. It should also be noted that the M−H−C angles in **1**−**7** (ca.140°) are more acute by 20°−30° than in those complexes with a confirmed M···H bonding interaction.[42]

Ligand $[L^3]^-$ which bears only a single *ortho* isopropyl substituent on all of its aryl groups was expected to provide clear evidence for the absence or presence of an attractive M···H−C interaction, since the isopropyl substituent might be oriented away from the metal ion or towards the axial coordination sites. The former proved to be the case, as revealed by the X-ray analysis of single crystals of $[L^3_2Ni_2](ClO_4)_2$ (**8**), which could be obtained from propionitrile/diethyl ether. In **8**, both nickel ions were again found in square planar $\{N_4\}$ coordination environments with almost planar five-membered chelate rings, and all bond lengths are in the expected regions (Figure 12). For each ligand $[L^3]^-$, the aryl substituents are on the same side of the coordination framework (isomer **E**, Scheme 4), and the isopropyl groups adopt the largest possible distance from the nickel ions. Due to the steric bulk of the isopropyl groups, opposing aryl rings are not fully parallel but are tilted by ca. 30 °C with respect to each other. Overall, the structure of **8** confirms that the system tends to relieve steric strain and to avoid any close M···H−C contacts if possible.

The ^{1}H NMR spectra of **8** in CD_3CN at 293−343 K revealed only very broad signals, indicative of a variety of dynamic processes in solution. The CH protons of the isopropyl groups resonate at ca. 2.3 ppm (at 293 K). Unfortunately, the poor solubility of **8** limits the range of solvents and temperatures for NMR spectroscopy, and satisfactory ^{13}C NMR spectra could not be obtained for **8**.

Electrochemistry

While no anodic processes were observed up to +1.8 V (all potentials relative to the SCE), the low-spin dinickel(II) complexes **3**, **5**, and **8** as well as the dipalladium complex **6** can be electrochemically reduced in acetonitrile or dichloromethane, respectively. Figure 13 depicts their cyclic voltammograms.

The dinickel complex **3** shows a reversible reduction at $E_{1/2}$ = −0.94 V, presumably giving the respective mixed-valent $Ni^{I}Ni^{II}$ compound. Further reduction is quasi-reversible with E_p^{red} = −1.25 V. The rather large separation of the two processes of around 130 mV (from an estimated "$E_{1/2}$" = −1.18 V for the second reduction wave) indicates significant stabilization of the mixed-valent species towards disproportionation ($K_{comp.}$ = 1.2 × 10^4).

Reduction of complexes **5** and **8** bearing isopropyl substituents at the aryl groups is quasi-reversible (E_p^{red} = −0.81 and −0.98 V, respectively), followed by a second irreversible process. The fully reduced species gives an oxidative wave at around −0.14 V or −0.30 V in the reverse scan. Apparently, the more sterically demanding isopropyl substituents lead to enhanced lability of the reduced compounds, and the methyl-substituted scaffold in **3** is best suited for accepting an additional electron in the antibonding nickel d_{xy} orbitals within the coordination plane.

The electrochemistry of the dipalladium complex **6** is quite similar to that of **5** (except for the lack of the oxidative wave in the back scan). Unexpectedly, however, the dipalladium complex **4** does not show any cathodic process

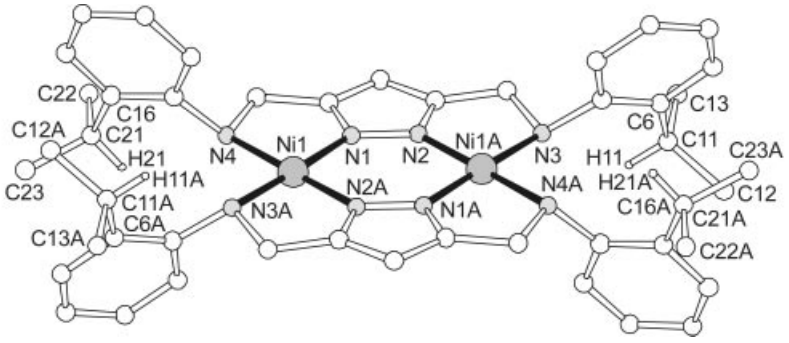

Figure 12. Molecular structure of the cation of **8**; in the interests of clarity only a few hydrogen atoms are shown; selected interatomic distances (Å) and bond angles (°): Ni1−N1 1.8364(12), Ni1−N2A 1.8372(12), Ni1−N3A 1.9697(12), Ni1−N4 1.9719(12), Ni1···Ni1A 3.853(2); N1−Ni1−N3A 178.69(5), N2A−Ni1−N4 176.84(5)

 © 2004 Wiley-VCH Verlag GmbH & Co. KGaA, Weinheim

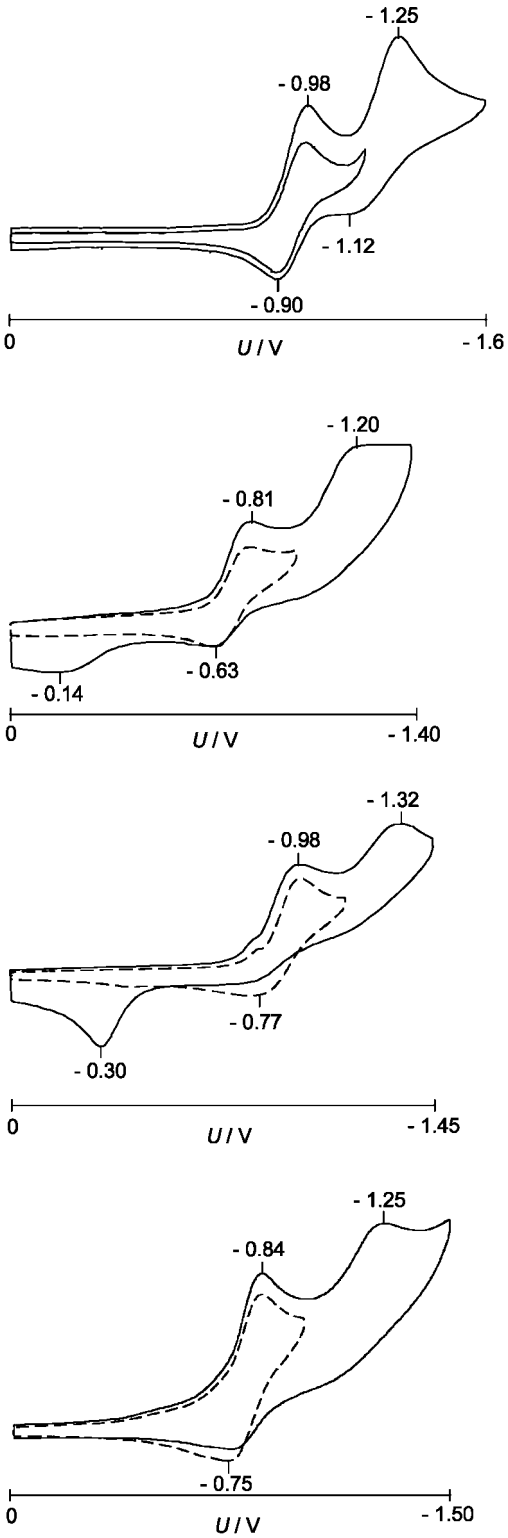

Figure 13. Cyclic voltammograms of **3** (top), **5** (second from top), **8** (second from bottom) and **6** (bottom) recorded on a platinum electrode in MeCN (**3**, **5**, **8**) or CH_2Cl_2 (**6**) containing 0.1 M $NnBu_4^+PF_6^-$; scan speed 200 mVs^{-1}

down to −2.5 V, but an irreversible oxidation at E_p^{ox} = +1.05 V. This corroborates the conclusions drawn from the NMR spectroscopic findings, i.e. the constitution of **4** in solution is most probably not identical to the structure observed in the solid state.

Conclusion

The anilinomethyl-appended pyrazolate ligands $[L^1]^-$, $[L^2]^-$ and $[L^3]^-$ yielded dinuclear type **A** complexes $[L_2M_2]^{2+}$ upon treatment with nickel(II) and palladium(II). Coordinating counter-anions such as chloride can bind to axial sites of the dinickel species in a solvent-dependent process, giving rise to five-coordinate metal ions. In the case of weakly coordinating anions, the metal ions were found in roughly square-planar environments with the structures being dictated by steric requirements due to the bulky aryl substituents. It is noteworthy that all complexes with four-coordinate (square planar) metal ions characterized crystallographically (i.e. complexes **3**, **4**, **5**, **6**, **7** and **8**) feature a (non-crystallographic) C_{2h}-type *meso* arrangement of the aryl groups, while the chiral D_2-type (compare Scheme 4) was not observed in the solid state. Only in the case of **2** was a less sterically favorable C_{2v} isomer enforced by the NH···Cl hydrogen bonds.

The tendency of the aryl groups to avoid each other and not to face each other in close proximity forces the methyl or isopropyl substituents in the aryl 2- and 6-positions to approach the metal ions from the axial directions. This leads to a drastic low-field shift of the respective ^{1}H NMR signals, e.g. δ = 7.86 ppm for the isopropyl-CH that come close to the low-spin nickel(II) ion in $[L^2_2Ni_2]^{2+}$ (**5**). In contrast, the remaining isopropyl-CH comes to lie within the field of the ring-current of the opposing aryl groups and resonates at very high field (δ = 1.86 ppm for **5**).

While the low-field NMR signature of protons close to the axial sites of d^8 metal ions has previously been considered indicative of three-center four-electron M···H−C hydrogen bonds involving the filled d_z^2 orbital of the metal ion, attractive M···H interactions were assumed not to be of major relevance in the present case. This was corroborated by the structure of $[L^3_2Ni_2]^{2+}$, where the single 2-isopropyl groups at each phenyl ring are rotated away from the metal. These phenomena and findings related to the sterically enforced proximity of aliphatic CH bonds to square-planar d^8 metal centers, as reported in the present work, may also be relevant to the characteristics of recent-generation late transition metal catalysts incorporating diamine and diimine ligands, which in many cases also bear bulky aryl substituents.

Experimental Section

General Remarks: Most manipulations were carried out under an dry nitrogen by employing standard Schlenk techniques. Solvents were dried according to established procedures. The ligands were synthesized according to the reported methods,[27] and all other chemicals were used as purchased. Microanalyses: Mikroanalytische Laboratorien des Organisch-Chemischen Instituts der Universität Heidelberg. IR spectra: Perkin−Elmer 983G; recorded as KBr

 © 2004 Wiley-VCH Verlag GmbH & Co. KGaA, Weinheim

pellets. UV/Vis spectra: Perkin−Elmer Lambda 19. FAB-MS spectra: Finnigan MAT 8230. NMR spectra: Bruker AC 200 at 200.13 (^{1}H) and 50.32 (^{13}C) MHz, or Bruker DRX 300 at 300.13 MHz (^{1}H) and 75.47 (^{13}C) MHz; solvent signal as chemical shift reference (CD_3CN δ_H = 1.94, δ_C = 118.1/1.2 ppm); where necessary, assignments were based on a series of 2D experiments. Cyclic voltammetry: PAR equipment, (potentiostat/galvanostat 273), in 0.1 M NBu_4PF_6/CH_3CN. Potentials in V on a glassy carbon electrode, referenced to the SCE at ambient temperature. Magnetic measurements: Bruker magnet B-E 15 C8, field controller B-H 15, variable temperature unit ER 4111 VT, Sartorius microbalance M 25 D-S. Experimental susceptibility data were corrected for the underlying diamagnetism.

Caution! *Although no problems were encountered in this work, perchlorate salts are potentially explosive and should be handled with proper precautions.*

General Synthesis of Complexes: For the syntheses of the complexes, the respective ligand (HL^1, HL^2, HL^3; approximately 1 mmol) was dissolved in THF (50 mL) and deprotonated with one equivalent of KO*t*Bu. After the reaction mixture had been stirred for 30 min, one equivalent of the metal salt {$NiCl_2{\cdot}6H_2O$ or $[Ni(H_2O)_6](ClO_4)_2$ or $[Pd(CH_3CN)_4](BF_4)_2$} was added and stirring continued for 15 h. The solvent was then removed under reduced pressure and the residue washed with light petroleum. Pure compounds were obtained by crystallization, i.e. by slow diffusion of light petroleum or diethyl ether into a solution of the complex as detailed below.

Complex 1: Single crystals were obtained from acetone/light petroleum (yield of crystalline material 183 mg; 42%). IR (KBr): $\tilde{\nu}_{max.}$ = 3242 w, 2955 w, 1590 w, 1512 w, 1464 vs, 1436 s, 1379 m, 1302 s, 1251 w, 1191 s, 1093 s, 1042 w, 974 w, 924 m, 900 m, 761 s, 618 w cm^{-1}. M.p. > 240 °C. UV/Vis (CH_3CN): λ (ε) = 226 (16600), 290 sh (7040), 397 (610), 495 (155), 643 nm (35). MS (FAB): *m*/*z* (%) = 819 (30) $[L^1_2Ni_2Cl]^+$, 782 (100) $[L^1_2Ni_2]^+$. $C_{42}H_{50}Cl_2N_8Ni_2$ (855.20): calcd. C 58.99, H 5.89, N 13.10; found C 58.99, H 6.34, N 12.89.

Complex 2: Single crystals were obtained from dichloromethane/light petroleum (yield of crystalline material 114 mg; 26%). IR (KBr): $\tilde{\nu}_{max.}$ = 2944 w, 1590 w, 1522 w, 1465 vs, 1439 s, 1380 m, 1307 s, 1172 s, 1095 s, 947 m, 902 w, 763 s, 724 w, 571 w cm^{-1}. M.p. > 240 °C. UV/Vis (CH_3CN): identical to the spectrum of **1**.

Complex 3: Single crystals were obtained from acetonitrile/diethyl ether (yield of crystalline material 430 mg; 88%). ^{1}H NMR (300 MHz, CD_3CN): δ = 1.08 (s, 12 H, CH_3), 3.37−3.49 (m, 4 H, CH_2), 4.08−4.30 (m, 4 H, CH_2), 4.17, 4.20 (s, 12 H, CH_3), 4.50 (s, 4 H, NH), 5.80 (s, 1 H, CH^{pz4}), 5.81 (s, 1 H, CH^{pz4}), 6.83 (m, 4 H, $CH^{Ph,m}$), 7.21 (t, ^3J = 7.5 Hz, 4 H, $CH^{Ph,p}$), 7.37 (d, ^3J = 7.5 Hz, 4 H, $CH^{Ph,m}$) ppm. ^{13}C NMR (300 MHz, CD_3CN): δ = 16.6 (CH_3), 21.9 (CH_3), 54.5 (CH_2), 97.0 (CH^{pz4}), 129.2 ($CH^{Ph,p}$), 130.1($CH^{Ph,m}$), 132.5 ($CH^{Ph,m}$), 132.9 ($CH^{Ph,m}$), 142.1, 142.4 (C^{ar}), 157.5, 157.6 ($C^{pz3/5}$) ppm. IR (KBr): $\tilde{\nu}_{max.}$ = 3349 m, 3226 m, 2951 m, 1622 m, 1463 m, 1443 m, 1382 w, 1366 w, 1308 m, 1259 w, 1214 w, 1137 vs, 1112 vs, 1084 vs, 951 w, 772 m, 624 s, 418 m cm^{-1}. M.p. > 240 °C. UV/Vis (CH_3CN): λ (ε) = 240 (14820), 300 (10560), 454 (185), 500 nm(175). MS (FAB): *m*/*z* (%) = 883 (90) $[L^1_2Ni_2ClO_4]^+$, 782 (100) $[L^1_2Ni_2]^+$. $C_{42}H_{50}Cl_2N_8Ni_2O_8$ (983.13): calcd. C 51.31, H 5.12, N 11.39; found C 50.83, H 5.41, N 11.44.

Complex 4: A few single crystals were obtained from dichloromethane/light petroleum. MS (FAB): *m*/*z* (%) = 877 (100) $[L^1_2Pd_2]^+$.

Complex 5: Single crystals were obtained from acetone/diethyl ether (yield of crystalline material 170 mg; 28%). ^{1}H NMR (300 MHz, CD_3CN, 233 K), only data for the major isomer are given: δ = 0.39 (d, ^3J = 6.0 Hz, 12 H, CH_3), 0.90 (d, ^3J = 6.0 Hz, 12 H, CH_3), 1.31 (d, ^3J = 6.0 Hz, 12 H, CH_3), 1.86 (sept, ^3J = 6.0 Hz, 4 H, CH*iPr*), 2.05 (d, ^3J = 6.0 Hz, 12 H, CH_3), 3.45 (dd, ^3J = 16.7/4.5 Hz, 4 H, CH_2), 4.31 (dd, ^3J = 16.7/7.8 Hz, 4 H, CH_2), 4.79 (br., s, NH), 5.75 (s, 2 H, CH^{pz4}), 6.98 (d, ^3J = 7.6 Hz, 4 H, $CH^{Ph,m}$), 7.35 (t, ^3J = 7.6 Hz, 4 H, $CH^{Ph,p}$), 7.55 (d, ^3J = 7.6 Hz, 4 H, $CH^{Ph,m}$), 7.86 (sept, ^3J = 6.0 Hz, 4 H, CH*iPr*) ppm. ^{13}C NMR (300 MHz, CD_3CN, 233 K): δ = 22.7 (CH_3), 25.4 (CH_3), 25.8 (CH_3), 26.0 (CH_3), 28.6 (CH*iPr*), 30.9 (CH*iPr*), 57.8 (CH_2), 99.0 ($CH^{pz,4}$), 126.0 ($CH^{Ph,m}$), 127.4 ($CH^{Ph,m}$), 130.2 ($CH^{Ph,p}$), 138.5 ($C^{Ph,1}$), 141.8 ($C^{Ph,2/6}$), 155.8 ($C^{pz3/5}$) ppm. IR (KBr): $\tilde{\nu}_{max.}$ = 3255 m, 2957 s, 2920 m, 2860 w, 1698 m, 1622 w, 1459 s, 1439 s, 1382 m, 1361 m, 1304 s, 1093 vs, 944 w, 931 w, 804 s, 760 m, 623 s, 527 w, 457 w, 419 w cm^{-1}. M.p. > 240 °C. UV/Vis (CH_3CN): λ (ε) = 235 (16560), 298 (8210), 447 (180), 507 nm (195). MS (FAB): *m*/*z* (%) = 1107 (70) $[L^2_2Ni_2(ClO_4)]^+$, 1006 (100) $[L^2_2Ni_2]^+$. $C_{58}H_{82}Cl_2N_8Ni_2O_8$ (1207.62): calcd. C 57.68, H 6.84, N 9.27; found C 57.76, H 7.63, N 9.59.

Complex 6: Single crystals were obtained from dichloromethane/light petroleum (yield of crystalline material 178 mg; 76% after starting from 0.37 mmol HL^2). ^{1}H NMR (300 MHz, CD_2Cl_2): δ = 0.58 (d, ^3J = 6.6 Hz, 6 H, CH_3), 1.04, 1.05 (d, ^3J = 6.6 Hz, 6 H, CH_3), 1.25, 1.30 (d, ^3J = 6.6 Hz, 6 H, CH_3), 1.82 (d, ^3J = 6.6 Hz, 6 H, CH_3), 2.04 (sept, ^3J = 6.6 Hz, 4 H, CH*iPr*), 3.84, 3.95 (dd, ^3J = 16.6/5.3 Hz, 4 H, CH_2), 4.63, 4.71 (dd, ^3J = 16.5/7.8 Hz, 4 H, CH_2), 4.84, 5.00 (sept, ^3J = 6.6 Hz, 4 H, CH*iPr*), 5.90, 6.05 (br., NH), 6.11, 6.22 (s, 2 H, $CH^{pz,4}$), 6.93 (m, 4 H, $CH^{Ph,m}$), 7.30 (m, 4 H, $CH^{Ph,p}$), 7.41 (m, 4 H, $CH^{Ph,m}$) ppm. ^{13}C NMR (300 MHz, CD_2Cl_2): δ = 23.0, 25.3, 25.5, 25.6, 25.8 (CH_3), 28.4 (CH*iPr*), 28.8 (CH*iPr*), 59.8 (CH_2), 97.9, 98.6 ($CH^{pz,4}$), 124.9, 125.0 ($CH^{Ph,m}$), 127.5, 127.6 ($CH^{Ph,m}$), 129.8, 130.0 ($CH^{Ph,p}$), 139.9, 140.3, 140.6, 140.8, 142.3 ($C^{Ph,1/2/6}$), 154.1 ($C^{pz,3/5}$) ppm. IR (KBr): $\tilde{\nu}_{max.}$ = 3421 m, 3291 m, 3249 m, 2954 m, 2918 m, 2863 m, 1730 w, 1625 m, 1456 s, 1382 m, 1361 m, 1304 s, 1272 w, 1250 w, 1089 vs, 963 s, 925 s, 802 s, 759 m, 625 m, 519 m, 465 m cm^{-1}. M.p. > 240 °C. UV/Vis (CH_2Cl_2): λ (ε) = 353 nm (4387). MS (FAB): *m*/*z* (%) = 1103 (60) $[L^2_2Pd_2]^+$, 656 (60) $[L^2Pd_2]^+$. $C_{58}H_{82}B_2F_8N_8Pd_2$ (1277.78): calcd. C 54.54, H 6.42, N 8.77; found C 53.43, H 6.59, N 9.10.

Complex 7: Single crystals were obtained from acetonitrile/diethyl ether (yield of crystalline material 204 mg; 37%). The bulk crystalline material is a 2:1 mixture of compounds **7** and **3**, according to the ratio of the NMR signals observed for L^1 and L^2. ^{1}H NMR (300 MHz, $CDCl_3$): δ = 0.68 (s, 6 H, CH_3*iPr*), 0.87 (s, 6 H, CH_3*iPr*), 1.09, 1.12 (s, 12 H, CH_3 of L^1), 1.41, 1.48 (d, ^3J = 6 Hz, 6 H, CH_3*iPr*), 1.85 (m, 1 H, CH*iPr*), 2.18 (m, 6 H, CH_3*iPr*), 3.36−3.49 (m, CH_2), 3.95, 4.04 (s, 2 H, NH), 4.17, 4.20 (s, 12 H, CH_3 of L^1), 4.09−4.52 (m, CH_2), 4.90, 5.01 (s, 2 H, NH), 5.82 (s, 2 H, CH^{pz} of L^1), 5.92 (s, 1 H, CH^{pz} of L^2), 6.80−6.90 (m, CH^{Ar}), 7.10−7.23, 7.36−7.49 (m, CH^{Ar} and 1 H, CH*iPr*), 7.66 (d, ^3J = 7.4 Hz, 2 H, CH^{Ar}) ppm. ^{13}C NMR (300 MHz, $CDCl_3$): δ = 15.9, 16.6 (CH_3 of L^1), 22.0, 22.2, 22.7, 22.9, 25.6, 26.8 (CH_3 of L^1, L^2), 28.4 (CH*iPr*), 30.6 (CH*iPr*), 54.4, 54.6 (CH_2 of L^1), 55.3, 57.4 (CH_2 of L^2), 97.1 (CH^{pz} of L^1), 98.1 (CH^{pz} of L^2), 125.8, 128.3, 129.2, 129.4, 130.1, 130.3, 130.7, 131.8, 132.5, 132.9 (CH^{ar}), 138.5, 138.9, 142.1, 142.4 (C^{ar}), 157.5, 157.6 ($C^{pz,3/5}$) ppm. IR (KBr): $\tilde{\nu}_{max.}$ = 3225 m, 2952 m, 2931 m, 2860 w, 1622 w, 1524 w, 1461 s, 1443 s, 1382 s, 1361 m, 1307 s, 1253 w, 1094 vs, 961 w, 805 m, 777 m, 623 s, 570 w, 459 w, 418 w cm^{-1}. M.p.> 240 °C. UV/Vis (CH_3CN): λ (ε) = 218 (30808), 298 (9705), 499 (217). MS (FAB): *m*/*z* (%) = 995 (80) $[L^1L^2Ni_2ClO_4]^+$, 894 (100) $[L^1L^2Ni_2]^+$.

 © 2004 Wiley-VCH Verlag GmbH & Co. KGaA, Weinheim

Table 1. Crystal data and refinement details for complexes **1**, **2**, **3**, **4**

	$[L^1_2Ni_2Cl_2]$ (**1**)	$[L^1_2Ni_2]Cl_2$ (**2**)	$[L^1_2Ni_2](ClO_4)_2$ (**3**)	$[L^1_2Pd_2](BF_4)_2$ (**4**)
Empirical formula	$C_{42}H_{50}Cl_2N_8Ni_2{\cdot}2[OC(CH_3)_2]$	$C_{42}H_{50}Cl_2N_8Ni_2{\cdot}4(CH_2Cl_2)$	$C_{42}H_{50}N_8O_8Cl_2Ni_2{\cdot}4(CH_3CN)$	$C_{42}H_{50}B_2F_8N_8Pd_2{\cdot}2(CH_2Cl_2, H_2O)$
M_r (g/mol)	971.35	1194.94	1147.39	1259.20
Crystal size (mm)	0.30 × 0.30 × 0.20	0.20 × 0.25 × 0.10	0.10 × 0.30 × 0.20	0.20 × 0.15 × 0.15
Crystal system	triclinic	monoclinic	triclinic	monoclinic
Space group	$P\bar{1}$	$C2/c$	$P\bar{1}$	$P2_1/c$
a (Å)	10.507(2)	32.664(7)	8.758(2)	13.909(3)
b (Å)	13.559(3)	13.841(3)	11.006(2)	10.012(2)
c (Å)	17.019(3)	11.991(2)	15.009(3)	19.084(4)
α (deg)	81.55(3)	90	107.32(3)	90
β (deg)	77.14(3)	103.00(3)	98.62(3)	108.71(3)
γ (deg)	88.63(3)	90	103.85(3)	90
Volume (Å^3)	2338.0	5282.3	1302.3	2517.2
Z	2	4	1	2
$\rho_{calcd.}$ (g/cm^3)	1.363	1.503	1.463	1.661
F(000)	1024	2464	600	1272
hkl range	−12−13, ±16, ±21	±42, ±17, ±15	±11, ±14, ±19	±18, ±12, −25−27
Temperature (K)	200	200	200	200
2θ range	$3.6 < 2\theta < 52.4$	$2.6 < 2\theta < 55$	$4.1 < 2\theta < 55.1$	$3.1 < 2\theta < 60.8$
Measured reflections	37920	44628	11835	11548
Unique reflections	9226	6057	5991	5793
Obsd. reflections $[I > 2\sigma(I)]$	5172	4382	4617	4900
Refined parameters	592	414	345	407
Residual electron density (e·Å^{-3})	0.55	0.60	0.67	1.66
$R1$ $[I > 2\sigma(I)]$	0.042	0.039	0.039	0.036
$wR2$ (all data)	0.105	0.096	0.099	0.094
Goodness-of-fit	0.966	0.997	1.071	1.080

Table 2. Crystal data and refinement details for complexes **5**, **6**, **7** and **8**

	$[L^2_2 Ni_2](ClO_4)_2$ (**5**)	$[L^2_2Pd_2](BF_4)_2$ (**6**)	$[L^1L^2Ni_2](ClO_4)_2$ (**7**)	$[L^3_2Ni_2](ClO_4)_2$ (**8**)
Formula	$C_{58}H_{82}N_8O_8Cl_2Ni_2{\cdot}1.4$ $[OC(CH_3)_2]$ 0.4 C_2H_5OH	$C_{58}H_{82}B_2F_8N_8Pd_2{\cdot}2$ (CH_2Cl_2)	$C_{50}H_{66}Cl_2N_8Ni_2O_8{\cdot}1.5$ (CH_3CN)	$C_{46}H_{58}Cl_2N_8Ni_2O_8{\cdot}2$ (C_2H_5CN)
M_r (g/mol)	1307.35	1447.59	1157.01	1149.48
Crystal size (mm)	0.08 × 0.20 × 0.30	0.06 × 0.23 × 0.38	0.10 × 0.10 × 0.05	0.35 × 0.26 × 0.24
Crystal system	triclinic	triclinic	orthorhombic	triclinic
Space group	$P\bar{1}$	$P\bar{1}$	$Pbca$	$P\bar{1}$
a (Å)	10.760(2)	11.4267(5)	17.380(4)	9.2380(1)
b (Å)	11.073(2)	12.3828(6)	18.230(4)	9.2919(1)
c (Å)	15.022(3)	13.4776(6)	35.150(7)	16.3793(3)
α (deg)	106.21(3)	80.048(3)	90	99.750(1)
β (deg)	96.44(3)	66.255(3)	90	96.833(1)
γ (deg)	101.36(3)	69.194(3)	90	98.877(1)
Volume (Å^3)	1658.2	1630.75	11137.0	1353.78(3)
Z	1	1	8	1
$\rho_{calcd.}$ (g/cm^3)	1.309	1.474	1.380	1.410
F(000)	697	744	4872	604
hkl range	±42, ±17, ±15	−13−15, ±16, 0−17	±23, ±25, ±49	−12−11, ±12. 0−21
Temperature (K)	200	173	200	173
2θ range	$3.9 < 2\theta < 52.0$	$3.3 < 2\theta < 56.8$	$3.4 < 2\theta < 60.3$	$4.52 < 2\theta < 56.64$
Measured reflections	11777	22195	29886	18243
Unique reflections	6132	8020	15258	6599
Obsd. reflections $[I > 2\sigma(I)]$	4487	6181	6187	5830
Refined parameters	392	541	735	468
Residual electron density (e·Å^{-3})	0.93	1.95	0.69	0.54
$R1$ $[I > 2\sigma(I)]$	0.052	0.054	0.079	0.032
$wR2$ (all data)	0.144	0.156	0.227	0.092
Goodness-of-fit	1.048	1.043	0.966	1.059

 © 2004 Wiley-VCH Verlag GmbH & Co. KGaA, Weinheim

Complex 8: Single crystals were obtained from acetonitrile/diethyl ether (yield of crystalline material 105 mg; 20%). ^{1}H NMR (300 MHz, $CDCl_3$, 333 K): δ = 1.03 (br. s, CH_3), 2.80 (br. s, CH*iPr*), 6.69 ($CH^{pz,4}$), 7.67, 7.96, 8.50 (br. s, CH^{Ph}) ppm, CH_2 not observed. ^{13}C NMR (300 MHz, $CDCl_3$): no signals observed. IR (KBr): $\tilde{\nu}_{max.}$ = 3425 w, 3226 s, 2935 s, 2921 m, 2879 w, 1484 s, 1437 m, 1383 m, 1359 w, 1312 s, 1237 w, 1112 vs, 1102 vs, 1088 vs, 1030 vs, 944 w, 929 w, 91 w, 763 s, 622 vs, 526 m, 461 w, 420 w cm^{-1}. M.p.> 240 °C. UV/Vis (CH_3CN): λ (ε) = 216 (28006), 242 (20310), 285 (7708), 477 (361). MS (FD): *m*/*z* (%) = 939 (100) $[L_2^3Ni_2(ClO_4)]^+$, 839 (10) $[L_2^3Ni_2]^+$. $C_{46}H_{58}Cl_2N_8Ni_2O_8$ (1039.29): calcd. C 53.16, H 5.63, N 10.78; found C 53.00, H 5.57, N 10.80.

X-ray Crystallographic Studies: The measurements for **1**, **2**, **3**, **4**, **5** and **7** were carried out with a Nonius Kappa CCD diffractometer and for **6** and **8** with a Bruker-AXS-CCD diffractometer, using graphite-monochromated Mo-K_α radiation. All calculations were performed using the SHELXT PLUS software package.[52] Structures were solved by direct methods with SHELXS-97 and refined with SHELXL-97. Atomic coordinates and thermal parameters of the non-hydrogen atoms were refined in fully or partially anisotropic models by full-matrix least-squares calculation based on F^2. In general the hydrogen atoms were placed in calculated positions and allowed to ride on the atoms to which they are attached. Table 1 and Table 2 shows a compilation of the data for the structure determinations.

CCDC-222584 (for **1**), -222585 (for **2**), -222586 (for **3**), -222587 (for **4**), -222588 (for **5**), -222589 (for **6**), -222590 (for **7**) and -222591 (for **8**) contain the supplementary crystallographic data for this paper. These data can be obtained free of charge at www.ccdc.cam.ac.uk/conts/retrieving.html [or from the Cambridge Crystallographic Data Center, 12 Union Road, Cambridge CB2 1EZ, UK; Fax: (internat.) +44-1223-336-033; E-mail: deposit@ccdc.cam.ac.uk].

Acknowledgments

F. M. sincerely thanks Prof. Dr. G. Huttner for his generous support and Dr. S. Dechert for valuable discussions. Funding from the DFG (SFB, 247, Graduiertenkolleg-Fellowship to J. C. R.) and the Fonds der Chemischen Industrie (F. M.) is gratefully acknowledged.

[1] K. D. Karlin, *Science* **1993**, *261*, 701−708.
[2] E. K. van den Beuken, B. L. Feringa, *Tetrahedron* **1998**, *54*, 12985−13011.
[3] H. Steinhagen, G. Helmchen, *Angew. Chem.* **1996**, *108*, 2489−2492; *Angew. Chem. Int. Ed. Engl.* **1996**, *35*, 2339−2342.
[4] O. Kahn, *Molecular Magnetism*, Wiley-VCH, Weinheim, **1993**.
[5] S. Trofimenko, *Progr. Inorg. Chem.* **1986**, *34*, 115−210.
[6] G. La Monica, G. A. Ardizzoia, *Progr. Inorg. Chem.* **1997**, *46*, 151−238.
[7] F. Meyer, S. Beyreuther, K. Heinze, L. Zsolnai, *Chem. Ber./Recl.* **1997**, *130*, 605−613.
[8] F. Meyer, P. Rutsch, *Chem. Commun.* **1998**, 1037−1038.
[9] T. Kamiusuki, H. Okawa, N. Matsumoto, S. Kida, *J. Chem. Soc., Dalton Trans.* **1990**, 195−198.
[10] C. W. Hahn, P. G. Rasmussen, J. Carlos Bayón, *Inorg. Chem.* **1992**, *31*, 1963−1965.
[11] J. Pons, X. López, J. Casabó, F. Teixidor, A. Caubet, J. Rius, C. Miravitlles, *Inorg. Chim. Acta* **1992**, *195*, 61−66.
[12] B. Mernari, F. Abraham, M. Lagrenee, M. Drillon, P. Legoll, *J. Chem. Soc., Dalton Trans.* **1993**, 1707−1711.
[13] F. Meyer, A. Jacobi, L. Zsolnai, *Chem. Ber./Recl.* **1997**, *130*, 1441−1447.
[14] M. Itoh, K.-I. Motoda, K. Shindo, T. Kamiusuki, H. Sakiyama, N. Matsumoto, H. Okawa, *J. Chem. Soc., Dalton Trans.* **1995**, 3635−3641.
[15] F. Escartí, C. Miranda, L. Lamarque, J. Latorre, E. García-España, M. Kumar, V. J. Arán, P. Navarro, *Chem. Commun.* **2002**, 936−937.
[16] T. G. Schenck, C. R. C. Milne, J. F. Sawyer, B. Bosnich, *Inorg. Chem.* **1985**, *24*, 2338−2344.
[17] T. Kamiusuki, H. Okawa, E. Kitaura, M. Koikawa, N. Matsumoto, S. Kida, H. Oshio, *J. Chem. Soc., Dalton Trans.* **1989**, 2077−2081.
[18] T. A. Kaden, *Coord. Chem. Rev.* **1999**, *190−192*, 371−389.
[19] J.-L. Chou, D.-N. Horng, J.-P. Chyn, K.-M. Lee, F. L. Urbach, G.-H. Lee, H.-L. Tsai, *Inorg. Chem. Commun.* **1999**, *2*, 392−395.
[20] S. Tanaka, M. Akita, *Angew. Chem.* **2001**, *113*, 2951−2953; *Angew. Chem. Int. Ed.* **2001**, *40*, 2865−2867.
[21] F. Meyer, K. Heinze, B. Nuber, L. Zsolnai, *J. Chem. Soc., Dalton Trans.* **1998**, 207−214.
[22] F. Meyer, E. Kaifer, P. Kircher, K. Heinze, H. Pritzkow, *Chem. Eur. J.* **1999**, *5*, 1617−1630.
[23] F. Meyer, I. Hyla-Kryspin, E. Kaifer, P. Kircher, *Eur. J. Inorg. Chem.* **2000**, 771−781.
[24] S. Buchler, F. Meyer, E. Kaifer, H. Pritzkow, *Inorg. Chim. Acta* **2002**, *337*, 371−386.
[25] J. C. Röder, F. Meyer, H. Pritzkow, *Chem. Commun.* **2001**, 2176−2177.
[26] J. C. Röder, G. Noel, F. Meyer, unpublished results.
[27] J. C. Röder, F. Meyer, M. Konrad, S. Sandhöfner, E. Kaifer, H. Pritzkow, *Eur. J. Org. Chem.* **2001**, 4479−4487.
[28] The angular structural parameter τ is defined as τ = (β − α)/60, where α and β represent two basal angles with β > α. It is a measure of the degree of trigonality: a perfect TB-5 structure is associated with τ = 1, while τ = 0 is expected for an idealized SPY-5 geometry: A. W. Addison, T. N. Rao, J. Reedijk, J. van Rijn, G. C. Verschoor, *J. Chem. Soc., Dalton Trans.* **1984**, 1349−1356.
[29] C. Janiak, *J. Chem. Soc., Dalton Trans.* **2000**, 3885−3896.
[30] C. J. O′Connor, *Inorg. Chem.* **1982**, *29*, 203−283.
[31] N_α refers to the temperature-independent paramagnetism [100 × 10^{-6} cm^3/mol per nickel(II) ion[29]]; all other parameters have their usual meaning. $\chi_{dim} = (Ng^2\mu_B{}^2/kT)\cdot[2\exp(2J/kT) + 10\exp(6J/kT)]/[1 + 3\exp(2J/kT) + 5\exp(6J/kT)]$; $\chi_{mono} = 2Ng^2\mu_B{}^2/3kT$; $R = \Sigma(\chi^{calcd.} - \chi^{obsd.})^2/\Sigma(\chi^{obsd.})^2$.
[32] P. Chaudhuri, H.-J. Küppers, K. Wieghardt, S. Gehring, W. Haase, B. Nuber, J. Weiss, *J. Chem. Soc., Dalton Trans.* **1988**, 1367−1370.
[33] L. Siegfried, T. A. Kaden, F. Meyer, P. Kircher, H. Pritzkow, *J. Chem. Soc., Dalton Trans.* **2001**, 2310−2315.
[34] J. Casabó, J. Pons, K. S. Siddiqi, F. Teixidor, E. Molins, C. Miravitlles, *J. Chem. Soc., Dalton Trans.* **1989**, 1401−1403.
[35] J. Pons, X. López, E. Benet, J. Casabó, *Polyhedron* **1990**, *9*, 2839−2845.
[36] V. P. Hanot, T. D. Robert, J. Kolnaar, J. G. Haasnoot, J. Reedijk, H. Kooijman, A. L. Spek, *J. Chem. Soc., Dalton Trans.* **1996**, 4275−4281.
[37] C. J. Ballhausen, A. D. Liehr, *J. Am. Chem. Soc.* **1959**, *81*, 538−542.
[38] L. Brammer, *Dalton Trans.* **2003**, 3145−3157.
[39] M. Brookhart, M. L. H. Green, *J. Organomet. Chem.* **1983**, *250*, 395−408.
[40] R. H. Crabtree, *Angew. Chem.* **1993**, *105*, 828−845; *Angew. Chem. Int. Ed. Engl.* **1993**, *32*, 789−806.
[41] D. Braga, F. Grepioni, E. Tedesco, K. Biradha, G. R. Desiraju, *Organometallics* **1997**, *16*, 1846−1856.
[42] A. Martín, *J. Chem. Ed.* **1999**, *76*, 578−583.
[43] J. Y. Saillard, R. Hoffman, *J. Am. Chem. Soc.* **1984**, *106*, 2006−2026.

 © 2004 Wiley-VCH Verlag GmbH & Co. KGaA, Weinheim

[44] A. Albinati, C. G. Anklin, F. Ganazzoli, H. Rüegg, P. S. Pregosin, *Inorg. Chem.* **1987**, *26*, 50−508.
[45] A. Albinati, C. Arz, P. S. Pregosin, *Inorg. Chem.* **1987**, *26*, 508−513.
[46] A. Albinati, P. S. Pregosin, F. Wombacher, *Inorg. Chem.* **1990**, *29*, 1812−1817.
[47] M. Bortolin, U. E. Bucher, H. Rüegger, L. M. Venanzi, A. Albinati, F. Lianza, S. Trofimenko, *Organometallics* **1992**, *11*, 2514−2521.
[48] I. C. M. Wehman-OoYevaar, D. M. Grove, H. Kooijman, P. van der Sluis, A. L. Spek, G. Van Koten, *J. Am. Chem. Soc.* **1992**, *114*, 9916−9924.
[49] J. M. Casas, L. R. Falvello, J. Fourníes, A. Martín, A. J. Welch, *Inorg. Chem.* **1996**, *35*, 6009−6014.
[50] T. Kawamoto, I. Nagasawa, H. Kuma, Y. Kushi, *Inorg. Chem.* **1996**, *35*, 2427−2432.
[51] T. W. Hambley, *Inorg. Chem.* **1998**, *37*, 3767−3774.
[52] G. M. Sheldrick, *SHELXL-97, Program for Crystal Structure Refinement*, University of Göttingen, **1997**; G. M. Sheldrick, *SHELXS-97, Program for Crystal Structure Solution*, University of Göttingen, **1997**.

Received October 23, 2003
Early View Article
Published Online March 9, 2004

 © 2004 Wiley-VCH Verlag GmbH & Co. KGaA, Weinheim

Structural Study of Novel Graphite−Lithium−Calcium Intercalation Compounds

Sébastien Pruvost,[a,b] Claire Hérold,*[a] Albert Hérold,[a] and Philippe Lagrange[a,b]

Keywords: Calcium / Electron microscopy / Graphite / Intercalation / Lithium / X-ray diffraction

Three new layered compounds were synthesised by immersing a pyrographite platelet in a molten Ca–Li alloy creating a new graphite intercalation compound family. The samples were studied by X-ray and neutron diffraction, revealing that the intercalated sheets are polylayered. The study of the 00*l* reflections allowed us to establish the *c*-axis stacking of these three phases. The α-phase exhibits a five-layered intercalated sheet which has something in common with a Li–Ca–Li–Ca–Li slice cut in the $CaLi_2$ structure ($ThMn_2$ Laves phase type). The β-phase, which is richer in metallic elements and with a greater repeat distance, possesses seven-layered intercalated sheets due to the splitting of the middle lithium plane in three. The third phase is a pseudo-binary compound, containing monolayered sheets and with a formula close to CaC_6. Electron microdiffraction allowed us to determine the 2D unit cell for each compound, all of which were commensurate with that of graphite. Charge transfer from the intercalate to the host lattice was evaluated for the three phases from *hk*0 data, leading to high values.

(© Wiley-VCH Verlag GmbH & Co. KGaA, 69451 Weinheim, Germany, 2004)

Introduction

Graphite exhibits a lamellar structure containing two-dimensional Van der Waals gaps, and it therefore acts as a host lattice for numerous reagents. It turns out that the alkali metals are excellent electron donors in order to intercalate into graphite. The intercalation of the pure alkali metal was reported a long time ago;[1] it leads to binary compounds whose stage varies with metal content. Indeed, when potassium, rubidium and caesium react with graphite, it is very easy to prepare the pure first-stage MC_8 (M = K, Rb, Cs) compounds, which contain a monoatomic metal layer in each interlayer space. On the other hand, the behaviour of graphite changes radically when a less electropositive element is added to the reactive alkali metal. For example, when a graphite sample is immersed in liquid potassium containing a small amount of sulfur, a ternary compound is formed whose intercalated sheets are poly-layered with potassium atoms in contact with graphene planes.[2] Moreover, these potassium-rich compounds are very stable in air.

In the case of lithium, the binary first-stage compound is rather different from the previous ones:[3] its metal content is higher, since its chemical formula is LiC_6. This compound is of great interest, due to its widespread use as the negative electrode material in Li-ion batteries.[4] One way to improve the batteries' capacity could be to increase the lithium content of the negative electrode, although the co-intercalation of lithium with another element seems to be very difficult. The data concerning the structure and the properties of the LiC_6 compound, in comparison with those of the heavy alkali metal compounds, are unfavourable to this co-intercalation because the repeat distance would be increased and part of the strong Li−Li interactions along the *c*-axis would be destroyed. Moreover, the synthesis of a ternary alkali metal compound requires the melting of the M−E mixture (M = alkali metal, E = co-intercalated element) or the partial solubility of M−E in the liquid metal. The melting points of most M−E mixtures are very high and the attack of graphite by lithium is very fast above 600 °C, with formation of lithium acetylide (Li_2C_2) and, of course, destruction of the graphene planes. Numerous experiments have been carried out associating lithium with various elements but generally only binary compounds are obtained.[5] Consequently, we tried to co-intercalate lithium with some elements that are able to intercalate into graphite by themselves. We chose the alkaline earth metals because their intercalation into graphite leads to first-stage MC_6 compounds (M = Ca, Sr, Ba)[6] rather close to LiC_6, despite the fact that the reaction is markedly more difficult, especially with calcium. These experiments led to the isolation of the first ternary graphite−lithium−third-element compounds, that were obtained associating lithium and calcium.[7] We report three new intercalation compounds, called α, β and γ, and their description is given below.

[a] Laboratoire de Chimie du Solide Minéral, UMR 7555, Université Henri Poincaré Nancy I
B. P. 239, 54506 Vandœuvre-lès-Nancy Cedex, France
E-mail: Claire.Herold@lcsm.uhp-nancy.fr
[b] Ecole Européenne d'Ingénieurs en Génie des Matériaux, Institut National Polytechnique de Lorraine,
6, rue Bastien-Lepage, B. P. 630, 54010 Nancy Cedex, France

Results and Discussion

Structure of the α Compound

The 00*l* diffraction diagram of this compound (Figure 1) gives a *c*-axis repeat distance of 776 pm. According to the dilatometric measurements, which give values of around 157%, it belongs to the first stage thus confirming the crystallographic data (the theoretical calculation leads to 132%). This difference is almost certainly due to the non-uniformity of the sample's faces. The repeat distance is quite characteristic of a poly-layered intercalated sheet. Indeed, the repeat distances are only 370 pm and 455 pm for both the binary compounds LiC_6 and CaC_6, respectively.[3,6]

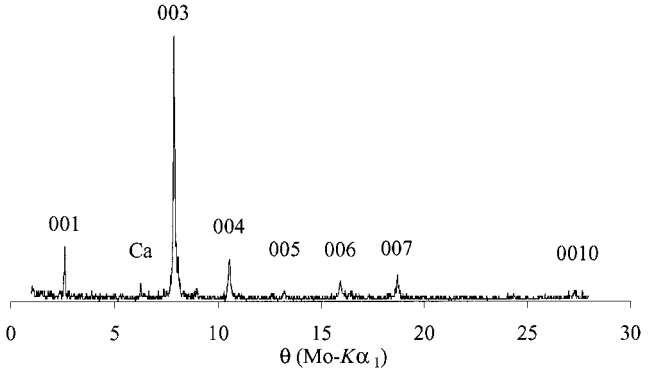

Figure 1. 00*l* X-ray diagram of the α compound

The study of lithium by X-ray diffraction is particularly difficult due to the presence of very few electrons in these atoms, therefore neutron diffraction experiments are often necessary in order to complete the data and allow us to calculate the *c*-axis atomic stacking.

Firstly, however, we will consider only the results obtained from the X-ray experiments. The Fourier transform of the 00*l* structure factors allowed us to produce the *c*-axis electronic density profile in the direct space. From a *c*-axis atomic stacking model, without taking the lithium atoms into account, we then plotted a second electronic density profile, which was compared to the previous one. When the best agreement had been obtained between both profiles (Figure 2), the atomic stacking model was considered to be a good description of the carbon and calcium positions along the *c*-axis. This model presents two superimposed symmetrical calcium layers in the graphitic interval, with a graphene—calcium layer distance of 238 pm, such that the calcium layer—calcium layer distance in the same graphitic interval reaches 300 pm. Moreover, the C/Ca ratio is equal to 2.3, in accordance with the results of the analyses.

Secondly, we used the neutron-diffraction data in order to take the lithium atoms into account. Using the same method, we obtained a final model with three additional lithium layers: one of them is placed at the centre of the

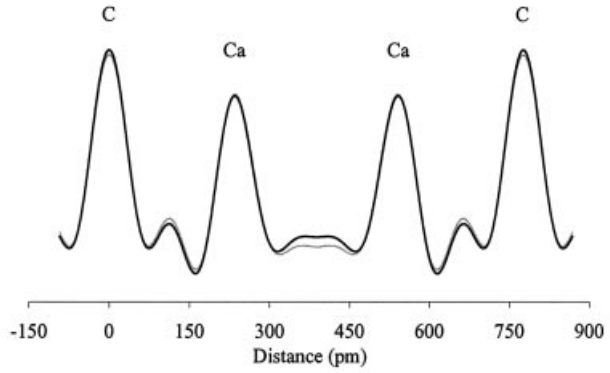

Figure 2. Electronic density profiles along the **c** axis of the α compound; black line: experimental data; grey line: calculated data; seven reflections are taken into account (residual factor R_{F00l} = 8.35%)

graphitic interval with two symmetrical layers between the graphene plane and the calcium layer. The graphite—lithium layer distance is estimated to be 160 pm. This result, nevertheless, remains qualitative, because it has been shown by nuclear microprobe analysis[8] that lithium distribution inside the compound is not really homogeneous. Consequently, it is not possible to attribute a well-defined metal content for each lithium layer. The lithium content is, however, higher in both of the symmetrical external layers.

Finally, the intercalated sheet appears as a five-layer, according to the Li−Ca−Li−Ca−Li sequence and we can clearly see that there are lithium atoms in contact with the graphene planes. Indeed, as is usual in these ternary compounds, the more electropositive element is localised close to the more electronegative one, in this case the carbon atoms.

The intercalation reaction into graphite is always an oxido-reduction. With electron donor species, graphite is reduced and the electron concentration of the graphene planes increases; the carbon−carbon distance simultaneously increases. The *hk*0 X-ray diagram allows us to determine this charge transfer between the intercalated species and the graphene layers, since measuring the angular position of the 110 reflection generated by the graphene planes very precisely is enough to be able to calculate this distance. Its value was compared to that of pristine graphite, and the increase of the carbon−carbon distance was deduced. For these measurements, diamond was used as an internal standard (the 220 reflection of the CFC diamond for our calculations). The d-spacing of the 110 reflection is equal to 125.2 pm for the ternary compound, whereas it only reaches 123 pm in pristine graphite. The corresponding increase of the C−C distance is of the order of 1.8%. Pietronero and Strässler[10] have established the following equation between this parameter and the charge transfer (f_c):

$$\Delta d_{C\text{-}C} = 0.157 f_c + 0.146 f_c^{3/2} + 0.236 f_c^2$$

 © 2004 Wiley-VCH Verlag GmbH & Co. KGaA, Weinheim

According to this relation, the electronic transfer reaches 0.111 electrons per carbon atom for the compound. In comparison, the corresponding value is only 0.07 electrons per carbon atom in the LiC_6 compound. In spite of the very large amount of intercalated metal, the charge transfer remains moderate, so that it is probable that there are metallic bonds within the intercalated sheets. These bonds could explain the unusual hardness of the samples.

The 2D organisation of the compound was observed by several techniques, including TEM (transmission electron microscopy) and XRD (*hk*0 reflections). The TEM study was carried out in a single-crystalline area of the sample. In order to be sure that this area is well representative of the compound, it was systematically observed by EDS (electron dispersive spectroscopy) measurements. The electron microdiffraction images gave the symmetry and the parameters of the 2D unit cell: it is rectangular with $a = 2000$ pm and $b = 430$ pm, and it is commensurate with the graphitic one after taking the charge transfer into account. The 110 graphitic reflection becomes the 830 one in this unit cell. Furthermore, the a and b parameters can be respectively written as $8a_G$ and $\sqrt{3}{\cdot}a_G$. Of course, in these expressions the value of a_G is not that corresponding to pristine graphite, but that obtained from the expanded graphene planes present in the ternary compound. The particular values of these parameters lead to a 2D unit cell that contains exactly 32 carbon atoms (Figure 3).

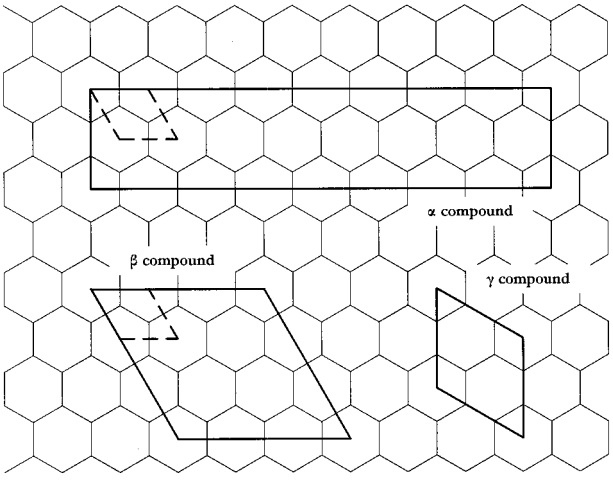

Figure 3. 2D unit cells of the α, β and γ compounds; dotted lines represent the 2D graphite unit cell

A rotating crystal image (Figure 4) allowed us to determine the value of the third parameter, which is twice the repeat distance, that is to say: $c = 1552$ pm. Consequently, the 3D unit cell of the compound is orthorhombic with the three previous parameters.

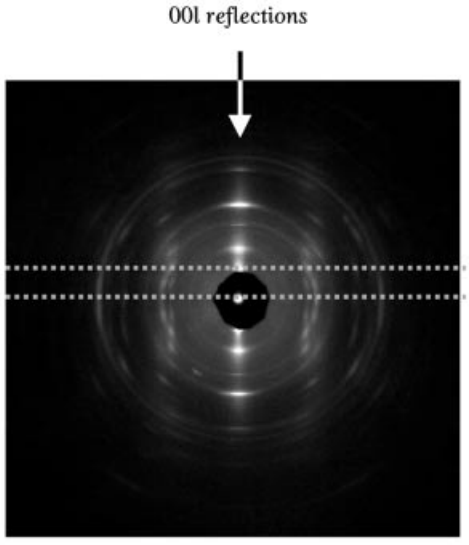

Figure 4. Rotating crystal image of the α compound; both dotted lines symbolise the equatorial stratum and stratum 2

It is interesting to compare the *c*-axis atomic stacking of the α ternary compound with the structure of the $CaLi_2$ binary solid alloy. $CaLi_2$ appears in the Ca−Li phase diagram[11,12] as the only definite compound. Its structure, first studied by Hellner and Laves[13] and later by Carfagno,[11] is hexagonal and isomorphic with the Laves's $ThMn_2$ phase with the following parameters: $a = 631.3$ pm and $c = 1028$ pm. Its space group is $P6_{3/m}mc$, with calcium atoms occupying the 4f sites and lithium atoms the 2a and 6h ones, such that each unit cell contains four $CaLi_2$ units. Along the *c*-axis, the structural arrangement of $CaLi_2$ can be described by a perfectly alternating sequence of calcium and lithium layers, in accordance with a Li−Ca−Li−Ca−Li five-layered intercalated sheet. As is shown in Figure 5, two possibilities exist in order to allow the formation of a *c*-axis five-layered sequence in the $CaLi_2$ solid alloy. The first slice (denoted A) seems to be more likely than the second one (denoted B) for two reasons. Firstly, in the A-slice the out-

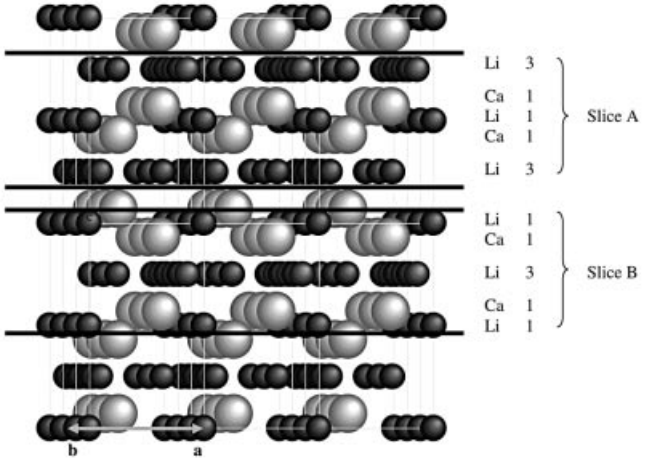

Figure 5. $CaLi_2$ structure and both possible slices

 © 2004 Wiley-VCH Verlag GmbH & Co. KGaA, Weinheim

side lithium layers contain a larger number of atoms than the internal lithium plane — an identical distribution was observed in the intercalated sheet, according to the neutron-diffraction data — whereas in the B-slice the metal content of the internal lithium layer is particularly high. Secondly, the calcium atoms are exactly superimposed in the B-slice, while they are shifted in the A-slice, therefore it is likely that this second arrangement is more stable for a 2D slice intercalated between graphene planes.

These comments present a great interest because we can observe that the intercalation into graphite of binary species often allows a comparison between the sequence of the intercalated sheets and the structure of the free binary species. In spite of the stress applied by the graphene planes, the atomic stacking in the intercalation compound could be identical to a slice judiciously cut off in the structure. Similar results were previously observed in several cases, for example potassium sulfide,[14] potassium amalgam[15] and sodium peroxide.[16,17]

A mixture containing the second stage compound (α type) and CaC_6 was also obtained but it was not possible to isolate this ternary phase. The value of its repeat distance is 1100 pm, that is to say approximately (776 + 335) pm. Therefore, this compound exhibits alternating occupied graphitic intervals (with the same atomic stacking as in the first stage α phase) and empty ones along the *c*-axis.

Structure of the β Compound

As described above, the 00*l* X-ray diffraction diagram (Figure 6) gives the repeat distance of this first-stage compound. It is much higher for this phase, since it reaches 970 pm (instead of 776 pm for α compound). There is an obvious connection between this high value and the very large lithium content of the phase, which possesses a C/Li ratio slightly lower than 2.

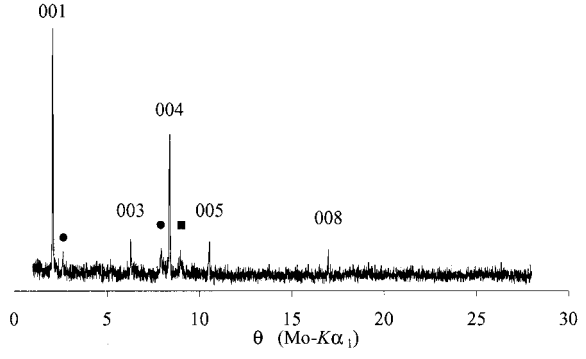

Figure 6. 00*l* X-ray diagram of the β compound; • α phase, ■ CaC_6

Using the previous method, it is possible to draw the experimental *c*-axis electronic density profile. This model then allows us to draw a second profile, and the comparison between both profiles leads to an improvement of this model until a better agreement was obtained. However, since this compound contains a lot of lithium, it is necessary in this case to take the lithium atoms into account. Indeed, their presence is clearly evident in Figure 7. The *c*-axis atomic stacking model contains seven layers, according to the Li−Ca−Li−Li−Li−Ca−Li sequence. The central lithium layer is very rich in metal (1.5 lithium atoms for every six carbon atoms), whereas the outer lithium planes (130 pm above and below) contain only 0.6 lithium atoms for every six carbon atoms. For this reason it is not easy to confirm the presence of these latter lithium layers by XRD, although the inter-calcium layer distance of 510 pm means that the calcium layers cannot surround only one lithium plane. This large value therefore confirms the presence of three central lithium layers. Both calcium planes contain 2.1 calcium atoms for every six carbons. Moreover, this very thick sheet is sandwiched between two lithium layers 650 pm away from one another, which contain one lithium atom for every six carbon atoms.

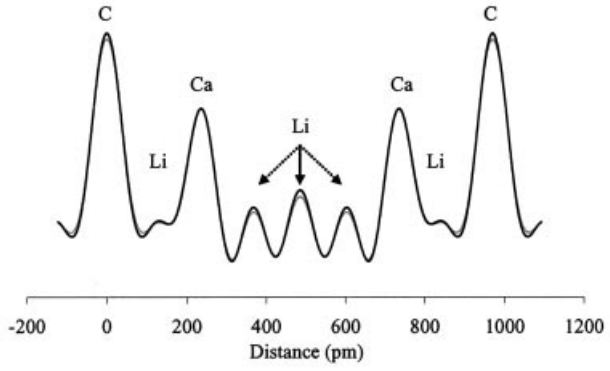

Figure 7. Electron-density profiles along the *c* axis of the β compound; black line: experimental data; grey line: calculated data; eight reflections are taken into account (residual factor R_{F00l} = 6.6%)

This intercalated sheet is extremely rich in metal and is consequently very thick. A similar phenomenon was observed previously in another system when we carried out the intercalation reaction of potassium−thallium alloys into graphite.[18] The amount of intercalated metal was also very high, as was the repeat distance, and the core of the intercalated sheet was also constituted by three metal layers, although with Tl−Tl−Tl stacking instead of Li−Li−Li stacking. In these cases it is generally not possible to establish a connection between the structure of the binary alloy and that of the poly-layered intercalated sheet.

The charge transfer between the graphene layers and intercalated species can also be measured by XRD using the positions of the *hk*0 reflections. In the graphene plane, the internal C−C distance reaches in this case 143.5 pm, instead of 142 pm in pristine graphite, meaning that the charge transfer is close to 0.07 electrons per carbon atom, which is about the same value as in LiC_6. This β ternary compound contains approximately five times as much metal as the binary compound, but nevertheless the electron transfer remains essentially unaltered. As above, this interesting result clearly emphasises the difficulty in correlating

 © 2004 Wiley-VCH Verlag GmbH & Co. KGaA, Weinheim

both phenomena: a high metal content does not inevitably lead to a sizeable charge transfer, because there are automatically metallic bonds in the intercalated sheet in order to maintain its cohesion. These latter, of course, strongly reduce this transfer.

The 2D unit cell of the compound was obtained by TEM and XRD (*hk*0 reflections) techniques. Both methods give the same results: Figure 8 shows the *hk*0 diffraction diagram, for which all the reflections can be easily indexed in a hexagonal two-dimensional unit cell identical to the graphitic one. Indeed, the value of its parameter is 745 pm, that is to say $3a_G$. From this value, one can see that this unit cell contains 18 carbon atoms (Figure 3).

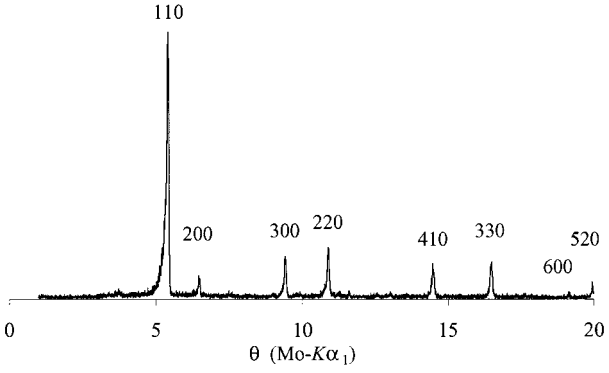

Figure 8. *hk*0 X-ray diagram of the β compound

Structure of the γ Compound

This first-stage compound exhibits a repeat distance that is much smaller than that of the previous ones (Figure 9). It has a value of only 454 pm, which is exactly the same as that of the CaC_6 binary intercalation compound. As expected, the study of the 00*l* reflections intensities (Fourier transform) shows unambiguously the presence of mono-layered intercalated sheets (Figure 10). This intercalated layer contains calcium atoms and its metal content corresponds accurately to a C/Ca ratio of six. It is basically the same compound as the CaC_6 binary, although it nevertheless contains a very small amount of lithium (1 atom-% of lithium), as was shown by nuclear microprobe measurements. This lithium amount is, of course, strictly invisible by XRD measurements. It is possible to consider this compound as a quasi-binary CaC_6 phase.

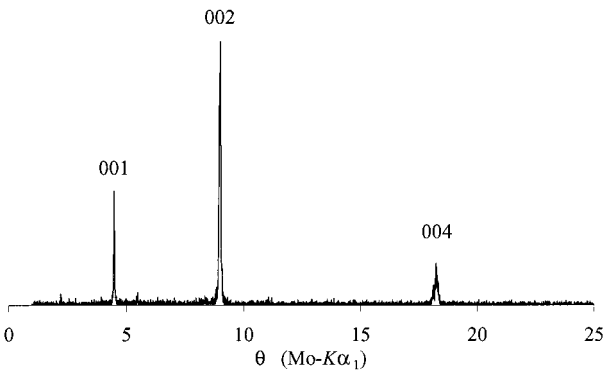

Figure 9. 00*l* X-ray diagram of the γ compound

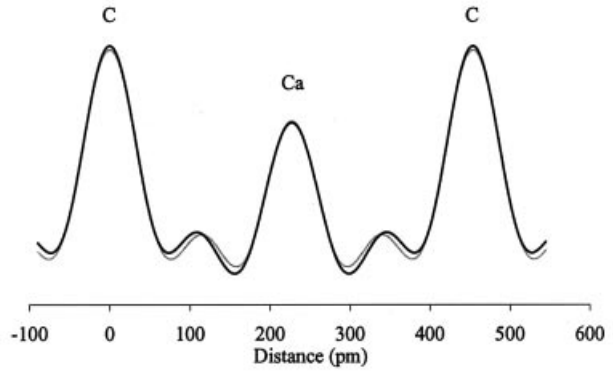

Figure 10. Electron-density profiles along the *c* axis of the γ compound; black line: experimental data; grey line: calculated data; five reflections are taken into account (residual factor R_{F00l} = 7.5%)

All its characteristics are exactly identical to that of the real binary.[6] The internal C−C distance of the graphene planes is equal to 125 pm, so that the charge transfer between the graphene and intercalated layers is close to 0.102 electrons per carbon atom. One can explain this high value for a binary compound as follows. Firstly, contrary to the alkali metals, calcium is divalent so that it is more easily able to release two electrons instead of one. Secondly, in a binary compound the intercalated sheet is mono-layered. Consequently the delocalised electrons, which are partially used in the ternaries in order to supply the internal cohesion of the poly-layered intercalated sheet by the means of metallic bonds, can in this case be wholly "absorbed" by the graphene layers. Indeed, the intercalated mono-layer does not need any internal cohesion, since it appears as a cation plane sandwiched between two macro-anionic planes: this situation is exactly the same as that observed in ionic salts, such as NaCl.

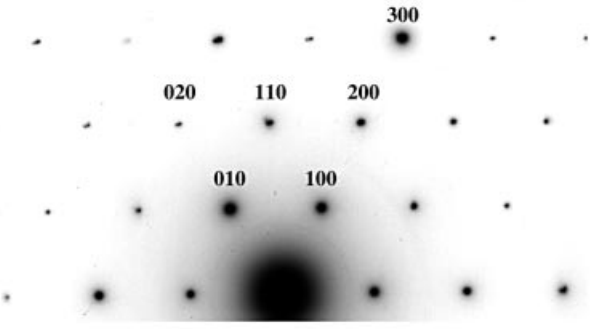

Figure 11. Electron-microdiffraction pattern of the γ compound; hexale lattice: *a* = 431 pm; the 110 reflection corresponds to the 100 reflection of graphite; the 300 reflection corresponds to the 110 reflection of graphite

 © 2004 Wiley-VCH Verlag GmbH & Co. KGaA, Weinheim

Figure 11 shows the reciprocal lattice observed using a TEM technique. The two-dimensional unit cell of the compound is hexagonal with a parameter of 431 pm (Figure 3). It is the same as the graphitic one, since $a = 3d_{C-C} = \sqrt{3}\cdot a_G$. This classic 2D arrangement is known as the "hexal structure".[3]

As has been mentioned above, this compound is essentially the CaC_6 binary compound, since the lithium content is exceedingly low. However, this is the first time that the binary has been isolated. Its synthesis makes use of the reaction between graphite and calcium vapour at high temperature, so that the vapour pressure is sufficient, but nevertheless not so high as to allow the attack of the metal on graphite, leading to acetylides. The reaction is strongly limited by this range of temperatures, so that the formation of CaC_6 in that case is just superficial. But using a calcium-lithium liquid alloy, we have prepared this compound in the bulk of the sample.

Two hypotheses can explain this phenomenon. Firstly, the interstitial lithium (even though its content is extremely low) is necessary in order to carry out the intercalation right through to the core, so that thermodynamically its role is very significant. Secondly, this novel method is able to give a bulk CaC_6 sample and makes use of a liquid, and not a vapour, as reagent, so that the reaction can be undertaken at low temperatures (350 °C) with a very concentrated reagent. In these conditions, the carburisation by lithium or calcium is completely avoided and the intercalation reaction becomes total. The interstitial lithium is dragged towards the graphitic intervals by calcium during its intercalation, and after reaction it is trapped inside the intercalated sheet, but it does not play a role in the stability of the compound. This second explanation is probably the most likely.

This interesting synthesis technique has been used previously with another binary system: the reaction between graphite and lithium−sodium liquid alloys leads to the quasi-pure LiC_6 compound.[19] This latter, however, was isolated using the vapour method, although its preparation is much easier by this second method. On the contrary, for CaC_6, the liquid method is absolutely essential in order to isolate this compound.

Conclusion

It has been shown that the co-intercalation of lithium and another element into graphite is very difficult since the thermodynamic parameters are not favourable for such a reaction. However, the first ternary graphite intercalation compounds containing lithium and a second metal were prepared from lithium−calcium alloys.

Two novel first-stage graphite−lithium−calcium compounds were isolated and a structural study was carried out with samples prepared from pyrolytic graphite platelets. They are very rich in metal and one of them particularly in lithium. Both ternaries possess poly-layered intercalated sheets, with roughly an alternate sequence of lithium and calcium. Lithium, the more electropositive, builds two layers in contact with graphene planes, the more electronegative. Between these lithium layers are sandwiched two monoatomic calcium layers, which surround a central lithium sheet (mono- or three-layered according to the compound). This atomic stacking is typical for such ternary intercalation compounds. The charge transfer caused by the oxido-reducing character of the reaction takes place in the interfaces of the host structure and the intercalated species, that is to say between the graphene planes and adjacent lithium.

The α compound can be considered as a slice of $CaLi_2$ crystal alloy. Indeed, this latter consists of an alternating *c*-axis lithium−calcium stacking, exactly similar to that present inside the intercalated sheet of the ternary compound.

The two-dimensional unit cells of these ternaries were established: they are both identical to the graphitic one, with rectangular or hexagonal symmetry according to the compound. The 3D unit cell of one of them was found.

The third compound contains a very low amount of lithium, such that it appears as a quasi-binary phase, which could be identified as CaC_6. The liquid-solid reaction used for this synthesis appears to be a better method for the preparation and isolation of bulk CaC_6.

Experimental Section

Synthesis: The synthesis of these novel ternary graphite−lithium−calcium intercalation compounds requires a rigorous experimental process, including several successive steps: purification of the reagents, formation of the reactive alloy, reaction and sample recovery. All the steps must be done in a glove box, under a very pure argon atmosphere. The purity of the reagents is one of the main factors influencing the synthesis of the ternary graphite−lithium−calcium compounds. The dendritic calcium used was distilled and exhibited a purity of 99.99%. The lithium, with an initial purity of 99.95%, required a further purification step, which was carried out in the glove box, after melting of the metal. The formation of the alloy is tricky, because its good homogeneity is absolutely essential for the preparation of the ternary compounds. In order to obtain pure ternary phases, we use Ca−Li alloys whose composition is well defined and varies according to the nature of the ternary compound. Both metals were mixed carefully in order to obtain a molten alloy that is as homogeneous as possible (the binary phase diagram shows a complete miscibility in the liquid state). Then, the pyrographite platelet was immersed in this liquid mixture in a tightly closed reactor. Lastly, the temperature of the reagents was raised to the appropriate value for several days: 350 °C for ten days when using an equimolar Ca−Li alloy (α compound); 350 °C for ten days when using a $CaLi_2$ alloy (β compound); and 350 °C for ten days when using an alloy whose composition is included between Ca_3Li and Ca_4Li (γ compound). After reaction, the sample obtained after removal of the alloy was introduced into a Pyrex or a Lindemann capillary tube (according to the size of the sample), which was sealed for characterisation of the sample by X-ray diffraction (XRD). The chemical formulae of these compounds were established by nuclear microprobe measurements,[8] because it is difficult to determine lithium concentration and distribution by classical methods such as Castaing microprobe, SEM and TEM. The formulae, which represent the composition of the bulk samples, are $Li_{0.4}Ca_{2.7}C_6$ for the α compound, $Li_{3.1}Ca_{2.1}C_6$

 © 2004 Wiley-VCH Verlag GmbH & Co. KGaA, Weinheim

for the β compound, and $Li_{0.07}CaC_6$ for the γ compound. It should be emphasised that the third compound (γ) has a very low lithium content, and it is so low that it appears to be almost a binary compound, close to the well-known CaC_6 phase.[6] On the other hand, the metal contents of the α and β compounds are much higher. The β compound in particular exhibits a very large lithium content (eight times richer than the α compound). It is probably the most metal-rich phase amongst the graphite intercalation compounds.

Structural Study: The compounds were studied by X-ray diffraction, using a specific technique because the samples are partially oriented. The host graphite sample used for the intercalation reaction is a platelet of highly oriented pyrolytic graphite (HOPG from Union Carbide). The *c*-axes of all elemental graphite crystals are mutually parallel but, within the graphene sheets, their *a* and *b* axes are randomly distributed. This structural particularity confers the properties of a single crystal along the *c* axis and the properties of a powder in the perpendicular plane. Consequently, it is very easy to observe the 00*l*, *hk*0 and *hkl* reflections with a device perfected in our laboratory.[9]

Acknowledgments

The authors wish to thank Sylvie Schneider for her contribution to X-ray diffraction measurements and especially for the rotating crystal image and Arsene Goukasov and Jean-Michel Kiat for neutron diffraction measurements.

[1] K. Fredenhagen, G. Cadenbach, *Z. Anorg. Allg. Chem.* **1926**, *158*, 249−263.
[2] P. Lagrange, in *Chemical Physics of Intercalation II* (Ed.: P. Bernier), Plenum Press: New York, **1993**, vol. 305, p. 303−310.
[3] D. Guérard, A. Hérold, *Carbon* **1975**, *13*, 337−345.
[4] J.-M. Tarascon, D. Guyomard, *Electrochim. Acta* **1993**, *38*, 1221−1231.
[5] S. Pruvost, C. Hérold, A. Hérold, P. Lagrange, *Carbon* **2003**, *41*, 1281−1289.
[6] D. Guérard, M. Chaabouni, P. Lagrange, M. El Makrini, A. Hérold, *Carbon* **1980**, *18*, 257−264.
[7] S. Pruvost, C. Hérold, J-F. Marêché, A. Hérold, P. Lagrange, in *Carbon '02*, Peking (China), **2002**, vol. P2−11, p. 172.
[8] S. Pruvost, P. Berger, C. Hérold, P. Lagrange, *Carbon*, manuscript to be published.
[9] B. Carton, PhD Thesis, Nancy University, **1971**.
[10] L. Pietronero, S. Strässler, *Phys. Rev. Lett.* **1981**, *47*, 593−596.
[11] D. G. Carfagno, PhD Thesis, Syracuse University, **1966**.
[12] C. W. Bale, A. D. Pelton, *Bull. Alloys Phase Diagr.* **1987**, *8*, 125−127.
[13] E. Hellner, F. Laves, *Z. Kristallogr.* **1943**, *105*, 135−143.
[14] F. Goutfer-Wurmser, C. Hérold, J-F. Marêché, P. Lagrange, *Mol. Cryst. Liq. Cryst* **1998**, *310*, 51−56.
[15] P. Lagrange, M. El Makrini, A. Hérold, *Rev. Chim. Miner.* **1983**, *19*, 229.
[16] M. El Gadi, A. Hérold, C. Hérold, J.-F. Marêché, P. Lagrange, *Mol. Cryst. Liq. Cryst.* **1994**, *244*, 29−34.
[17] M. El Gadi, A. Hérold, C. Hérold, J.-F. Marêché, P. Lagrange, *J. Solid State Chem.* **1997**, *131*, 282−289.
[18] P. Lagrange, B. Outti, J. Assouik, J. Clément, *Mater. Sci. Forum* **1992**, *91−93*, 295−299.
[19] D. Billaud, E. McRae, J-F. Marêché, A. Hérold, *Synth. Met.* **1981**, *3*, 21−26.

Received September 5, 2004
Early View Article
Published Online March 5, 2004

 © 2004 Wiley-VCH Verlag GmbH & Co. KGaA, Weinheim

Selective Reaction of Aminorhenium Complexes and the Formation of Cp-N-P Tridentate Complexes

Tein-Fu Wang,*[a] Tan-Ching Wang,[a] and Yuh-Sheng Wen[a]

Keywords: Rhenium / Cyclopentadienes / N ligands / P ligands / Tridentate ligands

Rhenium complexes containing cyclopentadienyl-aminophosphanyl tridentate ligands have been prepared starting from a cyclopentadienyl-amino bidentate complex in a controlled manner. Dehydrobromination of $[\eta^5{:}\eta^1\text{-}C_5H_4CH_2CH_2NH(CH_3)Re(CO)_2Br]^+$ (**2**) was carried out selectively at low temperature to give an exocyclic iminorhenium complex $[\eta^5{:}\eta^1\text{-}C_5H_4CH_2CH_2N(=CH_2)Re(CO)_2]$ (**5**). Selective *N*-methylation provided a cationic heterocyclopropane complex **8** which reacted with various nucleophiles (tBuNH$_2$, NaOCH$_3$, KPPh$_2$) to give precursors for tridentate complexes. A formal oxidation of the carbonyl ligand to a labile carbon dioxide ligand was accomplished by oxidation with peroxy acid. Intramolecular N ligand displacement furnished the Cp-N-P tridentate complex. The relative stability of the N, P and CO ligands was revealed when an η^3-allyl ligand was formed. The N ligand became detached from the metal rather than the P or CO ligands as the η^1-allyl was transformed to the corresponding η^3-allyl coordination mode.
(© Wiley-VCH Verlag GmbH & Co. KGaA, 69451 Weinheim, Germany, 2004)

Introduction

Transition metal Cp complexes containing an amino group functionalized side chain are of considerable current interest.[1] The majority of studies have concentrated on complex formation with early transition metals and their behavior as the ethylene polymerization catalysts.[2] Relatively little is known about the chemistry with low-valent transition metals. Amino groups have no π-acceptor capabilities, they coordinate only weakly to low-valent metals and form relatively labile complexes. Through chelation, several stable low-valent organometallic complexes have been realized.[3] With the strong electron donating amino group coordinated to the metal, the complexes show unprecedented chemical properties. We have reported aminorhenium complexes containing η^2-carbamoyl,[4] η^3-benzyl[5] and η^2-carbon dioxide[6] functionalities. These complexes are quite stable under ambient conditions and further exploration of the chemistry of this class of complexes is important.

In this study, we report some selective reactions of the aminorhenium complexes and ultimate conversion into the corresponding Cp-N-P tridentate complexes.[7] We introduce a new approach for promoting the carbonyl ligand substitution for the first time by an unprecedented peroxy acid oxidation. The synthesis and chemistry are reported herein.

[a] Institute of Chemistry, Academia Sinica, Taipei, Taiwan
E-mail: tfwang@chem.sinica.edu.tw

Results and Discussion

Selective Reactions of Iminorhenium Complexes

We have previously reported that treatment of the aminorhenium bromide **2** with a base at room temperature afforded the η^2-carbamoyl complex **4**.[4] When the reaction was carried out at 0 °C, however, a significant amount of the iminorhenium complex **5** was isolated (Scheme 1). The reaction presumably proceeds via the neutral intermediate **3**, followed by two competitive pathways. Migratory CO insertion gave complex **4**, while dehydrobromination gave complex **5**. We assumed that the CO migratory insertion might be more temperature dependent than that of the dehydrobromination. Low temperature reactions were therefore tested. Indeed, when **2** was treated with base at −78 °C, only the dehydrobromination products **5** and **6** (≈ 3%) were isolated. The exocyclic imino complex **5** and the endocyclic imino complex **6** that were formed presumably *via* kinetic control, could be easily differentiated by their ^{1}H NMR spectra. There are two imino protons (δ = 7.90 and 7.79 ppm) for **5**, while only one imino proton (δ = 7.68 ppm) and a methyl group (δ = 3.81 ppm) for **6**.

Unlike the aminorhenium complex **1** in which the alkylation occurred selectively at the rhenium center,[8] the methylation of the exocyclic iminorhenium complex **5** turned out to be non-selective. Both *Re*- and *N*-methylation compounds **7** and **8** were obtained (Scheme 1). The formation of the *Re*-methylation compound is faster than that of the *N*-methylation compound. When the reaction mixture was stirred longer, however, the *N*-methylation compound **7** disappeared gradually by virtue of reversibility and finally the iminium complex **8** was isolated in good yield. The im-

 © 2004 Wiley-VCH Verlag GmbH & Co. KGaA, Weinheim DOI: 10.1002/ejic.200300650

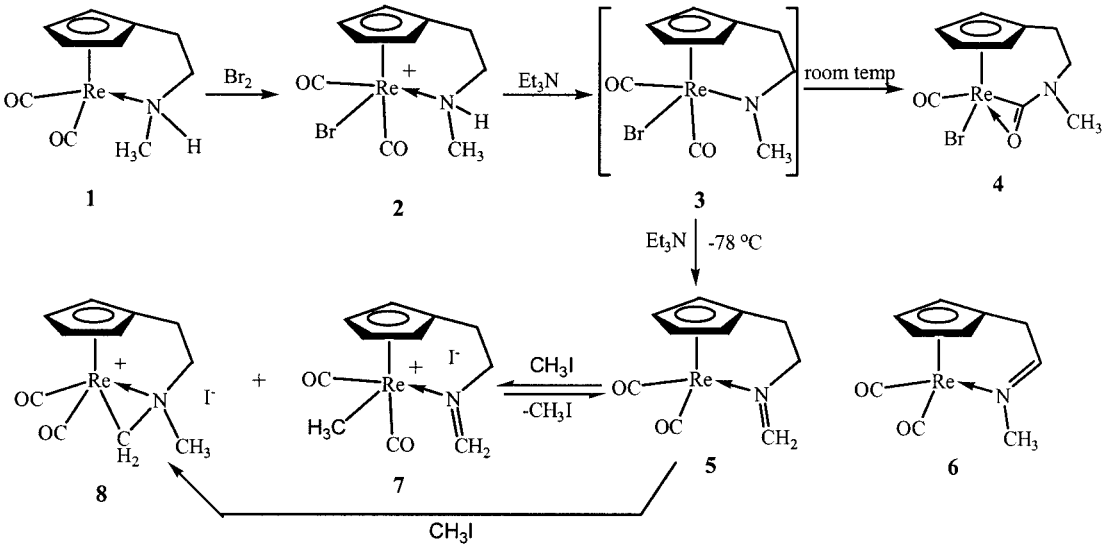

Scheme 1. Selective dehydrobromination and methylation

inium protons of **8** are shifted upfield to δ = 3.78 and 3.46 ppm, respectively, compared with δ = 8.42 and 8.11 ppm for complex **7**, suggesting that the iminium carbon is bonded to the metal center. The *N*-methyl resonance appeared at δ = 3.40 ppm indicating that the N ligand remains coordinated. The iminium ligand is therefore better viewed as a heterocyclopropane ring.

Reactions of the Cationic Complex 8 with Nucleophiles

Treatment of the cationic complex **8** with various nucleophiles (tBuNH$_2$, NaOCH$_3$) resulted in the opening of the heterocyclopropane ring to give the neutral complex **9** (Scheme 2). The physical properties of **9a** and **9b** are similar to those of *N*,*N*-disubstituted aminorhenium complexes that we have reported previously.[8] When **8** was treated with potassium diphenylphosphide, the phosphane-coordinated complex **10** was obtained. The terminal carbonyl stretching frequencies of **10** appeared at 1920 and 1848 cm^{-1} compared with 1894 and 1818 cm^{-1} in **9a**, and 1899 and 1823 cm^{-1} in **9b**. Higher energy shifts of the carbonyl stretching frequencies of **10** are consistent with the weaker electron donating ability of the phosphanyl group compared with that of the amino group. The *N*-methyl group of **10** appeared at δ = 2.30 ppm compared with δ = 3.08 ppm in **9a** and δ = 3.26 ppm in **9b** suggesting that the amino group of **10** is uncoordinated. The aminorhenium complex **9c** was assumed to be the initial reaction product. Phosphanyl groups are generally considered to be better ligands for low valent organometallic complexes than amino groups. The amino ligand of **9c** was therefore substituted intramolecularly by the newly generated phosphanyl group to give **10**. The intramolecular exchange of the two amino groups of **9a** was not observed. Unambiguous characterization of **10** was accomplished by a single-crystal X-ray diffraction study and Figure 1 shows an ORTEP diagram of **10**. The Re−P bond length is 2.331 Å, similar to those reported for neutral rhenium complexes (2.325−2.356 Å).[9] The carbonyl groups are bonded to the rhenium in a linear manner as indicated by the bond angles of 175.8° for Re−C10−O10 and 177.3° for Re−C11−O11.

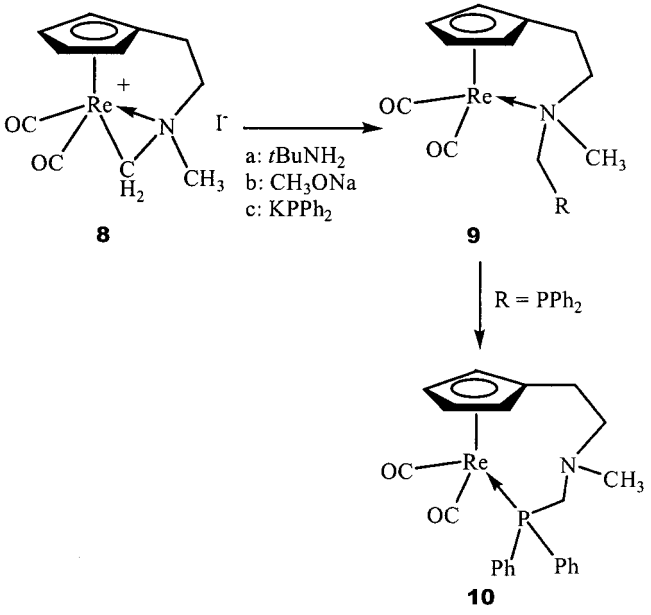

Scheme 2. Reactions of the heterocyclopropane complex **8** with nucleophiles

Formation of Cyclopentadienyl-Nitrogen-Phosphorous Tridentate Complexes

Formation of a Cp-N-P tridentate complex from the rhenium phosphane compound **10** requires removal of a carbonyl ligand. Photochemical[10] and trimethylamine *N*-oxide promoted[11] CO expulsion have been commonly used for the removal of terminal carbonyl ligands. However,

 © 2004 Wiley-VCH Verlag GmbH & Co. KGaA, Weinheim

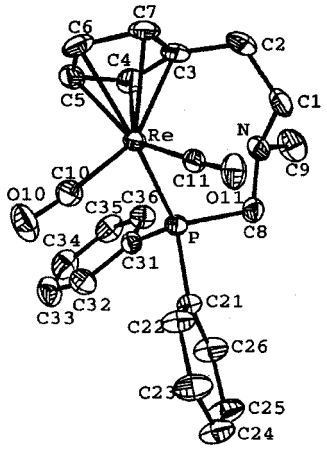

Figure 1. ORTEP diagram of **10**. Selective bond lengths (Å) and bond angles (°): Re−P 2.331(2), Re−C10 1.886(6), Re−C11 1.874(6); P−Re−C10 94.2(2), P−Re−C11 88.6(2), Re−C10−O10 175.8(6), Re−C11−O11 177.3(5)

these methodologies are not useful for complex **10**, owing to the relatively inert carbonyl groups (IR: $\tilde{\nu}$ = 1920, 1848 cm^{-1}). When **10** was treated with trimethylamine *N*-oxide or ultraviolet irradiation, only the starting material was recovered accompanied by some decomposition. It has been reported that an electron-rich aminorhenium complex such as **A** (Scheme 3), reacts with electrophilic peroxy acids to provide the CO_2 complex **B**.[6] Although the phosphanyl ligand is less electron donating than the amino ligand, we anticipated that the rhenium phosphane complex **10** would still be reactive enough with elctrophilic peroxy acids. Indeed, when **10** was treated with *m*-chloroperbenzoic acid, a carbonyl group disappeared immediately. Only one carbonyl stretch appeared at 1926 cm^{-1} in the resultant infrared spectrum. The resonance of the *N*-methyl group appeared at δ = 3.41 ppm in the ^1H NMR spectrum indicating that the amino group had become coordinated to the metal. A hydride appeared at δ = −6.15 suggesting that a Re−H bond had formed. The product was therefore proposed as the Cp-N-P tridentate complex **13** (Scheme 3). The reaction presumably proceeds through the rhenium carbon dioxide complex **11** followed by intramolecular amino group displacement of the labile CO_2 to give the neutral Cp-N-P tridentate complex **12**. The basic rhenium center picked up a proton and anion exchange furnished complex **13**.

Single crystals of **13** were obtained from a solution in acetone and methanol. An ORTEP drawing of **13** is shown in Figure 2. Both nitrogen and phosphorous are bonded to the metal with distances of 2.146 Å for Re−N and 2.363 Å for Re−P, respectively. The torsion angle of the heterocyclic 4−membered N−Re−P−C8 ring is 10.1°.

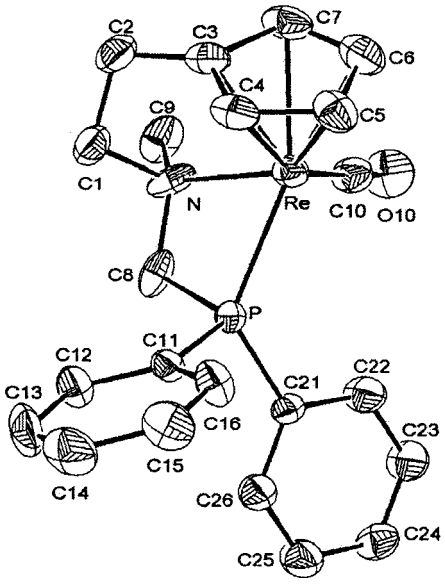

Figure 2. ORTEP drawing of the cationic part of **13**. Selective bond lengths (Å) and bond angles (°): Re−P 2.363(2), Re−N 2.146(7), P−C8 1.828(7), N−C8 1.467(11); P−Re−N 67.5(2), N−Re−C10 90.8(3), P−Re−C10 100.5(2)

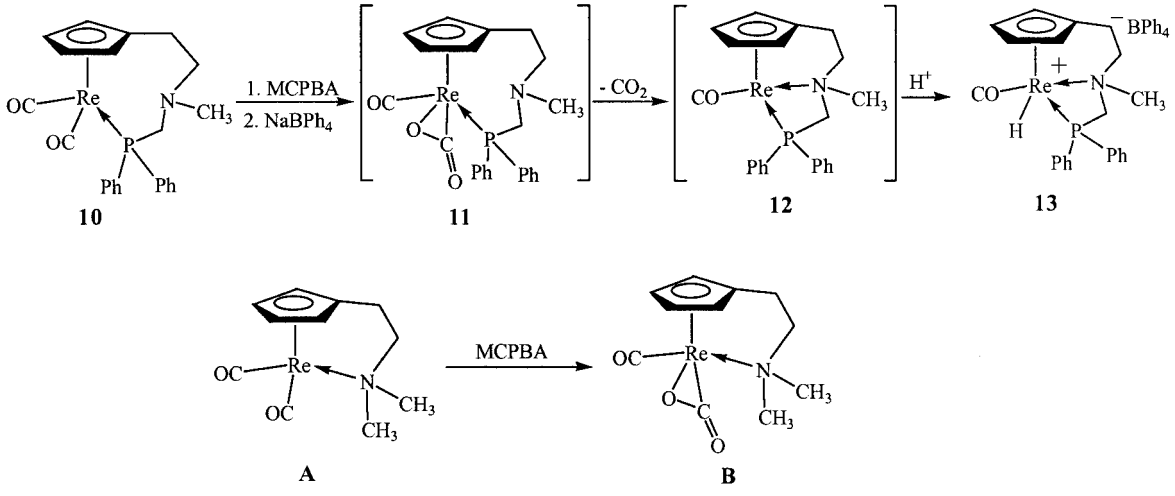

Scheme 3. Formation of a Cp-N-P tridentate complex

 © 2004 Wiley-VCH Verlag GmbH & Co. KGaA, Weinheim

Reaction of the Cp-N-P Tridentate Complex with Electrophiles

The spontaneous protonation of the neutral Cp-N-P tridentate complex **12** to give the cationic complex **13** prompted us to investigate nucleophilic reactions of **12** (Scheme 3). Complex **12** was regenerated from the cationic **13** by deprotonation with *n*BuLi. Treatment of **12** with various electrophiles (*N*-bromosuccinimide, methyl iodide, benzyl bromide) gave the expected products **14a**−**c** in excellent yield (Scheme 4). The spectroscopic properties of **14a**−**c** appeared similar to those of **13**. The *N*-methyl groups appeared at δ = 3.36−3.52 ppm in the ^{1}H NMR spectra suggesting that the amino groups remained coordinated. The Re−CH_3 methyl protons of **14b** and the Re-benzyl methylene protons of **14c** show ^3J couplings with the phosphorous indicating that the alkylations were successful and that the phosphanyl ligands remain coordinated to the metal. The carbonyl stretching appeared at 1918 cm^{-1} for both **14b** and **14c**. A relatively higher stretching frequency appeared at 1953 cm^{-1} for **14a**, consistent with the presence of the electronegative bromine on the metal. Complex **14a** could also be obtained by direct treatment of **13** with *N*-bromosuccinimide.

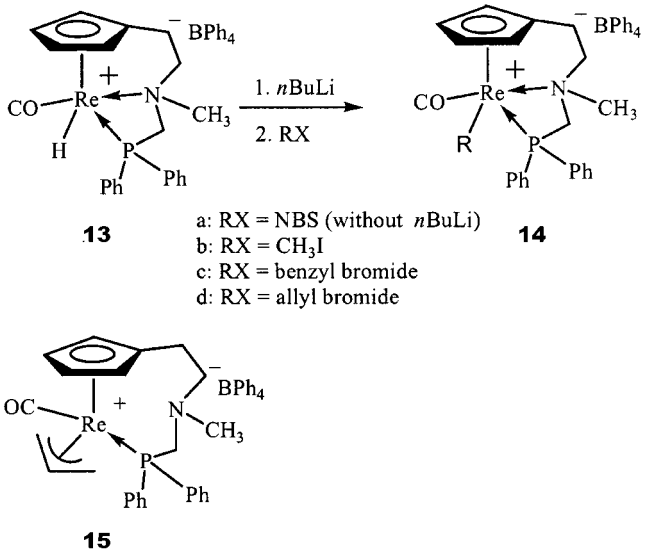

Scheme 4. Reaction of the tridentate complex **13** and selective removal of the N ligand

The reaction of **12** with allyl bromide doesn't stop at the η^1-allyl complex **14d**, but proceeds further to give the η^3-allyl complex **15**. Examination of the ^{1}H NMR spectrum showed that the N−CH_3 group appeared at δ = 1.98 ppm, indicating that the amino group had become detached from the metal. A single-crystal X-ray analysis confirmed this assignment. Figure 3 shows an ORTEP diagram of **15**. The allyl group is bonded to the rhenium in an η^3-fashion with bond lengths of 2.257, 2.200 and 2.244 Å, respectively. The rhenium−phosphorous bond length is 2.414 Å, slight longer than those in complexes **10** and **13**. The amino group was generally thought to be a better ligand than that of the phosphanyl ligand towards the cationic metal center. To our surprise, however, the amino group was expelled in preference to the phosphanyl or the CO groups when the η^3-allyl complex was formed.

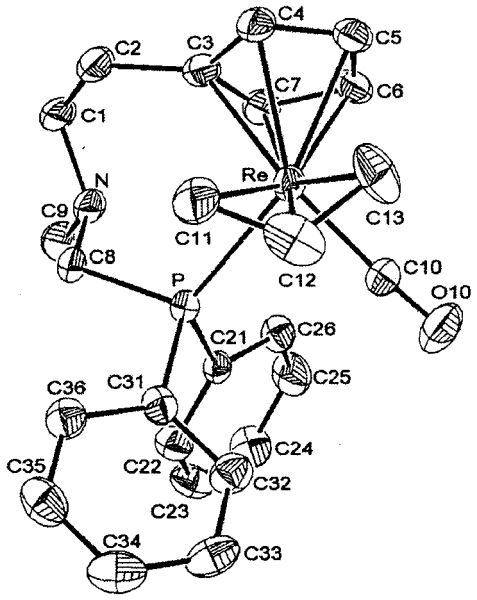

Figure 3. ORTEP drawing of the cationic part of **15**. Selective bond lengths (Å) and bond angles (°): Re−P 2.414(2), Re−C11 2.257(8), Re−C12 2.200(9), Re−C13 2.244(8); P−Re−C10 82.7(2), P−Re−C11 79.5(2), P−Re−C12 92.1(2), P−Re−C13 126.8(2), C11−C12−C13 119.0(8)

Conclusion

We have demonstrated that CO migratory insertion and dehydrobromination can be carried out selectively by temperature control. The CO migratory insertion of compound **3** was drastically reduced at low temperature thereby allowing selective dehydrobromination to give complex **5**. By learning that the rhenium-methylation is reversible, we successfully obtained the *N*-methylation complex **8** exclusively by prolonged reaction. Introduction of a P ligand was achieved by nucleophilic addition to the activated methylene group of the iminium ligand. Removal of a carbonyl ligand was demonstrated for the first time using a peroxy acid which formally oxidized the CO to a labile CO_2 ligand. Intramolecular ligand displacement furnished the Cp-N-P tridentate complex. It is worth noting that when the η^1-allyl was transformed to η^3-allyl, the N ligand of the cationic tridentate complex **14c** was detached from the metal to give **15**.

Experimental Section

General: Infrared solution spectra were recorded with a Perkin−Elmer 882 infrared spectrophotometer using 0.1 mm cells with CaF_2 windows. Melting points were determined using a Yanaco Model MP micro melting point apparatus and were uncor-

 © 2004 Wiley-VCH Verlag GmbH & Co. KGaA, Weinheim

rected. ^{1}H NMR (300 MHz), ^{13}C NMR (75 MHz) and ^{31}P{^{1}H} NMR (121 MHz) were obtained with a Bruker AC-300 FT spectrometer. For the assignment of ^{1}H and ^{13}C NMR spectroscopic data, the carbon bound to the nitrogen was designated as C^1 and the hydrogens on C^1 were designated as H^{1a} and H^{1b}. The next carbon was designated as C^2, and the hydrogen atoms on C^2 were designated as H^{2a} and H^{2b}. ^{1}H and ^{13}C chemical shifts are reported in parts per million (ppm) relative to Me_4Si and ^{31}P chemical shifts are relative to 85% H_3PO_4. Elemental analyses were obtained on a Perkin−Elmer 2400 CHN elemental analyzer.

Preparation of [η^5:η^1-$C_5H_4CH_2CH_2N(=CH_2)Re(CO)_2$]: 5 To a stirred solution of complex **1** (3.44 g, 9.44 mmol) in CH_2Cl_2 (120 mL) at 0 °C was added a solution of bromine in CH_2Cl_2 (18.9 mL, 0.5 M) slowly over 15 min. After stirring for an additional 5 min, the resultant orange-red solution was cooled in a dry ice-acetone bath. A solution of triethylamine (4.5 mL) in CH_2Cl_2 (45 mL) was then added slowly over 1 h using a syringe pump. After addition, the cooling bath was removed and the solution was stirred at room temperature for 30 min. Solvents were then evaporated under reduced pressure. The brown solid residue was chromatographed on silica gel using 20% followed by 30% ethyl acetate in hexane as eluents. The first yellow band was collected and concentrated to give yellow crystalline **5** (2.406 g, 70% yield). A slightly more polar fraction was collected to give yellow crystalline **6** (0.112 g, 3% yield).

Complex 5: R_f = 0.57 (50% EtOAc in hexane). M.p. 169−171 °C. IR (CH_2Cl_2): $\tilde{\nu}$ = 1908 s, 1835 s cm^{-1}. ^{1}H NMR ($CDCl_3$): δ = 7.90 (dt, J = 12.9, 1.4 Hz, 1 H, imine), 7.79 (dt, J = 12.9, 1.4 Hz, 1 H, imine), 5.31 (t, J = 2.0 Hz, 2 H, Cp), 5.06 (t, J = 2.0 Hz, 2 H, Cp), 4.34 (tt, J = 6.6, 1.4 Hz, 2 H), 2.18 (t, J = 6.6 Hz, 2 H) ppm. ^{13}C NMR ($CDCl_3$): δ = 203.6 (CO × 2), 165.4 (CH_2, imine), 119.6 (C, Cp), 84.0 (CH_2), 80.4 (CH × 2, Cp), 77.1 (CH × 2, Cp), 26.7 (CH_2) ppm. $C_{10}H_{10}NO_2Re$ (362.40): calcd. C 33.14, H 2.78, N 3.86; found C 33.31, H 2.62, N 3.95.

Complex 6: M.p. 192−195 °C (dec). IR (CH_2Cl_2): $\tilde{\nu}$ = 1907 s, 1830 s cm^{-1}. ^{1}H NMR ($CDCl_3$): δ = 7.70−7.67 (m, 1 H, imine), 5.51 (t, J = 2.0 Hz, 2 H, Cp), 5.07 (t, J = 2.0 Hz, 2 H, Cp), 3.82−3.80 (m, 3 H, CH_3), 3.18−3.15 (m, 2 H) ppm. ^{13}C NMR ($CDCl_3$): δ = 205.2 (CO × 2), 181.2 (CH, imine), 115.7 (C, Cp), 79.3 (CH × 2, Cp), 77.8 (CH × 2, Cp), 60.8 (CH_3), 35.8 (CH_2) ppm. $C_{10}H_{10}NO_2Re$ (362.40): calcd. C 33.14, H 2.78, N 3.86; found C 33.15, H 2.88, N, 3.56.

Preparation of 8: A suspension of complex **5** (0.875 g, 2.41 mmol) in CH_3I (15 mL) was heated under reflux for 5 days. Excess CH_3I was evaporated. The solids was washed four times with CH_2Cl_2 (5 mL × 4) to give 0.852 g (72% yield) of **8** as a yellow powder. M.p. 90 °C (dec). IR (CH_3CN): $\tilde{\nu}$ = 2030 s, 1953 s cm^{-1}. ^{1}H NMR (CD_3CN): δ = 6.41−6.39 (m, 1 H, Cp), 6.37−6.35 (m, 1 H, Cp), 6.16−6.14 (m, 1 H, Cp), 5.66−5.64 (m, 1 H, Cp), 4.29−4.22 (m, 1 H, H^{1a}), 4.09−3.98 (m, 1 H, H^{1b}), 3.78 (d, J = 1.7 Hz, 1 H, Re−CH_2^a), 3.46 (d, J = 1.7 Hz, 1 H, Re−CH^{2b}), 3.40 (s, 3 H, N−CH_3), 2.21−2.15 (m, 2 H, $H^{2\prime}$s) ppm. ^{13}C NMR (CD_3CN): δ = 200.9 (CO), 196.8 (CO), 122.0 (C, Cp), 97.8 (CH, Cp), 92.9 (CH, Cp), 88.7 (CH, Cp), 84.6 (CH, Cp), 77.3 (CH_2, C^1), 58.4 (CH_3), 30.7 (CH_2, Re−CH_2), 22.4 (CH_2, C^2) ppm. $C_{11}H_{13}INO_2Re$ (359.12): calcd. C 26.20, H 2.60, N 2.78; found C 26.04, H 2.75, N 3.03.

Preparation of 9a: To a stirred suspension of **8** (0.149 g, 0.29 mmol) in CH_2Cl_2 (10 mL) was added *tert*-butylamine (2 mL). The mixture was stirred at room temperature for 17 h. The resultant yellow solution was concentrated and the residue was flash chromatographed on silica gel using 10% followed by 20% ethyl acetate in hexane as eluents. A yellow band which appeared at R_f = 0.65 (30% EtOAc/hexane) was collected and concentrated to give a yellow solid 0.122 g (94% yield) of **9a**. M.p. 147−150 °C (dec). IR (CH_2Cl_2): $\tilde{\nu}$ = 1894 s, 1818 s cm^{-1}. ^{1}H NMR ($CDCl_3$): δ = 5.23−5.21 (m, 1 H, Cp), 5.13−5.11 (m, 1 H, Cp), 4.92−4.90 (m, 1 H, Cp), 4.89−4.87 (m, 1 H, Cp), 3.90 (d, J = 11.5 Hz, 1 H, −NCH_2^aN−), 3.80 (d, J = 11.5 Hz, 1 H, −NCH_2^bN−), 3.40−3.22 (m, 2 H, H^1), 3.08 (s, 3 H, N−CH_3), 2.29−2.14 (m, 2 H, H^2), 1.10 (s, 9 H, *t*Bu) ppm. ^{13}C NMR ($CDCl_3$): δ = 205.4 (CO × 2), 119.9 (C, Cp), 81.5 (CH, Cp), 79.0 (CH_2, NCH_2N), 78.3 (CH, Cp), 75.5 (CH, Cp), 74.3 (CH, Cp), 73.6 (CH_2, C^1), 56.4 (CH_3, N−CH_3), 50.2 (C, *t*Bu), 29.6 (CH_3 × 3, *t*Bu), 24.6 (CH_2, C^2) ppm. $C_{15}H_{23}N_2O_2Re$ (449.57): calcd. C 40.07, H 5.16, N 6.23; found C 39.98, H 5.14, N 5.85.

Preparation of 9b: A solution of sodium methoxide in methanol (0.9 mL, 25 wt%) was added to a stirred solution of **8** (95 mg) in methanol (10 mL) at room temperature. After stirring for 1.5 h, methanol was evaporated under reduced pressure. The residue was extracted with CH_2Cl_2, concentrated and flash chromatographed on silica gel using 10% followed by 30% EtOAc in hexane as eluents. A yellow band appeared at R_f = 0.62 (50% EtOAc/hexane) which was collected and concentrated to give the yellow crystalline complex **9b** (70 mg, 90% yield). M.p. 98−103 °C. IR (CH_2Cl_2): $\tilde{\nu}$ = 1899 s, 1823 s cm^{-1}. ^{1}H NMR ($CDCl_3$): δ = 5.25−5.23 (m, 1 H, Cp), 5.13−5.11 (m, 1 H, Cp), 4.95−4.93 (m, 1 H, Cp), 4.87−4.85 (m, 1 H, Cp), 4.35 (d, J = 8.5 Hz, 1 H, −OCH_2^a), 4.28 (d, J = 8.5 Hz, 1 H, −OCH_2^b), 3.50−3.41 (m, 2 H, H^1), 3.37 (s, 3 H), 3.26 (s, 3 H), 2.21−2.12 (m, 2 H, H^2) ppm. ^{13}C NMR ($CDCl_3$): δ = 204.6 (CO), 204.5 (CO), 119.6 (C, Cp), 97.0 (CH2, OCH2N), 80.3 (CH, Cp), 79.0 (CH, Cp), 74.9 (CH, Cp), 74.7 (CH, Cp), 73.0 (CH_2, C^1), 57.5 (CH_3, CH_3), 56.6 (CH_3), 24.7 (CH_2, C^2) ppm. $C_{12}H_{16}NO_3Re$ (408.47): calcd. C 35.28, H 3.95, N 3.43; found C 35.29, H 3.70, N 3.30.

Preparation of Complex 10: To a stirred suspension of **8** (1.955 g, 3.987 mmol) in THF (40 mL) at 0 °C was added a red solution of potassium diphenylphosphide in THF (10.4 mL, 0.5 M) over 5 min. After addition, the cold bath was removed and the mixture was stirred at room temperature for 30 min. and then solvents were evaporated under reduced pressure. The residue was purified chromatographically on silica gel using 10% followed by 20% EtOAc in hexane as eluents. A yellow band appeared at R_f = 0.59 (20% EtOAc/hexane) which was collected and concentrated to give **10** (1.705 g, 80% yield) as a white solid. M.p. 145−149 °C. IR (CH_2Cl_2): $\tilde{\nu}$ = 1920 s, 1848 s cm^{-1}. ^{1}H NMR ($CDCl_3$): δ = 7.55−7.49 (m, 4 H, Ph), 7.39−7.32 (m, 6 H, Ph), 5.22−5.20 (m, 2 H, Cp), 5.05−5.03 (m, 2 H, Cp), 3.68 (s, 2 H, −PCH_2N), 2.75−2.71 (m, 2 H, H^1), 2.38−2.34 (m, 2 H, H^2), 2.30 (s, 3 H, N−CH_3) ppm. ^{13}C NMR ($CDCl_3$): δ = 203.2 (d, $J_{C,P}$ = 7.5 Hz, CO × 2), 138.8 (d, $J_{C,P}$ = 46 Hz, C × 2, Ph), 132.2 (d, $J_{C,P}$ = 9.6 Hz, CH × 4, Ph), 129.4 (CH × 2, Ph), 128.0 (d, $J_{C,P}$ = 9.3 Hz, CH × 4, Ph), 103.5 (C, Cp), 88.7 (CH × 2, Cp), 78.5 (CH × 2, Cp), 63.8 (CH_2, C^1), 62.9 (d, $J_{C,P}$ = 52 Hz, CH_2, PCH_2), 45.9 (d, $J_{C,P}$ = 10.4 Hz, CH_3, N−CH_3), 26.6 (CH_2, C^2) ppm. ^{31}P NMR ($CDCl_3$): δ = 26.0 (s) ppm. $C_{23}H_{23}NO_2PRe$ (562.62): calcd. C 49.10, H 4.12, N 2.49; found C 49.24, H 3.92, N 2.28.

Preparation of Complex 13: To a stirred solution of **10** (1.414 g, 2.66 mmol) in CH_2Cl_2 (35 mL) at 0 °C was added *m*-chloroperbenzoic acid (0.67 g, 80%, 1.2 equiv.) in 3 portions over 5 min. The initially colorless solution became yellow immediately. After stirring for an additional 20 min, CH_2Cl_2 was evaporated. The residue was dissolved in CH_3OH (15 mL) and a solution of $NaBPh_4$ (1.1 g) in CH_3OH (5 mL) was then added. The yellow solid was collected

 © 2004 Wiley-VCH Verlag GmbH & Co. KGaA, Weinheim

using a centrifuge and washed three times with CH_3OH. The final yellow solid was recrystallized from a solution of acetone and methanol to give yellow crystalline **13** (1.377 g, 60%, yield). M.p. 190−196 °C. IR (acetone): $\tilde{\nu}$ = 1926 s cm^{-1}. ^1H NMR ([D$_6$]acetone): δ = 8.00−7.55 (m, 10 H, Ph), 7.36−7.30 (m, 8 H, Ph), 6.91 (t, *J* = 7.3 Hz, 8 H, Ph), 6.67 (t, *J* = 7.2 Hz, 4 H, Ph), 6.50 (dd, *J* = 15.3, 6.0 Hz, 1 H, PCH_2^a), 6.17−6.15 (m, 1 H, Cp), 5.76−5.67 (m, 3 H, Cp-H's and PCH_2^b), 4.95−4.93 (m, 1 H, Cp), 4.06−4.39 (m, 1 H, H^{1a}), 3.95−3.85 (m, 1 H, H^{1b}), 3.41 (s, 3 H, N−CH_3), 2.71−2.68 (m, 1 H, H^{2a}), 2.50−2.45 (m, 1 H, H^{2b}), −6.15 (d, *J* = 41 Hz, 1 H, Re−H) ppm. ^{31}P NMR ($CDCl_3$): δ = −42.7 ppm. $C_{46}H_{44}BNOPRe$ (854.86): calcd. C 64.63, H 5.19, N 1.64; found C 64.50, H 5.12, N 1.80.

Preparation of Complex 14a: To a stirred pale yellow solution of **13** (0.196 g, 0.23 mmol) in acetone (10 mL) at 0 °C was added *N*-bromosuccinimide (62 mg, 1.5 equiv.). After stirring for 5 min, the acetone was evaporated. The resultant solid was washed with diethyl ether several times and recrystallized from a solution of acetone and methanol to provide red crystals 168 mg (78% yield) of **14a**. M.p. 199−210 °C (dec). IR (acetone): $\tilde{\nu}$ = 1953 s cm^{-1}. ^1H NMR (CD_3CN): δ = 7.99−6.82 (m, 30 H, Ph), 6.63−6.61 (m, 1 H, Cp), 6.41−6.39 (m, 1 H, Cp), 5.92 (dd, *J* = 11.3, 4.2 Hz, 1 H, PCH_2^a), 5.65−5.63 (m, 1 H, Cp), 5.55−5.53 (m, 1 H, Cp), 5.48 (dd, *J* = 11.3, 4.5 Hz, 1 H, PCH_2^b), 3.82−3.77 (m, 1 H, H^{1a}), 3.62−3.56 (m, 1 H, H^{1b}), 3.36 (s, 3 H, N−CH_3), 2.30−2.26 (m, 2 H, $H^{2\prime}$s) ppm. ^{31}P NMR ([D$_6$]acetone): δ = −54.1 ppm. $C_{46}H_{43}BBrNOPRe$ (933.75): calcd. C 59.17, H 4.64, N 1.50; found C 59.20, H 4.42, N 1.72.

General Procedure for the Preparation of 14b and 14c: A solution *n*BuLi in hexane (1.6 M, 0.31 mL, 1.2 equiv.) was added to a stirred suspension of **13** (342 mg, 0.4 mmol) in THF (6 mL) at 0 °C over 1 min. After stirring for an additional 20 min, CH_3I (0.4 mL) or benzyl bromide (0.5 mL) was added to the resultant yellow-brown solution. The cooling bath was removed and the solution was stirred at room temperature for 1 h. The solution was concentrated under reduced pressure and the residues were washed twice with methanol then twice with diethyl ether. The solids were then recrystallized from a solution of acetone and hexane.

14b: Orange crystals, 271 mg (78% yield). M.p. 210−215 °C (dec.). IR (CH_3CN): $\tilde{\nu}$ =1918 s cm^{-1}. ^1H NMR ([D$_6$]acetone): δ = 8.10−7.31 (m, 18 H, Ph), 6.91 (t, *J* = 7.3 Hz, 8 H, Ph), 6.77 (t, *J* = 7.2 Hz, 4 H, Ph), 6.45 (dd, *J* = 15.1, 5.8 Hz, 1 H, PCH_2^a), 6.43−6.41 (m, 1 H, Cp), 6.34−6.32 (m, 1 H, Cp), 5.55 (dd, *J* = 15.1, 6.5 Hz, 1 H, PCH_2^b), 5.25−5.23 (m, 1 H, Cp), 4.88−4.86 (m, 1 H, Cp), 4.09 (br. dd, *J* = 12.1, 5.2 Hz, 1 H, H^{1a}), 3.90 (td, *J* = 12.1, 5.5 Hz, 1 H, H^{1b}), 3.52 (s, 3 H, N−CH_3), 2.67 (ddd, *J* = 14.4, 12.6, 5.2 Hz, 1 H, H^{2a}), 2.37 (ddd, *J* = 14.4, 5.4, 1.5 Hz, 1 H, H^{2b}), 0.48 (d, *J* = 12 Hz, 3 H, Re−CH_3) ppm. ^{31}P NMR ([D$_6$]acetone): δ = −36.6 ppm. $C_{47}H_{46}BNOPRe$ (868.88): calcd. C 64.97, H 5.34, N 1.61; found C 65.02, H 5.51, N 1.48.

14c: Orange crystals, 322 mg (85% yield). M.p. 165−170 °C (dec.). IR (CH_2Cl_2): $\tilde{\nu}$ =1918 s cm^{-1}. ^1H NMR ([D$_6$]acetone): δ = 8.22−6.72 (m, 35 H, Ph), 6.55−6.53 (m, 1 H, Cp), 6.48 (dd, *J* = 14.8, 5.6 Hz, 1 H, PCH_2^a), 6.29−6.27 (m, 1 H, Cp), 5.59 (dd, *J* = 14.8, 6.4 Hz, 1 H, PCH_2^b), 5.43−5.41 (m, 1 H, Cp), 4.10−4.06 (m, 1 H, H^{1a}), 3.98−3.92 (m, 1 H, H^{1b}), 3.65 (dd, *J* = 9.8, 7.3 Hz, 1 H, benzylic-H^a), 3.49 (s, 3 H, N−CH_3), 3.39−3.37 (m, 1 H, Cp), 2.78 (dd, *J* = 14, 9.8 Hz, 1 H, benzylic-H^b), 2.69−2.60 (m, 1 H, H^{2a}), 2.32−2.26 (m, 1 H, H^{2b}) ppm. ^{31}P NMR ($CDCl_3$): δ =

Table 1. Crystallographic data and structure refinements for **10**, **13** and **15**

Compound	**10**	**13**	**15**
Empirical formula	$C_{23}H_{23}NO_2PRe$	$C_{46}H_{43}BNOPRe$	$C_{49}H_{48}BNOPRe$
Formula mass	562.62	853.84	893.91
Crystal size (mm)	0.25 × 0.31 × 0.38	0.29 × 0.25 × 0.17	0.44 × 0.22 × 0.13
Color	colorless	yellow	yellow
Temp. (K)	293	293	293
Crystal system	monoclinic	monoclinic	monoclinic
Space group	$P2_1/c$	$P2_1$	$P2_1/c$
a (Å)	9.396(2)	9.8352(9)	17.6512(15)
b (Å)	13.264(1)	14.9626(8)	12.0400(9)
c (Å)	17.399(3)	13.5028(14)	18.8272(19)
α (°)	90	90	90
β (°)	103.50(1)	103.218(7)	90.968(8)
γ (°)	90	90	90
V (Å^3)	2108.5(5)	1934.4(3)	4000.6(6)
Z	4	2	4
$D_{calcd.}$ (g cm^{-3})	1.772	1.466	1.484
F(000)	1096	857.81	1803.61
λ (Mo-K_α) (Å)	0.71069	0.71069	0.71069
μ (Mo-K_α) (cm^{-1})	59.331	32.2	31.2
$T_{min.,max.}$	0.758, 1.00	0.391, 0.500	0.323, 0.500
Scan rate (°·min^{-1})	2.06−8.24	1.92−13.5	1.22−6.74
θ/2θ scan width (°)	0.70 + 0.35tanθ	0.76 + 0.39tanθ	0.60 + 0.35tanθ
$2\theta_{max}$ (°)	50	50	50
h,*k*,*l* range	(−11;10), (0;15), (0;20)	(−11;11), (−17;0), (−16;16)	(−20;20), (0;14), (0;21)
Unique reflns.	3698	3534	5814
Obsd. reflns. [$I > 2.0\sigma(I)$]	2893	3252	4102
Refined parameters	254	459	488
R_F;R_w	0.025; 0.028	0.023; 0.027	0.031; 0.035
GOF	1.31	1.44	1.51
$(\Delta\rho)_{max.,min.}$ (e·Å^{-3})	0.910; −0.690	0.910; −0.530	0.890; −0.980

 © 2004 Wiley-VCH Verlag GmbH & Co. KGaA, Weinheim

−36.5 ppm. $C_{53}H_{50}BNOPRe$ (944.98): calcd. C 67.36, H 5.33, N 1.48; found C 67.11, H 5.35, N 1.62.

Preparation of 15: A solution *n*BuLi in hexane (1.6 M, 0.13 mL, 1.2 equiv.) was added to a stirred suspension of **13** (144 mg, 0.168 mmol) in THF (3 mL) at 0 °C over 1 min. After stirring for an additional 20 min, allyl bromide (0.3 mL) was added to the resultant yellow-brown solution. The solution was stirred at room temperature for 1 h. Solvents were evaporated and the residues were washed twice with methanol. The solid obtained was recrystallized from a solution of CH_2Cl_2 (3 mL) and CH_3OH (5 mL) at room temperature. Pale yellow platelet crystals of the η^3-allyl complex **15** were collected (137 mg, 91% yield). M.p. 220−225 °C (dec.). IR (CH_2Cl_2): $\tilde{\nu}$ =1960 s cm^{-1}. ^1H NMR ([D_6]acetone): δ = 7.61−7.31 (m, 18 H, Ph), 6.91 (t, *J* = 7.4 Hz, 8 H, Ph), 6.76 (t, *J* = 7.2 Hz, 4 H, Ph), 6.40 (br., 1 H, Cp), 6.07 (br., 1 H, Cp), 5.90 (br., 1 H, Cp), 5.83 (br., 1 H, Cp), 4.20 (d, *J* = 14.5 Hz, 1 H, PCH_2^a), 4.00 (dd, *J* = 14.5, 1.5 Hz, 1 H, PCH_2^b), 3.14−2.79 (m, 9 H), 1.98 (s, 3 H, N−CH_3) ppm. ^{31}P NMR ([D_6]acetone): δ = 10.2 ppm. $C_{49}H_{48}BNOPRe$ (894.92): calcd. C 65.76, H 5.41, N 1.56; found C 65.58, H 5.70, N 1.62.

Crystal Structures of 10, 13 and 15: Single crystals of **10** were obtained from a solution of CH_2Cl_2 and hexane, **13** from a solution of acetone and methanol, and **15** from a solution of CH_2Cl_2 and methanol at room temperature, respectively. Diffraction measurements were made on an Enraf−Nonius CAD-4 automated diffractometer using graphite-monochromated Mo-K_α radiation (λ = 0.71069 Å) with the θ−2θ scan mode. The unit cells were determined and refined using 25 randomly selected reflections obtained with the automatic search, center, index, and least-squares routines. Lorentz/polarization and empirical absorption corrections based on three azimuthal scans were applied to the data. The space groups ($P2_1/c$ for both **10** and **15**, $P2_1$ for **13**) were determined from the systematic absences observed during data collection. All data reduction and refinements were carried out on a DecAlpha 3400/400 computer using the NRCVX program.[12] Structures were solved by direct methods and refined by a full-matrix least-squares routine[13] with anisotropic thermal parameters for all non-hydrogen atoms. The structures were refined by minimizing $\Sigma w|F_o - F_c|^2$, where $w = (1/\sigma^2)F_o$ was calculated from the counting statistics. Hydrogens were included in the structure factor calculations in their expected positions on the basis of idealized bonding geometries but were not refined in the least-squares procedure. The final cell parameters and data collection parameters are listed in Table 1.
CCDC-219541 (for **10**), -219542 (for **13**) and -219543 (for **15**) contain the supplementary crystallographic data for this paper. Copies of the data can be obtained free of charge on application to CCDC, 12 Union Road, Cambridge CB2 1EZ, UK [Fax: (internat.) + 44-1223-336-033; E-mail: deposit@ccdc.cam.ac.uk].

Acknowledgments

We are grateful to the National Science Council of Taiwan for financial support.

[1] P. Jutzi, T. Redeker, *Eur. J. Inorg. Chem.* **1998**, 663−674.
[2] [2a] F. Amor, J. Okuda, *J. Organomet. Chem.* **1996**, *520*, 245−248. [2b] D. D. Devour, F. J. Timmers, D. L. Hasha, R. K. Rosen, T. J. Marks, P. A. Deck, C. L. Stern, *Organometallics* **1995**, *14*, 3132−3134. [2c] A. Baretta, K. S. Chong, F. G. N. Cloke, A. Feigenbaum, M. L. H. Green, *J. Chem. Soc., Dalton Trans.* **1983**, 861−864. [2d] J. C. Flores, J. C. W. Chien, M. D. Rausch, *Organometallics* **1994**, *13*, 4141−4142. [2e] W. A. Herrmann, M. J. A. Morawietz, T. Priermeier, K. Mashima, *J. Organomet. Chem.* **1995**, *486*, 291−295. [2f] P. Jutzi, J. Kleimeier, *J. Organomet. Chem.* **1995**, *486*, 287−289. [2g] P. Jutzi, T. Redeker, H. G. Stammler, B. Neumann, *J. Organomet. Chem.* **1995**, *498*, 127−137.
[3] [3a] T. F. Wang, T. Y. Lee, Y. S. Wen, L. K. Liu, *J. Organomet. Chem.* **1991**, *403*, 353−358. [3b] T. F. Wang, T. Y. Lee, *J. Organomet. Chem.* **1992**, *423*, 31−38. [3c] T. F. Wang, Y. S. Wen, *J. Organomet. Chem.* **1992**, *439*, 155−162.
[4] T. F. Wang, C. C. Hwu, C. W. Tsai, Y. S. Wen, *Organometallics* **1998**, *17*, 131−138.
[5] T. F. Wang, C. C. Hwu, C. W. Tsai, Y. S. Wen, *J. Chem. Soc., Dalton Trans.* **1998**, 2091−2095.
[6] T. F. Wang, C. C. Hwu, C. W. Tsai, K. J. Lin, *Organometallics* **1997**, *16*, 3089−3090.
[7] [7a] A part of the results has been presented at the 220th American Chemical Society National Meeting at Washington D. C., August 20−24, **2000**, INOR−241. Recent publications concerning Cp-N-X tridentate complexes: [7b] S. Arndt, K. Beckerle, K. C. Hultzsch, P. J. Sinnema, P. Voth, T. P. Spaniol, P. Thomas, J. Okuda, *J. Mol. Catal. A* **2002**, *190*, 215−223. [7c] I. Fedushkin, S. Dechert, H. Schumann, *Organometallics* **2000**, *19*, 4066−4076. [7d] K. C. Hultzsch, P. Voth, K. Beckerle, T. P. Spaniol, J. Okuda, *Organometallics* **2000**, *19*, 228−243. [7e] F. Amor, A. Butt, K. E. duPlooy, E. Karen, T. P. Spaniol, J. Okuda, *Organometallics* **1998**, *17*, 5836−5849. [7f] J. Okuda, K. E. duPlooy, W. Massa, H. C. Kang, U. Rose, *Chem. Ber.* **1996**, *129*, 275−277. [7g] K. E. duPlooy, E. Karen, U. Moll, S. Wocadlo, W. Massa, J. Okuda, *Organometallics* **1995**, *14*, 3129−3131.
[8] T. F. Wang, C. Y. Lai, C. C. Hwu, Y. S. Wen, *Organometallics* **1997**, *16*, 1218−1223.
[9] [9a] W. K. Wong, W. Tam, C. E. Strouse, J. A. Gladysz, *J. Chem. Soc., Chem. Commun.* **1979**, 530−531. [9b] L. J. Alvey, O. Delacroix, C. Wallner, O. Meyer, F. Hampel, S. Szafert, T. Lis, J. A. Gladysz, *Organometallics* **2001**, *20*, 3087−3096.
[10] [10a] A. Wojcicki, *Adv. Organomet. Chem.* **1973**, *11*, 87−145. [10b] I. Bernal, J. D. Korp, W. A. Herrmann, R. Serrano, *Chem. Ber.* **1984**, *117*, 434−444. [10c] W. A. Herrmann, R. Serrano, J. Weichmann, *J. Organomet. Chem.* **1983**, *246*, C57−C60.
[11] M. O. Albers, N. J. Coville, *Coord. Chem. Rev.* **1984**, *53*, 227−259.
[12] E. J. Gabe, Y. LePage, J. P. Charland, F. L. Lee, P. S. White, *J. Appl. Crystallogr.* **1989**, *22*, 384−387.
[13] P. Main, in *Crystallographic Computing 3: Data Collection, Structure Determination, Proteins and Databases* (Eds.: G. M. Sheldrick, C. Krüger, R. Goddard), Clarendon Press: Oxford, **1985**, pp. 206−215.

Received September 14, 2003
Early View Article
Published Online March 9, 2004

 © 2004 Wiley-VCH Verlag GmbH & Co. KGaA, Weinheim

Strongly Nucleophilic Rh^I Centre in Square-Planar Complexes with Terdentate (κ^3) 2,2′:6′,2′′-Terpyridine Ligands: Crystallographic, Electrochemical and Density Functional Theoretical Studies

Boke C. de Pater,[a] Hans-Werner Frühauf,[a] Kees Vrieze,[a] René de Gelder,[b] Evert J. Baerends,[c] Drew McCormack,[c] Martin Lutz,[d] Anthony L. Spek,[d] and František Hartl*[a]

Keywords: Rhodium / Tridentate ligands / X-ray diffraction / Cyclic voltammetry / Density functional calculations

Rh^I-terpyridine complexes have been unambiguously formed for the first time. The 2,2′:6′,2′′-terpyridine (tpy), 4′-chloro-2,2′:6′,2′′-terpyridine (4′-Cl-tpy) and 4′-(*tert*-butyldimethylsilyl-*ortho*-carboranyl)-2,2′:6′,2′′-terpyridine (carboranyl-tpy) ligands were used for successful syntheses and characterisation of the corresponding Rh^I complexes with halide co-ligands, [Rh(X)(4′-Y-terpyridine)] (X = Cl, Y = H, Cl, carboranyl; X = Br, Y = H). All four neutral Rh-tpy complexes are square planar, with Rh–X bonds in the plane of the 4′-Y-terpyridine ligands. Full characterisation of these dark blue, highly air-sensitive compounds was hampered by their poor solubility in various organic solvents. This is mainly due to the formation of π-stacked aggregates, as evidenced by the crystal structure of [Rh(Cl)(tpy)]; in addition, [Rh(Cl)(carboranyl-tpy)] merely forms discrete dimers. The (bonding) properties of the novel Rh^I-terpyridine complexes have been studied with single-crystal X-ray diffraction, (time-dependent) density functional theoretical (DFT) calculations, far-infrared spectroscopy, electronic absorption spectroscopy and cyclic voltammetry. From DFT calculations, the HOMO of the studied Rh^I-terpyridine complexes involves predominantly the metal centre, while the LUMO resides on the terpyridine ligand. Absorption bands of the studied complexes in the visible region (400–900 nm) can be assigned to MLCT and MLCT/XLCT transitions. The relatively low oxidation potentials of [Rh(X)(tpy)] (X = Cl, Br) point to a high electron density on the metal centre. This makes the Rh^I-terpyridine complexes strongly nucleophilic and (potentially) highly reactive towards various (small) substrate molecules containing carbon–halide bonds.

(© Wiley-VCH Verlag GmbH & Co. KGaA, 69451 Weinheim, Germany, 2004)

Introduction

Transition metal complexes containing terdentate nitrogen ligands (N−N−N) are of great interest both in the field of supramolecular chemistry[1,2] and catalysis. For example,[3] $[Pd(Me)(N-N-N)]^+$ complexes react rapidly with CO and subsequently with norbornadiene to produce $[Pd\{C_7H_8C(O)Me\}(N-N-N)]^+$ on the road to metal-bound polyketone fragments. Notably, the highest insertion rates are for complexes containing highly rigid ligands, e.g. dipyrido[4,3-*b*;5,6-*b*]acridine.[4] According to theoretical calculations,[5] this is most probably due to the rigidity of the ligand causing an increased strain in the metal complex itself, thereby facilitating intermediate bidentate coordination of the N−N−N ligand. These interesting findings initiated investigation of isoelectronic Rh^I compounds. Haarman et al. reported novel compounds [Rh(Cl)(2,6-[$C(R^1)=N-R^2)_2C_5H_3N$], containing fairly flexible 2,6-diiminopyridine ligands.[6–8] These complexes react readily with alkyl halides and oxygen owing to a strongly nucleophilic Rh^I centre.[6] The present article extends these studies to complexes with stronger σ-donating[9] and more rigid terpyridine ligands.

Since the first report on 2,2′:6′,2′′-terpyridine (tpy) by Morgan and Burstall,[10,11] the coordination chemistry of this ligand and its derivatives has been widely studied. They exhibit variable coordination modes to transition metals, viz. terdentate,[1] bidentate,[1,2] or monodentate.[12] Although complexes with many late transition metals are known,[1] only a few Rh-terpyridine complexes have been prepared, all of which contain rhodium(II) or rhodium(III)

[a] Institute of Molecular Chemistry, University of Amsterdam, Nieuwe Achtergracht 166, 1018 WV Amsterdam, The Netherlands,
Fax: (internat.) +31-20-5256456
[b] Department of Inorganic Chemistry, Faculty of Science, University of Nijmegen,
Toernooiveld 1, 6525 ED Nijmegen, The Netherlands
[c] Department of Theoretical Chemistry, Free University Amsterdam,
De Boelelaan 1083, 1081 HV Amsterdam, The Netherlands
[d] Bijvoet Centre for Biomolecular Research, Department of Crystal and Structural Chemistry, University of Utrecht,
Padualaan 8, 3584 CH Utrecht, The Netherlands

centres.[12−18] Electrochemical studies revealed stable rhodium(IV)- and oxorhodium(V)-terpyridine species.[16] Some rhodium(I) intermediates with terpyridine ligands have been proposed to participate in catalytic cycles,[19] but their formation has never been unambiguously established.

We report here, for the first time, syntheses, structures, spectroscopic, redox and bonding properties of four mononuclear square-planar Rh^I-terpyridine complexes. Due to the planar tpy skeleton, these compounds exhibit a strong tendency to π-stacking, which implies their low solubility. This is the main factor complicating their characterisation. Consequently, the bulky *tert*-butyldimethylsilyl-*o*-carboranyl group was placed at the C(4′)-position of the tpy ligand of the Rh^I-terpyridine species in the hope that such a sterically demanding substituent would lead to an increase in solubility.

Results

Syntheses of Complexes [Rh(X)(4′-Y-tpy)] (X = Cl, Y = H (1), Cl (3), *tert*-butyldimethylsilyl-*o*-carboranyl (4); X = Br, Y = H (2)]

The novel complexes **1**−**4** (Scheme 1) have been prepared by a ligand displacement reaction (Scheme 2). Characterisation by NMR techniques was problematic due to the poor solubility of the complexes. After scanning for 20 h (using C_6D_6 as solvent), only complex **4** gave an acceptable ^1H NMR spectrum (Figure 1). The C(6,6′′)-H signals of **4** were hidden under the benzene signal. The B−H signals, presumably spread over the range of 2−4 ppm, were not observable. The ^1H spectrum also contained additional signals of a minor species, probably a degradation product, since complex **4** is far less stable in organic solvents than **1**−**3**. The solubility of **1**−**4** in CD_3CN is lower than that in benzene and no acceptable ^1H NMR spectrum could be recorded. Finally, although the solubility of **1**−**4** in [D_6]EtOH and [D_6]DMF is similar to that in benzene, the ^1H NMR spectra only exhibited very broad signals.

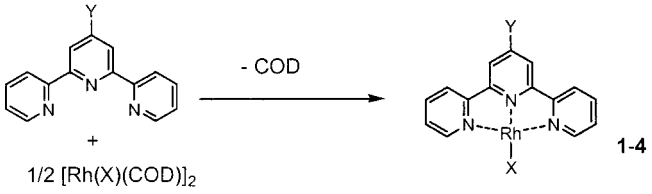

X = Cl (**1**,**3**,**4**), Br (**2**)
Y = H (**1**,**2**), Cl (**3**), *tert*-butyldimethylsilyl-*ortho*-carborane (**4**)
COD = cycloocta-1,5-diene

Scheme 2. Formation of complexes **1**−**4**

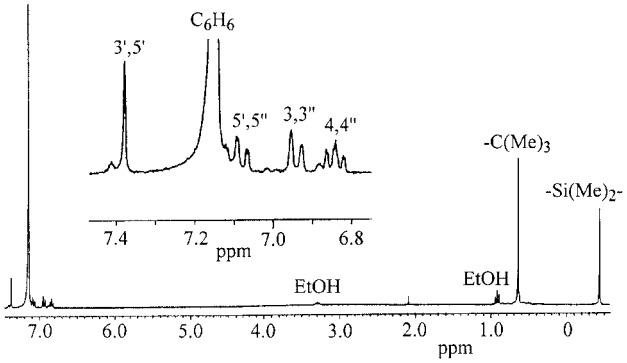

Figure 1. ^1H NMR spectrum of complex **4** in C_6D_6

X-ray Structures of Complexes 1 and 4

Molecules of complex **1** (Figure 2) are arranged in sheets that run parallel with the crystallographic *b*-axis (Figure 3). The sheets are 3.508(12) Å apart, which is considered as the thickness of the molecules. Neighbouring molecules in different sheets are in a staggered arrangement close to inversion symmetry. The distance between the sheets strongly indicates the presence of π-stacking (Figure 4). Within the sheets, short intermolecular distances are found between the chlorine atom and H5′ and H3′′ of a neighbouring molecule: H···Cl are 2.79 and 2.85 Å, and C−H···Cl angles 167° and 169°, respectively (Figure 5). These short distances

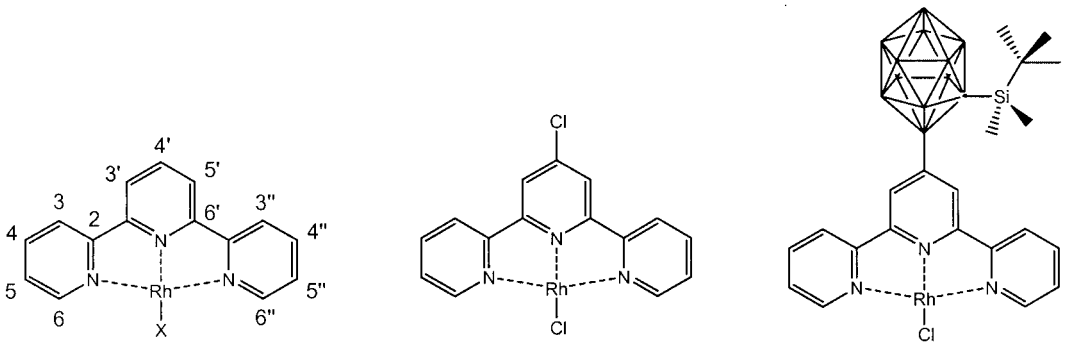

Scheme 1

 © 2004 Wiley-VCH Verlag GmbH & Co. KGaA, Weinheim

indicate "chelating" C−H···Cl hydrogen bonds that link the neighbouring molecules into a one-dimensional intermolecular hydrogen-bonding network. The hydrogen-bonded sheets are stacked in the crystallographic [101] direction (Figure 5). There are no short Rh−Rh′ contacts, the smallest distance being 4.896(2) Å. Selected bond lengths and angles in complex **1**, together with those in the ADF/BP-calculated complexes **1′** and **2′**, for comparison, are summarised in Table 1 and Table 2, respectively.

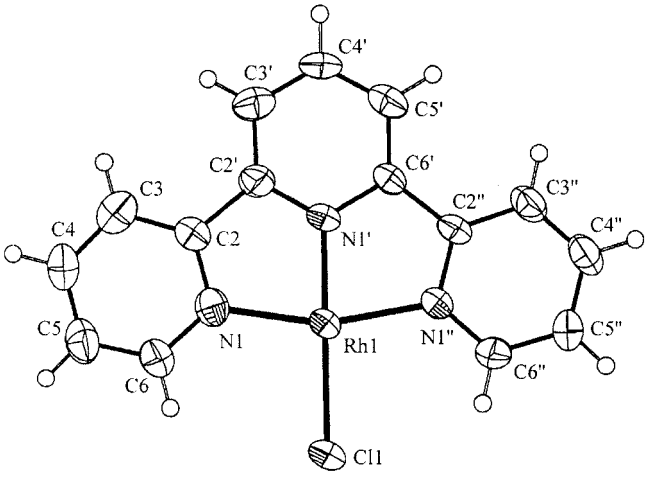

Figure 2. Displacement ellipsoid plot (50% probability level) of complex **1**

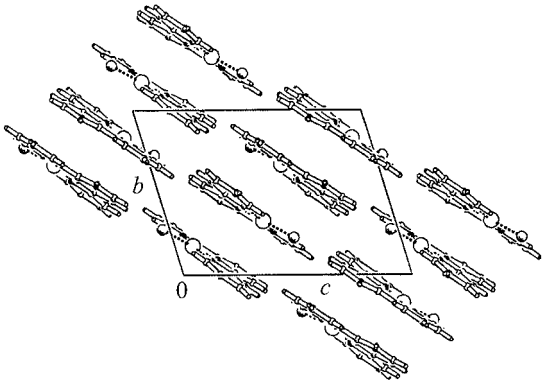

Figure 3. Molecular stacking in the crystal structure of complex **1**

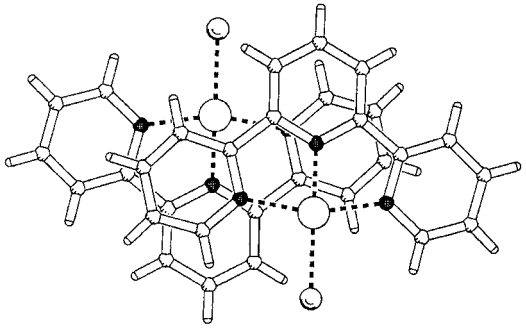

Figure 4. π-Stacking between two molecules in the crystal structure of complex **1**

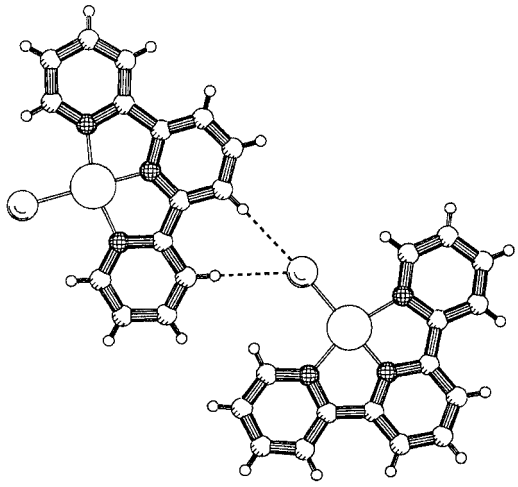

Figure 5. Hydrogen bonding in complex **1**

Table 1. Selected bond lengths (Å) for complexes **1** and **4**, and for geometry-optimised **1′** and **2′**

Bond length	**1**	**4**	**1′**	**2′**
Rh−X[a]	2.356(2)	2.369(2)	2.354	2.487
Rh−N1	2.026(7)	2.018(6)	2.048	2.057
Rh−N2	1.896(7)	1.890(6)	1.929	1.944
Rh−N3	2.019(7)	2.012(7)	2.048	2.057
N1−C1	1.336(12)	1.338(11)	1.350	1.350
N1−C5	1.362(12)	1.381(10)	1.381	1.381
N2−C6	1.360(11)	1.360(11)	1.371	1.370
N2−C10	1.354(11)	1.345(10)	1.371	1.370
N3−C11	1.367(11)	1.371(11)	1.381	1.381
N3−C15	1.347(11)	1.350(11)	1.350	1.350

[a] X = Cl for **1**, **4** and **1′**; Br for **2′**.

Table 2. Selected bond angles (°) for complexes **1** and **4**, and for geometry-optimised **1′** and **2′**.

Bond angles	**1**	**4**	**1′**	**2′**
X−Rh−N1[a]	99.5(2)	99.62(19)	99.8	100.2
X−Rh−N2	179.1(2)	175.1(2)	180.0	180.0
X−Rh−N3	99.1(2)	99.25(19)	99.8	100.2
N1−Rh−N2	80.8(3)	80.9(3)	80.2	79.8
N1−Rh−N3	161.3(3)	160.7(3)	160.3	159.6
N2−Rh−N3	80.5(3)	80.0(3)	80.2	79.8
Rh−N1−C1	128.9(7)	129.0(5)	127.7	127.8
Rh−N1−C5	113.2(6)	113.2(5)	113.5	113.6
C1−N1−C5	117.9(8)	117.8(6)	118.8	118.6
Rh−N2−C6	119.6(6)	118.8(5)	119.2	119.2
Rh−N2−C10	119.7(6)	120.1(5)	119.2	119.2
C6−N2−C10	120.7(8)	121.0(7)	121.6	121.6
Rh−N3−C11	113.5(5)	114.0(5)	113.5	113.6
Rh−N3−C15	128.6(6)	128.0(6)	127.7	127.8
C11−N3−C15	117.9(7)	117.9(7)	118.8	118.6

[a] X = Cl for **1**, **4** and **1′**; Br for **2′**.

Dark blue crystals of **4**, suitable for X-ray analysis, were grown from a saturated EtOH solution upon standing for three weeks at room temperature. In the solid state, the molecules (Figure 6) are packed in discrete dimers around the

 © 2004 Wiley-VCH Verlag GmbH & Co. KGaA, Weinheim

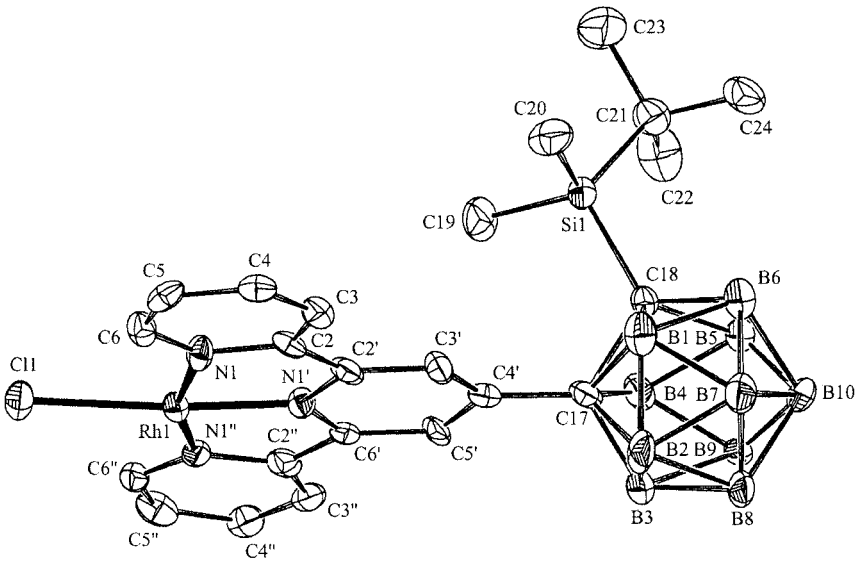

Figure 6. Displacement ellipsoid plot (50% probability level) of complex **4**. Hydrogen atoms and the disordered ethanol solvent molecule omitted for clarity

inversion centres (Figure 7), with Rh−Rh′ distances of 3.1503(13) Å. The packing of the dimers appears to be dominated by intermolecular hydrophobic interactions of the carborane residues, and by hydrophilic interactions of the Rh−Cl residues, with the disordered ethanol molecules also present in the structure. Apart from the interaction between the two halves of each dimer, no π-stacking is observed (Figure 8).

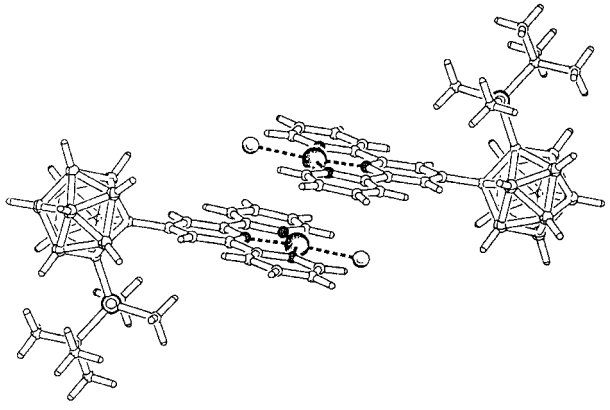

Figure 7. Dimer formation in the crystal structure of complex **4**. Symmetry operation i: $-x$, $1-y$, $1-z$

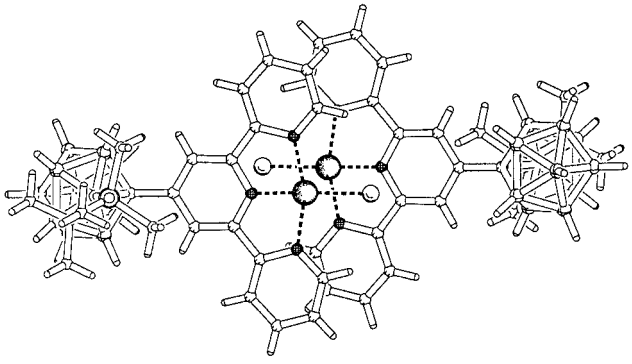

Figure 8. Perpendicular view of the aromatic system of complex **4**

FIR Spectra of Complexes 1 and 2

Generally, the IR ν(Rh−X) (X = Cl, Br) modes of pseudooctahedral $Rh^{III}X_3$-terpyridine complexes are difficult to assign.[20] The complexity of the FIR spectra of these complexes is largely attributed to the coupling of ν(Rh−X) and ν(Rh−N) modes, and to the difference between the ν(Rh−X) modes of the cis and trans halides.

Conversely, analysis of the square-planar Rh^{I}(X)-terpyridine complexes is easier. The FIR spectra of complexes **1** and **2** are similar, except for the ν(Rh−Cl) and ν(Rh−Br) bands (Figure 9). Assignment of ν(Rh−X) (X = Cl, Br for **1** and **2**, respectively) is straightforward: ν(Rh−Cl) at 256−260 cm^{-1} and ν(Rh−Br) at 188 cm^{-1}. The assignment of ν(Rh−Cl) is also supported by the observation of chlorine isotope splitting; the experimental value of 4 cm^{-1} (256 and 260 cm^{-1} for ^{37}Cl and ^{35}Cl, respectively) is similar to the calculated isotope splitting of 5 cm^{-1} ($K = 6.33\cdot10^{28}$ dyn cm^{-1} for $^{103}Rh-^{37}Cl$; 1 dyn = 10^{-3} N m^{-1} = 10^{-3} J).

The band pattern observed for complex **1** at 129 and 138 cm^{-1} is also considerably shifted to smaller wavenumbers for complex **2** (85 and 96 cm^{-1}). These bands are probably Rh−X bending vibrations (out-of-plane and in-plane).

Other absorption bands for **1** at 300−320, 220−230 and 153 cm^{-1} show only a minor shift to smaller wavenumbers for **2**, viz. 295−302, 214−226 and 141 cm^{-1}, respectively. These bands are attributed, without detailed analysis, to Rh−N/tpy vibrations.

DFT Study and Electronic Absorption Spectra of Complexes 1 and 2

Density functional theoretical calculations were performed on complexes **1** and **2**, restricted to a C_{2v}-symmetry

 © 2004 Wiley-VCH Verlag GmbH & Co. KGaA, Weinheim

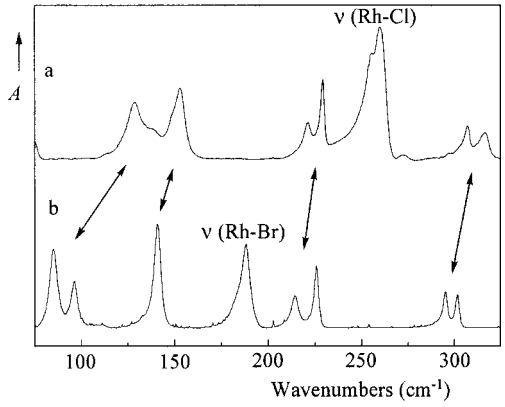

Figure 9. Far-IR spectra of complexes **1** (a) and **2** (b) dispersed in Nujol

square-planar arrangement. Only orbital contributions above 4% are incorporated in Table 3.

Table 3. Characteristics and one-electron energies of the HOMO-8 to LUMO+5 levels of [Rh(X)(tpy)] (**1**: X = Cl; **2**: X = Br), as calculated by the ADF/BP program; both complexes lie in the $x-y$ plane, and the Rh−X bond along the x-axis

MO	X	Energy (eV)	Terpyridine	Rh	X
Unoccupied orbitals					
$24a_1$	Cl	−1.170	31.3% ($18a_1$)	55.5% ($d_{x^2-y^2}$)	9.0% (p_x)
$26a_1$	Br	−1.350	30.2% ($18a_1$)	54.3% ($d_{x^2-y^2}$)	9.3% (p_x)
$11b_2$	Cl	−1.463	95.9% ($8b_2$)	−	−
$12b_2$	Br	−1.490	95.9% ($8b_2$)	−	−
$7a_2$	Cl	−2.057	92.1% ($6a_2$)	8.0% (d_{yz})	−
$8a_2$	Br	−2.084	92.2% ($6a_2$)	7.8% (d_{yz})	−
$10b_2$	Cl	−2.131	96.7% ($7b_2$)	−	−
$11b_2$	Br	−2.149	96.6% ($7b_2$)	−	−
$6a_2$	Cl	−2.998	95.8% ($5a_2$)	−	−
$7a_2$	Br	−3.026	95.7% ($5a_2$)	−	−
$9b_2$	Cl	−3.079	75.4% ($6b_2$)	18.3% (d_{xz})	−
$10b_2$	Br	−3.115	76.0% ($6b_2$)	17.6% (d_{xz})	−
Occupied orbitals					
$23a_1$	Cl	−4.119	−	77.6% (d_{z^2})	−
$25a_1$	Br	−4.129	−	78.0% (d_{z^2})	−
$19b_1$	Cl	−4.514	−	56.0% (d_{xy})	34.3% (p_y)
$20b_1$	Br	−4.500	−	49.6% (d_{xy})	41.1% (p_y)
$8b_2$	Cl	−4.519	26.3% (diff. b_2)	46.7% (d_{xz})	23.7% (p_z)
$9b_2$	Br	−4.501	24.6% (diff. b_2)	42.5% (d_{xz})	29.7% (p_z)
$5a_2$	Cl	−4.706	19.1% (diff. a_2)	77.5% (d_{yz})	−
$6a_2$	Br	−4.712	21.0% (diff. a_2)	77.9% (d_{yz})	−
$7b_2$	Cl	−6.105	−	22.4% (d_{xz})	70.0% (p_z)
$8b_2$	Br	−5.842	−	28.1% (d_{xz})	64.5% (p_z)
$18b_1$	Cl	−6.241	−	28.3% (d_{xy})	61.0% (p_y)
19b1	Br	−5.989	−	34.3% (d_{xy})	54.7% (p_y)
$4a_2$	Cl	−6.398	96.3% ($4a_2$)	−	−
$5a_2$	Br	−6.417	96.4% ($5a_2$)	−	−
$22a_1$	Cl	−6.602	10.6% ($18a_1$)	4.3% ($d_{x^2-y^2}$, s)	76.4% (p_x)
$24a_1$	Br	−6.327	9.2% ($18a_1$)	4.6% ($d_{x^2-y^2}$, s)	79.0% (p_x)
$6b_2$	Cl	−7.099	77.7% ($5b_2$)	−	−
$7b_2$	Br	−7.111	79.5% ($7b_2$)	−	−

The DFT calculations prove that variation of the ligand X (Cl and Br for complexes **1** and **2**, respectively) produces only small differences in orbital characters and energies

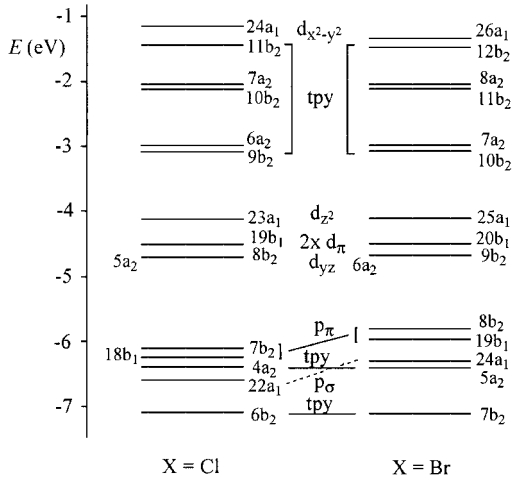

Figure 10. Relevant part of the MO diagrams of [Rh(X)(tpy)] (**1**: X = Cl; **2**: X = Br), as calculated with the ADF/BP program

(Table 3 and Figure 10). MO diagrams of complexes **1** and **2** clearly show that the comparable, predominantly Rh(d), orbitals of **1** and **2** (HOMO-1, -2, -3) have the same energies (except for empty $d_{x^2-y^2}$), which is also the case for the tpy-centred orbitals. Thus, the only comparable orbitals of **1** and **2** differing in energy are those with a predominant halide (p_π and p_σ) character (Figure 10). The variation of X in complexes **1** and **2** is reflected in the HOMO-4, HOMO-5 and HOMO-7 (X = Cl)/HOMO-6 (X = Br). These largely halide-based orbitals are ca. 0.3 eV lower in energy for complex **1** (X = Cl) than for **2** (X = Br).

According to the DFT calculations, the HOMO-1, HOMO-4 and HOMO-5 of **1** and **2** have significantly mixed X(p_π)/Rh(d_π) characters. Also, HOMO-2 of **1** and **2** is strongly mixed, tpy(π^*)/X(p_π)/Rh(d_π). In contrast, the HOMO and HOMO-3 of **1** and **2** are largely Rh(d_{z^2}) and Rh(d_{yz}), respectively, while HOMO-7 (X = Cl)/HOMO-6 (X = Br) has a predominantly halide (p_σ) character. As expected, the LUMO of **1** and **2** reside on the π^*(tpy) system, with some Rh(d_π) contribution. The higher-lying virtual orbitals of **1** and **2** are also almost exclusively localised on the π^*(tpy) system, except for LUMO+5, which is mainly Rh($d_{x^2-y^2}$).

Relevant electronic transitions (transition energies, wavelengths, oscillator strengths) of complexes **1** and **2** and their characters obtained from TD-DFT calculations are presented in Table 4 and Table 5, respectively. Apart from the first three excitations, only electronic transitions with oscillator strengths >0.015 have been incorporated.

The first seven single-electron transitions in Tables 4 and 5 are the same excitations from the comparable Rh(d) orbitals of complexes **1** and **2**. Single-electron transitions at higher energies are less similar owing to different characters of the molecular orbitals involved.

Experimental UV/Vis spectra and calculated electronic transitions for complexes **1** and **2** are shown in Figure 11 and Figure 12, respectively. The lowest seven single-electron transitions are highlighted, except for the forbidden transitions 1 of very low oscillator strengths.

 © 2004 Wiley-VCH Verlag GmbH & Co. KGaA, Weinheim

Table 4. Single-electron transitions of complex **1**, as calculated with the ADF/BP program

Transition		Energy (eV)	Wavelength (nm)	Oscillator strength	Character
1	$23a_1 \rightarrow 9b_2$ (1.00)	1.142	1086	0.0002	MLCT
2	$8b_2 \rightarrow 6a_2$ (0.80) $5a_2 \rightarrow 9b_2$ (0.20)	1.605	773	0.0051	MLCT/XLCT
3	$5a_2 \rightarrow 6a_2$ (0.64) $8b_2 \rightarrow 9b_2$ (0.35)	1.753	707	0.0009	MLCT
4	$5a_2 \rightarrow 9b_2$ (0.77) $8b_2 \rightarrow 6a_2$ (0.18)	1.872	662	0.0437	MLCT
5	$8b_2 \rightarrow 9b_2$ (0.49) $5a_2 \rightarrow 6a_2$ (0.28)	2.075	597	0.0327	MLCT/XLCT
6	$8b_2 \rightarrow 10b_2$ (0.89) $8b_2 \rightarrow 11b_2$ (0.03)	2.494	497	0.0194	MLCT/XLCT
7	$5a_2 \rightarrow 10b_2$ (0.81) $8b_2 \rightarrow 7a_2$ (0.09)	2.760	449	0.1018	MLCT
8	$8b_2 \rightarrow 11b_2$ (0.56) $7b_2 \rightarrow 9b_2$ (0.35)	3.242	382	0.0478	MLCT/XLCT
9	$4a_2 \rightarrow 9b_2$ (0.64) $19b_1 \rightarrow 24a_1$(0.16)	3.628	342	0.2444	intraligand
10	$4a_2 \rightarrow 6a_2$ (0.56) $6b_2 \rightarrow 9b_2$ (0.25)	3.898	318	0.0535	intraligand
11	$6b_2 \rightarrow 6a_2$ (0.51) $4a_2 \rightarrow 10b_2$ (0.31)	4.327	287	0.1278	intraligand
12	$4a_2 \rightarrow 7a_2$ (0.41) $6b_2 \rightarrow 9b_2$ (0.28)	4.396	282	0.0549	intraligand
13	$4a_2 \rightarrow 10b_2$ (0.54) $6b_2 \rightarrow 6a_2$ (0.27)	4.546	273	0.2673	intraligand
14	$4a_2 \rightarrow 7a_2$ (0.37) $6b_2 \rightarrow 9b_2$ (0.20)	4.558	272	0.0545	intraligand

Table 5. Single-electron transitions of complex **2**, as calculated with the ADF/BP program

Transition		Energy (eV)	Wavelength (nm)	Oscillator strength	Character
1	$25a_1 \rightarrow 10b_2$ (1.00)	1.112	1115	0.0002	MLCT
2	$9b_2 \rightarrow 7a_2$ (0.83) $6a_2 \rightarrow 10b_2$ (0.17)	1.556	795	0.0057	MLCT/XLCT
3	$6a_2 \rightarrow 7a_2$ (0.57) $9b_2 \rightarrow 10b_2$ (0.42)	1.713	724	0.0036	MLCT/XLCT
4	$6a_2 \rightarrow 10b_2$ (0.80) $9b_2 \rightarrow 7a_2$ (0.16)	1.831	677	0.0401	MLCT
5	$9b_2 \rightarrow 10b_2$ (0.44) $6a_2 \rightarrow 7a_2$ (0.35)	2.016	615	0.0411	MLCT/XLCT
6	$9b_2 \rightarrow 11b_2$ (0.91) $9b_2 \rightarrow 12b_2$ (0.03)	2.448	507	0.0205	MLCT/XLCT
7	$6a_2 \rightarrow 11b_2$ (0.82) $9b_2 \rightarrow 8a_2$ (0.06)	2.733	454	0.0830	MLCT
8	$8b_2 \rightarrow 10b_2$ (0.58) $6a_2 \rightarrow 8a_2$ (0.35)	2.893	429	0.0229	XLCT/MLCT
9	$6a_2 \rightarrow 8a_2$ (0.28) $8b_2 \rightarrow 10b_2$(0.19)	3.488	356	0.0285	MLCT/XLCT
10	$5a_2 \rightarrow 10b_2$ (0.76) $7b_2 \rightarrow 7a_2$ (0.08)	3.587	346	0.2229	intraligand
11	$5a_2 \rightarrow 7a_2$ (0.58) $7b_2 \rightarrow 10b_2$ (0.24)	3.882	319	0.0506	intraligand
12	$7b_2 \rightarrow 7a_2$ (0.55) $5a_2 \rightarrow 11b_2$ (0.29)	4.314	287	0.1409	intraligand
13	$8b_2 \rightarrow 12b_2$ (0.37) $7b_2 \rightarrow 10b_2$ (0.31)	4.329	286	0.0218	intraligand
14	$5a_2 \rightarrow 11b_2$ (0.57) $7b_2 \rightarrow 7a_2$ (0.24)	4.538	273	0.2338	intraligand

Assignment of the absorption bands in the UV/Visible region (250−900 nm) is facilitated by the TD-DFT calculations. The calculated electronic transitions of complex **1** match fairly well the experimental electronic absorption spectrum, except for transition 7 (Table 4). For complex **2** the deviations in the UV region are larger. The intense ab-

 © 2004 Wiley-VCH Verlag GmbH & Co. KGaA, Weinheim

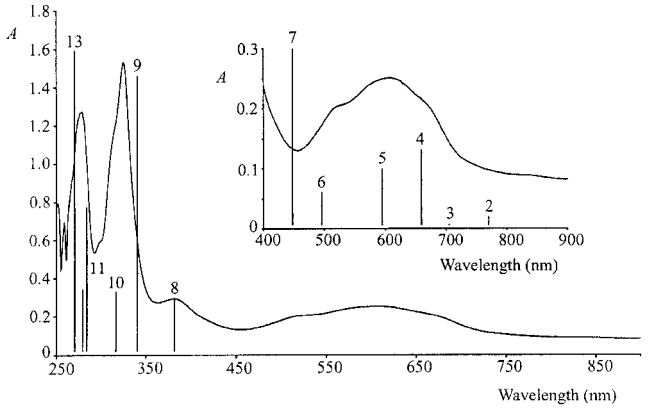

Figure 11. Electronic absorption spectrum of complex **1** (7.27×10^{-5} M) in EtOH. Major electronic transitions of complex **1**, as calculated by the ADF/BP method (Table 4)

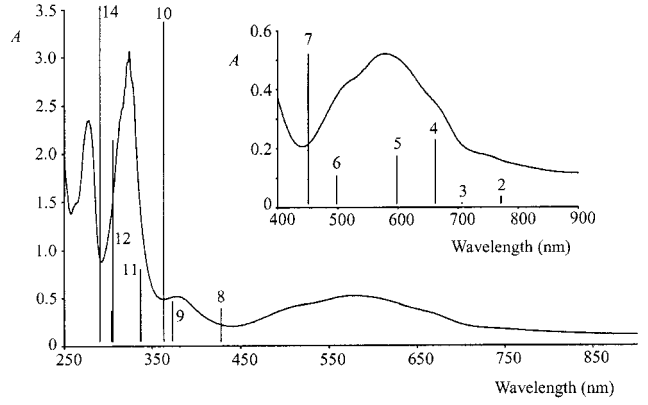

Figure 12. Electronic absorption spectrum of complex **2** (1.36×10^{-4} M) in EtOH. Major electronic transitions of complex **2**, as calculated by the ADF/BP method (Table 5)

sorption bands in the region 250−350 nm are predominantly due to intraligand tpy transitions. The pronounced composed absorption band in the 450−700 nm region encompasses mixed MLCT/XLCT (6, 5) and MLCT (4) transitions. Minor absorption bands in the region 700−900 nm belong to symmetry-forbidden (in a perfect square-planar coordination) MLCT (3), MLCT/XLCT (2) and MLCT (1; HOMO-to-LUMO) transitions.

Cyclic Voltammetry of Complexes 1 and 2

Solutions of complexes **1** and **2** in dry DMF, freshly prepared under an argon atmosphere, show very similar cyclic voltammograms. Therefore, only the cyclic voltammogram of complex **1** is depicted in Figure 13.

Electrochemical oxidation of complexes **1** and **2** is partly chemically reversible on the cyclic voltammetry time scale (ν = 100 mV s^{-1}) at room temperature (Figure 13). In accordance with DFT results (Table 3), this anodic process corresponds to a one-electron oxidation of the formal Rh^I centre to the corresponding Rh^{II} product. Further oxidation of $\mathbf{1}^+$ and $\mathbf{2}^+$ to the corresponding Rh^{III} species was not observed. The oxidation potentials of **1** and **2** show

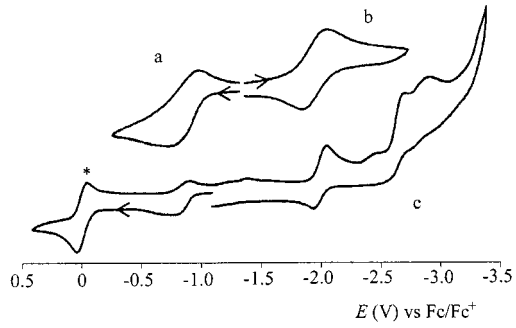

Figure 13. Cyclic voltammogram of complex **1** in DMF at a Pt disk electrode, ν = 100 mV s^{-1}: (a) Partly reversible one-electron oxidation of the Rh^I centre to Rh^{II} at T = 293 K; (b) reversible one-electron reduction of the tpy ligand at T = 233 K; (c) complete cyclic voltammogram at T = 293 K. Asterisk denotes the Fc/Fc^+ redox couple

negligible differences: $E_{1/2}$ (**1**) = −0.84 V vs. Fc/Fc^+; $E_{1/2}$ (**2**) = −0.83 V vs. Fc/Fc^+. This agrees with the DFT-calculated energies of the HOMO for both complexes, which differ merely by 0.01 eV (Table 3).

Electrochemical reduction of **1** and **2** is fully reversible on the cyclic voltammetry time scale at T = 233 K (ν = 100 mV s^{-1}) (Figure 13), being predominantly localised on the lowest π*(tpy) level (Table 3). Understandably, therefore, the reduction potentials of both complexes are nearly identical ($E_{1/2}$ (**1**) = −1.98 V and $E_{1/2}$ (**2**) = −1.97 V vs. Fc/Fc^+). The calculated LUMO energies of **1** and **2** differ to a slightly greater extent (0.036 eV).

Discussion

Syntheses of Complexes 1−4

Under the right reaction conditions, in particular with a suitable solvent, the studied Rh^I-terpyridine complexes are fairly simply synthesised, in nearly quantitative yields. The dark blue Rh^I-terpyridine products are highly air-sensitive and readily oxidise to yellow/red Rh^{III} species.

Having prepared complex **1** in toluene and washed it subsequently with hot THF, crystals were grown during gentle cooling of the combined THF phases. However, this method was unsuccessful for the crystallisation of the other studied Rh^I-terpyridine complexes. In contrast to complex **1**, complex **2** could not be synthesised in toluene; instead, only orange Rh^{III} species were formed. Complex **2** was only obtained in EtOH. Similar to complex **1**, complex **3** could be prepared in various organic solvents such as benzene, THF, Et_2O and EtOH. Attempts to synthesise the Rh−Br complex analogous to **3** only gave red oxidised products. Finally, despite the instability of the carboranyl-tpy unit in various organic solvents, complex **4** was stable for several weeks in EtOH and crystallised upon standing at room temperature.

X-ray Crystallographic Studies of Complexes 1 and 4

In contrast to the fairly facile syntheses of the studied Rh^I-terpyridine complexes, their characterisation is compli-

 © 2004 Wiley-VCH Verlag GmbH & Co. KGaA, Weinheim

cated by their low solubility in organic solvents. The crystal packing of various square-planar d^8 transition metal complexes containing rigid aromatic ligands is dominated by π−π stacking interactions,[21−23] leading to poor solubility and so hampering full characterisation. The distance between the sheets (3.508 Å) in the crystal of **1** is due to this type of π-stacking (Figure 3 and Figure 4).

Complex **4**, bearing the bulky carboranyl group,[24] was prepared to prevent such π-stacking. In the crystal, molecules of **4** are packed in discrete dimers with a Rh−Rh′ distance of 3.1503(13) Å, which is too long for a single bond but rather short for a non-bonding contact.[25] Clearly, the carboranyl group has resulted in a structure without strong π-stacking, the dimeric structure being apparently the highest degree of association possible with this ligand. Unfortunately, even this non-π-stacked complex does not dissolve well in organic solvents. Thus, preventing π-stacking is not a sufficient condition for increased solubility of Rh^I-terpyridine complexes.

Despite the dramatic difference in the packing of complexes **1** and **4**, the coordination geometries of the mononuclear units are very similar, and similar to isoelectronic Pd^{II} [26] and Pt^{II} [27] terpyridine complexes. The corresponding bond lengths (Table 1) and angles (Table 2) are almost the same. Rh−N distances for both **1** and **4** [1.891(6)−2.026(7) Å] are significantly shorter than (κ^1) Rh^{II}-terpyridine,[12] (κ^3) Rh^{II}-terpyridine[12] and (κ^3) Rh^I-diiminepyridine[6] complexes. For Rh^I-chloride complexes with the diiminepyridine ligands 2,6-bis(R^2-iminomethyl)pyridine and 2,6-bis(R^2-iminoethyl)pyridine (R^2 = *i*Pr, *t*Bu), Haarman et al. have shown that the angle between the N−N−N plane and the Rh−Cl axis is a useful measure of steric interactions between the R^2 groups and the chlorine atom.[6] In our study, these angles are 0.25(7)° for **1** and 3.4(3)° for **4**, which are much smaller than those found by Haarman et al. [5.34(16)−11.73(11)°]. We therefore conclude that steric interactions between the terpyridine ligand and the chlorine atom in complexes **1** and **4** are not significant.

FIR Spectra of Complexes 1 and 2

The Rh^I(X)-terpyridine complexes contain only a single Rh−X bond. This facilitates the analysis of their far-IR (FIR) spectra compared with those of $Rh^{III}(X)_3$-tpy[20] species. Assignment of ν(Rh−X) for **1** (256−260 cm^{-1}) and **2** (188 cm^{-1}) is straightforward. Bands at 129−138 cm^{-1} (**1**) and 85−96 cm^{-1} (**2**) are tentatively assigned to Rh−X bending vibrations. The influence of the Rh-metal oxidation state and of the absence/presence of axial halides on the ν(Rh−X) modes for Rh^I(X)-tpy and $Rh^{III}(X)_3$-tpy has not been thoroughly studied. Rh^I−X bonds are generally weaker than Rh^{III}−X bonds, due to stronger π-donation from X to Rh^{III} than to Rh^I metal ions. Therefore, the larger ν(Rh−X) wavenumbers reported for [$Rh(Cl)_3$(tpy)] (330−380 cm^{-1}) and [$Rh(Br)_3$(tpy)] (205−209 cm^{-1}) are reasonable.[20]

Bonding Properties of Complexes 1 and 2

The experimental and corresponding DFT calculated bond lengths and angles in complexes **1** and **2** (Table 1 and Table 2) are in good agreement. This confirms that the used GGA functional (Becke−Perdew), for geometry determination, and the chosen basis set for the DFT calculations, run by the ADF program, are adequate.

From the DFT calculations, the HOMO of complexes **1** and **2** is clearly located mainly on the Rh(d_{z^2}) orbital. This property, combined with the strong electron-donating nitrogen atoms coordinated at the Rh^I centre, makes complexes **1** and **2** extremely nucleophilic and, thereby, very reactive towards, e.g., oxygen and carbon−halogen bonds.[28] While the HOMO of **1** and **2** has a strong metal character, the LUMO is predominantly located on the π* system of the tpy ligand. The HOMO-1 and HOMO-2 can be characterised as antibonding combinations (π-interactions) of p(X) (X = Cl, Br) and d(Rh) orbitals. Both molecular orbitals are destabilised compared with the HOMO-3 that is mainly Rh(d_{yz}). HOMO-4 and HOMO-5 are bonding orbitals − π-interactions between p_π(X) and d_π(Rh) orbitals. HOMO-6 (X = Cl)/HOMO-7 (X = Br) have exclusively a ligand tpy character (like the HOMO-8). HOMO-7 (X = Cl)/HOMO-6 (X = Br) have predominantly a halide character (σ-interaction).

Complexes **1** and **2** feature comparable electronic transitions from orbitals of the same character (Table 4 and Table 5). The lowest seven excitations in both complexes correspond mutually very well. At higher energies, there is no longer a one-to-one relationship between the composition of the excited states of the Cl and Br complexes (**1** and **2**, respectively) in terms of one-electron transitions. After the seventh excitation, the Br p-orbitals play a more dominant role in the single-electron transitions for complex **2** than the Cl p-orbitals for complex **1**. This is mainly due to the difference in energy of the halide p-orbitals (Figure 10).

Regarding differences, for complex **2** an extra electronic transition (viz. 9, Table 5) has been calculated by the ADF/BP program, which has no counterpart in complex **1**. Furthermore, for complex **1**, the electronic transition 8 has a predominant MLCT character (Table 4), while the corresponding electronic transition 8 in complex **2** can better be assigned as XLCT (Table 5).

The MO diagrams of complexes **1** and **2** are very similar. Only the unoccupied predominantly Rh($d_{x^2-y^2}$) and occupied halide molecular orbitals of **1** and **2**, viz. LUMO+5, HOMO-4, HOMO-5 and HOMO-7 (X = Cl)/HOMO-6 (X = Br), slightly differ in energies (ca. 0.3 eV), as displayed by their molecular orbital diagrams in Figure 10. This rationalises the similar UV/Vis spectra and cyclic voltammograms of complexes **1** and **2**. Assignment of the UV/Vis absorption bands of **1** and **2** to particular types of electronic transitions is facilitated by the TD-DFT calculations. The most intense absorption bands in the UV region 250−350 nm are solely assigned as intraligand tpy transitions. The dominant and minor absorption bands and shoulders in the visible region 450−900 nm belong to mixed

 © 2004 Wiley-VCH Verlag GmbH & Co. KGaA, Weinheim

electronic transitions that vary in nature from pure MLCT to mixed XLCT/MLCT charge transfers (Tables 4 and 5). The HOMO−LUMO transition is not symmetry allowed (Table 3), resulting in a very low oscillator strength (Tables 4 and 5). Exclusive Rh-centred (d−d, LF) transitions are not observed. The only notable d−d contribution, of limited significance (16% to transition 9) has been calculated for complex **1** (Table 4).

Complexes **1** and **2** have fairly negative oxidation potentials, strongly indicating that the Rh^I metal centres indeed accommodate high electron densities. The one-electron oxidation of formally Rh^I to Rh^{II} at room temperature is partly reversible on the time scale of seconds. The relative stability of the Rh^{II} species can be ascribed to the high electron-donating capacity of the coordinated tpy and halide ligands. Notably, the subsequent oxidation of Rh^{II} to Rh^{III} was not observed in the available potential window.

At room temperature, the initial one-electron reduction of complexes **1** and **2** in DMF is also partly chemically reversible. A fully reversible scan (ν = 100 mV/s) was achieved at T = 233 K. Long lifetimes of radical anions of **1** and **2** result from the accommodation of the added electron in the π*(tpy) LUMO, as evidenced by the DFT calculations. The subsequent thermal reaction of the radical anions most likely involves release of the halide ligand to compensate for the high electron density at the metal centre. Slow halide dissociation also occurs with the radical anion of the much less electron-rich complex [RhCl(CO)(*i*Pr_2Ph-BIAN)] [*i*Pr_2Ph-BIAN = *N*,*N*′-1,2-bis(2,6-diisopropylphenylimino)acenaphthene].[29,30]

Conclusions

We report the first successful syntheses, characterisation and determination of properties of neutral rigid square-planar Rh^I-terpyridine complexes **1**−**4**. For the syntheses, an appropriate solvent is of crucial importance for each complex. Characterisation is difficult, primarily due to the low solubility (formation of π-stacked aggregates and discrete dimers) and high reactivity of the complexes, promoted by the high electron density on the Rh centre. The Rh^I-terpyridine complexes show no steric repulsion between the halides and the tpy ligand, as evidenced by the crystal structures. Variation of the halide ligand in complexes **1** and **2** (Cl and Br, respectively) has no significant influence on the electronic structure. Their HOMO is predominantly localised on the Rh^I centre (d_{z^2}), and the LUMO resides on the tpy ligand.

Experimental Section

General Remarks: The syntheses of the Rh^I-terpyridine complexes under study and all manipulations with them were strictly performed under an inert atmosphere of purified dry argon or nitrogen, using standard Schlenk techniques. Solvents and reagents were dried and purified by standard procedures.[31] ^{1}H NMR measurements were carried out at 294 K with a Bruker AMX 300 spectrometer operating at 300 MHz. Fast Atom Bombardment (FAB^+) mass spectra were obtained with a JEOL JMS SX/SX102A four-sector mass spectrometer, coupled to a JEOL MS-7000 data system. Samples were loaded in a matrix phase (glycerol) on a stainless steel probe and bombarded with xenon atoms (3 keV). During the high-resolution FAB MS measurements a resolving power of 5000 (10% valley definition) was used. CsI and glycerol served as calibration standards. Elemental analyses were performed by H. Kolbe Mikroanalytisches Laboratorium (Mülheim an der Ruhr, Germany) and Analytische Laboratorien GmbH (Lindlar, Germany).

The tpy and 4′-chloro-2,2′:6′,2′′-terpyridine (4′-Cl-tpy) ligands are commercially available (Aldrich). Precursor complexes $[Rh(X)(COD)]_2$ (X = Cl, Br; COD = cycloocta-1,5-diene)[32] and the ligand 4′-(*tert*-butyldimethylsilyl-*o*-carboranyl)-2,2′:6′,2′′-terpyridine (carboranyl-tpy)[33] were synthesised according to literature procedures.

[Rh(Cl)(Tpy)] (1): Solutions of tpy (1.0 g, 4.3 mmol) and $[Rh(Cl)(COD)]_2$ (1.0 g, 2.0 mmol) in toluene (50 mL) were mixed and stirred together at room temperature. After five minutes, a dark blue precipitate of complex **1** was formed. The product was filtered off, washed with hot THF (3×20 mL) and dried under reduced pressure. Yield 0.7 g (95%). Gentle cooling of the collected THF phases afforded needle-shaped dark blue crystals suitable for X-ray diffraction studies. A small portion of the solid was recrystallised from hot benzonitrile as dark blue leaflets that were used for elemental analysis. FAB^+ MS: *m*/*z* = 371.98 [M^+]. $C_{15}H_{11}ClN_3Rh$ (370.97): calcd. C 48.48, H 2.98, Cl 9.54, N 11.31; found C 48.60, H 3.04, Cl 9.80, N 11.43.

[Rh(Br)(tpy)] (2): A solution of tpy (0.024 g, 0.10 mmol) and $[Rh(Br)(COD)]_2$ (0.03 g, 0.05 mmol) in EtOH (20 mL) was stirred at room temperature for 5 to 10 min, having afforded a dark blue suspension. After filtration, the so-obtained dark blue solid was washed with EtOH (3×10 mL), followed by pentane (3×10 mL). The product was then dried under reduced pressure. Complex **2** was collected as a dark blue powder in nearly quantitative yield (20 mg). FAB^+ MS: *m*/*z* = 414.92 [M^+]. $C_{15}H_{11}BrN_3Rh$ (414.92): calcd. C 43.30, H 2.66, Br 19.20, N 10.10; found C 43.28, H 2.66, Br 19.32, N 10.06.

[Rh(Cl)(4′-Cl-tpy)] (3): Solutions of 4′-Cl-tpy (0.045 g, 0.17 mmol) and $[Rh(Cl)(COD)]_2$ (0.04 g, 0.08 mmol) in toluene (10 mL) were mixed at room temperature. After stirring for 5 to 10 min, a dark blue solid precipitated that was filtered off, washed with toluene (3×10 mL), pentane (3×10 mL), and dried under reduced pressure. Complex **3** was collected as a dark blue powder in nearly quantitative yield (32 mg). FAB^+ MS: *m*/*z* = 404.93 [M^+]. $C_{15}H_{10}Cl_2N_3Rh$ (404.93): calcd. C 44.37, H 2.48, Cl 17.46, N 10.35; found C 44.26, H 2.55, Cl 17.55, N 10.18.

[Rh(Cl)(carboranyl-tpy)] (4): A solution of carboranyl-tpy (0.2 g, 0.41 mmol) and $[RhCl(COD)]_2$ (0.1 g, 0.20 mmol) in EtOH (100 mL) was stirred for 6 h at room temperature. After standing for three weeks and decanting the dark purple supernatant liquid, dark blue crystals of **4** were collected. Yield 0.11 g (90%). ^{1}H NMR (300 MHz, C_6D_6, 20 °C): δ (ppm) = 7.38 (s, 2 H), 7.09 [t, $^3J_{H,H}$ = 8 Hz, 2 H, C(5,5′′)−H], 6.94 [d, $^3J_{H,H}$ = 8 Hz, 2 H, C(3,3′′)−H], 6.84 [t, $^3J_{H,H}$ = 7 Hz, 2 H, C(4,4′′)−H], 0.65 (s, *t*Bu), −0.43 [s, −Si(Me)$_2$−]. $C_{23}H_{35}B_{10}ClN_3SiRh{\cdot}CH_3CH_2OH$ (675.27): calcd. C 44.54, H 6.13, N 6.23; found C 44.32, H 6.03, N 6.31.

Complexes **1** and **3** could also be synthesised in organic solvents other than toluene, such as benzene, THF, Et_2O and EtOH. In contrast, the syntheses of complexes **2** and **4** were only successful

 © 2004 Wiley-VCH Verlag GmbH & Co. KGaA, Weinheim

in EtOH. Complexes **1**−**4** react rapidly with MeOH to produce unidentified red Rh^{III} species.

X-ray Structure Determination of Complexes 1 and 4: A dark blue single crystal was mounted on a capillary. Intensity data were collected at room temperature with an Enraf-Nonius CAD4 diffractometer, using the ω-2θ scan mode. Unit cell dimensions were determined from the angular setting of 25 reflections. Intensity data were corrected for Lorentz and polarisation effects. A semi-empirical absorption correction (ψ-scans)[34] was applied. The structures were solved by the program system DIRDIF,[35] using the program PATTY[36] to locate the rhodium atom, and refined with standard methods (refinement against F^2 of all reflections with SHELXL-97[37]), with anisotropic parameters for the non-hydrogen atoms. All hydrogen atoms were placed at calculated positions and refined riding on the parent atoms. A structure determination summary is presented in Table 6. PLATON[38] drawings of complexes **1** and **4** are shown in Figures 2 and 6, respectively. Selected bond lengths and angles for both crystal structures are given in Tables 1 and 2. CCDC-125107 (for **1**) and -125106 (for **4**) contain the supplementary crystallographic data for this paper. These data can be obtained free of charge at www.ccdc.cam.ac.uk/conts/retrieving.html [or from the Cambridge Crystallographic Data Centre, 12 Union Road, Cambridge CB2 1EZ, UK; Fax: (internat.) +44-1223-336-033; E-mail: deposit@ccdc.cam.ac.uk].

UV/Vis and FIR Spectra of Complexes 1 and 2: Electronic absorption spectra were measured with a HP 8453 diode-array spectrophotometer. Far-infrared (FIR) spectra were recorded between 75 and 375 cm^{-1} with a BOMEM DA3.02 FTIR spectrometer, using a polyethylene cell filled under an argon atmosphere. All FIR experiments used a globar light source and a helium-cooled germanium bolometer operating at 4.2 K. The spectra (128 scans) were recorded at 0.5 cm^{-1} resolution. Samples were dispersed in Nujol under an argon atmosphere.

Density Functional Theoretical (DFT) Study of Complexes 1 and 2: Density functional theory (DFT) was employed to determine the ground-state electronic structures of complexes **1** and **2**, and time-dependent density functional theory (TD-DFT) to describe the corresponding electronic transitions.[39−41] It is important to stress that the Kohn−Shan molecular orbitals, arising from DFT calculations, are physically meaningful,[42,43] and that the accuracy of excitation energies determined with TD-DFT is often similar to that of the most advanced ab initio methods.[44,45]

Calculations of geometry-optimised [Rh(Cl)(tpy)] (**1′**) and [Rh(Br)(tpy)] (**2′**) were performed with the Amsterdam Density Functional (ADF) program.[46] Crystallographic data of complex **1** were used to provide an initial estimate of the equilibrium geometry. Atomic coordinates were then projected onto a plane, and geometry optimisation was performed for the ground state. A separate optimisation was carried out for each molecule, with constrained planar geometry and C_{2v} symmetry.

For all calculations, including the geometry optimisation, the following basis sets were employed: for C, N, H, Cl and Br, an uncontracted triple-ζ Slater-type orbital (STO) basis with two polarisation functions; for Rh, an uncontracted triple-ζ STO basis with one polarisation function (5p). Core orbitals were frozen for C and N (1s), Cl (2s, 2p), Br (3s, 3p), and Rh (1s-3d).

Table 6. Crystallographic data and summary of the refinement for complexes **1** and **4**

Complex	**1**	**4**
Crystal colour	dark blue	dark blue
Crystal shape	irregular rod	plate
Crystal size, mm	0.41 × 0.19 × 0.12	0.38 × 0.30 × 0.05
Empirical formula	$C_{15}H_{11}ClN_3Rh$	$C_{23}H_{35}B_{10}ClN_3RhSi{\cdot}0.7\ C_2H_5OH$
M_w	371.63	660.34
T, K	293(2)	200
Radiation	Cu-K_α (graphite monochromator)	Mo-K_α (graphite monochromator)
Wavelength, Å	1.54184	0.71073
Crystal system	monoclinic	monoclinic
Space group	$P2_1/n$	$P2_1/c$
Unit cell dimensions	a = 9.5594(5) Å	a = 20.5101(15) Å
	b = 11.1190(5) Å, β= 107.936(4)°	b = 10.5314(11) Å, β= 99.674(8)°
	c = 13.0679(5) Å	c = 15.0070(15) Å
V, Å^3	1321.49(10)	3195.4(5)
Z	4	4
$D_{calcd.}$, g cm^{-3}	1.868	1.373
μ, mm^{-1}	12.233	0.68
F(000)	736	1353
Θ range for data collection, °	5.06 to 69.91	1.01 to 27.47
Index ranges	$0 \le h \le 11$, $-13 \le k \le 13$, $-15 \le l \le 15$	$-26 \le h \le 26$, $0 \le k \le 13$, $-19 \le l \le 13$
Reflections collected/unique	5096/2495 [R_{int} = 0.1058][a]	9900/7321 [R_{int} = 0.0568][a]
Reflections observed	1743 ([$I_o > 2\sigma(I_o)$])	3702 ([$I_o > 2\sigma(I_o)$])
Range of relat. transm. factors	1.463 and 0.77	0.98 and 0.93
Data/restraints/parameters	2495/0/181	7321/14/388
Goodness-of-fit on F^2	1.059	1.025
Final R indices [$I > 2\sigma(I)$][b] [c]	R_1 = 0.0569, wR_2 = 0.1465	R_1 = 0.0791, wR_2 = 0.1528
R indices (all data)	R_1 = 0.0888, wR_2 = 0.1638	R_1 = 0.1809, wR_2 = 0.1986
Diff. peak/hole, e·Å^{-3}	1.321/−1.142	0.92/−0.93

[a] $R_{int} = \Sigma|F_o^2 - F_o^2(\text{mean})|/\Sigma F_o^2$. [b] Unweighted agreement factor $R_1 = \Sigma||F_o| - |F_c||/\Sigma|F_o|$. [c] The weighted agreement factor $wR_2 = [\Sigma[w||F_o| - |F_c||^2/\Sigma w|F_o|^2]^{1/2}$, where $w = 4F^2/\sigma^2(F^2)$.

 © 2004 Wiley-VCH Verlag GmbH & Co. KGaA, Weinheim

To approximate the exchange-correlation potential, the generalised gradient approximation (GGA) was adopted, which employs the Becke gradient approximation for the exchange,[47] and Perdew approximation for correlation (ADF/BP).[48] After the geometry optimisation, calculations were performed for three different fragments of each complex molecule; the tpy ligand, Cl/Br and Rh. The ADF package allows the results of the fragment calculations to be used in ground-state calculations of each complete molecule, and the molecular orbitals (MOs) to be analysed in terms of the fragments' orbitals. In all calculations, C_{2v} symmetry was incorporated for the terpyridine ligand and the entire molecule. For the individual-atom fragments, spherical symmetry was imposed.

The ADF-RESPONSE module,[49] an extension of the ADF, was used to perform TD-DFT calculations, for the ground-state optimised geometry. These calculations provide excitation energies and relative contributions of individual occupied-to-virtual MO transitions to each excitation.

Cyclic Voltammetry of Complexes 1 and 2: Cyclic voltammetry was performed in a gas-tight cell under an inert atmosphere of dry argon. The cell was equipped with a Pt disk working electrode (apparent surface area of 0.42 mm^2), Pt wire auxiliary electrode, and Ag wire pseudoreference electrode. Before each experiment, the working electrode was carefully polished with a 0.25 μm grain diamond paste. Redox potentials are reported against the ferrocene/ferrocenium (Fc/Fc^+) redox couple, used as an internal reference standard.[50] Cyclic voltammetric experiments were performed with complexes **1** and **2** (10^{-4} M) in dry HPLC-grade dimethylformamide (DMF). The potential was controlled with a PAR Model 283 potentiostat equipped with positive feedback for ohmic drop compensation.

Acknowledgments

Prof. Anton W. Gal and Dr. Peter H. M. Budzelaar (University of Nijmegen) are thanked for their interest in this work and for their help with the syntheses.

[1] E. C. Constable, *Adv. Inorg. Chem. Rad.* **1986**, *30*, 69−121.
[2] E. C. Constable, *Prog. Inorg. Chem.* **1994**, *42*, 67−138.
[3] R. E. Rülke, V. E. Kaasjager, P. Wehman, A. L. Spek, C. J. Elsevier, P. W. N. M. van Leeuwen, K. Vrieze, *Organometallics* **1996**, *15*, 668−677.
[4] K. Vrieze, J. H. Groen, J. G. P. Delis, C. J. Elsevier, P. W. N. M. van Leeuwen, *New J. Chem.* **1997**, *21*, 807−813.
[5] J. H. Groen, A. de Zwart, M. J. M. Vlaar, J. M. Ernsting, P. W. N. M. van Leeuwen, K. Vrieze, H. Kooijman, W. J. J. Smeets, A. L. Spek, P. H. M. Budzelaar, Q. Xiang, R. P. Thummel, *Eur. J. Inorg. Chem.* **1998**, 1129−1143.
[6] H. F. Haarman, J. M. Ernsting, M. Kranenburg, H. Kooijman, N. Veldman, A. L. Spek, P. W. N. M. van Leeuwen, K. Vrieze, *Organometallics* **1997**, *16*, 887−900.
[7] H. F. Haarman, F. R. Bregman, P. W. N. M. van Leeuwen, K. Vrieze, *Organometallics* **1997**, *16*, 979−985.
[8] H. F. Haarman, J. W. F. Kaagman, W. J. J. Smeets, A. L. Spek, K. Vrieze, *Inorg. Chim. Acta* **1998**, *270*, 34−45.
[9] H.-W. Frühauf, Habilitation Thesis, University of Duisburg, Germany, **1980**.
[10] G. T. Morgan, F. H. Bursthall, *J. Chem. Soc.* **1932**, 20−30.
[11] G. T. Morgan, F. H. Bursthall, *J. Chem. Soc.* **1937**, 1649−1655.
[12] F. P. Pruchnik, F. Robert, Y. Jeannin, S. Jeannin, *Inorg. Chem.* **1996**, *35*, 4261−4263.
[13] F. P. Pruchnik, P. Jakimowicz, Z. Ciunik, J. Zakrzewska-Czerwinska, A. Opolski, J. Wietrzyk, E. Wojdat, *Inorg. Chim. Acta* **2002**, *334*, 59−66.
[14] W. K. Seok, H. N. Lee, M. Y. Kim, T. M. Klapotke, Y. Dong, H. Yun, *J. Organomet. Chem.* **2002**, *654*, 170−175.
[15] T. Yutaka, I. Mori, M. Kurihara, J. Mizutani, K. Kubo, S. Furusho, K. Matsumura, N. Tamai, H. Nishihara, *Inorg. Chem.* **2001**, *40*, 4986−4995.
[16] M. Y. Kim, W. K. Seok, Y. Dong, H. Yun, *Inorg. Chim. Acta* **2001**, *319*, 194−198.
[17] F. Odobel, J. P. Sauvage, A. Harriman, *Tetrahedron Lett.* **1993**, *34*, 8113−8116.
[18] M. E. Frink, D. Steven, H. A. Goodwin, R. J. Watts, P. C. Ford, *Inorg. Chem.* **1988**, *27*, 1283−1286.
[19] R. Marcec, *React. Kinet. Catal. Lett.* **1986**, *31*, 337−341.
[20] I. I. Bhayat, W. R. McWhinnie, *Spectrochim. Acta Part A* **1972**, *28*, 743−751.
[21] G. R. Cayley, D. W. Margerum, *J. Chem. Soc., Chem. Commun.* **1974**, 1002−1004.
[22] M. Chou, C. Creutz, D. Mahajan, N. Sutin, A. P. Zipp, *Inorg. Chem.* **1982**, *21*, 3989−3997.
[23] G. Arena, L. M. Scolaro, R. F. Pasternack, R. Romeo, *Inorg. Chem.* **1995**, *34*, 2994−3007.
[24] D. Armspach, E. C. Constable, C. E. Housecroft, M. Neuburger, M. Zehnder, *J. Organomet. Chem.* **1998**, *550*, 193−206.
[25] G. Aullón, P. Alemany, S. Alvarez, *Inorg. Chem.* **1996**, *35*, 5061−5067.
[26] G. M. Intille, C. E. Pfuger, W. A. Baker, *J. Cryst. Mol. Struct.* **1973**, *3*, 47−54.
[27] K. W. Jennette, J. T. Gill, J. A. Sadownick, S. J. Lippard, *J. Am. Chem. Soc.* **1976**, *98*, 6159−6168.
[28] B. C. de Pater, E. J. Zijp, H.-W. Frühauf, J. M. Ernsting, C. J. Elsevier, K. Vricze, P. H. M. Budzelaar, A. W. Gal, *Organometallics* **2004**, *23*, 269−279.
[29] E. Dova, K. Goubitz, A. van Langevelde, R. Driessen, T. Mahabiersing, R. Blaauw, R. Peschar, H. Schenk, *J. Synchrotron Rad.* **2001**, *8*, 1186−1190.
[30] T. Mahabiersing, H. Luyten, R. Nieuwendam, F. Hartl, *Collect. Czech. Chem. Commun.* **2003**, *68*, 1687−1709.
[31] D. D. Perrin, W. L. F. Armarego, *Purification of Laboratory Chemicals*, 3rd ed., Pergamon Press, Exeter, United Kingdom, **1988**.
[32] A. van der Ent, A. L. Onderdelinden, *Inorg. Synth.* **1990**, *28*, 90−92.
[33] D. Armspach, E. C. Constable, C. E. Housecroft, M. Neuburger, M. Zehnder, *New J. Chem.* **1996**, *20*, 331−335.
[34] A. C. T. North, D. C. Phillips, F. S. Mathews, *Acta Crystallogr., Sect. A* 1968, 24, 351−359.
[35] P. T. Beurskens, G. Beurskens, W. P. Bosman, R. de Gelder, S. Garcia-Granda, R. O. Gould, R. Istrael, J. M. M. Smits, *DIRDIF-96.* A computer program system for crystal structure determination by Patterson methods and direct methods applied to difference structure factors, Laboratory of Crystallography, University of Nijmegen, The Netherlands, **1996**.
[36] P. T. Beurskens, P. T. Admiraal, G. Behm, G. Beurskens, J. M. M. Smits, C. Smykalla, *Z. Kristallogr.* **1991**, Suppl. 4, 99.
[37] G. M. Sheldrick, *SHELXL-97*, Program for the refinement of crystal structures, University of Göttingen, Germany, **1997**.
[38] A. L. Spek, *PLATON, A Multipurpose Crystallographic Tool*, Utrecht University, Utrecht, The Netherlands, **2002**.
[39] M. Casida, *Recent Advances in Density Functional Methods*, World Scientific, Singapore, **1995**.
[40] E. K. U. Gross, W. Kohn, *Adv. Quantum Chem.* **1990**, *21*, 255−291.
[41] E. K. U. Gross, J. F. Dobson, M. Petersilka, *Density Functional Theory*, Springer, Heidelberg, Germany, **1996**.
[42] E. J. Baerends, O. V. Gritsenko, R. van Leeuwen, *Chemical Applications of Density Functional Theory*, American Chemical Society, Washington D. C., **1996**, vol. 629.
[43] E. J. Baerends, O. V. Gritsenko, *J. Phys. Chem. A* **1997**, *101*, 5383−5403.
[44] M. Grüning, O. V. Gritsenko, S. J. A. van Gisbergen, E. J. Baerends, *J. Chem. Phys.* **2001**, *114*, 652−660.
[45] P. R. T. Schipper, O. V. Gritsenko, S. J. A. van Gisbergen, E. J. Baerends, *J. Chem. Phys.* **2000**, *112*, 1344−1352.

 © 2004 Wiley-VCH Verlag GmbH & Co. KGaA, Weinheim

[46] G. te Velde, F. M. Bickelhaupt, E. J. Baerends, C. Fonseca Guerra, S. J. A. van Gisbergen, J. G. Snijders, T. Ziegler, *J. Comput. Chem.* **2001**, *22*, 931−967.
[47] A. Becke, *Phys. Rev. A* **1988**, *38*, 3098−3100.
[48] J. P. Perdew, *Phys. Rev. B* **1986**, *33*, 8822; see also Erratum: *Phys. Rev. B 1986, 34*, 7406).
[49] S. J. A. van Gisbergen, J. G. Snijders, E.-J. Baerends, *Comput. Phys. Commun.* **1999**, *118*, 119−138.
[50] G. Gritzner, J. Kůta, *Pure Appl. Chem.* **1984**, *56*, 461−466.

Received October 3, 2003
Early View Article
Published Online March 9, 2004

 © 2004 Wiley-VCH Verlag GmbH & Co. KGaA, Weinheim

Electrochemical Studies of Complexes with Oxo- or Hydroxo-Bridged $\{Mo_2(\mu\text{-}SMe)_3\}^+$ Centers: Cleavage of the Oxygen Bridge and Generation of Substrate-Binding Sites

Marc Le Hénanf,[a] Christine Le Roy,[a] Kenneth W. Muir,[b] François Y. Pétillon,[a] Philippe Schollhammer,[a] and Jean Talarmin*[a]

Keywords: Dinuclear complexes / Molybdenum / Electrochemical reduction / Oxo, hydroxo bridges / Protonations / Aqua ligands

The reduction of $[Mo_2(Cp)_2(\mu\text{-}SMe)_3(\mu\text{-}O)]^+$ (**1**$^+$) has been investigated by cyclic voltammetry and controlled-potential electrolysis in THF- and MeCN/NBu_4PF_6 without added acid or in the presence of various acids HX (HX: HTsO, CF_3CO_2H, HBF_4). Reduction in the presence of acid follows an $EC_{rev}E$ mechanism in which the intermediate chemical step is an acid-base equilibrium between **1** and $[Mo_2(Cp)_2(\mu\text{-}SMe)_3(\mu\text{-}OH)]^+$ (**2**$^+$). This electrochemical process is followed by protonation of the neutral μ-hydroxo complex **2** to afford different products which depend both on the solvent (THF or MeCN) and on the nature of the acid. Controlled-potential electrolysis of **1**$^+$ in the presence of HX (2 equiv.) leads to the generation of binding sites and finally gives products identical to those obtained from protonation of **2** by HX. The complex $[Mo_2(Cp)_2(\mu\text{-}SMe)_3(\mu\text{-}\eta^1,\eta^1\text{-}OCOCF_3)]$ (**3**) which can be obtained either by protonation of **2** by CF_3CO_2H or by reduction of **1**$^+$ in the presence of CF_3CO_2H, has been characterized crystallographically. In the presence of HBF_4 protonation of **1**$^+$ gives **2**$^{2+}$. The reactivity of **2**$^+$ and of the complexes $[Mo_2(Cp)_2(\mu\text{-}SMe)_3(H_2O)(TsO)]$ (**4**) and $[Mo_2(cp)_2(\mu\text{-}SMe)_3(H_2O)L]^+$ (L = H_2O or THF) (**6**$^+$), all of which contain a terminal aqua ligand, has also been investigated.
(© Wiley-VCH Verlag GmbH & Co. KGaA, 69451 Weinheim, Germany, 2004)

Introduction

We have previously reported various aspects of the chemistry and electrochemistry of dinuclear complexes in which the metal centers are held together by thiolate bridges.[1] We have shown that the dinuclear $\{[Mo_2(Cp)_2(\mu\text{-}SMe)_3]^+\}$ entity can sustain progressive reduction of nitrogenous substrates thus modeling, in vitro, key steps of the nitrogen fixation process.[2−7] The same dinuclear center also permits the conversion of alkynes to carbyne and alkyl groups[8] and the partial reduction of C≡N bonds.[9] These transformations are facilitated by the ability of the $\{[Mo_2(Cp)_2(\mu\text{-}SMe)_3]^+\}$ core to adapt to the different modes of coordination required by different substrates. Recently, we turned our attention to oxygen-containing complexes such as $[Mo_2(Cp)_2(\mu\text{-}SMe)_3(\mu\text{-}O)]^+$ (**1**$^+$) and $[Mo_2(Cp)_2(\mu\text{-}SMe)_3(\mu\text{-}OH)]$ (**2**) (respectively isoelectronic with the imido and amido complexes we studied previously[5,6]) to see whether they had potential as precursors to species with sites able to bind and reduce nitrate and nitrite.[10]

Much of the published work on dinuclear complexes containing oxo- and/or hydroxo bridges has been prompted by the implication of such centers in various biological processes.[11] Electrochemical studies have been published for iron, ruthenium and manganese compounds.[12−14] In the case of molybdenum it has been reported that chemical reduction of a dinuclear complex with terminal and bridging oxo groups in acidic aqueous media affords complexes with hydroxo or aqua ligands,[15] and electrochemical studies of complexes with the $Mo_2O_2(\mu\text{-}O)_2^{2+}$ core in various aqueous buffers have shown that the terminal oxo groups are reduced to aqua ligands.[16]

In this paper, we report detailed electrochemical studies of the reactivity at the oxygen bridges in **1**$^+$ and **2**. We show that by protonation of **2** or reduction of **1**$^+$ in acidic solution it is possible to generate coordination sites suitable for occupation by oxygen-donor ligands such as the trifluoroacetate anion. Related to this, the crystal and molecular structures of $[Mo_2(Cp)_2(\mu\text{-}SMe)_3(\mu\text{-}\eta^1,\eta^1\text{-}OCOCF_3)]$ are described. The reactivity at the μ-oxo and μ-hydroxo ligands is shown to be strongly affected by the (formal) oxidation state of the metal centers in the $\{Mo(\mu\text{-}SMe)_3\}$ core. We believe that these results, obtained for dimolybdenum species, may also provide a more general insight into the reactivity of oxo and hydroxo groups when they act in a bridging role at a dinuclear metal center.

[a] UMR CNRS 6521 Chimie, Electrochimie Moléculaires et Chimie Analytique, Université de Bretagne Occidentale
6 Av. V. Le Gorgeu, 29285 Brest Cedex, France
E-mail: jean.talarmin@univ-brest.fr
[b] Department of Chemistry, University of Glasgow
Glasgow G12 8QQ, UK

Results and Discussion

In order to examine the reactivity of the bridging oxo ligand the electrochemical reduction of $\mathbf{1}^+$ was investigated in the absence and presence of acid (tetrafluoroboric: HBF_4/H_2O or HBF_4/Et_2O; trifluoroacetic: CF_3CO_2H; *p*-toluenesulfonic: HTsO) using THF- or $MeCN/NBu_4PF_6$ as an electrolyte. Because the presence of acid is likely to lead to protonation at the oxygen bridge, we also investigated the reactivity of $[Mo_2(Cp)_2(\mu\text{-}SMe)_3(\mu\text{-}OH)]$ (**2**) with acids and its oxidative electrochemistry. For the sake of clarity, this topic is presented first.

1. Protonation and Oxidation of $[Mo_2(Cp)_2(\mu\text{-}SMe)_3(\mu\text{-}OH)]$ (2)

The μ-hydroxo complex **2** was prepared by our standard method[10] which involves treatment of $[Mo_2(Cp)_2(\mu\text{-}SMe)_3(\mu\text{-}Cl)]$[17] with an excess of KOH. This reaction produced samples of **2** contaminated with small amounts of other compounds. Repeated attempts to purify these samples failed because **2** has limited stability in solution and decomposes during column chromatography. The reactivity studies were therefore carried out with samples of **2** containing small quantities of impurities (see Figure 1,a).

Protonation of $[Mo_2(Cp)_2(\mu\text{-}SMe)_3(\mu\text{-}OH)]$, 2: Cleavage of the OH Bridge

The action of acid on **2** depends both on the solvent and on the nature of the acid. Addition of 1 equivalent of HBF_4 to a MeCN solution of **2** quantitatively[18] produced the known[4] bis(acetonitrile) complex $\mathbf{5}^+$, identified by its characteristic redox potentials (Scheme 1). Treatment of **2** with 1 equivalent of CF_3CO_2H in THF resulted in the quantitative[18] formation of $[Mo_2(Cp)_2(\mu\text{-}SMe)_3(\mu\text{-}\eta^1,\eta^1\text{-}OCOCF_3)]$ (**3**) (Scheme 1), which has been fully characterized (see Crystallographic and Experim. Sections). In both cases it is likely that initial protonation at the bridging hydroxide and binding of the conjugate base, or a solvent molecule, is followed by elimination of H_2O from the undetected aqua intermediate, $[Mo_2(Cp)_2(\mu\text{-}SMe)_3(H_2O)(L/X)]^{n+}$ [X = CF_3CO_2, n = 0; L = MeCN, n = 1], to give the observed products. It should be noted that the ammine analogue of the intermediate can be obtained by protonation of $[Mo_2(Cp)_2(\mu\text{-}SMe)_3(\mu\text{-}NH_2)]$ by trifluoroacetic acid in THF but is also detectable by cyclic voltammetry as an intermediate on the path to $\mathbf{5}^+$ {obtained by protonation of $[Mo_2(Cp)_2(\mu\text{-}SMe)_3(\mu\text{-}NH_2)]$ by HBF_4 in MeCN}.[5] The different lifetimes of the aqua- and ammine-containing species suggest that H_2O is more labile than NH_3 at the $\{Mo_2(Cp)_2(\mu\text{-}SMe)_3\}$ site.

Complex **2** also reacted with HTsO (Scheme 1). The reaction product **4** was formed quantitatively[18] but could not be isolated or characterized. Complex **4** was formulated as $[Mo_2(Cp)_2(\mu\text{-}SMe)_3(H_2O)(TsO)]$ by analogy with $[Mo_2(Cp)_2(\mu\text{-}SMe)_3(NH_3)(TsO)]$ which is formed through protonation of $[Mo_2(Cp)_2(\mu\text{-}SMe)_3(\mu\text{-}NH_2)]$ by HTsO in THF.[5] Since there was a possibility that the TsO^- anion could occupy a bridging position (due to the lability of the aqua ligand compared with NH_3), we investigated the reactivity and electrochemistry of **4** in order to obtain more information about the nature of this complex.

Treatment of **4** with different substrates (MeCN, *t*BuNC, Cl^-, $CF_3CO_2^-$), respectively, produced $[Mo_2(Cp)_2(\mu\text{-}SMe)_3(L)_2]^+$ (L = MeCN or *t*BuNC), $[Mo_2(Cp)_2(\mu\text{-}SMe)_3(\mu\text{-}Cl)]$ or $[Mo_2(Cp)_2(\mu\text{-}SMe)_3(\mu\text{-}\eta^1,\eta^1\text{-}OCOCF_3)]$

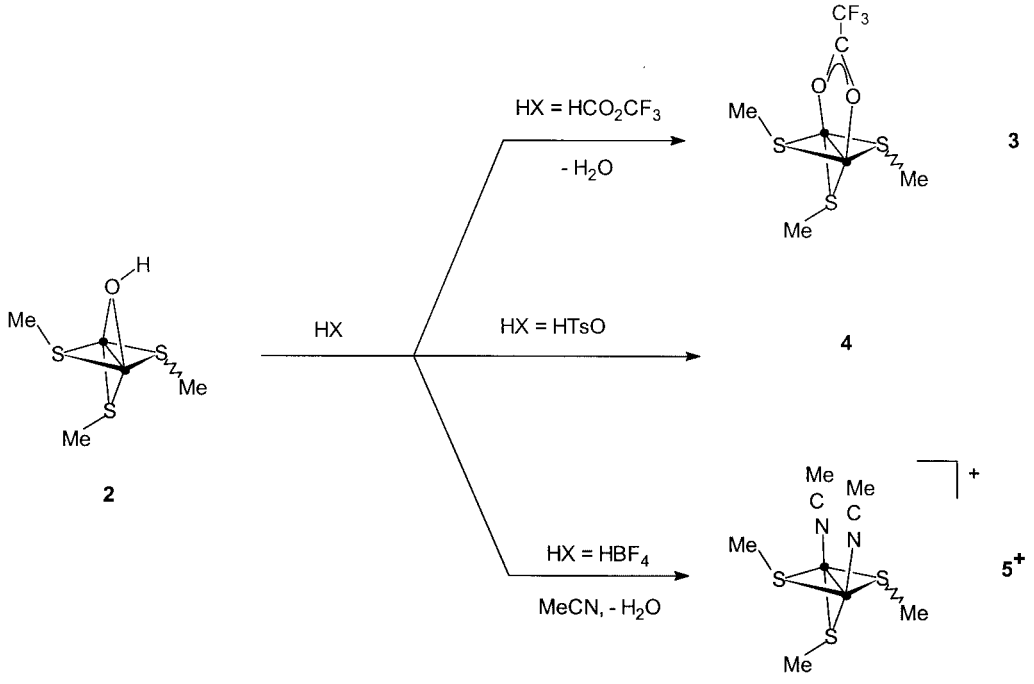

Scheme 1. • = Mo(Cp)

 © 2004 Wiley-VCH Verlag GmbH & Co. KGaA, Weinheim

Table 1 Redox potentials of the different complexes

Compound	Solvent	$E_{1/2}^{red1}$ [a] [V/Fc]	E_p^{red2} [V/Fc]	$E_{1/2}^{ox1}$ [V/Fc]	$E_{1/2}^{ox2}$ [V/Fc]
1$^+$	thf	−0.89	−1.9 (irr)	0.94 (irr)	−
	CH_3CN	−0.88	−1.7 (irr)	0.92 (irr)	−
	CH_2Cl_2	−0.86	−1.9 (irr)	1.1 (irr)	
2	thf	−3.1 (irr)	−	−0.63 (120)[b]	−0.34 (330)[b]
	CH_2Cl_2			−0.58 (80)[b]	−0.15 (150)[b]
3	thf	−2.87 (irr)		−0.35	0.35
4	thf	−2.48 (irr)		−0.51	0.14
6$^+$	thf	−2.5 (irr)		−0.46	0.20

[a] Potentials were determined by cyclic voltammetry at a vitreous carbon electrode and a scan rate of 0.2 V·s^{-1}; irr: irreversible. [b] ΔEp in mV (average) measured at v = 0.2 V·s^{-1}.

(**3**). These products were characterized by their redox potentials (refs.[4,19] and Table 1) and, for the latter two complexes, by the NMR spectra of the solids isolated after completion of the reaction. This demonstrates that **4** retains the $\{Mo_2(Cp)_2(\mu\text{-}SMe)_3\}$ core.

The electrochemical study of **4** provided indirect evidence for the presence of an aqua ligand in the complex. Firstly, the electrochemical reduction of **4** (E_{el} = −2.6 V, Pt cathode, 1 F·mol^{-1} **4**) produced the hydroxo complex **2** (Scheme 2). This can be shown by comparing the CV[20] of the catholyte (Figure 2, b) with that of **2** in the presence of TsO^- (Figure 1, b). The shapes of the CV curves in Figure 1(b) and Figure 2(b) arose from the reaction of complex **2**$^+$ generated at the electrode with TsO^-. This will be detailed below. The fact that **2** is generated by a one-electron reduction of **4** is consistent with the occurrence of an aqua ligand in the latter, but cannot be reconciled with **4** being $[Mo_2(Cp)_2(\mu\text{-}SMe)_3(\mu\text{-}OTs)]$. Secondly, the first oxidation of **4** ($E_{1/2}^{ox1}$ = −0.51 V, Table 1) shown in Figure 3(A) occurs according to an EC process[20,21] (the peak current ratio $(i_p^c/i_p^a)^{ox1}$ increases with increasing scan rates, and the product peak decreases accordingly). The product peak observed on the reverse scan can be suppressed in the presence of excess acid (Figure 3, B). This indicates that the electrochemical oxidation of **4** follows an EC_{rev} mechanism,[21] as shown in Scheme 2, the chemical step being a *reversible* proton loss from **4**$^+$. Since treatment of **2**$^+$ with HTsO afforded **4**$^+$ (see below), these results are entirely consistent with **4** being $[Mo_2(Cp)_2(\mu\text{-}SMe)_3(H_2O)(TsO)]$.

Treatment of **2** with 1 equivalent of HBF_4/H_2O in THF resulted in partial oxidation of the starting material. When the reaction was monitored by voltammetry at a rotating disc electrode, a reduction current was detected thereby showing that some **2**$^+$ had been produced. However, **2** was not entirely converted into **2**$^+$. Cyclic voltammetry of a solution of **2** in the presence of increasing amounts of HBF_4/H_2O (1−5 equiv.) showed that new redox systems slowly increased at the expense of those due to the **2**$^{2+}$/**2**$^+$ and **2**$^+$/**2** couples (see below, oxidation of **2**). The new product **6**$^+$ ($E_{1/2}^{ox1}$ = −0.46 V and $E_{1/2}^{ox2}$ = 0.20 V, Table 1),

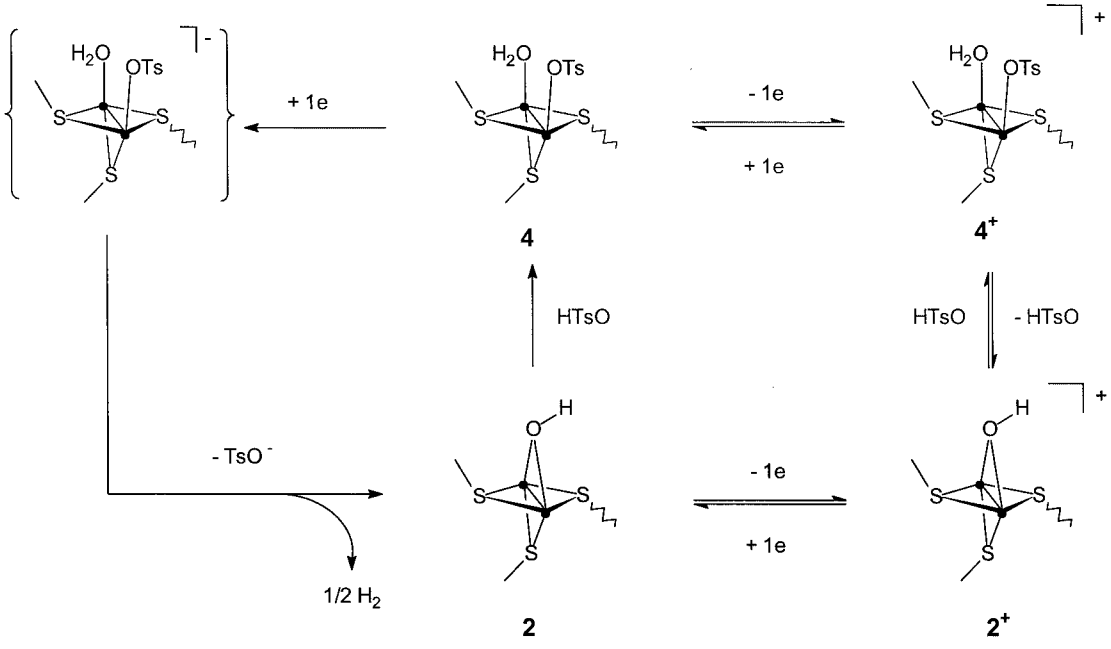

Scheme 2. • = Mo(Cp); methyl groups on the bridging S atoms are omitted

 © 2004 Wiley-VCH Verlag GmbH & Co. KGaA, Weinheim

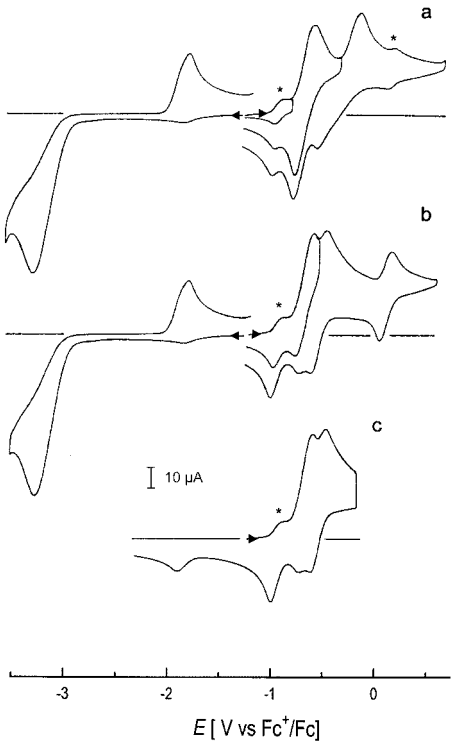

Figure 1. Cyclic voltammetry of $[Mo_2(Cp)_2(\mu\text{-}SMe)_3(\mu\text{-}OH)]$ **2** (ca. 1.2 mM) a) in the absence, and b) and c) in the presence of an excess NBu_4TsO. In scan c) the potential was held 10s at 0 V before scan reversal; under these conditions, the second (irreversible) reduction of $\mathbf{1}^+$ was observed on the reverse scan. The peaks marked with an asterisk are due to an impurity (THF/NBu_4PF_6; vitreous carbon electrode; scan rate $v = 0.2\ V{\cdot}s^{-1}$).

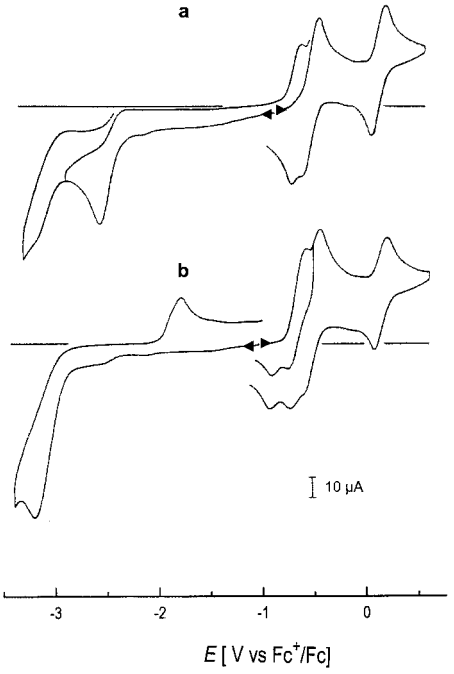

Figure 2. Cyclic voltammetry of $[Mo_2(Cp)_2(\mu\text{-}SMe)_3(H_2O)(TsO)]$ **4** (ca. 1.2 mM) a) before, and b) after electrolysis at −2.6 V (n = 1 $F{\cdot}mol^{-1}$ **4**) (THF/NBu_4PF_6; vitreous carbon electrode; scan rate $v = 0.2\ V{\cdot}s^{-1}$).

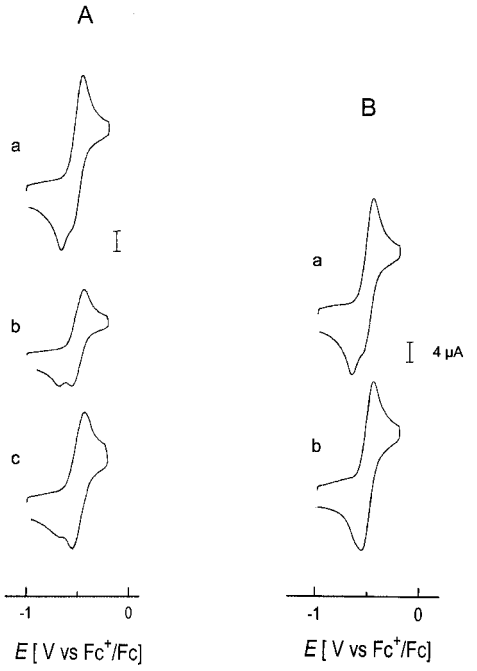

Figure 3. **A:** Cyclic voltammetry of $[Mo_2(Cp)_2(\mu\text{-}SMe)_3(H_2O)(TsO)]$ (**4**) (ca. 1.2 mM) at different scan rates a) 0.2 $V{\cdot}s^{-1}$, b) 0.5 $V{\cdot}s^{-1}$, c) 1 $V{\cdot}s^{-1}$; the current scale is 4 µA for a) and 10 µA for b) and c). **B:** Cyclic voltammetry of $[Mo_2(Cp)_2(\mu\text{-}SMe)_3(H_2O)(TsO)]$ (**4**) (ca. 1.2 mM) at $v = 0.2\ V{\cdot}s^{-1}$, a) in the absence and b) in the presence of an excess of HTsO (THF/NBu_4PF_6; vitreous carbon electrode)

obtained as a mixture of $\mathbf{6}^+$ and $\mathbf{6}^{2+}$, formed faster when HBF_4/Et_2O replaced HBF_4/H_2O in the reaction with **2**. Complex $\mathbf{6}^+$ decomposed on workup and could not be isolated or characterized by analytical methods. However, its reactivity with different substrates demonstrated the presence of labile ligand(s) bound to the metal centers of the conserved $\{[Mo_2(Cp)_2(\mu\text{-}SMe)_3]^+\}$ core and showed a striking similarity to that of complex **4**. Addition of chloride, trifluoroacetate or acetonitrile causes the quantitative conversion[18] of $\mathbf{6}^+$ to $[Mo_2(Cp)_2(\mu\text{-}SMe)_3(\mu\text{-}Cl)]$, **3** or $\mathbf{5}^+$, respectively. Furthermore, treatment of $\mathbf{6}^+$ with *t*BuNC produces the bis(isocyanide)[19] analogue of $\mathbf{5}^+$. Since the electrochemical behaviour of $\mathbf{6}^+$, and in particular its first oxidation step, is very similar to that of **4** (EC_{rev} process, see Scheme 2), and since treatment of $\mathbf{2}^+$ with HBF_4/H_2O afforded $\mathbf{6}^{2+}$ (see below), we have assigned $\mathbf{6}^+$ as $[Mo_2(Cp)_2(\mu\text{-}SMe)_3(H_2O)(L)]^+$, where L could be a molecule of water or THF.

Protonation at the µ-OH ligand of **2** by HX could initially produce an intermediate with an aqua bridge (Scheme 3, step A). Subsequent coordination of the conjugate base X^- (or that of a substrate such as MeCN or *t*BuNC) would shift the H_2O ligand from a bridging to a terminal position (Scheme 3, step B). Protonation of a hydroxo bridge in tris-bridged cobalt complexes was similarly assumed to involve a µ-aqua intermediate on the path to the final product which contained terminally coordinated H_2O molecules.[22,23] Although we are not aware of stable

 © 2004 Wiley-VCH Verlag GmbH & Co. KGaA, Weinheim

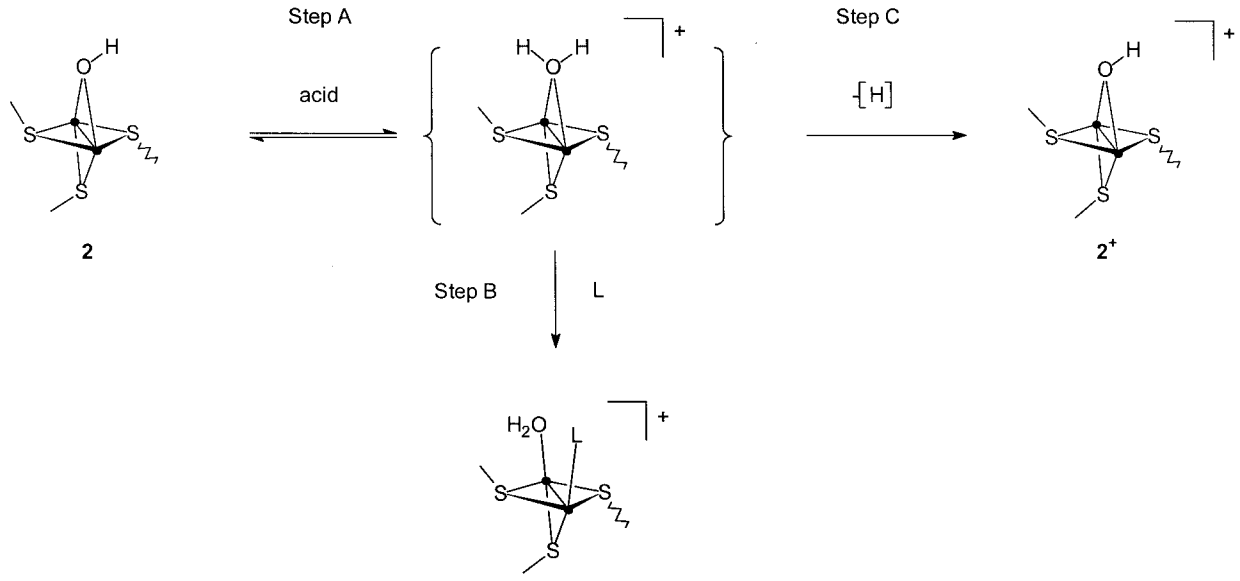

Scheme 3. • = Mo(Cp); L = MeCN, *t*BuNC, THF or H_2O (see text); methyl groups on the bridging S atoms are omitted

Mo(μ-H_2O)Mo compounds, ruthenium,[24−26] cobalt,[27] and nickel[27] complexes containing bridging water molecule(s) have been characterized crystallographically. In these complexes, the aqua bridge appears to be stabilized via hydrogen bonds to the oxygen atom of terminally coordinated carboxylate ligands.[24−27]

Alternatively, protonation at the oxygen of **2** with concerted binding of X^- would afford directly $[Mo_2(Cp)_2(\mu\text{-}SMe)_3(H_2O)(X)]$ (X = TsO or CF_3CO_2). This species was not detected when X = CF_3CO_2 but it was the final product **4** when X = TsO. In the absence of X^- or ligand L (protonation by HBF_4/H_2O in THF), treatment of **2** with protons led to two different types of reaction (oxidation and protonation). This suggests that two mechanisms are involved.

Although no kinetic measurements were performed, it appears that the rate of formation of $[Mo_2(Cp)_2(\mu\text{-}SMe)_3(H_2O)(L)]^+$ (Scheme 3), which is either a likely intermediate (L = MeCN, *t*BuNC) or the final product (L = H_2O or THF) of the protonation of **2** under different conditions, depends on the nature of both the acid (Scheme 3, step A) and of the nucleophile (Scheme 3, step B). The nature of the acid (HX) affects the concentration of the μ-aqua intermediate by perturbing the equilibrium constant [$K_{eq} = K_a^{HX}/K_a^{(\mu\text{-aqua})}$] and thus, the rate of the second-order reaction producing $[Mo_2(Cp)_2(\mu\text{-}SMe)_3(H_2O)(L)]^+$ (Scheme 3, step B). This is shown by the fact that **6**$^+$ was obtained more rapidly when **2** was treated with HBF_4/Et_2O instead of HBF_4/H_2O. The effect of the nucleophile can be demonstrated by the fact that $[Mo_2(Cp)_2(\mu\text{-}SMe)_3L_2]^+$ (L = MeCN, *t*BuNC) was obtained "instantly" when a THF solution of **2** was treated by HBF_4/H_2O in the presence of L, while **6**$^+$ (L = H_2O or THF) was formed slowly upon treatment of **2** with HBF_4/H_2O in THF in the absence of MeCN or *t*BuNC, even though the former reaction involves a supplementary step (substitution of H_2O by a second L molecule) with respect to the latter. Substrate binding to the metal center, consecutive to (or concerted with) the cleavage of one Mo−O bond of the μ-aqua intermediate, was faster when L= MeCN or *t*BuNC than when L = H_2O or THF. The formation of **2**$^+$ observed in the latter situation could arise by loss of a hydrogen atom from the μ-aqua intermediate (Scheme 3, step C). The fate of the hydrogen atom is not known.[28]

Electrochemical Oxidation of [Mo₂(Cp)₂(μ-SMe)₃(μ-OH)], 2. Reactivity of 2⁺

With either THF or CH_2Cl_2 as solvent, complex **2** undergoes two oxidation steps; for both, the anodic-to-cathodic peak separation (ΔE_p[20]) is smaller in CH_2Cl_2 than it is in THF (Table 1, Figure 1, a). Comparison of the first oxidation peak current [$(i_p{}^a)^{ox1}$][20] for equimolar CH_2Cl_2 solutions of **2** and of $[Mo_2(Cp)_2(\mu\text{-}SMe)_3(\mu\text{-}Cl)]$ (which undergoes a reversible one-electron oxidation in this solvent[4]) indicates that the first oxidation of **2** at ca −0.6 V involves one electron on the CV timescale.[29]

The current of the second oxidation of **2** ($E_{1/2}{}^{ox2} = -0.34$ V in THF, −0.15 V in CH_2Cl_2) is lower than that of the first step in both solvents [$i_p{}^{ox2}/i_p{}^{ox1} = 0.6$ (average) in THF]. The second oxidation of **2** is quasi-reversible,[21] the large peak-to-peak separation [in THF: ΔE_p = 330 mV (average) at 0.2 V·s^{-1}][20] suggesting that a chemical reaction takes place along with the electron-transfer. The small value of the rate constant of the heterogeneous electron-transfer (k_e ca 6·10^{-4} cm·s^{-1} as estimated from CV simulations[40]) could indicate substantial structural reorganization without compositional change of the complex. Alternatively, a concerted reaction involving solvent-binding in THF is possible, since the potential and the CV peak separation of the second oxidation step are substantially affected by the nature of the solvent (Table 1). The dication cannot, however,

 © 2004 Wiley-VCH Verlag GmbH & Co. KGaA, Weinheim

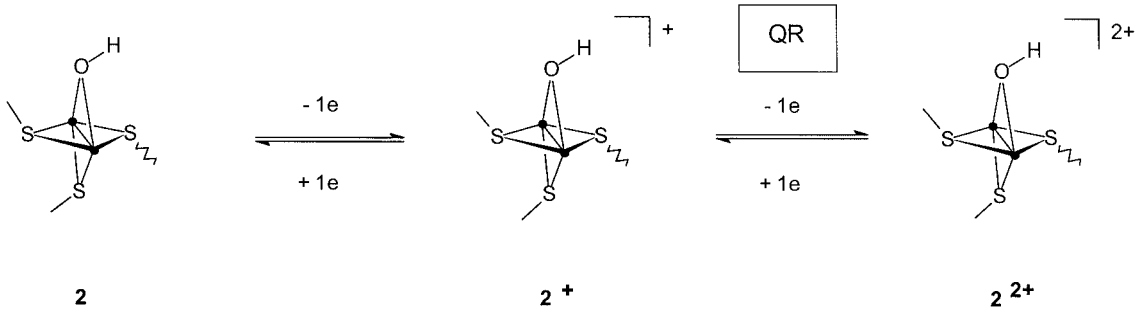

Scheme 4. • = Mo(Cp); QR = quasi-reversible electron-transfer

be isolated. The nature of the chemical step thus remains speculative and 2^{2+} will therefore be represented formally with a bridging hydroxide group in Scheme 4 and in the rest of the paper.

The reduction peak of **2** was not altered by tosylate, thereby demonstrating that **2** and TsO^- do not react. In contrast, the oxidative part of the CV of **2** in THF was strongly affected by the presence of tosylate (Figure 1, b). Indeed, the second oxidation of **2** was not detectable when TsO^- was present. Key features of the oxidation of **2** in the presence of TsO^- include the detection of the two oxidation systems of **4** and of the reduction of the oxo complex $\mathbf{1}^+$ on the reverse scan (Figure 1, b and c). A rationalization of these features in terms of a reaction between TsO^- and electrogenerated $\mathbf{2}^+$ is presented in Scheme 5.

This has been checked independently by treating a THF solution of $\mathbf{2}^+$ electrogenerated from $\mathbf{1}^+$ in the presence of 1 equivalent of HBF_4/H_2O [see below and Figures 4(a) and 6(b)] with different substrates (MeCN, *t*BuNC, $CF_3CO_2^-$, TsO^-). The expected products, $[Mo_2Cp)_2(\mu\text{-}SMe)_3(L)_2]^+$ (L = MeCN, *t*BuNC), **3** and **4**, respectively, were obtained along with $\mathbf{1}^+$ in a ratio close to 1:1. The equilibrium in Scheme 5, formally a hydrogen atom transfer, probably arises from the deprotonation of $\mathbf{2}^+$, see below. Consistent with this, the CV of **2** in the presence of an excess of $CF_3CO_2^-$ in THF shows that the first one-electron oxidation of **2** is replaced by a reversible two-electron transfer at around −0.7 V. This is indicative of the $EC_{rev}E$ mechanism[21] shown in Scheme 6. Deprotonation of $\mathbf{2}^+$ by $CF_3CO_2^-$ produces the reduced oxo complex **1** which is oxidized at a potential more negative than that of **2** (ECE mechanism). The reversibility of the intervening chemical reaction (see below for the reduction of $\mathbf{1}^+$ in the presence of CF_3CO_2H) confers reversibility on the redox process and ensures that its potential is intermediate between those of $\mathbf{2}/\mathbf{2}^+$ and $\mathbf{1}/\mathbf{1}^+$.

Complex $\mathbf{2}^+$ could also be protonated. Addition of 1 equivalent of HTsO to a THF solution of $\mathbf{2}^+$ produced $\mathbf{4}^+$ (Figure 4). Similarly, treatment of $\mathbf{2}^+$ with HBF_4/H_2O led to $\mathbf{6}^{2+}$. These results demonstrate that $\mathbf{2}^+$ can behave both as an acid and as a base.

2. Reduction of $[Mo_2(Cp)_2(\mu\text{-}SMe)_3(\mu\text{-}O)]^+$ ($\mathbf{1}^+$)

In the Absence of Acid

Complex $\mathbf{1}^+$ undergoes an irreversible oxidation and two reduction steps in CH_2Cl_2-, THF-, or MeCN/NBu_4PF_6 (Figure 5, a). The irreversible reduction around $E_p^{red} = -1.9$ V and the irreversible oxidation were not investigated. The potential of the first reduction is essentially independent of the solvent (Table 1). From the usual diagnostic criteria ($i_p^{red1}/v^{1/2}$ independent of scan rate, v; $(i_p^a/i_p^c)^{red1}$ close

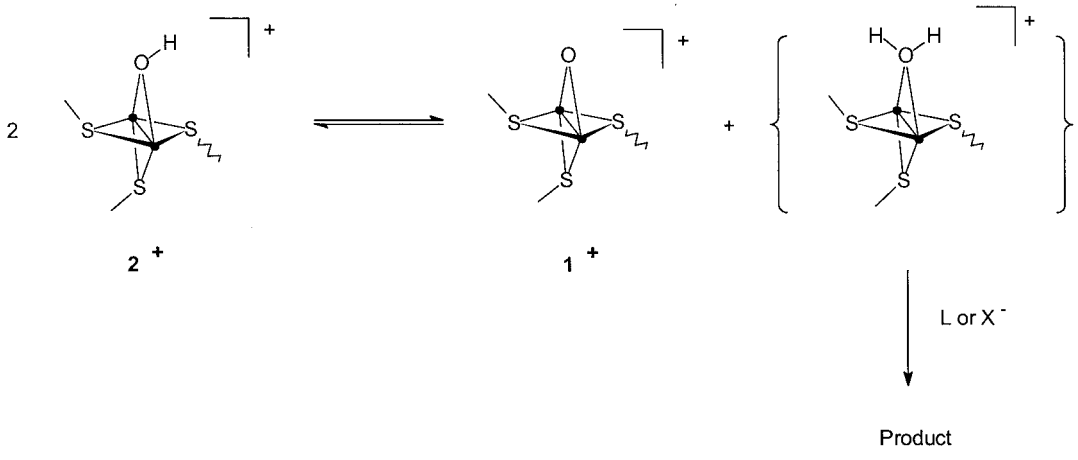

Scheme 5. • = Mo(Cp); methyl groups on the bridging S atoms are omitted

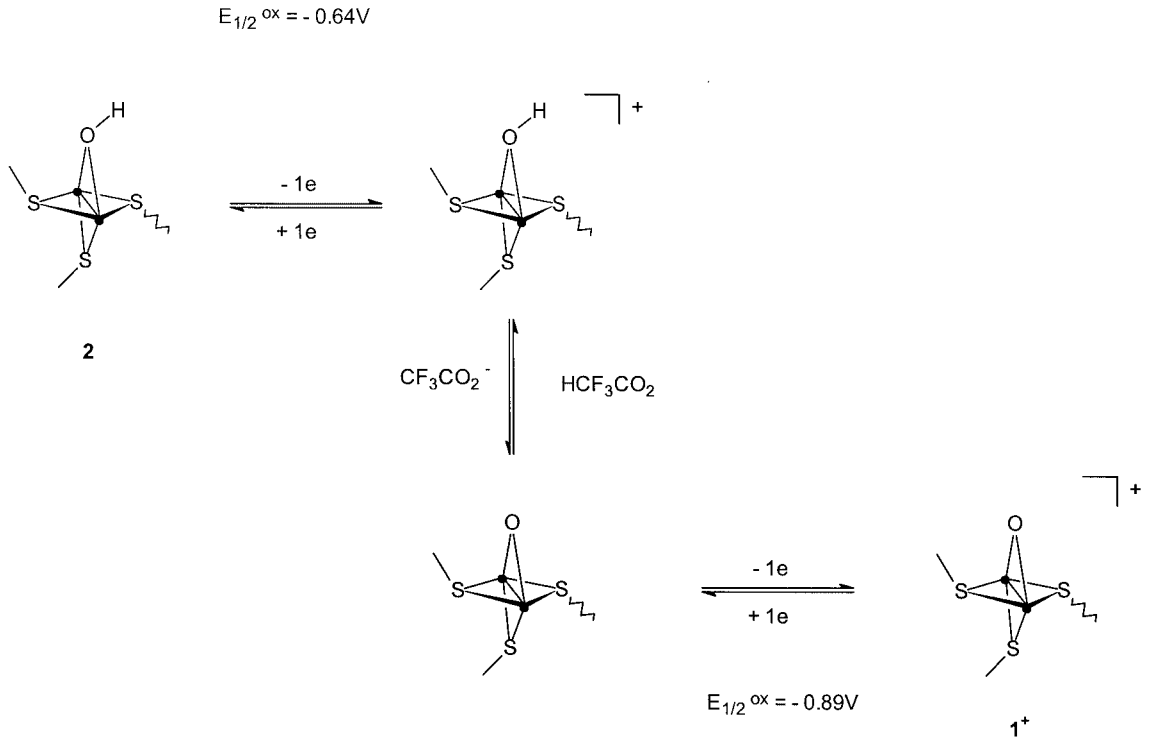

Scheme 6. • = Mo(Cp); methyl groups on the bridging S atoms are omitted

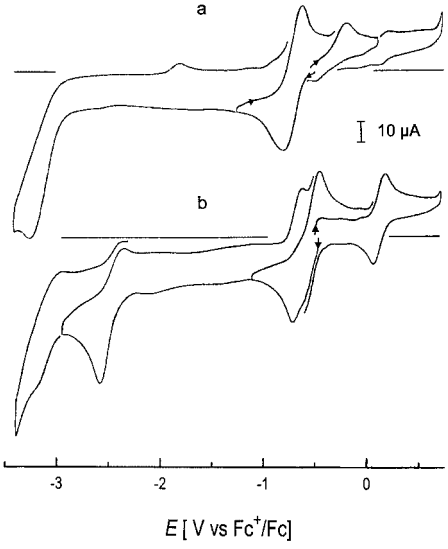

Figure 4. a) Cyclic voltammetry of $[Mo_2(Cp)_2(\mu\text{-}SMe)_3(\mu\text{-}OH)]^+$ ($\mathbf{2}^+$) generated by controlled-potential reduction (n = 1 F·mol^{-1} $\mathbf{1}^+$) of $\mathbf{1}^+$ (ca. 1.2 mM) in the presence of 1 equiv. HBF_4/H_2O; b) after addition of 1 equiv. HTsO to the solution in a). (THF/NBu_4PF_6; vitreous carbon electrode; scan rate v = 0.2 V·s^{-1})

vations have been made in the case of mononuclear imide and oxo complexes with the {Mo(dppe)$_2$} core.[30,31]

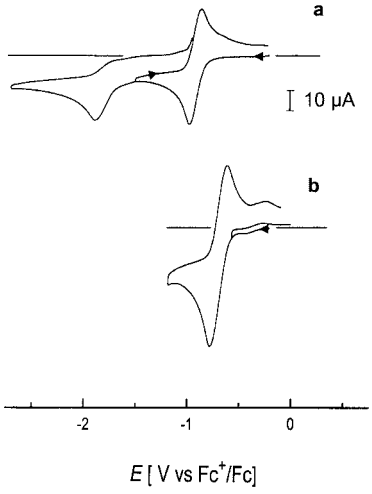

Figure 5. Cyclic voltammetry of $[Mo_2(Cp)_2(\mu\text{-}SMe)_3(\mu\text{-}O)]^+$ ($\mathbf{1}^+$) (ca. 1.5 mM) a) in the absence, and b) in the presence of 1 equivalent of HBF_4/H_2O (THF/NBu_4PF_6; vitreous carbon electrode; scan rate v = 0.2 V·s^{-1}).

to 1; ΔE_p ca 80mV),[21] the first reduction can be assigned to a reversible one-electron, diffusion-controlled step on the cyclic voltammetry timescale. The neutral oxo complex **1** is thus longer-lived than the isoelectronic imido derivative, since the reduction of $[Mo_2(Cp)_2(\mu\text{-}SMe)_3(\mu\text{-}NH)]^+$ was irreversible under the same conditions.[6] Similar obser-

Controlled-potential reduction of $\mathbf{1}^+$ in CH_2Cl_2/NBu_4PF_6 (E_{el} = −1.0 V, Pt cathode, n = 0.9 F·mol^{-1} $\mathbf{1}^+$ by coulometry) afforded **1** in essentially quantitative yield,[18] as shown by cyclic voltammetry of the catholyte. In contrast, **1** was not obtained in a THF electrolyte. Under these conditions electrolysis of $\mathbf{1}^+$ (ca. 1 F·mol^{-1} $\mathbf{1}^+$) afforded a product showing irreversible reduction and oxi-

 © 2004 Wiley-VCH Verlag GmbH & Co. KGaA, Weinheim

dation processes ($E_p^{red} = -1.92$ V; $E_p^{ox} = -0.30$ V) which we have not attempted to characterize.

Reduction of 1⁺ in the Presence of Acid

The products of controlled-potential electrolyses of **1**$^+$ performed in THF and in MeCN electrolytes in the presence of acid (CF_3CO_2H, HTsO, HBF_4/H_2O) were the same as those obtained by protonation of **2** (Scheme 1). This suggested that **2** might be an intermediate in the reduction of **1**$^+$ in acidic media. However, when HTsO (in THF) or HBF_4/H_2O (in THF or in MeCN) were used, the same products as in Scheme 1 could also be obtained by controlled-potential reduction of **1**$^+$ at a potential where **2** could not be generated. The formation of these products by different pathways prompted us into a detailed investigation of the reduction mechanisms of **1**$^+$ in the presence of acid.

Addition of small amounts of HBF_4/H_2O (≤ 1 equiv.) to a solution of **1**$^+$ in THF/NBu_4PF_6 resulted in the presence of a new reversible reduction around -0.7 V. The corresponding current increased with increasing acid concentration. Comparison of the peak current of **1**$^+$ in the absence of acid (Figure 5, a) to that of the reversible system at $E_{1/2}^{red} = -0.7$ V in the presence of 1 equivalent of acid (Figure 5, b) showed that two electrons are involved in the latter reduction. This arises from the observation that complex **1** generated at the electrode is protonated to **2**$^+$, which is reducible at a less negative potential than **1**$^+$ (ECE process). The reversibility of the observed (overall) two-electron reduction and the intermediate position of its potential relative to those of the **1**$^+$/**1** and **2**$^+$/**2** couples indicates that the chemical step (protonation of **1**) is reversible and that an $EC_{rev}E$ mechanism is operative (Scheme 7, path B). In agreement with Scheme 7, compound **2**$^+$ can be generated almost quantitatively[18] by controlled-potential reduction of **1**$^+$ in the presence of 1 equivalent of HBF_4/H_2O (THF/NBu_4PF_6; $E_{el} = -0.9$ V; Pt or graphite cathode, electrolysis interrupted after the passage of 1 F mol^{-1} **1**$^+$) (Figure 6, b).

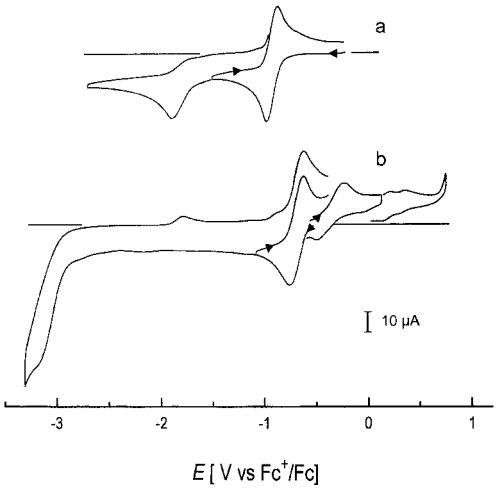

Figure 6. Cyclic voltammetry of $[Mo_2(Cp)_2(\mu\text{-}SMe)_3(\mu\text{-}O)]^+$ (**1**$^+$) (ca. 1.5 mM) a) before and b) after controlled-potential reduction ($E_{el} = -0.9$ V; $n = 1$ F·mol^{-1} **1**$^+$) in the presence of 1 equivalent of HBF_4/H_2O (see the solution in Figure 5,b) (THF/NBu_4PF_6; vitreous carbon electrode; scan rate $v = 0.2$ V·s^{-1}).

Further additions of HBF_4/H_2O (> 1 equiv.) to a THF solution of **1**$^+$ led to the increase of the quasi-reversible reduction of **2**$^{2+}$ at $E_{1/2}^{red} = -0.34$ V while the reversible couple was slightly suppressed (Figure 7). These obser-

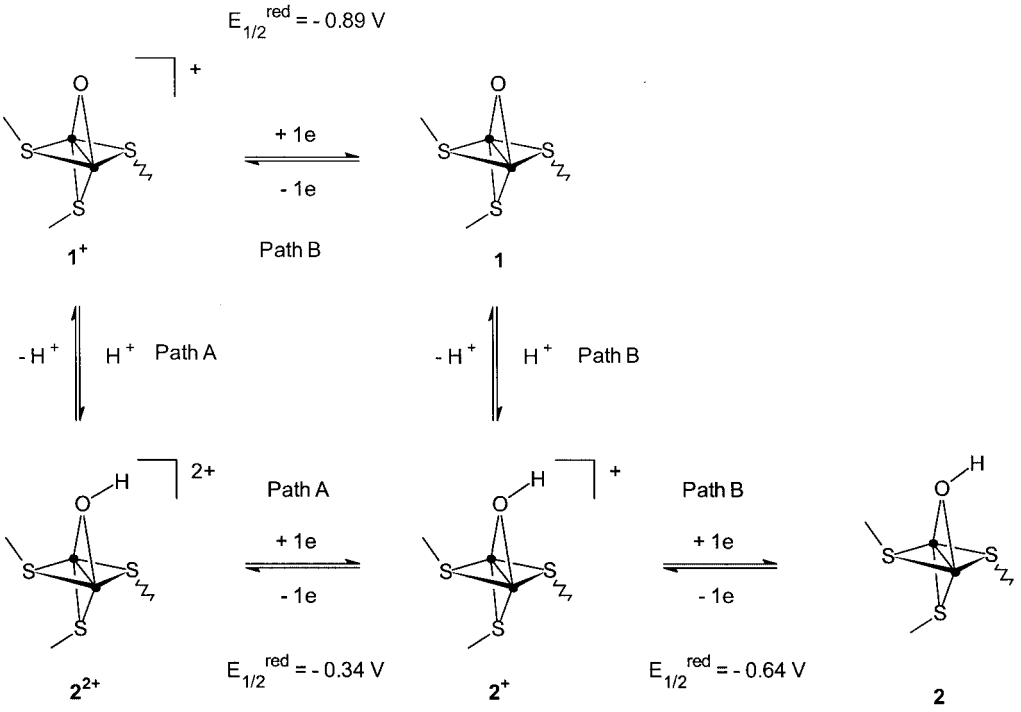

Scheme 7. • = Mo(Cp); methyl groups on the bridging S atoms are omitted

vations demonstrate that $\mathbf{1}^+$ can be protonated by HBF_4/H_2O in THF (Scheme 7, path A), which is reminiscent of the behavior of the imide analogue of $\mathbf{1}^+$ in acidic media, since protonation of the imide cation to the amide dication was also observed.[6] The protonation of $\mathbf{1}^+$ is reversible, since it is still possible to detect the irreversible oxidation of $\mathbf{1}^+$ in the presence of acid, with little modification of the corresponding peak current. The first steps of the reduction mechanism of $\mathbf{1}^+$ in the presence of HBF_4/H_2O are presented in Scheme 7. We believe that the reactions of $\mathbf{2}^+$ with substrates, which are depicted as hydrogen atom transfers in Scheme 5, actually arise from the acid-base equilibrium in Scheme 7, path B. Complex **1** formed by deprotonation of $\mathbf{2}^+$ would be oxidized by $\mathbf{2}^+$ in a homogeneous redox reaction ($E_{1/2}^{red}$ $\mathbf{2}^+ = -0.64$ V; $E_{1/2}^{ox}$ **1** $= -0.89$ V) producing **2** and $\mathbf{1}^+$. Protonation of **2** would then afford the μ-aqua intermediate (Scheme 8). The overall reaction in Scheme 8 is equivalent to the equilibrium in Scheme 5.

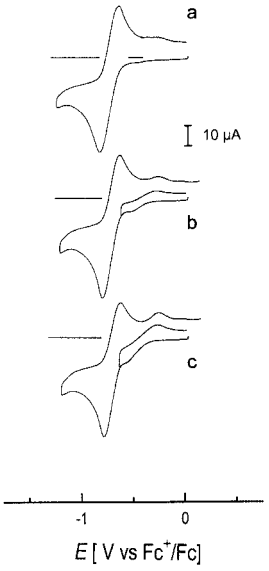

Figure 7. Cyclic voltammetry of $[Mo_2(Cp)_2(\mu\text{-}SMe)_3(\mu\text{-}O)]^+$ ($\mathbf{1}^+$) (ca. 1.4 mM) in the presence of a) 1 equivalent, b) 2 equivalents, and c) 3 equivalents of HBF_4/H_2O (THF/NBu_4PF_6; vitreous carbon electrode; scan rate $v = 0.2$ V·s^{-1}).

In addition to the increase of the $\mathbf{2}^{2+}/\mathbf{2}^+$ quasi-reversible reduction, addition of acid (> 2 equiv. HBF_4/H_2O) causes a gradual loss of reversibility of the two-electron reduction around −0.7 V, with $(i_p^a/i_p^c) < 1$ at slow scan rates. This shows the occurrence after the $EC_{rev}E$ mechanism of other chemical step(s) which eventually lead to $\mathbf{6}^+$. Controlled-potential electrolysis of $\mathbf{1}^+$ performed at −0.9 V (Pt cathode; $n = 2.2\pm0.2$ F·mol^{-1} $\mathbf{1}^+$ [32]) in the presence of an excess (> 3 equiv.) of HBF_4/H_2O effectively produces $\mathbf{6}^+$, characterized by two one-electron oxidation steps and by an irreversible reduction (Table 1). Electrolyses carried out at −0.5 V, a potential which does not permit the reduction of $\mathbf{2}^+$, also produced $\mathbf{6}^+$ after transfer of ca 2 F·mol^{-1} $\mathbf{1}^+$.[32] Under the latter conditions the formation of $\mathbf{6}^+$ occurs exclusively via reduction of $\mathbf{2}^{2+}$ and subsequent protonation of $\mathbf{2}^+$ (Schemes 7 and 9, path A). We have checked, in separate experiments, that addition of HBF_4/H_2O to a solution of $\mathbf{2}^+$ effectively produces $\mathbf{6}^{2+}$. The different mechanisms leading to the formation of the product, $\mathbf{6}^+$, are described by Schemes 7 and 9.

We have already mentioned that oxidation of $\mathbf{6}^+$ occurs according to an EC_{rev} process where the chemical step is a proton transfer. This protonation equilibrium (between $\mathbf{2}^+$

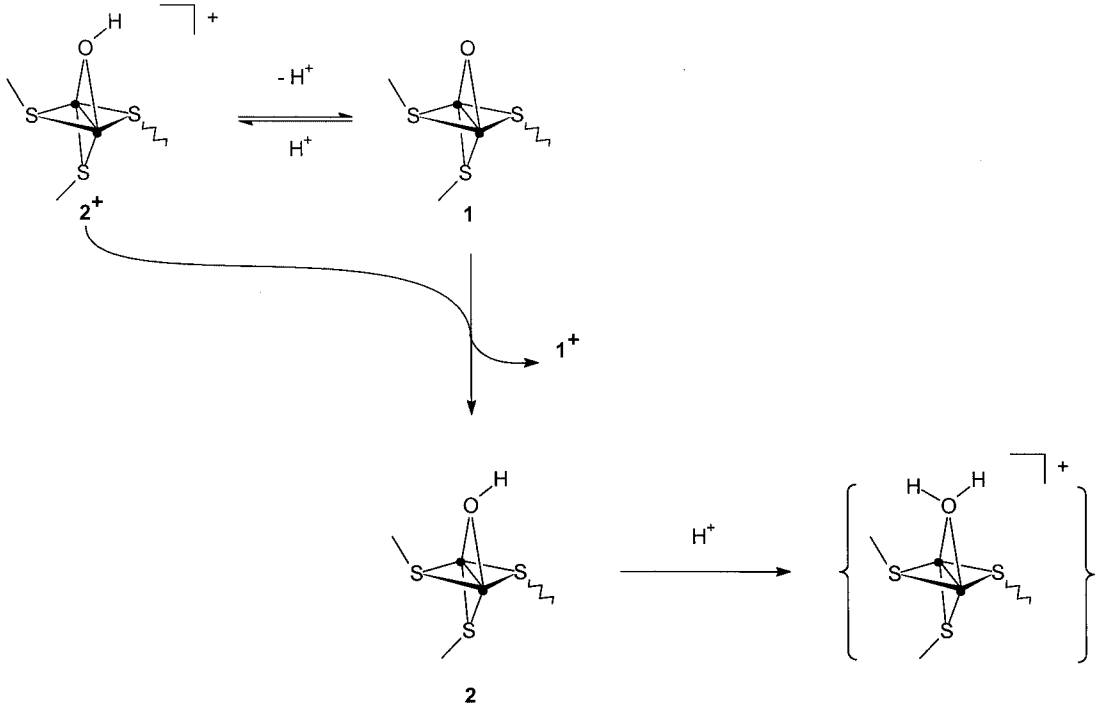

Scheme 8. • = Mo(Cp); methyl groups on the bridging S atoms are omitted

 © 2004 Wiley-VCH Verlag GmbH & Co. KGaA, Weinheim

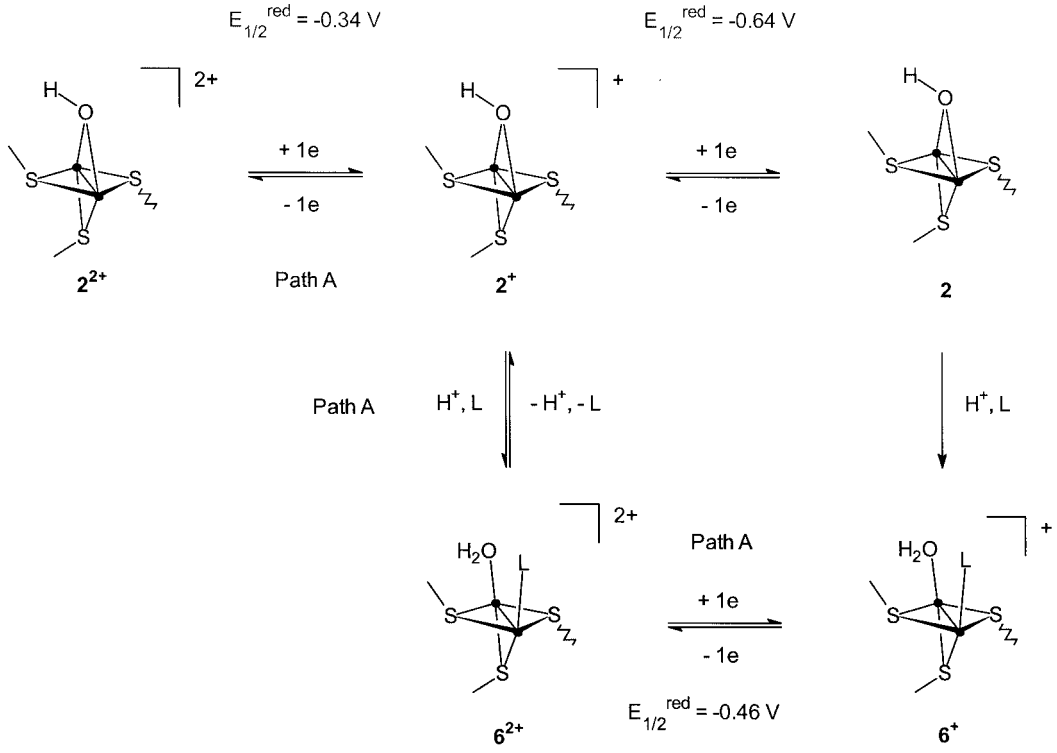

Scheme 9. • = Mo(Cp); methyl groups on the bridging S atoms are omitted

and $\mathbf{6}^{2+}$) is entirely consistent with the results of the electrochemical study of the reduction of $\mathbf{1}^{+}$ in the presence of HBF_4 (Scheme 9).

The electrochemical reduction of $\mathbf{1}^{+}$ in the presence of HBF_4/H_2O in MeCN follows the same type of mechanism as in THF (Schemes 7 and 9), except that the products $\mathbf{6}^{2+}$ and $\mathbf{6}^{+}$ are replaced by $\mathbf{5}^{2+}$ and $\mathbf{5}^{+}$, respectively.

In the presence of trifluoroacetic acid (2 equiv.; THF/NBu_4PF_6), the CV of $\mathbf{1}^{+}$ also shows a reversible overall two-electron reduction with $E_{1/2}^{red} = -0.72$ V, indicative of an $EC_{rev}E$ mechanism (see Scheme 6, Figure 8, a). The decrease of the anodic-to-cathodic peak current ratio $[(i_p^a/i_p^c)^{red}]$ with decreasing scan rates demonstrates that the $EC_{rev}E$ process is followed by one or more further chemical steps. Consistent with this observation, two reversible one-electron oxidations were detected at $E_{1/2}^{ox1} = -0.35$ V (Figure 8, a) and $E_{1/2}^{ox2} = 0.35$ V (not shown on Figure 8, a) on the reverse scan. These are due to $[Mo_2(Cp)_2(\mu\text{-}SMe)_3(\mu\text{-}\eta^1,\eta^1\text{-}OCOCF_3)]$ (**3**) as is evident by comparison with the redox potentials of an authentic sample of this complex. Controlled-potential electrolysis performed under these conditions at the potential of the reduction step (Pt cathode, 1.6 F·mol^{-1} $\mathbf{1}^{+}$) produced **3** almost quantitatively[18] (Figure 8, b). The nature of the product was confirmed by comparison of the ^1H and ^{19}F NMR spectra of the solid isolated from the catholyte to those of an authentic sample of **3** prepared independently and characterized crystallographically (see below).

The reduction of $\mathbf{1}^{+}$ in the presence of HTsO was also investigated. Addition of 1 equivalent of acid resulted in the

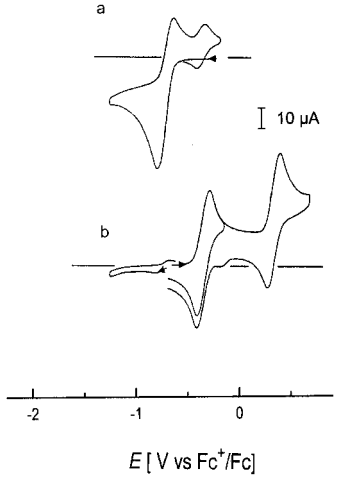

Figure 8. Cyclic voltammetry of $[Mo_2(Cp)_2(\mu\text{-}SMe)_3(\mu\text{-}O)]^{+}$ ($\mathbf{1}^{+}$) (ca. 1.4 mM) in the presence of 2 equivalents CF_3CO_2H a) before, and b) after controlled-potential reduction at −0.95 V (1.6 F·mol^{-1} $\mathbf{1}^{+}$) (THF/NBu_4PF_6; vitreous carbon electrode; scan rate $v = 0.2$ V·s^{-1})

presence of a reduction peak at −0.68 V. Comparison of the corresponding current with that of $\mathbf{1}^{+}$ in the absence of acid indicated that more than one electron is involved in the process. In contrast with the CV recorded in the presence of 1 equivalent of HBF_4/H_2O or CF_3CO_2H, the reduction is not fully reversible $[(i_p^a/i_p^c) < 1]$ and the redox systems of **4** were detected on the return scan. This is again consistent with an initial $EC_{rev}E$ mechanism, but in this case the prod-

 © 2004 Wiley-VCH Verlag GmbH & Co. KGaA, Weinheim

uct-forming reaction subsequent to the electrochemical process is faster than in previous examples. This might be due to two factors: (i) formation of the product requires less rearrangement for **4** than it does, for example, for **3** and (ii) formation of **4** is faster than that of $\mathbf{6}^+$ due to either a concerted attack of HTsO on **2** (and/or $\mathbf{2}^+$) or to a faster binding to the μ-aqua intermediate (see above) of TsO^- compared with L (L = H_2O or THF).

Controlled-potential electrolysis of $\mathbf{1}^+$ in the presence of 2 equivalents of HTsO produced **4** quantitatively[18] after transfer of ca 2 $F\cdot mol^{-1}$ $\mathbf{1}^+$. Since protonation of $\mathbf{2}^+$ by HTsO afforded $\mathbf{4}^+$ (Figure 4), two different pathways (similar to paths A and B in Scheme 9) can be followed. Evidence for the formation of $\mathbf{4}^+$ was obtained by voltammetry at the rotating disc electrode of the catholyte after the electrolysis was interrupted after passage of 1 $F\cdot mol^{-1}$ $\mathbf{1}^+$: this showed the presence of both **4** and $\mathbf{4}^+$ in the solution.

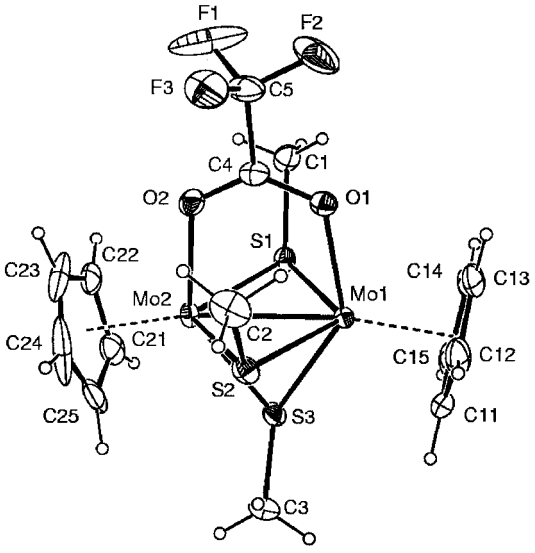

Figure 9. The molecular structure of $[Mo_2(cp)_2(\mu\text{-}SMe)_3(\mu\text{-}\eta^1,\eta^1\text{-}OCOCF_3)]$ (**3**) showing 20% ellipsoids

Solid State Structure of $[Mo_2(Cp)_2(\mu\text{-}SMe)_3(\mu\text{-}\eta^1,\eta^1\text{-}OCOCF_3)]$ (3)

The results of a single-crystal X-ray diffraction study of **3** (Figure 9, Table 2) confirmed the molecular structure proposed on the basis of the spectroscopic and analytical data presented in the Experim. Section. In particular, they demonstrate that the μ-hydroxo ligand in **2** has been replaced by a bridging trifluoroacetate group in **3**.

In the structure of **3** the two molybdenum atoms [Mo−Mo = 2.709(1) Å] are linked by four bridging ligands: three methylthiolates and a trifluoroacetate group. Each metal atom thereby attains a four-legged piano-stool coordination. This dinuclear structure is of a novel type in as much as that structurally characterized μ-carboxylato−Mo_2^{III} species are usually triply-bridged compounds with long Mo−Mo bonds e.g. in $[\{Mo_2(NC_6H_4CH_3)(S_2POEt_2)\}_2(\mu\text{-}S)(\mu\text{-}SR)(\mu\text{-}O_2CCF_3)]$ (R = H, Me),[33] and $[L_2Mo_2(\mu\text{-}O)(\mu\text{-}O_2CCH_3)_2]^{2+}$ (L = *N*,*N*′,*N*′′-trimethyl-1,4,7-triazacyclononane)[34] the Mo−Mo distances are 2.839(2), 2.844(1), and 2.885(1) Å, respectively. The Mo−Mo bond in the quadruply-bridged dinuclear molybdenum(IV) complex $[(Cp^*Mo)_2(\mu\text{-}O_2CMe)_2(\mu\text{-}PMe_2)(\mu\text{-}CH_3)]$ [Mo−Mo = 2.845(1) Å][35] is also significantly longer than that in **3**. However, Poli et al. recently reported a short Mo−Mo bond of 2.553(1) Å in the quadruply-bridged molybdenum(IV) complex $[(Cp^*Mo)_2(\mu\text{-}O)_2(\mu\text{-}O_2CMe)_2]$;[36] this contrasts with the long Mo−Mo bond [2.799(4) Å] found in the related triply-bridged molybdenum(IV) compound $[(Cp^*MoCl)_2(\mu\text{-}O)(\mu\text{-}Cl)(\mu\text{-}O_2COH)]$.[37] Metal−metal bonds in comparable thiolato-bridged bimetallic anions $[\{Mo(CO)_3\}_2(\mu\text{-}SR)_2(\mu\text{-}O_2CR')]^-$ {R = C_6H_5, *p*-ClC_6H_4; R′ = CMe_3, CF_3, $C(Me)=CH_2$}[38] where the molybdenum atoms are in low oxidation states (e.g. I) are much longer (ca. 2.91 Å) than that in **3**. It is clear, then, that the oxidation states of the metal atoms and the number and size of the bridging groups all play a part in bringing about the large variations

Table 2. Selected distances (Å) and angles (deg.) for $[Mo_2(cp)_2(\mu\text{-}SMe)_3(\mu\text{-}\eta^1,\eta^1\text{-}OCOCF_3)]$ (**3**)

Mo(1)−Mo(2)	2.709(1)	Mo(2)−O(2)	2.173(3)
Mo(1)−O(1)	2.174(3)	Mo(2)−S(1)	2.443(1)
Mo(1)−S(1)	2.430(1)	Mo(2)−S(2)	2.447(1)
Mo(1)−S(2)	2.446(1)	Mo(2)−S(3)	2.421(1)
Mo(1)−S(3)	2.429(1)	O(2)−C(4)	1.245(5)
O(1)−C(4)	1.258(5)	C(4)−C(5)	1.533(6)
Mo(2)−S(1)−Mo(1)	67.5(1)	O(2)−Mo(2)−Mo(1)	83.9(1)
Mo(2)−S(2)−Mo(1)	67.2(1)	O(2)−Mo(2)−S(1)	85.3(1)
Mo(2)−S(3)−Mo(1)	67.9(1)	O(2)−Mo(2)−S(2)	84.2(1)
O(1)−Mo(1)−Mo(2)	84.0(1)	O(2)−Mo(2)−S(3)	140.0(1)
O(1)−Mo(1)−S(1)	85.6(1)	C(4)−O(1)−Mo(1)	121.8(3)
O(1)−Mo(1)−S(2)	84.0(1)	C(5)−O(2)−Mo(2)	122.3(2)
O(1)−Mo(1)−S(3)	139.9(1)	O(1)−C(4)−O(2)	128.0(4)
O(1)−C(4)−C(5)	116.5(4)	O(2)−C(4)−C(5)	115.5(4)
O(1)−Mo(1)−Mo(2)−O(2)	0.2(1)	O(1)−Mo(1)−Mo(2)−S(3)	178.5(1)
O(1)−Mo(1)−Mo(2)−S(2)	−86.8(1)	O(1)−Mo(1)−Mo(2)−S(1)	88.7(1)

 © 2004 Wiley-VCH Verlag GmbH & Co. KGaA, Weinheim

in the Mo-Mo distances found in these μ-carboxylato complexes.[33,38]

The mean Mo−S bond length in **3** (2.436 Å) is comparable with values for other acetato−thiolato-bridged compounds, such as $[\{Mo_2(NC_6H_4CH_3)(S_2POEt_2)\}_2(\mu\text{-}S)(\mu\text{-}SR)(\mu\text{-}O_2CCF_3)]$,[33] and $[\{Mo(CO)_3\}_2(\mu\text{-}SR)_2(\mu\text{-}O_2CR')]^-$[38] (average 2.456 Å). However, the shorter Mo−Mo bond in **3** requires the Mo−S−Mo angles to be more acute (average 67.5°) than those in the above mentioned compounds (average 72.0°).[33,38] The structural features of the CF_3CO_2 ligand, in particular the nearly equal C(4)−O(1) and C(4)−O(2) bond lengths of 1.258(5) and 1.245(5) Å, are unexceptional[33−38] and indicate π-electron delocalization over the O(1), O(2), and C(4) atoms. The Mo−O distances of 2.174(3) and 2.173(3) Å indicate single bonds. They are significantly shorter than values in neutral, triply-bridged dimolybdenum(III) complexes with acetate ligands (average 2.267 Å),[33] but are close to those in neutral, quadruply-bridged dimolybdenum(IV) compounds (average 2.161 Å).[36]

The heavy atom skeleton of **3**, excluding C3 and F1−F3, has approximate mirror symmetry: none of the nine atoms Mo1, Mo2, S3, O1, O2, C4, C5, C13, and C23 lie more than 0.04 Å from their common plane.

Conclusion

This work has illustrated the reactivity both of bridging oxo and hydroxo ligands in acidic media and of aqua ligands. It leads to four main conclusions.

(A) We have shown that protonation at a μ-OH ligand in a dimolybdenum complex is possible. Depending on the conditions (nature of the conjugate base, presence of a π-acid ligand L), the product can either retain the protonated OH bridge as a terminally bonded H_2O ligand or give rise to a disubstituted complex after elimination of a water molecule. It follows that protonation of $[Mo_2(Cp)_2(\mu\text{-}SMe)_3(\mu\text{-}OH)]$ gives ready access to one or more coordination sites at the metal centers.

(B) The reactivity of $\mathbf{2}^+$, due to its amphoteric nature, is also quite rich. Protonation of $\mathbf{2}^+$ by HTsO or HBF_4/H_2O in THF produces $\mathbf{4}^+$ or $\mathbf{6}^{2+}$, respectively. On the other hand, the products obtained on addition of CF_3CO_2H to $\mathbf{2}^+$, that is $\mathbf{1}^+$ and **3**, result from the reaction of the trifluoroacetate anion with the μ-aqua complex (see Scheme 5), rather than from protonation of the μ-hydroxo cation. The equilibrium in Scheme 5, which is formally a hydrogen atom transfer, could result from an acid-base equilibrium between $\mathbf{2}^+$ and **1**, coupled to a redox reaction between these species (Scheme 8).

(C) Both the oxo cation, $\mathbf{1}^+$, and its reduced form, **1**, can be protonated. The difference in pK_a between the $\mathbf{2}^{2+}$ and $\mathbf{2}^+$ forms can be estimated from the thermochemical cycle in Scheme 7. This ΔpK_a value, which is approximate because of the quasi-reversible nature of the $\mathbf{2}^{2+}/\mathbf{2}^+$ couple, is around 11 units in MeCN [$E_{1/2}(\mathbf{2}^{2+}/\mathbf{2}^+) = -0.24$ V; $E_{1/2}(\mathbf{1}^+/\mathbf{1}) = -0.89$ V] and about 9 units in THF [$E_{1/2}(\mathbf{2}^{2+}/\mathbf{2}^+) = -0.34$ V; $E_{1/2}(\mathbf{1}^+/\mathbf{1}) = -0.89$ V]. Similarly, the ΔpK_a between the $\mathbf{2}^+$ and **2** forms can be estimated using the redox potentials of the $\mathbf{2}^+/\mathbf{2}$ and $\mathbf{1}/\mathbf{1}^-$ reduction steps; in this case, ΔpK_a is about 20 units. Although this figure is at best a rough estimate since the $\mathbf{1}/\mathbf{1}^-$ irreversible reduction is shifted from the thermodynamic potential, it nevertheless illustrates the dramatic effect of the metal core oxidation state on the acidity of the μ-OH proton.

Since $\mathbf{1}^+$ can be protonated by HBF_4/H_2O to give $\mathbf{2}^{2+}$ it is possible to generate coordination sites (and access to $\mathbf{6}^+$ or products derived therefrom) at a potential ca 0.4 V less negative than would be required in the absence of such a protonation step. This conclusion is important for any consideration of biological processes involving redox enzymes since the range of potentials accessible to natural reductants is restricted.

(D) We have also shown that electrochemical reduction of a species containing a terminal aqua ligand leads to a hydroxo bridge (with elimination of a hydrogen atom). Oxidation of a compound containing terminally bonded water also affords a bridging hydroxide after the release of a proton. This kind of redox-induced reactivity at a terminal aqua ligand could also be relevant to different types of enzyme-driven reactions.

Experimental Section

Methods and Materials: All the experiments were carried out under an inert atmosphere using Schlenk techniques for the syntheses. Tetrahydrofuran (THF) was purified as described previously.[6] Acetonitrile (Merck, HPLC grade) was used as received. The acids, *p*-toluenesulfonic (Prolabo), trifluoroacetic (Aldrich), fluoroboric (diethyl ether complex and aqueous solution, Aldrich), were used as received. The preparation and purification of the supporting electrolyte NBu_4PF_6 and the configuration of the electrochemical equipment were as described previously.[6] All the potentials (text, tables, figures) are quoted relative to the ferrocene−ferrocenium couple. Ferrocene was added as an internal standard at the end of the experiments. ^1H NMR spectra were recorded on a Bruker AC300 spectrometer. Shifts are relative to tetramethylsilane as an internal reference. Chemical analyses were carried out at the Centre de Microanalyses du CNRS, Vernaison. Complexes $[Mo_2(Cp)_2(\mu\text{-}SMe)_3(\mu\text{-}O)]^+$ ($\mathbf{1}^+$), $[Mo_2(Cp)_2(\mu\text{-}SMe)_3(\mu\text{-}OH)]$ (**2**), and $[Mo_2(Cp)_2(\mu\text{-}SMe)_3(L)_2]^+$ were synthesized as described previously.[4,10,19]

Synthesis of $[Mo_2(Cp)_2(\mu\text{-}SMe)_3(\mu\text{-}\eta^1,\eta^1\text{-}OCOCF_3)]$ (3): $[Mo_2(cp)_2(\mu\text{-}SMe)_3(MeCN)_2][BF_4]$ (100 mg, 0.158 mmol) and a 0.346 M solution (450 μL of) of $Et_4NCF_3CO_2/H_2O$ prepared by neutralization of a THF solution of CF_3CO_2H by Et_4NOH (40% in methanol) were added to THF (20 mL). After stirring for 5 minutes the dark red solution was evaporated to dryness. The residue was stirred with pentane (100 mL), the dark red solution was filtered, and pentane was evaporated under vacuum. After stirring in cold pentane and elimination of the solvent by filtration, the solid was vacuum dried. Yield 80 mg (0.139 mmol, 88%). C,H analysis for $C_{15}H_{19}O_2F_3S_3Mo_2$ (575.8): calcd. C, 31.3, H 3.3; found C 31.6, H 3.4. ^1H NMR, $(CD_3)_2CO$: δ = 5.36 (s, 10 H, C_5H_5), 1.53 (s, 3 H, SCH_3),1.38 (s, 3 H, SCH_3), 1.32 (s, 3 H, SCH_3). ^{19}F NMR $(CD_3)_2CO$: −73.9 (CF_3CO_2).

 © 2004 Wiley-VCH Verlag GmbH & Co. KGaA, Weinheim

X-ray Analysis: Crystals of $[Mo_2(Cp)_2(\mu\text{-}SMe)_3(\mu\text{-}\eta^1,\eta^1\text{-}OCOCF_3)]$ (**3**) were obtained at room temperature from a pentane solution. Measurements were made with a plate-shaped crystal, 0.30 × 0.30 × 0.03 mm, on a Nonius CAD4 diffractometer with Mo-K_α X-rays, λ = 0.71073 Å. Intensities were estimated from ω/2θ scans and corrected empirically for absorption from ψ-scans (transmission factors 0.640−0.953). The structure was solved by Patterson methods and refined by full-matrix least-squares on F^2 using all independent reflections with $2\theta < 60°$.[39] Hydrogen atoms rode on their parent carbon atoms. A single orientation parameter was refined for each methyl group.

Crystal data for **3**, $C_{15}H_{19}F_3Mo_2O_2S_3$; M = 576.36, monoclinic, space group $P2_1/c$, a = 12.8796(5), b = 9.0131(5), c = 16.8558(5) Å, β = 91.411(3)°, V = 1956.11(14) Å^3, Z = 4, T = 20 °C, $\rho_{calcd.}$ = 1.957 g cm^{-3}, μ(Mo-K_α) = 1.636 mm^{-1}, F(000) = 1136, 7166 reflections collected, 5675 unique (R_{int} = 0.0240), 229 parameters refined, $R1$ = 0.0705 and $wR(F^2)$ = 0.0903 over all 5675 data used in refinement. Extreme Δρ values: 0.79−0.67 e·Å^{-3}.

CCDC-216408 contains the supplementary crystallographic data for this paper. These data can be obtained free of charge via www.ccdc.cam.ac.uk/conts/retrieving.html or from the Cambridge Crystallographic Data Center, 12 Union Road, Cambridge CB2 1EZ, UK; Fax: + 44-1223-336-033; or E-mail: deposit@ccdc.cam.ac.uk.

Acknowledgments

The authors thank the CNRS (France), the EPSRC (UK), Université de Bretagne Occidentale and Glasgow University for financial support. The Conseil Régional de Bretagne is acknowledged for financial support of this work (PRIR, Operation n° 98CCO9) and for providing a studentship to M. L. H.

[1] F. Y. Pétillon, P. Schollhammer, J. Talarmin, K. W. Muir, *Coord. Chem. Rev.* **1998**, *178−180*, 203−247.
[2] P. Madec, K. W. Muir, F. Y. Pétillon, R. Rumin, Y. Scaon, P. Schollhammer, J. Talarmin, *J. Chem. Soc., Dalton Trans.* **1999**, 2371−2383.
[3] P. Schollhammer, E. Guénin, F. Y. Pétillon, J. Talarmin, K. W. Muir, D. S. Yufit, *Organometallics* **1998**, *17*, 1922−1924.
[4] F. Barrière, Y. Le Mest, F. Y. Pétillon, S. Poder-Guillou, P. Schollhammer, J. Talarmin, *J. Chem. Soc., Dalton Trans.* **1996**, 3967−3976.
[5] F. Y. Pétillon, P. Schollhammer, J. Talarmin, *J. Chem. Soc., Dalton Trans.* **1997**, 4019−4024.
[6] J. Y. Cabon, C. Le Roy, K. W. Muir, F. Y. Pétillon, F. Quentel, P. Schollhammer, J. Talarmin, *Chem. Eur. J.* **2000**, *6*, 3033−3042.
[7] F. Y. Pétillon, P. Schollhammer, J. Talarmin, K. W. Muir, *Inorg. Chem.* **1999**, *38*, 1954−1955; N. Le Grand, K. W. Muir, F. Y. Pétillon, C. J. Pickett, P. Schollhammer, J. Talarmin, *Chem. Eur. J.* **2002**, *8*, 3115−3127.
[8] P. Schollhammer, N. Cabon, J. F. Capon, F. Y. Pétillon, J. Talarmin, K. W. Muir, *Organometallics* **2001**, *20*, 1230−1242.
[9] P. Schollhammer, M. Pichon, K. W. Muir, F. Y. Pétillon, R. Pichon, J. Talarmin, *Eur. J. Inorg. Chem.* **1999**, 221−223.
[10] P. Schollhammer, M. Le Hénanf, C. Le Roy-Le Floch, F. Y. Pétillon, J. Talarmin, K. W. Muir, *J. Chem. Soc., Dalton Trans.* **2001**, 1573−1577.
[11] S. J. Lippard, *Angew. Chem. Int. Ed. Engl.* **1988**, *27*, 344−361; D. M. Kurtz, Jr., *Chem. Rev.* **1990**, *90*, 585−606; R. Than, A. A. Feldmann, B. Krebs, *Coord. Chem. Rev.* **1999**, *182*, 211−241; E. I. Solomon, *Inorg. Chem.* **2001**, *40*, 3656−3669.
[12] M. N. Collomb Dunand-Sauthier, A. Deronzier, A. Piron, *J. Electroanal. Chem.* **1999**, *463*, 119−122; M. N. Collomb, A. Deronzier, A. Richardot, J. Pécaut, *New J. Chem.* **1999**, *23*, 351−353.
[13] T. Tanase, N. Takeshita, S. Yano, I. Kinoshita, A. Ichimura, *New J. Chem.* **1998**, 927−929; T. Tanase, N. Takeshita, C. Inoue, M. Kato, S. Yano, K. Sato, *J. Chem. Soc., Dalton Trans.* **2001**, 2293−2302.
[14] Y. Sasaki, M. Suzuki, A. Nagasawa, A. Tokiwa, M. Ebihara, T. Yamagushi, C. Kabuto, T. Ochi, T. Ito, *Inorg. Chem.* **1991**, *30*, 4903−4908; A. Kikuchi, T. Fukumoto, K. Umakoshi, Y. Sasaki, A. Ichimura, *J. Chem. Soc., Chem. Commun.* **1995**, 2125−2126; T. Fukumoto, A. Kikuchi, K. Umakoshi, Y. Sasaki, *Inorg. Chim. Acta* **1998**, *283*, 151−159.
[15] K. Wieghardt, U. Bossek, A. Neves, B. Nuber, J. Weiss, *Inorg. Chem.* **1989**, *28*, 432−440; K. Wieghardt, M. Guttmann, P. Chaudhuri, W. Gebert, M. Minelli, C. G. Young, J. H. Enemark, *Inorg. Chem.* **1985**, *24*, 3151−3155.
[16] V. R. Ott, F. A. Schultz, *J. Electroanal. Chem.* **1975**, *59*, 47−60; V. R. Ott, F. A. Schultz, *J. Electroanal. Chem.* **1975**, *61*, 81−98; V. R. Ott, D. S. Swieter, F. A. Schultz, *Inorg. Chem.* **1977**, *16*, 2538−2545.
[17] M. B. Gomes de Lima, J. E. Guerchais, R. Mercier, F. Y. Pétillon, *Organometallics* **1986**, *5*, 1952−1964.
[18] The yield of the reaction of **2** with different acids was calculated by comparing the peak current of the reactant with that of the product, assuming identical diffusion coefficients. Similar procedures were used to estimate the yield of controlled-potential electrolyses, or that of the reaction of **4** or **6**$^+$ with different substrates.
[19] N. Cabon, E. Paugam, F. Y. Pétillon, P. Schollhammer, J. Talarmin, K. W. Muir, *Organometallics* **2003**, *22*, 4178−4180.
[20] The parameters i_p and E_p are the peak current and the peak potential of a redox process, respectively; $E_{1/2} = (E_p^a + E_p^c)/2$; E_p^a, i_p^a and E_p^c, i_p^c are the potential and the current of the anodic and of the cathodic peak of a reversible process, respectively; $\Delta E_p = E_p^a - E_p^c$; k_e (in cm/s) is the rate constant of the heterogeneous electron-transfer; an EC process comprises an electron-transfer step (E) followed by a chemical reaction (C). CV and CPE stand for cyclic voltammetry and controlled-potential electrolysis, respectively; v (V/s) is the scan rate in CV experiments.
[21] A. J. Bard, L. R. Faulkner, *Electrochemical Methods. Fundamentals and Applications*, Wiley, New York, **1980**, chapter 11, pp. 429−485; E. R. Brown, R. F. Large, in: *Techniques of Chemistry*, Volume I − *Physical Methods of Chemistry*, Part IIA (Ed.: A. Weissberger), Wiley, **1971**, chapter 6, pp. 423−530.
[22] W. H. Baur, K. Wieghardt, *J. Chem. Soc., Dalton Trans.* **1973**, 2669−2674.
[23] J. D. Edwards, K. Wieghardt, A. G. Sykes, *J. Chem. Soc., Dalton Trans.* **1974**, 2198−2204.
[24] C. Grünwald, M. Laubender, J. Wolf, H. Werner, *J. Chem. Soc., Dalton Trans.* **1998**, 833−839.
[25] B. K. Das, A. R. Chakravarty, *Inorg. Chem.* **1991**, *30*, 4978−4986.
[26] T. Arliguie, B. Chaudret, G. Chung, F. Dahan, *Organometallics* **1991**, *10*, 2973−2977.
[27] D. Lee, P.-L. Hung, B. Spingler, S. J. Lippard, *Inorg. Chem.* **2002**, *41*, 521−531.
[28] The design of the electrochemical cell used throughout did not allow the detection of H_2 (a possible product of the oxidation of **2** by protons) because a dinitrogen or argon stream was continuously circulating over the solution during the experiments.
[29] This statement is made on the reasonable assumption that the diffusion coefficients of the μ-OH and μ-Cl complexes are similar.
[30] Y. Alias, S. K. Ibrahim, M. A. Queiros, A. Fonseca, J. Talarmin, F. Volant, C. J. Pickett, *J. Chem. Soc., Dalton Trans.* **1997**, 4807−4815.
[31] D. L. Hughes, M. Y. Mohammed, C. J. Pickett, *J. Chem. Soc., Chem. Commun.* **1988**, 1481−1482.

 © 2004 Wiley-VCH Verlag GmbH & Co. KGaA, Weinheim

[32] The fact that *n* is slightly larger than the theoretical value (2.0) when the electrolysis potential is −0.9 V can be attributed to the fact that small amounts of $\mathbf{2}^{+}$ produced by protonation of **2** (see Schemes 5 and 8) are reduced back to **2**. The extra charge consumed thus results in the reduction of H^{+} to H[28] via the $\mathbf{2}^{+}/\mathbf{2}$ couple. When the electrolysis is performed at a potential which does not allow the $\mathbf{2}^{+} \rightarrow \mathbf{2}$ reduction ($E_{el} = -0.5$V), the charge consumed is $n \leq 2$ F·mol^{-1} $\mathbf{1}^{+}$.
[33] M. E. Noble, J. C. Huffman, R. A. D. Wentworth, *Inorg. Chem.* **1983**, *22*, 1756−1760; M. E. Noble, K. Folting, J. C. Huffman, R. A. D. Wentworth, *Inorg. Chem.* **1984**, *23*, 631−634.
[34] A. Neves, U. Bossek, K. Wieghardt, B. Nuber, J. Weiss, *Angew. Chem. Int. Ed. Engl.* **1988**, *27*, 685−687.
[35] J. H. Shin, G. Parkin, *Chem. Commun.* **1998**, 1273−1274.
[36] F. Demirhan, P. Richard, R. Poli, *Inorg. Chim. Acta* **2003**, *347*, 61−66.
[37] F. Bottomley, J. Chen, *Organometallics* **1992**, *11*, 3404−3411.
[38] G.-H. Pan, B.-T. Zhuang, Q. Wei, Z.-F. Zhou, S.-Q. Peng, K.-C. Wu, J.-T. Chen, *Chinese J. Struct. Chem.* **2001**, *20*, 381−383; G. Pan, B. Zhuang, J. Chen, *Acta Crystallogr. Sect. C* **1999**, *55*, 298−300; G. Pan, B. Zhuang, J. Chen, *Acta Crystallogr. Sect. C* **1998**, *54*, 1580−1582.
[39] Programs used: *SHELX97* − Programs for Crystal Structure Analysis (Release 97−2). G. M. Sheldrick, Institut für Anorganische Chemie der Universität Göttingen, Tammanstrasse 4, 3400 Göttingen, Germany, **1998**, *WinGX* − A Windows Program for Crystal Structure Analysis: L. J. Farrugia, *J. Appl. Crystallogr.* **1999**, *32*, 837.
[40] Programs used for CV simulations: ESP (Electrochemical Simulations Package v. 2.4) from Carlo Nervi (http://lem. ch. unito. it/chemistry/esp manual. html) or Virtual CV 1.0 (available on the worldwide web as vTLCv10.zip) from André Laouénan.

Received October 7, 2003
Early View Article
Published Online March 5, 2004

 © 2004 Wiley-VCH Verlag GmbH & Co. KGaA, Weinheim

The First (Trisulfoxide)metal Complexes: Synthesis and Crystal Structures of the 1D Lanthanide Coordination Polymers $[Ln(L)(MeOH)(NO_3)_3]_n$ and $\{[La(L)(DMF)_5](ClO_4)_3\}_n$ [L = 1,3,5-Tris(ethylsulfinyl)-2,4,6-trimethylbenzene, Ln = La^{III} and Nd^{III}]

Jian-Rong Li,[a] Xian-He Bu,*[a,b] and Ruo-Hua Zhang[a]

Keywords: Coordination polymers / Helical structures / Lanthanides / Sulfoxide

A new trisulfoxide ligand, 1,3,5-tris(ethylsulfinyl)-2,4,6-trimethylbenzene (L), was designed and synthesized, and treated with $Ln(NO_3)_3$ or $Ln(ClO_4)_3$ to produce three coordination polymers: $[Ln(L)(MeOH)(NO_3)_3]_n$ [where Ln = La^{III} (**1**); Nd^{III} (**2**)] and $\{[La(L)(DMF)_5](ClO_4)_3\}_n$ (**3**). Solid-state structures of all three complexes were determined by single-crystal X-ray diffraction. The three complexes have 1D helical-chain structures and complexes **1** and **2** are isostructural. To the best of our knowledge, these coordination polymers are the first examples of (trisulfoxide)metal complexes.
(© Wiley-VCH Verlag GmbH & Co. KGaA, 69451 Weinheim, Germany, 2004)

Introduction

In recent years, much effort has been invested in attempts to design and synthesize metal-organic coordination polymers having specific network topologies and potential applicable properties.[1,2] In this regard, the studies performed by us and others[3] on the construction of coordination architectures using flexible disulfoxide ligands and metal ions as building blocks have acquired some interesting results. We are, therefore, interested in further exploiting the multisulfoxide ligands. Such ligands may produce interesting coordination polymers because of their multiple coordination modes. As a continuation of this study, we designed a new trisulfoxide ligand, 1,3,5-tris(ethylsulfinyl)-2,4,6-trimethylbenzene (L) (see structure shown below), which is a simple tridentate ligand. Since each S atom is an asymmetric center, the tridentate L molecule should be a chiral bridging ligand. Therefore, the ligand may be used to construct non-centric framework polymers (or chiral crystals). To the best of our knowledge, (trisulfoxide)metal complexes have not yet been reported and the lanthanide complexes presented here are the first structurally characterized examples of metal complexes with such ligands. Herein, we report the synthesis and crystal structures of three novel lanthanide complexes with L, $[Ln(L)(CH_3OH)(NO_3)_3]_n$ [where Ln = La (**1**); Nd, (**2**)] and $\{[La(L)(DMF)_5](ClO_4)_3\}_n$ (**3**).

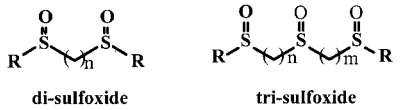

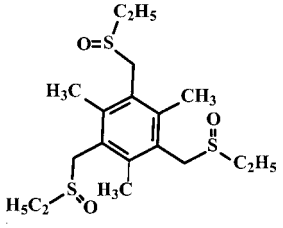

L

Results and Discussion

Synthesis and General Characterization

The ligand L was synthesized according to a similar method used for the synthesis of disulfoxide[4] and the product might have been a mixture containing several isomers of the trisulfoxides. The attempts for separation were not successful so the mixture was used directly to prepare the metal complexes. The IR data of L show the characteristic band of the sulfinyl group (S=O) at 1022 cm^{-1} and the C−S stretching vibration at 756 cm^{-1}.[5]

The complexes **1**−**3** were prepared by the reaction of L with $Ln(NO_3)_3{\cdot}nH_2O$ or $Ln(ClO_4)_3{\cdot}nH_2O$ in the presence of triethyl orthoformate (see Scheme 1). The complexes are soluble in DMF and DMSO, and slightly soluble in CH_3OH and CH_3CN, but almost insoluble in H_2O and acetone. The IR spectrum of each complex has a $\nu_{S=O}$ band at around 1000 cm^{-1}, which is shifted to a lower frequency than that of the free ligand (1022 cm^{-1}), indicating that the

[a] Department of Chemistry, Nankai University, Tianjin 300071, China
Fax: (internat.) +86-22-23502458
E-mail: buxh@nankai.edu.cn
[b] The State Key Laboratory of Rare Earth Materials Chemistry and Applications, Peking University, Beijing 100871, China

oxygen is coordinated to the Ln^{III} ions.[5] The existence of nitrate and perchlorate anions in the complexes was also confirmed by the IR spectra.

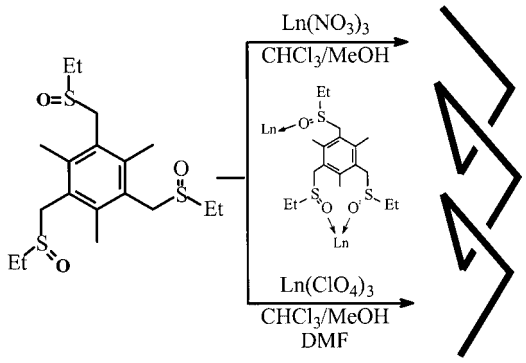

Scheme 1. Schematic representation of the formation of **1**−**3**

Description of the Crystal Structures

Complexes **1** and **2**, $[Ln(L)(CH_3OH)(NO_3)_3]_n$ [where Ln = La^{III} (**1**); Nd^{III} (**2**)], have isostructural, neutral helical-chain structures, with only minor differences in their geometry parameters, which reflect the normal lanthanide contraction. The coordination environments of the Ln^{III} centers in **1** and **2** are shown in Figure 1 (top, with **1** as a representative). Each Ln^{III} center is coordinated to three oxygen atoms of two distinct L ligands (one is mono-*O* and the other is chelating), six oxygen atoms of three bidentate nitrate groups and one oxygen atom of methanol to form a 4,4-bicapped square-antiprism geometry. Due to the small bite angle of the nitrate group, its oxygen atoms are closer than those of two independent L ligands, which makes their complexes have higher coordination numbers. In **1** and **2** the smallest chelating angles of the nitrate groups are 45.25° for **1** [O(9)−La(1)−O(7)] and 45.07° for **2** [O(32)−Nd(1)−O(31)]. Otherwise, one relatively short and one longer Ln−O (NO_3^-) bond [La(1)−O(9) = 2.629(6) Å and La(1)−O(7) = 2.926(7) Å for **1**, Nd(1)−O(32) = 2.541(6) Å and Nd(1)−O(31) = 2.947(6) Å for **2**] also show the binding of the oxygen atoms of this nitrate group, with the smaller chelating angle, to the Ln^{III} ions. In particular, for the La(1)−O(7) and Nd(1)−O(31) bonds, the interactions between the metal and the oxygen atom are week. The lengths of the bonds [2.436(6)−2.498(6) Å for **1** and 2.365(5)−2.437(5) Å for **2**] between the oxygen atoms of the sulfoxide moieties and the Ln^{III} ions are within the expected ranges and similar to those found in disulfoxide analogues,[3f] but significantly shorter than those of the nitrate groups [2.611(7)−2.926(7) Å for **1** and 2.541(6)−2.958(6) Å for **2**] or methanol [2.553(6) Å for **1** and 2.488(4) Å for **2**] in the same complex.

In **1** and **2**, each L links two adjacent Ln^{III} ions to form a 1D helical chain and the shortest Ln···Ln intrachain distance is 11.113 Å for **1** and 11.017 Å for **2**, as shown in Figure 1 (middle). In the chain the alternating Ln centers are located in a straight line and the alternating phenyl groups of the ligands are parallel to each other, while the

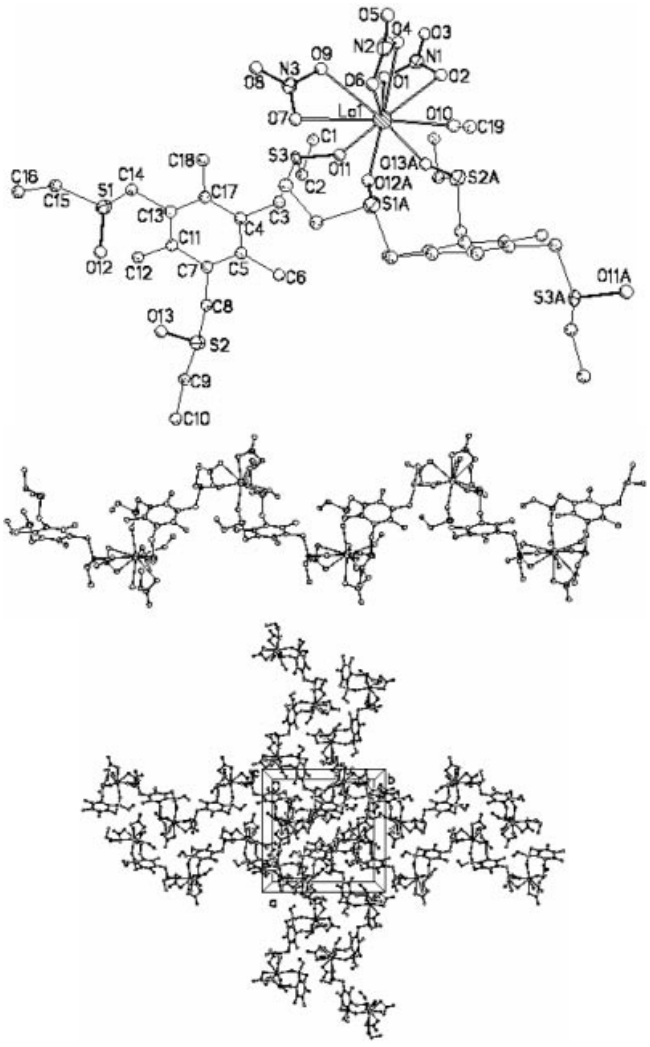

Figure 1. (Top) View of **1** showing the coordination environment of the center ion, (middle) the helical-chain structures of **1** (or **2**) and (bottom) crystal packing diagram in **1** (or **2**), only one position of the disordered sets of S atoms is shown

dihedral angle between two adjacent phenyl planes (namely, around one Ln center) is 66.6° for **1** and 64.5° for **2**, respectively. The 1D helical chain is related by a 4_1 helical axis, which passes through the alternating Ln^{III} ions. Furthermore, in the crystal packing of **1** and **2** the 1D chains are arranged parallel to each other in the *a* and *b* directions, respectively, to form planes. However, the chains in the adjacent planes are perpendicular to each other (see Figure 1 bottom).

The structure of **3** ($\{[La(L)(DMF)_5](ClO_4)_3\}_n$) consists of cationic, helical chains and perchlorate anions. Each chain contains the structural units $[La(L)(DMF)_5]^{3+}$, which are linked by L bridges. In each $[La(L)(DMF)_5]^{3+}$ unit, the La^{III} center is coordinated to eight oxygen atoms, of which three from two distinct L ligands and five from DMF (see Figure 2 top). The geometry of the La center approximates to a square antiprism. In **3** the La−O bond lengths are in the range of 2.4506(2)−2.5806(2) Å and are in the normal La−O bond-length range of eight-coordinate La^{III} com-

 © 2004 Wiley-VCH Verlag GmbH & Co. KGaA, Weinheim

plexes. The three distances of La−O(L) are basically equal and the average value is 2.4713(5) Å, which is slightly longer than that in **1** [2.4573(6) Å].

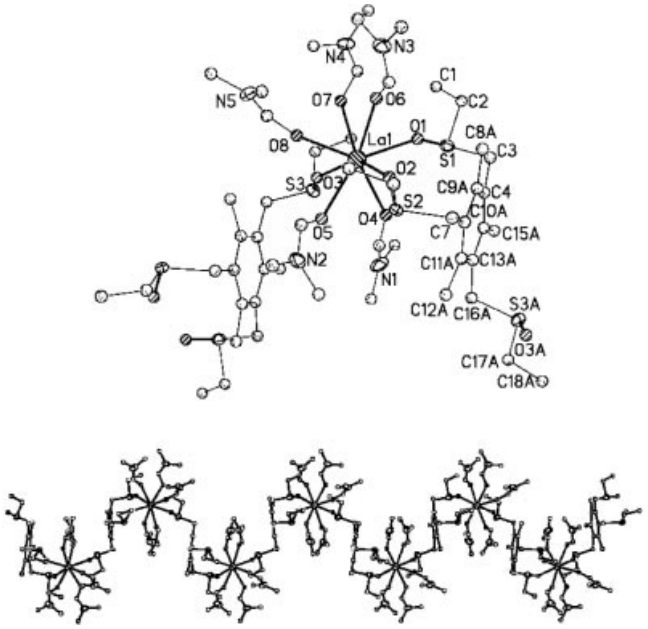

Figure 2. (Top) View of **3** showing the coordination environment of the center ion and (bottom) the helical-chain structure of **3**, only one position of the disordered sets of S atoms is shown

In **3**, the L ligands act as bridges that link adjacent metal ions to form a helical chain (see Figure 2 bottom) with an La···La separation of 10.313 Å. Within the chain, the alternating La^{III} ions are in a straight line, as in **1** and **2**, but all the phenyl groups are parallel to each other and related by a 2_1 helical axis, in contrast to **1** and **2**. Another difference is that in **3** all the chains are arranged parallel to each other along the *c* axis and the perchlorate ions are located among these chains.

In **1**−**3** the ligand is multidentate and displays two kinds of coordination mode: chelate bridging and mono-*O*-bridging. Each L ligand uses two of the sulfinyl moieties to chelate one Ln^{III} center to form a 10-membered ring and uses other one to bridge an adjacent Ln^{III} center. In **1**−**3**, although the trisulfoxide ligand is chiral due to its three S atoms displaying *S*,*R*,*R* (or *S*,*R*,*S*) configurations, in the crystal the presence of a 1:1 disorder for the sulfur atom (S, S′) of one of the sulfoxide moieties makes the configurations offset each other, which means that the complexes as a whole are not chiral. The S=O bond lengths are normal for sulfoxide moieties coordinated to metal ions and are similar to those in di- or mono-sulfoxide analogues.[6] In addition, and similarly to the lanthanide complexes with disulfoxide,[3c,3d] in **1**−**3** there are large M−O−S angles (140.1−168.8° for **1**, 143.6−156.1° for **2** and 147.1−150.6° for **3**) probably due to the high coordination number of the lanthanide ions, and the coordination configurations of the ligands are *trans*−*trans* (C−S−O−M torsion angles are 90−270°) as those in the previously reported disulfoxide lanthanide complexes.[3c−3g]

In summary, three 1D lanthanide-coordination polymers with trisulfoxide ligands were synthesized and structurally characterized. In the complexes, the trisulfoxide ligand shows tridentate linkage as well as mono-*O*-bridging and chelate-bridging coordination modes. Similarly to the disulfoxide ligands, the trisulfoxide ligands also act as bridges to link adjacent metal ions, which may allow the complexes to have higher dimensions. To the best of our knowledge, this is the first report on a trisulfoxide ligand used as a building block to construct coordination polymers. This study may not only open up a new researching domain for developing multisulfoxide-coordination chemistry, but will also offer a new type of organic building block for the construction of metal-organic coordination polymers.

Experimental Section

All the reagents used for synthesis and analyses were of analytical grade and used as received. Hydrated lanthanide nitrate and perchlorate were prepared from the corresponding oxides. Elemental analyses were performed on a Perkin−Elmer 240C analyzer. IR spectra (KBr pellets) were taken on an FT-IR 170SX (Nicolet) spectrometer. ^{1}H NMR spectra were measured on a Bruker AC-P500 spectrometer (300 MHz) at 25 °C with tetramethylsilane as the internal reference. The melting point measurement was taken on an X-4 melting point meter.

Syntheses of the Ligand: 1,3,5-Tris(bromomethyl)-2,4,6-trimethylbenzene was prepared according to a reported procedure.[7] 1,3,5-Tris(ethylthio)-2,4,6-trimethylbenzene was synthesized by the similar literature method.[8]

1,3,5-Tris(ethylsulfinyl)-2,4,6-trimethylbenzene (L): L was synthesized following a procedure similar to our previous work for synthesizing disulfoxides.[4] Nitric acid (63 %, 2 mL) was added dropwise to a vigorously stirred solution of 1,3,5-tris(ethylthio)-2,4,6-trimethylbenzene (10.3 g, 0.03 mol) in benzene (50 mL). After stirring for 24 h, the resulting mixture was added to a 15 % sodium hydrogen carbonate solution to adjust the pH value to ca. 7. The solid product was filtered and washed with distilled water, ethanol and diethyl ether successively. Yield 6.1 g, 52 %. M.p. 233−242 °C (mixture of isomers). $C_{18}H_{30}O_3S_3$ (390.15): calcd. C 55.35, H 7.74; found C 55.01, H 7.22. IR (cm^{-1}): 2887 (w), 2546 (w), 1455 (w), 1278 (m), 1022 (s), 962 (m), 864 (m), 756 (m), 689 (m), 639 (w), 580 (w). ^{1}H NMR (300 MHz): δ = 1.40 (t, 9 H, S−CH_2−CH_3), 2.82 (s, 9 H, Ph−CH_3), 4.04 (q, 6 H, S−CH_2−CH_3), 4.31 (s, 6 H, S−CH_2−Ph) ppm.

Preparation of Complexes: Caution! While we have experienced no problems in handling Ln^{III} perchlorates, these compounds should be handled with great caution because of their potential for explosion.

[Ln(L)(CH$_3$OH)(NO$_3$)$_3$]$_n$ [Ln = La (1); Nd (2)]: Triethyl orthoformate (3 mL) was added to a solution of L (117 mg, 0.3 mmol) in $CHCl_3$ (4 mL) and the mixture was stirred for ca. 20 min. Then $Ln(NO_3)_3{\cdot}nH_2O$ (0.2 mmol) in anhydrous methanol (4 mL) was added to the above mixture and further stirred at 70−80 °C for about 4 h. The mixture was cooled to room temperature and filtered. The filtrate was allowed to stand at room temperature for ca. one week and single crystals suitable for X-ray analysis were obtained. For **1**, yield 87 mg, 39 % based on L. $C_{19}H_{34}LaN_3O_{13}S_3$ (747.58): calcd. C 30.53, H 4.58, N 5.62; found C 30.11, H 4.27, N 5.40. IR (cm^{-1}):

 © 2004 Wiley-VCH Verlag GmbH & Co. KGaA, Weinheim

2917 (m), 2426 (w), 1636 (m), 1456 (m), 1384 (s), 1043 (m), 1001 (s), 970 (m), 839 (w), 678 (m). For **2**, yield 77 mg, 34 % based on L. $C_{19}H_{34}NdN_3O_{13}S_3$ (752.91): calcd. C 30.31, H 4.55, N 5.58; found C 30.14, H 4.21, N 5.24. IR (cm^{-1}): 2941 (m), 2426 (w), 1638 (s), 1457 (m), 1384 (s), 1042 (m), 1000 (s), 970 (m), 637 (m).

$\{[La(L)(DMF)_5](ClO_4)_3\}_n$ (3): Triethyl orthoformate (2 mL) was added to a solution of L (78 mg, 0.2 mmol) in $CHCl_3$ (3 mL) and the mixture was stirred for 20 min. $La(ClO_4)_3{\cdot}nH_2O$ (0.2 mmol) in anhydrous methanol (3 mL) was added to the mixture and a precipitate immediately appeared. The mixture was further stirred at about 60 °C for 30 min. Then, DMF was slowly added until the precipitate dissolved and the solution was filtered. The slow diffusion of diethyl ether into the filtrate resulted in the formation of single crystals in 23 % yield. $C_{33}H_{65}Cl_3LaN_5O_{20}S_3$ (1193.34): calcd. C 33.21, H 5.49, N 5.87; found C 33.04, H 5.21, N 5.48. IR (cm^{-1}): 2981 (m), 1647 (m), 1457 (w), 1384 (m), 1141 (s), 1121 (s), 1086 (m), 1001 (s), 636 (m).

Crystal Structure Determinations: Single-crystal X-ray diffraction measurements of **1**−**3** were carried out at 293(2) K on a Bruker−Smart 1000 CCD area detector with Mo-K_α radiation (λ = 0.71073 Å). The structures were solved by direct methods and refined by full-matrix least-square methods based on F^2 using the SHELXS-97 program.[9] All non-hydrogen atoms were refined anisotropically and the hydrogen atoms were added theoretically. In **1**−**3** one of the three sulfur atoms in each crystallographic asymmetry unit displays positional disorder, and was refined in a statistical two-site occupancy. CCDC-217187 to -217189 contain the supplementary crystallographic data for this paper. These data can be obtained free of charge at www.ccdc.cam.ac.uk/conts/retrieving.html [or from the Cambridge Crystallographic Data Centre, 12 Union Road, Cambridge CB2 1EZ, UK; Fax: (internat.) +44-1223/336-033; E-mail: deposit@ccdc.cam.ac.uk].

Crystal Data for 1: Tetragonal, space group $I4_1/cd$, $a = b =$ 18.215(4), c = 36.89(1) Å, V = 12241(5) Å^3, Z = 16, final refinement [$I > 2\sigma(I)$]: $R1$ = 0.0392, $wR2$ = 0.0882.

Crystal Data for 2: Tetragonal, space group $I4_1/cd$, $a = b =$ 17.9931(2), c = 36.7875(6) Å, V = 11910.0(3) Å^3, Z = 16, final refinement [$I > 2\sigma(I)$]: $R1$ = 0.0621, $wR2$ = 0.1565.

Crystal Data for 3: Monoclinic, space group $P2_1/c$, a = 11.897(4), b = 27.391(8), c = 16.288(5) Å, β = 91.841(5)°, V = 5305(3) Å^3, Z = 4, final refinement [$I > 2\sigma(I)$]: $R1$ = 0.0660, $wR2$ = 0.1417.

Acknowledgments

This work was financially supported by the Outstanding Youth Foundation of NSFC (No. 20225101).

[1] For recent reviews, see: [1a] O. R. Evans, W. Lin, *Acc. Chem. Res.* **2002**, *35*, 511−522. [1b] L. H. Gade, *Acc. Chem. Res.* **2002**, *35*, 575−582. [1c] B. Moulton, M. J. Zaworotko, *Chem. Rev.* **2001**, *101*, 1629−1658. [1d] M. Eddaoudi, D. B. Moler, H. Li, B. Chen, T. M. Reineke, M. O′Keeffe, O. M. Yaghi, *Acc. Chem. Res.* **2001**, *34*, 319−330. [1e] R. Robson, *J. Chem. Soc., Dalton Trans.* **2000**, 3735−3744. [1f] A. J. Blake, N. R. Champness, P. Hubberstey, W.-S. Li, M. A. Withersby, M. Schröder, *Coord. Chem. Rev.* **1999**, *183*, 117−138. [1g] C. Janiak, *Dalton* **2003**, 2781−2804.

[2] For examples: [2a] G. J. Halder, C. J. Kepert, B. Moubaraki, K. S. Murray, J. D. Cashion, *Science* **2002**, *298*, 1762−1765. [2b] R. Kitaura, S. Kitagawa, Y. Kubota, T. C. Kobayashi, K. Kindo, Y. Mita, A. Matsuo, M. Kobayashi, H.-C. Chang, T. C. Ozawa, M. Suzuki, M. Sakata, M. Takata, *Science* **2002**, *298*, 2358−2361. [2c] M. Oh, G. B. Carpenter, D. A. Sweigart, *Angew. Chem. Int. Ed.* **2003**, *42*, 2026−2028. [2d] H. Zhao, M. J. Bazile Jr., J. R. Galán-Mascarós, K. R. Dunbar, *Angew. Chem. Int. Ed.* **2003**, *42*, 1015−1018. [2e] W. Chen, H.-M. Yuan, J.-Y. Wang, Z. Y. Liu, J.-J. Xu, M. Yang, J.-S. Chen, *J. Am. Chem. Soc.* **2003**, *125*, 9266−9267. [2f] L. Pan, K. M. Adams, H. E. Hernandez, X. Wang, C. Zheng, Y. Hattori, K. Kaneko, *J. Am. Chem. Soc.* **2003**, *125*, 3062−3067. [2g] E. J. Cussen, J. B. Claridge, M. J. Rosseinsky, C. J. Kepert, *J. Am. Chem. Soc.* **2002**, *124*, 9574−9581. [2h] D.-L. Long; A. J. Blake, N. R. Champness, C. Wilson, M. Schröder, *Chem. Eur. J.* **2002**, *8*, 2026−2033. [2i] D. Guo, Y.-T. Li, C.-Y. Duan, H. Mo, Q.-J. Meng, *Inorg. Chem.* **2003**, *42*, 2519−2530. [2j] Y.-G. Li, N. Hao, E.-B. Wang, M. Yuan, C.-W. Hu, N.-H. Hu, H.-Q. Jia, *Inorg. Chem.* **2003**, *42*, 2729−2735.

[3] For examples: [3a] X.-H. Bu, W. Chen, S.-L. Lu, R.-H. Zhang, D.-Z. Liao, M. Shionoya, F. Brisse, J. Ribas, *Angew. Chem. Int. Ed.* **2001**, *40*, 3201−3203. [3b] X.-H. Bu, W. Chen, M. Du, R.-H. Zhang, *CrystEngComm.* **2001**, *3*, 131−133. [3c] X.-H. Bu, W. Weng, J.-R. Li, W. Chen, R.-H. Zhang, *Inorg. Chem.* **2002**, *41*, 413−415. [3d] X.-H. Bu, W. Weng, M. Du, W. Chen, J.-R. Li, R.-H. Zhang, L.-J. Zhao, *Inorg. Chem.* **2002**, *41*, 1007−1010. [3e] J.-R. Li, X.-H. Bu, R.-H. Zhang, *Inorg. Chem.* **2004**, *43*, 237−244. [3f] J.-R. Li, M. Du, X.-H. Bu, R.-H. Zhang, *J. Solid State Chem.* **2003**, *173*, 20−26. [3g] R.-H. Zhang, B.-Q. Ma, X.-H. Bu, H.-G. Wang, X.-K. Yao, *Polyhedron* **1997**, *16*, 1123−1127 and 1787−1792. [3h] J. D. Ayala, G. Bombieri, A. D. Pra, G. Vicentini, *Inorg. Chim. Acta* **1998**, *274*, 236−238. [3i] F.-C. Zhu, P.-X. Shao, X.-K. Yao, H.-G. Wang, *Inorg. Chim. Acta* **1990**, *171*, 85−88. [3j] J.-C. Bao, P.-X. Shao, R.-J. Wang, H.-G. Wang, X.-K. Yao, *Polyhedron* **1995**, *14*, 927−933. [3k] M. Calligaris, A. Melchior, S. Geremia, *Inorg. Chim. Acta* **2001**, *323*, 89−95. [3l] S. Geremia, M. Calligaris, S. Mestroni, *Inorg. Chim. Acta* **1999**, *292*, 144−146.

[4] R.-H. Zhang, Y.-L. Zhan, J.-T. Chen, *Synth. React. Inorg. Met.-Org. Chem.* **1995**, *25*, 283−292.

[5] H. B. Kagan, B. Ronan, *Rev. Heteroat. Chem.* **1992**, *7*, 92−103.

[6] M. Calligaris, O. Carugo, *Coord. Chem. Rev.* **1996**, *153*, 83−154.

[7] A. W. van der Made, R. H. van der Made, *J. Org. Chem.* **1993**, *58*, 1262−1263.

[8] X.-H. Bu, W.-F. Hou, M. Du, W. Chen, R.-H. Zhang, *Cryst. Growth Des.* **2002**, *2*, 303−307.

[9] G. M. Sheldrick, *SHELXTL-97*, Program for X-ray Crystal Structure Solution and Refinement, University of Göttingen, Germany, **1997**.

Received October 20, 2003
Early View Article
Published Online March 5, 2004

 © 2004 Wiley-VCH Verlag GmbH & Co. KGaA, Weinheim

A Molecular Tool for Measuring the Electron-Acceptor Ability of Ligands from Crystallographic Data

Francesco P. Fanizzi,*[a] Nicola Margiotta,[b] Maurizio Lanfranchi,[c] Antonio Tiripicchio,[c] Gianfranco Pacchioni,[d] and Giovanni Natile*[b]

Keywords: Ab initio calculations / NMR spectroscopy / Pi ligands / Platinum / X-ray diffraction

A method is proposed for the direct measurement of the π-acidity of ligands coordinated to a metal center. The four-coordinate complex [PtI_2(Me_2-phen)] (Me_2-phen = 2,9-dimethyl-1,10-phenanthroline) is unique since it behaves as a molecular trap and, in the presence of a nucleophile (L), one end of it dissociates to allow the L ligand to coordinate *trans* to the monocoordinated diamine. The coordination of the free end of the phenanthroline is impeded by the filled d orbitals of the metal lying in the same plane as the phenanthroline (d_{yz} and d_z^2 electrons assuming as x-axis that of the I–Pt–I vector). However, if the L ligand is a π-acid able to remove electron charge from the yz plane, the second end of the phenanthroline will also be able to interact with platinum. A linear correlation is found between the crystallographic N–Pt–L angle (180° in ideal square-planar species and 143° in a trigonal bipyramid with a bite angle for bidentate Me_2-phen of 74°) and the π-acceptor capacity of the L ligand as estimated by ab initio calculations. Alkenes and alkynes are found to be among the best π-acids and lead to a regular trigonal-bipyramidal five-coordinate species. CO appears to be only halfway in between the best π-acceptor ligands and those with smallest π-acidity. P-, S-, and N-donor ligands follow in that order without significant differences between sulfides and sulfoxides or between aliphatic amines and pyridine. The very small difference between aliphatic amines and pyridine has been confirmed by investigation of the rate of exchange between the two ends for monocoordinated phenanthroline by ^{1}H NMR spectroscopy. The activation energy ($\Delta G^{\ddagger}$) was found to be equal, within the experimental error, for the two types of *trans* ligands.
(© Wiley-VCH Verlag GmbH & Co. KGaA, 69451 Weinheim, Germany, 2004)

1. Introduction

The π-acceptor ability of a ligand is a key factor in determining its *trans* effect in substitution reactions involving square-planar complexes.[1] A π-acceptor ligand, one that is able to draw electron charge from the metallic center, stabilizes the trigonal-bipyramidal transition state in which the π-acceptor ligand, its *trans* ligand, and the incoming nucleophile share the trigonal plane. The accepted order of *trans*-labilizing ligands is: C_2H_4, CO > CN^- > NO_2^- > SCN^- > I^- > Br^- > Cl^- > NH_3 > OH^-.[2] This series has been derived mainly from kinetic experiments, however it would be highly desirable to have a direct means of measuring the ability of a ligand to favor the assembly of three ligands in the trigonal plane of a five-coordinate geometry.

In investigating the reaction of the sterically strained and highly reactive complexes [PtX_2(Me_2-phen)] (X = Cl, Br, I; Me_2-phen = 2,9-dimethyl-1,10-phenanthroline)[3,4] with an incoming nucleophile, it was found that, contrary to all expectations, no substitution takes place but, instead, simple addition of the extra ligand occurs, with formation of [PtX_2(Me_2-phen)(L)] species.[5–8] Depending upon the characteristics of the incoming ligand, the phenanthroline may become monodentate (and the platinum center still be four-coordinate) or can remain bidentate (and the platinum center become five-coordinate). Preliminary X-ray structural results concerning *trans*-[PtX_2(Me_2-phen)(L)] complexes (X = Cl, L = C_2H_4; X = I, L = CO, PPh_3, and PhNO) showed that the geometry of the complex can range from trigonal bipyramidal (L = ethylene) to square planar (L = PhNO).[5]

We have hypothesized that the structural data of this series of complexes can offer a direct way to rank the π-acceptor ability of L ligands and have extended the investigation to several L ligands comprising the most common S- (sulfides, sulfoxides) and N-donor ligands (aliphatic am-

[a] Dipartimento di Scienze e Tecnologie Biologiche ed Ambientali, Università di Lecce,
Via Monteroni 73100, Lecce, Italy
E-mail: fp.fanizzi@unile.it
[b] Dipartimento Farmaco-Chimico, Università degli Studi di Bari,
Via E. Orabona 4, 70125 Bari, Italy
E-mail: natile@farmchim.uniba.it
[c] Dipartimento di Chimica Generale ed Inorganica, Chimica Analitica, Chimica Fisica, Università di Parma,
Parco Area delle Scienze 17/A, 43100 Parma, Italy
[d] Dipartimento di Scienza dei Materiali, Università di Milano-Bicocca,
Via R. Cozzi 53, 20125 Milano, Italy

ines and pyridine). In this paper we combine accurate X-ray diffraction data of a wide series of *trans*-[$PtI_2(Me_2$-phen)(L)] complexes with the results of ab initio calculations to show that there is a linear relationship between the stereochemistry of the phenanthroline and the π-acidity of the *trans* ligand. The calculations are aimed at providing a quantum-mechanical rationale for the observed trends more than to give quantitative estimates of the observable properties.

The paper is organized as follows. In Section 2a we describe the synthesis and NMR studies of the complexes under investigation. Section 2b is dedicated to the structure of the complexes from X-ray diffraction measurements. Section 2c is devoted to the calculations and to the quantitative estimate of the π-acceptor ability of the L ligands. The existence of a direct correlation between the N−Pt−L angle and the π-acceptor ability is shown and discussed in the concluding Section 3.

2. Results

2a. Synthetic Aspects and NMR Measurements

[$PtI_2(Me_2$-phen)] (**1**) reacts instantaneously with an extra ligand (L) to give the corresponding addition product [$PtI_2(Me_2$-phen)(L)] (**2**). The addition reaction is quantitative for L = C_2H_4 (**a**), $C_2(C_6H_5)_2$ (**b**), CO (**c**), $P(C_6H_5)_3$ (**d**), $H_2(C_3H_7)N$ (**g**), and C_5H_5N (**h**). In the case of L = $(CH_3)_2SO$ (**e**) and $(CH_3)_2S$ (**f**) an excess of L ligand is required in order to obtain complete conversion into the addition product. The direct displacement of one end of the Me_2-phen ligand by the incoming ligand (L) by the usual S_N2 mechanism would place L *cis* to the monodentate Me_2-phen (upper row of Scheme 1). In some instances (L = PPh_3), such a species has been detected in solution, but not as the major reaction product. Moreover it is not an intermediate leading to the species with PPh_3 *trans* to monocoordinated Me_2-phen but it reacts further placing a second molecule of PPh_3 *trans* to the first one.[6] However, the L ligand is most commonly found *trans* to the monodentate Me_2-phen, an indication that one end of Me_2-phen is first released and the transient T-shaped three-coordinate species isomerizes from *cis* to *trans* conformation before addition of L (lower row of Scheme 1). Most of the data thus far accumulated indicate that such a dissociative mechanism can be operative even in four-coordinate square-planar complexes.[9−13]

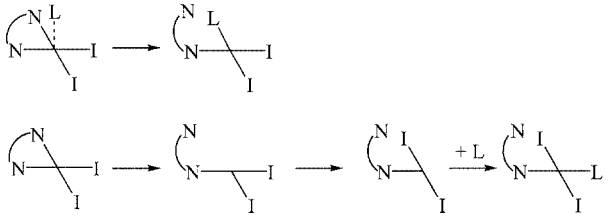

Scheme 1

It has been found that, depending upon the nature of the L ligand, the phenanthroline can assume the whole range of positions spanning from pure monodentate to perfectly symmetrical bidentate coordination. This aspect will be treated in detail in Section 2b devoted to the crystal structure analysis. NMR spectroscopy is not very informative in this respect since, even in the case of monocoordinated Me_2-phen, a fast rate of exchange between the free and coordinated ends can render the two halves of the phenanthroline equivalent on the NMR timescale, as in the case of five-coordinate species. However in the case of pyridine and *n*-propylamine complexes, the single set of proton resonances observed for Me_2-phen at room temperature is split into two sets (one for each inequivalent half of Me_2-phen) by lowering the temperature to 210 K (Table 1). In these two cases dynamic NMR spectroscopy[14,15] allowed to calculate the rate constants (k) for the exchange between the free and coordinated ends of the phenanthroline and, from the dependence of the rate constants upon the temperature, it was possible to evaluate the activation parameters ($\Delta H^{\ddagger}$, $\Delta S^{\ddagger}$, and therefrom $\Delta G^{\ddagger}$ at a given temperature T, $\Delta G^{\ddagger}_T$). $\Delta G^{\ddagger}_T$ corresponds to the free-energy difference between the ground state (the four-coordinate species) and the transition state (the latter is likely to be close to a transition species with both ends of the phenanthroline symmetrically bound to platinum).

The NMR spectra of [$PtI_2(Me_2$-phen)(py)] (**2g**) recorded at different temperatures (black lines) overlapped by the simulated spectra (grey lines) are reported in Figure 1. Plots of $\ln(k/T)$ versus $1/T$ are reported in Figure 2. Values of $\Delta H^{\ddagger} = 57 \pm 2$ kJ·mol^{-1}, $\Delta S^{\ddagger} = 20 \pm 2$ J·mol^{-1}·K^{-1}, and $\Delta G^{\ddagger}_{295} = 51 \pm 2$ kJ·mol^{-1} were found for the pyridine complex **2g**, while values of $\Delta H^{\ddagger} = 56 \pm 2$ kJ·mol^{-1}, $\Delta S^{\ddagger} = 14 \pm 2$ J·mol^{-1}·K^{-1}, and $\Delta G^{\ddagger}_{295} = 52 \pm 2$ kJ·mol^{-1} were found for the *n*-propylamine complex **2h**. The very small difference between the $\Delta G^{\ddagger}_{295}$ values for compounds **2g** and **2h** indicates that the ability to stabilize the trigonal bipyramidal transition state, and hence their π-acceptor capacity towards electrons confined in the trigonal plane, can be considered equivalent for the two ligands and, in general, for aliphatic amines and pyridine.

2b. Crystal Structures of Complexes 2a, 2e, 2f, 2g, and 2h

The molecular structures of **2a** (L = C_2H_4), **2e** (L = DMSO), **2f** (L = DMS), **2g** (L = Py), and **2h** (L = NH_2nPr) are depicted in Figure 3, 4, 5, 6, and 7, respectively. Selected bond lengths and angles are summarized in Table 2 for all compounds.

In **2a** the Pt atom presents a trigonal bipyramidal coordination geometry in which the two N atoms of the bidentate Me_2-phen ligand and the double bond of the ethylene molecule are the equatorial donors and the two iodine atoms the axial ligands (Figure 3). The complex has pseudo-C_{2v} symmetry with the pseudo-twofold axis passing through the midpoint of the ethylene ligand and the Pt atom. The bond lengths and angles in the coordination sphere are normal

 © 2004 Wiley-VCH Verlag GmbH & Co. KGaA, Weinheim

Table 1. ^{1}H NMR chemical shifts (ppm) for free Me_2-phen, [$PtI_2(Me_2$-phen)] (**1**), and [$PtI_2(Me_2$-phen)(L)] (**2**) complexes in $CDCl_3$ [a]

Compound	Temp. (K)	H(4/7)	H(5/6)	H(3/8)	CH_3(2/9)	L
Me_2-phen	298	8.11 d (8)	7.70 s	7.47 d (8)	2.93 s	–
[$PtI_2(Me_2$-phen)] (**1**)	298	8.33 d (8)	7.79 s	7.57 d (8)	3.25 s [7]	–
L = C_2H_4 (**2a**)	298	8.25 d (8)	7.85 s	7.79 d (8) [3]	3.44 s [7]	4.20 [71]
L = $(CH_3)_2SO$ (**2e**)	293	8.20 d (8)	7.76 s	7.46 d (8)	3.46 s [7]	4.04 [22]
L = $(CH_3)_2S$ (**2f**)	298	8.13 d (8)	7.75 s	7.60 d (8)	3.42 s [7]	2.83 s [42]
L = C_5H_5N (**2g**)	295	8.19 d (8)	7.78 s	7.63 d (8)	3.58 br	9.45 d (8) [33] (*o*), 7.75 t (*p*), 7.23 (*m*)
	213	H(4), 8.32 d (8)	H(5), 7.89 s	H(3), 7.70 d (8)	Me(2), 3.81 s	9.28 d (8) (*o*), 7.78 t (8) (*p*), 7.35 d (8) (*m*)
		H(7), 8.20 d (8)	H(6), 7.88 s	H(8), 7.62 d (8)	Me(9), 2.83 s	
L = $H_2(C_3H_7)N$ (**2h**)	293	8.09 d (8)	7.71 s	7.55 d (8)	3.45 br	1.00 t (8), 1.62 m (8), 3.16 m, 3.62 br
	203	H(4), 8.19 d (8)	H(5), 7.83 d	H(3), 7.64 d (8)	Me(2), 3.70 s [38]	0.87 t (8), 1.55 m, 3.10 m, 3.05 m
		H(7), 8.12 d (8)	H(6), 7.70 d	H(8), 7.59 d (8)	Me(9), 2.98 s	

[a] $J_{Pt,H}$ (Hz) in square brackets and $^3J_{H,H}$ (Hz) in parentheses when assignable, s = singlet, d = doublet, t = triplet, m = multiplet, br = broad, (*o*) = *ortho*, (*m*) = *meta*, and (*p*) = *para.*

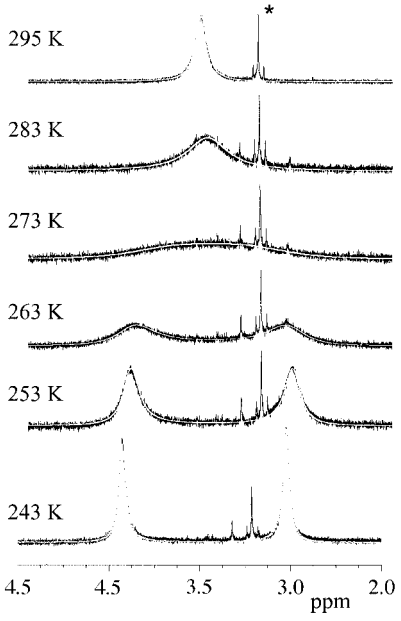

Figure 1. Experimental (black line) and simulated (grey line) ^{1}H NMR spectra (only the aliphatic region is shown) of [$PtI_2(Me_2$-phen)(py)] (**2g**) in $CDCl_3$ at different temperatures; the asterisk indicates the peak belonging to a small excess of the starting complex [$PtI_2(Me_2$-phen)] (**1**)

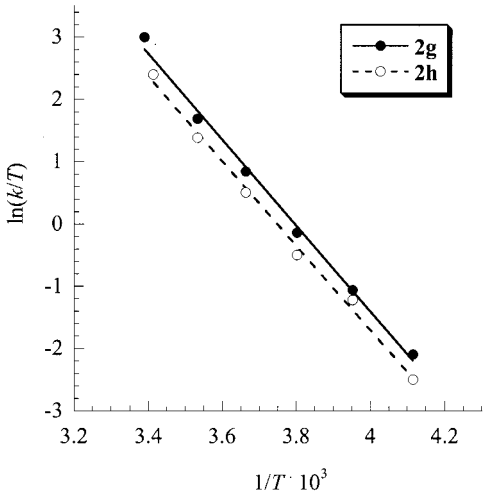

Figure 2. Plots of ln(*k*/T) as a function of 1/T for compounds **2g** and **2h** (*k* values obtained from the line shape analysis of the simulated NMR spectra)

and very similar to those found in the related dichloro derivative.[5]

In **2e** the L ligand is an S-coordinated DMSO molecule (Figure 4) while in **2f** it is dimethyl sulfide (Figure 5). In both complexes the Pt atom shows a slightly distorted square-planar coordination with the L ligand *trans* to the N1-coordinated phenanthroline; two *trans* iodo ligands complete the coordination sphere. In **2e** the orientation of the DMSO molecule is such that a methyl group is placed in the coordination plane [C(15)–S–Pt–I(1) torsion angle of 3.1(4)°] and is responsible for the increase in the S–Pt–I(1) angle with respect to the S–Pt–I(2) angle [96.47(8)° and 89.15(8)°, respectively]. The two Pt–I bond lengths are also significantly different [Pt–I(1) = 2.617(1) and Pt–I(2) = 2.650(1) Å]. A similar situation is found in **2f** [C(15)–S–Pt–I(1) torsion angle of 23.6(4)°, S–Pt–I(1) angle of 96.27(7)°, and S–Pt–I(2) angle of 85.90(7)°]. The phenanthroline is not perfectly planar but shows a certain degree of twist [displacements of the methyl carbon atoms C(13) and C(14) from the mean plane of the phenanthroline of 0.22(1) and −0.22(1) Å for **2e** and 0.25(1) and −0.18(1) Å for **2f**]. This type of phenanthroline deformation is also present in **2a**, but to a smaller extent [deviations from the mean plane of −0.16(1) and 0.14(1) Å for C(13) and C(14), respectively]. In both compounds **2e** and **2f** the Pt atom is slightly out of the mean coordination plane and displaced towards the N(2) atom of the phenanthroline [Pt···N(2) distance of 2.629(6) and 2.666(6) Å for **2e** and **2f**, respectively]. Thus the coordination can be defined as elongated square pyramidal (4+1). The degree of transition from four coordination to five coordination can be judged from the N(1)–Pt–S angle [170.58(17)° and 169.89(17)° for **2e** and

 © 2004 Wiley-VCH Verlag GmbH & Co. KGaA, Weinheim

Table 2. Selected bond lengths (Å) and angles (°) for **2a**, **2e**, **2f**, **2g**, and **2h**

Compound	$[PtI_2(Me_2\text{-phen})(C_2H_4)]$ (**2a**)	$[PtI_2(Me_2\text{-phen})(DMSO)]$ (**2e**)	$[PtI_2(Me_2\text{-phen})(DMS)]$ (**2f**)	$[PtI_2(Me_2\text{-phen})(py)]$ (**2g**)	$[PtI_2(Me_2\text{-phen})(NH_2nPr)]$ (**2h**)
Pt−I(1)	2.6169(13)	2.6171(14)	2.6239(14)	2.6286(13)	2.6310(12)
Pt−I(2)	2.6240(13)	2.6495(13)	2.6395(13)	2.6091(13)	2.6073(13)
Pt−L	1.957(3)[a]	2.200(2)	2.264(2)	2.026(5)	2.030(8)
Pt−N(1)	2.236(6)	2.108(6)	2.093(5)	2.037(4)	2.043(8)
Pt−N(2)	2.238(6)	2.629(6)	2.666(6)	2.684(5)	2.641(7)
I(1)−Pt−I(2)	179.32(3)	173.13(2)	175.39(2)	170.97(2)	171.03(3)
N(1)−Pt−I(1)	89.60(18)	86.05(18)	88.44(17)	92.07(13)	92.2(2)
N(1)−Pt−I(2)	90.05(18)	87.78(18)	88.79(17)	86.90(13)	90.4(2)
N(2)−Pt−I(1)	90.11(16)	92.21(14)	91.01(13)	88.58(12)	92.06(17)
N(2)−Pt−I(2)	90.35(16)	88.67(14)	91.57(13)	99.60(11)	96.90(17)
N(1)−Pt−L	143.1(4)[a]	170.58(17)	169.89(17)	176.52(17)	178.6(3)
N(1)−Pt−N(2)	74.1(2)	71.3(2)	71.1(2)	71.9(2)	72.4(3)
I(1)−Pt−L	90.3(4)[a]	96.47(8)	96.27(7)	91.40(14)	89.0(3)
I(2)−Pt−L	89.6(4)[a]	89.15(8)	85.90(7)	89.71(14)	88.3(3)

[a] With respect to the midpoint of the C=C bond.

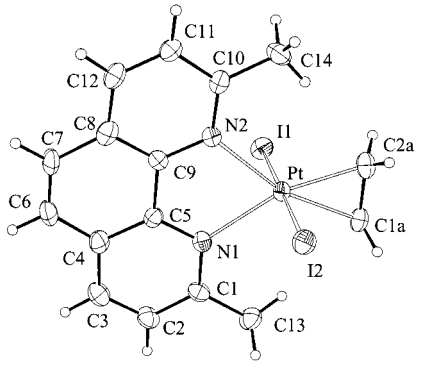

Figure 3. ORTEP view of the molecular structure of $[PtI_2(Me_2\text{-phen})(C_2H_4)]$ (**2a**), thermal ellipsoids are drawn at 30% probability level

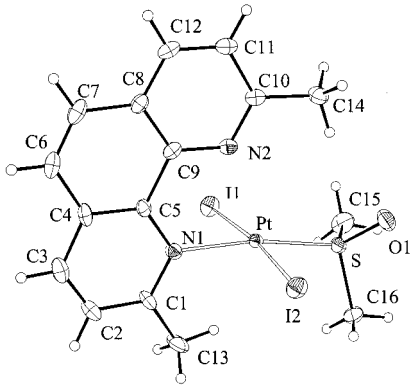

Figure 4. ORTEP view of the molecular structure of $[PtI_2(Me_2\text{-phen})(DMSO)]$ (**2e**), thermal ellipsoids are drawn at 30% probability level

2f, respectively]. The expected values are 180° for a regular square-planar species and 143° for a trigonal bipyramidal species in which the bite angle of the bidentate Me_2-phen lying in the trigonal plane is 74°. The Pt−N(1) bond lengths are similar within experimental errors [2.108(6) and 2.094(5) Å for **2e** and **2f**, respectively] and are in agreement with a comparable *trans* influence of the two ligands. In contrast, the Pt−S distances are significantly different [2.200(2) and 2.264(2) Å for **2e** and **2f**, respectively] reflecting the different oxidation state of the sulfur atom in DMSO and DMS.

The molecular structures of **2g** (L = py) and **2h** (L = NH_2nPr) are depicted in Figure 6 and 7, respectively. The square-planar coordination of the Pt atoms is less distorted than that observed in the previous two cases. The steric bulk of the pyridine and propylamine ligands with respect to the *cis* iodo ligand, is small, and therefore both I−Pt−L angles are close to 90°; this was not the case for the DMSO and DMS complexes previously considered. In **2g** there is an apparent interaction between the pyridine and the phenanthroline ligands so that the planes of the two ligands are

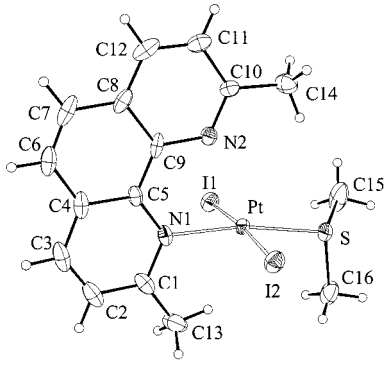

Figure 5. ORTEP view of the molecular structure of $[PtI_2(Me_2\text{-phen})(DMS)]$ (**2f**), thermal ellipsoids are drawn at 30% probability level

canted on the coordination plane in opposite directions and make a dihedral angle of 30.1(2)°. This steric interaction results in a greater twisting of the phenanthroline in **2g** than in **2e** and **2f** [displacement of the C(14) and C(13) carbon atoms from the mean plane of the phenanthroline of

 © 2004 Wiley-VCH Verlag GmbH & Co. KGaA, Weinheim

−0.35(1) Å and 0.19(1) Å, respectively]. In **2h** the propyl group of the $H_2(C_3H_7)N$ ligand extends into the half space of the coordination plane opposite to that of the N(2) atom and is *quasi* orthogonal to the coordination plane [I(1)−Pt−N(3)−C(15) torsion angle of −88.0(8)°]. The phenanthroline is perfectly planar and makes a dihedral angle of 88.4(1)° with the coordination plane. The degree of transition from four- to five-coordination is smaller in **2g** and **2h** than it was in **2e** and **2f**; moreover there is a small difference between **2g** and **2h** [N(1)−Pt−N(3) angles of 176.5(2)° and 178.6(3)° for **2g** and **2h**, respectively]. Despite the different hybridization of the L donor atom (sp^2 and sp^3 for **2g** and **2h**, respectively) the Pt−N(3) bond length is similar for the two compounds (Table 2). Also the *trans* influence appears to be rather similar for the two compounds as indicated by the values of the Pt−N(1) bond lengths, which are equal within experimental errors. Moreover the Pt−N(1) bond lengths are about 0.06 Å shorter in **2g** and **2h** than they were in **2e** and **2f**, consistent with a greater *trans* influence of S-donor ligands with respect to N-donor ligands.

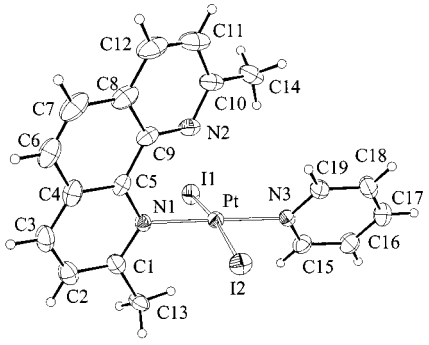

Figure 6. ORTEP view of the molecular structure of $[PtI_2(Me_2\text{-phen})(py)]$ (**2g**), thermal ellipsoids are drawn at 30% probability level

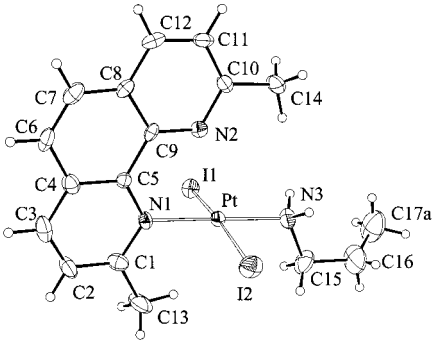

Figure 7. ORTEP view of the molecular structure of $[PtI_2(Me_2\text{-phen})(NH_2Pr^n)]$ (**2h**), thermal ellipsoids are drawn at 30% probability level

2c. Ab initio Calculations

Ab initio calculations were carried out with the aim of confirming that the observed solid-state molecular structures correspond to the computed ground-state structures and correlating the switch from a four-coordinate (monodentate Me_2-phen) to a five-coordinate structure (bidentate Me_2-phen) with the electronic properties of the L ligand. The calculations were performed at the Hartree−Fock level in order to take advantage of an energy partitioning described below and implemented at this level of theory in a computer code available to us. The use of the HF approach implies the neglect of correlation effects. While this certainly affects some of the computed properties, the physics of the interaction is properly described.

A direct comparison between the results of the geometry optimization and those of the X-ray structures is given in Table 3. In general, the agreement between the ab initio HF and the experimental results is good, in particular as far as the Pt−N(2) distance and the N(1)−Pt−L angle — the main parameters used to characterise the extent of the π-back bonding to L — are concerned. Only in the case of the CO complex does the computed structure not agree perfectly with the experimental structure: the Pt−N(2) distance and the N(1)−Pt−L angle are greater in the calculated than in the experimental geometries (by 0.10 Å and 10°, respectively). However, it should be mentioned that a change in the N(1)−Pt−C angle of 10° causes only a small change in the total energy (a few kJ/mol). For the Pt−L distances greater differences between calculated and experimental values (Table 3) have been observed for the sulfur- and phosphorus-donor ligands, but this is mainly due to the neglecting of correlation effects in the calculations. The fact that the calculations reproduce the experimental geometries correctly indicates that the electronic structure of each complex has been described in a satisfactory way even at the HF level.

Table 3. Optimal geometrical parameters for $[PtI_2(R_2\text{-phen})(L)]$ complexes (distances in Å, angles in degrees)

L[a]		Pt−N1	Pt−N2	N1−Pt−L	Pt−L
C_2H_4	exp.	2.24	2.24	143[b]	1.96
	calcd.	2.29	2.29	143[b]	2.14
C_2R_2[c]	exp.[d]	2.28	2.28	143[b]	2.01
	calcd.	2.29	2.29	143[b]	2.16
CO	exp.[e]	2.16	2.48	163	1.81
	calcd.	2.11	2.59	172	1.93
PR_3 [c]	exp.[e]	2.18	2.66	166	2.19
	calcd.	2.12	2.65	172	2.36
$(CH_3)_2SO$	exp.	2.11	2.63	171	2.20
	calcd.	2.05	2.65	178	2.47
$(CH_3)_2S$	exp.	2.09	2.67	170	2.26
	calcd.	2.07	2.64	173	2.47
C_5H_5N	exp.	2.04	2.68	177	2.03
	calcd.	2.08	2.67	171	2.12
H_2NR[f]	exp.	2.04	2.64	179	2.03
	calcd.	2.08	2.67	176	2.06

[a] R = H in the theoretical investigation (phen) and Me in the X-ray structural investigations (Me_2phen). [b] With respect to the midpoint of the C−C bond. [c] R = H in the theoretical and C_6H_5 (phenyl) in the X-ray structural investigation. [d] Experimental values.[8] [e] Experimental values.[5] [f] R = H in the theoretical and C_3H_7 (*n*-propyl) in the X-ray investigation.

 © 2004 Wiley-VCH Verlag GmbH & Co. KGaA, Weinheim

An energy decomposition technique, the CSOV method,[16,17] has been employed to analyze the HF wave function and to identify the relative values of the charge transfer from L to the PtI_2(phenanthroline) residue (hereafter referred to as σ-donation) and of the reverse process, charge transfer from PtI_2(phenanthroline) to L (π back-donation). The interaction energy of the complex is divided into the sum of intra-unit polarization and charge-transfer contributions. Details of the procedure are not given here and can be found elsewhere.[16,18] The extent of charge transfer can be deduced from two independent parameters: the first one is the contribution of each charge-transfer process to the interaction energy (E_{int} in kJ·mol^{-1}), and the second parameter is related to a wavefunction property, the dipole moment. With the assumed orientation of the I−Pt−I atoms along the *x* axis and the N−Pt−L groups along the *y* axis, the change in the *y* component of the dipole moment μ at each CSOV step ($\Delta\mu$) provides a direct measure of the charge flow from L to Pt and vice versa: a positive $\Delta\mu$ value indicates donation, a negative $\Delta\mu$ indicates back-donation. This is a much more reliable measure of the charge transfer than, for instance, the Mulliken charge.[18] Still, one has to keep in mind the qualitative nature of this partitioning.

The CSOV analysis allows the evaluation of the donating/back-donating properties of the ligands considered here (Table 4). As far as the donor properties are concerned, all ligands are good electron donors, as would be expected given the +2 formal oxidation state of the Pt atom. In more detail, the E_{int} values can be grouped into two domains: 180−230 and 130−160 kJ·mol^{-1}. Similarly, two ranges of $\Delta\mu$ values are clearly distinguishable: 0.59−0.65 (with a peak of 0.91 for PH_3) and 0.46−0.47 au. Therefore PH_3, CO, C_2H_2, and C_2H_4 are the strongest donors both from the E_{int} and $\Delta\mu$ values. In contrast C_5H_5N and NH_3 are the poorest donors in the series both from E_{int} and $\Delta\mu$. $(CH_3)_2SO$ and $(CH_3)_2S$ lie between the two groups since they fall in the group of poor donors according to E_{int} but in the group of strong donors according to $\Delta\mu$.

Table 4. Donation and back-donation contributions in [PtI_2(phen)(L)] complexes as derived from a CSOV analysis; E_{int} is the contribution to the total interaction energy and $\Delta\mu$ the change in dipole moment associated with the donation or back-donation mechanisms

	Donation		Back-donation	
L	E_{int} (kJ/mol)	$\Delta\mu$ (au)	E_{int} (kJ/mol)	Δμ (au)
C_2H_4	219	+0.61	175	−0.93
C_2H_2	181	+0.59	154	−0.80
CO	230	+0.61	93	−0.46
PH_3	207	+0.91	48	−0.23
$(CH_3)_2SO$	143	+0.65	39	−0.23
$(CH_3)_2S$	132	+0.63	32	−0.13
C_5H_5N	160	+0.46	51	−0.43
NH_3	146	+0.47	23	−0.11

The π-acceptor properties, on the other hand, are quite different for the various ligands; moreover in this case both E_{int} and $\Delta\mu$ give very similar descriptions (E_{int} was chosen in drawing Figure 8). Acetylene and ethylene exhibit the strongest back-donating contributions. CO is halfway in between the alkene and the alkyne on one side and the amine ligand on the other. All other ligands fall in between the CO and the amine. The direct correlation between the π-acidity of the L ligand, as determined by the CSOV analysis, and the coordination mode of the phenanthroline ligand is surprising: bidentate when L is a good π-acceptor able to decrease the electron density in the trigonal plane, monodentate in most of the other cases with the CO positioned halfway in between the two extremes (Figure 8).

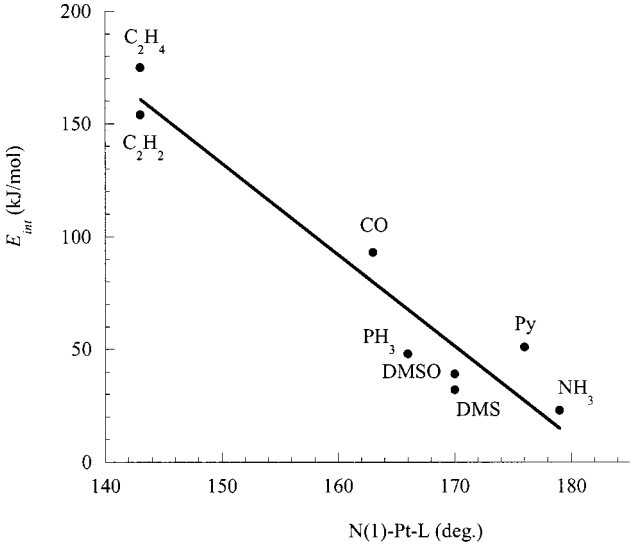

Figure 8. Plot of the computed π-acceptor ability of the L ligands (interaction energy E_{int}, Table 4) versus the experimental values of the N(1)−Pt−L angle (Table 3)

3. Discussion and Conclusion

The [PtI_2(Me_2-phen-*N*,*N*′)] system is characterized by an extremly high steric interaction between the *ortho* substituents of the phenanthroline and the *cis* halogen ligands.[3−7] The steric constrictions within the square-planar geometry can be released by displacement of one end of the phenanthroline and addition of an extra ligand, forming a *trans*-[PtI_2(Me_2-phen-*N*)(L)] species. The coordinated Me_2-phen can then assume an orthogonal orientation with respect to the coordination plane so as to minimize the steric interactions with the *cis* ligands.

The coordination of the free end of the phenanthroline from the top side (the *z* direction assuming the square plane to be *xy*) is prevented by filled d orbitals of the metal lying in the same plane as the phenanthroline (d_{yz} and d_{z^2} electrons assuming as *x* direction that of the I−Pt−I vector).[19] However if the L ligand is a π-acid able to remove electron charge from the *yz* plane, the second end of the phenanthroline can also interact with the metal center and the complex switch from a square-planar four-coordinate to a

 © 2004 Wiley-VCH Verlag GmbH & Co. KGaA, Weinheim

trigonal-bipyramidal five-coordinate geometry comprising all possible intermediate situations. The X-ray technique is ideally suited for the observation of ground-state structures, particularly when intermolecular interactions are weak. This is the case here since the two large iodo ligands in *trans* positions (*x* axis) shield the *yz* plane, leaving the Me_2-phen ligand free to ride on the metal center and to assume the position which corresponds to the minimum of energy.

Therefore a direct correlation appears to exist between the N(1)−Pt−L angle (180° in four-coordinate and 143° in five-coordinate environments) and the ability of the ligand to remove electron charge from the *yz* plane. Alkenes and alkynes are found to be among the best π-acids and lead to a regular five-coordinate species. On the other hand the CO ligand is found to have a π-acidity much weaker than that of alkenes and alkynes. In our opinion the main difference between CO and alkenes or alkynes is that in CO the π*-orbitals of the ligand are disposed end-on with respect to the metal center, while in the case of alkenes and alkynes the π*-orbitals are disposed side-on with respect to the metal. Therefore the overlap of the platinum d-orbitals with the π*-orbitals of the carbonyl ligand is smaller than that with the π*-orbitals of alkenes and alkynes.

As expected, the phosphane ligand is found to be a better π-acid than ligands with sulfur and nitrogen donor atoms.

There is no significant difference between sulfoxide and sulfide from a crystallographic point of view, although theoretical calculations indicate a slightly better π-electron acceptor capacity for the sulfoxide.

The difference between pyridine and *n*-propylamine is also rather small [N−Pt−L angles of 176.5(2)° and 178.6(3)° for C_5H_5N and $H_2(C_3H_7)N$, respectively]. This small difference contrasts with the theoretical calculations reporting a π-acidity for pyridine similar to that of the phosphane. A very likely explanation for this apparent contradiction is that the N−Pt−L angle measures the ability of the L ligand to remove electron charge only from the *yz* plane and, for steric constrictions, such an ability is very small for pyridine. In fact, in order to reduce the steric interaction with the *cis* ligands, the plane of the pyridine will tend to be orthogonal to the coordination plane (*xy* plane) and, as a consequence, the empty π*-orbitals of the pyridine will be set roughly orthogonal to the *yz* plane and therefore will be unable to remove electron density from the platinum d-orbitals lying in this plane. In contrast, theoretical calculations measure the overall back-donation from platinum to L and this can be significant for pyridine due to the circumstances that the empty π*-orbitals of the pyridine are coplanar with the filled d_{xy} orbital of the metal. Therefore, for a pyridine oriented *quasi* orthogonal to the coordination plane, only the X-ray structural analysis gives an accurate description of the electron-acceptor ability of this ligand with respect to metal d-electrons localized in the *yz* plane. The same molecular device also allows a direct measure of the free-energy difference between ground state (four-coordinate species with singly bonded Me_2-phen) and transition state (five-coordinate species with doubly bonded Me_2-phen) when the former configuration is sufficiently low in energy to allow detection, by NMR spectroscopy, of different signals for the two inequivalent halves of the Me_2-phen ligand. By measuring the rate constants at different temperatures for the exchange between the two ends of singly bonded Me_2-phen, it is possible to evaluate $\Delta G^{\ddagger}_{T}$ ($\Delta G^{\ddagger}_{T} = \Delta G^{\ddagger}$ at the temperature T). In the case of the two amine ligands considered here the calculated values of $\Delta G^{\ddagger}_{295}$ (51 ± 2 and 52 ± 2 kJ·mol^{-1} for pyridine and *n*-propylamine, respectively) are very similar and in good agreement with the similar π-acceptor capacities deduced from X-ray data.

It cannot be excluded, however, that the possibility that, by using bidentate ligands with a lower tendency to act as a chelate than 2,9-dimethyl-1,10-phenanthroline, it is possible to destabilize the five-coordinate geometry to such an extent that the rate of exchange between free and coordinated ends of the bidentate ligand becomes observable by NMR spectroscopy also for compounds having L ligands with higher π-acidity than amines.

4. Experimental Section

Starting Materials: Commercial reagent-grade chemicals, 2,9-dimethyl-1,10-phenanthroline (Me_2-phen), ethylene (C_2H_4) (**a**), dimethyl sulfoxide (DMSO) (**e**), dimethyl sulfide (DMS) (**f**), pyridine (py) (**g**), and *n*-propylamine (NH_2Pr^n) (**h**), were purchased from Aldrich and used without further purification. [PtI_2(Me_2-phen)] (**1**) was prepared by a previously reported procedure.[3]

Preparation of *trans*-[PtI_2(Me_2-phen)(L)] Complexes (2): For L = C_2H_4 (**2a**) a rubber bladder filled with ethylene gas was connected to a flask containing a solution of [PtI_2(Me_2-phen)] (**1**) (0.3 mmol) in CH_2Cl_2 (20 mL).[5] After 30 minutes stirring, addition of diethyl ether to the mixture caused the precipitation of a red solid which was collected, washed with diethyl ether, and dried in air, yield 90%. $C_{16}H_{16}I_2N_2Pt$ (**2a**; 685.2): calcd. C 28.1, H 2.4, N 4.1; found C 28.4, H 2.1, N 4.0.

The complexes with L = DMSO (**2e**) and DMS (**2f**) were synthesized according to a procedure reported previously.[8] Yield 90%. $C_{16}H_{18}I_2N_2OPtS$ (**2e**; 735.3): calcd. C 26.1, H 2.5, N 3.8; found C 26.2, H 2.6, N 3.7. $C_{16}H_{18}I_2N_2PtS$ (**2f**; 719.3): calcd. C 26.7, H 2.5, N 3.9; found C 26.7, H 2.6, N 3.8.

The complexes with L = py (**2g**) and NH_2nPr (**2h**) were synthesized by addition of a dichloromethane solution of the L ligand (0.3 mmol in 5 mL of solvent) to a solution containing the stoichiometric amount of [PtI_2(Me_2-phen)] (0.3 mmol) in the same solvent (15 mL). After 2 minutes stirring, addition of diethyl ether to the mixture caused the precipitation of a dark-red solid which was collected, washed with diethyl ether, and dried in air, yield 90%. $C_{19}H_{17}I_2N_3Pt$ (**2g**; 736.2): calcd. C 31.0, H 2.3, N 5.7; found C 30.8, H 2.4, N 5.5. $C_{17}H_{21}I_2N_3Pt$ (**2h**; 716.3): calcd. C 28.5, H 3.0, N 5.9; found C 28.3, H 3.1, N 5.7.

Crystals of the compounds suitable for X-ray structure determinations were obtained from solutions of the platinum complexes in chloroform. Diethyl ether was gently stratified upon the above solutions in order to induce crystallization.

Physical Measurements: ^{1}H NMR spectra were recorded on a Bruker AM 300 instrument equipped with a temperature control unit; the data are reported in Table 1. The spectral simulation was performed using D NMR6.[20] The methyl protons of the 2,9-substituted phenanthroline were used to analyse the exchange between

 © 2004 Wiley-VCH Verlag GmbH & Co. KGaA, Weinheim

the free and coordinated ends of singly bonded Me_2-phen (flipping of the Me_2-phen ligand) in compounds **2g** and **2h**. Values of $\Delta H^{\ddagger}$ and $\Delta S^{\ddagger}$ were calculated from plots of $\ln(k/T)$ against $1/T$. IR spectra were recorded as KBr pellets on Perkin−Elmer 283 and FT 1600 spectrophotometers.

X-ray Data Collection, Structure Determination, and Refinement for Complexes 2a, 2e, 2f, 2g, and 2h: The crystallographic data are summarized in Table 5. Accurate unit-cell parameters were determined by least-squares refinement of the setting angles of 30 randomly distributed and carefully centerd reflections with θ in the range 10−20°. The data collections were performed at 293 K on a Siemens AED diffractometer by using the $\theta/2\theta$ scan mode. One standard reflection was monitored every 100 measurements, no significant decay was noticed over the time of data collection for all the compounds. The structures were solved by direct methods (SIR92)[21] and refined by full-matrix least-squares based on F_o^2 (**2a**, **2f**, and **2h**) or F_o (**2e** and **2h**) using the SHELXL-97 program,[22] first with isotropic then with anisotropic thermal parameters for all the non-hydrogen atoms. A semi-empirical method of absorption correction was applied for all the compounds (maximum and minimum values for the transmission coefficient were 1.000 and 0.904 for **2a**, 1.000 and 0.903 for **2e**, 1.000 and 0.725 for **2f**, 1.000 and 0.908 for **2g** and 1.000 and 0.937 for **2h**).[23,24] All the hydrogen atoms were placed at their geometrically calculated positions and refined as "riding" on their parent carbon or nitrogen atoms, except those of the ethylene (**2a**), which were found and refined isotropically. For compound **2h** the methyl group of the propylamine ligand was found to be disordered over two positions with occupancy factors of 0.66 and 0.34, respectively.

CCDC-216146 to -216150 (**2a**, **2e**, **2f**, **2g**, and **2h**, respectively) contain the supplementary crystallographic data for this paper. These data can be obtained free of charge via www.ccdc.cam.ac.uk/conts/retrieving.html (or from the Cambridge Crystallographic Data Centre, 12 Union Road, Cambridge CB2 1EZ, UK; Fax: (internat.) + 44-1223/336-033; or E-mail: deposit@ccdc.cam.ac.uk).

Computational Details: Ab initio calculations were performed to obtain an internally consistent measure of the π-acceptor ability of the L ligands. This was done according to an energy decomposition technique, the Constrained Space Orbital Variation (CSOV), implemented in the computer code HONDO 8.5[25] at the Hartree−Fock (HF) level. For this reason the electronic structures of the *trans*-[PtI_2(phen)(L)] complexes were determined at the ab initio HF level. Recently, the CSOV method has been implemented also at the Density Functional Theory (DFT) level, and test calculations have shown that the qualitative trends obtained as to the extent of donation/back-donation processes are very similar at the HF and DFT levels.[26] Therefore we expect the conclusions of this analysis not to be affected by the use of an HF wavefunction and to be valid in general. Except for the heavy atoms Pt and I, where an Effective Core Potential (ECP) was used, all other atoms were treated at the all-electron level. 68- and 46-Electron relativistic ECP's were used for Pt and I, respectively.[27] The 2,9-dimethyl-1,10-phenanthroline ligand (Me_2-phen) was represented by a 1,10-phenanthroline (phen). The L ligands considered were: C_2H_4, C_2H_2, CO, H_3P, $(CH_3)_2SO$, $(CH_3)_2S$, C_5H_5N, and H_3N. The ligands actually present in the real compounds were: C_2H_4, $C_2(C_6H_5)_2$, CO, $(C_6H_5)_3P$, $(CH_3)_2SO$, $(CH_3)_2S$, C_5H_5N, and $H_2(C_3H_7)N$. Therefore in the calculation procedure alkyl and phenyl substituents were represented by H atoms to reduce the computational burden. In the analysis of the results one has to take into account that some small differences between theory and experiment can be due to the use of simplified ligands in the calculations. The basis sets were of double-zeta quality for the ECPs of the Pt and I atoms,[27] for the C and N atoms directly bound to Pt, and for the P and S atoms.[28] Polarization functions (*d*),[29] particularly important for second-row

Table 5. Summary of the X-ray Crystallographic Data for **2a**, **2e**, **2f**, **2g**, and **2h**

Compound	[PtI_2(Me_2-phen)-(C_2H_4)] (**2a**)	[PtI_2(Me_2-phen)-(DMSO)] (**2e**)	[PtI_2(Me_2-phen)-(DMS)] (**2f**)	[PtI_2(Me_2-phen)-(py)] (**2g**)	[PtI_2(Me_2-phen)-(NH_2Pr^n)] (**2h**)
Empirical formula	$C_{16}H_{16}I_2N_2Pt$	$C_{16}H_{18}I_2N_2OPtS$	$C_{16}H_{18}I_2N_2PtS$	$C_{19}H_{17}I_2N_3Pt$	$C_{17}H_{21}I_2N_3Pt$
Molecular weight	685.20	735.27	719.27	736.25	716.26
Crystal system	triclinic	triclinic	triclinic	triclinic	monoclinic
Space group	$P\bar{1}$	$P\bar{1}$	$P\bar{1}$	$P\bar{1}$	$P2_1/c$
a (Å)	7.878(5)	13.908(8)	8.411(6)	9.715(5)	9.883(5)
b (Å)	9.231(5)	8.987(6)	9.143(7)	10.299(5)	13.168(7)
c (Å)	12.739(7)	8.211(6)	13.241(8)	11.682(6)	16.290(9)
α (°)	80.40(2)	75.69(2)	82.81(2)	79.87(2)	90
β (°)	75.09(2)	74.10(2)	78.46(2)	69.03(2)	106.53(2)
γ (°)	75.46(2)	82.86(2)	76.85(2)	67.40(2)	90
V (Å^3)	861.4(9)	954.6(11)	968.1(12)	1006.6(9)	2032.4(19)
Z	2	2	2	2	4
λ (Mo-*Kα*)	0.71073	0.71073	0.71073	0.71073	0.71073
ρ(calcd) (Mg/m^3)	2.642	2.558	2.467	2.429	2.341
μ (mm^{-1})	11.724	10.697	10.541	10.043	9.945
θ range (°)	3.17−30.04	3.05−30.06	3.04−30.00	3.48−27.04	3.03−27.07
No. of reflns/obsd $F > 4\sigma(F)$	5006/2886	5586/4235	5632/4112	4401/3739	4803/2588
GOOF [a]	0.944	1.009	1.197	1.049	0.929
*R*1[a]	0.0444	0.0414	0.0312	0.0316	0.0339
*wR*2[a]	0.1233	0.1047	0.0696	0.0880	0.0677

[a] GOOF = $\{\Sigma[w(F_o^2 - F_c^2)^2]/(n-p)\}^{1/2}$; $R1 = \Sigma||F_o| - |F_c||/\Sigma|F_o|$; $wR2 = \{\Sigma[w(F_o^2 - F_c^2)^2]/\Sigma[w(F_o^2)^2]\}^{1/2}$; $w = 1/[\sigma^2(F_o^2) + (aP)^2 + bP]$, $P = [\max(F_o^2,0) + 2F_c^2]/3$.

 © 2004 Wiley-VCH Verlag GmbH & Co. KGaA, Weinheim

atoms like S and P,[18] were added to these atoms. All the remaining C and H atoms were treated by a MINI basis set.[30]

The geometry of the complexes was fully optimized by means of analytical gradients. Only one plane of symmetry was imposed: this is the plane containing the phenanthroline ligand and perpendicular to the straight line connecting the two iodo ligands (C_s symmetry). The L ligand was completely free to rotate and change position with respect to the phenanthroline. This is essential in order to guarantee that the calculations reproduce the correct geometry.

Acknowledgments

We thank the University of Bari, the Ministero dell'Istruzione Università e Ricerca (MIUR) (Cofin. N. 2001053898 and 2000 N. MMO3027791), the EC (COST Chemistry projects D20/0001/2000 and D20/0003/01) for support.

[1] F. Basolo, *Coord. Chem. Rev.* **1996**, *154*, 151−161, and references cited therein.
[2] F. A. Cotton, G. Wilkinson, C. A. Murillo, M. Bochmann. *Advanced Inorganic Chemistry*, 6th ed; Wiley-Interscience, John Wiley & Sons, New York, **1999**.
[3] F. P. Fanizzi, F. P. Intini, L. Maresca, G. Natile, M. Lanfranchi, A. Tiripicchio, *J. Chem. Soc., Dalton Trans.* **1991**, 1007−1015.
[4] R. J. H. Clark, F. P. Fanizzi, G. Natile, C. Pacifico, G. C. van Rooyen, D. A. Tocher, *Inorg. Chim. Acta* **1995**, *235*, 205−213.
[5] F. P. Fanizzi, L. Maresca, G. Natile, M. Lanfranchi, A. Tiripicchio, G. Pacchioni, *Chem. Commun.* **1992**, 333−335.
[6] F. P. Fanizzi, G. Natile, M. Lanfranchi, A. Tiripicchio, *Inorg. Chem.* **1994**, *33*, 3331−3339.
[7] F. P. Fanizzi, G. Natile, M. Lanfranchi, A. Tiripicchio, F. Laschi, P. Zanello, *Inorg. Chem.* **1996**, *35*, 3173−3182.
[8] F. P. Fanizzi, G. Natile, M. Lanfranchi, A. Tiripicchio, G. Pacchioni, *Inorg. Chim. Acta* **1998**, *275−276*, 500−509.
[9] A. Albinati, R. W. Kunz, C. J. Ammann, P. S. Pregosin, *Organometallics* **1991**, *10*, 1800.
[10] A. Gogoll, J. Ornebro, H. Grennberg, J. E. Bakwall, *J. Am. Chem. Soc.* **1994**, *116*, 3631−3632.
[11] R. Romeo, G. Alibrandi, *Inorg. Chem.* **1997**, *36*, 4822−4830.
[12] J. G. P. Delis, P. G. Aubel, K. Vrieze, P. W. N. M. van Leuwen, N. Veldman, A. L. Spek, F. J. R. van Neer, *Organometallics* **1997**, *16*, 2948.
[13] R. Romeo, L. Fenech, L. Monsù Scolaro, A. Albinati, A. Macchioni, C. Zuccaccia, *Inorg. Chem.* **2001**, *40*, 3293−3302.
[14] L. Lunazzi, G. Cerioni, K. U. Ingold, *J. Am. Chem. Soc.* **1976**, *98*, 7484−7488.
[15] K. G. Orrell, V. Sik, *Ann. Rep. NMR Spect.* **1993**, *27*, 103−171.
[16] P. S. Bagus, K. Hermann, C. W. Bauschlicher, *J. Chem. Phys.* **1984**, *80*, 4378−4386.
[17] P. S. Bagus, F. J. Illas, *Chem. Phys.* **1992**, *96*, 8962−8970.
[18] G. Pacchioni, P. S. Bagus, *Inorg. Chem.* **1992**, *31*, 4391−4398.
[19] Z. Lin, M. B. Hall, *Inorg. Chem.* **1991**, *30*, 646−651.
[20] D NMR6: *Calculation of NMR Spectra (I = 1/2) Subject to the Effects of Chemical Exchange.* J. H. Brown and C. H. Bushweller, University of Vermont, Burlington, Vermont, **1983**.
[21] A. Altomare, G. Cascarano, C. Giacovazzo, A. Gualiardi, M. C. Burla, G. Polidori, M. Camalli, *J. Appl. Crystallogr.* **1994**, *27*, 435−443.
[22] G. M. Sheldrick, SHELXL-97. *Program for Crystal Structure Determination.* University of Göttingen, Göttingen, Germany, **1997**.
[23] N. Walker, D. Stuart, *Acta Crystallogr., Sect. A* **1983**, *39*, 158−166.
[24] F. Ugozzoli, *Comput. Chem.* **1987**, *11*, 109−120.
[25] M. Dupuis, F. Johnston, A. Marquez, HONDO 8.5 for CHEMStation (IBM Co., Kingston, **1994**).
[26] A. M. Márquez, N. Lopez, M. García-Hernández, F. Illas, *Surf. Sci.* **1999**, *442*, 463−476.
[27] P. J. Hay, W. R. Wadt, *J. Chem. Phys.* **1985**, *82*, 270−283.
[28] J. Hehre, R. Ditchfield, J. A. Pople, *J. Chem. Phys.* **1972**, *56*, 2257−2261.
[29] *Gaussian Basis Sets for Molecular Calculations* (Ed.: S. Huzinaga), Physical Science Data, Vol. 16 (Elsevier, Amsterdam **1984**).
[30] H. Tatewaki, S. Huzinaga, *J. Comp. Chem.* **1980**, *1*, 205−228.

Received December 2, 2003
Early View Article
Published Online March 9, 2004

 © 2004 Wiley-VCH Verlag GmbH & Co. KGaA, Weinheim

The Ligating Ability of Functionalised Diaminodimethylsilanes towards Zirconium(IV)

Vincenzo Passarelli,*[a] Franco Benetollo,[a] and Pierino Zanella[a]

Keywords: Chelates / NMR spectroscopy / N,O ligands / Silanes / Zirconium

The functionalised diaminodimethylsilanes $SiMe_2[NH(CH_2)_nX]_2$ (X = NMe_2, n = 2, H_2L^1; n = 3, H_2L^2; X = OMe, n = 2, H_2L^3; n = 3, H_2L^4) have been synthesised by aminolysis of $SiMe_2Cl_2$ with $NH_2(CH_2)_nX$, and their ligating ability towards zirconium(IV) has been investigated. The syntheses of $[ZrY_2(L)]$ (Y = Cl, NMe_2, Me; L = L^1, L^2, L^3, L^4) are reported and the solid-state structures of some selected compounds determined by X-ray crystallography. In addition, the solution molecular structures of all the metal derivatives have been elucidated by variable-temperature multinuclear 1D/2D NMR spectroscopy, and the dynamics have been investigated in some selected cases.
(© Wiley-VCH Verlag GmbH & Co. KGaA, 69451 Weinheim, Germany, 2004)

Introduction

Due to the observed peculiar catalytic and structural properties of metal amide derivatives,[1] increasing attention has been devoted to the synthesis of novel compounds of this class. Silylamides of the type $NRSiR'_3$ are widely reported in the literature,[1a–1c] while only a limited number of papers are available[2] dealing with the ligating ability of diaminosilanes (**I**). Nevertheless, in the case of the zirconium derivatives, it appears that the substituents of the $SiMe_2N_2$ core, i.e. the hydrocarbyl groups on the nitrogen atoms, play a fundamental role in determining the nature of the product(s). For instance, the *tert*-butyl derivative $[Zr\{(NtBu)_2SiMe_2\}_2]$[2a] is mononuclear, while the isopropyl analogue is dinuclear,[2r] containing both bridging and terminal $SiMe_2(NiPr)_2$ amido ligands. In addition to the molecular structure of $[Zr\{(NiPr)_2SiMe_2\}_2]_2$,[2r] relevant to this paper are the crystallographically established pentacoordinate or hexacoordinate zirconium derivatives, namely $[Zr(NMe_2)_2(NHMe_2)\{(NAr)_2SiMe_2\}]$,[1d] $[ZrCl_2\{(NAr')_2SiMe_2\}(THF)_2]$[2p] and $[AlMe_2(THF)_2][Zr_2Cl_5\{(NAr')_2SiMe_2\}_2]$[2p] (Ar = 2,6-$Me_2C_6H_3$; Ar′ = 2,6-$iPr_2C_6H_3$). These results suggest that when the starting diaminosilane contains the $Si(NHR)_2$ moiety, the zirconium centre of the formally resulting $[ZrX_2\{(NR)_2SiMe_2\}]$ moiety is coordinatively unsaturated and therefore able to bond additional ligands, thus yielding mononuclear solvento species or ligand-bridged structures.

In light of this, it appeared of interest to synthesise novel functionalised diaminodimethylsilanes (**II**), containing potential ligating sites besides the SiN_2 moiety, investigate their ligating ability towards zirconium, and elucidate the molecular structure of the complexes both in solution and in the solid state.

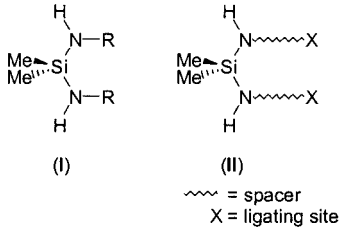

Results and Discussion

Synthesis of $SiMe_2[NH(CH_2)_nX]_2$ (H_2L; n = 2, 3; X = NMe_2, OMe) and Li_2L

The aminolysis of $SiMe_2Cl_2$ by $NH_2(CH_2)_nX$ (n = 2, 3; X = NMe_2, OMe) yields the diaminodimethylsilanes $SiMe_2[NH(CH_2)_nX]_2$ (**1**, H_2L^1, n = 2, X = NMe_2; **2**, H_2L^2, n = 3, X = NMe_2; **3**, H_2L^3, n = 2, X = OMe; **4**, H_2L^4, n = 3, X = OMe), the chlorides being removed as the ammonium salt $NH_2(CH_2)_nX{\cdot}HCl$ (see Scheme 1). The resulting silanes H_2L are readily deprotonated by MeLi (1:2 molar ratio) yielding the lithium salts Li_2L (Scheme 1).

[a] ICIS-CNR,
Corso Stati Uniti 4, 35127, Padova, Italy
Fax: (internat.) + 39-049-870-2911
E-mail: passarel@dcci.unipi.it
Supporting information for this article is available on the WWW under http://www.eurjic.org or from the author.

 © 2004 Wiley-VCH Verlag GmbH & Co. KGaA, Weinheim **DOI: 10.1002/ejic.200300700**

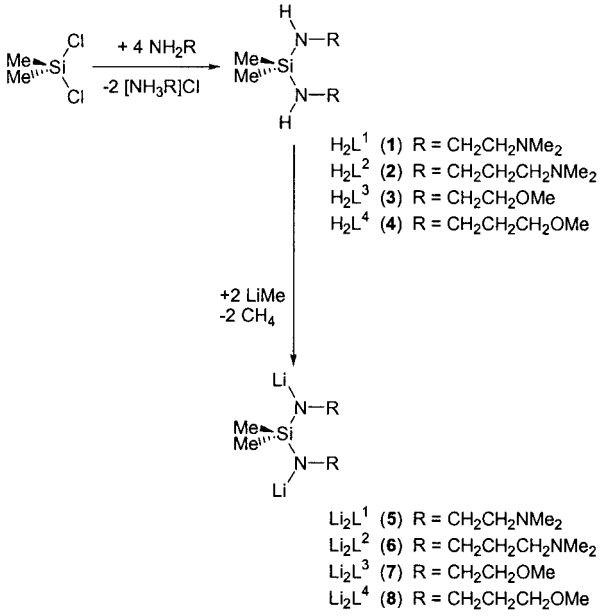

Scheme 1

The ^1H and ^{13}C NMR spectra of H_2L and Li_2L (L = L^1, L^2, L^3, L^4) show high-field resonances for the $SiMe_2$ group, while the peaks of the $NH(CH_2)_nX$ moiety are observed in the range δ = 1−4 ppm (^1H) and δ = 30−80 ppm (^{13}C). The ^{29}Si NMR resonances of the lithium salts Li_2L are high-field shifted with respect to H_2L due to the formal doubly negative charge on L in Li_2L.

Synthesis of $[ZrY_2(L)]$ (Y = Cl, Me, NMe_2; L = L^1, L^2, L^3, L^4)

The reaction of $ZrCl_4$ with Li_2L yields the dichloro derivatives $[ZrCl_2(L)]$ (**9**, L = L^1; **10**, L = L^2; **11**, L = L^3; **12**, L = L^4) as pure materials after recrystallisation from pentane at 249 K (Scheme 2).

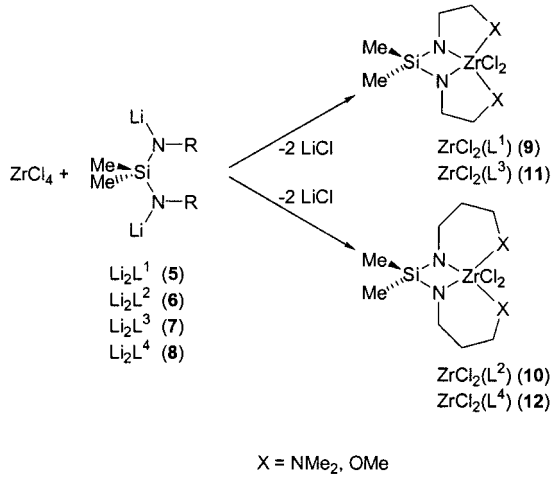

Scheme 2

The solid-state molecular structures of compounds **10** and **12** were determined by single-crystal X-ray diffraction analysis, showing the $ZrCl_2$ moiety to be coordinated to the tetradentate ligand L (Figure 1A and 1B). The arrangement of the donor atoms in **10** is intermediate between the *cis*- and *trans*-octahedral isomers[3a] [Cl(1)−Zr−Cl(2): 109.0(1)°; N(3)−Zr−N(4): 160.1(1)°; the dihedral angle between the ZrCl(1)Cl(2) and ZrN(1)N(2) planes is 28.3(1)°]. Compound **12** shows a more symmetric coordination sphere in which the tetradentate ligand defines the equatorial plane (containing the metal centre) and the chlorine ligands occupy opposite sites with respect to it [Cl(1)−Zr−Cl(2): 140.7(1)°; O−Zr−O′: 122.4(2)°; the dihedral angle between the ZrCl(1)Cl(2) and ZrNN′ planes is 90.0°].

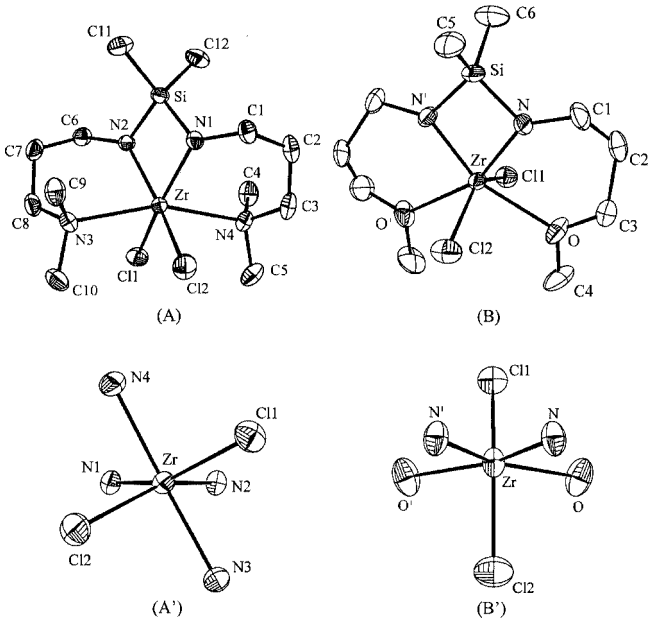

Figure 1. Molecular structures of (A) $[ZrCl_2(L^2)]$ (**10**) and (B) $[ZrCl_2(L^4)]$ (**12**)] with the numbering schemes adopted and the coordination polyhedra {$[ZrCl_2(L^2)]$ (A′); $[ZrCl_2(L^4)]$ (B′)}

As far as the SiN_2Zr moiety in **10** and **12** is concerned, similar bond lengths and angles (Table 1 and 2) have been observed in related compounds {e.g. Zr−N: 2.052 Å (av.); Si−N: 1.753 Å (av.) in $[Zr\{(NtBu)_2SiMe_2\}_2]$[2a]} and it is important to note that the shorter the Zr−N [**10**, Zr−N(1); Zr−N(2); **12**, Zr−N] and Si−N [**10**, Si−N(1); Si−N(2); **12**, Si−N] bond lengths, the wider the N−Zr−N [**10**, N(1)−Zr−N(2); **12**, N−Zr−N′] and N−Si−N angles [**10**, N(1)−Si−N(2); **12**, N−Si−N′; cf. Table 1, 2].

Concerning the neutral ligating sites NMe_2 and OMe, it should be noted that in agreement with the trends in zirconium(IV) compounds, the Zr−N distance is longer than the Zr−O one [**10**, Zr−N(3), 2.427(2) Å, 2.438(2) Å; **12**, Zr−O, 2.330(4) Å].[4]

Coordination polyhedra similar to **10** and **12** have already been observed for zirconium complexes[2p,5] but, to the best of our knowledge, **10** is the first structurally charac-

 © 2004 Wiley-VCH Verlag GmbH & Co. KGaA, Weinheim

Table 1. Selected bond lengths (Å) and angles (°) for $[ZrCl_2(L^2)]$ (**10**)

Zr−Cl(1)	2.507(1)	Zr−Cl(2)	2.510(1)
Zr−N(1)	2.059(2)	Zr−N(2)	2.059(2)
Zr−N(3)	2.427(2)	Zr−N(4)	2.438(2)
Si−N(1)	1.729(2)	Si−N(2)	1.728(2)
Si−C(11)	1.871(3)	Si−C(12)	1.866(3)
Cl(1)−Zr−Cl(2)	109.0(1)	Cl(1)−Zr−N(1)	153.9(1)
Cl(1)−Zr−N(2)	92.5(1)	Cl(1)−Zr−N(4)	83.4(1)
Cl(1)−Zr−N(3)	83.8(1)	Cl(2)−Zr−N(1)	91.3(1)
Cl(2)−Zr−N(2)	153.0(1)	Cl(2)−Zr−N(3)	84.6(1)
Cl(2)−Zr−N(4)	85.3(1)	N(1)−Zr−N(2)	73.9(1)
N(1)−Zr−N(3)	115.1(1)	N(1)−Zr−N(4)	82.2(1)
N(2)−Zr−N(3)	81.7(1)	N(2)−Zr−N(4)	114.0(1)
N(3)−Zr−N(4)	160.1(1)	N(1)−Si−N(2)	91.4(2)
N(1)−Si−C(11)	113.1(2)	N(1)−Si−C(12)	115.9(2)
N(2)−Si−C(11)	116.5(2)	N(2)−Si−C(12)	113.4(2)
C(11)−Si−C(12)	106.4(2)		

Table 2. Selected bond lengths (Å) and angles (°) for $[ZrCl_2(L^4)]$ (**12**)

Zr−Cl(1)	2.465(2)	Zr−Cl(2)	2.463(2)
Zr−N	2.024(4)	Zr−O	2.330(4)
Si−N	1.719(4)	Si−C(5)	1.858(9)
Si−C(6)	1.865(9)	N(1)−C(1)	1.450(3)
O−C(3)	1.354(3)	O−C(4)	1.424(8)
Cl(1)−Zr−Cl(2)	140.7(1)	Cl(1)−Zr−N	104.7(1)
Cl(2)−Zr−N	106.1(1)	Cl(1)−Zr−O	80.7(1)
Cl(2)−Zr−O	80.7(1)	O−Zr−N	80.9(2)
N−Zr−N′[a]	75.6(2)	O−Zr−O′[a]	122.4(2)
N−Si−C(5)	113.7(1)	N−Si−C(6)	113.6(1)
N−Si−N′[a]	92.4(3)	C(5)−Si−C(6)	109.3(5)

[a] Equivalent atom generated by $-x, y, z$.

terised hexacoordinate derivative containing a linear open-chain N_4 ligand bonded to the $ZrCl_2$ moiety. With regards to **12**, the molecular structure of the solvento zirconium derivative $[ZrCl_2\{(NAr)_2SiMe_2\}(THF)_2]$[2p] (Ar = 2,6-*i*$Pr_2C_6H_3$) is to be considered because of the strictly similar arrangement of the donor atoms, i.e. the zirconium, the oxygen and the nitrogen atoms define the equatorial plane, while the chlorides occupy the apical sites.

The solution molecular structures of **9**−**12** were investigated by NMR spectroscopy. The ^1H and ^{13}C NMR spectra show the expected patterns (see Exp. Sect.) and, relevant to the structure elucidation, the ^1H NMR resonances of the CH_2NMe_2 (**9**, **10**) and the CH_2OMe (**11**, **12**) moieties are shifted with respect to the uncomplexed ligands, thus indicating their coordination to the metal centre, and the two halves of the silane ligands, namely $SiN(CH_2)_nNMe_2$ and $SiN(CH_2)_nOMe$ are equivalent[3b] even at 188 K (^1H and ^{13}C NMR), suggesting the symmetric coordination[3a] of the ligand to the metal centre. The solution molecular structures of **9**−**12** should therefore be essentially similar to the solid-state structures of **10** and **12**.

In order to extend the class of the zirconium derivatives containing L^1 and L^2 the synthesis of complexes containing ancillary ligands other than Cl, namely Me and NMe_2, was investigated. The dimethyl derivatives $[ZrMe_2(L)]$ (**13**, L = L^1; **14**, L = L^2) were prepared by reacting $ZrMe_4$ (generated in situ by treating $ZrCl_4$ with MeLi, 1:4 molar ratio, 233 K) with H_2L (L = L^1, L^2, Scheme 3). Alternatively, **13** could be obtained from the reaction of **9** with MeLi (1:2 molar ratio, 233 K; Scheme 3). The products are extremely air and moisture sensitive and thermally unstable (samples of both **13** and **14** were found to decompose within one week, even if stored under dinitrogen at 249 K).

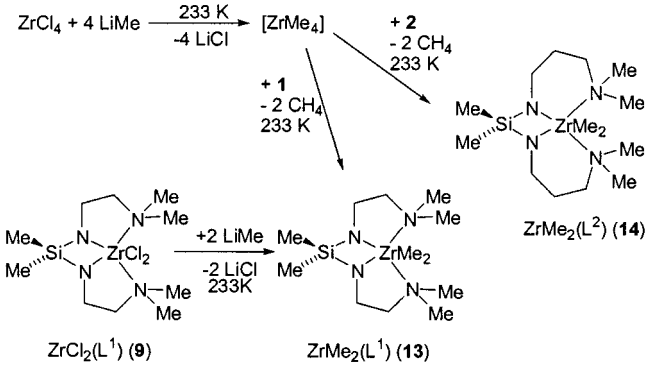

Scheme 3

Similar to $[ZrCl_2(L)]$, the ^1H and/or ^{13}C NMR resonances of the $CH_2N(CH_3)_2$ group of $[ZrMe_2(L)]$ (L = L^1, L^2) are shifted with respect to the uncomplexed ligands, thus proving the coordination of the neutral NMe_2 units to the zirconium centre. In addition, the equivalence of the two arms of the diaminosilane ligands (^1H, ^{13}C) indicates a symmetric coordination of the ligand.[3b]

The reaction of $[Zr(NMe_2)_4]$ with **1** yields the mixed amido derivative $[Zr(NMe_2)_2(L^1)]$ (**15**) as a microcrystalline solid, after removing all the volatiles from the reaction mixture (Scheme 4). Unfortunately, H_2L^2 reacts with $[Zr(NMe_2)_4]$ to give a mixture of products that we were unable to separate and characterise. However, $[Zr(NMe_2)_2(L^2)]$ (**16**) could be obtained as a pure material from the reaction of **10** with $LiNMe_2$ (1:2 molar ratio, Scheme 4); formation of the chloroamido derivative $[ZrCl(NMe_2)(L^2)]$ (**17**) was also observed in the course of the reaction. As a matter of fact, when **10** was treated with $LiNMe_2$ (1:1 molar ratio), **17** was isolated as a pure material in high yield, and the treatment of **17** with $LiNMe_2$ (1:1 molar ratio) yielded **16**.

The solid-state molecular structure of **15** was determined by X-ray diffraction analysis, showing the zirconium centre to be coordinated to the tetradentate dianionic ligand L^1 and to the dimethylamido ligands (Figure 2). To the best of our knowledge, $[Zr(NMe_2)_2(L^1)]$ (**15**) is the first structurally characterised hexacoordinate zirconium complex containing a linear open-chain N_4 ligand coordinated to the $Zr(NMe_2)_2$ moiety. The coordination polyhedron can be described as a distorted octahedron or a bicapped tetrahedron (amino NMe_2 groups capping two faces). In any case, the four donor atoms from the silane ligand define the equa-

 © 2004 Wiley-VCH Verlag GmbH & Co. KGaA, Weinheim

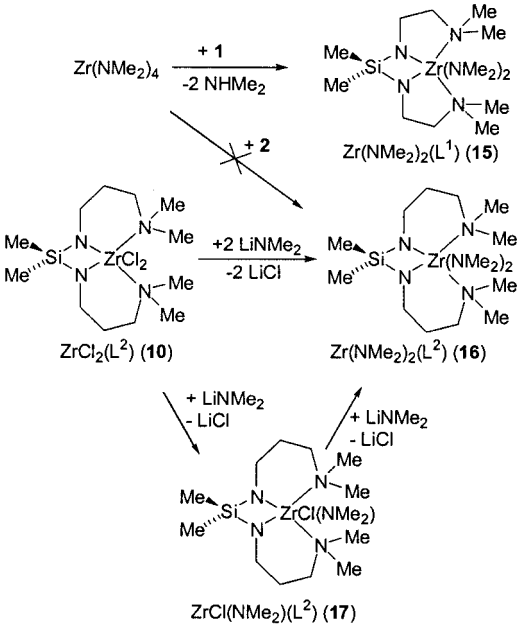

Scheme 4

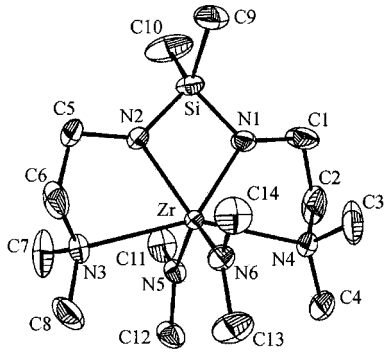

Figure 2. Molecular structure of $[Zr(NMe_2)_2(L^1)]$ (**15**) with the numbering scheme adopted

torial plane of the molecule and the dimethylamido groups occupy opposite coordination sites with respect to it. Concerning bond lengths and angles (Table 3), the Si−N(1), Si−N(2), Zr−N(1) and Zr−N(2) distances and the N(1)−Si−N(2) and N(1)−Zr−N(2) angles of the SiN_2Zr core are similar to those observed in **10**, **12** and related compounds (vide supra). The Zr−N(3) and Zr−N(4) distances [2.566(6), 2.580(7) Å, respectively] in **15** are longer than those in **10** [2.427(2), 2.438(2) Å, respectively], and we propose that the different hydrocarbon chains (the shorter ethylene one in **15** vs. the longer propylene one in **10**), the different arrangement of the tetradentate ligand (Figure 1 and 2), and the presence of the more sterically demanding dimethylamido ligand (with respect to Cl) might be responsible for this.

Table 3. Selected bond lengths (Å) and angles (°) for $[Zr(NMe_2)_2(L^1)]$ (**15**)

Zr−N(1)	2.103(6)	Zr−N(2)	2.117(6)
Zr−N(3)	2.566(6)	Zr−N(4)	2.580(7)
Zr−N(5)	2.075(6)	Zr−N(6)	2.084(6)
Si−N(1)	1.683(7)	Si−N(2)	1.684(7)
Si−C(9)	1.87(1)	Si−C(10)	1.85(1)
N(4)−Zr−N(1)	67.9(3)	N(4)−Zr−N(2)	136.7(2)
N(4)−Zr−N(3)	154.4(2)	N(4)−Zr−N(5)	84.2(2)
N(4)−Zr−N(6)	83.5(3)	N(1)−Zr−N(2)	69.1(3)
N(1)−Zr−N(5)	110.6(3)	N(1)−Zr−N(3)	137.7(3)
N(1)−Zr−N(6)	113.7(3)	N(2)−Zr−N(3)	68.8(3)
N(2)−Zr−N(5)	115.4(3)	N(2)−Zr−N(6)	110.1(3)
N(3)−Zr−N(5)	84.4(3)	N(3)−Zr−N(6)	84.5(3)
N(5)−Zr−N(6)	124.8(3)	N(1)−Si−N(2)	90.6(3)
N(1)−Si−C(9)	115.9(5)	N(1)−Si−C(10)	114.7(6)
N(2)−Si−C(9)	114.6(5)	N(2)−Si−C(10)	116.0(7)
C(9)−Si−C(10)	105.2(6)		

The ^1H and ^{13}C NMR spectra of $[Zr(NMe_2)_2(L)]$ (**15**, **16**) show only two (**15**) and three (**16**) methylene resonances, suggesting a symmetrical coordination[3b] of L to the $Zr(NMe_2)_2$ moiety, and, consequently, that the solid-state molecular structure of **15** is preserved in solution. A similar arrangement of the donor atoms can be proposed for **16** (vide infra).

As far as the chloroamido derivative $[ZrCl(NMe_2)(L^2)]$ (**17**) is concerned, only one ^{29}Si NMR signal (δ = −22.1 ppm) is observed, while the ^{13}C NMR spectrum shows three resonances for the methylene carbons atoms (even at 188 K), thus indicating that the ligand should be symmetrically coordinated to the metal centre.[3b] In addition: i) the $SiMe_2$ moiety yields two ^1H and two ^{13}C resonances, ii) non-equivalent methylene protons of both the CH_2NMe_2 and the $CH_2CH_2CH_2$ units are observed, and iii) the $SiNCH_2$ signal is broad and unresolved (Scheme 5), suggesting that the coordinated L^2 should approximately define a plane and the Cl and dimethylamido groups should occupy opposite coordination sites with respect to it (Scheme 5). This would make the two faces of the molecular plane nonequivalent. This is confirmed by the *negative* cross-peaks observed in the ^1H NOESY spectrum of **17** (298 K) between the resonances of the dimethylamido ligand (δ = 2.99 ppm) and the H*b* (δ = 1.56 ppm), H*c* (δ = 2.05 ppm) and Me′ (δ = 0.28 ppm) resonances, thus leading to the assignment given in Scheme 5.[6]

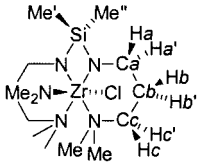

	δ_H (298 K)	δ_C (298 K)
	3.57 [Ha, Ha']	48.1 [C*a*]
	1.56 [H*b*], 1.40 [H*b*']	30.3 [C*b*]
	2.05 [Hc], 2.82 [Hc']	64.0 [Cc]
	0.28 [Me']	1.1 [Me']
	0.31 [Me"]	1.4 [Me"]

Scheme 5

Dynamics

Variable-temperature 1D/2D NMR spectra of selected compounds, namely LiL^2 (**6**), $[ZrCl_2(L^2)]$ (**10**), $[Zr(NMe_2)_2(L^1)]$ (**15**) and $[ZrCl(NMe_2)(L^2)]$ (**17**) showed that dynamic processes occur in solution, i.e. the inversion

 © 2004 Wiley-VCH Verlag GmbH & Co. KGaA, Weinheim

of the six-membered [MN_2C_3] ring (**6**, **10**) and rotation of the amido ligand NMe_2 around the Zr−N bond (**15**, **17**).

Six-Membered [MN_2C_3] Ring Inversion

Despite the different nature of Li_2L^2 (**6**) and [$ZrCl_2(L^2)$] (**10**), the L^2 ligand exhibits similar dynamics in both compounds, i.e. the inversion of the six-membered [MN_2C_3] ring. As far as **10** is concerned, its ^{1}H NMR spectrum is strongly affected by the temperature: at 188 K each methylene resonance in the ^{1}H NMR spectrum splits into two signals (Scheme 6, cf. ESI) and the two NMe_2 methyls are nonequivalent. As both the solid-state and the proposed solution structure of **10** indicate the presence of a six-membered ZrN_2C_3 ring, we are dealing here with the slowing down of its inversion — on lowering the temperature the exchange between the equatorial and axial positions of the ring slows down, thus making both the geminal methylene protons and the NMe_2 groups nonequivalent (Scheme 6). The correlation peaks in the COSY spectrum at 188 K are indicative of both the geminal and the vicinal couplings of the methylene protons, and the observed pattern of the resonances in the 1D ^{1}H NMR spectrum (188 K) indicates that both the geminal and vicinal (axial-axial) couplings are responsible for the structure of the signals (as estimated from the spectrum, the geminal and the vicinal coupling constants are similar, i.e. about 12 Hz, cf. ESI). Likewise, the ^{13}C NMR spectrum at 188 K shows six signals (δ = 68.6, 56.9, 55.2, 49.0, 35.0, 5.6 ppm) and the ^{1}H-^{13}C HMQC spectrum indicates that the methylene carbons (δ = 68.6, 55.2 and 35.0 ppm) bear two nonequivalent protons (δ = 3.27, 1.52; 4.06, 3.18; 1.20, 1.10 ppm, respectively; cf. Scheme 6).

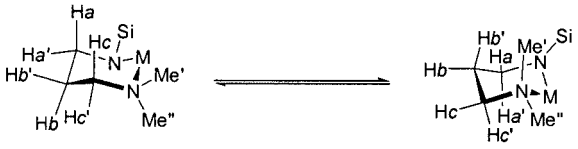

	δ_H (188 K)	
	M = Zr	M = Li
Ha, Ha'	4.06, 3.18	3.28 (broad)
Hb, Hb'	1.20, 1.10	1.36, 1.61
Hc, Hc'	3.27, 1.52	2.01, 2.30
Me', Me"	2.04, 2.68	1.99 (broad)

Scheme 6

A line-shape analysis[7] of the NMe_2 resonances has been carried out at different temperatures in order to obtain the kinetic constants of the ring inversion (cf. ESI) and the activation parameters [ΔH_{act} = (32.5 ± 0.7) kJ·mol^{-1}; ΔS_{act} = (−44 ± 3) J·mol^{-1}·K^{-1}]. The observed negative ΔS_{act} suggests that the ring inversion does not occur through a dissociative pathway, and that we are dealing with a cyclohexane-like ring inversion.

Despite the observation of one ^{7}Li peak and one ^{29}Si signal even at 188 K for **6**, the ^{1}H resonances of the $SiNCH_2$ and NCH_3 groups broaden and appear unresolved at 188 K; moreover, the ^{1}H resonances of both the CH_2NMe_2 and $CH_2CH_2CH_2$ groups split into two signals (Scheme 6), thus indicating that, independent of the coordination sphere around lithium, **6** should contain a six-membered LiN_2C_3 ring (Scheme 6), and that, as a consequence, the slowing down of ring inversion is responsible for the nonequivalence of the CH_2NMe_2 and $CH_2CH_2CH_2$ geminal protons and for the broadening of the $SiNCH_2$ and NCH_3 resonances (cf. Scheme 6 for assignment).

Zr−NMe_2 Rotation

The ^{1}H and ^{13}C NMR spectra of [$Zr(NMe_2)_2(L^1)$] (**15**) and [$ZrCl(NMe_2)(L^2)$] (**17**) at about 200 K show two resonances for the amido NMe_2 groups (Scheme 7), indicating that the two methyl groups experience different chemical environments at that temperature. As a matter of fact, the ^{1}H NOESY spectra of the compounds (**15**, 203 K; **17**, 193 K) show negative cross-peaks between the resonances of the $SiMe_2$ group and one of the amido NMe_2 methyl groups (**15**, δ = 3.03 ppm; **17**, δ = 2.94 ppm), and between the other amido NMe_2 methyl group (**15**, δ = 2.68 ppm; **17**, δ = 3.00 ppm) and the amino NMe_2 moiety, thus indicating that: i) one methyl group of the amido NMe_2 moiety points towards the $SiMe_2$ group, ii) the other one faces the coordinated NMe_2 unit (Scheme 7), similar to the solid-state structure of **15** (Figure 2), and iii) at these temperatures the rotation of the amido NMe_2 group is slow enough to prevent the exchange of the two methyl groups.

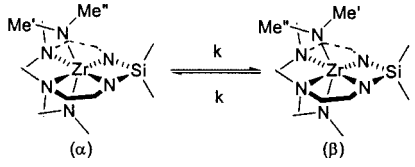

	δ_H (203 K)	δ_C (203 K)
Me' (α)	2.68	43.8
Me" (α)	3.03	44.5

(A)

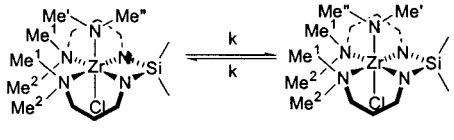

	δ_H (193 K)	δ_C (193 K)
Me' (α)	3.00	43.8
Me" (α)	2.94	46.0
Me^1	2.20	45.8
Me^2	2.15	45.6

(B)

Scheme 7

 © 2004 Wiley-VCH Verlag GmbH & Co. KGaA, Weinheim

In order to further elucidate the dynamics, a line-shape analysis of the methyl resonances was undertaken, and the kinetic constants and the activation parameters were calculated [**15**, ΔH_{act} = (61.5 ± 0.8) kJ·mol^{-1}; ΔS_{act} = (55 ± 3) J·mol^{-1}·K^{-1}; **17**, ΔH_{act} = (27 ± 1) kJ·mol^{-1}; ΔS_{act} = (−73 ± 7) J·mol^{-1}·K^{-1}].

As far as the exchange between the two methyls of the amido NMe_2 group in **15** and **17** is concerned, two mechanisms could be proposed: i) a distortion of the [ZrL] framework, allowing free rotation of the amido NMe_2 group (A in Scheme 8), or ii) dissociation of one amino NMe_2 moiety, yielding a pentacoordinate derivative in which the rotation of the amido NMe_2 group should be no longer restricted (B in Scheme 8).

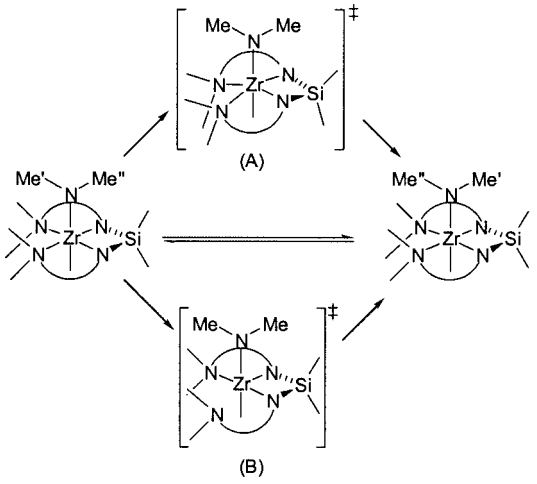

Scheme 8

Provided the activation entropy is negative for **17** and positive for **15** (vide supra), we propose that the exchange mechanisms are different for the two compounds and that the dissociative pathway (B in Scheme 8) is operative in **15**, while in **17** a distortion of the coordinated ligand should allow the exchange to occur (A in Scheme 8). In light of this, it is relevant that the activation enthalpy of **15** is about twice that of **17**, in agreement with the proposed dissociation of the Zr−N (amino) bond in **15** and the distortion in **17**. Moreover, L^2 is expected to be more flexible than L^1, due to the longer hydrocarbon chain between NMe_2 and SiN, and Cl is less sterically demanding than NMe_2, thus making the distortion of L in **17**, rather than in **15**, possible.[8]

Conclusions

The aminolysis of $SiMe_2Cl_2$ with the appropriate amine yields the functionalised diaminodimethylsilanes $SiMe_2[NH(CH_2)_nX]_2$ (H_2L, n = 2, 3; X = NMe_2, OMe, Scheme 9), which are able to coordinate to a ZrY_2 moiety, the zirconium derivatives of general formula $ZrY_2(L)$ (Scheme 9, **III**; Y = Cl, Me, NMe_2; L = L^1, L^2, L^3, L^4) being readily prepared according to the appropriate procedures.

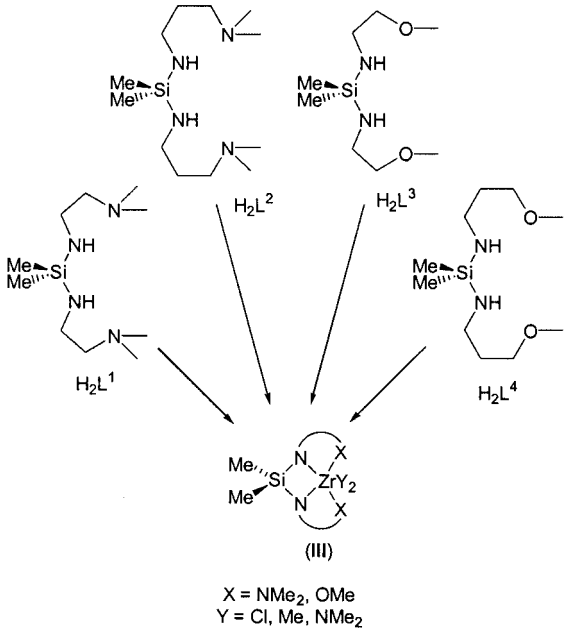

Scheme 9

The solid-state structures of selected compounds, namely $[ZrCl_2(L)]$ (L = L^2, L^4) and $[Zr(NMe_2)_2(L^1)]$, show that L is tetradentate, coordinating to the metal centre through both the $Si(NR)_2$ and the neutral X moieties (X = OMe, NMe_2; Scheme 9). The coordination polyhedra are strongly affected by the nature of the diaminosilane ligand and by the zirconium ancillary ligands. To the best of our knowledge, $[ZrCl_2(L^2)]$ and $[Zr(NMe_2)_2(L^1)]$ are the first examples of hexacoordinate zirconium complexes containing a linear open-chain N_4 tetradentate ligand coordinated to the ZrY_2 moiety (Y = Cl, NMe_2).

1D/2D multinuclear NMR spectroscopic investigations on the compounds $[ZrY_2(L)]$ have shown that L is tetradentate and symmetrically coordinated to the metal centre, similar to the solid-state structures. In addition, variable-temperature 1D/2D multinuclear NMR measurements have allowed the dynamics of some selected compounds to be investigated, the kinetics of the six-membered $[MN_2C_3]$ ring inversion in $[Li_2L^2]$ and $[ZrCl_2(L^2)]$, and the rotation of the dimethylamido ligand around the Zr−N bond in $[Zr(NMe_2)(L^1)]$ and $[ZrCl(NMe_2)(L^2)]$ being elucidated.

Experimental Section

General: All operations were carried out in a glove-box under an atmosphere of dinitrogen. Elemental analyses (C, H, N) were performed using a Fisons Instruments analyser (Mod. EA 1108); the chlorine content in the samples was determined by potentiometric titration using a standard solution of silver nitrate (Aldrich). NMR spectra were recorded with a Bruker AMX 300 spectrometer

 © 2004 Wiley-VCH Verlag GmbH & Co. KGaA, Weinheim

(300 MHz for ^{1}H). ^{1}H, ^{13}C and ^{29}Si NMR spectra are referenced to TMS; LiCl (1 M, D_2O) was used as reference for the ^{7}Li NMR spectra. Multiplicity is indicated as s (singlet), t (triplet), q (quadruplet), quint (quintuplet), m (multiplet). Variable-temperature NMR measurements were carried out on [D_8]toluene solutions.

Zirconium tetrachloride ($ZrCl_4$, Fluka) was washed with boiling toluene, then with pentane, dried in vacuo and stored under an atmosphere of dinitrogen. *N*,*N*-dimethylethylenediamine ($C_4H_{12}N_2$, Aldrich) was refluxed over BaO for one day, then distilled and stored under dinitrogen. *N*,*N*-dimethylpropanediamine ($C_5H_{14}N_2$, Aldrich), 3-methoxypropylamine ($C_4H_{11}NO$, Aldrich), 2-methoxyethylamine (C_3H_9NO, Aldrich), MeLi (Et_2O solution, 1.6 M, Aldrich) and dichlorodimethylsilane ($SiCl_2Me_2$, Aldrich) were used as received. $Zr(NMe_2)_4$ was prepared according to the published procedure.[9] $LiNMe_2$ was obtained as a colourless solid by bubbling $NHMe_2$ (Fluka) into an Et_2O solution of MeLi.

Synthesis of $SiMe_2[NH(CH_2)_nX_2]_2$ (H_2L; X = NMe_2, OMe; *n* = 2, 3): Only the synthesis of $SiMe_2(NHCH_2CH_2NMe_2)_2$ is reported in detail, the other reactions being carried out similarly. A pentane solution (50 mL) of $SiMe_2Cl_2$ (2.00 g, 15.5 mmol) was added dropwise to a pentane solution (50 mL) of $NH_2CH_2CH_2NMe_2$ (5.46 g, 61.9 mmol) and the prompt precipitation of a colourless solid was observed. After 12 h stirring, the suspension was filtered and the solid identified (vide infra) as $NH_2CH_2CH_2NMe_2$·HCl (3.77 g, 98% yield). The filtrate was evaporated to dryness and the residual liquid identified as $SiMe_2(NHCH_2CH_2NMe_2)_2$ (**1**, H_2L^1, colourless, 3.46 g, 96% yield). $C_{10}H_{28}N_4Si$ (232.44): calcd. C 51.7, H 12.1, N 24.1; found 52.0, H 12.0, N 24.0. ^{1}H NMR (C_6D_6, 298 K): δ = 0.17 (s, 3 H, $SiCH_3$), 1.22 (br., 1 H, NH), 2.18 (s, 6 H, NCH_3), 2.31 (t, $^3J_{H,H}$ = 6.1 Hz, 2 H, CH_2NMe$_2$), 2.94 (t, $^3J_{H,H}$ = 6.1 Hz, 2 H, $SiNCH_2$) ppm. ^{13}C NMR (C_6D_6, 298 K): δ = −1.20 ($SiCH_3$), 39.2 ($SiNCH_2$), 45.5 (NCH_3), 63.5 (*C*H_2NMe$_2$) ppm. ^{29}Si NMR (C_6D_6, 298 K): δ = −8.7 ppm.

$NH_2CH_2CH_2NMe_2$·HCl: $C_4H_{13}ClN_2$ (124.61): calcd. C 38.6, H 10.5, Cl 28.5, N 22.5; found C 38.5, H 10.3, Cl 28.7, N 22.5. ^{1}H NMR ($CDCl_3$, 298 K): δ = 2.20 (s, 6 H, NCH_3), 2.52 (t, $^3J_{H,H}$ = 6 Hz, 2 H, CH_2), 2.96 (t, $^3J_{H,H}$ = 6 Hz, 2 H, CH_2), 7.2 (br., 3 H, NH) ppm. ^{13}C NMR ($CDCl_3$, 298 K): δ = 37.7 (CH_2), 45.4 (CH_3), 57.1 (CH_2) ppm.

$SiMe_2(NHCH_2CH_2CH_2NMe_2)_2$ (2, H_2L^2): Colourless liquid (4.2 g, 92% yield). $C_{12}H_{32}N_4Si$ (260.50): calcd. C 55.3, H 12.4, N 21.5; found 55.0, H 12.5, N 21.3. ^{1}H NMR (C_6D_6, 298 K): δ = 0.10 (s, 3 H, $SiCH_3$), 0.63 (br., 1 H, NH), 1.52 (quint, $^3J_{H,H}$ = 6.2 Hz, 2 H, $CH_2CH_2CH_2$), 2.11 (s, 6 H, NCH_3), 2.23 (t, $^3J_{H,H}$ = 6.2 Hz, 2 H, CH_2NMe$_2$), 2.84 (t, $^3J_{H,H}$ = 6.2 Hz, 2 H, $SiNCH_2$) ppm. ^{13}C NMR (C_6D_6, 298 K): δ = −1.02 ($SiCH_3$), 33.0 ($CH_2CH_2CH_2$), 39.8 ($SiNCH_2$), 45.7 (NCH_3), 57.9 (*C*H_2NMe$_2$) ppm. ^{29}Si NMR (C_6D_6, 298 K): δ = −9.3 ppm.

$NH_2CH_2CH_2CH_2NMe_2$·HCl: $C_5H_{15}ClN_2$ (138.64): calcd. C 43.3, H 10.9, Cl 25.6, N 20.2; found C 42.9, H 11.0, Cl 21.0, N 20.5. ^{1}H NMR ($CDCl_3$, 298 K): δ = 1.81 (quint, $^3J_{H,H}$ = 6.0 Hz, 2 H, CH_2), 2.27 (s, 6 H, NCH_3), 2.52 (t, $^3J_{H,H}$ = 6.0 Hz, 2 H, NCH_2), 3.09 (t, 2 H, NCH_2, $^3J_{H,H}$ = 6.0 Hz), 6.1 (br., 3 H, NH) ppm.

$SiMe_2(NHCH_2CH_2OMe)_2$ (3, H_2L^3): Colourless liquid (2.5 g 90% yield). $C_8H_{22}N_2O_2Si$ (206.36): calcd. C 46.6, H 10.7, N 13.6; found 46.5, H 10.5, N 13.8. ^{1}H NMR (C_6D_6, 298 K): δ = 1.10 (br., 1 H, NH), 1.28 (s, 3 H, $SiCH_3$), 2.88 (q, $^3J_{H,H}$ = 5.40 Hz, 2 H, NCH_2), 3.14 (s, 3 H, OCH_3), 3.18 (t, $^3J_{H,H}$ = 5.4 Hz, 2 H, OCH_2) ppm. ^{13}C NMR (C_6D_6, 298 K): δ = −1.24 ($SiCH_3$), 41.1 (NCH_2), 58.4 (OCH_3), 76.1 (OCH_2) ppm. ^{29}Si NMR (C_6D_6, 298 K): δ = −8.0 ppm.

$NH_2CH_2CH_2OMe$·HCl: $C_3H_{10}ClNO$ (111.57): calcd. C 32.3, H 9.0, Cl 31.8, N 12.6; found C 32.2, H 9.2, Cl 31.7, N 12.4. ^{1}H NMR ($CDCl_3$, 298 K): δ = 3.16 (t, 2 H, OCH_2, $^3J_{H,H}$ = 5.1 Hz), 3.29 (s, 3 H, OCH_3), 3.62 (t, $^3J_{H,H}$ = 5.1 Hz, 2 H, NCH_2), 8.02 (br., 3 H, NH) ppm. ^{13}C NMR ($CDCl_3$, 298 K): δ = 39.3 (OCH_2), 58.8 (OCH_3). 68.0 (NCH_2) ppm.

$SiMe_2(NHCH_2CH_2CH_2OMe)_2$ (4, H_2L^4): Colourless liquid (3.7 g, 94% yield). $C_{10}H_{26}N_2O_2Si$ (234.41): calcd. C 51.2, H 11.2, N 12.0; found 51.5, H 11.0, N 11.9. ^{1}H NMR (C_6D_6, 298 K): δ = −0.04 (s, 3 H, $SiCH_3$), 0.56 (br., 1 H, NH), 1.54 (m, 2 H, CH_2), 2.76 (t, $^3J_{H,H}$ = 6.6 Hz, 2 H, NCH_2), 3.11 (s, 3 H, OCH_3), 3.24 (t, $^3J_{H,H}$ = 6.2 Hz, 2 H, OCH_2) ppm. ^{13}C NMR (C_6D_6, 298 K): δ = −1.23 ($SiCH_3$), 34.1 (CH_2), 38.6 (NCH_2), 58.3 (OCH_3), 70.7 (OCH_2) ppm. ^{29}Si NMR (C_6D_6, 298 K): δ = −8.9 ppm.

$NH_2CH_2CH_2CH_2OMe$·HCl: $C_4H_{12}ClNO$ (125.60): calcd. C 38.3, H 9.6, Cl 28.2, N 11.2; found C 38.4, H 10.0, Cl 28.0, N 11.0. ^{1}H NMR ($CDCl_3$, 298 K): δ = 2.02 (m, 2 H, CH_2), 3.15 (t, 2 H, NCH_2, $^3J_{H,H}$ = 6.5 Hz), 3.30 (s, 3 H, OCH_3), 3.52 (t, 2 H, OCH_2, 5.7 Hz), 8.2 (br., 3 H, NH) ppm. ^{13}C NMR ($CDCl_3$, 298 K): δ = 38.4 (CH_2), 58.8 (NCH_2), 61.6 (OCH_3), 70.3 (OCH_2) ppm.

Synthesis of $Li_2\{SiMe_2[N(CH_2)_nX]_2\}$ (Li_2L, X = NMe_2, OMe; *n* = 2, 3): Only the synthesis of $Li_2[SiMe_2(NCH_2CH_2NMe_2)_2]$ is reported in detail, the other reactions being similar. A solution of $SiMe_2(NHCH_2CH_2NMe_2)_2$ (1.50 g, 6.45 mmol) in Et_2O (25 mL) was treated with MeLi (1.6 M, in Et_2O, 8.1 mL, 13.0 mmol) at room temperature. Prompt gas evolution was observed and after 2 h stirring the solution was evaporated to dryness yielding a colourless solid identified as $Li_2[SiMe_2(NCH_2CH_2NMe_2)_2]$ (**5**, Li_2L^1, 1.45 g, 92% yield). $C_{10}H_{26}Li_2N_4Si$ (244.31): calcd. C 49.2, H 10.7, N 22.9; found C 49.0, H 11.0, N 23.0. ^{1}H NMR (C_6D_6, 298 K): δ = 0.33 (s, 3 H, $SiCH_3$), 2.06 (s, 6 H, NCH_3), 2.29 (t, $^3J_{H,H}$ = 5.4 Hz, 2 H, CH_2NMe$_2$), 3.32 (t, $^3J_{H,H}$ = 5.4, 2 H, $SiNCH_2$) ppm. ^{7}Li NMR (C_6D_6, 298 K): δ = 9.9 ppm. ^{13}C NMR (C_6D_6, 298 K): δ = 0.57 ($SiCH_3$), 44.4 ($SiNCH_2$), 44.8 (NCH_3), 68.3 (*C*H_2NMe$_2$) ppm. ^{29}Si NMR (C_6D_6, 298 K): δ = −9.5 ppm.

$Li_2[SiMe_2(NCH_2CH_2CH_2NMe_2)_2]$ (6, Li_2L^2): Colourless solid (1.2 g, 95% yield). $C_{12}H_{30}Li_2N_4Si$ (272.36): calcd. C 52.9, H 11.1, N 20.6; found C 53.0, H 11.0, N 20.8. ^{1}H NMR (C_6D_6, 298 K): δ = 0.27 (s, 3 H, $SiCH_3$), 1.51 (m, 2 H, $CH_2CH_2CH_2$), 2.06 (s, 6 H, NCH_3), 2.24 (m, 2 H, CH_2NMe$_2$), 3.37 (m, 2 H, $SiNCH_2$) ppm. ^{7}Li NMR (C_6D_6, 298 K): δ = 10.5 ppm. ^{13}C NMR (C_6D_6, 298 K): δ = 1.76 ($SiCH_3$), 34.7 ($CH_2CH_2CH_2$), 45.7 (NCH_3), 50.7 ($SiNCH_2$), 63.7 (*C*H_2NMe$_2$) ppm. ^{29}Si NMR (C_6D_6, 298 K): δ = −11.6 ppm.

$Li_2[SiMe_2(NCH_2CH_2OMe)_2]$ (7, Li_2L^3): Colourless solid (1.7 g, 90% yield). $C_8H_{20}Li_2N_2O_2Si$ (218.22): calcd. C 44.0, H 9.2, N 12.8; found C 44.2, H 9.1, N 12.7. ^{1}H NMR (C_6D_6, 298 K): δ = 0.28 (s, 3 H, $SiCH_3$), 3.15 (s, 3 H, OCH_3), 3.37 (t, $^3J_{H,H}$ = 4.5 Hz, 2 H, NCH_2), 3.44 (t, $^3J_{H,H}$ = 4.5 Hz, 2 H, OCH_2) ppm. ^{7}Li NMR (C_6D_6, 298 K): δ = 9.6 ppm. ^{13}C NMR (C_6D_6, 298 K): δ = 2.19 ($SiCH_3$), 47.6 (NCH_2), 58.5 (OCH_3), 80.5 (OCH_2) ppm. ^{29}Si NMR (C_6D_6, 298 K): δ = −11.1 ppm.

$Li_2[SiMe_2(NCH_2CH_2CH_2OMe)_2]$ (8, Li_2L^4): Colourless solid (1.0 g, 93% yield). $C_{10}H_{24}Li_2N_2O_2Si$ (246.28): calcd. C 48.8, H 9.8, N 11.4; found C 48.9, H 9.7, N 11.3. ^{1}H NMR (C_6D_6, 298 K): δ = 0.29 (s, 3 H, $SiCH_3$), 1.68 (m, 2 H, CH_2), 3.12 (s, 3 H, OCH_3), 3.27 (t, $^3J_{H,H}$ = 4.8 Hz, 2 H, NCH_2), 3.46 (m, 2 H, OCH_2) ppm. ^{7}Li NMR (C_6D_6, 298 K): δ = 10.2 ppm. ^{13}C NMR (C_6D_6, 298 K): δ = 1.01 ($SiCH_3$), 39.0 (CH_2), 48.9 (NCH_2), 59.6 (OCH_3), 77.4 (OCH_2) ppm. ^{29}Si NMR (C_6D_6, 298 K): δ = −11.0 ppm.

 © 2004 Wiley-VCH Verlag GmbH & Co. KGaA, Weinheim

Synthesis of [$ZrCl_2${SiMe[$N(CH_2)_nX$]}] [$ZrCl_2(L)$; X = NMe_2, OMe; *n* = 2, 3]: Only the synthesis of [$ZrCl_2(L^1)$] is reported in detail, the other ones being similar. A solution of Li_2L^1 (800 mg, 3.27 mmol) in Et_2O (30 mL) was cooled to 243 K and then $ZrCl_4$ (762 mg, 3.27 mmol) was added. After 3 h stirring at 243 K, the suspension was allowed to warm up to room temperature and then filtered (260 mg of colourless solid). The filtrate was evaporated to dryness and [$ZrCl_2${$SiMe_2(NCH_2CH_2NMe_2)_2$}] (**9**, 770 mg g, 60% yield) was obtained as a colourless solid after recrystallisation from pentane at 249 K. $C_{10}H_{26}Cl_2N_4SiZr$ (392.56): calcd. C 30.6, H 6.7, Cl 18.1, N 14.3; found C 31.0, H 6.5, Cl 18.0, N 14.0. ^{1}H NMR (C_6D_6, 298 K): δ = 0.23 (s, 3 H, $SiCH_3$), 2.35 (s, 6 H, NCH_3), 2.81 (t, $^3J_{H,H}$ = 5.4 Hz, 2 H, CH_2NMe_2), 3.37 (t, $^3J_{H,H}$ = 5.4 Hz, 2 H, $SiNCH_2$) ppm. ^{13}C NMR (C_6D_6, 298 K): δ = 0.11 ($SiCH_3$), 46.3 (NCH_3), 46.8 ($SiNCH_2$), 63.9 (CH_2NMe_2) ppm. ^{29}Si NMR (C_6D_6, 298 K): δ = −23.3 ppm.

[$ZrCl_2${$SiMe_2(NCH_2CH_2CH_2NMe_2)_2$}] [10, $ZrCl_2(L^2)$]: Colourless solid, recrystallised from pentane at 249 K (560 mg, 70% yield). $C_{12}H_{30}Cl_2N_4SiZr$ (420.61): calcd. C 34.3, H 7.2, Cl 16.9, N 13.3; found C 34.0, H 7.0, Cl 17.0, N 13.5. ^{1}H NMR (C_6D_6, 298 K): δ = 0.17 (s, 3 H, $SiCH_3$), 1.34 (m, 2 H, $CH_2CH_2CH_2$), 2.41 (s, 6 H, NCH_3), 2.59 (m, 2 H, CH_2NMe_2), 3.62 (m, 2 H, $SiNCH_2$) ppm. ^{13}C NMR (C_6D_6, 298 K): δ = 0.33 ($SiCH_3$), 29.9 ($CH_2CH_2CH_2$), 48.2 (NCH_3), 49.6 ($SiNCH_2$), 63.8 (CH_2NMe_2) ppm. ^{29}Si NMR (C_6D_6, 298 K): δ = −28.8 ppm.

[$ZrCl_2${$SiMe_2(NCH_2CH_2OMe)_2$}] [11, $ZrCl_2(L^3)$]: Colourless solid, recrystallised from pentane at 249 K (612 mg, 70% yield). $C_8H_{20}Cl_2N_2O_2SiZr$ (366.47): calcd. C 26.2, H 5.5, Cl 19.3, N 7.6; found C 26.0, H 5.5, Cl 19.5, N 7.6. ^{1}H NMR (C_6D_6, 298 K): δ = 0.41 (s, 3 H, $SiCH_3$), 3.48 (t, $^3J_{H,H}$ = 5.7 Hz, 2 H, NCH_2), 3.56 (s, 3 H, OCH_3), 3.58 (t, $^3J_{H,H}$ = 5.7 Hz, 2 H, OCH_2) ppm. ^{13}C NMR (C_6D_6, 298 K): δ = 1.24 ($SiCH_3$), 47.2 (OCH_3), 61.1 (NCH_2), 78.4 (OCH_2) ppm.

[$ZrCl_2${$SiMe_2(NCH_2CH_2CH_2OMe)_2$}] [12, $ZrCl_2(L^4)$]: Colourless solid, recrystallised from pentane at 249 K, 850 mg, 70% yield]. $C_{10}H_{24}Cl_2N_2O_2SiZr$ (394.52): calcd. C 30.4, H 6.1, Cl 18.0, N 7.1; found C 30.3, H 6.2, Cl 17.9, N 7.0. ^{1}H NMR (C_6D_6, 298 K): δ = 0.44 ($SiCH_3$), 1.77 (m, 2 H, CH_2), 3.23 (s, 3 H, OCH_3), 3.24 (t, $^3J_{H,H}$ = 5.6 Hz, 2 H, NCH_2), 3.55 (m, 2 H, OCH_2) ppm. ^{13}C NMR (C_6D_6, 298 K): δ = −1.02 ($SiCH_3$), 32.7 (CH_2), 48.1 (NCH_2), 60.5 (OCH_3), 76.9 (OCH_2) ppm.

Synthesis of $ZrMe_2${$SiMe_2[N(CH_2)_nNMe_2]_2$} [$ZrMe_2(L^1)$, *n* = 2; $ZrMe_2(L^2)$, *n* = 3] From $ZrMe_4$ and H_2L (L = L^1, L^2): Only the procedure yielding [$ZrMe_2(L^1)$] is reported in detail, the other reaction being similar. A solution of MeLi in Et_2O (1.6 M, 12.9 mL, 20.6 mmol) was added to 20 mL of Et_2O, cooled to 243 K and treated with $ZrCl_4$ (1.20 g, 5.15 mmol). After 1 h stirring at 243 K, H_2L^1 (1.20 g, 5.16 mmol) was added dropwise. After a further 2 h stirring at 243 K, the suspension was allowed to warm to room temperature and then filtered (820 mg of a colourless solid). The solution was evaporated to dryness yielding a pale-orange sticky material identified as [$ZrMe_2${$SiMe_2(NCH_2CH_2NMe_2)_2$}] (**13**, 1.72 g, 95% yield). $C_{12}H_{32}N_4SiZr$ (351.72): calcd. C 41.0, H 9.2, N 15.9; found C 41.2, H 9.0, N 16.0. ^{1}H NMR (C_6D_6, 298 K): δ = −0.12 (s, 3 H, $ZrCH_3$), 0.40 (s, 3 H, $SiCH_3$), 2.23 (s, 6 H, NCH_3), 2.61 (t, $^3J_{H,H}$ = 5.5 Hz, 2 H, CH_2NMe_2), 3.54 (t, $^3J_{H,H}$ = 5.5 Hz, 2 H, $SiNCH_2$) ppm. ^{13}C NMR (C_6D_6, 298 K): δ = 1.55 ($SiCH_3$), 33.2 ($ZrCH_3$), 46.3 (NCH_3), 46.4 ($SiNCH_2$), 65.3 (CH_2NMe_2) ppm. ^{29}Si NMR (C_6D_6, 298 K): δ = −22.4 ppm.

[$ZrMe_2${$SiMe_2(NCH_2CH_2CH_2NMe_2)_2$}] [14, $ZrMe_2(L^2)$]: Pale-yellow solid (950 mg, 90% yield). $C_{14}H_{36}N_4SiZr$ (379.77): calcd. C 44.3, H 9.6, N 14.8; found C 44.2, H 9.8, N 14.8. ^{1}H NMR (C_6D_6, 298 K): δ = −0.07 (s, 3 H, $ZrCH_3$), 0.41 (s, 3 H, $SiCH_3$), 1.62 (q, $^3J_{H,H}$ = 6.4 Hz, 2 H, $CH_2CH_2CH_2$), 2.01 (s, 6 H, NCH_3), 2.27 (t, $^3J_{H,H}$ = 6.4 Hz, 2 H, CH_2NMe_2), 3.58 (t, $^3J_{H,H}$ = 6.4 Hz, 2 H, $SiNCH_2$) ppm. ^{13}C NMR (C_6D_6, 298 K): δ = 59.3 (CH_2NMe_2), 47.3 ($SiNCH_2$), 45.7 (NCH_3), 34.0 ($CH_2CH_2CH_2$), 15.4 ($ZrCH_3$), 2.87 ($SiCH_3$) ppm.

From [$ZrCl_2(L^1)$] and MeLi: A solution of [$ZrCl_2(L^1)$] (212 mg, 0.54 mmol) in Et_2O was cooled to 243 K and treated with a solution of MeLi in Et_2O (1.6 M, 0.68 mL, 1.09 mmol), yielding a pale-yellow solution, which was allowed to slowly warm up to room temperature (about 30 min). The precipitation of a colourless solid was observed and the suspension was stirred at room temperature for 1 h. The solid was filtered off (42 mg) and the solvents were evaporated from the pale-yellow filtrate, yielding a pale-orange sticky material analytically and spectroscopically identified as [$ZrMe_2(L^1)$] (175 mg, 350 mg, 92% yield).

Synthesis of [$Zr(NMe_2)_2${$SiMe_2(NCH_2CH_2NMe_2)_2$}]: A toluene solution (25 mL) of $Zr(NMe_2)_4$ (452 mg, 1.69 mmol) was treated with H_2L^1 (395 mg, 1.70 mmol). After 2 h stirring, the solution was evaporated to dryness and the colourless residue identified as $Zr(NMe_2)_2$[$SiMe_2(NCH_2CH_2NMe_2)_2$] [**15**, $Zr(NMe_2)_2(L^1)$, 630 mg, 91% yield]. $C_{14}H_{38}N_6SiZr$ (409.80): calcd. C 41.0, H 9.3, N 20.5; found C 41.2, H 9.5, N 20.3. ^{1}H NMR (C_6D_6, 298 K): δ = 0.35 (s, 3 H, $SiCH_3$), 2.04 (s, 6 H, CH_2NCH_3), 2.39 (t, $^3J_{H,H}$ = 5.7 Hz, 2 H, CH_2NMe_2), 2.81 (s, 6 H, $ZrNCH_3$), 3.51 (t, $^3J_{H,H}$ = 5.7 Hz, 2 H, $SiNCH_2$) ppm. ^{13}C NMR (C_6D_6, 298 K): δ = 1.09 ($SiCH_3$), 44.2 ($ZrNCH_3$), 46.0 ($SiNCH_2$), 46.1 (CH_2NCH_3), 64.3 (CH_2NMe_2) ppm. ^{29}Si NMR (C_6D_6, 298 K): δ = −20.3.

Synthesis of [$ZrCl_{2-x}(NMe_2)_x${$SiMe_2(NCH_2CH_2CH_2NMe_2)_2$}] (*x* = 1, 2). Only the procedure yielding [$Zr(NMe_2)_2(L^2)$] is described, the other one being similar. A solution of [$ZrCl_2(L^2)$] (324 mg, 0.77 mmol) in Et_2O (25 mL) was treated with $LiNMe_2$ (79 mg, 1.55 mmol) and the prompt precipitation of a colourless solid was observed. After 30 min stirring, the suspension was filtered and the filtrate evaporated in vacuo to dryness yielding a colourless solid identified as [$Zr(NMe_2)_2${$SiMe_2(NCH_2CH_2CH_2NMe_2)_2$}] (**16**, 296 mg, 88% yield). $C_{16}H_{42}N_6SiZr$ (437.86): calcd. C 43.9, H 9.7, N 19.2; found C 44.0, H 10.0, N 19.0. ^{1}H NMR (C_6D_6, 298 K): δ = 0.46 (s, 3 H, $SiCH_3$), 1.69 (quint, $^3J_{H,H}$ = 6.4 Hz, 2 H, $CH_2CH_2CH_2$), 2.05 (s, 6 H, CH_2NCH_3), 2.32 (t, $^3J_{H,H}$ = 6.4 Hz, 2 H, CH_2NMe_2), 2.95 (s, 6 H, $ZrNCH_3$), 3.51 (t, $^3J_{H,H}$ = 6.4 Hz, 2 H, $SiNCH_2$) ppm. ^{13}C NMR (C_6D_6, 298 K): δ = 1.06 ($SiCH_3$), 32.7 (CH_2), 42.4 ($ZrNCH_3$), 46.8 (CH_2NCH_3), 47.8 ($SiNCH_2$), 61.0 (CH_2NMe_2) ppm. ^{29}Si NMR (C_6D_6, 298 K): δ = −24.7 ppm.

[$ZrCl(NMe_2)${$SiMe_2(NCH_2CH_2CH_2NMe_2)_2$}] [17, $ZrCl(NMe_2)(L^2)$]: Colourless solid (512 mg, 85% yield). $C_{14}H_{36}ClN_5SiZr$ (429.23): calcd. C 39.2, H 8.5, Cl 8.3, N 16.3; found C 39.0, H 8.4, Cl 8.0, N, 16.2. ^{1}H NMR (C_6D_6, 298 K): δ = 0.28 (s, 3 H, $SiCH_3$), 0.31 (s, 3 H, $SiCH_3$), 1.40 (br., 2 H, $CH_2CH_2CH_2$), 1.56 (br., 2 H, $CH_2CH_2CH_2$), 2.05 (m, 2 H, CH_2NMe_2), 2.28 (s, 12 H, CH_2NCH_3), 2.82 (m, 2 H, CH_2NMe_2), 2.99 (s, 6 H, $ZrNCH_3$), 3.57 (br., 4 H, $SiNCH_2$) ppm. ^{13}C NMR (C_6D_6, 298 K): δ = 1.1 ($SiCH_3$), 1.4 ($SiCH_3$), 30.3 (CH_2), 45.1 ($ZrNCH_3$), 48.1 ($SiNCH_2$), 48.2 (CH_2NCH_3), 64.0 (CH_2NMe_2) ppm. ^{29}Si NMR (C_6D_6, 298 K): δ = −22.1 ppm.

Crystal Structure determination of [$ZrCl_2(L^2)$] (10), [$ZrCl_2(L^4)$] (12) and [$Zr(NMe_2)_2(L^1)$] (15): Crystals of **10**, **12** and **15** were grown by slowly evaporating pentane (**10**, **15**) or Et_2O (**12**) from solutions of the compounds. The crystals were placed in Lindemann glass

 © 2004 Wiley-VCH Verlag GmbH & Co. KGaA, Weinheim

Table 4. Crystallographic data for $[ZrCl_2(L^2)]$ (**10**), $[ZrCl_2(L^4)]$ (**12**) and $[Zr(NMe_2)_2(L^1)]$ (**15**)

Compound	**10**	**12**	**15**
Chemical formula	$C_{12}H_{30}N_4Cl_2SiZr$	$C_{10}H_{24}N_2O_2Cl_2SiZr$	$C_{14}H_{38}N_6SiZr$
Molecular weight	420.61	394.52	409.80
Crystal system	monoclinic	orthorhombic	monoclinic
Space group	$P2_1/n$	*Cmca*	$P2_1/n$
a (Å)	10.349(2)	11.393(3)	16.121(3)
b (Å)	15.037(3)	17.033(3)	9.128(2)
c (Å)	13.110(3)	18.209(3)	16.308(3)
β (°)	106.41(4)		111.57(3)
V (Å^3)	1957.0(7)	3534(1)	2231.7(9)
Z	4	8	4
$D_{calcd.}$ (g cm^{-3})	1.428	1.483	1.220
F(000)	872	1616	872
μ(Mo-K_α) (mm^{-1})	0.893	0.989	0.553
Reflections collected	4500	2920	4848
Reflections observed [$I \geq 2\sigma(I)$]	4434	1825	4333
Final *R*1, *wR*2[a]	0.035; 0.089	0.059; 0.155	0.086; 0.180

[a] $R1 = \|\|F_o| - |F_c\|/|F_o|$; $wR2 = \{[w(F_o^2 - F_c^2)^2]/[w(F_o^2)^2]\}^{1/2}$.

capillaries and centred on a four-circle Philips PW1100 diffractometer using graphite-monochromated Mo-K_α radiation (λ = 0.71073 Å), at room temperature, following standard procedures. The diffraction data were corrected for Lorentz polarisation effects and for absorption, as described by North et al.[10]

The structures were solved by standard direct methods[11] and subsequently completed by Fourier syntheses. Non-hydrogen atoms were refined anisotropically in all the structures. The hydrogen atoms were introduced at the calculated positions with fixed isotropic thermal parameters (1.2 U_{equiv} of the parent carbon atom), except for the hydrogens of the CH_2 moiety of $ZrCl_2(L^2)$ (**10**), which were located from Fourier maps and refined isotropically. The C(2) carbon of **12** is disordered in two positions with an occupation factor of 0.5. Figure 1B shows only one of the two positions of C(2).

Structure refinement and final geometrical calculations were carried out with the SHELXL-97[12] program, implemented with the WinGX package.[13] Drawings were produced by using the ORTEP II program.[14] Crystallographic data are listed in Table 4. CCDC-207384 (**10**), -220157 (**12**) and -207385 (**15**) contain the supplementary crystallographic data for this paper. The data can be obtained free of charge at www.ccdc.cam.ac.uk/conts/retrieving.html [or from the Cambridge Crystallographic Data Centre, 12 Union Road, Cambridge CB2 1EZ, UK; Fax: (internat.) +44-1223/336-033; E-mail: deposit@ccdc.cam.ac.uk].

Acknowledgments

The authors thank Mrs Annarosa Moresco (ICIS-CNR, Padova) for the elemental analyses. VP is indebted to Prof. Fausto Calderazzo (Università di Pisa), Dr. Lorella Marchetti (Università di Pisa) and Dr. Sergio Tamburini (ICIS-CNR) for helpful discussions and insightful comments.

[1] [1a] R. Kempe, *Angew. Chem. Int. Ed.* **2000**, *39*, 468. [1b] G. J. P. Britovsek, V. C. Gibson, D. F. Wass, *Angew. Chem. Int. Ed.* **1999**, *38*, 429. [1c] L. H. Gade, *Chem. Commun.* **2000**, 173. [1d] V. C. Gibson, B. S. Kimberley, A. J. P. White, D. J. Williams, P. Howard, *Chem. Commun.* **1998**, 313.

[2] [2a] D. J. Brauer, H. Bürger, E. Essig, W. Geschwandtner, *J. Organomet. Chem.* **1980**, *190*, 343. [2b] W. D. Von Beiersdorf, D. J. Brauer, H. Bürger, *Z. Anorg. Allg. Chem.* **1981**, *475*, 56. [2c] H. Bürger, W. Geschwandtner, G. R. Liewald, *J. Organomet. Chem.* **1983**, *259*, 145. [2d] R. A. Jones, M. H. Seeberger, J. L. Atwood, W. E. Hunter, *J. Organomet. Chem.* **1983**, *247*, 1. [2e] D. J. Brauer, H. Bürger, W. Geschwandtner, G. R. Liewald, C. Krüger, *J. Organomet. Chem.* **1983**, *248*, 1. [2f] F. Preuss, E. Fuchslocher, W. S. Sheldrick, *Z. Naturforsch., Teil B* **1985**, *40*, 1040. [2g] M. Veith, H. Lange, A. Belo, O. Recktenwald, *Chem. Ber.* **1985**, *118*, 1600. [2h] D. J. Brauer, H. Bürger, G. R. Liewald, *J. Organomet. Chem.* **1986**, *307*, 177. [2i] D. J. Brauer, H. Bürger, G. R. Liewald, J. Wilke, *J. Organomet. Chem.* **1986**, *310*, 317. [2j] M. Veith, W. Frank, F. Töllner, H. Lange, *J. Organomet. Chem.* **1987**, *326*, 315. [2k] R. Buheitel, W. Milius, W. Schnick, *Z. Naturforsch., Teil B* **1996**, *51*, 1141. [2l] A. D. Horton, J. de With, *Organometallics* **1997**, *16*, 5424. [2m] F. J. Shattenmann, R. R. Schrock, W. M. Davis, *Organometallics* **1998**, *17*, 989. [2n] H. Schumann, J. Gottfriedsen, S. Dechert, F. Girgsdies, *Z. Anorg. Allg. Chem.* **2000**, *626*, 747. [2o] S.-J. Kim, I. N. Jung, B. R. Yoo, S. H. Kim, J. Ko, D. Byun, S. O. Kang, *Organometallics* **2001**, *20*, 2136. [2p] M. S. Hill, P. B. Hitchcock, *Organometallics* **2002**, *21*, 3258. [2q] S.-J. Kim, Y.-J. Lee, S. H. Kim, J. Ko, S. Cho, S. O. Kang, *Organometallics* **2002**, *21*, 5358. [2r] V. Passarelli, F. Benetollo, P. Zanella, G. Carta, G. Rossetto, *Dalton Trans.* **2003**, 1411.

[3] [3a] Assuming an octahedral coordination polyhedron for the metal centre in $ZrY_2(L)$, two coordination modes can be proposed, namely symmetric and asymmetric, and two isomers are postulable for the symmetric mode, namely *cis* and *trans* (vide infra). [3b] As far as the NMR-based solution molecular structure elucidation of $ZrY_2(L)$ is concerned, when symmetrically coordinated to the ZrY_2 moiety, L should show equivalent methylene (^{1}H, ^{13}C) resonances for the two $SiN(CH_2)_nX$ moieties. On the other hand, the two halves of the asymmetrically coordinated L should be nonequivalent.

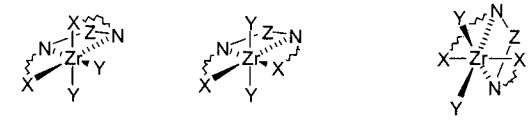

X = NMe_2, OMe; Y = Cl, Me, NMe_2; Z = $SiMe_2$

[4] As examples, Zr−N is 2.43 Å in [$ZrCl_4$(TMEDA)] (TMEDA = *N*,*N*,*N*′,*N*′-tetramethylethylenediamine) [cf. C. E. F. Rickard, M. W. Glenny, A. J. Nielson, *Acta Crystallogr., Sect. E (Struct. Rep. Online)*, **2003**, *59*, m183] and Zr−O(DME) is 2.33 Å in [$ZrCl_2(OSiPh_3)_2$(DME)] (DME = 1,2-dimethoxyethane) [cf. E. A. Babian, D. C. Hrnicr, S. G. Bott, J. L. Atwood, *Inorg. Chem.* **1986**, *25*, 4818].

[5] For examples of $ZrCl_2[N_4]$ complexes, see: [5a] S. B. Cortright, J. N. Johnston, *Angew. Chem. Int. Ed.* **2002**, *41*, 345. [5b] R. M. Porter, S. Winston, A. A. Danopoulos, M. B. Hursthouse, *J. Chem. Soc., Dalton Trans.* **2002**, 3290. [5c] J.-H. Huang, L.-S. Chi, R.-C. Yu, G. J. Jiang, W.-T. Yang, G.-H. Lee, S.-M. Peng, *Organometallics* **2001**, *20*, 5788. [5d] D. M. Dawson, D. A. Walker, M. Thornton-Pett, M. Bochmann, *J. Chem. Soc., Dalton Trans.* **2000**, 459. [5e] D. Wood, G. P. A. Yap, D. S. Richeson, *Inorg. Chem.* **1999**, *38*, 5788. [5f] B.-J. Deelman, P. B. Hitchcock, M. F. Lappert, W.-P. Leung, H.-K. Lee, T. C. W. Mak, *Organometallics* **1999**, *18*, 1444. [5g] A. J. Rogers, E. Solari, C. Floriani, A. Chiesi-Villa, C. Rizzoli, *J. Chem. Soc., Dalton Trans.* **1997**, 2385. For examples of $ZrCl_2[N_2O_2]$ complexes, see: [5h] P. E. O'Connor, D. J. Morrison, S. Steeves, K. Burrage, D. J. Berg, *Organometallics* **2001**, *20*, 1153. [5i] X. Zhang, Q. Zhu, I. A. Guzel, R. F. Jordan, *J. Am. Chem. Soc.* **2000**, *122*, 8093. [5j] L. H. Gade, S. Friedrich, D. J. M. Trisch, I. J. Scowen, M. McPartin, *Inorg. Chem.* **1999**, *38*, 5295. [5k] P. R. Woodman, I. J. Munslow, P. B. Hitchcock, P. Scott, *J. Chem. Soc., Dalton Trans.* **1999**, 4069. [5l] S. Brenner, R. Kempe, P. Arndt, *Z. Anorg. Allg. Chem.* **1995**, *621*, 2021.

[6] At room temperature the amino NMe_2 methyl groups are equivalent (^1H, ^{13}C), but at 193 K they yield two signals in agreement with the proposed molecular structure, suggesting exchange of the two methyl groups at room temperature.

[7] Harald Günther, "NMR spectroscopy", 2nd edition, John Wiley & Sons, Chichester, **1994**, p. 335.

[8] In principle, also electronic factors should be taken into account, specifically the Zr−NMe_2 π-bonding. Nevertheless, due to the similar nature of **15** and **17**, this contribution is expected to be similar in the two complexes, thus making the above-mentioned steric factors decisive in influencing the exchange mechanism.

[9] D. C. Bradley, I. M. Thomas, *J. Chem. Soc.* **1960**, 3857.

[10] A. T. C. North, D. C. Philips, F. S. Mathews, *Acta Crystallogr., Sect. A* **1968**, *24*, 351.

[11] A. Altomare, M. C. Burla, M. Camalli, G. L. Cascarano, C. Giacovazzo, A. Guagliardi, A. G. G. Moliterni, G. Polidori, R. Spagna, "SIR-97", *J. Appl. Crystallogr.* **1999**, *32*, 115.

[12] G. M. Sheldrick, "SHELXL-97", Program for the Refinement of Crystal Structures, University of Göttingen, Germany, **1997**.

[13] L. J. Farrugia, *J. Appl. Crystallogr.* **1999**, *32*, 837.

[14] L. J. Farrugia, "ORTEP3 for Windows", *J. Appl. Crystallogr.* **1997**, *30*, 565.

Received October 3, 2003
Early View Article
Published Online March 9, 2004

 © 2004 Wiley-VCH Verlag GmbH & Co. KGaA, Weinheim

Electronic Structures and Reactivities of Corrole−Copper Complexes

Inna Luobeznova,[a] Liliya Simkhovich,[a] Israel Goldberg,*[b] and Zeev Gross*[a]

Keywords: Copper / Cyclic voltammetry / Electronic structure / Porphyrinoids / Structure elucidation

The spectroscopic and electrochemical examination of the mononuclear copper complexes of 5,10,15-tris(pentafluorophenyl)corrole and 5,10,15-tris(2,6-dichlorophenyl)corrole (**1a** and **2a**, respectively) and of the corresponding dinuclear corrole dimers **1b** and **2b** reveal the existence of two almost degenerate electronic states. The lower state consists of copper(III) ions coordinated by closed-shell corrolato trianions and the higher state is composed of copper(II) ions chelated by open-shell corrolato dianions. The contributions from both states are evident in the molecular structure of monomeric and mononuclear **2a**, which displays a distorted square-planar coordination geometry around the metal ion and short Cu–N bond lengths typical of copper(III), together with some non-equivalence of the C_{α}–C_{meso} bond lengths that might reflect the open-shell character of the macrocycle. The latter state is most likely to be responsible for the dimerization process.

(© Wiley-VCH Verlag GmbH & Co. KGaA, 69451 Weinheim, Germany, 2004)

Introduction

Recent years have evidenced a real renaissance in the chemistry of corroles,[1,2] due to the introduction of three facile synthetic methodologies for preparation of triarylcorroles: the solvent-free condensation of pyrrole and aldehydes,[3] the modified Rothemund procedure,[4] and the condensation of dipyrromethane with aldehydes.[5,6] Among all the new corroles, the *meso*-pentafluorophenyl-substituted derivative H_3(tpfc) (**1** in Scheme 1) is by far the most intensively studied. This single corrole and its variants have been shown to support a large variety of metal ions (Cr,[7] Mn,[8] Fe,[9] Ru,[10] Co,[9,11] Rh,[9,12] Ni,[13] Pd,[12] Cu,[12] Zn,[14] Al,[15] Ga,[16] Ge,[9b] Sn,[9b] P[9b]) and many of these complexes have been fully characterized in several oxidation and coordination states. The novel features that were found for **1** and its metal complexes include very high fluorescence quantum yields,[13,14] easily achieved chirality,[10,12] potent catalytic activity,[17] facile methodologies for further functionalization,[18] and selective interactions with tumor cells.[19] Another important development is the introduction of corroles with *meso*-aryl groups that contain large *ortho*-phenyl substituents (Cl, CH_3), whose impact in affecting catalysis was demonstrated recently.[20]

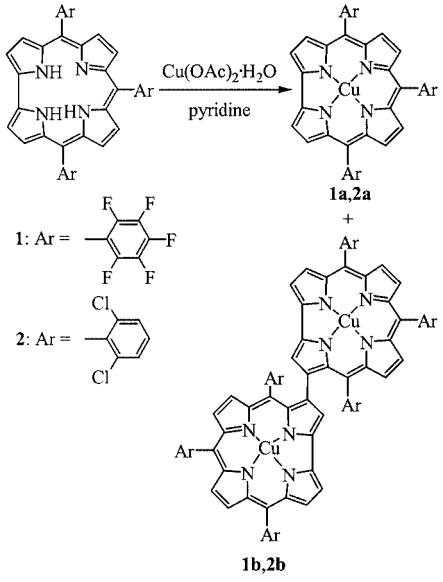

Scheme 1

One of the first metal ions inserted into the N_4 coordination core of corroles was copper,[21] but both the structural and electronic features of the complexes remained ill-defined for a very long time until, in 1997, Vogel and coworkers provided new insights into these issues by the isolation and full characterization of Cu(tetmc).[22a] This complex displays a square-planar coordination geometry, consistent with a d^8 copper(III) ion chelated by a closed-shell corrolato trianion. This appeared to be the ground state in solution as well, although the large shifts and broad signals of the resonances in the ^{1}H NMR spectra obtained at room

[a] Department of Chemistry and Institute of Catalysis Science and Technology, Technion − Israel Institute of Technology, Haifa 32000, Israel
Fax: (internat.) + 972-4-829-5703
E-mail: chr10zg@tx.technion.ac.il
[b] School of Chemistry, Tel Aviv University, Tel Aviv 69978, Israel
Fax: (internat.) + 972-3-640-9293
E-mail: goldberg@chemsg7.tau.ac.il

 © 2004 Wiley-VCH Verlag GmbH & Co. KGaA, Weinheim **DOI: 10.1002/ejic.200300806**

temperature clearly demonstrate that the electronic state with a copper(II) ion coordinated by an open-shell corrole (formally a dianion radical, but usually referred to as a corrole cation radical) is only slightly higher in energy. This coexistence of copper(III) and copper(II) radicals was also predicted by the DFT calculations of Ghosh et al.[22b] An additional complication exists in the electrochemistry of corrole−copper complexes, as demonstrated by Kadish and co-workers.[23] Reduction of Cu(oec) provided a simple copper(II) complex, but a dimeric product was formed upon oxidation. The latter was assigned as a non-covalent dimer held together by strong interactions between the π-systems of the corroles. This is reminiscent of the features of metalloporphyrin π-cation radicals,[24] although definite structural proof is still not available for corroles.

As part of our interest in the preparation and utilization of the metal complexes of **1**, isolation of its copper complex was one of the earliest goals that we wanted to achieve.[12] Insertion of copper proceeded well, but the corresponding complex, Cu(tpfc) (**1a**), was not stable in solution. Even carefully purified **1a** was converted within a few hours into a mixture of new complexes, which, according to mass spectrometry, are dimeric. This is reminiscent of our recent observation with the cobalt complexes of **1**: pentacoordinate [Co(tpfc)(PPh_3)] and hexacoordinate [Co(tpfc)(pyridine)$_2$] are very stable complexes, but the tetracoordinate Co(tpfc) is converted in high yield into a single isomer of a C−C-bound corrole dimer with two cobalt(III) ions.[11] This suggests that the complexes obtained from **1a** are analogous dimers, with a lower selectivity in the C−C bond formation being responsible for the observation of several isomers. In any case, the instability of **1a** in solution significantly hampered further research as it complicates the spectroscopic investigations and interferes with attempts to grow X-ray quality crystals. Because of these shortcomings, we have prepared the copper complex of 5,10,15-tris(2,6-dichlorophenyl)corrole [H_3(tdcc),[3a,3g] **2** in Scheme 1], anticipating that dimerization of this sterically protected corrole will be a less severe problem. Indeed, the much higher stability of monomeric **2a** allowed for its characterization by X-ray crystallography and the electronic states of the complexes were elucidated by a combination of spectroscopic methods and electrochemistry.

Results and Discussion

Synthesis

All the copper complexes were obtained from the reactions of the corresponding corrole with $Cu(OAc)_2{\cdot}H_2O$ in pyridine (Scheme 1). The insertion of copper was found to be a facile process for both **1** and **2**, proceeding to completion at room temperature within 30 min, and the red complexes **1a** and **2a** were obtained in 73 and 85% yield, respectively. The lower yield for the formation of **1a** was found to reflect its instability in solution: it is transformed into a mixture of green compounds within a few hours at room temp. All the green complexes display identical mass spectra, consistent with two copper ions coordinated by a dimeric corrole. This was confirmed by isolation of the major green complex (**1b**), whose spectroscopic features are consistent with the structure shown in Scheme 1. The other green complexes are most likely isomers of **1b** that differ in the identity of the carbon atoms that form the bond between the corroles. Three isomers are possible, even when only the more reactive carbon atoms of rings A and D are taken into account. The red complex **2a** is much more stable: only a minute amount of green dinuclear material is obtained when its solutions in CH_2Cl_2 are left for two weeks at room temp. This allowed us to grow X-ray quality crystals of **2a** and for its characterization by various spectroscopic methods. It was also possible to obtain appreciable amounts of the dinuclear complex **2b** (as a single isomer) by performing the copper insertion reaction at higher temperatures.

Electrochemistry

The cyclic voltammograms (CVs) of **1a** (freshly prepared) and **2a** displayed in Figure 1 show that the half-wave potentials of the former complex are more positive (easier to reduce and harder to oxidize) than for the latter, as expected for a corrole with more electron-withdrawing *meso* substituents. Based on a comparison with non-transition-metal complexes of **1**, wherein corrole-centered reductions occur below −1.0 V, the reduction waves [Cu(tpfc): $E_{1/2}$ = 0.22 V; Cu(tdcc): $E_{1/2}$ = 0.06 V] may be confidently assigned as reflecting metal-centered processes. The processes occurring with $E_{1/2}$ of 1.01 and 0.92 V for **1a** and **2a**, respectively, were assigned as reflecting corrole-centered oxidations based on the similarity of the oxidation potentials to that of gallium(III) complexes of **1** and **2**. The quite different spacing of the redox couples in **1a** (0.79 V) and **2a** (0.86 V) is also consistent with different centers involved in the reduction and oxidation processes. Taken together, the CVs of **1a** and **2a** indicate that while their reduction is metal-centered, the oxidation is corrole-centered. This was further confirmed

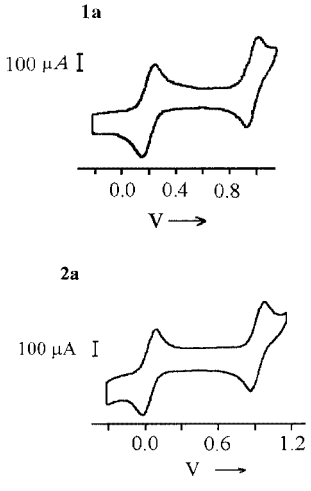

Figure 1. Cyclic voltammograms of Cu(tpfc) (**1a**: $E_{1/2}$ = 0.22 V and 1.01 V) and Cu(tdcc) (**2a**: $E_{1/2}$ = 0.06 and 0.92 V), in benzonitrile/5 × 10^{-4} M TBAP

 © 2004 Wiley-VCH Verlag GmbH & Co. KGaA, Weinheim

for **2a** by its chemical reduction ($Na_2S_2O_4$, EtOH/H_2O/Ar) and oxidation {[(4-Br-C_6H_5)N]$^+SbCl_6^-$, CH_2Cl_2}: the EPR spectra (see below for more details) are characteristic of corrole−copper(II) and −copper(III) radicals, respectively.

The CV of **2b** (Figure 2) shows that the subunits of the dinuclear dimeric corrole are not strongly interacting. Both the reduction and the oxidation waves are partially resolved, with $E_{1/2}$ = −0.17, 0.05 V and 0.82, 0.95 V, respectively. The similarities of the redox potentials of **2b** to those of **2a** suggest that the former complex undergoes stepwise reduction of the copper(III) ions at low potentials and stepwise oxidation of the corrole subunits at more positive potentials.

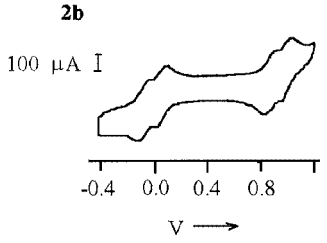

Figure 2. Cyclic voltammogram of the dinuclear corrole dimer **2b** ($E_{1/2}$ = −0.17, 0.05 V and 0.82, 0.95 V) in benzonitrile/5 × 10^{-4} M TBAP

Spectroscopy

Complexes **1a** and **2a** are EPR-silent and their NMR spectra at low temperature (Figure 3a, c) display resonances that are sharp enough to determine the characteristic vicinal coupling constants of the β-pyrrole hydrogen and the *meso*-C_6F_5 fluorine atoms ($J_{H,H} \approx 4$, $J_{F,F} \approx 23$ Hz). This data is consistent with expectations for diamagnetic square-planar d^8 complexes, suggesting that **1a** and **2a** contain low-spin copper(III) ions coordinated by closed-shell corroles. The first clue that this description might be oversimplified is that the ^{1}H NMR chemical shifts are at higher field (δ = 6.9−7.7 ppm) than in the corresponding free-base corroles and their complexes with other diamagnetic metal ions (δ = 8.2−9.2 ppm).[3−5,11,15,16] What is more, both the ^{1}H and the ^{19}F NMR resonances are much broader in the spectra recorded at higher temperatures (Figure 3b, d). These changes are fully reversible, suggesting a coexistence of dia- and paramagnetic electronic states, with the former being dominant at lower temperatures. There are three conceivable possibilities that might explain the indications for diamagnetism at low temperatures and paramagnetism at high temperatures: a low-spin vs. high-spin corrole−copper(III) complex, a dimeric (cofacial) vs. monomeric corrole−copper(II) radical, and a corrole−copper(III) complex vs. a corrole−copper(II) radical. The first suggestion is the least likely: the large ligand field stabilization energy (LFSE) of copper(III) enforces a d^8 low-spin configuration in square-planar geometry, while higher coordination numbers should actually be less populated at high temperatures. The second proposal is more probable, especially since similar temperature effects have been observed for porphyrin−copper(II) radicals. However, non-covalent dimerization of π-cation radical complexes (of porphyrins and corroles) is only effective in the absence of prohibitive steric effects.[24] This is not the case for **1a** and **2a**, as proven by the crystal structure of the latter (vide infra). Accordingly, the only reasonable explanation that remains is that the ground state of the corrole−copper(III) complex is only slightly lower in energy than that of the corrole−copper(II) radical (Scheme 2). The contribution of the latter state increases with temperature, exactly as proposed by Vogel and co-workers for the copper complex of β-alkyl-substituted

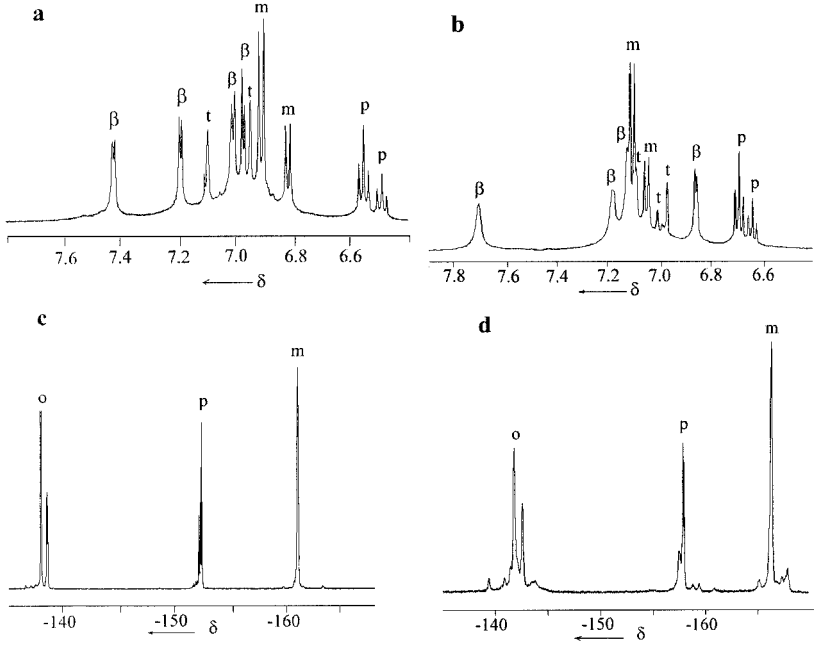

Figure 3. ^{1}H NMR spectra of **2a** at (a) 240 K and (b) 297 K (β = β-pyrrole CH, p = *para*-H, m = *meta*-H, t = [D_7]toluene), and ^{19}F NMR spectra of **1a** at (c) 240 K and (d) 355 K (o = *ortho*-F, p = *para*-F, m = *meta*-F), in [D_8]toluene

 © 2004 Wiley-VCH Verlag GmbH & Co. KGaA, Weinheim

corroles.[22] The small difference between the electronic states could also account for the apparent sensitivity of the electronic absorption spectra of triarylcorrole−copper complexes to substitution on the aryl groups.[25]

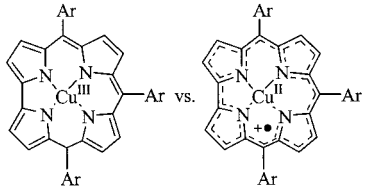

Scheme 2

The mass spectra of **1b** and **2b** correspond to $[(\mathbf{1a})_2-2H]$ and $[(\mathbf{2a})_2-2H]$, respectively, and are consistent with two copper ions coordinated by covalently bound corrole dimers (Scheme 1). The seven rather than eight β-pyrrole hydrogen atoms that are evident in the NMR spectra of **2b** (Figure 4) confirm the loss of two protons upon dimerization. What is more, since there is only a total number of seven different β-pyrrole hydrogen atoms in each of the complexes, substitution must have occurred at the same carbon atom in each of the subunits, otherwise 14 different β-pyrrole hydrogen atoms should be apparent. The same conclusion holds for **1b**, whose ^{19}F NMR spectrum (Figure 4) reveals three rather than six types of C_6F_5 rings. Unfortunately, we were not able to grow X-ray quality crystals of **1b** or **2b**. However, the independently demonstrated high reactivity of C3 in other metal complexes of corrole **1** and the full characterization of the cobalt(III) analog of **1b**,[11,18] suggest that the single bond in **1b** and **2b** is also between the C3 atoms of the subunits.

Since all isolated complexes are EPR-silent, we turned our attention to the spectra of the reduced and oxidized complexes. Chemical reduction of **2a** leads to a spectrum that is typical of copper(II) (Figure 5a). The spectrum is centered at $g = 2.033$, with a four-line hyperfine splitting due to the $I = {}^3/_2$ ^{63}Cu ion, with $a_{Cu} = 207.12$ G. The expected nine-line superhyperfine splitting from the ^{14}N atoms of the corrole is best seen in the high-field part of the spectrum, with $a_N = 17.64$ G. These values are similar to those obtained by Kadish and co-workers for $[(oec)Cu]^-$, where $a_{Cu} = 227$ G.[23,26] The spectrum of one-electron-oxidized **2a** ($[\mathbf{2a}]^+$) is very different (Figure 5b). It contains a single and quite sharp line, resembling that of the corrole−gallium(III) radical $[Ga(tpfc^{+\cdot})]^+$.[16] In addition, a comparison between the electronic spectra of $[\mathbf{2a}]^+$ and **2a** reveals that the Soret-like band of the former is less intense and blue-shifted and that it contains a new band at long

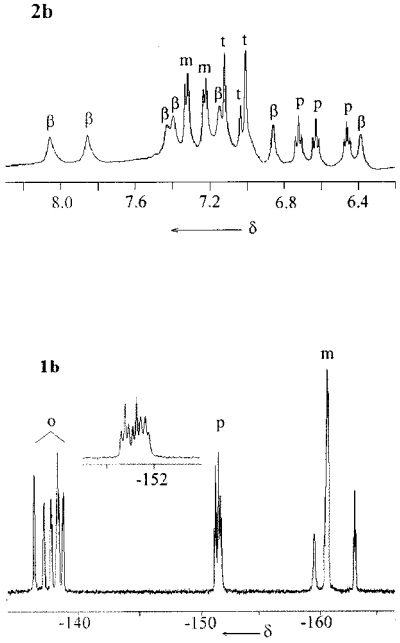

Figure 4. ^1H NMR spectrum of **2b** at 320 K (β = β-pyrrole CH, p = *para*-H, m = *meta*-H, t = $[D_7]$toluene), and ^{19}F NMR spectrum of **1b** at 275 K, in $[D_8]$toluene; inset: extension of the *para*-F resonances

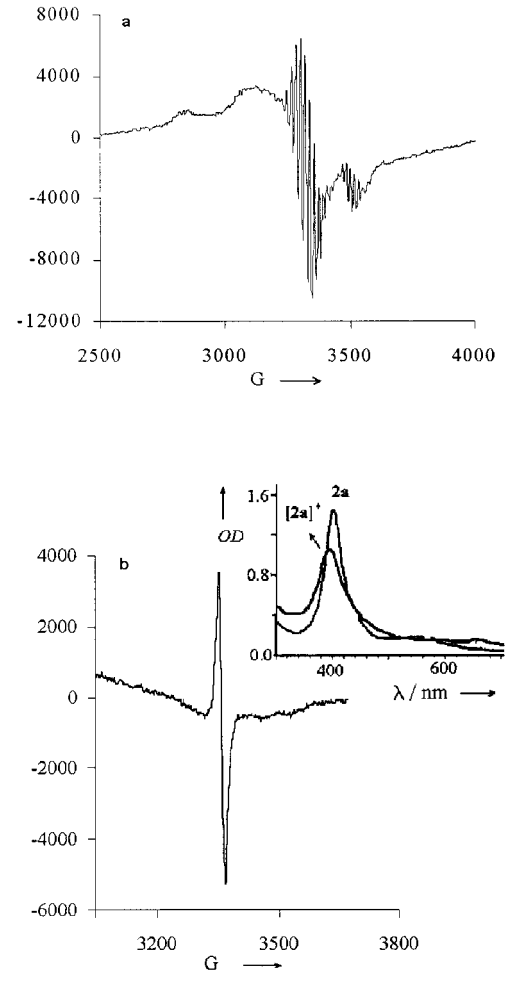

Figure 5. EPR spectra of (a) reduced **2a** (by $Na_2S_2O_4$ in EtOH/H_2O/Ar; instrument settings: power 20.070 mW, modulation frequency 100 kHz, modulation amplitude 10 G, $T = 150$ K) and (b) oxidized **2a** {by $[(BrC_6H_4)_3N]^+SbCl_6^-$, recorded in CH_2Cl_2; instrument settings: power 0.635 mW, modulation frequency 100 kHz, modulation amplitude 10 G, $T = 150$ K}; inset: UV/Vis spectra of **2a** and its oxidation product in CH_2Cl_2

 © 2004 Wiley-VCH Verlag GmbH & Co. KGaA, Weinheim

wavelengths (λ_{max} = 654 nm; Figure 5b, inset). This data allows for quite a confident identification of $[\mathbf{2a}]^+$ as a corrole−copper(III) cation radical. This is remarkably different from the situation for β-pyrrole-alkylated corroles, which dimerize to as yet unidentified products.[23]

Structural Aspects

The X-ray structure of **2a** determined at ca. 110 K is presented in Figure 6. There are two structurally similar but crystallographically independent molecules of the corrole in the asymmetric unit (labeled as unprimed and primed atoms). The 23-atom corrole macrocycle is significantly ruffled, the individual atoms deviating from the mean plane by between −0.28 and +0.21 Å in one species and between −0.22 and +0.23 Å in the other unit (the r.m.s. of these deviations is 0.13 Å). The copper ion resides at the center of the corrole ring and, as is commonly observed for porphyrinoid−copper systems (see below), is four-coordinate. The Cu−N(pyrrole) bond-length range is 1.874(3)−1.891(3) Å in one unit and 1.880(3)−1.890(3) Å in the other unit. In the crystal, the monomeric units of **2a** are arranged in columns along the *b* axis, alternating in their relative orientation (Figure 6b). The dihedral angle between the mean planes of neighboring corrole rings is 44°. This allows the copper center of any given moiety to form van der Waals contacts from above and below with one of the chlorine substituents of the adjacent corroles in the column. The corresponding contact distances are Cu···Cl′ 3.366 and 3.521 Å and Cu′···Cl 3.663 and 3.730 Å. There is no interaction between the antiparallel inversion-related columns in the triclinic crystal, and the *n*-heptane crystallization solvent is included between them. The Cu−N coordination distances in **2a** are similar to those observed in Cu(tetmc), the only other corrole−copper complex for which crystallographic data are available.[22] In the latter, the d^8 Cu^{III} ion is four-coordinate as well, and the observed Cu−N bonds are within 1.866−1.896 Å. However, due to the apparent π-π dimerization of the Cu(tetmc) molecules, at 3.43 Å between the parallel and overlapping units within the dimer, their central corrole framework is somewhat less corrugated (with deviations of individual atoms from the corrole plane confined within −0.21 to +0.17 Å, and r.m.s. deviation of 0.08 Å) than **2a**.

It is of further interest to compare the current findings with those observed for the copper complex of tetra(2,6-dichlorophenyl)porphyrin.[24b] In this compound the porphyrin ring is only slightly saddled (r.m.s. deviation of the porphyrin atoms from their mean plane is 0.11 Å), with the four-coordinate copper ion residing at the center of the ring. However, the Cu−N bonds within the porphyrin macrocycle (1.957−2.019 Å) are significantly longer than in the corrole. Adjacent porphyrin units in this structure are also markedly inclined with respect to each other, but no specific interaction is evident between them. Moreover, in many tetracoordinate Cu^{II} complexes of tetraarylporphyrins the Cu−N bond lengths are within a similar general range of 1.97−2.00 Å, irrespective of the intermolecular organization.[27] Based on the above, and related evidence from other square-planar $Cu^{III}-N_4$ complexes with noncyclic ligands,[28] we may thus safely conclude that the much shorter Cu−N bonds in **2a** are supportive of the corrole−copper(III) electronic state.

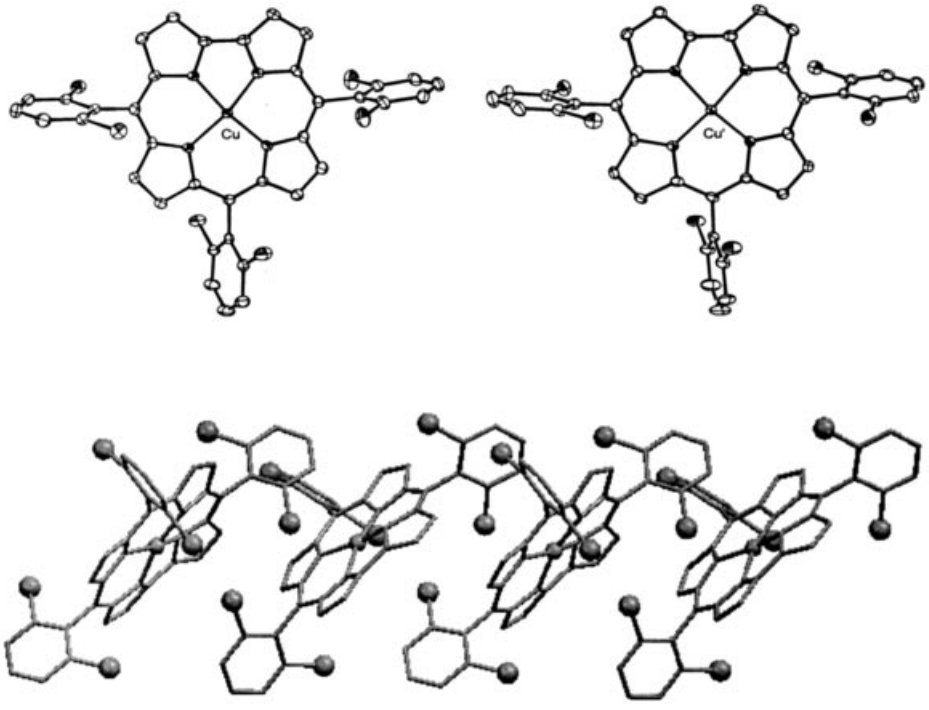

Figure 6. (top) ORTEP illustration of the two crystallographically independent corrole species of **2a** (the atomic displacement parameters are represented by 50% probability ellipsoids); (bottom) the columnar intermolecular organization of the corroles along the *b* axis of the crystal, showing that the corrole ring is approached from both sides by the chlorine substituents

 © 2004 Wiley-VCH Verlag GmbH & Co. KGaA, Weinheim

Another interesting comparison can be made with the copper complexes of octaethyltetraphenylporphyrin, where both the Cu^{II} and formally Cu^{III} complexes are available.[24c] In this case, due to the steric crowding around the molecular periphery caused by the substitution of eight alkyl and four aryl residues, the porphyrin core is severely distorted from planarity, adopting a highly puckered S4-saddle conformation. This seems to have little effect on the coordination distances of the copper ions positioned at the center, which are within 1.966−1.980 Å in the porphyrin−Cu^{II} complex and within 1.968−1.979 Å in the oxidized porphyrin−Cu perchlorate moiety, mostly due to the fact that the oxidation of this system is porphyin-centered rather than metal-centered.

In porphyrins, an alternation of shorter and longer bonds within the inner 16-membered ring π-network (comprised of the N, α-C and *meso*-C) atoms is one of the criteria for oxidation of the macrocycle.[29] Although not always present, it provides a strong indication that oxidation of the copper(II) complex of octaethyltetraphenylporphyrin affects the porphyrin rather than the metal ion, resulting in a porphyrin−Cu^{II} cation radical species. In the same context, we have examined the distribution of bond lengths within the two crystallographically independent corrole rings of **2a**, as displayed in Figure 7. The observed structure clearly

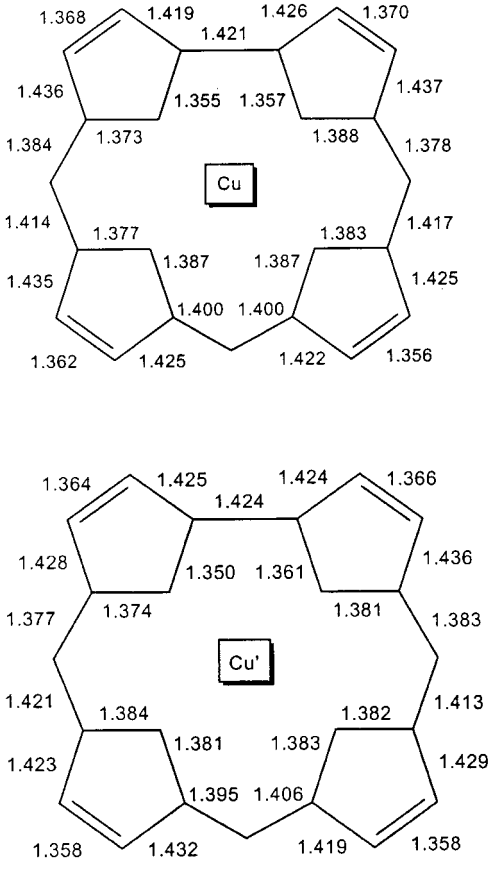

Figure 7. Observed distribution of bond lengths within the central corrole ring of **2a**; the estimated standard deviations for the shown values are 0.005 Å; two crystallographically independent species of the asymmetric unit are shown

shows a portion of an alternating bond length pattern in the "upper" section of the ring close to the C1−C19 bond. This pattern consists of systematically short C_α−N (av. 1.356 Å), long N−C_α (av. 1.379 Å), short C_α−C_{meso} (av. 1.380 Å) and long C_{meso}−C_α (av. 1.416 Å) bonds, while for a closed-shell fully delocalized corrolato trianion one might expect all bond lengths within the N−C_α and the C_{meso}−C_α sets to be equivalent. The observed structural data are thus consistent with the related spectroscopic evidence described above, that the paramagnetic corrole−copper(II) radical state contributes to the structure of **2a** even at the low applied temperature. A different aspect that is emphasized in Figure 7 is that the β-pyrrole bonds are much shorter than all other C−C bonds — they have the characteristics of non-aromatic double bonds. This is a common feature in all crystallographically characterized corroles,[9−11,20] apparently responsible for the facile electrophilic substitution at those positions.

In a broader sense, and of particular relevance to ongoing debates about the assignment of oxidation states in corrole complexes with transition metal ions,[9c,13,30] it is of interest to examine this aspect with the increasing number of crystallographically characterized complexes of **1** and **2**.[31] Accordingly, we have summarized the available data in Table 1.

Inspection of these data reveals that the differences in C_α−C_{meso} bond lengths are smallest in [Ga(tpfc)(py)] (average 0.004 Å), the prototype of closed-shell corrolato−metal complexes, and largest in **2a** (average 0.028 Å), for which the evidence for contribution of open-shell electronic states is the strongest. Within the limit of experimental errors (average ESD of the relevant bond lengths being 0.005 Å), the complexes may be classified by the average difference between C_α−C_{meso} bond lengths: less than 0.01 Å in [Co(tpfc)$(py)_2$], [Ga(tpfc)(py)], [Fe(tpfc)$(py)_2$], and [Ru(tpfc)NO], 0.01−0.014 Å in [Rh(tpfc)(PPh_3)(py)], [Rh(tpfc)(PPh_3)], and [Rh(tdcc)(PPh_3)(py)], and 0.019−0.028 Å in [Fe(tdcc)(NO)], [Fe(tpfc)(NO)], [Fe(tpfc)(Cl)], and [Cu(tdcc)]. Based on this criterion only, this could be indicative for ranking the complexes in terms of the contribution of open-shell electronic states therein. However, one must keep in mind that in all the corrole complexes the $C_{\beta\text{-pyrrole}}$−$C_{\beta\text{-pyrrole}}$ bonds are particularly short, the average differences in C_α−N bond lengths are quite similar, and that even the largest average difference between C_α−C_{meso} bond lengths (0.028 Å) is significantly smaller than in porphyrin radical complexes (> 0.04 Å).

Summary and Conclusions

The reactions of 5,10,15-tris(pentafluorophenyl)corrole and 5,10,15-tris(2,6-dichlorophenyl)corrole with $Cu(OAc)_2{\cdot}H_2O$ lead to the tetracoordinate mononuclear copper complexes **1a** and **2a**, respectively, which can be further transformed into the corresponding dinuclear corrole dimers **1b** and **2b**. All complexes are EPR-silent, and electrochemical measurements coupled with EPR spectroscopy revealed that their reduction and oxidation pro-

 © 2004 Wiley-VCH Verlag GmbH & Co. KGaA, Weinheim

Table 1. Differences in bond lengths [Å] between the carbon atoms bound to *meso*-carbon (C5, C10, C15) and nitrogen (N21, N22, N23, N24) atoms in various complexes of **1** (tpfc) and **2** (tdcc)

	C−C5−C	C−C10−C	C−C15−C	$C_\alpha-C_{meso}$, average	C−N21−C	C−N22−C	C−N23−C	C−N24−C	C_α−N, average	Ref.
Cu(tdcc)	0.030	0.011	0.044	0.028	0.020	0.001	0.003	0.024	0.012	this work
Rh(tdcc)(PPh_3)(py)	0.021	0.006	0.004	0.010	0.014	0.014	0.024	0.014	0.016	[20]
Rh(tpfc)(PPh_3)(py)	0.008	0.004	0.025	0.012	0.014	0.036	0.031	0.000	0.020	[20]
Rh(tpfc)(PPh_3)	0.017	0.018	0.007	0.014	0.004	0.008	0.018	0.024	0.013	[9a]
Fe(tdcc)(NO)	0.021	0.010	0.025	0.019	0.025	0.002	0.006	0.007	0.010	[9c]
Fe(tpfc)(NO)	0.027	0.000	0.043	0.023	0.020	0.004	0.020	0.006	0.013	[9c]
Fe(tpfc)$(py)_2$	0.009	0.007	0.002	0.006	0.031	0.015	0.010	0.024	0.020	[9b]
Fe(tpfc)(Cl)	0.026	0.007	0.040	0.024	0.003	0.004	0.005	0.015	0.007	[9a]
Ru(tpfc)NO	0.019	0.007	0.001	0.009	0.012	0.015	0.002	0.015	0.011	[10]
Co(tpfc)$(py)_2$	0.001	0.004	0.002	0.002	0.001	0.027	0.029	0.005	0.016	[11]
Ga(tpfc)(py)	0.000	0.003	0.009	0.004	0.007	0.023	0.018	0.007	0.014	[16]

cesses are metal- and corrole-centered, leading to corrole−copper(II) and −copper(III) radicals, respectively. The temperature-dependent NMR spectra of **1a** and **2a** revealed the existence of two almost degenerate electronic states. The diamagnetic ground states, favored at lower temperatures, were analyzed as consisting of copper(III) coordinated by closed-shell corrolato trianions and the paramagnetic state as being composed of copper(II) chelated by open-shell corrolato dianions. The contributions from both states are evident in the molecular structure of **2a**, which displays a distorted square-planar coordination geometry around the metal ion and short Cu−N bond lengths typical of copper(III), together with some non-equivalence of the $C_\alpha-C_{meso}$ bond lengths that might reflect the open-shell character of the macrocycle. The radical character is also likely to be responsible for the facile C−C coupling process that leads to the dimerization products. Nevertheless, the contribution of the copper(II) radical state is much lower than in analogous complexes of porphyrins and octaethylbilindione (a noncyclic tetrapyrrole with three protonated N atoms as in corroles),[32] where the Cu−N bonds are much longer. The latter case may be considered at the opposite extreme, based on its magnetic moment and the very large paramagnetic isotopic shifts in its NMR spectrum.

Experimental Section

Physical Methods: The ^1H and ^{19}F NMR spectra were recorded with a Bruker AM 200, operating at 200 MHz for ^1H and 188 MHz for ^{19}F, a Bruker AM 300, operating at 300 MHz for ^1H and 282 MHz for ^{19}F, or a Bruker AM 500, operating at 500 MHz for ^1H. Chemical shifts are reported in ppm relative to residual hydrogen atoms in the deuterated solvents: δ = 7.24, 7.15, 7.00 ppm for chloroform, benzene and toluene, respectively, for the ^1H NMR spectra and relative to $CFCl_3$ (δ = 0.00 ppm) in the ^{19}F NMR spectra. The electronic spectra were recorded with an HP 8452A diode array spectrophotometer and gas chromatographic analysis was performed with an HP-5890 GC equipped with an HP-5 capillary column and FID detector. Mass spectrometry was performed with a Finnigan mat TSQ 70 instrument with isobutane as carrier gas and IR measurements with an FT-IR Bruker Vector 22. The redox potentials were determined by cyclic voltammetry (CV) at ambient temperatures with a home-made voltammograph, using C_6H_5CN solutions, 0.05 M in tetra-*n*-butylammonium perchlorate (TBAP, Fluka, recrystallized three times from absolute ethanol) and about 0.5 mM in substrate. Ag/AgCl was used as the reference electrode. The other experimental conditions are reported in the captions of the corresponding spectra.

Materials: C_6H_5CN (BioLab Ltd.), dichloromethane (Bio-Lab Ltd.), pyridine (Merck), ethanol (Bio-Lab Ltd.), *n*-heptane (Carlo-Erba), *n*-hexane (Bio-Lab Ltd.), $Cu(OAc)_2{\cdot}H_2O$ (Riedel−de Haën), $Na_2S_2O_4$ (Merck), $(BrC_6H_4)_3NSbCl_6$ (Aldrich) and deuterated solvents (Aldrich and Cambridge Isotopes products) were used as received.

Synthetic Methods: The synthetic details for the preparation of H_3(tpfc) and H_3(tdcc) are provided in previous publications.[3a,3b,3e−3g]

Cu(tpfc) (1a) and the Dinuclear Complex 1b: An approximate threefold excess of $Cu(OAc)_2{\cdot}H_2O$ (66 mg, 0.34 mmol) was added to a solution of **1** (100 mg, 0.126 mmol) in pyridine (5 mL) in one portion. TLC examinations (silica gel; *n*-hexane/CH_2Cl_2, 2:1) revealed that the starting material was fully consumed at room temp. within 30 min. The solvents were evaporated from the red-green mixture and **1a** was obtained as a red powder (75 mg, 73% yield) after column chromatography (silica gel; *n*-hexane/CH_2Cl_2, 4:1), together with trace amounts of **1b**. When an identical reaction mixture was heated to reflux for 10 min, both **1a** (32 mg, 30% yield) and **1b** (42.8 mg, 40% yield) could be isolated by column chromatography (silica gel; *n*-hexane/CH_2Cl_2, 10:3). Complexes **1a** and **1b** could not be further purified by recrystallization because of their transformation (within hours) into a mixture of green compounds, all of which were analyzed by mass spectrometry as dinuclear complexes of dimeric corrole (isomers of **1b**).

1a: UV/Vis (benzene): λ_{max} ($\varepsilon \times 10^{-4}$) = 410 (6.17), 550 (0.81) nm. MS (DCI$^-$): *m*/*z* (%) = 856 (100) [M$^-$]. ^1H NMR (toluene, 500 MHz, room temp.): δ = 7.76 (br. s, 2 H), 7.23 (br. s, 2 H), 7.14 (br. s, 2 H), 6.93 (br. s, 2 H) ppm. ^1H NMR (toluene, 200 MHz, 233 K): δ = 7.67 (d, *J* = 3.99 Hz, 2 H), 7.32 (d, *J* = 3.98 Hz, 2 H), 7.23 (unresolved d, 2 H), 7.18 (unresolved d, 2 H) ppm. ^{19}F NMR ($CDCl_3$, 300 MHz, room temp.): δ = −137.11 (d, m, 4 F, *o*-F), −137.97 (m, 2 F, *o*-F), −152.12 (t, *J* = 21.2 Hz, 1 F, *p*-F), −152.35 (t, *J* = 21.2 Hz, 2 F, *p*-F), −160.89 (m, 6 F, *m*-F) ppm.

1b: UV/Vis (benzene): λ_{max} ($\varepsilon \times 10^{-4}$) = 412 (10.95), 566 (1.44) nm. MS (DCI$^-$): *m*/*z* (%) = 1710 (100) [M$^-$]. ^1H NMR ($CDCl_3$, 200 MHz, room temp.): δ = 7.84 (br. s, 2 H), 7.58 (br. s, 2 H), 7.33 (br. s, 2 H), 7.21 (br. s, 2 H), 7.14 (br. s, 2 H), 6.94 (m, 4 H) ppm.

 © 2004 Wiley-VCH Verlag GmbH & Co. KGaA, Weinheim

^{19}F NMR ([D$_8$]toluene, 300 MHz, room temp.): δ = −136.04 (s, 2 F, *o*-F), −136.98 (d, *J* = 21.17 Hz, 2 F, *o*-F), −137.56 (d, *J* = 21.17 Hz, 2 F, *o*-F), −138.12 (m, 4 F, *o*-F), −138.62 (d, *J* = 21.17 Hz, 2 F, *o*-F), −151.62 (t, *J* = 21.17 Hz, 2 F, *p*-F), −152.01 (dt, 4 F, *p*-F), −159.79 (s, 2 F, *m*-F), −160.81 (m, 8 F, *m*-F), −163.06 (t, *J* = 21.17 Hz, 2 F, *m*-F) ppm.

Cu(tdcc) (2a) and the Dinuclear Complex 2b: A threefold excess of $Cu(OAc)_2 \cdot H_2O$ (25 mg, 0.12 mmol) was added to a solution of **2** (30 mg, 0.04 mmol) in pyridine (5 mL) in one portion and mixed for 30 min at room temp. After solvent evaporation and column chromatography (silica gel; *n*-hexane/CH_2Cl_2, 4:1), **2a** was isolated as a red powder (26 mg, 85% yield). X-ray quality crystals were obtained by recrystallization from CH_2Cl_2/*n*-heptane. When an identical reaction mixture was heated to reflux for 30 min, **2a** (15 mg, 45% yield) and **2b** (14 mg, 42%% yield) were separated by column chromatography (silica gel; *n*-hexane/CH_2Cl_2, 10:3).

2a: UV/Vis (benzene): λ_{max} (ε × 10^{-4}) = 406 (4.71), 548 (0.56) nm. MS (DCI$^-$): *m*/*z* (%) = 794 (100) [M$^-$]. ^{1}H NMR (toluene, 500 MHz, room temp.): δ = 7.69 (br. s, 2 H), 7.26 (br. s, 2 H), 7.17 (br. s, 2 H), 6.86 (unresolved d, 2 H), 7.10 (d, *J* = 8 Hz, 4 H, *m*-H), 7.04 (d, *J* = 8 Hz, 2 H, *m*-H), 6.68 (t, *J* = 8.25 Hz, 2 H, *p*-H), 6.63 (t, *J* = 8.25 Hz, 1 H, *p*-H) ppm. ^{1}H NMR (toluene, 500 MHz, 240 K): δ = 7.43 (d, *J* = 4.37 Hz, 2 H), 7.19 (d, *J* = 4.37 Hz, 2 H), 7.01 (d, *J* = 4.77 Hz, 2 H), 6.97 (d, *J* = 4.77 Hz, 2 H), 6.92 (d, *J* = 8.34 Hz, 4 H, *m*-H), 6.83 (d, *J* = 8.34 Hz, 2 H, *m*-H), 6.56 (t, *J* = 8.25 Hz, 2 H, *p*-H), 6.50 (t, *J* = 8.25 Hz, 1 H, *p*-H) ppm.

2b: UV/Vis (benzene): λ_{max} (ε × 10^{-4}) = 410 (12.8), 560 (2.14) nm. MS (DCI$^-$): *m*/*z* (%) = 1584 (100) [M$^-$]. ^{1}H NMR (toluene, 500 MHz, room temp.): δ = 7.77 (br. s, 4 H), 7.64 (br. s, 4 H), 6.86 (d, *J* = 4 Hz, 4 H), 6.53 (unresolved d, 4 H), 7.19 (unresolved d, 6 H, *m*-H), 7.06 (unresolved d, 4 H, *m*-H), 6.67 (d, *J* = 8 Hz, 2 H, *m*-H), 6.68 (t, *J* = 8 Hz, 2 H, *p*-H), 6.58 (t, *J* = 8.25 Hz, 2 H, *p*-H), 6.40 (t, *J* = 8 Hz, 2 H, *p*-H) ppm. ^{1}H NMR (toluene, 500 MHz, 235 K): δ = 7.38 (br. s, 2 H), 7.33 (d, *J* = 3.97 Hz, 2 H), 7.26 (d, *J* = 3.97 Hz, 2 H), 6.85 (d, *J* = 4.37 Hz, 2 H), 6.73 (d, *J* = 4.77 Hz, 2 H), 6.44 (unresolved d, 2 H), 7.01 (unresolved d, 2 H), 6.98 (m, 6 H, *m*-H), 6.79 (m, 6 H, *m*-H), 6.54 (t, *J* = 8 Hz, 2 H, *p*-H), 6.54 (t, *J* = 8.25 Hz, 2 H, *p*-H), 6.25 (t, *J* = 8 Hz, 2 H, *p*-H) ppm. ^{1}H NMR (toluene, 500 MHz, 320 K): δ = 8.06 (br. s, 2 H), 7.86 (br. s, 2 H), 7.42 (br. s, 2 H), 7.38 (br. s, 2 H), 7.15 (br. s, 2 H), 6.86 (br. s, 2 H), 6.39 (br. s, 2 H), 7.32 (d, *J* = 7.9 Hz, 6 H, *m*-H), 7.23 (d, *J* = 7.8 Hz, 6 H, *m*-H), 6.72 (t, *J* = 8.07 Hz, 2 H, *p*-H), 6.63 (t, *J* = 8.07 Hz, 2 H, *p*-H), 6.45 (t, *J* = 8.07 Hz, 2 H, *p*-H) ppm.

Chemical Oxidation of [Cu(tdcc)] (2a): Solid $(BrC_6H_4)_3NSbCl_6$ (13 mg, 18 μmol) was added in one portion to a well-stirred solution of **2a** (5 mg, 6 μmol) in CH_2Cl_2. The color changed to yellow-green within a few minutes, after which the solution was filtered and used for the spectroscopic examinations.

Chemical Reduction of [Cu(tdcc)] (2a): A saturated solution of $Na_2S_2O_4$ (2 mg, 0.011 mmol) in H_2O (2 mL) was added in one portion to a 50-mL three-necked, round-bottomed flask containing a solution of **2a** (5 mg, 6 μmol) in ethanol (2 mL). The mixture was stirred under Ar for 5 min, during which time the color changed from red to green. This solution was used for the EPR measurements, still under Ar.

Electrochemistry: The cyclovoltammograms of the complexes were measured for approximately 0.5 mM substrate in 0.05 M TBAP/C_6H_5CN solutions at scan rates of 100 V/s with Ag/AgCl reference electrode. The redox potentials are reported vs. the ferrocene/ferrocenium redox couple observed at 0.4 V vs. Ag/AgCl.

X-ray Crystallography of [Cu(tdcc)] (2a): The crystalline sample of **2a** was covered with a thin layer of light oil and cooled to 110 K in order to minimize the escape of the volatile crystallization solvent and minimize thermal motion/structural disorder effects. The intensity data were corrected for absorption. The structure was solved and refined by standard crystallographic techniques. All non-hydrogen atoms of the corroles were refined anisotropically. The hydrogen atoms were located in calculated positions, and were refined using a riding model with fixed thermal parameters [U_{ij} = 1.2 U_{ij}(eq.) for the atom to which they are bonded]. Complex **2a** crystallized as an *n*-heptane solvate. $2C_{37}H_{17}Cl_6N_4Cu \cdot 1/2C_7H_{16}$, *M* = 1637.68, triclinic, space group $P\bar{1}$, *a* = 12.3630(2), *b* = 16.5760(3), *c* = 17.8710(4) Å, α = 93.615(1), β = 92.401(1), γ = 97.352(1)°, *V* = 3401.9(1) Å^3, *Z* = 2, *T* = 110(2) K, D_c = 1.599 g·cm^{-3}, μ(Mo-K_α) = 1.15 mm^{-1}, 15035 unique reflections to $2\theta_{max}$ = 56.6°, 902 refined parameters, R_1 = 0.055 for 120571 observations with $I > 2\sigma(I)$, R_1 = 0.096 (wR_2 = 0.108) for all unique data, $\Delta\rho \leq 0.64$ e/Å^3. The asymmetric unit consists of two corrole species and half of the *n*-heptane solvate molecule which is located on, and disordered about, a center of inversion. CCDC-206173 contains the supplementary crystallographic data for this paper. These data can be obtained free of charge at www.ccdc.cam.ac.uk/conts/retrieving.html [or from the Cambridge Crystallographic Data Centre, 12 Union Road, Cambridge CB2 1EZ, UK; Fax: (internat.) + 44-1223/336-033; E-mail: deposit@ccdc.cam.ac.uk].

Acknowledgments

This research was supported by the Israel Science Foundation under Grants 368/00 (Z. G.) and 68/01 (I. G.). A postdoctoral fellowship for L. S. by the Institute of Catalysis Science and Technology of the Technion is acknowledged as well.

[1] For reviews that cover the chemistry of corrole up to 1999, see: [1a] J. L. Sessler, S. J. Weghorn, in *Expanded, Contracted & Isomeric Porphyrins*, Pergamon, Oxford, **1997**, pp. 11−85. [1b] R. Paolesse, in *The Porphyrin Handbook*, vol. 2 (Eds.: K. M. Kadish, K. M. Smith, R. Guilard), Academic Press, New York, **2000**, chapter 11, pp. 201−231. [1c] K. M. Kadish, in *The Porphyrin Handbook*, vol. 2 (Eds.: K. M. Kadish, K. M. Smith, R. Guilard), Academic Press, New York, **2000**, chapter 12, pp. 233−295.

[2] For only the two triarylcorroles that were reported prior to 1999, see: [2a] N. M. Loim, E. V. Grishko, N. I. Pyshnograeva, E. V. Vorontsov, V. I. Sokolov, *Izv. Akad. Nauk. Ser. Khim.* **1994**, *5*, 925. [2b] E. Rose, A. Kossanyi, M. Quelquejeu, M. Soleilhavoup, F. Duwavran, N. Bernard, A. Lecas, *J. Am. Chem. Soc.* **1996**, *118*, 1567.

[3] [3a] Z. Gross, N. Galili, I. Saltsman, *Angew. Chem. Int. Ed.* **1999**, *38*, 1427. [3b] Z. Gross, N. Galili, L. Simkhovich, I. Saltsman, M. Botoshansky, D. Bläser, R. Boese, I. Goldberg, *Org. Lett.* **1999**, *1*, 599. [3c] L. Simkhovich, I. Goldberg, Z. Gross, *J. Inorg. Biochem.* **2000**, *80*, 235. [3d] E. Steene, T. Wondimagegn, A. Ghosh, *J. Inorg. Biochem.* **2002**, *88*, 113. [3e] L. Simkhovich, I. Goldberg, Z. Gross, *Org. Lett.* **2003**, *5*, 1241. [3f] J. P. Collman, R. A. Decreau, *Tetrahedron Lett.* **2003**, *44*, 1207. [3g] D. T. Gryko, B. Koszarna, *Org. Biomol. Chem.* **2003**, *1*, 350.

[4] [4a] R. Paolesse, L. Jaquinod, D. J. Nurco, S. Mini, F. Sagone, T. Boschi, K. M. Smith, *Chem. Commun.* **1999**, 1307. [4b] R. Paolesse, S. Nardis, F. Sagone, R. G. Khoury, *J. Org. Chem.* **2001**, *66*, 550.

[5] [5a] J.-W. Ka, C.-H. Lee, *Tetrahedron Lett.* **2000**, *41*, 4609. [5b] J.-W. Ka, W.-S. Cho, C.-H. Lee, *Tetrahedron Lett.* **2000**, *41*, 8121. [5c] D. T. Gryko, *Chem. Commun.* **2000**, 2243. [5d] D. T. Gryko, K. Jadach, *J. Org. Chem.* **2001**, *66*, 4267. [5e] R. P.

 © 2004 Wiley-VCH Verlag GmbH & Co. KGaA, Weinheim

Brinas, C. Bruckner, *Synlett* **2001**, *3*, 442. [5f] C. V. Asokan, S. Smeets, W. Dehaen, *Tetrahedron Lett.* **2001**, *42*, 4483. [5g] R. A. Decreau, J. P. Collman, *Tetrahedron Lett.* **2003**, *44*, 3323.

[6] For synthesis of corrole-like molecules, see: [6a] B. Sridevi, S. J. Narayanan, T. K. Chandrashekar, U. Englich, K. Ruhlandt-Senge, *Chem. Eur. J.* **2000**, *6*, 2554. [6b] B. Ramdhanie, C. L. Stern, D. P. Goldberg, *J. Am. Chem. Soc.* **2001**, *123*, 9447. [6c] M. Broering, C. Hell, *Chem. Commun.* **2001**, *22*, 2336.

[7] [7a] A. E. Meier-Callahan, H. B. Gray, Z. Gross, *Inorg. Chem.* **2000**, *39*, 3605. [7b] A. E. Meier-Callahan, A. J. Di Bilio, L. Simkhovich, A. Mahammed, I. Goldberg, H. B. Gray, Z. Gross, *Inorg. Chem.* **2001**, *40*, 6788.

[8] [8a] Z. Gross, G. Golubkov, L. Simkhovich, *Angew. Chem. Int. Ed.* **2000**, *39*, 4045. [8b] J. Bendix, G. Golubkov, H. B. Gray, Z. Gross, *Chem. Commun.* **2000**, 1957. [8c] G. Golubkov, J. Bendix, H. B. Gray, A. Mahammed, I. Goldberg, A. J. DiBilio, Z. Gross, *Angew. Chem. Int. Ed.* **2001**, *40*, 2132. [8d] S. P. de Visser, F. Ogliaro, Z. Gross, S. Shaik, *Chem. Eur. J.* **2001**, *7*, 4954.

[9] [9a] L. Simkhovich, N. Galili, I. Saltsman, I. Goldberg, Z. Gross, *Inorg. Chem.* **2000**, *39*, 2704. [9b] L. Simkhovich, A. Mahammed, I. Goldberg, Z. Gross, *Chem. Eur. J.* **2001**, *7*, 1041. [9c] L. Simkhovich, I. Goldberg, Z. Gross, *Inorg. Chem.* **2002**, *41*, 5433.

[10] L. Simkhovich, I. Luobeznova, I. Goldberg, Z. Gross, *Chem. Eur. J.* **2003**, *9*, 201.

[11] A. Mahammed, I. Giladi, I. Goldberg, Z. Gross, *Chem. Eur. J.* **2001**, *7*, 4259.

[12] L. Simkhovich, P. Iyer, I. Goldberg, Z. Gross, *Chem. Eur. J.* **2002**, *8*, 2595.

[13] Z. Gross, *J. Biol. Inorg. Chem.* **2001**, *6*, 733.

[14] Z. Gross, N. Galili, *Angew. Chem. Int. Ed.* **1999**, *38*, 2366.

[15] A. Mahammed, Z. Gross, *J. Inorg. Biochem.* **2002**, *88*, 305.

[16] J. Bendix, I. J. Dmochowski, H. B. Gray, A. Mahammed, L. Simkhovich, Z. Gross, *Angew. Chem. Int. Ed.* **2000**, *39*, 4048.

[17] [17a] Z. Gross, L. Simkhovich, N. Galili, *Chem. Commun.* **1999**, 599. [17b] L. Simkhovich, Z. Gross, *Tetrahedron Lett.* **2001**, *42*, 8089. [17c] J. Grodkowski, P. Neta, E. Fujita, A. Mahammed, Z. Gross, *J. Phys. Chem. A* **2002**, *106*, 4772. [17d] R. A. Eikey, S. I. Khan, M. M. Abu-Omar, *Angew. Chem. Int. Ed.* **2002**, *41*, 3592.

[18] [18a] A. Mahammed, I. Goldberg, Z. Gross, *Org. Lett.* **2001**, *3*, 3443. [18b] I. Saltsman, A. Mahammed, I. Goldberg, E. Tkachenko, M. Botoshansky, Z. Gross, *J. Am. Chem. Soc.* **2002**, *124*, 7411. [18c] Z. Gross, A. Mahammed, *J. Porphyrins Phthalocyanines* **2002**, *6*, 553.

[19] D. Aviezer, S. Cotton, M. David, A. Segev, N. Khaselev, N. Galili, Z. Gross, A. Yayon, *Cancer Res.* **2000**, *60*, 2973.

[20] L. Simkhovich, I. Goldberg, Z. Gross, *J. Porphyrins Phthalocyanines* **2002**, *6*, 439−444.

[21] [21a] A. W. Johnson, I. T. Kay, *J. Chem. Soc.* **1965**, *1620*. [21b] R. Grigg, A. W. Johnson, G. Shelton, *J. Chem. Soc., C* **1971**, 2287.

[22] [22a] S. Will, J. Lex, E. Vogel, H. Schmicker, J.-P. Gisselbrecht, C. Haubtmann, M. Bernard, M. Gross, *Angew. Chem. Int. Ed. Engl.* **1997**, *36,* 357*; Angew. Chem.* **1997**, *109*, 367. [22b] A. Ghosh, T. Wondimagegn, A. B. Parusel, *J. Am. Chem. Soc.* **2000**, *122*, 5100.

[23] K. M. Kadish, V. A. Adamian, E. Van Caemelbecke, E. Gueletii, S. Will, C. Erben, E. Vogel, *J. Am. Chem. Soc.* **1998**, *120*, 11986.

[24] [24a] Y. Ni, S. Lee, B. B. Wayland, *Inorg. Chem.* **1999**, *38*, 3947. [24b] N. Ehlinger, W. R. Scheidt, *Inorg. Chem.* **1999**, *38*, 1316. [24c] M. W. Renner, K.M. Barkigia, Y. Zhang, C. J. Medforth, K. M. Smith, J. Fajer, *J. Am. Chem. Soc.* **1994**, *116*, 8582.

[25] I. H. Wasbotten, T. Wondimagegn, A. Ghosh, *J. Am. Chem. Soc.* **2002**, *124*, 8104.

[26] The a_N of 3.3 G reported in the text of ref.[23] must be erroneous, as judged from examination of the relevant figure therein.

[27] R. Krishna Kumar, S. Balasubramanian, I. Goldberg, *Inorg. Chem.* **1998**, *37*, 541; Y. Diskin-Posner, S. Dahal, I. Goldberg *Angew. Chem. Int. Ed.* **2000**, *39*, 1288.

[28] [28a] R. Ruiz, C. Surville-Barland, A. Aukauloo, E. Anxolabehere-Mallart, Y. Journaux, J. Cano, M. C. Munoz, *J. Chem. Soc., Dalton Trans.* **1997**, 745. [28b] M. Melnik, M. Kabesova, *J. Coord. Chem.* **2000**, *50*, 323.

[29] W. R. Scheidt, *J. Biol. Inorg. Chem.* **2001**, *6*, 727.

[30] [30a] O. Zakharieva, V. Schunemann, M. Gerdan, S. Licoccia, S. Cai, F. A. Walker, A. X. Trautwein, *J. Am. Chem. Soc.* **2002**, *124*, 6636. [30b] A. Ghosh, P. R. Taylor, *Curr. Opin. Chem. Biol.* **2003**, *7*, 113. [30c] F. A. Walker, *Inorg. Chem.* **2003**, *42*, 4526.

[31] For another triarylcorrole−copper complex that was published while this manuscript was in the referee process, see: C. Bruckner, R. P. Brinas, J. A. Krause-Bauer, *Inorg. Chem.* **2003**, *42*, 4495.

[32] A. L. Balch, M. Mazzanti, B. C. Noll, M. M. Olmstead, *J. Am. Chem. Soc.* **1993**, *115*, 12206.

Received November 3, 2003
Early View Article
Published Online March 9, 2004

 © 2004 Wiley-VCH Verlag GmbH & Co. KGaA, Weinheim

The First Amine-Templated Layered Metal Selenates

D. Udayakumar,[a] Meenakshi Dan,[a] and C. N. R. Rao*[a]

Keywords: Open-framework / Selenium / Hydrothermal chemistry / Amines / Template synthesis

Although a few open-framework metal sulfates and selenites have been synthesized and characterized recently, it has not been possible to prepare the corresponding selenates, probably because of the instability of the +6 oxidation state of Se in alkaline media. We have been able to synthesize, for the first time, organically templated open-framework rare earth selenates with the general formula $0.5[C_2N_2H_{10}][Ln(H_2O)_2(SeO_4)_2]$ (**I**) (Ln = La, Nd or Pr) and $0.5[C_4N_2H_{14}][La(SeO_4)_2]\cdot 0.5H_2O$ (**II**), under hydrothermal conditions in an acidic medium. Crystal data: **I** (Ln = La): triclinic, space group = $P\bar{1}$, *M*r = 491.91, *a* = 7.0105(8) Å, *b* = 7.3772(9) Å, *c* = 9.526(1) Å, α = 82.014(2), β = 84.514(2), γ = 84.247(2)°, *V* = 483.76(1) Å^3, *Z* = 2; **II**: triclinic, space group = $P\bar{1}$, *M*r = 478.91, *a* = 5.94(2), *b* = 7.408(3), *c* = 11.048(2) Å, α = 86.899(2), β = 75.971(1), γ = 79.456(2)°, *V* = 463.7(2) Å^3, *Z* = 4. Being the first report of complex layered selenates, it is likely to stimulate efforts to synthesize other novel open-framework structures making use of the selenate ion as the building unit.
(© Wiley-VCH Verlag GmbH & Co. KGaA, 69451 Weinheim, Germany, 2004)

Introduction

A wide variety of organically templated inorganic open-framework materials are known today. Although metal silicates,[1] phosphates[2] and carboxylates[3−5] dominate this area, several organically templated open-framework metal sulfates[6−8] and selenites[9−11] have also been prepared more recently. The first organically templated layered selenite was synthesized by Harrison et.al,[9] followed by the reports of three-dimensional as well as other layered metal selenites.[10−11] To the best of our knowledge, no organically templated layered metal selenates are known hitherto. While the most stable oxidation state of S is +6 as in SO_4^{2-}, that of Se is +4 (SeO_3^{2-} or $Se_2O_5^{2-}$). The reduction potential of the SO_4^{2-}/SO_3^{2-} couple is 0.119V while that of the SeO_4^{2-}/SeO_3^{2-} couple is only 0.03V in alkaline media. This has direct implications on the stability of the compounds of oxy anions of selenium. Selenites are thus commonly obtained as products even though one may start with H_2SeO_4 as source of Se. This has been encountered by us in few instances[10] and it is probably because of this difficulty that it has not been possible to prepare open-framework metal selenates in the presence of amines. In this article, we report the first successful synthesis and characterization of organically templated open-framework lanthanum selenates, $0.5[C_2N_2H_{10}][Ln(H_2O)_2(SeO_4)_2]$ (**I**) (Ln = La, Nd or Pr) and $0.5[C_4N_2H_{14}][La(SeO_4)_2]\cdot 0.5H_2O$ (**II**), prepared hydrothermally under acidic conditions.

[a] Chemistry and Physics of Materials Unit and CSIR Center of Excellence in Chemistry, Jawaharlal Nehru Center for Advanced Scientific Research,
Jakkur P. O., Bangalore 560064, India

Results and Discussion

$0.5[C_2N_2H_{10}][Ln(H_2O)_2(SeO_4)_2]$ (I) (Ln = La, Nd or Pr)

We shall discuss the structure of the La compound as a representative of this isomorphous group of compounds. The asymmetric unit of **I** contains 14 non-hydrogen atoms of which twelve belong to the inorganic framework and two to the amine (ethylenediamine) as shown in Figure 1 (a). There are two crystallographically distinct Se atoms and a unique La atom, with half of the amine appearing in the asymmetric unit. The lanthanum atoms are nine-coordinate with seven oxygen atoms from two selenate anions [Se(1)X2, Se(2)X5] and two oxygen atoms from water ligands. Each La is connected to two neighboring La atoms by La−μ-O−La linkages, through three-coordinate oxygen atoms (O2 and O6). The Se(1)O_4 tetrahedron shares corners (O1 and O3) with two adjacent LaO_9 polyhedra. The remaining two oxygen atoms O7 and O8 are part of terminal Se=O groups. The Se2 atom forms five Se−O−La linkages via a two-coordinate O10 atom, and the three-coordinate O2 and O6 atoms. We thus observed three types of Se−O bonds: Se−O, Se=O and Se−μ_3-O, with average bonds lengths of 1.637 Å, 1.62 Å and 1.645 Å respectively. Bond Valence Sum (BVS) calculations for the La and Se atoms [La(1) = 3.13, Se(1) = 6.14 and Se(2) = 5.98] clearly show the oxidation states of the La and Se to be +3 and +6 respectively. The framework stoichiometry of $La(H_2O)_2(SeO_4)_2$ creates a net framework charge of −1, which is balanced by the presence of half of the diprotonated ethylenediamine.

The structure of **I** involves a two-dimensional covalently bonded framework built up of LaO_9 polyhedra and SeO_4 tetrahedra, the former being connected through La−μ_3-

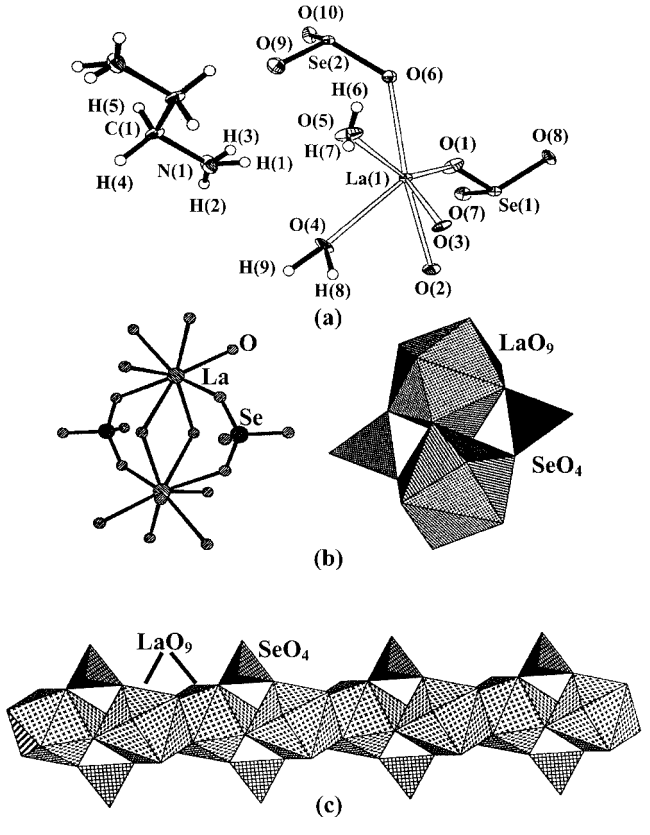

Figure 1. (a) ORTEP plot of $0.5[C_2N_2H_{10}][La(H_2O)_2(SeO_4)_2]$ (**I**); the asymmetric unit is labeled; thermal ellipsoids are given at the 50% probability level; (b) ball and stick, and polyhedral representation of the secondary building unit, SBU-4 in **I**; note the presence of two three-membered rings (La_2Se); c) connectivity between the SBU-4 units creating an infinite chain of edge-shared LaO_9 polyhedra

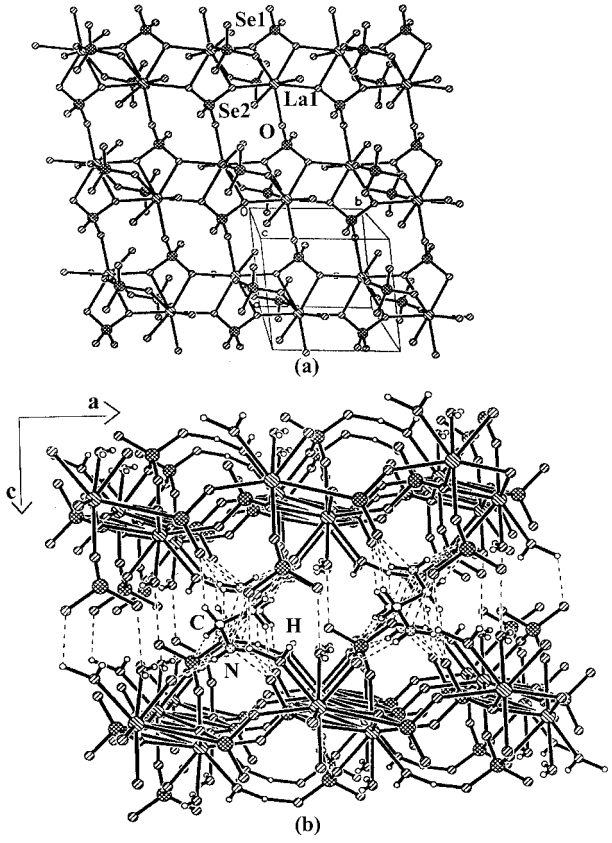

Figure 2. (a) Ball and stick representation of the inorganic layer of **I**, in the *ab* plane; note the presence of two different types of chains; (b) view down the crystallographic *b* axis showing the packing of layers in **I**; hydrogen-bonding interactions between the amine and the framework oxygen atoms are shown by dotted lines

O−La linkages. The topology of the layer in **I** can be described in terms of a secondary building unit (SBU), constructed by capping the two edge-shared LaO_9 polyhedra by two $Se(1)O_4$ groups as shown in Figure 1 (b). Such SBUs, described as SBU-4 by Ferey,[15] have been observed in several metal phosphate systems.[16] The SBU-4 units are linked by three-coordinate oxygen atoms (O2 and O6) forming an infinite chain-like structure consisting of edge-shared LaO_9 polyhedra propagating in a zig-zag fashion as shown in Figure 1 (c). Such a chain can be considered as a tetrahedrally decorated rutile type chain as in a recently reported FePO system.[17] The chains run parallel to the *b* axis and are covalently connected by the $Se(2)O_4$ groups via La−O−Se linkages creating edge-shared four-membered rings (ladder). The $Se(2)O_4$ units also share an edge with neighboring LaO_9 polyhedra along the chain, where as the $Se(1)O_4$ units are involved only in capping the LaO_9 polyhedra along the chain. The structure of **I** is thus made of two types of chains arranged in an ABAB fashion in the *ab* plane (Figure 2, a). The ethylenediamine cations occupy the interlayer sites, forming hydrogen bonds with the framework oxygen atoms (Figure 2, b).

$0.5[C_4N_2H_{14}][La(SeO_4)_2]\ 0.5H_2O$ (II)

The asymmetric unit of **II** (Figure 3, a) contains fifteen non-hydrogen atoms of which eleven belong to the inorganic framework and three to the amine (piperazine). There are two crystallographically distinct Se atoms and a unique La atom, with half of the amine appearing in the asymmetric unit. Two bidentate and five monodentate selenate anions give rise to the nine-coordination of the La atoms. In the framework structure, each lanthanum atom is connected to three neighboring lanthanum centers by La−μ-O−La linkages through three-coordinate oxygen atoms (O3, O4 and O8). The average La−O bond length is 2.61(8) Å. The Se1 atom makes four Se−O−La linkages with the three neighboring La atoms through a three-coordinate oxygen atom O3 ($Se-\mu_3-O-La_2$ bridge), and two two-coordinate oxygen atoms O1 and O5 (Se−O−La bridge). The Se2 atom is connected to four neighboring La atoms through Se−O−La linkages via two three-coordinate oxygen atoms, O4 and O8 ($Se-\mu_3-O-La_2$), and a two-coordinate oxygen atom, O2 (Se−O−La bridge). The O6 and O7 atoms form terminal Se=O groups. The average Se−O

 © 2004 Wiley-VCH Verlag GmbH & Co. KGaA, Weinheim

bond lengths, which are in the range 1.609(9)−1.665(8) Å, are in agreement with the literature value.[18,19] The coordination environments of La and Se are shown in Figure 3 (b). Bond Valence Sum (BVS) calculations show the La and Se atoms to be in +3 and +6 oxidation states, respectively. The framework stoichiometry of La $(SeO_4)_2$ creates a net framework charge of −1, which is compensated by the +1 charge of half of the diprotonated piperazine.

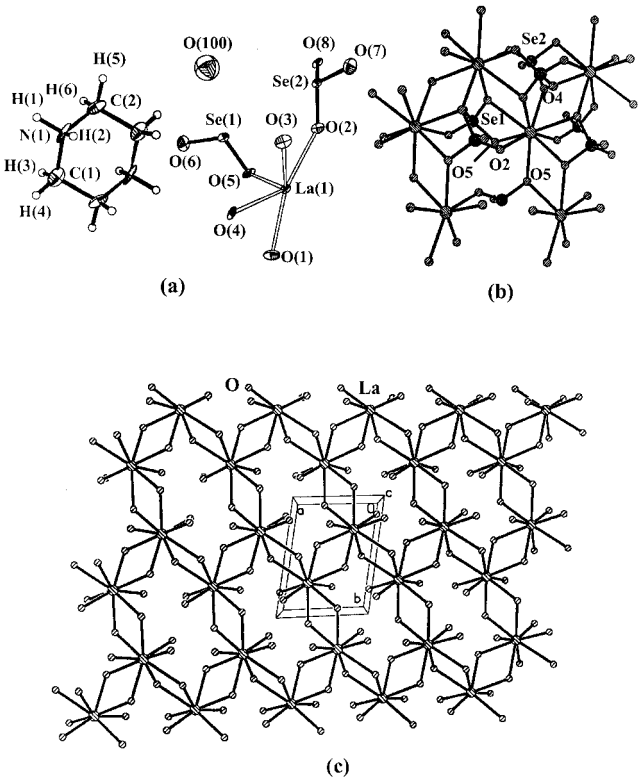

Figure 3. (a) ORTEP plot of $0.5[C_2N_2H_{14}][La(SeO_4)_2]\cdot 0.5H_2O$ (**II**); the asymmetric unit is labeled; thermal ellipsoids are given at the 50% probability level; (b) ball and stick representation showing the coordination environment of La and Se atoms in **II**; (c) the LaO layer in **II**; note the presence of six-membered rings made up of edge-shared LaO_9 polyhedra

The structure of **II** is constructed from macro-anionic framework layers of $[La(SeO_4)_2]^{-1}$, held together by hydrogen-bonding interactions with the amine molecules located in the interlamellar space. The structure involves LaO sheets formed by the edge-sharing LaO_9 polyhedra in the *ab* plane (Figure 3, c). The LaO_9 polyhedra are connected by La−μ-O−La linkages forming chains running parallel to the *b* axis with the alternate La atoms of the chains being bridged by La−μ-O−La linkages along the perpendicular direction. Such connectivity between the chains creates hexanuclear lanthanide rings as shown in Figure 3 (c). Along the chain two LaO_9 polyhedra are capped on either side by the $Se(2)O_4$ units alternatively, which are also connected to the two La atoms in the neighboring chains through a three-coordinate oxygen (O8). In the perpendicular direction, the bridging La atoms are capped by two $Se(1)O_4$ units which share an edge with a LaO_9 polyhedron of the neighboring chains. Accordingly, the SeO_4 units are involved in both capping and bridging the La atoms in the LaO sheets. Such a dual connectivity of the SeO_4 units produces corner-shared four-membered rings (La_2Se_2) propagating along the *a* direction as shown in Figure 4 (a).

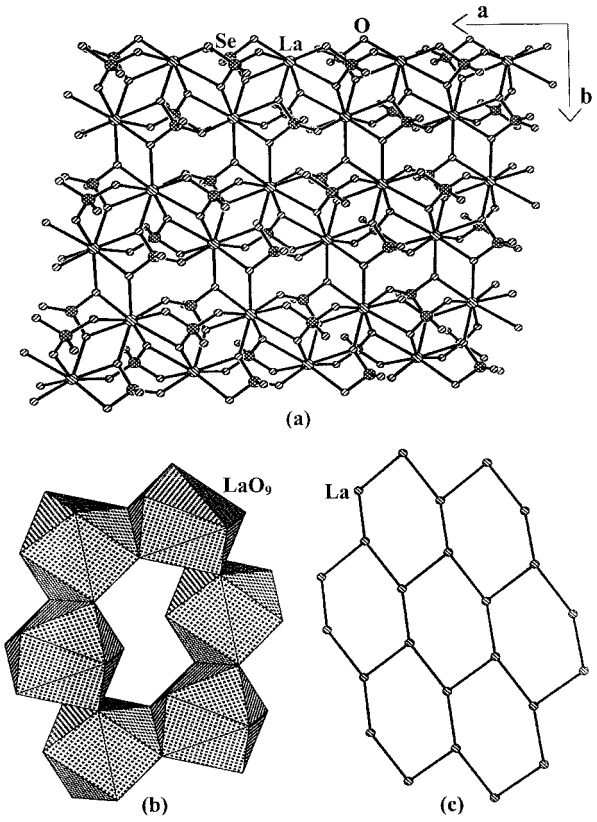

Figure 4. (a) The inorganic layer in **II**; note the capping and bridging of the LaO_9 dimers by two selenate units, resulting in corner-shared four-membered rings along the *a* axis; (b) polyhedral view of a hexanuclear lanthanide ring in **II**; (c) the (6,3) net in **II**

The thermogravimetric analyses (TGA) of **I** and **II** were carried out under N_2 from 30−900 °C at a heating rate of 5 °C/min. Compound **I** decomposes to the selenite in the temperature range 100−330 °C, with the removal of the amine, water and SeO_2 (wt.loss: calcd. 33.02%, obsd. 33.89%) which on further heating, decomposes to a mixture of La_2Se_3 and La_2O_3 (JC, PDS file, card nos: 22-0369, 19-0659), as indicated by the PXRD of the residue at 950 °C. Such thermal decomposition of selenate to selenite has been observed in the case of simple lanthanum selenate hydrates,[20] but the reduction to selenide is unusual. A similar decomposition scheme was observed for **II**, except that in the final stage, all the selenium was lost as SeO_2 to give La_2O_3 as the residue. The overall weight losses for **I** and **II** are 55.94% (calcd. 55.55%) and 57.25% (57.12%), respectively.

Besides being the first examples of two-dimensional organically templated metal selenates, **I** and **II** exhibit several

 © 2004 Wiley-VCH Verlag GmbH & Co. KGaA, Weinheim

interesting structural features. The La atoms are nine-coordinate in both **I** and **II**, but there are definitive differences between their structures. The layer structure of **I** is constructed from two types of chains: type A consisting of chains formed by the SBU-4 units and type B chains consisting of ladders, arranged in an ABAB fashion. **I** appears to be a unique case whereby the layer structure is formed by alternating chains of SBU-4 units and ladders. An important feature of **II** is the two-dimensional network of edge-sharing LaO_9 polyhedra to form a hexanuclear lanthanide ring (Figure 4, b). The hexanuclear lanthanide rings are surrounded by six similar rings resulting in the (6,3) net shown in Figure 4 (c). This is probably the first such layer architecture in the open-framework compounds containing XO_4^{2-} units. Similar rings containing twelve and 14 edge-shared MO_6 octahedra (M = Mn, Co) occur in metal-organic hybrid compounds containing dicarboxylate units.[21] These organic moieties covalently connect the neighboring metal atoms of the ring through C−O−M bonds. A similar connectivity occurs in **II** whereby the two selenate units connect the La atoms in a ring through Se−μ_3-O−La_2 linkages. The zig-zag chains made from edge-sharing LaO_9 polyhedra run parallel in **I** (Figure 2, b), but the chains in **II**, shifted along the *a* direction, are linked to form the LaO sheet in the *ab* plane (Figure 4, c).

Conclusion

In conclusion, the successful synthesis of amine-templated open-framework metal selenates with layered structures has been demonstrated. The results suggest that it may indeed be possible to prepare other complex metal selenates with 2-D and 3-D networks.

Experimental Section

Synthesis and Initial Characterization: Compounds **I** and **II** were synthesized by employing the hydrothermal method in the presence of organic amines. In a typical synthesis of **I** with Ln = La, $LaCl_3$ (0.25 g) was dissolved in water (2 mL) in a Teflon beaker. To this solution selenic acid (0.26 mL, 40 wt%) was added with stirring followed by ethylenediamine (0.08 mL) and the stirring continued for a further 20 min until a homogeneous gel was obtained. The resultant gel with the molar ratio $LaCl_3/H_2SeO_4/1.2en/111H_2O$ was transferred to a 7 mL capacity PTFE-lined stainless steel autoclave and heated at 150 °C for 48 h. The pH of the starting reaction mixture was 4, and there was no change in pH after the completion of the reaction. Colorless plate-like crystals of **I** were collected, washed with de-ionized water, and dried under ambient conditions. For the synthesis of the Nd and Pr analogues of compound **I**, Nd_2O_3 and $Pr_2(CO_3)_3$ were used as metal sources, respectively. The Nd analogue of **I** was obtained by heating a mixture of molar composition $Nd_2O_3/6H_2SeO_4/4en/600H_2O$ at 100 °C for 120 h whereas the Pr analogue of **I** was synthesized starting with the following mixture: $Pr_2(CO_3)_3$ (0.23 g), H_2SeO_4 (0.78 mL), en (0.1 mL), and H_2O (1.8 mL) at 150 °C for 48 h. For the synthesis of **II**, hydrothermal reactions were carried out at 150 °C for 70 h starting with the following composition, $LaCl_3$ (0.25 g, 1 mmol)/H_2SeO_4 (0.4 mL, 1.5 mmol)/PIP (0.17 g, 2 mmol)/H_2O (1.8 mL, 100 mmol) (PIP = piperazine). Initial characterization of both **I** and **II** was carried out by powder X-ray diffraction (PXRD), energy dispersive analysis of X-rays (EDAX), elemental CHN analysis and thermogravimetric analysis (TGA).

The compounds gave satisfactory elemental analysis. The experimental and calculated (in wt%) values for C, H, and N are as follows: **I** (Ln = La): calcd. C 2.43, N 2.80, H 1.84; found C 2.4, N 2.69, H 1.86; **II**: calcd. C 5.02, N 2.94, H 1.67; found: C 5.12, N 2.92, H 1.61. EDAX indicated that the ratios of Ln (Ln = La, Nd or Pr) and Se are 1: 2 for **I** and **II**, which is in agreement with

Table 1. Crystal data and structure refinement parameters **I** and **II**

	I[a]	**II**
Empirical formula	$0.5[C_2N_2H_{10}][La(H_2O)_2(SeO_4)_2]$	$0.5[C_4N_2H_{14}][La(SeO_4)_2]\cdot 0.5H_2O$
Crystal system	triclinic	triclinic
Space group	$P\bar{1}$	$P\bar{1}$
T [K]	293(2)	293(2)
a [Å]	7.0105(8)	5.94(2)
b [Å]	7.3772(9)	7.408(3)
c [Å]	9.526(1)	11.048(2)
α [°]	82.014(2)	86.899(2)
β [°]	84.514(2)	75.971(1)
γ [°]	84.247(2)	79.456(2)
Volume [Å^3]	483.76(1)	463.7(2)
Z	2	4
Formula mass	491.91	478.91
$\rho_{calcd.}$ [g cm^{-3}]	3.453	3.358
μ [mm^{-1}]	11.986	12.476
Total data collected	2032	1956
Unique data	1359	1316
λ(Mo-K_α) [Å]	0.071073	0.071073
R_{int}	0.0329	0.0383
R [$I > 2\sigma(I)$]	$R1$= 0.0435, $wR2$ = 0.1083[b]	R_1= 0.0456, wR_2= 0.1128
R (all data)	$R1$= 0.0482, $wR2$ = 0.1105	R_1= 0.0610, wR_2= 0.1193

[a] The lattice parameters of the corresponding Nd and Pr compounds were comparable. [b] $R1 = ||F_o| - |F_c||/|F_o|$; $wR2 = [\{w(F_o^2 - F_c^2)^2\}/\{w(F_o^2)^2\}]^{1/2}$, $w = 1/[\sigma^2(F_o)^2 + (aP)^2]$, $P = [F_o^2 + 2F_c^2]/3$, where a = 0.0710 for **I** and a = 0.0623 for **II**.

 © 2004 Wiley-VCH Verlag GmbH & Co. KGaA, Weinheim

the molecular formulae. The formula masses of **I** and **II** are 491.91 and 478.91, respectively.

Single-Crystal Structure Determination: Suitable single-crystals of each compound were carefully selected under a polarizing microscope and mounted on the tip of a thin glass fiber using cyanoacrylate (super glue) adhesive. Single-crystal structure determinations by X-ray diffraction were performed with a Siemens SMART-CCD diffractometer equipped with a normal focus, 2.4 kW sealed-tube X-ray source (Mo-K_α radiation, $\lambda = 0.71073$ Å) operating at 50 kV

Table 2. Selected bond lengths and angles for $0.5[C_2N_2H_{10}][La(H_2O)_2(SeO_4)_2]$ (**I**)

Moiety	Distance [Å]	Moiety	Angle [°]
La(1)−O(1)	2.449(7)	O(3)−La(1)−O(6)$^{\#2}$	77.1(2)
La(1)−O(2)	2.476(7)	O(10)$^{\#1}$−La(1)−O(6)$^{\#2}$	139.7(2)
La(1)−O(3)	2.498(7)	O(4)−La(1)−O(6)$^{\#2}$	140.4(3)
La(1)−O(10)$^{\#1}$	2.521(7)	O(5)−La(1)−O(6)$^{\#2}$	81.0(3)
La(1)−O(4)	2.556(8)	O(6)−La(1)−O(6)$^{\#2}$	65.5(3)
La(1)−O(5)	2.586(9)	O(1)−La(1)−O(2)$^{\#3}$	67.5(2)
La(1)−O(6)	2.609(7)	O(2)−La(1)−O(2)$^{\#3}$	63.7(3)
La(1)−O(6)$^{\#2}$	2.637(7)	O(3)−La(1)−O(2)$^{\#3}$	64.5(2)
La(1)−O(2)$^{\#3}$	2.842(7)	O(10)$^{\#1}$−La(1)−O(2)$^{\#3}$	147.8(2)
La(1)−Se(2)$^{\#2}$	3.4747(1)	O(4)−La(1)−O(2)$^{\#3}$	120.0(2)
Se(1)−O(7)	1.617(8)	O(5)−La(1)−O(2)$^{\#3}$	120.2(3)
Se(1)−O(1)	1.623(7)	O(6)−La(1)−O(2)$^{\#3}$	112.4(2)
Se(1)−O(8)	1.627(7)	O(6)$^{\#2}$−La(1)−O(2)$^{\#3}$	55.5(2)
Se(1)−O(3)$^{\#3}$	1.647(7)	O(1)−La(1)−Se(2)$^{\#2}$	74.3(2)
Se(2)−O(9)	1.608(8)	O(2)−La(1)−Se(2)$^{\#2}$	91.6(2)
Se(2)−O(10)	1.637(7)	O(3)−La(1)−Se(2)$^{\#2}$	67.1(2)
Se(2)−O(2)$^{\#4}$	1.646(7)	O(10)$^{\#1}$−La(1)−Se(2)$^{\#2}$	156.6(2)
Se(2)−O(6)	1.668(7)	O(4)−La(1)−Se(2)$^{\#2}$	134.7(2)
Se(2)−La(1)$^{\#2}$	3.4747(1)	O(5)−La(1)−Se(2)$^{\#2}$	100.2(2)
O(2)−Se(2)$^{\#5}$	1.646(7)	O(6)−La(1)−Se(2)$^{\#2}$	89.5(2)
O(2)−La(1)$^{\#3}$	2.842(7)	O(6)$^{\#2}$−La(1)−Se(2)$^{\#2}$	27.6(2)
O(3)−Se(1)$^{\#3}$	1.647(7)	O(2)$^{\#3}$−La(1)−Se(2)$^{\#2}$	27.98(1)
O(6)−La(1)$^{\#2}$	2.637(7)	O(7)−Se(1)−O(1)	109.2(4)
O(10)−La(1)$^{\#1}$	2.521(7)	O(7)−Se(1)−O(8)	111.3(4)
Moiety	Angle [°]	O(1)−Se(1)−O(8)	108.3(4)
		O(7)−Se(1)−O(3)$^{\#3}$	106.8(4)
O(1)−La(1)−O(2)	74.5(3)	O(1)−Se(1)−O(3)$^{\#3}$	112.2(4)
O(1)−La(1)−O(3)	131.4(2)	O(8)−Se(1)−O(3)$^{\#3}$	108.9(4)
O(2)−La(1)−O(3)	78.2(2)	O(9)−Se(2)−O(10)	112.7(4)
O(1)−La(1)−O(10)$^{\#1}$	85.2(3)	O(9)−Se(2)−O(2)$^{\#4}$	112.6(4)
O(2)−La(1)−O(10)$^{\#1}$	93.7(2)	O(10)−Se(2)−O(2)$^{\#4}$	109.3(4)
O(3)−La(1)−O(10)$^{\#1}$	136.3(2)	O(9)−Se(2)−O(6)	110.4(4)
O(1)−La(1)−O(4)	135.6(3)	O(10)−Se(2)−O(6)	110.2(4)
O(2)−La(1)−O(4)	72.5(3)	O(2)$^{\#4}$−Se(2)−O(6)	101.0(4)
O(3)−La(1)−O(4)	68.2(3)	O(9)−Se(2)−La(1)$^{\#2}$	128.0(3)
O(10)$^{\#1}$−La(1)−O(4)	68.4(3)	O(10)−Se(2)−La(1)$^{\#2}$	119.0(3)
O(1)−La(1)−O(5)	150.4(3)	O(2)$^{\#4}$−Se(2)−La(1)$^{\#2}$	54.1(3)
O(2)−La(1)−O(5)	135.1(3)	O(6)−Se(2)−La(1)$^{\#2}$	47.0(2)
O(3)−La(1)−O(5)	67.4(3)	Se(1)−O(1)−La(1)	144.6(4)
O(10)$^{\#1}$−La(1)−O(5)	92.0(3)	Se(2)$^{\#5}$−O(2)−La(1)	145.7(4)
O(4)−La(1)−O(5)	68.5(3)	Se(2)$^{\#5}$−O(2)−La(1)$^{\#3}$	97.9(3)
O(1)−La(1)−O(6)	75.3(2)	La(1)−O(2)−La(1)$^{\#3}$	116.3(3)
O(2)−La(1)−O(6)	148.2(2)	Se(1)$^{\#3}$−O(3)−La(1)	134.3(4)
O(3)−La(1)−O(6)	130.6(2)	La(1)−O(4)−H(8)	119(8)
O(10)$^{\#1}$−La(1)−O(6)	74.2(2)	La(1)−O(5)−H(5)	130(1)
O(4)−La(1)−O(6)	126.1(3)	Se(2)−O(6)−La(1)	129.5(4)
O(5)−La(1)−O(6)	75.6(3)	Se(2)−O(6)−La(1)$^{\#2}$	105.4(3)
O(1)−La(1)−O(6)$^{\#2}$	82.2(3)	La(1)−O(6)−La(1)$^{\#2}$	114.5(3)
O(2)−La(1)−O(6)$^{\#2}$	119.2(2)	Se(2)−O(10)−La(1)$^{\#1}$	141.4(4)

Organic moiety

Moiety	Distance [Å]	Moiety	Angle [°]
N(1)−C(1)	1.479(14)	N(1)−C(1)−C(1)$^{\#6}$	109.4(11)
C(1)−C(1)$^{\#6}$	1.55(2)		

Symmetry transformations used to generate equivalent atoms: $^{\#1}$ $-x, -y+1, -z+2$; $^{\#2}$ $-x+1, -y+1, -z+2$; $^{\#3}$ $-x+1, -y+2, -z+2$; $^{\#4}$ $x, y-1, z$; $^{\#5}$ $x, y+1, z$; $^{\#6}$ $-x, -y+1, -z+1$

 © 2004 Wiley-VCH Verlag GmbH & Co. KGaA, Weinheim

Table 3. Selected bond lengths and angles for $0.5[C_4N_2H_{14}][La(SeO_4)_2]\cdot 0.5H_2O$ (**II**)

Moiety	Distance [Å]	Moiety	Angle [°]	Moiety	Angle [°]
La(1)−O(1)	2.479(9)	O(1)−La(1)−O(2)	150.6(3)	O(8)#1−La(1)−O(4)$^{\#3}$	115.7(2)
La(1)−O(2)	2.480(8)	O(1)−La(1)−O(3)	140.4(3)	O(8)#2−La(1)−O(4)$^{\#3}$	57.0(2)
La(1)−O(3)	2.533(8)	O(2)−La(1)−O(3)	67.6(3)	O(1)−La(1)−O(3)$^{\#4}$	117.9(3)
La(1)−O(4)	2.534(7)	O(1)−La(1)−O(4)	73.2(3)	O(2)−La(1)−O(3)$^{\#4}$	78.1(3)
La(1)−O(5)	2.554(8)	O(2)−La(1)−O(4)	136.0(3)	O(3)−La(1)−O(3)$^{\#4}$	65.0(3)
La(1)−O(8)$^{\#1}$	2.605(7)	O(3)−La(1)−O(4)	71.5(3)	O(4)−La(1)−O(3)$^{\#4}$	70.4(2)
La(1)−O(8)$^{\#2}$	2.614(7)	O(1)−La(1)−O(5)	84.1(3)	O(5)−La(1)−O(3)$^{\#4}$	56.6(2)
La(1)−O(4)$^{\#3}$	2.665(8)	O(2)−La(1)−O(5)	85.8(3)	O(8)$^{\#1}$−La(1)−O(3)$^{\#4}$	119.1(2)
La(1)−O(3)$^{\#4}$	2.795(8)	O(3)−La(1)−O(5)	119.5(2)	O(8)$^{\#2}$−La(1)−O(3)$^{\#4}$	160.8(3)
O(4)−La(1)$^{\#3}$	2.665(8)	O(4)−La(1)−O(5)	100.9(3)	O(4)$^{\#3}$−La(1)−O(3)$^{\#4}$	125.2(2)
O(8)−La(1)$^{\#1}$	2.605(7)	O(1)−La(1)−O(8)$^{\#1}$	72.9(3)	La(1)−O(3)−La(1)$^{\#4}$	115.0(3)
O(8)−La(1)$^{\#5}$	2.614(7)	O(2)−La(1)−O(8)$^{\#1}$	77.8(3)	La(1)−O(4)−La(1)$^{\#3}$	115.7(3)
O(3)−La(1)$^{\#4}$	2.795(8)	O(3)−La(1)−O(8)$^{\#1}$	143.6(3)	La(1)$^{\#1}$−O(8)La(1)$^{\#5}$	116.7(3)
Se(1)−O(6)	1.609(9)	O(4)−La(1)−O(8)$^{\#1}$	144.8(3)	O(2)−Se(2)−O(7)	113.9(4)
Se(1)−O(1)$^{\#5}$	1.628(8)	O(5)−La(1)−O(8)$^{\#1}$	66.7(2)	O(2)−Se(2)−O(4)$^{\#4}$	111.9(4)
Se(1)−O(5)	1.645(8)	O(1)−La(1)−O(8)$^{\#2}$	81.3(3)	O(7)−Se(2)−O(4)$^{\#4}$	110.1(4)
Se(1)−O(3)$^{\#4}$	1.660(8)	O(2)−La(1)−O(8)$^{\#2}$	84.3(2)	O(2)−Se(2)−O(8)	109.4(4)
Se(2)−O(2)	1.600(8)	O(3)−La(1)−O(8)$^{\#2}$	101.3(3)	O(7)−Se(2)−O(8)	112.1(4)
Se(2)−O(7)	1.614(9)	O(4)−La(1)−O(8)$^{\#2}$	119.7(2)	O(4)$^{\#4}$−Se(2)−O(8)	98.6(4)
Se(2)−O(4)$^{\#4}$	1.657(7)	O(5)−La(1)−O(8)$^{\#2}$	130.0(2)	O(6)−Se(1)−O(1)$^{\#5}$	109.7(4)
Se(2)−O(8)	1.665(7)	O(8)$^{\#1}$−La(1)−O(8)$^{\#2}$	63.3(3)	O(6)−Se(1)−O(5)	110.5(5)
O(1)−Se(1)$^{\#2}$	1.628(8)	O(1)−La(1)−O(4)$^{\#3}$	76.7(3)	O(1)$^{\#5}$−Se(1)−O(5)	110.3(4)
O(3)−Se(1)$^{\#4}$	1.660(8)	O(2)−La(1)−O(4)$^{\#3}$	115.8(3)	O(6)−Se(1)−O(3)$^{\#4}$	113.5(4)
O(4)−Se(2)$^{\#4}$	1.657(7)	O(3)−La(1)−O(4)$^{\#3}$	72.4(2)	O(1)$^{\#5}$−Se(1)−O(3)$^{\#4}$	111.9(5)
		O(4)−La(1)−O(4)$^{\#3}$	64.3(3)	O(5)−Se(1)−O(3)$^{\#4}$	100.7(4)
		O(5)−La(1)−O(4)$^{\#3}$	158.4(3)		

Organic moiety Moiety	Distance [Å]	Moiety	Angle [°]
N(1)−C(2)	1.46(2)	N(1)−C(1)−C(2)$^{\#6}$	111.9(12)
N(1)−C(1)	1.47(2)	N(1)−C(2)−C(1)$^{\#6}$	112.4(11)
C(1)−C(2)$^{\#6}$	1.48(2)		
C(2)−C(1)$^{\#6}$	1.48(2)		

Symmetry transformations used to generate equivalent atoms: $^{\#1}$ $-x, -y, -z$; $^{\#2}$ $x+1, y, z$; $^{\#3}$ $-x+1, -y+1, -z$; $^{\#4}$ $-x, -y+1, -z$; $^{\#5}$: $x-1, y, z$; $^{\#6}$: $-x+1, -y, -z-1$

and 40 mA. The structures were solved by direct methods using SHELXS-86,[12] which readily revealed all the heavy atom positions (La, Se) and enabled us to locate the other non-hydrogen (C, N and O) positions from the difference Fourier maps. Empirical absorption corrections based on symmetry-equivalent reflections were applied using SADABS.[13] All the hydrogen positions were found in the difference Fourier maps. For the final refinements, hydrogen atoms for both the framework as well as the amine were placed geometrically and held in the riding mode. The last cycles of refinement included atomic positions, anisotropic thermal parameters for all the non-hydrogen atoms and isotropic thermal parameters for all the hydrogen atoms. However hydrogen positions for the extra-framework water (O100) for **II** were not included in the final refinement because of disorder at that site. Full-matrix least-squares structure refinement against $|F^2|$ was carried out using the SHELXTL-PLUS[14] package of programs. Details of the structure determinations and final refinements for **I** (M = La) and **II** are listed in Table 1. Selected bond lengths and bond angles in **I** and **II** are given in Tables 2 and 3, respectively. Various hydrogen-bonding interactions in **I** and **II** are listed in Table 4. The powder X-ray diffraction patterns of **I** and **II** were in good agreement with the simulated patterns based on single-crystal data, indicative of their phase purity. CCDC-212329 (**I**) and -212330 (**II**) contain the supplementary crystallographic data for this paper. These data can be

Table 4. Hydrogen-bonding interactions in **I** and **II**

Moiety	D−H [Å]	H···A [Å]	D···A [Å]	D−H···A [°]
I				
N(1)−H(1)···O(7)	0.92(2)	2.07(2)	2.83(2)	138.8(1)
N(1)−H(2)··· O(6)	0.92(2)	2.00(1)	2.92(1)	171.2(1)
C(1)−H(3)··· O(1)	0.99(2)	2.51(2)	3.31(2)	138.1(1)
C(1)−H(4)··· O(7)	0.99(2)	2.52(2)	3.24(2)	129.9(1)
C(2)−H(5) ···O(5)	0.99(2)	2.46(2)	3.44(2)	171.8(1)
N(1)−H(1)···O(100)	0.92(2)	2.23(1)	2.91(1)	130.7(1)
II				
N(1)−H(1)···O(9)	0.861(16)	2.501(14)	2.823(14)	103.1(11)
N(1)−H(2)···O(3)	0.860(16)	2.125(14)	2.981(14)	173.8(13)
N(1)−H(3)···O(9)	0.64(12)	2.29(12)	2.823(14)	143(14)
N(1)−H(3)···O(10)	0.64(12)	2.57(12)	3.048(14)	134(13)
*O(5)−H(6)···O(8)	0.71(14)	2.46(14)	3.049(15)	142(13)
O(5)−H(7)···O(8)	0.5(3)	2.4(3)	2.858(13)	158(38)
*O(4)−H(8)···O(8)	0.91(13)	2.17(13)	3.010(12)	153(11)
O(4)−H(9)···O(7)	1.04(15)	1.70(14)	2.709(12)	162(13)
C(1)−H(4)···O(9)	0.970(17)	2.327(15)	3.099(15)	136.0(11)

* Intramolecular hydrogen bonding

 © 2004 Wiley-VCH Verlag GmbH & Co. KGaA, Weinheim

obtained free of charge at www.ccdc.cam.ac.uk/conts/retrieving.html [or from the Cambridge Crystallographic Data Center, 12 Union Road, Cambridge CB2 1EZ, UK; Fax: (internat.) + 44-1223/336-033; E-mail: deposit@ccdc.cam.ac.uk].

Acknowledgments

The authors thank the DRDO (India) and the CSIR (India) for the support of this research work.

[1] [1a] D. W. Breck, *Zeolite Molecular Sieves*, John Wiley & Sons, New York, **1974**. [1b] W. M. Meier, D. H. Oslen, C. Baerlocher, *Atlas of Zeolite Structure Types*, Elsevier, London, **1996**.
[2] A. K. Cheetham, G. Ferry, T. Loiseau, *Angew. Chem.* **1999**, *111*, 3466−3492; *Angew. Chem. Int. Ed.* **1999**, *38*, 3268−3292.
[3] [3a] C. Livage, C. Egger, G. Ferey, *Chem. Mater.* **1999**, *11*, 1546−1550. [3b] T. M. Reineke, M. Eddaoudi, M. O'Keeffe, O. M. Yaghi, *Angew. Chem.* **1999**, *111*, 2712−271; *Angew. Chem. Int. Ed.* **1999**, *38*, 2590−2594. [3c] H. Li, M. Eddaoudi, T. L. Groy, O. L. Yaghi, *J. Am. Chem. Soc.* **1998**, *120*, 8571−8572.
[4] N. Guillou, S. Pastre, C. Livage, G. Ferey, *Chem. Commun.* **2002**, 2358−2359.
[5] R. Vaidhyanathan, S. Natarajan, C. N. R. Rao, *Chem. Mater.* **2001**, *13*, 185−191.
[6] [6a] A. Choudhury, J. Krishnamoorthy, C. N. R. Rao, *Chem. Commun.* **2001**, 2610−2611. [6b] Geo Paul, A. Choudhury, C. N. R. Rao, *J. Chem. Soc., Dalton Trans.* **2002**, 3859−3867. [6c] Geo Paul, A. Choudhury, C. N. R. Rao, *Angew. Chem. Int. Ed.* **2002**, *41*, 4297−4300. [6d] Geo Paul, A. Choudhury, C. N. R. Rao, *Chem. Commun.* **2002**, 1904−1905.
[7] Yan Xing, Zhan Shi, Guanghua Li, Wenqin Pang, *Dalton Trans.* **2003**, 940−943.
[8] [8a] A. J. Norquist, P. M. Thomas, M. B. Doran, Dermot O'Hare, *Chem. Mater.* **2002**, *14*, 5179−5984. [8b] P. M. Thomas, A. J. Norquist, M. B. Doran, Dermot O'Hare, *J. Mater. Chem.* **2003**, *13*, 88−92. [8c] T. Bataille, D. Louer, *J. Mater. Chem.* **2002**, *12*, 3487−3493.
[9] W. T. A. Harrison, M. L. F. Phillips, J. Stanchfield, T. M. Nenoff, *Angew. Chem. Int. Ed.* **2000**, *39*, 3808−3810.
[10] [10a] A. Choudhury, D. Udayakumar, C. N. R. Rao, *Angew. Chem. Int. Ed.* **2002**, *41*, 158−161. [10b] I. Pasha, A. Choudhury, C. N. R Rao, *Inorg. Chem.* **2003**, *42*, 409−415.
[11] D. Udayakumar, C. N. R. Rao, *J. Mater. Chem.* **2003**, *13*, 1635−1638.
[12] [12a] G. M. Sheldrick, *SHELXS-86, Program for crystal structure determination*, University of Göttingen, Göttingen, Germany, **1986**. [12b] M. Sheldrick, *Acta Crystallogr., Sect. A* **1990**, *35*, 467.
[13] G. M. Sheldrick, *SADABS, Siemens Area Detector Absorption Correction Program*, University of Göttingen, Germany, **1994**.
[14] G. M. Sheldrick, *SHELXTL-PLUS, Program for Crystal Structure Solution and Refinement*, University of Göttingen, Göttingen, Germany, **1993**.
[15] G. Ferey, *J. Fluorine Chem.* **1995**, *72*, 187−193.
[16] [16a] N. Simon, T. Loiseau, G. Ferey, *J. Mater. Chem.* **1995**, *9*, 585−590. [16b] F. Taulelle, T. Loiseau, J. Maquet, J. Livage, G. Ferey, *J. Solid State Chem.* **1993**, *105*, 191−196. [16c] W. Yan, J. Wu, Z. Shi, R. Xu, *Inorg. Chem.* **2001**, *40*, 379−383. [16d] G. Ferey, T. Loiseau, P. Laccore, F. Taulelle, *J. Solid State Chem.* **1993**, *105*, 179−190. [16e] T. Loiseau, G. Ferey, *J. Chem. Soc., Chem. Commun.* **1992**, 1179−1180.
[17] S. Mandal, S. Natarajan, J. M. Greneche, M. Riou-Cavellec, G. Ferey, *Chem. Mater.* **2002**, *14*, 3751−3757.
[18] M. L. Martinez, A. Rodriguez, L. Mestres, X. Solans, E. H. Bocanegra, *J. Solid State Chem.* **1990**, *89*, 88−93.
[19] M. Fleck, U. Kolitsch, B. Hertweck, G. Giester, M. Prem, A. Wohlschlager, *Z. Kristallogr.* **2002**, *217*, 1−7.
[20] M. S. Wickleder, *Chem. Rev.* **2002**, *102*, 2011−2087.
[21] [21a] R. Vaidhyanathan, S. Natarajan, C. N. R Rao, *J. Chem. Soc., Dalton Trans.* **2003**, 1459−1464. [21b] C. Livage, C. Egger, M. Nogues, G. Ferey, *J. Mater. Chem.* **1998**, *8*, 2743−2747. [21c] C. Livage, C. Egger, M. Nogues, G. Ferey, *Chem. Mater.* **1999**, *11*, 1546−1550.

Received October 3, 2003
Early View Article
Published Online March 9, 2004

 © 2004 Wiley-VCH Verlag GmbH & Co. KGaA, Weinheim

Iminohydroxamato Early and Late Transition Metal Halide Complexes − New Precatalysts for Aluminoxane-Cocatalyzed Olefin Insertion Polymerization

Alexander Krajete,[a] Georg Steiner,[a] Holger Kopacka,[a] Karl-Hans Ongania,[b] Klaus Wurst,[a] Marc O. Kristen,[c] Peter Preishuber-Pflügl,[d] and Benno Bildstein*[a]

Keywords: N,O ligands / N ligands / Chelates / Transition metals / Polymerization

We report on new families of non-metallocene metal precatalysts for olefin polymerization with titanium, zirconium, vanadium and nickel as the active metal sites. The novel ligand design concept is based on iminohydroxamic acids and their derivatives as the principal chelating units. Various anionic and neutral [*N*,*O*] and [*N*,*N*] ligand systems are easily accessible by a modular synthetic sequence of imidoyl chlorides with substituted hydroxylamines or hydrazines, respectively. Steric protection of the metal coordination site, a necessary requirement for suppression of chain termination pathways of non-metallocene catalysts, is brought about by bulky aryl substituents on the imino nitrogen atoms. Crystal structures of some of the hydroxamato ligands reveal interesting intermolecular hydrogen-bridged structures, whereas in the solid-state structure of one titanium precatalyst a five-membered chelate was observed, in line with the design principle of these systems. Preliminary ethylene polymerization studies with methylaluminoxane-activated metal complexes (M = Ti, Zr, V, Ni) show that the most active systems are [*N*,*O*]$NiBr_2$ catalysts containing neutral *O*-alkyl iminohydroxamate ligands.

(© Wiley-VCH Verlag GmbH & Co. KGaA, 69451 Weinheim, Germany, 2004)

Introduction

Olefin polymerization catalysis based on transition metal complexes containing non-cyclopentadienyl ligand frameworks is an extremely active research area[1] since the recent key discoveries of very active (i) (diimine)nickel[2] catalysts, (ii) [bis(imino)pyridine]iron[3] catalysts, and (iii) (salicylaldiminato)nickel[4] and -titanium[5] catalysts. These new systems show some significant advantages in comparison with the more familiar traditional Ziegler−Natta titanium/zirconium or Phillips chromium systems, including (i) simplified ligand design, (ii) metal centers ranging from early to late transition metals, (iii) decreased oxophilicity of the late transition metal complexes, allowing polymerizations and/or copolymerizations of polar monomers or even polymerizations in water,[6] (iv) access to new branched microstructures of the polymers due to "chain-walking" of the catalytically active species,[7] and (v) living polymerization of olefins,[8] giving precise control of polymer molecular weights and giving access to block copolymers and other new materials. Due to the economic importance of polyolefinic materials in general, academic and industrial research activity in this area is very high and an ever increasing number of catalyst improvements and developments are being published and/or patented.[1]

Here we introduce a new family of ligands based on the iminohydroxamate backbone and we report on their transition metal halide complexes as new precatalysts for methylaluminoxane (MAO) activated olefin polymerizations.[9] Our design principle is based on chelating [*N*,*O*] and [*N*,*N*] ligands in accordance with (salicylaldiminato)nickel and -titanium systems reported by the groups of Grubbs[4] and Fujita[5] (Scheme 1). Such salicylaldimine ligands form six-membered metal chelates and for steric protection they usually contain bulky aromatic imine moieties (in most cases 2,6-diisopropylphenyl) and sterically shielding groups in the *ortho* position of the oxygen donor site. In contrast, in our newly designed iminohydroxamate ligands, the metal chelate is an energetically favored five-membered ring and steric protection is provided by bulky arylimino substituents. This is similar to most non-cyclopentadienyl transition metal polymerization catalysts.[1] Scheme 1 outlines the chemical relationships between the parent iminohydroxamic acids (**A**), their *O*-alkyl esters (**B**), their *N*-mono- (**C**) and *N*,*N*-disubstituted amides (**D**), showing the large structural

[a] Institute of General, Inorganic and Theoretical Chemistry; University of Innsbruck,
Innrain 52a, 6020 Innsbruck, Austria
E-mail: benno.bildstein@uibk.ac.at
[b] Institute of Organic Chemistry, University of Innsbruck,
Innrain 52a, 6020 Innsbruck, Austria
[c] Basell Polyolefin GmbH,
67056 Ludwigshafen, Germany
[d] BASF Aktiengesellschaft,
67056 Ludwigshafen, Germany

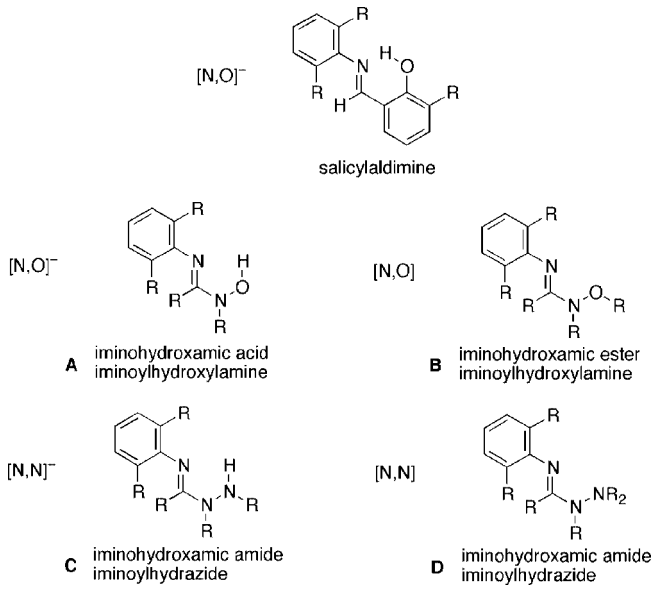

Scheme 1. Design principle of chelating [*N*,*O*] and [*N*,*N*] hydroxamate ligands

varieties possible and indicating the obvious ligand design opportunities in these [*N*,*O*] and [*N*,*N*] ligand families.

In a historical perspective, in situ generated hydroxamic acids are well known in qualitative organic analysis for their formation of magenta- or burgundy-colored Fe^{III} complexes,[10] a more or less specific color test for carboxylic acid derivatives in the presence of hydroxylamine. Simple (iminohydroxamato)metal complexes have been investigated for over 100 years,[11] mainly in spectrophotometric and pharmaceutical studies. However, no applications as olefin polymerization precatalysts have been reported up to now.

Results and Discussion

Synthesis and Characterization of Ligands

In general, ligand design is an essential part of the search for new and improved metal catalysts because steric bulk and stereoelectronic effects of the ligand architecture control the selectivity and activity of the metal complexes in their function as catalysts. From a preparative viewpoint the synthetic route should be straightforward, avoid tedious workup and separations, and should be of wide scope, thereby allowing parallel synthetic optimization.

The preparation of our new families of hydroxamate-based ligands fulfill these requirements (Scheme 2). *N*-Substituted benzamides **1a**−**1d** containing *N*-aryl groups with different substitution pattern are easily available in large quantities from the corresponding anilines and benzoyl chloride. Conversion into the corresponding imidoyl chlorides **2a**−**2d** can be brought about quantitatively by treatment with an excess of thionyl chloride employing standard published chemistry.[12] Usually these synthons were prepared in situ only, and used in the following reactions without being isolated. In one case, however, single crystals were obtained by chance (Table 2).

Figure 1 shows the molecular structure of **2a** in the solid state, clearly visible is the steric shielding of the imine functionality by the bulky *N*-(2,6-diisopropyl) group. As a result of the two *ortho*-alkyl substituents the aryl group is tilted by 80.56(10)° in relation to the imidoyl chloride plane, as anticipated and in line with our design principle of axial steric shielding brought about by bulky *N*-imino substituents (vide infra).

Iminohydroxamic acids **3a**−**3f** can be quite easily synthesized by iminoacylation of *N*-monosubstituted hydroxylamines. Similar chemistry has been reported earlier in the literature employing *N*-phenylhydroxylamine.[11b] As antici-

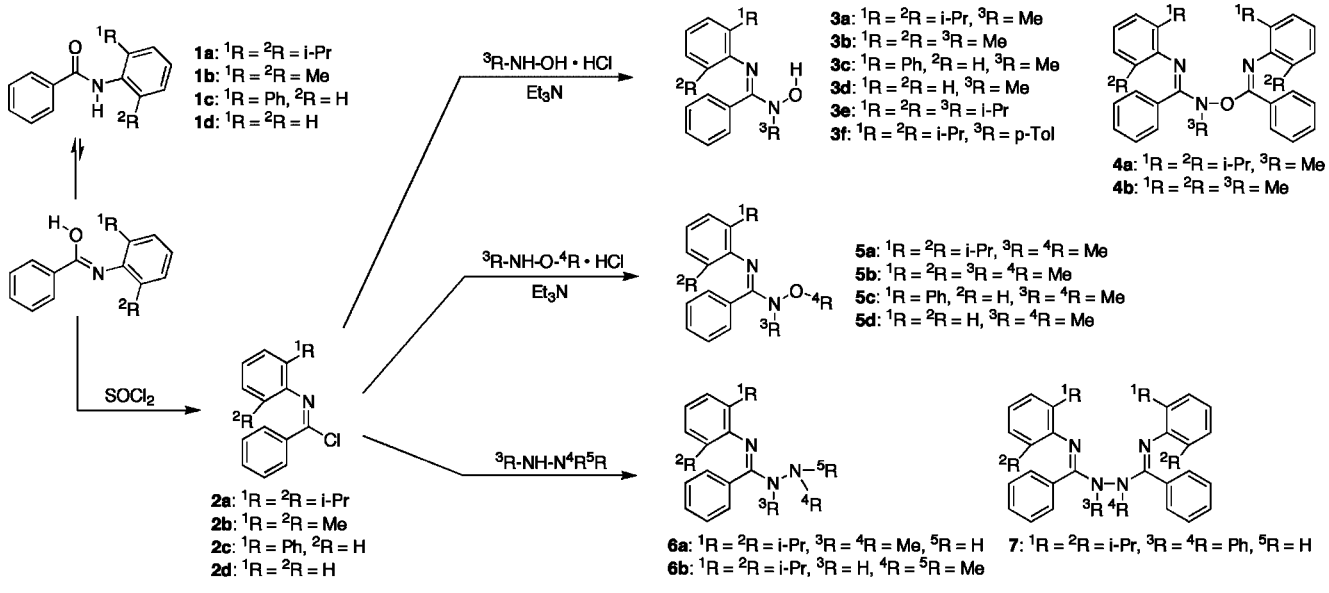

Scheme 2. Synthesis of iminohydroxamate ligands

 © 2004 Wiley-VCH Verlag GmbH & Co. KGaA, Weinheim

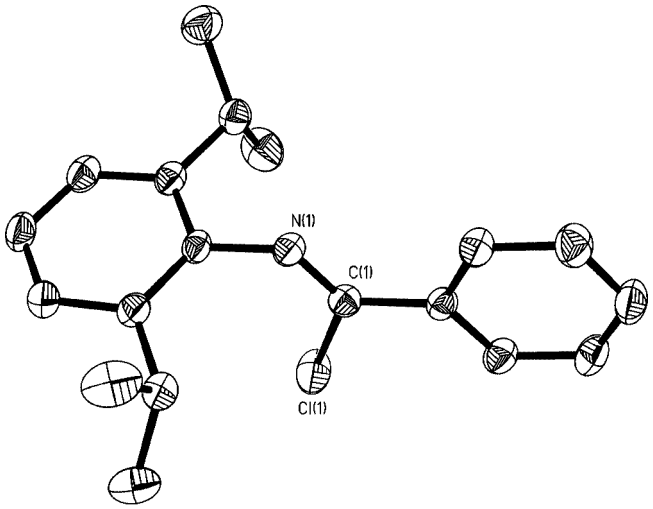

Figure 1. Molecular structure of **2a**; hydrogen atoms are omitted for clarity; selected bond lengths [pm]: Cl(1)−C(1) 178.0(2), C(1)−N(1) 124.8(2); tilt angles [°]: plane of phenyl ring versus plane Cl(1)−C(1)−N(1): 3.25(24); plane of 2,6-diisopropylphenyl ring versus Cl(1)−C(1)−N(1): 80.56(10)

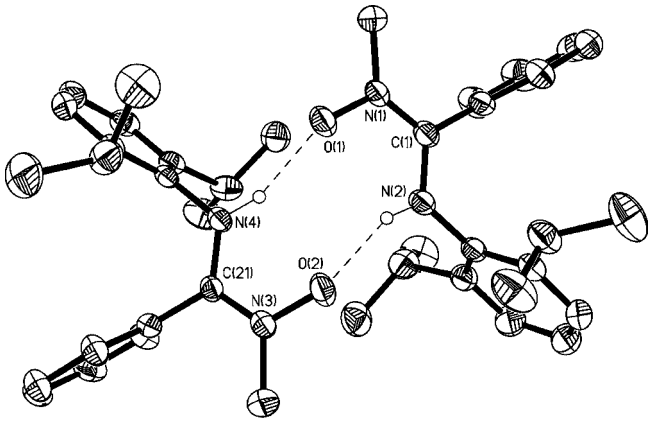

Figure 2. Molecular structure of **3a**; except for N−H−O hydrogen bonds, hydrogen atoms are omitted for clarity; selected bond lengths [pm]: C(1)−N(1) 131.2(3), N(1)−O(1) 134.5(3), C(1)−N(2) 133.8(3), C(21)−N(3) 131.1(3), N(3)−O(2) 134.6(3), C(21)−N(4) 134.4(3), N(2)−H(2N) 87(3), N(4)−H(4N) 91(3); tilt angles [°]: plane of phenyl ring of C(1) versus plane N(1)−C(1)−N(2): 83.48(15); plane of 2,6-diisopropylphenyl ring of N(2) versus plane N(1)−C(1)−N(2): 88.55(21); plane of phenyl ring of C(21) versus plane N(3)−C(21)−N(4): 75.17(15); plane of 2,6-diisopropylphenyl ring of N(4) versus plane N(3)−C(21)−N(4): 85.38(22)

pated, the more nucleophilic nitrogen atom is acylated first in these ambident substrates affording the desired ligands in isolated yields of 18−63%, followed by *O*-acylation which always occurs to a certain degree, dependent on the substitution pattern of the building blocks. Due to the much higher polarity of the mono(iminoacylated) hydroxamic acids **3a**−**3f** in comparison with the undesired *N*,*O*-bis(iminoacylated) side products, separation and purification of the hydroxamic acids can be conveniently accomplished by a simple filtration through a short silica column (see Exp. Sect.). In two cases, **4a** and **4b**, the undesired *N*,*O*-bis(iminoacylated) products were isolated and characterized spectroscopically.

In principle any hydroxylamine can be derivatized in this manner, including the parent unsubstituted hydroxylamine. However, the starting hydroxylamines containing one *N*-organo substituent were chosen because the *N*−H acidic site in these iminohydroxamic acids is blocked. This enables activation of the corresponding metal complexes with methylaluminoxane (vide infra) without undesired *N*-deprotonation or *N*-alumination, respectively.

Iminohydroxamic acids **3a**−**3f** are stable organic compounds and white to yellow in color. Relevant spectroscopic properties include characteristic IR stretching vibrations due to the imino groups ($\nu_{C=N}$ = 1598−1630 cm^{-1}), and diagnostic low-field ^{13}C NMR chemical shifts of the imino functionalities ($\delta_{C=N}$ = 147.7−150.5 ppm). The ν_{O-H} bands of the hydroxy groups (3600 to 3100 cm^{-1}) are very weak and broad in the IR spectra, due to line broadening and association. Also in the ^1H NMR spectra the signals of the hydroxy hydrogen atoms are usually not observed, due to exchange and overlapping with other signals (compare Exp. Sect.). For three of these iminohydroxamic acids, suitable single crystals for X-ray structural analyses were obtained (Figures 2−4).

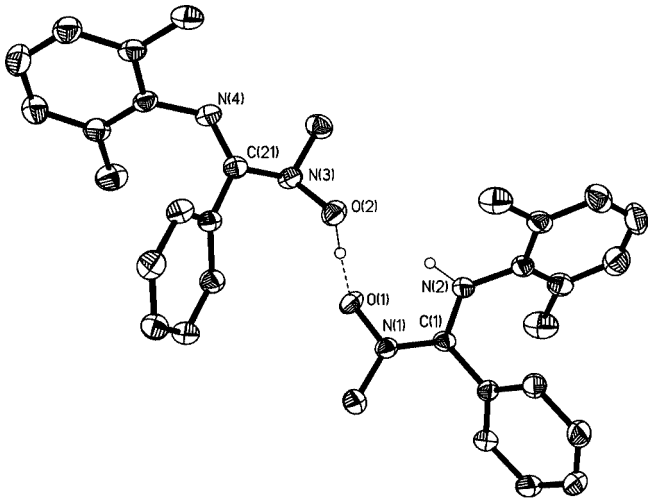

Figure 3. Molecular structure of **3b**; except for N−H and O−H hydrogen atoms, all other hydrogen atoms are omitted for clarity; selected bond lengths [pm]: C(1)−N(1) 130.6(3), N(1)−O(1) 135.1(2), C(1)−N(2) 135.7(3), C(21)−N(3) 139.0(3), N(3)−O(2) 142.2(2), C(21)−N(4) 128.1(3), N(2)−H(2N) 94(2), O(2)−H(2O) 106(3); tilt angles [°]: plane of phenyl ring of C(1) versus plane N(1)−C(1)−N(2): 62.26(13); plane of 2,6-dimethylphenyl ring of N(2) versus plane N(1)−C(1)−N(2): 70.93(16); plane of phenyl ring of C(21) versus plane N(3)−C(21)−N(4): 43.52(10); plane of 2,6-dimethylphenyl ring of N(4) versus plane N(3)−C(21)−N(4): 76.18(18)

A common feature in all three structures is the tilting of both aryl rings relative to the plane of the principal N=C−N−O unit. These tilt angles range from 43.5 to 83.5° for the *C*-phenyl ring, and from 34.0 to 88.6° for the substituted *N*-aryl moiety, respectively. Clearly the tilting in both cases is caused by steric crowding, especially in the latter case, due to the two *ortho*-alkyl groups on the *N*-aryl sub-

 © 2004 Wiley-VCH Verlag GmbH & Co. KGaA, Weinheim

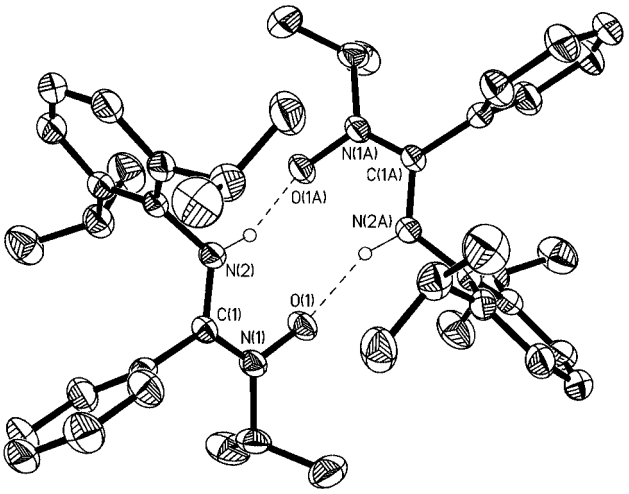

Figure 4. Molecular structure of **3e**; except for N−H−O hydrogen bonds, hydrogen atoms are omitted for clarity; selected bond lengths [pm]: C(1)−N(1) 130.5(4), N(1)−O(1) 134.0(3), C(1)−N(2) 135.9(4), N(2)−H(2N) 98(4); tilt angles [°]: plane of phenyl ring of C(1) versus plane N(1)−C(1)−N(2): 78.74(15); plane of 2,6-diisopropylphenyl ring of N(2) versus plane N(1)−C(1)−N(2): 34.02(23)

stituent. As anticipated, in all three structures, hydrogen-bridging plays a decisive role in the solid-state packing of the molecules. In all three structures two molecules are paired by one or two O−H−N hydrogen bonds. Interestingly, both possible tautomers of the iminohydoxamic acid functionality were observed, depending on the substitution pattern of the principal N=C−N−OH unit. Compounds **3a** and **3e** exist in the solid state solely in their zwitterionic iminium hydroxamate $^{+}$NH=C−N−O^{-} forms connected by two hydrogen bonds (see Figures 2 and 4), whereas in the case of compound **3b** both tautomers with only one hydrogen bond are present, the expected and "usual" neutral N=C−N−OH form and the unexpected and "exotic" zwitterionic $^{+}$NH=C−N−O^{-} form (Figure 3). It is quite clear, however, that this tautomerism is dominated by solid-state forces and in solution the position of equilibrium will be almost totally on the side of the uncharged normal iminohydroxamic acid species.

The synthesis of iminohydoxamic esters **5a**−**5d** can be very easily accomplished by iminoacylation of *N*,*O*-bis(alkylated) hydroxylamines (Scheme 2). The isolated yields of 78−94% are much higher than those of the iminohydroxamic acids discussed above, simply because there is only one nucleophilic site in the substrates. Ligands **5a**−**5d** are stable compounds which are white to yellow in color. Spectroscopically, the imine functionalities may be corroborated by their typical IR absorptions ($\nu_{C=N}$ = 1628−1636 cm^{-1}), shifted to higher wave numbers compared with the hydroxamic acids **3a**−**3f**, and by their ^{13}C NMR chemical shifts (δ = 160.8−162.8 ppm) which are also shifted to lower field in comparison with compounds **3a**−**3f**. The signals of the methyl groups of the ester functionalities were detected at δ = 3.38−3.54 ppm in the ^{1}H NMR spectra and at δ = 60.2−60.6 ppm in the ^{13}C NMR spectra; both sets of chemical shifts are in accordance with expectations at lower field in comparison with those of the *N*-alkyl substituents of **3a**−**3f** and **5a**−**5d**, respectively.

Amino derivatives of iminohydroxamic acids are accessible similarly by iminoacylation of hydrazines. In our hands, however, this chemistry was only possible for alkylated hydrazines affording ligands **6a** and **6b**, but on attempted mono(iminoacylation) of *N*,*N*′-diphenylhydrazine only the bis(derivative) **7** was obtained. This is a rather unfortunate result because diarylhydrazines can be easily synthesized from azobenzenes by reduction, and various substituted diarylhydrazines would allow a convenient stereoelectronic fine-tuning on the amino *N*-donor site of ligands of type **6**. The spectroscopic data of **6a**, **6b** and **7** are consistent with their structures with values similar to those of the other ligand families discussed above. As a minor issue, we note that the imidoyl hydrazide **6b** is the only ligand of all these compounds with an *N*−H substituent on the benzamidine moiety, in this case no protection of the *N*−H acidic moiety is present (vide infra).

Metal Complexes

[N,O] Iminohydroxamato Complexes

In principle, with tetravalent early transition metals, [*N*,*O*]MX_3 mono- and [*N*,*O*]$_2$MX_2 bis(complexes) should be accessible. Hence six differently substituted iminohydroxamic acids (**3a**−**3f**) and three different metal halides ($ZrCl_4$, $TiCl_4$, VCl_4) would afford a series of 36 different metal complexes. In this work, however, only selected examples from this rather large number of compounds were synthesized on a preparative scale (Scheme 3), based on the following criteria and objectives: (i) in order to compare the stereoelectronic influence of all six ligands **3a**−**3f**, all six zirconium mono(complexes) [*N*,*O*]$ZrCl_3$ **8a**−**8f** were synthesized, (ii) for comparing the difference between mono- and bis(complexes), one [*N*,*O*]$_2$$ZrCl_2$ complex (**9a**) was prepared, (iii) to study the effect of different metals, two additional complexes **10b** [M = Ti] and **11b** [M = V] with ligand **3b** were synthesized, and (iv) to facilitate characterization of the complexes by NMR spectroscopy we focused on the diamagnetic Zr and Ti complexes. Furthermore we note that [*N*,*O*]NiRL complexes (L = phosphane, R = alkyl or aryl) in analogy to Grubbs' (salicylaldiminato)Ni complexes[4] are also accessible, but unfortunately such compounds are very labile and, according to our preliminary results, decompose very quickly.

As anticipated, the synthesis of metal complexes of [*N*,*O*]H ligands **3a**−**3f** was rather simple. Deprotonation with *n*-butyllithium in THF followed by treatment with the appropriate transition metal halide afforded complexes **8a**−**11b** (Scheme 3) in isolated yields ranging from 64 to 95% (see Exp. Sect.). All the compounds are stable under dry and inert conditions. On exposure to air, however, they are quickly hydrolyzed as expected. The zirconium and titanium complexes **8a**−**10b** are diamagnetic and are yellow to orange in color, in contrast to the dark green vanadium complex **11b** which is strongly paramagnetic.

 © 2004 Wiley-VCH Verlag GmbH & Co. KGaA, Weinheim

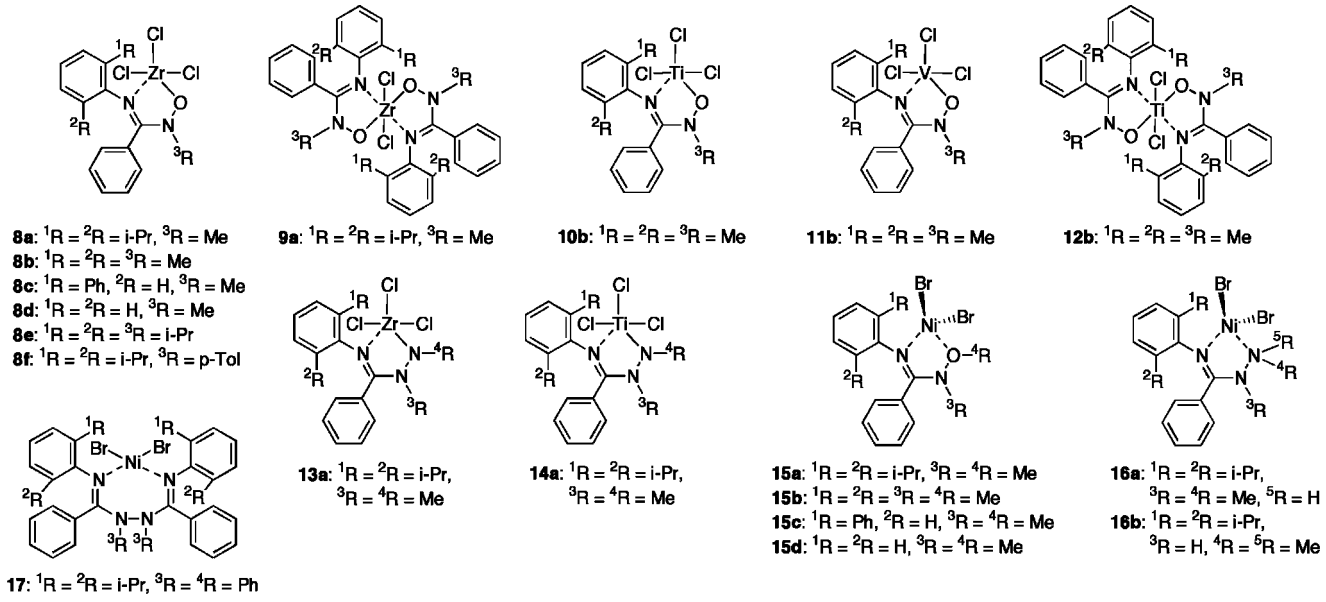

Scheme 3. Metal complexes of [*N*,*O*] and [*N*,*N*] iminohydroxamato ligands

The characterization of the diamagnetic compounds relies mainly on NMR spectroscopy. In the ^{13}C NMR spectra the coordinated imino functionalities ($\delta_{C=N}$ = 159−162 ppm) are shifted to lower field by approximately 10 ppm compared with the chemical shifts of the imine carbon signals of the free ligands ($\delta_{C=N}$ = 146−151 ppm). Other resonances were shifted as well, but to a much lesser degree. Most significantly, the ^1H and ^{13}C NMR spectra clearly show that the [*N*,*O*]$ZrCl_3$ mono(complexes) **8a**−**8f** exist predominantly as mixtures of isomers containing THF as an additional neutral ligand in an octahedral coordination environment. In principle, 4 pairs of chiral diastereoisomers are possible with these heterotopic [*N*,*O*] chelate ligands in combination with three chloride ions and one THF ligand (Scheme 4). Mono-Zr complexes containing the *N*-(2,6-diisopropylphenyl) substituent exist as one isomer (**8a**, **8e**, **8f**), whereas those with sterically less demanding *N*-aryl groups give rise to the observation of two diastereoisomers (**8b**, **8c**, **8d**) according to their NMR spectra (compare Exp. Sect.).

In contrast to the [*N*,*O*]$ZrCl_3$ complexes **8a**−**8f**, no coordinated THF was present in the titanium complex **10b**, most likely due to the smaller size of the lighter transition metal atom. Also, complex **9a** with two chelating [*N*,*O*] ligands had no coordinated THF, but four structural isomers of the theoretically possible 5 isomers (Scheme 5) were observed in this heterotopic and non-homoleptic complex.

In most of the zirconium compounds **8a**−**9a** (with the exception of **8a**, **8e**, **8f**) the occurrence of a mixture of isomers was clearly evident from NMR spectroscopy. On the one hand this is an expected and interesting stereochemical observation, on the other hand, however, it hampers further characterization of these complexes by X-ray crystallography. Unfortunately, under no circumstances we were able to obtain single crystals. In the case of the titanium complex

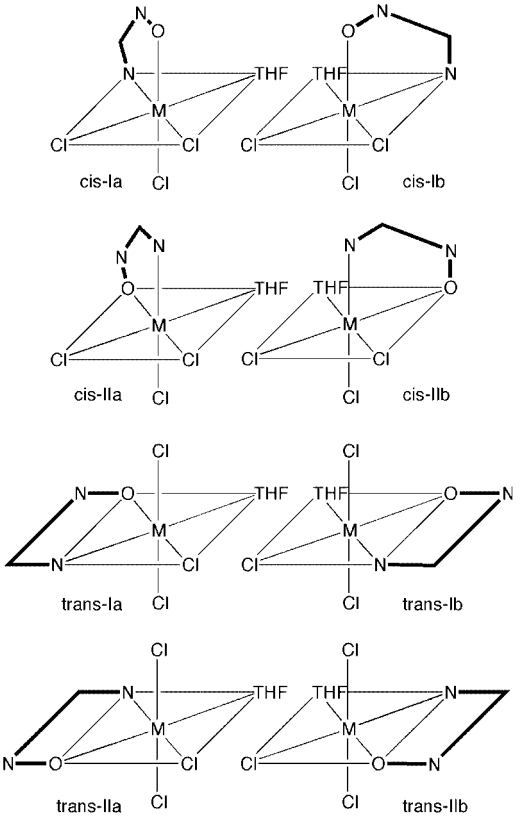

Scheme 4. Structural isomers of [*N*,*O*]$ZrCl_3$(THF) complexes

10b, however, suitable red single crystals grew after one year, together with some amorphous colorless material. Figure 5 shows the molecular structure of this crystalline material. Unexpectedly, the structure corresponds to the [*N*,*O*]$_2$-$TiCl_2$ bis complex **12b** which must have been formed from

 © 2004 Wiley-VCH Verlag GmbH & Co. KGaA, Weinheim

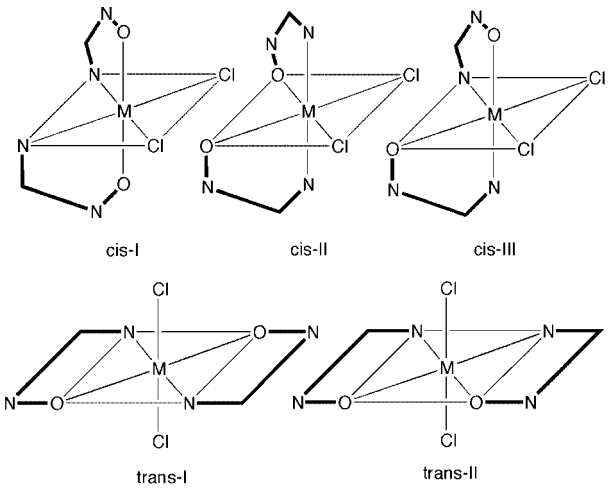

Scheme 5. Structural isomers of $[N,O]_2ZrCl_2$ complexes

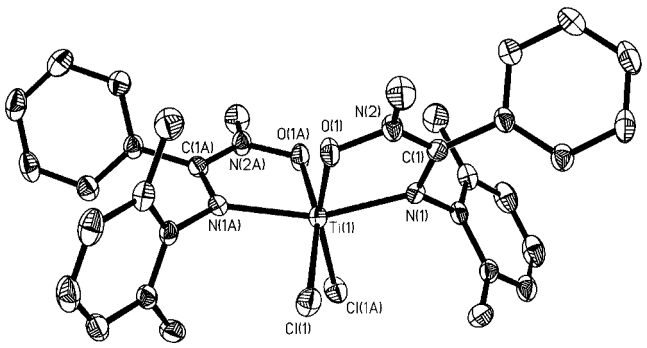

Figure 5. Molecular structure of **12b**; hydrogen atoms are omitted for clarity; selected bond lengths [pm]: Ti(1)−Cl(1) 231.97(7), Ti(1)−N(1) 210.83(18), Ti(1)−O(1) 192.44(17), C(1)−N(1) 132.9(3), C(1)−N(2) 132.4(3), N(2)−O(1) 136.1(3); selected angles [°]: Cl(1)−Ti(1)−Cl(1A) 90.22(4), O(1)−Ti(1)−O(1A) 95.10(12), N(1)−Ti(1)−O(1) 74.54(7), N(1)−Ti(1)−Cl(1) 105.26(5), O(1)−Ti(1)−Cl(1) 89.74(6), N(1)−Ti(1)−N(1A) 159.57(10), Ti(1)−N(1)−C(1) 115.12(15), N(1)−C(1)−N(2) 114.9(2), Ti(1)−O(1)−N(2) 120.79(13); tilt angle plane of phenyl group of C(1) versus plane N(1)−C(1)−N(2): 66.71(26); tilt angle of 2,6-dimethylphenyl group of N(1) versus plane N(1)−C(1)−N(2): 82.46(19)

the $[N,O]TiCl_3$ mono(complex) **10b** by ligand scrambling. Despite the obvious serendipity of this result, the molecular structure clearly demonstrates the chelating nature of the hydroxamato ligand **3b**, indicating that in all other cases such five-membered metal chelates are also present. Overall, the stereochemistry of **12b** corresponds to isomer *cis*-**II** of Scheme 5 with *cis*-oriented chloro ligands and *trans*-oriented imino donor sites of the heterotopic iminohydroxamato ligands. The coordination geometry at the central titanium atom is principally octahedral with only minor deviations from the ideal 90° (0.3−15.5°) and 180° (16.8−20.4°) angles. The bond lengths of the titanium atom to the nitrogen, oxygen, and chlorine atoms of the ligands are given in the caption of Figure 5. They are unexceptional and in the commonly observed range. In contrast to the more or less undistorted coordination geometry, the peripheral phenyl groups of the iminohydroxamato ligands are strongly tilted (66.7 and 82.5°) with respect to the hydroxamate plane, showing that steric shielding by the *N*-arylimino substituent is effective, in accordance with the general design principle of these olefin polymerization precatalysts (vide supra).

The syntheses of the imidoyl hydrazido complexes **13a** and **14a** are analogous to the preparation of the iminohydroxamato complexes discussed above (Scheme 3). Deprotonation of ligand **6a** in THF by *n*-butyllithium followed by treatment with $ZrCl_4$ or $TiCl_4$ in a 1:1 stoichiometric ratio afforded complexes **13a** and **14a**, respectively. Besides the additional *N*-methyl resonances, both compounds show NMR spectroscopic properties very similar to those of the iminohydroxamato complexes **8a**−**8f** and **10b**. Stereochemically, Zr complex **13a** exists as a mixture of two octahedral isomers containing one additional THF ligand (in analogy to the isomers in Scheme 4), whereas **14a** seems to be either five-coordinate or more likely a chloro-bridged dimer with no coordinated THF.

The synthesis of nickel(II) complexes starting from the neutral (non-acidic) iminohydroxamic esters **5a**−**5d**, imidoyl hydrazides **6a**−**6b** and **7** was very straightforward. Treatment with $NiBr_2$ in dichloromethane at room temperature overnight afforded the corresponding $[N,O]NiBr_2$ complexes **15a**−**15d** and $[N,N]NiBr_2$ complexes **16a**, **16b**, **17** in good yields (Scheme 3).

With the exception of **17**, which is a seven-membered chelate in contrast to all other complexes, all the Ni complexes are dark green or brown, air-sensitive and paramagnetic, thereby thwarting their characterization by NMR spectroscopy. In general, broad and shifted signals were observed in the ^1H NMR spectra and signal intensities in the ^{13}C NMR spectra were very low allowing, only in one case, the detection of the carbon resonances (see Exp. Sect.). The paramagnetism of these complexes clearly indicates a non-quadratic, non-planar coordination geometry and these compounds exist either as four-coordinate tetrahedrally distorted monomers or as bromo-bridged five-coordinate dimers. Clearly, crystal structures would provide the best information on the structures of these compounds, but despite many attempts with different solvents employing various crystallization procedures no suitable crystals could be obtained. On the other hand, the observed paramagnetism shows that steric shielding of the ligands is sufficient to distort the orientation of the bromo ligands from their preferred square-planar geometry, as in Grubbs'[4] and Brookhart's[2] $[N,O]$- and $[N,N]$Ni catalysts.

Polymerization Studies

The main question to be answered by this work is: "How active and selective are these newly designed catalyst families for the polymerization of olefins?" To evaluate the catalytic performance of complexes **8a**−**17** a standard polymerization procedure was applied. A steel autoclave containing a toluene solution of the precatalyst was activated with an excess of methylaluminoxane and at a temperature of 70 °C

 © 2004 Wiley-VCH Verlag GmbH & Co. KGaA, Weinheim

Table 1. Polymerization of ethylene (MAO as activator, 70 °C, 40 bar)

Complex (metal)	Amount precatalyst [mg]	Polymerization time [min]	Yield polymer [g]	Viscosity of polymer [dL/g]	Activity [g mmol^{-1} h^{-1} bar^{-1}]
8a (Zr)	4.8	30	9.5	9.51	50.2
8b (Zr)	6.0	30	12.0	14.01	45.1
8c (Zr)	1.5	35	4.8	11.41	68.4
8d (Zr)	0.9	60	6.7	24.95	78.7
8e (Zr)	1.2	90	11.9	4.43	88.4
8f (Zr)	2.0	75	8.8	8.76	51.3
9a (Zr)	4.0	90	9.4	41.38	30.6
10b (Ti)	4.0	60	7.4	54.33	18.8
11b (V)	8.0	90	6.2	19.18	5.3
13a (Zr)	1.4	45	6.2	15.6	76.8
14a (Ti)	1.7	15	1.0	–	28.0
15a (Ni)	3.9	5	7.25	3.62	302.8
16a (Ni)	2.7	90	1.0	2.15	3.3
16b (Ni)	1.4	90	1.3	2.57	8.4
17 (Ni)	1.8	90	1.7	2.50	14.6

ethylene was added up to a pressure of 40 bar, the reaction was allowed to proceed for 5−90 min while maintaining a 40 bar pressure by adjusting the feed of ethylene (Table 1, for further details see Exp. Sect.).

In terms of activity, all [*N*,*O*]- and [*N*,*N*]zirconium complexes showed a moderate activity of 30.6−88.4 g polyethylene × mmol^{-1} × catalyst × h^{-1} × bar^{-1}. The bis(complex) [*N*,*O*]$_2$ZrCl$_2$ (**9a**) had the lowest activity of all Zr complexes, clearly indicating that one ligand per metal center ([*N*,*O*]ZrCl$_3$) is superior to a 2:1 ratio. Changing the metal to either titanium or vanadium resulted in a significantly reduced activity with either the [*N*,*O*] or [*N*,*N*] ligand architecture. In the case of the nickel complexes, compound **15a** truly stands out as a precatalyst with a (very) high activity of 302.8, suggesting that neutral *O*-alkyl iminohydroxamate is the best ligand framework developed in this work. However, the long-term stability of the [*N*,*O*]NiBr$_2$ complexes **15a**−**15d** in their MAO-activated form has not yet been optimized and only with **15a** under short polymerization times was a polymer obtained, indicating fast deactivation pathways. Future work towards improvements of these systems will focus on altering the *O*-alkyl substituent to create better shielding of the active metal center and to increase the stability of the activated complex.

In terms of polymer properties, the polyethylene samples obtained by the zirconium catalyst family were very high molecular weight (Mv = 1.5 to 10 × 10^6 g/mol, derived from viscosity measurements) polymers with viscosities ranging from 4.43 to 54.33 dl/g, dependent on the substitution pattern of the ligands. In contrast, PE samples obtained from nickel complexes **15a**−**17** were of the HDPE type with no detectable branches and molar masses (Mv) of 1.0 to 2.5 × 10^5 g/mol.

In addition, polymerization of propylene and copolymerization of ethylene with *n*-hexene was briefly investigated. In both cases, only low activities below 150 g polymer × mmol^{-1} × catalyst × h^{-1} were achieved.

Summary and Conclusions

New bidentate chelate ligands based on an iminohydroxamate backbone architecture have been developed. These new ligands contain an imino nitrogen donor site with a substituted aryl group to effect steric shielding and an anionic or neutral oxygen or nitrogen donor site, respectively. The free ligands show interesting solid-state structures in which hydrogen bonding is responsible for unusual zwitterionic tautomeric structures. New metal complexes of zirconium, titanium, vanadium, and nickel have been synthesized and evaluated for their performance as olefin polymerization catalysts. Structurally, the five-membered metal chelates exist in most cases as a number of different octahedral stereoisomers in the case of early transition metals, and as tetragonally distorted paramagnetic four- or five-coordinated compounds in the case of nickel. Polymerization studies were performed in homogeneous solution using methylaluminoxane as the cocatalyst. These showed that [*N*,*O*]NiBr$_2$ complexes containing neutral iminohydroxamate with *O*-alkyl substituents are the most active systems of these various catalyst families. Further optimization of the ligand substitution pattern is expected to improve long term stability of the catalysts and the catalytic performance for applications on a technical scale.

Experimental Section

General: Commercially available starting materials were used as obtained. Solvents were dried, deoxygenated and saturated with argon according to standard procedures in organometallic chemistry. Reactions of air-sensitive materials were performed in Schlenk glassware under argon by techniques common in inorganic/organometallic chemistry. New compounds were characterized by IR, NMR, MS, etc. using current state-of-the-art procedures, details of instrumentation have been published previously.[13]

 © 2004 Wiley-VCH Verlag GmbH & Co. KGaA, Weinheim

Synthesis of Ligands

Representative Procedure for Iminohydroxamic Acids 3a−3f: A Schlenk tube was charged with *N*-(2,6-diisopropylphenyl)benzamide (**1a**, 1.9 g, 6.7 mmol) and an excess of thionyl chloride (10 mL). The mixture was heated to reflux for 1 h and the excess thionyl chloride was removed in a vacuum line, yielding a yellow oil of the corresponding imidoyl chloride **2a**. This material was dissolved in dry dichloromethane (20 mL). A second Schlenk vessel was charged with *N*-methylhydroxylamine hydrochloride (0.56 g, 6.7 mmol), dry ethanol (50 mL), and triethylamine (10 mL, 72 mmol). After the stirred mixture was cooled to −40 °C, a dropping funnel was attached to the Schlenk vessel, and a dichloromethane solution of imidoyl chloride **2a** (from above) was added dropwise over a period of 30 min. The mixture was warmed to room temperature and stirred at ambient temperature for further 60 min, resulting in a yellow suspension. Workup: the reaction mixture was hydrolyzed by addition of water (100 mL), the organic materials were extracted three times with diethyl ether, the combined organic layers were dried with Na_2SO_4 and the volatile materials were removed in a rotary evaporator yielding a semi-solid crude product consisting of *N*-(2,6-diisopropylphenyl)-*N*′-hydroxy-*N*′-methylbenzamidine (**3a**) and the apolar side product *N*-(2,6-diisopropylphenyl)-*N*′-{[2,6-diisopropylphenyl)imino]phenylmethoxy}-*N*′-methylbenzamidine (**4a**). To separate this mixture, the crude product mixture was dissolved in a small volume of dichloromethane and filtered through a short column of silica. In this manner, apolar **4a** (0.76 g, 1.3 mmol, 19.8% yield) could be removed by filtration, whereas the polar product **3a** remained immobilized on the column. Elution with ethanol and subsequent removal of ethanol in a rotary evaporator afforded 0.83 g of pure **3a** as an off-white solid in 40% yield.

All other iminohydroxamic acids **3** were prepared according to this procedure except that different benzamides and hydroxylamines were employed as starting materials. The bis(imino)-substituted hydroxylamines **4** (the apolar side product) were usually only separated and not isolated. Isolated yields of ligands **3** ranged from 18 to 63%, depending on the substitution pattern of the building blocks.

***N*-(2,6-Diisopropylphenyl)-*N*′-hydroxy-*N*′-methylbenzamidine (3a):** Starting materials: *N*-(2,6-diisopropylphenyl)benzamide (**1a**, 1.9 g, 6.7 mmol) and *N*-methylhydroxylamine hydrochloride (0.56 g, 6.7 mmol). Yield: 0.83 g (40%). IR (KBr): $\tilde{\nu}$ = 3065 (w), 2962 (m), 2869 (m), 1630 (s), 1586 (m), 1505 (m), 1470 (s), 1445 (m), 1432 (m), 1383 (m), 1324 (m), 1225 (m), 1187 (s), 1162 (m), 1105 (s), 1077 (w), 1044 (m), 971 (m), 917 (w), 807 (s), 780 (s), 758 (s), 700 (s) cm^{-1}. MS (FAB): *m*/*z* = 311 $[M + H]^+$. MS(EI, 70 eV): *m*/*z* = 310 $[M]^+$. ^1H NMR (300 MHz, $CDCl_3$): δ = 0.96 [d, $^3J_{H,H}$ = 6.6 Hz, 6 H, $CH(CH_3)_2$], 1.09 [d, $^3J_{H,H}$ = 6.2 Hz, 6 H, $CH(CH_3)_2$], 3.18 [sept, 2 H, 2 × $CH(CH_3)_2$], 3.47 (s, 3 H, NCH_3), 6.95 (m, 2 H, C_6H_5), 7.01−7.12 (m, 3 H, C_6H_5), 7.17−7.25 (m, 3 H, C_6H_3), not observed (s, 1 H, NOH) ppm. ^{13}C NMR (75.432 MHz, $CDCl_3$): δ = 21.9, 25.4, 28.2 $[CH(CH_3)_2]$, 43.7 (NCH_3), 123.2, 127.3, 127.8, 128.2, 128.9, 130.1, 131.9, 146.2 (C_6H_5, C_6H_3), 149.1 (C=N) ppm. $C_{20}H_{26}N_2O$ (310.44): calcd. C 77.38, H 8.44, N 9.20; found C 77.42, H 8.48, N 9.16.

***N*-(2,6-Diisopropylphenyl)-*N*′-{[(2,6-diisopropylphenyl)imino]-phenylmethoxy}-*N*′-methylbenzamidine (4a):** Starting materials: *N*-(2,6-diisopropylphenyl)benzamide (**1a**, 1.9 g, 6.7 mmol) and *N*-methylhydroxylamine hydrochloride (0.56 g, 6.7 mmol). Yield: 0.76 g (19.8%). IR (KBr): $\tilde{\nu}$ = 2970 (m), 2931 (m), 2869 (m), 1683 (s), 1630 (s), 1602 (m), 1590 (m), 1578 (m), 1492 (m), 1459 (m), 1436 (m), 1407 (w), 1383 (m), 1362 (w), 1328 (m), 1287 (w), 1264 (m), 1233 (m), 1185 (w), 1108 (m), 1063 (s), 1038 (m), 1030 (m), 1013 (s), 922 (w), 803 (m), 766 (s), 726 (m) cm^{-1}. MS (FAB): *m*/*z* = 574 $[M + H]^+$. ^1H NMR (300 MHz, $CDCl_3$): δ = 1.14−1.21 [m, 24 H, 4 × $CH(CH_3)_2$], 3.10, 3.42 [sept, 4 H, 4 × $CH(CH_3)_2$], 3.61 (s, 3 H, NCH_3), 6.46 (m, 2 H, C_6H_5), 6.91−7.90 (m, 16 H, C_6H_5, C_6H_3) ppm. ^{13}C NMR (75.432 MHz, $CDCl_3$): δ = 22.0, 23.7, 24.0, 28.9 $[CH(CH_3)_2]$, 39.7 (NCH_3), 122.9, 123.7, 127.1, 127.8, 127.9, 128.5, 128.8, 129.0, 129.3, 130.4, 131.8, 133.1, 142.1, 143.5, 146.4 (C_6H_5, C_6H_3), 154.5, 160.4 (C=N) ppm. $C_{39}H_{47}N_3O$ (573.82): calcd. C 81.63, H 8.26, N 7.32; found C 81.55, H 8.30, N 7.30.

***N*-(2,6-Dimethylphenyl)-*N*′-hydroxy-*N*′-methylbenzamidine (3b)** Starting materials: *N*-(2,6-dimethylphenyl)benzamide (**1b**, 2.30 g, 10.2 mmol) and *N*-methylhydroxylamine hydrochloride (1.30 g, 15.6 mmol). Yield: 1.63 g (63%). IR (KBr): $\tilde{\nu}$ = 1627 (s), 1590 (m), 1578 (m), 1505 (m), 1472 (m), 1445 (m), 1426 (m), 1341 (m), 1258 (m), 1237 (s), 1179 (s), 1158 (m), 1106 (m), 1092 (m), 1079 (w), 1048 (m), 1025 (m), 957 (s), 783 (s), 774 (s), 762 (s), 754 (s), 726 (s), 700 (s) cm^{-1}. MS (EI, 70 eV): *m*/*z* = 254 $[M]^+$. ^1H NMR (300 MHz, $CDCl_3$): δ = 2.16 (s, 6 H, 2 × CH_3), 3.47 (s, 3 H, NCH_3), 6.82−6.92 (m, 3 H, C_6H_3), 7.08−7.27 (m, 5 H, C_6H_5), not observed (s, 1 H, NOH) ppm. ^{13}C NMR (75.432 MHz, $CDCl_3$): δ = 18.6 (CH_3), 43.6 (NCH_3), 126.6, 127.7, 128.0, 128.2, 128.5, 130.1, 135.4, 135.5 (C_6H_5, C_6H_3), 149.0 (C=N) ppm. $C_{16}H_{18}N_2O$ (254.33): calcd. C 75.56, H 7.13, N 11.01; found C 75.62, H 7.18, N 10.93.

***N*-(2,6-Dimethylphenyl)-*N*′-{[(2,6-dimethylphenyl)imino]-phenylmethoxy}-*N*′-methylbenzamidine (4b):** Starting materials: *N*-(2,6-dimethylphenyl)benzamide (**1b**, 2.30 g, 10.2 mmol) and *N*-methylhydroxylamine hydrochloride (1.30 g, 15.6 mmol). Yield: 1.1 g (23%). IR (KBr): $\tilde{\nu}$ = 2919 (w), 1688 (s), 1644 (s), 1592 (m), 1580 (w), 1493 (w), 1466 (m), 1447 (m), 1405 (w), 1326 (s), 1293 (w), 1262 (m), 1246 (m), 1229 (m), 1216 (m), 1183 (w), 1104 (w), 1079 (s), 1069 (s), 1027 (m), 1013 (m), 922 (w), 787 (m), 768 (s), 756 (m), 741 (m), 697 (s), 675 (m) cm^{-1}. MS (EI, 70 eV): *m*/*z* = 461 $[M]^+$. ^1H NMR (300 MHz, $CDCl_3$): δ = 1.95, 2.20 (2 × s, 12 H, 4 × CH_3), 3.61 (s, 3 H, NCH_3), 6.25 (m, 2 H, C_6H_3), 6.67−6.96 (m, 6 H, C_6H_5 and C_6H_3), 7.05−7.22 (m, 5 H, C_6H_5) ppm. ^{13}C NMR (75.432 MHz, $CDCl_3$): δ = 18.5, 18.8 (CH_3), 39.4 (NCH_3), 122.3, 122.9, 127.0, 127.1, 127.6, 127.8, 127.9, 128.2, 128.7, 129.4, 129.5, 130.0, 130.5, 131.7, 133.6, 135.5, 144.6, 146.1 (C_6H_5, C_6H_3), 154.7, 161.5 (C=N) ppm. $C_{31}H_{31}N_3O$ (461.60): calcd. C 80.66, H 6.77, N 9.10; found C 80.71, H 6.80, N 9.08.

***N*-(Biphenyl-2-yl)-*N*′-hydroxy-*N*′-methylbenzamidine (3c):** Starting materials: *N*-(2-biphenyl)benzamide (**1c**, 2.62 g, 9.59 mmol) and *N*-methylhydroxylamine hydrochloride (1.28 g, 15.3 mmol). Yield: 1.39 g (48%). IR (KBr): $\tilde{\nu}$ = 3257 (w), 2946 (w), 1607 (s), 1580 (m), 1509 (s), 1488 (s), 1447 (m), 1436 (s), 1422 (s), 1393 (m), 1387 (m), 1243 (s), 1196 (s), 1073 (m), 963 (s), 783 (m), 770 (s), 756 (s), 743 (s), 698 (s) cm^{-1}. MS (EI, 70 eV): *m*/*z* = 302 $[M]^+$. ^1H NMR (300 MHz, $CDCl_3$): δ = 3.38 (s, 3 H, NCH_3), 6.48−6.51 (m, 1 H, C_6H_5), 6.89−7.02 (m, 4 H, C_6H_5), 7.11−7.14 (m, 1 H, C_6H_5), 7.25−7.42 (m, 8 H, C_6H_5), not observed (s, 1 H, NOH) ppm. ^{13}C NMR (75.432 MHz, $CDCl_3$): δ = 43.5 (NCH_3), 122.5, 124.0, 127.4, 127.5, 127.9, 128.7, 128.9, 129.0, 130.1, 130.7, 134.7, 135.5, 138.4 (C_6H_5, C_6H_4), 146.8 (C=N) ppm. $C_{20}H_{18}N_2O$ (302.38): calcd. C 79.44, H 6.00, N 9.26; found C 79.35, H 6.04, N 9.21.

***N*′-Hydroxy-*N*′-methyl-*N*-phenylbenzamidine (3d):** Starting materials: benzanilide (**1d**, 2.12 g, 10.8 mmol) and *N*-methylhydroxylamine hydrochloride (1.28 g, 15.3 mmol). Yield: 1.03 g (42%). IR

 © 2004 Wiley-VCH Verlag GmbH & Co. KGaA, Weinheim

(KBr): $\tilde{\nu}$ = 3049 (w), 2943 (w), 1615 (s), 1603 (s), 1574 (m), 1509 (s), 1482 (m), 1447 (m), 1428 (m), 1196 (s), 1160 (m), 1071 (w), 971 (s), 758 (s), 726 (s), 697 (s) cm^{-1}. MS (EI, 70 eV): *m*/*z* = 226 $[M]^+$. ^1H NMR (300 MHz, $CDCl_3$): δ = 3.47 (s, 3 H, NCH_3), 6.56 (d, 2 H, C_6H_5), 6.87 (t, 1 H, C_6H_5), 7.01 (t, 2 H, C_6H_5), 7.25 (d, 2 H, C_6H_5), 7.24−7.43 (m, 3 H, C_6H_5), not observed (s, 1 H, NOH) ppm. ^{13}C NMR (75.432 MHz, $CDCl_3$): δ = 43.4 (NCH_3), 121.0, 123.3, 127.8, 128.6, 129.0, 129.1, 130.4, 138.1 (C_6H_5), 146.7 (C=N) ppm. $C_{14}H_{14}N_2O$ (254.33): calcd. C 74.31, H 6.42, N 12.38; found C 74.24, H 6.27, N 12.34.

***N*-(2,6-Diisopropylphenyl)-*N*′-hydroxy-*N*′-isopropylbenzamidine (3e):** Starting materials: *N*-(2,6-diisopropylphenyl)benzamide (**1a**, 1.47 g, 6.7 mmol) and *N*-isopropylhydroxylamine hydrochloride (0.85 g, 7.6 mmol). Yield: 0.63 g (36%). IR (KBr): $\tilde{\nu}$ = 3433 (w), 3064 (w), 3006 (w), 2968 (s), 2948 (m), 2931 (m), 2867 (m), 1683 (w), 1598 (s), 1503 (s), 1461 (s), 1436 (m), 1385 (m), 1378 (m), 1360 (s), 1343 (w), 1335 (w), 1320 (w), 1256 (w), 1173 (s), 1123 (w), 1104 (w), 1067 (s), 1040 (w), 978 (m), 930 (w), 924 (w), 822 (w), 808 (s), 781 (m), 760 (s), 702 (s) cm^{-1}. MS(EI, 70 eV): *m*/*z* = 338 $[M]^+$. ^1H NMR (300 MHz, $CDCl_3$): δ = 0.98 [d, $^3J_{H,H}$ = 6.2 Hz, 6 H, $CH(CH_3)_2$], 1.11 [d, $^3J_{H,H}$ = 6.2 Hz, 6 H, $CH(CH_3)_2$], 1.37 [d, $^3J_{H,H}$ = 6.6 Hz, 6 H, $CH(CH_3)_2$], 3.16 [sept, 2 H, 2 × $CH(CH_3)_2$], 4.03 [sept, $^3J_{H,H}$ = 6.6 Hz, 1 H, $CH(CH_3)_2$], 6.95 (m, 2 H, C_6H_5), 7.02−7.12 (m, 3 H, C_6H_5), 7.20−7.27 (m, 3 H, C_6H_3), not observed (s, 1 H, NOH) ppm. ^{13}C NMR (75.432 MHz, $CDCl_3$): δ = 20.0, 21.9, 25.4, 28.2 [$CH(CH_3)_2$], 54.8 [$NCH(CH_3)_2$], 123.0, 127.5, 127.7, 128.3, 128.5, 129.9, 132.5, 145.9 (C_6H_5, C_6H_3), 148.1 (C=N) ppm. $C_{22}H_{30}N_2O$ (338.49): calcd. C 78.06, H 8.93, N 8.28; found C 78.00, H 8.95, N 8.24.

***N*-(2,6-Diisopropylphenyl)-*N*′-hydroxy-*N*′-(4-methylphenyl)-benzamidine (3f):** Starting materials: *N*-(2,6-diisopropylphenyl)benzamide (**1a**, 1.21 g, 4.3 mmol) and *N*-(4-methylphenyl)hydroxylamine (0.53 g, 4.3 mmol).[14] Yield: 0.30 g (18%). IR (KBr): $\tilde{\nu}$ = 2964 (s), 2927 (m), 2867 (m), 1600 (s), 1571 (s), 1507 (s), 1461 (s), 1322 (m), 1302 (w), 1285 (w), 1260 (m), 1239 (m), 1187 (w), 1106 (m), 1077 (w), 1044 (m), 818 (s), 787 (s), 776 (s), 758 (s), 697 (s) cm^{-1}. MS(FAB): *m*/*z* = 387 $[M + H]^+$. ^1H NMR (300 MHz, $CDCl_3$): δ = 0.90 [d, $^3J_{H,H}$ = 7.0 Hz, 6 H, $CH(CH_3)_2$], 2.19 (s, 3 H, $NC_6H_4CH_3$), 3.17 [sept, $^3J_{H,H}$ = 7.0 Hz, 2 H, 2 × $CH(CH_3)_2$], 6.82−6.91 (m, 4 H, C_6H_4, C_6H_3), 6.96−7.23 (m, 8 H, C_6H_4, C_6H_3), not observed (s, 1 H, NOH) ppm. ^{13}C NMR (75.432 MHz, $CDCl_3$): δ = 14.0, 20.6, 22.0, 22.5, 25.2, 29.4, 31.5 [CH_3, 2 × $CH(CH_3)_2$], 132.1, 137.4, 141.0, 145.4 (C_6H_3, C_6H_4), 150.5 (C=N) ppm. $C_{26}H_{30}N_2O$ (386.54): calcd. C 80.79, H 7.82, N 7.25; found C 80.86, H 7.83, N 7.26.

Representative Procedure for Iminohydroxamic Esters 5a−5d and Iminohydroxamic Amides 6a, 6b: A dichloromethane solution of imidoyl chloride **2a** (*c* = 0.108 g/ml or 0.36 mmol/ml, respectively) was prepared as described above. A second Schlenk vessel was charged with *N*-methyl-*O*-methylhydroxylamine hydrochloride (0.78 g, 8.0 mmol), dry ethanol (50 mL), and triethylamine (2.2 mL, 16 mmol). After the stirred mixture was cooled to −40 °C, a dropping funnel was attached to the Schlenk vessel, and a stoichiometric amount of a dichloromethane solution of imidoyl chloride **2a** was added dropwise over a period of 30 min. The mixture was warmed to room temperature and stirred at ambient temperature for further 60 min, resulting in a yellow suspension. Workup: the reaction mixture was hydrolyzed by addition of of water (100 mL), the organic material was extracted three times with diethyl ether, the combined organic layers were dried with Na_2SO_4, the volatile materials were removed in a rotary evaporator, yielding **5a** in 93% yield as a yellow viscous oil which solidified on drying in vacuo.

All other iminohydroxamic esters **5** and amides **6** were prepared according to this procedure, only different benzamides and hydroxylamines or hydrazines were employed as starting materials, respectively. Isolated yields of ligands **5** and **6** ranged from 78 to 99%, depending on the substitution pattern of the building blocks.

***N*-(2,6-Diisopropylphenyl)-*N*′-methoxy-*N*′-methylbenzamidine (5a):** Starting materials: *N*-(2,6-diisopropylphenyl)benzamide (**1a**, 1.98 g, 7.0 mmol) and *N*-methyl-*O*-methylhydroxylamine hydrochloride (0.53 g, 4.3 mmol). Yield: 2.11 g (93%). IR (KBr): $\tilde{\nu}$ = 2962 (m), 2931 (m), 1634 (s), 1602 (m), 1590 (m), 1461 (m), 1436 (m), 1360 (w), 1324 (m), 1256 (w), 1181 (w), 1104 (m), 1057 (w), 1030 (w), 1007 (m), 778 (m), 760 (m), 722 (w), 700 (s) cm^{-1}. MS(EI, 70 eV): *m*/*z* = 324 $[M]^+$. ^1H NMR (300 MHz, $CDCl_3$): δ = 0.91 [d, $^3J_{H,H}$ = 7.0 Hz, 6 H, $CH(CH_3)_2$], 1.06 [d, $^3J_{H,H}$ = 7.0 Hz, 6 H, $CH(CH_3)_2$], 2.89 [sept, $^3J_{H,H}$ = 7.0 Hz, 2 H, 2 × $CH(CH_3)_2$], 3.15 (s, 3 H, NCH_3), 3.49 (s, 3 H, OCH_3), 6.82−6.89 (m, 3 H, C_6H_3), 7.13 (s, 5 H, C_6H_5) ppm. ^{13}C NMR (75.432 MHz, $CDCl_3$): δ = 21.9, 23.9, 28.0 [2 × $CH(CH_3)_2$], 37.0 (NCH_3), 60.2 (OCH_3), 122.4, 122.5, 127.5, 128.1, 128.8, 137.1, 144.0 (C_6H_3, C_6H_5), 160.8 (C=N) ppm. $C_{21}H_{28}N_2O$ (324.47): calcd. C 77.74, H 8.70, N 8.63; found C 77.69, H 8.72, N 8.60.

***N*′-Methoxy-*N*′-methyl-*N*-(2,6-methylphenyl)benzamidine (5b):** Starting materials: *N*-(2,6-diisopropylphenyl)benzamide (**1a**, 2.07 g, 9.2 mmol) and *N*-methyl-*O*-methylhydroxylamine hydrochloride (0.90 g, 9.2 mmol). Yield: 2.33 g (94%). IR (KBr): $\tilde{\nu}$ = 2973 (m), 2930 (m), 1636 (s), 1591 (m), 1578 (m), 1466 (m), 1447 (m), 1325 (m), 1260 (m), 1101 (m), 1076 (m), 1051 (m), 1028 (m), 1007 (s), 783 (m), 766 (s), 727 (m), 700 (s) cm^{-1}. MS(EI, 70 eV): *m*/*z* = 268 $[M]^+$. ^1H NMR (300 MHz, $CDCl_3$): δ = 2.02 (s, 6 H, CH_3), 3.16 (s, 3 H, NCH_3), 3.52 (s, 3 H, OCH_3), 6.64−6.79 (m, 3 H, C_6H_3), 7.16 (s, 5 H, C_6H_5) ppm. ^{13}C NMR (75.432 MHz, $CDCl_3$): δ = 18.5 (CH_3), 37.2 (NCH_3), 60.3 (OCH_3), 121.9, 127.2, 127.5, 127.55, 127.6, 129.0, 134.0, 146.7 (C_6H_3, C_6H_5), 161.7 (C=N) ppm. $C_{17}H_{20}N_2O$ (268.36): calcd. C 76.09, H 7.51, N 10.44; found C 76.16, H 7.53, N 10.41.

***N*-(Biphenyl-2-yl)-*N*′-methoxy-*N*′-methylbenzamidine (5c):** Starting materials: *N*-(biphenyl-2-yl)benzamide (**1c**, 2.08 g, 7.6 mmol) and *N*-methyl-*O*-methylhydroxylamine hydrochloride (0.74 g, 7.6 mmol). Yield: 2.18 g (91%). IR (KBr): $\tilde{\nu}$ = 1628 (m), 1593 (m), 1578 (m), 1493 (m), 1474 (m), 1447 (m), 1431 (m), 1337 (m), 1267 (m), 1103 (m), 1074 (m), 1049 (m), 1030 (m), 1009 (m), 783 (m), 762 (m), 739 (s), 698 (s), 632 (m) cm^{-1}. MS (EI, 70 eV): *m*/*z* = 316 $[M]^+$. ^1H NMR (300 MHz, $CDCl_3$): δ = 3.03 (s, 3 H, NCH_3), 3.38 (s, 3 H, OCH_3), 6.68−7.27 (m, 14 H, C_6H_5, C_6H_4) ppm. ^{13}C NMR (75.432 MHz, $CDCl_3$): δ = 37.0 (NCH_3), 60.5 (OCH_3), 122.6, 122.8, 126.1, 127.3, 127.34, 127.6, 128.2, 128.5, 129.6, 129.9, 132.9, 133.2, 140.3, 147.1 (C_6H_5, C_6H_4), 161.9 (C=N) ppm. $C_{21}H_{20}N_2O$ (316.40): calcd. C 79.72, H 6.37, N 8.85; found C 79.66, H 6.39, N 8.83.

***N*′-Methoxy-*N*′-methyl-*N*-phenylbenzamidine (5d):** Starting materials: benzanilide (**1d**, 2.13 g, 10.8 mmol) and *N*-methyl-*O*-methylhydroxylamine hydrochloride (1.06 g, 10.8 mmol). Yield: 2.03 g (78%). IR (KBr): $\tilde{\nu}$ = 2932 (w), 1628 (m), 1591 (m), 1439 (m), 1335 (m), 1256 (m), 1103 (m), 1074 (m), 1028 (m), 1009 (m), 997 (m), 920 (m), 903 (m), 781 (s), 762 (s), 744 (s), 696 (s) cm^{-1}. MS (EI, 70 eV): *m*/*z* = 240 $[M]^+$. ^1H NMR (300 MHz, $CDCl_3$): δ = 3.16 (s, 3 H, NCH_3), 3.54 (s, 3 H, OCH_3), 6.60 (d, 2 H, C_6H_5), 6.79 (t, 1 H, C_6H_5), 7.03 (t, 2 H, C_6H_5), 7.20−7.28 (m, 5 H, C_6H_5) ppm. ^{13}C NMR (75.432 MHz, $CDCl_3$): δ = 37.0 (NCH_3), 60.6 (OCH_3),

 © 2004 Wiley-VCH Verlag GmbH & Co. KGaA, Weinheim

121.9, 122.1, 127.7, 128.2, 128.7, 128.8, 133.1, 149.7 (C_6H_5), 162.8 (C=N) ppm. $C_{15}H_{16}N_2O$ (240.30): calcd. C 74.97, H 6.71, N 11.66; found C 74.92, H 6.73, N 11.63.

***N*-(2,6-Diisopropylphenyl)-*N'*-methyl-*N'*-(methylamino)benzamidine (6a):** Starting materials: *N*-(2,6-diisopropylphenyl)benzamide (**1a**, 1.01 g, 3.6 mmol) and *N,N'*-dimethylhydrazine hydrochloride (0.55 g, 4.1 mmol). Yield: 1.10 g (94%). IR (KBr): $\tilde{\nu}$ = 3244 (w), 3062 (w), 3022 (w), 2973 (m), 2960 (m), 1609 (s), 1596 (s), 1586 (s), 1576 (s), 1492 (w), 1439 (m), 1382 (m), 1364 (s), 1329 (m), 1262 (m), 1183 (w), 1111 (m), 1069 (s), 1046 (m), 1025 (s), 924 (m), 845 (s), 824 (m), 808 (w), 799 (m), 772 (s), 760 (s), 714 (s), 700 (s) cm^{-1}. MS(EI, 70 eV): *m/z* = 323 $[M]^+$. ^1H NMR (300 MHz, $CDCl_3$): δ = 0.94 [d, $^3J_{H,H}$ = 7.0 Hz, 6 H, $CH(CH_3)_2$], 1.06 [d, $^3J_{H,H}$ = 6.6 Hz, 6 H, $CH(CH_3)_2$], 2.64 (s, 3 H, NCH_3), 2.90 (s, 3 H, NCH_3), 2.94 [sept, 2 H, 2 × $CH(CH_3)_2$], 6.78−6.86 (m, 3 H, C_6H_3), 7.01−7.14 (m, 5 H, C_6H_5), not observed (s, 1 H, NH) ppm. ^{13}C NMR (75.432 MHz, $CDCl_3$): δ = 21.8, 24.1, 28.1 [$CH(CH_3)_2$], 36.4, 39.2 (NCH_3), 122.1, 122.2, 127.8, 128.1, 128.8, 133.1, 138.2, 144.7 (C_6H_3, C_6H_5), 157.3 (C=N) ppm. $C_{21}H_{29}N_3$ (323.48): calcd. C 77.97, H 9.04, N 12.99; found C 78.01, H 9.07, N 13.02.

***N*-(2,6-Diisopropylphenyl)-*N'*-(dimethylamino)benzamidine (6b):** Starting materials: *N*-(2,6-diisopropylphenyl)benzamide (**1a**, 1.01 g, 3.6 mmol) and *N,N*-dimethylhydrazine (0.58 mL, 0.46 g, 7.7 mmol, excess). Yield: 1.15 g (99%), brown viscous oil. MS (EI, 70 eV): *m/z* = 323 $[M]^+$. ^1H NMR (300 MHz, $CDCl_3$): δ = 0.88 [d, $^3J_{H,H}$ = 6.9 Hz, 6 H, $CH(CH_3)_2$], 1.10 [d, $^3J_{H,H}$ = 6.9 Hz, 6 H, $CH(CH_3)_2$], 2.57 [s, 6 H, $N(CH_3)_2$], 3.13 (sept, $^3J_{H,H}$ = 6.9 Hz, 2 H, 2 × $CH(CH_3)_2$], 6.98−7.21 (m, 8 H, C_6H_3, C_6H_5), 7.95 (s, 1 H, NH) ppm. ^{13}C NMR (75.432 MHz, $CDCl_3$): δ = 21.9, 24.9, 26.3 [$CH(CH_3)_2$], 46.7 [$N(CH_3)_2$], 123.3, 126.9, 127.6, 128.5, 129.1, 132.9, 134.3, 145.2 (C_6H_3, C_6H_5), 159.7 (C=N) ppm. $C_{21}H_{29}N_3$ (323.48): calcd. C 77.97, H 9.04, N 12.99; found C 77.92, H 9.07, N 12.95.

***N*-(2,6-Diisopropylphenyl)-*N'*-{[(2,6-diisopropylphenyl)iminobenzyl]-phenylamino}benzamidine (7):** Starting materials: *N*-(2,6-diisopropylphenyl)benzamide (**1a**, 2.03 g, 7.2 mmol) and *N,N'*-diphenylhydrazine (1.40 g, 7.6 mmol). Yield: 0.42 g (16% based on limiting reagent **1a**). IR (KBr): $\tilde{\nu}$ = 2964 (m), 2929 (m), 2869 (m), 1627 (s), 1607 (s), 1589 (m), 1574 (s), 1497 (m), 1463 (m), 1443 (w), 1356 (w), 1328 (m), 1104 (w), 1057 (w), 1007 (w), 822 (w), 805 (w), 789 (w), 778 (w), 762 (w), 700 (m) cm^{-1}. MS(FAB): *m/z* = 712 $[M + H]^+$. ^1H NMR (300 MHz, $CDCl_3$): δ = 1.00 [d, 12 H, $^3J_{H,H}$ = 6.6 Hz, 2 × $CH(CH_3)_2$], 1.25 [d, $^3J_{H,H}$ = 6.6 Hz, 12 H, 2 × $CH(CH_3)_2$], 3.13 [sept, 4 H, 4 × $CH(CH_3)_2$], 6.92 (d, 4 H, C_6H_3), 7.04 (m, 8 H, C_6H_3, C_6H_5), 7.13−7.36 (m, 14 H, C_6H_5) ppm. ^{13}C NMR (75.432 MHz, $CDCl_3$): δ = 21.7, 25.5, 28.9 [$CH(CH_3)_2$], 123.8, 124.5, 124.6, 124.9, 127.5, 128.6, 128.8, 129.1, 129.3, 129.5, 129.7, 132.6, 135.3, 137.9, 145.3 (C_6H_3, C_6H_5), 164.9 (C=N) ppm. $C_{50}H_{54}N_4$ (711.01): calcd. C 84.46, H 7.66, N 7.88; found C 84.51, H 7.66, N 7.85.

Synthesis of Metal Complexes

Representative Procedure for Iminohydroxamato and Imidoyl Hydrazido Complexes 8a−14a: A Schlenk tube was charged with **3a** (0.28 g, 0.90 mmol) and dry, deoxygenated THF (20 mL). After the mixture was cooled to −80 °C, a 2.0 M *n*-pentane solution of *n*-butyllithium (0.90 mmol, 0.45 mL) was added through a syringe. The stirred mixture changed gradually in color from orange to dark red, indicating deprotonation of **3a**. After 1 h of stirring at −80 °C, $ZrCl_4$ (0.21 g, 0.90 mmol, 1 mol-equiv. in relation to **3a**) was added under protection from air and the external cooling bath was removed. Stirring was continued overnight, resulting in a brown solution. Workup: THF and other volatile materials were removed in a vacuum line, the brown residue was dissolved in dry, deoxygenated dichloromethane giving a brown solution and a precipitate of lithium chloride. The inorganic salt was removed by filtration through a Schlenk frit, the dichloromethane was removed in a vacuum line, and the residue was triturated with dry, deoxygenated *n*-hexane (10 mL) to remove apolar impurities from the solid product. The precipitate was allowed to settle, *n*-hexane was removed by pipette followed by drying in vacuo, affording the product as an orange air-sensitive powder in 90% yield.

Trichloro[*N*-(2,6-diisopropylphenyl)-*N'*-methyl-*N'*-oxybenzamidinato]zirconium(IV) (8a): Starting materials: **3a** (0.28 g, 0.90 mmol), *n*-butyllithium (0.90 mmol, 0.21 g), $ZrCl_4$ (0.90 mmol, 1 mol-equiv. in relation to **3a**). Yield: 0.41 g (90%) as an orange, air-sensitive powder. ^1H NMR (300 MHz, CD_2Cl_2): δ = 1.04 [d, 6 H, 2 × $CH(CH_3)_2$], 1.81 (br. s, 4 H, CH_2 of coordinating THF), 3.33 [m, 5 H, NCH_3, 2 × $CH(CH_3)_2$], 3.83 (br. s, 4 H, CH_2 of coordinating THF), 6.94−7.02 (m, 3 H, C_6H_3), 7.10−7.35 (m, 5 H, C_6H_5) ppm. ^{13}C NMR (75.432 MHz, CD_2Cl_2): δ = 24.2, 25.9, 28.1 [$CH(CH_3)_2$], 41.6 (NCH_3), 123.6, 124.2, 126.1, 128.5, 128.7, 129.1, 129.3, 129.4, 130.6, 143.9, 144.2 (C_6H_3, C_6H_5), 161.7 (C=N) ppm. $C_{20}H_{25}Cl_3N_2OZr{\cdot}THF$ = $C_{24}H_{33}Cl_3N_2O_2Zr$ (579.11): calcd. C 49.78, H 5.74, N 4.84; found C 49.67, H 5.70, N 4.77.

Trichloro[*N*-(2,6-dimethylphenyl)-*N'*-methyl-*N'*-oxybenzamidinato]zirconium(IV) (8b): Starting materials: **3b** (0.54 g, 2.12 mmol), *n*-butyllithium (2.4 mmol, 0.56 g), $ZrCl_4$ (2.4 mmol, 1.1 mol-equiv. in relation to **3b**). Yield: 0.82 g (86%) as an orange, air-sensitive powder. ^1H NMR (300 MHz, CD_2Cl_2): δ = 1.91 (br. s, 4 H, CH_2 of coordinating THF), 2.28, 2.31, 2.34, 2.39 (4 × s, 6 H, CH_3), 3.27, 3.33 (2 × s, 3 H, NCH_3), 3.85, 4.3 (2 × br. s, 4 H, CH_2 of coordinating THF), 6.83−7.37 (m, 8 H, C_6H_3, C_6H_5) ppm. ^{13}C NMR (75.432 MHz, CD_2Cl_2): δ = 18.7, 19.5, 19.7, 20.7, 20.9 (CH_3, THF), 39.5, 41.3, 41.9, 42.2 (NCH_3), 69.3 (THF), 125.5, 126.0, 127.2, 127.9, 128.0, 128.1, 128.4, 128.7, 128.9, 129.2, 130.1, 130.3, 130.4, 130.5, 130.9, 131.4, 133.1, 133.4, 133.8, 134.4, 134.7, 146.3 (C_6H_3, C_6H_5), 161.3 (C=N) ppm. $C_{16}H_{17}Cl_3N_2OZr{\cdot}THF$ = $C_{20}H_{25}Cl_3N_2O_2Zr$ (523.01): calcd. C 45.93, H 4.82, N 5.36; found C 45.87, H 4.79, N 5.31.

Trichloro[*N*-(biphenyl-2-yl)-*N'*-methyl-*N'*-oxybenzamidinato]zirconium(IV) (8c): Starting materials: **3c** (0.49 g, 1.62 mmol), *n*-butyllithium (1.7 mmol, 0.46 g), $ZrCl_4$ (2.0 mmol, 1.2 mol-equiv. in relation to **3c**). Yield: 0.71 g (88%) as an orange-brown, air-sensitive powder. ^1H NMR (300 MHz, CD_2Cl_2): δ = 1.88 (br. s, 4 H, CH_2 of coordinating THF), 2.33, 2.84, 2.97, 3.15 (4 × s, 3 H, NCH_3), 3.82, 4.56 (2 × br. s, 4 H, CH_2 of coordinating THF), 6.90−7.43 (m, 14 H, C_6H_4, C_6H_5) ppm. ^{13}C NMR (75.432 MHz, CD_2Cl_2): δ = 25.9 (THF), 41.1 (NCH_3), 69.2 (THF), 126.3, 127.2, 127.8, 127.9, 128.1, 128.5, 128.6, 128.7, 129.3, 129.4, 129.7, 130.2, 130.2, 131.2, 139.9, 144.5 (C_6H_4, C_6H_5), 160.9 (C=N) ppm. $C_{20}H_{17}Cl_3N_2OZr{\cdot}THF$ = $C_{24}H_{25}Cl_3N_2O_2Zr$ (571.05): calcd. C 50.48, H 4.41, N 4.91; found C 50.40, H 4.38, N 4.86.

Trichloro[*N'*-methyl-*N'*-oxybenzamidinato-*N*-phenyl]zirconium(IV) (8d): Starting materials: **3d** (0.34 g, 1.49 mmol), *n*-butyllithium (1.5 mmol, 0.41 g), $ZrCl_4$ (1.8 mmol, 1.2 mol-equiv. in relation to **3d**). Yield: 0.58 g (92%) as a yellow, air-sensitive powder. ^1H NMR (300 MHz, CD_2Cl_2): δ = 1.86 (br. s, 4 H, CH_2 of coordinating THF), 2.78, 3.32 (2 × s, 3 H, NCH_3), 3.84, 4.54 (2 × br. s, 4 H, CH_2 of coordinating THF), 6.92−7.35 (m, 10 H, C_6H_5) ppm. ^{13}C NMR (75.432 MHz, CD_2Cl_2): δ = 25.8 (THF), 40.0 (NCH_3), 125.2, 126.5, 128.3, 128.4, 128.6, 128.8, 129.0, 129.1, 129.2, 130.8,

 © 2004 Wiley-VCH Verlag GmbH & Co. KGaA, Weinheim

146.3 (C_6H_5), 159.3 (C=N) ppm. $C_{14}H_{13}Cl_3N_2OZr\cdot THF$ = $C_{18}H_{21}Cl_3N_2O_2Zr$ (494.96): calcd. C 43.68, H 4.28, N 5.66; found C 43.57, H 4.24, N 5.61.

Trichloro[*N*-(2,6-diisopropylphenyl)-*N*′-isopropyl-*N*′-oxybenzamidinato]zirconium(IV) (8e): Starting materials: **3e** (0.28 g, 0.83 mmol), *n*-butyllithium (0.82 mmol, 0.22 g), $ZrCl_4$ (0.90 mmol, 1.2 mol-equiv. in relation to **3e**). Yield: 0.28 g (64%) as a colorless, air-sensitive powder. ^{1}H NMR (300 MHz, CD_2Cl_2): δ = 1.00−1.45 [m, 15 H, 2 × $CH(CH_3)_2$, $NCH(CH_3)_2$], 1.61 [d, $^3J_{H,H}$ = 6.6 Hz, 3 H, $NCH(CH_3)_2$], 1.83, 2.10 (br. s, 4 H, CH_2 of coordinating THF), 3.28−4.02 [3 overlapping sept, 3 H, $NCH(CH_3)_2$], 3.76, 4.70 (br. s, 4 H, CH_2 of coordinating THF), 6.92−7.46 (m, 8 H, C_6H_3, C_6H_5) ppm. ^{13}C NMR (75.432 MHz, CD_2Cl_2): δ = 20.0, 20.1, 22.0, 23.8, 24.3, 25.9, 26.1, 16.3, 28.2, 29.0, 29.2 [$CH(CH_3)_2$], 55.1 [$NCH(CH_3)_2$], 123.5, 123.6, 123.8, 124.1, 126.1, 126.3, 127.9, 128.5, 128.6, 128.8, 129.0, 129.2, 129.6, 129.7, 130.5, 131.9, 143.8, 144.5, 146.9, 147.4, 155.0 (C_6H_3, C_6H_5), 162.0 (C=N) ppm. $C_{22}H_{29}Cl_3N_2OZr\cdot THF$ = $C_{26}H_{37}Cl_3N_2O_2Zr$ (607.17): calcd. C 51.43, H 6.14, N 4.61; found C 51.38, H 6.10, 4.56.

Trichloro[*N*-(2,6-diisopropylphenyl)-*N*′-4-methylphenyl-*N*′-oxybenzamidinato]zirconium(IV) (8f): Starting materials: **3f** (0.22 g, 0.56 mmol), *n*-butyllithium (0.60 mmol, 0.13 g), $ZrCl_4$ (0.56 mmol, 1.0 mol-equiv. in relation to **3f**). Yield: 0.29 g (90%) as a tan, air-sensitive powder. ^{1}H NMR (300 MHz, CD_2Cl_2): δ = 1.05−1.35 [m, 12 H, 2 × $CH(CH_3)_2$], 1.82, 1.97 (br. s, 4 H, CH_2 of coordinating THF), 2.27 (s, 3 H, CH_3), 3.20, 3.40 [2 × sept, 2 H, $CH(CH_3)_2$], 3.77, 4.48 (br. s, 4 H, CH_2 of coordinating THF), 6.77−7.67 (m, 12 H, C_6H_3, C_6H_4, C_6H_5) ppm. $C_{26}H_{29}Cl_3N_2OZr\cdot THF$ = $C_{30}H_{37}Cl_3N_2O_2Zr$ (655.21): calcd. C 54.99, H 5.69, N 4.28; found C 55.06, H 5.73, N 4.25.

Dichlorobis[*N*-(2,6-diisopropylphenyl)-*N*′-methyl-*N*′-oxybenzamidinato]zirconium(IV) (9a): Starting materials: **3a** (0.65 g, 2.08 mmol), *n*-butyllithium (2.04 mmol, 0.21 g), $ZrCl_4$ (0.90 mmol, 0.5 mol-equiv. in relation to **3a**). Yield: 0.54 g (77%) as a tan, air-sensitive powder. ^{1}H NMR (300 MHz, CD_2Cl_2): δ = 0.23, 0.34. 0.29. 1.04 [4 × d, $^3J_{H,H}$ = 6.6 Hz, 24 H, 4 × $CH(CH_3)_2$], 2.89 [sept, 2 H, 2 × $CH(CH_3)_2$], 3.18 [sept, 2 H, 2 × $CH(CH_3)_2$], 3.40, 3.54, 3.60, 3.97 (4 × s, 6 H, NCH_3), 6.80−7.29 (m, 16 H, C_6H_3, C_6H_5) ppm. ^{13}C NMR (75.432 MHz, CD_2Cl_2): δ = 24.5, 25.1, 25.9, 26.2, 27.9, 28.1 [$CH(CH_3)_2$], 43.6 (NCH_3), 123.5, 124.2, 124.8, 125.8, 127.7, 127.9, 128.3, 128.3, 128.7, 129.0, 129.4, 130.0, 130.3, 143.3, 143.5, 145.5 (C_6H_3, C_6H_5), 159.8 (C=N) ppm. $C_{40}H_{50}Cl_2N_2O_2Zr$ (752.98): calcd. C 63.81, H 6.69, N 3.72; found C 63.95, H 6.72, N 3.70.

Trichloro[*N*-(2,6-dimethylphenyl)-*N*′-methyl-*N*′-oxybenzamidinato]-titanium(IV) (10b): Starting materials: **3b** (0.44 g, 1.73 mmol), *n*-butyllithium (1.9 mmol, 0.68 g), $TiCl_4$ (2.0 mmol, 1.2 mol-equiv. in relation to **3b**). Yield: 0.67 g (95%) as an orange, air-sensitive powder. ^{1}H NMR (300 MHz, CD_2Cl_2): δ = 2.13, 2.34 (2 × s, 6 H, CH_3), 3.40, 3.49, 3.63 (3 × s, 3 H, NCH_3), 6.85 (m, 3 H, C_6H_3), 7.12−7.41 (m, 5 H, C_6H_5) ppm. ^{13}C NMR (75.432 MHz, CD_2Cl_2): δ = 19.6, 20.4 (CH_3), 30.0, 39.2, 41.5 (NCH_3), 125.8, 126.0, 128.1, 128.5, 128.7, 129.0, 129.3, 131.0, 131.7, 133.2, 133.5, 145.4, 149.9 (C_6H_3, C_6H_5), 160.3 (C=N) ppm. $C_{16}H_{17}Cl_3N_2OTi$ (407.56): calcd. C 47.15, H 4.20, N 6.87; found C 47.07, H 4.16, N 6.82.

Trichloro[*N*-(2,6-dimethylphenyl)-*N*′-methyl-*N*′-oxybenzamidinato]-vanadium(IV) (11b): Starting materials: **3b** (0.40 g, 1.56 mmol), *n*-butyllithium (1.7 mmol, 0.2 mL), VCl_4 (1.9 mmol, 1.2 mol-equiv. in relation to **3b**). Yield: 0.67 g (95%) as a dark green, air-sensitive powder. Due to strong paramagnetism no informative NMR spectra were obtained. $C_{16}H_{17}Cl_3N_2OV$ (410.62): calcd. C 46.80, H 4.17, N 6.82; found C 45.72, H 4.25, N 6.70.

Trichloro[*N*-(2,6-diisopropylphenyl)-*N*′-methylamino-*N*′-methylbenzamidinato]zirconium(IV) (13a): Starting materials: **6a** (0.52 g, 1.61 mmol), *n*-butyllithium (1.6 mmol, 0.49 g), $ZrCl_4$ (2.1 mmol, 1.3 mol-equiv. in relation to **6a**). Yield: 0.71 g (85%) as a yellow, air-sensitive powder. ^{1}H NMR (300 MHz, CD_2Cl_2): δ = 0.93−1.24 [4 × d, 12 H, 2 × $CH(CH_3)_2$], 1.82 (br. s, 4 H, CH_2 of coordinating THF), 2.94, 3.07, 3.18, 3.29 [4 × s, sept, 5 H, NCH_3, 2 × $CH(CH_3)_2$], 3.39, 3.48, 3.57, 3.89 (4 × s, 3 H, NCH_3), 3.84, 4.56 (2 × br. s, 4 H, CH_2 of coordinating THF), 6.90−7.60 (m, 8 H, C_6H_3, C_6H_5) ppm. ^{13}C NMR (75.432 MHz, CD_2Cl_2): δ = 21.8, 22.6, 24.2, 25.3, 25.9, 27.0, 28.2, 29.2 [$CH(CH_3)_2$], 34.9, 38.8, 40.4 (NCH_3), 123.0, 124.0, 124.3, 128.3, 128.6, 128.9, 129.5, 129.7, 129.8, 133.0, 143.8, 144.0, 146.1 (C_6H_3, C_6H_5), not observed: (C=N) ppm. $C_{21}H_{28}Cl_3N_3Zr\cdot THF$ = $C_{25}H_{36}Cl_3N_3Zr$ (576.16): calcd. C 52.12, H 6.30, N 7.29; found C 52.06, H 6.26, N 7.21.

Trichloro[*N*-(2,6-diisopropylphenyl)-*N*′-methylamino-*N*′-methylbenzamidinato]titanium(IV) (14a): Starting materials: **6a** (0.40 g, 1.24 mmol), *n*-butyllithium (1.24 mmol, 0.49 g), $TiCl_4$ (1.5 mmol, 1.2 mol-equiv. in relation to **6a**). Yield: 0.56 g (95%) as a green, air-sensitive powder. ^{1}H NMR (300 MHz, CD_2Cl_2): δ = 1.05 [d, $^3J_{H,H}$ = 6.9 Hz, 6 H, $CH(CH_3)_2$], 2.93 [sept, $^3J_{H,H}$ = 6.9 Hz, 2 H, $CH(CH_3)_2$], 3.38 (s, 3 H, NCH_3), 4.38 (s, 3 H, NCH_3), 6.99−7.36 (m, 8 H, C_6H_3, C_6H_5) ppm. ^{13}C NMR (75.432 MHz, CD_2Cl_2): δ = 23.9, 25.3, 28.6 [$CH(CH_3)_2$], 38.0, 45.2 (NCH_3), 123.8, 128.0, 128.7, 128.9, 129.0, 131.4, 141.2, 150.9 (C_6H_3, C_6H_5), 160.0 (C=N) ppm. $C_{21}H_{28}Cl_3N_3Ti$ (476.71): calcd. C 52.91, H 5.92, N 8.81; found C 53.03, H 5.88, N 8.75.

Representative Procedure for Iminohydroxylamino and Hydrazido Complexes 15a−17: A Schlenk tube was charged with **5a** (0.97 g, 3.0 mmol), dibromo(dimethoxethane)nickel(II) (1.25 g, 3.1 mmol) and dry, deoxygenated dichloromethane (20 mL). The mixture was stirred overnight, resulting in a dark green solution/suspension. Workup: dry dichloromethane (60 mL) was added, the solution was filtered through a Schlenk frit, the green solution was concentrated in a vacuum line, and the residue was dried in vacuo affording a green air-sensitive powder in 94% yield.

Dibromo[*N*-(2,6-diisopropylphenyl)-*N*′-methoxy-*N*′-methylbenzamidinato]nickel(II) (15a): Starting materials: **5a** (0.97 g, 3.0 mmol), $NiBr_2\cdot$DME (1.25 g, 3.1 mmol). Yield: 1.53 g (94%) as a green, paramagnetic, air-sensitive powder. ^{1}H NMR (300 MHz, CD_2Cl_2): δ = 1.10−1.49 [br. m, 12 H, $CH(CH_3)_2$], 2.97−3.56 [br. m, 8 H, $CH(CH_3)_2$, NCH_3, OCH_3], 6.80−8.30 (br. m, 8 H, C_6H_3, C_6H_5) ppm. ^{13}C NMR (75.432 MHz, CD_2Cl_2): due to paramagnetism, only very weak signals were observed. $C_{21}H_{28}Br_2N_2NiO$ (542.96): calcd. C 46.45, H 5.20, N 5.16; found C 46.52, H 5.25, N 5.07.

Dibromo[*N*-(2,6-dimethylphenyl)-*N*′-methoxy-*N*′-methylbenzamidinato]nickel(II) (15b): Starting materials: **5b** (0.79 g, 2.94 mmol), $NiBr_2\cdot$DME (1.17 g, 2.94 mmol). Yield: 1.08 g (66%) as a green, paramagnetic, air-sensitive powder. ^{1}H NMR (300 MHz, CD_2Cl_2): δ = 2.75 [br. s, 12 H, $CH(CH_3)_2$], 3.99 [br. m, 8 H, $CH(CH_3)_2$, NCH_3, OCH_3], 6.80−7.70 (br. m, 8 H, C_6H_3, C_6H_5) ppm. ^{13}C NMR (75.432 MHz, CD_2Cl_2): due to paramagnetism, no informative signals were observed. $C_{17}H_{20}Br_2N_2NiO$ (486.86): calcd. C 41.94, H 4.14, N 5.75; found C 42.02, H 4.16, N 5.70.

Dibromo[*N*-(biphenyl-2-yl)-*N*′-methoxy-*N*′-methylbenzamidinato]-nickel(II) (15c): Starting materials: **5c** (0.87 g, 2.75 mmol), $NiBr_2\cdot$DME (1.10 g, 2.75 mmol). Yield: 1.43 g (97%) as a green,

 © 2004 Wiley-VCH Verlag GmbH & Co. KGaA, Weinheim

paramagnetic, air-sensitive powder. ^{1}H NMR (300 MHz, CD_2Cl_2): only one very broad signal from δ = −4 to +24 ppm centered at δ = 12.0 ppm was observed. ^{13}C NMR (75.432 MHz, CD_2Cl_2): due to paramagnetism, no informative signals were observed. $C_{21}H_{20}Br_2N_2NiO$ (534.90): calcd. C 47.15, H 3.77, N 5.24; found C 47.04, H 3.81, N 5.18.

Dibromo[*N*′-methoxy-*N*′-methyl-*N*-phenylbenzamidinato]nickel(II) (15d): Starting materials: **5d** (0.62 g, 2.58 mmol), $NiBr_2$·DME (1.03 g, 2.58 mmol). Yield: 0.70 g (59%) as a green, paramagnetic, air-sensitive powder. ^{1}H NMR (300 MHz, CD_2Cl_2): δ = 0.07, 0.87, 1.27, 4.33 (4 × br. s, 6 H, NCH_3, OCH_3), 6.84−9.96 (br. m, 10 H, C_6H_5) ppm. ^{13}C NMR (75.432 MHz, CD_2Cl_2): due to paramagnetism, no informative signals were observed. $C_{15}H_{16}Br_2N_2NiO$ (458.80): calcd. C 39.27, H 3.52, N 6.11; found C 39.19, H 3.56, N 6.06.

Dibromo[*N*-(2,6-diisopropylphenyl)-*N*′-methylamino-*N*′-methylbenzamidinato]nickel(II) (16a): Starting materials: **6a** (0.44 g, 1.36 mmol), $NiBr_2$·DME (0.56 g, 1.4 mmol). Yield: 0.70 g (95%) as a brown, paramagnetic, air-sensitive powder. ^{1}H NMR (300 MHz, CD_2Cl_2): δ = −0.16, 1.76, 5.16, 5.41 [4 × br. s, 20 H, $CH(CH_3)_2$, NCH_3, OCH_3], 15.38, 19.63, 22.57 (3 × br. s, 8 H, C_6H_3,C_6H_5) ppm. ^{13}C NMR (75.432 MHz, CD_2Cl_2): due to paramagnetism, no informative signals were observed. $C_{21}H_{29}Br_2N_3Ni$ (541.98): calcd. C 46.54, H 5.39, N 7.75; found C 46.40, H 5.44, N 7.67.

Dibromo[*N*-(2,6-diisopropylphenyl)-*N*′-(dimethylamino)benzamidinato]nickel(II) (16b): Starting materials: **6b** (0.52 g, 1.6 mmol), $NiBr_2$·DME (0.70 g, 1.8 mmol). Yield: 0.66 g (76%) as a brown, slightly paramagnetic, air-sensitive powder. ^{1}H NMR (300 MHz, CD_2Cl_2): δ = 0.89, 0.95, 1.08, 2.04, 2.40, 3.47, 5.99 [6 × br. s, 21 H, $CH(CH_3)_2$, NCH_3, NH], 7.11, 7.14, 7.39, 7.82, 8.19, 8.48, 8.57, 8.96 (8 × br. s, 8 H, C_6H_3, C_6H_5) ppm. ^{13}C NMR (75.432 MHz, CD_2Cl_2): δ = 13.1, 21.8, 22.2, 24.7, 29.8, 30.7 [$CH(CH_3)_2$], 50.8 (NCH_3), 124.0, 126.0, 127.7, 129.7, 131.2, 131.7, 135.5, 140.0, 143.8 (C_6H_3, C_6H_5), not observed: (C=N) ppm. $C_{21}H_{29}Br_2N_3Ni$ (541.98): calcd. C 46.54, H 5.39, N 7.75; found C 46.58, H 5.32, N 7.70.

Dibromo[*N*-2,6-diisopropylphenyl-*N*′-({[(2,6-diisopropylphenyl)-imino]benzyl}phenylamino)benzamidino]nickel(II) (17): Starting materials: **7** (0.26 g, 0.37 mmol), $NiBr_2$·DME (0.17 g, 0.40 mmol). Yield: 0.30 g (88%) as a pale green, air-stable powder. ^{1}H NMR (300 MHz, CD_2Cl_2): δ = 1.07 [d, $^3J_{H,H}$ = 6.9 Hz, 12 H, $CH(CH_3)_2$], 1.31 [d, $^3J_{H,H}$ = 6.6 Hz, 12 H, $CH(CH_3)_2$], 3.14 [sept, 4 H, $CH(CH_3)_2$], 6.97 (d, 4 H, C_6H_3), 7.09 (d, 8 H, C_6H_5), 7.18−7.39 (m, 14 H, C_6H_3, C_6H_5) ppm. ^{13}C NMR (75.432 MHz, CD_2Cl_2): δ = 21.8, 26.7, 29.5 [$CH(CH_3)_2$], 124.2, 125.1, 125.3, 125.4, 127.5, 127.9, 128.1, 129.1, 129.2, 129.7, 129.8, 130.2, 133.1, 135.5, 138.4, 145.9 (C_6H_3, C_6H_5), 165.5 (C=N) ppm.

Table 2. Crystallographic data for **2a**, **3a**, **3b**, **3e**, **12b**

Compound	**2a**	**3a**	**3b**	**3e**	**12b**
Empirical formula	$C_{19}H_{22}ClN$	$C_{20}H_{26}N_2O \times 0.75H_2O \times 0.5EtOH$	$C_{16}H_{18}N_2O$	$C_{22}H_{30}N_2O \times 0.5H_2O$	$C_{32}H_{34}Cl_4N_4O_2Ti \times CH_2Cl_2$
Formula mass	299.83	346.97	254.32	347.49	710.36
Crystal system	monoclinic	monoclinic	triclinic	orthorhombic	monoclinic
Space group	$P2_1/c$ (No. 14)	$P2_1/c$ (No. 14)	$P\bar{1}$ (No. 2)	*Pbcn* (No. 60)	*C*2/*c* (No. 15)
a [pm]	849.30(4)	1385.87(5)	999.74(8)	1610.5(1)	1705.81(4)
b [pm]	2683.84(9)	1688.70(7)	1096.61(8)	1661.4(2)	1542.57(3)
c [pm]	807.69(4)	1813.58(5)	1404.0(1)	1579.4(1)	1580.06(3)
α [°]	90	90	67.673(4)	90	90
β [°]	113.381(2)	93.683(2)	87.115(4)	90	122.569(2)
γ [°]	90	90	87.317(4)	90	90
Z	4	8	4	8	4
V [nm^3]	1.68986(13)	4.2356(3)	1.42140(18)	4.2260(6)	3.50384(13)
$\rho_{calcd.}$ [Mg·m^{-3}]	1.178	1.088	1.188	1.092	1.347
T [K]	233(2)	223(2)	223(2)	223(2)	233(2)
μ [mm^{-1}]	0.220	0.070	0.075	0.068	0.584
F(000)	640	1508	544	1512	1472
Color, habit	colorless prism	colorless prism	colorless prism	colorless prism	red prism
Crystal size [mm]	0.4 × 0.35 × 0.3	0.4 × 0.3 × 0.2	0.39 × 0.13 × 0.12	0.3 × 0.15 × 0.08	0.2 × 0.12 × 0.08
θ range for data collection [°]	2.61−23.50	1.90−21.00	2.01−22.00	1.76° to 19.94	1.94−24.00
Index ranges	$-9 \le h \le 0$ $-29 \le k \le 30$ $-8 \le l \le 9$	$0 \le h \le 13$ $-16 \le k \le 17$ $-18 \le l \le 18$	$0 \le h \le 10$ $-11 \le k \le 11$ $-14 \le l \le 14$	$0 \le h \le 15$ $-15 \le k \le 15$ $-15 \le l \le 15$	$-13 \le h \le 19$ $-12 \le k \le 15$ $-15 \le l \le 15$
Reflections collected	5162	17026	6271	12806	9665
Independent reflections	2316 (R_{int} = 0.0251)	4516 (R_{int} = 0.0434)	3468 (R_{int} = 0.0304)	1950 (R_{int} = 0.1025)	2759 (R_{int} = 0.0322)
Reflections with $I > 2\sigma(I)$	1970	3531	2501	1380	2299
Absorption correction	none	none	none	none	none
Refinement method	full-matrix least squares on F^2	full-matrix least squares on F^2	full-matrix least squares on F^2	full-matrix least squares on F^2	full-matrix least squares on F^2
Data/restraints/parameters	2316/0/192	4516/0/506	3468/0/358	1950/0/246	2759/0/221
Goodness-of-fit on F^2	1.044	1.047	1.045	1.033	1.037
Final *R* indices [$I > 2\sigma(I)$]	R_1 = 0.0410 wR_2 = 0.0995	R_1 = 0.0489 wR_2 = 0.1226	R_1 = 0.0467 wR_2 = 0.1211	R_1 = 0.0501 wR_2 = 0.1175	R_1 = 0.0397 wR_2 = 0.0990
R indices (all data)	R_1 = 0.0513 wR_2 = 0.1050	R_1 = 0.0674 wR_2 = 0.1304	R_1 = 0.0728 wR_2 = 0.1323	R_1 = 0.0814 wR_2 = 0.1313	R_1 = 0.0516 wR_2 = 0.1050
Extinction coefficient	0.015(3)	0.0074(8)	0.017(3)	0.0060(10)	
Largest diff. peak/hole [e nm^{-3}]	166/−261	202/−144	343/−160	292/−132	335/−335

 © 2004 Wiley-VCH Verlag GmbH & Co. KGaA, Weinheim

$C_{50}H_{54}Br_2N_4Ni$ (929.50): calcd. C 64.61, H 5.86, N 6.03; found C 64.72, H 5.90, N 5.98.

Crystallography: Single-crystal X-ray measurements and structure determinations of **2a**−**3a**, **3b**, **3e**, **12b** (Table 2). The data collection was performed with a Nonius−Kappa CCD instrument equipped with graphite-monochromated Mo-K_α radiation (λ = 0.71073 Å) and a nominal crystal to area detector distance of 36 mm. Intensities were integrated using DENZO and scaled with SCALEPACK.[15] Several scans in φ and ω directions were made to increase the number of redundant reflections, which were averaged in the refinement cycles. This procedure replaces an empirical absorption correction. The structures were solved with direct methods (SHELXS 86) and refined against F^2 (SHELX 97).[16] Hydrogen atoms at carbon atoms were added geometrically and refined using a riding model. Hydrogen atoms at nitrogen and oxygen atoms of compounds **3a**, **3b**, **3e** were located and refined isotropically. All non-hydrogen atoms were refined with anisotropic displacement parameters. CCDC-213598 (for **2a**), -213599 (**3a**), -213600 (**3b**), -213601 (**3e**) and -213602 (**2b**) contain the supplementary crystallographic data for this paper. These data can be obtained free of charge at www.ccdc.cam.ac.uk/conts/retrieving.html [or from the Cambridge Crystallographic Data Center, 12 Union Road, Cambridge CB2 1EZ, UK; Fax: (internat.) + 44-1223/336-033; E-mail: deposit@ccdc.cam.ac.uk].

Polymerizations: All polymerization studies and polymer characterizations were performed at Basell/BASF AG in Ludwigshafen, Germany. Ethylene polymerization: a dry 1000-mL steel autoclave was charged under strict exclusion of air with toluene (400 mL) and a small amount (1−6 mg, compare Table 1) of precatalyst **8a**−**17**. A 30% toluene solution of methylaluminoxane (MAO) was added (2 mL) and the temperature of the autoclave was kept constant at 70 °C. Ethylene gas was added up to a pressure of 40 bar and the reaction was allowed to proceed for 5−75 minutes, depending on the activity of the catalyst. After the polymerization time given in Table 1, the reaction was terminated by releasing the pressure in the autoclave. The solid polymer was isolated by filtration, washed with methanol, and dried in vacuo. Propylene polymerization: conditions were similar as those in ethylene polymerizations, but propylene was used as monomer. Ethylene/*n*-hexene copolymerizations: conditions were similar as in ethylene homopolymerizations, but in addition to the other reagents *n*-hexene (12.5 mL) was employed.

[1] Recent reviews: [1a] V. C. Gibson, S. K. Spitzmesser, *Chem. Rev.* **2003**, *103*, 283. [1b] S. Mecking, *Angew. Chem.* **2001**, *113*, 550; *Angew. Chem. Int. Ed.* **2001**, *40*, 534−540. [1c] S. D. Ittel, L. K. Johnson, M. Brookhart, *Chem. Rev.* **2000**, *100*, 1169. [1d] S. Mecking, *Coord. Chem. Rev.* **2000**, *203*, 325. [1e] G. J. P. Britovsek, V. C. Gibson, D. F. Wass, *Angew. Chem.* **1999**, *111*, 448.

[2] L. K. Johnson, C. M. Killian, M. Brookhart, *J. Am. Chem. Soc.* **1995**, *117*, 6414.

[3] [3a] B. L. Small, M. Brookhart, A. M. A. Bennett, *J. Am. Chem. Soc.* **1998**, *120*, 4049. [3b] G. J. P. Britovsek, V. C. Gibson, B. S. Kimberley, P. J. Maddox, S. J. McTavish, G. A. Solan, A. J. P. White, D. J. Williams, *Chem. Commun.* **1998**, 849.

[4] [4a] T. R. Younkin, E. F. Connor, J. I. Henderson, S. K. Friedrich, R. H. Grubbs, D. A. Bansleben, *Science* **2000**, *287*, 460. [4b] E. B. Coughlin, S. D. Ittel, J. Feldman, L. Wang, A. M. A. Bennett, E. Hauptmann, L. K. Johnson, A. Parthasarathy, R. D. Simpson, WO9830609, **1998**.

[5] [5a] S. Matsui, M. Mitani, J. Saito, Y. Tohi, H. Makio, H. Tanaka, T. Fujita, *Chem. Lett.* **1999**, 1263. [5b] H. Makio, N. Kashiwa, T. Fujita, *Adv. Synth. Catal.* **2002**, *344*, 477.

[6] [6a] A. Held, F. M. Bauers, S. Mecking, *Chem. Commun.* **2000**, 301. [6b] A. Tomov, J. P. Broyer, R. Spitz, *Macromol. Symp.* **2000**, *150*, 53. [6c] S. Mecking, A. Held, F. M. Bauers, *Angew. Chem.* **2002**, *114*, 564.

[7] Z. Guan, *Chem. Eur. J.* **2002**, *8*, 3087.

[8] G. W. Coates, P. D. Hustad, S. Reinartz, *Angew. Chem. Int. Ed.* **2002**, *41*, 2237.

[9] [9a] B. Bildstein, A. Krajete, M. O. Kristen (BASF AG), DE 10206116, **2002**. [9b] B. Bildstein, A. Krajete, M. O. Kristen (BASF AG), DE 10206113, **2002**.

[10] A. Vogel, *Vogel's Textbook of Practical Organic Chemistry, Including Qualitative Organic Analysis*, Longman Inc., New York, **1978**, p. 1075.

[11] [11a] H. Ley, P. Krafft, *Ber. Dtsch. Chem. Ges.* **1907**, *40*, 697; and references cited therein. [11b] L. H. Briggs, R. C. Cambie, I. C. Dean, P. S. Rutledge, *Aust. J. Chem.* **1976**, *29*, 357.

[12] R. T. Boere, V. Klassen, G. Wolmershäuser, *J. Chem. Soc., Dalton Trans.* **1998**, 4147.

[13] B. Bildstein, M. Malaun, H. Kopacka, K. Wurst, M. Mitterböck, K.-H. Ongania, G. Opromolla, P. Zanello, *Organometallics* **1999**, *18*, 4325.

[14] S. Blechert, *Liebigs Ann. Chem.* **1985**, 673.

[15] Z. Otwinowski, W. Minor, *Methods Enzymol.* **1997**, *276*, 307.

[16] G. M. Sheldrick, *Program package SHELXTL V.5.1*, Bruker Analytical X-ray Instruments, Inc., Madison, USA, **1997**.

Received June 26, 2003
Early View Article
Published Online March 9, 2004

 © 2004 Wiley-VCH Verlag GmbH & Co. KGaA, Weinheim

Synthesis and Monitoring of α-$Bi_2Mo_3O_{12}$ Catalyst Formation using Thermo-Raman Spectroscopy

Anil Ghule,[a] Shin-Hwa Tzing,[a] Jia-Yaw Chang,[a] Kalyani Ghule,[a] Hua Chang,[a] and Yong Chien Ling*[a]

Keywords: Thermo-Raman spectroscopy / Thermochemistry / Dehydration / Phase transformations / Bismuth / α-$Bi_2Mo_3O_{12}$ catalyst

Thermo-Raman spectroscopy was used to monitor the dehydration and phase transformations of $Bi_2Mo_3O_{12}\cdot 5H_2O$. The hydrated forms $Bi_2Mo_3O_{12}\cdot 5H_2O$, $Bi_2Mo_3O_{12}\cdot 4.75H_2O$, $Bi_2Mo_3O_{12}\cdot 3H_2O$, $Bi_2Mo_3O_{12}\cdot 2H_2O$, and anhydrous $Bi_2Mo_3O_{12}$ were observed during dehydration in the wavelength range from 200 to 1400 cm^{-1}. Representative Raman spectra of these compounds are reported for the first time. The thermo-Raman intensity thermogram showed a systematic dehydration in four steps, and the differential thermo-Raman intensity thermogram confirmed this. Thermogravimetry, differential thermogravimetry, and differential scanning calorimetry results were in harmony with the results of the thermo-Raman spectroscopy. Additionally, the dehydration resulting in formation of anhydrous $Bi_2Mo_3O_{12}$ (amorphous $Bi_2Mo_3O_{12}$ phase) and the final transformation into the α-$Bi_2Mo_3O_{12}$ phase was observed to be a dynamic thermal process. The slow, controlled heating rate produced α-$Bi_2Mo_3O_{12}$ catalyst with a particle size averaging 200 nm. The catalyst formed was further characterized by Fourier transform infrared spectroscopy, X-ray diffraction, time of flight SIMS, transmission electron microscopy, and energy-dispersive X-ray analysis.
(© Wiley-VCH Verlag GmbH & Co. KGaA, 69451 Weinheim, Germany, 2004)

Introduction

Bismuth molybdates (α-$Bi_2Mo_3O_{12}$, β-$Bi_2Mo_2O_9$, and γ-Bi_2MoO_6 phases) are very popular and widely studied catalysts because of their commercial importance.[1] Extensive investigation of their ability to catalyze the selective oxidation and ammoxidation of alkenes[1−4] and hydrogen sulfide[5] has been carried out. The importance of bismuth molybdates is not limited to catalysis since they also show interesting physical properties with potential technological applications. Vannier et al.[6] reported $Bi_{26}Mo_{10}O_{69}$ as being the first unidimensional bismuth-based oxide ion conductor. Bismuth molybdates also show good optical quality with a wide transmission window between 0.415 and 5.2 μm.[7] Additionally, single crystals with large photon-phonon scattering cross-sections have attracted increasing interest as acousto-optical materials. They possess low optic and acoustic absorptions, good mechanical properties, and chemical stability (e.g. insolubility in water).[8,9] The tetragonal phases of thin-film bismuth-derived compounds are efficient photoconductors[10] and thin films of bismuth molybdates are effective gas sensors showing potential applications in breathalyzer devices.[11]

Bismuth molybdate catalyst systems have been structurally characterized,[12] and studied extensively by different techniques such as X-ray absorption,[13] X-ray diffraction,[14] neutron diffraction,[15] time-of-flight SIMS,[16] electron diffraction techniques,[17] high-resolution electron microscopy and vibrational spectroscopy.[18−20] Raman spectroscopy has proved to be an effective tool for the characterization of the structures of transition metal oxides in the bulk and two-dimensional surface phases.[21] Thus, a systematic study has been made of Raman stretching frequency, bond length, and bond strength empirical correlations. However, all these studies concentrated on the α-$Bi_2Mo_3O_{12}$ phase and little attention has been paid to $Bi_2Mo_3O_{12}\cdot 5H_2O$ and the other hydrated species, which could be important in optics and acoustic applications. The catalytic α-$Bi_2Mo_3O_{12}$ phase used in earlier studies was usually prepared by co-precipitation,[22] sol-gel methods,[23] solid-state reactions,[20] spray drying,[24] high-temperature calcination of solid mixtures or several other methods.[25] However, co-precipitation techniques result in co-precipitation of pure hydroxides and also precipitate bismuth with polymerized Mo ions. Solid-state reactions yield byproducts (phases) formed as a result of non-stoichiometric compositions,[26] and thus require several high-temperature calcination steps and regrinding to give a single, selective phase of the catalyst. Attempts to use mechanical mixtures have been made because of co-operative catalytic effects in multiphase systems where individual catalytic phases were prepared separately before mixing. Occasionally, pure forms, often contaminated with small amounts (ca. 2%) of other phases, have been reported.[27] Thus, monitoring of the

[a] Department of Chemistry, National Tsing Hua University, Hsinchu, Taiwan 30043, Republic of China
Fax: (internat.) + 886-35711082
E-mail: ycling@mx.nthu.edu.tw

preparation process is important to obtain selectively a single phase. This should enable a clarification of the roles and stabilities of individual bismuth molybdate phases during selective oxidations.

Thermogravimetry (TG), differential thermal analysis (DTA), and differential scanning calorimetry (DSC) are techniques generally used to study the thermal properties of solid samples in dynamic and static thermal processes.[28] However, these techniques fail to provide direct information about the phases and their compositions during a dynamic process. Thermo-Raman spectroscopy (TRS) is a useful technique in which successive collection of Raman spectra yields many details about a dynamic thermal process. The compositional changes of all the intermediates and phase transformations can be easily monitored and identified on a time scale of seconds and in temperature increments of one degree. The Raman intensity and the derivative of the Raman intensity of the characteristic band are plotted as a function of temperature and are the thermo-Raman intensity (TRI) and differential thermo-Raman intensity (DTRI) thermograms, respectively. These provide detailed quantitative information about the compositional changes and phase transformations[29] and can be compared with thermograms from TG, DTA, and DSC. Thus, thermo-Raman spectroscopy should be an ideal technique for monitoring and study of the morphological and compositional changes occurring during heating and calcinations.

In this work, the compositional variations of $Bi_2Mo_3O_{12}\cdot 5H_2O$ were observed by thermo-Raman spectroscopy in the temperature range from 25 to 600 °C. Spectral variation monitored in the H_2O and MoO_4^{2-} regions revealed four dehydrations resulting in formation of $Bi_2Mo_3O_{12}\cdot 4.75H_2O$, $Bi_2Mo_3O_{12}\cdot 3H_2O$, $Bi_2Mo_3O_{12}\cdot 2H_2O$, and $Bi_2Mo_3O_{12}$, respectively. Characteristic Raman spectra representing all the intermediates were obtained. The TRI thermogram and DTRI thermogram for the H_2O bands were plotted revealing four steps of dehydration with a proportionate loss of water in each step. The TG thermogram showed loss of 9% weight for the entire dehydration process suggesting loss of five H_2O molecules, with differential thermogravimetry (DTG) thermograms showing dips at 95, 148, 190, and 221 °C. Formation of anhydrous $Bi_2Mo_3O_{12}$ (amorphous $Bi_2Mo_3O_{12}$) in the temperature range from 290 to 320 °C was followed by transformation to the α-$Bi_2Mo_3O_{12}$ phase, which was identified by its Raman spectrum in the temperature range from 320 to 345 °C. This resulting α-$Bi_2Mo_3O_{12}$ phase was subjected to morphological and phase purity characterization.

Results and Discussion

Thermograms

The TG thermogram of $Bi_2Mo_3O_{12}\cdot 5H_2O$ in the temperature range from 25 to 600 °C is shown in Figure 1(a). It indicates a weight loss of 9% for the entire dehydration process suggesting the loss of five water molecules (calculated weight loss for five water molecules = 9.1%). The TG thermogram shows weight losses of 0.5% or 0.25 water molecules (T = 90−100 °C to form $Bi_2Mo_3O_{12}\cdot 4.75H_2O$), 3.5% or 1.9 water molecules (T = 100−165 °C to form $Bi_2Mo_3O_{12}\cdot 3H_2O$), 5.4% or 2.93 molecules (T = 165−200 °C to form $Bi_2Mo_3O_{12}\cdot 2H_2O$), and 9% or 4.94 water molecules (T = 200−290 °C to form anhydrous $Bi_2Mo_3O_{12}$) in the first, second, third, and fourth steps of dehydration, respectively. The entire dehydration process extended up to 290 °C. The observed weight losses were in close agreement with the theoretical weight losses of 0.5, 3.6, 5.4, and 9.1%, in the respective dehydration steps. Further heating gave a slight loss in weight upon transformation into the α-$Bi_2Mo_3O_{12}$ phase. This might be due to the diffusion of lattice oxygen atoms to the surface and its subsequent loss, as the bulk is known to act as an oxygen carrier.[1]

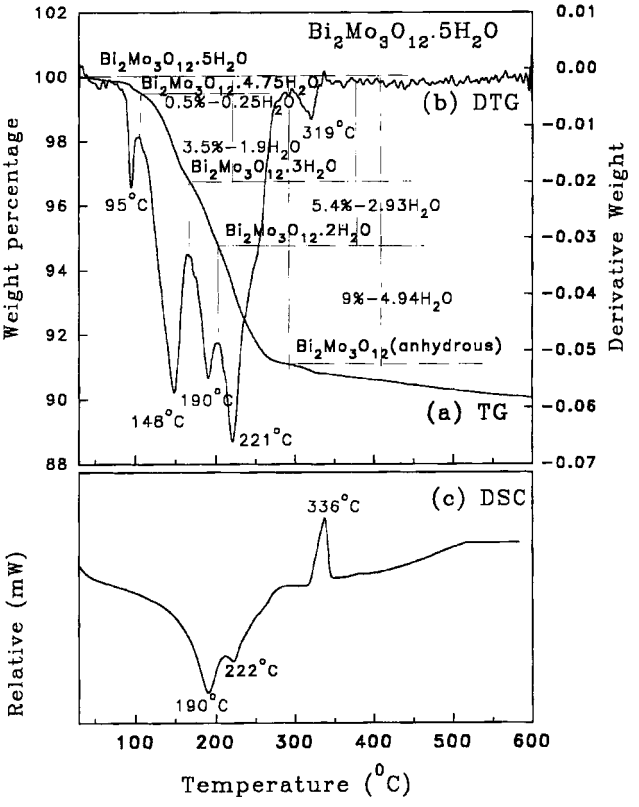

Figure 1. (a) TG, (b) DTG, and (c) DSC thermograms from 25 to 600 °C starting from $Bi_2Mo_3O_{12}\cdot 5H_2O$

The DTG thermogram, which is the derivative of the TG thermogram, is shown in Figure 1(b). It shows dips at 95, 148, 190, and 221 °C indicating maximum weight losses during the first, second, third, and fourth dehydration steps, respectively. A slight shoulder at 250 °C to the dip at 221 °C is due to the prolonged fourth step of dehydration. The dip at 319 °C is assigned to the transformation from the anhydrous form to the α-$Bi_2Mo_3O_{12}$ phase. No further information could be extracted at higher temperatures.

There are several reports about the presence of the hydrated species. Murakami and Imai[30] reported the presence of $Bi_2Mo_3O_{12}\cdot 4.75H_2O$ and anhydrous $Bi_2Mo_3O_{12}$ (amorphous) based on thermogravimetric (TG) analysis.

 © 2004 Wiley-VCH Verlag GmbH & Co. KGaA, Weinheim

The amorphous phase formation occurred at 150 °C based on the X-ray diffraction pattern, contradicting their TGA data, which indicated a transition at 250 °C. Yinjie and Aimin[31] estimated the presence of $Bi_2Mo_3O_{12}\cdot 3.86H_2O$ based on their TGA data. Thus, it was of interest to determine the different hydrated species of $Bi_2Mo_3O_{12}\cdot 5H_2O$.

The DSC thermogram of $Bi_2Mo_3O_{12}\cdot 5H_2O$ in the temperature range from 25 to 600 °C is shown in Figure 1(c). It has a broad endotherm at 190 °C accounting for the first three dehydration steps and an endotherm at 222 °C for the fourth dehydration step . The sharp exotherm at 336 °C (enthalpy = −22.6 J/g) is as a result of the phase transformation from the amorphous phase to the α-$Bi_2Mo_3O_{12}$ phase. The DSC thermogram also shows that the entire dehydration process extends up to 290 °C, in contrast to the earlier report by Murakami and Imai.[30]

Thermo-Raman Studies

Extensive theoretical considerations and experimental studies have shown that vibrational spectroscopy of powdered samples provides information not only about the phases, but also about the size, shape, and state of aggregation of the particles that constitute the powder.[32] Assuming the internal and external modes of the sample to be independent of one another, the internal modes of metal oxide molecules within the unit cell of a crystal occur in the medium- and high-frequency regions (> 400 cm^{-1} for the MoO_4^{2-} species). External modes, including translational and librational modes, occur at lower frequencies (< 400 cm^{-1}). This helps in identification and assignment of species based on their characteristic Raman spectra. The internal modes in the range from 400 to 1200 cm^{-1} provide information about the environment around the MoO_4^{2-} ions. The free molybdate ion, MoO_4^{2-}, is tetrahedral with point group T_d symmetry. It has four vibrational modes $\nu_1(A_1)$, $\nu_2(E)$, $\nu_3(T_2)$, and $\nu_4(T_2)$. The stretching modes connect $\nu_1(A_1)$ and $\nu_3(T_2)$, while the bending modes connect $\nu_2(E)$ and $\nu_4(T_2)$. In addition, the α-$Bi_2Mo_3O_{12}$ phase contains three different tetrahedra which might result in different band positions. Matsuura et al.[18] reported six bands around 900 and 800 cm^{-1} attributed to the stretching modes of each tetrahedral species. Theobald et al.,[15] in their XANES experiments, observed that the Mo^{6+} ions in

Table 1. Raman bands for $Bi_2Mo_3O_{12}\cdot 5H_2O$, $Bi_2Mo_3O_{12}\cdot 4.75H_2O$, $Bi_2Mo_3O_{12}\cdot 3H_2O$ $Bi_2Mo_3O_{12}\cdot 2H_2O$, anhydrous $Bi_2Mo_3O_{12}$, and α-$Bi_2Mo_3O_{12}$

$Bi_2Mo_3O_{12}$ $5H_2O$ 25 °C	$Bi_2Mo_3O_{12}$ $4.75H_2O$ 100 °C	$Bi_2Mo_3O_{12}$ $3H_2O$ 165 °C	$Bi_2Mo_3O_{12}$ $2H_2O$ 200 °C	$Bi_2Mo_3O_{12}$ (anhydrous) 290 °C	α-$Bi_2Mo_3O_{12}$ 450 °C	Assignment[a]
		3549 w[b]	3542 w			
		3502 w	3502 w	3521 w		
3453 s	3451 s	3462 s	3458 w			
		3305 w				H_2O
3265 m	3285 w	3273 w				(stre.vib.)
		3233 w	3220 w	3220 w		
					996 s	
					959 w	
920 s	920 s	920 s	920 s	928 m		
				905 m	899 s	Mo−O
866 s	866 s	866 s	864 s			stre.vib.
				844 w		
			820 w		824 s	
684 w	684 w	684 w		681 w	669 s	
649 s	649 s	649 s	657 m			
525 s	525 s	525 s	525 m			
					542 w	Bi−O stre.
499 w	499 w	501 w			504 m	vib.
					495 w	Mo_2O_2 dioxo
467 w	467 w	467 w				
418 s	418 s	418 s	420 m			
374 s	374 s	374 s	374 m	374 w	370 s	
352 w	352 m	352 w				Mo−O
342 w		342 w	342 w		340 w	bend./wag.
324 w	322 w	322 w			324 w	and external
292 w	289 w	291 w			289 s	vib. modes
267 w	267 w	267 w				

[a] Refs.[12,21] [b] s = strong, m = medium, w = weak, and stre. vib. = stretching vibrations.

 © 2004 Wiley-VCH Verlag GmbH & Co. KGaA, Weinheim

α-$Bi_2Mo_3O_{12}$ are surrounded by five oxygen atoms in an asymmetric Mo−O_5 coordination environment, with an average Mo−O interatomic distance of 1.91 Å. However, the Fourier transform EXAFS data revealed a substantial structural complexity. The irregular oxygen coordination about the Mo^{6+} ions results in three peaks at 1.26, 1.53, and 1.97Å. The more distant Bi and Mo cations around this molybdenum give rise to three peaks at 2.86, 3.30, and 3.65 Å, which are due to Mo···Mo, Mo···Bi, and Mo···Mo/Bi back scatterings, respectively.[13] Generally, in dynamic thermal process within crystals, structural distortions may occur, which lower the symmetry causing shifting and splitting of the bands. Raman bands for $Bi_2Mo_3O_{12}$ fall between 200 and 1200 cm^{-1} and are assigned as in Table 1. The broad band in the range from 3200 to 3600 cm^{-1} is due to lattice H_2O (antisymmetric and symmetric OH stretching).[21]

Dehydration

First Dehydration

Figure 2(A)(a) shows the characteristic Raman spectrum of $Bi_2Mo_3O_{12}·5H_2O$ at 25 °C in the H_2O region from 3000 to 3700 cm^{-1}. The two broad bands at 3453 and 3265 cm^{-1} at 25 °C represent the lattice H_2O. As the temperature rises above 60 °C, these bands shift to 3451 and 3285 cm^{-1}, respectively, as $Bi_2Mo_3O_{12}·4.75H_2O$ forms during the first dehydration step. The characteristic Raman spectrum of $Bi_2Mo_3O_{12}·4.75H_2O$ in the water region is shown in Figure 2(A)(b) (100 °C). The actual transformation occurs in the temperature range from 60 to 75 °C, where the weakly bound water molecule (water of crystallization) is easily lost.

The corresponding characteristic Raman spectrum of $Bi_2Mo_3O_{12}·5H_2O$ at 25 °C in the MoO_4^{2-} region (from 200 to 1200 cm^{-1}) is shown in Figure 2(B)(a). A slight decrease in intensity of the two bands at 920 and 866 cm^{-1} is observed with the rise in temperature to 100 °C. The bands at 684, 649, 525, 499, 467, 418, 374, 352, 342, 292, and 267 cm^{-1} show a slight broadening. No distinct changes in spectrum and symmetry of MoO_4^{2-} were observed since only a small amount of water is lost in this step. Among the noticeable changes, the weak band at 499 cm^{-1} appears as a shoulder to the band at 525 cm^{-1} and the doublet at 352 and 342 cm^{-1} disappears as the temperature rises above 60 °C. These spectral changes were especially evident in the temperature range from 60 to 75 °C and are represented in the characteristic spectrum of $Bi_2Mo_3O_{12}·4.75H_2O$ shown in Figure 2(B)(b). The first dehydration is the transformation from $Bi_2Mo_3O_{12}·5H_2O$ to $Bi_2Mo_3O_{12}·4.75H_2O$. To the best of our knowledge, no crystal data are available for $Bi_2Mo_3O_{12}·5H_2O$. However, the structure of $Bi_2Mo_3O_{12}·5H_2O$ could be similar to that of $Bi_2Mo_3O_{12}·4.75H_2O$ (reported by Murakami and Imai,[30]) based on the similarity of their Raman spectra. The crystal structure of $Bi_2Mo_3O_{12}·4.75H_2O$ has a monoclinic unit cell, with lattice parameters calculated to be a = 6.334, b = 11.593, c = 5.777 Å and β = 113.166° as indexed from the X-ray diffraction pattern.

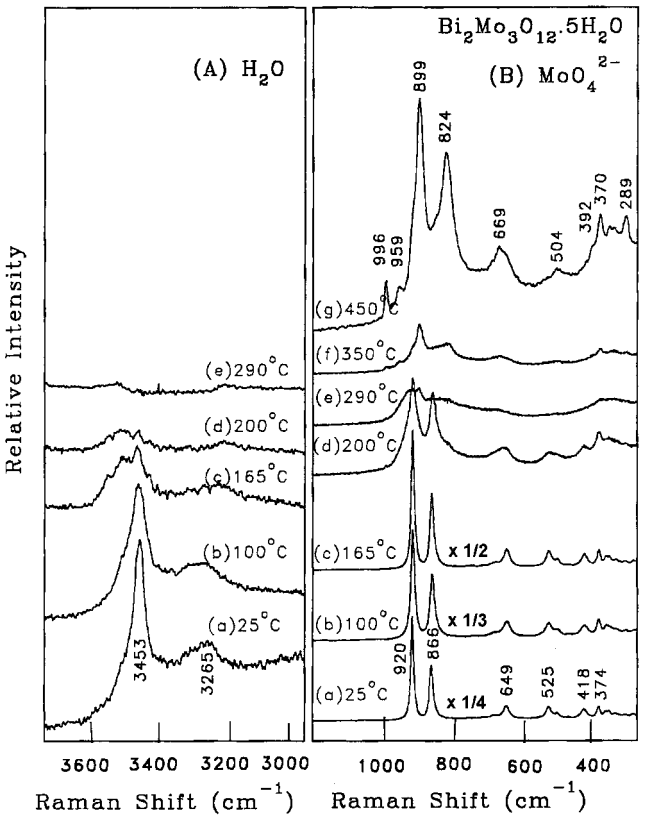

Figure 2. Characteristic thermo-Raman spectra of $Bi_2Mo_3O_{12}·5H_2O$ during the dehydration and of the intermediate hydrated species observed: (a) $Bi_2Mo_3O_{12}·5H_2O$ (25 °C; intensity reduced 4 times); (b) $Bi_2Mo_3O_{12}·4.75H_2O$ (100 °C; intensity reduced 3 times); (c) $Bi_2Mo_3O_{12}·3H_2O$ (165 °C; intensity reduced 2 times); (d) $Bi_2Mo_3O_{12}·2H_2O$ (200 °C); (e) $Bi_2Mo_3O_{12}$ (290 °C); (f) $Bi_2Mo_3O_{12}$ amorphous phase (350 °C); (g) α-$Bi_2Mo_3O_{12}$ (450 °C) in (A) the H_2O region from 3000 to 3700 cm^{-1} and (B) the MoO_4^{2-} region from 200 to 1200 cm^{-1}

Second Dehydration

The spectral variations in the H_2O region for the second dehydration in the temperature range from 100 to 165 °C were observed and the characteristic Raman spectrum of $Bi_2Mo_3O_{12}·3H_2O$ is shown in Figure 2(A)(c). The broad band at 3451 cm^{-1} further broadens and shifts to 3462 cm^{-1} as the temperature rises above 128 °C. Two broad bands at 3549 and 3502 cm^{-1} emerge and become distinct with the rise in temperature to 165 °C. The broad band at 3285 cm^{-1}splits into bands at 3305, 3273, and 3233 cm^{-1}. Overall, a decrease in intensity of the H_2O bands was observed with major spectral changes in the temperature range from 128 to 132 °C.

Similar changes were observed in the MoO_4^{2-} region for the second dehydration in the temperature range from 100 to 165 °C, and the characteristic Raman spectrum of $Bi_2Mo_3O_{12}·3H_2O$ is shown in Figure 2(B)(c). The bands observed at 920 and 866 cm^{-1} show a notable decrease in intensity as the temperature rises to 165 °C. The singlet at 351 cm^{-1}, observed at 100 °C, splits into two bands at 352 and 342 cm^{-1} as the temperature rises above 128 °C. The

 © 2004 Wiley-VCH Verlag GmbH & Co. KGaA, Weinheim

band at 322 cm^{-1} becomes distinct and the bands at 289 and 263 cm^{-1} shift to 291 and 267 cm^{-1}, respectively. The spectral changes in the temperature range from 128 to 132 °C correspond to a second dehydration to form $Bi_2Mo_3O_{12}·3H_2O$ from $Bi_2Mo_3O_{12}·4.75H_2O$. The two water molecules lost below 165 °C are attributed to the water of crystallization. To the best of our knowledge, the Raman spectrum of $Bi_2Mo_3O_{12}·3H_2O$ is reported here for the first time and crystal structure data for $Bi_2Mo_3O_{12}·3H_2O$ are yet to be reported. However, based on the similarity of their Raman spectra, its structure is expected to be similar to $Bi_2Mo_3O_{12}·4.75H_2O$ with a slight variation in lattice parameters. Yinjie and Aimin,[31] reported the crystal structure of $Bi_2Mo_3O_{12}·3.86H_2O$ as monoclinic, with lattice parameters calculated to be a = 6.338, b = 11.658, c = 5.787 Å and β = 113.168° as indexed from the X-ray diffraction pattern.

Third Dehydration

Spectral variations were observed in the H_2O region for the third dehydration in the temperature range from 165 to 200 °C with a transformation temperature at 192 °C. The characteristic Raman spectrum of $Bi_2Mo_3O_{12}·2H_2O$ obtained after the third dehydration is shown in Figure 2(A)(d). The spectrum at 165 °C shows broad bands at 3549 and 3462 cm^{-1}. These bands gradually shift to 3542 and 3458 cm^{-1}, respectively, with the rise in temperature above 190 °C. The band at 3502 cm^{-1} further broadens and the weak bands at 3305 and 3273 cm^{-1} disappear as the temperature approaches 200 °C. The weak band at 3233 cm^{-1} shifts to 3220 cm^{-1}.

Spectral variations were also observed in the MoO_4^{2-} region for the third dehydration step in the temperature range from 165 to 200 °C and the characteristic spectrum of $Bi_2Mo_3O_{12}·2H_2O$ is shown in Figure 2(B)(d). The band at 920 cm^{-1} broadens and drastically decreases in intensity. A shoulder at 820 cm^{-1} to the band at 864 cm^{-1} starts appearing at 193 °C and gradually resolves as the temperature rises to 200 °C. The band at 649 cm^{-1} broadens and shifts to 657 cm^{-1} and the shoulder at 684 cm^{-1} gradually disappears as the temperature rises to 200 °C. Similarly, the band at 525 cm^{-1} becomes weak and the shoulder at 501 cm^{-1} and the weak band at 467 cm^{-1} disappear. The doublet at 352 and 342 cm^{-1} merges to form a broad singlet at 342 cm^{-1}. The lower modes at 322, 291, and 267 cm^{-1} also disappear as the temperature rises to 200 °C. The major changes observed in the spectra indicate the drastic change in symmetry of MoO_4^{2-}, even though only one water molecule is lost in this step, resulting in the transformation from $Bi_2Mo_3O_{12}·3H_2O$ to $Bi_2Mo_3O_{12}·2H_2O$. This shows that the water molecule evolved in this third dehydration must be different from the two water molecules evolved in the previous dehydrations and that it is associated directly with the structural composition. It is assigned as a water of constitution. The crystal structure of $Bi_2Mo_3O_{12}·2H_2O$ is yet to be reported.

Fourth Dehydration

The spectral variations in the H_2O region for the fourth dehydration in the temperature range from 200 to 290 °C were monitored and the characteristic Raman spectrum for anhydrous $Bi_2Mo_3O_{12}$ is shown in Figure 2(A)(e). The weak, broad bands observed at 3542, 3502, 3458, and 3220 cm^{-1} gradually disappear when the temperature reaches 290 °C. This indicates a complete loss of water to form anhydrous $Bi_2Mo_3O_{12}$. The Raman spectral profile appears almost flat.

Similarly, spectral changes were clearly observed in the MoO_4^{2-} region for the fourth dehydration in the temperature range from 200 to 290 °C with a transformation temperature observed at 220 °C. The characteristic Raman spectra of the anhydrous $Bi_2Mo_3O_{12}$ is shown in Figure 2(B)(e). The broad band at 920 cm^{-1} gradually shifts to 928 cm^{-1} and a new band at 905 cm^{-1} starts to appear as the temperature rises above 220 °C. The band at 864 cm^{-1} and its shoulder at 820 cm^{-1} disappear and a broad band at 844 cm^{-1} appears as the temperature approaches 290 °C. The band at 657 cm^{-1} decreases in intensity and shifts to 681 cm^{-1}. The weak bands at 525 and 420 cm^{-1} disappear and the weak bands at 374 and 342 cm^{-1} broaden and decrease in intensity as the temperature rises to 290 °C. Major spectral changes observed in the temperature range from 220 to 240 °C are the result of the fourth dehydration where $Bi_2Mo_3O_{12}·2H_2O$ transforms to anhydrous $Bi_2Mo_3O_{12}$. The crystal structure of anhydrous $Bi_2Mo_3O_{12}$ has not been reported. However, an X-ray diffraction pattern recorded contained no measurable peaks suggesting that the powder is amorphous (data not shown).

Phase Transformations

Figure 2(B)(f) shows the representative spectral variations in the MoO_4^{2-} region from 200 to 1200 cm^{-1} for the onset of crystallization of the α-$Bi_2Mo_3O_{12}$ phase from the $Bi_2Mo_3O_{12}$ amorphous phase. The crystallization process began at 312 °C. The spectrum at 350 °C shows traces of the amorphous phase as well as the α-$Bi_2Mo_3O_{12}$ phase. The weak bands at 996, 959, 504, 374, and 289 cm^{-1} are due to the α-$Bi_2Mo_3O_{12}$ phase whereas the sharp bands at 905, 672, and 328 cm^{-1} represent the amorphous phase. The band at 928 cm^{-1} (290 °C) shifts to 905 cm^{-1} as the temperature approaches 350 °C. A further increase in temperature to 450 °C, as in Figure 2(B)(g), shows sharp bands at 996, 959, 899, 824, 669, 504 370, 340, 324, and 289 cm^{-1} characteristic of the α-$Bi_2Mo_3O_{12}$ phase. A major shift in the band at 905 cm^{-1} to 899 cm^{-1} was observed. There were no further spectral changes up to 600 °C indicating a complete transformation into the pure α-$Bi_2Mo_3O_{12}$ phase. The crystal structure of the α-$Bi_2Mo_3O_{12}$ phase (scheelite structure) has been extensively studied and reported to be monoclinic (trigonal-bipyramidal or distorted tetrahedral) with space group $P2_1/c$ and unit cell parameters a = 7.685, b = 11.491, c = 11.929 Å with characteristic edge β = 115.40°.[33] The crystal structure, reported by Cesari et

 © 2004 Wiley-VCH Verlag GmbH & Co. KGaA, Weinheim

al.,[34] shows that the α-$Bi_2Mo_3O_{12}$ phase consists of two kinds of twin tetrahedra $\alpha_1\alpha_1$ and $\alpha_2\alpha_3$, one of which ($\alpha_1\alpha_1$) contains a center of symmetry; α_1 and α_2 have Bi ions adjacent to the tetrahedra, while there is a Bi ion vacancy in the α_3 tetrahedron. In all cases, there are three different and distorted tetrahedra, resulting in complicated absorption bands.

Intensity Variation

The thermo-Raman intensity (TRI) and the derivative of the thermo-Raman intensity (DTRI) of the water bands in the range from 3100 to 3700 cm^{-1} from 25 to 300 °C were plotted as shown in Figure 3(a) and (b), respectively. Based on the TGA information, the loss in intensity is equated with loss of five molecules of water. Slopes in the TRI thermogram indicate loss of water and plateaus imply intermediate formation. The TRI thermogram shows four slopes and four plateaus corresponding to four steps of dehydration. The temperature range, percentage reduction in intensity (between two intermediates), equivalent number of molecules of water lost and dip observed in the DTRI during each step of dehydration are tabulated in Table 2. The entire dehydration process extended up to 290 °C and no further decrease in intensity was observed, indicating completion of the dehydration. The slight temperature variations in the starting and end point of each of the dehydration steps in the TRS and TGA can be attributed to the different physical properties monitored by these techniques. TRS monitors the surface of the sample whilst TGA monitors the bulk. However, the end point of the completion of the dehydration process was the same for both techniques.

Band Shift

Figure 4 shows the shifts of the bands at 920 and 866 cm^{-1} plotted as a function of temperature (from 25 to 600 °C). No noticeable shift in the band at 866 cm^{-1} was observed until it gradually disappeared during the fourth step of dehydration. A similar trend was observed for the characteristic band at 920 cm^{-1}, although it showed a gradual shift to 928 cm^{-1} during the fourth step of dehydration. This clearly indicates that a major structural transformation occurs during the fourth dehydration, where two water molecules (water of constitution) are lost, distorting the structure and the environment around the MoO_4^{2-} ions. Furthermore, a drastic shift of the band from 928 to 905 cm^{-1} was observed around 310 °C during the onset of crystallization towards the formation of α-$Bi_2Mo_3O_{12}$ phase. As the temperature rose above 310 °C the band shifted gradually to 899 cm^{-1} after which no further shift was noted marking completion of transformation into the α-$Bi_2Mo_3O_{12}$ phase.

Characterization of the α-$Bi_2Mo_3O_{12}$ Phase

Morphological characteristics depend on the rate of heating and calcination time. The particle size is important and

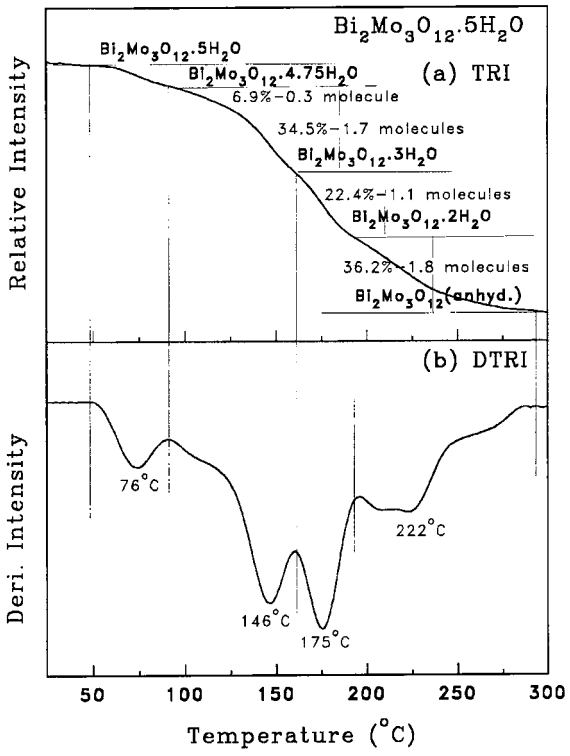

Figure 3. (a) Thermo-Raman intensity (TRI) thermogram and (b) differential thermo-Raman intensity (DTRI) thermogram for the stretching bands of H_2O during dehydration of $Bi_2Mo_3O_{12}\cdot 5H_2O$ in the temperature range from 25 to 300 °C

governs the activity and selectivity of bismuth molybdates, which must provide sufficient lattice oxide ions during catalytic redox cycles.[35]

Fourier Transform Infrared Spectroscopy

Figure 5 shows the FT-IR spectra of as-synthesized $Bi_2Mo_3O_{12}\cdot 5H_2O$ and the α-$Bi_2Mo_3O_{12}$ phase (sample collected at 450 °C). The IR spectra and the bands of the α-$Bi_2Mo_3O_{12}$ phase are in agreement with those observed by Matsuura et al.[18] The major difference observed was the disappearance of water bands and the bands at 1189 and 1879 cm^{-1}. In addition, a drastic decrease in intensity was noted in the spectra of the α-$Bi_2Mo_3O_{12}$ phase with a major splitting around 900 cm^{-1}.

X-ray Diffraction (XRD)

The XRD patterns of $Bi_2Mo_3O_{12}\cdot 5H_2O$ and the α-$Bi_2Mo_3O_{12}$ phase are shown in Figure 6. The XRD pattern of the amorphous phase contains no diffraction peaks (data not shown). The crystalline nature of $Bi_2Mo_3O_{12}\cdot 5H_2O$ and the α-$Bi_2Mo_3O_{12}$ phase is demonstrated by the presence of distinct diffraction peaks. However, notable changes in the diffraction patterns between the two crystalline forms was observed which agrees with the considerable spectral changes observed in our thermo-Raman study. The diffraction pattern of pure α-$Bi_2Mo_3O_{12}$ is in close agreement with that reported by Li and Cheng.[5] Measurement of the XRD

 © 2004 Wiley-VCH Verlag GmbH & Co. KGaA, Weinheim

Table 2. TRI and DTRI data obtained during dehydration of $Bi_2Mo_3O_{12}·5H_2O$

Dehydration	Temperature. range [°C]	Intensity drop (% of H_2O)	H_2O molecules [equiv.]	DTRI endotherm [°C]
First step ($Bi_2Mo_3O_{12}·5H_2O$ to $Bi_2Mo_3O_{12}·4.75H_2O$)	50−95	6.9	0.3	76
Second step ($Bi_2Mo_3O_{12}·4.75H_2O$ to $Bi_2Mo_3O_{12}·3H_2O$)	100−160	34.5	1.7	146
Third step ($Bi_2Mo_3O_{12}·3H_2O$ to $Bi_2Mo_3O_{12}·2H_2O$)	165−190	22.4	1.1	175
Fourth step ($Bi_2Mo_3O_{12}·2H_2O$ to anhyd. $Bi_2Mo_3O_{12}$)	190−290	36.2	1.8	222

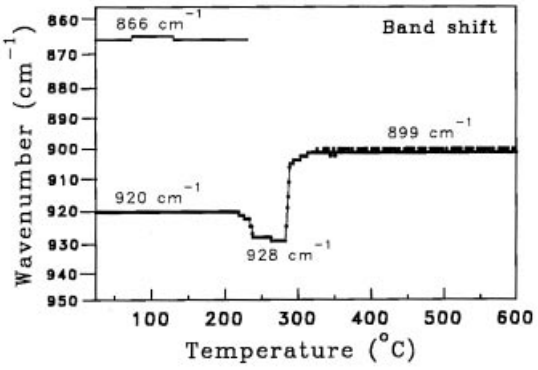

Figure 4. Band-shift measurements for the bands at 920 and 866 cm^{-1} of $Bi_2Mo_3O_{12}·5H_2O$ observed in the temperature range from 25 to 600 °C

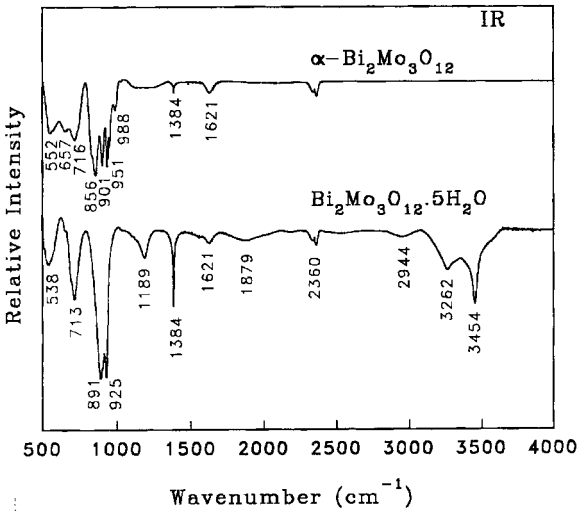

Figure 5. Fourier transform infrared spectra of as-synthesized $Bi_2Mo_3O_{12}·5H_2O$ and α-$Bi_2Mo_3O_{12}$ in the range from 500 to 4000 cm^{-1}

patterns of the intermediate hydrated species should be of interest for a better comparison with the data obtained from thermo-Raman spectroscopy. Ideally, an in situ measurement of the temperature dependence of the XRD spectrum over the temperature range of interest is required to obtain accurate data.

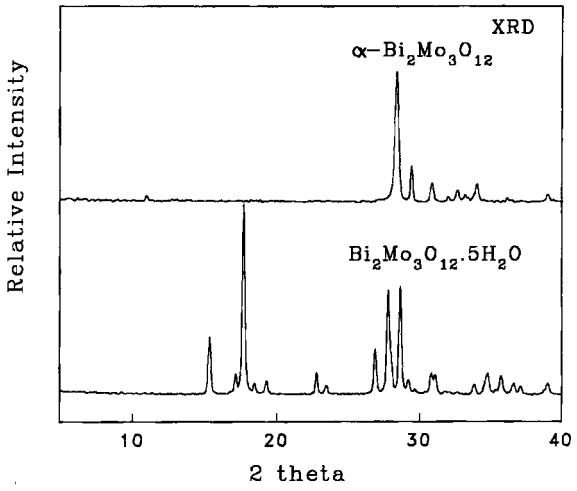

Figure 6. XRD pattern of as-synthesized $Bi_2Mo_3O_{12}·5H_2O$ and α-$Bi_2Mo_3O_{12}$ (heated to 450 °C)

Time of Flight Secondary Ionization Mass Spectrometry (TOF SIMS)

The positive ion static TOF-SIMS spectrum of the α-$Bi_2Mo_3O_{12}$ phase was also recorded and is presented in Figure 7. The observed spectral pattern and the $Bi_3O_4^+/Bi^+$ ratio of 0.0004 are in close agreement with that previously reported for the α-$Bi_2Mo_3O_{12}$ phase.[16] Considering the sensitivity of TOF-SIMS, the phase purity of α-$Bi_2Mo_3O_{12}$ can be confirmed. However, the peaks at m/z = 487 and 565 reported by Weng et al.[16] were not observed.

Electron Microscopic Study and EDS Analysis

Electron microscopy is extensively used for structural, chemical (composition), and morphological studies (grain size, crystallinity, and phase identification). Figure 8(a) shows a TEM image of the α-$Bi_2Mo_3O_{12}$ phase obtained after controlled heating to 450 °C at a rate of 5 °C·min^{-1}. The distribution of the particle size was in the range of several hundreds of nanometers (avg. 200 nm) as observed from the particle size distribution profile deduced from TEM images [Figure 8,(b)]. However, in most of the earlier reports where the calcination step probably involved fast heating rates, the particle size was reported to be in the

 © 2004 Wiley-VCH Verlag GmbH & Co. KGaA, Weinheim

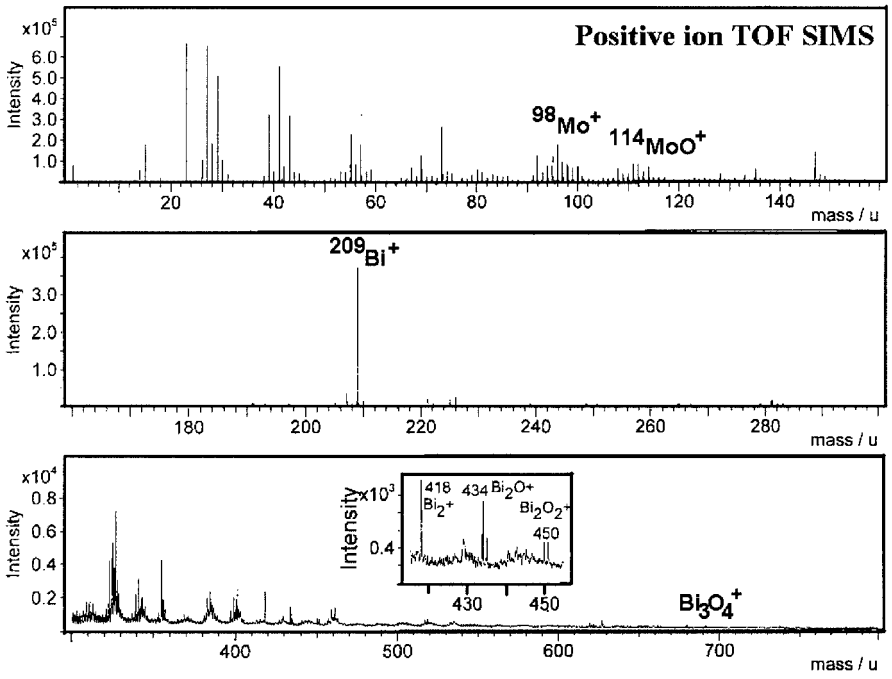

Figure 7. Positive ion TOF-SIMS spectra of α-$Bi_2Mo_3O_{12}$ (heated to 450 °C)

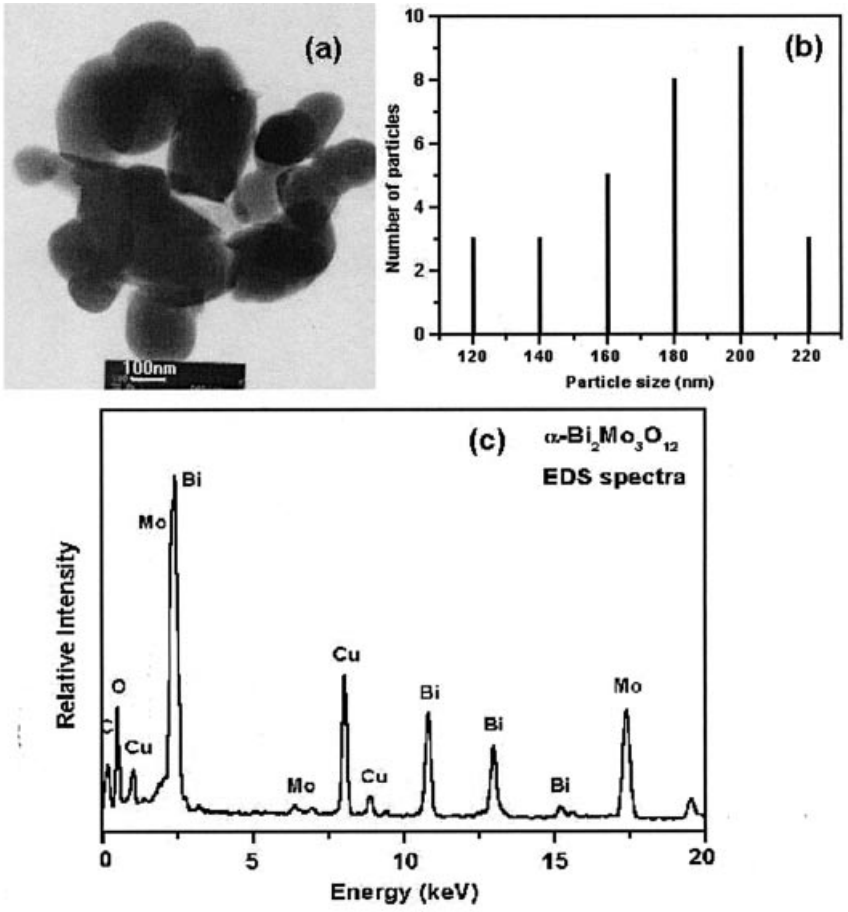

Figure 8. Morphological and compositional characterization of α-$Bi_2Mo_3O_{12}$ (heated to 450 °C): (a) TEM image indicating the particle size and surface characteristics; (b) particle size distribution profile; (c) EDS spectra showing the composition of the α-$Bi_2Mo_3O_{12}$ formed (atomic ratio Bi/Mo ≈ 2:3)

 © 2004 Wiley-VCH Verlag GmbH & Co. KGaA, Weinheim

micrometer range (100−400 μm).[36] EDS is useful for quantitative analysis. EDS measurements were carried out on $Bi_2Mo_3O_{12}·5H_2O$, α-$Bi_2Mo_3O_{12}$ (heated at 450 °C), and α-$Bi_2Mo_3O_{12}$ (heated at 550 °C). The presence of bismuth, molybdenum, and oxygen was examined and a representative EDS spectrum of α-$Bi_2Mo_3O_{12}$ (heated at 550 °C) is shown in Figure 8(c). The bismuth and molybdenum contents, and the Bi/Mo ratios in all the samples were identical. The atomic ratio of Bi/Mo was observed to be 43:57 which is in close agreement with the molar ratios of Bi_2O_3/$Na_2MoO_4·2H_2O$ in the starting solution.

According to AFM, XRD, and XPS experiments carried out by Yanina and Smith,[37] a loss of Mo was observed on heating to temperatures higher than 500 °C in dry air or air with 2.3% H_2O due to volatilization. This resulted in precipitation of traces of γ-Bi_2MoO_6 and β-$Bi_2Mo_2O_9$ on the surface of the α-$Bi_2Mo_3O_{12}$ catalyst. However, no such changes were observed in our experiments even though the heating was performed in the presence of air. This might be due to the slow and controlled heating rate used in our experiment. Additionally, TOF-SIMS data also support the presence of the α-$Bi_2Mo_3O_{12}$ phase. This provides evidence for the formation of the pure form of the α-$Bi_2Mo_3O_{12}$ catalyst under a controlled heating rate in the presence of air. In addition, the particle size observed from TEM images lies in the hundreds of nanometers range, suggesting that the controlled heating rate is also important in governing the particle size of the catalyst.

Conclusion

A systematic study of the dehydration and phase-transformation processes of $Bi_2Mo_3O_{12}·5H_2O$ was carried out using thermo-Raman spectroscopy in the temperature range from 25 to 600 °C. Three different hydrated species, $Bi_2Mo_3O_{12}·4.75H_2O$, $Bi_2Mo_3O_{12}·3H_2O$, $Bi_2Mo_3O_{12}·2H_2O$, and anhydrous $Bi_2Mo_3O_{12}$ were observed as intermediates, based on the spectral variations observed in the H_2O and MoO_4^{2-} absorption regions during temperature increments of 1 °C. Characteristic Raman spectra of these hydrated species have been reported for the first time. The TRI thermogram for the H_2O bands supported the results revealing four dehydration steps with a proportionate loss of water in each step. The DTRI thermogram was also in harmony with the TRI and TGA data. The phase transformation of anhydrous $Bi_2Mo_3O_{12}$ to the α-$Bi_2Mo_3O_{12}$ phase was also observed and characterized by other techniques. Slow and controlled heating resulted in the α-$Bi_2Mo_3O_{12}$ phase without precipitating γ-Bi_2MoO_6 and β-$Bi_2Mo_2O_9$ phases and the particle size thus obtained was in the range of a few hundreds of nanometers as observed from the morphological characterization. The characterization of the α-$Bi_2Mo_3O_{12}$ phase by XRD, EDS, and FTIR for phase purity was further supported by TOF-SIMS analysis. The fact that the thermo-Raman spectroscopy setup could detect all the dehydration steps involved and also the transformation to the α-$Bi_2Mo_3O_{12}$ phase indicates its sensitivity and potential future applications in monitoring catalyst formation if a commercial instrument can be developed.

Experimental Section

Sample Preparation: Bi_2O_3 (Aldrich Chem., WI, USA) and $Na_2MoO_4·2H_2O$ (Riedel−de Haën, Seelze, Germany) were used as received without further purification. Bi_2O_3 and $Na_2MoO_4·2H_2O$ (1:3 molar ratio) were dissolved in 1 M nitric acid and stirred vigorously at 60 °C until a slurry was obtained. This slurry was cooled, filtered, and the residue washed thoroughly with distilled water until the washings reached pH = 6. The sample was dried at room temperature to ensure the retention of water of hydration. This sample was lightly ground prior to analysis.

Thermo-Raman Study: The Raman spectra were obtained using laser excitation at a wavelength of 514.5 nm (50 mW) from an argon ion laser (Coherent, Innova 100-15). A filter was used to remove the plasma lines. The scattered light was collected at right angles, dispersed by a single spectrometer (Spex, 0.5 m) with a resolution of 2 cm^{-1} and detected by a CCD camera (Princeton Instruments, 1024 × 1024 pixels). A notch filter was set in front of the spectrometer to remove the Rayleigh scattered light. The sample was placed in a sample holder and mounted on the thermocouple in a homemade oven in stationary air. The temperature of the oven was programmed to increase from 25 to 600 °C at a rate of 5 °C min^{-1}. Thermo-Raman spectra were collected continuously during heating without disturbing the sample. The exposure time of the CCD was set such that the temperature range covered by each spectrum was 1 °C. Overall, 575 spectra were collected and their reproducibility checked in the spectral range from 200 to 1400 cm^{-1} for MoO_4^{2-} whilst 275 spectra in the range from 2900 to 3900 cm^{-1} were collected for H_2O. A BASIC computer program was written to systematically determine the intensity variation for TRI thermogram and the band-shift measurements.

Characterization: A thermogravimetric analyzer (Perkin−Elmer TGA6) was used to record the thermogram in the temperature range from 25 to 600 °C with a heating rate of 5 °C·min^{-1} in a flow of air at 20 mL·min^{-1}. The DSC thermogram of the same sample was recorded with a Setaram DSC131 in a crimped aluminum crucible in the temperature range from 25 to 550 °C with a heating rate of 5 °C·min^{-1} in a flow of air at 30 mL·min^{-1}. Fourier transform infrared spectroscopy was carried out with a Bomem Hartmann & Braun (MB-series) spectrometer. The X-ray diffraction patterns of the product were measured with a Material Analysis and Characterization (MAC) advanced powder X-ray diffractometer using Cu-$K_{\alpha 1}$ radiation (1.54056 Å). Positive TOF SIMS (ION-TOF) measurements were performed using pulsed Ga^+ ions (15 keV) and a post-acceleration of 10 kV. The analysis area of 100 μm × 100 μm with data acquisition time of 200 s was used for static TOF-SIMS conditions. The best resolution obtained was $M/\Delta M \approx 8000$. The powders were pressed on to the carbon tape supported on a clean Si wafer. Excess particles were removed by blowing with compressed air such that the layer thickness was minimal. The particle morphology was studied by transmission electron microscopy (TEM) (Philips, Tecnai 20) working at a 200 kV accelerating voltage. A drop of sample suspension, which had been previously dispersed in methanol by ultrasonication, was placed on the microgrid and dried before microscopy study. The elemental composition of the material was analyzed by energy-dispersive X-ray analysis (EDS) (Philips, Tecnai 20).

 © 2004 Wiley-VCH Verlag GmbH & Co. KGaA, Weinheim

Acknowledgments

This work was supported by the National Science Council of the Republic of China (NSC91-2113-M007-056).

[1] [1a] R. K. Grasselli, *Handbook of Heterogeneous Catalysis* (Eds.: G. Ertl, H. Knözinger, J. Weitkamp), Wiley-VCH, Weinheim, **1997**, vol. 5. [1b]T. D. Snyder, G. C. Hill, Jr., *Catal. Rev. Sci. Eng.* **1989**, *31*, 43−95. [1c] R. K. Grasselli, J. D. Burrington, J. F. Brazdil, *Faraday Discuss. Chem. Soc.* **1982**, *72*, 203−223.
[2] C. N. Satterfield, *Heterogeneous Catalysis in Industrial Practice*, McGraw Hill, New York, **1991**.
[3] [3a] J. L. Callahan, R. K. Grasselli, E. C. Milberger, H. A. Strecker, *Ind. Eng. Chem. Prod. Res. Develop.* **1970**, *9*, 134−142. [3b] J. M. M. Millet, H. Ponceblanc, G. Coudurier, J. M. Herrmann, J. C. Vedrine, *J. Catal.* **1993**, *142*, 381−391.
[4] [4a] B. C. Gates, J. R. Katzer, G. C. A. Schuit, *Chemistry of Catalytic Processes*, McGraw Hill, New York, United States **1979**, chapter 4. [4b] G. W. Keulks, L. D. Krenzke, T. M. Notermann, *Adv. Catal.* **1978**, *27*, 183−225. [4c] R. K. Grasselli, J. D. Burrington, *Adv. Catal.* **1981**, *30*, 133−163. [4d] Y. Moro-Oka, W. Ueda, *Adv. Catal.* **1994**, *40*, 233−273. [4e] M. M. Bettahar, G. Costentin, L. Savary, J. C. Lavalley, *Appl. Catal. A.* **1996**, *145*, 1−48.
[5] K. T. Li, W. D. Cheng, *Appl. Catal. A: Gen.* **1996**, *142*, 315−326.
[6] R. N. Vannier, F. Abraham, G. Nowogrocki, G. Mairesse, *J. Solid State Chem.* **1999**, *142*, 294−304.
[7] V. Marinova, M. Veleva, *Opt. Mater.* **2002**, *19*, 329−333.
[8] D. K. Biegelsen, T. Chen, J. C. Zesch, *J. Appl. Phys.* **1975**, *46*, 941−942.
[9] K. Y. Kang, P. H. Her, M. S. Jang, H. K. Kim, H. L. Park, D. Finotello, M. H. W. Chan, *Solid State Commun.* **1988**, *67*, 723−724.
[10] T. Sekiya, A. Tsuzuki, Y. Torii, *Mater. Res. Bull.* **1985**, *21*, 601−608.
[11] N. Hykaway, W. M. Sears, R. F. Frindt, S. R. Morrison, *Sens. Actuators* **1988**, *15*, 105−118.
[12] F. D. Hardcastle, I. E. Wachs, *J. Phys. Chem.* **1991**, *95*, 10763−10772.
[13] M. R. Antonio, R. G. Teller, D. R. Sandstrom, M. Mehicic, J. F. Brazdil, *J. Phys. Chem.* **1988**, *92*, 2939−2944.
[14] [14a] A. F. Van den Elzen, G. D. Rieck, *Mater. Res. Bull.* **1975**, *10*, 1163−1168. [14b] Z. Wuzong, D. A. Jefferson, M. Alario-Franco, J. M. Thomas, *J. Phys. Chem.* **1987**, *91*, 512−514.
[15] F. Theobald, A. Laarif, A. W. Hewat, *Mater. Res. Bull.* **1985**, *20*, 653−665.
[16] L. T. Weng, P. Bertrand, O. Tirions, M. Devillers, *Appl. Surf. Sci.* **1996**, *99*, 185−196.
[17] D. J. Buttrey, D. A. Jefferson, J. M. Thomas, *Philos. Mag. A* **1986**, *53*, 897−906.
[18] I. Matsuura, R. Schut, K. Hirakawa, *J. Catal.* **1980**, *63*, 152−166.
[19] J. M. Stencel, *Raman Spectroscopy for Catalysis*, Van Nostrand Reinhold, New York, **1990**, vol. 2.
[20] T. Ono, N. Ogata, R. L. Kuczkowski, *J. Catal.* **1998**, *175*, 185−193.
[21] [21a] K. Nakamoto, *Infrared and Raman Spectra of Inorganic and Coordination Compounds*, 3rd ed, Wiley, New York, **1978**. [21b] L. Dixit, D. L. Gerrard, H. J. Bowley, *Appl. Spectrosc. Rev.* **1986**, *22*, 189−249.
[22] [22a] Ph. A. Batist, J. F. H. Bouwens, G. C. A. Schuits, *J. Catal.* **1972**, *25*, 1−11. [22b] B. Grzybowska, J. Haber, J. Komorek, *J. Catal.* **1972**, *25*, 25−32.
[23] J. D. Grunwaldt, M. D. Wildberger, T. Mallat, A. Baiker, *J. Catal.* **1998**, *177*, 53−59.
[24] I. VanDriessche, R. Mouton, S. Hoste, *Mater. Res. Bull.* **1996**, *31*, 979−992.
[25] F. Trifiro, H. Hoser, R. D. Scarle, *J. Catal.* **1972**, *25*, 12−24.
[26] D. J. Buttrey, T. Vogt, B. D. White, *J. Solid State Chem.* **2000**, *155*, 206−215.
[27] E. Godard, E. M. Gaigneaux, P. Ruiz, B. Delmon, *Catal. Today* **2000**, *61*, 279−285.
[28] W. W. Wendlandt, *Thermal Analysis*, 3rd ed., Wiley, New York, **1986**.
[29] [29a] H. Chang, P. J. Huang, *Anal. Chem.* **1997**, *69*, 1485−1491. [29b] A. Ghule, R. Murugan, H. Chang, *Inorg. Chem.* **2001**, *40*, 5917−5923. [29c] A. Ghule, R. Murugan, H. Chang, *Thermochim. Acta* **2001**, *371*, 127−135.
[30] Y. Murakami, H. Imai, *J. Mater. Sci. Lett.* **1990**, *10*, 107−108.
[31] S. Yinjie, Z. Aimin, *J. Radioanal. Nucl. Chem.* **1998**, *231*, 17−20.
[32] C. J. Serna, M. Ocana, J. E. Iglesias, *J. Chem. Phys.* **1987**, *C20*, 473−484.
[33] [33a] A. F. Van den Elzen, G. D. Rieck, *Acta Crystallogr., Sect. B* **1973**, *29*, 2433−2436. [33b] S. Miyazawa, A. Kawana, H. Koizumi, H. Iwasaki, *Mater. Res. Bull.* **1974**, *9*, 41−52.
[34] M. Cesari, G. Perego, A. Zazzetta, G. Manara, B. Notari, *J. Inorg. Nucl. Chem.* **1971**, *33*, 3595−3597.
[35] [35a] Y. H. Han, W. Ueda, Y. Moro-Oka, *Appl. Catal. A* **1999**, *176*, 11−16. [35b] N. Arora, G. Deo, I. E. Wachs, A. M. Hirt, *J. Catal.* **1996**, *159*, 1−13.
[36] P. Boutry, R. Montarnal, J. Wrzyszcz, *J. Catal.* **1969**, *13*, 75−82.
[37] S. V. Yanina, R. L. Smith, *J. Catal.* **2003**, *213*, 151−162.

Received August 28, 2003
Early View Article
Published Online March 5, 2004

 © 2004 Wiley-VCH Verlag GmbH & Co. KGaA, Weinheim

Linear Multinuclear Ru^{II} Photosensitizers

Simona Vaduvescu[a] and Pierre G. Potvin*[a]

Keywords: Ruthenium / Tridentate ligands / Bridging ligands / Electron transfer / Photochemistry

Four ditopic bridging ligands, containing 2,2′:6′,2′′-terpyridine and 2,6-dipyrazinylpyridine (dpp) metal-binding units attached through *p*- or *m*-phenylene linkages, have been incorporated into eight mono-, di- and trinuclear linear Ru^{II} complexes. These were characterized by UV/Vis spectroscopy and cyclic voltammetry, and by their ability to undergo light-induced electron transfers to methylviologen. The dpp-bearing complexes were more difficult to prepare but were superior sensitizers, a fact attributable to longer excited state lifetimes and an electrostatically favored reductive quenching pathway.

(© Wiley-VCH Verlag GmbH & Co. KGaA, 69451 Weinheim, Germany, 2004)

Introduction

Ruthenium(II)−polypyridine complexes act as light absorption sensitizers,[1] a characteristic that can be put to use in solar energy conversion and storage applications. A critical limitation on the photo-responsiveness is the concentration of the sensitizer's excited state that can be achieved, and this notably depends on the excited state lifetime (τ) and on the extinction coefficient (ε) for the metal-to-ligand charge transfer (MLCT) absorption that leads to the excited state. One approach to improving the photoactivity is to increase the number of metal atoms in the sensitizer and the probability of light absorption. Dendritic assemblies epitomize this idea,[2] but electrostatic considerations make them unattractive because their globular structures and high charges would impede electron transfers to positively charged acceptors, such as methylviologen (MV^{2+}), and/or, in the case of neutral or anionic acceptors, would facilitate the energy-wasting reverse electron transfer that regenerates the initial states. The effect of charge repulsion can be minimized with linear multinuclear arrays, where an end-on approach by an electron acceptor is minimally affected by repulsions from the more distal metal centers. Hence, the electrostatics can be relatively insensitive to the sensitizer chain length while the light absorption would increase with chain length.

We have recently communicated the preparation and characterization of a linear trinuclear Ru^{II} complex in which the "back-to-back" bis(terpy) ligand **A** bridges the metal centers. This material was assessed as a photosensitizer relative to the mono- and dinuclear analogues.[3] In the above-mentioned report, the assessment used measurements of the rates of formation of the methylviologen radical cation ($MV^{\cdot+}$) from methylviologen (MV^{2+}) in CH_3CN in the presence of a sacrificial reductant (triethanolamine) according to a set protocol.[4] Comparisons were also made with $[Ru(\mathbf{ttpy})_2]^{2+}$ (**ttpy** = 4′-*p*-tolyl-2,2′:6′,2′′-terpyridine), a related complex of known τ (0.95 ns in CH_3CN).[5] This paper provides full details of that work and extends it by exploring the photoactivity of several new complexes of related bridging ligands, namely the *meta* isomer of **A** (ligand **B**) and the dipyrazinylpyridine (dpp) analogues of **A** and **B** (ligands **C** and **D**). It was anticipated that the *meta* linkages

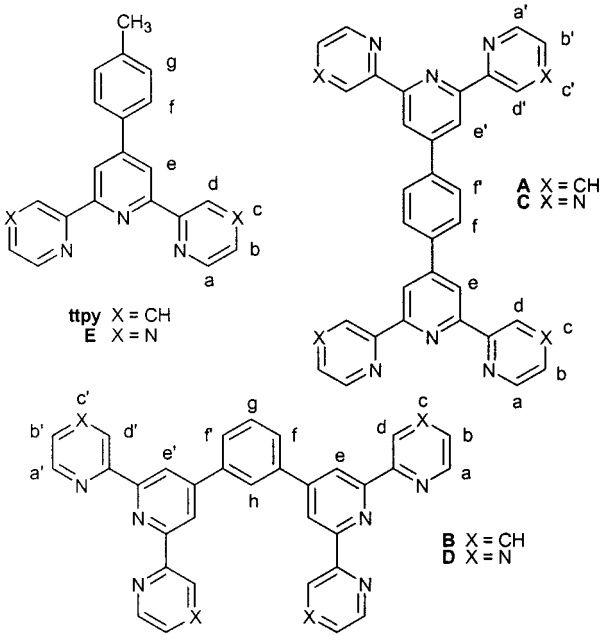

[a] Department of Chemistry, York University,
4700 Keele Street, Toronto, ON M3J 1P3, Canada
Fax: (internat.) + 1-416-736-5936
E-mail: pgpotvin@yorku.ca
Supporting information for this article is available on the WWW under http://www.eurjic.org or from the author.

of **B** and **D** would enable electrostatically easier access, by MV^{2+}, to the areas between metal atoms in di- and trinuclear complexes and to the central metal atoms in trinuclear cases, while the dpp ligands would be expected to promote longer τ values.[6]

Results and Discussion

Synthesis

Bis(terpyridine) **A** is known, and has been prepared by two routes.[7,8] We prepared it by the one-pot method developed for the synthesis of dpp ligands,[6] and recently applied this to other terpy-based materials.[9] In this remarkable reaction, a total of seven reactant molecules condense and expel six molecules of H_2O, then undergo two cycles of aerial dehydrogenation. The isolated yield (39%) was entirely similar to those of the previous preparations but with less effort and in less time. The linkage isomer **B** was produced under the same conditions from isophthalaldehyde and in a similar yield (37%).[10] Its X-ray crystal structure showed a lack of co-planarity consistent with the absence of a resonance pathway of communication between terpy units. Its NMR spectra showed a single set of pyridine signals, which implies free rotation about the terpy-to-linker bonds. A useful spectroscopic marker for the complexes of **A** and **B** was the most downfield ^{1}H NMR signal, i.e. the singlet from the central pyridine 3′/5′-H (at δ = 8.83 ppm in free **A**; δ = 8.84 ppm in free **B**).

By similar reactions with acetylpyrazine, the bis(dpp) ligands **C** and **D** were obtained in isolated yields of 42% and 37%, respectively. Those materials are soluble only in trifluoroacetic acid (TFA) and could not be properly recrystallized. Their NMR spectra in [D]TFA were inconclusive, but their identities were confirmed by EI-MS and, for **C**, by conversions to Ru^{II} complexes (see below).

The monotopic **ttpy** was used as a terminal ligand. It could also be prepared by the one-pot method from acetylpyridine and *p*-tolualdehyde in 46% yield after recrystallization, while a 70% yield was obtained by our earlier, two-step method.[11]

[Ru(**ttpy**)Cl_3][12] was activated with $AgBF_4$,[13] then treated with 1 equiv. of **A** to form [(**ttpy**)Ru(**A**)]$(PF_6)_2$ in 70% yield, after chromatography and anion exchange. In contrast, [Ru(**A**)$_2$]$(PF_6)_2$ was obtained in only 40% yield, by treatment of $RuCl_3$ with 2 equiv. of **A**; 2 equiv. of [(**ttpy**)Ru(**A**)]$(PF_6)_2$ and 1 equiv. of $RuCl_3$ were heated in 1,2-ethanediol to form the trinuclear complex [(**ttpy**)Ru(**A**)Ru(**A**)-Ru(**ttpy**)]$(PF_6)_6$ in 87% yield, after anion exchange and recrystallization. The dinuclear analogue [(**ttpy**)Ru(**A**)-Ru(**ttpy**)]$(PF_6)_4$ was needed for comparative purposes. It is a known species[14] which we prepared from 2 equiv. of $AgBF_4$-activated [(**ttpy**)$RuCl_3$] and **A** in a yield of 19% (not optimized), after anion exchange, chromatography and a second cycle of anion exchange.

^{1}H and COSY NMR spectroscopy were used to confirm the structures. Complexation was indicated by a strong upfield migration of the doublets from 6-H, which juts out above the plane of the perpendicular ligand and experiences the effect of its ring current. Two sets of terpy signals were obtained with [Ru(**A**)$_2$]$(PF_6)_2$, including singlets for 3′/5′-H at δ = 9.14 ppm and 8.98 ppm for the complexed and free terpy units, respectively, and the phenylene singlet of **A** was replaced by a pair of doublets in this less symmetrical species. Though [(**ttpy**)Ru(**A**)]$(PF_6)_2$ has been previously reported,[15] it was characterized only by NMR spectroscopy. Here, three sets of partially overlapping terpy signals were evident, including three distinct 3′/5′-H singlets at δ = 9.12, 9.02 and 8.97 ppm for bound **A**, **ttpy** and free **A** terpyridine units, respectively, as well as phenylene doublets. With the trinuclear complex [(**ttpy**)Ru(**A**)Ru(**A**)Ru(**ttpy**)]$(PF_6)_6$, three sets of terpy ^{1}H NMR signals were expected but the majority overlapped considerably, reflecting the similarities in the three ligand environments, including those from the phenylene spacer, which appeared together as one large singlet. However, the three distinct central pyridine 3′/5′-H singlets at lowfield positions (δ = 9.23, 9.21 and 9.06 ppm) confirmed the lack of symmetry and metal coordination. [(**ttpy**)Ru(**A**)Ru(**ttpy**)]$(PF_6)_4$ showed only two sets of terpy signals reflecting the higher symmetry, including a phenylene singlet and 3′/5′-H singlets at δ = 9.19 and 9.05 ppm for metal-bound terpy units of **A** and **ttpy**, respectively.

An entirely analogous sequence from the *m*-linked ligand **B** led to PF_6^- salts of [(**ttpy**)Ru(**B**)]$^{2+}$, [(**ttpy**)Ru(**B**)Ru(**B**)-Ru(**ttpy**)]$^{6+}$ and [(**ttpy**)Ru(**B**)Ru(**ttpy**)]$^{4+}$. The yields were slightly lower than in the *p*-linked cases (65%, 70% and 17%, respectively). In the latter preparation, we found that [Ru(**ttpy**)$_2$]$^{2+}$ was a contaminant, presumably arising from a ligand exchange process. This contaminant and the reduced yields imply some resistance to coordinate to **B**, in comparison with **A**, perhaps due to steric encumbrance or increased repulsions between metal centers. The dinuclear [(**ttpy**)Ru(**B**)Ru(**ttpy**)]$^{4+}$ also appeared as a side-product in the preparation of [(**ttpy**)Ru(**B**)]$^{2+}$ and necessitated chromatographic purification. The ^{1}H NMR spectra of the **B** complexes were very similar to those of the **A** series, except for the singlet-doublet-triplet pattern from the *m*-phenylene linkage, and showed only one set of pyridine signals per distinct terpy unit, again consistent with free rotation of the terpy units about the linkage.

The reactions with the pyrazine-containing ligands were less straightforward. Attempted preparation of [(**ttpy**)Ru(**C**)]$^{2+}$ from (**ttpy**)$RuCl_3$ and **C** in ethane-1,2-diol produced only the ligand-exchange product [Ru(**ttpy**)$_2$]$^{2+}$, owing to the poor solubility of **C**. Using TFA as a co-solvent was helpful, and the best solvent found was a TFA/ethane-1,2-diol (5:1) mixture that led to a 70% yield of [(**ttpy**)Ru(**C**)]$(PF_6)_2$ after anion exchange and chromatography. The ^{1}H NMR spectra differ from those of the all-terpy series in that the lowest field signals are now due to the pyrazinyl 3/3′′-H instead of the pyridine 3′/5′-H. The pyrazinyl 5-H and 6-H are weakly coupled but COSY spectroscopy revealed a long-range W-coupling between 3-H and 5-H. The dinuclear species [(**ttpy**)Ru(**C**)Ru(**ttpy**)]$(PF_6)_4$ was obtained in 20% yield from Ag^+-activated [(**ttpy**)$RuCl_3$]

 © 2004 Wiley-VCH Verlag GmbH & Co. KGaA, Weinheim

and **C** in a mixture of TFA and ethane-1,2-diol. Chromatography was required to separate the desired material from the now abundant $[Ru(\mathbf{ttpy})_2]^{2+}$ impurity. The ^1H NMR spectrum was similar to that of the mononuclear analogue, simplified by symmetry, and COSY spectroscopy was used to identify one pyrazinyl 3-H singlet, two pyridine 3′/5′-H singlets and one phenylene singlet, all consistent with the structure. Unfortunately, all attempts at preparing the trinuclear analogue failed, producing only a brown-black, paramagnetic material. Similarly, all complexation reactions with ligand **D** failed as well. Treatment of $[(\mathbf{ttpy})RuCl_3]$ with 1 equiv. of **D** also produced a paramagnetic product. With 0.5 equiv., $[Ru(\mathbf{ttpy})_2]^{2+}$ was the major product and the desired dinuclear species was only a minor constituent detectable by NMR spectroscopy and ESI-MS. It became obvious that the *m*-phenylene linkage and the lower basicity of dpp units, relative to terpy, decreased the reactivity of the ligand. An alternate route was attempted to circumvent the latter problem. Treatment of $RuCl_3$ with 0.5 equiv. of **D** in EtOH provided a brown-black precipitate, putatively $[Cl_3Ru(\mathbf{D})RuCl_3]$, but treatment of this with **ttpy** in ethane-1,2-diol to produce the dinuclear compound led to $[Ru(\mathbf{ttpy})_2]^{2+}$ as the only detectable product.

As is common with aromatic materials and Ru complexes, elemental analyses often return correct H compositions but low C and/or N compositions, even in the presence of extra oxidation catalyst, presumably due to incomplete combustion and/or the formation of stable carbides and nitrides. Mass and isotopic distribution analyses (ESI, MALDI or high resolution MALDI) were used to confirm the structural assignments. Fortunately, the precipitation of PF_6^- salts enabled purification, which was made evident by chromatographic homogeneity and the absence of extraneous NMR peaks.

UV/Vis Spectroscopy

The electronic spectra of all complexes in CH_3CN showed intense π-π* bands below 350 nm and MLCT bands ($\lambda_{max.}$) at 490−500 nm, reported in Table 1, in complete analogy with $[Ru(\mathbf{ttpy})_2]^{2+}$.[16] In addition, the complexes of **C** showed shoulders near 450 nm. With the *p*-linked ligands **A** and **C**, the position of $\lambda_{max.}$ drifted slightly toward the red with an increasing number of metal centers, while $\lambda_{max.}$ remained constant with the *m*-linked ligand **B**. Relative to $[Ru(\mathbf{ttpy})_2]^{2+}$, each added dpp or terpy unit and each added metal center constitutes an electron-withdrawing group. The drift with a *p*-linkage is likely a result of electron withdrawal on the ligands' π systems and stabilization of the ligand π* orbitals, relative to the metal-centered orbitals. The lack of such a drift with the *m*-linkage is probably owing to the absence of a resonance path for electronic transmission, and the 2 nm shift in $\lambda_{max.}$ with $[(\mathbf{ttpy})Ru(\mathbf{B})]^{2+}$ then represents the inductive contribution of an added terpy unit. At the same time, the ε values grew upon increasing the number of metal atoms, as expected. It is interesting to note that the ε values of all the mononuclear complexes $[(\mathbf{ttpy})RuL]^{2+}$ (L = **A**−C) are larger than for the homoleptic case, where L = **ttpy**. This is even more pronounced with the homoleptic $[Ru(\mathbf{A})_2]^{2+}$ ($\lambda_{max.}$ = 496 nm, ε = 42700 $M^{-1}\cdot cm^{-1}$). Because the MLCT $\lambda_{max.}$ values are all of lower energies than with $[Ru(\mathbf{ttpy})_2]^{2+}$, it is reasonable to conclude that the bridging ligands have lower π* orbital energies than does the terminal ligand **ttpy**, and are therefore the repositories of the excited electron density.

Electrochemistry

The results of cyclic voltammetry are also reported in Table 1. As is typical for complexes of this nature,[14,17] the new complexes show single reversible oxidation waves at potentials that are practically insensitive to chain length and at least two reduction waves that are somewhat less constant. Owing to their additional nitrogen atoms, the two complexes of **C** show particularly positive $E(Ru^{III/II})$ potentials, lying between the value for the homoleptic dpp complex $[Ru(\mathbf{E})_2]^{2+}$ (+1.62 V)[6] and that for the bis(terpy) complex $[Ru(\mathbf{ttpy})_2]^{2+}$ (+1.25 V).[18] The first reduction potentials of the new complexes are all positive compared with that of $[Ru(\mathbf{ttpy})_2]^{2+}$. Along with the spectroscopic evidence, this suggests that reduction adds an electron to the bridging ligands, rather than to the terminal **ttpy** whose π* orbital is evidently at a higher energy.

In accordance with the more negative reductions of the terpy-based ligands, we can assign the first and second reduction waves shown by the complexes of **C** to reductions

Table 1. Key spectroscopic, electrochemical and photochemical data

Compound[a]	$\lambda_{max.}$ [nm]	ε [104 $M^{-1}\cdot cm^{-1}$]	E_{ox} [V vs. SCE]	E_{red} [V vs. SCE]	k_f [10^{-5} s^{-1}]	k_q [10^{-3} s^{-1}]	χ [mM]	$\Delta G^{\ddagger}_{FET}$ [eV]	$\Delta G^{\ddagger}_{RET}$ [eV]
$[(\mathbf{ttpy})_2Ru]^{2+}$	490[b]	1.55[b]	1.25[c]	−1.24,[c] −1.42[d]	1.12(1)[e]	8.8(6)[e]	11(4)[e]	0.24	0.22
$[(\mathbf{ttpy})Ru(\mathbf{A})]^{2+}$ [f]	496	3.27	1.27	−1.18, −1.42	1.93(18)	7.4(9)	26(4)	0.25	0.23
$[\{(\mathbf{ttpy})Ru\}_2\mathbf{A}]^{4+}$ [f]	502	5.98	1.27[g]	−1.18, −1.45[g]	1.086(2)	2.40(16)	45(3)	0.29	0.25
$[\{(\mathbf{ttpy})Ru(\mathbf{A})\}_2Ru]^{6+}$ [f]	504	7.33	1.27	−1.03, −1.23	1.339(5)	3.67(1)	36.3(2)	0.32	0.26
$[(\mathbf{ttpy})Ru(\mathbf{B})]^{2+}$	492	2.61	1.28	−1.22, −1.44	1.01(5)	2.5(3)	40(5)	0.25	0.23
$[\{(\mathbf{ttpy})Ru\}_2\mathbf{B}]^{4+}$	492	3.70	1.28	−1.18, −1.45	1.98(4)	4.2(3)	47(3)	0.30	0.25
$[\{(\mathbf{ttpy})Ru(\mathbf{B})\}_2Ru]^{6+}$	492	6.96	1.28	−1.18, −1.37	0.95(3)	3.79(11)	25(1)	0.33	0.27
$[(\mathbf{ttpy})Ru(\mathbf{C})]^{2+}$	456, 504	1.48, 2.01	1.48	−0.86, −1.25, −1.65	3.48(2)	7.0(3)	50(2)	0.38	0.32
$[\{(\mathbf{ttpy})Ru\}_2\mathbf{C}]^{4+}$	454, 506	2.54, 3.33	1.49	−0.85, −1.25, −1.65	2.31(13)	4.7(13)	49(13)	0.42	0.34

[a] Uncertainties in least significant digits appear in brackets. [b] From Mikel and Potvin.[16] [c] From Kalyanasundaram et al.[18] [d] In DMSO, from Constable et al.[31] [e] From Potvin et al.[4] [f] From Vaduvescu and Potvin.[3] [g] From Collin et al.[14]

 © 2004 Wiley-VCH Verlag GmbH & Co. KGaA, Weinheim

of the relatively electron-poor bridging and electron-rich terminal ligands, respectively. Since $E(Ru^{III/II}) - E(L^{0/-})$ is known to correlate with the MLCT energy,[19] the higher-energy MLCT bands of the **C** complexes can then be assigned to Ru→**ttpy** transitions, and the lower-energy bands to Ru → **C** transitions. With these pairings, the correlation is fairly good ($r^2 > 0.92$).

Photochemistry

Under visible light irradiation and in the presence of triethanolamine (TEOA) as a sacrificial reductant, Ru^{II} complexes are able to generate the methylviologen radical cation ($MV^{\cdot+}$) from methylviologen (MV^{2+}) to different degrees. In real-life photoredox applications, there would be no sacrificial donor present, but the excited state could be reductively quenched at an electrode surface or by a reversibly reduced electron relay molecule such as MV^{2+} at an illuminated organic-aqueous interface. Comparisons between sensitizers in terms of the kinetic parameters governing this process have previously enabled us to probe steric, electrostatic and solvent effects on activity,[16,20,21] and we wished, in the present work, to probe the effect of increasing the Ru chain length *N*. Using our standard protocol,[4] we measured the time courses of $MV^{\cdot+}$ development at room temperature in CH_3CN at 600 nm with a sensitizer concentration of 4×10^{-5} M. The key results presented in Table 1 are the first-order rate constants k_f and k_q for $MV^{\cdot+}$ formation and anaerobic quenching, respectively, and the anaerobic yields χ, given by $k_f[MV^{2+}]_0/(k_f + k_q)$. The usual mechanism is oxidative quenching of the excited state of the sensitizer ($Ru^{II*} + MV^{2+} \rightarrow Ru^{III} + MV^{\cdot+}$) followed by reverse electron transfer to (quenching of) $MV^{\cdot+}$ ($Ru^{III} + MV^{\cdot+} \rightarrow Ru^{II} + MV^{2+}$), or competitive trapping ($Ru^{III} + TEOA \rightarrow Ru^{II} + TEOA^{\cdot+}$) which allows $MV^{\cdot+}$ to accumulate. Additionally, Table 1 reports estimates of $\Delta G^{\ddagger}_{FET}$ and $\Delta G^{\ddagger}_{RET}$, the Marcus activation energies for the forward and reverse electron transfers, respectively, for end-on approaches by $MV^{2+/\cdot+}$ to the terminal metals. Their computations and the values for electrostatically less favorable approaches are detailed in the Supporting Information (see also the footnote on the first page of this article).

All of the new complexes are better sensitizers than $[Ru(\mathbf{ttpy})_2]^{2+}$,[4] with higher k_f and χ values. This may reflect generally longer τ values owing to a greater π-delocalization and π^* stabilization in the bridging ligands which, as discussed earlier, are the preferred sites for the excited electrons. Clearly, there is variation between the **A** and **B** series, in spite of similarities in structures, properties (E_{ox}, E_{red}, λ, ε/N) and even $\Delta G^{\ddagger}$ values. Part of the success of $[\{(\mathbf{ttpy})Ru\}_2\mathbf{B}]^{4+}$ relative to the **A** analogue may be due to easier access to the areas between the metal atoms, but this advantage does not appear to carry forward to the trinuclear case.

Because of similar properties *within* a ligand series and virtually identical structures at the metal termini, we can make the a priori assumption that the differences in sensitizer activities within a series should be largely electrostatic and not photophysical in origin, an assumption which our results should confirm or deny. The constant k_f incorporates the concentration of excited state species (Ru^{II*}) and will depend on $\Delta G^{\ddagger}_{FET}$, which contains the electrostatic barrier to the forward electron transfer which increases with increasing *N*, while k_q incorporates the concentration of the Ru^{III} photoproduct and depends on $\Delta G^{\ddagger}_{RET}$, which contains the corresponding electrostatic barrier. The constants k_q and k_f, however, are linked because a higher k_f leads to a higher concentration of Ru^{III} and therefore a higher k_q. Both, then, also depend on the photophysical properties that govern the production of Ru^{II*}, including ε and τ. However, the ratio k_q/k_f ($= [MV^{2+}]_0/\chi - 1$) was previously shown to equal $k_r[MV^{2+}]_0/k_t[TEOA]_0$,[4] where k_r and k_t are the second-order rate constants for the reactions of the Ru^{III} photoproduct with the $MV^{\cdot+}$ co-product (reverse electron transfer) and with TEOA (trapping), respectively. This ratio is therefore a measure of the competition between the non-productive and productive fates of the Ru^{III} form of the sensitizer. The first constant, k_r, will vary within a series according to $\exp(-\Delta G^{\ddagger}_{RET})$, while k_t involves encounters with the neutral TEOA and should remain constant within a series. Hence, if the sensitizers within a series only differed in electrostatic terms, k_q/k_f should steadily decrease as $\Delta G^{\ddagger}_{RET}$ steadily increases with *N*. The values in Table 1 reveal that this is not so, with $[\{(\mathbf{ttpy})Ru\}_2\mathbf{A}]^{4+}$ and $[\{(\mathbf{ttpy})Ru(\mathbf{B})\}_2Ru]^{6+}$ being particularly outstanding. Moreover, k_f should vary with $\varepsilon \exp(-\Delta G^{\ddagger}_{FET})$, but $\ln(k_f/\varepsilon)$ does not uniformly decrease as $\Delta G^{\ddagger}_{FET}$ increases. These findings imply that the sensitizers within a series also differ in their photophysical characteristics, such as τ, orbital overlap, approach geometry or approach distance, which this study cannot probe. Nevertheless, Table 1 identifies the most effective sensitizers $[\{(\mathbf{ttpy})Ru(\mathbf{A})\}_2Ru]^{6+}$, $[\{(\mathbf{ttpy})Ru\}_2\mathbf{B}]^{4+}$, and especially the two complexes of **C**, as meriting further study.

The two **C**-containing complexes show higher activities in spite of having the highest barriers $\Delta G^{\ddagger}_{FET}$. They probably benefit from longer τ values than the all-terpy complexes of **A** and **B** because the first dpp complex, $[Ru(\mathbf{E})_2]^{2+}$, showed a longer τ (18 ns at 667 nm)[6] than its terpy analogue $[Ru(\mathbf{ttpy})_2]^{2+}$ (0.95 ns at 640 nm).[22] In addition, the redox potentials for the **C**-containing complexes lie about 0.2 V more positive of those of the other complexes and this is probably sufficient to enable reductive quenching (formally $Ru^{II*} + TEOA \rightarrow Ru^{I} + TEOA^{\cdot+}$), as was the case in other complexes with high E_{ox} values.[23–25] Reductive quenching has an electrostatic advantage over oxidative quenching because it involves initial encounters with neutral TEOA instead of cationic MV^{2+}, and because the wasteful reverse electron transfer (formally $Ru^{I} + TEOA^{\cdot+} \rightarrow Ru^{II} + TEOA$) is electrostatically disfavored relative to the forward reaction, whereas the opposite is true in oxidative quenching ($Ru^{III} + MV^{\cdot+} \rightarrow Ru^{II} + MV^{2+}$). Moreover, the $TEOA^{\cdot+}$ by-product can be deprotonated in an alkaline medium ($TEOA^{\cdot+} \rightarrow H^+ + H_{-1}TEOA^{\cdot}$) to generate a reducing species[26] that is depleted by O_2.[4] This consumption of $TEOA^{\cdot+}$ further reduces the probability of reverse electron transfer, thereby leaving more of the re-

 © 2004 Wiley-VCH Verlag GmbH & Co. KGaA, Weinheim

duced form of the sensitizer able to produce $MV^{\cdot+}$ (Ru^{I} + $MV^{2+} \rightarrow Ru^{II}$ + $MV^{\cdot+}$) in electrostatically more favorable encounters than is the case in oxidative quenching. These combined electrostatic advantages would contribute to a faster net accumulation of the ultimate photoproduct, $MV^{\cdot+}$, as witnessed with ligand **C**.

Conclusion

Ditopic bridging ligands can be assembled in a one-pot reaction and incorporated into short, linear multinuclear assemblies that act as photosensitizers in spite of electrostatic repulsions. The photochemical experiments have identified $[\{(\mathbf{ttpy})Ru(\mathbf{A})\}_2Ru]^{6+}$, $[\{(\mathbf{ttpy})Ru\}_2\mathbf{B}]^{4+}$ and both complexes of **C** as candidates for photophysical studies, in order to elucidate the origins of the difference in behavior between the **A** series and the **B** series and the origin of the better activity for the **C** series. However, the dpp-containing ligands **C** and **D** were fraught with solubility and reactivity problems that need to be addressed. An obvious improvement to the general design is to add negatively charged groups to the peripheries which can constitute binding sites for positively charged electron acceptors such as MV^{2+} since this has proven to be of great benefit in mononuclear species.[21] However, the ideal linear multinuclear sensitizer will absorb light anywhere along the chain and relay the excited electron to the ends (the so-called antenna effect), where electrostatic repulsions with acceptors can be minimized. Another improvement would therefore be to use the most electron-poor ligands at the termini.

Experimental Section

General Remarks: NMR spectroscopic data were obtained with a Bruker AMX 400 MHz spectrometer in CD_3CN (unless indicated otherwise) at 25 °C and are reported relative to $SiMe_4$. The signal assignments were made on the basis of COSY spectra and use the position letters appearing in the structural diagrams. A Kratos Profile mass spectrometer was used for EI-MS acquisitions. MALDI-MS data were acquired with a Voyager-DE STR MALDI/TOF instrument and ESI-MS data with a Sciex Targa 6000E MS/MS system. High resolution MALDI-MS (HR-MALDI-MS) was performed by the McMaster Regional Center for Mass Spectrometry, Hamilton, ON, Canada with a Micromass TofSpec 2E instrument. UV/Vis spectra were obtained at room temperature with a Hewlett−Packard 8452A diode array spectrophotometer, with 10^{-5} M solutions in spectroscopic-grade solvents. Cyclic voltammetry was performed with a Cypress System three-electrode configuration consisting of a reference Ag/AgCl wire electrode and platinum wire working and auxiliary electrodes, using CH_3CN distilled from P_2O_5 and stored over 4-Å molecular sieves, in solutions containing 0.1 M n-Bu_4NPF_6. Half-wave potentials were calculated as the average of the cathodic and anodic peak potentials.[27] The current-scan rate dependence was evaluated for each sample to check the reversibility, and ferrocene was added at the end of each run as an internal reference (+0.425 V vs. SCE in CH_3CN).[28] Photochemical data were obtained using the apparatus and data treatment described earlier,[4] with stirred CH_3CN solutions containing the sensitizer (4×10^{-5} M), $MV(PF_6)_2$ (0.01 M) and triethanolamine (0.05 M). Reagents and spectroscopic-grade solvents (Sigma−Aldrich) were used directly. Anhydrous solvents were purchased in Sigma−Aldrich Sure-seal bottles. All other solvents were reagent-grade quality (Caledon Chemical Ltd.) and used directly. $[Ru(\mathbf{ttpy})Cl_3]$ was prepared in 71% yield by a literature method[12], with its identity verified by ESI-MS [m/z (%) = 531 (100)]. Thin-layer chromatography was used to monitor reactions and chromatography and was carried out on Macherey−Nagel Polygram Sil G/UV silica gel plates and Alox N/UV alumina plates. Column chromatography was performed employing silica gel (ca. 200−400 mesh, 60 Å) or neutral alumina (ca. 150 mesh, 58 Å), both from Sigma−Aldrich. Elemental analyses were performed by Guelph Chemical Laboratories Ltd., Guelph, ON, Canada.

4′-*p*-Tolyl-2,2′:6′,2"-terpyridine (ttpy): 2-Acetylpyridine (1.00 g, 8.3 mmol) was added to a solution of *p*-tolualdehyde (0.50 g, 4.2 mmol) in CH_3OH (32 mL). 15% aq. KOH (2.9 mL) and conc. NH_4OH (29 mL) were then added to the solution and vigorous stirring was maintained for 3 d. The yellow precipitate that formed was removed by vacuum filtration, washed with water to neutral pH and dissolved in $CHCl_3$ (40 mL). The solution obtained was washed with H_2O (3 × 30 mL). The organic fraction was dried with $MgSO_4$ and freed of solvent in vacuo. The residue was recrystallized from $CHCl_3/Et_2O$ to yield 0.61 g (46%) of **ttpy**, m.p. 168 °C. ^1H NMR ($CDCl_3$): δ = 8.77 (2 s, 4 H, *a* + *e*), 8.71 (d, $^3J_{H,H}$ = 8 Hz, 2 H, *d*), 7.92 (dd, 2 H, *c*), 7.87 (d, $^3J_{H,H}$ = 7.9 Hz, 2 H, *f*), 7.39 (dd, $^3J_{H,H}$ = 5 Hz, 2 H, *b*), 7.35 (d, $^3J_{H,H}$ = 7.9 Hz, 2 H, *g*), 2.46 (s, 3 H, CH_3) ppm. EI-MS: m/z (%) = 324 (100) [$M^{\cdot+}$], in agreement with the literature data.[11,29,30]

1,4-Bis(2,2′:6′,2"-terpyridin-4′-yl)benzene (A): The same procedure as for **ttpy** was applied, using 2-acetylpyridine (1.00 g, 8.3 mmol) and terephthalaldehyde (0.2764 g, 2.1 mmol) at reflux for 48 h. Recrystallization from $CHCl_3$ and CH_3OH yielded 0.4427 g of **A** (39%), m.p. > 300 °C. ^1H NMR ($CDCl_3$): δ = 8.83 (s, 4 H, *e*), 8.79 (d, $^3J_{H,H}$ = 4.2 Hz, 4 H, *a*), 8.74 (d, $^3J_{H,H}$ = 7.0 Hz, 4 H, *d*), 8.09 (s, 4 H, *f*), 7.92 (dd, $^3J_{H,H}$ = 7.0 Hz, 4 H, *c*), 7.39 (dd, $^3J_{H,H}$ = 4.2 Hz, 4 H, *b*) ppm. MALDI-MS: m/z (%) = 541 (100) [M^+]. $C_{36}H_{24}N_6$ (540.6): calcd. C 79.98, H 4.47, N 15.54; found C 79.57, H 4.73, N 12.31.

1,4-Bis(2,6-dipyrazinylpyridin-4-yl)benzene (C): A mixture of acetylpyrazine (500 mg, 4.1 mmol) and terephthalaldehyde (135 mg, 1.0 mmol) in CH_3OH (50 mL) containing 15% aq. KOH (1.2 mL) and conc. NH_4OH (11.5 mL) was vigorously stirred while heating to reflux for 48 h. The precipitate formed was removed by vacuum filtration and washed with water to neutral pH. The compound proved to be soluble only in TFA and insoluble in all common organic solvents. It was dried under vacuum and a yield of 42% (0.2285 g) was obtained, m.p. > 300 °C. EI-MS: m/z (%) = 545 (100) [M^+]. $C_{32}H_{20}N_{10}$ (544.6): calcd. C 70.58, H 3.70, N 25.72; found C 69.90, H 3.80, N 25.10.

1,3-Bis(2,6-dipyrazinylpyridin-4-yl)benzene (D): The same procedure as for **C** with isophthalaldehyde produced 0.2013 g (37% yield) of **D**, which was similarly insoluble, m.p. > 300°C. EI-MS: m/z (%) = 545 (100) [M^+]. $C_{32}H_{20}N_{10}$ (544.6): calcd. C 70.58, H 3.70, N 25.72; found C 69.93, H 3.81, N 25.13.

$[Ru(A)_2](PF_6)_2$: A solution of **A** (80.0 mg, 0.15 mmol) in DMF (10 mL) was added to a solution of $RuCl_3 \cdot 3H_2O$ (19.4 g, 0.07 mmol) in DMF (10 mL) and the mixture was heated to reflux under Ar for 24 h. Addition of the cooled red solution to a saturated aqueous solution of NH_4PF_6 precipitated the product as a red solid. Purification by column chromatography (alumina; CH_3CN/satd. KNO_3/H_2O, 7:1:0.5, containing 1% $N(C_2H_5)_3$] pro-

 © 2004 Wiley-VCH Verlag GmbH & Co. KGaA, Weinheim

duced 41.2 mg (40%). ^{1}H NMR: δ = 9.14 (s, 4 H, *e*), 8.98 (s, 4 H, *e′*), 8.82 (m, 8 H, *a′*, *d′*), 8.74 (d, $^3J_{H,H}$ = 8 Hz, 4 H, *d*), 8.45 (d, $^3J_{H,H}$ = 7.8 Hz, 4 H, *f*), 8.36 (d, $^3J_{H,H}$ = 7.8 Hz, 4 H, *f′*), 8.10 (t, $^3J_{H,H}$ = 7 Hz, 4 H, *c′*), 8.01 (t, $^3J_{H,H}$ = 7 Hz, 4 H, *c*), 7.57 (m, 8 H, *b′*, *a*), 7.24 (t, $^3J_{H,H}$ = 7 Hz, 4 H, *b*) ppm. MALDI-MS: *m*/*z* (%) = 593 (100) [M^{2+}]. $C_{72}H_{48}F_{12}N_{12}P_2Ru$ (1472.3): calcd. C 58.74, H 3.29, N 11.42; found C 59.15, H 3.49, N 10.89.

[(ttpy)Ru(A)](PF$_6$)$_2$: A mixture of [Ru(**ttpy**)Cl$_3$] (55.0 mg, 0.1 mmol) and $AgBF_4$ (62.5 mg, 0.3 mmol) was heated to reflux in acetone (25 mL) for 3 h. The AgCl precipitate was filtered off and the volume of the resultant violet solution was halved under reduced pressure. DMF (15 mL) was added and the remaining acetone removed. The resultant solution was added to a pre-heated (80 °C) solution of **A** (84.0 mg, 0.15 mmol) in DMF (25 mL) and the mixture was heated to reflux under Ar for 2 h. The cooled red solution was added to a saturated aqueous solution of NH_4PF_6. The red precipitate was collected by vacuum filtration, washed with water (3 × 30 mL) and Et_2O (3 × 30 mL), and freed of solvent under vacuum. Column chromatography (alumina; CH_3CN/satd. KNO_3/H_2O, 31:2:1, containing 0.66% $N(C_2H_5)_3$] and re-precipitation (NH_4PF_6) afforded 87.8 mg (70% yield) of [(**ttpy**)Ru(**A**)](PF$_6$)$_2$. The ^{1}H NMR spectroscopic data are in agreement with literature data.[15] ESI-MS: *m*/*z* (%) = 483 (100) [M^{2+}]. $C_{58}H_{41}F_{12}N_9P_2Ru$ (1255.0): calcd. C 55.51, H 3.29, N 10.04; found C 55.86, H 3.50, N 9.77.

[(ttpy)Ru(B)](PF$_6$)$_2$: This complex was prepared by the same procedure as with **A**, using [Ru(**ttpy**)Cl$_3$] (55.0 mg, 0.1 mmol), $AgBF_4$ (62.5 mg, 0.3 mmol), DMF (10 mL), ligand **B**[10] (84.0 mg, 0.15 mmol) in DMF (15 mL), previously heated to 80 °C, and heating at reflux under Ar for 2 h. Workup, chromatography and re-precipitation (NH_4PF_6) as before afforded a yield of 65% (0.0816 g) of [(**ttpy**)Ru(**B**)](PF$_6$)$_2$. ^{1}H NMR: δ = 9.13 (s, 2 H, **B**-*e*), 9.00 (s, 4 H, **B**-*e′*, **ttpy**-*e*), 8.78 (m, 4 H, **B**-*a′*, **B**-*d′*), 8.70 (d, $^3J_{H,H}$ = 4.5 Hz, 2 H, **B**-*d*), 8.65 (d, $^3J_{H,H}$ = 8 Hz, 2 H, **ttpy**-*d*), 8.33 (m, 2 H, **B**-*f*/*f′*), 8.21 (m, 2 H, **B**-*g*, **B**-*h*), 8.12 (m, 4 H, **ttpy**-*f*, **B**-*c′*), 7.97 (m, 4 H, **B**-*c*, **ttpy**-*c*), 7.60 (m, 4 H, **ttpy**-*g*, **B**-*b′*), 7.45 (m, 4 H, **B**-*a*, **ttpy**-*a*), 7.21 (2 t, 4 H, **B**-*b*, **ttpy**-*b*), 2.54 (s, 3 H, CH_3) ppm. ESI-MS: *m*/*z* (%) = 482 (75) [M^{2+}]. $C_{58}H_{41}F_{12}N_9P_2Ru$ (1255.0): calcd. C 55.51, H 3.29, N 10.04; found C 55.86, H 3.49, N 9.68.

[(ttpy)Ru(C)](PF$_6$)$_2$: This complex was prepared by the same procedure as for **A**, using [Ru(**ttpy**)Cl$_3$] (112.0 mg, 0.2 mmol) and $AgBF_4$ (125.0 mg, 0.6 mmol) in acetone (40 mL), complete removal of the acetone, 1,2-ethanediol (15 mL) instead of DMF, **C** (170.0 mg, 0.3 mmol) in TFA (25 mL) and heating to reflux under Ar for 3 h. Workup, chromatography (CH_3CN/satd. KNO_3/H_2O, 50:2:1) and re-precipitation (NH_4PF_6) as before afforded a yield of 70% (0.1763 g) of [(**ttpy**)Ru(**C**)](PF$_6$)$_2$. ^{1}H NMR: δ = 9.99 (s, 2 H, **C**-*d′*), 9.91 (s, 2 H, **C**-*d*), 9.31 (s, 2 H, **C**-*e*), 9.03 (s, 2 H, **C**-*e′*), 8.97 (s, 2 H, **ttpy**-*e*), 8.79 (m, 4 H, **C**-*b′*, **C**-*a′*), 8.69 (d, $^3J_{H,H}$ = 7.7 Hz, 2 H, **ttpy**-*d*), 8.49 (d, $^3J_{H,H}$ = 8.5 Hz, 2 H, **C**-*f*), 8.39 (m, 4 H, **C**-*a*, **C**-*f′*), 8.16 (d, $^3J_{H,H}$ = 7 Hz, 2 H, **ttpy**-*f*), 8.02 (t, 2 H, **ttpy**-*c*), 7.62 (m, 4 H, **ttpy**-*g*, **C**-*b*), 7.41 (d, $^3J_{H,H}$ = 5 Hz, 2 H, **ttpy**-*a*), 7.23 (t, 2 H, **ttpy**-*b*), 2.58 (s, 3 H, CH_3) ppm. HR-MALDI-MS: *m*/*z* (%) = 969.237 (100); $[RuC_{54}H_{37}N_{13}]^{2+}$ requires 969.044. $C_{54}H_{37}F_{12}N_{13}P_2Ru$ (1259.0): calcd. C 51.52, H 2.96, N 14.46; found C 52.20, H 3.56, N 13.94.

[(ttpy)Ru(A)Ru(ttpy)](PF$_6$)$_4$: This complex was prepared by the same procedure as for [(**ttpy**)Ru(**A**)](PF$_6$)$_2$, using [Ru(**ttpy**)Cl$_3$] (53.0 mg, 0.1 mmol), $AgBF_4$ (77.5 mg, 0.3 mmol) in acetone (25 mL), DMF (10 mL), **A** (27.0 mg, 0.05 mmol) in DMF (10 mL), and heating at reflux under Ar for 3 h. Workup as before afforded a yield of 19% (18.7 mg) of [(**ttpy**)Ru**A**Ru(**ttpy**)](PF$_6$)$_4$. ^{1}H NMR: δ = 9.19 (s, 4 H, **A**-*e*), 9.05 (s, 4 H, **ttpy**-*e*), 8.78 (d, $^3J_{H,H}$ = 8 Hz, 4 H, **A**-*d*), 8.71 (d, $^3J_{H,H}$ = 8 Hz, 4 H, **ttpy**-*d*), 8.62 (s, 4 H, **A**-*f*), 8.17 (d, $^3J_{H,H}$ = 7.6 Hz, 4 H, **ttpy**-*f*), 8.03 (m, 8 H, **A**-*c*, **ttpy**-*c*), 7.64 (d, $^3J_{H,H}$ = 7.5 Hz, 4 H, **ttpy**-*g*), 7.51 (m, 8 H, **A**-*a*, **ttpy**-*a*), 7.26 (m, 8 H, **A**-*b*, **ttpy**-*b*), 2.58 (s, 6 H, CH_3) ppm. ESI-MS: *m*/*z* (%) = 348 (75) [M^{4+}].

[(ttpy)Ru(B)Ru(ttpy)](PF$_6$)$_4$: This complex was prepared by exactly the same procedure as for [(**ttpy**)Ru(**A**)Ru(**ttpy**)](PF$_6$)$_4$, using [Ru(**ttpy**)Cl$_3$] (52.6 mg, 0.1 mmol), $AgBF_4$ (79.3 mg, 0.3 mmol) and **B**[10] (28.0 mg, 0.05 mmol), affording a yield of 17% (16.7 mg) of [(**ttpy**)Ru(**B**)Ru(**ttpy**)](PF$_6$)$_4$. ^{1}H NMR: δ = 9.27 (s, 4 H, **B**-*e*), 9.02 (s, 4 H, **ttpy**-*e*), 8.80 (d, $^3J_{H,H}$ = 7.3 Hz, 4 H, **B**-*d*), 8.68 (d, $^3J_{H,H}$ = 8.3 Hz, 4 H, **ttpy**-*d*), 8.47 (m, 4 H, **B**-*f*, **B**-*g*, **B**-*h*), 8.13 (d, $^3J_{H,H}$ = 7.6 Hz, 4 H, **ttpy**-*f*), 7.99 (m, 8 H, **B**-*c*, **ttpy**-*c*), 7.60 (d, $^3J_{H,H}$ = 7.6 Hz, 4 H, **ttpy**-*g*), 7.48 (m, 8 H, **B**-*a*, **ttpy**-*a*), 7.23 (m, 8 H, **B**-*b*, **ttpy**-*d*), 2.55 (s, 6 H, CH_3) ppm. ESI-MS: *m*/*z* (%) = 347 (100) [M^{4+}]. $C_{80}H_{58}F_{24}N_{12}P_4Ru_2$ (1969.4): calcd. C 48.79, H 2.97, N 8.53; found C 48.24, H 3.45, N 8.45.

[(ttpy)Ru(C)Ru(ttpy)](PF$_6$)$_4$: This was prepared by the same procedure as for [(**ttpy**)Ru(**C**)](PF$_6$)$_2$, using [Ru(**ttpy**)Cl$_3$] (96.0 mg, 0.2 mmol) and $AgBF_4$ (130.0 mg, 0.6 mmol) in acetone (25 mL), ethane-1,2-diol (10 mL), and a solution of **C** (50.0 mg, 0.1 mmol) in TFA (5 mL) and ethane-1,2-diol (10 mL), with heating to reflux under Ar for 24 h in the presence of *N*-methylmorpholine (2 drops). Workup, chromatography (CH_3CN/satd. KNO_3/H_2O, 7:1:0.5), to remove the minor impurity of [Ru(**ttpy**)$_2$](PF$_6$)$_2$, and re-precipitation (NH_4PF_6) as before afforded a yield of 20% (39.5 mg) of [(**ttpy**)Ru(**C**)Ru(**ttpy**)](PF$_6$)$_4$. ^{1}H NMR: δ = 9.84 (s, 4 H, **C**-*d*), 9.34 (s, 4 H, **C**-*e*), 9.04 (s, 4 H, **ttpy**-*e*), 8.70 (d, $^3J_{H,H}$ = 8 Hz, 4 H, **ttpy**-*d*), 8.64 (s, 4 H, **C**-*f*), 8.41 (d, 4 H, **C**-*a*), 8.16 (d, $^3J_{H,H}$ = 7.9 Hz, 4 H, **ttpy**-*f*), 8.03 (t, $^3J_{H,H}$ = 7.5 Hz, 4 H, **ttpy**-*c*), 7.64 (m, 8 H, **C**-*b*, **ttpy**-*g*), 7.42 (d, $^3J_{H,H}$ = 5 Hz, 4 H, **ttpy**-*a*), 7.23 (t, $^3J_{H,H}$ = 6 Hz, 4 H, **ttpy**-*b*), 2.57 (s, 6 H, CH_3) ppm. HR-MALDI-MS: *m*/*z* (%) = 1393.297 (60), $[Ru_2C_{76}H_{54}N_{16}]^{4+}$ requires 1393.509. $C_{76}H_{54}F_{24}N_{16}P_4Ru_2$ (1973.4): calcd. C 46.26, H 2.76, N 11.36; found C 46.75, H 3.07, N 11.55.

[(ttpy)Ru(A)Ru(A)Ru(ttpy)](PF$_6$)$_6$: To a solution of $RuCl_3 \cdot 3H_2O$ (9.0 mg, 0.03 mmol) in ethane-1,2-diol (30 mL) was added [(**ttpy**)-Ru(**A**)](PF$_6$)$_2$ (90.0 mg, 0.07 mmol) and *N*-methylmorpholine (9 drops). Ths solution was heated to reflux under Ar for 24 h. The addition of the cooled red solution to a saturated aqueous solution of NH_4PF_6 precipitated the product as a red solid. Recrystallization using CH_3CN/Et_2O of the red solid yielded the desired pure product in 87% yield (75.8 mg). ^{1}H NMR: δ = 9.23 (s, 4 H, **A**-*e*), 9.21 (s, 4 H, **A**-*e′*), 9.06 (s, 4 H, **ttpy**-*e*), 8.79 (2 t, 8 H, **A**-*d*, **A**-*d′*), 8.71 (d, $^3J_{H,H}$ = 7.9 Hz, 4 H, **ttpy**-*d*), 8.64 (s, 8 H, **A**-*f*, **A**-*f′*), 8.17 (d, $^3J_{H,H}$ = 7.4 Hz, 4 H, **ttpy**-*f*), 8.03 (m, 12 H, **A**-*c*, **A**-*c′*, **ttpy**-*c*), 7.64 (d, $^3J_{H,H}$ = 7.4 Hz, 4 H, **ttpy**-*g*), 7.58 (d, $^3J_{H,H}$ = 5.3 Hz, 4 H, **A**-*a*), 7.52 (m, 8 H, **A**-*a′*, **ttpy**-*a*), 7.28 (m, 12 H, **A**-*b*, **A**-*b′*, **ttpy**-*b*), 2.58 (s, 6 H, CH_3) ppm. ESI-MS: *m*/*z* (%) = 339.2 (70) [M^{6+}]. $C_{116}H_{82}F_{36}N_{18}P_6Ru_3$ (2901.0): calcd. C 48.03, H 2.85, N 8.69; found C 47.52, H 2.89, N 7.89.

[(ttpy)Ru(B)Ru(B)Ru(ttpy)](PF$_6$)$_6$: The same procedure used for [(**ttpy**)Ru(**A**)Ru(**A**)Ru(**ttpy**)](PF$_6$)$_6$ was applied using [(**ttpy**)-Ru(**B**)](PF$_6$)$_2$ (100 mg, 0.07 mmol) and $RuCl_3 \cdot 3H_2O$ (11 mg, 0.03 mmol), to produce the desired pure product in 70% yield (61 mg). ^{1}H NMR: δ = 9.29 (s, 4 H, **B**-*e*), 9.27 (s, 4 H, **B**-*e′*), 9.05 (s, 4 H, **ttpy**-*e*), 8.81 (2 t, $^3J_{H,H}$ = 9.3 Hz, 8 H, **B**-*d*, **B**-*d′*), 8.71 (d, $^3J_{H,H}$ = 8 Hz, 4 H, **ttpy**-*d*), 8.54 (m, 4 H, **B**-*f*, **B**-*f′*), 8.16 (d, $^3J_{H,H}$ = 8 Hz, 4 H, **ttpy**-*f*), 8.02 (m, 16 H, **B**-*c*, **B**-*c′*, **ttpy**-*c*, **B**-*g*, **B**-*h*), 7.63

 © 2004 Wiley-VCH Verlag GmbH & Co. KGaA, Weinheim

(d, $^3J_{H,H}$ = 8 Hz, 4 H, **ttpy**-*g*), 7.58 (d, $^3J_{H,H}$ = 5 Hz, 4 H, **B**-*a*), 7.52 (m, 8 H, **B**-*a′*, **ttpy**-*a*), 7.30 (m, 12 H, **B**-*b*, **B**-*b′*, **ttpy**-*b*), 2.58 (s, 6 H, CH_3) ppm. ESI-MS: *m*/*z* (%) = 338.5 (70) [M^{6+}]. $C_{116}H_{82}F_{36}N_{18}P_6Ru_3{\cdot}2H_2O$ (2937.1): calcd. C 47.44, H 2.95, N 8.58; found C 47.60, H 2.94, N 8.25.

Acknowledgments

The authors thank A. B. P. Lever for access to instruments and the Natural Sciences and Engineering Council of Canada for funding.

[1] V. Balzani, F. Barigelletti, L. De Cola, *Top. Curr. Chem.* **1990**, *158*, 31−71.
[2] S. Bodige, A. S. Torres, D. J. Maloney, D. Tate, G. R. Kinsel, A. K. Walker, F. M. MacDonnell, *J. Am. Chem. Soc.* **1997**, *119*, 10364−10369.
[3] S. Vaduvescu, P. G. Potvin, *Inorg. Chem.* **2002**, *41*, 4081−4083.
[4] P. G. Potvin, P. U. Luyen, F. Al-Mutlaq, *New J. Chem.* **2001**, *25*, 839−846.
[5] J.-P. Sauvage, J.-P. Collin, J.-C. Chambron, S. Guillerez, C. Coudret, V. Balzani, F. Barigelletti, L. De Cola, L. Flamigni, *Chem. Rev.* **1994**, *94*, 993−1019.
[6] R. Liegghio, P. G. Potvin, A. B. P. Lever, *Inorg. Chem.* **2001**, *40*, 5485−5486.
[7] F. Kröhnke, *Synthesis* **1976**, 1−24.
[8] E. C. Constable, A. M. W. Cargill Thompson, *J. Chem. Soc., Dalton Trans.* **1992**, 3467−3475.
[9] L. Masciello, P. G. Potvin, *Can. J. Chem.* **2003**, *81*, 209−218.
[10] S. Vaduvescu, P. G. Potvin, *Acta Crystallogr., Sect. E* **2003**, *59*, o483−o484.
[11] C. Chamchoumis, P. G. Potvin, *J. Chem. Res. (M)* **1998**, 870−875.
[12] B. P. Sullivan, J. M. Calvert, T. J. Meyer, *Inorg. Chem.* **1980**, *19*, 1404−1407.
[13] M. Beley, J.-P. Collin, R. Louis, B. Metz, J.-P. Sauvage, *J. Am. Chem. Soc.* **1991**, *113*, 8521−8522.
[14] J.-P. Collin, P. Laine, J.-P. Launay, J.-P. Sauvage, A. Sour, *J. Chem. Soc., Chem. Commun.* **1993**, 434−435.
[15] F. Barigelletti, L. Flamigni, V. Balzani, J.-P. Collin, J.-P. Sauvage, A. Sour, E. C. Constable, A. M. W. Cargill Thompson, *J. Am. Chem. Soc.* **1994**, *116*, 7692−7699.
[16] C. Mikel, P. G. Potvin, *Polyhedron* **2002**, *21*, 49−54.
[17] A. El-ghayoury, A. Harriman, A. Khatyr, R. Ziessel, *J. Phys. Chem. A* **2000**, *104*, 1512−1523.
[18] K. Kalyanasundaram, M. K. Nazeeruddin, M. Grätzel, G. Viscardi, P. Savarino, E. Barni, *Inorg. Chim. Acta* **1992**, *198*, 831−839.
[19] A. Juris, V. Balzani, F. Barigelletti, S. Campagna, P. Belser, A. von Zelewsky, *Coord. Chem. Rev.* **1988**, *84*, 85−277.
[20] C. Mikel, P. G. Potvin, *Inorg. Chim. Acta* **2001**, *325*, 1−8.
[21] P. G. Potvin, P. U. Luyen, J. Bräckow, *J. Am. Chem. Soc.* **2003**, *125*, 4894−4906.
[22] F. Barigelletti, L. Flamigni, V. Balzani, J.-P. Collin, J.-P. Sauvage, A. Sour, E. C. Constable, A. M. W. Cargill Thompson, *J. Chem. Soc., Chem. Commun.* **1993**, 942−944.
[23] D. R. Prasad, M. Z. Hoffman, *J. Am. Chem. Soc.* **1986**, *108*, 2568−2573.
[24] N. Kitamura, Y. Kawanishi, S. Tazuke, *Chem. Lett.* **1983**, 1185−1188.
[25] P. J. Delaive, J. T. Lee, H. Abruna, H. W. Sprintschnik, T. J. Meyer, D. G. Whitten, *Adv. Chem. Ser.* **1977**, *168*, 28−43.
[26] K. Kalyanasundaram, J. Kiwi, M. Grätzel, *Helv. Chim. Acta* **1978**, *61*, 2720−2730.
[27] A. J. Bard, L. R. Faulkner, *Electrochemical Methods*, John Wiley & Sons, New York, **1980**.
[28] B. J. Coe, J. A. Harris, K. Clays, A. Persoon, K. Wostyn, B. S. Brunschweig, *Chem. Commun.* **2001**, 1548−1549.
[29] W. Spahni, G. Calzaferri, *Helv. Chim. Acta* **1984**, *67*, 450−454.
[30] J.-P. Collin, S. Guillerez, J.-P. Sauvage, F. Barigelletti, L. De Cola, L. Flamigni, V. Balzani, *Inorg. Chem.* **1991**, *30*, 4230−4238.
[31] E. C. Constable, A. M. W. Cargill Thompson, D. A. Tocher, M. A. M. Daniels, *New J. Chem.* **1992**, *16*, 855−867.

Received May 28, 2003
Early View Article
Published Online March 5, 2004

 © 2004 Wiley-VCH Verlag GmbH & Co. KGaA, Weinheim

EurJIC
European Journal of Inorganic Chemistry

Issue 9/2004

Pages 1771–1970

Papers available ahead of print in Early View at www.interscience.wiley.com

Earliest available Table of Contents:
Automatically, free of charge by e-mail through
www.interscience.wiley.com/alerts

COVER PICTURE

The cover picture shows the calix[6]arene-based tris(imidazole) ligand coordinated to divalent metal ions. These supramolecular edifices mimic enzyme environments. These funnel complexes present an exchangeable coordination site located in the heart of the hydrophobic cavity of the calixarene. The interplay between the strength of the host–guest noncovalent interactions and the flexibility of the system allows a variety of geometries for the metal complexes, either tetrahedral, trigonal-bipyramidal or square-pyramidal. Details are discussed in the article by O. Reinaud et al. on p. 1817ff.

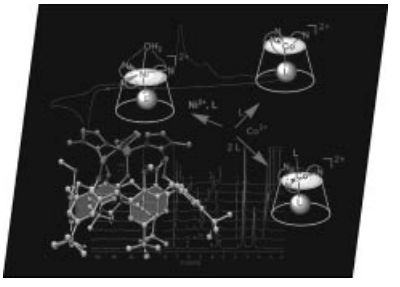

SHORT COMMUNICATIONS

Contents

1785 **B. Yang, M. Mo, H. Hu, C. Li, X. Yang, Q. Li, Y. Qian***

A Rational Self-Sacrificing Template Route to β-Bi_2O_3 Nanotube Arrays

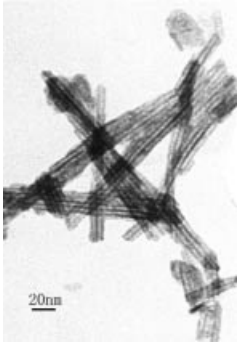

Keywords: Bismuth oxide / Nanostructures / Nanotubes / Synthesis design

 © 2004 Wiley-VCH Verlag GmbH & Co. KGaA, Weinheim

1788 **S. M. Ng, C. Yin, C. H. Yeung, T. C. Chan, C. P. Lau***

Ruthenium-Catalyzed Hydrogenation of Carbon Dioxide to Formic Acid in Alcohols

Keywords: Ruthenium / Hydrogenation / Alcohols / Carbon dioxide / Formic acid

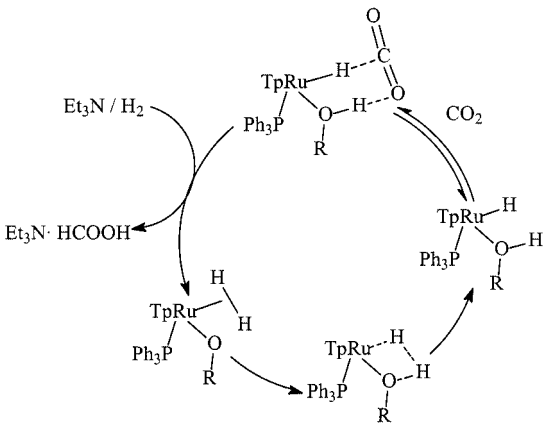

1794 **D. V. Konarev,* I. S. Neretin, G. Saito,* Y. L. Slovokhotov, A. Otsuka, R. N. Lyubovskaya**

Multicomponent Ionic Complexes of Cobalt(II) Tetraphenylporphyrin with C_{60} Fullerides – Transition from the σ-Bonded [($Co^{II}TPP$)·(C_{60}^-)] Anion to Nonbonded $Co^{II}TPP$ and $C_{60}^{\cdot -}$ Components

Keywords: Fullerenes / Porphyrinoids / Crystal engineering / Solid-state structures / IR and EPR spectroscopy

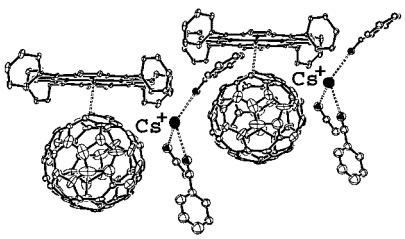

1799 **J. El Haskouri, S. Cabrera, C. Guillem, J. Latorre, A. Beltrán, M. D. Marcos, C. J. Gómez-García, D. Beltrán, P. Amorós***

One-Pot Synthesis of Superparamagnetic CoO-MCM-41 Nanocomposites with Uniform and Highly Dispersed Magnetic Nanoclusters

Keywords: Mesoporous materials / Nanocomposites / Superparamagnetism / Nanoparticles / Nanotechnology

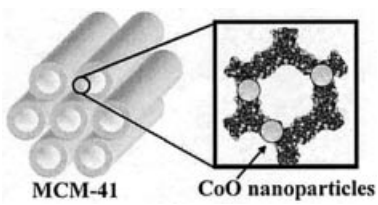

1804 **J. El Haskouri, C. Guillem, J. Latorre, A. Beltrán, D. Beltrán, P. Amorós***

The First Pure Mesoporous Aluminium Phosphonates and Diphosphonates – New Hybrid Porous Materials

Keywords: Hybrid materials / Mesoporous / Template synthesis / Aluminium / Phosphonates

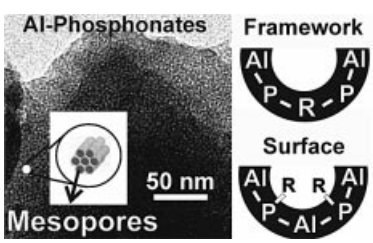

 © 2004 Wiley-VCH Verlag GmbH & Co. KGaA, Weinheim

1808 **G. Novitchi, J.-P. Costes,* B. Donnadieu**

Synthesis and Structure of 1-D Heterometallic Thiocyanato-Bridged $Cu^{II}Gd^{III}$ Polymers with Ferromagnetic Properties

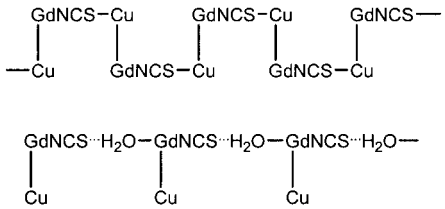

Keywords: Heterometallic complexes / Copper / Lanthanides / Magnetic properties

1813 **Y.-Q. Tian, H.-J. Xu, L.-H. Weng, Z.-X. Chen, D.-Y. Zhao,* X.-Z. You***

$[Cu^{I}(im)]_{\infty}$: Is this Air-Stable Copper(I) Imidazolate ($8^{2}10$)-Net Polymer the Species Responsible for the Corrosion-Inhibiting Properties of Imidazole with Copper Metal?

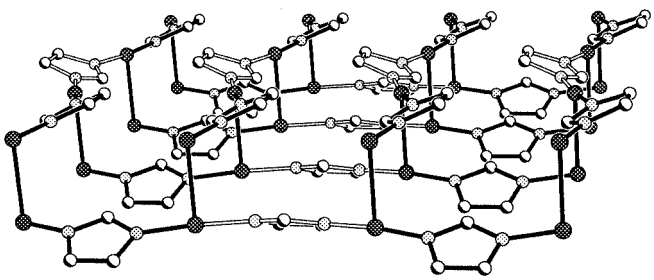

Keywords: Coordination polymers / Copper / Heterocycles / N ligands / Solvothermal synthesis

FULL PAPERS

1817 **O. Sénèque, M. Campion, M. Giorgi, Y. Le Mest, O. Reinaud***

Funnel Complexes with Co^{II} and Ni^{II}: New Probes into the Biomimetic Coordination Ability of the Calix[6]arene-Based Tris(imidazole) System

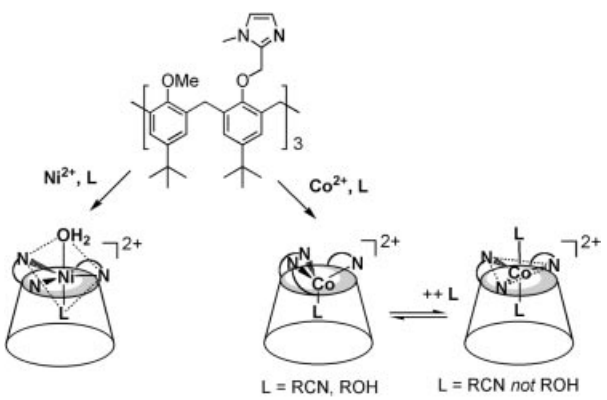

Keywords: Bioinorganic chemistry / Calixarenes / Cobalt / N ligands / Nickel

1827 **Z. Mazej,* P. Benkič, A. Tressaud, B. Žemva**

Palladium Chemistry in Anhydrous HF/AsF_5 Superacid Medium

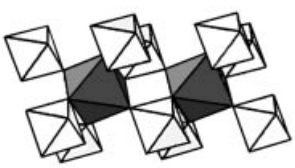

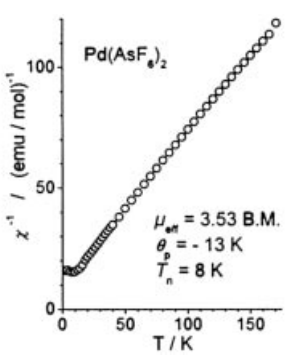

Keywords: Palladium / Fluorine / Superacids / Structure elucidation / Magnetic properties

 © 2004 Wiley-VCH Verlag GmbH & Co. KGaA, Weinheim

1835 **M. Jupa, G. Kickelbick, U. Schubert***

Methacrylate-Substituted Titanium-Yttrium Mixed-Metal Oxo Clusters

Keywords: Cluster compounds / Yttrium / Titanium / Organic-inorganic hybrids / Hydrogen bonding / Alkoxides

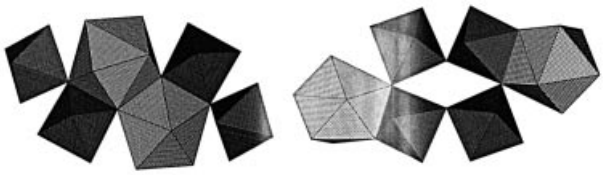

1840 **V. G. Vaidyanathan, B. U. Nair***

Nucleobase Oxidation of DNA by (Terpyridyl)chromium(III) Derivatives

Keywords: Chromium / DNA cleavage / Photo cleavage / Terpyridyl ligands

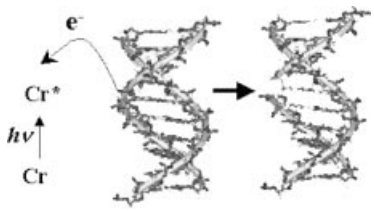

1847 **D. Sellmann, R. Prakash,* F. W. Heinemann**

Activation of H_2 and CO by Sulfur-Rich Nickel Model Complexes for [NiFe] Hydrogenases and CO Dehydrogenases

Keywords: Hydrogenases / H_2 activation / Nickel / N ligands / S ligands

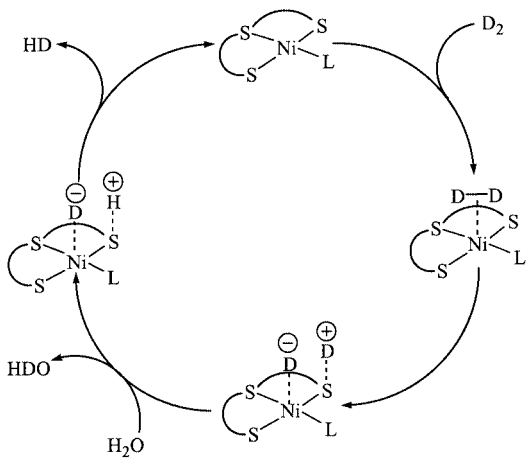

1859 **H. Grisaru, V. G. Pol, A. Gedanken,* I. Nowik**

Preparation and Characterization of Cu_2SnSe_4 Nanoparticles Using a Microwave-Assisted Polyol Method

Keywords: Nanoparticles / Microwave heating / Polyol method / Copper / Tin / Selenium

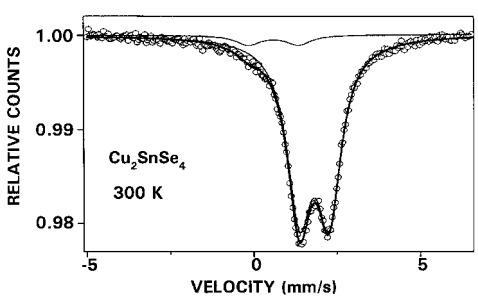

1865 **D. Rais, I. R. Gould, R. Vilar,* A. J. P. White, D. J. Williams**

Structural and Theoretical Studies of New Ruthenium-Amidato Complexes with Phenanthroline Ligands Containing H-Bonding Groups

Keywords: Chelates / Tridentate ligands / Ligand design / Ruthenium / pi interactions

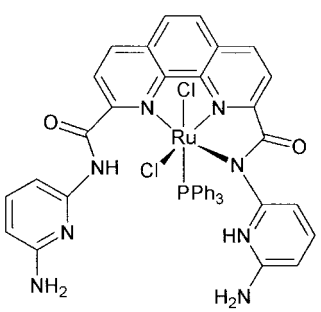

 © 2004 Wiley-VCH Verlag GmbH & Co. KGaA, Weinheim

1873 **B. Baruah, S. P. Rath, A. Chakravorty***

A Novel Pentacoordinated Dioxovanadium(V) Salicylaldiminate: Solvent Specific Crystallization of Dimorphs with Contrasting Coordination Geometries, Ligand Conformations and Supramolecular Architectures

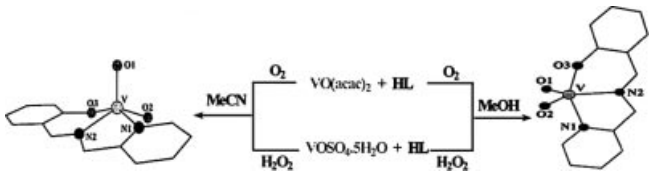

Keywords: Vanadium / O ligands / Dimorphism / Supramolecular architecture

1879 **J. C. Toledo, H. A. S. Silva, M. Scarpellini, V. Mori, A. J. Carmago, M. Bertotti, D. W. Franco***

Ruthenium Tetraammines as a Model of Nitric Oxide Donor Compounds

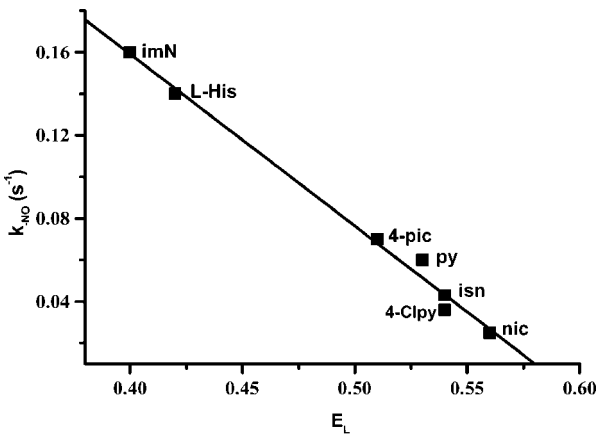

Keywords: Nitric oxide / Ruthenium / NO donor / N-heterocyclic ligands

1886 **I. Muga, J. M. Gutiérrez-Zorrilla,* P. Vitoria, P. Román, L. Lezama, J. I. Beitia**

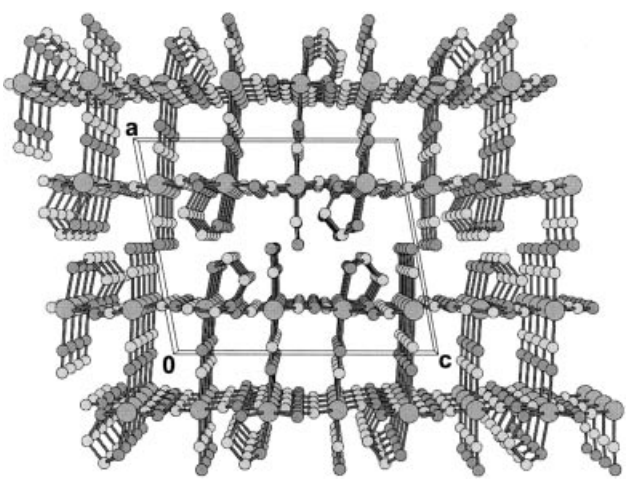

Unusual Two-Dimensional Nickel(II) Complexes Based on $[Ni(dien)]^{2+}$ and $[M(CN)_4]^{2-}$ Building Blocks (M = Ni, Pd and Pt) − Synthesis, Structural Diversity and Magnetic Properties

Keywords: Nickel / Palladium / Platinum / Cyanides / Bridging ligands

1894 **J. Huang, S.-A. Li, D.-F. Li, D.-X. Yang, W.-Y. Sun,* W.-X. Tang**

Carboxy Ester Hydrolysis Promoted by a Dicopper(II) Macrocyclic Polyamine Complex with Hydroxypropyl Pendant Groups

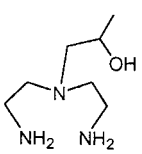

L^1

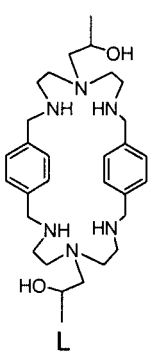

L

Keywords: Copper / Hydrolysis / Macrocyclic ligands / Mass spectrometry / Potentiometric titrations

 © 2004 Wiley-VCH Verlag GmbH & Co. KGaA, Weinheim

1902 **C. Bolzati, F. Refosco, A. Cagnolini, F. Tisato,* A. Boschi, A. Duatti, L. Uccelli, A. Dolmella, E. Marotta, M. Tubaro**

Synthesis, Solution-State and Solid-State Structural Characterization of Monocationic Nitrido Heterocomplexes $[M(N)(DTC)(PNP)]^+$ (M = ^{99}Tc, Re; DTC = Dithiocarbamate; PNP = Heterodiphosphane)

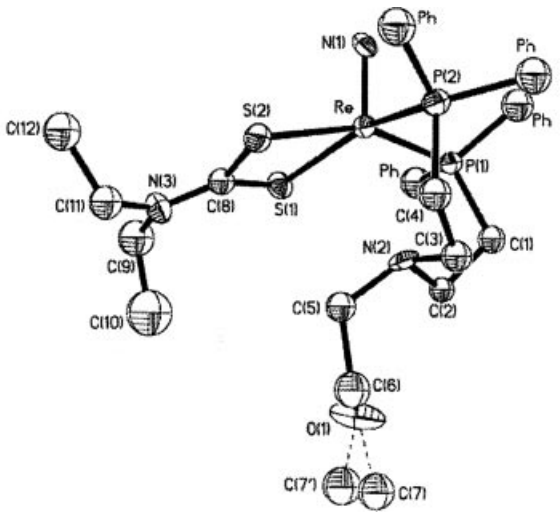

Keywords: Technetium / Rhenium / Radiopharmaceuticals / NMR spectroscopy / P ligands

1914 **A. Martín, M. Mena,* M. C. Morales-Varela, C. Santamaría**

Deprotonation of μ_3-Methylidyne Groups on a Ti_3O_3 Support: A Way to Build Oxotitanocubanes Containing Alkali and Alkaline-Earth Metals

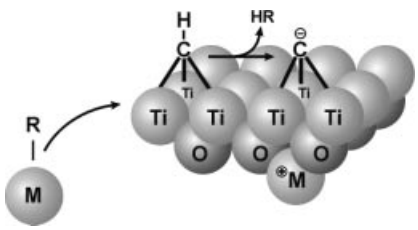

Keywords: Alkali metals / Alkaline earth metals / Alkylidyne complexes / Oxo ligands / Titanium

1922 **G. Albertin,* S. Antoniutti, A. Bacchi, B. Fregolent, G. Pelizzi**

New Nitrosylrhenium Hydrides as Precursors of "Diazo" Complexes: Preparation of Hydrazine and Diazene Derivatives

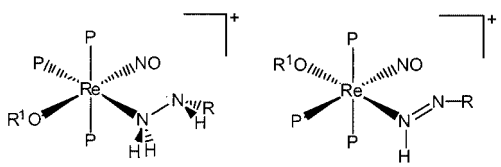

R = H, CH_3, C_6H_5; R^1 = CH_3, C_2H_5; P = phosphane

Keywords: Diazene / Hydrazine / P ligands / N ligands / Rhenium

1939 **L. Truflandier, C. J. Marsden, C. Freund, B. Martin-Vaca, D. Bourissou***

Theoretical Investigation of Group 4 Constrained-Geometry Complexes Featuring Phosphazene and Phosphinimido Arms

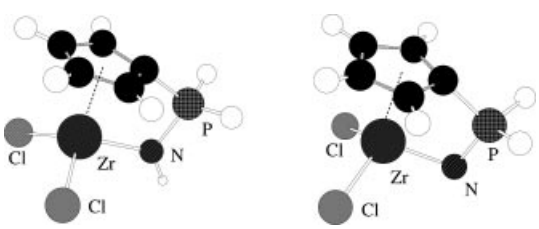

Keywords: Cations / Density functional calculations / Ligand Effects / Phosphorus / Zirconium

 © 2004 Wiley-VCH Verlag GmbH & Co. KGaA, Weinheim

1948 **Q.-Z. Yang, Q.-X. Tong, L.-Z. Wu, Z.-X. Wu, L.-P. Zhang, C.-H. Tung***

Switch of the Lowest Excited-States of Terpyridylplatinum(II) Acetylide Complexes Bearing Amino or Azacrown Moieties by Proton and Cations

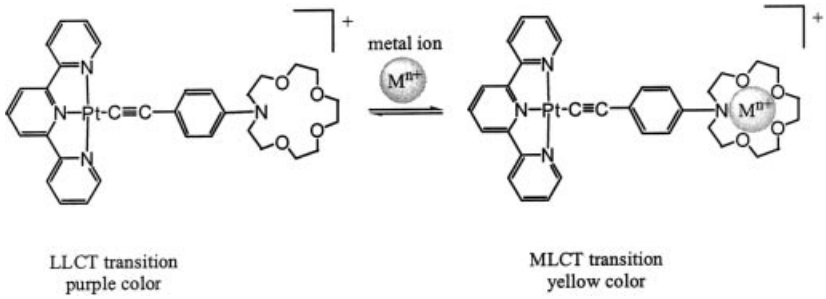

Keywords: Crown compounds / N ligands / Platinum / Sensors

1955 **C. González-Arellano, E. Gutiérrez-Puebla, M. Iglesias, F. Sánchez***

Easy Synthesis of New Chiral Tridentate Schiff Bases and Their Use as [N,N,O] Ligands for Ni and Pd Complexes − Catalytic Behaviour versus Hydrogenation Reactions

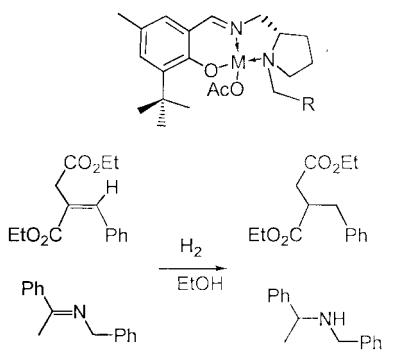

Keywords: Palladium / Nickel / Chiral Schiff bases / Hydrogenation / Tridentate ligands

1963 **S. Tanase, E. Bouwman,* J. Reedijk, W. L. Driessen, M. Ferbinteanu, M. Huber, A. M. Mills, A. L. Spek**

Synthesis and Structural Studies of Two New Base Adducts of Bis(2,4-pentanedionato)cobalt(II)

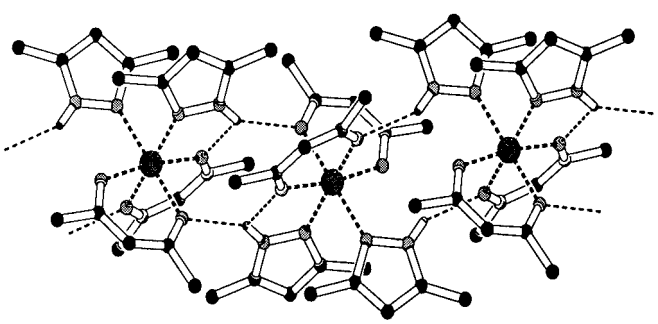

Keywords: Cobalt / 2,4-Pentanedione / 3,5-Dimethylpyrazole / Dimethylethanolamine / Coordination modes

 © 2004 Wiley-VCH Verlag GmbH & Co. KGaA, Weinheim

A Rational Self-Sacrificing Template Route to β-Bi_2O_3 Nanotube Arrays

Baojun Yang,[a,b] Maosong Mo,[a] Hanmei Hu,[a] Cun Li,[a] Xiaogang Yang,[a] Qiaowei Li,[a] and Yitai Qian*[a]

Keywords: Bismuth oxide / Nanostructures / Nanotubes / Synthesis design

Arrayed β-Bi_2O_3 nanotubes (NTs) were synthesized for the first time through a rational "self-sacrificing template" route, simply by oxidizing the precursor metallic bismuth NT arrays in air at 200–220 °C for 14–18 h. XRD, TEM, and HRTEM characterizations show that the prepared β-Bi_2O_3 samples are all phase pure and the β-Bi_2O_3 NTs have uniform diameters of approximately 3–6 nm and lengths up to several micrometers. The optical absorption and photoluminescence (PL) characteristics of the prepared samples were investigated.

(© Wiley-VCH Verlag GmbH & Co. KGaA, 69451 Weinheim, Germany, 2004)

Introduction

The discovery of carbon nanotubes (NTs) in 1991 has lead to a fruitful and growing interest in NTs for both basic and application-oriented industrial research.[1] Over the past years, various template-directing synthetic methods have been used to generate tubular forms of different oxides. For example, template-assisted soft chemistry routes have lead to the synthesis of VO_x,[2] TiO_2,[3] and SiO_2[4] NTs; pre-structured materials (including carbon NTs and polymer fibers) have been employed as structure-directing templates for tubular forms of SiO_2, Al_2O_3, V_2O_5,[5] TiO_2,[6] MoO_3, RuO_2,[7] ZrO_2,[8] and SnO_2;[9] porous aluminum oxide and polymer membrane templates for NTs or ordering arrays of oxide NTs[10] have also been used.

Bismuth trioxide (Bi_2O_3) and various bismuth-containing materials are very important in modern solid-state technology, owing to their peculiar physical properties (electrical, optical, and excellent ionic conductivity, etc.). They are widely used in gas sensors,[11] optoelectronic devices, optical coatings, transparent ceramic glass manufacturing,[12] cathode ray tubes,[13] as catalysts for the soft oxidation of hydrocarbons,[14] and so on. This special interest explains the great effort devoted to the investigation of Bi_2O_3 polymorphs over the last years.

Bi_2O_3 shows four main structures that are denoted by α-, β-, γ-, and δ-Bi_2O_3.[15] Among them, the tetragonal β-Bi_2O_3, which has a distorted defect-fluorite structure, is a metastable phase at ambient conditions, and usually transforms into the stable monoclinic α-Bi_2O_3 at about 870 K. The formation of the tetragonal β-Bi_2O_3 is observed at about 920 K on cooling the high-temperature cubic-phase δ-Bi_2O_3, although several synthetic procedures for obtaining these materials at relatively low temperatures have been reported.[14–16]

Recently, we have developed an aqueous chemical route to synthesize bamboo raft-like bismuth NT arrays at room temperature.[17] Herein, we also report on a novel "self-sacrificing template" approach for the synthesis of crystalline tetragonal β-Bi_2O_3 NT arrays, by oxidizing the precursor bismuth NT arrays directly in air at 200–220 °C. To the best of our knowledge, this is the first time that a method for the synthesis of β-Bi_2O_3 NTs has been reported.

Results and Discussion

Figure 1 shows a typical XRD pattern of a prepared sample. All the intensive and sharp reflection peaks can be indexed to a pure tetragonal phase (space group: $C\bar{4}b2$)

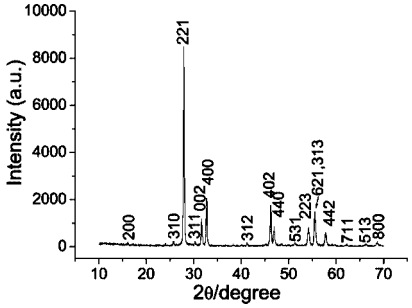

Figure 1. Typical XRD pattern of the prepared β-Bi_2O_3 samples

[a] Structure Research Laboratory and Department of Chemistry, University of Science and Technology of China, Hefei, Anhui 230026, P. R. China
Fax: (internat.) +86-551-3607402
E-mail: ytqian@ustc.edu.cn
[b] The School of Chemical Engineering, Hefei University of Technology, Hefei, Anhui 230009, P. R. China
Fax: (internat.) +86-551-2902956
E-mail: lhmybigy@mail.ustc.edu.cn

of crystalline β-Bi_2O_3. The calculated cell constants are a = 10.94 Å and c = 5.64 Å [the root mean square value (RMS) is 1.5×10^{-4}] and are in good agreement with the literature values of a = 10.93 Å and c = 5.62 Å (JC,PDS 74−1374). This XRD pattern indicates that the oxidization of metallic bismuth is complete and phase-pure crystalline β-Bi_2O_3 products can be obtained under the present synthetic conditions.

The morphologies and the size of the prepared samples were characterized by TEM. As shown in Figure 2 (see a, b, and c), a significant amount of the sample dispersed on the TEM copper grids exhibited nanotubular morphology, although other block-like morphologies also appeared. All of the β-Bi_2O_3 NTs are straight with uniform diameters of approximately 3−6 nm and lengths up to several micrometers. Most of them are also surprisingly aligned together, side by side, along the axial direction, in a similar way to that of the precursor metallic Bi NT arrays, to form bamboo raft-like NT arrays. This phenomenon suggests that the precursor bismuth NT arrays may serve as self-sacrificing templates and maintain their original tubular morphology in the oxidizing process. The SAED pattern, of a "bamboo raft", indicates the crystalline nature of the NT array (see a, the inset of Figure 2). The concentric diffraction rings could be indexed outwards as [110], [311], and [400] diffractions of tetragonal β-Bi_2O_3. Figure 2 (d) shows a representative HRTEM image of a section of a "bamboo raft". The lattice fringes are perpendicular to the axial direction of the NTs; the fringe spacing is about 7.8 Å, close to the interplanar spacing of the [110] lattice planes of the tetragonal β-Bi_2O_3. This means that the axial direction of the NTs is along the normal direction of the [110] lattice planes of the tetragonal β-Bi_2O_3.

Figure 2 (see e) shows the typical optical absorption spectrum of a prepared β-Bi_2O_3 sample, along with the PL of the same sample (λ_{exe} = 291 nm). The band edge is found to be around 3.90 eV (318 nm) and it shifts to much higher energy than that of the bulk bandgap at 2.58 eV.[15] The material also exhibits photoluminescence. A Stokes shift is observed; such effects have been attributed to either band-edge emission or shallow-trap emission in recent publications.[18]

Here, the use of precursor metallic bismuth NT arrays is crucial to the formation of β-Bi_2O_3 NT arrays. The reaction between the precursor metallic bismuth and oxygen in air can be simply formulated as:Bi (NT arrays) + O_2 (in air) → β-Bi_2O_3 (NT arrays)

In this reaction, the precursor metallic Bi NT arrays may serve as "self-sacrificing templates" which maintain their original tubular morphology in the oxidizing process, thus resulting in the formation of the β-Bi_2O_3 NT arrays.

The materials and experimental conditions have significant effects on the formation of the β-Bi_2O_3 NT arrays. Under similar experimental conditions, almost no Bi_2O_3 is formed after oxidization (24 h) by using commercial Bi powder (about 200 mesh) instead of the precursor metallic Bi NT arrays. On the other hand, the relatively low melting point of metallic Bi (273.1 °C) greatly limited the selection

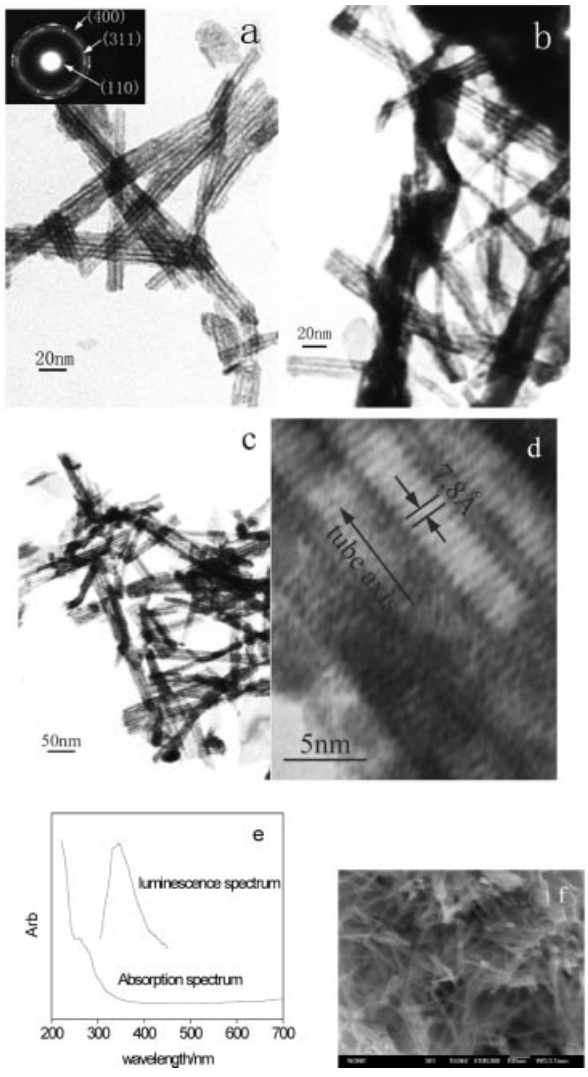

Figure 2. Typical TEM images (a, b, c), HRTEM image (d), UV/Vis absorption, PL spectra (e) of theprepared β-Bi_2O_3 samples and FESEM image (f) of the Bi precursor

of reaction temperature for our experiments. When the reaction temperature is below 160 °C, a mixture of β-Bi_2O_3 and unreacted metallic Bi was detected by XRD . When the reaction temperature was above 240 °C, a great deal of block-like and a small amount of tube-like β-Bi_2O_3 was observed by TEM. This phenomenon can be simply explained as follows: the precursor metallic Bi NTs may have a lower melting point than the bulk Bi due to the well-known small-size effects. When the experimental temperature (above 240 °C) is close to the melting point of the Bi precursor, local melting and aggregation of the precursor may occur before oxidization, which may further result in the formation of block-like β-Bi_2O_3. Based on the results mentioned above, we believe that the ratio of the NTs in the final β-Bi_2O_3 products can be greatly affected by varying the temperature of thermal oxidization of the Bi precursor. Thus, the optimal experimental temperature we selected is 200−220 °C. Under these conditions, the precursor metallic Bi NT arrays

 © 2004 Wiley-VCH Verlag GmbH & Co. KGaA, Weinheim

may keep their origin tubular morphology during oxidization, and once the β-Bi_2O_3 NTs are formed, the tubular morphology of β-Bi_2O_3 could be kept due to its thermal stability, which is higher than that of the Bi NTs.

Conclusion

In summary, we have presented a simple self-sacrificing template route for the synthesis of β-Bi_2O_3 NT arrays, by oxidizing the precursor Bi NT arrays. The prepared β-Bi_2O_3 samples are all phase-pure and stable at room temperature. This method requires no complex apparatus or technique and the conditions are much more mild, which makes it possible to produce β-Bi_2O_3 NTs on a large scale. The present study supplies a novel route to synthesize phase-pure β-Bi_2O_3, enlarges the family of oxide NTs, and may provide a facile method for the synthesis of other one-dimensional oxide nanomaterials.

Experimental Section

Reactions and Conditions: All reagents used in our experiments were analytically pure, purchased from Shanghai Chemicals Co. (China), and used without further purification. The precursor metallic bismuth NT arrays were prepared following a prodecure found in the literature,[17] as shown in Figure 2 (see f). A high proportion of the precursor sample exhibits 1D morphology with lengths from several hundred nanometers to several micrometers. TEM observations show that the 1D morphology is in fact present as nanotubular arrays (special TEM images and descriptions have been shown in our previously published paper).[17] Then, an appropriate amount of the prepared precursor bismuth powder was transferred into a ceramic boat. The boat was placed into the center of a temperature-controlled electrothermal oven (DHG-9076A) in which the temperature was previously kept at 200−220 °C (dry air), and maintained for 14−18 h. After the reaction was complete, the boat was taken out and the yellow powder obtained was immediately sealed in a small glass bottle filled with anhydrous alcohol to prevent direct contact with carbon dioxide in air (see Figure 3). The samples were characterized by X-ray powder diffraction (XRD), which was recorded on a Japan Rigaku Dmax-γA X-ray powder diffractometer with graphite-monochromatized Cu-K_α radiation (λ = 1.54178 Å). Transmission electron microscopy (TEM) images and high-resolution transmission electron microscopy (HRTEM) images were obtained with a JEOL-2010 transmission electron microscope, employing an accelerating voltage of 200 kV. Field-emission scanning electron microscope (FESEM) images were taken on a field-emission microscope (JEOL JSM-6700F, 15 kV). UV/Vis absorption spectra were recorded on a Shimadzu UV-2401PC UV/Vis spectrophotometer. Photoluminescence spectroscopy was carried out on a Shimadzu RF-5301PC spectrofluorophotometer with an Xe lamp at room temperature.

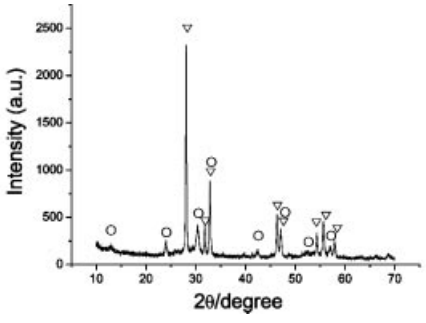

Figure 3. Typical XRD pattern of a prepared β-Bi_2O_3 sample exposed directly to air for about two hours (the triangle represent β-Bi_2O_3, the circle represent $Bi_2O_2CO_3$)

Acknowledgments

This work was financially supported from the National Natural Science Funds and the 973 Projects of China.

[1] [1a] S. Iijima, *Nature* **1991**, *354*, 56−58. [1b] G. R. Patzke, F. Krumeich, R. Nesper, *Angew. Chem. Int. Ed.* **2002**, *41*, 2446−2461.
[2] [2a] M. E. Spahr, P. Bitterli, R. Nesper, M. Müller, F. Krumeich, H.-U. Nissen, *Angew. Chem.* **1998**, *37*, 1263−1265. [2b] F. Krumeich, H.-J. Muhr, M. Niederberger, F. Bieri, B. Schnyder, R. Nesper, *J. Am. Chem. Soc.* **1999**, *121*, 8324−8331.
[3] S. Kobayashi, K. Hanabusa, N. Hamasaki, M. Kimura, H. Shirai, *Chem. Mater.* **2000**, *12*, 1523−1525.
[4] [4a] H. P. Lin, C. Y. Mou, S. B. Liu, *Adv. Mater.* **2000**, *12*, 103−106. [4b] J. H. Jung, Y. Ono, S. Shinkai, *Langmuir* **2000**, *16*, 1643−1649.
[5] B. C. Satishkumar, A. Govindaraj, E. M. Vogl, L. Baumallick, C. N. R. Rao, *J. Mater. Res.* **1997**, *12*, 604−606.
[6] R. A. Caruso, J. H. Schattka, A. Greiner, *Adv. Mater.* **2001**, *13*, 1577.
[7] B. C. Satishkumar, A. Govindaraj, M. Nath, C. N. R. Rao, *J. Mater. Chem.* **2000**, *10*, 2115−2119.
[8] C. N. R. Rao, B. C. Satishkumar, A. Govindaraj, *Chem. Commun.* **1997**, 1581−1582.
[9] W. Q. Han, A. Zettl, *J. Am. Chem. Soc.* **2003**, *125*, 2062−2063.
[10] [10a] C. R. Martin, *Science* **1994**, *266*, 1961−1966. [10b] J. C. Hulteen, C. R. Martin, *J. Mater. Chem.* **1997**, *7*, 1075−1087. [10c] B. Cheng, E. T. Samulki, *J. Mater. Chem.* **2001**, *11*, 2901−2902.
[11] [11a] Z. N. Adamian, H. V. Abovian, V. M. Aroutiounian, *Sens. and Actuators B* **1996**, 35−36, 241−243. [11b] E. Kanazawa, G. Sakai, K. Shimanoe, Y. Kanmura, Y. Teraoka, N. Miura, N. Yamazoe, *Sens. and Actuators B* **2001**, *77*, 72−77.
[12] L. Leontie, M. Caraman, M. Delibas, G. I. Rusu, *Mater. Res. Bull.* **2001**, *36*, 1629−1637.
[13] M. Yamamoto, M. Koitabashi, H. Kimura, *Jpn. J. Appl. Phys.* **2001**, *40*, 4691−4695.
[14] A. N. Romanov, D. P. Shashkin, E. V. Khaula, *Russ. J. Inorg. Chem.* **2000**, *45*, 500−503.
[15] [15a] P. Shuk, H.-D. Wiemhöfer, U. Guth, W. Göpel, M. Greenblatt, *Solid State Ionics* **1996**, *89*, 179−196. [15b] S. K. Blower, C. Greaves, *Acta Crystallogr., Sect. C* **1988**, *44*, 587−589.
[16] [16a] X. L. Chen, W. Eysel, *J. Solid State Chem.* **1996**, *127*, 128−130. [16b] O. Monnereau, L. Tortet, P. Llewellyn, F. Rouquerol, G. Vacquier, *Solid State Ionics* **2003**, *157*, 163−169.
[17] B. J. Yang, C. Li, H. M. Hu, X. G. Yang, Q. W. Li, Y. T. Qian, *Eur. J. Inorg. Chem.* **2003**, 3699−3702.
[18] W. T. Dong, C. S. Zhu, *J. Phys. Chem. Solids* **2003**, *64*, 265−271.

Received December 24, 2003

 © 2004 Wiley-VCH Verlag GmbH & Co. KGaA, Weinheim

Ruthenium-Catalyzed Hydrogenation of Carbon Dioxide to Formic Acid in Alcohols

Siu Man Ng,[a] Chuanqi Yin,[a] Chi Hung Yeung,[a] Tak Chung Chan,[a] and Chak Po Lau*[a]

Keywords: Ruthenium / Hydrogenation / Alcohols / Carbon dioxide / Formic acid

Catalytic hydrogenation of CO_2 to formic acid with the (solvento)metal hydride complex, $TpRu(PPh_3)(CH_3CN)H$ [Tp = hydrotris(pyrazolyl)borate], in various alcohols was studied. High-pressure NMR monitoring of the catalytic reaction in non-acidic methanol shows that the observable intermediate is a formate complex resulting from CO_2 insertion into the Ru–H bond and is stabilized by the hydrogen-bonding interaction between the formato ligand and a methanol molecule. However, in the case of the acidic alcohol, CF_3CH_2OH, the observable intermediates are $[TpRu(PPh_3)(CH_3CN)_2]^+$-$CF_3CH_2O^-$ and the alkyl carbonate complex, $TpRu(PPh_3)(\eta^2$-$O_2COCH_2CF_3)$, which are formed by the reaction of CO_2 with the alkoxide species, $TpRu(PPh_3)(CH_3CN)(OCH_2CF_3)$, generated by a very facile reaction between $TpRu(PPh_3)(CH_3CN)H$ and CF_3CH_2OH. We propose that the productive catalytic cycles of the reactions conducted in a variety of alcohols are similar to the one we formulated for the catalytic hydrogenation of CO_2 in hydrous THF. The formic acid is produced by the transfer of a hydride and a proton from the transient alcohol hydride intermediate, $TpRu(PPh_3)(ROH)H$, to an approaching CO_2 molecule. The activity of $TpRu(PPh_3)(CH_3CN)H$ is higher in CF_3CH_2OH than in methanol and other non-acidic alcohols and it is probably due to the enhanced electrophilicity of the carbon atom of CO_2, which results from the strong interaction between the proton of the highly acidic alcohol in $TpRu(PPh_3)(CF_3$-$CH_2OH)H$ and an oxygen atom of CO_2. The electrophilic carbon atom of CO_2 could in turn abstract the hydride from Ru–H in a more facile manner.

(© Wiley-VCH Verlag GmbH & Co. KGaA, 69451 Weinheim, Germany, 2004)

Introduction

Transition-metal-catalyzed CO_2 hydrogenation to formic acid remains an area of interest, as it provides a promising approach for utilizing carbon dioxide as a raw material for large-scale chemical synthesis.[1] Although it has been known for some time that addition of water to active Pd,[2] Rh,[3] and Ru[4] systems is effective in enhancing the catalytic hydrogenation of CO_2 to formic acid, no compelling experimental and theoretical data had been provided to explain the positive "water effect" until the publication of our recent work on the promoting effect of water in the catalytic hydrogenation CO_2 with the ruthenium complex $TpRu(PPh_3)(CH_3CN)H$ (**1**) [Tp = hydrotris(pyrazolyl)borate]. With the support of high-pressure NMR spectroscopy and theoretical calculations, we proposed a reaction mechanism to account for the "water effect". The key intermediate in the catalytic cycle is an (aquo)ruthenium hydride species, $TpRu(PPh_3)(H_2O)H$, which is generated through ligand displacement by H_2O. It transfers a hydride and a proton of the coordinated H_2O to the approaching CO_2 molecule to give formic acid and is converted into a transient hydroxo species, which then associates an H_2 molecule to regenerate $TpRu(PPh_3)(H_2O)H$ by σ-metathesis between the hydroxo and the η^2-H_2 ligands.[5]

Continuing our investigation on the catalytic hydrogenation of CO_2 to formic acid with **1**, we studied the **1**-catalyzed reactions in alcohols. The accelerating effects of certain alcohols on the hydrogenation of carbon dioxide, catalyzed by (trimethylphosphane)ruthenium complexes, have recently been reported.[6]

[a] Department of Applied Biology and Chemical Technology, The Hong Kong Polytechnic University
Hung Hom, Kowloon, Hong Kong, China
Fax: (internat.) + 852-2364-9932
E-mail: bccplau@inet.polyu.edu.hk

Results and Discussion

Hydrogenation of Carbon Dioxide to Formic Acid with 1

We have previously learned that **1** catalyzes the hydrogenation of carbon dioxide to yield formic acid with a low turnover number in anhydrous THF (see Entry 1, Table 1), but the catalytic activity of **1** was greatly enhanced when 5% (by volume) of water was added to the system (Entry 2, Table 1).[5] Perusal of Table 1 reveals significant increase in the catalytic activity of **1** in alcohols too (relative to that of **1** in anhydrous THF), although the enhancement effects are not as large as in THF/H_2O, except for the acidic alcohol, CF_3CH_2OH. In the catalytic reactions using alcohols as solvents, the yields of the ester side products are very low. Also noteworthy is the trend of decreasing turnover numbers of

 © 2004 Wiley-VCH Verlag GmbH & Co. KGaA, Weinheim DOI: 10.1002/ejic.200300847

Table 1. Hydrogenation of CO_2 to formic acid with $TpRu(PPh_3)(CH_3CN)H$ (**1**) in alcohols

Entry[a]	Solvent	Turnover no. of formic acid[b]	Turnover no. of ester[b]
1	THF	30	–
2	THF/H_2O[c]	720	–
3	THF/H_2O[c,d]	250	
4	CH_3OH	388	75
5	C_2H_5OH	230	11
6	C_2H_5OH[d]	127	4
7	n-C_3H_7OH	213	12
8	i-C_3H_7OH	141	–
9	t-C_4H_9OH	72	15
10	CF_3CH_2OH	1815	–

[a] Typical reaction conditions: catalyst 0.013 mmol; NEt_3 2 mL; solvents 20 mL; total pressure 50 atm (CO_2/H_2 = 1:1); temperature 100 °C; reaction time 16 h. [b] Turnover no: mol of product/mol of complex. [c] THF/H_2O (19 mL/1 mL). [d] Reaction time 4 h.

formic acid with increasing bulkiness of the alcohols (Entries 4−9, Table 1).

In Situ High-Pressure NMR Studies

To gain more insight into the mechanisms of the catalytic CO_2-hydrogenation reactions by **1** in alcohols, we carried out a series of in situ high-pressure NMR studies.

(a) Reaction of 1 with CO_2 in Methanol/THF

A $CH_3OH/[D_8]THF$ (1:1 by volume) solution of **1** in a 5-mm Wilmad pressure-valved NMR tube was pressurized with 6 atm of $^{13}CO_2$ at room temperature. The $^{31}P\{^1H\}$ NMR spectrum of the resulting solution recorded after 10 min shows the disappearance of **1** and the presence of a new complex **2** which gives a singlet at δ = 52.9 ppm. The $^1H\{^{13}C\}$ NMR spectrum of the same solution clearly shows the set of nine peaks pertaining to the Tp ligand. A singlet at δ = 2.30 ppm, integrated for 3 H, is assignable to the coordinated CH_3CN, a singlet (1 H) at δ = 7.63 ppm can be attributed to the hydrogen atom of a formate ligand. This signal is split into a doublet in the ^{13}C-coupled ^1H NMR spectrum by the formato carbon atom, half of it is unfortunately masked by the peaks of the Tp and PPh_3 ligands. The $^{13}C\{^1H\}$ NMR spectrum of the solution exhibits a singlet at δ = 174.7 ppm, pertaining to the formato carbon atom, which is split into a doublet in the ^1H-coupled ^{13}C NMR spectrum with an H-C coupling constant of 194.9 Hz. If the ^{31}P, ^1H, and ^{13}C NMR spectroscopic data of **2** are taken together, it is obvious that the ligand set of the complex consists of a Tp, a PPh_3, a formate, and an acetonitrile ligand. With reference to our recently reported formate complex, $TpRu(PPh_3)(CH_3CN)(\eta^1\text{-}OCHO)$, generated by CO_2 insertion into the Ru−H bond of **1** in anhydrous THF, and $TpRu(PPh_3)(CH_3CN)(\eta^1\text{-}OCHO)\cdot H_2O$, which is formed by the reaction of **1** with CO_2 in hydrous THF and stabilized by hydrogen-bonding interactions between the formato ligand and a water molecule,[5] we propose that the molecular formula of **2** is $TpRu(PPh_3)(CH_3CN)(\eta^1\text{-}OCHO)\cdot HOCH_3$. The formato ligand in **2** is hydrogen-bonded to a methanol molecule. Unfortunately, we have not been able to observe any downfield-shifted OH proton signals due to the hydrogen-bonded CH_3OH, probably because of its undergoing rapid exchange with the molecules in the bulk, or because the signal is masked by the large number of peaks due to the Tp and phosphane ligands in the region.

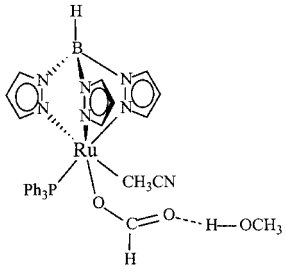

2

Attempts to synthesize **2** on a preparative scale by treating **1** with pressurized CO_2 were frustrated by its decomposition to the hydride species and some intractable materials during workup, in which the CO_2 pressure has to be removed. Similar problems were encountered in our previous efforts to isolate the formate complexes, $TpRu(PPh_3)(CH_3CN)(\eta^1\text{-}OCHO)$ and $TpRu(PPh_3)(CH_3CN)(\eta^1\text{-}OCHO)\cdot H_2O$.[5] Treatment of the chloro complex $TpRu(PPh_3)(CH_3CN)Cl$ with sodium formate also resulted in the formation of the hydride complex **1** as the major product. It seems that all these (Tp)ruthenium formate species are only stable under CO_2 pressure.

(b) Reaction of 1 with CO_2 and H_2 in Methanol/THF

A $CH_3OH/[D_8]THF$ (1:1 by volume) solution of **1** containing 20 equiv. of Et_3N was pressurized with 6 atm of $^{13}CO_2$ and H_2 in a 5-mm Wilmad pressure-valved NMR tube; the $^{31}P\{^1H\}$ and ^1H NMR spectra of the solution taken within 10 min at room temperature shows the disappearance of **1** and the formation of **2**. A minute amount of formic acid, indicated by a very small doublet at δ = 8.60 ppm ($J_{C,H}$ = 189 Hz) in the ^1H NMR spectrum, was formed. After heating the tube at 100 °C for 3 h, ^1H NMR spectroscopy showed a very significant increase of the formic acid signal. In the downfield region, in addition to the set of peaks pertaining to the Tp ligand of **2**, some minute peaks were also visible. The $^{31}P\{^1H\}$ spectrum, however, shows only one singlet due to **2**. The CO_2-hydrogenation reaction was basically complete within 3 h because the ^1H NMR spectrum taken 3 h later did not show any visible increase in the formic acid signal. It is, however, worth noting that, after heating the solution at 100 °C for 2 d, the ^1H NMR spectrum showed that the amount of formic acid decreased, while the downfield region of the spectrum became relatively complex, indicating the presence of a few sets of Tp signals. A doublet of doublets ($J_{H,P}$ = 26.4, $J_{C,H}$ = 9.3 Hz) is observed in the upfield region at δ = −11.81 ppm, which can be assigned to the carbonyl hydride

 © 2004 Wiley-VCH Verlag GmbH & Co. KGaA, Weinheim

complex $TpRu(PPh_3)(CO)H$ (**3**), which we have previously reported.[7] The $^{31}P\{^1H\}$ spectrum exhibits a major singlet at $\delta = 52.9$ ppm, which is due to **2**. A singlet at $\delta = 66.1$ ppm is assignable to **3**, while the singlet at $\delta = 30.9$ ppm is identified as the signal of triphenylphosphane oxide, which was probably formed by CO_2 oxidation of PPh_3. A number of small, unidentified signals can be observed in the region between the signals of **2** and **3**. After heating at 100 °C for 3 d, a further decrease in the amount of formic acid was evidenced by ^1H NMR spectroscopy and a set of Tp signals of $TpRu(PPh_3)(CO)H$ (**3**) was observed in the downfield region. The hydride signal of **3** also shows enhanced intensity. The $^{31}P\{^1H\}$ NMR spectrum was also simplified, showing a major peak at $\delta = 66.1$ ppm, which is due to **3**. The phosphane oxide peak at $\delta = 30.9$ ppm and an unidentified peak at $\delta = 63.3$ ppm are the only two minor signals in the spectrum. In our previous work, high-pressure NMR spectroscopy monitoring of the catalytic CO_2 hydrogenation with **1** in hydrous THF revealed that the carbonyl hydride complex **3** was the major ruthenium-containing species after prolonged heating at 100 °C. Moreover, in the course of the reaction, a very small amount of $TpRu(PPh_3)(H_2)H$ (**4**)[7] was also detected by ^1H NMR spectroscopy. Independent NMR experiments showed that **4** reacted slowly with formic acid in $[D_8]$THF to yield $TpRu(PPh_3)(CO)H$. We believe that in the course of the **1**-catalyzed CO_2 hydrogenation in $CH_3OH/[D_8]$THF, the carbonyl hydride complex **3** was formed by the reaction of $TpRu(PPh_3)(H_2)H$ (**4**) with formic acid and the dihydrogen hydride species was present in such low concentration that it eluded detection by NMR spectroscopy. Examples relevant to the formation of **3** can be found in the literature.[8−10] An authentic sample of **3** was found to be inactive in catalyzing CO_2 hydrogenation in methanol.

Reaction of CF_3CH_2OH with 1

In view of the superiority of CF_3CH_2OH in promoting the CO_2-hydrogenation reaction, studies to gain insight into its role in the catalytic reaction were carried out. The ^1H NMR spectrum taken a few minutes after the dissolution of **1** in $CF_3CH_2OH/[D_8]$THF (1:1 by volume) in a 5-mm Wilmad pressure-valved NMR tube showed that the alkoxide complex $TpRu(PPh_3)(CH_3CN)(OCH_2CF_3)$ (**5**) was formed and **1** was no longer detectable. The spectrum shows a new set of nine peaks pertaining to the Tp ligand. A singlet at $\delta = 2.27$ ppm integrated for 3 H is assignable to the coordinated acetonitrile. Two multiplets, each integrated for 1 H, are observed at $\delta = 3.04$ and 3.45 ppm; these peaks can be attributed to the methylene hydrogen atoms of the coordinated $-OCH_2CF_3$ group. A singlet at $\delta = 4.65$ ppm signals the presence of free hydrogen. The trifluoroalkoxo ligand was verified by ^{19}F NMR spectroscopy, which shows the signal of $-OCH_2CF_3$ as a triplet at $\delta = -75.05$ ppm ($J_{H,F} = 10$ Hz). The $^{31}P\{^1H\}$ NMR spectrum shows a singlet at $\delta = 52.8$ ppm.

Formation of **5** probably resulted from protonation of the hydrido ligand of **1** by CF_3CH_2OH via a dihydrogen-bonded intermediate $Tp(PPh_3)(CH_3CN)$ $Ru-H\cdots H-OCH_2CF_3$ and the η^2-dihydrogen complex (see Scheme 1). The relevancy of dihydrogen bonding to the protonation reaction is suggested by independent NMR studies involving reactions of **1** with limited amounts of CF_3CH_2OH. Upon addition of 1.5 and 7.5 equiv. of CF_3CH_2OH to $[D_8]$toluene solutions of **1**, the ^1H NMR spectra of the solutions show that the hydride signal of **1** becomes broadened and shifted upfield by 0.16 and 0.63 ppm, respectively. Variable-temperature T_1 measurements for the hydrido ligand of **1** yielded a T_1(min) of 252 ms (at 400 MHz and 235 K) and 65 ms (at 400 MHz and 233 K) for the **1**/1.5 equiv. CF_3CH_2OH and the **1**/7.5 equiv. CF_3CH_2OH solutions, respectively. The two T_1(min) values are much lower than that of the hydrido ligand of **1** in $[D_8]$toluene in the absence of CF_3CH_2OH (540 ms at 400 MHz and 257 K). These T_1(min) measurements thus suggest the presence of $Ru-H\cdots H-OCH_2CF_3$ dihydrogen-bonding interaction. Reactions of acidic alcohols with transition-metal hydride complexes to generate $M-H\cdots H-OR$ dihydrogen-bonded species are well documented.[11] For example, a dynamic equilibrium between the dihydrogen-bonded ruthenium hydride species and the η^2-dihydrogen complex $(dppm)_2HRu-H\cdots H-OR$ $[(dppm)_2HRu(H_2)]^+OR^-$ is established in the presence of phenol. The more acidic alcohol, hexafluoro-2-propanol, shifts the equilibrium to the side of the η^2-dihydrogen complex and eventually yields the alkoxide complex $(dppm)_2Ru[OCH(CF_3)_2]_2$.[11c]

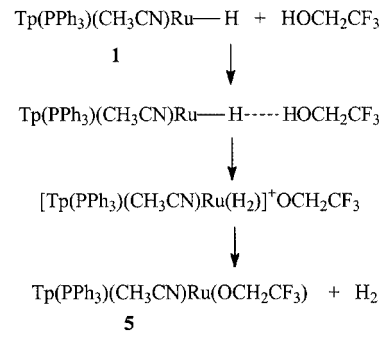

Scheme 1

Attempts to synthesize **5** on a preparative scale, unfortunately, were not successful, due to its decomposition into some intractable materials during the workup processes. It seems that **5** is only stable in CF_3CH_2OH solutions.

Reaction of $TpRu(PPh_3)(CH_3CN)(OCH_2CF_3)$ (5) with CO_2

Et_3N (20 equiv.) was added to a $CF_3CH_2OH/[D_8]$THF solution of **5**; $^{31}P\{^1H\}$ NMR spectroscopy indicated that **5** was unaffected by the base. The solution was then subjected to 8 atm of CO_2 at room temperature; NMR spectroscopy showed that **5** was converted into a 1:1 mixture of $[TpRu(PPh_3)(CH_3CN)_2]^+$ (**6**) and another complex **7** after 2 h. Complex **6**, which we have previously reported,[12] can

 © 2004 Wiley-VCH Verlag GmbH & Co. KGaA, Weinheim

be easily identified by ^1H and $^{31}P\{^1H\}$ NMR spectroscopy. The ^1H NMR spectrum of the mixture clearly shows two sets of signals (six peaks each) in the downfield region, one of which pertaining to the Tp ligand of complex **6**, while the other set belongs to the Tp ligand of **7**. A six-peak pattern for the Tp ligand implies that two of the three legs *trans* to the Tp ligand in an octahedral configuration are equivalent. The assumption that the two legs in **7** are due to the bidentate alkyl carbonato ligand $CF_3CH_2OCO_2^-$ is supported by the ^{13}C NMR study of an identical reaction using $^{13}CO_2$ in place of the unlabeled carbon dioxide. The ^{13}C NMR spectrum of the resulting solution shows a characteristic carbonate singlet resonance at δ = 172.3 ppm. Since only one carbonate signal was detected in the ^{13}C NMR spectrum, the counterion of **6** is not a free alkyl carbonato anion but it is the alkoxide anion $CF_3CH_2O^-$, which is confirmed by ^{19}F NMR spectroscopy showing a triplet signal at $\delta = -76.02$ ($J_{H,F}$ = 10 Hz). The methylene hydrogen signals of the $CF_3CH_2OCO_2$ ligand are unfortunately masked by a huge peak in the ^1H NMR spectrum due to the free alcohol. The $^{31}P\{^1H\}$ spectrum of the solution shows two singlets: one at δ = 50.8 ppm pertaining to **6** and another one at δ = 63.9 ppm, ascribable to the phosphane ligand of **7**. When all the NMR spectroscopic data are taken together, **7** can be identified as the alkyl carbonato complex $TpRu(PPh_3)(\eta^2\text{-}O_2COCH_2CF_3)$. Apparently, **7** was formed by CO_2 insertion into the $Ru-OCH_2CF_3$ bond of **5** [see Equation (1)]. Insertion of CO_2 into metal−oxygen bonds of metal alkoxides and phenoxides to form metal carbonate species is well documented.[13]

$$\underset{\mathbf{5}}{2\ TpRu(PPh_3)(CH_3CN)(OCH_2CF_3)} + CO_2 \longrightarrow [TpRu(PPh_3)(CH_3CN)_2]^+\ CF_3CH_2O^- + TpRu(PPh_3)(\eta^2\text{-}O_2COCH_2CF_3) \quad (1)$$

$$\mathbf{6.CF_3CH_2O^-} \qquad\qquad \mathbf{7}$$

Reaction of 1 with CO_2/H_2 in $CF_3CH_2OH/[D_8]THF$

A $CF_3CH_2OH/[D_8]THF$ (1:1 by volume) solution of **1** containing 20 equiv. of Et_3N was pressurized with 6 atm of CO_2 and H_2 at room temperature in a 5-mm Wilmad pressure-valved NMR tube. The $^{31}P\{^1H\}$ NMR spectrum taken 1 h later at room temperature indicates the formation of a 1:1 mixture of **6** and **7**. ^1H NMR spectroscopy shows, in addition to **6** and **7**, a small amount of formic acid, evidenced by a small singlet at δ = 8.42 ppm. A few hours later, ^1H NMR measurements showed that the amount of formic acid increased, and it also suggested the presence of a minute amount of $TpRu(PPh_3)(CO)H$ (**3**), as evidenced by a very small doublet at $\delta = -11.83$ ppm ($J_{H,P}$ = 26.8 Hz). After heating the NMR tube at 100 °C for 1 d, it was found by ^1H and $^{31}P\{^1H\}$ studies that **6** and **7** disappeared and **3** was the only ruthenium complex present in the solution.

Mechanism of CO_2 Hydrogenation in Non-Acidic Alcohols

Our high-pressure NMR studies show that reactivity of **1** in the CO_2-hydrogenation reaction in methanol is very similar to that in hydrous THF and it is therefore reasonable to propose that the mechanism of **1**-catalyzed CO_2-hydrogenation reactions in non-acidic alcohols (Entries 4−9, Table 1) is analogous to that of the catalysis in hydrous THF. Therefore, in analogy to the active aquo hydride species $TpRu(PPh_3)(H_2O)H$ in hydrous THF, the key intermediate in the catalytic cycle **A** (see Scheme 2) is the transient alcohol hydride species **8**, which is mainly formed by displacement of the acetonitrile ligand of **1** by ROH. The interaction of the OH proton of the alcohol in **8** with one of the oxygen atoms of the approaching CO_2 increases the electrophilicity of the carbon atom, which is then able to abstract the hydride from Ru−H. The turnover numbers of the catalytic reactions decrease with increasing bulkiness of the alcohols (Entries 3−7, Table 1) and this observation supports the fact that the availability of **8** might have a large effect on the overall efficiency of the catalytic system. It is more difficult for a hindered alcohol to displace the acetonitrile ligand of **1**. In view of the detection of a small amount of $TpRu(PPh_3)(H_2)H$ (**4**) by NMR spectroscopy in our previous study of **1**-catalyzed CO_2 hydrogenation in hydrous THF, we propose that **4** is present in a minute amount in the alcohols, although it has not been successfully detected by NMR spectroscopy. Reaction of $TpRu(PPh_3)(H_2)H$ with formic acid to yield $TpRu(PPh_3)(CO)H$ was verified by an independent experiment.

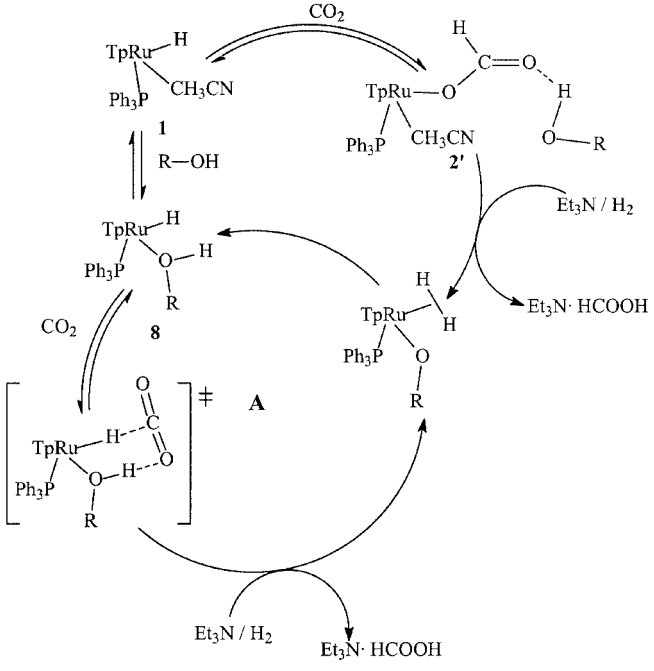

Scheme 2

 © 2004 Wiley-VCH Verlag GmbH & Co. KGaA, Weinheim

Mechanism of CO_2 Hydrogenation in Acidic Alcohol CF_3CH_2OH

Unlike the CO_2-hydrogenation reaction in methanol, no metalloformate intermediate is observable in the course of the catalysis in CF_3CH_2OH because complex **1** reacts rapidly with the acidic alcohol to form the metal alkoxide **5**, which then reacts with CO_2 to give the observable intermediate species $[TpRu(PPh_3)(CH_3CN)_2]^+$ (**6**) and $TpRu(PPh_3)(\eta^2\text{-}O_2COCH_2CF_3)$ (**7**). Although the observable intermediates in the catalyses in methanol and CF_3CH_2OH are different, we propose that the sequence in cycle **B** (see Scheme 3), which is basically identical to the catalytic cycle **A** of Scheme 2, is the productive route for the catalytic process in trifluoroethanol. Under H_2 pressure, a minute quantity of the active alcohol hydride species $TpRu(PPh_3)(CF_3CH_2OH)H$ (**9**) might be generated through the alkoxo dihydrogen intermediate $TpRu(PPh_3)(OCH_2CF_3)(H_2)$. The much higher catalytic activity of **1** in CF_3CH_2OH than in the non-acidic alcohols is probably related to the much stronger interaction of the proton of the coordinated CF_3CH_2OH in **9** with an oxygen atom of CO_2, which enhances significantly the positive charge at the carbon atom of the molecule, making the hydride abstraction from Ru−H facile. Again, the final ruthenium complex $TpRu(PPh_3)(CO)H$ results from the reaction of formic acid with $TpRu(PPh_3)(H_2)H$ (**4**) after prolonged heating. The action of H_2 on the alkyl carbonato intermediate **7** is believed to be one of the routes to generate **4**, although the sequence of the reaction is unknown.

Conclusion

Continuing our study on the promoting effect of water in the **1**-catalyzed hydrogenation of CO_2 to formic acid, we have studied the effect of alcohols on the catalysis. Our study suggests that, although the NMR-detectable intermediates in the catalysis in methanol (and probably in other non-acidic alcohols) and in acidic CF_3CH_2OH are different, the catalytic cycles of CO_2 hydrogenation in both cases are probably identical. The key species of the catalytic process, $TpRu(PPh_3)(ROH)H$, is the alcohol analogue of the aquo hydride complex that we have proposed for our previously studied hydrous THF system. The exceptionally

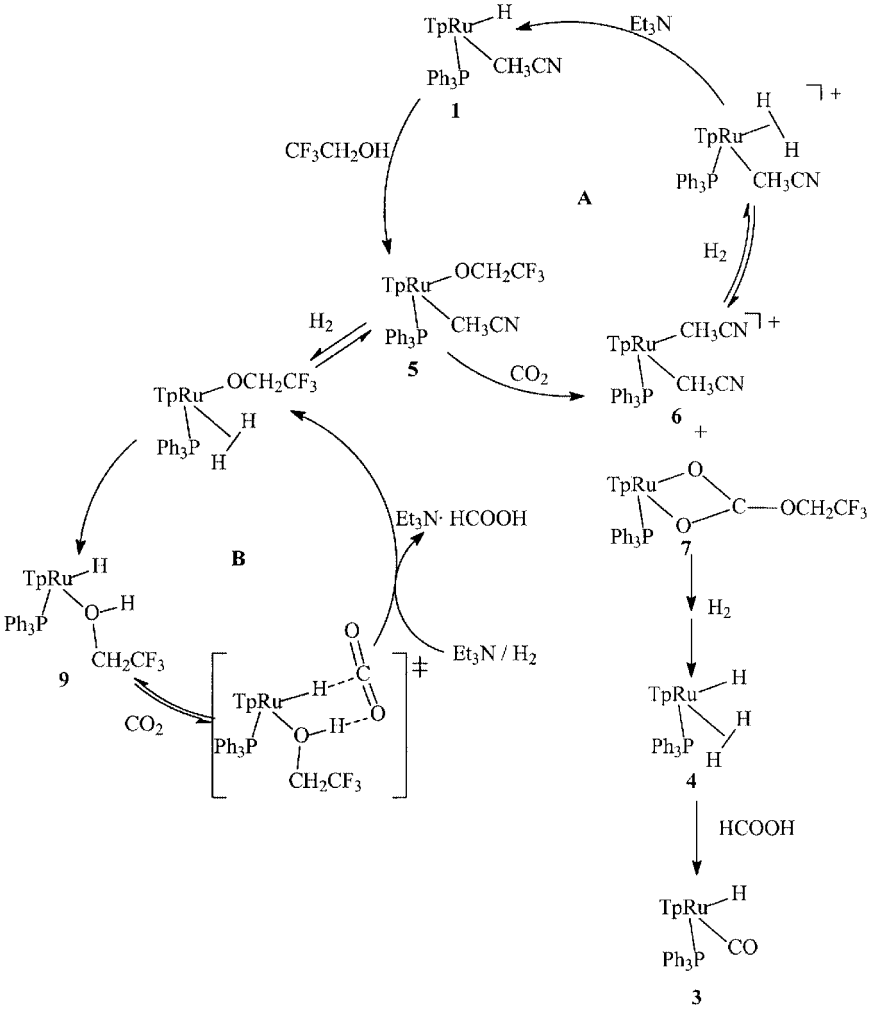

Scheme 3

 © 2004 Wiley-VCH Verlag GmbH & Co. KGaA, Weinheim

high promoting effect of CF_3CH_2OH among the alcohols studied is due to the stronger interaction of the highly acidic hydrogen of the trifluoroethanol in $TpRu(PPh_3)(CF_3CH_2OH)H$ with an oxygen atom of the approaching CO_2, greatly enhancing the electrophilicity of the carbon atom of the molecule, and enabling its abstraction of the hydride from Ru−H.

Experimental Section

General Remarks: Ruthenium trichloride, $RuCl_3·3H_2O$, pyrazole, and sodium borohydride were obtained from Aldrich. Triphenylphosphane was purchased from Merck and was recrystallized from ethanol before use. The complex $TpRu(PPh_3)(CH_3CN)H$ was synthesized according to published procedures.[13] Solvents were distilled under dry nitrogen with appropriate drying agents.[14] High-purity hydrogen gas and carbon dioxide were supplied by Hong Kong Oxygen. ^1H NMR spectra were obtained with a Bruker DPX 400 spectrometer. Chemical shifts are reported relative to residual protons of the deuterated solvents. ^{31}P, ^{19}F, and ^{13}C NMR spectra were recorded with a Bruker DPX 400 spectrometer at 161.70, 376.31 and 100.60 MHz, respectively. ^{31}P NMR chemical shifts were externally referenced to 85 % H_3PO_4 in D_2O. ^{19}F NMR chemical shifts were externally referenced to $CFCl_3$ in $CDCl_3$. ^{13}C NMR chemical shifts were internally referenced to the residual peak of the deuterated solvents. High-pressure NMR studies were carried out in commercial 5-mm Wilmad pressure-valved NMR tubes.

Safety Warning: It is advisable not to add more than 12 atm of gas(es) to the 5-mm Wilmad pressure-valved NMR tubes at room temperature.

Catalytic Hydrogenation of CO_2 with $TpRu(PPh_3)(CH_3CN)H$ (1): The reactions were performed in a 100-mL stainless steel autoclave. In a typical run, about 0.013 mmol of **1** in 20 mL of alcohol and 2 mL of NEt_3 was added to the autoclave. After being flushed with H_2 three times, the system was heated whilst stirring at 100 °C under 50 atm of CO_2/H_2 (1:1). At the end of the required length of time, the autoclave was cooled rapidly and vented carefully. The formic acid in the resulting solution was analyzed by ^1H NMR spectroscopy. The relative intensities of the formato hydrogen signal of the product and the formato hydrogen signal of the internal standard (DMF) were measured, and with the help of a calibration curve, the turnover number of the catalysis was derived.

Acknowledgments

We thank the Hong Kong Research Grant Council (Project No. PolyU5188/00P) for financial support.

[1] [1a] A. Behr, *Carbon Dioxide Activation by Metal Complexes*, VCH, Weinheim, Germany, **1988**. [1b] *Enzymatic and Model Carboxylation and Resuction Reactions for Carbon Dioxide Utilization* (Eds.: M. Aresta, J. V. Schloss), NATO ASI Series C, No. 314, Kluwer Academic, Dordrecht, The Netherlands, **1990**. [1c]P. G. Jessop, T. Ikariya, R. Noyori, *Chem. Rev.* **1995**, *95*, 259−272. [1d] W. Leitner, *Angew. Chem. Int. Ed. Engl.* **1995**, *34*, 2207−2221. [1e] W. Leitner, *Coord. Chem. Rev.* **1996**, *153*, 247−247.

[2] Y. Inoue, H. Izumida, Y. Sasaki, H. Hashimoto, *Chem. Lett.* **1976**, 863−864.

[3] J.-C. Tsai, K. M. Nicholas, *J. Am. Chem. Soc.* **1992**, *114*, 5117−5124.

[4] P. G. Jessop, Y. Hsiao; T. Ikariya, R. Noyori, *J. Am. Chem. Soc.* **1996**, *118*, 344−355.

[5] C. Yin, Z. Xu, S.-Y. Yang, S. M. Ng; K. Y. Wong, Z. Lin, C. P. Lau, *Organometallics* **2001**, *20*, 1216−1222.

[6] [6a] P. Munshi, A. D. Main, J. C. Linehan, C.-C. Tai, P. G. Jessop, *J. Am. Chem. Soc.* **2002**, *124*, 7963−7971. [6b] C. A. Thomas, R. J. Bonilla, Y. Huang, P. G. Jessop, *Can. J. Chem.* **2001**, *79*, 719−724.

[7] Y.-Z. Chen, W. C. Chan, C. P. Lau, H. S. Chu, H. L. Lee, G. Jia, *Organometallics* **1997**, *16*, 1241−1246.

[8] M. A. McLoughlin, N. L. Keder, W. T. Harrison, R. J. Flesher, H. A. Mayer, W. C. Kaska, *Inorg. Chem.* **1999**, *38*, 3223−3227.

[9] C. S. Yi, N. Liu, *Organometallics* **1995**, *14*, 2616−2617.

[10] H. Koinuma, Y. Yoshida, H. Hirai, *Chem. Lett.* **1975**, 1223−1226.

[11] [11a] E. S. Shubina, N. V. Belkova, A. A. Krylov, E. V. Vorontsov, L. M. Epstein, D. G. Gusev, M. Niedermann, H. Berke, *J. Am. Chem. Soc.* **1996**, *118*, 1105−1112. [11b] N. V. Belkova, E. S. Shubina, A. V. Ionidis, L. M. Epstein, H. Jacobsen, A. Messmer, H. Berke, *Inorg. Chem.* **1997**, *36*, 1522−1525. [11c] J. A. Ayllón, C. Gervaux, S. Sabo-Etienne, B. Chaudret, *Organometallics* **1997**, *16*, 2000−2002. [11d] Y. Guari, J. A. Allyón, S. Sabo-Etienne, B. Chaudret, *Inorg. Chem.* **1998**, *37*, 640−644. [11e] S. Gründemann, S. Ulrich, H.-H. Limbach, N. S. Golubev, G. S. Denisov, L. M. Epstein, S. Sato-Etienne, B. Chaudret, *Inorg. Chem.* **1999**, *38*, 2550−2551. [11f] E. I. Gutsul, N. V. Belkova, M. S. Sverdlov, L. M. Epstgein, E. S. Shubina, V. I. Bakhmutov, T. N. Gribanova, R. M. Minyaev, C. Bianchini, M. Peruzzini, F. Zanobini, *Chem. Eur. J.* **2003**, *9*, 2219−2228.

[12] W. C. Chan, C. P. Lau, Y.-Z. Chen, Y.-Q. Fang, S. M. Ng, G. Jia, *Organometallics* **1997**, *16*, 34−44.

[13] [13a] H. S. Kim, J. J. Kim, B. G. Lee, O. S. Jung, H. G. Jang, S. O. Kang, *Angew. Chem. Int. Ed.* **2000**, *39*, 4096−4098. [13b] T. Tsuda, S. I. Sanada, K. Ueda, T. Saegusa, *Inorg. Chem.* **1976**, *15*, 2329−2332. [13c] D. J. Darensbourg, M. W. Holtcamp, G. E. Struck, M. S. Zimmer, S. A. Niezgoda, P. Rainey, J. B. Robertson, J. D. Draper, J. H. Reibenspies, *J. Am. Chem. Soc.* **1999**, *121*, 107−116. [13d] D. J. Darensbourg, K. M. Sanchez, J. H. Reibenspies, A. L. Rheingold, *J. Am. Chem. Soc.* **1989**, *111*, 7094−7103. [13e] D. J. Darensbourg, K. M. Sanchez, A. L. Rheingold, *J. Am. Chem. Soc.* **1987**, *109*, 290−292.

[14] D. R. Perrin, W. L. Armanego, *Purification of Laboratory Chemicals*, 2nd ed., Pergmon, Oxford, U.K., **1980**.

Received November 18, 2003

 © 2004 Wiley-VCH Verlag GmbH & Co. KGaA, Weinheim

Multicomponent Ionic Complexes of Cobalt(II) Tetraphenylporphyrin with C_{60} Fullerides − Transition from the σ-Bonded [($Co^{II}TPP$)·(C_{60}^{-})] Anion to Nonbonded $Co^{II}TPP$ and $C_{60}^{\cdot-}$ Components

Dmitri V. Konarev,*[a,b] Ivan S. Neretin,[c] Gunzi Saito,*[a] Yury L. Slovokhotov,[c] Akihiro Otsuka,[a,d] and Rimma N. Lyubovskaya[b]

Keywords: Fullerenes / Porphyrinoids / Crystal engineering / Solid-state structures / IR and EPR spectroscopy

New multicomponent ionic complexes containing [(Cation$^+$)·(C_{60}^-)] fullerides and neutral $Co^{II}TPP$ molecules were obtained [the cations are Cs^+ (**1**), tetramethylammonium $(CH_3)_4N^+$ (**2**) and *N*-methylpyridinium *N*-$MePy^+$ (**3**)]. The crystal structure of **1** determined from single-crystal X-ray diffraction analysis contains chains of alternating $Co^{II}TPP$ and $C_{60}^{\cdot-}$ units with voids accommodating solvated [(Cs^+)·($C_6H_5CN)_{1.64}$]·CH_3CN counter cations. Relatively long Co···C distances between $Co^{II}TPP$ and $C_{60}^{\cdot-}$ in **1** (2.55–3.05 Å) indicate the absence of noticeable bonding of $Co^{II}TPP$ and $C_{60}^{\cdot-}$. This is consistent with the EPR spectrum of **1**, which manifests two EPR signals with g = 2.0009 and 2.4982 attributable to $C_{60}^{\cdot-}$ and $Co^{II}TPP$, respectively. In contrast to **1**, complexes **2** and **3** contain EPR-silent, σ-bonded [($Co^{II}TPP$)·(C_{60}^-)] anions. The influence of the size of counter cations on the stability of σ-bonded [($Co^{II}TPP$)·(C_{60}^-)] anions in ionic [(Cation$^+$)·($Co^{II}TPP$)·(C_{60}^-)] complexes is analyzed.

(© Wiley-VCH Verlag GmbH & Co. KGaA, 69451 Weinheim, Germany, 2004)

Introduction

Fullerene C_{60}-based compounds possess unique magnetic, conductive, and photoactive properties.[1,2] From this variety of compounds, fullerene assemblies with metal-containing porphyrins are of special interest due to possible applications in energy transducers and the modeling of artificial photosynthesis.[2,3] About several tens of fullerene donor−acceptor complexes ranging from molecular to ionic ones,[4−9] as well as covalently and noncovalently linked dyads and triads[3] were obtained with metal octaethyl- and tetraphenylporphyrins. In this context it is very important to understand the metal−fullerene interaction that occurs in such assemblies. Neutral fullerenes are considered to be relatively weak ligands when they coordinate with metal-containing porphyrins.[8,9] Among different metalloporphyrins only iron(II), iron(III), and cobalt(II) tetraphenylporphyrins form short M···C(C_{60}) contacts of 2.58−2.63, 2.57, and 2.58−2.69 Å, respectively, with C_{60}.[10−13] These contacts are shorter than the sum of the van der Waals radii of the M and C atoms, but essentially longer than typical M···C distances when a strong M···C bond is formed, for example, in alkylcobalamins (1.99−2.03 Å).[14]

The preparation of the multicomponent ionic complexes [{$Cr^I(C_6H_6)_2^{\cdot+}$}·($Co^{II}TPP$·fullerene$^-$)·($C_6H_4Cl_2$)] allows us to study the interaction of cobalt(II) tetraphenylporphyrin with fullerene radical anions of C_{60}, C_{70}, and $C_{60}CN_2$. It turned out that the fullerene radical anions are bound more strongly to $Co^{II}TPP$ than neutral fullerenes and form unusual diamagnetic σ-bonded ($Co^{II}TPP$·fullerene$^-$) anions with shortened Co···C(fullerene$^-$) distances of 2.28−2.32 Å.[13,15] However, these interatomic distances are longer than those for the strong M···C bond in alkylcobalamins and indicate a relatively weak σ-bond in ($Co^{II}TPP$·fullerene$^-$) anions. Therefore, the dissociation of these anions could be expected. Indeed, the study of another multicomponent ionic complex with bulkier tetrakis(dimethylamino)ethylene — [(TDAE$^{\cdot+}$)·($Co^{II}TPP$·C_{60}^-)] — indicates the presence of diamagnetic σ-bonded [$Co^{II}TPP$·C_{60}^-] anions in the 2−190 K range, which dis-

[a] Division of Chemistry, Graduate School of Science, Kyoto University,
Sakyo-ku, Kyoto 606-8502, Japan
Fax: (internat.) + 81-75-753-4035
E-mail: saito@kuchem.kyoto-u.ac.jp
konarev@kuchem.kyoto-u.ac.jp
[b] Institute of Problems of Chemical Physics RAS,
Chernogolovka, Moscow region 142432, Russia
Fax: (internat.) + 7-096-5155420
E-mail: konarev@icp.ac.ru
[c] Institute of Organoelement Compounds RAS,
28 Vavilov St., 119991, Moscow, Russia
Fax: (internat.) + 7-095-1355085
E-mail: slov@ineos.ac.ru
[d] Research Center for Low Temperature and Materials Sciences, Kyoto University,
Sakyo-ku, Kyoto 606-8502, Japan
Supporting information for this article is available on the WWW under http://www.eurjic.org or from the author.

 © 2004 Wiley-VCH Verlag GmbH & Co. KGaA, Weinheim **DOI: 10.1002/ejic.200300874**

sociate to paramagnetic and EPR-active, nonbonded Co^{II}-TPP and $C_{60}^{\cdot-}$ components at temperatures higher than 190 K.[16]

Here we report on new multicomponent ionic complexes containing [Cation$^+$·C_{60}^{-}] fullerides and neutral Co^{II}TPP, where the cations are Cs^+ (in **1**), tetramethylammonium $(CH_3)_4N^+$ (in **2**), and *N*-methylpyridinium *N*-MePy$^+$ (in **3**). The crystal structure of [(Cs^+)·$(Co^{II}TPP)$·$(C_{60}^{\cdot-})$·$(C_6H_5CN)_{1.64}$·$(C_6H_4Cl_2)_{0.36}$·CH_3CN] (**1**), the IR and EPR spectra of **1**, [{$(CH_3)_4N^+$}·$(Co^{II}TPP·C_{60}^{-})$·(C_6H_5CN)·$(C_6H_4Cl_2)$] (**2**), and [(*N*-MePy$^+$)·$(Co^{II}TPP·C_{60}^{-})$·$(C_6H_4Cl_2)_{1.2}$] (**3**) are presented. For the first time, the complex containing nonbonded Co^{II}TPP and $C_{60}^{\cdot-}$ components in the 4−290 K range is described and its properties are compared with those of the complexes containing diamagnetic σ-bonded [$Co^{II}TPP·C_{60}^{-}$] anions.

Results and Discussion

The resulting complexes are presented in Table 1. Crystals of **1**−**3** were obtained by diffusion of *n*-hexane into a solution containing the corresponding [Cation$^+$·$C_{60}^{\cdot-}$] salts and Co^{II}TPP in anaerobic conditions. The crystal structure of **1** was studied at 110 K.[17] Two crystallographically independent Co^{II}TPP molecules are located in inversion centers, whereas $C_{60}^{\cdot-}$, Cs^+, and the solvent C_6H_5CN, $C_6H_4Cl_2$, and CH_3CN molecules are in general positions. The $C_{60}^{\cdot-}$ units are disordered between two orientations (40:60 occupancy) related to each other by their rotation about the noncrystallographic fourfold axis passing through the molecular centroid and the midpoints of two 6−6 bonds.

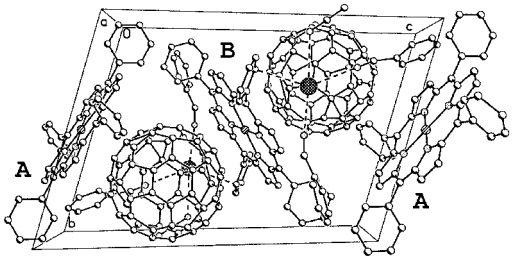

Figure 1. The crystal structure of **1**; the disordered $C_6H_4Cl_2$ molecules are omitted; only the major orientation of $C_{60}^{\cdot-}$ is shown

The main structural motif of the complex is a zigzag chain of alternating Co^{II}TPP and $C_{60}^{\cdot-}$ molecules (Figure 1). Similar motifs were found in the neutral complexes of fullerenes with both metal-containing and metal-free tetraphenylporphyrins.[5−7,13] Each C_{60} unit forms shortened contacts with two Co^{II}TPP molecules (Figure 1). The shortest Co···C(C_{60}) contacts are in the 2.55−3.07 Å range for both orientations of C_{60}. These contacts are of the σ-type (Figure 2); however, they are longer than those in the σ-bonded diamagnetic [$Co^{II}TPP·fullerene^{-}$] anions (fullerene: C_{60} and $C_{60}CN_2$; 2.28−2.32 Å)[13,15] and close to those in the neutral complexes of Fe^{II}, Fe^{III}, and Co^{II}TPP with C_{60} (2.57−2.69 Å)[10−13]. Thus, in contrast to the previously studied ionic complexes [{$Cr^{I}(C_6H_6)_2^{\cdot+}$}$_{1.7}$·{$(Co^{II}TPP·C_{60})_2$}$^{1.7-}$·$(C_6H_4Cl_2)_{3.3}$] and [$(TDAE^{\cdot+})$·$(Co^{II}TPP·C_{60}^{-})$], **1** contains nonbonded Co^{II}TPP and $C_{60}^{\cdot-}$ components at 110 K. The weakness of the Co···$C_{60}^{\cdot-}$ bonding in **1** is also justified by the rotation disorder of the $C_{60}^{\cdot-}$ radical anions, whereas they are ordered in the complex [{$Cr^{I}(C_6H_6)_2^{\cdot+}$}$_{1.7}$·{$(Co^{II}TPP·C_{60})_2$}$^{1.7-}$·$(C_6H_4Cl_2)_{3.3}$].[13] A dihedral angle of 63.8° between the planes of the porphyrin macrocycles of **A** and **B** (Figure 1) is larger in **1** than those in the neutral complexes of tetraphenylporphyrins with fullerenes: 39.0° in [$Cu^{II}TPP·C_{70}$·$(C_6H_5Me)_{1.5}$·$(Cl_2C=CHCl)_{0.5}$];[6] 44.1° in [$Co^{II}TPP·C_{60}$·$(C_6H_4Cl_2)_{2.5}$],[13] and 45.3° in [$H_2TPP·C_{60}$·$(C_6H_5Me)_3$].[5]

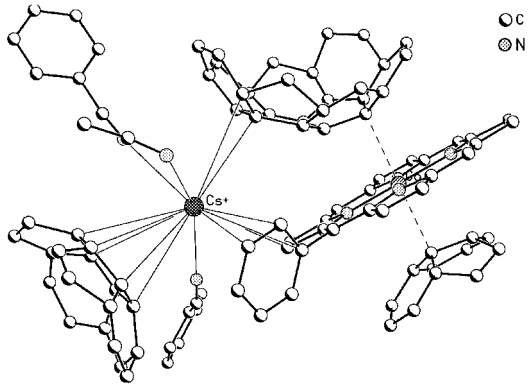

Figure 2. Coordination surrounding of the Cs^+ cation and the cobalt atom of Co^{II}TPP in the crystal structure of **1**; the disordered $C_6H_4Cl_2$ molecules are omitted; only the major orientation of $C_{60}^{\cdot-}$ is shown

Table 1. The data for crystals of **1**−**3**

No.	Complex	Elemental analysis found/calcd. C	H,	N,	Cl,	Difference (%)[a]	Shape
1	$Cs·Co^{II}TPP·C_{60}·(C_6H_5CN)_{1.64}(C_6H_4Cl_2)_{0.36}·CH_3CN$	According to X-ray diffraction data					prisms
2	{$(CH_3)_4N$}·$(Co^{II}TPP·C_{60})$·(C_6H_5CN)·$(C_6H_4Cl_2)$	81.36/ 82.30	3.02/ 2.94	4.66/ 5.04	3.67/ 4.26	7.29/ 3.54 (Co), 1.92 (O)	prisms
3	*N*-MePy·$Co^{II}TPP·C_{60}$·$(C_6H_4Cl_2)_{1.2}$	81.14/ 82.98	2.72/ 2.42	4.12/ 4.15	4.99/ 5.05	7.03/ 3.50 (Co), 1.90 (O)	prisms

[a] The difference (100 %) − (C, H, N, Cl %).

 © 2004 Wiley-VCH Verlag GmbH & Co. KGaA, Weinheim

Cesium cations occupy the voids in the $Co^{II}TPP$ and $C_{60}^{\cdot-}$ packing and have an irregular environment. The coordination sphere of Cs^+ (Figure 2) involves nitrogen atoms of one CH_3CN and two disordered C_6H_5CN molecules, six carbon atoms from a hexagonal facet of one $C_{60}^{\cdot-}$ in one orientation or five carbon atoms from a pentagonal facet in the other orientation, two carbon atoms of a 6−6 bond of another closest $C_{60}^{\cdot-}$ (in both orientations), and four carbon atoms from phenyl substituents of $Co^{II}TPP$. The total number of carbon and nitrogen atoms coordinated to Cs^+ is 15; the Cs···N distances are in the 3.05−3.21 Å range and the Cs···C distances in the 3.43−3.86 Å range. However, the (Cs^+)···$(C_{60}^{\cdot-})$ interaction is unable to lower the rotational disorder of $C_{60}^{\cdot-}$. In other Cs^+-containing compounds (according to the Cambridge Structural Database) the coordination number of Cs varies between 14−19, the Cs···N distances are in the range 3.07−3.30 Å, and the Cs···C distances are in the range 3.44−3.69 Å. Cesium fulleride Cs_6C_{60}[18] provides an example of a carbon-only coordination sphere of Cs that contains 22 atoms with Cs···C(C_{60}) distances of 3.37−3.69 Å.

Fullerene radical anions are located in pairs isolated from one another by the $Co^{II}TPP$ molecules and the $[(Cs^+)\cdot(C_6H_5CN)_{1.64}\cdot(C_6H_4Cl_2)_{0.36}\cdot CH_3CN]$ aggregates. A center-to-center distance between two $C_{60}^{\cdot-}$ radical anions in the pair is 9.88 Å and the interfullerene C···C distances are in the range 3.07−3.48 Å. The intercenter and the interfullerene C···C contacts in the pair of $C_{60}^{\cdot-}$ are slightly shorter than those in van der Waals neutral complexes of C_{60}.[19] It is quite unusual that in spite of the rather short C···C contacts between $C_{60}^{\cdot-}$, they are not dimerized at temperatures as low as 110 K, whereas in various ionic complexes of C_{60} with metallocenes, such dimerization is observed even at 160−250 K.[20]

The porphyrin macrocycle of $Co^{II}TPP$ retains its planar shape (the root-mean-square deviation of atoms from the mean plane in the porphyrin macrocycle is only 0.017 and 0.015 Å for molecules **A** and **B** in Figure 1, respectively). Such conformation is characteristic of most of the metal-containing tetraphenylporphyrins in the complexes with C_{60}.[5−7,13] The cobalt atom of $Co^{II}TPP$ does not deviate from the mean plane of the porphyrin macrocycle towards the fullerene indicating the absence of noticeable Co···C($C_{60}^{\cdot-}$) bonding in **1**. On the contrary, these deviations are essentially larger (0.091−0.113 Å) in $[\{Cr^I(C_6H_6)_2^{\cdot+}\}\cdot(Co^{II}TPP\cdot fullerene^-)\cdot C_6H_4Cl_2]$ (fullerene: C_{60} and $C_{60}CN_2$).[13,15]

Thus, complex **1** differs from the previously studied multicomponent ionic complexes of $Co^{II}TPP$ with C_{60}^- by the presence of nonbonded $Co^{II}TPP$ and $C_{60}^{\cdot-}$ components. The IR and EPR spectra of **1** support this assertion.

The IR spectrum of **1** is a superposition of the spectra of neutral $Co^{II}TPP$, $C_{60}^{\cdot-}$, and solvent molecules.[21] The position of the $F_{1u}(4)$ C_{60} mode at 1397 cm^{-1} coincides with those for other radical anion salts of C_{60} with a −1 charge on the C_{60} molecule.[22,23] The integral intensity of the $F_{1u}(2)$ mode at 576 cm^{-1} is also essentially higher than that of the $F_{1u}(1)$ mode at 526 cm^{-1}. The bands attributable to "silent" modes of C_{60} are not observed in the spectrum of **1**[21] indicating the retention of $C_{60}^{\cdot-}$ symmetry and the absence of noticeable σ-bonding between $Co^{II}TPP$ and $C_{60}^{\cdot-}$ at room temperature (RT = 290 K). On the contrary, the formation of σ-bonded ($Co^{II}TPP\cdot C_{60}^-$) anions in $[\{Cr^I(C_6H_6)_2^{\cdot+}\}_{1.7}\cdot\{(Co^{II}TPP\cdot C_{60})_2\}^{1.7-}\cdot(C_6H_4Cl_2)_{3.3}]$ results in the appearance of weak additional bands due to C_{60} symmetry breaking.[13]

The EPR spectrum of **1** contains two intense EPR signals with g = 2.0009 [Figure 3 (a)] and 2.4982 [(Figure 3 (b)] and the line halfwidth (ΔH) of 4.78 and 51.2 mT, respectively. The total integrated intensity of these signals corresponds to approximately two spins per one formula unit. On the contrary, the σ-bonded ($Co^{II}TPP\cdot C_{60}^-$) anions are diamagnetic and EPR silent.[13,15,16] The first signal in **1** is unambiguously attributed to the nonbonded $C_{60}^{\cdot-}$ radical anions. The line halfwidth of this signal monotonically decreases down to 0.3 mT at 4 K. Such behavior is also characteristic of the EPR signal from $C_{60}^{\cdot-}$. The second signal can be attributed to $Co^{II}TPP$ with S = 1/2 ground state. This signal is essentially different from that of the parent porphyrin $Co^{II}TPP$ (the asymmetric signal with $g_\perp$ = 3.322 and g_{II} = 1.798)[24] and similar to the EPR signals from $Co^{II}TPP$ in the neutral complexes with fullerenes C_{60}, C_{70}, and $C_{60}CN_2$ (the asymmetric signals with $g_\perp$ = 2.51−2.64 and ΔH = 15−30 mT, g_{II} = 2.28−2.42 and ΔH = 31−45 mT).[13] The difference implies that the EPR signal in **1** is a symmetric Lorentzian line down to 4 K, whereas the EPR signals in the neutral complexes with fullerenes are asymmetric and contain two components down to 4 K. The g-factor of the EPR signal of $Co^{II}TPP$ in **1** shifts to smaller values as the temperature decreases

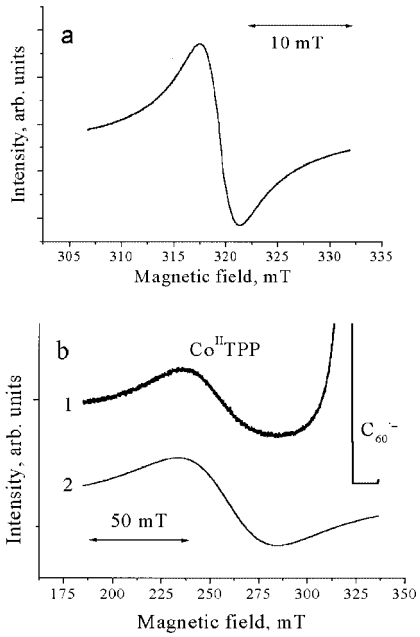

Figure 3. EPR spectrum of polycrystalline **1** at T = 290 K; (a) the signal attributable to $C_{60}^{\cdot-}$; (b) the signals attributable to $Co^{II}TPP$ and $C_{60}^{\cdot-}$ (1); the simulation of the signal from $Co^{II}TPP$ by one Lorentzian line is shown below (2)

 © 2004 Wiley-VCH Verlag GmbH & Co. KGaA, Weinheim

and the line halfwidth becomes narrower (g = 2.3785 and ΔH = 41.5 mT at 4 K).

When Rb was used instead of Cs, in the absence of CH_3CN, the complex [(Rb^+)·$Co^{II}TPP$·$(C_{60}^{\cdot-})$] did not crystallize. We used the reaction of cationic metathesis to substitute the Rb^+ counter cations for other small cations such as Me_4N^+ (in **2**) and *N*-$MePy^+$ (in **3**). The crystallization of these complexes by the diffusion of *n*-hexane affords [(Me_4N^+)·$(Co^{II}TPP$·$C_{60}^-)$·(C_6H_5CN)·$(C_6H_4Cl_2)$] (**2**), and [$(N$-$MePy^+)$·$(Co^{II}TPP$·$C_{60}^-)$·$(C_6H_4Cl_2)_{1.2}$] (**3**). The IR spectra of **2** and **3** justify their ionic ground state (the spectra manifest the absorption bands attributable to $C_{60}^{\cdot-}$) and show additional silent modes of C_{60} due to its symmetry breaking.[21] The EPR spectra of **2** and **3**, in contrast to **1**, show no signals from 290 down to 4 K indicating the formation of diamagnetic and EPR-silent σ-bonded ($Co^{II}TPP$·C_{60}^-) anions, which are stable in the 4−290 K range.

Thus, two extreme cases can be found in **1**−**3**. Complex **1** contains nonbonded $Co^{II}TPP$ and $C_{60}^{\cdot-}$ components in the 4−290 K range, whereas complexes **2** and **3** contain σ-bonded ($Co^{II}TPP$·C_{60}^-) anions stable in the 4−290 K range. Previously studied ionic [$\{Cr^I(C_6H_6)_2^{\cdot+}\}_{1.7}$·$\{(Co^{II}TPP$·$C_{60})_2\}^{1.7-}$·$(C_6H_4Cl_2)_{3.3}$][13] and [$(TDAE^{\cdot+})$·$(Co^{II}TPP$·$C_{60}^-)$][16] are intermediates between **1**, and complexes **2** and **3**. At low temperatures they contain σ-bonded [$Co^{II}TPP$·C_{60}^-] anions. The broadening of the EPR signal above 200 K in [$\{Cr^I(C_6H_6)_2^{\cdot+}\}_{1.7}$·$\{(Co^{II}TPP$·$C_{60})_2\}^{1.7-}$·$(C_6H_4Cl_2)_{3.3}$] can be associated with the appearance of a small contribution from nonbonded $Co^{II}TPP$ and $C_{60}^{\cdot-}$.[16] Evident dissociation of σ-bonded ($Co^{II}TPP$·C_{60}^-) anions to nonbonded $Co^{II}TPP$ and $C_{60}^{\cdot-}$ components is observed in [$(TDAE^{\cdot+})$·$(Co^{II}TPP$·$C_{60}^-)$] above 190 K, and it is accompanied by an increase of the magnetic moment, the essential broadening of the EPR line, and the shift of its *g*-factor to larger values. At 290 K approximately 20 % of total $Co^{II}TPP$ and $C_{60}^{\cdot-}$ exists in a nonbonded state.[16]

The temperature ranges of the existence of σ-bonded ($Co^{II}TPP$·C_{60}^-) anions in the ionic multi-component complexes of $Co^{II}TPP$ with C_{60}^- and the counter cations used are listed in Table 2. The complexes are given in Table 2 in order of increasing size of the counter cations. The increase in the size of counter cations is seen to destabilize the σ-bonded [$Co^{II}TPP$·C_{60}^-] anions. The use of large cations like Cs^+ solvated by one CH_3CN and nearly two C_6H_5CN molecules forces the units $Co^{II}TPP$ and $C_{60}^{\cdot-}$ apart, and does not allow them to approach each other so closely to form a Co···C($C_{60}^{\cdot-}$) σ-bond. Thus, in spite of the obvious ability of $Co^{II}TPP$ and $C_{60}^{\cdot-}$ to form σ-bonds, steric factors (namely, the size of the counter cations) also determine the possibility of the formation of σ-bonded [$Co^{II}TPP$·C_{60}^-] anions. Similarly, in ionic charge transfer complexes of C_{60} with metallocenes, the stability of single-bonded $[C_{60}^-]_2$ dimers varies in a wide range (the beginning of dissociation is in the 160−250 K range) and is determined by the size of the donor and even the solvent molecules involved in the complex.[20]

Experimental Section

General Remarks: $Co^{II}TPP$ and Me_4NI were purchased from Aldrich. *N*-MePyI was obtained by the reaction of Py with MeI and then recrystallized from *N*,*N*-dimethylformamide. C_{60} of 99.98 % purity was purchased from MTR Ltd. All solvents were distilled under argon: *o*-dichlorobenzene ($C_6H_4Cl_2$) over CaH_2, benzonitrile (C_6H_5CN) over Na/benzophenone under reduced pressure, acetonitrile over CaH_2, P_2O_5, and K_2CO_3. The solvents were degassed prior to use and were stored in a glove box. All manipulations during the synthesis and isolation of the crystals of **1**−**3** were carried out in a MBraun 150B-G glove box; the content of H_2O and O_2 was less than 1 ppm. The crystals were stored in the glove box and sealed in 2 mm quartz tubes for EPR measurements under 10^{-5} Torr. KBr pellets for IR measurements were also prepared in the glove box. UV-Vis-NIR spectra were measured on a Shimadzu-3100 spectrometer in the 240−2600 nm range. FT-IR spectra were measured with KBr pellets on a Perkin−Elmer 1000 Series spectrometer (400−7800 cm^{-1}). EPR spectra were recorded down to 4 K with a JEOL JES-TE 200 X-band ESR spectrometer equipped with a JEOL ES-CT470 cryostat.

Synthesis: The crystals of **1**−**3** were obtained by the diffusion of *n*-hexane into a solution containing the corresponding [$C_{60}^{\cdot-}$·Cation$^+$] salt and $Co^{II}TPP$ porphyrin complex. The diffusion was carried out in a glass tube of 1.5 cm in diameter and 40 mL volume with a ground glass plug. The crystals of **1**−**3** were formed as large black prisms of up to 1 × 1 × 0.5 mm^3. The composition of the compounds was determined from X-ray diffraction on a single crystal for **1** and by elemental analysis for **2** and **3** (Table 1). In **2** and **3**, the difference [(100 %)-(C, H, N, Cl, %)] exceeds the calculated content of metals (Co and Cr) indicating the addition of oxygen to the complexes during the elemental analysis. Indeed, the complexes are sensitive to oxygen. The addition of ap-

Table 2. The temperature ranges in which σ-bonded ($Co^{II}TPP$·C_{60}^-) anions exist in ionic multicomponent complexes

Complex	The temperature in which σ-bonded ($Co^{II}TPP$·C_{60}^-) anions exist, (K)	Counter cation
$\{(CH_3)_4N^+\}$·($Co^{II}TPP$·C_{60}^-)·(C_6H_5CN)·$(C_6H_4Cl_2)$	4−290	$(CH_3)_4N^+$
$(N$-$MePy^+)$·($Co^{II}TPP$·C_{60}^-)·$(C_6H_4Cl_2)_{1.2}$	4−290	N-$MePy^+$
$\{Cr^I(C_6H_6)_2^{\cdot+}\}_{1.7}$·$\{(Co^{II}TPP$·$C_{60})_2\}^{1.7-}$·$(C_6H_4Cl_2)_{3.3}$	4−290, probable appearance of contribution from nonbonded $Co^{II}TPP$ and ($C_{60}^{\cdot-}$) above 200 K	$Cr^I(C_6H_6)_2^{\cdot+}$
$(TDAE^{\cdot+})$·($Co^{II}TPP$·C_{60}^-)	4−190	$TDAE^{\cdot+}$
(Cs^+)·$Co^{II}TPP$·$(C_{60}^{\cdot-})$·$(C_6H_5CN)_{1.64}(C_6H_4Cl_2)_{0.36}$·$CH_3CN$	does not exist	(Cs^+)·$(C_6H_5CN)_{1.64}$·CH_3CN

 © 2004 Wiley-VCH Verlag GmbH & Co. KGaA, Weinheim

proximately one O_2 molecule per one formula unit of the complex is observed. Thus, the calculated C, H, N, and Cl (%) content was corrected for the composition (Formula unit:O_2). We assumed that oxygenation occurring during elemental analysis was extrinsic and omitted oxygen throughout the manuscript.

Complex 1: The cesium salt of fullerene $(Cs^+)\cdot(C_{60}^{\cdot-})$ was obtained by the dissolution of C_{60} (25 mg, 0.035 mmol) with Cs (5.2 mg, 0.038 mmol) in benzonitrile which was stirred for 2 hours at 60 °C. The purity of the salt was justified by the presence of characteristic $(C_{60}^{\cdot-})$ absorption bands in the solution NIR spectrum. The solution was cooled down to room temp. filtered, and $C_6H_4Cl_2$ and CH_3CN were added (the $C_6H_4Cl_2/C_6H_5CN/CH_3CN$ volume ratio is 50:45:5, the total volume is 20 mL). $Co^{II}TPP$ (23.5 mg, 0.035 mmol) was dissolved in this solution at 60 °C; the resulting solution was cooled down to room temp., filtered into a glass tube and layered with *n*-hexane (20 mL). Crystals of **1** that precipitated after 1 month were washed with *n*-hexane and dried (yield 31 mg, 50 %).

Complexes 2 and 3: Complexes **2** and **3** were obtained similarly. The $(Rb^+)\cdot(C_{60}^{\cdot-})$ complex was obtained by the dissolution of C_{60} (100 mg, 0.14 mmol) with Rb (13.2 mg, 0.152 mmol) in benzonitrile (40 mL) at 60 °C by stirring for 2 hours. The solution was cooled down to room temp. and filtered. The purity of the $(Rb^+)\cdot(C_{60}^{\cdot-})$ salt was justified by the solution NIR spectrum. The solution 10 mL) containing of $(Rb^+)\cdot(C_{60}^{\cdot-})$ was treated with an excess of tetramethylammonium iodide (**2**) or *N*-methylpyridinium iodide (**3**) at 60 °C. After 4 hours the solution was cooled down, filtered, and mixed with $C_6H_4Cl_2$ at a 50:50 volume ratio (the total volume was 20 mL). $Co^{II}TPP$ (23.5 mg, 0.035 mmol) was dissolved in the obtained solution at 60 °C, allowed to cool to room temp., filtered into a glass tube and layered with *n*-hexane (20 mL). Crystals of **2** and **3** that precipitated after 1 month were washed with *n*-hexane and dried (yield 30 mg, 50% for **2**; 34.6 mg, 60% for **3**).

X-ray Crystallographic Study: X-ray diffraction data were collected at 110 K on a Bruker SMART CCD diffractometer with an area detector (sealed tube, Mo-K_α radiation, $\lambda = 0.71073$ Å). A series of three ω scans with a 0.3° frame width were collected. Reflection intensities were integrated using the SAINT program.[25] The structure was solved with direct methods using SHELXTL program package[26] and refined by full-matrix least-squares on F^2. The ordered non-hydrogen atoms were refined anisotropically. Hydrogen atoms were placed in calculated positions and refined within the "riding atom" model. Both C_6H_5CN molecules are statistically substituted by $C_6H_4Cl_2$ ones per 20 % and 16 %. One of the $Co^{II}TPP$ phenyl rings is also disordered between two positions in a 40:60 ratio.

Acknowledgments

The work was supported by the COE Research on Elements Science 12CE2005, JSPS, and the RFBR grants N 03−03−32699a and 02−03−33225a.

[1] D. V. Konarev, R. N. Lyubovskaya, *Russ. Chem. Reviews* **1999**, *68*, 19−38.
[2] N. S. Sariciftci, A. J. Heeger, *in Handbook of Organic Conductive Molecules and Polymers*, (Ed. H. S. Nalwa), John Wiley & Sons Ltd., **1997**, *1*, 414.
[3] D. M. Guldi, *Chem. Soc. Rev.* **2002**, *31*, 22−36.
[4] M. M. Olmstead, D. A. Costa, K. Maitra, B. C. Noll, S. L. Phillips, P. M. Van Calcar, A. L. Balch, *J. Am. Chem. Soc.* **1999**, *121*, 7090−7097.
[5] P. D. W. Boyd, M. C. Hodgson, C. E. F. Rickard, A. G. Oliver, L. Chaker, P. J. Brothers, R. D. Bolskar, F. S. Tham, C. A. Reed, *J. Am. Chem. Soc.* **1999**, *121*, 10487−10495.
[6] D. V. Konarev, I. S. Neretin, Y. L. Slovokhotov, E. I. Yudanova, N. V. Drichko, Y. M. Shul′ga, B. P. Tarasov, L. L. Gumanov, A. S. Batsanov, J. A. K. Howard, R. N. Lyubovskaya, *Chem. Eur. J.* **2001**, *7*, 2605−2616.
[7] D. V. Konarev, A. Y. Kovalevsky, X. Li, I. S. Neretin, A. L. Litvinov, N. V. Drichko, Y. L. Slovokhotov, P. Coppens, R. N. Lyubovskaya, *Inorg. Chem.* **2002**, *41*, 3638−3646.
[8] A. Pénicaud, J. Hsu, C. A. Reed, A. Koch, K. Khemani, P.-M. Allemand, F. Wudl, *J. Am. Chem. Soc.* **1991**, *113*, 6698−6700.
[9] J. Stinchcombe, A. Pénicaud, P. Bhyrappa, P. D. V. Boyd, C. A. Reed, *J. Am. Chem. Soc.* **1993**, *115*, 5212−5217.
[10] S. Mikami, K. Sugiura, E. Asato, Y. Maeda, Y. Sakat, *The* P*roceeding of the conference "The 19th Fullerene General Symposium*", Kiryu, Japan, July 27−28, **2000**, p. 40.
[11] D. R. Evans, N. L. P. Fackler, Z. Xie, C. E. F. Rickard, P. D. W. Boyd, C. A. Reed, *J. Am. Chem. Soc.* **1999**, *121*, 8466−8474.
[12] T. Ishii, R. Kenehama, N. Aizawa, M. Yamashita, H. Matsuzaka, K. Sugiura, H. Miyasaka, T. Kodama, K. Kukuchi, I. Ikemoto, H. Tanaka, K. Marumoto, S.-I. Kuroda, *J. Chem. Soc., Dalton Trans.* **2001**, 2975−2980.
[13] D. V. Konarev, S. S. Khasanov, A. Otsuka, Y. Yoshida, R. N. Lyubovskaya, G. Saito, *Chem. Eur. J.* **2003**, *9*, 3837−3848.
[14] M. Rossi, J. P. Glusker, L. Randaccio, M. F. Summers, P. J. Toscano, L. G. Marzilli, *J. Am. Chem. Soc.* **1985**, *107*, 1729−1738.
[15] D. V. Konarev, S. S. Khasanov, A. Otsuka, Y. Yoshida, G. Saito, *J. Am. Chem. Soc.* **2002**, *124*, 7648−7649.
[16] D. V. Konarev, I. S. Neretin, G. Saito, Y. L. Slovokhotov, A. Otsuka, R. N. Lyubovskaya, *Dalton Trans.* **2003**, 3886−3891.
[17] Crystallographic data for **1**: $C_{119.64}H_{40.64}Cl_{0.72}CoCsN_{6.64}$, $M_r = 1788.23$ g·mol^{-1}, black prisms, triclinic, $P\bar{1}$, $a = 13.553(3)$, $b = 14.096(4)$, $c = 20.734(5)$ Å, $\alpha = 105.108(5)$, $\beta = 106.148(5)$, $\gamma = 92.160(5)°$, $V = 3642(1)$ Å^3, $Z = 2$, $d_{calcd.} = 1.631$ g·cm^{-3}, $T = 110$ K, $\mu = 0.82$ mm^{-1}, $F(000) = 1798$, max. $2\theta = 50.0°$, $R_{int} = 0.0338$ for 30069 measured and 12793 unique reflections, $R[I > 2\sigma(I)] = 0.1215$, $wR_2 = 0.2731$, GooF = 0.818. CCDC-224942 contains the supplementary crystallographic data for this paper. These data can be obtained free of charge at www.ccdc.cam.ac.uk/conts/retrieving.html [or from the Cambridge Crystallographic Data Centre, 12, Union Road, Cambridge CB2 1EZ, UK; fax: (internat.) +44-1223-336-033; E- mail: deposit@ccdc.cam.ac.uk].
[18] O. Zhou, J. E. Fischer, N. Coustel, S. Kycia, Q. Zhu, A. R. McGhie, W. J. Romanow, J. P. McCauley Jr, A. B. Smith III, D. E. Cox, *Nature* **1991**, *351*, 462−464.
[19] D. V. Konarev, R. N. Lyubovskaya, N. V. Drichko, E. I. Yudanova, Y. M. Shul′ga, A. L. Litvinov, V. N. Semkin, B. P. Tarasov, *J. Mat. Chem.* **2000**, 803−818.
[20] D. V. Konarev, S. S. Khasanov, G. Saito, A. Otsuka, Y. Yoshida, R. N. Lyubovskaya, *J. Am. Chem. Soc.* **2003**, *125*, 10074−10083.
[21] see Supporting Information.
[22] V. N. Semkin, N. G. Spitsina, S. Krol, A. Graja, *Chem. Phys. Lett.* **1996**, *256*, 616−622.
[23] T. Picher, R. Winkler, H. Kuzmany, *Phys. Rev. B, Solid State* **1994**, *49*, 15879−15889.
[24] J. M. Assour, *J. Chem. Phys.* **1965**, *43*, 2477−2489.
[25] *SMART and SAINT, Area detector control and integration software*, Version 6.01, Bruker Analytical X-ray Systems, Madison, WI, **1999**.
[26] *SHELXTL, An integrated system for solving, refining and displaying crystal structures from diffraction data*, Version 5.10, Bruker Analytical X-ray Systems, Madison, WI, USA, **1997**.

Received November 26, 2003

 © 2004 Wiley-VCH Verlag GmbH & Co. KGaA, Weinheim

One-Pot Synthesis of Superparamagnetic CoO-MCM-41 Nanocomposites with Uniform and Highly Dispersed Magnetic Nanoclusters

Jamal El Haskouri,[a] Saúl Cabrera,[b] Carmen Guillem,[a] Julio Latorre,[a] Aurelio Beltrán,[a] M. Dolores Marcos,[d] Carlos J. Gómez-García,[c] Daniel Beltrán,[a] and Pedro Amorós*[a]

Keywords: Mesoporous materials / Nanocomposites / Superparamagnetism / Nanoparticles / Nanotechnology

Superparamagnetic CoO-MCM-41 mesoporous nanocomposites, with variable cobalt amounts, in the form of well-dispersed CoO-like clusters, were prepared in a large compositional range by a one-step reproducible procedure employing co-hydrolysis and co-condensation of the inorganic precursors in a water/triethanolamine medium.
(© Wiley-VCH Verlag GmbH & Co. KGaA, 69451 Weinheim, Germany, 2004)

Introduction

The growing interest on uniform nanometric particles is related to the novel properties associated with systems that are intermediate in size between isolated atoms or molecules and bulk materials.[1] These properties extend the interest in nanostructured materials not only to evident areas, such as microelectronics or catalysis, but also to more original applications, such as the separation of magnetically-labelled biomolecules. In fact, magnetic nanomaterials are currently considered the most promising candidates for data-storage devices, due to the possibility of exploiting the quantum-tunnelling of magnetization effect, which is typical of nanomagnets.[2] Notwithstanding, the special properties of nanoparticulate materials strongly depend on morphological aspects. Control of the size and shape of the particles and the attainment of good dispersity levels are essential requirements.[2] In addition, the use of nanoparticles is limited because of their tendency to form large aggregates, which means that the properties associated with the nanometer range are lost. A well-known solution to overcome this problem consists in the dispersion and/or encapsulation of the nanoparticles in an inert matrix. Indeed, nanosized magnetic materials have been produced by using polymers as a support.[3,4] In this context, silica-based micro- and mesoporous solids, such as zeolites and MCM-41-like materials, are attracting increasing attention as a way to stabilize highly dispersed metal or metal oxide particles.[5] In practice, the functionality of the M41 mesoporous solids has been greatly expanded in recent years by incorporating organic groups or inorganic elements in the pore voids and/or inside the silica walls. Thus, in the search for magnetic materials, a diversity of guest species (semiconductors, metals, metal oxides, clusters, organic molecules, and even single-molecule magnets) have been hosted in the M41 matrices.[6−14] There are relatively few studies concerning Co-containing related materials. These studies are basically focussed on catalytic applications and involve materials in which the cobalt load was carried out after the matrix synthesis.[15−19] As far as we know, there are only two previous publications dealing with the magnetic properties of nanometric cobalt oxides hosted in MCM-41 solids, and, in both cases, the nanocomposites were prepared by post-synthesis impregnation treatments.[20,21] Although soaking really is a common procedure for functionalizing mesoporous silicas, this approach is multistep and, more importantly, frequently leads to necking or even blocking of the pore system.

We report here on a one-pot, reproducible surfactant-assisted procedure yielding superparamagnetic CoO-MCM-

[a] Institut de Ciència dels Materials (ICMUV), Universitat de València,
P. O. Box 2085, 46071 València, Spain
Fax: (internat) + 34-96-3543633
E-mail: pedro.amoros@uv.es
[b] Laboratorio de Sólidos y Química Teórica, Instituto de Investigaciones Químicas UMSA,
Cota-Cota, Calle n° 27, La Paz, Bolivia
E-mail: solidos@megalink.com
[c] Instituto de Ciencia Molecular, Universidad de Valencia,
Doctor Moliner 50, 46100 Burjassot (Valencia), Spain
Fax: (internat) + 34-96-3544859
E-mail: carlos.gomez@uv.es
[d] Departamento de Química, Universidad Politécnica de Valencia,
Camino de Vera s/n, 46071 Valencia, Spain
Fax: (internat) + 34-96-3879349
E-mail: mmarcos@qim.upv.es

41 mesoporous nanocomposites, in which the high dispersion of the CoO-like nanoclusters inside the silica walls is maintained for a high compositional range (up to Si/Co = 23 molar ratio) without blocking of the mesopore system.

Results and Discussion

Mesoporous materials of the MCM-41 type that are rich in CoO-like nanoclusters were synthesized through a one-pot approach using CTABr as a surfactant in a $TEAH_3$–water medium (CTABr = cetyltrimethylammonium bromide; $TEAH_3$ = triethanolamine). The molar ratio of the reagents in the starting solution was 2 Si: *x* Co: 7 $TEAH_3$: 0.50 NaOH/ 0.50 CTABr: 180 H_2O (see Table 1). Our synthesis strategy is based on the use of complexes containing $TEAH_3$ ligands as hydrolytic inorganic precursors. Under basic conditions, and working in an excess of $TEAH_3$, this method unifies the precursor nature (by forming metal-atranes) and it favours the preparation (through co-hydrolysis) of mixed oxides displaying a high chemical homogeneity.[22] Moreover, this approach overcomes, as far as possible, problems related to restrictions on the final stoichiometry. In any case, we should not forget that the replacement of silicon atoms by divalent transition metal cations in a silica matrix is a thermodynamically unfavourable process, and phase segregation must be expected a priori. Thus, the preparative technique is designed to optimize the dispersion of the Co-guest species in the mesoporous host matrix.

EPMA data show that all the samples are chemically homogeneous at micrometric level (spot area about 1μm). Furthermore, only one type of particle morphology, with a hexagonal microstructure that becomes progressively distorted as the Co content increases, is observed in the TEM images of each sample (see Figure 1). Also, the absence of XRD peaks (characteristic of cobalt oxides) at high 2θ values confirms that no extra wall-phase segregation occurs. Hence, at the present scale, which is limited by these techniques, the samples can be considered CoO-MCM-41 monophasic systems. Consequently, the maximum expected dimensions of the possible CoO-like aggregates should be close to the pore-wall size.

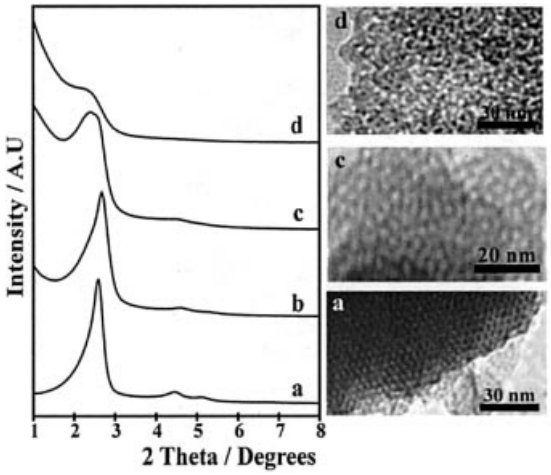

Figure 1. XRD patterns and selected TEM images of CoO-MCM-41 samples; (a) Si/Co = 155; (b) Si/Co = 98; (c) Si/Co = 49; (d) Si/Co = 23

All the samples show XRD patterns that are characteristic for mesoporous hexagonal MCM-41 materials, with at least one strong peak in the low-angle zone and two additional small reflections (exception made of the sample with Si/Co = 23) at higher 2θ values. Nevertheless, the quality and definition of the XRD patterns diminishes as the Co content increases. This evolution indicates progressive lowering of order in the pore array as the cobalt content increases, from ordered hexagonal through disordered hexagonal to wormhole-like systems. The trend is clearly confirmed by the TEM micrographs (see Figure1). Additionally the cell parameter increases with the Co content (see Table 1), an effect typically induced by an effective incorporation of heteroelements in the pore wall of the mesoporous silicas.[23] This behaviour probably results form the interaction of the heteroelement in the growing of the silica network in one-pot (co-hydrolysis) synthesis methods. In our case it could be attributed to a poor charge matching between the CTABr and silica moieties due to the cobalt species, which, in turn, would constitute an indirect probe of the incorporation of cobalt in the pore walls. On the contrary, in mesoporous silicas with metal oxide nanoparticles filling the pores or coating the pore surfaces, prepared through post synthesis treatments, the a_0 value does not significantly depend on the nanoparticle amount.[13,14,17]

Table 1. Co content and selected physical data for CoO-MCM-41

Si/Co (solid)[a]	a_0 [nm][b]	Pore size [nm]	S_{BET} [$m^2\ g^{-1}$]	Pore-wall thickness [nm]
155	3.80	2.50	908.5	1.30
98	3.80	2.48	662.0	1.32
49	4.09	2.47	526.3	1.63
23	4.14	2.50	478.6	1.64

[a] Values averaged from the EPMA of about 40 different particles. [b] Calculated cell parameters assuming an MCM-41 type hexagonal cell.

 © 2004 Wiley-VCH Verlag GmbH & Co. KGaA, Weinheim

The loss of X-ray intensity observed in the XRD, corresponding to the solid with the highest Co content, must be attributed to a significant loss of order more than to phase-cancellation phenomena, which are associated with the introduction of scattering material into the pores or to a partial collapse of the mesostructure. In fact, as indicated above, the observation by TEM of a single type of particle of homogeneous morphology containing mesopores allows us to discard the presence of collapsed bulk materials.

Mesoporosity is evaluated by N_2 adsorption−desorption isotherms (see Figure 2). All the curves display one well-defined step at intermediate P/P_0 values typical of type IV isotherms. Although incorporation of Co results in a gradual decrease of the surface area, the high surface area and porosity, characteristic of the MCM-41 silica, are retained in all cases. Moreover, the fact that the pore size remains practically constant as the cobalt content increases, together with the absence of significant hysteresis loops in the isotherms, indicates that no necking or blocking of the pore system occurs. The thickness of the pore walls (estimated from XRD and porosity data) increases with the Co content, which explains the decrease of the S_{BET}. Thus, it is reasonable to propose that CoO nanoclusters are incorporated into the silica walls.

The UV/Vis spectra of some selected CoO-MCM-41 samples dehydrated at 400 °C are shown in Figure 3. All the spectra display a strong absorption in the visible region

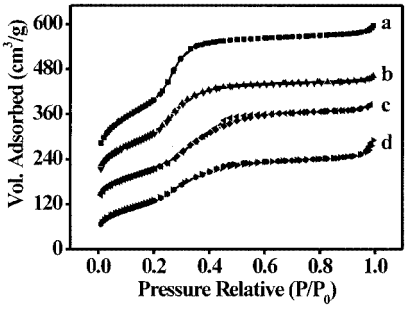

Figure 2. N_2 adsorption−desorption isotherms (curves are shifted for clarity) of CoO-MCM-41 samples; (a) Si/Co = 155; (b) Si/Co = 98; (c) Si/Co = 49; (d) Si/Co = 23

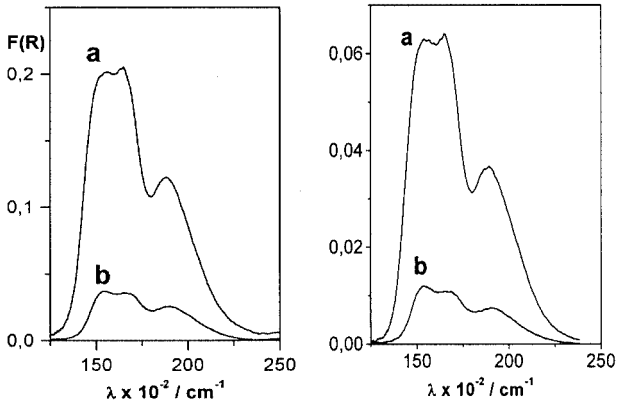

Figure 3. UV/Vis spectra of CoO-MCM-41 Si/Co = 23 (left) and Si/Co = 98 (right); (a) dehydrated sample; (b) hydrated sample

(15000−20000 cm^{-1}) with three maxima at around 15000, 17000 and 19000 cm^{-1}. This triplet can be unambiguously assigned to the $^4A_2(F) \rightarrow {}^4T_1(P)$ transition of cobalt(II) ions in tetrahedral oxygen environments, which allows us to discard the presence of Co^{III} atoms. In all cases, the characteristic blue colour of the materials is typical of tetrahedral $Co^{II}O_4$ sites. The intensity of this band significantly decreases with hydration, and it recovers reversibly by posterior drying. This behaviour clearly indicates that a certain proportion of the tetrahedral cobalt atoms becomes octahedrally coordinated by water uptaking and lies on the surface of the pore wall. Taking into account the large difference between the absorption molar coefficients of the bands due to electronic transitions associated to octahedral vs. tetrahedral Co^{II} sites, it can be reasonably assumed that the area under the vis curve is proportional to the number of non-hydrated tetrahedral cobalt centres. With this simplification, we can estimate the ratio of "surface" (water accessible)-to-"bulk" (inaccessible) Co ions by the intensity variation of the band after hydration. Remarkably, this ratio is practically constant and close to 2:7, irrespective of the cobalt content in the sample. This result strongly suggests that the nature of the CoO clusters does not depend on the Co concentration in the sample and supports the existence of a regular interaction of the clusters with the pore walls that become progressively distorted by increasing the cluster concentration.

The results of the magnetic measurements offer definitive evidence for the fact that the particle size remains constant, independent of the Si/Co molar ratio. Thus, all the samples show identical behaviour: (i) a sharp increase of the DC magnetic susceptibility below 12−17 K; (ii) a frequency-dependent AC signal with maxima at 4−7 K in the in-phase signal (χ') and at 3−5 K in the out-of-phase signal (χ''; see Figure 4); (iii) deviations in the zero-field-cooled and field-cooled susceptibilities below 10−15 K, with a remnant magnetization that vanishes at around 15 K for all the samples; and (iv) hysteresis cycles in the isothermal magnetization at low temperatures. All these features suggest a superparamagnetic behaviour with a blocking temperature

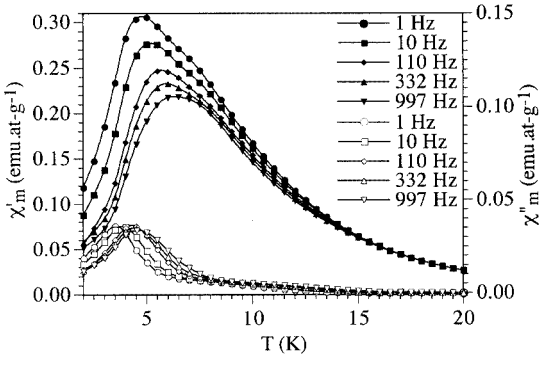

Figure 4. Thermal variation of χ' (filled symbols, scale on the left) and χ'' (empty symbols, scale on the right) at different frequencies for the sample with Si/Co = 49

 © 2004 Wiley-VCH Verlag GmbH & Co. KGaA, Weinheim

Table 2. CoO particle size determined from magnetic measurements

Si/Co (solid)	T_B [K][a]	E_a [K]	D [nm][b]
155	13	123.1	2.0
49	14	107.2	1.9
23	16	105.8	1.9

[a] Defined as the temperature at which $\chi'' \neq 0$. [b] Diameter determined from the E_a data ($E_a = K \cdot V$).

of around 15 K (see Table 2). It should be noted that possible spin-glass behaviour is excluded since the conditions for a spin-glass system are not fulfilled and the activation energies obtained from the frequency dependence of the maxima in χ'' (see below) are much lower than those expected for spin-glass systems.[19]

A way of estimating the particle size is to use the relationship between the activation energy of the blocking process of the resultant moments on the particles (E_a) and the particle volume (V), that is, $E_a = K \cdot V$, where K is the energy density of the magnetic anisotropy.[17] With the activation energies (E_a ca. 90−120 K, see Table 2) obtained from the Arrhenius law for the temperatures of the maxima in χ'' (T_m) as a function of the frequency (ν), $\nu = \nu_0 \cdot \exp(-E_a/kBT_m)$, and taking $K = 3.8 \cdot 10^6$ erg·cm^{-3},[20] we can estimate that the particle sizes are between 1.8 and 2.0 nm (see Table 2).

In any case, the relevant conclusion from the magnetic and spectroscopic studies is that, regardless of the Si/Co ratio, the CoO particles are similar and homo-disperse with sizes close to 2 nm. Assuming that the structure is sphalerite, these nanoclusters should contain around 200 CoO units. Taking the "nonaccessible"-to-"accessible" Co ratio found by spectroscopy into account, we postulate a model for these CoO-MCM-41 nanocomposites in which the CoO nanodomains are partially embedded (about 25 %) in the silica matrix.

Conclusion

In summary, we present a simple one-pot surfactant-assisted approach for obtaining superparamagnetic mesoporous materials with high cobalt content and well-dispersed uniform CoO nanoparticles within the inorganic walls, without blocking of the pore system. The homogeneity in size, nature and dispersion of the CoO nanoparticles can be explained by the fact that the growing process of the nucleated CoO species, generated by the hydrolysis of the Co precursor, is blocked by the relatively slower condensation of the mesostructured silica network. In short (in the experimental Si/Co concentrations) the time consumption for the nucleation and growing of the CoO particles is constant and limited by the silica polymerisation process. These materials may be described as nanocomposites of CoO clusters on mesoporous silicas. The nanometric organization of highly dispersed and accessible CoO nanodomains could be of catalytic interest in Fischer−Tropsch and ODH processes.

Experimental Section

CoO-MCM-41 Mesoporous Nanocomposites: The molar ratio of the reagents in the starting solution was 2 Si: x Co: 7 $TEAH_3$: 0.50 NaOH/ 0.50 CTABr: 180 H_2O (Table 1). In a typical synthesis leading to the Si/Co = 49 mesoporous material, 0.49 g of NaOH were dissolved at 60 °C in 20 mL of $TEAH_3$. After a few minutes, 10.5 mL of TEOS and 0.20 g of $CoCl_2$ were added whilst stirring, and the mixture was heated at 150 °C for 5 min. The resulting solution was cooled down to 100 °C, and 4.68 g of CTABr were added while stirring. Then, 80 mL of water were added with vigorous stirring at 60 °C. After a few minutes, a pale-blue suspension resulted, and it was aged at room temperature for 24 hours. The resulting powder was filtered off, washed with water and ethanol, and air dried. Finally, to open the mesopore system, the surfactant was removed by calcination at 550 °C in the course of 5 hours under air atmosphere.

All samples were analyzed and characterized by electron probe microanalysis (EPMA, Philips SEM-515), XRD techniques (Seifert 3000TT diffractometer; Cu-K_α radiation), TEM (Philips CM10 microscope), N_2 adsorption−desorption isotherms (Micromeritics ASAP2010), UV/Vis spectroscopy (UV-250 1PC Shimadzu), magnetic susceptibility measurements (DC and AC magnetic fields) and isothermal magnetization (PPMS-9 and SQUID susceptometer MPMS-XL-5, Quantum Design).

Acknowledgments

This research was supported by the Spanish Ministerio de Ciencia y Tecnología under grants MAT2000-1387-C021 and MAT2002-04239-C03-02. J. E. H. thanks the Spanish Ministerio de Educación y Ciencia for a post-doctoral grant.

[1] A. P. Alivisatos, *Science* **1996**, *271*, 933−937.
[2] T. Hyeon, *Chem. Commun.* **2003**, 927−934, and references cited therein.
[3] I.-W. Park, M. Yoon, Y. M. Kim, Y. Kim, H. Yoon, H. J. Song, V. Volkov, A. Avilov, Y. J. Park, *Solid State Commun.* **2003**, *126*, 385−389.
[4] J. Ramos, A. Millán, F. Palacio, *Polymer* **2000**, *41*, 8461−8464.
[5] F. Schüth, A. Wingen, J. Sauer, *Microporous Mesoporous Mater.* **2001**, *44*, 465−476.
[6] C. Yang, H.-S. Sheu, K.-J. Chao, *Adv. Funct. Mater.* **2002**, *12*, 143−148.
[7] N. R. B. Coleman, M. A. Morris, T. P. Spakling, J. D. Holmes, *J. Am. Chem. Soc.* **2001**, *123*, 187−188.
[8] F. Gao, Q. Lu, X. Llu, Y. Yan, D. Zhao, *Nano Lett.* **2001**, *1*, 743−748.
[9] T. Coradin, J. Larionova, A. A. Smith, G. Rogez, R. Clérac, C. Guérin, G. Blondin, R. E. P. Winpenny, C. Sanchez, T. Mallah, *Adv. Mater.* **2002**, *14*, 896−898.
[10] K. Moller, T. Bein, *Chem. Mater.* **1998**, *10*, 2950−2963, and references cited therein.
[11] A. Jentys, N. H. Pham, H. Vinek, M. Englisch, J. A. Lercher, *Microporous Mater.* **1996**, *6*, 13−17.
[12] S. Murray, M. Trudeau, D. M. Antonelli, *Adv. Mater.* **2000**, *12*, 1339−1342.
[13] R. Köhn, D. Paneva, M. Dimitrov, T. Tsoncheva, I. Mitov, C. Minchev, M. Fröba, *Microporous Mesoporous Mater.* **2003**, *63*, 125−137.
[14] R. Köhn, M. Fröba, *Catal. Today* **2001**, *68*, 227−236.

 © 2004 Wiley-VCH Verlag GmbH & Co. KGaA, Weinheim

[15] A. F. Gross, M. R. Diehl, K. C. Beverly, E. K. Richman, S. H. Tolbert, *J. Phys. Chem. B* **2003**, *107*, 5475−5482.
[16] S. Suvanto, J. Hukkamäki, T. T. Pakkanen, T. A. Pakkanen, *Langmuir* **2000**, *16*, 4109−4115.
[17] M. Wei, K. Okabe, H. Arakawa, Y. Teraoka, *New. J. Chem.* **2002**, *26*, 20−23.
[18] D. Yin, W. Li, W. Yang, H. Xiang, Y. Sun, B. Zhing, S. Peng, *Microporous Mesoporous Mater.* **2001**, *47*, 15−24.
[19] A. Vinu, J. Dedecek, V. Murugesan, M. Hartmann, *Chem. Mater.* **2002**, *14*, 2433−2435.
[20] M. Sato, S. Takada, S. Kohiki, T. Babasaki, H. Deguchi, M. Oku, M. Mitome, *Appl. Phys. Lett.* **2000**, *77*, 1194−1196.
[21] S. Takada, M. Fujii, S. Kohiki, T. Babasaki, H. Deguchi, M. Mitome, M. Oku, *Nano Lett.* **2001**, *1*, 379−382.
[22] S. Cabrera, J. El Haskouri, C. Guillem, J. Latorre, A. Beltrán, D. Beltrán, M. D. Marcos, P. Amorós, *Solid State Sci.* **2000**, *2*, 405−420.
[23] A. Sayari, *Chem. Mater.* **1996**, *8*, 248−257.
[24] J. A. Mydosh "*Spin Glasses: an Experimental Introduction*", Taylor and Francis, London, **1993**.
[25] M. Gruyters, *J. Magn. Magn. Mater.* **2002**, *248*, 248−257.

Received December 1, 2003

 © 2004 Wiley-VCH Verlag GmbH & Co. KGaA, Weinheim

The First Pure Mesoporous Aluminium Phosphonates and Diphosphonates – New Hybrid Porous Materials

Jamal El Haskouri,[a] Carmen Guillem,[a] Julio Latorre,[a] Aurelio Beltrán,[a] Daniel Beltrán,[a] and Pedro Amorós*[a]

Keywords: Hybrid materials / Mesoporous / Template synthesis / Aluminium / Phosphonates

Organophosphorus moieties have been incorporated into mesoporous ALPOs through a one-pot surfactant-assisted procedure leading, for the first time, to periodic mesoporous aluminium phosphonates and diphosphonates. The number of organic groups on the surface or in the network can be modulated continuously up to the maximum incorporation level of the respective organophosphorus entities (100 %).
(© Wiley-VCH Verlag GmbH & Co. KGaA, 69451 Weinheim, Germany, 2004)

Introduction

Since the discovery of three-dimensional aluminium phosphates (ALPOs),[1] the chemistry of open metal phosphates and phosphonates was extensively explored in the search for expanding microporous availability.[2] Organophosphorus reagents have been used as both anionic species able to construct layered or open structures[2] (one-pot) and coupling agents[3] for the preparation of hybrid materials based on metal oxides (grafting). Interest in these materials is currently related to the broad range of their potential applications in fields such as catalysis, molecular sieves and biomedical sciences.[4] The current trend of expanding pore sizes by using supramolecular templates has been successfully adapted for obtaining MCM-41-like aluminium phosphates.[5] Notwithstanding, reports on organically modified mesoporous phosphates are very scarce when compared to those dealing with hybrid organosilicas.[6] In fact, once the preparation of mesoporous silicas began to be controlled, a key objective was the functionalisation of the walls with organic groups (housed in the pore space or embedded in the walls).[6] In contrast, as far as we know, there are only three publications in which mixed mesoporous phosphate-phosphonate (containing Ti[7] and Zr[8]) or mesoporous phosphate-diphosphonate (based on Al[9]) materials are described. In the case of the Ti[7] and Zr[8] derivatives, by using terminal RPO_3 substituting groups, the phosphonate incorporation to the final materials is limited (< 50 %) and restricted to the pore surface. Dealing with the Al-containing solid, although diphosphonate moieties with bridged methylene groups have been used to connect the Al centres (in the mesostructured solid), the thermal evolution of the surfactant to prepare the corresponding mesoporous material leads to a significant degradation of diphosphonate moieties that decompose into terminal RPO_3 and phosphate groups. Hence, this solid must be understood as a mixed phosphate–phosphonate–diphosphonate mesoporous material constructed, as stated by the author, from aluminophosphate-like domains interconnected through bridged organic groups instead of a pure mesoporous aluminium-diphosphonate.[9]

Results and Discussion

We report here a generalised one-pot method that has allowed us to prepare for the first time pure mesoporous aluminium phosphonates and diphosphonates (henceforth denoted as UVM-9 for University of Valencia Materials) showing that a good selection of reagents, conditions and procedures allow the full extension of the ALPO derivatives to as broad a family as mesoporous organosilicas. In fact, a great variety of terminal organic groups [$(RO)_{4-n}Si-R'_n$, $1 \leq n \leq 3$] have been incorporated into the silica matrix through cohydrolysis or post-treatments. In any case, these terminal groups are usually housed in the pore space.[6] As an alternative, a novel strategy based on the use of bridge-bonded silsesquioxanes [$(RO)_3-Si-R'-Si(OR)_3$] leads to the incorporation of the organic functional groups embedded in the silica walls (PMO materials).[11] Thus, surface and framework organic modifications have been carried out by using RPO_3^{2-} terminal phosphonates [instead of $R'Si(OR)_3$][6] or $^{2-}O_3P-R-PO_3^{2-}$-bridged diphosphonates [instead of $(RO)_3-Si-R'-Si(OR)_3$],[10] respectively. Our method al-

[a] Institut de Ciència dels Materials (ICMUV), Universitat de València,
P. O. Box 2085, 46071-València, Spain
Fax: (internat) + 34-96-3543633
E-mail: pedro.amoros@uv.es
Supporting information for this article is available on the WWW under http://www.eurjic.org or from the author.

 © 2004 Wiley-VCH Verlag GmbH & Co. KGaA, Weinheim **DOI: 10.1002/ejic.200400071**

lows the progressive incorporation of organic groups, which originates from organic-free ALPOs to pure mesoporous aluminium phosphonates or diphosphonates (100 % of organophosphorus groups) through ALPOs with organically modified surfaces (terminal phosphonates) and/or frameworks (bridged diphosphonates).

The procedure is based on the use of a simple and commercial structural-directing agent (CTABr = cetyltrimethylammonium bromide) and a complexing polyalcohol (2,2′,2′′-nitrilotriethanol = TEAH3), which has proved its capability to harmonise the rates of the hydrolytic reactions of the aluminium species in water−phosphoric acid media and the subsequent processes of self-assembling with the surfactant aggregates.[11] The same general procedure has been used for obtaining solids with diphosphonates (using ethylenephosphonic acid), phosphonates (using methylphosphonic acid) or mixed phosphate−phosphonate/diphosphonate derivatives (starting from mixtures of phosphoric and organophosphorus acids; see Exp. Sect.). In all cases, the molar ratio of the reagents was adjusted to 2 Al/3 P (H_3PO_4 + phosphonic acid)/8 TEAH3/0.52 CTABr/270 H_2O. Table 1 summarises the main synthesis variables and physical data.

EPMA shows that all UVM-9 samples are chemically homogeneous (spot area ca. 1 μm) and have a constant and well defined composition. In all cases, UVM-9 solids containing diphosphonate groups show Al/P proportions close to the idealised Al/P molar ratio (1:1), typical of stoichiometric ALPOs, in contrast to the aluminium phosphate−phosphonate materials previously described (Al/P = 1.37[9]), while deviations from the Al/P ratio have been observed when monophosphonate groups were present. This fact indicates that the UVM-9 solids may basically be regarded as aluminophosphonates rather than a compound consisting, to a significant degree, of alumina domains connected through organophosphorus moieties. Moreover, the high-angle XRD patterns do not show peaks associated to segregated bulk phases. Based on these facts and taking into account the difficulty to condense phosphate, phosphonate and/or diphosphonate groups among them (leading to P−O−P bonds) under aqueous conditions, we can propose that the UVM-9 materials display a regular distribution of Al and P atoms along the pore walls. The high chemical homogeneity and dispersion achieved for Al and P atoms indicates that the good reactivity control previously reached with Al-TEAH3 complexes as an aluminium source in water/phosphoric media is maintained when phosphoric acid is partially or totally replaced by phosphonic or diphosphonic acids.

Elemental CNH analysis of all mesoporous UVM-9 samples reveals that they are nitrogen-free materials. This fact confirms the efficiency of the soft surfactant extraction procedure we have used. Moreover, the absence of signals associated to surfactant molecules in the ^{13}C NMR spectra supports the total CTA^+ evolution. Thus, CNH analysis allows an estimation of the content of organic groups in the final mesoporous materials to be calculated (see Table 1). The phosphonate/phosphate molar ratio in the materials containing diphosphonate species is close to that present in the mother liquor (samples 5 and 7), but it significantly drops when monophosphonates are involved (samples 2 and 3). Very likely, this difference is related to the capability of the phosphate and diphosphonate groups to act as network building blocks (bridging Al atoms); a role that monophosphate groups do not play (RPO_3^{2-} groups are necessarily terminal). As in the case of the PMO organosilicas, the bridging nature of the diphosphonates and their ability to interact through six O atoms allows their easy incorporation as network-forming groups. For this reason, the isolation of practically stoichiometric (Al/P = 1) diphosphonate materials is possible. Without prejudice to the observed preferential incorporation of the phosphate groups vs. monophosphonate groups, the existence of pure Al-monophosphonates (sample 4) and Al-diphosphonates (sample 7) is proof of the cooperative ability of the organophosphorus and aluminium moieties to construct stable networks around the surfactant aggregates. This last result accords well with previous results on organosilicas (with terminal organic groups), suggesting an upper functionalisation limit of about 40 %;[12] probably because at least 50 % of SiO_4^{3-} units is required to stabilise the pore wall network. Effectively, the intrinsic compositional nature of the UVM-9 materials (Al/P ≈ 1:1) warrants the presence of a similar amount of network-forming groups. Indeed, the slightly higher aluminium content in the Al-monophosphonates (Al/P = 1.15−1.25:1), should be viewed as a requirement for the pore wall stabilisation.

^{31}P MAS NMR spectra (Figure 1) confirm the incorporation of phosphate and phosphonate groups and provide useful information on their evolution as the functionalis-

Table 1. Selected synthetic and physical data for UVM-9 mesoporous organophosphonates

Sample	Phosphonic acid used	Solution (%)[a]	Solid (%)[b]	Al/P[c]	d_{100} (XRD)/nm	S_{BET} ($m^2 \cdot g^{-1}$)	BJH pore (nm)	Pore vol. ($cm^3 \cdot g^{-1}$)
1	–	–	–	1.10(2)	4.86	633.2	3.23	0.70
2	$CH_3PO(OH)_2$	50	22.3	1.25(2)	4.95	703.6	2.84	0.75
3	$CH_3PO(OH)_2$	75	45.8	1.15(2)	5.09	793.9	2.69	0.71
4	$CH_3PO(OH)_2$	100	100	1.24(2)	6.13	674.9	3.33	0.75
5	$(OH)_2OP\text{-}(CH_2)_2\text{-}PO(OH)_2$	50	54.2	0.97(2)	4.96	655.0	3.41	0.86
6	$(OH)_2OP\text{-}(CH_2)_2\text{-}PO(OH)_2$	75	78.1	1.00(2)	5.33	712.8	3.26	0.85
7	$(OH)_2OP\text{-}(CH_2)_2\text{-}PO(OH)_2$	100	100	1.11(2)	6.09	674.9	3.32	0.63

[a] P(phosphonate)/P(total) molar ratio (%) in the starting solution. [b] Values estimated from CNH analysis and referred to the P(phosphonate)/P(total) molar ratio (%) in the final UVM-9 solids. [c] Values averaged from EPMA of about 50 particles.

 © 2004 Wiley-VCH Verlag GmbH & Co. KGaA, Weinheim

ation level increases. The spectrum of sample 1 (ALPO) shows a broad signal centred at −25 ppm, which can be attributed to tetrahedral phosphates connected to aluminium centres.[5] As expected, according to the CNH analysis, the spectra clearly show the evolution of the P environments as the phosphonic/phosphoric acid ratio increases (samples 2−4 and 5−7); the intensity of the signals associated with the phosphate groups decreases while that of the signals characteristic of the phosphonate increases (10−22 ppm range).[13] Finally, the spectra of samples 4 and 7 (Al-methylphosphonate and Al-ethylenediphosphonate, respectively) only display the ^{31}P signal typical of phosphonate groups. Hence, while samples 2, 3, 5 and 6 present two different phosphorus environments, the UVM-9 materials with a functionalisation level of 100 % (samples 4 and 7) show only one environment for the P atoms both before and after (mesoporous) surfactant evolution. The small ^{31}P signal shifts observed in the NMR spectra can be associated to different parameters such as the proportion of octahedral aluminium sites and OH groups bonded to the P atoms and also to the presence of variable water amounts inside the mesopores.[14] In our case, the soft chemical treatment used to extract the surfactant allows us to maintain the chemical integrity of methylphosphonate and ethylenediphosphonate groups in the final mesoporous solids. This strategy avoids the degradation of the bridged diphosphonate.[9] All UVM-9 materials have ^{27}Al MAS NMR spectra that include two resonance signals at approximately $\delta = 0$ and 50 ppm (see Supporting Information; see also the footnote on the first page of this article). These signals are indicative of six- and four-coordinate Al centres, respectively. In the case of ALPO (sample 1), the majority of the Al centres are in tetrahedral sites. The proportion of octahedral Al sites increases as more of the phosphonate or diphosphonate groups are incorporated, and finally they become dominant in samples 4 and 7 where a significant amount of hydroxyl groups, probably bonded to aluminium atoms, would be required to balance the charge. Moreover, the coordination of the aluminium atoms at the pore surface should be increased by water molecules.

Selected XRD patterns of UVM-9 samples are shown in Figure 2. All materials display XRD patterns with at least one strong peak at low 2θ values (associated with the [100] reflection if a hexagonal cell is assumed), which is typical of periodic mesoporous materials. The shift of the d_{100} peak at low 2θ values as the content of organophosphorus groups increases suggests that both phosphonates and diphosphonates should be effectively incorporated into the inorganic walls. The resolution from the background of this intense peak decreases with increasing functionalisation level. Such an evolution indicates that incorporation of phosphonate or diphosphonate groups implies a progressive lowering of order in the pore system from hexagonal partially ordered (sample 1) to clearly disordered materials (samples 4 and 7). TEM micrographs (Figure 3) fully correlate to

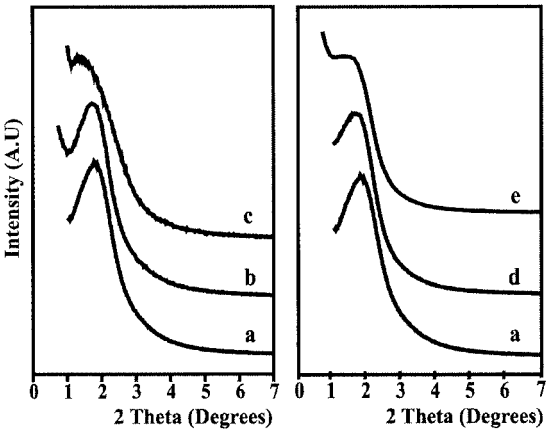

Figure 2. Selected XRD patterns of UVM-9 materials: (a) sample 1; (b) sample 3; (c) sample 4; (d) sample 5; (e) sample7

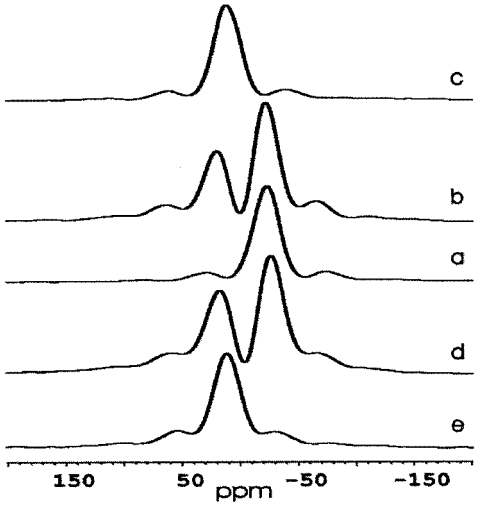

Figure 1. ^{31}P MAS NMR spectra of selected dehydrated samples: (a) sample 1; (b) sample 3; (c) sample 4; (d) sample 5; (e) sample 7

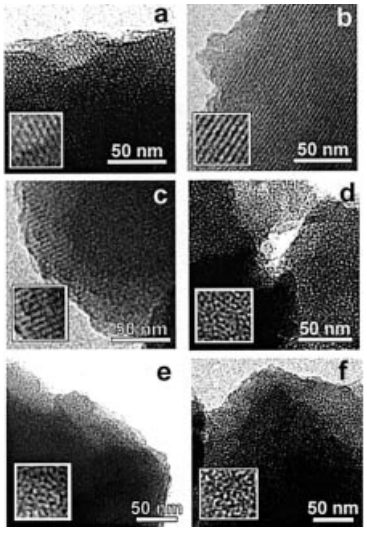

Figure 3. Representative TEM images of UVM-9 materials: (a) sample 1; (b) sample 2; (c) sample 5; (d) sample 3; (e) sample 4; (f) sample 7; the insets show enlarged (× 2) images

 © 2004 Wiley-VCH Verlag GmbH & Co. KGaA, Weinheim

XRD observations. Whereas small domains with partially ordered hexagonal (H_d) mesopore arrays are observed in the ALPO (sample 1) and materials with low amounts of organophosphorus moieties, the solids having medium and high proportions of phosphonate or diphosphonate groups show disordered topologies. On the other hand, all UVM-9 samples show one well-defined step in their N_2 adsorption−desorption curves, characteristic of type IV isotherms (see Supporting Information). Although XRD and TEM data suggest that a progressive loss of order occurs as the amount of organophosphorus moieties increases, the relatively sharpness of these steps (unusual in nonsilica based materials) indicates a reasonable uniformity of the mesopores. A high surface area and pore volume are retained in all UVM-9 solids.

Conclusion

In short, periodic mesoporous aluminium phosphonates and diphosphonates (100 % of organophosphorus groups) have been synthesised for the first time through a generalised surfactant-assisted procedure. This method is applicable to the preparation of materials including other cations (different from Al) and/or phosphonic acids, which implies in turn new opportunities for applications of mesoporous phosphates. The control of the pore size and the wall properties such as hydrophobicity and the easy incorporation of organic functional groups attached to the P atoms confers on this new family of hybrid porous materials potential interest in areas such as chemical sensors, separations, catalysis and environmental sciences.

Experimental Section

UVM-9 Mesoporous Hybrid Materials: A typical synthesis leading to sample 7 (a pure Al-diphosphonate) is as follows: 1) $Al(OBus)_3$ (12.7 mL) was slowly added to liquid TEAH3 (26.2 mL) and heated at 150 °C to give aluminium atrane complexes (compounds containing TEAH3 ligands); 2) after cooling this solution to 110 °C, CTABr (4.68 g) were added; 3) the resulting solution was cooled to 60 °C and mixed with a solution of 1,2-ethylenediphosphonic acid (7.03 g in 120 ml water). After a few minutes a white powder precipitated out and was filtered off, washed with water and ethanol and air dried. Finally, the surfactant was extracted from the obtained powder with an acetic acid/ethanol solution (ca. 1 g of powder, 16 mL of acetic acid and 130 mL of ethanol; t = 24 h, at room temperature). The final porous material was separated by filtration, washed with ethanol and air dried.

All samples were characterised by CNH elemental analysis and electron probe microanalysis EPMA (Philips SEM-515), ^{13}C, ^{27}Al and ^{31}P MAS NMR (Varian Unity-300), XRD (Seifert 3000TT diffractometer using Cu-K_α radiation), TEM (JEOL JEM-1010 operating at 100 kV) and N_2 adsorption-desorption isotherms (ASAP2010).

Acknowledgments

Financial support by the Spanish Ministerio de Ciencia y Tecnología (under grants MAT2000-1387-C01-01 and MAT2003-08568-C03-01) is acknowledged. JEH thanks the MEC for a post-doctoral grant.

[1] A S. T. Wilson, B. M. Lok, C. A. Messina, T. R. Cannon, E. M. Flanigan, *J. Am. Chem. Soc.* **1982**, *104*, 1146−1147.
[2] A. K. Cheetham, G. Ferey, T. Loiseau, *Angew. Chem. Int. Ed.* **1999**, *38*, 3268−3292.
[3] G. Guerrero, P. Mutin, A. Vioux, *Chem. Mater.* **2001**, *13*, 4367−4373.
[4] [4a] G. O. Rocha, J. Rocha, Z. Lin, *Catal. Lett.* **2003**, *89*, 69−74. [4b] R. Michel, J. W. Lussi, G. Csucs, I. Reviakine, G. Danuser, B. Kettere, J. Hubbell, M. Textor, N. D. Spencer, *Langmuir* **2002**, *18*, 3281−3287.
[5] [5a] M. Tiemann, M. Fröba, *Chem. Mater.* **2001**, *13*, 3211−3217. [5b] F. Schüth, *Chem. Mater.* **2001**, *13*, 3184−3195.
[6] A. Sayari, S. Hamoudi, *Chem. Mater.* **2001**, *13*, 3151−3168.
[7] A. Bhaumik, S. Inagaki, *J. Am. Chem. Soc.* **2001**, *123*, 691−696.
[8] N. Ren, Y. Tang, Y. J. Wang, S. H. Hu, A. G. Dong, W. M. Hua, Y. H. Yue, J. Y. Shen, *Chem. Lett.* **2002**, 1036−1037.
[9] T. Kimura, *Chem. Mater.* **2003**, *15*, 3742−3744.
[10] B. J. Melde, B. T. Holland, C. F. Blanford, A. Stein, *Chem. Mater.* **1999**, *11*, 3302−3308.
[11] [11a] S. Cabrera, J. El Haskouri, C. Guillem, J. Latorre, A. Beltrán, D. Beltrán, M. D. Marcos, P. Amorós, *Solid State Sci.* **2000**, *2*, 405−420. [11b] S. Cabrera, J. El Haskouri, C. Guillem, A. Beltrán, D. Beltrán, S. Mendioroz, D. Marcos, P. Amorós, *Chem. Commun.* **1999**, 333−334.
[12] S. L. Burkett, S. D. Sims, S. Mann, *Chem. Commun.* **1996**, 1367−1368.
[13] C. Serre, G. Ferey, *Inorg. Chem.* **2001**, *40*, 5350−5353.
[14] Y. Z. Khimyak, J. Klinowski, *Phys. Chem. Chem. Phys.* **2000**, *2*, 5275−5285.

Received January 28, 2004

 © 2004 Wiley-VCH Verlag GmbH & Co. KGaA, Weinheim

Synthesis and Structure of 1-D Heterometallic Thiocyanato-Bridged $Cu^{II}Gd^{III}$ Polymers with Ferromagnetic Properties

Ghenadie Novitchi,[a] Jean-Pierre Costes,*[a] and Bruno Donnadieu[a]

Keywords: Heterometallic complexes / Copper / Lanthanides / Magnetic properties

Reaction of the tetracoordinate CuL_A and CuL_B complexes with $Gd(NCS)_3$ leads to two unique one-dimensional $\{Cu–Gd\}_n$ thiocyanato-bridged (I) and hydrogen-bonded (II) polymers, depending on the periphery of the L_A and L_B ligands, with ferromagnetic properties.

(© Wiley-VCH Verlag GmbH & Co. KGaA, 69451 Weinheim, Germany, 2004)

Introduction

The synthesis and the design of solid-state architectures with ferromagnetic ordering is one of the major challenges in magnetochemistry.[1–4] The controlled assembly of these structural units in the solid state is determined by a number of factors: (i) coordination bonding,[5] (ii) versatile hydrogen-bonding interaction[6] (iii) π-π-stacking[7] and (iv) electrostatic interactions.[8] Thiocyanates with orbitals oriented in various directions have been used to build up coordination networks for two different reasons. On the one hand, they can furnish directional conformation to structures, owing to linear coordination modes as well as π-π overlapping interactions;[9] on the other hand, they can provide different super-exchange pathways, transmitting magnetic interactions between paramagnetic metal centres, owing to the diversity of their bonding modes.[10]

We have previously shown that ferromagnetic interactions are predominant in Cu–Gd complexes.[11] The linking of these units through intermolecular ferromagnetic interactions could yield high-spin species. So far, only tetranuclear entities have been obtained.[12,13] In the present study, we report on the synthesis, crystal structure and magnetic properties of one heterometallic coordination polymer and one hydrogen-bonded polymer, which are based on the Cu^{II}-Gd^{III} core, on thiocyanate ligands and on water molecules.

Results and Discussion

The reaction of 3-ethoxysalicylaldehyde and propylenediamine or 2,2-dimethylpropylenediamine in methanol (2:1 molar ratio), followed by addition of $CuOAc_2{\cdot}H_2O$, yielded the "compartmental complex ligands" $CuL_A{\cdot}H_2O$ and $CuL_B{\cdot}H_2O$.[14] These complexes possess a convenient O_2-O_2 metal-binding site, made of two phenoxide and two ethoxy oxygen atoms, which are able to accommodate 4f ions. Heterometallic Cu^{II}-Gd^{III} complexes were synthesized by reaction of the "compartmental complex ligands" CuL_A and CuL_B with $Gd(NCS)_3$ in acetone. $Gd(NCS)_3$ was prepared by metathesis with equimolar, warm solutions of $Gd(NO_3)_3$ /$6H_2O$ and KNCS in acetone (see Scheme 1).

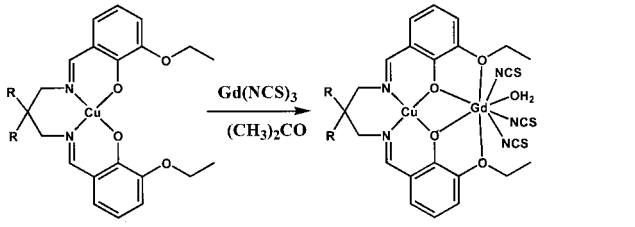

CuL_A R=H; CuL_B R=CH_3

$[L_ACuGd(NCS)_3H_2O]{\cdot}2(CH_3)_2CO$ (I)

$[L_BCuGd(NCS)_3H_2O(CH_3)_2CO]$ (II)

Scheme 1

The IR spectra of the two complexes are nearly identical. The C=N stretching vibrations are observed at 1603 and 1610 cm^{-1}. Very strong bands (2076, 2054 cm^{-1}) corresponding to coordinated thiocyanate anions are observed for **I** and **II**. The splitting indicates the different structural functions of the thiocyanate ligands.[15]

The structures of **I** and **II** were studied by X-ray diffraction methods at 180 K.[16] The structure of complex **I** is shown in Figure 1 (top). Cu^{II} is bound to two imino nitrogen and to two phenoxide oxygen atoms of the deprotonated L_A ligand. The Cu^{II} and Gd^{III} centres are bridged by two phenoxide oxygens, with a Cu–Gd distance of 3.460(1) Å. The copper-atom deviation from the least-squares N_2O_2 plane, formed by the four coordinating

[a] Laboratoire de chimie de coordination du CNRS,
205 route de Narbonne, 31077 Toulouse Cedex, France
E-mail: costes@lcc-toulouse.fr
[b] Department of Chemistry Moldova State University,
A. Mateevici str. 60, 2009 Chisinau, Moldova

 © 2004 Wiley-VCH Verlag GmbH & Co. KGaA, Weinheim **DOI: 10.1002/ejic.200300957**

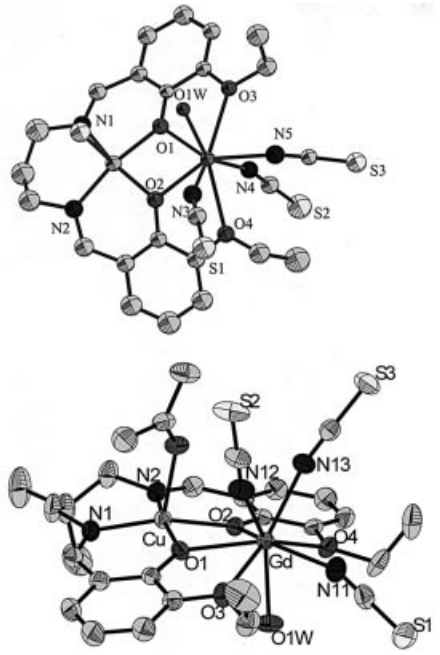

Figure 1. Views of the $\{LCuGd(NCS)_3H_2O\}$ units, **I** (top) and **II** (bottom); hydrogen atoms and solvent molecules are omitted for clarity

atoms, is −0.135(2) Å. The axial site is occupied by the sulfur atom of an NCS group, belonging to a neighbouring molecule (Cu−S = 2.744(2) Å]. The Gd^{III} centre is eight-coordinate, with three nitrogen atoms from the thiocyanate ligands, four oxygen atoms from the "compartmental complex ligand'' CuL_A, and one from a water molecule. The CuO_2Gd segment is not planar: the dihedral angle between the CuO1O2 and GdO1O2 planes is equal to 17.1(2)°. The molecules form zigzag chains through Cu(SCN)Gd′ bridges (see Figure 2). It is worth mentioning the π-π stacking interactions at 3.65(8), between two neighbouring chains.

The structure of **II** consists of $L_BCu^{II}Gd^{III}$ binuclear units (see Figure 1, bottom), in which the metal ions are doubly bridged by the phenoxide oxygen atoms. Acetone occupies the apical position in the copper-coordination sphere, with a Cu−O bond length of 2.293(2) Å. As in **I**, the copper(II) ion is situated in the inner N_2O_2 site of the Schiff-base ligand, L_B^{2-}. The Cu atom is displaced from this equatorial plane towards the apical position by 0.14(1) Å. The Cu−Gd distance is 3.454(1) Å and the dihedral angle between the GdO1O2 and CuO1O2 planes is 19.18(4)°. The Gd atom in **II** is again eight-coordinate ($N_3O_4O_w$). The supramolecular arrangement of the heteronuclear unit $\{L_BCuGd(NCS)_3H_2O\}$ is realised with hydrogen bonds that connect the coordinated water molecule to two sulfur atoms of thiocyanate ligands belonging to neighbouring molecules [$O1_W\cdots S2$ = 3.197(3); $O1_W\cdots S3$ = 3.292(3) Å (see Figure 3)].

The magnetic behaviour of **I** is shown in Figure 4 (top), as the thermal variation of the $\chi_M T$ product; χ_M is the molar susceptibility corrected for diamagnetism. At 300 K, $\chi_M T$ for I is equal to 8.4 $cm^3\ mol^{-1}\ K$, which corresponds to the value expected for two uncoupled metal ions. Lowering the temperature causes $\chi_M T$ to increase to 9.8 $cm^3\ mol^{-1}\ K$ at 7 K. This value compares well with that of 9.85 $cm^3\ mol^{-1}\ K$, expected for an $S = 4$ spin state, resulting from ferromagnetic coupling between Cu^{II} ($S = 1/2$) and Gd^{III} ($S = 7/2$) and assuming that $g_{Cu} = g_{Gd} = 2$.

A quantitative analysis for **I** was performed employing an expression derived from the spin-only Hamiltonian $H = -J_1 S_{Cu} S_{Gd}$. Taking into consideration the g values associated with the low-lying levels E(4) = 0 [$g_4 = (7g_{Gd} + g_{Cu})$/

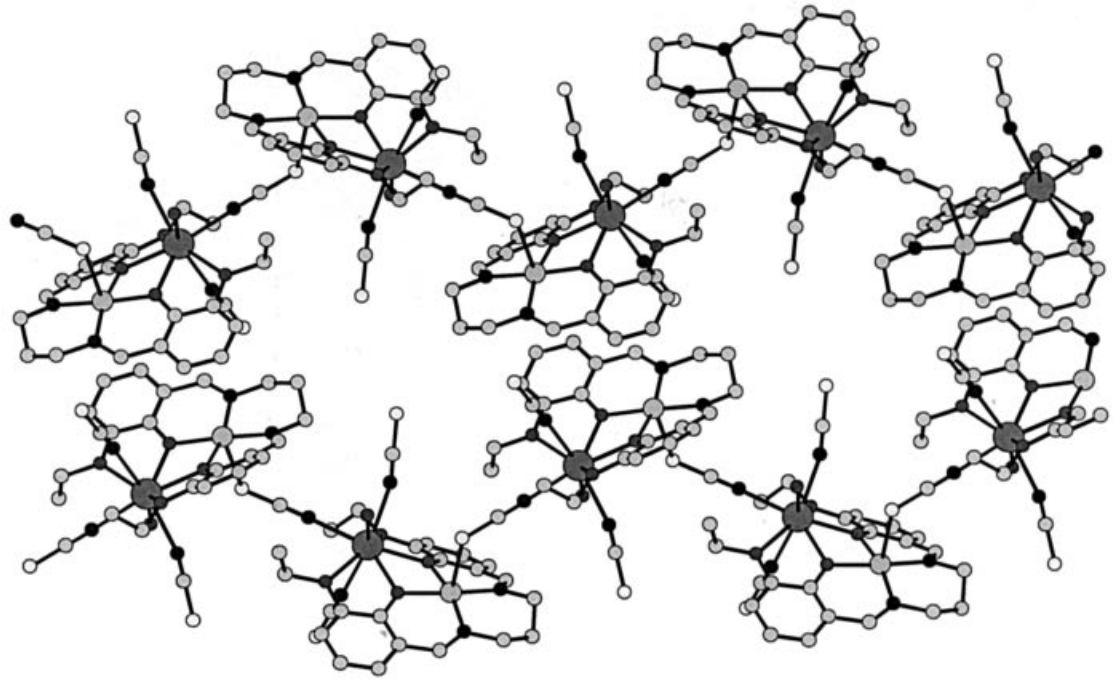

Figure 2. Stack of the polymeric **I** molecules; hydrogen atoms and solvent molecules are omitted for clarity

 © 2004 Wiley-VCH Verlag GmbH & Co. KGaA, Weinheim

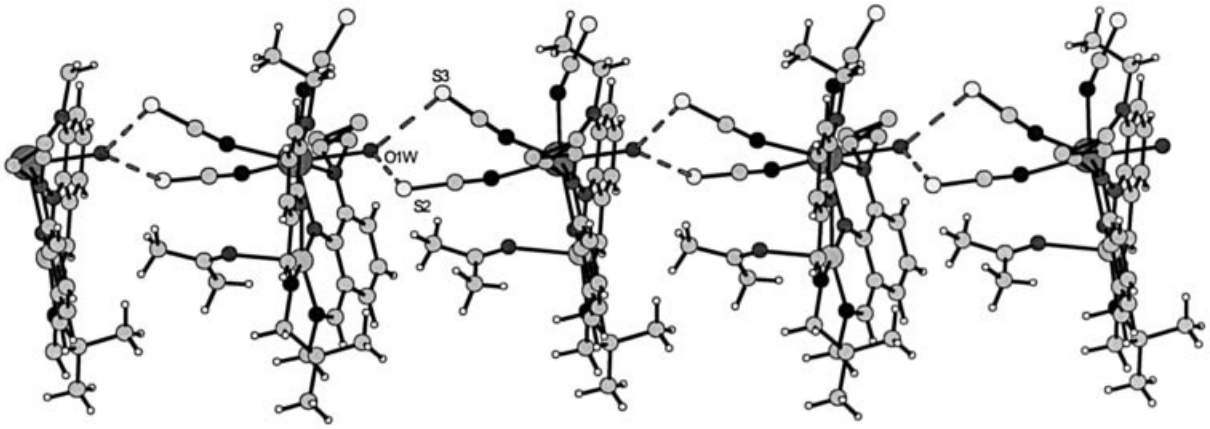

Figure 3. A portion of the hydrogen-bonded chain in **II**

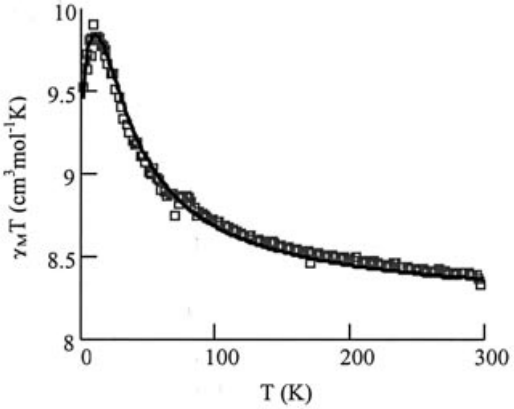

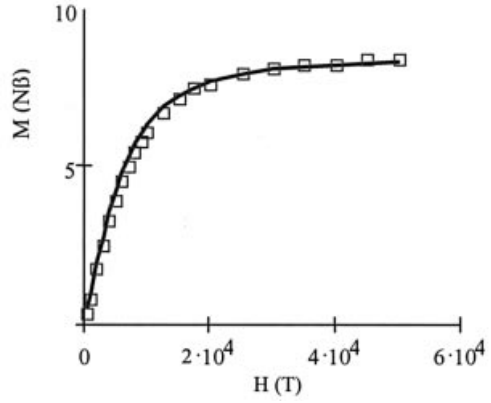

Figure 4. Magnetic behaviour of complex **I** between 2 and 300 K ($\chi_M T$ vs. T plot) and at 0.1 T (top), the solid line corresponds to the best fit; field dependence of the magnetization for compound **II** at 2 K (bottom), the solid line corresponds to the $S = 4$ ground state

8] and E(3) = $4J_1$ [$g_3 = (9g_{Gd} - g_{Cu})/8$],[17] the following expression [Equation (1)] is obtained:

$$\chi_d T = \frac{4N\beta^2 T}{\kappa(T-\theta)} \cdot \frac{15g_4^2 + 7g_3^2 \cdot \exp(-\frac{4J_1}{kT})}{9 + 7 \cdot \exp(-\frac{4J_1}{kT})} \quad (1)$$

Least-squares fitting of the experimental data led to the following set of parameters: $g_{Gd} = 1.99$, $g_{Cu} = 2.04$, $J_1 = 9.20\ cm^{-1}$, $\theta = -0.11$ for **I** and $g_{Gd} = 1.99$, $g_{Cu} = 2.02$, $J_1 = 5.5\ cm^{-1}$, $\theta = -0.14$ for **II**. The agreement factors R [$R = \Sigma(\chi T_{calc} - \chi T_{obs})^2/\Sigma(\chi T_{obs})^2$ are equal to 2×10^{-5} and 3×10^{-5}, respectively. From these values, it is clear that, from a magnetic point of view, these chain complexes behave as single dinuclear units.

For a better estimation of the magnetic interaction in the heterometallic Cu−Gd 1D chain, **I**, we adopted the model previously developed in the literature, in which the dimeric unit is assumed to act as an effective S_d classical-spin system.[18]

$$S_d = \frac{-1 + \sqrt{1 + 4\left(\chi_d T / 0{,}1251\bar{g}^2\right)}}{2} \quad (2)$$

The ladder chain can then be treated as a linkage of dimers and its contribution, χ_{chain}, to the total magnetic susceptibility, χ, according to Fisher's model[19] using the Drillon function,[20] is determined by Equation (3).

$$\chi_{chain} = \frac{Ng^2\beta^2 S_d(S_d+1)}{3k_B T} \cdot \frac{1+u}{1-u}$$
$$u = \coth\left[\frac{2J_2 S_d(S_d+1)}{k_B T}\right] - \frac{kT}{2J_2 S_d(S_d+1)} \quad (3)$$

where J_2 is the inter-dimer coupling constant. Least-squares fitting of the experimental data for **I** leads to a J_2 value of $-0.003\ cm^{-1}$. A similar result can be obtained for **II**. This very weak J_2 value confirms, as expected, that the dinuclear model can be retained to study the magnetic behaviour of these chain complexes. Indeed, the copper magnetic orbital is of the $d_{x^2-y^2}$ type while the interaction with

 © 2004 Wiley-VCH Verlag GmbH & Co. KGaA, Weinheim

the gadolinium ion occurs via the axially coordinated SCN ligand, in a region of very low spin density. The experimental values of magnetization for **I** and **II**, measured at 2.0 K, are correctly fitted by the Brillouin function for an $S = 4$ spin state, which confirms the ferromagnetic nature of the Cu−Gd interaction and the dinuclear character of these polymers (see Figure 4, bottom).

In conclusion, we have shown that heterobimetallic chains are obtained by using thiocyanate ligands. Depending on the ligand coordinating the Cu and Gd ions, the arrangement of the dinuclear units furnishes chains involving either Gd−Gd bridges through hydrogen bonding (**II**) or Cu−Gd bridges through NCS binding (**I**). These types of binding could be responsible for weak antiferromagnetic interactions in the present complexes, **I** and **II**. Nevertheless, from a supramolecular point of view, we have demonstrated that a change at the periphery of the ligand complex can drastically change the assembling mode of the heterodinuclear complexes.

Experimental Section

All starting materials and solvents were purchased from Aldrich and were used without further purification. Elemental analyses (C, H, N) were carried out by the Service de Microanalyse du Laboratoire de Chimie de Coordination, Toulouse. Magnetic susceptibility data were collected on powdered samples of a SQUID-based sample magnetometer on a Quantum Design model MPMS instrument. All data were corrected for diamagnetism of the ligands, estimated from Pascal's constants.[21]

$[L_ACuGd(NCS)_3H_2O]\cdot 2(CH_3)_2CO$ (I): $CuL_A\cdot H_2O$ (0.5 mmol), dissolved in acetone (50 mL), was added slowly to an acetone solution (20 mL) of $Gd(NCS)_3$ (0.5 mmol) under vigorous stirring. After partial evaporation of the solvent, blue-green crystals were formed. They were separated by filtration, washed with cold acetone and air dried. $C_{30}H_{38}CuGdN_5O_5S_3$ (897.62):calcd. C 40.14, H 4.27, N 7.80; found C 40.42, H 4.41, N 7.85.

$[L_BCuGd(NCS)_3H_2O(CH_3)_2CO]$ (II): prepared following a similar procedure. $C_{29}H_{36}CuGdN_5O_6S_3$ (867.60): calcd. C 40.15, H 4.18, N 8.07; found C 40.95, H 4.23, N 8.11.

Acknowledgments

G. N. is grateful to the NATO for financial support.

[1] [1a] O. Kahn, *Molecular Magnetism*, VCH Publishers, New York, **1993**. [1b] *Magnetism: A Supramolecular Function, NATO ASI series C484* (Ed. O. Kahn), Kluwer Academic Publishers, Dordrecht, **1996**. [1c]O. Kahn, *Adv. Inorg. Chem.* **1996**, *4*, 179. [1d] O. Kahn, *Struct. Bonding* (*Berlin*) **1987**, *68*, 89.

[2] [2a] C. Benelli, D. Gatteschi, *Chem. Rev.* **2002**, *102*, 2369. [2b] *Molecular Magnetic Materials* (Eds. D. Gatteschi, O. Kahn, J. S. Miller, F. Palacio), *NATO ASI Series*, Kluwer, Dordrecht, The Netherlands, **1991**. [2c]J. S. Miller, A. J. Epstein, *Chem. Eng. News* **1995**, 30.

[3] [3a] M. Sakamoto, K. Manseki, H. Okawa, *Coord. Chem. Rev.* **2001**, *219*, 379. [3b] H. Okawa, H. Furutachi, D. E. Fenton, *Coord. Chem. Rev.* **1998**, *174*, 51.

[4] C. Piguet, C. Edder, S. Rigaut, G. Bernardinelli, J.-C. G. Bunzli, G. Hopfgarther, *J. Chem. Soc., Dalton Trans.* **2000**, 3999.

[5] J.-M. Lehn: *Supramolecular Chemistry: Concepts and Perspectives*, VCH, Weinheim, **1995**. [5b]C. Janiak, *Dalton Trans.* **2003**, 2781. [5c] M. J. Zaworotko, *Chem. Commun.* **2001**, 1. [5d] B. Moulton, E. B. Rather, M. J. Zaworotko, *Cryst. Eng.* **2001**, *4*, 309. [5e] P. Losier, M. J. Zaworotko, *Angew. Chem. Int. Ed. Engl.* **1996**, *35*, 2779;.

[6] [6a] T. Steiner, *Angew. Chem. Int. Ed.* **2002**, *41*, 48. [6b] H. W. Roesky, M. Andruh, *Coord. Chem. Rev.* **2003**, *236*, 91. [6c] C. M. R. Juan, B. Lee, *Coord. Chem. Rev.* **1999**, *183*, 43. [6d] T. N. Guru Row, *Coord. Chem. Rev.* **1999**, *183*, 81;.

[7] [7a] V. Russell, M. Scudder, I. Dance, *J. Chem. Soc., Dalton Trans.* **2001**, 789. [7b] C. Janiak, *J. Chem. Soc., Dalton Trans.* **2000**, 3885. [7c] I. Unamuno, J. M. Gutierrez-Zorrilla, A. Luque, P. Roman, L. Lezama, R. Calvo, T. Rojo, *Inorg. Chem.* **1998**, *37*, 6452. [7d] M.-C. Tse, K.-K. Cheung, M. C.-W. Chan, C.-M. Che, *Chem. Commun.* **1998**, 3245.

[8] [8a] P. D. Beer, P. A. Gale, *Angew. Chem. Int. Ed.* **2001**, *40*, 486. [8b] P. D. Beer, P. A. Gale, G. Z. Chen, *J. Chem. Soc., Dalton Trans.* **1999**, 1897. [8c] Y.-B. Dong, M. D. Smith, R. C. Layland, H.-C. zur Loye, *J. Chem. Soc., Dalton Trans.* **2000**, 775. [8d] D. S. Reddy, K. Panneerselvam, T. Pilati, G. R. Desiraju, *J. Chem. Soc., Chem. Commun.* **1993**, 661.

[9] [9a] J.-C. Liu, G.-C. Guo, J.-S. Huang, X.-Z. You, *Inorg. Chem.* **2003**, *42*, 235. [9b] J. Tercero, C. Diaz, J. Ribas, E. Ruiz, J. Mahia, M. Maestro, *Inorg. Chem.* **2002**, *41*, 6780. [9c] S. A. Barnett, A. J. Blake, N. R. Champness, C. Wilson, *Chem. Commun.* **2002**, *15*, 1640.

[10] [10a] V. G. Makhankova, O. Yu. Vassilyeva, V. N. Kokozay, B. W. Skelton, L. Sorace, D. J. Gatteschi, *J. Chem. Soc., Dalton Trans.* **2002**, *22*, 4253. [10b] L. Licun, L. Daizheng, L. Songyan, J. Zonghui, Y. Shiping, *Inorg. Chem. Commun.* **2003**, *6*, 225. [10c] S. Sailaja, K. R. Reddy, M. V. Rajasekharan, C. Hureau, E. Riviere, J. Cano, J.-J. Girerd, *Inorg. Chem.* **2003**, *42*, 180.

[11] [11a] J. P. Costes, F. Dahan, A. Dupuis, *Inorg. Chem.* **2000**, *39*, 165. [11b] J. P. Costes, F. Dahan, A. Dupuis, J. P. Laurent, *Inorg. Chem.* **2000**, *39*, 169.

[12] J. P. Costes, F. Dahan, *C. R. Acad. Sci. Paris* **2001**, *4*, 97.

[13] T. Kido, S. Nagasato, Y. Sunatsuki, N. Matsumoto, *Chem. Commun.* **2000**, 2113; T. Kido, Y. Ikuta, Y. Sunatsuki, Y. Ogawa, N. Matsumoto, N. Re, *Inorg. Chem.* **2003**, *42*, 398.

[14] $CuL_A\cdot H_2O$ experimental analysis: $C_{21}H_{26}CuN_2O_5$ (449.99): calcd. C 56.05, H 5.82, N 6.23; found C 56.47, H, 5.53, N 6.31. $CuL_B\cdot H_2O$ experimental analysis: $C_{23}H_{30}CuN_2O_5$ (478.04): calcd. C 57.79, H 6.33, N 5.86; found C 57.67, H 5.46, N 5.90.

[15] K. Nakamoto *Infrared and Raman Spectra of Inorganic and Coordination Compound*, Fifth Edition Wiley, **1997**.

[16] Crystal data for **I**: $C_{30}H_{38}CuGdN_5O_7S_3$ $M_r = 897.62$ monoclinic; $P2_1/n$; $Z = 4$; $a = 13.347(5)$, $b = 15.344(5)$, $c = 17.930(5)$ Å; $\beta = 93.316(5)°$; $V = 3666(2)$ Å^3; $T = 180(2)$ K; 20945 reflections measured; 5252 independent ($R_{int} = 0.0561$); final residuals $R_1 = 0.0435$ [with $I > 2\sigma(I)$], $wR_2 = 0.0697$ (all data). Crystal data for **II**: $C_{29}H_{36}CuGdN_5O_6S_3$ $M_r = 867.60$ orthorhombic; P_{cab}; $Z = 8$; $a = 16.8845(10)$, $b = 19.5134(13)$, $c = 21.6665(18)$ Å; $V = 7138.5(9)$Å^3; $T = 180(2)$ K; 54516 reflections measured; 6968 independent ($R_{int} = 0.0447$), final residuals $R_1 = 0.0319$, [with $I > 2\sigma(I)$], $wR_2 = 0.0748$ (all data). Structure solution and refinement were performed using the SHELXS-97 and SHELX97 programs, respectively. CCDC-220473 for **I** and -220474 for **II** contain the supplementary crystallographic data for this paper. These data can be obtained free of charge at www.ccdc.cam.ac.uk/conts/retrieving.html [or from the Cambridge Crystallographic Data Centre, 12 Union Road, Cambridge CB2 1EZ, UK; Fax: (internat.) + 44-1223/336-033; E-mail: deposit@ccdc.cam.ac.uk].See also http://www. rsc.org/suppdata/cc/b3/b/ for crystallographic data in CIF or other electronic format.

[17] [17a] M. L. Kahn, T. M. Rajendiran, Y. Jeannin, C. Mathoniere, O. Kahn, *C. R. Acad. Sci. Paris, Serie II c, Chimie* **2000**, *3*, 131. [17b] J.-P. Costes, F. Dahan, A. Dupuis, J.-P. Laurent, *Inorg.*

 © 2004 Wiley-VCH Verlag GmbH & Co. KGaA, Weinheim

Chem. **1996**, *35*, 2400. [17c] J.-P. Costes, F. Dahan, A. Dupuis, J.-P. Laurent, *Inorg. Chem.* **1997**, *36*, 3429. [17d] J.-P. Costes, F. Dahan, A. Dupuis, J.-P. Laurent, *New. J. Chem.* **1998**, 1525.
[18] B. Chiari, A. Cinti, L. David, F. Ferraro, D. Gatteschi, O. Piovesana, P. F. Zanazzi, *Inorg. Chem.* **1996**, *35*, 7413.
[19] [19a] M. E. Fisher, *Am. J. Phys.* **1964**, *32*, 343. [19b] R. Deorges, J. J. Borràs-Almenar, E. Coronado, J. Curély, M. Drillon, *One-Dimension Magnetism: An Overview of the Models. In Magnetism: Molecules to Materials* (Eds: J. S. Miller, M. Drillon, Wiley-VCH, **2001**, 1. [19c]H.-Z. Kou, B. C. Zhou, S. Gao, D.-Z. Liao, R.-J. Wang, *Inorg. Chem.* **2003**, *42*, 5604.
[20] M. Drillon, E. Coronado, D. Beltran, R. Georges, *Chem. Physics.* **1983**, *79*, 449.
[21] P. Pascal, *Ann. Chim. Phys.* **1910**, *19*, 5.

Received December 22, 2003

 © 2004 Wiley-VCH Verlag GmbH & Co. KGaA, Weinheim

$[Cu^{I}(im)]_{\infty}$: Is this Air-Stable Copper(I) Imidazolate ($8^2$10)-Net Polymer the Species Responsible for the Corrosion-Inhibiting Properties of Imidazole with Copper Metal?

Yun-Qi Tian,[a,b,c] Hai-Jun Xu,[a] Lin-Hong Weng,[b] Zhen-Xia Chen,[b] Dong-Yuan Zhao,*[b] and Xiao-Zeng You*[a]

Keywords: Coordination polymers / Copper / Heterocycles / N ligands / Solvothermal synthesis

An air-stable two-dimensional (2D) copper(I) imidazolate polymer, $[Cu^{I}(im)]_{\infty}$ (**1**), with a d^{10}-d^{10} interaction, was synthesized solvothermally and structurally characterized by X-ray crystallography: a = 8.069(2), b = 8.068(2), c = 13.425(3) Å, β = 99.414(3)°, monoclinic, $C2/c$. This is the first example of an air-stable copper(I) imidazolate polymer that may play a significant role in the corrosion-inhibition mechanism of imidazole (or its derivatives) with copper metal.
(© Wiley-VCH Verlag GmbH & Co. KGaA, 69451 Weinheim, Germany, 2004)

Introduction

Imidazolate is an important ligand since it participates in the construction of the active sites of various bioenzymes, such as superoxide dismutase (SOD)[1] and cytochrome c.[2] As an exobidentate ligand, imidazolate can form metal coordination polymers,[3,4] a good example being the cobalt(II) imidazolate polymer,[4] which is a potential metal-organic porous material since its extended polymorphic framework demonstrates not only the necessary relatively high thermal stability but also a zeolitic porous structure. Moreover, according to recent publications,[5] imidazole and its derivatives are of interest as corrosion inhibitors for copper metal and its alloys. Despite extensive studies on the issue, until now it is still questionable which mechanism is adequate to explain the inhibition of copper corrosion by imidazole, in particular what is the substance formed on the surface of the copper metal. It is generally thought that a Cu^{II}-based imidazolate polymer may form a strong anti-corrosion layer[6] since copper(II) imidazolate polymers are known to afford five different polymorphs that show different spectroscopic and structural properties.[3a] However, there are also researchers who regard a Cu^{I}-based imidazolate polymer (or monomer) as the anti-corrosion substance[7] even though an air-stable copper(I) imidazolate polymer was, until now, unknown [Masciocchi et al. have reported a copper(I) imidazolate polymer whose structure, and even its cell parameters, are still not known due to the poor X-ray powder diffraction pattern of the easily oxidizable sample[3b]]. Here we describe an air-stable 2D copper(I) imidazolate polymer, $[Cu(im)]_{\infty}$ (**1**), whose structure should be different from Masciocchi's species since its simulated XRPD pattern from a single crystal (Figure S3) is very different from the XRPD pattern measured by Masciocchi et al.[8]

[a] State Key Laboratory of Coordination Chemistry, Coordination Chemistry Institute, Nanjing University, Nanjing 210093, P. R. China
Fax: (internat.) + 86-25-331-4502
E-mail: xyz@nju.edu.cn
[b] Department of Chemistry, Fudan University 200433 Shanghai, China
Fax: (internat.) + 86-21-6564-2036
E-mail: dyzhao@fudan.edu.cn
[c] Department of Chemistry, Liaoning University 110036 Shenyang, China
Fax: (internat.) + 86-24-6220-2053
E-mail: ytian588@sina.com.cn
Supporting information for this article is available on the WWW under http://www.eurjic.org or from the author.

Results and Discussion

The reaction of $Cu(CH_3COO)_2{\cdot}4H_2O$ (1.0 g, 5 mmol) with imidazole (0.68 g, 10 mmol) in 3-methyl-1-butanol (MB; 30 mL) under solvothermal conditions at 140 °C gave golden transparent single crystals that were suitable for X-ray diffraction. The elemental analysis reveals a copper(I) compound formulated as $C_3H_3N_2Cu$ {$[Cu(im)]_{\infty}$, **1**}. Although the yield of the substance is very low, its synthesis is reproducible. An EPR measurement on a sample of the compound exposed to air for almost half a year demonstrates that the substance remains unchanged. The formation of a copper(I) compound from a copper(II) precursor may be due to a redox reaction between the precursor and the reductive organic solvent under the solvothermal conditions employed. In order to compare Masciocchi's species with our air-stable compound spectroscopically, it was also prepared in our laboratory. However, we could not charac-

terize it spectroscopically since the white polymer rapidly turned blue after being formed in acetonitrile, especially upon removal of the solvent.

X-ray crystallography showed that the copper(I) ions in the crystal of **1** are bridged by imidazolates in a *trans* manner[3b] (Cu−N: 1.867 Å) forming infinite 1D chains. The parallel chains run along the [110] direction and intersect with those running along the [1−10] direction in a Cu−Cu (d^{10}-d^{10}) interaction, forming the 2D sheet of a typical ($8^2$10) net (Figures 1 and 2).[9] Within the imidazolate-bridged chains, the distance between adjacent Cu···Cu centers is 5.75 Å, while between the intersected chains the nearest Cu−Cu distance is 2.783 Å, slightly shorter than two times 1.40 Å, which is the van der Waals radius of copper, and 0.23 Å longer than the Cu−Cu distance in Cu metal (2.56 Å). Within the sheet, if the imidazolato ring planes in the chains running along [110] vary in +22.3° and 157.7° dihedral angles alternately with the *ab* plane, those imidazolato rings in the chains along [1−10] should vary in −22.3° and −157.7° dihedral angles alternately with the *ab* plane. In other words, the dihedral angles between adjacent imidazolato ring planes in all the chains are ±44.6°, and imidazolato rings with the same orientation are parallel to each other between the parallel chains.

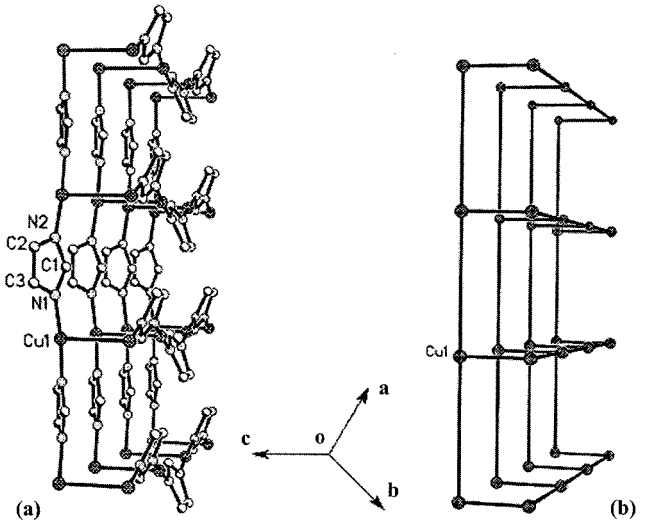

Figure 1. Cu−Cu (d^{10}-d^{10}) interaction forming a 2D sheet: (a) ball-and-stick diagram of $[Cu(im)]_\infty$ (**1**) (hydrogen atoms are omitted for clarity); (b) ($8^2$10) net of **1**, the spheres represent Cu atoms and the sticks represent imidazolates

In the crystal, these ($8^2$10) sheets are parallel to the *ab* plane and separated by 1/2*c* along the *c* axis. However, the imidazolato ring planes are not always parallel to each other between the parallel intersheet chains. Therefore, the imidazolato rings in the asymmetric unit of the crystal are statistically disordered, with dihedral angles of +22.3° and +157.7° (or −22.3° and −157.7°) relative to the *ab* plane (Figure 3).This phenomenon is not due to molecular thermal vibration. The layer structure depicted in Figures 1 and 2 is to be expected bearing in mind that copper(I) usually has a linear coordination geometry when it is coordinated

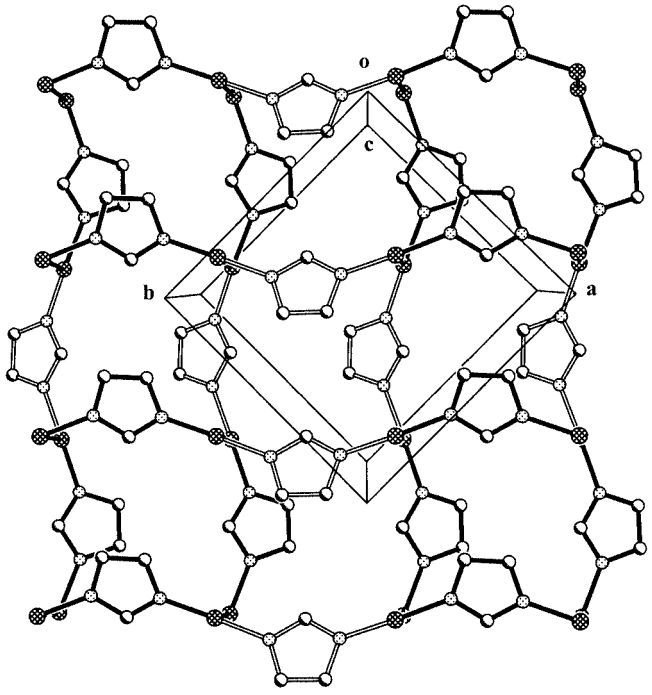

Figure 2. View of $[Cu(im)]_\infty$ (**1**) along the [001] direction; the imidazolate rings with solid or open bonds are those in the asymmetric unit

to deprotonated imidazole molecules, as is also observed in $[CoCu_2(im)_4]_\infty$,[10] and that molecules in parallel will suffer from the smallest degree of steric interaction (Figure 3).

It has been reported that the geometrical constraints of some ligands can produce Cu^I clusters and oligomers with a d^{10}-d^{10} interaction[11] that have an even shorter Cu−Cu distance than the Cu−Cu separation in Cu metal. Nevertheless, extended Hückel MO calculations have shown that the Cu−Cu interactions in these compounds are only weakly attractive.[12] Since imidazolate possesses none of the above-mentioned geometrical constraints, the short Cu−Cu distance in **1** is due only to the weakly attractive Cu−Cu interaction. Therefore, the Cu−Cu d^{10}−d^{10} interaction should be the same as those in the Cu^I clusters or oligomers.

Coordination polymers resulting from d^{10}-d^{10} interactions in Au^I [13] and Ag^I [3b,14] complexes with geometrically unconstrained ligands have already been reported. Of them, polymeric silver(I) imidazolate has a 3D structure constructed from one-dimensional $[Ag(im)]_\infty$ chains in a *cis-trans-cis-trans* sequence through these d^{10}-d^{10} interactions.[3b] However, the copper(I) imidazolate polymer reported here is only a 2D structure due to the relatively large dihedral angles between adjacent imidazolato rings in the chains {±44.6° in $[Cu(im)]_\infty$ and ±8° in $[Ag(im)]_\infty$} that prevent the copper(I) ions between the sheets from bonding to each other to form a 3D structure. Nevertheless, this is the first reported copper(I) coordination polymer resulting from a d^{10}-d^{10} interaction, and it may give a clue as to why imidazole and its N-substituted derivatives are good corrosion inhibitors for copper metal.[6c] We propose that the

 © 2004 Wiley-VCH Verlag GmbH & Co. KGaA, Weinheim

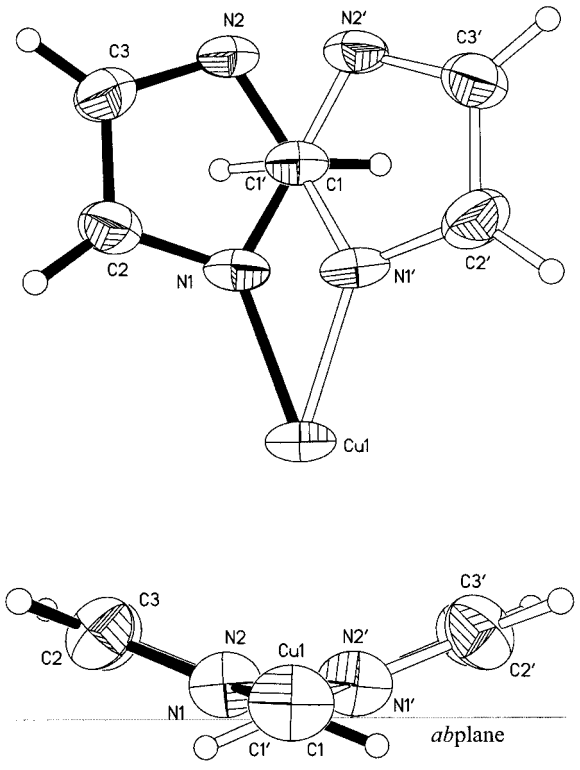

Figure 3. ORTEP drawing of the asymmetric unit of **1** showing the position disorder of the imidazolate rings; thermal ellipsoids are at the 30% probability level; top: view of the molecule along [001]; bottom: view of the molecule along [1−10]; the disordered imidazolate rings each have 30% occupancy

copper(I) imidazolate polymer (or monomer) may form an anti-corrosion layer on the copper metal surface and that the stability of this layer is enhanced by a Cu−Cu (d^{10}-d^{10}) interaction between the copper(I) polymer (or monomer) and the copper surface. Paradies et al. have reported a Cu−Cu distance of 2.85 Å in their EXAFS studies[15] on colloidal copper with adsorbed imidazole. However, although they were surprised by the result they did not give any reasonable explanation. Therefore, the air-stable copper(I) polymer with Cu−Cu bonds, in combination with the EXAFS results of Paradies et al., is good evidence that a copper(I) imidazolate polymer (or monomer) produces the anti-corrosive effect with copper metal[15] (Scheme 1), since Cu−Cu (d^{10}-d^{10}) interactions cannot be formed in a Cu^{II}-based imidazolate polymer. We suppose that if the inhibition were actually based on a Cu^{II}-related polymer layer, the hydrophobic interactions between the polymer (or monomer) and the copper surface should play a key role. However, such a copper(II) imidazolate polymer should not be formed under acidic conditions. Copper(II) *N*-substituted imidazolate monomers also cannot form the anti-corrosion layer since such monomers are water-soluble under acidic conditions. In fact, imidazole inhibits copper corrosion even in 1 M HNO_3 [5] and *N*-substituted imidazoles are even better inhibitors than imidazole itself in acidic solution.[6c] Therefore, it is reasonable for us to propose the copper(I) imidazolate as the anti-corrosion substance. However, the role of the Cu−Cu interactions must be stressed as they not only prevent the Cu^{I} complex from being oxidized to Cu^{II}, but they also bind the Cu^{I} complex polymer (or monomer) tightly to the copper metal surface. Without these Cu−Cu interactions a copper(I) imidazolate polymer may even be air-sensitive and therefore not able to provide the anti-corrosion effect. We propose that Masciocchi's white species may be a copper(I) imidazolate polymer without Cu−Cu interactions.

Conclusion

An air-stable copper(I) imidazolate polymer containing ($8^2$10) nets due to Cu−Cu (d^{10}-d^{10}) interactions can be synthesized under solvothermal conditions. This is the first structurally characterized copper(I) imidazolate polymer and is the only structural example supporting the proposal that a copper(I) imidazolate polymer (or monomer) produces the anti-corrosive effect of imidazole with copper metal.

Experimental Section

General Remarks: Imidazole, copper(II) acetate monohydrate and 3-methyl-1-butanol were purchased from commercial sources and used without further purification. Elemental analyses for C, H and N were performed with a Perkin−Elmer 240 analyzer. FT-IR spectra were measured from KBr pellets.

$[Cu^{I}(Im)]_{\infty}$ (1): $Cu(OAc)_2 \cdot H_2O$ (0.50 g, 5 mmol) and imidazole (0.68 g, 10 mmol) were added to 30 mL of 3-methyl-1-butanol. After stirring at room temperature for 12 h, this heterogeneous mixture was transferred into a Teflon-lined autoclave (34 mL). The autoclave was then sealed and heated at 140 °C for 24 h. After cooling to room temperature, golden crystals of **1** mixed with a large amount of amorphous substance (the XRPD pattern is shown in Figure S3) were collected, washed three times with 15 mL of ethanol and dried in vacuo. About 0.05 g of **1** was separated by

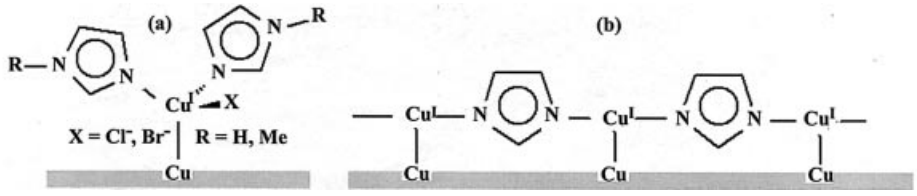

Scheme 1. The proposed layer structure of copper(I) imidazolate polymer or *N*-substituted imidazole monomer adsorbed on the copper surface by Cu−Cu (d^{10}-d^{10}) interactions: (a) the anti-corrosive substance formed by copper(I) and *N*-substituted imidazole or imidazole in acidic condition; (b) the anti-corrosive substance formed by copper(I) and deprotonated imidazole

 © 2004 Wiley-VCH Verlag GmbH & Co. KGaA, Weinheim

hand [yield ca. 8% based on the $Cu(Ac)_2 \cdot H_2O$ used]. $C_3H_3CuN_2$ (130.62): calcd. C 27.58, H 2.30, N 21.45; found C 27.24, H 2.45, N 21.30. IR (KBr pellet): $\tilde{\nu}$ = 3124 cm^{-1} (w), 1574 (s), 1486 (vs, sh), 1313 (m, sh), 1239 (m, sh), 1179 (w, sh), 1089 (vs, sh), 960 (w), 819 (m), 750 (m), 665 (m).

X-ray Crystallographic Study: $C_3H_3CuN_3$ (**1**), M = 130.42, monoclinic, space group $C2/c$, a = 8.069(2), b = 8.068(2), c = 13.425(3) Å, β = 99.414(3)°, V = 862.24(4) $Å^3$, Z = 2, D_c = 2.012 $Mg \cdot m^{-3}$, μ(Mo-K_α) = 4.877 mm^{-1}, F(000) = 512, GOF = 1.000. A total of 936 reflections were collected of which 803 were unique (R_{int} = 0.0156). $R1$ and $wR2$ were 0.0229 and 0.0468, respectively, for 92 parameters and 936 reflections [$I > 2\sigma(I)$]. CCDC-220508 contains the supplementary crystallographic data for this paper. These data can be obtained free of charge at www.ccdc.cam.ac.uk/conts/retrieving.html [or from the Cambridge Crystallographic Data Centre, 12 Union Road, Cambridge CB2 1EZ, UK; Fax: (internat.) + 44-1223-336-033; E-mail: deposit@ccdc.cam.ac.uk].

Acknowledgments

This work was supported by State Key Project of Fundamental Research of China (No. G200077500 and G200048001) and Postdoctoral Foundation of PRC and Shanghai City.

[1] [1a] I. Fridovich, *Annu. Rev. Biochem.* **1995**, *64*, 97−112. [1b] I. Bertini, L. Banci, M. Piccioli, *Coord. Chem. Rev.* **1990**, *100*, 67−103.
[2] J. T. Landrum, C. A. Reed, K. Hatano, W. R. Schneidt, *J. Am. Chem. Soc.* **1978**, *37*, 3232−3234.
[3] [3a] N. Masciocchi, S. Bruni, E. Cariati, F. Cariati, S. Galli, A. Sironi, *Inorg. Chem.* **2001**, *40*, 5897−5905 and references cited therein. [3b] N. Masciocchi, M. Moret, P. Cairati, A. Sironi, G. A. Ardizzoia, G. L. Monica, *J. Chem. Soc., Dalton Trans.* **1995**, *10*, 1671−1675. [3c] N. Masciocchi, G. A. Ardizzoia, S. Brenna, F. Castelli, S. Galli, A. Maspero, A. Sironi, *Chem. Commun.* **2003**, 2018−2019.
[4] [4a] Y.-Q. Tian, C.-X. Cai, Y. Ji, X.-Z. You, S.-M. Peng, G.-S. Lee, *Angew. Chem. Int. Ed.* **2002**, *41*, 1384−1386. [4b] Y.-Q. Tian, C.-X. Cai, X.-M. Ren, C.-Y. Duan, Y. Xu, S. Gao, X.-Z. You, *Chem. Eur. J.* **2003**, *9*, 5673−5685.
[5] W.-J. Lee, *Mater. Sci. Eng.* **2003**, *A384*, 217−226, and references cited therein.
[6] [6a] K. T. Carron, G. Xue, M. L. Lewis, *Langmuir* **1991**, *7*, 2−4. [6b] V. Sirtori, L. Lombardi, G. Redaelli, *J. Electron. Mater.* **1997**, *26*, 459−462. [6c] R. Gašparac, E. Stupnišek-Lisac, *Corrosion* **1999**, *55*, 1031−1039.
[7] See, for example: K. Aramaki, T. Sumiyoshi, H. Nishihara, *Corros. Sci.* **1991**, *32*, 593−607.
[8] Powder Diffraction File, ICDD, Swarthmore, PA, PDF No. 52-2401.
[9] S. R. Batten, R. Robson, *Angew. Chem. Int. Ed.* **1998**, *37*, 1460−1494.
[10] Unpublished crystal data for $[CoCu_2(im)_4]_\infty$: $a = b$ = 10.9513(15), c = 6.3063(13) Å, space group $P42_1c$. For view of crystal structure see Figure S2.
[11] P. Pyykkö, *Chem. Rev.* **1997**, *97*, 597−636.
[12] [12a] K. M. Merz, R. Hoffmann, *Inorg. Chem.* **1988**, *27*, 2120−2127 and references cited therein. [12b] J. Back, J. Strähle, *Angew. Chem. Int. Ed. Engl.* **1985**, *24*, 409−410.
[13] E. Colacio, F. Lloret, R. Kivekäs, J. Suárez-Varela, M. R. Sundberg, *Chem. Commun.* **2002**, 592−593.
[14] O. Yaghi, H.-L. Li, *J. Am. Chem. Soc.* **1996**, *118*, 295−296.
[15] H. H. Paradies, M. Thies, U. Hinze, *Rigaku J.* **1996**, *13*, 16−22.

Received December 10, 2003

 © 2004 Wiley-VCH Verlag GmbH & Co. KGaA, Weinheim

Funnel Complexes with Co^{II} and Ni^{II}: New Probes into the Biomimetic Coordination Ability of the Calix[6]arene-Based Tris(imidazole) System

Olivier Sénèque,[a] Morgane Campion,[b] Michel Giorgi,[c] Yves Le Mest,[b] and Olivia Reinaud*[a]

Keywords: Bioinorganic chemistry / Calixarenes / Cobalt / N ligands / Nickel

The coordination properties of the calix[6]arene-based tris(imidazole) ligand $X_6Me_3Imme_3$ were further explored with Co^{II} and Ni^{II}. This imidazole system stabilizes tetrahedral mononuclear Co^{II} complexes with an exchangeable fourth exogenous ligand (water, alcohol, amide) located at the heart of the hydrophobic calixarene cavity. With a weak donor ligand such as a nitrile, both four-coordinate tetrahedral and five-coordinate trigonal bipyramidal complexes were obtained. The latter contains a second nitrile molecule *trans* to the included guest nitrile. These complexes were characterized in solution as well as in the solid state. The Ni^{II} complexes are square-based pyramidal five-coordinate edifices with a guest nitrile inside the cavity and a water molecule outside. A comparison with previously described Zn^{II} and Cu^{II} complexes emphasizes the flexibility of this ligand. A comparison with carbonic anhydrase, a mononuclear zinc enzyme with a tris(histidine) coordination core, shows that $X_6Me_3Imme_3$ displays many structural features of this enzyme except for the *cis* coordination of the exogenous ligands.
(© Wiley-VCH Verlag GmbH & Co. KGaA, 69451 Weinheim, Germany, 2004)

Introduction

Coordination of metal ions by nitrogen donors is ubiquitous in metalloenzyme active sites. This has been a tremendously rich source of inspiration for coordination chemists, and over the last 25 years or so the syntheses of countless poly-aza ligands have been developed and their coordination chemistry explored. The tris(histidine) motif, frequently encountered in the case of zinc and copper enzymes,[1,2] has guided the architecture of the tri-aza ligands. Among the most famous artificial tripodal systems are the tris(pyrazolyl)borates,[3] also called scorpionate ligands, and triazacyclononanes.[4,5] However, the use of tris(imidazole) ligands, although closer to the tris(histidine) core, is somewhat rare in the modeling of active sites.[6−8]

In recent years we have described a novel supramolecular system based on a calix[6]arene bearing three nitrogen arms. Upon coordination to Cu^{I},[9,10] Cu^{II} [11,12] or Zn^{II} [13,14] the calixarene structure becomes constrained in a cone conformation accessible to a guest molecule. The most biomimetic ligand of the series, a tris(imidazole)-based system, provided the first structurally characterized model for the aqua dicationic tetrahedral Zn^{II} center found in hydrolytic enzymes.[15] The Cu^{I} complexes were able to bind CO reversibly, just as Cu^{I} enzymes do.[10]

A usual probe for the coordinating ability and flexibility of enzymatic active sites is the substitution of the native metal by other metals displaying different coordination requirements. As we were interested in further exploring the new perspectives offered by our supramolecular system and evaluating its flexibility as well as the geometrical constraints that it is able to provide on the metal ion coordination core, we decided to study its ability to bind to other first-row elements. In this paper, we describe the synthesis, characterization and host-guest behavior of Co^{II} and Ni^{II} complexes obtained with the tris(imidazole)-based system $X_6Me_3Imme_3$. A comparison with Zn^{II} and Cu^{II} complexes as well as with carbonic anhydrase, a zinc enzyme prototype,[16,17] highlights this ligand's biomimetic behavior.

Results

Synthesis and Characterization of a Tetrahedral Co^{II}-Aqua Complex

The calix[6]arene-based tris(imidazole) ligand $X_6Me_3Imme_3$ [13] was reacted with $[Co^{II}(H_2O)_6(ClO_4)_2]$ in THF.

[a] Laboratoire de Chimie et Biochimie Pharmacologiques et Toxicologiques, UMR CNRS 8601, Université René Descartes, 45 rue des Saints Pères, 75270 Paris cedex 06, France
Fax: (internat.) +33-1-4286-2183
E-mail: reinaud@biomedicale.univ-paris5.fr
[b] Laboratoire de Chimie, Electrochimie Moléculaires et Chimie Analytique, UMR CNRS 6521, Université de Bretagne Occidentale,
CS 93837, 6 av. Victor Le Gorgeu, 29237 Brest cedex 3, France
[c] Laboratoire de Cristallochimie, UMR CNRS 6517, Centre Scientifique Saint-Jérôme,
av. Escadrille Normandie-Niemen, 13397 Marseille cedex 20, France
Supporting information for this article is available on the WWW under http://www.eurjic.org or from the author.

Upon addition of 1.1 equivalents of $X_6Me_3Imme_3$ to the pale pink cobalt solution, the color immediately changed to an intense purple. Precipitation with Et_2O led to a purple solid. Its IR spectrum attested to the presence of the perchlorate counterions, and its elemental analysis was in good agreement with a 1:1 ligand/Co ratio. The magnetic moment at 300 K was assessed by the Evans method in $CDCl_3$.[18,19] The measured value of 4.6(2) μ_B,[20] although exceeding the spin-only value of 3.87 μ_B for $S = 3/2$, falls in the typical range for high-spin cobalt(II) complexes.[21] The UV/Vis spectrum in CH_2Cl_2 exhibits three bands between 450 and 650 nm with extinction coefficients above 300 $M^{-1}\cdot cm^{-1}$ characteristic of the $^4A_2 \rightarrow {}^4T_1(P)$ d-d transitions of a tetrahedral (Td) high-spin cobalt(II) ion.[21,22]

In $CDCl_3$, the ^1H NMR spectrum of the complex (Figure 1A) displays well-defined isotropically shifted resonances in the $\delta = 0-90$ ppm spectral window, with the expected number of signals for a C_{3v} symmetrical species, thereby suggesting the coordination of all three imidazoles to Co^{II}. The assignment of the resonances was performed by integration of the peaks and comparison with similar complexes obtained with ligands bearing ethyl substituents instead of methyl on the phenyoxyl or imidazolyl rings.[10] Two sets of signals could be distinguished: the imidazole protons (OCH_2, NCH_3 and both ImH) are shifted downfield in the $\delta = 15-80$ ppm region, whereas the protons of the calixarene skeleton (ArH, *t*Bu, $ArCH_2Ar$, OMe) appear in the diamagnetic region with chemical shifts quite similar to those of the parent diamagnetic zinc(II) complex (Figure 1B).

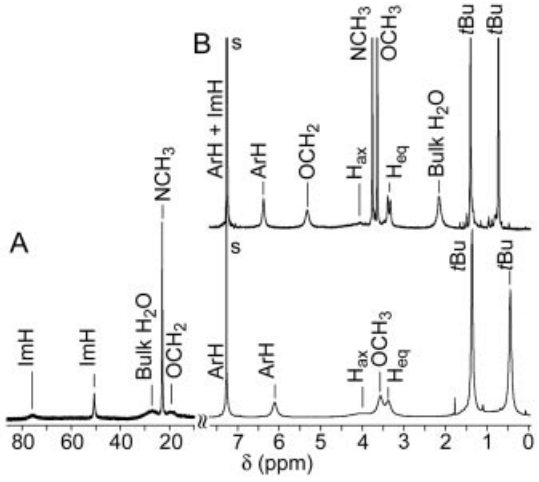

Figure 1. ^1H NMR spectra (250 MHz, 300 K, $CDCl_3$) of (A) $[Co(X_6Me_3Imme_3)(H_2O)](ClO_4)_2$ and (B) $[Zn(X_6Me_3Imme_3)(H_2O)\cdot(H_2O)](ClO_4)_2$; the residual solvent peak is labeled "s"

The very small shifts observed for the calixarene protons are highly suggestive of a tetrahedral geometry, for which the magnetic susceptibility is isotropic and the Fermi-contact interaction, which propagates along covalent bonds, is the only contribution to the hyperfine shift (no dipolar contribution).[19] Indeed, in this system, the calixarene protons are separated from the cobalt ion by at least eight bonds.

Since no other ligand beside water is available in a non-coordinating solvent such as THF, diethyl ether or chloroform, in agreement with all the above described spectroscopic data, we conclude that the isolated species is a tetrahedral cobalt(II) complex in which a water molecule is the fourth ligand, as was found in the parent zinc complex (Scheme 1).[23]

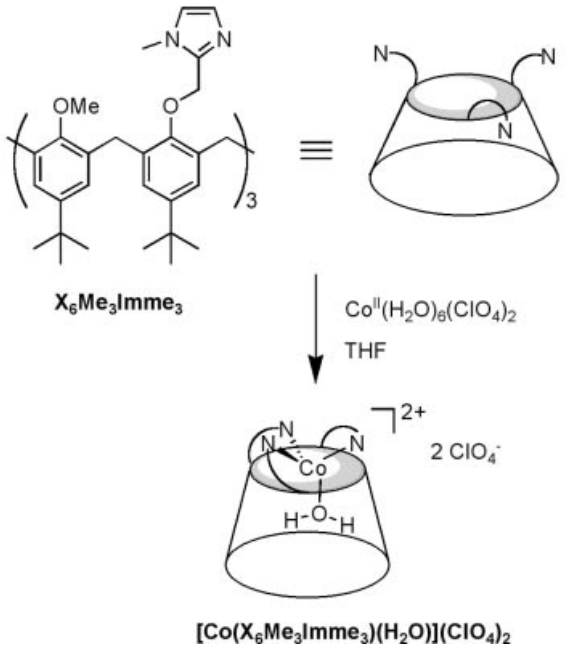

Scheme 1. Formation of the tetrahedral Co^{II}-aqua complex

Host/Guest Chemistry: A Solid-State Study

X-ray quality crystals of the complex $[Co(X_6Me_3Imme_3)(CH_3COCH_3)](ClO_4)_2$ were obtained by slow diffusion of Et_2O into a solution of the aqua complex in acetone. Three other complexes $[Co(X_6Me_3Imme_3)(L)](ClO_4)_2$ (L = DMF, EtOH and EtCN) were crystallized using the same procedure, but with the addition of about 10 equivalents of L to the acetone solution.

All four complexes display a nearly tetrahedral cobalt(II) ion coordinated by the three imidazole rings of the calixarene ligand, which stands in a flattened-cone conformation (Figure 2, Table 1). The fourth ligand, L, sits inside the calixarene cavity. Two perchlorate ions attest to the dicationic nature of the complexes. The average $Co-N_{Im}$ distances are short and very similar in all complexes (2.003, 2.003, 2.004 and 2.000 Å for L = Me_2CO, DMF, EtOH and EtCN, respectively). The bond between the metal ion and the coordinating atom of the guest ligand is also quite short, thereby reflecting the high Lewis acidity of the metal center in such a tetrahedral dicationic environment. Supramolecular interactions are observed between the calixarene host cavity and the guest ligand L. The structure of the acetone complex displays several CH···π interactions: each methyl group of the guest selectively faces an anisole ring at a short perpen-

 © 2004 Wiley-VCH Verlag GmbH & Co. KGaA, Weinheim

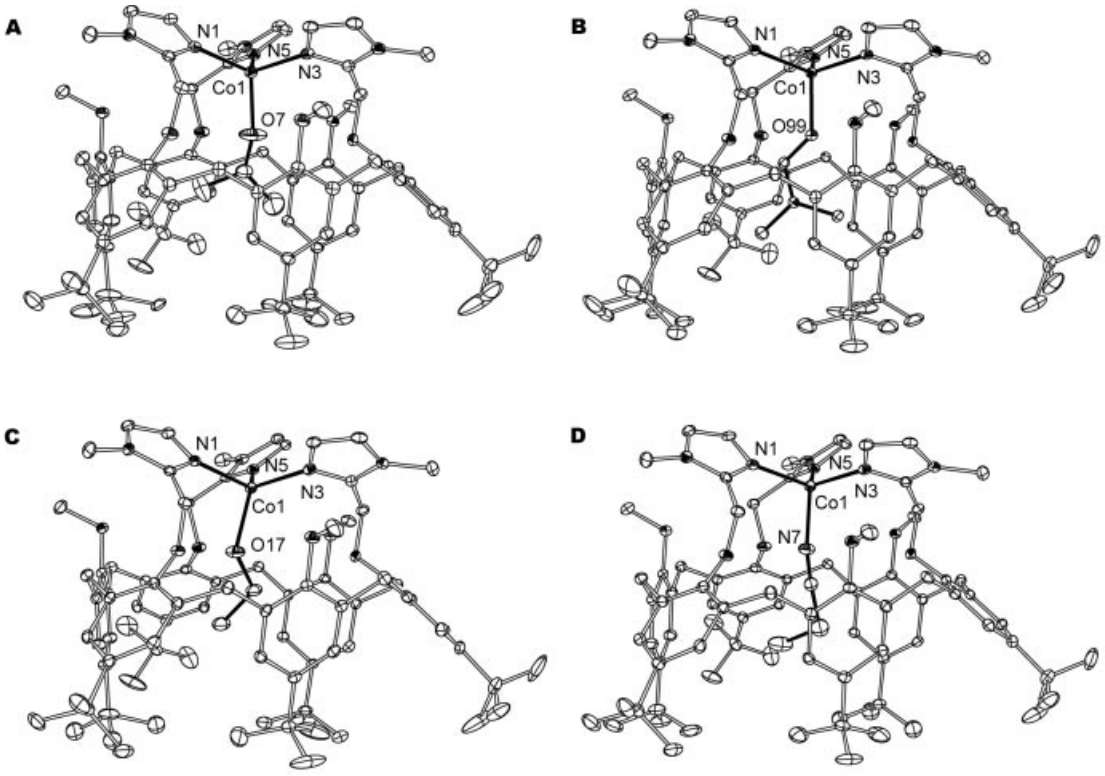

Figure 2. X-ray structures of tetrahedral complexes $[Co(X_6Me_3Imme_3)(L)](ClO_4)_2$ showing ellipsoids at 20% probability; L = (A) Me_2CO, (B) DMF, (C) EtOH, (D) EtCN; hydrogen atoms, perchlorate counterions and solvent of crystallization are omitted for clarity

Table 1. Selected bond lengths (Å) and angles (°) for complexes $[Co(X_6Me_3Imme_3)(L)](ClO_4)_2$

L	Bond length (Å)		Angles (°)			
Me_2CO	Co1−N1	2.000(4)	N1−Co1−N3	117.27(15)	O7−Co1−N1	114.0(3)
	Co1−N3	2.005(4)	N1−Co1−N5	105.95(16)	O7−Co1−N3	104.5(2)
	Co1−N5	2.004(4)	N3−Co1−N5	108.57(16)	O7−Co1−N5	106.0(2)
	Co1−O7	1.925(4)				
DMF	Co1−N1	1.994(3)	N1−Co1−N3	118.72(10)	O99−Co1−N1	108.38(10)
	Co1−N3	1.991(3)	N1−Co1−N5	106.81(10)	O99−Co1−N3	103.07(10)
	Co1−N5	2.025(2)	N3−Co1−N5	110.08(11)	O99−Co1−N5	109.54(10)
	Co1−O99	1.929(2)				
EtOH	Co1−N1	2.008(3)	N1−Co1−N3	116.41(13)	O17−Co1−N1	97.3(14)
	Co1−N3	2.005(3)	N1−Co1−N5	106.60(13)	O17−Co1−N3	113.96(16)
	Co1−N5	1.999(3)	N3−Co1−N5	107.37(14)	O17−Co1−N5	114.99(14)
	Co1−O17	1.986(3)				
EtCN	Co1−N1	1.996(3)	N1−Co1−N3	119.14(13)	N1−Co1−N7	105.97(16)
	Co1−N3	2.002(3)	N1−Co1−N5	106.37(13)	N3−Co1−N7	107.04(14)
	Co1−N5	2.003(3)	N3−Co1−N5	110.40(12)	N5−Co1−N7	107.32(15)
	Co1−N7	1.956(4)				

dicular distance, C···Ar, of 3.23 and 3.30 Å. With L = DMF, the guest methyl groups also appear selectively oriented towards an aromatic ring [d(C···Ar) = 3.37 and 3.45 Å] and an additional CH···π contact is observed between the O=C−H group and an anisole ring (3.90 Å). For L = EtOH and EtCN, CH···π interactions with both CH_2 and CH_3 groups are observed. In the case of the EtOH adduct, a hydrogen bond between the coordinated hydroxy group and one oxygen linked to an imidazole arm [*d*(O,O) = 2.78 Å] further stabilizes the edifice. Finally, it is noteworthy that the average distances between two *t*Bu groups in the "out" position (those of the aromatic rings bearing imidazole) are almost identical in all four complexes (12.89 Å, 12.67 Å, 12.70 Å and 12.81 Å for L = CH_3COCH_3, DMF, EtOH and EtCN, respectively) whereas those between two *t*Bu groups in the "in" position differ significantly (6.39 Å, 7.07 Å, 6.30 Å and 6.83 Å, respectively). This shows that coordination to Co^{II} ion freezes the positions of the *p*-*t*Bu-ArO-CH_2Im moieties, the equality of the *t*Bu−*t*Bu distances reflecting the equality of the $Co-N_{Im}$ bond lengths and geometry in the four complexes. In contrast, the positions of *p*-*t*Bu-ArOMe are adjusted by the supramolecular system

 © 2004 Wiley-VCH Verlag GmbH & Co. KGaA, Weinheim

in order to optimize the size of the cavity and the stabilizing interactions with the guests.

In addition to these four tetrahedral complexes, another complex was crystallized from pure MeCN by Et_2O vapor diffusion. The structure (Figure 3, Table 2) shows a cobalt ion surrounded by five ligands in a distorted trigonal bipyramidal geometry (TBP, $\tau = 0.69$).[24] The three imidazole moieties of $X_6Me_3Imme_3$ sit in the equatorial positions and the two axial positions are occupied by MeCN molecules, one of them being buried inside the calixarene cavity and the other lying outside. The average $Co-N_{Im}$ and Co−N7 (inner nitrile) bond lengths are longer (2.053 and 2.078 Å, respectively) in this complex than in the tetrahedral EtCN adduct. The Co−N8 distance (2.171 Å) reveals that the outer nitrile is bound more weakly to Co than the inner one.

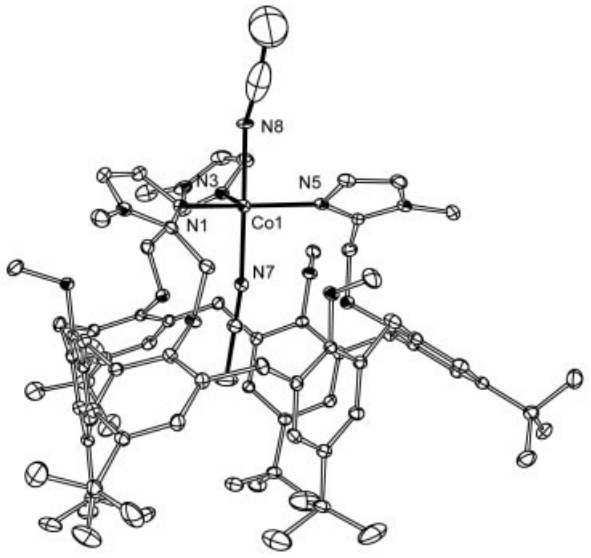

Figure 3. X-ray structure of $[Co(X_6Me_3Imme_3)(MeCN)_2](ClO_4)_2$ showing ellipsoids at 20% probability; hydrogen atoms, perchlorate counterions and solvent of crystallization are omitted for clarity

Table 2. Selected bond lengths (Å) and angles (°) for $[Co(X_6Me_3Imme_3)(MeCN)_2](ClO_4)_2$

Bond length (Å)			
Co1−N1	2.046(4)	Co1−N7	2.078(4)
Co1−N3	2.053(4)	Co1−N8	2.171(4)
Co1−N5	2.061(4)		
Angles (°)			
N1−Co1−N3	110.00(15)	N5−Co1−N7	93.76(14)
N1−Co1−N5	133.15(15)	N1−Co1−N8	84.95(15)
N3−Co1−N5	115.88(15)	N3−Co1−N8	89.93(16)
N1−Co1−N7	91.10(15)	N5−Co1−N8	86.13(15)
N3−Co1−N7	95.12(15)	N7−Co1−N8	174.43(17)

Thus, these structures confirm that the $X_6Me_3Imme_3$ system can stabilize dicationic tetrahedral cobalt(II) complexes with a guest in the cavity. The inner aqua ligand that is present in the complex isolated during the synthesis in a non-coordinating solvent is easily displaced by a coordinating molecule. In the specific case of MeCN, coordination of a second nitrile ligand was evidenced, yielding a five-coordinate species. This was further studied in solution.

Host/Guest Chemistry: UV/Vis and ^{1}H NMR Spectroscopic Studies in Solution

In solution the host/guest behavior of the calix[6]arene-Co^{II} system towards alcohols, nitriles and amides was monitored by UV/Vis and ^{1}H NMR spectroscopy by adding aliquots of these coordinating co-solvents, L, to a CH_2Cl_2 or $CDCl_3$ solution of $[Co(X_6Me_3Imme_3)(H_2O)](ClO_4)_2$. With L = EtOH, the extinction coefficients of the three $^4A_2 \rightarrow {}^4T_1(P)$ d-d transitions increased until a plateau was reached with ε values of 280, 400 and 450 $M^{-1}\cdot cm^{-1}$ at 524, 566 and 593 nm, respectively. An isosbestic point was observed at 615 nm, demonstrating the presence of only two species in solution. When increasing amounts of EtOH were introduced into an NMR tube containing a solution of $[Co(X_6Me_3Imme_3)(H_2O)](ClO_4)_2$ in $CDCl_3$ (approx. 10^{-2} M), resonances characteristic of a new complex progressively appeared while those of the aqua complex diminished. The profile of the new species resembled that of the tetrahedral aqua complex and remained unchanged whatever the EtOH concentration, with constant shifts for all signals. Here again, the signals of the calixarene structure were weakly hyperfine-shifted compared to the zinc analogue. Although the bound EtOH resonances were not located, these UV/Vis and NMR titrations are in agreement with the progressive exchange of the aqua ligand by EtOH until complete formation of the tetrahedral $[Co(X_6Me_3Imme_3)(EtOH)]^{2+}$ complex. A similar behavior was observed with other alcohols (*n*PrOH and *i*PrOH).

With MeCN as a co-solvent, no isosbestic point was observed during the UV/Vis titration, suggesting that more than two species are present. Two steps were observed in the evolution of the electronic spectra. Upon addition of MeCN, the apparent extinction coefficients of three $^4A_2 \rightarrow {}^4T_1(P)$ bands first increased to over 500 $M^{-1}\cdot cm^{-1}$, then subsequently decreased, down to a plateau with lower ε values (170, 260 and 230 $M^{-1}\cdot cm^{-1}$ at 530, 566 and 595 nm, respectively). This can be interpreted as the successive formation of a four-coordinate complex, namely $[Co(X_6Me_3Imme_3)(MeCN)]^{2+}$, as shown by the increase of ε values, and then a five-coordinate one, $[Co(X_6Me_3Imme_3)(MeCN)_2]^{2+}$ becoming predominant at a high $MeCN/CH_2Cl_2$ ratio, in agreement with the decrease of ε, with final values lower than 300 $M^{-1}\cdot cm^{-1}$. ^{1}H NMR spectroscopy confirmed this observation (Figure 4). When aliquots of MeCN were added to a $CDCl_3$ solution of the aqua complex (approx. 10^{-2} M), additional sharp resonances developed, attesting to the coordination of MeCN to Co^{II}. At substoichiometric MeCN concentration, the CH_3 resonance of a bound MeCN was detected at $\delta \approx 40$ ppm; the new OCH_2, NCH_3 and ImH signals were close to those of the aqua complex. Upon further addition of MeCN, the

 © 2004 Wiley-VCH Verlag GmbH & Co. KGaA, Weinheim

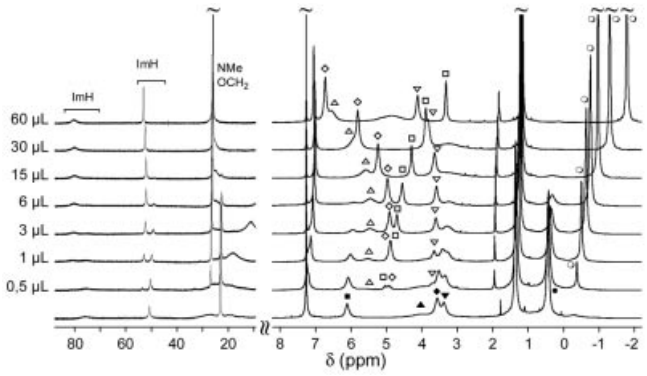

Figure 4. Evolution of ^{1}H NMR spectrum (250 MHz, 300 K) after successive additions of aliquots of acetonitrile (CH_3CN for the first spectrum, CD_3CN for the others) to a $CDCl_3$ solution of complex $[Co(X_6Me_3Imme_3)(H_2O)](ClO_4)_2$ (initial concentration: 12 mM); protons of the cobalt-aqua complex are indicated by filled symbols (ArH^1: ν, $ArCH_{ax}H_{eq}Ar$: ▲, $ArCH_{ax}H_{eq}Ar$: ▼, OCH_3: ◆, tBu^1: •) and those of the new species with open symbols (ArH^1: □, $ArCH_{ax}H_{eq}Ar$: Δ, $ArCH_{ax}H_{eq}Ar$: ▽, OCH_3: ★, tBu^1: ○); ArH^1 and tBu^1 belong to the anisole rings; the small shift of the aqua complex resonances during the titration is ascribed to a small change in the magnetic susceptibility of the solvent (spectra were calibrated with respect to residual $CHCl_3$) as they all shift the same way

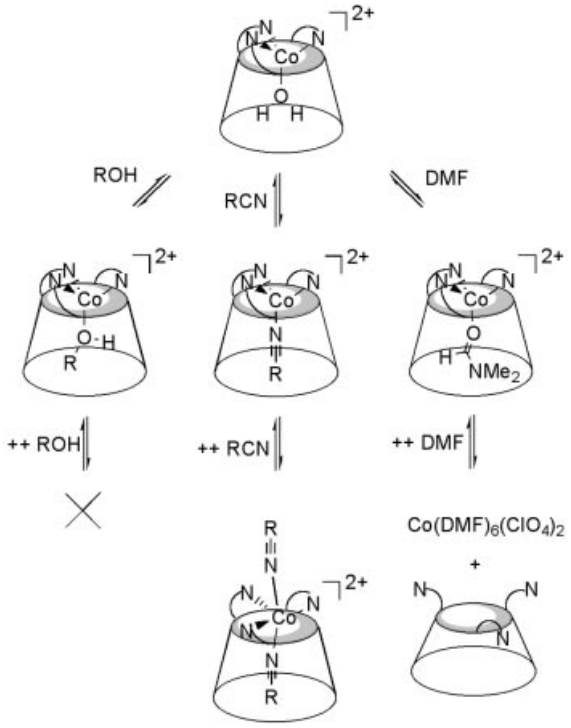

Scheme 2. Reaction of complex $[Co(X_6Me_3Imme_3)(H_2O)]^{2+}$ with small coordinating organic molecules

guest resonance moved upfield, whereas some protons belonging to the calixarene structure shifted upfield (one *t*Bu and one ArH) and others shifted downfield (OMe and $ArCH_{ax}H_{eq}Ar$). In addition, the larger the MeCN concentration, the larger the shifts, which stands in strong contrast to the experiment with EtOH described above. In accordance with the UV/Vis titration, this attests to the formation of two different species that are in fast equilibrium on the NMR timescale. The up- and downfield shifts observed for the calix structure are indicative of a dipolar contribution to their hyperfine shifts, and, thus, of an anisotropy in the magnetic susceptibility consistent with a five-coordinate complex. All these observations account for an equilibrium between a four-coordinate tetrahedral nitrile complex, predominant at low MeCN concentration, and a five-coordinate bis(nitrile) complex, predominant at high MeCN concentration (Scheme 2).

In order to evaluate the geometry of the five-coordinate species, the experimental hyperfine chemical shifts measured in CD_3CN, δ^{HF}_{exp} (see Table 3), were compared to the theoretical value δ^{HF}_{calc} calculated from the X-ray structure of $[Co(X_6Me_3Imme_3)(MeCN)_2]^{2+}$. A TBP complex is known to display an axial anisotropy in the magnetic susceptibility ($\chi_z \neq \chi_{xy}$, z being the nitrile−Co−nitrile axis) with a dipolar shift given by $\delta^{dip} = A \times [3 \times \cos^2(\theta) - 1]/r^3_{Co-H}$ (r_{Co-H} is the distance between the cobalt ion and a proton and θ the angle between Co−H and the anisotropy

Table 3. Hyperfine chemical shifts δ^{HF}_{calc} calculated from the X-ray structure of complex $[Co(X_6Me_3Imme_3)(MeCN)_2](ClO_4)_2$ and experimental values δ^{HF}_{exp}

Protons	r_{Co-H} (Å)	θ (°)[a]	δ^{HF}_{calc} (ppm)[b]	δ_{Zn} (ppm)[c]	δ_{Co} (ppm)[d]	δ^{HF}_{exp} (ppm)[e]
tBu^1 [f]	9.33	23.2	2.10	0.74	−1.55	2.29
tBu^2 [f]	10.54	53.9	0.04	1.40	1.27	0.13
H_{eq}	6.78	60.4	−0.95	3.45	4.41	−0.96
OCH_3	6.32	76.8	−3.70	3.58	6.95	−3.37
H_{ax}	5.32	62.4	−2.63	4.16	6.95	−2.79
ArH^1	7.32	36.1	2.72	6.47	3.72	2.75
ArH^2	8.32	54.7	0.01	7.39	7.34	0.05

[a] Atoms N7, Co1 and N8 are not perfectly aligned in the X-ray structure; θ is taken as the mean value of angles Co−N7 and Co−N8 axis. [b] $\delta^{HF}{}_{calc} = \delta^{dip} = A \times (3 \times \cos^2(\theta) - 1)/r_{Co-H}{}^3$. $1/A = 9.05 \times 10^{-4}$ according to Figure 5. [c] δ_{Zn} is the chemical shift observed for the diamagnetic complex $[Zn(X_6Me_3Imme_3)(CD_3CN)](ClO_4)_2$ in CD_3CN.[14] [d] δ_{Co} is the chemical shift observed for the paramagnetic complex $[Co(X_6Me_3Imme_3)(CD_3CN)_2](ClO_4)_2$ in CD_3CN. [e] $\delta^{HF}{}_{exp} = \delta_{Zn} - \delta_{Co}$. [f] Resonances related to the anisole moieties are noted as ^{1} and the others as ^{2}.

 © 2004 Wiley-VCH Verlag GmbH & Co. KGaA, Weinheim

axis). For *t*Bu, $ArCH_{ax}H_{eq}Ar$, OCH_3 and ArH, the Fermi-contact contribution is zero and thus $\delta^{HF}_{calc} = \delta^{dip}$. The plot of $(3 \times \cos^2(\theta) - 1]/r^3_{Co-H}$ versus δ^{HF}_{exp} displayed in Figure 5 shows a nice linear relationship; the δ^{HF}_{calc} and δ^{HF}_{exp} values are reported in Table 3.

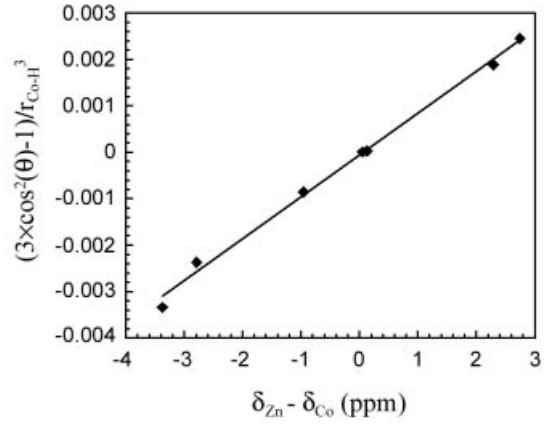

Figure 5. Plot of $(3 \times \cos^2(\theta) - 1]/r^3_{Co-H}$ vs. δ^{HF}_{exp}; $y = x \times 9.05 \times 10^{-4}$; $R = 0.997$

The excellent agreement between the values calculated from the X-ray structure and those measured by NMR spectroscopy confirms the existence of a bipyramidal $[Co(X_6Me_3Imme_3)(MeCN)_2]^{2+}$ species in solution. A similar behavior was observed with EtCN, but no evidence for an interaction between PhCN and the aqua complex could be found.

Interaction with DMF was monitored by UV/Vis spectroscopy as for ROH and RCN. First, upon addition of DMF to the CH_2Cl_2 solution of the Co-aqua complex, the extinction coefficients of three $^4A_2 \rightarrow {}^4T_1(P)$ bands increased (up to a maximum over 500 $M^{-1}\cdot cm^{-1}$) attesting to the formation of tetrahedral $[Co(X_6Me_3Imme_3)(DMF)]^{2+}$. This was confirmed by ^1H NMR spectroscopy at low DMF concentration (coordinated DMF was identified at δ_{COH} = 135 ppm, δ_{CH_3} = 23.2 and 22.8 ppm). In the second part of the titration, the bands near 500 nm broadened and their intensities decreased. The final spectrum, in nearly pure DMF, displays a broad transition between 450 and 700 nm with ε_{max} = 25 $M^{-1}\cdot cm^{-1}$, characteristic of $[Co(DMF)_6(ClO_4)_2]$. All this accounts for the formation of a tetrahedral Co-DMF complex followed by demetallation at high DMF concentration (Scheme 2).

Electrochemistry

The electrochemical behavior of the tris(imidazole)-Co^{II} complex was examined under a nitrogen atmosphere in acetonitrile. Cyclic voltammetry showed a totally irreversible Co^{II}/Co^{I} reduction peak at $E_p(red) = -1.8$ V,[25] together with metal deposition at the electrode, as evidenced by an anodic redissolution peak on the reverse scan. A very broad irreversible oxidation wave was observed at $E_p(ox) \approx 1.3$ V, ascribed to ligand oxidation. The same behavior was observed in dichloromethane. No interaction with O_2 could be evidenced. This indicates that the calix[6]arene-based tris(imidazole) system cannot stabilize any other oxidation state than Co^{II}. This was confirmed by the fact that all attempts to reduce the Co^{II} with a chemical reagent ($NaBH_4$ or $CoCp_2$) were unsuccessful, leading to decomplexation.

Synthesis and Characterization of a Five-Coordinate Ni^{II} Complex

Reaction of the tris(imidazole) ligand $X_6Me_3Imme_3$ with one equivalent of $[Ni(H_2O)_6(ClO_4)_2]$ in a THF/MeCN mixture,[26] followed by precipitation with Et_2O, yielded a green solid. IR spectroscopy and elemental analysis were consistent with the formula $[Ni(X_6Me_3Imme_3)(MeCN)(H_2O)](ClO_4)_2$. X-ray quality crystals were obtained by slow diffusion of Et_2O into an acetone/acetonitrile solution of the complex. The molecular structure (Figure 6) displays a five-coordinate nickel(II) ion in a distorted square-based pyramid geometry (SBP, $\tau = 0.45$).[24] The base of the pyramid is formed by two imidazole arms of the calixarene ligand, one acetonitrile molecule, buried in the conic cavity of the calixarene, and a water molecule, *trans* to the acetonitrile guest. The axial ligand is the third imidazole arm. The Ni−O7 bond is slightly longer than the four Ni−N bonds (see Table 4). The coordinated water is part of a hydrogen bonding network implying a second water molecule and an Et_2O molecule [*d*(O7,O16) = 2.688 Å and *d*(O16,O17) = 2.833 Å].

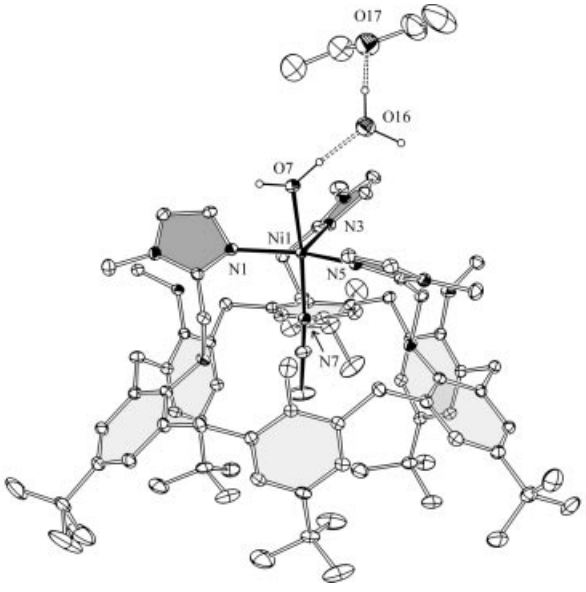

Figure 6. X-ray structure of $[Ni(X_6Me_3Imme_3)(MeCN)(H_2O)](ClO_4)_2\cdot H_2O\cdot Et_2O$ showing ellipsoids at 20% probability; some hydrogen atoms, perchlorate counterions and solvent of crystallization are omitted for clarity; all hydrogen atoms were located experimentally except those of the acetonitrile molecule

The magnetic moment of this Ni^{II} complex assessed by the Evans method in CD_3CN is 3.1(1) μ_B, which corresponds to a high-spin Ni^{2+} ion in a tetragonal environment.[27,28] Its UV/Vis spectrum in MeCN with five broad bands and weak extinction coefficients ε is suggestive of an SBP geometry. The ^1H NMR spectrum in CD_3CN presents

 © 2004 Wiley-VCH Verlag GmbH & Co. KGaA, Weinheim

Table 4. Selected bond lengths (Å) and angles (°) for $[Ni(X_6Me_3Imme_3)(MeCN)(H_2O)](ClO_4)_2$

Bond lengths (Å)			
Ni1−N1	2.029(3)	Ni1−N7	2.024(3)
Ni1−N3	2.029(3)	Ni1−O7	2.077(2)
Ni1−N5	2.053(3)		
Angles (°)			
N1−Ni1−N3	104.36(11)	N5−Ni1−N7	93.53(10)
N1−Ni1−N5	146.40(11)	N1−Ni1−O7	84.69(10)
N3−Ni1−N5	108.34(11)	N3−Ni1−O7	91.70(10)
N1−Ni1−N7	91.46(10)	N5−Ni1−O7	86.79(10)
N3−Ni1−N7	94.44(11)	N7−Ni1−O7	173.41(11)

few resonances in the $\delta = -200$ to 200 ppm range. However, the diamagnetic region contains peaks attributable to $ArCH_2Ar$, ArH and *t*Bu, close to those of the tris(imidazole)Zn^{II} complex.[14] This shows that the dipolar contribution to the chemical shift is negligible and agrees with the non-degenerate $^3B_1$ ground state.[29] A putative attribution[30] of the UV/Vis data in MeCN is given in Table 5.

Table 5. UV/Vis data in MeCN of $[Ni(X_6Me_3Imme_3)(MeCN)(H_2O)](ClO_4)_2$

λ (nm)	ε ($M^{-1}\cdot cm^{-1}$)	Transition
325	65	$^3B_1 \rightarrow {}^3E(P)$
400	31	$^3B_1 \rightarrow {}^3A_2(P)$
617	11	$^3B_1 \rightarrow {}^3E$
545	4	$^3B_1 \rightarrow {}^3B_2$
965	5	$^3B_1 \rightarrow {}^3E$

The electrochemical behavior of the Ni^{II} complex was studied in acetonitrile under nitrogen. Cyclic voltammetry showed no oxidation wave up to 1.8 V. An irreversible reduction peak, corresponding to Ni^{II}/Ni^{I} was observed at $E_p(red) = -1.35V$ with Ni^0 deposition at the electrode, as shown by the redissolution peak on the reverse scan. In benzonitrile, the reduction wave was broader and shifted to −1.45 V indicating a slower reduction process. However, the Ni^{I} state was not stable enough to yield a reversible reduction, even at high scan-rates. Similar to cobalt, the calix[6]arene-based tris(imidazole) system does not appear to be capable of stabilizing nickel ions in any other oxidation state than +2.

Discussion and Conclusion

The calix[6]arene-based tris(imidazole) ligand $X_6Me_3Imme_3$ thus appears particularly well suited for the stabilization of Co^{II} and Ni^{II} complexes, but not for higher or lower oxidation states. All complexes display a host/guest behavior, with a preferential binding of the exogenous organic ligand inside the hydrophobic cavity of the calixarene.

As previously described with Cu^{II}, reaction of the N_3 ligand with Ni^{II} yields five-coordinate complexes with an SBP environment. Also, in both cases, the organic ligand (RCN) is selectively bound in the heart of the hydrophobic calixarene cavity whereas a water molecule, standing outside, caps the structure.

With Co^{II}, four-coordinate species that strongly resemble the parent Zn^{II} complexes were characterized. Indeed, the aqua complex resulting from the synthesis in a non-coordinating solvent was easily exchanged for various small molecules L (alcohol, nitrile or amide), yielding novel tetrahedral complexes with included L. In the specific case of L = RCN, the four-coordinate Co complex was found to be in equilibrium with a trigonal bipyramidal species containing a second nitrile ligand bound outside the cavity and *trans* to the first one. Interestingly, such a five-coordinate species could not be evidenced with L = H_2O or ROH. This can be explained by the lower σ-donor ability of RCN compared to water or alcohol and by its π-acceptor character. Indeed, its first binding weakens the Co^{II} electronic density, thereby enhancing its affinity for a fifth ligand.[31]

A comparison of the X-ray structural parameters of the five-coordinate acetonitrile complexes of each of these metal ions is given in Table 6. Zinc and cobalt are in a TBP geometry whereas copper and nickel are in an SBP geometry. This follows the tendency generally observed for these metal ions in a five-coordinate environment.[27,28] As expected because of its lack of a crystal field, zinc is closer to pure TBP. On the other hand, there is a strong axial

Table 6. Comparison between complexes $[M^{II}(X_6R_3ImR_3)(MeCN)(L)]^{2+}$ (R = Me or Et) with M = Zn, Cu, Ni (L = H_2O) and Co (L = MeCN)

Compound	Geometry[a]	τ[b]	$d(M,L_{ax})$[c] (Å)	$d(M,L_{eq})$[c] (Å)
$[Zn^{II}(X_6Et_3Imet_3)(MeCN)(H_2O)]^{2+}$ [d]	TBP	0.86	2.13 $(MeCN)_i$ [e] 2.37 $(H_2O)_o$	2.03
$[Co^{II}(X_6Me_3Imme_3)(MeCN)(MeCN)]^{2+}$	TBP	0.69	2.08 $(MeCN)_i$ 2.17 $(MeCN)_o$	2.05
$[Cu^{II}(X_6Me_3Imme_3)(MeCN)(H_2O)]^{2+}$ [f]	SBP	0.49	2.19 (Imme)	2.01
$[Ni^{II}(X_6Me_3Imme_3)(MeCN)(H_2O)]^{2+}$	SBP	0.45	2.05 (Imme)	2.04

[a] TBP: trigonal bipyramid, SBP: square-based pyramid. [b] τ quantifies the distortion between ideal TBP (τ = 1) and SBP (τ = 0) geometries.[24] [c] $d(M,L_{ax})$ is the distance between metal and axial ligand and $d(M,L_{eq})$ is the mean distance between metal and equatorial ligands. [d] $X_6Et_3Imet_3$ is the OEt and NEt analogue of $X_6Me_3Imme_3$. See supporting information for the X-ray structure of the complex. [e] "*i*" refers to the ligand included in the calixarene cavity and "*o*" to the external one. [f] See ref.[11]

 © 2004 Wiley-VCH Verlag GmbH & Co. KGaA, Weinheim

distortion in the case of copper due to the Jahn−Teller effect, which does not exist for nickel.

It thus appears that the calix[6]arene-based tris(imidazole) ligand is flexible enough to allow the metal ion to adopt the most favorable geometry, although it precludes a six-coordinate environment. The position of the acetonitrile guest in the cavity does not seem to be influenced by the nature of the metal ion, as variations of the CH_3···Ar, C···O and N···O distances remain minor (± 0.015 Å). This shows that the calixarene/guest interaction is relatively strong and that the nitrogen arms are flexible enough to accommodate the metal ion with a fixed calixarene conformation. This flexibility is reminiscent of what has been observed in carbonic anhydrase.[16,17] In its native form, this enzyme presents a mono-zinc active site, with a tetrahedral environment provided by three histidine residues and a water molecule. For the Co^{II}-substituted protein, both four- and five-coordinate metal centers have been characterized, whereas Cu^{II} is in a TBP environment and Ni^{II} octahedral. Hence, like the calixarene-based system, carbonic anhydrase favors a tetrahedral environment for Zn and can stabilize both four- and five-coordinate Co^{II} species. For copper, the two systems differ in the geometry of the metal ion. This shows that the calixarene system is more flexible than the enzyme active site as it does not constrain Cu^{II} in a TBP geometry. On the other hand, the enzyme active site can provide an octahedral environment for Ni, which seems to be precluded by the calixarene system. In conclusion, comparison with carbonic anhydrase confirms that the calixarene-based supramolecular system is a good model for Michaelis adducts, reproducing many structural aspects encountered in natural active sites but not the *cis* coordination of the exogenous ligands. We are currently working on controlling the fifth (outer) coordination site.

Experimental Section

Material and Methods: All solvents and reagents were obtained commercially. THF was distilled from over sodium/benzophenone under argon. CH_2Cl_2 and MeCN were distilled from over CaH_2 under argon. ^1H NMR spectra were recorded on a Bruker ARX 250 spectrometer. Electrochemical experiments were carried out under a dry dioxygen-free atmosphere (N_2) in a dry-box manufactured by Jacomex. The electrochemical cell was specifically designed to fit the rotating disk electrode (EDI Tacussel) for a minimum volume of solution in the main compartment. The auxiliary and reference (ferrocenium/ferrocene = Fc^+/Fc) electrodes were in separate compartments connected to the main compartment through ground joints terminated by frits (Vycor tips from PAR). For voltammetric measurements, a platinum disk (diameter = 2 mm) was employed, and the electrolyses were performed with the same electrode, but rotated, equipped with a 4 mm diameter disk. A model PAR 173 potentiostat equipped with a PAR 179 digital coulometric unit, was monitored by a PAR 175 programmer. The chart recorder was a T-2Y SEFRAM ENERTEC. IR spectra were recorded on a Perkin−Elmer 783 spectrometer. UV/Vis spectra were recorded on a SAFAS UVmc^2 spectrophotometer. Elemental analyses were performed at the Institut de Chimie des Substances Naturelles, France.

Safety Note. Caution! *Although we have not encountered any problems, please note that perchlorate salts of metal complexes with organic ligands are potentially explosive and should be handled only in small quantities with appropriate precautions.*

Table 7. Crystallographic data for the four-coordinate complexes $[Co(X_6Me_3Imme_3)(L)](ClO_4)_2$

L	Me_2CO	DMF	EtOH	EtCN
Formula	$C_{90}H_{120}Cl_2CoN_6O_{16}$	$C_{90}H_{121}Cl_2CoN_7O_{16}$	$C_{89}H_{120}Cl_2CoN_6O_{16}$	$C_{90}H_{119}Cl_2CoN_7O_{15}$
Temp. (K)	193	193	193	193
Crystal colour	Purple	Purple	Purple	Purple
Crystal size (mm^3)	0.4 × 0.4 × 0.3	0.3 × 0.3 × 0.2	0.4 × 0.4 × 0.3	0.4 × 0.3 × 0.2
Mol. mass	1671.81	1686.77	1658.73	1668.75
Crystal system	Triclinic	Triclinic	Triclinic	Triclinic
Space group	$P\bar{1}$	$P\bar{1}$	$P\bar{1}$	$P\bar{1}$
a (Å)	13.687(1)	13.8246(4)	13.6243(7)	13.6902(6)
b (Å)	16.140(1)	16.1590(4)	16.0153(7)	16.1470(7)
c (Å)	22.739(2)	22.3976(7)	22.803(1)	22.5562(7)
α (°)	88.444(4)	88.029(1)	88.782(2)	88.021(2)
β (°)	78.274(4)	78.934(1)	78.078(2)	78.648(2)
γ (°)	68.267(5)	68.358(1)	68.444(2)	68.713(2)
V (Å^3)	4562.4(6)	4560.6(2)	4519.6(4)	4551.4(3)
Z	2	2	2	2
ρ(calcd.) (g·cm^{-3})	1.22	1.23	1.21	1.21
μ(Mo-K_α) (cm^{-1})	3.12	3.13	3.11	3.11
θ range (°)	3−26	5−27	6−26	2−26
No. of unique data	15914	16643	16325	16803
No. parameters refined	1045	1166	1134	1031
No. refl. in refinement	15914	16643	16325	16803
R [$F^2 > 4\sigma F^2$]	0.104	0.086	0.080	0.087
wR[a]	0.213[b]	0.181[c]	0.173[d]	0.244[e]
Goodness of fit	1.081	0.992	0.976	1.07
Residual Fourier (e·Å^{-3})	0.71, −0.86	1.15, −1.31	0.83, −0.78	1.07, −1.41

[a] $P = (F_o^2 + 2F_c^2)/3$ for [b] $w = 1/[\sigma^2(F_o^2) + (0.0701P)^2 + 12.398P]$. [c] $w = 1/[\sigma^2(F_o^2) + (0.0924P)^2 + 9.1861P]$. [d] $w = 1/[\sigma^2(F_o^2) + (0.0619P)^2 + 15.9154P]$. [e] $w = 1/[\sigma^2(F_o^2) + (0.1696P)^2 + 6.8382P]$.

 © 2004 Wiley-VCH Verlag GmbH & Co. KGaA, Weinheim

Table 8. Crystallographic data for five-coordinate complexes $[Co(X_6Me_3Imme_3)(MeCN)_2](ClO_4)_2$ and $[Ni(X_6Me_3Imme_3)(MeCN)(H_2O)](ClO_4)_2$

Compound	$[Co(X_6Me_3Imme_3)(MeCN)_2](ClO_4)_2$	$[Ni(X_6Me_3Imme_3)(MeCN)(H_2O)](ClO_4)_2$
Formula	$C_{94}H_{127}Cl_2CoN_9O_{16}$	$C_{93}H_{131}Cl_2N_7NiO_{18}$
Temp. (K)	173	193
Crystal colour	Purple	Green
Crystal size (mm^3)	0.4 × 0.3 × 0.3	0.4 × 0.4 × 0.2
Mol. mass	1768.94	1764.66
Crystal system	Monoclinic	Monoclinic
Space group	$P2_1/c$	$P2_1/c$
a (Å)	22.4259(5)	22.583(1)
b (Å)	16.3266(4)	16.337(1)
c (Å)	26.6529(5)	26.626(1)
β (°)	93.580(1)	93.913(1)
V ($Å^3$)	9739.6(4)	9800.5(8)
Z	4	4
ρ(calcd.) ($g.cm^{-3}$)	1.206	1.196
μ(Mo-K_α) (cm^{-1})	3.0	3.18
θ range (°)	5−25	2−33
No. of unique data	16989	22948
No. parameters refined	1150	1090
No. refl. in refinement	16989	22948
R [$F^2 > 4\sigma F^2$]	0.098	0.087
wR[a]	0.214[b]	0.196[c]
Goodness of fit	1.144	1.062
Residual Fourier ($e·Å^{-3}$)	0.54, −0.59	0.71, −0.59

[a] $P = (F_o^2 + 2Fc^2)/3$ for [b] $w = 1/[\sigma^2(F_o^2) + (0.08P)^2 + 25.50P]$. [c] $w = 1/[\sigma^2(F_o^2) + (0.081P)^2 + 15.1143P]$.

$[Co(X_6Me_3Imme_3)(H_2O)](ClO_4)_2$: Under an argon atmosphere, dry THF (2 mL) was added to a mixture of $[Co(H_2O)_6(ClO_4)_2]$ (36.6 mg, 0.10 mmol) and $X_6Me_3Imme_3$ (143 mg, 0.11 mmol).[13] The purple solution was stirred for one hour at room temperature and the product precipitated with Et_2O (5 mL). The solid was separated from the supernatant by centrifugation and washed with Et_2O. It was further purified by dissolution in CH_2Cl_2 and precipitation with pentane (twice) then dried under vacuum to yield a purple solid (138 mg, 85%). M.p. > 250 °C (decomp). ^1H NMR (250 MHz, $CDCl_3$, 298 K): δ = 0.44 (s, 27 H, *t*Bu), 1.35 (s, 27 H, *t*Bu), 3.37 (s, 6 H, Ar-αCH_{eq}), 3.56 (s, 9 H, OCH_3), 3.5−4.5 (br. s, 6 H, Ar-αCH_{ax}), 6.10 (s, 6 H, ArH), 7.26 (s, 6 H, ArH), 18−22 (br., 6 H, Im-αCH_2), 22.9 (br., 9 H, NCH_3), 50.5 (br., 3 H, ImH), 70−80 (br., 3 H, ImH). μ_{eff} = 4.6(1) μ_B. UV/Vis (CH_2Cl_2): λ (ε) = 523 (230), 564 (336), 592 nm (339 $M^{-1}·cm^{-1}$). IR (KBr): $\tilde{\nu}$ = 3460 (H_2O), 1505, 1487, 1462, 1421, 1398, 1367, 1110 (ClO_4^-), 628 (ClO_4^-) cm^{-1}. $C_{84}H_{110}Cl_2CoN_6O_{15}·3H_2O$ (1627.7): calcd. C 61.98, H 7.18, N 5.16; found C 61.75, H 6.91, N 4.83.

$[Ni(X_6Me_3Imme_3)(MeCN)(H_2O)](ClO_4)_2$: Under an argon atmosphere, dry MeCN (0.25 mL) and THF (1 mL) were added to a mixture of $[Ni(H_2O)_6(ClO_4)_2]$ (30.7 mg, 0.084 mmol) and $X_6Me_3Imme_3$ (109 mg, 0.084 mmol).[13] The green solution was stirred for 30 minutes at room temperature and the product precipitated with Et_2O (6 mL). The solid was separated from the supernatant by centrifugation and washed with Et_2O. It was further purified by dissolution in MeCN and precipitation with Et_2O then dried under vacuum to yield a green solid (105 mg, 75%). M.p. > 270 °C (decomp). μ_{eff} = 3.1(1) μ_B. UV/Vis (CH_2CN): λ (ε) = 400 (sh, 31), 617 (11), 965 nm (5 $M^{-1}·cm^{-1}$). IR (KBr): $\tilde{\nu}$ = 3400 (H_2O), 1483, 1462, 1363, 1113 (ClO_4^-), 626 (ClO_4^-) cm^{-1}. $C_{86}H_{113}Cl_2N_7NiO_{15}·2H_2O$ (1410.5): calcd. C 62.58, H 7.15, N 5.94; found C 62.17, H 6.86, N 6.12.

X-ray Structure Determinations:[32] Crystallographic data for $[Co(X_6Me_3Imme_3)(L)](ClO_4)_2$ (L = Me_2CO, DMF, EtOH and EtCN), $[Co(X_6Me_3Imme_3)(MeCN)_2](ClO_4)_2$ and $[Ni(X_6Me_3Imme_3)(MeCN)(H_2O)](ClO_4)_2$ are listed in Table 7 and 8. Diffraction data were collected on a Bruker−Nonius−KappaCCD diffractometer.[33] Structures were solved by direct methods and refined using the program SHELXL-97.[34]

Acknowledgments

The authors gratefully acknowledge financial support from the CNRS, Ministère de la Recherche (doctoral fellowship for O.S.) and Conseil Régional de Bretagne (doctoral fellowship for M. C.).

[1] W. N. Lipscomb, S. Sträter, *Chem. Rev.* **1996**, *96*, 2375.
[2] *Handbook on Metalloproteins* (Eds.: I. Bertini, A. Sigel, H. Siegel), Marcel Dekker Inc., New York, **2001**.
[3] S. Trofimenko, *Scorpionates*, Imperial College Press, London, **1999**.
[4] K Wieghardt, P. Chaudhury, *Prog. Inorg. Chem.* **1988**, *35*, 329.
[5] W. B. Tolman, *Acc. Chem. Res.* **1997**, *30*, 227 and references cited therein.
[6] M. N. G. James, R. S. Brown, *J. Am. Chem. Soc.* **1981**, *103*, 6947.
[7] C. Kimblin, W. E. Allen, G. Parkin, *J. Chem. Soc., Chem. Commun.* **1995**, 1813.
[8] C. Place, J.-L. Zimmermann, E. Mulliez, G. Guillot, C. Bois, J.-C. Chottard, *Inorg. Chem.* **1998**, *37*, 4030.
[9] S. Blanchard, L. Le Clainche, M.-N. Rager, B. Chansou, J.-P. Tuchagues, A. F. Duprat, Y. Le Mest, O. Reinaud, *Angew. Chem. Int. Ed.* **1998**, *37*, 2732; *Angew. Chem.* **1998**, *110*, 2861.
[10] Y. Rondelez, O. Sénèque, M.-N. Rager, A. F. Duprat, O. Reinaud, *Chem. Eur. J.* **2000**, *6*, 4218.
[11] L. Le Clainche, M. Giorgi, O. Reinaud, *Inorg. Chem.* **2000**, *39*, 3436.
[12] L. Le Clainche, Y. Rondelez, O. Sénèque, S. Blanchard, M. Campion, M. Giorgi, A. F. Duprat, Y. Le Mest, O. Reinaud, *C. R. Acad. Sci. Paris, Serie IIc, Chem.* **2000**, *3*, 811.

 © 2004 Wiley-VCH Verlag GmbH & Co. KGaA, Weinheim

[13] O. Sénèque, M.-N. Rager, M. Giorgi, O. Reinaud, *J. Am. Chem. Soc.* **2000**, *122*, 6183.
[14] O. Sénèque, Y. Rondelez, L. Le Clainche, C. Inisan, M.-N. Rager, M. Giorgi, O. Reinaud, *Eur. J. Inorg. Chem.* **2001**, 2597.
[15] O. Sénèque, M.-N. Rager, M. Giorgi, O. Reinaud, *J. Am. Chem. Soc.* **2001**, *123*, 8442.
[16] K. HÅkansson, M. Carlsson, L. A. Svensson, A. Liljas, *J. Mol. Biol.* **1992**, *227*, 1192.
[17] K. Håkansson, A. Wehnert, A. Liljas, *Acta Crystallogr. Sect. D* **1994**, *50*, 93.
[18] D. F. Evans, *J. Chem. Soc.* **1959**, 2003.
[19] I. Bertini, C. Luchinat, *Coord. Chem. Rev.* **1996**, *150*, 1.
[20] Due to the high molecular mass of this cobalt(II) complex, it was necessary to evaluate the diamagnetic contribution with the zinc(II) complex of the same ligand.
[21] L. Banci, A. Bencini, C. Benelli, D. Gatteschi, C. Zanchini, in *Structure and Bonding*, vol. 57 (Ed.: P. J. Sadler), Springer-Verlag, Berlin, Heidelberg, **1982**, p. 37.
[22] For four-coordinate Co^{II}, $\varepsilon > 300$ $M^{-1}\cdot cm^{-1}$; for five-coordinate Co^{II} $50 < \varepsilon < 300$ $M^{-1}\cdot cm^{-1}$ and for six-coordinate Co^{II} $\varepsilon < 50$ $M^{-1}\cdot cm^{-1}$. See: A. B. P. Lever, *Inorganic Electronic Spectroscopy (5th ed.)*, Elsevier, Amsterdam, **1984**.
[23] By analogy with the Zn complex, it seems very likely that a second water molecule, hydrogen bonded to the aqua ligand, occupies the calixarene cavity.
[24] A. W. Addison, T. N. Rao, J. Reedijk, J. van Rijn, G. C. Verschoor, *J. Chem. Soc., Dalton Trans.* **1984**, 1349.
[25] Potentials are reported versus Fc^+/Fc.
[26] Reaction in pure THF led to a thick non-homogeneous reaction mixture.
[27] F. A. Cotton, G. Wilkinson, *Advanced Inorganic Chemistry*, 5th ed., Wiley, New York, **1998**.
[28] N. N. Greenwood, A. Earnshaw, *Chemistry of the Elements*, Pergamon Press, Oxford, **1984**.
[29] This Ni^{II}-nitrilo-aqua complex is soluble in acetone, acetonitrile or a chloroform/acetonitrile mixture but totally insoluble in ethanol and pure chloroform or dichloromethane.
[30] L. Sacconi, F. Mani, A. Bencini, in *Comprehensive Coordination Chemistry*, vol. 5 (Ed.: G. Wilkinson), Pergamon Press, Oxford, **1987**, 1.
[31] It was not possible to study the host/guest property of the $X_6Me_3Imme_3$-Ni^{II} system because of its poor solubility in non-coordinating solvents. We have already noticed with other $X_6Me_3N_3$-M^{II} systems that the addition of a small excess of coordinating molecule enhances solubility: in these systems, the complexes seem to be maintained in solution by the included guest exchange. The low solubility might be related to the great inertia of Ni^{II} for the exchange of its ligands.
[32] CCDC-193247 for $[Co(X_6Me_3Imme_3)(CH_3COCH_3)](ClO_4)_2$, -193249 for $[Co(X_6Me_3Imme_3)(DMF)](ClO_4)_2$, -193240 for $[Co(X_6Me_3Imme_3)(EtOH)](ClO_4)_2$, -193241 for $[Co(X_6Me_3Imme_3)(EtCN)](ClO_4)_2$, -193248 for $[Co(X_6Me_3Imme_3)(MeCN)_2](ClO_4)_2$, and -193246 for $[Ni(X_6Me_3Imme_3)(MeCN)(H_2O)](ClO_4)_2$ contain the supplementary crystallographic data for this paper. Copies of the data can be obtained free of charge on application to CCDC, 12 Union Road, Cambridge CB2 1EZ, UK [Fax: (internat.) +44-1223-336-033; E-mail: deposit@ccdc.ac.uk].
[33] Bruker-Nonius B. V., Röntgenweg 1, 2624 BD Delft, P. O. Box 811, 2600 AV Delft, The Netherlands.
[34] G. M. Sheldrick, *SHELXL-97, a program for the refinement of crystal structures*; University of Göttingen, Germany, **1997**.

Received October 30, 2003
Early View Article
Published Online March 9, 2004

 © 2004 Wiley-VCH Verlag GmbH & Co. KGaA, Weinheim

Palladium Chemistry in Anhydrous HF/AsF_5 Superacid Medium

Zoran Mazej,*[a] Primož Benkič,[a] Alain Tressaud,[b] and Boris Žemva[a]

Keywords: Palladium / Fluorine / Superacids / Structure elucidation / Magnetic properties

Pd metal dissolves in anhydrous HF (aHF) acidified with AsF_5 in the presence of F_2 at ≈298 K to give a blue-green solution from which green $Pd(AsF_6)_2$ can be isolated. The latter was also prepared by the interaction of PdF_2 and AsF_5 in aHF or by the reaction between PdO and F_2 in aHF acidified with AsF_5. Powdered $Pd(AsF_6)_2$ slowly loses AsF_5 in a dynamic vacuum. It can therefore be isolated from solution at $T < 253$ K. Single-crystals of $Pd(AsF_6)_2$ were prepared by solvothermal synthesis from a $Pd/AsF_5/F_2$/aHF mixture at 393 K. $Pd(AsF_6)_2$ is triclinic with a = 500.9(5), b = 538.3(5), c = 864.9(9) pm, α = 74.46(3), β = 89.97(4), γ = 62.47(2)°, V = 0.1972(3) nm^3, and Z = 1, space group $P\bar{1}$ (No. 2). The six-coordinate Pd atoms (coordinated with fluorine) are well separated by isolated AsF_6 units. In the 2–175 K temperature range $Pd(AsF_6)_2$ follows the Curie–Weiss law with μ_{eff} = 3.53 B.M., T_n = 8 K and θ_p= −13 K. Because of cation-anion interactions, the AsF_6^- anions deviate from ideal O_h symmetry. The reduced symmetry can be seen in vibrational spectra, where splitting of the anion vibrational modes can be observed. The oxidation of Pd metal or PdO with F_2 in neutral aHF yielded Pd_2F_6. No reaction was observed between Pd, PdO or Pd_2F_6 and AsF_5 in aHF. All attempts to prepare $PdFAsF_6$ were unsuccessful.

(© Wiley-VCH Verlag GmbH & Co. KGaA, 69451 Weinheim, Germany, 2004)

Introduction

Ususally, self-ionization of pure anhydrous hydrogen fluoride (aHF) yields solvated protons $H^+_{(solv)}$ (the acid) and solvated fluoride anions $F^-_{(solv)}$ (the base).[1] On addition of Lewis bases (fluoro bases) or acids (fluoro acids) to aHF, a massive displacement in aHF self-ionization occurs. In this way it is possible to adjust the acidity (or basicity) of aHF. Addition of Lewis bases (donors of F^-, e.g. CsF) causes an enhancement of the F^- concentration, that is, an increase in basicity (a decrease in acidity) and, conversely, addition of Lewis acids (acceptors of F^-, e.g. AsF_5) causes a lowering of the F^- concentration and consequently an increase in acidity (decrease in basicity) of aHF. In absolutely pure aHF, the concentration of $F^-_{(solv)}$ equals that of $H^+_{(solv)}$ and aHF is neutral. We can talk about acidic, neutral and basic aHF, expressions which are generally accepted in fluorine chemistry and are also generally valid for any other solvent (including water) which can be acidic, neutral or basic.[1] The acidity (or basicity) of the solvent is important for the generation of desired oxidation states of transition metals.[1–6] The oxidation of noble metals by elemental fluorine conveniently shows the influence of acidity of aHF on the final oxidation state of the noble metal in the products. Basic aHF, with a high concentration of $F^-_{(solv)}$, favours anion formation with the metal in a high oxidation state, whereas acidic aHF, with a low concentration of $F^-_{(solv)}$, favours compounds with the metal in a cationic form and a low oxidation state.[7,8] In neutral aHF, binary fluorides are formed.

In previous investigations it was found that oxidation of palladium metal by elemental fluorine in basic aHF yielded the Pd(IV) high oxidation state in the PdF_6^{2-} anion (Li_2PdF_6 [8], K_2PdF_6,[8] $(NH_4)_2PdF_6$ [7]), whereas in acidic aHF (acidified with SbF_5) the final product of oxidation, i.e. $Pd(SbF_6)_2$,[8] contained a low-oxidation state Pd^{II} cation. Our preliminary results showed that clear blue-green solutions of the Pd^{II} salt [$Pd(AsF_6)_2$], when treated with alkali fluoride in aHF, gave a light-brown precipitate of a new variety of PdF_2 (low-temperature form),[9] while the same procedure on $Pd(SbF_6)_2$ gave the previously known lilac rutile-type form of PdF_2.[8] For that reason we decided to study palladium chemistry in AsF_5/aHF superacid media in more detail. The aim of this work was to find out what happens when palladium metal and different palladium compounds (i.e. PdO, PdF_2 and Pd_2F_6) are treated with aHF acidified with AsF_5 (a Lewis acid weaker than SbF_5) in the presence or absence of elemental fluorine. The results of investigations of palladium chemistry in neutral aHF are also reported.

[a] Jožef Stefan Institute, Department of Inorganic Chemistry and Technology,
Jamova 39, 1000 Ljubljana, Slovenia
Fax: (internat.) +386-1-423-2125
E-mail: zoran.mazej@ijs.si
[b] ICMCB-CNRS, 87,
Avenue Dr. A. Schweitzer, 33608 Pessac Cedex, France
Fax: (internat.) +33-5-40002761
E-mail: tressaud@icmcb.u-bordeaux.fr

Results and Discussion

Syntheses

AsF_5 is able to oxidize 3*d*-metals at room temperature using AsF_3 or anhydrous hydrogen fluoride (aHF) as the solvent, giving $M(AsF_6)_2$, $MFAsF_6$ or $M(AsF_6)_2{\cdot}2AsF_3$ types of compounds.[10] In contrast, the use of elemental fluorine is necessary for the oxidation of 4*d*− and 5*d*−metals,[7,8] including palladium, in aHF acidified with AsF_5. In the superacidic system AsF_5/aHF, palladium was slowly oxidized and finally completely dissolved yielding a green-blue solution of solvated Pd^{2+} cations, from which green $Pd(AsF_6)_2$ was isolated [Equation (1)]

$$\underset{m = 2.5\text{-}8,\ n = 1\text{-}2}{Pd + mAsF_5 + nF_2} \xrightarrow{aHF} Pd(AsF_6)_2 + (m\text{-}2)AsF_5 + (n\text{-}1)F_2 \quad (1)$$

There was no noticeable difference in the course of the reactions when different forms of Pd metal were used (Pd black, gray or sponge). In some experiments with Pd and AsF_5 in aHF we observed a green-blue solution, indicating a possible reaction. Later we discovered, however, that the reason lay in impure AsF_5 contaminated by traces of fluorine. When superacid AsF_5/aHF was first treated with hydrogen and then allowed to react with palladium, no such coloring of the liquid phase was observed.

PdO does not dissolve in an AsF_5/aHF superacidic system, contrary to some other oxides of 3*d*- and 5*f*-transition metals which can yield oxonium salts.[11,12] On addition of elemental fluorine to a suspension of PdO in AsF_5/aHF, the reaction proceeds with formation of a green-blue solution from which $Pd(AsF_6)_2$ can be isolated [Equation (2)].

$$\underset{m = 8,\ n = 1.3}{PdO + mAsF_5 + nF_2} \xrightarrow{aHF} Pd(AsF_6)_2 + (m\text{-}2)AsF_5 + (n\text{-}1)F_2 + 0.5O_2 \quad (2)$$

$Pd(AsF_6)_2$ can be prepared directly by the reaction between PdF_2 and AsF_5 in aHF [Equation (3)].

$$\underset{m = 3}{PdF_2 + mAsF_5} \xrightarrow{aHF} Pd(AsF_6)_2 + (m\text{-}2)AsF_5 \quad (3)$$

For the first two reactions [Equations (1) and (2)] the amount of fluorine is very important. In the literature it has been reported that addition of fluorine to a solution of AgF_2 in AsF_5/aHF causes the partial oxidation of Ag^{II} to Ag^{III} and formation of $(Ag^{II}F)_2(Ag^{III}F_4)AsF_6$.[13] On prolonged exposure to F_2 of the highly aHF−soluble $Au(SbF_6)_2$, part of the Au^{II} is oxidized to Au^{III}, yielding mixed−valence, poorly soluble $Au^{II}(SbF_6)_2Au^{II}(Au^{III}F_4)_2$.[5] If the excess of fluorine in reactions (1) and (2) is too great, black aHF−insoluble mixed-oxidation state Pd_2F_6, i.e. $Pd^{II}(Pd^{IV}F_6)$,[14] is formed besides aHF−soluble $Pd(AsF_6)_2$ [Equation (4)].

$$\underset{m = 2.5\text{-}8,\ n = 4}{Pd + mAsF_5 + nF_2} \xrightarrow{aHF} \begin{matrix} x\,Pd(AsF_6)_2 \\ (1\text{-}x)Pd_2F_6 \end{matrix} \quad (4)$$

The precipitation of black Pd_2F_6 also occurred when fluorine was added to a clear green−blue solution of solvated Pd^{2+} in AsF_5/aHF. Reactions between Pd or PdO and F_2 in neutral aHF also yielded Pd_2F_6 [Equation (5)].

$$\begin{matrix} 2Pd \\ 2PdO \end{matrix} \xrightarrow{+\,nF_2 \ \text{in aHF}} \begin{matrix} Pd_2F_6 + (n\text{-}3)F_2 \\ Pd_2F_6 + (n\text{-}3)F_2 + O_2 \end{matrix} \quad (5)$$

$n = 12\text{-}18$

Even when PdO and F_2 in aHF were left to react for a longer time (48 days) than Pd and F_2 in aHF (4 days), unchanged PdO was still present in the solid and only ≈60 mol % of starting PdO was converted into Pd_2F_6. It is also worth noting that there was no sign of any reaction between PdF_2 and F_2 in aHF, even after several days, probably due to kinetic reasons.

The formation of Pd_2F_6 shows that the oxidation of Pd metal by fluorine can also partly proceed to Pd(IV) in acidic aHF [Equation (4)] as well as in basic[7,8] and neutral aHF media [Equation (5)].

This is in agreement with previous results showing that, by using a stronger oxidizer (KrF_2) than fluorine in neutral or acid aHF (acidified with AsF_5), all Pd is oxidized to $Pd^{IV}F_4$.[15] The main driving forces for the formation of $Pd(AsF_6)_2$ or $PdPdF_6$ are the fluoride ion affinities of AsF_5 (PdF_4) and the lattice energy differences between PdF_2 and the complex fluoroanion salts $Pd(AsF_6)_2$ ($PdPdF_6$). Since even PdF_4 prepared in situ does not react with AsF_5 [15] and precipitates on addition of AsF_5 to aHF solutions of PdF_6^{2-} alkali metal salts,[16] it can be concluded that the Lewis acidity (fluoroacidity or fluoride ion affinity) of PdF_4 is weaker than that of AsF_5. The driving force for the formation of Pd_2F_6 (PdF_2+PdF_4), despite the presence of the stronger fluoro acid AsF_5, is its high lattice energy. This explains why AsF_5 is not able to precipitate PdF_4 from Pd_2F_6 although it has a higher fluoride ion affinity than PdF_4.

Solvated Pd^{II} in green-blue solutions of $Pd(AsF_6)_2$ can, on the other hand, be easily oxidized or reduced, yielding finely powdered Pd_2F_6 or Pd metal, respectively [Equation (6)].

$$Pd^{2+}{}_{(solv.)}\ \text{in}\ AsF_5/aHF \begin{matrix} \xrightarrow{+\,nF_2} 0.5Pd_2F_6 + 2AsF_5 + (n\text{-}1.5)F_2 \\ \xrightarrow{+\,nH_2} Pd + 2HF + 2AsF_5 + (n\text{-}1)H_2 \end{matrix} \quad (6)$$

Additionally it was found that Pd_2F_6 can also be reduced by hydrogen in aHF yielding powdered Pd metal [Equation (7)].

 © 2004 Wiley-VCH Verlag GmbH & Co. KGaA, Weinheim

$$Pd_2F_6 + nH_2 \xrightarrow{aHF} 2Pd + 6HF + (n\text{-}3)H_2 \quad (7)$$

To prepare pure $Pd(AsF_6)_2$ according to reactions (1), (2) and (3), the temperature of recovery from solution is important. It was found that $Pd(AsF_6)_2$ releases AsF_5 in a dynamic vacuum. Pure $Pd(AsF_6)_2$ can be isolated from solution in aHF by pumping away volatiles at temperatures lower than 253 K. At room temperature, the isolated products had varied compositions "$PdF_x(AsF_6)_{2-x}$" with $0 < x \leq 1$ depending on temperature, time of isolation and vacuum conditions. For all compositions, the X−ray powder diffraction patterns showed only lines which could be attributed to $Pd(AsF_6)_2$. Even the X−ray powder pattern of the phase close to a "$PdFAsF_6$" composition was the same as that of $Pd(AsF_6)_2$. We also tried to prepare $PdFAsF_6$ by displacing a weak acid from its alkali metal salt, similar to that reported for $AgFBiF_6$ from $Ag(BiF_6)_2$ [17] but, instead of $PdFAsF_6$, a mixture of $Pd(AsF_6)_2$ and a low-temperature modification of PdF_2 [9] was always obtained [Equation (8)].

$$Pd(AsF_6)_2 + KPF_6 \xrightarrow{aHF} 0.5Pd(AsF_6)_2 + 0.5PdF_2 + KAsF_6 + PF_5 \quad (8)$$

On the basis of these results we conclude that phases with compositions $PdF_x(AsF_6)_{2-x}$ ($0 < x \leq 1$) are mixtures of $Pd(AsF_6)_2$ and PdF_2 and not mixtures of $Pd(AsF_6)_2$ and $PdFAsF_6$. The possible preparation and existence of $PdFAsF_6$ is thus still in question. The instability of $Pd(AsF_6)_2$ in a dynamic vacuum could be a consequence of the inadequate fluoroacidity of AsF_5. When a stronger fluoroacid SbF_5 (FIA[SbF_5,g] ≈ −506 (± 63) kJ/mol)[18] was used instead of AsF_5 (FIA[AsF_5,g] ≈ −421 (± 22) kJ/mol)[18] the resultant $Pd(SbF_6)_2$ was stable at room temperature.[8] However care must be exercised in this type of comparison, in that the relative volatilities of AsF_5 and SbF_5 are also important factors in the stabilities of the resultant $Pd(AsF_6)_2$ and $Pd(SbF_6)_2$.

Crystal Structure of $Pd(AsF_6)_2$

$Pd(AsF_6)_2$ crystallizes in the same structural category as many other compounds obtained in the systems MF_2/XF_5 (M = transition metal, XF_5 = Lewis acid), e.g. $Mn(SbF_6)_2$,[19] $Ag(XF_6)_2$, X = Sb,[20] Nb,[21] Ta,[21] Bi,[17] $Au(SbF_6)_2$.[5] Pertinent crystallographic data are given in Exp. Sect.

A view of the crystal structure of $Pd(AsF_6)_2$ perpendicular to the slab that contains all palladium atoms in the same plane is shown in Figure 1. Pd atoms are in octahedral environments of fluorine, and PdF_6 octahedra are connected through their vertices to six AsF_6 units on either side of the plane formed by the Pd atoms. There are only van der Waals contacts of fluorine atoms between neighboring slabs and the network is a derivative of the $CdCl_2$ structural type. The structure can be alternatively described as being derived from the $LiSbF_6$ type (ordered ReO_3) with ordered vacancies (□) for half of the cationic sites, i.e. $Pd_{0.5}\square_{0.5}AsF_6$.

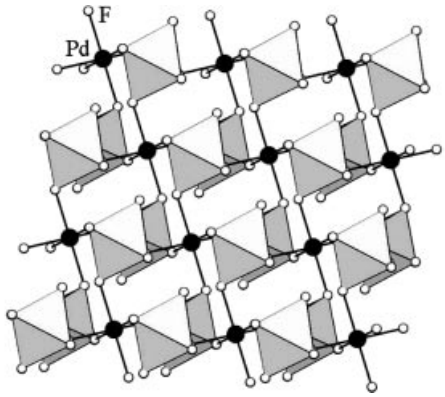

Figure 1. Part of the crystal structure of $Pd(AsF_6)_2$ perpendicular to the slab containing the palladium atoms.

The six-fold coordination of Pd^{II} in $Pd(AsF_6)_2$ is different from similar Ag and Au compounds in which, due to the Jahn−Teller effect, the metal octahedral environments are so distorted that coordination around Ag^{II} and Au^{II} is better described as square-planar rather than octahedral. The Pd−F bond lengths [218.3(5)−219.0(5) pm] of hexacoordinated Pd^{II} are slightly longer than the Pd−F bond lengths in PdF_2 [9,22,23] (Figure 2, Table 1).

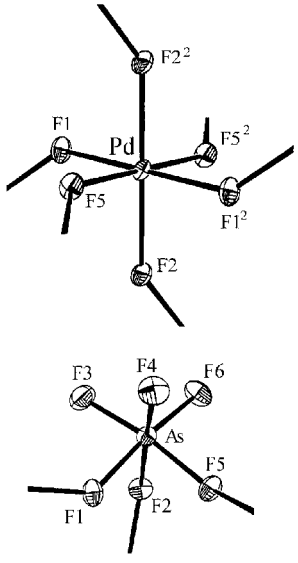

Figure 2. Coordination of the Pd^{II} atom and AsF_6 unit (thermal ellipsoids are shown at the 50% probability level)

The AsF_6^- anions are highly distorted by their interaction with the cation (Figure 2, Table 1). Consequently three As−F bonds with bridging fluorine atoms are considerably longer [179.8(5), 178.6(5), 176.8(5) pm] than the other three As−F bonds with non−bridging fluorine atoms [166.3(5), 167.9(3), 168.8(5) pm]. From the gross distortion of the AsF_6^- unit, it is evident that Pd^{II} strongly attracts the fluorine ligands of the surrounding AsF_6 species. The reason

 © 2004 Wiley-VCH Verlag GmbH & Co. KGaA, Weinheim

Table 1. Selected bond lengths (pm) and angles (°); symmetry codes used to generate equivalent atoms: $-x$, $-y$, $-z$; due to the center of inversion at the Pd center, the coordination of Pd is completed by $F1^2$, $F2^2$ and $F5^2$

As−F1	179.8(5)	F1−As−F2	84.5(2)	F3−As−F4	95.1(3)
As−F2	176.8(5)	F1−As−F3	88.4(3)	F3−As−F5	172.1(2)
As−F3	167.8(5)	F1−As−F4	89.1(3)	F3−As−F6	96.2(3)
As−F4	168.8(5)	F1−As−F5	84.6(3)		
As−F5	178.6(5)	F1−As−F6	173.5(2)	F4−As−F5	88.4(3)
As−F6	166.3(5)			F4−As−F6	95.0(3)
		F2−As−F3	90.4(3)		
		F2−As−F4	171.5(2)	F5−As−F6	90.6(3)
Pd−F1	218.9(5)	F2−As−F5	85.4(2)		
Pd−F2	219.0(5)	F2−As−F6	90.9(2)	Pd−F1−As	134.7(3)
Pd−F5	218.3(5)			Pd−F2−As	143.5(3)
				Pd−F5−As	138.0(3)

must be due to the high effective nuclear charge (i.e, the charge density; Z^+/r ratio) of the Pd^{II} cation.

Magnetic Properties of $Pd(AsF_6)_2$

Because of the peculiar d^8 electronic configuration of divalent palladium, the Pd^{II} based fluoro-compounds may exhibit either paramagnetic or diamagnetic behavior depending on whether the configuration of the transition element is high-spin or low-spin, respectively. The corresponding coordination numbers are so various that this element has been called an "inorganic chameleon".[24] $MPdF_4$ (M = Ca, Sr, Ba, Pb) and $M'MPdF_5$ compounds (M′ = K, Rb, Cs) are examples of the latter, low-spin case, in which the Pd^{II} has a square planar environment.[24] In the former case, Pd^{II} exhibits a regular octahedral coordination, as in rutile-type PdF_2 and $PdM^{IV}F_6$ phases (M^{IV} = Pd, Pt) derived from ReO_3 structures by cationic ordering.[25] Due to the ordering of Pd electronic orbitals, ferromagnetism occurs in these Pd_2F_6-derived materials. An intermediate case is that of $CsPd_2F_5$, in which half of the Pd^{II} centers are in a high-spin configuration and the other half in a low−spin state.[26]

$Pd(AsF_6)_2$ is paramagnetic and the reciprocal susceptibility follows the Curie−Weiss law with a Weiss constant of −13 K and possible three dimensional ordering below 8 K (C = 1.56 and μ_{eff} = 3.53 B.M.) (Figure 3). The absence of 3D interactions over a large temperature range is in agreement with the structural features. Pd atoms are isolated from each other and there is thus no possible Pd−F−Pd superexchange coupling. The average μ_{eff} is considerably higher than the calculated μ_{eff} considering only spin (2.83 B.M). Such high values of μ_{eff} were also previously reported for palladium fluorosulfates [$Pd(SO_3F)_2$: 3.39 B.M.,[27,28] $Pd(M^{IV}(SO_3F)_6]$: 3.45 B.M. for M = Pd,[27−29] 3.37 B.M. for M = Pt[29] and 3.60 B.M. for M = Sn[29]].

It should be noted that a second Pd^{II} compound with a similar formula, i.e. $Pd(SbF_6)_2$, is structurally related to $Pd(AsF_6)_2$. A preliminary crystal structure was reported,[30] but was incomplete possibly because of twinning of the crystals. The only difference is that in $Pd(SbF_6)_2$, a disordered distribution of Pd^{II} occurs in all octahedral sites. Magnetic data have been determined[8,31] over the range 2−82 K (at 82 K $Pd(SbF_6)_2$ has a μ_{eff} = 3.09 B.M.).

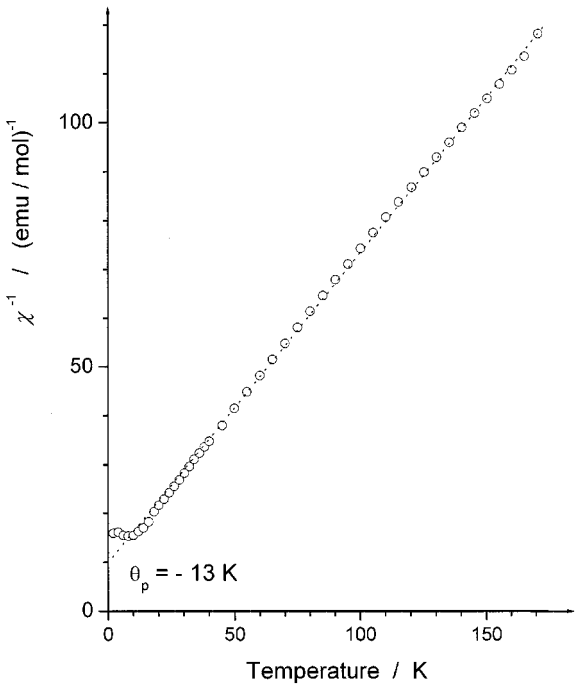

Figure 3. Temperature dependence of the reciprocal magnetic susceptibility of $Pd(AsF_6)_2$

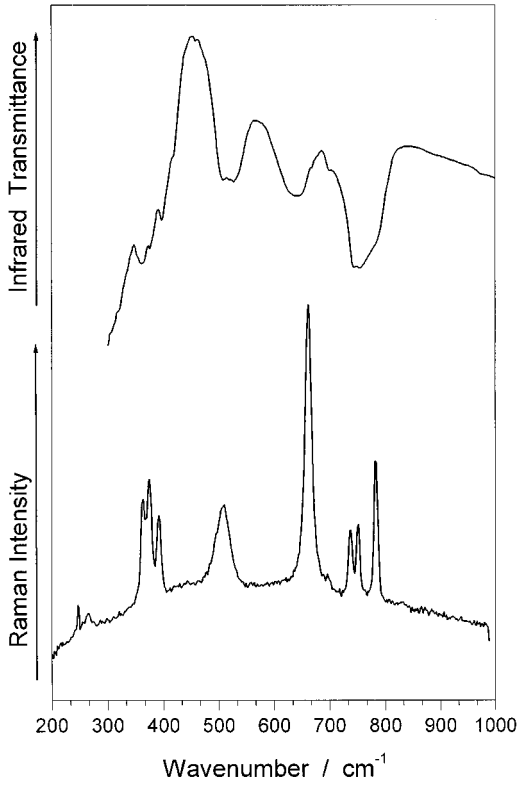

Figure 4. IR and Raman spectra of $Pd(AsF_6)_2$

 © 2004 Wiley-VCH Verlag GmbH & Co. KGaA, Weinheim

Vibrational Spectra of $Pd(AsF_6)_2$

More bands were observed in the vibrational spectra than would be expected for a regular AsF_6^- anion with O_h symmetry (Figure 4), consistent with a highly distorted AsF_6 octahedral structure in solid $Pd(AsF_6)_2$. The bands in the region 640−790 cm^{-1} can be assigned to $As-F_{terminal}$ stretching modes. Bands in the region 490−530 cm^{-1}, which are weaker than the stretching ones for terminal fluorine atoms, are typical for species where one fluorine bridges two different atoms,[1] and can be readily assigned to As−F−Pd stretching modes. Bands below 400 cm^{-1} were assigned to deformation and lattice modes (Table 2).

Table 2. Vibrational spectra of $Pd(AsF_6)_2$

IR[a]	Raman	Partial assignments[b]
782(sh)	784(40)	As−F_t stretching modes
759(vs)	751(25)	As−F_t stretching modes
745(vs)		As−F_t stretching modes
	737(20)	As−F_t stretching modes
701(w)	699(5)	As−F_t stretching modes
	662(100)	As−F_t stretching modes
641(s, br)		As−F_t stretching modes
528(s)		As−F−Pd stretching modes
509(s)	509(30)	As−F−Pd stretching modes
	495(sh)	As−F−Pd stretching modes
399(w)	393(20)	deformation modes
377(w)	374(50)	deformation modes
362(w)	366(35)	deformation modes
	264(5)	lattice modes
	246(10)	lattice modes

[a] Intensities are given in parentheses; w = weak, m = medium, s = strong, vs. = very strong, sh = shoulder. [b] F_t = terminal (non-bridging) fluorine atom.

Conclusion

In this study we have investigated the reactions of Pd metal and different Pd compounds (PdF_2, PdO, Pd_2F_6) with AsF_5, with or without elemental fluorine, in liquid aHF. The observed reactions follow the general scheme for the dependence of the generation of low- or high-oxidation states of transition metals on the acid-base properties of the solvent. In neutral aHF, the binary fluoride Pd_2F_6 is formed, whereas acidic aHF favors the metal in a cationic form in the low oxidation state, with formation of $Pd(AsF_6)_2$. Additionally it was found that the oxidation of Pd metal by fluorine can also partly proceed to Pd(IV) in acidic aHF. It can be concluded that Pd_2F_6 is thermodynamically favorable but kinetically unfavorable relative to $Pd(AsF_6)_2$.

The partial oxidation of Pd with elemental fluorine to Pd(IV) in acidic or neutral aHF and formation of Pd_2F_6 ($Pd^{II}Pd^{IV}F_6$) with no further oxidation to PdF_4 is more likely a consequence of unfavorable thermodynamics than kinetics. For the latter, the main reason lies in aHF insoluble Pd_2F_6 which has to be oxidized by fluorine in aHF to insoluble PdF_4. However, if KrF_2 [15] or ultraviolet photolyzed F_2 [32] are used instead of elemental F_2 in liquid aHF then Pd_2F_6 is quantitatively converted into PdF_4. Treatment of Pd with KrF_2 in aHF is energetically favorable because of the lower heat of atomization of KrF_2 (97.8 kJ·mol^{-1}) in comparison with elemental fluorine (157.7±0.4 kJ·mol^{-1}), making it a better low-temperature source of fluorine atoms.[33] In the case of the reaction of ultraviolet photolyzed F_2 and Pd in aHF, UV-irradiation provides the energy for the cleavage of the chemical bonds in F_2 and access to atomic fluorine.

The solubility of the reactants and products is not always the governing factor for the generation of the desired oxidation states of transition metals in liquid aHF. For example, elemental fluorine oxidizes MnF_2 in aHF yielding only pure MnF_3. In the presence of a UV source, MnF_2 is completely oxidized by photodissociated F_2 in aHF to MnF_4.[34] The same thing happens if KrF_2 is used as the oxidizing agent.[35] However, the suppression of kinetic barriers (insolubility of reactants and products) has a great influence on the preparation of LnF_4 (Ln = Pr, Tb) in liquid aHF. Reactions between LnF_3 and elemental F_2 in aHF at room temperature were incomplete even in the presence of ultraviolet light and gave mixtures of LnF_3 and LnF_4. However when the corresponding Ln oxides were used as starting materials LnF_4 were obtained in a quantitative yields, because the coatings of the reaction products on the surface of the solid reagents were destroyed by gas evolution, thereby accelerating the process.[36]

When oxidation of Pd by elemental fluorine is carried out in basic aHF (*A*F/aHF systems; *A* = alkali metal) with a high concentration of $F^-_{(solv)}$, the forming Pd(IV) instantaneously dissolves as PdF_6^{2-}. Although Pd^{II} is formed as an intermediate it has to compete with a stronger Lewis base, i.e. A^+ for the formation of PdF_6^{2-} salts.

The crystal structure of $Pd(AsF_6)_2$ confirms the presence of highly distorted AsF_6^- anions as predicted by vibrational spectroscopy. It is composed of 2D slabs containing Pd atoms in the center and AsF_6 groups on either side. Only van der Waals bonding exists between neighboring slabs. The network can be described as being based on the $CdCl_2$ structural type or the $LiSbF_6$ type (ordered ReO_3), with ordered vacancies (□) for half the cationic sites, i.e. $Pd_{0.5}□_{0.5}AsF_6$. As found by single-crystal X-ray analyses and X-ray powder diffraction, this structure is adopted by most of the known compounds with formula $M^{II}(X^{V}F_6)_2$ (*M* = transition metal; *X* = As, Sb, Bi, Nb, Ta). Two exceptions are $Mn(AsF_6)_2$ [37] and $Pd(NbF_6)_2$.[38]

The paramagnetic behavior of $Pd(AsF_6)_2$ is in good agreement with the structural data because no Pd−F−Pd superexchange interaction is possible.

Experimental Section

Apparatus and Reagents: Volatile materials (AsF_5, PF_5, aHF) were manipulated in an all-PTFE vacuum line equipped with PTFE valves. Non-volatile materials were manipulated in a dry-box (M.

 © 2004 Wiley-VCH Verlag GmbH & Co. KGaA, Weinheim

Braun). The residual water in the atmosphere within the dry-box never exceeded 1 ppm. The reactions were carried out in translucent fluorocarbon polymer (FEP) reaction vessels (height 250−300 mm with inner diameter 15.5 mm and outer diameter 18.75 mm) equipped with PTFE body valves and PTFE coated stirring bars. Reaction vessels combined from two FEP tubes in a T-shape manner and equipped with PTFE body valves were used in some experiments. Each reaction vessel was pre-treated with F_2 (to about 1 bar) for several hours before use.

Pd black (Alfa Products, 99.9%), Pd black (Aldrich, 99.9%), Pd gray (Johnson Matthey & Co-limited, 99.9%), Pd gray (Merck, 99.9%), Pd sponge (Aldrich, 99.9), PdO (Cerac Incorporated, 99.99%), and KF (Ventron, 99.9%) were used as supplied. AsF_5 was synthesized by pressure fluorination of arsenic trioxide with elemental fluorine in a nickel reactor at 573 K as described for the synthesis of PF_5.[39] KPF_6 was prepared from KF and PF_5 in aHF. The lilac rutile form of PdF_2 was prepared as described.[40] Fluorine was used as supplied (Solvay, 99.98%). Anhydrous HF (Praxair, 99.9%) was treated with K_2NiF_6 for several hours prior to use.

CAUTION: aHF, AsF_5, and PF_5 should only be handled in a well-ventilated hood, and protective clothing should be worn at all times!

Instrumentation: Infrared spectra were recorded on a Perkin−Elmer FTIR 1710 spectrometer on powdered samples between AgCl plates in a leak-tight brass cell. Raman spectra were recorded on a Renishaw Raman Imaging Microscope System 1000, with a He−Ne laser of wavelength 632.8 nm. X-ray powder diffraction patterns were obtained using the Debye−Scherrer technique with Ni-filtered Cu-K_α radiation. Samples were loaded into quartz capillaries (0.3 mm) in a dry-box.

Chemical Analyses: Palladium was determined by complexometric titration;[41−43] total fluoride ion content was determined with a fluoride ion selective electrode;[44,45] AsF_6^- species were determined gravimetrically as insoluble tetraphenylarsonium salts;[46,47] arsenic was determined by the ICP method.[48] The results of chemical analyses are given in mass percentages.

Syntheses

General Procedure: Starting materials were loaded into an FEP reaction vessel in a glove box. aHF and, when necessary, AsF_5 were condensed onto solid reactants at 77 K, which were then brought to room temperature. Fluorine was added when needed. The reaction mixtures were vigorously agitated and after some time volatiles were pumped away. Isolated products were characterized by mass balance, chemical analysis, vibrational spectroscopy, X-ray powder diffraction patterns (XRPD-pattern) and/or magnetic measurements.

Reaction between Pd and F_2 in aHF: Reaction mixture: Pd (0.242 g, 2.27 mmol) and F_2 (13.99 mmol) in aHF (6 mL). After 4 days no visible change was observed (colorless liquid was present above a black solid). Final mass: 0.401 g (calcd. for Pd_2F_6: 0.371 g). XRPD-pattern and Raman spectrum (563 cm^{-1}, 281 cm^{-1} and 213 cm^{-1}) corresponded to Pd_2F_6. Pd_2F_6 (326.8): calcd. F 34.88, Pd 65.12; found F 34.6, Pd 63.9.

Reaction between PdO and F_2 in aHF: Reaction mixture: PdO (0.191 g, 1.56 mmol) and F_2 (12.92 mmol) in aHF (4 mL). After 48 days no visible change was observed (colorless liquid was present above a black solid). Pd_2F_6 (326.8): calcd. F 34.88; found F 23.4. XRPD-pattern showed a mixture of PdO and Pd_2F_6.

Reaction between PdF_2 and F_2 in aHF: Reaction mixture: rutile form of PdF_2 (0.275 g, 1.90 mmol) and F_2 (12.92 mmol) in aHF (4 mL). After 13 days, the liquid was colorless and starting PdF_2 remained as an insoluble brown solid, characterized by XRPD-pattern. PdF_2 (144.4): calcd. F 26.32, Pd 73.68; found F 26.9, Pd 72.1.

Reactions between Pd and AsF_5 in aHF: Two experiments were carried out. In the first experiment, a reaction mixture of Pd (0.110 g) and AsF_5 (2.000 g) in aHF (4 mL) was prepared. After 3 days a green-blue solution was observed above unchanged Pd metal. The Raman spectrum of the solution showed a strong band at 703 cm^{-1}, which could be attributed to $As_2F_{11}^-$. After 42 days the volatile components were pumped away. The XRPD-pattern of the isolated solid showed only Pd metal. Chemical analysis showed 4.78% As in the isolated solid.

In the second experiment a solution of AsF_5 (2.000 g) in aHF (3 mL) was treated with 4 bar of hydrogen. After one day of intensive stirring the solution was cooled to 77 K, and volatile components were pumped away. The mixture of AsF_5/aHF was then brought to room temperature and condensed onto Pd metal (0.118 g, 1.11 mmol). The Raman spectrum of the liquid phase showed a strong band at 703 cm^{-1}. After 42 days the liquid phase was still colorless. The XRPD−pattern of the isolated solid showed it to consist of metallic Pd. Pd (106.4): calcd. Pd 100; found Pd 98.2.

Reaction between PdO and AsF_5 with and without F_2 in aHF: Reaction mixture: PdO (0.182 g, 1.49 mmol) and AsF_5 (11.77 mmol) in aHF (4 mL). The Raman spectrum of the solution showed a strong band at 703 cm^{-1}. After 8 days the liquid phase was still colorless. Because there was no sign of reaction, F_2 (1.96 mmol) was added to the reaction vessel. The liquid phase became green-blue over few hours. Within 13 days a clear green-blue solution was obtained. Volatiles were pumped away at 253 K. Final mass of isolated green solid: 0.799 g [calcd. for $Pd(AsF_6)_2$: 0.726 g]. $Pd(AsF_6)_2$ (484.2): calcd. Pd 21.97; F 47.09; As 30.94; AsF_6 78.03; found Pd 21.4; F 46.3; As 33.3; AsF_6 76.0 [corresponding to molar ratio: n(Pd):n(As):n(AsF_6):n(F) = 1.0:2.2:2.0:12.1].

Reaction between PdF_2 and AsF_5 in aHF: Immediately after warming to room temperature, a reaction mixture of PdF_2 (0.270 g,1.87 mmol) and AsF_5 (5.90 mmol) in aHF (4 mL) became green-blue in color. After three days, some of the volatiles were pumped away at room temperature until 1 mL of solution was left. Finally, all volatiles were pumped away over 6 days at 243 K. Final mass of the green solid: 0.913 g, calcd. for $Pd(AsF_6)_2$: 0.906 g. $Pd(AsF_6)_2$ (484.2): calcd. Pd 21.97, F 47.09, AsF_6 78.03; found Pd 21.7, F 46.3, AsF_6 76.6.

Reaction between Pd_2F_6 and AsF_5 in aHF: Reaction mixture: Pd_2F_6 (0.138 g, 0.84 mmol) and AsF_5 (3.53 mmol) in aHF (6 mL). After 6 days the liquid phase was still colorless, and the insoluble solid was black. The XRPD-pattern and Raman spectrum (563, 283 and 215 cm^{-1}) of the isolated solid showed only starting Pd_2F_6. Pd_2F_6 (326.8): calcd. F 34.88; found F 34.9.

Reactions between Pd and AsF_5 in aHF in the Presence of Fluorine: Many experiments were performed with different forms of Pd. Only two typical ones will be described. Reaction mixture: Pd (0.292 g, 2.74 mmol), AsF_5 (7.06 mmol) and F_2 (4.95 mmol) in aHF (10 mL). After one hour the color of the solution became green−blue. After 5 days a clear green-blue solution was obtained. Volatiles were pumped away at room temperature. The final mass of isolated grayish−green solid was 1.246 g, corresponding to a

 © 2004 Wiley-VCH Verlag GmbH & Co. KGaA, Weinheim

molar ratio $n(PdF_2):n(AsF_5)$ = 1:1.87. $Pd(AsF_6)_2$ (484.2): calcd. Pd 21.97, F 47.09, As 30.94, AsF_6 78.03; found Pd 23.2, F 45.3, As 30.6, AsF_6 76.1 [corresponding to molar ratio $n(PdF_2):n(AsF_5)$ = 1:1.87]. In other experiments different final molar ratios $n(PdF_2):n(AsF_5)$ were obtained giving "$PdF_x(AsF_6)_{2-x}$" where $0 < x \leq 1$ depending on the temperature and time of isolation and vacuum conditions. Reaction mixture: Pd (0.281 g, 2.64 mmol), AsF_5 (20.56 mmol) and F_2 (3.53 mmol) in aHF (8 mL). After 5 days a clear green−blue solution was obtained. Volatiles were pumped away for 10 days at 253 K. The isolated solid product was green. $Pd(AsF_6)_2$ (484.2): calcd. Pd 21.97, F 47.09, As 30.94, AsF_6 78.03; found Pd 21.4, F 46.1, As 33.8, AsF_6 77.3 [corresponding to molar ratio n(Pd):n(As):$n(AsF_6):n$(F) = 1.0:2.2:2.0:12.1].

Reaction between Pd and AsF_5 in aHF in the Presence of a Large Excess of Fluorine: Reaction mixture: Pd (0.326 g, 3.06 mmol), AsF_5 (25.15 mmol) and F_2 (11.95 mmol) in aHF (8 mL). After bringing the reaction mixture to room temperature, the color of the liquid phase changed to green-blue. After 10 days a clear green−blue solution was visible above an insoluble black solid. The solution was decanted. The mass of black solid was 0.359 g. Its Raman spectrum (565, 291 and 219 cm^{-1}) showed only Pd_2F_6. The XRPD-pattern of green solid isolated from decanted solution showed only $Pd(AsF_6)_2$.

Reaction between Pd_2F_6 and H_2 in aHF: Pd_2F_6 (0.239 g, 1.46 mmol) was suspended in HF (7 mL) and agitated intensively at room temperature. Immediately after addition of hydrogen the sample deposited on the bottom of the reaction vessel despite intensive stirring. The final pressure of hydrogen was 3.7 bar. After one day volatiles were pumped away at room temperature. Final mass: 0.169 g (calcd. for Pd: 0.155 g). Pd (106.4): calcd. Pd 100; found Pd 97.8. The XRPD-pattern showed Pd metal.

Reduction and Oxidation of Solvated Pd^{2+} Dissolved in AsF_5/aHF: A clear green blue solution was prepared from Pd (0.133 g, 1.26 mmol), AsF_5 (3.700 g, 21.78 mmol) and F_2 (1.50 mmol) in aHF (8 mL). The excess fluorine was pumped away at 77 K. After addition of 2 bar of hydrogen at room temperature, the liquid phase became colorless over 10 minutes. A metallic, shiny solid precipitated on the walls of reaction vessel. Volatiles were pumped away at room temperature. Final mass: 0.167 g. Chemical analysis: % Pd, 92.5,% As, 4.2. The XRPD-pattern showed only Pd metal.

A green blue solution of Pd metal was prepared as above. After addition of elemental fluorine, a black solid started to precipitate. The amount of insoluble solid increased with time and the intensity of the green-blue color of the liquid phase decreased. The XRPD-pattern of the isolated solid showed only Pd_2F_6.

Attempted Synthesis of $PdFAsF_6$: A T-shaped FEP reactor with two PTFE valves as described before[49] was loaded with Pd (0.155 g, 1.46 mmol) in one arm and KPF_6 (0.266 g, 1.46 mmol) in the other. aHF (about 4 mL), AsF_5 (2 g) and F_2 (1.60 mmol) were condensed onto the Pd and in the other arm aHF (3 mL) was condensed onto KPF_6, yielding a colorless solution. After one day the Pd metal completely dissolved, yielding a blue-green solution. Volatiles were pumped away at 253 K and fresh aHF was added. The solution of KPF_6 in aHF was slowly poured onto the clear solution of $Pd(AsF_6)_2$ in aHF. A light-brown solid immediately precipitated. After two days a green-blue solution was visible above the light-brown solid. The solution was decanted. The XRPD-pattern of the insoluble brown solid corresponded to the low-temperature form of PdF_2.[9] The XRPD-pattern and Raman spectrum of the solid precipitated from the decanted solution showed a mixture of $KAsF_6$ and $Pd(AsF_6)_2$.

Preparation of Single-Crystals of $Pd(AsF_6)_2$ and Structure Determination: The crystal structure of $Pd(AsF_6)_2$ was first determined on our single-crystals with the help of Dr. H. Borrmann, Max Planck Institut für Chemische Physik fester Stoffe, Dresden, Germany. Later the determination of the crystal structure of $Pd(AsF_6)_2$ was repeated on new crystals. All crystallographic data presented in this paper are from repeated crystal structure determinations.

Single-crystals of $Pd(AsF_6)_2$ were prepared by solvothermal syntheses. The reaction between Pd (0.110 g, 1.03 mmol), AsF_5 (1.5 g, 8.83 mmol), aHF (0.050 g) and F_2 (1.5 mmol) was carried out in a special stainless steel autoclave with a PTFE liner (V = 6 mL). After entering all reactants into the autoclave it was heated to 393 K for 43 days. After cooling to ambient temperature all volatiles were quickly pumped away. A large piece of brown solid was found inside. When it was broken up, blue-green crystals of $Pd(AsF_6)_2$ were found inside. Single-crystals were selected in a dry-box and mounted in 0.3 mm quartz capillaries.

Single-crystal data from $Pd(AsF_6)_2$ were collected on a Mercury CCD area detector coupled with a Rigaku AFC7S diffractometer using monochromated MoK_α radiation. Data were corrected for Lorentz, polarization, and absorption effects and processed using the Rigaku Crystalclear software suite program package.[50] The structure was solved by direct methods[51] and expanded using Fourier techniques. Some details of the single-crystal data collection, data processing, and refinement are given in Table 3. Further details of the crystal-structure investigation may be obtained from the Fachinformationzentrum Karlsruhe, 76344 Eggenstein-

Table 3. Crystal data and structure refinement for $Pd(AsF_6)_2$

Formula	$Pd(AsF_6)_2$
Crystal system	triclinic
Space group	$P\bar{1}$ (No.2)
Unit cell dimensions (pm,°)	a = 500.9(5)
	b = 538.3(5)
	c = 864.9(9)
	α = 74.46(3)
	β = 89.97(4)
	γ = 62.47(2)
V (nm^3)	0.1972(3)
$D_{calcd.}$ (gcm^{-3})	4.079
Z	1
Molecular mass ($gmol^{-1}$)	484.24
Wavelength (pm)	71.069
Temperature (K)	293(2)
θ range for data collection (°)	$2.47 \leq \theta \leq 29.00$
Index ranges	$-6 \leq h \leq 6$, $-6 \leq k \leq 6$, $-6 \leq l \leq 11$
Reflections collected	898
Independent reflections	796 (R_{int} = 0.0256)
Observed reflections [$I > 2\sigma(I)$]	762
Refinement method	Full matrix least-squares on F^2
Data/restraints/parameters	796/0/70
Absorption correction	multi-scan
Absorption coefficient (mm^{-1})	10.864
Goodness-of-fit on F^2	1.061
R indices (all data)	$R1$ = 0.0615, $wR2$ = 0.1620
Final R indices [$I > 2\sigma(I)$]	$R1$ = 0.0602, $wR2$ = 0.1599

[a] $R1 = \Sigma||F_o| - |F_c||/\Sigma|F_o|$, $wR2 = \Sigma[w(F_o^2-F_c^2)^2/\Sigma[w(F_o^2)^2]^{1/2}$, GOF = $\Sigma[w(F_o^2-F_c^2)^2/(N_o-N_p)]^{1/2}$, where N_o = no. of reflections and N_p = no. of refined parameters.

 © 2004 Wiley-VCH Verlag GmbH & Co. KGaA, Weinheim

Leopoldshafen, Germany, on quoting the depository number CSD-413415.

Magnetic Measurements: Cylindrical screw-capped sample containers ($V \approx 0.5$ mL, $m \approx 0.250$ mg) for magnetic measurements of $Pd(AsF_6)_2$ were made of Kel-F (polytrifluorochloroethylene) and were additionally tightened with PTFE gaskets. Prior to their use, both the container and Kel-F packing tool were made passive with elemental fluorine. The field dependence of the magnetization was measured for various temperatures in the 4.2−300 K range using a SQUID magnetometer (MPMS-5S, Quantum Design).

Acknowledgments

The authors are indebted to J. Darriet for fruitful help with magnetic measurements and Maja Ponikvar for chemical analyses. The authors gratefully acknowledge the financial support of the Ministry of Education, Science and Sport of the Republic of Slovenia and the financial support of the French-Slovenian scientific cooperation program PROTEUS.

[1] T. A. O'Donnell, *Superacids and Acidic Melts as Inorganic Chemical Reaction Media*, VCH Publishers, New York, **1993**.
[2] B. Žemva, *C. R. Acad. Sc. Paris Serie II* **1998**, *1*, 151−156.
[3] T. A. O'Donnell, *Eur. J. Inorg. Chem.* **2001**, 21−34.
[4] I. C. Hwang, K. Seppelt, *Z. Anorg. Allg. Chem.* **2002**, *628*, 765−769.
[5] F. G. Herring, G. Hwang, K. C. Lee, F. Mistry, P. S. Phillips, H. Willner, F. Aubke, *J. Am. Chem. Soc.* **1992**, *114*, 1271−1277.
[6] S. H. Elder, G. M. Lucier, F. J. Hollander, N. Bartlett, *J. Am. Chem. Soc.* **1997**, *119*, 1020−1026.
[7] J. H. Holloway, E. G. Hope, C. D. Puxley, *Eur. J. Solid State Inorg. Chem.* **1996**, *33*, 821−829.
[8] G. Lucier, S. H. Elder, L. Chacón, N. Bartlett, *Eur. J. Solid State Inorg. Chem.* **1996**, *33*, 809−820.
[9] Z. Mazej, A. Tressaud, J. Darriet, *J. Fluorine Chem.* **2001**, *110*, 139−143.
[10] K. Lutar, H. Borrmann, A. Jesih, B. Žemva, *Acta Chim. Slov.* **1999**, *46*, 213−228.
[11] Z. Mazej, P. Benkič, K. Lutar, B. Žemva, *J. Fluorine Chem.* **2001**, *112*, 173−178.
[12] K. Lutar, B. Žemva, H. Borrmann, *Eur. J. Solid State Inorg. Chem.* **1996**, *33*, 957−969.
[13] C. Shen, B. Žemva, G. M. Lucier, O. Graudejus, J. A. Allman, N. Bartlett, *Inorg. Chem.* **1999**, *38*, 4570−4577.
[14] A. Tressaud, M. Wintenberger, N. Bartlett, P. Hagenmuller, *C. R. Acad. Sc. Paris Serie C* **1976**, *282*, 1069−1072.
[15] Z. Mazej, K. Lutar, B. Žemva, *Acta Chim. Slov.* **1999**, *46*, 229−238.
[16] W. J. Casteel Jr., D. H. Lohmann, N. Bartlett, *J. Fluorine Chem.* **2001**, *112*, 165−171.
[17] G. Lucier, J. Müzenberg, W. J. Casteel Jr., N. Bartlett, *Inorg. Chem.* **1995**, *34*, 2692−2698.
[18] H. D. B. Jenkins, H. K. Roobottom, *Inorg. Chem.* **2003**, *42*, 2886−2893.
[19] P. Benkič, Z. Mazej, *Z. Anorg. Allg. Chem.* **2001**, *627*, 1952−1957.
[20] D. Gantar, I. Leban, B. Frlec, J. H. Holloway, *J. Chem. Soc., Dalton Trans.* **1987**, 2379−2383.
[21] B. G. Müller, *Angew. Chem. Int. Ed. Engl.* **1987**, *26*, 689−690.
[22] A. Tressaud, J. L. Soubeyroux, H. Touhara, G. Demazeau, F. Langlais, *Mater. Res. Bull.* **1981**, *16*, 207−214.
[23] N. Bartlett, R. Maitland, *Acta Crystallogr.* **1958**, *11*, 747−748.
[24] B. G. Müller, *Angew. Chem. Int. Ed. Engl.* **1987**, *26*, 1081−1097.
[25] A. Tressaud, N. Bartlett, *J. Solid State Chem.* **2001**, *162*, 333−340.
[26] N. Ruchaud, J. Grannec, A. Tressaud, *Z. Anorg. Allg. Chem.* **1995**, *621*, 1958−1962.
[27] K. C. Lee, F. Aubke, *Can. J. Chem.* **1977**, *55*, 2473−2477.
[28] M. S. R. Cader, R. C. Thompson, F. Aubke, *Chem. Phys. Letters.* **1989**, *164*, 438−440.
[29] K. C. Lee, F. Aubke, *Can. J. Chem.* **1979**, *57*, 2058−2064.
[30] B. G. Müller, *Proceedings, 11th European Symposium on Fluorine Chem.*, Bled, Slovenia, **1995**, Abstracts, p. 127.
[31] M. S. R. Cader, F. Aubke, *Can. J. Chem.* **1989**, *67*, 1700−1707.
[32] Z. Mazej, unpublished results and PhD Thesis, University of Ljubljana, **2000**.
[33] G. J. Schrobilgen, *Noble-Gas Chemistry; in Encyclopaedia of Physical Science and Technology*, Third Edition, Vol. 10, Academic Press, **2002**.
[34] Z. Mazej, *J. Fluorine Chem.* **2002**, *114*, 75−80.
[35] K. Lutar, A. Jesih, B. Žemva, *Polyhedron* **1988**, *7*, 1217−1219.
[36] Z. Mazej, *J. Fluorine Chem.* **2002**, *118*, 127−129.
[37] H. Borrmann, K. Lutar, B. Žemva, *Inorg. Chem.* **1997**, *36*, 880−882.
[38] M. Kraus, M. Müller, R. Fischer, R. Schmidt, D. Koller, B. G. Müller, *J. Fluorine Chem.* **2000**, *101*, 165−171.
[39] A. Jesih, B. Žemva, *Vestn. Slov. Kem. Drus.* **1986**, *33*, 25−28.
[40] B. G. Müller, R. Hoppe, *Mater. Res. Bull.* **1972**, *7*, 1297−1306.
[41] G. Schwarzenbach, H. Flaschka, *Complexometric Titrations*, Methuen, London, **1969**, p. 250.
[42] D. D. Perrin, *Masking and Demasking of Chemical Reactions*, Wiley-Interscience, New York, **1970**, p. 33.
[43] R. Pribil, *Applied Complexometry*, Pergamon Press, London, Vol. 5, **1982**, pp. 194−197.
[44] J. Koryta, *Anal. Chim. Acta* **1972**, *61*, 329.
[45] A. K. Covington, *Ion-Selective Electrode Methodology*, vol. II, CRC Press Inc., Florida, **1984**, pp. 76−80.
[46] H. M. Dess, R. W. Parry, *J. Am. Chem. Soc.* **1957**, *79*, 1589−1591.
[47] A. Vogel, *Textbook of Quantitative Inorganic Analysis*, Longman, London, **1978**.
[48] P. W. J. M. Boumans, *Inductively Coupled Plasma Emission Spectroscopy*, Part 1, Wiley-Interscience, New York, **1987**.
[49] Z. Mazej, K. Lutar, *J. Fluorine Chem.* **2001**, *107*, 63−69.
[50] *CrystalClear,* Rigaku Corporation, Woodlands, Texas, USA, **1999**.
[51] G. M. Sheldrick, *SHELX97-2*, University of Göttingen, Germany, **1997**.

Received September 27, 2003
Early View Article
Published Online March 23, 2004

 © 2004 Wiley-VCH Verlag GmbH & Co. KGaA, Weinheim

Methacrylate-Substituted Titanium-Yttrium Mixed-Metal Oxo Clusters

Myhedin Jupa,[a] Guido Kickelbick,[a] and Ulrich Schubert*[a]

Keywords: Cluster compounds / Yttrium / Titanium / Organic-inorganic hybrids / Hydrogen bonding / Alkoxides

Upon reaction of titanium propoxide and yttrium 2-methoxyethoxide with a sevenfold excess of methacrylic acid, three different mixed-metal clusters were obtained, depending on the titanium to yttrium alkoxide ratio. Clusters of the type $Ti_4Y_2(\mu_3\text{-}O)_4(\mu_2\text{-methacrylate})_{12}(\mu_1\text{-methacrylate})_2L_2$ (L = $MeOCH_2CH_2OH$ or methacrylic acid), with two $[TiO_6]$ octahedra condensed to a zigzag chain of two $[YO_8]$ dodecahedra and two $[TiO_6]$ octahedra, were formed when the Ti/Y ratio in the precursor mixture was ≥ 3.5. The structure of $Ti_4Y_2O_4(OMc)_{12}(OCH_2CH_2OMe)_2(McOH)_2$ obtained with a Ti/Y ratio of 2 in the precursor mixture, consists of a ring of four corner-sharing $[TiO_6]$ octahedra to which two $[YO_8]$ dodecahedra are condensed.

(© Wiley-VCH Verlag GmbH & Co. KGaA, 69451 Weinheim, Germany, 2004)

Introduction

The traditional sol-gel route to inorganic-organic hybrid polymers, in which the organic and inorganic entities are connected by covalent bonds, is based on molecular precursors of the general composition $(RO)_nM-X-A$ with a hydrolyzable group $(RO)_nM$, and a polymerizable organic group A connected by an inert spacer X. In a typical preparative protocol the precursors are first reacted with water. After formation of the inorganic network, the organic groups A are polymerized or crosslinked to form oligomeric or polymeric organic structures. Modification of the type, structure and proportions of the organic and inorganic constituents allows, in principle, tailoring of the properties of the resulting hybrid polymer. A special challenge of increasing importance is to tailor also structural features of the hybrid materials, especially the dimension (especially on a nanometer scale), geometry and mutual arrangement of the organic and inorganic building blocks.

Such a structural control is hardly possible with the traditional procedure. It is more easily reached when the formation of the inorganic and organic structures is done at different times in clearly separated reaction steps. Hydrolysis and condensation of metal or semi-metal alkoxides may lead to structurally defined molecular cage compounds (clusters), instead of oligomers or polymers with broad size distributions, if the reaction with water is performed in a very controlled manner. Such clusters can be used for the preparation of inorganic-organic hybrid polymers as structurally well-defined oligomeric building blocks. In order to connect the clusters with polymeric organic structures, the cluster surface must be covered with reactive organic groups (polymerizable groups, for example).

We previously synthesized a variety of methacrylate-substituted mono- (Ti, Zr, Hf, Nb, Ta), di- (Ti/Zr, Ti/Hf) and trimetallic (Ti/Zr/Hf) oxo/alkoxo clusters of different size and shape for this purpose.[1] It was shown that the cluster type has a distinct influence on the properties of the resulting hybrid materials;[2] the origin of this effect is not yet known. The methacrylate-substituted metal oxo clusters can be obtained in high yields by reaction of metal alkoxides with methacrylic acid (McOH). The formation of the clusters can be rationalized by the sequence of three reactions. One or more alkoxide ligands of the starting alkoxide $M(OR)_x$ are first substituted by methacrylate groups to give $M(OR)_{x-n}(OMc)_n$. Water is generated in situ by esterification of excess methacrylic acid with alcohol (either liberated by the substitution reaction or present as solvent)[3] and hydrolyzes all or part of the remaining alkoxide groups. The very slow in situ production of water allows a very controlled growth of clusters $M_nO_x(OR/OH)_y(OMc)_z$, the size and shape of which can be influenced to a certain degree by the reaction conditions. The most important parameter is the metal alkoxide/carboxylic acid ratio,[4] and a second parameter is the type of alkoxide group in the parent alkoxide.[5]

In this article we report the preparation of three methacrylate-substituted titanium-yttrium mixed-metal oxo clusters obtained by this route, viz. $Ti_4Y_2O_4(OMc)_{14}(MeOCH_2CH_2OH)_2$ (**1**), $Ti_4Y_2O_4(OMc)_{14}(McOH)_2$ (**2**) and $Ti_4Y_2O_4(OMc)_{12}(OCH_2CH_2OMe)_2(McOH)_2$ (**3**), and their structural characterization.

Results and Discussion

We have previously prepared a series of mixed Ti/Zr oxide clusters, viz. $Ti_2Zr_4O_4(OBu)_2(OMc)_{14}$ (Ti_2Zr_4),

[a] Institute of Materials Chemistry, Vienna University of Technology,
Getreidemarkt 9/165, 1060 Wien, Austria

$Ti_4Zr_2O_4(OBu)_6(OMc)_{10}$ (Ti_4Zr_2), $Ti_4Zr_4O_6(OBu)_4(OMc)_{16}$ and $Ti_2Zr_6O_6(OMc)_{20}$, and related Ti/Hf and Ti/Zr/Hf clusters, by reacting titanium and zirconium (hafnium) butoxide mixtures with methacrylic acid in different molar ratios.[6,7] The same procedure was used in the present work to prepare Ti/Y clusters from $Ti(O\textit{n}Pr)_4$ and $Y(OCH_2CH_2OMe)_3$. The latter alkoxide, with a decameric ring structure,[8] was employed as a ca. 11% solution in 2-methoxyethanol. The metal alkoxide [$Ti(OR)_4$ + $Y(OME)_3$]/methacrylic acid molar ratio (OME = OCH_2CH_2OMe)was kept at about 1:7 in each experiment, but the $Ti(OR)_4/Y(OME)_3$ ratio was varied from 2:1 to 3.5:1 and 18:1. Each precursor composition resulted in a different mixed-metal cluster **1**−**3** which was isolated in high yields in each case and structurally characterized by single crystal diffraction. The NMR spectra, both in benzene solution and in the solid state, are of little diagnostic value, because only one group of signals is observed for each type of ligand.

Interestingly, each of the clusters **1**−**3** has the general composition $Ti_4Y_2O_4X_{14}(HY)_2$ (X,Y = OMc and/or OME) despite the different Ti/Y ratio in the precursor mixture. The clusters differ by the distribution of X and Y, and by the arrangement of the titanium and yttrium polyhedra as discussed in the following.

Cluster **1** was obtained from a $Ti(OR)_4/Y(OME)_3$ ratio of 3.5. An X-ray structure analysis revealed that the composition of **1** is $Ti_4Y_2(\mu_3\text{-}O)_4(\mu_2\text{-}OMc)_{12}(\mu_1\text{-}OMc)_2(MeOCH_2CH_2OH)_2$. The structure of **1** (Figure 1, Table 1) is very similar to that of Ti_4Zr_2 [= $Ti_4Zr_2(\mu_3\text{-}O)_4(\mu_2\text{-}OMc)_{10}(\mu_2\text{-}OBu)_2(\mu_1\text{-}OBu)_2$] (Figure 2).

The common structural motive of the hexanuclear clusters Ti_2Zr_4 and Ti_4Zr_2 is a zigzag chain of two central [ZrO_8] dodecahedra and two terminal [TiO_6] tetrahedra. Two additional [ZrO_8] dodecahedra (in Ti_2Zr_4) or [TiO_6] octahedra (in Ti_4Zr_2) are condensed to the zirconium atoms of the main chain by a shared edge. The central structural motif of **1** is the same zigzag chain as in Ti_4Zr_2 with [YO_8] instead of [ZrO_8] dodecahedra. The main structural difference is that the additional [TiO_6] octahedra are condensed to the main chain via corners.

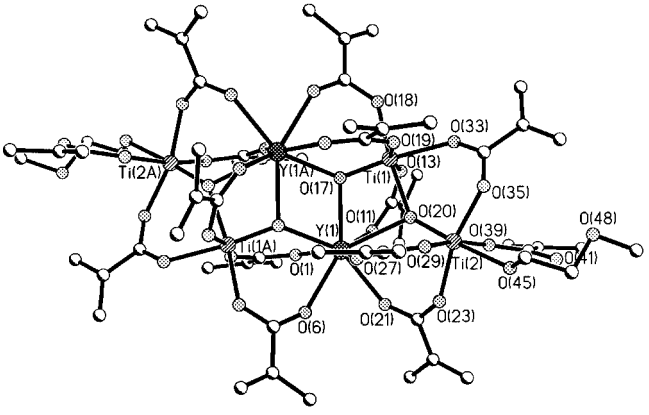

Figure 1. Molecular structure of $Ti_4Y_2O_4(OMc)_{14}(MeOCH_2CH_2OH)_2$ (**1**)

Table 1. Bond lengths [pm] and angles [deg] for **1** (* = $-x+1, -y+1, -z+1$)

Y(1)−Ti(1)	333.59(6)	Ti(2)−O(35)	199.3(2)
Y(1)−Ti(1)*	372.62(6)	Ti(2)−O(39)	195.6(2)
Y(1)−Y(1)*	388.16(5)	Ti(2)−O(45)	218.0(2)
Ti(1)−O(13)	198.7(2)	Y(1)−O(1)	229.2(2)
Ti(1)−O(17)	171.9(2)	Y(1)−O(6)	235.4(2)
Ti(1)−O(18)	195.8(2)	Y(1)−O(11)	233.6(2)
Ti(1)−O(19)	201.1(2)	Y(1)−O(17)	233.0(2)
Ti(1)−O(20)	202.3(2)	Y(1)−O(17)*	235.8(2)
Ti(1)−O(33)	212.2(2)	Y(1)−O(20)	250.6(2)
Ti(2)−O(20)	173.4(2)	Y(1)−O(21)	231.6(2)
Ti(2)−O(23)	197.0(2)	Y(1)−O(27)	231.4(2)
Ti(2)−O(29)	198.8(2)		
O(1)−Y(1)−O(27)	148.73(7)	O(13)−Ti(1)−O(19)	165.95(9)
O(21)−Y(1)−O(17)	141.26(7)	O(18)−Ti(1)−O(20)	172.49(8)
O(27)−Y(1)−O(11)	139.52(7)	O(17)−Ti(1)−O(33)	172.38(9)
O(17)−Y(1)−O(6)	144.57(7)	O(23)−Ti(2)−O(35)	165.09(9)
O(11)−Y(1)−O(6)	130.69(7)	O(20)−Ti(2)−O(45)	174.45(9)
O(21)−Y(1)−O(17)*	149.25(7)	Ti(1)−O(17)−Y(1)	110.01(8)
O(11)−Y(1)−O(17)*	130.56(7)	Ti(1)−O(17)−Y(1)*	131.45(9)
O(1)−Y(1)−O(20)	140.29(6)	Y(1)−O(17)−Y(1)*	111.76(7)
O(6)−Y(1)−O(20)	137.31(7)	Ti(2)−O(20)−Ti(1)	136.96(11)
O(17)*−Y(1)−O(20)	121.42(6)	Ti(2)−O(20)−Y(1)	125.48(9)
		Ti(1)−O(20)−Y(1)	94.29(7)

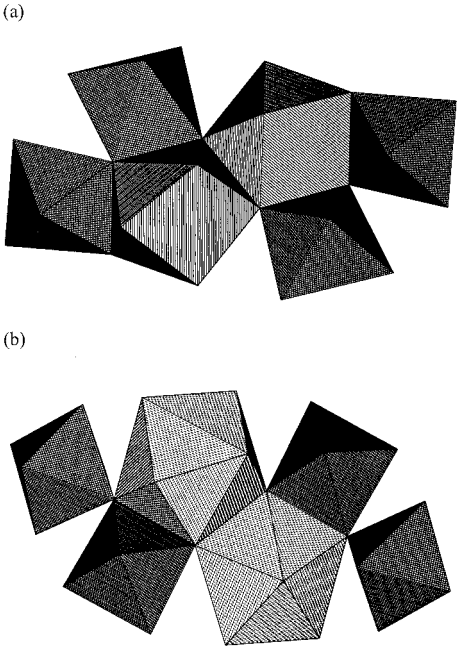

Figure 2. Cluster cores of connected polyhedra in $Ti_4Zr_2O_4(OBu)_6(OMc)_{10}$ (Ti_4Zr_2) (a) and **1/2** (b). The central polyhedra are eight-coordinate Zr or Y, and the terminal polyhedra six-coordinate Ti

While the sum of the metal coordination numbers in Ti_4Zr_2 and **1** is the same, the total metal charge in **1** is smaller by two units [Y^{III} instead of Zr^{IV}). That means that two of the 16 ligands in **1** must be neutral, i.e. must be coordinated in their protonated form. The protonated ligands are clearly identified by comparing the Ti−O and Y−O distances. The Ti−O distance associated with the OME group in **1** [Ti(2)−O(45) 218.0(2) pm] is much longer

 © 2004 Wiley-VCH Verlag GmbH & Co. KGaA, Weinheim

than comparable Ti−OR distances *trans* to a μ_3-oxo ligand [for example, Ti−OPr 180.3(2) in $Ti_3O(OPr)_9(OOCPh)_2$,[9] 179.3(3) in $Ti_6O_4(OEt)_8(OAc)_8$,[10] or 178.7(2) in $Ti_4O_2(OiPr)_6(OMc)_6$ [5]]. Thus, O(45) *trans* to the μ_3-oxo group at Ti(2) is the oxygen atom of a coordinated alcohol rather than an alkoxide ligand. The alcoholic hydrogen atom at O(45) undergoes an intramolecular hydrogen bond with the non-coordinated oxygen atom O(41) of the neighboring μ_1-OMc ligand [O(41)−O(45) 259.4 pm]. The presence of a weakly coordinating ROH ligand also manifests itself in the very short Ti(2)−O(20) distance [173.4(2) pm] [for comparison, Ti-μ_3-O distances *trans* to Ti−OR are 185.6(2) in $Ti_3O(OPr)_9(OOCPh)_2$, 209.9(1) in $Ti_6O_4(OEt)_8(OMc)_8$ and 208.9(2) in $Ti_4O_2(OiPr)_6(OMc)_6$].

A very similar cluster was obtained when the $Ti(OR)_4/Y(OME)_3$ ratio in the starting mixture was 18. The structure of **2** (Figure 2 and 3, Table 2) is basically the same as that of **1** with coordinated methacrylic acid molecules instead of the coordinated alcohols [i.e., $Ti_4Y_2(\mu_3\text{-}O)_4(\mu_2\text{-}OMc)_{12}(\mu_1\text{-}OMc)_2(McOH)_2$]. This can be rationalized by the smaller concentration of methoxyethanol in the starting mixture due to the low portion of $Y(OME)_3$ (which is employed as a solution in methoxyethanol).

Table 2. Bond lengths [pm] and angles [deg] for **2** (*: $-x+1, -y, -z+1$)

Ti(2)−Y(1)	333.85(6)	Ti(2)−O(37)	201.1(2)
Y(1)−Y(1)*	386.35(6)	Ti(2)−O(49)	202.0(2)
Ti(1)−O(1)	212.6(2)	Ti(2)−O(50)	194.6(2)
Ti(1)−O(7)	198.0(3)	Y(1)−O(13)	234.6(2)
Ti(1)−O(19)	198.8(3)	Y(1)−O(21)	228.5(2)
Ti(1)−O(25)	197.4(3)	Y(1)−O(27)	231.3(2)
Ti(1)−O(31)	199.2(3)	Y(1)−O(42)	234.9(2)
Ti(1)−O(49)	173.3(2)	Y(1)−O(47)	228.3(2)
Ti(2)−O(48)	172.0(2)	Y(1)−O(48)	232.0(2)
Ti(2)−O(15)	199.0(3)	Y(1)−O(48)*	235.8(2)
Ti(2)−O(33)	212.7(2)	Y(1)−O(49)	255.1(2)
O(25)−Ti(1)−O(7)	169.58(11)	O(13)−Y(1)−O(48)*	127.15(8)
O(19)−Ti(1)−O(31)	163.52(11)	O(47)−Y(1)−O(49)	143.68(8)
O(49)−Ti(1)−O(1)	174.10(12)	O(42)−Y(1)−O(49)	132.29(8)
O(15)−Ti(2)−O(37)	166.86(10)	O(48)*−Y(1)−O(49)	123.39(7)
O(50)−Ti(2)−O(49)	172.21(10)	Ti(2)−O(48)−Y(1)	110.59(10)
O(48)−Ti(2)−O(33)	173.03(10)	Ti(2)−O(48)−Y(1)*	132.48(11)
O(47)−Y(1)−O(27)	147.33(9)	Y(1)−O(48)−Y(1)*	111.37(8)
O(21)−Y(1)−O(48)	140.14(8)	Ti(1)−O(49)−Ti(2)	137.10(13)
O(27)−Y(1)−O(13)	139.65(8)	Ti(1)−O(49)−Y(1)	125.80(11)
O(48)−Y(1)−O(42)	142.57(9)	Ti(2)−O(49)−Y(1)	93.10(8)
O(13)−Y(1)−O(42)	136.40(9)	C(43)*−O(50)−Ti(2)	130.5(2)
O(21)−Y(1)−O(48)*	149.29(8)		

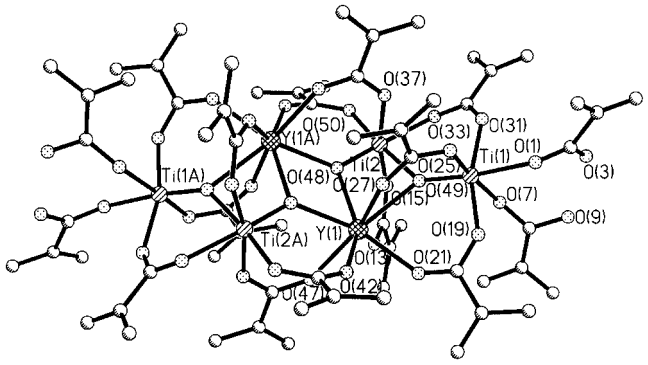

Figure 3. Molecular structure of $Ti_4Y_2O_4(OMc)_{14}(McOH)_2$ (**2**)

The coordinated methacrylic acid molecules are coordinated via the oxygen atom of their C=O double bond, while the OH hydrogen atom once again forms a hydrogen bond to the non-coordinated oxygen atom of the neighboring μ_1-OMc ligand [O(3)−O(9) 222.1(11) pm]. The Ti(1)−O(1) distance of the (neutral) methacrylic acid ligand [212.6(2) pm] is clearly longer than that of the (anionic) μ_1-methacrylate ligand [Ti(1)−O(7) 198.0(3) pm].

When the $Ti(OR)_4/Y(OME)_3$ ratio in the precursor mixture was lowered to 2, cluster **3** was obtained. The blueprint of **3** is completely different from that of **1** and **2**, although cluster **3** has the same overall composition as **1** (i.e. clusters **1** and **3** are geometric isomers). The neutral (protonated) ligand in **3** is McOH rather than $HOCH_2CH_2OMe$, as in **1**. This shift in protons results in dramatic structural changes. The structure (Figure 4, Table 3) consists of a ring of four corner-sharing [TiO_6] octahedra to which two [YO_8] dodecahedra are condensed (Figure 5). This arrangement of the polyhedra implies that only two of the oxo ligands are μ_3 [O(26)], while the other two oxo ligands are μ_2 [O(39)].

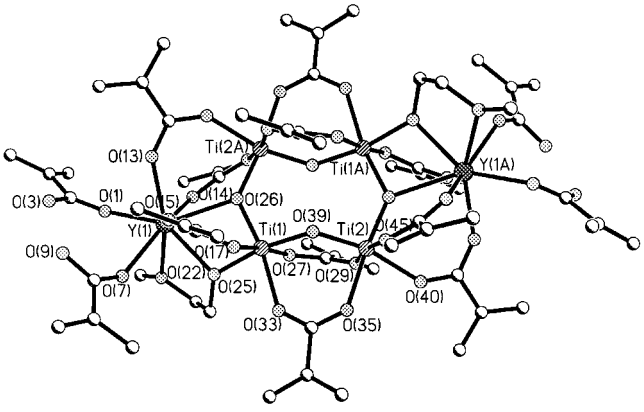

Figure 4. Molecular structure of $Ti_4Y_2O_4(OMc)_{12}(OCH_2CH_2OMe)_2(McOH)_2$ (**3**)

As in **2**, the neutral ligands are methacrylic acid molecules. However, in **3** both the monodentate OMc and HOMc ligands are bonded to the yttrium atoms. The methacrylic acid ligands are again coordinated via the oxygen atom of their C=O double bonds, and there is again a hydrogen bond between the OH hydrogen atom of the methacrylic acid and the non-coordinated oxygen atom of the neighboring μ_1-OMc ligand [O(3)−O(9) 240.8 pm].

Due to two oxo ligands now being μ_2 (rather than μ_3 as in **1** and **2**), each OCH_2CH_2OMe ligand in **3** must now occupy three coordination sites. In fact, the alkoxy oxygen atom [O(25)] bridges Ti(1) and Y(1), and the ether oxygen [O(22)] additionally coordinates to Y(1), thus **3** is $Ti_4Y_2(\mu_3\text{-}O)_2(\mu_2\text{-}O)_2(\mu_2\text{-}OMc)_{10}(\mu_1\text{-}OMc)_2(\mu,\eta^2\text{-}OCH_2CH_2OMe)_2(McOH)_2$.

 © 2004 Wiley-VCH Verlag GmbH & Co. KGaA, Weinheim

Table 3. Bond lengths [pm] and angles [deg] for **3** (*: $-x$, $-y$, $-z+1$)

Ti(1)−Ti(2)	338.62(9)	Ti(2)−O(39)	178.1(2)
Y(1)−Ti(1)	338.20(7)	Ti(2)−O(40)	204.6(2)
Y(1)−O(26)	251.9(2)	Ti(2)−O(45)	196.9(3)
Ti(1)−O(17)	197.5(2)	Y(1)−O(1)	228.3(3)
Ti(1)−O(25	194.2(2)	Y(1)−O(7)	233.4(3)
Ti(1)−O(26)	184.4(2)	Y(1)−O(13)	223.9(3)
Ti(1)−O(27)	204.4(2)	Y(1)−O(14)	232.6(3)
Ti(1)−O(33)	208.2(2)	Y(1)−O(15)	235.4(3)
Ti(1)−O(39)	185.3(2)	Y(1)−O(22)	250.4(3)
Ti(2)−O(26)*	187.3(2)	Y(1)−O(25)	230.1(2)
Ti(2)−O(29)	203.3(3)	Y(1)−O(26)	251.9(2)
Ti(2)−O(35)	207.4(3)		
O(39)−Ti(1)−O(25)	169.27(10)	O(14)−Y(1)−O(15)	142.70(9)
O(17)−Ti(1)−O(27)	174.44(11)	O(13)−Y(1)−O(22)	146.33(10)
O(26)−Ti(1)−O(33)	168.72(10)	O(15)−Y(1)−O(22)	136.14(9)
O(45)−Ti(2)−O(29)	170.67(11)	O(1)−Y(1)−O(26)	148.76(11)
O(39)−Ti(2)−O(40)	165.55(11)	O(7)−Y(1)−O(26)	130.95(10)
O(26)*−Ti(2)−O(35)	173.84(10)	Ti(1)−O(26)−Ti(2)*	131.14(12)
O(13)−Y(1)−O(25)	142.15(9)	Ti(1)−O(26)−Y(1)	100.48(10)
O(1)−Y(1)−O(25)	141.37(10)	Ti(2)*−O(26)−Y(1)	126.29(11)
O(14)−Y(1)−O(7)	145.82(11)	Ti(2)−O(39)−Ti(1)	137.43(13)

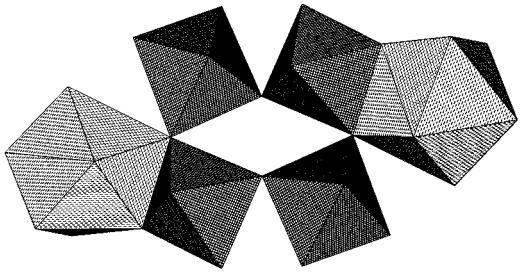

Figure 5. Cluster core of connected polyhedra in $Ti_4Y_2O_4(OMc)_{12}(OCH_2CH_2OMe)_2(McOH)_2$ (**3**). The central polyhedra are six-coordinate Ti and the terminal eight-coordinate Y.

Conclusions

Titanium-yttrium mixed-metal oxo clusters capped by polymerizable methacrylate ligands were prepared by reaction of mixtures of $Ti(OnPr)_4$ and $Y(OCH_2CH_2OMe)_3$ with methacrylic acid. Only the ratio between the two alkoxides was varied while the metal alkoxide/methacrylic acid ratio was kept constant. This procedure resulted in two different cluster types. At a Ti/Y ratio of 2 in the precursor mixture, the cluster $Ti_4Y_2O_4(OMc)_{12}(OCH_2CH_2OMe)_2(McOH)_2$ (**3**) was formed with a ring of four corner-sharing [TiO_6] octahedra as the central structural motive to which two [YO_8] dodecahedra are condensed. At a Ti/Y ratio $\geq$ 3.5, clusters of the type $Ti_4Y_2O_4(OMc)_{14}L_2$ (**1**: L = $MeOCH_2CH_2OH$, **2**: L = McOH) were formed. The basic structural motive is a zigzag chain of two central [YO_8] dodecahedra and two terminal [TiO_6] octahedra to which two additional [TiO_6] octahedra are condensed. The second cluster type is very similar to the previously obtained titanium-zirconium mixed-metal clusters $Ti_2Zr_4O_4(OBu)_2(OMc)_{14}$ and $Ti_4Zr_2O_4(OBu)_6(OMc)_{10}$. The formation of the two different Ti/Y oxo clusters is difficult to rationalize in terms of reactivity of the two alkoxide precursors. It must be kept in mind, however, that the $Ti(OPr)_4/Y(OME)_3$ precursor combination is more complicated than in previous syntheses of methacrylate-substituted oxo clusters: (i) An alcoholic solvent was involved, since $Y(OME)_3$ was employed as a methoxyethanol solution. Thus, when the $Y(OME)_3$ proportion was varied, the amount of methoxyethanol was also varied. It is well-known that the use of 2-methoxyethoxy groups changes sol-gel reactions of metal alkoxides significantly due to the coordination ability of the ether oxygen. (ii) The alkoxide ligands of the two metal precursors were different, and alkoxide exchange reactions may occur prior to reaction with the acid and/or water.

Another noteworthy feature of the clusters **1**−**3** is the presence of monodentate carboxylate ligands and coordinated alcohol or acid molecules. Both types of ligands are always in a *cis* position at the same metal. This allows the formation of a hydrogen bond between the alcoholic or carboxylic OH group and the C=O group of the monodentate methacrylate ligand, which probably stabilizes this unusual ligand combination. A similar situation was previously observed in the clusters $Zr_6(OH)_4O_4(OOCR)_{12}(n$PrOH) (R = Ph, CMe=$CH_2$).[11] The question whether conversion of a bidentate carboxylate ligand to a monodentate ligand, with concomitant coordination of a neutral ligand to the opened coordination site, is connected with the reactivity of the clusters is currently under investigation.

Experimental Section

All operations were carried out in Schlenk tubes under argon. $Ti(OPr)_4$ (98% in propanol) and $Y(OCH_2CH_2OMe)_3$ (11% in methoxyethanol) were used as received.

$Ti_4Y_2O_4(OMc)_{14}(MeOCH_2CH_2OH)_2$ (1): An amount of methacrylic acid (1.02 g, 11.8 mmol) was added dropwise at room temperature to a stirred mixture of $Ti(OPr)_4$ (0.38 g, 1.32 mmol) (98% in propanol) and 0.39 mmol of $Y(OCH_2CH_2OMe)_3$ (1.11 g of a ca. 11% methoxyethanol solution). After 7 days at room temperature, 0.31 g of colorless crystals were formed (87% yield relative to Y). The crystals were separated and dried at in vacuo. $C_{62}H_{86}O_{36}Ti_4Y_2$ (1776.7): calcd. C 41.9, H 4.9, TiO_2/Y_2O_3 30.6; found C 42.1, H 4.6, TiO_2/Y_2O_3 32.8 (TGA). IR-ATR: $\tilde{\nu}$ = 2927 (w, CH), 1668 (w, C=C), 1566 (s, sh, COO), 1464 (s), 1424 (s), 1270 (s), 1129 (m), 1031 (m), 978 (m,$CH_{C=CH_2}$), 849 (m), 797 (m) cm^{-1}.

$Ti_4Y_2O_4(OMc)_{14}(McOH)_2$ (2): An amount of methacrylic acid (2.57 g, 29.9 mmol) was added dropwise at room temperature to a stirred mixture of $Ti(OPr)_4$ (1.11 g, 3.8 mmol) (98% in propanol) and 0.21 mmol of $Y(OCH_2CH_2OMe)_3$ (0.60 g of a ca. 11% methoxyethanol solution). After 8 days at room temperature, 0.23 g of colorless crystals were formed (quantitative yield relative to Y). The crystals were separated and dried at in vacuo. $C_{64}H_{82}O_{36}Ti_4Y_2$ (1796.7): calcd. C 42.8, H 4.6, TiO_2/Y_2O_3, 30.2; found C 41.6, H 4.7, TiO_2/Y_2O_3, 32.4 (TGA). IR-ATR: $\tilde{\nu}$ = 2927 (w, CH), 1642 (w, C=C), 1546 (s, sh, COO), 1454 (s), 1405 (s, sh), 1241 (s), 1112 (m), 1007 (m), 940 (m, $CH_{C=CH_2}$), 827 (m), 764 (m) cm^{-1}.

$Ti_4Y_2O_4(OMc)_{12}(OCH_2CH_2OMe)_2(McOH)_2$ (3): Methacrylic acid (0.74 g, 8.6 mmol) was added dropwise at room temperature to a

 © 2004 Wiley-VCH Verlag GmbH & Co. KGaA, Weinheim

Table 4. Crystallographic and structural parameters of **1**−**3**

	1	**2**	**3**
Empirical formula	$C_{62}H_{86}O_{36}Ti_4Y_2$	$C_{64}H_{82}O_{36}Ti_4Y_2$	$C_{62}H_{86}O_{36}Ti_4Y_2$
Molecular mass	1776.7	1796.7	1776.7
Crystal system, space group	triclinic, $P\bar{1}$	triclinic, $P\bar{1}$	triclinic, $P\bar{1}$
a [pm]	1136.6(1)	1145.83(7)	1117.1(1)
b [pm]	1283.3(1)	1249.25(8)	1366.1(2)
c [pm]	1493.2(1)	1448.52(9)	1409.2(2)
α [deg]	91.410(2)	84.884(1)	71.659(2)
β [deg]	103.669(2)	82.250(1)	75.690(2)
γ [deg]	110.698(2)	76.971(1)	76.208(2)
Volume [pm^3]	$1965.6(3)\cdot10^6$	$1997.9(2)\cdot10^6$	$1947.6(4)\cdot10^6$
Z/calcd. density [$g\cdot cm^{-3}$]	1/1.492	1/1.493	1/1.513
μ [mm^{-1}]	1.932	1.902	1.950
Crystal size [mm]	0.42 × 0.31 × 0.23	0.30 × 0.24 × 0.18	0.39 × 0.23 × 0.19
2θ range	2.69−28.32	2.44−30.06	2.27−28.33
Reflections coll./unique	13838/9523	15837/11271	13818/9496
Data/parameters	9523/485	11271/479	9496/469
GOF	1.024	1.024	1.007
*R*1 [$I > 2\sigma(I)$]	0.0438	0.0572	0.0553
*wR*2	0.1090	0.1469	0.1357
Largest diff. peak and hole [$e\cdot Å^{-3}$]	0.716/−0.315	1.024/−0.630	1.103/−0.452

stirred mixture of $Ti(OPr)_4$ (0.23 g, 0.8 mmol, 98% in propanol) and $Y(OCH_2CH_2OMe)_3$ (0.39 mmol, 1.13 g of a ca. 11% methoxyethanol solution). After 3 days at room temperature, 0.31 g of colorless crystals were formed (87% yield relative to Y). The crystals were separated and dried in vacuo. $C_{62}H_{86}O_{36}Ti_4Y_2$ (1776.7): calcd. C 41.9, H 4.9, TiO_2/Y_2O_3, 30.6; found C 41.9, H 4.7, TiO_2/Y_2O_3, 32.3 (TGA). IR-ATR: $\tilde{\nu}$ = 2926 (w, CH), 1644 (w, C=C), 1571 (s, COO), 1455 (s), 1387 (s, sh), 1369 (s), 1236 (s), 1103 (m), 1065 (m), 1006 (m), 938 (m, $CH_{C=CH_2}$), 826 (m), 736 (m) cm^{-1}.

X-ray Structure Analyses of 1−3: See also Tables 1−4. Selected crystals were mounted on a Bruker AXS SMART diffractometer with an APEX CCD area detector. Graphite-monochromated Mo-K_α radiation (71.073 pm) was used for all measurements. The crystal-to-detector distance was 5.00 cm. A hemisphere of data was collected by a combination of three sets of exposures at 173 K. Each set had a different φ angle for the crystal, and each exposure took 20 s and covered 0.3° in ω. The data were corrected for polarization and Lorentz effects, and an empirical absorption correction (SADABS) was applied. The cell dimensions were refined with all unique reflections. The structure was solved by direct methods (SHELXS-86). Refinement was carried out with the full-matrix least-squares method based on F^2 (SHELXL-93) with anisotropic thermal parameters for all non-hydrogen atoms. Hydrogen atoms were inserted in calculated positions and refined riding with the corresponding atom. In **2**, O(48) is disordered and was refined with a 0.5:0.5 occupation of O(48) and O48(A). Crystallographic data (excluding structure factors) for the structures of **1**−**3** have been deposited at the Cambridge Crystallographic Data Centre as supplementary publication no. CCDC-220753 (**1**), -220751 (**2**), -220752 (**3**). Copies of the data can be obtained free of charge on application to CCDC, 12 Union Road, Cambridge CB2 1EZ, UK [Fax: (internat.) + 44-1223-336033; E-mail: deposit@ccdc.cam.ac.uk].

Acknowledgments

We thank the Fonds zur Förderung der wissenschaftlichen Forschung (FWF), Vienna, for the support of this work.

[1] Review articles: F. Ribot, C. Sanchez, *Comments, Inorg. Chem.* **1999**, *20*, 327. G. Kickelbick, U. Schubert, *Monatsh. Chem.* **2001**, *132*, 13. U. Schubert, *Chem. Mater.* **2001**, *13*, 3487. U. Schubert, *J. Sol-Gel Sci. Technol.*, in press.
[2] S. Gross, V. Di Noto, G. Kickelbick, U. Schubert, *Mat. Res. Soc., Symp. Proc.* **2002**, *726*, 47.
[3] G. Kickelbick, M. P. Feth, H. Bertagnolli, M. Puchberger, D. Holzinger, S. Gross, *J. Chem. Soc., Dalton* **2002**, 3892.
[4] B. Moraru, S. Gross, G. Kickelbick, G. Trimmel, U. Schubert, *Monatsh. Chem.* **2001**, *132*, 993.
[5] B. Moraru, N. Hüsing, G. Kickelbick, U. Schubert, P. Fratzl, H. Peterlik, *Chem. Mater.* **2002**, *14*, 2732.
[6] B. Moraru, G. Kickelbick, U. Schubert, *Eur. J. Inorg. Chem.* **2001**, 1295.
[7] S. Gross, G. Kickelbick, M. Puchberger, U. Schubert, *Monatsh. Chem.* **2003**, *134*, 1053.
[8] O. Poncelet, L. G. Hubert-Pfalzgraf, J. C. Daran, R. Astier, *J. Chem. Soc., Chem. Commun.* **1989**, 1846.
[9] I. Mijatovic, G. Kickelbick, M. Puchberger, U. Schubert, *New J. Chem.* **2003**, *27*, 3.
[10] I. Gautier-Luneau, A. Mosset, J. Galy, *Z. Kristallogr.* **1987**, *180*, 83.
[11] G. Kickelbick, P. Wiede, U. Schubert, *Inorg. Chim. Acta* **1999**, *284*, 1.

Received October 1, 2003
Early View Article
Published Online March 23, 2004

 © 2004 Wiley-VCH Verlag GmbH & Co. KGaA, Weinheim

Nucleobase Oxidation of DNA by (Terpyridyl)chromium(III) Derivatives

Vaidyanathan Ganesan Vaidyanathan[a] and Balachandran Unni Nair*[a]

Keywords: Chromium / DNA cleavage / Photo cleavage / Terpyridyl ligands

The chromium(III) complexes $[Cr(ttpy)_2](ClO_4)_3$ (**1**) and $[Cr(Brphtpy)_2](ClO_4)_3$ (**2**), containing the terpyridyl derivatives ttpy and Brphtpy [ttpy = *p*-tolylterpyridine; Brphtpy = (*p*-bromophenyl)terpyridine] have been synthesized and characterized by ESI-MS, electronic spectroscopy, and cyclic voltammetry. Absorption titration and thermal denaturation studies reveal that both complexes are moderate binders of calf thymus DNA (CT DNA), while viscosity measurements show that they bind with partial intercalation. Binding of the two chromium complexes to DNA and mononucleotides dGMP, dAMP, dCMP, and dTMP decreases the emission intensity of complex **2**. However, the emission intensity of complex **1** is quenched only by DNA and the nucleotides dGMP and dAMP. Excited state potentials of both **1** and **2** have been estimated to be 1.65 and 1.85 V vs. NHE. These results demonstrate that **2** is a stronger photooxidant than **1**, and other (diimine)chromium complexes, and that it can oxidize nucleobases. The photonuclease activity of **1** and **2** has been confirmed by gel electrophoresis.

(© Wiley-VCH Verlag GmbH & Co. KGaA, 69451 Weinheim, Germany, 2004)

Introduction

The interaction of various metal ions with DNA has been investigated in great detail to understand the mode of binding of metal ions to DNA. Changes in ligand structure can alter the DNA binding properties of metalloporphyrins, Schiff-base−Mn^{III} complexes, phenanthroline−Cu^{II} complexes, and macrocyclic Ni^{II} complexes.[1−13] We have reported previously the influence of ligand structure on the DNA binding properties of Cr^{III} complexes.[14−18] A main offshoot of these studies has been the development of metal complexes that cleave DNA. Synthetic reagents that cleave DNA are of considerable interest as tools for molecular biologists − such cleavage has led to the development of both sequence-specific nucleases and footprinting agents. The redox properties of various transition metal complexes have been exploited for DNA cleaving. The anticancer drug bleomycin relies on a metal redox center for its DNA-cleaving reaction.[19−20] Polypyridyl complexes of oxoruthenium(IV) are efficient oxidative DNA-cleaving agents.[21] Another class of DNA-cleaving agents are those activated by light. Indeed, light-activated metal complexes have some distinct experimental advantages as they can be added to a protein−DNA complex and remain inert until photoactivation. One, therefore, has control over the timing of these reactions and hence the potential to examine protein−DNA interactions directly with some time resolution. (Polypyridyl)metal complexes of d^6 systems, such as Ru^{II}, Rh^{III}, and Co^{III}, are used extensively as photophysical probe and as photochemical agents because of their room-temperature luminescence.[22−26] Because these complexes are coordinatively saturated, there is no opportunity for reactions other than electron and energy transfer. Thus cleavage of DNA by complicated hydrogen atom or oxo transfer pathways is unlikely, and the binding modes of the complexes can be studied exclusively. Coordinatively saturated phenanthrenequinone diimine (phi) complexes of Rh^{III}, $[Rh(phi)(bpy)_2]^{3+}$, are conformationally selective photocleaving agents.[24−26] Surprisingly, despite its extensive photochemistry, Cr^{III} complexes have found little use as photoprobes for nucleic acids. Even though certain Cr^{III} complexes exhibit nuclease activity, the photochemistry of only some diimine complexes, such as $[Cr(bpy)_3]^{3+}$, $[Cr(phen)_3]^{3+}$, $[Cr(phen)_2(dppz)]^{3+}$, and $[Cr(TMP)_3]^{3+}$, has been investigated in the presence of DNA because of their strong room-temperature luminescence ($^2E_g \rightarrow {}^4A_{2g}$ phosphorescence).[27−29] We report here the synthesis and characterization of the terpyridyl−Cr^{III} complexes **1** and **2** and the photocleavage of DNA in the presence of these complexes.

[a] Department of Physical and Inorganic Chemistry, Central Leather Research Institute,
Adyar, Chennai 600 020, India
Fax: (internat.) + 91-44-24911589
E-mail: bcunchem@rediffmail.com

Results and Discussion

Synthesis and Characterization

The chromium(III) complexes **1** and **2** were synthesized by the reaction of $[Cr(H_2O)_6]^{2+}$ and the corresponding ligand under nitrogen followed by air oxidation. Both complexes showed satisfactory elemental analyses and IR spectra. Their authenticity was confirmed by their ESI mass spectra.

 © 2004 Wiley-VCH Verlag GmbH & Co. KGaA, Weinheim **DOI: 10.1002/ejic.200300718**

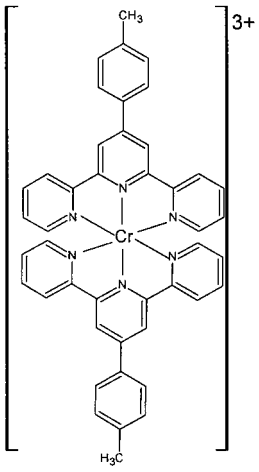

1

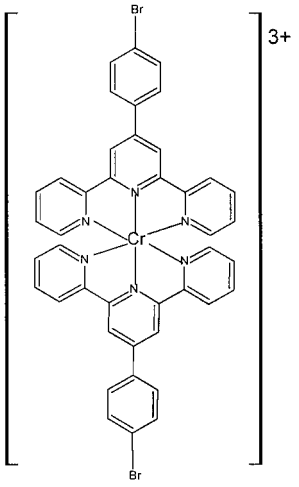

2

Table 1. Ground-state absorption spectral details of aqueous solutions of $[Cr(tpy)_2]^{3+}$, $[Cr(ttpy)_2]^{3+}$, and $[Cr(Brphtpy)_2]^{3+}$

$[Cr(tpy)_2]^{3+}$ λ [nm] (log ε)	$[Cr(ttpy)_2]^{3+}$ (**1**) λ [nm] (log ε)	$[Cr(Brphtpy)_2]^{3+}$ (**2**) λ [nm] (log ε)
225 (4.79)	225 (4.38)	225 (4.95)
ca. 239 (4.64)	ca. 239 (4.27)	ca. 239 (4.89)
267 (4.49)	267 (4.13)	267 (4.77)
ca. 286 (4.32)	ca. 286 (4.24)	ca. 286 (4.86)
315 (4.04)	315 (4.01)	315 (4.71)
327 (4.12)	327 (4.05)	327 (4.77)
348 (4.22)	348 (4.09)	348 (4.84)
364 (4.23)	364 (4.12)	364 (4.82)
422 (3.31)	422 (1.3)	422 (2.2)
443 (3.35)	443 (1.12)	443 (2.1)
473 (3.15)	473 (0.87)	473 (1.96)

Like other polypyridyl and terpyridyl complexes of Cr^{III}, complexes **1** and **2** exhibit multiple absorbances between 200 and 800 nm (Table 1), as well as ligand-centered absorbances at 285 and 287 nm, respectively. The visible absorption bands can be attributed to ligand field transitions. The lowest energy ligand field transition for complex **1** appears at 576 nm and the same transition for **2** appears at 564 nm. Other ligand field transitions occur at 481 and 450 nm for complex **1** and at 472 and 442 nm for **2**. Both complexes are electrochemically active and exhibit multiple reduction processes. Their cyclic voltammograms show well-separated reduction waves at −0.19, −0.5, −0.96, −1.913, and −2.196 V (for **1**) and −0.14, −0.45, −0.94, −1.767, and −2.20 V (for **2**) (Figure 1). The first three electrochemical waves are reversible one-electron processes with ΔE_p = 58−65 mV at all scan rates (Table 2). The first two reduction potentials at −0.18 and −0.5 V (**1**) and −0.14 and −0.45 V (**2**) could be due to two reversible one-electron reduction processes arising from Cr^{III}/Cr^{II} and Cr^{II}/Cr^{I} couples, respectively. For $Cr(tpy)_2{}^{3+}$, the Cr^{III}/Cr^{II} and Cr^{II}/Cr^{I} couples are reported to be at −0.28 and −0.69 V vs. SCE, respectively.[30] The less negative reduction potential observed here for these complexes, compared with the parent terpyridyl ligand, could be due to the substituent effect on the terpyridyl ligand. In the present case, on substituting tolyl and bromophenyl group to the terpyridyl ligand, the metal-centered redox potentials shift toward more positive values than for the parent terpyridyl complex of chromium.

DNA Binding Experiments

Absorption Titration of Chromium Complex with Calf Thymus DNA

Interaction of the complexes with DNA was investigated by monitoring the absorption spectra of the complexes in the presence and absence of DNA (Figure 2). The absorption maxima of both chromium(III) complexes are shifted by 3−5 nm in the presence of DNA. A noticeable hypochromicity arises due to interaction of the two chromium complexes with DNA. The intraligand transitions show a decrease in intensity to the maximum of 22% for complex **1** and 19% for complex **2** on addition of an incremental amount of DNA. These spectroscopic changes suggest that there are interactions between the metal complexes and DNA. Such hypochromicity has been attributed to intercalative binding.[31] Notably, the hypochromicities of the peaks are lower than those of classical intercalators such as ethidium bromide and $[Ru(phen)_2(dppz)]^{2+}$ whose percentage hypochromicities are > 25%.[32] The binding constants of the complexes with DNA have been measured from absorption titration as reported earlier.[15] Intrinsic binding constants for complexes **1** and **2** with DNA calculated to be $3.1\pm0.2\times10^3$ and $1.252\pm0.2\times10^4$ M^{-1}, respectively, which are lower than the 10^6-10^7 M^{-1} of classical intercalators,[32] but similar to some of the chromium and ruthenium complexes, which prefer surface binding to DNA.[14−18] These results indicate that the preferred binding mode of complexes **1** and **2** to DNA is surface binding or electrostatic interaction.

Viscosity Measurements

A critical test for a binding model in solution in the absence of crystallographic structural data is hydrodynamic measurement, which is more sensitive to the length change of nucleic acid. Of the hydrodynamic measurements, viscosity measurements provide a tool for the study of metal−DNA interaction since optical studies provide necessary but not sufficient clues to support the binding model. Generally, classical intercalators increase the viscosity of DNA due to the accommodation of the ligand between the base pairs of the helix. In contrast, non-classical intercalators could bend or kink the DNA helix, reduce its effective length and concomitantly its viscosity. Here, the viscosity of CT DNA increased with increasing concentration of **1** and **2** (Figure 3). Such a trend is typical of intercalators. However, since complexes **1** and **2** have octahedral geometry and the ligands are not strictly coplanar one can expect only partial intercalation of these molecules between the DNA bases.

 © 2004 Wiley-VCH Verlag GmbH & Co. KGaA, Weinheim

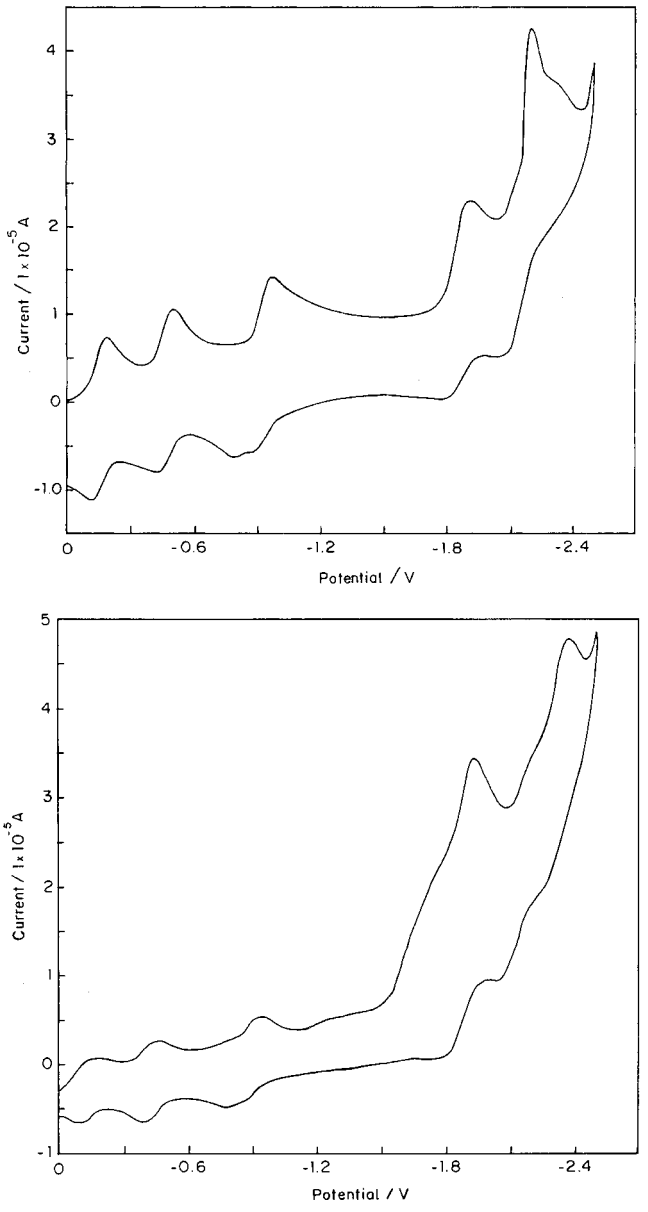

Figure 1. Cyclic voltammogram of the complexes **1** (top) and **2** (bottom) in CH_3CN (0.1 M TBAP as supporting electrolyte, scan rate = 100 mV/s)

Thermal Denaturation Study

The melting of DNA can be used to distinguish between those molecules that bind by intercalation and those that bind externally, i.e. electrostatically. Two parameters can be derived from the thermal denaturation curves of DNA, namely the melting temperature (T_m) at which 50% of the DNA has become single-stranded, and the curve width (σ_T), the temperature range within which 10−90% of the denaturation occurs.[33] DNA melting revealed ΔT_m values of calf thymus DNA in the presence of complexes **1** and **2** of 3±0.5 and 5±0.5 °C, respectively; $\Delta\sigma_T$ values for the duplex in the presence of **1** and **2** were 3±0.5 and 5±0.5 °C, respectively. Generally, one would expect a much larger increase in T_m and σ_T for classical intercalators, e.g. ethidium bromide, which shows an increase in the T_m of DNA of 14 °C and a curve width of 22 °C.[34] The magnitude of the increase in T_m and σ_T for DNA in the presence of **1** and **2** indicates that their interaction with DNA is non-intercalative binding. This is also reflected in the binding constant.

Table 2. Half-wave potentials and peak current ratio of the chromium complexes **1** and **2** compared with the parent compound $[Cr(tpy)_2]^{3+}$

Complex	E_{pc}	E_{pa}	ΔE [mV]	i_{pc}/i_{pa}
$[Cr(tpy)_2]^{3+}$ [a]	−0.177	−0.114	58	1.06
	−0.576	−0.518	58	1.02
	−1.085	−1.022	63	1.03
$[Cr(ttpy)_2]^{3+}$ (**1**)	−0.189	−0.129	62	1.12
	−0.5	−0.443	57	1.14
	−0.968	−0.908	60	1.17
	−1.913	−1.830	83	1.13
	−2.196	−2.158	38	1.99
$[Cr(Brphtpy)_2]^{3+}$ (**2**)	−0.140	−0.084	56	1.1
	−0.451	−0.394	57	1.09
	−0.943	−0.88	63	1.08
	−1.767	−1.705	62	1.59
	−2.198	−2.160	38	1.81

[a] This complex also shows two ligand-centered redox waves with $E_{1/2}$ of −1.99 and −2.37 V.

Luminescence Study

Aqueous solutions of the complexes **1** and **2** emit strongly at room temperature. In aqueous solution, complexes **1** and **2** show strong emission bands ($^2E_g \rightarrow {}^4A_{2g}$) at 773 nm and 707 nm, respectively, on excitation at 340 nm. The emission spectral bands, which represent the 0−0 transition of $^2E_g \rightarrow {}^4A_{2g}$, are only slightly sensitive to the nature of ligand substituents with diimine systems. For example, on substitution of a phenyl group on the bipyridyl ligand, there is a red-shift of 14 nm in the emission spectra of the corresponding chromium complex. $[Cr(tpy)_2]^{3+}$ shows a red-shift of 42 nm in the emission bands compared with $[Cr(bpy)_3]^{3+}$.[35] The $^2E_g \rightarrow {}^4A_{2g}$ band is seen at 728 nm for $[Cr(bpy)_3]^{3+}$ but occurs at 770 nm for $[Cr(tpy)_2]^{3+}$. Interestingly, substituting the bromophenyl group on the terpyridyl ligand results in a drastic blue-shift in the emission band of $[Cr(Brphtpy)_2]^{3+}$, by 63 nm compared with the parent (terpyridyl)chromium complex. However, a *p*-tolylterpyridyl substituent yields a red-shift of 3 nm in the emission maxima compared with the emission maxima of $[Cr(tpy)_2]^{3+}$. Generally, the binding of a luminescent compound to DNA or polynucleotides leads to an increase in the emission and excited state lifetime due to the rigidity of DNA microenvironment and protection from solvent quenching. The influence of DNA on the emission of **1** and **2** has been examined. Interestingly, the emission intensity of the complexes is quenched by the addition of incremental amounts of DNA, in contrast to $[Cr(bzimpy)_2]^+$.[36] Effects of nucleotides dGMP, dAMP, dCMP, and dTMP on the emission intensity of **1** and **2** have also been examined. The emission intensity of complex **1** at 773 nm was quenched by

 © 2004 Wiley-VCH Verlag GmbH & Co. KGaA, Weinheim

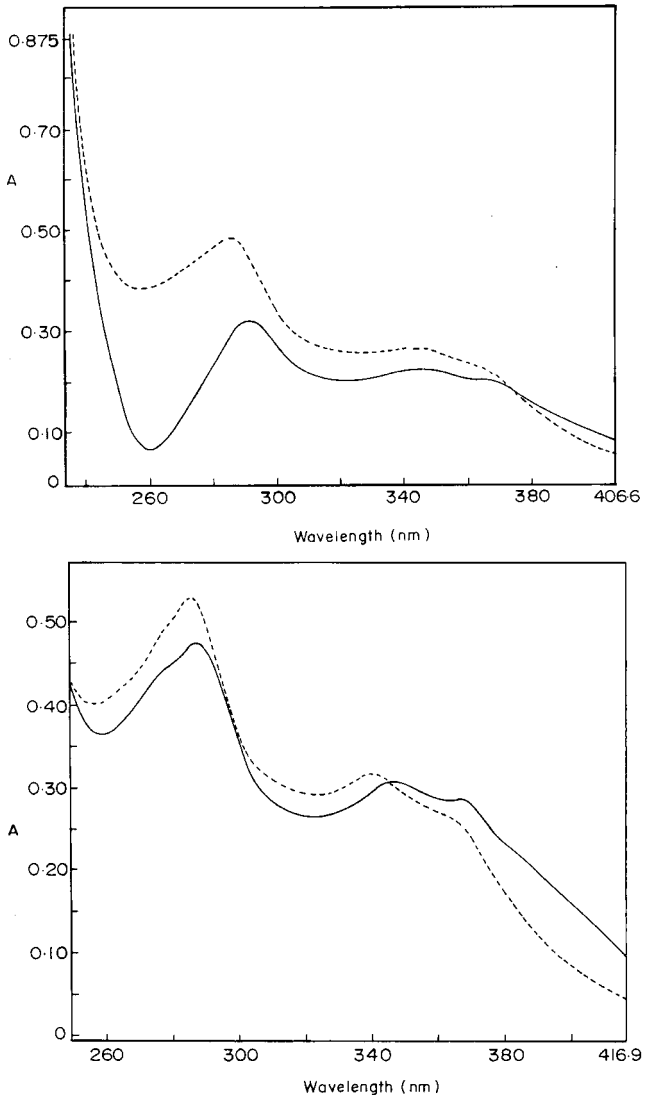

Figure 2. Absorption spectra of **1** (top) and **2** (bottom) in the absence (---) and presence (—) of increasing amounts of CT DNA; [Cr] = 10 μM; [DNA] = 0−220 μM

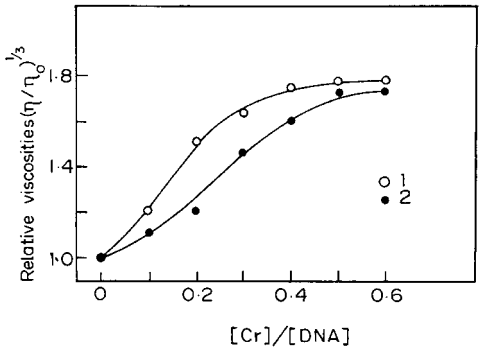

Figure 3. Effect of increasing $[Cr(ttpy)_2]^{3+}$ (**1**) and $[Cr(Brphtpy)_2]^{3+}$ (**2**) on the relative viscosity of DNA

dGMP and dAMP, but not affected by dCMP and dTMP (Figure 4, top). Conversely, the emission intensity complex **2** was quenched by all four mononucleotides (Figure 4, bottom). Stern−Volmer plots for steady-state emission intensity quenching are expected to be a straight line for dynamic quenching. Figure 4 (top and bottom), show plots with upward curvature at higher nucleotide concentrations. Such behavior indicates an additional deactivation pathway involving static quenching, attributed in this case to nucleotide-bound chromium(III) complex. To probe the mechanism for the quenching of the complexes **1** and **2** by DNA and mononucleotides, the excited state potentials were calculated using Equation (1), where $E°(Cr^{3+}/Cr^{2+})$ is the ground-state reduction potential and $E_{0-0}(Cr^{3+}/Cr^{2+})$ is the potential calculated from the emission energy. The excited state potentials for complexes **1** and **2** were calculated as +1.65 V and +1.85 V vs. NHE, respectively. The excited state potential of complex **1** is higher than that of dGMP (1.29 V) and dAMP (1.4 V) but similar to those of dCMP (1.53 V) and dTMP (1.63 V).[37] However, for complex **2**, $E°(*Cr^{3+}/Cr^{2+})$ is much higher than that of all the four nucleotides. Hence, the quenching process clearly could be due to electron transfer from a nucleobase to an excited state complex. Such luminescent quenching has been reported for various ruthenium compounds as well as chromium complexes containing diimine systems. However, in the present investigation, chromium(III) complexes having a triimine system, such as the (*p*-bromophenyl)terpyridyl derivative, exhibited a much higher excited-state oxidizing power than complex **1** and also diimine−Cr^{III} systems such as $[Cr(bpy)_3]^{3+}$, $[Cr(phen)_3]^{3+}$, and $[Cr(TMP)_3]^{3+}$. Notably, coordination of triimine ligands like ttpy and Brphtpy gives chromium complexes with a much higher excited state potential than that observed for the diimine−Cr^{III} complexes such as $[Cr(bpy)_3]^{3+}$, $[Cr(phen)_3]^{3+}$, and $[Cr(TMP)_3]^{3+}$, whose excited state potentials are in the range of 1.2−1.5 V.

$$E°(*Cr^{3+}/Cr^{2+}) = E°(Cr^{3+}/Cr^{2+}) - E_{0-0}(Cr^{3+}/Cr^{2+}) \quad (1)$$

Photonuclease Activity

One possible consequence of electron transfer from a nucleobase to a molecule in the ground state or excited state is a single strand break of DNA. This process is generally demonstrated by gel electrophoresis of plasmid DNA, because the conversion of the supercoiled, closed circular form of plasmid DNA into an open circular form, induced by a single strand nick, is easily monitored. To support the electron transfer from the nucleobase to the excited state of a chromium(III) complex, we have carried out gel electrophoresis of plasmid DNA after irradiating it in the presence of the complexes **1** and **2**. On excitation of complexes **1** and **2** at 340 nm in the presence of supercoiled plasmid DNA, a single strand break was observed (lanes 4 and 5 of Figure 5). DNA cleavage was not observed for the complex with DNA without irradiation (lanes 2 and 3). A possible role of singlet oxygen has also been ruled out in the present case because the strand break was not inhibited by the addition of a singlet oxygen scavenger such as sodium azide (lanes 6 and 7); furthermore, reactions carried out in D_2O

 © 2004 Wiley-VCH Verlag GmbH & Co. KGaA, Weinheim

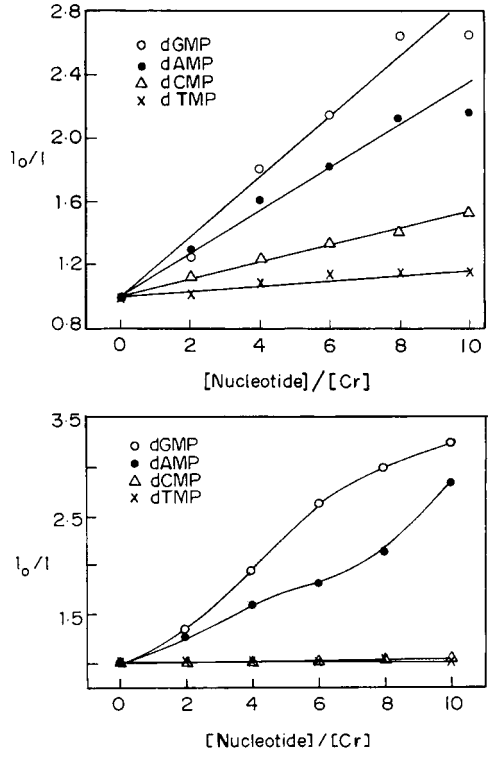

Figure 4. Relative emission intensity of the complexes **1** (bottom) and **2** (top) in the presence of mononucleotides; [Cr]= 10 μM; [nucleotides] = 20−100 μM

showed no enhancement in cleavage reaction (not shown). From the above observations, it is assumed that formation of a radical cation of guanine by electron transfer to the excited state of the complex plays a key role in this damage event since the guanine base is the most oxidizable base of all the four bases. Similar photonuclease activity has also been reported for photooxidizing agents such as $[Ru(TAP)_3]^{2+}$, $[Ru(bzimpy)_2]^{2+}$, $[Ru(bpz)_3]^{2+}$, and $[Ru(bpz)_2(DPPZ)]^{2+}$.[38−41]

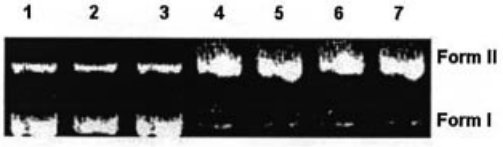

Figure 5. Photoinduced cleavage of pBR 322 DNA by complex **1** and **2** (20 μM) following 340 nm photolysis for 20 min at 25 °C (0.8% agarose gel); form I: supercoiled plasmid; form II: nicked plasmid; lane 1: control DNA; lane 2: DNA + **1**; lane 3: DNA + **2**; lane 4: DNA + **1** + *hv*; lane 5: DNA + **2** + *hv*; lane 6: DNA + **1** + NaN_3 (2 mM) + *hv*; lane 7: DNA + **2** + NaN_3 (2 mM) + *hv*

Conclusions

The cations $[Cr(ttpy)_2]^{3+}$ and $[Cr(Brphtpy)_2]^{3+}$ exhibit very high excited-state oxidizing power and bring about electron transfer from DNA bases to the excited state of the complex. These complexes also bring about cleavage of plasmid DNA upon photoirradiation. Such photonuclease activity by metal complexes can be exploited to develop footprinting agents in molecular biology.

Experimental Section

Chemicals: 2-Acetylpyridine and *p*-tolualdehyde were obtained from Sigma Aldrich chemicals and used as received. *p*-Bromobenzaldehyde was purchased from Lancaster chemicals, and used as received. Calf thymus DNA, Hepes, Tris, and mononucleotides were obtained from SRL chemicals, Mumbai. The stock solution of DNA was prepared by stirring the sample, dissolving in Hepes buffer (10 mM, pH = 7.0), at 4 °C. The solution was then dialyzed exhaustively against buffer for 48 h and filtered using a membrane filter obtained from Sartorius (0.45 μm). Filtered DNA solution in the buffer gave a UV absorbance ratio A_{260}/A_{280} of about 1.9, indicating that the DNA was sufficiently free from protein.[42] The concentration of DNA was determined by using the molar absorption coefficient of 6600 $M^{-1}\cdot cm^{-1}$ at 260 nm.[43] The stock solution of the Cr^{III} complex was prepared in water and its concentration estimated according to a reported procedure.[44] All solvents used were of analytical grade, received from Ranbaxy, Mumbai, and were used without further purification. All experiments were carried out in Hepes buffer at pH = 7.0 in Milli Q water.

Methods: UV/Vis spectra of the chromium(III) complexes and DNA binding studies were recorded with a Perkin−Elmer Lambda 35 double beam spectrophotometer at 25 °C. Elemental analyses were performed using a Heraeus-CHN-Rapid Analyzer at RSIC, IIT, Madras. Emission spectra were recorded with a Hitachi 650-40 spectrofluorimeter. Electrospray ionisation (ESI) mass spectra of the complexes were recorded with a Hewlett Packard 1100 mass spectrometer equipped with an electron spray source. Infrared spectra of the complex were recorded with a Perkin−Elmer FT-IR spectrometer. Cyclic voltammetry experiments were performed with an EG and G PAR 173 potentiostat/Galvanostat analyzer. Tetrabutylammonium perchlorate (TBAP) was used as supporting electrolyte. A standard three-electrode system was used, consisting of a glassy carbon as working electrode, platinum electrode as auxiliary electrode and a saturated calomel solution as reference electrode (SCE).

Synthesis of $[Cr(ttpy)_2](ClO_4)_3$ (1): The ligand ttpy was prepared according to a literature procedure.[45] Subsequently, ttpy (0.646 g, 2 mmol), dissolved in methanol (10 mL), was taken and purged with nitrogen for 20 min. To this a deaerated solution of the ligand, a $[Cr(H_2O)_6]^{2+}$ solution (1 mmol), was added under nitrogen. The resulting brown solution was then bubbled with air for 3 h. The resultant orange-yellow compound was filtered off and recrystallized from a mixture of acetone/water (2:1). The recrystallized product was then filtered off, washed with diethyl ether, and dried under vacuum. ESI-MS: m/z = 696 $[M - 2H^+ - 3ClO_4]^+$. $C_{44}H_{34}Cl_3CrN_6O_{12}$ (997.12): calcd. C 53.00, H 3.44, N 8.43, Cr 5.21; found C 52.85, H 3.32, N 8.38, Cr 5.11.

Synthesis of $[Cr(Brphtpy)_2](ClO_4)_3$ (2): The ligand Brphtpy was prepared according to a literature procedure.[46] The chromium(III) complex was synthesized according to the above procedure, using Brphtpy in place of ttpy. ESI-MS: m/z = 826 $[M - 2H^+ - 3ClO_4]^+$. $C_{42}H_{28}Br_2Cl_3CrN_6O_{12}$ (1126.86): calcd. C 44.70, H 2.50, N 7.46; Cr, 4.61; found C 44.75, H 2.41, N 7.38; Cr, 4.43.

Caution! Although we had no difficulty during working, perchlorate salts are potentially explosive! Utmost care should be exercised in handling perchlorate salts.

 © 2004 Wiley-VCH Verlag GmbH & Co. KGaA, Weinheim

DNA Binding Studies: Electronic spectra of Cr^{III} complexes were monitored in the presence and absence of DNA. The binding constants for the interaction of Cr^{III} complexes with DNA were obtained from absorption titration data. A fixed amount of the complex (10 μM) was titrated with increasing amounts of DNA, over the range 20−220 μM. The binding constant was then determined using Equation (2), where ε_A, ε_F, and ε_B correspond to A_{obsd}/[Cr], the molar absorption coefficient for the free chromium complex and the molar absorption coefficient for the chromium complex in the fully bound form, respectively. A plot of [DNA]/($\varepsilon_A - \varepsilon_F$) vs. [DNA], gives K_b as the ratio of the slope to intercept.

$$[DNA]/(\varepsilon_A - \varepsilon_F) = [DNA]/(\varepsilon_B - \varepsilon_F) + 1/K_b(\varepsilon_B - \varepsilon_F) \quad (2)$$

Thermal denaturation studies were conducted in a Perkin−Elmer Lambda 35 spectrophotometer equipped with thermostatted cell holder. The temperature was controlled by a Peltier system (±0.1 °C). The absorbance at 260 nm was monitored for DNA in the absence and the presence of the complexes. Viscometric experiments were carried out using an Ostwald-type viscometer (2 mL capacity), thermostated in a water bath maintained at 25±1 °C. Flow rates of buffer (10 mM), DNA (150 μM), and DNA in the presence of Cr^{III} complex at various concentrations (15−90 μM) were measured with a manually operated timer at least three times to agree within 1 s. The viscosity was calculated according to $\eta = (t - t_0)/t_0$, where t_0 is the flow time for the buffer and t is the observed flow time for DNA in the presence and absence of the complex. Plots of $(\eta/\eta_0)^{1/3}$ vs. R (R = [complex]/[DNA]) were constructed from the viscosity measurements.[47] Steady-state emission spectra of complexes **1** and **2** in the presence of DNA were recorded. The concentration of complexes was fixed (10 μM) while that of DNA was varied from 20 to 100 μM. The Cr^{III} complexes were excited at 340 nm and the emission intensity of the complexes **1** and **2** monitored at 773 and 707 nm, respectively. Time-resolved fluorescence for the complexes was determined using a picosecond-laser-excited TCSPC spectrometer. The excitation source was a tunable Ti-Sapphire laser (Tsunami, Spectrophysics, USA) with a pulse width of < 2 ps and repetition rate of 82 MHz. Samples were excited at 340 nm and the emission monitored using an MCP-PMT (Hamamatsu-C 4878) detector. The decay traces were deconvoluted using a non-linear least-squares analysis with IBH software.

Gel electrophoresis of plasmid DNA (pBR322 DNA) was carried out with a reaction mixture (25 μL) containing plasmid DNA (4 μL of 200 μg·mL^{-1}), a solution of complex **1** and **2** (5 μL of 0.1 mM) and remaining buffer. NaN_3 solution (5 μL) was then added to one of the samples. Metal/DNA solutions were preincubated for 1 h in the dark and the samples were kept in a spectrofluorimeter sample chamber. The sample was then irradiated at 340±5 nm for 20 min and subsequently analyzed by 0.8% agarose gel electrophoresis (Tris/boric acid/EDTA buffer, pH = 8.0) at 50 V for 4 h. The gel was stained with 0.5 μg·mL^{-1} ethidium bromide and then illuminated under a UV lamp and photographed with Polaroid film using a Kodak DC-40 digital camera.

Acknowledgments

V. G. V. thanks CSIR for a research fellowship. The authors thank the National Centre for Ultrafast Processes for providing the facilities to carry out time-resolved fluorescence experiments.

[1] D. J. Gravert, J. H. Griffin, *Inorg. Chem.* **1996**, *35*, 4837−4847.
[2] C. J. Burrows, J. G. Muller, G. T. Poulter, S. E. Rokita, *Acta Chem. Scand.* **1996**, *50*, 337−344.
[3] R. F. Pasternack, P. Garrity, B. Ehrlich, C. B. Davis, E. J. Gibbs, G. Orloff, A. Giartosio, C. Turano, *Nucleic Acids Res.* **1986**, *14*, 5919−5931.
[4] R. F. Pasternack, E. J. Gibbs, J. J. Villafranca, *Biochemistry* **1983**, *22*, 2406−2414.
[5] C. J. Burrows and S. E. Rokita, in: *Metal Ions in Biological Systems* (Eds.: A. Sigel and H. Sigel), Marcel Dekker, New York, **1996**, vol. 33, p. 537−560.
[6] J. G. Muller, R. P. Hickerson, R. J. Perez, C. J. Burrows, *J. Am. Chem. Soc.* **1997**, *119*, 1501−1506.
[7] J. G. Muller, P. Zheng, S. E. Rokita, C. J. Burrows, *J. Am. Chem. Soc.* **1996**, *118*, 2320−2325.
[8] C. J. Burrows, S. E. Rokita, *Acc. Chem. Res.* **1994**, *27*, 295−301.
[9] X. Chen, C. J. Burrows, S. E. Rokita, *J. Am. Chem. Soc.* **1992**, *114*, 322−325.
[10] J. G. Muller, X. Chen, A. C. Dadiz, S. E. Rokita, C. J. Burrows, *J. Am. Chem. Soc.* **1992**, *114*, 6407−6411.
[11] J. G. Muller, X. Chen, A. C. Dadiz, S. E. Rokita, C. J. Burrows, *Pure Appl. Chem.* **1993**, *65*, 545−550.
[12] L. E. Marshall, D. R. Graham, K. A. Reich, D. S. Sigman, *Biochemistry* **1981**, *20*, 244−250.
[13] J. M. Veal, K. Merchant, R. L. Rill, *Biochemistry* **1991**, *30*, 1132−1140.
[14] R. Vijayalakshmi, M. Kanthimathi, V. Subramanian, B. U. Nair, *Biochem. Biophys. Res. Commun.* **2000**, *271*, 731−734.
[15] R. Vijayalakshmi, M. Kanthimathi, V. Subramanian, B. U. Nair, *Biochim. Biophys. Acta* **2000**, *1475*, 157−162.
[16] R. Vijayalakshmi, A. Dhathathreyan, V. Subramanian, B. U. Nair, T. Ramasami, *Langmuir* **1999**, *15*, 2898−2900.
[17] R. Vijayalakshmi, V. Subramanian, B. U. Nair, *J. Biomol. Struct. Dyn.* **2002**, *19*, 1063−1069.
[18] V. G. Vaidyanathan, R. Vijayalakshmi, V. Subramanian, B. U. Nair, *Bull. Chem. Soc. Jpn.* **2002**, *75*, 1143−1149.
[19] R. M. Burger, J. Peisach, S. B. Horwitz, *J. Biol. Chem.* **1981**, *256*, 11636−11644.
[20] H. Kuromochi, K. Takahashi, T. Takita, H. Umezawa, *J. Antibiot. (Tokyo)* **1981**, *34*, 576−582.
[21] N. Grover, H. H. Thorp, *J. Am. Chem. Soc.* **1991**, *113*, 7030−7031.
[22] J. M. Kelly, M. J. Murphy, D. J. McConnell, C. OhUigin, *Nucleic Acids Res.* **1985**, *13*, 167−184.
[23] L. A. Lipscomb, F. X. Zhou, S. R. Presnell, R. J. Woo, M. E. Peek, R. R. Plaskon, L. D. Williams, *Biochemistry* **1996**, *35*, 2818−2823.
[24] D. B. Hall, R. E. Holmin, J. K. Barton, *Nature* **1996**, *382*, 73−75.
[25] J. K. Barton, A. T. Danishefsky, J. M. Goldberg, *J. Am. Chem. Soc.* **1984**, *106*, 2172−2176.
[26] J. K. Barton, A. L. Raphel, *J. Am. Chem. Soc.* **1984**, *106*, 2466−2468.
[27] R. T. Watson, N. Desai, J. Wildsmith, J. F. Wheeler, N. A. P. Kane-Maguire, *Inorg. Chem.* **1999**, *38*, 2683−2687.
[28] K. D. Barker, B. R. Benoit, J. A. Bordelon, R. J. Davis, A. S. Delmas, O. V. Mytykh, J. T. Petty, J. F. Wheeler, N. A. P. Kane-Maguire, *Inorg. Chem. Acta* **2001**, *322*, 74−78.
[29] N. A. P. Kane-Maguire, J. F. Wheeler, *Coord. Chem. Rev.* **2001**, *211*, 145−162.
[30] R. P. Bonomo, S. Musumeci, E. Rizzarelli, S. Samartano, *Gazz. Chim. Ital.* **1974**, *104*, 1067−1074.
[31] X.-H. Zou, B.-H. Ye, H. Li, Q.-L. Zhang, H. Chao, J.-G. Liu, L.-N. Ji, X.-Y. Li, *J. Biol. Inorg. Chem.* **2001**, *6*, 143−150.
[32] A. E. Friedmann, J. C. Chambron, J. P. Sauvage, N. J. Turro, J. K. Barton, *J. Am. Chem. Soc.* **1990**, *112*, 4960−4962.

 © 2004 Wiley-VCH Verlag GmbH & Co. KGaA, Weinheim

[33] J. M. Kelly, A. B. Tossi, D. J. McConnell, C. OhUigin, *Nucleic Acids Res.* **1985**, *13*, 6017−6034.
[34] G. A. Neyhart, N. Grover, S. R. Smith, W. A. Kalsbeck, T. A. Fairley, M. Cory, H. H. Thorp, *J. Am. Chem. Soc.* **1993**, *115*, 4423−4428.
[35] N. Serpone, M. A. Jamieson, M. S. Henry, M. Z. Hoffman, F. Bolletta, M. Maestri, *J. Am. Chem. Soc.* **1979**, *101*, 2907−2916.
[36] V. G. Vaidyanathan, B. U. Nair, *Eur. J. Inorg. Chem.* **2003**, 3633−3638.
[37] C. J. Burrows, J. G. Muller, *Chem. Rev.* **1998**, *98*, 1109−1152.
[38] J. M. Kelly, D. J. McConnell, C. OhUigin, A. B. Tossi, A. Kirsch-De Mesmaeker, A. Masschelein, J. Nasielski, *J. Chem. Soc., Chem. Commun.* **1987**, *24*, 1821−1823.
[39] J. P. Lecomte, A. Kirsch-De Mesmaeker, J. M. Kelly, A. B. Tossi, H. Gorner, *Photochem. Photobiol.* **1992**, *55*, 681−689.
[40] A. Kirsch-De Mesmaeker, G. Orellama, J. K. Barton, N. J. Turro, *Photochem. Photobiol.* **1990**, *52*, 461−472.
[41] V. G. Vaidyanathan, B. U. Nair, *J. Inorg. Biochem.* **2002**, *91*, 405−412.
[42] J. Marmur, *J. Mol. Biol.* **1961**, *3*, 208−218.
[43] R. Reichmann, S. A. Rice, C. A. Thomas, P. Doty, *J. Am. Chem. Soc.* **1954**, *76*, 3047−3053.
[44] K. Lingane, R. Peesok, *Anal. Chem.* **1948**, *20*, 425−428.
[45] J. P. Collin, S. Guillerez, J. P. Sauvage, F. Barigelletti, L. D. Cola, L. Flamigni, V. Balzani, *Inorg. Chem.* **1991**, *30*, 4230−4238.
[46] W. Spahni, G. Calzaferri, *Helv. Chim. Acta* **1984**, *67*, 450−454.
[47] G. Cohen, H. Eisenberg, *Biopolymers* **1969**, *8*, 45−55.

Received October 10, 2003
Early View Article
Published Online March 23, 2004

 © 2004 Wiley-VCH Verlag GmbH & Co. KGaA, Weinheim

Activation of H_2 and CO by Sulfur-Rich Nickel Model Complexes for [NiFe] Hydrogenases and CO Dehydrogenases[‡]

Dieter Sellmann,[a][†] Raju Prakash,*[a] and Frank W. Heinemann[a]

Keywords: Hydrogenases / H_2 activation / Nickel / N ligands / S ligands

Reactions of the trinuclear complexes [Ni($^{R}S_3$)]$_3$ [$^{H}S_3^{2-}$ = bis(2-mercaptophenyl)sulfide(2–) (**1a**) or $^{si}S_3^{2-}$ = bis(2-mercapto-3-trimethylsilylphenyl)sulfide(2–) (**1b**)] with nucleophiles L (L = NHP*n*Pr$_3$, NHPCy$_3$, NHSPh$_2$, P*n*Pr$_3$) afforded the corresponding mononuclear complexes [Ni(L)($^{R}S_3$)] [R = si = SiMe$_3$; L = NHP*n*Pr$_3$ (**2b**); L = NHPCy$_3$ (**3a**,**b**); L = NHSPh$_2$ (**4a**,**b**); L = P*n*Pr$_3$ (**5a**)]. X-ray structural determinations showed that **2b**, **3a**, **3b**, **4a**, and **5a** exhibit tetrahedrally distorted planar [Ni(L)($^{R}S_3$)] fragments. Complex **2b** dimerizes through intermolecular N–H···N hydrogen bonding. In contrast to **2b**, complexes **3a** and **4a** exhibit intramolecular hydrogen bonds between thiol groups and NH protons. Complexes **2**–**4** possess weakly acidic NH protons and undergo D$^+$/NH exchange reactions with D_2O or CD_3OD. Complexes **2**–**4** and [Ni(S*t*Bu)($^{R}S_3$)]$^-$ (**9a**,**b**) also catalyze D_2/H$^+$ exchange in [D_8]THF/H_2O under an elevated pressure of D_2 (18 bar), as confirmed by ^{1}H NMR spectroscopy. It is proposed that D_2 heterolysis is achieved through attack of the Lewis-acidic nickel centers and the Brönsted-basic sulfur atoms at an η^2-D_2 ligand. Complexes **9a** and **9b** are the first sulfur-only nickel complexes that enable the modeling of the [NiFe] hydrogenase catalyzed D_2/H$^+$ exchange reaction. Evidence for labile five-coordinate [Ni(CO)(L)($^{R}S_3$)] has been found in the reaction between [Ni(L)($^{R}S_3$)] complexes and CO. The CO adducts of complexes with nitrogenous ligands L such as N_3^-, NHPR$_3$ (R = *n*Pr$_3$, Cy$_3$), or NHSPh$_2$ showed rapid consecutive reactions. The reaction between Et$_4$N[Ni(N_3)($^{si}S_3$)] (**8b**) and CO gave Et$_4$N[Ni(NCO)($^{si}S_3$)] (**10b**), whereas reactions between **2**–**4** and CO afforded only **1a** or **1b**. Mechanisms are suggested which have the formation of reactive five-coordinated [Ni(CO)(L)($^{R}S_3$)] intermediates in common.

(© Wiley-VCH Verlag GmbH & Co. KGaA, 69451 Weinheim, Germany, 2004)

Introduction

Modeling active sites in metalloenzymes is the motivation for the synthesis of low-molecular-weight complexes that exhibit the structural and reactivity features of the enzyme centers.[1] A key feature of the active sites of hydrogenases and CO dehydrogenases are nickel atoms in sulfur-dominated coordination spheres.[1–5] X-ray structural determinations of several [NiFe] hydrogenases[2,3] and two CO dehydrogenases[4,5] have established that the active sites contain four-coordinate nickel atoms in tetrahedrally distorted planar coordination spheres of sulfur atoms[2–5] (Figure 1). These centers are generally accepted to be the location of the reactions catalyzed by hydrogenases [Equation (1a), (1b)] and CO dehydrogenases [Equation (2)].

$$2\,H^+ + 2\,e^- \rightleftharpoons H_2 \quad (1a)$$

$$H_2 \rightleftharpoons H^+ + H^- \quad (1b) \qquad (1)$$

$$CO + H_2O \rightleftharpoons CO_2 + 2\,H^+ + 2\,e^- \qquad (2)$$

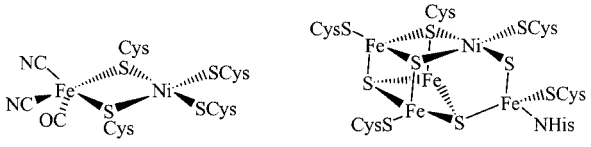

Figure 1. Schematic structures of the active centers in fully reduced [NiFe] hydrogenase from *D. vulgaris* Miyazaki[2] (left) and the CO dehydrogenase from *C. hydrogenoformans*[4,5] (right)

Catalysis of the reactions in Equations (1) and (2) makes hydrogenases and CO dehydrogenases essential for energy metabolism in nature. Low-molecular-weight nickel complexes with sulfur-dominated coordination spheres and reactivity towards H_2, CO, or CO_2 thus have considerable significance for gaining closer insights into the mechanisms of the reactions according to Equations (1) and (2), and for the development of competitive catalysts. Such complexes,

[‡] Transition Metal Complexes with Sulfur Ligands, 160. Part 159: D. Sellmann, K. P. Peters, F. W. Heinemann, *Eur. J. Inorg. Chem.*, **2004**, 581–590.

[a] Institut für Anorganische Chemie der Universität Erlangen-Nürnberg,
Egerlandstrasse 1, 91058 Erlangen, Germany
Fax: (internat.) + 49-(0)9131/85-27367
E-mail: prakash@anorganik.chemie.uni-erlangen.de

[†] Deceased.

however, are extremely rare. [Ni(L)($^{R}S_3$)] is one of the very few examples of complexes of type **A**, in which $^{R}S_3$ denotes the tridentate sulfur ligands $^{H}S_3^{2-}$ [bis(2-mercaptophenyl)sulfide(2−)] or $^{si}S_3^{2-}$ [bis(2-mercapto-3-trimethylsilylphenyl)sulfide (2−)] and L neutral or anionic ligands, such as PR_3, HNP*n*Pr$_3$, Cl^-, N_3^-, or S*t*Bu$^-$.[6−9]

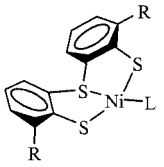

A [Ni(L)($^{R}S_3$)]

Recent findings that the neutral phosphorane imine complex [Ni(NHP*n*Pr$_3$)($^{H}S_3$)] catalyzes the heterolytic activation of H_2 [Equation (1b)][6] and the anionic complex [Ni(N_3)($^{H}S_3$)]$^-$ reacts with CO to give [Ni(NCO)($^{H}S_3$)]$^-$ [7] prompted us to explore this type of complex in greater detail. This paper focuses on the synthesis and characterization of [Ni(L)($^{H}S_3$)] and its analogous [Ni(L)($^{si}S_3$)] complexes, and their reactivity towards H_2. In addition, we extend our investigation towards the reactivity of [Ni(L)($^{R}S_3$)] complexes with CO in an effort to identify the possible five-coordinate intermediate species by means of spectroscopic techniques.

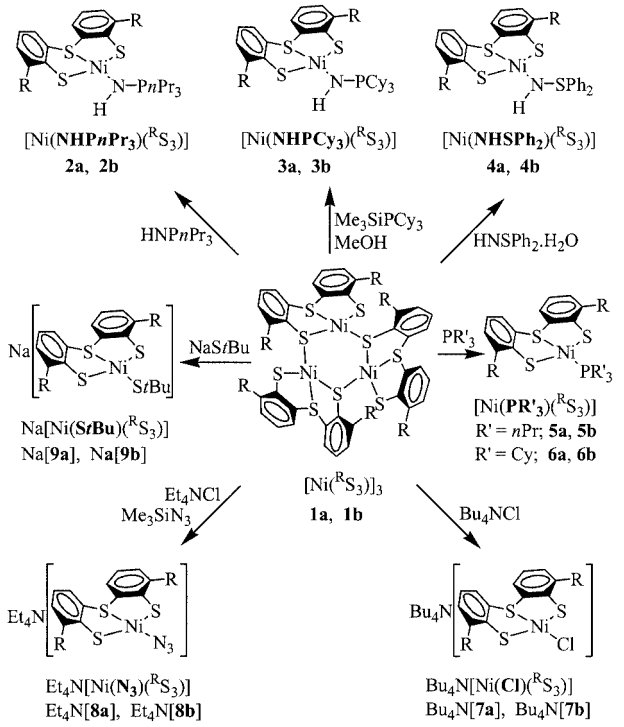

Scheme 1. Synthesis of [Ni(L)($^{R}S_3$)] complexes (R = H → **a**; R = $SiMe_3$ → **b**)

Results and Discussion

Synthesis and Characterization of [Ni(L)($^{H}S_3$)] and [Ni(L)($^{si}S_3$)] Complexes

[Ni(L)($^{R}S_3$)] complexes containing different ligands L are a prerequisite for probing the influence of L upon the potential activation of H_2 and CO. Scheme 1 summarizes the synthesis of such [Ni(L)($^{R}S_3$)] complexes. The letters **a** and **b** always designate the unsubstituted (R = H) and substituted (R = $SiMe_3$ = si) complexes, respectively. For the sake of completeness, Scheme 1 also includes complexes **2a**, **5b**, **6a**/**6b**, Bu$_4$N[**7a**/**7b**], and Et$_4$N[**8b**], which have been reported previously.[8,9] In most cases, the new complexes were obtained by cleavage of the trinuclear starting complexes [Ni($^{R}S_3$)]$_3$ (**1a**,**b**) with nucleophiles L.

Treatment of **1b** with NHP*n*Pr$_3$ in THF gave purple [Ni(NHP*n*Pr$_3$)($^{si}S_3$)] (**2b**) in analogy to the known synthesis of **2a**. The bulkier phosphorane imine $HNPCy_3$ had to be generated in situ through methanolysis of $Me_3SiNPCy_3$ and treated with **1a** and **1b** to afford [Ni(NHPCy$_3$)($^{R}S_3$)] (**3a**,**b**). These reactions could be monitored visually by the color change of the THF suspension (**1a**) or THF solution (**1b**) from red-brown to purple-red. Complex **1b** reacted much faster than complex **1a**.

Diphenylsulfimine, $HNSPh_2$, can potentially coordinate through either its nitrogen or sulfur atom. Reactions of **1a** and **1b** in THF with equimolar amounts of diphenylsulfimine hydrate, $NHSPh_2{\cdot}H_2O$, afforded the first examples of sulfimine sulfur-only nickel complexes as red-brown [Ni(NHSPh$_2$)($^{H}S_3$)] (**4a**) and dark-red [Ni(NHSPh$_2$)($^{si}S_3$)] (**4b**). The X-ray structure determination of **4a** proved that $HNSPh_2$ coordinates to the nickel atom through its N atom like the phosphorane imines.[8c]

Red-yellow crystals of [Ni(P*n*Pr$_3$)($^{H}S_3$)] (**5a**) formed instantaneously when a black-brown THF suspension of **1a** was treated with an equivalent amount of P*n*Pr$_3$. The analogous synthesis of **5b** could be carried out in homogeneous phase in THF. The chloro complexes Bu$_4$N[Ni(Cl)($^{H}S_3$)] (Bu$_4$N[**7a**]) and Bu$_4$N[Ni(Cl)($^{si}S_3$)] (Bu$_4$N[**7b**]) were obtained from **1a** and **1b** with Bu$_4$NCl. The anions **7a** and **7b** were required as precursors for the synthesis of the azido complexes Et$_4$N[Ni(N_3)($^{H}S_3$)] (Et$_4$N[**8a**]) and Et$_4$N[Ni(N_3)($^{si}S_3$)] (Et$_4$N[**8b**]), which formed from the reaction of **1a** and **1b**, respectively, with Et$_4$NCl and subsequent reaction with Me_3SiN_3. The sodium derivatives Na[Ni(S*t*Bu)($^{H}S_3$)] (Na[**9a**]) and Na[Ni(S*t*Bu)($^{si}S_3$)] (Na[**9b**]) were obtained from **1a** and **1b** with NaS*t*Bu, similar to the formation of similar Bu$_4$N derivatives reported in the literature.[8,9]

All new complexes were isolated in analytically pure form, are soluble in THF, CH_2Cl_2, acetone, DMF, or DMSO, and were characterized by IR and NMR spectroscopy, and mass spectrometry. The molecular structures of **2b**, **3a**, **3b**, **4a**, and **5a** were determined by X-ray crystallography.

The IR (KBr) spectra of the complexes exhibit absorption patterns typical for complexes with [Ni($^{H}S_3$)] or [Ni($^{si}S_3$)] fragments. The HNPR$_3$ and $HNSPh_2$ ligands of **2**−**4** give rise to sharp ν(NH) bands in the region

 © 2004 Wiley-VCH Verlag GmbH & Co. KGaA, Weinheim

3365−3200 cm^{-1} and ν(NP) or ν(NS) bands in the region 995−915 cm^{-1}. The ν(NH), ν(NP), and ν(NS) bands correspond to those of $HNPR_3$ [10] and $HNSPh_2$ [11] complexes reported previously. In comparison to the ν(NH) band of free $HNPnPr_3$ (3368 cm^{-1}), the ν(NH) band in **2b** (3298 cm^{-1}) is significantly red-shifted. Similarly, the ν(NH) band of **4a** (3202 cm^{-1}) and **4b** (3210 cm^{-1}) appears at lower wavenumbers than that of free $HNSPh_2$ (3306 cm^{-1}).[11b] The solid-state IR spectra of **3a** and **4a** also contain weak bands at 2560 cm^{-1} (**3a**) and 2559 cm^{-1} (**4a**), indicating the existence of N−H···S(thiolate) bridges. Such hydrogen-bond bridges were confirmed by the X-ray structure determinations.

As judged by their well-resolved NMR spectra, the complexes are diamagnetic. The ^1H NMR spectra of all complexes show a characteristic splitting pattern for the aromatic protons, consisting of either four or three multiplets depending on the fragment [Ni($^HS_3$)] or [Ni($^{si}S_3$)]. In **4a** and **4b**, some of these aromatic multiplets are superimposed by SPh_2 signals. The $SiMe_3$ protons in the [Ni(L)($^{si}S_3$)] complexes give rise to a sharp singlet in the region between δ = 0.5 and 0.3 ppm. The ^1H and ^{13}C NMR spectra are consistent with the C_s symmetry of all complexes in solution. The NH singlet signals of **2a/b**, **3a/b**, and **4a/b** appear in the high-field region between δ = 0.9 and −1.9 ppm, and their chemical shifts are solvent-dependent. They are always shifted to higher fields when compared with the NH singlets of free $HNPnPr_3$ (δ = 0.51 ppm) or $HNSPh_2$ (δ = 1.12 ppm), possibly indicating a decrease of NH acidity of the $HNPR_3$ and $HNSPh_2$ ligands. It should be noted that the NH protons exhibit slightly lower shifts in the [Ni(L)($^{si}S_3$)] complexes **2b**, **3b**, and **4b** than in the corresponding [Ni(L)($^HS_3$)] complexes **2a**, **3a**, and **4a**. This might indicate a slightly higher NH acidity of the [Ni(L)($^{si}S_3$)] complexes, caused by the electron-withdrawing effect of the $SiMe_3$ groups.

The NH shifts of the $HNPR_3$ and $HNSPh_2$ complexes allowed us to determine whether the N−P and N−S bonds in $HNPR_3$ and $HNSPh_2$ exhibit single- or double-bond character. Protons at sp^2-hybridized N atoms in HN=X compounds (X = NH, NO, CH_2, CR_2) such as diazene, nitroxyl, methyleneimines, or ketimines usually exhibit strong low-field shifts (δ = 10−20 ppm), both in the free and coordinated state.[12] The high-field NH shifts of the $HNPR_3$ and $HNSPh_2$ complexes **2**−**4** (δ = 0.9 to −1.9 ppm) thus rather resemble the NH shifts in hydrazine and ammonia complexes and indicate N−P and N−S single bonds with sp^3-hybridized N atoms. These considerations suggest the ylidic structures **I** and **II** for the $HNPR_3$ and $HNSPh_2$ ligands.

I

II

In agreement with these structures, the ^1H and ^{13}C NMR spectra of the $HNPR_3$ and $HNSPh_2$ complexes **2**−**4** do not show any splitting of the signals when the temperature was lowered to −80 °C, indicating a free rotation of the PR_3 and SPh_2 fragments around the N−P or N−S bonds, as well as of the NH groups around the Ni−N bonds.

X-ray Crystal Structure Determinations

The molecular structures of [Ni($NHPnPr_3$)($^{si}S_3$)] (**2b**), [Ni($NHPCy_3$)($^HS_3$)] (**3a**), [Ni($NHPCy_3$)($^{si}S_3$)] (**3b**), [Ni($NHSPh_2$)($^HS_3$)] (**4a**), and [Ni($PnPr_3$)($^HS_3$)] (**5a**) were determined by X-ray structure analysis. Figure 2 depicts the molecular structures and Table 1 lists selected distances and angles.

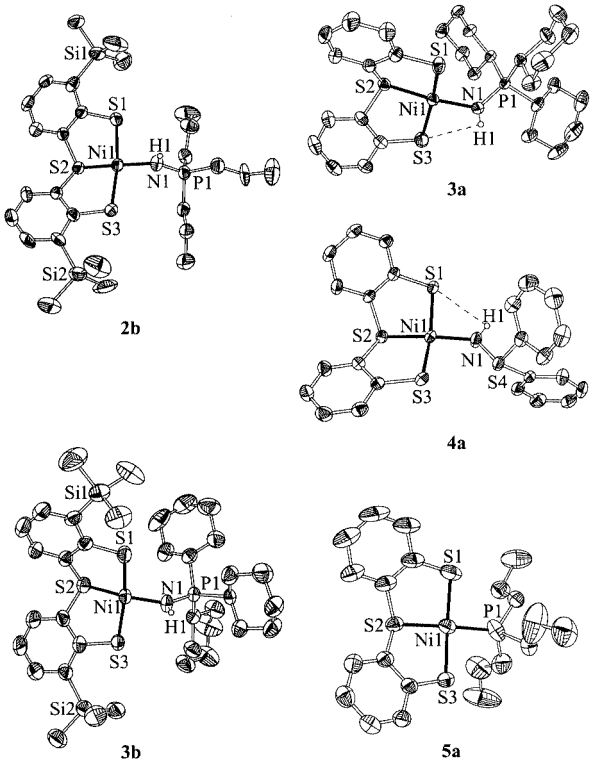

Figure 2. Thermal ellipsoid plots of [Ni($NHPnPr_3$)($^{si}S_3$)] (**2b**), [Ni($NHPCy_3$)($^HS_3$)] (**3a**), [Ni($NHPCy_3$)($^{si}S_3$)] (**3b**), [Ni($NHSPh_2$)($^HS_3$)] (**4a**), [Ni($PnPr_3$)($^HS_3$)] (**5a**) (50% probability ellipsoids; H atoms, except for *N*-bound ones, omitted)

The unit cells of all complexes contain discrete molecules whose four-coordinate nickel atoms exhibit a tetrahedrally distorted planar coordination, as evidenced by the non-linear S1−Ni1−S3 and S2−Ni1−L angles. This tetrahedral distortion can be traced back to the sp^3 hybridization of the central thioether sulfur atom in the $^RS_3$ ligands. It leads to a butterfly shape of the nickel−sulfur fragments, the characteristic topology of which also causes a very short Ni−S(thioether) distance of 208−213 pm, which is distinctly shorter than the Ni−S(thiolate) distances (216−220 pm).[7−9]

The Ni−N distances of **2b** [190.6(7) pm], **3a** [193.1(3) pm)], **3b** [192.3(4) pm], and **4a** [189.5(2) pm] are similar to that of [Ni($NHPnPr_3$)($^HS_3$)] (**2a**) reported previously,[8c] and indicate the presence of Ni−N single bonds. They are all considerably shorter than the Ni−N distances observed in

 © 2004 Wiley-VCH Verlag GmbH & Co. KGaA, Weinheim

Table 1. Selected bond lengths [pm] and angles [°] for $[Ni(NHPnPr_3)(^{si}S_3)]$ (**2b**), $[Ni(NHPCy_3)(^{H}S_3)]$ (**3a**), $[Ni(NHPCy_3)(^{si}S_3)]$ (**3b**), $[Ni(NHSPh_2)(^{H}S_3)]$ (**4a**), $[Ni(PnPr_3)(^{H}S_3)]$ (**5a**)

Compound	**2b**	**3a**	**3b**	**4a**	**5a**
Ni1−S1	216.8(3)	218.7(1)	217.0(2)	221.6(1)	216.3(1)
Ni1−S2	208.9(3)	210.7(1)	211.0(2)	211.7(1)	214.1(1)
Ni1−S3	219.9(3)	217.8(1)	217.0(2)	217.7(1)	217.4(1)
Ni1−N1	190.6(7)	193.1(3)	192.3(4)	189.5(2)	219.0(2)[a]
N1−P1	160.5(7)	160.9(3)	159.8(5)	159.5(2)[b]	
N1−H1	86	73(4)	86	80(3)	
S1−Ni1−S2	89.3(1)	89.41(3)	89.97(7)	87.46(3)	90.25(5)
S1−Ni1−S3	166.4(2)	162.02(4)	159.50(8)	160.27(3)	164.10(5)
S1−Ni1−N1	91.1(2)	96.60(9)	91.2(2)	91.55(8)	93.05(5)[a]
S2−Ni1−S3	87.2(1)	88.90(4)	89.83(7)	90.71(3)	88.74(4)
S2−Ni1−N1	172.1(2)	165.83(9)	168.5(2)	165.62(8)	170.77(4)[a]
S3−Ni1−N1	94.2(2)	89.23(8)	93.1(2)	94.95(8)	90.42(5)[a]
Ni1−N1−P1	128.3(4)	128.4(2)	127.3(3)	125.4(2)[b]	
Ni1−N1−H1	116	114(4)	116	122(2)	

[a] N1=P1. [b] P1=S4.

other diamagnetic four-coordinate Ni^{II} complexes (201−203 pm).[10a,13] The Ni−P distances of $[Ni(PnPr_3)(^{H}S_3)]$ (**5a**) [219.0(2) pm] and previously reported $[Ni(PR_3)(^{R}S_3)]$ complexes (R = Me, Ph or Cy) lie in the same range of 219−221 pm.[8,9] The N−P distances (160 pm) of **2b**, **3a**, and **3b** are identical within the limit of the 3σ criterion. Hydrogen bonds are observed for **2b**, **3a**, and **4a**. Figure 3 illustrates that N−H···N bridges lead to the formation of dimers of $[Ni(NHPnPr_3)(^{si}S_3)]$ (**2b**) which possesses crystallographically imposed inversion symmetry. The hydrogen bonds are concluded from the distances H1···N1a (246 pm) and N1···N1a [322(2) pm], which are shorter than the sum of the corresponding van der Waals radii (N = 155 pm; H = 120 pm).[14] With respect to the hydrogen bonds, complex **2b** contrasts with the analogous complex $[Ni(NHPnPr_3)(^{H}S_3)]$ (**2a**) which contains the parent ligand $^{H}S_3^{2-}$. Complex **2a** also dimerizes in the solid state, however through N−H···S(thiolate) bridges rather than N−H···N bridges.[8c]

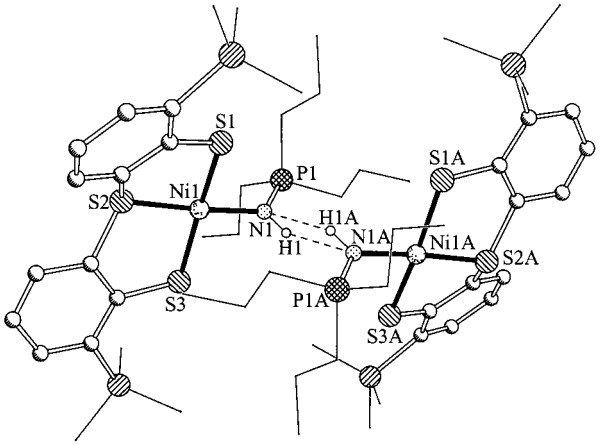

Figure 3. View of the N−H···N hydrogen bond dimers of $[Ni(NHPnPr_3)(^{si}S_3)]$ (**2b**) (H atoms, except for *N*-bound ones, omitted)

Intramolecular N−H···S(thiolate) bridges are found in $[Ni(NHPCy_3)(^{H}S_3)]$ (**3a**) and $[Ni(NHSPh_2)(^{H}S_3)]$ (**4a**). This can be deduced from the distances H1···S3 in **3a** [269(5) pm] and H1···S1 in **4a** [283(3) pm] as well as the distances N1···S3 in **3a** [289.1(3) pm] and N1···S1 in **4a** [295.5(2) pm], which are shorter than the sum of van der Waals radii (N = 155 pm; H = 120 pm; S = 180 pm).[14] No hydrogen bonds are found in $[Ni(NHPCy_3)(^{si}S_3)]$ (**3b**).

Reactions with Molecular Hydrogen

The heterolytic cleavage of H_2 into H^+ and H^- according to Equation (1b) and formation of HD from H_2 and D_2O, respectively, is one of the key reactions catalyzed by hydrogenases. Such a heterolytic H_2 cleavage and H_2/D^+ or D_2/H^+ exchange reaction could be proved to be catalyzed by the phosphorane imine and sulfimine complexes. The NH−R′ ligands (R′ = P*n*Pr$_3$, PCy$_3$, SPh$_2$) in these complexes are excellent probes for unambiguously establishing the H_2 or D_2 heterolysis because they have weakly acidic NH protons that exchange for D^+. Such an NH/D^+ exchange was similarly observed for the complexes **2a/b**, **3a/b**, and **4a/b** according to Equation (3).

$$[Ni(NH\text{-}R)(^{R}S_3)] + D^+ \longrightarrow [Ni(ND\text{-}R)(^{R}S_3)] + H^+ \quad (3)$$

A concentrated CD_2Cl_2/CH_2Cl_2 solution of the respective complex was treated with D_2O or CD_3OD, and the NH/D^+ exchange was monitored by $^1H/^2D$ NMR spectroscopy. In the course of 5−20 min, the NH signals of the starting complexes (between δ = 0.80 and −1.96 ppm) disappeared, while the ND signals of the resulting deuterated product complexes could be observed at the same region in the ^2D NMR spectrum. After completion of the reactions, the solvents were removed in vacuo; ν(ND) bands in the region of 2480−2420 cm^{-1} of the IR (KBr) spectra of the residues further corroborated the formation of the deuterated complexes.

The D_2/NH exchange was probed with complexes **2b**, **3a/3b**, and **4a/4b** and the formation of HD was monitored by ^1H NMR spectroscopy. In high-pressure NMR tubes, concentrated CD_2Cl_2 or [D$_8$]THF solutions of **2b**, **3a/3b**, and **4a/4b** were pressurized with D_2 (18 bar). ^1H NMR spectra recorded at regular time intervals showed the appearance of the 1:1:1 triplets of HD ($J_{H,D}$ = 42.5 Hz) formed according to Equation (4). The HD triplets in the region of δ = 4.2−4.8 ppm reached maximum intensity after 80 h in the case of **2b** and 120 h in the case of **4a**.

$$[Ni(NH\text{-}R)(^{R}S_3)] + D_2 \longrightarrow [Ni(ND\text{-}R)(^{R}S_3)] + HD \quad (4)$$

The reactions in Equations (3) and (4) thus prove that the $[Ni(NHR')(^{R}S_3)]$complexes **2b**, **3a**, **3b**, **4a**, and **4b** catalyze the heterolytic cleavage of D_2 and the exchange of molecular hydrogen with protons that ultimately result from protic solvents such as H_2O or CH_3OH. In a further experiment

 © 2004 Wiley-VCH Verlag GmbH & Co. KGaA, Weinheim

we therefore tried to combine these reactions. Initially, we chose the complex **3b** because it proved to have the highest stability towards methanolysis leading to $[Ni(^{si}S_3)]_3$ and free $NHPCy_3$. In a high-pressure NMR tube, a concentrated CD_2Cl_2 solution of **3b** and MeOH (50 μL) was pressurized with D_2 (18 bar) and the reaction was monitored by ^1H NMR spectroscopy. Unfortunately, due to the large signals of the MeOH protons the HD signal could not be identified. However, repeating this experiment by changing the solvent to $[D_8]THF$ and the proton source to H_2O yielded a favorable result. A ^1H NMR spectrum of **3b** recorded after 4 d showed the appearance of the 1:1:1 triplets ($J_{H,D}$ = 42.5 Hz) of HD in the region of δ = 4.2−4.8 ppm. Interestingly, the intensity of the triplet increases with an increase in reaction time and nearly triples in size after 15 d. The complexes **2a**, **2b**, **3a**, **4a**, and **4b** also exhibit the same behavior.

These positive results prompted us to extend our investigations to complexes Bu_4N[**9a**] and Bu_4N[**9b**] as, like in the active sites of [NiFe] hydrogenases, they exhibit all-sulfur nickel coordination. These complexes were investigated first in the form of their sodium salts Na[**9a**] and Na[**9b**]. In a high-pressure NMR tube, a concentrated solution of Na[**9a**] or Na[**9b**] in a $[D_8]THF/H_2O$ (50 μL) mixture was pressurized with D_2 (18 bar) and the reaction was monitored by ^1H NMR spectroscopy at various time intervals. Figure 4 depicts the ^1H NMR spectra of the HD region of Na[**9a**] in $[D_8]THF/H_2O$ with D_2 pressure at various time intervals. The ^1H NMR spectrum of Na[**9a**] recorded after 1 d does not show any new peaks (Figure 4a), while after 5 d it shows a small 1:1:1 triplet of HD ($J_{H,D}$ = 42.5 Hz) in the region between δ = 4.8 and 4.2 ppm (Figure 4b). The concomitant formation of HDO could not be identified due to the large H_2O signal. However, the intensity of the HD triplet increases with increasing reaction time (Figure 4b−d). The reaction was prolonged for 15 d and the intensity of the HD triplet was enhanced to three times that of the initial one, suggesting that the reaction is catalytic. Compound Na[**9b**] undergoes an identical reaction but is more active, giving rise to HD formation in a shorter reaction time (initial HD triplet showed up after 4 d). It is worth mentioning that the complexes remain intact even after 15 d of reaction time. Identical experiments performed without either the complexes Na[**9b**] and Na[**9b**] or H_2O did not show any HD signals. These results unambiguously prove that the reaction is catalytic and the heterolytic cleavage of D_2 must take place at the nickel center via a five-coordinated D_2 intermediate species.

These results suggest that the D_2 heterolysis is achieved through the concerted action of the Lewis-acidic nickel center and the Brönsted-basic thiol atoms upon η^2-D_2 ligands. The resulting acidic thiol deuteron exchanges with the H_2O proton to give HDO. The thiol proton and nickel deuteride ion combine to give HD. Release of HD in the consecutive step leaves $[Ni(L)(^RS_3)]$ intact, which can then add another molecule of D_2 to complete the reaction cycle (Scheme 2). It is worthwhile to note that Na[**9a**] and Na[**9b**] are the first completely characterized sulfur-only nickel

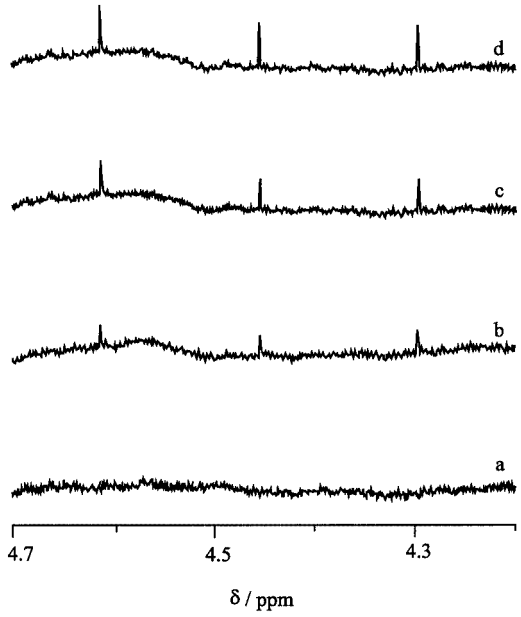

Figure 4. ^1H NMR spectra of the HD region of Na[Ni(S*t*Bu)($^HS_3$)] Na[**9a**] in $[D_8]THF/H_2O$ under D_2 (18 bar), recorded after: (a) 1, (b) 5, (c) 10, and (d) 15 d

complexes that model the [NiFe] hydrogenase catalyzed D_2/H^+ exchange reaction.

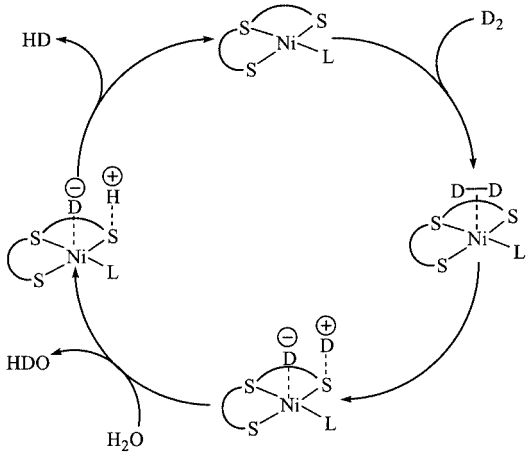

Scheme 2. Mechanism of $[Ni(L)(^RS_3)]$-catalyzed D_2/H_2O exchange reaction

Reactions with CO

Coordination of CO to tetrahedrally distorted planar $[NiS_4]$ sites is postulated as the primary key step in CO dehydrogenase reactions[15] and is possibly responsible for the inhibition of [NiFe] hydrogenases by CO.[16] Complexes exhibiting $[Ni(CO)(S_4)]$ cores, however, have never been identified or isolated. Recently, the five-coordinate carbonyl−Ni^I−chalcogenate complexes $[Ni(DAPA)(EPh)_2(CO)]^-$ {DAPA = 2,6-bis[1-(phenylimino)ethyl]pyridine; E = S or Se} and the first five-coordinate carbonyl−Ni^{II}−thiolate complex $[Ni(PS3^*)(CO)]^-$ [PS3* =

 © 2004 Wiley-VCH Verlag GmbH & Co. KGaA, Weinheim

tris(3-phenyl-2-thiophenyl)phosphane] were reported.[17] For this reason, the reaction of the nickel complexes [Ni(L)($^{R}S_3$)] (**2**−**9**) with CO was investigated. They all possess at least [NiS_3] cores, and it has been pointed out previously[8,9] that the characteristic tetrahedral distortion of [Ni(L)($^{R}S_3$)] complexes could be crucial for their capability to add a fifth ligand.

The distances and angles in the [Ni($^{R}S_3$)] cores of all the complexes investigated are almost identical, although the reactivity of the individual [Ni(L)($^{R}S_3$)] complexes towards CO proved to be extremely different, clearly showing the decisive influence of the coligands L. The influence of the R substituents of the $^{R}S_3$ ligands is evidenced by the fact that the [Ni(L)($^{si}S_3$)] complexes always reacted faster than their [Ni(L)($^{H}S_3$)] counterparts.

Because the S*t*Bu$^-$ complex [Ni(S*t*Bu)($^{H}S_3$)]$^-$ (**9a**) has an all-sulfur coordination sphere, it was investigated first in form of its sodium salt Na[**9a**]. Bubbling CO gas through a THF solution of Na[**9a**] for 3−5 min gave rise to a ν(CO) band in the IR spectrum at 2131 cm^{-1}. When this solution was stored under CO for 24 h, a second ν(CO) band appeared at 2040 cm^{-1}. These bands were assigned to [Ni(CO)(S*t*Bu)($^{H}S_3$)]$^-$ (2131 cm^{-1}) and [$Ni(CO)_4$] (2040 cm^{-1}) which form according to Equation (5).

$$[Ni(S\mathit{t}Bu)(^{H}S_3)]^- + CO \xrightarrow{5\ min} [Ni(CO)(S\mathit{t}Bu)(^{H}S_3)]^- \xrightarrow[24\ h]{+\ exc.\ CO} \mathit{t}BuS\text{–}S\mathit{t}Bu + [^{H}S_3]_x + [Ni(CO)_4] \quad (5)$$

The reduction of Ni^{II} to Ni^0 is possibly initiated by the reductive elimination of the (labile) S*t*Bu$^-$ ligand. This is suggested by the observation that the substitutionally inert phosphane complex [Ni(PCy_3)($^{si}S_3$)] does not yield [$Ni(CO)_4$] when treated with CO (vide infra).

The ν(CO) assignment was corroborated by the following experiments. Purging the solutions with N_2 for 10 min led to complete disappearance of the ν(CO) bands. This indicated that the first step yielding [Ni(CO)(S*t*Bu)($^{H}S_3$)]$^-$ is reversible. Carrying out the experiment [according to Equation (5)] with ^{13}CO gave rise to ν(CO) bands at 2085 cm^{-1} ([Ni(^{13}CO)(S*t*Bu)($^{H}S_3$)]$^-$) and 1995 cm^{-1} ([Ni($^{13}CO)_4$]). The isotopic shifts of 45 cm^{-1} agree with theoretical expectations. Formation of the five-coordinate intermediate [Ni(CO)(S*t*Bu)($^{H}S_3$)]$^-$ was further corroborated by monitoring the reaction by ^{13}C NMR spectroscopy. The ^{13}C NMR spectrum shows that treatment of a [D_8]THF solution of Na[**9a**] with ^{13}CO (5 bar) in a medium-pressure NMR tube gave rise to ^{13}C NMR signals at δ = 198.5, 192.1, and 184.7 ppm, which could be assigned to [Ni(^{13}CO)(S*t*Bu)($^{H}S_3$)]$^-$, [Ni($^{13}CO)_4$], and free ^{13}CO, respectively. This assignment was checked by recording the ^{13}C NMR spectra of ^{13}CO and [$Ni(CO)_4$] in [D_8]THF. In summary, these results suggest that nickel thiolate complexes with a tetrahedrally distorted planar [NiS_4] core can reversibly coordinate CO, but afford [$Ni(CO)_4$] when treated with an excess of CO for longer periods of time.

In the next step, the influence of the phosphane coligands upon CO coordination was probed with [Ni(PCy_3)($^{si}S_3$)](**6b**). When CO was bubbled through a THF solution of **6b** according to Equation (6), a ν(CO) band appeared at 2135 cm^{-1} in the IR spectrum. Purging the solution with a stream of N_2 led to disappearance of the ν(CO) band and **6b** was regained. This result suggests that [Ni(PR_3)($^{R}S_3$)] complexes can also reversibly add CO. In addition, the ν(CO) frequency of [Ni(CO)(PCy_3)($^{si}S_3$)] at 2135 cm^{-1} is similar to that of [Ni(CO)(S*t*Bu)($^{H}S_3$)]$^-$ (2131 cm^{-1}), indicating that the electron density at the nickel atom is a little lower in the neutral phosphane than in the anionic S*t*Bu$^-$ complex. However, the relatively high wavenumbers indicate a weak binding of the CO ligands, rationalizing their reversible coordination.

$$[Ni(PCy_3)(^{si}S_3)] \underset{+\ N_2,\ -\ CO}{\overset{+\ CO}{\rightleftharpoons}} [Ni(CO)(PCy_3)(^{si}S_3)] \quad (6)$$

The coligands S*t*Bu$^-$ or PCy_3 in the [Ni(L)($^{R}S_3$)] complexes [Ni(S*t*Bu)($^{H}S_3$)]$^-$ (**9a**) and [Ni(PCy_3)($^{Si}S_3$)] (**6b**) do not react with CO, either in the free or complexed state, whereas the nitrogen-containing ligands $NHPR_3$, $NHSPh_2$, and N_3^- show a distinctly different behavior. In the free state they, too, do not react with CO, however, when functioning as ligands in the [Ni(L)($^{R}S_3$)] complexes **2**−**4** and **8b**, they undergo rapid reactions with equimolar amounts of CO. This demonstrates that the reactions are mediated by the [Ni($^{R}S_3$)] fragments, and indicates that both CO and nitrogenous ligands can be activated.

From the mechanistic point of view, the reaction between Et_4N[Ni(N_3)($^{si}S_3$)] (**8b**) and CO can be rationalized best. In THF solution, complex **8b** is thermally stable and resistant to UV photolysis (150 W Hg lamp) over extended periods of time (3 d). When treated with equimolar amounts of CO gas in the dark, however, it rapidly transforms into the NCO complex Et_4N[Ni(NCO)($^{si}S_3$)] (**10b**) and N_2, and complex **10b** could be isolated in nearly quantitative yield (92%). Monitoring the reaction by IR spectroscopy demonstrated that the ν(N_3) band of **8b** at 2037 cm^{-1} continuously decreases in intensity while the ν(NCO) band of **10b** at 2227 cm^{-1} increases.

The analogous reaction of the $^{H}S_3$ complex Bu_4N-[Ni(N_3)($^{H}S_3$)] (Bu_4N[**8a**]) with CO afforded Bu_4N-[Ni(NCO)($^{H}S_3$)][7] and enabled us to detect a short-lived [Ni(CO)(N_3)($^{H}S_3$)]$^-$ intermediate, with a ν(CO) band at 2129 cm^{-1} by IR spectroscopy. Such an intermediate could not be found in the reaction between Et_4N[**8b**] and CO, probably owing to the greater reactivity of **8b** and its intermediates. However, the close analogy between Bu_4N[**8a**] and Et_4N[**8b**] suggests identical mechanisms for their reaction with CO [Equation (7)].

Coordination of CO to the [Ni(N_3)($^{R}S_3$)]$^-$ anion leads to activation of CO and N_3^-, release of N_2 and formation of the NCO complex. Related mechanisms have previously

 © 2004 Wiley-VCH Verlag GmbH & Co. KGaA, Weinheim

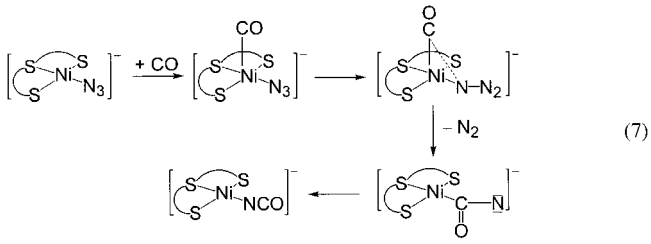

(7)

been suggested for four-coordinate azido(phosphane) complexes of Pd^{II}, Pt^{II}, Rh^{I} and Ir^{I}.[18] The phosphorane imine complexes **2a/2b**, **3a/3b**, and the sulfimine complexes **4a/4b** also react quickly with CO under standard conditions (1 bar, 20 °C). However, the mechanisms of the reactions are less obvious. When a stream of CO was bubbled through CH_2Cl_2 solutions of **2a/2b**, **3a/3b**, or **4a/4b**, the parent complexes $[Ni(^{R}S_3)]_3$ (**1a** or **1b**) formed and could be isolated in high yields. When the CH_2Cl_2 solutions were each treated with 1 equiv. of CO gas, the reactions proceeded more slowly, and monitoring of the reactions by IR and NMR spectroscopy, and mass spectrometry, yielded hints as to the nature of the intermediates. Experiments with the respective $[Ni(L)(^{H}S_3)]$ and $[Ni(L)(^{si}S_3)]$ complexes complemented each other. For example, after addition of 1 equiv. of CO, the IR spectrum of the CH_2Cl_2 solution of the phosphorane imine complex $[Ni(NHP\textit{n}Pr_3)(^{H}S_3)]$ (**2a**) shows a weak band at 2146 cm^{-1}. This band disappeared in the course of 25 h, and a new band at 2227 cm^{-1} developed simultaneously; its intensity increased over 45 h and then decreased again, while $[Ni(^{H}S_3)]_3$ (**1a**) started precipitating from the solution (Figure 5). The weak band at 2040 cm^{-1} corresponds to the side product $[Ni(CO)_4]$ that forms and disappears during the reaction. The same IR spectroscopic behavior was found for CH_2Cl_2 solutions of $[Ni(NHP\textit{n}Pr_3)(^{si}S_3)]$ (**2b**).

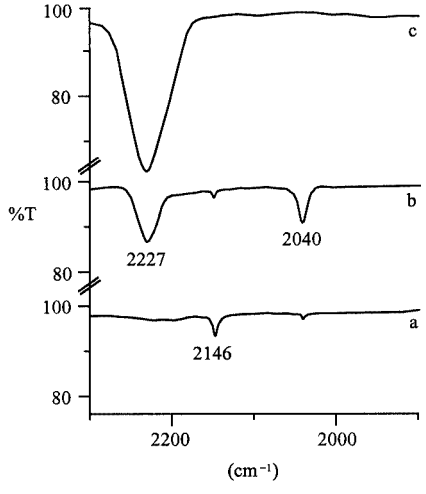

Figure 5. IR spectroscopic monitoring of the reaction between equimolar amounts of $[Ni(NHP\textit{n}Pr_3)(^{H}S_3)]$ (**2a**) and CO in CH_2Cl_2 solution; the spectra were recorded after (a) 3, (b) 20, and (c) 48 h

The ^1H NMR spectrum of **2a** in CD_2Cl_2 shows the NH signal at $\delta = -1.82$ ppm. After injecting an equimolar amount of CO, this NH signal gradually broadens and disappears and a new doublet appears at $\delta = 4.85$ ppm ($J_{P,H}$ = 550 Hz). Similarly, in the ^{31}P NMR spectrum of **2a**, the signal at $\delta = 50.8$ ppm disappears gradually in the presence of CO and a new peak appears at $\delta = 55.1$ ppm. This new peak, in turn, vanishes over the course of 30 h to give a new low-intensity doublet at $\delta = 34.2$ ppm ($J_{P,H}$ = 527 Hz). All ^1H and ^{31}P NMR signals disappear when $[Ni(^{H}S_3)]_3$ (**1a**) precipitates from the solution. These findings can be interpreted as follows: the initial step is the coordination of CO to give a five-coordinate $[Ni(CO)(NHP\textit{n}Pr_3)(^{H}S_3)]$ intermediate showing a ν(CO) band at 2146 cm^{-1} (^{31}P NMR: $\delta = 55.1$ ppm). As above, the high frequency of this band indicates that the CO is only weakly bound. Subsequently, the intramolecular nucleophilic addition of the N atom of $NHP\textit{n}Pr_3$ to CO is followed by the removal of $P\textit{n}Pr_3$ to give an unstable acylimide species. Then, the deprotonation of the N–H bond by the free $P\textit{n}Pr_3$ gives $[HP\textit{n}Pr_3]^+$ (doublet in the ^1H and ^{31}P NMR spectra) and the acyl azide complexes. A similar reactivity has already been reported in coordinated phosphanylamine complexes of Ni^{II} and free PMe_3 to give $[HPMe_3]^+$.[10a] These acyl azides can rearrange to give $[HP\textit{n}Pr_3][Ni(NCO)(^{H}S_3)]$ [ν(NCO) = 2227 cm^{-1}] according to Equation (8). Unlike $Et_4N[Ni(NCO)(^{si}S_3)]$ (**10b**), $[HP\textit{n}Pr_3][Ni(NCO)(^{H}S_3)]$ is unstable and undergoes further reactions to give **1a** as the final product. Monitoring the reactions of the $^{si}S_3$ complex **2b** by ^1H and ^{31}P NMR spectroscopy only showed the replacement of the signals of **2b** by those of **1b**, but did not allow us to draw further conclusions. All attempts to isolate the intermediate species were unsuccessful, even at −78 °C.

After addition of 1 equiv. of CO, the IR spectrum of the CH_2Cl_2 solution of the sulfimine complex $[Ni(NHSPh_2)(^{H}S_3)]$ (**4a**) shows a weak band at 2148 cm^{-1}. This band disappeared over the course of 1 h, and simultaneously a new band appeared at 2185 cm^{-1}, whose intensity increased over 5 h and then decreased again, while $[Ni(^{H}S_3)]_3$ (**1a**) started precipitating from the solution. The same IR spectroscopic behavior was found for CH_2Cl_2 solutions of $[Ni(NHSPh_2)(^{si}S_3)]$ (**4b**). The $SiMe_3$ substituents of **4b** were also used as a spectroscopic probe. The ^1H NMR spectra of the reactions in CD_2Cl_2 show that the $SiMe_3$ singlet of **4b** at $\delta = 0.36$ ppm broadens slightly and is replaced by the two singlets of $[Ni(^{si}S_3)]_3$ (**1b**) at $\delta = 0.55$ and 0.08 ppm.

These findings are interpreted in the following way. The primary step is again the coordination of CO to give a five-coordinate $[Ni(CO)(NHSPh_2)(^{R}S_3)]$ intermediate showing a ν(CO) band at 2148 cm^{-1}. Subsequent reaction between CO and the $HNSPh_2$ ligands leads to deoxygenation of CO resulting in $OSPh_2$ and coordinated HC=N or HN=C ligands, which give rise to the band at 2185 cm^{-1}. Transition metal complexes with HCN or HNC ligands show ν(CN) bands in the region of 2200–2100 cm^{-1}.[19] Subsequent decoordination of the HCN ligands results in the formation of $[Ni(^{R}S_3)]_3$ [Equation (9)].

 © 2004 Wiley-VCH Verlag GmbH & Co. KGaA, Weinheim

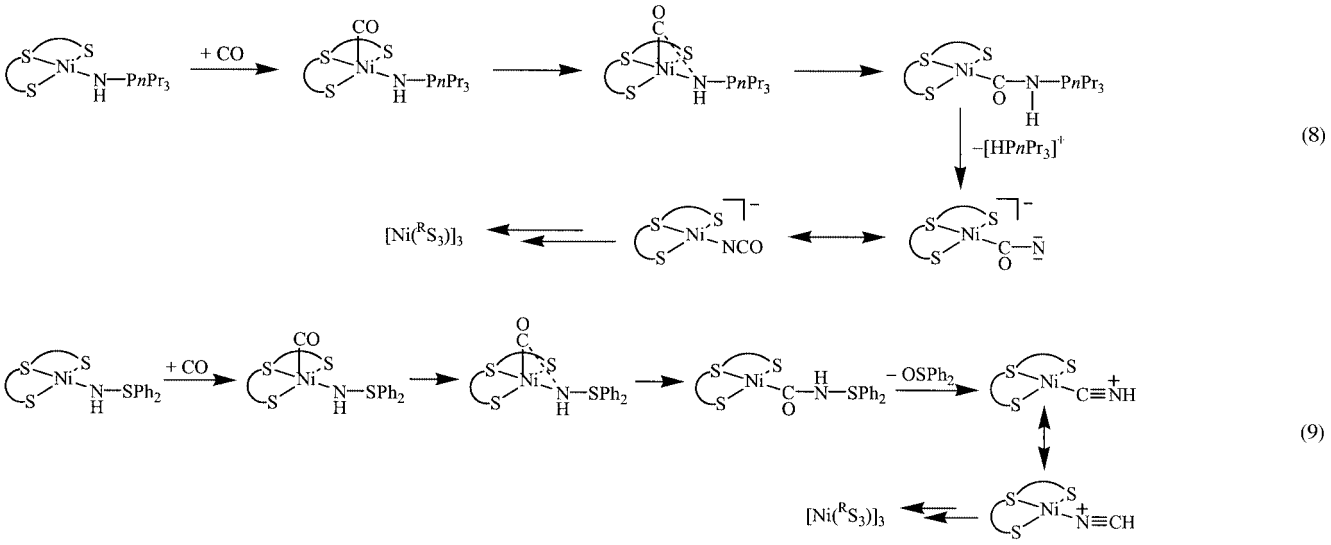

(8)

(9)

The mass spectra of the reaction solutions recorded when the band at 2185 cm^{-1} had attained maximum intensity support this interpretation. These spectra exhibit peaks at $m/z = 202$ assignable to $OSPh_2$ and at 335 (**4a**) or 479 (**4b**), which are compatible with the formation of $[Ni(HCN)(^{R}S_3)]$ complexes.

Table 2 summarizes the ν(CO) frequencies of the CO adducts initially formed and demonstrates that complexes with $^{H}S_3$ and $^{Si}S_3$ ligands show identical ν(CO) frequencies. Therefore, the sometimes remarkably different reaction rates of $^{H}S_3$ and $^{si}S_3$ complexes might be caused by differences in solubility rather than by changes in the electronic properties. Anionic complexes give rise to lower ν(CO) frequencies than neutral complexes. This trend of ν(CO) frequencies is well known from classical carbonylmetal complexes, and it strongly suggests that structurally similar five-coordinate $[Ni(CO)(L)(^{R}S_3)]$ species form in all cases. These five-coordinate species can reversibly dissociate CO or undergo rapid consecutive reactions if L is a nitrogenous species having lone-pairs at the N donor such as azide or the ylidic $HNPR_3$ and $HNSPh_2$ ligands. The subsequent reactions lead to conversion of CO and the nitrogenous ligand. The final products, which could be isolated, depend on the nitrogenous ligands. If they release inert species such as N_2 in the case of azide, the resulting NCO^- complexes $[Ni(NCO)(^{R}S_3)]^-$ can be isolated in good yields. In the case of the phosphorane imine or sulfimine complexes, an analogous cleavage of N−P or N−S bonds yields species that are still highly reactive and go on reacting until the stable trinuclear $[Ni(^{R}S_3)]_3$ complexes form.

It should be noted that the ν(CO) frequencies of all five-coordinate intermediates (Table 2) are relatively high and, in some cases, even slightly higher than that of free CO in the gas phase (2143 cm^{-1}). Additional measurements corroborated that these bands do not result from dissolved CO.

The CO adducts of the phosphorane imine and sulfimine complexes thus belong to the class of "non-classical" carbonylmetal complexes which can exhibit ν(CO) frequencies of up to 2280 cm^{-1}.[20] The high ν(CO) frequencies of these complexes are rationalized by a subtle interplay of σ-donor, π-acceptor and semipolar contributions in the M−CO bonds.[21] In accordance with this rationalization, the results obtained here show that binding CO to $[Ni(L)(^{R}S_3)]$ complexes not only enhances the polarity of the CO bond but also increases the susceptibility of CO towards attack by nucleophiles. This may be a reason why coordination of CO to the $[NiS_4]$ core of CO dehydrogenase centers can enable the CO/CO_2 conversion according to Equation (2) (vide infra).

Table 2. ν(CO) frequencies of the primary five-coordinate species $[Ni(CO)(L)(^{R}S_3)]$ resulting from $[Ni(L)(^{R}S_3)]$ and CO (1 bar) at 20 °C

Complex	ν(CO) [cm^{-1}]	Reaction type
$Bu_4N[Ni(N_3)(^{H}S_3)]$ (Bu_4N[**8a**])[a]	2129[b]	irr.
$Et_4N[Ni(N_3)(^{si}S_3)]$ (Et_4N[**8b**])	–	–
Na[Ni(S*t*Bu)($^{H}S_3$)] (Na[**9a**])	2131[b]	rev.
$Ni(PCy_3)(^{si}S_3)]$ (**6b**)	2135[b]	rev.
$Ni(NHPnPr_3)(^{H}S_3)]$ (**2a**)	2146[c]	irr.
$Ni(NHPnPr_3)(^{si}S_3)]$ (**2b**)	2146[c]	irr.
$Ni(NHPCy_3)(^{H}S_3)]$ (**3a**)	2146[c]	irr.
$Ni(NHPCy_3)(^{si}S_3)]$ (**3b**)	2146[c]	irr.
$Ni(NHSPh_2)(^{H}S_3)]$ (**4a**)	2148[c]	irr.
$Ni(NHSPh_2)(^{si}S_3)]$ (**4b**)	2148[c]	irr.

[a] Ref.[7] [b] In THF. [c] In CH_2Cl_2.

Conclusion

In the quest for sulfur−nickel complexes that enable us to model the reactivity features and key intermediates of [NiFe] hydrogenases and CO dehydrogenases, $[Ni(L)(^{R}S_3)]$ complexes were synthesized, completely characterized, and investigated with regard to their reactivity towards H_2 and CO. All $[Ni(L)(^{R}S_3)]$ complexes exhibit sulfur-dominated and tetrahedrally distorted square-planar coordination

 © 2004 Wiley-VCH Verlag GmbH & Co. KGaA, Weinheim

spheres. Complexes **4a** and **4b** are rare examples of sulfimine complexes and are the first sulfimine complexes with only sulfur as ancillary coligands. Introduction of the $^{si}S_3$ ligand enabled us to overcome the solubility problems frequently encountered with nickel complexes of the $^{H}S_3$ parent ligand.

It has been demonstrated that the phosphorane imine and sulfimine complexes **2**−**4** possess weakly acidic NH protons and catalyze D_2/NH exchange reactions through heterolysis of D_2. The D_2/H^+ exchange reaction between D_2 and protons from H_2O is also catalyzed by complexes **2**−**4** and **9**. These reactions unambiguously prove that the D_2/H^+ exchange is catalytic in nature. The D_2 heterolysis most likely proceeds through attack of the Lewis-acidic nickel and Brönsted-basic sulfur atoms at η^2-D_2 ligands. It is worthwhile to note that **9a** and **9b** are the first completely characterized sulfur-only nickel complexes that enable us to model the [NiFe] hydrogenase catalyzed D_2 heterolysis and D_2/H^+ exchange reactions.

Coordination of CO to four-coordinate nickel centers in sulfur coordination spheres is assumed to be the decisive step in the activation of CO catalyzed by CO dehydrogenases. Evidence for labile five-coordinate [Ni(CO)(L)($^{R}S_3$)] has been found in the reactions of CO with [Ni(L)($^{R}S_3$)] complexes containing neutral and anionic ligands L. The CO adducts of complexes with nitrogenous ligands L such as N_3^-, $NHPR_3$, or $NHSPh_2$ showed rapid consecutive reactions demonstrating the activation of CO and ligands L. In extrapolation of these findings it can be hypothesized that simultaneous coordination of CO and H_2O to [Ni($^{R}S_3$)] fragments possibly enables the biological CO dehydrogenase reaction.

Experimental Section

General Methods: Unless noted otherwise, all reactions and manipulations were carried out under nitrogen at room temperature using standard Schlenk techniques. Reaction solutions were stirred continuously. Solvents were freshly dried and distilled before use. As far as possible, reactions were monitored by IR or NMR spectroscopy. Physical measurements were carried out with the following instruments: IR (KBr discs or CaF_2 cuvettes, solvent bands were compensated for): Perkin−Elmer 983, 1620 FT-IR and 16PC FT-IR. NMR: Jeol JMM-GX 270, Jeol JMM-EX 270, and Lambda LA 400 with the residual protio-solvent signal used as an internal reference. Chemical shifts are quoted in the δ scale (downfield shifts are positive) relative to tetramethylsilane (^{1}H, ^{13}C{^{1}H} NMR) or 85% H_3PO_4 (^{31}P{^{1}H} NMR). MS: Jeol MSTATION 700 spectrometer. Elemental analysis: Carlo Erba EA 1106 or 1108 analyzer. Me_3SiCl, $HNSPh_2{\cdot}H_2O$, Et_4NCl, and Bu_4NCl were purchased from either Aldrich or Fluka. HNP*n*Pr_3, $Me_3SiNPCy_3$,[22] [Ni($^{H}S_3$)]$_3$ (**1a**), [Ni(NHP*n*Pr_3)($^{H}S_3$)] (**2a**), [Ni(PCy_3)($^{H}S_3$)] (**6a**), Bu_4N[Ni(Cl)($^{H}S_3$)] (Bu_4N[**7a**]), and Bu_4N[Ni(N_3)($^{H}S_3$)] (Bu_4N[**8b**]) were prepared as described in the literature.[8] The syntheses of [Ni($^{si}S_3$)]$_3$ (**1b**), Et_4N[Ni(N_3)($^{si}S_3$)] (Et_4N[**8b**]), [Ni(P*n*Pr_3)($^{si}S_3$)] (**5b**), [Ni(PCy_3)($^{si}S_3$)] (**6b**), and Bu_4N[Ni(Cl)($^{si}S_3$)] (Bu_4N[**7b**]) were described in our previous paper.[9]

[Ni(NHP*n*Pr_3)($^{si}S_3$)] (2b): HNP*n*Pr_3 (0.52 mL, 2.35 mmol) was added to a solution of [Ni($^{si}S_3$)]$_3$ (**1b**; 800 mg, 0.59 mmol) in THF (10 mL), and the color changed from black-brown to purple-red in the course of about 6 h. The solution was filtered after 15 h, the purple-red filtrate was reduced in volume to 3 mL and layered with CH_3CN (20 mL). Pink crystals precipitated at −25 °C which were separated after 10 d, washed with cold CH_3CN and dried in vacuo. Yield: 765 mg (69%). $C_{27}H_{46}NNiPS_3Si_2$ (626.71): calcd. C 51.75, H 7.40, N 2.23, S 15.35; found C 51.88, H 7.53, N 2.10, S 15.21. IR (KBr): $\tilde{\nu}$ = 3298 [ν(NH)], 995 [ν(NP)] cm^{-1}. ^{1}H NMR (269.7 MHz, [D$_8$]THF): δ = 7.57 (d, $J_{H,H}$ = 7.9 Hz, 2 H, C_6H_3), 7.19 (d, $J_{H,H}$ = 6.8 Hz, 2 H, C_6H_3), 6.84 (t, $J_{H,H}$ = 7.6 Hz, 2 H, C_6H_3), 2.04 (m, 6 H, PCH_2), 1.73 (m, 6 H, PCH_2CH_2), 1.08 (t, $J_{H,H}$ = 6.9 Hz, 9 H, $PCH_2CH_2CH_3$), 0.38 (s, 18 H, $SiMe_3$), −1.06 (s, 1 H, NH) ppm. ^{13}C NMR (67.8 MHz, [D$_8$]THF): δ = 159.9, 139.6, 134.8, 134.3, 129.0, 121.3 (C_6H_3), 29.7 (d, $^1J_{P,C}$ = 62.9 Hz), 15.7 (d, $J_{P,C}$ = 3.3 Hz), 15.5 (d, $J_{P,C}$ = 16.1 Hz, P*n*Pr_3), −0.7 ($SiMe_3$) ppm. ^{31}P NMR (161.8 MHz, [D$_8$]THF): δ = 50.3 (P*n*Pr_3) ppm. MS (FD, THF): *m*/*z* = 626 [Ni(NHP*n*Pr_3)($^{si}S_3$)]$^+$.

[Ni(NHPCy_3)($^{H}S_3$)] (3a): A solution of $Me_3SiNPCy_3$ (825 mg, 2.24 mmol) in THF (5 mL) and MeOH (1 mL) was added to a black-brown suspension of [Ni($^{H}S_3$)]$_3$ (**1a**; 525 mg, 0.57 mmol) in THF (15 mL). A purple-red solution formed which was concentrated to dryness after 15 h. The purple-red residue was redissolved in THF (10 mL), and traces of undissolved materials were removed by filtration. The filtrate was reduced in volume to 3 mL, layered with CH_3CN (30 mL) and stored at −25 °C. Pink microcrystals precipitated which were separated after 3 days, washed with cold CH_3CN and Et_2O, and dried in vacuo. Yield: 815 mg (79%). $C_{30}H_{42}NNiPS_3$ (602.54): calcd. C 59.80, H 7.03, N 2.32, S 15.96; found C 59.82, H 7.19, N 2.35, S 15.58. IR (KBr): $\tilde{\nu}$ = 3364 [ν(NH)], 978 [ν(NP)] cm^{-1}. ^{1}H NMR (269.7 MHz, [D$_8$]THF): δ = 7.58 (d, $J_{H,H}$ = 7.6 Hz, 2 H, C_6H_4), 7.20 (d, $J_{H,H}$ = 7.9 Hz, 2 H, C_6H_4), 6.97 (t, $J_{H,H}$ = 7.1 Hz, 2 H, C_6H_4), 6.83 (t, $J_{H,H}$ = 7.1 Hz, 2 H, C_6H_4), 2.23−1.32 (m, 33 H, PCy_3), −1.88 (s, 1 H, NH) ppm. ^{13}C NMR (67.8 MHz, [D$_8$]THF): δ = 154.2, 134.2, 129.6, 128.5, 128.0, 121.9 (C_6H_4), 35.3 (d, $^1J_{P,C}$ = 55.3 Hz), 27.8, 27.5 (d, $^3J_{P,C}$ = 15 Hz), 26.9 (PCy_3) ppm. ^{31}P NMR (161.8 MHz, [D$_8$]THF): δ = 59.2 (PCy_3) ppm. MS (FD, THF): *m*/*z* = 602 [Ni(NHPCy_3)($^{H}S_3$)]$^+$.

[Ni(NHPCy_3)($^{si}S_3$)] (3b): A solution of $Me_3SiNPCy_3$ (272 mg, 0.74 mmol) in THF (5 mL) and MeOH (1 mL) was added to a solution of [Ni($^{si}S_3$)]$_3$ (**1b**; 300 mg, 0.22 mmol) in THF (15 mL), and the color changed from black-brown to purple-red in the course of about 3 h. After 15 h, the solution was concentrated to dryness to give a purple-red residue, which was redissolved in THF (10 mL). Undissolved material was removed by filtration. The filtrate was reduced in volume to 3 mL, layered with CH_3CN (30 mL) and stored at −25 °C. Pink microcrystals precipitated which were separated after 4 d, washed with cold CH_3CN and Et_2O, and dried in vacuo. Yield: 412 mg (83%). $C_{36}H_{58}NNiPS_3Si_2$ (746.90): calcd. C 57.89, H 7.83, N 1.87, S 12.88; found C 57.47, H 7.44, N 1.80, S 12.63. IR (KBr): $\tilde{\nu}$ = 3364 [ν(NH)], 985 [ν(NP)] cm^{-1}. ^{1}H NMR (269.7 MHz, [D$_8$]THF): δ = 7.56 (d, $J_{H,H}$ = 7.9 Hz, 2 H, C_6H_3), 7.18 (d, $J_{H,H}$ = 7.1 Hz, 2 H, C_6H_3), 6.82 (t, $J_{H,H}$ = 7.5 Hz, 2 H, C_6H_3), 2.35−1.30 (m, 33 H, PCy_3), 0.38 (s, 18 H, $SiMe_3$), −1.62 (s, 1 H, NH) ppm. ^{13}C NMR (67.8 MHz, $CDCl_3$): δ = 158.0, 139.5, 134.2, 133.2, 127.9, 126.8 (C_6H_3), 34.3 (d, $^1J_{P,C}$ = 49.5 Hz), 27.0 (d, $^2J_{P,C}$ = 6.8 Hz), 26.7 (d, $^3J_{P,C}$ = 2.7 Hz), 25.9 (PCy_3), −0.5 ($SiMe_3$) ppm. ^{31}P NMR (161.8 MHz, [D$_8$]THF): δ = 54.5 (PCy_3) ppm. MS (FD, THF): *m*/*z* = 746 [Ni(NHPCy_3)($^{si}S_3$)]$^+$.

[Ni(NHSPh_2)($^{H}S_3$)] (4a): $HNSPh_2{\cdot}H_2O$ (425 mg, 1.93 mmol) was added to a black-brown suspension of **1a** (500 mg, 0.54 mmol) in THF (10 mL). The resulting suspension was stirred for 12 h, in the course of which it became red-brown. The solution was filtered,

 © 2004 Wiley-VCH Verlag GmbH & Co. KGaA, Weinheim

the filtrate reduced in volume to about 3 mL and layered with Et_2O (20 mL). Dark red crystals precipitated at −25 °C, which were separated after 7 d, washed with Et_2O and dried in vacuo. Yield: 680 mg (82%). $C_{24}H_{19}NNiS_4$ (508.38): calcd. C 56.70, H 3.77, N 2.75, S 25.23; found C 56.82, H 3.91, N 2.71, S 25.07. IR (KBr): $\tilde{\nu}$ = 3202 [ν(NH)], 924 [ν(NS)] cm^{-1}. ^1H NMR (269.7 MHz, [D$_8$]THF): δ = 7.75−7.40 (m, 12 H, C_6H_4, SPh_2), 7.21 (d, $J_{H,H}$ = 7.5 Hz, 2 H, C_6H_4), 7.00 (t, $J_{H,H}$ = 6.5 Hz, 2 H, C_6H_4), 6.85 (t, $J_{H,H}$ = 6.4 Hz, 2 H, C_6H_4), 0.89 (s, 1 H, NH) ppm. ^{13}C NMR (67.8 MHz, [D$_8$]THF): δ = 153.0, 134.6, 132.4, 131.8, 130.4, 130.0, 128.9, 128.4, 127.8, 122.4 (C_6H_4, SPh_2) ppm. MS (FD, THF): *m*/*z* = 508 [Ni(NHSPh$_2$)(^{H}S$_3$)]$^+$.

[Ni(NHSPh$_2$)(^{si}S$_3$)] (4b): A solution of $HNSPh_2 \cdot H_2O$ (128 mg, 0.58 mmol) in THF (5 mL) was added to a solution of **1b** (250 mg, 0.18 mmol) in THF (10 mL) and the color changed from black-brown to brown-red in the course of about 6 h. The solution was filtered after 12 h, reduced in volume to 3 mL and layered with pentane (20 mL). Dark-red microcrystals precipitated at −25 °C which were separated after 7 d, washed with pentane and dried in vacuo. Yield: 282 mg (78%). $C_{30}H_{35}NNiS_4Si_2$ (652.75): calcd. C 55.20, H 5.40, N 2.15, S 19.65; found C 55.91, H 5.90, N 2.28, S 19.02. IR (KBr): $\tilde{\nu}$ = 3210 [ν(NH)], 916 [ν(NS)] cm^{-1}. ^1H NMR (269.7 MHz, [D$_8$]THF): δ = 7.75−7.40 (m, 12 H, C_6H_3, SPh_2), 7.19 (d, $J_{H,H}$ = 6.1 Hz, 2 H, C_6H_3), 6.84 (t, $J_{H,H}$ = 6.8 Hz, 2 H, C_6H_3), 0.83 (s, 1 H, NH), 0.36 (s, 18 H, $SiMe_3$) ppm. ^{13}C NMR (67.8 MHz, [D$_8$]THF): δ = 159.2, 139.8, 134.9, 134.8, 132.3, 131.8, 130.4, 129.3, 128.4, 121.6 (C_6H_3, SPh_2), −0.4 ($SiMe_3$) ppm. MS(FD, THF): *m*/*z* = 653 [Ni(NHSPh$_2$)(^{si}S$_3$)]$^+$.

[Ni(P*n*Pr$_3$)(^{H}S$_3$)] (5a): P*n*Pr$_3$ (0.3 mL, 1.49 mmol) was added to a black-brown suspension of **1a** (445 mg, 0.48 mmol) in THF (10 mL). In the course of about 10 min, a red-yellow solution formed which was filtered after 1 h. The filtrate was reduced in volume to 2 mL, layered with hexane (20 mL) and stored at −25 °C. Dark red crystals precipitated which were separated after 2 d, washed with hexane and dried in vacuo. Yield: 645 mg (95%). $C_{21}H_{29}NiPS_3$ (467.33): calcd. C 53.97, H 6.26, S 20.58; found C 54.06, H 6.38, S 20.37. ^1H NMR (269.7 MHz, $CDCl_3$): δ = 7.66 (dd, $J_{H,H}$ = 1.2, 8.1 Hz, 2 H, C_6H_4), 7.39 (d, $J_{H,H}$ = 1.3, 7.9 Hz, 2 H, C_6H_4), 7.09 (dt, $J_{H,H}$ = 1.3, 7.9 Hz, 2 H, C_6H_4), 6.98 (dt, $J_{H,H}$ = 1.4, 7.3 Hz, 2 H, C_6H_4), 1.72 (m, 6 H, PCH_2), 1.65 (m, 6 H, PCH_2CH_2), 1.04 (t, $J_{H,H}$ = 6.6 Hz, 9 H, $PCH_2CH_2CH_3$) ppm. ^{13}C NMR (100.4 MHz, $CDCl_3$): δ = 152.1(d, $^3J_{P,C}$ = 12.5 Hz), 132.4, 129.8, 128.5, 127.4, 122.5 (C_6H_4), 25.4 (d, $^1J_{P,C}$ = 26.4 Hz), 17.8 (d, $J_{P,C}$ = 1.7 Hz), 16.0 (d, $J_{P,C}$ = 14.0 Hz) (P*n*Pr$_3$) ppm. ^{31}P NMR (161.8 MHz, $CDCl_3$): δ = 13.5 (P*n*Pr$_3$) ppm. MS (FD, THF): *m*/*z* = 467 [Ni(P*n*Pr$_3$)(^{H}S$_3$)]$^+$.

D$^+$/NH Exchange Reactions of 2a/2b, 3a/3b, and 4a/4b with D_2O or CD_3OD: In an NMR tube, D_2O or CD_3OD (50 μL) was added to a saturated solution of the respective complex (ca. 50 mg) in CD_2Cl_2 or CH_2Cl_2. The reactions were monitored by recording the $^1H/^2D$ NMR spectra and measuring the intensity of the NH or ND signals. After completion of the reactions (5−20 min), the solvents were removed in vacuo and the resulting residue was identified by IR (KBr) spectroscopy. The deuterated complexes each exhibited a ν(ND) band in the region 2480−2420 cm^{-1}.

D$_2$/NH Exchange Reactions of 2b, 3a/3b, and 4a/4b with D_2 and Identification of HD: In a high-pressure NMR tube (524-PV-1, Wilmad, USA), a concentrated solution of the respective complex (ca. 50 mg) in CD_2Cl_2 or [D$_8$]THF was pressurized with D_2 (18 bar). The reactions were monitored by recording ^1H NMR spectra. The formation of HD gave rise to a 1:1:1 triplet ($J_{H,D}$ = 42.5 Hz) in the region of δ = 4−5 ppm after 80−120 h.

D$_2$/H$_2$O Exchange Reaction of 2a/2b, 3a/3b, 4a/4b, and Na[9a]/Na[9b]: In a high-pressure NMR tube, a concentrated solution of the respective complex (ca. 50 mg) in [D$_8$]THF, after addition of H_2O (50 μL), was pressurized with D_2 (18 bar). The reactions were monitored by recording ^1H NMR spectra at regular time intervals for 15 d. The formation of HD gave rise to a 1:1:1 triplet ($J_{H,D}$ = 42.5 Hz) in the region of δ = 4−5 ppm.

Et$_4$N[Ni(NCO)(^{si}S$_3$)] (10b) from Et$_4$N[Ni(N$_3$)(^{si}S$_3$)] (8b) and CO: CO gas (16.5 mL, 0.74 mmol) was injected into a Schlenk tube in the dark containing a solution of **8b** (450 mg, 0.72 mmol) in THF (10 mL) and fitted with a septum. The color of the solution changed from purple to dark-red in the course of ca 15 h. The solution was filtered after 24 h, reduced in volume to ca. 2 mL and layered with pentane (20 mL). Dark-red microcrystals precipitated at −25 °C which were separated after 4 d, washed with pentane and dried in vacuo. Yield: 412 mg (92%). $C_{27}H_{44}N_2NiOS_3Si_2$ (623.73): calcd. C 51.99, H 7.11, N 4.49, S 15.42; found C 52.41, H 7.43, N 4.27, S 15.38. IR (KBr): $\tilde{\nu}$ = 2227 [ν(NCO)] cm^{-1}. ^1H NMR (269.7 MHz, [D$_8$]acetone): δ = 7.63 (d, $J_{H,H}$ = 7.9 Hz, 2 H, C_6H_3), 7.20 (d, $J_{H,H}$ = 7.1 Hz, 2 H, C_6H_3), 6.89 (t, $J_{H,H}$ = 7.9 Hz, 2 H, C_6H_3), 3.42 (m, 8 H, NCH_2), 1.29 (t, $J_{H,H}$ = 7.3 Hz, 12 H, NCH_2CH_3), 0.35 (s, 18 H, $SiMe_3$) ppm. ^{13}C NMR (67.8 MHz, [D$_8$]acetone): δ = 160.4, 139.7, 135.0, 133.9 (C_6H_3), 132.0 (NCO), 129.1, 121.4 (C_6H_3), 53.1, 7.7 (Et_4N), −0.5 ($SiMe_3$) ppm.

[Ni(^{H}S$_3$)]$_3$ (1a) from [Ni(NHR)(^{H}S$_3$)] [R = P*n*Pr$_3$ (2a), PCy$_3$ (3a), SPh$_2$ (4a)] and CO. General Procedure: An equimolar amount of CO was injected into a Schlenk tube containing a CH_2Cl_2 solution (ca. 10 mL) of the respective complex and fitted with a septum. In the course of several hours, depending on the complex, the color of the CH_2Cl_2 solution changed from purple or yellow-red to dark-red. Subsequently, dark-brown microcrystals of **1a** precipitated, which were separated, washed with MeOH and/or pentane and dried in vacuo.

[Ni(^{H}S$_3$)]$_3$ (1a) from 2a and CO: From 215 mg (0.445 mmol) of **2a** and 10.0 mL (0.446 mmol) of CO. The reaction was complete after 50 h. Yield: 93 mg (67%). $C_{36}H_{24}Ni_3S_9$ (921.25): calcd. C 46.94, H 2.63, S 31.33; found C 46.81, H 2.56, S 30.83. MS (FD, DMF): *m*/*z* = 921 [Ni(^{H}S$_3$)]$_3^+$, 614 [Ni(^{H}S$_3$)]$_2^+$.

[Ni(^{H}S$_3$)]$_3$ (1a) from 3a and CO: From 210 mg (0.348 mmol) of **3a** and 7.85 mL (0.350 mmol) of CO gas. Reaction time 78 h. Yield: 79 mg (74%).

[Ni(^{H}S$_3$)]$_3$ (1a) from 4a and CO: From 200 mg (0.393 mmol) of **4a** and 8.9 mL (0.397 mmol) of CO gas. Reaction time 5 h. Yield: 94 mg (78%).

[Ni(^{si}S$_3$)]$_3$ (1b) from [Ni(NHR)(^{si}S$_3$)] [R = P*n*Pr$_3$ (2b), PCy$_3$ (2b), SPh$_2$ (4b)] and CO. General Procedure: An equimolar amount of CO was injected into a Schlenk tube containing a CH_2Cl_2 solution (ca. 10 mL) of the respective complex and fitted with a septum. In the course of several hours, depending on the complex, the color of the CH_2Cl_2 solution changed from purple or yellow-red to red-brown. The solution was filtered, reduced in volume to ca. 2 mL and layered with MeOH (20 mL). Dark-red crystals of **1b** precipitated at −25 °C, which were separated after 3−7 d, washed with MeOH and dried in vacuo.

[Ni(^{si}S$_3$)]$_3$ (1b) from 2b and CO: From 185 mg (0.295 mmol) of **2b** and 6.7 mL (0.299 mmol) of CO gas. Reaction time 40 h. Yield: 81 mg (61%).

[Ni(^{si}S$_3$)]$_3$ (1b) from 3b and CO: From 224 mg (0.300 mmol) of **3b** and 6.8 mL (0.304 mmol) of CO gas. Reaction time 65 h. Yield: 87 mg (64%).

 © 2004 Wiley-VCH Verlag GmbH & Co. KGaA, Weinheim

Table 3. Selected crystallographic data for [Ni(NHP*n*Pr$_3$)(^{si}S$_3$)] (**2b**), [Ni(NHPCy$_3$)(^{H}S$_3$)] (**3a**), [Ni(NHPCy$_3$)(^{si}S$_3$)] (**3b**), [Ni(NHSPh$_2$)(^{H}S$_3$)] (**4a**), and [Ni(P*n*Pr$_3$)(^{H}S$_3$)] (**5a**)

	2b	**3a**	**3b**	**4a**	**5a**
Empirical formula	$C_{27}H_{46}NNiPS_3Si_2$	$C_{30}H_{42}NNiPS_3$	$C_{36}H_{58}NNiPS_3Si_2$	$C_{24}H_{19}NNiS_4$	$C_{21}H_{29}NiPS_3$
M_r (g mol^{-1})	626.69	602.51	746.87	508.35	467.30
Crystal system	triclinic	monoclinic	orthorhombic	monoclinic	orthorhombic
Space group	$P\bar{1}$	$P2_1/c$	$P2_12_12_1$	$P2_1/c$	$Pbca$
a [pm]	1154.8(2)	1084.2(1)	1107.4(1)	1295.2(1)	1231.9(1)
b [pm]	1659.7(2)	1452.1(1)	1532.1(2)	1536.0(2)	1640.8(1)
c [pm]	1913.2(3)	1937.8(1)	2383.9(2)	1126.8(1)	2295.4(2)
α [°]	73.43(1)	90	90	90	90
β [°]	84.60(1)	105.40(1)	90	101.08(1)	90
γ [°]	76.20(1)	90	90	90	90
V [nm^3]	3.4118(9)	2.9413(4)	4.0446(7)	2.1999(4)	4.6397(6)
Z	4	4	4	4	8
$\rho_{calcd.}$ [g cm^{-3}]	1.220	1.361	1.227	1.535	1.338
μ [mm^{-1}]	0.886	0.947	0.758	1.274	1.179
Crystal size [mm]	0.30 × 0.18 × 0.06	0.60 × 0.55 × 0.42	0.70 × 0.50 × 0.10	0.60 × 0.55 × 0.42	0.70 × 0.62 × 0.44
2θ range [°]	3.6−50.0	3.5−56.0	3.4−52.0	4.1−58.0	3.5−54.0
T_{min}/T_{max}	−	0.321/0.360	0.385/0.441	0.189/0.250	0.168/0.222
Measd. refl.	12546	8815	8876	7153	6197
Indep. refl.	10615	7086	7956	5846	5067
Obsd. refl.	4824	4806	5464	4241	3487
Ref. parameters	649	451	403	347	266
Max/min resid. density [e·nm^{-3}]	462/−446	397/−328	342/−452	390/−311	482/−756
$R1$;[a] $wR2$[b][%]	7.63; 17.80	4.88; 11.32	6.48; 16.30	3.88; 8.49	4.87; 12.15
Abs. struct. parameter	−	−	0.03(2)	−	−

[a] [$I > 2\sigma(I)$]. [b] All data.

[Ni(^{si}S$_3$)]$_3$ (1b) from 4b and CO: From 112 mg (0.172 mmol) of **4b** and 3.9 mL (0.174 mmol) of CO gas. Reaction time 3 h. Yield: 62 mg (80%).

Monitoring the Reactions of 2a/2b, 3a/3b, and 4a/4b with CO by ^{1}H and ^{31}P NMR Spectroscopy: An equimolar amount of CO was injected into an NMR tube containing the solution of the respective complex (ca. 50 mg) in CD_2Cl_2 (ca. 0.6 mL) and fitted with a septum. ^{1}H and ^{31}P NMR spectra were recorded at regular time intervals.

X-ray Structure Determination of [Ni(NHP*n*Pr$_3$)(^{si}S$_3$)] (2b), [Ni(NHPCy$_3$)(^{H}S$_3$)] (3a), [Ni(NHPCy$_3$)(^{si}S$_3$)] (3b), [Ni(NHSPh$_2$)(^{H}S$_3$)] (4a), and [Ni(P*n*Pr$_3$)(^{H}S$_3$)] (5a): In the course of 10 d, red-brown blocks of **2b** crystallized at −25 °C from a saturated THF solution of **2b** layered with CH_3CN. In an NMR tube at −25 °C, in the course of 3 d dark-red blocks of **3a** crystallized from a $CDCl_3$ solution of **3a** layered with Et_2O. Red-violet plates of **3b** crystallized from a hot CH_3CN solution (65 °C) of **3b**, which was slowly cooled to −30 °C. Red-brown crystals of **4a** were grown in the course of 7 d from a saturated CH_2Cl_2 solution of **4a** that was layered with hexane at −30 °C. Red-brown blocks of **5a** crystallized from a concentrated THF solution of **5a**, which was layered with hexane at −30 °C. Suitable single crystals were either embedded in protective perfluoro polyether oil or sealed in glass capillaries under N_2. Data were collected at 210 K (**2b** and **5a**), 220 K (**3a** and **4a**), or 295 K (**3b**) with a Siemens P4 diffractometer using Mo-K_α radiation (λ = 71.073 pm), a graphite monochromator, and the ω-scan technique. With the exception of **2b**, semiempirical absorption corrections using ψ-scans were performed. All structures were solved by direct methods, and full-matrix least-squares refinement was carried out on F^2 using SHELXTL NT 5.1.[23] All non-hydrogen atoms were refined anisotropically. The hydrogen atoms of **3a** and **4a** were located in a difference Fourier map and were either refined with a fixed common isotropic displacement parameter (**3a**) or were refined isotropically (**4a**). In all other compounds, the H atoms were geometrically positioned with isotropic displacement parameters being 1.5-times U(eq) of the corresponding C or N atom. One of the *n*-propyl groups of **5a** is disordered. Two alternative sites were refined giving site-occupancy factors of 0.711(8) (site A) and 0.289(8) (site B). The unit cell of **2b** contains two symmetrically independent molecules. Selected crystallographic data are summarized in Table 3.[24]

Acknowledgments

Support of these investigations by the Deutsche Forschungsgemeinschaft (SFB 583: "Redoxaktive Metallkomplexe") and the Fonds der Chemischen Industrie is gratefully acknowledged. We thank Prof. Dr. Horst Kisch for his fruitful discussions.

[1] [1a] J. Arnold, *Prog. Inorg. Chem.* **1995**, *43*, 353. [1b] W.-F. Liaw, Y.-C. Horng, D.-S. Qu, C.-Y. Ching, G.-H. Lee, S.-M. Peng, *J. Am. Chem. Soc.* **1997**, *119*, 9299−9300. [1c] H. Wang, C. Y. Ralston, D. S. Patil, R. M. Jones, W. Gu, M. Verhagen, M. Adams, P. Ge, C. Riordan, C. A. Marganian, P. Mascharak, J. Kovacs, C. G. Miller, T. J. Collins, S. Brooker, P. D. Croucher, K. Wang, E. I. Stiefel, S. P. Cramer, *J. Am. Chem. Soc.* **2000**, *122*, 10544−10552.

[2] Y. Higuchi, H. Ogata, K. Miki, N. Yasuoka, T. Yagi, *Structure (London)* **1999**, *7*, 549−556.

[3] E. Garcin, X. Vernede, E. C. Hatchikian, A. Volbeda, M. Frey, J. C. Fontecilla-Camps, *Structure (London)* **1999**, *7*, 557−566.

[4] H. Dobbek, V. Svetlitchnyi, L. Gremer, R. Huber, O. Meyer, *Science* **2001**, *293*, 1281−1285.

[5] C. L. Drennan, J. Heo, M. D. Sintchak, E. Schreiter, P. W. Ludden, *Proc. Natl. Acad. Sci. USA* **2001**, *98*, 11973−11978.

[6] D. Sellmann, F. Geipel, M. Moll, *Angew. Chem.* **2000**, *112*, 570−572; *Angew. Chem. Int. Ed.* **2000**, *39*, 561−563.

 © 2004 Wiley-VCH Verlag GmbH & Co. KGaA, Weinheim

[7] D. Sellmann, F. Geipel, F. W. Heinemann, *Chem. Eur. J.* **2000**, *6*, 4279−4284.
[8] [8a] D. Sellmann, D. Häußinger, F. W. Heinemann, *Eur. J. Inorg. Chem.* **1999**, 1715−1725. [8b] D. Sellmann, F. Geipel, F. W. Heinemann, *Eur. J. Inorg. Chem.* **2000**, 271−279. [8c] D. Sellmann, F. Geipel, F. W. Heinemann, *Eur. J. Inorg. Chem.* **2000**, 59−63.
[9] D. Sellmann, R. Prakash, F. Geipel, F. W. Heinemann, *Eur. J. Inorg. Chem.* **2002**, 2138−2146.
[10] [10a] L. Crociani, F. Tisato, F. Refosco, G. Bandoli, B. Corain, L. M. Venanzi, *J. Am. Chem. Soc.* **1998**, *120*, 2973−2974. [10b] K. Dehnicke, M. Krieger, W. Massa, *Coord. Chem. Rev.* **1999**, *182*, 19−65. [10c] T. Grob, B. Neumüller, K. Harms, F. Schmock, A. Greiner, K. Dehnicke, *Z. Anorg. Allg. Chem.* **2001**, *627*, 1928−1931.
[11] [11a] G. Urban, W. Beck, *Z. Naturforsch., Teil B* **1982**, *37*, 1101−1103. [11b] R. E. Cramer, K. A. N. S. Ariyaratne, J. W. Gilje, *Z. Anorg. Allg. Chem.* **1995**, *621*, 1856−1864. [11c] P. F. Kelly, A. M. Z. Slawin, *Chem. Commun.* **1999**, 1081−1082. [11d] P. F. Kelly, S.-M. Man, A. M. Z. Slawin, K. W. Waring, *Polyhedron.* **1999**, *18*, 3173−3179. [11e] D. Sellmann, F. Geipel, F. W. Heinemann, *Z. Anorg. Allg. Chem.* **2001**, *627*, 1034−1038.
[12] [12a] B. Kersting, P. Suter, H. Vahrenkamp, *Z. Anorg. Allg. Chem.* **1998**, *624*, 787−791. [12b] D. Sellmann, E. Thallmair, *J. Organomet. Chem.* **1979**, *164*, 337−352.
[13] M. Krieger, R. O. Gould, J. Pebler, K. Dehnicke, *Z. Anorg. Allg. Chem.* **1998**, *624*, 781−786.
[14] A. Bondi, *J. Phys. Chem.* **1964**, *68*, 441−451.
[15] [15a] S. W. Ragsdale, M. Kumar, *Chem. Rev.* **1996**, *96*, 2515−2540. [15b] J. Xia, Z. Hu, C. V. Popesue, P. A. Lindahl, E. Münck, *J. Am. Chem. Soc.* **1997**, *119*, 8301−8312. [15c] C. Davidson, S. B. Choudhury, Z. Gu, K. Bose, W. Roseboom, S. P. J. Albracht, M. J. Maroney, *Biochemistry* **2000**, *39*, 7468−7479.
[16] [16a] R. P. Happe, W. Roseboom, S. P. J. Albracht, *Eur. J. Biochem.* **1999**, *259*, 602−608. [16b] H. Ogata, Y. Mizoguchi, N. Mizuno, K. Miki, S.-i. Adachi, N. Yasuoka, T. Yagi, O. Yamauchi, S. Hirota, Y. Higuchi, *J. Am. Chem. Soc.* **2002**, *124*, 11628−11635.
[17] [17a] C. A. Marganian, H. Vazir, N. Baidya, M. M. Olmstead, P. K. Mascharak, *J. Am. Chem. Soc.* **1995**, *117*, 1584−1594. [17b] D. H. Nguyen, H.-F. Hsu, M. Millar, S. A. Koch, *J. Am. Chem. Soc.* **1996**, *118*, 8963−8964.
[18] W. Beck, *J. Organomet. Chem.* **1990**, *383*, 141−160.
[19] W. P. Fehlhammer, M. Fritz, *Chem. Rev.* **1993**, *93*, 1243−1280.
[20] J. Lupinetti, G. Frenking, S. H. Strauss, *Angew. Chem.* **1998**, *110*, 2229−2232; *Angew. Chem. Int. Ed.* **1998**, *37*, 2113−2116.
[21] S. H. Strauss, *J. Chem. Soc., Dalton Trans.* **2000**, 1−6.
[22] [22a] W. Buchner, W. Wolfsberger, *Z. Naturforsch., Teil B* **1974**, *29*, 328−334. [22b] L. Birkofer, S. M. Kim, *Chem. Ber.* **1964**, *97*, 2100−2101.
[23] *SHELXTL NT 5.1*, Bruker AXS, Inc., Madison, WI, U. S. A., **1998**
[24] CCDC-213454 (**2b**), -213455 (**3a**), -213456 (**3b**), -213457 (**4a**) and -213458 (**5a**) contain the supplementary crystallographic data for this paper. These data can be obtained free of charge at www.ccdc.cam.ac.uk/conts/retrieving.html [or from the Cambridge Crystallographic Data Centre, 12 Union Road, Cambridge CB2 1EZ, UK; Fax: (internat.) + 44-1223/336-033; E-mail: deposit@ccdc.cam.ac.uk].

Received October 22, 2003
Early View Article
Published Online March 18, 2004

 © 2004 Wiley-VCH Verlag GmbH & Co. KGaA, Weinheim

Preparation and Characterization of Cu_2SnSe_4 Nanoparticles Using a Microwave-Assisted Polyol Method

Haviv Grisaru,[a] V. G. Pol,[a] Aharon Gedanken,*[a] and Israel Nowik[b]

Keywords: Nanoparticles / Microwave heating / Polyol method / Copper / Tin / Selenium

The microwave-assisted polyol method has been applied to the preparation of nanosized Cu_2SnSe_4. Cheap materials such as CuCl (or $CuCl_2{\cdot}2H_2O$), Sn and Se were used as starting materials. Polyethylene glycol (PEG) is the only solvent in which the reaction takes place and the materials did not react in ethylene glycol, tri-, or tetraethylene glycol. Mössbauer spectroscopic measurements revealed a single doublet whose isomer shift of 1.81 mm/s is typical of that seen in tetravalent covalent tin semiconductors. The final product was characterized by X-ray powder diffraction, transmission electron microscopy (TEM), high resolution TEM (HR-TEM), scanning electron microscopy (SEM), X-ray photoelectron spectroscopy (XPS) and electron paramagnetic resonance (EPR) spectroscopy.
(© Wiley-VCH Verlag GmbH & Co. KGaA, 69451 Weinheim, Germany, 2004)

Introduction

In recent years, there has been special interest in new multinary metal chalcogenido materials.[1−3] These compounds have the specific properties that are required for technological devices and have been used in optoelectronic devices, lasers and solar cells.[4,5] The compound Cu_2SnSe_4, or more precisely $Cu_2Sn\square Se_4$, where □ denotes the cation vacancy that is included to maintain the same number of cations and anion sites, belongs to one of the families of fourfold defect derivatives of the $A^{II}B^{VI}$ binary semiconductors.[6] It is expected, that in order to maintain an average of four valence electrons per lattice site, the copper atoms should be divalent (Cu^{+2}) in Cu_2SnSe_4.

The multinary metal chalcogenides can be divided into two main groups. In the first group the metal is an alkali metal, and these materials can be prepared either by reactive-flux methods at temperatures between 300−600 °C or by the solvothermal method at relatively low temperatures.[2,7] The second group of multinary metal chalcogenides consists mostly of transition metals instead of alkali metals. These compounds can be synthesized by a simple combination of the elements followed by heating to high temperatures for a prolonged period of time.[8] Marcano and co-workers[9] have prepared ingots of Cu_2SnSe_4 by the vertical Bridgman−Stockbarger technique. The mixture of Cu, Sn and Se, in the ratio of 2:1:4 was sealed in an evacuated quartz ampoule, and heated to 1150 °C for 24 h. Later, it was annealed at 500 °C for 120 h and then cooled to room temperature. Bulk compounds with large sized particles have been prepared using this method, but it is unsuitable for the synthesis of nanomaterials.

Recently, two solvothermal reactions were described by Qian's group.[10,11] B. Li et al.[10] prepared Cu_2SnSe_4 nanocrystals at 140 °C for 15 h using $CuCl_2{\cdot}2H_2O$, $SnCl_2{\cdot}2H_2O$ and Se as the reagents and Q. Li et al.[11] also synthesized nanocrystals in a similar solvothermal process using $CuCl_2{\cdot}2H_2O$, Sn, and Se as the reactants in ethylenediamine (en) at 180 °C for 12 h. They also investigated the effect of different solvents on the formation of the product. Ethylenediamine, diethylamine, benzene, and ethanol were examined as solvents in a sealed autoclave maintained at 140 °C for 15 h. The disadvantage of this method is the need for relatively high pressures and prolonged heating.

In our continuing effort to prepare semiconducting nanoparticles we have developed a general method, the so-called microwave-assisted polyol method, which is general and very efficient. We have applied this method to the preparation of binary and ternary nanosized chalcogenides (selenides and tellurides).[12−14] In most experiments the microwave reaction is complete within a few minutes, the maximum duration being one hour.

The polyol method has been developed over the past two decades and has been applied to the preparation of submicrometer nanoparticles of the easily reducible transition metals.[15] This method is based on alcohols (such as ethylene glycol as well as other glycols) reducing metallic cations to form the corresponding metals. In almost all the reactions, the polyol also plays the role of the solvent.

The application of microwaves to inorganic chemistry began only in the late 1980s.[16] Ethylene glycol (and other glycols) has been proposed as a solvent for microwave di-

[a] Department of Chemistry, Bar-Ilan University, Ramat-Gan 52900, Israel
E-mail: gedanken@mail.biu.ac.il
[b] The Racah Institute of Physics, The Hebrew University, Jerusalem 91904, Israel

electric heating because it is highly susceptible to microwave radiation due to its high permanent dipole and high dissipation factor.[17] An added advantage is that ethylene glycol is a good reducing agent only at high temperatures. The metallic particles that are produced as intermediates in the polyol reaction are also susceptible to microwave radiation, and therefore undergo rapid heating. While the solvent temperature is expected to be that of boiling ethylene glycol, it is likely that the temperature in the reaction cell will be much higher than that of the surrounding liquid. Mingos and Whittaker[18] recently reported that high boiling point alcohols are superior solvents in microwave-assisted reactions because they help prevent arcing, which is known to lead to the decomposition of solvents resulting in carbon and carbonaceous residues. Arcing is considered the main source of the high levels of impurities that are found in the end-products.

In this study, the microwave-assisted polyol method has been shown to be an excellent method for the preparation of Cu_2SnSe_4 nanoparticles. Their crystal structure, morphology, and properties have been investigated using various analytical techniques, and the results are reported below.

Results and Discussion

Powder XRD Studies

The XRD patterns of the prepared and annealed products are shown in Figure 1 (a and b), respectively. The prepared product was not obtained as clean Cu_2SnSe_4 but as a mixture of about 90% Cu_2SnSe_4 (face-centered cubic, PDF: 78−0600), and 10% $SnSe_2$ (PDF: 23−0602), the latter being obtained as a secondary phase. To purify the material, the mixture was heated at 450 °C for 12 h. The X-ray diffraction patterns of the annealed product are presented in Figure 1 (b). No evidence for any impurity was detected and only diffractions characteristic of polycrystalline Cu_2SnSe_4 (PDF: 78−0600) were indexed. To check for other impurities in the annealed compound, we carried out an elemental analysis for carbon and hydrogen. It was found that the levels of carbon and hydrogen impurities after the annealing of Cu_2SnSe_4 were less than 0.2%. The Scherrer equation was used to calculate the particle dimensions.[19] The sizes of the Cu_2SnSe_4 particles are ≈ 40 nm. The calculated lattice parameter found for the compound is a = 5.71 Å. These results are in agreement with previously published data.[9−11] Additional analyses were conducted in order to verify the stoichiometry of the heated sample. Elemental analysis is especially important for Cu_2SnSe_4, because of the secondary phase that was observed for the prepared material. The stoichiometric ratio of Cu:Sn:Se in the annealed sample, measured using EDS, is 2.01:1:3.3. The EDS results show a deficiency of Se. It cannot be claimed that the product is Cu_2SnSe_3 because the positions of the diffraction peaks of this compound are very different from those of Cu_2SnSe_4.[20] For example, Cu_2SnSe_3 has a remarkably intense diffraction peak at 2θ = 36.50°, which was not observed in our measurements. By analyzing the XRD and the EDS measurements we confirmed Cu_2SnSe_4 to be the sole product of the heated sample.

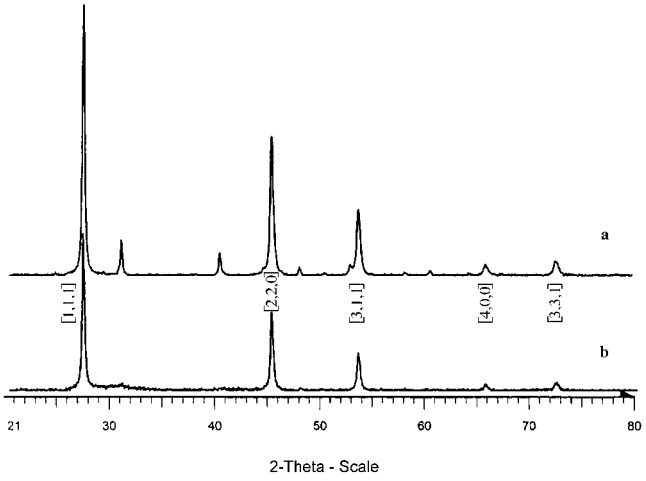

Figure 1. Powder XRD patterns of: (a) Cu_2SnSe_4 compound prepared in PEG and (b) annealed face-centered cubic product after heating at 450 °C for 12 h

TGA Measurements

The thermogravimetric measurements of the prepared product in the temperature range of 30 to 600 °C revealed two main mass losses. The first loss was ca. 1.6% and occurred in the temperature range of 240−450 °C. This loss can be attributed to the removal of PEG from the surface of the product. A second mass decrease of 4.3% was seen over the range 480−600 °C. This loss may perhaps be due to the removal of $SnSe_2$.

Electron Microscopy Studies (TEM, SEM and HR-TEM)

The morphology of the heated sample was studied by TEM and SEM measurements. The TEM image of Cu_2SnSe_4 is shown in Figure 2. The diameters of most of the particles are in the 30−50 nm range. We also observed agglomerated particles with an average diameter of about 150 nm. The prepared nanoparticles were also found to be

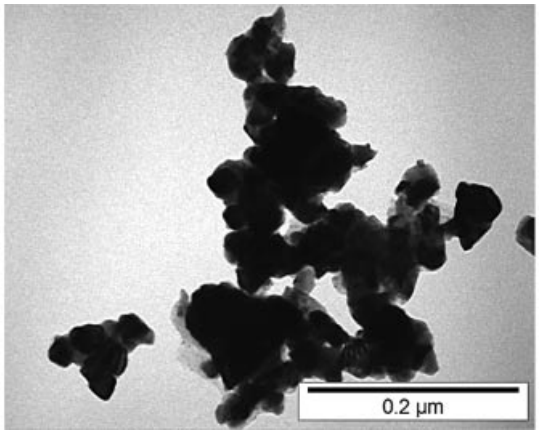

Figure 2. TEM image of the heated Cu_2SnSe_4 sample

 © 2004 Wiley-VCH Verlag GmbH & Co. KGaA, Weinheim

aggregated and the aggregation mode changed only slightly upon annealing. The size of the individual particles, of 30−50 nm, is in agreement with the results calculated from the XRD data. The polycrystalline nature of Cu_2SnSe_4 was established from electron diffraction measurements. The SEM micrograph of the product (Figure 3) is consistent with the overall view of the TEM image. It also showed aggregated nanoparticles resulting in large clusters.

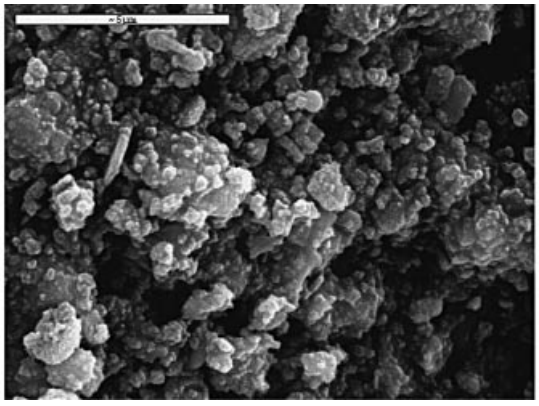

Figure 3. SEM image of the heated Cu_2SnSe_4 sample (scale bar equal to 5 μm)

The HR-TEM is depicted in Figure 4 and provides further evidence for the identification of the product as Cu_2SnSe_4. The micrograph shown in Figure 4 is a picture of the edge of the Cu_2SnSe_4 particle. The image was recorded along the [111] zone. It illustrates the perfect arrangements of the atomic layers and the lack of defects. The measured distance between these [111] lattice planes is 0.315 nm, which is very close to the distance between the planes reported in the literature (0.328 nm) for the face-centered cubic lattice of Cu_2SnSe_4 (PDF: 78−0600). An outer amorphous shell was also observed at the edge of the nanocrystalline Cu_2SnSe_4 particles and is marked by an arrow. The thickness of this shell measured for many particles is approximately 1 nm. The Fast Fourier Transform filtered (FFT) image of this lattice is shown in the insert.

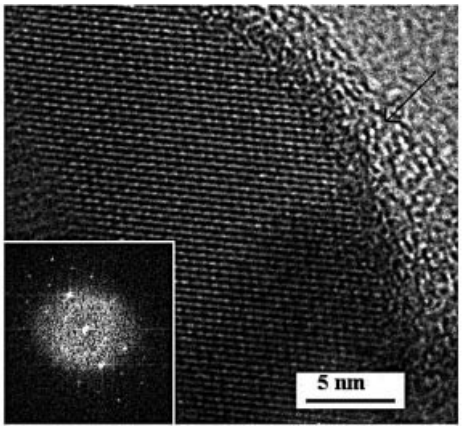

Figure 4. HR-TEM image of the heated Cu_2SnSe_4 sample. The FFT image of this lattice and the computer generated diffraction pattern is shown in the insert

The aggregated nature of the product was also evident from BET measurements. The surface area measured was 5.7 m^2g^{-1}.The surface area for a 40 nm sphere of Cu_2SnSe_4, assuming a density of 5.1 gcm^{-3}, was calculated as 29.4 m^2g^{-1}. This indicates the aggregated nature of the product. However, the aggregated initially prepared material or the aggregated annealed material both form colloidal solutions upon dissolving in 2-mercaptoethanol.

XPS Measurements

X-ray photoelectron spectroscopy (XPS) is known to probe only the surface of the particles. In XPS, excitation by X-rays enables core atomic levels to be probed, and the resultant chemical shift provides an indication of the oxidation state of the surface materials. In Figure 5 (a) we present the wide XPS spectrum of the heated sample. The overall XPS spectrum of the Cu_2SnSe_4 nanoparticles is in agreement with previously published data.[11] The binding energies obtained in the XPS analysis were corrected for specimen charging by referencing the C 1s to 285.2 eV, and are presented in Table 1. Peaks for carbon and oxygen were also observed, and we have assigned them to organic impurities adsorbed on the surface of the powders due to solvent decomposition. The XPS picture of the peaks of the doublet of Sn in Cu_2SnSe_4 nanoparticles is shown in Figure 5 (b). The energy of the Sn $3d_{5/2}$ band is 486.6 eV, and is probably an average value between that of Sn^{+4} in SnO_2 (486.9 eV) and that of Sn^{+2} in SnO (486.3 eV).[21,22] According to the recent literature, Sn undergoes a chemical shift of at least 0.4 eV when reduced from Sn^{+4} to Sn^{+2}.[23] We have attributed the presence Sn^{+2} ions to the reduction that the Sn^{+4} undergoes upon X-ray irradiation. Similar examples are well documented in the literature.[24,25] It can therefore be concluded that the XPS measurements cannot confirm unequivocally that the oxidation state of Sn in the prepared or annealed materials is Sn^{+4}. We therefore required another spectroscopic tool in order to determine the oxidation state of the Sn in the heated sample.

Mössbauer Spectroscopic Measurements

In order to verify our conjecture that the oxidation state of Sn in the heated sample of Cu_2SnSe_4 nanoparticles is +4, Mössbauer spectroscopic measurements were performed. The Mössbauer spectrum of Cu_2SnSe_4 at room temperature is shown in Figure 6. A similar spectrum was obtained at 90 K. The spectrum was analyzed in terms of two quadrupole doublets, one corresponding to Cu_2SnSe_4 (isomer shift: 1.81 mm/s relative to $BaSnO_3$, and quadrupole splitting: 0.90 mm/s), while the second (less than 5%) is perhaps due to an Sn^{+2} impurity, which was also observed in the XPS spectrum. The value obtained for the isomer shift of ^{119}Sn in Cu_2SnSe_4 is typical of Sn^{+4} in essentially covalent semiconductors,[26] and quite similar to the $SnSe_2$ system.[27] This conclusion leads to the determination of the oxidation state of the copper as +2 in Cu_2SnSe_4. The oxidation states of the Sn and Cu as determined by Mössbauer spectroscopy are bulk properties, which are different from the surface values.

 © 2004 Wiley-VCH Verlag GmbH & Co. KGaA, Weinheim

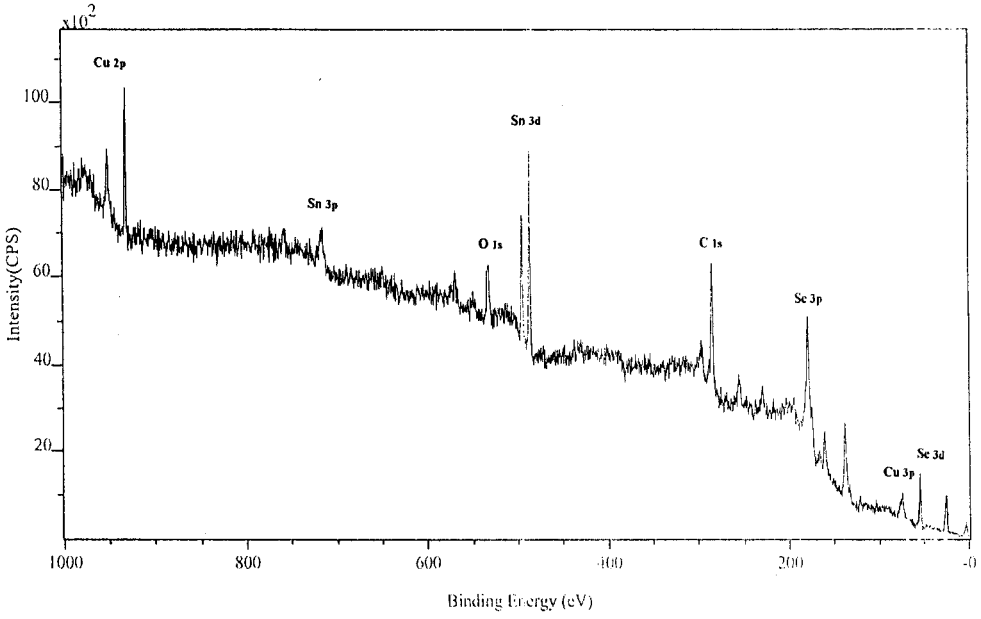

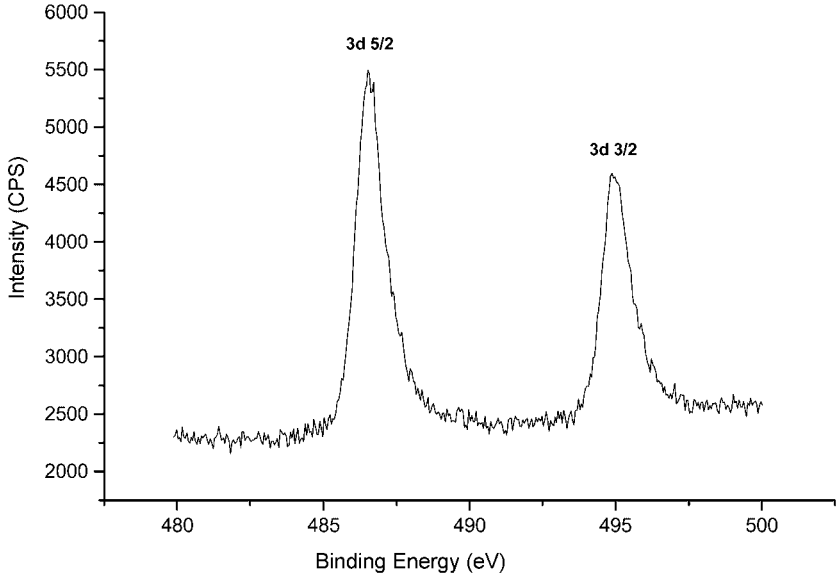

Figure 5. a) Wide XPS spectrum of the Cu_2SnSe_4 heated sample; b) the XPS picture of the peaks of the doublet of Sn in Cu_2SnSe_4 nanoparticles

Table 1. Spin orbit components and respective binding energies of the elements in Cu_2SnSe_4 nanoparticles

Elements	Cu	Sn	Se
Spin orbit component	2p 3/2 2p 1/2	3d 5/2 3d 3/2	3d
B.E. (eV)	932.3 952.1	486.6 494.6	54.7

EPR Measurements

The electron paramagnetic resonance (EPR) spectrum of the heated sample of Cu_2SnSe_4 nanoparticles was measured at room temperature (not shown here). The Cu_2SnSe_4

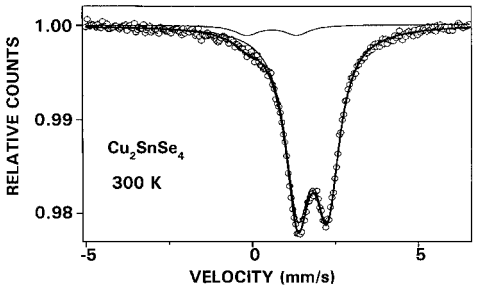

Figure 6. The ^{119}Sn Mössbauer spectrum of Cu_2SnSe_4 nanoparticles at room temperature

 © 2004 Wiley-VCH Verlag GmbH & Co. KGaA, Weinheim

sample showed a peak-to-peak separation (ΔHpp) of 320 G and a *g* value 2.178. The *g* factor is equal to 2.00232 for the unbound electron.[28] The paramagnetic resonance signal in Cu_2SnSe_4 is associated with the paramagnetic nature of Cu^{+2}. This is consistent with the fact that copper atoms should be divalent in Cu_2SnSe_4 in accordance with the Sn oxidation state of +4 obtained from the Mössbauer measurements. The experimental *g* value of 2.178 for this sample is within the experimental error of the *g* values reported for Cu^{+2}.[29]

Reaction Mechanism

The main question regarding the preparation of Cu_2SnSe_4 is the mechanism of its formation. In previous work, we proposed a mechanism for the formation of $CuInSe_2$ (CIS) and $CuInTe_2$ (CIT) nanoparticles.[14] The proposed mechanism was based on the fact that the reduced metallic particles react with a second metallic element and with the chalcogenide under microwave irradiation in order to form a ternary chalcogenide compound. For the above-mentioned compounds, CIS and CIT, the additional metallic element was indium. We refer to these reactions as "wet solid-state reactions". A control experiment in which metallic copper powder, an In^{+3} salt, and Se (or Te) reacted together (Cu/In^{3+}/Se or Te), did not result in ternary chalcogenides (a binary copper selenide was obtained instead).

Copper(I) or copper(II) are known from previous experiments to be reduced by the ethylene glycol to the corresponding metallic nanoparticles. This was demonstrated when CuCl or $CuCl_2$ were treated with EG in the absence of Se and Sn, yielding copper nanoparticles as the sole products. In the current reaction, both copper(I) and copper(II) yielded the same product, Cu_2SnSe_4, when treated with Sn and Se. The mixture reacted in the microwave field forming Cu_2SnSe_4 nanoparticles. As in previous cases, we have attributed the ability of the two metals (Cu and Sn) to reduce Se to their strong interaction with microwave radiation. The experiments to reduce tin salts under the same reaction conditions were unsuccessful. In another control experiment, metallic copper powder, a Sn^{+2} salt, and Se reacted together but did not yield the ternary compound (instead a binary copper selenide was obtained). We also tried to synthesize Cu_2SnTe_4 using the same starting materials but replacing Se with Te but only copper telluride was obtained. We could not find any report in the literature of the synthesis of bulk or nanoparticles of Cu_2SnTe_4.

Finally, we discuss the role of the PEG in this reaction. We could not synthesize Cu_2SnSe_4 when Cu^{II} or Cu^{I} was treated with Sn and Se in ethylene glycol, triethylene, or tetraethylene glycol. The only solvent *in* which these materials react and *with* which these materials react is PEG. We have attributed these observations to the higher boiling temperature of PEG (around 400 °C) compared with those of ethylene glycol (198 °C) and the other glycols.

Conclusions

Cu_2SnSe_4 nanoparticles have been prepared by using the microwave-assisted polyol method. Two routes have been suggested for the synthesis. The starting materials did not react when ethylene glycol, tri-, or tetraethylene glycol were used as solvents. They did react, however, when PEG was used as a solvent, and the reaction took 2 h. The sizes of the nanoparticles measured from transmission electron microscopy are in the range of 30−50 nm, which is in agreement with the results calculated from the XRD data.

Experimental Section

Materials: All reagents were of the highest purity. Elemental Se, Sn, copper(I) chloride, $CuCl_2{\cdot}2H_2O$, polyethylene glycol (PEG) (MW = 400 g/mol), and 2-mercapto ethanol were all purchased from Aldrich and used without further purification.

Instrumentation: The X-ray diffraction patterns of the products were recorded using a Bruker AXS D8 Advance Powder X-ray Diffractometer (using Cu-K_α radiation, λ = 0.15418 nm at 40 kV/40 mA) with a secondary graphite crystal monochromator. The transmission electron micrographs (TEM) were obtained with a JEOL-JEM 100SX microscope, working at an 80 kV accelerating voltage, and a JEOL-2010 HR-TEM instrument using an accelerating voltage of 200 kV. EDS measurements were conducted using an X-ray microanalyzer (Oxford Scientific) built on a JSM-840 Scanning Electron Microscope (JEOL). Elemental analyses (Carbon) were carried out with an EA 1110 CHNS-O instrument. Thermogravimetric analyses (TGA) were performed with a Mettler−Toledo TGA/SDTA851 instrument using nitrogen or argon as the purging gas with a scanning rate of 5 °C/min. X-ray photoelectron spectra (XPS) were measured with an AXIS, HIS 165, Kratos Analytical, ULTRA instrument. Mössbauer spectroscopic studies of a Cu_2SnSe_4 sample were performed using a $Ba^{119m}SnO_3$ source (10 mCi) and a conventional constant acceleration Mössbauer drive. Electron paramagnetic resonance (EPR) spectra were recorded with a Bruker EPR spectrometer (ER083 CS) operating at X-band (υ = 9.77 GHz), with a 100-kHz magnetic field modulation. The Brunauer−Emmett−Teller (BET) surface area measurements were performed using a Micromeritics (Gemini 2375) surface area analyzer. The nitrogen adsorption and desorption isotherms were measured at a temperature of 77 K after heating the sample at 100 °C for 1 h.

Microwave-assisted reactions were conducted in a domestic microwave oven, Kenwood-900 W, 2.45 × 10^9 Hz working frequency, modified with a refluxing system. In all the experiments the microwave oven worked in the following cycling mode: on for 21 s, off for 9 s, and the total power was always 900 W. This cycling mode was chosen in order to prevent the violent "bump" boiling of the solvent. All reactions were conducted under a flow of nitrogen.

Preparation of Cu_2SnSe_4: CuCl (0.197 g, 2 mmol) was dissolved in PEG (50 mL) by gentle heating in the microwave oven for approximately 1 minute. The stoichiometric quantities of Sn (0.118 g, 1 mmol), and Se (0.315 g, 4 mmol) powder were then added. The system was purged for 10 minutes with nitrogen and then the microwave reactor was turned on. The process was carried out for 2 h.

In the post reaction treatment, the product was centrifuged once at 9500 rpm with the mother liquor to separate the powder from the liquid, and was then washed a few times with ethanol at 20 °C at 9500 rpm. The product was then dried overnight under vacuum. The sample was annealed under argon for 12 h at 450 °C.

 © 2004 Wiley-VCH Verlag GmbH & Co. KGaA, Weinheim

Another attempt to fabricate Cu_2SnSe_4 nanoparticles was carried out using $CuCl_2 \cdot 2H_2O$ (0.341 g, 2 mmol) instead of CuCl under the same conditions as in the first route. The results discussed can be applied to samples prepared by either of these methods.

Acknowledgments

Prof. A. Gedanken thanks the German Ministry of Science through the Deutsche-Israel Program (DIP) for supporting this research. The assistance of Dr. Y. Gofer with the XPS measurements is gratefully acknowledged. The authors are also grateful to Prof. Z. Malik of the Faculty of Life Sciences for extending the use of his facilities to us, and to Dr. Y. Grinblat and Dr. T. Tamary of the Chemistry Department for their assistance with TEM and HR-TEM measurements.

[1] F. J. Disalvo, *Science* **1991**, *247*, 649.
[2] W. S. Sheldrick, M. Wachhold, *Angew. Chem. Int. Ed. Engl.* **1997**, *36*, 206.
[3] *Ternary Diamond Like Semiconductors* (Eds.: L. I. Berger, V. D. Prochukhan), Consultanta Bureau, New York, **1969**.
[4] L. K. Samanta, D. K. Ghosh, G. C. Bhar, *Phys. Stat. Sol., A* **1986**, *93*, k5.
[5] L. K. Samanta, D. K. Ghosh, in *Proceedings 2nd Asia and Pacific Phys. Conference SAPPC*, Raman Research Institute, Bangalore (India), January 13−17, **1986**.
[6] Ternary and Multinary Compounds, J. M. Delgado, *Inst. Phys. Conf. Ser.* **1998**, *152*, 45; Institute of Physics, Bristol.
[7] M. G. Kanatzidis, A. C. Sutorik, *Prog. Inorg. Chem.* **1995**, *43*, 151.
[8] M. E. Badding, F. J. Disalvo, *Inorg. Chem.* **1990**, *29*, 3952.
[9] G. Marcano, C. Rincón, G. Marín, R. Tovar, G. Delgado, *J. Appl. Phys.* **2002**, *92*, 1811.
[10] B. Li, Y. Xie, J. Huang, Y. Qian, *Solid State Ionics* **1999**, *126*, 359.
[11] Q. Li, Y. Ding, X. Liu, Y. Qian, *Mater. Res. Bull.* **2001**, *36*, 2649.
[12] J. Zhu, O. Palchik, S. Chen, A. Gedanken, *J. Phys. Chem. B* **2000**, *104*, 7344; R. Kerner, O. Palchik, A. Gedanken, *Chem. Mater.* **2001**, *13*, 1413; O. Palchik, R. Kerner, A. Gedanken, A. M. Weiss, M. A. Slifkin, V. Palchik, *J. Mater. Chem.* **2001**, *11*, 874.
[13] H. Grisaru, O. Palchik, A. Gedanken, V. Palchik, M. A. Slifkin, A. M. Weiss, Y. Rozenfeld Hacohen, *Inorg. Chem.* **2001**, *40*, 4814; H. Grisaru, O. Palchik, A. Gedanken, V. Palchik, M. A. Slifkin, A. M. Weiss, *J. Mater. Chem.* **2002**, *12*, 339.
[14] H. Grisaru, O. Palchik, A. Gedanken, V. Palchik, M. A. Slifkin, A. M. Weiss, *Inorg. Chem.* **2003**, *42*, 7148.
[15] G. M. Chow, K. L. Kurihara, D. Ma, C. R. Feng, P. E. Schoen, L. J. Martinez-Miranda, *Appl. Phys. Lett.* **1997**, *70*, 2315; F. Fiévet, J. P. Lagier, M. Figlarz, *MRS Bull.* **1989**, 29. December; M. S. Hegde, D. Larcher, L. Dupont, B. Beaudoin, K. Tekaia-Elhsissen, J. M. Tarascon, *Solid State Ionics* **1997**, *93*, 33.
[16] D. M. P. Mingos, *Res. Chem. Intermed.* **1994**, *20*, 85; D. M. P. Mingos, *Chem. Ind.,* **1994**, 1 August, p. 596; D. R. Baghurst, D. M. P. Mingos, *J. Chem. Soc., Chem. Commun.* **1992**, 674; D. M. P. Mingos, D. R. Baghurst, *Chem. Soc. Rev.* **1991**, 20, 1; S. Caddic, *Tetrahedron* **1995**, *51*, 10403.
[17] C. Gabriel, S. Gabriel, E. H. Grant, B. S. J. Halstead, D. M. P. Mingos, *Chem. Soc. Rev.* **1998**, *27*, 213.
[18] A. G. Whittaker, D. M. P. Mingos, *J. Chem. Soc., Dalton Trans.* **2000**, 1521; A. G. Whittaker, D. M. P. Mingos, *J. Chem. Soc., Dalton Trans.* **1995**, 2073.
[19] *X-ray Diffraction Procedures*, (Eds.: H. Klug, L. Alexander), John Wiley & Sons, New York, **1962**, p. 125.
[20] G. Marcano, C. Rincón, L. M. de Chalbaud, D. B. Bracho, G. S. Pérez, *J. Appl. Phys.* **2001**, *90*, 1847; G. Marcano, L. M. de Chalbaud, C. Rincón, G. S. Pérez, *Mater. Lett.* **2002**, *53*, 151.
[21] N. Graciela Valente, L. A. Arrúa, L. E. Cadús, *Appl. Catal. A* **2001**, *205*, 201.
[22] C. D. Wagner, A. V. Naumkin, A. Kraut-Vass, J. W. Allison, C. J. Powell, J. R. Rumble Jr., *NIST X-ray Photoelectron Spectroscopy Database 20*, Version 3.3 (Web Version), **2003**.
[23] Y. Okamoto, K. Oh-Hiraki, T. Imanaka, S. Teranishi, *J. Catal.* **1981**, *71*, 99.
[24] D. A. Cleary, D. R. Baer, *Chem. Mater.* **1992**, *4*, 112.
[25] Z. M. Liu, X. L. Zhou, J. M. White, *Chem. Phys. Lett.* **1992**, *198*, 615; X. L. Zhou, P. M. Blass, B. E. Koel, J. M. White, *Surf. Sci.* **1992**, 271, 452; X. L. Zhou, J. M. White, *J. Chem. Phys.* **1990**, *92*, 5612.
[26] P. A. Flinn, in *Mössbauer Isomer Shifts*, (Eds.: G. K. Shenoy, F. E. Wagner), North-Holland Publishing, **1978**, p. 599−602.
[27] R. H. Herber, A. E. Smelkinson, M. J. Sienko, L. F. Schneemeyer, *J. Chem. Phys.* **1978**, *68*, 3705.
[28] *Instrumental Methods of Analysis*, 5th ed., H. H. Willard, L. Merrit Jr., J. A. Dean, Van Nostrand, New York, **1974**.
[29] S. K. Dutta, M. Shang, G. Ferraudi, *Inorg. Chim. Acta* **2001**, *312*, 226.

Received October 28, 2003
Early View Article
Published Online March 18, 2004

 © 2004 Wiley-VCH Verlag GmbH & Co. KGaA, Weinheim

Structural and Theoretical Studies of New Ruthenium-Amidato Complexes with Phenanthroline Ligands Containing H-Bonding Groups

Daniela Rais,[a] Ian R. Gould,[a] Ramón Vilar,*[a] Andrew J. P. White,[a] and David J. Williams[a]

Keywords: Chelates / Tridentate ligands / Ligand design / Ruthenium / pi interactions

The syntheses, characterization and coordination chemistry of two new 1,10-phenanthroline-based ligands are presented here. Crystallographic studies have shown that both molecules display hydrogen-bonding and π–π stacking interactions, generating interesting supramolecular assemblies in the solid state. The reactions of these ligands with $[RuCl_2(PPh_3)_3]$ have been performed and two new ruthenium-amidato complexes have been prepared. In both cases, the presence of a pyridyl group in the ligand backbone favours the deprotonation of one of the carboxyamido moieties leading to a tridentate coordination mode of the ligands. The structural characterization of one of the ruthenium complexes is also reported.

(© Wiley-VCH Verlag GmbH & Co. KGaA, 69451 Weinheim, Germany, 2004)

Introduction

Transition metal complexes featuring *N*-amidato [−NRC(=O)R′] ligands are relatively less common than those containing other *N*-based species such as amines (−NR_3) or amides (−NR_2). Nevertheless, increasing interest has recently been paid to *N*-amidato-containing systems due to their role as models for the interactions between metal centres and proteins.[1] To date, studies have largely focused on iron- and copper-amidato species[2,3] because of their biological relevance, and on cobalt systems due to their interesting catalytic properties.[4] Although some reports exist on the chemistry of *N*-amidato-ruthenium complexes, these have mainly dealt with pentaaminoruthenium amido species. Examples of compounds where the carboxyamido moiety is part of a more complex coordination environment are somewhat rare. However, the ability of ruthenium to participate in a wide range of catalytic and photochemical processes[5] coupled with the stability, ease of preparation and strong σ-donating properties of the amidato ligands have contributed to the renewed interest in these systems.[6,7] Synthetic and structural information on Ru^{II} and Ru^{III} complexes of deprotonated *N*-aryl-2-pyridinecarboxamide ligands has been reported by Bhattacharya[6] while Wright has investigated a series of Ru^{II} complexes of doubly deprotonated *N*,*N*′-bis(6-methyl-2-pyridinyl)-2,6-pyridinedicarboxamide.[7] In this context, the pendant pyridine moieties were found to interact with appropriately positioned ruthenium-bound molecules, thereby mimicking many metalloenzymes that influence the reactivity of bound substrates through interactions with the metal centre and functional groups present on the nearby protein backbone. The general ability of *N*-amidato ligands to stabilize metals in high coordination states was further confirmed by the generation and characterization of the Ru^{IV} species $[RuL_2]\cdot H_2O$ [H_2L = *N*,*N*′-bis(2-phenyl)-2,6-pyridinedicarboxamide].

As part of our interest in the chemistry of transition metal complexes that possess hydrogen bonding capabilities,[8] we have recently focused our efforts on the synthesis of 2,9-carboxyamido-substituted phenanthroline molecules. Metal complexes with hydrogen-bonding properties are of great interest due to their applications in the design of molecular receptors[9] as well as in the fields of crystal engineering[10] and supramolecular catalysis.[11] Herein we report the synthesis and characterization of two phenanthroline-carboxamide ligands (H_2L1 and L2 in Scheme 1) and the products resulting from their reactions with $[RuCl_2(PPh_3)_3]$.

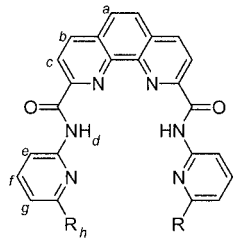

R = NH_2, **L1**; H, **L2**

Scheme 1

[a] Department of Chemistry, Imperial College London, South Kensington, London SW7 2AY, UK
Fax: (internat.) + 44-20-7594-5804
E-mail: r.vilar@ic.ac.uk

Results and Discussion

Synthesis of Phenanthroline-Based Ligands H_2L1 and L2

The two molecules *N*,*N*′-bis(2-amino-6-pyridyl)-1,10-phenanthroline-2,9-carboxamide (in its protonated form, H_2L1) and *N*,*N*′-bis(2-pyridyl)-1,10-phenanthroline-2,9-carboxyamide (L2) (Scheme 1) were obtained in good yields (60 and 91 %, respectively) by reaction of 1,10-phenanthroline-2,9-dicarbonyl chloride (prepared from neocuproine by previously reported methods[12]) with the corresponding amine.

The new compounds were characterized by analytical and spectroscopic means. The IR spectra of the two species showed broad bands centred at $\tilde{\nu}$ = 3326 and 3333 cm^{-1} for H_2L1 and L2, respectively, which were assigned to the ν(NH) band of the carboxyamido groups. In the ^1H NMR spectra, the CO−N*H* proton was found to resonate as a singlet at δ = 10.33 and 11.17 ppm for H_2L1 and L2, respectively. A single set of resonances was observed for the two halves of the molecules indicating their equivalence on the NMR time scale.

The structural features of the newly synthesized molecules were elucidated by performing single-crystal X-ray analyses. It should be noted that attempts to crystallise the protonated H_2L1 species were not successful; instead, a very small number of single crystals of the deprotonated form of this compound (i.e. L1) were obtained and structurally characterised. This suggests that, although the bulk of the material is isolated as the diprotonated form (see below) a small amount of the neutral form is also present (which forms single crystals).

In the solid state L1 has a nonplanar hemi-helical conformation, there being a significant twist of the phenanthroline unit with rings **B** and **D** inclined by approximately 9° (see Figure 1). One of the amide groups [associated with N(16)] is held in an almost co-planar arrangement with its adjacent phenanthroline pyridyl ring **B** by an intramolecular N−H···N hydrogen-bond (**f** in Figure 1); rings **A** and **B** are inclined by approximately 3°. By contrast, the other amide group is rotated substantially out of plane, the torsional twists about C(11)−C(24) and N(25)−C(26) being approximately 24 and 33°, respectively [cf. ca. 4 and 3° about C(2)−C(15) and N(16)−C(17)]. However, these rotations are in opposite senses such that rings **D** and **E** which are inclined by approximately 8°, are in a stepped relationship to each other. This second amide group is not intramolecularly hydrogen-bonded to its adjacent phenanthroline pyridyl ring **D** (N···H 2.40 Å), entering instead into intermolecular hydrogen-bonding with the carbonyl oxygen atom of the "first" amide of a centrosymmetrically related counterpart (**b** in Figure 2). There is also an intermolecular N−H···N hydrogen bond between the N(23) terminal amino group of one molecule and the pyridyl nitrogen atom N(18) of another across an independent inversion centre (**a** in Figure 2). These interactions, combined with π−π stacking interactions **c** and **d**, create a continuous "staircase-like" chain of alternating hemi-helices that progresses along the crystallographic *a* direction. Adjacent chains are cross-linked by N−H···O hydrogen bonds between the other terminal amide group N(32) in one chain and the carbonyl oxygen O(24) of the next [N···O, H···O 3.00, 2.10 Å; N−H···O 175°].

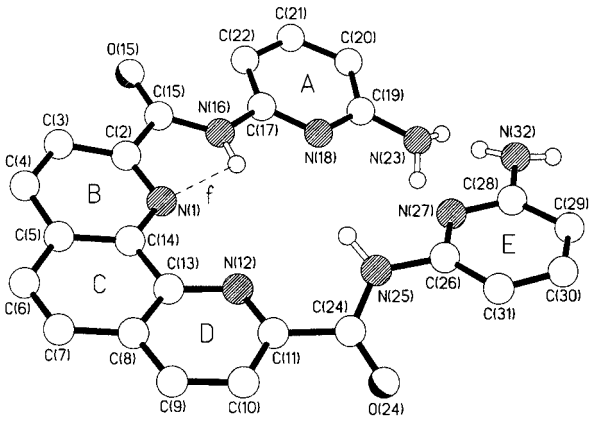

Figure 1. Molecular structure of L1; the intramolecular N−H···N hydrogen bond **f** has N···N, H···N 2.69, 2.24 Å and N−H···N 111°; the nonbonded N(23)···N(32) separation is 3.47 Å

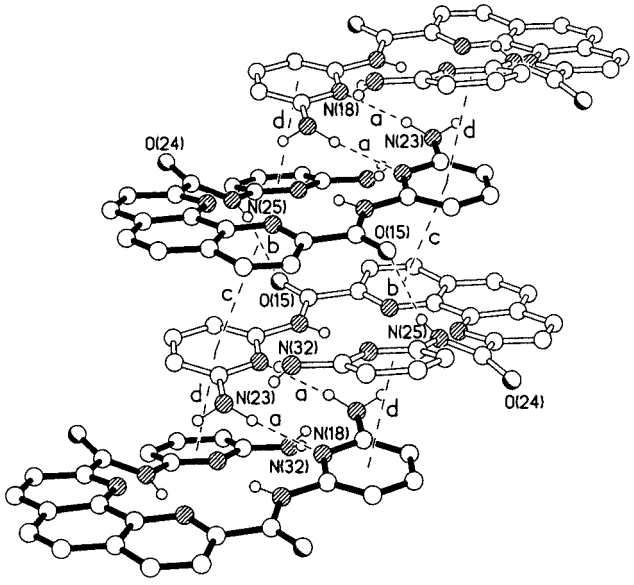

Figure 2. Part of one of the continuous "staircases" in the solid-state structure of L1; the hydrogen bonding geometries [N···X, H···X (Å), N−H···X (°)] are **a** 3.08, 2.18, 174; **b** 2.97, 2.16, 149; the centroid···centroid separations are **c** 3.58 Å and **d** 3.67 Å, the interacting rings being inclined by 3 and 19°, respectively

The related molecule L2 has a similar conformation but with a smaller distortion of the central phenanthroline ring system-rings **B** and **D** being inclined by approximately 4° (see Figure 3). Rings **A** and **B** are inclined by approximately 9°, and **D** and **E** by approximately 35°. The two amide groups, however, are both essentially co-planar with, and intramolecularly N−H···N hydrogen bonded to (**f** and **g** in Figure 3), their adjacent phenanthroline pyridyl rings; the torsional twists about C(11)−C(23) and C(2)−C(15) are

 © 2004 Wiley-VCH Verlag GmbH & Co. KGaA, Weinheim

approximately 2 and 11°, respectively. The molecules pack to form continuous stacks along the crystallographic *a* direction (Figure 4), there being a parallel π−π stacking interaction between ring **B** of one molecule and its centrosymmetrically related counterpart in another (centroid···centroid and mean interplanar separations of 3.87 and 3.57 Å, respectively). The other stacking interaction is more unusual, and involves an orthogonal approach of the amide N($p\pi$) orbital of N(24) in one molecule to ring **C** of another and *vice versa* across an independent inversion centre; the N···centroid distance **b** is 3.42 Å and the N···centroid vector is inclined by approximately 86° to the {C(23)−N(24)−C(25)} plane.

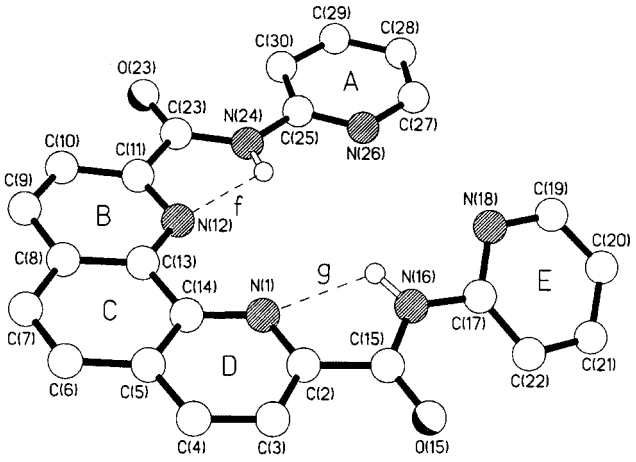

Figure 3. Molecular structure of L2; the intramolecular N−H···N hydrogen bonding geometries [N···N, H···N (Å), N−H···N (°)] are **f** 2.65, 2.16, 114; **g** 2.67, 2.21, 111

Synthesis of $[RuCl_2(L1)(PPh_3)]$ (1)

Reaction of $[RuCl_2(PPh_3)_3]$ with H_2L1 in a DMF/toluene solvent mixture led to isolation of complex $[RuCl_2(L1)(PPh_3)]$ (**1**) in 84% yield (Scheme 2). The initially dark brown suspension was refluxed for 4 hours under a N_2 atmosphere, turning dark purple after approximately 30 min. Filtration of the suspension yielded **1** as a dark purple powder.

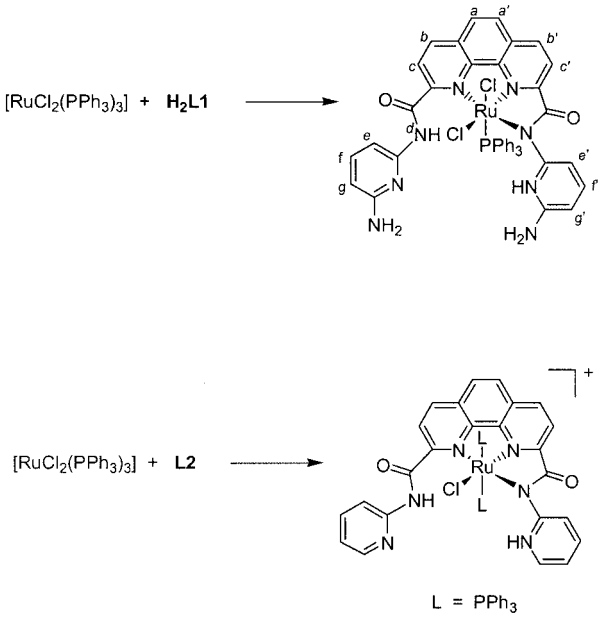

Scheme 2

The new compound was found to be air stable and could be characterized by means of IR, $^{31}P\{^1H\}$ and ^1H NMR spectroscopy, FAB^+ mass spectrometry and elemental analyses. The formulation based on the analytical and spectroscopic data was further confirmed by a single-crystal X-ray structural determination. Suitable crystals were obtained by layering diethyl ether onto a solution of **1** in DMF.

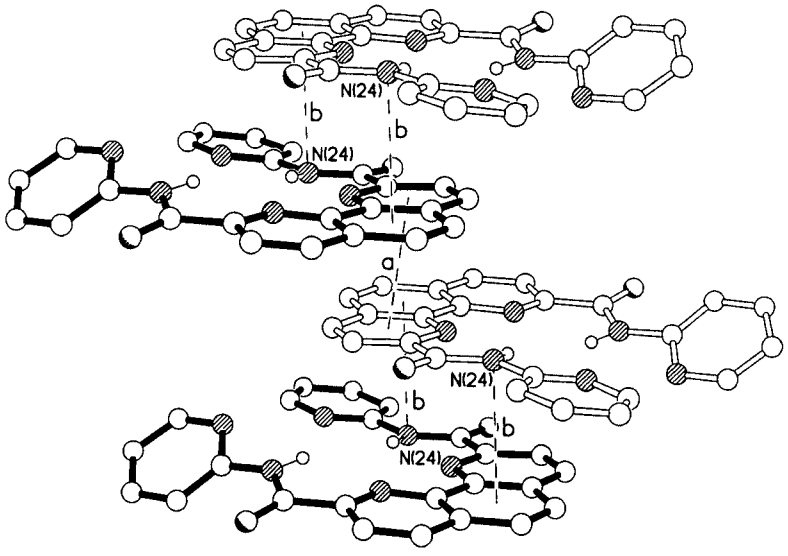

Figure 4. Part of one of the continuous stacks of molecules in the structure of L2; the centroid···centroid separation **a** is 3.87 Å and the N···centroid distance **b** is 3.42 A

 © 2004 Wiley-VCH Verlag GmbH & Co. KGaA, Weinheim

The X-ray analysis showed L1 to be coordinated to the ruthenium centre in an asymmetric tridentate fashion, forming two coordinative Ru−N bonds with the phenanthroline nitrogen atoms and a Ru−N amidato bond with a deprotonated carboxyamido unit, the amido proton having been transferred to N(18) of the adjacent aminopyridine ring (Figure 5).

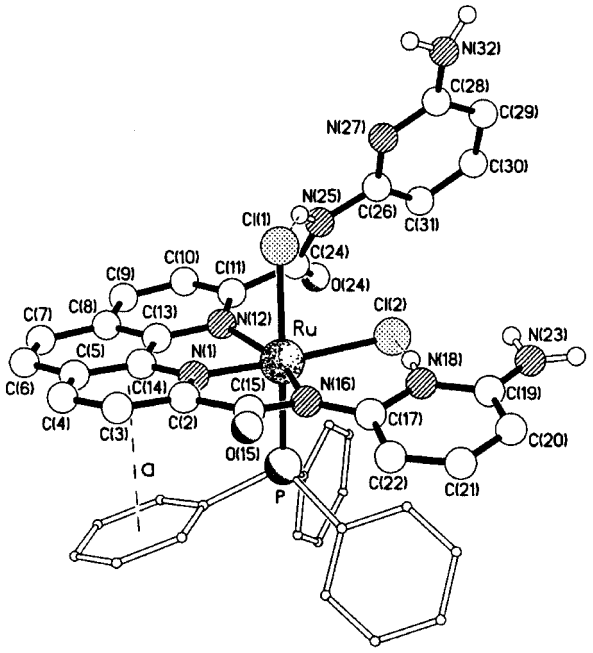

Figure 5. Molecular structure of $[RuCl_2(L1)(PPh_3)]$ (**1**); the centroid···centroid separation **a** is 3.47 Å and the rings are inclined by approximately 16°

The coordinated amido arm of the ligand lies within the equatorial coordination plane, the torsional twists about C(2)−C(15) and N(16)−C(17) being approximately 5 and 17°, respectively, a geometry that facilitates an intramolecular N−H···Cl hydrogen bond from the pyridinium nitrogen N(18) to the equatorially coordinated chloride Cl(2) [N···Cl, H···Cl 2.99, 2.12 Å; N−H···Cl 163°]. By contrast the other arm is rotated substantially out of plane−the torsional twists about C(11)−C(24) and N(25)−C(26) are approximately 54 and 12°, respectively, thereby directing the amide N−H group towards the axially coordinated chloride Cl(1); here the N−H···Cl hydrogen bond is noticeably weaker [N···Cl, H···Cl 3.36, 2.55 Å; N−H···Cl 150°]. The phenanthroline unit has a warped geometry very similar to that seen in the free ligand, the two pyridyl rings being inclined by approximately 10°. The geometry at ruthenium is distorted octahedral with *cis* angles in the range 77.4(2) to 93.0(1)°, the most acute angles being associated with the five-membered chelate rings (see Table 1 and Table 2) which are coplanar to within 0.06 Å. There is a substantial distortion of the *trans* N(12)−Ru−N(16) angle [156.8(2)°] which is a consequence of the geometrical constraints of the chelating ligand. The Ru−N(1) bond [1.951(5) Å] is, as expected, significantly shorter than those to N(12) [2.163(5) Å] and N(16) [2.156(5) Å]. The Ru−Cl(1) bond [2.469(2) Å], *trans* to P, is noticeably shorter than that to Cl(2) [2.493(1) Å] *trans* to N(1). It is interesting to note that the asymmetric chelating mode of the ligand is also reflected in an asymmetric pattern of bonding within the phenanthroline ring system−for example, though the N(1)−C(2) [1.332(8) Å] and N(1)−C(14) [1.340(8) Å] bond lengths are the same, those between N(12)−C(13) [1.392(7) Å] and N(12)−C(11) [1.329(8) Å] differ significantly. A similar (but expected) asymmetry is seen between the two amide groups, with the C−N bond in the deprotonated amide [C(15)−N(16) 1.380(8) Å] being significantly elongated compared with its counterpart [C(24)−N(25) 1.327(9) Å]. This asymmetry is also observed in the solution ^{1}H NMR spectra and in the solid-state infrared spectra (vide infra). The orientation of the triphenylphosphane is to some extent influenced by an intramolecular π−π stacking interaction (**a** in Figure 5) between one of the phosphane phenyl rings and the N(1) pyridyl ring of the phenanthroline. The only inter complex interaction of note is a π−π stacking interaction between the N(12) containing pyridyl ring of the phenanthroline unit in one molecule and the N(18) aminopyridinium ring of another, the centroid···centroid separation is 3.65 Å and the rings are inclined by approximately 14°. The only other noteworthy intermolecular interactions are N−H···O hydrogen bonds between the terminal amine groups and included dimethylformamide (DMF) solvent molecules. The N(32) amino group is involved in two N−H···O hydrogen bonds to the oxygen atoms of two centrosymmetrically related DMF molecules, linking pairs of complexes [N···O, H···O (Å), N−H···O (°); 2.95, 2.07, 167; 3.02, 2.13, 170]. The other terminal amino group [N(23)] forms a single hydrogen bond to an independent DMF solvent molecule [N···O, H···O 2.69, 1.81 Å, N−H···O 165°].

Table 1. Selected bond lengths (Å) for L1 and **1**

	L1	1		L1	1
Ru−Cl(1)	−	2.469(2)	Ru−Cl(2)	−	2.4929(14)
Ru−P	−	2.294(2)	Ru−N(1)	−	1.951(5)
Ru−N(12)	−	2.163(5)	Ru−N(16)	−	2.156(5)
N(1)−C(2)	1.331(3)	1.332(8)	N(1)−C(14)	1.357(3)	1.340(8)
C(2)−C(15)	1.502(3)	1.491(9)	C(11)−N(12)	1.327(3)	1.329(8)
C(11)−C(24)	1.510(3)	1.521(9)	N(12)−C(13)	1.362(3)	1.392(7)
C(13)−C(14)	1.454(3)	1.417(8)	C(15)−O(15)	1.226(3)	1.229(8)
C(15)−N(16)	1.353(3)	1.380(8)	C(24)−O(24)	1.223(3)	1.241(8)
C(24)−N(25)	1.348(3)	1.327(9)			

Table 2. Selected bond angles (°) for **1**

Cl(1)−Ru−Cl(2)	88.52(5)	P−Ru−Cl(1)	179.19(5)
P−Ru−Cl(2)	92.26(6)	N(1)−Ru−N(16)	77.4(2)
N(1)−Ru−N(12)	79.7(2)	N(16)−Ru−N(12)	156.8(2)
N(1)−Ru−P	91.4(2)	N(16)−Ru−P	91.0(2)
N(12)−Ru−P	92.97(14)	N(1)−Ru−Cl(1)	87.8(2)
N(16)−Ru−Cl(1)	88.60(14)	N(12)−Ru−Cl(1)	87.08(14)
N(1)−Ru−Cl(2)	176.3(2)	N(16)−Ru−Cl(2)	102.44(14)
N(12)−Ru−Cl(2)	100.26(13)		

 © 2004 Wiley-VCH Verlag GmbH & Co. KGaA, Weinheim

The ligand's asymmetric coordination was reflected in the IR spectrum of complex **1** which showed two different carbonyl absorptions: the one at $\tilde{\nu}$ = 1683 cm^{-1} was assigned to the CO stretching of the noncoordinated carboxamide while the one at $\tilde{\nu}$ = 1638 cm^{-1} was attributed to the CO stretching of the *N*-coordinated amidato group, in agreement with values reported in the literature for analogous *N*-bound amidato ligands (see the calculations section for a discussion of these values). Several bands were observed in the N−H bond stretching region but their assignment was found to be problematic given the numerous N−H groups present in the molecule; only after quantum mechanical calculations were performed it was possible to assign these values (see calculations section). The $^{31}P\{^{1}H\}$ NMR spectrum showed a singlet at δ = 45.0 ppm, shifted downfield with respect to the starting material ($[RuCl_2(PPh_3)_3]$, 42.0 ppm). The ^{1}H NMR spectrum of **1** in $[D_6]$DMF displayed an extremely complicated pattern in the aromatic region, consistent with the asymmetric coordination of the ligand to the ruthenium centre (as shown in the solid-state structure). The N−H group of the noncoordinated carboxamide was observed as a singlet at δ = 10.58 ppm while a signal at δ = 13.74 ppm was assigned to the pyridinium proton.

Synthesis of *trans*-[RuCl(L2)(PPh_3)$_2$]Cl (*trans*-2)

By analogy with the synthesis of **1**, the reaction of $[RuCl_2(PPh_3)_3]$ with one equivalent of L2 was investigated. However, instead of the expected $[RuCl_2(L2)(PPh_3)]$ a complex with formula $[RuCl(L2)(PPh_3)_2]Cl$ was obtained (Scheme 2). Upon mixing the reactants in DMF/toluene, a deep purple solution was immediately formed. The mixture was stirred at room temperature for 2 hours yielding a dark purple precipitate. The $^{31}P\{^{1}H\}$ NMR spectrum of the solid in $[D_2]$-dichloromethane showed two doublets at δ = 49.7 and 39.6 ppm ($J_{P,P}$ = 36.0 Hz), indicating the presence of two nonequivalent phosphane ligands in this species. However, during the course of the NMR studies it was observed that the compound was not stable since a dark purple solid precipitated few minutes after the $[D_2]$-dichloromethane solution (originally highly coloured and perfectly clear) had been prepared. After 1 hour the entire soluble compound had been transformed into the dichloromethane-insoluble product and no $^{31}P\{^{1}H\}$ NMR signal could be detected in the supernatant solution. The resulting purple solid was isolated by filtration and analyzed by $^{31}P\{^{1}H\}$ NMR and IR spectroscopy, FAB^+ mass spectrometry and elemental analyses. On the basis of the spectroscopic and analytical data, the compound was formulated as *trans*-$[RuCl(L2)(PPh_3)_2]Cl$ (*trans*-**2**).

The $^{31}P\{^{1}H\}$ NMR spectrum of *trans*-**2** in $[D_6]$DMF showed the presence of a singlet resonance at δ = 25.5 ppm, in contrast to the value of 43.0 ppm observed for **1**. The chemical shift of 25.5 ppm is consistent with previously reported data for ruthenium complexes where two triphenylphosphane ligands are *trans* to each other (and *cis* to chlorides and chelating *N*-ligands).[13] The formulation of *trans*-**2** was further supported by FAB^+ mass spectrometry which showed a molecular ion peak a.m.u. at 1081 corresponding to $[RuCl(L2)(PPh_3)_2]^+$. The IR spectrum of *trans*-**2** was also consistent with the proposed formulation showing two bands at $\tilde{\nu}$ = 1690 and 1648 cm^{-1} that were assigned to the carbonyl stretching modes of a nondeprotonated amide (i.e. the noncoordinated one) and a coordinated amidato group, respectively, on the basis of quantum-mechanical calculations (see below). The asymmetric coordination of ligand L2 in complex *trans*-**2** found support in the ^{1}H NMR spectrum of the compound, which showed a very complicated pattern for the protons on the phenanthroline and the pyridine moieties and the presence of two different CO-N*H* resonances (whose values were consistent with that of a noncoordinated carboxamide and a protonated pyridine group). Elemental analyses agreed with the proposed formulation.

The identity of the solid obtained during the first stage of the reaction between L2 and $[RuCl_2(PPh_3)_3]$ is uncertain. However, the available spectroscopic and analytical data [$^{31}P\{^{1}H\}$ NMR spectrum, elemental analyses and FAB^+ mass spectrum] are compatible with a formulation of the purple powder as *cis*-$[RuCl(L2)(PPh_3)_2]Cl$ (*cis*-**2**). It is reasonable to propose that compound *cis*-**2** is formed as the kinetic product of the reaction and isolated as a solid due to its insolubility in the reaction medium. However, once in either dichloromethane or DMF solution, it rapidly converts to its thermodynamically more stable isomer *trans*-**2**.

Quantum-Mechanical Calculations

To gain a better understanding of the nature of the ruthenium-amidato complexes and be able to rationalize some of their spectroscopic and structural parameters, a quantum mechanical study of complexes **1** and **2** was carried out. It was also of interest to compare the relative energy of the *cis* and *trans* isomers of complex **2**.

Selected structural parameters for compounds **1** and *trans*-**2** are reported in Table 3 and Table 4. It can be seen that the calculated structure of **1** is in reasonably good agreement with that determined crystallographically (see Tables 1 and 2). The calculated molecular structure of *trans*-**2** is shown in Figure 6, the bond lengths and angles around the ruthenium centres being in good agreement with the crystallographic data of **1**. As would be expected, the largest difference between the calculated structures of **1** and *trans*-**2** is observed in the bond length between the Ru and the P atoms due to the different *trans* influence of the chloride (in **1**) and the phosphane (in *trans*-**2**).

Minima have been obtained for both *cis*-**2** and *trans*-**2** and, as expected on steric grounds, the *trans* isomer is calculated to be more stable than the *cis* isomer by ca. 30 kcal mol^{-1}. These findings sustain our hypothesis that *cis*-**2** may indeed be the kinetic product of the reaction of L2 and $[RuCl_2(PPh_3)_3]$ which, however, easily coverts to its thermodynamically more stable isomer *trans*-**2**.

Inspection of the vibrational modes of **1** shows good correlation with the experimental data. There are two distinct carbonyl absorptions: one at $\tilde{\nu}$ = 1661 cm^{-1}, corresponding to the CO stretch of the noncoordinated carboxamide (cf. experimental $\tilde{\nu}$ = 1683 cm^{-1}), while the CO of the

 © 2004 Wiley-VCH Verlag GmbH & Co. KGaA, Weinheim

Table 3. (a) Selected bond lengths (Å) for **1** and *trans*-**2**

	1	*trans*-**2**		**1**	*trans*-**2**
Ru−Cl(1)	2.473	−	Ru−Cl(2)	2.617	−
Ru−P	2.369	2.480	Ru−N(1)	1.964	1.980
Ru−N(12)	2.211	2.185	Ru−N(16)	2.189	2.191
N(1)−C(2)	1.340	1.338	N(1)−C(14)	1.359	1.359
C(2)−C(15)	1.484	1.488	C(11)−N(12)	1.347	1.347
C(11)−C(24)	1.515	1.510	N(12)−C(13)	1.389	1.385
C(13)−C(14)	1.422	1.420	C(15)−O(15)	1.251	1.248
C(15)−N(16)	1.390	1.403	C(24)−O(24)	1.254	1.249
C(24)−N(25)	1.354	1.357			

Table 4. Selected bond angles (°) for **1** and *trans*-**2**

	1	*trans*-**2**		**1**	*trans*-**2**
Cl(1)−Ru−Cl(2)	94.10	−	P−Ru−Cl(1)	176.40	−
P−Ru−Cl(2)	82.30	82.06	N(1)−Ru−N(16)	77.27	77.55
N(1)−Ru−N(12)	79.33	79.07	N(16)−Ru−N(12)	154.90	156.60
N(1)−Ru−P	93.23	90.80	N(16)−Ru−P	96.80	90.40
N(12)−Ru−P	95.80	90.73	N(1)−Ru−Cl(1)	90.40	−
N(16)−Ru−Cl(1)	94.46	−	N(12)−Ru−Cl(1)	85.22	−
N(1)−Ru−Cl(2)	175.52	172.83	N(16)−Ru−Cl(2)	102.84	103.12
N(12)−Ru−Cl(2)	101.21	103.13			

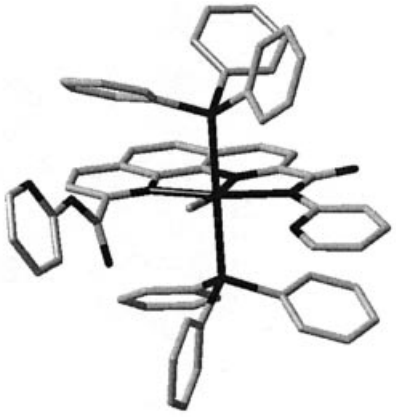

Figure 6. Calculated molecular structure of $[RuCl(L2)(PPh_3)_2]Cl$ (**2**)

N−coordinated amidato group is identified by two bands at $\tilde{\nu}$ = 1651 and 1648 cm^{-1} (cf experimental $\tilde{\nu}$ = 1638 cm^{-1}). We have also identified a very distinct N−H stretch at $\tilde{\nu}$ = 3062 cm^{-1} (cf. experimental $\tilde{\nu}$ = 3050 cm^{-1}), associated with the protonated pyridine group which forms a hydrogen bond with Cl(2). A second strong stretching frequency at $\tilde{\nu}$ = 3244 cm^{-1} (cf. experimental $\tilde{\nu}$ = 3234 cm^{-1}), is associated with the N−H bond of the noncoordinated amide [i.e. N(25)−H] which forms a hydrogen bond to the apical Cl(1) chloride.

We observe the same vibrational progression in *trans*-**2** with the carboxamide CO stretch at $\tilde{\nu}$ = 1669 cm^{-1}, the amidato CO at $\tilde{\nu}$ = 1657 cm^{-1}, the N−H···Cl (from the protonated pyridine group) at $\tilde{\nu}$ = 3048 cm^{-1} and the N−H (from the noncoordinated amide) at $\tilde{\nu}$ = 3442 cm^{-1} (cf. experimental $\tilde{\nu}$ = 1683, 1648, 3048 and 3342 cm^{-1}, respectively). It is worth noting that the frequency associated with the N−H of the noncoordinated amide in *trans*-**2** (calculated value of $\tilde{\nu}$ = 3442 cm^{-1}) is larger than the frequency associated with the same moiety in compound **1** (calculated value of $\tilde{\nu}$ = 3244 cm^{-1}). This is not surprising since in **1** the N−H group of the noncoordinated amide is hydrogen-bonding to the apical chloride of the complex weakening the bond and hence lowering the stretching frequency.

Conclusions

Two new phenanthroline-carboxamide ligands have been prepared and fully characterised. Crystallographic studies have shown that both ligands display various supramolecular interactions in the solid state. Particularly interesting are those observed for L1 where a combination of H-bonding and π−π stacking interactions create a continuous "staircase-like" chain of alternating hemi-helices. The reactions of H_2L1 and L2 with $[RuCl_2(PPh_3)_3]$ result in the formation of two different type of complexes. While the reaction with H_2L1 yields $[RuCl_2(L1)(PPh_3)]$ (**1**), the reaction with L2 leads to formation of *trans*-$[RuCl(L2)(PPh_3)_2]Cl$ (*trans*-**2**). The difference in reactivity could be due to the fact that, while **2** is formed from the neutral ligand L2, **1** is prepared using the hydrochloride salt of L1 (i.e. H_2L1) and hence there is a different concentration of chloride anions in the reaction mixtures. It is also possible that the difference could result from the sterically more demanding nature of L1 (due to the presence of the amino group in position 6 of the pyridine ring) in comparison to L2. However, in both cases the deprotonation of one of the carboxyamido moieties leads to the formation of a ruthenium-amidato bond and consequent tridentate coordination mode of the ligands. Structural characterisation of complex **1** has confirmed this coordination mode. On the basis of our results, we propose that the generation of complex *trans*-**2** takes place through a process in which the corresponding *cis* isomer (presumably kinetically favoured) is likely to be initially formed. However, this isomer rapidly rearranges to the thermodynamically more stable *trans*-**2** once it is dissolved in an appropriate solvent. Quantum mechanical calculations indicate that *trans*-**2** is indeed thermodynamically more stable than *cis*-**2** supporting the experimental observations. Furthermore, these calculations have allowed us to make a detailed assignment of some of the stretching frequencies observed in the IR spectrum of the new complexes. The experimental and calculated structural parameters for compound **1** are in good agreement.

Experimental Section

General: All manipulations were carried out in an atmosphere of purified and dry N_2 using standard Schlenk line techniques unless otherwise stated. Solvents were dried from the appropriate drying agent, degassed and stored under N_2. All commercially available solid starting materials were not further purified. ^1H and $^{31}P\{^1H\}$

 © 2004 Wiley-VCH Verlag GmbH & Co. KGaA, Weinheim

NMR spectra were recorded on a JEOL-EX270 spectrometer (δ = 270.17 and 109.38 MHz, respectively) with TMS and H_3PO_4, respectively, as internal references. IR spectra were recorded on Research Series FT-IR using KBr disks in the range 4000−500 cm^{-1}.

Protonated Form of *N,N′*-Bis(2-amino-6-pyridyl)-1,10-phenanthroline-2,9-carboxamide (H_2L1): A solution of 2,6-diaminopyridine (2.5 g, 22.8 mmol) in CH_2Cl_2 (50 cm^3) was added dropwise to a suspension of 1,10-phenanthroline-2,9-dicarbonyl chloride (1.21 g, 3.8 mmol) in CH_2Cl_2 (50 cm^3) over 1 hour. A pale yellow precipitate formed immediately. The suspension was stirred overnight at room temperature. The mixture was filtered and the resulting precipitate washed with ethanol to extract excess amine, yielding H_2L1 as a pale yellow solid. Yield 1.2 g (60%). $C_{24}H_{18}N_8O_2$·2HCl (523): calcd. C 55.07, H 3.82, N 21.42; found C 55.02, H 3.86, N 21.51. IR (KBr): $\tilde{\nu}$ = 3443 (s), 3399 (m) (NH_2), 3326 (s) (CO−*NH*), 1680 (vs) (CO), 1644 (m), 1605 (m), 1580 (m) (C=N). ^{1}H NMR ([D_6]DMSO): δ = 10.33 (s, CO−N*H*, 1 H), 8.83 (d, H_b, $^3J_{H,H}$ = 8.4 Hz, 1 H), 8.57 (d, H_c, $^3J_{H,H}$ = 8.4 Hz, 1 H), 8.25 (s, H_a, 1 H), 7.53−7.40 (m, H_e, H_f, 2 H), 6.35 (d, H_g, $^3J_{H,H}$ = 5.7 Hz, 1 H), 5.82 (s, NH_2, 2 H) (see Scheme 1 for assignments). FAB$^+$−MS: *m*/*z* = 451 [M − 2HCl]$^+$

***N,N′*-Bis(2-pyridyl)-1,10-phenanthroline-2,9-carboxamide (L2):** A solution of 2-aminopyridine (1.75 g, 18.64 mmol) in CH_2Cl_2 (20 cm^3) was added dropwise to a suspension of 1,10-phenanthroline-2,9-dicarbonyl chloride (1.43 g, 4.7 mmol) in CH_2Cl_2 (20 cm^3). A dark brown solution formed immediately and was stirred at room temperature overnight yielding a white precipitate. The suspension was filtered and the precipitate washed with EtOH (3×10 cm^3) to extract the excess amine, yielding L2 as an off-white powder. Yield: 1.06 g, (91%). $C_{24}H_{16}N_6O_2$ (420): calcd. C 68.57, H 3.81, N 20.0; found C 68.48, H 3.95, N 19.73. IR (nujol): $\tilde{\nu}$ = 3353 (w), 3333 (w) (CO−*NH*), 1690 (vs) (C=O), 1587 (w), 1574 (w) (C=N). ^{1}H NMR ($CDCl_3$): δ = 11.17 (s, CO−*NH*, 1 H), 8.64 (d, H_b, $^3J_{H,H}$ = 8.4 Hz, 1 H), 8.49−8.43 (m, H_c, H_e, H_h, 3 H), 7.95 (s, H_a, 1 H), 7.81 (t, H_f, $^3J_{H,H}$ = 8.6 Hz, 1 H), 7.16−7.13 (m, broad, H_g, 1 H) (see Scheme 1 for assignments). FAB$^+$−MS: *m*/*z* = 421 MH^+.

[$RuCl_2$(L1)(PPh_3)] (1): Solid [$RuCl_2(PPh_3)_3$] (0.72 g, 0.75 mmol) was added to a solution of H_2L1 (0.34 g, 0.66 mmol) in a mixture of DMF/toluene (in a 1:5 ratio). The brown mixture was refluxed for 4 hours turning purple after ca 30 minutes then stirred overnight at room temperature. The suspension was then filtered and the precipitate washed several times with toluene and diethyl ether yielding **1** as a dark purple solid. Yield: 0.493 g, (84%). $C_{42}H_{33}Cl_2N_8O_2PRu$ (884.1): calcd. C 57.01, H 3.73, N 12.67; found calcd. C 57.07, H 3.68, N 12.67. IR (KBr): $\tilde{\nu}$ = 3234 (m) (CO−*NH*, noncoordinated carboxamide), 3050 (m) (py*H*), 1683 (s) (CO, noncoordinated carboxamide), 1638 (vs) (CO, *N*−bound amidato group). ^{1}H NMR ([D_6]DMF): 13.74 (s, py*H*, 1 H), 10.58 (s, CO−*NH*, 1 H), 8.41 (d, $H_{b'}$, $^3J_{H,H}$ = 8.3 Hz, 1 H), 7.97 (d, $H_{c'}$, $^3J_{H,H}$ = 8.3 Hz, 1 H), 7.94−7.81 (m, H_e, $H_{e'}$, H_g, $H_{g'}$ 4 H), 7.79 (s, H_a and $H_{a'}$, 2 H), 7.63 (d, H_b, $^3J_{H,H}$ = 8.3 Hz, 1 H), 7.46 (d, H_c, $^3J_{H,H}$ = 8.3 Hz, 1 H), 7.37 (t, H_f, $^3J_{H,H}$ = 8.3 Hz, 1 H), 7.25 (t, H_f, $^3J_{H,H}$ = 8.0 Hz, 1 H), 6.93−6.71 (m, PPh_3, 20 H) (see Scheme 2 for assignment); ^{31}P{^{1}H} NMR ([D_6]DMF): δ = 45.0; FAB$^+$−MS: *m*/*z* = 885 [M]$^+$, 849 [Ru(L1)(PPh_3)Cl]$^+$, 813 [Ru(L1)(PPh_3)]$^+$, 550 [Ru(L1)]$^+$.

***trans*-[RuCl(L2)(PPh_3)$_2$]Cl (*trans*-2):** Solid [$RuCl_2(PPh_3)_3$] (0.51 g, 0.53 mmol) was added to a solution of **L2** (0.22 g, 0.53 mmol) in a mixture of DMF/toluene (in a 1:5 ratio). A dark violet solution formed immediately and after few minutes a dark purple precipitate started forming. The suspension was stirred for 2 hours and the solid formed filtered off. The precipitate was washed several times with toluene and diethyl ether. The solid was re-dissolved in CH_2Cl_2 yielding a purple solution. After a few minutes the solution

Table 5. Crystal data, data collection and refinement parameters for compounds $\mathbf{L_1}$, $\mathbf{L_2}$ and **1**[a]

	L1	**L2**	**1**
Empirical formula	$C_{24}H_{18}N_8O_2$	$C_{24}H_{16}N_6O_2$	$C_{42}H_{33}N_8O_2PCl_2Ru$
Solvent	−	−	2 Me_2NCHO
Molecular mass	450.5	420.4	1030.9
Colour, habit	yellow needles	colourless prisms	very dark claret rhombs
Crystal size / mm	0.50 × 0.08 × 0.07	0.93 × 0.27 × 0.17	0.50 × 0.33 × 0.30
Temperature / K	293	293	183
Crystal system	monoclinic	orthorhombic	monoclinic
Space group	$P2_1/c$ (no. 14)	*Pbca* (no. 61)	$P2_1/n$ (no. 14)
a (Å)	9.176(1)	7.433(1)	12.922(1)
b (Å)	14.203(1)	23.051(3)	17.280(3)
c (Å)	16.309(1)	23.356(3)	21.165(4)
β / deg	102.53(1)	−	98.77(2)
V / Å^3	2075.0(3)	4001.8(9)	4671(1)
Z	4	8	4
D_c / g cm^{-3}	1.442	1.396	1.466
Radiation used	Cu-K_α	Cu-K_α	Cu-K_α[b]
μ / mm^{-1}	0.802	0.762	4.55
θ range / deg	4.2−60.0	3.8−60.0	3.3−60.0
No. of unique reflections measured	3076	2970	6893
observed, $\|F_o\| > 4\sigma(\|F_o\|)$	2423	2039	5022
Absorptions correction	−	−	empirical
Max. min. transmission	−	−	0.67, 0.20
No. of variables	332	298	603
R_1, wR_2 [c]	0.039, 0.095	0.046, 0.106	0.057, 0.126

[a] Details in common: graphite monochromated radiation, refinement based on F^2. [b] Rotating anode source. [c] $R_1 = \Sigma\|\|F_o| - |F_c\|/\Sigma|F_o|$; $wR_2 = \{\Sigma[w(F_o^2 - F_c^2)^2]/\Sigma[w(F_o^2)^2]\}^{1/2}$; $w^{-1} = \sigma^2(F_o^2) + (aP)^2 + bP$.

 © 2004 Wiley-VCH Verlag GmbH & Co. KGaA, Weinheim

started to loose its colour and a dark purple solid precipitated. This solid was filtered and washed several times with CH_2Cl_2 to yield *trans*-**2** as a pure compound. Yield: 0.378 g (64%). $C_{60}H_{46}Cl_2N_6O_2P_2Ru$ (1116.1): calcd. C 64.45, H 4.12, N 7.52; found C 63.92, H 4.07, N 6.94. IR (KBr): $\tilde{\nu}$ = 3342 (w) (CO−*NH*, noncoordinated carboxamide), 3048 (w) (py*H*), 1690 (vs) (CO, noncoordinated carboxamide), 1648 (vs) (CO, *N*−bound amidato group), 1604 (m), 1573 (s) (C=N); $^{31}P\{^1H\}$ NMR (CD_2Cl_2): δ = 25.5 ppm. FAB$^+$−MS: *m/z* = 1081 $[M - Cl]^+$, 783 $[Ru(L2)(PPh_3)]^+$, 521 $[Ru(L2)]^+$.

Crystallography: Table 5 provides a summary of the crystallographic data for compounds L1, L2 and **1**. Data were collected on Siemens P4 diffractometers using ω-scans. The structures were solved by direct methods and refined based on F^2 using the SHELXTL program system.[14] CCDC-191577 (for L1), -191578 (for **1**) and -191579 (for L2) contain the supplementary crystallographic data for this paper. These data can be obtained free of charge at www.ccdc.cam.ac.uk/conts/retrieving.html [or from the Cambridge Crystallographic Data Centre, 12 Union Road, Cambridge CB2 1EZ, UK; Fax: (internat.) +44-1223-336-033; E-mail: deposit@ccdc.cam.ac.uk].

Computational Details

Ab initio molecular orbital calculations on compound **1** and the *cis* and *trans* isomers of compound **2** were performed All three molecules have been subjected to geometry optimisation using density functional theory (DFT) at the B3LYP level of theory[15−17] using the 3−21G* basis set.[18] The structures were model built with no reference to the crystal structure of compound **1**. All stationary points have been characterised as minima by calculation and inspection of the vibrational modes. We have not scaled the vibrational frequencies reported in this paper. All calculations were performed with Gaussian 98.[17]

Acknowledgments

The Department of Chemistry at Imperial College is gratefully acknowledged for a Teaching Assistantship Grant (D. R.).

[1] H. Sigel, R. B. Martin, *Chem. Rev.* **1982**, *82*, 385.
[2] [2a] D. S. Marlin, P. K. Mascharak, *Chem. Soc. Rev.* **2000**, *29*, 69 and references cited therein. [2b] A. K. Patra, J. M. Rowland, D. S. Marlin, E. Bill, M. M. Olmstead, P. K. Mascharak, *Inorg. Chem.* **2003**, *42*, 6812.
[3] E. Kimura, H. Kurosaki, Y. Kurogi, M. Shionoya, M. Shiro, *Inorg. Chem.* **1992**, *31*, 4314.
[4] T. J. Collins, *Acc. Chem. Res.* **1994**, *27*, 279 and references cited therein.
[5] See for example: S. Dutta, P. K. Bhattacharya, *J. Mol Cat. A: Chem.* **2002**, *188*, 45.
[6] [6a] S. Dutta, S. Pal, P. K. Bhattacharya, *Polyhedron* **1999**, *18*, 2157. [6b] S. Dutta; P. K. Bhattacharya, E. R. T. Tiekink, *Polyhedron* **2001**, *20*, 2027. [6c] A. K. Singh, V. Balamurugan, R. Mukherjee, *Inorg. Chem.* **2003**, *42*, 6497.
[7] S. M. Redmore, C. E. F. Rickard, S. J. Webb, L. J. Wright, *Inorg. Chem.* **1997**, *36*, 4743.
[8] [8a] S.-T. Cheng, E. Doxiadi, R. Vilar, A. J. P. White, D. J. Williams, *J. Chem. Soc., Dalton Trans.* **2001**, 2239. [8b] H. A. Burkill, R. Vilar, A. J. P. White, D. J. Williams, *J. Chem. Soc., Dalton Trans.* **2002**, 837.
[9] [9a] M. S. Luth, E. Freisinger, B. Lippert, *Chem. Eur. J.* **2001**, *7*, 2104. [9b] C. R. Bondy, P. A. Gale, S. J. Loeb, *Chem. Commun.* **2001**, 729. [9c] H. Aït-Haddou, S. L. Wiskur, V. M. Lynch, E. V. Anslyn, *J. Am. Chem. Soc.* **2001**, *123*, 11296. [9d] S. Aoki, K. Iwaida, N. Hanamoto, M. Shiro, E. Kimura, *J. Am. Chem. Soc.* **2002**, *124*, 5256. [9e] J. S. Disch, R. J. Staples, T. E. Concolino, T. E. Haas, E. V. Rybak-Akimova, *Inorg. Chem.* **2003**, *42*, 6749.
[10] [10a] A. D. Burrows, C.-W. Chan, M. M. Chowdhry, J. E. McGrady, D. M. P. Mingos, *Chem. Soc. Rev.* **1995**, *24*, 329 and references cited therein. [10b] M. T. Allen, A. D. Burrows, M. F. Mahon, *J. Chem. Soc., Dalton Trans.* **1999**, 215. [10c] A. D. Burrows, D. M. P. Mingos, A. J. P. White, D. J. Williams, *J. Chem. Soc., Dalton Trans.* **1996**, 3805. [10d] L. Brammer, J. C. M. Rivas, R. Atencio, S. Y. Fang, F. C. Pigge, *J. Chem. Soc., Dalton Trans.* **2000**, 3855.
[11] Examples of biomimetic models of metallo-enzymes which use H-bonding for recognition are: [11a] K. Matsumura, M. Endo, M. Komiyama, *J. Chem. Soc., Chem. Commun.* **1994**, 2019. [11b] W. C. Putman, J. K. Bashkin, *Chem. Commun.* **2000**, 767. [11c] S. Matsuda, A. Ishikubo, A. Kuzuya, M. Yashiro, M. Komiyama, *Angew. Chem. Int. Ed.* **1998**, *37*, 3284.
[12] [12a] C. J. Chandler, L. W. Deady, J. A. Reiss, *J. Heterocyclic Chem.* **1981**, *18*, 599. [12b] P. T. Kaye, K. W. Wellington, *Synth. Commun.* **2001**, *31*, 799.
[13] A. A. Batista, M. O. Santiago, C. L. O. Donnici, I. S. Moreira, P. C. Healy, S. J. Berners-Price, S. L. Queiroz, *Polyhedron* **2001**, *20*, 2123.
[14] *SHELXTL PC* version 5.03, Siemens Analytical X-ray Instruments, Inc., In Madison, WI, **1994**; *SHELXTL PC* version 5.1, Bruker AXS, Madison, WI, **1997**.
[15] C. Lee, W. Yang, R. G. Parr, *Phys. Rev. B* **1988**, *37*, 785.
[16] B. Miehlich, A. Savin, H. Stoll, H. Preuss, *Chem. Phys. Lett.* **1989**, *157*, 200.
[17] A. D. Becke, *J. Chem. Phys.* **1993**, *98*, 5648.
[18] [18a] J. S. Binkley, J. A. Pople, W. J. Hehre, *J. Am. Chem. Soc.* **1980**, *102*, 939. [18b] M. S. Gordon, J. S. Binkley, J. A. Pople, W. J. Pietro, W. J. Hehre, *J. Am. Chem. Soc.* **1982**, *104*, 2797. [18c] W. J. Pietro, M. M. Francl, W. J. Hehre, D. J. Defress, J. A. Pople, J. S. Binkley, *J. Am. Chem. Soc.* **1982**, *104*, 5039. [18d] K. D. Dobbs, W. J. Hehre, *J. Comp. Chem.* **1986**, *7*, 359. [18e] K. D. Dobbs, W. J. Hehre, *J. Comp. Chem.* **1987**, *8*, 861. [18f] K. D. Dobbs, W. J. Hehre, *J. Comp. Chem.* **1987**, *8*, 880.
[19] Gaussian 98, Revision A.11.3, M. J. Frisch, G. W. Trucks, H. B. Schlegel, G. E. Scuseria, M. A. Robb, J. R. Cheeseman, V. G. Zakrzewski, J. A. Montgomery, Jr., R. E. Stratmann, J. C. Burant, S. Dapprich, J. M. Millam, A. D. Daniels, K. N. Kudin, M. C. Strain, O. Farkas, J. Tomasi, V. Barone, M. Cossi, R. Cammi, B. Mennucci, C. Pomelli, C. Adamo, S. Clifford, J. Ochterski, G. A. Petersson, P. Y. Ayala, Q. Cui, K. Morokuma, N. Rega, P. Salvador, J. J. Dannenberg, D. K. Malick, A. D. Rabuck, K. Raghavachari, J. B. Foresman, J. Cioslowski, J. V. Ortiz, A. G. Baboul, B. B. Stefanov, G. Liu, A. Liashenko, P. Piskorz, I. Komaromi, R. Gomperts, R. L. Martin, D. J. Fox, T. Keith, M. A. Al-Laham, C. Y. Peng, A. Nanayakkara, M. Challacombe, P. M. W. Gill, B. Johnson, W. Chen, M. W. Wong, J. L. Andres, C. Gonzalez, M. Head-Gordon, E. S. Replogle, and J. A. Pople, Gaussian Inc., Pittsburgh, PA, **2002**.

Received November 3, 2003
Early View Article
Published Online March 18, 2004

 © 2004 Wiley-VCH Verlag GmbH & Co. KGaA, Weinheim

A Novel Pentacoordinated Dioxovanadium(v) Salicylaldiminate: Solvent Specific Crystallization of Dimorphs with Contrasting Coordination Geometries, Ligand Conformations and Supramolecular Architectures

Bharat Baruah,[a] Sankar Prasad Rath,[a] and Animesh Chakravorty*[a,b]

Keywords: Vanadium / O ligands / Dimorphism / Supramolecular architecture

The reaction of the tridentate salicylaldimine of 2-picolylamine, $C_6H_4(OH)CHNCH_2C_5H_4N$ (HL), with bis(acetylacetonato)oxovanadium(IV) at room temperature under oxygen (or with $VOSO_4 \cdot 5H_2O$ plus H_2O_2) furnished crystalline greenish-yellow α-VO_2(L) and green β-VO_2(L) from methanol (or ethanol) and acetonitrile (or dichloromethane), respectively. The dimorphs give rise to the same solution species as revealed by spectroscopic data (UV/Vis, ^{1}H and ^{51}V NMR). Both forms react with 3,5-bis(*tert*-butyl)catechol (H_2dbcat) furnishing the known pseudooctahedral complex VO(L)(dbcat). In the α form the V(L) fragment is planar and the VO_3N_2 coordination sphere is distorted trigonal bipyramidal (τ = 0.55) with the two oxo oxygen atoms and the azomethine nitrogen atom defining the trigonal plane. In β-VO_2(L) the V(L) moiety, like that in VO(L)(dbcat), is not planar but consists of two planar parts rotated away from each other along the C–N single bond. In this case the coordination sphere is distorted square pyramidal (τ = 0.20) with the three donor sites of the L ligand and an oxo oxygen atom defining the tetragonal plane. Both the α and β crystal lattices consist of dimers which associate further to form supramolecules. The noncovalent intradimer and interdimer bonding interactions are predominantly of aromatic π-π stacking (aryl···pyridyl and pyridyl···pyridyl) and C–H···O hydrogen bonding (azomethine···oxo and aryl···phenolato) types in the α and β dimorphs, respectively. It is proposed that the low polarizability of methanol promotes π-π stacking of planar V(L) fragments, resulting in crystallization of the α form. When the polarizability is relatively high, as in acetonitrile, the β form crystallizes. The geometrically isomeric coordination spheres of the α and β forms are sustained by the respective supramolecular architectures. The Schiff base HL′ of 2-hydroxynapthaldehyde and 2-picolylamine has also afforded two forms of VO_2(L′) in the same manner as for VO_2(L).
(© Wiley-VCH Verlag GmbH & Co. KGaA, 69451 Weinheim, Germany, 2004)

Introduction

The long-standing interest in the structure and properties of mononuclear VO_2^+ complexes[1] has multiplied with the emergence of bioinorganic linkages to the RNase transition state,[2] vanadium dependent haloperoxidase[3,4] and insulin mimicry.[5] The coordination number of the metal in VO_2^+ complexes can be six,[1,6] but the focus of the present work is on pentacoordinate species of type VO_2(tridentate), which have attracted special attention in recent years. The geometry of structurally characterized compounds of the latter type is (relatively rarely) distorted trigonal bipyramidal (dtbp, α form, as shown in **1**),[7] the common geometry being distorted square pyramidal (dsp, β form, as in **2**).[8−10] The latter geometry is particularly relevant in the context of the RNase transition state[2] and haloperoxidase activity.[3]

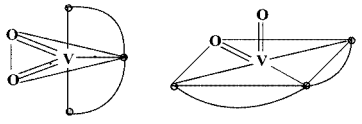

dtbp (α form) dsp (β form)

1 **2**

In the present work we report the synthesis and characterization of a remarkable pentacoordinate VO_2^+ system which has been isolated in two distinct crystalline forms by merely varying the solvent employed in the synthesis. The solid-state structural features of the dimorphs (which otherwise display identical chemical composition and solution properties) differ dramatically in coordination geometry, ligand conformation and supramolecular architecture. To the best of our knowledge, structural dimorphism of the present type is unprecedented in VO_2^+ solid-state chemistry.

[a] Department of Inorganic Chemistry, Indian Association for the Cultivation of Science,
Kolkata 700 032, India
[b] Jawaharlal Nehru Centre for Advanced Scientific Research,
Bangalore 560064, India
Fax: (internat.) +91-33-2473-2805
E-mail: icac@mahendra.iacs.res.in

Results and Discussion

Synthesis of Dimorphs

The tridentate ligand concerning us in this work is the salicylaldimine of 2-picolylamine (HL, **3**). It reacted smoothly with $VO(acac)_2$ in methanol solution at room temperature in the presence of oxygen, furnishing in excellent yield a greenish-yellow crystalline complex of composition $VO_2(L)$, designated as the α dimorph.

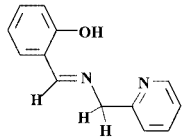

HL

3

A similar reaction occurred in acetonitrile solution to give the β dimorph; this complex had the same composition, but was green. The same dimorphs were also synthesized by reacting $VOSO_4{\cdot}5H_2O$ with HL using hydrogen peroxide as the oxidant (Scheme 1). The possible role of the solvent in crystallization of specific dimorphs will be considered later.

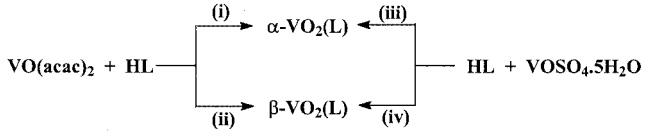

Scheme 1. Synthesis of dimorphic $VO_2(L)$ at room temperature; (i) MeOH, O_2; (ii) MeCN, O_2; (iii) MeOH, H_2O_2; (iv) MeCN, H_2O_2

Spectra and Solution Behaviour

Spectral data are given in the Exp. Sect. Both forms display two V=O stretches near 920 and 940 cm^{-1} (KBr disk), consistent with *cis* geometry of the VO_2 moiety. Both dimorphs are insoluble except in solvents like *N*,*N*-dimethylformamide and dimethyl sulfoxide. The pale yellow solutions display identical UV/Vis spectra (within experimental error), and display a band at 395 nm. In dimethyl sulfoxide solutions the two forms give rise to identical ^{51}V NMR spectra, with a signal at $\delta = -535$ ppm. The well-resolved ^1H NMR spectra of both the α and β forms in $[D_6]$dimethyl sulfoxide are also superimposable. Thus, α-$VO_2(L)$ and β-$VO_2(L)$ must give rise to the same species in mobile solution.

Reaction with a Catechol

In dichloromethane suspension, both α and β-$VO_2(L)$ react [as shown in Equation (1)] with aromatic diols such as 3,5-di-*tert*-butylcatechol (H_2dbcat) furnishing the violet complex VO(L)(dbcat) (**4**), which is already known from the reaction of $VO(acac)_2$ with HL and H_2dbcat in air.[11] The conformation of the L ligand in VO(L)(dbcat) has close similarities to that in β-$VO_2(L)$; the significance of this is considered later.

$$VO_2(L) + H_2dbcat \rightarrow VO(L)(dbcat) + H_2O \quad (1)$$

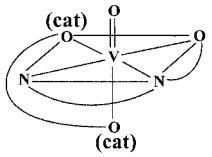

4

Structure

The α and β dimorphs have distinctive crystal, molecular and supramolecular structures. They belong respectively to the monoclinic and triclinic crystal systems. Molecular views are given in Figure 1 and 2; selected bond parameters are listed in Table 1. In both forms, the VO_2 fragment has a *cis* geometry and the tridentate ligand is meridionally disposed. The coordination sphere is of type VO_3N_2. The metal−ligand bond lengths in the two forms are equal to within 0.02 Å. However, there are major differences in the coordination geometry, V(L) conformation and noncovalent intermolecular interactions.

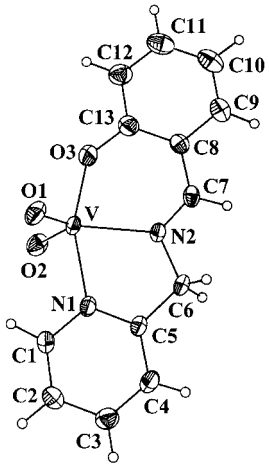

Figure 1. Perspective view and atom labeling scheme of α-$VO_2(L)$. All non-hydrogen atoms are represented by 30% thermal probability ellipsoids

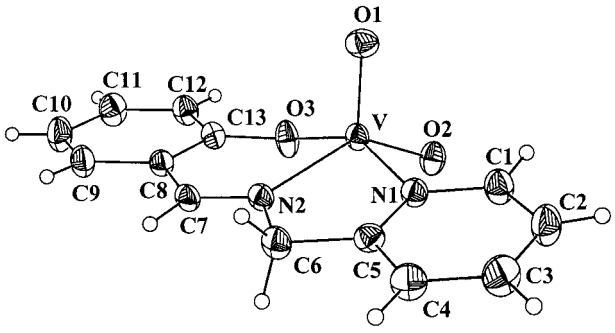

Figure 2. Perspective view and atom labeling scheme of β-$VO_2(L)$. All non-hydrogen atoms are represented by 30% thermal probability ellipsoids

 © 2004 Wiley-VCH Verlag GmbH & Co. KGaA, Weinheim

Table 1. Selected bond lengths [Å] and angles [°] for α-VO_2(L) and β-VO_2(L)

	α-VO_2(L)	β-VO_2(L)
V−O(1)	1.617(2)	1.613(2)
V−O(2)	1.615(2)	1.627(2)
V−O(3)	1.901(2)	1.903(2)
V−N(1)	2.113(2)	2.134(2)
V−N(2)	2.129(2)	2.145(2)
O(1)−V−O(2)	109.4(1)	109.2(1)
O(1)−V−O(3)	100.2(1)	105.5(1)
O(2)−V−O(3)	100.7(1)	97.1(1)
O(1)−V−N(1)	90.9(1)	98.2(1)
O(1)−V−N(2)	123.0(1)	109.4(1)
O(2)−V−N(1)	92.3(1)	89.4(1)
O(2)−V−N(2)	125.8(1)	139.7(1)
O(3)−V−N(1)	159.0(1)	151.7(1)
O(3)−V−N(2)	83.8(1)	83.4(1)
N(1)−V−N(2)	75.2(1)	74.2(1)

Coordination Geometry

In the α form, the V(L) fragment constitutes a plane (mean deviation, 0.03 Å), which makes a dihedral angle of 90.5 with the VO_2 plane. The double bonds in the latter fragment constrain the O1−V−O2 angle to about 109°, as is generally observed among pentacoordinated VO_2 complexes.[7−10]

An important feature of the α structure is that the metal atom is shifted only by about 0.1 Å from the O1−O2−N2 plane towards the O3 atom, and the N2 atom is approximately symmetrically positioned with respect to the Ol and O2 atoms, the O1−V−N2 and O2−V−N2 angles being 123.0(1) and 125.8(1)°, respectively [N2···O1, 3.301(7) Å and N2···O2, 3.341(7) Å]. The rigidity of the L ligand constrains the O3−V−N1 angle to 159.0(1)°.

The coordination geometry of α-VO_2(L) is thus best described as dtbp (trigonal plane O1−O2−N2). The τ parameter[12] (equal to Δ/60°, where Δ is the difference between the largest and the next-to-largest ligand−metal−ligand angles) is a useful geometrical discriminator; Δ = 60, τ = 1 for idealized tbp and Δ = 0, τ = 0 for idealized sp).[12] The τ value of α-VO_2(L) is 0.55. In representative structures of VO_2(tridentate) species the τ values generally lie well below 0.50 and in most cases below 0.40.[7−10] Thus α-VO_2(L) approaches the tbp geometry more closely than any other known member of the VO_2(tridentate) family.

The V(L) moiety in the β form is not planar and it actually consists of two highly planar fragments: C1−C6, N1, V (plane A, mean deviation, 0.01 Å) and C7−C13, N2, O3 (plane B, mean deviation, 0.02 Å). Plane A is rotated away from plane B by 11.2° along the C6−N2 bond. The metal atom is shifted from plane B by 0.53 Å, and thus the six-membered chelate ring is folded by 20.4° along the N2···O3 line.

Whereas the rigid O1−V−O2 angle remains virtually unchanged near 109°, V(L) nonplanarity results in major changes in the other angles at the metal compared to those in the α form. Thus, the O1−V−N2 angle decreases by about 14° to 109.4(1)° and the O2−V−N2 angle increases by a similar amount to 139.7(1)°. The O3−V−N1 angle is also contracted by about 7° to 151.7(1)°. The net result of these angular changes is that the O2, O3, N1 and N2 atoms in the β form constitute an approximate tetragonal plane, from which the metal atom is displaced by 0.51 Å towards the O1 atom. Therefore, the coordination geometry in the β form can be aptly described as dsp, which is also consistent with its low τ value of 0.20.

The structure of β-VO_2(L) bears certain qualitative similarities to that[11] of pseudooctahedral V(L)(dbcat) **4**. A significant feature is that the nonplanar V(L) fragment in **4** also consists of two planar fragments of types A and B (dihedral angle 19.7°). The approximate tetragonal plane is again of N_2O_2 type from which the metal atom is displaced towards the oxo atom (by 0.28 Å). The nonplanarity of the V(L) fragment appears to be crucial for achieving a tetragonal equator, be it in β-VO_2(L) or in VO(L)(dbcat).

Aromatic Stacking and Hydrogen Bonding: Dimers and Supramolecules

All the hydrogen atoms in both α-VO_2(L) and β-VO_2(L) were directly located by difference Fourier maps. Both the lattices consist of dimers, which associate further to form supramolecules. The noncovalent intradimer and interdimer bonding interactions are primarily of the π-π stacking and C−H···O hydrogen-bonding type. These interactions can be seen in the partial packing diagrams shown in Figure 3 and 4; the relevant distances are listed in Table 2.

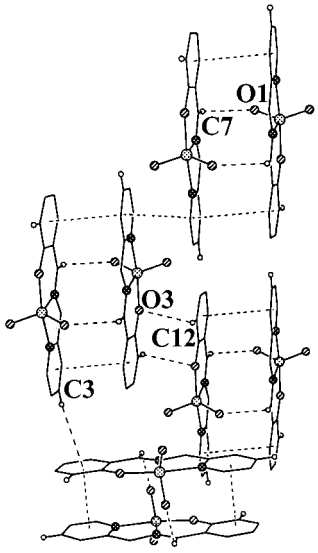

Figure 3. Supramolecular structure of the α-VO_2(L) lattice; hydrogen atoms other than H3, H7 and H12 have been omitted for clarity and noncovalent interactions are indicated by dotted lines

In the α dimers the (virtually parallel) V(L) planes are held together by a pair of aryl···pyridyl π-π interactions and a pair of azomethine···oxo (C7−H7···O1) hydrogen bonding interactions(Figure 3). The distance between the centroids of the overlapping aryl and pyridyl rings (ar···py in Table 2), 3.716(7) Å, is consistent[13,14] with the presence of an attractive π-π interaction. The ar···py line subtends an

 © 2004 Wiley-VCH Verlag GmbH & Co. KGaA, Weinheim

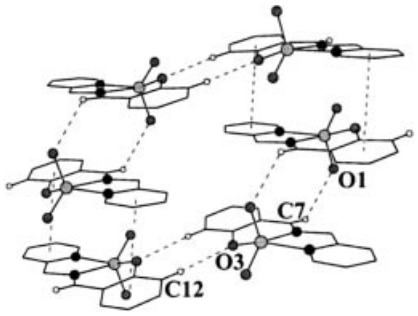

Figure 4. Supramolecular structure of the β-VO_2(L) lattice. Hydrogen atoms other than H7 and H12 have been omitted for clarity and noncovalent interactions are indicated by dotted lines

Table 2. Distances [Å] and angles [°] characterizing aromatic π-π stacking and C−H···O hydrogen bonding in the two dimorphs

	α-VO_2(L)	β-VO_2(L)
ar···py[a]	3.716(7)	3.752(7)
py···py[a]	3.520(6)	–
C(7)···O(1)	3.185(7)	3.063(6)
H(7)···O(1)	2.62(9)	2.51(8)
C(12)···O(3)	3.550(7)	3.431(6)
H(12)···O(3)	2.95(8)	2.56(9)
C(7)−H(7)···O(1)	120(1)	123(1)
C(12)−H(12)···O(3)	123(1)	176(1)

[a] ar = aryl ring centroid; py = pyridyl ring centroid.

angle of 10.4° with the aryl ring normal, and 10.8° with the pyridyl ring normal. The offset of the parallel rings is thus small, signifying strong stacking. In metal complexes of pyridyl ligands π-π stacking is usually associated with a larger offset (about 20°).[13] The bond parameters of the C7−H7···O1 fragment (Table 2) are consistent with the presence of significant hydrogen bonding. The accepted ranges are 3.0−3.5 Å (C···O), 2.3−3.0 Å (H···O) and 100−180° (C−H···O).[15−18]

Interdimer bonding in the α form consists of a relatively strong pyridyl···pyridyl π−π overlap [py···py, 3.520(6) Å] with a very small offset (5.6°), and aryl···phenol (C12−H12···O3) hydrogen bonding which is significantly weaker than the intradimer C7−H7···O1 bonding. There is also a weak interdimer edge-to-face interaction[13,17,19] between the pyridyl C3−H3 and aryl fragments, the centroid of the latter being 3.31(9) Å and 3.889(8) Å away from the H3 and C3 atoms, respectively. The C3−H3···ar angle is 124°. The C10 carbon atom of the aryl ring lies closest to H3 [distance 2.91(8) Å].

The nonplanarity of the V(L) fragment in the β form results in increased intradimer aryl···pyridyl separation, marginalizing the π-π interaction [ar···py, 4.086(8) Å]. On the other hand, the azomethine function now lies closer to the O1 atom, thus resulting in stronger intradimer C7−H7···O1 hydrogen bonds than in the α dimer (Table 2). The interdimer association is also dominated by the relatively strong hydrogen bonding which occurs between the aryl and phenolato functions, the site of action being the nearly linear C12−H12···O3 moiety. Interdimer aryl···pyridyl stacking (offset 19.9°) also contributes to supramolecule formation in the β form.

Solvent Specific Crystallization

In summary, π-π stacking and C−H···O hydrogen bonding are the respective dominant features in the supramolecular architectures of the α and β forms of VO_2(L). This provides some insight into the possible nature of the role of solvent in dimorph crystallization. It is known that solvents like water and small alcohols with low polarizability and high cohesive interaction lead to aggregation of lipophilic molecular π surfaces in solutes.[13,20] It is therefore logical to propose that such effects lead to π-π stacking in the case of VO_2(L), with consequent crystallization of the α form from methanol (we have found ethanol to be just as effective). The planar V(L) configuration and the associated dtbp geometry may very well be the consequence of maximization of the π-π stacking interactions in the lattice. The tendency towards lipophilic aggregation is considerably diminished in solvents of significantly higher polarizability such as acetonitrile (dichloromethane is found to behave similarly);[20c] in these cases the β form crystallizes, with a structure dominated by polar interactions (viz. strong C−H···O hydrogen bonding) rather than π-π stacking. This is best achieved when the V(L) configuration is nonplanar and consequently the coordination geometry is dsp. The synthesis of α and β forms of VO_2(L) is an instance of solvent-directed crystal engineering. The two geometrical isomeric coordination spheres are sustained by their characteristic supramolecular architectures.

On the basis of the above logic we expected that 2-hydroxynapthaldimine(HL′, **5**) of 2-picolylamine should also yield dimorphs. Indeed, two forms of VO_2(L′) have been isolated by the same procedures employed for the VO_2(L) dimorphs.

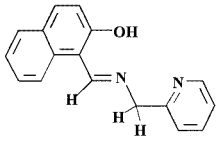

HL′

5

Selected characterization data is given in the Exp. Sect. Unfortunately, neither α-VO_2(L′) nor β-VO_2(L′) afforded single crystals suitable for structure determination. A search for other examples of the VO_2(tridentate) family showing similar dimorphism is continuing.

Conclusions

A remarkable case of solvent-directed crystal engineering has been revealed in the synthesis of VO_2(L) in dimorphic α and β forms, isolated from methanol and acetonitrile, respectively.

 © 2004 Wiley-VCH Verlag GmbH & Co. KGaA, Weinheim

The two forms differ strongly in both their coordination geometries (dtbp versus dsp) and supramolecular architecture (aromatic π-π stacking versus C−H···O hydrogen bonding), the former being a consequence of the latter.

This solvent-specific dimorph crystallization is qualitatively consistent with relative polarizability; the $VO_2(L')$ dimorphs appear to be similar to those of $VO_2(L)$.

Experimental Section

General: Bis(acetylacetonato)oxovanadium(IV) was prepared by literature methods.[21] 2-Picolylamine, salicylaldehyde, 2-hydroxynapthaldehyde and acetylacetone were obtained from Aldrich. Vanadyl sulfate pentahydrate was purchased from Loba Chemie (India) and 30% hydrogen peroxide was obtained from S. D. Fine Chem. (India). All other chemicals and solvents were of analytical grade and were used as received. Spectra were recorded using the following equipment: IR (KBr disk), Nicolet Magna 750 Series II spectrometer. UV/Vis, Shimadzu UVPC 1601 spectrometer. ^{1}H NMR, Bruker FT 300 MHz spectrometer (assignments were based on chemical shifts and spin-spin structures) and ^{51}V NMR, Varian 78.8 MHz spectrometer ($VOCl_3$ external reference). A Perkin−Elmer 240C elemental analyzer was used for microanalysis (C, H, N).

HL: 2-Picolylamine (0.885 g, 8.2 mmol) was added to a solution of salicylaldehyde (1 g, 8.2 mmol) in ethanol (15 mL). After refluxing the mixture for half an hour, the solvent was removed in a rotary evaporator and the yellow oil thus obtained used without further purification.

HL′: Prepared similarly, using 2-hydroxynapthaldehyde in place of salicylaldehyde.

α-VO_2(L): A solution of HL (0.159 g, 0.75 mmol) in methanol (5 mL) was added to a solution of $VO(acac)_2$ (0.2 g, 0.75 mmol) in methanol (50 mL). Pure oxygen was bubbled through the deep red solution for 5 h with stirring. The greenish-yellow precipitate that appeared was filtered off, washed with dichloromethane, and dried in vacuo over fused $CaCl_2$. Yield: 0.171 g (77%). $C_{13}H_{11}N_2O_3V$ (294.18): calcd. C 53.08, H 3.77, N 9.52; found C 53.14, H 3.85, N 9.58. IR (KBr): $\tilde{\nu}$ = 921, 939 (s, V=O), 1621 (s, C=N) cm^{-1}. UV/Vis (DMF): $\lambda_{max.}$ (ε, M^{-1}·cm^{-1}) = 395 nm (1810). ^{1}H NMR ([D$_6$]DMSO): δ = 5.60 (s, 2 H, −CH_2−), 9.06 (s, 1 H, −CH=N), 8.95 (br., 1 H, −C_6H_4), 8.15 (t, J = 6.0 Hz, 1 H, −C_6H_4), 7.80 (d, J = 6.0 Hz, 1 H, −C_6H_4), 7.52 (t, J = 7.5 Hz, 1 H, −C_6H_4), 7.64 (t, J = 6.0 Hz, 2 H, −C_5H_4N), 6.87 ppm (d, J = 6.0 Hz, 2 H, −C_5H_4N) ppm. ^{51}V NMR ([D$_6$]DMSO): δ = −535 ppm.

Synthesis from $VOSO_4$·5H_2O: 30% Hydrogen peroxide (1 mL) was added to a suspension of $VOSO_4$·5H_2O (0.2 g, 0.79 mmol) in methanol (50 mL). 15 min of stirring resulted in the formation of an orange-red solution, to which a solution of HL (0.168 g, 0.79 mmol) in methanol (5 mL) was added. The dark-brown solution was kept undisturbed in air at room temperature. After 24 h, the crystalline product deposited was filtered off, washed with methanol and dried in vacuo under fused $CaCl_2$. This afforded 0.168 g (72%) of α-VO_2(L).

β-VO_2(L): Prepared as for α-VO_2(L), but using acetonitrile instead of methanol. Yield: 0.164 (74%). $C_{13}H_{11}N_2O_3V$ (294.18): calcd. C 53.08, H 3.77, N 9.52; found C 53.19, H 3.82, N 9.57. IR (KBr): $\tilde{\nu}$ = 918, 939 (s, V= O), 1626 (s, C=N) cm^{-1}. UV/Vis (DMF): $\lambda_{max.}$ (ε, M^{-1}·cm^{-1}) = 395 nm (1789). ^{1}H NMR ([D$_6$]DMSO): δ = 5.60 (s, 2 H, −CH_2−), 9.06 (s, 1 H, −CH=N), 8.95 (br., 1 H, −C_6H_4), 8.15 (t, J = 6.0 Hz, 1 H, −C_6H_4), 7.80 (d, J = 6.0 Hz, 1 H, −C_6H_4), 7.52 (t, J = 7.5 Hz, 1 H, −C_6H_4), 7.64 (t, J = 6.0 Hz, 2 H, −C_5H_4N), 6.87 ppm (d, J = 6.0 Hz, 2 H, −C_5H_4N) ppm. ^{51}V NMR ([D$_6$]DMSO): δ = −535 ppm.

Synthesis from $VOSO_4$·5H_2O: Prepared as for α-VO_2(L), but using acetonitrile instead of methanol. Yield: 0.174 g (75%).

α-VO_2(L′): Prepared as for α-VO_2(L), but using HL′ instead of HL. Yield: 0.197 g (76%). $C_{17}H_{13}N_2O_3V$ (344.24): calcd. C 59.32, H 3.81, N 8.14; found C 59.38, H 3.89, N. 8.17. IR (KBr): $\tilde{\nu}$ = 925, 941 (s, V=O), 1626 (s, C=N) cm^{-1}. UV/Vis (DMF): $\lambda_{max.}$ (ε, M^{-1}·cm^{-1}) = 412 nm (2068). ^{1}H NMR ([D$_6$]DMSO): δ = 5.76 (s, 2 H, −CH_2−), 9.89 (s, 1 H, −CH=N), 8.94 (d, J = 6.0 Hz, 1 H, −$C_{10}H_6$), 8.42 (d, J = 6.0 Hz, 1 H, −$C_{10}H_6$), 8.21 (t, J = 6.0 Hz, 1 H, −$C_{10}H_6$), 8.09 (d, J = 9.0 Hz, 1 H, −$C_{10}H_6$), 7.42 (t, J = 7.5 Hz, 1 H, −$C_{10}H_6$), 7.14 (d, J = 9.0 Hz, 1 H, −$C_{10}H_6$), 7.88 (t, J = 7.5 Hz, 2 H, −C_5H_4N), 7.65 (d, J = 9.0 Hz, 2 H, −C_5H_4N) ppm.

Synthesis of α-VO_2(L′) from $VOSO_4$·5H_2O: Prepared as for α-VO_2(L), but using HL′ instead of HL. Yield 0.193 g (71%).

β-VO_2(L′): Prepared as for α-VO_2(L′), but using acetonitrile instead of methanol. Yield: 0.183 g (71%). $C_{17}H_{13}N_2O_3V$ (344.24): calcd. C 59.32, H 3.81, N 8.14; found C 59.34, H 3.85, N. 8.15. IR (KBr): $\tilde{\nu}$ = 923, 942 (s, V=O), 1623 (s, C=N) cm^{-1}. UV/Vis (DMF): $\lambda_{max.}$ (ε, M^{-1}·cm^{-1}) = 412 nm (2026). ^{1}H NMR ([D$_6$]DMSO): δ = 5.76 (s, 2 H, −CH_2−), 9.89 (s, 1 H, −CH=N), 8.94 (d, J = 6.0 Hz, 1 H, −$C_{10}H_6$), 8.42 (d, J = 6.0 Hz, 1 H, −$C_{10}H_6$), 8.21 (t, J = 6.0 Hz, 1 H, −$C_{10}H_6$), 8.09 (d, J = 9.0 Hz, 1 H, −$C_{10}H_6$), 7.42 (t, J = 7.5 Hz, 1 H, −$C_{10}H_6$), 7.14(d, J = 9.0 Hz, 1 H, −$C_{10}H_6$), 7.88 (t, J = 7.5 Hz, 2 H, −C_5H_4N), 7.65 (d, J = 9.0 Hz, 2 H, −C_5H_4N) ppm.

Synthesis of β-VO_2(L′) from $VOSO_4$·5H_2O: Prepared as for α-VO_2(L′), but using acetonitrile instead of methanol. Yield: 0.201 g (74%).

Conversion of VO_2(L) to VO(L)(dbcat): 3,5-Bis(*tert*-butyl)catechol (H_2dbcat) (0.076 g, 0.34 mmol) was added to a suspension of either form of VO_2(L) (0.10 g, 0.34 mmol) in dichloromethane (20 mL). The mixture was stirred for 8 h and the violet-coloured solution concentrated and left to evaporate in the air. The crystalline product thus obtained was washed with cold methanol and dried in vacuo over fused $CaCl_2$. Yield: 0.134 g (76%). This complex was found to be identical in all respects with that reported earlier.[11]

Crystal Structure Determination: Single crystals of α-VO_2(L) and β-VO_2(L) were obtained directly during synthesis but without stirring of the oxygen-saturated reaction mixture (vide supra). The undisturbed solution deposited suitable single crystals within a few days. Data were collected with a Nicolet R3m/V four-circle diffractometer with graphite-monochromated Mo-K_α radiation (λ = 0.71073 Å) using the ω-scan technique ($3 \le 2\theta \le 48°$ for both the α and β forms). All data were corrected for Lorentz polarization, and an empirical absorption correction[22] was performed on each set of data on the basis of the azimuthal scans of six reflections. All calculations of data reduction, structure solution and refinement were done with the programs of SHELXTL, version 5.03.[23] The two structures were solved by direct methods and refined by full-matrix least-squares on F^2. All non-hydrogen atoms were refined anisotropically. All the hydrogen atoms in two structures were located in the difference Fourier maps. Significant crystal data are listed in Table 3. Supplementary crystallographic data have been deposited.

 © 2004 Wiley-VCH Verlag GmbH & Co. KGaA, Weinheim

CCDC-168305 [for α-VO_2(L)] and -168304 [for β-VO_2(L)] contain the supplementary crystallographic data for this paper. These data can be obtained free of charge at www.ccdc.cam.ac.uk/conts/retrieving.html [or from the Cambridge Crystallographic Data Centre, 12 Union Road, Cambridge CB2 1EZ, UK; Fax: (internat.) +44-1223-336-033; E-mail: deposit@ccdc.cam.ac.uk].

Table 3. Crystallographic data for α-VO_2(L) and β-VO_2(L)

	α-VO_2(L)	β-VO_2(L)
Empirical formula	$C_{13}H_{11}N_2O_3V$	$C_{13}H_{11}N_2O_3V$
Mr [g·mol^{-1}]	294.18	294.18
Crystal size [mm]	0.40 × 0.30 × 0.20	0.40 × 0.30 × 0.25
T [K]	293(2)	293(2)
Crystal system	monoclinic	triclinic
Space group	$P2_1/n$ (no. 14)	$P\bar{1}$ (no. 2)
a (Å)	10.723(2)	7.798(2)
b (Å)	10.270(2)	8.363(2)
c (Å)	11.944(2)	9.585(2)
α [°]	–	80.92(3)
β [°]	108.36(3)	89.47(3)
γ [°]	–	82.76(3)
V (Å^3)	1248.4(4)	612.3(2)
Z	4	2
Calcd. density [g·cm^{-3}]	1.565	1.596
μ [mm^{-1}]	0.799	0.814
R_{int}	0.0189	0.0085
Reflections measured	2115	1985
Independent reflections	1970	1929
R_1 [$I > 2\sigma(I)$]	0.0336	0.0279
wR_2 [$I > 2\sigma(I)$]	0.0759	0.0766
Goodness of fit on F^2	1.087	1.101

Acknowledgments

We acknowledge financial support received from the Department of Science and Technology and Council of Scientific and Industrial Research, New Delhi. We are thankful to Prof. G. K. Lahiri for help.

[1] [1a] W. R. Scheidt, D. M. Collins, J. L. Hoard, *J. Am. Chem. Soc.* **1971**, *93*, 3873−3877. [1b] W. R. Scheidt, R. Countryman, J. L. Hoard, *J. Am. Chem. Soc.* **1971**, *93*, 3878−3882. [1c] W. R. Scheidt, C. Tasi, J. L. Hoard, *J. Am. Chem. Soc.* **1971**, *93*, 3867−3872. [1d] R. E. Drew, F. W. B. Einstein, S. E. Gransden, *Can. J. Chem.* **1974**, *52*, 2184−2189.

[2] [2a] R. N. Lindquist, J. L. Lynn, G. E. Lienhard, *J. Am. Chem. Soc.* **1973**, *95*, 8762−8768. [2b] B. Borah, C. Chen, W. Egan, M. Miller, A. Wlodawer, J. C. Cohen, *Biochemistry* **1985**, *24*, 2058−2067.

[3] [3a] R. I. De la Rosa, M. J. Clague, A. Butler, *J. Am. Chem. Soc.* **1992**, *114*, 760−761. [3b] D. Rehder, *Coord. Chem. Rev.* **1990**, *182*, 297−322. [3c] A. G. J. Lightenbarg, R. Hage, B. L. Feringa, *Coord. Chem. Rev.* **2003**, *237*, 89−101.

[4] A. Butler, in *Bioinorganic Catalysis* (Eds.: J. Reedjik, E. Bouwman), Marcel Dekker, New York, **1999** 2nd ed., chapter 5.

[5] D. C. Crans, L. Yang, J. A. Alfano, L.-H. Chi, W. Jin, M. Mahroof-Tahir, K. Robbins, M.-M. Tolue, L. K. Chan, A. J. Plante, R. Z. Grayson, G. R. Willsky, *Coord. Chem. Rev.* **2003**, *237*, 13−22.

[6] [6a] A. Kojima, K. Okazaki, S. Ooi, K. Saito, *Inorg. Chem.* **1983**, *22*, 1168−1174. [6b] A. Giacomelli, C. Floriani, A. O. D. S. Duarte, A. C-Villa, C. Guastini, *Inorg. Chem.* **1982**, *21*, 3310−3316. [6c] S. G. Brand, N. Edelstein, C. J. Hawkins, G. Shalimoff, M. R. Snow, *Inorg. Chem.* **1990**, *29*, 434−438. [6d] G. Suss-Fink, S. Stanislas, G. B. Shul'pin, G. V. Nizova, H. Stoeckli-Evans, A. Neels, C. Bobillier, S. Claude, *J. Chem. Soc., Dalton Trans.* **1999**, 3169−3175.

[7] [7a] L. M. Mokry, C. J. Carrano, *Inorg. Chem.* **1993**, *32*, 6119−6121. [7b] G. Asgedom, A. Sreedhara, J. Kivikaski, E. Kolehmainen, C. P. Rao, *J. Chem. Soc., Dalton Trans.* **1996**, 93−97. [7c] M. R. Maurya, S. Khurana, W. Zhang, D. Rehder, *Eur. J. Inorg. Chem.* **2002**, 1749−1760.

[8] [8a] N. Galesic, M. Siroki, *Acta Crystallogr., Sect. B* **1979**, *35*, 2931−2937. [8b] N. Galesic, M. Siroki, *Acta Crystallogr., Sect. C* **1984**, *40*, 378−381.

[9] [9a] K. Nakajima, N. Tokida, M. Kojima, J. Fujita, *Bull. Chem. Soc. Jpn.* **1992**, *65*, 1725−1727. [9b] S. Dutta, P. Basu, A. Chakravorty, *Inorg. Chem.* **1993**, *32*, 5343−5348. [9c] V. Vergopoulous, W. Priebsch, M. Fritzsche, D. Rehder, *Inorg. Chem.* **1993**, *32*, 1844−1849. [9d] G. Asgedom, A. Sreedhara, J. Kivikoski, J. Valkonen, C. P. Rao, *J. Chem. Soc., Dalton Trans.* **1995**, 2459−2466. [9e] A. G. Lightenbarg, A. L. Spek, R. Hage, B. L. Feringa, *J. Chem. Soc., Dalton Trans.* **1999**, 659−661.

[10] [10a] L. Yang, A. Conr, O. P. Anderson, D. C. Crans, *Inorg. Chem.* **2002**, *41*, 6322−6331. [10b] M. R. Maurya, S. Khurana, W. Zhang, D. Rehder, *J. Chem. Soc., Dalton Trans.* **2002**, 3015−3023. [10c] M. R. Maurya, S. Khurana, Shailendra, A. Azam, W. Zhang, D. Rehder, *Eur. J. Inorg. Chem.* **2003**, 1996−1973. [10d] W. Plass, H.-P. Yozgatli, *Z. Anorg. Allg. Chem.* **2003**, *629*, 65−70. [10e] W. Plass, *Coord. Chem. Rev.* **2003**, *237*, 205−212.

[11] B. Baruah, S. Das, A. Chakravorty, *Inorg. Chem.* **2002**, *41*, 4502−4508.

[12] A. W. Addison, T. N. Rao, J. Reedjik, J. van Rijn, G. C. Verschoor, *J. Chem. Soc., Dalton Trans.* **1984**, 1349−1356.

[13] C. Janiak, *J. Chem. Soc., Dalton Trans.* **2000**, 3885−3896.

[14] H. W. Roesky, M. Andruh, *Coord. Chem. Rev.* **2003**, *236*, 91−119.

[15] G. R. Desiraju, *Acc. Chem. Res.* **1991**, *24*, 290−296.

[16] L. Jiang, L. Lai, *J. Biol. Chem.* **2002**, *277*, 37732−37740.

[17] G. R. Desiraju, T. Steiner, *The Weak Hydrogen Bond in Structural Chemistry and Biology*, Oxford University Press, New York, **1999**.

[18] C. Janiak, T. G. Scharmann, *Polyhedron* **2003**, *22*, 1123−1133.

[19] H. Suezawa, T. Yoshida, Y. Umezawa, S. Tsuboyama, M. Nishio, *Eur. J. Inorg. Chem.* **2002**, 3148−3155.

[20] [20a] C. A. Hunter, *Chem. Soc. Rev.* **1994**, 101−109. [20b] C. A. Hunter, *Angew. Chem. Int. Ed. Engl.* **1993**, *32*, 1584−1586. [20c] D. B. Smithrud, F. Diederich, *J. Am. Chem. Soc.* **1990**, *112*, 339−343.

[21] R. A. Rowe, M. M. Jones, *Inorg. Synth.* **1957**, *5*, 113−116.

[22] A. C. T. North, D. C. Phillips, F. S. Mathews, *Acta Crystallogr., Sect. A* **1968**, *24*, 351−359.

[23] G. M. Sheldrick, *SHELXTL*, version 5.03, Siemens Analytical Instruments, Inc., Madison, WI, **1994**.

Received August 30, 2003
Early View Article
Published Online March 23, 2004

 © 2004 Wiley-VCH Verlag GmbH & Co. KGaA, Weinheim

Ruthenium Tetraammines as a Model of Nitric Oxide Donor Compounds

José Carlos Toledo,[a] Hildo A. S. Silva,[a] Marciela Scarpellini,[a] Vânia Mori,[b] Ademir J. Camargo,[a] Mauro Bertotti,[b] and Douglas W. Franco*[a]

Dedicated to our friend and colleague Luiz Manoel Aleixo in memoriam

Keywords: Nitric oxide / Ruthenium / NO donor / N-heterocyclic ligands

The nitric oxide liberation from *trans*-$[Ru(NH_3)_4(L)(NO)]^{3+}$ (where L = py, 4-pic, isn, nic, L-His, 4-Clpy, imN) after one-electron-chemical or electrochemical reduction was investigated through spectroscopic and electrochemical techniques, reaction-product analysis and quantum-mechanic calculations. These complexes can be formally viewed as a $Ru^{II}(NO^+)$ species and the reduction site is located on the NO ligand. The $E°$ for the *trans*-$[Ru^{II}(NH_3)_4(L)(NO^+)]^{3+}$/*trans*-$[Ru^{II}(NH_3)_4(L)(NO)]^{2+}$ redox process ranges from 0.072 V vs. NHE (nic) to –0.118 V vs. NHE (imN). The specific rate constants for NO dissociation from *trans*-$[Ru^{II}(NH_3)_4(L)(NO)]^{2+}$, evaluated through double-step chronoamperometry, range from 0.025 s^{-1} (nic) to 0.160 s^{-1} (ImN) at 25 °C. The $[Ru^{II}NO^+/Ru^{II}NO^0]$ redox potential and the specific rate constant (k_{-NO}), key steps for designing nitrosyl complexes as NO-donor drug prototypes, proved to be controlled by a judicious choice of the ligand (L) trans to NO.

(© Wiley-VCH Verlag GmbH & Co. KGaA, 69451 Weinheim, Germany, 2004)

Introduction

Since the physiological roles of nitric oxide (NO) were discovered,[1,2] a great deal of effort has been put into the development of NO-carrier drugs.[3,4] The great affinity of d^6 and d^5 low-spin-metal complexes for NO and the versatility of NO on its own right as a ligand[5–7] make the nitrosyl complexes a good alternative for such a proposal.[8,9] Indeed, many metal complexes have been suggested as both promising NO scavengers and NO donors.[10–17] In general, the bonding between a d^6 low-spin-metal center and NO, which preferably assumes the MNO^+ form, is remarkably strong.[5,6] Therefore, for tailoring NO-donor compounds, procedures to generate MNO^0 species, in which NO is labile, are essential. Strategies involving photochemistry[18,19] and reduction activation[20] of nitrosyl complexes have been proposed as alternatives.

In this context, the photochemical[9,21,22] and reductive pathways[9,15,16] to induce NO liberation in *trans*-$[Ru(NH_3)_4(L)(NO)]^{3+}$ complex ions have been explored. This is a promising system, since these complexes are generally resistant to air oxidation and are water-soluble and robust under physiological conditions.[21,22] Furthermore, it is well-known that ammine ligands localized in the equatorial positions are inert towards substitution reactions,[23] allowing the control of the NO reactivity in relation to the properties of the ligand trans to NO. This paper reports on the activation of the *trans*-$[Ru(NH_3)_4L(NO)]^{3+}$ species, (where L = N-heterocyclic ligands) to induce NO release through reduction. Two main requirements for these complexes to work as NO donors in biological media are: i) the reduction potential of coordinated NO must be accessible to biological reducing agents; ii) it is necessary to control the dissociation of NO^0 from the intermediate *trans*-$[Ru(NH_3)_4L(NO)]^{2+}$. As described here, both requirements can be fulfilled by means of a judicious choice of L.

Results and Discussion

The systems dealt with in this study, the *trans*-$[Ru(NH_3)_4(L)(NO)]^{3+}$ complex ions, are EPR silent. In addition, their ν_{NO} is always higher than 1900 cm^{-1} and the Ru–N–O angle obtained by X-ray crystallography is close to 180°: *trans*-$[Ru(NH_3)_4(nic)(NO)](SiF_6)_3$ (177.0°),[21] *trans*-$[Ru(NH_3)_4(H_2O)(NO)]Cl_3$ (178.1°),[24] *trans*-$[Ru(NH_3)_4(4\text{-pic})(NO)](SiF_6)(BF_4)\cdot H_2O$ (178.6°) and *trans*-$[Ru(NH_3)_4P(OEt)_3(NO)](CF_3COO)_3$ (174.9°).[25] Based on these properties, it is reasonable to assign the $[Ru^{II}NO^+]$ formula to all these *trans*-$[Ru(NH_3)_4(L)(NO)]^{3+}$ complexes. The result of the reaction with hydroxide ions, always yielding the corresponding nitro compound,[9,21,22,26] *trans*-$[Ru(NH_3)_4(L)(NO_2)]^+$, confirms the nitrosonium character of the NO ligand in such species.

[a] Instituto de Química de São Carlos, Universidade de São Paulo, Av. Trabalhador SãoCarlense 400, 13560-970 São Carlos, Brazil
Fax: (internat.) +55-16-2739976
E-mail: douglas@iqsc.usp.br
[b] Instituto de Química, Universidade de São Paulo, Av. Prof. Lineu Prestes 748, 05508900 São Paulo, Brazil

It is well-known that nitrosyl complexes in aqueous solution react with hydroxide ions yielding the respective nitro compounds (see Equation 1), depending on both the pH of the solution and the nature of L.[5,6,21,22,26] Since nitro compounds are not expected to exhibit the hypotensive effect observed in nitrosyl complexes, the equilibrium established between the two species, *trans*-$[Ru(NH_3)_4L(NO)]^{3+}$ and *trans*-$[Ru(NH_3)_4L(NO_2)]^{+}$, in physiological pH, is a fundamental factor to be considered when utilizing nitrosyl complexes as nitric oxide donors. According to the K_{eq} data[9,21,22,26] for Equation 1, the *trans*-$[Ru(NH_3)_4L(NO)]^{3+}$ form accounts for more than 98 % of the nitrosyl complexes at pH 7.

$$trans\text{-}[Ru(NH_3)_4L(NO)]^{3+} + 2\,OH^- \overset{K_{eq}}{\rightleftharpoons} trans\text{-}[Ru(NH_3)_4L(NO_2)]^{+} + H_2O \quad (1)$$

Cyclic voltammograms of *trans*-$[Ru(NH_3)_4(L)(NO)]^{3+}$ aqueous solutions show only one monoelectronic redox process between −0.6 V and 1.0 V versus SCE,[21,22] which was attributed to the couple $Ru^{II}NO^+/Ru^{II}NO^0$, in Equation (2):

$$trans\text{-}[Ru^{II}(NH_3)_4(L)(NO^+)]^{3+} + e^- \longrightarrow trans\text{-}[Ru^{II}(NH_3)_4(L)(NO^0)]^{2+} \quad (2)$$

DFT computation[27] for *trans*-$[Ru^{II}(NH_3)_4(L)(NO^+)]^{3+/2+}$ (where L = NH_3, Cl^-, OH^-, py and pz), indicates that the LUMO is always predominantly on the π* of NO (68−70%), although the HOMO is dependent on the nature of L: 90−95 % Ru (dxy) for L = NH_3, Cl^-, OH^- and 100 % L (πL) for L = pyridine and pyrazine. Thus, the one-electron reduction of these complexes is expected to generate $[Ru^{II}NO^0]$ species. Indeed, the coordinated NO radical have been detected through electron paramagnetic-resonance spectroscopy[28] for the reduced form of the *trans*-$[Ru(NH_3)_4(H_2O)(NO)]^{3+}$ ion. Considering the structural and chemical similarities among all title complexes, such behavior is expected to be general for the whole series. A similar EPR spectrum[28] was also observed for the one-electron reduced species of *trans*-$[RuPP(Cl)(NO)]^{2+}$ PP = $(C_2H_5)_2P(CH_2)_2P(C_2H_5)_2$ or $(C_6H_5)_2P(CH_2)_2P(C_6H_5)_2$, *trans*-$[Ru(cyclam)(Cl)(NO)]^{2+}$ and $[Ru(bipy)_2(Cl)(NO)]^{2+}$.[29]

The reduced species, *trans*-$[Ru(NH_3)_4(L)(NO)]^{2+}$, releases NO^0 according to Equation (3).

$$trans\text{-}[Ru(NH_3)_4(L)(NO)]^{2+} + H_2O \longrightarrow trans\text{-}[Ru(NH_3)_4(L)(H_2O)]^{2+} + NO^0 \quad (3)$$

The presence of free NO in solution, after reduction of the nitrosyl complexes, was detected by cyclic voltammetric and differential-pulse polarographic experiments ($E°$ NO^+/NO^0 = +0.80 V vs. SCE).[30−32] The presence of the resulting aqua species, *trans*-$[Ru(NH_3)_4(L)(H_2O)]^{2+}$, was also evident from the electronic spectra and voltammetric behavior. Furthermore, the resulting solutions are EPR silent at liquid nitrogen temperature.

The *trans*-$[Ru(NH_3)_4L(NO)]^{2+}$ ions were generated through chemical [Cd(Hg) and Eu^{II}] or electrochemical reduction. Figure 1 shows typical UV/Vis spectra for *trans*-$[Ru(NH_3)_4(py)(NO)]^{3+}$, when the solution is electrolyzed in a spectroelectrochemical experiment as a function of time. The observed bathochromic shift (from λ_{226} and λ_{267} to λ_{256} and λ_{330})[33] is consistent with the lower π-acceptor ability of the NO^0 ligand relative to the NO^+ ligand. The appearance of a band at 406 nm during the experiment is in agreement with the formation of *trans*-$[Ru(NH_3)_4(py)(H_2O)]^{2+}$, since this species absorbs strongly in this region (ε_{406} = 3.4 × 10^3 M^{-1} cm^{-1}).[32]

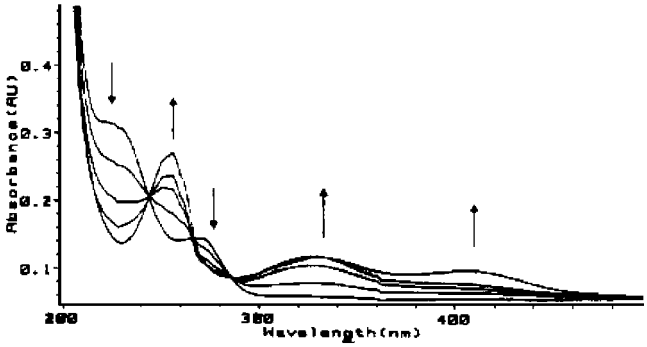

Figure 1. UV/Vis spectra for solutions containing *trans*-$[Ru(NH_3)_4(py)(NO)]^{2+}$ ions subjected to electrolysis as a function of time (applied potential: −0.40 V vs. SCE; μ = 0.1 $NaCF_3COO$; T = 15 °C, [Ru] = 5.0 × 10^{-4} M)

As expected, the chemical reduction of the *trans*-$[Ru(NH_3)_4L(NO)]^{3+}$ ions using Eu^{II} ions or Cd(Hg) also produces the respective aqua species. Differential-pulse polarographic experiments of *trans*-$[Ru(NH_3)_4(py)(NO)]^{3+}$ solutions show that after the addition of Eu^{II} ions ($E°$ = −0.60 V vs. SCE), the reduction wave corresponding to the $Ru^{II}NO^+/Ru^{II}NO^0$ redox process completely disappears with the simultaneous formation of a redox wave, which corresponds to the Ru^{III}/Ru^{II} couple in *trans*-$[Ru(NH_3)_4(py)(H_2O)]^{2+}$. In addition, the IR spectrum of the resulting solution does not show the easily identifiable NO-stretching frequency at 1931 cm^{-1}, indicating that the NO ligand is no longer present in the ruthenium-coordination sphere.

The rate-constant values for NO dissociation were determined by double-potential-step chronoamperometry (see Table 1) and are consistent with the rate law:

d/dt [*trans*-$[Ru(NH_3)_4(L)(H_2O)]^{2+}$] = k_{-NO} [*trans*-$[Ru(NH_3)_4(L)(NO)]^{2+}$]

According to the data shown in Table 1, the rate constants for NO dissociation in *trans*-$[Ru(NH_3)_4(L)(NO)]^{2+}$ ions vary from 0.025 s^{-1} (isn) to 4.00 s^{-1} (imC) at 25 °C. The sequence of k_{-NO} as a function of L increases as follows: pic ≈ nic ≈ H_2O ≈ py < L-His ≈ imN < pz < imC, which is the same sequence observed for water[34] or

 © 2004 Wiley-VCH Verlag GmbH & Co. KGaA, Weinheim

Table 1. Specific rate constants for NO^0 dissociation from *trans*-$[Ru(NH_3)_4(L)(NO)]^{2+}$, $[Ru^{II}NO^+/Ru^{II}NO^0]$ redox potential and electrochemical ligand parameters

Ion complex	[a] k_{-NO} (s^{-1})	$E^{0'}_{(NO+/NO)}$ (V vs. NHE)	ΣE_L
[b] *trans*-$[Ru(NH_3)_4(nic)(NO)]^{2+}$	0.025	0.072[21]	0.56
[b] *trans*-$[Ru(NH_3)_4(isn)(NO)]^{2+}$	0.043	0.052[21]	0.54
[b] *trans*-$[Ru(NH_3)_4(4\text{-pic})(NO)]^{2+}$	0.070	−0.008	0.51
[b] *trans*-$[Ru(NH_3)_4(4\text{-Clpy})(NO)]^{2+}$	0.030	0.012	0.54
[c] *trans*-$[Ru(NH_3)_4(H_2O)(NO)]^{2+}$	0.040[24]	−0.148[24]	0.32
[b] *trans*-$[Ru(NH_3)_4(py)(NO)]^{2+}$	0.060	0.012[21]	0.53
[b] *trans*-$[Ru(NH_3)_4(\text{L-His})(NO)]^{2+}$	0.140	−0.108[22]	0.42
[b] *trans*-$[Ru(NH_3)_4(imN)(NO)]^{2+}$	0.160	−0.118[22]	0.40
[b] *trans*-$[Ru(NH_3)_4(pz)(NO)]^{2+}$	0.070	0.112[21]	0.61
[c] *trans*-$[Ru(NH_3)_4(imC)(NO)]^{2+}$	4.000[20]	−0.298[20]	–
[c] *trans*-$[Ru(NH_3)_4P(OEt)_3(NO)]^{2+}$	0.980[25]	0.142[25]	0.68

[a] ($\mu = 0.1$, $NaCF_3COO$; $T = 25$ °C; [Ru] = 1.0×10^{-3} M, pH = 5). [b] Estimated by chronoamperometric method; most of the reported values are the average of at least three determinations; uncertainty of ± 15%. [c] Estimated by cyclic voltammetric method (Nicholson and Shain).

sulfate[32] lability in *trans*-$[Ru(NH_3)_4L(Y)]^{2+}$ complexes (where L = N-heterocyclic ligand, Y = H_2O or SO_4^{2-}).

According to the dissociative pathway for octahedral complexes, NO labilization should reflect the affinity of the *trans*-$[Ru(NH_3)_4(L)(H_2O)]^{2+}$ complex ions for the NO ligand and should be directly connected to the effective ruthenium charge in these complexes. Due to the similarities of the ion complexes studied, the ruthenium effective charge could be discussed on the basis of the electronic properties of the trans N-heterocyclic ligands. It is well-accepted that the higher the π-withdrawing ability of L, the more positive the redox potential of the $Ru^{III/II}$ couple and, therefore, the lower the specific rate constant for the dissociation of the ligand leaving. Since the $M^{n+/(n-1)+}$ redox potential is an indication of the metal-center-effective charge, it is expected that the higher the *trans*-$[Ru(NH_3)_4(L)(H_2O)]^{3+/2+}$ redox potential,[35] the lower the k_{-NO} value. Indeed, as observed for other leaving ligands, a linear tendency ($k_{-NO}/s^{-1} = -0.7 \times E^\circ$ *trans*-$[Ru(NH_3)_4(L)(H_2O)]^{3+/2+} + 0.07$; $R = 0.97$; pyrazine value not considered) is observed when the *trans*-$[Ru(NH_3)_4(L)(H_2O)]^{3+/2+}$ redox potential is plotted against the k_{-NO} values (see Figure 2). The ligand electrochemical parameter (E_L), introduced by Lever,[36] is known to be helpful in predicting the metal redox potential and we expected to find a correlation between the k_{-NO} values and the sum of E_L (ΣE_L) (see Table 1). This correlation exists and as can be observed in Figure 3 ($k_{-NO}/s^{-1} = -0.81 \times \Sigma E_L + 0.48$; $R = 0.997$, pyrazine value not considered). Since E_L values for a large number of N-heterocyclic ligands are available in the literature,[36] this correlation could become a very convenient tool for estimating the rate constants for NO dissociation from *trans*-$[Ru(NH_3)_4(L)(NO)]^{2+}$ species.

As observed in Table 1, the values for NO dissociation when L = pz, imC and $P(OEt)_3$ do not follow the trend observed for the other N-heterocyclic ligands (see Figure 3). The imC and $P(OEt)_3$ properties differ substantially from the N-based ligands as they are coordinated through carbon and phosphorus atoms, respectively. The trans labilizing effect of these two ligands is notable and therefore their

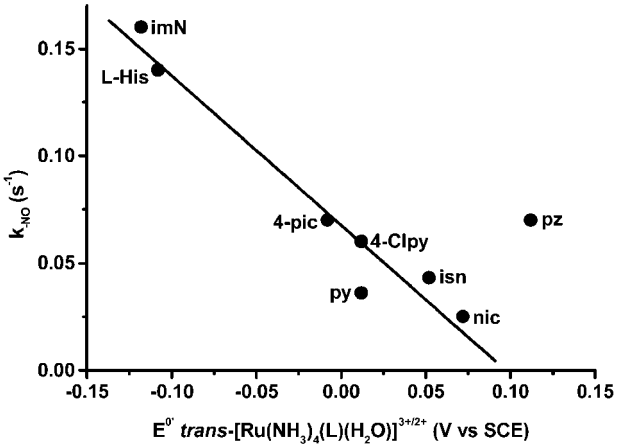

Figure 2. Correlation between the k_{-NO} values and $E^{\circ'}$ *trans*-$[Ru(NH_3)_4(L)(H_2O)]^{3+/2+}$ (V vs. SCE)

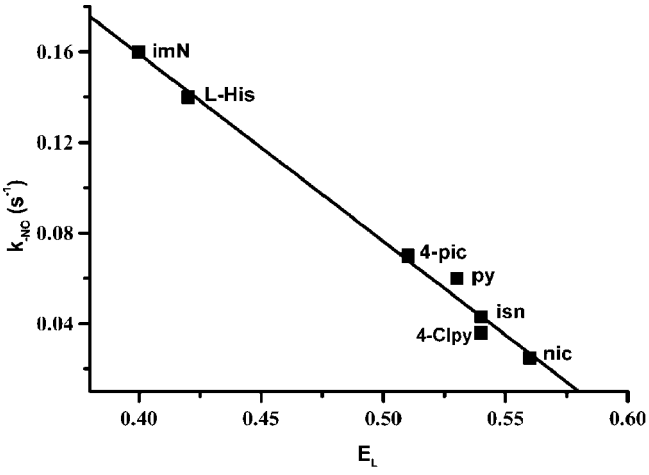

Figure 3. Correlation between the k_{-NO} values and ΣE_L ($\Sigma E_L = 4 \times E_L$ NH_3 + E_L L)

complexes do not fit the correlation implied by Figure 3 [imC and $P(OEt)_3$ values were omitted for clarity]. The behavior of the pyrazine ligand has not yet been understood

 © 2004 Wiley-VCH Verlag GmbH & Co. KGaA, Weinheim

and is currently under investigation in our laboratory. However, the same behavior has been observed for pyrazine derivatives in studies on sulfate dissociation from *trans*-$[Ru(NH_3)_4(L)(SO_4)]$ (L = N-heterocyclic ligands).[32]

From the discussion above, it is clear that the $[Ru^{II}NO^+/Ru^{II}NO^0]$ reduction potential is one of the key steps in activating nitrosyl complexes to release NO. If the target is to tailor a compound that can be activated in vivo through reduction, the $[Ru^{II}NO^+/Ru^{II}NO^0]$ redox potential must be in a range suitable to reducing agents present in the biological medium. The $[Ru^{II}NO^+/Ru^{II}NO^0]$ redox potential for the nitrosyl complexes dealt with here (Table 1) ranges from −0.118 for L = imN to 0.072 V vs. NHE for L = nic, suggesting that all these complexes could be reduced by biological reducing agents[37] such as NADH, the flavin coenzymes $FADH_2$ and $FMNH_2$ and iron sulfur proteins. Recent studies have suggested that the *trans*-$[Ru(NH_3)_4P(OC_2H_5)_3(NO)]^{3+}$ nitrosyl complex can be reduced by mitochondrial reducing power[38] and that this compound exhibits an effective hypotensive effect in mice.[15,16] This biological activity is attributed to its NO-donor ability. The $[Ru^{II}NO^+/Ru^{II}NO^0]$ redox potential for *trans*-$[Ru(NH_3)_4L(NO)]^{3+}$ complexes was shown to be sensitive to the nature of the ligand L, trans to NO. This was expected, since the most accessible site for reduction in these complexes is localized on the nitrosyl ligand. Thus, the NO electronic density and therefore the $[Ru^{II}NO^+/Ru^{II}NO^0]$ redox potential are a function of the competition between the axial ligands, NO and L, on the ruthenium 4dπ electron density. Indeed, a correlation between the *trans*-$[Ru(NH_3)_4L(NO)]^{3+/2+}$ and the respective aqua species *trans*-$[Ru(NH_3)_4L(H_2O)]^{3+/2+}$ redox potential was observed. In addition, a linear correlation was also observed plotting the *trans*-$[Ru(NH_3)_4L(NO)]^{3+/2+}$ redox potential and the ligand electrochemical parameters ΣE_L (Table 1) for L = N-heterocyclic ligands.[39] This correlation is valuable since E_L is available in the literature and was proved to be useful in previously estimating the *trans*-$[Ru(NH_3)_4L(NO)]^{3+/2+}$ redox potential.

It is important to stress that, depending on the electronic characteristics of L, the latter could be displaced instead of NO. In complexes where Cl^- is localized trans to NO,[24,25] as in *trans*-$[Ru(NH_3)_4(Cl)(NO)]^+$, *trans*-[Ru(cyclam)-$(Cl)(NO)]^+$ and *trans*-[Ru(dppe)$(Cl)(NO)]^+$, chloride is preferentially released before NO.

In contrast to the inertia of the $Ru^{II}NO^+$ species, the lability of NO in $Ru^{II}NO^0$ species seems to be common in species where L is a π-acid and should reflect the strength of the Ru−NO bond in both species. To investigate the origin of this different behavior, DFT computations for *trans*-$[Ru(NH_3)_4(L)(NO)]^{3+}$ and *trans*-$[Ru(NH_3)_4(L)(NO)]^{2+}$ (L = py) were performed. The results obtained in terms of bond lengths and bond angles are similar to those reported for the two systems:[40] $[Ru(CN)_5(NO)]^{2-}$ and $[Ru(CN)_5(NO)]^{3-}$,[41] $[Ru(NH_3)_5(NO)]^{3+}$ and $[Ru(NH_3)_5$-$(NO)]^{2+}$ (Table 2).

The MO composition (see Table 3) for *trans*-$[Ru(NH_3)_4(L)(NO)]^{3+}$ shows that the π interaction between Ru^{II} and NO^+ consists of a combination of the filled d_{xy} and d_{xz} orbitals (Ru) and the double degenerate, empty π* orbitals of nitric oxide besides the p_y* orbitals of pyridine: HOMO-5 (Ru d_{xy} 33 %, NO p_y 11 %, py p_y 54 %) and HOMO-6 (Ru d_{xz} 69 %, NO p_z 22 %, py p_z 6 %). Figure 4 (left) shows the HOMO-6 graphical representation of *trans*-$[Ru(NH_3)_4(py)(NO)]^{3+}$. The percentage [11−22 % (π* NO)] in the HOMO-5 and HOMO-6 orbitals is consistent with the well-known back bonding from Ru^{II} to NO^+, while 54 % for py (p_y) in the HOMO-5 orbital, which could be considered responsible for the influence of the *trans* ligand on the NO electronic density, is reflected on the $[Ru^{II}NO^+/Ru^{II}NO^0]$ redox potential and ν_{NO}, as observed.

As expected, the LUMO and LUMO+1 for the *trans*-$[Ru(NH_3)_4(L)(NO)]^{3+}$ complexes [an example of these molecular orbitals is shown in Figure 4 (right)] are antibonding with relation to the Ru−NO π-bond. These π-antibonding orbitals are predominantly on NO π* (66−69 %) (Table 3), which is in agreement with the formation of *trans*-$[Ru(NH_3)_4(L)(NO)]^{2+}$ as a result of *trans*-$[Ru(NH_3)_4(L)(NO)]^{3+}$ one-electron reduction and with the additional electron occupying one of these π* MOs. Indeed, a similar DFT MO calculation performed on *trans*-$[Ru(NH_3)_4(L)(NO)]^{2+}$ agrees with this prediction and the singly occupied MO (HOMO) and the LUMO, which correspond to the LUMO and LUMO+1 of *trans*-$[Ru(NH_3)_4(L)(NO)]^{3+}$, respectively, are composed of HOMO Ru (d_{xz}) 35 %, NO (p_z) 50 % and py (p_z) 13 % and LUMO Ru (d_{xy}) 28 %, NO (p_y) 70 % and py (p_y) 2 %. As expected from previous DFT calculations for the $[Ru(CN)_5(NO)]^{3-}$ and $[Ru(NH_3)_5(NO)]^{2+}$ systems,[40,41] a pronounced bend of 139° in the Ru−N−O angle is observed (Table 2). Although, a π-bonding interaction between Ru and NO still exists, that is, HOMO-3 and HOMO-4 [see Table 4 and an orbital representation in Figure 5 (left)], this Ru−*N*−O bending induces a considerable

Table 2. Selected theoretical bond lengths and angles calculated by DFT for (nitrosyl)ruthenium complexes

Complex	Ru−NO (Å)	N−O (Å)	Ru−*N*−O (deg)	Ref.
trans-$[Ru(NH_3)_4(py)(NO)]^{3+}$	1.820	1.130	180.0	this work
trans-$[Ru(NH_3)_4(py)(NO)]^{2+}$	1.910	1.174	139.0	this work
trans-$[Ru(NH_3)_4(nic)(NO)]^{3+}$	1.775	1.137	179.4	[42]
trans-$[Ru(NH_3)_5(NO)]^{3+}$	1.808	1.153	172.8	[40]
trans-$[Ru(NH_3)_5(NO)]^{2+}$	1.894	1.216	137.1	[40]
$[Ru(CN)_5(NO)]^{3+}$	1.770	1.176	180.0	[41]
$[Ru(CN)_5(NO)]^{2+}$	1.893	1.221	144.9	[41]

 © 2004 Wiley-VCH Verlag GmbH & Co. KGaA, Weinheim

Table 3. Selected MO contribution in percentage for *trans*-$[Ru(NH_3)_4(py)(NO)]^{3+}$

			trans-$[Ru(NH_3)_4(py)(NO)]^{3+}$			
	eV	symm	Ru	NO	NH_3	L
LUMO	−15.2	π*	23 (d_{xy})	66 (p_y)	3	8 (p_y)
HOMO	−15.2	π*	26 (d_{xz})	69 (p_z)	4	1
HOMO-1	−18.3	nonbonding	0	0	4	96 (p_z)
HOMO-2	−18.8	nonbonding	4 (d_{xz})	5 (p_z)	4	87 (p_z)
HOMO-3	−19.7	nonbonding	68 (d_{z^2},$d_{x^2-y^2}$)	1	4	25 (s)
HOMO-4	−20.2	π*L	23 ($d_{x^2-y^2}$)	5 (s)	1	71 (p_x)
HOMO-5	−20.5	π	33 (d_{xy})	11 (p_y)	3	54 (s,p_x,p_y)
HOMO-6	−20.6	π	69 (d_{xz})	22 (p_z)	4	6 (p_z)

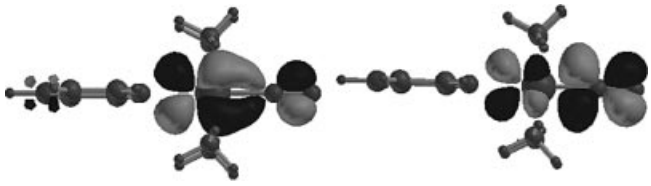

Figure 4. Molecular orbital description of a (nitrosyl)metal complex; (left) HOMO-6: ligand π interaction between Ru (either d_{xy} and d_{xz}) and NO π* orbitals (p_y* and p_z*); (right) LUMO: antiligand π interaction between Ru (either d_{xy} and d_{xz}) and the NO π* orbitals (p_y* and p_z*)

reduction of Ru and NO π-bonding [compare Figure 4 (left) and 5 (left)].

As a consequence, Ru−NO bond weakening is expected and it is comprehensible that the nitric oxide ligand is much more susceptible to dissociation in the *trans*-$[Ru(NH_3)_4(L)(NO)]^{2+}$ species than in the the oxidized analogues. Although, the HOMO and the LUMO for *trans*-$[Ru(NH_3)_4(L)(NO)]^{2+}$ ions, which were totally antibonding

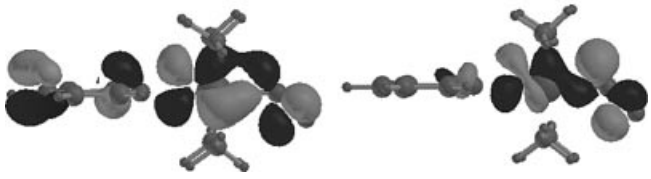

Figure 5. Molecular orbital interaction in a bent (nitrosyl)metal complex; (left) HOMO-3: bending the NO ligand minimizes the overlap between the metal orbitals (either d_{xy} and d_{xz}) and the NO π* orbitals (either p_y* and p_z*); (right) HOMO: the antibonding character presents a compensatory bonding interaction between the NO (p_z*) and the metal (d_{xz}) orbitals as Ru−*N*−O bend

MOs for *trans*-$[Ru(NH_3)_4(L)(NO)]^{3+}$ (LUMO and LUMO+1, respectively), assume a partial bonding character, they do not seem to be strong enough to keep the metal-coordination sphere intact, as observed. The calculated Ru−NO bond lengths for *trans*-$[Ru(NH_3)_4(L)(NO)]^{3+}$ (1.82 Å) and *trans*-$[Ru(NH_3)_4(L)(NO)]^{2+}$ (1.91 Å) are in agreement with the Ru−NO bond weakening (Table 2) and they are accompanied by a measurable lengthening of the N−O bond, from 1.130 Å to 1.174 Å (Table 2), which is consistent since the HOMO for the *trans*-$[Ru(NH_3)_4(py)(NO)]^{2+}$ ion has a considerable population and its composition is predominant on NO π* orbitals. As shown in Table 2, Ru−NO and N−O bond lengthening is usual as the same is also observed for $[Ru(CN)_5(NO)]^{3-}$ and $[Ru(NH_3)_5(NO)]^{2+}$ systems.[40,41]

Conclusion

The *trans*-$[Ru(NH_3)_4L(NO)]^{3+}$ complex ions are better described as formally $Ru^{II}NO^+$ and they are stable towards substitution reactions. Following activation by one-electron reduction, species having a labile NO^0 ligand are produced, which makes these compounds good NO-donor drug prototypes.

The rate of NO dissociation from the *trans*-$[Ru(NH_3)_4(L)(NO)]^{2+}$ and the *trans*-$[Ru(NH_3)_4L(NO)]^{3+/2+}$ redox potential, could be modulated by a judicious choice of the ligand, L. These two critical steps for NO-donor-drug designing can be predicted by plots of k_{-NO} versus ΣE_L and from the *trans*-$[Ru(NH_3)_4L(NO)]^{3+/2+}$ redox potential versus ΣE_L, respectively.

Table 4. Selected MO contribution in percentage for *trans*-$[Ru(NH_3)_4(py)(NO)]^{2+}$

			trans-$[Ru(NH_3)_4(py)(NO)]^{+2}$			
	eV	symm	Ru	NO	NH_3	L
LUMO	−9.7	π*	28 (d_{xy})	70 (p_y)	0	2 (p_y)
HOMO	−12.9	π*	35 (d_{xz})	50 (p_z)	2	13 (p_y)
HOMO-1	−14.1	nonbonding	87 (d_{z^2}; $d_{x^2-y^2}$)	0	5	8
HOMO-2	−14.5	nonbonding	0	0	3	97 (p_z,p_y)
HOMO-3	−14.5	π	44 (d_{xz})	26 (p_z)	2	28 (p_z)
HOMO-4	−14.5	π	58 (d_{xy})	20 (p_y)	3	19 (p_y,p_x)
HOMO-5	−15.3	π*L	24 (d_{xz})	6 (p_z)	2	68 (p_z)

 © 2004 Wiley-VCH Verlag GmbH & Co. KGaA, Weinheim

Experimental Section

Chemicals and Reagents: High purity chemicals (Aldrich) were used as supplied. $RuCl_3$ was obtained from Johnson Matthey. All solvents were purified following the known procedures.[43] Doubly distilled water was used throughout the experiments. All preparations and measurements were performed under argon. $[Ru(NH_3)_5Cl]Cl_2$,[44] *trans*-$[Ru(NH_3)_4(SO_2)(Cl)]Cl$,[45,46] *trans*-$[Ru(NH_3)_4(SO_4)(L)]Cl$[47] and *trans*-$[Ru(NH_3)_4(L)(NO)](BF_4)_3$[21,22] were prepared as described previously. ESR spectra were recorded in a Bruker ESP 300 E spectrophotometer at the temperature of liquid nitrogen. Electrochemical measurements were performed in both an EG&G Princeton Applied Research model 264A Par and an Autolab potentiostat/galvanostat PGSTAT30. Experiments were conducted using a glassy carbon or gold disks as working electrodes, a saturated calomel electrode (SCE) as a reference electrode and a platinum wire as an auxiliary electrode. The supporting electrolyte consisted of an aqueous buffer solution (pH = 5.0 at μ = 0.1 maintained with $NaCH_3COO/CH_3COOH$) kept under argon atmosphere during measurements. Electrolysis experiments were performed on an EG&G PARC model 173/interface model 276 potentiostat/galvanostat using an optically transparent gold minigrid as a working electrode, Ag/AgCl as a reference electrode and a platinum wire as auxiliary electrode, in a 0.1 cm quartz cell. Spectral changes during the electrolysis were recorded in an HP 8453 diode-array spectrophotometer.

Infrared spectra in aqueous solution (pH = 4) were performed in a calcium fluoride cell in an FTIR Bomen MB-102 spectrometer.

Kinetic experiments were conducted by double-potential-step chronoamperometry. The potential was briefly stepped from a value in which the compound is not reduced at the electrode surface to one in which the reduction proceeds at diffusion-controlled rate. After a period of time, the potential was stepped back to a potential in which the reduced form is oxidized. The kinetic information is obtained from the ratio between the currents measured on both potential steps as a function of time and by comparing these data with those obtained from working curves described in the literature.[48]

All the calculations were performed using the Gaussian 98 suite of programs.[49] The starting molecular geometries were obtained at the UHF/3−21G level of theory.[50−52] The final molecular geometry optimizations were performed using the Kohn−Shan density functional theory (DFT)[53−56] with the 6−31(d) basis set for the H, C, N, O, and P atoms, and an effective core potential LanL2DZ[57−59] for the Ru atom and the Becke three-parameters hybrid exchange-correlation functional known as B3LYP.[60−62] The analytical evaluation of the derivative matrix cartesian coordinates of the second energy (Hessian matrix) at the same level of approximation confirmed the nature of the minimum of the potential surface points associated to the optimized structures.

Acknowledgments

The authors would like to acknowledge Bruce R. McGarvey for reading the manuscript and the Brazilian foundations FAPESP (processes numbers 1999/07109−9, 99/11252−1 and 01/08563−7), CNPq and Capes for their financial support and also Johnson Matthey for supplying the $RuCl_3$ compound.

[1] L. J. Ignarro, *Pharmacol. Res.* **1989**, *6*, 651−659.
[2] S. Moncada, R. M. J. Palmer, E. A. Higgs, *Pharm. Rev.* **1991**, *43*, 109−142.
[3] M. J. Clarke, *Coord. Chem. Rev.* **2003**, *236*, 209−233.
[4] P. G. Wang, M. Xian, X. P. Tang, X. J. Wu, Z. Wen, T. W. Cai, A. J. Janczuk, *Chem. Rev.* **2002**, *102*, 1091−1134.
[5] F. Bottomley, *Reaction of Coordinated Ligands* (Ed: P. S. Braterman) Plenum Press, New York **1992**, chapter 3.
[6] G. B. Richter-Addo, P. Legzdins, *Metal Nitrosyls*, New York Ed, New York, **1992**, 271−333.
[7] T. W. Hayton, P. Legzdins, W. B. Sharp, *Chem. Rev.* **2002**, *102*, 935−991.
[8] C. S. Allardyce, P. J. Dyson, *Platinum Met. Rev.* **2001**, *45*, 62−69.
[9] E. Tfouni, M. H. Krieger, B. R. McGarvey, D. W. Franco, *Coord. Chem. Rev.* **2002**, *236*, 57−69.
[10] S. P. Fricker, *Platinum Met. Rev.* **1995**, *39*, 150−159.
[11] S. P. Fricker, E. Slade, N. A. Powell, O. J. Vaughan, G. R. Henderson, B. A. Murrer, I. L. Megson, S. K. Bisland, F. W. Flitney, *Br. J. Pharmacol.* **1997**, *122*, 1441−1449.
[12] Y. Chen, R. E. Shepherd, *J. Inorg. Biochem.* **1997**, *68*, 183−193.
[13] B. R. Cameron, M. C. Darkes, H. Yee, M. Olsen, S. P. Fricker, R. T. Skerlj, G. J. Bridger, N. A. Davies, M. T. Wilson, D. J. Rose, J. Zubieta, *Inorg. Chem.* **2003**, *42*, 1868−1876.
[14] B. R. Cameron, M. C. Darkes, I. R. Baird, R. T. Skerlj, Z. L. Santicci, S. P. Fricker, *Inorg. Chem.* **2003**, *42*, 4102−4108.
[15] B. F. Barros, J. C. Toledo Jr., D. W. Franco, E. Tfouni, M. H. Krieger, *Biochem., Pharmacol. Clin. Aspects Nitric Oxide* **2002**, *7*, 50−56.
[16] A. S. Torsoni, B. F. Barros, J. C. Toledo Jr., M. Hawn, M. H. Krieger, E. Tfouni, D. W. Franco, *Biochem., Pharmacol. Clin. Aspects Nitric Oxide* **2002**, *6*, 247−254.
[17] O. Siri, A. Tabard, P. Pullumbi, R. Guilard, *Inorg. Chim. Acta* **2003**, *350*, 633−640.
[18] P. C. Ford, J. Bourassa, K. Miranda, B. Lee, I. Lorkovic, S. Boggs, S. Kudo, L. Laverman, *Coord. Chem. Rev.* **1998**, *171*, 185−202.
[19] P. C. Ford, I. M. Lorkovic, *Chem. Rev.* **2002**, *102*, 993−1017.
[20] L. G. F. Lopes, A. Wieraszko, Y. EL-Sherif, M. J. Clarke, *Inorg. Chim. Acta* **2001**, *312*, 15−22.
[21] S. S. S. Borges, C. U. Davanzo, E. E. Castellano, J. Z-Schpector, S. C. Silva, D. W. Franco, *Inorg. Chem.* **1998**, *37*, 2670−2677.
[22] M. G. Gomes, C. U. Davanzo, S. C. Silva, L. G. F. Lopes, R. H. A. Santos, D. W. Franco, *J. Chem. Soc., Dalton Trans.* **1998**, *37*, 601−607.
[23] P. C. Ford, *Coord. Chem. Rev.* **1970**, *5*, 75−89.
[24] C. W. B. Bezerra, S. C. Silva, M. T. P. Gambardella, R. H. A. Santos, L. M. A. Plicas, E. Tfouni, D. W. Franco, *Inorg. Chem.* **1999**, *38*, 5660−5667.
[25] L. G. F. Lopes, E. E. Castellano, J. Z-Schpector, A. G. Ferreira, C. U. Davanzo, M. J. Clarke, D. W. Franco, *in preparation*.
[26] F. Roncaroli, M. E. Ruggiero, D. W. Franco, G. L. Estiú, J. A. Olabe, *Inorg. Chem.* **2002**, *41*, 5760 −5769.
[27] S. I. Gorelsky, S. C. Silva, A. B. P. Lever, D. W. Franco, *Inorg. Chim. Acta* **2000**, *300*, 698−708.
[28] B. R. McGarvey, A. A. Ferro, E. Tfouni, C. W. B. Bezerra, I. Bagatin, D. W. Franco, *Inorg. Chem.* **2000**, *39*, 3577−3581.
[29] R. W. Callahan, T. J. Meyer, *Inorg. Chem.* **1977**, *16*, 574−581.
[30] Y. Chen, F. T. Lin, R. E. Shepherd, *Inorg. Chem.* **1999**, *38*, 973−983.
[31] V. Mori, J. C. Toledo Jr., H. A. S. Silva, D. W. Franco, M. Bertotti, *J. Electroanal. Chem.* **2003**, *547*, 9−15.
[32] H. A. S. Silva, B. R. McGarvey, R. H. A. Santos, M. Bertotti, V. Mori, D. W. Franco, *Can. J. Chem.* **2001**, *79*, 679−687.
[33] D. R. Lang, J. A. Davis, L. G. F. Lopes, A. A. Ferro, L. C. G. Vasconcellos, D. W. Franco, E. Tfouni, A. Wieraszko, M. J. Clarke, *Inorg. Chem.* **2000**, *39*, 2294−2300.
[34] S. S. Isied, H. Taube, *Inorg. Chem.* **1976**, *15*, 3070−3075.
[35] D. W. Franco, *Coord. Chem. Rev.* **1992**, *119*, 199−225.
[36] A. B. P. Lever, *Inorg. Chem.* **1990**, *29*, 1271−1285.
[37] L. Stryer, *Biochemistry 2nd Ed.,* W. H. Freeman and Company: New York, **1981**,235−254.

 © 2004 Wiley-VCH Verlag GmbH & Co. KGaA, Weinheim

[38] J. C. Toledo Jr., L. G. F. Gonzaga, A. A. Alves, L. P. Silva, D. W. Franco, *J. Inorg. Biochem.* **2002**, *89*, 267−271.
[39] L. G. F. Lopes, M. G. Gomes, S. S. S. Borges, D. W. Franco, *Aust. J. Chem.* **1998**, *51*, 865−866.
[40] M. Wanner, T. Scheiring, W. Kaim, L. D. Slep, L. M. Baraldo, J. A. Olabe, E. J. Baerends, *Inorg. Chem.* **2001**, *40*, 5704−5707.
[41] J. C. Patterson, I. M. Lorkovic, P. C. Ford, *Inorg. Chem.* **2003**, *42*, 4902−4908.
[42] C. Kim, I. Novozhilova, M. S. Goodman, K. A. Bagley, P. Coppens, *Inorg. Chem.* **2000**, *39*, 5791−5795.
[43] D. D. Perrin, W. L. F. Armarego, D. P. Perrin, *Purification of Laboratory Chemicals*, 3 rd ed, Pergamon Press: New York, **1983**, 65−310.
[44] A. D. Allen, F. Bottomley, R. D. Harris, V. P. Reinslau, C. V. Senoff, *Inorg. Synth.* **1970**, *12*, 2−11.
[45] K. Gleu, W. Breuel, K. Z. Rehm, *Z. Anorg. Allg. Chem.* **1938**, *235*, 201−208.
[46] L. H. Vogt, J. L. Katz, S. E. Wiberley, *Inorg. Chem.* **1965**, *4*, 1157−1163.
[47] G. M. Brown, J. E. Sutton, H. Taube, *J. Am. Chem. Soc.* **1978**, *100*, 2767−2774.
[48] A. J. Bard, L. A. Faulkner, *Electrochemical Methods: Fundamentals and Applications*, John Wiley & Sons, New York, **1980**, 176−183.
[49] M. J. Frisch, G. W. Trucks, H. B. Schlegel, G. E. Scuseria, M. A. Robb, J. R. Cheeseman, V. G. Zakrzewski, J. A. Montgomery, Jr., R. E. Stratmann, J. C. Burant, S. Dapprich, J. M. Millam, A. D. Daniels, K. N. Kudin, M. C. Strain, O. Farkas, J. Tomasi, V. Barone, M. Cossi, R. Cammi, B. Mennucci, C. Pomelli, C. Adamo, S. Cli. ord, J. Ochterski, G. A. Petersson, P. Y. Ayala, Q. Cui, K. Morokuma, D. K. Malick, A. D. Rabuck, K. Raghavachari, J. B. Foresman, J. Cioslowski, J. V. Ortiz, B. B. Stefanov, G. Liu, A. Liashenko, P. Piskorz, I. Komaromi, R. Gomperts, R. L. Martin, D. J. Fox, T. Keith, M. A. Al-Laham, C. Y. Peng, A. Nanayakkara, C. Gonzalez, M. Challacombe, P. M. W. Gill, B. Johnson, W. Chen, M. W. Wong, J. L. Andres, C. Gonzalez, M. Head-Gordon, E. S. Replogle, J. A. Pople, *Gaussian 98*, Revision A.6, Gaussian, Inc., Pittsburgh, PA (**1998**).
[50] C. C. J. Roothan, *Rev. Mod. Phys.* **1951**, *23*, 69−75.
[51] J. A. Pople, R. K. Nesbet, *J. Chem. Phys.* **1954**, *22*, 571−572.
[52] R. McWeeny, G. Dierksen, *J. Chem. Phys.* **1968**, *49*, 4852−4856.
[53] P. Hohenberg, W. Kohn, *Phys. Rev. Sect. B* **1964**, *136*, 864−871.
[54] W. Kohn, L. J. Sham, *Phys. Rev. Sect. A* **1965**, *140*, 1133−1138.
[55] A. D. Becke, *J. Chem. Phys.* **1993**, *98*, 5648−5652.
[56] R. G. Parr, W. Yang, *Density-Functional Theory of Atoms and Molecules*, Oxford Univ. Press, Oxford, **1989**, 142−197.
[57] P. J. Hay, W. R. Wadt, *J. Chem. Phys.* **1985**, *82*, 270−283.
[58] W. R. Wadt, P. J. Hay, *J. Chem. Phys.* **1985**, *82*, 284−298.
[59] P. J. Hay, W. R. Wadt, *J. Chem. Phys.* **1985**, *82*, 299−310.
[60] A. D. Becke, *J. Chem. Phys.* **1993**, *98*, 5648−5652.
[61] C. Lee, W. Yang, R. G. Parr, *Phys. Rev. Sect. B* **1988**, *37*, 785−789.
[62] A. D. Becke, *Phys. Rev. A* **1988**, *38*, 3098−3100.

Received September 29, 2003
Early View Article
Published Online March 23, 2004

 © 2004 Wiley-VCH Verlag GmbH & Co. KGaA, Weinheim

Unusual Two-Dimensional Nickel(II) Complexes Based on $[Ni(dien)]^{2+}$ and $[M(CN)_4]^{2-}$ Building Blocks (M = Ni, Pd and Pt) − Synthesis, Structural Diversity and Magnetic Properties

Iñaki Muga,[a] Juan M. Gutiérrez-Zorrilla,*[a] Pablo Vitoria,[a] Pascual Román,[a] Luis Lezama,[a] and Javier I. Beitia[a]

Keywords: Nickel / Palladium / Platinum / Cyanides / Bridging ligands

Three novel polymeric compounds $[Ni(dien)Ni(CN)_4]_n(H_2O)_n$ (**1**), $[Ni(dien)Pd(CN)_4]_n$ (**2**), and $[Ni(dien)Pt(CN)_4]_n$ (**3**) were synthesised by reaction of $[\{Ni(dien)(H_2O)\}_2(\mu\text{-ox})](PF_6)_2$ with $[M(CN)_4]^{2-}$ (M = Ni, Pd, Pt) in aqueous solution. The structure of these compounds contains two $[Ni(dien)]^{2+}$ cationic units bridged by two $[M(CN)_4]^{2-}$ anions in a *cis* fashion, generating a square-shaped $[Ni_2–M_2]$ metal core. The different linking modes between the cores afford a 2D bilayer with encapsulated water in compound **1** and corrugated layers in compounds **2** and **3**. These coordination modes are compared to the different bridging modes of tetracyanometalate-containing compounds retrieved from the CSD database. The three compounds present a very weak antiferromagnetic coupling between the octahedrally coordinated Ni^{II} ions.
(© Wiley-VCH Verlag GmbH & Co. KGaA, 69451 Weinheim, Germany, 2004)

Introduction

The design and synthesis of molecular magnetic materials have been the focus of increasing attention over the past three decades.[1] So, the study of magnetic interactions in di- and polynuclear complexes, as a function of structural and electronic factors, is still a main challenge in inorganic chemistry. Significant research has been devoted to analyzing the role of the cyanide group as a bridging ligand, both from an experimental[2] and a theoretical[3] point of view. Because it is a good exchange pathway between paramagnetic centres, it is widely employed in the preparation of molecular magnetic materials.[4]

Cyanometalate anions have been extensively used as design elements in supramolecular systems, where they can act as bridging ligands to form high dimensionality coordination polymers with transition metal cations.[5] An approach to the synthesis of these materials is the use of $[M(CN)_4]^{2-}$ groups in conjunction with a transition-metal-ion complex, due to the ability of the cyanide group to connect various central atoms, for building molecular assemblies with various degrees of dimensionality. As can be seen in Table 1, a wide structural diversity can be found in compounds containing bridging tetracyanometalate anions.[6] In this context, it is worth underlining the works of Shore et al.[7] on polymeric systems based on lanthanides, with a variety of Lewis bases and tetracyanometalate anions, and those of Long et al.[8] on cubic-cluster systems. Furthermore, some Hofmann clathrates present cooperative spin-crossover behaviour.[9]

The work described here is part of our research program on the chemistry of first-row transition metal oxalate and cyanide complexes.[10] We employed the nickel dinuclear precursor, $[\{Ni(dien)(H_2O)\}_2(\mu\text{-ox})](PF_6)_2$, due to the lability of its water molecules, which may be replaced by a plethora of ligands. In this paper we report the synthesis, vibrational study, crystal structure and magnetic properties of the following polymeric compounds: $[Ni(dien)Ni(CN)_4]_n(H_2O)_n$ (**1**), $[Ni(dien)Pd(CN)_4]_n$ (**2**), and $[Ni(dien)Pt(CN)4]_n$ (**3**), obtained from the above-mentioned precursor and the cyano complexes $[Ni(CN)_4]^{2-}$, $[Pd(CN)_4]^{2-}$ and $[Pt(CN)_4]^{2-}$, respectively.

Results and Discussion

Synthesis and Spectroscopic Studies

In the synthesis of Ni^{II} complexes based on bridging oxalate and tetracyanometalates, the dinuclear cationic complex $[\{Ni(dien)(H_2O)\}_2(\mu\text{-ox})]^{2+}$ was used as a precursor, owing to the lability of its water molecules, which may be substituted by a plethora of ligands, such as pseudohalide ligands and cyanometalates. As can be seen in Scheme 1, the reaction of the precursor with $[M(CN)_4]^{2-}$ (M = Ni, Pd, Pt) gives at first an insoluble precipitate, which correspond to the polymeric compounds $[\{Ni(dien)M(CN)_4\}]_n$, and then the trinuclear molecular compounds $[\{Ni(dien)\}_2(\mu\text{-ox})\{M(CN)_4\}]$.[6d,10b] The formation of com-

[a] Departamento de Química Inorgánica, Facultad de Ciencias, Universidad del País Vasco, Apartado 644, 48080 Bilbao, Spain
E-mail: qipguloj@lg.ehu.es
Supporting information for this article is available on the WWW under http://www.eurjic.org or from the author.

 © 2004 Wiley-VCH Verlag GmbH & Co. KGaA, Weinheim **DOI: 10.1002/ejic.200300696**

Table 1. Bridging modes of group 10 tetracyanometalates

Coordination 2			
Structure	Description[a]	No.	Ref.
	trans 0D, trinuclear monomer [M'MM']; M: Ni, Pt; M': Fe, Re, Ho [{Fe(dppe)(Cp)}$_2${Pt(CN)$_4$}] (QAFLAK)	3	6a
	trans 1D, chain [M'M]$_n$; M: Ni, Pd, Pt; M': Ni, Cu, Ag, Sm, Yb [Cu(en)$_2${Ni(CN)$_4$}]$_n$ (HEGBIE)	11	6b
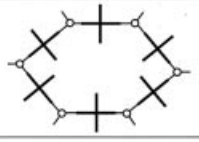	*trans* 2D, plane [M'$_6$M$_6$]$_n$; M: Ni, Pt; M': Eu, Yb [Eu(dmf)$_5${Ni(CN)$_4$}]$_n$ (YEQRIV)	2	6c
	cis 0D, trinuclear monomer [M'MM']; M: Ni, Pd, Pt; M': Ni, Cu [{Ni(dien)}$_2${Ni(CN)$_4$}(ox)] (RIHBEP)	4	6d
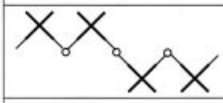	*cis* 1D, chain [M'M]$_n$; M: Ni; M': Ni [Ni(en)$_2${Ni(CN)$_4$}]$_n$ (SIFKOH)	1	6e
	double *cis* 0D, tetranuclear monomer [M'M$_2$M']; M: Pt; M': Cu [{Cu(bpy)(H$_2$O)}$_2${Pt(CN)$_4$}$_2$] (HIPHOD)	1	6f
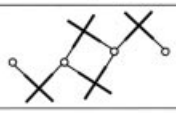	*cis*-double *cis* 1D, chain [M'M$_2$M'M]$_n$; M: Pd, Pt; M': Nd, Eu [{Nd(H$_2$O)$_6$}$_2${Pd(CN)$_4$}$_3$]$_n$ (PIJPON)	2	6g
	trans-double *cis* 1D, chain [M'M$_2$M'M]$_n$; M: Ni, Pd; M': Ce, Sm, Eu, Er, Yb [Yb(H$_2$O)(dmf)$_4$}$_2${Pd(CN)$_4$}$_3$]$_n$ (GOMTUX)	7	6h
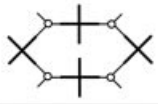	double *trans*-double *cis* 1D ladder [M'$_4$M$_4$]$_n$; M: Ni, Pd, Pt; M': Y, Sm, Eu, Gd, Ho, Yb [Sm(dmf)$_5$}$_2${Pd(CN)$_4$}$_3$]$_n$ (JAQBOS)	7	6i

Coordination 3			
Structure	Description[b]	No.	Ref.
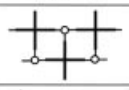	1D, ladder [M'M]$_n$; M: Ni, Pt; M': Eu [Eu(dmf)$_4${Ni(CN)$_4$}]$_n$ (TOJXIZ)	2	6j
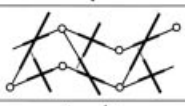	2D, bilayer [M'$_3$M$_3$]$_n$; M: Ni; M': Cu [Cu(dap){Ni(CN)$_4$}]$_n$ (WODBAS)	1	6k
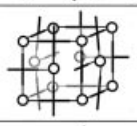	3D, cubic cluster [M'$_{12}$M$_{12}$]; M: Ni; M': Cr [{Cr(Me$_3$-tacn)}$_{12}${Ni(CN)$_4$}$_{12}$]$^{12+}$ (OFOQUV)	1	6l
	2D, bilayer [M'$_2$M$_2$]; M: Ni; M': Ni [Ni(dien){Ni(CN)$_4$}]$_n$ (**1**)	1	This work
Coordination 4			
	0D nonanuclear monomer [M'$_4$M]; M: Ni; M': Ni [{Ni$_2$L(CN)}$_4${Ni(CN)$_4$}]$^{6+}$ (NEPFAP)	1	6m
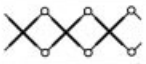	1D, chain [M'M$_2$M']; M: Ni; M': Cu [{Cu(medpt)}$_2$Ni(CN)$_4$}]$_n^{2n+}$ (RAKJUI)	2	6n
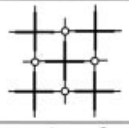	2D, plane [M'M]$_n$; M: Ni; M': Mn, Fe, Ni [Fe(NH$_3$)$_2${Ni(CN)$_4$}]$_n$ (COQSAC)	7	6o
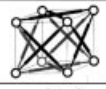	3D, cubic cluster [M'$_8$M$_6$]; M: Ni; M': Cr, Mo [{Cr(Me$_3$-tacn)}$_8${Ni(CN)$_4$}$_6$]$^{12+}$ (RAHYOO)	7	2a
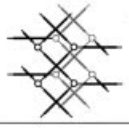	3D network [M'M]$_n$; M: Pt; M': Cu [Cu{Pt(CN)$_4$}]$_n^n$ (JEJFAF)	1	6p

[a] Coordination mode, dimensionality, abbreviated formula, example, CSD refcode. [b] Dimensionality, abbreviated formula, example, CSD refcode

pound **1**, by using KCN as starting material, is probably a consequence of the high stability of the $[Ni(CN)_4]^{2-}$ complex, which leads to the initial formation of the tetracyanonickelate(II) anion when cyanide salt is added to a solution of the precursor.

The IR and Raman spectra of the compounds displaying the stretching vibrations associated to the CN group are shown in Figure 1. The similitude between the spectra of compounds **2** and **3** suggests that the coordination modes of the tetracyanometalate anions are very similar and quite different from that observed in compound **1**. Besides, as the number of independent $[M(CN)_4]^{2-}$ groups increases (one for **1** and two for **2** and **3**), the number of CN stretching-vibration bands also becomes greater.

Crystal Structures

The crystal structures of the compounds present two-dimensional arrangements, based on $[Ni(dien)]^{2+}$ cationic fragments, bridged by $[M(CN)_4]^{2-}$ groups.

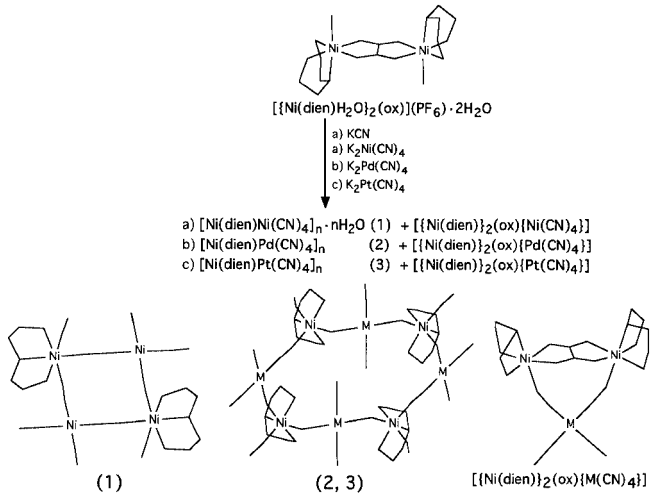

Scheme 1

 © 2004 Wiley-VCH Verlag GmbH & Co. KGaA, Weinheim

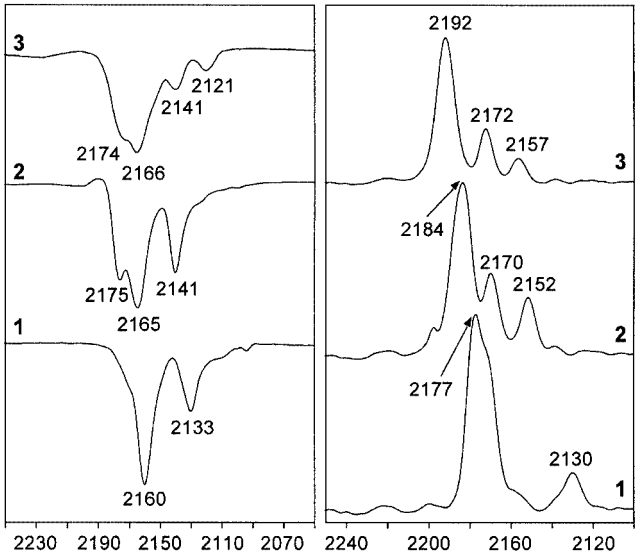

Figure 1. IR (left) and Raman (right) spectra of the compounds

[Ni(dien){Ni(CN)$_4$}]$_n$(H$_2$O)$_n$ (1)

The asymmetric unit of compound **1** consists of one $[Ni(dien)]^{2+}$ unit, one $[Ni(CN)_4]^{2-}$ anion and a water molecule, as illustrated in Figure 2. Selected bond lengths and angles are listed in Table 2. The structure of this compound contains two $[Ni(dien)]^{2+}$ cationic groups, bridged by two $[Ni(CN)_4]^{2-}$ anions in a *cis* fashion, generating a square-shaped $[Ni_2-Ni_2]$ metal core. Each core is linked to another four cores through cyano groups, creating a two-dimensional bilayer parallel to the (011) plane (see Figure 3). In this arrangement, the distorted octahedral environment of Ni1 is set up by three nitrogen atoms from a diethylenetriamine ligand in *fac* and three nitrogen atoms from the corresponding cyanide ligands; thereby, each tetracyanonickelate anion connects three $[Ni(dien)]^{2+}$ moieties and the remaining uncoordinated cyano groups are parallel or antiparallel to the [100] direction giving rise to CN-rich hydrophilic regions (see Figure 4). The water molecule remains encapsulated inside the bilayer and is weakly hydrogen-bonded to the N atoms of the dien ligands. The bilayers are held together by hydrogen bonds, which involve the N1 and

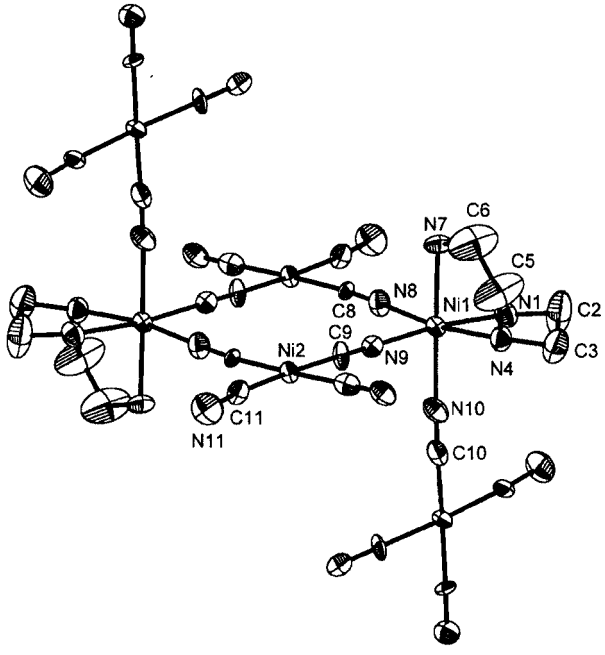

Figure 2. ORTEP view of the metallic core in compound **1** together with the atom labelling

Table 2. Selected bond lengths [Å] and angles [°] for compounds **1**–**3**

Compound	**1**	**2**	**3**
Ni1 coordination sphere:			
Ni1–N1	2.099(7)	2.125(4)	2.12(2)
Ni1–N4	2.104(8)	2.116(4)	2.12(2)
Ni1–N7	2.093(7)	2.074(4)	2.09(2)
Ni1–N8	2.056(9)	2.058(4)	2.09(2)
Ni1–N9	2.099(9)	2.108(4)	2.13(2)
Ni1–N10	2.095(9)	2.106(4)	2.14(2)
N1–Ni1–N4	81.8(3)	81.4(2)	80.7(6)
N1–Ni1–N7	94.8(3)	94.5(2)	95.7(6)
N1–Ni1–N8	92.0(3)	91.7(2)	92.9(6)
N1–Ni1–N9	172.8(3)	168.8(2)	168.8(7)
N1–Ni1–N10	86.2(3)	84.2(2)	83.3(6)
N4–Ni1–N7	81.8(3)	82.2(2)	82.4(6)
N4–Ni1–N8	170.7(3)	168.4(2)	168.5(6)
N4–Ni1–N9	92.5(3)	90.7(2)	91.9(5)
N4–Ni1–N10	95.6(3)	99.3(2)	98.8(6)
N7–Ni1–N8	92.1(3)	89.0(2)	88.8(6)
N7–Ni1–N9	88.6(3)	92.3(2)	91.7(6)
N7–Ni1–N10	177.0(3)	177.7(2)	178.3(5)
N8–Ni1–N9	94.3(3)	97.4(2)	95.7(6)
N8–Ni1–N10	90.8(3)	89.2(2)	89.9(6)
N9–Ni1–N10	90.1(3)	89.3(2)	89.4(6)
Ni coordination plane:			
Ni2–C8	1.86(1)		
Ni2–C9	1.853(9)		
Ni2–C10	1.84(1)		
Ni2–C11	1.857(9)		
C8–Ni2–C9	87.6(4)		
C8–Ni2–C10	177.5(4)		
C8–Ni2–C11	93.3(4)		
C9–Ni2–C10	90.0(4)		
C9–Ni2–C11	177.3(5)		
C10–Ni2–C11	89.1(4)		
Pd and Pt coordination planes:		M = Pd	M = Pt
M1–C9		2.013(4)	1.97(2)
M1–C10		1.990(4)	1.99(2)
M2–C8		1.989(5)	2.01(1)
M2–C11		1.988(5)	1.98(2)
C9–M1–C10		91.0(2)	92.4(8)
C9–M1–C9′		180.0(2)	180.0(6)
C9–M1–C10′		89.0(2)	87.6(8)
C10–M1–C10′		180.0(–)	180.0(–)
C8–M1–C11		85.9(2)	95.3(9)
C8–M1–C8′		180.0(3)	180.0(9)
C8–M1–C11′		94.1(2)	84.7(9)
C11–M1–C11′		180.0(–)	180.0(–)

 © 2004 Wiley-VCH Verlag GmbH & Co. KGaA, Weinheim

N7 atoms belonging to the same dien ligand and the N11 atom of the uncoordinated cyano group (see Table 3).

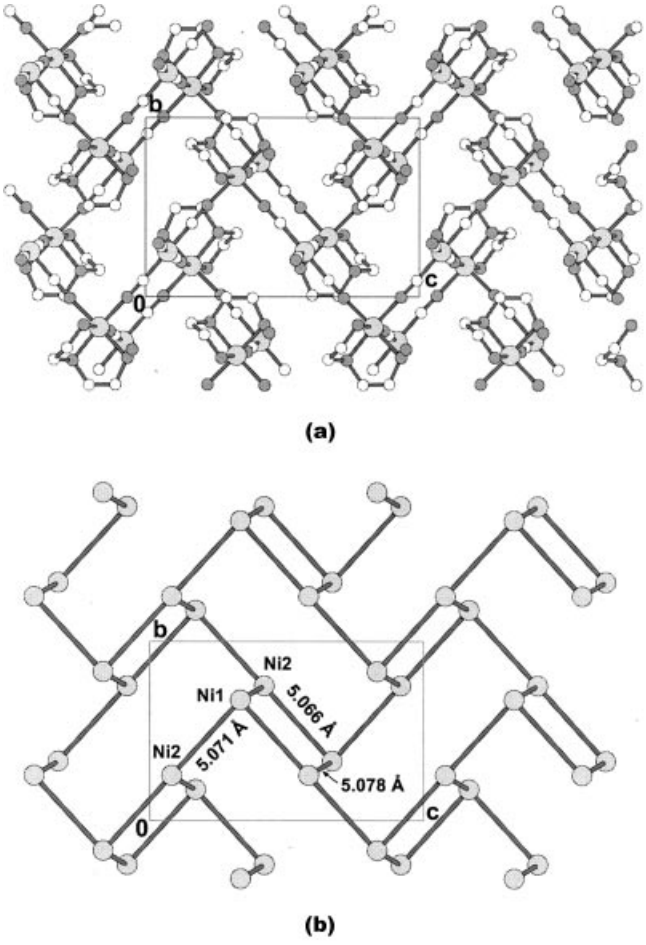

Figure 3. Compound **1**: (a) projection along the *a* axis of the bilayer; (b) metallic skeleton formed by cyanide-bridged Ni atoms with indication of the Ni···Ni distances shorter than 6 Å (water molecules are omitted for clarity)

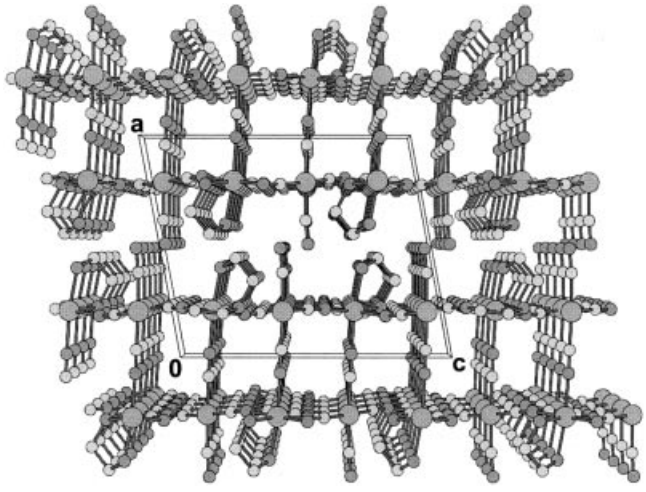

Figure 4. Perspective view of compound **1** along the *b* axis showing the cyanide terminal-rich area between two adjacent bilayers

Table 3. Hydrogen contacts for compounds **1**−**3**

	1		**2**	**3**
N1···N11[a]	3.13(1)	N1···N11[b]	3.488(7)	3.54(3)
N4···O1 (intra)	3.114(9)	N4···N10[c]	3.383(6)	3.36(2)
N7···N11[a]	3.184(9)	N7···N11[d] (intra)	3.050(6)	3.04(3)
N7···O1[e] (intra)	3.44(1)	N7···N11[b]	3.152(7)	3.12(3)

[a] Symmetry codes: $1 + x, y, z$. [b] $1 - x, 2 - y, 1 - z$. [c] $1 - x, 1 - y, 2 - z$. [d] $x, y - 1, z$. [e] $x, 1/2 - y, z - 1/2$; "intra" means intralamellar hydrogen bonds.

[Ni(dien){Pd(CN)$_4$}]$_n$ (2) and [Ni(dien){Pt(CN)$_4$}]$_n$ (3)

Compounds **2** and **3** are isostructural and the asymmetric unit of both consists of one *fac*-$[Ni(dien)]^{2+}$ cationic group and two centrosymmetric $[M(CN)_4]^{2-}$ anions, as illustrated in Figure 5 [M = Pd (**2**), Pt (**3**)]. Selected bond lengths and angles are listed in Table 2. The repeating molecular unit of **2** and **3** is similar to that of compound **1**: two $[Ni(dien)]^{2+}$ moieties bridged by two $[M(CN)_4]^{2-}$ anions in a *cis* mode, generating a $[Ni_2-M_2]$ metal core. Nevertheless, some differences between the two metallic cores, concerning the dien orientation around the nickel atoms, can be appreciated. Thus, in compound **1**, the N4 dien atom occupies an equatorial position with respect to the metallic core, whereas in compounds **2** and **3** its position is axial. Moreover, these metallic cores form ribbons running along the [010] direction, where each tetracyanometalate(II) group connects four $[Ni(dien)]^{2+}$ cations, as in compound $\{[\{Cu(medpt)\}_2Ni(CN)_4]\}(ClO_4)_2\}_n$.[6n] These ribbons are linked by $[M(CN)_4]^{2-}$ anions that are bound to the Ni^{2+} centres through the cyanide bridges in a *trans* fashion to generate a puckered sheet along the (011) plane (see Figure 6). The 2D planes are connected by hydrogen bonds in a weakly held 3D array (see Figure 7), which involves all dien N atoms and the uncoordinated N11 atoms of the M2 centres together with the N10 atom (see Table 3).

Bridging Modes of [M(CN)$_4$]$^{2-}$ Anions

A total of 60 compounds, containing tetracyanometalates as bridging units, were retrieved from the Cambridge Structural Database. Table 1 summarizes their bridging modes and main features (coordination modes, dimensionality, abbreviated formula and CSD refcode of a representative example). More than half present coordination 2, a bridging mode that usually gives 1D arrangements, in which the metal is usually a lanthanide. Coordination 3 is only present in four cases with variable dimensionality. Although compound **1** shows coordination 3, its structure stands for a new packing mode. Coordination 4 is mainly present in cubic clusters and square-planar arrangements. On the other hand, in compounds **2** and **3**, the tetracyanometalate anions present two coordination modes, 4 to form ribbons along one direction and 2 in order to connect the ribbons in a corrugated layer.

 © 2004 Wiley-VCH Verlag GmbH & Co. KGaA, Weinheim

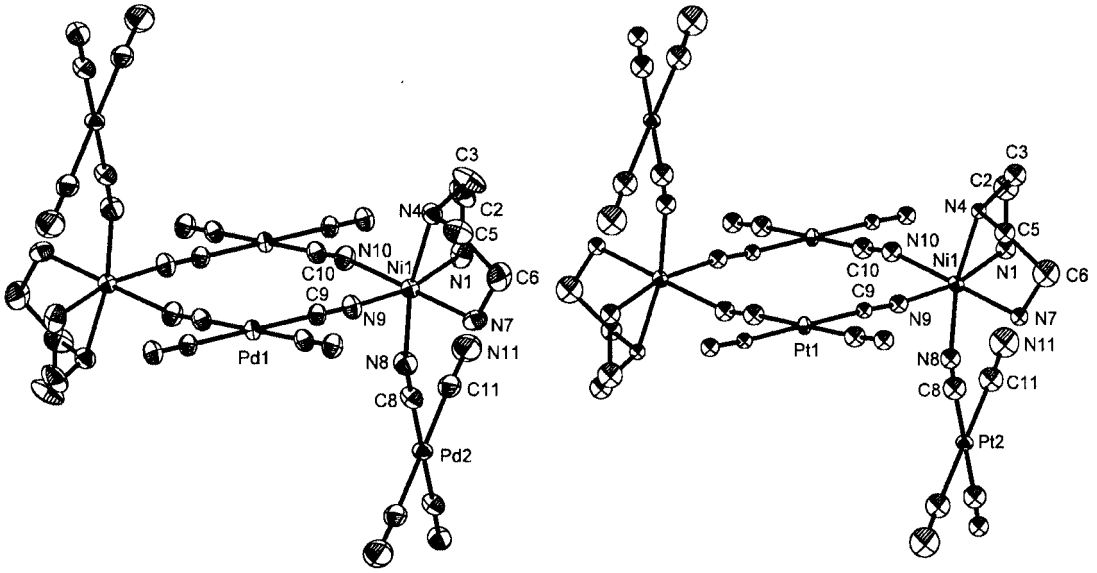

Figure 5. ORTEP views of the metallic core in compounds **2** (left) and **3** (right)

Magnetic Measurements

The temperature dependence of the magnetic susceptibilities of compounds **1**−**3** was measured in the temperature range 5−300 K. Plots of $\chi_m T$ and $\chi_m{}^{-1} T$ vs. T were deposited (see Supporting Information). The thermal evolution of χ_m satisfies the Curie−Weiss law at high temperatures. The values of C and θ are equal to 1.14 $cm^3 \cdot K \cdot mol^{-1}$ and −0.8 K, respectively, for compound **1**, 1.13 and −0.9 for **2** and 1.16 and −0.6 for **3**. These results, together with the continuous decrease in the $\chi_m T$ values, is indicative of antiferromagnetic exchange coupling in the compounds. On the basis of the crystal structures, the compounds were treated as 2D square-planar Heisenberg systems with S = 1 and only magnetic interactions between the nickel(II) ions inside the layers were considered. It was possible to fit the χ_m experimental values using the analytical expression reported by Lines[11] for a 2D square-planar Heisenberg system, from a high-temperature expansion series studied by Rushbrooke and Wood [Equation (1)], where $x = J/kT$, A = 5.333333, B = 9.777778, C = 9.481482, D = 19.06173, E = 45.08971, F = 25.46392.[12]

$$\chi = \frac{2Ng^2\beta^2}{3kT}\left[1 + Ax + Bx^2 + Cx^3 + Dx^4 + Ex^5 + Fx^6\right]^{-1} \quad (1)$$

The least-squares fittings to the experimental data (J = −0.10 cm^{-1} and g = 2.134 for compound **1**, −0.11 and 2.127 for **2** and −0.08 and 2.150 for **3**) show the presence of very weak antiferromagnetic interactions between the paramagnetic nickel ions within each layer through the diamagnetic $[M(CN)_4]^{2-}$ groups.

On the other hand, octahedrally coordinated Ni^{II} compounds frequently exhibit large zero-field splittings of the $^3A_2$ ground state that, qualitatively, produce similar effects to those of antiferromagnetic interactions. In this sense, we have tried to fit the experimental data to the analytical equation for magnetic susceptibility, calculated by application of van Vleck's equation. However, no satisfactory fit could be obtained using that expression and the calculated curves show that the experimental decrease of the magnetic effective moment starts at higher temperatures that those predicted by this simple model (deposited as Supporting Information). Therefore, we can conclude that magnetic exchange is the dominant term in the magnetic properties of compounds **1**−**3**, even if the obtained J values could be somewhat overestimated, due to the possible influence of the Ni^{II} single-ion zero-field splitting.

Conclusions

The reaction between group 10 tetracyanometalates and the cationic complex $[\{Ni(dien)(H_2O)\}_2(\mu\text{-ox})]^{2+}$ leads to the formation of the title polymeric compounds, followed by the trinuclear molecular compounds $[\{Ni(dien)\}_2(\mu\text{-ox})\{M(CN)_4\}]$. Compound **1** contains an encapsulated water molecule, while compounds **2** and **3** are anhydrous and isostructural.

The repeating molecular unit for the three compounds consists of two $[Ni(dien)]^{2+}$ cationic building blocks bridged by two $[M(CN)_4]^{2-}$ anions in a *cis* mode, generating a $[Ni_2-M_2]$ metal core. Nevertheless, some structural differences between both metallic cores could be appreciated, concerning the dien orientation around the nickel atoms and the dihedral angle between the metallic core and the $[M(CN)_4]^{2-}$ groups. This fact could be explained by the different types of hydrogen-bonding present in the compounds, which are strongly influenced by the presence of the water molecule of compound **1**.

These compounds present two novel bridging modes for tetracyanometalate groups. Compound **1** could be used as

 © 2004 Wiley-VCH Verlag GmbH & Co. KGaA, Weinheim

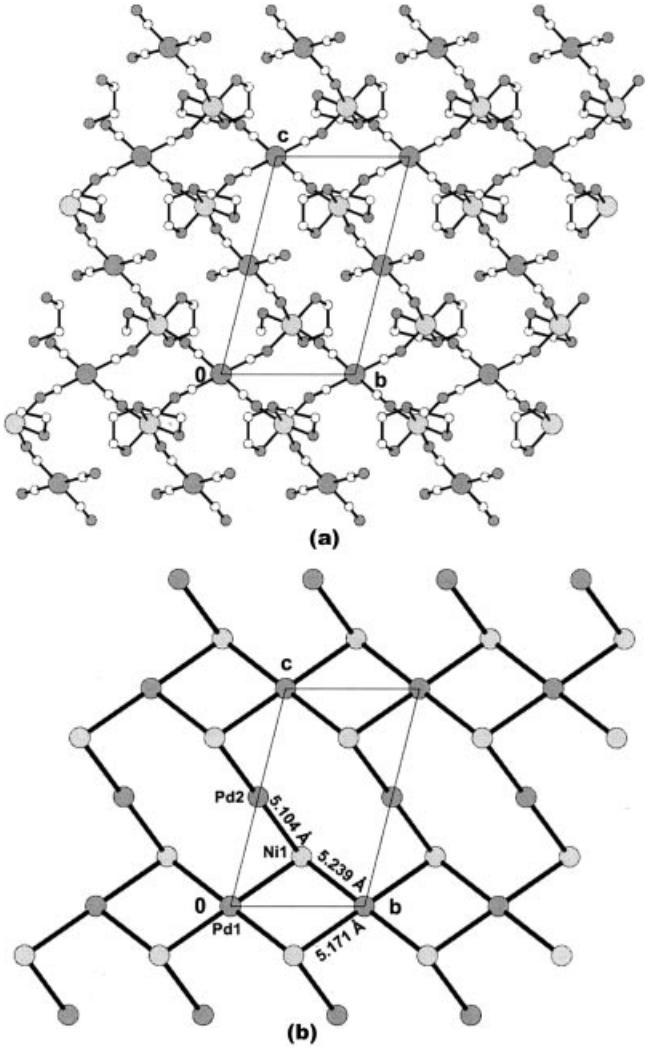

Figure 6. Compound **2**: (a) projection along the *a* axis of a corrugated layer; (b) metallic skeleton formed by cyanide-bridged Ni and Pd atoms with indication of the Ni···Pd distances shorter than 6 Å

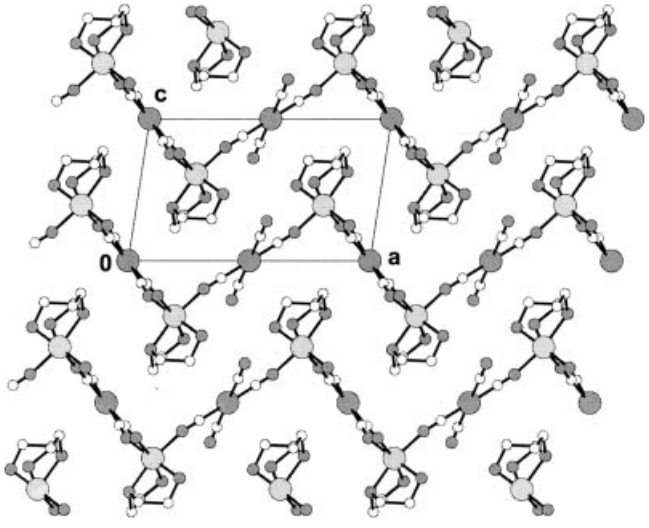

Figure 7. Arrangement of corrugated layers in compound **2**

an intercalation precursor, due to the special arrangement of the uncoordinated cyanide groups of the $[Ni(CN)_4]^{2-}$ anions. On the other hand, compounds **2** and **3** present two types of bridging modes for the tetracyanometalate groups (coordination numbers 2 and 4), giving rise to a structure containing corrugated layers.

The very low values in the coupling constants confirm the poor exchanging capabilities of the tetracyanometalate groups.

Experimental Section

General: Potassium cyanide (KCN; Fluka), potassium tetracyanonickelate $\{K_2[Ni(CN)_4]$; Aldrich$\}$, potassium tetracyanopalladate $\{K_2[Pd(CN)_4]$; Aldrich$\}$, and potassium tetracyanoplatinate $\{K_2[Pt(CN)_4]$; Aldrich$\}$ were used as purchased without further purification. The complex $[\{Ni(dien)(H_2O)\}_2(\mu\text{-ox})](PF_6)_2$ was prepared using a previously described method.[13] Infrared spectra for solid samples were obtained as KBr pellets with a Mattson 1000 FT-IR spectrometer. Raman spectra were measured as pressed pellets using a dispersive micro-probe Renishaw spectrometer, equipped with a high-power 785 nm excitation laser of 500 mW nominal output power. Filters were used to reduce the laser power at the sample to 10 or 1 %. For each spectrum 5−10 scans were collected and the acquisition times ranging from 100 to 300 s. Magnetic susceptibility measurements on polycrystalline samples were performed in the temperature range 5−300 K with a Quantum Design MPMS-7 SQUID magnetometer. The magnetic field used in the experiments was of 0.1 T, a value at which the magnetization versus magnetic-field curve was still linear at 5.0 K. Experimental susceptibility values were corrected for the diamagnetic contributions of the constituent atoms, evaluated from Pascal's constants ($-185\cdot10^{-6}$, $-187\cdot10^{-6}$ and $-201\cdot10^{-6}$ cm^3/mol for compounds **1**−**3**, respectively), and for the temperature-independent paramagnetism (estimated to be $200\cdot10^{-6}$ cm^3/mol).

Synthesis of $[Ni(dien)\{Ni(CN)_4\}]_n(H_2O)_n$ (1): This compound precipitated as a highly insoluble pink residue when KCN (0.25 g, 3.84 mmol) was added, whilst stirring, to an aqueous solution (50 mL) of the precursor complex, $[\{Ni(dien)(H_2O)\}_2(\mu\text{-ox})](PF_6)_2$ (1.42 g, 1.84 mmol). An alternative method involved mixing aqueous solutions of $K_2[Ni(CN)_4]$ (0.058 g, 0.24 mmol) and the precursor (0.36 g, 0.475 mmol). After removing the pink precipitate by filtration, the solvent was refluxed for 20 min and single crystals of compound **1** appeared after one week, yield 0.062 g (75%). $C_8H_{13}N_7Ni_2\cdot H_2O$ (342.69): calcd. C 28.04; H 4.41; N 28.61; found C 27.54; H 4.26; N 28.44.

Synthesis of $[Ni(dien)\{Pd(CN)_4\}]_n$ (2): This compound was obtained as a insoluble pink residue when the precursor (0.25 g, 0.324 mmol) was added to an aqueous solution (20 mL) of $K_2[Pd(CN)_4]$ (0.115 g, 0.40 mmol), yield 0.10 g (65%). Single crystals of this compound were obtained by slow diffusion in a test tube of a methanolic solution of $K_2[Pd(CN)_4]$, into an aqueous solution of the precursor. $C_8H_{13}N_7NiPd$ (372.36): calcd. C 25.81; H 3.52; N 26.33; found C 25.56; H 3.58; N 26.08.

Synthesis of $[Ni(dien)\{Pt(CN)_4\}]_n$ (3): Following the same procedure, compound **3** was prepared as a violet precipitate by using $K_2[Pt(CN)_4]$ (0.051 g, 0.136 mmol) and the precursor (0.25 g, 0.324 mmol), yield 0.035 g (55%). Single crystals of compound **3** were obtained by slow diffusion in a test tube of a methanolic solution of $K_2[Pt(CN)_4]$ into an aqueous solution of the precursor.

 © 2004 Wiley-VCH Verlag GmbH & Co. KGaA, Weinheim

$C_8H_{13}N_7NiPt$ (461.05): calcd. C 20.84; H 2.84; N 21.27; found. C 20.55; H 3.00; N 20.94.

X-ray Crystallographic Studies: Single crystals suitable for X-ray analysis were obtained for the three compounds. Data collections for **1** and **3** were performed with a STOE IPDS diffractometer, equipped with graphite-monochromated Mo-K_α radiation (λ = 0.71073 Å) and an image-plate detector. A total of 200 frames (oscillation range of 1°/frame and exposure time 5 min/frame) were collected, which were processed and corrected for Lorentz and polarization effects with the Stoe IPDS X-RED software package.[14] Indexes and unit-cell refinement were based on all observed reflections from ten frames collected with an oscillation range of 1°/frame and exposure time of 3 min/frame. Data for compound **2** were taken at room temperature with an Xcalibur single-crystal diffractometer (graphite-monochromated Mo-K_α radiation, λ = 0.71073 Å) fitted with a Sapphire CCD detector. A total of 764 frames of data were collected with an exposure time of 10 s/frame, using the ω-scan technique with a frame width of $\Delta\omega = 0.6°$. Data frames were processed (unit cell determination, intensity data integration and correction for Lorentz and polarization effects) using the CrysAlis software package.[15] Visual inspection of the frames collected clearly indicated that compounds **2** and **3** crystallize as non-merohedral twins in the triclinic space group $P\bar{1}$. For compound **2**, an initial orientation matrix and initial cell parameters were obtained by indexing and post-refinement with the CrysAlis software package. This orientation matrix only indexed ca.75 % of the total data. The reflections not indexed by this orientation matrix were then extracted from the measured CCD images and indexed. Both orientation matrices are related by a twofold rotation around the [100] direction in reciprocal space. All frames were then evaluated twice using the CrysAlis software. An HKLF4 reflection file was first output using the data from the major component to aid in the solution of the structure. After the structure was solved, both data sets were given different batch numbers for SHELXL-97 refinement with HKLF5. Overlapping reflections occur twice in the reflection list with the indices of both domains. The twin refinement was performed with SHELXL-97 using the data in HKLF5 format and refinement of batch scale factors. Symmetry-equivalent reflections were not merged (SHELXL-97 procedure); all measured intensities were treated as independent data in the refinement. The refinement resulted in a ratio of 77.0(2):23.0(2) for the two twin domains. Following the same procedure, but using the Stoe IPDS software, the twin law for compound **3** was determined and found to be the same as for **2**. Due to the lower quality of the data collected for compound **3**, only the intensities from the major component of the twin were used for solution and refinement of the structure. All structures were solved using a combination of Patterson and direct methods.[16] Either all non-hydrogen atoms (compounds **1** and **2**) or metal atoms only (compound **3**) were refined anisotropically by the full-matrix least-squares method. Hydrogen atoms of the dien ligands were placed in calculated positions and refined with a riding model. SHELXL-97[17] was used for all structure refinements. Neutral atom scattering factors and anomalous dispersion factors were taken from the literature.[18] Experimental details and crystal data for compounds **1**−**3** are given in Table 4. The April 2003 release of the Cambridge Structural Database[19] was used in this work to obtain the different bridging modes of the group 10

Table 4. Crystal data and data collection parameters for compounds **1**−**3**

Compound	**1**	**2**	**3**
Empirical formula	$C_8H_{13}N_7Ni_2{\cdot}H_2O$	$C_8H_{13}N_7NiPd$	$C_8H_{13}N_7NiPt$
Formula mass	342.69	372.36	461.05
Crystal system	monoclinic	triclinic	triclinic
Space group	$P2_1/c$	$P\bar{1}$	$P\bar{1}$
a [Å]	11.439(3)	7.283(1)	7.289(2)
b [Å]	8.839(2)	7.437(1)	7.447(2)
c [Å]	13.747(3)	12.589(1)	12.553(3)
α [°]	90	75.01(1)	74.92(2)
β [°]	100.60(3)	80.01(1)	79.84(3)
γ [°]	90	83.7581)	84.27(3)
V [Å^3]	1366.2(5)	647.2(1)	646.6(2)
Z	4	2	2
F(000)	704	368	432
$D_{calcd.}$ [g·cm^{-3}]	1.666	1.911	2.368
Crystal shape	prism	prism	prism
Crystal colour	pale violet	violet	violet
Crystal size [mm]	0.20 × 0.15 × 0.10	0.21 × 0.16 × 0.07	0.16 × 0.15 × 0.04
Diffractometer	STOE IPDS	Xcalibur	STOE IPDS
Temperature [K]	293(2)	293(2)	293(2)
Radiation [Å]	0.71073	0.71073	0.71073
μ [mm^{-1}]	2.755	2.833	12.252
Monochromator	graphite	graphite	graphite
Scan mode	φ oscillation	ω	φ oscillation
θ limits [°]	2.75−25	2.84−30	2.84−30.38
hkl range	−13 to 13; −9 to 10; −16 to 16	−10 to 10; −10 to 10; −17 to 17	−10 to 10; −10 to 10; −17 to 16
No. of unique reflections	2389	6251	2675
No. of observed data	801 [$I = 2\sigma(I)$]	4746 [$I = 2\sigma(I)$]	1148 [$I = 2\sigma(I)$]
No. of parameters	158	158	82
$\Delta\rho_{max}/\Delta\rho_{min}$ [e·Å^{-3}]	0.43/−0.53	2.57/−0.93	2.95/−3.55
R_1 [obsd. rflns.]	0.0426	0.0476	0.0596
wR_2 [all rflns.]	0.0683	0.1300	0.1310

 © 2004 Wiley-VCH Verlag GmbH & Co. KGaA, Weinheim

tetracyanometalates. All searches were restricted to those CSD entries that satisfied the following secondary search criteria: (a) error-free after CSD evaluation procedures, (b) no reported structural disorder and (c) perfect matching of their chemical and crystallographic connectivity representations. CCDC-220434 (**1**), -220435 (**2**), -220436 (**3**) contain the supplementary crystallographic data for this paper. These data can be obtained free of charge at www.ccdc.cam.ac.uk/conts/retrieving.html [or from the Cambridge Crystallographic Data Centre, 12 Union Road, Cambridge CB2 1EZ, UK; Fax: (internat.) + 44-1223/336-033; E-mail: deposit@ccdc.cam.ac.uk].

Acknowledgments

This work was supported by Ministerio de Ciencia y Tecnología (MAT2002-03166) and Universidad del País Vasco (9/UPV 00169.310-15329/2003).

[1] [1a] *Magnetic Molecular Materials* (Eds.: D. Gatteschi, O. Khan, J. S. Miller, F. Palacio), Kluwer, Dordrecht, **1991**. [1b] *Molecular Magnetism* (Ed: O. Khan),Wiley-VCH, New York, **1993**. [1c]S. Decurtins, H. W. Schmalle, R. Pellaux, P. Fischer, A. Hauser, *Mol. Cryst. Liq. Cryst.* **1997**, *305*, 227. [1d] J. S. Miller, J. L. Manson, *Acc. Chem. Res.* **2001**, *34*, 563. [1e] E. Coronado, F. Palacio, J. Veciana, *Angew. Chem. Int. Ed.* **2003**, *42*, 2570.

[2] [2a] P. A. Berseth, J. J. Sokol, M. P. Shores, J. L. Heinrich, J. R. Long, *J. Am. Chem. Soc.* **2000**, *122*, 9655. [2b] K. M. Anderson, N. G. Connelly, E. Llamas-Rey, A. G. Orpen, R. L. Paul, *Chem. Commun.* **2001**, 1734. [2c] P. V. Bernhardt, B. P. Macpherson, M. Martinez, *J. Chem. Soc., Dalton Trans.* **2002**, 1435. [2d] R. Lescoueezec, J. Vaissermann, F. Lloret, M. Julve, M. Verdaguer, *Inorg. Chem.* **2002**, *41*, 5943. [2e] C. P. Berlingette, J. A. Smith, J. R. Galán-Mascarós, K. R. Dunbar, *C. R. Chim.* **2002**, *5*, 665.

[3] [3a] A. Rodriguez-Fortea, P. Alemany, S. Alvarez, E. Ruiz, A. Scuiller, C. Decroix, V. Marvaud, J. Vaissermann, M. Verdaguer, I. Rosenman, M. Julve, *Inorg. Chem.* **2001**, *40*, 5868. [3b] J. K. Bera, P. Szalay, K. R. Dunbar, *Inorg. Chem.* **2002**, *41*, 3429.

[4] [4a] M. S. El Fallah, E. Rentschler, A. Caneschi, R. Sessoli, D. Gatteschi, *Angew. Chem. Int. Ed. Engl.* **1996**, *35*, 1947. [4b] M. Verdaguer, A. Bleuze, V. Marvaud, J. Vaissermann, M. Seuleiman, C. Deplanches, A. Scuiller, C. Train, R. Garde, G. Gelly, C. Lomenech, I. Rosenman, P. Veillet, C. Cartier, F. Villain, *Coord. Chem. Rev.* **1999**, *190−192*, 1023. [4c] M. Ohba, H. Okawa, *Coord. Chem. Rev.* **2000**, *198*, 313. [4d] R. Clerac, F. A. Cotton, S. P. Jeffery, C. A. Murillo, X. Wang, *Inorg. Chem.* **2001**, *40*, 1265. [4e] J. A. Smith, J. R. Galan-Mascaros, R. Clerac, J. S. Sun, X. Ouyang, K. R. Dunbar, *Polyhedron* **2001**, *20*, 1727. [4f] E. Colacio, M. Ghazi, H. Stoeckli-Evans, F. Lloret, J. M. Moreno, C. Perez, *Inorg. Chem.* **2001**, *40*, 4876. [4g] H. Okawa, M. Ohba, *Bull. Chem. Soc. Jpn.* **2002**, *75*, 1191. [4h] A. Figuerola, C. Diaz, J. Ribas, V. Tangoulis, J. Granell, F. Lloret, J. Mahia, M. Maestro, *Inorg. Chem.* **2003**, *42*, 641.

[5] [5a] T. Mallah, S. Thiebaut, M. Verdaguer, P. Veillet, *Science* **1993**, *262*, 1554. [5b] M. Ohba, N. Maruono, H. Okawa, T. Enoki, J. Latour, *J. Am. Chem. Soc.* **1994**, *116*, 11566. [5c] W. R. Entley, G. S. Girolami, *Science* **1995**, *268*, 397. [5d] O. Sato, T. Iyoda, A. Fujishima, K. Hashimoto, *Science* **1996**, *271*, 49. [5e] H. Miyasaka, N. Matsumoto, H. Okawa, N. Re, E. Gallo, C. Floriani, *J. Am. Chem. Soc.* **1996**, *118*, 981. [5f] H. Vahrenkamp, A. Geiss, G. N. Richardson, *J. Chem. Soc., Dalton Trans.* **1997**, 3643. [5g] J. Cernak, M. Orendac, I. Potocnak, J. Chomic, A. Orendacova, J. Skorsepa, A. Feher, *Coord. Chem. Rev.* **2002**, *224*, 51. [5h] R. Eckhardt, H. Hanika-Heidl, R. D. Fischer, *Chem. Eur. J.* **2003**, *9*, 1795. [5i] C. C. Chang, B. Pfennig, A. B. Bocarsly, *Coord. Chem. Rev.* **2000**, *208*, 33.

[6] [6a] G. N. Richardson, U. Brand, H. Vahrenkamp, *Inorg. Chem.* **1999**, *38*, 3070. [6b] H. Yuge, T. Iwamoto, *J. Chem. Soc., Dalton Trans.* **1994**, 1237. [6c] B. Du, E. A. Meyers, S. G. Shore, *Inorg. Chem.* **2001**, *40*, 4353. [6d] I. Muga, J. M. Gutiérrez-Zorrilla, A. Luque, P. Román, F. Lloret, *Inorg. Chem.* **1997**, *36*, 743. [6e] J. Cernak, J. Chomic, P. Domiano, O. Ori, G. D. Andreetti, *Acta Crystallogr., Sect. C* **1990**, *46*, 2103. [6f] L. Falvello, M. Tomas, *Chem. Commun.* **1999**, 273. [6g] U. Klement, *Z. Kristallogr.* **1993**, *208*, 285. [6h] J. Liu, E. A. Mayers, S. G. Shore, *Inorg. Chem.* **1998**, *37*, 5410. [6i] D. W. Knoeppel, J. Liu, E. A. Meyers, S. G. Shore, *Inorg. Chem.* **1998**, *37*, 4828. [6j] D. W. Knoeppel, S. D. Shore, *Inorg. Chem.* **1996**, *35*, 5328. [6k] J. Cernak, J. Lipkowski, *Monatsh. Chem.* **1999**, *130*, 1195. [6l] J. J. Sokol, M. P. Shores, J. R. Long, *Inorg. Chem.* **2002**, *41*, 3052. [6m] F. Meyer, R. F. Winter, E. Kaifer, *Inorg. Chem.* **2001**, *40*, 4597. [6n] T. K. Maji, P. S. Mukherjee, G. Mostafa, E. Zangrando, N. R. Chaudhuri, *Chem. Commun.* **2001**, 1368. [6o] T. Kitazawa, Y. Gomi, M. Takahashi, M. Takeda, *Mol. Cryst. Liq. Cryst. Sci. Technol., Sect. A* **1998**, *311*, 167. [6p] R. W. Gable, B. F. Hoskins, R. Robson, *J. Chem. Soc., Chem. Commun.* **1990**, 762.

[7] [7a] B. Du, E. A. Meyers, S. G. Shore, *Inorg. Chem.* **2000**, *39*, 4639. [7b] J. Liu, D. W. Knoeppel, S. Liu, E. A. Meyers, S. G. Shore, *Inorg. Chem.* **2001**, *40*, 2842.

[8] J. J. Sokol, M. P. Shores, J. R. Long, *Angew. Chem. Int. Ed.* **2001**, *40*, 236.

[9] V. Niel, J. M. Martínez-Agudo, M. C. Muñoz, A. B. Gaspar, J. A. Real, *Inorg. Chem.* **2001**, *40*, 3838.

[10] [10a] I. Muga, J. M. Gutiérrez-Zorrilla, P. Vitoria, A. Luque, M. Insausti, P. Román, F. Lloret, *Eur. J. Inorg. Chem.* **2000**, 2541. [10b] I. Muga, J. M. Gutiérrez-Zorrilla, P. Vitoria, P. Román, F. Lloret, *Polyhedron* **2002**, *21*, 2631. [10c] P. Vitoria, I. Muga, J. M. Gutiérrez-Zorrilla, A. Luque, P. Román, L. Lezama, F. J. Zúñiga, F. J. Beitia, *Inorg. Chem.* **2003**, *42*, 960.

[11] M. E. Lines, *J. Phys. Chem. Solids* **1970**, *31*, 101.

[12] G. S. Rushbrooke, P. J. Wood, *Molec. Phys.* **1958**, *1*, 257.

[13] I. Muga, P. Vitoria, J. M. Gutiérrez-Zorrilla, A. Luque, C. Guzmán, P. Román, *Acta Crystallogr., Sect. C* **2002**, *58*, m81.

[14] Stoe, *X-RED, Data Reduction for STADI4 and IPDS*, Revision 1.08, Stoe & Cie, Darmstadt, Germany, **1996**.

[15] Oxford Diffraction, CrysAlis, *CCD and RED*, Version 1.70, Oxford Diffraction Ltd, Oxford, UK, **2003**.

[16] P. T. Beurskens, G. Beurskens, R. de Gelder, S. García-Granda, R. O. Gould, R. Israel, J. M. M. Smits, "The DIRDIF99 Program System", *Technical Report of the Crystallography Laboratory*, University of Nijmegen, The Netherlands, **1999**.

[17] G. M. Sheldrick, *SHELXL-97*, University of Göttingen, Germany, **1997**.

[18] *International Tables for X-ray Crystallography*; Kynoch Press, Birmingham, England, **1974**, vol. IV.

[19] F. H. Allen, *Acta Crystallogr., Sect. B* **2002**, *58*, 380.

Received October 1, 2003
Early View Article
Published Online March 23, 2004

 © 2004 Wiley-VCH Verlag GmbH & Co. KGaA, Weinheim

Carboxy Ester Hydrolysis Promoted by a Dicopper(II) Macrocyclic Polyamine Complex with Hydroxypropyl Pendant Groups

Jin Huang,[a] Shu-An Li,[a] Dong-Feng Li,[a] De-Xi Yang,[a] Wei-Yin Sun,*[a] and Wen-Xia Tang[a][†]

Keywords: Copper / Hydrolysis / Macrocyclic ligands / Mass spectrometry / Potentiometric titrations

A dinuclear Cu^{II} complex containing a hexaaza macrocyclic ligand bearing two 2-hydroxypropyl pendants, 3,6,9,16,19,22-hexaaza-6,19-bis(2-hydroxypropyl)tricyclo-[22.2.2.2^{11,14}]triaconta-1,11,13,24,27,29-hexaene (L), was synthesized. The title complex $[Cu_2(H_{-2}L)Cl_2]\cdot 6.5H_2O$ was isolated as a blue crystal, orthorhombic, space group *Fddd*, with a = 16.4581(12), b = 32.248(2), c = 35.830(2) Å, V = 19017(2) Å^3, Z = 16, $R1$ = 0.0690, and $wR2$ = 0.1546 [$I > 2\sigma(I)$]. The protonation constants of Cu_2L were determined by potentiometric titration, and it was found that the alcoholic hydroxypropyl group of the complex Cu_2L exhibits low pK_a values of pK_{a1} = 7.31, pK_{a2} = 7.83 at 25 °C. The hydrolysis kinetics of 4-nitrophenyl acetate (NA) promoted by the title complex have also been studied. The pH-rate profile for Cu_2L gave a sigmoidal curve and showed a second-order rate constant of 0.39 ± 0.02 M^{-1} s^{-1} in 10% CH_3CN/H_2O(v/v), which is greater than that of the dinuclear Cu^{II} complex formed by a hexaaza macrocycle without pendants. The reason for the higher catalytic activity of the title complex is discussed. We found that the volume of nucleophile RO^- can effect the hydrolysis of the carboxy ester, the nucleophilicity of RO^- and the Lewis acidity of the metal macrocycle also affect the carboxy ester hydrolysis.

(© Wiley-VCH Verlag GmbH & Co. KGaA, 69451 Weinheim, Germany, 2004)

Introduction

Metal hydroxides and metal alkoxides play important roles in hydrolytic metalloenzymes. Metal hydroxides have been implicated in the carbonic anhydrase catalyzed hydration of carbon dioxide[1] as well as in the carboxypeptidase-catalyzed hydrolysis of amides.[2] The role of the metal ions in the activation of proximate alcoholic OH groups is well documented in natural metalloenzymes. The key role of the metal atom in promoting hydrolysis appears to be the intramolecular delivery of the nucleophile. By virtue of its Lewis acidity, the metal ion reduces the pK_a of a coordinated water molecule, thereby producing a good nucleophile at neutral pH. In addition, the hydration sphere normally associated with water molecules in bulk solution does not interfere with nucleophilic attack in an inner-sphere reaction.[3]

Kimura's group discovered that the pendant alcohol can be deprotonated to form a Zn^{II}-bound alkoxide anion, which acts as a strong nucleophile at physiological pH.[4,5] Chin's group has investigated the reactivities and mechanisms of copper(II) hydroxide and copper(II) alkoxide for the cleavage of phosphate diesters, and discovered that the copper(II) alkoxide-promoted transesterification path is two orders of magnitude faster than the hydrolysis path, i.e., the copper(II) hydroxide path.[6] A mechanistic study of Cu^{II}-catalyzed ester hydrolysis has yielded a variety of kinetic behaviors and proposed active species. We use a macrocycle dinucleating ligand with two hydroxypropyl pendants (L in Scheme 1) to further explore the influence of the alcohol pendant on the behavior of the corresponding Cu^{II} complexes. Here, we report the crystal structure of the dinuclear Cu^{II} complex of L. The stability constants of Cu^{II} complexes of L and carboxy ester hydrolysis were also investigated. Indeed, we found that the catalytic activity of Cu_2L is higher than that of the dicopper complex with a macrocyclic ligand without hydroxy pendants. Our results indicate that the volume of nucleophile RO^-, the nucleophilicity and the Lewis acidity of the metal macrocycle may effect the carboxy ester hydrolysis.

Results and Discussion

Structure Description of $[Cu_2(H_{-2}L)Cl_2]\cdot 6.5H_2O$

The compound crystallizes in the orthorhombic system with space group *Fddd* and consists of a neutral unit of $[Cu_2(H_{-2}L)Cl_2]$ and six and a half water molecules of crystallization. Selected bond lengths and bond angles relevant to the Cu^{II} coordination sphere are given in Table 1.

[a] Coordination Chemistry Institute, State Key Laboratory of Coordination Chemistry, Nanjing University,
Nanjing 210093, China
Fax: (internat.) + 86-25/331-4502
E-mail: chem1121@netra.nju.edu.cn
[†] Deceased.

Supporting information for this article is available on the WWW under http://www.eurjic.org or from the author.

 © 2004 Wiley-VCH Verlag GmbH & Co. KGaA, Weinheim **DOI: 10.1002/ejic.200300452**

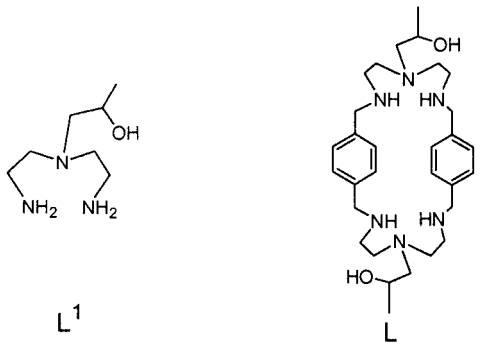

Scheme 1

Table 1. Select bond lengths [Å] and angles [°] for $[Cu_2(H_{-2}L)Cl_2]\cdot 6.5H_2O$

Cu1−Cl1	2.2486(15)	Cu1−N3	2.056(4)
Cu1−N1	2.018(5)	Cu1−O1	2.177(4)
Cu1−N2	2.087(4)		
N1−Cu1−Cl1	173.93(16)	N2−Cu1−O1	105.28(17)
N1−Cu1−N2	84.28(19)	N3−Cu1−Cl1	98.39(15)
N1−Cu1−N3	85.4(2)	N3−Cu1−N2	128.81(18)
N1−Cu1−O1	81.63(18)	N3−Cu1−O1	122.46(16)
N2−Cu1−Cl1	96.93(14)	O1−Cu1−Cl1	92.32(12)

As illustrated in Figure 1, each macrocycle binds two Cu^{II} ions by its diethylenetriamine moieties, which provide three nitrogen atoms to each Cu^{II} ion; the rest of the coordinated atoms are a chloride anion and an oxygen atom from the hydroxypropyl pendant. The Cu1 atom deviates 0.216 Å from the trigonal equatorial plane formed by O1, N2 and N3 towards the Cl ion with N3−Cu1−N2 = 128.81°, N3−Cu1−O1 = 122.46° and N2−Cu1−O1 = 105.28°, while the axial positions are occupied by N1 of the macrocycle and Cl1 with an N1−Cu1−Cl1 angle of 173.93°, and Cu1−N1 and Cu1−Cl1 bond lengths of 2.018 and 2.249 Å, respectively. The distortion (Δ) of the coordination polyhedron from an ideal trigonal bipyramid (Δ = 0) to a square pyramid (Δ = 1) has been calculated according to the method reported by Muetterties[7] and Galy.[8] The Δ value of 0.086 indicates that each Cu ion has a coordination geometry much closer to a trigonal bipyramid in the pentacoordinate environment. The distance between two Cu^{II} ions is 8.128 Å, which is similar to those observed in other dicopper(II) macrocyclic complexes.[9] With the center-to-center distance of 5.662 Å, the two phenyl rings form a dihedral angle of 83.3° to each other. Additionally, the two hydroxypropyl arms are located on the same sides of the plane defined by the nitrogen atoms and the phenyl groups of the macrocyclic ligand, thus ligand L in the title complex has a boat-like (*syn*) conformation.

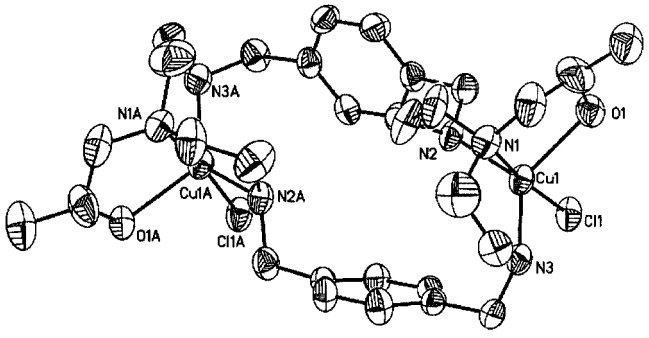

Figure 1. ORTEP drawing (30% probability ellipsoids) of $[Cu_2(H_{-2}L)Cl_2]\cdot 6.5H_2O$; hydrogen atoms and water molecules are omitted for clarity

We noticed that the Cu^{II}−O(ROH) bond length (2.177 Å) in the title complex is shorter than the Cu^{II}−O distance of 2.186 Å in the dicopper complex of a 26-membered macrocycle ligand with two hydroxyethyl groups.[9] Since shorter water oxygen−copper bonds always lead to greater acidity, and hence to lower pK_a values,[6] the discrepancy in the structure between these two Cu^{II}−macrocycle complexes may be responsible for the different deprotonation behavior.

Complexation Constants of L with Cu^{II}

The complexation constants of the species formed by L and Cu^{II} in a 1:2 [L/Cu^{II}] system with I = 0.10 M ($NaNO_3$) in aqueous solution at 298 K have been determined by potentiometric titration (6 equiv. of HCl added to acidify the pure ligand before titration). As shown in Figure S1 (see Supporting Information), when 2 equiv. of Cu^{II} are added to the solution, the titration reveals two inflexions at a = 6 and a = 8 (a is the number of mol of NaOH added per mol of ligand), respectively. The inflexion at a = 6 corresponds to the completion of the neutralization of the six ammonium ions in the diethylenetramine moieties, which are easily deprotonated to form dinuclear complexes. The inflection at a = 8 indicates the further deprotonation of two titratable protons from two hydroxypropyl pendants bound to the Cu^{II}.

To rationalize the model selection and data process, several different analysis processes were conducted and evaluated. In the first case, the deprotonated species were set to be the dinuclear complexes of $[Cu_2H_{-1}L]^{3+}$ and $[Cu_2H_{-2}L]^{2+}$. In the second case, the deprotonated species were set for both dinuclear and mononuclear complexes; i.e., the species CuL, CuHL, CuH_2L, Cu_2L, $[Cu_2H_{-1}L]^{3+}$, $[Cu_2H_{-2}L]^{2+}$ and $[CuH_{-1}L]^{+}$ were included. In the third case, all possible deprotonated species and hydroxide species were included. In the third case, reasonable results were given by BEST, with a σ-fit value optimized to be 0.028. However, in other cases, the σ-fit values are all larger than 0.2. Thus, we chose the third case as the most rational one.

Figure 2 displays the species distribution as a function of pH at a total Cu^{II} concentration of 2 mM and a total L concentration of 1 mM at 25 °C. As shown in Figure 2, $[CuH_2L]^{4+}$, $[Cu_2L]^{4+}$, $[Cu_2H_{-1}L]^{3+}$, $[Cu_2H_{-2}L]^{2+}$, $[Cu_2H_{-2}L(OH)]^{+}$ and $[Cu_2H_{-2}L(OH)_2]$ exist as the major Cu^{II} complex species under the employed experiment conditions, and the other species were less than 1 ppm in concentration. The dinuclear complex $[Cu_2L]^{4+}$ is the predominant species over the pH range of 5−6.5. The monodepro-

 © 2004 Wiley-VCH Verlag GmbH & Co. KGaA, Weinheim

tonated $[Cu_2H_{-1}L]^{3+}$ has a favourable pH of 7.4, above which it is gradually converted into $[Cu_2H_{-2}L]^{2+}$, $[Cu_2H_{-2}L(OH)]^{+}$, $[Cu_2H_{-2}L(OH)_2]$; $[Cu_2H_{-2}L]^{2+}$ predominates at pH values of about 8.5, and this is in accordance with the X-ray crystal structure analysis. To illustrate the process clearly, the stepwise complexation of L with Cu^{II} via these species is shown in Scheme 2. ES-MS data (shown in Figure 3a) for the complex in 10% CH_3CN/H_2O (v/v) at a pH of about 6.0 in aqueous solution evidence the stable existence of $[Cu_2LCl_2]^{2+}$ (m/z = 362.1) and $[Cu_2LCl_3]^{+}$ (m/z = 759.0). The stable existence of these species indicates that the dinuclear complex $[Cu_2L]^{4+}$ is the predominant species at a pH of about 6.0.

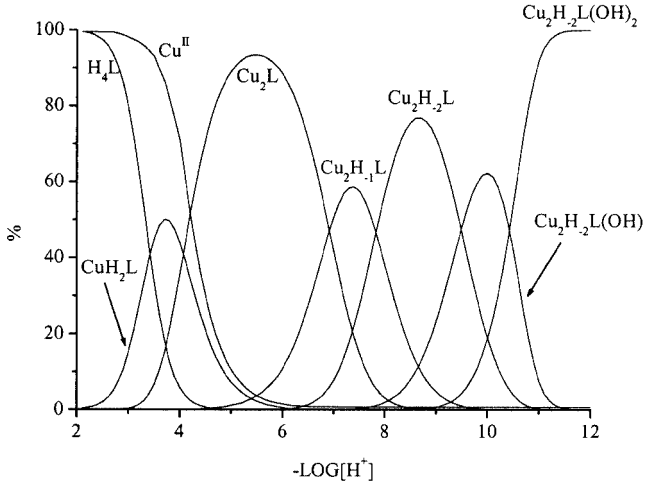

Figure 2. Species distribution graph as a function of pH for the 1 mM L + 2 mM Cu^{II} system at 25 °C and I = 0.10 M ($NaNO_3$)

The program BEST was used to analyze the titration data, and the obtained log K and the deprotonation constant pK_a for the Cu^{II} complexes with L at 25 °C are listed in Table 2. The most significant finding from Table 2 is the rather facile deprotonation of the alcoholic function with pK_a = 7.31 at 25 °C, which is lower than that found by Kimura et al.[4] for the Zn^{II} complex of 1-(2-hydroxyethyl)-1,5,9-triazacyclodecane (pK_a = 7.40 at 25 °C) and a dicopper complex of a 26-membered macrocyclic ligand with two hydroxyethyl pendants (pK_a = 7.60).[9] This lower pK_a value implies that the title complex is a strong enough nucleophile hydroxyethyl pendants (pK_a = 7.60).[9] This lower pK_a value implies that the title complex is a strong enough nucleophile to attack an ester bond in catalytic hydrolysis.

Hydrolysis of 4-Nitrophenyl Acetate

The reactivity of the dinuclear complex toward the hydrolysis of phosphate ester or carboxy ester has also been checked. Since phospho monoesters undergo slow hydrolysis with the complex, we only describe the hydrolytic cleav-

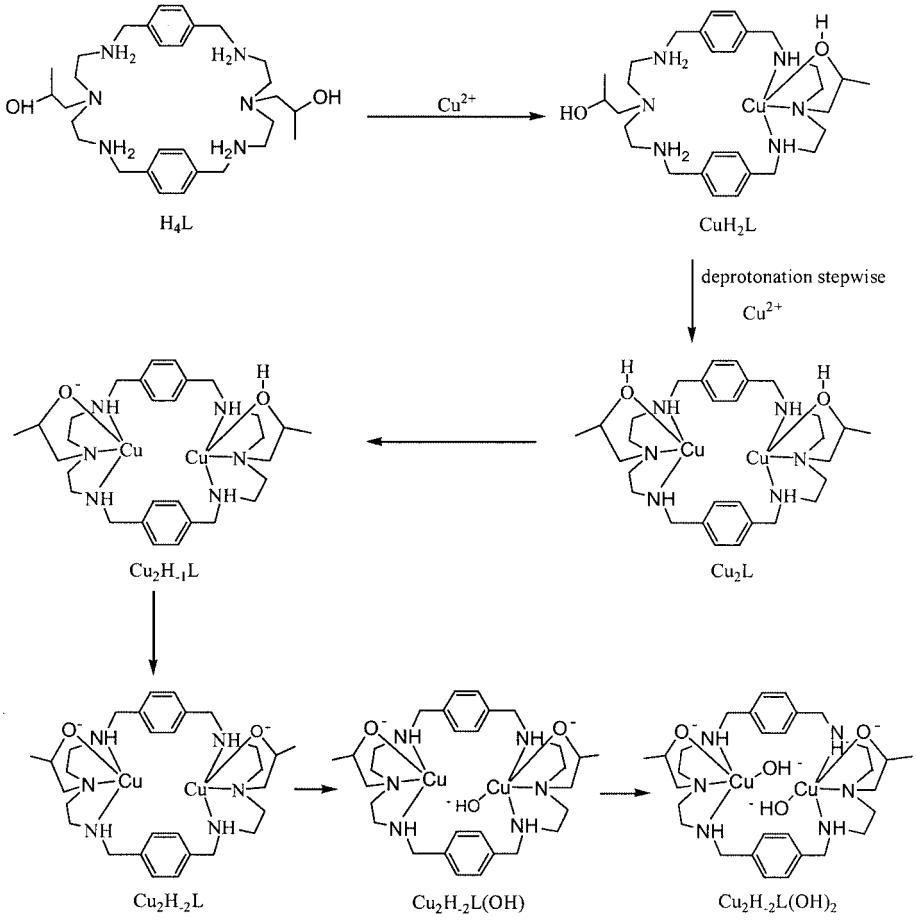

Scheme 2

 © 2004 Wiley-VCH Verlag GmbH & Co. KGaA, Weinheim

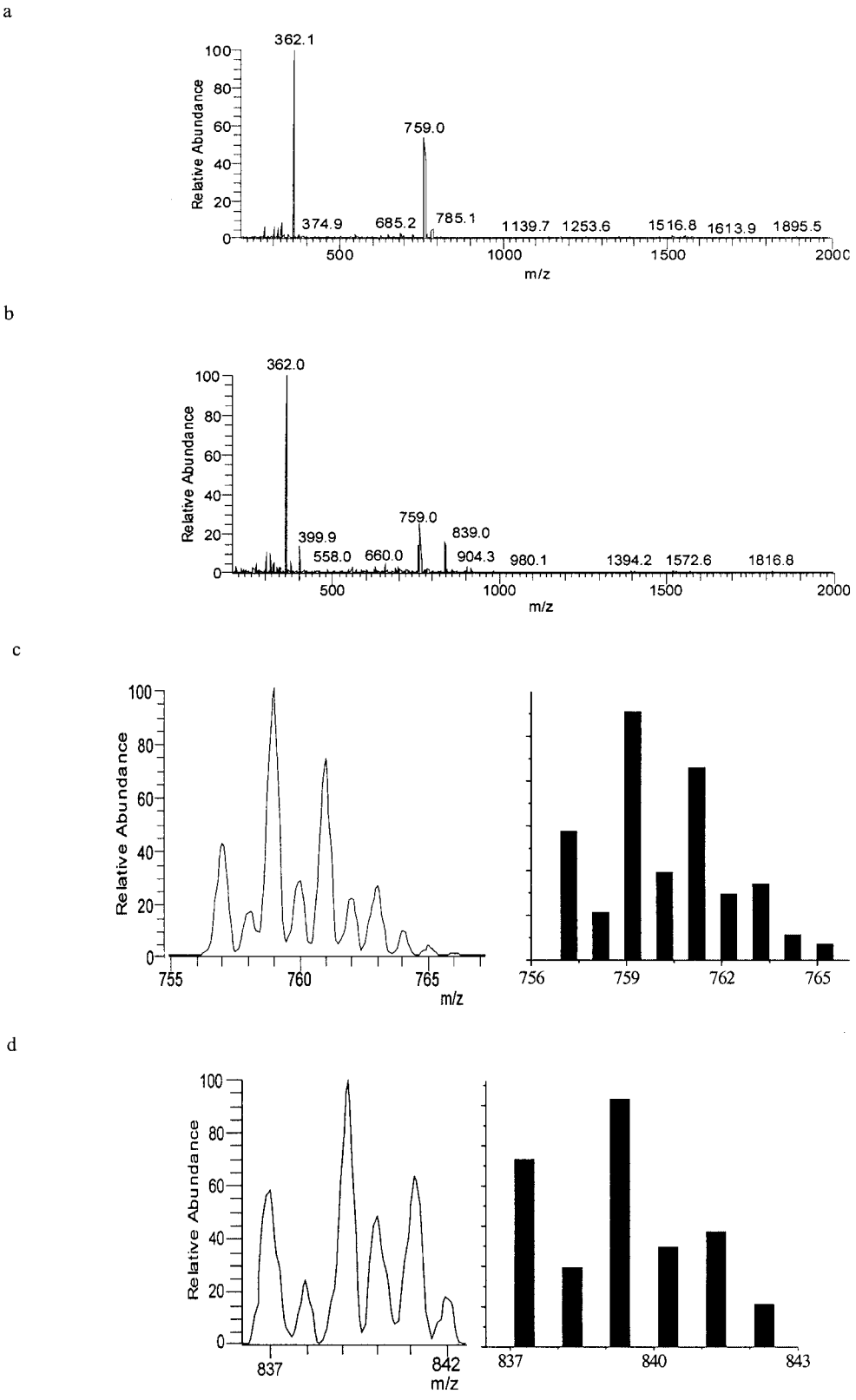

Figure 3. (a) Electrospray mass spectrum of the complex at pH ≈ 6 and 10% CH_3CN/H_2O (v/v) solution; the peak at m/z = 362.1 is assigned to $[Cu_2LCl_2]^{2+}$, m/z = 759.0 is assigned to $[Cu_2LCl_3]^{+}$; (b) electrospray mass spectrum for the mixture of Cu_2L/NA = 1:1 at pH ≈ 6 and 10% CH_3CN/H_2O (v/v) solution; the peak at m/z = 836.9 is assigned to $[IaH_{-2}Cl(CH_3OH)_2]^{+}$; (c) comparison of the observed (traces) and calculated (bars) isotopic distributions for the peak at m/z = 759.0 in the ES-MS data of the complex; (d) comparison of the observed (traces) and calculated (bars) isotopic distributions for the peak at m/z = 836.9 in the ES-MS data for the mixture of equimolecular Cu_2L and NA

 © 2004 Wiley-VCH Verlag GmbH & Co. KGaA, Weinheim

Table 2. Complexation constants and deprotonation constants for Cu^{II} complexes with I = 0.1 M ($NaNO_3$) at 25 °C

Symbol	Equilibrium quotient	log$K$
log$K$(CuL)	[CuL]/[Cu][L]	15.17 (0.03)
log$K$(CuHL)	[CuHL]/[CuL][H]	8.57 (0.02)
log$K$(CuH_2L)	[CuH_2L]/[CuHL][H]	5.76 (0.03)
log$K$(Cu_2L)	[Cu_2L]/[CuL][Cu]	6.83 (0.025)
pK_{a1}	[$Cu_2H_{-1}L$][H]/[Cu_2L]	7.31 (0.05)
pK_{a2}	[$Cu_2H_{-2}L$][H]/[$Cu_2H_{-1}L$]	7.83 (0.06)
pK_{a3}	[$Cu_2H_{-2}L(OH)$][H]/[$Cu_2H_{-2}L$]	9.48 (0.03)
pK_{a4}	[$Cu_2H_{-2}L(OH)_2$][H]/[$Cu_2H_{-2}L(OH)$]	10.56 (0.02)

age of 4-nitrophenyl acetate (NA). The activity of the dinuclear species has been investigated by monitoring the hydrolysis of NA (0.4−1.0 mM) promoted by Cu_2L at different concentrations (0.5−2.0 mM) at pH = 7.3−9.3, as described in the Exp. Sect. The spontaneous hydrolysis of NA by buffered solution was subtracted from the Cu complex promoted hydrolysis. A second-order kinetics of Cu_2L promotion NA hydrolysis was observed at different pH values. The initial rate constant, k_{in}, observed rate constant, k_{obs}, the spontaneous hydrolysis constant, v_{buffer}, and second-order constant, k_{cat}, are defined as follows:

$v_{total} = v_{Cu} + v_{buffer} = k_{in}[NA]$
$v_{buffer} = (k_{OH^-}[OH^-] + ...)\cdot[NA]$
$v_{Cu} = k_{NA}\cdot[Cu^{II}complex]_{total}\cdot[NA] = k_{cat}\cdot[Cu_2H_{-2}L][NA]$

The first-order constant k_{obs} [s^{-1}] is calculated from the slope of the straight line v_{Cu} vs. [NA]. The plot of k_{obs} vs. $[Cu^{II}\ complexes]_{total}$ gives a straight line with the slope denoted as k_{cat} ($M^{-1}s^{-1}$).[6] The second-order rate constant k_{cat} for Cu_2L is 0.39 $M^{-1}s^{-1}$ at pH = 9.5 (shown in Figure 4), where $[Cu_2H_{-2}L]^{2+}$ is the main species in aqueous solution.

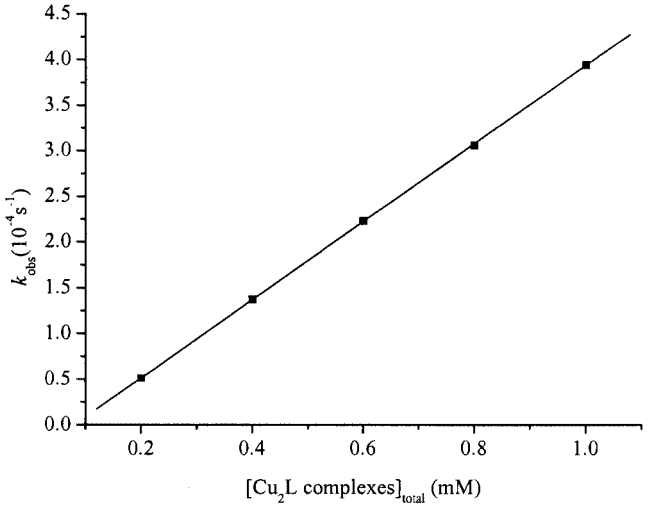

Figure 4. Dependence of k_{obs} on [total Cu^{II} complexes] at pH = 0 9.5, ionic strength 0.1 M ($NaNO_3$), and at 25 °C in the presence of 10% CH_3CN/H_2O (v/v); correlation coefficient > 0.99

To examine whether the whole process is a catalytic hydrolysis or transesterification, we followed the release of NP up to more than one cycle with the NA concentration set at 6.0 mM and the Cu^{II} complex concentration at only 0.2 mM in buffer solution (pH = 9.0) by monitoring the absorbance at 400 nm at 25 °C. The resulting v_{total} vs. time curve reveals that the rate constant for Cu_2L is identical to the initial rate constant determined above. Thus, the mechanism is catalytic hydrolysis. The second-order constants k_{cat} are plotted as a function of pH, and the resulting sigmoidal curve is shown in Figure 5. This curve is characteristic of a kinetic process controlled by an acid/base equilibrium with an inflexion at pH ≈ 8.75, and, as shown in Figure 2, $[CuH_{-2}L]^{2+}$ is the major species in aqueous solution at pH ≈ 8.7. Therefore, the main promoter species is proposed to be the deprotonated species $[CuH_{-2}L]^{2+}$. Different from the reported dicopper complex of a 26-membered macrocyclic ligand with two hydroxyethyl pendants,[9] the maximum value of k_{cat} for Cu_2L appears at pH ≈ 9.0 because the concentration of $[CuH_{-2}L]^{2+}$ species decreases significantly when the solution's pH is higher than 9.0. As with the reported dicopper complex,[9] the value of k_{cat} increases further when the solution's pH is higher than 9.5 because the doubly deprotonated species is still the major component.

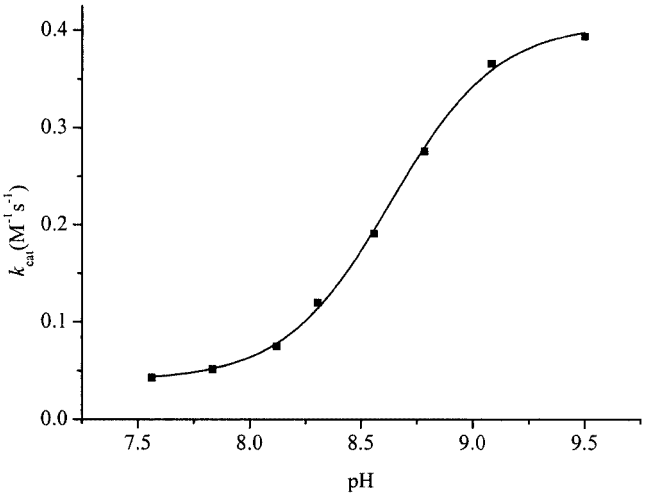

Figure 5. pH/rate profile for the second-order rate constant of NA hydrolysis with the Cu_2L complex at 25 °C and I = 0.1 M ($NaNO_3$) in 10% CH_3CN/H_2O (v/v)

In the course of catalytic NA hydrolysis, we suspected that a transient "acetyl intermediate" is formed, which then disappears very rapidly to give the final product acetate anion and Cu_2L. At pH values of 6 or lower, the intermediate can exist in aqueous solution for long time and it will disappear quickly when the pH of the solution is adjusted to 8.8.[10] A non-buffered solution (pH ≈ 6) of Cu_2L/NA = 1:1 in 10% CH_3CN/H_2O (v/v) was analyzed by ES-MS (shown in Figure 3b). When compared to Figure 3a, a new peak at m/z = 839.0 appears after the addition of NA and this peak is assigned to the intermediate $[\mathbf{Ia}H_{-2}Cl(CH_3OH)]^+$ (Scheme 3). On this basis, we propose

 © 2004 Wiley-VCH Verlag GmbH & Co. KGaA, Weinheim

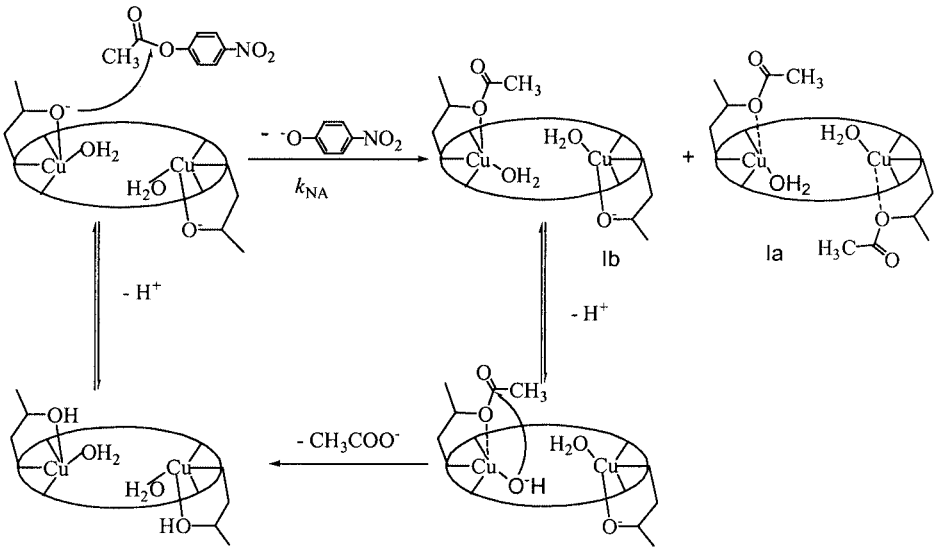

Scheme 3

the overall possible catalytic reaction depicted in Scheme 3, with the initial formation of an "acyl intermediate" being the slowest step. The formation of a similar intermediate was also observed by the groups of Kimura, Bencini and ourselves in NA hydrolysis catalyzed by Zn^{II} complexes.[4,10–12]

Comparing the kinetic data for Cu_2L and other dicopper(II) macrocyclic complexes, we found that the rate constant for Cu_2L is similar to that of a dicopper complex of a 26-membered macrocyclic ligand with two hydroxyethyl pendants (0.41 $M^{-1}s^{-1}$), and approximately 14 times higher than the Cu^{II} complex of the macrocyclic ligand without hydroxy pendants (0.027 $M^{-1}s^{-1}$).[9] These results suggest that a Cu^{II}-bound alkoxide is a better nucleophile than a Cu^{II}-bound hydroxide. The similar hydrolysis rate constants of Cu_2L and the reported dicopper hydroxyethyl macrocycle complex[9] may be related to this. The substitution of 2-hydroxypropyl for hydroxyethyl increases the nucleophilicity of the metal macrocycle and thus increases the hydrolysis rate constant, while the addition of a methyl group can increase the nucleophilic reaction's steric constraint and does not benefit the nucleophilic attack. The other reason may be the Lewis acidity of the metal complex. This trend of increasing Lewis acidity with increasing macrocycle size can be observed through the comparison of the pK_a of Cu_2L (pK_{a1} = 7.31, pK_{a2} = 7.83) and a reported dicopper complex of a hydroxyethyl macrocycle (pK_{a1} = 7.60, pK_{a2} = 8.07).[9] Since Cu_2L is a stronger Lewis acid than the Cu^{II} hydroxyethyl macrocycle complex, Cu_2L is expected to activate the coordinated carboxy ester toward nucleophilic attack to a greater degree than the other complex, although as the metal complex becomes a stronger Lewis acid, the nucleophilicity of the coordinated hydroxide decreases.

Conclusions

A new dinuclear Cu^{II} complex of a macrocyclic ligand with two 2-hydroxypropyl pendants has been synthesized. X-ray crystal analysis reveals that the two pendant alcohol groups are deprotonated to bind two Cu^{II} ions, which both adopt a trigonal-bipyramid geometry with a Cu···Cu distance of 8.129 Å. The solution complexation studied by potentiometric titration on the Cu^{II} complexes of L has revealed that $[Cu_2H_{-2}L]^{2+}$ is the major species when the pH of an aqueous solution is around 8.7, which is in accordance with the X-ray crystal analysis result. The 4-nitrophenyl acetate hydrolysis promoted by Cu_2L shows a second-order rate constant of 0.39 $M^{-1}s^{-1}$, which is approximately 14 times higher than that of the dicopper macrocycle complex without hydroxy pendants, while it is similar to that of a similar Cu^{II} complex of a macrocycle with hydroxyethyl pendants, which suggests that a Cu^{II}-bound alkoxide is a better nucleophile than a Cu^{II}-bound hydroxide. In spite of the volume of RO^-, the nucleophilicity and the Lewis acidity of the metal macrocycle can also effect the carboxy ester hydrolysis.

Experimental Section

Instrumentation and Materials: C, H and N analyses were performed with a Perkin–Elmer 240C elemental analyzer. ES mass spectra were obtained with a Finnigan MAT LCQ ES mass spectrometer with an *m*/*z* range of 2000. A CH_3OH/water (1:1) mixture was used as the solvent, and the concentration used in the experiment was 1.0 μmol/L. 1-[Bis(2-aminoethyl)amino]-2-propanol (L^1, Scheme 1) was prepared as described previously.[13] The other reagents were of analytical grade from commercial sources and were used without further purification. The synthesis of L and its Cu^{II}

 © 2004 Wiley-VCH Verlag GmbH & Co. KGaA, Weinheim

complex is shown in Scheme 4. L was synthesized as a mixture of diastereomers by $NaBH_4$ reduction of the corresponding Schiff base obtained from the [2 + 2] condensation between 1-[bis(2-aminoethyl)amino]-2-propanol (L^1) and terephthaldehyde similar to the reported procedures,[9] and then the Cu_2L complex was synthesized by reaction of L with $CuCl_2$.

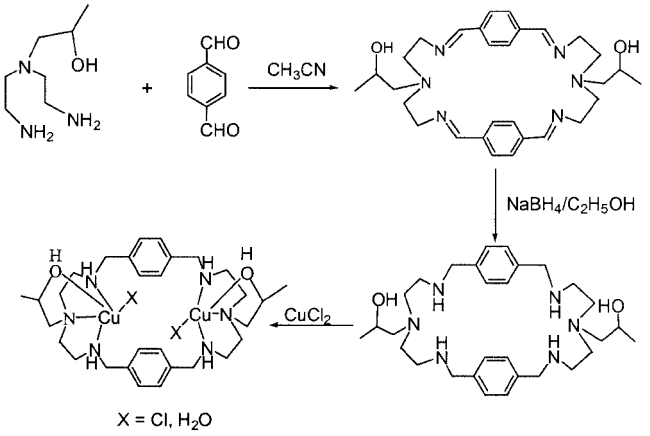

Scheme 4

Preparation of the Dinuclear Copper Complex $[Cu_2(H_{-2}L)Cl_2]\cdot 6.5H_2O$: A solution of L (0.0512 g, 0.10 mmol) in H_2O (2 mL) was added dropwise with stirring to an aqueous solution (2 mL) containing $CuCl_2\cdot 2H_2O$ (0.0341 g, 0.20 mmol), at 25 °C, to give a blue solution (pH ≈ 8.5). After being stirred for 2 h, the reaction mixture was filtered. Blue polyhedral crystals were obtained by slow evaporation of the solvents from the filtered solution for several days at ambient temperature. $[Cu(H_{-2}L)Cl_2]\cdot 6.5H_2O$ (839.83): calcd. C 43.09, H 6.94, N 10.13; found C 43.07, H 6.82, N 10.05.

X-ray Crystallographic Study of $[Cu_2(H_{-2}L)Cl_2]\cdot 6.5H_2O$: Diffraction data for the crystal were collected with a Siemens SMART CCD system equipped with monochromated Mo-K_α radiation (λ = 0.71073 Å) at room temperature in the range of $2.20° \le \theta \le 25.00°$. Data integration and empirical absorption corrections were carried out with the SAINT[14] and SADABS[15] programs. The structure was solved by direct methods (SHELXS 97) and refined on F^2 by full-matrix least-squares techniques (SHELXL 97).[16] All the non-H atoms were refined anisotropically. Hydrogen atoms were introduced in calculated positions and treated as riding atoms using the SHELXL-97 default parameters. All of the crystalline water molecules were found to be disordered and the site occupancy factors (s.o.f.s) for these oxygen atoms (O1W, O2W, O3W, O1W′, O2W′, O3W′, O4W, O5W, O6W) are 0.5, 0.25, 0.25, 0.5, 0.5, 0.25, 0.5, 0.5 and 0.25, respectively. The O5W atom is located on the twofold axis. The crystallographic data and details of the data collection are summarized in Table 3. CCDC-210142 contains the supplementary crystallographic data for this paper. These data can be obtained free of charge at www.ccdc.cam.ac.uk/conts/retrieving.html [or from the Cambridge Crystallographic Data Centre, 12 Union Road, Cambridge CB2 1EZ, UK; Fax: (internat.) + 44-1223/336-033; E-mail: deposit@ccdc.cam.ac.uk].

Potentiometric Measurements: Potentiometric experiments were conducted with an Orion 91−04 glass combination pH electrode and an Orion microprocessor analyzer/901 at 25 °C. All solutions were carefully protected from air by a stream of humidified nitrogen. Standard NaOH (0.1 M, CO_2 free) was added by a spiral micro-injector. The $CuCl_2$ solution was calibrated by standard EDTA, and doubly distilled water with a pH of about 6 was used. The temperature of the cell was controlled by a thermostat. K_w was chosen as 13.69 for 25 °C, 0.1 M $NaNO_3$ was contained to adjust the ionic strength to 0.1 M. Solutions containing 1 mM L with or without 2 mM $CuCl_2\cdot 2H_2O$ were titrated to pH > 11. The complexation and protonation constants were calculated using the program BEST.[17] All data represent the average of at least two independent experiments and all the sigma fit values have been reduced to less than 0.03 after optimization.

Table 3. Summary of crystal data, data collection and refinement for $[Cu_2(H_{-2}L)Cl_2]\cdot 6.5H_2O$

Empirical formula	$C_{30}H_{61}Cl_2Cu_2N_6O_{8.5}$
Formula mass	839.83
λ [Å]	0.71073
Crystal system	orthorhombic
Space group	*Fddd*
a [Å]	16.4581(12)
b [Å]	32.248(2)
c [Å]	35.830(2)
V [Å^3]	19017(2)
Z	16
ρ [g cm^{-1}]	1.173
Measured reflections	21787
Unique reflections	4034 (R_{int} = 0.0613)
Observed reflections [$I > 2\sigma(I)$]	2288
μ [mm^{-1}]	1.051
Goodness-of-fit on F^2	1.026
$R1$,[a] $wR2$[b] [$I > 2\sigma(I)$]	0.0694, 0.1566
Largest difference peak/hole [e Å^{-3}]	0.578/−0.339

[a] $R1 = \Sigma||F_o| - |F_c||/\Sigma|F_o|$; $wR2 = \{\Sigma[w(F_o^2 - F_c^2)^2]/\Sigma[w(F_o^2)^2]\}^{1/2}$. [b] $w = 1/[(F_o^2)^2 + (0.0354P)^2 + 0.0000P]$, where $P = (F_o^2 + 2F_c^2)/3$.

Kinetic Studies: The hydrolysis rate of 4-nitrophenyl acetate (NA) was measured by an initial slope method by monitoring the increase in the 400-nm absorption of the released 4-nitrophenolate in 10% CH_3CN/H_2O (v/v) aqueous solution at 25.0 ± 0.5 °C with a UV-3100 spectrophotometer by using the procedures reported previously.[9,10] Buffered solutions containing Tris buffer (pH = 7.3−9.0) or CHES buffer (pH = 9.3−9.6) were used, and the ionic strength was adjusted to 0.10 M with 1.0 M $NaNO_3$. The initial rate determination was carried out according to the typical procedure previously reported by Kimura and ourselves.[4,5,9,10,18] NA and Cu^{II} complex were mixed in the buffered solution, the UV absorption increase at 400 nm was recorded immediately and monitored generally until 2% formation of 4-nitrophenolate. The observed first-order rate constant k_{obs} [s^{-1}] was calculated from the decay slope of 4-nitrophenolate release rate vs. [NA] and the slope of k_{obs} vs. $[Cu^{II}\ complex]_{total}$ was denoted as the second-order rate constant k_{NA} [M^{-1}s^{-1}]. All the experiments were conducted at least twice, and the tabulated data represent the average of these experiments.

Acknowledgments

This work was supported by the National Natural Science Foundation of China.

 © 2004 Wiley-VCH Verlag GmbH & Co. KGaA, Weinheim

[1] [1a] A. E. Eriksson, T. A. Jones, A. Liljas, *Proteins: Struc. Funct. Gen.* **1988**, *4*, 274−282. [1b] S. K. Nair, D. W. Christianson, *J. Am. Chem. Soc.* **1991**, *113*, 9455−9458.
[2] D. W. Christianson, W. N. Lipscomb, *Acc. Chem. Res.* **1989**, *22*, 62−69.
[3] K. A. Deal, J. N. Burstyn, *Inorg. Chem.* **1996**, *35*, 2792−2798.
[4] E. Kimura, I. Nakamura, T. Koike, M. Shionaoya, Y. Kodama, T. Ikeda, T. Shiro, *J. Am. Chem. Soc.* **1994**, *116*, 4764−4771.
[5] T. Koile, S. Kajitan, I. Nakamura, E. Kimura, M. Shiro, *J. Am. Chem. Soc.* **1995**, *117*, 1210−1219.
[6] M. J. Young, D. Wajnon, R. C. Hynes, J. Chin, *J. Am. Chem. Soc.* **1995**, *117*, 9441−9447.
[7] E. L. Mutterties, L. J. Guggenberger, *J. Am. Chem. Soc.* **1974**, *96*, 1748−1756.
[8] J. Galy, J. I. Bonnet, S. Anderson, *Acta Chem. Scand., Ser. A* **1979**, *33*, 383−389.
[9] S. A. Li, J. Xia, D. X. Yang, Y. Xu, D. F. Li, M. F. Wu, W. X. Tang, *Inorg. Chem.* **2002**, *42*, 1807−1815.
[10] J. Xia, Y. Xu, S. A. Li, K. B. Yu, W. X. Tang, *Inorg. Chem.* **2001**, *40*, 2394−2401.
[11] C. Bazzicalpi, A. Bencini, E. Berni, A. Bianchi, V. Fedi, V. Fusi, C. Giorgi, P. Paoletti, B. Valtancoli, *Inorg. Chem.* **1999**, *38*, 4115−4122.
[12] S. A. Li, D. X. Yang, D. F. Li, J. Huang, W. X. Tang, *New. J. Chem.* **2002**, *26*, 1831−1837.
[13] Dow Chemical Co. Fr. 2112697, 1972-07-28; from *Chem. Abstr.* **1973**, *78*, 124002g).
[14] *SAINT*, version 4.0, Data Integration Software, Bruker AXS, Inc., Madison, WI, **1997**.
[15] G. M. Sheldrick, *SADABS*, version 2.01, Empirical Absorption Correction Program, University of Göttingen, **1996**.
[16] G. M. Sheldrick, *SHELXTL*, version 5.10, Program for Crystal Structure Determinations, Siemens Industrial Automation, Inc., Madison, WI, **1997**.
[17] A. E. Martell, R. J. Motekaitis, *Determination and uses of stability constants*, 2nd ed., VCH, New York, **1989**.
[18] E. Kimura, E. Kikuta, *J. Biol. Inorg. Chem.* **2000**, *5*, 139.

Received July 10, 2003
Early View Article
Published Online March 18, 2004

 © 2004 Wiley-VCH Verlag GmbH & Co. KGaA, Weinheim

Synthesis, Solution-State and Solid-State Structural Characterization of Monocationic Nitrido Heterocomplexes $[M(N)(DTC)(PNP)]^+$ (M = ^{99}Tc, Re; DTC = Dithiocarbamate; PNP = Heterodiphosphane)

Cristina Bolzati,[a] Fiorenzo Refosco,[a] Aldo Cagnolini,[a] Francesco Tisato,*[a] Alessandra Boschi,[b] Adriano Duatti,[b] Licia Uccelli,[b] Alessandro Dolmella,[c] Ester Marotta,[d] and Michela Tubaro[d]

Keywords: Technetium / Rhenium / Radiopharmaceuticals / NMR spectroscopy / P ligands

Mono-cationic nitrido heterocomplexes of general formula $[M(N)(DTC)(PNP)]^+$ (where M is ^{99}Tc or Re, DTC is the monoanionic form of a dithiocarbamate ligand, and PNP is a diphosphane ligand with a tertiary amine-containing five-membered spacer) were prepared by ligand-exchange reactions with the labile precursors $[M(N)Cl_2(PPh_3)_2]$ in dichloromethane/alcohol mixtures. The molecular structure of the representative rhenium complex $[Re(N)(dedc)(pnp2)][PF_6]$ (**1**) displays a distorted, square-pyramidal geometry with the dithiocarbamate sulfur and the diphosphane phosphorus atoms spanning the four coordination positions on the equatorial plane. If the additional interactions between the nitrido nitrogen and the weakly bonded *trans N*-diphosphane heteroatom, the molecular geometry can be viewed as pseudo-octahedral. The structure in solution, as established by multinuclear NMR spectroscopy and ESI spectrometry, is monomeric, and identical to that shown in the solid state. Replacement of the phenyl groups on the phosphorous atoms in complexes **1**, **2**, **5**, and **6** with alkyl groups modified neither the course of the reaction nor the composition of the resulting complexes. These results, together with the observation that no symmetrical complexes containing two identical bidentate ligands were produced in these reactions, strongly supports the conclusion that a mixed coordination sphere, composed by a combination of π-donor and π-acceptor atoms around the $[M{\equiv}N]^{2+}$ group, constitutes a highly stable system. Compounds containing dangling alkyl-substituted groups in the outer sphere (**3**, **4**, **7**, and **8**) were fully characterized by multinuclear NMR spectroscopy and ESI mass spectrometry.

(© Wiley-VCH Verlag GmbH & Co. KGaA, 69451 Weinheim, Germany, 2004)

Introduction

Radioactive isotopes of the two elements technetium and rhenium play an important role in nuclear medicine for diagnostic and therapeutic applications. In particular, the γ-emitting radionuclide ^{99m}Tc has almost ideal properties (E_γ = 142 keV, $t_{1/2}$ = 6.06 h) for the imaging of internal organs. Similarly, the β-emitting radionuclide ^{188}Re is currently considered to be an important candidate for the development of therapeutic agents for the treatment of degenerative diseases. Selective uptake into the target organ is one of the key issues that should be always considered in the development of effective diagnostic or therapeutic agents. Ultimately, this requires the design of radiopharmaceuticals possessing specific molecular features. Metal complexes of technetium and rhenium characterized by a selective reactivity toward a selected set of coordinating atoms are currently attracting much interest as suitable precursors for the design and preparation of new radiopharmaceuticals.[1−3] These complexes can be viewed as being composed of a robust metal-containing fragment with a few substitution-labile coordination positions, spanned by some weakly bound ancillary ligands. It turns out that these ancillary substituents can be easily replaced by ligands which only carry a specific set of coordinating atoms. The metal unit, therefore, manifests a selective reactivity towards a specific class of ligands, and is almost completely inert towards other types of reagents. Examples of this specific class include the low-valent aqua-carbonyl $[Tc^I(CO)_3(OH_2)_3]^+$ complex[4,5] and high-valent, nitrido-diphosphane $[Tc(N)(PNP)Cl_2]$ complexes.[6,7] In these complexes, the $[Tc(CO)_3]^+$ and $[Tc(N)(PNP)]^{2+}$ fragments are the stable molecular units. In contrast, the water and halide

[a] Istituto di Chimica Inorganica e delle Superfici − C.N.R., Area della Ricerca, Corso Stati Uniti, 4, 35127 Padua, Italy
Fax: (internat.) +39-049-8702911
E-mail: tisato@icis.cnr.it
[b] Laboratory of Nuclear Medicine, Department of Clinical & Experimental Medicine, University of Ferrara, Via L. Borsari, 46, 44100 Ferrara, Italy
[c] Department of Pharmaceutical Sciences, University of Padua, Via Marzolo, 5, 35131 Padua, Italy
[d] ISTM − C.N.R., Area della Ricerca, Corso Stati Uniti, 4, 35127 Padua, Italy

 © 2004 Wiley-VCH Verlag GmbH & Co. KGaA, Weinheim **DOI: 10.1002/ejic.200300666**

ligands can be efficiently substituted by a series of bi-functional tridentate σ-donor ligands (L) and bidentate π-donor ligands (L′), respectively, to yield mixed heterocomplexes of the type $[Tc(CO)_3(L)]^+$ [8,9] and [Tc(N)(PNP)(L′)].[10,11]

In the last few years, we have investigated the design of nitrido-containing species by exploiting the strong electrophilic character exhibited by the $[M(N)(PNP)]^{2+}$ metal fragment, which selectively reacts with nucleophilic bidentate ligands having a π-donor set of coordinating atoms. In particular, emphasis was placed on bidentate ligands containing both heteroatomic chelating sites (such as cysteine, thiocarboxylic acids, and aminothiols) and homoatomic sites (such as dithiols and dithiocarbamates). For example, small peptides having a terminal cysteine residue have been efficiently labeled with the $[^{99m}Tc(N)(PNP)]^{2+}$ complex at a high-specific-activity level.[10] A cysteine-conjugated 2-methoxyphenylpiperazine ligand was linked to the same metal fragment to investigate the binding affinity of the resulting heterocomplex for 5-HT_{1A} receptors in the central nervous system.[12]

Within the class of homoatomic bidentate ligands, monoanionic dithiocarbamates (DTC) were found to possess a strong affinity for the $[^{99m}Tc(N)(PNP)]^{2+}$ complex. Reactions with these ligands, carried out at tracer level (μM concentrations), yielded mono-cationic nitrido heterocomplexes, thought to be of general formula $[^{99m}Tc(N)(DTC)(PNP)]^+$. Biological evaluation of these new products demonstrated that they selectively accumulate in the myocardium of rats. For some derivatives, retention in this region was accompanied by a very fast blood, lung and liver clearance, suggesting that these tracers could be potentially utilized for obtaining SPECT myocardial images of superior quality compared to those obtained using currently available commercial agents.[13,14] The elucidation of the molecular structure of these compounds, therefore, appears to be of utmost importance for the comprehension of their peculiar biological properties. For this reason, we synthesized and structurally characterized a series of nitrido heterocomplexes of technetium and rhenium, obtained by treating the nitrido precursors $[M(N)Cl_2(PNP)]$ (M = Re, Tc) with the appropriate dithiocarbamate ligand.

The present study describes the synthesis, and solid-state and solution-state determination of the molecular structure of ^{99}Tc and Re mono-cationic compounds $[M(N)(DTC)(PNP)]^+$, where DTC indicates the derivatives diethyldithiocarbamate (dedc) and *N*,*N*′-bis(ethoxyethyl)dithiocarbamate (dbodc), and PNP represents the diphosphane ligands bis[(diphenylphosphanyl)ethyl]methoxyethyl-

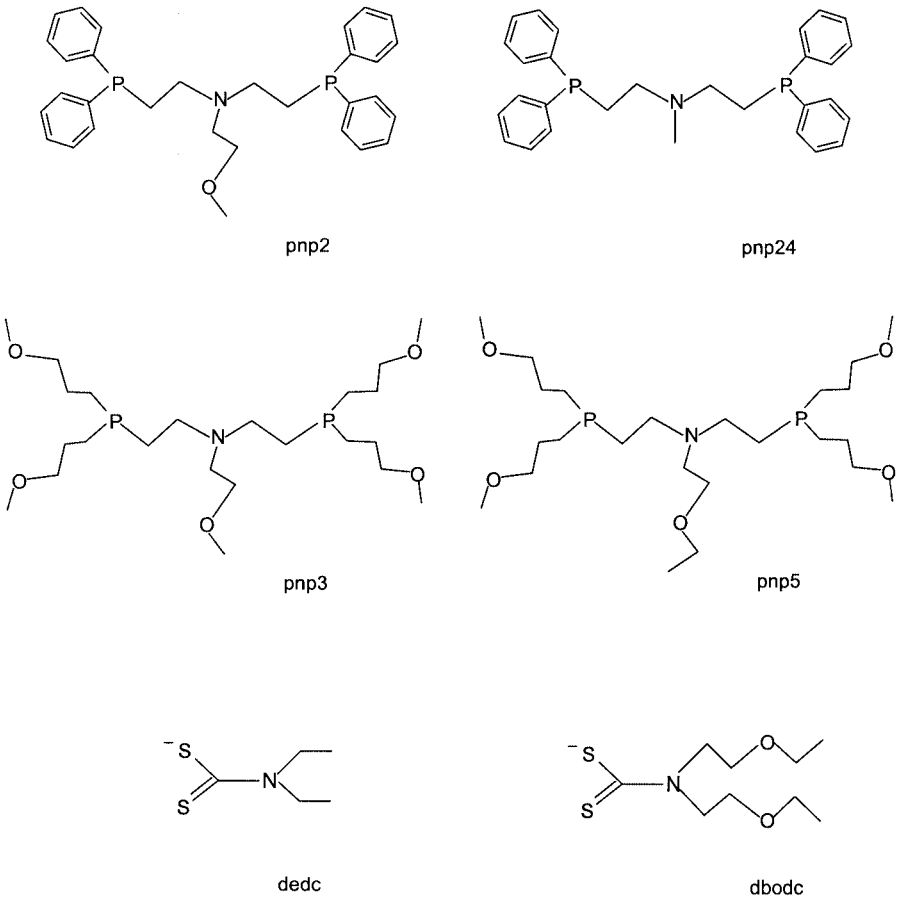

Figure 1. PNP and DTC ligands utilized in this study

 © 2004 Wiley-VCH Verlag GmbH & Co. KGaA, Weinheim

amine (pnp2), bis[(diphenylphosphanyl)ethyl]methylamine (pnp24), bis[(dimethoxypropylphosphanyl)ethyl]methoxyethylamine (pnp3) and bis[(dimethoxypropylphosphanyl)-ethyl]ethoxyethylamine (pnp5). The dithiocarbamate and heterodiphosphane ligands utilized here are depicted in Figure 1, and the molecular structure of the $[M(N)(DTC)(PNP)]^+$ complexes is outlined in Figure 2.

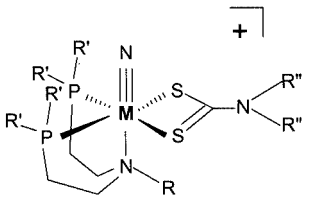

Complex	PNP	DTC
$[Re(N)(dedc)(pnp2)]^+$ **1**	$R = (CH_2)_2OCH_3$ $R' = Ph$	$R'' = CH_2CH_3$
$[Re(N)(dedc)(pnp24)]^+$ **2**	$R = CH_3$ $R' = Ph$	$R'' = CH_2CH_3$
$[Re(N)(dedc)(pnp3)]^+$ **3**	$R = (CH_2)_2OCH_3$ $R' = (CH_2)_3OCH_3$	$R'' = CH_2CH_3$
$[Re(N)(dbodc)(pnp5)]^+$ **4**	$R = (CH_2)_2OCH_2CH_3$ $R' = (CH_2)_3OCH_3$	$R'' = (CH_2)_2OCH_2CH_3$
$[Tc(N)(dedc)(pnp2)]^+$ **5**	$R = (CH_2)_2OCH_3$ $R' = Ph$	$R'' = CH_2CH_3$
$[Tc(N)(dedc)(pnp24)]^+$ **6**	$R = CH_3$ $R' = Ph$	$R'' = CH_2CH_3$
$[Tc(N)(dbodc)(pnp3)]^+$ **7**	$R = (CH_2)_2OCH_3$ $R' = (CH_2)_3OCH_3$	$R'' = (CH_2)_2OCH_2CH_3$
$[Tc(N)(dbodc)(pnp5)]^+$ **8**	$R = (CH_2)_2OCH_2CH_3$ $R' = (CH_2)_3OCH_3$	$R'' = (CH_2)_2OCH_2CH_3$

Figure 2. Sketch of the molecular structure of $[M(N)(TDC)(PNP)]^+$ complexes

Results and Discussion

Synthesis of Technetium and Rhenium Complexes

Technetium and rhenium nitrido heterocomplexes containing one diphosphane and one dithiocarbamate ligand bound to the same Tc≡N group were prepared by a one-pot procedure, as shown in Scheme 1. Reaction of equimolar amounts of $[M(N)Cl_2(PPh_3)_2]$ and the relevant diphosphane ligand in dichloromethane/ethanol yielded the intermediate precursor $[M(N)Cl_2(PNP)]$, which in turn provided the mixed-ligand complex on treatment with a slight excess of dithiocarbamate. Formation of the corresponding bis-substituted complexes with two identical polydentate ligands was not observed, even when 3:1 or 1:3 PNP/DTC ratios were used.

The reaction was faster for the technetium species, and afforded nearly quantitative yields. The preparation of the rhenium analogues required more drastic conditions (i.e. prolonged reflux), and yields dropped sharply, owing to the concomitant production of unstable side-products.

Characterization of the Complexes

The complexes were characterized by elemental analysis, spectroscopic methods and, in the case of complex **1**, X-ray diffraction. The IR spectra of both **1** and **2** exhibit bands of medium intensity at ca. 1060 cm^{-1}, attributable to the $\nu_{Re\equiv N}$ stretching vibration. Complex **1** displays an additional strong vibration at 840 cm^{-1}, characteristic of the hexafluorophosphate counter-anion.

X-ray Crystal Structure of $[Re(N)(dedc)(pnp2)][PF_6]$ (1)

Figure 3 shows the molecular structure of complex **1**, together with the essential numbering scheme. Relevant bond lengths and angles are given in Table 1. Crystallographic and structure refinement data are summarized in Table 2 (see Exp. Sect.).

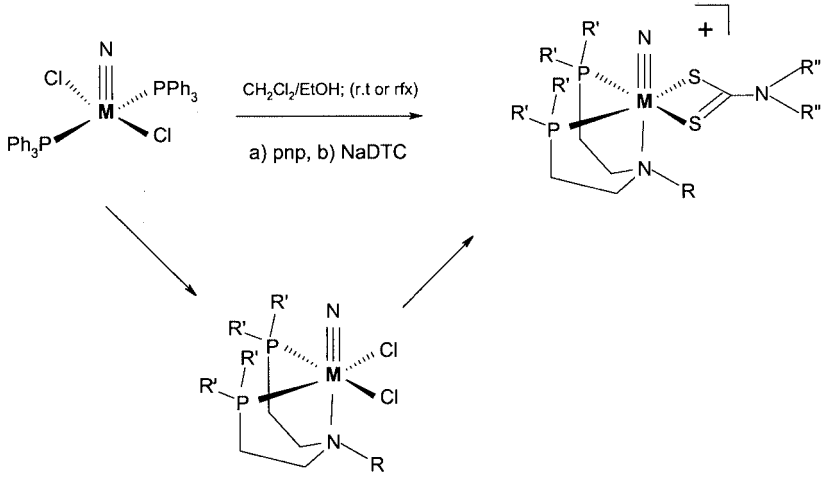

Scheme 1. Reaction pathway for the preparation of mixed nitride-M(V) heterocomplexes **1**–**8**

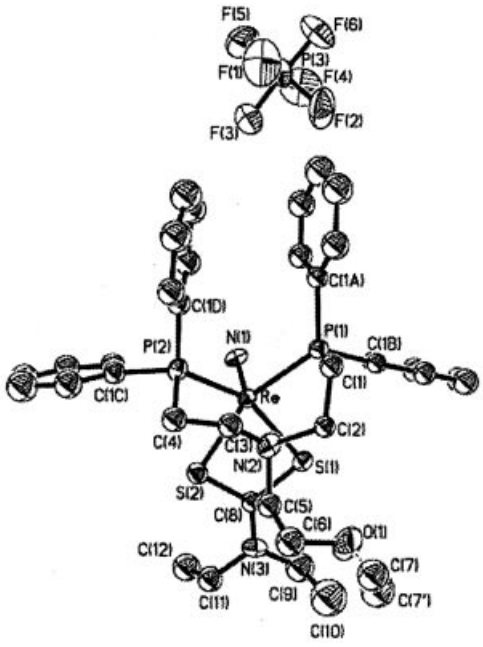

Figure 3. An ORTEP view of complex **1** with essential atom numbering. Hydrogen atoms have been omitted for clarity; displacement ellipsoids have been drawn at the 40% probability level

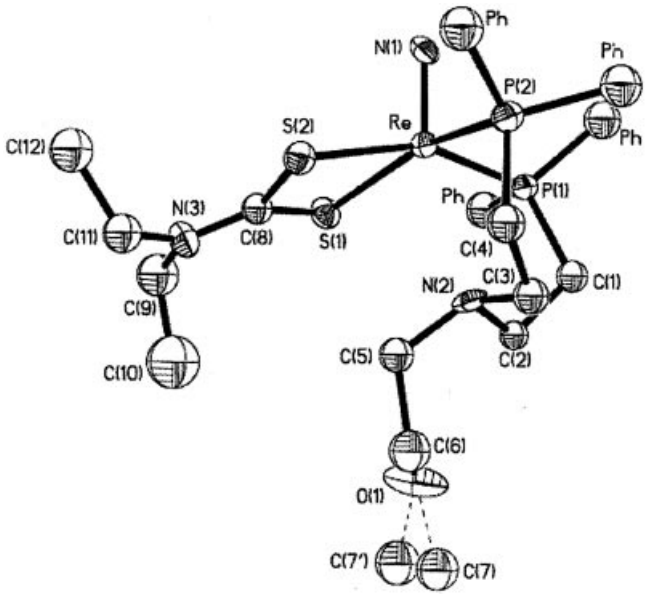

Figure 4. A close view of complex **1**. The phenyl rings have been replaced by pseudo atoms labelled as Ph. The C(7) atom position is split in two positions, each with an occupancy factor of 0.5

Table 1. Selected Bond lengths (Å) and Angles (°) for complex **1**

Re−S(1)	2.425(3)	Re−S(2)	2.413(3)
Re−P(1)	2.408(3)	Re−P(2)	2.396(3)
Re−N(1)	1.660(9)	Re···N(2)	2.73(1)
S(1)−C(8)	1.75(1)	S(2)−C(8)	1.72(1)
S(1)−Re−S(2)	72.5(1)	N(1)−Re−P(1)	93.3(4)
P(1)−Re−P(2)	101.2(1)	N(1)−Re−P(2)	96.8(3)
N(1)−Re−S(1)	105.4(3)	N(1)−Re···N(2)	164.4(5)
N(1)−Re−S(2)	106.4(4)	S(1)−C(8)−S(2)	110.9(7)

Crystalline **1** is made up of well-separated mono-cationic units and PF_6^- anions, which do not show any interaction below the sum of the van der Waals radii. The environment around the Re atom is square pyramidal, or pseudo-octahedral if we consider the additional weak interaction of N(2) with the metal, with the base plane defined by the P(1), S(1), S(2) and P(2) atoms (Figure 4).

None of these atoms deviate more than 0.02 Å from the mean plane, whereas Re is located 0.41 Å above the plane, towards N(1). The Re≡N(1) distance of 1.660(9) Å is close to the average of 1.675 Å found for terminal nitride-Re^V compounds (29 entries in the Cambridge Structural Database[15]). A similar search for the diphenylphosphinorhenium(v) synthon gave an average value of 2.484 Å for the Re^V-PPh_2R bond (25 entries), a distance markedly longer than those found for **1** [for which Re−P(1) and Re−P(2) are 2.408(3) and 2.396(3) Å, respectively). This shortening can be ascribed to the cationic nature of the complex, as previously observed for similar [Re(N)(pnp2)(L)][BF_4] and [Re(N)(pnp2)(POP)][BF_4] compounds (L = *S*-methyl 2-methyldithiocarbazate monoanion, POP = bis[(diphenylphosphanyl)ethyl]ether).[7] The S(1)−Re−S(2) bite angle of 72.5(1)° and the Re−S(1) and Re−S(2) bond lengths of 2.425(3) and 2.413(3) Å are in agreement with the reported data (average Re−S distance and S−Re−S angle of 2.433 Å and 71.3°, respectively).

The position assumed by the phenyl rings bound to the phosphorous atoms deserves comment. The two facing phenyl groups (labeled as A and D in Figure 3) adopt the so-called "parallel displaced" arrangement, characterized by the X(A) and X(D) centroid distance of 4.11 Å, and the C(1A)−X(A)−X(D)−C(1D) "twist angle" of 24.1°. These values corroborate the hypothesis of a possible role for π-bonds in stabilizing the *cis*-P coordination. On the other hand, the two rings bound to each phosphorous atom are roughly orthogonal to each other, with dihedral angles of 83.9° and 103.9° between the mean planes of A and B, and C and D, respectively. The A, B, C, and D phenyl rings have dihedral angles with the S_2P_2 equatorial plane of 93.3, 117.0, 114.7, and 69.3,°respectively. This plane has a dihedral angle of 13.6° to the dithiocarbamate plane [sp^2 geometry at N(3)], defined by the six S(1), S(2), C(8), N(3), C(9), and C(11) atoms. The methylene carbons of the diphosphane chain, C(1), C(4), C(2), and C(3), are located, respectively, at 1.69, 1.81, 2.64 and 2.64 Å below the mean S_2P_2 basal plane, whereas N(2) faces this plane at the intermediate distance of 2.29 Å. This additional metal−N(2) interaction provides further thermodynamic stability to the system and contributes to the kinetic inertness shown by this class of mixed nitrido heterocomplexes.

ESI Mass Spectrometry

The ESI mass spectra of the rhenium complexes **1**−**4** each show a peak corresponding to the molecular ion with

 © 2004 Wiley-VCH Verlag GmbH & Co. KGaA, Weinheim

no additional detectable fragments, indicating the high stability of the cation in the oxidative/reductive conditions typical of ESI experiments. To gain further information on the ligand-rhenium bond strengths, a series of collision experiments was undertaken. Such collisions (performed with an ion trap) inidicate the presence of decomposition channels with a low critical energy; the eventual products represent the more energetically favored pathways. For complex **4**, under these conditions, many fragment ions become detectable (as summarized in Scheme 2). The related collision-induced decomposition pathway is illustrated in Scheme 3. Collision of the molecular cation (m/z = 933) produces abundant fragments at m/z = 755 and 727, both corresponding to the unexpected loss of phosphorous-containing residues originating from the pnp5 ligand. As shown in Scheme 3, the resulting species at m/z = 727 most likely adopt a five-coordinate structure (the common arrangement for nitrido-containing rhenium compounds), in which a native bidentate *P*,*N*-phosphinoamine ligand shares the coordination positions around the Re=N group with the dithiocarbamate unit. It should be noted that this first fragmentation is identical to that exhibited by the isostructural technetium complex **8**, which was separately investigated in a previous study.[16]

No variation in the first collision-induced fragmentation profile is observed for any of the complexes investigated,

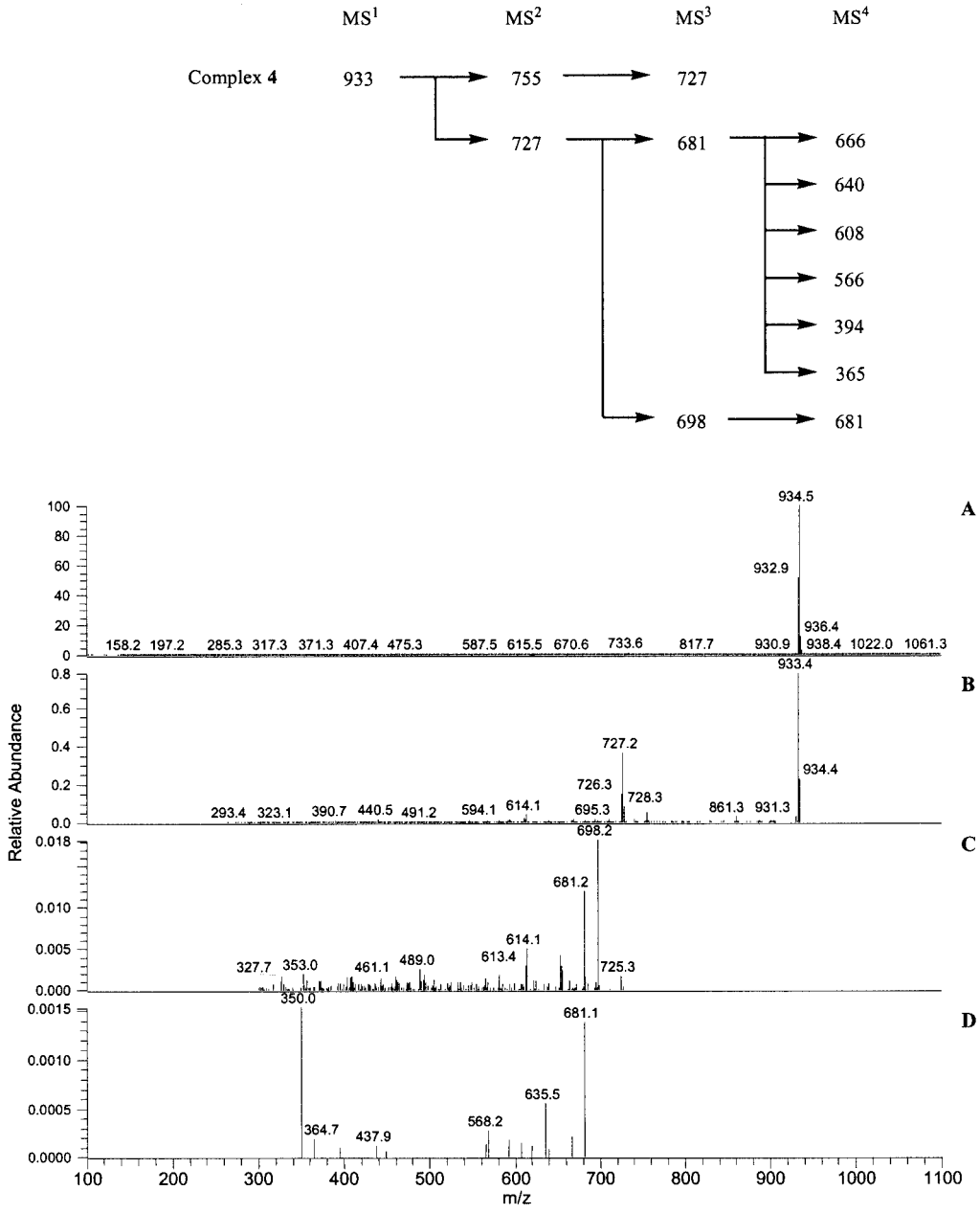

Scheme 2. MS^n data for complex **4** obtained by resonant excitation of the indicated precursor ion and of the main collision-generated fragment ions; below, **A**) ESI-MS spectrum of compound **4**; **B**) MS^2 spectrum of the molecular ion (m/z = 727); **C**) MS^3 spectrum of product ion at m/z = 698; **D**) MS^3 spectrum of the product ion at m/z = 681

 © 2004 Wiley-VCH Verlag GmbH & Co. KGaA, Weinheim

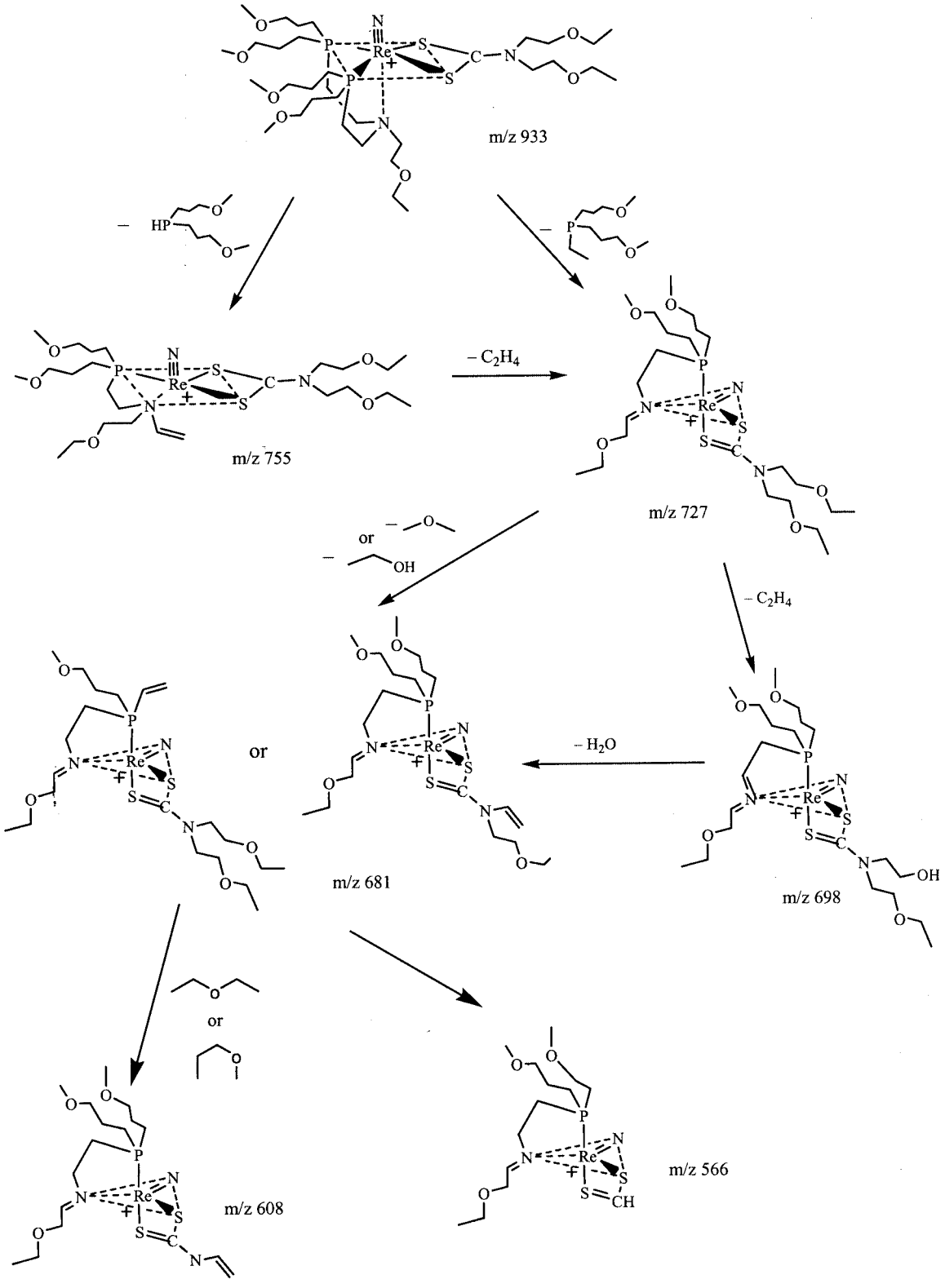

Scheme 3. Fragmentation scheme proposed to rationalize the collision-induced decomposition behavior of complex **4**

either by decreasing the bulkiness at the dithiocarbamate ligand (bdodc → dedc, **4** → **3**), replacing dangling methoxyethyl substituents at the diphosphane phosphorous with rigid phenyl groups (pnp3 → pnp2, **3** → **1**), or by diminishing the steric hindrance at the *N*-diphosphinoamine function (pnp2 → pnp24, **1** → **2**).

Further MS^n experiments implied the loss of ethanol followed by release of other groups originating from the di-

 © 2004 Wiley-VCH Verlag GmbH & Co. KGaA, Weinheim

thiocarbamate and/or the phosphinoamine ligands. In the latter case, the substituents begin to play a significant role in the decomposition pathways. For example, dedc complexes 1−3 always retain the dithiocarbamate ligand intact, in contrast to the dbodc complex **4**, which undergoes cleavage of the C−N bond C−N, with retention of carbon disulfide. Moreover, the bidentate P,N-phosphinoamine ligand in complexes **1** and **2** releases the diarylalkylphosphane arm and retains the amine group, whereas the reverse is observed for complexes **3** and **4**, which carry the more strongly donating trialkylphosphanes.

Multinuclear NMR Spectroscopy

The remarkable downfield shift of the ^{31}P signal from negative values typical of uncoordinated diphosphanes to positive values for these complexes is diagnostic of metal-phosphorus coordination. Consistent with the expected magnetic equivalence of the two diphosphane phosphorus atoms, complexes 1−8 exhibit a singlet in the ^{31}P NMR spectrum, the peak profile being narrow ($\nu_{1/2} \approx 25$ Hz) in the case of rhenium and broad ($\nu_{1/2} \approx 350$ Hz) in the case of technetium.

One-dimensional proton and carbon spectra are quite complicated owing to the presence of overlapping methyl and methylene signals. However, the use of several two-dimensional experiments including homonuclear ^{1}H-^{1}H COSY and heteronuclear ^{1}H-^{13}C HETCOR makes the assignment of each signal possible. By way of example, COSY and HETCOR maps and the corresponding proton and carbon spectra for the technetium complex **8** are shown in Figure 5.

The assignment was determined as follows. Methyl carbons may be distinguished from methylene carbons with the ^{13}C DEPT-135 experiment (as shown in the bottom right

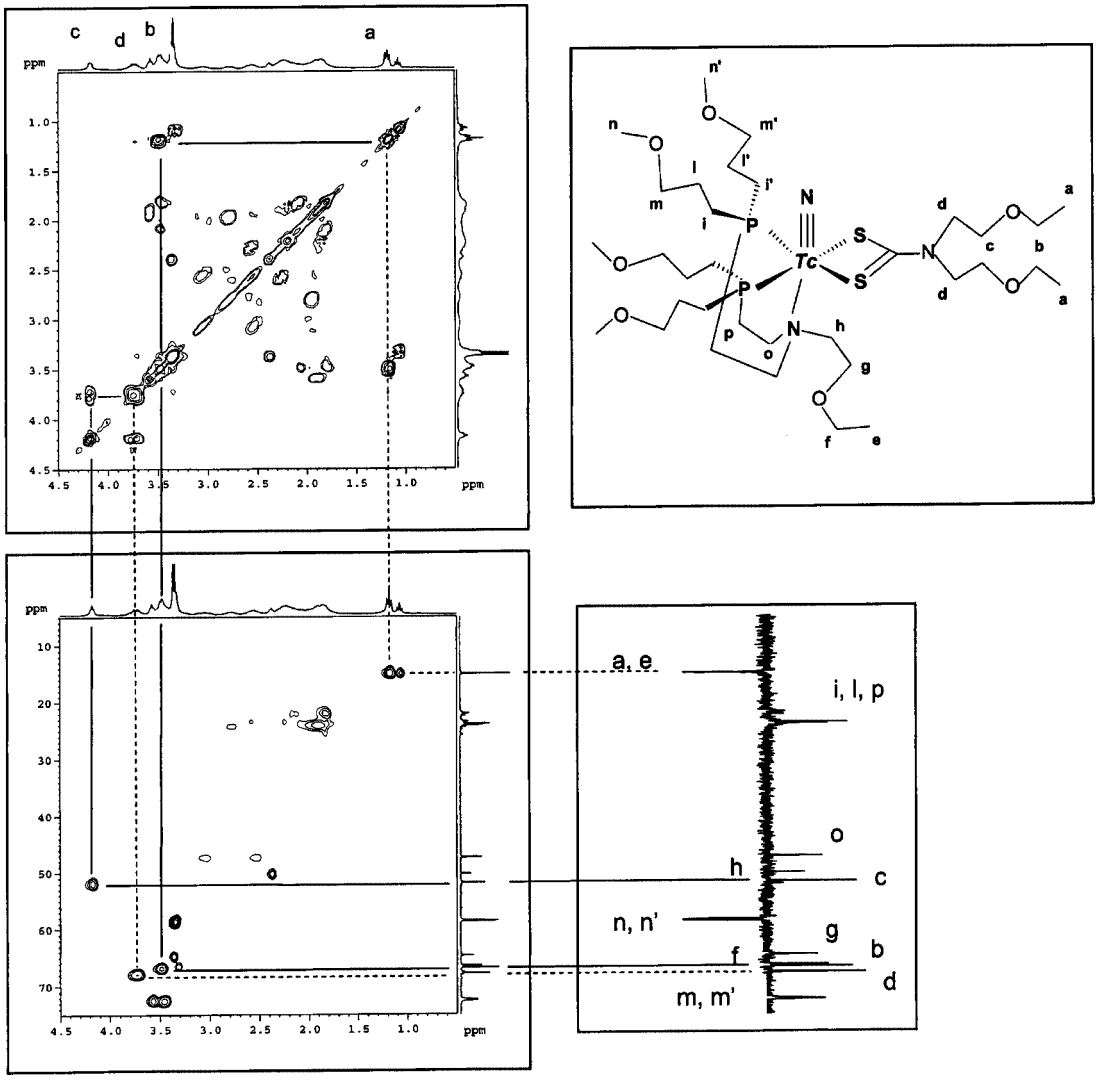

Figure 5. NMR spectra and maps of complex **8**; ^{1}H-^{1}H COSY spectrum (top left); ^{1}H-^{13}C HETCOR spectrum (bottom left); ^{13}C-DEPT 135 spectrum (bottom right); atom numbering scheme (top right); example of interpretation: carbon **b** is connected (solid line) with methylene protons **b** (multiplet at ca. 3.5 ppm) through a unique spot in the HETCOR map; protons **b** are coupled with methyl protons **a** (triplet at ca 1.20 ppm) in the COSY map; protons **a** are in turn connected with carbon **a** (dotted line) through another spot in the HETCOR map; the same interpretation strategy is applied for carbon and protons **c** and **d**, and for the other networks

 © 2004 Wiley-VCH Verlag GmbH & Co. KGaA, Weinheim

diagram in Figure 5), the former being phased "down" (on the left of the spectrum, as shown) and the latter being phased "up" (on the right of the spectrum). The downfield-shifted methyl carbons correspond to the terminal methoxy groups of the phosphane substituents (C-n and C-n′); the splitting is determined by the relative *syn* and *anti* orientation of each substituent with respect to the Tc≡N core. The upfield-shifted methyl signal in the carbon spectrum consists of two overlapping signals (split correctly into two components in the proton spectrum), due to the presence of two chemically inequivalent ethoxy groups (Me-a and Me-e). The related methylene protons of the terminal ethoxy groups CH_2-b and CH_2-f, as well as the methylene network of the dithiocarbamate (CH_2-c and CH_2-d) are distinguished in the COSY spectrum. Analogously, the methylene chain of the pendant *N*-diphosphane ethoxyethyl fragment (CH_2-h and CH_2-g) shows cross peaks in the COSY spectrum, as well as two distinct peaks in the HETCOR spectrum. Regarding the terminal methoxy groups Me-n and Me-n′ outlined above, the diphosphane methoxypropyl chains are oriented *syn* and *anti* with respect to the Tc≡N core, giving two distinct proton networks (i, l and m, and i′, l′ and m′). The peaks due to the bridging diphosphane methylene protons (o and p) are widely separated and show a cross-peak in the COSY spectrum. The diastereotopic nature of the bridging methylene protons is clear from the HETCOR map, which shows two distinct spots for each bridging carbon.

Comments

The efficient synthesis of mono-cationic heterocomplexes $[M(N)(DTC)(PNP)]^+$ (M = Tc, Re) described here provides a clear example of reactions able to form complexes containing two different polydentate ligands coordinated to the same Tc≡N group. As previously noted for the similar compound $[M(N)(L)(POP)]^+$ [L = *S*-methyl 2-methyldithiocarbazate mono-anion, POP = bis[(diphenylphosphanyl)ethyl]ether],[7] the remarkable stability of this class of complexes results from a balance of π-acceptor and π-donor properties provided by the combination of the diphosphane and dithiocarbamate ligands bound to the same $[M{\equiv}N]^{2+}$ group. The exclusive formation of the mixed complexes $[M(N)(DTC)(PNP)]^+$, without the concomitant production of the symmetrical species $[M(N)(DTC)_2]$, is attributed to the strong electrophilic character of the metal fragment $[M(N)(PNP)]^{2+}$. This electrophilic character results from removal of electronic density from the two residual positions of the five-coordinate arrangement determined by the two π-acceptor atoms. As a consequence, these two bonding sites are activated only towards soft, π-donor atoms, and the whole metal fragment $[M(N)(PNP)]^{2+}$ becomes strongly stabilized upon substitution with an appropriate bidentate π-donor ligand. The additional contact between the metal center and the PNP diphosphane nitrogen helps to explain the remarkable kinetic inertness demonstrated by these class of heterocomplexes toward transchelation by other chelating agents.[14] In this regard, it should be mentioned that diphosphanes incorporating merely methylene groups in the spacer or diphosphanes carrying a quaternary ammonium group in the middle of the spacer yielded only mixtures from which the isolation of stable compounds was unsuccessful, thus supporting the view that contact of the lone pair of the amine nitrogen with the metal is important.

The high chemical stability of mono-cationic $[M(N)(DTC)(PNP)]^+$ heterocomplexes is also partially responsible for their interesting biological properties. These complexes showed selective localization into the myocardium of rats and retention in this region for a prolonged time.[13,14] Modification of the outer sphere pendant groups was found to influence both the kinetics of uptake by the heart and clearance from the background organs, giving unprecedentedly high heart/liver and heart/lung uptake ratios.[14] Hence, the prototype agent $[^{99m}Tc(N)(dbodc)(pnp5)]^+$ was proposed as a potential candidate for the development of a new myocardial perfusion tracer.[17] These findings prompted us to prepare and characterize macroscopic amounts of the corresponding ^{99}Tc and Re complexes with the aim to elucidate their molecular structure. As outlined in Figure 4, the solid-state geometry exhibited by the representative rhenium complex **1** is distorted square pyramidal [or pseudo-octahedral if we consider the additional Re−N(2) contact]. However, the flexiblity of the methoxypropyl groups made it impossible to grow crystals suitable for X-ray diffraction studies. Therefore, we were forced to characterize alkyldiphosphane-containing compounds in the solution state by means of combined mass spectrometry and multinuclear NMR investigations. These experiments confirmed that the molecular structure of these complexes (shown in Figures 2 and 5) is monomeric and, most importantly, identical to that shown by the aryldiphosphane-containing species (Figure 4). In particular, the diphosphane phosphorous atoms, as well as the pendant arms of the dithiocarbamate unit, were found to be magnetically equivalent, whereas the

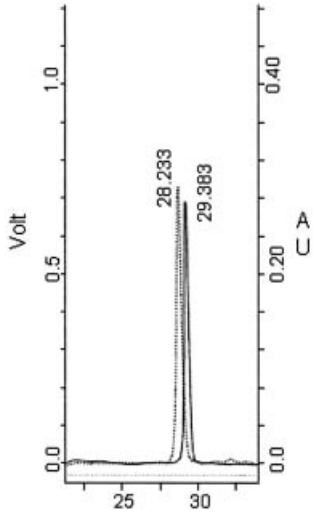

Figure 6. HPLC co-injection profiles for the complexes $[^{99m}Tc(N)(dbodc)(pnp5)]^+$ and $[^{99}Tc(N)(dbodc)(pnp5)]^+$ **8** (solid line, radiometric trace; dashed line, UV/Vis trace)

 © 2004 Wiley-VCH Verlag GmbH & Co. KGaA, Weinheim

methoxypropyl substituents on the phosphorous atoms were magnetically inequivalent, and oriented *syn* and *anti* with respect to the terminal nitrido group.

Strong support for the conclusion that the chemical nature of the complex $[^{99m}Tc(N)(dbodc)(pnp5)]^+$ (prepared at tracer level) is similar to that of the corresponding ^{99m}Tc analogue (isolated in macroscopic amounts) was obtained by comparison of their chromatographic profiles after HPLC co-injection. As shown in Figure 6, the two species co-eluted at 29.38 min (radiometric trace) and at 28.23 min (UV/Vis trace).

Conclusion

A new family of cationic mixed nitrido heterocomplexes of general formula $[M(N)(DTC)(PNP)]^+$, where M is ^{99}Tc or Re, DTC is the mono-anionic form of a dithiocarbamate ligand and PNP is a heterodiphosphane incorporating a tertiary amine group in a five-membered spacer, has been synthesized and completely characterized both in the solid and in the solution state. The molecular structure of this class of mixed complexes is best described as pseudo-octahedral, with the diphosphane ligand facing the dithiocarbamate unit on the equatorial plane. The terminal nitrido and the weakly bound heterodiphosphane nitrogen complete the octahedron in a reciprocal *trans*-axial arrangement. The peculiar combination of π-acceptor phosphorous and π-donor sulfur around the M≡N group ensures remarkable thermodynamic stability and associated high kinetic inertness towards transchelation reactions. One of these complexes prepared at tracer level, $[^{99m}Tc(N)(dbodc)(pnp5)]^+$, has shown interesting biological properties in animal models.

Experimental Section

General Remarks: ***Caution!*** ^{99}Tc is a weak β-emitter (E_β = 0.292 MeV, $t_{1/2} = 2.12 \times 10^5$ years). All manipulations were carried out in laboratories approved for low-level radioactivity using monitored hoods and glove-boxes. When handled in milligram amounts, ^{99}Tc does not present a serious health hazard since common laboratory glassware provides adequate shielding. Bremsstrahlung radiation is not a significant problem due to the low-energy of the β-particles. However, normal radiation safety procedures must be used at all times, especially with solid samples, to prevent contamination and inhalation. Methanolic solutions (concentration ca. 2×10^{-6} M) were used for mass spectrometric measurements (ESI). For a 50-minute analysis at a flow-rate of 5 μL/min, the amount of ^{99}Tc injected into the mass spectrometer led to a radioactivity level lower than the environmental background.

Technetium (as $[NH_4][^{99}TcO_4]$) was obtained from Oak Ridge National Laboratory. Samples were dissolved in water and treated with excess aqueous ammonia and 30% H_2O_2 at 80 °C prior to use to eliminate residual TcO_2. Solid samples of purified ammonium pertechnetate were obtained by slow evaporation of the solvent at 40 °C. Literature methods were applied to prepare the starting compounds $[M(N)Cl_2(PPh_3)_2]$[18,19] and the intermediate species $[M(N)Cl_2(PNP)]$.[7] Finely powdered rhenium was obtained as a gift from H. C. Starck GmbH, Germany. Samples were first oxidized to perrhenate and then reduced to suitable Re^V compounds prior to use. Diethyldithiocarbamate sodium salt (dedcNa) was purchased from Aldrich Chimica and *N,N′*-bis(ethoxyethyl)dithiocarbamate sodium salt (dbodcNa) was prepared according to literature methods or obtained from Alchemy, Italy.[20] Aryl diphosphanes (pnp2 and pnp24) and alkyl diphosphanes (pnp3 and pnp5) were synthesized as reported previously[21,22] or purchased from Argus Chemicals, Italy. Aryl diphosphanes are stable both as solids and in solution, but alkyl diphosphanes are air and moisture sensitive, and should be handled carefully under a nitrogen atmosphere and stored under nitrogen at −20 °C to avoid oxidation of the tertiary diphosphane to the corresponding diphosphaneoxide. Common laboratory solvents and other chemicals were used as received.

Elemental analyses (C, H, N, S) were performed on a Carlo−Erba 1106 elemental analyzer. FT IR spectra were recorded on a Nicolet 510P Fourier-transform spectrometer in the range 4000−400 cm^{-1} in KBr mixtures using a Spectra-Tech diffuse-reflectance collector accessory for technetium compounds and on a Mattson 3030 Fourier-transform spectrometer in the range 4000−400 cm^{-1} in KBr pellets for rhenium compounds. Proton and ^{31}P NMR spectra were collected on a Bruker AC-300 instrument, using $SiMe_4$ as an internal reference (for ^1H) and 85% aqueous H_3PO_4 as an external reference (for ^{31}P). Mass spectrometric measurements were performed with a LCQ DECA instrument (ThermoFinnigan, Palo Alto, CA, USA) using ca. 5×10^{-6} M methanol solutions of rhenium complexes **1−4**, which were injected by a syringe pump at a flow rate of 5 μL/min. MS^n experiments were performed by selection of the ionic species of interest followed by collision with He inside the ion trap (He pressure 10^{-4} Torr) accomplished by resonant excitation. The supplementary rf voltage was in the range 0.25−4.00 V. Thin-layer chromatography (TLC) was performed using plates from Merck (Silica gel 60 F 254).

Ligands

Diphosphanes and Dithiocarbamates: The diphosphane ligands utilized in this work were prepared according to published methods.[21,22] The full NMR characterizations of these diphosphanes and of the branched dithiocarbamate Nadbodc are detailed below.

Bis[(diphenylphosphanyl)ethyl]methoxyethylamine (pnp2): ^1H NMR (300 MHz, Me_4Si, $CDCl_3$): δ = 2.07 [m, 4 H, N−(CH_2−CH_2−PPh_2)$_2$], 2.59 [m, 4 H + 2 H, N−(CH_2−CH_2−PPh_2)$_2$ and N−CH_2−CH_2−O−CH_3], 3.20 (s, 3 H, N−CH_2−CH_2−O−CH_3), 3.26 (t, ^3J = 9 Hz, 2 H; N−CH_2−CH_2−O−CH_3), 7.30−7.40 (−PPh_2, 20 H) ppm. ^{13}C NMR (300 MHz, Me_4Si, $CDCl_3$): δ = 25.0 (d, $^1J_{C,P}$ = 13 Hz; N−CH_2−CH_2−PPh_2), 50.1 (d, $^2J_{C,P}$ = 35 Hz; N−CH_2−CH_2−PPh_2), 52.8 (s, N−CH_2−CH_2−O−CH_3), 58.7 (s, N−CH_2−CH_2−OCH_3), 70.7 (s, N−CH_2−CH_2−OCH_3), 128.4 (d, $^3J_{C,P}$ = 8 Hz), 128.5 (s), 132.7 (d, $^2J_{C,P}$ = 22 Hz), 138.4 (d, $^1J_{C,P}$ = 8 Hz) (aromatic *C*) ppm. ^{31}P NMR (300 MHz, 85% H_3PO_4, $CDCl_3$): δ = −21.5 (s).

Bis[(diphenylphosphanyl)ethyl]methylamine (pnp24): ^1H NMR (300 MHz, Me_4Si, $CDCl_3$): δ = 2.14 [m, 4 H, N−(CH_2−CH_2−PPh_2)$_2$], 2.24 (s, 3 H, N−CH_3), 2.48 [m, 4 H, N−(CH_2−CH_2−PPh_2)$_2$], 7.30−7.41 (−PPh_2, 20 H) ppm. ^{13}C NMR (300 MHz, Me_4Si, $CDCl_3$): δ = 22.1 (d, $^1J_{C,P}$ = 18 Hz; N−CH_2−CH_2−PPh_2), 39.6 (s, N−CH_3), 52.7 (d, $^2J_{C,P}$ = 29 Hz, N−CH_2−CH_2−PPh_2), 128.9 (d, $^3J_{C,P}$ = 7 Hz), 129.5 (s), 132.7 (d, $^1J_{C,P}$ = 20 Hz), 135.6 (d, $^2J_{C,P}$ = 9 Hz) (aromatic *C*) ppm. ^{31}P NMR (300 MHz, 85% H_3PO_4, $CDCl_3$): δ = −21.5 (d) ppm.

Bis[(dimethoxypropylphosphanyl)ethyl]methoxyethylamine (pnp3): ^1H NMR (300 MHz, Me_4Si, $CDCl_3$): δ = 1.36−1.75 (4 H +16 H,

 © 2004 Wiley-VCH Verlag GmbH & Co. KGaA, Weinheim

N−(CH2−CH2)2−[P−(CH2−CH2−CH2−O−CH3)2]2), 2.62 [m, 2 H +4 H, CH3−O−CH2−CH2−N−(CH2−CH2)2−P], 3.30 (s, 3 H +12 H, O−CH3), 3.38 (t, 3J = 9 Hz, 8 H, P−CH2−CH2−CH2−O−CH3), 3.42 (t, 3J = 9 Hz, 2 H, N−CH2−CH2−O−CH3) ppm. 13C NMR (300 MHz, Me4Si, CDCl3): δ = 23.4 (d, 1JC,P = 12 Hz, P−CH2−CH2−CH2−O−CH3), 24.2 [d, 1JC,P = 13 Hz; P−(CH2−CH2)2−N], 26.0 (d, 2JC,P = 13 Hz; P−CH2−CH2−CH2−O−CH3), 50.9 [d, 2JC,P = 21 Hz; P−(CH2−CH2)2−N], 52.5 (s, N−CH2−CH2−O−CH3), 58.5 (s, P−CH2−CH2−CH2−OCH3), 58.9 (s, N−CH2−CH2−OCH3), 71.1 (s, N−CH2−CH2−OCH3), 73.4−73.6 (P−CH2−CH2−CH2−OCH3) ppm. 31P NMR (300 MHz, 85% H3PO4, CDCl3): δ = − 34.4 (s).

Bis[(dimethoxypropylphosphanyl)ethyl]ethoxyethylamine (pnp5): 1H NMR (300 MHz, Me4Si, CDCl3): δ = 1.19 (t, 3J = 7 Hz, 3 H, P2N−CH2−CH2−O−CH2−CH3), 1.45 (m, 8 H, P−CH2−CH2−CH2−O−CH3), 1.54 [m, 4 H, (P−CH2−CH2)2N−), 1.68 [m, 8 H, P(CH2−CH2−CH2−O−CH3)2], 2.65 [m, 4 H + 2 H, P−(CH2−CH2)2−N−CH2−CH2−O−CH2−CH3], 3.33 [s, 12 H, P(CH2−CH2−CH2−O−CH3)2], 3.40 [t, 3J = 6 Hz, 8 H, P−(CH2−CH2−CH2−O−CH3)2], 3.49 (m, 2 H + 2 H, >N−CH2−CH2−O−CH2−CH3) ppm. 13C NMR (CDCl3, ppm): δ = 15.1 (s, >N−CH2−CH2−O−CH2−CH3), 23.4 (d, 1JC,P = 12 Hz; P−CH2−CH2−CH2−O−CH3), 24.3 [d, 1JC,P = 12 Hz; P−(CH2−CH2)2−N], 26.0 (d, 2JC,P = 14 Hz; P−CH2−CH2−CH2−O−CH3), 51.0 [d, 1JC,P = 21 Hz; P−(CH2−CH2)2−N], 52.5 (s, >N−CH2−CH2−O−CH2−CH3), 58.5 (s, P−CH2−CH2−CH2−O−CH3), 66.5 (s, >N−CH2−CH2−O−CH2−CH3), 69.0 (s, >N−CH2−CH2−O−CH2−CH3), 73.4 and 73.6 (P−CH2−CH2−CH2−O−CH3) ppm. 31P NMR (300 MHz, 85% H3PO4, CDCl3): δ = − 31.7 (s).

***N,N′*-Bis(ethoxyethyl)dithiocarbamate Sodium Salt (Nadbodc):** 1H NMR (300 MHz, D2O): δ = 1.20 [t, 6 H, S2CN(CH2−CH2−O−CH2−CH3)2], 3.62 [q, 4 H, S2CN(CH2−CH2−O−CH2−CH3)2], 3.85 [t, 4 H, S2CN(CH2−CH2−O−CH2−CH3)2], 4.29 [t, 4 H, S2CN(CH2−CH2−O−CH2−CH3)2] ppm. 13C NMR (300 MHz, D2O ppm): δ = 17.1 [s, S2CN(CH2−CH2−O−CH2−CH3)2], 57.2 [s, S2CN(CH2−CH2−O−CH2−CH3)2], 69.6 and 69.9 [s, S2CN(CH2−CH2−O−CH2−CH3)2], 213.9 [s, S2CN(CH2−CH2−O−CH2−CH3)2].

Synthesis of Technetium and Rhenium Complexes: A general one-pot procedure was adopted for the preparation of both technetium and rhenium complexes.

[M(N)(DTC)(PNP)][Cl] (M = 99Tc, Re) (1−8): A solution of the appropriate diphosphane (0.05 mmol) in ethanol (10 mL) was added under a nitrogen atmosphere to a three-neck round-bottomed flask containing a suspension of [M(N)Cl2(PPh3)2] (0.05 mmol) in dichloromethane (10 mL). The mixture was stirred for 60 min at room temperature (or at reflux for rhenium complexes) to give a clear bright yellow solution. A solution of DTC sodium salt (0.055 mmol) in ethanol (5 mL) was added, and, after reflux for an additional 60 min (overnight reflux is necessary for rhenium complexes), the yellow solution was cooled and the solvent removed by a gentle stream of nitrogen. The residue was treated with dichloromethane (5 mL) and a white precipitate was separated by filtration. The filtrate was again evaporated to dryness to give a pale yellow solid residue (for compounds containing aryl diphosphanes), or a yellow oil (for compounds containing alkyl diphosphanes). Technetium complexes **5** and **6** were purified by treating the residue with ethanol (3 mL). A yellow precipitate was collected by filtration, washed with diethyl ether (4 × 5 mL) and dried under vacuum. The oily products **7** and **8** were placed under vacuum overnight to afford pure compounds as a yellow-orange oils (yield >90%). For all rhenium complexes, column chromatography (described below) was necessary to separate the pure species. The filtrate was evaporated to dryness and then re-dissolved in the minimum amount of chloroform. The resulting solution was loaded onto a silica column (diameter 2 cm, length 30 cm) previously conditioned with chloroform. Elution was conducted with chloroform (100 mL) followed by a mixture of ethanol/chloroform/toluene/0.5 M ammonium acetate (5:3:3:0.5) to provide the pure compounds in low-to-moderate yields (25−40%). The light yellow residue obtained after chromatography of complex **1** was dissolved in methanol (2 mL) and added to an excess of NH_4PF_6 in methanol (3 mL). Trituration with diethyl ether (20 mL) yielded a yellow-orange powder, which was filtered off, washed with diethyl ether (2 × 5 mL) and dried under vacuum.

[Re(N)(dedc)(pnp2)][PF6] (1): $C_{36}H_{45}F_6N_3OP_3S_2Re$ (993.0): calcd. C 43.54, H 4.57, N 4.23, S 6.45; found C 43.72, H 4.51, N 4.41, S 6.63. IR (KBr): $\tilde{\nu}$ = 1434 cm^{-1} (s), 1100 (s, Re−P), 1061 [m, Re(N)], 840 (vs, PF_6), 693 (s). 1H NMR ($CDCl_3$, ppm): δ = 1.27 [t, 6 H, $S_2CN(CH_2-CH_3)_2$], 2.53 (t, 2 H, $P_2N-CH_2-CH_2-O-CH_3$), 3.00−3.51 [8 H, $(P-CH_2-CH_2)_2N-$], 3.27 (s, 3 H, $P_2N-CH_2-CH_2-O-CH_3$), 3.57 (t, 2 H, $P_2N-CH_2-CH_2-O-CH_3$), 3.70 [m, 4 H, $S_2CN(CH_2-CH_3)_2$], 6.95−7.94 (20 H, C_6H_5-P) ppm. 13C NMR ($CDCl_3$, ppm): δ = 12.5 [s, $S_2CN-(CH_2-CH_3)_2$], 25.1 [d, $J_{C,P}$ = 14 Hz; $P-(CH_2-CH_2)_2N-$], 45.0 (s, $S_2CN(CH_2-CH_3)_2$], 49.5 [s, $P(CH_2-CH_2)_2N-$], 50.9 (s, $P_2N-CH_2-CH_2-O-CH_3$), 58.9 (s, $P_2N-CH_2-CH_2-O-CH_3$), 67.2 (s, $P_2N-CH_2-CH_2-O-CH_3$), 128.8−134.0 (C_6H_5-P), 215.8 [s, $S_2CN-(CH_2-CH_3)_2$] ppm. 31P NMR ($CDCl_3$, ppm): δ = 18.3 (s), −144.0 (septet, PF_6). ESI MS (*m/z*): 848 $[M]^+$. Yield 35%.

[Re(N)(dedc)(pnp24)][Cl] (2): $C_{34}H_{41}ClN_3P_2ReS_2$ (839.4): calcd. C 48.64, H 4.92, N 5.00, S 7.64; found C 48.78, H 5.01, N 5.21, S 7.88. 1H NMR ($CDCl_3$, ppm): δ = 1.28 [t, 6 H, $S_2CN(CH_2-CH_3)_2$], 2.09 (s, 3 H, $N-CH_3$), 2.86−3.56 [8 H, $(P-CH_2-CH_2)_2N-$], 3.70 [m, 4 H, $S_2CN(CH_2-CH_3)_2$], 6.96−7.95 (20 H, C_6H_5-P) ppm. 13C NMR ($CDCl_3$, ppm): 12.5 [s, $S_2CN-(CH_2-CH_3)_2$], 24.2 [d, $-P-(CH_2-CH_2)_2N-$], 44.6 (s, $N-CH_3$), 45.2 [s, $S_2CN(CH_2-CH_3)_2$], 50.3 [s, $P(CH_2-CH_2)_2N-$], 128.9−132.4 (C_6H_5-P), 212.5 [s, $S_2CN-(CH_2-CH_3)_2$] ppm. 31P NMR ($CDCl_3$, ppm): δ = 18.8 (s). ESI MS (*m/z*): 804 $[M]^+$. Yield 25%.

[Re(N)(dedc)(pnp3)][Cl] (3): $C_{28}H_{61}ClN_3O_5P_2ReS_2$ (867.5): calcd. C 38.76, H 7.09, N 4.84, S 7.39; found C 39.01, H 7.16, N 4.98, S 7.59. 1H NMR ($CDCl_3$, ppm): δ = 1.37 [t, 6 H, $S_2CN(CH_2-CH_3)_2$], 1.73 [m, 4 H, $P(CH_2-CH_2-CH_2-O-CH_3)_{2endo}$], 1.85 [m, 4 H, $P(CH_2-CH_2-CH_2-O-CH_3)_{2exo}$], 2.04 [m, 2 H + 2 H, $(P-CH_2-CH_2)_2N-_{endo}$ and $P(CH_2-CH_2-CH_2-O-CH_3)_2$], 2.31 [m, 4 H, $P(CH_2-CH_2-CH_2-O-CH_3)_2$], 2.42 (t, 2 H, $P_2N-CH_2-CH_2-O-CH_3$), 2.66 [m, 2 H, $(P-CH_2-CH_2)_2N-_{endo}$], 2.70 [m, 2 H, $P(CH_2-CH_2-CH_2-O-CH_3)_2$], 2.93 [m, 2 H, $(P-CH_2-CH_2)_2N-_{exo}$], 3.20 (s, 3 H, $P_2N-CH_2-CH_2-O-CH_3$), 3.22 [m, 2 H, $(P-CH_2-CH_2)_2N-_{exo}$], 3.35 [s, 6 H, $P(CH_2-CH_2-CH_2-O-CH_3)_{2endo}$], 3.37 [s, 6 H, $P(CH_2-CH_2-CH_2-O-CH_3)_{2exo}$], 3.38 (m, 2 H, $P_2N-CH_2-CH_2-O-CH_3$), 3.50 [m, 4 H, $P(CH_2-CH_2-CH_2-O-CH_3)_{2endo}$], 3.59 [m, 4 H, $P(CH_2-CH_2-CH_2-O-CH_3)_{2exo}$], 3.82 [m, 4 H, $S_2CN(CH_2-CH_3)_2$] ppm. 13C NMR ($CDCl_3$, ppm): δ = 12.6 (s, $S_2CN-(CH_2-CH_3)_2$], 22.9−26.1 [2 s and 3 d, $P(CH_2-CH_2-CH_2-O-CH_3)_{2endo/exo}$, $(P-CH_2-CH_2)_2N-$ and $P(CH_2-CH_2-CH_2-O-CH_3)_2$], 45.3 [s, $S_2CN(CH_2-CH_3)_2$], 48.7 [s, $P(CH_2-CH_2)_2N-$], 50.3 (s, $P_2N-CH_2-CH_2-O-CH_3$), 58.5 and 58.7 [2 s, $P(CH_2-CH_2-CH_2-O-CH_3)_2$], 58.8 (s, $P_2N-CH_2-CH_2-O-CH_3$), 66.9 (s, $P_2N-CH_2-CH_2-O-CH_3$),

 © 2004 Wiley-VCH Verlag GmbH & Co. KGaA, Weinheim

72.3−72.5 [m, $P(CH_2-CH_2-CH_2-O-CH_3)_2$] ppm. ^{31}P NMR ($CDCl_3$, ppm): δ = 13.4 (s). ESI MS (*m*/*z*): 832 $[M]^+$. Yield 30%.

[Re(N)(dbodc)(pnp5)][Cl] (4): $C_{33}H_{71}ClN_3O_7P_2ReS_2$ (969.7): calcd. C 40.90, H 7.38, N 4.33, S 6.61; found C 41.08, H 7.46, N 4.28, S 6.86. ^1H NMR ($CDCl_3$, ppm): δ = 1.09 (t, 3 H, $P_2N-CH_2-CH_2-O-CH_2-CH_3$), 1.19 [t, 6 H, $S_2CN(CH_2-CH_2-O-CH_2-CH_3)_2$], 1.78 [m, 4 H, $P(CH_2-CH_2-CH_2-O-CH_3)_{2endo}$], 1.87 [m, 4 H, $P(CH_2-CH_2-CH_2-O-CH_3)_{2exo}$], 2.04 [m, 2 H, $(P-CH_2-CH_2)_2N-_{endo}$], 2.06 and 2.31 [m, 2 H + 4 H, $P(CH_2-CH_2-CH_2-O-CH_3)_2$], 2.45 (t, 2 H, $P_2N-CH_2-CH_2-O-CH_2-CH_3$), 2.67 [m, 2 H, $P(CH_2-CH_2-CH_2-O-CH_3)_2$], 2.70 [m, 2 H, $(P-CH_2-CH_2)_2N-_{endo}$], 2.90 [m, 2 H, $(P-CH_2-CH_2)_2N-_{exo}$], 3.23 [m, 2 H, $(P-CH_2-CH_2)_2N-_{exo}$], 3.32 (q, 2 H, $P_2N-CH_2-CH_2-O-CH_2-CH_3$), 3.35 [s, 6 H, $P(CH_2-CH_2-CH_2-O-CH_3)_{2endo}$], 3.37 [s, 6 H, $P(CH_2-CH_2-CH_2-O-CH_3)_{2exo}$], 3.39 (m, 2 H, $P_2N-CH_2-CH_2-O-CH_2-CH_3$), 3.50 [q + m, 4 H + 4 H, $S_2CN(CH_2-CH_2-O-CH_2-CH_3)_2$ + $P(CH_2-CH_2-CH_2-O-CH_3)_{2endo}$], 3.59 [m, 4 H, $P(CH_2-CH_2-CH_2-O-CH_3)_{2exo}$], 3.76 [m, 4 H, $S_2CN(CH_2-CH_2-O-CH_2-CH_3)_2$], 4.10 [m, 4 H, $S_2CN(CH_2-CH_2-O-CH_2-CH_3)_2$] ppm. ^{13}C NMR ($CDCl_3$, ppm): δ = 15.1 [s, $S_2CN-(CH_2-CH_2-O-CH_2-CH_3)_2$ + $P_2N-CH_2-CH_2-O-CH_2-CH_3$], 23.9−26.1 [2 s and 3 d, $P(CH_2-CH_2-CH_2-O-CH_3)_{2endo/exo}$, $(P-CH_2-CH_2)_2N-$)], 48.7 [s, $P(CH_2-CH_2)_2N-$], 50.4 (s, $P_2N-CH_2-CH_2-O-CH_2-CH_3$), 51.9 [s, $S_2CN(CH_2-CH_2-O-CH_2-CH_3)_2$], 58.5 and 58.7 [2 s, $P(CH_2-CH_2-CH_2-O-CH_3)_2$], 64.7 (s, $P_2N-CH_2-CH_2-O-CH_2-CH_3$), 66.5 (s, $P_2N-CH_2-CH_2-O-CH_2-CH_3$), 66.9 [s, $S_2CN-(CH_2-CH_2-O-CH_2-CH_3)_2$], 67.8 [s, $S_2CN-(CH_2-CH_2-O-CH_2-CH_3)_2$], 72.3−72.5 [m, $P(CH_2-CH_2-CH_2-O-CH_3)_2$], 220.2 [s, $S_2CN-(CH_2-CH_2-O-CH_2-CH_3)_2$] ppm. ^{31}P NMR ($CDCl_3$, ppm): δ = 13.4 (s). ESI MS (*m*/*z*): 933 $[M]^+$. Yield 30%.

[Tc(N)(dedc)(pnp2)][Cl] (5): $C_{36}H_{45}ClN_3P_2S_2Tc$ (780.2): calcd. C 54.30, H 5.69, N 5.28, S 8.05; found C 54.62, H 5.59, N 5.33, S 8.32. ^1H NMR ($CDCl_3$, ppm): δ = 1.22 (t, 6 H, $S_2CN(CH_2-CH_3)_2$], 2.45 (t, 2 H, $P_2N-CH_2-CH_2-O-CH_3$), 2.96−3.46 [8 H, $(P-CH_2-CH_2)_2N-$], 3.22 (s, 3 H, $P_2N-CH_2-CH_2-O-CH_3$), 3.50 (t, 2 H, $P_2N-CH_2-CH_2-O-CH_3$), 3.75 [m, 4 H, $S_2CN(CH_2-CH_3)_2$], 6.96−7.89 (20 H, C_6H_5-P) ppm. ^{13}C NMR ($CDCl_3$, ppm): δ = 12.5 [s, $S_2CN-(CH_2-CH_3)_2$], 24.0 [d, $J_{C,P}$ = 14 Hz; $P-(CH_2-CH_2)_2N-$], 44.8 [s, $S_2CN(CH_2-CH_3)_2$], 48.5 [s, $P(CH_2-CH_2)_2N-$], 50.9 (s, $P_2N-CH_2-CH_2-O-CH_3$), 58.9 (s, $P_2N-CH_2-CH_2-O-CH_3$), 67.4 (s, $P_2N-CH_2-CH_2-O-CH_3$), $S_2CN(CH_2-CH_3)_2$] ppm. ^{13}C NMR NMR ($CDCl_3$, ppm): δ = 29.9 (bs). Yield 80%.

[Tc(N)(dedc)(pnp24)][Cl] (6): $C_{34}H_{41}ClN_3OP_2S_2Tc$ (768.1): calcd. C 54.28, H 5.49, N 5.58, S 8.52; found C 54.63, H 5.71, N 5.39, S 8.23. ^1H NMR ($CDCl_3$, ppm): 1.23 (t, 6 H, $N-CH_2-CH_3$), 1.98 (s, 3 H, $N-CH_3$), 2.23−3.35 [8 H, $(P-CH_2-CH_2)_2-N-$], 3.72 (m, 4 H, $N-CH_2-CH_3$), 6.97−7.89 (20 H, H_{arom}) ppm. ^{13}C NMR ($CDCl_3$, ppm): δ = 12.5 [s, $S_2CN-(CH_2-CH_3)_2$], 23.5 [d, $-P-(CH_2-CH_2)_2N-$], 43.5 (s, $N-CH_3$), 44.9 [s, $S_2CN(CH_2-CH_3)_2$], 49.8 [s, $P(CH_2-CH_2)_2N-$], 128.9−132.3 (C_6H_5-P), 210.5 [s, $S_2CN-(CH_2-CH_3)_2$] ppm. ^{31}P NMR ($CDCl_3$, ppm): δ = 34.4 (bs). Yield 78%.

[Tc(N)(dbodc)(pnp3)][Cl] (7): $C_{32}H_{69}ClN_3O_7P_2S_2Tc$ (868.3): calcd. C 44.25, H 8.01, N 4.84, S 7.38; found C 44.22, H 8.22, N 4.77, S 7.55. ^1H NMR ($CDCl_3$, ppm): δ = 1.15 [t, 6 H, $S_2CN(CH_2-CH_2-O-CH_2-CH_3)_2$], 1.84 [m, 4 H, $P(CH_2-CH_2-CH_2-O-CH_3)_{2endo}$], 1.90 [m, 4 H, $P(CH_2-CH_2-CH_2-O-CH_3)_{2exo}$], 2.10 [m, 2 H, $(P-CH_2-CH_2)_2N-_{endo}$], 2.14 and 2.24 [m, 2 H + 4 H, $P(CH_2-CH_2-CH_2-O-CH_3)_2$], 2.35 (t, 2 H, $P_2N-CH_2-CH_2-O-CH_3$), 2.54 [m, 2 H, $P(CH_2-CH_2-CH_2-O-CH_3)_2$], 2.56 [m, 2 H, $(P-CH_2-CH_2)_2N-_{endo}$], 2.76 [m, 2 H, $(P-CH_2-CH_2)_2N-_{exo}$], 3.03 [m, 2 H, $(P-CH_2-CH_2)_2N-_{exo}$], 3.14 (s, 3 H, $P_2N-CH_2-CH_2-O-CH_3$), 3.29 (t, 2 H, $P_2N-CH_2-CH_2-O-CH_3$), 3.31 [s, 6 H, $P(CH_2-CH_2-CH_2-O-CH_3)_{2endo}$], 3.33 [s, 6 H, $P(CH_2-CH_2-CH_2-O-CH_3)_{2exo}$], 3.40 (m, 2 H, $P_2N-CH_2-CH_2-O-CH_2-CH_3$), 3.45 [q + m, 4 H +4 H, $S_2CN(CH_2-CH_2-O-CH_2-CH_3)_2$ + $P(CH_2-CH_2-CH_2-O-CH_2-CH_3)_{2endo}$], 3.55 [m, 4 H, $P(CH_2-CH_2-CH_2-O-CH_3)_{2exo}$], 3.69 [m, 4 H, $S_2CN(CH_2-CH_2-O-CH_2-CH_3)_2$], 4.14 [m, 4 H, $S_2CN(CH_2-CH_2-O-CH_2-CH_3)_2$] ppm. ^{13}C NMR ($CDCl_3$, ppm): δ = 15.0 [s, $S_2CN-(CH_2-CH_2-O-CH_2-CH_3)_2$], 22.0−24.4 [2 s and 3 d, $P(CH_2-CH_2-CH_2-O-CH_3)_{2endo/exo}$, + $(P-CH_2-CH_2)_2N-$], 47.4 [s, $P(CH_2-CH_2)_2N-$], 50.2 (s, $P_2N-CH_2-CH_2-O-CH_3$), 51.9 [s, $S_2CN(CH_2-CH_2-O-CH_2-CH_3)_2$], 58.6 and 58.7 [2 s, $P(CH_2-CH_2-CH_2-O-CH_3)_2$], 66.8 (s, $P_2N-CH_2-CH_2-O-CH_3$), 67.0 [s, $S_2CN-(CH_2-CH_2-O-CH_2-CH_3)_2$], 67.8 [s, $S_2CN-(CH_2-CH_2-O-CH_2-CH_3)_2$], 72.3−72.5 [m, $P(CH_2-CH_2-CH_2-O-CH_3)_2$], 213.8 [s, $S_2CN-(CH_2-CH_2-O-CH_2-CH_3)_2$].$^{31}P$ NMR ($CDCl_3$, ppm): δ = 29.9 (bs). Yield 85%.

[Tc(N)(dbodc)(pnp5)][Cl] (8): $C_{33}H_{71}ClN_3O_7P_2S_2Tc$ (882.4): calcd. C 44.91, H 8.11, N 4.76, S 7.27; found C 45.32, H 8.33, N 4.67, S 7.44. ^1H NMR ($CDCl_3$, ppm): δ = 1.07 (t, 3 H, $P_2N-CH_2-CH_2-O-CH_2-CH_3$), 1.18 [t, 6 H, $S_2CN(CH_2-CH_2-O-CH_2-CH_3)_2$], 1.84 [m, 4 H, $P(CH_2-CH_2-CH_2-O-CH_3)_{2endo}$], 1.90 [m, 4 H, $P(CH_2-CH_2-CH_2-O-CH_3)_{2exo}$], 2.10 [m, 2 H, $(P-CH_2-CH_2)_2N-_{endo}$], 2.14 and 2.24 [m, 2 H + 4 H, $P(CH_2-CH_2-CH_2-O-CH_3)_2$], 2.38 (t, 2 H, $P_2N-CH_2-CH_2-O-CH_2-CH_3$), 2.53 [m, 2 H, $P(CH_2-CH_2-CH_2-O-CH_3)_2$], 2.56 [m, 2 H, $(P-CH_2-CH_2)_2N-_{endo}$], 2.77 [m, 2 H, $(P-CH_2-CH_2)_2N-_{exo}$], 3.04 [m, 2 H, $(P-CH_2-CH_2)_2N-_{exo}$], 3.32 (q, 2 H, $P_2N-CH_2-CH_2-O-CH_2-CH_3$), 3.34 [s, 6 H, $P(CH_2-CH_2-CH_2-O-CH_3)_{2endo}$], 3.36 [s, 6 H, $P(CH_2-CH_2-CH_2-O-CH_3)_{2exo}$], 3.40 (m, 2 H, $P_2N-CH_2-CH_2-O-CH_2-CH_3$), 3.50 [q + m, 4 H + 4 H, $S_2CN(CH_2-CH_2-O-CH_2-CH_3)_2$] + $P(CH_2-CH_2-CH_2-O-CH_3)_{2endo}$, 3.59 [m, 4 H, $P(CH_2-CH_2-CH_2-O-CH_3)_{2exo}$], 3.72 [m, 4 H, $S_2CN(CH_2-CH_2-O-CH_2-CH_3)_2$], 4.17 [m, 4 H, $S_2CN(CH_2-CH_2-O-CH_2-CH_3)_2$] ppm. ^{13}C NMR ($CDCl_3$, ppm): δ = 15.1 [s, $S_2CN-(CH_2-CH_2-O-CH_2-CH_3)_2$ + $P_2N-CH_2-CH_2-O-CH_2-CH_3$], 22.0−24.4 [2 s and 3 d, $P(CH_2-CH_2-CH_2-O-CH_3)_{2endo/exo}$, + $(P-CH_2-CH_2)_2N-$], 47.4 [s, $P(CH_2-CH_2)_2N-$], 50.3 (s, $P_2N-CH_2-CH_2-O-CH_2-CH_3$), 51.9 [s, $S_2CN(CH_2-CH_2-O-CH_2-CH_3)_2$], 58.6 and 58.7 [2 s, $P(CH_2-CH_2-CH_2-O-CH_3)_2$], 64.7 (s, $P_2N-CH_2-CH_2-O-CH_2-CH_3$), 66.5 (s, $P_2N-CH_2-CH_2-O-CH_2-CH_3$), 66.7 [s, $S_2CN-(CH_2-CH_2-O-CH_2-CH_3)_2$], 67.8 [s, $S_2CN-(CH_2-CH_2-O-CH_2-CH_3)_2$], 72.3−72.6 [m, $P(CH_2-CH_2-CH_2-O-CH_3)_2$], 214.0 [s, $S_2CN-(CH_2-CH_2-O-CH_2-CH_3)_2$] ppm. ^{31}P NMR ($CDCl_3$, ppm): δ = 30.2 (bs). ESI MS (*m*/*z*): 847 $[M]^+$. Yield 89%.

X-ray Crystallographic Study: Single crystals of complex **1** were grown by slow evaporation from DMSO solutions as light yellow blocks. Pertinent crystallographic data and structure refinement data are summarized in Table 2. The data set was collected at room temperature on a Nicolet Siemens R3m /V diffractometer with graphite-monochromatized Mo-K_α radiation. Cell parameters were obtained by fitting a set of 50 high-angle reflections. After Lorentz, polarization and absorption corrections (Ψ-scans method), the structure was solved using the SHELXTL NT computer program[23] and refined with SHELXL-97[24] by the full-matrix least-

 © 2004 Wiley-VCH Verlag GmbH & Co. KGaA, Weinheim

Table 2. Crystallographic data for complex **1**

Formula	$C_{36}H_{45}F_6N_3OP_3ReS_2$
Formula mass	993.0
Cryst. syst.	monoclinic
Space group	$P2_1/c$ (No. 14)
a, Å	11.730(2)
b, Å	30.234(6)
c, Å	11.732(2)
β, °	93.44(3)
V, Å^3	4153(1)
Z, $D_{calcd.}$, g cm^{-3}	4; 1.588
μ (Mo-K_α), (cm^{-1})	32.0
T (°C)	23
λ (Mo-K_α), Å	0.71073
Θ_{max}, °	24
Obsd. reflections [$I > 2\sigma(I)$]	4809
$R1$[a]	0.053
$wR2$[b]	0.121
GOF[c]	1.045

[a] $R1 = \Sigma|F_o| - |F_c|/\Sigma|F_o|$. [b] $wR2 = \{\Sigma[w\ (F_o^2 - F_c^2)^2]/\Sigma[w(F_o^2)^2]\}^{1/2}$. [c] GOF = $\{\Sigma[w\ (F_o^2 - F_c^2)^2]/(n - p)\}^{1/2}$ (n = reflections; p = parameters).

squares technique based on F^2. Figures were drawn with the ORTEP II program.[25] The final difference map was featureless, apart from a relevant residue in the vicinity of C(7) atom, indicating a possible second position [C(7′)]. This model was refined satisfactorily with occupancies of ca. 0.5. Anisotropy was applied only to non−carbon atoms to assure a good reflections/parameters ratio. CCDC-220372 contains the supplementary crystallographic data for this paper. These data can be obtained free of charge at www.ccdc.cam.ac.uk/conts/retrieving.html [or from the Cambridge Crystallographic Data Centre, 12 Union Road, Cambridge CB2 1EZ, UK; Fax: (internat.) + 44-1223-336-033; E-mail: deposit@ccdc.cam.ac.uk].

Acknowledgments

The authors are grateful to Nihon Medi-Physics, Tokio, Japan, for financial support of this work, and to A. Moresco for elemental analyses.

[1] S. Jurisson, J. D. Lydon, *Chem. Rev.* **1999**, *99*, 2205−2218.
[2] S. Liu, D. S. Edwards, *Chem. Rev.* **1999**, *99*, 2235−2268.
[3] A. Duatti, *Technetium in Chemistry and Nuclear Medicine −5*; SG Editoriali, Padova, **1999**, 3−17.
[4] R. Alberto, R. Schibli, A. Egli, A. P. Schubiger, W. A. Hermann, G. Artus, U. Abram, T. Kaden, *J. Organomet. Chem.* **1995**, *493*, 119−127.
[5] R. Alberto, R. Schibli, R. Waibel, U. Abram, A. P. Schubiger, *Coord. Chem. Rev.* **1999**, *190−192*, 901−919.
[6] C. Bolzati, A. Boschi, A. Duatti, S. Prakash, L. Uccelli, G. Bandoli, F. Tisato, F. Refosco, *J. Am. Chem. Soc.* **2000**, *122*, 4510−4511.
[7] C. Bolzati, A. Boschi, L. Uccelli, F. Tisato, F. Refosco, A. Cagnolini, A. Duatti, S. Prakash, G. Bandoli, A. Vittadini, *J. Am. Chem. Soc.* **2002**, *124*, 11468−11479.
[8] A. Egli, R. Alberto, L. Tannahill, R. Schibli, U. Abram, A. Schaffland, R. Waibel, D. Tourwè, L. Jeannin, K. Iterbeke, A. P. Schubiger, *J. Nucl. Med.* **1999**, *40*, 1913−1917.
[9] R. Waibel, R. Alberto, J. Willuda, R. Finnern, R. Schibli, A. Stichelberger, A. Egli, U. Abram, J.-P. Mach, A. Pluckthun, A. P. Schubiger, *Nat. Biotechnol.* **1999**, *17*, 897−901.
[10] A. Boschi, C. Bolzati, E. Benini, E. Malagò, L. Uccelli, A. Duatti, A. Piffanelli, F. Refosco, F. Tisato, *Bioconjugate Chem.* **2001**, *12*, 1035−1042.
[11] F. Refosco, C. Bolzati, A. Duatti, F. Tisato, L. Uccelli, *Recent Res. Devel. Inorganic Chem.* **2000**, *2*, 89−98.
[12] C. Bolzati, A. Mahmood, E. Malagò, A. Boschi, L. Uccelli, M. Friebe, A. G. Jones, A. Duatti, *Technetium in Chemistry and Nuclear Medicine −6*; SGEditoriali, Padova, **2002**, 369−374.
[13] A. Boschi, C. Bolzati, L. Uccelli, A. Duatti, E. Benini, F. Refosco, F. Tisato, A. Piffanelli, *Nucl. Med. Commun.* **2002**, *23*, 689−693.
[14] A. Boschi, L. Uccelli, C. Bolzati, A. Duatti, N. Sabba, E. Moretti, G. Di Domenico, G. Zavattini, F. Refosco, M. Giganti, *J. Nucl. Med.* **2003**, *44*, 806−814.
[15] F. H. Allen, J. E. Davies, J. J. Galloy, O. Johnson, O. Kennard, C. F. Macrae, E. M. Mitchell, J. M. Smith, D. G. Watson, *J. Chem. Info. Comp. Sci.* **1991**, *31*, 187; Cambridge Crystallographic Database (Version 5.22 of October **2001**).
[16] E. Marotta, F. Tisato, F. Refosco, C. Bolzati, M. Porchia, P. Traldi, *Rapid Commun. Mass Spectr.* **2003**, *17*, 1−4.
[17] A. Duatti, C. Bolzati, L. Uccelli, F. Refosco, F. Tisato, **1998,** PCT Int. Appl. WO98 27,100 (Cl. CO7F9/50).
[18] U. Abram, B. Lorenz, L. Kaden, D. Scheller, *Polyhedron* **1988**, *7*, 285.
[19] J. Chatt, C. D. Falck, G. J. Leigh, R. J. Paske, *J. Chem. Soc., A* **1969**, 2288.
[20] R. Pasqualini, A. Duatti, E. Bellande, V. Comazzi, V. Brucato, D. Hoffschir, D. Fagret, M. Comet, *J. Nucl. Med.* **1994**, *35*, 334−341.
[21] R. Morassi, L. Sacconi, *J. Chem. Soc., A* **1971**, 492−496.
[22] C. Bianchini, J. A. Casares, M. Peruzzini, A. Romerosa, F. Zanobini, *J. Am. Chem. Soc.* **1996**, *118*, 4585−4595.
[23] G. M. Sheldrick, *SHELXTL NT*, Version 5.10; Bruker AXS Inc.: Madison, WI, **1999**.
[24] G. M. Sheldrick, *SHELXL-97*, *Program for Crystal Structure Refinement*, University of Göttingen: Germany, **1997**.
[25] C. K. Johnson, *ORTEP*, Report ORNL-5138, Oak Ridge National Laboratory, Oak Ridge, TN, **1976**.

Received September 25, 2003
Early View Article
Published Online March 31, 2004

 © 2004 Wiley-VCH Verlag GmbH & Co. KGaA, Weinheim

Deprotonation of μ_3-Methylidyne Groups on a Ti_3O_3 Support: A Way to Build Oxotitanocubanes Containing Alkali and Alkaline-Earth Metals

Avelino Martín,[a] Miguel Mena,*[a] María del Carmen Morales-Varela,[a] and Cristina Santamaría[a]

Keywords: Alkali metals / Alkaline earth metals / Alkylidyne complexes / Oxo ligands / Titanium

The μ_3-methylidyne group of the complex [{TiCp*(μ-O)}$_3$(μ_3-CH)] (**1**) (Cp* = η^5-C_5Me_5) was deprotonated by amides of the group 1 elements, [MN(SiMe$_3$)$_2$] (M = Li, Na, K, Rb, Cs) to form the oxoheterometallocubane complexes [M(μ_3-O)$_3${Ti$_3$Cp*$_3$(μ_3-C)}] [M = Li (**3**), Na (**4**), K (**5**), Rb (**6**), Cs (**7**)]. Similar treatments of **1** with the alkaline-earth amides [M{N(SiMe$_3$)$_2$}$_2$(thf)$_2$] (M = Mg, Ca, Sr) afforded the heterometallocubane derivatives [{(thf)$_x$(Me$_3$Si)$_2$NM}(μ_3-O)$_3${Ti$_3$Cp*$_3$(μ_3-C)}] [M = Mg, *x* = 0, (**8**); Ca, *x* = 1, (**9**); Sr, *x* = 1, (**10**)] in high yields. The addition of ligands such as cyclopentadiene (C_5H_6) or pentamethylcyclopentadiene (C_5Me_5H) to the compounds **3**–**7** allowed recovery of the μ_3-methylidyne oxocomplex **1**. The analogous reaction of **8**–**10** with C_5H_6 caused the displacement of the amide fragment to give the heterometallocubanes [(CpM)(μ_3-O)$_3${Ti$_3$Cp*$_3$(μ_3-C)}] [M = Mg (**11**), Ca (**12**), Sr (**13**)], while C_5Me_5H reacts only with **9** and **10** to give the compounds [(Cp*M)(μ_3-O)$_3${Ti$_3$Cp*$_3$(μ_3-C)}] [M = Ca (**14**), Sr (**15**)]. Furthermore, heating of the species **8**–**10** in the presence of the starting complex **1** produced amine elimination and afforded the corner-shared heterometallodicubanes [M{(μ_3-O)$_3$Ti$_3$Cp*$_3$(μ_3-C)}$_2$] [M = Mg (**16**), Ca (**17**), Sr (**18**)]. Treatment of **1** with the amide [Ba{N(SiMe$_3$)$_2$}$_2$(thf)$_2$] or dialkyl derivatives of magnesium [MgR$_2$(thf)$_2$] (R = CH_2Ph, *t*Bu) and barium [Ba(CH_2Ph)$_2$] provided the corner-shared metallodicubanes [M{(μ_3-O)$_3$Ti$_3$Cp*$_3$-(μ_3-C)}$_2$] [M = Mg(**16**), Ba(**19**)]. The molecular structures of complexes **9**, **16**, **17** and **18** have been established by single-crystal X-ray analyses.

(© Wiley-VCH Verlag GmbH & Co. KGaA, 69451 Weinheim, Germany, 2004)

Introduction

Our efforts to explore the behavior of alkylidyne groups on a trinuclear support in the complexes [{TiCp*(μ-O)}$_3$(μ_3-CR)] [R = H (**1**), Me (**2**)],[1] as a molecular approach to hydrocarbon-metal(oxo) surface interactions, have revealed surprising and unprecedented chemical reactivity. Thus, we have shown that metal carbonyl hydrides,[2] carbon monoxide,[3] isocyanides,[3] ketones,[4] *N*-benzylidene(phenyl)amine,[5] amines, diamines and the imine Ph_2C=NH[6] are incorporated into the Ti_3O_3 core by transformation of the alkylidyne units. In these systems, the role of the oxygen atoms is considerable, bridging the titanium atoms firmly and enhancing the cooperative effect between them but we do not have evidence for its direct participation in those processes. Furthermore, in the course of our studies we have discovered other kinds of reactivity for the complexes [{TiCp*(μ-O)}$_3$(μ_3-CR)] [R = H (**1**), Me (**2**)] as preorganized neutral tridentate six electron donor ligands without implication of the alkylidyne groups.[7] In fact, they provide an effective route to heterometallocubanes upon treatment with appropriate metal carbonyl complexes, where the metal carbonyl fragment shares electron density with the titanium atoms. Therefore the [(μ_3-CR)Ti$_3$Cp*$_3$(μ_3-O)$_3$M(CO)$_n$] cores of these oxoheterometallocubanes are discrete models for studying the oxide-to-metal catalyst-support interaction.

Recently, we have communicated the intercalation of alkali metal ions into layered organometallic titanium oxides by treatment of the complex [{TiCp*(μ-O)}$_3$(μ_3-CH)] (**1**) with alkali metal (Li, Na, K) alkyls and amides.[8] This process takes place with the incorporation of the alkali metal at the free vertex of the incomplete cube-type core Ti_3O_3C and the deprotonation of the μ_3-methylidyne ligand. Consequently, the active cooperation between the oxo and alkylidyne groups is possible in the singular chemistry of the complexes [{TiCp*(μ-O)}$_3$(μ_3-CR)].

We have expanded this preliminary study and herein we describe the behavior of the complex [{TiCp*(μ-O)}$_3$(μ_3-CH)] (**1**) towards alkali and alkaline-earth dialkylamides and alkyls.

Results and Discussion

When the complex [{TiCp*(μ-O)}$_3$(μ-CH)] (**1**) was treated with the alkyl derivatives [MR] (M = Li, R = CH_2SiMe_3, CH_2CMe_3, *n*Bu; M = Na, K, R = *t*Bu) at room temperature or with the amides [MN(SiMe$_3$)$_2$] (M = Li,

[a] Departamento de Química Inorgánica, Universidad de Alcalá, Campus Universitario, 28871 Alcalá de Henares-Madrid, Spain
Fax: (internat.) + 34-91-885-4683
E-mail: miguel.mena@uah.es

 © 2004 Wiley-VCH Verlag GmbH & Co. KGaA, Weinheim **DOI: 10.1002/ejic.200300840**

Na, K), at 60 °C overnight in a 1:1 ratio in toluene or hexane, the compounds **3**−**5** were obtained (70−90%) (see Scheme 1). On the other hand, the amides $[MN(SiMe_3)_2]$ (M = Rb, Cs), react with complex **1** in a 1:1 ratio at 60 °C in tetrahydrofuran to give the derivatives **6** and **7** in high yields (70−80%). The isolated solids were found to be stable under argon at room temperature and practically insoluble in common solvents such as toluene, hexane and dichloromethane, with the exception of tetrahydrofuran, which allowed their NMR spectroscopic characterization.

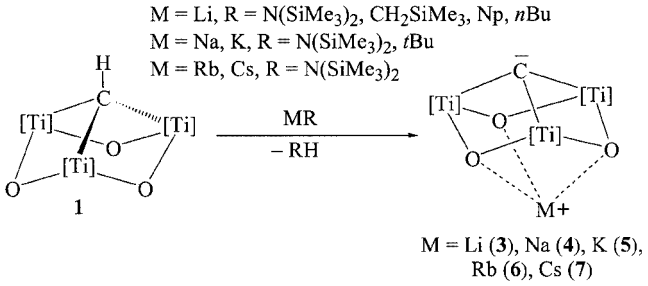

Scheme 1. Reaction of **1** with alkaline amide and alkyl reagents. [Ti] = $Ti(\eta^5\text{-}C_5Me_5)$

The ^1H and ^{13}C NMR spectra in $[D_8]$tetrahydrofuran, of these species, show signals assignable to equivalent η^5-C_5Me_5 groups and singlets for the apical μ_3-carbon atoms in the range 577−587 ppm, consistent with symmetrical structures in solution and the removal of the protons of the μ_3-methylidyne fragments.

To unequivocally probe the existence of the μ_3-carbido group, the reactions of **3**−**7** with MeI in $[D_6]$benzene were performed, which slowly yielded the μ_3-ethylidyne complex $[Ti_3Cp^*_3(\mu_3\text{-}O)_3(\mu_3\text{-}CMe)]$ (**2**). In a similar way, addition of ligands with acidic protons such as C_5H_6 or C_5Me_5H to the compounds **3**−**7** in $[D_6]$benzene caused the protonation of the carbide species and recovery of the μ_3-methylidyne complex **1**.

The X-ray diffraction study of **3** was reported in a previous communication and showed a dimeric structure in the solid state.[8] The lithium atoms are incorporated at the free vertex of the deprotonated oxoalkylidyne **1** derivative and two cube-type cores LiO_3Ti_3C are directly linked through two Li−O bonds.

In an attempt to extend our studies on the incorporation of s-block metals into the preorganized structure of **1**, we have also designed reactions with alkaline-earth derivatives. With this aim, we chose as starting reagents the dialkylamides $[M\{N(SiMe_3)_2\}_2(thf)_2]$ (M = Mg, Ca, Sr, Ba) and the dialkyls $[MgR_2(thf)_2]$ (R = CH_2Ph, *t*Bu) and $[Ba(CH_2Ph)_2]$.

The reactions of **1** with equimolecular amounts of $[M\{N(SiMe_3)_2\}_2(thf)_2]$ (M = Mg, Ca, Sr) also appeared to take place through the deprotonation of the μ_3-methylidyne group and amine elimination, to give soluble green microcrystalline solids of the complexes **8**−**10** in high yields (82−95%). The X-ray diffraction study of **9** and the analytical and spectroscopic data of all compounds support the structures shown in Scheme 2.

The structure of **9** was determined by a single-crystal X-ray diffraction study (Figure 1). Geometrical parameters

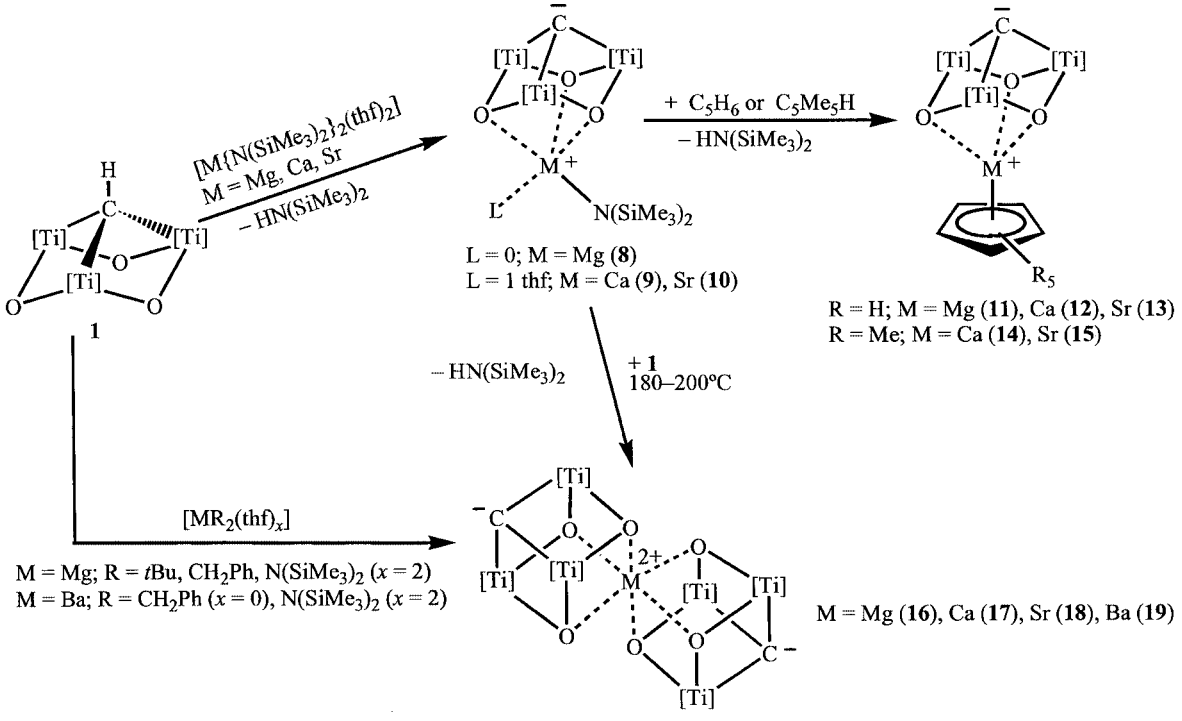

Scheme 2. Reactivity of **1** with alkaline-earth metal reagents. [Ti] = $Ti(\eta^5\text{-}C_5Me_5)$

 © 2004 Wiley-VCH Verlag GmbH & Co. KGaA, Weinheim

are summarized in Table 1. At first sight, the core of the molecular structure can be described as a cube in which the metallic centers alternate their positions with the oxygen and carbon atoms. The titanium atoms exhibit three-legged stool environments, while the calcium atom is five-coordinate with three sites occupied by the tridentate ligand, [{TiCp*(μ-O)}$_3$(μ-C)], and the remainder of the coordination sphere being filled by one amide group and one tetrahydrofuran molecule.

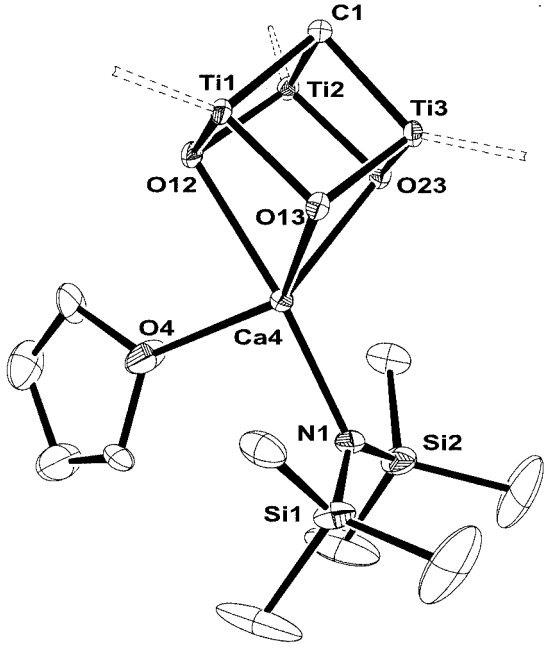

Figure 1. Simplified view of the molecular structure of **9** in the crystal

Table 1. Selected averaged lengths (Å) and angles (°) for complex **9**

Ti−C(1)	1.963(4)	N(1)−Ca(4)	2.291(4)
Ti−O	1.895(3)	O(4)−Ca(4)	2.376(4)
O(13)−Ca(4)	2.427(3)	Ca(4)···Ti	3.232(1)
O(23)−Ca(4)	2.425(3)	Ti···Ti	2.756(1)
O(12)−Ca(4)	2.483(3)	N(1)−Si	1.684(4)
Ti−C(1)−Ti	89.2(2)	Ti−O−Ti	93.3(1)
Ti−O−Ca(4)	95.4(1)	O−Ti−O	96.6(1)
N(1)−Ca(4)−O(4)	92.3(1)	O−Ti−C(1)	88.6(2)
N(1)−Ca(4)−O(23)	114.4(1)	Si(1)−N(1)−Ca(4)	115.1(2)
N(1)−Ca(4)−O(13)	114.4(1)	Si(1)−N(1)−Si(2)	129.7(2)
N(1)−Ca(4)−O(12)	173.8(1)	Si(2)−N(1)−Ca(4)	115.0(2)
O(23)−Ca(4)−O(13)	71.3(1)	O(4)−Ca(4)−O(23)	133.0(2)
O(4)−Ca(4)−O(12)	81.5(1)	O(4)−Ca(4)−O(13)	133.2(2)
O(13)−Ca(4)−O(12)	70.4(1)	O(23)−Ca(4)−O(12)	70.5(1)

Distances from the calcium to the oxygen atoms of the preorganized ligand are in the range of 2.425(3)−2.483(3) Å, the latter corresponding to a *trans* position of the calcium to the amido group. These distances are similar to those seen in other calcium complexes found in the literature with higher coordination numbers.[9] In the same way, the calcium−nitrogen bond length of 2.291(4) Å is close to that found for complexes containing the Ca−N(SiMe$_3$)$_2$ moiety.[10] The Ti−C(1) bond length, 1.963 Å (av.), is shorter than those shown in [{TiCp*(μ-O)}$_3$(μ-CH)] (**1**) [Ti−C(1) = 2.10 Å av.],[1b,1c] **2** [Ti−C(1) = 2.12 Å av.][1a,1c] and the oxoheterometallodicubane [{Li(μ$_3$-O)$_3$[Ti$_3$(η^5-C$_5$Me$_5$)$_3$(μ$_3$-C)]}$_2$] (Ti−C$^-$ 2.055 Å av.),[8] and close to that in the zwitterionic derivative [{Ti(η^5-C$_5$Me$_5$)(μ-O)}$_3${μ$_3$-η^2-C$^-$C(Me)N$^+$(2,6-Me$_2$C$_6$H$_3$)}] (Ti−C$^-$ 2.017(5) Å].[3]

The ^{1}H NMR spectra for complexes **8**−**10** in [D$_6$]benzene each show only one signal assignable to the η^5-C$_5$Me$_5$ groups due to the rotation of the organometallic ligand around the metallic center, analogous to the situation found in other similar compounds.[11] In the ^{13}C NMR spectra of these complexes the singlets for the apical carbides at very low field (δ = 588−598 ppm) are particularly noteworthy.

Again, the chemical evidence for the existence of the μ$_3$-carbido groups in **8**−**10** was obtained by their treatment with MeI in [D$_6$]benzene, which quantitatively afforded the μ$_3$-ethylidyne complex [Ti$_3$Cp*$_3$(μ-O)$_3$(μ$_3$-CMe)] (**2**).

Unlike the alkali metal complexes **3**−**7**, the reactions of compounds **8**−**10** with cyclopentadiene (C$_5$H$_6$) did not involve carbide protonation, but led to the metathesis reaction of the amide group to give the new heterometallocubane derivatives [(CpM)(μ$_3$-O)$_3${Ti$_3$Cp*$_3$(μ$_3$-C)}] [M = Mg (**11**), Ca (**12**), Sr (**13**)]. The analogous reaction with pentamethylcyclopentadiene (C$_5$Me$_5$H) afforded the compounds [(Cp*M)(μ$_3$-O)$_3${Ti$_3$Cp*$_3$(μ$_3$-C)}] [M = Ca (**14**), Sr (**15**)]. Pentamethylcyclopentadiene did not react, however, with the magnesium compound **8**, probably due to the steric hindrance and lower acidity of the C$_5$Me$_5$H ligand. The compounds **11**−**15** were isolated as green solids in good yields and the analytical and spectroscopic data are in agreement with the formulations given in Scheme 2.[12]

Compounds **11**, **12**, **13** and **14** are soluble in hydrocarbon and aromatic solvents, which allowed their NMR spectroscopic characterization. The strontium compound **15**, however, is scarcely soluble in benzene, toluene or tetrahydrofuran. The presence of the apical μ$_3$-carbido in all the cases was confirmed by ^{13}C NMR spectroscopy in [D$_6$]benzene, a singlet in the range δ = 580−594 ppm being observed in each case.

On the other hand, the elimination of the amido group could also be achieved by thermal treatment (over 150 °C) of **8**−**10** in toluene with one equivalent of the starting complex [{TiCp*(μ-O)}$_3$(μ$_3$-CH)] (**1**), producing green solids identified as the corner-shared double heterometallocubanes species [M{(μ-O)$_3$Ti$_3$Cp*$_3$(μ$_3$-C)}$_2$] M = Mg (**16**), Ca (**17**), Sr (**18**).[13] These complexes are insoluble in all the usual solvents such as toluene, hexane and even tetrahydrofuran. Fortunately, after numerous trials their solid-state structures were determined by X-ray diffraction (vide infra).

The complex [Mg{(μ-O)$_3$Ti$_3$Cp*$_3$(μ$_3$-C)}$_2$] (**16**) could also be obtained in 80−87% yield by irradiation or heating of a toluene solution of **1** and [Mg(CH$_2$Ph)$_2$(thf)$_2$] or [Mg*t*Bu$_2$(thf)$_2$]. In both cases, the reaction occurred with alkane elimination. Similar thermal treatment of **1** with [Ba{N(SiMe$_3$)$_2$}$_2$(thf)$_2$] in toluene at 100 °C for two days or with [Ba(CH$_2$Ph)$_2$] at 90 °C overnight afforded the oxoheterometallodicubane barium analogue, in good yield

 © 2004 Wiley-VCH Verlag GmbH & Co. KGaA, Weinheim

(66−78%), [Ba{(μ-O)$_3$Ti$_3$Cp*$_3$(μ$_3$-C)}$_2$] (**19**), as a microcrystalline green solid, which was insoluble in practically all solvents.

X-ray Crystal Structures of 16, 17 and 18

The solid-state structures of **16**, **17** and **18** determined from X-ray diffraction data are comprised of two trinuclear [Ti$_3$Cp*$_3$O$_3$C] units that are joined to each other by an alkaline-earth metal atom, which lies on the center of symmetry. In this arrangement, the tridentate organometallic ligands are situated in alternate positions relative to the pentamethylcyclopentadienyl groups in each case .

As shown in Figure 2, the geometry around the central metal atom can be described as distorted octahedral in each case. An examination of the values of the bond lengths and angles for these complexes (see Table 2) reveals an increasing distortion from magnesium to strontium, with the latter being best described as a trigonal antiprism with wider O−M−O intercube and closer intracube angles. The distance M−O increases in the same way, in agreement with the increasing size of the atomic radii of the central atom upon descending the group. In the case of calcium [Ca−O = 2.435(4) Å av., **17**], this value is close to that mentioned above for the metallocubane compound **9** [Ca−O = 2.445(3) Å av.]. The M−O bond lengths in the magnesium and strontium derivatives are in the expected ranges for oxocomplexes with high numbers of oxygen atoms.[14]

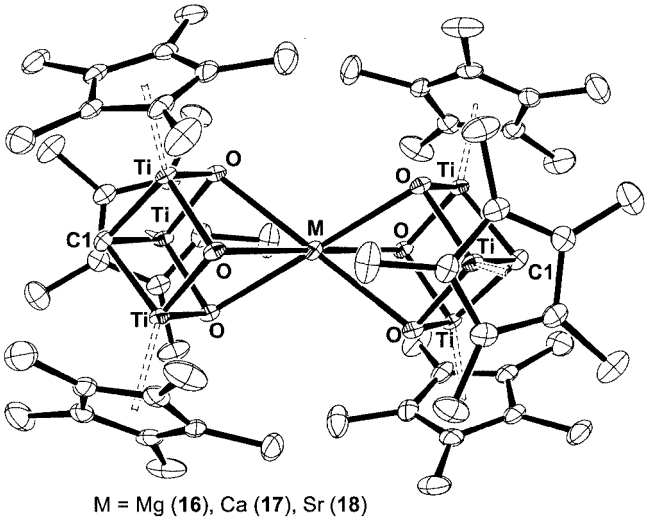

Figure 2. Simplified view of the molecular structures of **16**, **17** and **18**

The Ti−C(1) bond lengths decrease from magnesium to strontium [Mg = 2.020(10) Å av., Ca = 1.990(7) Å av., Sr = 1.970(2) Å av.], consistent with the higher steric requirement of the metal center. In all cases, these bond lengths are slightly shorter than those shown in **1** [Ti−C(1) = 2.10 Å av.][1b,1c] and **2** [Ti−C(1) = 2.12 Å av.],[1a,1c] and in the same range as those found in the zwitterionic derivative [{Ti(η^5-C$_5$Me$_5$)(μ-O)}$_3${μ$_3$-η^2-C$^-$C(Me)N$^+$(2,6-Me$_2$C$_6$H$_3$)}] [Ti−C$^-$ 2.017(5) Å].[3]

Table 2. Selected averaged distances (Å) and angles (°) for **16**, **17** and **18**

	M = Mg, **16**	M = Ca, **17**	M = Sr, **18**
Ti−O	1.905(6)	1.907(4)	1.896(2)
Ti−C(1)	2.020(10)	1.990(7)	1.970(2)
Ti···Ti	2.815(3)	2.780(2)	2.756(1)
M−O	2.174(6)	2.435(4)	2.585(2)
Ti···M	2.995(2)	3.230(2)	3.383(1)
O−Ti−O	92.1(3)	96.2(2)	97.2(1)
Ti−O−Ti	95.2(3)	93.6(2)	93.2(1)
M−O−Ti	94.2(2)	95.4(2)	96.9(1)
Ti−C1−Ti	88.3(4)	88.5(3)	88.1(1)
O−M−O[a]	78.2(3)−101.8(2)	71.2(2)−108.8(2)	66.8(1)−113.2(1)

[a] The narrower values correspond to the O−M−O angles of the same cube.

Conclusion

As outlined in the introduction, the active cooperation between the oxo and methylidyne groups is possible in the singular trinuclear chemistry of titanium. The results presented here demonstrate the peculiar behavior of the μ_3-methylidyne complex [{TiCp*(μ-O)}$_3$(μ$_3$-CH)] (**1**) with alkali and alkaline-earth metal amides and alkyls. In all cases, the processes go via the alkylidyne deprotonation and the anchorage of the group 1 or 2 cation metal on the [Ti$_3$O$_3$] system to form heterometallocubane or corner-shared heterometallodicubane species.

Experimental Section

General Remarks: All syntheses and subsequent manipulations of the described compounds were carried out with the exclusion of air and moisture using Schlenk or glovebox techniques. Solvents were carefully dried from the appropriate drying agents and distilled prior to use.

[{TiCp*(μ-O)}$_3$(μ$_3$-CH)] (**1**) was synthesized according to the published procedures.[1a,1c] *n*BuLi was purchased from Aldrich as a 1.6 M solution in hexane. [LiCH$_2$SiMe$_3$] and [LiNp] were prepared as described in the literature,[15] as were [Na*t*Bu] and [K*t*Bu].[16] [MN(SiMe$_3$)$_2$] (M = Li, Na, K) were purchased from Aldrich and used as supplied. [MN(SiMe$_3$)$_2$] (M = Rb, Cs),[17] [MgR$_2$(thf)$_2$] (R = CH$_2$Ph,[18] *t*Bu[19]), [Ba(CH$_2$Ph)$_2$],[20] and [M{N(SiMe$_3$)$_2$}$_2$(thf)$_2$], (M = Mg,[21] Ca,[22] Sr,[22] Ba[22]) were prepared following the literature methods. Pentamethylcyclopentadiene and dicyclopentadiene were purchased from Aldrich.

Elemental analyses (C,H,N) were performed with a Heraeus CHN-O-RAPID and/or Perkin−Elmer 2400-Serie II C, H, N, S/O instrument. IR spectra were obtained in KBr pellets by using an FT-IR Perkin−Elmer SPECTRUM 2000 spectrophotometer. NMR spectra were recorded with a Varian 300 spectrometer. Chemical shifts are given in ppm (δ) downfield from TMS (δ = 0.0) using the residual protons or carbon atoms of the solvent as an internal reference. Thermal reactions were carried out in a Roth autoclave model III (300 mL), with heater model 30S (20−300 °C) and temperature regulator model DR 500.

 © 2004 Wiley-VCH Verlag GmbH & Co. KGaA, Weinheim

Preparation of [Li(μ$_3$-O)$_3${Ti$_3$Cp$_3$*(μ$_3$-C)}] (3): *n*BuLi (0.35 mL, 0.56 mmol) was added to a solution of **1** (0.35 g, 0.57 mmol) in hexane (40 mL) in a 100-mL Carius tube. The reaction mixture was stirred at room temperature overnight. The green solid was then filtered, washed with hexane and vacuum dried to afford 0.33 g of **3** (Yield: 93%). ^{1}H NMR (300 MHz, [D$_8$]tetrahydrofuran, 20 °C, TMS): δ = 1.99 (s, C$_5$*Me*$_5$) ppm. ^{13}C{^{1}H} NMR (300 MHz, [D$_8$]tetrahydrofuran, 20 °C, TMS): δ = 12.0 (C$_5$*Me*$_5$), 115.3 (*C*$_5$Me$_5$), 581.4 (μ$_3$-*C*) ppm. IR (KBr, cm^{-1}): ṽ = 2907 (s), 2856 (vs), 1491 (w), 1437 (s), 1373 (s), 1023 (m), 801 (w), 681 (vs), 616 (vs), 464 (w), 416 (s). $C_{31}H_{45}LiO_3Ti_3$ (616.27): calcd. C 60.42, H 7.36; found C 60.81, H 7.59.

Preparation of [Na(μ$_3$-O)$_3${Ti$_3$Cp$_3$*(μ$_3$-C)}] (4): A 100-mL Carius tube was charged with **1** (0.30 g, 0.49 mmol), [NaN(SiMe$_3$)$_2$] (0.09 g, 0.49 mmol), and hexane (40 mL). The reaction mixture was heated at 60 °C overnight and the red solid formed was filtered, washed with hexane and dried under vacuum to give 0.26 g of **4** (Yield: 83%). ^{1}H NMR (300 MHz, [D$_8$]tetrahydrofuran, 20 °C, TMS): δ = 1.95 (s, C$_5$*Me*$_5$) ppm. ^{13}C{^{1}H} NMR (300 MHz, [D$_8$]tetrahydrofuran, 20 °C, TMS): δ = 11.7 (C$_5$*Me*$_5$), 115.4 (*C*$_5$Me$_5$), 586.7 (μ$_3$-*C*) ppm. IR (KBr, cm^{-1}): ṽ = 2907 (vs), 2850 (vs), 1493 (w), 1437 (s), 1372 (s), 1023 (m), 795 (w), 681 (vs), 621 (vs), 467 (w), 411 (s). $C_{31}H_{45}NaO_3Ti_3$ (632.32): calcd. C 58.88, H 7.17; found C 58.65, H 7.45.

Preparation of [K(μ$_3$-O)$_3${Ti$_3$Cp$_3$*(μ$_3$-C)}] (5): In a similar fashion to **4**, a solution of **1** (0.30 g, 0.49 mmol) and [KN(SiMe$_3$)$_2$] (0.10 g, 0.49 mmol) in hexane (40 mL) was heated at 60 °C overnight. The red solid formed was filtered and dried under vacuum to give 0.23 g of **5** (Yield: 72%). ^{1}H NMR (300 MHz, [D$_8$]tetrahydrofuran, 20 °C, TMS): δ = 1.94 (s, C$_5$*Me*$_5$) ppm. ^{13}C{^{1}H} NMR (300 MHz, [D$_8$]tetrahydrofuran, 20 °C, TMS): δ = 11.5 (C$_5$*Me*$_5$), 115.1 (*C*$_5$Me$_5$), 582.0 (μ$_3$-*C*) ppm. IR (KBr, cm^{-1}): ṽ = 2910 (vs), 2857 (vs), 1597 (w), 1495 (w), 1439 (s), 1375 (s), 1247 (w), 1067 (w), 916 (m), 899 (m), 852 (s), 784 (vs), 680 (s), 624 (m), 573 (m), 411 (s). $C_{31}H_{45}KO_3Ti_3$ (648.43): calcd. C 57.42, H 6.99; found C 56.99, H 7.10.

Preparation of [Rb(μ$_3$-O)$_3${Ti$_3$Cp$_3$*(μ$_3$-C)}] (6): In a 100-mL Carius tube with a valve were placed [{TiCp*(μ-O)}$_3$(μ$_3$-CH)] (**1**) (0.50 g, 0.82 mmol), [RbN(SiMe$_3$)$_2$] (0.20 g, 0.82 mmol) and tetrahydrofuran (40 mL). The reaction mixture was heated at 60 °C and stirred overnight. The red solution was then filtered, and the solvent removed under vacuum to afford 0.46 g of **6** (Yield: 81%). ^{1}H NMR (300 MHz, [D$_8$]tetrahydrofuran, 20 °C, TMS): δ = 1.94 (s, C$_5$*Me*$_5$) ppm. ^{13}C{^{1}H} NMR (300 MHz, [D$_8$]tetrahydrofuran, 20 °C, TMS): δ = 11.7 (C$_5$*Me*$_5$), 115.1 (*C*$_5$Me$_5$), 579.5 (μ$_3$-*C*) ppm. IR (KBr, cm^{-1}): ṽ = 2905 (vs), 2854 (s), 1493 (w), 1431 (m), 1375 (s), 1260 (w), 1023 (w), 800 (w), 776 (w), 657 (vs), 630 (vs), 583 (m), 436 (m), 382 (m). $C_{31}H_{45}O_3RbTi_3$ (694.80): calcd. C 53.59, H 6.53; found C 53.02, H 6.85.

Preparation of [Cs(μ$_3$-O)$_3${Ti$_3$Cp$_3$*(μ$_3$-C)}] (7): The preparation was similar to that for **6** from [{TiCp*(μ-O)}$_3$(μ$_3$-CH)] (**1**) (0.50 g, 0.82 mmol), [CsN(SiMe$_3$)$_2$] (0.24 g, 0.82 mmol) and tetrahydrofuran (40 mL). The light red solid of **7** was obtained in a 73% yield (0.44 g). ^{1}H NMR (300 MHz, [D$_8$]tetrahydrofuran, 20 °C, TMS): δ = 1.94 (s, C$_5$Me$_5$) ppm. ^{13}C{^{1}H} NMR (300 MHz, [D$_8$]tetrahydrofuran, 20 °C, TMS): δ = 11.6 (C$_5$*Me*$_5$), 114.7 (*C*$_5$Me$_5$), 577.3 (μ$_3$-*C*) ppm. IR (KBr, cm^{-1}): ṽ = 2908 (s), 2856 (s), 1494 (w), 1438 (w), 1373 (w), 1261 (w), 1021 (w), 800 (w), 681 (vs), 628 (s), 476 (w), 418 (s). $C_{31}H_{45}CsO_3Ti_3$ (742.24): calcd. C 50.16, H 6.11; found C 49.08, H 6.45.

Preparation of [{(Me$_3$Si)$_2$NMg}(μ$_3$-O)$_3${Ti$_3$Cp$_3$*(μ$_3$-C)}] (8): A solution of compound **1** (0.20 g, 0.33 mmol) and [Mg{N(SiMe$_3$)$_2$}$_2$(thf)$_2$] (0.16 g, 0.33 mmol) in toluene (30 mL) was placed in a 100-mL Carius-tube. The ampoule was sealed under vacuum by flame and the reaction mixture was heated at 180 °C for two days. The solution was then filtered, and the solvent removed to afford **8** as a green microcrystalline solid. Yield: 0.21 g, 82%. ^{1}H NMR (300 MHz, [D$_6$]benzene, 20 °C, TMS): δ = 0.40 [s, 18 H, N(Si*Me*$_3$)$_2$], 2.04 (s, 45 H, C$_5$*Me*$_5$); ^{13}C{^{1}H} NMR (300 MHz, [D$_6$]benzene, 20 °C, TMS): δ = 6.3 [N(Si*Me*$_3$)], 11.8 (C$_5$*Me*$_5$), 120.6 (*C*$_5$Me$_5$), 598.3 (μ$_3$-*C*) ppm. IR (KBr, cm^{-1}): ṽ = 2940 (s), 2909 (vs), 2858 (s), 1491 (w), 1435 (m), 1377 (s), 1242 (s), 1001 (vs), 931 (w), 888 (s), 829 (vs), 789 (s), 752 (m), 670 (vs), 610 (vs), 467 (m), 430 (s). $C_{37}H_{63}MgNO_3Si_2Ti_3$ (794.03): calcd. C 55.97, H 8.00, N 1.76; found C 55.99, H 8.39, N 1.73.

Preparation of [{(thf)(Me$_3$Si)$_2$NCa}(μ$_3$-O)$_3${Ti$_3$Cp$_3$*(μ$_3$-C)}] (9): A solution of **1** (0.50 g, 0.82 mmol) and [Ca{N(SiMe$_3$)$_2$}$_2$(thf)$_2$] (0.41 g, 0.82 mmol) in hexane (50 mL) was placed in a 100-mL Carius-tube with Young's valve. The reaction mixture was heated at 90 °C for 36 h. The green solution was then filtered, and the solvent was removed under vacuum to give **9** as a green powder (0.68 g, 94%). The slow evaporation of the solvent from a concentrated solution in hexane led to single-crystals of **9** suitable for an X-ray analysis. ^{1}H NMR (300 MHz, [D$_6$]benzene, 20 °C, TMS): δ = 0.34 [s, 18 H, N(Si*Me*$_3$)$_2$], 1.36 (m, 4 H, thf), 2.12 (s, 45 H, C$_5$*Me*$_5$), 3.87 (m, 4 H, thf) ppm. ^{13}C{^{1}H} NMR (300 MHz, [D$_6$]benzene, 20 °C, TMS): δ = 5.8 [N(Si*Me*$_3$)$_2$], 12.1 (C$_5$*Me*$_5$), 24.9 and 70.4 (thf), 118.9 (*C*$_5$Me$_5$), 592.7 (μ$_3$-*C*) ppm. IR (KBr): ṽ = 2944 (m), 2909 (s), 2856 (m), 1493 (w), 1437 (m), 1376 (m), 1256 (m), 1057 (s), 1027 (s), 931 (w), 879 (m), 793 (s), 675 (vs), 615 (s), 467 (m), 423 (m). $C_{41}H_{71}CaNO_4Si_2Ti_3$ (881.91): calcd. C 55.84, H 8.12, N 1.59; found C 56.27, H 8.12, N 1.30.

Preparation of [{(thf)(Me$_3$Si)$_2$NSr}(μ$_3$-O)$_3${Ti$_3$Cp$_3$*(μ$_3$-C)}] (10): Compound **10** was prepared similarly to **9** from **1** (0.40 g, 0.66 mmol), [Sr{N(SiMe$_3$)$_2$}$_2$(thf)$_2$] (0.36 g, 0.66 mmol) and hexane (50 mL). The solution was heated at 90 °C for 36 h. The green solution was filtered, and the solvent was removed to yield 0.58 g (95%) of **10** as a crystalline green solid. ^{1}H NMR (300 MHz, [D$_6$]benzene, 20 °C, TMS): δ = 0.32 [s, 18 H, N(Si*Me*$_3$)$_2$], 1.32 (m, 4 H, thf), 2.13 (s, 45 H, C$_5$*Me*$_5$), 3.77 (m, 4 H, thf) ppm. ^{13}C{^{1}H} NMR (300 MHz, [D$_6$]benzene, 20 °C, TMS): δ = 5.6 [N(Si*Me*$_3$)$_2$], 12.0 (C$_5$*Me*$_5$), 25.0 and 69.8 (thf), 118.5 (*C*$_5$Me$_5$), 588.0 (μ$_3$-*C*) ppm. IR (KBr): ṽ = 2910 (s), 2860 (s), 1493 (w), 1441 (m), 1377 (m), 1254 (m), 1178 (w), 1037 (m), 932 (w), 818 (s), 678 (vs), 615 (s), 467 (w), 421 (m). $C_{41}H_{71}NO_4Si_2SrTi_3$ (929.45): calcd. C 52.98, H 7.70, N 1.51; found C 53.24, H 8.10, N 1.32.

Preparation of [(CpMg)(μ$_3$-O)$_3${Ti$_3$Cp$_3$*(μ$_3$-C)}] (11): Addition of cyclopentadiene (25 μL, 0.38 mmol) to a solution of **8** (0.30 g, 0.38 mmol) and heating in toluene (30 mL) at 70 °C overnight led to the product **11** as a green solid in 73% yield (0.19 g). ^{1}H NMR (300 MHz, [D$_6$]benzene, 20 °C, TMS): δ = 2.03 (s, 45 H, C$_5$*Me*$_5$), 6.49 (s, 5 H, C$_5$*H*$_5$) ppm. ^{13}C{^{1}H} NMR (300 MHz, [D$_6$]benzene, 20 °C, TMS): δ = 11.7 (C$_5$*Me*$_5$), 106.3 (*C*$_5$H$_5$), 120.5 (*C*$_5$Me$_5$), 594.3 (μ$_3$-*C*) ppm. IR (KBr): ṽ = 2909 (s), 2857 (m), 1494 (w), 1435 (m), 1375 (m), 1246 (m), 1025 (w), 789 (vs), 672 (vs), 618 (m), 419 (m). $C_{36}H_{50}MgO_3Ti_3$ (698.74): calcd. C 61.88, H 7.21; found C 61.10, H 7.75.

Preparation of [(CpCa)(μ$_3$-O)$_3${Ti$_3$Cp$_3$*(μ$_3$-C)}] (12): Compound **12** was prepared in a similar way to **11** from **9** (0.50 g, 0.57 mmol) and cyclopentadiene (40 μL, 0.60 mmol) in toluene (40 mL) at room temperature. After 2 h, 0.34 g of dark green solid **12** (84% yield) was obtained. ^{1}H NMR (300 MHz, [D$_6$]benzene, 20 °C, TMS): δ = 2.06 (s, 45 H, C$_5$*Me*$_5$), 6.44 (s, 5 H, C$_5$*H*$_5$) ppm. ^{13}C{^{1}H} NMR

 © 2004 Wiley-VCH Verlag GmbH & Co. KGaA, Weinheim

(300 MHz, [D$_6$]benzene, 20 °C, TMS): δ = 11.8 (C_5Me_5), 110.3 (C_5H_5), 119.1 (C_5Me_5), 588.3 (μ_3-*C*) ppm. IR (KBr): $\tilde{\nu}$ = 3078 (w), 2908 (s), 2857 (m), 1493 (w), 1436 (m), 1375 (m), 1259 (w), 1068 (w), 1024 (m), 788 (vs), 735 (s), 676 (vs), 619 (s), 466 (w), 419 (m), 396 (m). $C_{36}H_{50}CaO_3Ti_3$ (714.51): calcd. C 60.52, H 7.05; found C 60.96, H 7.44.

Preparation of [(CpSr)(μ_3-O)$_3${Ti$_3$Cp$_3$*(μ_3-C)}] (13): Cyclopentadiene (40 μL, 0.60 mmol) was added to a solution of **10** (0.50 g, 0.54 mmol) in toluene (40 mL) and kept at room temperature. After 2 h, **13** was isolated as a green solid in 76% yield (0.31 g) by removing the solvent. ^{1}H NMR (300 MHz, [D$_6$]benzene, 20 °C, TMS): δ = 2.14 (s, 45 H, C_5Me_5), 6.36 (s, 5 H, C_5H_5) ppm. ^{13}C{^{1}H} NMR (300 MHz, [D$_6$]benzene, 20 °C, TMS): δ = 12.0 (C_5Me_5), 108.9 (C_5H_5), 117.6 (C_5Me_5), 591.6 (μ_3-*C*) ppm. IR (KBr): $\tilde{\nu}$ = 2909 (s), 2858 (s), 1493 (w), 1437 (m), 1377 (m), 1259 (w), 1068 (w), 1025 (w), 788 (vs), 735 (s), 675 (vs), 608 (s), 466 (w), 421 (m). $C_{36}H_{50}O_3SrTi_3$ (762.05): calcd. C 56.74, H 6.61; found C 56.76, H 6.88.

Preparation of [(Cp*Ca)(μ_3-O)$_3${Ti$_3$Cp$_3$*(μ_3-C)}] (14): Pentamethylcyclopentadiene (55 μL, 0.35 mmol) was added to a solution of **9** (0.30 g, 0.34 mmol) in hexane (40 mL). The reaction mixture was heated at 90 °C for 6 h to afford a green solution. The solvent was removed under vacuum and the product was isolated in 75% yield (0.20 g). ^{1}H NMR (300 MHz, [D$_6$]benzene, 20 °C, TMS): δ = 2.04 (s, 45 H, C_5Me_5), 2.21 (s, 15 H, C_5Me_5) ppm. ^{13}C{^{1}H} NMR (300 MHz, [D$_6$]benzene, 20 °C, TMS): δ = 11.2 and 11.8 (C_5Me_5), 114.3 and 119.4 (C_5Me_5), 588.6 (μ_3-*C*) ppm. IR (KBr): $\tilde{\nu}$ = 2962 (m), 2910 (s), 2855 (m), 1495 (w), 1438 (m), 1375 (m), 1259 (w), 1084 (m), 1020 (m), 790 (vs), 733 (m), 676 (vs), 615 (m), 467 (m), 420 (m). $C_{41}H_{60}CaO_3Ti_3$ (784.64): calcd. C 62.76, H 7.71; found C 63.07, H 7.96.

Preparation of [(Cp*Sr)(μ_3-O)$_3${Ti$_3$Cp$_3$*(μ_3-C)}] (15): Compound **15** was prepared similarly to **14** from **10** (0.30 g, 0.32 mmol) and C_5Me_5H (50 μL, 0.32 mmol) in hexane (40 mL). The solution was heated at 90 °C for 6 h to yield 0.22 g of **15** as a green microcrystalline solid (82% yield). ^{1}H NMR (300 MHz, [D$_6$]benzene, 20 °C, TMS): δ = 2.03 (s, 45 H, C_5Me_5), 2.17 (s, 15 H, C_5Me_5) ppm. ^{13}C{^{1}H} NMR (300 MHz, [D$_6$]benzene, 20 °C, TMS): δ = 11.5 and 12.4 (C_5Me_5), 114.0 and 118.8 (C_5Me_5), 580.0 (μ_3-*C*) ppm. IR (KBr): $\tilde{\nu}$ = 2964 (m), 2910 (s), 2586 (m), 1495 (w), 1439 (m), 1375 (m), 1258 (w), 1081 (m), 1022 (m), 790 (vs), 731 (m), 678 (vs), 616 (s), 468 (m), 420 (m). $C_{41}H_{60}O_3SrTi_3$ (832.19): calcd. C 59.18, H 7.27; found C 59.72, H 7.49.

Preparation of [Mg{(μ-O)$_3$Ti$_3$Cp*$_3$(μ_3-C)}$_2$]·C$_7$H$_8$ (16). Method A: [{TiCp*(μ-O)}$_3$(μ_3-CH)] (**1**) (0.50 g, 0.82 mmol), [Mg(CH$_2$Ph)$_2$(thf)$_2$] (0.14 g, 0.41 mmol) or [Mg*t*Bu$_2$(thf)$_2$] (0.12 g, 0.41 mmol) and toluene (50 mL) were placed in a Carius tube with Young's valve. The argon atmosphere pressure was reduced and the reaction mixture was irradiated with an ultraviolet lamp for 2 days. The green solution was then filtered and cooled to 4 °C to afford **16** as green crystals suitable for an X-ray diffraction analysis. After several crystallizations the isolated product was dried under vacuum giving a total yield of 80% (0.44 g) in the reaction with [Mg(CH$_2$Ph)$_2$(thf)$_2$] and 87% (0.48 g) with [Mg*t*Bu$_2$(thf)$_2$]. **Method B:** In a 100-mL Carius tube **1** (0.12 g, 0.19 mmol) and **8** (0.15 g, 0.19 mmol) were dissolved in toluene (20 mL) and then the ampoule was sealed under vacuum by flame. The solution was heated at 200 °C for 2 days. Slow crystallization led to green needles of **16** (0.20 g, 79%) which were vacuum dried. IR (KBr, cm^{-1}): $\tilde{\nu}$ = 2906 (vs), 2848 (vs), 1494 (m), 1437 (s), 1374 (s), 1261 (w), 1023 (m), 858 (s), 786 (s), 729 (s), 676 (m), 607 (vs), 464 (w), 424 (s). $C_{69}H_{98}MgO_6Ti_6$ (1335.12): calcd. C 62.07, H 7.40; found C 62.28, H 7.57.

Preparation of [{M{(μ_3-O)$_3$Ti$_3$Cp*$_3$(μ_3-C)}$_2$] [M = Ca (17), Sr (18)]: The preparations of **17** and **18** were similar to that of **16**. **1** (0.10 g, 0.17 mmol) and **9** (0.15 g, 0.17 mmol) or **10** (0.15 g, 0.16 mmol) in toluene (20 mL) react at 180 °C over 36 h to afford **17** or **18**, respectively, as green needles (Yields: 0.18 g, 84% **17**; 0.15 g, 71% **18**).

17: IR (KBr): $\tilde{\nu}$ = 2908 (s), 2858 (s), 1489 (w), 1437 (m), 1384 (m), 1376 (m), 1257 (w), 1025 (w), 790 (m), 675 (vs), 606 (s), 464 (m), 425 (m). $C_{62}H_{90}CaO_6Ti_6$ (1258.75): calcd. C 59.16, H 7.21; found C 59.58, H 7.20.

18: IR (KBr): $\tilde{\nu}$ = 2908 (s), 2857 (m), 1492 (w), 1439 (m), 1376 (m), 1025 (w), 790 (w), 675 (vs), 608 (vs), 467 (m), 426 (s). $C_{62}H_{90}O_6SrTi_6$ (1306.29): calcd. C 57.01, H 6.94; found C 57.07, H 6.95.

Preparation of [Ba{(μ_3-O)$_3$Ti$_3$Cp*$_3$(μ_3-C)}$_2$] (19): This complex can be synthesized either by thermal treatment at 100 °C for two days of a solution of [{TiCp*(μ-O)}$_3$(μ_3-CH)] (**1**) (0.40 g, 0.65 mmol) and [Ba{N(SiMe$_3$)$_2$}$_2$(thf)$_2$] (0.20 g, 0.33 mmol) in toluene (50 mL) or by heating at 90 °C overnight a solution of **1** (0.30 g, 0.49 mmol) and [Ba(CH$_2$Ph)$_2$] (0.08 g, 0.24 mmol). Following this, the reaction mixture was repeatedly concentrated, cooled and filtered to afford a green microcrystalline solid identified as **19** (Yield: 0.22−0.35 g, 66−78%). IR (KBr): $\tilde{\nu}$ = 2911 (vs), 2858 (s), 1493 (w), 1436 (m), 1377 (s), 1262 (w), 1103 (m), 1023 (m), 795 (vs), 668 (m), 616 (s), 394 (m). $C_{62}H_{90}BaO_6Ti_6$ (1356.00): calcd. C 54.92, H 6.69; found C 54.40, H 6.96.

X-ray Crystallographic Studies of Complexes 9, 16, 17 and 18

X-ray quality crystals of **16** were grown as described in the Exp. Sect. Crystals were mounted in glass capillaries in a random orientation and transferred to an Enraf−Nonius CAD4 diffractometer for characterization and data collection at room temperature. Crystals of complexes **9**, **17** and **18** were grown as described in the Exp. Sect., removed from the Schlenk vessels and covered with a layer of a viscous perfluoropolyether (Fomblin®Y). A suitable crystal was selected with the aid of a microscope, attached to a glass fiber, and immediately placed in the low temperature nitrogen stream of the diffractometer. The intensity data sets were collected at 100 K on a Bruker−Nonius KappaCCD diffractometer equipped with an Oxford Cryostream 700 unit. Crystallographic data for all the complexes are presented in Table 3.

The structures were solved using the WINGX package[23] by direct methods (SHELXS-97) and refined by least-squares against F^2 (SHELXL-97).[24]

Complex **9** exhibited severe disorder both in the pentamethylcyclopentadienyl rings and in the coordinated THF molecule, two sites with 50% occupancy were found for all the disordered atoms. Only the carbon atoms of the C31−C40 pentamethylcyclopentadienyl ring were isotropically refined, the rest of the non-hydrogen atoms were refined anisotropically. The hydrogen atoms were not added.

All non-hydrogen atoms of **16**, except the methyl carbon atoms C14, C15 and C16 of one pentamethylcyclopentadienyl ring and those of the disordered solvent, were anisotropically refined. Only the hydrogen atoms of the pentamethylcyclopentadienyl rings were included, positioned geometrically and refined by using a riding model.

Complex **17** also exhibited disorder in both molecules of the solvent and C16, all these atoms were refined with 50% of occupan-

 © 2004 Wiley-VCH Verlag GmbH & Co. KGaA, Weinheim

Table 3. Crystal data and structure refinement for **9**, **16**, **17** and **18**

Compound	**9**	**16**	**17**	**18**
Empirical formula	$C_{41}H_{71}CaNO_4Si_2Ti_3$	$C_{62}H_{90}MgO_6Ti_6{\cdot}2C_7H_8$	$C_{62}H_{90}O_6CaTi_6{\cdot}2\ C_7H_8$	$C_{62}H_{90}O_6SrTi_6$
Molecular mass	881.95	1427.32	1443.09	1306.36
Temperature [K]	100(2)	293(2)	100(2)	100(2)
Wavelength (Mo-K_α)	0.71073 Å	0.71073	0.71073	0.71073
Crystal system	triclinic	orthorhombic	orthorhombic	monoclinic
Space group	$P\bar{1}$	*Pnnm*	*Pnmn*	*C2/c*
a (Å); α (°)	11.310(1); 89.97(1)	14.409(5)	14.508(4)	19.707(2)
b (Å); β (°)	12.729(1); 89.95(1)	15.099(7)	15.2028(4)	14.026(3); 95.886(10)
c (Å); γ (°)	16.223(2); 88.85(1)	16.640(8)	16.421(4)	22.539(4)
Volume [Å^3]; Z	2335.0(4); 2	3620(3); 2	3621.9(13); 2	6197.2(18); 4
$\rho_{calcd.}$ [g·cm^{-3}]	1.254	1.309	1.323	1.400
μ(Mo-K_α) [mm^{-1}]	0.699	0.688	0.750	1.635
F(000)	940	1508	1524	2720
Crystal size [mm]	0.441 × 0.267 × 0.150	0.24 × 0.22 × 0.18	0.65 × 0.50 × 0.27	0.34 × 0.30 × 0.28
Diffractometer	Bruker−Nonius KappaCCD	Enraf−Nonius CAD4	Bruker−Nonius KappaCCD	Bruker−Nonius KappaCCD
θ Range	5.03 to 27.50	3.05 to 25.03°	4.85 to 29.79°	5.08 to 27.51°
Index ranges	$-14 \le h \le 14$	$-17 \le h \le 0$	$-18 \le h \le 18$	$-25 \le h \le 25$
	$-16 \le k \le 16$	$0 \le k \le 17$	$-21 \le k \le 21$	$-18 \le k \le 18$
	$0 \le l \le 21$	$-19 \le l \le 0$	$-19 \le l \le 18$	$-29 \le l \le 29$
Collected reflections	47913	3583	48804	50676
Independent reflections	10507 [*R*(int) = 0.001]	3307 [*R*(int) = 0.001]	4286 [*R*(int) = 0.2009]	7091 [*R*(int) = 0.1071]
Observed data [$I > 2\sigma(I)$]	6700	1788	3044	5829
Goodness-of-fit on F^2	0.939	1.135	1.101	1.094
Final *R* indices [$I > 2\sigma(I)$]	*R*1 = 0.071, *wR*2 = 0.178	*R*1 = 0.108, *wR*2 = 0.291	*R*1 = 0.095, *wR*2 = 0.242	*R*1 = 0.035, *wR*2 = 0.079
R indices (all data)	*R*1 = 0.125, *wR*2 = 0.212	*R*1 = 0.190, *wR*2 = 0.350	*R*1 = 0.132, *wR*2 = 0.274	*R*1 = 0.052, *wR*2 = 0.086
Largest diff. peak and hole [e·Å^{-3}]	1.879 and −0.992	0.992 and −0.827	1.292 and −1.378	0.490 and −0.476

cies. All the hydrogen atoms were included, positioned geometrically and refined by using a riding model except those linked to disordered atoms.

Complex **18** crystallized without solvent molecules. All non-hydrogen atoms were refined anisotropically. The hydrogen atoms were directly located in the difference Fourier maps and isotropically refined.

CCDC-223163 to -223166 contain the supplementary crystallographic data for this paper. These data can be obtained free of charge at www.ccdc.cam.ac.uk/conts/retrieving.html [or from the Cambridge Crystallographic Data Center, 12 Union Road, Cambridge CB2 1EZ, UK; Fax: (internat.) + 44-1223-336-033; E-mail: deposit@ccdc.cam.ac.uk].

Acknowledgments

This work was supported by the Ministerio de Ciencia y Tecnología (BQU2001−1499) and the Comunidad de Madrid (07N/0091/2002). M. C. M.-V. wishes to thank the Comunidad de Madrid for a doctoral fellowship.

[1] [1a] R. Andrés, M. Galakhov, A. Martín, M. Mena, C. Santamaría, *Organometallics* **1994**, *13*, 2159−2163. [1b] R. Andrés, M. Galakhov, A. Martín, M. Mena, C. Santamaría, *J. Chem. Soc., Chem. Commun.* **1995**, 551−552. [1c] R. Andrés, PhD thesis, Universidad de Alcalá, Madrid (Spain), **1995**.

[2] R. Andrés, M. Galakhov, A. Martín, M. Mena, C. Santamaría, *J. Chem. Soc., Chem. Commun.* **1995**, 551−552.

[3] R. Andrés, M. Galakhov, M. P. Gómez-Sal, A. Martín, M. Mena, C. Santamaría, *Chem. Eur. J.* **1998**, *4*, 1206−1213.

[4] M. Galakhov, M. Mena, C. Santamaría, *Chem. Commun.* **1998**, 691−692.

[5] M. P. Gómez-Sal, A. Martín, M. Mena, M. C. Morales, C. Santamaría, *Chem. Commun.* **1999**, 1839−1840.

[6] R. Andrés, M. Galakhov, M. P. Gómez-Sal, A. Martín, M. Mena, M. C. Morales-Varela, C. Santamaría, *Chem. Eur. J.* **2002**, *8*, 805−811.

[7] A. Abarca, M. Galakhov, P. Gómez-Sal, A. Martín, M. Mena, J. M. Poblet, C. Santamaría, J. P. Sarasa, *Angew. Chem.* **2000**, *112*, 544−547; *Angew. Chem. Int. Ed.* **2000**, *39*, 534−537.

[8] J. Gracia, A. Martín, M. Mena, M. C. Morales-Varela, J.-M. Poblet, C. Santamaría, *Angew. Chem.* **2003**, *115*, 957−960; *Angew. Chem. Int. Ed.* **2003**, *42*, 927−930.

[9] See as a few examples: [9a] K. Kubo, E. Yamamoto, N. Kato, A. Mori, *Acta Crystallogr., Sect. C: Cryst. Struct. Commun.* **1999**, *55*, 1819−1821. [9b] M. Westerhausen, S. Schneiderbauer, H. Piotrowski, M. Suter, H. Noth, *J. Organomet. Chem.* **2002**, *643*, 189−193. [9c] K. Kunze, L. Bihry, P. Atanasova, M. J. Hampden-Smith, E. N. Duesler, *Chem. Vap. Deposition* **1996**, *2*, 105.

[10] [10a] M. Westerhausen, M. Hartmann, N. Makropoulos, B. Wieneke, M. Wieneke, W. Schwarz, D. Stalke, *Z. Naturforsch., Teil B* **1998**, *53*, 117−125. [10b] M. Westerhausen, R. Low, W. Schwarz, *J. Organomet. Chem.* **1996**, *513*, 213−229. [10c] D. J. Burkey, E. K. Alexander, T. P. Hanusa, *Organometallics* **1994**, *13*, 2773−2786. More examples can be found in the Cambridge Crystallographic Data Base: F. H. Allen, *Acta Crystallogr., Sect. B* **2002**, *58*, 380−388.

[11] A. Abarca, M. V. Galakhov, J. Gracia, A. Martín, M. Mena, J.-M. Poblet, J. P. Sarasa, C. Yélamos, *Chem. Eur. J.* **2003**, *9*, 2337−2346.

[12] The compounds **14** and **15** were also detected by ^{1}H NMR in the thermolysis of solutions of **9** and **10**, respectively.

[13] Also, complexes **16**−**18** can be obtained in lower yield by thermal treatment (170−200 °C) of compounds **8**−**10**.

 © 2004 Wiley-VCH Verlag GmbH & Co. KGaA, Weinheim

[14] For magnesium: [14a] S. Chadwick, U. Englich, K. Ruhlandt-Senge, *Inorg. Chem.* **1999**, *38*, 6289−6293. [14b]A. D. Bond, R. A. Layfield, J. A. MacAllister, M. McPartlin, J. M. Rawson, D. S. Wright, *Chem. Commun.* **2001**, 1956−1957. For strontium: [14c] W. Paw, T. H. Baum, Kin-Chung Lam, A. L. Rheingold, *Inorg. Chem.* **2000**, *39*, 2011−2014. [14d] S. R. Drake, S. A. S. Miller, M. B. Hursthouse, K. M. A. Malik, *Polyhedron* **1993**, *12*, 1621−1634. More examples can be found in the Cambridge Crystallographic Data Base: F. H. Allen, *Acta Crystallogr. Sect. B* **2002**, *58*, 380−388.
[15] C. Tessiers-Youngs, O. T. Beachley Jr., *Inorg. Synth.* **1986**, *24*, 95−97.
[16] C. Schade, W. Bauer, P. von R. Schleyer, *J. Organomet. Chem.* **1985**, *295*, C25−C28.
[17] F. T. Edelmann, F. Pauer, M. Wedler, D. Stalke, *Inorg. Chem.* **1992**, *31*, 4143−4146.
[18] R. R. Schrock, *J. Organomet. Chem.* **1976**, *122*, 209−225.
[19] [19a] G. E. Coates, J. A. Heslop, *J. Chem. Soc., Chem. Commun.* **1968**, *A*, 514. [19b] C. W. Kamienski, J. F. Eastham, *J. Organomet. Chem.* **1967**, *8*, 535−541.
[20] A. Weeber, S. Harder, H. H. Brintzinger, K. Knoll, *Organometallics* **2000**, *19*, 1325−1332.
[21] K. W. Henderson, J. F. Allan, A. R. Kennedy, *Chem. Commun.* **1997**, 1149−1150.
[22] D. C. Bradley, M. B. Hursthouse, A. A. Ibrahim, K. M. A. Malik, M. Motevalli, R. Möseler, H. Powell, J. D. Runnades, A. C. Sullivan, *Polyhedron* **1990**, *9*, 2959−2964.
[23] L. J. Farrugia, WinGX.-A Windows Program for Crystal Structure Analysis, University of Glasgow, Glasgow, **1998**.
[24] G. M. Sheldrick, SHELX97, Program for Crystal Structure Analysis (Release 97−2), University of Göttingen, Germany, **1998**.

Received November 12, 2003
Early View Article
Published Online March 30, 2004

 © 2004 Wiley-VCH Verlag GmbH & Co. KGaA, Weinheim

New Nitrosylrhenium Hydrides as Precursors of "Diazo" Complexes: Preparation of Hydrazine and Diazene Derivatives

Gabriele Albertin,*[a] Stefano Antoniutti,[a] Alessia Bacchi,[b] Barbara Fregolent,[a] and Giancarlo Pelizzi[b]

Keywords: Diazene / Hydrazine / P ligands / N ligands / Rhenium

The reaction of $[ReCl_2(OCH_3)(NO)(PPh_3)_2]$ with phosphane in the presence of $NaBH_4$ gives different dihydride $[ReH_2(NO)\{PPh_2(OEt)\}_3]$ (**1**) and alkoxy-hydride $[ReH(OR^1)(NO)P_3]$ (**2**, **3**) [$R^1 = CH_3$, C_2H_5; P = $PPh(OEt)_2$, $P(OEt)_3$] derivatives depending on the nature of the phosphane and the solvent used. The protonation reactions of the new hydrides with Brønsted acid were performed and led to thermally unstable $[Re(OR^1)(\eta^2\text{-}H_2)(NO)P_3]^+$ (**2***, **3***) dihydrogen cations. Hydrazine complexes $[ReH(RNHNH_2)(NO)\{PPh_2(OEt)\}_3]BPh_4$ (**4**) (R = H, CH_3,C_6H_5) and $[Re(OR^1)(RNHNH_2)(NO)P_3]BPh_4$ (**5**, **6**) [$R^1 = CH_3$, C_2H_5; R = H, CH_3,C_6H_5; P = $PPh(OEt)_2$] were prepared by allowing the hydrides $[ReH_2(NO)P_3]$ and $[ReH(OR^1)(NO)P_3]$ to react first with triflic acid and then with hydrazine. The complexes were characterized spectroscopically and by the X-ray crystal structure determination of $[Re(OC_2H_5)(NH_2NH_2)(NO)\{PPh(OEt)_2\}_3]BPh_4$ (**5a**). Oxidation of the hydrazine complexes **4**–**6** was studied with $Pb(OAc)_4$ at –30 °C and, depending on the nature of the hydrazine and the stoichiometry of the complexes, led to aryldiazene $[ReH(C_6H_5N{=}NH)(NO)\{PPh_2(OEt)\}_3]BPh_4$ (**7c**), $[Re(OC_2H_5)(C_6H_5N{=}NH)(NO)\{PPh(OEt)_2\}_3]BPh_4$ (**8c**), methyldiazene $[ReH(CH_3N{=}NH)(NO)\{PPh_2(OEt)\}_3]BPh_4$ (**7b**) and a mixture of methyldiazene $[Re(OCH_3)(CH_3N{=}NH)(NO)\{PPh_2(OEt)\}_3]BPh_4$ (**9b**) and methyleneimine $[Re(OCH_3)(\eta^1\text{-}NH{=}CH_2)(NO)\{PPh_2(OEt)\}_3]BPh_4$ (**9*b**) derivatives. Mono- and binuclear aryldiazene complexes $[ReH(ArN{=}NH)(NO)\{PPh_2(OEt)\}_3]BPh_4$ (**10**), $[\{ReH(NO)[PPh_2(OEt)]_3\}_2(\mu\text{-}HN{=}NAr{-}ArN{=}NH)](BPh_4)_2$ (**11**), $[Re(OR^1)(ArN{=}NH)(NO)P_3]BPh_4$ (**12**, **14**, **16**) and $[\{Re(OR^1)(NO)P_3\}_2(\mu\text{-}HN{=}NAr{-}ArN{=}NH)](BPh_4)_2$ (**13**, **15**) [$R^1 = CH_3$, C_2H_5; P = $PPh(OEt)_2$, $P(OEt)_3$; Ar = C_6H_5, 4-$CH_3C_6H_4$; Ar-Ar = 4,4′-C_6H_4-C_6H_4] were also prepared by allowing hydrides $[ReH_2(NO)[PPh_2(OEt)]_3]$ and $[ReH(OR^1)(NO)P_3]$ to react with mono- and bis-aryldiazonium cations.
(© Wiley-VCH Verlag GmbH & Co. KGaA, 69451 Weinheim, Germany, 2004)

Introduction

The chemistry of transition metal complexes containing partially reduced dinitrogen ligands such as aryldiazenido, ArN_2, diazene, RN=NH, or hydrazine, $RNHNH_2$, has developed considerably in the past 25 years,[1−3] not only because of the similarity of these derivatives with the intermediates in nitrogen fixation, but also for the interesting reactivity modes and structural properties that this class of compounds may exhibit.[1−4]

Among the metal centers used to bind diazo molecules, rhenium plays a prominent role and a number of studies on aryldiazenido [Re]−N_2Ar complexes have been reported.[5] Less attention, however, has been devoted to hydrazine and diazene chemistry. A glance through the literature shows, in fact, that hydrazine or substituted hydrazine complexes are rather rare and include, apart from the pioneering work on $[Re(NCO)(CO)_2(NH_2NH_2)P_2]$ (P = tertiary phosphane) complexes,[6] only two papers[7] on $[ReCp^*Me_3(NH_2NH_2)]CF_3SO_3$ (Cp* = pentamethylcyclopentadienyl) and $[Re(NH_2NH_2)(CO)_3(PPh_3)_2]CF_3SO_3$ hydrazine derivatives, and another on the substituted hydrazine complex $[ReCl_2(PPh_3)_2\{NNC(O)Ph\}\{H_2NNHC(S)Ph\}]$.[8]

Only a few studies on aryldiazene complexes have been reported and include, apart from chelate organodiazene complexes[9] such as $[ReCl(HN{=}Npy)(NNpy)(PPhMe_2)_2]^+$, $[ReCl_2(NNC_4H_2N_2CF_3)(HN{=}NC_4H_2N_2CF_3)(PPh_3)]$, and $[ReCl_3(NNC_5H_4NH)(HN{=}NC_5H_4N)]$, only two types[10] of stable aryldiazene complexes — $[Re(\eta^5\text{-}C_5H_5)(CO)_2(HN{=}NR)]$ (R = 4-$CH_3C_6H_4$, 4-$CH_3OC_6H_4$) and $[Re(NH{=}NPh)(CO)_3(PPh_3)]BF_4$.

We are active in this field[3] and have recently reported[11,12] on the synthesis and reactivity of aryldiazene and hydrazine complexes of rhenium stabilized by mixed phosphane-carbonyl ligands of the type $[Re(ArN{=}NH)(CO)_nP_{5-n}]BPh_4$ and $[Re(RNHNH_2)(CO)_nP_{5-n}]BPh_4$ [P = $P(OEt)_3$, $PPh(OEt)_2$ and PPh_2OEt; $n = 1-4$] obtained from the hydride $[ReH(CO)_nP_{5-n}]$[13] as precursor. We now extend these studies to include nitrosyl and phosphane as supporting ligands with the aim both to increase the knowledge of the "diazo" chemistry of rhenium and to determine

[a] Dipartimento di Chimica, Università Ca′ Foscari di Venezia, Dorsoduro, 2137, 30123 Venezia, Italy
[b] Dipartimento di Chimica Generale ed Inorganica, Chimica Analitica, Chimica Fisica, Università di Parma, Parco Area delle Scienze, 17/a, 43100 Parma, Italy

 © 2004 Wiley-VCH Verlag GmbH & Co. KGaA, Weinheim **DOI: 10.1002/ejic.200300665**

the influence of these ligands on the stability and on the properties of both diazene and hydrazine derivatives. The precursors for these syntheses needed to be mixed-ligand hydride complexes with the phosphanes $P(OEt)_3$, $PPh(OEt)_2$, PPh_2OEt and nitrosyl, whose synthesis has not previously been reported.[14,15] We therefore began to study how to prepare rhenium hydrides containing both phosphane and nitrosyl ligands to use as precursors in diazo chemistry. The results of these studies, which include the preparation of new rhenium hydrides and their use as precursor for the synthesis of new diazene and hydrazine complexes, are reported here.

Results and Discussion

Preparation of Hydride Complexes

The outcome of the reaction of the dichloro complex $[ReCl_2(OCH_3)(NO)(PPh_3)_2]$ with phosphanes and $NaBH_4$ depends on the nature of the phosphorus ligands and the solvent used, as shown in Schemes 1 and 2.

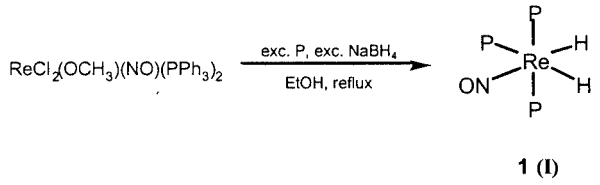

1 (I)

Scheme 1. P = PPh_2OEt

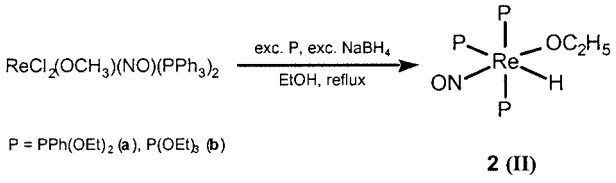

P = $PPh(OEt)_2$ (**a**), $P(OEt)_3$ (**b**)

2 (II)

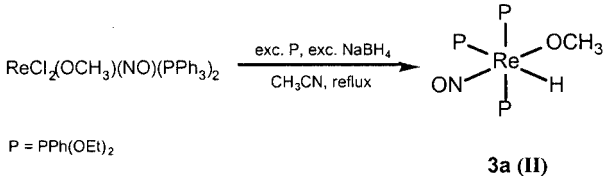

P = $PPh(OEt)_2$

3a (II)

Scheme 2

In the presence of ethoxydiphenylphosphane PPh_2OEt, the reaction of $[ReCl_2(OCH_3)(NO)(PPh_3)_2]$ with $NaBH_4$ in ethanol proceeds to give the dihydride $[ReH_2(NO)P_3]$ (**1**; P = PPh_2OEt) which was isolated as white microcrystals in about 83% yield (Scheme 1). In the presence of $PPh(OEt)_2$ and $P(OEt)_3$ the reaction proceeds to give exclusively the monohydride $[ReH(OC_2H_5)(NO)P_3]$ (**2**) [P = $PPh(OEt)_2$ (**a**), $P(OEt)_3$ (**b**)] containing the ethoxide group OC_2H_5 as a supporting ligand (Scheme 2). The presence of this OC_2H_5 ligand in the final complex **2** as well as the absence of traces of the dihydride $[ReH_2(NO)P_3]$ in the raw reaction product prompted us to use a different solvent for the reaction. The reaction of $[ReCl_2(OCH_3)(NO)(PPh_3)_2]$ with $NaBH_4$ in acetonitrile, in the presence of $PPh(OEt)_2$ and $P(OEt)_3$, however, also only gives the monohydride $[ReH(OCH_3)(NO)P_3]$ (**3**) [P = $PPh(OEt)_2$ (**a**)] which, in this case, contains the OCH_3 group as a ligand. The hydride was isolated as a stable solid with $PPh(OEt)_2$ (**3a**), while with $P(OEt)_3$ only an oily product was obtained (Scheme 2). The reaction of $[ReCl_2(OCH_3)(NO)(PPh_3)_2]$ with $NaBH_4$, in the presence of ethoxydiphenylphosphane PPh_2OEt, in acetonitrile solvent was also performed and gave the dihydride $[ReH_2(NO)P_3]$ (**1**), as in the reaction in ethanol but with a lower yield.

These results seem to indicate that the nature of the phosphane ligand determines the stoichiometry of the hydride obtained from the reaction of $[ReCl_2(OCH_3)(NO)(PPh_3)_2]$ with $NaBH_4$. The dihydride **1** can be obtained under all conditions with PPh_2OEt, which is a bulkier ligand[16] than $PPh(OEt)_2$ and $P(OEt)_3$, but less π-acid, while only the alkoxy-monohydrides $[ReH(OR^1)(NO)P_3]$ (**2**, **3**) were obtained with the ligands $PPh(OEt)_2$ and $P(OEt)_3$. The good π-acceptor ability[16] of these latter phosphanes probably requires the presence of an alkoxy ligand bonded to an $\{ReNO\}^6$-metal fragment[17] for the stabilization of the complexes. The nature of the solvent is important in determining the type of OR^1 group in the monohydride species.

Although a number of mono- and polyhydride complexes of rhenium have been reported,[14,15] few of them contain phosphanes as an ancillary ligand and none, to the best of our knowledge, an alkoxy group. The use of $[ReCl_2(OCH_3)(NO)(PPh_3)_2]$ as a precursor in the reaction with phosphanes and $NaBH_4$ allows the synthesis of new types of nitrosyl-hydride complexes to be achieved.

The hydride complexes **1**−**3** are white diamagnetic solids that are stable in air and in solution in the more common organic solvents, where they behave as non-electrolytes. Analytical and spectroscopic data (Table 1) support the proposed formulation and a geometry in solution was also established. The IR spectrum of $[ReH_2(NO)(PPh_2OEt)_3]$ (**1**) show two ν_{ReH} bands at 1914 and 1841 cm^{-1} suggesting a mutually *cis* position of the two hydride ligands. A strong band at 1637 cm^{-1} attributed to the ν_{NO} of the nitrosyl ligand is also present. In the temperature range between +20 and −80 °C the $^{31}P\{^1H\}$ NMR spectra of the complex appear as an AB_2 multiplet, in agreement with the presence of two magnetically equivalent phosphanes that are different to the third. The ^1H NMR spectrum confirms the presence of the hydride ligand showing, besides the signals of the PPh_2OEt groups, a multiplet between δ = −2 and −4 ppm. Taking into account the AB_2 pattern of the ^{31}P NMR spectra, the hydride multiplet can be simulated using an AB_2XY model (X, Y = H) with the parameters reported in Table 1. This model involves two inequivalent hydride ligands, one hydride with two very similar $J_{P,H}$ values, while the other has different $J_{P,H}$ values (29.5 and 39.8 Hz). On the basis of these data a geometry of type **I** (Scheme 1) can reasonably be proposed for the dihydride complex.

 © 2004 Wiley-VCH Verlag GmbH & Co. KGaA, Weinheim

Table 1. IR and NMR spectroscopic data of the rhenium complexes

Compound	IR[a] (cm^{-1})	Assignment	^1H NMR[b] δ (*J*/Hz)	Assignment	Spin system	$^{31}P\{^1H\}$ NMR[b] [c] δ (*J*/Hz)
$[ReH_2(NO)\{PPh_2(OEt)\}_3]$ (**1**)	1914 m	ν(ReH)	3.59 m	CH_2	AB_2	$\delta_A = 118.3$
	1841 m		3.06 qnt			$\delta_B = 117.5$
	1637 s	ν(NO)	1.17 t	CH_3		$J_{A,B} = 14.5$
			1.00 t			
			AB_2XY spin system	ReH		
			$\delta_X = -2.08$			
			$\delta_Y = -3.95$			
			$J_{A,X} = 29.5$			
			$J_{A,Y} = 39.8$			
			$J_{B,X} = 28.6$			
			$J_{B,Y} = 28.7$			
			$J_{X,Y} = 6.20$			
$[ReH(OC_2H_5)(NO)\{PPh(OEt)_2\}_3]$ (**2a**)	1832 m	ν(ReH)	4.21−3.70 m	CH_2 phos	A_2B	$\delta_A = 142.3$
	1635 s	ν(NO)	2.82 q	CH_2		$\delta_B = 135.0$
			1.34 t	CH_3 phos		$J_{A,B} = 19.6$
			1.27 t			
			1.25 t			
			0.018 t	CH_3		
			A_2BX spin system	ReH		
			$\delta_X = 0.26$			
			$J_{A,X} = 26.0$			
			$J_{B,X} = 92.5$			
$[Re(\eta^2\text{-}H_2)(OC_2H_5)(NO)\{PPh(OEt)_2\}_3]BF_4$ (**2*a**)			4.19−3.88 m[d]	CH_2 phos	A_2B[d]	$\delta_A = 147.4$
			2.92 q	CH_2		$\delta_B = 144.9$
			1.38 t	CH_3 phos		$J_{A,B} = 16.6$
			1.34 t			
			0.31 t	CH_3		
$[ReH(OC_2H_5)(NO)\{P(OEt)_3\}_3]$ (**2b**)	1864 m	ν(ReH)	4.03 m[e]	CH_2 phos		126.5 s, br
	1657 s	ν(NO)	3.27 q	CH_2		
			1.23 t	CH_3 phos	A_2B[e]	$\delta_A = 127.8$
			1.20 t			$\delta_B = 126.4$
			0.55 t	CH_3		$J_{A,B} = 27.1$
			A_2BX spin system	ReH		
			$\delta_X = 0.86$			
			$J_{A,X} = 8.0$			
			$J_{B,X} = 36.1$			
$[ReH(OCH_3)(NO)\{PPh(OEt)_2\}_3]$ (**3**)	1848 s	ν(ReH)	3.90 m	CH_2	A_2B	$\delta_A = 141.6$
	1650 s	ν(NO)	2.81 s	CH_3O		$\delta_B = 135.3$
			1.30 t	CH_3		$J_{A,B} = 19.2$
			1.27 t			
			A_2BX spin system	ReH		
			$\delta_X = 0.51$			
			$J_{A,X} = 26$			
			$J_{B,X} = 92$			
$[Re(\eta^2\text{-}H_2)(OCH_3)(NO)\{PPh(OEt)_2\}_3]BF_4$ (**3***)			4.05 m	CH_2	A_2B[d]	$\delta_A = 148.0$
			3.84 m			$\delta_B = 144.7$
			2.56 s	CH_3O		$J_{A,B} = 17.0$
			1.37 t	CH_3		
			1.33 t			
			1.28 t			
$[ReH(NH_2NH_2)(NO)\{PPh_2(OEt)\}_3]BPh_4$ (**4a**)	3341 w	ν(NH)	5.75 br	NH_2	AB_2	$\delta_A = 110.0$
	3304 w		3.74 br	NH_2		$\delta_B = 101.1$
	3215 m		3.45 br	CH_2		$J_{A,B} = 13.0$
	1683 s	ν(NO)	3.10 qnt			
			1.06 t	CH_3		
			0.58 t			
			AB_2X spin system	ReH		
			$\delta_X = -3.48$			
			$J_{A,X} = 30$			
			$J_{B,X} = 20$			
$[ReH(CH_3NHNH_2)(NO)\{PPh_2(OEt)\}_3]BPh_4$ (**4b**)	3609 w	ν(NH)	5.60 br	NH_2	AB_2	$\delta_A = 110.8$
	3289 w		4.13 br	NH		$\delta_B = 100.6$
	1683 s	ν(NO)	3.51 m	CH_2		$J_{A,B} = 15.5$
			3.16 qnt			
			2.47 d	CH_3 hydraz		
			$J_{H,H} = 6$			
			1.12 t	CH_3		
			0.63 t			
			AB_2X spin system	ReH		
			$\delta_X = -3.40$			
			$J_{A,X} = 20$			
			$J_{B,X} = 32$			

 © 2004 Wiley-VCH Verlag GmbH & Co. KGaA, Weinheim

Table 1. *(continued)*

Compound	IR[a] (cm^{-1})	Assignment	^1H NMR[b] δ (*J*/Hz)	Assignment	Spin system	$^{31}P\{^1H\}$ NMR[b] [c] δ (*J*/Hz)
$[ReH(C_6H_5NHNH_2)(NO)\{PPh_2(OEt)\}_3]BPh_4$ (**4c**)	3601 m	ν(NH)	6.71 br, m	NH_2	AB_2	$\delta_A = 109.8$
	3289 m		6.53 br, m	NH		$\delta_B = 101.6$
	3217 w		3.41 m	CH_2		$J_{A,B} = 14.5$
	1690 s	ν(NO)	3.14 qnt			
			0.97 t	CH_3		
			0.66 t			
$[Re(OC_2H_5)(NH_2NH_2)(NO)\{PPh(OEt)_2\}_3]BPh_4$ (**5a**)	3356 m	ν(NH)	5.61 br	NH_2	AB_2	$\delta_A = 128.3$
	3329 m		4.00 m	CH_2 phos		$\delta_B = 122.6$
	3270 m		3.58 m			$J_{A,B} = 22.8$
	1690 s	ν(NO)	3.21 q	CH_2		
			1.26 t	CH_3 phos		
			1.22 t			
			1.01 t			
			0.81 t	CH_3		
$[Re(OC_2H_5)(CH_3NHNH_2)(NO)\{PPh(OEt)_2\}_3]CF_3SO_3$ (**5b$_2$**)	3335 m	ν(NH)	5.84 br	NH_2	AB_2	$\delta_A = 128.1$
	3302 m		4.00 m	CH_2 phos		$\delta_B = 122.9$
	3217 w		3.56 m			$J_{A,B} = 24.0$
	1690 s	ν(NO)	3.32 q	CH_2		
			2.81 d	CH_3 hydraz		
			$J_{H,H} = 6$			
			1.34 t	CH_3 phos		
			1.30 t			
			1.12 t			
			0.88 t	CH_3		
$[Re(OC_2H_5)(C_6H_5NHNH_2)(NO)\{PPh(OEt)_2\}_3]BPh_4$ (**5c**)	3375 m	ν(NH)	6.34 m	NH_2	AB_2	$\delta_A = 131.5$
	3302 m		3.86 m	CH_2 phos		$\delta_B = 123.1$
	3237 w		3.69 m			$J_{A,B} = 23.6$
	1696 s	ν(NO)	3.41 q	CH_2		
	1618 m	δ(NH_2)	1.27 t	CH_3 phos		
			1.25 t			
			1.22 t			
			0.88 t	CH_3		
$[Re(OCH_3)(NH_2NH_2)(NO)\{PPh(OEt)_2\}_3]BPh_4$ (**6a**)	3368 w	ν(NH)	5.73 br	NH_2	AB_2	$\delta_A = 127.8$
	3322 m		3.97 m	CH_2		$\delta_B = 122.2$
	3270 m		3.44 m			$J_{A,B} = 23.1$
	1683 s	ν(NO)	3.23 s	CH_3O		
			1.35 t	CH_3		
			1.31 t			
			1.10 t			
$[Re(OCH_3)(CH_3NHNH_2)(NO)\{PPh(OEt)_2\}_3]BPh_4$ (**6b**)	3323 m	ν(NH)	5.75 s br	NH_2	AB_2	$\delta_A = 127.6$
	3296 m		3.96 m	CH_2		$\delta_B = 122.6$
	1670 s	ν(NO)	3.65 m			$J_{A,B} = 23.4$
			3.45 s	CH_3O		
			3.30 m, br	NH		
			2.78 d	CH_3 hydraz		
			$J_{H,H} = 6$			
			1.36 t	CH_3		
			1.33 t			
			1.11 t			
$[Re(OCH_3)(C_6H_5NHNH_2)(NO)\{PPh(OEt)_2\}_3]BPh_4$ (**6c**)	3302 m	ν(NH)	6.31 s, br	NH_2	AB_2	$\delta_A = 131.0$
	3243 w		3.86 m	CH_2		$\delta_B = 122.5$
	1697 s	ν(NO)	3.50 m			$J_{A,B} = 23.9$
	1604 m	δ(NH_2)	3.28 s	CH_3O		
			1.24 t	CH_3		
			1.20 t			
$[ReH(CH_3N{=}NH)(NO)\{PPh_2(OEt)\}_3]BPh_4$ (**7b**)	1696 s	ν(NO)	15.74 d, br	NH	AB_2	$\delta_A = 109.9$
			4.17 s	$CH_3N{=}$		$\delta_B = 101.7$
			3.67 q	H hydride		$J_{A,B} = 16.0$
			$J_{P,Hcis} = 6$			
			$J_{P,Htrans} = 6$			
			3.29 m	CH_2		
			3.14 m			
			1.02 t	CH_3		
			0.92 t			
$[ReH(C_6H_5N{=}NH)(NO)\{PPh_2(OEt)\}_3]BPh_4$ (**7c**)	1736 s	ν(NO)	17.32 d, br	NH	AB_2	$\delta_A = 117.0$
			3.66 q	H hydride		$\delta_B = 105.7$
			$J_{P,Hcis} = 6$			$J_{A,B} = 16.0$
			0.90 t			
$[Re(OC_2H_5)(C_6H_5N{=}NH)(NO)\{PPh(OEt)_2\}_3]BPh_4$ (**8c**)	1729 s	ν(NO)	17.26 d, br	NH	A_2B	$\delta_A = 133.2$
			3.90 m	CH_2		$\delta_B = 132.6$
			1.34 t	CH_3		$J_{A,B} = 18.9$

 © 2004 Wiley-VCH Verlag GmbH & Co. KGaA, Weinheim

Table 1. *(continued)*

Compound	IR[a] (cm^{-1})	Assignment	^1H NMR[b] δ (*J*/Hz)	Assignment	Spin system	$^{31}P\{^1H\}$ NMR[b] [c] δ (*J*/Hz)
			1.27 t			
			1.23 t			
			1.17 t			
$[Re(OCH_3)(CH_3N{=}NH)(NO)\{PPh(OEt)_2\}_3]BPh_4$ (**9b**)[f]	1723 s	ν(NO)	18.73 d	HN=N	AB_2	δ_A = 133.1
+	1690 s		15.68 d	HN=C		δ_B = 127.6
$[Re(OCH_3)(\eta^1\text{-}NH{=}CH_2)(NO)\{PPh(OEt)_2\}_3]BPh_4$ (**9*b**) [f]			4.06 s, br	CH_2=N		$J_{A,B}$ = 26.0
			3.85 m	CH_2		
			3.73 s	CH_3N=	AB_2	δ_A = 132.6
			3.30 s	CH_3O		δ_B = 126.7
			1.31 m	CH_3		$J_{A,B}$ = 28.0
$[ReH(C_6H_5N{=}NH)(NO)\{PPh_2(OEt)\}_3]BPh_4$ (**10c**)	1729 s	ν(NO)	13.83 d	NH	AB_2	δ_A = 112.1
			13.61 d			δ_B = 111.1
			3.55−3.25 m	CH_2		$J_{A,B}$ = 24.0
			AB_2X spin system	H hydride		
			δ_X = 2.83		AB_2	δ_A = 108.5
			$J_{A,X}$ = 29.5			δ_B = 93.2
			$J_{B,X}$ = 20.0			$J_{A,B}$ = 19.5
			1.03 t	CH_3		
			0.83 t			
			0.78 t			
			0.66 t			
$[ReH(C_6H_5N{=}^{15}NH)(NO)\{PPh_2(OEt)\}_3]BPh_4$ (**10c$_1$**)	1723 s	ν(NO)	13.84 dd	NH	AB_2Y	δ_A = 112.1
			J^{15}_{NH} = 65			δ_B = 111.1
			13.62 dd			$J_{A,B}$ = 24.1
			J^{15}_{NH} = 64.0			$J_{A,Y}$ = 28.8
			3.55−3.25 m	CH_2		$J_{B,Y}$ = 2.2
			AB_2X spin system	H hydride		
			δ_X = 2.82		AB_2Y	δ_A = 108.9
			$J_{A,X}$ = 29.0			δ_B = 93.5
			$J_{B,X}$ = 19.7			$J_{A,B}$ = 19.5
			1.01 t	CH_3		$J_{A,Y}$ = 39.3
			0.85 t			$J_{B,Y}$ = 1.8
			0.79 t			
			0.68 t			
$[ReH(4\text{-}CH_3C_6H_5N{=}NH)(NO)\{PPh_2(OEt)\}_3]BPh_4$ (**10d**)	1729 s, br	ν(NO)	13.62 d, br	NH	AB_2	δ_A = 112.2
	1705 sh		13.45 d, br			δ_B = 111.3
			3.62−3.20 m	CH_2		$J_{A,B}$ = 23.0
			2.40 s	CH_3 *p*-tolyl		
			2.38 s		AB_2	δ_A = 108.7
			1.18−0.65 m	CH_3		δ_B = 92.1
						$J_{A,B}$ = 18.1
$[\{ReH(NO)[PPh_2(OEt)]_3\}_2(\mu\text{-}4,4'\text{-}HN{=}NHC_6H_4\text{-}C_6H_4N{=}NH)](BPh_4)_2$ (**11a**)	1696 s	ν(NO)	13.45 d, br	NH	AB_2	δ_A = 112.1
			3.45 m	CH_2		δ_B = 110.6
			AB_2X spin system	H hydride		$J_{A,B}$ = 24.3
			δ_X = 2.93			
			$J_{A,X}$ = 20.4			
			$J_{B,X}$ = 29.4			
			0.84 t	CH_3		
			0.81 t			
$[\{ReH(NO)[PPh_2(OEt)]_3\}_2\text{-}(\mu\text{-}4,4'\text{-}H^{15}N{=}NC_6H_4\text{-}C_6H_4N{=}^{15}NH)](BPh_4)_2$ (**11a$_1$**)	1696 s	ν(NO)	13.44 dd	NH	AB_2Y	δ_A = 112.6
			J^{15}_{NH} = 64.0			δ_B = 111.3
			3.45 m	CH_2		J_{AB} = 24.3
			AB_2X spin system	H hydride		J_{AY} = 29.1
			δ_X = 2.95			J_{BY} = 1.0
			$J_{A,X}$ = 20.0			
			$J_{B,X}$ = 29.5			
			0.85 m	CH_3		
$[Re(OC_2H_5)(C_6H_5N{=}NH)(NO)\{PPh(OEt)_2\}_3]BF_4$ (**12c**)	1736 s	ν(NO)	13.67 d, br	NH	AB_2	δ_A = 127.1
			3.96 m	CH_2		δ_B = 116.7
			3.78 m			$J_{A,B}$ = 26.0
			1.24 t	CH_3		
			1.20 t			
			1.15 t			
$[Re(OC_2H_5)(NO)(C_6H_5N{=}^{15}NH)\{PPh(OEt)_2\}_3]BF_4$ (**12c$_1$**)	1734 s	ν(NO)	13.68 dd	NH	AB_2Y	δ_A = 127.1
			J^{15}_{NH} = 64.5			δ_B = 116.8
			3.96 m	CH_2		$J_{A,B}$ = 26.0
			3.78 m			$J_{A,Y}$ = 43.5
			1.25 t	CH_3		$J_{B,Y}$ = 4.0
			1.13 t			
$[Re(OC_2H_5)(4\text{-}CH_3C_6H_4N{=}NH)(NO)\{PPh(OEt)_2\}_3]BF_4$ (**12d**)	1722 s	ν(NO)	13.47 d, br	NH	AB_2	δ_A = 127.3
			3.93 m	CH_2		δ_B = 116.9
			3.60 m			$J_{A,B}$ = 26.0
			2.43 s	CH_3 *p*-tolyl		

 © 2004 Wiley-VCH Verlag GmbH & Co. KGaA, Weinheim

Table 1. *(continued)*

Compound	IR[a] (cm^{-1})	Assignment	^1H NMR[b] δ (*J*/Hz)	Assignment	Spin system	$^{31}P\{^1H\}$ NMR[b] [c] δ (*J*/Hz)
			1.25 t	CH_3		
			1.22 t			
			1.13 t			
$[\{Re(OC_2H_5)(NO)[PPh(OEt)_2]_3\}_2(\mu\text{-}4,4'\text{-}HN{=}NC_6H_4{-}C_6H_4N{=}NH)](BF_4)_2$ (**13a**)	1728 s	ν(NO)	13.77 d, br	NH	AB_2	$\delta_A = 127.5$
			13.66 d, br			$\delta_B = 117.3$
			4.00 m	CH_2		$J_{A,B} = 26.1$
			3.68 m			
			1.31 t	CH_3	AB_2	$\delta_A = 127.3$
			1.28 t			$\delta_B = 117.0$
			1.24 t			$J_{A,B} = 26.2$
			1.21 t			
$[\{Re(OC_2H_5)(NO)[PPh(OEt)_2]_3\}_2(\mu\text{-}4,4'\text{-}H^{15}N{=}NC_6H_4{-}C_6H_4N{=}{}^{15}NH)](BF_4)_2$ (**13a$_1$**)	1729 s	ν(NO)	13.79 dd	NH	AB_2Y	$\delta_A = 127.6$
			$J^{15}_{NH} = 64.5$			$\delta_B = 117.3$
			13.65 dd			$J_{A,B} = 26.2$
			$J^{15}_{NH} = 64.5$			$J_{A,Y} = 45.0$
			4.00 m	CH_2		$J_{B,Y} = 4.0$
			3.66 m			
			1.30 t	CH_3	AB_2Y	$\delta_A = 127.4$
			1.25 t			$\delta_B = 117.1$
			1.24 t			$J_{A,B} = 26.1$
			1.21 t			$J_{A,Y} = 45.2$
						$J_{B,Y} = 4.0$
$[Re(OCH_3)(4\text{-}CH_3C_6H_4N{=}NH)(NO)\{PPh(OEt)_2\}_3]BPh_4$ (**14d**)	1736 s	ν(NO)	13.67 d, br	NH	AB_2	$\delta_A = 127.3$
			13.52 d, br			$\delta_B = 116.9$
			3.98 m	CH_2		$J_{AB} = 25.6$
			3.70 m			
			2.51 s	CH_3	AB_2	$\delta_A = 126.9$
			2.46 s			$\delta_B = 117.2$
			1.32 t	CH_3 phos		$J_{A,B} = 26.0$
			1.29 t			
			1.27 t			
			1.24 t			
			1.17 t			
$[\{Re(OCH_3)(NO)[PPh(OEt)_2]_3\}_2(\mu\text{-}4,4'\text{-}HN{=}NC_6H_4{-}C_6H_4N{=}NH)](BPh_4)_2$ (**15a**)	1742 s	ν(NO)	13.76 d, br	NH	AB_2	$\delta_A = 126.9$
			13.63 d, br			$\delta_B = 116.7$
			4.00 m	CH_2		$J_{A,B} = 26.3$
			3.72 m			
			1.32 t	CH_3	AB_2	$\delta_A = 127.1$
			1.26 t			$\delta_B = 116.8$
			1.20 t			$J_{AB} = 24.5$
$[\{Re(OCH_3)(NO)[PPh(OEt)_2]_3\}_2(\mu\text{-}4,4'\text{-}H^{15}N{=}NC_6H_4{-}C_6H_4N{=}{}^{15}NH)](BPh_4)_2$ (**15a$_1$**)	1736 s	ν(NO)	13.76 dd	NH	AB_2Y	$\delta_A = 127.4$
			$J^{15}_{NH} = 64.0$			$\delta_B = 117.1$
			13.63 dd			$J_{A,B} = 26.4$
			$J^{15}_{NH} = 64.0$			$J_{A,Y} = 45.1$
			4.00 m	CH_2		$J_{B,Y} = 2.9$
			3.75 m			
			1.31 t	CH_3	AB_2Y	$\delta_A = 127.0$
			1.25 t			$\delta_B = 116.7$
			1.20 t			$J_{A,B} = 26.0$
						$J_{A,Y} = 45.0$
						$J_{B,Y} = 3.0$
$[Re(OC_2H_5)(4\text{-}CH_3C_6H_4N{=}NH)(NO)\{P(OEt)_3\}_3]BF_4$ (**16d**)	1722 s	ν(NO)	14.03 d, br	NH	AB_2	$\delta_A = 108.3$
			4.10 m	CH_2		$\delta_B = 96.3$
			2.49 s	CH_3 *p*-tolyl		$J_{A,B} = 36.5$
			1.32 t	CH_3		
			1.25 t			

[a] In KBr pellets. [b] In CD_2Cl_2 at 25 °C unless otherwise noted. [c] Positive shift downfield from 85% H_3PO_4. [d] At −30 °C. [e] At −70 °C. [f] $^{13}C\{^1H\}$ NMR (CD_2Cl_2): δ = 165−121 (m, Ph), 64.0 (br, s, $CH_2{=}NH$), 63.0 (m, CH_2), 62.5 (s, $CH_3N{=}NH$), 16.6 (m, CH_3) ppm.

The infrared spectra of the alkoxide complexes [Re-H(OR^1)(NO)P$_3$] (**2**, **3**) show only one medium-intensity band at 1864−1832 cm^{-1} attributed to ν_{ReH} of the hydride ligand and one strong absorption at 1657−1635 cm^{-1} due to the ν_{NO} of the nitrosyl group. In the temperature range between +20 and −80 °C the $^{31}P\{^1H\}$ NMR spectra appear, for each of the hydrides, as an A_2B multiplet in agreement with the presence of two magnetically equivalent phosphanes that are different from the third. The ^1H NMR spectra confirm the presence of both the hydride and the alkoxide ligand showing, besides the signals of the phosphane protons, a multiplet at δ = 0.86−0.26 ppm attributed to the hydride ligand and the characteristic signals of either an OC_2H_5 or an OCH_3 group. The multiplet of the hydride can be easily simulated using an A_2BX model (X = H) with the parameters reported in Table 1. The values of the two $J_{P,H}$ coupling constants deduced from this simulation are rather different between each other and suggest that the hy-

 © 2004 Wiley-VCH Verlag GmbH & Co. KGaA, Weinheim

dride occupies a *trans* position with respect to one phosphane and a *cis* position with respect to the other two. On this basis a geometry of type **II** (Scheme 2) can be reasonably proposed in solution for all the monohydride $[ReH(OR^1)(NO)P_3]$ (**2**, **3**) derivatives.

Protonation Reactions

The protonation reaction of the new hydrides **1**−**3** with Brønsted acids was studied in an NMR tube at temperatures between +20 and −80 °C. The results are summarized in Scheme 3.

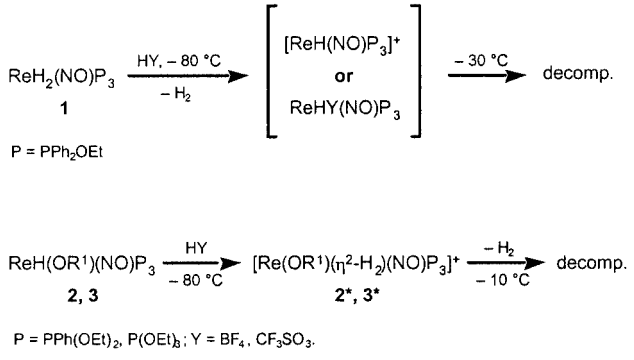

Scheme 3

Addition of an equimolar amount of CF_3SO_3H or $HBF_4{\cdot}Et_2O$ to a solution of the dihydride $[ReH_2(NO)P_3]$ (**1**) in CD_2Cl_2 at −80 °C causes a change in the ^1H and ^{31}P NMR spectra of the solution with evolution of H_2 at this temperature. The formation of H_2 suggests that the protonation forms a dihydrogen $[ReH(\eta^2\text{-}H_2)(NO)P_3]^+$ intermediate[18] which is unstable to the loss of H_2 even at −80 °C, yielding either a coordinatively unsaturated $[ReH(NO)P_3]^+$ cation or a neutral $[ReHY(NO)P_3]$ species (Y = BF_4 or CF_3SO_3). The formation of a dichloromethane complex[19] of the type $[ReH(CH_2Cl_2)(NO)P_3]^+$, however, cannot be excluded. These complexes are thermally unstable and decompose above −30 °C, preventing their isolation in the solid state. The loss of H_2 at low temperatures (−70 °C) was also observed in the protonation with CF_3COOH of similar[15c] $[ReH_2(CO)(NO)L_2]$ [L = P(*i*Pr)$_3$, P(O*i*Pr)$_3$] hydride complexes which yield, in this case, the trifluoroacetate $[ReH(OOCCF_3)(CO)(NO)L_2]$ derivatives.

The protonation of the alkoxy-hydride $[ReH(OR^1)(NO)P_3]$ (**2**, **3**) with CF_3SO_3H or $HBF_4{\cdot}Et_2O$ at −80 °C proceeds with the disappearance of the hydride multiplet in the ^1H NMR spectra at δ = 0.86−0.26 ppm and a simultaneous change in chemical shift of all the other signals of both the phosphanes and the alkoxide groups. The $^{31}P\{^1H\}$ NMR spectra also show the disappearance of the A_2B multiplet of the hydride precursor and the appearance of a new A_2B pattern (Table 1). These data may be interpreted on the basis of the formation of a dihydrogen[18] complex of the type $[Re(OR^1)(\eta^2\text{-}H_2)(NO)P_3]^+$ obtained by the attack of the acid on the hydride ligand. In the ^1H NMR spectra, however, no signal attributable to the η^2-H_2 resonance was clearly observed, and this may make the presence of the dihydrogen complex uncertain. In order to obtain further information, we increased the temperature of the sample and observed no change in the profile of the spectra until −10 °C. At this temperature a signal at δ = 4.58 ppm due[20] to free H_2 appears in the ^1H NMR spectra, which increases in intensity with time with the simultaneous lowering of all the other signals. The ^{31}P NMR spectra also show a decrease in the intensity of the A_2B multiplet and the formation of decomposition products near −10 °C. The appearance of free H_2 as the temperature is increased seems to confirm the formation of the $[Re(OR^1)(\eta^2\text{-}H_2)(NO)P_3]^+$ (**2***, **3***) dihydrogen cation whose η^2-H_2 signal is probably masked by the intense methyl multiplet of the phosphane ligands. The chemical shift of the η^2-H_2 ligand,[18] in fact, generally falls at lower values than those of the related hydride precursor, making the signal, in our case, probably superimposed by the methyl multiplet of the phosphane. The formation of the dihydrogen complexes **2*** and **3*** also indicates that among the three potential sites for protonation in $[ReH(OR^1)(NO)P_3]$ complexes — the alkoxy, the hydride or the NO — the hydride is probably the most accessible and affords the corresponding η^2-H_2 complex. Unfortunately, this species is thermally unstable and the loss of H_2 already at −10 °C prevents its isolation in the solid state.

Preparation of Hydrazine Complexes

The unstable complexes formed by the protonation of the hydrides **1**−**3** are either coordinatively unsaturated or contain one labile ligand (Y or η^2-H_2) and should therefore react easily with the appropriate ligands, allowing the synthesis of new complexes. This reaction does occur with hydrazine and a series of new complexes was prepared and characterized (Schemes 4 and 5).

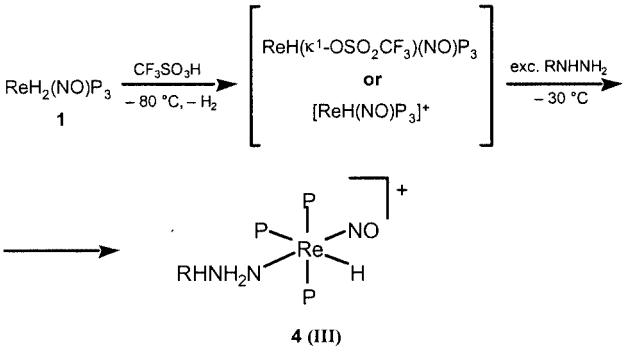

Scheme 4. P = PPh_2OEt; R = H (**a**), CH_3 (**b**), C_6H_5 (**c**)

The new hydrazine complexes **4a**−**c**, **5a**−**c**, **6a**−**c** were isolated in good yields as BPh_4^- salts and are white or pale-yellow solids that are stable in air and in solution in polar organic solvents, where they behave as 1:1 electrolytes.[21] Their characterization is supported by analytical and spectroscopic data (IR, NMR, Table 1) and by the X-ray crystal structure determination (Table 2) of the derivative $[Re(OC_2H_5)(NH_2NH_2)(NO)\{PPh(OEt)_2\}_3]BPh_4$ (**5a**).

 © 2004 Wiley-VCH Verlag GmbH & Co. KGaA, Weinheim

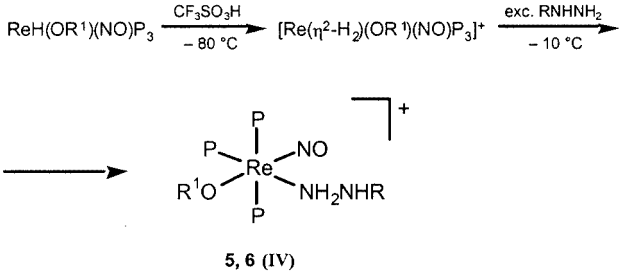

Scheme 5. P = $PPh(OEt)_2$; R = C_2H_5 (**5**), CH_3 (**6**); R^1 = H (**a**), CH_3 (**b**), C_6H_5 (**c**)

Table 2. Crystal data and structure refinement for $[Re(OCH_2CH_3)(NH_2NH_2)(NO)\{PPh(OEt)_2\}_3]^+$ (**5a**)

Empirical formula	$C_{56}H_{74}BN_3O_8P_3Re$
Molecular mass	1207.10
Temperature	293(2) K
Wavelength	0.71069 Å
Crystal system	monoclinic
Space group	$P2_1/n$
Unit cell dimensions	a = 9.6930(10) Å
	b = 18.093(3) Å β = 84.276(3)°
	c = 33.710(5) Å
Volume	5882.4(14) Å^3
Z	4
Density (calculated)	1.363 Mg/m^3
Absorption coefficient	2.199 mm^{-1}
F(000)	2480
θ range for data collection	1−26°
Index ranges	$-11 \le h \le 11$, $-22 \le$
	$k \le 22$, $-41 \le l \le 39$
Reflections collected	50057
Independent reflections	11598 [R(int) = 0.0969]
Refinement method	Full-matrix least-squares on F^2
Data/restraints/parameters	11598/1/576
Goodness-of-fit on F^2	1.182
Final R indices [$I > 2\sigma(I)$]	$R1$ = 0.0722, $wR2$ = 0.1125
R indices (all data)	$R1$ = 0.1319, $wR2$ = 0.1309

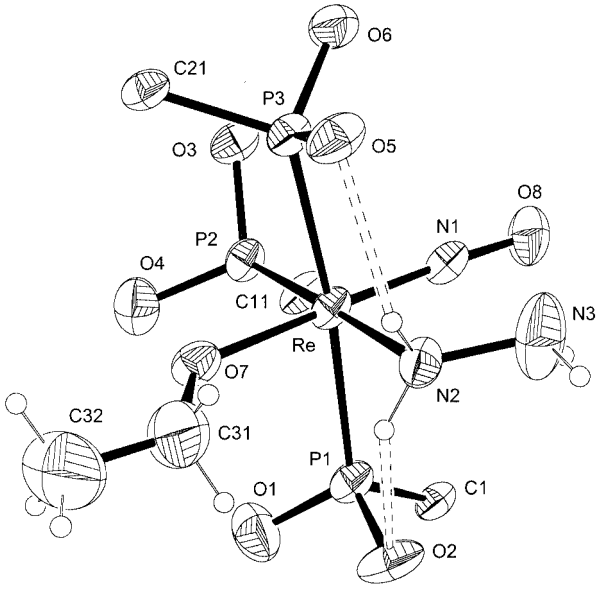

Figure 1. Perspective view and labelling scheme of the cation $[Re(OC_2H_5)(NH_2NH_2)(NO)\{PPh(OEt)_2\}_3]^+$ in the crystal structure of **5a**; thermal ellipsoids at the 30% level; phenyl and ethyl groups of phosphane ligands are omitted for clarity; intramolecular hydrogen bonds are dashed

Table 3. Selected bond lengths (Å) and angles (°) for compound **5a**

Re−N(1)	1.763(7)	Re−P(1)	2.418(2)
Re−O(7)	2.016(5)	Re−P(3)	2.443(2)
Re−N(2)	2.256(6)	N(1)−O(8)	1.215(8)
Re−P(2)	2.352(2)	N(2)−N(3)	1.44(1)
N(1)−Re−O(7)	176.2(3)	P(2)−Re−P(1)	91.35(8)
N(1)−Re−N(2)	92.0(3)	N(1)−Re−P(3)	95.0(2)
O(7)−Re−N(2)	84.3(2)	O(7)−Re−P(3)	84.1(2)
N(1)−Re−P(2)	89.7(2)	N(2)−Re−P(3)	86.9(2)
O(7)−Re−P(2)	94.0(2)	P(2)−Re−P(3)	92.96(8)
N(2)−Re−P(2)	178.3(2)	P(1)−Re−P(3)	169.87(8)
N(1)−Re−P(1)	94.2(2)	O(8)−N(1)−Re	174.2(6)
O(7)−Re−P(1)	86.4(2)	N(3)−N(2)−Re	114.1(5)
N(2)−Re−P(1)	88.5(2)		

The molecular structure adopted by the cation in the solid state is shown in Figure 1, along with the labelling scheme. The metal coordination is octahedral, with the nitrosyl ligand placed *trans* to the ethoxy group, while the hydrazine molecule is coordinated *trans* to a phosphane. The ligands NO^+, NH_2NH_2 and $CH_3CH_2O^-$ are in a *mer* arrangement, and two more phosphanes complete the coordination. The relevant bond lengths and angles for the cationic complex are in Table 3.

The hydrazine ligand is in a Z configuration relative to the nitrosyl molecule and is almost perfectly coplanar with it [N1−Re−N2−N3 = 2.5(6)°]. The Re−N2 and N2−N3 bonds (Table 3) are typical of coordination by a single σ-bond via the terminal -NH_2 group, with a bonding geometry similar to that observed previously for the coordination of methylhydrazine to rhenium [Re−N = 2.235(3), N−N = 1.445(4) Å].[3d] The nitrosyl bonding mode [Re−N1 = 1.763(7), N1−O8 = 1.215(9) Å] agrees with the average geometry found in the literature {e.g. Re−N = 1.765, N−O = 1.200 Å in $[ReCl_3(NO)(PPh_3)_2]$}.[22] The ethoxy group is also roughly coplanar with the hydrazine, and the α-carbon is oriented towards N2 [C31−O7−Re−N2 = −12.8(8)°].

The Re−P bond *trans* to the hydrazine ligand is significantly shorter [Re−P2 = 2.352(2) Å] than the Re−P bond of the phosphanes *trans* to each other [Re−P3 = 2.443(2) and Re−P1 = 2.418(2) Å, respectively], which are similar to those observed for *trans* $PPh(OEt)_2$ groups bonded to rhenium, ranging between 2.41 and 2.46 Å.[3d] This trend has already been observed in $[ReCl(CH_3N_2)(CH_3NHNH_2)\{PPh(OEt)_2\}_3]BPh_4$,[3d] where the Re−P distance *trans* to the methylhydrazine [2.362(1) Å] is remarkably

 © 2004 Wiley-VCH Verlag GmbH & Co. KGaA, Weinheim

shorter than those observed for the phosphanes situated *trans* to each other [2.406(1) and 2.412(1) Å]. As also pointed out in the above paper, the Re−P elongation is supported by a system of intramolecular hydrogen bonds between the hydrazine NH groups and the ethoxy substituents carried by the adjacent phosphanes [N2···O5 = 2.871(9) Å, N2−H···O5 = 131.6(4)°, N2···O2 = 2.941(9) Å, N2−H···O2 = 139.2(4)°], and is accompanied by a bending of the phosphanes P1 and P3 towards the hydrazine [P3−Re−N2 = 86.9(2)° and P1−Re−N2 = 88.5(2)°].

The IR spectra of all the hydrazine complexes **4**−**6** show, besides the bands of the phosphane and the BPh_4 anion, a strong absorption at 1697−1670 cm^{-1} due to the ν_{NO} of the nitrosyl ligand and three or four medium-intensity bands between 3609 and 3215 cm^{-1} attributed to the ν_{NH} of the hydrazine ligand. In some compounds the δ_{NH_2} band is also observed at 1630−1620 cm^{-1}.

The presence of the hydrazine ligand is confirmed by the ^1H NMR spectrum, which show the characteristic broad multiplets between δ = 6 and 3 ppm (Table 1) of the NH_2 and NH protons of the $RNHNH_2$ ligand. Integration measurements and ^1H COSY experiments confirm the proposed attributions.

In the ^1H NMR spectra of complexes $[ReH(RNHNH_2)(NO)P_3]BPh_4$ (**4**) one multiplet at δ = −3.40 and at −3.48 ppm is also present, attributed to the hydride ligand, and can be simulated by using an AB_2X (X = H) model with the parameters reported in Table 1. The two $J_{P,H}$ coupling constants have different values (20 and 30 Hz) which suggests that the hydride should be *trans* to one phosphane and *cis* to the other two. In the temperature range between +20 and −80 °C the $^{31}P\{^1H\}$ NMR spectra appear as an AB_2 multiplet, in agreement with the presence of two magnetically equivalent phosphanes that are different from the third. On this basis a geometry of type **III** can be reasonably proposed for the hydride-hydrazine complexes **4**.

The ^1H NMR spectra of the alkoxy derivative **5** and **6** show, besides the signals of the phosphanes and of the hydrazine, the resonance of the OR^1 ligands, which appear as a triplet and a quadruplet for OC_2H_5 and as a singlet for OCH_3. The $^{31}P\{^1H\}$ NMR spectra also indicate that for these complexes an AB_2 multiplet is present. These data, however, do not allow us to unambiguously assign a geometry for the alkoxy complexes although, by analogy with the solid state, a complex of type **IV** can reasonably be proposed. The preparation of complexes **4**−**6** highlights the fact that both hydride $[ReH(NO)P_3]$ and alkoxy $[Re(OR^1)(NO)P_3]$ nitrosyl fragments can bind the hydrazine molecule to give stable derivatives that can be isolated.

Oxidation of Hydrazine Complexes

The oxidation reaction of the hydrazine complexes **4**−**6** with $Pb(OAc)_4$ was studied extensively and the results are summarized in Schemes 6 and 7.

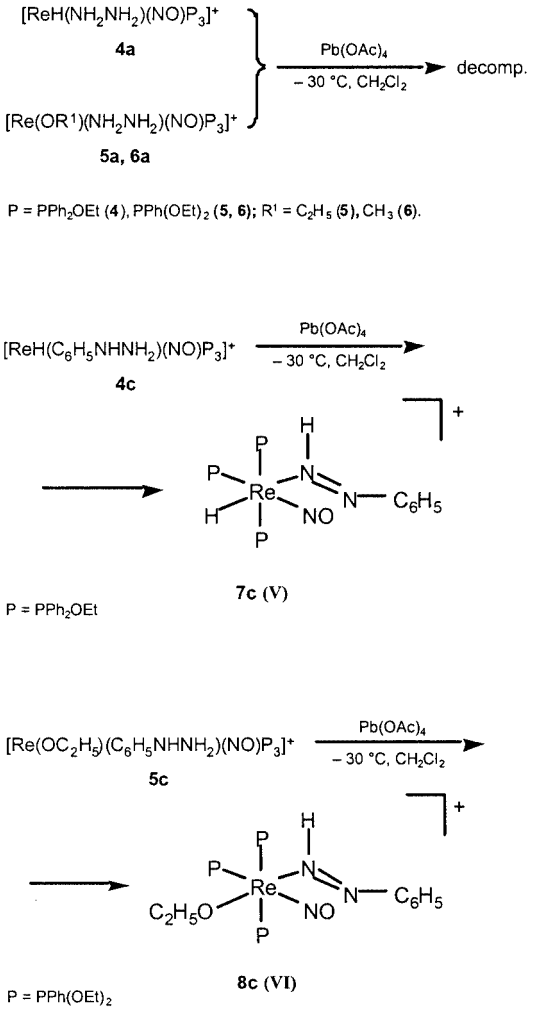

Scheme 6

The outcome of the oxidation reactions depends on the nature of both the metal fragment and the hydrazine used. The NH_2NH_2 complexes **4a**, **5a** and **6a** do not give any diazene complexes in the reaction with $Pb(OAc)_4$ and only decomposition products were obtained. The reaction proceeds with a color change of the reaction mixture but probably leads to unstable species. Instead, the phenylhydrazine is selectively oxidized in both the hydride (**4c**) and the ethoxy (**5c**) derivatives to the corresponding phenyldiazene compounds (**7c** and **8c**, respectively), which were isolated in the solid state and characterized. Surprisingly, the reaction of methylhydrazine gives the methyldiazene complex **7b** in the oxidation of the hydride $[ReH(CH_3NHNH_2)(NO)P_3]^+$ (**4b**), while a mixture of the methyldiazene complex $[Re(OCH_3)(CH_3N{=}NH)(NO)P_3]^+$ (**9b**) and the methyleneimine[11] complex $[Re(OCH_3)(\eta^1\text{-}NH{=}CH_2)(NO)P_3]^+$ (**9*b**) was obtained in the reaction with the methoxy-methylhydrazine derivative $[Re(OCH_3)(CH_3NHNH_2)(NO)P_3]^+$ (**6b**). The hydride-methyldiazene complex **7b** was isolated in the solid state and in a pure form, whereas the two compounds **9b** and **9*b** were obtained as a mixture and were not sepa-

 © 2004 Wiley-VCH Verlag GmbH & Co. KGaA, Weinheim

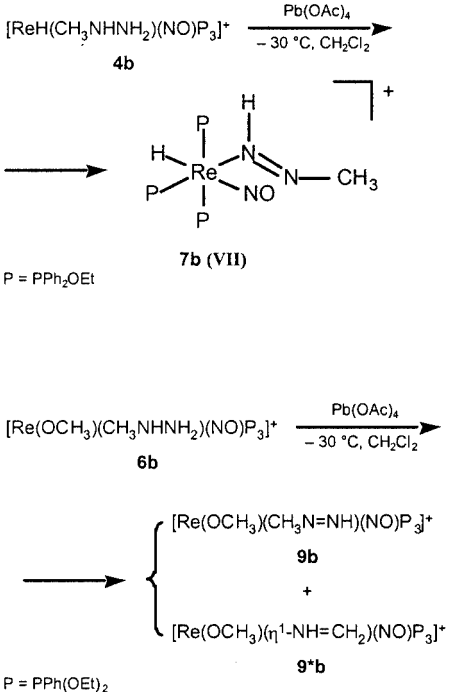

Scheme 7

rated. The spectroscopic data, however, strongly support their formulation (see below).

The different behavior of the hydrazine complexes towards oxidation may be explained by taking into account that, whereas coordinated aryldiazenes[1−3] are generally stable and can be easily isolated, 1,2-diazene complexes [M]−NH=NH are rare and few metal fragments are able to stabilize the unstable NH=NH species.[23] Our $[ReH(NO)P_3]$ and $[Re(OR^1)(NO)P_3]$ fragments are not among these, although they are able to stabilize the methyldiazene $CH_3N{=}NH$ giving **7b** and **9b**. Furthermore, the oxidation of methylhydrazine bonded to the $[Re(OCH_3)(NO)P_3]$ fragment with $Pb(OAc)_4$ shows a second example of a new reaction[11] of coordinated methylhydrazine, which can give both methyldiazene and methyleneimine η^1-NH=CH_2 species. This reaction depends on the nature of the metal fragment, and only in the case of the alkoxy precursor $[Re(OCH_3)(CH_3N{=}NH)(NO)P_3]^+$ were both **9b** and **9*b** obtained; with the hydride derivative $[ReH(CH_3N{=}NH)(NO)P_3]^+$ only the formation of methyldiazene **7b** was observed. These results show that the substitution of only one ligand — H^- with OCH_3^- — in the rhenium nitrosyls changes the nature of the reaction course in the oxidation of the methylhydrazine ligand with $Pb(OAc)_4$. Furthermore, a comparison with related carbonyl complexes[11] highlights the fact that both the nitrosyl $[Re(OCH_3)(CH_3NHNH_2)(NO)P_3]^+$ and the carbonyl $[Re(CH_3NHNH_2)(CO)_2P_3]^+$ methylhydrazine derivatives react with $Pb(OAc)_4$ to give a mixture of η^1-NH=CH_2 and $CH_3N{=}NH$ complexes. A different behavior is shown by the hydride-nitrosyl $[ReH(CH_3NHNH_2)(NO)P_3]^+$ cation, which only gives the methyldiazene **7b**. Studies were also carried out to identify the product of the reaction with $Pb(OAc)_4$ in order to obtain information on a possible reaction path giving **9*b**. Unfortunately, apart from acetic acid and traces of NH_3, no other nitrogen-containing products were unambiguously identified in the reaction mixture and therefore no proposal can be made about the mechanism of the reaction, which involves the cleavage of the N−N bond of methylhydrazine to give an η^1-NH=CH_2 species.

Good analytical data were obtained for all the diazene complexes **7**−**9** which are pale-yellow solids stable in air and in solutions of polar organic solvents, where they behave as 1:1 electrolytes.[21] The IR and NMR spectra (Table 1) support the proposed formulation and a geometry in solution was also established. The presence of the diazene ligand is confirmed by the ^1H NMR spectra, which show the characteristic, slightly broad NH signal at δ = 16−18 ppm.

In the ^1H NMR spectra of the complexes $[ReH(RN{=}NH)(NO)P_3]BPh_4$ (**7b**, **7c**) a quadruplet at δ = 3.68−3.67 ppm also appears, which can be attributed to the hydride ligand coupled to the phosphorus nuclei of the phosphanes. This attribution was confirmed by ^1H, ^{31}P NMR spectra and HMQC experiments. The two $J_{P,H}$ coupling constants have the same value of 6 Hz, suggesting that the hydride should be in the same position relative to all the phosphane ligands. It should also be noted that the chemical shifts of the hydride fall at very high frequencies as compared to known rhenium hydrides,[14,15] and this feature may be due to the combined influences of both the diazene and the NO ligands. In the temperature range between +20 and −80 °C the $^{31}P\{^1H\}$ NMR spectra of **7b** and **7c** appear as AB_2 multiplets, in agreement with the presence of two magnetically equivalent phosphanes that are different from the third. These data do not allow us to unambiguously assign a geometry to the complexes. However, further information comes from a comparison of the IR spectra of the diazene compounds **7b** and **7c** with those of the precursors **4b** and **4c**, which shows that the ν_{NO} values are similar for **4b** and **7b** (1683 and 1696 cm^{-1}, respectively) whereas a higher value is found in the phenyldiazene complex $[ReH(C_6H_5N{=}NH)(NO)P_3]BPh_4$ (**7c**) (ν_{NO} = 1736 cm^{-1}) than in the precursor **4c** (1690 cm^{-1}). This high ν_{NO} value for **7c** seems to indicate that the NO ligand is *trans* to a good π-acceptor ligand such as the phosphane and therefore, taking into account the ^1H and the ^{31}P NMR spectra, a geometry such as **V** can be proposed. In the methyldiazene complex **7b** the NO group should be *trans* to a σ-donor ligand as in a type-**VII** geometry.

The IR spectrum of the alkoxy complex $[Re(OC_2H_5)(C_6H_5N{=}NH)(NO)P_3]BPh_4$ (**8c**) shows the ν_{NO} at higher value (1729 cm^{-1}) than its hydrazine precursor **5c** (1685 cm^{-1}) suggesting, also in this case, the mutually *trans* position of NO and one phosphane ligand. Taking into account that the ^{31}P NMR spectra is an A_2B multiplet, a type-**VI** geometry may be proposed.

The IR spectrum of the oxidation product of $[Re(OCH_3)(CH_3NHNH_2)(NO)P_3]BPh_4$ (**6b**) shows two ν_{NO} bands at 1723 and 1650 cm^{-1} and two AB_2 multiplets in the $^{31}P\{^1H\}$ NMR spectra, suggesting the presence of two

 © 2004 Wiley-VCH Verlag GmbH & Co. KGaA, Weinheim

compounds formulated as a mixture of $[Re(OCH_3)(CH_3N{=}NH)(NO)P_3]^+$ (**9b**) and $[Re(OCH_3)(\eta^1\text{-}NH{=}CH_2)(NO)P_3]^+$ (**9*b**). The ^1H NMR spectra show, besides the phosphane and BPh_4 signals, two slightly broad signals at $\delta = 18.69$ and 15.73 ppm attributed to two NH groups. A singlet at $\delta = 3.73$ ppm and a slightly broad signal at $\delta = 4.05$ ppm are also present. The singlet at $\delta = 3.73$ ppm is correlated to the broad signal at $\delta = 18.69$ ppm (^1H COSY experiment) and can be attributed to the $CH_3N{=}NH$ group. An APT experiment confirmed this attribution. The slightly broad signal at $\delta = 4.05$ ppm is correlated to the proton resonance at $\delta = 15.73$ ppm (^1H COSY) and an APT experiment indicated a CH_2 group attributable to the $CH_2{=}NH$ ligand. The $^{13}C\{^1H\}$ spectra show, besides the signals of the phosphane and BPh_4 anion, two singlets at $\delta = 62.5$ and 64.0 ppm, and HMBC and HMQC experiments allow the attribution of these carbon resonances to the $CH_3N{=}NH$ and $CH_2{=}NH$ groups, respectively, and are thus in agreement with the proposed formulation for the mixture of the two compounds **9b** and **9*b**. These attributions, indeed, are strongly supported by a comparison with the data we previously reported on methyleneimine $[Re(\eta^1\text{-}NH{=}CH_2)(CO)P_4]BPh_4$ and methyldiazene $[Re(CH_3N{=}NH)(CO)P_4]BPh_4$ complexes.[11] In conclusion, although the two compounds **9b** and **9*b** cannot be separated, the strong similarity of their spectroscopic data with those of known complexes[11] supports their proposed formulation.

Reactions with Aryldiazonium Cations

The synthesis of the aryldiazene complexes **7c** and **8c** prompted us to test whether analogous compounds can be prepared by the insertion reaction of aryldiazonium cations into the Re−H bond of our hydrides **1**−**3**. The reaction was studied extensively and the results can be summarized in Schemes 8 and 9.

Aryldiazonium cations react quickly with an equimolar amount of dihydride $[ReH_2(NO)P_3]$ to give the aryldiazene complexes **10**, which were isolated and characterized as BPh_4 salts. The reaction was also studied in the presence of an excess of ArN_2^+ to test whether the insertion of two diazonium salts can take place giving bis(aryldiazene) complexes. Although the reaction proceeds, the solid obtained contains several products which decomposed during crystallization and were not separated. The NMR spectra reveal the presence of new diazene complexes besides **10**, but also of large amounts of decomposition products which prevent any further investigation.

Bis(aryldiazonium) cations $[N_2Ar{-}ArN_2]^{2+}$ also react with the hydride $[ReH_2(NO)P_3]$ yielding the binuclear complexes **11** containing the bis(diazene) $NH{=}NAr{-}ArN{=}NH$ as a bridging unit (Scheme 8).

Parallel to the behavior of the dihydride, the hydride-alkoxy complexes $[ReH(OR^1)(NO)P_3]$ also react with both mono- $[ArN_2]^+$ and bis(aryldiazonium) $[N_2Ar{-}ArN_2]^{2+}$ cations to give the corresponding aryldiazene derivatives **12**−**16**, which were isolated and characterized (Scheme 9).

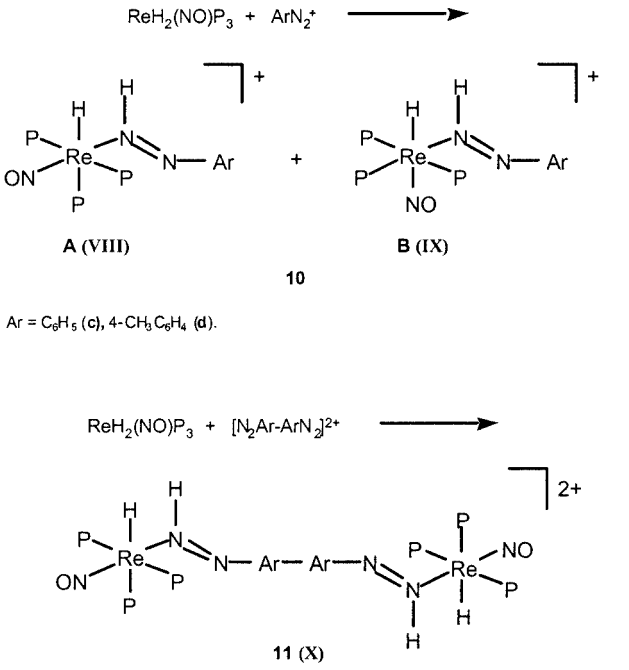

Scheme 8. P = PPh_2OEt

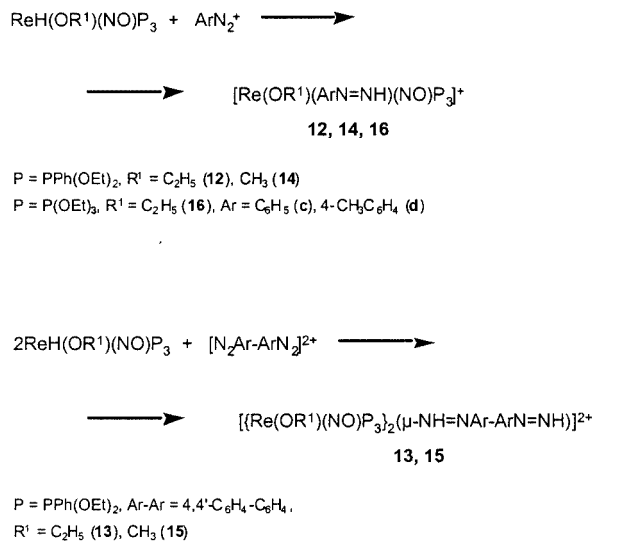

Scheme 9

These results highlight that the same aryldiazene complexes of rhenium (**7c** and **10c**) and (**8c** and **12c**) can be prepared both by the oxidation of the arylhydrazine derivative with $Pb(OAc)_4$ and by the insertion of an aryldiazonium cation into the Re−H bond of the appropriate hydride. The two methods, however, give isomers with a different geometry, as will be discussed below. Furthermore, a comparison of the results obtained in the reaction of our nitrosyl hydrides **1**−**3** with ArN_2^+ with those we[12] previously reported on the carbonyls $[ReH(CO)_nP_{5-n}]$ shows that, in both cases, aryldiazene rhenium complexes can be obtained by "apparent" insertion of aryldiazonium cations into the

 © 2004 Wiley-VCH Verlag GmbH & Co. KGaA, Weinheim

Re−H bond of all the hydride species. The reaction seems to be general for both the carbonyl and nitrosyl hydrides yielding stable aryldiazene complexes. Some differences, however, were observed in the reaction with bis(aryldiazonium) salts, which allow, in the case of carbonyls $[ReH(CO)_nP_{5-n}]$ containing the bulky PPh_2OEt ligand, the preparation of "diazo-diazene" $[Re(CO)_nP_{5-n}(HN{=}NAr{-}ArN{\equiv}N)]^{2+}$ (n = 1, 2) derivatives[12] through the insertion of only one end of the $^+N_2Ar{-}ArN_2^+$ ligand with the hydride. The same mononuclear compounds were not obtained with the nitrosyl-hydride $[ReH_2(NO)(PPh_2OEt)_3]$ which gives exclusively binuclear bis(aryldiazene) derivatives, under all conditions.

The aryldiazene complexes **10**, **11**, **14** and **15** were isolated with the BPh_4 anion whereas the ethoxy derivatives **12**, **13** and **16** were obtained as BF_4 salts. All are yellow or pale-yellow solids, stable in air and in solution in polar organic solvents where they behave as 1:1 or 2:1 electrolytes, respectively. Some decomposition was observed for the alkoxy derivatives **12**, **13** and **16** in solutions of ethanol. Analytical and spectroscopic data (Table 1) support the proposed formulation for the complexes and for the hydride-diazene derivatives **10** and **12** a geometry in solution can also be established.

The ^1H NMR spectra of the cations $[ReH(ArN{=}NH)(NO)P_3]^+$ (**10**) show two slightly broad signals in the high-frequency region (δ = 13.84−13.45 ppm) attributed to two diazene protons. This attribution is confirmed by the spectra of the labeled complex **10c$_1$** which show two high-frequency doublets centered at the same chemical shift of the two slightly broad signals of unlabeled **10c** and with a $^1J^{15}_{N,H}$ coupling constant of 65 Hz, in agreement with the presence of two diazene ligands. This is also confirmed by the $^{15}N\{^1H\}$ NMR spectrum of **10c$_1$** which shows two AB_2Y (Y = ^{15}N) multiplets at δ = −2.57 and at δ = −8.70 ppm (Table 4) due to the coupling with the phosphorus nuclei. Because the compounds contain only one aryldiazene ligand, the presence of two NH signal may suggest the existence of two isomers. This was confirmed by the ^{31}P NMR spectra, which show two AB_2 multiplets which can be simulated using the parameters reported in Table 1. The formation of two isomers for **10** is not unexpected due to the chemical non-equivalence of the two hydrides in the $[ReH_2(NO)P_3]$ precursors which give two isomers through the insertion of only one ArN_2^+ into each of the two Re−H bonds. Whether or not an isomerization may be excluded, the insertion should only give the two isomers **A** and **B** (Scheme 8) which were isolated in a 30:70 ratio. This ratio is probably related to the different insertion rate of ArN_2^+ into the two different hydrides.

In the ^1H NMR spectra of **10c** one AB_2X (X = H) multiplet at δ = 2.83 ppm is also present which can be attributed to one of the hydride ligands. The H^- signal of the other isomer probably overlaps the multiplet of the methylene protons, as well as those of **10d**. Furthermore, the ν_{NO} band observed in the IR spectrum appears slightly broad in **10c** and also contains a shoulder in **10d** in agreement with the presence of more nitrosyl compounds. These data confirm the formulation proposed for the hydride-aryldiazene complexes, but do not allow us to unambiguously propose a geometry in solution. However, a comparison of the spectroscopic data of **10c** with those of the related complex **7c** obtained by the oxidation of phenylhydrazine shows different chemical shift values for both the NH proton signals and the ^{31}P nucleus suggesting that the complex **7c** has a geometry that is different from those of the two isomers. Since a geometry of type **V** (Scheme 6) for **7c** had been proposed and the structure of the $[ReH(ArN{=}NH)(NO)P_3]^+$ complex can be discussed in terms of only three geometries, it follows that **VIII** and **XI** should be proposed for the two isomers **A** and **B** of complexes **10**.

The ^1H and ^{31}P NMR spectra of the dinuclear complexes **11** indicate the presence of only one isomer. In fact, only one diazene signal at δ = 13.45 ppm is present in the ^1H NMR spectrum of **11a**, which is split into a doublet with a $^1J^{15}_{N,H}$ coupling constant of 64 Hz in the labeled compound **11a$_1$**. In the ^1H NMR spectrum one AB_2X (X = H) multiplet, simulated with the parameters reported in

Table 4. $^{15}N\{^1H\}$ NMR spectroscopic data for selected rhenium compounds

Compound	$^{15}N\{^1H\}$ NMR[a] δ (J/Hz)
$[ReH(C_6H_5N{=}^{15}NH)(NO)\{PPh_2(OEt)\}_3]BPh_4$ (**10c$_1$**)	AB_2Y spin system δ_Y = −2.57 $J_{A,Y}$ = 28.8 $J_{B,Y}$ = 2.0 AB_2Y spin system δ_Y = −8.70 $J_{A,Y}$ = 39.3 $J_{B,Y}$ = 2.0
$[\{ReH(NO)[PPh_2(OEt)]_3\}_2(\mu\text{-}4,4'\text{-}H^{15}N{=}NC_6H_4{-}C_6H_4N{=}^{15}NH)](BPh_4)_2$ (**11a$_1$**)	AB_2Y spin system δ_Y = −3.0 $J_{A,Y}$ = 29.1 $J_{B,Y}$ = 1.0
$[Re(OC_2H_5)(NO)\{PPh(OEt)_2\}_3(C_6H_5N{=}^{15}NH)]BF_4$ (**12c$_1$**)	AB_2Y spin system δ_Y = −7.9 $J_{A,Y}$ = 44.0 $J_{B,Y}$ = 4.0
$[\{Re(OC_2H_5)(NO)[PPh(OEt)_2]_3\}_2(\mu\text{-}4,4'\text{-}H^{15}N{=}NC_6H_4{-}C_6H_4N{=}^{15}NH)](BF_4)_2$ (**13a$_1$**)	AB_2Y spin system δ_Y = −8.20 $J_{A,Y}$ = 45.0 $J_{B,Y}$ = 4.0 AB_2Y spin system δ_Y = −12.2 $J_{A,Y}$ = 45.0 $J_{B,Y}$ = 4.0
$[\{Re(OCH_3)(NO)[PPh(OEt)_2]_3\}_2(\mu\text{-}4,4'\text{-}H^{15}N{=}NC_6H_4{-}C_6H_4N{=}^{15}NH)](BPh_4)_2$ (**15a$_1$**)	AB_2Y spin system δ_Y = −8.05 $J_{A,Y}$ = 45.0 $J_{B,Y}$ = 3.0 AB_2Y spin system δ_Y = −12.4 $J_{A,Y}$ = 45.0 $J_{B,Y}$ = 2.9

[a] In CD_2Cl_2 at 25 °C. Positive shifts downfield from $CH_3{}^{15}NO_2$.

 © 2004 Wiley-VCH Verlag GmbH & Co. KGaA, Weinheim

Table 1, is also present which was attributed to the hydride ligand. The two $J_{P,H}$ coupling constants deduced from the spectra have different values of 20.4, 29.4 Hz, respectively, suggesting that the hydride should be in *trans* to one phosphane and *cis* to the other two. In the temperature range between +20 and −80 °C the ^{31}P NMR spectra show only one AB_2 multiplet in agreement with the presence of only one isomer with two magnetically equivalent phosphanes that are different from the third. On the basis of these data a geometry of type **IX** can reasonably be proposed for the binuclear complex **11a**.

The formation of only one isomer with the bis(aryldiazonium) cation may be explained on the basis of the faster insertion rate of the aryldiazonium cation into one of the two Re−H bonds which affords, in the case of the dinuclear complexes, only traces of the other isomers that were discarded by crystallization.

The ^1H NMR spectra of the alkoxy complexes **12**−**16** confirm the presence of the diazene ligand showing the characteristic high-frequency NH signal which splits into a doublet in the ^{15}N-labeled complexes (Table 1). In the spectra the characteristic resonance of the alkoxy OR^1 ligand is also present, along with the signals of the phosphane and BPh_4 anion. The $^{31}P\{^1H\}$ NMR spectra show, for some complexes, the presence of only one AB_2 multiplet, while two AB_2 multiplets are present in the spectra of **13**, **14** and **15**, suggesting the probable presence of two isomers. These data support the proposed formulation for the complexes but, in the absence of an X-ray determination, do not allow us to unambiguously propose a geometry in solution for these aryldiazene derivatives.

Conclusion

In this contribution we have reported the synthesis of new rhenium nitrosyl hydrides of the $[ReH_2(NO)P_3]$ and $[ReH(OR^1)(NO)P_3]$ type containing both phosphane and alkoxy groups as supporting ligands. Their protonation with Brønsted acids allows thermally unstable η^2-H_2 complexes to be obtained. Both classical and non-classical rhenium hydrides behave with an easy entry into "diazo" chemistry and allow the synthesis of the first hydrazine and diazene complexes stabilized by nitrosyl ligands. The structural parameters for one hydrazine complex, $[Re(OC_2H_5)(NH_2NH_2)(NO)\{PPh(OEt)_2\}_3]BPh_4$, are also reported. Reactivity studies also show that aryldiazene $[ReH(ArN{=}NH)(NO)P_3]BPh_4$ and $[Re(OR^1)(ArN{=}NH)(NO)P_3]BPh_4$ complexes can be prepared both by insertion of an aryldiazonium cation into the Re−H bond of an appropriate hydride and by the oxidation of the related arylhydrazine derivatives with $Pb(OAc)_4$. Furthermore, the oxidation of the methylhydrazine complex $[Re(OCH_3)(CH_3NHNH_2)(NO)\{PPh(OEt)_2\}_3]BPh_4$ with $Pb(OAc)_4$ shows a new example of formation of a methyleneimine $[Re(OCH_3)(\eta^1\text{-}NH{=}CH_2)(NO)\{PPh(OEt)_2\}_3]BPh_4$ derivative.

Experimental Section

General: All synthetic work was carried out under an inert atmosphere using standard Schlenk techniques or in a Vacuum Atmospheres dry box. Once isolated, the complexes were found to be relatively stable in air, but were stored under an inert atmosphere at −25 °C. All solvents were dried over appropriate drying agents, degassed on a vacuum line and distilled into vacuum-tight storage flasks. The phosphanes $PPh(OEt)_2$ and PPh_2OEt were prepared by the method of Rabinowitz and Pellon,[24] whereas $P(OEt)_3$ was an Aldrich product, purified by distillation under nitrogen. Diazonium salts were obtained in the usual way.[25] The related di-diazonium salts $[N_2Ar{-}ArN_2](BF_4)_2$ (Ar−Ar = 4,4′-C_6H_4-C_6H_4) were prepared by treating the amine precursors H_2NAr-$ArNH_2$ with $NaNO_2$ as described in the literature for the common monodiazonium salts.[25] The labeled diazonium tetrafluoroborate $[C_6H_5N{\equiv}^{15}N]BF_4$ and $[4,4'\text{-}^{15}N{\equiv}NC_6H_4{-}C_6H_4N{\equiv}^{15}N](BF_4)_2$ were prepared from $Na^{15}NO_2$ (99% enriched, CIL) and the appropriate amine. The hydrazines $C_6H_5NHNH_2$, $C_6H_5CONHNH_2$ and CH_3NHNH_2 were Aldrich products and used as received. Hydrazine (NH_2NH_2) was prepared by decomposition of hydrazine cyanurate (Fluka) following the reported method.[26] High-grade (99.99%) lead(IV) acetate was purchased from Aldrich. Other reagents were purchased from commercial sources in the highest available purity and used as received. Infrared spectra were recorded on a Nicolet Magna 750 FT-IR spectrophotometer. NMR spectra (^1H, ^{13}C, ^{31}P, ^{15}N) were obtained on Bruker AC200 or Avance 300 spectrometers at temperatures varying between −90 and +30 °C, unless otherwise noted. ^1H and ^{13}C chemical shifts are referenced to internal tetramethylsilane, while $^{31}P\{^1H\}$ chemical shifts are reported with respect to 85% H_3PO_4, with downfield shifts considered positive. ^{15}N NMR spectra are referenced to external $CH_3{}^{15}NO_2$, with downfield shifts considered positive. The SwaN-MR software package[27] was used to treat NMR spectroscopic data. The conductivities of 10^{-3} M solutions of the complexes in CH_3NO_2 at 25 °C were measured with a Radiometer CDM 83 instrument.

Synthesis of Complexes: $[ReCl_2(OCH_3)(NO)(PPh_3)_2]$ was prepared following a reported method.[15a]

$[ReH_2(NO)(PPh_2OEt)_3]$ (1): An excess of PPh_2OEt (2.05 mL, 8.9 mmol) and then an excess of $NaBH_4$ (0.404 g, 10.68 mmol) in 15 mL of ethanol were added to a suspension of $[ReCl_2(OCH_3)(NO)(PPh_3)_2]$ (1.5 g, 1.78 mmol) in 30 mL of ethanol. Upon refluxing the reaction mixture both a color change of the solution from red-brown to yellow and the separation of a yellow solid were observed. After about 90 min of reflux the mixture was cooled and the solid obtained was filtered and crystallized from CH_2Cl_2 and ethanol; yield 1.34 g (83%). $C_{42}H_{47}NO_4P_3Re$ (908.96): calcd. C 55.5, H 5.2, N 1.5; found C 55.7, H, 5.3, N 1.4.

$[ReH(OC_2H_5)(NO)P_3]$ (2) [P = $PPh(OEt)_2$ (a), $P(OEt)_3$ (b)]: An excess of the appropriate phosphane (12 mmol) and then an excess of $NaBH_4$ (0.45 g, 12 mmol) in 15 mL of ethanol were added to a suspension of $[ReCl_2(OCH_3)(NO)(PPh_3)_2]$ (2 g, 2.37 mmol) in 45 mL of ethanol. The reaction mixture was refluxed for 1 h, cooled to room temperature, filtered and concentrated to about 20 mL by evaporation of the solvent under reduced pressure. At this point, the method to obtain solid samples of the complexes depends on the nature of the phosphane ligand. In the case of $PPh(OEt)_2$ yellow crystals of **2a** were obtained by cooling the resulting solution to −25 °C. These were filtered and dried under vacuum. In the case of $P(OEt)_3$, the solid obtained by cooling the solution to −25 °C gave PPh_3. Finally, by further concentrating

 © 2004 Wiley-VCH Verlag GmbH & Co. KGaA, Weinheim

and cooling of the solution, yellow crystals of **2b** separated out, which were filtered and dried under vacuum; yield 1.58 g for **2a** (78%); 0.36 g for **2b** (20%).
2a: $C_{32}H_{51}NO_8P_3Re$ (856.88): calcd. C 44.9, H 6.0, N 1.6; found C 44.7, H 6.0, N 1.5.
2b: $C_{20}H_{51}NO_{11}P_3Re$ (760.74): calcd. C 31.6, H 6.8, N 1.8; found C 31.4, H 6.9, N 1.8.

[ReH(OCH$_3$)(NO){PPh(OEt)$_2$}$_3$] (3): An excess of $PPh(OEt)_2$ (2.76 g, 12 mmol) and then an excess of $NaBH_4$ (0.45 g, 12 mmol) in 20 mL of CH_3CN were added to a solution of $[ReCl_2(OCH_3)(NO)(PPh_3)_2]$ (2 g, 2.37 mmol) in 30 mL of CH_3CN. The reaction mixture was refluxed for about 2 h and then the solvent was removed by evaporation under reduced pressure. The oil obtained was treated with 8 mL of ethanol and the resulting solution, after filtration, was allowed to stand at −25 °C. A yellow-green solid slowly separated out which was filtered and crystallized from CH_2Cl_2 and ethanol; yield 1.04 g (52%). $C_{31}H_{49}NO_8P_3Re$ (842.85): calcd. C 44.2, H 5.9, N 1.7; found C 44.3, H 5.7, N 1.6.

[ReH(RNHNH$_2$)(NO)(PPh$_2$OEt)$_3$]BPh$_4$ (4) [R = H (a), CH$_3$ (b), C$_6$H$_5$ (c)]: An equimolar amount of CF_3SO_3H (9.7 μL, 0.11 mmol) was added to a solution of $[ReH_2(NO)(PPh_2OEt)_3]$ (100 mg, 0.11 mmol) in 8 mL of CH_2Cl_2 cooled to −196 °C. The reaction mixture was warmed to about −10 °C, stirred for 1 h and then an excess of the appropriate hydrazine (0.22 mmol) was added. After two hours of stirring at −10 °C, the solvent was removed under reduced pressure to give an oil which was treated with ethanol (2 mL) containing an excess of $NaBPh_4$ (75 mg, 0.22 mmol). A yellow solid slowly separated out from the resulting solution which was filtered and crystallized from CH_2Cl_2 and ethanol; yield 93 mg for **4a** (67%), 91 mg for **4b** (65%), 100 mg for **4c** (98%).
4a: $C_{66}H_{70}BN_3O_4P_3Re$ (1259.2): calcd. C 63.0, H 5.6, N 3.3; found C 63.2, H 5.7, N 3.2. Λ_M = 48.7 Ω^{-1} mol^{-1} cm^2.
4b: $C_{67}H_{72}BN_3O_4P_3Re$ (1273.3): calcd. C 63.2, H 5.7, N 3.3; found C 63.0, H 5.6, N 3.2. Λ_M = 51.8 Ω^{-1} mol^{-1} cm^2.
4c: $C_{72}H_{74}BN_3O_4P_3Re$ (1335.3): calcd. C 64.8, H 5.6, N 3.2; found C 64.6, H 5.7, N 3.1. Λ_M = 50.3 Ω^{-1} mol^{-1} cm^2.

[Re(OC$_2$H$_5$)(RNHNH$_2$)(NO){PPh(OEt)$_2$}$_3$]BPh$_4$ (5) [R = H (a), C$_6$H$_5$ (c)]: An equimolar amount of CF_3SO_3H (10.3 μL, 0.117 mmol) was added to a solution of $[ReH(OC_2H_5)(NO)\{PPh(OEt)_2\}_3]$ (100 mg, 0.117 mmol) in 8 mL of CH_2Cl_2 cooled to −196 °C and the reaction mixture brought to 0 °C and stirred for 1 h. The solution was cooled to −196 °C again and an excess of the appropriate hydrazine (0.24 mmol) added. The reaction mixture was brought to 0 °C, stirred for about 2 h and then the solvent removed under reduced pressure. The solid obtained was treated with ethanol (3 mL) containing an excess of $NaBPh_4$ (85 mg, 0.25 mmol). A pale-yellow solid slowly separated out from the resulting solution, which was filtered and crystallized from CH_2Cl_2 and ethanol; yield 80 mg for **5a** (55%), 86 mg for **5c** (58%).
5a: $C_{56}H_{74}BN_3O_8P_3Re$ (1207.2): calcd. C 55.7, H 6.2, N 3.5; found C 55.5, H 6.3, N 3.5. Λ_M = 49.5 Ω^{-1} mol^{-1} cm^2.
5c: $C_{62}H_{78}BN_3O_8P_3Re$ (1283.2): calcd. C 58.0, H 6.1, N 3.3; found C 57.8, H 6.0, N 3.3. Λ_M = 51.4 Ω^{-1} mol^{-1} cm^2.

[Re(OC$_2$H$_5$)(CH$_3$NHNH$_2$)(NO){PPh(OEt)$_2$}$_3$]CF$_3$SO$_3$ (5b$_2$): This complex was prepared following the method used for the related BPh_4 complex **5a** by reacting $[ReH(OC_2H_5)(NO)\{PPh(OEt)_2\}_3]$ first with CF_3SO_3H and then with an excess of CH_3NHNH_2 in CH_2Cl_2 as a solvent. After the reaction was finished, the solvent was removed under reduced pressure to give a pale-yellow solid which was triturated with ethanol (1.5 mL). A yellow solid slowly separated out from the resulting solution, which was cooled to −25 °C to complete the precipitation. The solid was filtered, washed with cold ethanol and dried under vacuum; yield 52 mg (42%). $C_{34}H_{56}F_3N_3O_{11}P_3ReS$ (1051.01): calcd. C 38.9, H 5.4, N 4.0; found C 39.0, H 5.5, N 3.9. Λ_M = 78.5 Ω^{-1} mol^{-1} cm^2.

[Re(OCH$_3$)(RNHNH$_2$)(NO){PPh(OEt)$_2$}$_3$]BPh$_4$ (6) [R = H (a), CH$_3$ (b), C$_6$H$_5$ (c)]: These complexes were prepared exactly like the related ethoxy complexes **5a** and **5c** by reacting $[ReH(OCH_3)(NO)\{PPh(OEt)_2\}_3]$ first with CF_3SO_3H and then with an excess of the appropriate hydrazine. After precipitation with $NaBPh_4$ in ethanol, the yields were 95 mg for **6a** (65%), 89 mg for **6b** (63%) and 101 mg for **6c** (68%).
6a: $C_{55}H_{72}BN_3O_8P_3Re$ (1193.1): calcd. C 55.4, H 6.1, N 3.5; found C 55.2, H 6.0, N 3.5. Λ_M = 54.8 Ω^{-1} mol^{-1} cm^2.
6b: $C_{56}H_{74}BN_3O_8P_3Re$ (1207.2): calcd. C 55.7, H 6.2, N 3.5; found C 55.6, H 6.3, N 3.4. Λ_M = 53.3 Ω^{-1} mol^{-1} cm^2.
6c: $C_{61}H_{76}BN_3O_8P_3Re$ (1269.2): calcd. C 57.7, H 6.0, N 3.3; found C 57.9, H 6.2, N 3.3. Λ_M = 49.6 Ω^{-1} mol^{-1} cm^2.

[ReH(CH$_3$N=NH)(NO)(PPh$_2$OEt)$_3$]BPh$_4$ (7b) and [ReH(C$_6$H$_5$N=NH)(NO)(PPh$_2$OEt)$_3$]BPh$_4$ (7c): A sample of the appropriate hydrazine complex $[ReH(RNHNH_2)(NO)(PPh_2OEt)_3]BPh_4$ (**4**) (R = CH_3 or C_6H_5; 0.07 mmol) was placed in a three-necked 25-mL round-bottomed flask fitted with a solid-addition sidearm containing an equimolar amount of $Pb(OAc)_4$ (31 mg, 0.07 mmol). The system was evacuated, CH_2Cl_2 (10 mL) was added, the solution cooled to −30 °C and the $Pb(OAc)_4$ was added portionwise over 10−20 min. The reaction mixture was then allowed to warm to 0 °C, stirred for 10 min and the solvent removed under reduced pressure. The oil obtained was treated at 0 °C with ethanol (2 mL) containing $NaBPh_4$ (34 mg, 0.10 mmol). A white solid slowly separated out upon stirring the resulting solution at 0 °C, which was filtered and crystallized at 0 °C from CH_2Cl_2 and ethanol; yield 64 mg for **7b** (72%) and 65 mg for **7c** (70%).
7b: $C_{67}H_{70}BN_3O_4P_3Re$ (1271.2): calcd. C 63.3, H 5.6, N 3.3; found C 63.1, H 5.4, N 3.2. Λ_M = 49.9 Ω^{-1} mol^{-1} cm^2.
7c: $C_{72}H_{72}BN_3O_4P_3Re$ (1333.3): calcd. C 64.9, H 5.4, N 3.2; found C 64.6, H 5.3, N 3.0. Λ_M = 52.1 Ω^{-1} mol^{-1} cm^2.

[Re(OC$_2$H$_5$)(C$_6$H$_5$N=NH)(NO){PPh(OEt)$_2$}$_3$]BPh$_4$ (8c): This complex was prepared exactly like the related complexes **7** by oxidation of the phenylhydrazine derivative $[Re(OC_2H_5)(C_6H_5NHNH_2)(NO)\{PPh(OEt)_2\}_3]BPh_4$ (**5c**) with $Pb(OAc)_4$ at −30 °C; yield 56 mg (62%). $C_{62}H_{76}BN_3O_8P_3Re$ (1281.2): calcd. C 58.1, H 6.0, N 3.3; found C 57.9, H 6.1, N 3.2. Λ_M = 52.0 Ω^{-1} mol^{-1} cm^2.

[Re(OCH$_3$)(CH$_3$N=NH)(NO){PPh(OEt)$_2$}$_3$]BPh$_4$ (9b) and [Re(OCH$_3$)(η^1-NH=CH$_2$)(NO){PPh(OEt)$_2$}$_3$]BPh$_4$ (9*b): These complexes were obtained as a mixture by oxidation of the methylhydrazine compound $[Re(OCH_3)(CH_3NHNH_2)(NO)\{PPh(OEt)_2\}_3]BPh_4$ (**6b**) with $Pb(OAc)_4$ at −30 °C following the method used for the related **7** and **8** complexes.

[ReH(ArN=NH)(NO)(PPh$_2$OEt)$_3$]BPh$_4$ (10) [Ar = C$_6$H$_5$ (c), 4-CH$_3$C$_6$H$_4$ (d)]: Solid samples of $[ReH_2(NO)(PPh_2OEt)_3]$ (0.1 g, 0.11 mmol) and the appropriate aryldiazonium salt $[ArN_2]BF_4$ (0.11 mmol) were placed into a 25-mL three-necked round-bottomed flask. The mixture was cooled to −196 °C and CH_2Cl_2 (8 mL) slowly added. The reaction mixture was allowed to warm to room temperature, stirred for about 8 h and then the solvent removed under reduced pressure. The oil obtained was treated with ethanol (2 mL) containing an excess of $NaBPh_4$ (75 mg, 0.22 mmol). A yellow solid slowly separated out from the resulting solution which was filtered and crystallized from CH_2Cl_2 and ethanol; yield 107 mg for **10c** (73%) and 105 mg for **10d** (71%).

 © 2004 Wiley-VCH Verlag GmbH & Co. KGaA, Weinheim

10c: $C_{72}H_{72}BN_3O_4P_3Re$ (1333.3): calcd. C 64.9, H 5.4, N 3.2; found C 64.8, H 5.5, N 3.0. Λ_M = 49.4 Ω^{-1} mol^{-1} cm^2.
10d: $C_{73}H_{74}BN_3O_4P_3Re$ (1347.3): calcd. C 65.1, H 5.5, N 3.1; found C 65.3, H 5.6, N 3.0. Λ_M = 53.8 Ω^{-1} mol^{-1} cm^2.

[ReH(C_6H_5N=^{15}NH)(NO)(PPh_2OEt)$_3$]BPh_4 (10c$_1$): This complex was prepared exactly like the related compound **10** using the labeled diazonium salt [$C_6H_5N{\equiv}^{15}N$]BF_4; yield 95 mg (65%).

[{ReH(NO)(PPh_2OEt)$_3$}$_2$(μ-4,4′-HN=NC_6H_4-C_6H_4N=NH)]-(BPh_4)$_2$ (11a): Solid samples of [ReH_2(NO)(PPh_2OEt)$_3$] (0.1 g, 0.11 mmol) and the bis(aryldiazonium) salt [4,4′-$N_2C_6H_4$-$C_6H_4N_2$](BF_4)$_2$ (21 mg, 0.055 mmol) were placed into a 25-mL three-necked flask. The mixture was cooled to −196 °C and CH_2Cl_2 (12 mL) added. The reaction mixture was brought to room temperature, stirred for about 12 h and then the solvent removed by evaporation under reduced pressure. The oil obtained was triturated with ethanol (3 mL) containing an excess of $NaBPh_4$ (75 mg, 0.22 mmol). A red solid separated out from the resulting solution which was filtered and crystallized from CH_2Cl_2 and ethanol; yield 217 mg (74%). $C_{144}H_{142}B_2N_6O_8P_6Re_2$ (2664.6): calcd. C 64.9, H 5.4, N 3.2; found C 64.7, H 5.5, N 3.2. Λ_M = 115 Ω^{-1} mol^{-1} cm^2.

[{ReH(NO)(PPh_2OEt)$_3$}$_2$(μ-4,4′-H^{15}N=NC_6H_4−C_6H_4-N=^{15}NH)](BPh_4)$_2$ (11a$_1$): This complex was prepared exactly like the related compound **11a** using the labeled bis(aryldiazonium) salt [4,4′-^{15}N≡NC_6H_4−$C_6H_4N{\equiv}^{15}$N](BF_4)$_2$; yield 194 mg (66%).

[Re(OC_2H_5)(ArN=NH)(NO){PPh(OEt)$_2$}$_3$]BF_4 (12) [Ar = C_6H_5 (c), 4-$CH_3C_6H_4$ (d)]: Equimolar amounts of [ReH(OC_2H_5)-(NO){PPh(OEt)$_2$}$_3$] (100 mg, 0.117 mmol) and the appropriate aryldiazonium salt [ArN_2]BF_4 (0.117 mmol) were placed into a 25-mL three-necked flask. The mixture was cooled to −196 °C and CH_2Cl_2 (8 mL) added. The reaction mixture was brought to room temperature, stirred for 8 h and then the solvent was removed under reduced pressure. The oil obtained was triturated with diethyl ether (10 mL) until a pale-yellow solid separated out, which was filtered and dried under vacuum; yield 112 mg for **12c** (91%) and 109 mg for **12d** (88%).
12c: $C_{38}H_{56}BF_4N_3O_8P_3Re$ (1048.8): calcd. C 43.5, H 5.4, N 4.0; found C 43.4, H 5.5, N 3.9. Λ_M = 88.7 Ω^{-1} mol^{-1} cm^2.
12d: $C_{39}H_{58}BF_4N_3O_8P_3Re$ (1062.8): calcd. C 44.1, H 5.5, N 4.0; found C 44.23, H 5.37, N 4.02. Λ_M = 93.1 Ω^{-1} mol^{-1} cm^2.

[Re(OC_2H_5)(NO)(C_6H_5N=^{15}NH){PPh(OEt)$_2$}$_3$]BF_4 (12c$_1$): This complex was prepared exactly like the related compound **12c** using the labeled aryldiazonium salt [$C_6H_5N{\equiv}^{15}$N]BF_4; yield 104 mg (85%).

[{Re(OC_2H_5)(NO)[PPh(OEt)$_2$]$_3$}$_2$(μ-4,4′-HN=NC_6H_4−C_6H_4N=NH)](BF_4)$_2$ (13a): This complex was prepared following the method used for the related mononuclear compound **12** by reacting [ReH(OC_2H_5)(NO){PPh(OEt)$_2$}$_3$] with [4,4′-$N_2C_6H_4$-$C_6H_4N_2$](BF_4)$_2$ in CH_2Cl_2 with a reaction time of 12 h; yield 218 mg (89%). $C_{76}H_{110}B_2F_8N_6O_{16}P_6Re_2$ (2095.6): calcd. C 43.6, H 5.3, N 4.0; found C 43.7, H 5.2, N 3.9. Λ_M = 188 Ω^{-1} mol^{-1} cm^2.

[{Re(OC_2H_5)(NO)[PPh(OEt)$_2$]$_3$}$_2$(μ-4,4′-H^{15}N=NC_6H_4−C_6H_4N=^{15}NH)](BF_4)$_2$ (13a$_1$): This complex was prepared exactly like the related compound **13a** using the labeled bis(aryldiazonium) salt [4,4′-^{15}N≡NC_6H_4-$C_6H_4N{\equiv}^{15}$N](BF_4)$_2$; yield 206 mg (84%).

[Re(OCH_3)(4-$CH_3C_6H_4$N=NH)(NO){PPh(OEt)$_2$}$_3$]BPh_4 (14d): Solid samples of [ReH(OCH_3)(NO){PPh(OEt)$_2$}$_3$] (100 mg, 0.119 mmol) and the diazonium salt [4-$CH_3C_6H_4N_2$]BF_4 (23 mg, 0.119 mmol) were placed into a 25-mL three-necked round-bottomed flask and the mixture cooled to −196 °C. Dichloromethane (8 mL) was added and the reaction mixture brought to room temperature and stirred for 9 h. The solvent was removed under reduced pressure to give an oil which was treated with ethanol (2 mL) containing an excess of $NaBPh_4$ (82 mg, 0.24 mmol). A yellow solid slowly separated out from the resulting solution which was filtered and crystallized from CH_2Cl_2 and ethanol; yield 126 mg (83%). $C_{62}H_{76}BN_3O_8P_3Re$ (1281.2): calcd. C 58.1, H 6.0, N 3.3; found C 58.2, H 5.9, N 3.2. Λ_M = 52.7 Ω^{-1} mol^{-1} cm^2.

[{Re(OCH_3)(NO)[PPh(OEt)$_2$]$_3$}$_2$(μ-4,4′-HN=NC_6H_4−C_6H_4-N=NH)](BPh_4)$_2$ (15a): This complex was prepared following the method used for the related mononuclear compound **14d** by reacting [ReH(OCH_3)(NO){PPh(OEt)$_2$}$_3$] with the bis(aryldiazonium) salt [4,4′-$N_2C_6H_4$-$C_6H_4N_2$](BF_4)$_2$ in CH_2Cl_2 for about 13 h; yield 205 mg (68%). $C_{122}H_{146}B_2N_6O_{16}P_6Re_2$ (2532.4): calcd. C 57.9, H 5.8, N 3.3; found C 57.7, H 5.7, N 3.4. Λ_M = 113 Ω^{-1} mol^{-1} cm^2.

[{Re(OCH_3)(NO)[PPh(OEt)$_2$]$_3$}$_2$(μ-4,4′-H^{15}N=NC_6H_4−C_6H_4N=^{15}NH)](BPh_4)$_2$ (15a$_1$): This complex was prepared exactly like the related compound **15a** using the labeled bis(aryldiazonium) salt [4,4′-^{15}N≡NC_6H_4-$C_6H_4N{\equiv}^{15}$N](BF_4)$_2$; yield 196 mg (65%).

[Re(OC_2H_5)(4-$CH_3C_6H_4$N=NH)(NO){P(OEt)$_3$}$_3$]BF_4 (16d): Equimolar amounts of solid samples of [ReH(OC_2H_5)(NO){P(OEt)$_3$}$_3$] (100 mg, 0.13 mmol) and [4-$CH_3C_6H_4N_2$]BF_4 (27 mg, 0.13 mmol) were placed in a 25-mL three-necked round-bottomed flask and the mixture cooled to −196 °C. Dichloromethane (8 mL) was added and the reaction mixture brought to 0 °C and stirred for 9 h. The solvent was removed under reduced pressure to give an oil which was triturated with diethyl ether (7 mL). A pale-yellow solid slowly separated out which was filtered and dried under vacuum; yield 103 mg (82%). $C_{27}H_{58}BF_4N_3O_{11}P_3Re$ (966.69): calcd. C 33.6, H 6.1, N 4.4; found C 33.7, H 6.2, N 4.3. Λ_M = 89.4 Ω^{-1} mol^{-1} cm^2.

Protonation Reactions: The protonation of the hydrides [ReH_2(NO)(PPh_2OEt)$_3$] (**1**) and [ReH(OR^1)(NO)P_3] (**2**, **3**) was carried out in a 5-mm NMR tube at temperatures of between −80 and +20 °C. A typical experiment involved the preparation, in an argon-filled dry-box, of a solution of the appropriate hydride (0.04 mmol) in CD_2Cl_2 (0.5 mL). The solution was placed in a screw-cap NMR tube, cooled to −80 °C, and then an equivalent amount (0.04 mmol, 3.5 μL) of CF_3SO_3H was added. The tube was transferred into the NMR probe (pre-cooled to −80 °C) and the ^{1}H and ^{31}P NMR spectra of the solution were recorded.

X-ray Crystal Structure Determination of [Re(OC_2H_5)-(NH_2NH_2)(NO){PPh(OEt)$_2$}$_3$]BPh_4 (5a): A pale-yellow single crystal was mounted on a glass fiber and X-ray diffraction data were collected on a Bruker-Siemens SMART AXS 1000 equipped with CCD detector, using graphite monochromated Mo-K_α radiation (λ = 0.71069 Å). Data collection details are: crystal to detector distance = 5.0 cm, 2424 frames collected (complete sphere mode), time per frame = 30 s, oscillation Δω = 0.300°. Crystal decay resulted negligible. Data reduction was performed up to d = 0.90 Å with the SAINT package[28] and data were corrected for absorption effects by the SADABS[29] procedure (T_{max} = 1.000, T_{min} = 0.746). The phase problem was solved by direct methods[30] and refined by full-matrix least-squares on all F^2,[31] implemented in the WinGX package.[32] Anisotropic displacement parameters were refined for all non hydrogen atoms, while hydrogen atoms were introduced in calculated positions, except for hydrazine hydrogens, which were located from Fourier maps and refined isotropically. Use of the Cambridge Crystallographic Database[33] facilities was made for

 © 2004 Wiley-VCH Verlag GmbH & Co. KGaA, Weinheim

structure discussion. The final map was featureless. Data collection and refinement results are summarized in Table 2.

CCDC-220153 contains the supplementary crystallographic data for this paper. These data can be obtained free of charge at www.ccdc.cam.ac.uk/conts/retrieving.html [or from the Cambridge Crystallographic Data Centre, 12 Union Road, Cambridge CB2 1EZ, UK; Fax: (internat.) + 44-1223/336-033; E-mail: deposit@ccdc.cam.ac.uk].

Acknowledgments

The financial support of MIUR (Rome), PRIN 2002, is gratefully acknowledged. We thank Daniela Baldan for technical assistance.

[1] [1a] D. Sutton, *Chem. Rev.* **1993**, *93*, 995−1022. [1b] H. Zollinger, *Diazo Chemistry II*, VCH, Weinheim, Germany, **1995**. [1c]H. Kisch, P. Holzmeier, *Adv. Organomet. Chem.* **1992**, *34*, 67−109.

[2] [2a] B. F. G. Johnson, B. L. Haymore, J. R. Dilworth, in *Comprehensive Coordination Chemistry* (Eds.: G. Wilkinson, R. D. Gillard, J. A. McCleverty), Pergamon Press, Oxford, UK, **1987**, vol. 2, pp. 130−141. [2b]R. A. Henderson, G. J. Leigh, C. Pickett, *Adv. Inorg. Chem. Radiochem.* **1983**, *27*, 197−292. [2c] W. A. Nugent, B. L. Haymore, *Coord. Chem. Rev.* **1980**, *31*, 123−175.

[3] [3a] G. Albertin, S. Antoniutti, A. Bacchi, M. Boato, G. Pelizzi, *J. Chem. Soc., Dalton Trans.* **2002**, 3313−3320. [3b] G. Albertin, S. Antoniutti, E. Bordignon, E. Visentin, *Inorg. Chem.* **2001**, *40*, 4565−4567. [3c] G. Albertin, S. Antoniutti, E. Bordignon, G. Perinello, *J. Organomet. Chem.* **2001**, *625*, 217−230. [3d] G. Albertin, S. Antoniutti, A. Bacchi, E. Bordignon, F. Miani, G. Pelizzi, *Inorg. Chem.* **2000**, *39*, 3283−3293. [3e] G. Albertin, S. Antoniutti, A. Bacchi, D. Barbera, E. Bordignon, G. Pelizzi, P. Ugo, *Inorg. Chem.* **1998**, *37*, 5602−5610, and references cited therein. [3f] G. Albertin, S. Antoniutti, A. Bacchi, E. Bordignon, F. Busatto, G. Pelizzi, *Inorg. Chem.* **1997**, *36*, 1296−1305.

[4] [4a] X. Yan, R. J. Batchelor, F. W. B. Einstein, X. Zhang, R. Nagelkerke, D. Sutton, *Inorg. Chem.* **1997**, *36*, 1237−1246. [4b] D. Sellmann, K. Engl, F. W. Heinemann, J. Sieler, *Eur. J. Inorg. Chem.* **2000**, 1079−1089.

[5] [5a] A. R. Cowley, J. R. Dilworth, P. S. Donnelly, *Inorg. Chem.* **2003**, *42*, 929−931. [5b] M. T. A. R. S. da Costa, J. R. Dilworth, M. T. Duarte, J. J. R. F. da Silva, A. M. Galvão, A. J. L. Pombeiro, *J. Chem. Soc., Dalton Trans.* **1998**, 2405−2410. [5c] A. Garcia-Minsal, D. Sutton, *Organometallics* **1996**, *15*, 332−336. [5d] D. J. Rose, K. P. Maresca, P. B. Kettler, Y.-D. Chang, V. Soghomomian, Q. Chen, M. J. Abrams, S. K. Larsen, J. Zubieta, *Inorg. Chem.* **1996**, *35*, 3548−3558. [5e] B. Coutinho, J. R. Dilworth, P. Jobanputra, R. M. Thompson, S. Schmid, J. Strähle, C. M. Archer, *J. Chem. Soc., Dalton Trans.* **1995**, 1663−1669. [5f] A. Cusanelli, D. Sutton, *Organometallics* **1995**, *14*, 4651−4660. [5g] A. Cusanelli, R. J. Batchelor, F. W. B. Einstein, D. Sutton, *Organometallics* **1994**, *13*, 5096−5112. [5h] P. B. Kettler, Y.-D. Chang, J. Zubieta, *Inorg. Chem.* **1994**, *33*, 5864−5871. [5i] S. W. Carr, X. L. R. Fontaine, B. L. Shaw, *J. Chem. Soc., Dalton Trans.* **1987**, 3067−3071. [5j] H. M. Ali, G. J. Leigh, *J. Chem. Soc., Dalton Trans.* **1986**, 213−215. [5k] C. F. Barrientos-Penna, A. B. Gilchrist, A. H. Klahn-Oliva, A. J. L. Hanlan, D. Sutton, *Organometallics* **1985**, *4*, 478−485. [5l] J. R. Dilworth, S. A. Harrison, D. R. M. Walton, E. Schweda, *Inorg. Chem.* **1985**, *24*, 2594−2595.

[6] J. T. Moelwyn-Hughes, A. W. B. Garner, A. S. Howard, *J. Chem. Soc. (A)* **1971**, 2361−2370.

[7] [7a] M. G. Vale, R. R. Schrock, *Organometallics* **1991**, *10*, 1661−1662. [7b] T.-Y. Cheng, J. C. Peters, G. L. Hillhouse, *J. Am. Chem. Soc.* **1994**, *116*, 204−207.

[8] A. Moehlenkamp, R. Mattes, *Z. Naturforsch., Teil B* **1992**, *47*, 969.

[9] [9a] P. Perez-Lourido, J. Romero, J. A. Garcia-Vasquez, A. Souza, K. P. Maresca, J. Zubieta, *Inorg. Chem.* **1999**, *38*, 1511−1519. [9b] M. Hirsch-Kuchma, T. Nicholson, A. Davison, W. M. Davis, A. G. Jones, *Inorg. Chem.* **1997**, *36*, 3237−3241. [9c] M. Hirsch-Kuchma, T. Nicholson, A. Davison, W. M. Davis, A. G. Jones, *J. Chem. Soc., Dalton Trans.* **1997**, 3185−3188. [9d] T. Nicholson, J. Cook, A. Davison, D. J. Rose, K. P. Maresca, J. A. Zubieta, A. G. Jones, *Inorg. Chim. Acta* **1996**, *252*, 421−426. [9e] P. B. Kettler, Y.-D. Chang, Q. Chen, J. A. Zubieta, M. J. Abrams, S. K. Larsen, *Inorg. Chim. Acta* **1996**, *252*, 427−430. [9f] P. B. Kettler, Y.-D. Chang, Q. Chen, J. A. Zubieta, M. J. Abrams, S. K. Larsen, *Inorg. Chim. Acta* **1995**, *231*, 13.

[10] [10a] C. F. Barrientos-Penna, F. W. B. Einstein, T. Jones, D. Sutton, *Inorg. Chem.* **1982**, *21*, 2578−2585. [10b] C. F. Barrientos-Penna, C. F. Campana, F. W. B. Einstein, T. Jones, D. Sutton, A. S. Tracey, *Inorg. Chem.* **1984**, *23*, 363−368. [10c] R. Melenkivitz, J. S. Southern, G. L. Hillhouse, T. E. Concolino, L. M. Liable-Sands, A. L. Rheingold, *J. Am. Chem. Soc.* **2002**, *124*, 12068−12069.

[11] [11a] G. Albertin, S. Antoniutti, M. T. Giorgi, *Eur. J. Inorg. Chem.* **2003**, 2855−2866. [11b] G. Albertin, S. Antoniutti, A. Bacchi, E. Bordignon, M. T. Giorgi, G. Pelizzi, *Angew. Chem.* **2002**, *114*, 2296; *Angew. Chem. Int. Ed.* **2002**, *41*, 2192−2194.

[12] G. Albertin, S. Antoniutti, A. Bacchi, G. B. Ballico, E. Bordignon, G. Pelizzi, M. Ranieri, P. Ugo, *Inorg. Chem.* **2000**, *39*, 3265−3279.

[13] G. Albertin, S. Antoniutti, S. Garcia-Fontán, R. Carballo, F. Padoan, *J. Chem. Soc., Dalton Trans.* **1998**, 2071−2081.

[14] For rhenium polyhydrides see: [14a] D. Gusev, A. Llamazares, G. Artus, H. Jacobsen, H. Berke, *Organometallics* **1999**, *18*, 75−89. [14b] D. M. Heynekey, C. E. Radzewich, M. H. Voges, B. M. Schomber, *J. Am. Chem. Soc.* **1997**, *119*, 4172−4181. [14c] Y. Kim, H. Deng, J. C. Gallucci, A. Wojcicki, *Inorg. Chem.* **1996**, *35*, 7166−7173. [14d] A. L. Ondracek, W. Wu, P. E. Fanwick, R. A. Walton, *Inorg. Chem.* **1996**, *35*, 5249−5253. [14e] X. L. R. Fontaine, T. P. Layzell, B. L. Shaw, *J. Chem. Soc., Dalton Trans.* **1994**, 917−924. [14f] M. Kohli, D. J. Lewis, R. L. Luck, J. V. Silverton, K. Sylla, *Inorg. Chem.* **1994**, *33*, 883. [14g] M. Leeaphon, K. Rohl, R. J. Thomas, P. E. Fanwick, R. A. Walton, *Inorg. Chem.* **1993**, *32*, 5562−5568. [14h] D. Michos, X.-L. Luo, J. A. K. Howard, R. H. Crabtree, *Inorg. Chem.* **1992**, *31*, 3914−3916. [14i] Y. Kim, H. Deng, D. W. Meek, A. Wojcicki, *J. Am. Chem. Soc.* **1990**, *112*, 2798−2800. [14j] F. A. Cotton, R. L. Luck, *J. Am. Chem. Soc.* **1989**, *111*, 5757−5761. [14k] K. A. Earl, G. Jia, P. A. Maltby, R. H. Morris, *J. Am. Chem. Soc.* **1991**, *113*, 3027−3039. [14l] D. M. Heynekey, B. M. Schomber, C. E. Radzewich, *J. Am. Chem. Soc.* **1994**, *116*, 4515−4516.

[15] The known nitrosyl rhenium hydrides are of the types $[ReH_2(NO)(PPh_3)_3]$, $[ReH_2(NO)(CO)P_2]$ and $[ReH(NO)_2P_2]$ [P = PMe_3, $PiPr_3$, $P(OiPr)_3$]: [15a] T. S. Cameron, K. R. Grundy, K. N. Robertson, *Inorg. Chem.* **1982**, *21*, 4149−4155. [15b] N. V. Belkova, E. S. Shubina, A. V. Ionidis, L. M. Epstein, H. Jacobsen, A. Messmer, H. Berke, *Inorg. Chem.* **1997**, *26*, 1522−1525. [15c] S. Feracin, T. Bürgi, V. I. Bakhmutov, I. Eremenko, E. V. Vorontsov, A. B. Vimenits, H. Berke, *Organometallics* **1994**, *13*, 4194−4202. [15d] D. G. Gusev, D. Nietlispach, I. L. Eremenko, H. Berke, *Inorg. Chem.* **1993**, *32*, 3628−3636.

[16] [16a] C. A. Tolman, *Chem. Rev.* **1977**, *77*, 313−348. [16b] M. M. Rahman, H.-Y. Lin, K. Eriks, A. Prock, W. P. Giering, *Organometallics* **1989**, *8*, 1−7.

[17] J. H. Enemark, R. D. Feltham, *Coord. Chem. Rev.* **1974**, *13*, 339−406.

[18] [18a] G. J. Kubas, *Acc. Chem. Res.* **1988**, *21*, 120−128. [18b] P. G. Jessop, R. H. Morris, *Coord. Chem. Rev.* **1992**, *121*, 155−284. [18c] R. H. Crabtree, *Angew. Chem. Int. Ed. Engl.* **1993**, *92*, 789−805. [18d] D. M. Heynekey, W. J. Oldham Jr., *Chem. Rev.* **1993**, *93*, 913−926.

[19] J. Huhmann-Vincent, B. L. Scott, G. J. Kubas, *Inorg. Chem.* **1999**, *38*, 115−124, and references cited therein.

 © 2004 Wiley-VCH Verlag GmbH & Co. KGaA, Weinheim

[20] R. H. Crabtree, M. Lavin, L. Bonneviot, *J. Am. Chem. Soc.* **1986**, *108*, 4032−4037.
[21] W. G. Geary, *Coord. Chem. Rev.* **1971**, *7*, 81−122.
[22] T. J. Bartczak, W. Czurak, J. O. Dziemagegielewski, B. Machura, A. Jankowska, J. Kusz, J. Warczewski, *Polyhedron* **1999**, *18*, 2313−2320.
[23] [23a] M. R. Smith III, T.-Y. Cheng, G. L. Hillhouse, *J. Am. Chem. Soc.* **1993**, *115*, 8638−8642. [23b] T.-Y. Cheng, A. L. Ponce, A. L. Rheingold, G. L. Hillhouse, *Angew. Chem. Int. Ed. Engl.* **1994**, *33*, 657−659. [23c] T.-Y. Cheng, J. C. Peters, G. L. Hillhouse, *J. Am. Chem. Soc.* **1994**, *116*, 204−207.
[24] R. Rabinowitz, J. Pellon, *J. Org. Chem.* **1961**, *26*, 4623−4626.
[25] A. I. Vogel, *Practical Organic Chemistry*, 3rd ed., Longmans, Green and Co., New York, **1956**.
[26] E. Nachbaur, G. Leiseder, *Monatsh. Chem.* **1971**, *102*, 1718−1723.
[27] G. Balacco, *J. Chem. Inf. Comput. Sci.* **1994**, *34*, 1235−1241.
[28] SAINT: SAX, *Area Detector Integration*, Siemens Analytical instruments INC., Madison, Wisconsin, USA.
[29] G. Sheldrick *SADABS: Siemens Area Detector Absorption Correction Software*, University of Göttingen, Germany, **1996**.
[30] A. Altomare, M. C. Burla, M. Camalli, G. Cascarano, C. Giacovazzo, A. Guagliardi, A. G. Moliterni, G Polidori, R. Spagna, *Sir97: A New Program For Solving And Refining Crystal Structures*, Istituto di Ricerca per lo Sviluppo di Metodologie Cristallografiche C N R, Bari, Italy, 1997.
[31] G. Sheldrick, *Shelxl97. Program for structure refinement*, University of Göttingen, Germany, **1997**.
[32] L. J. Farrugia, *J. Appl. Crystallogr.* **1999**, *32*, 837−838.
[33] F. H. Allen, O. Kennard, R. Taylor, *Acc. Chem. Res.* **1983**, *16*, 146−153.

Received September 25, 2003
Early View Article
Published Online March 31, 2004

 © 2004 Wiley-VCH Verlag GmbH & Co. KGaA, Weinheim

Theoretical Investigation of Group 4 Constrained-Geometry Complexes Featuring Phosphazene and Phosphinimido Arms

Lionel Truflandier,[a] Colin J. Marsden,[a] Christelle Freund,[b] Blanca Martin-Vaca,[b] and Didier Bourissou*[b]

Keywords: Cations / Density functional calculations / Ligand Effects / Phosphorus / Zirconium

Density functional calculations are reported for the neutral and cationic forms of the "CpPN" zirconium complexes **E** and **F** featuring a phosphazene and phosphinimido pendant arm, respectively.

(© Wiley-VCH Verlag GmbH & Co. KGaA, 69451 Weinheim, Germany, 2004)

Introduction

The past 15 years have witnessed tremendous developments in the design and application of non-metallocene complexes as olefin polymerization catalysts.[1] Spectacular achievements have been reported for the *ansa*-monocyclopentadienylsilylamido group IV catalysts, initially developed by Bercaw[2a] and Okuda,[2b] the so-called constrained-geometry catalysts (CGC) **A** (Scheme 1). Abstraction of one of the X ligands surrounding the metal centre provides the corresponding unsaturated d^0 cationic complexes $\mathbf{A}^+$ that are generally agreed to be the catalytically active species in olefin polymerization.[3] The applications of CGC catalysts are based not only on their electronic unsaturation, but also on their sterically unhindered reactive sites, combined with rigidity of the molecular framework and thermal stability. Of special interest is that the coordination of linear α-olefins is facilitated, allowing for their incorporation into polyethylene.

Numerous structural analogues of the initial "CpSiN" catalyst **A** have already been investigated by varying the nature of the cyclopentadienyl ligand,[4] the bridging unit,[5] the metal substituents[6] and/or by replacing the amido group with another type of donor.[7–9] Although phosphorus-containing complexes such as **B**–**D** have attracted considerable attention,[10] the incorporation of a phosphazene or phosphinimido unit in constrained-geometry

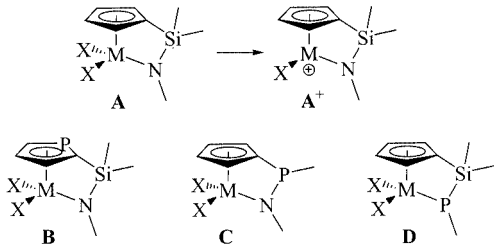

Scheme 1. Structure of "CpSiN" complexes **A** and $\mathbf{A}^+$ and representative examples of related phosphorus-containing systems **B**–**D**

complexes has not yet been investigated. These phosphorus-containing nitrogen-based moieties are, however, common ligands for transition metals, whose properties can be readily be tuned by varying their substituents. Due to the highly polarized $N^{\delta-}P^{\delta+}$ bond, phosphazenes ($R_3P{=}NR$)[11] are rather "hard" sp^2-nitrogen donors that have recently been successfully involved in ethylene oligomerisation[12a] as well as asymmetric cyclopropanation[12b,12c] and allylic substitution.[12d] Phosphinimido ligands ($R_3P{=}N^-$)[13] possess a particularly versatile coordination chemistry. Their coordination to a single transition metal can involve from two to six electrons and result in linear as well as bent geometries. Their analogy with cyclopentadienyl ligands has been pointed out by Dehnicke[14] and has been investigated by Stephan and co-workers for group IV complexes.[15]

Here we report the theoretical investigation of two new "CpPN" models **E** and **F** (Scheme 2), featuring a pendant phosphazene and phosphinimido unit, respectively. DFT calculations were performed in order to determine if these constrained-geometry complexes deserve to be studied experimentally. For both models, the geometries of the neutral complexes as well as of their cationic analogues (derived by

[a] Laboratoire de Physique Quantique du CNRS (UMR, 5626), IRSAMC, Université Paul Sabatier
118, route de Narbonne, 31062 Toulouse Cedex 04, France
Fax: (internat.) +33-5/6155-6065
[b] Laboratoire Hétérochimie Fondamentale et Appliquée du CNRS (UMR, 5069), Université Paul Sabatier
118, route de Narbonne, 31062 Toulouse Cedex 04, France
Fax: (internat.) +33-5-6155-8204
E-mail: dbouriss@chimie.ups-tlse.fr

Supporting information for this article is available on the WWW under http://www.eurjic.org or from the author.

halide abstraction) were optimized. The resulting structural data and charges are discussed and compared with those of a model silicon-based complex of type **A**. During this study, particular emphasis has been placed upon the coordination of the phosphazene arm as well as substituent effects in complexes **E**.

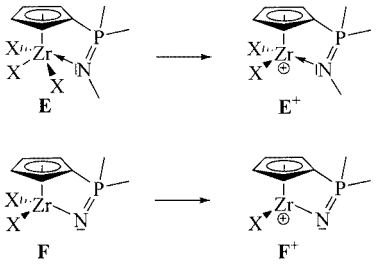

Scheme 2. Structure of the phosphazene- and phosphinimido-based constrained geometry complexes **E** and **F**

Results and Discussion

Complexes featuring a pendant phosphazene unit were first investigated both in the parent form and for various substitution patterns. Replacement of the phosphazene unit by a phosphinimido moiety was then studied for the parent form. For both model complexes, halide dissociation was evaluated geometrically and energetically.

Complexes Featuring a Pendant Phosphazene Unit $[R_2P(\eta^5\text{-}C_5H_4)(R'N)ZrX_3]$ and $[R_2P(\eta^5\text{-}C_5H_4)(R'N)ZrX_2]^+$

Parent Complex $[H_2P(\eta^5\text{-}C_5H_4)(HN)ZrCl_3]$ (1)

Two energy minima were located on the potential energy hypersurface. The corresponding complexes **1** and **1*** are represented in Scheme 3, and selected geometric parameters are collected in Table 1.

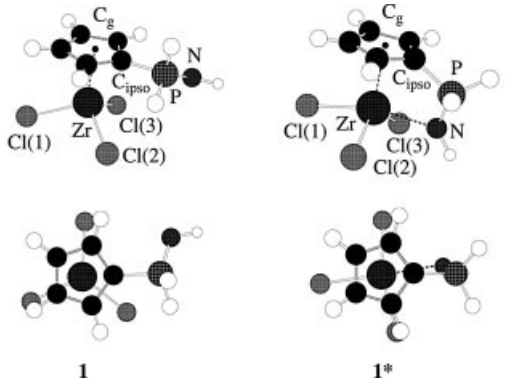

Scheme 3. Schematic representation (side and top views) of the B3LYP-optimized geometry of complexes **1** and **1***

In complex **1**, the phosphazene arm is in a position *cis* to the metal centre relative to the cyclopentadienyl ring (Cp) (torsion angle $Zr-C_{ipso}-P-N$: 64.0° where C_{ipso} is the substituted carbon of the Cp ring), but not coordinated to the zirconium centre, as indicated by the Zr−N distance (4.085 Å). The environment around the zirconium centre is very similar to that of the model complex $[CpZrCl_3]$ (**2**), which is a more or less distorted tetrahedral geometry ("three-legged piano-stool"). As expected, the distance between the centroid (C_g) of the Cp ring and the metallic centre (2.265 Å) is almost identical (2.242 Å) to that observed for **2**.

The geometric parameters predicted for complex **1*** clearly indicate the rotation of the phosphazene arm (torsion angle $Zr-C_{ipso}-P-N$: 10.9°) and the presence of a Zr−N interaction. Considering the centroid (C_g), the three chlorides and the nitrogen atom, the environment around the metal can be depicted by a pseudo-square-pyramidal ("four-legged piano-stool"[16]) or trigonal bipyramidal structure. The constrained-geometry structure is indicated by the pyramidalization of C_{ipso} (sum of the bond angles Σ = 352.9° and $C_g-C_{ipso}-P$ angle = 158.1°). As a consequence, the C_g-Zr distance for **1*** (2.341 Å) is significantly longer than that predicted for **1** (2.265 Å). The Zr−Cl distances are also elongated (**1***: 2.425 Å on average; **1**: 2.373 Å), but there is no preferential elongation of the Zr−Cl bond in a position *trans* to the phosphazene unit in **1*** (2.432 Å). The N−Zr bond (2.357 Å) is notably longer than that predicted for the unconstrained complex $[CpZrCl_3(HN{=}PH_3)]$ (**3**) (2.252 Å) and the N−P bond length in **1*** (1.613 Å) is half-way between those of **1** (1.587 Å) and **3** (1.633 Å). All these data suggest only a weak coordination of the pendant arm.

The bonding interaction between the phosphazene and transition metal can be represented by two schematic forms **Ea** and **Eb** (Scheme 4). The phosphazene behaves only as a σ-donor in **Ea**, but both as a σ- and π-donor in **Eb**.[17] The contribution of both σ- and π-type interactions in **1*** is clearly apparent from the appropriate orbitals localized according to the Boys method[18] (Scheme 5).

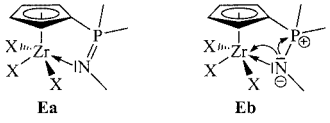

Scheme 4. Schematic representations of complex **E**

Scheme 5. Isosurfaces for the localized molecular orbitals associated with σ and π N−Zr overlaps

The coordination strength of the phosphazene arm may be estimated by the energy difference between **1** and **1***. The

 © 2004 Wiley-VCH Verlag GmbH & Co. KGaA, Weinheim

phosphazene coordination was found to be favoured by ca. 8.4 kcal/mol[19] (free enthalpy difference at 298 K, taking into account the vibrational and entropic corrections). This rather small value might result from the geometric constraint associated with the phosphazene coordination, or alternatively can be inherent to the coordination of the phosphazene to the $CpZrCl_3$ fragment. The latter hypothesis is supported by the only slightly larger value predicted for the coordination of the parent phosphazene $HN{=}PH_3$ to $CpZrCl_3$ leading to the unconstrained complex $[CpZrCl_3(HN{=}PH_3)]$ (**3**; free enthalpy difference of 10.2 kcal/mol).

Substituent Effects: Complexes [$R_2P(\eta^5\text{-}C_5H_4)(R'N)\text{-}ZrX_3$] (4−7)

Variation of the halide, phosphorus and nitrogen substituents was first investigated separately by geometry optimizations of complexes **4**-R, **5**-R′ and **6**. For each complex, two energy minima were located on the potential energy hypersurface. The following discussion will be focussed on structures **4***−**6*** featuring a phosphazene-zirconium interaction (Table 2). The C_{ipso} pyramidalization and $C_g{-}C_{ipso}{-}P$ bond angles are very similar in all complexes, suggesting that the geometric constraint is imposed by the framework and is essentially unaffected by the substituents. More significant modifications are observed for the Zr−N and N−P bond lengths. As far as the phosphorus substituents are concerned (complexes **4***-R), the Zr−N bond length decreases and the P−N bond length increases in the series $Cl/H/NH_2/CH_3/C_6H_5$. The pronounced P−N bond shortening and Zr−N distance elongation on going from H to Cl can readily be related to the strong electron-withdrawing inductive effect (-I) of the chlorine atoms, which significantly decreases the electron density at the nitrogen[20] and thus weakens the phosphazene-zirconium interaction. In contrast, the NH_2 (+M), CH_3 (+I) and C_6H_5 (+M) donor substituents (+M and +I for electron-donating mesomeric and inductive effects, respectively) increase the $N^{\delta-}P^{\delta+}$ polarity of the P=N bond[20] and thereby reinforce the phosphazene coordination. With regard to the nitrogen substituents, almost no structural modifications were observed with a methyl group, whereas introduction of an amino group induces a shortening of the Zr−N distance and an elongation of the P−N bond length. By analogy with that discussed for the phosphorus substituents, these modifications can be related to the +M effect of the amino group. Lastly, replacement of the chlorine by iodine atoms at zirconium (complex **6***) results in only negligible geometric modifications.

Susbtituent effects on the coordination strength of the phosphazene arm were then evaluated quantitatively. For all complexes **4**−**6**, except **4**-NH_2 (see below), the second minimum located on the energy surface is strongly related to **1**, with no interaction between the phosphazene and zirconium centre. As discussed previously, the coordination energy was thus obtained from the free enthalpy energy difference between the two energy minima (Table 3).

No energy minimum without interaction could be located for R = NH_2. Indeed, a stabilizing interaction between the

Table 1. Selected bond lengths (Å) and bond angles (°) for complexes **1**, **1*** and **2**

Complex	$C_g{-}Zr$[a]	Zr−Cl(1)[b]	Cl(2)−Zr−Cl(1)[b]
$[H_2P(\eta^5\text{-}C_5H_4)(HN)ZrCl_3]$ (**1**)	2.265	2.378	103.3
$[H_2P(\eta^5\text{-}C_5H_4)(HN)ZrCl_3]$ (**1***)	2.341	2.432	90.5
$[(\eta^5\text{-}C_5H_4)ZrCl_3]$ (**2**)	2.242	2.378	105.2

[a] C_g denotes the centroid of the Cp ring. [b] See Scheme 3 for the notation (1, 2).

Table 2. Selected bond lengths (Å) and bond angles (°) for complexes $[R_2P(\eta^5\text{-}C_5H_4)(R'N)ZrX_3]$ (**1***, **4***-R, **5***-R′, **6*** and **7***)

Complex	Zr−N	N−P	Zr−X(1)[a]	Zr−X(2)	Zr−X(3)	$C_g{-}Zr{-}N$[b]	$C_g{-}C_{ipso}{-}P$[c]	$C_{ipso}{-}P{-}N$	Σ[d]	$Zr{-}C_{ipso}{-}P{-}N$
1* (R = R′ = H, X = Cl)	2.357	1.613	2.432	2.428	2.414	91.2	158.1	98.4	352.9	10.9
4*-R (R′ = H, X = Cl)										
Cl	2.456	1.578	2.411	2.405	2.405	90.9	159.4	100.7	353.9	0.6
NH_2	2.319	1.616	2.441	2.438	2.475	91.2	159.2	95.9	353.0	18.1
CH_3	2.307	1.625	2.443	2.448	2.426	91.7	158.6	96.7	352.9	9.6
C_6H_5	2.298	1.626	2.447	2.429	2.453	91.1	158.3	96.5	353.0	1.6
5*-R′ (R = H, X = Cl)										
CH_3	2.340	1.617	2.437	2.435	2.421	92.2	157.6	99.1	352.6	13.4
NH_2	2.297	1.628	2.438	2.432	2.431	91.5	158.3	96.8	352.9	1.0
6* (R = R′ = H, X = I)	2.306	1.617	2.853	2.870	2.843	92.7	157.5	98.0	352.5	11.2
7* (R = C_6H_5, R′ = CH_3, X = I)	2.245	1.639	2.885	2.879	2.894	94.6	157.7	96.7	352.9	4.0

[a] See Scheme 3 for the notation (1, 2, 3). [b] C_g denotes the centroid of the Cp ring. [c] C_{ipso} denotes the substituted carbon of the Cp ring. [d] Sum of bond angles around C_{ipso}.

 © 2004 Wiley-VCH Verlag GmbH & Co. KGaA, Weinheim

Table 3. Estimated free enthalpy for the phosphazene-zirconium interaction ($\Delta_rG°_{N-Zr\ interaction}$) in complexes $[R_2P(\eta^5\text{-}C_5H_4)(R'N)ZrX_3]$ (**1***, **4***-R, **5***-R′, **6*** and **7***); negative values of $\Delta_rG°_{N-Zr\ interaction}$ imply energetically favourable N−Zr interactions

Complex	Method 1[a]	Method 2[b]	Method 3[b]
1* (R = R′ = H, X = Cl)	−8.39	15.63	−8.49
4*-R (R′ = H, X = Cl)			
Cl	−2.50	47.35	3.71
NH_2	−8.05	8.98	−14.44
CH_3	−14.68	6.54	−15.06
C_6H_5	−16.94	11.77	−15.33
5*-R′ (R = H, X = Cl)			
CH_3	−10.38	16.00	−10.40
NH_2	−15.78	9.56	−16.54
6* (R = R′ = H, X = I)	−9.86	14.39	−9.73
7* (R = C_6H_5, R′ = Me, X = I)	−19.48	9.40	−19.57

[a] Method 1 refers to the energy difference between the two energy minima, with and without an N−Zr interaction. [b] Methods 2 and 3 refer to the isodesmic reactions 1 and 2, respectively.

zirconium centre and one of the amino substituents at the phosphorus was observed for **4**-NH_2 (Scheme 6). As a consequence, the coordination strength cannot be accurately estimated in this case by the energy difference between **4**-NH_2 and **4***-NH_2.

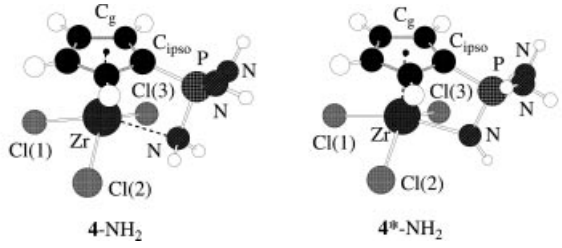

Scheme 6. Schematic representation of the B3LYP-optimized geometry of complexes **4**-NH_2 and **4***-NH_2

To circumvent this difficulty, we chose to evaluate the coordination energies through an isodesmic reaction.[21,22] The coordination exchange between the anionic ligands $(Cp)^-$ and $(Cp-PR_2=NR')^-$ was investigated first [Equation (1)]. The coordination was found to be endothermic $\{\Delta_rG°_{N-Zr\ interaction}$ [Equation (1)] $> 0\}$ and the predicted values differ significantly from those obtained previously (Table 3). This divergence has tentatively been attributed to an electronic delocalization phenomenon, $C_{ipso} \rightarrow P$, within $(Cp-PR_2=NR')^-$. To confirm this hypothesis, coordination exchange between the corresponding neutral (protonated) ligands was then investigated [Equation (2)]. The resulting $\Delta_rG°_{N-Zr\ interaction}$ [Equation (2)] values are now in very good agreement with those obtained previously (Method 1). Methods 1 and 3 differ significantly only in the case of **4***-Cl, the value of $\Delta_rG°_{N-Zr\ interaction}$ [Equation (2)] having probably been overestimated in this case due to the strong −I effect of the chlorine atoms. For all other complexes, these two methods are almost perfectly correlated (slope: 0.97, correlation factor: 0.984), so that the coordination energy for R = NH_2 estimated using Equation (2) (14.4 kcal/mol) is likely to be reliable.

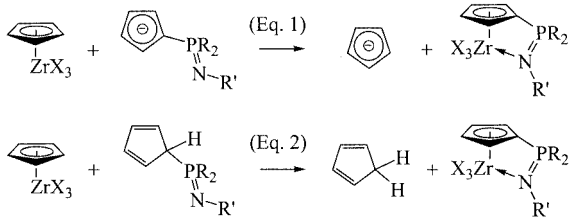

The value of $\Delta_rG°_{N-Zr\ interaction}$ was found to be negative for all complexes **4***−**6*** (from −16.9 to −2.5 kcal/mol). However, the phosphazene-zirconium interaction weakens significantly when chlorine atoms are introduced at phosphorus (**4***-Cl: −2.5 kcal/mol compared to −8.4 kcal/mol for **1***), in agreement with previously discussed structural modifications. To a first approximation, the values of $\Delta_rG°_{N-Zr\ interaction}$ are inversely proportional to the Zr−N bond lengths. Indeed, the substituents that induce the shorter Zr−N distances (NH_2, CH_3 and C_6H_5 at phosphorus, NH_2 at nitrogen) are associated with the larger coordination strengths (**4***-NH_2: 14.4, **4***-CH_3: 14.7, **4***-C_6H_5: 16.9, **5***-NH_2: 15.8 kcal/mol).

A more sophisticated complex was then studied in order to determine whether the various substituents have additive effects or not. A combination of iodine at zirconium, phenyl at phosphorus and methyl at nitrogen (complex **7***) results in the shortest N−Zr bond length (2.245 Å) and longest N−P bond length (1.639 Å) among all the complexes investigated (Table 2). The corresponding value of $\Delta_rG°_{N-Zr\ interaction}$ (given by the energy difference between **7** and **7*** i.e. 19.5 kcal/mol) is more than twice as large as that for the parent complex (Table 3). This result suggests that the various substituents indeed have additive effects. This is further corroborated by the validity of Equation (3), in which the overall substituent effect in **7*** is expressed by the combination of related single-site terms (20.1 kcal/mol).

 © 2004 Wiley-VCH Verlag GmbH & Co. KGaA, Weinheim

$$\Delta_r G^\circ_{\text{N-Zr interaction}}(\mathbf{7^*}) \approx \Delta_r G^\circ_{\text{N-Zr interaction}}(\mathbf{1^*}) + \Delta_r G^\circ_{\text{effect}}(C_6H_5) + \Delta_r G^\circ_{\text{effect}}(CH_3) + \Delta_r G^\circ_{\text{effect}}(I) \quad \text{(Eq. 3)}$$

with $\Delta_r G^\circ_{\text{effect}}(C_6H_5) = \Delta_r G^\circ_{\text{N-Zr interaction}}(\mathbf{4^*}\text{-}C_6H_5) - \Delta_r G^\circ_{\text{N-Zr interaction}}(\mathbf{1^*})$,

$\Delta_r G^\circ_{\text{effect}}(CH_3) = \Delta_r G^\circ_{\text{N-Zr interaction}}(\mathbf{5^*}\text{-}CH_3) - \Delta_r G^\circ_{\text{N-Zr interaction}}(\mathbf{1^*})$,

$\Delta_r G^\circ_{\text{effect}}(I) = \Delta_r G^\circ_{\text{N-Zr interaction}}(\mathbf{6^*}) - \Delta_r G^\circ_{\text{N-Zr interaction}}(\mathbf{1^*})$.

Cationic Complexes $[R_2P(\eta^5\text{-}C_5H_4)(R'N)ZrX_2]^+$ (1^+ and 4^+-7^+)

Calculations were then performed on the cationic complexes obtained by dissociation of one of the halides. The coordination of the phosphazene arm is strongly favoured here by the high electrophilicity of the metallic centre. Accordingly, a single minimum was located on the energy hypersurface for the parent system $\mathbf{1^+}$ (Scheme 7, Table 4). The zirconium centre adopts a pseudo-tetrahedral geometry with C_s symmetry (planar environment around the nitrogen atom and eclipsed conformation of the phosphazene arm: Zr−C_{ipso}−P−N dihedral angle of 0.2°). As expected, the halide dissociation induces a significant shortening of the Zr−N bond ($\mathbf{1^+}$: 2.166 Å compared to **1***: 2.357 Å) associated with a slight elongation of the N−P bond ($\mathbf{1^+}$: 1.647 Å compared to **1***: 1.613 Å). These modifications appear to have limited impact upon the coordination geometry, as suggested by the value of the C_g−C_{ipso}−P bond angle ($\mathbf{1^+}$: 154.9° compared to **1***: 158.1°).

The bridging $(R_2P)^+$ and (R_2Si) fragments are isolobal, and the cationic phosphorus-bridged complex $\mathbf{1^+}$ was thus also compared to the neutral silicon-bridged complex $[H_2Si(\eta^5\text{-}C_5H_4)(HN)ZrCl_2]$ (**8**) (Table 5). Since the phosphorus and silicon atoms are almost identical in size, the geometric constraint is very similar (C_g−C_{ipso}−P bond angle for **8**: 154.5°). But, as expected, the Zr−N bond is shorter in the neutral complex **8** (2.054 Å), which formally features a strongly donating silylamido arm.

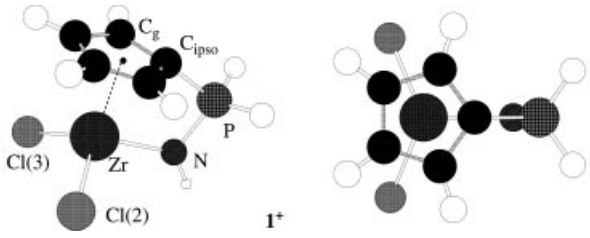

Scheme 7. Schematic representation (side and top views) of the B3LYP-optimized geometry of complex $\mathbf{1^+}$

According to NBO calculations (Table 6), the natural charges for the (NH) and (PH_2) fragments remain almost identical upon halide dissociation. In fact, the positive charge of $\mathbf{1^+}$ mainly develops on the metal centre (0.92 for the $ZrCl_2$ fragment in $\mathbf{1^+}$ compared to 0.16 for the $ZrCl_3$ fragment in **1***). Interestingly, the charge distribution in $\mathbf{1^+}$ is half-way between those of the neutral and cationic silicon-bridged complexes $[H_2Si(\eta^5\text{-}C_5H_4)(HN)ZrCl_2]$ (**8**) and $[H_2Si(\eta^5\text{-}C_5H_4)(HN)ZrCl]^+$ ($\mathbf{8^+}$) (0.74 for the $ZrCl_2$ fragment in **8** and 1.52 for the ZrCl fragment in $\mathbf{8^+}$). Complex $\mathbf{1^+}$, represented by schematic forms $\mathbf{E^+a-c}$ (Scheme 8), can

Table 4. Selected bond lengths (Å) and bond angles (°) for complexes $[R_2P(\eta^5\text{-}C_5H_4)(R'N)ZrX_2]^+$ ($\mathbf{1^+}$, $\mathbf{4^+}$-R, $\mathbf{5^+}$-R′, $\mathbf{6^+}$ and $\mathbf{7^+}$)

Complex	Zr−N	N−P	Zr−X(2)[a]	Zr−X(3)	C_g−Zr−N[b]	C_g−C_{ipso}−P[c]	C_{ipso}−P−N	Σ[d]	Zr−C_{ipso}−P−N
$\mathbf{1^+}$ (R = R′ = H, X = Cl)	2.166	1.647	2.341	2.340	95.9	154.9	97.0	351.4	0.2
$\mathbf{4^+}$-R (R′ = H, X = Cl)									
Cl	2.191	1.625	2.335	2.335	96.1	155.3	97.9	352.0	0.1
NH_2	2.147	1.652	2.349	2.352	95.4	156.8	94.5	352.4	2.3
CH_3	2.139	1.665	2.350	2.349	95.8	156.0	94.8	351.9	0.3
C_6H_5	2.128	1.671	2.355	2.360	96.0	156.4	94.0	352.1	0.6
$\mathbf{5^+}$-R′ (R = H, X = Cl)									
CH_3	2.150	1.651	2.347	2.346	96.8	154.4	97.8	352.1	0.3
NH_2	2.144	1.664	2.348	2.348	95.5	155.5	95.4	351.9	0.2
$\mathbf{6^+}$ (R = R′ = H, X = I)	2.164	1.646	2.724	2.734	96.2	154.7	97.1	351.3	0.1
$\mathbf{7^+}$ (R = C_6H_5, R′ = CH_3, X = I)	2.108	1.680	2.745	2.756	97.0	156.2	94.0	352.0	2.6

[a] See Scheme 7 for the notation (2, 3). [b] C_g denotes the centroid of the Cp ring. [c] C_{ipso} denotes the substituted carbon atom of the Cp ring. [d] Sum of bond angles around C_{ipso}.

Table 5. Selected bond lengths (Å) and bond angles (°) for complexes $[H_2Si(\eta^5\text{-}C_5H_4)(HN)ZrCl_2]$ (**8**) and $[H_2Si(\eta^5\text{-}C_5H_4)(HN)ZrCl]^+$ ($\mathbf{8^+}$)

Complex	Zr−N	N−Si	Zr−Cl	C_g−Zr−N[a]	C_g−C_{ipso}−Si[b]	C_{ipso}−Si−N	Σ[c]	Zr−C_{ipso}−Si−N
$[H_2Si(\eta^5\text{-}C_5H_4)(HN)ZrCl_2]$ (**8**)	2.054	1.756	2.399	98.6	154.5	92.5	350.2	0.0
$[H_2Si(\eta^5\text{-}C_5H_4)(HN)ZrCl]^+$ ($\mathbf{8^+}$)	2.005	1.798	2.341	99.6	152.7	90.3	349.6	0.3

[a] C_g denotes the centroid of the Cp ring. [b] C_{ipso} denotes the substituted carbon atom of the Cp ring. [c] Sum of bond angles around C_{ipso}.

 © 2004 Wiley-VCH Verlag GmbH & Co. KGaA, Weinheim

Table 6. NBO charges[7] for selected fragments of the parent complexes **1***, **1**$^+$, **8**, **8**$^+$, **9**$^-$, **9** and **9**$^+$

Complex	$ZrCl_n$	NH/N	PH_2/SiH_2	Cp
$[H_2P(\eta^5\text{-}C_5H_4)(HN)ZrCl_3]$ (**1***)	0.16	−0.90	1.39	−0.65
$[H_2P(\eta^5\text{-}C_5H_4)(HN)ZrCl_2]^+$ (**1**$^+$)	0.92	−0.88	1.49	−0.54
$[H_2Si(\eta^5\text{-}C_5H_4)(HN)ZrCl_2]$ (**8**)	0.74	−0.97	1.04	−0.81
$[H_2Si(\eta^5\text{-}C_5H_4)(HN)ZrCl]^+$ (**8**$^+$)	1.52	−0.92	1.12	−0.72
$[H_2P(\eta^5\text{-}C_5H_4)(N)ZrCl_3]^-$ (**9**$^-$)	−0.18	−1.31	1.28	−0.78
$[H_2P(\eta^5\text{-}C_5H_4)(N)ZrCl_2]$ (**9**)	0.68	−1.30	1.35	−0.73
$[H_2P(\eta^5\text{-}C_5H_4)(N)ZrCl]^+$ (**9**$^+$)	1.45	−1.25	1.44	−0.64

thus be considered as the cationic version of the "CpSiN" complex **A**.

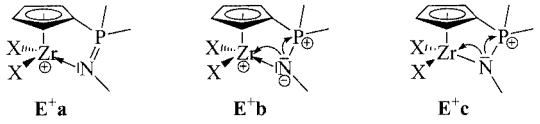

Scheme 8. Schematic representations of complex **E**$^+$

The cationic complexes **4**$^+$−**6**$^+$ featuring the various substitution patterns were then studied (Table 4). The resulting structural modifications are very similar to those observed for the neutral precursors **4***−**6***. Comparison of the free enthalpies for the halide dissociation at 298 K in the gas phase [Equation (4)] yields a quantitative determination of the substituent effects (Table 7). As expected, the ionic dissociation of the neutral complexes **1*** and **4***−**6*** is highly endothermic. The absolute values for $\Delta_rG^\circ_{Zr-X\ dissociation}$ cannot be discussed properly, since solvation and counteranion effects were not taken into account, although comparisons give more insight into the substituent effects. With regard to changes in the nature of the substituent at phosphorus (complexes **4**$^+$-R), $\Delta_rG^\circ_{Zr-X\ dissociation}$ decreases along the series Cl > H > NH_2 > CH_3 > C_6H_5 with a maximum variation of 23.3 kcal/mol. The least and most favourable patterns for the halide dissociation are encountered by introduction of chlorine atoms and phenyl groups, respectively. These results parallel those observed for the phosphazene coordination (see above), and indeed, the influence of the phosphorus substituents on the Zr−X dissociation is nicely correlated with that on the N−Zr interaction (Scheme 9). In marked contrast, introduction of an amino group at the nitrogen atom (**5***-NH_2) induces a strong reinforcement of the Zr−N interaction, but only a small variation of $\Delta_rG^\circ_{Zr-X\ dissociation}$. In other words, the substituents at nitrogen have a much less pronounced effect on $\Delta_rG^\circ_{Zr-X\ dissociation}$ than those at phosphorus. Lastly, the halide dissociation is obviously more favourable for **6**$^+$ (X = iodine) than for **1**$^+$ (X = chlorine). Here again substituent effects are basically cumulative. Association of the most favourable substituents results in a decrease in $\Delta_rG^\circ_{Zr-X\ dissociation}$ by 37.4 kcal/mol for **7**$^+$ compared to **1**$^+$.

Table 7. Estimated free enthalpy change for the halide dissociation from neutral complexes $[R_2P(\eta^5\text{-}C_5H_4)(R'N)ZrX_3]$ (**1***, **4***-R, **5***-R′, **6*** and **7***) to the related cationic complexes $[R_2P(\eta^5\text{-}C_5H_4)(R'N)ZrX_2]^+$ (**1**$^+$, **4**$^+$-R, **5**$^+$-R′, **6**$^+$ and **7**$^+$)

Complex	$\Delta_rG^\circ_{Zr-X\ dissociation}$
1$^+$ (R = R′ = H, X = Cl)	117.9
4$^+$-R (R′ = H, X = Cl)	
Cl	126.7
NH_2	110.7
CH_3	110.2
C_6H_5	103.4
5$^+$-R′ (R = H, X = Cl)	
CH_3	115.7
NH_2	119.7
6$^+$ (R = R′ = H, X = I)	95.3
7$^+$ (R = C_6H_5, R′ = CH_3, X = I)	80.5

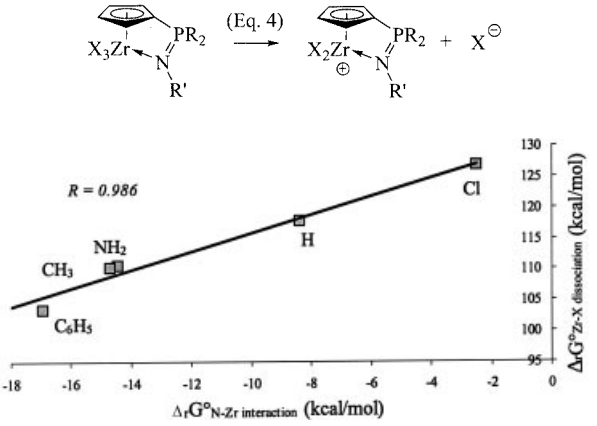

Scheme 9. Correlation of the influence of the phosphorus substituents on the N−Zr interaction and Zr−X dissociation; $\Delta_rG^\circ_{N-Zr\ interaction}$ determined with Method 1, except for R = NH_2 (Method 3)

Complexes Featuring a Pendant Phosphinimido Unit $[H_2P(\eta^5\text{-}C_5H_4)(N)ZrCl_3]^-$ (**9**$^-$), $[H_2P(\eta^5\text{-}C_5H_4)(N)ZrCl_2]$ (**9**) and $[H_2P(\eta^5\text{-}C_5H_4)(N)ZrCl]^+$ (**9**$^+$)

Calculations were then carried out on the related complexes **9**$^-$, **9** and **9**$^+$ featuring the dianionic ligand $(Cp-PR_2=N)^{2-}$ and the $ZrCl_3^+$, $ZrCl_2^{2+}$ and $ZrCl^{3+}$ fragments, respectively (Scheme 10). The presence of the strongly donating phosphinimido unit clearly favours the N−Zr interaction, which was observed for all these complexes.

Coordination of $(Cp-PR_2=N)^{2-}$ to the $ZrCl_3^+$ fragment does not induce the spontaneous dissociation of one chloride from the zirconium coordination sphere, and the anionic complex **9**$^-$ remains an energy minimum. The zirconium in **9**$^-$ adopts a pseudo-square-pyramidal environment, and the imido is inherently bent (Zr−*N*−P: 102.2°). The major difference concerns the N−Zr bond length, which is, as expected, considerably shorter in **9**$^-$ (2.075 Å) than in **1*** (2.357 Å). The reinforcement of this N−Zr interaction induces some increase in the geometry constraint, as illustrated by the bending of the $C_g-C_{ipso}-P$ bond angle (**8**$^-$: 149.6° compared to **1***: 158.1°). According to the NBO analysis, the excess negative charge is distributed over the $ZrCl_3$ fragment (−0.18) and the nitrogen atom (−1.31), in agreement with schematic structures **9**$^-$**a** and **9**$^-$**c** (Scheme 10).

 © 2004 Wiley-VCH Verlag GmbH & Co. KGaA, Weinheim

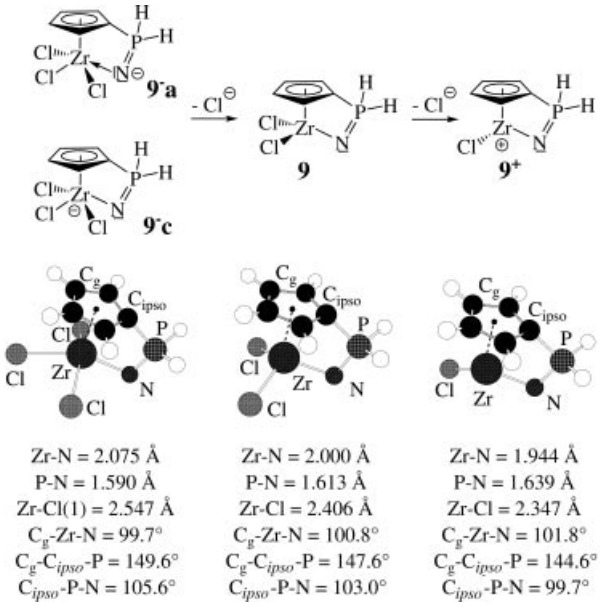

Scheme 10. Structure, schematic representation and selected geometric data of the B3LYP-optimized complexes **9**$^-$, **9** and **9**$^+$

Not surprisingly, dissociation of one chlorine leads to the neutral complex **9**, featuring a pseudo-tetrahedral geometry. Chlorine dissociation is much more favourable for **9** ($\Delta_rG°_{Zr-X\ dissociation}$ = 18.9 kcal/mol) than for **1*** (117.9 kcal/mol). The N−Zr bond length (2.000 Å) is shorter than that of **9**$^-$, but the difference is significantly smaller than that predicted for the phosphazene-containing complexes **1**. Dissociation of a second chlorine affords the cationic complex **9**$^+$ featuring a pyramidal zirconium centre[23] and a yet shorter N−Zr bond length (1.944 Å).

Complexes **9** and **9**$^+$ are strongly related to the silicon-bridged systems **8** and **8**$^+$. The N−Zr bond lengths are only slightly shorter and the geometry constraint marginally higher in the phosphorus-bridged complexes. This analogy is corroborated by the similarity of both the NBO charges for the $ZrCl_2$ (**9**: 0.68/**8**: 0.74) and ZrCl (**9**$^+$: 1.45/ **8**$^+$: 1.52) fragments (Table 6) and the free enthalpies calculated for **9** → **9**$^+$ (155.2 kcal/mol) and **8** → **8**$^+$ (159.7 kcal/mol).

Lastly, phosphinimido-based complexes **F** were compared with their phosphinamido-based isomers **C**.[10b] Isomerization between (NH)-aminophosphanes [R_2P-(NH)R′] and (PH)-phosphazenes [R_2(PH)=NR′] is indeed a well-known process, including in metal complexes.[24] Calculations were thus carried out on model complexes of type **C** and, accordingly, the phosphinamido complexes **10** and **10**$^+$ are predicted to be 25.7 and 20.6 kcal/mol more stable than the related phosphinimido complexes **9** and **9**$^+$ (Scheme 11). These values are in the same range as that reported by Schoeller for the free ligands $(H_2P\text{-}NH)^-$ and $(H_3P{=}N)^-$ (31 kcal/mol in favour of the NH tautomer).[24d] The stabilization of the PH tautomer usually observed upon metal coordination is thus strongly balanced in this case by the ensuing increase in the geometric constraints (from **9** to **10** and **9**$^+$ to **10**$^+$, the N−Zr and N−P bonds are noticeably elongated and the bending of C_{ipso} is significantly released).

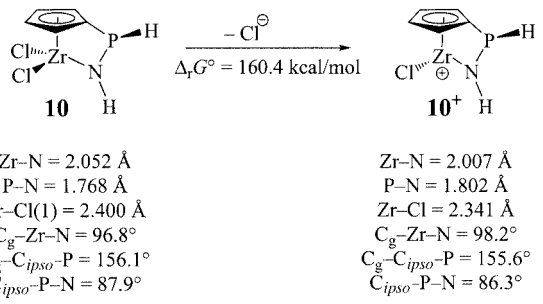

Scheme 11. Structure and selected geometric data of the B3LYP-optimized complexes **10** and **10**$^+$

Concluding Remarks

Theoretical investigations of phosphazene- and phosphinimido-based complexes **E** and **F** reveal numerous similarities but also noticeable differences with the "CpSiN" catalysts **A**. In particular, NBO natural charges suggest a significantly higher metal electrophilicity for **E** than for **A** (the positive charge is mainly localized on the $ZrCl_2$ fragment). Substituent effects are predicted to be additive and they influence strongly the structure and properties of both neutral and cationic complexes **E** and **E**$^+$. Their influences on the N−Zr coordination strength and Zr−X dissociation appear to be strongly correlated, at least with respect to the nature of the phosphorus substituents. Phosphinimido-based complexes **F** are geometrically and electronically strongly related to the "CpSiN" catalysts **A**, but significantly more constrained than the related phosphinamido complexes **C**. Accordingly tautomerization of the parent complexes **9** → **10** and **9**$^+$ → **10**$^+$ is predicted to be energetically favoured.

These results as a whole suggest that constrained-geometry complexes featuring phosphazene and phosphinimido arms might indeed be interesting alternatives for the "CpSiN" catalysts. Accordingly, the interaction of complexes **E** and **F** with alkenes clearly deserves to be studied, and detailed investigations in this field are planned.

Computational Details

All calculations were carried out with the Gaussian 98[25] suite of programs at the DFT level of theory using the hybrid functional B3LYP as implemented in that program.[26,27] Halide, phosphorus, silicon and zirconium atoms were treated with the Averaged Relativistic Effective Core Potentials (AREPs) optimized by the Dresden-Stuttgart-Bonn group (Cl, I, P, Si[28] and Zr[29]). Basis sets adapted to the AREPs augmented with a d polarization function were used for the atoms of the *p*-block (exp_P = 0.387, exp_{Si} = 0.284,[30] exp_{Cl} = 0.643, exp_I = 0.730[31]) and an f polarization function was used for the zirconium atom (exp_{Zr} = 0.975[32]). Carbon, nitrogen and hydrogen were treated with an all-electron double-ζ 6-31G(d,p) basis set.[33] Geometry optimiza-

 © 2004 Wiley-VCH Verlag GmbH & Co. KGaA, Weinheim

tions were performed without spatial symmetry constraints and the nature of the extrema was verified by analytical calculations of vibrational frequencies. The atomic charges were obtained by NBO analyses.[34]

Acknowledgments

Thanks are due to the CNRS, UPS and French Ministry of Research and New Technologies (ACI JC4091) for financial support of this work.

[1] [1a] A. L. McKnight, R. M. Waymouth, *Chem. Rev.* **1998**, *98*, 2587. [1b] G. J. P. Britovsek, V. C. Gibson, D. F. Wass, *Angew. Chem. Int. Ed.* **1999**, *38*, 429. [1c] V. C. Gibson, S. K. Spitzmesser, *Chem. Rev.* **2003**, *103*, 283.

[2] [2a] P. J. Shapiro, E. Bunel, W. P. Schaefer, J. E Bercaw, *Organometallics* **1990**, *9*, 867. [2b] J. Okuda, *Chem. Ber.* **1990**, *123*, 1649.

[3] For theoretical investigation of CGC mechanistic aspects, see: [3a] T. K. Woo, P. M. Margl, J. C. W. Lohrenz, P. E. Blöchl, T. Ziegler, *J. Am. Chem. Soc.* **1996**, *118*, 13021. [3b] G. Lanza, I. L. Fragalà, T. J. Marks, *Organometallics* **2001**, *20*, 4006. [3c] G. Lanza, I. L. Fragalà, T. J. Marks, *Organometallics* **2002**, *21*, 5594.

[4] [4a] S. Feng, J. Klosin, W. J. Kruper Jr, M. H. McAdon, D. R. Neithamer, P. N. Nickias, J. T. Patton, D. R. Wilson, K. A. Abboud, C. L. Stern, *Organometallics* **1999**, *18*, 1159. [4b] A. J. Ashe, X. G. Fang, J. W. Kampf, *Organometallics* **1999**, *18*, 1363. [4c] J. Klosin, W. J. Kluper Jr, P. N. Nickias, G. R. Roof, P. De Waele, K. A. Abboud, *Organometallics* **2001**, *20*, 2663.

[5] [5a] P. J. Sinnema, L. v. d. Veen, A. L. Spek, N. Veldman, J. H. Teuben, *Organometallics* **1997**, *16*, 4245. [5b] P. T. Gomes, M. L. H. Green, A. M. Martins, *J. Organomet. Chem.* **1998**, *551*, 133. [5c] L. Duda, G. Erker, R. Fröhlich, F. Zippel, *Eur. J. Inorg. Chem.* **1998**, 1153. [5d] D. van Leusen, D. J. Beestra, B. Hessen, J. H. Teuben, *Organometallics* **2000**, *19*, 4084. [5e] H. Braunschweig, C. von Koblinski, U. Englert, *Chem. Commun.* **2000**, 1049. [5f] K. Kunz, G. Erker, S. Döring, R. Fröhlich, G. Kehr, *J. Am. Chem. Soc.* **2001**, *123*, 6181. [5g] K. Kunz, G. Erker, S. Döring, S. Bredeau, G. Kehr, R. Fröhlich, *Organometallics* **2002**, *21*, 1031. [5h] V. V. Kotov, E. V. Avtomonov, J. Sundermeyer, K. Harms, D. A. Lemenovskii, *Eur. J. Inorg. Chem.* **2002**, 678.

[6] J. Jin, D. R. Wilson, E. Y. X. Chen, *Chem. Commun.* **2002**, 708.

[7] [7a] F. Amor, A. Butt, D. E. du Plooy, T. P. Spaniol, J. Okuda, *Organometallics* **1998**, *17*, 5836. [7b] J. Okuda, T. Eberle, T. P. Spaniol, V. Piquet-Faure, *J. Organomet. Chem.* **1999**, *591*, 127. [7c] J. T. Park, S. C. Yoon, B. J. Bae, W. S. Seo, I. H. Suh, T. K. Han, J. R. Park, *Organometallics* **2000**, *19*, 1269.

[8] For simultaneous variation of the bridging unit and donor site, see: [8a] Y. X. Chen, P. F. Fu, C. L. Stern, T. J. Marks, *Organometallics* **1997**, *16*, 5958. [8b] K. Kunz, G. Erker, G. Kehr, R. Fröhlich, H. Jacobsen, H. Berke, O. Blacque, *J. Am. Chem. Soc.* **2002**, *124*, 3316. [8c] T. Ishiyama, T. Mizuta, K. Miyoshi, H. Nakazawa, *Organometallics* **2003**, *22*, 1096. [8d] L. E. Turner, M. G. Thorn, P. E. Fanwick, I. P. Rothwell, *Chem. Commun.* **2003**, 1034.

[9] For doubly bridged complexes, see: [9a] W. A. Herrmann, M. J. A. Morawietz, T. Priermeier, *Angew. Chem. Int. Ed. Engl.* **1994**, *33*, 1946. [9b] J. Cano, P. Royo, M. Lanfranchi, M. A. Pellinghelli, A. Tiripicchio, *Angew. Chem. Int. Ed.* **2001**, *40*, 2495. [9c] J. Cano, P. Royo, H. Jacobsen, O. Blacque, H. Berke, E. Herdtweck, *Eur. J. Inorg. Chem.* **2003**, 2463.

[10] [10a] S. J. Brown, X. Gao, D. G. Harrison, L. Koch, R. E. v. H. Spence, G. P. A. Yap, *Organometallics* **1998**, *17*, 5445. [10b] V. V. Kotov, E. V. Avtomonov, J. Sundermeyer, K. Harms, D. A. Lemenovskii, *Eur. J. Inorg. Chem.* **2002**, 678. [10c] G. Altenhoff, S. Bredeau, G. Erker, G. Kehr, O. Kataeva, R. Fröhlich, *Organometallics* **2002**, *21*, 4084.

[11] M. Witt, H. W. Roesky, *Chem. Rev.* **1994**, *94*, 1163.

[12] [12a] M. Sauthier, F. Leca, R. Fernando de Souza, K. Bernardo-Gusmão, L. F. T. Queiroz, L. Toupet, R. Réau, *New J. Chem.* **2002**, *26*, 630. [12b] M. T. Reetz, E. Bohres, R. Goddard, *Chem. Commun.* **1998**, 935. [12c] J. M. Brunel, O. Legrand, S. Reymond, G. Buono, *J. Am. Chem. Soc.* **1999**, *121*, 5807. [12d] M. Sauthier, J. Forniés-Cámer, L. Toupet, R. Réau, *Organometallics* **2000**, *19*, 553.

[13] [13a] K. Dehnicke, M. Krieger, W. Massa, *Coord. Chem. Rev.* **1999**, *182*, 19. [13b] H. J. Cristau, M. Taillefer, N. Rahier, *J. Organomet. Chem.* **2002**, *646*, 94.

[14] [14a] T. Rubenstahl, F. Weller, S. Wacadlo, W. Massa, K. Dehnicke, *Z. Anorg. Allg. Chem.* **1995**, *621*, 953. [14b] S. Anfang, K. Harms, F. Weller, O. Borgmeier, H. Lueken, H. Schilder, K. Dehnicke, *Z. Anorg. Allg. Chem.* **1998**, *624*, 159.

[15] [15a] D. W. Stephan, J. C. Stewart, F. Guérin, R. E. v. H. Spence, W. Xu, D. G. Harrison, *Organometallics* **1999**, *18*, 1116. [15b] D. W. Stephan, F. Guérin, R. E. v. H. Spence, L. Koch, X. Gao, S. J. Brown, J. W. Swabey, Q. Wang, W. Xu, P. Zoricak, D. G. Harrison, *Organometallics* **1999**, *18*, 2046. [15c] J. E. Kickham, F. Guérin, J. C. Stewart, D. W. Stephan, *Angew. Chem. Int. Ed.* **2000**, *39*, 3263. [15d] F. Guérin, C. L. Beddie, D. W. Stephan, R. E. v. H. Spence, R. Wurz, *Organometallics* **2001**, *20*, 3466. [15e] N. Yue, E. Hollink, F. Guérin, D. W. Stephan, *Organometallics* **2001**, *20*, 4424. [15f] C. Ong, J. Kickham, S. Clemens, F. Guérin, D. W. Stephan, *Organometallics* **2002**, *21*, 1646. [15g] J. Kickham, F. Guérin, D. W. Stephan, *J. Am. Chem. Soc.* **2002**, *124*, 11486. [15h] D. W. Stephan, J. C. Stewart, F. Guérin, S. Courtenay, J. Kickham, E. Hollink, C. Beddie, A. Hoskin, T. Graham, P. Wie, R. E. v. H. Spence, W. Xu, L. Koch, X. Gao, D. G. Harrison, *Organometallics* **2003**, *22*, 1937. [15i] L. P. Spencer, R. Altwer, P. Wei, L. Gelmini, J. Gauld, D. W. Stephan, *Organometallics* **2003**, *22*, 3841.

[16] P. Kubáček, R. Hoffmann, Z. Havlas, *Organometallics* **1982**, *1*, 180.

[17] K. A. O. Starzewski, H. T. Dieck, *Inorg. Chem.* **1979**, *18*, 3307.

[18] S. F. Boys, *Rev. Mod. Phys.* **1960**, *32*, 296.

[19] At the suggestion of one of the referees, a few tests were performed with a larger basis set including diffuse functions either on nitrogen alone or both on nitrogen and carbon [6-31+G(d,p) instead of 6-31G(d,p)]. Changes of less than 0.01 Å were observed for the N−Zr bond lengths of complex **1*** and the coordination strengths decreased by only 1 kcal/mol.

[20] W. C. Lu, C. C. Sun, *J. Mol. Struct. (Theochem)* **2002**, *593*, 1.

[21] P. George, C. W. Bock, M. Trachtman, *J. Chem. Ed.* **1988**, *61*, 225.

[22] W. J. Hehre, R. Ditchfield, L. Radom, J. A. Pople, *J. Am. Chem. Soc.* **1970**, *92*, 4796.

[23] L. Perrin, L. Maron, O. Eisenstein, *Faraday Discuss.* **2003**, *124*, 25.

[24] [24a] G. Schick, A. Loew, M. Nieger, K. Airola, E. Niecke, *Chem. Ber.* **1996**, *129*, 211. [24b] G. Schick, M. Raab, D. Gudat, M. Nieger, E. Niecke, *Angew. Chem. Int. Ed.* **1998**, *37*, 2390. [24c] S. Schulz, M. Raab, M. Nieger, E. Niecke, *Organometallics* **2000**, *19*, 2616. [24d] M. Raab, A. Sundermann, G. Schick, A. Loew, M. Nieger, W. W. Schoeller, E. Niecke, *Organometallics* **2001**, *20*, 1770. [24e] S. Schulz, T. Bauer, M. Nieger, I. Krossing, *Chem. Commun.* **2002**, 1422. [24f] T. Bauer, S. Schulz, M. Nieger, U. Kessler, *Organometallics* **2003**, *22*, 3134.

[25] M. J. Frisch, G. W. Trucks, H. B. Schlegel, G. E. Scuseria, M. A. Robb, J. R. Cheeseman, V. G. Zakrzewski, J. A. Montgomery, R. E. Stratemann, J. C. Burant, S. Dapprich, J. M. Millam, A. D. Daniels, K. N. Kudin, M. C. Strain, O. Farkas, J. Tomasi, V. Barone, M. Cossi, R. Cammi, B. Mennucci, C. Pomelli, C. Adamo, S. Clifford, J. Ochterski, G. A. Peterson, P. Y. Ayala, Q. Cui, K. Morokuma, D. K. Malick, A. D. Rabuck, K. Raghavachari, J. B. Foresman, J. Ciolowski, J. V. Ortiz, B. B. Stefanov, G. Liu, A. Liashenko, P. Piskorz, I. Nanayakkara, C.

 © 2004 Wiley-VCH Verlag GmbH & Co. KGaA, Weinheim

Gonzalez, M. Challacombe, P. M. W. Gill, B. G. Johnson, W. Chen, M. W. Wong, J. L. Andres, M. Head-Gordon, E. S. Replogle, et J. A. Pople. Gaussian 98, Revision A7, Gaussian Inc., Pittsburgh, PA, **1998**.
[26] A. D. Becke, *J. Chem. Phys.* **1993**, *98*, 5648.
[27] C. Lee, W. Yang, R. G. Parr, *Phys. Rev.* **1988**, *37*, B785.
[28] A. Bergner, M. Dolg, W. Kuechle, H. Stoll, H. Preuss, *Mol. Phys.* **1993**, *80*, 1431.
[29] D. Andrae, U. Haeussermann, M. Dolg, H. Stoll, H. Preuss, *Theor. Chim. Acta* **1990**, *77*, 123.
[30] A. Höllwarth, M. Böhme, S. Dapprich, A. W. Ehlers, A. Gobbi, V. Jonas, K. F. Köhler, R. Stegmann, A. Veldkamp, G. Frenking, *Chem. Phys. Lett.* **1993**, *208*, 237.
[31] L. Maron, C. Teichteil, *Chem. Phys.* **1998**, *237*, 105.
[32] A. W. Ehlers, M. Böhme, S. Dapprich, A. Gobbi, A. Höllwarth, V. Jonas, K. F. Kölher, R. Stegmann, A. Veldkamp, G. Frenking, *Chem. Phys. Lett.* **1993**, *208*, 111.
[33] W. J. Hehre, R. Ditchfield, J. A. Pople, *J. Chem. Phys.* **1972**, *56*, 2257.
[34] [34a] NBO version 3.1. [34b]A. E. Reed, F. Weinhold, *J. Chem. Phys.* **1983**, *78*, 1736. [34c] A. E. Reed, F. Weinhold, *J. Chem. Phys.* **1983**, *78*, 4066. [34d] A. E. Reed, R. B. Weinstock, F. Weinhold, *J. Chem. Phys.* **1985**, *83*, 735. [34e] A. E. Reed, L. A. Curtis, F. Weinhold, *Chem. Rev.* **1988**, *88*, 899. [34f] E. D. Glendening, A. E. Reed, J. E. Carpenter, F. Weinhold, *J. Mol. Struct. (Theochem)* **1988**, *169*, 41. [34g] J. P. Foster, F. Weinhold, *J. Am. Chem. Soc.* **1988**, *102*, 7211.

Received October 21, 2003
Early View Article
Published Online March 30, 2004

 © 2004 Wiley-VCH Verlag GmbH & Co. KGaA, Weinheim

Switch of the Lowest Excited-States of Terpyridylplatinum(II) Acetylide Complexes Bearing Amino or Azacrown Moieties by Proton and Cations

Qing-Zheng Yang,[a] Qing-Xiao Tong,[a] Li-Zhu Wu,*[a] Zi-Xin Wu,[a] Li-Ping Zhang,[a] and Chen-Ho Tung*[a]

Keywords: Crown compounds / N ligands / Platinum / Sensors

The investigation of the synthesis and unique photophysical properties of two terpyridylplatinum(II) acetylide complexes [Pt(terpy)(C≡CC_6H_4-4-R)] where terpy is 2,2′:6′,2′′-terpyridyl and R = $N(CH_3)_2$ (**1**) or *N*-15-monoazacrown-5 (**2**) has been carried out. These complexes exhibit an absorption band in the region of 460–650 nm in neutral or basic solution that corresponds to a ligand-to-ligand charge transfer (LLCT) transition from the amino-substituted acetylide to the terpyridyl acceptor. In acidic solutions the complexes show the lowest-energy absorption band at 380–500 nm, which is assignable to a dπ(Pt)→π*(terpy) metal-to-ligand charge transfer (MLCT) transition. In acidic media the complexes are emissive with quantum yields of 1×10^{-3} to 2×10^{-3}, and lifetimes of 20–50 ns. Compound **2** may complex metal cations through its azacrown ether moiety. For Na^+, Ba^{2+}, Ca^{2+} and Mg^{2+}, a 1:1 binding mode with log *K*s of 2.52 to 4.18 was observed. As in the case of acidic solution, the cation-bound complex also features the lowest-lying MLCT excited state.
(© Wiley-VCH Verlag GmbH & Co. KGaA, 69451 Weinheim, Germany, 2004)

Introduction

The creation of host molecules that can selectively recognize specific guest molecules at their receptor site and produce a measurable physical change has been the subject of intense study.[1,2] Of particular interest is the design of molecules that show dramatic and reversible changes in color and/or luminescence in the visible spectral region upon exposure to specific substrates.[3−6] In this context square-planar platinum(II) complexes show considerable promise due to their rich and medium-sensitive spectroscopic and photophysical behavior.[7−10] In particular, alkynyl complexes of platinum(II) have received much attention because these complexes generally display bright luminescence with high quantum yields and long lifetimes, and a number of excellent studies have been performed.[11−23] Che and co-workers[11] reported a luminescent platinum(II) acetylide complex with aromatic diimine ligands in 1994. The [Pt(C≡CPh)$_2$(phen)] (phen = 1,10-phenanthroline) complex exhibits intense emission in fluid solution at room temperature, which was attributed to a triplet metal-to-ligand charge transfer [^{3}MLCT: dπ(Pt) → π*(phen)] excited state. Later on, Eisenberg and co-workers,[12−14] and Schanze and co-workers[15] investigated the excited-state properties of a series of complexes of the type [Pt(C≡C−Ar)$_2$(diimine)], where diimine is a series of 2,2′-bipyridine or 1,10-phenanthroline ligands and C≡C−Ar is a series of substituted arylacetylide ligands. They systematically examined the influence of the electronic demand of the diimine and arylacetylide ligands on the properties of the MLCT excited state, and revealed that in most cases the photophysics of the complexes is dominated by the energetically low-lying dπ(Pt) → π*(diimine) ^{3}MLCT state. Some of the complexes also feature a low-lying triplet intraligand (^{3}IL) ππ* excited state that is derived from transitions between π-type orbitals localized largely on the arylacetylide ligands.[16] Recently, Che and co-workers have used diiminepalatinum(II) bis(arylacetylide) complexes as emitters in organic light-emitting devices.[17,18]

The photoluminescence of [*trans*-Pt(C≡CR)$_2$](PEt_3)$_2$, where R = H or phenyl, in the solid state and frozen glass solution at 77 K was investigated by Demas and co-workers.[19] The emission was assigned as arising from a charge transfer excited state involving Pt d_{z^2} and acetylide π* orbitals. Yam and co-workers reported the luminescence of branched alkynylplatinum(II) complexes containing the [PtCl(C≡CC_6H_4C≡C)(PEt_3)$_2$] moiety, and suggested that the emission originates from a mixed π → π* (C≡CR) intraligand (IL)/$d_{z(Pt)}$ → π* (C≡CR) MLCT triplet state with predominantly IL character.[20] The photophysics of terpyridylplatinum(II) acetylide complexes and tridentate cyclometalated platinum(II) complexes bearing σ-alkynyl ligands was also reported.[21−23] Yam and co-workers investigated the photophysics and electrochemistry of a series of terpyridylplatinum(II) acetylide complexes with the general for-

[a] Technical Institute of Physics and Chemistry, the Chinese Academy of Sciences,
Beijing 100101, P. R. China
Fax: (internat.) +86-10-6487-9375
E-mail: chtung@mail.ipc.ac.cn
lzwu@mail.ipc.ac.cn

 © 2004 Wiley-VCH Verlag GmbH & Co. KGaA, Weinheim DOI: 10.1002/ejic.200300878

mula $[Pt(C{\equiv}CC_6H_4R)(terpy)]PF_6$, and found that the emission energies depend on the nature of the acetylide ligands with different substituents on the phenyl ring:[21] an electron-withdrawing group on the phenyl ring increases the emission energy. Our laboratory has reported the photoluminescence of a series of 4′-*p*-tolyl-terpyridylplatinum(II) acetylide complexes.[22] These complexes exhibit long-lived emission from the ^{3}MLCT states with high emission quantum yields. The complexes bearing (C≡CR) ligands with R = alkyl in dichloromethane solution at room temperature show lifetimes greater than 10 μs and emission quantum yields greater than 0.25. We found that the cyclometalated platinum(II) complexes [Pt(C^N^N)(C≡CC_6H_4R)] where HC^N^N = 6-phenyl-4-*p*-tolyl-2,2′-bipyridine, also show photoluminescence with long lifetimes.[23]

Although the spectroscopic properties of alkynylplatinum(II) complexes have been extensively studied,[11−23] the utilization of such complexes for applications in molecular recognition and chemosensing work is rare.[21] In this paper we describe the syntheses and unique photophysical properties of two terpyridylplatinum(II) acetylide complexes [Pt(C≡ CC_6H_4-4-R)(terpy)] where R = $N(CH_3)_2$ (**1**) or *N*-15-monoazacrown-5 (**2**; Scheme 1). The amino groups in these complexes serve as proton receptors. In neutral or basic solutions, **1** and **2** are non-emissive and their low-energy absorption arises from a ligand-to-ligand charge transfer (LLCT) transition from the amino-substituted acetylide to the terpyridyl acceptor with a deep purple color. Upon protonation, these complexes display luminescence and their MLCT dπ→ π*(terpy) transition becomes the lowest energy absorption and the solutions are yellow in color. Thus, these complexes can be utilized as a chemosensor for proton detection by monitoring the changes both in luminescence and color. Significantly, the azacrown moiety in complexes **2** can also serve as metal-ion receptor. Upon complexing a metal cation, its ^{1}LLCT excited state shifts energetically to be above the ^{1}MLCT excited state, hence producing color changes from deep purple to yellow. Thus, **2** can also be employed as a chemosensor for the detection of metal ions. To the best of our knowledge, this is the first example to use the switch of the lowest excited state from the ^{3}LLCT to the ^{3}MLCT state of metal complexes for chemosensors.

Results and Discussion

Synthesis

The synthetic strategy for making the terpyridylplatinum(II) acetylide complexes is based on a CuI-catalyzed chloride-to-acetylide metathesis. Complexes **1** and **2** were prepared by reaction of [PtCl(terpy)]Cl with two equivalents of 4-(dimethylamino)phenylacetylene and 4-ethynylphenyl-*N*-15-monoazacrown-5 ether, respectively, in DMF in the presence of CuI and triethylamine at room temperature. After the metathesis reaction with KBF_4 for **1** or $LiClO_4$ for **2**, and recrystallization of the crude products by vapor diffusion of diethyl ether into an acetonitrile solution, **1** and **2** were obtained as dark-blue crystals in 70−76% yield. The identity of complexes **1** and **2** was confirmed by ^{1}H NMR spectroscopy, MS spectrometry and satisfactory elemental analyses. For comparison, the complex [Pt(C≡CC_6H_5)(terpy)]ClO_4 (**3**; Scheme 1) was also synthesized by a similar procedure.

Crystal Structure of Complex 1

A dark-blue single-crystal of dimensions 0.05 × 0.2 × 0.5 mm^3 in a glass capillary was used for data collection at 296 K on a Bruker Smart1000 X-ray diffractometer. The molecular structure and perspective drawing of the complex are depicted in Figure 1. The crystal belongs to the triclinic crystal system of centrosymmetric space group $P\bar{1}$ with unit cell parameters of a = 9.4033(8) Å, b = 11.0229(10) Å, c = 12.4015(11) Å; α = 101.619(2)°, β = 106.128(2)°, γ = 103.441(2)°, Important bond lengths and angles are given in Table 1. The coordination geometry about the platinum is essentially square planar with the bond from platinum to the central nitrogen atom of the terpyridine ligand slightly shorter than that to the other two outer nitrogen atoms, as is required by the steric demands of the terpyridine ligand. All the Pt−N distances are in the range found for typical platinum(II) terpyridine complexes.[21,28,29] The N−Pt−N angles [N(1)−Pt(1)−N(2): 80.59(17); N(2)−Pt(1)−N(3): 80.63(18); N(1)−Pt(1)−N(3): 161.18(19)] deviate from the idealized values of 90° and 180° as a consequence of the geometric constraints imposed by the terpyridyl ligands. The Pt−C bond length is 1.977 Å, which compares well with a value of 1.98 Å for other terpyridylplatinum(II) ace-

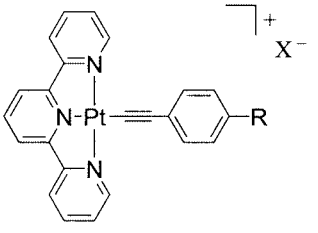

1. R = $N(CH_3)_2$ $X^- = BF_4^-$

2. R = 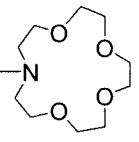 $X^- = ClO_4^-$

3. R = H $X^- = ClO_4^-$

Scheme 1

 © 2004 Wiley-VCH Verlag GmbH & Co. KGaA, Weinheim

tylide complexes.[21] The C≡C bond length of 1.193 Å is similar to those of the other related platinum(II) acetylide complexes.[12,21,30] The phenyl ring of the acetylide ligand is almost coplanar to the platinum-terpyridine plane, with a dihedral angle of 4.5°. The crystal packing of **1** reveals a head-to-tail stacking between pairs of complex cations. The intermolecular Pt···Pt distance of 8.146 Å and the intermolecular separation of 6.718 Å between the terpy ligand and the phenyl group of the acetylide moiety are suggestive of a lack of intermolecular interactions between the metal centers and the aromatic groups.

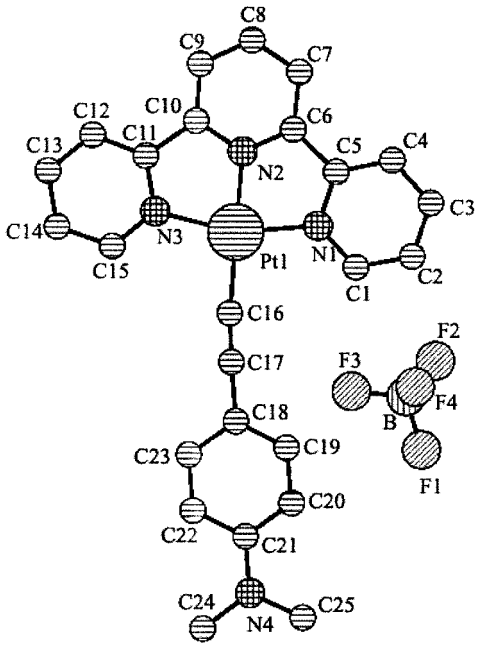

Figure 1. Perspective drawing of complex **1** with atomic numbering. (30% probability ellipsoids)

Table 1. Important bond lengths (Å) and bond angles (°) for complex **1**

Pt(1)−N(1)	2.004(4)	Pt(1)−N(2)	1.956(4)
Pt(1)−N(3)	2.014(5)	Pt(1)−C(16)	1.977(6)
C(16)−C(17)	1.193(8)	N(1)−Pt(1)−N(2)	80.59(17)
N(1)−Pt(1)−N(3)	161.18(19)	N(1)−Pt(1)−C(16)	98.3(2)
N(2)−Pt(1)−N(3)	80.63(18)	N(2)−Pt(1)−C(16)	178.00(19)
N(3)−Pt(1)−C(16)	100.5(2)	Pt(1)−C(16)−C(17)	173.7(5)

Absorption Spectra

Figure 2 presents the UV/Vis spectra of complexes **1** and **2** in acetonitrile solution. For comparison, the absorption spectrum of **3** is also shown in Figure 2. All the complexes exhibit intense vibronic-structured absorption bands at wavelengths below 350 nm, with extinction coefficients (ε) of the order of 10^4 $dm^3 \cdot mol^{-1} \cdot cm^{-1}$, and a less-intense band at 380−500 nm (centered at ca. 410, 411 and 432 nm with ε = 2860, 2950 and 4410 $dm^3 \cdot mol^{-1} \cdot cm^{-1}$ for **1**, **2** and **3** respectively). Significantly, complexes **1** and **2** show a moderately intense low-energy absorption band in the region of 460−650 nm (absorption maximum λ_{max} = 535 and 548 nm, ε = 4920 and 5370 $dm^3 \cdot mol^{-1} \cdot cm^{-1}$ for **1** and **2**, respectively). Complex **3** does not show such a band. The absorption spectral properties are found to follow Beer's Law at concentrations below 1×10^{-3} $mol \cdot dm^{-3}$, suggesting that no significant complex aggregation occurs. With reference to previous spectroscopic work on terpyridylplatinum(II) complexes,[21,22,31−34] the absorption bands at wavelengths below 350 nm are assigned to the intraligand (IL) transition of terpyridyl and acetylide ligands, while the absorption band at 380−500 nm is ascribed to the $d\pi(Pt) \rightarrow \pi^*$ (terpy) MLCT transition. The low-energy absorption band in the region of 460−650 nm for **1** and **2** is tentatively assigned to the LLCT transition from the amino-substituted acetylide ligand to the terpyridyl acceptor. This assignment is based on the following observations. First, the energy of the band increases with solvent polarity. For example, λ_{max} of the band for **1** is blue-shifted from 595 nm in dichloromethane to 535 nm in acetonitrile. This suggests that the ground state of the complex is more polar than its excited state, and is consistent with the notion that in the ground state the acetylide ligand is carbanionic in nature, and in the LLCT excited state the terpyridyl-acetylide ligands are like a diradical. Second, we have performed cyclic voltammetry studies on complexes **1** and **3** in acetonitrile. Both complexes exhibit two quasi-reversible cathodic waves in the potential region −0.8 to −1.5 V vs. SCE. By analogy to previous studies on other terpyridylplatinum(II) complexes,[21,22] these waves are ascribed to the reduction of the terpyridyl ligand with some mixing of the Pt^{II} character. Complex **3** displays an irreversible anodic wave with E_p at +1.22 V vs. SCE which has been assigned to a metal-centered oxidation from Pt^{II} to Pt^{III} by Yam and co-workers.[21] On the other hand, for complex **1** we observed an irreversible anodic wave near +0.63 V vs. SCE. Upon addition of an acid to the solution, this wave disappeared. Cyclic voltammetry of the uncomplexed ligand, *p*-(dimethylamino)-phenylacetylene exhibits a similar anodic wave at a slightly more positive potential (ca. +0.85 V vs. SCE). Thus, we

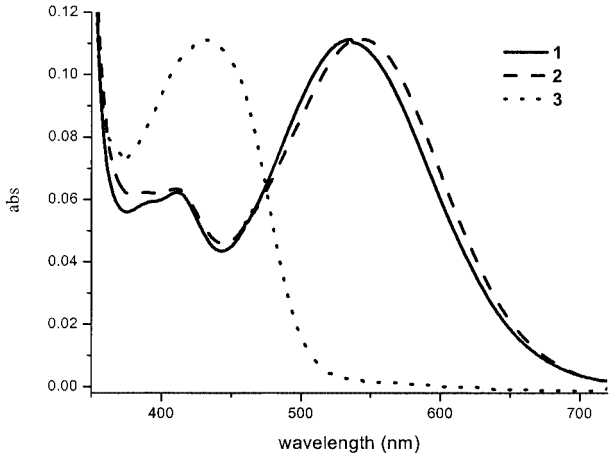

Figure 2. The normalized absorption spectra of complexes **1**−**3** in acetonitrile solutions at room temperature

 © 2004 Wiley-VCH Verlag GmbH & Co. KGaA, Weinheim

assign the wave near +0.63 V to the oxidation of the amino-substituted acetylide ligand. Obviously, the LLCT transition in **1** should be at lower energy than the MLCT transition. Third, the lowest energy absorption band (λ_{max} = 535 and 548 nm) for **1** and **2** is red-shifted by more than 100 nm compared with that of **3** (λ_{max} = 432 nm). This observation is not consistent with the assignment of the 535 and 548 nm bands to a MLCT transition, because it has been established[12,21] that variation of the acetylide in platinum(II) acetylide complexes does not lead to very large changes in the Pt-based HOMO and the terpyridyl-based LUMO, hence it is not expected to affect the energy of the MLCT transition very much.

An Acid/Base-Controlled Molecular Switch based on Complexes 1 and 2

An initial observation when working with an acetonitrile solution of complex **1** was the change of the deep-purple color in neutral solution to yellow when exposed to a micromolar concentration of HBF_4. Such a dramatic color change, especially the large blue-shift of the absorption band in a dilute acidic medium, prompted an investigation of the nature of the acid-dependent absorption. Figure 3 shows the absorption spectra of complex **1** (3.87×10^{-5} mol·dm^{-3}) in acetonitrile as a function of added HBF_4. Upon addition of HBF_4 to the solution, the decrease in the absorption band at 535 nm is accompanied by a growth in the band with a maximum at 418 nm. Isosbestic points are observed at 457, 358, 344, 337 and 279 nm, indicative of the presence of only two absorbing species in the solution. The insert in Figure 3 shows a plot of the absorbance at 535 nm vs. the concentration of added HBF_4. Similar changes in the absorption spectrum were observed for complex **2** upon addition of HBF_4. In contrast, addition of HBF_4 to a solution of complex **3** in acetonitrile causes no marked changes in the absorption. These observations are evidently attributed to the protonation of the amino group in the acetylide ligands for complexes **1** and **2**. As the amino receptor is protonated in the presence of HBF_4, its electron-donating ability is decreased. This would dramatically lower the HOMO of the acetylide ligand. The Pt-based HOMO would also be lowered, but the extent of this lowering is expected to be much less than that of the acetylide ligand (Scheme 2). As a result, the LLCT transition from the amino-substituted acetylide ligand to the terpyridyl acceptor shifts to higher energy, and the dπ(Pt) → π*(terpy) MLCT transition becomes the lowest-energy transition.

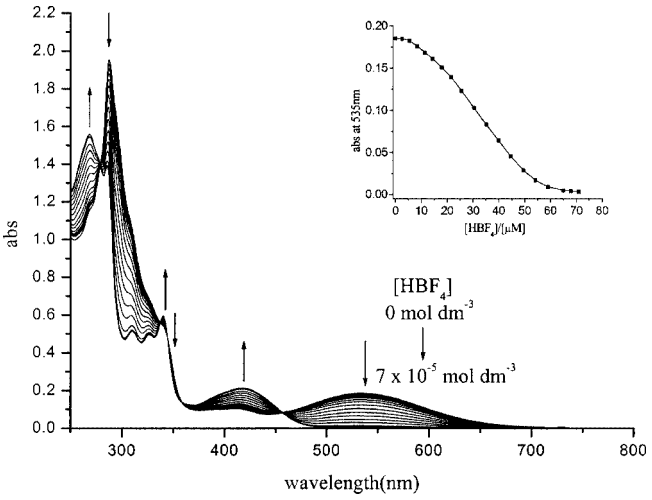

Figure 3. Absorption spectrum changes of complex **1** (3.87×10^{-5} mol·dm^{-3}) upon addition of various concentrations ($0-7 \times 10^{-5}$ mol·dm^{-3}) of HBF_4 in acetonitrile; the insert gives the titration curve for the plot of the absorbance at 535 nm vs. the concentration of HBF_4

The change in the luminescence response of complexes **1** and **2** towards protons was found to be even more pronounced. In neutral or basic solution **1** and **2** are non-emissive. The lack of emission upon excitation of the MLCT band is attributed to the transfer of the electron pair on the amino groups to the Pt^{III} metal center, resulting in an LLCT excited state. Because of the low energy, the ^{3}LLCT excited state decays via a non-radiative pathway. However, in acidic medium **1** and **2** exhibit a structureless emission band centered at about 560 nm. Figure 4 shows the change in the emission spectrum of **1** as a function of HBF_4 concentration. Throughout the titration, the excitation wavelength corresponds to the isosbestic point found at 457 nm in Figure 3. The emission intensity is noticeably

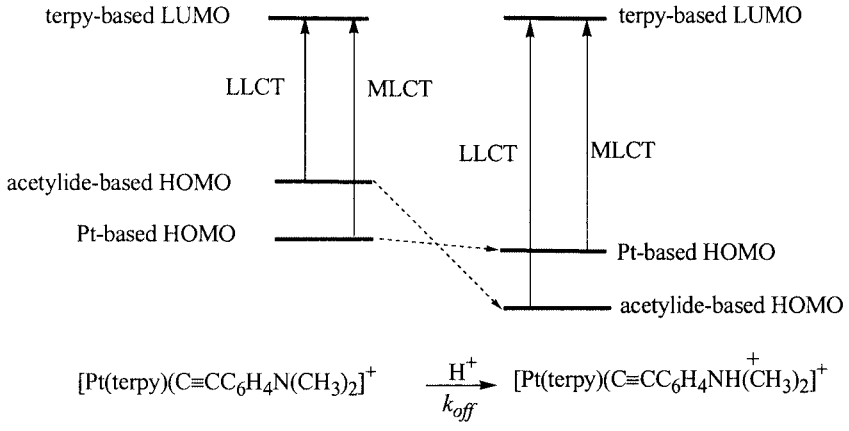

Scheme 2

 © 2004 Wiley-VCH Verlag GmbH & Co. KGaA, Weinheim

enhanced upon increasing HBF_4 concentration, with saturation observed toward the end of the titration, while the shape and energy of the emission band remain unchanged. With reference to previous work on the emission of terpyridylplatinum(II) complexes,[21,22,29,31] this emission is assigned as being derived from the $d\pi(Pt)\rightarrow\pi^*$(terpy) ^{3}MLCT excited state. The insert in Figure 4 shows a plot of the emission intensity at 560 nm against the concentration of HBF_4. The emission quantum yields of **1** and **2** in their protonated form were measured to be 0.001 and 0.002, respectively, and their lifetimes 0.02 and 0.05 μs, respectively. Similar to the absorption studies, control experiments with complex **3** under the same conditions showed no change in the emission character upon addition of HBF_4. Evidently, the emission of complexes **1** and **2** upon addition of HBF_4 originates from protonation of the amino group. As mentioned above, upon protonation the ^{3}MLCT excited state becomes the lowest state and displays luminescence.

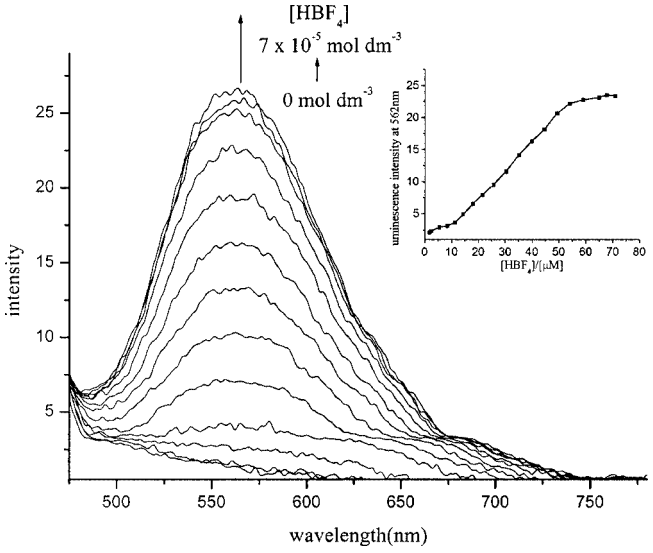

Figure 4. Luminescence spectrum changes of **1** (3.87×10^{-5} mol·dm^{-3}) upon addition of various concentrations ($0-7 \times 10^{-5}$ mol·dm^{-3}) of HBF_4 in acetonitrile; the insert shows the luminescence intensity at 560 nm as a function of HBF_4 concentration

The changes in absorption and emission behavior for complexes **1** and **2** are fully reversible. For example, subsequent addition of a base (e.g. triethylamine) to the acidic solution of **1** in acetonitrile led to the observation of a reverse trend: the luminescence was gradually quenched, and the absorbance at 418 nm dropped, with a concomitant rise in the absorption at 535 nm. Eventually the LLCT band in the absorption spectrum was totally recovered, and the solution became deep purple again. This result is indicative of the reversible nature of the protonation and deprotonation processes for the amino group in complexes **1** and **2**.

Cation-Binding Properties of Complex 2

Alkali and alkaline earth metal cations have profound effects on the absorption spectrum of **2**. Addition of Na^+, Ba^{2+}, Ca^{2+} or Mg^{2+}, as their perchlorate salts, to a solution of **2** in acetonitrile leads to dramatic changes in the absorption spectrum. Figure 5 presents the changes in the UV/Vis spectrum of **2** upon addition of Ca^{2+}. The lowest energy band at 548 nm decreases monotonically throughout the addition, while the band at 390−470 nm concomitantly grows-in with increasing Ca^{2+} concentration. Well-defined isosbestic points at 465, 375, 347, 342 and 283 nm were clearly observed. The solution becomes yellow at the end of the titration. Similar results were observed upon addition of other cations to the solution of **2**. This phenomenon evidently arises from the complexation of the cation with the azacrown ether receptor in the acetylide ligand, which decreases the electron-donating ability of the acetylide ligand, hence lowering the acetylide-based HOMO. Thus, the LLCT transition from the azacrown-containing acetylide ligand to the terpyridyl acceptor shifts to higher energy, and the $d\pi(Pt)\rightarrow\pi^*$(terpy) MLCT transition becomes the lowest energy absorption. Indeed, control experiments with the crown-free analogues **1** and **3** showed no such absorption spectrum changes upon addition of the cations under identical conditions. The insert in Figure 5 shows the plot of $A_0/(A_0 - A)$ vs. $[Ca^{2+}]^{-1}$, where A and A_0 refer to the absorbance at 548 nm for complex **2** in the presence and absence of Ca^{2+}, respectively. The straight line suggests that the complexation of the cation to the azacrown ether is in a 1:1 ratio. The bonding constants (log *K*s) determined from such plots for the cations are Na^+ (2.52), Ba^{2+} (3.01), Ca^{2+} (4.18) and Mg^{2+} (3.76), and their absolute values are very similar to those of other aza-15-crown-5 ionophores reported in the literature.[35]

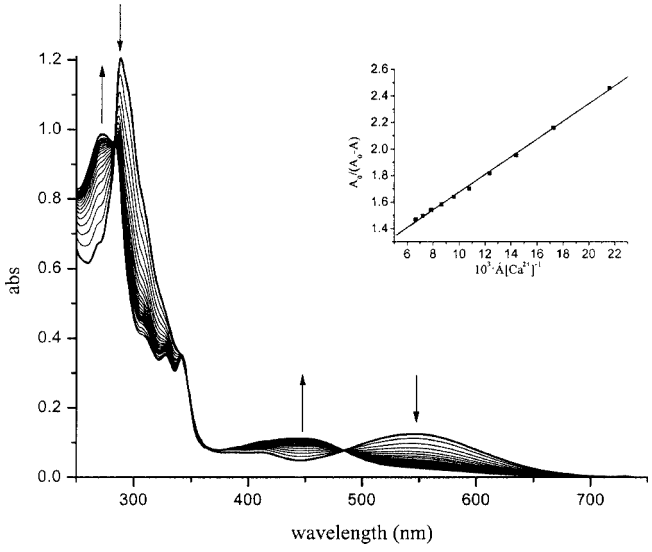

Figure 5. Absorption spectrum changes of **2** upon addition of various concentrations of Ca^{2+} in acetonitrile solution; the insert shows the plot of $A_0/(A_0 - A)$ vs. $[Ca^{2+}]^{-1}$

Complexation of cations with the azacrown ether receptor in **2** also affects the MLCT transition. We noted that the λ_{max} of the MLCT band of **2** complexed with the cations shifts to the blue side along the series Na^+ (481 nm),

 © 2004 Wiley-VCH Verlag GmbH & Co. KGaA, Weinheim

Ba^{2+} (470 nm), Ca^{2+} (446 nm) and Mg^{2+} (430 nm). This reflects the difference in the strength of the ion-dipole interaction between the cations and the crown nitrogen. A strong interaction will further reduce the electron-donating ability of the acetylide and would make the metal center in **2** less electron-rich, and hence decrease the dπ(Pt)-orbital energy and cause the MLCT transition to occur at higher energy. It is well-known that the charge densities[36] of the metal ions increase in the following order: Na^+ (0.10) < Ba^{2+} (0.13) < Ca^{2+} (0.24) < Mg^{2+} (0.75). Mg^{2+} has the highest charge density in the series of metal ions studied in this work, and its value is considerably larger than the other cations. As a result, the interaction between Mg^{2+} and the crown nitrogen would be strongest, and complexation with this cation leads to the highest energy of the MLCT transition among the **2**·M^{n+} complexes.

In contrast to protonated **1** and **2**, complexation with metal cations does not cause luminescence from complex **2**, although the ^{3}MLCT state becomes the lowest energy excited state after complexation, as reflected in the absorption spectrum changes. This lack of emission may be interpreted by a kinetic model (Scheme 3) proposed by Schanze[37] for explanation of ion effect on the photophysics of a Re^I complex. In this scheme (N^N^N) and (C≡CPhAc) represent, respectively, the terpyridyl ligand and the acetylide with monoazacrown in complex **2**. Excitation of the **2**·M^{n+} complex produces the ^{1}MLCT state, which undergoes an intersystem crossing to the ^{3}MLCT state. Since the metal center in MLCT excited states (Pt^{III}) is much more electrophilic than that in the ground state (Pt^{II}), the charge density on the amino group will be reduced. This in turn decreases the binding ability of the azacrown, leading to the dissociation of the crown-complexed cation from the azacrown within the lifetime of the MLCT state. Thus, in addition to the normal radiative and non-radiative pathways, the ^{3}MLCT state of **2**·M^{n+} can also decay by a non-radiative pathway involving the dissociation of the crowned cation (k_{off}) followed by rapid internal conversion into the ^{3}LLCT state (k_{ic}). As a result, no emission could be detected from the acetonitrile solution of **2**·M^{n+}. The K_{off} values can be estimated by reference to the lifetime of the ^{3}MLCT state of protonated **2**. Assuming the deprotonation of **2**·H^+ in its ^{3}MLCT state is not competitive with the normal ^{3}MLCT decay rate, the lifetime (τ_1) of the ^{3}MLCT state of protonated **2** can be used to estimate the "normal" decay rate [$1/(k_r + k_{nr})$] of the ^{3}MLCT state of **2**·M^{n+}; k_{off} can then be obtained approximately from the lifetime (τ_2) of the ^{3}MLCT state of the **2**·M^{n+} complexes.

$$k_{off} = 1/\tau_2 - 1/\tau_1$$

The limiting value for the lifetime measurements in our instruments is > 0.2 ns, thus τ_2 for the complexes of **2** with cations is smaller than 0.2 ns. The emission lifetime (τ_1) of protonated **2** was measured to be 50 ns, as mentioned above. The k_{off} values obtained should therefore be greater than 5×10^9 s^{-1} for the cation-crowned complexes.

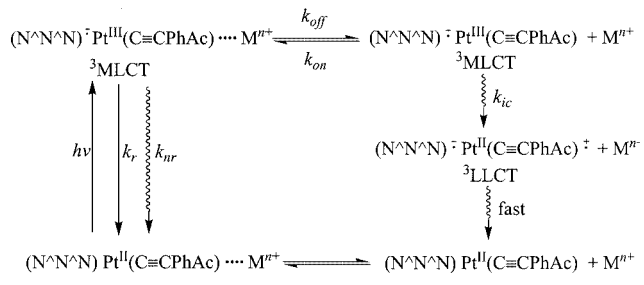

Scheme 3

Conclusion

Two terpyridylplatinum(II) acetylide complexes, one having an amino group and the other containing a monoazacrown moiety in their acetylide ligand, were prepared and their medium-sensitive photophysical properties were investigated. Incorporation of the amino or azacrown group into the acetylide destabilizes the HOMO of this ligand, hence in neutral or basic solutions the low-energy absorption of these complexes arises from the LLCT transition from the acetylide ligand to the terpyridyl acceptor. These complexes are non-emissive due to the fast non-radiative decay of the ^{3}LLCT excited state. Upon protonation of the amino group the HOMO of the acetylide ligand is lowered, thus the LLCT transition shifts to high energy, and the dπ(Pt)→π* (terpy) MLCT transition becomes the lowest energy absorption. In this case, the ^{3}MLCT state displays luminescence with a reasonably high quantum yield and long lifetime. Complexing a metal cation with the azacrown in complex **2** also results in a switch between the LLCT and MLCT transitions and dramatic absorption spectrum changes. The lack of emission for the cation-bound **2** is due to the dissociation of the crowned cation from the azacrown within the lifetime of the ^{3}MLCT state, and the rapid internal conversion from the ^{3}MLCT to the ^{3}LLCT states for the cation-free complex. These complexes can be utilized for molecular recognition and chemosensors specific for detection of proton and metal cations.

Experimental Section

Materials: 4-(Dimethylamino)phenylacetylene and [PtCl(terpy)]Cl·$2H_2O$ were prepared by literature methods.[24,25] 4-Ethynylphenyl-*N*-15-azacrown-5 ether was synthesized by a modified literature method.[24,26] Acetonitrile was distilled after refluxing for 3 h in the presence of P_2O_5. Other reagents were of analytical grade and used as received.

[Pt{C≡CC_6H_4-4-N$(CH_3)_2$}(terpy)]BF_4 (1): A mixture of [Pt(terpy)Cl]Cl·$2H_2O$ (100 mg, 0.19 mmol), CuI (10 mg), 4-(dimethylamino)phenylacetylene (55 mg, 0.38 mmol), 3 mL of DMF, and 4 mL of trimethylamine was sonicated under nitrogen for 8 h. An excess of an aqueous solution of KBF_4 was then added to the mixture. Dark-blue crystals were obtained after stirring for 1 h. The product was isolated, washed with water and diethyl ether. Subsequent recrystallization by diffusion of diethyl ether vapor into an acetonitrile solution of the product gave **1** as dark-blue crystals. Yield: 96 mg (76%). FAB-MS: *m/z* = 572 [M^+]. ^{1}H NMR ([D_6]DMSO): δ = 2.93 (s, 6 H), 6.68 (d, *J* = 8.4 Hz, 2 H), 7.34 (d,

 © 2004 Wiley-VCH Verlag GmbH & Co. KGaA, Weinheim

J = 8.2 Hz, 2 H), 7.95 (t, J = 6.3 Hz, 2 H), 8.58 (m, 7 H), 9.21(d, J = 5.1 Hz, 2 H). $C_{25}H_{21}BF_4N_4Pt\cdot0.5H_2O$ (668.36): calcd. C 44.92, H 3.29, N 8.39; found C 44.87, H 3.59, N 8.58.

[Pt(C≡CC$_6$H$_4$-4-*N*-15-monoazacrown-5)(terpy)]ClO$_4$ (2): The synthesis of **2** was similar to that for complex **1**, except 4-ethynylphenyl-*N*-15-azacrown-5 ether was used in place of 4-(dimethylamino)phenylacetylene, and $LiClO_4$ was used in place of KBF_4. Yield: 110 mg (70%). FAB-MS: m/z = 746 [M^+]. ^{1}H NMR ([D$_6$]DMSO): δ = 3.64−3.82 (m, 20 H), 6.76 (d, J = 8.8 Hz, 2 H), 7.40 (d, J = 8.8 Hz, 2 H), 8.00 (t, J = 6.1 Hz, 2 H), 8.56−8.73 (m, 7 H), 9.16 (d, J = 5.1 Hz, 2 H). $C_{33}H_{35}ClN_4O_8Pt\cdot0.5H_2O$ (855.21): calcd. C 46.35, H 4.24, N 6.55; found C 46.32, H 4.18, N 6.15.

Physical Measurements and Instrumentation: UV/Vis spectra were obtained on a Shimadzu UV-1601PC spectrophotometer. Steady-state emission spectra were recorded on a Perkin Elmer LS50B spectrofluorometer. Elemental analysis was performed on a Carlo Erba 1106 elemental analyzer. ^{1}H NMR spectra were recorded on a Bruker-400 FT NMR spectrometer with chemical shifts (in ppm) relative to tetramethylsilane. FAB-MS spectra were run on a KYKY-ZHP mass spectrometer. X-ray analysis was performed on a Bruker Smart1000 X-ray diffractometer. Excited-state lifetimes were measured using a conventional laser system. The excitation source was the 355 nm line from the output of a Nd:YAG laser (third harmonic, 10 ns). All solutions were purged with argon for 15 min for emission spectra and lifetime measurements. The quantum yields of the emission were obtained by the optical dilute method using a degassed acetonitrile solution of $[Ru(bpy)_3](PF_6)_2$ as a reference (Φ = 0.062).[22] The ion-binding constants for **2** were calculated from the Hildebrand−Benesi equation: [27]

$$A_0/(A_0 - A) = A_0/\alpha[\text{complex } \mathbf{2}] + (A_0/\alpha[\text{complex } \mathbf{2}]\ Ks)\cdot(1/[M^{n+}])$$

where A and A_0 are the absorbance for complex **2** in the presence and absence of a metal ion, respectively, α is the ratio of complexation between complex **2** and the cation and Ks is the binding constant.

Crystallographic data for the structure reported in this paper have been deposited with the Cambridge Crystallographic Data Centre as supplementary publication No. CCDC-199962. Copies of the data can be obtained free of charge on application to CCDC, 12 Union Road, Cambridge CB2 1EZ, UK [Fax: (internat.) +44-1223/336-033; E-mail: deposit@ccdc.cam.ac.uk].

Acknowledgments

Financial support from the Ministry of Science and Technology of China (Grant Nos. G2000078104 and G2000077502) and the National Science Foundation of China (Nos. 20332040, 20333080, 20125207, 20272066, 20202013) is gratefully acknowledged. We also thank Dr. Jia-Hong Zhou for the cyclic voltammetry measurements, Prof. Wen Li for the emission lifetime measurements, and Prof. Ming Xiong and Mr. Guowu Li for the determination of the single crystal structure.

[1] J.-M. Lehn, *Supramolecular Chemistry, Concepts and Perspective*, VCH, Weinheim, **1995**.
[2] *Chemosensors of Ion and Molecular Recognition* (Eds.: J.-P. Desvergne, A. W. Czarnik), Kluwer, Dordrecht, **1997**, vol. 492.
[3] *Fluorescent Chemosensors for Ions and Molecule Recognition* (Ed.: A. W. Czarnik), Am. Chem. Soc., Washington DC, **1993**.
[4] A. P. de Silva, H. Q. Gunaratne, T. Gunnlaugsson, A. J. M. Huxley, C. P. McCoy, J. T. Rademacher, T. E. Rice, *Chem. Rev.* **1997**, *97*, 1515.
[5] D. H. Lee, J. H. Im, S. U. Son, Y. K. Chung, J.-I. Hong, *J. Am. Chem. Soc.* **2003**, *125*, 7752.
[6] M. S. Han, D. H. Kim, *Angew. Chem. Int. Ed.* **2002**, *41*, 3809.
[7] K. H. Wong, M. C. W. Chan, C. M. Che, *Chem. Eur. J.* **1999**, *5*, 2845.
[8] L.-Z. Wu, T. C. Cheung, C. M. Che, K. K. Cheung, M. H. W. Lam, *Chem. Commun.* **1998**, 1127.
[9] X.-H. Li, L.-Z. Wu, L.-P. Zhang, C.-H. Tung, C.-M. Che, *Chem. Commun.* **2001**, *21*, 2280.
[10] M. Kato, A. Omura, A. Toshikawa, S. Kishi, Y. Suginmoto, *Angew. Chem. Int. Ed.* **2002**, *41*, 3183.
[11] C.-W. Chan, L.-K. Cheng, C.-M. Che, *Coord. Chem. Rev.* **1994**, *132*, 87.
[12] M. Hissler, W. B. Connick, D. K. Geiger, J. E. McGarrah, D. Lipa, R. J. Lachiocotte, R. Eisenberg, *Inorg. Chem.* **2000**, *39*, 447.
[13] M. Hissler, J. E. McGarrah, W. B. Connick, D. K. Geiger, S. D. Cummings, R. Eisenberg, *Coord. Chem. Rev.* **2000**, *208*, 115.
[14] J. E. McGarrah, Y.-J. Kim, M. Hissler, R. Eisenberg, *Inorg. Chem.* **2001**, *40*, 4510.
[15] C. E. Whittle, J. A. Weinstein, M. W. George, K. S. Schanze, *Inorg. Chem.* **2001**, *40*, 4053.
[16] I. E. Pomestchenko, C. R. Luman, M. Hissler, R. Ziessel, F. N. Castellano, *Inorg. Chem.* **2003**, *42*, 1394.
[17] S.-C. Chan, M. C. W. Chan, Y. Wang, C.-M. Che, K.-K. Cheung, N. Zhu, *Chem. Eur. J.* **2001**, *7*, 4180.
[18] W. Lu, B.-X. Mi, M. C. W. Chan, Z. Hui, N. Zhu, S.-T. Lee, C.-M. Che, *Chem. Commun.* **2002**, 206.
[19] L. Sacksteder, E. Baralt, B. A. Degraff, C. M. Lukehart, J. N. Demas, *Inorg. Chem.* **1991**, *30*, 2468.
[20] V. W. W. Yam, C. H. Tao, L. Zhang, C. M. C. Wong, K. K. Cheung, *Organometallics* **2001**, *20*, 453.
[21] V. W.-W. Yam, R. P. L. Tang, K. M. C. Wong, K. K. Cheung, *Organometallics* **2001**, *20*, 4476.
[22] Q.-Z. Yang, L.-Z. Wu, Z.-X. Wu, L.-P. Zhang, C.-H. Tung, *Inorg. Chem.* **2002**, *41*, 5653.
[23] Z.-X. Wu, L.-Z. Wu, Q.-Z. Yang, L.-P. Zhang, C.-H. Tung, *Chin. J. Chem.* **2003**, *21*, 196.
[24] K. A. Leonard, M. I. Nelen, L. T. Anderson, S. L. Gibson, R. Hilf, M. R. Detty, *J. Med. Chem.* **1999**, *42*, 3942.
[25] M. Howe-Grant, S. J. Lippard, *Inorg. Synth.* **1980**, *20*, 101.
[26] C.-T. Chen, W.-P. Huang, *J. Am. Chem. Soc.* **2002**, *124*, 6246 and references cited therein.
[27] H. A. Benesi, J. H. Hildebrand, *J. Am. Chem. Soc.* **1949**, *71*, 2703.
[28] B. C. Tzeng, W. F. Fu, C. M. Che, H. Y. Chao, K. K. Cheung, S. M. Peng, *J. Chem. Soc., Dalton Trans.* **1999**, 1017.
[29] S. W. Lai, M. C. W. Chan, K. K. Cheung, C.-M. Che, *Inorg. Chem.* **1999**, *38*, 4262.
[30] C. J. Adams, S. L. James, X. Liu, P. R. Raithby, L. J. Yellowless, *J. Chem. Soc., Dalton Trans.* **2000**, 63.
[31] T. K. Aldridge, E. M. Stacy, D. R. McMillin, *Inorg. Chem.* **1994**, *33*, 722.
[32] J. A. Bailey, G. M. Hill, R. E. Marsh, V. M. Miskowski, W. P. Schaefer, H. B. Gray, *Inorg. Chem.* **1995**, *34*, 4591.
[33] G. Arena, G. Calogero, S. Campagna, L. M. Scolaro, V. Ricevuto, R. Romeo, *Inorg. Chem.* **1998**, *37*, 2763.
[34] D. R. McMillin, J. J. Moore, *Coord. Chem. Rev.* **2002**, *229*, 113.
[35] W. Burgermeister, R. Winkler-Oswatitsch, *Top. Curr. Chem.* **1977**, *69*, 91.
[36] The charge density (ρ) is defined as the amount of electronic charge per unit volume. It is given here by $\rho = g/(4/3\ \pi\ r^3)$ where g is the formal charge (+1 or +2) and r is the Shannon ion radius. The following values of r (Å) were used: Na^+ (1.32), Mg^{2+} (0.86), Ca^{2+} (1.26), Ba^{2+} (1.56): R. D. Shannon, *Acta Crystallogr.* **1976**, *32*, 751.
[37] D. B. MacQueen, K. S. Schanze, *J. Am. Chem. Soc.* **1991**, *113*, 6108.

Received November 17, 2003
Early View Article
Published Online March 30, 2004

 © 2004 Wiley-VCH Verlag GmbH & Co. KGaA, Weinheim

Easy Synthesis of New Chiral Tridentate Schiff Bases and Their Use as [N,N,O] Ligands for Ni and Pd Complexes − Catalytic Behaviour versus Hydrogenation Reactions[‡]

Camino González-Arellano,[a,b] Enrique Gutiérrez-Puebla,[a] Marta Iglesias,*[a] and Félix Sánchez*[b]

Keywords: Palladium / Nickel / Chiral Schiff bases / Hydrogenation / Tridentate ligands

The chiral [N,N,O] tridentate unsymmetrical Schiff bases **3**–**5** (aryl = phenyl, 1-naphthyl, 2-naphthyl) were synthesised easily in high purity and good yields. All the organic compounds were characterised by elemental analysis, mass spectrometry, IR, ^{1}H and ^{13}C NMR spectroscopy. Palladium(II) and nickel(II) Schiff-base complexes were prepared as air-stable solids. Because the [N,N,O] ligand is tridentate after deprotonation of the –OH group, the coordination of the metal ion is completely stereospecific and gives rise to only one diastereoisomer. The X-ray crystal structures of the complexes [Ni(**3**)(OAc)] and [Pd(**4**)(OAc)] were determined. These complexes were shown to be very active catalysts (TOF up to 10^6 h^{-1}) for the hydrogenation of olefins and imines under mild conditions.
(© Wiley-VCH Verlag GmbH & Co. KGaA, 69451 Weinheim, Germany, 2004)

Introduction

The development of efficient catalytic asymmetric reactions is one of the most challenging tasks in current synthetic chemistry, much effort having been devoted to the creation of new chiral N-ligands and their metal complexes for evaluation in advanced asymmetric catalysis.[1] The condensation of an amine and an aldehyde, to form Schiff bases, was one of the earliest reported reactions in chemistry;[2] these compounds are now an important class of ligands in coordination chemistry, and have been studied extensively[3] because of their selectivity for various metal ions. Jacobsen and Katsuki have developed tetradentate salen ligands, now one of the most intensely studied classes of bis-chiral Schiff bases, able to coordinate easily to a wide variety of metals. The interest in such bases has increased since the discovery of manganese(III) salen complexes, which are excellent catalysts for the enantiomeric epoxidation of unfunctionalized alkenes;[4] the development of chiral salen metal complexes and catalysts in the last decade has therefore shown a very rapid growth.[5] Chiral salen-containing complexes are now used as catalysts for a variety of enantioselective reactions such as oxidation, aziridination, cyclopropanation, Diels−Alder cyclisation, and hydrogenation.[6]

In this report, we focus on new simpler chiral Schiff-base ligands containing pyrrolidinylamino functionalities (in place of one of the phenolic groups on salen ligands), the synthesis of the complexes [Pd(**L**)(OAc)] (**LPd**), [Ni(**L**)(OAc)] (**LNi**), as well as the X-ray crystal structures of **3Ni** and **4Pd**. The method we have developed should allow the easy synthesis of a wide variety of chiral Schiff-base ligands. The iminophenoxy ligands were designed to coordinate to Pd^{II} and Ni^{II}; the amino substituent could be varied in order to improve the stability of the complexes in the catalytic hydrogenation of alkenes and imines.

Results and Discussion

Synthesis of Ligands

The synthesis of chiral ligands **3**−**5** is based on the condensation of enantiomerically pure (*S*)-(1-benzylpyrrolidin-2-yl)methylamine (**2a**), (*S*)-[1-(1-naphthylmethyl)pyrrolidin-2-yl]methylamine (**2b**) and (*S*)-[1-(2-naphthylmethyl)pyrrolidin-2-yl]methylamine (**2c**) with 3-*tert*-butyl-2-hydroxy-5-methylbenzaldehyde (**1**) in the presence of 3 Å molecular sieves (Scheme 1). The chiral amines **2b** and **2c** were synthesized from (*S*)-proline in a simple sequence of reactions (Scheme 2), with the chiral centre remaining unmodified. The preparation of the benzyl analogue **2a** was efficiently

[‡] Preliminary results were presented in the 6th International Symposium on Catalysis Applied to Fine Chemicals (Delft, 2003).

[a] Instituto de Ciencia de Materiales de Madrid, CSIC, Cantoblanco, 28049 Madrid, Spain
Fax: (internat.) +34-913720623
E-mail: marta.iglesias@icmm.csic.es
[b] Instituto de Química Orgánica General, CSIC, Juan de la Cierva, 3, 28006 Madrid, Spain,
Fax: (internat.) +34-915644853
E-mail: felix-iqo@iqog.csic.es

carried out by the procedure published by us previously.[7] Compounds **3−5** were characterised by elemental analysis (C, H, N), ^{1}H and ^{13}C NMR and mass spectrometry. In the ^{1}H NMR spectra, the OH protons appear at δ = 9.80 ppm (for **4**) and the imine protons appear as singlets at δ = 8.18 (for **3**), 8.00 (for **4**) and 8.30 (for **5**) ppm. NOE experiments indicate unequivocally that the ligands prefer the *anti* configuration.

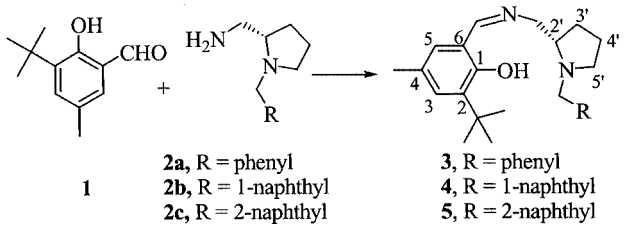

Scheme 1. General synthesis of chiral Schiff bases **3−5**

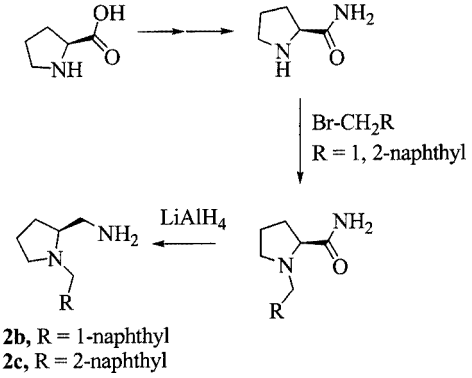

Scheme 2. Synthesis of chiral amine precursors

Synthesis of the Complexes

The interest in making new salen-type ligands lies in their ability to form stable complexes with transition metals, thus serving as potential precursors for homogeneous catalysis of a variety of reactions.[5,8] We decided to use a chiral catalyst employing a chiral ligand in which the stereogenic centres are in close proximity to the metal (Scheme 3); chiral predetermination was observed for all of the palladium and nickel complexes.[9] When the chiral ligands are coordinated to the metal, two chiral centres are introduced, at the coordinated nitrogen atom and at the metal. From the ORTEP diagrams and the NMR spectroscopic data, we can deduce that the coordination of the metal ion is completely stereospecific, and gives rise to only one of the two possible diastereoisomers.

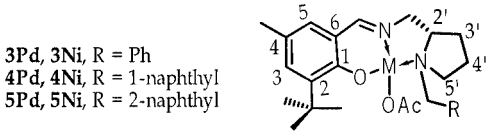

Scheme 3. General structural formulae of complexes **3Pd, 3Ni**, **4Pd**, **4Ni**, **5Pd** and **5Ni**

All the complexes were prepared by addition of the divalent metal salts [$Pd(OAc)_2$, $Ni(OAc)_2$] to an ethanolic solution of ligand; one of the acetate groups is displaced by the phenolic anion whereas the amine and imine nitrogen atoms coordinate to the metal in a square planar arrangement (Scheme 3). The complexes, which were precipitated from EtOH, were obtained with high purity and in high yields as microcrystalline stable solids, which are soluble in organic solvents. The structures of all the complexes were confirmed by elemental analysis (C, H, N and M), IR spectroscopy, and ^{1}H and ^{13}C NMR spectroscopy. They were also characterised by electro-spray mass spectrometry. The ES-MS spectra of complexes show the molecular ion peaks, [M^+], and peaks from the fragments due to elimination of the acetate ion [$M^+ - OAc$]. All assignments were confirmed by good agreement between the observed and calculated isotopic distributions.

Infrared and Electronic Spectra

IR stretching frequencies were used to characterize the binding of the imine nitrogen. Bands at 1600 cm^{-1} were assigned to the $\nu_{C=C}$ and $\nu_{C=N}$ vibrations, shifted to lower wavenumbers (relative to the free ligands) due to N-coordination of the imine.[10] The absence of the ν_{O-H} band (present in the spectra of the free ligands at ca. 3430 cm^{-1}) is in accordance with loss of the hydroxyl proton. The IR spectra also show strong bands at 1290 and ca. 1500 cm^{-1}; these were assigned to the symmetric and asymmetric ν_{COO} bands, respectively, in agreement with the values expected for monocoordinate acetate ligands.[11] New bands in the 500−600 cm^{-1} region were ascribed to ν_{M-O}.

The electronic absorption spectra for all complexes in the 200−800 nm range were obtained using 10^{-3} to 10^{-5} M solutions in ethanol. The complexes show several band maxima in the UV region, assigned to the intraligand π→π* and n→π* transitions in the aromatic ring and the azomethine group and the charge-transfer transitions.[12] The higher molar extinction coefficient of the bands in the 260−350 nm range may be due to the coincidence of the charge transfer, d→π* and intraligand π→π* and n→π* transitions. The bands in the 400−450 nm region correspond to the d→d transitions expected for planar complexes[13] and MLCT bands.

NMR Spectra

The diamagnetic palladium and nickel complexes were characterised by ^{1}H and ^{13}C NMR spectroscopy. All assignments were based on several correlations in the 2D spectra, and are fully consistent with the structures depicted in Scheme 3. In all cases, the spectra show the simultaneous occurrence of two sets of signals, which are attributable to the substituted benzaldimine entity and the aliphatic part of the ligand. In the ^{1}H NMR spectra all the resonances were high-field shifted compared to the uncoordinated ligand, and they were in agreement with metallation of the ligand and coordination of the metal atom to the imine nitrogen atom. The most noticeable shifts observed were

 © 2004 Wiley-VCH Verlag GmbH & Co. KGaA, Weinheim

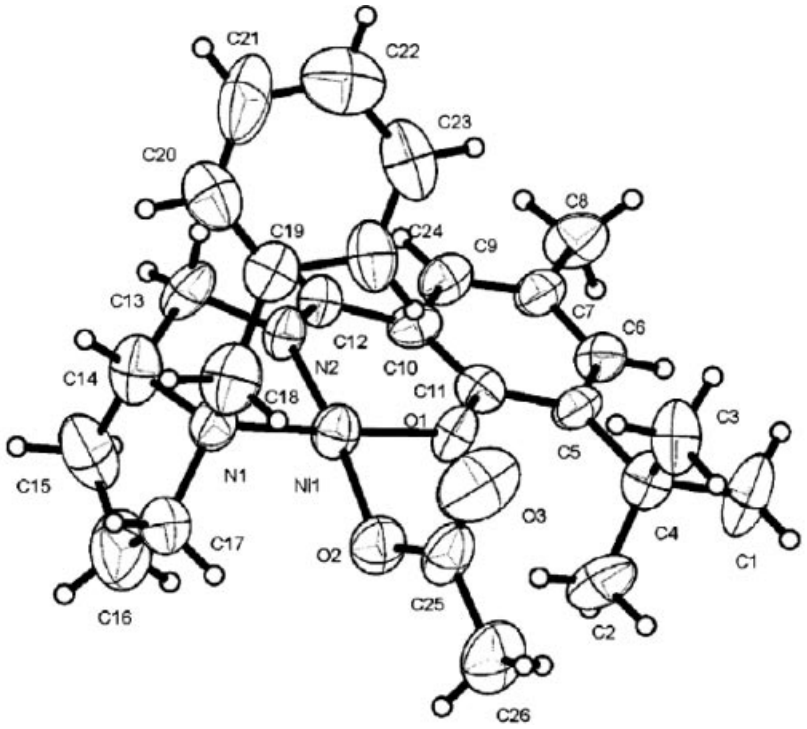

Figure 1. Molecular structure of **3Ni**, with labelling scheme; only one molecule has been shown for clarity

those for C*H*=N, CH=NCH_2, H-2′ and H-5′. Deprotonation of the hydroxyl group was confirmed by the absence of OH resonances in the ^{1}H NMR spectrum. The resonance corresponding to the C*H*=N proton appears as a singlet (δ = 7.9−7.2 ppm), shifted to high field due to the coordination of the imine group to the metal atom through the lone pair of the nitrogen atom.[14] The ^{1}H NMR spectrum shows the *Me*COO protons as a singlet at δ = 2.10 ppm. The ^{13}C NMR spectra show that the signals assigned to the *C*=N carbons are shifted to high-field and those due to C-1 shifted downfield (to δ ≈ 162 ppm), confirming that metallation had occurred.

Crystal Structure Studies of 3Ni and 4Pd

Suitable crystals were grown by slowly evaporating an ethanolic solution of the complex. The molecular structures are shown in Figure 1 and Figure 2. Crystal data are given in Table 4, and selected bond lengths and angles with estimated standard deviations are shown in Table 1.

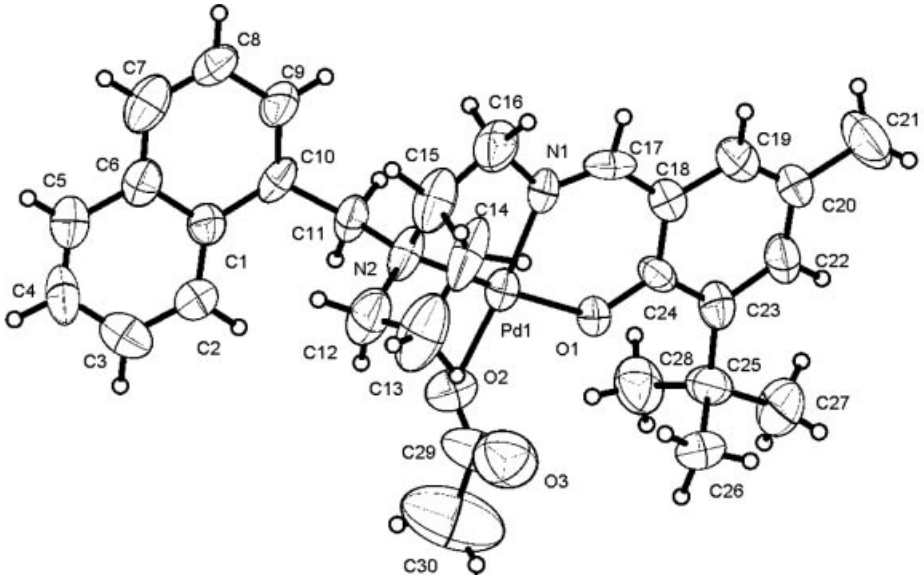

Figure 2. Molecular structure of **4Pd**, with labelling scheme

 © 2004 Wiley-VCH Verlag GmbH & Co. KGaA, Weinheim

Table 1. Selected bond lengths (Å) and angles (°) for complexes **3Ni** and **4Pd**

3Ni		**4Pd**	
Ni(1)−O(1)	1.825(5)	Pd(1)−O(1)	1.975(5)
Ni(1)−N(1)	1.947(6)	Pd(1)−N(2)	2.072(6)
Ni(1)−O(2)	1.851(6)	Pd(1)−O(2)	2.054(8)
Ni(1)−N(2)	1.834(7)	Pd(1)−N(1)	1.925(8)
Ni(2)−O(4)	1.863(6)		
Ni(2)−N(4)	1.941(6)		
Ni(2)−O(5)	1.863(6)		
Ni(2)−N(3)	1.841(7)		
O(1)−Ni(1)−N(2)	93.3(3)	N(1)−Pd(1)−O(1)	94.1(3)
O(1)−Ni(1)−O(2)	87.4(2)	O(1)−Pd(1)−O(2)	89.2(3)
N(2)−Ni(1)−O(2)	170.7(3)	N(1)−Pd(1)−O(1)	175.3(3)
O(1)−Ni(1)−N(1)	176.1(3)	O(1)−Pd(1)−N(2)	175.4(3)
N(2)−Ni(1)−N(1)	87.7(3)	N(1)−Pd(1)−N(2)	83.0(3)
O(2)−Ni(1)−N(1)	92.3(3)	O(2)−Pd(1)−N(2)	93.5(3)
O(3)−Ni(2)−N(3)	94.5(3)		
O(3)−Ni(2)−O(4)	86.7(2)		
N(3)−Ni(2)−O(4)	169.3(3)		
O(3)−Ni(2)−N(4)	176.0(3)		
N(3)−Ni(2)−N(4)	88.0(3)		
O(4)−Ni(2)−N(4)	91.5(3)		

The structure consists of ML(OAc) molecules; each asymmetric unit of **3Ni** contains two crystallographically independent molecules (only one molecule is shown). The absolute configuration is assigned on the basis of known chirality of the amine used. The ligands are tridentate, and bond to the M^{II} atom by the deprotonated phenolic oxygen atom (O_{phe}) and the imine (N_{im}) and tertiary amine nitrogens (N_{am}); each metal also coordinates to one acetate group. The geometry of metal coordination sphere is distorted square planar, and the sum of the angles around the metal atom is 360.7(4)° for the Ni complex and 359.8(4)° for the Pd complex. The angles between adjacent atoms in the coordination sphere are close to the expected value of 90°, with the most noticeable distortions found for the N−M−N angle, due to chelation [N(2)−Ni(1)−N(1): 87.7(3)°, N(3)−Ni(2)−N(4): 88.0(3)°, N(1)−Pd−N(2): 83.0(3)°]. The $M-O_{phe}$, $M-N_{im}$ and $M-N_{am}$ distances were found to be 1.825, 1.863; 1.834, 1.841 and 1.947, 1.941 [Ni(1), Ni(2)] for **3Ni** and 1.975, 1.925 and 2.072 for **4Pd** in good agreement with the literature values.[15] Furthermore, the pyrrolidine metal distances [$M-N_{am}$: 1.947(6) for the free ligand, 1.941(6) for **3Ni** and 2.072(6) Å for **4Pd**] are longer than the $M-N_{im}$ distances, despite the fact that amine nitrogen atoms usually show stronger coordination than imine nitrogen atoms. This effect, however, is probably caused by greater steric hindrance of the tertiary amine nitrogen compared to the mono-substituted imine nitrogen. The coordinated atoms lie exactly in plane (the maximum deviation from least-squares plane is 0.002 Å) and are arranged at the corners of an irregular quadrilateral, reflecting the difficulty that the ligand has in spanning the square-planar coordination positions. The structures contain one six-membered and one five-membered chelate ring. The six-membered metallacycle containing the imino moiety is practically coplanar with the O(1)−O(2) coordination plane [dihedral angles 8.21(0.27)° for Ni(1), 10.07(0.27)° for Ni(2) in **3Ni**, 7.13(0.46)° for **4Pd**]. The five-membered metallacycle is in an envelope conformation, on C(15) for **4Pd**, and on C(14) [Ni(1)] and C(40′) [Ni(2)] for **3Ni**. The pyrrolidine rings are also in an envelope conformation. In **3Ni**, the 1-benzylpyrrolidine group of the ligand **3** is in close proximity to the nickel ion.

Catalytic Hydrogenation

These structurally well-defined Ni^{II} and Pd^{II} complexes enable us to explore their application to catalytic hydrogenation. The hydrogenation of the simple alkenes **I** and **II**, the functionalized alkenes **III**−**V** and the imines **VI** and **VII** (Figure 3) with Pd and Ni complexes were carried out under standard conditions (EtOH, 4 atm. H_2, 40 °C). The results are summarised in Table 2 and Table 3.

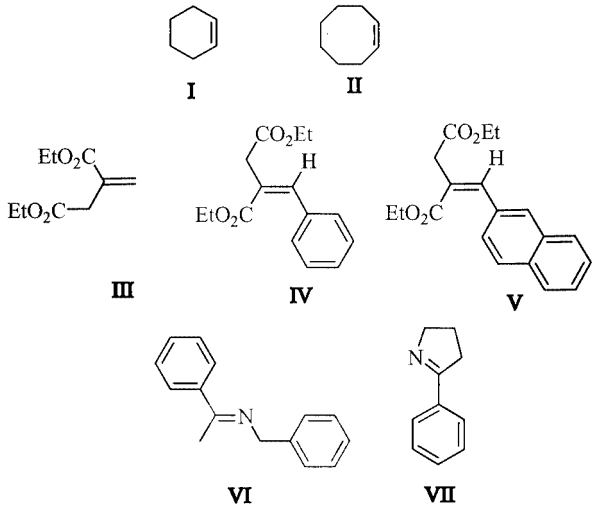

Figure 3. Substrates used in the hydrogenation reactions

Table 2. Turnover rates for catalytic hydrogenation with ligand **3** (TOF: h^{-1}; Conditions: 4 atm, 40 °C, S/C ratio 1000:1)

Substrate	Pd	Ni
I	5460	4020
II[a]	25500	22800
III	3360	2400
IV	640	220
V	153	117
VI	3240	4800
VII	167	93

[a] S/C ratio 10000:1.

The nature of the metal center has an influence on the catalytic activity. In general, the palladium catalysts were more active than their nickel analogues when **3** was used as ligand under our conditions; the nickel complexes were the most active when **4** or **5** were used. The complexes **4Pd**, **4Ni**, **5Pd** and **5Ni** contain naphthyl groups as substituents in the pyrrolidinyl group, and display TOFs of 8×10^5 to 10^6 h^{-1} for the hydrogenation of cyclooctene (**II**) and 3−5

 © 2004 Wiley-VCH Verlag GmbH & Co. KGaA, Weinheim

Table 3. Turnover rates for catalytic hydrogenation with ligands **4** and **5** (TOF: h^{-1}; Conditions: 4 atm, 40 °C S/C ratio 100000:1).

Catalyst	II	VI
4Pd	842760	337500
4Ni	964320	410940
5Pd	684000	309240
5Ni	961920	461520

$\times 10^5$ h^{-1} for imine **VI**. This may be due to the closeness of the phenyl group to the metal (Figures 1 and 2). Use of these Pd and Ni complexes led to quantitative conversion of the olefins under the hydrogenation conditions employed. No palladium black or nickel was formed in any of the hydrogenation reactions. Low enantiomeric excesses (< 10% *ee*) resulted in all cases, as shown by ^{1}H NMR spectroscopy and chiral GCMS of the reaction mixtures.

The accumulated evidence concerning the mechanisms of homogeneously catalysed hydrogenations indicates that there are three principal modes of hydrogen activation: oxidative addition, and homolytic or heterolytic hydrogen cleavage. In the case of the Pd and Ni complexes, heterolytic cleavage is preferred to a hydride intermediate, which would have to involve charge separation without any oxidation of the metal.[16]

Conclusion

A series of chiral [N,N,O] tridentate Schiff bases were synthesised with high purity and in good yield. Treatment of these ligands with palladium(II) and nickel(II) acetate in EtOH gave only one diastereoisomer of the respective air-stable complexes. These complexes were shown to be active catalysts for hydrogenation, with high reactivity under mild conditions (TOF up to 10^6 h^{-1}). These simple catalysts, especially the cheaper Ni complexes, are a real alternative to conventional Pd catalysts for hydrogenation in industrial processes.

Experimental Section

General Remarks: All preparations of metal complexes were carried out under nitrogen by conventional Schlenk techniques. Solvents were carefully degassed before use. C, H, N analyses were carried out by the analytical department of the Institute of Materials Science (C.S.I.C.) with a perkin-Elmer 240C apparatus. Metal contents were analysed by atomic absorption using Perkin−Elmer Analyst 300 atomic absorption and Plasma ICP Perkin−Elmer 40 spectrometers. IR spectra were recorded with a Nicolet XR60 spectrophotometer (range 4000−200 cm^{-1}) in KBr pellets. ^{1}H NMR and ^{13}C NMR spectra were taken on Varian XR300 and Bruker 200 spectrometers. Chemical shifts are referred to tetramethylsilane (internal standard). Optical rotation values were measured using the sodium-D line (589 nm) with a Perkin−Elmer 241 MC polarimeter. Gas chromatography analysis was performed using a Hewlett−Packard 5890 II apparatus with a flame ionisation detector in a cross-linked methylsilicone column.

2-*tert*-Butyl-4-methyl-6-[(*E*)-({[(2*S*)-1-benzylpyrrolidin-2-yl]methyl}-imino)methyl]phenol (3): A solution of (*S*)-(1-benzylpyrrolidin-2-yl)methylamine (**2a**) (380 mg, 2 mmol) in ethanol (20 mL) was added to a solution of 3-*tert*-butyl-5-methylsalicylaldehyde (384 mg, 2 mmol) in ethanol (20 mL) at room temperature over a period of 30 min with stirring. The solvent was removed under vacuum, and the residue purified by flash chromatography (hexane:EtOAc, 5:1) to give a yellow oil (640 mg). Yield 88%. $[\alpha]_D^{25} = -14.3$ (c = 0.5, EtOH). $C_{24}H_{32}N_2O$ (364): calcd. C 79.1, H 8.8, N 7.7; found C 78.9, H 8.6, N 7.4. IR (film, cm^{-1}): $\tilde{\nu}$ = 1628, 1592 (C=C + C=N). UV/Vis (λ, nm): 221, 262, 332. ^{1}H NMR ($CDCl_3$, ppm): δ = 8.18 (s, C*H*=N), 7.10−7.20 (m, 5 H_{arom}, H_{Bzl}), 7.05−7.00 (m, H_{arom}), 6.82−6.77 (m, H_{arom}), 3.95, 3.35 (d, J_{AB} = 13.4 Hz, CH_2Ph), 3.69−3.61 (m, CH=NCH_2), 3.45−3.35 (m, CH=NCH_2), 2.94−2.85 (m, $H^{5'a}$); 2.83−2.73 (m, $H^{2'}$), 2.24−2.12 (m, CH_3, $H^{5'b}$), 1.98−1.87 (m, $H_{3'a}$), 1.71−1.54 (m, $H^{3'b}$, $H^{4'a,b}$), 1.35 [s, C(CH_3)$_3$] ppm. ^{13}C NMR ($CDCl_3$): δ = 166.23 (*C*H=N), 158.35 (C_1), 139.75 (C_{arom}), 137.17 (C^6), 130.27 (C^5), 129.40 (C_2), 128.78 (C_{arom}), 128.17 (C_{arom}), 126.81 (C_{arom}), 126.30 (C^3), 118.47 (C^4), 64.20 ($C^{2'}$), 63.87 (CH=NCH_2), 59.32 (CH_2Ph), 54.67 ($C^{5'}$), 34.70 [*C*(CH$_3$)$_3$], 29.59 ($C^{3'}$), 29.40 [C(*C*H$_3$)$_3$], 22.84 ($C^{4'}$), 20.61 (CH_3). MS (EI) (*m*/*z*, %): 364 (1) [M^+]; 160 (M^+ − 184, 100); 91 (M^+ − 69, 47).

[(2*S*)-1-(1-Naphthylmethyl)pyrrolidin-2-yl]methylamine (2b): K_2CO_3 (1.38 g, 10 mmol) and 1-bromomethylnaphthalene[17] (2.21 mg, 10 mmol) were added to a solution of pyrrolidin-2-carboxamide[18] (114 mg, 1 mmol) in acetonitrile (30 mL). The mixture was stirred for 24 h and purified by flash chromatography (eluant: hexane), to provide (2*S*)-1-(1-naphthylmethyl)pyrrolidine-2-carboxamide. Yield 70%. M.p. 159−161 °C. $[\alpha]_D^{25} = -5.1$ (c = 0.9, $CHCl_3$). $C_{16}H_{18}N_2O$ (254): calcd. C 75.6, H 7.1, N 11.0; found C 75.3, H 7.3, N 10.9. IR (KBr, cm^{-1}): $\tilde{\nu}$ = 3393 (NH), 1650 (C=O). ^{1}H NMR ($CDCl_3$, ppm): δ = 8.10−8.00 (m, H_{arom}), 7.80−7.60 (m, 2 H_{arom}), 7.50−7.20 (m, 4 H_{arom}), 6.80−6.70 (m, NH_2), 4.87−4.68 (m, NH_2), 4.20−3.98 (m, $CH_2^{naphthyl}$), 3.21−2.97 (m, $H^{2'}$, $H^{5'a}$), 2.54−2.37 (m, $H^{5'b}$), 2.30−2.10 (m, $H^{3'a}$), 1.95−1.63 (m, $H^{3'b}$, $H^{4'a}$), 1.22−1.10 (m, $H^{4'b}$). ^{13}C NMR ($CDCl_3$): δ = 179.91 (*C*=O), 136.21 (C_{arom}), 135.71 (C_{arom}), 133.94 (C_{arom}), 130.81 (C_{arom}), 130.24 (C_{arom}), 128.98 (C_{arom}), 128.12 (C_{arom}), 127.60 (C_{arom}), 127.35 (C_{arom}), 125.28 (C_{arom}), 69.57 ($C^{2'}$), 60.07 ($CH_2^{naphthyl}$), 57.04 ($C^{5'}$), 32.81 ($C^{3'}$), 26.24 ($C^{4'}$). MS (EI) (*m*/*z*, %): 210 (56), 141 (100).

$LiAlH_4$ (3.8 g, 100 mmol) was added to a solution of (2*S*)-1-(1-naphthylmethyl)pyrrolidine-2-carboxamide (2.54 g, 10 mmol) in THF (15 mL), and the mixture stirred at reflux for 12 h. After workup, **2b** was obtained as a yellow oil. Yield 97%. $[\alpha]_D^{25} = -29.6$ (c = 0.9, $CHCl_3$). $C_{16}H_{20}N_2$ (240): calcd. C 80.0, H 8.3, N 11.7; found C 80.1, H, 8.6, N 11.5. IR (film, cm^{-1}): $\tilde{\nu}$ = 3368 (NH). ^{1}H NMR ($CDCl_3$, ppm): δ = 8.30−8.20 (m, H_{arom}), 7.95−7.67 (m, 2 H_{arom}), 7.60−7.28 (m, 4 H_{arom}), 4.41, 3.72 (2 H, J_{AB} = 13 Hz, $CH_2^{naphthyl}$), 2.95−2.87 (m, $H^{5'a}$), 2.80−2.74 (m, CH_2NH_2), 2.73−2.61 (m, $H^{2'}$), 2.37−2.20 (m, $H^{5'b}$), 2.04−1.89 (m, $H^{3'a}$), 1.78−1.62 (m, $H^{3'b}$, $H^{4'a,b}$) ppm. ^{13}C NMR ($CDCl_3$): δ = 128.45 (C_{arom}), 127.70 (C_{arom}), 126.69 (C_{arom}), 125.76 (C_{arom}), 125.65 (C_{arom}), 125.52 (C_{arom}), 125.48 (C_{arom}), 125.20 (C_{arom}), 124.15 (C_{arom}), 124.05 (C_{arom}), 66.12 ($C^{2'}$); 57.48 ($CH_2^{naphthyl}$), 55.05 ($C^{5'}$), 44.33 (CH_2NH_2), 28.10 ($C^{3'}$), 23.24 ($C^{4'}$). MS (EI) (*m*/*z*, %): 212 (90); 141 (100).

2-*tert*-Butyl-4-methyl-6-[(*E*)-({[(2*S*)-1-(1-naphthylmethyl)pyrrolidin-2-yl]methyl}imino)methyl]phenol (4): The method and conditions described for the synthesis of **3** were used. Reaction of 3-*tert*-butyl-5-methylsalicylaldehyde (384 mg, 2 mmol) with [(2*S*)-1-(1-naph-

 © 2004 Wiley-VCH Verlag GmbH & Co. KGaA, Weinheim

thylmethyl)pyrrolidin-2-yl]methylamine (**2b**) (480 mg, 2 mmol), and flash chromatography (hexane/ethyl acetate) gave **4** as a yellow oil in 52% yield. $[\alpha]_D^{25} = -17.6$ (c = 0.9, $CHCl_3$). $C_{28}H_{34}N_2O$ (414): calcd. C 81.1, H 8.3, N 6.7; found C 79.9, H 8.4, N 6.5. IR (film, cm^{-1}): $\tilde{\nu}$ = 1628, 1592 (C=C + C=N). UV/Vis (λ, nm): 240, 266, 349. ^{1}H NMR ($CDCl_3$, ppm): δ = 9.80 (s, O*H*), 8.22−8.18 (m, $H_{arom,}$), 8.00 (s, CH=N), 7.78−7.66 (m, 2 H_{arom}), 7.43−7.29 (m, H_{arom}), 7.03−7.01 (m, H_{arom}), 6.74−6.71 (m, H_{arom}) 4.33, 3.82 (d, J_{AB} = 13 Hz, $CH_2^{naphthyl}$), 3.70−3.61 (m, CH=NC*H*$_2$), 3.36−3.32 (m, CH=NC*H*$_2$), 2.93−2.80 (m, H$^{2',5'a}$), 2.33−2.16 (m, C*H*$_3$, H$^{5'b}$), 2.05−1.90 (m, H$^{3'a}$), 1.78−1.57 (m, H$^{3'b}$, H$^{4'a,b}$), 1.36 [s, C(CH$_3$)$_3$] ppm. ^{13}C NMR ($CDCl_3$): δ = 165.33 (*C*H=N); 157.32 (C$^{1\ arom}$), 136.09 (C_{arom}), 134.75 (C_{arom}), 134.39 (C_{arom}), 132.73 (C_{arom}), 130.43 (C_{arom}), 129.43 (C_{arom}), 128.46 (C_{arom}), 127.35 (C_{arom}), 126.77 (C_{arom}), 125.72 (C_{arom}), 124.78 (C_{arom}), 124.57 (C_{arom}), 124.24 (C_{arom}), 123.60 (C_{arom}), 117.42 (C_{arom}), 63.95 (C$^{2'}$), 62.72 (CH=N*C*H$_2$), 56.93 ($CH_2^{naphthyl}$), 54.14 (C$^{5'}$), 33.70 [*C*(CH$_3$)$_3$], 28.68 (C$^{3'}$), 28.38 [C(*C*H$_3$)$_3$], 22.02 (C$^{4'}$), 19.65 (CH$_3$). MS (EI) (*m*/*z*, %): 414 (2) [M$^+$]; 210 (25); 141 (100).

[(2*S*)-1-(2-Naphthylmethyl)pyrrolidin-2-yl]methylamine (2c): K_2CO_3 (1.38 g, 10 mmol) and 2-bromomethylnaphthalene (2.21 mg, 10 mmol) were added to a solution of pyrrolidin-2-carboxamide (114 mg, 1 mmol) in acetonitrile (30 mL). The mixture was stirred for 24 h and purified by flash chromatography (hexane/ethyl acetate), to provide (2*S*)-1-(2-naphthylmethyl)pyrrolidin-2-carboxamide as a white solid. Yield 72%. M.p. 140−143 °C. $[\alpha]_D^{25} = -35.0$ (c = 1, $CHCl_3$). $C_{16}H_{18}N_2O$ (254): calcd. C 75.6, H 7.1, N 11.0; found C 75.2, H 7.0, N 11.2. IR (KBr, cm^{-1}): $\tilde{\nu}$ = 3401 (NH); 1632 (C=O). ^{1}H NMR ($CDCl_3$, ppm): δ = 7.85−7.63 (m, 4 H_{arom}), 7.51−7.22 (m, 3 H_{arom}), 6.02−5.90 (m, NH_2), 4.11, 3.62 (d, J_{AB} = 13 Hz, $CH_2^{naphthyl}$), 3.28−2.23 (m, H$^{2'}$), 3.07−3.01 (m, H$^{5'a}$), 2.44−2.34 (m, H$^{5'b}$), 2.31−2.20 (m, H$^{3'a}$), 2.05−1.97 (m, H$^{3'b}$), 1.84−1.72 (m, H$^{4'a,b}$) ppm. ^{13}C NMR ($CDCl_3$): δ = 178.08 (C=O); 136.04 (C_{arom}); 133.28 (C_{arom}), 132.66 (C_{arom}), 128.14 (C_{arom}), 127.66 (C_{arom}), 127.62 (C_{arom}), 127.15 (C_{arom}), 126.77 (C_{arom}), 126.13 (C_{arom}), 125.77 (C_{arom}), 67.44 (C$^{2'}$), 59.95 ($CH_2^{naphthyl}$), 53.87 (C$^{5'}$), 30.60 (C$^{3'}$), 24.03 (C$^{4'}$). MS (EI) (*m*/*z*, %): 210 (48); 141 (100).

$LiAlH_4$ (3.8 g, 100 mmol) was added to a solution of (2*S*)-1-(2-naphthylmethyl)pyrrolidin-2-carboxamide (2.54 g, 10 mmol) in THF (15 mL) and the mixture stirred at reflux temperature for 12 h. After workup, **2c** was obtained as a yellow oil (2.54 g, 10 mmol). Yield 91%. $[\alpha]_D^{25} = -39.9$ (c = 0.8, $CHCl_3$). $C_{16}H_{20}N_2$ (240): calcd. C 80.0; H; 8.3; N; 11.6; found C 79.8; H 8.4; N 11.5. IR (film, cm^{-1}): $\tilde{\nu}$ = 3361 (NH). ^{1}H NMR ($CDCl_3$, ppm): δ = 7.93−7.70 (m, 4 H_{arom}), 7.54−7.40 (m, 3 H_{arom}), 4.17, 3.48 (d, J_{AB} = 14.4 Hz, $CH_2^{naphthyl}$), 3.04−2.90 (m, H$^{5'a}$), 2.83−2.74 (m, C*H*$_2$NH$_2$), 2.65−2.56 (m, H$^{2'}$), 2.32−2.20 (m, H$^{5'b}$), 2.20−1.87 (m, H$^{3'a}$), 1.82−1.62 (m, H$^{3'b}$, H$^{4'a,b}$) ppm. ^{13}C NMR ($CDCl_3$): δ = 137.48 (C_{arom}), 133.32 (C_{arom}), 132.60 (C_{arom}), 127.81 (C_{arom}), 127.62 (C_{arom}), 127.60 (C_{arom}), 127.18 (C_{arom}), 126.91 (C_{arom}), 125.86 (C_{arom}), 125.43 (C_{arom}), 65.60 (C$^{2'}$), 59.28 ($CH_2^{naphthyl}$), 54.67 (C$^{5'}$), 44.12 (*C*H$_2$NH$_2$), 27.96 (C$^{3'}$), 22.96 (C$^{4'}$). MS (EI) (*m*/*z*, %): 212 (96); 141 (100).

2-*tert*-Butyl-4-methyl-6-[(*E*)-({[(2*S*)-1-(2-naphthylmethyl)pyrrolidin-2-yl]methyl}imino)methyl]phenol (5): The method and conditions described for the synthesis of **4** were used. Reaction of 3-*tert*-butyl-2-hydroxy-5-methylbenzaldehyde (384 mg, 2 mmol) with [(2*S*)-1-(2-naphthylmethyl)pyrrolidin-2-yl]methylamine (**2c**) (480 mg, 2 mmol), and flash chromatography (hexane/ethyl acetate) gave **5** as a yellow oil in 58% yield. $[\alpha]_D^{25} = -37.4$ (c = 0.9, $CHCl_3$). $C_{28}H_{34}N_2O$ (414): calcd. C 81.1, H 8.3, N 6.8; found C 81.1, H 8.3, N 6.4. IR (film, cm^{-1}): $\tilde{\nu}$ = 1628, 1594 (C=C + C=N). UV/Vis (λ, nm): 240, 266, 334. ^{1}H NMR ($CDCl_3$, ppm): δ = 8.30−8.19 (m, C*H*=N), 7.86−7.71 (m, 4 H_{arom}), 7.51−7.40 (m, 3 H_{arom}), 7.12−7.09 (m, H^3); 6.86−6.81 (m, H^5); 4.18, 3.58 (d, J_{AB} = 19 Hz, $CH_2^{naphthyl}$), 3.82−3.40 (m, CH=NC*H*$_2$), 3.10−2.80 (m, H$^{2'}$, H$^{5'a}$), 2.36−2.24 (m, C*H*$_3$, H$^{5'b}$), 2.10−1.88 (m, H$^{3'a}$), 1.82−166 (m, H$^{3'b}$, H$^{4'a,b}$), 1.41 [s, C(C*H*$_3$)$_3$] ppm. ^{13}C NMR ($CDCl_3$): δ = 166.75 (CH=N), 158.74 (C^1), 137.88 (C_{arom}), 137.54 (C_{arom}), 133.83 (C_{arom}), 133.12 (C_{arom}), 130.72 (C_{arom}), 129.88 (C_{arom}), 128.23 (C_{arom}), 128.16 (C_{arom}), 128.03 (C_{arom}), 127.71 (C_{arom}), 127.46 (C_{arom}), 126.76 (C_{arom}), 126.27 (C_{arom}), 125.88 (C_{arom}), 118.85 (C_{arom}), 64.82 (C$^{2'}$), 64.38 (CH=N*C*H$_2$), 60.02 ($CH_2^{naphthyl}$), 55.33 (C$^{5'}$), 35.16 [*C*(CH$_3$)$_3$], 30.04 (C$^{3'}$), 29.83 [C(*C*H$_3$)$_3$], 23.36 (C$^{4'}$), 21.08 (CH$_3$). MS (EI) (*m*/*z*, %): 414 (2) [M$^+$]; 210 (100); 141 (95).

Preparation of Metal Complexes. General Method: An solution of $Pd(OAc)_2$ or $Ni(OAc)_2$ in ethanol (0.5 mmol/15 mL) was added to a solution of the ligand in EtOH (15 mL) at room temperature. The resulting mixture was stirred under reflux for 4 hours, cooled to room temperature and then concentrated under vacuum. The residue was washed several times with diethyl ether, dried and filtered to afford the complex in almost quantitative yield.

[Pd(3)(OAc)] (3Pd): M.p. 218−220 °C. $[\alpha]_D^{25} = -34.8$ (c = 1, EtOH). $C_{26}H_{34}N_2O_3Pd$ (528): calcd. C 59.0, H 6.4, N 5.3, Pd 20.1; found C 58.6, H 6.6, N 5.1, Pd 19.8. IR (KBr, cm^{-1}): $\tilde{\nu}$ = 1614−1600 (C=C + C=N), 557 (Pd−O). UV/Vis (λ, nm) = 235, 259, 289, 420. ^{1}H NMR ($CDCl_3$, ppm): δ = 7.79−7.72 (m, 2 H_{arom}), 7.41−7.32 (m, 3 H_{arom}), 7.23 (s, CH=N), 7.11−7.07 (m, H_{arom}), 6.74 (s, H_{arom}), 4.82, 4.13 (d, J_{AB} = 9 Hz, CH_2Ph), 3.57−3.48 (m, CH=NC*H*$_2$, H$^{5'a}$), 3.29−3.20 (m, CH=NC*H*$_2$), 3.10−3.00 (m, H$^{4'a}$), 2.78−2.65 (m, H$^{2'}$), 2.50−2.40 (m, H$^{5'b}$), 2.17 (s, CH$_3$), 2.10−2.03 (m, OOCC*H*$_3$), 1.98−1.87 (m, H$^{3'a,b}$), 1.86−1.75 (m, H$^{4'b}$), 1.26 [s, C(C*H*$_3$)$_3$]. ^{13}C NMR ($CDCl_3$): δ = 178.26 (−OO*C*CH$_3$), 162.88 (*C*−O−Pd), 159.84 (*C*H=N), 140.66, 133.68, 131.99, 131.89, 130.65, 129.10, 128.74, 122.64, 119.94 (C_{arom}), 65.41 (*C*$^{2'}$), 63.12 (CH=N*C*H$_2$), 61.77 (CH_2Ph), 58.71 (C$^{5'}$), 35.36 [*C*(CH$_3$)$_3$], 29.37 [C(*C*H$_3$)$_3$], 27.48 (C$^{3'}$), 23.72 (CH$_3$), 22.57 (C$^{4'}$), 20.33 (OOC*C*H$_3$). MS$^+$ (EI) (*m*/*z*, %): 469 (M$^+$ − Ac, for ^{106}Pd), 471 (M$^+$ − Ac, for ^{108}Pd), 473(M$^+$ − Ac, for ^{110}Pd), 467 (M$^+$ − Ac, for ^{104}Pd), 465 (M$^+$ − Ac, for ^{102}Pd).

[Ni(3)(OAc)] (3Ni): M.p. 153−156 °C. $[\alpha]_D^{25} = -2.8$ (c = 1, EtOH). $C_{26}H_{34}N_2O_3Ni$ (481): calcd. C 64.8, H 7.0, N 6.0, Ni 12.3; found C 64.6, H 7.4, N 5.9, Ni 11.9. IR (KBr, cm^{-1}): $\tilde{\nu}$ = 1612−1590 (C=C + C=N), 554 (Ni−O). UV/Vis (λ, nm): 230, 264, 345, 425. ^{1}H NMR ($CDCl_3$, ppm): δ = 8.21 (s, 2 H_{arom}), 7.75 (s, H_{arom}), 7.42−7.35 (m, 2H_{arom}, CH=N), 6.93 (s, H_{arom}), 6.56 (s, H_{arom}), 4.90, 3.83 (d, J_{AB} = 10.5 Hz, CH_2Ph), 3.78−3.70 (m, H$^{5'a}$), 3.45 (s, H$^{4'a}$), 3.25−3.12 (m, CH=NC*H*$_2$), 2.98−2.83 (m, CH=NC*H*$_2$), 2.37−2.27 (m, H$^{2'}$), 2.18−2.07 (m, C*H*$_3$, OCOCC*H*$_3$, H$^{4'b}$, H$^{3'a}$), 1.95−1.83 (m, H$^{5'b}$, H$^{3'b}$), 1.23 [s, C(C*H*$_3$)$_3$] ppm. ^{13}C NMR ($CDCl_3$): δ = 178.33 (OO*C*CH$_3$); 162.13 (*C*−O−Ni); 161.69 (*C*H=N), 141.12, 132.34, 132.23, 131.97, 128.95, 128.77, 128.67, 122.74, 119.67 (C_{arom}), 62.22 (C$^{2'}$), 61.36 (CH=N*C*H$_2$), 59.29 (*C*H$_2$Ph), 56.65 (C$^{5'}$), 34.88 [*C*(CH$_3$)$_3$], 29.13 [C(*C*H$_3$)$_3$], 27.85 (C$^{3'}$), 24.53 (CH$_3$), 22.91 (C$^{4'}$), 20.36 (OOC*C*H$_3$). MS$^+$ (EI) (*m*/*z*, %): 422 (M$^+$, ^{59}Ni); 423 (M$^+$, ^{60}Ni).

[Pd(4)(OAc)] (4Pd): Yield 65%. M.p. 211−215 °C. $[\alpha]_D^{25} = -4.3$ (c = 0.5, $CHCl_3$). $C_{30}H_{36}N_2O_3Pd$ (578): calcd. C 62.3, H 5.9, N 4.8, Pd 18.3; found C 62.0, H 6.2, N 5.1, Pd 17.7. IR (KBr, cm^{-1}): $\tilde{\nu}$ = 1616−1598 (C=C + C=N), 514 (Pd−O). UV/Vis (λ, nm): 243, 288, 423. ^{1}H NMR ($CDCl_3$, ppm): δ = 8.27−8.10 (m, H_{arom}), 7.90−7.77 (m, H_{arom}, CH=N), 7.60−7.38 (m, H_{arom}), 7.12−7.02

 © 2004 Wiley-VCH Verlag GmbH & Co. KGaA, Weinheim

(m, H_{arom}), 6.72−6.66 (m, H_{arom}), 5.20, 4.95 (d, J_{AB} = 16 Hz, $CH_2^{naphthyl}$), 3.77−3.37 (m, $H^{5'a}$, CH=NCH_2), 3.22−2.76 (m, $H^{2'}$, CH=NCH_2), 2.17−2.05 (m, $H^{5'b}$, CH_3, OCOCH_3), 1.93−1.47 (m, $H^{3'a,b}$, $H^{4'a,b}$), 1.34−1.21 [s, C(CH_3)$_3$] ppm. ^{13}C NMR ($CDCl_3$): δ = 178.80 (O*C*OCH$_3$), 163.33 (*C*−O−Pd), 160.33 (CH=N), 133.72, 131.93, 131.39, 131.06, 130.77, 130.53, 129.39, 129.30, 128.22, 127.51, 126.60 (C_{arom}), 125.51 123.97 123.11 120.40 (C_{arom}), 65.42 ($C^{2'}$), 63.29 (CH=NCH_2), 60.11 ($C^{5'}$), 58.75 ($CH_2^{naphthyl}$), 35.79 [*C*(CH$_3$)$_3$], 29.78 [C(*C*H$_3$)$_3$], 27.47 ($C^{3'}$), 24.14 ($C^{4'}$), 23.16 (CH_3), 20.76 (OCO*C*H$_3$). MS$^+$ (EI) (*m*/*z*, %): 519 (M^+ − Ac, for ^{106}Pd); 521 (M^+ − Ac, for ^{108}Pd); 523 (M^+ − Ac, for ^{110}Pd); 517 (M^+ − Ac, for ^{104}Pd); 515 (M^+ − Ac, for ^{102}Pd).

[Ni(4)(OAc)] (4Ni): Yield 75%. M.p. 218−222 °C. $[\alpha]_D^{25}$ = −1.9 (*c* = 0.9, $CHCl_3$). $C_{30}H_{36}N_2O_3Ni$ (531): calcd. C 67.8, H 6.8, N 5.4, Ni 11.1; found C 67.6, H 7.0, N 5.3, Ni 10.9. IR (KBr, cm^{-1}): $\tilde{\nu}$ = 1614−1600 (C=C + C=N), 518 (Ni−O). UV/Vis (λ, nm): 245, 267, 346, 428. ^{1}H NMR ($CDCl_3$, ppm): δ = 8.41−8.32 (m, 2 H_{arom}), 7.92−7.83 (m, 2 H_{arom}), 7.67−7.45 (m, 3 H_{arom}), 7.34 (s, CH=N), 6.97−6.91 (m, H_{arom}), 6.62−6.57 (m, H_{arom}), 5.15−5.02 (m, $CH_2^{naphthyl}$), 3.80−3.64 (m, $H^{4'a}$), 4.15−3.83 (m, $H^{5'a}$), 3.45−3.20 (m, $H^{5'b}$, CH=NCH_2), 3.01−2.82 (m, CH=NCH_2), 2.57−2.38 (m, $H^{2'}$), 2.23−2.12 (m, OCOCH$_3$, $H^{3'a}$), 2.05 (s, CH_3), 1.95−1.56 (m, $H^{3'b}$, $H^{4a,b}$), 1.40−1.12 [s, C(CH_3)$_3$] ppm. ^{13}C NMR ($CDCl_3$): δ = 178.75 (O*C*OCH$_3$), 162.61 (*C*−O−Ni), 162.20 (*C*H=N), 141.50, 134.18, 133.80, 132.70, 131.2, 130.40, 129.32, 129.09, 128.69, 127.38, 126.54, 125.57, 124.11, 123.15, 120.13 (C_{arom}), 62.37 ($C^{2'}$); 61.70 (CH=N*C*H$_2$), 57.06 ($CH_2^{naphthyl}$), 54.18 ($C^{5'}$), 35.32 [*C*(CH$_3$)$_3$], 30.09 [C(*C*H$_3$)$_3$], 29.60 ($C^{3'}$), 28.11 (CH_3), 24.85 ($C^{4'}$), 20.79 (OCO*C*H$_3$). MS$^+$ (EI) (*m*/*z*, %): 472 (M^+ − Ac, for ^{59}Ni), 473 (M^+ − Ac, for ^{60}Ni).

[Pd(5)(OAc)] (5Pd): Yield 65%. M.p. 208−211 °C. $[\alpha]_{435}^{25}$ = +1.9 (*c* = 0.9, $CHCl_3$). $C_{30}H_{36}N_2O_3Pd$ (578): calcd. C 62.3, H 5.9, N 4.8, Pd 18.3, found C 62.0, H 6.0, N 5.2, Pd 17.9. IR (KBr, cm^{-1}): $\tilde{\nu}$ = 1618−1599 (C=C + C=N), 514 (Pd−O). UV/Vis (λ, nm): 245, 290, 424. ^{1}H NMR ($CDCl_3$, ppm): δ = 8.10−8.03 (m, H_{arom}), 8.00−7.96 (m, CH=N), 7.85−7.75 (m, 4 H_{arom}), 7.50−7.38 (m, 2 H_{arom}), 7.18−7.16 (m, H_{arom}), 7.07−7.02 (m, H_{arom}), 4.95, 4.26 (d, J_{AB} = 13.8 Hz, $CH_2^{naphthyl}$), 3.60−3.37 (m, $H^{5'a}$, CHN=CH_2), 3.24−3.15 (m, CH=NCH_2), 2.83−2.71 (m, $H^{2'}$), 2.58−2.42 (m, $H^{5'b}$), 2.17−2.04 (m, OCOCH$_3$, CH_3), 1.97−1.83 (m, $H^{3'a,b}$, $H^{4'a,b}$), 1.40−1.25 [s, C(CH_3)$_3$] ppm. ^{13}C NMR ($CDCl_3$): δ = 176.23 (O*C*OCH$_3$), 160.92 (C−O−Pd), 157.81 (CH=N), 138.70, 131.63 130.95, 129.38, 128.62, 127.53, 127.19, 126.68, 126.50, 126.07, 125.75, 124.87, 124.60, 121.14, 117.91 (C_{arom}), 63.62 ($C^{2'}$), 61.23 (CH=N*C*H$_2$), 59.98 ($CH_2^{naphthyl}$), 56.85 ($C^{5'}$); 33.39 [*C*(CH$_3$)$_3$], 28.88 [C(*C*H$_3$)$_3$], 27.38 ($C^{3'}$), 25.50 (CH_3), 21.78 ($C^{4'}$), 18.34 (OCO*C*H$_3$). MS$^+$ (EI) (*m*/*z*, %): 519 (M^+ − Ac, for ^{106}Pd); 521 (M^+ − Ac, for ^{108}Pd); 523 (M^+ − Ac, for ^{110}Pd); 517 (M^+ − Ac, for ^{104}Pd); 515 (M^+ − Ac, for ^{102}Pd).

[Ni(5)(OAc)] (5Ni): Yield 73%. M.p. 223−226 °C. $[\alpha]_D^{25}$ = −0.7 (*c* = 0.9, $CHCl_3$). $C_{30}H_{36}N_2O_3Ni$ (531): calcd. C 67.8, H 6.8, N 5.3, Ni 11.1; found C 67.6, H 7.0, N 5.3, Ni 11.5. IR (KBr, cm^{-1}): $\tilde{\nu}$ = 1612−1600 (C=C + C=N), 540 (Ni−O). UV/Vis (λ, nm): 241, 267, 346, 428. ^{1}H NMR ($CDCl_3$, ppm): δ = 8.70−8.60 (m, H_{arom}), 8.30−8.27 (s, H_{arom}), 7.93−7.85 (s, CH=N), 7.85−7.75 (m, 3 H_{arom}), 7.50−7.38 (m, 2 H_{arom}), 6.92−6.85 (m, H^3), 6.55−6.48 (m, H^5), 5.00, 3.91 (d, J_{AB} = 16.3 Hz, $CH_2^{naphthyl}$), 3.80−3.64 (m, $H^{4'a}$), 3.45−3.35 (m, $H^{5'a}$), 3.18−3.07 (m, CH=NCH_2), 2.91−2.80 (m, CH=NCH_2), 2.38−2.27 (m, $H^{2'}$), 2.17−2.00 (m, OCOCH$_3$, $H^{3'a}$, $H^{5'b}$), 1.98−1.75 (m, CH_3, $H^{3'b}$, $H^{4'b}$), 1.00−0.96[s, C(CH_3)$_3$]

Table 4. Crystallographic data for complexes **3Ni** and **4Pd**

	3Ni	**4Pd**
Empirical formula	$C_{26}H_{34}N_2NiO_3$	$C_{30}H_{36}N_2O_3Pd$
Molecular mass	481.26	579.01
T [K]	296(2)	296(2)
λ [Å]	0.71073	0.71073
Crystal system	monoclinic	orthorhombic
Space group	*C*2	$P2_12_12_1$
a (Å)	36.337(4)	7.9823(12)
b (Å)	9.0865(9)	10.6063(16)
c (Å)	15.5821(16)	32.171(5)
β [°]	103.878(2)	
V (Å^3)	4994.7(9)	2723.7(7)
Z	8	4
D (calcd.) [g/cm^3]	1.280	1.412
μ [mm^{-1}]	0.805	0.714
F(000)	2048	1200
Crystal size [mm]	0.40 × 0.15 × 0.10	0.16 × 0.16 × 0.12
θ range [°]	3.65 to 31.10	3.84 to 26.40
Index ranges	$-49 \le h \le 52$, $-11 \le k \le 13$, $-21 \le l \le 20$	$-9 \le h \le 9$, $0 \le k \le 13$, $0 \le l \le 40$
Reflections collected	15515	5315
Independent reflections	9891 [R_{int} = 0.0867]	5315 [R_{int} = 0.0000]
Completeness to θ [%]	81.1	97.7
Absorption correction	Multi-scan (SADABS)	Multi-scan (SADABS)
Refinement method	Full-matrix least-squares on F^2	Full-matrix least-squares on F^2
Data/restraints/parameters	9891/1/588	5315/0/331
Goodness-of-fit on F^2	0.805	1.047
Final *R* indices [$I > 2\sigma(I)$]	$R1$ = 0.0653, $wR2$ = 0.1561	$R1$ = 0.0683, $wR2$ = 0.1156
R indices (all data)	$R1$ = 0.1665, $wR2$ = 0.1814	$R1$ = 0.1399, $wR2$ = 0.1295
Absolute structure parameter	0.02(6)	0.08(6)
Extinction coefficient	0.0000(2)	0.0044(7)
Largest diff. peak and hole [e·Å^3]	2.283 and −0.325	1.101 and −0.491

 © 2004 Wiley-VCH Verlag GmbH & Co. KGaA, Weinheim

ppm. ^{13}C NMR ($CDCl_3$): δ = 163.50 (C−O−Ni), 163.25 (*C*H=N), 142.63, 134.77, 134.52, 133.67, 132.71, 131.70, 130.75, 130.10, 130.00, 129.52, 129.22, 128.21, 128.01, 124.17, 121.14 (C_{arom}), 64.10 ($C^{2'}$), 63.07 (CHN=*C*H_2), 61.23 ($CH_2^{naphthyl}$), 58.56 ($C^{5'}$), 32.32 [*C*$(CH_3)_3$], 30.63 [C(*C*$H_3)_3$], 29.39 ($C^{3'}$), 25.97 (CH_3), 24.45 ($C^{4'}$), 21.79 (OCO*C*H_3). MS^+ (EI) (*m*/*z*, %): 472 (M^+ − Ac, for ^{59}Ni); 473 (M^+ − Ac, for ^{60}Ni).

Catalytic Experiments: The catalytic properties of the Pd and Ni complexes with respect to hydrogenation were examined under conventional conditions for batch reactions in a 100 mL reactor (Autoclave Engineers) at 40 °C, using 4 atm. hydrogen pressure and a metal/substrate molar ratio of 1/1000. The progress of the reaction and the optical purity (*ee*) of the hydrogenated product were monitored by gas chromatography with a chiral glass capillary column {stationary phase: a mixture of methyl silicone (OV-1701) and methylsilicone heptakis[2,3-dipentyl-6-(*tert*-butyldimethylsilyl)]-β-cyclodextrin}.[19]

X-ray Crystallography: Three-dimensional, room temperature X-ray data were collected on a Bruker−Siemens Smart CCD diffractometer equipped with a normal focus, 2.4 kW sealed tube X-ray source (molybdenum, λ = 0.71073 Å) operating at 50 kV and 20 mA. Data were collected over a quadrant of the reciprocal space by a combination of two frame sets. The cell parameters were determined and refined by least-squares fit of all the reflections collected. Each frame exposure time was 10 s covering 0.3° in ω. The crystal-to-detector distance was 6.05 cm. Coverage of the unique set was over 81.1% (**3Ni**), 97.7% (**4Pd**), complete to at least 31.10° (Ni), 26.40° (Pd) in θ. The first 50 frames were re-collected at the end of the data collection to monitor crystal decay; this showed a drop in the intensities to about 60% of their initial values. The Flack *x* parameters were 0.02(6) and 0.08(6), indicative of a correct absolute structure. The structure was solved by Multan and Fourier methods using SHELXTL.[20] Full matrix least-square refinement was carried out by using SHELXTL[20] minimising $w(F^2_o - F^2_c)^2$. The crystal of **3Ni** showed a very poor spectrum at high angles; thus, about 18% of the reflections gave negative intensities after the integration process. Because of this, only positive reflections (81.1%) were taken into account. Weighted *R* factors (*Rw*) and all goodness of fit parameters *S* are based on F^2, conventional *R* factors (*R*) are based on *F*. Crystal data are given in Table 4.

CCDC-218738 (for **4Pd**) and -218739 (for **3Ni**) contains the supplementary crystallographic data for this paper. These data can be obtained free of charge at www.ccdc.cam.ac.uk/conts/retrieving.html [or from the Cambridge Crystallographic Data Centre, 12 Union Road, Cambridge CB2 1EZ, UK; Fax: (internat.) +44-1223-336-033; E-mail: deposit@ccdc.cam.ac.uk].

Acknowledgments

Financial support by the Dirección General de Investigación Científica y Técnica of Spain (Project MAT2000−1768-C02−02) is gratefully acknowledged.

[1] F. Fache, E. Schulz, M. L. Tommasino, M. Lemaire, *Chem. Rev.* **2000**, *100*, 2159−2231.
[2] H. Schiff, *Ann. Suppl.* **1864**, *3*, 343.
[3] G. Shing, P. A. Shing, A. K. Sen, K. Shing, S. N. Dubey, R. N. Handa, J. Choi, *Synth. React. Inorg. Met.-Org. Chem.* **2002**, *32*, 171−187.
[4] [4a] T. Katsuki, in *Catalytic Asymmetric Synthesis* (Ed.: I. Ojima), John Wiley & Sons, New York, **2000**, chapter 6, p. 287. [4b] E. N. Jacobsen, M. H. Wu, in *Comprehensive Asymmetric Catalysis II* (Eds.: E. N. Jacobsen, A. Pfaltz, H. Yamamoto), Springer Verlag, New York, **1999**, chapter 18, p. 649. [4c]K. Smith, C. Liu, *Chem. Commun.* **2002**, 886−887.
[5] [5a] L. Canali, D. C. Sherrington, *Chem. Soc. Rev.* **1999**, *28*, 85−93. [5b] D. A. Atwood, M. J. Harvey, *Chem. Rev.* **2001**, *101*, 37−52.
[6] [6a] Y. N. Ito, T. Katsuki, *Bull. Chem. Soc. Jpn.* **1999**, *72*, 603−619. [6b] V. Ayala, A. Corma, M. Iglesias, F. Sánchez, *J. Catal.*, in press.
[7] [7a] M. J. Alcón, M. Iglesias, F. Sánchez, I. Viani, *J. Organomet. Chem.* **2000**, *601*, 284−292. [7b] M. T. Rispens, O. J. Gelling, A: H. De Vries, A. Meetsma, F. van Bolhuis, B. L. Feringa, *Tetrahedron* **1996**, *52*, 3521−3546.
[8] F. Lake, C. Moberg, *Eur. J. Org. Chem.* **2002**, 3179−3188 and references cited therein.
[9] U. Knof, A. von Zelewsky, *Angew. Chem. Int. Ed.* **1999**, *38*, 302−322 and references cited therein.
[10] [10a] H. Onoue, I. Moritani, *J. Organomet. Chem.* **1972**, *43*, 431−436. [10b] H. Onoue, K. Minami, K. Nakagawa, *Bull. Chem. Soc. Jpn.* **1970**, *43*, 3480−3485.
[11] K. Nakamoto, *IR and Raman Spectra of Inorganic and Coordination Compounds*, 5th ed., Wiley & Sons, New York, **1997**.
[12] T. N. Sorrell, W. E. Allen, P. S. White, *Inorg. Chem.* **1995**, *34*, 952.
[13] A. B. P. Lever, *Inorganic Electronic Spectroscopy*, Elsevier, Amsterdam, **1984**.
[14] Y. Ustynyuk, V. A. Chertkov, J. V. Barinov, *J. Organomet. Chem.* **1971**, *29*, C53.
[15] [15a] T. Koga, H. Furutachi, T. Nakamura, N. Fusita, M. Ohba, K. Takahashi, H. Okawa, *Inorg. Chem.* **1998**, *37*, 989−996. [15b] S. Uozumi, H. Furutachi, M. Ohba, H. Okawa, D. E. Fenton, K. Shindo, S. Murata, D. J. Kitko, *Inorg. Chem.* **1998**, *37*, 6281−6287.
[16] Heterolytic cleavage of hydrogen by Pd complexes has been proposed before: K. Kaneda, T. Manaka, *Trends Org. Chem.* **1991**, *2*, 109. This is reinforced from our experiments using more polar and protic acid media, which show a significant increase in reaction rate, probably resulting from charge separation during the formation of intermediate species (more detailed studies for establishing reaction pathways are in progress).
[17] [17a] M. S. Newman, S. I. Kosak, *J. Org. Chem.* **1949**, *14*, 375−381. [17b] T. A. Thornton, G. A. Ross, D. Patil, K. Mukaida, J. O Warnick, N. F. Woolsey, D. E Bartak, *J. Am. Chem. Soc.* **1989**, *111*, 2434−2440.
[18] [18a] M. Jun, C. Liu, *J. Coord. Chem.* **1975**, *5*, 1. [18b] M Jun, C. Liu, *Inorg. Chem.* **1975**, *14*, 2310−2314. [18c] A. Corma, M. Iglesias, C. del Pino, F. Sánchez, *J. Organomet. Chem.* **1992**, *431*, 233−246. [18d] A. Carmona, A. Corma, M. Iglesias, F. Sánchez, *Inorg. Chim. Acta* **1996**, *244*, 79−85. [18e] A. Carmona, A. Corma, M. Iglesias, F. Sánchez, *Inorg. Chim. Acta* **1996**, *244*, 239−245.
[19] E. Miranda, F. Sánchez, J. Sanz, M. I. Jiménez, I. Martínez-Castro, *J. High-Resol. Chromatogr.* **1998**, *21*, 225−233.
[20] G. M. Sheldrick, *SHELXTL program for the refinement of crystal structures*, University of Göttingen, Germany, **1997.**

Received September 5, 2003
Early View Article
Published Online March 31, 2004

 © 2004 Wiley-VCH Verlag GmbH & Co. KGaA, Weinheim

Synthesis and Structural Studies of Two New Base Adducts of Bis(2,4-pentanedionato)cobalt(II)

Stefania Tanase,[a] Elisabeth Bouwman,*[a] Jan Reedijk,[a] Willem L. Driessen,[a] Marilena Ferbinteanu,[b] Martina Huber,[c] Allison M. Mills,[d] and Anthony L. Spek[d]

Keywords: Cobalt / 2,4-Pentanedione / 3,5-Dimethylpyrazole / Dimethylethanolamine / Coordination modes

The syntheses, spectroscopic properties and crystal structures of two new base adducts of bis(2,4-pentanedionato)cobalt(II) with 3,5-dimethylpyrazole (Hdmpz) (**1**) and dimethylethanolamine (Hdmea) (**2**) are described. The crystal structures of both compounds contain monomeric Co^{II} complexes with *cis*-distorted octahedral environments, even for the monodentate Hdmpz ligand which is quite unique. These mononuclear complexes are linked by hydrogen bonds between the anionic 2,4-pentanedionato groups and the neutral Hdmpz or Hdmea ligands. The low-temperature polycrystalline-powder EPR spectra display unresolved metal hyperfine coupling. The *g* values are anisotropic in both cases; the anisotropy is larger for the Hdmea adduct. Interesting insights into the coordination effects were gained with the help of electron-density descriptors (Laplacian of density and Natural Bond Orbitals). This revealed a slight deviation of the coordinating lone pairs of the pentanedionato ligands from the Co–O axis, as well as a nonstandard hybrid composition. (© Wiley-VCH Verlag GmbH & Co. KGaA, 69451 Weinheim, Germany, 2004)

Introduction

The β-diketonato complexes of cobalt(II) are of interest in the field of coordination chemistry as structural prototypes and because of their tendency to form unanticipated oligomeric structures where the metal centre achieves a coordination number greater than four. Bis(acetylacetonato)cobalt(II) is a very common and easily accessible coordination complex, which exists as a tetranuclear complex in nonpolar solvents.[1] If a small amount of some neutral donor ligand (L) is introduced into a solution of the tetrameric $Co(acac)_2$ in a noncoordinating solvent, complex equilibria involving the following types of compounds are established: $[Co(acac)_2]_4$, $[Co(acac)_2L]$, $[Co(acac)_2L]_2$ and $[Co(acac)_2L_2]$.[2] Thus, upon treatment of $[Co(acac)_2]_4$ with pyridine (py), the compound *trans*-$[Co(acac)_2py_2]$ was isolated and its structure determined.[3] Similarly, *trans*-$[Co(acac)_2L_2]$ compounds (where L represents water, 6-methylquinoline, imidazole and 2-aminopyridine) were also prepared and their crystal structures reported.[4−7] With water as the donor molecule, two intermediate products were isolated: $[Co(acac)_2(H_2O)]_2$ and $[Co(acac)_2]_3(H_2O)$.[8,9] The crystal structures of both are derived from that of the tetrameric complex $[Co(acac)_2]_4$.

Our current interest in the autoxidation drying mechanism occurring in alkyd paints,[10,11] which involves cobalt complexes that are present as additives, led us to investigate the coordination chemistry and the catalytic activity of bis(2,4-pentanedionato)cobalt(II) in the presence of some organic ligands as possible co-catalysts.[12] In this context, it is of interest to probe the stability and reactivity of such adducts and additional information can be gained by contrasting the properties of chelating ligands, constrained to adopt *cis* geometry, with those of monodentate ligands, which typically yield *trans* complexes.[13]

In this paper, the syntheses, crystal structures and spectroscopic properties of *cis*-$[Co(acac)_2(Hdmpz)_2]$ (**1**) and $[Co(acac)_2(Hdmea)]$ (**2**) are described. Both complexes are new base adducts of bis(2,4-pentanedionato)cobalt(II) with Hdmpz (3,5-dimethylpyrazole) or Hdmea (dimethylethanolamine). Furthermore, compound **1** offers an interesting chromophore, distinguished as having the anisotropy of π effects in the N−Co−N moiety qualitatively different (in-plane) as compared to those encountered in chelating diamines (perpendicular to the N−Co−N plane).

[a] Leiden Institute of Chemistry, Gorlaeus Laboratories, Leiden University
P. O. Box 9502, 2300 RA Leiden, The Netherlands
Fax: (internat.) + 31-71-527-4451
E-mail: bouwman@chem.leidenuniv.nl
[b] University of Bucharest, Faculty of Chemistry, Department of Inorganic Chemistry,
Dumbrava Rosie 23, Bucharest 70254, Romania
[c] Leiden University, Department of Molecular Physics,
2300 RA Leiden, The Netherlands
[d] Bijvoet Center for Biomolecular Research, Utrecht University,
Padualaan 8, 3584 CH, Utrecht, The Netherlands

 DOI: 10.1002/ejic.200300708 © 2004 Wiley-VCH Verlag GmbH & Co. KGaA, Weinheim

Results and Discussion

Synthetic and Spectroscopic Studies

The compounds *cis*-[Co(acac)$_2$(Hdmpz)$_2$] (**1**) and [Co(acac)$_2$(Hdmea)] (**2**) were obtained in good yields by adding a stoichiometric amount of either Hdmpz or Hdmea to a solution of anhydrous cobalt acetylacetonate in toluene. Suitable crystals were obtained by slow evaporation of the solvent. Although compound **1** appeared to be unstable in solution (see below), the reaction that forms the oxidized product is sufficiently slow to allow the crystallisation of the pure cobalt(II) complex. The IR spectra of both compounds show the bands expected for the organic ligands coordinated to the cobalt centre. In particular, the peak at $\tilde{\nu}$ = 3348 cm^{-1} observed in the IR spectrum of **2**, indicates the presence of the protonated ligand Hdmea.

The solid-state electronic spectra of both compounds show two principal regions of absorption, as expected for octahedral Co^{II} complexes. The absorption spectrum of compound **1** is dominated by a broad band with a maximum at 1170 nm and a multicomponent band at 510 nm which together suggest the presence of pseudo-octahedral high spin Co^{II} centres. Compound **2** has a similar absorption spectrum with two main bands, one at 1125 nm and the other at 502 nm. These two bands correspond to the $^4T_{1g}(F)\rightarrow{}^4T_{2g}(F)$ and $^4T_{1g}(F)\rightarrow{}^4T_{1g}(P)$ transitions. The multiple structure of the band near 500 nm arises from a number of effects, but primarily from the admixture of spin-forbidden transitions to doublet states mainly derived from ^2G and ^2H.[14]

Study of the complexation reaction that occurs upon adding Hdmpz or Hdmea to [Co(acac)$_2$(H$_2$O)$_2$] in various solvents (methanol, ethanol, acetone, benzene and toluene) reveals that compounds with the composition [Co(acac)$_2$(Hdmpz)$_2$] or [Co(acac)$_2$(Hdmea)] are formed, irrespective of the nature of the solvent used. The electronic spectrum of the violet solution of **1** is typical for a distorted octahedral Co^{II} compound and it shows similar features as observed for other base adducts of bis(2,4-pentanedionato)-cobalt(II).[2,14] When a toluene solution of **1** is stored in a closed atmosphere it gradually transforms into a red colour over a number of days. The electronic spectrum of the red solution shows a broad absorption band with the maximum at 560 nm that is characteristic for an octahedral cobalt(III) species (Figure 1);[14] however, traces of cobalt(II) might still be present. This transformation suggests the oxidation of Co^{II} to Co^{III} and indicates that the complex *cis*-[Co(acac)$_2$(Hdmpz)$_2$] is unstable in solution. Red crystals have been isolated, but these thin plates are prone to stacking faults. Although X-ray diffraction data were collected for one of the plates, the stacking disorder could not be resolved. However, a preliminary crystal structure solution revealed the presence of the cobalt ion surrounded by two 2,4-pentanedionato groups and two neutral Hdmpz ligands in the *trans* positions, showing that the assumed oxidation of Co^{II} to Co^{III} in **1** is accompanied by a *cis*/*trans* isomerisation process. Complex **2** does not display such solution redox behaviour.

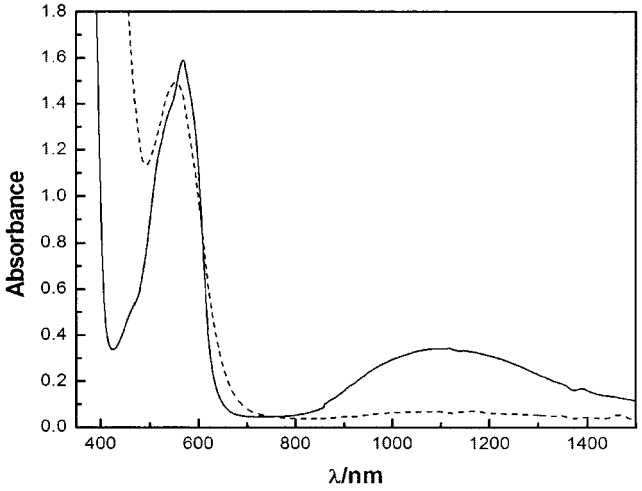

Figure 1. Spectral changes observed for a toluene solution of compound **1**; (a) just after preparation (—); (b) after 12 d (---)

Crystal Structures

The structures of **1** and **2** were determined by X-ray crystallography. Selected bond lengths and angles are listed in Table 1.

As shown in Figure 2, the crystal structure of **1** consists of isolated *cis*-[Co(acac)$_2$(Hdmpz)$_2$] molecules. To the best of our knowledge, this is the first base adduct of bis(2,4-pentanedionato)cobalt(II) to contain the two monodentate ligands in *cis* positions. The cobalt ion is in a distorted octahedral environment; it is coordinated by four oxygen atoms from two chelating acetylacetonato groups and two nitrogen atoms from two monodentate Hdmpz ligands. The Co−O bond lengths, in the range 2.0571(17)−2.0978(18) Å, are similar to those reported for *trans*-[Co(acac)$_2$L$_2$] complexes. The Co−N bonds of 2.159(2) and 2.166(2) Å are shorter than the corresponding Co−N bonds in *trans*-[Co(acac)$_2$L$_2$] complexes with L = pyridine,[5] 6-methylquinoline[4] and 2-aminopyridine,[6] but are longer than those observed for other Co^{II} complexes with 3,5-dimethylpyrazole.[15,16] The most interesting feature of the crystal structure of **1** is the presence of hydrogen bonds that may play an important role in the stabilisation of the *cis* configuration of the monodentate ligands. The details of these interactions are presented in Table 2. The NH groups of both Hdmpz ligands each participate in one intramolecular and one intermolecular hydrogen bond. Thus, molecules of **1** are linked into one-dimensional chains along the *c*-direction by the propagation of two bifurcated hydrogen bonds of the N−H···(O)$_2$ type (Figure 3). The closest separation between the metal ions of neighbouring molecules is 6.1035(5) Å.

The molecular structure of [Co(acac)$_2$(Hdmea)] (**2**) is similar to that of **1** concerning the topology of the Co(acac)$_2$ moiety and the position of the donor atoms (Figure 4). The base adduct **2** is constrained to adopt the *cis* configuration due to the chelating nature of Hdmea. The Co^{II} ion has a distorted octahedral coordination sphere consisting of four oxygen atoms from two acetylacetonato

 © 2004 Wiley-VCH Verlag GmbH & Co. KGaA, Weinheim

Table 1. Selected bond lengths [Å] and angles [°] for compounds **1** and **2**

cis-[Co(acac)$_2$(Hdmpz)$_2$] (**1**)		[Co(acac)$_2$(Hdmea)] (**2**)	
Co1−O16	2.088(2)	Co1−O16	2.060(10)
Co1−O17	2.0571(17)	Co1−O17	2.036(7)
Co1−O26	2.0978(18)	Co1−O26	2.05(2)
Co1−O27	2.0604(17)	Co1−O27	2.070(8)
Co1−N32	2.159(2)	Co1−O31	2.15(2)
Co1−N42	2.166(2)	Co1−N34	2.237(7)
O16−Co1−O17	88.63(7)	O16−Co1−O17	89.2(4)
O16−Co1−O26	94.20(7)	O16−Co1−O26	97.9(7)
O16−Co1−O27	85.55(7)	O16−Co1−O27	89.6(5)
O16−Co1−N32	174.86(8)	O16−Co1−O31	89.8(8)
O16−Co1−N42	90.13(8)	O16−Co1−N34	167.84(12)
O17−Co1−O26	86.64(7)	O17−Co1−O26	92.7(8)
O17−Co1−O27	171.79(7)	O17−Co1−O27	178.61(7)
O17−Co1−N32	87.62(8)	O17−Co1−O31	91.5(8)
O17−Co1−N42	98.88(7)	O17−Co1−N34	87.9(3)
O26−Co1−O27	88.01(8)	O26−Co1−O27	88.0(8)
O26−Co1−N32	89.10(8)	O26−Co1−O31	171.24(13)
O26−Co1−N42	173.97(8)	O26−Co1−N34	94.0(7)
O27−Co1−N32	98.52(8)	O27−Co1−O31	88.0(8)
O27−Co1−N42	86.93(7)	O27−Co1−N34	93.2(3)
N32−Co1−N42	86.97(8)	O31−Co1−N34	78.5(7)

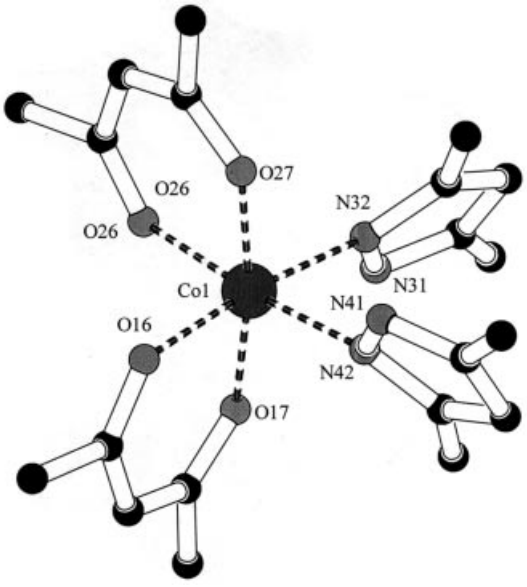

Figure 2. Pluton projection and atomic labels for *cis*-[Co(acac)$_2$(Hdmpz)$_2$] (**1**); hydrogen atoms are omitted for clarity

Table 2. Hydrogen bond details (distances [Å] and angles [°]) for compounds **1** and **2**

Donor−H···Acceptor	D−H	H···A	D···A	D−H···A
cis-[Co(acac)$_2$(Hdmpz)$_2$]:				
N(31)−H(31)···O(17)	0.88	2.63	3.030(3)	109
N(31)−H(31)···O(26)[a]	0.88	2.22	3.013(3)	151
N(41)−H(41)···O(27)	0.88	2.59	2.992(3)	109
N(41)−H(41)···O(16)[b]	0.88	2.28	3.067(3)	149
[Co(acac)$_2$(Hdmea)]:				
O(31)−H(31)···O(27)[c]	0.86(3)	1.87(5)	2.72(5)	170(30

[a] Symmetry transformations used to generate equivalent atoms: 2 − *x*, 1 − *y*, 1 − *z*. [b] 2 − *x*, 1 − *y*, −*z*. [c] − *x*, 1 − *y*, −*z*.

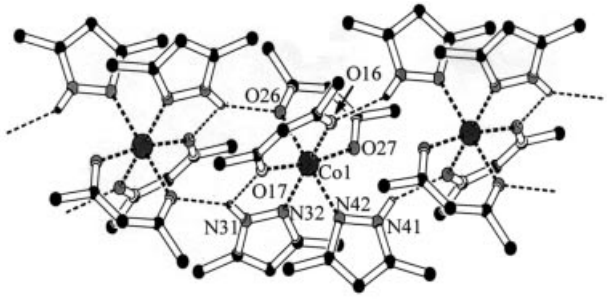

Figure 3. View of **1** showing the one-dimensional hydrogen-bonded chain

groups, as well as one oxygen and one nitrogen atom from a chelating Hdmea ligand. The Co−O bond lengths involving the 2,4-pentanedionato anions are in the range 2.036(7)−2.070(8) Å, slightly shorter than those in **1**; however, the Co1−O31 bond of 2.15(2) Å is longer. The Co1−N34 bond of 2.237(7) Å is significantly longer than the Co−N distances observed in **1**. In the crystal structure of **2**, the molecules are packed as dimers, as shown in Figure 4. Two strong O−H···O hydrogen bonds involving the

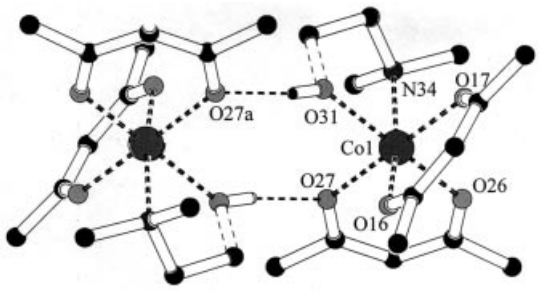

Figure 4. Atomic labels and view of the hydrogen-bonded dimer in **2**; only the major conformation of the disordered Hdmea ligand is shown

 © 2004 Wiley-VCH Verlag GmbH & Co. KGaA, Weinheim

OH groups of the Hdmea molecules and 2,4-pentanedionato O atoms link each pair of molecules (Table 2). The separation between the metal ions of neighbouring molecules is 5.47(9) Å.

EPR Spectroscopy and Magnetic Properties

The EPR spectra of polycrystalline *cis*-[Co(acac)$_2$(Hdmpz)$_2$] and [Co(acac)$_2$(Hdmea)] recorded at 4.2 K are shown in Figure 5. As previously observed for *trans* adducts of bis(2,4-pentanedionato)cobalt(II),[17] the large anisotropy of cobalt(II) complexes is such that the intermolecular exchange interactions do not cause exchange narrowing and the signals of individual molecules are resolved. However, the high- and low-field features are very broad, due to unresolved metal hyperfine coupling. Assuming an effective $S = 1/2$ ground state and neglecting interactions between the two Co^{II} ions, the following *g*-values are obtained;[18] for **1** they are: $g_1 = 2.1$, $g_2 = 2.5$ and $g_3 = 6.5$; for **2** they are: $g_1 = 1.9$, $g_2 = 4.3$ and $g_3 = 10.7$. The large variation of the *g*-values is expected in view of the high sensitivity of the *g*-values of Co^{II} with respect to any weak distortion of the ligand field. The average *g*-value ($<g>$) of complex **1** ($<g> = 3.7$) is similar to those observed for distorted octahedral cobalt(II) complexes. For such complexes, $<g> = 4.3$ and *g*-tensor components in the range from 1.5 to 7 have been reported.[19] For compound **2**, $<g> = 5.6$ and g_3 are larger than usual.

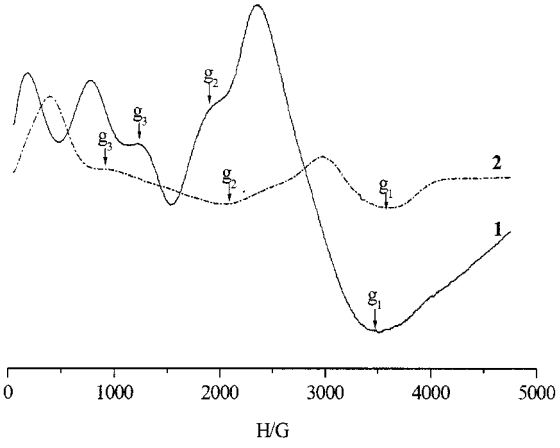

Figure 5. EPR spectra of polycrystalline powders of **1** and **2** recorded at 4.2 K and 9 GHz

The magnetic properties of **1** and **2** were investigated in the range 5−300 K. The $\chi_m T$ product at room temperature is 1.92 emu·K·mol^{-1} for **1** and 2.19 emu·K·mol^{-1} for **2**. Both values are slightly larger than the spin-only value for an isolated high-spin Co^{II} centre (1.875 emu·K·mol^{-1} for $S = 3/2$ assuming $g_{Co} = 2$) because of the orbital contribution. The $\chi_m T$ curves of both compounds exhibit a continuous decrease as the temperature is lowered from 300 to 5 K. Such behaviour, characteristic for Co^{II} complexes, is essentially due to single-ion anisotropy which may be combined with minor contributions from antiferromagnetic exchange between the Co^{II} centres by hydrogen bonds.

Electron Structure Analysis of the Ligand Binding in Complexes 1 and 2

A synoptic perception of the coordination bonding is obtained using the Laplacian of electron density and the density difference maps drawn in the ligand planes. The following results are based on the unrestricted DFT-B3LYP calculation with the 6-31G basis set.[20,21] The Laplacian pattern of each coordinated ligand [Figure 6 (a−c)] is in its gross part similar to those of the free ligands. The metal ion is mapped in complexes by areas with $\nabla^2\rho > 0$, corresponding to the electron-density depletion due to its ionic positive status.[22,23] The Laplacian can in principle detect the location of the lone pairs among the areas with $\nabla^2\rho > 0$. Figure 6 (a−c) shows, however, that the lone pairs are not very prominent at the oxygen donors, but are more pronounced at the nitrogen donor atoms. A similar aspect is observed comparing the different donor atoms of the amino alcohol ligand Hdmea. This may be due to the high chemical hardness of the oxygen atoms as compared to nitrogen atoms (the resistance of the electron cloud to deformations).

The formation of lone pairs in the valence shell is revealed in a rather spectacular way by taking the difference of the electron density of the ligand in the complex and that of the free ligand (taken in the same location and with the same geometry). In these representations [Figure 6 (d−f)] the lone pairs are detected as density depletion areas (dashed, grey contours). This is practically a direct visualisation of the density flow corresponding to the donation of the lone pair towards the metal ion.

Another method suitable for the detection and the analysis of lone pairs is the Natural Bond Orbital theory.[24,25] The orbital pictures in Figure 7 were drawn with the "molekel" PC program.[26] Surprisingly, for the 2,4-pentanedionato ligand it was found that the coordinating lone pairs have a content of about *s*(10 %)*p*(90 %) [see λ_1(O) and λ_1(O′) in Figure 7], rather than the *s*(33 %)*p*(67 %) character of the expected sp^2 hybrids. Besides, the λ_1 hybrids are not perfectly aligned along the Co−O axis, which has a deviation of about 10° inward of the chelating ring. The noncoordinating lone pairs at the oxygen atoms (denoted λ_2 in Figure 7) have approximately an *s*(50 %)*p*(50 %) composition and are inclined toward the metal ion with an angle of about 100° (instead of the expected 120°). The higher content in *p* character at the coordinating lone pairs λ_1(O) may be interpreted as favourable to the coordination process, because the lower ionisation potential of the *p* shell as compared to *s* ensures a better σ-donor action. This effect occurs at the expense of a lower *p* content at λ_2. The hybrid of the oxygen atom devoted to the σ(C−O) bond has approximately *s*(40 %)*p*(60 %) composition, which is closer to the expected sp^2 scheme. The composition of the hybrids around the oxygen atom in the M−O−C plane practically sums up to the total sp^2 content. Surprisingly, the abovementioned nonstandard compositions of lone pairs represent a real electronic structure effect that remains quali-

 © 2004 Wiley-VCH Verlag GmbH & Co. KGaA, Weinheim

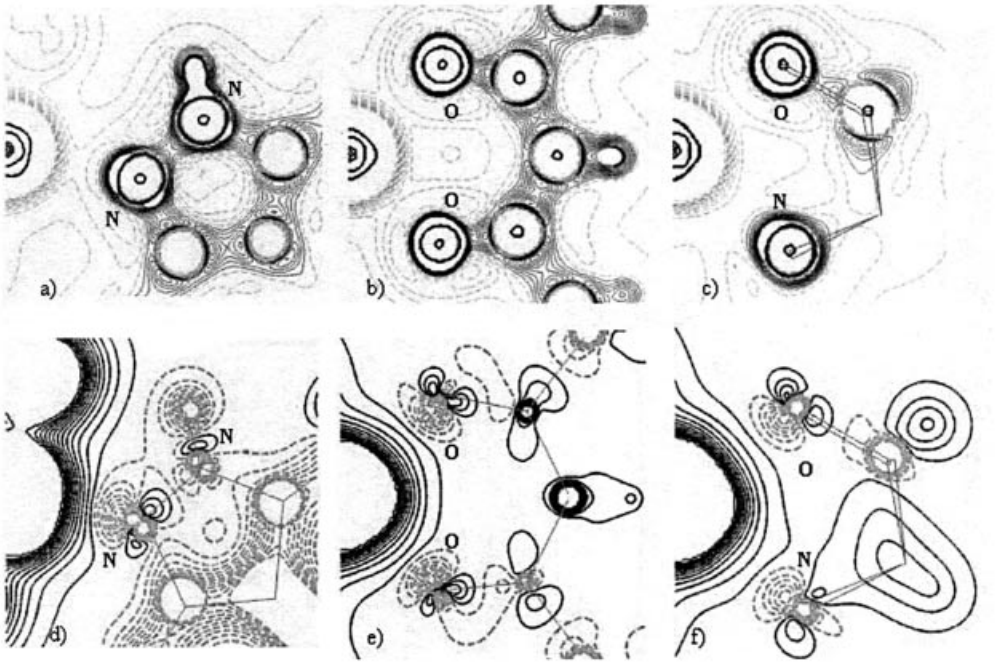

Figure 6. The electron-density descriptors applied to the ligands in complexes **1** and **2**: (a), (b) and (c) the Laplacian density maps in the CoNN, CoOO and CoON coordination planes of pyrazole, acac and amino alcohol Hdmea, respectively; in (d), (e) and (f) the electron density difference maps (complex minus free ligand) are presented for the same series of ligands; the acac ligand shown is taken from complex **1**, the situation for complex **2** being quite similar; in all the figures the dark, continuous lines correspond to density accumulation, dashed lines to depletion areas

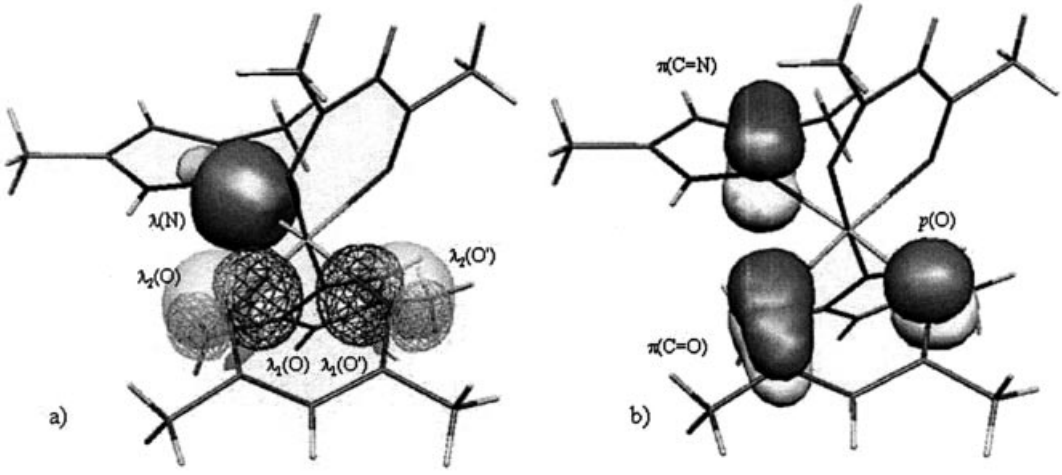

Figure 7. a) The σ-type lone pairs and b) *p*-π coordinating bond orbitals of the 2,4-pentanedionato and pyrazole ligands resulting from the application of NBO analysis on **1**

tatively stable at different levels of calculation. The calculated situation does not offend the concept of sp^2 hybridisation.

Keeping in mind that the sp^2 concept is only a qualitative or average rule, a careful look at the data offered by NBO analysis provides interesting new information for chemical intuition. It should be noted that the regular sp^2 hybridisation at a symmetric AX_3 triangular substitution of a main group central atom means that the three necessary orbitals are decided by symmetry to be one *s* plus two *p* (in plane) orbitals. The sp^2 notation is a convention concerning, in fact, the sum of hybrid compositions. Each of the equivalent hybrids can be more precisely noted $s^{1/3}p^{2/3}$, namely with *s*(33.33 %)*p*(66.67 %) composition. When the substituents at the central atom are of a different chemical nature, the electronegativity difference is a supplementary factor that determines the *s*/*p* content of each hybrid (keeping the total sp^2 composition). In the same respect, when the angles between substituents differ from the ideal 120°, the detailed composition should vary due to trigonometric reasons in order to accomplish the orientation of the hybrids along the bond. In certain circumstances the electronegativity versus

 © 2004 Wiley-VCH Verlag GmbH & Co. KGaA, Weinheim

geometric factors may result in slight deviations of the hybrid orbitals from the bond axis, as is the case in the coordinating lone pair.

Conclusion

The synthesis and characterisation of two new base adducts of bis(2,4-pentanedionato)cobalt(II) with 3,5-dimethylpyrazole (Hdmpz) and dimethylethanolamine (Hdmea) are reported. The crystal structures of **1** and **2** show mononuclear Co^{II} complexes with *cis*-distorted octahedral geometries; these complexes are linked by hydrogen bonds between the coordinated 2,4-pentanedionato anions and the neutral Hdmpz or Hdmea ligands. In solution, compound **1** is kinetically unstable. Its slow oxidation into a Co^{III} complex is accompanied by a *cis*/*trans* isomerization. In contrast, complex **2** does not display this behaviour. In subsequent studies the results presented here will be applied to the investigation of the antioxidant properties of these complexes as antiskinning agents in alkyd paints. The properties of chelating ligands, constrained to adopt *cis* geometry, may be compared with those of monodentate ligands, which typically yield *trans* complexes except in the case of the Hdmpz complex reported here. Interesting particularities of the lone pair topology at the pentanedionato ligands were revealed with the help of various analyses based on DFT calculations.

Experimental Section

General Remarks: All chemicals were of reagent grade, and were used as received. The anhydrous cobalt acetylacetonate was synthesised as previously reported.[27] All experiments were carried out in air. Elemental analyses for C, H and N were performed with a Perkin−Elmer 2400 Series II analyzer. Infrared spectra (4000−300 cm^{-1}) were recorded with a Perkin−Elmer Paragon 1000 FTIR spectrometer equipped with a Golden Gate ATR device, using the reflectance technique. UV/Vis spectra were obtained with a Perkin−Elmer Lambda 900 spectrophotometer using the diffuse reflectance technique, with MgO as the reference. X-band EPR spectra were recorded with a Bruker Elexsys 680 spectrometer using a rectangular cavity with an Oxford flow cryostat. Magnetic susceptibility measurements (5−300 K) were carried out at 1000 G using a Quantum Design MPMS-5 5T SQUID magnetometer. Data were corrected for magnetisation of the sample holder and for diamagnetic contributions, which were estimated from the Pascal constants.

[Bis(acetylacetonato)bis(3,5-dimethylpyrazole)Co^{II}] (1): Compound **1** was synthesised by adding 3,5-dimethylpyrazole (0.384 g, 4 mmol) to a hot solution of anhydrous cobalt acetylacetonate (0.513 g, 2 mmol) in toluene (20 mL) and stirring for 1 h. The resulting solution was allowed to stand at room temperature; violet crystals of **1** formed overnight. These were collected by filtration, washed with methanol and dried in air. Yield 0.75 g (83%). $C_{20}H_{30}CoN_4O_4$ (449.81): calcd. C 53.40, H 6.66, N 12.44; found C 53.63, H 6.32, N 12.66. IR: $\tilde{\nu}$ = 3284 (N−H), 2923 (C−H), 1595 (C=N), 1571 (C−O), 1516 (C−C), 1357 (C−H), 1014 (C−H), 765 (C−H) cm^{-1}. UV/Vis/NIR: $\tilde{\nu}_{max}$ = 8547, 19607 cm^{-1}.

[Bis(acetylacetonato)(dimethylethanolamine)Co^{II}] (2): Compound **2** was synthesised by adding *N*,*N*-dimethylethanolamine (0.178 g, 2 mmol) to a hot solution of anhydrous cobalt acetylacetonate (0.513 g, 2 mmol) in toluene (20 mL) and stirring for 1 h. The resulting solution was allowed to stand at room temperature for 5 d during which time red crystals formed. These were collected by filtration, washed with diethyl ether and dried in air. Yield 0.92 g (67 %). $C_{14}H_{25}CoNO_5$ (346.02): calcd. C 48.59, H 7.22, N 4.04; found C 48.03, H 6.90, N 4.23. IR: $\tilde{\nu}$ = 3348 (O−H), 2918 (C−H),

Table 3. Crystallographic data for compounds **1** and **2**

	cis-[$Co(acac)_2(Hdmpz)_2$] (**1**)	[$Co(acac)_2(Hdmea)$] (**2**)
Empirical formula	$C_{20}H_{30}CoN_4O_4$	$C_{14}H_{25}CoNO_5$
Formula mass	449.41	346.28
Crystal system	triclinic	triclinic
Space group	$P\bar{1}$ (no. 2)	$P\bar{1}$ (no. 2)
a [Å]	9.8218(2)	7.824(11)
b [Å]	10.3638(2)	10.36(2)
c [Å]	12.1242(3)	12.0(2)
α [°]	97.558(1)	105.4(4)
β [°]	98.579(1)	104.5(3)
γ [°]	117.369(1)	98.21(18)
V [$Å^3$]	1055.22(4)	885(15)
Z	2	2
$D_{calcd.}$ [g cm^{-1}]	1.41	1.30
μ(Mo-$K_α$) [mm^{-1}]	0.847	0.988
Crystal size [mm]	0.450 × 0.045 × 0.045	0.40 × 0.40 × 0.08
T [K]	150	293
Data collected	17051	8245
Unique data	4829	4064
R_{int}	0.086	0.033
$R(F)$ [$I > 2σ(I)$]	0.050	0.035
$R_w(F^2)$	0.100	0.110
S	0.96	1.08
$Δρ_{min}$, $Δρ_{max}$ [e·$Å^{-3}$]	−0.43, 0.43	−0.37, 0.33

 © 2004 Wiley-VCH Verlag GmbH & Co. KGaA, Weinheim

2820 (C−H), 1654 (C−N), 1575 (C−O), 1557 (C−C), 1386 (C−H), 1015 (C−H), 751 (C−H) cm^{-1}. UV/Vis/NIR: $\tilde{\nu}_{max}$ = 8889, 19920 cm^{-1}.

X-ray Crystal Structure Analysis: Intensity data for a single crystal were collected using Mo-K_α radiation (λ = 0.71073 Å) with either a Nonius Kappa CCD diffractometer with a rotating anode as for **1**, or with an Enraf−Nonius CAD4 diffractometer with a sealed tube for **2**. A correction for absorption was considered unnecessary in both cases. The structures were solved by automated Patterson methods using DIRDIF99,[28] and were refined on F^2 by least-squares procedures using SHELXL-97.[29] All non-hydrogen atoms were refined with anisotropic displacement parameters. The hydroxy hydrogen atom in **2** was refined freely with an isotropic displacement parameter. All other hydrogen atoms were constrained to idealised geometries and allowed to ride on their carrier atoms with an isotropic displacement parameter related to the equivalent displacement parameter of their carrier atoms. In **2**, the Hdmea ligand is disordered over two conformations, with refined relative occupancies of 0.845(5):0.155. Structure validation and molecular graphics preparation were performed with the PLATON package.[30] Crystallographic data are presented in Table 3. CCDC-219606 (for **1**) and -219607 (for **2**) contain the supplementary crystallographic data for this paper. These data can be obtained free of charge at www.ccdc.cam.ac.uk/conts/retrieving.html [or from the Cambridge Crystallographic Data Centre, 12 Union Road, Cambridge CB2 1EZ, UK; Fax: (internat.) + 44-1223-336-033; E-mail: deposit@ccdc.cam.ac.uk].

Acknowledgments

Financial support was provided by the Dutch Ministry of Economic Affairs (BTS 98141). This work was also supported in part (A. M. M. and A. L. S.) by the Netherlands Foundation of Chemical Research with financial aid from the Netherlands Organisation for Scientific Research (CW-NWO). M. F. acknowledges financial support of the Roumanian National Council of Research (CNCSIS grant no. 703-33618/2002). We gratefully acknowledge Mr. S. Gorter for the X-ray data collection for compound **2**.

[1] F. A. Cotton, C. A. Elder, *Inorg. Chem.* **1965**, *4*, 1145−1151.
[2] J. P. Fackler, *Inorg. Chem.* **1963**, *2*, 266−270.
[3] R. C. Elder, *Inorg. Chem.* **1968**, *7*, 1117−1123.
[4] G. J. Bullen, *Acta Crystallogr.* **1959**, *12*, 703−708.
[5] M. B. Hursthouse, K. M. A. Malik, J. E. Davies, J. H. Harding, *Acta Crystallogr., Sect. B* **1978**, *34*, 1355−1357.
[6] M. Doring, M. Meinert, E. Uhlig, L. Dahlenburg, R. Fawzi, *Z. Anorg. Allg. Chem.* **1991**, *598*, 71−82.
[7] M. Doring, W. Ludwig, E. Uhlig, S. Wocadlo, U. Muller, *Z. Anorg. Allg. Chem.* **1992**, *611*, 61−67.
[8] F. A. Cotton, C. A. Elder, *Inorg. Chem.* **1966**, *5*, 423−429.
[9] F. A. Cotton, R. Eiss, *J. Am. Chem. Soc.* **1968**, *90*, 38−46.
[10] S. Tanase, J.-C. Hierso, E. Bouwman, J. Reedijk, J. Bieleman, J. ter Borg, A. Schut, *New J. Chem.* **2003**, *27*, 854−859.
[11] S. T. Warzeska, M. Zonneveld, R. van Gorkum, W. J. Muizebelt, E. Bouwman, J. Reedijk, *Prog. Org. Coat.* **2002**, *44*, 243−248.
[12] S. Tanase, E. Bouwman, J. Reedijk, *Appl. Catal.*, *A* **2004**, *259*, 101−107.
[13] R. E. Colborn, M. F. Garbauskas, C. I. Hejna, *Inorg. Chem.* **1988**, *27*, 3661−3663.
[14] A. B. P. Lever, *Inorganic Electronic Spectroscopy*, Elsevier Science B. V., Amsterdam, **1986**.
[15] C. G. van Kralingen, J. Reedijk, *J. Chem. Soc., Chem. Commun.* **1976**, *14*, 533−533.
[16] A. R. Oki, J. Sanchez, R. J. Mogan, T. J. Emge, *J. Coord. Chem.* **1995**, *36*, 63−69.
[17] A. Bencini, C. Benelli, D. Gatteschi, C. Zanchini, *Inorg. Chem.* **1980**, *19*, 3027−3030.
[18] A. Abragam, B. Beaney, *Electronic Paramagnetic Resonance*, Clarendon Press, Oxford, **1970**.
[19] L. Banci, C. Benelli, D. Gatteschi, *Inorg. Chem.* **1981**, *20*, 4397−4400.
[20] The discussed calculation results are based on the experimental geometries. However, optimisisation of the molecular geometry was performed, finding a satisfactorily agreement with the experimental one. For **1** the mean deviation in computed vs. experimental bond lengths and angles is 0.011 Å and 0.274°, respectively. For **2**, these values are 0.009 Å and 0.221°. The good ab initio retrieval of experimental structures proves the reliability of the applied computation technique, in spite of the average level of sophistication.
[21] M. W. Schmidt, K. K. Baldridge, J. A. Boatz, S. T. Elbert, M. S. Gordon, J. H. Jensen, S. Koseki, N. Matsunaga, K. A. Nguyen, S. J. Su, T. L. Windus, *J. Comput. Chem.* **1993**, *14*, 1347−1363.
[22] R. F. W. Bader, *Acc. Chem. Res.* **1985**, *18*, 9−15.
[23] R. F. W. Bader, *Atoms in Molecules − A Quantum Theory*, Oxford University Press, Oxford, **1990**.
[24] A. E. Reed, L. A. Curtiss, F. Weinhold, *Chem. Rev.* **1988**, *88*, 899−926.
[25] A. E. Glendening, A. E. Reed, J. E. Carpenter, F. Weinhold, *NBO Version 3.1*, Theoretical Chemistry Institute, University of Wisconsin, Madison, **2001**.
[26] P. Flukiger, H. P. Luthi, S. Portmann, J. Weber, *MOLEKEL 4.3: An Interactive Molecular Graphics Tool*, Swiss Centre for Scientific Computing, Manno, Switzerland, **2000−2002**.
[27] F. A. Cotton, R. H. Holm, *J. Am. Chem. Soc.* **1960**, *82*, 2979−2983.
[28] P. T. Beurskens, G. Beurskens, R. de Gelder, S. García-Granda, R. O. Gould, R. I. Israel, J. M. M. Smits, *The DIRDIF99 Program System, Technical Report of the Crystallography Laboratory*, University of Nijmegen, The Netherlands, **1999**.
[29] G. Sheldrick, *SHELXL-97*, University of Göttingen, Germany, **1997**.
[30] A. L. Spek, *PLATON, A Multi-purpose Crystallographic Tool*, Utrecht University, The Netherlands, **2002**.

Received October 7, 2003
Early View Article
Published Online March 31, 2004

 © 2004 Wiley-VCH Verlag GmbH & Co. KGaA, Weinheim

EurJIC
European Journal of Inorganic Chemistry

Issue 10/2004

Pages 1971–2188

Papers available ahead of print in Early View at www.interscience.wiley.com

Earliest available Table of Contents:
Automatically, free of charge by e-mail through
www.interscience.wiley.com/alerts

COVER PICTURE

The cover picture shows the characteristic crystal form of elemental bismuth in the background and a perspective view of the crystal structure $Bi(Bi_9)[NbCl_6]_3$ containing three-capped trigonal prismatic Bi_9^{5+} clusters. The Bi^+ cations in the channels made up of the octahedral halometalate anions are disordered and can be treated in different ways in the crystallographic description. A remarkable feature of the compound is the paramagnetic behaviour, which shows the presence of Nb in the less common oxidation state +IV. Details are discussed in the article by J. Beck and T. Hilbert on p. 2019ff.

SHORT COMMUNICATIONS

Contents

1985 **A. Bacchi,* E. Bosetti, M. Carcelli, P. Pelagatti, D. Rogolino**

The Structural Role of the Triflate Anion in the Non-Covalent Silver Polymer $[Ag(LOH)_2(CF_3SO_3)(CH_3CN)]$ {LOH = α-(4-Pyridyl)-benzhydrol}

Keywords: Crystal engineering / Non-covalent interactions / Hydrogen bonds / Molecular tectonics / Silver compounds

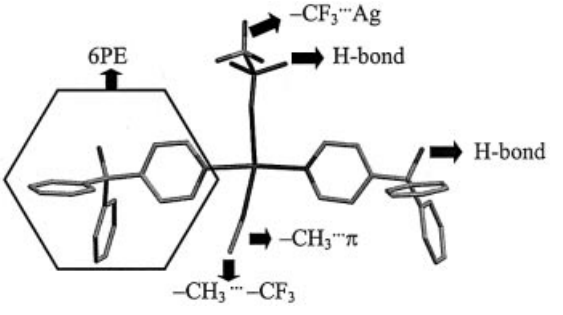

 © 2004 Wiley-VCH Verlag GmbH & Co. KGaA, Weinheim

1992 **J. Wang, A. K. J. Dick, M. G. Gardiner,* B. F. Yates, E. J. Peacock, B. W. Skelton, A. H. White**

Lanthanide(II) and -(III) Porphyrinogens. Rational Synthesis and Derivatisation of Mononuclear, Alkali-Metal-Free Lanthanide(II) and -(III) *meso*-Octaalkylporphyrinogen Complexes

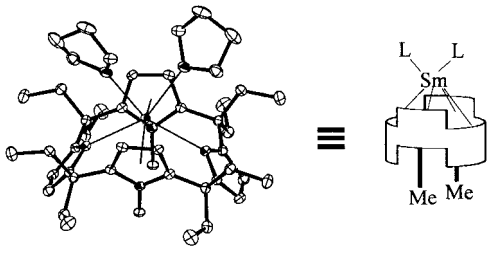

Keywords: Lanthanides / Macrocyclic ligands / Metallocenes / Porphyrinoids / Samarium

1996 **T. Mehdoui, J.-C. Berthet,* P. Thuéry, M. Ephritikhine***

Clear-Cut Lanthanide(III)/Actinide(III) Differentiation in Coordination of Pyrazine to Tris(cyclopentadienyl) Complexes of Cerium and Uranium, Involving Reversible $U^{III} \rightarrow U^{IV}$ Oxidation

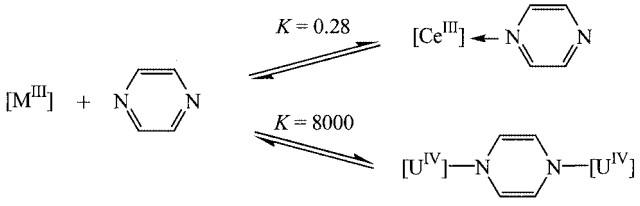

Keywords: Actinides / Lanthanides / Nitrogen ligands / Selective complexation

2001 **S. Rau,* R. Fischer, M. Jäger, B. Schäfer, S. Meyer, G. Kreisel, H. Görls, M. Rudolf, W. Henry, J. G. Vos**

Regioselective Functionalization of Tetrabromophenanthroline−Ruthenium Complexes

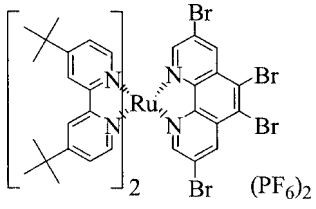

Keywords: Ruthenium / Nucleophilic substitution / Phenanthroline

2004 **S.-T. Zheng, J. Zhang, G.-Y. Yang***

$[\{Zn(enMe)_2\}_2(enMe)_2\{Zn_2As_8V_{12}O_{40}(H_2O)\}]\cdot 4H_2O$: A Hybrid Molecular Material Based on Covalently Linked Inorganic Zn−As−V Clusters and Transition Metal Complexes via enMe Ligands

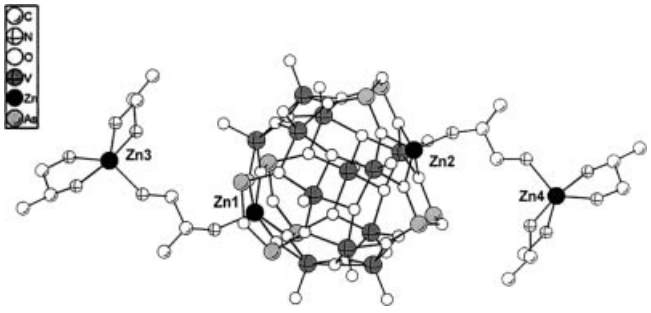

Keywords: Polyoxometalate / Vanadium / Arsenic / Zinc / Inorganic−organic hybrids

 © 2004 Wiley-VCH Verlag GmbH & Co. KGaA, Weinheim

2008 **M. C. Aragoni,* M. Arca, N. R. Champness, A. V. Chernikov, F. A. Devillanova, F. Isaia, V. Lippolis, N. S. Oxtoby, G. Verani, S. Z. Vatsadze, C. Wilson**

Designed Assembly of Low-dimensional Molecular Units: Novel Neutral Coordination Polymers Based on (Phosphonodithioato)Ni^{II} Complexes

Keywords: Phosphonodithioates / Bipyridyl ligands / Crystal engineering / Coordination polymers / X-ray diffraction

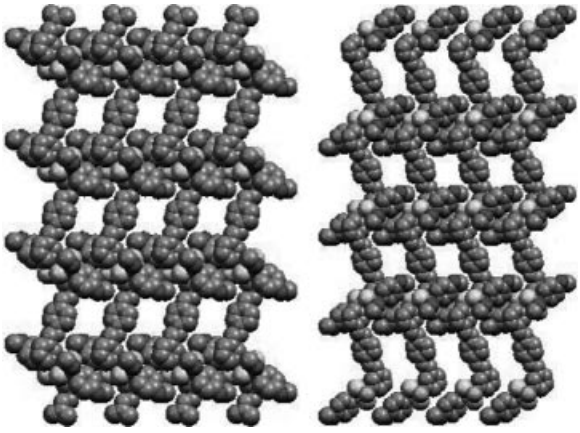

2013 **S. Masi, S. Top,* L. Boubekeur, G. Jaouen,* S. Mundwiler, B. Spingler, R. Alberto***

Direct Synthesis of Tricarbonyl(cyclopentadienyl)-rhenium and Tricarbonyl(cyclopentadienyl)technetium Units from Ferrocenyl Moieties − Preparation of 17α-Ethynylestradiol Derivative bearing a Tricarbonyl(cyclopentadienyl)technetium Group

Keywords: Technetium / Rhenium / Estradiol / Radiopharmaceuticals / Bioorganometallics

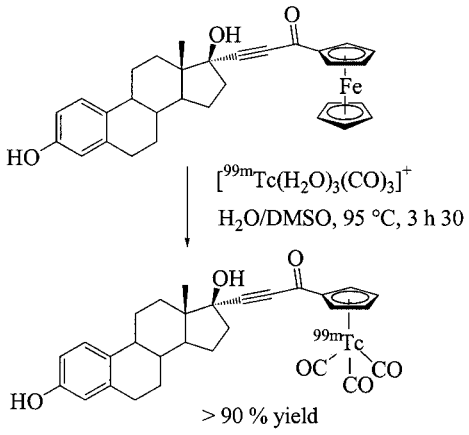

FULL PAPERS

2019 **J. Beck,* T. Hilbert**

Crystal Structure and Magnetic Properties of $Bi(Bi_9)[NbCl_6]_3$, a New Member of the Structure Family $Bi(Bi_9)[MX_6]_3$, and the Crystal Structure of $Bi_8[Ta_2O_2Br_7]_2$

Keywords: Bismuth / Niobium / Tantalum / Magnetic properties / X-ray diffraction

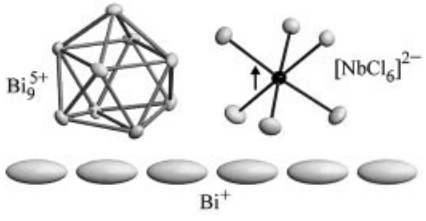

2027 **A. R. Silva, M. Martins, M. M. A. Freitas, J. L. Figueiredo, C. Freire,* B. de Castro**

Anchoring of Copper(II) Acetylacetonate onto an Activated Carbon Functionalised with a Triamine

Keywords: Copper / Schiff bases / Activated carbon / Anchoring / EPR spectroscopy

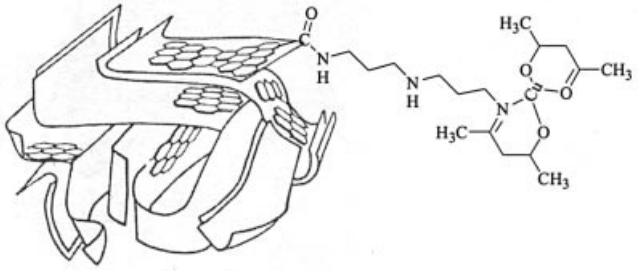

 © 2004 Wiley-VCH Verlag GmbH & Co. KGaA, Weinheim

2036 **D. Jabbour, B. Keita, I.-M. Mbomekalle, L. Nadjo,* U. Kortz**

Investigation of Multi-Nickel-Substituted Tungstophosphates and Their Stability and Electrocatalytic Properties in Aqueous Media

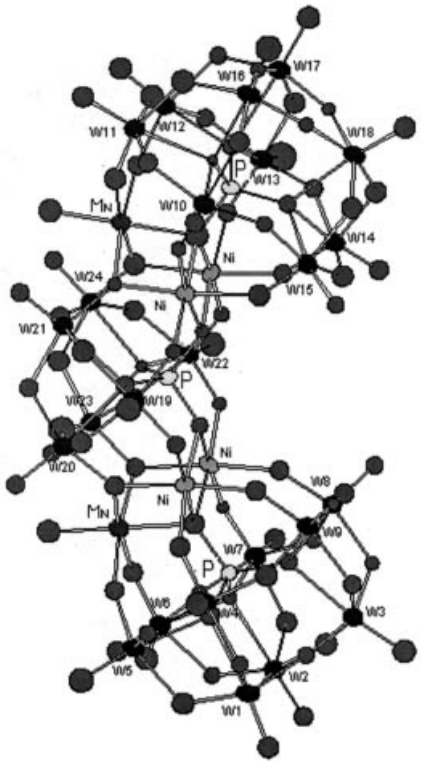

Keywords: Electrochemistry / Nickel / Polyoxometallates / Sandwich complexes / UV/Vis spectroscopy

2045 **M. Hogenbirk, G. Schat, F. J. J. de Kanter, O. S. Akkerman, F. Bickelhaupt,* H. Kooijman, A. L. Spek**

Investigations on the Reactivity of Bis(bromomagnesio)trimethylsilylmethane – Molecular Structure of a Tebbe-Type Spiro-Organomagnesium Compound

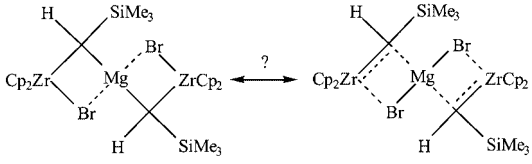

Keywords: Magnesium / Zirconium / Metallocenes / Metallacycles / Structure elucidation

2053 **K. Heinze,* V. Jacob, C. Feige**

Oxidative Addition of RX to Soluble and Polymer-Bound Molybdenum Carbonyl Complexes

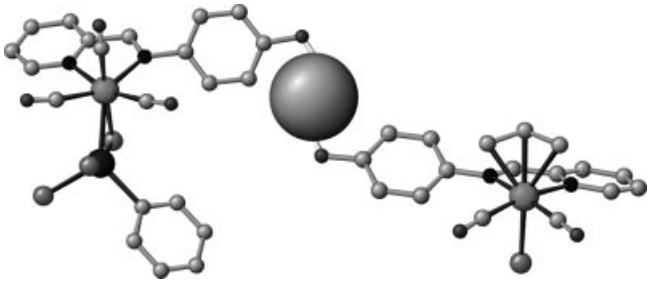

Keywords: Allyl Ligands / Molybdenum / Polymer-bound complexes / Solid-phase synthesis

2062 **U. Vogel, K.-C. Schwan, M. Scheer***

Reactivity of a Phosphanylalane Complex towards Lewis Bases

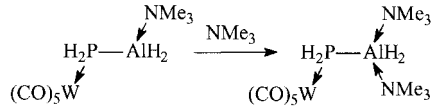

Keywords: Aluminum / Phosphorus / Hydrides / Reactivity / Lewis bases

 © 2004 Wiley-VCH Verlag GmbH & Co. KGaA, Weinheim

2066 **W.-Y. Wong,* G.-L. Lu, L. Liu, J.-X. Shi, Z. Lin**

Synthesis, Structures and Luminescent Properties of σ-Alkynyl Complexes of Orthomercuriated Schiff Bases

Keywords: Alkyne ligands / Luminescence / Mercury / Schiff bases

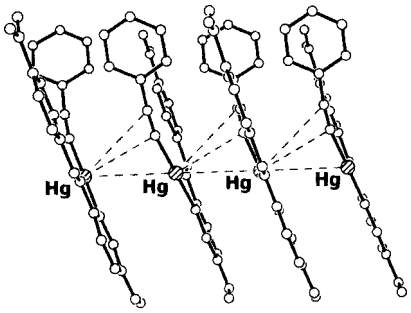

2078 **J. Díez, M. P. Gamasa,* J. Gimeno, Y. Rodríguez, S. García-Granda**

Five- and Six-Coordinate Ruthenium(II) Complexes Containing the Bidentate Phosphane (−)-*N*,*N*-Bis(diphenylphosphanyl)-(*S*)-1-phenylethylamine [(*S*)-peap]: X-ray Crystal Structure of the First 16-Electron Ruthenium Complex Bearing a Four-Membered Ring [RuCl{κ^2-*P*,*P*-(*S*)-peap}$_2$][SbF_6]·$C_2H_4Cl_2$

Keywords: Ruthenium / (*S*)-peap ligand / Five-coordinate complexes / Octahedral complexes

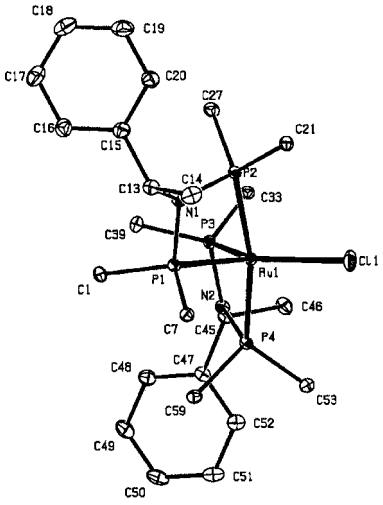

2086 **M. Vetrichelvan, Y.-H. Lai,* K. F. Mok**

3,11,19-Trithia[3.3.3]pyridinophane: Structural Diversity in Its Transition Metal Complexes

Keywords: Coordination polymers / Macrocycles / Structural diversity / Transition metals / Zwitterions

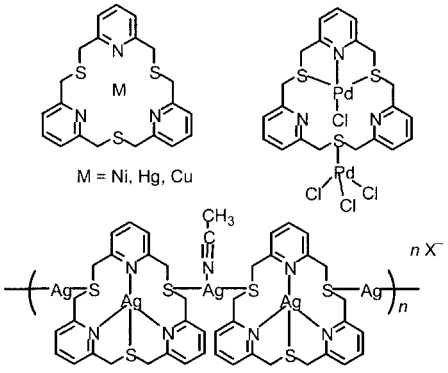

2096 **J.-C. Dai, X.-T. Wu,* S.-M. Hu, Z.-Y. Fu, J.-J. Zhang, W.-X. Du, H.-H. Zhang, R.-Q. Sun**

Crystal Engineering of the Coordination Architecture of Metal Polycarboxylate Complexes by Hydrothermal Synthesis: Assembly and Characterization of Four Novel Cadmium Polycarboxylate Coordination Polymers Based on Mixed Ligands

Keywords: Cadmium / Coordination polymers / Crystal engineering / Hydrothermal synthesis / Mixed ligands / Structural topology

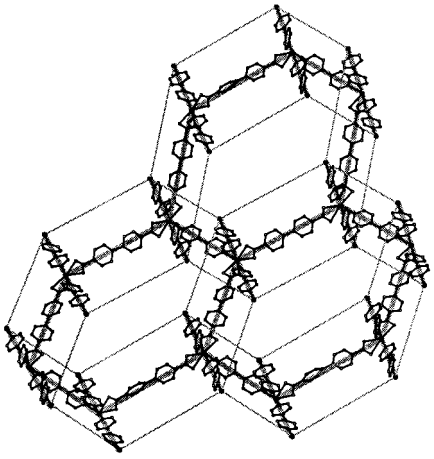

 © 2004 Wiley-VCH Verlag GmbH & Co. KGaA, Weinheim

2107 **J.-P. Djukic,* C. Michon, D. Heiser, N. Kyritsakas-Gruber, A. de Cian, K. H. Dötz, M. Pfeffer**

The Reaction of Diazocyclopentadienyl Compounds with Cyclomanganated Arenes as a Route to Ligand-Appended Cymantrenes

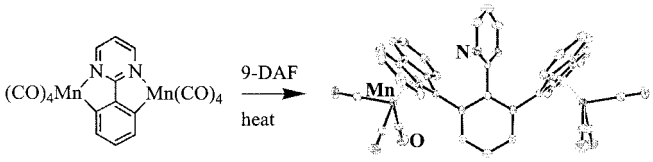

9-DAF: 9-diazofluorene

Keywords: Diazo compounds / Cyclopentadienyl ligands / Insertion / Manganese / Ligand design

2123 **P. L. Shutov, S. S. Karlov,* K. Harms, A. V. Churakov, J. Lorberth, G. S. Zaitseva**

Reaction of $[In(NEt_2)_3]_2$ with $N(CH_2CH_2N\text{-}SiMe_3H)_3$: Synthesis and Characterization of New Azaindatranes and Azaindocane

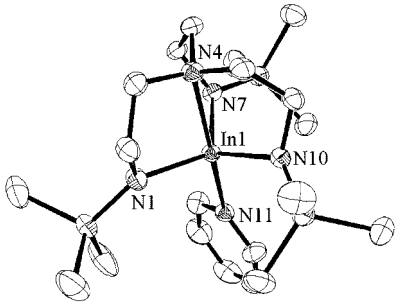

Keywords: N ligands / Indium / Tripodal ligands / Amides

2130 **W. Han, L. Yi, Z.-Q. Liu, W. Gu, S.-P. Yan,* P. Cheng, D.-Z. Liao, Z.-H. Jiang**

Synthesis and Characterisation of Two Supramolecular Polymers $[CuAg_4(CN)_6(tacn)]_n$ and $[CuAu_2(CN)_4(tacn)]_n$ Containing Metal−Metal Interactions

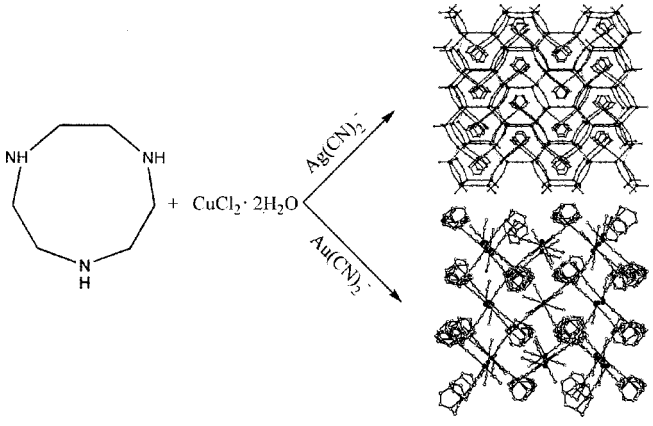

Keywords: Silver / Gold / Macrocyclic ligands / Metal−metal interactions

2137 **K. Kawabata, M. Nakano, H. Tamura, G. Matsubayashi***

Properties of Organometallic Sulfur-Rich Dithiolate Complexes $[M(L)(C_8H_4S_8)]$ (M = Rh^{III} and Ir^{III}; L = η^5-C_5H_5 and η^5-C_5Me_5) and Their Oxidation

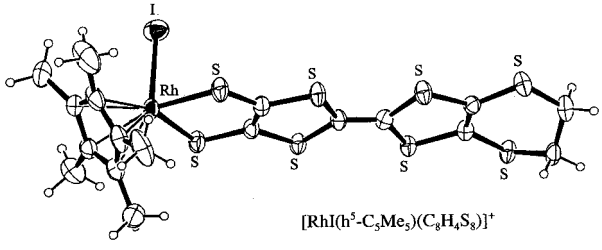

$[RhI(h^5\text{-}C_5Me_5)(C_8H_4S_8)]^+$

Keywords: Electrical conductivity / EPR spectroscopy / Iridium / Oxidation / Rhodium / S ligands / X-ray diffraction

 © 2004 Wiley-VCH Verlag GmbH & Co. KGaA, Weinheim

2144 **D. Sun, R. Cao,* W. Bi, X. Li, Y. Wang, M. Hong**

Self-Assembly of Novel Silver Polymers Based on Flexible Sulfonate Ligands

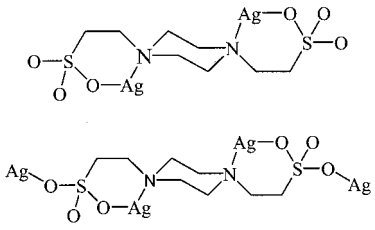

Keywords: Self-assembly / Silver / Sulfonate / Polymers

2151 **R. Müller, E. Hübner, N. Burzlaff***

Ruthenium(II) Complexes Bearing Carboxylato and 2-Oxocarboxylato Ligands

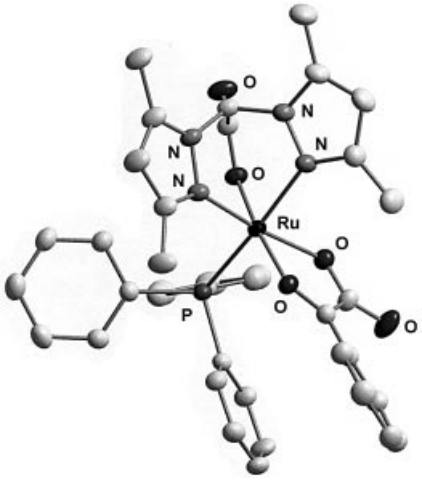

Keywords: Scorpionate ligands / Ruthenium / Bioinorganic chemistry / Tripodal ligands

2160 **T. Gáti, A. Simon, G. Tóth,* A. Szmigielska, A. M. May, K. M. Pietrusiewicz, S. Moeller, D. Magiera, H. Duddeck***

Bis(phosphane oxide) Adducts of $Rh_2(MTPA)_4$ − Kinetics and Chirality Discrimination

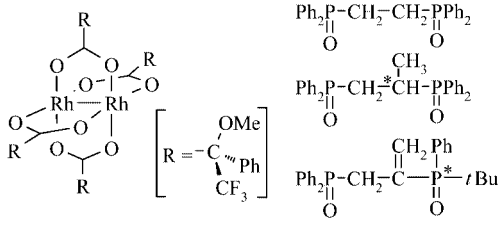

Keywords: Rhodium / Phosphane ligands / NMR spectroscopy / Complexation modes / Chiral discrimination

2167 **L. Zhou, Y. Yao, Y. Zhang, M. Xue, J. Chen, Q. Shen***

Synthesis and Characterization of Homoleptic Lanthanide Guanidinate Complexes and Their Catalytic Activity for the Ring-Opening Polymerization of Trimethylene Carbonate

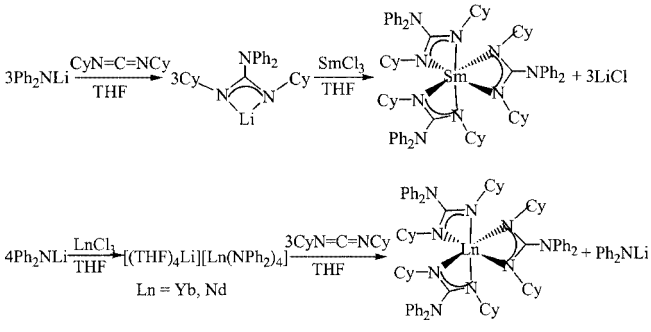

Keywords: Insertion / Lanthanides / N ligands / Polymerization

 © 2004 Wiley-VCH Verlag GmbH & Co. KGaA, Weinheim

2173 **V. Videva, A.-S. Chauvin, S. Varbanov, C. Baux, R. Scopelliti, M. Mitewa, J.-C. G. Bünzli***

Cobalt(II), Nickel(II), Copper(II), and Zinc(II) Complexes with a *p-tert*-Butylcalix[4]arene Fitted with Phosphinoyl Pendant Arms

Keywords: Calix[4]arene / Transition metals / Stability constants / X-ray diffraction / Polynuclear compounds

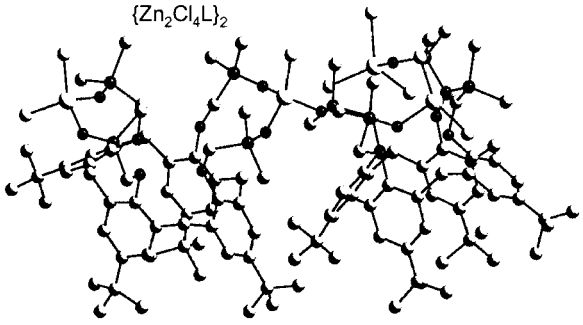

2180 **Y.-T. Cheng, H.-L. Chen, S.-Y. Tsai, C.-C. Su,* H.-S. Tsang, T.-S. Kuo, Y.-C. Tsai, F.-L. Liao, S.-L. Wang**

Structure, Bonding, and Tyrosinase-Like Reactivity of Copper Complexes Coordinated by Mononucleating Tridentate N−O−N Type Ligands

Keywords: Enzyme models / N,O ligands / Copper / Oxidations

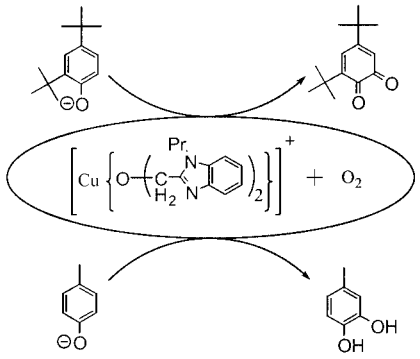

 © 2004 Wiley-VCH Verlag GmbH & Co. KGaA, Weinheim

The Structural Role of the Triflate Anion in the Non-Covalent Silver Polymer $[Ag(LOH)_2(CF_3SO_3)(CH_3CN)]$ {LOH = α-(4-Pyridyl)benzhydrol}

Alessia Bacchi,*[a] Elsa Bosetti,[a] Mauro Carcelli,[a] Paolo Pelagatti,[a] and Dominga Rogolino[a]

Keywords: Crystal engineering / Non-covalent interactions / Hydrogen bonds / Molecular tectonics / Silver compounds

$Ag(CF_3SO_3)$ was reacted with the ligand α-(4-pyridyl)benzhydrol (LOH) in order to build a mixed organic/inorganic analogue of wheel-and-axle diols. In the resulting $[Ag(LOH)_2(CF_3SO_3)(CH_3CN)]$ complex, the metal is four-coordinate, with two pyridines *trans* each other and a triflate and an acetonitrile group completing a sawhorse geometry. The main structural motif is based on the strongest and most directional tectons, the coordination bond Ag–O and the hydrogen bonds –OH···O–S–O···HO–. Secondly, the sixfold phenyl embrace, $CH_3\cdots\pi$, $CH_3\cdots CF_3$ and Ag···F tectons also direct the crystal assembly. A new synthon originating from the combination of the S–O···HO–, the $\pi\cdots CH_3$ and the $CH_3\cdots CF_3$ individual tectons is identified. The structural roles of the anion and of the solvent are discussed.
(© Wiley-VCH Verlag GmbH & Co. KGaA, 69451 Weinheim, Germany, 2004)

Introduction

We are currently pursuing the engineering of crystalline systems built by combining photoactivatable triphenylmethanol derivatives with metal centers structured in porous networks.

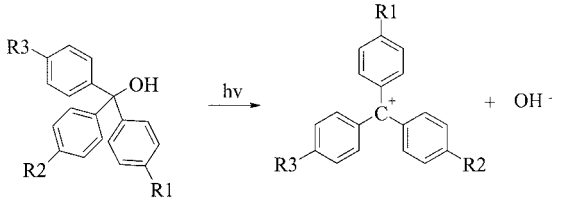

Scheme 1

Triphenylmethanol derivatives (TPMs) (Scheme 1) are actively studied because they show C−OH photocleavage, accompanied by an intense chromatic change on irradiation by UV/Visible light both in polar solvents and in the solid state.[1] Furthermore, compounds with the general formula Ar_3X−OH (X = C, Si, Ge) have a propensity to crystallize giving trimeric or tetrameric molecular aggregates based on hydrogen-bonded −OH clusters, and they also frequently form clathrate compounds with hydrogen-bond acceptor solvent molecules.[2] Remarkable clathrating properties are shown also by the diol derivatives of the general formula $HOC(Ar)_2$-L-$(Ar)_2COH$, where L is a suitable rigid organic spacer,[3a] the so-called "wheel-and-axle" systems.

Our purpose is to incorporate a metal center into the L spacer of the $HOC(Ar)_2$-L-$(Ar)_2COH$ host framework, in order to combine the clathrating nature of the diol organic matrix with the potential host-guest reactivity triggered by the inorganic functionality (Scheme 2). The coordination of a metal center at the peripheral rim of the TPM molecule could tune the electronic properties of the chromophore and concomitantly drive the organization of the crystal architecture.

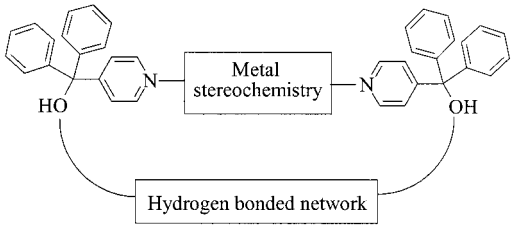

Scheme 2

Our approach to the rational design of these architectures is based on the molecular tectonics method,[4] in which the crystal structure is deconvoluted in the contributions of the single inorganic and organic building blocks, which are separately analyzed and optimized.

The first step in modeling these organic-inorganic "wheel-and-axle" complexes consists in the introduction of a transition metal as a bridge between two aromatic rings; this aim is pursued by synthesizing the transition metal complexes of the ligand α-(4-pyridyl)benzhydrol (LOH, Scheme 2).[5] Here, we report and analyze the solid-state arrangement of the new silver complex $[Ag(LOH)_2$-

[a] Dipartimento di Chimica Generale ed Inorganica, Chimica Analitica, Chimica Fisica, University of Parma,
Parco Area delle Scienze 17A, 43100 Parma, Italy
E-mail: alessia.bacchi@unipr.it

(OTf)(CH_3CN)], with the aim of establishing a hierarchy in the importance and robustness of the supramolecular motifs observed in the compound and of elucidating the structural role of the counteranion. Currently, we also report our first results on the supramolecular organization of two $Ag(LOH)_2^+$ complexes with weakly coordinating anions, BF_4^- and PF_6^-.[6]

The analysis of the relevant interactions in the crystal packing of [$Ag(LOH)_2$(OTf)(CH_3CN)] will follow the scheme: (i) search for hydrogen bonds involving the −OH donor; (ii) search for short contacts (less than the sum of the van der Waals radii); among the above short contacts, detect weak hydrogen bonds, π interactions, aromatic···aromatic association; (iii) heuristic search for other supramolecular long range arrangements, such as multiple phenyl embrace and long F···Ag contacts, to complete the metal environment; (iv) analysis of the combination of the patterns to determine recurrent motifs for the structure, in comparison also to other $Ag(LOH)_2^+$ complexes.[6]

Results and Discussion

[$Ag(LOH)_2$(OTf)(CH_3CN)] is obtained by reacting LOH with an excess of $Ag(CF_3SO_3)$. The complex is stable in the solid state in the dark, while its solution slowly releases silver. The spectroscopic characterization does not show any remarkable feature: in the ^1H NMR spectrum, the protons H4 and H5 of the pyridyl ring are deshielded with respect to the free ligand, and the singlet assigned to the acetonitrile molecule is present (δ = 2.00 ppm); in the IR spectrum, there are the typical bands assigned to the triflate anion. Crystals suitable for X ray diffraction analysis were obtained from the mother liquor within a couple of days.

The metal is coordinated to two pyridine N_{py} atoms, one oxygen atom of the anion and to one acetonitrile molecule (Figure 1), in a sawhorse geometry already observed for similar Ag complexes[7] [N2−Ag−O2 = 127.7(4)°]. The acetonitrile molecule is loosely bound, in fact the Ag−N2 distance [2.650(9) Å] is one of the longest ever observed in the solid state for $Ag-N{\equiv}C-CH_3$ coordination. The Ag atom, the CH_3CN and CF_3SO_3 ligands are placed on a symmetry plane that cuts the complex perpendicularly to the $N_{py}-Ag-N_{py}$ vector.

In a related work,[6] we found that in [$Ag(LOH)_2$]BF_4 and [$Ag(LOH)_2$]PF_6 the silver ion coordinates linearly two ligand molecules. In [$Ag(LOH)_2(CF_3SO_3)(CH_3CN)$], a new element is introduced into the organization of the crystal structure around the $[Ag(LOH)_2]^+$ unit; namely, the metal atom also employs covalent bonds to expand its supramolecular environment by directly coordinating the anion and the acetonitrile molecule. Scheme 3 shows the geometric descriptors chosen to represent the conformation of the complex. Selected parameters are: the dihedral angle between pyridines (ψ: C4−N1−N1′−C4′), the orientation of the C−OH vectors with respect to the adjacent pyridine (φ: O1−C1−C2−C3 and O1′−C1′−C2′−C3′), and the reciprocal orientation of the two C−OH vectors (χ: O1−C1−C1′−O1′). The classification of the triaryl groups has been made following Dance's analysis of triphenylphosphanes,[8] by calculating the torsion angles $C_{(ortho)}-C_{(ipso)}-C_{(sp3)}-O$ for each ring (labeled so that |torsion| < 90°), and then considering the cases: *rotor* (20° < |T1| ≈ |T2| ≈ |T3| < 70°, same sign), *anti-rotor* (20° < |T1| ≈ |T2| ≈ |T3| < 70°, opposite sign), *parallel flipper* (|T1| < 20°, T2 ≈ −T3), *orthogonal flipper* (70° < |T1| < 90°,

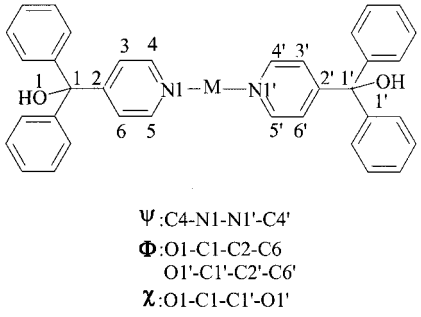

Scheme 3

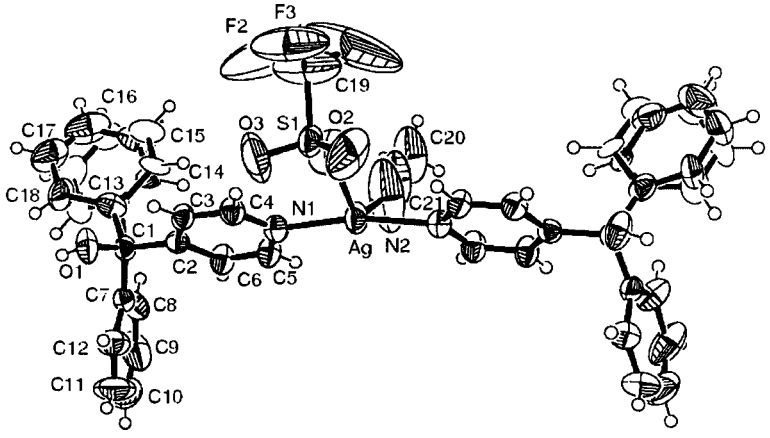

Figure 1. Molecular structure and labelling of the independent unit of [$Ag(LOH)_2(CF_3SO_3)(CH_3CN)$]; Ag, O2, S1, C19, F3, N2, C20 and C21 are on a mirror plane; phenyl C13−C18 is disordered over two orientations

 © 2004 Wiley-VCH Verlag GmbH & Co. KGaA, Weinheim

Table 1. Molecular conformation and supramolecular organization of the $[Ag(LOH)_2(OTf)(CH_3CN)]$ complex; *top*: ψ = reciprocal pyridine orientation, φ = orientation of the C−OH vector relative to the adjacent pyridine ring, χ = reciprocal orientation of the two C−OH vectors, T1, T2, T3 = conformation of the triaryl group, following Dance;[8] T1 refers to the pyridine ring and T2 to the ring involved in the NC−CH_3···π contact; T3 is presented for both disordered conformers (a) and (b); *bottom*: supramolecular tectons belong to three classes: metal environment (4+1 coordination), hydrogen bond (−OH···O−S−O···HO− motif), and weak directional interactions [CH_3···CF_3, CH_3···π, sixfold phenyl embrace (6PE)]; symmetry operations: (i) *x*, 3/2 − *y*, *z*; (ii) 1 − *x*, 2 − *y*, −*z*; (iii) *x* + 1, *y*, *z*; (iv) *x* + 1, *y*, *z* + 1; (v) 2 − *x*, 2 − *y*, 1 − *z*; (vi) *x*, 5/2 − *y*, *z*; (vii) 2 − *x*, *y* − 1/2, 1 − *z*

Molecular conformation (°)	ψ (C4−N1−N1′−C4′)	φ (O1−C1−C2−C3)	χ (O1−C1−C1′−O1′)	T1	T2	T3
	0.00	−24.3(5)	0.00	−24.3(5)	−35.1(5)	−69.8(7)(a) −38.0(8)(b)

Supramolecular organization (Å,°)	Metal environment			H-bond	Weak directional interactions		
	Ag−N_{py}	Ag···O	Ag···N_{solv}	Ag···CF_3	O−H···O D···A <DHA	CH_3···F	CH_3···π	6PE O−C1Ar_3···Ar_3C1−O
	Ag···N1 2.191(3)	Ag···O2 2.529(5)	Ag···N2 2.650(9)	Ag···F3(iii) 3.542(6)	O1−H···O3(ii) 2.849(5) 171(5)	C20···F3(iv) 3.00(1)	C20···C9(v) 3.552(7)	C1···C1(v) 6.535(7)
	Ag···N1(i) 2.191(3)	N1−Ag−O2 93.90(8)	N1−Ag−N2 90.86(9)	N1−Ag−F3(iii) 84.56(8)			C20···C9(vii) 3.552(7)	O1−C1···C1(v) 175.9(2)
	N1−Ag−N1(i) 168.7(2)		O2−Ag−N2 127.7(4)	O2−Ag−F3(iii) 117.3(2)				O1(v)−C1(v)···C1 175.9(2)
				N2−Ag−F3(iii) 115.0(3)				

T2 ≈ −T3). Table 1 lists the results of the conformational analysis and contains the key features of the supramolecular arrangement; symmetry operations cited in the text are also reported in Table 1. The pyridine rings are coplanar (Ψ = 0°), while the −OH groups deviate by Φ = −24.3(5)° from the pyridine plane. The complex exhibits the *syn* configuration for the two −OH groups (χ = 0°), in contrast with the *anti* configuration usually found in similar cases;[6,13] this will be related to the crystal packing in the course of the discussion. The triaryl group has a regular rotor conformation, with *T*1, *T*2 and *T*3 values falling in the range indicated by Dance.[8]

The coordination of the anion and acetonitrile group can be considered as the first stage of the supramolecular organization of the $[Ag(LOH)_2]^+$ unit; the analysis of the assembly of the $[Ag(LOH)_2(OTf)(CH_3CN)]$ molecules follows the steps outlined in the introduction.

(i) The −OH donors are strongly linked to the triflate acceptors of adjacent molecules by OH···O hydrogen bonds [O1···O3(ii) = 2.849(5) Å, O1−H···O3(ii) = 171(5)°]: the $[Ag(LOH)_2(OTf)(CH_3CN)]$ molecule uses its two −OH groups to hydrogen bond with the two triflate groups of a pair of adjacent molecules related by a twofold screw axis; concomitantly each triflate anion accepts two hydrogen bonds from the −OH groups of two adjacent molecules, generating the −OH···O−S−O···HO− tecton, with a OH···OH(vi) distance of 7.544(6) Å. The overall arrangement consists of a double strand along the *b* axis (Figure 2).

(ii) The short contacts (Table 1) involve the methyl group of the acetonitrile ligand, which is sandwiched between two aromatic rings giving two symmetric CH_3···π[9] interactions [C20···C9(v,vii) = 3.552(7) Å, H20···C9(v,vii) = 2.87 Å, H···π = 2.76 Å]. The two aromatic rings belong to a pair of triaryl groups in an adjacent double strand. The same methyl group also interacts with the triflate bridging the two aryl groups by means of a CH_3···CF_3 interaction [C20···F3(iv) = 3.00(1) Å]. Both interactions connect the double strands in a sheet (Figure 3). A short non-bonded H···H(vi) distance (2.36 Å, vi = *x*, 5/2 − *y*, *z*) between two almost coplanar aromatic rings which belong to the pair of molecules held together by the triflate bridge is also present in the structure. The local mirror symmetry would impose a much shorter contact between the two H atoms facing each other (1.66 Å), but this distance is relaxed by tilting the rings out of the common plane and introducing local disorder.

(iii) A sixfold phenyl embrace[10] [6PE, C1···C1(v) = 6.535(7) Å, O1−C1···C1(v) = 175.9(2)°] is formed between triaryl groups that are also involved in the CH_3···π interactions (Figure 4). The rotor conformation of the triaryl groups fits well in the 6PE and dictates the reciprocal orientation of the rings also involved in the H···H contact. Recently it has been shown by Bader and co-workers[11] that short H−H contacts between hydrogen atoms with similar charges can contribute up to 10 kcal/mol to the stabilization of the system where they occur. The assignment of stabiliz-

 © 2004 Wiley-VCH Verlag GmbH & Co. KGaA, Weinheim

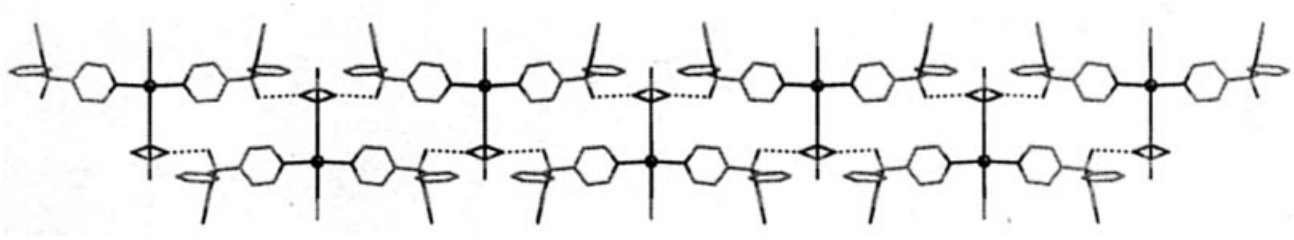

Figure 2. Association of the −OH···O−S−O···HO− tectons in double strands

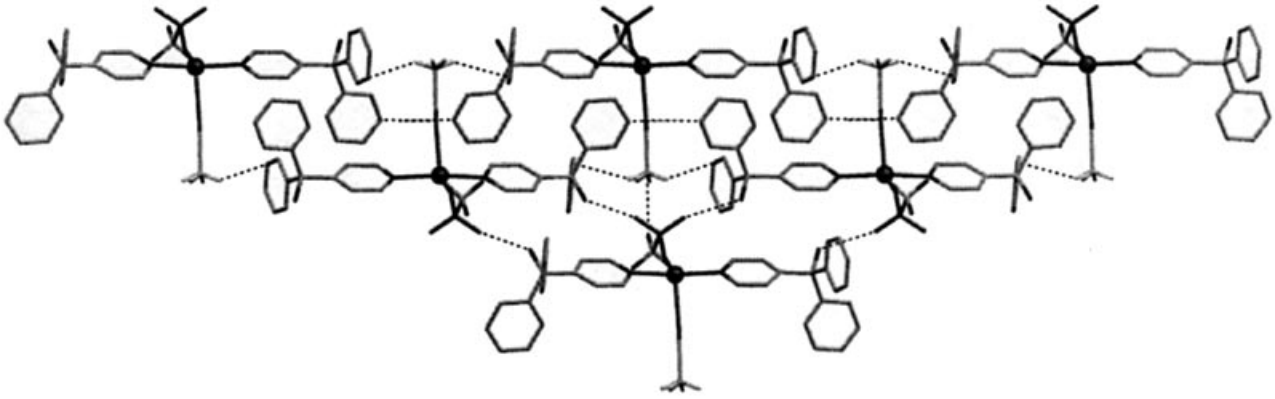

Figure 3. Association of the hydrogen-bonded double strands in sheets, via $CH_3\cdots\pi$ and $CH_3\cdots CF_3$ interactions (dashed); the short H···H contacts are also dashed (2.36 Å)

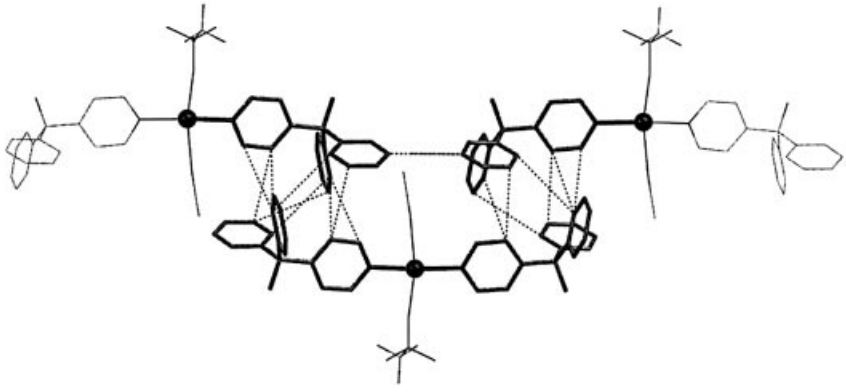

Figure 4. Sixfold phenyl embrace (6PE) involving molecules in the sheets shown in Figure 3; C···C contacts are dashed; the H···H short interaction is also shown

ing character to a short H−H interaction relies on the analysis of the experimental electron-density topology; in the absence of such evidence, it can be noted that the observed contact results from the balance of a local compression required to optimize the 6PE geometry in the presence of mirror symmetry, and a consequent rearrangement due to local overcrowding. The stabilization arising from the 6PE geometry can equal up to 20 kcal mol^{-1},[12] and this could counterbalance the possible repulsion between symmetry-related aromatic rings, whilst the H−H stabilization could justify a slight distortion from the best 6PE geometry.

Finally, an examination of the metal environment shows that a long Ag···F3(iii) [3.542(6) Å] contact completes the silver environment giving a distorted trigonal bipyramidal geometry [O2−Ag···F3(iii) = 117.3(2)°, N2−Ag···F3(iii) = 115.0(3)°].

(iv) The main structural motif, the double strand, is based on the strongest and most directional tectons, the coordination bond Ag−O and the hydrogen bonds −OH···O−S−O···HO− involving the cation and the anion. The first useful observation to interpret and rationalize the supramolecular arrangement of $[Ag(LOH)_2(OTf)(CH_3CN)]$ is that the coordination of the anion to the $[Ag(LOH)_2]^+$ structural unit sets the concomitant presence of a pair of hydrogen-bond donors (LOH) and a pair of hydrogen-bond acceptors ($-SO_3^-$) on the complex neutral molecule. The molecule is divided into two halves, each one bearing a −OH and a $-S-O^-$ function and behaving as a self-complementary moiety. Each half of the $[Ag(LOH)_2(OTf)]$ unit

 © 2004 Wiley-VCH Verlag GmbH & Co. KGaA, Weinheim

[−Ag(OSO)(LOH)] thus presents the requirements for self-association, which may be triggered by an inversion center or by some twofold rotation relating two adjacent molecules (see a in Scheme 4). Also the basic $[Ag(LOH)_2]^+$ cation, found in $[Ag(LOH)_2]BF_4$ and $[Ag(LOH)_2]PF_6$, bears two −OH groups, both potential hydrogen bond donors and acceptors, but in that case the self-association could be disfavored for two reasons: cation···cation repulsion, and the relatively poor accepting nature of alcoholic −OHs. We can consider the dimeric system defined by the association of two centrosymmetric [−Ag(OSO)(LOH)] moieties as the basic tecton for building the structural motif based on hydrogen bonds. The association of the tectons in the double strands of collinear complexes (see b in Scheme 4) is governed by the nature of the anion: since the triflate fuses two $-S-O^-$ acceptors together, in the *cis* position relative to the metal, the complex must present a *syn* configuration of the C−OH vectors ($\chi = 0°$, Table 1) in order to pair all the donors and all the acceptors in the self-complementary structure. Different motifs could be engineered by choosing a single hydrogen-bond acceptor X (formation of dimers, with unsaturated terminal −OH groups) or a pair of single hydrogen-bond acceptors as *trans* ligands (formation of chains with *anti* configuration of the complex, $\chi = 180°$) (see c in Scheme 4). Both cases have been studied for Pd complexes.[13]

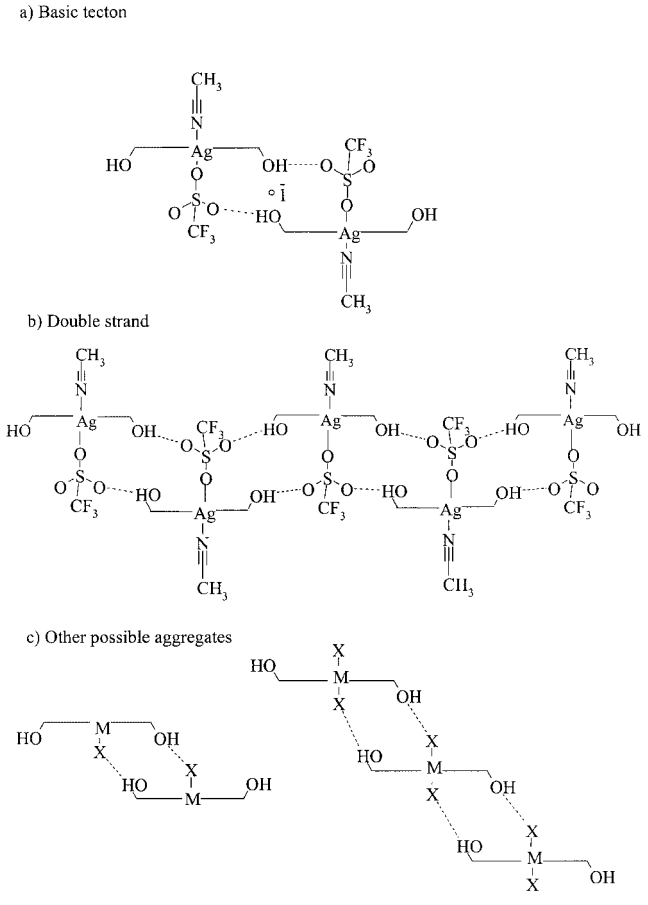

Scheme 4

The association of the double strands described above, built by the coordination bond Ag−O and the hydrogen bonds −OH···O−S−O···HO−, is governed by the formation of a 6PE tecton, which holds the strands together in sheets. The sheets are also held together by the solvent, which adopts a structuring role, through the coordination bond Ag−N and the short $CH_3\cdots\pi$ and $CH_3\cdots CF_3$ interactions .

Finally, the sheets interact using the Ag···F tecton, involving the anion. To investigate the role of the anion and of the solvent in the crystal organization of $[Ag(LOH)_2(OTf)(CH_3CN)]$, the local environment of the triflate anion was examined, see Figure 5. It appears that the combination of the S−O···HO−, the $\pi\cdots CH_3$, and the $CH_3\cdots CF_3$ individual tectons gives rise to a tetrafunctional cyclic pattern that is very similar to the one already observed in the related complexes $[Ag(LOH)_2]BF_4$ and $[Ag(LOH)_2]PF_6$ (Scheme 5).[6] In these complexes there are two basic independent supramolecular tectons (the OH···F−X−F···HO pattern and the cyclic pattern involving Ag···F, Ag···π and −OH···F interactions around the metal), which concur in creating two packing motifs: a chain motif, generated by hydrogen bonds around the anions $[\cdots F-X-F\cdots HO\cap Ag\cap OH\cdots F-X-F\cdots]_n$, and a layer motif, generated by the repetition of the Ag···F···HO−C-π cycle around the metal centers.

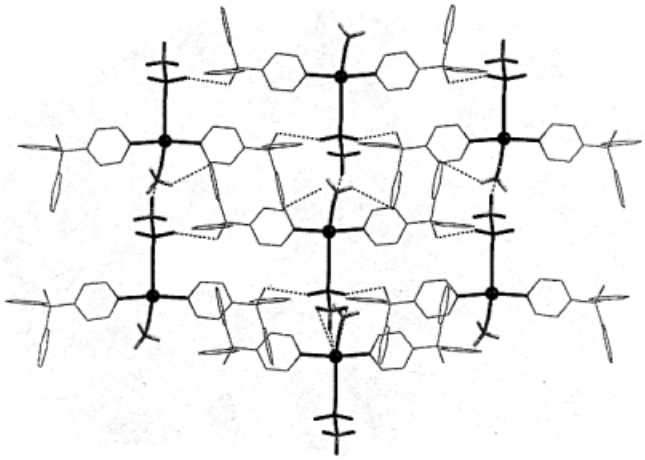

Figure 5. Structural role of the coordinated triflate anion; two mirror-related tetrafunctional cyclic patterns are organized by combining the S−O···HO−, the $\pi\cdots CH_3$ and the $CH_3\cdots CF_3$ individual tectons

In the present case, the methyl group of the acetonitrile plays the structural function of the Ag atoms in the above complexes, by bridging a triarylcarbinol group and the related hydrogen-bonded anion (Scheme 6). A pair of tetrafunctional cyclic patterns surround the anion in a mirror symmetry linking five molecules together: one covalently coordinated to the anion, two coordinated through hydrogen bonds, one through $CF_3\cdots CH_3$ interactions, and one through a $CF_3\cdots Ag$ long contact. The long axes of the five $Ag(pyridine)_2$ systems are approximately parallel.

 © 2004 Wiley-VCH Verlag GmbH & Co. KGaA, Weinheim

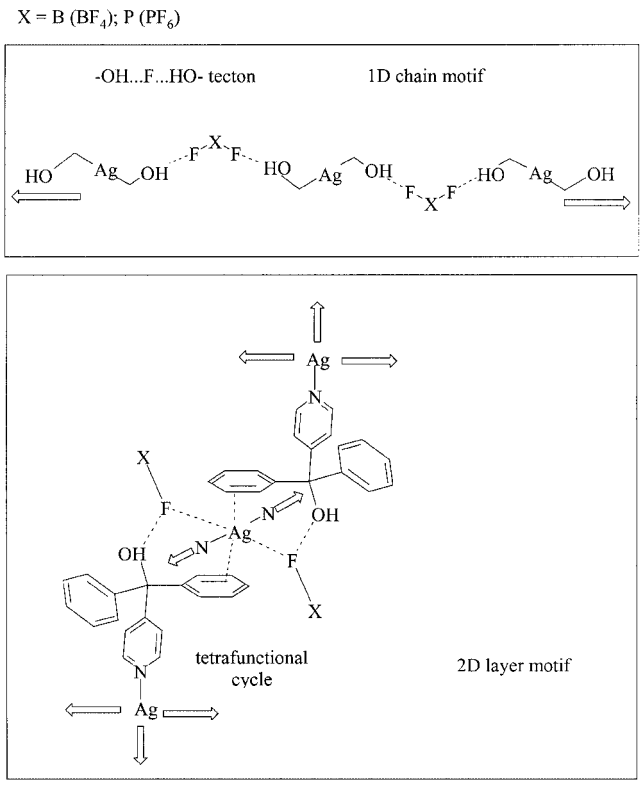

Scheme 5

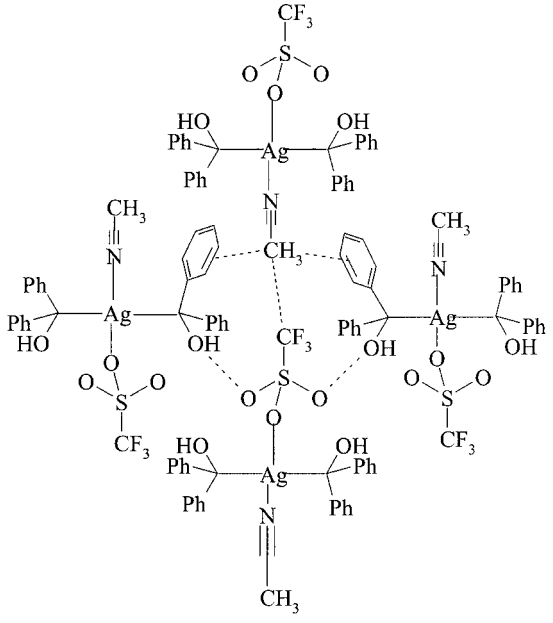

Scheme 6

Conclusions

In $[Ag(LOH)_2(OTf)(CH_3CN)]$, the structural role of the anion is expressed through the coordination to the metal, with the concomitant presence of the acetonitrile molecule. We have uncoupled the function of the two LOH ligands by observing that the anion triggers the formation of the double strands of collinear complexes in the *syn* configuration: this results in a non-covalent supramolecular polymer.[14] The solvent assists in the stabilization of the association of the strands in sheets. The most striking feature of the solid-state arrangement of $[Ag(LOH)_2(OTf)(CH_3CN)]$ is the plasticity of the molecule in response to the structural function of the anion, which allows for the tuning of both the coordination geometry and the configuration of the terminal −OH groups in order to achieve the best self-complementary shape, thus giving the multitude of diverse interactions highlighted in the course of the analysis.

Experimental Section

Synthesis: A solution of LOH (62 mg, 0.237 mmol) in THF (40 mL) was added to a solution of $Ag(CF_3SO_3)$ (61 mg, 0.237 mmol) in CH_3CN (10 mL). The solution was stirred for 3 hours; diethyl ether was added until a white precipitate formed. The mixture was filtered and the precipitate was washed with diethyl ether. Yield 72%, m.p. > 123 °C (dec.). Colorless crystals suitable for X-ray analysis were obtained by cooling mother liquors. $C_{39}H_{33}AgF_3N_3O_5S$ (820.372): calcd. C 57.09, H 4.02, N 5.12, S 3.90; found C 56.61, H 4.11, N 5.55, S 3.94. ^{1}H NMR (300 MHz, $CDCl_3$, 25 °C): δ= 8.57 (d, $^3J_{H,H}$ = 6 Hz, 4 H, C(4)−H + C(5)−H), 7.57 (d, $^3J_{H,H}$ = 6 (Hz), 4 H, C(3)−H + C(6)−H), 7.33−7.23 (m, 20 H, Ar), 3.09 (br., 2 H, −OH), 2.00 (s, 3 H, CH_3CN). IR [KBr (cm^{-1})]: ν(OH): 3458 (m), ν(CN): 2255 (m), ν(SO): 1267 (m).

Crystallographic Analysis: Mo-K_α radiation (λ = 0.71073 Å), T = 293 K (SMART AXS 1000 CCD diffractometer). Lorentz and polarization corrections were applied.[15] Structure solved by direct methods using SIR97 [16] and refined by full-matrix least-squares on all F^2 using SHELXL-97,[17] implemented in the WingX package.[18] Hydrogen atoms located on Fourier difference maps and refined isotropically except for the disordered parts, where they have been introduced in idealized positions. Anisotropic displacement parameters refined for all non-hydrogen atoms. The phenyl group C13−C18 is disordered over two equally populated orientations, in order to release steric overcrowding due to a crystallographic mirror plane passing close to C17. The removal of the mirror plane and the modeling of the structure in the corresponding $P2_1$ space group did not result in a unique conformation of the ring. Hydrogen bonds have been analyzed with SHELXL-97[17] and PARST97.[19] Crystal data: $C_{39}H_{33}AgF_3N_3O_5S$, 0.10 × 0.08 × 0.03 mm, monoclinic, space group $P2_1/m$, a = 8.4826(7), b = 21.475(2), c = 10.5455(9) Å, β = 101.144(2)°, V = 1884.8(3) Å^3, ρ = 1.446 Mg·m^{-3}, 2369 unique reflections, 1958 observed [$I > 2\sigma(I)$], 318 parameters, $R1$ = 0.0355, $wR2$ = 0.0933 [on $I > 2\sigma(I)$] and $R1$ = 0.0453, $wR2$ = 0.0978 (on all data). For the analysis of the organization of supramolecular tectons in the observed structures and for comparison with literature data, extended use has been made of the software of the Cambridge Structural Database (CSD).[20] The van der Waals radii used for assigning threshold values to intermolecular contacts are (Å): Ag 1.72, C 1.70, F 1.47, H 1.20, N 1.55, O 1.52, S 1.80 (taken from CSD reference values). CCDC-226532 contains the supplementary crystallographic data for this paper. These data can be obtained free of charge at www.ccdc.cam.ac.uk/conts/retrieving.html [or from the Cambridge Crystallographic Data Centre, 12 Union Road, Cambridge CB2 1EZ, UK; Fax: (internat.) +44-1223-336-033; E-mail: deposit@ccdc.cam.ac.uk].

 © 2004 Wiley-VCH Verlag GmbH & Co. KGaA, Weinheim

[1] [1a] E. O. Holmes, *J. Phys. Chem.* **1966**, 1037−1046. [1b] M. Irie, *J. Am. Chem. Soc.* **1983**, *105*, 2078−2079. [1c] S. Abbruzzetti, M. Carcelli, P. Pelagatti, D. Rogolino, C. Viappiani, *Chem. Phys. Letters* **2001**, *344*, 387−394.
[2] [2a] S. A. Bourne, L. R. Nassimbeni, K. Skobiridis, E. Weber, *J. Chem. Soc., Chem. Commun.* **1991**, 282−283. [2b] S. A. Bourne, L. Johnson, C. Marais, L. R. Nassimbeni, E. Weber, K. Skobridis, F. Toda, *J. Chem. Soc., Perkin Trans. 2* **1991**, 1707−1713. [2c] K. Eckardt, H. Paulus, H. Fuess, N. Onoda-Yamamuto, R. Ikeda, A. Weiss, *J. Incl. Phenom. Macrocyclic Chem.* **1999**, *35*, 431−449. [2d] N. Hayashi, T. Mori, K. Matsumoto, *Chem. Commun.* **1998**, 1905−1906. [2e] E. Weber, K. Skobridis, I. Goldberg, *J. Chem. Soc., Chem. Commun.* **1989**, 1195−1197. [2f] E. Weber, K. Skobridis, A. Wierig, I. Goldberg, *J. Incl. Phenom. Macrocyclic Chem.* **1997**, *28*, 163−179.
[3] [3a] F. Toda, *Comprehensive Supramolecular Chemistry,* D. D. MacNicol, F. Toda, R Bishop Ed., Pergamon, Oxford, UK, **1996**, vol. 6, p. 465−516. [3b]E. Weber, K. Skobridis, A. Wierig, L. R. Nassimbeni, L. Johnson, *J. Chem. Soc., Perkin Trans. 2* **1992**, 2123−2130. [3c] L. Johnson, L. R. Nassimbeni, E. Weber, K. Skobridis, *J. Chem. Soc., Perkin Trans. 2* **1992**, 2131−2136. [3d] A. Gavezzotti, *Chem. Eur. J.* **2000**, 2288−2294.
[4] S. Mann, *Nature* **1993**, *365*, 499−505.
[5] C. Glidewell, G. Ferguson, *Acta Crystallogr., Sect. C* **1994**, *50*, 924−928.
[6] A. Bacchi, E. Bosetti, M. Carcelli, P. Pelagatti, D. Rogolino, *New J. Chem.* submitted.
[7] D. Venkataraman, S. Lee, J. S. Moore, *Chem. Mater* **1996**, *8*, 2030−2040.
[8] I. Dance, M. Scudder, *J. Chem. Soc., Dalton Trans.* **2000**, 1579−1585.
[9] Y. Umezawa, S. Tsuboyama, K. Honda, J. Uzawa, M. Nishio, *Bull. Chem. Soc. Jpn.* **1998**, *71*, 1207−1213.
[10] M. Scudder, I. Dance, *J. Chem. Soc., Dalton Trans.* **2000**, 2909−2915.
[11] C. F. Matta, J. Hernàndez-Trujillo, T.-H. Tang, R. F. W. Bader, *Chem. Eur. J.* **2003**, 1940−1951.
[12] I. Dance, M. Scudder, *J. Chem. Soc., Chem. Commun.* **1995**, 1039−1040.
[13] E. Bosetti, *Tesi di Laurea in Chimica*, University of Parma, Anno Accademico, **2001−2002**.
[14] F. Huang, F. R. Fronczek, H. W. Gibson, *Chem. Commun.* **2003**, 1480−1481.
[15] [15a] SAINT: SAX, Area Detector Integration, Siemens Analytical instruments INC., Madison, Wisconsin, USA. [15b] SADABS: Siemens Area Detector Absorption Correction Software: G. Sheldrick, University of Göttingen, Germany, **1996**.
[16] Sir97: A new Program For Solving And Refining Crystal Structures: A. Altomare, M. C. Burla, M. Camalli, G. Cascarano, C. Giacovazzo, A. Guagliardi, A. G. Moliterni, G. Polidori, R. Spagna, Istituto di Ricerca per lo Sviluppo di Metodologie Cristallografiche CNR, Bari, **1997**.
[17] Shelxl97: Program for structure refinement: G. Sheldrick, University of Göttingen, Germany, **1997**.
[18] L. J. Farrugia, *J. Appl. Crystallogr.* **1999**, *32*, 837−838.
[19] M. Nardelli, *J. Appl. Crystallogr.* **1995**, *28*, 659.
[20] [20a] F. H. Allen, O. Kennard, R. Taylor, *Acc. Chem. Res.* **1983**, *16*, 146−153. [20b] I. J. Bruno, J. C. Cole, P. R. Edgington, M. Kessler, C. F. Macrae, P. McCabe, J. Pearson, R. Taylor, *Acta Crystallogr., Sect. B* **2002**, *58*, 389−397.

Received December 12, 2003

 © 2004 Wiley-VCH Verlag GmbH & Co. KGaA, Weinheim

Lanthanide(II) and -(III) Porphyrinogens − Rational Synthesis and Derivatisation of Mononuclear, Alkali-Metal-Free Lanthanide(II) and -(III) *meso*-Octaalkylporphyrinogen Complexes

Jun Wang,[a] Andrew K. J. Dick,[a] Michael G. Gardiner,*[a] Brian F. Yates,[a] Evan J. Peacock,[b] Brian W. Skelton,[c] and Allan H. White[c]

Keywords: Lanthanides / Macrocyclic ligands / Metallocenes / Porphyrinoids / Samarium

Modifying the porphyrinogen framework in lanthanide porphyrinogen complexes by *trans*-*N*,*N*′-dimethylation results in Sm^{II} and Sm^{III} derivatives that are remarkably simple in structure and formulation, and are amenable to highly controllable further reaction chemistry. The Sm^{II} bis(tetrahydrofuran) adduct, Sm^{III} chloride and bis(trimethylsilyl)amide complexes have been synthesised and characterised by elemental analysis, ^1H and ^{13}C NMR spectroscopy and X-ray crystal structure determinations.

(© Wiley-VCH Verlag GmbH & Co. KGaA, 69451 Weinheim, Germany, 2004)

Introduction

The metallo-*meso*-octaalkylporphyrinogen complexes of the lanthanides reported to date are structurally diverse, and their unique reactivities have highlighted a range of important potential applications in the area of small-molecule activation and catalysis.[1] The reactivities of Sm^{II} and Sm^{III} complexes have been noted in some cases to exceed those of decamethylsamarocenes, which to date have been the mainstay of organolanthanide-based synthetic transformations and catalysis. Invariably, these complexes have featured (i) the retention of alkali metals arising from metathetical exchange synthetic pathways, and/or (ii) two lanthanides binding within the macrocyclic cavity. These features are clearly the result of the four acidic N−H moieties of the pyrrole units and/or the divergent nature of the macrocyclic cavity in the 1,3-alternate conformation typically adopted when binding large metals by an $\eta^5{:}\eta^1{:}\eta^5{:}\eta^1$- binding mode. The inclusion of alkali metals in these complexes can, in some cases, be seen to have added to the stabilising framework that led to the trapping of reactive species such as $(N_2)^{2-}$, $(N_2)^{4-}$, $(C_2)^{2-}$ and $(C_2H_4)^{2-}$ in stoichiometric reactions.[1b−1h] However, the incorporation of alkali metals (and halides) is generally regarded as limiting the catalytic utility of organolanthanides, as it can lead to the occupation of vital metal coordination sites or, at least, to poorly defined catalytically active species. Significantly, lanthanoid complexes based on tetraanionic porphyrinogens have also proven difficult to derivatise. Indeed, the reaction of the Y^{III} complex $[(THF)_2LiY(L)\cdot LiOEt]$ (where H_4L = *meso*-octaethylporphyrinogen **1**) with lithium reagents led to loss of yttrium from the porphyrinogen.[1a] A single Sm^{III} alkyl complex in which the alkyl group is not involved in bridging with an alkali metal is known, $[(THF)_4(Cl)Li_3(\mathbf{1}-4H)SmMe]$, but its subsequent chemistry is influenced by the incorporation of the alkali metal.[1i] Thus, access to "simple" lanthanocene analogues of the archetypical motif $(L)_nLn^{II/III}R$(solvent) [where $(L)_n$ = a dianionic porphyrinogen-containing unit and R = solvent, alkyl, amide, hydride etc.], often implied in catalysis, has not been realised in the porphyrinogen chemistry of the lanthanide metals. Perhaps then, the full potential of metalloporphyrinogen complexes has not been established in the absence of such desired complexes?

We recently reported that improved structural control is possible through *N*-alkylation of the porphyrinogens by the synthesis of the dipotassium complex **3** derived from *trans*-*N*,*N*′-dimethyl-*meso*-octaethylporphyrinogen **2**.[2] The schematic representation of **3** highlights the steric restraints that the *N*-methyl substituents impose on the macrocyclic cavity in the 1,3-alternate macrocyclic conformation that allows only one potassium cation to bind within the cavity. We report herein the rational synthesis of the first mononuclear, alkali-metal-free metalloporphyrinogens of a lanthanide(II) and -(III) metal, derived from the modified porphyrinogen **2** by metathetical exchange reactions and subsequent derivatisation involving oxidation and halide/amide exchange.

[a] School of Chemistry, University of Tasmania
Private Bag 75, Hobart, TAS 7001, Australia
Fax: (internat.) +61 3-6226-2404
E-mail: michael.gardiner@utas.edu.au
[b] Central Science Laboratory, University of Tasmania
Private Bag 74, Hobart, TAS 7001, Australia
[c] Chemistry Department, University of Western Australia
Crawley, WA 6009, Australia

 © 2004 Wiley-VCH Verlag GmbH & Co. KGaA, Weinheim **DOI: 10.1002/ejic.200300965**

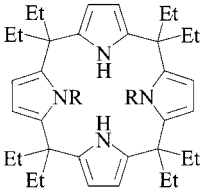

1 (R = H), **2** (R = Me)

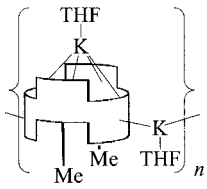

3

Results and Discussion

Complexes **4**−**6** were synthesised according to the route shown in Scheme 1. The reaction of **3** with SmI_2 in THF afforded a brown solution of the Sm^{II} complex **4**, which was isolated in high yield as dark purple/brown crystals. Complex **4** was also prepared in low yield by the reaction of the dilithium complex derived from **2**, $(\mathbf{2}-2H)Li_2$, with $[(\eta^5\text{-}C_5Me_5)_2Sm(THF)_2]$ in toluene, where the driving force is presumably the precipitation of the insoluble $[\{(\eta^5\text{-}C_5Me_5)Li\}_n]$. The Sm^{II} complex **4** was oxidised to the Sm^{III} chloride **5** by reaction with *t*BuCl in THF/toluene, which precipitates nearly quantitatively as a brown/red solid, that could be recrystallised from toluene. The Sm^{III} amide **6** was prepared by the reaction of **5** with sodium bis(trimethylsilyl)-amide in THF and isolated as orange crystals in high yield from a solution of the same color. Complexes **4**−**6** were characterised by ^1H and ^{13}C NMR spectroscopy,[3] microanalysis and X-ray crystal structure determinations.[4]

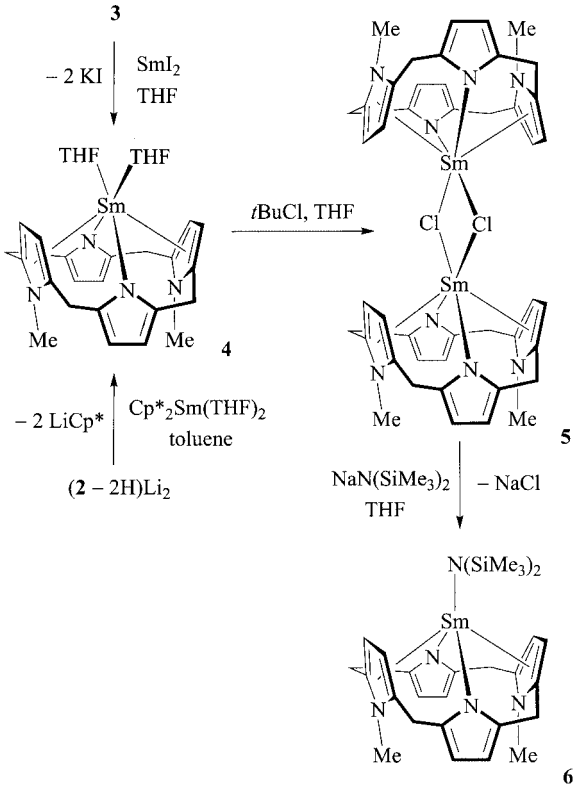

Scheme 1. Synthesis of Sm^{II} and Sm^{III} complexes (*meso*-octaethyl groups omitted for clarity)

The ^1H NMR chemical shifts of **4** and **6** were highly influenced by the paramagnetic shift influence of the $Sm^{II/III}$ centers, covering a wide chemical shift range of 42.19 to −21.07 ppm for the Sm^{II} complex **4** at 25 °C, and a narrower range of 6.10 to −0.17 ppm for the Sm^{III} complex **6** at 25 °C. Variable-temperature ^1H NMR experiments established rigid macrocycle conformations for **4** and **6** in toluene, on the basis of the Curie−Weiss Law being obeyed in the temperature range −50 to 50 °C. The ^{13}C NMR chemical shifts of **4** and **6** revealed only slight paramagnetic shift influences. The poor solubility of **5** prevented NMR spectroscopic studies.

The crystal structures of **4**−**6** (Figures 1, 2, and 3), show the Sm centers bound within the macrocyclic cavities by η^5:η^1:η^5:η^1- binding modes. Of particular note are the eclipsed η^5-interactions to the neutral *N*-methylpyrrole units, with σ-contacts being through the anionic pyrrolide units. η^5-Bound neutral pyrrole units are uncommon,[5] and unknown in lanthanide chemistry. They are a forced constraint, resulting from either the macrocyclic ring strain or steric interference of the *N*-methyl substituents, which is likely to feature in other bonding situations in which large-radii metals are hosted within the macrocycle. The macrocycle is formally a 16-electron donor, 4 greater than the bis-(cyclopentadienyl) ligand set. The Sm−centroid distance in **4** [2.75_6 Å] is longer than in **5** and **6** [2.63_4 and 2.65_3 Å, respectively], reflecting the relative sizes of Sm^{II} and Sm^{III}. The ensuing conformational changes to the macrocycle are mainly restricted to the "metallocene bend angle", being $154.4_3°$ in **4** and in the range $160.0_8-162.3_1°$ in **5** and **6** (N−Sm−N angles are within 120.5 ± 1° for **4**−**6**). The Sm^{III} centers in **5** and **6** reside deeper in the macrocyclic cavities as a result. The Sm−N distances in **4**−**6** also correlate with the Sm oxidation states and are greatly influenced (± 0.13 Å) by the details of the chloride and amide coordination in **5** and **6** (vide infra). The metallocene bend angle in **4** is much larger than in $[(\eta^5\text{-}C_5Me_5)_2Sm(THF)_2]$ ($136.7_0°$),[6] but the small β-pyrrole H substituents in **4** effectively result in a wider coordination arc available for ligand binding in the region of the η^5- bound pyrrole rings, relative to the samarocene. Conversely, the O−Sm−O angle in **4**, 70.13(6)°, is smaller than in $[(\eta^5\text{-}C_5Me_5)_2Sm(THF)_2]$, 82.7(4)°, indicating reduced space for additional ligand binding in the region of the σ-bound pyrrolide units, compared with the samarocene.

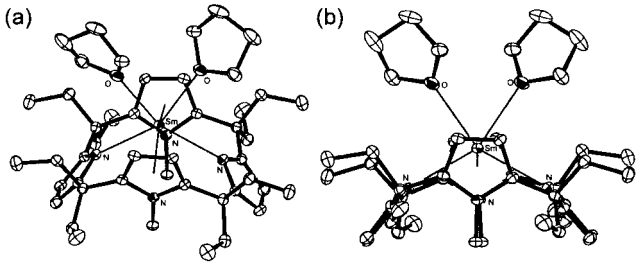

Figure 1. Structure of **4**: (a) general view of **4**, (b) "side" view of **4**

 © 2004 Wiley-VCH Verlag GmbH & Co. KGaA, Weinheim

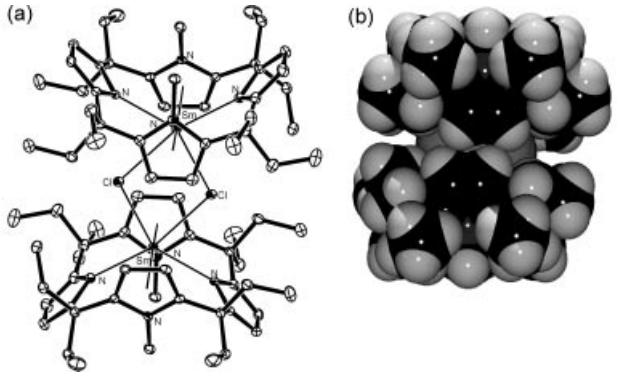

Figure 2. Structure of **5**: (a) general view of **5**, (b) space-filling "side" view of **5**

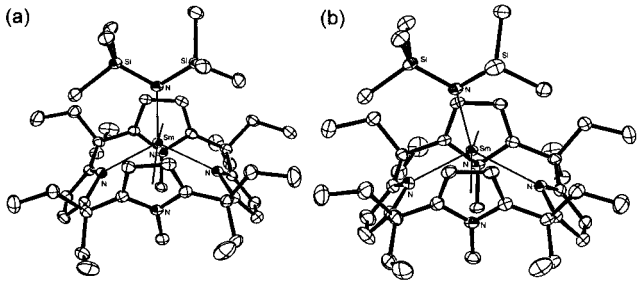

Figure 3. Structure of **6**: (a) general view of a molecule of **6** with a symmetrically bound amide, (b) general view of a molecule of **6** with a "tilted" amide

Both single- and two-fold additional coordination is known for Sm^{II} and Sm^{III} complexes of tetraanionic porphyrinogens, and is seemingly influenced by conformational changes in the macrocycle caused by additional binding of alkali metals and counter-anions in the macrocyclic cavity.[1] Complexes **4** and **5** feature two-fold coordination through THF molecules and two μ_2-Cl ligands, respectively, and **6** displays single-fold coordination through the amide ligand (see Figures 1, 2, and 3).

The Sm−O distances in **4** [2.655(1) Å] are crystallographically equivalent. The Sm−Cl distances in **5** are markedly different [2.7511(5) and 2.9290(5) Å], which is a consequence of the steric interactions between the macrocycles [see Figure 2(b)]. A long terminal Sm−Cl bond [3.15(2) Å] has been reported for a porphyrinogen complex.[1b] The disparate Sm−N(pyrrolide) distances in **5** [2.488(2) and 2.538(2) Å], are also a consequence of the asymmetrically bound chlorides, the former "*trans*" to the short Sm−Cl bond. Decamethylsamarocene(III) chloride forms both a monomeric THF adduct, $[(\eta^5\text{-}C_5Me_5)_2Sm(Cl)(THF)]$, and a more "open" Cl-bridged trimer, $[\{(\eta^5\text{-}C_5Me_5)_2Sm(\mu\text{-}Cl)\}_3]$,[7] whereas non-peralkylated samarocenes, e.g. $[\{[\eta^5\text{-}1,3\text{-}(Me_3Si)_2C_5H_3]_2Sm(\mu\text{-}Cl)\}_2]$, dimerise by symmetrical $(\mu_2\text{-}Cl)_2$-bridging (Sm−Cl = 2.758(2) and 2.771(2) Å].[8]

In addition to the coordination of the Sm center through the nitrogen center of the amide in **6**, one of the three crystallographically independent molecules exhibits a highly "tilted" amide ligand, diagnostic of a putative weak agostic interaction involving a NSiMe unit, [see Figure 3(b)]. The relevant parameters are: Sm···N 2.314(2), Sm···Si 3.3856(7), Sm···C 3.338(3) Å, Sm−N−Si 113.3(1), N−Si−C 109.5(1)°, and, for the opposite NSiMe unit: Sm···Si 3.6762(9), Sm···C 4.059(3) Å, Sm−N−Si 129.94(9), N−Si−C 114.8(1)°. The Sm···γ-methyl distance is substantially longer than in bona fide agostic interactions of lanthanocene amides featuring a single agostic interaction from a tilted amide, e.g. 2.901(8) Å for $[\{\eta^5,\eta^5\text{-}C_5H_4Si(Me)_2C_{13}H_8\}DyN(SiMe_3)_2]$, but this should be placed in the context of the shorter Dy−N distance of 2.207(5) Å relative to **6**.[9] γ-Agostic interactions in "symmetrically bound" lanthanocene amides where two NSiMe units are inclined towards the metal center, e.g. $[(\eta^5\text{-}C_5Me_5)_2SmN(SiMe_3)_2]$,[10] feature NSiMe···Sm geometries (Sm···N 2.301(3), Sm···Si 3.40_2, Sm···C 3.24_9 Å, Sm−N−Si 115.7_5, N−Si−C 106.3_5°) similar to those for the silyl group nearest the Sm center in the tilted amide of **6**. Steric interactions between the amide and the macrocycle (absent in lanthanocene amides — recall the discussion of the small O−Sm−O angle in **4**) may be limiting further development of agostic interactions in **6**, or indeed the higher coordination number from the modified porphyrinogen may negate the tendency for the agostic interaction. The putative weak agostic interaction in **6** is "*trans*" to a closely bound σ-bound pyrrolide [Sm−N 2.470(2) Å] [cf. opposite counterpart, 2.604(2) Å]. In comparison, asymmetry is absent in molecules of **6** having non-tilted amides [2.514−2.543(2) Å]. We have yet to delineate the steric and electronic effects on the structure of **6**, and the tendency for the agostic interaction remains an important matter of discussion, of relevance to the reactivity of lanthanide(II) and -(III) complexes of the modified porphyrinogen **2**.

The preparation of the Sm^{II} and Sm^{III} complexes in this report has demonstrated that improved composition, structure and reactivity control is achievable by efforts to match the charge (in its deprotonated form) and steric restraints of a modified porphyrinogen to the metal ions under study. The "simplicity" of the prepared complexes makes this clear. Despite substantial electronic differences that could be expected to exist between the modified porphyrinogen complexes **4**−**6** and both lanthanocenes and unmodified porphyrinogen complexes (viz. η^5-interactions to neutral pyrrole units) we have demonstrated that imperative structure and reactivity patterns relevant to catalytic applications are common to both systems. A rigid macrocycle conformation in solution for **6** is evident from NMR experiments, thus the macrocycle promises to be an extremely well-defined non-participative ligand for subsequent reactivity studies and applications for which "$(\eta^5\text{-}C_5Me_5)_2Ln^{II/III}R$" systems are utilised. We are continuing synthetic, reactivity and computational studies of this new class of "metallocenes" and related modified porphyrinogen complexes.

Experimental Section

Compound 4: Potassium metal (0.16 g, 4.1 mmol) was added to a solution of **2**[11] (1.14 g, 2.00 mmol) in THF (80 mL) and refluxed

 © 2004 Wiley-VCH Verlag GmbH & Co. KGaA, Weinheim

for 6 h. SmI_2 (0.10 M solution in THF, 20 mL, 2.0 mmol) was added dropwise to the crude stirred slurry of **3** over 20 min and allowed to stir for 12 h. The reaction mixture was filtered and the purple solution concentrated in vacuo to ca. 20 mL, giving dark purple/brown crystals (1.38 g, 80 %). ^{1}H NMR (399.694 MHz, [D$_6$]benzene, 25 °C): δ = −21.07 (m, 4 H, CH_2), −8.15 (t, 12 H, CH_3), −4.89 (m, 4 H, CH_2), 0.93 (t, 12 H, CH_3), 1.12 (s, 4 H, =CH, pyrA), 1.26 (m, 4 H, CH_2), 4.51 (br. s, 8 H, CH_2, THF), 5.17 (m, 4 H, CH_2), 10.83 (br. s, 8 H, OCH_2, THF), 19.22 (s, 4 H, =CH, pyrB), 42.91 ppm (s, 6 H, NCH_3) ppm. ^{13}C NMR (100.512 MHz, [D$_6$]benzene, 25 °C): δ = 10.8 (2 × CH_3), 21.3 (CH_2), 32.0 (CH_2), 44.3 (=CH, pyrA), 50.0 (CEt_2), 68.2 (=CH, pyrB), 108.7 (=CR, pyrB), 188.0 ppm (=CR, pyrA) ppm. $C_{46}H_{70}N_4O_2Sm$ (861.43): calcd. C 64.14, H 8.19, N 6.50; found C 63.98, H 8.27, N 6.43.

Alternative preparation of compound 4: *n*BuLi (6.0 mL, 9.6 mmol) was added to a stirred solution of **2** (2.0 g, 3.5 mmol) in toluene (60 mL) at 0 °C. A colorless solid immediately formed and the mixture was left to stir for 6 h at 50 °C. After being allowed to settle at 20 °C, the solvent was removed by cannula, the colorless solid washed with hexane (20 mL) and dried in vacuo. Toluene (25 mL) was added to a stirred mixture of $[(\eta^5\text{-}C_5Me_5)_2Sm(THF)_2]$[6] (400 mg, 0.718 mmol) and the above-described crude lithium reagent (416 mg, 0.714 mmol) at 20 °C. The mixture was then heated at 50 °C for 4 h to give a dark purple/brown solution. The solution was filtered to remove a colorless solid and the toluene removed in vacuo to give a purple/brown solid. Recrystallisation from THF gave dark purple/brown crystals (163 mg, 27 %) that, by ^{1}H NMR spectroscopy, were identical to the product prepared by the alternative route.

Compound 5: A solution of *t*BuCl (0.093 g, 1.0 mmol) in THF (10 mL) was added to a stirred solution of **4** (0.86 g, 1.0 mmol) in toluene (50 mL) dropwise over 5 minutes and left to stir for 1 h. The resulting pale brown solid was filtered, washed with toluene and dried in vacuo (0.68 g, 91 %). MS (EI): *m*/*z* (%) = 755 (14) [M^+], 726 (64) [M^+ − Et], 568 (33) [$\mathbf{2}^+$], 539 (100) [$\mathbf{2}^+$ − Et]. $C_{38}H_{54}ClN_4Sm$ (752.68): calcd. C 60.64, H 7.23, N 7.44; found C 60.68, H 7.18, N 7.39.

Compound 6: A solution of *t*BuCl (0.093 g, 1.0 mmol) in THF (10 mL) was added to a stirred solution of **4** (0.86 g, 1.0 mmol) in toluene (50 mL) dropwise over 5 minutes and left to stir for 1 h. $NaN(SiMe_3)_2$ (1.0 M solution in THF, 1.0 mL, 1.0 mmol) was added to the mixture and stirring was continued for 12 h. The solution was filtered and concentrated to ca. 15 mL to give orange crystals (0.64 g, 73 %). ^{1}H NMR (399.694 MHz, [D$_6$]benzene, 25 °C): δ = −0.17 (m, 12 H, CH_3), 0.75 (m, 12 H, CH_3), 0.87 (m, 4 H, CH_2), 1.08 (s, 18 H, CH_3), 1.37 (m, 4 H, CH_2), 1.95 (m, 8 H, CH_2), 3.74 (s, 4 H, =CH, pyrMe), 4.87 (s, 6 H, NMe), 6.10 (s, 4 H, = CH, pyr) ppm. ^{13}C NMR (100.512 MHz, [D$_6$]benzene, 25 °C): δ = 7.9 ($SiCH_3$), 8.1 (CH_3), 8.3 (CH_3), 23.1 (CH_2), 28.7 (CH_2), 36.6 (NCH_3), 41.7 (CEt_2), 100.2 (=CH, pyrMe), 103.5 (=CH, pyr) 139.8 (=CR, pyrMe), 149.9 (=CR, pyr) ppm. $C_{44}H_{72}N_5Si_2Sm$ (877.61): calcd. C 60.22, H 8.27, N 7.98; found C 60.10, H 8.36, N 7.94.

Acknowledgments

We thank the Australian Research Council for financial support of this research and Dr. Gary Fallon, Monash University, for measurement of the 123 K X-ray diffraction data.

[1] [1a] J. Jubb, S. Gambarotta, R. Duchateau, J. H. Teuben, *J. Chem. Soc., Chem. Commun.* **1994**, 2641−2642. [1b] T. Dubé, S. Gambarotta, G. P. A. Yap, *Organometallics* **2000**, *19*, 4820−4827. [1c] E. Campazzi, E. Solari, C. Floriani, R. Scopelliti, *Chem. Commun.* **1998**, 2603−2604. [1d] J. Jubb, S. Gambarotta, *J. Am. Chem. Soc.* **1994**, *116*, 4477−4478. [1e] E. Campazzi, E. Solari, R. Scopelliti, C. Floriani, *Chem. Commun.* **1999**, 1617−1618. [1f] T. Dubé, S. Gambarotta, G. P. A. Yap, *Angew. Chem.* **1999**, *111*, 1507−1510; *Angew. Chem. Int. Ed.* **1999**, *38*, 1432−1435. [1g] T. Dubé, J. Guan, S. Gambarotta, G. P. A. Yap, *Chem. Eur. J.* **2001**, *7*, 374−381. [1h] J. I. Song, S. Gambarotta, *Angew. Chem.* **1995**, *107*, 2319−2321; *Angew. Chem. Int. Ed. Engl.* **1995**, *34*, 2141−2142. [1i] T. Dubé, S. Gambarotta, G. Yap, *Organometallics* **2000**, *19*, 121−126.

[2] J. Wang, M. G. Gardiner, E. J. Peacock, B. W. Skelton, A. H. White, *Dalton Trans.* **2003**, 161−162.

[3] Full ^{1}H and ^{13}C assignments for **6** were made by gCOSY, gHMBC and gNOESY and VT ^{1}H NMR spectroscopy. The *Me*N ^{13}C resonance of **4** could not be located. A low signal-to-noise ratio caused by paramagnetic line broadening in the gCOSY, gHMQC and gHMBC spectra of **4** did not allow full assignment of ^{1}H and ^{13}C resonances (unique assignment of the pyrrolide and *N*-methylpyrrole units and no conformational information was obtained). Full details of the NMR analyses will be published separately.

[4] Crystallographic data for **4**−**6**: recorded at 123 K (for **4** and **5**) and 150 K (for **6**), with Mo-K_α (0.71073 Å) radiation: **4**: orthorhombic, space group *Pbcn*, *a* = 21.3197(2), *b* = 10.5498(1), *c* = 18.5892(2) Å, *V* = 4181.06(7) Å^3, *Z* = 4, *R* = 0.024 for 4197 [$I > 2\sigma(I)$] data and *wR* = 0.069 for 5187 all data; **5**: monoclinic, space group *C*2/*c*, *a* = 19.4523(2), *b* = 13.8795(1), *c* = 26.9726(3) Å, β = 106.1366(4)°, *V* = 6995.37(12) Å^3, *Z* = 4, *R* = 0.026 for 6738 [$I > 2\sigma(I)$] data and *wR* = 0.050 for 8572 all data; **6**: triclinic, space group $P\bar{1}$, *a* = 12.1952(7), *b* = 23.2630(10), *c* = 24.728(2) Å, α = 88.925(2), β = 78.125(2), γ = 75.229(2)°, *V* = 6634.0(7) Å^3, *Z* = 6, *R* = 0.042 for 41973 [$I > 2\sigma(I)$] data and *wR* = 0.049 for 65461 all data. CCDC 219394−219396 (**4**−**6**) contain the supplementary crystallographic data for this paper. These data can be obtained free of charge via www.ccdc.cam.ac.uk/conts/retrieving.html (or from the Cambridge Crystallographic Data Centre, 12, Union Road, Cambridge CB2 1EZ, UK; fax: +44 1223-336033; or deposit@ccdc.cam.ac.uk).

[5] For review articles on π-bound pyrrole/pyrrolide interactions, see: [5a] M. O. Senge, *Angew. Chem.* **1996**, *108*, 2051−2053; *Angew. Chem. Int. Ed. Engl.* **1996**, *35*, 1923−1925. [5b] K. H. Pannell, B. L. Kalsotra, C. Párkanyi, *J. Heterocyclic Chem.* **1978**, *15*, 1057−1081.

[6] W. J. Evans, J. W. Grate, H. W. Choi, I. Bloom, W. E. Hunter, J. L. Atwood, *J. Am. Chem. Soc.* **1985**, *107*, 941−946.

[7] [7a] W. J. Evans, J. W. Grate, K. R. Levan, I. Bloom, T. T. Peterson, R. J. Doedens, H. Zhang, J. L. Atwood, *Inorg. Chem.* **1986**, *25*, 3614−3619. [7b] W. J. Evans, D. K. Drummond, J. W. Grate, H. Zhang, J. L. Atwood, *J. Am. Chem. Soc.* **1987**, *109*, 3928−3936.

[8] Z. Xie, K. Chui, Q. Yang, T. C. Mak, J. Sun, *Organometallics* **1998**, *17*, 3937−3944.

[9] C. Qian, W. Nie, J. Sun, *Organometallics* **2000**, *19*, 4134−4140.

[10] W. J. Evans, R. A. Keyer, J. W. Ziller, *Organometallics* **1993**, *12*, 2618−2633.

[11] Y. Furusho, H. Kawasaki, S. Nakanishi, T. Aida, T. Takata, *Tetrahedron Lett.* **1998**, *39*, 3537−3541.

Received December 24, 2003

 © 2004 Wiley-VCH Verlag GmbH & Co. KGaA, Weinheim

Clear-Cut Lanthanide(III)/Actinide(III) Differentiation in Coordination of Pyrazine to Tris(cyclopentadienyl) Complexes of Cerium and Uranium, Involving Reversible $U^{III} \rightarrow U^{IV}$ Oxidation

Thouraya Mehdoui,[a] Jean-Claude Berthet,*[a] Pierre Thuéry,[a] and Michel Ephritikhine*[a]

Keywords: Actinides / Lanthanides / Nitrogen ligands / Selective complexation

In contrast to the $[Ce(C_5H_4R)_3]$ complexes (where R = *t*Bu, $SiMe_3$), which react with pyrazine to give the Lewis base adducts $[Ce(C_5H_4R)_3(pyz)]$ (where R = *t*Bu **1**, $SiMe_3$ **2**), the uranium analogues are oxidized by the azine molecule to the dinuclear U^{IV} complexes $[\{U(C_5H_4R)_3\}_2(\mu\text{-pyz})]$ (R = *t*Bu **3**, $SiMe_3$ **4**). The U–N distances of approximately 2.32 Å in the crystal structures of **3** and **4** are characteristic of U^{IV}–N bond lengths of terminally-coordinated amide groups. The formation constants of **1** and **3** in THF at 23 °C are 0.28(6) and $8(1) \times 10^3$, respectively, permitting the clear differentiation between the two metallocenes by means of the nitrogen ligand.
(© Wiley-VCH Verlag GmbH & Co. KGaA, 69451 Weinheim, Germany, 2004)

Introduction

The separation of trivalent minor actinides (An) from trivalent lanthanides (Ln) is a challenging goal in the management of nuclear waste; this key step in the advanced reprocessing of spent nuclear fuels would permit the subsequent transmutation of the long-lived americium and curium radionuclides into short-lived isotopes, by neutron bombardment.[1] A number of extractant molecules have been designed and tested for the selective complexation of An^{III} ions in solution; polydentate aromatic amines proved to be the most promising.[2] The better affinity of these molecules for An^{III} rather than Ln^{III} ions is generally explained by the stronger interaction between the softer (or less hard) 5f ion and the nitrogen atom. The greater stability of the An−N bond, in relation to its more covalent character, would result from π back donation of the f orbitals into the π* orbitals of the aromatic ligand, which is less likely in the lanthanide counterpart.[3] This assumption was consolidated after our recent studies on the complexation of the organometallic compounds $[M(C_5H_4R)_3]$ (where M = Ce, U; R = *t*Bu, $SiMe_3$) with various azines, which revealed that the selectivity of the nitrogen ligand in favour of U^{III} is proportional to its π-accepting ability, measured by its reduction potential.[4] Since extensive π back donation would eventually lead to metal oxidation and formation of an An^{IV}−N bond, a conceptual question arising from these results then concerned the possibility of clearly differentiating the trivalent actinide form the lanthanide ions by a reversible oxido-reduction reaction between the An^{III} compound and the extractant molecule. This scenario, which would open new routes to the selective complexation of An^{III} over Ln^{III} ions and the discrimination of minor actinides (americium and curium), should turn out to be successful as the formation of the An^{IV} complex is thermodynamically favoured over that of the simple An^{III} and Ln^{III} Lewis base adducts. Here we demonstrate the feasibility of such a process by presenting the distinct behaviour of the uranium and cerium compounds $[M(C_5H_4R)_3]$ (M = Ce, U; R = *t*Bu, $SiMe_3$) in the presence of pyrazine.

Results and Discussion

Addition of pyrazine (pyz) to a solution of $[Ce(C_5H_4R)_3]$ in THF led to an equilibrium between $[Ce(C_5H_4R)_3(THF)]$

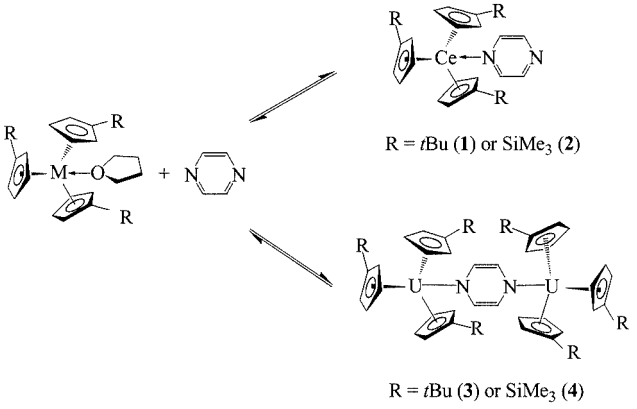

Scheme 1. The distinct reactions of $[M(C_5H_4R)_3]$ (M = Ce, U) with pyrazine

[a] Service de Chimie Moléculaire, DSM, DRECAM, CNRS URA 331, CEA/Saclay,
91191 Gif-sur-Yvette, France
E-mail: ephri@drecam.cea.fr
berthet@drecam.cea.fr

 © 2004 Wiley-VCH Verlag GmbH & Co. KGaA, Weinheim **DOI: 10.1002/ejic.200400133**

and $[Ce(C_5H_4R)_3(pyz)]$ (see Scheme 1). The formation constants K_{CeL} of the pyrazine adducts were calculated by using Equation (1), where C_0 is the initial concentration of $[Ce(C_5H_4R)_3(THF)]$, n the number of molar equivalents of pyrazine added to the solution, and x_{CeL} the molar fraction of $[Ce(C_5H_4R)_3(pyz)]$, which was determined from the ^1H NMR spectra of the mixtures.

$$K_{CeL} = [Ce(C_5H_4R)_3(pyz)]/[Ce(C_5H_4R)_3(THF)][pyz] = x_{CeL}/C_0(1 - x_{CeL})(n - x_{CeL}) \quad (1)$$

The formation constants at 23 °C of $[Ce(C_5H_4tBu)_3(pyz)]$ (**1**) and $[Ce(C_5H_4SiMe_3)_3(pyz)]$ (**2**) in THF are equal to 0.28(6) and 0.23(2), respectively. These constants are smaller than those measured for the equilibrating formation of **1** and **2** from $[Ce(C_5H_4R)_3]$ and pyrazine in toluene [0.44(3) and $1.4(1) \times 10^2$],[4] because of the competing coordination of THF to the Lewis acidic metal centre. The formation constants of **1** and **2** in toluene are quite similar to those of $[Ce(C_5H_4R)_3(3,5\text{-}Me_2pyz)]$ [0.33(3) and $1.6(1) \times 10^2$ for R = *t*Bu and $SiMe_3$, respectively] which are themselves lower than those of the uranium analogues [1.5(1) and $1.5(2) \times 10^3$]. The slightly greater stability of the U^{III} compounds was explained by the presence of a π backbonding interaction between the uranium atom and the 3,5-dimethylpyrazine ligand.[4]

In striking contrast with dimethylpyrazine, pyrazine reacted with two molar equivalents of $[U(C_5H_4R)_3]$ in toluene to give the dinuclear compounds $[\{U(C_5H_4R)_3\}_2(\mu\text{-pyz})]$ (R = *t*Bu **3**; R = $SiMe_3$ **4**) in quantitative yields. The mononuclear species $[U(C_5H_4R)_3(pyz)]$ could not be detected, even after further addition of free pyrazine. The ^1H NMR spectra of **3** and **4** exhibit three signals, of relative intensities 54:12:12, corresponding to the six equivalent C_5H_4R groups and a single resonance attributed to the four equivalent protons of the nitrogen ligand. These uranium complexes were stable in the toluene or pentane solutions from which they were isolated as black powders after evaporation. It is noteworthy that the complexes $[\{U(C_5H_4R)_3\}_2(\mu\text{-pyz})]$ (R = H or Me) were synthesized in a similar way from $[U(C_5H_4R)_3(THF)]$ and pyrazine and, in the absence of structural information, were considered as π-bridged dimers of U^{III}.[5]

Black crystals of $[\{U(C_5H_4tBu)_3\}_2(\mu\text{-pyz})]\cdot 0.5pyz$ (**3**·0.5pyz) and $[\{U(C_5H_4SiMe_3)_3\}_2(\mu\text{-pyz})]\cdot 2pyz$ (**4**·2pyz) were obtained by cooling concentrated solutions of $[U(C_5H_4R)_3]$ and excess pyrazine in pentane. The crystal structures of **3** and **4** are very similar; **3** is shown in Figure 1 with selected bond lengths and angles. The two $U(C_5H_4R)_3$ fragments are bridged by a pyrazine ring, coordinated through its nitrogen atoms; the middle of the U−U′ segment in **4** is an inversion centre. The pyrazine rings are planar within ±0.019(6) and ±0.001(3) Å in **3** and **4**, respectively. The U(1) and U(2) atoms in **3** are located out of the plane, on the same side, at a distance of 0.075(13) and 0.257(12) Å, respectively; because of the imposed symmetry, U and U′ in **4** are on either side of the plane, at a distance of 0.071(9) Å. The U−N distances of 2.323(6) and 2.325(6) Å in **3**, and 2.318(4) Å in **4**, are much shorter than those measured in the series of trivalent $[U(C_5H_4R)_3(azine)]$ complexes, which vary from 2.646(4) Å in $[U(C_5H_4SiMe_3)_3(lutidine)]$ to 2.688(7) Å in $[U(C_5H_4SiMe_3)_3(pyrimidine)]$;[4] they are also 0.34 Å shorter than the average U−N(pyrazine) distance in $[UI_3(tpza)(MeCN)]$ {tpza = tris[(2-pyrazinyl)methyl]amine}.[3a] In fact, the U−N distances in **3** and **4** are in the range of U^{IV}−N bond lengths of terminally-coordinated amide groups[6] and are, in particular, similar to that of 2.29(2) Å in $[U(C_5H_5)_3(NPh_2)]$.[7] Concomitantly with the oxidation of the metal centre, the pyrazine ligand in **3** and **4** appears to be reduced to its dianionic form, since the average C−N and C−C distances of 1.405(5) and 1.340(5) Å are, respectively, longer and shorter than those in the free or coordinated neutral molecule, which are typically equal to 1.34 and 1.38 Å. These distances are equal to 1.33(2) and 1.37(2) Å in the Yb^{III} complex $[\{Yb(C_5H_5)_3\}_2(\mu\text{-pyz})]$,[8] and to 1.339(1) and 1.378(6) Å in $[Ce(C_5H_4tBu)_3(pyz)]$.[4]

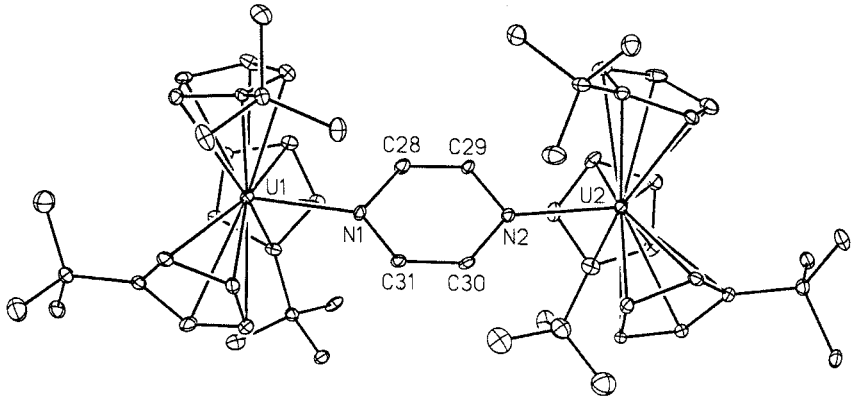

Figure 1. View of $[\{U(C_5H_4tBu)_3\}_2(\mu\text{-pyz})]$; hydrogen atoms are omitted for clarity; only one position of the disordered C_5H_4tBu group is represented; the displacement ellipsoids are drawn at the 10 % probability level; selected bond lengths (Å) and angles (°), the corresponding values for $[\{U(C_5H_4SiMe_3)_3\}_2(\mu\text{-pyz})]$ are given in brackets: U(1)−N(1) 2.323(6) [2.318(4)], U(2)−N(2) 2.325(6), N(1)−C(28) 1.406(11) [1.410(6)], N(1)−C(31) 1.399(9) [1.411(6)], N(2)−C(29) 1.399(10), N(2)−C(30) 1.404(10), C(28)−C(29) 1.335(12) [1.342(7)], C(30)−C(31) 1.344(11); Cp−U(1)−Cp 110.6−124.3 [114.9−118.0], Cp−U(2)−Cp 115.7−117.1, Cp−U(1)−N(1) 94.4−107.7 [98.6−102.3], Cp−U(2)−N(2) 99.2−103.8; Cp is the centroid of the C_5H_4R rings

 © 2004 Wiley-VCH Verlag GmbH & Co. KGaA, Weinheim

The crystal structures of **3** and **4** clearly revealed that the remarkable difference between the reactions of $[U(C_5H_4R)_3]$ and $[Ce(C_5H_4R)_3]$ with pyrazine is related to the actual $U^{III} \rightarrow U^{IV}$ oxidation; this process is clearly favoured by the electron richness of the trivalent metallocenes. Reduction of pyrazine with the divalent lanthanide compounds $[Yb(C_5Me_5)_2(OEt_2)]$[9] and $[Sm\{HB(3,5\text{-}Me_2\text{-}pyrazolyl)_3\}_2]$[10] has also been reported, but the products have not been identified. The distinct reactions of pyrazine and dimethylpyrazine with $[U(C_5H_4R)_3]$ should be related to their reduction potentials $E_{1/2}$ which are equal to −2.17 and −2.28 V vs. Ag/AgCl, respectively.[11] Thus, azine molecules with $E_{1/2}$ values higher than about −2.2 V vs. Ag/AgCl should be reduced by the trivalent metallocenes, while the less reducible ones should give the simple U^{III} Lewis base adducts.

Most notably, compounds **3** and **4** were found to undergo reversible reductive elimination of pyrazine in coordinating solvents, like THF and pyridine. The equilibrium between $[U(C_5H_4R)_3(THF)]$, free pyrazine and $[\{U(C_5H_4R)_3\}_2(\mu\text{-pyz})]$ in THF (Scheme 1) was studied by ^1H NMR spectroscopy, and the formation constants K_{U2L} of the dinuclear compounds were determined from Equation (2), where C_0 is the initial concentration of $[U(C_5H_4R)_3(THF)]$, n the number of molar equivalents of pyrazine and x_{U2L} the molar fraction of **3** or **4**. This expression is simplified to Equation (3) for $n = 0.5$ (stoichiometric ratio).

$$K_{U2L} = [\{U(C_5H_4R)_3\}_2(\mu\text{-pyz})]/[U(C_5H_4R)_3(THF)]^2[pyz]$$
$$K_{U2L} = x_{U2L}(1 + x_{U2L})^2/C_0^2(1 - x_{U2L})^2[n(1 + x_{U2L}) - x_{U2L}] \quad (2)$$

$$K_{U2L} = 2x_{U2L}(1 + x_{U2L})^2/C_0^2(1 - x_{U2L})^3 \ (n = 0.5) \quad (3)$$

The values of K_{U2L} at 23 °C are $8(1) \times 10^3$ and $1.5(1) \times 10^2$ for **3** and **4**, respectively. The difference between these constants reflects the more important electron richness of the $[U(C_5H_4tBu)_3]$ fragment, with respect to $[U(C_5H_4SiMe_3)_3]$,[4] which has a double beneficial effect on the reaction: it impedes the competitive coordination of THF and favours the oxidation of the U^{III} centre. The K_{U2L}/K_{CeL} ratios of 2.8×10^4 and 6.5×10^2, for R = *t*Bu and $SiMe_3$, respectively, are considerably higher than those found in the case of the complexation of $[M(C_5H_4R)_3]$ (M = Ce or U) with various azines in toluene, which do not exceed the value of nine for the reactions of $[M(C_5H_4SiMe_3)_3]$ with 3,5-dimethylpyrazine.[4] The distinct nature of the reactions of $[Ce(C_5H_4R)_3]$ and $[U(C_5H_4R)_3]$ with pyrazine is also reflected in the thermodynamic parameters ΔH and ΔS corresponding to the formation of $[Ce(C_5H_4R)_3(pyz)]$ and $[\{U(C_5H_4R)_3\}_2(\mu\text{-pyz})]$ in THF, which were determined from the van't Hoff diagrams (see Table 1). The difference between the enthalpies of formation of **1** and **3** is as high as 54 kJ·mol^{-1}, whereas the corresponding $\Delta(\Delta H)$ values for the $[M(C_5H_4R)_3(azine)]$ adducts (M = Ce, U) range from 3 to 17 kJ·mol^{-1}.[4]

Table 1. Values of K, $-\Delta H$ (kJ·mol^{-1}) and $-\Delta S$ (J·mol^{-1} K^{-1}) for the formation of the complexes in THF

Compound	K	$-\Delta H$	$-\Delta S$
$[Ce(C_5H_4tBu)_3(pyz)]$ (**1**)	0.28(6)	0(3)	12(7)
$[Ce(C_5H_4SiMe_3)_3(pyz)]$ (**2**)	0.23(2)	19(2)	79(5)
$[\{U(C_5H_4tBu)_3\}_2(\mu\text{-pyz})]$ (**3**)	$8(1) \times 10^3$	54(5)	109(20)
$[\{U(C_5H_4SiMe_3)_3\}_2(\mu\text{-pyz})]$ (**4**)	$1.5(1) \times 10^2$	35(3)	76(15)

As expected from the thermodynamic parameters, the competition reactions of $[Ce(C_5H_4R)_3]$ and $[U(C_5H_4R)_3]$ with pyrazine in THF favoured the formation of the dinuclear uranium compounds **3** and **4**. Thus, the ^1H NMR spectrum of an equimolar mixture of the two trivalent metallocenes $[M(C_5H_4tBu)_3]$ (C_0 = 0.049 M) in the presence of 0.5 molar equivalent of pyrazine {which is identical to that of a 2:1 mixture of $[Ce(C_5H_4tBu)_3]$ and **3**} showed that 45 % of the U^{III} complex was transformed into **3**, while the quantity of **1** was too small to be measured; the molar fraction of **1** should be less than 5×10^{-3}, from Equation (1). In the presence of 9 molar equivalents of pyrazine, 90 % of $[U(C_5H_4tBu)_3]$ and 17 % of $[Ce(C_5H_4tBu)_3]$ were converted into **3** and **1**, respectively. Similar experiments with $[U(C_5H_4SiMe_3)_3]$ and $[Ce(C_5H_4SiMe_3)_3]$ showed that pyrazine is less efficient in the differentiation of these metallocenes, since 18 molar equivalents of the nitrogen ligand were necessary for a 45 % conversion of the U^{III} complex into **4**, and 12 % of **2** were also formed.

Conclusion

The reactions of $[Ce(C_5H_4R)_3]$ and $[U(C_5H_4R)_3]$ with pyrazine are very different because the former is a Lewis acid−Lewis base reaction whereas the latter is a redox reaction. These two reactions led to the equilibrium between $[M(C_5H_4R)_3(THF)]$ (M = Ce and U), $[Ce(C_5H_4R)_3(pyz)]$ (R = *t*Bu **1**; R = $SiMe_3$ **2**) and $[\{U(C_5H_4R)_3\}_2(\mu\text{-pyz})]$ (R = *t*Bu **3**; R = $SiMe_3$ **4**) in THF solution. The greater stability of the dinuclear U^{IV} compounds **3** and **4** with respect to the Ce^{III} complexes **1** and **2** permits a clear differentiation of the two metallocenes by means of the nitrogen ligand. As expected from an oxidation process, the selectivity in favour of uranium(III) is backed by an increased electron density on the metal centre. Oxidation of U^{III} can be seen as the ultimate result of extensive π back donation of the metal orbitals into the π* orbitals of the aromatic ring, which is thought to play a major role in the selective complexation of An^{III} over Ln^{III} ions by nitrogen ligands. It is, however, important to note that Am^{III} and Cm^{III} are less easily oxidized than U^{III}; their extraction based on a redox process would be rendered possible if their oxidation potentials were lowered by using anionic and/or neutral donor ligands, or by operating in specific media, like ionic liquids.

Experimental Section

General: All reactions were carried out under argon (< 5 ppm oxygen or water) using standard Schlenk-vessel and vacuum line tech-

 © 2004 Wiley-VCH Verlag GmbH & Co. KGaA, Weinheim

niques or in a glove box. Solvents were dried by standard methods and distilled immediately before use; deuterated toluene and THF (Eurisotop) were distilled from over Na/K alloy and stored over 3 Å molecular sieves. Pyrazine (Aldrich) was used as received; the metallocenes $[M(C_5H_4tBu)_3]$ (M = Ce,[12] U[13]) and $[M(C_5H_4SiMe_3)_3]$ (M = Ce,[12] U[14]) and the pyrazine adducts **1** and **2**[4] were prepared by published methods. The ^{1}H NMR spectra were recorded on a Bruker DPX 200 instrument and referenced internally using the residual protio-solvent resonances relative to tetramethylsilane (δ = 0 ppm). Elemental analyses were performed by Analytische Laboratorien at Lindlar (Germany).

Synthesis of 3 and 4: A flask was charged with $[U(C_5H_4tBu)_3]$ (200 mg, 0.33 mmol) and pyrazine (26.6 mg, 0.33 mmol) in pentane (15 mL). After 3 h at 20 °C, the dark blue solution deposited a black powder of **3**; a greater quantity of precipitate was obtained after cooling at −78 °C for 3 h. The product was then filtered off and dried under vacuum. Yield: 134 mg (63 %). ^{1}H NMR (200 MHz, [D$_8$]toluene): δ = −70.26 (4 H, pyz), −13.67 (12 H, C_5H_4R), −12.91 (12 H, C_5H_4R), 0.85 (54 H, C_5H_4R) ppm. $C_{58}H_{82}N_2U_2$ (1283): calcd. C 54.29, H 6.40, N 2.18; found C 54.44, H 6.25, N 2.31. The same reaction with $[U(C_5H_4SiMe_3)_3]$ gave **4** in 65 % yield. ^{1}H NMR (200 MHz, [D$_8$]toluene): δ = −69.79 (4 H, pyz), −15.24 (12 H, C_5H_4R), −10.68 (12 H, C_5H_4R), 0.24 (54 H, C_5H_4R).

Determination of the Formation Constants K_{CeL}: An NMR tube was charged with a 0.1 M solution of $[Ce(C_5H_4R)_3]$ in [D$_8$]THF. Under fast exchange conditions, successive addition of pyrazine lead to the displacement of the three resonances of the metallocene towards the limit positions corresponding to the complete formation of $[Ce(C_5H_4R)_3(pyz)]$. The observed chemical shifts for the C_5H_4R ligands, δ_{obs}, are a weighted average of the chemical shifts of these cyclopentadienyl groups in $[Ce(C_5H_4R)_3(THF)]$ and $[Ce(C_5H_4R)_3(pyz)]$, δ_{Ce} and δ_{CeL}, proportional to their relative concentrations, according to $\delta_{obs} = (1 - x_{CeL})\delta_{Ce} + x_{CeL}\delta_{CeL}$, in which x_{CeL} is the molar fraction of $[Ce(C_5H_4R)_3(pyz)]$; the values of x_{CeL} were thus obtained by $x_{CeL} = (\delta_{obs} - \delta_{Ce})/(\delta_{CeL} - \delta_{Ce})$.[4] After each addition of pyrazine, the complexation reactions were monitored by recording the ^{1}H NMR spectra from +23 to −30 °C with intervals of 5 °C. For a 0.146 M solution of $[Ce(C_5H_4tBu)_3(THF)]$ at 23 °C, ^{1}H NMR (200 MHz, [D$_8$]THF): δ_{Ce} = −3.29 (27 H), 11.22 (6 H), 11.72 (6 H) ppm; δ_{CeL} = −3.17 (27 H), 10.17 (6 H), 12.39 (6 H) ppm; δ_{obs} (n = 11.5) = −3.23 (27 H), 10.83 (6 H), 11.91 (6 H) ppm. For a 0.100 M solution of $[Ce(C_5H_4SiMe_3)_3(THF)]$ at 23 °C, ^{1}H NMR (200 MHz, [D$_8$]THF): δ_{Ce} = −0.97 (27 H), 6.75 (6 H), 10.03 (6 H) ppm; δ_{CeL} = −1.52 (27 H), 6.88 (6 H), 10.95 (6 H) ppm; δ_{obs} (n = 14.5) = −1.10 (27 H), 6.76 (6 H), 10.25 (6 H) ppm. The K_{CeL} constants and the corresponding ΔH and ΔS values are given in Table 1.

Determination of the Formation Constants K_{U2L}: In a typical experiment, an NMR tube was charged with a 0.037 M solution of $[U(C_5H_4tBu)_3]$ in [D$_8$]THF. ^{1}H NMR (200 MHz, [D$_8$]THF): δ = −23.16 (6 H), −7.76 (27 H), −2.85 (6 H) ppm. After addition of pyrazine, new signals corresponding to **3** appeared. ^{1}H NMR (200 MHz, [D$_8$]THF): δ = −72.95 (4 H, pyz), −14.93 (12 H, C_5H_4R), −12.97 (12 H, C_5H_4R), 0.76 (54 H, C_5H_4R) ppm. In the presence of 0.5 molar equivalent of pyrazine, the spectrum was identical to that obtained by dissolving **3** in [D$_8$]THF, showing the presence of $[U(C_5H_4tBu)_3(THF)]$ and **3** in relative proportions of 55:45. Similarly, an NMR tube was charged with a 0.025 M solution of $[U(C_5H_4SiMe_3)_3]$ in [D$_8$]THF. ^{1}H NMR (200 MHz, [D$_8$]THF): δ = −17.61 (6 H), −5.97 (6 H), −4.03 (27 H) ppm. Addition of 0.5 molar equivalent of pyrazine had practically no influence on these signals, in agreement with the fact that **4** is almost totally dissociated into $[U(C_5H_4SiMe_3)_3(THF)]$ and pyrazine in THF. After addition of 8.8 molar equivalents of pyrazine, new signals corresponding to **4** appeared. ^{1}H NMR (200 MHz, [D$_8$]THF): δ = −73.73 (4 H, pyz), −16.25 (12 H, C_5H_4R), −10.84 (12 H, C_5H_4R), −0.16 (54 H, C_5H_4R) ppm. The two complexes $[U(C_5H_4SiMe_3)_3(THF)]$ and **4** were in relative proportions of 70:30. The K_{U2L} constants and the corresponding ΔH and ΔS values are given in Table 1.

X-ray Crystallography: The data were collected at 100(2) K on a Nonius Kappa-CCD area detector diffractometer[15] using graphite-monochromated Mo-K_α radiation (λ = 0.71073 Å). The crystals were introduced in glass capillaries with a protecting "Paratone-N" oil (Hampton Research) coating. The unit cell parameters were determined from ten frames, then refined on all data. A 180° φ-range was scanned with 2° steps during data collection, with a crystal-to-detector distance fixed to 28 mm. The data were processed with DENZO-SMN.[16] The structures were solved by direct methods (**3**) or Patterson map interpretation (**4**) with SHELXS-97 and subsequent Fourier-difference synthesis and refined by full-matrix least-squares on F^2 with SHELXL-97.[17] Absorption effects were corrected empirically with the program DELABS from PLATON.[18] One C_5H_4tBu group in compound **3** was found to be disordered over two positions sharing two aromatic and one terminal methyl carbon atom, which were refined with occupancy parameters constrained to sum to unity and with some restraints on bond lengths and displacement parameters. Some short intramolecular C···C contacts result from the imperfect location of the disordered parts. The solvent pyrazine molecule in **3** is disordered around a symmetry centre and the position of the nitrogen atom was not determined. All non-hydrogen atoms were refined with anisotropic displacement parameters. Hydrogen atoms were introduced at calculated positions (except in the disordered parts when present) and were treated as riding atoms with a displacement parameter equal to 1.2 (CH) or 1.5 (CH_3) times that of the parent atom. The molecular plot was drawn with SHELXTL.[19] CCDC-231705 (**3**·0.5pyz) and -231706 (**4**·2pyz) contain the supplementary crystallographic data for this paper. These data can be obtained free of charge at www.ccdc.cam.ac.uk/conts/retrieving.html [or from the Cambridge Crystallographic Data Centre, 12, Union Road, Cambridge CB2 1EZ, UK; Fax: (internat.) +44-1223-336-033; E-mail: deposit@ccdc.cam.ac.uk].

Crystal Data for 3·0.5pyz: $C_{60}H_{84}N_3U_2$, M = 1323.36 g mol^{-1}, monoclinic, $P2_1/c$, a = 15.9661(6), b = 10.6364(4), c = 31.6769(11) Å, β = 94.115(2)°, U = 5365.6(3) Å^3, Z = 4, μ(Mo-K_α) = 6.068 mm^{-1}, 35622 reflections measured, 10137 unique (R_{int} = 0.086) which were used in all calculations. Final R values: R_1 = 0.047, wR_2 = 0.105 (all data).

Crystal Data for 4·2pyz: $C_{60}H_{90}N_6Si_6U_2$, M = 1539.98 g mol^{-1}, triclinic, $P\bar{1}$, a = 11.0619(7), b = 11.1804(6), c = 15.1358(10) Å, α = 105.831(3), β = 105.869(3), γ = 103.017(4)°, U = 1638.86(19) Å^3, Z = 1, μ(Mo-K_α) = 5.084 mm^{-1}, 11306 reflections measured, 5732 unique (R_{int} = 0.038) which were used in all calculations. Final R values: R_1 = 0.030, wR_2 = 0.073 (all data).

[1] [1a] *Actinides and Fission Products Partitioning and Transmutation. Status and Assessment Report.* NEA/OECD Report; NEA/OECD: Paris, **1999**. [1b] *Actinides and Fission Products Partitioning and Transmutation.* Proceedings of the Fifth International Information Exchange Meeting, Mol, Belgium, 25−27 Nov 1998, NEA/OECD Report, Paris, **1999**.

 © 2004 Wiley-VCH Verlag GmbH & Co. KGaA, Weinheim

[2] [2a] K. L. Nash, *Solvent Extr. Ion Exch.* **1993**, *11*, 729−768. [2b] K. L. Nash, *Separation Chemistry for Lanthanides and Trivalent Actinides*, in *Handbook on the Physics and Chemistry of Rare Earths. Lanthanides/Actinides: Chemistry* (Eds.: K. A. Gschneidner Jr., L. Eyring, G. R. Choppin, G. H. Lander), Elsevier Science, Amsterdam, **1994**, vol. 18, 197.

[3] [3a] M. Mazzanti, R. Wietzke, J. Pécaut, J. M. Latour, P. Maldivi, M. Remy, *Inorg. Chem.* **2002**, *41*, 2389−2399. [3b] J. C. Berthet, C. Rivière, Y. Miquel, M. Nierlich, C. Madic, M. Ephritikhine, *Eur. J. Inorg. Chem.* **2002**, 1439−1446. [3c] J. C. Berthet, Y. Miquel, P. B. Iveson, M. Nierlich, P. Thuéry, C. Madic, M. Ephritikhine, *J. Chem. Soc., Dalton Trans.* **2002**, 3265−3272.

[4] T. Mehdoui, J. C. Berthet, P. Thuéry, M. Ephritikhine, *Dalton Trans.* **2004**, 579−590.

[5] C. W. Eigenbrot, K. N. Raymond, *Polyhedron* **1982**, *1*, 417−419.

[6] [6a] J. C. Berthet, C. Boisson, M. Lance, J. Vigner, M. Nierlich, M. Ephritikhine, *J. Chem. Soc., Dalton Trans.* **1995**, 3019−3025. [6b] J. C. Berthet, M. Ephritikhine, *Coord. Chem. Rev.* **1998**, *178−180*, 83−116.

[7] R. E. Cramer, U. Engelhardt, K. Higa, J. W. Gilje, *Organometallics* **1987**, *6*, 41−45.

[8] E. C. Baker, K. N. Raymond, *Inorg. Chem.* **1977**, *16*, 2710−2714.

[9] D. J. Berg, J. M. Boncella, R. A. Andersen, *Organometallics* **2002**, *21*, 4622−4631.

[10] I. Lopes, R. Dias, A. Domingos, N. Marques, *J. Alloys Compds* **2002**, *344*, 60−64.

[11] B. J. Tabner, J. R. Yandle, *J. Chem. Soc. A* **1968**, 381−388.

[12] S. D. Stults, R. A. Andersen, A. Zalkin, *Organometallics* **1990**, *9*, 115−122.

[13] S. D. Stults, R. A. Andersen, A. Zalkin, *Organometallics* **1990**, *9*, 1623−1629.

[14] J. G. Brennan, R. A. Andersen, A. Zalkin, *Inorg. Chem.* **1986**, *25*, 1756−1760.

[15] *Kappa-CCD Software*, Nonius BV, Delft, The Netherlands, **1998**.

[16] Z. Otwinowski, W. Minor, *Methods Enzymol.* **1997**, *276*, 307−326.

[17] G. M. Sheldrick, *SHELXS-97* and *SHELXL-97*, University of Göttingen, Germany, **1997**.

[18] A. L. Spek, *PLATON*, University of Utrecht, The Netherlands, **2000**.

[19] G. M. Sheldrick, *SHELXTL*, Version 5.1, Bruker AXS Inc., Madison, WI, USA, **1999**.

Received February 18, 2004

 © 2004 Wiley-VCH Verlag GmbH & Co. KGaA, Weinheim

Regioselective Functionalization of Tetrabromophenanthroline−Ruthenium Complexes

Sven Rau,*[a] Reinald Fischer,[a] Michael Jäger,[a] Bernhard Schäfer,[a] Susann Meyer,[b] Günter Kreisel,[b] Helmar Görls,[a] Manfred Rudolf,[a] William Henry,[c] and Johannes G. Vos[c]

Keywords: Ruthenium / Nucleophilic substitution / Phenanthroline

Structural, photophysical and photochemical characterization and reactivity of a novel polypyridyl ruthenium complex based on 3,5,6,8-tetrabromophenanthroline are discussed.

(© Wiley-VCH Verlag GmbH & Co. KGaA, 69451 Weinheim, Germany, 2004)

Signal storage at a molecular level is a great challenge for chemistry.[1] The possibility of connecting different functionalities selectively to one ligand of a metal complex may open the route towards higher integrated molecular units capable of processing various external stimuli in a predesignated order. The implementation of this concept demands ligands with a multitude of potential connecting groups which can selectively be transformed.[2] 3-bromo- and 3,8-dibromophenanthrolines have proved useful for the preparation of mononuclear[3] and multiheteronuclear complexes.[4] These systems have found applications ranging from DNA photoprobes,[5] to metalloligands in catalysis.[6] A very useful and well-established feature of these bromophenanthroline−ruthenium complexes is their susceptibility towards nucleophilic aromatic substitution.[7]

We have improved the bromination reaction of phenanthroline first published by Dénes and Chira,[8] which allows for the selective formation of 3,5,6,8,-tetrabromophenanthroline (Br_4phen) in a one-step multigram reaction, Figure 1.[8]

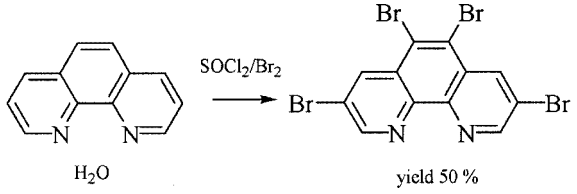

Figure 1. Improved preparation of 3,5,6,8-tetrabromophenanthroline (Br_4phen)

Br_4phen readily forms a complex with $[tbbpy]_2RuCl_2$ resulting in $[(tbbpy)_2Ru(Br_4phen)]^{2+}$, **1**. The structural characterization using two-dimensional NMR spectroscopy suggests that a symmetrical complex is formed as indicated by the presence of only two signals for the four phenanthroline-based protons. ^{13}C, HSQC, and HMBC spectroscopy allows the complete assignment of all signals in the ^1H- and ^{13}C NMR spectra, which together with mass spectroscopy suggests that Br_4phen coordinates in a similar fashion as the unsubstituted phenanthroline. The X-ray crystallographic characterization confirms this assumption, and as seen from Table 1 shows no significant differences compared with the parent complex $[(tbbpy)_2Ru(phen)]^{2+}$, **2** (see Supporting Information). The molecular structure is depicted in Figure 2.

Table 1. Bond lengths (Å) and angles (°)

	1	**2**
Ru−N1	2.046(5)	2.055(4)
Ru−N2	2.060(5)	2.056(5)
Ru−N3	2.064(5)	2.053(4)
Ru−N4	2.052(5)	2.055(4)
Ru−N5	2.047(5)	2.060(4)
Ru−N6	2.071(5)	2.074(4)
C2−Br1	1.891(6)	–
C5−Br2	1.883(6)	–
N1−Ru−N2	79.27(19)	79.9(2)
N3−Ru−N4	78.21(19)	77.88(16)
N5−Ru−N6	78.25(19)	78.99(16)

[a] Institut für Anorganische und Analytische Chemie, Friedrich-Schiller-Universität,
07743 Jena, Germany
E-mail: Sven.Rau@uni-jena.de
[b] Institut für Technische Chemie und Umweltchemie, Friedrich-Schiller-Universität,
07743 Jena, Germany
[c] National Centre for Sensor Research, School of Chemical Sciences, Dublin City University,
Dublin 9, Ireland

Supporting information for this article is available on the WWW under http://www.eurjic.org or from the author.

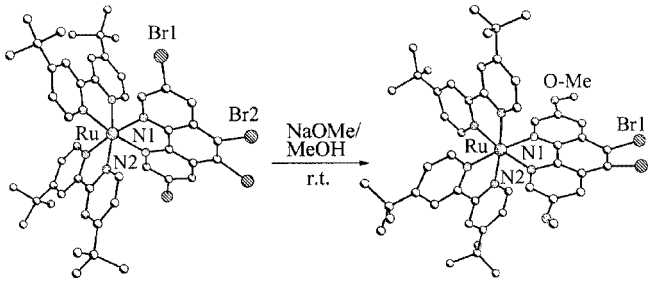

Figure 2. Regioselective nucleophilic substitution of **1** with NaOMe leading to **3**; molecular structure of **1**; anions and hydrogen atoms omitted, and the structural motif of **3** confirming the regioselective substitution

Reaction of **1** with NaOMe at room temperature in methanol leads to the selective formation of one product that contains two bromine and two new methoxy functions, as confirmed by ESI-MS. The fact that the positions of all the bipyridine-based signals in the ^{1}H NMR spectra did not change, together with the presence of only one new signal at $\delta = 4.15$ ppm for the methoxy function, suggests the formation of a symmetrical species where substitution at the phenanthroline moiety has taken place. The regioselective formation of the 5,6-dibromo-3,8-dimethoxyphenanthroline ruthenium complex **3** could be confirmed by a structural motive depicted in Figure 2.

Photophysical investigation of compounds **1** to **3** suggests that tetrabromo substitution lowers the electron density of the phenanthroline ligand considerably. The absorption and emission wavelength of **1** are red-shifted relative to **2**, see Table 2. This finding correlates well with the data obtained for the oxidation potential of $Ru^{II/III}$, which clearly shows that the four bromine substituents significantly decrease the electron density at the metal center (difference of 137 mV). Introduction of the methoxy groups increases the electron density, as expected.[9] The introduction of two methoxy groups has a pronounced influence on the photophysical properties, and this is in agreement with an electron-donating substituent.

Table 2. Photophysical and electrochemical properties of complexes **1**−**3** in acetonitrile

Compound	$E_{1/2}$ ox in V (vs. Fc/Fc$^+$)	λ_{max} in nm	λ_{em} in nm
1	0.92	470	680
2	0.783	444	610
3	0.845	450	615

In conclusion, rutheniumpolypyridyl complexes based on the ligand Br_4phen are readily obtainable. Most importantly a regioselective nucleophilic substitution with NaOMe at the 3,8-position is possible. It is evident from the conventional reactivity of bromine-substituted aromatics that **1** and **3** are potentially very interesting synthons in itself, opening the possibility to derivatise the previously not easily accessible 5,6-position. Initial investigations on the photochemical reactivity of **3** using ion exchange HPLC suggest that Br_2OMe_2phen is very photolabile.

Experimental Section

All solvents used for spectroscopic measurements were of Uvasol (Merck) grade. All other reagents were of HPLC grade. *cis*-[Ru(tbbpy)$_2$Cl$_2$]·2H$_2$O,[10] was prepared by standard procedures. All reagents for synthesis, $RuCl_3 \cdot 3H_2O$ (Chempur), 1,10-phenanthroline (Aldrich) and all other materials were commercially available and of reagent grade.

3,5,6,8-tetrabromophenanthroline (Br_4phen): 1,10-phenanthroline monohydrate (4.0 g, 20 mmol) was dissolved in $SOCl_2$ (200 mL). Freshly distilled Br_2 (9.3 g, 120 mmol) was carefully added. This mixture was refluxed for 31 h and cooled to room temperature, and the bright yellow precipitate was filtered off (3,5,6,8,-tetrabromophenanthroline). The precipitate was washed with aqueous NH_3 until a colorless solution was obtained. The white solid was recrystallized from toluene. ^{1}H NMR ($CDCl_3$): $\delta = 9.16$ (2 H, d), 8.91 (2 H, d) ppm. ^{13}C NMR ($CDCl_3$): $\delta = 122.0$, 125.1, 129.6, 139.0, 143.6, 152.4 ppm. MS (DCI with H_2O): 497 [M + H$^+$] 417 (M − Br + H$^+$), 338 (M − Br_2 + H$^+$), 257 (M$^+$ − Br_3). Yield 5.22 g (52% based on phen).

Synthesis of [(tbbpy)$_2$Ru(Br_4phen)](PF$_6$)$_2$ (1): 3,5,6,8-Tetrabromo-1,10-phenanthroline (1.15 g, 2.32 mmol) and [(tbbpy)$_2$RuCl$_2$] (1.5 g, 2.11 mmol) were refluxed in a mixture of ethanol (80 mL) and H_2O (20 mL) for 8 hours. The crude reaction mixture was filtered, washed twice with ethanol/H_2O (80:20), and the combined filtrate was concentrated to the half volume. On addition of NH_4PF_6 and stirring at room temperature for 1 hour, the crude product precipitated. Recrystallization from acetone/water gave the desired product. Crystals suitable for X-ray analysis were obtained from acetone/water. ^{1}H NMR ([D$_6$]DMSO): $\delta = 8.997$ [4,7, 2 H, s (lc)], 8.792 [3′′, 2 H, s (lc)], 8.788 [3′, 2 H, s (lc)], 8.055 [2,9, 2 H, s (lc)], 7.599 [5′′, 2 H, d (lc)], 7.527 (6′,6′′, 4 H, m), 7.310 [5′, 2 H, d (lc)], 1.391 [CH$_3$(*tert*-butyl), 18 H, s], 1.362 [CH$_3$(*tert*-butyl), 18 H, s] ppm. MS (Micro-ESI in $CHCl_3$ + methanol); *m*/*z* (relative intensity) with matching isotope pattern: 1279 (100) (**1** + PF_6), 1201 (34) (**1** − Br + PF_6), 567 (51) (**1**$^{2+}$). Crystal data for **1**: $[C_{48}H_{52}Br_4N_6Ru]^{2+} \cdot 2\,[PF_6]^-$, $M = 1423.61$ g mol^{-1}, bordeaux-red prism, size 0.02 × 0.02 × 0.01 mm, tetragonal, space group $I4_1/a$, $a = b = 32.5281(3)$, $c = 20.5151(4)$ Å, $V = 21706.6(5)$ Å^3, $T = -90$ °C, $Z = 16$, $\rho_{calcd.} = 1.742$ g cm^{-3}, μ (Mo-K_α) = 33.74 cm^{-1}, psi-scan, trans(min): 0.5565, trans(max): 0.7367, $F(000) = 11264$, 20023 reflections in $h(-42/42)$, $k(-29/29)$, $l(-19/26)$, measured in the range $2.66° \le \Theta \le 27.49°$, completeness $\Theta_{max} = 99.8\%$, 12423 independent reflections.

Synthesis of [(tbbpy)$_2$Ru(phen)](PF$_6$)$_2$ (2): 1,10-phenanthroline (0.018 g, 0.09 mmol) and [(tbbpy)$_2$RuCl$_2$] (0.06 g, 0.085 mmol) were reacted and purified according to **1**. Yield 96 mg (95%). Crystals suitable for X-ray analysis were obtained from acetone/water. ^{1}H NMR ([D$_3$]acetonitrile): $\delta = 8.613$ [4,7, 2 H, s (lc)], 8.504 [3′, 2 H, s (lc)], 8.456 [3′′, 2 H, s (lc)], 8.299 (5,6, 2 H, s), 8.058 [2,9, 2 H, s (lc)] 7.753 (3,8, 2 H, m), 7.705 (6′, 2 H, d), 7.463 [5′, 2 H, d (lc)], 7.405 (6′′, 2 H, d), 7.200 [5′′, 2 H, d (lc)], 1.437 [CH$_3$(*tert*-butyl), 18 H, s], 1.322 [CH$_3$(*tert*-butyl), 18 H, s] ppm. MS FAB in nba *m*/*z* (relative intensity) with matching isotope pattern: 980 (22) (**2** + PF_6); 834 (15) (**2**). Crystal data for **2**: $[C_{48}H_{56}N_6Ru]^{2+} \cdot 2\,[PF_6]^- \cdot 2\,C_3H_6O$, $M = 1224.15$ g mol^{-1}, red-brown prism, size 0.12 × 0.10 × 0.09 mm, triclinic, space group $P\bar{1}$, $a = 12.1999(7)$, $b =$

 © 2004 Wiley-VCH Verlag GmbH & Co. KGaA, Weinheim

13.3243(7), c = 18.989(1) Å, α = 76.854(2), β = 74.819(3), γ = 78.206(3)°, V = 2866.3(3) Å^3, T = −90 °C, Z = 2, $\rho_{calcd.}$ = 1.418 g cm^{-3}, μ (Mo-K_α) = 4.13 cm^{-1}, psi-scan, trans(min): 0.9521, trans(max): 0.9637, F(000) = 1264, 19624 reflections in h(−15/15), k(−17/14), l(−24/24), measured in the range 2.11° ≤ Θ ≤ 27.44°, completeness Θ_{max} = 97.4%, 12753 independent reflections.

Synthesis of [(tbbpy)$_2$Ru(OMe$_2$Br$_2$phen)](PF$_6$)$_2$ (3): 1 (200 mg, 0.14 mmol), was dissolved in a solution of freshly prepared NaOMe (1 M) in MeOH (100 mL). The solution was stirred for 6 h and H_2O (200 mL) was added. The pH of the solution was slowly adjusted to 7 by adding dilute HCl. The resulting opaque orange solution was extracted with CH_2Cl_2 until colorless, and the solvent was removed from the combined organic phases. The precipitate was dissolved in a minimal amount of EtOH and concentrated aqueous NH_4PF_6 added. The precipitate was recrystallized from acetone/water. Yield 170 mg (90%). ^{1}H NMR ([D$_6$]acetone): δ = 8.879 [3′, 2 H, s (lc)], 8.844 [3′′, 2 H, s (lc)], 8.174 [4,7, 2 H, s (lc)], 7.939 (6′, 2 H, d), 7.845 [2,9, 2 H, s (lc)], 7.828 (6′′, 2 H, d), 7.618 [5′, 2 H, d (lc)], 7.397 [5′′, 2 H, d (lc)], 4.156 [CH$_3$(OMe), 6 H, s], 1.428 [CH$_3$(*tert*-butyl), 18 H, s], 1.367 [CH$_3$(*tert*-butyl), 18 H, s] ppm . MS FAB in nba *m*/*z* (relative intensity) with matching isotope pattern: 1181 (5) (**3** + PF$_6$); 1035 (5) (**3**). Crystal data for **3**: $C_{52}H_{61}Br_2F_{12}N_6O_2P_2Ru$, M = 1304.72 g mol^{-1}, red prism, size 0.02 × 0.02 × 0.01 mm, monoclinic, space group $P2_1/n$, a = 13.983(3), b = 39.063(5), c = 10.4711(15) Å, β = 100.945(13)°, V = 5615.4(17) Å^3, T = −153 °C, Z = 4, $\rho_{calcd.}$ = 1.543 g cm^{-3}, μ(Mo-K_α) = 6.22 cm^{-1}, F(000) = 2654, 21731 reflections in h(−15/13), k(−45/45), l(−12/12), measured in the range 1.52° ≤ Θ ≤ 14.56°, completeness Θ_{max} = 72.1%, 6903 independent reflections.

CCDC-216455 and -216456 contain the supplementary crystallographic data for this paper. These data can be obtained free of charge via www.ccdc.cam.ac.uk/conts/retrieving.html (or from the Cambridge Crystallographic Data Centre, 12 Union Road, Cambridge CB2 1EZ, UK; Fax: + 44-1223-336-033; E-mail: deposit@ccdc.cam.ac.uk).

Acknowledgments

Financial support for this work from the Deutsche Forschungsgemeinschaft SFB 436 and a grant to S.R. is gratefully acknowledged. We would like to thank Prof. D. Walther for helpful discussions and encouragement.

[1] V. Balzani, A. Credi, M. Venturi, *Molecular Devices and Machines*, Wiley-VCH, Weinheim, **2003**.
[2] A. C. Laemmel, J. P. Collin, J. P. Sauvage, G. Accorsi, N. Amaroli, *Eur. J. Inorg. Chem.* **2003**, 467.
[3] Y. Tor, *Synlett* **2002**, *7*, 1043, and references cited therein.
[4] P. J. Connors, D. Tzalis, A. L. Dunnick, Y. Tor, *Inorg. Chem.* **1998**, *37*, 1121.
[5] D. J. Hurley, Y. Tor, *J. Am. Chem. Soc.* **2002**, *124*, 13231.
[6] M. Osawa, M. Hoshino, Y. Wakatsuki, *Angew. Chem. Int. Ed.* **2001**, *113*, 3580.
[7] D. Tzalis, Y. Tor, *Angew. Chem. Int. Ed., Engl.* **1997**, *36*, 2666.
[8] V. Dénes, R. Chira, *J. Prak. Chem.* **1978**, *320*, 172.
[9] The electrochemical investigation shows different currents for oxidation and reduction of the ruthenium center of **3** suggesting an involvement of the methoxy function as observed previously: L. O'Brien, M. Duati, S. Rau, A. L. Guckian, T. E. Keyes, N. M. Boyle, A. Serr, H. Görls, J. G. Vos, *Dalton Trans.* **2004**, 514.
[10] S. Rau, M. Ruben, T. Büttner, C. Temme, S. Dautz, H. Görls, M. Rudolph, D. Walther, A. Brodkorb, M. Duati, C. O'Connor, J. G. Vos, *J. Chem. Soc., Dalton Trans.* **2000**, 3649.

Received February 27, 2004

 © 2004 Wiley-VCH Verlag GmbH & Co. KGaA, Weinheim

$[\{Zn(enMe)_2\}_2(enMe)_2\{Zn_2As_8V_{12}O_{40}(H_2O)\}]\cdot 4H_2O$: A Hybrid Molecular Material Based on Covalently Linked Inorganic Zn−As−V Clusters and Transition Metal Complexes via enMe Ligands

Shou-Tian Zheng,[a] Jie Zhang,[a] and Guo-Yu Yang*[a,b]

Keywords: Polyoxometalate / Vanadium / Arsenic / Zinc / Inorganic−organic hybrids

A novel zinc-substituted polyoxovanadate, $[\{Zn(enMe)_2\}_2(enMe)_2\{Zn_2As_8V_{12}O_{40}(H_2O)\}]\cdot 4H_2O$ **1** (enMe = 1,2-diaminopropane), which is built up from $Zn_2As_8V_{12}O_{40}(H_2O)$ clusters and $Zn(enMe)_2$ complexes, and further connected together by *trans*-enMe ligands, has been hydrothermally prepared and characterized by X-ray crystallography. The study of the magnetic susceptibility of **1** demonstrates the presence of antiferromagnetic interaction between V^{IV} cations in **1**.
(© Wiley-VCH Verlag GmbH & Co. KGaA, 69451 Weinheim, Germany, 2004)

Introduction

The design and synthesis of inorganic−organic hybrid materials have been of great interest for their unusual topological properties and potential applications in the fields of catalysis, biochemistry, magnetism and material science.[1−4] In recent years, the design of inorganic−organic hybrid polyoxometalates (POMs) made possible architectures that contribute to the increasing understanding of the methods that control the synergistic interaction between organic and inorganic chemical compositions.[1] A number of transition metal (TM) coordination complex-linked POMs with one-, two- and three-dimensional inorganic−organic hybrid frameworks, as well as some POMs-supported TM complexes have been reported.[5−15] In general, the early transition metals (TMs), especially V, Mo, and W, are flexible and are able to form POMs by using various coordination geometries (from regular and distorted octahedra and square pyramids to tetrahedra) in their highest or mixed oxidation states;[16] however, in contrast, the post TMs, such as Cu^{2+}, Zn^{2+}, and Cd^{2+}, tend to form various TM coordination complexes in which they act as the countercations, the decorated fragments or bridging units in inorganic−organic hybrid POMs. Since the post TMs exhibit extensive coordination chemistry involving a variety of organic ligands, the post TM-substituted POMs may, in principle, incorporate appropriate organic ligands. This offers opportunity for making new inorganic−organic hybrid complexes containing an inorganic cluster backbone decorated with organic functionalities. Such compounds are much less developed. We are currently exploring the potential of this approach in order to obtain some POMs with unusual structures and properties. This report describes the hydrothermal synthesis and characterization by IR and EPR spectroscopy, TGA, elemental analysis, magnetic properties and single-crystal X-ray structure analysis of the first zinc-substituted polyoxovanadate: $[\{Zn(enMe)_2\}_2(enMe)_2\{Zn_2As_8V_{12}O_{40}(H_2O)\}]\cdot 4H_2O$ **1**, in which *trans*-enMe molecules serve as bridges between the inorganic Zn−As−V clusters and $Zn(enMe)_2$ complexes.

Results and Discussion

Single-crystal X-ray analysis reveals that compound **1** is a neutral zinc-substituted polyoxovanadate: $[\{Zn(enMe)_2\}_2(enMe)_2\{Zn_2As_8V_{12}O_{40}(H_2O)\}]\cdot 4H_2O$. As shown in Figure 1, an unusual feature of **1** is that two Zn^{2+} take the place of two VO^{2+} groups located between the As_2O_5 units of the well-known $[As_8V_{14}O_{42}(X^{n-})]^{(8-n)-}$ (X = SO_4^{2-}, SO_3^{2-}, 0.5 H_2O) anion[17,18] and form a new metal cluster anion $[Zn_2As_8V_{12}(H_2O)]^{4-}$. Each $[Zn_2As_8V_{12}O_{40}(H_2O)]^{4-}$ anion is then decorated by two novel TM complexes $[(enMe)Zn(enMe)_2]^{2+}$ to generate an unprecedented inorganic−organic cluster **1**. In the structure of **1**, four crystallographically distinct zinc sites display two different coordination environments: $NZn(1,2)O_4$ square pyramids and distorted $N_2Zn(3,4)N_3$ trigonal bipyramids. The equatorial positions of the $NZnO_4$ square pyramids are occupied by four μ_3-O atoms linked to neighboring OVO_4 square pyramids and four As atoms [Zn−O = 2.007(8)−2.076(7) Å],

[a] Coordination and Hydrothermal Chemistry Group, State Key Laboratory of Structural Chemistry, Fujian Institute of Research on the Structure of Matter, Chinese Academy of Sciences,
Fuzhou, Fujian 350002, China
[b] State Key Laboratory of Coordination Chemistry, Nanjing University,
Nanjng, Jiangsu 210093, China
Fax: (internat.) +86-591-371-0051
E-mail: ygy@ms.fjirsm.ac.cn

 © 2004 Wiley-VCH Verlag GmbH & Co. KGaA, Weinheim **DOI: 10.1002/ejic.200400019**

and the axial position is occupied by one N atom from a enMe ligand [Zn−N = 2.030(10) Å]. Two distorted N_2ZnN_3 trigonal bipyramids are defined by five N donors of three enMe ligands, respectively, with the Zn−N bond lengths of 2.071(10)−2.203(10) Å. All V centers have a distorted OVO_4 square pyramidal environment with V−O bond lengths in the usual range, 1.596(8)−1.622(7) Å for the terminal oxygen atoms and 1.919(7)−2.007(7) Å for μ_3-O atoms. In the As_2O_5 fragments, the As−O distances vary from 1.741(8) to 1.805(8) Å.

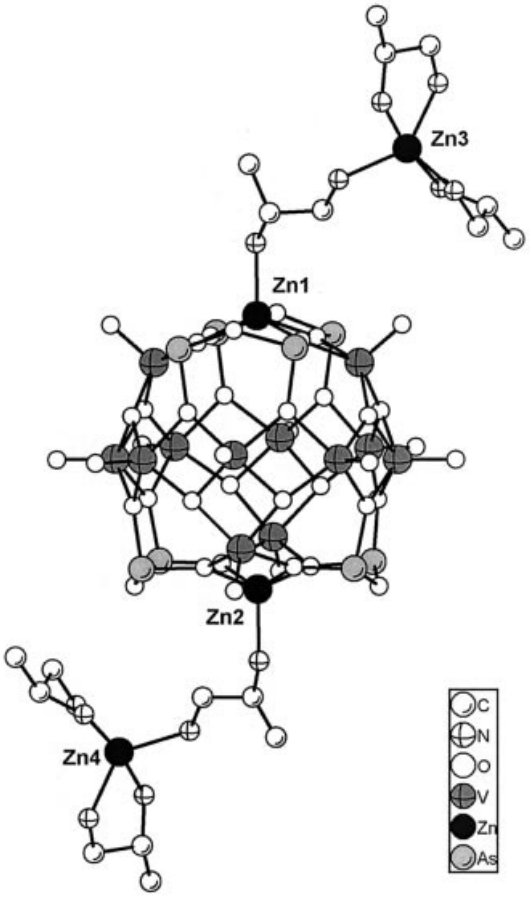

Figure 1. Molecular drawing of **1** (all H atoms are omitted for clarity)

Another unusual feature of **1** is the coordination modes of enMe. There are two types of configuration modes for *cis*- and *trans*-enMe. The *cis*-enMe molecules act as a bidentate chelating ligand and coordinate to the Zn(3) and Zn(4) atoms to form $Zn(enMe)_2$ fragments, while the *trans*-enMe molecules bridge the Zn center of the Zn−As−V cluster and $Zn(enMe)_2$ fragment in an end-to-end fashion, acting as a pillar between the polyoxoanion and the TM coordination fragment. To the best of our knowledge, this linking mode between polyoxoanion and TM coordination fragment in **1** has not been described in other polyoxometalates to date, although the topology of the $\{Zn(enMe)_2\}(enMe)$ group has already been described by Khan et al. in the free complex $[Zn_2(en)_5]^{2+}$.[15]

In compound **1**, each zinc-substituted polyoxovanadium cluster joins eight other adjacent clusters through strong hydrogen bonds between the amine nitrogen atoms and the oxygen atoms, thus resulting in an interesting three-dimensional supramolecular array (Figure 2).

On the basis of valence sum (Σ_s) calculations[19] in **1**, the oxidation states of all V atoms are +4 (Σ_s = 3.972-4.146), the eight As atoms are +3 (Σ_s = 3.043-3.176), and the four Zn atoms are +2 (Σ_s = 1.944−2.096). The EPR spectrum of **1** at liquid nitrogen temperatures shows that the *g* value is 1.9476, corresponding to the signal of V^{4+}. This is consistent with the results from the valence sum calculations.

The thermogravimetric study of compound **1**, which was carried out under a flow of nitrogen and at a heating rate of 10 °C min^{-1}, indicates that the weight loss of **1** cannot be completely divided into distinct stages. The whole stage, which occurs from 45 to 795 °C, is attributed to the loss of H_2O, enMe and the sublimation of As_2O_3. Assuming that the residue corresponds to VO_2 and ZnO, the observed weight loss (50.41%) is in good agreement with the calculated value (50.13%).[20,21]

The variable temperature magnetic susceptibility of **1** was measured between 5 and 300 K. The magnetism may be attributed solely to the presence of V^{4+} ions ($3d^1$, S = 1/2). Figure 3 shows the magnetic behavior of **1** in the form of a reciprocal molar susceptibility (χ_M^{-1}) and $\chi_M T$ vs. temperature. The $\chi_M T$ at room temperature, 1.23 emu K mol^{-1} (3.10 μ_B), is much lower than that expected for 12 uncoupled S = 1/2 spins with g = 2 (4.5 emu K mol^{-1}, 6.0 μ_B). This lower value is similar to that reported for $[V^{IV}{}_8V^{V}{}_4As_8O_{40}(HCOO-)]^{2-}$ or $[H_3KV^{V}{}_8V^{IV}{}_4As_3O_{39}(AsO_4)]^{6-}$ polyoxovanadate (1.2−1.26 emu K mol^{-1}),[22,23] corresponding to four uncoupled electrons (1.5 emu K mol^{-1} for g = 2, 3.46 μ_B). The fact that compound **1** has a much lower χT value at high temperature suggests that there is a possibility that at least eight electrons are already completely paired at room temperature, while the remaining four are unpaired, an observation which is similar to those seen in polyoxovanadates containing V^{IV} centers.[24,25] In compound **1**, all the equatorial vanadium atoms are bridged by one μ-oxo and a μ-arsenato group with a mean distance of 3.014 Å. The capped V atoms are connected to equatorial vanadium atoms through two different exchange pathways. One pathway is formed by a single μ-oxo bridge with a large V−V distance with a mean of 3.733 Å, while the other is formed by two μ-oxo groups with short V−V distance (2.903 Å). It is well-known[26] that μ-oxo bridges are more effective in transmitting antiferromagnetic exchange interactions between several transition metal elements, generally the extent of the coupling in dioxo-bridges is expected to be stronger than for single bridges, and the short metal-metal distance associated to these bridges gives the possibility of direct V−V overlap. The short distances of neighboring V···V pairs with dioxo-bridges, V1···V6 [2.900 Å], V3···V7 [2.895 Å], V8···V11 [2.903 Å] and V9···V10 [2.917 Å], lie in the range expected

 © 2004 Wiley-VCH Verlag GmbH & Co. KGaA, Weinheim

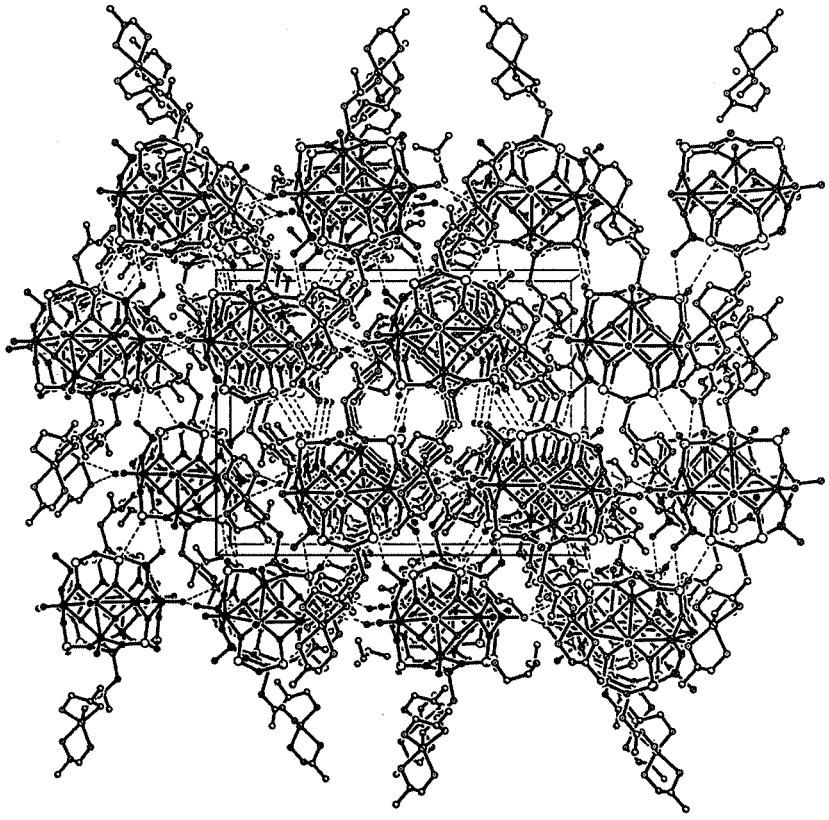

Figure 2. Packing of compound **1** down *a*-axis showing the intercluster hydrogen bonds (water molecules and all H atoms are omitted for clarity)

for strong antiferromagnetic coupling,[27] thus, it is reasonable to assume that these four pairs of vanadium centers between equatorial and capped sites are in the ground $S = 0$ state at relatively high temperature due to the very strong antiferromagnetic coupling provided by the di-μ-oxo bridge, leaving four uncoupled vanadium centers at the equator of the cluster in an approximate square arrangement. On cooling from room temperature, the $\chi_M T$ value decreases slowly until 50 K and then sharply falls to a minimum value of 0.4 cm^3 K mol^{-1} (1.79 μ_B) at 5 K, indicative of antiferromagnetic coupling between the remaining vanadium centers. This dominant antiferromagnetic character is in agreement with a negative Weiss constant ($\theta = -10$ K) obtained from a linear fitting of $\chi_M{}^{-1}$ vs. T using the Curie−Weiss equation. The susceptibility data at low temperature were analyzed using expressions[28,29] for an $S = 1/2$ tetramer based on the Heisenberg Hamiltonian $H = -J(\boldsymbol{S}_1 \cdot \boldsymbol{S}_2 + \boldsymbol{S}_2 \cdot \boldsymbol{S}_3 + \boldsymbol{S}_3 \cdot \boldsymbol{S}_4 + \boldsymbol{S}_4 \cdot \boldsymbol{S}_1)$, the intercluster interactions were included in the model in the molecular field approximation $\chi = \chi_{cluster}/[1 - (2zJ'/Ng^2\beta^2)\,\chi_{cluster}]$.[30] The best fit was obtained with $J = -3.59\ cm^{-1}$, $zJ' = -1.85\ cm^{-1}$, $g = 1.79$ and $R = 8.13 \times 10^{-4}$ for 36 observations at $T \leq 100$ K. R is the agreement factor defined as $\Sigma i[(\chi_M T)_{obs}(i) - (\chi_M T)_{cal}(i)]^2/\Sigma i\,[(\chi_M T)_{obs}(i)]^2$.

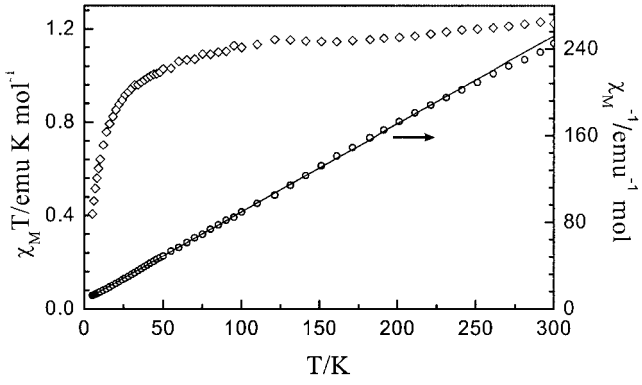

Figure 3. The temperature dependence of reciprocal magnetic susceptibility $\chi_M{}^{-1}$ (circle) and the product $\chi_M T$ (diamond) for complex **1**

Conclusion

In this communication we show the first zinc-substituted inorganic−organic hybrid polyoxovanadium cluster. This is a rare complex in which the organonitrogen ligand serves

 © 2004 Wiley-VCH Verlag GmbH & Co. KGaA, Weinheim

as a bridge between the metal oxide cluster and the TM coordination fragment. The results demonstrate the potential of post TM-substituted POMs as molecular building blocks for the construction of novel inorganic−organic materials. The substituted Zn centers can also be replaced with other TM ions.[31] Further investigation in this area is in progress.

Experimental Section

Synthesis and Initial Characterization: In a typical synthesis, a mixture of V_2O_5 (0.3 g, 1.66 mmol), As_2O_3 (0.36 g, 1.82 mmol), $ZnAc_2{\cdot}4H_2O$ (1.0 g, 3.98 mmol), enMe (1.1 mL, 14.86 mmol) and H_2O (10 mL, 555.56 mmol), in a molar ratio of 4:4.5:10:37:1389 was stirred under ambient conditions. The resulting gel was sealed in a Teflon-lined steel autoclave and heated at 180 °C for 7 days, and then cooled to room temperature. The resulting product, consisting of single crystals in the form of brown blocks, was recovered by filtration, washed with distilled water and dried in air. Yield 0.553 g (76.1% based on V). Elemental analysis showed that the sample contains 8.02, 2.58, and 6.42 wt% of C, H, and N, respectively, in good agreement with the expected values of 8.09, 2.67, and 6.38 wt%, respectively, on the basis of the empirical formula given by the single-crystal structure analysis. IR (KBr pellet ν/cm^{-1}): 3318 (s), 3262 (s), 2964 (m), 1587 (s), 1458 (w), 1390 (w), 1016 (s), 983 (vs), 718 (vs), 637(s), 460 (s).

X-ray Crystallography

$[\{Zn(enMe)_2\}_2(enMe)_2\{Zn_2As_8V_{12}O_{40}(H_2O)\}]{\cdot}4H_2O$ (1): Monoclinic, space group $P2_1/n$ (no.14), a = 14.9617(6), b = 19.1992(8), c = 24.9403(11) Å, β = 90.050(1)°, V = 7164.2(5) Å^3, Z = 4, D_c = 2.454 g cm^{-3}, $F(000)$ = 5128, M = 2646.98, S = 1.116, T = 293 K. λ(Mo-K_α) = 0.71073 E, θ range 1.34−25.03°. Bruker Smart CCD diffractometer. ω and scan. 12308 reflections are unique, 8482 reflections with $I > 2\sigma(I)$ were used in the refinement and the calculation of R_1 and wR_2. The last successful full-matrix least-squares refinement with anisotropic thermal parameters for all non-hydrogen atoms converged to R_1 = 0.0631, wR_2 = 0.1209. The positions of hydrogen atoms were calculated in ideal positions and not refined. The structure was solved by direct methods.

CCDC-221503 contains the supplementary crystallographic data for this paper. These data can be obtained free of charge at www.ccdc.cam.ac.uk/conts/retrieving.html [or from the Cambridge Crystallographic Data Centre, 12 Union Road, Cambridge CB2 1EZ, UK; Fax: (internat.) + 44-1223/336-033; E-mail: deposit@ccdc.cam.ac.uk].

Acknowledgments

This work was supported by the NSF of China (Grant No. 20271050 and 20171045), and the Talents Program of Chinese Academy of Sciences.

[1] P. J. Hagrman, D. Hagrman, J. Zubieta, *Angew. Chem. Int. Ed.* **1999**, *38*, 2638−2684.
[2] A. K. Cheetham, G. Férey, T. Loiseau, *Angew. Chem. Int. Ed.* **1999**, *38*, 3268−3292.
[3] R. Finn, J. Zubieta, *Chem. Commun.* **2000**, 1321−1322.
[4] Polyoxometalates in: *Chem. Rev.* **1998**, *98*, 1−387.
[5] D. Hagrman, C. Zubieta, D. J. Rose, J. Zubieta, R. C. Haushalter, *Angew. Chem. Int. Ed., Engl.* **1997**, *36*, 873−876.
[6] C. L. Pan, J. Q. Xu, G. H. Li, D. Q. Chu, T. G. Wang, *Eur. J. Inorg. Chem.* **2003**, 1514−1517.
[7] P. J. Zapf, C. J. Warren, R. C. Haushalter, J. Zubieta, *Chem. Commun.* **1997**, 1543−1544.
[8] C. D. Wu, C. Z. Lu, H. H. Zhuang, J. S. Huang, *Inorg. Chem.* **2002**, *41*, 5636−5637.
[9] J. Lu, E. H. Shen, M. Yuan, Y. G. Li, E. B. Wang, C. W. Hu, L. Xu, J. Peng, *Inorg. Chem.* **2003**, *42*, 6956−6958.
[10] J. Q. Xu, R. Z. Wang, G. Y. Yang, Y. H. Xing, D. M. Li, W. M. Bu, L. Ye, Y. G. Fan, G. D. Yang, Y. Xing, Y. H. Lin, H. Q. Jia, *Chem. Commun.* **1999**, 983−984.
[11] M. I. Khan, *J. Solid. State Chem.* **2000**, *152*, 105−112.
[12] S. T. Zheng, J. Zhang, G. Y. Yang, *Chem. Lett.* **2003**, *32*, 810−811.
[13] D. Hagrman, P. J. Zapf, J. Zubieta, *Chem. Commun.* **1998**, 1283−1284.
[14] B. Z. Lin, S. X. Liu, *Chem. Commun.* **2002**, 2126−2127.
[15] M. I. Khan, E. Yohannes, R. J. Doedens, *Inorg. Chem.* **2003**, *42*, 3125−3129.
[16] A. Müller, *Nature* **1991**, *352*, 115−115.
[17] A. Müller, J. Döring, *Z. Anorg. Allg. Chem.* **1991**, *595*, 251−274.
[18] G. H. Huan, M. A. Greaney, A. J. Jacobson, *J. Chem. Soc., Chem. Commun.* **1991**, 260−261.
[19] I. D. Brown, D. Altermatt, *Acta Crystallogr., Sect. B* **1985**, *41*, 244−247.
[20] G. Paul, A. Choudhury, R. Nagarajan, C. N. R. Rao, *Inorg. Chem.* **2003**, *42*, 2004−2013.
[21] X. B. Cui, Y. Q. Sun, G. Y. Yang, *Inorg. Chem. Commun.* **2003**, *6*, 259−261.
[22] A. L. Barra, D. Gatteschi, B. S. Tsukerbaltt, J. Döring, A. Müller, L. C. Brunel, *Inorg. Chem.* **1992**, *31*, 5132−5134.
[23] D. Gatteschi, B. Tsukerblatt, A. L. Barra, L. C. Brunel, A. Müller, J. Döring, *Inorg. Chem.* **1993**, *32*, 2114−2117.
[24] A. Müller, F. Peters, M.T. Pope, D. Gatteschi, *Chem. Rev.* **1998**, *98*, 239−272.
[25] A. Müller, R. Sessoli, E. Krickemeyer, H. Bögge, J. Meyer, D. Gatteschi, L. Pardi, J. Westphal, K. Hovemeier, R. Rohlfing, J. Döring, F. Hellweg, C. Beugholt, M. Schmidtmann, *Inorg. Chem.* **1997**, *36*, 5239−5250.
[26] A.L. Barra, D. Gatteschi, L. Pardi, A. Müller, J. Döring, *J. Am. Chem. Soc.* **1992**, *114*, 8509−8514.
[27] T. Yamase, M. Suzuki, K. Ohtaka, *J. Chem. Soc., Dalton Trans.* **1997**, 2463−2472.
[28] Y. Rodriguez-Martin, C. Ruiz-Perez, J. Sanchiz, F. Lloret, M. Julve, *Inorg. Chim. Acta* **2001**, *318* 159−165.
[29] G. Alzuet, J. A. Real, J. Borrás, R. Santiago-García, S. García-Granda, *Inorg. Chem.* **2001**, *40*, 2420−2423.
[30] R. L. Carlin, *Magnetochemistry*, Springer, Berlin, **1986**.
[31] During preparation of this Communication, another new POM cluster $[Cd(en)_2]_2[\{Cd(en)\}_2As^{III}_8V^{IV}_{12}O_{40}]$ which incorporates a pair of $Cd(en)^{2+}$ groups was successfully obtained as crystals. The single-crystal X-ray diffraction reveals that this compound possesses a 1-D chain structure constructed from Cd-substituted POMs and $Cd(en)_2$ coordination complex fragments.

Received January 11, 2004

 © 2004 Wiley-VCH Verlag GmbH & Co. KGaA, Weinheim

Designed Assembly of Low-dimensional Molecular Units: Novel Neutral Coordination Polymers Based on (Phosphonodithioato)Ni^{II} Complexes

M. Carla Aragoni,*[a] Massimiliano Arca,[a] Neil R. Champness,[b] Aleksey V. Chernikov,[c] Francesco A. Devillanova,[a] Francesco Isaia,[a] Vito Lippolis,[a] Neil S. Oxtoby,[b] Gaetano Verani,[a] Sergey Z. Vatsadze,[c] and Claire Wilson[b]

Keywords: Phosphonodithioates / Bipyridyl ligands / Crystal engineering / Coordination polymers / X-ray diffraction

The reactions of phosphonodithioato complexes [Ni(ROdtp)$_2$] [where ROdtp = (4-MeOPh)(RO)PS$_2$; R = Et, Me] with 4,4′-bipy and *N*,*N*′-bis-(3-pyridinylmethylene)benzene-1,4-diamine (bdpy), respectively, yield the 1:1 coordination polymers [Ni(EtOdtp)$_2$(bipy)]$_8$ and [Ni(MeOdtp)$_2$(bdpy)]$_\infty$, whose syntheses and single-crystal X-ray diffraction analyses are reported.

(© Wiley-VCH Verlag GmbH & Co. KGaA, 69451 Weinheim, Germany, 2004)

Introduction

Crystal engineering is an important form of supramolecular synthesis, which utilises the understanding of intermolecular interactions in the design of new solids with desired physical and chemical properties.[1] In this view, the involvement of transition metals in crystal engineering can introduce specific physical properties,[2] such as optical properties,[3] electrical conductivity and magnetism,[4] and allows us to exploit a well-established know-how, based on the principles of coordination chemistry.[5] The most employed approach to coordination polymers with predetermined molecular architecture is the rational self-assembly of cleverly selected, multifunctional ligands and metal ions.[6] However, the nature of the counterion, the choice of the solvent, and various phenomena, such as supramolecular isomerism and interpenetration, introduce some uncertainty into the outcome of a particular experiment.[7] In this regard, by reducing the degrees of freedom of the system, for instance by using *cis*-protected metal blocks in place of the "naked" metal ions,[8] or by using a neutral, coordinatively unsaturated metal complex, less uncertainty can be expected. Moreover, the use of neutral synthons leads to self-reliant supramolecular assemblies, which do not require the presence of a counterion. Therefore, the use of suitable coordination compounds as molecular building blocks[9] is a logical extension of the self-assembly approach and is becoming an important synthetic strategy, as attested by the extensive work done on the use of di- and tricarboxylic acids to link adjacent equatorial sites in dimetal units and, more recently, on the use of axial linking to connect simple oligomers to form one- and two-dimensional polymers.[10] However, apart from the massive work on metal carboxylates,[10] this strategy remains largely untapped. Our aim in this study is to exploit this building strategy by using neutral coordinatively unsaturated (phosphonodithioato)Ni^{II} complexes, [Ni(ROdtp)$_2$], [where ROdtp = (4-MeOPh)(RO)PS$_2$; R = Me (**1**), Et (**2**)] and bipyridyl-type ligands as neutral building blocks.[11]

Results and Discussion

Recently, following the one-step reaction between alcohols and diorgano-dithiadiphosphetane disulfides (ArPS$_2$)$_2$ (where Ar = 4-MeOPh, Ph), in the presence of nickel chloride, square planar phosphonodithioato complexes have been synthesised.[12]

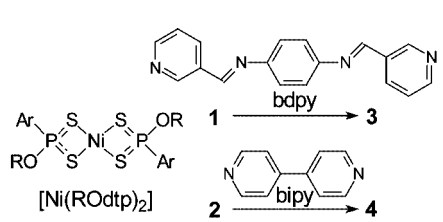

R = Me (**1**), Et (**2**); Ar = 4-MeOPh

[a] Dipartimento di Chimica Inorganica ed Analitica, Cittadella Universitaria,
S.S. 554 bivio Sestu, 09042 Monserrato, CA, Italy
Fax: (internat.) +39-0706754456
E-mail: aragoni@unica.it
[b] School of Chemistry, The University of Nottingham, University Park, Nottingham,
NG7 2RD, UK
[c] Department of Chemistry, M. V. Lomonosov Moscow State University,
Moscow, 119899, Russia

 © 2004 Wiley-VCH Verlag GmbH & Co. KGaA, Weinheim **DOI: 10.1002/ejic.200400089**

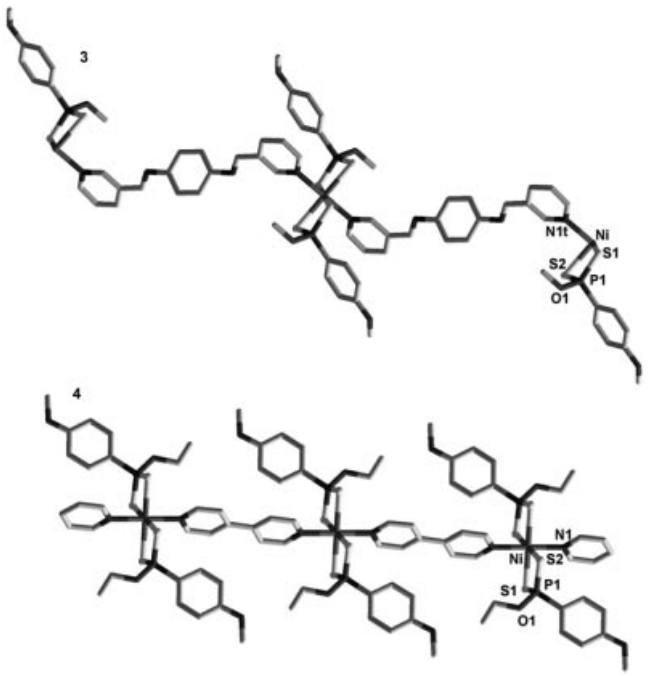

Figure 1. Linear and zigzag polymeric chains of compounds **3** and **4**; hydrogen atoms have been omitted for clarity

The reactivity of these complexes towards pyridine ligands to form octahedral adducts has been studied both in solution and in the solid state,[13] and given the high values of the formation constants of the corresponding adducts,[14] we decided to exploit the tendency of these square-planar (dtp)Ni complexes to be axially coordinated by N−R−N multidentate ligands, such as bidentate bipyridyl-based spacers, to form [Ni(ROdtp)$_2$]−(N−R−N)−[Ni(ROdtp)$_2$]−(N−R−N)− neutral polymers. We report here the synthesis and the structural characterisation of the 1:1 coordination polymers [Ni(MeOdtp)$_2$(bdpy)]$_\infty$ (**3**) and [Ni-(EtOdtp)$_2$(bipy)]$_\infty$ (**4**), obtained by treating [Ni(MeOdtp)$_2$] (**1**) with *N*,*N*′-bis-(3-pyridinylmethylene)-benzene-1,4-diamine (bdpy), and [Ni(EtOdtp)$_2$] (**2**) with 4,4′-bipyridine (bipy), respectively. The bipy and bdpy spacers differ not only in the directionality of the two nitrogen donor atoms, but also in the distance between the N donor atoms, which is of about 7.2 and 14.1 Å for bipy and bdpy, respectively. In both **3** and **4** the nickel ion displays a distorted octahedral environment and the two bidentate phosphonodithioato units occupy the equatorial positions. Each pyridine unit of both bipy and bdpy is axially coordinated to the Ni^{II} ion of two [Ni(ROdtp)$_2$] units [Ni−N, **3**: 2.129(3) Å; **4**: 2.136(2)], thus forming polymeric structures.

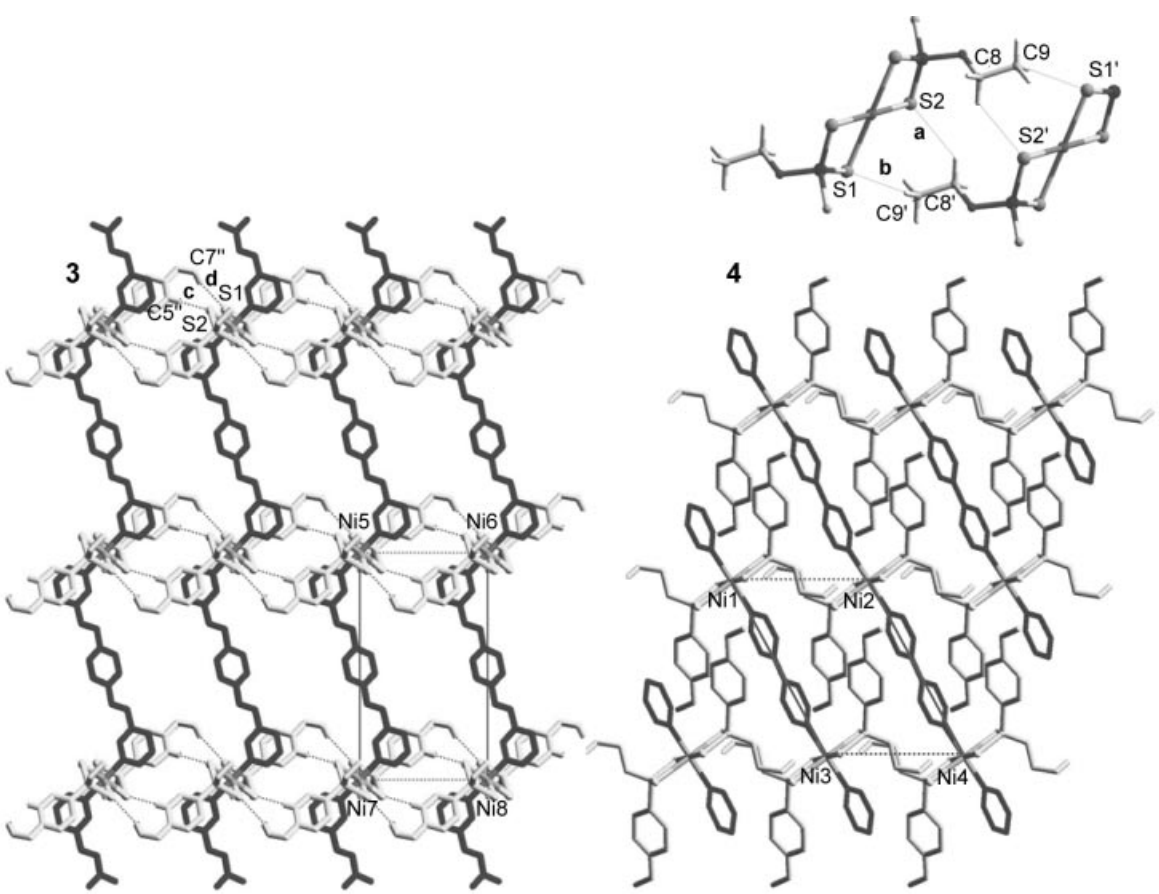

Figure 2. 2D grids viewed down the crystallographic axes *c* and *b* for **3** and **4**, respectively; bipy and bdpy are shaded to evidence the coordination polymers; interactions **a**···**b** (enlarged at the top for clarity reasons) and **c**···**d** connect adjacent chains: **a** S2···C8′ 3.76, H···S 2.96 Å; **b** S1···C9′ 3.90, H···S 3.01 Å; **c** S2···C5′′ 3.74, H···S 2.80 Å; **d** S1···C7′′ 4.00, H···S 3.05 Å; Ni1···Ni2 8.12; Ni1···Ni3 11.38; Ni5···Ni6 10.02, Ni5···Ni7 16.72 Å. Ni2−Ni1−Ni3 60°; Ni5−Ni6−Ni7 90°; ′: 1 + x, *y*, *z*; ′′: −x, −*y*, −*z*; hydrogen atoms except those involved in the described interactions have been omitted for clarity

 © 2004 Wiley-VCH Verlag GmbH & Co. KGaA, Weinheim

The coordination of the pyridyl bases causes an increase in the Ni−S bond lengths [**1**: 2.2330(6), 2.2340(6); **2**: 2.2197(8), 2.2225(8); **3**: 2.4729(9), 2.4997(9); **4**: 2.4646(10), 2.4763(8) Å] and variations in the bond angles in the PS_2Ni metallacycle [S1−Ni−S2, **1**: 88.24(2), **2**: 88.14(3), **3**: 82.19(3), **4**: 82.54(2)°; S1−P−S2, **1**: 102.15(3), **2**: 101.57(4), **3**: 110.16(5), **4**: 109.43(4)°]. These variations closely resemble those found in analogous molecular adducts between phosphonodithioato complexes and pyridine derivatives.[13]

The main, common, structural feature of **3** and **4** is the presence of $[Ni(ROdtp)_2]-N-R-N-[Ni(ROdtp)_2]-N-R-N-$ neutral parallel chains running in linear and zigzag lines with an Ni−Ni distance, through coordinate bonds, of 16.72 and 11.38 Å for **3** and **4**, respectively (see Figure 1). It is interesting to note that in **3** and **4** the 4-MeOPh rings bound to the phosphorus atom show different torsion angles with respect to the P−S bonds [**3**: S2−P−C1−C2 164.4(3)°; **4**: S1−P−C1−C2 99.1(2)°]. Moreover, the orientations of the 4-MeOPh groups with respect to the pyridyl rings in **3** and **4** are different: the mean planes of the two types of rings form an angle of 19.7° in the case of **3**, and 72.5° in the case of **4** (Figure 1). Weak hydrogen bonds, especially of the C−H···S type,[15] between the phosphonodithioato units connect the linear polymers in 2D rectangular and rhombic grids in the case of **3** and **4**, respectively, due to the different geometries of the spacers (see Figure 2). In the case of **3**, the grids feature openings of about 10 × 17 Å; however, in the crystal lattice two sets of symmetry-equivalent parallel and specular grids, shifted by *a*/2, *b*/2, *c*/2, pack in such a way that the bulky nodes of one net are complementary to the spaces within the other net (see Figure 3). Moreover, the sheets interact through weak hydrogen bonds between the bdpy and ROdtp units generating a three-dimensional network. In contrast, in the case of **4**, due to the short length of the bipy rods, the rhombic grids, arising from hydrogen bonding of the chains, do not have enough room to host anything else but the 4-MeOPh rings of two different ligand units (Figure 2).

In conclusion, the use of neutral (phosphonodithioato)Ni^{II} complexes, with predefined coordination sites, as molecular building blocks and suitable bipyridyl-based spacers allows us to assemble one-dimensional coordination polymers. The architecture of the polymers strongly depends on the geometrical features of the spacers and on the weak hydrogen bonds involving the substituents at the

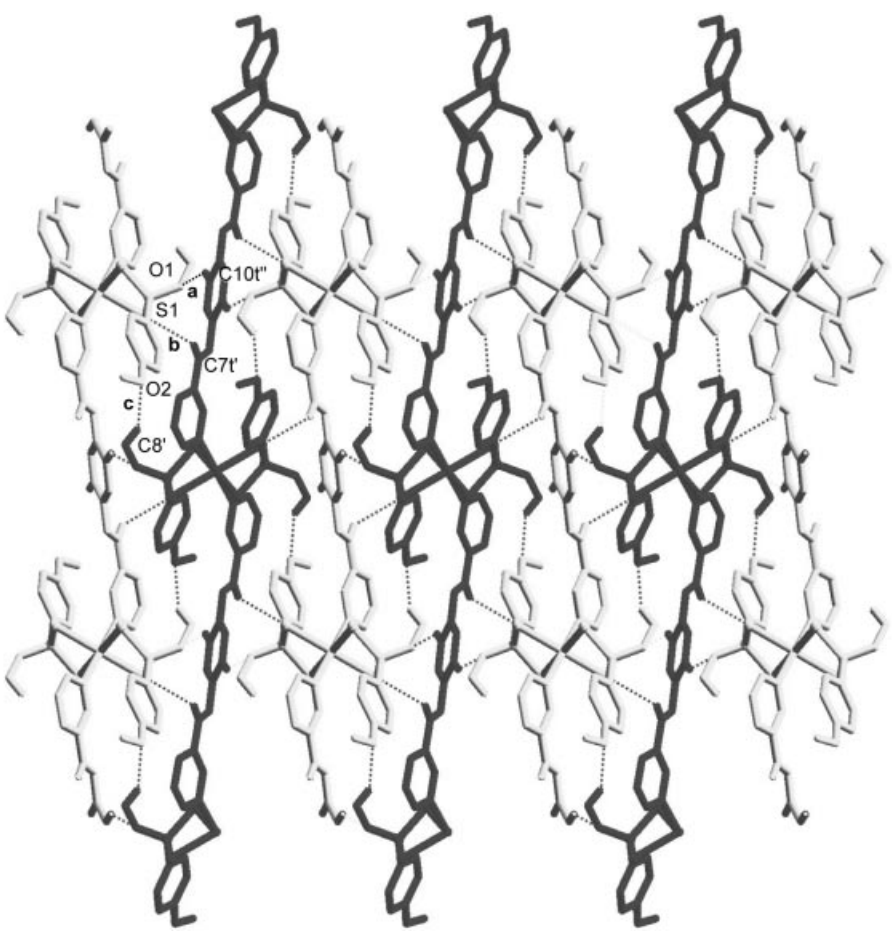

Figure 3. 2D view (*bc* plane) of **3** showing the complementary arrangement of the two sets of grids (dark and light) formed by H bonding of the chains. Hydrogen interactions: **a** O1···C10t′′ 3.42, H···O 2.61 Å; **b** S1···C7t′ 3.80, H···S 2.99 Å; **c** O2···C8′ 3.17, H···O 2.35 Å; ′: −x − 1/2, y − 1/2, −z − 1/2; ′′: x + 1/2, −y + 3/2, z + 1/2; hydrogen atoms except those involved in the described interactions have been omitted for clarity.

 © 2004 Wiley-VCH Verlag GmbH & Co. KGaA, Weinheim

phosphorus atoms, which play an important role in the packing of the molecules. Further systematic work is now in progress in our laboratories with the aim of studying the effects of the structural features of building blocks on the resulting supramolecular structures.

Experimental Section

Materials and Methods: Solvents and reagents were Aldrich products and used as purchased. The degree of purity of each compound was checked by CHNS and TLC analyses. Elemental analyses were performed with an EA1108 CHNS-O Fisons instrument. Infrared spectra were recorded on a Bruker IFS55 spectrometer at room temperature using a flow of dried air. Far-IR (500−50 cm^{-1}) spectra (resolution 2 cm^{-1}) were recorded as polythene pellets with a Mylar beam splitter and polythene windows. Middle-IR spectra (resolution 2 cm^{-1}) were recorded as KBr pellets, with a KBr beam splitter and KBr windows. FT-Raman spectra were recorded on the solid sample, dispersed in a KBr matrix (resolution of 2 cm^{-1}) on a Bruker RFS100 FT-Raman spectrometer, fitted with an In-Ga-As detector (room temperature) operating with a Nd-YAG laser (excitation wavelength 1064 nm) with an 180° scattering geometry, at an excitation power of 350 mW.

Syntheses: *N*,*N*′-Bis-(3-pyridinylmethylene)benzene-1,4-diamine (bdpy) was synthesised by an adaptation of literature procedures.[16] Compounds **1** and **2** were prepared as previously reported.[12]

$[Ni(MeOdtp)_2(bdpy)]_\infty$ (3): 1 (26.4 mg, 0.05 mmol) and bdpy (14.6 mg, 0.05 mmol) were reacted at 100 °C in a high-pressure Aldrich tube in 40 mL of a MeOH/$CHCl_3$ (1:1 v/v) mixture. After the reagents had completely dissolved, the reaction mixture was slowly cooled to room temperature. **3** (20.6 mg, 0.025 mmol, 50 % yield) was obtained as bright green crystals; m.p. 190 °C (decomp.). $C_{34}H_{34}N_4O_4P_2S_4Ni$ (811.55): calcd. C 50.3, H 4.2, N 6.9, S 15.8; found C 50.3, H 4.2, N 7.0, S 15.6. FT-IR: 1700 w, 1653 mw, 1625 ms, 1593 vs, 1541 mw, 1498 s, 1456 ms, 1365 mw, 1319 mw, 1305 m, 1295 ms, 1255 vs, 1182 s, 1112 vs, 1006 vs, 893 ms, 835 s, 800 s, 777 vs, 694 s, 659 vs, 645 s, 623 s, 546 vs, 525 m, 438 m, 418 mw, 383 m, 353 w, 326 w, 302 w, 280 mw, 267 w, 247 w, 227 mw, 203 w, 172 mw, 151 m, 140 mw, 121 mw, 101 m, 91 w cm^{-1}. FT-Raman (solid state, relative intensities in parentheses related to the highest peak taken equal to 10.0): 3054 (0.4), 1630 (2.6), 1582 (10.0), 1429 (0.6), 1320 (0.2), 1193 (2.1), 1157 (3.4), 1111 (0.7), 1034 (1.0), 984 (0.5), 892 (0.2), 824 (0.2), 664 (0.2), 545 (0.9), 399 (0.3), 265 (0.7), 136 (2.1), 89 (2.8) cm^{-1}.

$[Ni(EtOdtp)_2(bipy)]_\infty$ (4): 2 (10.2 mg, 0.018 mmol) and bipy (4.8 mg, 0.03 mmol) were reacted at 100 °C in a high-pressure Aldrich tube in 35 mL of an EtOH/$CHCl_3$ (1:1 v/v) mixture. After the reagents had completely dissolved, the reaction mixture was slowly cooled to room temperature. The product was obtained quantitatively as tiny yellow-green needles. M.p.: 230 °C (decomp.). $C_{28}H_{32}N_2O_4P_2S_4Ni$ (709.45): calcd. C 47.4, H 4.5, N 3.9, S 18.1; found C 47.4, H 4.2, N 4.0, S 17.4. FT-IR : 1598 vs, 1568 m, 1531 mw, 1500 s, 1484 m, 1455 m, 1440 m, 1403 ms, 1389 mw, 1297 s, 1259 vs, 1216 m, 1178 ms, 1114 vs, 1064 m, 1029 vs, 949 vs, 830 m, 810 ms, 784 s, 728 mw, 660 ms, 646 s, 628 ms, 545 s, 521 mw, 500 w, 475 w, 438 m, 383 m, 353 w, 326 w, 302 w, 279 mw, 254 w, 247 w, 227 mw, 203 w, 176 w, 151 m, 140 mw, 121 mw, 101 m, 91 w cm^{-1}. FT-Raman (solid state, relative intensities in parentheses related to the highest peak taken equal to 10.0): 3066 (1.2), 3045 (1.5), 2941 (1.6), 2924 (1.6), 1604 (8.7), 1284 (10.0), 1113 (5.7), 1062 (3.1), 1018 (8.1), 659 (1.7), 633 (1.1), 545 (5.8), 379 (0.9), 359 (1.5), 101 (9.3), 68 (6.7) cm^{-1}.

X-ray Crystal Structure Determination: Data collection for **3** was performed on a Bruker SMART APEX CCD area detector diffractometer with graphite-monochromated Mo-K_α radiation (λ = 0.71073 Å), equipped with an Oxford Cryosystems open-flow cryostat.[17] Data collection for **4** was performed on a Siemens SMART CCD diffractometer with a monochromated synchrotron radiation (λ = 0.68710 Å, ω rotation with narrow frames) using a silicon 111 monochromator, at 120(2) K. SADABS corrections were applied for **3**, while no absorption corrections were applied for **4**. The structures were solved by direct methods using SHELXS-97[18] and all non-hydrogen atoms were located using subsequent difference Fourier methods.[19] Hydrogen atoms were placed in calculated positions and thereafter allowed to ride on their parent atoms, except for the methyl groups for **4**, which were located by difference Fourier methods and treated as rigid rotors. All crystal structure diagrams were prepared using the OLEX program.[20]

Compound 3: $C_{34}H_{34}N_4NiO_4P_2S_4$, monoclinic, space group $P2_1/n$, a = 10.016(2) Å, b = 16.724(3) Å, c = 11.412(2) Å, β = 103.902(4)°, V = 1855.6(11) $Å^3$, Z = 2, $D_{calcd.}$ = 1.452 Mg/m^3. R = 0.0465, wR = 0.0908 for 2670 observed independent data.

Compound 4: $C_{28}H_{32}N_2NiO_4P_2S_4$, triclinic, space group $P\bar{1}$, a = 8.13(3) Å, b = 9.910(3) Å, c = 10.126(3) Å, α = 89.479(7), β = 76.330(5), γ = 77.675(6)°, V = 773.0(4) $Å^3$, Z = 1, $D_{calcd.}$ = 1.524 Mg/m^3. R = 0.0397, wR = 0.0884 for 2981 observed independent data.

CCDC-227421 for **3** and CCDC-227422 for **4** contain the supplementary crystallographic data for this paper. These data can be obtained free of charge at www.ccdc.cam.ac.uk/conts/retrieving.html [or from the Cambridge Crystallographic Data Centre, 12 Union Road, Cambridge CB2 1EZ, UK; Fax: (internat.) +44-1223/336-033; E-mail: deposit@ccdc.cam.ac.uk].

Acknowledgments

We would like to thank the EPSRC and RFBR 03−03−32401 for funding and for provision of X-ray diffractometers.

[1] G. R. Desiraju, *Chem. Commun.* **1997**, 1475−1482.
[2] B. Moulton, M. J. Zaworotko, *Curr. Opin. Solid State Mater. Sci.* **2002**, *6*, 117−123.
[3] C. Chen, K. S. Suslick, *Coord. Chem. Rev.* **1993**, *128*, 293−316.
[4] O. Kahn, *Magnetism: A Supramolecular Function*; Kluwer Academic Publishers, Dordrecht, The Netherlands, **1996**; P. S. Mukherjee, S. Konar, E. Zangrando, T. Mallah, J. Ribas, N. R. Chaudhuri, *Inorg. Chem.* **2003**, *42*, 2695−2703; T. Ishida, T. Kawakami, S. Mitsubori, T. Nogami, K. Yamaguchi, H. Iwamura, *J. Chem. Soc., Dalton Trans.* **2002**, 3177−3186; J. Koo, D. Kim, Y.-S. Kim, Y. Do, *Inorg. Chem.* **2003**, *42*, 2983−2987.
[5] C. Janiak, *Dalton Trans.* **2003**, 2781−2804.
[6] M. P. Froster, A. K. Cheetham, *Angew. Chem. Int. Ed.* **2002**, *41*, 457−459; A. N. Khlobystov, A. J. Blake, N. R. Champness, D. A. Lemenovskii, A. G. Majouga, N. V. Zyk, M. Schröder, *Coord. Chem. Rev.* **2001**, *222*, 155−192; L. Carlucci, G. Ciani, D. M. Proserpio, S. Rizzato, *Chem. Commun.* **2001**, 1198−1199; O. V. Dolomanov, A. J. Blake, N. R. Champness, M. Schröder, C. Wilson, *Chem. Commun.* **2003**, 682−683; L. Carlucci, G. Ciani, D. M. Proserpio, S. Rizzato, *J. Chem. Soc., Dalton Trans.* **2000**, 3821−3828; R. Robson, *J. Chem. Soc., Dalton Trans.* **2000**, 3735−3744.
[7] S. A. Bourne, J. Lu, B. Moulton, M. J. Zaworotko, *Chem. Commun.* **2001**, 861−862; T. L. Henningar, D. C. Macquarrie, P.

 © 2004 Wiley-VCH Verlag GmbH & Co. KGaA, Weinheim

Losier, R. D. Rogers, M. J. Zaworotko, *Angew. Chem. Int. Ed. Engl.* **1997**, *36*, 972−973; S. R. Batten, R. Robson, *Angew. Chem. Int. Ed.* **1998**, *37*, 1460−1494.

[8] M. Fujita, *Chem. Soc. Rev.* **1998**, *27*, 417−425; B. Olenyuk, A. Fechtenkötter, P. J. Stang, *J. Chem. Soc., Dalton Trans.* **1998**, 1707−1728; D. K. Chand, M. Fujita, K. Biradha, S. Sakamoto, K. Yamaguchi, *Dalton Trans.* **2003**, 2750−2756; S. Leininger, B. Olenyuk, P. J. Stang, *Chem. Rev.* **2000**, *100*, 853−907.

[9] M. O'Keeffe, M. Eddaoudi, H. Li, T. Reineke, O. M. Yaghi, *J. Solid State Chem.* **2000**, *152*, 3−20.

[10] B. Rather, M. J. Zaworotko, *Chem. Commun.* **2003**, 830−831; B. Moulton, H. Abourahma, M. W. Bradner, J. Lu, G. J. McManus, M. J. Zaworotko, *Chem. Commun.* **2003**, 1342−1343; N. L. Rosi, M. Eddaoudi, J. Kim, M. O'Keeffe, O. M. Yaghi, *Cryst Eng Comm.* **2002**, *4*, 401−404; F. A. Cotton, C. Lin, C. A. Murillo, *J. Chem. Soc., Dalton Trans.* **2001**, 499−501; F. A. Cotton, C. Lin, C. A. Murillo, *Chem. Commun.* **2001**, 11−12; M. E. Braun, C. D. Steffek, J. Kim, P. G. Rasmussen, O. M. Yaghi, *Chem. Commun.* **2001**, 2532−2533. W. Mori, S. Takamizawa, *J. Solid State Chem.* **2000**, *152*, 120−129.

[11] To the best of our knowledge, the only comparable compound, which was structurally characterized, is the polymer complex of the nickel xanthate with 4,4′-bipyridine, isolated in two different conformations: R. W. Gable, B. F. Hoskins, G. Winter, *Inorg. Chim. Acta* **1985**, *96*, 151−159; R.-G. Xiong, Z. Yu, C.-M. Liu, X.-Z. You, *Polyhedron* **1997**, *16*, 2667−2671.

[12] M. C. Aragoni, M. Arca, F. Demartin, F. A. Devillanova, C. Graiff, F. Isaia, V. Lippolis, A. Tiripicchio, G. Verani, *Eur. J. Inorg. Chem.* **2000**, 2239−2244, and refs. therein; M. C. Aragoni, M. Arca, F. A. Devillanova, J. Ferraro, V. Lippolis, G. Verani, *Can. J. Chem.* **2001**, *79*, 1483−1491; V. G. Albano, M. C. Aragoni, M. Arca, C. Castellari, F. Demartin, F. A. Devillanova, F. Isaia, V. Lippolis, L. Loddo, G. Verani, *Chem. Commun.* **2002**, *11*, 1170−1171.

[13] M. C. Aragoni, M. Arca, F. Demartin, F. A. Devillanova, C. Graiff, F. Isaia, V. Lippolis, A. Tiripicchio, G. Verani, *J. Chem. Soc., Dalton Trans.* **2001**, 2671−2677, and refs. therein.

[14] Formation equilibrium constants of the adducts between [Ni(-ROdtp)$_2$] and py: log β_{eq} = 3.20; *o*-NH_2py: log β_{eq} = 1.88; *m*-NH_2py: log β_{eq} = 3.46; *p*-NH_2py: log β_{eq} = 4.71, determined by means of spectrophotometric measurements [ref. 13].

[15] H. Borrmann, I. Persson, M. Sandström, C. M. V. Stålhandske, *J. Chem. Soc., Perkin Trans. 2* **2000**, 393−402.

[16] D. Grasso, G. Buemi, S. Fasone, C. Gandolfo, *Croat. Chem. Acta* **1981**, *54*, 85−90.

[17] J. Cosier, A. M. Glazer, *J. Appl. Crystallogr.* **1986**, *19*, 105.

[18] G. M. Sheldrick, SHELXS-97, University of Göttingen, Germany, **1997**.

[19] G. M. Sheldrick, SHELXL-97, University of Göttingen, Germany, **1997**.

[20] O. V. Dolomanov, A. J. Blake, N. R. Champness, M. Schröder, *J. Appl. Cryst.* **2003**, *36*, 1283−1284.

Received February 3, 2004

 © 2004 Wiley-VCH Verlag GmbH & Co. KGaA, Weinheim

Direct Synthesis of Tricarbonyl(cyclopentadienyl)rhenium and Tricarbonyl(cyclopentadienyl)technetium Units from Ferrocenyl Moieties − Preparation of 17α-Ethynylestradiol Derivatives Bearing a Tricarbonyl(cyclopentadienyl)technetium Group

Stéphane Masi,[a] Siden Top,*[a] Leila Boubekeur,[a] Gérard Jaouen,*[a] Stefan Mundwiler,[b] Bernhard Spingler,[b] and Roger Alberto*[b]

Keywords: Technetium / Rhenium / Estradiol / Radiopharmaceuticals / Bioorganometallics

The preparation of new tricarbonyl(cyclopentadienyl)rhenium and tricarbonyl(cyclopentadienyl)technetium derivatives is described. The approach used was applied to a cold target model, 17α-ethynylestradiol substituted at the 17α position by a ketotricarbonyl(cyclopentadienyl)rhenium group. The novel organometallic reaction applied here, when extended to potential radiopharmaceuticals, consists of a cyclopentadienyl-ligand transfer between ketoferrocenes and *fac*-$[^{99m}Tc(H_2O)_3(CO)_3]^+$ in a water/DMSO 1:1 mixture. This reaction lead to the synthesis of a new estradiol derivative, labeled with ^{99m}Tc. The synthesis of another product was performed by using $[^{99}TcCl_3(CO)_3]^{2-}$ as the Tc precursor and its X-ray crystal structure was determined. In each case high yields were obtained.
(© Wiley-VCH Verlag GmbH & Co. KGaA, 69451 Weinheim, Germany, 2004)

Introduction

The synthesis of new radiolabeled estrogen derivatives has generated much interest during the last decade.[1] The design of new molecules labeled with technetium, ^{99m}Tc, or rhenium, ^{188}Re, for imaging and therapy of breast tumors, respectively, is of current interest since most of the compounds prepared have not yet shown enough affinity or selectivity towards estrogen receptors (ER) and, in addition, their synthesis is rather circuitous. Many different systems have been envisaged for the labeling of ligands with technetium or rhenium. One general approach is the coordination of a Tc^V moiety through chelation with heteroatom systems, but the molecules obtained are not always stable in solution.[1,2] Therefore, we have elaborated an organometallic approach, in which a low-oxidation-state-rhenium core is tethered to a cyclopentadienyl (Cp) ligand.[3] The organometallic tether using this ligand seems to be particularly attractive. This group has the advantage of being lipophilic, fairly small in size and very robust. Furthermore, this approach can be easily extended to the preparation of tricarbonyl(cyclopentadienyl)technetium compounds because Re and Tc complexes exhibit very similar chemical behavior.

The search for an easy route to $CpM(CO)_3$ complexes (where M = Re, Tc) bearing a functional substituent on the Cp ring, with the purpose of being compatible with the handling of radioactive compounds, has attracted much interest.[4] Wenzel reported a unique double ligand-transfer reaction where the technetium source is $[^{99m}TcO_4]^-$.[5] More recently, Alberto et al. reported the preparation of different $[(R\text{-}Cp)^{99m}Tc(CO)_3]$ molecules (R = ketone), where the *fac*-$[^{99m}Tc(H_2O)_3(CO)_3]^+$ compound, generated in physiological media, is the ^{99m}Tc precursor.[6] With regard to rhenium, Top et al. reported various syntheses of $[(R'\text{-}Cp)Re(CO)_3]$ molecules (R′ = organic fragment) based on the use of $[Re(CO)_6][BF_4]$ with particular monosubstituted ferrocene compounds in DMSO. This method is compatible with aqueous media as we obtained promising results in a water/DMSO 1:1 mixture.[7]

The first step in the transformation of $[Re(CO)_6][BF_4]$ in DMSO seems to be the departure of three carbonyl ligands from the $[Re(CO)_6]^+$ cation. Thus, we postulated the formation of the *fac*-$[Re(DMSO)_3(CO)_3]^+$intermediate. It is believed that *fac*-$[Re(DMSO)_3(CO)_3]^+$ may react with the cyclopentadienyl ligands the same way that *fac*-$[^{99m}Tc(H_2O)_3(CO)_3]^+$ does.[6,7] Combining these aspects, we decided to extend our work with ferrocene derivatives and the $[Re(CO)_6]^+$ cation to the preparation of [(R-

[a] Laboratoire de Chimie et Biochimie des Complexes Moléculaires, Ecole Nationale Supérieure de Chimie de Paris, UMR C.N.R.S. 7576,
11, rue Pierre et Marie Curie, 75231 Paris Cédex 05, France
Fax: (internat.) +33-1-43-26-00-61
E-mail: Jaouen@ext.jussieu.fr
[b] Institute of Inorganic Chemistry, University of Zürich
Winterthurerstrasse 190, 8057 Zürich, Switzerland
Fax: (internat.) +41-1-635-68-03
E-mail: ariel@aci.unizh.ch
Supporting information for this article is available on the WWW under http://www.eurjic.org or from the author.

Cp)^{99m}Tc(CO)$_3$] from the same ferrocene derivatives and using *fac*-[^{99m}Tc(H$_2$O)$_3$(CO)$_3$]$^+$ as the reagent.

Results and Discussion

The ketoferrocene **1** was first used as a model for the reaction between [Re(CO)$_6$][BF$_4$] and *fac*-[^{99m}Tc(H$_2$O)$_3$(CO)$_3$]$^+$. It was prepared from ferrocene and *p*-anisoyl chloride following the procedure described in the literature.[8] The reaction with [Re(CO)$_6$]$^+$ was carried out by heating the DMSO solution of **1** and [Re(CO)$_6$]$^+$ at 160 °C for 30 min and **2** was obtained in 65 % yield (see Scheme 1).

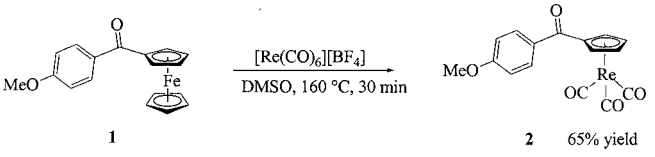

Scheme 1. Ligand-transfer reaction between ketoferrocene **1** and the hexacarbonylrhenium cation

In the hormone series, the ferrocenyl-β-estradiol derivative, **3**, was prepared. The amidoferrocene **4**, prepared according to the Weinreb method,[9] was reacted with the lithium compound generated from 17α-ethynylestradiol, diprotected with methylmethoxy (MOM) to produce **3** (see Scheme 2). Heating **3** with [Re(CO)$_6$][BF$_4$] in DMSO for one hour affords the rhenium compound **5** in 41 % yield.

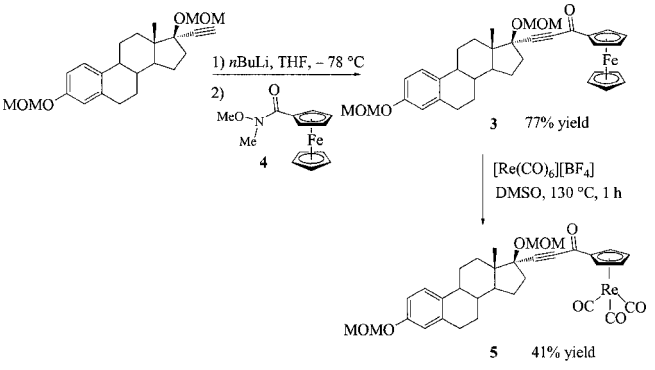

Scheme 2. Synthesis of tricarbonyl(cyclopentadienyl)rhenium derivative **5**

The removal of the methoxymethyl groups was achieved by using BCl$_3$ in dichloromethane (see Scheme 3). The rhenium compound **6** and the ferrocenyl derivative **7** were obtained in good yields. Compound **6** had already been prepared by another method.[10] Heating the unprotected ferrocenyl steroid **7** with [Re(CO)$_6$][BF$_4$] also gives the rhenium complex **6** but in low yield (12 %) (see Scheme 4).

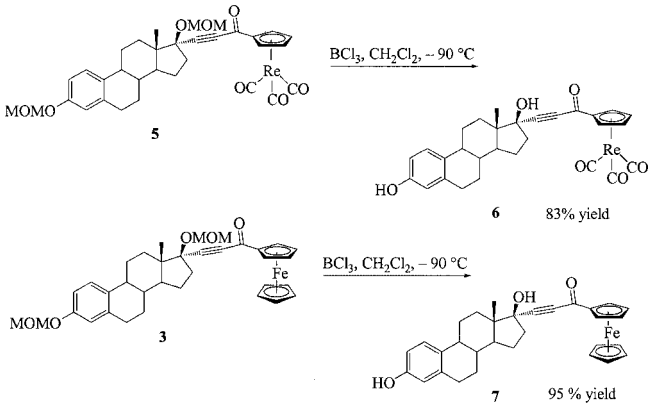

Scheme 3. Deprotection of the ethynyl estradiol derivatives

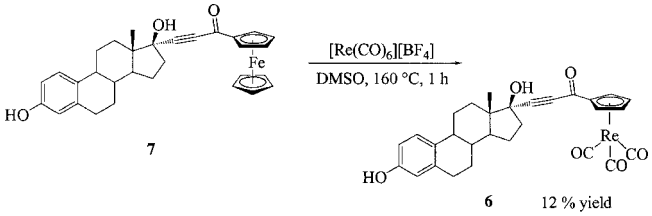

Scheme 4. Ligand-transfer reaction between **7** and the rhenium-hexacarbonyl cation

Since the chemistry of Re is similar to that of Tc, the above reaction between [Re(CO)$_6$]$^+$ and the ferrocenyl derivative may be adapted to Tc analogs. Recently, Alberto et al. have found a very convenient synthetic method for [^{99m}Tc(H$_2$O)$_3$(CO)$_3$]$^+$ starting from ^{99m}TcO$_4^-$.[11] Therefore, it would be interesting to use the reagent [^{99m}Tc(H$_2$O)$_3$(CO)$_3$]$^+$ in the exchange reaction. According to the procedure already described for the reaction of *fac*-[^{99m}Tc(H$_2$O)$_3$(CO)$_3$]$^+$ with NaCp derivatives,[6] an aliquot of 0.5 mL of an aqueous solution containing [^{99m}Tc(H$_2$O)$_3$(CO)$_3$]$^+$ (nM–μM range) was mixed with 0.5 mL of a DMSO solution, where an excess of **1** had been previously dissolved (1.5–2 μmol). The mixture was heated at 95 °C and the reaction was monitored by HPLC (high-pressure liquid chromatography) equipped with a γ radiodetector. The expected complex, **8a**, was formed in > 80 % radiochemical yield after heating for 4 h (see Scheme 5). The presence of **8a** (^{99m}Tc) was confirmed by comparing its HPLC chromatogram, measured by γ-detection, with the HPLC chromatogram of the analogous cold compound, **2** (Re). Due to the very low concentration of the ^{99m}Tc species, characterization is only possible by chromatographic comparison.

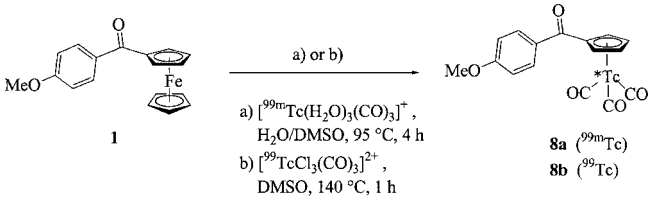

Scheme 5. Synthesis of a cyclopentadienyltechnetium derivative from the corresponding ferrocene precursor

 © 2004 Wiley-VCH Verlag GmbH & Co. KGaA, Weinheim

After the successful formation of **8a** from *fac*-$[^{99m}Tc(H_2O)_3(CO)_3]^+$, we attempted to synthesize **8** on a larger scale, in order to identify it with more accuracy. Starting from $[^{99}TcCl_3(CO)_3]^{2-}$, larger quantities of complex **8** can be produced and handled because the long half-life of ^{99}Tc results in weak radiation of this isotope. Thus, **1** was treated in 0.5 mL of DMSO at 140 °C with $[^{99}TcCl_3(CO)_3][Et_4N]_2$. Within 1 h, **8b** had formed in about 74 % yield and was crystallized from a diethyl ether/hexane 2:1 solution. The reaction was monitored with HPLC equipped with a β radiodetector. The retention time of the isolated **8b** (^{99}Tc) is very close to that of **8a** (^{99m}Tc) (24.3 min for **8b** and 24.4 min for **8a**, respectively), thus proving the identity of **8a**. The structure of **8b** was elucidated by an X-ray study. An ORTEP representation of this complex is given in Figure 1.

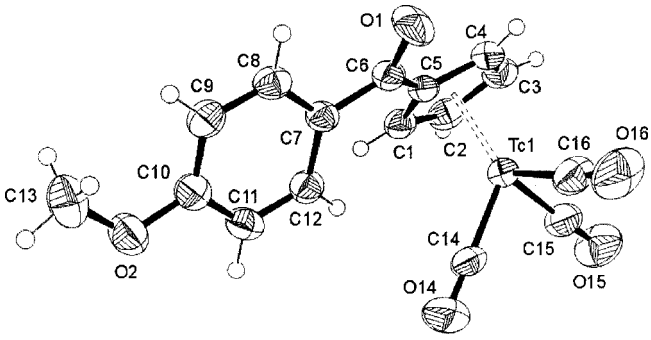

Figure 1. Ortep plot of **8b**, ellipsoids drawn with 50 % probability

We next applied the reaction between ketoferrocene compounds and the reagent *fac*-$[^{99m}Tc(H_2O)_3(CO)_3]^+$ to steroid **7** and obtained molecule **9** with excellent yields. Thus, using the conditions described above with **1** and heating for 3 h 30 min, allowed us to form **9** in quantitative yield (> 90%) (see Scheme 6). It is remarkable that such a mild and efficient reaction has never been reported for the synthesis of molecules belonging to the class of ethynylestradiol. Additionally, it is noteworthy that our approach for the labeling of ^{99m}Tc on (bio)organic molecules constitutes a real improvement, with regard to the transformations of ferrocene derivatives into corresponding tricarbonyl(cyclopentadienyl)technetium derivatives, described in the literature.[5,12]

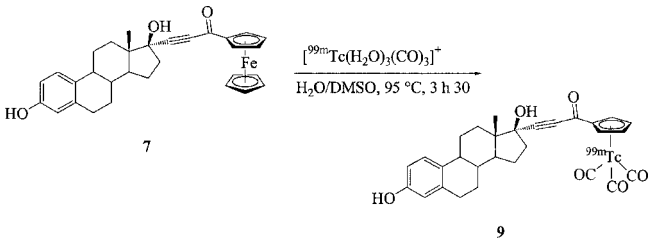

Scheme 6. Synthesis of a novel 17α-ethynyl estradiol derivative labeled with ^{99m}Tc, in a water/DMSO 1:1 mixture at atmospheric pressure

Conclusion

In summary, we have presented the synthesis of new complexes bearing tricarbonyl(cyclopentadienyl)rhenium or tricarbonyl(cyclopentadienyl)technetium functionalities, where the target molecules belong to the estradiol series. In addition, the first synthesis of tricarbonyl(cyclopentadienyl)-technetium derivatives from the organometallic aqua complex *fac*-$[^{99m}Tc(H_2O)_3(CO)_3]^+$ and ferrocene-containing compounds has been successfully investigated. Thanks to this convenient method, the efficient radiochemical synthesis of a novel 17α-ethynylestradiol derivative can be achieved in aqueous media under mild conditions, without protecting the estradiol substituents. On the basis of these encouraging results, the reaction should be useful in the development of a wide variety of radiolabeled compounds in aqueous media.

Experimental Section

DMSO was used without any purification. TLC chromatography was performed on silica gel 60-GF254. Infrared spectra were recorded on an IR-FT BOMEM Michelson-100 spectrometer. ^1H- and ^{13}C NMR spectra were recorded on 200 MHz and 400 MHz Bruker spectrometers. Mass spectrometry was performed with a Nermag R 10−10C spectrometer. Melting points were measured with a Kofler device. Elemental analyses were performed by the regional microanalysis department of Université Pierre et Marie Curie.

1: $AlCl_3$ (0.477 g, 3.49 mmol) was added to a 5 mL dichloromethane solution of ferrocene (0.5 g, 2.69 mmol). *p*-Anisoyl chloride (0.305 g, 1.79 mmol) was then added dropwise and the resulting solution was stirred for 4 h at room temperature. The mixture was hydrolyzed with water (40 mL) and the aqueous solution was extracted with diethyl ether (3 × 80 mL). All the organic fractions were combined, dried over magnesium sulfate, filtered and the solvents evaporated. The compound was purified by a silica-gel plate (dichloromethane) to give **1** (0.18 g, 31% yield); m.p. 74−76 °C. ^1H NMR (200 MHz, $CDCl_3$): δ = 3.82 (s, 3 H, -OCH_3), 4.13 (s, 5 H, Cp), 4.49 (s, 2 H, 2,5-H of C_5H_4), 4.83 (s, 2 H, 3,4-H of C_5H_4), 6.89 (d, *J* = 8.0 Hz, 2 H, Ar), 7.88 (d, *J* = 8.0 Hz, 2 H, Ar) ppm. ^{13}C NMR (50 MHz, $CDCl_3$): δ = 55.4 (-OCH_3), 70.1 (C_{Cp}), 71.4 (C_{Cp}), 72.1 (C_{Cp}), 113.4 (C_{Ar}), 130.4 (C_{Ar}), 162.4 (C_{Ar}), 197.3 (CO) ppm. IR (CH_2Cl_2): $\tilde{\nu}$ = 1635 (ν_{CO}) cm^{-1}. MS (EI): *m*/*z* = 56 $[Fe]^+$, 77, 92, 121, 135 $[M - Fc]^+$, 171, 277, 320 $[M]^+$.

2: $[Re(CO)_6][BF_4]$ (0.073 g, 0.166 mmol) was dissolved in DMSO (1 mL) in a 5 mL round-bottomed flask equipped with a magnetic stirring bar. Compound **1** (0.166 g, 0.518 mmol) was added and the solution was heated for 30 min at 160 °C. The mixture was allowed to warm to room temperature and then water (10 mL) was added. The product was extracted with dichloromethane (2 × 50 mL). The organic phase was washed, dried ($MgSO_4$), filtered and concentrated. The mixture was purified by chromatography on a silica-gel plate (ethyl acetate/petroleum ether 1:7) to give **2** (0.051 g, 65 % yield); m.p. 186 °C. ^1H NMR (200 MHz, $CDCl_3$): δ = 3.88 (s, 3 H, -OCH_3), 5.45 (t, *J* = 2.2 Hz, 2 H, 3,4-H of C_5H_4), 6.05 (t, *J* = 2.2 Hz, 2 H, 2,5-H of C_5H_4), 6.95 (d, *J* = 8.0 Hz, 2 H, Ar), 7.83 (d, *J* = 8.0 Hz, 2 H, Ar) ppm. ^{13}C NMR (50 MHz, $CDCl_3$): δ = 55.4 (-OCH_3), 85.1 (2 C_{Cp}), 89.4 (2 C_{Cp}), 113.8 (2 C_{Ar}), 130.8 (2

 © 2004 Wiley-VCH Verlag GmbH & Co. KGaA, Weinheim

C_{Ar}) ppm. IR (CH_2Cl_2): $\tilde{\nu}$ = 2030 s, 1938 s, 1652 w (ν_{CO}) cm^{-1}. MS (EI): *m/z* = 386 [M − 3 CO]$^+$, 412, 442 [M − CO]$^+$, 469 [M]$^+$. $C_{16}H_{11}O_5Re$ (469.46): calcd. C 40.93, H 2.36; found C 40.97, H 2.29.

4: The synthesis of **4** was performed using the procedure for the preparation of *N*-methoxy-*N*-methylamides (see reference [9]). Oxalyl chloride (7.250 g, 57 mmol) was added to ferrocenecarboxylic acid (0.550 g, 2.39 mmol) placed in a Schlenk tube and cooled in an ice bath. The mixture was stirred for 3 h, then the excess oxalyl chloride was removed under vacuum. Chloroform (20 mL) was added, followed by addition of *N*,*O*-dimethylhydroxyamine hydrochloride (0.260 g, 2.63 mmol). Anhydrous pyridine (0.420 g, 5.26 mmol) was added dropwise to the mixture, cooled in an ice bath. The mixture was stirred for 2 h 30 min to allow the temperature to rise to room temperature. Then, dichloromethane (200 mL) was added and the solution obtained was washed with a saturated K_2CO_3 solution, dried over magnesium sulfate, filtered and the solvents were evaporated. The compound obtained was crystallized in pentane to give **4** (0.524 g, 83 % yield); m.p. 28 °C. ^{1}H NMR (200 MHz, $CDCl_3$): δ = 3.31 (s, 3 H, -NCH_3), 3.74 (s, 3 H, -$NOCH_3$), 4.22 (s, 5 H, Cp), 4.39 (t, *J* = 1.8 Hz, 2 H, 3,4-H of C_5H_4), 4.91 (t, *J* = 1.8 Hz, 2 H, 2,5-H of C_5H_4) ppm. ^{13}C NMR (50 MHz, $CDCl_3$): δ = 33.4 (-NCH_3), 61.0 (-$NOCH_3$), 69.5 (C_{Cp}), 70.6 (C_{Cp}), 71.0 (C_{Cp}), 73.0 (C_{Cp}), 171.0 (CO) ppm. IR (CH_2Cl_2): $\tilde{\nu}$ = 1616 s (ν_{CO}) cm^{-1}. MS (EI): *m/z* = 56 [Fe]$^+$, 65 [Cp]$^+$, 121 [FeCp]$^+$, 129, 185 [Fc]$^+$, 213 [FcCO]$^+$, 273 [M]$^{+\cdot}$. $C_{13}H_{15}FeNO_2$ (273.05): calcd. C 57.17, H 5.54, N 5.13; found C 57.02, H 5.73, N 5.15.

3: In a Schlenk tube, 17α-ethynylestradiol diprotected with a methoxymethyl group (0.665 g, 1.73 mmol) was dissolved in THF (6 mL) and cooled to −78 °C. *n*BuLi (0.8 mL, 2.05 mmol, 2.5 M solution in hexane) was added dropwise and the mixture was stirred for 1 h. By that time the temperature had risen to −50 °C. Then, a solution of **4** (0.429 g, 1.57 mmol) in THF (4 mL) was added dropwise. After 15 min of stirring, the ice bath was removed and the stirring was maintained for two more hours . Then, dichloromethane (200 mL) was added and the solution obtained was washed with water, dried over magnesium sulfate, filtered and the solvents were evaporated. The crude product was purified by chromatography on a silica-gel plate (diethyl ether/petroleum ether 1:1) to give **3** (77 %); m.p. 102 °C. ^{1}H NMR (200 MHz, $CDCl_3$): δ = 0.99 (s, 3 H, CH_3-18), 2.88 (m, 2 H, H-6), 3.47 (s, 3 H, -OCH_3), 3.48 (s, 3 H, -OCH_3), 4.28 (s, 5 H, Cp), 4.61 (t, *J* = 2 Hz, 2 H, 3,4-H of C_5H_4), 4.90 (d, *J* = 6.6 Hz, 1 H, -OCH_2O-17), 4.94 (t, *J* = 2 Hz, 2 H, 3,4-H of C_5H_4), 5.13 (d, *J* = 6.6 Hz, 1 H, -OCH_2O-17), 5.16 (s, 2 H, -OCH_2O-3), 6.79 (d, *J* = 2.6 Hz, 1 H, H-4), 6.84 (dd, *J* = 8.4, 2.6 Hz, 1 H, 2-H), 7.24 (d, *J* = 8.4 Hz, 1 H, 1-H) ppm. ^{13}C NMR (50 MHz, $CDCl_3$): δ = 13.0 (C-18), 29.6 (C-6), 23.1, 26.3, 27.3, 33.5 and 37.3 (C-7, C-11, C-12, C-15 and C-16), 39.1, 43.7, 49.3 (C-8, C-9 and C-14), 48.5 (C-13), 55.8 and 56.0 (2 MeO-3), 70.3 and 73.3 (C_{Cp}), 85.4 and 87.4 (C_{Cp} and C-17), 91.0, 93.9 and 94.4 (C-19, C-20, and -OCH_2O-), 113.7 (C-2), 116.2 (C-4), 126.3 (C-1), 133.5 (C-10), 137.9 (C-5), 155.1 (C-3) ppm. IR (CH_2Cl_2): $\tilde{\nu}$ = 2207 w ($\nu_{C\equiv C}$), 1623 s (ν_{CO}) cm^{-1}. MS (EI): *m/z* = 45 [CH_2OCH_3]$^+$, 596 [M]$^{+\cdot}$. MS (IC, DCI/NH_3): *m/z* = 597 [M + H]$^+$. $C_{35}H_{40}FeO_5$ (596.22): calcd. C 70.47, H 6.76; found C 70.17, H 7.17.

5: [$Re(CO)_6$][BF_4] (0.540 g, 1.22 mmol) was dissolved in DMSO (1 mL) in a 5 mL round-bottomed flask equipped with a magnetic stirring bar. Compound **3** (0.640 g, 1.07 mmol) was added and the solution was heated for 1 h at 130 °C. The mixture was allowed to warm to room temperature and then water (10 mL) was added. The product was extracted with dichloromethane (2 × 150 mL). The organic phase was washed, dried ($MgSO_4$), filtered and concentrated. The mixture was purified by chromatography on a silica-gel plate (ethyl acetate/petroleum ether 1:5) to give **5** (0.331 g, 41 % yield); m.p. 119 °C. ^{1}H NMR (400 MHz, $CDCl_3$): δ = 0.94 (s, 3 H, CH_3-18), 2.85 (m, 2 H, H-6), 3.43 (s, 3 H, -OCH_3), 3.47 (s, 3 H, -OCH_3), 4.84 (d, *J* = 7.2 Hz, 1 H, -OCH_2O-17), 4.99 (d, *J* = 7.2 Hz, 1 H, -OCH_2O-17), 5.15 (s, 2 H, -OCH_2O-3), 5.41 (m, 2 H, 3,4-H of C_5H_4), 6.21 (m, 2 H, 2,5-H of C_5H_4), 6.78 (d, 1 H, 4-H), 6.83 (dd, *J* = 8.4 Hz, 1 H, 2-H), 7.20 (d, *J* = 8.4 Hz, 1 H, 1-H) ppm. ^{13}C NMR (100 MHz, $CDCl_3$): δ = 13.2 (C-18), 29.8 (C-6), 23.1, 26.3, 27.2, 33.7 and 37.4 (C-7, C-11, C-12, C-15 and C-16), 39.1, 43.5 and 49.5 (C-8, 9 and C-14), 48.8 (C-13), 56.0 (2 CH_3O), 85.1 and 85.4 (C_{Cp} and C-17), 85.5, 89.2 and 89.3 (C_{Cp}), 94.0 (-OCH_2O-17), 94.5 (-OCH_2O-3), 94.3 and 96.5 (C-19 and C-20), 113.8, 116.3 and 126.5 (C-1, C-2, and C-4), 133.4 (C-10), 138.0 (C-5), 155.1 (C-3), 171.3 (CO, ketone), 191.4 (Re-CO) ppm. IR (CH_2Cl_2): $\tilde{\nu}$ = 2205 w ($\nu_{C\equiv C}$), 2032 s, 1940 vs, 1642 w (ν_{CO}) cm^{-1}. MS (EI): ^{187}Re *m/z* = 45 [CH_2OCH_3]$^+$, 746 [M]$^+$. MS (IC, DCI/NH_3): ^{187}Re *m/z* = 747 [M + H]$^+$, 764 [M + NH_4]$^+$. $C_{33}H_{35}O_8Re$ (746.19): calcd. C 53.14, H 4.73; found C 53.07, H 5.00.

6: The deprotection of **5** was carried out according to a procedure described in the literature.[13] Under an inert atmosphere, **5** (0.070 g, 0.094 mmol) was dissolved in 8 mL of dichloromethane. The solution was cooled to −90 °C and BCl_3 (1 mL, 1 M in CH_2Cl_2) was added dropwise. A rapid evolution of the color from beige to orange was observed. The solution was stirred for 30 min, the temperature of the cooling bath was thus −30 °C. The bath was removed and dichloromethane (150 mL) was poured into the mixture. This organic phase was washed with water (50 mL) and neutralized with 50 mL of K_2CO_3 (10 %). The organic phase was washed, dried ($MgSO_4$), filtered and concentrated. The mixture was purified by silica-gel chromatography (diethyl ether/petroleum ether 2:1) to give **6** (0.051 g, 83% yield); m.p. 156 °C. ^{1}H NMR (200 MHz, $CDCl_3$): δ = 0.95 (s, 3 H, CH_3-18), 2.75 (m, 2 H, 6-H), 5.78 (m, 2 H, 3,4-H of C_5H_4), 6.34 (m, 2 H, 2,5-H of C_5H_4), 6.53 (d, 1 H, 4-H), 6.59 (dd, 1 H, 2-H), 7.09 (d, 1 H, 1-H) ppm. ^{13}C NMR (100 MHz, $CDCl_3$): δ = 12.8 (C-18), 23.1 (C-15), 26.3, 27.1 (C-7 and C-11), 29.6 (C-6), 33.3 (C-16), 39.0 and 39.4 (C-12 and C-8), 43.5 (C-9), 48.1 (C-13), 50.3 (C-14), 80.4 (C-17), 85.5 and 89.4 (4 C_{Cp}), 83.0, 96.3 and 96.6 (1 C_{Cp} and C≡C), 112.8 (C-2), 115.3 (C-4), 126.7 (C-1), 132.3 (C-10), 138.3 (C-5), 153.5 (C-3), 171.4 (CO), 191.5 (Re-CO) ppm. IR (CH_2Cl_2): $\tilde{\nu}$ = 2033 s, 1943 vs, 1653 w (ν_{CO}) cm^{-1}. MS (IC, DCI/NH_3): ^{187}Re *m/z* = 659 [M + H]$^+$, 676 [M + NH_4]$^+$. $C_{29}H_{27}O_6Re$ + 1 Et_2O (732.21): calcd. C 54.16, H 5.10; found C 54.35, H 5.01.

7: The deprotection of **3** was carried out according to the procedure described above for the deprotection of **5**. The crude material was purified by silica-gel chromatography (diethyl ether/petroleum ether 1:1) to give **7** (0.081 g, 95% yield); m.p. 143 °C. ^{1}H NMR (200 MHz, $CDCl_3$): δ = 0.97 (s, 3 H, CH_3-18), 2.84 (m, 2 H, 6-H), 4.28 (s, 5 H, Cp), 4.63 (t, 2 H, 3,4-H of C_5H_4), 4.93 (t, 2 H, 2,5-H of C_5H_4), 6.59 (d, 1 H, 4-H), 6.64 (dd, *J* = 8.4 Hz, 1 H, 2-H), 7.17 (d, *J* = 8.4 Hz, 1 H, 1-H) ppm. ^{13}C NMR (100 MHz, $CDCl_3$): δ = 12.8 (C-18), 23.0 (C-15), 26.3, 27.3 (C-7 and C-11), 29.6 (C-6), 33.2 (C-16), 39.0 and 39.3 (C-12 and C-8), 43.5 (C-9), 47.9 (C-13), 50.2 (C-14), 70.6 (C_{cp} and 2 $C_{cp'}$), 73.7 (2 $C_{cp'}$), 80.1 (C-17), 84.9 and 94.8 (1 $C_{Cp'}$ and C≡C), 112.8 (C-2), 115.3 (C-4), 126.5 (C-1), 131.8 (C-10), 137.9 (C-5), 153.9 (C-3), 181.7 (CO) ppm. IR (CH_2Cl_2): $\tilde{\nu}$ = 1623 s (ν_{CO}) cm^{-1}. MS (EI): *m/z* = 43, 73, 147, 207, 221, 281, 508 [M]$^{+\cdot}$. $C_{31}H_{32}FeO_3$ + H_2O (526.43): calcd. C 70.72, H 6.52; found C 71.33, H 6.78.

 © 2004 Wiley-VCH Verlag GmbH & Co. KGaA, Weinheim

6 from 7: The compound **6** was also prepared according to the procedure described above for the synthesis of **2** or **5** (see also Scheme 4). 12 % yield of **6** was obtained.

8a: 0.5 mL of an aqueous solution containing the starting material $[^{99m}Tc(H_2O)_3(CO)_3]^+$ was prepared as described in the literature.[11] Compound **1** (0.6 mg, 1.9 μmol) in 0.5 mL of DMSO was added to the aqueous solution. Subsequent heating at 95 °C for 4 h afforded **8a** in an overall yield of > 80%.

8b: Compound **1** (0.0170 g, 0.053 mmol) in 0.5 mL of DMSO was added to $[NEt_4]_2[TcCl_3(CO)_3]$ (0.0225 g, 0.041 mmol) in a Schlenk tube equipped with a magnetic stirring bar. The mixture was heated for 1 h at 140 °C, yielding a brownish precipitate containing the product, as shown by HPLC analysis. The crude product was purified by column chromatography on a silica-gel plate (ethyl acetate/petroleum ether 1:7). Yield: 74 %. The product was dissolved in a diethyl ether/hexane 2:1 solution, slow evaporation of the solvents gave crystals suitable for an X-ray study. ^{1}H NMR (200 MHz, $CDCl_3$): δ = 3.89 (s, 3 H, -OCH_3), 5.37 (t, J = 2.4 Hz, 2 H, 3,4-H of C_5H_4), 6.01 (t, J = 2.4 Hz, 2 H, 2,5-H of C_5H_4), 6.96 (d, J = 9.0 Hz, 2 H, Ar), 7.84 (d, J = 9.0 Hz, 2 H, Ar) ppm. ^{13}C NMR (50 MHz, $CDCl_3$): δ = 55.5 (-OCH_3), 87.0 (2 C_{Cp}), 91.85 (2 C_{Cp}), 113.8 (2 C_{Ar}), 130.7 (2C_{Ar}), 163.2 (CO, ketone) ppm. ^{99}Tc NMR (740 Hz, $CDCl_3$): δ = −2478 ppm. IR (KBr): $\tilde{\nu}$ = 2040 s, 1957 vs, 1930 vs, 1631 w (ν_{CO}) cm^{-1}. MS (FAB): m/z = 382 $[M]^+$.

X-ray Crystal-Structure Determination of 8b: ($C_{16}H_{11}O_4Tc$), orange needle, 0.3 × 0.1 × 0.1 mm^3, Stoe IPDS diffractometer, λ = 0.71073 Å, φ oscillation scan, monoclinic, space group $P21/c$, a = 18.2751(5), b = 13.1242(8), c = 6.1913(17) Å, β = 90.380(11)°, V = 1484.9(4) Å^3, Z = 4, $D_{calcd.}$ = 1.634 g cm^{-3}, $R_1(I \geq 2\sigma(I)]$ = 0.0437, $wR_2(F^2, I \geq 2\sigma(I)]$ = 0. 0995 for 2595 data (total 14235 reflections collected, 4435 independent (R_{int} = 0.0984), 2595 observed (I, ≥ 2σ(I)]), θ range: 3.10 to 30.55°, completeness 97.4 %, 200 parameters, refinement with SHELXL-97[14] against F^2, calculated positions of hydrogen atoms, no absorption correction, μ = 0.981 mm^{-1}. CCDC-209247 contains the supplementary crystallographic data for this paper. These data can be obtained free of charge at www.ccdc.cam.ac.uk/conts/retrieving.html [or from the Cambridge Crystallographic Data Centre, 12 Union Road, Cambridge CB2 1EZ, UK; Fax: (internat.) +44-1223/336-033; E-mail: deposit@ccdc.cam.ac.uk].

9: 0.5 mL of an aqueous solution containing the starting material $[^{99m}Tc(H_2O)_3(CO)_3]^+$ was prepared as described in the literature.[11] Compound **7** (0.8 mg, 1.6 μmol) in 0.5 mL of DMSO was added to the aqueous solution. Subsequent heating at 95 °C for 3 h 30 min afforded **9** in an overall yield of > 90%.

Acknowledgments

Financial support from the Ministry of Research (S. M. grant), the Centre National de la Recherche Scientifique, and COST D20 (WG, 007) is gratefully ackowledged. Part of this study is financially supported by the Bundesamt für Bildung und Wissenschaft (COST 99.0055) and gratefully acknowledged.

[1] [1a] F. Wust, H. Spies, B. Johannsen, *Bioorg. Med. Chem. Lett.* **1996**, *22*, 2729−2734. [1b] M. Reisgys, F. Wust, R. Alberto, R. Schibli, P. A. Schubiger, H. J. Pietzsch, H. Spies, B. Johannsen, *Bioorg. Med. Chem. Lett.* **1997**, *17*, 2243−2246. [1c] F. Wust, D. Scheller, H. Spies, B. Johannsen, *Eur. J. Inorg. Chem.* **1998**, 789−793. [1d] J. B. Arterburn, C. Corona, K. Venkateswara Rao, K. E. Carlson, J. A. Katzenellenbogen, *J. Org. Chem.* **2003**, *68*, 7063−7070.

[2] [2a] S. S. Jurisson, J. D. Lydon, *Chem. Rev.* **1999**, *99*, 2205−2218. [2b] R. C. Mease, C. Lambert, *Semin. Nucl. Med.* **2001**, XXXI, 278−285.

[3] S. Top, H. El Hafa, A. Vessieres, J. Quivy, J. Vaissermann, D. W. Hugues, M. J. McGlinchey, J.-P. Mornon, E. Thoreau, G. Jaouen, *J. Am. Chem. Soc.* **1995**, *117*, 8372−8380.

[4] [4a] G. Jaouen, S. Top, A. Vessières, R. Alberto, *J. Organomet. Chem.* **2000**, *600*, 23−36. [4b] F. Le Bideau, M. Salmain, S. Top, G. Jaouen, *Chem. Eur. J.* **2001**, *7*, 2289−2294.

[5] M. Wenzel, *J. Labelled Compd. Radiopharm.* **1992**, *31*, 641−650.

[6] J. Wald, R. Alberto, K. Ortner, L. Candreia, *Angew. Chem. Int. Ed.* **2001**, *40*, 3062−3066.

[7] S. Top, S. Masi, G. Jaouen, *Eur. J. Inorg. Chem.* **2002**, 1848−1853.

[8] A. F. Cunningham, *Organometallics* **1994**, *13*, 2480−2485.

[9] S. Nahm, S. Weinreb, *Tetrahedron Lett.* **1981**, *22*, 3815−3818.

[10] T. W. Spradau, J. A. Katzenellenbogen, *Bioorg. Med. Chem. Lett.* **1998**, *8*, 3235−3240.

[11] R. Alberto, K. Ortner, N. Wheatley, R. Schibli, A. P. Schubiger, *J. Am. Chem. Soc.* **2001**, *123*, 3135−3136.

[12] M. Wenzel, C. Klinge, *J. Labelled Compd. Radiopharm.* **1994**, *34*, 981−987.

[13] D. R. William, P. D. Lowder, Y.-U. Gu, *Tetrahedron Lett.* **2000**, *41*, 9397−9401.

[14] Sheldrick, G. M. SHELXL-97, University of Göttingen: Germany, **1997**.

Received October 14, 2003

 © 2004 Wiley-VCH Verlag GmbH & Co. KGaA, Weinheim

Crystal Structure and Magnetic Properties of $Bi(Bi_9)[NbCl_6]_3$, a New Member of the Structure Family $Bi(Bi_9)[MX_6]_3$, and the Crystal Structure of $Bi_8[Ta_2O_2Br_7]_2$

Johannes Beck*[a] and Tobias Hilbert[a]

Keywords: Bismuth / Niobium / Tantalum / Magnetic properties / X-ray diffraction

Bi and Bi^{III} halides comproportionate to form subvalent cationic Bi clusters of various size and shape that can be stabilized in the solid state in the presence of suitable complex ions. Transition metal chlorides and bromides of group 4 elements lead to compounds of the $Bi(Bi_9)[MX_6]_3$ family, of which all members with M = Zr, Hf; X = Cl, Br are known. At 550 K Bi, $BiCl_3$ and $NbCl_5$, surprisingly, yield the isotypic $Bi^+(Bi_9^{5+})([NbCl_6]^{2-})_3$ containing Nb^{IV} formed by reduction of Nb^V. The crystal structure [hexagonal; $P6_3/m$; a = 1377.1(2), c = 1065.5(2) pm; Z = 2] contains Bi_9^{5+} clusters, octahedral $[NbCl_6]^{2-}$ and disordered Bi^+ ions. The low, temperature-dependent paramagnetic moment (76 K: 0.99 B.M.; 295 K: 1.22 B.M.) confirms the reduction of Nb to the +IV state. $Bi_8[Ta_2O_2Br_7]_2$, formed by a trace of H_2O in a reaction of Bi, $BiBr_3$ and $TaBr_5$ at 570 K, adopts a new structure type [tetragonal; $P4/mnc$; a = 1448.0(1), c = 1830.6(2) pm; Z = 4] and consists of square-antiprismatic Bi_8^{2+} clusters and one-dimensional polymeric bromooxotantalate(V) anions.
(© Wiley-VCH Verlag GmbH & Co. KGaA, 69451 Weinheim, Germany, 2004)

Introduction

Bismuth was one of the first elements for which subvalent species with oxidation states between 0 and +III were studied systematically. The series of discrete, homonuclear cations Bi^+, Bi_2^{4+}, Bi_3^+, Bi_5^+, Bi_5^{3+}, Bi_6^{2+}, Bi_8^{2+}, and Bi_9^{5+} has made bismuth the classical example of naked clusters among the main group elements. Because of these exceptional properties bismuth has been called "The Wonder Metal".[1] The tricapped trigonal-prismatic Bi_9^{5+} is the largest known molecular cluster of bismuth. It was first characterized in the binary subchloride Bi_6Cl_7 together with polymeric chlorobismuthate(III) anions of composition $[Bi_3Cl_{14}]^{5-}$,[2,3] and later also in the ternary phase $Bi(Bi_9)[HfCl_6]_3$.[4] With tetrachloroaluminate counterions bismuth tends to form smaller clusters such as the square-antiprismatic Bi_8^{2+} in $Bi_8[AlCl_4]_2$ [3,5,6] and the trigonal-bipyramidal Bi_5^{3+} in $Bi_5[AlCl_4]_3$.[5,7] Subsequent studies focused on replacing $[AlCl_4]^-$ with other anions and led to the preparation of several compounds like Bi_6Br_7,[8] $Bi(Bi_9)[ZrBr_6]_3$,[9] $Bi(Bi_9)[ZrCl_6]_3$ [10] and $Bi_5[GaCl_4]_3$.[11] New clusters, Bi_2^{4+} in $Bi_2[M_4X_8]$ (M = Al, Ga; X = S, Se)[12] and Bi_5^+/Bi_6^{2+} in $Bi_{34}Ir_3Br_{37}$ [13] were found in the thus far unexplored ternary systems.

Numerous articles deal with theoretical approaches to explain the bonding situation in these predominantly deltahedral clusters. The structures of Bi_5^{3+} and Bi_8^{2+} can be understood as *closo* and *arachno* clusters that fulfill Wade's rules.[14] The nine-atomic Bi_9^{5+} shows substantial deviation from the predicted structure of a monocapped square antiprism, which is adopted by the isoelectronic Zintl ion Sn_9^{4-}.[15] The actual three-capped trigonal-prismatic structure is related to a *closo* structure. Elongation along the threefold axis is the result of the antibonding character of the HOMO. The molecular geometries and electron configuration of different main group element clusters have been compared in several reviews.[16,17] The high degree of electron delocalization in the polyhedral clusters was recently termed "three-dimensional" or "spherical" aromaticity.[18,19]

We intended to expand the structure family $Bi(Bi_9)[MX_6]_3$ and to obtain new structure types by a varied cation/anion ratio using anions with a lower charge. We chose $NbCl_5$ as Lewis acid, since hexachloroniobates(V) are suitable for stabilizing naked clusters such as chalcogen polycations.[20,21] Thus, a compound composed of polycationic Bi clusters and $[NbCl_6]^-$ ions was expected. Instead, $Bi^+(Bi_9^{5+})([NbCl_6]^{2-})_3$ was obtained under reduction to Nb^{IV}. A special feature of this structure type of the general formula $Bi(Bi_9)[MX_6]_3$ is the occurrence of Bi^+ ions as a one-dimensional chain in a wide channel made up of $[MX_6]^{2-}$ anions. Alternative split-position models for these one-dimensionally disordered Bi^+ ions will be discussed. Finally, a new structure type is presented: $Bi_8[Ta_2O_2Br_7]_2$, which contains the known square-antiprismatic Bi_8^{2+} ions and a new bromooxotantalate(V) ion.

[a] Institut für Anorganische Chemie der Rheinischen Friedrich-Wilhelm-Universität Bonn,
Gerhard-Domagk-Straße 1, 53121 Bonn, Germany
Fax: (internat.) + 49-228-735660
E-mail: j.beck@uni-bonn.de

Results and Discussion

Syntheses of $Bi(Bi_9)[NbCl_6]_3$ and $Bi_8[Ta_2O_2Br_7]_2$

A common method for synthesizing polycationic bismuth clusters is the crystallization as tetrachloroaluminates from NaCl/$AlCl_3$ melts. This involves the difficulty of separating the crystals from the solidified melt. Compounds containing polyatomic bismuth clusters are also available by chemical vapor deposition. We avoided a melt by applying relatively low reaction temperatures compared with those described in the literature.[9] The two compounds presented here can be seen as arising from comproportionation of elemental bismuth and the corresponding trihalide, since Bi_6Cl_7 or Bi_6Br_7 can be isolated as a subvalent intermediate, followed by a Lewis acid/base reaction of these intermediates with the respective metal halide.

$$9\ Bi + BiCl_3 + 3\ NbCl_5 \rightarrow Bi(Bi_9)[NbCl_6]_3$$

Even under optimized conditions the yields did not exceed 30%. Apparently, a multicomponent equilibrium involving Bi, $BiCl_3$, bismuth subhalides, transition metal halide and gas phase species is present, which prevents higher conversion rates. Removing the $Bi(Bi_9)[NbCl_6]_3$ crystals from the reaction mixture led to a second yield of about the same amount. Large pure samples are hard to obtain by this method. The bismuth subchloride Bi_6Cl_7 is formed as black crystals under the same conditions and must be separated mechanically. This is complicated by the various crystal forms of Bi_6Cl_7 which makes visual distinction from crystals of $Bi(Bi_9)[NbCl_6]_3$ difficult.

$Bi_8[Ta_2O_2Br_7]_2$ was obtained only in small yield by partial hydrolysis of $TaBr_5$. An overall reaction equation can be written, although the attempts to repeat the reaction with stoichiometric amounts of oxygen, introduced into the reaction system either via Ta_2O_5 or by short exposure of the reaction mixture to air were unsuccessful.

$$22\ Bi + 2\ BiBr_3 + 12\ TaBr_5 + 12\ H_2O \rightarrow 3\ Bi_8[Ta_2O_2Br_7]_2 + 24\ HBr$$

Crystal Structure of $Bi(Bi_9)[NbCl_6]_3$

$Bi(Bi_9)[NbCl_6]_3$ crystallizes isotypically to $Bi(Bi_9)[HfCl_6]_3$,[4] $Bi(Bi_9)[ZrBr_6]_3$,[9] and $Bi(Bi_9)[ZrCl_6]_3$.[10] All compounds that adopt this structure type are built of a close packing of two sorts of discrete molecular ions: triply μ_4-capped trigonal-prismatic Bi_9^{5+} cations and octahedral $[MX_6]^{2-}$ anions (Figure 1). The projection along the crystallographic *c*-axis (Figure 2) shows that each Bi_9 cluster is surrounded by six MX_6 octahedra in a coplanar arrangement. As in hexagonal closest sphere packing, six further anions are in a trigonal arrangement placed below and above. The hexahalometalate anions form wide channels that are centered around the cell edges and run perpendicular to the hexagonal plane. The channels are ca. 630 pm in diameter and are filled with columns of disordered Bi^+ ions (vide infra).

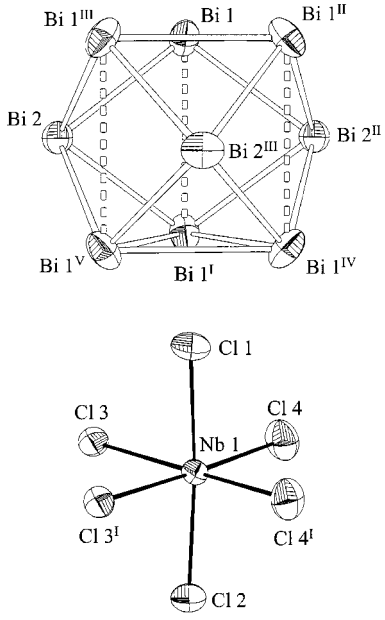

Figure 1. Bi_9^{5+} cluster and the $[NbCl_6]^{2-}$ ion in $Bi(Bi_9)[NbCl_6]_3$; displacement ellipsoids are scaled to enclose 50% probability density;[44] symmetry operations: I: *x*, *y*, 0.5 − *z*; II: 1 − *y*, *x* − *y*, *z*; III: 1 − *x* + *y*, 1 − *x*, *z*; IV: 1 − *y*, *x* − *y*, 0.5 − *z*, V: 1 − *x* + *y*, 1 − *x*, 0.5 − *z*; selected bond lengths [pm]: Bi(1)−Bi(2)/Bi(2)−Bi(1^I) 308.7(1), Bi(1)−Bi(2^{II})/Bi(2)−Bi($1^{III/V}$) 311.1(1), Bi(1)−Bi($1^{II/III}$) 324.3(1), Bi(1)−Bi(1^I) 373.8(1); Nb−Cl(1) 239.7(5), Nb−Cl(2) 239.8(5), Nb−Cl(3) 248.7(3), Nb−Cl(4) 234.8(3)

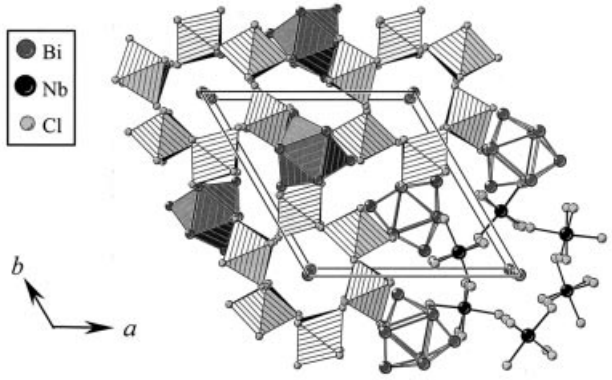

Figure 2. Unit cell of $Bi(Bi_9)[NbCl_6]_3$ in a perspective projection along the *c*-axis; the drawing combines shaded polyhedra and ball-and-stick models

The tri-capped trigonal-prismatic Bi_9^{5+} has crystallographic C_{3h} symmetry and is defined by two independent Bi atoms. Bi−Bi bonds, with the exception of the non-bonding prism edges (373.8 pm), have an average length of 314.7 pm. This agrees well with the literature values.[4] The difference between Bi−Bi bond lengths from a capping Bi(2) atom to the four corresponding Bi(1) atoms in the prism vertices is only 0.8%. This small irregular capping indicates only small distortions from the approximately fulfilled D_{3h} symmetry of the cluster ion.

Cl−Nb−Cl angles of the $[NbCl_6]^{2-}$ ion deviate by less than 3° from rectangularity; the Nb−Cl bonds, however, show considerable alternation in their lengths, between

 © 2004 Wiley-VCH Verlag GmbH & Co. KGaA, Weinheim

234.8 and 248.7 pm. Both Cl(3) atoms of the $[NbCl_6]^{2-}$ ion, which have the longest Nb−Cl bonds, take a bridging position over edges of the cluster cation, with the shortest Bi−Cl distances of 333.5 pm. Distortions of the hexachloro metalate anions in this structure type from the ideal octahedral shape reflect the electrophilic properties of the Bi_9^{5+} clusters.

Disorder of the Bi^+ Ions in the Structure Type $Bi(Bi_9)[MX_6]_3$

Several crystal structures with a one-dimensional disorder of atoms or ions located in channels are known. $Bi_{5,6}Ni_5I$[22] contains double-walled channels of nickel and bismuth atoms. Their central axis is filled with a coaxial string of disordered Bi atoms that, statistically, occupy only every fifth possible site. Other examples include the compounds Th_7S_{12},[23] $K_2Sn_5Cl_{12}$ [24] and several apatite[25] and hollandite type structures.[26] With $Bi(Bi_9)[NbCl_6]_3$ the electron density along the *c*-axis is sufficient for only two additional Bi^+ ions per unit cell. X-ray experiments gave no direct evidence for disorder in the form of diffuse scattering. Precession photographs and imaging plate exposures did not show any continuous streaks in the reciprocal lattice along *c**.

The split-position model involves 14 closely neighbored atomic positions along one translation period on the sixfold axis in (0,0,*z*). Of the four independent split sites position C has the highest occupation factor (Figure 3). This marked preference might be due to the almost octahedral coordination with Cl atoms of the surrounding hexahalometalate(IV) ions (d_{Bi-Cl}: 3 × 320 pm, 3 × 337 pm). To measure the interaction between the various Bi(3) sites and the neighboring anions we calculated the electrostatic potential for a hypothetical atom in (0,0,*z*) using the program MAPLE (Madelung Part of Lattice Energy).[27] The results show only a very flat modulation of the potential in the center of the channel, while even small shifts of the dummy atom towards one of the $[NbCl_6]^{2-}$ octahedra increased its potential significantly (Figure 4). The tendency to localization on one particular split position is expected to be small. The closest distance between sixfold axes is 1377 pm, and no correlation can be expected for the parallel running chains.

The origin of the elongated displacement ellipsoids in the refinements with anisotropic displacement parameters was examined by low-temperature X-ray diffraction. One set of independent reflections was collected at 223 and 173 K. The temperature dependence of the mean-square displacement parameters of the disordered Bi(3) and of Bi(1), a fully occupied atom site making up the Bi_9 cluster, is represented in Figure 5. For a thermally vibrating atom one expects a linear decrease of the mean square displacements, to approximately zero when extrapolated to 0 K. Bi(1) shows such regular behavior, while Bi(3) behaves differently. While the unusual long axis of the displacement ellipsoid diminishes on decreasing temperature, the two symmetry-equivalent short axes perpendicular to the crystallographic *c*-axis, however, turned out to be temperature-independent. For both low-temperature data sets, difference Fourier maps

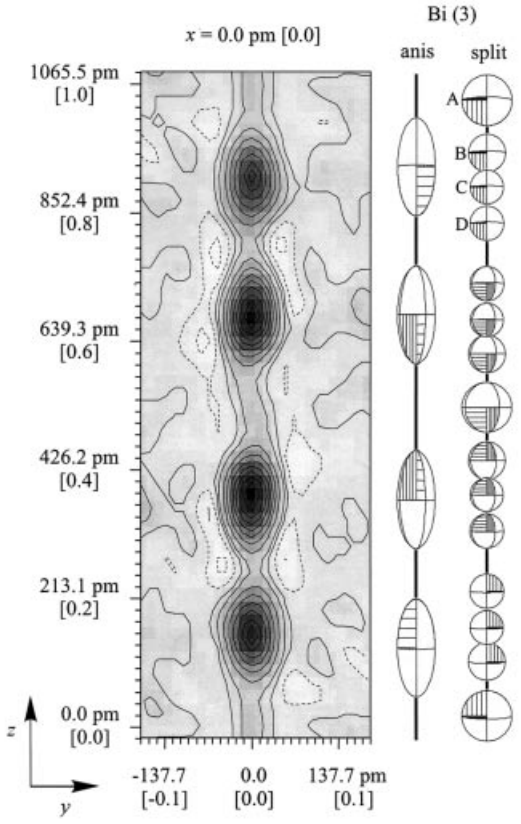

Figure 3. Difference Fourier electron density plot along the unit cell edge [001] in the structure of $Bi(Bi_9)[NbCl_6]_3$ − based on a structure model that was complete apart from the disordered Bi atoms in (0,0,*z*) and representations of the split positions and the disorder model for the Bi(3) site; displacement ellipsoids and spheres are scaled to enclose a 50% probability density

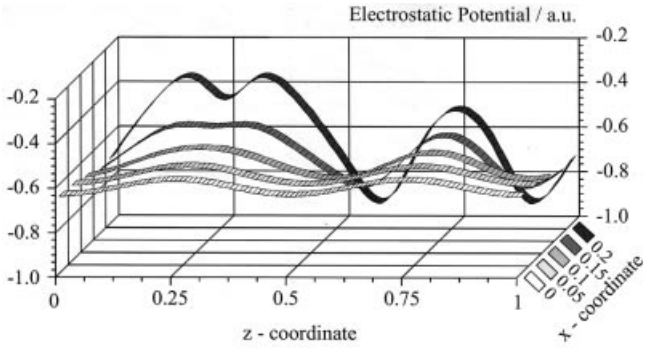

Figure 4. Electrostatic potential (arbitrary units) for a hypothetical atom on a site (0,0,*z*) under the influence of the anionic environment of $[NbCl_6]^{2-}$ ions in $Bi(Bi_9)[NbCl_6]_3$; since the dummy atom was assumed to be uncharged negative potentials indicate favorable positions for positively charged ions

show a contraction of the electron density maxima for the Bi(3) positions, but a diffuse density along the *c*-axis remains. Thus, elongation of the Bi(3) ellipsoids can not be attributed solely to a dynamical vibration phenomenon.

While previous structure determinations of compounds of this family[4,9] left it unclear whether the distribution of

 © 2004 Wiley-VCH Verlag GmbH & Co. KGaA, Weinheim

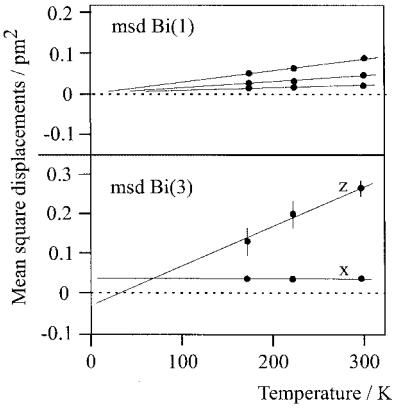

Figure 5. Temperature dependence of the mean square displacements of the atoms Bi(1) and Bi(3) in $Bi(Bi_9)[NbCl_6]_3$; errors of $\pm 3\sigma$ are indicated by vertical lines when bigger than the diameter of the dots

the disordered Bi ions should be interpreted as isolated Bi^+ ions or if two ions are associated in Bi_2^{2+} pairs with a bond length of ca. 300 pm, cationic Bi_2 dumbbells have been discovered in the phases $Bi_2M_4X_8$ (M = Al, Ga; X = S, Se).[12] The average Bi−Bi distances in the Bi_2^{4+} ions is 314 pm. Shorter Bi−Bi bonds are found in dibismuthanes with arene ligands, e.g. in Bi_2Ph_4 (d_{Bi-Bi} = 299 pm)[28] or in dibismuthenes ($d_{Bi=Bi}$ = 282 pm).[29] The presence of Bi_2^{2+} dumbbells may explain the distances (296 pm) between neighboring split atom positions in the ordered structure model of $Bi(Bi_9)[NbCl_6]_3$. The centers of gravity of these diatomic molecules are at (0,0,0) and (0,0,1/2). However, the intermolecular distance is only 237 pm, and only every second position can be statistically occupied by Bi_2^{2+}.

For $Bi_2[M_4X_8]$ (M = Al, Ga; X = S, Se) the Raman stretching vibration of the Bi_2^{4+} dumbbells is at 108 cm^{-1}.[12] Examination of $Bi(Bi_9)[ZrCl_6]_3$ and $Bi(Bi_9)[ZrBr_6]_3$ as easily obtainable model compounds for the structure type $Bi(Bi_9)[MX_6]_3$, and of Bi_6Cl_7, by IR and Raman spectroscopy show only a few lines in the region below 500 cm^{-1} {$Bi(Bi_9)[ZrCl_6]_3$: IR: $\tilde{\nu}$ = 289, 232, 162, 142, 112; Raman: $\tilde{\nu}$ = 224, 197, 158, 108, 93; $Bi(Bi_9)[ZrBr_6]_3$: IR: $\tilde{\nu}$ = 223, 189, 142, 108; Raman: $\tilde{\nu}$ = 170, 140, 106; Bi_6Cl_7: IR: $\tilde{\nu}$ = 422, 367, 212, 144, 107 cm^{-1}}. Comparison of $Bi(Bi_9)[ZrCl_6]_3$ and $Bi(Bi_9)[ZrBr_6]_3$ reveals a large drift for some of the IR absorption bands and some Raman lines. This indicates that the bands at 289, 232, 197, 162/158 cm^{-1} for $Bi(Bi_9)[ZrCl_6]_3$, and the bands at 223, 189, 170 cm^{-1} $Bi(Bi_9)[ZrBr_6]_3$ are attributable to vibration modes of the $[ZrX_6]^{2-}$ octahedra. The lines around 140 and 108 cm^{-1} appear for both compounds in the IR and Raman spectra but are also observed for Bi_6Cl_7. Since all three compounds contain Bi_9^{5+} clusters, these lines can, probably, be attributed to vibrations of the cluster ions. Distinct vibration bands attributable to Bi_2^{2+} groups are not present.

Neither of the two models, discrete Bi^+ ions or dinuclear Bi_2^{2+} ions, can be assigned on the basis of the present diffraction experiments and vibrational spectra.

Thermomagnetic Properties of $Bi(Bi_9)[NbCl_6]_3$

Analysis of the magnetic measurement unequivocally confirms the expected oxidation state of Nb^{IV}. The substance shows paramagnetic behavior, which is in contrast to the diamagnetic properties of $Bi(Bi_9)[HfCl_6]_3$ [4] and directly reflects the electronic state of the niobium atom. The effective magnetic moment at room temperature is well below the 1.72 B.M. for a spin-isolated single electron. Further, the simple Curie−Weiss law cannot be applied because the determined magnetic moment displays a distinct temperature dependency: its values increase from 0.99 at 76 K to 1.22 B.M. at 295 K per magnetic ion Nb^{IV} (Figure 6). Comparable behavior has been reported for other d^1-systems, e.g. in the compounds $M_2[NbCl_6]$ (M = Rb, Cs)[30] and $[N(C_2H_5)_4]_2[NbCl_6]$.[31]

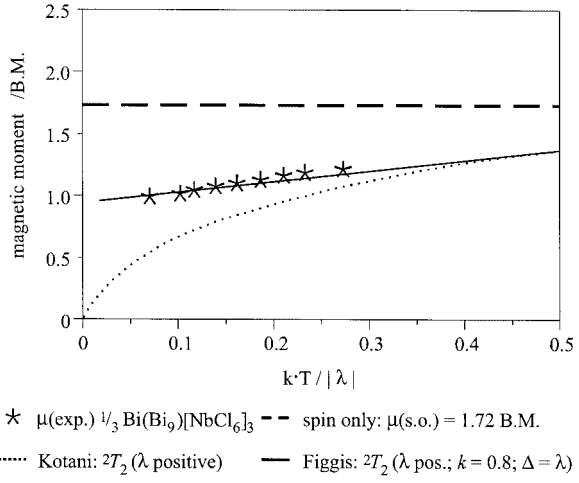

Figure 6. Temperature dependence of the effective magnetic moment of $Bi(Bi_9)[NbCl_6]_3$ scaled to a single magnetic Nb^{IV} ion; experimental data are set in relation to different theoretical approaches

The magnetic properties can be interpreted in terms of the models introduced by Kotani[32] and Figgis.[33] The effective magnetic moment arising from the $^2T_{2g}$ ground state of a transition metal complex ion in a centric symmetry ligand field depends upon several ligand field parameters: the spin-orbit coupling constant λ ($\lambda_{Nb^{IV}}$ = 750 cm^{-1} [34]), the orbital separation Δ between levels of the $^2T_{2g}$ term created by an axial ligand field, and the so-called orbital reduction factor k, which takes into consideration the delocalization of t_{2g} electrons into the orbitals of the ligand atoms.[35] The simplified Kotani model only takes into account the spin-orbit coupling, disregarding any distortion of the octahedral ions (k = 1 and Δ = 0 cm^{-1}). For the temperature dependence of the magnetic moments of $Bi(Bi_9)[NbCl_6]_3$ the best fit is reached in a model with Δ = 750 cm^{-1} and k = 0.8, reflecting the marked distortion of the $[NbCl_6]^{2-}$ polyhedra (Figure 6).

Crystal Structure of $Bi_8[Ta_2O_2Br_7]_2$

The structure contains square-antiprismatic Bi_8^{2+} clusters formerly known exclusively in $Bi_8[AlCl_4]_2$.[3] The coun-

 © 2004 Wiley-VCH Verlag GmbH & Co. KGaA, Weinheim

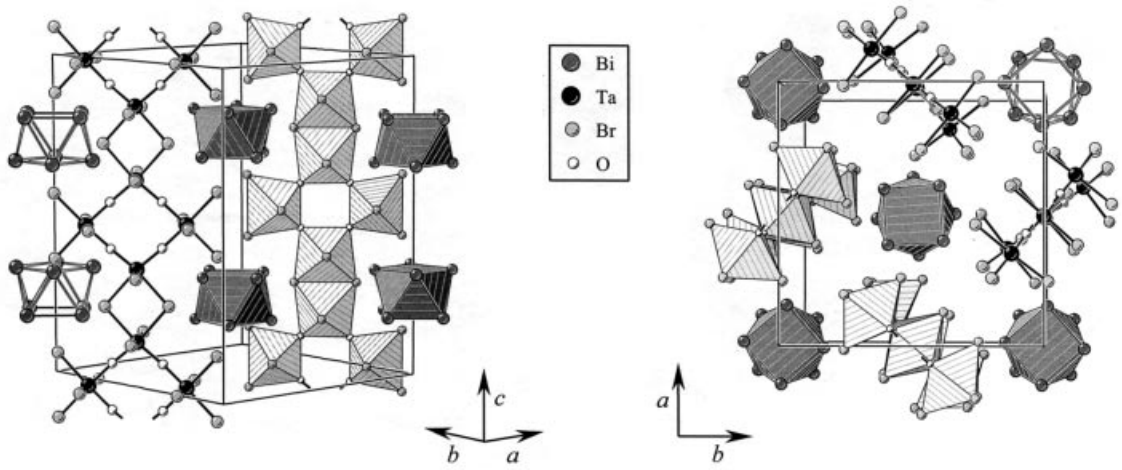

Figure 7. Unit cell of $Bi_8[Ta_2O_2Br_7]_2$ in two different views, along [110] and [001]; the drawing combines shaded polyhedra and ball-and-stick representations

terion is a novel, one-dimensional polymeric bromooxotantalate(v). Stacks of bismuth clusters and anionic chains are arranged in a tetragonal rod-packing along the crystallographic *c*-axis. Figure 7 shows two different views of the unit cell, along and perpendicular to the chains.

The Bi_8^{2+} cation has C_4 symmetry and is defined by two independent bismuth sites (Figure 8). The square faces are coplanar. Their twisting angle of 45.5° and the small difference in bond lengths [Bi(1) face: 312.6 pm; Bi(2) face: 311.7 pm] indicate only small distortions from the higher symmetrical point group D_{4d} (Table 1). Due to the lower charge per atom (*cpa*) the average Bi−Bi bond of 310.7 pm for Bi_8^{2+} (*cpa* = +0.25) is significantly shorter than the 314.7 pm observed for Bi_9^{5+} (*cpa* = +0.55). The cluster has to be considered as "naked" since the shortest anion−cation contacts are beyond 365 pm, and there are no intermolecular Bi−Bi distances shorter than 617 pm. The structure of the Bi_8^{2+} cluster ion in $Bi_8[Ta_2O_2Br_7]_2$ is very closely related to the cluster ion in $Bi_8[AlCl_4]_2$ [3,5,6] where Bi_8^{2+} has C_s symmetry and is generated by five crystallographically independent Bi atoms. There is a significant difference in the interionic intercations. In contrast to $Bi_8[Ta_2O_2Br_7]_2$ the shortest contacts between Bi atoms of neighboring Bi_8^{2+} ions in $Bi_8[AlCl_4]_2$ are only 390 and 410 pm, which indicate weak interactions between the clusters.

After $Te_4[Ta_2OBr_{10}]$[18] and $(NH_4)_2[Ta_3O_5Br_7]$,[36] $[Ta_2O_2Br_7]^-$ is only the third crystallographically characterized bromooxotantalate(v) reported. In contrast to $[Ta_2OBr_{10}]^{2-}$ ($Te_4[Nb_2OCl_{10}]$[37]) and $[Ta_3O_5Br_7]^{2-}$ {$(NH_4)_2[Nb_3O_5Cl_7]$[38]} no isostructural Nb/Cl analogue is known for $[Ta_2O_2Br_7]^-$. This anion consists of two symmetrically independent TaO_2Br_4 octahedra. Four vertex-sharing octahedra are connected by common oxygen atoms. The resulting tetrameric cyclic subunits are linked by common edges via four μ_2-Br atoms and form a one-dimensional polymeric anionic string (Figure 8). With Ta−O distances of 187 and 190 pm and Ta−O−Ta angles of 175.1° the oxygen bridges are nearly linear and symmetric. These

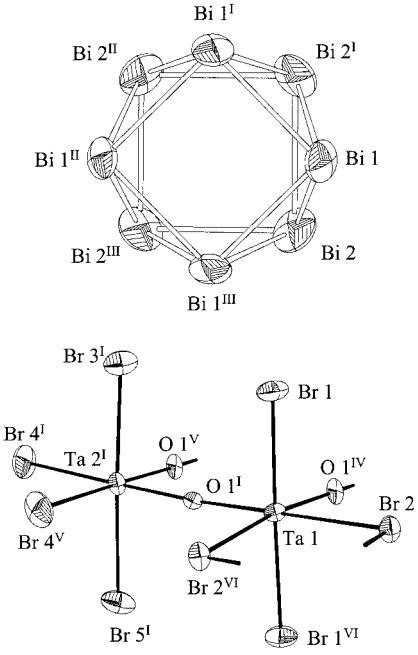

Figure 8. Bi_8^{2+} cluster and a section of the polymeric $[Ta_2O_2Br_7]^-$ ion in $Bi_8[Ta_2O_2Br_7]_2$; displacement ellipsoids are scaled to enclose 50% probability density;[44] symmetry operations: I: *y*, −*x*, *z*; II: −*x*, −*y*, *z*; III: −*y*, *x*, *z*; IV: 1 − *y*, *x*, *z*, V: *y*, −*x*, −*z*; VI: 1 − *x*, −*y*, *z*; selected bond lengths [pm]: Bi(1)−Bi(2) 308.7(3), Bi(1)−Bi(2^{I})/Bi(2)−Bi(1^{III}) 309.9(3), Bi(2)−Bi($2^{I/III}$) 311.7(2), Bi(1)−Bi($1^{I/III}$) 312.6(2); Ta(1)−O($1^{I/IV}$) 187(2), Ta(1)−Br(1) 2 × 248.5(2), Ta(1)−Br(2) 2 × 273.1(2), Ta(2)−O(1) 2 × 190(2), Ta(2)−Br(3^{I}) 249.5(4), Ta(2)−Br(4) 2 × 251.5(3), Ta(2)−Br(5) 253.5(4)

geometric parameters agree well with the Ta−O (188 pm) and linear Ta−O−Ta group in $[Ta_2OBr_{10}]^{2-}$.[18] Significantly shorter than the sum of the covalence radii of 209 pm,[39] the Ta−O bonds of both ions show strong indications of partial π-bonding. The four Ta−Br bonds of each tantalum atom in $[Ta_2O_2Br_7]^-$ vary substantially, between 248.5 and 273.1 pm for Ta(1), but only between 249.5 and 253.4 pm for Ta(2). This marked deviation reflects the

 © 2004 Wiley-VCH Verlag GmbH & Co. KGaA, Weinheim

Table 1. Atomic coordinates, equivalent isotropic thermal displacement parameters B_{eq} [10^4 pm^2] and site occupation factors (*sof*) for the atoms in $Bi(Bi_9)[NbCl_6]_3$ and $Bi_8[Ta_2O_2Br_7]_2$; superscript sp refers to the split model, anis to the refinement with anisotropic displacement parameters

Atom	sof	*x*/*a*	*y*/*b*	*z*/*c*	B_{eq}
$Bi(Bi_9)[NbCl_6]_3$					
Bi(1)	1	0.51925(5)	0.21288(5)	0.07459(6)	3.38(2)
Bi(2)	1	0.48518(7)	0.37178(8)	0.25	3.16(2)
Nb(1)	1	0.6595(2)	0.7805(2)	0.25	1.98(3)
Cl(1)	1	0.4969(5)	0.8016(6)	0.25	3.6(1)
Cl(2)	1	0.8122(5)	0.7436(5)	0.25	2.89(8)
Cl(3)	1	0.5665(3)	0.6326(3)	0.0874(3)	2.47(6)
Cl(4)	1	0.7411(4)	0.9161(4)	0.0912(3)	3.57(7)
Bi(3A)^{sp}	0.07(2)	0	0	0	6(2)
Bi(3B)^{sp}	0.123(9)	0	0	0.087(2)	3.5(3)
Bi(3C)^{sp}	0.249(9)	0	0	0.142(1)	2.8(2)
Bi(3D)^{sp}	0.11(1)	0	0	0.201(2)	2.9(3)
Bi(3)^{anis}	0.495(4)	0	0	0.1389(6)	8.8(2)
$Bi_8[Ta_2O_2Br_7]_2$					
Bi(1)	1	0.15223(9)	0.0110(2)	0.1899(2)	5.47(5)
Bi(2)	1	0.1002(2)	0.1146(2)	0.3315(2)	6.57(5)
Ta(1)	1	0.5	0	0.13797(7)	1.13(3)
Ta(2)	1	0.12155(9)	0.34983(9)	0	1.43(3)
Br(1)	1	0.3862(2)	0.1276(2)	0.1495(2)	2.33(5)
Br(2)	1	0.5881(2)	0.0881(2)	0.25	1.66(6)
Br(3)	1	−0.0161(3)	0.2462(3)	0	2.86(8)
Br(4)	1	0.1944(2)	0.2558(2)	−0.1001(3)	3.22(7)
Br(5)	1	0.2571(3)	0.4605(3)	0	3.10(9)
O(1)	1	0.065(1)	0.425(1)	0.072(1)	1.4(3)

bridging character of Br(2) and the terminal character of all other Br atoms. In the dinuclear ion $[Ta_2OBr_{10}]^{2-}$ the static *trans* effect elongates the Ta−Br bonds *trans* to the allenic linear Ta=O=Ta group by 12 pm. This elongation, which is expected especially for the Br(4) atoms, is not present in $[Ta_2O_2Br_7]^-$.

Experimental Section

General: All compounds were handled in an argon-filled glove box. Reactions were carried out in evacuated and sealed glass ampoules (1.4 cm in diameter and 10−15 cm long), which were placed in horizontal tube furnaces. The ampoules were dried at 600 K before use. $BiCl_3$, $BiBr_3$, $NbCl_5$, and $TaBr_5$ were prepared from the elements as described[40] and sublimated under vacuum prior to use. Bismuth powder (Riedel−de Haën) was used without further treatment.

$Bi(Bi_9)[NbCl_6]_3$: A glass ampoule was filled under anhydrous conditions with Bi, $BiCl_3$ and $NbCl_5$ in the molar ratio 8:2:3 (310 mg in total). The ampoule was then evacuated, sealed and placed asymmetrically in a tube furnace that was heated to 550 K. The hot end of the ampoule contained the starting mixture; the empty end was at 535 K. Within several days black crystals formed on top of the mixed reagents and on the glass walls of the hot side of the ampoule. Even after several weeks, no conversion of more than about 30% was observed. When the product was mechanically removed and the remaining reaction mixture mortared, and again subjected to the same reaction conditions, a second crop of crystals of comparable yield was obtained. Larger crystals, suitable for X-ray investigations, formed at the glass walls of the warmer parts of the ampoule.

$Bi_8[Ta_2O_2Br_7]_2$: Traces of H_2O in the ampoule were responsible for the formation of $Bi_8[Ta_2O_2Br_7]_2$ in a reaction of Bi, $BiBr_3$ and $TaBr_5$ (molar ratio 8:2:3, 262 mg in total). A few black crystals of $Bi_8[Ta_2O_2Br_7]_2$ with the typical form of needles with a square cross section were obtained within 4 d in a temperature gradient from 570 to 550 K.

Bi_6Cl_7, $Bi(Bi_9)[ZrCl_6]_3$, and $Bi(Bi_9)[ZrBr_6]_3$: Used as reference samples for vibrational spectroscopy, were prepared from Bi and $BiCl_3$, $ZrCl_4$, and $ZrBr_4$, respectively, according to literature procedures.[3,9,10]

Crystal Structure Analyses: Since all compounds are moisture-sensitive the selected crystals were sealed under argon in glass capillaries. Crystallographic data and further details of the data collection and refinement (Table 2) and the positional parameters of the atoms (Table 1) are given here. Data collections were performed with a STOE IPDS image plate diffractometer equipped with a graphite monochromator and Mo-K_α radiation at room temperature and at low temperature using a cold nitrogen stream. All reflection intensities were corrected for Lorentz and polarization effects, and a numerical absorption correction was applied to each data set. The crystal shapes were optimized with the aid of the program HABITUS.[41] The program DIAMOND[26] was used for the graphical representations of the structures. Further details of the crystal structure analyses have been deposited at the Fachinformationzentrum Karlsruhe, 76344 Eggenstein-Leopoldshafen, Germany, and are available by quoting the authors, the literature citation and the deposit number CSD-410927 for $Bi(Bi_9)[NbCl_6]_3$, and CSD-410929 for $Bi_8[Ta_2O_2Br_7]_2$.

$Bi(Bi_9)[NbCl_6]_3$: In analogy to the isotypic compounds,[4,9] precession photographs showed the expected hexagonal crystal system with Laue class 6/*m*. The serial reflection condition 00*l*, only present for $l = 2n$, led to the space groups $P6_3/m$ or $P6_3$, of which the centrosymmetric space group was confirmed by structure analyses. A preliminary structure model, containing the atoms of the Bi_9 clusters and the $NbCl_6$ ions, was obtained by Patterson methods[42] and refined against F^2 by full-matrix least-squares calculations with anisotropic displacement parameters for all atoms.[43] A further difference Fourier calculation showed a high remaining electron density distributed along the edge of the unit cell at (0,0,*z*) with a diffuse maximum at $z/c \approx 0.1$ (Figure 3), which could be interpreted as two additional Bi^+ ions in each unit cell. Problems arise as the symmetry of the site 4*e* (0,0,*z*) generates four equivalent Bi atoms instead of two, and adjacent atoms come too close, with Bi−Bi distances just above 200 pm. Previously, a structure model implying disorder with four half-occupied Bi sites was used for $Bi(Bi_9)[HfCl_6]_3$ [4] and $Bi(Bi_9)[ZrBr_6]_3$.[9] As reported for these two crystal structures, refinement with anisotropic displacement parameters resulted in strongly elongated, "zeppelin-shaped" thermal ellipsoids for the Bi^+ ions. Further difference peaks between the positions of the disordered bismuth ions, especially on (0,0,0), allow refinement to a slightly modified structure model: four closely neighbored split positions in the interval (0,0,0) to (0,0,$^1/_4$) form a linear arrangement of partially occupied atom positions. Because of their proximity only isotropic displacement parameters could be refined for the split atoms. The site occupation factors have been refined without restraints and add up to 2.08(4) Bi atoms per unit

 © 2004 Wiley-VCH Verlag GmbH & Co. KGaA, Weinheim

Table 2. Crystallographic data and details of structure refinement for the compounds $Bi(Bi_9)[NbCl_6]_3$ and $Bi_8[Ta_2O_2Br_7]_2$ (standard deviations in parentheses)

	$Bi(Bi_9)[NbCl_6]_3$	$Bi_8[Ta_2O_2Br_7]_2$
Empirical formula	$Bi_{10}Cl_{18}Nb_3$	$Bi_8Br_{14}O_4Ta_4$
Crystal system	hexagonal	tetragonal
Space group	$P6_3/m$	$P4/mnc$
Lattice constants	$a = 1377.1(2)$, $c = 1065.5(2)$ pm	$a = 1448.0(1)$, $c = 1830.6(2)$ pm
Unit cell volume	$V = 1749.8(3)\cdot10^6$ pm^3	$V = 3838.4(5)\cdot10^6$ pm^3
Number of formula units	$Z = 2$	$Z = 4$
Density (calculated)	$\rho = 5.706$ g·cm^{-3}	$\rho = 6.192$ g·cm^{-3}
Crystal dimensions	$0.095 \times 0.076 \times 0.475$ mm	$0.08 \times 0.09 \times 0.25$ mm
Diffractometer/radiation/temperature	Stoe Image Plate IPDS/Mo-K_α, $\lambda = 71.073$ pm/293 K	Stoe Image Plate IPDS/Mo-K_α, $\lambda = 71.073$ pm/293 K
Range of data collection	$9.5° \le 2\theta \le 56.3°$	$5.2° \le 2\theta \le 51.9°$
hkl range	$-18 \le h \le 18$; $-18 \le k \le 17$; $-13 \le l \le 13$	$-17 \le h \le 17$; $-17 \le k \le 17$; $-21 \le l \le 21$
Number of data collected	15926	27355
Number of unobserved reflections ($I \le 0$)	781	3297
Number of independent reflections/R_m	1471/0.098	1877/0.116
Number of reflections in least-squares	1471	1864; 13 reflections omitted
Absorption coefficient	$\mu = 523.9$ cm^{-1}	$\mu = 624.6$ cm^{-1}
Absorption correction/crystal shape[41]	numerical/11 faces	numerical/13 faces
Min./max. transmission T	0.0524/0.0788 anisotropic/isotropic split	0.0176/0.0600
Number of refined parameters	57/64	75
Ratio reflection/parameters	26/23	25
Extinction coefficient[43]	0.00351(6)/0.00351(6)	0.00011(2)
R values	0.068/0.066	0.085
$R(\|F\|)$ for all reflections	0.050/0.045	0.050
$R(\|F\|)$ [$F_o > 4\sigma(F_o)$]	1119/1119 reflections	988 reflections
$wR(F^2)$ for all reflections	0.068/0.066	0.118
Largest difference peak and hole [10^{-6} pm^{-3}]	+4.53 and −1.97/+3.40 and −1.93	+11.41/−2.32

cell. Although this alternative structure model slightly reduced the residual electron density, it had no significant effect on the overall quality of the refinement. The positions of the other atoms remained unchanged within their standard deviations.

$Bi_8[Ta_2O_2Br_7]_2$: Precession photographs showed the tetragonal crystal system with Laue class 4/*mmm*. Reflection conditions led to the space groups *P*4/*mnc* or *P*4*nc*, of which the centrosymmetric one was confirmed through structure analysis. The structure was solved by direct methods[42] and refined against F^2 by full-matrix least-squares calculations with anisotropic displacement parameters for all atoms.[43] A relatively large residual electron density was located at the origin of the unit cell. However, all attempts to include an atom at this position in the calculations did not enhance the quality of the structure refinement.

Magnetic Measurements: The thermomagnetic properties of $Bi(Bi_9)[NbCl_6]_3$ were determined on a sample (176 mg) of selected single crystals over the temperature range 76−295 K using a Faraday susceptometer. Measurements at several field forces showed no significant dependence. A diamagnetic correction was applied on the data. The purity of the sample was checked by powder X-ray diffractometry. Only a small impurity of Bi_6Cl_7 (ca. 5%) could be detected in the diffractogram.

Vibrational Spectroscopy: Infrared and Raman spectra were recorded using a Bruker IFS113V and a Bruker RFS100 spectrometer, respectively. For infrared spectroscopy, samples were prepared in a glove box as KBr discs. For Raman measurements, samples were finely ground with KBr in a mass ratio of 1:1 and placed in glass capillaries (1 mm diameter). We could not record a Raman spectrum of Bi_6Cl_7 as, even on cooling the sample capillary to 123 K, the compound decomposed in the laser beam.

Acknowledgments

Support of this work by the Deutsche Forschungsgemeinschaft and the Fonds der Chemischen Industrie is gratefully acknowledged.

Note added in proof (March 8, 2004): The synthesis and crystal structure of $Bi(Bi_9)[NbCl_6]_3$ was reported recently by: A. N. Kuznetsov, P. I. Naumenko, B. A. Popovkin, L. Kloo, *Russ. Chem. Bull.* **2003**, *52*, 2100−2104. The presence of Nb^{IV} was confirmed by the paramagnetic behaviour.

[1] J. D. Corbett, *Prog. Inorg. Chem.* **1976**, *21*, 129−158.
[2] A. Hershaft, J. D. Corbett, *J. Chem. Phys.* **1961**, *36*, 551−553; A. Hershaft, J. D. Corbett, *Inorg. Chem.* **1963**, *2*, 979−985; R. M. Friedman, J. D. Corbett, *Inorg. Chim. Acta* **1973**, *7*, 525−527.
[3] J. Beck, C. J. Brendel, L. Bengtsson-Kloo, B. Krebs, M. Mummert, A. Stankowski, S. Ulvenlund, *Chem. Ber.* **1996**, *129*, 1219−1226.
[4] R. M. Friedman, J. D. Corbett, *Inorg. Chem.* **1973**, *12*, 1134−1139.
[5] J. D. Corbett, *Inorg. Chem.* **1968**, *7*, 198−208.
[6] B. Krebs, M. Hucke, C. Brendel, *Angew. Chem.* **1982**, *94*, 453−454; *Angew. Chem. Int. Ed. Engl.* **1982**, *21*, 445−446.
[7] B. Krebs, M. Mummert, C. Brendel, *J. Less-Common Met.* **1986**, *116*, 159−168.

 © 2004 Wiley-VCH Verlag GmbH & Co. KGaA, Weinheim

[8] H. von Benda, A. Simon, W. Bauhofer, *Z. Anorg. Allgem. Chem.* **1978**, *438*, 53−67.
[9] A. N. Kutznetsov, A. V. Shevel'kov, S. I. Troyanov, B. A. Popovkin, *Russ. J. Inorg. Chem.* **1996**, *41*, 920−923, translated from *Zh. Neorg. Khim.* **1996**, *41*, 958−961; A. N. Kuznetsov, A. V. Shevel'kov, B. A. Popovkin, *Russ. J. Coord. Chem.* **1998**, *24*, 861−866, translated from *Koord. Khim.*
[10] A. N. Kutznetsov, A. V. Shevel'kov, B. A. Popovkin, *Russ. J. Coord. Chem.* **1998**, *24*, 861−866, translated from *Koord. Khim.* **1998**, *24*, 919−924.
[11] S. Ulvenlund, K. Ståhl, L. Bengtsson-Kloo, *Inorg. Chem.* **1996**, *35*, 223−230.
[12] H. Kalpen, W. Hönle, M. Somer, U. Schwarz, K. Peters, H. G. von Schnering, R. Blachnik, *Z. Anorg. Allgem. Chem.* **1998**, *624*, 1137−1147.
[13] M. Ruck, *Z. Anorg. Allgem. Chem.* **1998**, *624*, 521−528.
[14] K. Wade, *Adv. Inorg. Chem. Radiochem.* **1976**, *18*, 1; K. Ichikawa, T. Yamamaka, A. Takamaken, R. Glaser, *Inorg. Chem.* **1997**, *36*, 5284.
[15] J. Corbett, P. A. Edwards, *J. Am. Chem. Soc.* **1977**, *99*, 3313−3317.
[16] T. F. Fässler, in *Metal Clusters in Chemistry* (Eds.: P. Braunstein, L. A. Oro, P. R. Raithby), Wiley-VCH, Weinheim, Germany, **1998**.
[17] J. D. Corbett, *Chem. Rev.* **1985**, *85*, 383−397; J. D. Corbett, *Struct. Bonding* ***1997****, 87*, 157.
[18] A. Hirsch, Z. Chen, H. Jiao, *Angew. Chem.* **2001**, *113*, 2916−2920.
[19] A. N. Kutznetsov, L. Kloo, M. Lindsjö, J. Rosdahl, H. Stoll, *Chem. Eur. J.* **2001**, *7*, 2821−2828.
[20] J. Beck, A. Fischer, *Z. Anorg. Allgem. Chem.* **1997**, *623*, 780−784.
[21] J. Beck, G. Bock, *Z. Naturforsch., Teil B* **1996**, *51*, 119−126.
[22] M. Ruck, *Z. Anorg. Allgem. Chem.* **1995**, *621*, 2034−2042.
[23] W. H. Zachariasen, *Acta Crystallogr.* **1949**, *2*, 288−291.
[24] H. P. Beck, H. Nau, *Z. Anorg. Allgem. Chem.* **1988**, *558*, 193−200.
[25] J. M. Hughes, M. Cameron, K. D. Crowley, *Am. Min.* **1990**, *75*, 295−304.
[26] J. E. Post, R. B. Von Dreele, P. R. Buseck, *Acta Crystallogr., Sect. B* **1982**, *38*, 1056−1065.
[27] R. Hübenthal, R. Hoppe, *MAPLE, Programm zur Berechnung von Kristallstrukturen, ECoN und Mefir*, University Gießen, Germany, **1993**.
[28] F. Calderazzo, R. Poli, G. Pelizzi, *J. Chem. Soc., Dalton Trans.* **1984**, 2365−2369.
[29] N. Tokitoh, Y. Arai, R. Okazaki, S. Nagase, *Science* **1997**, *277*, 78−80.
[30] V. T. Kalinnikov, N. P. Lipatova, O. D. Ubozhenko, A. A. Zharkikh, *Dokl. Akad. Nauk SSSR* **1973**, *210*, 107.
[31] G. W. A. Fowles, D. J. Tidmarsh, R. A. Walton, *Inorg. Chem.* **1969**, *8*, 631−638.
[32] M. Kotani, *J. Phys. Soc., Jpn.* **1949**, *4*, 293.
[33] B. N. Figgis, *Trans. Faraday Soc.* **1961**, *57*, 198; B. N. Figgis, J. Lewis, *Progr. Inorg. Chem.* **1964**, *6*, 37−239.
[34] T. M. Dunn, *Trans. Faraday Soc.* **1961**, *57*, 1441.
[35] M. Gerloch, J. R. Miller, *Progr. Inorg. Chem.* **1968**, *10*, 1−47.
[36] K.-P. Frank, Dissertation, University Tübingen, Germany **1983**.
[37] M. J. Collins, R. J. Gillespie, J. W. Kolis, J. F. Sawyer, *Acta Crystallogr., Sect. C* **1987**, *43*, 2033−2036.
[38] U. Reusch, E. Schweda, *Z. Anorg. Allg. Chem.* **1997**, *623*, 805−809.
[39] L. Pauling, *The Nature of the Chemical Bond*, Cornell University Press, Ithaca, USA, **1960**.
[40] G. Brauer, *Handbuch der präparativen Anorganischen Chemie*, 3rd ed., Ferdinand Enke Verlag, Stuttgart, Germany, **1981**.
[41] W. Herrendorf, H. Bärnighausen, *HABITUS, Program for Numerical Absorption Correction*, University Karlsruhe, Germany, **1993**.
[42] G. M. Sheldrick, *SHELXS-86, Program for Crystal Structure Determination*, University Göttingen, Germany, **1986**.
[43] G. M. Sheldrick, *SHELXL-93, Program for Crystal Structure Refinement*, University Göttingen, Germany, **1993**.
[44] *DIAMOND, Visual Information System for Crystal Structures*, Crystal Impact Comp., Bonn, Germany, **1996**.

Received September 11, 2003
Early View Article
Published Online March 31, 2004

 © 2004 Wiley-VCH Verlag GmbH & Co. KGaA, Weinheim

Anchoring of Copper(II) Acetylacetonate onto an Activated Carbon Functionalised with a Triamine

Ana Rosa Silva,[a] Magda Martins,[a] M. Madalena A. Freitas,[b,c] José Luís Figueiredo,[b] Cristina Freire,*[a] and Baltazar de Castro[a]

Keywords: Copper / Schiff bases / Activated carbon / Anchoring / EPR spectroscopy

Copper(II) acetylacetonate was anchored onto a triamine functionalised activated carbon by Schiff condensation using a four-step procedure: (i) oxidation of activated carbon with nitric acid; (ii) treatment with thionyl chloride to convert carbon surface carboxylic acids into acyl chlorides; (iii) condensation of acyl chloride functionalities with amine groups of bis(3-aminopropyl)amine (*trien*); and (iv) Schiff condensation between free amine groups of bound *trien* with the oxygen atoms of acetylacetonate coordinated to the copper(II) ion. The same complex was also anchored to the unmodified activated carbon and to the acyl chloride functionalised carbon prepared in (ii). The resulting carbon-based materials were characterised by elemental analysis, surface techniques (SEM and XPS), temperature programmed desorption, and nitrogen adsorption at 77 K and EPR spectroscopy for the materials with copper(II) complexes. Data from all techniques provided evidence for (i) the covalent binding of *trien* to acyl chloride functionalities; and (ii) the irreversible attachment of $[Cu(acac)_2]$ to all carbon-based materials. Data for the materials with copper(II) proved conclusively that only the immobilisation procedure based on Schiff condensation with *trien* led to copper(II) complexes in which the metal centre remains four-coordinate.

(© Wiley-VCH Verlag GmbH & Co. KGaA, 69451 Weinheim, Germany, 2004)

Introduction

Aziridines are very important intermediates in organic synthesis and copper(II) acetylacetonate has been described as a very efficient homogeneous catalyst for the aziridination of olefins.[1] Copper(II) Schiff-base complexes have also been used as homogeneous catalysts in the aziridination of olefins,[2] as well as in the cyclopropanation of olefins,[3] oxidation of sulfides to sulfoxides[4] and in the peroxidative oxidation of phenol to dihydroxy benzynes.[5] Currently, transition metal complexes with Schiff-base ligands (*salen*) are the subject of intense research as they present high activity, chemoselectivity and enantioselectivity in a large range of catalytic processes.[6]

The last decade has witnessed a growing interest in the heterogenisation of homogeneous metal complexes using several types of supports,[6−10] with the aim to overcome some limitations of homogeneous catalysts − separation from the reaction media and subsequent recycling. Initially the complexes were ion exchanged or adsorbed on the porous supports and, consequently, could be susceptible to leaching.[10−12] More recently, several grafting and tethering procedures have been developed to covalently attach transition metal complexes to organic polymers,[8] silica, zeolites and other micro and mesoporous inorganic materials.[7,9,10]

Activated carbons and other carbon materials are widely used as catalysts and as supports for metals in its reduced state,[13,14] and few reports have appeared in the last years on the heterogenisation of homogeneous metal complexes, mainly of noble metals with simple ligands, to be used in hydrogenation and hydroformylation reactions.[15−17] Nevertheless, activated carbons present several advantages when compared to inorganic supports;[13] they are thermally stable, resistant to chemical attack in acid and basic media and, generally, of low cost.[13] On the other hand, several thermal and chemical processes can be used to tailor the porous structure and the type and concentration of specific oxygen surface groups.[13,18] These groups can be used as building blocks to bridge the metal complex to the support, and their variety allows for the use of various immobilisation procedures. Iron−phthalocyanine complexes supported by impregnation on carbon[19] and activated carbon blacks[20] have been used as heterogeneous catalysts in the oxidation of alkanes, but no reference to leaching or

[a] REQUIMTE/Departamento de Química, Faculdade de Ciências, Universidade do Porto,
4169-007 Porto, Portugal
Fax: (internat.) + 351-22-6082959
E-mail: acfreire@fc.up.pt
[b] Laboratório de Catálise e Materiais, Departamento de Engenharia Química, Faculdade de Engenharia, Universidade do Porto,
4200-465 Porto, Portugal
[c] Instituto Superior de Engenharia, Instituto Politécnico do Porto,
4200-072 Porto, Portugal

reuse was made, despite the method used being susceptible to leaching of the active phase. Anchorage of copper(II) and cobalt(II) acetylacetonates to surface groups of an activated carbon using a diamine as linking agent has also been reported, and resulting materials have not only proved to be efficient heterogeneous catalysts in the oxidation of pinane, but were also resistant to leaching of the complexes.[21]

We are pursuing the development of several strategies for the immobilisation of functionalised Schiff-base transition metal complexes onto activated carbons in order to gather information on whether the modifications of their surface groups can lead to a more efficient anchoring without loss of catalytic activity of the complex, with the overall aim of optimising procedures to prepare carbon-based heterogeneous catalysts. Recently, we have reported the anchoring of nickel(II) Schiff-base complexes onto activated carbon using two different routes;[22,23] in the first a linking agent, cyanuric chloride, was used to react with hydroxyl groups on both the activated surface and the metal complex;[22] and in the second, two metal complexes bearing uncoordinated amine groups were anchored onto an activated carbon functionalised with an acyl chloride that acted as the anchoring building block functionality.[23] The direct anchoring of a copper(II) Schiff-base complex functionalised with uncoordinated hydroxyl groups was achieved[24] and the process was applied to the heterogenisation of their manganese(III) counterparts, which were shown to act as efficient and reusable heterogeneous catalysts in the epoxidation of styrene,[25,26] with similar styrene epoxide chemoselectivities as the corresponding homogeneous phase reactions.[25,26,27]

Copper(II) complexes with pentadentate N_3O_2 Schiff bases have also been encapsulated in zeolites[28,29] and in aluminium pillared layered clays using the ship in a bottle procedure,[30,31] by reaction of copper(II) acetylacetonate with bis(3-aminopropyl)amine (*trien*), and using the simultaneous pillaring and copper(II) complex encapsulation in a montmorilonite.[32] In the present work, we report an extension of these procedures in which copper(II) acetylacetonate is irreversibly anchored onto a chemically oxidised activated carbon functionalised with *trien* by Schiff condensation between the free amine groups of *trien* covalently attached to the activated carbon surface (see Scheme 1) with the oxygen atoms of acetylacetonate coordinate to copper(II) (see Scheme 2). To assess the effectiveness of this method we have compared its anchoring efficiency with those obtained by direct adsorption onto unmodified oxidised activated carbon and onto a carbon functionalised with acyl chloride groups. In order to get information on the effect of the various treatments on the surface chemical and physical properties of the carbon materials, these were characterised by proximate and elemental analysis, surface techniques (scanning electron microscopy and X-ray photoelectron spectroscopy), nitrogen adsorption at 77 K, and thermal methods (temperature-programmed desorption). Copper(II) carbon-based materials were also characterised by electron paramagnetic resonance, which can provide information on the changes in the coordination sphere of the metal centre.

Results and Discussion

Immobilisation of copper(II) acetylacetonate onto the activated carbon was performed in four steps: (i) oxidation of the activated carbon with nitric acid, (ii) reaction with $SOCl_2$, (iii) functionalisation with *trien*, bis(3-aminopropyl)-amine, and then (iv) anchoring of the complex onto the modified carbon. The materials obtained after the first two steps of the anchoring procedure (carbon A2 and A3) have been extensively characterised by us in a previous report,[23] and thus the characterisation and discussion will be focused on the new materials obtained from the two last steps.

Functionalisation of Thionyl-Chloride-Modified Activated Carbon with Bis(3-aminopropyl)amine (*trien*)

Composition and Texture

The proximate and elemental analyses of carbon materials are collected in Table 1. The volatile matter and the nitrogen and hydrogen content increase when carbon A3 is modified with *trien* (Table 1), suggesting that *trien* reacted with the activated carbon surface groups and therefore was covalently attached to the activated carbon surface. This is also supported by a decrease, relative to carbon A3, of 16% in the micropore volume and of 19% in the larger pore area (Table 2), arising from the presence of a relatively voluminous compound at the surface of the activated carbon.

Table 1. Proximate and elemental analyses for carbon-based materials.

Carbon atom	Proximate analysis (wt.-%) volatiles	C_{fixed}	ash	Elemental analysis (wt.-%) C	H	N
A1	8.81	89.44	1.74	92.69	0.44	0.45
A2	11.78	87.28	0.95	91.04	0.36	0.73
A3	21.11	78.37	0.52	89.31	1.12	0.51
A4	23.78	76.19	0.03	88.57	1.49	1.20
A5	19.29	79.51	1.20	87.57	1.08	1.17

Table 2. Textural properties for carbon-based materials

Carbon	V_{micro}[a] ($cm^3\ g^{-1}$)	S_{me}[a] ($m^2\ g^{-1}$)	$V_{0.95}$[b] ($cm^3\ g^{-1}$)	V_{meso}[c] ($cm^3\ g^{-1}$)
A1	0.359	122	0.527	0.168
A2	0.347	122	0.516	0.169
A3	0.303	255	0.581	0.278
A4	0.255	207	0.514	0.259
A5	0.222	74	0.330	0.107

[a] Calculated by the *t*-method. [b] Pore volume at $p/p_0 = 0.95$. [c] Subtraction of the total pore volume, at $p/p_0 = 0.95$, and of the microporous volume.

 © 2004 Wiley-VCH Verlag GmbH & Co. KGaA, Weinheim

X-ray Photoelectron Spectroscopy

There is a significant increase in the nitrogen content following the introduction of *trien* in carbon A3, which is accompanied by a decrease in the chlorine content as can be seen in Table 3. This indicates that reaction between the amine groups of the triamine and the acyl chloride functionalities has occurred, with formation of new amide groups and loss of hydrogen chloride (Scheme 1, a). A superficial loss of oxygen is also observed which may be explained by Schiff condensation between the amine groups and the surface carbonyl groups (Scheme 1, b, see TPD section, below), that increases the effectiveness of the *trien* anchoring process.

Table 3. Area under the XPS bands in the O 1s, N 1s, Cl 2p, C 1s, and Cu $2p_{3/2}$ regions of the carbon-based materials

Carbon atom	Atomic % O	N	Cl	C	Cu	O/C	N/C	Cl/C	N/Cu
A1	7.66	0.58	0.86	90.41	–	0.0847	0.0064	0.0095	–
A2	20.27	0.58	0.13	78.61	–	0.2578	0.0074	0.0017	–
A3	10.98	0.60	3.03	84.84	–	0.1294	0.0071	0.0357	–
A4	9.01	3.64	1.81	85.06	–	0.106	0.0428	0.0213	–
A5	14.01	4.48	2.20	78.16	0.66	0.1792	0.0573	0.0281	6.8

The Cl 2p spectrum of carbon A4 exhibits bands at the same binding energy as those found in the parent material (Figure 1, a), thus providing evidence that not all surface acyl chloride functionalities have reacted with the amine groups of *trien*. A new band is also observed at about 199 eV, which corresponds to chloride ions produced in the reaction of acyl chloride with amine groups (Scheme 1, a).

The spectra of carbons A3 and A4 in the O 1s region are similar (Figure 1, b), but that of carbon A4 shows a very slight band broadening, which may suggest an increase in the amount of oxygen atoms in different chemical environments resulting from the new amide ligation (Scheme 1, a).

The XPS spectrum of carbon A4 in the N 1s region (Figure 1, c) presents an almost symmetrical large band, centred at about 400 eV, which corresponds to different types of nitrogen atoms present at the surface of the carbon material – primary amines, secondary amines, amides and imines (Scheme 1).[33]

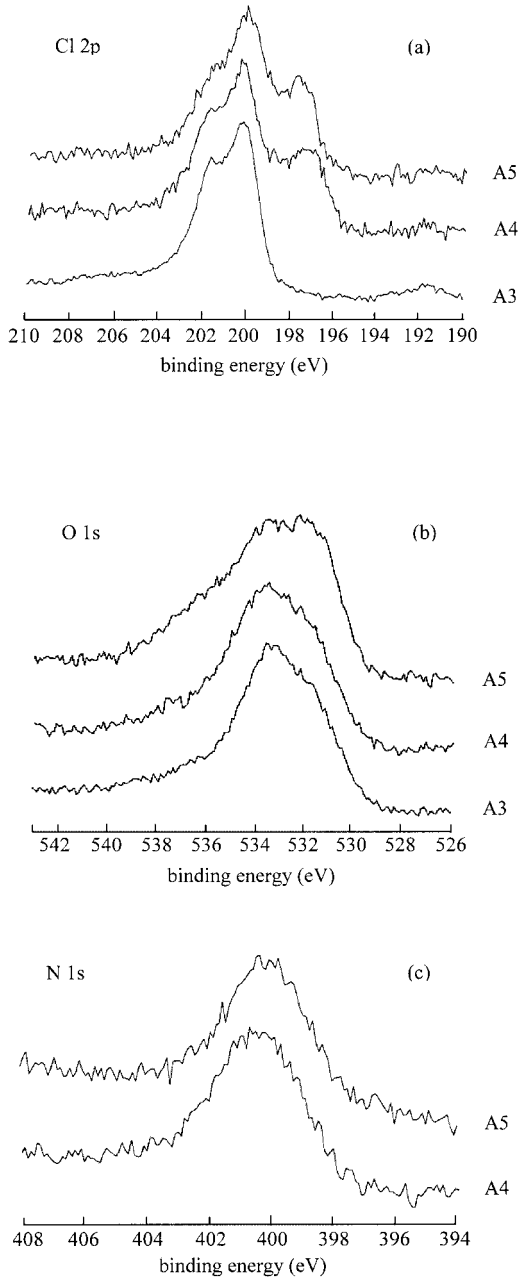

Figure 1. High resolution XPS spectra of carbon-based materials in the regions: a) Cl 2p; b) O 1s, and c) N 1s

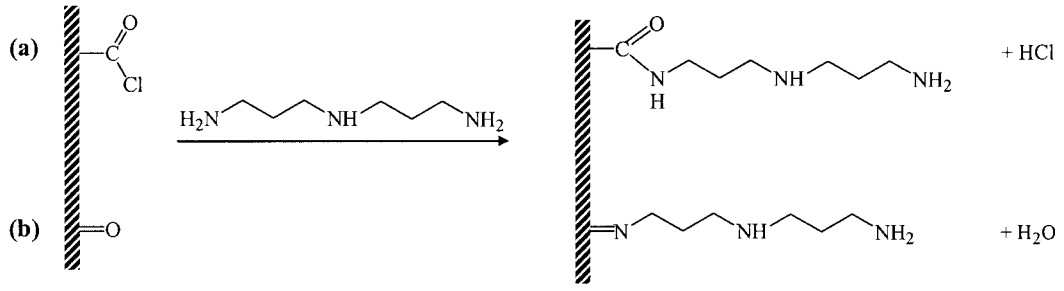

Scheme 1. Anchoring of *trien* onto acyl chloride functionalised activated carbon

 © 2004 Wiley-VCH Verlag GmbH & Co. KGaA, Weinheim

Temperature Programmed Desorption (TPD)

The TPD profiles for the $m/z = 28$ and $m/z = 44$ fragments of carbon atoms A3−A5 are represented in Figure 2, and the areas under the peaks for all carbon-based materials are collected in Table 4. We have already described in a previous report[23] that oxidation of activated carbons with nitric acid increases the number of carboxylic acid groups which are observed at 560 K in the $m/z = 44$ TPD profile.

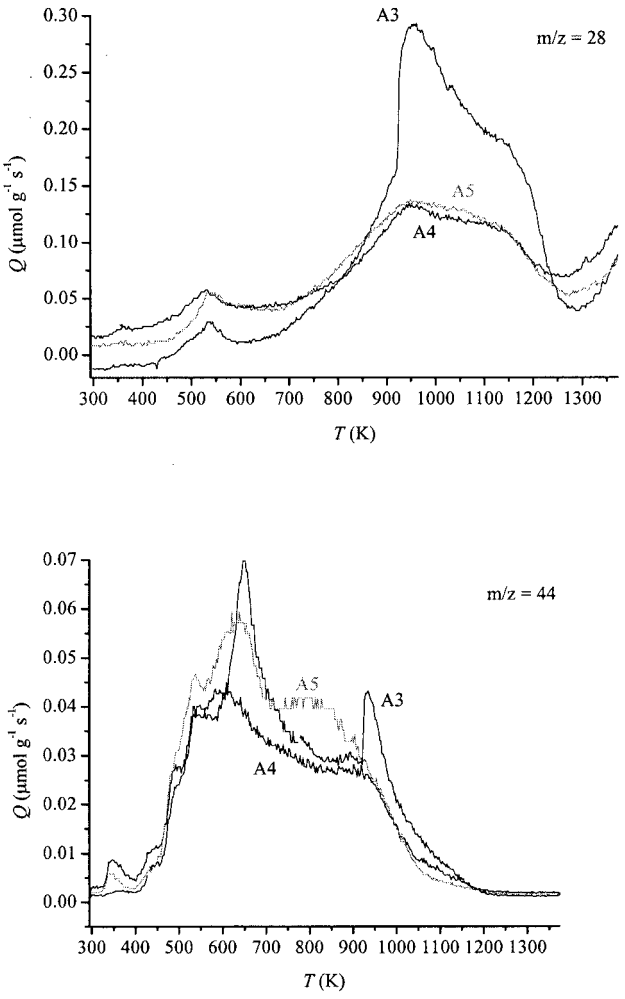

Figure 2. TPD profiles for the fragments $m/z = 28$ and 44 for A3−A5 carbon-based materials

Table 4. Amounts of fragments with $m/z = 28$ and $m/z = 44$ released during the TPD experiments, obtained by integration of the areas under the peaks, for the carbon-based materials

Carbon atom	$m/z = 28$ (μmol g^{-1})	$m/z = 44$ (μmol g^{-1})	$m/z = 28 + 44$ (μmol g^{-1})
A1	476	140	616
A2	1046	374	1420
A3	1270	245	1515
A4	712	201	913
A5	787	254	1041
A6	1041	314	1355
A7	1014	259	1273

These bands disappear after reaction with thionyl chloride, giving rise to a new intense band at 960 K in the $m/z = 28$ TPD profile, which has been attributed to the acyl chloride functionalities.[23] These functionalities decompose to carbon monoxide, but at lower temperature than the carbonyl/quinone functionalities (1100 K) due to the electron density withdrawing effect of chlorine atom. Introduction of the triamine at the surface of carbon A3 causes a significant decrease in intensity of the band at 960 K in the $m/z = 28$ TPD profile (Figure 2). This phenomenon was also observed upon the attachment of nickel(II) complexes functionalised with amines onto an activated carbon surface with acyl chloride functionalities and was attributed to the reaction between the amine groups and the acyl chloride groups, with the formation of amide ligations.[23] The same explanation is presupposed for the decrease in intensity of this band after the reaction of amine groups of *trien* with acyl chloride surface groups (Scheme 1, a).

There is also a significant intensity decrease in the high temperature region of the $m/z = 28$ TPD profile (Figure 2, b) assigned to carbonyl groups, which may be attributed to Schiff condensation reactions between these groups and the amines (Scheme 1, b), in accordance with the results of XPS analysis (vide supra).

Anchoring of the Copper(II) Acetylacetonate onto the Modified Activated Carbons

Evidence for the effective anchorage of the copper complexes onto the surface of carbon A4 is provided by noting that (a) the blue colour of complex solution disappears during the adsorption reaction, and (b) colourless solutions are obtained when the material is purified by Soxhlet extraction.

Adsorption of copper(II) acetylacetonate (toluene solutions) onto carbons A2 and A3 was also performed using similar experimental conditions and a decrease in the blue colour of solution was observed. During the purification steps of these materials no colour due to copper(II) complexes were observed in the washing solutions, suggesting that the adsorbed copper(II) acetylacetonate was not leached.

Copper content of carbons A5−A7 was determined by ICP-AES and from this it was possible to calculate the loading (mass of copper/mass of carbon × 100) and the efficiency of adsorption (amount of adsorbed complex/amount in original solution × 100) which are both summarised in Table 5. The data shows that metal loading in A6 and A7 are similar, but are about half of that in A5, with a similar pattern for the efficiency of adsorption. These results clearly indicate that functionalisation of the activated carbon surface with a triamine increases the efficiency of copper(II) acetylacetonate immobilisation.

Composition and Texture

A comparison of the results of proximate and elemental analyses of carbon A5 with those of its precursor (carbon

 © 2004 Wiley-VCH Verlag GmbH & Co. KGaA, Weinheim

Table 5. ICP-AES results for copper containing carbon-based materials

Carbon atom	n_i[a] (μmol g^{-1})	Cu (wt-%)	n_f[b] (μmol g^{-1})	η[c] (%)	N/Cu[d]
A5	145	0.779 (3.12)[e]	123	85	6.8
A6	168	0.396	62	37	–
A7	114	0.382	60	53	–

[a] n_i = initial $[Cu(acac)_2]$ mol (solution)/weight activated carbon. [b] n_f = adsorbed $[Cu(acac)_2]$ moles/weight activated carbon. [c] $\eta = n_f \times 100/n_i$. [d] N/Cu (atomic ratio) =[N(wt%) × relative atomic mass(Cu)]/[Cu(wt%) × relative atomic mass(N)]; N(wt%) from Table 1. [e] Copper weight% calculated from XPS in Table 3. Weight Cu% = atomic% Cu × Ar(Cu)/[atomic% O × Ar(O) + atomic% N × Ar(N) + atomic% Cl × Ar(Cl) + atomic% C × Ar(C) + atomic% Cu × Ar(Cu)].

A4) show an increase in ash content, and a decrease in hydrogen content. The first is due to the presence of copper(II) in the material, and the second further supports the immobilisation of $[Cu(acac)_2]$ by the processes represented in Scheme 2, due to loss of water during Schiff condensation.

The decrease of volatile matter after complex anchorage may be attributed to the inclusion of *trien* in the copper(II) coordination sphere (Scheme 2), which increases its stability relative to that of *trien* bound only to the activated carbon surface.

The immobilisation of copper(II) acetylacetonate onto carbon A4 causes pore blockage and thus a decrease in pore volume. The observation that the decrease (59%) in wide pore volume is much larger than that observed (13%) in micropore volume suggests that the metal complexes are anchored preferentially onto the mesopore and macropore surface.

X-ray Photoelectron Spectroscopy

High resolution XPS spectra of carbons A3−A5 in the O 1s region are depicted in Figure 1, and the areas under the high resolution XPS peaks in the regions O 1s, N 1s, Cl 2p, C 1s, and Cu $2p_{3/2}$ are summarised in Table 3.

When $[Cu(acac)_2]$ is immobilised onto the activated carbon functionalised with *trien* there is an increase in oxygen and copper surface content (Table 3), but no significant changes are observed in the XPS spectra, with the exception of the O 1s XPS profile, for which an increase in intensity of the lower energy band (531.6 eV) is observed (Figure 1). Since we reported that oxygen atoms coordinated to transition metal cations possess similar O 1s binding energies,[22−26] this increase may be assigned to oxygen atoms from $[Cu(acac)_2]$.

By using the Cu atomic% from XPS and converting to Cu wt% we get 3.12 (Table 5), a value that when compared with Cu wt% from bulk analysis (0.779), indicates that the complexes are located preferentially at the outer pores.

An atomic ratio N/Cu of 6.8 is obtained by both XPS (Table 3) and elemental analysis (Table 5), which provides an indication that the anchoring mechanism of $[Cu(acac)_2]$ is the same within the matrix. The atomic ratio N/Cu for anchored complexes must lie between 3 and 6 (Scheme 2), thus the observed value is consistent with the presence of uncomplexed *trien*, but does not provide any conclusive information on *trien* binding to copper.

Temperature Programmed Desorption

Carbons A4 and A5 exhibit TPD profiles that are practically identical for $m/z = 28$ and slightly different for $m/z = 44$ (Figure 2), which suggests that the main anchoring process takes place by reaction with the amine groups immobilised at the carbon A4 surface, and that direct complex anchoring to the oxygen groups on the carbon surface must be virtually absent. The small differences in the $m/z = 44$ profile between A5 and A4 carbons may be assigned to fragments arising from decomposition of acetylacetonate ligand.

This result must be contrasted with the changes in the TPD profiles of carbon atoms A6 and A7, which exhibit a decrease in band intensity when compared with those of their precursors (A2 and A3) (Figures 3 and 4, respectively). For A6, those corresponding to carbonyl/quinone groups

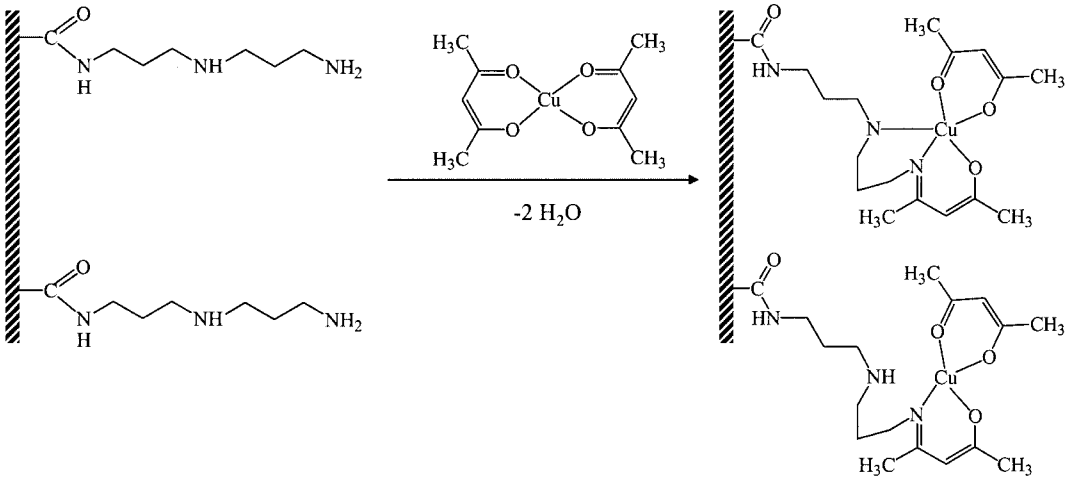

Scheme 2. Proposed structures for the anchored copper(II) acetylacetonate onto *trien* functionalised activated carbon

 © 2004 Wiley-VCH Verlag GmbH & Co. KGaA, Weinheim

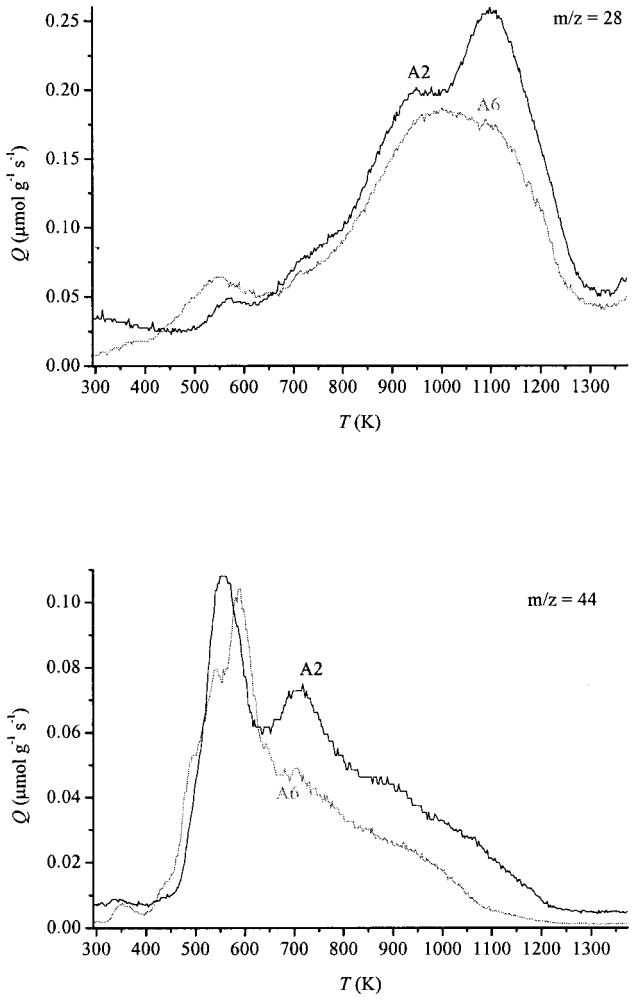

Figure 3. TPD profiles for the fragments m/z = 28 and 44 for A2 and A6 carbon-based materials

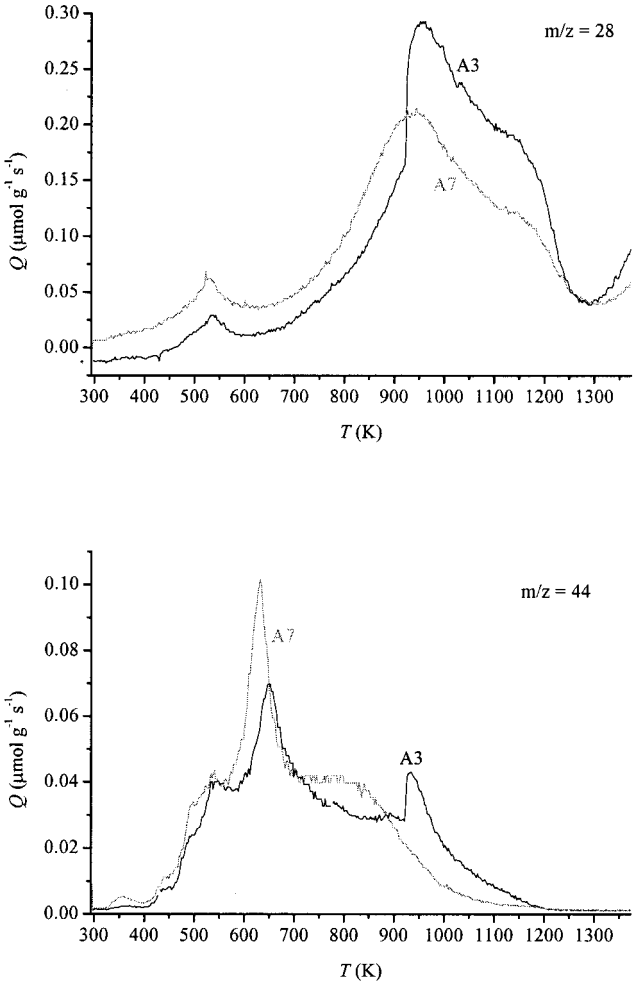

Figure 4. TPD profiles for the fragments m/z = 28 and 44 for A3 and A7 carbon-based materials

(higher temperatures in the m/z = 28 profile)[18] and to lactones and anhydrides (m/z = 44 profile).[18] A similar pattern is also observed for A7, but the most characteristic feature is the decrease in the band which was assigned to acyl chloride functionalities.[23] These changes suggest direct anchoring [Cu(acac)$_2$] to surface functional groups of the activated carbons and we propose that it takes place by axial coordination of the copper(II) complex to these surface groups.

Electronic Paramagnetic Resonance

Carbon A5 exhibits an EPR spectrum of axial type which shows hyperfine splitting in the lowest magnetic field region, due to the interaction of the unpaired electron with the copper nucleus (^{65}Cu/^{63}Cu I = 3/2) (Figure 5, a). The EPR spectrum is typical of magnetically diluted copper(II) species, despite the large band broadening, which indicates that [Cu(acac)$_2$] is regularly distributed within the carbon matrix, which acts as a diamagnetic host.

The similarity between the EPR spectrum of carbon A5 with those observed for free [Cu(acac)$_2$] (Figure 5, b) and [Cu(acac)$_2$*trien*] (Figure 5, c) complexes allows the same

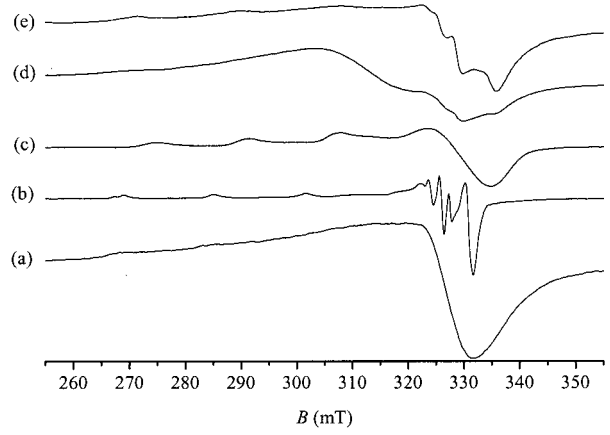

Figure 5. EPR spectra (ν = 9.41 GHz) at 120 K for: (a) carbon A5, 1% in KBr; (b) [Cu(acac)$_2$], frozen methanol solution; (c) [Cu(acac)$_2$-*trien*], frozen methanol solution; (d) A7, 5% in KBr, and (e) carbon A6, 5% in KBr

orientation scheme for the tensor axes: $g_1 = g_z$, $g_2 = g_x$, $g_3 = g_y$, where g_1 and g_3 refer to the lowest and highest magnetic fields g values (obviously, $A_1 = A_z$, $A_2 = A_x$, and $A_3 = A_y$);[34,35] in this context, as $g_z > g_x$, g_y, the ground

 © 2004 Wiley-VCH Verlag GmbH & Co. KGaA, Weinheim

Table 6. EPR data for the free and supported $[Cu(acac)_2]$ complex

Sample	g or g_z	$g_\perp$ or g_x; g_y	g_{av}[a]	A[b] or A_z	$A_\perp$[b] or A_x; A_y	Ref.
$[Cu(acac)_2]/CHCl_3$	2.285	2.042	2.123	175	28.2	[34]
$[Cu(acac)_2]$/dmf	2.293	2.061	2.138	172	13.1	[34]
$[Cu(acac)_2]$/methanol	2.290	2.067	2.141	165.0	15.4	[29]
$[Cu(acac)_2$*trien*]/methanol	2.243	2.050	2.144	174.9	12.0	[29]
A5	2.288	2.063	2.138	165.7	25.7;25.7	[c]
A6	2.251	2.044; 2.050	2.115	178.7	25.7;25.7	[c]
A7	[d]	[d]	[d]	[d]	[d]	[c]

[a] $gav = 1/3(g + 2\,g_\perp)$ or $g_{av} = 1/3(gz + gx + gy)$. [b] The values are expressed in 10^{-4} cm^{-1}. [c] This work. [d] Not simulated.

state proposed for $[Cu(acac)_2]$ anchored onto activated carbon functionalised with *trien* is d_{xy}.[35]

The values of tensors g and A obtained by simulation are compiled in Table 6, as well as the values for similar copper(II) free complexes. It must be pointed out that band broadening can be attributed not only to solid state effects, but also to the presence of distinct copper(II) species with very similar structures, a consequence of the different copper coordination spheres that arise from the anchorage (Scheme 2). The existence of several species for which the g and A values are very similar makes it impossible to resolve individual spectra and the EPR simulated values must be taken as average values. Nevertheless, a careful comparison with g an A values for free copper(II) complexes can provide insights into the possible structures of the anchored complexes.

The g value of carbon atom A5 is similar to those of $[Cu(acac)_2]$ in several solvents where axial coordination is incipient or nonexistent (Table 6), suggesting that the majority of *trien* based anchored complexes are four-coordinate (probably with some tetrahedral distortion) and with no axial coordination to the nitrogen of the secondary amine of *trien* (Scheme 2). However, direct anchoring of $[Cu(acac)_2]$ by axial coordination to carbon surface groups cannot be ruled out on the basis of the EPR data, as axial coordination and tetrahedral distortion of the equatorial plane may cause similar changes in the EPR spectra.[36,37]

The EPR spectrum of carbon atom A7 (Figure 5, d) is more complex, and as it can be interpreted assuming the existence of an octahedral species (strong axial coordination to carbon surface groups), either with pseudo isotropic EPR signals or low intensity magnetic interactions between vicinal copper(II) centres, its full interpretation was not further pursued.

In contrast, the EPR spectrum of carbon atom A6 (Figure 5, e) is similar to that of A5, thus also typical of magnetically diluted species, and for which the same orientation scheme for the g and A tensor can be used, and a d_{xy} ground state proposed. However, as the g value is similar to that of $[Cu(acac)_2$*trien*] (Table 6), axial coordination of the copper(II) atom to the carbon surface groups is proposed.

Conclusion

Direct anchoring of copper(II) acetylacetonate onto an oxidised activated carbon can be achieved using either the unmodified or an acyl chloride functionalised form (Scheme 1), but in either case direct coordination of the copper(II) centres to carbon surface groups takes place. The copper(II) complex can also be immobilised in activated carbons functionalised with acyl chlorides to which bis(3-aminopropyl)amine have been immobilised, thus making the available amine groups distant from the carbon surface, which are able to covalently attach $[Cu(acac)_2]$ by amide ligations, formed by Schiff condensation of the unbound amines with the oxygen atoms of the acetylacetonate ligands.

In all methods the complexes are bound to the carbon surface and thus leaching of complexes is prevented, but the anchoring method that uses *trien* has two significant advantages. On the one hand it allows for the loading of the copper(II) complex to be larger than the other methods by a factor of two, and more importantly the separation of the copper centres from the carbon surface which implies that the majority of the anchored complexes remain four-coordinate. This latter aspect is of crucial importance if these heterogeneous materials, with anchored copper(II) complexes, are to be used to catalyse reactions for which $[Cu(acac)_2]$ acts as a homogeneous catalyst. This means that the tethered complexes retain the same coordination sphere as that in solution, making these materials very promising heterogeneous catalysts for the aziridination of olefins.

Experimental Section

Materials: The starting carbon material was a NORIT ROX 0.8 activated carbon (rodlike pellets with 0.8 mm diameter and 5 mm length). This material has a pore volume of 0.695 $cm^3 \cdot g^{-1}$ determined by porosimetry (corresponding to meso and macropores), an ash content of 2.6% (w/w), an iodine number of 1000 and the mercury and helium densities are 0.666 and 2.11 $g \cdot cm^{-3}$, respectively. The activated carbon was purified by Soxhlet extraction with HCl 2 $mol \cdot dm^{-3}$ for 6 hours, washed with deionised water until pH 6−7 and then dried in an oven at 150 °C for 13 hours, under vacuum (carbon A1).

All reagents and solvents used in the modification of the activated carbon and in the anchoring of the copper(II) complex were purified by distillation, except for copper(II) acetylacetonate, which was used as received. Copper(II) acetylacetonate and bis(3-aminopropyl)-amine (*trien*) were from Aldrich, and thionyl chloride, toluene and all other chemicals were from Merck (pro analysi).

$[Cu(acac)_2]$, XPS spectrum (eV): C 1s, 285.0 and 287.2; O 1s, 532.0; Cu $2p_{3/2}$, 934.8.

 © 2004 Wiley-VCH Verlag GmbH & Co. KGaA, Weinheim

Functionalisation of Activated Carbon

Oxidation of Activated Carbon: The purified NORIT ROX 0.8 activated carbon (carbon A1; 22.0 g) was refluxed with a 5 mol·dm^{-3} solution of nitric acid (600 cm^3) for 7 hours. The oxidised carbon was extensively washed with deionised water until pH 6−7 and then dried in an oven at 150 °C for 13 hours, under vacuum (carbon A2).[18,23]

Reaction with Thionyl Chloride ($SOCl_2$): The oxidised activated carbon (12.0 g) was refluxed with 40 cm^3 of a 5% (v/v) solution of thionyl chloride in toluene for 5 hours, extensively washed with toluene, and then purified by Soxhlet extraction with toluene for 2 hours, and finally dried in an oven at 150 °C for 13 hours, under vacuum (carbon A3).[23,38]

Functionalisation with Bis(3-aminopropyl)amine (Trien): Carbon A3 (3.0 g) was refluxed with a solution containing 390 μmol of bis(3-aminopropyl)amine (*trien*) in 40 cm^3 toluene for 4 hours, then filtered and extensively washed with toluene. The material was also Soxhlet extracted for 2 hours with toluene and dried in an oven at 150 °C for 13 hours, under vacuum (carbon A4).

Anchoring of [Cu(acac)$_2$] onto the A4 Carbon: The activated carbon functionalised with *trien* (A4, 2.0 g) was added to 100 cm^3 of a solution of [Cu(acac)$_2$] in toluene (290 μmol), and the mixture was refluxed for 5 hours; during the reflux a progressive disappearance of the solution colour was observed. The resulting material was extensively washed with toluene and then purified by Soxhlet extraction with toluene for 7 hours, and dried in an oven at 150 °C for 13 hours, under vacuum (carbon A5).

Anchoring of [Cu(acac)$_2$] onto the A2 Carbon: The oxidised activated carbon A2 (2.0 g) was added to 100 cm^3 of a solution of [Cu(acac)$_2$] in toluene (335 μmol), and the mixture was refluxed for 5 hours, and a progressive disappearance of the solution colour was also observed. The resulting material, carbon A6, was extensively washed with toluene and then purified by Soxhlet extraction with toluene for 7 hours, and dried in an oven at 150 °C for 13 hours, under vacuum (carbon A6).

Anchoring of [Cu(acac)$_2$] onto the A3 Carbon: The activated carbon functionalised with acyl chloride groups (A3, 2.0 g) was added to 100 cm^3 of a solution of [Cu(acac)$_2$] in toluene (229 μmol), the mixture was refluxed for 5 hours, and a progressive disappearance of the solution colour was observed. The resulting material was extensively washed with toluene and then purified by Soxhlet extraction with toluene for 7 hours, and dried in an oven at 150 °C for 13 hours, under vacuum (carbon A7).

Physico-Chemical Measurements

X-ray photoelectron spectroscopy was carried out at "Centro de Materiais da Universidade do Porto" (Portugal), in a VG Scientific ESCALAB 200A spectrometer using a non-monochromatized Mg-*Kα* radiation (1253.6 eV). The metal complex was compressed into a pellet prior to the XPS study. In order to correct for possible deviations caused by electric charge on the samples, the C 1s line at 284.6 eV was taken as internal standard.[39,40]

The textural characterisation of carbon-based materials was based on the N_2 adsorption isotherms, which were determined at 77 K with a Coulter Omnisorp 100 CX apparatus. The samples were degassed at 350 °C (A1) or at 120 °C (all other samples) until a final vacuum of 10^{-6} Torr was reached. The volume (V_{micro}) and mesopore surface area (S_{me}) were determined by the *t*-method, using the standard isotherm for carbon materials proposed by Reinoso et al.[41] The pore volume at $p/p_0 = 0.95$ ($V_{0.95}$) was estimated from the N_2 uptake (using the value of 0.8081 as the density of N_2 in its normal liquid state); the porosity volume, other than that due to the micropores (which accounts for most of mesopores − V_{me}), was calculated by subtracting the micropore volume, (V_{micro}), obtained by the *t*-method at $p/p_0 = 0.95$, ($V_{0.95}$), from the pore volume.[42]

Elemental analysis of C, H, and N were performed with a Carlo−Erba EA 1108 Elemental Analyzer. Metal analysis was performed by Kingston Analytical Services, U.K.

The thermograms were recorded with a Mettler TA 4000 thermal analyser, using a heating rate of 5 K·min^{-1} and a flow rate of the N_2 carrier gas of 200 cm^3·min^{-1}. The TPD profiles were obtained with a custom built set-up, consisting of a U-shaped tubular microreactor, placed inside an electrical furnace. The flow rate of the helium carrier gas (25 cm^3·min^{-1}) and the heating rate of the furnace (5 K·min^{-1}) were controlled with appropriate units. The masses at $m/z = 28$ and 44 were monitored with a Spectramass Dataquad quadrupole mass spectrometer.

EPR spectra of powdered samples diluted in KBr (5%) were obtained with an X band Bruker ESP 300 E spectrometer, at room temperature and at 120 K. The spectra were calibrated with diphenylpicrylhydrazyl (dpph) with $g = 2.0037$, and the magnetic field was calibrated using Mn^{II} in MgO. Typical experimental conditions were − modulation frequency: 100 kHz; modulation amplitude: 9 G; microwave power: 5 mW. The EPR parameters were obtained by simulation using the program Win EPR Simfonia (Bruker) assuming axial or rhombic Spin Hamiltonians. The reported values of $g_\perp$ (or g_x and g_y) and $A_\perp$ (or A_x and A_y) are less accurate because of their dependence on the used line widths (20−60 G).

Acknowledgments

The authors are indebted to Dr. Carlos Sá (CEMUP) for assistance with XPS analysis and to NORIT N.V., Amersfoort, Netherlands, for providing the activated carbon. A. R. S. thanks "Fundação para a Ciência e Tecnologia" (Lisboa) and the European Social Fund for a fellowship.

[1] D. A. Evans, M. M. Faul, M. T. Bilodeau, *J. Org. Chem.* **1991**, *56*, 6744−6746.
[2] Z. Li, K. R. Conser, E. N. Jacobsen, *J. Am. Chem. Soc.* **1993**, *115*, 5326−5327.
[3] C.-M. Che, H.-L. Kwong, W.-C. Chu, K.-F. Cheng, W.-S. Lee, H.-S. Yu, C.-T. Yeung, K.-K. Cheung, *Eur. J. Inorg. Chem.* **2002**, 1456−1463.
[4] S. Bunce, R. J. Cross, L. J. Farrugia, S. Kunchandy, L. L. Meason, K. W. Muir, M. O′Donnell, R. D. Peacock, D. Stirling, S. J. Teat, *Polyhedron* **1998**, *17*, 4179−4187.
[5] C. R. Jacob, S. P. Varkey, P. Ratnasamy, *Microporous Mesoporous Mater.* **1998**, *22*, 465−474.
[6] L. Canali, D. C. Sherrington, *Chem. Soc. Rev.* **1999**, *28*, 85−93.
[7] Q.-H. Fan, Y.-M. Li, A. S. C. Chan, *Chem. Rev.* **2002**, *102*, 3385−3466.
[8] N. E. Leadbeater, M. Marco, *Chem. Rev.* **2002**, *102*, 3217−3274.
[9] C. E. Song, S. Lee, *Chem. Rev.* **2002**, *102*, 3495−3524.
[10] D. Brunel, N. Belloq, P. Sutra, A. Cauvel, M. Laspéras, P. Moreau, F. Di Renzo, A. Galarneau, F. Fajula, *Coord. Chem. Rev.* **1998**, *178−180*, 1085−1108.
[11] J. S. Rafelt, J. H. Clark, *Catal. Today* **2000**, *57*, 33−44.
[12] I. W. C. E. Arends, R. A. Sheldon, *Appl. Catal. A* **2001**, *212*, 175−187.

 © 2004 Wiley-VCH Verlag GmbH & Co. KGaA, Weinheim

[13] F. Rodríguez-Reinoso, *Carbon* **1998**, *36*, 159−175.
[14] A. J. Bird, in: *Catalyst Supports and Supported Catalysts* (Ed. A. B. Stiles), Butterworths, Boston, **1987**, chapter 5.
[15] P. C. L′Argentière, E. A. Cagnola, D. A. Liprandi, M. C. Román-Martínez, C. Salinas-Martínez de Lecea, *Appl. Catal. A* **1998**, *172*, 41−48.
[16] J. A. Díaz-Auñón, M. C. Román-Martínez, C. Salinas-Martínez de Lecea, P. C. L′Argentière, E. A. Cagnola, D. A. Liprandi, M. E. Quiroga, *J. Mol. Catal. A: Chem.* **2000**, *153*, 243−256.
[17] J. A. Díaz-Auñón, M. C. Román-Martínez, C. Salinas-Martínez de Lecea, *J. Mol. Catal. A* **2001**, *170*, 81−93.
[18] J. L. Figueiredo, M. F. R. Pereira, M. M. A. Freitas, J. J. M. Órfão, *Carbon* **1999**, *37*, 1379−1389.
[19] R. C. Sosa, R. F. Parton, P. E. Neys, O. Lardinois, P. A. Jacobs, P. G. Rouxhet, *J. Mol. Catal. A* **1996**, *110*, 141−151.
[20] R. F. Parton, P. E. Neys, P. A. Jacobs, R. C. Sosa, P. G. Rouxhet, *J. Catal.* **1996**, *164*, 341−346.
[21] A. Valente, A. M. Botelho do Rego, M. J. Reis, I. F. Silva, A. M. Ramos, J. Vital, *Appl. Catal. A* **2001**, *207*, 221−228.
[22] A. R. Silva, C. Freire, B. de Castro, M. M. A. Freitas, J. L. Figueiredo, *Microporous Mesoporous Mater.* **2001**, *46*, 211−221.
[23] A. R. Silva, M. Martins, M. M. A. Freitas, A. Valente, C. Freire, B. de Castro, J. L. Figueiredo, *Microporous Mesoporous Mater.* **2002**, *55*, 275−284.
[24] A. R. Silva, C. Freire, B. de Castro, M. M. A. Freitas, J. L. Figueiredo, *Langmuir* **2002**, *18*, 8017−8024.
[25] A. R. Silva, J. Vital, J. L. Figueiredo, C. Freire, B. de Castro, *New J. Chem.* **2003**, *27*, 1511−1517.
[26] A. R. Silva, J. L. Figueiredo, C. Freire, B. de Castro, *Microporous Mesoporous Mater.*, **2004**, *68*, 83−89.
[27] A. R. Silva, C. Freire, B. de Castro, *New J. Chem.*, **2004**, *28*, 253−260.
[28] I. N. Neves, C. Freire, A. N. Zakhárov, B. de Castro, J. L. Figueiredo, *Colloids Surf. A. Physicochem. Eng. Aspects* **1996**, *115*, 249−256.
[29] R. Ferreira, M. Silva, C. Freire, B. de Castro, J. L. Figueiredo, *Microporous Mesoporous Mater.* **2000**, *38*, 391−401.
[30] R. Ferreira, C. Freire, B. de Castro, A. P. Carvalho, J. Pires, M. Brotas de Carvalho, *Eur. J. Inorg. Chem.* **2002**, 3032−3038.
[31] J. Pires, J. Francisco, A. P. Carvalho, M. Brotas de Carvalho, A. R. Silva, C. Freire, B. de Castro, *Langmuir*, in press.
[32] A. P. Carvalho, C. Castanheira, B. Cardoso, J. Pires, A. R. Silva, C. Freire, B. de Castro, M. Brotas de Carvalho, *J. Mater. Chem.*, **2004**, *14*, 374−379.
[33] R. J. J. Janssen, H. van Bekkum, *Carbon* **1995**, *33*, 1021−1027.
[34] A. H. Maki, B. R. McGarvey, *J. Chem. Phys.* **1958**, *29*, 31−34.
[35] H. R. Gersmann, J. D. Swalen, *J. Chem. Phys.* **1962**, *36*, 3221−3233.
[36] J. I. Zink, R. S. Drago, *J. Am. Chem. Soc.* **1972**, *94*, 4550−4554.
[37] H. Yokoi, A. W. Addison, *Inorg. Chem.* **1977**, *16*, 1341−1349.
[38] J. C. Lennox, R. W. Murray, *J. Electroanal. Chem.* **1977**, *78*, 395−401.
[39] J. F. Moulder, W. F. Stickle, P. E. Sobol, K. D. Bomben, in: *Handbook of X-ray Photoelectron Spectroscopy* (Ed. J. Chastain), Perkin−Elmer, **1992**.
[40] Y. M. Xie, P. M. A. Sherwood, *Chem. Mater.* **1990**, *2*, 293−299.
[41] F. Rodríguez-Reinoso, J. M. Martin-Martinez, C. Prado-Burguet, B. McEnaney, *J. Phys. Chem.* **1987**, *91*, 515−516.
[42] Z. Hu, M. P. Srinivasan, *Microporous Mesoporous Mater.* **2001**, *43*, 267−275.

Received October 29, 2003
Early View Article
Published Online April 1, 2004

 © 2004 Wiley-VCH Verlag GmbH & Co. KGaA, Weinheim

Investigation of Multi-Nickel-Substituted Tungstophosphates and Their Stability and Electrocatalytic Properties in Aqueous Media

Darine Jabbour,[a] Bineta Keita,[a] Israel-Martyr Mbomekalle,[a] Louis Nadjo,*[a] and Ulrich Kortz[b]

Keywords: Electrochemistry / Nickel / Polyoxometallates / Sandwich complexes / UV/Vis spectroscopy

Several sandwich-type polyoxometallates based on the trivacant $[PW_9O_{34}]^{9-}$ fragment with different Ni nuclearities were selected. Their stability and redox behaviour in aqueous media were evaluated by UV/Vis spectroscopy and cyclic voltammetry as a function of pH with the aim of finding the conditions under which these compounds could be suitable candidates for electrocatalytic processes. Two polyoxoanions — $[Ni_3Na(H_2O)_2(PW_9O_{34})_2]^{11-}$ and (to a lesser extent) $[Ni_4Mn_2P_3W_{24}O_{94}]^{17-}$ — were found to be stable over a wide pH domain, while $[Ni_4(H_2O)_2(PW_9O_{34})_2]^{10-}$ requires the pH to be greater than 4 for its stability. The other derivatives are only suitable for solid-state studies. The stable polyoxoanions were tested for their activity in the electrocatalytic reduction of nitrate. The results suggest unambiguously that an increase in the number of Ni centres within these sandwich-type polyanions has a beneficial effect on the electrocatalytic process.

(© Wiley-VCH Verlag GmbH & Co. KGaA, 69451 Weinheim, Germany, 2004)

Introduction

Polyoxometallate ions are gaining widespread attention owing to their possible applications in catalysis, electrocatalysis, medicine, materials science, photochemistry, analytical chemistry and magnetochemistry.[1−5] The impetus was partly triggered by the pioneering remark by Baker[6] that monosubstituted heteropolyanions can be considered as the analogues of metallated porphyrins, and used in catalytic processes with the advantage, over their organic counterparts, of thermal stability, robustness and inertness toward oxidizing environments. With regard to their electrochemistry and, correspondingly, their use in electrocatalysis, we are currently studying the parameters, which eventually in conjunction with pH effects, could improve the catalytic properties of heteropolyanions (HPAs). The incentive behind this search is to trigger those energetically favourable cathodic processes that require several electrons for their effectiveness by reduced HPAs.[7−11] Among several possibilities, substitution effects on the polyoxometallates are considered with attention: the location of the metal atom in the framework; the nature and number of substituents are expected to influence more or less the interactions between the electroactive centres within the HPA molecule.

The present paper is devoted to a study of the effects of the accumulation of nickel centres in HPAs on their stability and electrocatalytic behaviour. Several reasons have dictated this choice. Recently, we have demonstrated, for the first time to the best of our knowledge, that Cu^{2+}- or Ni^{2+}-containing HPAs are the only monosubstituted polyoxoanions to be effective in the electrocatalytic reduction of nitrate in mildly acidic aqueous media.[12] Also, we have shown that the accumulation of Cu^{2+} centres within HPAs is useful in enhancing the catalytic properties of the polyoxometallate.[13] Specifically, a comparison of the catalytic activity of $\alpha\beta\beta\alpha$-$(Cu^{II}OH_2)_2Cu^{II}_2(H_4AsW_{15}O_{56})_2^{18-}$ based on the novel Wells−Dawson complex $H_4AsW_{18}O_{62}^{7-}$ [14] with those of the analogous monosubstituted Cu-HPAs demonstrated a favourable effect of the accumulation of Cu centres in the electrocatalytic reduction of nitrate; hence the idea that multi-nickel derivatives might be interesting in this respect. A large family of Ni-substituted tungstophosphates with a sandwich-type structure is known[15] and some other structures exist as well.[16−19] Novel polyoxoanions are often difficult to obtain owing to the fact that the mechanism of formation is far from well understood. Numerous sandwich-type compounds have been synthesised and characterised since the pioneering work of Weakley et al.,[20] but the nickel-containing Keggin derivative $[Ni_4(H_2O)_2(PW_9O_{34})_2]^{10-}$ has been isolated only recently under severely controlled experimental conditions to avoid or minimize other side products.[18] The synthesis con-

[a] Laboratoire de Chimie Physique, UMR 8000, CNRS, Electrochimie et Photoélectrochimie, Université Paris-Sud, Bâtiment 420,
91405 Orsay Cedex, France
Fax: (internat.) + 33-1-69154328
E-mail: nadjo@lcp.u-psud.fr
[b] School of Engineering and Science, International University Bremen
P. O. Box 750561, 28725 Bremen Germany

 © 2004 Wiley-VCH Verlag GmbH & Co. KGaA, Weinheim **DOI: 10.1002/ejic.200300830**

ditions suggest strongly that some species might be stable only in narrow pH domains in solution. Our choice of (PW_9O_{34})-based derivatives allows us to study several species with different nuclearities. However, there are also complications that have been reviewed recently, for example the existence of multiple isomers and their transformation pathways.[21] It has been demonstrated recently that the triferric sandwich-type complex $[Fe_2(FeOH_2)(NaOH_2)(P_2W_{15}O_{56})_2]^{14-}$ is significantly more stable than its diferric and tetraferric analogues.[22] The unique coordination environment of its single external iron site and the incorporated sodium ion most likely play an important, stabilizing role. This observation suggests that the nuclearity and the geometry of the incorporated transition metal centres might also influence the stability of other sandwich-type polyanions. Finally, the aforementioned catalytic activity of a monosubstituted Ni-HPA towards nitrate[12] and the diversity of multi-nickel HPAs available at present justify the search for a unified view of their behaviour in aqueous media.

Results and Discussion

Selection of Relevant Heteropolyanions

All polyanions studied here are derived from the Keggin fragment $[PW_9O_{34}]^{9-}$. The trilacunary $[A,\beta\text{-}PW_9O_{34}]^{9-}$ ($A,\beta\text{-}PW_9$) and the monolacunary $[\alpha\text{-}PW_{11}O_{39}]^{7-}$ (PW_{11}) were synthesised according to literature procedures.[23,24] Preparation of $[B,\alpha\text{-}PW_9O_{34}]^{9-}$ ($B,\alpha\text{-}PW_9$) was accomplished from $A,\beta\text{-}PW_9$ by heating according to the procedure first reported by Finke and co-workers[25] and then by Domaille.[24] The solution behaviour of the various isomers of the mono- and trilacunary Keggin species can be helpful for understanding possible transformation pathways of the Ni-containing compounds of interest. The following polyoxoanions were synthesised by literature methods and thoroughly characterised as pure samples. The mixed nickel/manganese-substituted $[Ni_4Mn_2P_3W_{24}O_{94}]^{17-}$ constitutes a novel polyanion:[27] $[H_2PW_9Ni_4O_{34}(OH)_3(H_2O)_6]^{2-}$ ($Ni_4H_2PW_9$);[19] $[Ni_3(H_2O)_3PW_{10}O_{39}H_2O]^{7-}$ (Ni_3PW_{10});[18] $[Ni_4(H_2O)_2(PW_9O_{34})_2]^{10-}$ ($Ni_4P_2W_{18}$);[18] $[Ni_9(OH)_3(H_2O)_6(HPO_4)_2(PW_9O_{34})_3]^{16-}$ ($Ni_9P_3W_{27}$);[18] $[Ni_3Na(H_2O)_2(PW_9O_{34})_2]^{11-}$ ($Ni_3P_2W_{18}$);[15,26] $[Ni_4Mn_2P_3W_{24}O_{94}]^{17-}$ ($Mn_2Ni_4P_3W_{24}$).[27] Also $[Ni_4(H_2O)_2(P_2W_{15}O_{56})_2]^{16-}$ ($Ni_4P_4W_{30}$)[28] will be considered for a brief comparison. The structures of $Ni_4H_2PW_9$, Ni_3PW_{10}, $Ni_4P_2W_{18}$, $Ni_9P_3W_{27}$, $Ni_3P_2W_{18}$, $Mn_2Ni_4P_3W_{24}$, and $Ni_4P_4W_{30}$ are shown in Scheme 1.

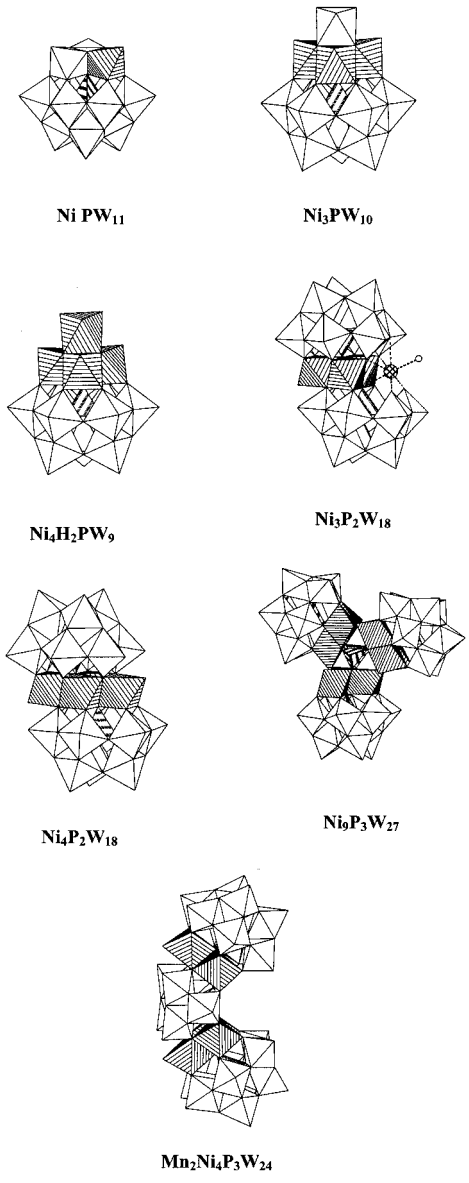

Scheme 1. Structures of polyanions $Ni_4H_2PW_9$, Ni_3PW_{10}, $Ni_4P_2W_{18}$, $Ni_9P_3W_{27}$, $Ni_3P_2W_{18}$, $Mn_2Ni_4P_3W_{24}$, and $Ni_4P_4W_{30}$

Cyclic Voltammetry (CV) Study of Selected Multi-Nickel HPAs in pH 3 Sulfate Medium

The cyclic voltammograms of the various electroactive species were monitored as a function of time. Therefore, their recording was started shortly after addition of the relevant HPA to the previously deaerated supporting electrolyte. The choice of CV in this issue stems from our primary interest to detect stable electroactive species that constitute the sole useful candidates for electrocatalysis. Three main classes will be discussed: two compounds — $Ni_3P_2W_{18}$ and $Mn_2Ni_4P_3W_{24}$ — are stable over a wide pH domain; $Ni_4P_2W_{18}$ requires pH values higher than 4 for its stability; no pH domain could be found for an appreciable stability of $Ni_4H_2PW_9$, Ni_3PW_{10} and $Ni_9P_3W_{27}$.

$[H_2PW_9Ni_4O_{34}(OH)_3(H_2O)_6]^{2-}$ ($Ni_4H_2PW_9$)

The very first voltanmmogram of $Ni_4H_2PW_9$ shows a composite reduction wave located between −0.600 V and

 © 2004 Wiley-VCH Verlag GmbH & Co. KGaA, Weinheim

−0.900 V vs. SCE. (Figure 1A). The proton reduction wave which followed this immediately is not shown. Roughly 10 min after the addition of $Ni_4H_2PW_9$ to the solution a modification of the voltammetric pattern was observed, characterised by two main features: (i) the whole voltammogram experiences a shift to positive potential; (ii) the two waves become better and better defined and separated. For the sake of clarity, only the "initial" cyclic voltammogram and those recorded after 30 min and 4 h are shown in Figure 1A. The two waves are attributed to the reduction of W^{VI} centres. This hypothesis was confirmed by controlled potential electrolysis. The cyclic voltammograms recorded after more than 4 h are nearly identical to that recorded after 4 h, except for a small increase of the second wave at the expense of the first one. It should be noted that the first wave remains slightly composite. The next issue concerns the nature of the new product(s). In particular, the possibility that one or several Ni^{2+} ions are lost from the new complexes should be considered. As a matter of fact, the present transformations resemble those of B,α-PW_9. In the supporting electrolyte used here, it was checked that B,α-PW_9 is rapidly converted into a species whose cyclic voltammogram is identical to that of PW_{11}, in agreement with the literature.[21] In contrast, Figure 1B indicates a difference of 58 mV between the potentials of the first reduction peaks of the transformation products of $Ni_4H_2PW_9$ and B,α-PW_9, the former complex being the more negative of the two. Finally, Figure 1C shows that the new complex from $Ni_4H_2PW_9$ has a cyclic voltammogram very close to that of $[PW_{11}O_{39}Ni(H_2O)]^{5-}$ ($PW_{11}Ni$).

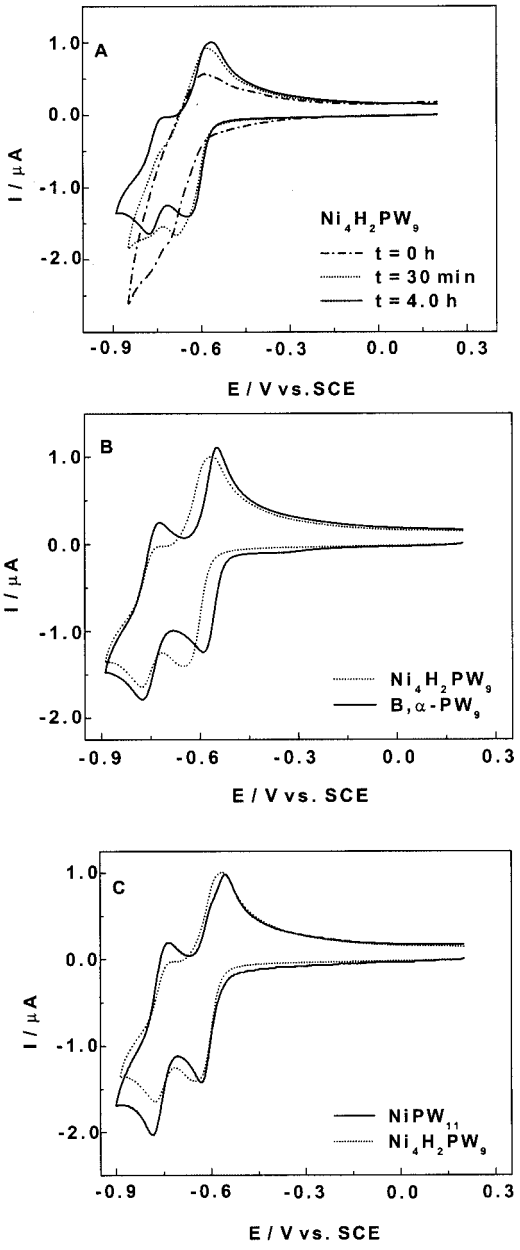

Figure 1. A: Cyclic voltammetry monitoring of the transformations of 2×10^{-4} M $Ni_4H_2PW_9$ as a function of time; medium 0.2 M Na_2SO_4 + H_2SO_4 (pH = 3); scan rate: 10 mV·s^{-1}; working electrode: polished glassy carbon; reference electrode: SCE; B: superimposition of the final cyclic voltammetry patterns for $Ni_4H_2PW_9$ and B,α-PW_9; the experimental conditions are the same as in A; C:) superimposition of the final cyclic voltammetry patterns for $Ni_4H_2PW_9$ and $NiPW_{11}$; the experimental conditions are the same as in A; for further details see text

Comparison with Other Multi-Nickel Derivatives

The "initial" cyclic voltammogram of Ni_3PW_{10} is different from that of $Ni_4H_2PW_9$; its conversion ends up in $NiPW_{11}$ in roughly 5 h (Figure 2A). The trimeric $Ni_9P_3W_{27}$ is also unstable in the pH 3 medium (0.2 M Na_2SO_4 + H_2SO_4) and its conversion is relatively fast. The first-wave current increases at the expense of the second one, which has a larger current intensity than the first wave and which is composite. Figure 2B shows, in superimposition, the "initial" cyclic voltammogram of $Ni_9P_3W_{27}$ and that recorded after 1.5 h. A longer duration does not bring about substantial changes in this cyclic voltammogram. The final pattern is different from that of $NiPW_{11}$, except for the first wave, which shows a peak located at the same potential in the two systems. However, no conclusion can be drawn at this stage (vide infra UV/Vis studies). For $Ni_4P_2W_{18}$, the "initial" cyclic voltammogram comprises a first composite wave, followed by a second wave close to the reduction of protons (Figure 2C). This pattern does not resemble any of the preceding ones. However, a very slow and gradual transformation of the cyclic voltammogram is observed as a function of time; in particular, the current intensity of the second wave decreases significantly, while the wave itself becomes better and better defined, with a gradual move of its reduction peak potential in the negative direction. In Figure 2C the "initial" cyclic voltammogram and those recorded after 3 h and 9 h are compared. Even after 9 h of transformation of $Ni_4P_2W_{18}$ the first wave remains slightly composite, which could indicate the presence of a mixture of products. No attempt was made to identify these other products but it is likely that the mixture contains $Ni_3P_2W_{18}$. This assumption is supported by Figure 2D, which compares the last cyclic voltammogram recorded with $Ni_4P_2W_{18}$ to that of $Ni_3P_2W_{18}$. Such a possibility is reminiscent of the aforementioned higher stability of the triferric

 © 2004 Wiley-VCH Verlag GmbH & Co. KGaA, Weinheim

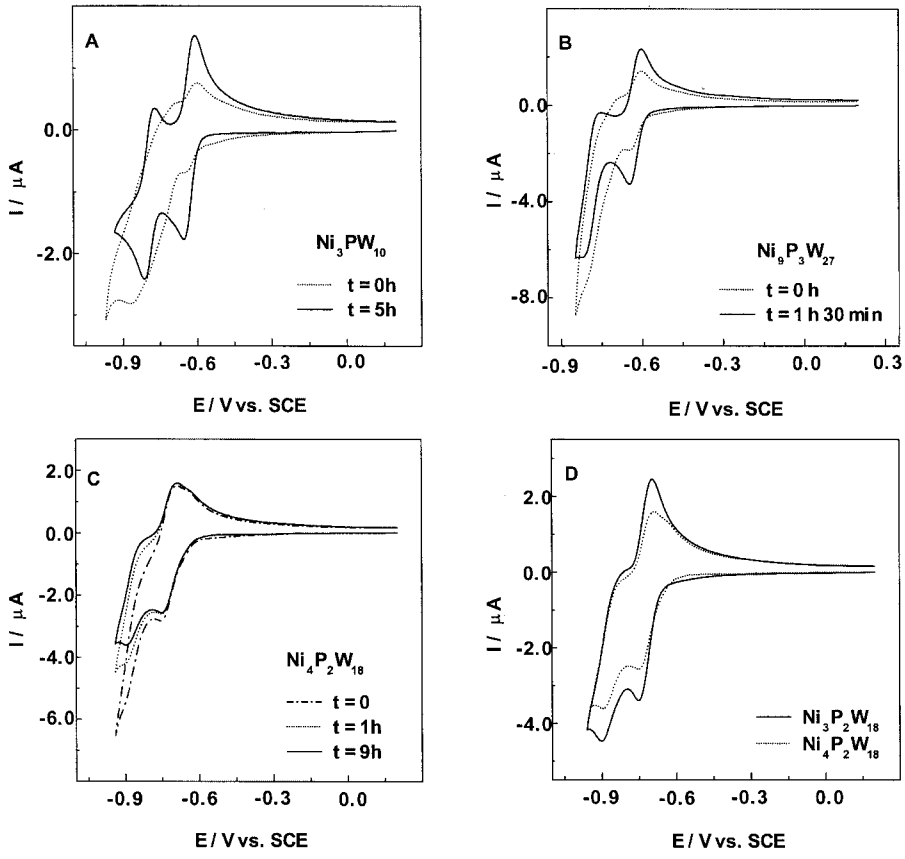

Figure 2. A: Comparison of the "initial" and "final" cyclic voltammograms of 2×10^{-4} M Ni_3PW_{10}; medium 0.2 M Na_2SO_4 + H_2SO_4 (pH = 3); scan rate: 10 $mV \cdot s^{-1}$; working electrode: polished glassy carbon; reference electrode: SCE; B: superimposition of the "initial" cyclic voltammogram of $Ni_9P_3W_{27}$ and that recorded after 1.5 h; the experimental conditions are the same as in A; C: cyclic voltammetry monitoring of the transformations of 2×10^{-4} M $Ni_4P_2W_{18}$ as a function of time; the experimental conditions are the same as in A; for further details see text; D: superimposition of the "final" cyclic voltammogram of $Ni_4P_2W_{18}$ with that of the stable $Ni_3P_2W_{18}$; the experimental conditions are the same as in A

sandwich complex $[Fe_2(FeOH_2)(NaOH_2)(P_2W_{15}O_{56})_2]^{14-}$ than its diferric and tetraferric analogues.[22] These complexes show remarkable differences in their junction connectivities. The tetrairon-substituted $[Fe_2(FeOH_2)_2(P_2W_{15}O_{56})_2]^{12-}$ has two β-junctions, the diiron-substituted $[Fe_2(NaOH_2)_2(P_2W_{15}O_{56})_2]^{16-}$ has two α-junctions and the triiron-substituted $[Fe_2(FeOH_2)(NaOH_2)(P_2W_{15}O_{56})_2]^{14-}$ has one β-junction and one α-junction.[22,29–31] The junction connectivity of the Keggin-based $Ni_3P_2W_{18}$ is ααβα[15] and therefore in complete agreement with the triiron Wells–Dawson derivative of Hill et al.[22] The unique coordination environment of the single external Ni site and the incorporated sodium ion seem to enhance the stability of the trinickel species, in analogy with the triiron derivative. Provisionally, it is worth recalling that $Ni_3P_2W_{18}$ is stable in the present medium, as reported previously.[15,26]

In summary, all of the above Ni-substituted tungstophosphates can be distinguished from each other, provided their very first cyclic voltammograms are recorded shortly after dissolution in the supporting electrolyte. With the exception of $Ni_3P_2W_{18}$ and $Mn_2Ni_4P_3W_{24}$ all polyoxoanions studied here are unstable upon standing in the pH 3 sulfate medium.[15,27] The slow transformation of $Ni_4P_2W_{18}$ in this pH 3 medium is also worth noting.

Influence of Counteranions

In the case of $Ni_4H_2PW_9$ it was checked that replacement of the countercation Na^+ by Li^+ in the supporting electrolyte has a negligible influence on the observed electrochemical processes. Therefore, in the following study of the influence of the counteranion and the pH of the electrolyte we selected the sodium counterion in all cases. This study was performed with $Ni_4H_2PW_9$ as a representative polyoxometallate. The choice of anions was restricted to those classically used in the electrochemistry of HPAs, namely ClO_4^-, $H_2PO_4^-$, CH_3COO^- and Cl^-; SO_4^{2-} has already been studied above. For easier comparisons, all the experiments were carried out at pH = 3 with 0.4 M Na^+.

The cyclic voltammogram of $Ni_4H_2PW_9$ also changes as a function of time for $H_2PO_4^-$ and CH_3COO^-, resulting in a mixture of electroactive products, and $NiPW_{11}$ appears to be the main product. To illustrate this conclusion, Figure 3A shows in superimposition the so-called "final state" cyclic voltammograms recorded in the presence of these two

 © 2004 Wiley-VCH Verlag GmbH & Co. KGaA, Weinheim

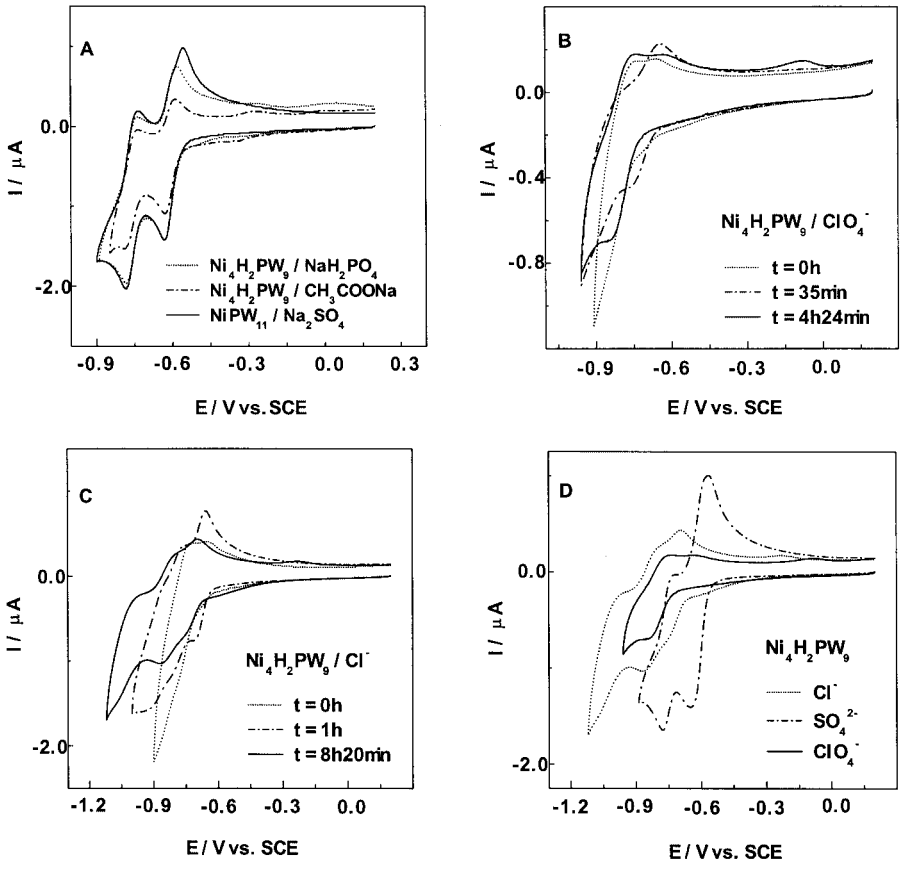

Figure 3. A: Superimposition of the so-called "final state" cyclic voltammograms recorded for 2×10^{-4} M $Ni_4H_2PW_9$ in pH 3 phosphate (0.4 M NaH_2PO_4 + H_3PO_4) and acetate (0.4 M CH_3COONa + CH_3COOH) media (pH = 3), respectively, and the cyclic voltammogram of $NiPW_{11}$ in sulfate medium (pH = 3); scan rate: 10 $mV \cdot s^{-1}$; working electrode: polished glassy carbon; reference electrode: SCE; B: cyclic voltammetry monitoring of the transformations of 2×10^{-4} M $Ni_4H_2PW_9$ as a function of time in the presence of 0.4 M $NaClO_4$ + $HClO_4$ (pH = 3); the experimental conditions are the same as in A; C: cyclic voltammetry monitoring of the transformations of 2×10^{-4} M $Ni_4H_2PW_9$ as a function of time in the presence of 0.4 M NaCl + HCl (pH = 3); the experimental conditions are the same as in A; D: superimposition of the "final" cyclic voltammograms of 2×10^{-4} M $Ni_4H_2PW_9$ observed in the presence of sulfate, chloride and perchlorate anions (pH = 3), respectively; the experimental conditions are the same as in A; for further details see text

anions and the cyclic voltammogram of $NiPW_{11}$ in sulfate medium. The transformation yield into $NiPW_{11}$ is smaller with CH_3COO^-. The presence of this anion induces an important formation of secondary species, as could be detected by their electroactivity between 0 and −0.4 V. It should also be noted that these "final states" were obtained after 2 h and 3 h for CH_3COO^- and $H_2PO_4^-$, respectively.

More intricate observations are made for $Ni_4H_2PW_9$ in the presence of ClO_4^- or Cl^- as illustrated in Figure 3B and C, respectively. These figures represent the "initial" cyclic voltammogram in superimposition with two other selected states; as a matter of fact, even after more than 6.5 h of standing, no "final state" could be reached. It is clear, however, that several electroactive species are formed irrespective of which of the two anions is present. Figure 3D compares the cyclic voltammograms recorded after 6.5 h in the presence of ClO_4^- and Cl^- with that recorded as a "final state" in sulfate medium. The remarkable influence of the two counteranions is obvious. The more marked effect is seen in the presence of ClO_4^- for which a small composite wave is observed, followed by the proton reduction wave (not shown).

In short, $Ni_4H_2PW_9$ is converted into respectable amounts of $NiPW_{11}$ in the presence of SO_4^{2-}, $H_2PO_4^-$ and CH_3COO^-. The transformation yield is similar for SO_4^{2-} and $H_2PO_4^-$, but is smaller for CH_3COO^-. No attempt was made to identify the secondary products. In contrast to this first group of anions, more complex observations are made in the presence of ClO_4^- and Cl^-; in their presence, $Ni_4H_2PW_9$ is gradually converted into various products with decreased overall electroactivity. This trend is representative of the main observations in the series of unstable multi-nickel compounds, except for $Ni_4P_2W_{18}$. The behaviour of the latter is illustrated in Figure 4, where the voltammograms obtained in the presence of SO_4^{2-}, ClO_4^- and Cl^- are compared. Unlike the other compounds of the series, no new electroactive species is detected in the explored potential domain. The two well-behaved waves recorded in the pH 3 sulfate medium undergo a general move in the negative potential direction, with a slight distortion of the second wave. Such behaviour has been observed previously for a large selection of stable Keggin and Wells−Dawson HPAs and has been ascribed to the buffer capacity of the electrolytes as a function of the coun-

 © 2004 Wiley-VCH Verlag GmbH & Co. KGaA, Weinheim

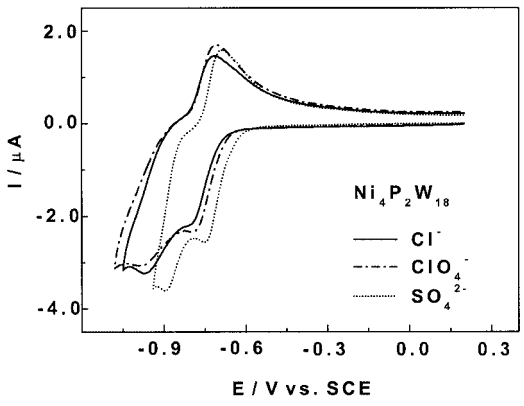

Figure 4. Superimposition of the "final" cyclic voltammograms of 2×10^{-4} M $Ni_4P_2W_{18}$ observed in the presence of sulfate, chloride and perchlorate anions (pH = 3), respectively; scan rate: 10 $mV \cdot s^{-1}$; working electrode: polished glassy carbon; reference electrode: SCE; for further details see text

teranion present in the medium.[32] Again, the clear observation of this phenomenon indicates a relatively large stability of $Ni_4P_2W_{18}$ in the pH 3 media.

UV/Vis Investigations

This study was performed as a function of pH. $Ni_4H_2PW_9$ was selected as a representative example showing the main UV/Vis features repeatedly encountered with all the other compounds. Only the observations at pH = 3 (0.2 M Na_2SO_4 + H_2SO_4) are shown. Typically, a 4.3×10^{-5} M solution of $Ni_4H_2PW_9$ in a 1.00-cm optical-path quartz cuvette was monitored as a function of time by UV/Vis spectroscopy between 380 and 200 nm. Figure 5A shows the evolution of the spectrum over 10 h. The general variation trends of the absorbance are sketched by arrows and indicate a transformation of the complex. The very first spectrum recorded does not go through the apparent isosbestic point in Figure 5A. It was checked that the variation of absorbance remains negligible from 10 h to 24 h, thus indicating that a complex stable in the pH 3 medium is already obtained. Figure 5B shows the initial spectrum of $Ni_4H_2PW_9$ and the final spectrum recorded after 24 h of standing. This last spectrum peaks at 252 nm. As it was checked previously that B,α-PW_9 is rapidly converted, in the supporting electrolyte used here, into a species whose cyclic voltammogram is identical to that of PW_{11}, we wondered whether the final complex from $Ni_4H_2PW_9$ could be the lacunary species PW_{11}, the UV/Vis spectrum of which peaks at 248 nm. However, this peak is preceded by a shoulder located between 280 and 260 nm, which rules out the presence of this lacunary complex. In contrast, the spectrum of an authentic sample of $NiPW_{11}$, which is stable in the pH 3 medium, peaks at 252 nm and has exactly the same shape as the spectrum recorded after 24 h shown in Figure 5B. These observations are in complete agreement with the conclusions from the CV investigations.

In short, the initial spectrum observed with each of the multi-nickel-substituted tungstophosphates of this work

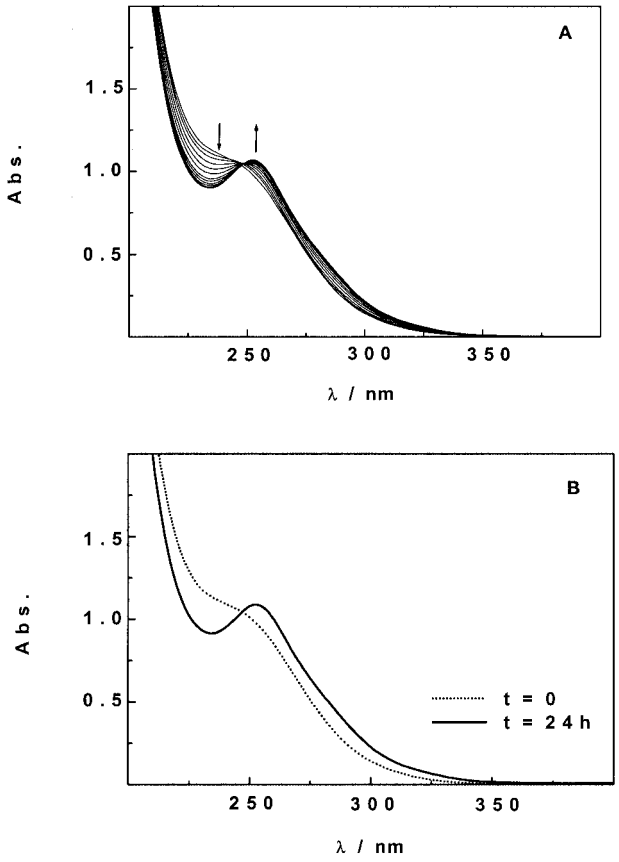

Figure 5. UV/Vis spectra of 4.3×10^{-5} M $Ni_4H_2PW_9$, recorded in a pH 3 medium (0.2 M Na_2SO_4 + H_2SO_4) with a 1.00-cm optical-path quartz cuvette; A: evolution of the spectrum with time; the arrows indicate the direction of variation of the absorbance with time; B: the initial spectrum and that recorded after 24 h of standing; for further details see text

was clearly different from those of $NiPW_{11}$ or $[PW_{11}O_{39}]^{7-}$. Long-term UV/Vis spectra and CV experiments on solutions aged for appropriate durations converge to indicate that the transformations of $Ni_4H_2PW_9$ and Ni_3PW_{10} end up, at least partly, in $NiPW_{11}$. Also, UV/Vis spectroscopy confirms the presence of $NiPW_{11}$ as a decomposition product of $Ni_9P_3W_{27}$, a conclusion already suggested by CV experiments.

Influence of pH

The pH influence was studied for all selected HPAs All solutions, except for the 0.5 M H_2SO_4 (pH = 0.33) solution, contained Na^+ at a concentration of 0.4 M as the major cation, in order to avoid any possibility of cation effect. The compositions of these media are indicated in the Exp. Sect.

Unstable HPAs

The polyanions $Ni_4H_2PW_9$, Ni_3PW_{10}, and $Ni_9P_3W_{27}$ are unstable at all pH values studied in this work. Occasionally, identification of a major transformation product by CV was achieved.

 © 2004 Wiley-VCH Verlag GmbH & Co. KGaA, Weinheim

Media of pH ≤ 3

In 0.5 M H_2SO_4 (pH = 0.33) $Ni_4H_2PW_9$ is not stable and precipitates gradually. In pH 1 and 2 media (0.2 M Na_2SO_4 + H_2SO_4), its current intensity for the whole pattern decreases steadily, without any other significant modifications of the CV characteristics, nor any appearance of significant new waves. The decomposition products are probably not electroactive in these two media. The decomposition is noted to be faster the higher the proton concentration. Also, the decompositions of Ni_3PW_{10} and $Ni_9P_3W_{27}$ are so fast at pH = 2 that further studies at lower pH were not carried out. For instance, CV monitoring of the transformation of Ni_3PW_{10} shows its concentration to decrease by a factor of two in less than 2 h; no new wave was observed, which indicates that the decomposition products do not show any electrochemical activity in this medium. In contrast, the decomposition of $Ni_9P_3W_{27}$ is characterised by several new waves indicating the presence of various electroactive species.

Media of pH ≥ 3

In pH 4 or 5 buffer media $Ni_4H_2PW_9$, Ni_3PW_{10} and $Ni_9P_3W_{27}$ are converted into $PW_{11}Ni$ as the major product, with Ni_3PW_{10} being by far the most unstable. At pH = 6, only $Ni_4H_2PW_9$ is slowly converted (7 h) into $NiPW_{11}$ as the major product. Compounds resulting from decomposition of Ni_3PW_{10} and $Ni_9P_3W_{27}$ have cyclic voltammograms with characteristics close to those of $NiPW_{11}$; these cyclic voltammograms might feature isomers of $NiPW_{11}$. At pH = 7, the three complexes and $NiPW_{11}$ exhibit ill-defined cyclic voltammograms, with a steady decrease in current and no new waves appearing.

The preceding sections have revealed that $Ni_4P_2W_{18}$ must be considered as a special case among the series of unstable multi-nickel species. Figure 6 illustrates the evolution of the cyclic voltammograms of $Ni_4P_2W_{18}$ as a function of pH. As expected, this polyanion behaves differently from the other three unstable HPAs as a function of pH variation. The transformation at pH < 3 leads to the same (not fully identified) product as observed in the pH 3 medium. The only difference is the faster kinetics at lower pH. The steady decrease of the transformation kinetics with increasing pH values could explain why $Ni_4P_2W_{18}$ is stable at pH > 4. The tendency for separation of waves with decreasing pH is not unusual in polyoxometallate electrochemistry.[33] Anyhow, despite the limited pH stability domain for $Ni_4P_2W_{18}$, the behaviour of this polyanion is distinctly more favourable than that of the Wells−Dawson analogue $[Ni_4(H_2O)_2(P_2W_{15}O_{56})_2]^{16-}$ ($Ni_4P_4W_{30}$) described by Ruhlmann and co-workers, for which slow degradation was observed during any titration between pH = 1 and 6.[28]

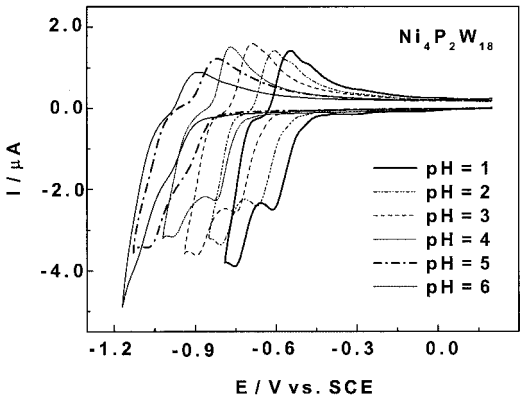

Figure 6. Superimposition of the "final" cyclic voltammograms of 2×10^{-4} M $Ni_4P_2W_{18}$ observed as a function of pH; scan rate: 10 mV·s^{-1}; working electrode: polished glassy carbon; reference electrode: SCE; for further details see text

Stable Multi-Nickel HPAs: Preliminary Evaluation of Electrocatalytic Processes

The representatives of this group are $Ni_3P_2W_{18}$ and $Mn_2Ni_4P_3W_{24}$, to which $Ni_4P_2W_{18}$ can be added at pH > 4. The electrochemistry of the two "fully" stable species at pH = 3 and 5 has been described in detail previously.[15,27] However, in order to envision electrocatalytic applications we decided to investigate the stability and redox behaviour of these polyanions from pH = 0 to 7 by UV/Vis spectroscopy and CV. The stability conclusions were deduced from the comparison of the UV/Vis spectra run on the freshly prepared solution and on the same solution after standing for 24 h. This duration is much longer than necessary for an electrochemical characterisation, but was considered useful to envision electrocatalytic applications. The results indicate that $Ni_3P_2W_{18}$ is very stable from pH = 1 to 6. The stability domain of $Mn_2Ni_4P_3W_{24}$ ranges from pH = 2 to 6. However, even at pH = 7 its decomposition is not very fast and reaches only 34% of the starting complex after 24 h. The characteristics of the W centres within the complexes were monitored by cyclic voltammetry as a function of time and pH. The results confirm the stability of the two HPAs. In agreement with previous observations at pH = 3 and 5,[15,27] the redox behaviour of the W centres is pH-dependent. Figure 7A shows the evolution of the cyclic voltammogram of $Ni_3P_2W_{18}$ for pH = 1−6. The curve for pH = 3 fits perfectly in the scheme, but it has been published previously[15] and is therefore omitted here for clarity. Coulometric determinations have also already been performed at pH = 3 and 5 and indicate that the first wave features an overall four-electron/four-proton process.[15] From a more qualitative point of view, the evolution of cyclic voltammograms with pH is illustrative of a behaviour frequently encountered in multi-electron/multi-proton processes. The distribution of the formal potentials and pK_a values of the various intermediate species will determine the broadness of the corresponding waves (and the current intensity of the wave). The same parameters will favour the merging of waves (or eventually their splitting) when their displacements as a function of pH are different. A remarkable example of such behaviour has been described recently in the electrochemistry of the tetrameric polyanion $[H_7P_8W_{48}O_{184}]^{33-}$.[33]

 © 2004 Wiley-VCH Verlag GmbH & Co. KGaA, Weinheim

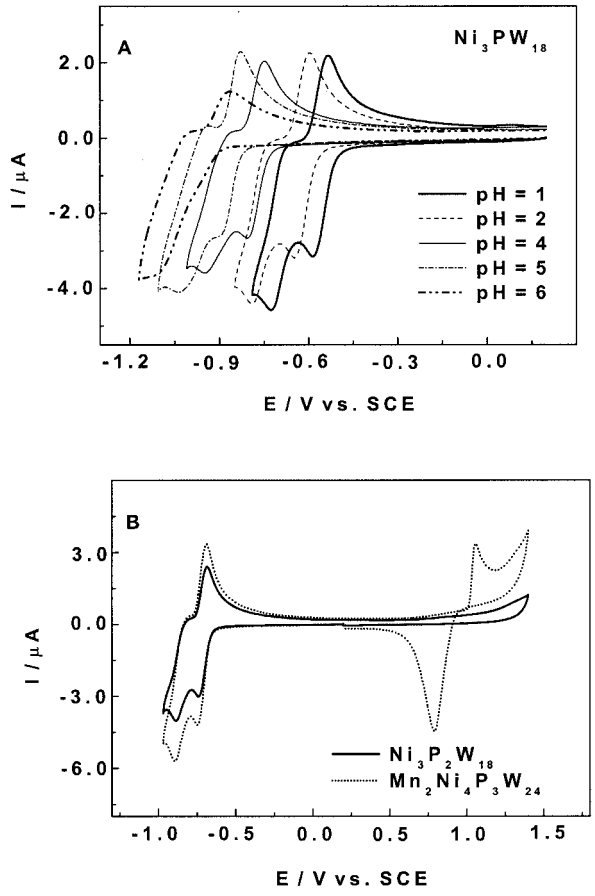

Figure 7. A: Superimposition of the cyclic voltammograms of 2×10^{-4} M $Ni_3P_2W_{18}$ observed as a function of pH; scan rate: 10 $mV \cdot s^{-1}$; working electrode: polished glassy carbon; reference electrode: SCE; B: comparison of the cyclic voltammograms of 2×10^{-4} M $Ni_3P_2W_{18}$ and $Mn_2Ni_4P_3W_{24}$ at pH = 3 (0.2 M Na_2SO_4 + H_2SO_4); for further details see text

Figure 7B compares the cyclic voltammograms of $Ni_3P_2W_{18}$ and $Mn_2Ni_4P_3W_{24}$ at pH = 3. The redox processes of the Mn centres in the latter complex do not require further comments. For both polyanions the W-centred redox processes are very similar in shape, with the current intensities being larger for $Mn_2Ni_4P_3W_{24}$ than for $Ni_3P_2W_{18}$. Coulometry in the pH 3 sulfate medium indicates a six-electron process for the first W wave of $Mn_2Ni_4P_3W_{24}$. These trends comply with expectations if it is assumed that all relevant parameters in the electrochemistry of the two complexes are close or even equal, except for their different diffusion coefficients.

Cyclic voltammetry was used to evaluate the activity of $Ni_3P_2W_{18}$ and $Mn_2Ni_4P_3W_{24}$ in the electrocatalytic reduction of nitrate. The choice of the substrate is tricky, as nitrate is difficult to reduce. To the best of our knowledge, the only examples where HPAs have proven to be useful in this system have been described recently by our group.[12,13,34] For this purpose, the excess parameter is an operational parameter defined as $\gamma = C^{\circ}_{NO_3^-}/C^{\circ}_{HPA}$ where C° designates the concentration of the relevant species. The electrocatalysis is characterised by the catalytic efficiency, CAT, defined as: $CAT = 100 \times [I_{(HPA+NO_3^-)} - I^d_{(HPA)}]/I^d_{(HPA)}$, where $I_{(HPA+NO_3^-)}$ is the peak current for reduction of the heteropolyanion (HPA) in the presence of NO_3^- and $I^d_{(HPA)}$ is the corresponding diffusion peak current for the HPA alone. CAT values are sufficient to compare the efficiencies for a given electrocatalytic process either for one compound as a function of pH or for two compounds under the same experimental conditions. However, it must be recognized that a more detailed comparison would necessitate determination of the nature and yields of the final products, which is beyond the scope of this work. As a first example, CAT values were measured in the presence of $Ni_3P_2W_{18}$ for the electrocatalytic reduction of nitrate in a pH 2 sulfate medium. CAT was measured at −0.840 V and varied from 2098 to 2733 for $\gamma = 500$ and 1000, respectively. These values indicate an efficient electrocatalysis of the reduction of nitrate by $Ni_3P_2W_{18}$ at pH = 2. Furthermore, several tests with NO_2^- and/or with NO under the aforementioned conditions confirm that these species are easily reduced electrocatalytically at substantially less negative potentials than nitrate.[35] Insofar as nitrite and NO are known to appear as intermediates in the reduction of nitrate by various metals, the present results suggest that highly reduced species should be obtained in the electrocatalytic reduction of nitrate in the presence of $Ni_3P_2W_{18}$. Also, the number of accumulated electrons in the polyoxoanion framework at the potential where the transformation of nitrate takes place is large enough for a complete reduction, which supports also the assumption of reduction of intermediates.

The media of pH = 3 and 5 were selected to compare the efficiencies of $Ni_3P_2W_{18}$ and $Mn_2Ni_4P_3W_{24}$, respectively, in the electrocatalytic reduction of nitrate because the latter complex is not very stable at pH = 2. Whatever the pH, $Mn_2Ni_4P_3W_{24}$ was found to be the more efficient of the two complexes: its CAT values were four and seven times larger at pH = 3 and 5, respectively, than those measured for $Ni_3P_2W_{18}$ under the same conditions.

The results for these two complexes were compared with the efficiencies obtained with $Ni_4P_2W_{18}$ and $NiPW_{11}$ in the pH 5 medium where all these complexes are stable. The efficiencies for $Ni_3P_2W_{18}$ and $Ni_4P_2W_{18}$ turned out to be comparable. In contrast, $NiPW_{11}$ shows a negligibly small activity toward the electrocatalytic reduction of nitrate in this medium.

Finally, comparisons of the efficiencies of several Ni-substituted tungstophosphates vis-à-vis the catalytic electroreduction of nitrate suggest that an increase of the number of Ni centres incorporated in stable sandwich-type polyoxoanions has a very beneficial effect.

Concluding Remarks

Several conclusions emerge from this work. The stability of a large variety of Ni-containing sandwich-type polyoxoanions has been investigated by electrochemistry in aqueous media. Such an evaluation is necessary in order to detect those species suitable for solid-state studies. Simul-

 © 2004 Wiley-VCH Verlag GmbH & Co. KGaA, Weinheim

taneously, such a study permits the selection of good candidates for electrocatalysis applications along with the appropriate pH conditions. At least two complexes turned out to be stable over a fairly wide pH domain. To the best of our knowledge such a broad, comparative overview has not been performed previously. The remarkable stability of the Keggin-based $Ni_3P_2W_{18}$ must be emphasised and is reminiscent of that demonstrated by Hill and co-workers for the Wells−Dawson-based triiron analogue.[22] Concerning electrocatalysis perspectives, it is worth noting that reduction of the W centres in the present complexes provides an appreciable electron reservoir under conditions where modification of electrode surfaces does not take place. The accumulated electrons in the HPA framework might therefore be useful for various electrocatalytic processes.

Experimental Section

General Methods and Materials: Pure water was used throughout. It was obtained by passing through a RiOs 8 unit followed by a Millipore-Q Academic purification set. H_2SO_4, Na_2SO_4, HCl, NaCl, $HClO_4$, $NaClO_4$, CH_3CO_2H, CH_2ClCO_2H, CH_3CO_2Na, H_3PO_4, NaH_2PO_4 were of high-purity grade and were used as purchased (Prolabo) without further purification. The UV/Vis spectra were recorded with a Perkin−Elmer Lambda 19 spectrophotometer from 600 to 200 nm using solutions that contained 2.5×10^{-5} M or 4.3×10^{-5} M of the relevant HPA. The measurements were performed in matched 1.000-cm optical-path quartz cuvettes. The preparation and characterisation of $Ni_4H_2PW_9$, Ni_3PW_{10}, $Ni_4P_2W_{18}$, $Ni_9P_3W_{27}$, $Ni_3P_2W_{18}$, and $Ni_4P_4W_{30}$ have already been described in detail.[15,18,19,26,28] The synthesis and characterisation of the novel polyanion $Mn_2Ni_4P_3W_{24}$ are described elsewhere.[27]

Electrochemical Experiments: The same media as for UV/Vis spectroscopy were used for electrochemistry, but the HPA concentration was at least 2×10^{-4} M. All cyclic voltammograms were recorded at a scan rate of 10 $mV \cdot s^{-1}$, unless otherwise stated. The solutions were deaerated thoroughly for at least 30 min with pure argon and kept under a positive pressure of this gas during the experiments. The source, mounting and polishing of the glassy carbon (GC, Tokai, Japan) electrodes has been described previously.[36] The glassy carbon samples had a diameter of 3 mm. The electrochemical setup was an EG & G 273 A driven by a PC with the M270 software. Potentials are quoted against a saturated calomel electrode (SCE). The counter electrode was a platinum gauze of large surface area. All experiments were performed at laboratory temperature.

Acknowledgments

This work was supported by the CNRS (UMR, 8000) and the University Paris XI. U. K. thanks the American University of Beirut, Lebanon, where he was employed when this collaboration started.

[1] M. T. Pope, *Heteropoly- and Isopolyoxometallates*, Springer-Verlag, Berlin, **1983**.
[2] M. T. Pope, A. Müller, *Angew. Chem. Int. Ed. Engl.* **1991**, *30*, 34−48.
[3] *Polyoxometallates: From Platonic Solids to Anti-Retroviral Activity* (Eds.: M. T. Pope, A. Müller), Kluwer, Dordrecht, The Netherlands, **1994**.
[4] Topical issue on polyoxometallates (Guest Ed.: C. L. Hill): *Chem. Rev.* **1998**, *98*, 1−389.
[5] *Polyoxometallate Chemistry: From Topology via Self-Assembly to Applications* (Eds.: M. T. Pope, A. Müller), Kluwer, Dordrecht, The Netherlands, **2001**.
[6] L. C. Baker, *Plenary Lecture Proc. XV Int. Conf. Coord. Chem.* **1973**, Moscow.
[7] R. Contant, M. Abbessi, J. Canny, A. Belhouari, B. Keita, L. Nadjo, *Inorg. Chem.* **1997**, *36*, 4961−4967.
[8] R. Contant, M. Abbessi, J. Canny, B. Keita, A. Belhouari, L. Nadjo, *Eur. J. Inorg. Chem.* **2000**, 567−574.
[9] B. Keita, Y. W. Lu, L. Nadjo, R. Contant, M. Abbessi, J. Canny, M. Richet, *J. Electroanal. Chem.* **1999**, *477*, 146−157.
[10] B. Keita, F. Girard, L. Nadjo, R. Contant, J. Canny, M. Richet, *J. Electroanal. Chem.* **1999**, *478*, 76−82.
[11] B. Keita, A. Belhouari, L. Nadjo, R. Contant, *J. Electroanal. Chem.* **1998**, *442*, 49−57.
[12] B. Keita, E. Abdeljalil, L. Nadjo, R. Contant, R. Belghiche, *Electrochem. Commun.* **2001**, *3*, 56−62.
[13] B. Keita, I. M. M. Mbomekalle, L. Nadjo, R. Contant, *Electrochem. Commun.* **2001**, *3*, 267−273.
[14] I. M. M. Mbomekalle, B. Keita, L. Nadjo, R. Contant, N. Belai, M. T. Pope, *Inorg. Chim. Acta* **2003**, *342*, 219−228.
[15] U. Kortz, I. M. Mbomekalle, B. Keita, L. Nadjo, P. Berthet, *Inorg. Chem.* **2002**, *41*, 6412−6416 and references cited therein.
[16] W. H. Knoth, P. J. Domaille, R. L. Harlow, *Inorg. Chem.* **1986**, *25*, 1577−1584.
[17] C. J. Gomez-Garcia, E. Coronado, L. Ouahab, *Angew. Chem. Int. Ed. Engl.* **1992**, *31*, 649−651.
[18] J. M. Clemente-Juan, E. Coronado, J. R. Glan-Mascaros, C. J. Gomez-Garcia, *Inorg. Chem.* **1999**, *38*, 55−63.
[19] U. Kortz, A. Tézé, G. Hervé, *Inorg. Chem.* **1999**, *38*, 2038−2042.
[20] T. J. R. Weakley, H. T. Evans Jr., J. S. Showell, G. F. Tourné, C. M. Tourné, *J. Chem. Soc., Chem. Commun.* **1973**, 139−140.
[21] R. Contant, G. Hervé, *Rev. Inorg. Chem.* **2002**, *22*, 63−111.
[22] T. M. Anderson, X. Zhang, K. I. Hardcastle, C. L. Hill, *Inorg. Chem.* **2002**, *41*, 2477−2487.
[23] R. Contant, *Can. J. Chem.* **1987**, *65*, 568−573.
[24] P. J. Domaille, *Inorg. Synth.* **1990**, *27*, 100−104.
[25] R. G. Finke, M. Droege, J. R. Hutchinson, O. J. Gansow, *J. Am. Chem. Soc.* **1981**, *103*, 1587−1589.
[26] I. M. Mbomekalle, B. Keita, L. Nadjo, P. Berthet, *Inorg. Chem. Commun.* **2003**, *6*, 435−438.
[27] I. M. Mbomekalle, B. Keita, M. Nierlich, U. Kortz, P. Berthet, L. Nadjo, *Inorg. Chem.* **2003**, *42*, 5143−5152.
[28] L. Ruhlmann, L. Nadjo, J. Canny, R. Contant, R. Thouvenot, *Eur. J. Inorg. Chem.* **2002**, 975−986.
[29] X. Zhang, T. M. Anderson, Q. Chen, C. L. Hill, *Inorg. Chem.* **2001**, *40*, 418−419.
[30] X. Zhang, C. L. Hill, *Chem. Ind.* **1998**, *75*, 519−524.
[31] X. Zhang, Q. Chen, D. C. Duncan, C. Campana, C. L. Hill, *Inorg. Chem.* **1997**, *36*, 4208−4215.
[32] B. Keita, Y. W. Lu, L. Nadjo, R. Contant, *Eur. J. Inorg. Chem.* **2000**, 2463−2471.
[33] B. Keita, Y. W. Lu, L. Nadjo, R. Contant, *Electrochem. Commun.* **2000**, *2*, 720−726.
[34] R. Belghiche, R. Contant, Y. W. Lu, B. Keita, M. Abbessi, L. Nadjo, J. Mahuteau, *Eur. J. Inorg. Chem.* **2002**, 1410−1414.
[35] A. Belhouari, B. Keita, L. Nadjo, R. Contant, *New J. Chem.* **1998**, 83−86.
[36] B. Keita, F. Girard, L. Nadjo, R. Contant, J. Canny, M. Richet, *J. Electroanal. Chem.* **2001**, *508*, 70−80.

Received November 7, 2003
Early View Article
Published Online April 1, 2004

 © 2004 Wiley-VCH Verlag GmbH & Co. KGaA, Weinheim

Investigations on the Reactivity of Bis(bromomagnesio)trimethylsilylmethane – Molecular Structure of a Tebbe-Type Spiro-Organomagnesium Compound

Marijke Hogenbirk,[a,b] Gerrit Schat,[a] Franciscus J. J. de Kanter,[a] Otto S. Akkerman,[a] Friedrich Bickelhaupt,*[a] Huub Kooijman,[c] and Anthony L. Spek[c][‡]

Keywords: Magnesium / Zirconium / Metallocenes / Metallacycles / Structure elucidation

The reactivity of the 1,1-di-Grignard reagent $Me_3SiCH(MgBr)_2$ (**8**) towards transition metal dihalides has been investigated. While most transformations were sluggish and gave no well-defined products, the reaction of **8** with $[Cp_2ZrCl_2]$ in a 1:1 ratio gave, in low yield, the novel spiro-organomagnesium compound $[Cp_2ZrCHSiMe_3(\mu\text{-}Br)]_2Mg$ (**12**), which is stable at room temperature and does not disproportionate on addition of dioxane. An X-ray crystal structure determination has shown that, in the solid state, **12** is present as the C_2 symmetric stereoisomer **12a**; it is sterically very crowded due to the trimethylsilyl substituents. Partial metalla-alkene character is indicated by the short zirconium–carbon bonds, and agostic zirconium–hydrogen interactions by the short zirconium–hydrogen distances (Zr···H–C) and small $^1J_{C,H}$ coupling constants. In benzene solution, equilibrium between **12a** and its C_1 symmetric stereoisomer **12b** was detected by ^1H and ^{13}C NMR spectroscopy.
(© Wiley-VCH Verlag GmbH & Co. KGaA, 69451 Weinheim, Germany, 2004)

Introduction

Organometallic reagents carrying two metals at the same carbon atom are often not easily accessible, but they are of interest both because of their intriguing structures and their synthetic applications. A well-known example is Tebbe's reagent (**1**), which is conveniently obtained from titanocene dichloride and trimethylaluminium[1] (Scheme 1); it has found application, for example, in Wittig-type olefinations of ketones.[1,2] We have reported the synthesis of **3**,[3,4] the magnesium analogue of **1**, from bis(bromomagnesio)methane (**2**)[3,5–9] and titanocene dichloride. The chemistry of **2** and of other 1,1-di-Grignard reagents has been reviewed.[10–13]

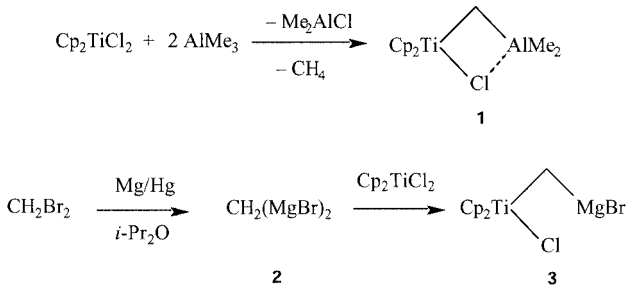

Scheme 1

Like **1** or related 1,1-bismetal-substituted reagents, **3** reacts with alkenes or alkynes to give titanacyclobutanes (**4**) or titanacyclobutenes (**5**), respectively (Scheme 2).[3] Reaction with trimethylphosphane yields the carbene complex **6**.[14] Of special interest here is the elimination of magnesium halide from **3** by evaporation of an ethereal solution followed by dissolution in toluene, which gave, based on its analytical data, $MgBr_2(CH_2TiCp_2)_2$ which was tentatively formulated as the spiro-organomagnesium compound **7**.[4]

Few known derivatives of **2** carry additional substituents at the carbon atom. We previously prepared the mono- and bis(trimethylsilyl)-substituted derivatives **8**[15] and **9**,[16] respectively (Scheme 3). However, silyl substitution stabilizes these di-Grignard reagents considerably. In particular, **9** was extremely sluggish to react even with benzophenone, and attempted reactions with metal dihalides were unproductive. The low reactivity was ascribed both to steric protection and to electronic stabilization of the negatively charged central carbon atom by silicon.[15,16]

Not surprisingly, the reactivity of **8** was intermediate between those of **2** and **9**. Thus, **8** did react with chlorotrimethylstannane; with benzophenone, it gave the expected Wittig-type product 1,1-diphenyl-2-trimethylsilylethene.[15]

[‡] Correspondence concerning the crystallography should be addressed to this author.
[a] Scheikundig Laboratorium, Vrije Universiteit, De Boelelaan 1083, 1083 HV Amsterdam, The Netherlands
Fax: (internat.) + 31-20-4447488
E-mail: bickelhpt@few.vu.nl
[b] Present address: Akzo Nobel, N.V. Organon, Molenstraat 110, P. O. Box 20, 5340 BH Oss, The Netherlands
[c] Bijvoet Center for Biomolecular Research, Utrecht University, Padualaan 8, 3584 CH Utrecht, The Netherlands

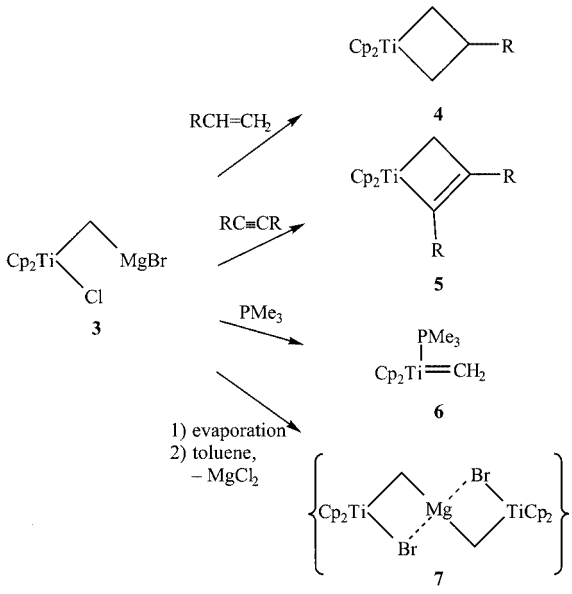

Scheme 2

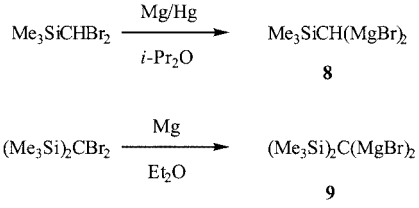

Scheme 3

Thus, we have investigated possible applications of **8**, analogous to those depicted in Schemes 1 and 2, to access the corresponding trimethylsilyl-substituted derivatives.

Results and Discussion

Reactions of $Me_3SiCH(MgBr)_2$ (8)

In analogy to the preparation of 1,3-dimetallacyclobutanes from **2**,[3,10–13] one of our main goals was the reaction of a group 4 metallocene dichloride [Cp_2MCl_2] (M = Ti, Zr, Hf) with **8** in a ratio of 1:2 to obtain the formal 1,3-di-Grignard reagent **10** which was then to be converted with the same (or a different) metal dichloride into the desired 1,3-dimetallacyclobutane **11** (Scheme 4). However, despite considerable efforts, including variation of solvents, reaction conditions etc., complicated reaction mixtures were obtained; even attempted interception of **10** with chlorotrimethylgermane did not furnish clear-cut results.

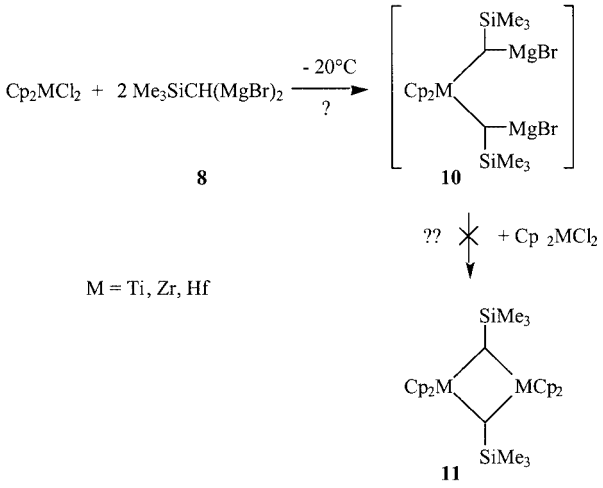

Scheme 4

In contrast, the reaction of [Cp_2ZrCl_2] with **8** in a 1:1 ratio gave an unforeseen product; after workup and purification, **12** was isolated by crystallization from a saturated toluene solution upon standing at room temperature for several weeks. The yield was low; the ^1H NMR spectrum of the crude product revealed several other compounds that could not be identified. A possible reaction pathway via the "Tebbe-type" reagent **13** is depicted in Scheme 5.

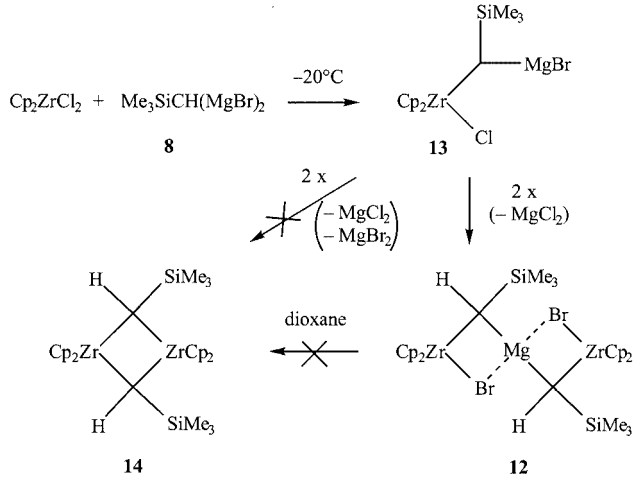

Scheme 5

Although there is no direct evidence for the occurrence of **13**, we assume it is formed by substitution of one of the chlorides of zirconocene dichloride by one of the two organomagnesium functions of **8**. Possibly, in the process of evaporating the reaction mixture and extracting the residue with toluene, **13** undergoes a partial "Schlenk equilibrium" by elimination of $MgCl_2$. Remarkably, the expected second Schlenk equilibrium step under elimination of $MgBr_2$ to furnish the 1,3-dizirconacyclobutane **14** does not proceed, neither from **13** nor from **12**. The latter reaction was tried separately by addition of dioxane to a solution of previously isolated **12**; however, **12** remained unchanged.

 © 2004 Wiley-VCH Verlag GmbH & Co. KGaA, Weinheim

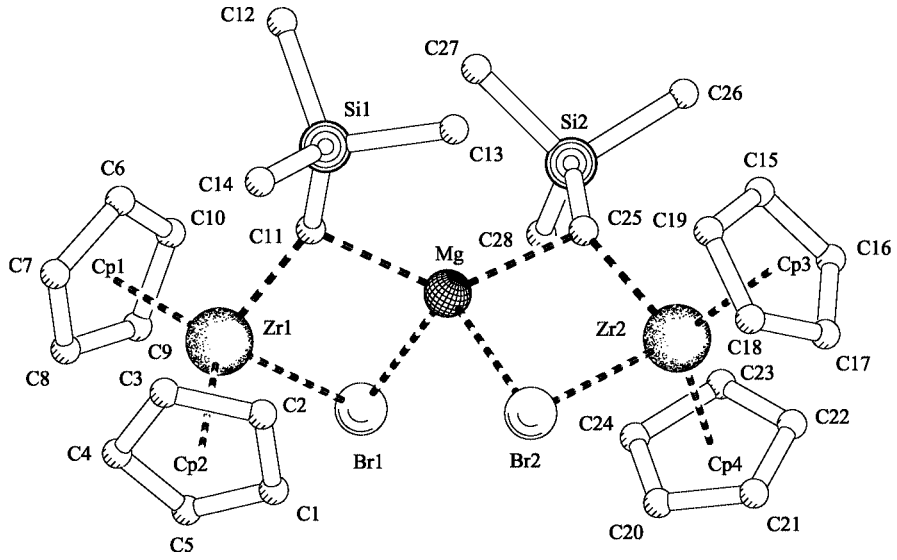

Figure 1. PLUTON[29] drawing of **12**; hydrogen atoms have been excluded for clarity; Cp indicates the center of a five-membered ring

Molecular Structure of $[Cp_2ZrCHSiMe_3(\mu\text{-}Br)]_2Mg$ (12) in the Crystal

From a saturated solution of **12** in toluene, crystals were obtained after standing for two months at room temperature. The pale yellow-orange rectangular crystals were collected and transferred to Lindemann-glass capillaries under a nitrogen atmosphere; the capillaries were then sealed by melting off. The X-ray crystal structure was determined (Figure 1). Selected bond lengths, nonbonded contacts, bond angles, and torsion angles are presented in Table 1−4, respectively.

Table 1. Selected bond lengths of **12**

[a]	Bond length [Å]		Bond length [Å]
Zr(1)−Cp(1)[a]	2.227(4)	Mg−Br(1)	2.672(3)
Zr(1)−Cp(2)[a]	2.239(4)	Mg−Br(2)	2.626(3)
Zr(2)−Cp(3)[a]	2.236(5)	Mg−C(11)	2.188(8)
Zr(2)−Cp(4)[a]	2.222(5)	Mg−C(25)	2.188(8)
Zr(1)−Br(1)	2.7232(11)	Si(1)−C(11)	1.851(8)
Zr(2)−Br(2)	2.7236(11)	Si(2)−C(25)	1.837(8)
Zr(1)−C(11)	2.147(7)		
Zr(2)−C(25)	2.160(7)		

[a] Cp(centroid).

Table 2. Selected nonbonded contacts of **12**

Contact	D(A−B)[a] [Å]	Σ(A−B)[b]	Δ[c] [Å]
Zr(1)···Si(1)	3.779(2)	4.46	−0.68
Zr(2)···Si(2)	3.740(3)	4.46	−0.72
Zr(1)···H(111)	2.496(7)	3.56	−1.06
Zr(2)···H(251)	2.546(7)	3.56	−1.01
C(6)···H(111)	2.722(11)	2.90	−0.18
C(15)···H(251)	2.721(13)	2.90	−0.18

[a] D(A−B) = measured distance between A and B. [b] Σ(A−B) = sum of radii of A and B; contact radii according to: A. Bondi, *J. Phys. Chem.* **1964**, *68*, 441, or covalent radii +0.8 Å. [c] Δ = D − Σ.

Table 3. Selected bond angles of **12**

Bond angle	[°]	Bond angle	[°]
Br(1)−Zr(1)−C(11)	91.7(2)	Zr(1)−C(11)−H(111)	99.1(6)
Zr(1)−C(11)−Mg	97.0(3)	Zr(1)−C(11)−Si(1)	141.8(4)
Zr(1)−Br(1)−Mg	73.99(6)	Si(1)−C(11)−H(111)	101.7(7)
C(11)−Mg−Br(1)	92.2(2)	Si(1)−C(11)−Mg	112.0(4)
Zr(2)−C(25)−Mg	97.0(3)	H(111)−C(11)−Mg	96.4(7)
Zr(2)−Br(2)−Mg	74.96(7)	Si(2)−C(25)−H(251)	105.5(7)
C(25)−Mg−Br(2)	93.9 (2)	Si(2)−C(25)−Mg	112.6(4)
Zr(1)−Mg−Zr(2)	157.09(9)	H(251)−C(25)−Mg	91.2(6)
Br(1)−Mg−Br(2)	103.80(9)	C(11)−Mg−Br(1)	92.2(2)
C(11)−Mg−C(25)	132.6(3)	C(11)−Mg−Br(2)	117.5(2)
Cp(1)··Zr(1)··Cp(2)	129.48(16)	Zr(2)−C(25)−Si(2)	138.6(4)
Cp(3)··Zr(1)··Cp(4)	128.76(19)		

Although the distances and angles in the two four-membered 1,3-metallacycles that constitute **12** are not equal, the compound has nearly C_2-symmetry. The "C_2"-axis passes through magnesium, perpendicular to the Zr(1)−Zr(2) vector, bisecting the Br−Mg−Br angle. As discussed below, in solution, **12** occurs as two equilibrating stereoisomers, **12a** and **12b**. Presumably, **12a** corresponds to the crystal structure, the only difference being that it *does* possess perfect C_2-symmetry, presumably due to time averaging.

Complex **12** is solvent-free, so the magnesium atom is not stabilized by coordinating diethyl ether molecules! This situation is unknown for monomeric organomagnesium compounds; rather, unsolvated organomagnesium compounds tend to crystallize in the form of polymeric ladder-type structures.[17,18] Nevertheless, the magnesium does show the usual tetracoordination with two carbon atoms and two bromine atoms forming the coordination sphere. The geometry around magnesium is distorted tetrahedral, the smallest angle being C−Mg−Br in the four-membered

 © 2004 Wiley-VCH Verlag GmbH & Co. KGaA, Weinheim

Table 4. Selected torsion angles of **12**

Torsion angle	[°]	Torsion angle	[°]
Zr(1)−Br(1)−Mg−C(11)	−15.3(2)	Zr(2)−Br(2)−Mg−C(25)	−10.4(2)
Zr(1)−C(11)−Mg−Br(1)	18.9(2)	Zr(2)−C(25)−Mg−Br(2)	12.8(2)
C(11)−Zr(1)−Br(1)−Mg	15.6(2)	C(25)−Zr(2)−Br(2)−Mg	10.5(2)
Si(1)−C(11)−Mg−Br(1)	173.5(3)	Si(2)−C(25)−Mg−Br(2)	163.2(3)
Si(1)−C(11)−Zr(1)−Br(1)	−158.6(6)	Si(2)−C(25)−Zr(2)−Br(2)	−148.8(6)
Mg−C(11)−Zr(1)−Br(1)	−18.5(2)	Mg−C(25)−Zr(2)−Br(2)	−12.3(2)
H(111)−C(11)−Zr(1)−Br(1)	79.1(6)	H(251)−C(25)−Zr(2)−Br(2)	80.4(7)
H(111)−C(11)−Mg−Br(1)	−81.1(6)	H(251)−C(25)−Mg−Br(2)	−89.2(6)
Zr(1)−Br(1)−Mg−Br(2)	103.69(8)	Zr(2)−Br(2)−Mg−Br(1)	106.64(8)
Zr(1)−C(11)−Mg−Br(2)	−87.9(3)	Zr(2)−C(25)−Mg−Br(1)	−94.4(2)
Zr(1)−Br(1)−Mg−C(25)	−155.2(2)	Zr(2)−Br(2)−Mg−C(11)	−153.5(2)
Zr(1)−C(11)−Mg−C(25)	146.6(3)	Zr(2)−C(25)−Mg−C(11)	146.4(3)
Si(1)−C(11)−Mg−Br(2)	66.7(4)	Si(2)−C(25)−Mg−Br(1)	56.0(4)
Si(1)−C(11)−Mg−C(25)	−58.8(5)	Si(2)−C(25)−Mg−C(11)	−63.2(5)

rings [92.2(2) and 93.9(2)], the largest one C(11)−Mg−C(25) (132.6°).

Crowding due to the trimethylsilyl substituents at the methine carbon atoms in combination with the cyclopentadienyl ligands at the zirconium atoms appears to be a prominent feature in the structure of **12**. The *trans*-orientation of the trimethylsilyl substituents reduces the crowding. They stick in between the neighboring cyclopentadienyl rings such that they minimize close contacts with these ligands. In addition, the Zr−C−Si angles are very large (average 140°). As a result, the silicon−carbon bonds form relatively small angles with the average planes of their metallacycle, as evidenced by the torsion angles Si(1)−C(11)−Mg−Br(1), Si(1)−C(11)−Zr(1)−Br(1), Si(2)−C(25)−Mg−Br(2), and Si(2)−C(25)−Zr(2)−Br(2) of 173.5(3)°, −158.6(6)°, 163.2(3)°, and −148.8(6)°, respectively; consequently, the trimethylsilyl substituents are close to the (approximate!) plane of the four-membered rings to which they are attached. However, the close Zr−Si contacts of 3.76 Å (Table 2, mean value) indicate that a really favorable orientation is not achieved as the sum of their contact radii is 4.46 Å. Due to this steric repulsion, the cyclopentadienyl groups are not bonded symmetrically to the zirconium atoms; the Zr−C(Cp) distances range from 2.48 to 2.56 Å.

Apparently, the sterically demanding trimethylsilyl groups also influence the geometry of the two four-membered rings. Firstly, these rings are not planar, as evidenced by the torsion angles Zr(1)−Br(1)−Mg−C(11) of −15.3(2)° and Zr(2)−Br(2)−Mg−C(25) of −10.4(2)°; in contrast, the four-membered ring is planar in the neopentyl-substituted Tebbe reagent $Cp_2ZrCH(CH_2CMe_3)AlCl$[19] (i.e. the zirconium derivative of **1**, in which the methylene group is substituted by the sterically *even more demanding* neopentyl group). Secondly, the two rings are not oriented orthogonally with respect to each other, as indicated by the angle of 85.53(17°) between their average planes. Finally, the axes of these average planes are bent towards each other, the Zr−Mg−Zr angle being 157.09(9)°. Despite these strong steric interactions **12** is, remarkably, thermally quite stable.

In addition to its rather unique spiro-Tebbe character, a closer analysis of the data for **12** reveals an intriguing duality of structural features. At first sight, **12** might be described as a dialkylmagnesium compound. This is in line with the seemingly normal Mg−C bond lengths of 2.188(8)Å, the usual range being 2.17−2.19Å.[17,18] In addition, the wide C−Mg−C angle of 132.6(3)° falls within the normal range (120−140°). Bonds to more electronegative ligands such as oxygen are smaller than tetrahedral; here, the negative ligand is bromine, and the Br−Mg−Br angle of 103.80(9)° fits into the general trend.

However, the Zr−C bonds [2.147(7) and 2.160(7)Å] are ca. 0.15 Å shorter than those in related compounds with "normal" σ-bonds between zirconium(IV) and sp^3-hybridized carbon atoms {[$Cp_2ZrMeCl$]: 2.35 and 2.36 Å;[20] [Cp_2ZrMe_2]: 2.280(5) and 2.273(5) Å;[20] [$Cp_2Zr\{CH(SiMe_3)_2\}Ph$]: 2.329(6)[21]}. Even the Zr−C bond in [$Cp_2Zr(\mu\text{-}\eta^1,\eta^2\text{-}Me_3SiCCPh)(\mu\text{-}Cl)AlMe_2$], in which an sp^2-hybridized carbon is σ-bonded to zirconium, is slightly longer [2.186 (3) Å].[22] The repulsion between the trimethylsilyl groups and the cyclopentadienyl ligands would be expected to lengthen the Zr−C bond.[21] We explain these short Zr−C bonds by invoking a certain amount of metalla-alkene character. A partial double bond will shift the hybridization of carbon from sp^3 towards sp^2 with concomitant bond shortening; in addition, the bond may be shortened by hyperconjugative interactions with silicon.[16] In addition, the Zr−C−Si angle will increase and so create more space for the trimethylsilyl groups; indeed, the Zr−C−Si angle is large [141.8(4)° and 138.6(4)°]. Conversely, the Zr−Br bond lengths are long (Zr1−Br1: 2.7232(11)Å, Zr2−Br2: 2.7236(11)Å]; most Zr−Br bonds are about 2.60 Å. We found only one other example of a long Zr−Br bond involving tetracoordinate zirconium: [$Cp_2ZrBr\{C(SiMe_3)=CHPh)\}$][23] [2.721(1) Å]. All this structural information suggests a description in terms of a loose complex **12′** between [$Cp_2Zr=CHSiMe_3$] and $MgBr_2$ (Scheme 6).

However, the situation is not so clear cut. The metalla-alkene/Lewis-acid character in "Tebbe-type" reagents such as **1**, involving titanium and zirconium in combination with

 © 2004 Wiley-VCH Verlag GmbH & Co. KGaA, Weinheim

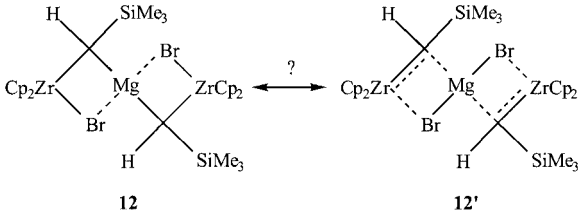

Scheme 6

aluminium, has been discussed on the basis of NMR spectroscopic data, reactivity patterns, and theoretical calculations.[19,25–27] The general conclusion is that the metal–carbene character is not very pronounced for titanium and even less so for zirconium.

As indicated above, the Mg–C bond lengths of 2.188(8) Å seems to fit better with **12** as a dialkylmagnesium.[17,18] For a loose interaction as in **12′**, the bond would be expected to be even longer, and this effect should be enhanced by steric congestion. However, these observations may be interpreted differently by looking at the structure of **9** $[(MeSi_3)_2C(MgBr{\cdot}2THF)_2]$[16] which has rather short Mg–C bonds (2.10–2.14 Å), even though two large trimethylsilyl groups and two large MgBr·2THF functions exert considerable steric pressure around the central carbon. Electrostatic effects which find their origin in the substitution of carbon by four electropositive elements (2 magnesiums, 2 silicons) have been invoked to explain the short Mg–C bonds in **9**.[16] With **12′**, similar factors might play a role, though to a lesser extent: the inherently loose interaction between magnesium and carbon is partly stabilized by polarizing effects due to zirconium and silicon. Conversely, the chemical shift of the bridging carbon in the four-membered ring, $\delta(^{13}C)$ = 153.7 ppm, is not indicative of strong metalla-alkene character, which is usually concomitant with a much more deshielded shift, as illustrated by the Ti=*C*H_2 carbon in **6** with $\delta(^{13}C)$ = 285.2 ppm.[14] The slightly elongated Mg–Br bonds (average 2.65 Å) are compatible with both **12** (μ-bridging between two metals)[17,18] and **12′** (loose interaction of $[Cp_2Zr{=}CHSiMe_3]$ with the Lewis acid $MgBr_2$).

A thorough theoretical analysis is clearly required, which was beyond the scope of the present investigation. From of the qualitative arguments discussed here, we propose that the structure of the compound is intermediate between the two extreme models, which is indicated by the resonance relation depicted in Scheme 6; apparently, **12** is preponderant, but contributions from **12′** are clearly indicated.

Another aspect to discuss briefly is a weak agostic interaction[24,25] between zirconium and the α-CH bond; **12** has short M···H distances and small $^1J_{C,H}$ coupling constants, both of which are characteristic of M···H–C agostic interactions. The Zr···H distances [2.496(7) and 2.546(7) Å] are more than 1 Å shorter than the sum of their contact radii, and $^1J_{C,H}$ = 91.4 Hz is small, though in the upper range for sp^3-hybridized agostic systems (60–90 Hz).

However, two caveats seem appropriate. First, the positions of the α-hydrogens – as light atoms next to the heavy zirconium – were restrained during refinement. Although the C–H moiety as a whole was allowed to reorient itself, the C–H bond was fixed at the ideal value of 0.98 Å. This makes the position of these hydrogens slightly less reliable. Typical β-agostic contacts are shorter, as exemplified by *d*(Zr···H) = 2.19 Å in $[Cp_2ZrBr(CSiMe_3{=}CHPh)]$.[23] Even so, the Zr···H contacts in **12** indicate a weak agostic interaction. Secondly, with regard to the small $^1J_{C,H}$ = 91.4 Hz, one has to consider that substitution of an sp^3-hybridized carbon by electropositive elements increases the s-character in the C–M bonds, and thus reduces s-contribution to the C–H bonds. For instance, we observed $^1J_{C,H}$ = 104.4 Hz for the joint effect of magnesium and silicon in Me_3Si-CH_2MgBr, while the additional silicon in $(Me_3Si)_2$-CHMgBr (**8**) further decreases $^1J_{C,H}$ to 93.1 Hz. However, against this background, it is unlikely that the small $^1J_{C,H}$ = 91.4 Hz of **12** can be fully accounted for by the effect of only three electropositive substituents on carbon (Mg, Zr, Si).

Finally, the X-ray crystal structure of **12** supports the previously suggested hypothetical assignment[4] of an analogous spiro-magnesium structure to **7** (Scheme 2).

Structure of 12 in Solution

Crystals of **12** dissolved in C_6D_6 for NMR analysis showed two species, **12a** and **12b**, in equilibrium; directly after dissolution, **12a** was the dominant species. Its simple ^{1}H NMR spectrum is indicative of C_2 symmetry: δ = 7.43 (s, 2 H, C*H*), 6.09 (s, 10 H, Cp), 5.94 (s, 10 H, Cp), 0.43 (s, 18 H, $SiMe_3$) ppm. Such a spectrum is also in line with the C_2 symmetric structure **12c** (Scheme 7). The immediate appearance of this spectrum after dissolving crystals of **12**, which have been proven to have the (approximate) C_2 structure (Figure 1), strongly suggests that the species in solution is **12a**; its ideal C_2 symmetry must be due to rapid time averaging. This structure assignment is further supported by inspection of models that reveal that the alternative conceivable C_2 isomer **12c** would experience severe steric hindrance because it has two trimethylsilyl groups at the two four-membered rings that point directly towards each other.

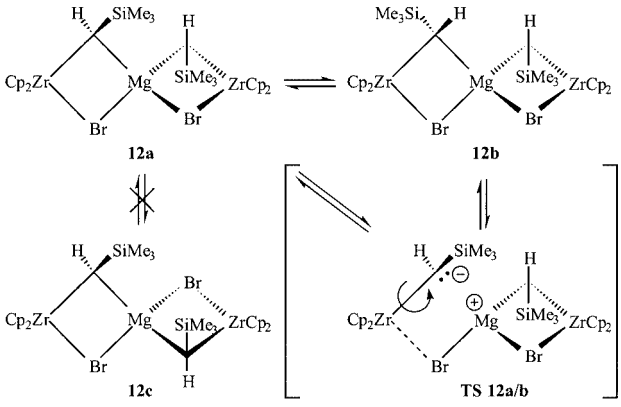

Scheme 7

 © 2004 Wiley-VCH Verlag GmbH & Co. KGaA, Weinheim

Compound **12b** is, apparently, an isomer of **12a**, but it has C_1 symmetry, as evidenced by two methine proton signals [δ = 7.80 and 7.17 ppm (2 s, 2 H)], four cyclopentadienyl signals at δ = 6.14, 6.04, 5.95 and 5.94 ppm (4 s, 20 H) and two trimethylsilyl signals at δ = 0.43 and 0.40 ppm (2 s, 18 H). The isomeric relation is in line with the chemical shifts of **12b** all being in the same range as the corresponding signals of **12a**; moreover, **12b** must contain a $MgBr_2$ unit because this species could not be removed from the solution on treatment with THF or dioxane, and free $MgBr_2$ would have precipitated in C_6D_6.

As mentioned above, crystals of **12**, when dissolved in C_6D_6, formed a mixture of **12a** and **12b** where the initial concentration of **12b** was very low. After standing for several days at room temperature, an equilibrium ratio of **12a/12b** = 1.14 was reached. At higher temperatures, the amount of **12a** increased (Table 5); this change was reversible. Below room temperature, the composition of the mixture showed no further changes; apparently, the rate of isomerization was too low.

Table 5. Equilibrium constants and equilibration times of **12a/b** in C_6D_6

T (K)[a]	K (**12a/12b**)	Equilibrium time[b]
293	1.14	several days
313	4.33	50 h
328	4.91	8.5 h
343	4.29	4 h

[a] Equilibrium constants K are based on the integrals of the cyclopentadienyl groups in the ^{1}H NMR spectra. [b] Time required to reach equilibrium when dissolving **12** at 293 K and warming to the temperature cited.

A pathway for the interconversion between **12a** and **12b** is tentatively proposed (Scheme 7). Formally, the transformation involves the interchange of the orientation of H and Me_3Si in one of the two four-membered rings (shown for the left ring in Scheme 7). The process must be intramolecular as the reactive metalla-alkene units could not be liberated by coordination of magnesium bromide upon addition of dioxane. Furthermore, the position of the equilibrium is concentration independent; at 313 K, in a separate experiment with a diluted solution of the **12a/b** mixture, the same reaction rate and equilibrium constant as in the undiluted experiment were found. We propose that, in **12a** or **12b**, one of the carbon−magnesium bonds is cleaved such that the formal $Cp_2Zr-CHSiMe_3^-$ substructure can rotate around the Zr−C bond, followed by reclosure of the C−Mg bond; simultaneous cleavage of the Zr−Br bond, with formation of the more or less free metalla-alkene [$Cp_2Zr{=}CHSiMe_3$], can be excluded as it should lead to decomposition with formation of free $MgBr_2$ and dimerization of [$Cp_2Zr{=}CHSiMe_3$] to give **14** (Scheme 5).

The temperature dependence of the equilibrium between **12a** and **12b** was studied by ^{1}H NMR spectroscopy with a sample in a sealed NMR tube (Table 5); at higher temperatures, the equilibrium shifted in favor of **12a**. Consequently, we expected the highest **12a/b** ratio at 343 K, but this was not observed. It is not clear what caused this deviation as the compounds did not decompose; for several measurements of the same NMR sample at higher temperatures the **12a/b** ratio returned to the initially determined K of 1.14 at 20°C. In view of this anomaly, the interpretation of these results must remain speculative and we refrain from a quantitative analysis; however, some qualitative conclusions may be justified. Thus, **12b** appears to be enthalpically more stable than **12a**. This seemed surprising as, intuitively, one would assume that **12a** with its two bulky trimethylsilyl groups *trans* at the two four-membered rings will experience less steric hindrance than **12b**, where they are somewhat closer; however, inspection of models suggests that in both isomers the trimethylsilyl groups do not interfere directly with each other. Conversely, the trimethylsilyl groups of **12b** can adopt a favorable position between the bulky cyclopentadienyl groups with less distortion of the two four-membered rings, and less concomitant strain, than those of **12a**. In contrast, the reaction entropy appears to favor **12a**; given the close similarity of the two isomers, we have at present no satisfactory explanation for this effect.

Conclusion

In line with earlier results on the reduced reactivity of organomagnesium reagents that carry electropositive substituents at the organometallic carbon atom,[15,16] the 1,1-di-Grignard reagent $Me_3SiCH(MgBr)_2$ (**8**) reacts sluggishly with transition metal dihalides and, mostly, gave no well-defined products. An exception is the reaction of **8** with [Cp_2ZrCl_2] (1:1) which, in low yield, furnished the novel spiro-organomagnesium compound [$Cp_2ZrCHSiMe_3(\mu\text{-}Br)]_2Mg$ (**12**). Compound **12** is stable at room temperature and does not disproportionate on addition of dioxane. An X-ray crystal structure determination showed that, in the solid state, **12** is present as the C_2 symmetric stereoisomer **12a**; it is sterically very crowded due to the trimethylsilyl substituents. Partial metalla-alkene character is indicated by the short zirconium−carbon bonds, and agostic zirconium−hydrogen interactions by the short zirconium−hydrogen distances (Zr···H−C) and small $^1J_{C,H}$ coupling constants. In benzene solution, an equilibrium between **12a** and its C_1 symmetric stereoisomer **12b** was detected by ^{1}H and ^{13}C NMR spectroscopy.

Experimental Section

General Remarks: Experiments with **8** and **12** were performed using high-vacuum sealed glass apparatus.[26] Solvents were dried before use by distillation from a liquid Na−K alloy. For spectroscopy, the solvent was first removed from a sample by distillation with liquid nitrogen, followed by evacuation; subsequently, the residue was redissolved in a deuterated solvent in a high-vacuum system and, finally, the NMR tube was sealed. NMR spectra were measured with a Bruker WM 250 spectrometer. GCMS analysis was per-

 © 2004 Wiley-VCH Verlag GmbH & Co. KGaA, Weinheim

formed on a Hewlett Packard 5890 GC/5970 MS combination with a 50 m Chrompack CP Sil 5 column.

2,2,6,6-Tetracyclopentadienyl-3,7-bis(trimethylsilyl)-1,5-dibroma-4-magnesa-2,6-dizirconaspiro[3.3]heptane (12): In a sealed glass vessel, **8**[15] (0.202 mmol) was dissolved in 2-methyltetrahydrofuran (10 mL). [Cp_2ZrCl_2] (59 mg, 0.202 mmol) was then added to this solution at −20 °C, resulting in a colorless solution. After 50 min stirring at −20 °C, the mixture was still colorless and homogeneous. The vessel was then warmed to +5 °C and, after 25 min, the mixture turned light yellow. Subsequently, the vessel was warmed and kept at room temperature for 4 h. The reaction mixture was yellow, and no precipitation was observed. After a further 17 h at room temperature, the solution became yellow-brownish. The solvent was then removed by distillation and pumping. The resultant residue was partly crystalline, partly oily. It was extracted with toluene to give a brownish solution, which was decanted from the precipitate of salts. Attempts to prepare crystals on cooling this solution (at −10 °C or −80 °C) failed. Toluene was removed by distillation into a vessel cooled by liquid nitrogen; a yellow oil was left in which crystals formed after several weeks. These were then washed with hexane; the light yellow hexane solution was decanted. The residue was made solvent free by distillation with liquid nitrogen and then toluene was added. Some precipitate (probably magnesium salts) formed, and the solution was decanted. After several further weeks at room temperature, a few pale yellow-orange crystals precipitated from this solution; they were used for X-ray crystal structure determination and for NMR measurements. The mother liquor, which contained mainly **12** (NMR analysis), was treated with dioxane. A small amount of a white precipitate ($MgBr_2$) formed, but NMR analysis of an aliquot revealed that no apparent change had taken place. **12a:** ^{1}H NMR (250 MHz, C_6D_6, ref.C_6D_5H δ = 7.17 ppm): δ = 7.43 (s, 2 H, methine), 6.09 (s, 10 H, Cp), 5.94 (s, 10 H, Cp), 0.43 (s, 18 H, Me) ppm. ^{13}C NMR (62.9 MHz, C_6D_6, ref.C_6D_6 δ = 128.0 ppm): δ = 153.3 (d, $^1J_{C,H}$ = 91.4 Hz, methine), 111.4 (dquint., $^1J_{C,H}$ = 172.5, $J_{C,H}$ = 6.9 Hz, Cp), 110.1 (dquint., $^1J_{C,H}$ = 173.1, $J_{C,H}$ = 6.8 Hz, Cp), 6.4 (q, $^1J_{C,H}$ = 117.2 Hz, Me) ppm. **12b:** ^{1}H NMR (250 MHz, C_6D_6, ref.C_6D_5H δ = 7.17 ppm): δ = 7.80 (s, 1 H, methine), 7.17 (s, 1 H, methine), 6.14 (s, 5 H, Cp), 6.04 (s, 5 H, Cp), 5.95 (s, 5 H, Cp), 5.94 (s, 5 H, Cp), 0.43 (s, 9 H, Me), 0.40 (s, 9 H, Me) ppm. ^{13}C NMR (62.9 MHz, C_6D_6, ref.C_6D_6 δ = 128.0 ppm): δ = 152.5 (d, $^1J_{C,H}$ = 88.5 Hz, methine), 145.6 (d, $^1J_{C,H}$ = 90.3 Hz, methine), 111.8 (dquint., $^1J_{C,H}$ = 172.7, $^1J_{C,H}$ = 6.7 Hz, Cp), 111.5 (dquint., $^1J_{C,H}$ = 173, $J_{C,H}$ = 7 Hz, Cp), 110.7 (dquint., $^1J_{C,H}$ = 173.2, $J_{C,H}$ = 6.8 Hz, Cp), 109.9 (dquint., $^1J_{C,H}$ = 173.1, $J_{C,H}$ = 6.7 Hz, Cp), 6.9 (q, $^1J_{C,H}$ = 117.2 Hz, Me), 6.2 (q, $^1J_{C,H}$ = 117.2 Hz, Me) ppm.

X-ray Crystal Structure Determination of 12: $C_{28}H_{40}Br_2MgSi_2Zr_2$. M = 799.35, pale orange crystal, 0.21 × 0.23 × 0.40, monoclinic, space group $P21/c$ (no. 14) with a = 14.7539(5), b = 12.3679(4), c = 17.8513(7) Å; β = 93.83(3)°, V = 3250.1(2) Å^3, Z = 4, $\rho_{calcd.}$ = 1.633 g·cm^{-3}, $F(000)$ = 1592, μ(Mo-K_α) = 3.17 mm^{-1}. Of the 9029 reflections measured on an Enraf−Nonius CAD4-T diffractometer, on a rotating anode [λ(Mo-K_α) = 0.71073 Å, T = 295 K, $\theta_{max.}$ = 27.5°], 7430 were unique (R_{int} = 0.029); 4477 reflections with $I > 2.5\sigma(I)$ were used in the structure solution and refinement. Application of empirical and analytical absorption correction algorithms on the measured data had no significant effect. A final model without absorption correction was therefore preferred. The structure was solved with Patterson methods (SHELXS-86[27]); 317 parameters were refined with SHELX-76,[28] including anisotropic displacement parameters for all non-hydrogen atoms. Hydrogen atoms were placed at calculated positions, riding on their carrier atoms, with the exception of hydrogen atoms bonded to C11 and C25 (the carbon atoms bonded to Mg, Br, and Zr). The coordinates of these hydrogen atoms were allowed to refine, albeit that the C−H bond length was constrained to the ideal value of 0.98 Å. Final figures of merit are R = 0.054, R_w = 0.073, S = 2.94. Residual density was in the range −1.34, 1.13 e·Å^3. CCDC-222722 contains the supplementary crystallographic data for this paper. These data can be obtained free of charge at www.ccdc.cam.ac.uk/conts/retrieving.html [or from the Cambridge Crystallographic Data Centre, 12 Union Road, Cambridge CB2 1EZ, UK; Fax: (internat.) +44-1223-336-033; E-mail: deposit@ccdc.cam.ac.uk].

Acknowledgments

This work was supported in part (ALS) by the Council for the Chemical Sciences of the Netherlands Organization for Scientific Research (CW-NWO).

[1] F. N. Tebbe, G. W. Parshall, G. S. Reddy, *J. Am. Chem. Soc.* **1978**, *100*, 3611−3613.
[2] S. H. Pine, R. Zahler, D. A. Evans, R. H. Grubbs, *J. Am. Chem. Soc.* **1980**, *102*, 3270−3272.
[3] J. W. Bruin, G. Schat, O. S. Akkerman, F. Bickelhaupt, *Tetrahedron Lett.* **1983**, *24*, 3935−3936.
[4] B. J. J. van de Heisteeg, G. Schat, O. S. Akkerman, F. Bickelhaupt, *Tetrahedron Lett.* **1987**, *28*, 6493−6496.
[5] G. Emschwiller, *C. R. Acad. Sci. Paris* **1926**, *183*, 665.
[6] F. Bertini, P. Grasselli, G. Zubiani, G. Cainelli, *Tetrahedron* **1970**, *26*, 1281, and ref. cited.
[7] J. W. Bruin, G. Schat, O. S. Akkerman, F. Bickelhaupt, *J. Organomet. Chem.* **1985**, *288*, 13−25.
[8] B. J. J. van de Heisteeg, G. Schat, O. S. Akkerman, F. Bickelhaupt, *J. Organomet. Chem.* **1986**, *308*, 1−10.
[9] B. J. J. van de Heisteeg, G. Schat, O. S. Akkerman, F. Bickelhaupt, in *Organometallic Syntheses* (Eds.: R. B. King, J. J. Eisch), Elsevier, Amsterdam, **1988**, Vol. 4, 389−391.
[10] F. Bickelhaupt, *Angew. Chem.* **1987**, *99*, 1020−1035; *Angew. Chem. Int. Ed. Engl.* **1987**, *26*, 990.
[11] F. Bickelhaupt, *J. Organomet. Chem.* **1994**, *475*, 1−14.
[12] K. C. Kennon, G. R. Krow, in *Handbook of Grignard Reagent*s (Eds.: G. S. Silverman, P. E. Rakita), Marcel Dekker, New York, **1996**, 497−526.
[13] F. Bickelhaupt, in *Grignard Reagents, New Developments* (Ed.: H. G. Richey), Wiley, Chichester, **2000**, 367−393.
[14] B. J. J. van de Heisteeg, G. Schat, O. S. Akkerman, F. Bickelhaupt, *J. Organomet. Chem.* **1986**, *108*, C25−C28.
[15] B. J. J. van de Heisteeg, G. Schat, M. A. G. M. Tinga, O. S. Akkerman, F. Bickelhaupt, *Tetrahedron Lett.* **1986**, *27*, 6123−6324.
[16] M. Hogenbirk, G. Schat, M. A. G. M. Tinga, O. S. Akkerman, F. Bickelhaupt, W. J. J. Smeets, A. L. Spek, *J. Am. Chem. Soc.* **1992**, *114*, 6195−6198.
[17] H. L. Uhm, in *Handbook of Grignard Reagent*s (Eds.: G. S. Silverman, P. E. Rakita), Marcel Dekker, New York, **1996**, 117−144.
[18] F. Bickelhaupt in *Grignard Reagents, New Developments* (Ed.: H. G. Richey), Wiley, Chichester, **2000**, 298−328.
[19] U. Klabunde, F. N. Tebbe, G. W. Parshall, R. L. Harlow, *J. Mol. Cat.* **1980**, *8*, 37−51.
[20] W. E. Hunter, D. C. Hrncir, R. Vann Bynum, R. A. Penttila, J. L. Atwood, *Organometallics* **1983**, *2*, 750−755.
[21] J. Jeffery, M. F. Lappert, N. T. Luong-Thi, J. L. Atwood, W. E. Hunter, *J. Chem. Soc., Chem. Commun.* **1978**, 1081−1083.

 © 2004 Wiley-VCH Verlag GmbH & Co. KGaA, Weinheim

[22] G. Erker, R. Zwettler, C. Krüger, R. Noe, S. Werner, *J. Am. Chem. Soc.* **1990**, *112*, 9620−9621.
[23] I. Hyla-Kryspin, R. Gleiter, C. Krüger, R. Zwettler, G. Erker, *Organometallics* **1990**, *9*, 517−523.
[24] M. Brookhart, M. L. H. Green, *J. Organomet. Chem.* **1983**, *285*, C5−C8.
[25] M. Brookhart, M. L. H. Green, L.-L. Wong, *Prog. Inorg. Chem.* **1988**, *36*, 1−124.
[26] A. D. Vreugdenhil, C. Blomberg, *Recl. Trav. Chim. Pays Bas* **1963**, *83*, 453−460.
[27] G. M. Sheldrick, *SHELXS-86* Program for crystal structure determination, University of Göttingen, Germany, **1986**.
[28] G. M. Sheldrick, *SHELX-76* Program for crystal structure determination and refinement, University of Göttingen, Germany, **1976**.
[29] A. L. Spek, PLATON, A multi-purpose crystallographic tool, Utrecht University, The Netherlands, **2003**; Internet: http://www.cryst.chem.uu.nl/platon/

Received November 6, 2003
Early View Article
Published Online April 1, 2004

 © 2004 Wiley-VCH Verlag GmbH & Co. KGaA, Weinheim

Oxidative Addition of RX to Soluble and Polymer-Bound Molybdenum Carbonyl Complexes

Katja Heinze,*[a] Volker Jacob,[a] and Christian Feige[a]

Keywords: Allyl Ligands / Molybdenum / Polymer-bound complexes / Solid-phase synthesis

Oxidative addition of $PhSnCl_3$ or allyl halides to molybdenum tetracarbonyl complexes proceeds both in solution and on polymer matrices. The structures of the soluble Mo^{II} complexes have been determined by single-crystal X-ray diffraction in the solid state and by NMR and IR spectroscopy in solution. The identity and stability of the polymer-bound complexes have been elucidated by spectroscopic techniques directly on the solid support and by releasing the complexes from the support.

(© Wiley-VCH Verlag GmbH & Co. KGaA, 69451 Weinheim, Germany, 2004)

Introduction

Homogeneous organometallic catalysis has several advantages over heterogeneous catalysis as the activity and selectivity can be tuned by the choice of suitable ligands. On the other hand soluble catalysts are more difficult to separate and to handle than the technically well-established heterogeneous ones. A promising strategy to combine the advantages of both catalyst types is the immobilisation of active metal complexes on supports, which can be separated by filtration. However, many of the heterogeneous systems are very difficult to characterise and are not well understood. Improved characterisation should lead to better reproducibility, whereas understanding on a molecular level, if possible, can help to improve existing concepts and to develop new catalytic systems.[1] This is even more important as some stoichiometric and catalytic reactions performed on polymer matrices give different results from the reactions performed in a homogeneous phase.[2] A polymer matrix can confer higher stability to reactive intermediates,[3,4] can stabilise catalytically active species ("site isolation" effect [5−7]) and thus lead to higher activity, but can also reduce catalyst activity and influence catalyst selectivity,[8] even enantioselectivity.[9] Thus it is desirable to identify and control the species bound to the polymer support.

As part of our program to synthesise and characterise metal complexes bound to a solid support[10−12] we investigated the transformation of polymer-bound Mo^0 complexes to Mo^{II} complexes by oxidative addition of RX and elimination of carbon monoxide. The oxidative addition of RX to Mo^0 is one of the first steps in the synthesis of the precatalyst of the molybdenum(0)-catalysed allylic alkylation developed by Trost et al.[13−15] This catalytic reaction has become an important tool in asymmetric organic synthesis. Control of catalyst regioselectivity and enantioselectivity has been achieved by designing suitable ligands and using suitable metal catalyst precursors.[13−16] Microwave flash heating has been employed to improve catalyst activity and the immobilisation of the nucleophile on a solid support has been reported.[17] An allylpalladium phosphane complex has been anchored to a polystyrene/poly(ethylene glycol) graft copolymer and has been used for the palladium-catalysed allylic substitution.[18] An allylmolybdenum complex has been synthesised on a solid support and released from the solid phase for biolabelling purposes.[19]

The solid-phase reaction system employed here allows the synthesis of metal complexes on an insoluble polystyrene/divinyl benzene copolymer, the transformation of these complexes on the support and finally release of the product complexes from the support under mild conditions to prove their identity and integrity.[11,12]

Results and Discussion

The Solid-Phase Synthesis of 3a−6a via 3b−6b and Solution Synthesis of 3a−6a

For the solid-phase synthesis the bidentate Schiff-base ligand **1a** was attached to polystyrene/2% divinyl benzene by a silyl ether linker to yield the immobilised ligand **1b** (Scheme 1).[10−12] This silyl ether can be cleaved by fluoride ions under mild conditions compatible with metal complexes.[11,12]

[a] Anorganisch-Chemisches Institut der Universität Heidelberg
Im Neuenheimer Feld 270, 69120 Heidelberg, Germany
Fax.: (internat.) + 49-(0)6221-545707
E-mail: katja.heinze@urz.uni-heidelberg.de

Supporting information for this article is available on the WWW under http://www.eurjic.org or from the author.

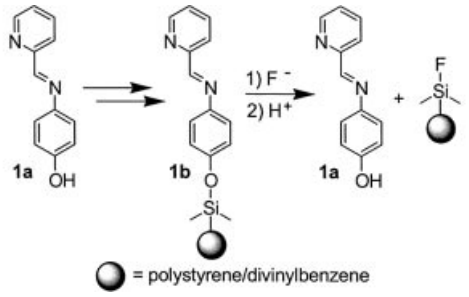

Scheme 1. Immobilisation of ligand **1a** and release of **1a** from the polymer

Solid-State Structures of 3a·Et_2O, 4a·THF, 5a·THF and 5a

The heterobimetallic complex **3a** crystallises in the monoclinic space group $P2_1/c$ with inclusion of one diethyl ether molecule (Figure 1, Table 1). The solvent molecule is attached to the complex by an O−H···O hydrogen bond (O1···O100 2.74 Å). Hydrogen bonds from the hydroxy group of the Schiff-base ligand to solvent molecules have been previously observed.[20] The molybdenum atom is seven-coordinate and the tin atom is five-coordinate with one chlorine atom occupying a bridging position between the two metal atoms. The coordination geometry around

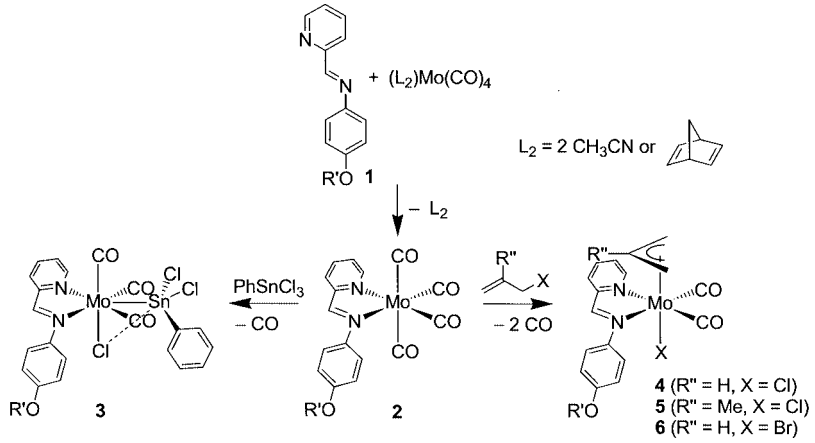

Scheme 2. Solid-phase and solution syntheses of **3**−**6** [a: R′ = H; b: R′ = polystyrene−Si(*i*Pr)$_2$]

The synthesis of Mo^{II} complexes from Mo^0 complexes on the solid phase and in solution is depicted in Scheme 2. The tetracarbonyl complexes **2a** and **2b** were prepared from the soluble ligand **1a** or the immobilised ligand **1b** and an $Mo(CO)_4$ source.[11] Oxidative addition of RX gives the seven-coordinate heterobimetallic complexes **3a** and **3b** with concomitant loss of one equivalent of carbon monoxide (RX = $PhSnCl_3$)[11] and the allyl complexes **4a**−**6a** and **4b**−**6b** [RX = CH_2CHCH_2Cl, $CH_2C(CH_3)CH_2Cl$, CH_2CHCH_2Br] with loss of two equivalents of carbon monoxide.

Release of the immobilised complexes from the solid support is accomplished by fluoridolysis of the silyl ether linker followed by protonation of the anionic complexes with acetic acid (Scheme 3).

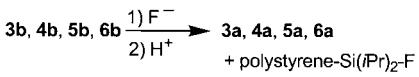

Scheme 3. Cleavage of the complexes from the solid support

All soluble complexes **3a**−**6a** have been completely characterised by spectroscopic methods and the solid-state structures of **3a**−**5a** have been determined by X-ray crystallography. The immobilised complexes **3b**−**6b** have been analysed by IR spectroscopy, diffuse reflection UV/Vis spectroscopy and thermogravimetric analysis.

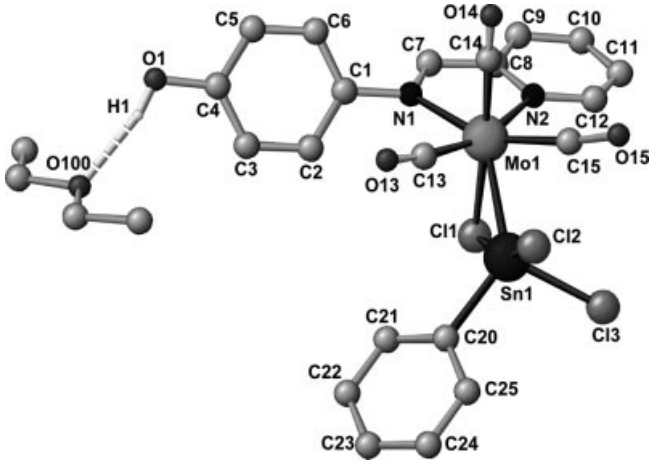

Figure 1. Structure of 3a·Et_2O in the solid state

molybdenum can be described as capped octahedral with the tin atom occupying the seventh position above an octahedral face defined by the bridging chloride Cl1 and two carbon atoms (C13 and C15). The angles between the atoms defining the capped face are larger (104−109°) than the angles between the atoms defining the opposite triangular face (73−96°). Thus, the octahedral symmetry is distorted to accommodate the seventh ligand — similar to the structure of [(bpy)Mo(CO)$_3$Cl(SnCl$_2$CH$_3$)].[21]

 © 2004 Wiley-VCH Verlag GmbH & Co. KGaA, Weinheim

Table 1. Selected bond lengths [Å] and angles [°] of **3a**·Et_2O, **4a**·THF, **5a**·THF and **5a**

	3a·Et_2O	**4a**·THF	**5a**·THF	**5a**
Mo1−N1	2.229(2)	2.2732(15)	2.291(2)	2.275(3)
Mo1−N2	2.230(2)	2.2230(16)	2.219(2)	2.247(3)
Mo1−C13	1.982(3)	1.959(2)	1.962(3)	1.958(5)
Mo1−C14	1.976(3)	1.970(2)	1.967(3)	1.955(5)
Mo1−C15	1.983(3)	–	–	–
Mo1−Cl1	2.5409(10)	2.5073(9)	2.5150(8)	2.5149(12)
Mo1−Sn1	2.7154(7)	–	–	–
Mo1−C16	–	2.322(2)	2.319(3)	2.325(4)
Mo1−C17	–	2.208(2)	2.243(2)	2.248(4)
Mo1−C18	–	2.309(2)	2.315(2)	2.304(4)
N1−Mo1−N2	73.17(8)	73.31(5)	73.33(7)	73.43(12)
N1−Mo1−C13	91.10(10)	170.31(7)	169.31(9)	168.71(15)
N1−Mo1−C14	90.46(10)	106.44(7)	105.91(9)	105.30(15)
N1−Mo1−C15	154.33(10)	–	–	–
N1−Mo1−Cl1	84.67(6)	80.97(4)	81.50(5)	79.54(9)
N1−Mo1−Sn1	136.26(6)	–	–	
N1−Mo1−C16	–	114.18(7)	116.89(9)	117.39(15)
N1−Mo1−C17	–	82.14(7)	85.11(9)	85.55(13)
N1−Mo1−C18	–	81.37(7)	83.41(9)	83.69(15)
N2−Mo1−C13	162.57(10)	100.34(7)	100.69(9)	100.69(16)
N2−Mo1−C14	95.91(11)	168.53(7)	168.21(8)	168.95(15)
N2−Mo1−C15	86.96(10)	–	–	–
N2−Mo1−Cl1	81.99(6)	81.15(4)	80.17(5)	82.62(9)
N2−Mo1−Sn1	126.98(5)	–	–	–
N2−Mo1−C16	–	81.16(7)	82.76(9)	82.58(16)
N2−Mo1−C17	–	86.90(7)	88.09(9)	87.49(14)
N2−Mo1−C18	–	120.51(7)	121.71(8)	120.80(14)
C13−Mo1−C14	76.34(13)	78.28(8)	78.08(10)	78.57(18)
C13−Mo1−C15	105.69(13)	–	–	–
C13−Mo1−Cl1	104.43(9)	90.91(6)	88.81(8)	90.24(12)
C13−Mo1−Sn1	69.74(8)	–	–	–
C13−Mo1−C16	–	71.19(9)	70.19(10)	70.45(17)
C13−Mo1−C17	–	105.12(8)	103.76(10)	104.04(16)
C13−Mo1−C18	–	108.29(8)	107.26(10)	107.57(18)
C14−Mo1−C15	75.30(12)	–	–	–
C14−Mo1−Cl1	175.07(8)	87.48(6)	88.07(7)	86.35(12)
C14−Mo1−Sn1	120.32(8)	–	–	–
C14−Mo1−C16	–	108.80(8)	107.50(10)	107.27(18)
C14−Mo1−C17	–	104.49(8)	103.62(10)	103.42(17)
C14−Mo1−C18	–	70.30(8)	69.38(9)	69.45(17)
C15−Mo1−Cl1	108.95(8)	–	–	–
C15−Mo1−Sn1	68.94(8)	–	–	–
Cl1−Mo1−Sn1	64.20(2)	–	–	–
C16−Mo1−C17	–	36.16(8)	35.73(10)	35.61(16)
C16−Mo1−C18	–	61.76(9)	61.52(10)	60.95(18)
C17−Mo1−C18	–	36.08(8)	36.32(9)	35.96(16)
C16−C17−C18	–	115.4(2)	114.1(2)	113.6(4)
H1···A	1.92(3)[a]	2.38(3)[b]	2.45(4)[b]	2.37(4)[b]
O1···A	2.738[a]	3.118[b]	3.145[b]	3.121[b]
O1−H1···A	166(4)[a]	176(3)[b]	179(4)[b]	175(4)[b]
C3−C4−O1−H1	1.6	−177.4	−178.7	−1.2
C7−N1−C1-C2	123.4(3)	−146.2(2)	−147.9(2)	−144.3(4)

[a] A = O100. [b] A = Cl1.

The allyl complex **4a** crystallises in the monoclinic space group $P2_1/c$ with inclusion of one THF molecule. Unlike the structure of **3a** the solvent molecule is isolated from the molybdenum complex. Instead, the hydroxy group of the ligand forms a hydrogen bond to the chloro ligand of a neighbouring molecule (Figure 2). The molecules are thus connected by O−H···Cl hydrogen bonds (O1···Cl1 3.12 Å) and form a chain consisting of alternating enantiomeric complexes along the *c*-axis (*c* glide plane).

The methallyl complex **5a** can be crystallised with and without inclusion of solvent molecules (**5a**·THF and **5a**). In the former pseudo-polymorph the THF molecule is isolated from the complex molecules which are connected by O−H···Cl hydrogen bonds (O1···Cl1 3.15 Å) to give the same motif as the allyl complex **4a** with the chain going along the crystallographic *n* axis. (Figure 3).

The solvent-free pseudo-polymorph of **5a** also displays an O−H···Cl hydrogen bonding motif (O1···Cl1 3.12 Å, Figure 4). Here the complexes form a helix along the crystallographic twofold axis and thus the helices consist of molecules with like stereochemistry (homochiral chain). A further difference is observed for the orientation of the OH group of the ligand in the pseudo-polymorphs **5a**·THF and **5a**: in the former structure the OH bond points away from the metal centre (torsion angle C3−C4−O1−H1 −178.7°, Figure 3) and in the latter it points towards the metal centre (torsion angle C3−C4−O1−H1 −1.2°, Figure 4) as a consequence of the arrangement of the molecules. Obviously the mere presence (**4a**·THF, **5a**·THF) or absence of solvent molecules (**5a**) controls the hetero- or homochirality of the chains without affecting the mode of connection. The O−H···Cl hydrogen bond indeed appears to be the most stable one in this system as no hydrogen bonds between the OH group and solvent molecules {as found for example for **3a** or [(**1a**)$Mo(CO)_3(PPh_3)$]·Et_2O[20]} or metal-bound carbonyl groups [as found for example in complexes {[(**1a**)$M(CO)_3(CNR)$];[20,22] M = Cr, Mo, W} are observed. DFT calculations for **4a** and **5a** with a water molecule (as a model hydrogen donor) hydrogen-bonded to chloride, to the carbonyl ligands, and to the hydroxo group show that the first hydrogen-bonded system is the most stable (although the calculated relative energies might not be be very accurate due to the basis set superposition error BSSE,[23] see Supporting Information).

Properties of 3a, 4a, 5a and 6a

The hydrogen bonding present in the solid-state structures of **3a**, **4a** and **5a** is also confirmed by the signals of the ν_{OH} vibrations at 3444, 3265 and 3256 cm^{-1} in the IR spectra. For the bromo derivative **6a** this band is found at 3173 cm^{-1} which also indicates a hydrogen-bonded structure in the solid state.

Complex **3a** shows three ν_{CO} absorption bands both in solution (Figure 5) and in the solid state, at similar energies, proving that only one isomer is present in solution which most likely has the same geometry as in the solid state (Figure 1).

The signals of the symmetric and asymmetric carbonyl stretching vibrations of the allyl complexes **4a**−**6a** are found at around 1950 and 1874 cm^{-1} (Table 2) at similar energies to the signals of complexes with phenanthroline ligands where the bidentate ligand occupies two equatorial positions, but at considerably higher energies than the sig-

 © 2004 Wiley-VCH Verlag GmbH & Co. KGaA, Weinheim

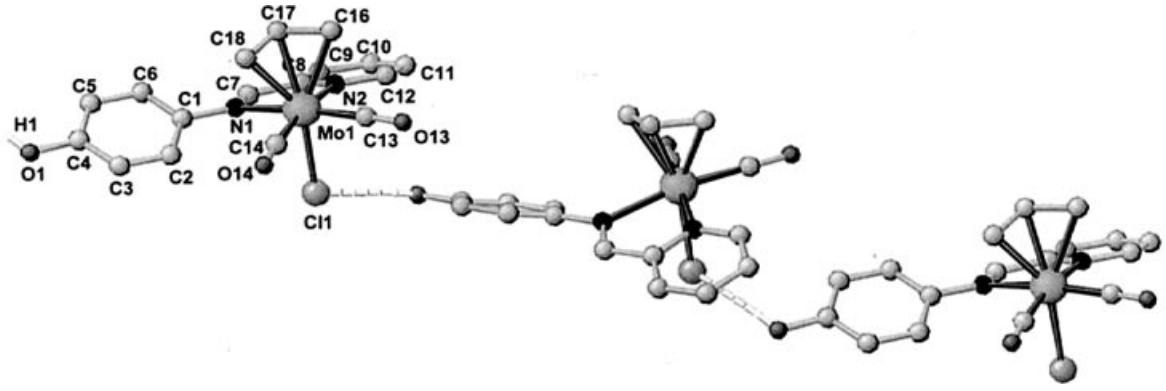

Figure 2. Structure of **4a**·THF in the solid state

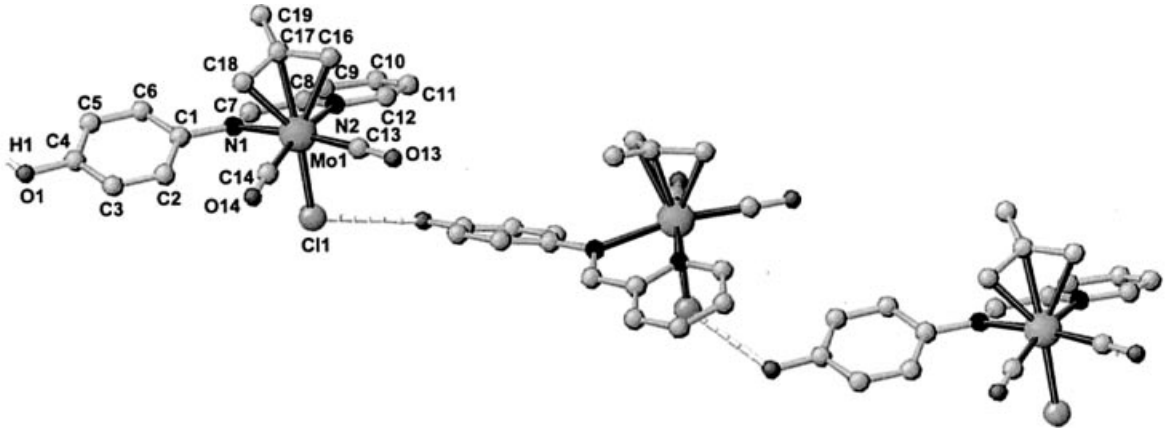

Figure 3. Structure of **5a**·THF in the solid state

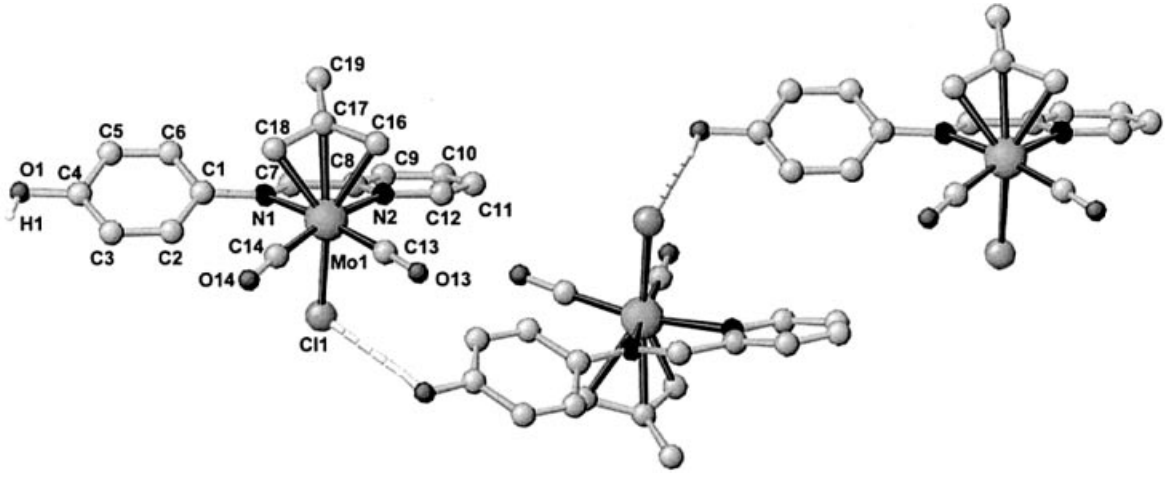

Figure 4. Structure of **5a** in the solid state

nals of complexes where the bidentate ligand occupies one equatorial and one axial position.[24] Thus the IR data suggest that **1a** exclusively coordinates at two equatorial positions in **4a**−**6a** in solution.[24,25]

For the allyl complexes **4a**−**6a** the symmetric and asymmetric carbonyl stretching vibrations are shifted slightly to lower energy in the solid state than in solution (Table 2; $\Delta\tilde{\nu}_{sym/asym}$ = 3/6, 7/11 and 14/11 cm^{-1} for **4a**, **5a** and **6a**). The same shift is predicted by DFT calculations on **4a** and **5a** upon addition of a water molecule hydrogen bonded to the chloro ligand — $\Delta\tilde{\nu}_{sym/asym}$ = 5/9 and 5/10 cm^{-1} for **4a** and **5a**, respectively — explaining the shift by the hydrogen bond to the rather remote chloro ligand. For hydrogen bonds to metal-coordinated carbonyl groups larger shifts are observed experimentally and predicted theoretically[20,22] (for water attached to carbonyl groups of **4a** and **5a** $\Delta\tilde{\nu}_{sym/asym}$ = 9−10/30−36 cm^{-1} are calculated, see Supporting Information).

 © 2004 Wiley-VCH Verlag GmbH & Co. KGaA, Weinheim

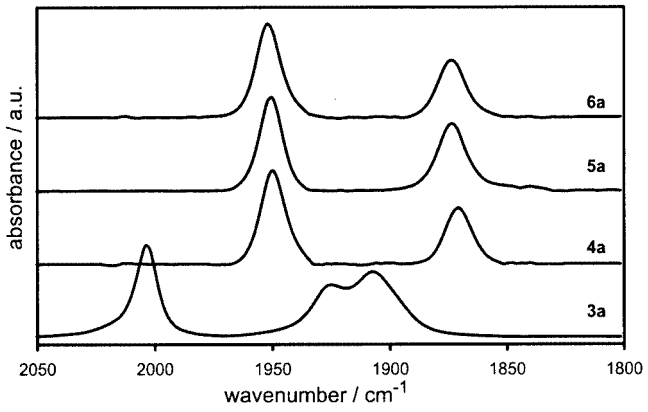

Figure 5. IR spectra of **3a**−**6a** in THF

Table 2. Characteristic IR absorptions of **3a**−**6a**

	$\tilde{\nu}_{CO}$ (cm^{-1})[a]	$\tilde{\nu}_{CO}$ (cm^{-1})[b]	$\tilde{\nu}_{OH}$ (cm^{-1})[b]
3a	2003, 1925, 1907[c]	2009, 1926, 1905[c]	3444
4a	1950, 1871[d]	1947, 1865[d]	3265
5a	1951, 1874[d]	1944, 1863[d]	3256
6a	1952, 1874[d]	1938, 1863[d]	3173

[a] In THF. [b] In CsI. [c] Totally symmetric vibration of all three CO ligands, symmetric vibration of the equatorial CO ligands, asymmetric vibration of the equatorial CO ligands, respectively. [d] Symmetric vibration of the equatorial CO ligands, asymmetric vibration of the equatorial CO ligands, respectively.

In the UV/Vis spectra all complexes display π-π* transitions of the Schiff-base ligand at around 356 nm (Figure 6, Table 3). The seven-coordinate complex **3a** has an MLCT absorption band at λ = 474 nm and is irreversibly reduced at E = −850 mV (Table 3). The allyl complexes **4a**−**6a** show MLCT absorption bands between 500 and 620 nm (Figure 6). The allyl and halide ligands influence the energy of the MLCT absorption according to their electron-donating and -withdrawing properties. The same consideration applies for the potentials of the metal-centred oxidations, as **5a** and **6a** are easier to oxidise than **4a**.

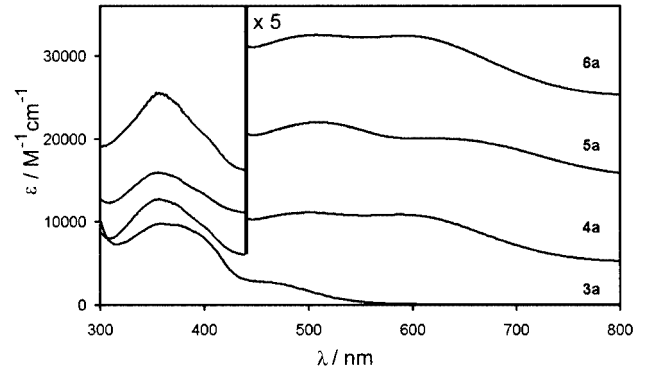

Figure 6. UV/Vis spectra of **3a**−**6a**

The solution structures of the complexes **4a**−**6a**, i.e. the orientations of the allyl ligands with respect to the Schiff-base ligands, have been determined by ^{1}H and ^{13}C NMR spectroscopy (Table 4 and 5). In the ^{1}H NMR spectra the allyl complexes **4a** and **6a** display an ABCDX pattern for the signals of the allyl ligand and **5a** shows an ABCD pattern, both of which suggest static structures in solution (e.g. absence of η^3-η^1-η^3 rearrangements of the allyl ligands). In the NOESY spectra, in addition to cross-peaks between intraligand protons (allyl and Schiff-base ligand), cross-peaks between allyl protons and Schiff-base ligand protons are observed (Figure 7). These observations show that the η^3-allyl ligands are oriented with the open face towards the carbonyls, which is the same orientation as found in the solid state for **4a** and **5a**. This is substantiated by the similar solution and solid state IR spectra of **4a**, **5a** and **6a** (Table 2).

Polymer-Bound Complexes 3b−6b

All polymer-bound complexes were characterised by IR and diffuse reflection UV/Vis spectroscopy and thermogravimetric analysis (Table 6).[11,12]

The IR spectra of the immobilised complexes **3b**−**6b** are shown in Figure 8. In addition to the intense signals of vibrations of the polymer backbone, signals in the characteristic ν_{CO} region are observed. These data compare well with those for the soluble complexes **3a**−**6a** (Table 2 and 6) confirming the presence of immobilised carbonyl complexes with the same stereochemistry as found in the solid state and in solution.

The UV/Vis absorption maxima of resins **3b**−**6b** (Figure 9) are shifted to lower energy than their solution counterparts (Table 3 and 6) but the trend of the MLCT transitions λ_{max}(**3**) << λ_{max}(**4**) < λ_{max}(**6**) < λ_{max}(**5**) is the same for the soluble and polymer-bound complexes. A similar behaviour has been observed for soluble and immobilised Mo^0 complexes.[11,12]

The thermal stability of **3b**−**6b** has been investigated by thermogravimetric analysis. For **3b** a larger weight loss of

Table 3. UV/Vis spectroscopic and cyclovoltammetric data of **3a**−**6a**

	λ_{max}/nm (ε/M^{-1} cm^{-1})			$E_{1/2}$/mV (ΔE/mV)[a]
3a	358 (9755)[b]	474 (2515)[b]		−850 mV (irr.; reverse scan: +40 mV)
4a	354 (7710)[c]	501 (1220)[c]	590 (1175)[c]	610 (100)
5a	356 (5920)[c]	510 (1400)[c]	620 (1010)[c]	515 (110)
6a	357 (10600)[c]	507 (1500)[c]	594 (1480)[c]	605 (90)

[a] 10^{-3} M in 0.1 M (nBu$_4$N)PF$_6$/CH$_2$Cl$_2$, vs. SCE. [b] In CH$_2$Cl$_2$. [c] In THF.

 © 2004 Wiley-VCH Verlag GmbH & Co. KGaA, Weinheim

Table 4. ^{1}H NMR spectroscopic data of **3a**−**6a**

	3a[a]	**4a**[b]	**5a**[b]	**6a**[b]
Ph	7.38 (m), 8.00 (m)	–	–	–
H[a]	–	2.5[c]	2.20 (d, J = 3.2 Hz)	2.5[c]
H^b	–	1.00 (d, J = 8.7 Hz)	1.04 (s)	1.04 (d, J = 8.0 Hz)
H^c	–	1.22 (d, J = 8.7 Hz)	1.22 (s)	1.28 (d, J = 8.0 Hz)
H^d	–	3.14 (bs)	2.84 (d, J = 3.2 Hz)	3.15 (bs)
R	–	3.3−3.4 (m)[d]	1.30 (s)[e]	3.37 (bs)[d]
H^{3,5}	6.87 (d, J = 8.4 Hz)	6.90 (d, J = 7.9 Hz)	6.91 (d, J = 8.4 Hz)	6.90 (d, J = 8.0 Hz)
H^{2,6}	7.41 (d, J = 8.4 Hz)	7.47 (d, J = 7.9 Hz)	7.32 (d, J = 8.4 Hz)	7.51 (d, J = 8.0 Hz)
H^{11}	7.78 (pt)	7.71 (bs)	7.68−7.75 (m)	7.70 (bs)
H$^{9/H10}$	8.09 (d, J = 7.2 Hz), 8.21 (pt)	8.1−8.2 (m)	8.2−8.3 (m)	8.2−8.3 (m)
H^{12}	9.10 (d, J = 4.8 Hz)	8.82 (d, J = 3.8 Hz)	8.79 (d, J = 5.4 Hz)	8.82 (d, J = 4.0 Hz)
H^7	8.64 (s)	8.71 (s)	8.82 (s)	8.71 (s)
OH	8.87 (s)	9.90 (s)	9.93 (s)	9.89 (s)

[a] In [D$_8$]THF. [b] In [D$_6$]DMSO. [c] Under solvent signal. [d] H^{17}. [e] H^{19}.

Table 5. ^{13}C NMR spectroscopic data of **3a**−**6a**

	3a[a]	**4a**[b]	**5a**[b]	**6a**[b]
Ph	143.8,[c] 129.2,[d] 130.6,[e] 136.2[f]	–	–	–
C^{16}	–	56.6	54.2	55.6
C^{17}	–	74.2	82.9	74.7
C^{18}	–	53.8	52.7	53.1
C^{19}	–	–	19.6	–
C^1	149.8	142.8	142.7	143.0
C^{2,6}	124.4	124.3	124.5	124.4
C^{3,5}	116.7	116.3	116.4	116.2
C^4	154.1	153.9	154.0	154.0
C^7	166.6	164.4	164.2	164.3
C^8	157.9	158.8	159.0	158.8
C^9	130.4	129.9	130.2	130.0
C^{10}	141.7	140.0	140.0	139.9
C^{11}	130.0	128.3	128.3	128.2
C^{12}	154.3	152.8	152.5	153.0
CO	215.1/224.9/227.7	227.6/228.2	227.6/228.4	226.8/227.4

[a] In [D$_8$]THF. [b] In [D$_6$]DMSO. [c] C-*ipso*. [d] C-*ortho*, $^2J_{Sn,C}$ = 87 Hz. [e] C-*para*, $^4J_{Sn,C}$ = 18 Hz. [f] C-*meta*, $^3J_{Sn,C}$ = 61 Hz.

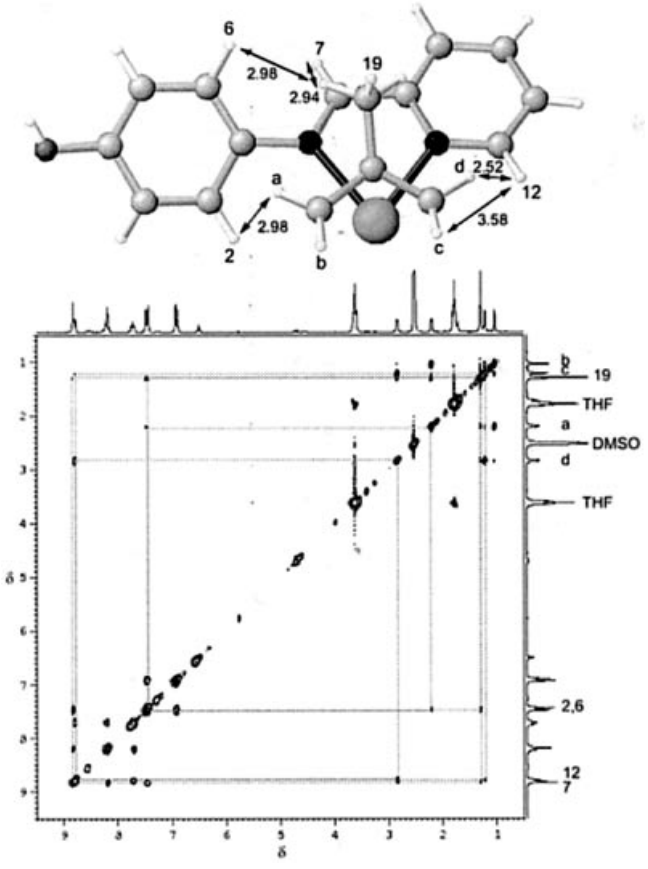

Figure 7. Relevant NOE contacts and distances [Å] (solid-state structure) between protons of the allyl ligand and the Schiff-base ligand in complex **5a** (top); NOESY spectrum of **5a**·THF in [D$_6$]DMSO (bottom)

6.1% is observed at 200 °C, which can be accounted for by a loss of three carbon monoxide ligands and one chloro ligand, while the immobilised allyl complexes **4b**−**6b** only lose coordinated carbonyl ligands up to 200 °C (Table 6). Carbon monoxide loss has also been detected for immobilised Mo^0 carbonyl complexes.[12] These data show that these complexes are formed quantitatively on the solid support and that allyl complexes are thermally more stable than the seven-coordinate molybdenum-tin complex.

Treating the resins **3b**−**6b** with tetra-*n*-butylammonium fluoride in dichloromethane (Scheme 3) results in deeply coloured solutions of the deprotonated complexes **3a**$^-$−**6a**$^-$ which were characterised by IR spectroscopy (Table 7). The signals of the ν_{CO} vibrations of **3a**$^-$−**6a**$^-$ are shifted to lower energy relative to the signals of the neutral parent complexes **3a**−**6a** (Table 2), as expected.

After washing the resins and concentrating the filtrates careful acidification with acetic acid yields solutions of the complexes **3a**−**6a**. In all cases no spectroscopic evidence was observed for the formation of side products, confirming the identity and stability of the polymer-bound complexes.

 © 2004 Wiley-VCH Verlag GmbH & Co. KGaA, Weinheim

Table 6. Analytical data of polymer-bound complexes **3b**−**6b**

	ν_{CO} (cm^{-1})	λ_{max} (nm)	$\Delta m/m$ (exp.) (%)[a]	$\Delta m/m$ (calcd.) (%)[b]
3b	2008, 1930, 1912	449, 533 (sh)	6.1	6.03
4b	1953, 1871	460 (sh), 673	3.2	3.24
5b	1953, 1878	460 (sh), 708, 810 (sh)	3.1	3.21
6b	1952, 1872	460 (sh), 699	3.1	3.16

[a] At 200°C. [b] The theoretical amount of weight loss is calculated according to the following formula: $\Delta m/m = 100 * (n_{CO} * M_{CO} + n_{Cl} * M_{Cl})/(M_{resin} + M_{complex\ fragment})$ with $n_{CO} = 3$ and $n_{Cl} = 1$ (**3b**), $n_{CO} = 2$ and $n_{Cl} = 0$ (**4b**, **5b**, **6b**), $M_{CO} = 28$ g mol^{-1}, $M_{Cl} = 35.5$ g mol^{-1}, $M_{resin} = 1500$ g mol^{-1} (resin loading 0.5 mmol g^{-1}), $M_{complex\ fragment} = 482.1$ [**3b**: $PhSnCl_3Mo(CO)_3$], 228.5 [**4b**: $C_3H_5ClMo(CO)_2$], 242.5 [**5b**: $C_4H_7ClMo(CO)_2$] and 272.9 [**6b**: $C_3H_5BrMo(CO)_2$] g mol^{-1} giving $\Delta m/m = 6.03$, 3.24 , 3.21 and 3.16%, respectively.

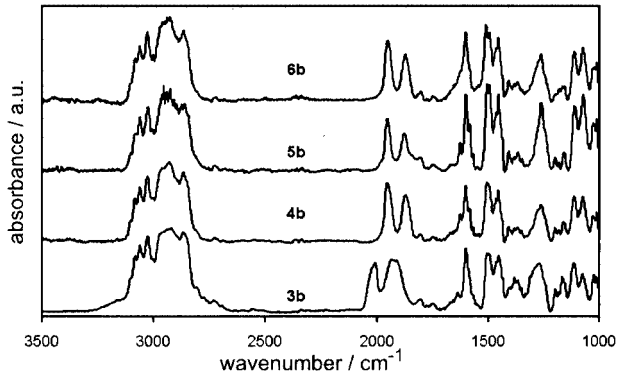

Figure 8. IR spectra of resins **3b**−**6b**

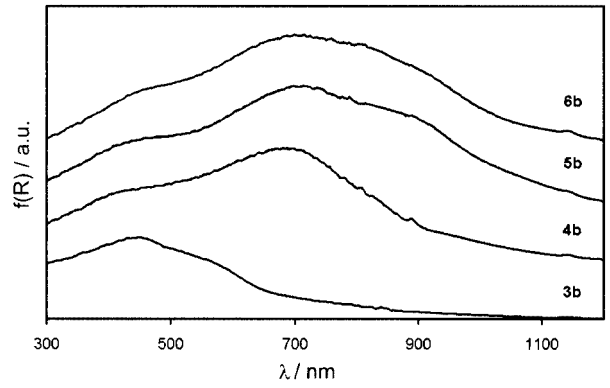

Figure 9. Diffuse reflection UV/Vis spectra of resins **3b**−**6b**

Table 7. Characteristic IR absorptions of **3a**$^-$−**6a**$^-$ in THF

	ν_{CO} (cm^{-1})
3a	1992, 1915, 1895[a]
4a	1943, 1861[b]
5a	1945, 1864[b]
6a	1946, 1864[b]

[a] Totally symmetric vibration of all three CO ligands, symmetric vibration of the equatorial CO ligands, asymmetric vibration of the equatorial CO ligands, respectively. [b] Symmetric vibration of the equatorial CO ligands, asymmetric vibration of the equatorial CO ligands, respectively.

Conclusion

Oxidative addition of RX ($PhSnCl_3$ or allyl halides) to the molybdenum tetracarbonyl complexes **2a**/**2b** furnishes the molybdenum(II) complexes **3a**−**6a**/**3b**−**6b**.

The stereochemistry of the complexes has been elucidated by single-crystal X-ray diffraction in the solid state and by NMR and IR spectroscopy in solution. The bimetallic molybdenum-tin complex **3a** has a capped octahedral coordination geometry with the tin occupying the seventh position above an octahedral face. The allyl complexes **4a**−**6a** have an octahedral coordination geometry with the bidentate Schiff-base ligand occupying two equatorial positions and the η^3-allyl ligand oriented with the open face towards the carbonyl ligands.

The reactions with polymer-bound complexes proceed quantitatively, as shown by IR spectroscopy and thermogravimetric analysis. The stereochemistry of the polymer-bound complexes **3b**−**6b** is the same as for the soluble complexes **3a**−**6a** in solution and in the solid state. The stability and identity of polymer-bound complexes has been demonstrated by release of the complexes from the polymer. These results pave the way for the immobilisation of active and selective molybdenum catalysts for (enantioselective) allylic alkylation reactions on polymeric supports.

Experimental Section

Unless noted otherwise, all manipulations were carried out under argon by means of standard Schlenk techniques. All solvents were dried by standard methods and distilled under argon prior to use. Complexes **1a**−**3a** and **1b**−**3b** were prepared by a literature method.[11,12] All other reagents were used as received from commercial sources.

NMR: Bruker Avance DPX 200 at 200.15 MHz (^1H), 50.323 MHz (^{13}C) at 303 K; chemical shifts (δ) in ppm with respect to residual solvent peaks as internal standards: $[D_6]DMSO$ (^1H: δ = 2.49 ppm; ^{13}C: δ = 39.7 ppm), $[D_8]THF$ (^1H: δ = 1.73, 3.58 ppm; ^{13}C: δ = 25.5, 67.7 ppm). IR spectra were recorded on a BioRad Excalibur FTS 3000 spectrometer using CaF_2 cells or CsI disks. UV/Vis/NIR spectra were recorded on a Perkin−Elmer Lambda 19 instrument with 0.2 cm cells (Hellma, suprasil). DRS-UV/Vis spectra were measured with the same instrument using the Perkin−Elmer inte-

 © 2004 Wiley-VCH Verlag GmbH & Co. KGaA, Weinheim

grating sphere and poly(tetrafluoroethylene) as reference. Cyclic voltammetry was performed using a glassy carbon electrode, a platinum electrode and an SCE electrode, 10^{-3} M in 0.1 M nBu$_4$NPF$_6$/CH$_2$Cl$_2$, potentials are given relative to that of SCE. Mass spectra were recorded on a Finnigan MAT 8400 spectrometer with a matrix of 4-nitrobenzyl alcohol (FAB). Elemental analyses were performed by the microanalytical laboratory of the Organic Chemistry Department, University of Heidelberg. Thermogravimetric measurements were carried out on a Mettler TC 15; heating rate: 10 K min^{-1} under argon from 30−800 °C.

Solution Syntheses of 4a−6a: The appropriate 3-halopropene (2 mmol) was added to a solution of **2a** (406 mg, 1 mmol) in THF (30 mL). The solution was heated under reflux until IR spectroscopy indicated disappearance of the bands of **2a** and complete formation of the product (3−4 h). The solvent was removed under reduced pressure and the crude product was washed with diethyl ether and recrystallised from THF/diethyl ether or CH$_2$Cl$_2$/diethyl ether.

4a: Yield: 311 mg, 0.73 mmol (73%). C$_{17}$H$_{15}$ClMoN$_2$O$_3$ (426.71): calcd. C 47.85, H 3.54, N 6.57; found C 48.04, H 3.79, N 6.40. MS (FAB): *m/z* (%) = 428 (100) [M$^+$ + H], 393 (41) [M$^+$ − Cl], 372 (97) [M$^+$ − 2CO].

5a: Yield: 366 mg, 0.83 mmol (83%). C$_{18}$H$_{17}$ClMoN$_2$O$_3$·THF (440.73·THF): calcd. C 51.52, H 4.91, N 5.46; found C 51.32, H 5.20, N 5.86. MS (FAB): *m/z* (%) = 442 (42) [M$^+$ + H], 407 (21) [M$^+$ − Cl], 386 (100) [M$^+$ − 2CO].

6a: Yield: 419 mg, 0.89 mmol (89%). C$_{17}$H$_{15}$BrMoN$_2$O$_3$·0.5THF (471.16·0.5THF): calcd. C 44.99, H 3.78, N 5.52; found C 45.18, H 4.02, N 5.27. MS (FAB): *m/z* (%) = 472 (12) [M$^+$ + H], 393 (100) [M$^+$ − Br], 416 (23) [M$^+$ − 2CO].

Solid-Phase Synthesis of 4b−6b: The appropriate 3-halopropene (1 mmol) was added to a suspension of **2b** (500 mg, 0.25 mmol) in THF (30 mL). The suspension was heated under reflux until IR spectroscopy of a polymer sample indicated formation of the product and complete conversion of the starting complex (8−10 h). The dark polymer was isolated by filtration, washed with THF and diethyl ether and dried in vacuo.

Cleavage procedure: A solution of tetra-*n*-butylammonium fluoride TBAF·3H$_2$O (2 equivalents) in THF was added to a suspension of the appropriate resin in THF (10 mL). The suspension was stirred for 6 h at room temperature. IR spectroscopy of the solution indicated release of the anionic complexes **4a**$^-$**−6a**$^-$. The mixture was filtered and the polymer was washed with THF until the solution was colourless. The combined filtrates were acidified with acetic acid giving **4a−6a** in 60%, 52% and 71% yield, respectively, based on the loading of **1b**. After cleavage, mass spectrometry of the remaining silyl fluoride polymer indicated complete removal of the complexes.[10]

Computational Methods: Density functional calculations were carried out with the Gaussian98/DFT[26] program series. The B3LYP formulation of density functional theory was used employing the LanL2DZ basis set.[26] Harmonic vibrational frequencies and infrared intensities were calculated by numerical second derivatives using analytically calculated first derivatives. Frequencies are not scaled.

Crystallographic Structure Determinations: The measurements were carried out on an Enraf−Nonius Kappa CCD diffractometer using graphite monochromated Mo-K_α radiation. The data were processed using the standard Nonius software.[27] All calculations were performed using the SHELXT PLUS software package. Structures were solved using direct or Patterson methods with the SHELXS-97 program and refined with the SHELXL-97 program.[28] Graphical handling of the structural data during refinement was performed using XMPA[29] and WinRay.[30] Atomic coordinates and anisotropic thermal parameters of the non-hydrogen atoms were refined by full-matrix least-squares calculations. Data relating to the structure determinations are collected in Table 8.

Table 8. X-ray crystallographic data of complexes **3a**·Et$_2$O, **4a**·THF, **5a**·THF and **5a**.

	3a·Et$_2$O	**4a**·THF	**5a**·THF	**5a**
Formula	C$_{25}$H$_{25}$Cl$_3$N$_2$O$_5$SnMo	C$_{21}$H$_{23}$ClN$_2$O$_4$Mo	C$_{22}$H$_{25}$ClN$_2$O$_4$Mo	C$_{18}$H$_{17}$ClN$_2$O$_3$Mo
Molecular mass	754.45	498.80	512.83	440.73
Crystal dimension/mm	0.20 × 0.10 × 0.10	1.00 × 0.50 × 0.25	0.30 × 0.30 × 0.20	0.25 × 0.10 × 0.10
Crystal system	monoclinic	monoclinic	monoclinic	monoclinic
Space group (no.)	$P2_1/c$ (14)	$P2_1/c$ (14)	$P2_1/n$ (14)	$P2_1/n$ (14)
a (Å)	7.6940(15)	10.568(2)	13.128(3)	8.939(2)
b (Å)	31.704(6)	10.403(2)	10.566(2)	16.163(3)
c (Å)	12.171(2)	19.905(4)	15.603(3)	12.729(3)
β (°)	101.09(3)	103.32(3)	91.73(3)	103.45(3)
Cell volume (Å^3)	2913.4(10)	2137.9(7)	2163.3(7)	1788.3(6)
Molecular units per cell	4	4	4	4
μ (mm^{-1})	1.599	0.768	0.761	0.902
Density (calcd.) (g cm^{-3})	1.720	1.550	1.575	1.637
T (K)	200	200	200	200
Scan range (2Θ)	3.6−60.1	3.9−30.1	4.0−61.1	4.1−55.0
Scan speed (sec frame^{-1})	10	8	6	30
Measured reflections	16483	14311	11494	6728
Unique reflections	8499	6158	6206	3971
Obs. reflections ($I \geq 2\sigma$)	5933	4945	5096	2670
Parameters refined	398	354	371	294
Max. resid. elec. density (e·Å^{-3})	0.64/−0.72	0.71/−0.67	1.10/−0.95	0.72/−0.57
Agreement factors	R_1 = 3.9%	R_1 = 3.1%	R_1 = 4.5%	R_1 = 4.7%
(F^2 refinement)	R_w = 7.8%	R_w = 7.7%	R_w = 12.0%	R_w = 11.4%

 © 2004 Wiley-VCH Verlag GmbH & Co. KGaA, Weinheim

CCDC-225156−225159 (**3a**·Et_2O, **4a**·THF, **5a**·THF and **5a**) contains the supplementary crystallographic data for this paper. These data can be obtained free of charge at www.ccdc.cam.ac.uk/conts/retrieving.html [or from the Cambridge Crystallographic Data Centre, 12 Union Road, Cambridge CB2 1EZ, UK; Fax: (internat.) +44-1223/336-033; E-mail: deposit@ccdc.cam.ac.uk].

Acknowledgments

This work was supported by the Deutsche Forschungsgemeinschaft and the Fonds der Chemischen Industrie. The permanent, generous support from Prof. Dr. G. Huttner is gratefully acknowledged. We thank Michela Doria for preparative assistance.

[1] *Chiral Catalyst Immobilisation and Recycling* (Eds.: E. De Vos, I. F. J. Vankelecom, P. A. Jacobs), **2000**, Wiley-VCH, Weinheim.
[2] S. Bräse, D. Enders, J. Köbberling, F. Avemaria, *Angew. Chem.* **1998**, *110*, 3614−3614; *Angew. Chem. Int. Ed.* **1998**, *37*, 3413−3415.
[3] R. Zanaletti, M. Freccero, *Chem. Commun.* **2002**, 1908−1909.
[4] S. Dahmen, S. Bräse, *Angew. Chem.* **2000**, *112*, 3827−3830; *Angew. Chem. Int. Ed.* **2000**, *39*, 3681−3683.
[5] P. Hodge, *Chem. Soc. Rev.* **1997**, *26*, 417−424.
[6] B. Pugin, *J. Mol. Catal. A* **1996**, *107*, 273−279.
[7] R. Grubbs, C. P. Lau, R. Cukier, C. Brubaker Jr., *J. Am. Chem. Soc.* **1977**, *99*, 4517−4518.
[8] X.-W. Yang, J.-H. Sheng, C.-S. Da, H.-S. Wang, W. Su, R. Wang, A. S. C. Chan, *J. Org. Chem.* **2000**, *65*, 295−296.
[9] B. Altava, M. I. Burguete, J. M. Fraile, J. I. García, S. V. Luis, J. A. Mayoral, M. J. Vicent, *Angew. Chem.* **2000**, *112*, 1563−1566; *Angew. Chem. Int. Ed.* **2000**, *39*, 1503−1506.
[10] K. Heinze, U. Winterhalter, T. Jannack, *Chem. Eur. J.* **2000**, *6*, 4203−4210.
[11] K. Heinze, *Chem. Eur. J.* **2001**, *7*, 2922−2932.
[12] K. Heinze, J. B. Toro, *Angew. Chem.* **2003**, *115*, 4671−4674; *Angew. Chem. Int. Ed.* **2003**, *42*, 4533−4536.
[13] B. M. Trost, I. Hachiya, *J. Am. Chem. Soc.* **1998**, *120*, 1104−1105.
[14] B. M. Trost, S. Hildbrand, K. Dogra, *J. Am. Chem. Soc.* **1999**, *121*, 10416−10417.
[15] F. Glorius, A. Pfaltz, *Org. Lett.* **1999**, *1*, 141−144.
[16] M. Palucki, J. M. Um, D. A. Conlon, N. Yusada, D. L. Hughes, B. Mao, J. Wang, P. J. Reider, *Adv. Synth. Catal.* **2001**, *343*, 46−50.
[17] N.-F. K. Kaiser, U. Bremberg, M. Larhed, C. Moberg, A. Hallberg, *Angew. Chem.* **2000**, *112*, 3742−3744; *Angew. Chem. Int. Ed.* **2000**, *39*, 3595−3598.
[18] Y. Uozumi, H. Danjo, T. Hayashi, *Tetrahedron Lett.* **1997**, *38*, 3557−3560.
[19] D. R. van Staveren, N. Metzler-Nolte, *Chem. Commun.* **2002**, 1406−1407.
[20] K. Heinze, *J. Chem. Soc., Dalton Trans.* **2002**, 540−547.
[21] M. Elder, D. Hall, *Inorg. Chem.* **1969**, *8*, 1268−1273.
[22] K. Heinze, V. Jacob, *J. Chem. Soc., Dalton Trans.* **2002**, 2379−2385.
[23] W. Koch, M. C. Holthausen, *A Chemist's Guide to Density Functional Theory*, Wiley-VCH, Weinheim, **2001**.
[24] M. P. T. Sjögren, H. Frisell, B. Åkermark, *Organometallics* **1997**, *16*, 942−950.
[25] P. Espinet, R. Hernando, G. Iturbe, F. Villafañe, G. A. Orpen, I. Pascual, *Eur. J. Inorg. Chem.* **2000**, 1031−1038.
[26] M. J. Frisch, G. W. Trucks, H. B. Schlegel, G. E. Scuseria, M. A. Robb, J. R. Cheeseman, V. G. Zakrzewski, J. A. Montgomery, Jr., R. E. Stratmann, J. C. Burant, S. Dapprich, J. M. Millam, A. D. Daniels, K. N. Kudin, M. C. Strain, O. Farkas, J. Tomasi, V. Barone, M. Cossi, R. Cammi, B. Mennucci, C. Pomelli, C. Adamo, S. Clifford, J. Ochterski, G. A. Petersson, P. Y. Ayala, Q. Cui, K. Morokuma, D. K. Malick, A. D. Rabuck, K. Raghavachari, J. B. Foresman, J. Cioslowski, J. V. Ortiz, B. B. Stefanov, G. Liu, A. Liashenko, P. Piskorz, I. Komaromi, R. Gomperts, R. L. Martin, D. J. Fox, T. Keith, M. A. Al-Laham, C. Y. Peng, A. Nanayakkara, C. Gonzalez, M. Challacombe, P. M. W. Gill, B. Johnson, W. Chen, M. W. Wong, J. L. Andres, C. Gonzalez, M. Head-Gordon, E. S. Replogle, J. A. Pople, *Gaussian 98, Revision A.6*, Gaussian, Inc., Pittsburgh PA, **1998**; http://www.gaussian.com.
[27] R. Hooft, Collect, Data Collection Software, Nonius, The Netherlands, **1998**; http://www.nonius.com.
[28] G. M. Sheldrick, *SHELXS-97, Program for Crystal Structure Solution*, University of Göttingen, Germany, **1997**; http://www.shelx.uni-ac.gwdg.de/shelx/index.html; G. M. Sheldrick, *SHELXL-97, Program for Crystal Structure Refinement*, University of Göttingen, Germany, **1997**; http://www.shelx.uni-ac.gwdg.de/shelx/index.html; *International Tables for X-ray Crystallography*, Kynoch Press, Birmingham, U. K., **1974**, vol. 4.
[29] L. Zsolnai, G. Huttner, *XPMA*, University of Heidelberg, Germany, **1998**; http://www.rzuser.uni-heidelberg.de/~il1/laszlo/xpm.html.
[30] R. Soltek, G. Huttner, *WinRay*, University of Heidelberg, Germany, **1999**; http://www.uni-heidelberg.de/institute/fak12/AC/huttner/frame/frame_soft.html.

Received December 5, 2003
Early View Article
Published Online April 1, 2004

 © 2004 Wiley-VCH Verlag GmbH & Co. KGaA, Weinheim

Reactivity of a Phosphanylalane Complex towards Lewis Bases

Ulf Vogel,[a] Karl-Christian Schwan,[a] and Manfred Scheer*[a]

Dedicated to Prof. R. Schmutzler on the occasion of his 70th birthday

Keywords: Aluminum / Phosphorus / Hydrides / Reactivity / Lewis bases

The reactivity of the Lewis acid/base stabilized complex of phosphanylalane $[(CO)_5W(H_2PAlH_2{\cdot}NMe_3)]$ (**1**) towards the Lewis bases THF and NMe_3 has been investigated. The reaction with THF leads to decomposition of the complex. One of the decomposition products was identified as containing the anion $[\{(CO)_5W\}_2PH_2]^-$ (**2**). This anion could be synthesized independently by reaction of $[(CO)_5WPH_3]$ with KH in the presence of $[(CO)_5W(THF)]$ and was isolated as the tetraphenylphosphonium salt $[Ph_4P][\{(CO)_5W\}_2PH_2]$ (**2a**). The treatment of **1** with NMe_3 leads to the formation of $[(CO)_5W(H_2PAlH_2{\cdot}2\,NMe_3)]$ (**3**) containing a five-coordinate aluminum atom. Compound **3** exhibits a fast exchange of the NMe_3 ligands in solution containing an excess of NMe_3. The products were characterized by spectroscopic methods and X-ray crystallography.

(© Wiley-VCH Verlag GmbH & Co. KGaA, 69451 Weinheim, Germany, 2004)

Introduction

Compounds containing bonds between group 13 and group 15 elements are especially interesting due to their potential use as molecular precursors for the generation of thin films of group 13/15 semiconductors. Compounds of the type $(R_2EE'R'_2)_n$ (R, R′: organic substituents, E′: group 13 element, E: group 15 element) have been intensively investigated[1] and usually form oligomeric structural frameworks. These compounds are monomeric if they possess bulky R and R′ groups to block the intermolecular aggregation. To obtain monomers, the steric influence of the substituents can be neglected if both a Lewis base is coordinated at the group 13 element and the group 15 element still possesses bulky substituents or if, besides the Lewis base at the group 13 element, the lone pair of the group 15 element is occupied by a Lewis acid. Examples of the former mode are the compounds $[Mes_2EAlH_2{\cdot}NMe_3]$,[2] obtained by the treatment of $ClAlH_2{\cdot}NMe_3$ with $LiEMes_2$ (E = P, As), and $[(Me_3Si)_2EAlMe_2{\cdot}dmap]$[3] synthesized by treating oligomers of the type $[Me_2AlE(Me_3Si)_2]_n$ (E = P, As; n = 2, 3) with the Lewis base *N*,*N*′-dimethylaminopyridine (dmap). We developed the latter concept of monomeric group 13/15 compounds by the stabilization of the hydrogen substituted parent compounds $[(CO)_5W(PH_2E'H_2{\cdot}NMe_3)]$ (**1**: E′ = Al, **2**: E′ = Ga, **3**: E′ = B). These phosphanylalane and -gallane complexes were synthesized by a hydrogen elimination reaction,[4] whereas the boron compound was accessible by a salt elimination route.[5] Herein we report on the reactivity of **1** towards the Lewis bases THF and NMe_3, respectively.

[a] Institut für Anorganische Chemie, Universität Karlsruhe (TH), 76128 Karlsruhe, Germany
Fax: (internat.) + 49-(0)721-6087021
E-mail: mascheer@chemie.uni-karlsruhe.de

Results and Discussion

Decomposition of 1 in THF

Upon dissolving in THF, **1** reacted with vigorous H_2 evolution [Equation (1)]. The ^{31}P NMR spectrum of the reaction mixture gave some hints of the possible formation of an anionic complex with the formula of **2**. The $^{31}P\{^1H\}$ NMR spectrum of the reaction mixture shows two main P containing products as single peaks having tungsten satellites which split into triplets when the proton coupled spectrum was recorded. Compound **2** shows a triplet at −267.7 ppm ($^1J_{P,H}$ = 268, $^1J_{W,P}$ = 146 Hz). The other product, whose structure could not be assigned yet, shows a triplet at −100.3 ppm ($^1J_{P,H}$ = 340, $^1J_{W,P}$ = 220 Hz). The ratio of the integrals of the tungsten satellites towards the central peak of **2** suggests that two tungsten atoms are bound to each phosphorus atom as in $[\{(CO)_5W\}_2PH_2]^-$. By adding Ph_4PBr to the mixture of reaction (1) some yellow crystals appeared which were identified crystallographically by their unit cell to be $[Ph_4P][\{(CO)_5W\}_2PH_2]$ (**2a**) (cf. discussion below).

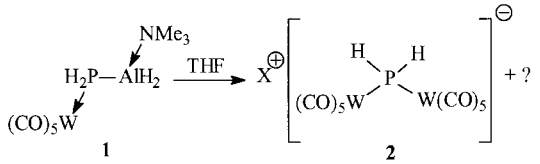

1 **2** (1)

 © 2004 Wiley-VCH Verlag GmbH & Co. KGaA, Weinheim DOI: 10.1002/ejic.200300637

In order to develop a more efficient approach to **2a** it was synthesized by the reaction of $[(CO)_5WPH_3]$ with KH in the presence of $[(CO)_5W(THF)]$ [Equation (2)]. Cation exchange using PPh_4Br and crystallization from CH_2Cl_2/*n*-hexane afforded pure $[PPh_4][\{(CO)_5W\}_2PH_2]$ (**2a**) which showed identical NMR spectra to the decomposition product **2**. The IR spectrum of **2a** revealed a PH stretching absorption at 2306 cm^{-1} as well as three CO valence stretching modes at 2048, 1930 and 1872 cm^{-1} for the two $W(CO)_5$ moieties showing a local C_{4v} symmetry.

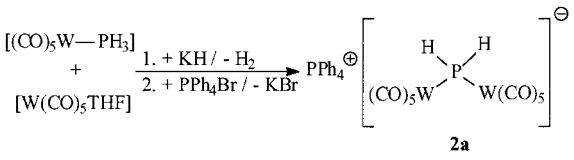

2a (2)

The X-ray Crystal Structure Analysis of 2a

The molecular structure of **2a** shows a $[PPh_4]^+$ cation and a $[\{(CO)_5W\}_2PH_2]^-$ anion. An ORTEP plot of the anion is depicted in Figure 1, while selected bond lengths and angles are listed in Table 1.

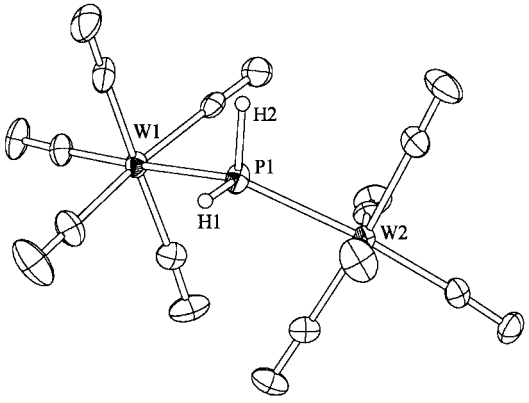

Figure 1. Molecular structure of the anion of **2a** in the crystal (ORTEP plot, 50% probability displacement ellipsoids)

Table 1. Selected bond lengths [Å] and angles [°] for **2a**

W1−P	2.579(2)	W2−P	2.580(2)
W−C_{trans} [a]	1.978(8)	W−C_{cis} [a]	2.029(9)
W1−P−W2	126.79(7)		

[a] Averaged bond lengths.

The anion of **2a** (Figure 1) shows a PH_2 group which is coordinated to two $W(CO)_5$ moieties. The W−P bond lengths are 2.579(2) and 2.580(2) Å, respectively, and the W1−P−W2 angle is 126.79(7)°. Comparison of these values with the compounds $[Cp(CO)_3W(\mu\text{-}PPh_2)W(CO)_5]$ [W−P−W 118.4(1)°; W−P 2.626(3) Å],[6] $[Cp(CO)_2Fe(\mu\text{-}PPh_2)W(CO)_5]$ (W−P−Fe 118.42(6)°; W−P 2.581(1) Å][7] and $[Et_4N][Cp'(CO)_2Mn(\mu\text{-}PPh_2)W(CO)_5]$ (Cp′ = η^5-C_5H_4Me) [W−P−Mn 119.8(1)°; W−P 2.622(3) Å][8] show that, in particular, the W−P−W angle is significantly larger in **2a**. This can be explained by the low steric shielding of the H substituents at the P atom. Complex **2a** represents the first parent compound (R = H) of the class $[(L_nM)_2PR_2]^-$, which exists amongst only a few organic substituted examples.[8]

Reaction of 1 with NMe_3

In contrast to the reaction with THF, **1** did not show decomposition when allowed to react with the nitrogen-centered Lewis base NMe_3. The product of this reaction is complex **3** which contains a pentacoordinated Al atom in a trigonal bipyramidal arrangement containing two NMe_3 molecules [Equation (3)]. A similar reaction is also known from $H_3Al{\cdot}NMe_3$ with NMe_3 which forms the adduct $H_3Al{\cdot}2\ NMe_3$,[9] exhibiting a trigonal bipyramidal coordinated aluminum atom.[10] The solid-state Raman spectrum of **3** showed bands in the region of the terminal CO stretching frequencies as well as for the PH valence at 2331 and 2315 cm^{-1} and one AlH stretch at 1744 cm^{-1}. The EI-mass spectrum did not show a molecular ion peak. However, $[(CO)_5WPH_2AlH_2{\cdot}NMe_3]^+$ was detected as the ion with the highest mass. Moreover, signals for its degradation, resulting from CO and NMe_3 loss were also found. The $^{31}P\{^1H\}$ NMR spectrum of **3** shows a singlet at $\delta = -251$ ppm which exhibits tungsten satellites ($^1J_{W,P}$ = 149 Hz). The ^1H NMR spectrum reveals a doublet for the PH_2 protons at $\delta = 1.58$ ppm ($^1J_{P,H}$ = 268 Hz), a singlet for the NMe_3 groups at $\delta = 1.71$ ppm and a broad signal for the AlH_2 protons at $\delta = 3.15$ ppm.

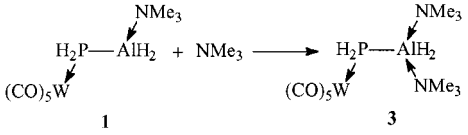

1 **3** (3)

In the presence of an excess of trimethylamine, **3** shows dynamic behavior in solution which can be attributed to fast exchange of the coordinated trimethylamine molecules. The variable temperature ^1H NMR spectra are shown in Figure 2. At low temperatures two signals can be detected for the NMe_3 groups: one can be assigned to coordinated (A) and one to free trimethylamine (B). With rising temperature, the two signals are shifted towards each other, and at the coalescence temperature of ca. −45 °C only one broad signal is observed. At higher temperatures only one signal is detected for coordinated and free trimethylamine (C). For this process the free activation enthalpy at the coalescence temperature was calculated to be 45.3 kJ·mol^{-1}.

The Solid-State Structure of 3

The solid-state structure of **3** was determined by a single-crystal X-ray diffraction study. Selected bond lengths and angles are reported in Table 2. An ORTEP plot of the molecular structure of **3** is depicted in Figure 3. The central motif of the crystal structure of **3** is a H_2AlPH_2 moiety which is connected to a $W(CO)_5$ fragment by the P atom. Two NMe_3 molecules are coordinated to the Al atom,

 © 2004 Wiley-VCH Verlag GmbH & Co. KGaA, Weinheim

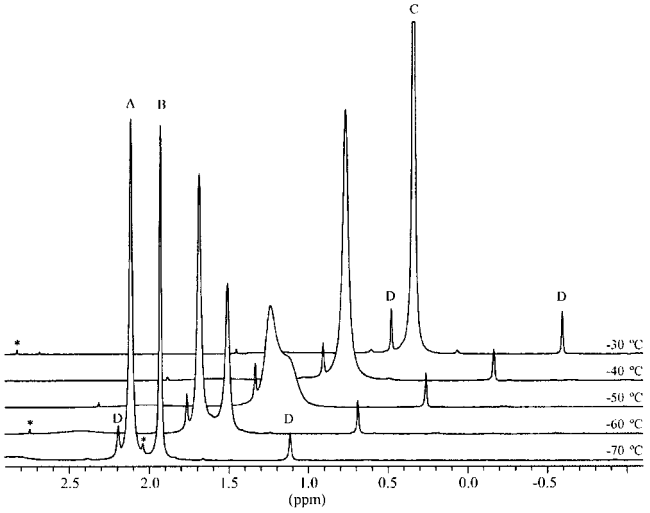

Figure 2. Variable temperature ^{1}H NMR spectra of a mixture of **3** and an excess of NMe_3 in CD_2Cl_2; at −70 °C the spectrum shows signals for coordinated NMe_3 (A), free NMe_3 (B) and the PH_2 protons (D); at −30 °C only the PH_2 protons and one signal for NMe_3 (C) are detected; impurities are marked with *

Table 2. Selected bond lengths [Å] and angles [°] for **3**

W−P	2.566(1)	P−Al	2.432(2)
Al−N1	2.160(4)	Al−N2	2.155(4)
W−C_{trans} [a]	1.988(5)	W−C_{cis} [a]	2.034(5)
Al−P−W	128.58(6)	N1−Al−P	94.7(1)
N2−Al−P	94.2(1)	N1−Al−N2	171.1(2)

[a] Averaged bond lengths.

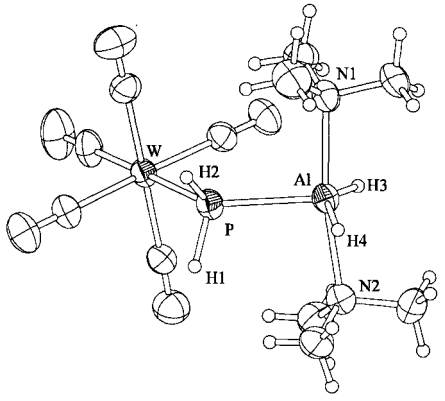

Figure 3. Molecular structure of **3** in the crystal (ORTEP drawing, 50% probability displacement ellipsoids)

which thus exhibits a coordination number of five in a distorted trigonal bipyramidal arrangement. Both trimethylamine ligands occupy the apical positions of the trigonal bipyramid with similar Al−N bond lengths of 2.160(4) and 2.155(4) Å, respectively. The N1−Al−N2 angle is 171.1(2)°. At 2.432(2) Å the Al−P bond length in **3** is significantly longer than in **1** [2.377(1) Å],[4] although in both compounds the aluminum atom is pentacoordinate (**1** reveals an intermolecular dimerization via H bridges). The longer Al−P bond in **3** can be attributed to the steric shielding at the aluminum atom by the second NMe_3 group. The slightly longer P−W bond (**3**: 2.566(1) Å, **1**: 2.549(1) Å] and the larger W−P−Al angle (**3**: 128.58(6)°, **1**: 118.44(4)°] in **3** further support this explanation.

Conclusion

The results have shown that the Lewis-acid/base stabilized phosphanylalane is very sensitive towards reactions with different Lewis bases. The ability of the Al atom to achieve pentacoordination enables firstly an addition of the Lewis base which leads, depending upon its nature, to stable adducts (as in the case of NMe_3) or to decomposition as in the case of THF via cleavage of the Al−P bond and removal of the Al moiety.

Experimental Section

General Remarks: All manipulations were carried out under an atmosphere of dinitrogen using standard Schlenk techniques. All solvents were dried via standard procedures and distilled freshly before use. NMe_3 was dried by condensing it over Na/benzophenone at −78 °C and stirring the mixture until the solution showed a dark blue color. PPh_4Br was heated to 100 °C in vacuo for one hour to remove traces of moisture. $[(CO)_5W(H_2PAlH_2{\cdot}NMe_3)]$ (**1**) was prepared according to our published method.[4] All NMR spectra were recorded on a Bruker AC 250 spectrometer with δ referenced to external $SiMe_4$ (^{1}H) or H_3PO_4 (^{31}P), respectively. IR spectra were measured on a Bruker IFS 28 instrument and Raman spectra on a Bruker FRA 106 spectrometer. All mass spectra were recorded on a Varian MAT 711 instrument at 70 eV.

$[Ph_4P][\{(CO)_5W\}_2PH_2]$ (2a): To a solution of $[(CO)_5W(THF)]$, which was produced by irradiating $[W(CO)_6]$ (352 mg, 1.00 mmol) in THF (50 mL), $[(CO)_5WPH_3]$ (358 mg, 1.00 mmol) and KH (40 mg, 1.00 mmol) were added subsequently. After the gas evolution had ceased the mixture was stirred for three hours to ensure complete reaction. To the clear yellow solution solid PPh_4Br (419 mg, 1.00 mmol) was added resulting in the formation of a white solid which was separated by filtration. The filtrate was reduced to dryness in vacuo and the remaining residue dissolved in CH_2Cl_2 (10 mL). After removal of the insoluble material by filtration the solution was layered with *n*-hexane (20 mL) affording yellow crystals of **2a** after two days. Yield 643 mg (63%). IR (CH_2Cl_2): $\tilde{\nu}$ = 3055 (m), 2987 (w), 2306 (w), 2048 (m), 1930 (vs), 1872 (s), 1440 (m), 1422 (m), 1271 (vs), 1259 (vs), 1109 (w), 896 (w) cm^{-1}. ^{1}H NMR (250 MHz, CD_2Cl_2): δ = 1.91 (d, $^1J_{P,H}$ = 268 Hz, 2 H, PH_2), 7.52−7.92 (m, 20 H, PPh_4) ppm. ^{31}P{^{1}H} NMR (101 MHz, CD_2Cl_2): δ = −267.7 (s, $^1J_{P,W}$ = 146 Hz, PH_2), 23.0 (s, PPh_4) ppm. ^{31}P NMR (101 MHz, CD_2Cl_2): δ = −267.7 (t, $^1J_{P,H}$ = 268, $^1J_{P,W}$ = 146 Hz, PH_2), 23.0 (s, PPh_4) ppm.

$[(CO)_5W(H_2PAlH_2{\cdot}2\,NMe_3)]$ (3): NMe_3 (0.36 mmol) was condensed into a solution of $[(CO)_5W(H_2PAlH_2{\cdot}NMe_3)]$ (53 mg, 0.12 mmol) in *n*-hexane (20 mL) at −196 °C. The reaction mixture was allowed to warm to ambient temperature over 20 minutes. Any insoluble material formed was removed by filtration, and the solution was kept at −20 °C. Light yellowish colored crystals of **3** were formed over two days. Yield 32 mg (53%). Raman (solid state): $\tilde{\nu}$ = 3004 (w), 2977 (m), 2929 (m), 2905 (m), 2855 (m), 2788 (w), 2331 (m), 2315 (m), 2063 (s), 1956 (vs), 1936 (w), 1904 (s), 1880 (w), 1744 (w, br), 821 (w), 435 (m), 434 (m), 116 (m) cm^{-1}. ^{1}H NMR

 © 2004 Wiley-VCH Verlag GmbH & Co. KGaA, Weinheim

Table 3. Crystallographic data for **2a** and **3**

	2	**3**
Empirical formula	$C_{34}H_{22}O_{10}P_2W_2$	$C_{11}H_{22}AlN_2O_5PW$
M_r	1020.16	504.11
T [K]	200(1)	200(1)
Crystal size	0.20 × 0.15 × 0.02	0.30 × 0.20 × 0.10
Space group	$P2_1/n$	$P2_1/n$
Crystal system	monoclinic	monoclinic
a (Å)	14.231(3)	11.559(2)
b (Å)	14.377(3)	10.957(2)
c (Å)	17.742(4)	15.371(3)
α [°]	90	90
β [°]	92.10(3)	102.11(3)
γ [°]	90	90
V [A^{-3}]	3627.7(12)	1903.4(7)
Z	4	4
d_c [g cm^{-3}]	1.868	1.759
μ_c [mm^{-1}]	6.478	6.216
2θ range [°]	$3.64 \le 2\theta \le 52.00$	$5.18 \le 2\theta \le 52.00$
hkl range	$-17 \le h \le 17$,$-16 \le k \le 15$,$-21 \le l \le 21$	$-13 \le h \le 14$,$-13 \le k \le 13$,$-17 \le l \le 18$
Data/restraints/parameters	6631/0/441	3519/0/200
No. of unique data	6631 (R_{int} = 0.0594)	3519 (R_{int} = 0.1318)
Independent reflections [$I > 2\sigma(I)$]	4879	3256
Goodness-of fit on F^2	0.903	1.056
R_1 [a], wR_2 [b] [$I > 2\sigma(I)$]	0.0340, 0.0732	0.0325, 0.0856
R_1 [a], wR_2 [b] [all data]	0.0522, 0.0774	0.0346, 0.0867
Largest diff. peak/hole [e·$Å^{-3}$]	1.041, −1.364	1.665, −2.111

[a] $R = ||F_o| - |F_c||/|F_o|$. [b] $wR_2 = [w(F_o^2 - F_c^2)^2]/[(F_o^2)^2]^{1/2}$

(250 MHz, [D$_8$]toluene, −50 °C): δ = 1.58 (d, $^1J_{P,H}$ = 268 Hz, 2 H, PH_2), 1.71 (s, 18 H, NMe_3), 3.15 (br. s, 2 H, AlH_2) ppm. $^{31}P\{^1H\}$ NMR (101 MHz, [D$_8$]toluene, −70 °C): δ = −251 (s, $^1J_{P,W}$ = 149 Hz, PH_2) ppm. ^{31}P NMR (101 MHz, [D$_8$]toluene, −70 °C): δ = −251 (t, $^1J_{P,W}$ = 268, $^1J_{P,W}$ = 149 Hz, PH_2) ppm. EI-MS (70 °C): *m*/*z* = 445 ($M^+ - NMe_3$, 1%), 417 ($M^+ - NMe_3 - CO$, 1%), 386 ($M^+ - 2\ NMe_3$, 2%), 358 ($M^+ - 2\ NMe_3 - CO$, 13%), 330 ($M^+ - 2\ NMe_3 - 2\ CO$, 5%), 302 ($M^+ - 2\ NMe_3 - 3\ CO$, 16%), 302 ($M^+ - 2\ NMe_3 - 3\ CO$, 16%), 272 ($M^+ - 2\ NMe_3 - 4\ CO - 2\ H$, 16%), 244 ($M^+ - 2\ NMe_3 - 5\ CO - 2\ H$, 11%).

Variable Temperature NMR of 3: In a typical experiment [$(CO)_5W(H_2PAlH_2{\cdot}2\ NMe_3)$] (30 mg, 0.06 mmol) was weighed into an NMR tube, and NMe_3 (0.18 mmol) was condensed into the tube at −196 °C. CD_2Cl_2 was then condensed into the tube, and it was sealed in vacuo. After variable temperature NMR measurements, starting from −70 °C, the samples decompose slowly at room temperature.

X-ray Crystallographic Studies: Crystal structure analyses of **2a** and **3** were performed on a STOE IPDS diffractometer with Mo-K_α radiation (λ = 0.71073 Å). The structures were solved by direct methods with the program SHELXS-97,[11a] and full-matrix least-squares refinements on F^2 using SHELXL-97[11b] were performed with anisotropic displacements for non-H atoms. Hydrogen atoms at the carbon atoms were located in idealized positions and refined isotropically according to the riding model. The hydrogen atoms at the phosphorus and aluminum atoms were freely refined. Further details of the structural refinements are given in Table 3.
CCDC-218817 and -218818 contain the supplementary crystallographic data for this paper. These data can be obtained free of charge at www.ccdc.cam.ac.uk/conts/retrieving.html [or from the Cambridge Crystallographic Data Center, 12, Union Road, Cambridge CB2 1EZ, UK; Fax: (internat.) +44-1223-336-033; E-mail: deposit@ccdc.cam.ac.uk].

Acknowledgments

This work was comprehensively supported by the Deutsche Forschungsgemeinschaft and the Fonds der Chemischen Industrie.

[1] Selected reviews: P. P. Power, *Chem. Rev.* **1999**, *99*, 3463−3503; R. T. Paine, H. Nöth, *Chem. Rev.* **1995**, *95*, 343−379; S. Schulz, *Coord. Chem. Rev.* **2001**, *215*, 1−37; R. L. Wells, *Coord. Chem. Rev.* **1992**, *112*, 273−291.
[2] D. A. Atwood, L. Contreras, A. H. Cowley, R. A. Jones, M. A. Mardones, *Organometallics* **1993**, *12*, 17−18.
[3] F. Thomas, S. Schulz, M. Nieger, *Eur. J. Inorg. Chem.* **2001**, 161−166.
[4] U. Vogel, M. Scheer, *Angew. Chem.* **2001**, *113*, 4541−4544; *Angew. Chem. Int. Ed.* **2001**, *40*, 4409−4412.
[5] U. Vogel, K.-C. Schwan, P. Hoemensch, M. Scheer, *Chem. Eur. J.* **2003**, *9*, 515−519.
[6] S.-G. Shyu, W.-J. Wu, Y.-S. Wen, S.-M. Peng, G.-H. Lee, *J. Organomet. Chem.* **1995**, *489*, 113−122.
[7] S.-G. Shyu, P.-J. Lin, T.-Y. Dong, Y.-S. Wen, *J. Organomet. Chem.* **1993**, *460*, 229−236.
[8] J. T. Lin, A. C. Yeh, Y. C. Chou, T. Y. R. Tsai, Y. S. Wen, *J. Organomet. Chem.* **1995**, *486*, 147−154.
[9] E. Wiberg, H. Graf, R. Usón, *Z. Anorg. Allg. Chem.* **1953**, *272*, 221−232.
[10] G. W. Fraser, N. N. Greenwood, B. P. Straughan, *J. Chem. Soc.* **1963**, 3742−3749; C. W. Heitsch, C. E. Nordman, R. W. Parry, *Inorg. Chem.* **1963**, *2*, 508−512.
[11] [11a] G. M. Sheldrick, *SHELXS-97*, University of Göttingen, **1997**. [11b] G. M. Sheldrick, *SHELXL-97*, University of Göttingen, **1997**.

Received July 9, 2003
Early View Article
Published Online March 5, 2004

 © 2004 Wiley-VCH Verlag GmbH & Co. KGaA, Weinheim

Synthesis, Structures and Luminescent Properties of σ-Alkynyl Complexes of Orthomercuriated Schiff Bases

Wai-Yeung Wong,*[a] Guo-Liang Lu,[a] Li Liu,[a] Jian-Xin Shi,[a,b] and Zhenyang Lin[c]

Keywords: Alkyne ligands / Luminescence / Mercury / Schiff bases

A novel series of σ-alkynyl complexes of orthomercuriated Schiff bases of substituted benzylideneanilines and anthracenylmethyleneanilines were synthesised in good yields by alkynylation of the mercuric chlorides of the appropriate Schiff bases with terminal alkynes RC≡CH (R = Ph, ferrocenyl, *p*-ferrocenylphenyl) at room temperature in a basic medium. All the new compounds generally displayed good solubility in polar organic solvents and their identities were completely elucidated by various spectroscopic methods. The X-ray crystal structures of these acetylide-functionalised compounds represent the first structurally characterised examples of such alkynylmercury(II) complexes and confirmed that the alkynylmercury(II) moiety is directed to the *ortho* position of the *N*-phenyl ring of the Schiff bases. In one instance, the crystal structure reveals that a loose 1D polymeric aggregate is formed for the first time through a combination of weak intermolecular Hg···Hg and Hg···η^2-C≡C interactions to afford an infinite zigzag chain of Hg atoms supported by acetylide linkages. All the complexes in this study were found to exhibit rich luminescence and solution redox behaviour and correlation of these data with the theoretical calculations by the density functional theory was made.
(© Wiley-VCH Verlag GmbH & Co. KGaA, 69451 Weinheim, Germany, 2004)

Introduction

The synthesis, structure and luminescence properties of transition metal complexes of alkynyl ligands have attracted enormous attention in the past two decades.[1] Metal alkynyls are common for many transition metals, particularly those of groups 8−11, and their chemistry has been developed extensively.[1,2] The interest in the study of mono-, di- and polynuclear gold(I) σ-acetylide complexes stems not only from their rich photochemistry but also from the observation of weak intermolecular d^{10}-d^{10} Au···Au interactions which can play important roles in materials science and crystal engineering.[3] In many cases, it is the combination of the complementary intermolecular forces of aurophilic interactions, hydrogen bonding, π−π stacking and other non-covalent interactions that determines the solid-state luminescent properties of these materials. In contrast to the large body of work on alkynylgold(I) compounds, the chemistry of group 12 metal alkynyls, especially d^{10} alkynylmercury(II) compounds, has not been so thoroughly investigated, and related research work on the isoelectronic mercury(II) system is still in its infancy.[4] Although mercury(II) acetylides were reported as early as the 1920s, they are limited to those of simple alkyl- and arylmercury derivatives.[5] Indeed, mono- and dialkynylmercury complexes have been shown to be useful in the analysis of toxic mercury(II) species[6] and to be valuable building blocks for the synthesis of luminescent metal-organic polymers and supramolecular aggregates.[4]

Very recently, a comprehensive program was launched in our laboratory to develop the chemistry of alkynylmercury complexes. We have reported a new class of bis(alkynyl)mercury(II) complexes incorporating a series of aromatic groups.[4d,4e] These molecules were shown to display a rich photophysical behaviour and interesting structural properties. The crystal structures of [MeHgC≡CRC≡CHgMe] (R = thiophene-2,5-diyl, [2,2′]-bithiophene-5,5′-diyl) reveal the formation of a loose polymeric structure in each case through weak intermolecular non-covalent Hg···Hg interactions.[4e] The solid-state aggregation of [Hg(C≡CR)$_2$] (R = Ph, SiMe$_3$) has been discussed by Nicholson et al. in which both mercuriophilic and Hg-η^2-C$_2$ interactions appear to contribute to the supramolecular aggregation process.[4b] π-Coordination of some transition metal ions to bis-alkynylmercury complexes has also been explored recently in which some compounds reveal weak anion···cation interactions and the structure of $\{[Hg(C{\equiv}CTol)_2Ag][BF_4]\}_n$ shows a polymeric skeleton comprised of helices cross-linked by C−H···π in-

[a] Department of Chemistry, Hong Kong Baptist University
Waterloo Road, Kowloon Tong, Hong Kong SAR, P.R. China
Fax: (internat.) +852-3411-7348
E-mail: rwywong@hkbu.edu.hk
[b] Department of Chemistry, Zhongshan University
Guangzhou 510275, P.R. China
[c] Department of Chemistry, The Hong Kong University of Science and Technology,
Clearwater Bay, Hong Kong SAR, P.R. China
Supporting information for this article is available on the WWW under http://www.eurjic.org or from the author.

 © 2004 Wiley-VCH Verlag GmbH & Co. KGaA, Weinheim **DOI: 10.1002/ejic.200300677**

teractions.[4a] In the pursuit of unsymmetrical diorganomercurials bearing an alkynyl ligand, we set out a strategy to synthesise some σ-acetylide complexes of orthomercuriated Schiff bases.[7] Perusal of the literature suggested that there were no examples of such kinds of alkynylmercury(II) compounds and their structures and luminescence behaviour have not been described before. We present here the synthesis and structural characterisation of the first σ-alkynyl complexes of orthomercuriated Schiff bases of substituted benzylideneanilines and anthracenylmethyleneanilines. The luminescence and electrochemical properties of these complexes have been examined.

Results and Discussion

Syntheses and Spectroscopic Properties

Condensation reactions of *p*-nitrobenzaldehyde and 9-anthraldehyde with the respective *para*-substituted anilines readily afforded the Schiff bases **1a**, **1b**, **2a** and **2b** in high yields.[7b] The mercuric chloride precursors of the corresponding Schiff bases (**3a**, **3b**, **4a** and **4b**) were prepared by in situ reaction of the Schiff bases with one molar equivalent of mercuric acetate in dry MeOH under reflux for 4 h, followed by the addition of lithium chloride (Scheme 1). The products were precipitated from the reaction mixture and isolated in very good overall yields.

The general alkynylation routes leading to new compounds **5**−**12** are shown in Scheme 1. Based on the classical dehydrohalogenation method,[3h,4d,4e] room temperature reactions of the orthomercuriated derivatives with a slight excess of the terminal alkynes RC≡CH (R = Ph, Fc, *p*-FcC_6H_4, where Fc = ferrocenyl) in THF in the presence of NaOMe in MeOH furnished compounds **5**−**12** in 82−87% yields. Pure samples of these products were obtained after extraction of the crude compounds with hot $CHCl_3$ followed by subsequent recrystallisation from CH_2Cl_2/hexane. Compounds **5**−**12** were isolated as air-stable yellow to yellow-brown solids. They exhibit fairly good solubility in chlorinated solvents such as CH_2Cl_2 and $CHCl_3$ and the solubility of the complex is enhanced by increasing the chain length of the alkoxy group from MeO to $C_{16}H_{33}O$. They were satisfactorily characterised by elemental analyses, IR, MS, ^1H and ^{13}C NMR spectroscopy.

All the spectroscopic data of new compounds are in agreement with their proposed structures. Each of the IR spectra of **5**−**12** displays a characteristic absorption band in the range 2137−2141 cm^{-1} corresponding to the ν(C≡C) stretching modes. The ^1H NMR spectra of **1**−**12** all show features pertaining to the protons of the aromatic and other organic groups. The position of the mercury atom in **5**−**12** was determined by ^1H NMR spectroscopy. The four *C*-phenyl protons for each of **5**−**8** consists of a group of left-right symmetrical multiplet peaks in the aromatic region typical of a four-spin AA′BB′ system at lower field due to the electron-withdrawing effect of the NO_2 group. At higher field, the two doublets and a doublet of doublets which belong to the three-spin AMX system correspond to the three *N*-phenyl protons. Such spectral assignments show that mercuriation takes place at the *ortho* position of the *N*-phenyl ring rather than at the *ortho* position of the *C*-phenyl ring. The ^{13}C NMR spectra of the σ-acetylide complexes show two resonances for the sp carbon atoms of the C≡C units in which the chemical-shift values are virtually unaffected upon varying the substituents; assignment of these ^{13}C signals was made by analogy with other similar acetylide compounds.[4a,5c] In each case, we can detect the respective molecular ion peak $[M]^+$ or $[MH]^+$ in the FAB mass spectra,

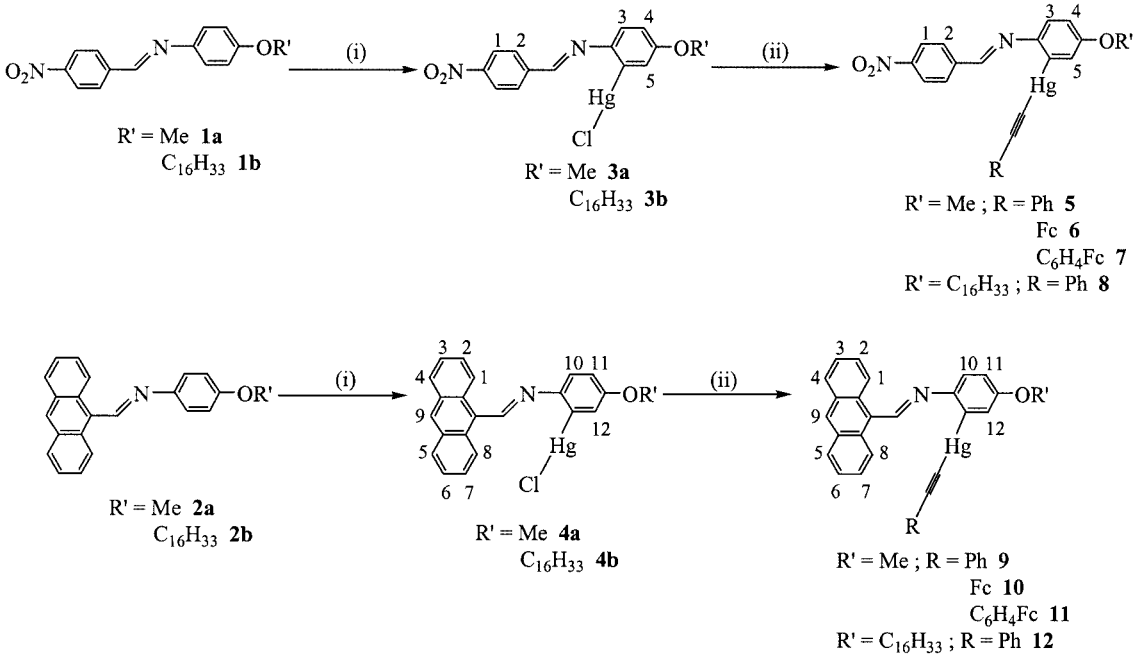

Scheme 1. Reagents and conditions: (i) $Hg(OAc)_2$ followed by LiCl; (ii) RC ≡ CH, NaOH/MeOH

 © 2004 Wiley-VCH Verlag GmbH & Co. KGaA, Weinheim

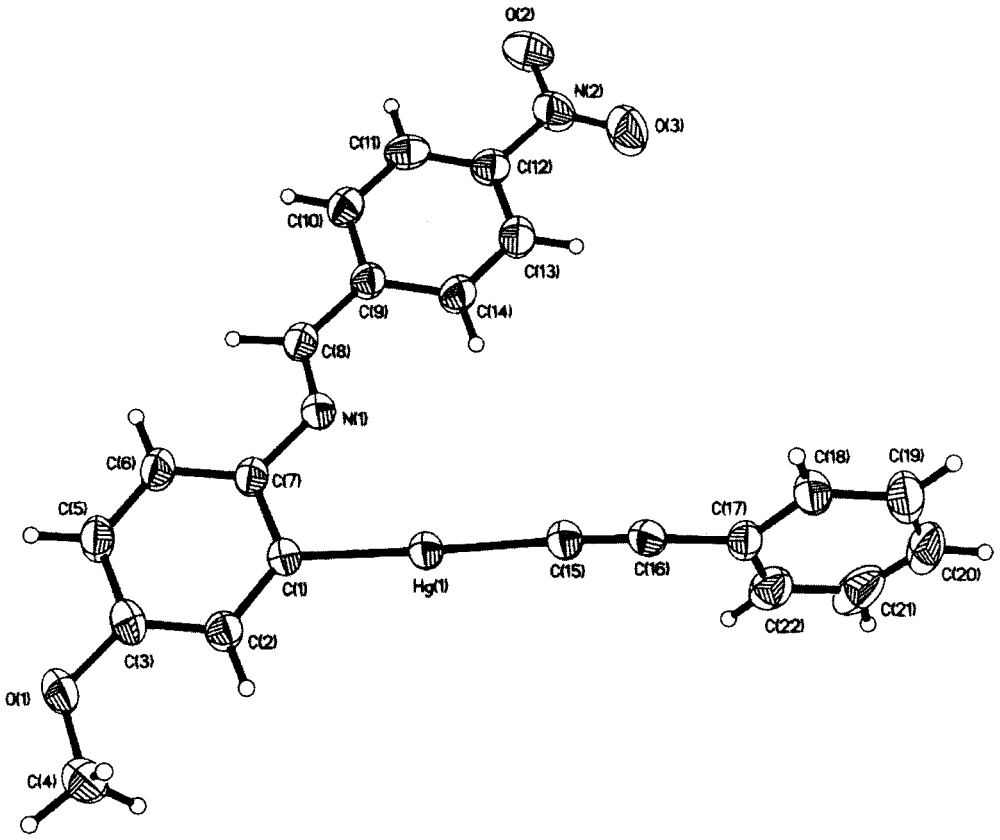

Figure 1. Molecular structure of **5**, with thermal ellipsoids shown at the 25% probability level

and for **5**−**12** we also observe the peaks corresponding to the detachment of the HgC≡CR groups.

Crystal-Structure Analysis

The molecular structures of complexes **5** (Figure 1), **6** (Figure 2), **7** (Figure 3), **9** (Figure 4), and **10** (Figure 5) are shown, and selected structural parameters are listed in Table 1. In each case, the crystal structure shows an unsymmetrical diorganomercurial species in which the Hg^{II} centre is σ bonded to an alkynyl ligand as well as an *ortho*-carbon atom of the *N*-phenyl ring of the corresponding Schiff base. The geometry about the Hg atom in each case is very similar, with the Hg^{II} centre being two-coordinate and essentially linear [$C(sp^2)-Hg-C(sp)$ 177.6(4)−179.3(4)°]. The Hg−C(sp) bonds are similar in length to those in other Hg^{II} acetylide compounds.[4,8] The near linearity of the Hg−C≡C fragment is confirmed from the Hg(1)−C(sp)−C(sp) angles [170.2(6)−178.5(13)°] and the slight deviations from 180° for **5** and **6** are consistent with the presence of short intermolecular interactions (vide infra). The C≡C bond lengths span the narrow range of 1.162(16)−1.196(9) Å, typical of other known Hg^{II} acetylides.[8] The Hg···N nonbonded contacts, which range from 2.860 to 3.126 Å, and the Hg(1)−$C(sp^2)$−$C(sp^2)$ bond angles [112.3(4)−118.2(9)°], which are less than 120°, suggest the opportunity for a secondary N→Hg intramolecular interaction with a four-membered ring. The presence of such weak Hg···N contacts can be justified based on the currently acceptable van der Waals radius of each element.[9] The present structural investigations corroborate the proposed reaction mechanism, in which the mercuriation at the *ortho* position of the *N*-phenyl ring was facilitated by the imino moiety upon formation of a coordination complex with $Hg(OAc)_2$ in the first step, followed by a subsequent electrophilic substitution at the *ortho* position of the *N*-phenyl ring.[7b]

Examination of the crystal packing diagram for each compound reveals the involvement of various intermolecular contacts in their structures. Interestingly, there is a strong tendency for the molecules in **5** to aggregate, and the lattice structure of **5** is highlighted by the presence of extensive non-covalent Hg···Hg and Hg···η^2-C≡C interactive vectors, which link up the molecular units to form a loose polymeric structure. Such a polymeric aggregate shows a zigzag 1D chain of Hg atoms with an Hg···Hg interaction distance of ca. 3.959 Å between adjacent molecules; the average Hg−Hg−Hg bond angle is 135.9° (Figure 6). To the best of our knowledge, this represents the first structurally characterised example of a mercury(II) acetylide compound exhibiting infinite polymeric chains of Hg atoms, although it is known that crystals such as $Hg_3(AlCl_4)_2$ and Hg_3AsF_6 also contain zigzag mercury chains in their lattices.[4c,10] A similar chain-like structure supported by alkynyl ligands is also found for silver(I) in $[(Me_3P)AgC{\equiv}CR]_\infty$ (R = Ph, $SiMe_3$).[11] While the Hg···Hg contacts in **5** indicate that each of the individual interac-

 © 2004 Wiley-VCH Verlag GmbH & Co. KGaA, Weinheim

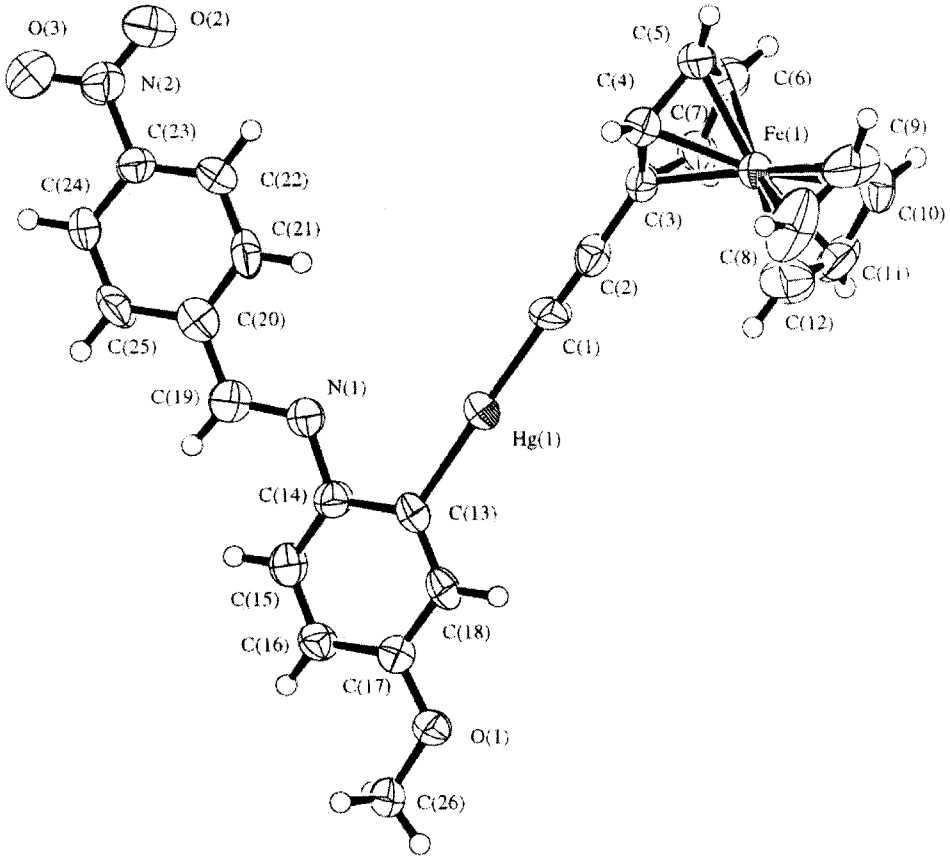

Figure 2. Molecular structure of **6**, with thermal ellipsoids shown at the 25% probability level

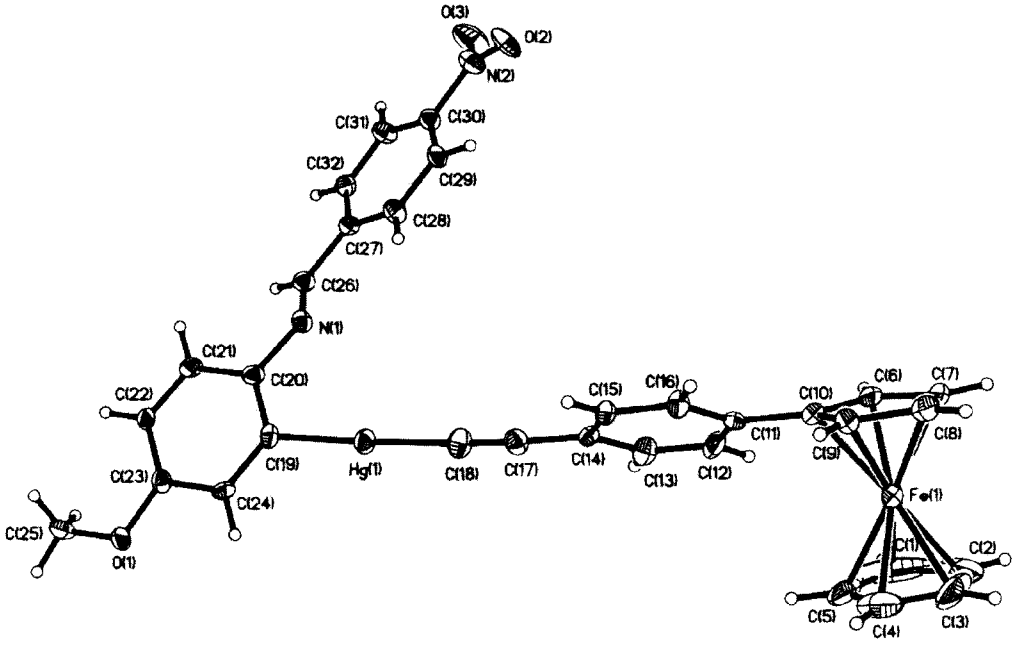

Figure 3. Molecular structure of **7**, with thermal ellipsoids shown at the 25% probability level

tions is relatively weak, it is the large number of them that play a supramolecular role and generate a significant driving force for solid-state aggregation. We believe that such mercuriophilic forces are more than just van der Waals interactions in these chemical systems. The intermolecular distances from the Hg atom to C_α [Hg(1)···C(15)] and C_β [Hg(1)···C(16)] are 3.398 and 3.783 Å, respectively, which compare well with the values quoted for [Hg(C≡CR)$_2$] (R = Ph, SiMe$_3$)[4b] but are significantly longer than the intramolecular distances found in some heterometallic

 © 2004 Wiley-VCH Verlag GmbH & Co. KGaA, Weinheim

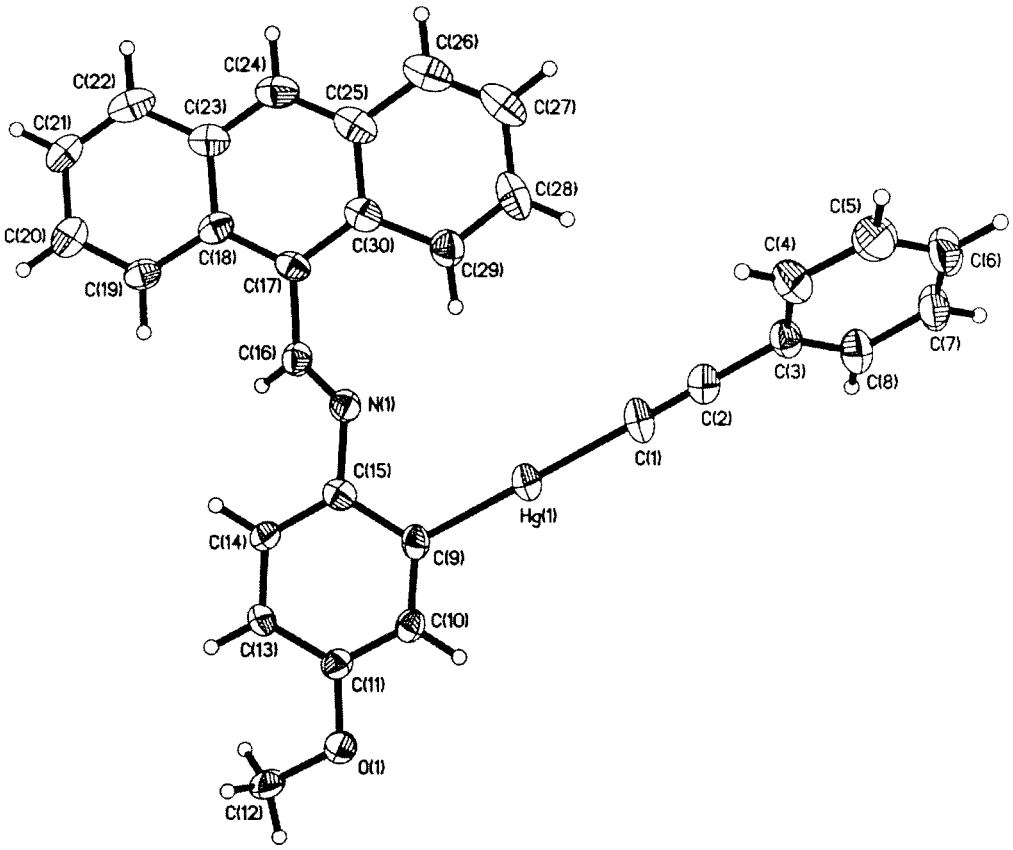

Figure 4. Molecular structure of **9**, with thermal ellipsoids shown at the 25% probability level

bis(η^2-alkyne)mercury complexes.[4g][4h] While the closest intermolecular contacts in **6** are attributed to the hydrogen-bonding interactions [O(1)···H(15) 2.44 Å; O(2)···H(15) 2.72 Å), the weak mercuriophilic (4.21 Å) and Hg···η^2-C≡C attractions [Hg(1)···C(1) 3.41 Å; Hg(1)···C(2) 3.57 Å) also contribute to the overall intermolecular packing. The van der Waals radius of mercury has been the subject of much debate and a value of up to 2.2 Å has been proposed recently,[4c,7a,9] which is conceived to be a better estimate than the value quoted by Bondi in 1964.[12] In light of this, the observed Hg···Hg separations which are similar to the values of 3.71−4.25 Å for [Hg(C≡CR)$_2$] (R = Ph, SiMe$_3$)[4b] are towards the upper limit of those accepted as representing metallophilic interactions and are consistent with other previous interpretations.[4e,4f] For **7**, **9** and **10**, the Hg···Hg and Hg···C≡C interactions become unimportant and the nearest intermolecular contacts involve the Hg centre, the methoxy oxygen atom and a hydrogen atom from the aromatic rings. These contacts arise from Hg(1)···H(25) (3.372 Å), Hg(1)···O(1) (3.698 Å) and O(2)···H(32) (2.376 Å) interactions for **7**, whereas each molecular unit of **9** is linked to two adjacent units through short Hg(1)···O(1) contacts (3.084 Å). Presumably because of the greater steric bulk of both anthryl and ferrocenyl rings, there are no other significant short contacts for **10** other than the Hg(1)···H(25) interactions (2.921 Å). None of these five structures show close π−π stacking of the arene rings in the solid state.

Absorption and Luminescence Properties

The electronic absorption and emission data of our compounds are given in Table 2. In general, these orthomercuriated complexes absorb strongly in the range 383−413 nm. The dependence of the solution absorption spectra on the nature of the original Schiff bases suggests that the transitions are mainly π−π* ligand-centred, and the apparent insensitivity of the low-energy absorption bands towards the ancillary groups R on the mercury centre (cf. **5**, **6** and **7**) precludes a metal-centred origin for these transitions.[4e] We also note that the lowest-energy absorption features show slight bathochromic shifts when the alkynylmercury(II) fragments are introduced at the *ortho* position of the Schiff bases (cf. **2a** and **9**), reflecting a certain degree of through-metal π-delocalisation due to metal-to-ligand back-donation to the π*(C≡CR) orbital. Hence, the electronic absorption spectra are probably dominated by intraligand π−π* transitions, but possibly mixed with a small contribution from the metal in the HOMO and the LUMO.[13] The π,π* character of the electronic states involved is consistent with the molecular orbital calculations. Figure 7 depicts the contour plots of the HOMOs and LUMOs for **2a**, **9** and **10**, showing the common bonding features in the frontier region. The HOMOs and LUMOs for the three complexes resemble each other and correspond to the π and π* orbitals of the conjugated organic unit. The substituents HgC≡CPh in **9** and HgC≡CFc in **10** only af-

 © 2004 Wiley-VCH Verlag GmbH & Co. KGaA, Weinheim

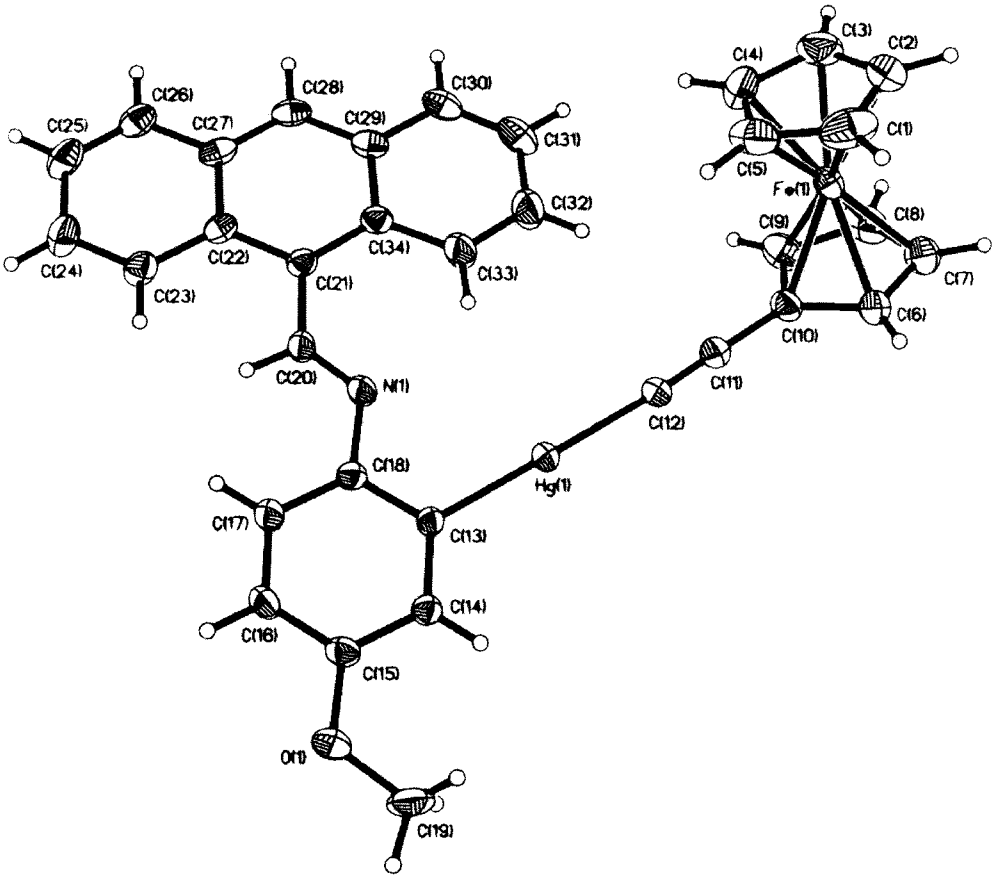

Figure 5. Molecular structure of **10**, with thermal ellipsoids shown at the 25% probability level

Table 1. Selected bond lengths (Å) and angles (°) for **5**, **6**, **7**, **9** and **10**

	5	**6**	**7**	**9**	**10**
Hg(1)−C(sp^2)	2.057(6)	2.08(1)	2.081(8)	2.061(11)	2.054(3)
Hg(1)−C(sp)	2.016(7)	2.02(1)	2.023(9)	2.047(12)	2.045(4)
C(sp)−C(sp)	1.196(9)	1.18(1)	1.182(11)	1.162(16)	1.169(5)
C(imine)−N(1)	1.258(9)	1.28(1)	1.254(10)	1.257(14)	1.196(5)
Fe(1)−ring(Cp)		1.6408	1.6509		1.6523
Fe(1)−ring(C_5H_4)		1.6375	1.6416		1.6564
Hg(1)···N(1)	2.860	3.049	3.041	3.126	2.999
$C(sp^2)$−Hg(1)−C(sp)	178.3(3)	179.3(4)	177.6(4)	179.0(5)	178.83(15)
Hg(1)−C(sp)−C(sp)	170.2(6)	173(1)	177.7(9)	178.5(13)	175.5(4)
$C(sp^2)$−N(1)−$C(sp^2)$	123.2(6)	120(1)	120.1(7)	119.1(9)	123.2(4)
Hg(1)−$C(sp^2)$−$C(sp^2)$	112.3(4)	117.4(8)	116.0(6)	118.2(9)	117.6(2)
$C(sp^2)$−$C(sp^2)$−N(1)[a]	115.2(5)	115.7(10)	118.4(7)	118.6(10)	115.6(3)

[a] sp^2 carbon atoms of the *N*-phenyl ring.

fect the energies of those orbitals above the LUMO and below the HOMO. The second LUMO for both **9** and **10** has significant contribution from the Hg's empty p orbitals. The presence of the ferrocenyl group in **10** introduces the two Fe(d_δ) orbitals as the second and third HOMOs (we define the δ-type d orbital by viewing the orbitals along the Ct−Fe−Ct direction where Ct is the centre of each cyclopentadienyl ring). The order of calculated HOMO−LUMO gaps **2a** (3.40 eV) > **10** (3.33 eV) > **9** (3.17 eV) is in line with our experimental observations.

Complexes **5**−**12** were found to exhibit luminescence in the solid state at 290 and 11 K (Table 2). There is little change in the emission spectra upon variation of the excitation wavelength, indicating that a single emissive state or multiple states in equilibrium is (are) responsible for the observed emission. The emission energy is dependent on the nature of the structure of the Schiff bases (Figure 8), but does not vary much with respect to the identity of R′. The striking similarity of the emission peak shapes of these σ-alkynyl complexes and those of their parent Schiff bases

 © 2004 Wiley-VCH Verlag GmbH & Co. KGaA, Weinheim

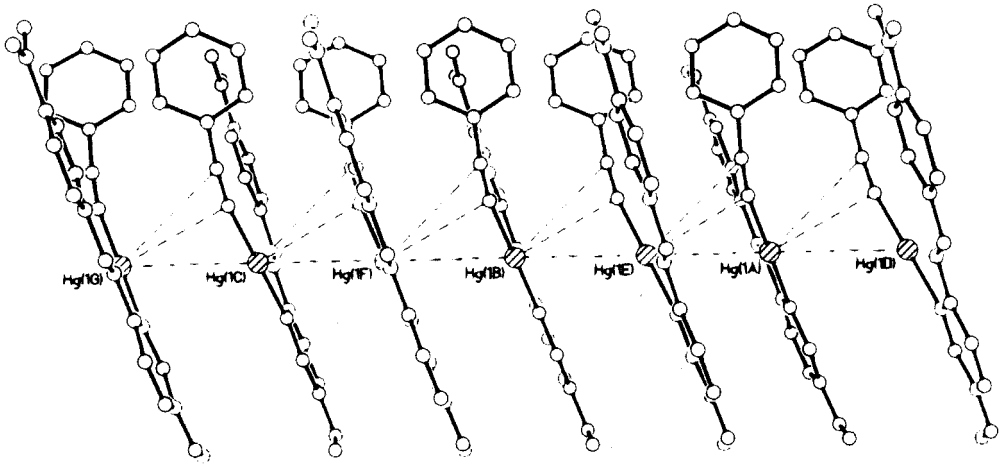

Figure 6. Crystal packing diagram for **5** showing the polymeric chain of Hg atoms aggregated through Hg···Hg and Hg···η^2-C≡C intermolecular contacts; all hydrogen atoms are omitted for clarity

and organomercuric chlorides are suggestive of a ligand-dominated emissive state, and the lowest emissive states in these complexes can tentatively be assigned as metal-perturbed intraligand $\pi-\pi^*$ transitions. The emission energies of the complexes in the solid state at 11 K roughly follow the order **9** > **5**, **10** > **6** and **12** > **8**, which is in agreement with the electron-withdrawing ability of the nitro group in the latter which tends to reduce the HOMO−LUMO gap. However, compounds **7** and **11** were found to be weakly emissive both in solution and as solids, and the appearance of the low-energy emission bands as broad shoulders or weak peaks makes it difficult for one to determine their exact maxima for comparative studies. In most cases, the marked red shift in the emission wavelengths for the solid-state spectra is a manifestation of the formation of aggregates in the ground state due to the presence of intermolecular interactions in the solid lattice, which is not present in solution (vide supra).[3b,13]

Electrochemistry

Table 3 collects the electrochemical data for our complexes in CH_2Cl_2. Each of the cyclic voltammograms of **5**−**12** essentially shows an irreversible oxidation wave (+0.77 to +1.11 V) which is suggested to arise from Schiff-base ligand-centred oxidation since the potentials within the same ligand class are found to have similar values. For the NO_2-substituted Schiff bases and their organomercury complexes, we observe one quasi-reversible reduction couple which can be attributed to reduction of the nitro moiety; these $E_{1/2}$ values (−1.41 to −1.45 V) are almost invariant of the structures. For each of **6**, **7**, **10** and **11**, the cyclic voltammogram is also characterised by one quasi-reversible oxidation wave due to the ferrocenyl electrophore that is present. The ferrocenyl oxidation potential is less anodic for **7** (+0.07 V) and **11** (+0.06 V) than for **6** (+0.13 V) and **10** (+0.10 V) because of the greater degree of electron delocalisation along the metal-capped ethynyl bridges with an additional C_6H_4 unit which would increase the ease of oxidation.

Concluding Remarks

This report has demonstrated that orthomercuriated Schiff bases are useful precursors to afford a range of luminescent diorganomercurial σ-alkynyl compounds. Structural characterisations of complexes **5**, **6**, **7**, **9** and **10** are particularly interesting and constitute the first examples of this type. The results also provide further evidence for the existence of N→Hg intramolecular coordination and the fact that the initial mercuriation step occurs at the *ortho* position of the *N*-phenyl ring instead of the *C*-phenyl ring. Depending on the geometric and steric properties of the end groups anchored on the alkynyl unit and the type of Schiff base employed, we were able to build up polymeric mercury(II) acetylide systems in the solid state aggregated through Hg···Hg and Hg···η^2-C≡C secondary interactions. Such a supramolecular aggregation process is best favoured for orthomercuriated molecules with the least steric bulk, such as **5**. The absorption and emission properties of **5**−**12** are dominated by mildly mercury-perturbed organic $\pi-\pi^*$ transitions, which are consistent with the results obtained from theoretical calculations. A comparison of the *p*-nitrophenyl and 9-anthryl substituents illustrates that the emission maximum is bathochromically shifted in the presence of the electron-accepting NO_2 group in the former case.

Experimental Section

General Procedures: All reactions were conducted under an atmosphere of dry nitrogen with the use of standard Schlenk techniques. Solvents for preparative work were dried and distilled before use. IR spectra were obtained using a Nicolet FTIR-550 spectrometer. NMR spectra were recorded on a JEOL JNM-EX 270 or a Varian Inova 400 MHz FT NMR spectrometer. Fast atom bombardment (FAB) mass spectra were recorded on a Finnigan-SSQ 710 spectrometer. Electronic absorption spectra were measured with a HP 8453 UV/Vis spectrometer. For emission spectral measurements, the 325 nm line of a He-Cd laser was used as an excitation source. The luminescence spectra were analysed by a 0.25 m focal length

 © 2004 Wiley-VCH Verlag GmbH & Co. KGaA, Weinheim

Table 2. Photophysical data of orthomercuriated complexes

Complex	Absorption[b] λ_{max}/nm ($\varepsilon/10^4$ $M^{-1}\cdot cm^{-1}$)	Emission[a] Medium (T/K)	λ_{em} (nm)
1a	261 (1.4), 383 (1.6)	CH_2Cl_2 (290)	478
		solid (290)	575
		solid (11)	600
1b	267 (2.8), 384 (2.8)	CH_2Cl_2 (290)	470
		solid (290)	570
		solid (11)	595
2a	252 (3.8), 400 (1.4)	CH_2Cl_2 (290)	467
		solid (290)	565
		solid (11)	560
2b	254 (3.9), 405 (1.9)	CH_2Cl_2 (290)	470
		solid (290)	555
		solid (11)	560
3a	267 (1.4), 383 (1.6)	CH_2Cl_2 (290)	455
		solid (290)	601
		solid (11)	623
3b	268 (1.2), 385 (1.3)	CH_2Cl_2 (290)	448, 465 sh, 534 sh
		solid (290)	568
		solid (11)	555
4a	252 (3.4), 404 (1.1)	CH_2Cl_2 (290)	440
		solid (290)	550
		solid (11)	533, 567
4b	254 (3.2), 308 (0.6), 410 (0.9)	CH_2Cl_2 (290)	439, 468, 498 sh
		solid (290)	530
		solid (11)	526, 561
5	253 (2.5), 387 (1.4)	CH_2Cl_2 (290)	456
		solid (290)	563
		solid (11)	569, 610
6	277 (1.8), 387 (1.1)	CH_2Cl_2 (290)	469 sh, 533
		solid (290)	425 sh, 602
		solid (11)	602
7	269 (2.6), 298 (2.4), 389 (1.2)	CH_2Cl_2 (290)	452 vw
		solid (290)	434, 510 sh
		solid (11)	420, 436, 520 sh
8	255 (3.2), 389 (1.6)	CH_2Cl_2 (290)	461
		solid (290)	556
		solid (11)	558
9	248 (3.8), 307 (0.7), 410 (1.1)	CH_2Cl_2 (290)	447
		solid (290)	552
		solid (11)	535, 570
10	274 (2.9), 406 (0.9)	CH_2Cl_2 (290)	466
		solid (290)	573
		solid (11)	575
11	262 (5.0), 304 (2.2), 408 (0.7)	CH_2Cl_2 (290)	465 vw
		solid (290)	435, 575 vw
		solid (11)	435, 578 vw
12	248 (3.7), 310 (0.7), 413 (1.3)	CH_2Cl_2 (290)	452
		solid (290)	540
		solid (11)	534, 571

[a] Excitation wavelength is 325 nm. sh = shoulder. vw = very weak. [b] All absorption spectra were recorded in CH_2Cl_2 at 290 K.

double monochromator with a Peltier cooled photomultiplier tube and processed with a lock-in amplifier. For the low temperature experiments, samples were mounted in a closed-cycle cryostat (Oxford CC1104) in which the temperature can be adjusted from 10 to 330 K. Cyclic voltammetry experiments were performed with a Princeton Applied Research (PAR) model 273A potentiostat. A conventional three-electrode configuration consisting of a glassy-carbon working electrode, a Pt-wire counter electrode and a Ag/$AgNO_3$ reference electrode was used at a scan rate of 100 mV s^{-1}. The solvent in all measurements was deoxygenated CH_2Cl_2 and the supporting electrolyte was 0.1 M $[Bu_4N]PF_6$. Ferrocene was added as an internal standard after each set of measurements and all potentials reported were quoted with reference to the ferrocene-ferrocenium couple. Unless otherwise stated, all reagents were from commercial sources and used as received. The compounds **1a**,[7b] **3a**,[7b] ethynylferrocene[14] and *p*-ethynylphenylferrocene[15] were prepared according to the reported procedures. The synthesis of **3b**, **4a** and **4b** was described in the supplementary materials. Density functional calculations at the B3LYP level[16] were performed on **2a**, **9** and **10** on the basis of their experimentally determined geometries obtained from crystallographic data. The basis set used for C, O, N and H atoms was 6−31G,[17] while effective core potentials with a LanL2DZ basis set[18] were employed for Fe and Hg atoms. The Gaussian 98 program was used for the calculations.[19]

 © 2004 Wiley-VCH Verlag GmbH & Co. KGaA, Weinheim

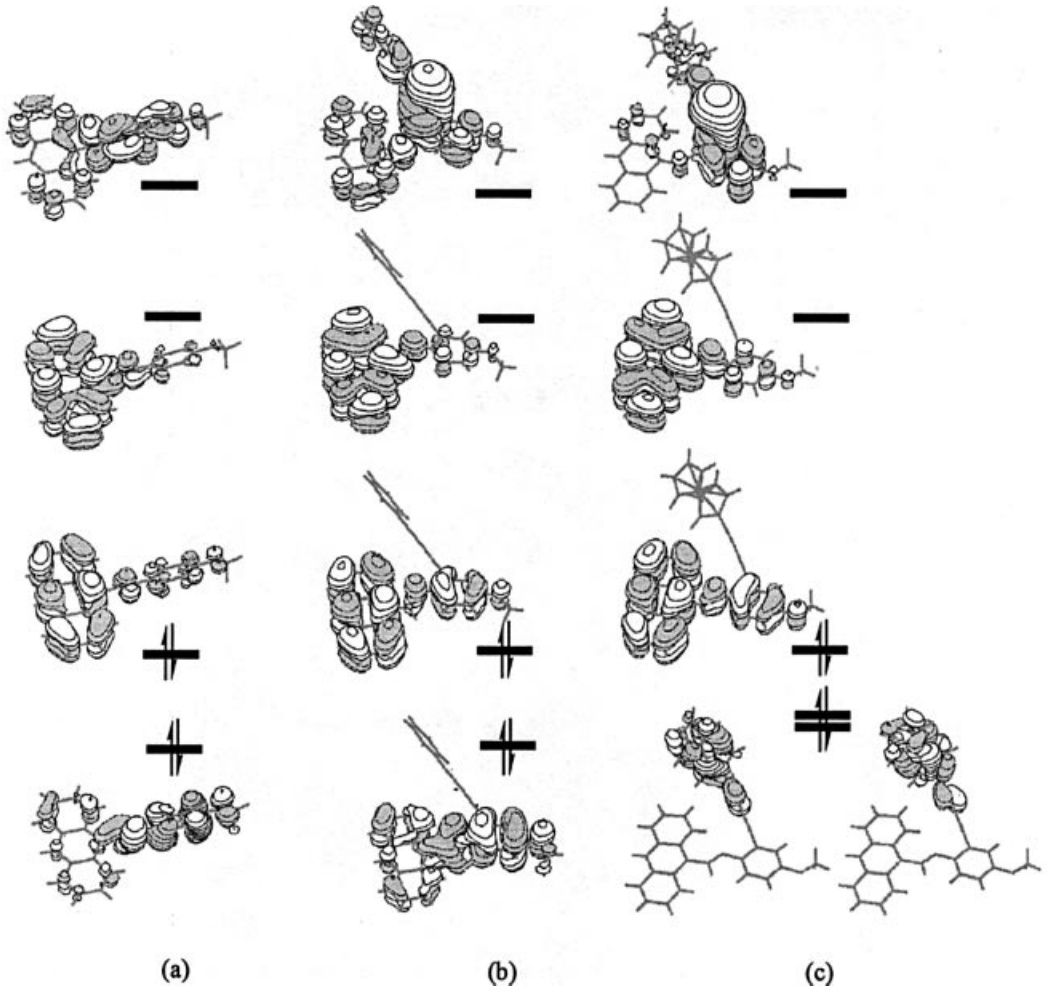

Figure 7. Spatial plots of the highest occupied (HOMO) and lowest unoccupied (LUMO) molecular orbitals for (a) **2a**, (b) **9** and (c) **10**

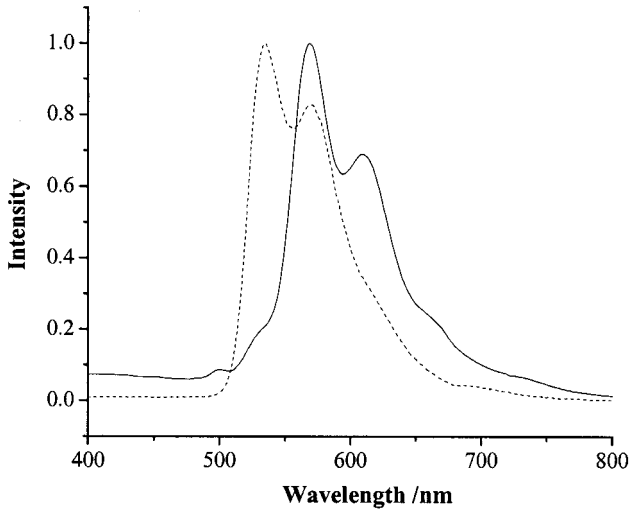

Figure 8. Solid-state emission spectra of **5** (solid line) and **9** (dashed line) at 11 K

Caution! *Organomercurials are extremely toxic, and appropriate handling conditions should be used for their generation and disposal.*

General Procedures for the Synthesis of σ-Alkynyl Complexes of Orthomercuriated Schiff Bases 5−12: Basic MeOH was added dropwise to a mixture of each of the mercuric chloride derivatives (**3a**, **3b**, **4a** or **4b**, 0.10 mmol) and two molar equivalents of RC≡CH (R = Ph, Fc or *p*-FcC_6H_4) in THF. In a typical run, a 0.5 M solution of NaOH in MeOH (5 mL, 1.00 mmol) was added to the mixture of **3a** (49.1 mg, 0.10 mmol) and PhC≡CH (0.022 mL, 0.20 mmol) in THF (5 mL). The resulting mixture was stirred for 3 h at room temperature before all the volatile components were removed under reduced pressure. The residue was extracted with hot $CHCl_3$ and the yellow extract was then filtered through a thick layer of Celite. After evaporation of solvent, the crude product was recrystallised from CH_2Cl_2/hexane to afford an essentially pure yellow solid in high yield.

Compound 5: Yellow solid. Yield 86% (47.9 mg). IR (KBr): ν(CH=N) = 1621 and ν(C≡C) = 2141 cm^{-1}. ^1H NMR ($CDCl_3$): δ = 3.85 (s, 3 H, Me), 6.88 (dd, $J_{H,H}$ = 2.7, 8.9 Hz, 1 H, H_4), 7.08 (d, $J_{H,H}$ = 2.7 Hz, 1 H, H_5), 7.32−7.35 (m, 3 H, Ph), 7.47 (d, $J_{H,H}$ = 8.9 Hz, 1 H, H_3), 7.51−7.54 (m, 2 H, Ph), 8.05 (d, $J_{H,H}$ = 8.8 Hz, 2 H, H_2), 8.32 (d, $J_{H,H}$ = 8.8 Hz, 2 H, H_1), 8.70 (s, 1 H, CH=N) ppm. ^{13}C NMR ($CDCl_3$): δ = 55.58 (Me), 106.46, 115.03 (C≡C), 117.18, 122.16, 122.84, 124.00, 128.18, 128.24, 128.92, 131.94, 132.10, 141.68, 148.79, 148.84, 152.71, 159.24 (Ar), 162.54 (CH=N) ppm.

 © 2004 Wiley-VCH Verlag GmbH & Co. KGaA, Weinheim

Table 3. Redox data for orthomercuriated compounds and their organic precursors

Compound	Oxidation[a] E_{pa} ($E_{1/2}$)/V	Reduction[b] $E_{1/2}$/V
1a	+1.11	−1.43
1b	+1.07	−1.41
2a	+0.82	
2b	+0.78	
3a	+1.10	−1.44
3b	+1.08	−1.42
4a	[c]	
4b	+0.87	
5	+1.11	−1.42
6	+1.09 (+0.13)	−1.41
7	+1.04 (+0.07)	−1.42
8	+1.04	−1.45
9	+1.07, +0.78	
10	+0.79 (+0.10)	
11	+0.77 (+0.06)	
12	+1.07, +0.77	

[a] E_{pa} refers to the anodic peak potential of the irreversible oxidation wave. $E_{1/2} = (E_{pa} + E_{pc})/2$ where E_{pa} and E_{pc} are the anodic and cathodic peak potentials of the quasi-reversible oxidation couple due to the ferrocenyl group, respectively. [b] $E_{1/2}$ refers to the half-wave potential of the quasi-reversible reduction wave. [c] Limited solubility.

FAB MS: *m*/*z* = 557 [M$^+$]. $C_{22}H_{16}HgN_2O_3$ (557): calcd. C 47.44, H 2.90, N 5.03; found C 47.15, H 2.83, N 4.99.

Compound 6: Brownish-yellow solid. Yield 81% (53.9 mg). IR (KBr): ν(CH=N) = 1617 and ν(C≡C) = 2137 cm^{-1}. ^{1}H NMR ($CDCl_3$): δ = 3.85 (s, 3 H, Me), 4.22 (t, $J_{H,H}$ = 1.8 Hz, 2 H, C_5H_4), 4.24 (s, 5 H, C_5H_5), 4.49 (t, $J_{H,H}$ = 1.8 Hz, 2 H, C_5H_4), 6.87 (dd, $J_{H,H}$ = 2.8, 8.9 Hz, 1 H, H_4), 7.07 (d, $J_{H,H}$ = 2.8 Hz, 1 H, H_5), 7.46 (d, $J_{H,H}$ = 8.9 Hz, 1 H, H_3), 8.06 (d, $J_{H,H}$ = 8.9 Hz, 2 H, H_2), 8.32 (d, $J_{H,H}$ = 8.9 Hz, 2 H, H_1), 8.69 (s, 1 H, CH=N) ppm. ^{13}C NMR ($CDCl_3$): δ = 55.56 (Me), 64.67, 68.75, 70.18, 71.89 (Fc), 106.11, 115.03 (C≡C), 117.28, 122.33, 124.09, 128.34, 129.06, 141.84, 148.95, 149.07, 152.90, 159.38 (Ar), 162.82 (CH=N) ppm. FAB MS: *m*/*z* = 665 [M$^+$]. $C_{26}H_{20}FeHgN_2O_3$ (665): calcd. C 46.97, H 3.03, N 4.21; found C 46.88, H 2.81, N 4.09.

Compound 7: Yellow solid. Yield 84% (62.2 mg). IR (KBr): ν(CH=N) = 1618 and ν(C≡C) = 2137 cm^{-1}. ^{1}H NMR ($CDCl_3$): δ = 3.87 (s, 3 H, Me), 4.05 (s, 5 H, C_5H_5), 4.36 (t, $J_{H,H}$ = 1.8 Hz, 2 H, C_5H_4), 4.67 (t, $J_{H,H}$ = 1.8 Hz, 2 H, C_5H_4), 6.90 (dd, $J_{H,H}$ = 2.8, 8.8 Hz, 1 H, H_4), 7.10 (d, $J_{H,H}$ = 2.8 Hz, 1 H, H_5), 7.45 (s, 4 H, C_6H_4), 7.49 (d, $J_{H,H}$ = 8.8 Hz, 1 H, H_3), 8.08 (d, $J_{H,H}$ = 9.0 Hz, 2 H, H_2), 8.35 (d, $J_{H,H}$ = 9.0 Hz, 2 H, H_1), 8.72 (s, 1 H, CH=N) ppm. FAB MS: *m*/*z* = 740 [M$^+$]. $C_{32}H_{24}FeHgN_2O_3$ (740): calcd. C 51.87, H 3.26, N 3.78; found C 52.01, H 3.04, N 3.50.

Compound 8: Yellow solid. Yield 82% (63.0 mg). IR (KBr): ν(CH=N) = 1621 and ν(C≡C) = 2140 cm^{-1}. ^{1}H NMR ($CDCl_3$): δ = 0.87 (m, 3 H, Me), 1.25−1.55 [m, 26 H, $(CH_2)_{13}$], 1.80 (quint., $J_{H,H}$ = 6.8 Hz, 2 H, OCH_2CH_2), 3.99 (t, $J_{H,H}$ = 6.8 Hz, 2 H, OCH_2), 6.87 (dd, $J_{H,H}$ = 2.9, 8.9 Hz, 1 H, H_4), 7.06 (d, $J_{H,H}$ = 2.9 Hz, 1 H, H_5), 7.32−7.34 (m, 3 H, Ph), 7.46 (d, $J_{H,H}$ = 8.9 Hz, 1 H, H_3), 7.51−7.54 (m, 2 H, Ph), 8.05 (d, $J_{H,H}$ = 8.9 Hz, 2 H, H_2), 8.32 (d, $J_{H,H}$ = 8.9 Hz, 2 H, H_1), 8.70 (s, 1 H, CH=N) ppm. ^{13}C NMR ($CDCl_3$): δ = 14.24, 22.75, 22.79, 26.12, 29.35, 29.44, 29.48, 29.67, 29.69, 29.74, 29.78, 31.66, 32.00, 68.38 ($C_{16}H_{33}$), 106.48, 115.65 (C≡C), 117.14, 122.70, 122.87, 124.02, 128.18, 128.27, 128.90, 132.10, 132.13, 141.74, 148.61, 148.78, 152.48, 158.91 (Ar), 162.56 (CH=N) ppm. FAB MS: *m*/*z* = 768 [M$^+$]. $C_{37}H_{46}HgN_2O_3$ (768): calcd. C 57.91, H 6.04, N 3.65; found C 57.72, H 5.88, N 3.39.

Compound 9: Yellow solid. Yield 88% (53.9 mg). IR (KBr): ν(CH=N) = 1624 and ν(C≡C) = 2141 cm^{-1}. ^{1}H NMR ($CDCl_3$): δ = 3.88 (s, 3 H, Me), 6.96 (dd, $J_{H,H}$ = 2.7, 8.9 Hz, 1 H, H_{11}), 7.11 (d, $J_{H,H}$ = 2.7 Hz, 1 H, H_{12}), 7.27−7.29 (m, 3 H, Ph), 7.42−7.53 (m, 4 H, $H_{2,3,6,7}$), 7.60 (d, $J_{H,H}$ = 8.9 Hz, 1 H, H_{10}), 7.64−7.67 (m, 2 H, Ph), 8.04 (d, $J_{H,H}$ = 8.4 Hz, 2 H, $H_{4,5}$), 8.54 (s, 1 H, CH=N), 8.87 (d, $J_{H,H}$ = 8.9 Hz, 2 H, $H_{1,8}$), 9.85 (s, 1 H, H_9) ppm. ^{13}C NMR ($CDCl_3$): δ = 55.64 (Me), 106.08, 114.98 (C≡C), 117.35, 122.35, 123.10, 124.80, 125.29, 126.91, 127.22, 127.93, 128.13, 128.97, 130.54, 130.65, 131.24, 132.06, 132.84, 151.16, 156.22, 158.47 (Ar), 160.68 (CH=N) ppm. FAB MS: *m*/*z* = 613 [M$^+$]. $C_{30}H_{21}HgNO$ (613): calcd. C 58.87, H 3.46, N 2.29; found C 58.50, H 3.19, N 2.03.

Compound 10: Yellow-brown solid. Yield 82% (59.1 mg). IR (KBr): ν(CH=N) = 1622 and ν(C≡C) = 2140 cm^{-1}. ^{1}H NMR ($CDCl_3$): δ = 3.88 (s, 3 H, Me), 4.16−4.17 (m, 7 H, C_5H_5 + C_5H_4), 4.41 (t, $J_{H,H}$ = 1.9 Hz, 2 H, C_5H_4), 6.96 (dd, $J_{H,H}$ = 2.9, 8.6 Hz, 1 H, H_{11}), 7.10 (d, $J_{H,H}$ = 2.9 Hz, 1 H, H_{12}), 7.50−7.70 (m, 5 H, $H_{2,3,6,7,10}$), 8.05 (d, $J_{H,H}$ = 8.4 Hz, 2 H, $H_{4,5}$), 8.55 (s, 1 H, CH=N), 8.89 (d, $J_{H,H}$ = 8.9 Hz, 2 H, $H_{1,8}$), 9.86 (s, 1 H, H_9) ppm. ^{13}C NMR ($CDCl_3$): δ = 55.61 (Me), 68.51, 70.06, 70.19, 71.75 (Fc), 105.55, 114.94 (C≡C), 117.42, 122.50, 124.94, 125.39, 127.07, 127.30, 129.09, 129.14, 130.63, 130.76, 131.36, 151.37, 156.32, 158.62 (Ar), 161.01 (CH=N) ppm. FAB MS: *m*/*z* = 721 [M$^+$]. $C_{34}H_{25}FeHgNO$ (721): calcd. C 56.72, H 3.50, N 1.95; found C 56.55, H 3.40, N 1.78.

Compound 11: Yellow-brown solid. Yield 87% (69.3 mg). IR (KBr): ν(CH=N) = 1622 and ν(C≡C) 2138 cm^{-1}. ^{1}H NMR ($CDCl_3$): δ = 3.89 (s, 3 H, Me), 4.03 (s, 5 H, C_5H_5), 4.33 (t, $J_{H,H}$ = 1.6 Hz, 2 H, C_5H_4), 4.64 (t, $J_{H,H}$ = 1.6 Hz, 2 H, C_5H_4), 6.97 (dd, $J_{H,H}$ = 2.8, 8.8 Hz, 1 H, H_{11}), 7.13 (d, $J_{H,H}$ = 2.8 Hz, 1 H, H_{12}), 7.35−7.41 (m, 4 H, $H_{2,3,6,7}$), 7.50−7.54 (m, 2 H, C_6H_4), 7.61 (d, $J_{H,H}$ = 8.8 Hz, 1 H, H_{10}), 7.64−7.68 (m, 2 H, C_6H_4), 8.06 (d, $J_{H,H}$ = 8.0 Hz, 2 H, $H_{4,5}$), 8.56 (s, 1 H, CH=N), 8.89 (d, $J_{H,H}$ = 8.8 Hz, 2 H, $H_{1,8}$), 9.86 (s, 1 H, H_9) ppm. ^{13}C NMR ($CDCl_3$): δ = 55.61 (Me), 66.48, 69.26, 69.41, 69.68 (Fc), 106.58, 115.03 (C≡C), 117.46, 120.24, 122.46, 124.92, 125.40, 125.74, 127.04, 127.34, 129.07, 130.65, 130.76, 131.35, 132.19, 132.88, 139.59, 151.35, 156.41, 158.62 (Ar), 160.90 (CH=N) ppm. FAB MS: *m*/*z* = 796 [M$^+$]. $C_{40}H_{29}FeHgNO$ (796): calcd. C 60.35, H 3.67, N 1.76; found C 60.02, H 3.43, N 1.59.

Compound 12: Yellow solid. Yield 80% (65.8 mg). IR (KBr): ν(CH=N) = 1624 and ν(C≡C) = 2141 cm^{-1}. ^{1}H NMR ($CDCl_3$): δ = 0.87 (m, 3 H, Me), 1.26−1.49 [m, 26 H, $(CH_2)_{13}$], 1.83 (quint., $J_{H,H}$ = 6.5 Hz, 2 H, OCH_2CH_2), 4.02 (t, $J_{H,H}$ = 6.5 Hz, 2 H, OCH_2), 6.96 (dd, $J_{H,H}$ = 2.8, 8.7 Hz, 1 H, H_{11}), 7.10 (d, $J_{H,H}$ = 2.8 Hz, 1 H, H_{12}), 7.27−7.29 (m, 3 H, Ph), 7.42−7.53 (m, 4 H, $H_{2,3,6,7}$), 7.58−7.68 (m, 3 H, H_{10} + Ph), 8.04 (d, $J_{H,H}$ = 8.4 Hz, 2 H, $H_{4,5}$), 8.54 (s, 1 H, CH=N), 8.88 (d, $J_{H,H}$ = 8.9 Hz, 2 H, $H_{1,8}$), 9.86 (s, 1 H, H_9) ppm. ^{13}C NMR ($CDCl_3$): δ = 14.23, 22.78, 26.16, 29.43, 29.45, 29.53, 29.69, 29.72, 29.74, 29.79, 32.00, 68.40 ($C_{16}H_{33}$), 106.08, 115.62 (C≡C), 117.27, 122.89, 123.15, 124.82, 125.26, 126.92, 127.18, 127.89, 128.11, 128.94, 130.46, 130.63, 131.23, 132.06, 133.06, 150.90, 155.99, 158.09 (Ar), 160.66 (CH=N) ppm. FAB MS: *m*/*z* = 823 [M$^+$]. $C_{45}H_{51}NHgO$ (823): calcd. C 65.71, H 6.25, N 1.70; found C 65.50, H 6.02, N 1.43.

X-ray Crystallography: Yellow to orange crystals of the compounds suitable for X-ray diffraction analyses were grown by slow evapor-

 © 2004 Wiley-VCH Verlag GmbH & Co. KGaA, Weinheim

Table 4. Crystal data for complexes **5**, **6**, **7**, **9** and **10**

	5	**6**	**7**	**9**	**10**
Empirical formula	$C_{22}H_{16}HgN_2O_3$	$C_{26}H_{20}FeHgN_2O_3$	$C_{32}H_{24}FeHgN_2O_3$	$C_{30}H_{21}HgNO$	$C_{34}H_{25}FeHgNO$
Formula mass	556.96	664.89	740.97	612.07	719.99
Crystal system	Monoclinic	Monoclinic	Monoclinic	Hexagonal	Monoclinic
Space group	$P2_1/c$	$P2_1/a$	$P2_1/n$	$P6_5$	$P2_1/c$
a (Å)	13.703(3)	7.655(7)	7.5643(6)	26.103(2)	15.2962(9)
b (Å)	19.968(4)	21.831(5)	34.412(3)	26.103(2)	12.7602(7)
c (Å)	7.3386(15)	13.584(5)	10.3974(8)	5.9421(8)	13.5800(8)
α (°)	90	90	90	90	90
β (°)	104.96(3)	100.78(5)	104.827(2)	90	95.6590(10)
γ (°)	90	90	90	120	90
V (Å^3)	1940.1(7)	2230(1)	2616.4(4)	3506.3(7)	2637.7(3)
Z	4	4	4	6	4
μ (Mo-K_α) (mm^{-1})	7.958	7.576	6.453	6.607	6.392
F(000)	1064	1280	1440	1776	1400
T (K)	293	301	293	293	293
Reflections collected	11378	4343	15655	17552	14902
Unique reflections	4379	4028	6129	4068	5893
R_{int}	0.0296	0.0270	0.0827	0.1228	0.0253
Observed reflections [$I > n\sigma(I)$]	2787 (n = 2.0)	2706 (n = 1.5)	3056 (n = 2.0)	3180 (n = 2.0)	4672 (n = 2.0)
Final R indices [$I > n\sigma(I)$][a]	$R1$ = 0.0336	R = 0.047	$R1$ = 0.0489	$R1$ = 0.0510	$R1$ = 0.0284
	$wR2$ = 0.0740	R_w = 0.044	$wR2$ = 0.0908	$wR2$ = 0.1081	$wR2$ = 0.0716

[a] $R = R1 = \Sigma||F_o| - |F_c||/\Sigma|F_o|$. $R_w = [\Sigma w(|F_o| - |F_c|)^2/\Sigma w(F_o)^2]^{1/2}$. $wR2 = [\Sigma w(|F_o^2| - |F_c^2|)^2/\Sigma w|F_o^2|^2]^{1/2}$.

ation of the solvents from their respective solutions in a hexane/CH_2Cl_2 mixture. Geometric and intensity data were collected using graphite-monochromated Mo-K_α radiation (λ = 0.71073 Å) on a Rigaku AFC7R diffractometer (**6**) and Bruker AXS SMART CCD area-detector (for the rest). Absorption corrections based on the ψ-scan method[20] (**6**) or SADABS program[21] (for the other four compounds) were applied. The structure was solved by the direct methods (SIR92[22] for **6**, SHELXTL[23] for the rest) in conjunction with standard difference Fourier techniques and subsequently refined by full-matrix least-squares analyses. All non-hydrogen atoms were assigned with anisotropic displacement parameters. Hydrogen atoms were generated in their idealised positions and allowed to ride on the respective carbon atoms. Crystallographic data for the alkynylmercury complexes are collected in Table 4. For **2a**, the crystal and other experimental details are given in the Supporting Information.

CCDC-217511 to -217516 (for **2a**, **5**, **6**, **7**, **9** and **10**, respectively) contain the supplementary crystallographic data for this paper. These data can be obtained free of charge at www.ccdc.cam.ac.uk/conts/retrieving.html or from the Cambridge Crystallographic Data Centre, 12, Union Road, Cambridge CB2 1EW, UK [Fax: (internat.) +44-1223/336-033; E-mail: deposit@ccdc.cam.ac.uk].

Acknowledgments

This work was supported by a CERG Grant from the Research Grants Council of the Hong Kong SAR, P.R. China (Project No. HKBU 2048/01P) and a Faculty Research Grant from Hong Kong Baptist University (Grant No. FRG/99−00/II-58).

[1] [1a] N. J. Long, C. K. Williams, *Angew. Chem.* **2003**, *115*, 2690−2722; *Angew. Chem. Int. Ed.* **2003**, *42*, 2586−2617. [1b] I. Manners, *Angew. Chem.* **1996**, *108*, 1712−1731; *Angew. Chem. Int. Ed. Engl.* **1996**, *35*, 1602−1621. [1c] R. P. Kingsborough, T. M. Swager, *Prog. Inorg. Chem.* **1999**, *48*, 123−231. [1d] P. Nguyen, P. Gómez-Elipe, I. Manners, *Chem. Rev.* **1999**, *99*, 1515−1548. [1e] V. W.-W. Yam, *Acc. Chem. Res.* **2002**, *35*, 555−563. [1f] U. H. F. Bunz, *Angew. Chem.* **1996**, *108*, 1047−1049; *Angew. Chem. Int. Ed. Engl.* **1996**, *35*, 969−971.

[2] [2a] V. W.-W. Yam, *Chem. Commun.* **2001**, 789−796. [2b] V. W.-W. Yam, K. K.-W. Lo, K. M.-C. Wong, *J. Organomet. Chem.* **1999**, *578*, 3−30. [2c] T. B. Peters, J. C. Bohling, A. M. Arif, J. A. Gladysz, *Organometallics* **1999**, *18*, 3261−3263. [2d] W. Mohr, J. Stahl, F. Hampel, J. A. Gladysz, *Inorg. Chem.* **2001**, *40*, 3263−3264. [2e] M. I. Bruce, B. C. Hall, B. D. Kelly, P. J. Low, B. W. Skelton, A. H. White, *J. Chem. Soc., Dalton Trans.* **1999**, 3719−3728. [2f] M. Guillemot, L. Toupet, C. Lapinte, *Organometallics* **1998**, *17*, 1928−1930. [2g] A. Sakurai, M. Akita, Y. Moro-oka, *Organometallics* **1999**, *18*, 3241−3244. [2h] O. Lavastre, J. Plass, P. Bachmann, S. Guesmi, C. Moinet, P. H. Dixneuf, *Organometallics* **1997**, *16*, 184−189. [2i] M. C. B. Colbert, J. Lewis, N. J. Long, P. R. Raithby, A. J. P. White, D. J. Williams, *J. Chem. Soc., Dalton Trans.* **1997**, 99−104. [2j] W.-Y. Wong, C.-K. Wong, G.-L. Lu, *J. Organomet. Chem.* **2003**, *671*, 27−34. [2k] W.-Y. Wong, C.-K. Wong, G.-L. Lu, A. W.-M. Lee, K.-W. Cheah, J.-X. Shi, *Macromolecules* **2003**, *36*, 983−990. [2l] W.-Y. Wong, C.-K. Wong, G.-L. Lu, K.-W. Cheah, J.-X. Shi, Z. Lin, *J. Chem. Soc., Dalton Trans.* **2002**, 4587−4594. [2m] N. Chawdhury, A. Köhler, R. H. Friend, W.-Y. Wong, J. Lewis, M. Younus, P. R. Raithby, T. C. Corcoran, M. R. A. Al-Mandhary, M. S. Khan, *J. Chem. Phys.* **1999**, *110*, 4963−4970. [2n] Y.-Y. Lin, S.-W. Lai, C.-M. Che, K.-K. Cheung, Z. Y. Zhou, *Organometallics* **2002**, *21*, 2275−2282.

[3] [3a] R. J. Puddephatt, *Chem. Commun.* **1998**, 1055−1062. [3b] R. J. Puddephatt, *Coord. Chem. Rev.* **2001**, *216−217*, 313−332. [3c] H. Schmidbaur, *Chem. Soc. Rev.* **1995**, *24*, 391−400. [3d] C.-M. Che, H.-Y. Chao, V. M. Miskowski, Y. Li, K.-K. Cheung, *J. Am. Chem. Soc.* **2001**, *123*, 4985−4991. [3e] W. Lu, H.-F. Xiang, N. Zhu, C.-M. Che, *Organometallics* **2002**, *21*, 2343−2346. [3f] H.-Y. Chao, W. Lu, Y. Li, M. C. W. Chan, C.-M. Che, K.-K. Cheung, N. Zhu, *J. Am. Chem. Soc.* **2002**, *124*, 14696−14706. [3g] M. I. Bruce, B. C. Hall, B. W. Skelton, M. E. Smith, A. H. White, *J. Chem. Soc., Dalton Trans.* **2002**, 995−1001. [3h] P. Li, B. Ahrens, K.-H. Choi, M. S. Khan, P. R. Raithby, P. J. Wilson, W.-Y. Wong, *CrystEngCommun.* **2002**, *4*, 405−412.

[4] [4a] D. Rais, D. M. P. Mingos, R. Vilar, A. J. P. White, D. J. Williams, *Organometallics* **2000**, *19*, 5209−5217. [4b] S. J. Faville, W. Henderson, T. J. Mathieson, B. K. Nicholson, *J. Or-*

 © 2004 Wiley-VCH Verlag GmbH & Co. KGaA, Weinheim

ganomet. Chem. **1999**, *580*, 363−369. [4c] P. Pyykkö, *Chem. Rev.* **1997**, *97*, 597−636 and references cited therein. [4d] W.-Y. Wong, K.-H. Choi, G.-L. Lu, J.-X. Shi, P.-Y. Lai, S.-M. Chan, Z. Lin, *Organometallics* **2001**, *20*, 5446−5454. [4e] W.-Y. Wong, K.-H. Choi, G.-L. Lu, Z. Lin, *Organometallics* **2002**, *21*, 4475−4481. [4f] W.-Y. Wong, L. Liu, J.-X. Shi, *Angew. Chem.* **2003**, *115*, 4198−4202; *Angew. Chem. Int. Ed.* **2003**, *42*, 4064−4068. [4g] J. R. Berenguer, J. Forniés, E. Lalinde, A. Martin, M. T. Moreno, *J. Chem. Soc., Dalton Trans.* **1994**, 3343−3348. [4h] D. Zhang, D. B. McConville, C. A. Tessier, W. J. Youngs, *Organometallics* **1997**, *16*, 824−825.

[5] [5a] J. R. Johnson, W. L. McEwen, *J. Am. Chem. Soc.* **1926**, *48*, 469−476. [5b] Y. Imai, K. Aida, *Bull. Chem. Soc. Jpn.* **1979**, *52*, 2875−2879. [5c] A. Sebald, B. Wrackmeyer, *Spectrochim. Acta* **1982**, *38A*, 163−173.

[6] [6a] D. Fabbri, M. Lombardo, C. Trombini, I. Vassura, *Appl. Organomet. Chem.* **1995**, *9*, 713−718. [6b] D. Fabbri, C. Trombini, *Chromatographica* **1994**, *39*, 246−248. [6c] F. Bolletta, D. Fabbri, M. Lombardo, L. Prodi, C. Trombini, N. Zaccheroni, *Organometallics* **1996**, *15*, 2415−2417.

[7] [7a] K. R. Flower, V. J. Howard, S. Naguthney, R. G. Pritchard, J. E. Warren, A. T. McGown, *Inorg. Chem.* **2002**, *41*, 1907−1912. [7b] K. Ding, Y. Wu, H. Hu, L. Shen, X. Wang, *Organometallics* **1992**, *11*, 3849−3856 and references cited therein. [7c] H. B. Singh, W. R. McWhinnie, *J. Chem. Soc., Dalton Trans.* **1985**, 821−825.

[8] [8a] E. Gutierrez-Puebla, A. Vegas, S. Garcia-Blanco, *Acta Crystallogr., Sect. B* **1978**, *34*, 3382−3384. [8b] C. Hartbaum, G. Roth, H. Fischer, *Eur. J. Inorg. Chem.* **1998**, 191−202. [8c] B. F. Hoskins, R. Robson, E. E. Sutherland, *J. Organomet. Chem.* **1996**, *515*, 259−260. [8d] I. Ghosh, R. Mishra, D. Poddar, A. K. Mukherjee, M. Mukherjee, R. Bhattacharyya, *Chem. Commun.* **1996**, 435−436.

[9] S. S. Batsanov, *J. Chem. Soc., Dalton Trans.* **1998**, 1541−1545 and references cited therein.

[10] [10a] C. X. Cui, M. Kertesz, *Inorg. Chem.* **1990**, *29*, 2568−2575. [10b] R. D. Ellison, H. A. Levy, K. W. Fung, *Inorg. Chem.* **1972**, *11*, 833−836. [10c] I. D. Brown, B. D. Cutforth, C. Davies, R. J. Gillespie, P. R. Irehrod, J. E. Vekris, *Can. J. Chem.* **1974**, *52*, 791−793.

[11] [11a] P. W. R. Corfield, H. M. M. Shearer, *Acta Crystallogr.* **1966**, *20*, 502−508. [11b] C. Brasse, P. R. Raithby, M.-A. Rennie, C. A. Russell, A. Steiner, D. S. Wright, *Organometallics* **1996**, *15*, 639−644.

[12] A. Bondi, *J. Phys. Chem.* **1964**, *68*, 441−451.

[13] M. J. Irwin, J. J. Vittal, R. J. Puddephatt, *Organometallics* **1997**, *16*, 3541−3547.

[14] M. Rosenblum, N. Brawn, J. Papenmeier, M. Applebaum, *J. Organomet. Chem.* **1966**, *6*, 173−180.

[15] C. Simionescu, T. Lixandru, I. Mazilu, L. Tataru, *J. Organomet. Chem.* **1976**, *113*, 23−28.

[16] [16a] A. D. Decke, *J. Chem. Phys.* **1993**, *98*, 5648−5652. [16b] B. Miehlich, A. Savin, H. Stoll, H. Preuss, *Chem. Phys. Lett.* **1989**, *157*, 200−206. [16c] C. Lee, W. Yang, G. Parr, *Phys. Rev. B* **1988**, *37*, 785−789.

[17] P. C. Hariharan, J. A. Pople, *Theor. Chim. Acta* **1973**, *28*, 213−222.

[18] P. J. Hay, W. R. Wadt, *J. Chem. Phys.* **1985**, *82*, 299−310.

[19] M. J. Frisch, G. W. Trucks, H. B. Schlegel, G. E. Scuseria, M. A. Robb, J. R. Cheeseman, V. G. Zakrzewski, J. A. Montgomery, Jr., R. E. Stratmann, J. C. Burant, S. Dapprich, J. M. Millam, A. D. Daniels, K. N. Kudin, M. C. Strain, O. Farkas, J. Tomasi, V. Barone, M. Cossi, R. Cammi, B. Mennucci, C. Pomelli, C. Adamo, S. Clifford, J. Ochterski, G. A. Petersson, P. Y. Ayala, Q. Cui, K. Morokuma, D. K. Malick, A. D. Rabuck, K. Raghavachari, J. B. Foresman, J. Cioslowski, J. V. Ortiz, B. B. Stefanov, G. Liu, A. Liashenko, P. Piskorz, I. Komaromi, R. Gomperts, R. L. Martin, D. J. Fox, T. Keith, M. A. Al-Laham, C. Y. Peng, A. Nanayakkara, C. Gonzalez, M. Challacombe, P. M. W. Gill, B. Johnson, W. Chen, M. W. Wong, J. L. Andres, C. Gonzalez, M. Head-Gordon, E. S. Replogle, J. A. Pople, *Gaussian 98* (Revision A. 5), Gaussian, Inc., Pittsburgh, PA **1968**.

[20] A. C. T. North, D. C. Phillips, F. S. Mathews, *Acta Crystallogr., Sect. A* **1968**, *24*, 351−359.

[21] G. M. Sheldrick, SADABS, Empirical Absorption Correction Program, University of Göttingen, Germany, **1997**.

[22] A. Altomare, M. C. Burla, M. Camalli, M. Cascarano, C. Giacovazzo, A. Guagliardi, G. Polidori, *J. Appl. Crystallogr.* **1994**, *27*, 435−436.

[23] G. M. Sheldrick, SHELXTL™, Reference manual, v5.1, Madison, WI, **1997**.

Received September 27, 2003
Early View Article
Published Online April 1, 2004

 © 2004 Wiley-VCH Verlag GmbH & Co. KGaA, Weinheim

Five- and Six-Coordinate Ruthenium(II) Complexes Containing the Bidentate Phosphane (−)-*N*,*N*-Bis(diphenylphosphanyl)-(*S*)-1-phenylethylamine [(*S*)-peap]: X-ray Crystal Structure of the First 16-Electron Ruthenium Complex Bearing a Four-Membered Ring $[RuCl\{\kappa^2\text{-}P,P\text{-}(S)\text{-peap}\}_2][SbF_6]\cdot C_2H_4Cl_2$

Josefina Díez,[a] M. Pilar Gamasa,*[a] José Gimeno,[a] Yolanda Rodríguez,[a] and Santiago García-Granda[b]

Dedicated to Professor José Vicente Soler on the occasion of his 60th birthday

Keywords: Ruthenium / (*S*)-peap ligand / Five-coordinate complexes / Octahedral complexes

The complex *trans*-$[RuCl_2\{\kappa^2\text{-}P,P\text{-}(S)\text{-peap}\}_2]$ (**1**) has been stereoselectively prepared by the treatment of a stoichiometric mixture of complex $[RuCl_2(DMSO)_4]$ (DMSO = dimethyl sulfoxide) and (*S*)-peap [(*S*)-peap = (–)-*N*,*N*-bis(diphenylphosphanyl)-(*S*)-1-phenylethylamine] in refluxing toluene. Irradiation of a dichloromethane solution of **1** with a UV lamp (400 W) at –15 °C affords the complex *cis*-$[RuCl_2\{\kappa^2\text{-}P,P\text{-}(S)\text{-peap}\}_2]$ (**2**). The thermodynamically stable *trans* isomer **1** has also been obtained by heating complex **2** in toluene. The reaction of **1** with $AgSbF_6$ in dichloromethane yields the complex $[RuCl\{\kappa^2\text{-}P,P\text{-}(S)\text{-peap}\}_2][SbF_6]$ (**3**), the first 16-electron cationic ruthenium complex bearing a four-membered chelate diphosphane ligand which has been fully characterized including its X-ray crystal structure. The reaction of unsaturated derivative **3** with CO gives the six-coordinate complex *cis*-$[RuCl(CO)\{\kappa^2\text{-}P,P\text{-}(S)\text{-peap}\}_2][SbF_6]$ (**4**) in a stereoselective manner, which slowly transforms into *trans*-$[RuCl(CO)\{\kappa^2\text{-}P,P\text{-}(S)\text{-peap}\}_2][SbF_6]$ (**5**) in a dichloromethane solution. The reaction of $[RuCl\{\kappa^2\text{-}P,P\text{-}(S)\text{-peap}\}_2][BF_4]$ with 1-phenyl-2-propyn-1-ol in 1,2-dichloroethane (60 °C) affords the allenylidene derivative *trans*-$[RuCl(=C=C=CHPh)\{\kappa^2\text{-}P,P\text{-}(S)\text{-peap}\}_2][BF_4]$ (**6**). The *cis*-$[Ru(acac)\{\kappa^2\text{-}P,P\text{-}(S)\text{-peap}\}_2][SbF_6]$ (**7**) is prepared by reaction of **3** and Na[acac].

(© Wiley-VCH Verlag GmbH & Co. KGaA, 69451 Weinheim, Germany, 2004)

Introduction

Six-coordinate ruthenium(II)diphosphane complexes $[RuX_2(P-P)_2]$ (X = halide), and especially the unsaturated five-coordinate derivatives $[RuX(P-P)_2]^+$, have attracted increasing attention in recent years, due in part to their potential interest involving homogeneous catalysis.[1] The 18-e six-coordinate diphosphane complexes, containing five- and six-membered chelate rings, can dissociate one of the halide ligands to give the unsaturated systems $[RuX(P-P)_2]^+$. Only a few of them have been characterized by X-ray crystallography i.e., $[RuCl(dppe)_2]^+$ [dppe = 1,2-bis(diphenylphosphanyl)ethane],[2] $[RuCl(dcpe)_2]^+$ [dcpe = 1,2-bis(dicyclohexylphosphanyl)ethane],[3] $[RuCl(bnpe)_2]^+$ [bnpe = 1,2-bis(1-naphthylphenylphosphanyl)ethane],[1e] $[RuX(dppp)_2]^+$ [dppp = 1,3-bis(diphenylphosphanyl)propane] (X = Cl,[4] F[5]). Apparently, the tendency to dissociate increases as the ring size of the chelate increases in the order six- > five- >> four-membered. So, diphosphane ligands, Ph_2PYPPh_2 [Y = CH_2, C=CH_2, CMe_2, N(R)], which form four-membered chelate rings, exclusively give six-coordinate *cis*- or *trans*-mononuclear complexes[6,7] and no examples of 16-electron five-coordinate cationic complexes have been reported to date.[8]

Continuing our interest in the chemistry of ruthenium complexes containing enantiopure bis(diphenylphosphanyl-)amine ligands,[9] we report in this paper the synthesis of the first 16-electron cationic ruthenium complex bearing a four-membered chelate diphosphane ligand namely $[RuCl\{\kappa^2\text{-}P,P\text{-}(S)\text{-peap}\}_2][SbF_6]$ (**3**), which has been fully characterized including its X-ray crystal structure. The precursor six-coordinate complex *trans*-$[RuCl_2\{\kappa^2\text{-}P,P\text{-}(S)\text{-peap}\}_2]$ (**1**), its *cis* isomer (**2**) and analogous cationic derivatives, *cis*-$[RuCl(CO)\{\kappa^2\text{-}P,P\text{-}(S)\text{-peap}\}_2][SbF_6]$ (**4**), *trans*-

[a] Instituto Universitario de Química Organometálica "Enrique Moles" (Unidad Asociada al CSIC), Departamento de Química Orgánica e Inorgánica, Facultad de Química, Universidad de Oviedo,
33071 Oviedo, Spain
Fax: (internat.) +34-985-103446
E-mail: pgb@sauron.quimica.uniovi.es
[b] Departamento de Química Física y Analítica, Facultad de Química, Universidad de Oviedo,
33071 Oviedo, Spain

[RuCl(CO){κ²-*P*,*P*-(*S*)-peap}₂][SbF₆] (**5**), *trans*-[RuCl(=C=C=CHPh){κ²-*P*,*P*-(*S*)-peap}₂][BF₄] (**6**) and [Ru(acac){κ²-*P*,*P*-(*S*)-peap}₂][SbF₆] (**7**) have also been prepared.

Results and Discussion

Synthesis of *trans*-[RuCl₂{κ²-*P*,*P*-(*S*)-peap}₂] (1) and *cis*-[RuCl₂{κ²-*P*,*P*-(*S*)-peap}₂] (2)

The complex *trans*-[RuCl₂{κ²-*P*,*P*-(*S*)-peap}₂] (**1**) is stereoselectively prepared by the treatment of a stoichiometric mixture of complex [RuCl₂(DMSO)₄] (DMSO = dimethyl sulfoxide) and (*S*)-peap [(−)-*N*,*N*-bis(diphenylphosphanyl)-(*S*)-1-phenylethylamine] in refluxing toluene. The complex **1** has been isolated as an air stable yellow solid (78%) (Scheme 1).

Irradiation with a UV lamp (400 W) of a dichloromethane solution of complex **1** at −15 °C for 1 h leads to an orange solution from which complex *cis*-[RuCl₂{k²-*P*,*P*-(*S*)-peap}₂] (**2**) can be isolated as an air stable orange solid (92%) (Scheme 1).

The complexes **1**−**2** are soluble in chlorinated solvents and insoluble in hexane and have been characterized by IR and NMR (^{1}H, ^{31}P{^{1}H} and ^{13}C{^{1}H}) spectroscopy (details are given in the Exp. Sect.). A sharp absorption band, assignable to the symmetrical vibration of the P-*N*−P group, is observed at ca. 850−870 cm^{-1} in the IR spectra.[10]

The ^{31}P{^{1}H} NMR spectrum of **1** shows a singlet signal at δ = 78.5, which is clearly downfield with respect to that of the free ligand (δ = 55.3 ppm, br), the deshielding ($\Delta\delta = \delta_{complex} - \delta_{ligand} = +23.2$) being intermediate to those found in the analogous *trans*-[RuCl₂{κ²-*P*,*P*−Ph₂PN(R)PPh₂}₂] [R = *i*Pr (Δδ = +27.1); H (Δδ = +18.0)].[7b] The ^{31}P{^{1}H} NMR spectrum of **2** shows two triplets (A_2X_2 spin system) at 72.57 and 87.73 ppm ($^2J_{P,P'}$ = 31.1 Hz) indicating that a single diastereoisomer, Δ(*S*,*S*) or Λ(*S*,*S*), is formed.[11] These signals can be assigned to the axial (P *trans* to P) and equatorial (P *trans* to Cl) phosphorus nuclei, respectively. Only one of the two diastereoisomers, Δ(*S*,*S*), is drawn in Scheme 1. Completion of the *trans*- to *cis*-isomerization is determined by the disappearance of the singlet resonance of complex **1** and the simultaneous appearance of two new signals assigned to complex **2**.

cis- to *trans*-Rearrangements

Complexes **1** and **2** undergo either *trans*/*cis* isomerization under thermal or photochemical conditions. The *cis* isomer **2** can be quantitatively converted into the thermodynamically stable *trans* isomer by heating in toluene (5 h) (Scheme 1).[12] The *cis*- to *trans*-isomerization does not take place at room temperature. It is interesting to note that the formation of the kinetically controlled *cis* isomer was not observed during the thermal synthesis of **1** starting from [RuCl₂(DMSO)₄] and (*S*)-peap. It can be suggested that if the *cis* isomer is actually formed in solution during the process, it immediately isomerizes to the thermodynamically more stable *trans* isomer **1**. On the other hand, the *trans*- to *cis*-rearrangement takes place by irradiation with a UV lamp as has been seen above. On the contrary, complexes [RuX₂{κ²-*P*,*P*−Ph₂PYPPh₂}₂] (X = halide; Y = CH₂,[13] C=CH₂ [14] or NH[8a]) undergo *trans*- to *cis*-isomerization by heating the *trans* isomers in refluxing chlorobenzene or 1,2-dichloroethane, and the reverse *cis*- to *trans* photochemical rearrangement has also been described for *cis*-[RuCl₂(dppm)₂].[13b] The factors responsible for determining the thermodynamically preferred forms of the *trans*/*cis* isomers are not entirely clear. Sullivan and Meyer argued, in the case of *cis*/*trans*-[RuCl₂(dppm)₂][13b] that the *cis* isomer is thermodynamically stable since it is stabilized by π-donation from the Cl atom through the Ru center to a *trans*-P atom, whereas this favorable interaction is not possible in the *trans* isomer. At present, we have no explanation

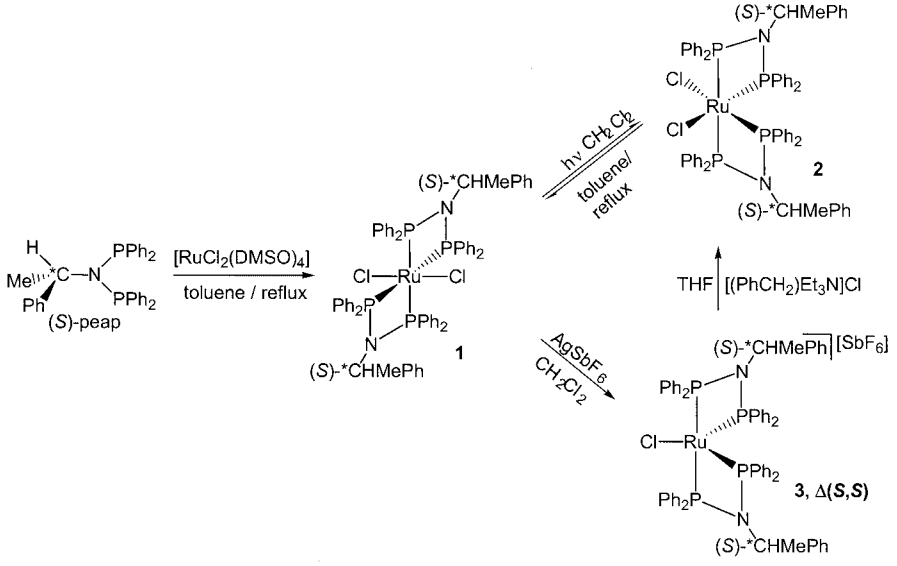

Scheme 1

 © 2004 Wiley-VCH Verlag GmbH & Co. KGaA, Weinheim

for the different results obtained in our case, with the auxiliary ligand (*S*)-peap.

Electrochemical Behavior of Complexes 1 and 2

In order to compare the electrochemical properties of *trans*/*cis* isomers with those of the $[RuX_2(P-P)_2]$ analogues, the electrochemical behavior of *trans*- and *cis*-$[RuCl_2\{\kappa^2$-*P*,*P*-(*S*)-peap$\}_2]$ complexes has been studied by cyclic voltammetry in CH_2Cl_2 solutions. All potentials are referenced to a silver-wire electrode. It was found that the *trans* isomer **1** undergoes one-electron oxidation [a chemically and electrochemically reversible process under the experimental conditions ($E_{1/2} = 1/2(E_p^{ox} + E_p^{red}) = 0.61$ V)], while the $E_{1/2}$ values for the analogous *trans* derivatives with dppm and $Ph_2N(R)PPh_2$ (R = H, Me) are 0.42 [13b] and 0.175−0.240 V,[7b] respectively. This means that the (*S*)-peap ligand is a much better stabilizing ligand for +2 oxidation state than dppm and the other bis(diphenylphosphanyl)amines. A second, chemically irreversible wave, corresponding to the Ru^{IV}/Ru^{III} couple, appears for all of the *trans*-ruthenium(III) complexes [for Ru^{III} complex containing the (*S*)-peap ligand at 1.25 V]. On the other hand, the *cis* isomer **2** only exhibits an irreversible anodic wave ($E_p^{ox} = 1.19$ V), while two waves are observed for *cis*-$[RuCl_2(dppm)_2]$ and *cis*-$[RuCl_2(\{\kappa^2$-*P*,*P*−$Ph_2N(Me)PPh_2)]$, the first one being chemically reversible, ($E_{1/2} = 0.79$ and 0.35 V, respectively) and the second one chemically irreversible.

The oxidation wave from the *cis* isomer **2** is at a higher potential than the corresponding *trans* isomer **1**. This increasing potential in going from the *trans* to the *cis* isomer is well established in ruthenium(II) chemistry.[7b,13b]

Synthesis of Five-Coordinate Complex $[RuCl\{k^2$-*P*,*P*-(*S*)-peap$\}_2][SbF_6]$ (3)

Complex **1** reacts with $AgSbF_6$ in dichloromethane at room temperature to give, after filtration of AgCl, the cationic complex $[RuCl\{\kappa^2$-*P*,*P*-(*S*)-peap$\}_2][SbF_6]$ (**3**) isolated as an air stable red solid (93%) (Scheme 1). Analogous tetrafluoroborate (BF_4) and triflate (OSO_2CF_3) salts can be obtained similarly. Conversely, Higgins has recently reported that the treatment of *trans*-$[RuCl_2\{\kappa^2$-*P*,*P*-$Ph_2PYPPh_2\}_2]$ (Y = C=CH_2, NH) in 1,2-dichloroethane at room temperature with $AgBF_4$ or $AgOSO_2CF_3$ gives the *trans*-$[RuCl\{\kappa^2$-*P*,*P*-$Ph_2PYPPh_2\}_2(\mu$-Cl)Ag]X (X = BF_4, OSO_2CF_3) and no AgCl precipitate is formed.[14b]

Complex **3** has been fully characterized by elemental analyses, IR and NMR (^1H, $^{31}P\{^1H\}$ and $^{13}C\{^1H\}$) spectroscopy (details are given in the Exp. Sect.) as well as an X-ray diffraction study (see below). All the data suggest the formation of only one diastereoisomer. In particular, the $^{31}P\{^1H\}$ NMR spectrum shows two pseudotriplets (A_2X_2 spin system) at $\delta = 69.63$ (P_{ax}) and 101.67 (P_{eq}) (t, $^2J_{P,P'} = 42.3$ Hz)[15] which are consistent with the formation of a sole diastereoisomer with a stereochemically rigid trigonal-bipyramidal structure (TBP). This pattern remains unchanged over a wide temperature range (193 to 353 K) in dichloromethane or 1,2-dichloroethane solution, indicating that a dynamic process involving an equilibrium between the two diastereoisomers $\Delta(S,S)$ and $\Lambda(S,S)$ is unlikely.

The five-coordinate species seems to remain unchanged in more concentrated solutions since no change in the chemical shifts is observed. Therefore, an equilibrium between the monomer and the chloride-bridged dimer, as observed for the complex $[RuCl(\kappa^2$-*P*,*N*−$Ph_2PCH_2CH_2$-2-py$)_2]^+$ can be discarded.[16] In addition, the solutions maintain the typical red colour due to pentacoordinate species.[17]

To the best of our knowledge, **3** is the first example of a five-coordinate ruthenium(II) complex with four-membered chelate ligands that could be isolated and characterized by an X-ray diffraction analysis. Several attempts to prepare analogous complexes having diphosphane ligands Ph_2YPPh_2 (Y = CH_2, C=CH_2; NH) have been reported in the literature, but they did not lead to pure products.[8a] Steric and electronic effects apparently cooperate in stabilizing the Lewis-acidic 16-electron complex **3** containing the bulkier phosphane (*S*)-peap.

Structure of Complex $[RuCl\{\kappa^2$-*P*,*P*-(*S*)-peap$\}_2]$-$[SbF_6]\cdot C_2H_4Cl_2$ (3)

The structure of the pentacoordinate complex $[RuCl\{\kappa^2$-*P*,*P*-(*S*)-peap$\}_2][SbF_6]$ has been determined by a single X-ray analysis. Suitable crystals have been obtained by slow diffusion of pentane into a solution of complex **3** in 1,2-dichloroethane. ORTEP type views of the cation of complex **3** are shown in Figure 1 and selected bond lengths and angles are collected in Table 1.

The five coordinate cation $[RuCl\{\kappa^2$-*P*,*P*-(*S*)-peap$\}_2]^+$ displays a distorted trigonal-bipyramidal structure (Y-shaped)[18] with the bidentate (*S*)-peap ligands spanning axial and equatorial positions and the chloride atom occupying the remaining equatorial position as expected for π-stabilized 16-electron complexes.[1e,11] The P(4)−Ru−P(2) [167.87(3)°], Cl−Ru−P(4) [95.65(3)°] and Cl−Ru−P(2) [96.39(3)°] angles are indicative of a distorted TBP geometry. The Y-equatorial plane is further distorted, with an angle P(3)−Ru−P(1) of 99.76(3)°, and two different P−Ru−Cl angles [P(1)−Ru−Cl [136.61(4)°] and P(3)−Ru−Cl [123.53(4)°], as already observed in pentacoordinate ruthenium systems with other diphosphanes.[1e,2,3] The angle between the planes defined by [P(1), P(3), Ru] and [Cl, P(1), P(3)] is 1.55(2)°, indicating that the ruthenium atom is slightly displaced towards P(2) from the equatorial plane. The bite angles P(1)−Ru−P(2) [69.32(3)°] and P(3)−Ru−P(4) [69.61(3)°] of the chelate (*S*)-peap ligands show values similar to those found in the complex $[RuH(\eta^5$-$C_9H_7)\{\kappa^2$-*P*,*P*-(*S*)-peap$\}]$ [70.44(12)°].[9]

The distance Ru−Cl [2.3722(9) Å] lies in the range found for analogous five coordinate diphosphane complexes, like $[RuCl(dppe)_2]^+$,[2] and $[RuCl(dcpe)_2]^+$,[3] and is ca. 0.05 Å shorter than those observed in *trans*-$[RuCl_2\{\kappa^2$-*P*,*P*−$Ph_2PN(R)PPh_2\}_2]$ (R = Me, *i*Pr),[7b] a feature that supports the chloride ligand-to-metal π-donation. Other typical features are the shorter Ru−P_{eq} distances, [Ru−P(1) 2.2425(8) and Ru−P(3) 2.2265(9) Å], compared with the

 © 2004 Wiley-VCH Verlag GmbH & Co. KGaA, Weinheim

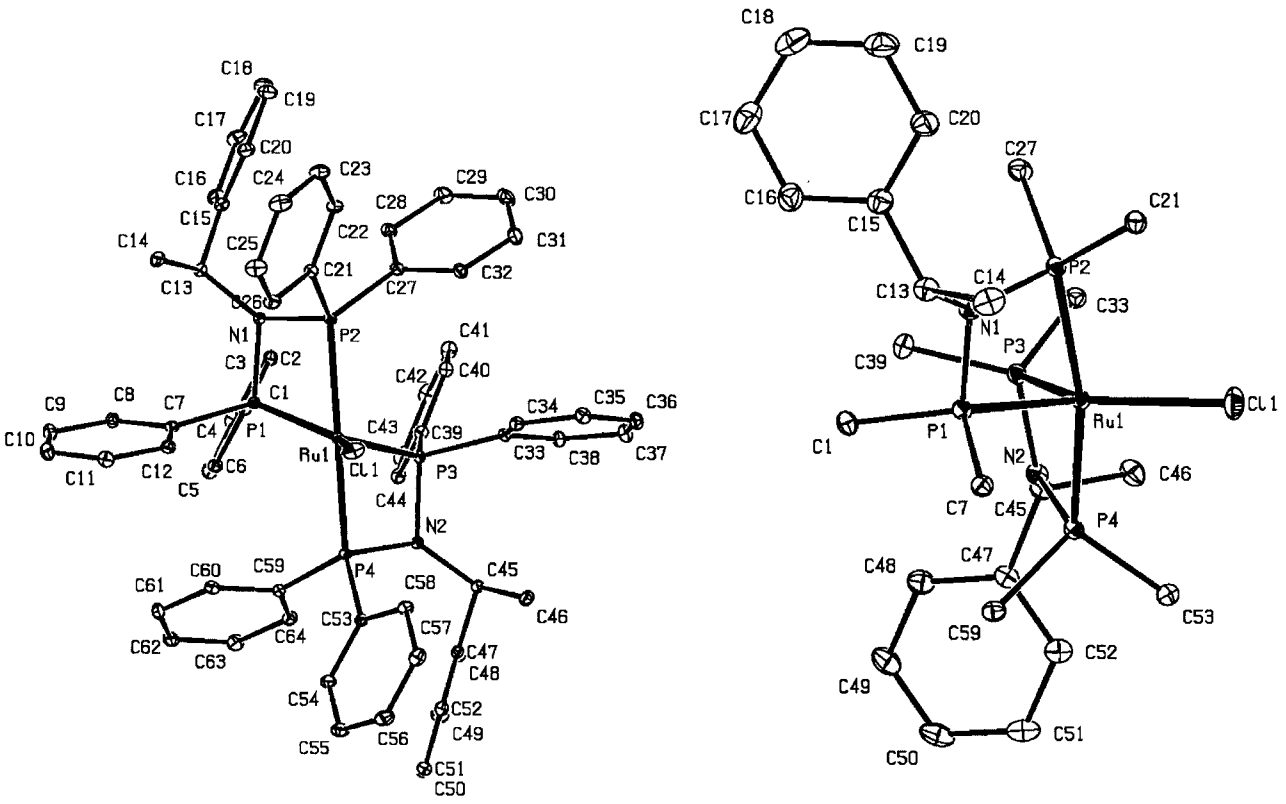

Figure 1. ORTEP type views of the molecular structure of the [RuCl{κ²-*P,P*-(*S*)-peap}₂][SbF_6]·$C_2H_4Cl_2$ (**3**); hexafluoroantimoniate anion and $C_2H_4Cl_2$ molecule have been omitted for clarity; (left) view of cation complex projected along the Ru−Cl vector, drawn at 10% probability level; (right) view of cation complex projected perpendicular to the Ru−Cl vector, drawn at 30% probability level; for clarity, only the C *ipso* of the aryl groups of PPh_2 are depicted

Ru−P_{ax} ones [Ru−P(2) 2.3768(8) and Ru−P(4) 2.3726(8) Å], thus suggesting that the former form strong phosphorous metal-dative bonds.[5,11] Usual Ru^{II}−P distances for phosphane ligands are in the range of 2.35−2.40 Å. Therefore it appears that these P_{eq} atoms as well as the chloride ligand make up for the electron deficiency of the ruthenium(II).

The configuration at the ruthenium atom is Δ [diastereoisomer Δ(*S,S*)]. Analogously, only one diastereoisomer, Λ(*S,S*), was found for complex [RuCl(bnpe)₂][PF_6] [bnpe = (*S,S*)-1,2-bis(1-naphthylphenylphosphanyl)ethane] whose structure was determined by an X-ray study.[1e] So, complex [RuCl{κ²-*P,P*-(*S*)-peap}₂][SbF_6] (**3**) is a five-coordinate system both, in the solid state and in solution (in ^{31}P NMR) and only one diastereoisomer has been found.

The catalytic activity of unsaturated complex **3** in the hydrogen transfer reaction of acetophenone has been investigated. The reaction has been performed in 2-propanol at 82 °C, in the presence of NaOH (acetophenone/cat/NaOH, 500:1:24) and monitored by gas chromatography. The ketone is rapidly reduced with 91% conversion in 1 h. Unfortunately, the enantioselective process fails because the (*S*)-peap ligand does not promote, in this case, any chiral induction. The remote location of the chiral centers from the reaction site might explain the lack of enantioselectivity.[19]

Synthesis of Cationic Complexes *cis*-[RuCl(CO){κ²-*P,P*-(*S*)-peap}₂][SbF_6] (4), *trans*-[RuCl(CO){κ²-*P,P*-(*S*)-peap}₂][SbF_6] (5), *trans*-[RuCl(=C=C=CHPh){κ²-*P,P*-(*S*)-peap}₂][BF_4] (6) and *cis*-[Ru(acac){κ²-*P,P*-(*S*)-peap}₂][SbF_6] (7)

As expected, the unsaturated complex **3** reacts with carbon monoxide at 1 atm to stereoselectively form the corresponding six-coordinate complex *cis*-[RuCl(CO){κ²-*P,P*-(*S*)-peap}₂][SbF_6] (**4**) (93%). Complex **4** slowly isomerizes in CH_2Cl_2 solution to give, quantitatively, the isomer *trans*-[RuCl(CO){κ²-*P,P*-(*S*)-peap}₂][SbF_6] (**5**) (Scheme 2).

These complexes are air stable pale yellow solids. Spectroscopic data (IR, ^1H, $^{31}P\{^1H\}$ and $^{13}C\{^1H\}$ NMR) support the proposed formulation. In particular, the IR spectra of complexes **4** and **5** show a strong ν(CO) absorption at 1997 and 1982 cm^{-1}, respectively. The $^{31}P\{^1H\}$ NMR spectra exhibit the expected pattern ABMX system for **4** (see Exp. Sect.) and a multiplet centered at δ = 72.83 ppm, typical of a closely spaced A_2B_2 system, occurs for **5**.

Similar *cis*- to *trans*-isomerization has been observed in analogous diphosphane complexes, i.e. [RuCl(CO)-(dcpe)₂]⁺,[20] and [RuCl(CO)(dppm)₂]⁺.[8a]

Complex [RuCl{κ²-*P,P*-(*S*)-peap}₂][BF_4] has also proven to be an excellent precursor for stabilized unsaturated car-

 © 2004 Wiley-VCH Verlag GmbH & Co. KGaA, Weinheim

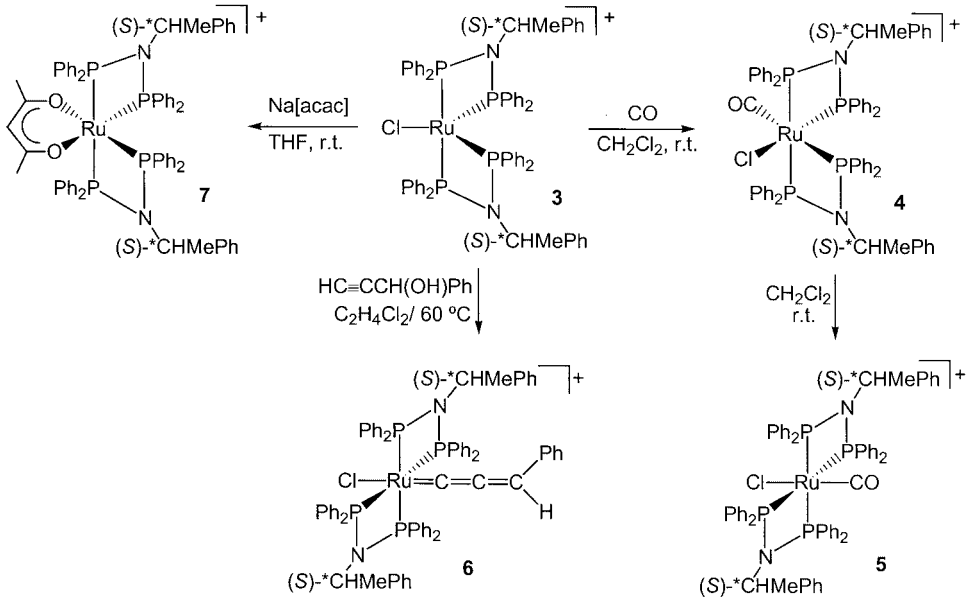

Scheme 2

bene complexes. Thus, the treatment of 1-phenyl-2-propyn-1-ol with [RuCl{κ²-*P*,*P*-(*S*)-peap}$_2$][BF_4] in 1,2-dichloroethane (60 °C) affords the allenylidene derivative *trans*-[RuCl(=C=C=CHPh){κ²-*P*,*P*-(*S*)-peap}$_2$][BF_4] (**6**) (76%) (Scheme 2). The formation of the allenylidene complex **6** requires heating the reaction at 60 °C for four hours in a minimum amount of solvent (around 0.5 mL for a 0.1 mmol scale) and an excess of alkynol (complex **3**/alkynol, 1:5). The synthesis of **6**, under more dilute conditions, does not go to completion but formation of decomposition products is observed. Probably, the higher steric requirement of the allenylidene fragment leads directly to the thermodynamically stable *trans* complex **6** and the *cis* isomer is not observed.

Analytical and spectroscopic data (IR, ^{1}H, ^{31}P{^{1}H} and ^{13}C{^{1}H} NMR) support the proposed formulation. Significantly, the ^{13}C{^{1}H} NMR spectrum of **6** is in agreement with the presence of the cumulene moiety, showing the expected resonances for C_α (δ = 322.32 ppm, pseudo triplet, $^2J_{C,P}$ = 14.8 Hz), C_β (δ = 218.14 ppm, s) and C_γ (δ = 150.11 ppm, s).[21] In addition the IR spectrum shows a strong absorption at 1939 cm^{-1} assigned to the ν(C=C=C) vibration.

The reaction of complex **3** with Na[acac] gives the complex [Ru(acac){κ²-*P*,*P*-(*S*)-peap}$_2$][SbF_6] (**7**) wherein the [acac]$^-$ acts as an anionic bidentate chelate ligand (see Scheme 2). Complex **7** is isolated as an air stable yellow solid in 81% yield. Spectroscopic data (IR, ^{1}H, ^{31}P{^{1}H} and ^{13}C{^{1}H} NMR) are in accordance with the proposed formulation. The ^{31}P{^{1}H} NMR spectrum of **7** shows two triplets (A_2X_2 spin system) at 68.50 and 83.11 ppm ($^2J_{P,P}$ = 34.9 Hz) and suggest the formation of the *cis* product. Complex **3** also reacts with an excess of [$(PhCH_2)Et_3N$]Cl to yield the 18-electron *cis* isomer **2**, the preparation of which has been described above (Scheme 1).

Experimental Section

General Conditions: The reactions were carried out under dry nitrogen using standard Schlenk techniques. Solvents were dried by standard methods and distilled under nitrogen before use. The complex [$RuCl_2(DMSO)_4$][22] and $(Ph_2P)_2N$[(*S*)-*CHMePh] [(*S*)-peap][23] were prepared by literature methods. Infrared spectra were recorded with a Perkin−Elmer FT-1720-Y spectrometer using KBr disks. The conductivities were measured at room temperature, in *ca* 5 × 10^{-4} mol·L^{-1} acetone solutions, with a Jenway PCM3 conductimeter. C, H and N analyses were carried out with a Perkin−Elmer 240-B microanalyzer (inconsistent analyses are found for complexes **2**, **4**−**6** due to incomplete combustion). Mass spectra (FAB) were recorded using a VG-Autospec spectrometer, operating in the positive mode; 3-nitrobenzyl alcohol (NBA) was used as the matrix. NMR spectra were recorded with a Bruker AC300 (DPX-300 or AV-300) instrument at 300 MHz (^{1}H), 121.5 MHz (^{31}P) or 75.4 MHz (^{13}C) or a Bruker AC200 instrument at 200 MHz (^{1}H), 81.01 MHz (^{31}P) or 50.32 MHz (^{13}C), using $SiMe_4$ or 85% H_3PO_4 as standards.

Synthesis

Synthesis of *trans*-[$RuCl_2${κ²-*P*,*P*-(*S*)-peap)}$_2$] (1): A mixture of [$RuCl_2(DMSO)_4$] (0.98 g, 2 mmol) and (*S*)-peap (1.958 g, 4 mmol) in 60 mL of toluene was heated under reflux for 3 h. The solvent was removed under reduced pressure and the yellow precipitate was washed with toluene and diethyl ether. The crude solid was recrystallized from dichloromethane/pentane, yielding 1.80 g of the solid **1** (78%). MS (FAB): *m*/*z* = 1150 [M$^+$ − 1], 1115 [M$^+$ − Cl − 1], 1079 [M$^+$ − 2 Cl − 1] (correct isotope patterns observed for each fragment). IR (KBr): $\tilde{\nu}$ = 853 cm^{-1} (s, PNP). ^{31}P{^{1}H} NMR

 © 2004 Wiley-VCH Verlag GmbH & Co. KGaA, Weinheim

(CD_2Cl_2): δ = 78.5 (s) ppm. ^1H NMR ($CDCl_3$): δ = 1.45 (d, $J_{H,H}$ = 7.1 Hz, 6 H, *CCH_3), 5.14 (m, 2 H, *CH), 6.72−7.76 (m, 50 H, PPh_2, *CPh) ppm. $^{13}C\{^1H\}$ NMR (CD_2Cl_2): δ = 23.44 (s, *C*CH_3), 62.45 (s, *C), 126.37−136.77 (PPh_2, *C*Ph*), 142.08 (s, *CC_{ipso}) ppm. $C_{64}H_{58}Cl_2N_2P_4Ru{\cdot}CH_2Cl_2$ (**1**·CH_2Cl_2) (1150.99·CH_2Cl_2): calcd. C 63.17, H 4.89, N 2.27; found C 63.76, H 4.88, N 2.05.

Synthesis of *cis*-[$RuCl_2${κ²-*P,P*-(*S*)-peap}$_2$] (2): A solution of complex **1** (0.345 g, 0.5 mmol) in 80 mL of dichloromethane was irradiated at −15 °C with a UV lamp (400 W) for 1 h. The solvent was removed to dryness and the product recrystallized from dichloromethane/diethyl ether yielding 0.317 g of **2** (92%). IR (KBr): $\tilde{\nu}$ = 849 cm^{-1} (s, PNP). $^{31}P\{^1H\}$ NMR (CD_2Cl_2): δ = 72.57 (t, $^2J_{P,P'}$ = 31.1 Hz, 2 P_{ax}), 87.73 (t, $^2J_{P,P'}$ = 31.1 Hz, 2 P_{eq}) ppm. ^1H NMR (CD_2Cl_2): δ = 1.33 (d, $J_{H,H}$ = 7.2 Hz, 6 H, *CCH_3), 4.75 (m, 2 H, *CH), 6.38−8.26 (m, 50 H, PPh_2, *CPh) ppm. $^{13}C\{^1H\}$ NMR (CD_2Cl_2): δ = 23.26 (s, *C*CH_3), 61.87 (s, *C), 125.15−139.07 (PPh_2, *C*Ph*), 140.69 (s, *CC_{ipso}) ppm.

Synthesis of [RuCl{κ²-*P,P*-(*S*)-peap}$_2$][SbF_6] (3): A mixture of complex **1** (1.15 g, 1 mmol) and $AgSbF_6$ (0.344 *g*, 1.1 mmol) was stirred at room temperature in 50 mL of dichloromethane for 1 h in the absence of light. The solution, whose color changed from yellow to red, was filtered through celite and the solvent removed to dryness. The oil obtained was recrystallized from diethyl ether to yield 1.26 g of complex **3** as a red solid (93%). The corresponding tetrafluoroborate (BF_4) or triflate (OSO_2CF_3) salts could be similarly prepared. MS (FAB): *m*/*z* = 1116 [M $^+$], 1080 [M^+ − Cl] (correct isotope patterns observed for each fragment). IR (KBr): $\tilde{\nu}$ = 849 (s, PNP), 658 cm^{-1} (s, SbF_6^-). Conductivity (acetone, 20 °C): 148 Ω^{-1} cm^2 mol^{-1}. $^{31}P\{^1H\}$ NMR (CD_2Cl_2): δ = 69.63 (t, $^2J_{P,P'}$ = 42.3 Hz, 2 P_{ax}), 101.67 (t, $^2J_{P,P'}$ = 42.3 Hz, 2 P_{eq}) ppm. ^1H NMR (CD_2Cl_2): δ = −0.06 ppm (d, $J_{H,H}$ = 7.2 Hz, 6 H, *CCH_3), 3.90 (m, 2 H, *CH), 6.49−7.70 (m, 50 H, PPh_2, *CPh) ppm. $^{13}C\{^1H\}$ NMR (CD_2Cl_2): δ = 21.25 (s, *C*CH_3), 64.42 (s, *C), 124.88−136.55 (PPh_2, *C*Ph*), 140.36 (s, *CC_{ipso}) ppm. $C_{64}H_{58}ClF_6N_2P_4RuSb{\cdot}0.5CH_2Cl_2$ (**3**·0.5CH_2Cl_2) (1351.27·0.5CH_2Cl_2): calcd. C 55.58, H 4.27, N 2.01; found C 55.52, H 4.68, N 1.73.

Synthesis of *cis*-[RuCl(CO){κ²-*P,P*-(*S*)-peap}$_2$][SbF_6] (4): Complex **3** (0.676 g, 0.5 mmol) was dissolved in 20 mL of dichloromethane, and CO gas was bubbled though the solution for 5 minutes. The solution immediately changed from red to colorless. The solvent was removed to dryness and the crude product recrystallized from dichloromethane/diethyl ether to yield 0.641 g of the pale yellow solid **4** (93%). IR (KBr): $\tilde{\nu}$ = 1997 (s, CO), 876 (m, PNP), 658 cm^{-1} (s, SbF_6^-). Conductivity (acetone, 20 °C): 126 $\Omega^{-1}{\cdot}cm^2{\cdot}mol^{-1}$. $^{31}P\{^1H\}$ NMR (CD_2Cl_2): ABMX system, δ = 55.79 [P_{eq} (P_M)], 63.63 [P_{ax} (P_A)], 68.26 [P_{ax} (P_B)], 76.79 [P_{eq} (P_X)] (J_{AB} = 270.2, J_{BM} = 54.4, J_{AX} = 51.3, J_{AM} = 28.0, J_{MX} = 21.7, J_{BX} = 18.6) ppm. ^1H NMR (CD_2Cl_2): δ = 0.73 (d, $J_{H,H}$ = 6.8 Hz, 3 H, *CCH_3), 0.83 (d, $J_{H,H}$ = 7.1 Hz, 3 H, *CCH_3), 4.44 (m, 2 H, *CH), 6.28−7.99 (m, 50 H, PPh_2, *CPh) ppm.

Synthesis of *trans*-[RuCl(CO){κ²-*P,P*-(*S*)-peap}$_2$][SbF_6] (5): Complex **4** (0.414 g, 0.3 mmol) was dissolved in 40 mL of dichloromethane and the solution was stirring at room temp. for 5 days until its complete conversion into the *trans* isomer. The solvent was removed to dryness and the crude product recrystallized from dichloromethane/diethyl ether yielding 0.393 g of **5** (95%). MS (FAB): *m*/*z* = 1144 [M $^+$], 1116 [M^+ − CO], 1080 [M^+ − CO − Cl] (correct isotope patterns observed for each fragment). IR (KBr): $\tilde{\nu}$ = 1982 (s, CO), 877 (m, PNP), 658 cm^{-1} (s, SbF_6^-). Conductivity (acetone, 20 °C): 126 $\Omega^{-1}{\cdot}cm^2{\cdot}mol^{-1}$. $^{31}P\{^1H\}$ NMR ($CDCl_3$): δ = 72.83 (m) ppm. ^1H NMR (CD_2Cl_2): δ = 1.18 (d, $J_{H,H}$ = 6.8 Hz, 6 H, *CCH_3), 4.84 (m, 2 H, *CH), 6.90−7.65 (m, 50 H, PPh_2, *CPh) ppm. $^{13}C\{^1H\}$ NMR (CD_2Cl_2): δ = 23.52 (s, *C*CH_3), 65.24 (s, *C), 128.19−135.52 (PPh_2, *C*Ph*), 140.03 (s, *CC_{ipso}), 198.09 (t, $^2J_{C,P}$ = 11.8 Hz, CO) ppm.

Synthesis of *trans*-[RuCl(=C=C=CHPh){κ²-*P,P*-(*S*)-peap}$_2$][BF_4] (6): To a mixture of complex [RuCl{κ²-*P,P*-(*S*)-peap}$_2$][BF_4] (0.120 g, 0.1 mmol) in 0.5 mL of 1,2-dichloroethane, the alkynol HC≡CCH(OH)Ph (0.66 g, 0.5 mmol) was added. The reaction mixture was heated at 60 °C for 4 h and the solution color changed from red to scarlet. The addition of 30 mL of diethyl ether lead to the precipitation of a scarlet solid which was washed with diethyl ether (3 × 10 mL) and vacuum-dried to yield 0.1 g of complex **6** (76%). IR (KBr): $\tilde{\nu}$ = 1939 (s, C=C=C), 1059 (br. s, BF_4^-), 864 cm^{-1} (m, PNP). Conductivity (acetone, 20 °C): 125 $\Omega^{-1}{\cdot}cm^2{\cdot}mol^{-1}$. $^{31}P\{^1H\}$ NMR (CD_2Cl_2): δ = 70.30 (m), 73.36 (m) ppm. ^1H NMR (CD_2Cl_2): δ = 1.36 (d, $J_{H,H}$ = 7.2 Hz, 6 H, *CCH_3), 5.10 (m, 2 H, *CH), 6.97−7.73 (m, 55 H, PPh_2, *CPh, C_γPh), 8.38 (s, 1 H, C_γH) ppm. $^{13}C\{^1H\}$ NMR (CD_2Cl_2): δ = 23.75 (s, *C*CH_3), 64.53 (s, *C), 127.88−135.80 (PPh_2, *C*Ph*, C_γ*Ph*), 140.54 (s, *CC_{ipso}), 142.49 (s, $C_\gamma C_{ipso}$), 150.11 (s, C_γ), 218.14 (s, C_β), 322.32 (t, $^2J_{C,P}$ = 14.8 Hz, Ru=C_α) ppm. $C_{73}H_{64}BClF_4N_2P_4Ru$ (1316.44): calcd. C 66.60, H 4.90, N 2.13; found C 65.85, H 4.83, N 1.63.

Synthesis of [Ru(acac){κ²-*P,P*-(*S*)-peap}$_2$][SbF_6] (7): A mixture of complex **3** (0.676 g, 0.5 mmol) and Na[acac] (0.122 g, 1 mmol) in 10 mL of tetrahydrofuran was stirred at room temp. for 1 h. The solution was then evaporated to dryness and the residue obtained was extracted with CH_2Cl_2 and filtered through celite. The concentration of the resulting solution to ca. 2 mL followed by the addition of 20 mL of hexane precipitated a pale yellow solid, which was washed with hexane (2 × 20 mL) and dried in vacuo, yielding 0.573 g of **7** (81%). MS (FAB): *m*/*z* = 1179 [M $^+$], 1080 [M^+ − acac] (correct isotope patterns observed for each fragment). IR (KBr): $\tilde{\nu}$ = 1580, 1518 (s, acac), 872 cm^{-1} (m, PNP), 658 (s, SbF_6^-). Conductivity (acetone, 20 °C): 117 $\Omega^{-1}{\cdot}cm^2{\cdot}mol^{-1}$. $^{31}P\{^1H\}$ NMR (CD_2Cl_2): δ = 68.50 (t, $^2J_{P,P'}$ = 34.9 Hz, 2 P_{ax}), 83.11 (t, $^2J_{P,P'}$ = 34.9 Hz, 2 P_{eq}) ppm. ^1H NMR (CD_2Cl_2): δ = 0.73 (d, $J_{H,H}$ = 6.7 Hz, 6 H, *CCH_3), 1.69 (s, 6 H, 2COCH_3), 4.32 (m, 2 H, *CH), 4.38 (s, 1 H, CH), 6.49−7.87 (m, 50 H, PPh_2, *CPh) ppm. $^{13}C\{^1H\}$ NMR (CD_2Cl_2): δ = 23.64 (s, *C*CH_3), 27.98 (s, 2CO*C*H_3), 63.00 (s, *C), 99.34 (s, CH), 127.55−137.06 (PPh_2, *C*Ph*), 140.12 (s, *CC_{ipso}), 186.61 (s, 2CO) ppm.

Electrochemical Measurements: The electrochemical experiments were performed with an EG&G PAR potentiostat/galvanostat model 273. Cyclic voltammetry measurements were carried out in a two-compartment three-electrode cell. The working electrode was a platinum disc electrode probed by a Luggin capillary connected to a silver-wire pseudo-reference electrode, a platinum auxiliary electrode was employed. Electrochemical solutions contained 0.1 M [NBu_4][PF_6] and 10^{-3} M complex in dichloromethane. Solutions were purged and maintained under nitrogen. The scan rate was 100 $mV{\cdot}s^{-1}$. All values are referenced to an internal $[Fe(\eta^5\text{-}C_5H_5)_2]^{+/0}$ couple ($E°$ = 0.59 V).

General Procedure for Hydrogen Transfer Reaction: Acetophenone (5 mmol) and complex **3** (0.01 mmol) were placed in a three-bottomed Schlenk flask under dry nitrogen and 2-propanol (50 mL) was added. The solution was heated at 82 °C and the corresponding amount of base from a 0.080 M solution in 2-propanol was added after 15 min. The reaction was monitored by gas chromatography. 1-phenylethanol, acetophenone and acetone were the only products detected.

 © 2004 Wiley-VCH Verlag GmbH & Co. KGaA, Weinheim

X-ray Structure Determination of 3·$C_2H_4Cl_2$: X-ray suitable single crystals were obtained by slow diffusion of pentane into a solution of complex **3** in 1,2-dichloroethane. Diffraction data were recorded with a Nonius Kappa CCD single-crystal diffractometer. The crystal distance was fixed at 29 mm, and 1100 frames were collected using the oscillation method, φ and ω−scans with 2° oscillation and 40 s exposure time per frame. Data collection strategy was calculated with the program Collect.[24] Data reduction and cell refinement were performed with the programs HKL Denzo and Scalepack.[25] Unit cell dimensions were determined from 11743 reflections. All data completeness was 99.4%. Data collection, crystal, and refinement parameters are collected in Table 1. The structure was solved by DIRDIF-96.[26] An empirical absorption correction was applied using XABS2.[27] Anisotropic least-squares refinement was carried out with SHELXL-97.[28] All non-hydrogen atoms, were anisotropically refined. H atoms were geometrically placed and their coordinates were refined riding on their parent atoms with isotropic displacement parameters set to 1.2 times the U_{eq} of the atoms to which they are attached (1.5 for methyl groups). The final cycle of full-matrix least-squares refinement based on 11860 reflections and 742 parameters converged to final values of R_1 [$F^2 > 2\sigma(F^2)$] = 0.0324. Atomic scattering factors were taken from International Tables for X-ray Crystallography.[29] The function minimized was $([\Sigma wF_o^2 - F_c^2)^2/\Sigma w(F_o^2)^2]^{1/2}$ where $w = 1/[\sigma^2(F_o^2) + (00498P)^2 + 2.3959P]$ where P = (Max. $(F_o^2 + 2F_c^2)/3$ with $\sigma^2(F_o^2)$ from counting statistics. Geometrical calculations were made with PARST.[30] The crystallographic plots were made with PLATON.[31] CCDC-216434 contains the supplementary crystallographic data for this paper. These data can be obtained free of charge at www.ccdc.cam.ac.uk/conts/retrieving.html [or from the Cambridge Crystallographic Data Center, 12 Union Road, Cambridge CB2 1EZ, UK; Fax: (internat.) +44−1223/336−033; E-mail: deposit@ccdc.cam.ac.uk].

Table 1. Crystal data and structure refinement for 3·$C_2H_4Cl_2$

Empirical formula	$C_{66}H_{62}Cl_3F_6N_2P_4RuSb$
Formula mass	1450.23
Temperature (K)	200(2)
Wavelength (Å)	1.54180
Crystal system	monoclinic
Space group	$P2_1$
a (Å)	11.8362(2)
b (Å)	17.8946(4)
c (Å)	15.1354(2)
α (deg)	90
β (deg)	94.697(1)
γ (deg)	90
V (Å^3)	3195.0(1)
Z	2
$D_{calcd.}$ (g cm^{-3})	1.507
Abs. coeff. (mm^{-1})	7.859
F(000)	1464
Crystal size (mm)	0.25 × 0.15 × 0.12
Radiation	Cu-K_α
Monochromator	graphite
θ range for data collecn (deg)	2.93 to 69.93
Index ranges	$-14 \le h \le 14$, $-20 \le k \le 21$, $-18 \le l \le 18$
Number of rflns. collected	131810
Number of independent rflns.	11860 [R(int) = 0.076]
Completeness to 2θ = 69.93 θ	99.4%
Refinement method	full-matrix least-squares on F^2
Number of data/restraints/params	11860/1/748
Goodness-of-fit on F^2	1.044
Final R indices [$I > 2\sigma(I)$]	R_1 = 0.0321, wR_2 = 0.0824
R Indices (all data)	R_1 = 0.0341, wR_2 = 0.0837
Absolute structure parameter	0.008(4)
Largest diff. peak and hole	0.949 and −0.973 e·Å^{-3}

Table 2. Selected bond lengths (Å) and angles (°) for complex 3·$C_2H_4Cl_2$

Distances	
Ru−Cl	2.3722(9)
Ru−P(1)	2.2425(8)
Ru−P(2)	2.3768(8)
Ru−P(3)	2.2265(9)
Ru−P(4)	2.3726(8)
Angles	
P(1)−Ru−Cl	136.61(4)
P(3)−Ru−Cl	123.53(4)
P(2)−Ru−Cl	96.39(3)
P(4)−Ru−Cl	95.65(3)
P(3)−Ru−P(1)	99.76(3)
P(4)−Ru−P(2)	167.87(3)
P(1)−Ru−P(2)	69.32(3)
P(3)−Ru−P(4)	69.61(3)
P(1)−Ru−P(4)	102.59(3)
P(3)−Ru−P(2)	102.19(3)

Acknowledgments

This work was supported by the Ministerio de Ciencia y Tecnología (MCT, Project BQU 2000−0227).

[1] Complexes [$RuCl_2(P-P)_2$] are active catalysts in: [1a] Hydrogenation of carbon dioxide: C.-C. Tai, J. Pitts, J. C. Linehan, A. D. Main, P. Munshi, P. G. Jessop, *Inorg. Chem.* **2002**, *41*, 1606−1614. [1b] Synthesis of *N*,*N*-dimethylformamide and methyl formate: O. Kröcher, R. A. Köppl, A. Baiker, *Chem. Commun.* **1997**, 453−454. [1c] Hydrogenation of olefins: T. Suárez, B. Fontal, D. García, *J. Mol. Catal.* **1986**, *34*, 163−171. Five-coordinate complexes are active catalysts in: [1d] $[RuCl(dppp)_2]^+$ [dppp = 1,3-bis(diphenylphosphanyl)propane], the epoxidation of olefins: F. Maran, A. Morvillo, N. D′Alessandro, M. Bressan, *Inorg. Chim. Acta* **1999**, *288*, 122−125 and references cited therein. [1e] $[RuCl(bnpe)_2]^+$ [bnpe = 1,2-bis(1-naphthylphenylphosphanyl)ethane], the epoxidation and cyclopropanation of olefins: R. M. Stoop, C. Bauer, P. Setz, M. Wörle, T. Y. H. Wong, A. Mezzetti, *Organometallics* **1999**, *18*, 5691−5700. [1f] $[RuCl(chiraphos)_2]^+$ [chiraphos = (*S*,*S*)-3,4-bis(diphenylphosphanyl)butane], the nucleophilic fluorination of activated alkyl halides in the presence of TlF as the fluoride source: P. Barthazy, A. Togni, A. Mezzetti, *Organometallics* **2001**, *20*, 3472−3477.

[2] B. Chin, A. J. Lough, R. H. Morris, C. T. Schweitzer, C. D'Agostino, *Inorg. Chem.* **1994**, *33*, 6278−6288.

[3] A. Mezzetti, A. Del Zotto, P. Rigo, N. B. Pahor, *J. Chem. Soc., Dalton Trans.* **1989**, 1045−1052.

[4] A. A. Batista, L. A. Centeno-Cordeiro, G. Oliva, *Inorg. Chim. Acta* **1993**, *203*, 185−191.

[5] P. Barthazy, R. M. Stoop, M. Wörle, A. Togni, A. Mezzetti, *Organometallics* **2000**, *19*, 2844−2852.

[6] The X-ray crystal structure of complexes *trans*-[$RuX_2(\kappa^2$-*P*,*P*-$Ph_2PYPPh_2)_2$] have been reported: [6a] Y = CH_2: A. R. Chakravarty, F. A. Cotton, W. Schwotzer, *Inorg. Chim. Acta* **1984**, *84*, 179−185. [6b] Y = CMe_2: J. V. Barkley, J. C. Grimshaw, S. J.

 © 2004 Wiley-VCH Verlag GmbH & Co. KGaA, Weinheim

Higgins, P. B. Hoare, M. K. McCart, A. K. Smith, *J. Chem. Soc., Dalton Trans.* **1995**, 2901−2908.

[7] The X-ray crystal structure of complexes *trans*-[$RuCl_2\{\kappa^2$-*P,P*-$Ph_2PN(R)PPh_2\}_2$] have been reported: [7a] R = *i*Bu, Y. Lu, Z. Zhang, W. Zhao, H. Wang, Y. Ma, *Chin. J. Struct. Chem. (Jiegou Huaxue)* **1993**, *12*, 129. [7b] R = Me, *i*Pr: M. S. Balakrishna, R. Panda, J. T. Mague, *Polyhedron* **2003**, *22*, 587−593. [7c] R = *o*-C_6H_4OMe: K. G. Gaw, M. B. Smith, A. M. Z. Slawin, *New. J. Chem.* **2000**, *24*, 429−435. To the best of our knowledge the synthesis of chiral derivatives has been not reported.

[8] [8a] The preparation of cationic complexes [$RuCl\{\kappa^2$-*P,P*-$Ph_2PYPh_2\}_2$]$^+$ (Y = CH_2, C=CH_2, NH) have been recently attempted, but they were isolated only as mixtures along with the corresponding *cis*-chloride six-coordinate complexes [$RuCl_2\{\kappa^2$-*P,P*−$R_2PYPR_2\}_2$]: S. J. Higgins, A. La Pensée, C. A. Stuart, J. M. Charnock, *J. Chem. Soc., Dalton Trans.* **2001**, 902−910. [8b] An $CDCl_3$ solution equilibrium between *trans*-[$RuCl_2$(2,2-dppp)$_2$] and [RuCl(2,2-dppp)$_2$]Cl (2,2-dppp = 2,2-bis(diphenylphosphanyl)propane) has been proposed by ^{31}P NMR spectroscopy: see ref.[6b]

[9] K. Bieger, J. Díez, M. P. Gamasa, J. Gimeno, M. Pavlišta, Y. Rodríguez-Álvarez, S. García-Granda, R. Santiago-García, *Eur. J. Inorg. Chem.* **2002**, 1647−1656.

[10] [10a] A. Badía, L. R. Falvello, R. Navarro, E. P. Urriolabeitia, *J. Organomet. Chem.* **1997**, *547*, 121−128. [10b] M. S. Balakrishna, V. Sreenivasa, S. S. Krishnamurthy, J. F. Nixon, J. C. T. R. Burckett St Laurent, *Coord. Chem. Rev.* **1994**, *129*, 1−90.

[11] P. Barthazy, M. Wörle, H. Rüegger, A. Mezzetti, *Inorg. Chem.* **2000**, *39*, 4903−4912.

[12] Two mechanism pathways accounting for the intramolecular rearrangements of metal chelate complexes can be considered: i) metal-ligand bond cleavage to give a five-coordinate species and, ii) a twisting mechanism that would result in rearrangement without cleavage of any metal-ligand bonds: E. L. Muetterties, *J. Am. Chem. Soc.* **1968**, *90*, 5097−5102.

[13] [13a] Y. Zhu, M. O. Wolf, G. P. A. Yap, *Inorg. Chem.* **1997**, *36*, 5483−5487. [13b] B. P. Sullivan, T. J. Meyer, *Inorg. Chem.* **1982**, *21*, 1037−1040.

[14] [14a] J. V. Barkley, S. J. Higgins, M. K. McCart, T. J. Pounds, *Inorg. Chem.* **1997**, *36*, 6188−6196. [14b] S. J. Higgins, C. A. Stuart, A. Mills, *Inorg. Chem. Commun.* **2000**, *3*, 208−210.

[15] The high-frequency signal is attributed to the equatorial P nucleus according with the assignments in other pentacoordinate complexes [$RuX(P-P)_2$]$^+$: J. C. Briggs, C. A. McAuliffe, G. Dyer, *J. Chem. Soc., Dalton Trans.* **1984**, 423−427. See also refs.[3,5]

[16] L. Costella, A. Del Zotto, A. Mezzetti, E. Zangrando, P. Rigo, *J. Chem. Soc., Dalton Trans.* **1993**, 3001−3008.

[17] B. N. Chaudret, D. J. Cole-Hamilton, R. S. Nohr, G. Wilkinson, *J. Chem. Soc., Dalton Trans.* **1977**, 1546−1557.

[18] J. F. Riehl, Y. Jean, O. Eisenstein, M. Pélissier, *Organometallics* **1992**, *11*, 729−737.

[19] Navarro and co-workers have also found no stereoselective induction in the stoichiometric reactions of complexes [Pt(acac)$\{\kappa^2$-P,*P*-(*S*)-peap)][ClO_4] and *cis*-[$PtCl_2\{\kappa^2$-P,*P*-(*S*)-peap$\}$] with amino acids (coordination reaction) or diazo derivatives (insertion reaction): A. Badía, R. Navarro, E. P. Urriolabeitia, *J. Organomet. Chem.* **1998**, *554*, 105−112.

[20] A. Mezzetti, A. Del Zotto, P. Rigo, *J. Chem. Soc., Dalton Trans.* **1990**, 2515−2520.

[21] V. Cadierno, M. P. Gamasa, J. Gimeno, *Eur. J. Inorg. Chem.* **2001**, 571−591.

[22] I. P. Evans, A. Spencer, G. W. Wilkinson, *J. Chem. Soc., Dalton Trans.* **1973**, 204−209.

[23] R. P. K. Babu, S. S. Krishnamurthy, M. Nethaji, *Tetrahedron: Asymmetry* **1995**, *6*, 427−438.

[24] Collected, Nonius BV, Delft, **1997−2000**.

[25] Z. Otwinowski, W. Minor, *Methods Enzymol.* **1997**, *276*, 307−326.

[26] P. T. Beurskens, G. Admiraal, G. Beurskens, W. P. Bosman, S. García-Granda, R. O. Gould, J. M. M. Smits, C. Smykalla, *The DIRDIF Program System; Technical Report; Crystallographic Laboratory*; University of Nijmegen: Nijmegen, The Netherlands, **1996**.

[27] XABS2: S. Parkin, B. Moezzi, H. Hope, *J. Appl. Crystallogr.* **1995**, *28*, 53−58.

[28] G. M. Sheldrick, *SHELXL-97, Program for the Refinement of Crystal Structures*, University of Göttingen, **1997**.

[29] *International Tables for X-ray Crystallography*, Kynoch Press: Birmingham, present distributor: Kluwer Academic Publishers, Dordrecht, U. K., **1974**, vol IV.

[30] M. Nardelli, *Comput. Chem.* **1983**, *7*, 95−98.

[31] A. L. Spek, *PLATON, a multipurpose crystallographic tool*, Utrecht University, Utrecht, The Netherlands, **2003**.

Received October 20, 2003
Early View Article
Published Online April 1, 2004

 © 2004 Wiley-VCH Verlag GmbH & Co. KGaA, Weinheim

3,11,19-Trithia[3.3.3]pyridinophane: Structural Diversity in Its Transition Metal Complexes

Muthalagu Vetrichelvan,[a] Yee-Hing Lai,*[a] and Kum Fun Mok[a]

Keywords: Coordination polymers / Macrocycles / Structural diversity / Transition metals / Zwitterions

The pyridine-containing aza-thia macrocycle 3,11,19-trithia-[3.3.3]pyridinophane (**10**) and its complexes with Ni^{II}, Pd^{II}, Cu^{I}, Ag^{I} and Hg^{II} were synthesised and their crystal structures were determined. The Ni^{II} and Hg^{II} complexes (**11**, **12**) are mononuclear with **10** serving as an unusual quinquedentate ligand. The Cu^{I} complex **13** is also mononuclear with **10** being tetra-coordinated to a tetrahedral Cu^{I}. Palladium(II) forms a binuclear complex **14** which exists as an inorganic zwitterion and both Pd^{II} metal ions adopt the expected square-planar geometry with facial coordination. Silver(I) forms one-dimensional coordination polymers (**15** and **16**) with **10** and these exhibit two different coordination modes, namely tetrahedral and trigonal planar. It was found that the macrocycle **10** did not show any selectivity among a series of metal ions. The electronic and redox properties of several complexes were studied.
(© Wiley-VCH Verlag GmbH & Co. KGaA, 69451 Weinheim, Germany, 2004)

Introduction

Crystal engineering remains one of the most fascinating areas of research in modern inorganic chemistry. It has given rise to many remarkable structures by using transition metals through the development of coordination polymers, the construction of molecular architectures and the self-assembly of complex molecular structures.[1−12] The coordination chemistry of pyridine-containing macrocycles is of particular interest due to the effective coordination ability of pyridine.[13] Parallel to this, binuclear macrocyclic complexes have also attracted much attention as catalysts and models for certain metalloenzymes.[14,15] There is also a need to understand the nature and extent of metal-metal interactions. Schröder et al.[16−18] and others[19−22] have reported a series of coordination polymers derived from Ag^{I} and thioether macrocycles **1**−**5** as well as other functionalised thioether macrocycles.[23,24] The search for appropriate organic building blocks for the construction of coordination polymers and the study of binuclear complexes led us to investigate the ligand **10**. The intramolecular layout of the three pyridine rings in **10** means that it is able to form a cone-like conformation similar to that of calixarenes and thus **10** was expected to exhibit interesting complexation properties.

We report herein a new synthetic route to the macrocycle **10** and the preparation of a series of its transition metal complexes **11**−**16**. The solid-state structures of the metal complexes, their electronic and redox properties and an extraction study of the macrocycle are discussed. To the best of our knowledge, complexes **15** and **16** are the first examples of one-dimensional Ag^{I} coordination polymers exhibiting two different coordination geometries with the same macrocyclic ligand. The palladium complex **14** is dinuclear and exists as an inorganic zwitterion while Cu^{I}, Ni^{II} and Hg^{II} form mononuclear complexes **11**−**13** having different degrees of coordination.

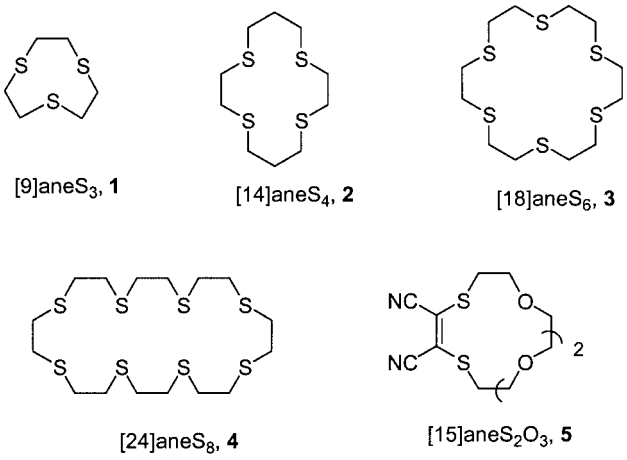

Results and Discussion

Syntheses

The macrocycle **10** was previously isolated as a side-product in a reaction between bis(bromomethyl)pyridine and

[a] Department of Chemistry, National University of Singapore, 3 Science Drive 3, Singapore 117543
Fax: (internat.) + 65-6779-1691
E-mail: chmlaiyh@nus.edu.sg
Supporting information for this article is available on the WWW under http://www.eurjic.org or from the author.

 © 2004 Wiley-VCH Verlag GmbH & Co. KGaA, Weinheim DOI: 10.1002/ejic.200300835

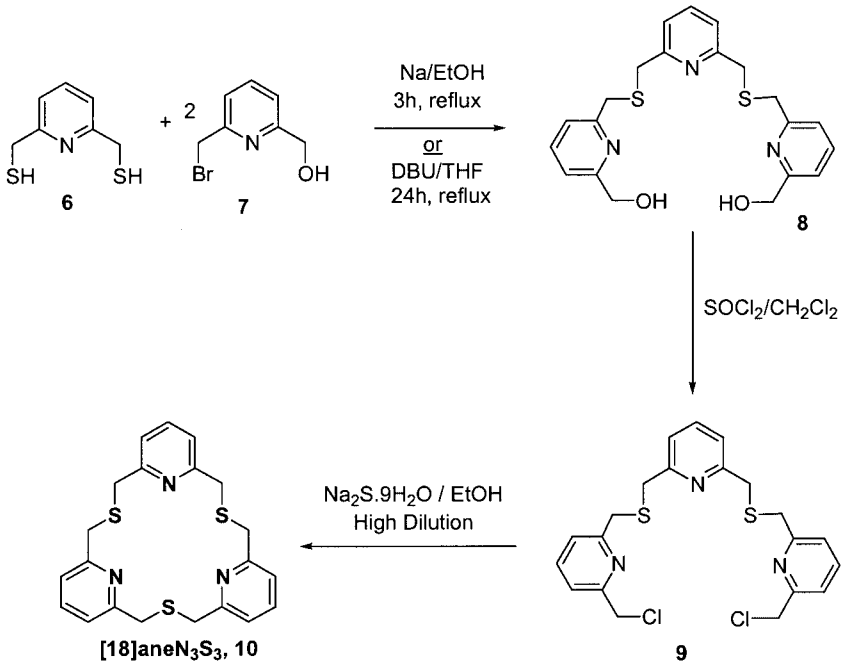

Scheme 1. Synthetic scheme for the preparation of the macrocycle **10**

thioacetamide.[25] An improved synthetic route to **10** was employed in this work starting from known precursors[26] **6** and **7** (Scheme 1) giving a 50% overall yield of **10**. The reaction between **6** and **7** to afford the diol **8** could be achieved in two ways: in the presence of DBU/THF or with Na/ethanol. The latter was found to need a shorter reaction time and gave a higher yield of **8**. Treatment of the diol **8** with thionyl chloride gave the dichloride **9** in a 90% yield. The macrocycle [18]aneN$_3$S$_3$ **10** was isolated in a 70% yield via an intramolecular coupling reaction of **9** with sodium sulfide under high-dilution conditions.[27,28]

The metal complexes **11**−**16** (Figure 1) of the macrocycle **10** were prepared by reactions of the ligand with the appropriate metal salts, respectively; details are given in the Exp. Sect.

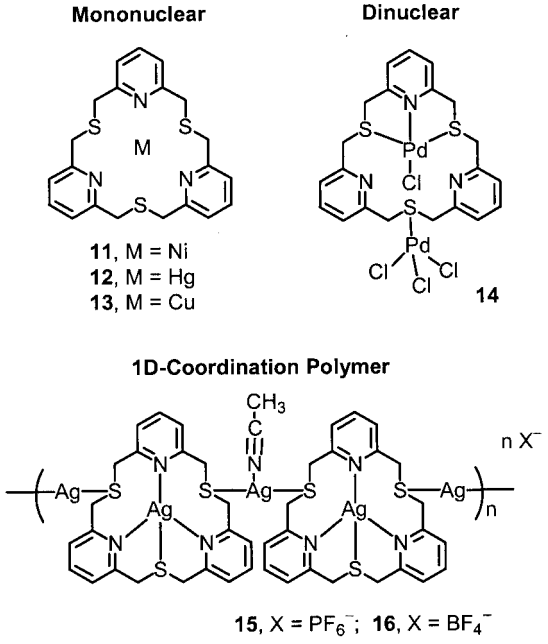

Figure 1. Structural diversity of complexes **11**−**16**

Structure Description of [Ni(10)(ClO$_4$)$_2$] (11)

In the crystal structure of the nickel complex **11** (Figure 2), the nickel centre is five-coordinate. Although the macrocycle **10** has six donor atoms, a rare pentacoordinate nickel is observed in this case, which is probably due to a relatively large macrocyclic cavity. The asymmetric unit contains two independent halves of the molecule. The ORTEP diagram of the complex is shown in Figure 2 (left) and selected bond lengths and bond angles are given in Table 1 and Table 2, respectively.

The geometric parameter τ, which is equal to zero for a perfect square pyramid and becomes unity for a perfect trigonal bipyramid,[29] was calculated to be about 0.65, thus indicating that the nickel in complex **11** adopts a distorted trigonal bipyramidal geometry. Three pyridine nitrogens form a trigonal plane and two of the benzylic sulfur atoms occupy the axial positions of the trigonal bipyramids. Pentacoordination is relatively rare for Ni^{II}, which more often forms either high-spin octahedral or low-spin square-planar complexes.[30] In addition, Ni^{II} complexes with pentadentate ligands are often hexacoordinate due to bonding

 © 2004 Wiley-VCH Verlag GmbH & Co. KGaA, Weinheim

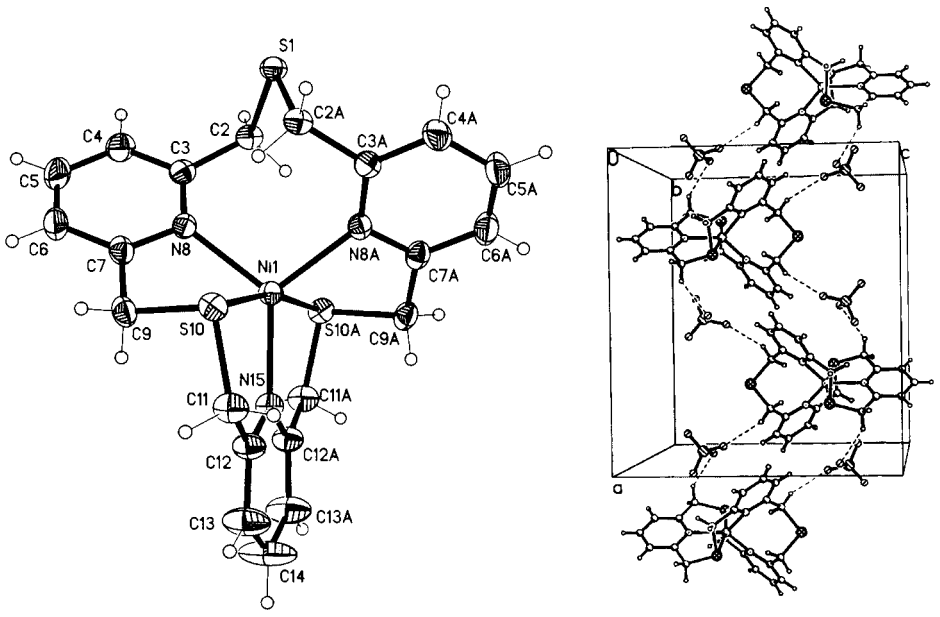

Figure 2. (left) ORTEP drawing of the Ni^{II} complex **11**; (right) packing diagram of complex **11** along the *b*-axis

to a solvent molecule or an anion.[31] A ligand with a 15- or 16-membered ring offers an ideal cavity for a six-coordinate nickel ion. The 18-membered ring in **10** is supposedly sufficiently large for this purpose. In the novel Ni^{II} complex **11**, a pentacoordinate nickel is unusually entrapped by a hexadentate macrocycle. This may be due to unfavourable steric interactions or geometrical strain developed in the ligand if all six donor groups in **11** are bonded to the Ni^{II} ion in an octahedral arrangement.[32] In addition hydrogen bonding may play a role in stabilizing the helical structure of the complex in the crystal packing [Figure 2 (right)] thus discouraging the utilisation of the sixth coordination position of the metal centre. This, we believe, is an unusual type of geometry rarely reported in the literature.

The Ni−N and Ni−S bond lengths in **11** are similar to those reported in the literature.[33] The Ni−N bond lengths are typical of high-spin Ni^{II} complexes with nitrogen donor atoms.[30] The perchlorate anions have the expected tetrahedral geometry although the variation in bond lengths and angles and the large thermal parameters suggest that some degree of disorder is present.

The packing diagram of **11** in the solid state along the *b*-axis is shown in Figure 2 (right). The adjacent molecules are linked through weak intermolecular hydrogen bonding of the type Cl−O···H−C via the benzylic C−H of the pyridine units and the oxygen atom of the perchlorate anions. The adjacent molecules are in an antiparallel array and thereby the overall crystal packing appears as a helix involving two types of hydrogen bonding, with typical bond lengths[34−36] of 2.500Å and 2.473 Å, respectively. Such hydrogen bonding has been found to be important in influencing the nature of the molecular packing in solid-state structures.[37] There is, however, no interaction between two adjacent helices in the crystal packing of **11**.

Structure Description of [Hg(10)(ClO_4)$_2$] (12)

A mononuclear mercury(II) complex of formula Hg(10)(ClO_4)$_2$ is formed when either a 1:2 or a 1:1 ratio of macrocycle **10** and metal salt were used. The X-ray structure of the complex shows that the mercury is coordinated to three pyridine nitrogens and two thioether sulfurs of the macrocycle. The geometric parameter τ for the mercury complex is 0.48, which indicates a distorted square-pyramidal geometry. The ORTEP diagram of the complex is shown in Figure 3 and Table 1 and 2 list the bond lengths and bond angles around the metal ion. One of the thioether sulfurs is not coordinated and it is in an exodentate position even after complexation. Three pyridine nitrogens form a perfect trigonal plane and two of the thioether sulfurs occupy approximately axial positions. The bond angles are very distorted due to two additional interactions of the metal ion with oxygens of the two perchlorate anions. The O···Hg distances are about 3.283 and 3.198 Å, which are too long to be considered as bonding interactions.[38] Due to these weak Hg···O interactions, the mercury ion is pseudo-seven coordinate. The N_{py}−Hg distances in the macrocycle are somewhat shorter than reported earlier.[39]

Similar to the nickel analogue, the mercury complex has four five-membered rings and one nine-membered ring which may explain the difference in bond angles and bond lengths. In the solid state, there are some weak interactions between mercury and oxygen atoms of the perchlorate anions. In addition to that, hydrogen bonding of the type -C···H-, with a bond length of 2.483 Å, is also present between the benzylic hydrogen and the oxygen of the perchlorate anions. Due to these interactions, a chain-like structure is formed.

 © 2004 Wiley-VCH Verlag GmbH & Co. KGaA, Weinheim

Table 1. Selected bond lengths (Å) with e.s.d.'s in parentheses for complexes **11**−**16**

Complex **11**			
Ni(1)−N(8)	2.088(3)	Ni(1)−N(8A)	2.088(3)
Ni(1)−N(15)	2.130(5)	Ni(1)−S(10)	2.385(1)
Ni(1)−S(10A)	2.385(1)	Ni(2)−N(23)	2.077(3)
Ni(2)−N(23A)	2.077(3)	Ni(2)−N(30)	2.119(5)
Ni(2)−S(25)	2.379(1)	Ni(2)−S(25A)	2.379(1)
Complex **12**			
Hg(1)−N(9)	2.332(4)	Hg(1)−N(18)	2.363(4)
Hg(1)−N(27)	2.401(4)	Hg(1)−S(20)	2.553(2)
Hg(1)−S(2)	2.577(1)		
Complex **13**			
Cu(1)−N(18)	2.002(4)	Cu(1)−N(9)	2.112(4)
Cu(1)−N(27)	2.132(4)	Cu(1)−S(2)	2.315(2)
Cu(2)−N(48)	2.001(4)	Cu(2)−N(57)	2.112(5)
Cu(2)−N(39)	2.135(5)	Cu(2)−S(32)	2.311(1)
Complex **14**			
Pd(1)−Cl(2)	2.297(2)	Pd(1)−Cl(3)	2.305(2)
Pd(1)−S(2)	2.305(1)	Pd(1)−Cl(1)	2.316(2)
Pd(2)−N(18)	1.988(3)	Pd(2)−S(11)	2.240(1)
Pd(2)−S(20)	2.275(2)	Pd(2)−Cl(4)	2.292(1)
Complex **15**			
Ag(1)−N(27)	2.213(3)	Ag(1)−N(9)	2.398(3)
Ag(1)−N(18)	2.436(4)	Ag(1)−S(11)	2.532(1)
Ag(2)−N(30)	2.245(5)	Ag(2)−S(2)A	2.517(2)
Ag(2)−S(20)	2.545(1)		
Complex **16**			
Ag(1)−N(1)	2.211(4)	Ag(1)−N(2)	2.350(4)
Ag(1)−N(3)	2.383(4)	Ag(1)−S(3)	2.541(1)
Ag(2)−N(1S)	2.286(6)	Ag(2)−S(2)	2.486(1)
Ag(2)−S(1A)	2.551(1)		

Table 2. Selected bond angles (°) with e.s.d.'s in parentheses for complexes **11**−**16**

Complex **11**			
N(8)−Ni(1)−N(8A)	105.72(3)	N(8A)−Ni(1)−N(15)	127.14(9)
N(8)−Ni(1)−N(15)	127.14(9)	N(8A)−Ni(1)−S(10A)	80.24(1)
N(8)−Ni(1)−S(10A)	108.73(10)	N(15)−Ni(1)−S(10A)	82.79(3)
N(8A)−Ni(1)−S(10)	108.73(10)	N(8)−Ni(1)−S(10)	80.24(1)
N(15)−Ni(1)−S(10)	82.79(3)	S(10A)−Ni(1)−S(10)	165.57(6)
N(23)−Ni(2)−N(23B)	106.73(19)	N(23)−Ni(2)−N(30)	126.64(9)
N(23B)−Ni(2)−N(30)	126.64(9)	N(23)−Ni(2)−S(25B)	107.27(9)
N(23B)−Ni(2)−S(25B)	81.25(9)	N(30)−Ni(2)−S(25B)	83.03(3)
N(23)−Ni(2)−S(25)	81.25(9)	N(23B)−Ni(2)−S(25)	107.27(9)
N(30)−Ni(2)−S(25)	81.03(3)	S(25B)−Ni(2)−S(25)	166.06(6)
Complex **12**			
N(9)−Hg(1)−N(18)	110.38(1)	N(9)−Hg(1)−N(27)	125.87(1)
N(18)−Hg(1)−N(27)	123.73(1)	N(9)−Hg(1)−S(20)	120.91(1)
N(18)−Hg(1)−S(20)	74.72(1)	N(27)−Hg(1)−S(20)	77.83(1)
N(9)−Hg(1)−S(2)	74.43(1)	N(18)−Hg(1)−S(2)	121.4(1)
N(27)−Hg(1)−S(2)	76.71(1)	S(20)−Hg(1)−S(2)	154.51(5)
Complex **13**			
N(18)−Cu(1)−N(9)	119.87(2)	N(18)−Cu(1)−N(27)	120.81(2)
N(9)−Cu(1)−N(27)	100.48(2)	N(18)−Cu(1)−S(2)	133.52(1)
N(9)−Cu(1)−S(2)	87.09(1)	N(27)−Cu(1)−S(2)	85.64(1)
N(48)−Cu(2)−N(57)	120.84(2)	N(48)−Cu(2)−N(39)	119.95(2)
N(57)−Cu(2)−N(39)	97.45(2)	N(48)−Cu(2)−S(32)	135.70(2)
N(57)−Cu(2)−S(32)	85.37(2)	N(39)−Cu(2)−S(32)	87.00(2)
Complex **14**			
Cl(2)−Pd(1)−Cl(3)	179.69(5)	Cl(2)−Pd(1)−S(2)	94.14(4)
Cl(3)−Pd(1)−S(2)	86.08(4)	Cl(2)−Pd(1)−Cl(1)	89.94(5)
Cl(3)−Pd(1)−Cl(1)	89.83(5)	S(2)−Pd(1)−Cl(1)	175.09(4)
N(18)−Pd(2)−S(11)	87.58(10)	N(18)−Pd(2)−S(20)	86.49(10)
S(11)−Pd(2)−S(20)	168.39(5)	S(20)−Pd(2)−Cl(4)	95.94(6)
Complex **15**			
N(27)−Ag(1)−N(9)	117.68(1)	N(27)−Ag(1)−N(18)	117.86(1)
N(9)−Ag(1)−N(18)	104.77(1)	N(27)−Ag(1)−S(11)	149.58(8)
N(9)−Ag(1)−S(11)	78.65(9)	N(18)−Ag(1)−S(11)	78.02(9)
N(30)−Ag(2)−S(2)A	119.0(2)	N(30)−Ag(2)−S(20)	111.6(2)
S(2)A−Ag(2)−S(20)	129.08(3)		
Complex **16**			
N(1)−Ag(1)−N(2)	119.27(2)	N(1)−Ag(1)−N(3)	118.32(1)
N(2)−Ag(1)−N(3)	102.02(1)	N(1)−Ag(1)−S(3)	148.30(1)
N(2)−Ag(1)−S(3)	79.08(1)	N(3)−Ag(1)−S(3)	78.16(1)
N(3)−Ag(1)−S(3)	78.16(1)	N(1S)−Ag(2)−S(2)	124.93(2)
N(1S)−Ag(2)−S(1A)	99.50(2)	S(2)−Ag(2)−S(1A)	135.11(4)

Close inspection of the complex crystal structure along the *c*-axis shows that there are six complex cations and six perchlorate anions packed alternately, resulting in a six-membered cyclic ring. The structure forms a hexagonal-shaped space, which may be useful for specific guests.

Structure Description of [Cu(10)(PF_6)] (13)

Similar to the nickel complex, the copper complex **13** also has two independent formula units present in one asymmetric unit. The basic molecular geometries are essentially identical, although some insignificant differences in bond lengths and bond angles are observed. The ORTEP diagram of the complex is shown in Figure 4 (left) and Table 1 and 2 provides selected bond lengths and bond angles.

Two exodentate sulfurs are not coordinated to the copper(I) and all attempts to form a coordination polymer containing other metal ions as a bridge between the molecules by using these non-coordinated sulfurs failed. The molecule itself looks like a model of a person, with two exodentate sulfurs as two folded arms, one pyridine as its head and another two pyridines as two legs, as can be easily visualized from the space-filling diagram in Figure 4 (right).

The Cu^I ion is encapsulated by the ligand **10** bonding directly to three pyridine nitrogens (N9, N18 and N27 in Cu1 and N39, N48 and N57 in Cu2) and one thioether sulfur (S2 in Cu1 and S32 in Cu2). The remaining two sulfurs are not coordinated to the copper metal and are found at an average non-bonding distance of 4.0 Å. The Cu^I ion

 © 2004 Wiley-VCH Verlag GmbH & Co. KGaA, Weinheim

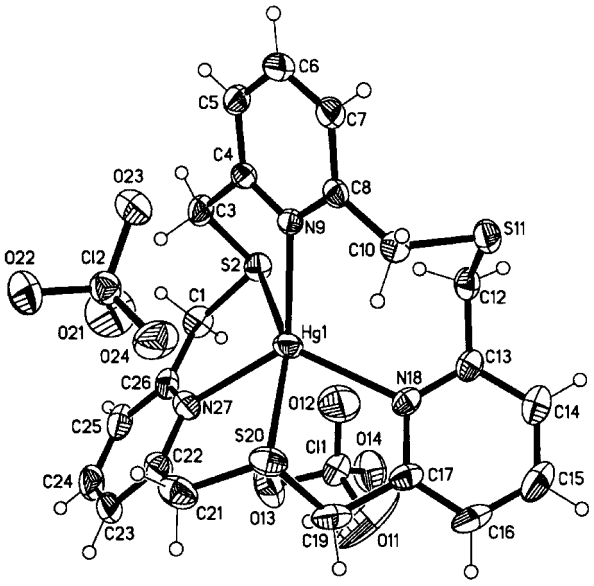

Figure 3. ORTEP drawing of the mercury complex **12**

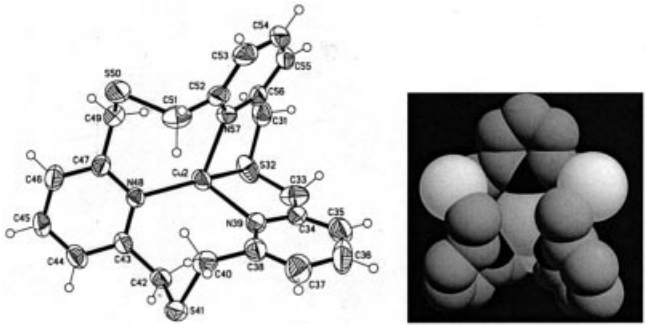

Figure 4. (left) ORTEP drawing of the copper(I) complex **13**; (right) space-filling model of **13** (hydrogen atoms omitted for clarity)

is in a tetrahedral environment with N−Cu−N angles ranging from 119.87(2) to 120.81(2)° for the eight-membered rings and S−Cu−N angles ranging from 85.64(1) to 87.09(1)° for the five-membered rings. The Cu−N and Cu−S distances are in the expected range.[40−43] In the solid-state, the molecules are not discrete but form a network structure through some hydrogen bonding and weak interactions.

Structure Description of [10(PdCl)($PdCl_3$)] (14)

The X-ray structure of the complex confirms the binuclear complex of formula [(**10**(PdCl)($PdCl_3$)]. Figure 5 shows an ORTEP diagram of the complex and Table 1 lists selected bond lengths for the metal coordination environment. The two palladium centres are not encapsulated by the ligand but are in a facial coordination. This may be because the cavity of the macrocycle is too small to accommodate two palladium metal ions or to avoid the steric interaction between the metal ions.

Each macrocyclic ligand coordinates to two palladium ions and the structure comprises two different distorted square-planar geometries. In Site A, Pd(1) is coordinated to only one sulfur [Pd−S(2) 2.306 Å] and three chlorine anions (Pd−Cl 2.297, 2.305 and 2.316 Å) and in Site B the metal ion is coordinated to one pyridine nitrogen (Pd−N 1.988 Å), two of the three sulfurs (Pd−S 2.240, 2.275 Å) and one chloride anion (Pd−Cl 2.291 Å). Thus the macrocycle acts simultaneously as a tridentate (NS_2) and a monodentate (S) ligand. The remaining two pyridine nitrogens are not coordinated to the palladium metal and are oriented away from it, with non-bonding distances of Pd(2)−N(27) 3.635 Å and Pd(2)−N(9) 3.752 Å. The Pd−N, Pd−S and Pd−Cl distances are within the expected range.[44,45]

The distance between palladium and the non-bonded nitrogens [N(9) and N(27)] is sufficiently large to permit the atoms to be non-interacting, but the nature of the macrocyclic ligand defines a limit for the furthest distance of the non-bonded nitrogens. A value of about 3.6 Å is intermediate between the normal distances for an inner-sphere or coordinated ligand (ca. 2.0 Å) and an outer-sphere or non-coordinated ligand (ca. 4.0 Å). This type of environment may cause unusual and interesting effects in the solution studies.[46] Pd(1) deviates from the mean square plane (S2, Cl1, Cl2, Cl3) by about 0.024 Å, and Pd(2) deviates by about 0.049 Å. It is of interest to note the differences in the Pd−Cl distances found for both coordination sites. Interestingly, the charges of the two palladium centres [Pd(1) and Pd(2)] in each neutral molecule are −1 and +1, respectively, resulting in an inorganic zwitterion.

The intramolecular distance between the two palladium atoms is about 6.9 Å and a short inter-ionic distance of 4.1 Å is observed between palladiums in adjacent dimeric units within the unit cell. These distances are much longer than the 2.751 Å in palladium metal[33] and preclude any metal-metal interaction. When viewed along the *a*-axis, successive layers of the complexes are arranged in an antiparallel fashion [see Figure 6 (left)]. This is due to some hydrogen bonding and other weak interactions[34−37] in the crystal lattice that are listed in Table 1 and 2. In this complex, the three pyridine rings are arranged in a cone-like conformation, as seen in Figure 6 (right). In the crystal packing and along the *c*-axis there are rectangular voids of about 13.3 Å due to these interactions and π-π stacking (3.347 Å to 4.168 Å) of the pyridine rings. Water molecules are also involved in the weak hydrogen-bonding networks.

Structure Description of [(10)$Ag_2(CH_3CN)(PF_6)_2]_\infty$ (15) and [(10)$Ag_2(CH_3CN)(BF_4)_2]_\infty$ (16)

X-ray analysis of complex **15** shows that it is a one-dimensional coordination polymer. The ORTEP diagram of the asymmetric unit of the coordination polymer is shown in Figure 7 (top). One Ag^I resides in the cavity of the macrocycle, coordinated by three N and one S donors; it adopts a distorted tetrahedral geometry with (N,S)−Ag−(S,N)

 © 2004 Wiley-VCH Verlag GmbH & Co. KGaA, Weinheim

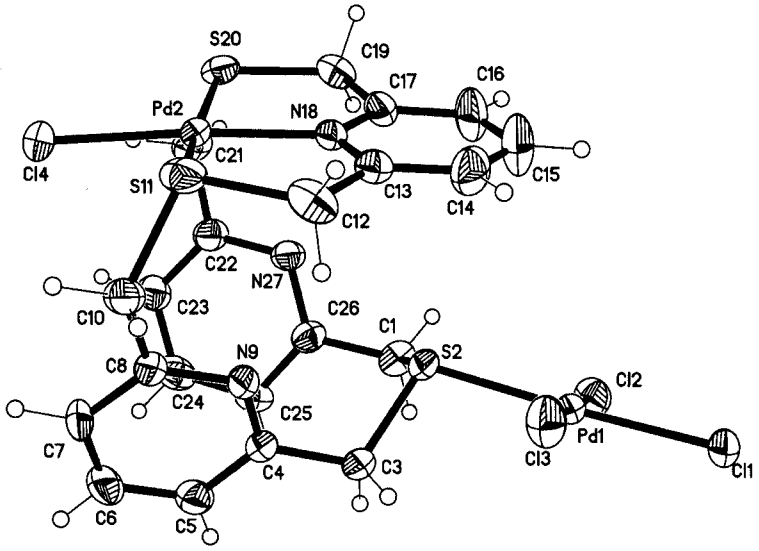

Figure 5. ORTEP diagram of the binuclear palladium complex **14**

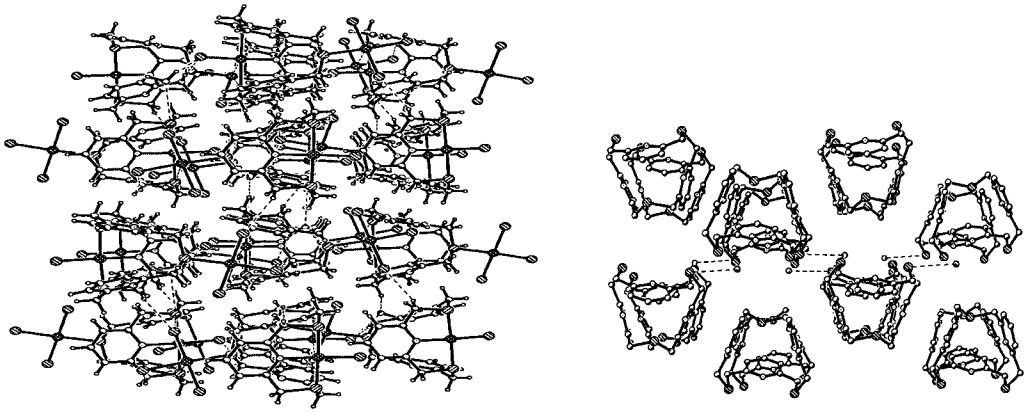

Figure 6. (left) Packing in complex **14** showing the molecules arranged into antiparallel sheets along the *a*-axis; (right) cone conformation in the packing of complex **14**

angles ranging from 78.02(9) to 149.58(8)°, Ag−N bond lengths between 2.213(3) and 2.436(4) Å and an Ag−S distance of 2.532(1) Å. The second Ag^{I} is coordinated to two S-donors from two different macrocyclic molecules with distances of 2.454(1) and 2.517(1) Å and an acetonitrile solvent molecule(Ag−N−C−CH_3 2.245 Å), with a trigonal planar geometry. The silver-acetonitrile nitrogen atom distance of 2.245 Å falls in the range of 2.18−2.33 Å reported previously.[47] Consequently all six donors of each macrocyclic molecule are engaged in coordination. The second Ag^{I} deviates by about 0.13 Å from the trigonal plane. Two different modes of coordination in a single silver complex are uncommon and the two modes of coordination are shown in Figure 7 (bottom).

Adjacent linear chains are arranged an antiparallel manner, most likely stabilized by the π-π stacking interaction of the pyridine rings. The distance between the π-π pyridine rings is about 3.6 Å, close enough for an interaction. The PF_6 counteranion is situated nicely in the voids between adjacent linear polymer layers and the linear polymers are arranged in a zig-zag fashion along the *c*-axis. Selected bond lengths and bond angles are summarised in Table 1 and 2.

The four-coordinate Ag1 has a long-range interaction with two fluorine atoms of the counterion (Ag1···F 3.379 and 3.562 Å) and hence a pseudo-octahedral geometry is observed. The trigonal planar geometry of the Ag(2) centre is stabilized by interaction of one of the fluorine atoms of

 © 2004 Wiley-VCH Verlag GmbH & Co. KGaA, Weinheim

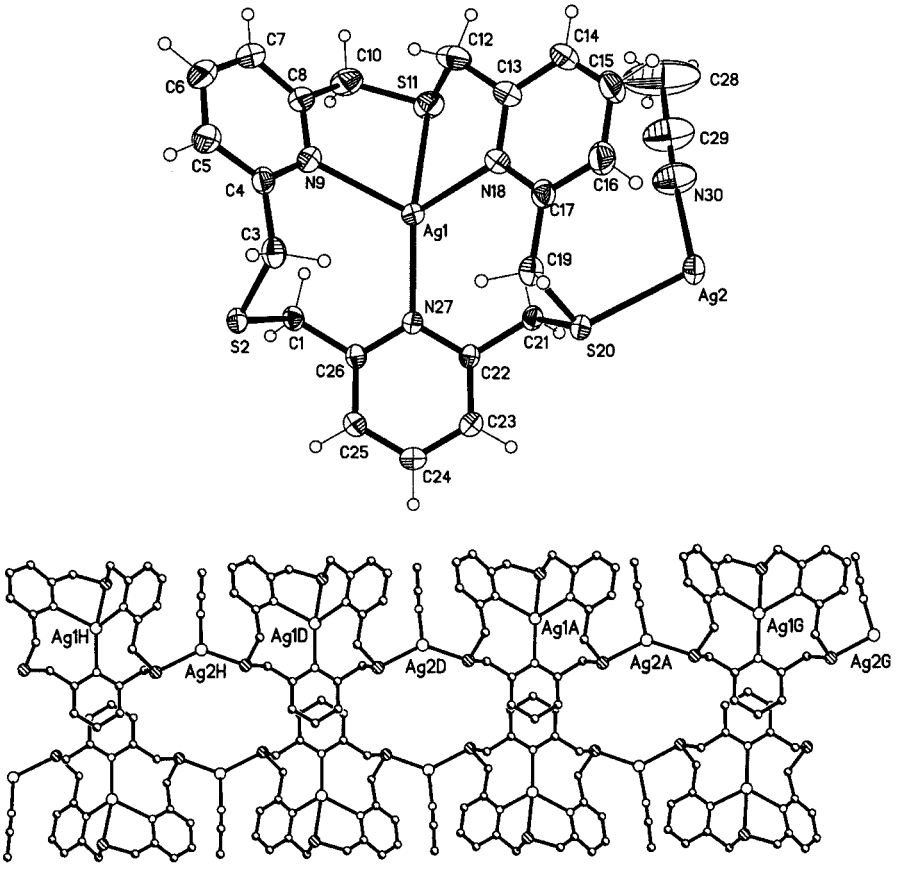

Figure 7. (top) ORTEP diagram of an asymmetric unit of the coordination polymer **15**; (bottom) the two coordination modes of silver in the coordination polymer **15**

the counterion PF_6, at a distance of 2.883 Å, resulting in a pseudo four-coordination. A polymeric disilver complex with two different geometries (tetrahedral and linear) was reported previously[48] with a small macrocycle. To the best of our knowledge, this is the first example of a polymeric complex with a pyridine-containing macrocycle with two different modes of four- and three-coordination. The distance between Ag1 and Ag2 is 5.742 Å and the intermolecular distance between Ag2 and Ag1 of the adjacent macrocycle is about 5.9 Å, which is significantly longer than the sum of their van der Waals radii.

There is no major difference in the X-ray structure when the metal salt is changed from $AgPF_6$ to $AgBF_4$. The complex formed with $AgBF_4$ is also a coordination polymer, with two different coordination modes of silver, with the formula $C_{23}H_{24}Ag_2B_2F_8N_4S_3$. One of the fluorine atoms in BF_4 in the complex **16** is disordered. The bond lengths and bond angles are similar to those of complex **16** listed in Table 1 and 2. The intra- and intermolecular Ag−Ag distances (5.865 Å and 5.657 Å respectively) are different from those in complex **15**. No good quality single crystals could be obtained when $AgNO_3$ was used.

UV/Vis and Redox Properties of the Complexes

The UV/Vis absorption spectrum data of the dinuclear palladium complex is given in the Exp. Sect. The palladium complex is orange and shows an absorption maximum at 374 nm with a further intense absorption band at 272 nm. A peak of this type is absent in most mononuclear complexes and seems to be characteristic of dinuclear palladium complexes, possibly arising from a metal-metal interaction. From previous work the absorption at 272 nm can be assigned to the spin-allowed $4d_{\sigma^*} \rightarrow 5p_\sigma$ transition.[49] The p_σ orbital is a hybrid of the $5p_z$(Pd) and π* (ligand) orbitals. Whether this kind of interaction would lead to some net metal-metal bonding still remains uncertain.

The redox properties of complexes **15** and **16** have been studied by cyclic voltammetry in acetonitrile solution with tetrabutylammonium perchlorate as the supporting electrolyte. Two irreversible reductions are observed at −1.1 and −0.25 V for complex **15** and −1.4 and −0.35 V for complex **16** together with an intense desorption spike at 0 V at a scan rate of 200 $mV \cdot s^{-1}$. Both reductions correspond to a one-electron transfer of Ag^I to Ag^0. No oxidation waves are observed in the cyclic voltammograms up to +2.0 V. However, for complex **15** there is an oxidation peak observed at −1.25 V. Similar potential ranges have been reported for related macrocyclic silver complexes.[50]

Extraction Studies

The complexing abilities of the macrocycle **10** with the selected metal cations Ag^I, Cd^{II}, Cu^{II}, Co^{II}, Hg^{II}, Ni^{II}, Pb^{II}

 © 2004 Wiley-VCH Verlag GmbH & Co. KGaA, Weinheim

and Zn^{II} were assessed by solvent extraction of the metal chlorides from aqueous solutions into chloroform. The procedure was based on the method used by Kumar et al. and Nishimura et al., in their investigation of mixed nitrogen and sulfur/oxygen-donor cyclophanes.[51,52] The extraction results, presented in Table 3, indicate that the macrocycle has poor selectivity and it extracts all the metals appreciably. Among these metals, macrocycle **10** exhibits a slightly higher preference for Ni^{II}. The observed extraction selectivity order is $Ni^{II} > Co^{II} > Zn^{II} > Pb^{II} > Cu^{II} > Cd^{II} > Hg^{II} > Ag^{I}$.

Table 3. Relative selectivity in extraction of metal ions by macrocycle **10**

Metal ion	Cd^{II}	Cu^{II}	Co^{II}	Pb^{II}	Hg^{II}	Ni^{II}	Ag^{I}	Zn^{II}
% Extraction	76	77	84	78	69	89	50	83

Conclusions

A hexadentate macrocyclic ligand containing mixed donor atoms, namely [18]aneN_3S_3 (**10**), has been synthesised by a new synthetic route and characterised by analytical and spectroscopic methods. The Ni^{II}, Pd^{II}, Pt^{II}, Cu^{I}, Ag^{I} and Hg^{II} complexes **11**−**16** of **10** have been prepared and their crystal structures investigated by X-ray crystallography. From the X-ray crystal structures of the complexes, **10** forms mononuclear complexes with nickel, copper and mercury metal ions, a binuclear complex with palladium and coordination polymers with silver. Both nickel and mercury adopt an unusual geometry due to the ligand conformation. The binuclear palladium complex exists as an unusual inorganic zwitterion and a cone conformation of the macrocycle was achieved upon metal ion complexation. The silver complex formed a one-dimensional coordination polymer with two different modes of coordination of silver. Changing the anion of the silver salt does not result in any structural changes in the silver complex. The electronic spectra of the complexes were also investigated. The extraction ability of the macrocycle shows a slightly higher preference for nickel(II). The solid-state packing diagrams in the X-ray structures of the complexes were explained by hydrogen bonding and other weak interactions.

Experimental Section

Materials and Physical Measurements: ^1H and ^{13}C NMR spectra were recorded on a Bruker ACF 300 Fourier-transform spectrometer. All chemical shifts are reported in ppm downfield from a tetramethylsilane internal standard. Mass spectra were recorded on a VG Micromass 7035 spectrometer at 70 eV in electron impact mode. Elemental analyses were performed by the Chemical and Molecular Analysis Centre, Department of Chemistry, National University of Singapore. The electronic spectra were recorded using a HP 8452A diode-array UV/Vis spectrophotometer. Cyclic voltammograms were recorded using a single compartment three-electrode cell. A platinum disc of 3 mm in diameter was used as a working electrode. The counter electrode consisted of a platinum wire. All the potentials were measured against the Ag/AgCl couple. An EG&G Princeton Applied Research 273 potentiostat, controlled by M270 software, was used to measure all the electrochemical data. Acetonitrile used for electrochemical studies was triply distilled under nitrogen from calcium hydride and stored over 4-Å molecular sieves. Tetrabutylammonium perchlorate employed as a supporting electrolyte was vacuum dried for 24 h prior to use. All solutions were purged with dry argon for 15 minutes prior to any electrochemical study. The following compounds were prepared according to the literature: 2,6-bis(mercaptomethyl)pyridine (**6**),[53] and 2-bromomethyl-6-hydroxymethylpyridine (**7**).[54]

CAUTION! *Perchlorate salts are potentially explosive and should be handled with care.*

2,6-Bis[(6-hydroxymethyl-2-pyridylmethyl)sulfanylmethyl]pyridine (8): Compound **6** (1.00 g, 5.85 mmol) was added to a solution of sodium ethoxide prepared by dissolving sodium metal (0.27 g, 11.70 mmol) in anhydrous EtOH (200 mL) and the mixture was stirred for 1 h. A solution of compound **7** (2.35 g, 11.70 mmol) in anhydrous EtOH (75 mL) was then added dropwise over 2 h while the reaction mixture was maintained at solvent refluxing temperature. The reaction mixture was allowed to stir for an additional 2 h and cooled to room temperature. The solvent was removed under reduced pressure yielding an orange oil. The crude product was extracted with CH_2Cl_2 and the organic phase was washed with water followed by saturated sodium chloride solution. The solvent was removed and the residue was chromatographed on silica gel (hexane/acetone, 1:1) to give the desired diol **8** as colourless crystals. Yield: 1.95 g (81%); m.p. 83−85 °C. MS: *m*/*z* = 413.2 [M^+]. ^1H NMR ($CDCl_3$): δ = 7.50−7.60 (m, 3 H), 7.20−7.30 (m, 4 H), 7.10 (d, *J* = 7.62 Hz, 2 H), 4.71 (s, 4 H), 4.30 (br., 2 H), 3.82 (s, 4 H), 3.80 (s, 4 H) ppm. ^{13}C NMR ($CDCl_3$): δ = 158.9, 157.8, 157.3, 137.2, 121.6, 121.3, 118.6, 64.5, 37.2, 37.0 ppm.

2,6-Bis[(6-chloromethyl-2-pyridylmethyl)sulfanylmethyl]pyridine (9) Thionyl chloride (1.04 g, 8.71 mmol, 20% excess) was added slowly with a syringe to a solution of the diol **8** (1.50 g, 3.63 mmol) in CH_2Cl_2 (75 mL) and the mixture was stirred for 6 h at room temperature. A saturated solution of $NaHCO_3$ (50 mL) was added and the mixture was stirred for 1 h. The organic layer was separated and dried. The solvent was removed under reduced pressure yielding brown oil which solidified on standing at 0 °C. Yield: 1.50 g (91%). ^1H NMR ($CDCl_3$): δ = 7.62 (m, 2 H), 7.52 (t, *J* = 7.62 Hz, 1 H), 7.30 (m, 4 H), 7.20 (d, *J* = 7.62 Hz, 2 H), 4.60 (s, 4 H), 3.76 (s, 4 H), 3.72 (s, 4 H) ppm. ^{13}C NMR: δ = 158.3, 157.8, 156.0, 137.5, 122.5, 121.3, 120.8, 53.3, 37.3, 37.2 ppm. Dichloride **9** decomposes slowly upon standing and was therefore used for the following reaction without further purification.

3,11,19-Trithia[3.3.3]pyridinophane (10): A catalytic amount of NaOH was added to a solution of $Na_2S{\cdot}9H_2O$ (0.58 g, 2.40 mmol) in 95% ethanol (250 mL). This was maintained under N_2 at room temperature and a solution of **9** (1.10 g, 2.40 mmol) in EtOH (100 mL) was added dropwise over a period of 6 h. The resulting mixture was then heated to reflux for 6 h. The bulk of the EtOH was removed under reduced pressure and the residue was extracted with chloroform. The organic layer was washed with 0.1 M aqueous NaOH followed by water and dried. The solvent was removed and the residue was recrystallised from acetone to give compound **10**. Yield: 0.68 g (68%); m.p. 158−160 °C. $C_{21}H_{21}N_3S_3$ (411.60): calcd. C 61.28, H 5.15, N 10.21; found C 60.57, H 5.34, N 10.20. MS: *m*/*z* = 411.1 [M^+]. ^1H NMR ($CDCl_3$): δ = 7.59 (t, *J* = 7.62 Hz, 3 H), 7.27 (d, *J* = 7.62 Hz, 6 H), 3.81 (s, 12 H) ppm. ^{13}C NMR: δ = 157.7, 137.4, 120.7, 36.7 ppm.

 © 2004 Wiley-VCH Verlag GmbH & Co. KGaA, Weinheim

Complex 11: A solution of $Ni(ClO_4)_2 \cdot 6H_2O$ (72.0 mg, 0.18 mmol) in acetonitrile (5 mL) was added to a solution of **10** (40.0 mg, 0.09 mmol) in CH_2Cl_2 (5 mL). The mixture was stirred for 4 h. Slow concentration of the solution gave green crystals of complex **11**. Yield: 53.0 mg (82%). $C_{21}H_{21}N_3NiS_3(ClO_4)_2 \cdot 2H_2O \cdot (CH_2Cl_2)_2$ (960.04): calcd. C 30.03, H 3.25, N 4.38, S 10.02; found C 25.92, H 3.64, N 4.40, S 9.85. FAB-MS: *m*/*z* = 469 [Ni·**10**].

Complex 12: A solution of $Hg(ClO_4)_2 \cdot 6H_2O$ (39.0 mg, 0.10 mmol) in methanol (5 mL) was added to a solution of **10** (20.0 mg, 0.05 mmol) in CH_2Cl_2 (5 mL). A colourless solid precipitated immediately. Diffusion of diethyl ether into a solution of the complex **12** in acetonitrile resulted in isolation of colourless crystals of **12**. Yield: 23.0 mg (60%). $C_{21}H_{21}HgN_3S_3(ClO_4)_2 \cdot 2H_2O$ (847.14): calcd. C 29.77, H 2.95, N 4.96, S 11.36; found C 29.17, H 2.45, N 4.84, S 10.96. FAB-MS: *m*/*z* = 610.9 [Hg·**10**].

Complex 13: $Cu(CH_3CN)_4(PF_6)$ (37.0 mg, 0.10 mmol) was added to a solution of **10** in a mixture of CH_2Cl_2 (5 mL) and methanol (5 mL). The reaction mixture was stirred for 3 h and the solution was concentrated. Slow addition of diethyl ether precipitated light grey crystals of the copper(I) complex **13**. Yield: 29.0 mg (96%); m.p. 136−138 °C (dec.). $C_{21}H_{21}CuF_6N_3PS_3$ (620.13): calcd. C 40.67, H 3.41, N 6.78, S 15.51; found C 42.10, H 3.63, N 7.01, S 15.65. FAB-MS: *m*/*z* = 474.0 [Cu·**10**].

Complex 14: A mixture of **10** (40.0 mg, 0.09 mmol) in CH_2Cl_2 (10 mL) was added to $[PdCl_2(CH_3CN)_2]$ (52.0 mg, 0.18 mmol) in methanol (10 mL) and the mixture was stirred at room temperature for 6 h. On standing dark-orange crystals of complex **14** precipitated from the solution. Yield: 68.0 mg (91%); m.p. 212−215 °C (dec.). $C_{21}H_{21}Cl_4N_3Pd_2S_3 \cdot H_2O$ (784.28): calcd. C 32.16, H 2.95, N 5.35; found C 32.18, H 2.93, N 4.93. FAB-MS: *m*/*z* = 517.0 [Pd·**10**], 552.5 [Pd·**10**·Cl], 624.0 [Pd_2·**10**·H], 658.0 [Pd_2·**10**·Cl]. UV/Vis: λ_{max} (ε) = 272 (13658), 374 nm (23030 $M^{-1}\,cm^{-1}$).

Complex 15: A solution of $AgNO_3$ (25.0 mg, 0.14 mmol) in acetonitrile (5 mL) was added to a solution of **10** (30.0 mg, 0.07 mmol) in CH_2Cl_2 (5 mL) and the mixture was stirred for 4 h. Addition of a large excess of NH_4PF_6 followed by partial removal of the solvent afforded a white solid. Recrystallisation of this solid from methanol gave a light-sensitive colourless precipitate. Colourless crystals of complex **15** were obtained by diffusion of diethyl ether into a solution of **15** in acetonitrile. Yield: 60.0 mg (86%); m.p. 154−156 °C (dec.). ^1H NMR (CD_3CN): δ = 7.88 (t, *J* = 7.62 Hz, 3 H), 7.47 (d, *J* = 7.62 Hz, 6 H), 4.10 (s, 12 H) ppm. ^{13}C NMR: δ = 157.7, 140.5, 124.8, 38.3 ppm. FAB-MS: *m*/*z* = 518.0 [Ag·**10**], 625.9 [Ag_2·**10**·H].

Complex 16: A solution of $AgBF_4$ (15.0 mg, 0.16 mmol) in acetonitrile (5 mL) was added to a solution of **10** (30.0 mg, 0.08 mmol) in CH_2Cl_2 (5 mL) and the mixture was stirred for 4 h. Slow concentration of the solution gave colourless crystals of complex **16**. Yield: 55.0 mg (90%); m.p. 144−146 °C (dec.). ^1H NMR (CD_3CN): δ = 7.87 (t, *J* = 7.62 Hz, 3 H), 7.46 (d, *J* = 7.62 Hz, 6 H), 4.02 (s, 12 H) ppm. ^{13}C NMR: δ = 157.8, 140.4, 124.7, 38.2 ppm. FAB-MS: *m*/*z* = 518.0 [Ag·**10**], 605.0 [Ag·**10**·BF_4], 711.9 [Ag_2·**10**·BF_4·H].

Crystallographic Data Collection and Refinement: Details of the crystal data and refinement of the structures are given in Table 4. Data collection was performed at 293 K using graphite-monochromated Mo-K_α radiation (λ = 0.71073 Å) on a Siemens CCD diffractometer. Structures were solved by Patterson or direct methods. All non-hydrogen atoms were refined anisotropically, except for those of solvent molecules where present. Refinement was done by full-matrix least- squares based on F^2 using SHELXL-93.[55] Hydrogen atoms were introduced at a fixed distance from carbon atoms and their isotropic thermal parameters were based on a riding mode of the parent atoms.

Table 4. Crystallographic data for complexes **11**−**16**

	11	**12**	**13**	**14**	**15**	**16**
Chemical formula	$C_{21}H_{21}Cl_2N_3NiO_8S_3$	$C_{21}H_{21}Cl_2HgN_3O_8S_4$	$C_{21}H_{21}CuF_6N_3PS_3$	$C_{21}H_{23}Cl_4N_3OPd_2S_3$	$C_{23}H_{24}Ag_2F_{12}N_4P_2S_3$	$C_{23}H_{24}Ag_2B_2F_8N_4S_3$
Molecular mass	669.20	811.08	620.10	784.20	958.32	842.00
T (K)	293(2)	293(2)	293(2)	293(2)	293(2)	223(2)
λ (Å)	0.71073	0.71073	0.71073	0.71073	0.71073	0.71073
Crystal system	orthorhombic	monoclinic	triclinic	monoclinic	triclinic	triclinic
Space group	Pnna	$P2_1/c$	$P\bar{1}$	$P2_1/n$	$P\bar{1}$	$P\bar{1}$
a (Å)	16.4967(2)	14.3417(6)	10.6984(9)	12.3992(6)	9.2186(1)	9.0413(2)
b (Å)	22.1884(1)	12.3088(5)	15.4046(1)	14.5148(7)	11.2790(2)	11.021(2)
c (Å)	14.6190(1)	14.8581(6)	16.6414(1)	14.3996(6)	16.9920(2)	14.667(3)
α (°)	90.0	90.0	114.333(2)	90.0	108.726(1)	96.548(4)
β (°)	90.0	92.872(2)	96.459(2)	92.093	94.227(1)	101.866(4)
γ (°)	90.0	90.0	90.262(2)	90.0	92.723(1)	96.730(4)
V (Å^3)	5351.07(8)	2619.59(1)	2479.2(4)	2589.8(2)	1663.95(4)	1405.9(5)
Z	8	4	4	4	2	2
ρ (Mg/cm^3)	1.661	2.057	1.661	2.011	1.913	1.989
μ (mm^{-1})	1.210	6.371	1.260	2.066	1.552	1.693
F (000)	2736	1576	1256	1544	940	828
Crystal size (mm^3)	0.32 × 0.18 × 0.15	0.20 × 0.14 × 0.11	0.15 × 0.12 × 0.10	0.20 × 0.20 × 0.08	0.20 × 0.20 × 0.05	0.68 × 0.50 × 0.14
θ range (°)	1.67 to 27.09	1.42 to 27.49	1.45 to 30.03	2.13 to 30.92	1.91 to 28.34	1.88 to 25.00
Index ranges	$-20 \le h \le 16$	$-18 \le h \le 18$	$-15 \le h \le 15$	$-16 \le h \le 17$	$-11 \le h \le 12$	$-10 \le h \le 10$
	$-28 \le k \le 26$	$-15 \le k \le 10$	$-21 \le k \le 21$	$-20 \le k \le 20$	$-14 \le k \le 15$	$-13 \le k \le 13$
	$-18 \le l \le 18$	$-17 \le l \le 19$	$-23 \le l \le 23$	$-10 \le l \le 19$	$-22 \le l \le 22$	$-17 \le l \le 17$
Reflections collected	30061	17925	28159	21186	15423	11550
Independent reflections	5767 *R*(int) = 0.0559	5894 *R*(int) = 0.0495	13929 *R*(int) = 0.0367	7547 *R*(int) = 0.0273	7885 *R*(int) = 0.0177	4953 v(int) = 0.0699
Max and min transmission	0.942 and 0.658	0.694 and 0.496	0.928 and 0.692	0.928 and 0.701	0.928 and 0.770	0.675 and 0.418
Data/restraints/parameters	5766/0/347	5894/0/343	13929/0/631	7547/0/304	7883/27/451	4953/108/392
Goodness of fit on F^2	1.061	0.758	0.958	0.982	1.042	1.172
Final *R* indices	*R*1 = 0.0539	*R*1 = 0.0374	*R*1 = 0.0807	*R*1 = 0.0460	*R*1 = 0.0422	*R*1 = 0.0559
[$I > 2\sigma(I)$]	*wR*2 = 0.1274	*wR*2 = 0.0568	*wR*2 = 0.2339	*wR*2 = 0.1157	*wR*2 = 0.1154	*wR*2 = 0.1482
R indices	*R*1 = 0.0903	*R*1 = 0.0750	*R*1 = 0.1490	*R*1 = 0.0668	*R*1 = 0.0568	*R*1 = 0.0586
(all data)	*wR*2 = 0.1522	*wR*2 = 0.0624	*wR*2 = 0.2582	*wR*2 = 0.1239	*wR*2 = 0.1263	*wR*2 = 0.1512
Largest difference peak and hole (e·Å^{-3})	0.814 and −0.556	1.378 and −0.734	0.864 and −0.483	1.301 and −1.119	1.057 and −0.583	0.957 and −0.786

 © 2004 Wiley-VCH Verlag GmbH & Co. KGaA, Weinheim

Acknowledgments

This work was supported by the National University of Singapore, Singapore (NUS) with grant no. R-143-000-026-112. M.V. thanks the NUS for a research scholarship. Assistance from the technical staff of the Department of Chemistry, NUS, is gratefully acknowledged.

[1] A. J. Blake, N. R. Champness, P. Hubberstey, W. S. Li, M. A. Withersby, M. Schröder, *Coord. Chem. Rev.* **1999**, *183*, 117−138.
[2] P. J. Stang, B. Olenyuk, *Acc. Chem. Res.* **1997**, *30*, 502−518.
[3] N. R. Champness, M. Schröder, *Curr. Opin. Solid State Mater. Sci.* **1998**, *3*, 419−424.
[4] O. M. Yaghi, H. Li, C. Davis, D. Richardson, T. L. Groy, *Acc. Chem. Res.* **1998**, *31*, 474−484.
[5] G. R. Desiraju, *Angew. Chem. Int. Ed. Engl.* **1995**, *34*, 2311−2317.
[6] G. R. Desiraju, *Crystal Engineering: Design of Organic Solids*, Elsevier, Amsterdam, **1989**.
[7] H. W. Yin, L. M. Tran, E. E. Pullen, R. Daniel, M. L. Louise, E. C. Thomas, A. L. Rheingold, *Inorg. Chem.* **1999**, *38*, 6234−6239.
[8] S. Sailaja, M. V. Rajasekaran, *Inorg. Chem.* **2001**, *39*, 4586−4590.
[9] L. Fabbrizi, A. Poggi, *Transition Metals in Supramolecular Chemistry*, Kluwer Academic Publishers: Dordrecht, The Netherlands, **1994**.
[10] R. Thaimattam, F. Xue, J. A. R. P. Sarma, T. C. W. Mak, G. R. Desiraju, *J. Am. Chem. Soc.* **2001**, *123*, 4432−4445.
[11] M. Hong, W. Su, R. Cao, W. Zhang, J. Lu, *Inorg. Chem.* **1999**, *38*, 600−602 and references therein.
[12] S. Yusaku, K. S. Takayoshi, M. Masahiko, M. Munakata, *J. Chem. Soc., Dalton Trans.* **1999**, 2737−2741.
[13] G. R. Newkome, J. D. Sauer, J. M. Roper, D. C. Hager, *Chem. Rev.* **1977**, *77*, 513−597.
[14] F. H. Fry, P. Jensen, C. M. Kepert, L. Spiccia, *Inorg. Chem.* **2003**, *42*, 5637−5644 and references therein.
[15] S. A. Li, J. Xia, D. X. Yang, Y. Xu, D. F. Li, M. F. Wu, W. X. Tang, *Inorg. Chem.* **2002**, *41*, 1807−1815 and references therein.
[16] A. J. Blake, W. S. Li, V. Lippolis, M. Schröder, *Chem. Commun.* **1997**, 1943−1944 and references therein.
[17] A. J. Blake, D. Collison, R. O. Gould, G. Reid, M. Schröder, *J. Chem. Soc., Dalton Trans.* **1993**, 521−531.
[18] A. J. Blake, M. Schröder, *Adv. Inorg. Chem.* **1990**, *35*, 1−80.
[19] A. J. Blake, N. R. Champness, S. M. Howdle, P. B. Webb, *Inorg. Chem.* **2000**, *39*, 1035−1038 and references therein.
[20] P. J. Blower, J. A. Clarkson, S. C. Rawle, J. R. Hartman, R. E. Wolf Jr., R. Yagbasan, S. G. Bott, S. R. Cooper, *Inorg. Chem.* **1989**, *28*, 4040−4046.
[21] S. C. Rawle, S. R. Cooper, *Struct. Bonding* **1990**, *72*, 1−72.
[22] L. R. Hanton, C. Richardson, W. T. Robinson, J. M. Turnbull, *Chem. Commun.* **2000**, 2465−2466 and references therein.
[23] M. Munakata, L. P. Wu, M. Yamamoto, T. Kuroda-Sowa, M. Maekawa, *J. Chem. Soc., Dalton Trans.* **1995**, 3215−3220.
[24] R. Alberto, D. Angst, U. Abram, K. Ortner, T. A. Kaden, P. August, *Chem. Commun.* **1999**, 1513−1514 and references therein.
[25] F. Vöegtle, F. Ley, *Chem. Ber.* **1983**, *116*, 3000−3002.
[26] S. J. Loeb, K. D. L. Smith, *Inorg. Chem.* **1993**, *32*, 1297−1300.
[27] J. Buter, R. M. Kellogg, *J. Org. Chem.* **1981**, 4481−4485.
[28] J. Buter, R. M. Kellogg, *Org. Synth.* **1987**, *65*, 150−158.
[29] A. W. Addision, T. N. Rao, J. Reedijk, J. van Rijn, G. C. Verschoor, *J. Chem. Soc., Dalton Trans.* **1984**, 1349−1356.
[30] L. Sacconi, F. Mani, A. Bencini, in *Comprehensive Coordination Chemistry* (Eds.: G. Wilkinsen, R. D. Gillard, J. A. McCleverty), Pergamon Press: New York, **1987**, 5, 86.
[31] J. G. Gilbert, A. W. Addison, R. J. Butcher, *Inorg. Chim. Acta* **2000**, *308*, 22−30.
[32] R. Morassi, I. Bertini, L. Sacconi, *Coord. Chem. Rev.* **1973**, *11*, 343−402.
[33] P. A. Duckworth, F. S. Stephens, K. P. Wainwright, K. D. V. Veerasuria, S. B. N. Wild, *Inorg. Chem.* **1989**, *28*, 4531−4535.
[34] G. R. Desiraju, *Acc. Chem. Res.* **1996**, *29*, 441−449.
[35] P. G. Jones, B. Aherns, *Chem. Commun.* **1998**, 2307−2308.
[36] T. Steiner, *Chem. Commun.* **1997**, 727−728.
[37] T. C. Deivaraj, J. J. Vittal, *J. Chem. Soc., Dalton Trans.* **2001**, 322−328.
[38] A. McAuley, T. W. Whitecombe, M. J. Zaworotko, *Inorg. Chem.* **1991**, *30*, 3513−3520.
[39] D. C. Bebout, A. E. DeLanoy, D. E. Ehmann, M. E. Kastner, D. A. Parrish, R. J. Butcher, *Inorg. Chem.* **1998**, *37*, 2952−2959.
[40] A. M. W. C. Thompson, I. Blandfors, H. Redfearn, J. C. Jeffery, M. D. Ward, *J. Chem. Soc., Dalton Trans.* **1997**, 2661−2666.
[41] B. D. Groot, S. J. Loeb, *Inorg. Chem.* **1989**, *28*, 3573−3578.
[42] B. D. Groot, G. R. Giesbrecht, S. J. Loeb, G. K. H. Shimizu, *Inorg. Chem.* **1991**, *30*, 177−182.
[43] F. R. Fronczek, P. J. Schilling, S. F. Watkins, V. K. Majestic, G. R. Newcomb, *Inorg. Chim. Acta* **1996**, *246*, 119−123 and references therein.
[44] K. Wieghardt, H. J. Kuppers, E. Raabe, C. Kruger, *Angew. Chem. Int. Ed. Engl.* **1986**, *25*, 1136−1138.
[45] R. A. Newman, D. S. Martin, R. F. Dallinger, W. H. Woodruff, A. E. Stiegman, C. M. Che, W. P. Schaefer, V. M. Miskowski, H. B. Gray, *Inorg. Chem.* **1991**, *30*, 4647−4654.
[46] G. Hunter, A. McAuley, T. W. Whitecombe, *Inorg. Chem.* **1988**, *27*, 2634−2639.
[47] H. Adams, N. A. Bailey, P. Bertrand, S. R. Collinson, D. E. Fenton, S. J. Kitchen, *Inorg. Chim. Acta* **1996**, *250*, 139−148.
[48] H. J. Drexler, M. Grotjahn, E. Kleinpeter, H. J. Holdt, *Inorg. Chim. Acta* **1999**, *285*, 305−308.
[49] H. K. Yip, T. F. Lai, C. M. Che, *J. Chem. Soc., Dalton Trans.* **1991**, 1639−1641.
[50] A. J. Blake, W. S. Li, V. Lippolis, A. Taylor, M. Schröder, *J. Chem. Soc., Dalton Trans.* **1998**, 2931−2938 and references therein.
[51] S. Kumar, M. S. Hundal, G. Hundal, P. Singh, V. Bhalla, H. Singh, *J. Chem. Soc., Perkin Trans. 2* **1998**, 925−932.
[52] S. Inokuma, K. Kimura, T. Funaki, J. Nishimura, *Heterocycles* **2001**, *54*, 123−130.
[53] E. C. Constable, A. C. King, P. R. Raithby, *Polyhedron* **1998**, *17*, 4275−4289.
[54] M. Newcomb, J. M. Timko, D. M. Walba, D. J. Cram, *J. Am. Chem. Soc.* **1977**, *99*, 6392−6398.
[55] G. M. Sheldrick, SHELXL 93, *Program for Crystal Structure Refinement*, University of Göttingen, **1993**.

Received November 12, 2003
Early View Article
Published Online April 1, 2004

 © 2004 Wiley-VCH Verlag GmbH & Co. KGaA, Weinheim

Crystal Engineering of the Coordination Architecture of Metal Polycarboxylate Complexes by Hydrothermal Synthesis: Assembly and Characterization of Four Novel Cadmium Polycarboxylate Coordination Polymers Based on Mixed Ligands

Jing-Cao Dai,[a,b] Xin-Tao Wu,*[a] Sheng-Min Hu,[a] Zhi-Yong Fu,[a] Jian-Jun Zhang,[a] Wen-Xin Du,[a] Han-Hui Zhang,[c] and Rui-Qing Sun[c]

Keywords: Cadmium / Coordination polymers / Crystal engineering / Hydrothermal synthesis / Mixed ligands / Structural topology

Four novel compounds, $[Cd(tp)(bpp)]_n$ (**1**), $[Cd(tp)(bpy)]_n$ (**2**), $[\{Cd_4(bpa)_4(bpy)_6\}\cdot(bpy)_{0.5}\cdot 7H_2O]_n$ (**3**) and $[Cd_2\{(Htp)(tp)_{1.5}\}(bpe)]_n$ (**4**) [tp = terephthalate, bpp = 1,3-bis(4-pyridyl)propane, bpy = 4,4′- bipyridine, bpa = 4,4′-biphenyldicarboxylate, bpe = 1,2-bis(4-pyridyl)ethane], of cadmium(II) polycarboxylate coordination polymers based on mixed ligands were obtained by a hydrothermal method. Complex **1** ($C_{21}H_{18}CdN_2O_4$) crystallizes in the orthorhombic *Pbca* space group [a = 11.9401(0) Å, b = 16.8148(3) Å, c = 20.2743(3) Å, and Z = 8]. Complex **2** ($C_{18}H_{12}CdN_2O_4$) belongs to the monoclinic *C2/m* space group [a = 20.299(3) Å, b = 10.720(1) Å, c = 11.764(2) Å, β = 110.944(2)°, and Z = 6]. Complex **3** ($C_{121}H_{98}Cd_4N_{13}O_{23}$) belongs to the monoclinic $P2_1/c$ space group [a = 23.2208(0) Å, b = 11.8103(1) Å, c = 45.4670(6) Å, β = 104.516(1)°, and Z = 4]. Complex **4** ($C_{32}H_{23}Cd_2N_2O_{10}$) belongs to the monoclinic $P2_1/n$ space group [a = 6.9896(1) Å, b = 22.6294(1) Å, c = 19.7738(3)Å, β = 99.380(1)°, and Z = 4].The Cd^{II} centers in the four compounds are bridged by mixed polycarboxylate ligands with bpy and related species to form the twofold parallel interpenetration topology of an undulating 2D 4^4 net for **1**, a twofold interpenetration topology of a 3D α-Po net for **2**, a fourfold interpenetration topology of a 3D 5-connected borazone 4^66^4 net for **3** and an interesting 3D spiral pipe-like structure with a bolt for **4**. These four compounds exhibit strong fluorescent emissions at 549 and 582 nm (λ_{ex} = 532 nm) for **1**, 493 nm (λ_{ex} = 360 nm) for **2**, 413 and 424 nm (λ_{ex} = 315 nm) for **3** and 350 nm (λ_{ex} = 220 nm) for **4** in the solid state at room temperature. These are novel structural topologies and could be significant in the field of photoactive materials.
(© Wiley-VCH Verlag GmbH & Co. KGaA, 69451 Weinheim, Germany, 2004)

Introduction

There has been an enormous growth in the crystal engineering of coordination-polymeric solids in recent decades owing to their intriguing applications, including catalysis, nonlinear optics, sensors, magnetism and molecular recognition.[1−10] Although a number of new coordination-polymeric solids with beautiful architectures and interesting topologies based on the assembly of bridging ligands and metal centers using the principles of crystal engineering have been reported,[11−31] a rational synthesis strategy to manipulate the assembly of donor and acceptor building blocks to generate desired supramolecular architectures is still one of the great challenges in this areas. For the design of coordination-polymeric solids that mimic mineral architectures such as quartz, clays and zeolites, an effective strategy is the choice of rigid "tecton" ligands containing O- or N-donors to bind metal centers as building blocks of the extended framework used to construct novel supramolecular architectures.[32,33] Polycarboxylates are often employed as bridging ligands to construct porous coordination polymers due to their versatile coordination modes and high structural stability.[7,8,26,34−53] These polymeric solids can be essentially regarded as a class of metal polycarboxylate salts. Hence, the structures of the resulting compounds are influenced by the degree of deprotonation, the coordination modes and capabilities, the sizes and shape of the polycarboxylic acids, as well as by the coordination sphere of the metal centers. Thus, it is possible to synthesise polymeric frameworks with interesting topologies through the appropriate choice of ligand, and tailoring and manipulation of the reaction conditions, including pH, temperature, stoichiometry, and the addition of templates or structure-directing agents.[26,33−46] In order to resolve the poor solubility of

[a] State Key Laboratory of Structural Chemistry, Fujian Institute of Research on the Structure of Matter, Chinese Academy of Sciences,
Fuzhou, Fujian 350002, China
E-mail: wxt@ms.fjirsm.ac.cn
[b] Institute of Materials Physical Chemistry, Huaqiao University, Quanzhou, Fujian 362011, China
[c] Department of Chemistry, Fuzhou University, Fuzhou, Fujian 350002, China

 © 2004 Wiley-VCH Verlag GmbH & Co. KGaA, Weinheim **DOI: 10.1002/ejic.200300850**

reactants and products, the hydrothermal reaction technique offers a powerful synthetic route to prepare polymeric solids with better crystallinity[7,54] than traditional solution techniques such as evaporation, diffusion and cooling etc. In most cases, water is not only a solvent but also acts as a competing ligand in these hydrothermal reactions. An interesting phenomenon can be observed whereby many coordination polymers constructed from polycarboxylate ligands usually contain water molecules as terminal or bridging ligands in the coordination sphere of the metal, thus increasing the variety of the assembled structural topology of the polymers. It is therefore possible to obtain metal polycarboxylates with novel coordination architectures of diverse sizes and shapes by use of other suitable compounds with different steric demands and ligating capabilities as the competing bridging ligand to substitute the water ligands mentioned above. Taking account of the potential of these approaches, we have embarked on a program aimed at using mixed ligands containing O- and N-donors to prepare coordination-polymeric solids that mimic mineral architectures. Herein, we report four interesting examples of coordination polymeric architectures based upon mixed bridging ligands: $[Cd(tp)(bpp)]_n$ (**1**), $[Cd(tp)(bpy)]_n$ (**2**), $[\{Cd_4(bpa)_4(bpy)_6\}\cdot(bpy)_{0.5}\cdot 7H_2O]_n$ (**3**), and $[Cd_2\{(Htp)(tp)_{1.5}\}(bpe)]_n$ (**4**) [tp = terephthalate, bpp = 1,3-bis(4-pyridyl)propane, bpy = 4,4′- bipyridine, bpa = 4,4′-biphenyldicarboxylate, bpe = 1,2-bis(4-pyridyl)ethane]. X-ray single-crystal analyses show that these four polymers possess novel structural topologies, namely the twofold parallel interpenetration topology of an undulating 2D 4^4 net for **1**, the twofold interpenetration topology of a 3D α-Po net for **2**, the fourfold interpenetration topology of a 3D 5-connected borazone 4^66^4 net for **3** and an interesting 3D spiral pipe-like structure with a bolt for **4**. The compounds display strong fluorescent emissions at 549 and 582 nm (λ_{ex} = 532 nm) for **1**, 493 nm (λ_{ex} = 360 nm) for **2**, 413 and 424 nm (λ_{ex} = 315 nm) for **3** and 350 nm (λ_{ex} = 220 nm) for **4** in the solid state at room temperature, implying that they may be excellent candidates for potential photoactive materials.

Results and Discussion

Synthesis and Characterization

The four coordination polymers were obtained in a similar way. The appropriate acidity or basicity of the reactants for deprotonation of polycarboxylates is very important for preparing these four compounds, as is the case for some other metal polycarboxylate coordination polymers reported in our earlier studies.[26] These four compounds were also prepared at different pHs: compound **1** at pH 5.5, compound **2** at pH 9.1, compound **3** at pH 8.0 and compound **4** at pH 5.6. We tried to prepare these four compounds at different pHs but without success. Besides the pH, a suitable steric geometry of the reactants is also very important for fabrication of the resulting coordination architectures. As described in the Exp. Sect., although the synthesis conditions are very similar, only a small difference in the steric demands of the reactants, for example between bpp and bpe, results in the different coordination architectures of compounds **1** and **4**. In addition, the synthesis of compounds **1** and **4** cannot be performed in the absence of $(Ph_3PCH_2Ph)Cl$, while another supramolecular isomer of compound **2**, reported by Chen,[21] was obtained when the synthesis of compound **2** was carried out in the absence of hexamethylenetetraamine, even though neither $(Ph_3PCH_2Ph)Cl$ nor hexamethylenetetraamine are found as ligands or guests in the resulting coordination polymers. This suggests that both $(Ph_3PCH_2Ph)Cl$ and hexamethylenetetraamine play a template or structure-directing role in the construction of the resulting coordination architectures.

The elemental analysis data for the four compounds are in good agreement with the formulas $[Cd(tp)(bpp)]_n$ (**1**), $[Cd(tp)(bpy)]_n$ (**2**), $[\{Cd_4(bpa)_4(bpy)_6\}\cdot(bpy)_{0.5}\cdot 7H_2O]_n$ (**3**) and $[Cd_2\{(Htp)(tp)_{1.5}\}(bpe)]_n$ (**4**). The IR spectra of these compounds show the characteristic bands of the dicarboxylate groups in the usual region[55] at 1400−1375 cm^{-1} for the symmetric vibration and at 1610−1539 cm^{-1} for the asymmetric vibration, as well as the bands of the bpp ligand at 2953, 2939, 2860, 1616, 1504 and 1429 cm^{-1} for **1**, the bands of the bpy ligand at 1491 cm^{-1} for **2**, the bands of the bpy or bpa ligand at 1585, 1489, 3082 and 3055 cm^{-1} for **3**, and the bands of the bpe ligand at 1504, 1551, 1574, 3051 and 2929 cm^{-1} for **4**. The splitting of $\nu_{asym}(CO_2)$ in both **2** and **4** confirms that the carboxylate groups have a variety of coordination fashions. Moreover, for **4**, the peak at 1705 cm^{-1} suggests the presence of a protonated carboxylate group. These proposals are consistent with the crystal structures. The TGA traces for **1**, **2** and **4** show that the decomposition of the three compounds occurs at ca. 297−524 °C, 373−587 °C and 210−600 °C, respectively. The TGA trace for **3** shows an obvious weight loss starting at about 50 °C up to 100 °C to give a total weight loss of ca. 5.4%, corresponding to the loss of seven water molecules per formula unit (calcd. 4.9%). Subsequent to this no obvious weight loss occurs for **3** up to 186.9 °C, followed by an obvious weight loss up to 271.9 °C to give a total weight loss of ca. 2.9% corresponding to the loss of 0.5 bpy molecules per formula unit (calcd. 3.1%). Complete decomposition of **3** occurs at 271.9 °C and finishes at ca. 511 °C. This is consistent with the structure of **3** and suggests that the framework of **3** possesses a similar thermal stability to the above three compounds.

Crystal Structures

X-ray single-crystal analysis revealed that the crystal structure of **1** is a twofold parallel interpenetration topology of a 2D 4^4 network polymer. As shown in Figure 1, the fundamental building unit of **1** is composed of a six-coordinate Cd^{II} center, a tp ligand and a bpp ligand, in which each Cd center is coordinated in a distorted tetrahedral geometry to two tp ligands and two bpp ligands through two chelating carboxylate groups (O1, O2 and O3a, O4a) [Cd−O: 2.254(3)−2.444(3) Å] and two nitrogen donors (N1, N2b) [Cd−N: 2.295(3) Å]. Each tp and bpp ligand is

 © 2004 Wiley-VCH Verlag GmbH & Co. KGaA, Weinheim

bridged to two different Cd centers, which provides the 4-linking nodes resulting in an interesting square-grid motif with a window of about 11.9 × 11.1 Å (Figure 1). No guest molecules are found in this square grid. The square-grid motifs are linked to each other to form a typical 2D 4^4 network.[8,14,32,56] Neither tp ligands nor bpp ligands bridging to the same Cd center are coplanar; the N−Cd−N bond angle is 98.57(12)°, while the angle between two adjacent tp ligands chelated to the same Cd center is 132.5°. This 2D 4^4 network is interesting as the 4-linking nodes come from a tetrahedral geometry rather than from a pseudo-octahedral geometry; 4-linking nodes of tetrahedral geometry usually result in adamantoid networks. Due to the N−Cd−N bond angle of 98.57(12)° and the flexibility of the bpp ligands, an interesting pipe-comb-like 2D layer structure with a channel of about 11.4 × 11.1 Å occurs in this single 4^4 network along the *ab* plane (Figure 2). Moreover, the 4-linking nodes allow the 2D 4^4 network to have the undulating nature of the square grid polycatenated by another independent, symmetry-related 4^4 network, thus showing a twofold parallel interpenetration topology (Figure 3). This interpenetration means that the effective voids in the crystal structure of **1** actually have a volume of only 58.1 $Å^3$, which is 1.4% of the unit-cell volume, even though the single 4^4 network contains a big window and channel as described above.

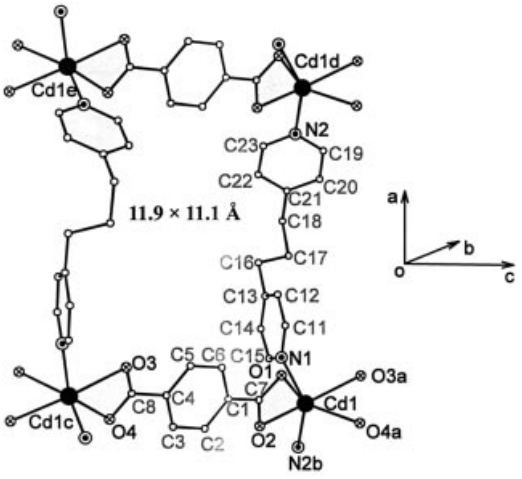

Figure 1. A drawing of **1** depicting the coordination environment around the Cd^{II} center to form a typical 4^4 net with a 11.9 × 11.1 Å window; the hydrogen atoms are omitted for clarity: (*a*) *x*, −*y* + 1/2, *z* + 1/2; (*b*) *x* − 1, *y*, *z*; (*c*) *x*, −*y* + 1/2, *z* − 1/2; (*d*) *x* + 1, *y*, *z*; (*e*) *x* + 1, −*y* + 1/2, *z* − 1/2

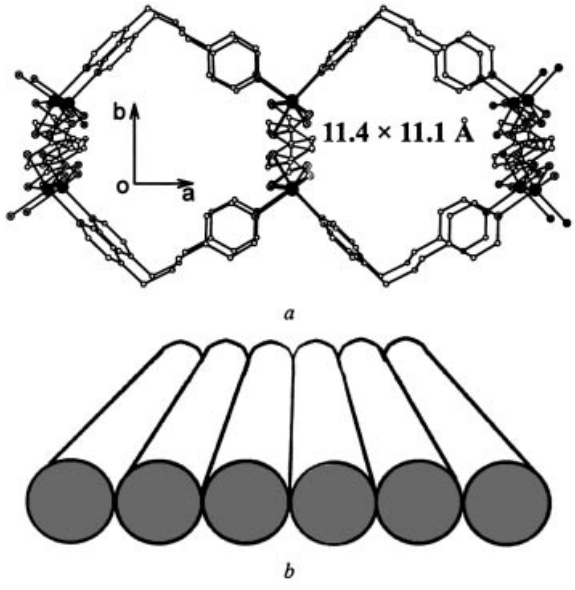

Figure 2. (a) A view of a single 4^4 net along the *ab* plane in **1** showing an interesting pipe-comb-like 2D layer structure with an 11.4 × 11.1 Å channel; the hydrogen atoms are omitted for clarity; (b) schematic diagram showing a pipe-comb-like 2D layer motif based upon **1**

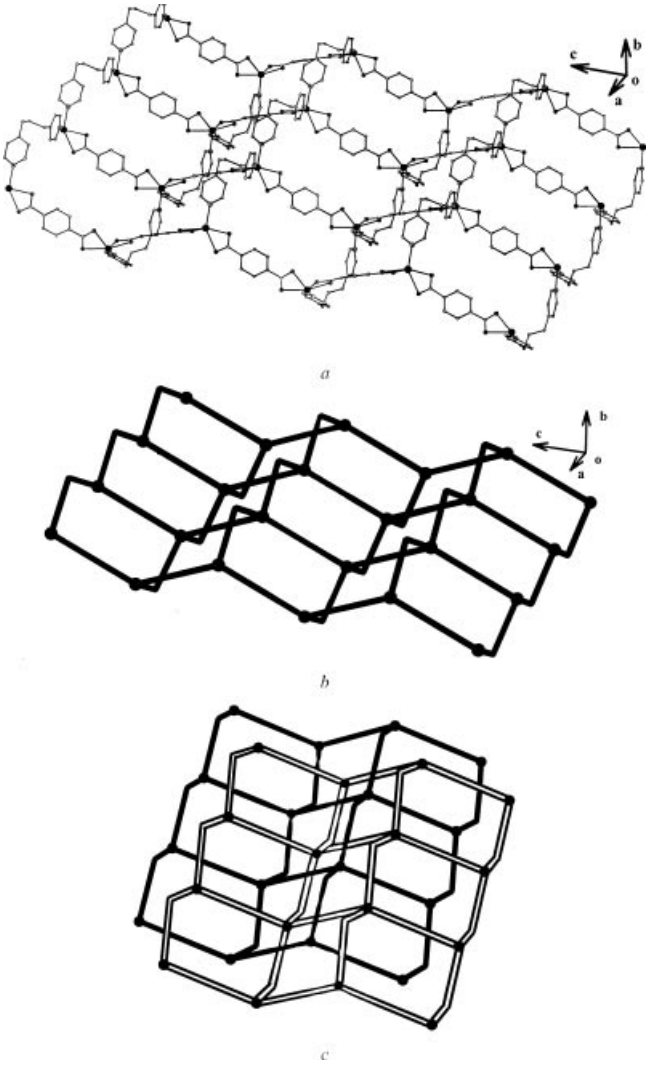

Figure 3. (a) The undulating nature of a single 4^4 net in **1**; the hydrogen atoms are omitted for clarity; (b) schematic diagram of **1**; (c) the twofold parallel interpenetration topology of **1**

The crystal structure of **2** consists of two independent six-coordinate Cd^{II} centers (Cd1, Cd2) that are bridged by

 © 2004 Wiley-VCH Verlag GmbH & Co. KGaA, Weinheim

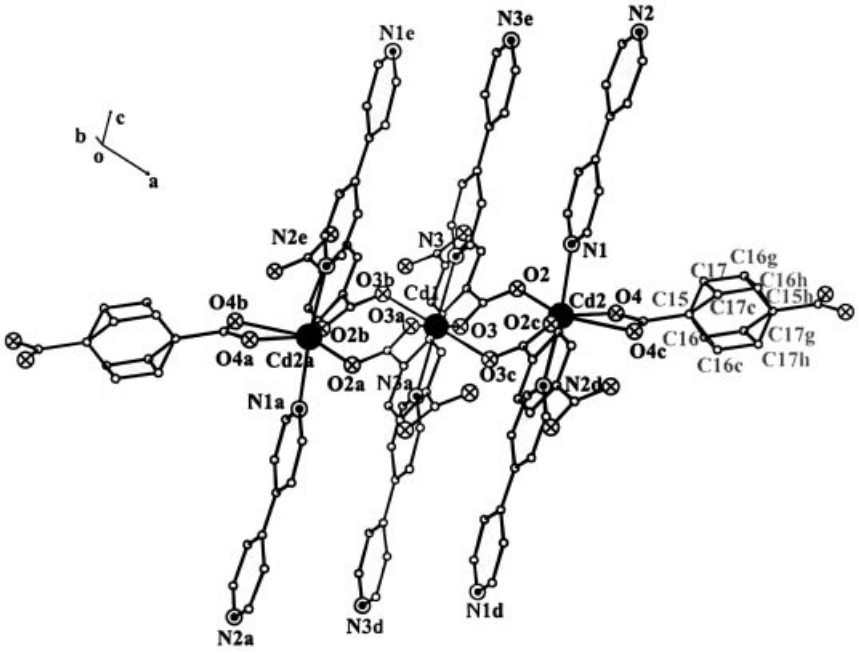

Figure 4. The coordination environment around the Cd^{II} centers in **2**; the hydrogen atoms are omitted for clarity: (*a*) $-x, -y, -z$; (*b*) $-x, y, -z$; (*c*) $x, -y, z$; (*d*) $x, y, z-1$; (*e*) $-x, -y, -z+1$; (*g*) $-x+1, y, -z+1$; (*h*) $-x+1, -y, -z+1$

two bis-bidentate tp ligands, the distance between the two metal centers (Cd1···Cd2) being 4.099 Å (Figure 4). The Cd1 center is in a distorted octahedral coordination sphere completed by two nitrogen atoms (N3, N3a) [Cd1−N: 2.342(12) Å] of two bpy ligands as the apices and four oxygen atoms (O3, O3a, O3b and O3c) [Cd1−O: 2.304(9) Å] in the equatorial positions; these oxygen atoms come from four bis-bidentate carboxylate groups of four different tp ligands. The Cd2 center also lies in a distorted octahedral coordination sphere, and is coordinated by two nitrogen atoms (N1, N2d) [Cd2−N: 2.338(14)−2.366(12) Å] of the other two bpy ligands as the apices and four oxygen atoms [Cd2−O: 2.231(8)−2.399(10) Å] in the equatorial positions, two (O2, O2c) of which are from two bridging bis-bidentate carboxylate groups of two different tp ligands, and the other two (O4, O4c) belong to a chelating carboxylate group of a tp ligand, whose aromatic ring shows positional disorder over two sites (C15, C16, C17g, C15h, C16h, C17c and C15, C16c, C17h, C15h, C16g, C17; see Figure 4). These two Cd^{II} centers (Cd1, Cd2) as well as Cd2a, an equivalent atom related to the Cd2 center, are bridged to construct a linear trinuclear $\{Cd_3O_{12}N_6\}$ cluster. In this way, the trinuclear $\{Cd_3O_{12}N_6\}$ clusters are interconnected through tp ligands to yield an interesting rectangular sheet

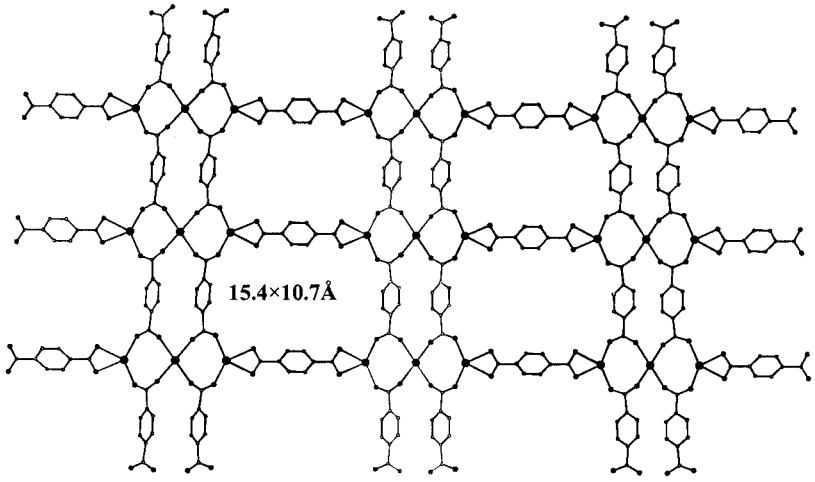

Figure 5. A view of the 2D rectangular {Cd(tp)} sheet subunit with a window of 15.4 × 10.7 Å in **2**; the hydrogen atoms are omitted for clarity

 © 2004 Wiley-VCH Verlag GmbH & Co. KGaA, Weinheim

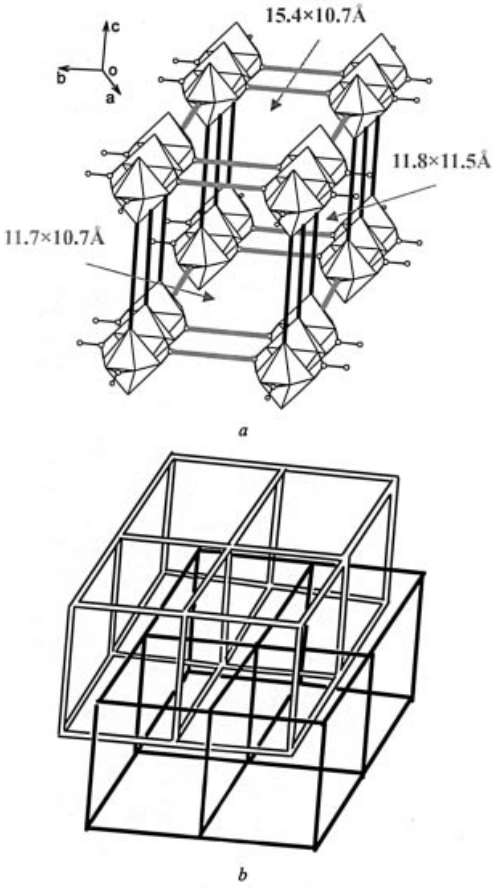

Figure 6. (a) A view depicting a 3D α-Po net topology in **2** assembled by the rectangular sheet subunits and bpy pillars (gray lines indicate the tp struts, black lines represent bpy struts); (b) the twofold interpenetration topology of **2**

with a window of 15.4 × 10.7 Å (Figure 5), which is different from similar reported structures.[21] The rectangular sheets are further pillared by bpy ligands to form a box-like 3D supramolecular architecture, a topology attributed to the α-Po net (Figure 6a), and the whole crystal structure of **2** exhibits twofold interpenetration (Figure 6b).

The crystal structure of **3** is a 3D porous framework composed of a well-separated host polymer, guest bpy molecules and lattice water molecules. There are four independent seven-coordinate Cd^{II} centers in the building unit of **3**, and the coordination sphere of each seven-coordinate Cd^{II} center is equivalent (Figure 7). In the host polymer, each seven-coordinate Cd^{II} center lies in a distorted pentagonal bipyramidal sphere, completed by two pairs of oxygen donors of two chelating carboxylate groups from two separate bpa ligands and three nitrogen donors from three different bpy ligands, in which two bpa and a bpy ligands are in the equatorial positions with the other two bpy ligands as the apices (Figure 7). Every bpa and bpy ligand links to two Cd^{II} centers through two chelating carboxylate groups and two nitrogen donors, respectively. Due to the angles between two adjacent bpa ligands and between bpa and bpy ligands coordinated to the same Cd^{II} center in the equatorial plane (130.5° and 112.6°, respectively), the Cd^{II} center and the bridging ligands actually form a slightly distorted trigonal-bipyramidal subunit, which has seldom been observed in metal-organic polymers.[32] In the crystal, these subunits are arranged to generate a honeycomb-like 3D supramolecular architecture, an unprecedented 5-connected borazone $4^6 6^4$ net topology,[57,58] with giant hexagonal channels about 30.5 × 24.8 Å across (Figure 8). To the best of our knowledge, this structural topology is still very rare

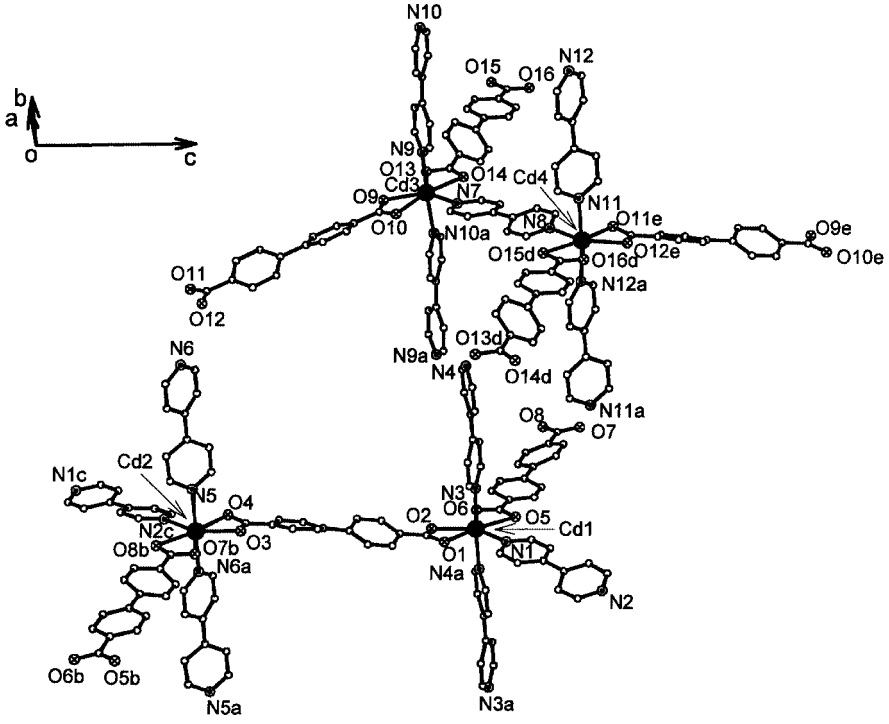

Figure 7. A view of **3** depicting the coordination environment around the Cd^{II} centers; hydrogen atoms, guest bpy and water molecules are omitted for clarity: (*a*) $x, y - 1, z$; (*b*) $x - 1, -y - 3/2, z - 1/2$; (*c*) $x, -y - 3/2, z - 1/2$; (*d*) $x - 1, y, z$; (*e*) $x, -y + 1/2, z + 1/2$

 © 2004 Wiley-VCH Verlag GmbH & Co. KGaA, Weinheim

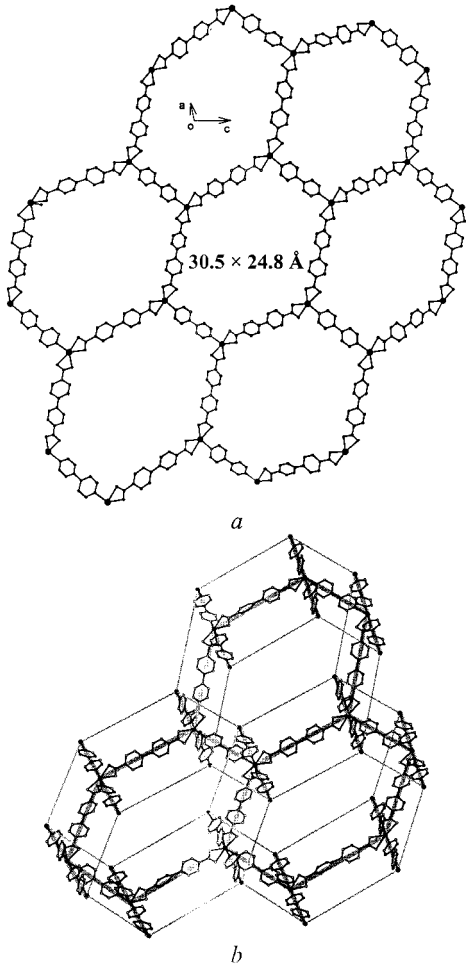

Figure 8. (*a*) A projective view along the *b* axis showing the honeycomb-like channels with a giant hexagonal cavity of about 30.5 × 24.8 Å in **3**; the hydrogen atoms and guests are omitted for clarity; (*b*) schematic topology of the 5-connected borazone $4^6 6^4$ net of **3**

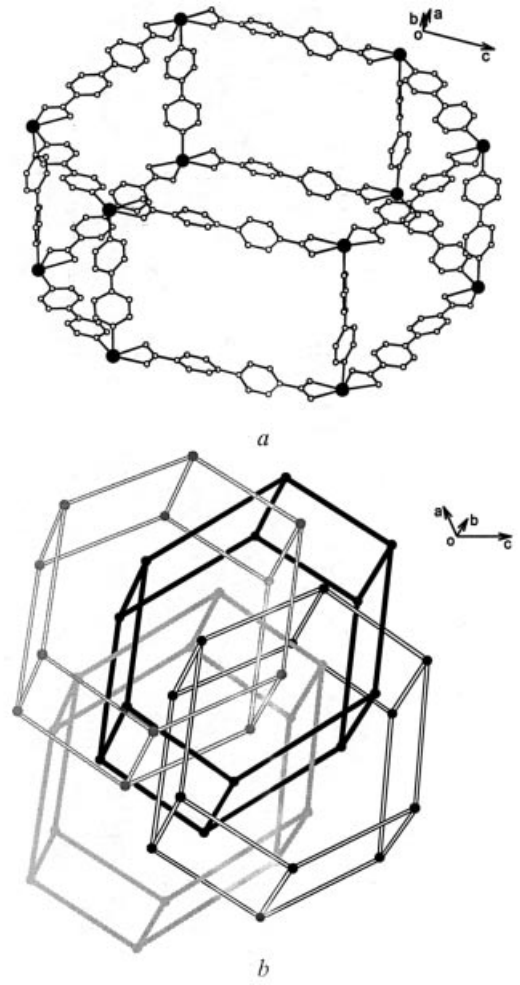

Figure 9. (*a*) A single hexagonal unit of the 3D honeycomb-like architecture in **3**;(*b*) the fourfold interpenetrating model of **3**

in coordination polymer chemistry.[32,58] Each hexagonal channel has a giant cavity of about 30.5 × 24.8 Å, while the actual crystal structure of compound **3** is a fourfold interpenetrating 3D supramolecular architecture (Figure 9). The resulting effective cavities, after removal of encapsulated guests − aqua and bpy molecules — in **3** has a volume of about 2609 $Å^3$, which is only 22% of the unit-cell volume.

The local coordination environment around the Cd^{II} centers in **4** is depicted in Figure 10. The two crystallographically distinct Cd^{II} centers (Cd1, Cd2) are each coordinated in a distorted octahedral sphere by five oxygen donors (O1, O21, O22, O24b and O12a for Cd1; O2, O11, O22, O23d and O24d for Cd2) and one nitrogen donor (N1 for Cd1; N2c for Cd2), in which the oxygen donors are from the carboxylate groups of four different tp ligands and the nitrogen donor is from a separate bpe ligand. Four different tp ligands bridge two Cd^{II} centers alternately in three different coordination fashions − chelating/bridging bis-bidentate, bis-bidentate and bidentate to form Cd-tp chains along the *a* axis (Figure 11a). Extension of these Cd-tp chains along the *ac* plane therefore gives a novel 2D abatis-like sheet (see b in Figure 11). These adjacent 2D abatis-like sheets are further crosslinked in a staggered fashion through bridging bpe ligands to generate an interesting 3D spiral pipe-like structure with a bolt (Figure 12). Although there is no interpenetration or incorporated guest molecule in **4**, the actual crystal structure has an effective void of an only 107 $Å^3$, which is 3.5% of the unit cell volume, due to the bolt described above.

Fluorescent Properties

To study the fluorescent properties of these four polymeric solids, the emission spectra of **1**−**4** were recorded for a polycrystalline sample of each of these materials in the solid state at ambient temperature. Intense fluorescent emissions at 549 and 582 nm (λ_{exc} = 532 nm) for **1**, 493 nm (λ_{exc} = 360 nm) for **2**, 413 and 424 nm (λ_{exc} = 315 nm) for **3** and 350 nm (λ_{exc} = 220 nm) for **4**, were observed, which can be assigned to ligand-to-metal charge transfer (LMCT) transitions. It is noticeable that compound **2** exhibits a quenching of the fluorescence with τ = 5.44 ns. This suggests that **2** may be an excellent candidate for potential photoactive material.

 © 2004 Wiley-VCH Verlag GmbH & Co. KGaA, Weinheim

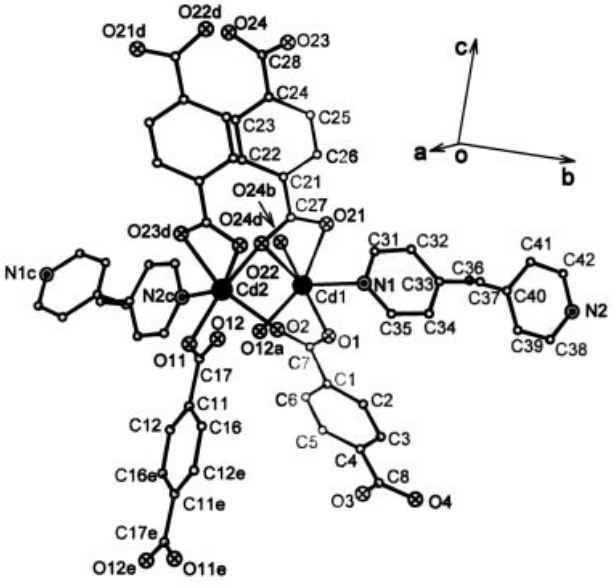

Figure 10. The local coordination of Cd^{II} centers in **4**; the hydrogen atoms are omitted for clarity: (*a*) $x - 1, y, z$; (*b*) $-x, -y, -z + 2$; (*c*) $-x - 3/2, y - 1/2, -z + 3/2$; (*d*) $-x + 1, -y, -z + 2$; (*e*) $-x + 1, -y, -z + 1$

Experimental Section

General Remarks: All the syntheses were performed in Parr Teflon-lined stainless steel autoclaves under autogenous pressure. Chemicals were purchased commercially and used as received without further purification. Infrared spectra were recorded on a Magna 750 spectrometer as KBr pellets. The C, H, O and N elemental microanalyses were carried out with a Vario EL III elemental analyzer. Fluorescent data were collected on an Edinburgh FL-FS920 TCSPC system at the Spectroscopy Lab of Fuzhou University, and TGA (thermal gravimetric analysis) was performed under nitrogen with a heating rate of 10 °C·min^{-1} using a TA5200/MDSC2910 system at the Thermal Analysis Lab of Huaqiao University. The pore-volume analysis was perfomed with the PLATON software package.[59]

[Cd(tp)(bpp)]$_n$ (1): Compound **1** was synthesized hydrothermally from the reaction of cadmium acetate dihydrate (1.5 mmol), H_2tp (1 mmol), bpp (1.075 mmol), $(Ph_3PCH_2Ph)Cl$ (1 mmol) and water (5 mL) in a molar ratio of 3:2:2.15:1:556 at 200 °C for 4 days. The mixture was then cooled at a rate of about 3.5 °C·h^{-1} to give a 32% yield of **1** (228.8 mg), based on Cd, as colorless block crystals, which were collected by hand and washed with water and absolute alcohol. $C_{21}H_{18}CdN_2O_4$ (474.77): calcd. C 53.12, H 3.82, N 5.90, O 13.48; found C 53.39, H 3.32, N 5.43, O 13.67. IR (KBr pellet): $\tilde{\nu}$ = 3401 cm^{-1} (w, br), 3064 (vw), 2953 (w), 2939 (w), 2860 (w),

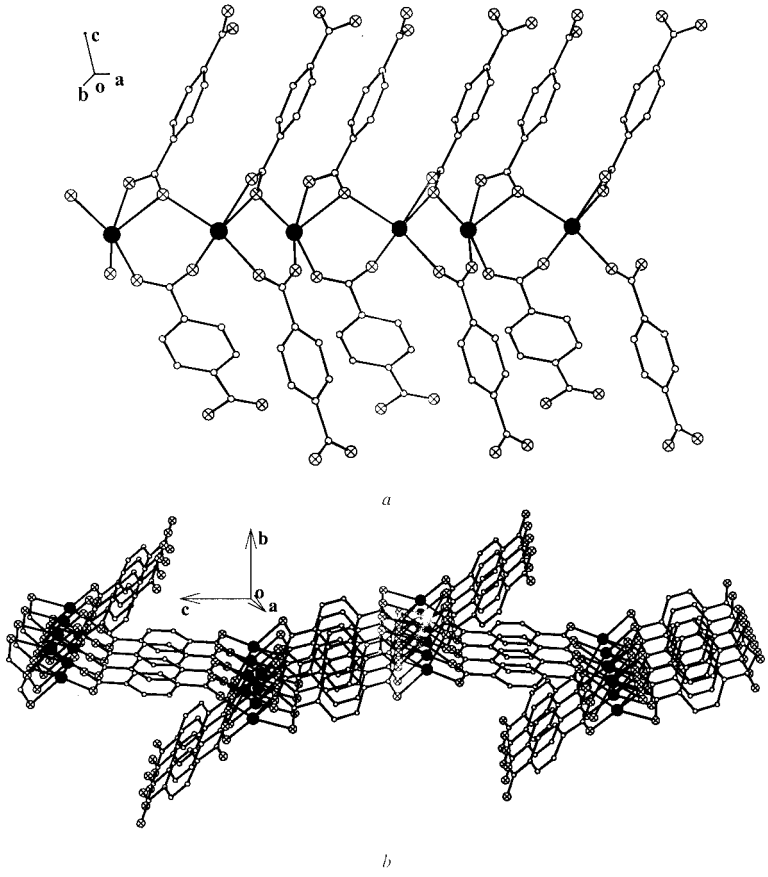

Figure 11. A view showing (a) the Cd-tp chains in **4** extended along the *ac* plane to generate (b) a novel 2D abatis-like sheet subunit; the hydrogen atoms are omitted for clarity.

 © 2004 Wiley-VCH Verlag GmbH & Co. KGaA, Weinheim

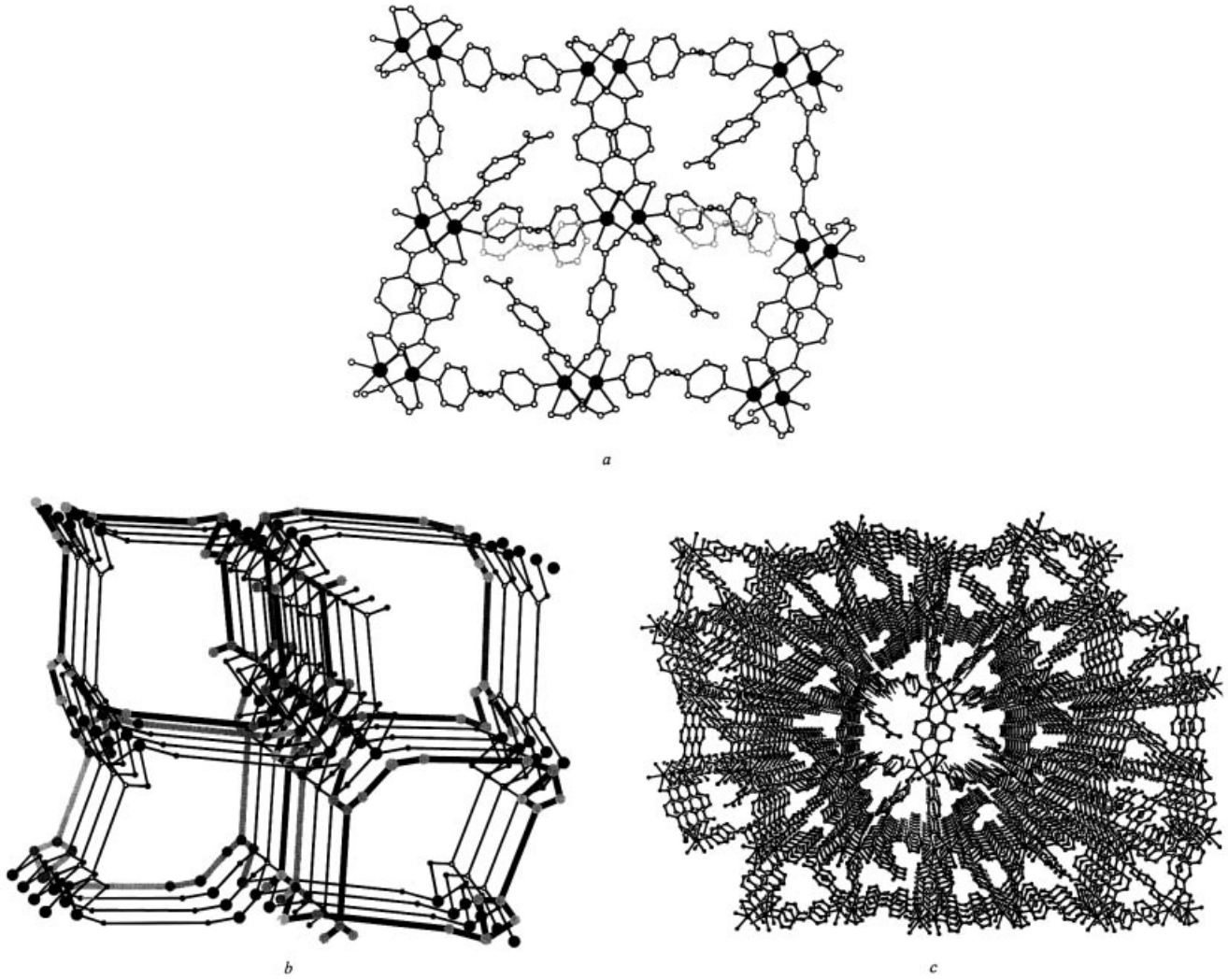

Figure 12. (a) An interesting 3D spiral pipe-like structure with a bolt in **4** constructed by 2D abatis-like sheet subunits with bpe bridging ligands; (b) 3D spiral pipe-like structure motif based on **4**, the bolts are omitted for clarity; (c) perspective view of the 3D architecture in **4** along the *a* axis

Table 1. Crystal parameters, data collections and structure refinements for **1**−**4**

Compound	**1**	**2**	**3**	**4**
Formula	$C_{21}H_{18}CdN_2O_4$	$C_{18}H_{12}CdN_2O_4$	$C_{121}H_{98}Cd_4N_{13}O_{23}$	$C_{32}H_{23}Cd_2N_2O_{10}$
Molecular mass	474.77	432.69	2551.72	820.32
Crystal system	orthorhombic	monoclinic	monoclinic	monoclinic
Space group	*Pbca*	*C*2/*m*	$P2_1/c$	$P2_1/n$
a (Å)	11.9401(0)	20.299(3)	23.2208(0)	6.9896(1)
b (Å)	16.8148(3)	10.720(1)	11.8103(1)	22.6294(1)
c (Å)	20.2743(3)	11.764(2)	45.4670(6)	19.7738(3)
α (°)	90	90	90	90
β (°)	90	110.944(2)	104.516(1)	99.380(1)
γ (°)	90	90	90	90
V (Å^3)	4070.48(9)	2390.6(6)	12071.0(2)	3085.81(7)
Z	8	6	4	4
ρ_{calc} (g·cm^{-3})	1.549	1.803	1.404	1.766
T (K)	293(2)	293(2)	293(2)	293(2)
μ (cm^{-1})	1.101	1.396	0.768	1.440
λ (Mo-$K_α$) (Å)	0.71073	0.71073	0.71073	0.71073
Collected reflections	14577	3808	35409	10386
Independent reflections	3600	2227	21219	5360
Observed reflections	2581 (>2σ*I*)	1215 (>2σ*I*)	13274 (>2σ*I*)	4468 (>2σ*I*)
R_{int}	0.0354	0.0554	0.0400	0.0232
R[a]	0.0306	0.0720	0.0725	0.0352
R_w [b] [c]	0.0710	0.1604	0.2014	0.0875

[a] $R = (F_o - F_c)/F_o$. [b] $R_w = \{w[(F_o^2 - F_c^2)^2]/w[(F_o^2)^2]\}^{1/2}$. [c] $w = 1/[\sigma^2(F_o^2) + (aP)^2 + bP]$, where $P = (F_o^2 + 2F_c^2)/3$.

 © 2004 Wiley-VCH Verlag GmbH & Co. KGaA, Weinheim

1957 (vw), 1709 (w), 1616 (vs), 1556 (vs), 1504 (s), 1429 (s), 1385 (vs), 1296 (m), 1225 (m), 1182 (w), 1074 (w,sh), 1026 (w,sh), 889 (w), 839 (s), 810 (m), 777 (w), 752 (vs), 729 (m), 613 (m), 577 (m), 528 (w), 511 (w), 480 (m), 451 (w).

[Cd(tp)(bpy)]$_n$ (2): Similar to the preparation of **1**, the hydrothermal reaction of cadmium acetate dihydrate (1.5 mmol), H_2tp (1 mmol), bpy (1 mmol), hexamethylenetetraamine (1 mmol) and water (5 mL) in a molar ratio of 3:2:2:2:556 was performed at 200 °C for 4 days, then the reactant was cooled to a rate of about 3.5 °C·h^{-1} to give about a 10% yield of **2** (64.8 mg), based on Cd, as brown block crystals, which were separated by hand from the reaction mixture and washed with water and absolute alcohol. The sample was allowed to dry in air and was found to be indefinitely stable. $C_{18}H_{12}CdN_2O_4$ (432.69): calcd. C 49.96, H 2.80, N 6.47, O 14.79; found C 49.77, H 2.41, N 6.31, O 14.48. IR (KBr pellet): $\tilde{\nu}$ = 3419 cm^{-1} (w, br), 3055 (w), 1603 (m), 1566 (vs), 1491 (w), 1400 (s), 1375 (s), 1221 (m), 1076 (m), 1043 (w), 1014 (m), 887 (vw), 823 (m), 806 (m), 744 (m), 727 (w), 631 (m), 509 (w).

[{Cd$_4$(bpa)$_4$(bpy)$_6$}·(bpy)$_{0.5}$·7H$_2$O]$_n$ (3): Similar to the synthesis of **1**, the hydrothermal reaction of cadmium acetate dihydrate (1.5 mmol), H_2bpa (1 mmol), bpy·2H_2O (1 mmol), $NaOC_2H_5$ (4 mmol) and H_2O (5 mL) in a molar ratio of 3:2:2:8:556 was performed at 200 °C for 4 days, then the reactant was cooled to a rate

Table 2. Selected bond lengths (Å) for **1**−**4**

Compound **1**[a]			
Cd(1)−O(1)	2.444(3)	Cd(1)−O(4a)	2.254(3)
Cd(1)−O(2)	2.271(3)	Cd(1)−N(1)	2.295(3)
Cd(1)−O(3a)	2.392(3)	Cd(1)−N(2b)	2.295(3)
Compound **2**[b]			
Cd(1)−O(3)	2.304(9)	Cd(2)−O(4)	2.399(10)
Cd(1)−N(3)	2.342(12)	Cd(2)−N(1)	2.366(12)
Cd(2)−O(2)	2.231(8)	Cd(2)−N(2d)	2.338(14)
Compound **3**[c]			
Cd(1)−O(1)	2.549(2)	Cd(3)−O(9)	2.335(3)
Cd(1)−O(2)	2.337(3)	Cd(3)−O(10)	2.551(3)
Cd(1)−O(5)	2.617(3)	Cd(3)−O(13)	2.323(3)
Cd(1)−O(6)	2.288(3)	Cd(3)−O(14)	2.488(3)
Cd(1)−N(1)	2.367(3)	Cd(3)−N(7)	2.380(3)
Cd(1)−N(3)	2.378(3)	Cd(3)−N(9)	2.378(3)
Cd(1)−N(4a)	2.351(3)	Cd(3)−N(10a)	2.378(3)
Cd(2)−O(3)	2.338(3)	Cd(4)−O(11e)	2.473(3)
Cd(2)−O(4)	2.580(3)	Cd(4)−O(12e)	2.363(3)
Cd(2)−O(7b)	2.342(3)	Cd(4)−O(15d)	2.589(3)
Cd(2)−O(8b)	2.528(3)	Cd(4)−O(16d)	2.268(3)
Cd(2)−N(2c)	2.364(3)	Cd(4)−N(8)	2.361(3)
Cd(2)−N(5)	2.360(3)	Cd(4)−N(11)	2.371(3)
Cd(2)−N(6a)	2.392(4)	Cd(4)−N(12a)	2.377(3)
Compound **4**[d]			
Cd(1)−O(1)	2.262(3)	Cd(2)−O(2)	2.177(4)
Cd(1)−O(12a)	2.192(3)	Cd(2)−O(11)	2.214(3)
Cd(1)−O(21)	2.415(3)	Cd(2)−O(22)	2.464(3)
Cd(1)−O(22)	2.395(3)	Cd(2)−O(23d)	2.304(3)
Cd(1)−O(24b)	2.453(3)	Cd(2)−O(24d)	2.449(3)
Cd(1)−N(1)	2.282(4)	Cd(2)−N(2c)	2.278(4)

[a] a: x, $-y + 1/2$, $z + 1/2$; b: $x - 1$, y, z. [b] d: x, y, $z - 1$. [c] a: x, $y - 1$, z; b: $x - 1$, $-y - 3/2$, $z - 1/2$; c x, $-y - 3/2$, $z - 1/2$; d: $x - 1$, y, z; e: x, $-y + 1/2$, $z + 1/2$. [d] a: $x - 1$, y, z; b: $-x$, $-y$, $-z + 2$; c: $-x - 3/2$, $y - 1/2$, $-z + 3/2$; d: $-x + 1$, $-y$, $-z + 2$.

Table 3. Selected bond angles (°) for **1**−**4**[a]

Compound **1**			
O(4a)−Cd(1)−O(2)	113.25(12)	N(1)−Cd(1)−O(3a)	83.77(12)
O(4a)−Cd(1)−N(1)	138.51(12)	N(2b)−Cd(1)−O(3a)	105.46(15)
O(2)−Cd(1)−N(1)	105.72(12)	O(4a)−Cd(1)−O(1)	103.29(11)
O(4a)−Cd(1)−N(2b)	94.13(13)	O(2)−Cd(1)−O(1)	55.33(10)
O(2)−Cd(1)−N(2b)	91.62(11)	N(1)−Cd(1)−O(1)	87.10(11)
N(1)−Cd(1)−N(2b)	98.57(12)	N(2b)−Cd(1)−O(1)	146.54(11)
O(4a)−Cd(1)−O(3a)	54.75(12)	O(3a)−Cd(1)−O(1)	107.94(14)
O(2)−Cd(1)−O(3a)	159.19(15)		
Compound **2**			
O(3a)−Cd(1)−O(3)	180.0(5)	O(2c)−Cd(2)−O(2)	128.7(6)
O(3a)−Cd(1)−O(3b)	104.0(5)	O(2c)−Cd(2)−N(2d)	94.1(3)
O(3)−Cd(1)−O(3b)	76.0(5)	O(2)−Cd(2)−N(2d)	94.1(3)
O(3a)−Cd(1)−O(3c)	76.0(5)	O(2c)−Cd(2)−N(1)	83.4(3)
O(3)−Cd(1)−O(3c)	104.0(5)	O(2)−Cd(2)−N(1)	83.4(3)
O(3b)−Cd(1)−O(3c)	180.0(5)	N(2d)−Cd(2)−N(1)	173.9(4)
O(3a)−Cd(1)−N(3a)	96.7(3)	O(2c)−Cd(2)−O(4)	140.2(4)
O(3)−Cd(1)−N(3a)	83.3(3)	O(2)−Cd(2)−O(4)	89.5(4)
O(3b)−Cd(1)−N(3a)	96.7(3)	N(2d)−Cd(2)−O(4)	93.9(4)
O(3c)−Cd(1)−N(3a)	83.3(3)	N(1)−Cd(2)−O(4)	91.6(4)
O(3a)−Cd(1)−N(3)	83.3(3)	O(2c)−Cd(2)−O(4c)	89.5(4)
O(3)−Cd(1)−N(3)	96.7(3)	O(2)−Cd(2)−O(4c)	140.2(4)
O(3b)−Cd(1)−N(3)	83.3(3)	N(2d)−Cd(2)−O(4c)	93.9(4)
O(3c)−Cd(1)−N(3)	96.7(3)	N(1)−Cd(2)−O(4c)	91.6(4)
N(3a)−Cd(1)−N(3)	180.0(6)	O(4)−Cd(2)−O(4c)	51.0(5)
Compound **3**			
O(6)−Cd(1)−O(2)	87.46(9)	O(13)−Cd(3)−O(9)	87.89(11)
O(6)−Cd(1)−N(4a)	89.55(10)	O(13)−Cd(3)−N(9)	86.18(11)
O(2)−Cd(1)−N(4a)	93.17(10)	O(9)−Cd(3)−N(9)	96.95(12)
O(6)−Cd(1)−N(1)	136.80(9)	O(13)−Cd(3)−N(7)	135.75(10)
O(2)−Cd(1)−N(1)	135.72(9)	O(9)−Cd(3)−N(7)	136.32(10)
N(4a)−Cd(1)−N(1)	89.24(11)	N(9)−Cd(3)−N(7)	89.23(11)
O(6)−Cd(1)−N(3)	91.98(10)	O(13)−Cd(3)−N(10a)	95.33(12)
O(2)−Cd(1)−N(3)	90.43(11)	O(9)−Cd(3)−N(10a)	88.05(12)
N(4a)−Cd(1)−N(3)	176.15(11)	N(9)−Cd(3)−N(10a)	174.83(12)
N(1)−Cd(1)−N(3)	87.22(11)	N(7)−Cd(3)−N(10a)	86.24(12)
O(6)−Cd(1)−O(1)	140.18(9)	O(13)−Cd(3)−O(14)	52.55(11)
O(2)−Cd(1)−O(1)	53.06(9)	O(9)−Cd(3)−O(14)	139.60(11)
N(4a)−Cd(1)−O(1)	96.79(9)	O(9)−Cd(3)−O(10)	53.37(10)
N(1)−Cd(1)−O(1)	82.74(9)	N(9)−Cd(3)−O(10)	94.09(10)
N(3)−Cd(1)−O(1)	84.28(9)	N(7)−Cd(3)−O(10)	83.14(10)
O(6)−Cd(1)−O(5)	52.50(10)	N(10a)−Cd(3)−O(10)	87.84(10)
O(2)−Cd(1)−O(5)	139.87(10)	O(14)−Cd(3)−O(10)	166.15(11)
N(4a)−Cd(1)−O(5)	84.88(11)	O(13)−Cd(3)−C(55)	27.19(13)
N(1)−Cd(1)−O(5)	84.39(9)	O(9)−Cd(3)−C(55)	114.91(13)
N(3)−Cd(1)−O(5)	93.26(11)	N(9)−Cd(3)−C(55)	86.27(13)
O(1)−Cd(1)−O(5)	167.00(10)	N(7)−Cd(3)−C(55)	108.61(13)
O(3)−Cd(2)−O(7b)	88.11(11)	N(10a)−Cd(3)−C(55)	92.82(13)
O(3)−Cd(2)−N(5)	93.18(12)	O(14)−Cd(3)−C(55)	25.41(13)
O(7b)−Cd(2)−N(5)	96.02(13)	O(10)−Cd(3)−C(55)	168.25(13)
O(3)−Cd(2)−N(2c)	136.74(10)	O(16d)−Cd(4)−N(8)	136.92(10)
O(7b)−Cd(2)−N(2c)	134.84(10)	O(16d)−Cd(4)−O(12e)	83.70(11)
N(5)−Cd(2)−N(2c)	87.84(12)	N(8)−Cd(4)−O(12e)	139.16(11)
O(3)−Cd(2)−N(6a)	87.89(12)	O(16d)−Cd(4)−N(11)	91.96(12)
O(7b)−Cd(2)−N(6a)	90.19(13)	N(8)−Cd(4)−N(11)	87.73(12)
N(5)−Cd(2)−N(6a)	173.72(13)	O(12e)−Cd(4)−N(11)	96.31(13)
N(2c)−Cd(2)−N(6a)	87.15(13)	O(16d)−Cd(4)−N(12a)	91.54(12)
O(3)−Cd(2)−O(8b)	140.35(10)	N(8)−Cd(4)−N(12a)	86.32(12)
O(7b)−Cd(2)−O(8b)	52.31(10)	O(12e)−Cd(4)−N(12a)	89.02(13)
N(5)−Cd(2)−O(8b)	89.43(12)	N(11)−Cd(4)−N(12a)	173.92(13)
N(2c)−Cd(2)−O(8b)	82.87(10)	O(16d)−Cd(4)−O(11e)	136.69(11)
N(6a)−Cd(2)−O(8b)	93.69(12)	N(8)−Cd(4)−O(11e)	86.23(10)
O(3)−Cd(2)−O(4)	51.92(11)	O(12e)−Cd(4)−O(11e)	53.00(12)
O(7b)−Cd(2)−O(4)	139.79(11)	N(11)−Cd(4)−O(11e)	93.65(11)
N(5)−Cd(2)−O(4)	90.99(11)	N(12a)−Cd(4)−O(11e)	87.21(10)
N(2c)−Cd(2)−O(4)	84.83(10)	O(16d)−Cd(4)−O(15d)	52.81(11)
N(6a)−Cd(2)−O(4)	84.80(11)	N(8)−Cd(4)−O(15d)	84.23(10)
O(8b)−Cd(2)−O(4)	167.66(10)	O(12e)−Cd(4)−O(15d)	136.51(11)
N(9)−Cd(3)−O(14)	89.06(12)	N(11)−Cd(4)−O(15d)	86.33(11)

 © 2004 Wiley-VCH Verlag GmbH & Co. KGaA, Weinheim

Table 3. *(Continued)*

N(7)−Cd(3)−O(14)	83.42(10)	N(12a)−Cd(4)−O(15d)	91.83(10)
N(10a)−Cd(3)−O(14)	87.95(13)	O(11e)−Cd(4)−O(15d)	170.45(11)
O(13)−Cd(3)−O(10)	141.07(11)		
Compound **4**			
O(12a)−Cd(1)−O(1)	87.38(15)	O(2)−Cd(2)−O(23d)	157.81(18)
O(12a)−Cd(1)−N(1)	113.42(15)	O(11)−Cd(2)−O(23d)	100.56(14)
O(1)−Cd(1)−N(1)	88.13(14)	N(2c)−Cd(2)−O(23d)	92.27(13)
O(12a)−Cd(1)−O(22)	105.45(13)	O(2)−Cd(2)−O(24d)	103.33(17)
O(1)−Cd(1)−O(22)	103.42(13)	O(11)−Cd(2)−O(24d)	100.92(13)
N(1)−Cd(1)−O(22)	139.91(12)	N(2c)−Cd(2)−O(24d)	146.80(12)
O(12a)−Cd(1)−O(21)	159.46(13)	O(23d)−Cd(2)−O(24d)	55.29(10)
O(1)−Cd(1)−O(21)	100.01(13)	O(2)−Cd(2)−O(22)	82.37(14)
N(1)−Cd(1)−O(21)	86.14(12)	O(11)−Cd(2)−O(22)	165.52(13)
O(22)−Cd(1)−O(21)	54.28(10)	N(2c)−Cd(2)−O(22)	80.89(12)
O(12a)−Cd(1)−O(24b)	85.80(12)	O(23d)−Cd(2)−O(22)	91.86(11)
O(1)−Cd(1)−O(24b)	165.57(13)	O(24d)−Cd(2)−O(22)	92.24(10)
N(1)−Cd(1)−O(24b)	82.95(12)	O(2)−Cd(2)−C(28d)	131.05(18)
O(22)−Cd(1)−O(24b)	90.66(10)	O(11)−Cd(2)−C(28d)	103.75(14)
O(21)−Cd(1)−O(24b)	90.72(11)	N(2c)−Cd(2)−C(28d)	118.83(14)
O(2)−Cd(2)−O(11)	88.69(17)	O(23d)−Cd(2)−C(28d)	27.13(12)
O(2)−Cd(2)−N(2c)	107.81(18)	O(24d)−Cd(2)−C(28d)	28.25(11)
O(11)−Cd(2)−N(2c)	91.12(14)	O(22)−Cd(2)−C(28d)	90.70(11)

[a] See footnotes to Table 2 for symmetry operations for each compound.

of about 3.5 °C·h^{-1}. The resulting primrose needle crystals were separated by hand from the reaction mixture and washed with water and absolute alcohol to give about a 39% yield of **1** (373.0 mg) based on Cd. $C_{121}H_{98}Cd_4N_{13}O_{23}$ (2551.7): calcd. C 56.95, H 3.87, N 7.14, O 14.42; found C 56.92, H 2.97, N 7.17, O 14.18. FT-IR (KBr pellet): $\tilde{\nu}$ = 3390 cm^{-1} (s), 3082 (w), 3055 (w), 1942 (w), 1585 (s), 1539 (s), 1489 (m), 1385 (s), 1219 (s), 1176 (w), 1105 (w), 1074 (m), 1043 (w), 1005 (s), 833 (s), 806 (s), 775 (s), 764 (s), 729 (w), 702 (w), 677 (m), 629(s), 567 (w), 492 (m).

$[Cd_2\{(Htp)(tp)_{1.5}\}(bpe)]_n$ (4): Similar to the synthesis of **1**, the hydrothermal reaction of cadmium acetate dihydrate (1.5 mmol), H_2tp (1 mmol), bpe (1 mmol), $(Ph_3PCH_2Ph)Cl$ (0.5 mmol) and water (5 mL) in a molar ratio of 3:2:2:1:556 was performed at 200 °C for 4 days, then the reactant was cooled at a rate of about 3.5 °C·h^{-1}. The resulting colorless crystals were separated by hand from the reaction mixture and then washed with water and absolute alcohol to give about a 37% yield of **4** (227.2 mg) based on Cd. $C_{32}H_{23}Cd_2N_2O_{10}$ (820.32): calcd. C 46.85, H 2.83, N 3.41, O 19.50; found C 46.78, H 2.12, N 3.51, O 19.72. IR (KBr pellet): $\tilde{\nu}$ = 3051 cm^{-1} (vw), 2929 (vw), 2617 (vw), 2480 (vw), 1954 (vw), 1705 (s), 1610 (vs), 1574 (vs), 1551 (vs), 1504 (s), 1394 (vs), 1313 (m), 1242 (s), 1111 (m), 1072 (m), 1016 (m), 881 (w), 831 (m), 777 (m), 735 (s), 677 (w), 633(w), 544 (m), 513 (m), 445 (w).

Crystallographic Studies: Intensity data for the four compounds were collected at 293(2) K on a Siemens Smart CCD area-detector diffractometer with Mo-K_α radiation (λ = 0.71073Å) and a graphite monochromator using the ω-scan mode. Data reductions and absorption corrections were performed with the SMART and SADABS software packages, respectively. The structures were solved by direct methods using SHELXS-97[60] and were refined by full-matrix least-squares methods using SHELXL-97.[61] Anisotropic displacement parameters were refined for all non-hydrogen atoms except for the disordered benzene ring of tp molecules. No attempt was made to locate the hydrogen atoms of water and disordered atoms; the other hydrogen atoms were added in the riding model and not refined. Final $R = (F_o - F_c)/F_o$, $R_w = \{w[(F_o^2 - F_c^2)^2]/w[(F_o^2)^2]\}^{1/2}$, with $w = 1/[\sigma^2(F_o^2) + (aP)^2 + bP]$ [where $P = (F_o^2 + 2F_c^2)/3$]. The structure reliability factors for **2** and **3** were not satisfactory (R = 0.0720 and 0.0725, respectively), probably as a result of the presence of disordered tp molecules and guest water and not refined. The crystallographic data are summarized in Table 1, and selected bond lengths and bond angles of the three compounds are listed in Tables 2 and 3, respectively.

CCDC-224384 to -224387 (for compounds **1**−**4**) contain the supplementary crystallographic data for this paper. These data can be obtained free of charge via www.ccdc.cam.ac.uk/conts/retrieving.html (or from the Cambridge Crystallograghic Data Centre, 12 Union Road, Cambridge CB2 1EZ, UK; Fax: (internat.) + 44-1223-336-033; E-mail: deposit@ccdc.cam.ac.uk).

Acknowledgments

This research was supported by grants from the State Key Laboratory of Structural Chemistry, Fujian Institute of Research on the Structure of Matter, Chinese Academy of Sciences (CAS), the National Ministry of Science Foundation of China (001CB1089), the National Science Foundation of China (20333070, 20273073 and 90206040), and the Science Foundation of CAS and Fujian Province for research funding support (2002F014).

[1] J. M. Lehn, *Supramolecular Chemistry*, VCH, Weinheim, **1995**.
[2] R. Robson, in *Comprehensive Supramolecular Chemistry*, Pergamon, New York, **1996**, chapter 22, p. 733.
[3] R. Robson, B. F. Abrahams, S. R. Batten, R. W. Gable, B. F. Hoskins, J. Liu, *Supramolecular Architecture*, ACS publications, Washington, DC, **1992**, chapter 19, p. 449.
[4] B. F. Abrahams, B. F. Hoskins, R. Robson, *J. Am. Chem. Soc.* **1991**, *113*, 3606.
[5] Q. Wang, X. Wu, W. Zhang, T. Sheng, P. Lin, J. Li, *Inorg. Chem.* **1999**, *38*, 2223.
[6] O. M. Yaghi, G. Li, *Angew. Chem. Int. Ed. Engl.* **1995**, *34*, 207.
[7] O. M. Yaghi, H. Li, C. Davis, D. Richardson, T. L. Groy, *Acc. Chem. Res.* **1998**, *31*, 474.
[8] M. Eddaoudi, D. B. Moler, H. Li, B. Chen, M. O'Keeffe, O. M. Yaghi, *Acc. Chem. Res.* **2001**, *34*, 319.
[9] M. P. Byrn, C. J. Curtis, Y. Hsiou, S. I. Khan, P. A. Sawin, A. Terzis, C. E. Strouse, in *Solid-State Supramolecular Chemistry: Crystal Engineering, Comprehensive Supramolecular Chemistry* (Eds.: D. D. MacNicol, F. Toda, R. Bishop); Elsevier, Oxford, U. K., **1996**; *6*, p. 715.
[10] F. Wurthner, A. Sautter, *Chem. Commun.* **2000**, 445.
[11] G. R. Desiraju, *Crystal Engineering, The Design of Organic Solids*, Elsevier, Amsterdam, **1989**.
[12] C. B. Aakeroy, *Acta Crystallogr., Sect. B* **1977**, *53*, 569.
[13] M. J. Plater, M. R. St. J. Foreman, T. Gelbrich, M. B. Hursthouse, *J. Chem. Soc., Dalton Trans.* **2000**, 1995.
[14] M. Fujita, Y. J. Kwon, S. W. Ashizu, K. Ogura, *J. Am. Chem. Soc.* **1994**, *116*, 1151.
[15] M. Fujita, K. Ogura, *Bull. Chem. Soc. Jpn.* **1996**, *69*, 1471.
[16] M. Fujita, Y. J. Kwon, Y. O. Sasaki, K. Yamaguchi, K. Ogura, *J. Am. Chem. Soc.* **1995**, *117*, 7287.
[17] P. J. Stang, B. Olenyuk, *Acc. Chem. Res.* **1997**, *30*, 502.
[18] X.-M. Chen, M.-L. Tong, Y.-J. Luo, Z.-N. Chen, *Aust. J. Chem.* **1996**, *49*, 835.
[19] M.-L. Tong, X.-M. Chen, X.-L. Yu, T. C. W. Mak, *J. Chem. Soc., Dalton Trans.* **1998**, 5.
[20] M.-L. Tong, B.-H. Ye, J.-W. Cai, X.-M. Chen, S. W. Ng, *Inorg. Chem.* **1998**, *37*, 2645.
[21] J. Tao, M.-L. Tong, X.-M. Chen, *J. Chem. Soc., Dalton Trans.* **2000**, 3669.
[22] M.-L. Tong, H.-J. Chen, X.-M. Chen, *Inorg. Chem.* **2000**, *39*, 2235.

 © 2004 Wiley-VCH Verlag GmbH & Co. KGaA, Weinheim

[23] J.-C. Dai, S.-M. Hu, X.-T. Wu, Z.-Y. Fu, W.-X. Du, H.-H. Zhang, R.-Q. Sun, *New J. Chem.* **2003**, *27*, 914.
[24] Z.-Y. Fu, X.-T. Wu, J.-C. Dai, S.-M. Hu, W.-X. Du, H.-H. Zhang, R.-Q. Sun, *Eur. J. Inorg. Chem.* **2002**, 2730.
[25] Z.-Y. Fu, X.-T. Wu, J.-C. Dai, L.-M. Wu, C.-P. Cui, S.-M. Hu, *Chem. Commun.* **2001**, 1856.
[26] J.-C. Dai, X.-T. Wu, Z.-Y. Fu, C.-P. Cui, S.-M. Hu, W.-X. Du, L.-M. Wu, H.-H. Zhang, R.-Q. Sun, *Inorg. Chem.* **2002**, *41*, 1391.
[27] Z.-Y. Fu, X.-T. Wu, J.-C. Dai, S.-M. Hu, W.-X. Du, *New J. Chem.* **2002**, *26*, 978.
[28] K. N. Power, T. L. Hennigar, M. J. Zaworotko, *New J. Chem.* **1998**, 177.
[29] L. R. MacGillivray, S. Subramanian, M. Zaworotko, *J. Chem. Soc., Chem. Commun.* **1994**, 1325.
[30] R. W. Gable, B. F. Hoskins, R. Robson, *J. Chem. Soc., Chem. Commun.* **1990**, 1677.
[31] L. Carlucci, G. Ciani, D. M. Proserpio, A. Sironi, *J. Chem. Soc., Chem. Commun.* **1994**, 2755.
[32] M. J. Zaworotko, *Chem. Commun.* **2001**, 1.
[33] J.-C. Dai, X.-T. Wu, Z.-Y. Fu, S.-M. Hu, W.-X. Du, C.-P. Cui, L.-M. Wu, H.-H. Zhang, R.-Q. Sun, *Chem. Commun.* **2002**, 12.
[34] O. M. Yaghi, H. Li, T. L. Groy, *J. Am. Chem. Soc.* **1996**, *118*, 9096.
[35] C. Livage, C. Egger, M. Nogues, G. Ferey, *J. Mater. Chem.* **1998**, *8*, 2743.
[36] S. O. H. Gutschke, M. Molinier, A. K. Powell, P. T. Wood, *Angew. Chem. Int. Ed. Engl.* **1997**, *36*, 991.
[37] S. S.-Y. Chui, S. M.-F. Lo, J. P. H. Charmant, A. G. Orpen, L. D. Williams, *Science* **1999**, *283*, 1148.
[38] M. Eddaoudi, J. Kim, N. Rosi, D. Vodak, J. Wachter, M. O′Keeffe, O. M. Yaghi, *Science* **2002**, *295*, 469.
[39] B. Chen, M. Eddaoudi, S. T. Hyde, M. O'Keeffe, O. M. Yaghi, *Science* **2001**, *291*, 1021.
[40] H. Li, M. Eddaoudi, M. O′Keeffe, O. M. Yaghi, *Nature* **1999**, *402*, 276.
[41] R. H. Groeneman, L. R. MacGillivray, J. L. Atwood, *Chem. Commun.* **1998**, 2735.
[42] H. J. Choi, T. S. Lee, M. P. Suh, *Angew. Chem. Int. Ed.* **1999**, *38*, 1405.
[43] H. Li, C. E. Davis, T. L. Groy, D. G. Kelley, O. M. Yaghi, *J. Am. Chem. Soc.* **1998**, *120*, 21856.
[44] O. R. Evans, W. Lin, *Inorg. Chem.* **2000**, *39*, 2189.
[45] L. Pan, N. Ching, X. Huang, J. Li, *Inorg. Chem.* **2000**, *39*, 5333.
[46] F. A. Cotton, L. M. Daniels, C. Lin, C. A. Murillo, *Chem. Commun.* **1999**, 841.
[47] O. M. Yaghi, C. E. Davis, G. Li, H. Li, *J. Am. Chem. Soc.* **1997**, *119*, 2861.
[48] C. Daiguebonne, O. Guilloa, Y. Gerault, A. Lecerf, K. Boubekeur, *Inorg. Chim. Acta* **1999**, *284*, 139.
[49] H. J. Choi, M. P. Suh, *J. Am. Chem. Soc.* **1998**, *120*, 10622.
[50] D. J. Plaut, K. M. Lund, M. D. Ward, *Chem. Commun.* **2000**, 769.
[51] O. M. Yaghi, H. Li, *J. Am. Chem. Soc.* **1996**, *118*, 295.
[52] O. M. Yaghi, H. Li, *J. Am. Chem. Soc.* **1995**, *117*, 10401.
[53] G. B. Gardner, D. Venkataraman, J. S. Moore, S. Lee, *Nature* **1995**, *374*, 792.
[54] S. Feng, R. Xu, *Acc. Chem. Res.* **2001**, *34*, 239.
[55] L. J. Bellamy, *The Infrared Spectra of Complex Molecules:* John Wiley & Sons, New York, **1958**.
[56] S. R. Batten, R. Robson, *Angew. Chem. Int. Ed.* **1998**, *37*, 1460.
[57] L. Pan, N. Ching, X. Huang, J. Li, *Chem. Commun.* **2001**, 1064.
[58] M. O'Keeffe, M. Eddaoudi, H. Li, T. Reineke, O. M. Yaghi, *J. Solid State Chem.* **2000**, *152*, 3.
[59] A. L. Spek, *PLATON, A Multipurpose Crystallographic Tool*, Utrecht University, Utrecht, The Netherlands, **2003**.
[60] G. M. Sheldrick, *SHELXS-97, Program for X-ray Crystal Structure Solution*; University of Göttingen: Göttingen, Germany, **1997**.
[61] G. M. Sheldrick, *SHELXL-97*, Pr*ogram for X-ray Crystal Structure Refinement*; University of Göttingen: Göttingen, Germany, **1997**.

Received November 18, 2003
Early View Article
Published Online April 1, 2004

 © 2004 Wiley-VCH Verlag GmbH & Co. KGaA, Weinheim

The Reaction of Diazocyclopentadienyl Compounds with Cyclomanganated Arenes as a Route to Ligand-Appended Cymantrenes

Jean-Pierre Djukic,*[a] Christophe Michon,[a] Dirk Heiser,[b] Nathalie Kyritsakas-Gruber,[c] André de Cian,[c] Karl Heinz Dötz,[b] and Michel Pfeffer[a]

Keywords: Diazo compounds / Cyclopentadienyl ligands / Insertion / Manganese / Ligand design

The thermolysis of various cyclomanganated arenes in the presence of 5-diazocyclopentadiene, 7-diazoindene or 9-diazofluorene afforded the corresponding arenes tethered with cymantrenyl, benzocymantrenyl or dibenzocymantrenyl groups in fair to good yields. This reaction implies a multifacetted mechanism that consists of three steps: the insertion of an alkylidene moiety into a C–Mn bond, a C_{Ar}–C bond formation and several haptotropic ring-slippages. The coupling reaction has proven to be particularly efficient with $Mn(CO)_4$ chelates derived from acetylarenes and nitrogen-containing heterocycles. In one case of a 2-phenyl-2-oxazoline complex, the coupling with 9-diazofluorene yields a new η^1-dibenzocymantrene complex in which the $Mn(CO)_4$ moiety is chelated and is part of a six-membered metallacycle. The results of this study are mainly supported by the molecular structures of nine new complexes obtained by X-ray diffraction analyses.

(© Wiley-VCH Verlag GmbH & Co. KGaA, 69451 Weinheim, Germany, 2004)

Introduction

We recently reported the thermolytic coupling of cyclomanganated compounds with non-cyclic diazoalkanes, which may efficiently yield new spiralenes.[1] We also showed that the same experiments carried out with 9-diazofluorene could lead to the corresponding tethered η^5-fluorenyl complex resulting from the insertion of a fluorenylidene into the $C_{Ar}-Mn$ bond of the substrate [Equation (1)].[1a] Such an insertion reaction of an alkylidene ligand into a $C_{Ar}-Mn$ bond of a cyclomanganated compound, which leads to an appended dibenzocymantrene derivative, was unprecedented, although similar insertions of alkylidenes were already known but never thoroughly applied to a wide range of substrates. The first reactions of that kind were between diazocyclopentadiene and $(CO)_5MnX$ (X = Cl, Br, I), and yielded halocymantrenes, as reported by Shaver and later by Herrmann.[2] More recently, a series of reactions involving carbonylrhenium complexes were disclosed by Katzenellenbogen and co-workers[3] who were focusing on the synthesis of cyrhetrenes (Re analogues of cymantrenes) for various applications as contrast agents in imaging.[4] Both cymantrenes and their Re analogues can be used as labels for biomolecules[5,6] and in radiopharmaceuticals.[7]

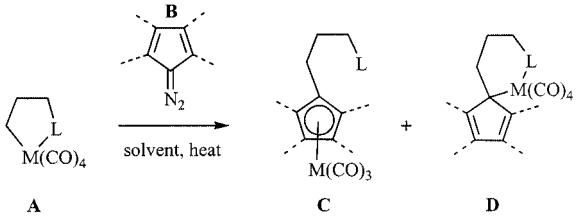

A C D (1)

Our previous results indicated that cymantrenes or -rhetrenes with either an η^5- or an η^1-bonding mode [**C** and **D**, Equation (1)] and appended with various internal ligands can be easily synthesised from readily available cyclomanganated complexes [**A**, Equation (1)] and 9-diazofluorene [**B**, Equation (1)]. One potential application of such complexes could be as chelating ligands for homogeneous catalysis.[8] Indeed, appended cyclopentadienyl-type ligands have received a great deal of attention and are widely investigated for the design of organometallic complexes of both early and late transition metals, which are expected to be active catalysts in various transformations such as the

[a] CNRS UMR 7513, Laboratoire de Synthèses Métallo-induites, 4 rue Blaise Pascal, 67000 Strasbourg, France
Fax: (internat.) + 33-3-90245001
E-mail: djukic@chimie.u-strasbg.fr
[b] Kekulé Institut für Organische Chemie und Biochemie der Universität Bonn,
Gerhard-Domagk Straße 1, 53121 Bonn, Germany
Fax: (internat.) + 49-228-73-5813
E-mail: doetz@uni-bonn.de
[c] Service d'Analyse par Diffraction des Rayons X, Institut de Chimie de Strasbourg,
4 rue Blaise Pascal, 67000 Strasbourg, France
Supporting information for this article is available on the WWW under http://www.eurjic.org or from the author.

Ziegler−Natta polymerisation.[9] These valuable appended Cp-like ligands can be synthesized by several different methods. In this article we disclose our recent findings on the investigation of the reactivity of a series of cyclomanganated compounds towards 1-diazocyclopentadiene, 7-diazoindene and 9-diazofluorene. With the support of various examples, we show that arenes tethered by cymantrenes can be efficiently synthesised by a multi-facetted reaction consisting of three steps: the insertion of an alkylidene moiety into a C−Mn bond, C_{Ar}−C bond formation and a series of haptotropic ring-slippages. We further show that the supposedly temperature-sensitive diazocyclopentadiene and diazoindene react efficiently as alkylidene sources even at temperatures as high as 100 °C.

Results and Discussion

The Preparation of 5-Diazocyclopentadiene (1a), 7-Diazoindene (1b), and 9-Diazofluorene (1c)

The poor reputation of diazomethane has thrown a shadow of suspicion on all the members of this class of reagents, although recent research has contributed to give a better and friendlier image, at least, to diazocyclopentadienes. For instance, natural diazofluorenes, such as some kinamycins, are active antitumor and antibiotic agents as they display some capabilities to cleave DNA,[10,11] and diazocyclopentadiene (**1a**) has been found to regulate ethylene production in tomatoes.[12]

When we decided to synthesise **1a**−**c**, most of the problems we encountered were not related to the putative explosive and unstable nature of diazoalkanes, which is not marked for most aryl-substituted diazoalkanes, but rather to their purification. The chemical stability and the feasibility of the targeted reagents conditioned our choice of synthetic pathway among all the known methods (Scheme 1). There are several different ways to introduce the diazo function that were compiled and detailed in pertinent reviews or books several years ago; these procedures will therefore not be detailed here.[13]

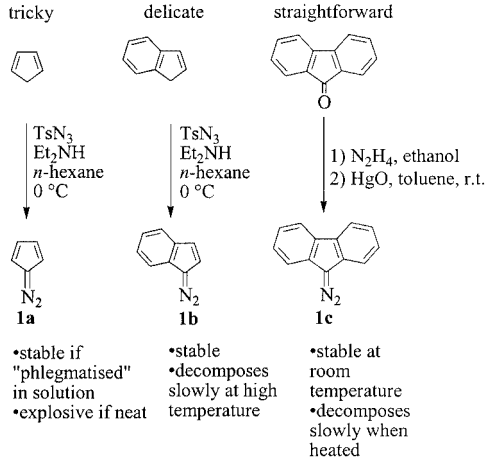

Scheme 1

An efficient synthesis of 9-diazofluorene (**1c**) was achieved by oxidation of the commercially available fluorenone hydrazone by yellow mercury(II) oxide (or activated manganese dioxide).[14] This reaction afforded a stable, deep-purple crystalline compound that can be stored at −10 °C for months. The thermal decomposition of this reagent in solution in toluene mostly produces the corresponding azines and alkenes.[15]

The synthesis of diazoindene **1b** was performed by applying the method described by Weil and Cais,[16] and improved by Rewicki and Tuchscherer by the diazo-transfer reaction of tosyl azide with a large excess of freshly distilled indene in the presence of diethylamine at 0 °C.[17] This reagent can also be obtained from a Bamford−Stevens-type transformation[18] of the indenone tosylhydrazone[19] prepared in several steps[20] from indanone. This diazoalkane is quite unstable and decomposes slowly in a non-explosive manner above 0 °C. When synthesised it can be stored for weeks if cooled to a temperature lower than −20 °C. In our hands, **1b** was formed in high yields and had to be extracted from a crude mixture that mostly contained limited amounts of insoluble tosylamide and large amounts of unchanged indene. The extraction and isolation of a highly enriched sample of diazoindene implied two critical and crucial steps, as already discussed by Herrmann and coworkers: (1) the removal of the large amounts of unchanged indene by distillation under reduced pressure, which had to be carried out carefully with mild and slow heating of the crude mixture in an oil-bath, and (2) a low-temperature (−10 °C) chromatographic separation on silica gel of the red-orange diazoindene **1b** from the brownish tar formed during step (1).

The synthesis of diazocyclopentadiene (**1a**) first reported by Doering and DePuy in 1953[21] and later improved by Weil and Cais and by Regitz and Liedhegener,[22] was even more tricky, although still possible. It was based on the above-mentioned diazo-transfer reaction between tosyl azide and freshly cracked cyclopentadiene in the presence of diethylamine in hexane at 0 °C. Because of its sensitive nature we did not attempt to isolate diazocyclopentadiene (**1a**) neat; it was handled instead in solution in an aliphatic solvent. It could be readily extracted from the crude reaction medium and purified by a low-temperature chromatographic separation on silica gel to remove tosylamide that was formed during the diazo-transfer reaction. The concentration of **1a** was readily assessed, as advocated by Weil and Cais, by a gravimetric titration of the phosphazine obtained from reaction of an aliquot of the mother solution with triphenylphosphane.

The Reaction of Monomanganated Complexes with 1a−c

It has long been known that cyclomanganated complexes of formula *cis*-[(LC)Mn(CO)$_4$] (LC: carbanionic chelating ligand) can undergo the replacement of one carbonyl ligand by a σ-donor ligand upon heating (Scheme 2).[23] In every reported case the incoming ligand occupies the axial position formerly occupied by the displaced carbonyl ligand, although this does not mean that the thermolysis of tetra-

 © 2004 Wiley-VCH Verlag GmbH & Co. KGaA, Weinheim

carbonylmanganese chelates proceeds by the selective expulsion of one of the axial ligands. Although the mechanism of this thermolytic decarbonylation is still not known, a thermodynamic control is probably responsible for the formation of a *fac*-tricarbonylmanganese chelate.

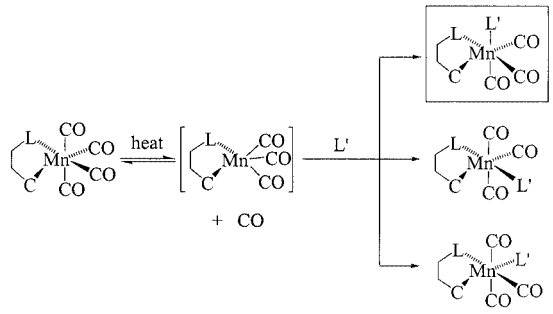

Scheme 2

Among all the possible adducts that may arise from the coordination of a donor ligand to the electron-deficient Mn^I centre, only the facial stereoisomer presents three *trans* influences that may significantly contribute to the stabilisation of the complex. When the exogenous ligand is a diazoalkane, we previously proposed that its coordination to Mn leads to a zwitterionic transient species — a manganese ylide — that evolves by elimination of N_2 to give a metallaalkylidene intermediate. A *cis* migration of the aromatic carbon atom bonded to the manganese atom creates a C−C bond between the exogenous alkylidene fragment and the chelate. At this point, we previously showed that the fluorenylidene species not only inserts into the carbon−metal bond, but the chelate itself is dismantled by the cleavage of the Mn−L bond, which is followed by a series of haptotropic shifts. In most cases, the final compounds are the corresponding [(η^5-fluorenyl)$Mn(CO)_3$] complexes **2a**−**d** and **2g**.

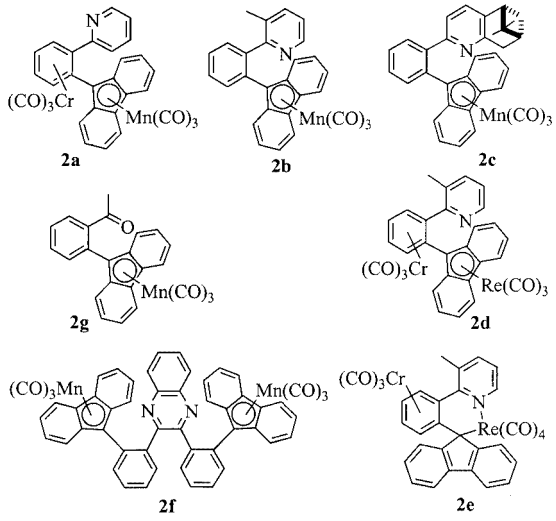

In the case of the rhenium(I) complex **2d**, we showed that it could undergo a haptotropic shift upon reaction with dissolved CO to give the [(η^1-fluorenyl)$Re(CO)_4$] complex **2e**. To check the validity of this coupling reaction with substrates containing various sorts of internal ligands, we decided to address the reactivity of diazocyclopentadienyl compounds such as **1a**−**c** with complexes **3**−**10**. Each thermolytic coupling reaction was carried out with an excess of the diazoalkane in order to compensate for the loss of reagent caused by a concomitant thermo-promoted conversion into azines and olefins. The course of the reaction could also be monitored by IR spectroscopy. The reaction was generally stopped when the characteristic four carbonyl-ligand stretching vibration bands generated by the $M(CO)_4$ group of the substrate completely faded out and were replaced by the characteristic two CO A_1 and E stretching vibration bands of the final product arising from the *fac*-$Mn(CO)_3$ fragment.

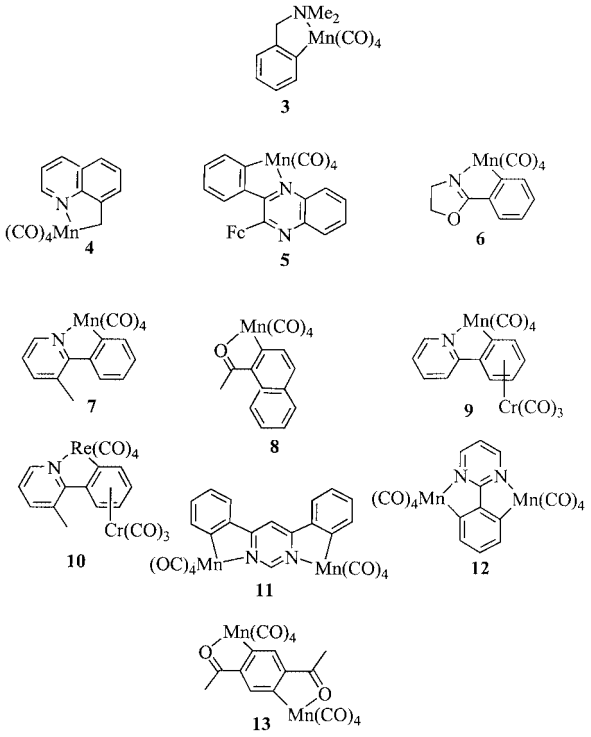

We first focussed our attention on the reactivity of **3** with **1c** [Equation (2) and Table 1, Entry 1]. Unfortunately, every attempted reaction between these two reagents led to the decomposition of **3** into dark-brown intractable compounds. More promising results were obtained with **4** [Equation (3)] and **5** [Equation (4)], which reacted readily and cleanly with **1c** to yield the corresponding substituted (η^5-fluorenylidene)$Mn(CO)_3$ complexes **4a** and **5a** (Table 1, Entries 2 and 3). The treatment of complex **6** with an excess of **1c** yielded a new brownish tetracarbonylmanganese chelate that was later identified by crystallographic means as complex **6a**, an analogue of **2e** [Equation (5) and Table 1, Entry 4]. The former plausibly arises from the carbonylation of the corresponding (η^5-fluorenyl)$Mn(CO)_3$ precursor, which was not isolated or detected in the crude mixture.

 © 2004 Wiley-VCH Verlag GmbH & Co. KGaA, Weinheim

Table 1. Experimental conditions used for the thermolytic coupling of diazocyclopentadienes **1a–c** with cyclomanganated aromatic compounds **3–13**

Entry	Substrate	R_2CN_2	*T* [°C]	Solvent(s)	Product(s)	Isolated yields (%)
1	**3**	**1c**	50	pentane/toluene	**3a**	–
2	**4**	**1c**	100	heptane/toluene	**4a**	70
3	**5**	**1c**	70	hexane/toluene	**5a**	63
4	**6**	**1c**	80	cyclohexane/toluene	**6a**	74
5	**7**	**1a**	100	heptane/hexane	**7a**	67
6	**7**	**1b**	70	hexane/cyclohexane	**7b**	87
7	**8**	**1b**	100	heptane/toluene	**8a**	76
8	**9**	**1a**	100	heptane/cyclohexane	**9a**	66
9	**9**	**1b**	80	cyclohexane/toluene	*u*-**9b**/*l*-**9b** (4:1)	55
10	**10**	**1a**	100	heptane/hexane	**10a**	71
11	**11**	**1c**	100	heptane/toluene	**11a**	84
12	**12**	**1c**	110	toluene	**12a**	61
13	**13**	**1c**	70	hexane/toluene	**13a**	> 90

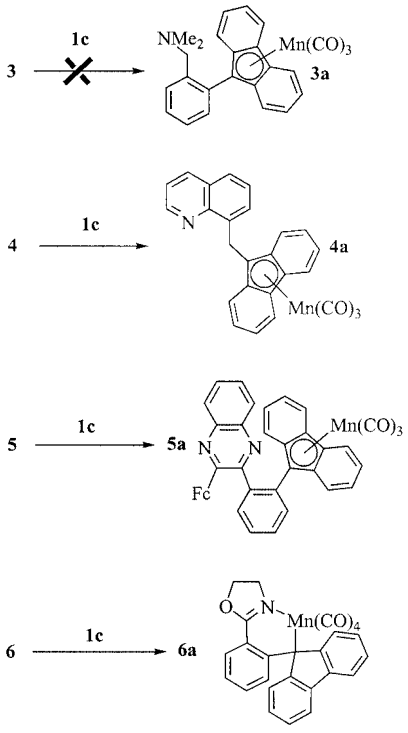

(2)

(3)

(4)

(5)

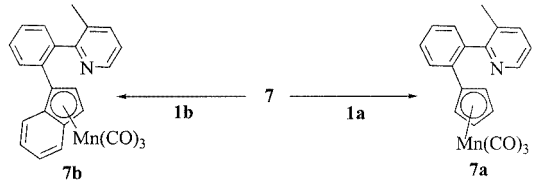

Scheme 3

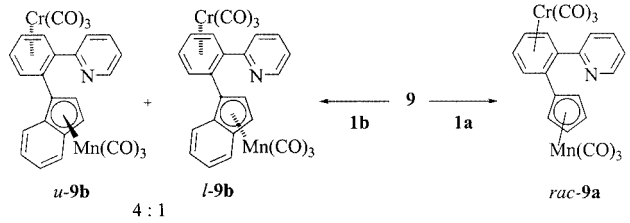

Scheme 4

treated with **1b**; complex **7** yielded **7b** (Scheme 3 and Table 1, Entry 6). The latter displayed a surprising dynamic behaviour when analysed by NMR spectroscopy in $CDCl_3$. A sample of **7b** dissolved in $CDCl_3$ was analysed at various sub-ambient temperatures until the resolution of the spectrum was sufficient to assume that a slow exchange had been reached. At 243 K we observed two sets of signals belonging to two isomers of this tris(aromatic) organometallic compound in a 1:3 ratio (Figure 1). Figure 1 displays the two signals of the olefinic protons of the indenyl fragment and their dependence on temperature. At first we thought that one of the two species might result from a combination of reversible coordination of the internal pyridyl group to the Mn^I centre and a haptotropic shift — or ring slippage[24] — from an η^5 to an η^3 mode, which indeed should cancel out the isochronicity of the three carbonyl ligands of the $Mn(CO)_3$ moiety.

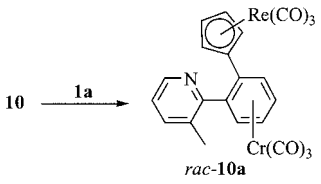

(6)

Complexes **7** (Scheme 3), **9** (Scheme 4) and **10** [Equation (6)] reacted readily with **1a** to give the corresponding substituted (η^5-cyclopentadienyl)$Mn(CO)_3$ complexes **7a**, **9a** and **10a**, respectively (Table 1, Entries 5, 8 and 10). Similar results were obtained when the same substrates were

A ^{13}C NMR spectrum recorded at −30 °C displayed only one intense signal at δ = 225 ppm, which is rather consistent with a rapidly rotating $M(CO)_3$ group (Figure 2). We therefore deduced that the observed dynamic effect was probably the consequence of a conformational equilibrium

 © 2004 Wiley-VCH Verlag GmbH & Co. KGaA, Weinheim

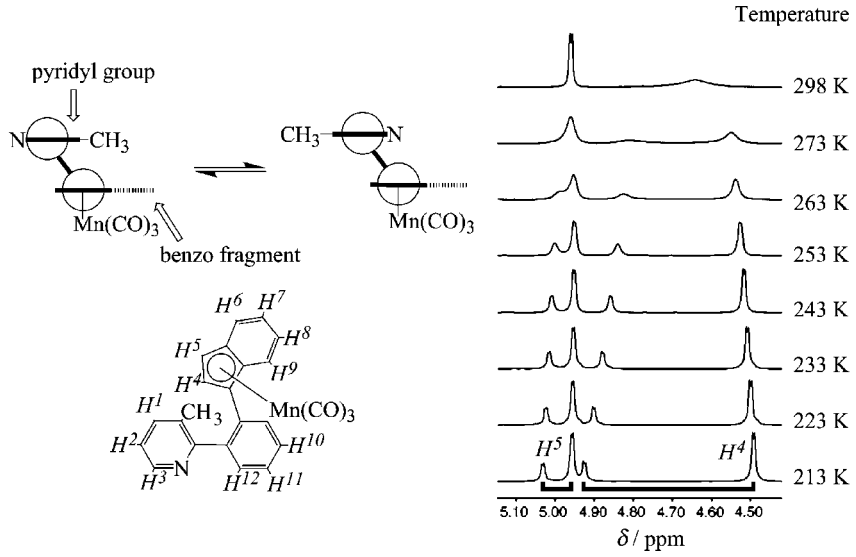

Figure 1. Temperature dependence of the ^{1}H NMR spectrum of **7b** in $CDCl_3$; enlargement of the olefinic indenyl protons region; the temperature dependency plausibly stems from a conformational equilibrium between two unequally populated conformers, whose Newman-type projections are depicted

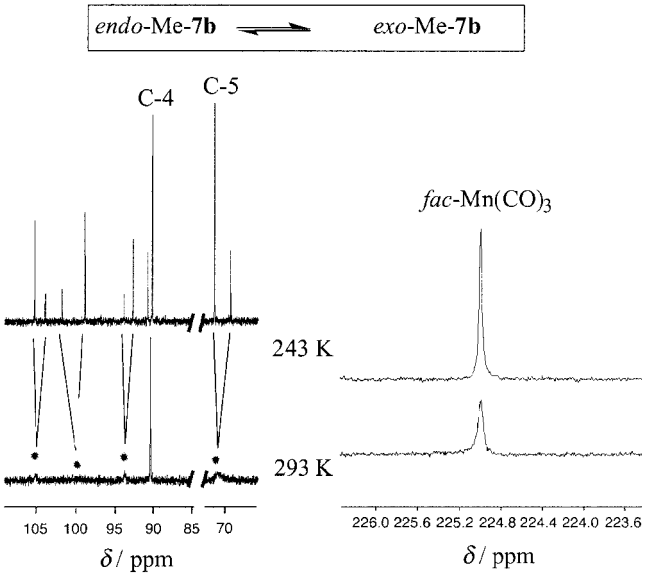

Figure 2. Temperature dependence of the ^{13}C NMR spectrum of **7b** in $CDCl_3$; enlargements of the areas of resonance of the η^5-bonded indenyl ^{13}C atoms (left) and of the $Mn(CO)_3$ fragment (right)

involving the rotation of the disubstituted pyridyl group. Such a conformational equilibrium should likely involve two conformers differing only in the orientation of the pyridyl group, which should place the methyl group either *endo* or *exo* with respect to the rest of the molecule (Figure 1). Strikingly, the ^{13}C NMR signals belonging to the indenyl group are distinguishable as sharp singlets only when the temperature drops down to 243 K. They appear as two sets of five signals between δ = 65 and 110 ppm (Figure 2). At room temperature, only the signal of the olefinic carbon atom C-4 (connected to 4-H) is well resolved since the difference in chemical shift between the two corresponding signals amounts to only 0.6 ppm at the slow exchange rate (Figure 2). From the analysis of the cross-peak correlation between the two sets of signals, a two-dimensional ^{1}H-^{1}H ROESY experiment carried out at 243 K allowed us to confirm that within the timescale of ^{1}H NMR a slow exchange exists between two unequally populated species (see Supporting Information). Unfortunately, we could not deduce any clue as to the structure of the major conformer because of the intricate mixing of the cross-peak correlations generated by pure nuclear Overhauser effects with those arising from the chemical exchange.

The reaction of complex **9** with **1b** yielded the two diastereomers *u*-**9b** and *l*-**9b** in a 4:1 ratio (Scheme 4 and Table 1, Entry 9). The predominance of *u*-**9b**, whose structure was firmly ascertained by X-ray diffraction analyses (vide infra), can be explained by the intervention of a late transition state in which the Mn-to-indenyl electronic interaction would define the activation barrier of the alkylidene insertion step. This is a proposal somewhat similar to that made for the mechanism of formation of "spiralenes".[1b] Indeed, prior to insertion, the indenylidene ligand may adopt several conformations, among which only two are rel-

 © 2004 Wiley-VCH Verlag GmbH & Co. KGaA, Weinheim

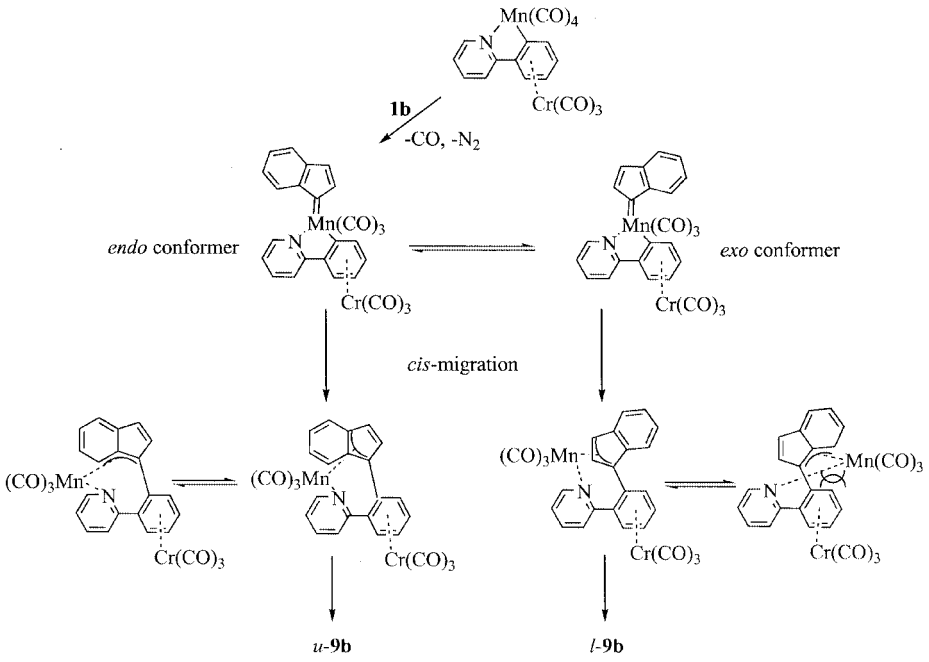

Scheme 5

evant for the *cis*-migration step: on the one hand, the benzo fragment of the indenylidene is placed at an *endo* position, and on the other the same fragment is found at an *exo* position with respect to the chelate (Scheme 5).

Upon insertion of the indenylidene, the formation of the carbon−carbon bond is accompanied by the creation of a vacant coordination site at the manganese centre that can be filled by an interaction with the π-system of the indenyl species. The ratio between the two products illustrates the intracyclic strains, which are putatively lower in the *endo* stereoisomer than in the *exo* isomer.

Complex **8** successfully reacted with an excess of **1b** to yield the aromatic ketone **8a** in good yield [Equation (7) and Table 1, Entry 7].

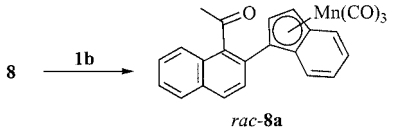

(7)

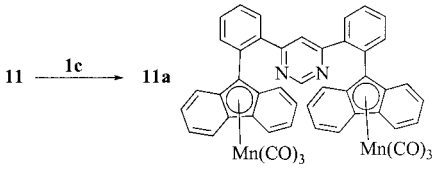

(8)

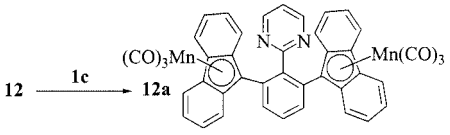

(9)

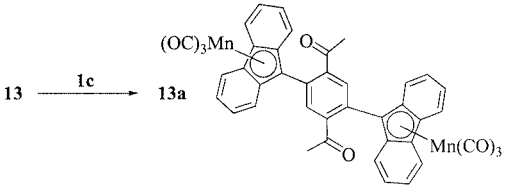

(10)

The Reaction of Dimanganated Complexes with 1c

Complexes **11** and **12**, derived from pyrimidine, were treated with an excess of **1c** and gave the corresponding dinuclear complexes **11a** and **12a** in good yields [Equations (8) and (9), Table 1, Entries 11 and 12]. Both complexes could be purified by column flash chromatography in spite of their polarity. The reaction of **13** with **1c** under the same conditions also afforded the corresponding dimetallic product **13a**, which precipitated immediately [Equation (10), Table 1, Entry 13].

This complex displays a pronounced insolubility even in polar solvents such as tetrahydrofuran, which prevented its purification by chromatography and its full characterisation by NMR spectroscopy. Its IR spectrum measured with a KBr pellet displays the expected stretching bands related to the $Mn(CO)_3$ group at $\tilde{\nu}$ = 2013 and 1926 cm^{-1} and that related to the ketone functions at $\tilde{\nu}$= 1694 cm^{-1}.

Structural and Spectroscopic Properties of Complexes 4−8a, 9b and 10−12a

Most of the new complexes reported here crystallised readily. In this article, we present the structures obtained by

 © 2004 Wiley-VCH Verlag GmbH & Co. KGaA, Weinheim

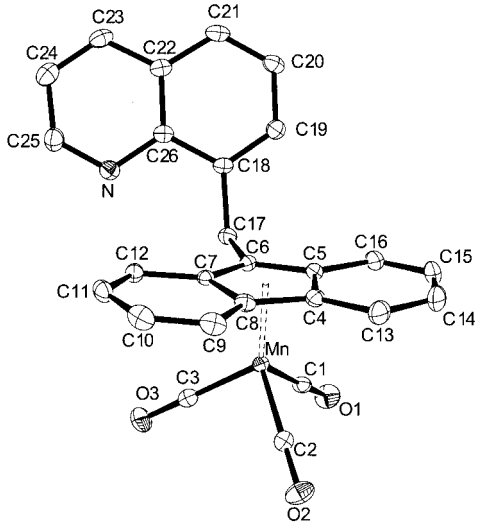

Figure 3. ORTEP diagram of compound **4a**, with the atom numbering scheme; hydrogen atoms have been omitted for clarity; the ellipsoids are drawn at the 30% probability level; selected interatomic distances [Å]: Mn−C6 2.126(2), Mn−C5 2.189(2), Mn−C8 2.202(2), Mn−C2 1.803(3), Mn−C1 1.783(3), Mn−C3 1.780(3), C6−C17 1.507(3), C6−C7 1.439(3), C8−C4 1.449(3)

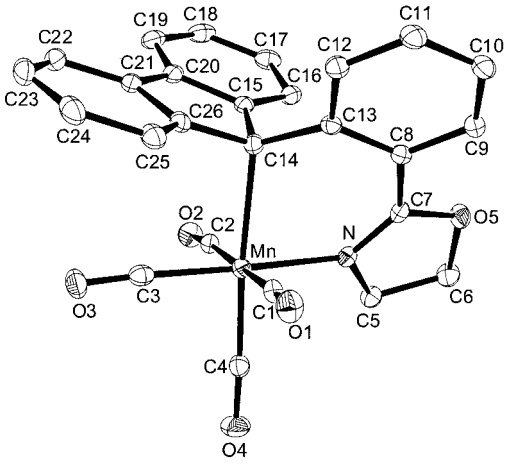

Figure 5. ORTEP diagram of compound **6a**, with the atom numbering scheme; the molecule of solvent and hydrogen atoms have been omitted for clarity; the ellipsoids are drawn at the 30% probability level; selected interatomic distances [Å] and angles [°]: Mn−C14 2.251(2), Mn−C1 1.869(2), Mn−C2 1.868(3), Mn−C3 1.821(3), Mn−N, 2.042(2), N−C7 1.285(3), O5−C7 1.348(3); N−Mn−C14 84.36(2), C8−C13−C12 116.6(2), C15−C14−C26 102.4(2)

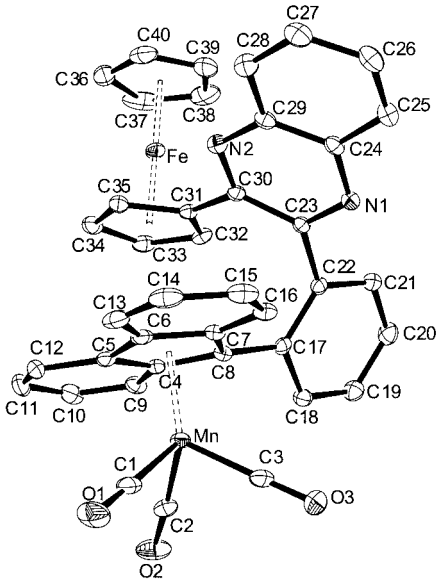

Figure 4. ORTEP diagram of compound **5a**, with the atom numbering scheme; the molecule of solvent and hydrogen atoms have been omitted for clarity; the ellipsoids are drawn at the 30% probability level; selected interatomic distances [Å] and angles [°]: Mn−C1 1.789(4), Mn−C2 1.786(3), Mn−C3 1.792(4), Mn−C4 2.181(3), Mn−C5 2.198(3), Mn−C6 2.203(3), Mn−C7 2.191(3), Mn−C8 2.157(3), Fe−C31 2.060(3), C8−C17 1.480(4), $centroid_{Fc}$−$centroid_{fluorene}$ 3.792(4); C1−Mn−C2 90.9(1), C1−Mn−C3 93.2(2), C2−Mn−C3 91.8(1)

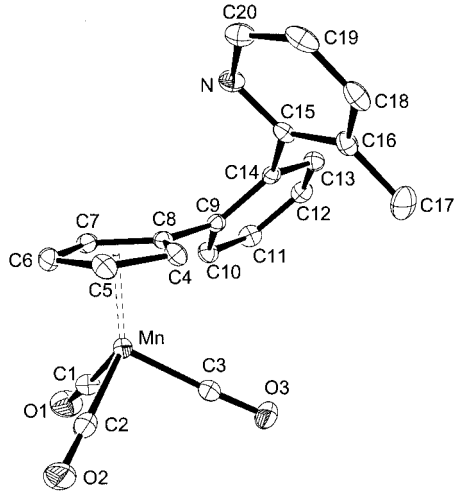

Figure 6. ORTEP diagram of compound **7a**, with the atom numbering scheme; atoms of hydrogen have been omitted for clarity; the ellipsoids are drawn at the 30% probability level; selected interatomic distances [Å] and angles [°]: Mn−C1 1.787(2), Mn−C2 1.804(3), Mn−C3 1.779(2), Mn−C8 2.154(2), Mn−C4 2.145 (2), Mn−C5 2.137(2), C8−C9 1.488(3); C4−C8−C7 106.4(2)

X-ray diffraction analyses for **4a** (Figure 3), **5a** (Figure 4), **6a** (Figure 5), **7a** (Figure 6), **8a** (Figure 7), **9a** (Figure 8), *u*-**9b** (Figure 9), **11a** (Figure 10) and **12a** (Figure 11). Main acquisition and refinement data are collected at the end of the Exp. Sect.; ORTEP diagrams of the relevant structures are given in the relevant figure, along with the atom numbering scheme and selected geometrical information.

In most structures where the Mn centre is bonded to the cyclopentadienyl moiety, there are disparities among the Mn−C_{Ar} bond lengths that reveal a sensitivity of the $Mn(CO)_3$ moiety to steric hindrance (Table 2). In η^5-fluorenyl complexes (Figures 3, 4, 10 and 11) the C_{ipso}−Mn distance can vary from 2.126(2) to 2.157(3) Å while the other C_{Ar}−Mn bonds remain unaffected, with an interatomic distance of about 2.195 Å. In a similar way, with η^5-indenyl complexes, the largest variation of the carbon−manganese distances is noticed for the C_{ipso}−Mn and $<C_{olefinic}-Mn>$ distances from 2.139(2) to 2.155(4) Å and from 2.126(2) to 2.141(2) Å in **8a** (Figure 7) and **9b** (Figure 9), respectively.

 © 2004 Wiley-VCH Verlag GmbH & Co. KGaA, Weinheim

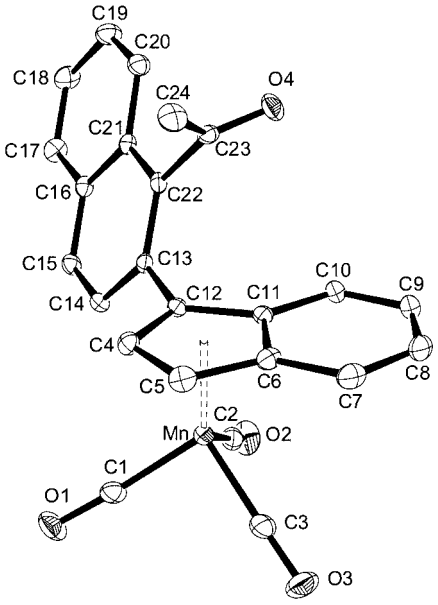

Figure 7. ORTEP diagram of compound **8a**, with the atom numbering scheme; atoms of hydrogen have been omitted for clarity; the ellipsoids are drawn at the 30% probability level; selected interatomic distances [Å] and angles [°]:Mn−C12 2.139(2), C12−C13 1.484(3), C22−C23 1.516(3), C23−O4 1.211(2); C4−C12−C11 106.4(2)

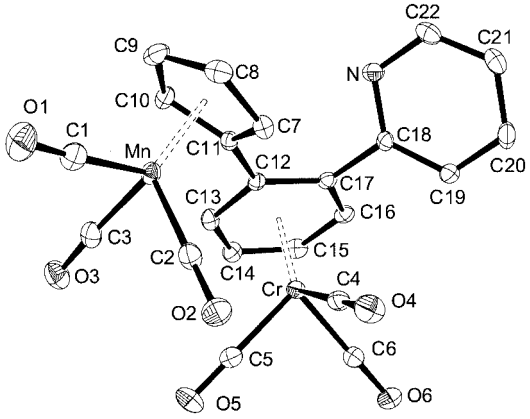

Figure 8. ORTEP diagram of compound *rac*-**9a**, with the atom numbering scheme; the molecule of solvent and hydrogen atoms have been omitted for clarity; the ellipsoids are drawn at the 30% probability level; selected interatomic distances [Å]: Cr−C12 2.240(4), Cr−C17 2.215(3), Cr−C15 2.217(4), Mn−C11 2.167(4), Mn−C9 2.137(4), Mn−C7 2.144(4), C17−C18 1.506(5), C11−C12 1.484(5)

Again the C_{Ar}−Mn bond lengths remain almost unaffected and remain at an average value of 2.202 Å.

Likewise, within the η^5-cyclopentadienyl complexes the disparity existing between C_{Cp}−Mn bond lengths is larger and directly related to the presence of bulky groups such as $Cr(CO)_3$ in the close vicinity of the $Mn(CO)_3$ group. For instance, in **7a** the C_{ipso}−Mn and the C4−Mn interatomic distances are the longest, with values of 2.154(2) and 2.145(2) Å, respectively, whereas the C(5−7)−Mn bond lengths are all equal to 2.137(2) Å (Figure 6). More dramatic distortions are observed in the dinuclear complex **9a**, in which C_{ipso}−Mn is the largest C_{Cp}−Mn distance with a value of 2.167(4) Å and C9−Mn is the smallest distance with a value of 2.137(4) Å (Figure 8). In the (η^6-aryl)tricarbonylchromium fragment the largest C−Cr distance is Cr−C12, with a value of 2.240(4) Å, whereas the remaining C(13−17)−Cr distances amount to about 2.216 Å.

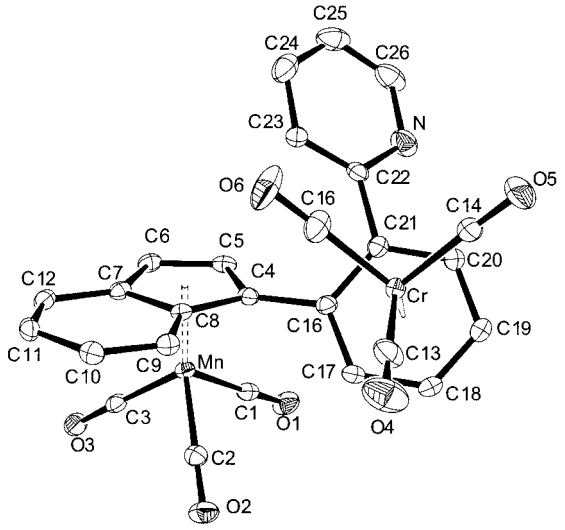

Figure 9. ORTEP diagram of compound *u*-**9b**, with the atom numbering scheme; atoms of hydrogen have been omitted for clarity; the ellipsoids are drawn at the 30% probability level; selected interatomic distances [Å]: Mn−C4 2.155(2), Mn−C5 2.138(2), Mn−C6 2.144(2), Cr−C16 2.259(2)

If we look closely at the reported structures of cymantrenes and benzo- and dibenzocymantrenes stored in the Cambridge Structural Database (CSD), we notice that the centroid−Mn distance clearly increases from cyclopentadienyl- to fluorenyl-type ligands. As already mentioned, and revealed previously by Calhorda and Veiros, this relative increase of the metal−cyclopentadienyl ligand distances stems from intrinsically different metal-to-π-system bonding modes, which is truly η^5 in Cp derivatives and seemingly more η^3-η^2 in indenyl derivatives.[24,25] The C_{ipso}−Mn distances seem much more sensitive to a factor such as steric hindrance than to changes in the electronic properties of neighbouring substituents. This can be readily assessed by the relative dispersion of the C_{ipso}−Mn distances collected from the CSD for monosubstituted cymantrenes.[26] Table 3 lists the statistical data related to centroid−Mn and C_{ipso}−Mn distances of 20 structures of monosubstituted cymantrenes deposited with the CSD.[27] For the benzo and dibenzo analogues, only two and three examples, respectively, have been selected based on their substitution pattern and their structural analogy with the complexes reported herein (Table 4).

In complex **6a**, the Mn atom sits in an octahedral environment (Figure 5). The manganese atom is chelated by the pentacyclic ligand and is included in a slightly twisted six-membered metallacycle consisting of atoms N, C7, C8, C13, C14 and Mn. The ^{13}C NMR analysis of a solution of this compound at room temperature reveals a dynamic

 © 2004 Wiley-VCH Verlag GmbH & Co. KGaA, Weinheim

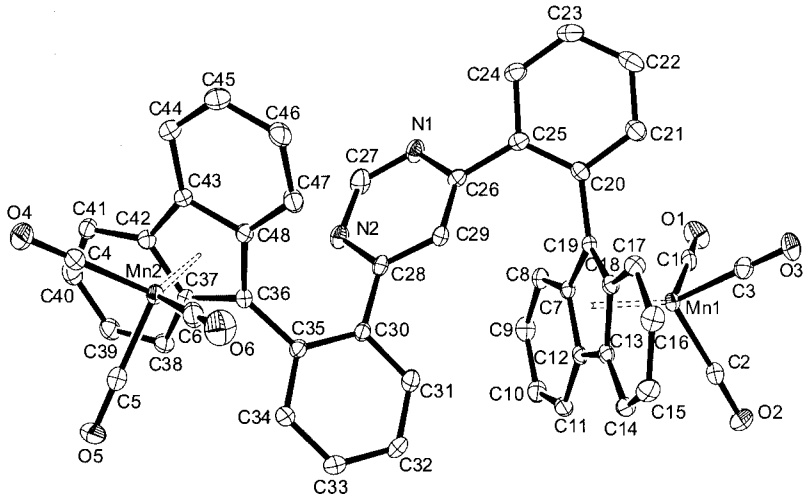

Figure 10. ORTEP diagram of compound **11a**, with the atom numbering scheme; the molecule of solvent and hydrogen atoms have been omitted for clarity; the ellipsoids are drawn at the 30% probability level; selected interatomic distances [Å] and angles [°]: Mn1−C1 1.798(4), Mn1−C2 1.793(4), Mn1−C3 1.793(4), Mn1−C7 2.194(3), Mn1−C12 2.187(3), Mn1−C13 2.197(4), Mn1−C18 2.191(4), Mn1−C19 2.155(4); C1−Mn1−C2 94.1(2), C1−Mn1−C3, 91.3(2); C1−Mn1−C7, 90.8(2)

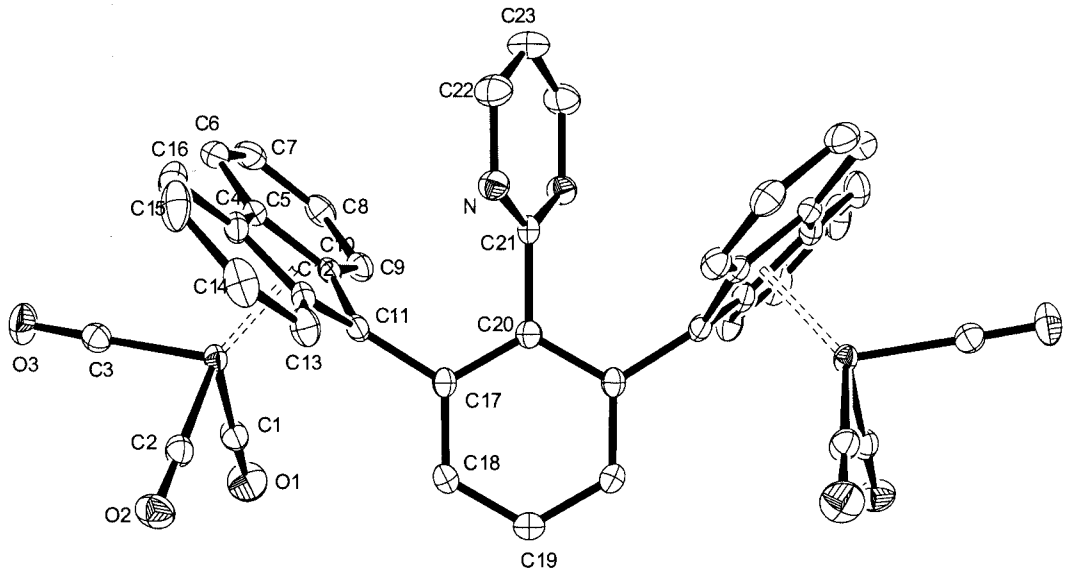

Figure 11. ORTEP diagram of compound **12a**, with the atom numbering scheme; atoms of hydrogen have been omitted for clarity; the ellipsoids are drawn at the 30% probability level; selected interatomic distances [Å] and angles [°]: Mn−C1 1.790(3), Mn−C2 1.787(3), Mn−C3 1.811(3), Mn−C4 2.205(3), Mn−C5 2.210(2), Mn−C10 2.198(2), Mn−C11 2.135(2), Mn−C12 2.191(2); C1−Mn−C2 92.2(1), C1−Mn−C3 93.0(1), C2−Mn−C3 91.4(1)

Table 2. Structural parameters for the cyclopentadienyl-to-manganese bonding interaction in compounds **4a**, **5a**, **7a**−**9a**, **9b**, **11a**−**12a**

Coordination mode[a]	η^5-Fl				η^5-In		η^5-Cp	
Compound	**4a**	**5a**	**11a**	**12a**	**8a**	*u*-**9b**	**7a**	*rac*-**9a**
C_{ipso}−Mn [Å]	2.126(2)	2.157(3)	2.155(4)	2.135(2)	2.139(2)	2.155(4)	2.154(2)	2.167(4)
$<C_{Ar}-Mn>$ [Å]	2.195(2)	2.193(2)	2.192(4)	2.201(3)	2.198(2)	2.207(2)		
<C−Mn> [Å]					2.126(2)	2.141(2)	2.139(3)	2.144(4)
<centroid−Mn> [Å]	1.805(2)	1.811(3)	1.807(4)	1.814(3)	1.782(2)	1.797(2)	1.771(3)	1.778(4)

[a] Abbreviations: Fl = fluorenyl; In = indenyl; Cp = cyclopentadienyl.

 © 2004 Wiley-VCH Verlag GmbH & Co. KGaA, Weinheim

Table 3. Mn−centroid and Mn−C_{ipso} statistical distances obtained from 20 structures of monosubstituted cymantrenes deposited with the Cambridge Structural Database[27]

	<Centroid−Mn> [Å]	C_{ipso}−Mn [Å]
Minimum	1.752	2.120
Maximum	1.784	2.185
Points	20	20
Mean	1.767	2.144
Median	1.766	2.147
Std. deviation	0.007	0.017
Variance	0.00005	0.00031
Std. error	0.001	0.004
Skewness	0.04	0.34

Table 4. Mn−centroid and Mn−C_{ipso} distances in structures of benzo- and dibenzocymantrenes deposited with the Cambridge Structural Database[27b,27c]

CSD refcodes	Centroid−Mn [Å]	C_{ipso}−Mn [Å]	R
Benzocymantrene:			
BINCMN	1.791	2.127	Br
TURNID	1.799	2.155	[(η^6-C_6H_5)Cr-$(CO)_3$]
Dibenzocymantrene:			
BAHFEW	1.823	2.147	C_6H_4
MIYXAT	1.801	2.122	H
ZUKLOG	1.813	2.154	Ph

behaviour. The four carbonyl ligands give rise to three very broad and poorly resolved ^{13}C signals at δ = 213.6, 213.0 and 211.8 ppm. Decreasing the temperature to −50 °C allowed the detection of sharper signals at δ = 213.9, 212.7 and 211.51 ppm, but did not allow us to distinguish separate signals for the two non-isochronous axial carbonyl ligands. This dynamic behaviour possibly stems from the conformational changes of the six-membered metallacycle that imply a partial rotation of the organic ligand around the C14−Mn axis via a transition state wherein the Mn−N bond is eclipsed by the C14−C13 bond. A similar broadening was observed in the ^1H NMR spectra, although we could not assign this exactly. To the best of our knowledge **6a** is only the second example of a carbonyl(η^1-fluorenyl)-manganese complex that has been characterised by X-ray diffraction analyses.[28] The Mn−C distance of 2.254(2) Å is in the range reported for similar compounds.[29]

In the crystalline state the homodimetallic complex **11a** (Figure 10) consists of a pentaaromatic distorted helix of 1,2- and 1,3-disubstituted arenes. The distance between the two Mn atoms is ca. 1 nm (10.7 Å). In this compound the helical arrangement optimises the electrostatic repulsion and minimises the steric interactions. The C_2-symmetric compound **12a** (Figure 11) is a rare case of a 1,2,3-heterotrisubstituted arene with an encapsulated heterocyclic aromatic ligand. In this compound the pyrimidyl ring stands almost perpendicular to the trisubstituted benzene. The two metal centres are about 0.9 nm apart.

Conclusion

Cyclomanganated aromatic compounds are generally readily accessible by the thermolysis of (alkyl)pentacarbonylmanganese compounds in the presence of an aromatic ligand. Such complexes have been studied for their reactivity towards various inorganic and organic reagents. Most interesting are those reactions that yield new organomanganese compounds and allow further chemical or physical investigations. We have shown here a valuable synthetic method for appended cymantrenes that could be of interest in various domains such as the design of polytopic ligands for homogeneous catalysts or in the preparation of coordination polymers from bidentate ligands containing two dibenzocymantrenyl substituents.[1a] Most coupling reactions with diazocyclopentadienyl compounds gave excellent yields of cymantrenes when the manganated substrate contained a pyridyl ring, a parent heterocycle or a ketone as internal donor ligand. In all other cases, the course of the reaction was not clear and definitely deserves more attention. We have shown that dinuclear substrates could also react even when the steric congestion is important, as in the case of one di-*ortho*-manganated 2-phenylpyrimidine.

The release of the cyclopentadienyl ligand, or in other words the removal of the $Mn(CO)_3$ fragment, is seemingly readily achievable by applying the method recently suggested by Jaouen and co-workers.[30] In a preliminary experiment, the photolysis of complex **2b** in MeOH efficiently afforded compound **14** [Equation (11)] as a white solid in 71% yield.

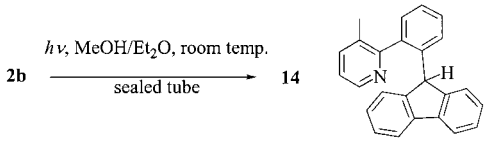

(11)

In summary, two synthetic steps are necessary to convert an aromatic compound into a polycyclic tethered cymantrene. Both the cyclomanganation and the coupling steps involve neutral reagents and are overall relatively efficient.

Experimental Section

General Remarks: All experiments were carried out under dry argon with dry and degassed solvents. The (η^6-arene)tricarbonylchromium complexes were synthesised according to published procedures.[1b] Ligands such as 2-phenylpyrimidine,[31] 4,6-diphenylpyrimidine[32] and 2-ferrocenyl-3-phenylquinoxaline[33] as well as tetracarbonyl[8-(methyl-κ$C^{l'}$)quinoline-κN]manganese(I) (**4**)[34] were synthesised according to published procedures. Other ligands were purchased from commercial sources and used without further purification. NMR spectra were acquired with Bruker DRX 500 (^1H and ^{13}C nuclei) and AC 300 (^1H nucleus) spectrometers at room temperature unless otherwise stated. Chemical shifts are reported in ppm downfield of $SiMe_4$. IR spectra were measured with a Perkin−Elmer FT spectrometer. Mass spectra were recorded at

 © 2004 Wiley-VCH Verlag GmbH & Co. KGaA, Weinheim

the Service of Mass Spectrometry of University Louis Pasteur (FAB+PEG matrix) or at the Analytical Centre of the Chemical Institute of the University of Bonn (EI). Elemental analyses were performed at the Service d'Analyses of the "Institut de Chimie de Strasbourg" and at the analytical centre of the "Institut Charles Sadron" in Strasbourg.

***p*-Tosyl Azide:** *p*-Toluenesulfonyl chloride (85 g, 0.45 mol) was added to a stirred solution of sodium azide (35 g, 0.54 mol) in a mixture of 35 mL of water and 500 mL of absolute ethanol. The resulting mixture was stirred overnight. After this time, 500 mL of water was added and the resulting slurry was extracted with diethyl ether. The organic phases were combined and dried with magnesium sulfate and then stripped of solvent under reduced pressure to afford a pale yellow oil.

5-Diazocyclopentadiene (1a): Freshly cracked cyclopentadiene (6.6 g, 0.1 mol), *p*-tosyl azide (19.7 g, 0.1 mol) and diethylamine (7.3 g, 10.4 mL, 0.1 mol) were dissolved in 50 mL of distilled acetonitrile and stirred under argon at 3 °C for 96 h. The resulting brownish reaction mixture was extracted with 300 mL of *n*-hexane and the organic phase was washed with 200 mL of water. The organic phase was washed twice with an aqueous solution of KOH (6% mass) and with water. The combined organic phases were dried with $MgSO_4$ and concentrated by the removal of half of the solvents under reduced pressure. The resulting solution was then loaded on the top of a column of SiO_2 packed in *n*-hexane and cooled to −10 °C. A large orange band containing the product was eluted with *n*-hexane and the corresponding solution was concentrated to 30 mL and titrated with triphenylphosphane. Thus, a 2-mL aliquot of mother solution was added to a solution of triphenylphosphane (1.8 g, 6 mmol) in diethyl ether and stirred under argon for 15 min. To the resulting mixture, 30 mL of *n*-hexane was added and the mixture stirred for an additional 15 min. The resulting orange precipitate was filtered off, washed with 40 mL of hexane and 30 mL of pentane, and dried under vacuum. The amount of cyclopentadienonetriphenylphosphazine (0.37 g, 1.04 mmol) recovered from this gravimetric titration gave an approximate concentration of 0.52 M of 5-diazocyclopentadiene. Yield: 1.44 g, 16%.

Diazoindene (1b): Freshly distilled indene (27.4 g, 0.236 mol) and *p*-tosyl azide (44.3 g, 0.224 mol) were dissolved in diethylamine (50 mL) and stirred at 0 °C under argon for 72 h. The resulting mixture was extracted with *n*-hexane and the organic phases washed with water and brine. The organic phases were combined, dried with Na_2SO_4 and concentrated under a reduced pressure of ca. 20 Torr at 30 °C. The resulting solution was distilled under a reduced pressure of 9 Torr, using a Vigreux column to improve the separation of the components of the raw mixture. A large fraction of indene was distilled at a temperature of 58 ± 4 °C. To avoid any explosive behaviour, the boiler was heated with an oil bath that was warmed slowly and whose temperature was homogenised by gentle stirring. The distillation of indene was stopped as soon as the temperature at the head of the Vigreux column started to fall. The boiler was then swiftly cooled to room temperature and the remaining residue separated by chromatography on an SiO_2 column refrigerated at 4 °C and packed in *n*-hexane. A red band containing the product was eluted with dry and distilled *n*-hexane. Removal of the solvent under reduced pressure afforded a red oil consisting of 92% of diazoindene and 8% of unchanged indene. This oil could be kept over long periods of time provided it was kept at a temperature lower than −20 °C. Yield: 15%.

9-Diazofluorene (1c): 9-Fluorenone hydrazone (1.0 g, 5.3 mmol) was dissolved in 75 mL of toluene and yellow mercuric oxide (3.41 g, 15.8 mmol) was added. The resulting suspension was stirred for 1 d, filtered and the filtrate dried with $MgSO_4$. The removal of solvents under reduced pressure afforded **1c** as a purple-red stable solid. Yield: 0.948 g, 94%.

General Procedure for the Reaction of 1a−c with Cyclometalated Arenes: The cyclometalated substrate was dissolved in a mixture of *n*-heptane and toluene and the resulting solution was brought to reflux. A solution of diazoalkane in toluene was added dropwise from a syringe and the resulting solution was stirred for an additional period of time. The solvents were then evaporated to dryness. The residue was dissolved in dichloromethane and SiO_2 was added. The suspension was stripped of solvent under reduced pressure and the coated silica gel was loaded on the top of a refrigerated SiO_2 column packed in *n*-hexane.

8-[1′-(Dibenzocymantren-1-yl)methyl]quinoline (4a): From **4** (0.32 g, 1 mmol), a 1:1 mixture of *n*-heptane (7 mL) and toluene (7 mL), and a solution of **1c** (0.4 g, 2.1 mmol) in toluene (4 mL). Addition 25 min, stirring for an additional 35 min. An initial SiO_2 column chromatography (60 μm, 5 °C) gave a raw sample of **4a** contaminated with various organic pollutants upon elution with pure dichloromethane. A second chromatographic separation (0 °C) with a different grade of SiO_2 (15−25 μm) gave **4a** after elution with dichloromethane/*n*-hexane (1:1). Yield: 0.35 g (70%). $C_{26}H_{16}MnNO_3$ (445.3): calcd. C 70.12, H 3.62, N 3.15; found C 69.79; H 3.54, N 3.01. IR (CH_2Cl_2): ṽ: 2015 vs, 1931 s cm^{-1}. ^1H NMR (300 MHz, $CDCl_3$): δ = 9.09 (d, ^3J = 2.9 Hz, 1 H), 8.17 (d, ^3J = 7.8 Hz, 1 H), 8.11 (m, 2 H), 7.66 (d, ^3J = 8.1 Hz, 4 H), 7.49 (m, 1 H), 7.20 (m, 4 H), 7.12 (d, ^3J = 7.0 Hz, 1 H), 5.31 (s, 2 H) ppm. ^{13}C NMR (125 MHz, $CDCl_3$, 263 K): δ = 225.5 (3 CO), 149.7, 146.4, 138.3, 136.7, 128.3, 127.8, 127.7, 126.6, 126.4, 125.3, 124.6, 123.6, 121.5, 107.2, 93.6, 77.7, 26.4 ppm.

Tetracarbonyl[2-ferrocenyl-3-(phenyl-κ$C^{2'}$)-quinoxaline-(κN^1)]-manganese(I) (5): 2-Ferrocenyl-3-phenylquinoxaline (0.37 g, 0.95 mmol) and $(PhCH_2)Mn(CO)_5$ (0.3 g, 1.1 mmol) were dissolved in a mixture of cyclohexane (10 mL) and toluene (5 mL). The resulting mixture was brought to reflux for 9 h, the solvents removed under reduced pressure and the resulting residue redissolved in dichloromethane. Silica gel was added to this solution and the suspension was stripped of solvent to afford a coated silica gel residue that was loaded on the top of a refrigerated (6 °C) SiO_2 column packed in *n*-hexane. A red band containing the product was eluted with a 1:1 mixture of *n*-hexane and dichloromethane. Compound **5** could be recovered as a red powder upon removal of the solvents under reduced pressure. Yield: 0.34 g, 65%. $C_{28}H_{17}FeMnN_2O_4$ (556.2): calcd. C 60.47, H 3.08, N 5.03; found C 60.18, H 3.14, N 4.90. IR (CH_2Cl_2): ṽ: 2075 w, 1993 vs, 1978 s, 1936 m cm^{-1}. ^1H NMR (400 MHz, $CDCl_3$): δ = 8.50 (d, ^3J = 7.9 Hz, 1 H), 8.11 (d, ^3J = 7.1 Hz, 1 H), 8.05 (d, ^3J = 7.3 Hz, 1 H), 7.72 (m, 2 H), 7.55 (d, ^3J = 8.2 Hz, 1 H), 7.20 (t, ^3J = 7.3 Hz, 1 H), 6.90 (t, ^3J = 7.6 Hz, 1 H), 4.98 (t, ^3J = 2.0 Hz, 2 H), 4.47 (t, ^3J = 1.9 Hz, 2 H), 4.05 (s, 5 H) ppm. ^{13}C NMR (100 MHz, $CDCl_3$): δ = 221.1 (CO), 214.3 (CO), 213.9 (2 CO), 178.9, 162.2, 153.4, 148.6, 141.9, 141.2, 140.7, 131.3, 130.0, 129.9, 129.7, 129.4, 126.7, 122.7, 85.3, 71.6 (2 C), 70.4 (5 C), 69.9 (2 C) ppm.

3-[2′-(Dibenzocymantren-1-yl)phenyl]-2-ferrocenylquinoxaline (5a): From **5** (0.124 g, 0.22 mmol), 10 mL of cyclohexane, 1 mL of toluene and a solution of **1c** (0.09 g, 0.47 mmol) in 2 mL of toluene. Addition for 20 min, additional stirring for 40 min. Chromatography on an SiO_2 column (6 °C) gave **5a** after elution with a 70:30 mixture of *n*-hexane/acetone. Deep red powder. Yield: 0.11 g (74%). $C_{40}H_{25}FeMnN_2O_3 \cdot 1/2CH_2Cl_2$ (734.8): calcd. C 60.80, H 3.44, N

 © 2004 Wiley-VCH Verlag GmbH & Co. KGaA, Weinheim

3.42; found C 60.81, H 3.40, N 3.53. IR (CH_2Cl_2): ṽ: 2016 s, 1934 s cm^{-1}. ^1H NMR (500 MHz, $CDCl_3$, 263 K): δ = 8.18 (d, ^3J = 4.5 Hz, 1 H), 8.01 (d, ^3J = 8.4 Hz, 1 H), 7.96 (t, ^3J = 4.6 Hz, 1 H), 7.86 (d, ^3J = 8.6 Hz, 1 H), 7.78 (m, 3 H), 7.64 (t, ^3J = 8.4 Hz, 2 H), 7.58 (t, ^3J = 7.6 Hz, 1 H), 7.01 (m, 2 H), 6.95 (m, 1 H), 6.79 (t, ^3J = 7.6 Hz, 1 H), 6.66 (d, ^3J = 8.8 Hz, 1 H), 6.24 (t, ^3J = 7.6 Hz, 1 H), 4.24 (s, 1 H), 3.91 (s, 1 H), 3.83 (s, 1 H), 3.74 (s, 5 H), 3.44 (s,1 H) ppm. ^{13}C NMR (125 MHz, $CDCl_3$, 263 K): δ = 225.3 (3 CO), 154.1, 152.1, 141.3, 141.1, 139.7, 135.0, 131.9, 130.1, 129.8, 129.7, 129.1, 128.7, 128.6, 127.9, 127.1, 125.2, 125.1, 124.8, 124.6, 124.3, 124.1, 123.2, 107.4, 103.2, 95.5, 90.9, 82.1, 81.5, 71.2, 70.1, 69.7, 69.6 (5 C), 68.2 ppm.

Tetracarbonyl[2-(phenyl-κ*C*^{2})-2-oxazoline-κ*N*]manganese(I) (6): 2-Phenyl-2-oxazoline and $(PhCH_2)Mn(CO)_5$ were dissolved in *n*-heptane and the resulting mixture was boiled for 9 h. The resulting suspension was stripped of solvent and the residue loaded on the top of an SiO_2 column packed in *n*-hexane. A pale yellow band was eluted with a 1:1 mixture of *n*-hexane/CH_2Cl_2, and the resulting solution stripped of solvents to afford a yellow powder. Yield: 1.61 g, 71%. M.p.: 106 °C. $C_{13}H_8MnNO_5$ (313.1): calcd. C 49.86, H 2.58, N 4.47; found C 49.70, H 2.61, N 4.45. HRMS: calcd. for $C_{13}H_8MnNO_5$ 312.9782; found 312.9782. IR (*n*-hexane): ṽ = 2077 w, 1991 vs, 1982 m, 1943 s cm^{-1}. ^1H NMR (500 MHz, $CDCl_3$): δ = 7.96 (ddd, $^3J_{H,H}$ = 7.4, $^4J_{H,H}$ = 1.0, $^5J_{H,H}$ = 0.6 Hz, 1 H), 7.52 (ddd, $^3J_{H,H}$ = 7.6, $^4J_{H,H}$ = 1.5, $^5J_{H,H}$ = 0.6 Hz, 1 H), 7.35 (td, $^3J_{H,H}$ = 7.4, $^4J_{H,H}$ = 1.5 Hz, 1 H), 7.14 (ddd, $^3J_{H,H}$ = 7.6, $^3J_{H,H}$ = 7.4, $^4J_{H,H}$ = 1.0 Hz, 1 H), 4.75 (t, $^2J_{H,H}$ = 9.4 Hz, 2 H, N-CH_2), 3.82 (dd, $^2J_{H,H}$ = 9.6, $^2J_{H,H}$ = 9.3 Hz, 2 H, OCH_2) ppm. ^{13}C NMR (125 MHz, $CDCl_3$): δ = 219.6 (MnCO), 215.3 (MnCO), 213.3 (2 MnCO), 179.0, 175.3, 141.8, 133.6, 131.8, 126.7, 123.7, 71.3 (NCH_2), 54.1 (OCH_2) ppm. EI-MS: *m*/*z* = 313 [M^+], 285 [M^+ − CO], 257 [M^+ − 2 CO], 229 [M^+ − 3 CO], 157 [M^+ − 4 CO − C_3H_4NO − H], 147 [M^+ − $Mn(CO)_4$ + H].

Tetracarbonyl{9-[2′-(2′′-oxazolin-2′′-yl-κ*N*$^{3''}$)phenyl]-fluorenyl-κ*C*^{9}}manganese(I) (6a): From **6** (782 mg, 2.5 mmol), *n*-hexane (10 mL) and a solution of **1c** (5 mmol) in toluene (17.5 mL). Addition 60 min, stirring for an additional 60 min. Chromatography on SiO_2 (5 °C) gave a brownish mixture containing mainly **6a** after elution with *n*-hexane/dichloromethane (1:1). A second chromatographic separation gave a brown-yellow solution of **6a**. Yield: 0.76 mg (63%). The air sensitivity of **6a** prevented its complete characterisation by elemental analysis. HRMS: calcd. for $C_{25}H_{16}MnNO_4$ [M − CO] 449.0459; found 449.0453. IR (*n*-hexane): ṽ = 2071 w, 1993 vs, 1986 s, 1940 s cm^{-1}. ^1H NMR (300 MHz, CD_2Cl_2): δ = 7.96 (d, $^3J_{H,H}$ = 7.6 Hz, 2 H, $H_{fluorene}$), 7.89 (dd, $^3J_{H,H}$ = 7.6, $^4J_{H,H}$ = 1.2 Hz, 1 H, H_{Ph}), 7.45 (d, $^3J_{H,H}$ = 7.6 Hz, 2 H, $H_{fluorene}$), 7.25 (m, 7 H), 4.75 (dd, $^2J_{H,H}$ = 9.8, $^3J_{H,H}$ = 9.5 Hz, 2 H, NCH_2), 4.01 (dd, $^2J_{H,H}$ = 9.8, $^3J_{H,H}$ = 9.5 Hz, 2 H, O-CH_2) ppm. ^1H NMR (500 MHz, $CDCl_3$, −50 °C): δ = 8.04 (d, $^3J_{H,H}$ = 7.6 Hz, 2 H), 7.86 (d, $^3J_{H,H}$ = 7.6 Hz, 1 H), 7.50 (br. s, 2 H), 7.36 (m, 3 H), 7.30 (m, 3 H), 7.21 (t, $^3J_{H,H}$ = 7.6 Hz, 1 H), 4.83 (t, $J_{H,H}$ = 9.6 Hz, 2 H, NCH_2), 4.01 (t, $J_{H,H}$ = 9.6 Hz, 2 H, OCH_2) ppm. ^{13}C NMR (125 MHz, $CDCl_3$, 293 K): δ = 213.7 (MnCO), 213.1 (MnCO), 211.7 (2 MnCO), 169.4 (OC=N), 157.6, 157.6 (2 C), 150.4, 133.5, 133.5 (2 C), 133.2, 130.2, 126.8, 126.1, 126.1, 125.0, 122.9, 122.8, 122.8, 120.8, 120.8, 120.1, 120.1, 67.5 (NCH_2), 61.1 (OCH_2), 52.2 ppm. ^{13}C NMR (125 MHz, $CDCl_3$, 263 K): δ = 213.9 (MnCO), 212.7 (MnCO), 211.5 (2 MnCO), 168.8 (O-C=N), 157.3, 157.3 (2C), 149.4, 133.0, 133.0 (2 C), 132.9, 130.1, 126.5, 126.0, 126.0, 125.1, 122.4, 122.3, 122.3, 120.7, 120.7, 119.9, 119.9 (2 C), 67.4 (NCH_2), 61.0 (OCH_2), 51.5 (C-9) ppm. ^{13}C NMR (125 MHz, $CDCl_3$, 223 K): δ = 213.7 (MnCO), 212.9 (MnCO), 211.6 (2 MnCO), 169.1 (OC=N), 157.4, 157.4 (2 C), 150.0, 133.3, 133.3 (2 C), 133.2, 130.2, 126.6, 126.1, 126.1, 125.1, 122.7, 122.6, 122.6, 120.8, 120.8, 120.0, 120.0 (2 C), 67.4 (NCH_2), 61.0 (OCH_2), 51.9 (C-9) ppm. EI-MS: *m*/*z* = 449 [M^+ − CO], 421 [M^+ − 2 CO], 393 [M^+ − 3 CO], 369 [M^+ − 4 CO].

2-[2′-(Cymantren-1′′-yl)phenyl]-3-methylpyridine (7a): From **7** (0.205 g, 0.61 mmol), *n*-heptane (10 mL) and a solution of **1a** in *n*-hexane (2 mL, 1.04 mmol, 0.52 M). Addition 5 min and stirring for an additional 25 min. Chromatography on hydrated SiO_2 (5 °C) gave **7a** upon elution with a mixture of *n*-hexane and acetone (4:1). Canary-yellow powder. Yield: 0.149 g (66%). $C_{20}H_{14}MnNO_3$ (275.2): calcd. C 64.70, H 3.80, N 3.77; found C 64.51, H 3.68, N, 3.70. IR (CH_2Cl_2): ṽ = 2020 s, 1934 s cm^{-1}. ^1H NMR (300 MHz, $CDCl_3$): δ = 8.51 (d, ^3J = 4.8 Hz, 1 H), 7.54 (d, ^3J = 7.7 Hz, 1 H), 7.50 (d, ^3J = 7.5 Hz, 1 H), 7.41 (t, ^3J = 7.1 Hz, 1 H), 7.35 (t, ^3J = 7.0 Hz, 1 H), 7.23 (m, 2 H), 4.53 (m, 4 H), 2.02 (s, 3 H) ppm. ^{13}C NMR (125 MHz, $CDCl_3$, 263 K): δ = 224.9 (3 CO), 158.8, 146.9, 139.2, 138.1, 132.0, 131.2, 129.9, 129.5, 128.4, 128.0, 122.9, 103.1, 84.6, 84.3, 82.0, 80.7, 19.2 ppm.

[1-(Acetyl-κ*O*)naphthyl-κ*C*^{2}]tetracarbonylmanganese(I) (8): $(PhCH_2)Mn(CO)_5$ (1.43 g, 5 mmol) and 1-acetylnaphthalene (1.02 g, 6 mmol) were dissolved in *n*-heptane (20 mL) and refluxed for 15 h. The resulting mixture was stripped of solvents and the residue subjected to flash chromatography on SiO_2. Compound **8** was eluted with a 1:1 mixture of dichloromethane/*n*-hexane. Yellow solid. Yield: 0.93 g (56%). $C_{16}H_9MnO_5 \cdot 1/2CH_2Cl_2$ (378.7): calcd. C 54.62, H 2.66; found C 54.65, H 2.71. HR-MS: calcd. for $C_{16}H_9MnO_5$ 335.9830; found 335.9831. IR (*n*-hexane): ṽ = 2082 m, 1997 vs, 1946 s, 1562 w cm^{-1}. ^1H NMR (300 MHz, $CDCl_3$): δ = 8.31 (d, ^3J = 8.8 Hz, 1 H), 8.27 (d, ^3J = 8.3 Hz, 1 H), 7.93 (d, ^3J = 8.1 Hz, 1 H), 7.81 (d, ^3J = 8.0 Hz, 1 H), 7.60 (t, ^3J = 7.7 Hz, 1 H), 7.47 (t, ^3J = 7.5 Hz, 1 H), 3.03 (s, 3 H) ppm. ^{13}C NMR (100 MHz, $CDCl_3$): δ = 220.6 (CO), 215.1 (CO), 213.2 (CO), 210.9 (CO), 210.2 (CO), 140.7, 138.3, 134.2, 133.4, 132.4, 130.5, 128.1, 124.7, 121.7, 32.2 ppm. EI-MS: *m*/*z* = 336 [M], 280 [M − 2 CO], 252 [M − 3 CO], 224 [M − 4 CO], 196 [M − 5 CO], 170 [M − Mn − 4 CO].

1-Acetyl-2-(benzocymantren-1′-yl)naphthalene (8a): From **8** (0.2 g, 0.6 mmol), *n*-heptane (5 mL), toluene (5 mL) and **1b** (0.2 g, 1.4 mmol) in toluene (3 mL). Addition 30 min and stirring for an additional 30 min. Chromatography on a hydrated SiO_2 column (5 °C), elution with pure dichloromethane. Canary-yellow powder. Yield: 0.19 g (76%). $C_{24}H_{15}MnO_4$ (422.3): calcd. C 68.26, H 3.58: found C 68.12, H 3.40. IR (KBr): ṽ = 2017 vs, 1942 s, 1925 s, 1694 m cm^{-1}. ^1H NMR (400 MHz, $CDCl_3$): δ = 8.02 (d, ^3J = 8.5 Hz, 2 H), 7.96 (m, 1 H), 7.76 (m, 1 H), 7.57 (m, 3 H), 7.49 (d, ^3J = 8.7 Hz, 1 H), 7.23 (t, ^3J = 7.4 Hz, 1 H), 7.16 (t, ^3J = 7.4 Hz, 1 H), 5.36 (d, ^3J = 2.7 Hz, 1 H), 5.25 (d, ^3J = 2.8 Hz, 1 H), 2.08 (s, 3 H) ppm. ^{13}C NMR (100 MHz, $CDCl_3$): δ = 224.6 (3 CO), 206.9 (CO), 141.0, 133.1, 130.4, 129.8, 128.7, 128.6, 128.0, 127.9, 127.0, 126.6, 126.2, 124.6, 122.9, 105.9, 100.4, 92.8, 90.7, 77.4, 72.1, 32.8 ppm.

2-[2′-(Benzocymantren-1′′-yl)phenyl]-3-methylpyridine (7b): From **7** (0.22 g, 0.79 mmol) cyclohexane (15 mL), **1b** (0.24 g, 1.7 mmol) and *n*-hexane (3 mL). Addition 10 min, stirring for an additional 50 min. Chromatography on SiO_2 (5 °C), elution with *n*-hexane/acetone (70:30). Red waxy solid. Yield: 0.24 g (87%). $C_{24}H_{16}MnNO_3 \cdot 1/2CH_2Cl_2$ (463.7): calcd. C 63.45, H 3.69, N 3.02; found C 63.92, H 3.86, N 3.05. HRMS (FAB$^+$): calcd. for $C_{24}H_{17}NMnO_3$ [M^+] 422.058888; found 422.058890. IR (CH_2Cl_2): ṽ = 2018 vs, 1934 s cm^{-1}. ^1H NMR (300 MHz, $CDCl_3$, 298 K):

 © 2004 Wiley-VCH Verlag GmbH & Co. KGaA, Weinheim

δ = 8.38 (m, 1 H), 8.02 (d, ^3J = 7.5 Hz, 1 H), 7.57 (t, ^3J = 7.6 Hz, 1 H), 7.48 (t, ^3J = 7.5 Hz, 1 H), 7.41 (d, ^3J = 8.5 Hz, 1 H), 7.36 (m, 2 H), 7.29 (d, ^3J = 7.7 Hz, 1 H), 7.03 (m, 3 H), 4.96 (d, ^3J = 2.9 Hz, 1 H), 4.65 (m, 1 H), 1.74 (s, 3 H) ppm. ^{13}C NMR (125 MHz, $CDCl_3$, 293 K): δ = 225.0, 158.8, 146.7 (C-3), 141.2, 137.7 (C-1), 132.8, 131.8 (2 C), 129.8, 128.6, 128.3, 126.9 (broad), 125.9 (2 C), 123.0 (broad), 122.4, 105.0 (broad), 100.0 (broad), 93.7 (broad), 90.4 (C_5), 71.0 (broad), 19.1 (CH_3, broad) ppm. Major conformer: ^{1}H NMR (500 MHz, $CDCl_3$, 243 K): δ = 8.45 (d, ^3J = 4.0 Hz, $H_{pyridyl}$), 8.04 (d, ^3J = 7.5 Hz, H_{phenyl}), 7.58 (t, ^3J = 7.3 Hz, H_{phenyl}), 7.52 (d, ^3J = 8.8 Hz, H6), 7.49 (t, ^3J = 7.5 Hz, H_{phenyl}), 7.41 (d, ^3J = 8.6 Hz, 9-H), 7.37 (d, ^3J = 7.2 Hz, H_{phenyl}), 7.32 (d, ^3J = 10.8 Hz, $H_{pyridyl}$), 7.16 (t, ^3J = 7.5 Hz, H_7), 7.12 (t, ^3J = 7.1 Hz, $H_{pyridyl}$), 7.06 (t, ^3J = 7.7 Hz, 8-H), 4.95 (d, ^3J = 2.5 Hz, 5-H), 4.51 (d, ^3J = 2.6 Hz, 4-H), 1.55 (s, 3 H, CH_3) ppm. ^{13}C NMR (125 MHz, $CDCl_3$, 243 K): δ = 224.9 (3 CO), 158.5, 146.6 (C-3), 140.8, 137.8 (C-1), 132.3, 131.8, 131.5, 129.5, 128.5, 128.2, 127.5, 126.2, 125.8, 122.5, 122.2, 105.2, 98.8, 92.6, 90.1 (C-5), 71.4 (C-4), 18.9 ppm. FAB-MS$^+$: *m*/*z* = 422 [M$^+$], 337 [M − 3 CO], 282 [M − Mn − 3 CO]. Minor conformer: ^{13}C NMR (125 MHz, $CDCl_3$, 243 K): δ = 224.9 (3 CO), 158.2, 146.7, 140.5, 137.8, 132.9, 131.7, 131.6, 129.9, 128.6, 128.2, 125.8, 125.7, 124.8, 124.2, 122.4, 103.8, 101.7, 93.8, 90.8, 69.3, 19.5 ppm.

Complex 9a: From **9** (0.2 g, 0.44 mmol), heptane (10 mL) and **1a** (2.1 mL, 1.1 mmol, 0.52 M). Addition 7 min, additional stirring for 30 min. Chromatography on hydrated SiO_2 (5 °C), elution with *n*-hexane/acetone (4:1). Canary yellow solid. Yield: 0.145 g (67%). $C_{22}H_{12}CrMnNO_6$ (493.3): calcd. C 53.57, H 2.45, N 2.84; found C 53.84, H 2.78, N 2.69. IR (CH_2Cl_2): ṽ = 2025 s, 1971 vs, 1939 s, 1899 m cm^{-1}. ^{1}H NMR (300 MHz, $CDCl_3$): δ = 8.62 (d, ^3J = 4.2 Hz, 1 H), 7.68 (t, ^3J = 7.8 Hz, 1 H), 7.35 (d, ^3J = 7.9 Hz, 1 H), 7.30 (m, 1 H), 5.75 (d, ^3J = 6.1 Hz, 1 H), 5.52 (m, 2 H), 5.45 (t, ^3J = 5.7 Hz, 1 H), 5.29(m, 1 H), 4.64 (m, 1 H), 4.52 (m, 1 H), 4.26 (m, 1 H) ppm. ^{13}C NMR (125 MHz, $CDCl_3$, 263 K): δ = 232.4 [3CO (Cr)], 224.0 [3 CO (Mn)], 154.5, 149.3, 136.4, 126.7, 123.6, 110.4, 104.0, 99.2, 94.8, 94.3, 92.2, 91.6, 88.0, 86.4, 82.4, 79.8 ppm.

Complexes *u*-9b and (*rel*)-*l*-9b: From **9** (0.2 g, 0.4 mmol), cyclohexane (10 mL), toluene (1 mL) and a solution of **1b** (0.12 g, 0.9 mmol) in toluene (3 mL). Addition 20 min, stirring for an additional 25 min. Chromatography on SiO_2 (−5 °C), *u*- and (*rel*)-*l*-**9b** were eluted with *n*-hexane/acetone (70:30). ^{1}H NMR spectroscopy indicated that the two diastereomers are in a 78:22 ratio. Conversion: 0.13 g (55%). $C_{26}H_{14}CrMnNO_6$ (543.3): calcd. C 57.48, H 2.60, N 2.58; found C 57.67, H 2.42, N 2.65. IR (CH_2Cl_2): ṽ = 2023 s, 1970 vs, 1937m, 1899 m cm^{-1}. *u*-**9b**: ^{1}H NMR (300 MHz, $CDCl_3$, 298 K): δ = 8.42 (d, ^3J = 4.8 Hz, 1 H), 7.36 (d, ^3J = 8.7 Hz, 1 H), 7.25 (m,1 H), 7.19 (t, ^3J = 6.5 Hz, 1 H), 7.00 (m, 3 H), 6.85 (t, ^3J = 7.6 Hz, 1 H), 6.02 (d, ^3J = 6.4 Hz, 1 H), 5.90 (d, ^3J = 6.4 Hz, 1 H), 5.65 (t, ^3J = 6.3 Hz, 1 H), 5.59 (t, ^3J = 6.4 Hz, 1 H), 5.54 (d, ^3J = 3.0 Hz, 1 H), 5.14 (d, ^3J = 3.0 Hz, 1 H) ppm. ^{13}C NMR (125 MHz, $CDCl_3$, 263 K): δ = 232.5 [$Cr(CO)_3$], 224.0 [$Mn(CO)_3$], 154.2, 149.1, 135.7, 126.8, 126.7, 125.6, 125.1, 123.2, 122.7, 112.5, 105.0, 103.2, 101.9, 99.0, 93.6, 93.5, 92.8, 91.1, 90.5, 69.5 ppm. (*rel*)-*l*-**9**: ^{1}H NMR (300 MHz, $CDCl_3$, 298 K): δ = 8.55 (d, ^3J = 5.4 Hz, 1 H), 7.97 (d, ^3J = 8.9 Hz, 1 H), 7.49 (m, 2 H), 7.30 (t, ^3J = 7.8 Hz, 1 H), 7.13 (m, 1 H), 6.91 (m, 2 H), 6.10 (d, ^3J = 6.4 Hz, 1 H), 5.96 (d, ^3J = 6.2 Hz, 1 H), 5.65 (t, ^3J = 6.3 Hz, 1 H), 5.59 (t, ^3J = 6.4 Hz, 1 H), 5.04 (d, ^3J = 3.4 Hz, 1 H), 4.49 (d, ^3J = 3.1 Hz, 1 H) ppm. ^{13}C NMR (125 MHz, $CDCl_3$, 263 K): δ = 232.6 [$Cr(CO)_3$], 224.1 [$Mn(CO)_3$], 154.5, 149.4, 136.0, 128.0 (2 C), 126.4, 126.3, 123.5, 123.4, 109.7, 105.5, 105.4, 99.0, 93.6, 93.5, 92.8, 91.1, 90.5, 69.5 ppm.

Complex 10a: From **10** (0.2 g, 0.44 mmol), heptane (10 mL) and a solution of **1a** (1.9 mL, 1.0 mmol, 0.52 M) in *n*-hexane, added in 3 fractions: 1 mL was added over 7 min, followed by an additional 0.45 mL after 1 h of reaction, and finally 0.45 mL after 2 h of reaction. The reaction mixture was then stirred for an additional hour. Chromatography on SiO_2 (5 °C), elution of **10a** with *n*-hexane/acetone (9:1). Yellow powder. Yield: 0.112 g, 71%. $C_{23}H_{14}CrNO_6Re$ (638.6): calcd. C 43.26, H 2.21, N 2.19; found C 43.05, H 2.45, N 2.02. IR (CH_2Cl_2): ṽ = 2026 s, 1972 vs, 1928 s, 1901 m cm^{-1}. ^{1}H NMR (300 MHz, $CDCl_3$): δ = 8.53 (d, ^3J = 4.2 Hz, 1 H), 7.55 (t, ^3J = 7.6 Hz, 1 H), 7.28 (m, 1 H), 5.65 (m, 1 H), 5.49 (t, ^3J = 5.6 Hz, 1 H), 5.41 (d, ^3J = 6.6 Hz, 1 H), 5.38 (d, ^3J = 6.2 Hz, 1 H), 5.32 (t, ^3J = 5.8 Hz, 1 H), 5.20 (m, 1 H), 4.98 (m, 1 H), 4.84 (m, 1 H), 2.19 (s, 3 H) ppm. ^{13}C NMR (125 MHz, $CDCl_3$, 263 K): δ = 232.4 [$Cr(CO)_3$], 193.5 [$Re(CO)_3$], 152.9, 147.3, 138.4, 132.6, 124.0, 102.0, 93.9, 92.1 (2 C), 91.9, 89.8 (2 C), 88.1, 87.8, 83.9, 82.6, 19.8 ppm.

[4,6-(Diphenyl-κ*C*$^{2'}$,κ*C*$^{2''}$)pyrimidine-(κ*N*^{1},κ*N*^{2})]bis(tetracarbonylmanganese(I)] (11): 4,6-Diphenylpyrimidine (0.4 g, 1.7 mmol) and $(PhCH_2)Mn(CO)_5$ (1.48 g, 5.2 mmol) were dissolved in a mixture of *n*-heptane (10 mL) and toluene (10 mL) and the resulting mixture heated to reflux for 11 h. The mixture was then stripped of its solvents, the residue was dissolved in dichloromethane and SiO_2 was added to this solution. After removal of the solvent under reduced pressure, the coated silica gel was loaded on the top of an SiO_2 column packed in *n*-hexane and refrigerated at 6 °C. A large band containing pure compound **11** was eluted with dichloromethane/*n*-hexane (3:2). Yellow powder. Yield: 0.71 g, 73%. $C_{24}H_{10}Mn_2N_2O_8$ (564.2): calcd. C 51.09, H 1.79, N 4.96; found C 50.97, H 1.46, N 5.03. IR (CH_2Cl_2): ṽ = 2082 w, 2000 vs, 1985 s, 1937 m cm^{-1}. ^{1}H NMR (300 MHz, [D$_6$]acetone): δ = 9.70 (s, 1 H), 8.79 (s, 1 H), 8.44 (d, ^3J = 7.3 Hz, 2 H), 8.01 (d, ^3J = 7.4 Hz, 2 H), 7.42 (t, ^3J = 7.3 Hz, 2 H), 7.29 (t, ^3J = 7.5 Hz, 2 H) ppm. ^{13}C NMR (100 MHz, $CDCl_3$): δ = 221.1 (CO), 214.7 (CO), 214.0 (2 CO), 180.2, 173.0, 166.4, 145.4, 142.2, 133.2, 128.3, 125.4, 109.2 ppm.

4,6-Bis[2′-(dibenzocymantren-1′′-yl)phenyl]pyrimidine (11a): From **11** (0.2 g, 0.35 mmol), *n*-heptane (5 mL), toluene (5 mL) and a solution of **1c** (0.27 g, 1.42 mmol) in toluene (3 mL). Addition 25 min, stirring for an additional 35 min. Chromatography on SiO_2 (6 °C), **11a** was eluted with pure acetone. Yellow powder. Yield: 0.25 g, 84%. $C_{42}H_{22}N_2Mn_2O_6 \cdot 1/3CH_2Cl_2$ (788.8): calcd. C 64.48, H 2.90, N 3.55; found C 64.38, H 2.97, N 3.61. IR (CH_2Cl_2): ṽ = 2016 s, 1935 s cm^{-1}. ^{1}H NMR (300 MHz, $CDCl_3$): δ = 8.23 (d, ^3J = 7.7 Hz, 2 H), 8.08 (s, 1 H), 8.06 (d, ^3J = 8.2 Hz, 4 H), 7.67 (t, ^3J = 7.6 Hz, 2 H), 7.43 (t, ^3J = 7.6 Hz, 2 H), 7.17 (t, ^3J = 7.3 Hz, 4 H), 7.04 (m, 8 H), 6.71 (d, ^3J = 7.8 Hz, 2 H), 6.29 (s, 1 H) ppm. ^{13}C NMR (125 MHz, $CDCl_3$, 263 K): δ = 224.9 (3 CO), 165.2, 157.3, 139.4, 136.3, 130.6, 130.5, 129.5, 128.8, 128.2, 125.1, 124.8, 123.0, 120.6, 107.2, 92.9, 83.3 ppm.

[2-(Phenyl-κ*C*$^{2'}$,κ*C*$^{2''}$)pyrimidine-(κ*N*^{1},κ*N*^{2})]bis(tetracarbonylmanganese(I)] (12): 2-Phenylpyrimidine (0.79 g, 5.06 mmol) and $(PhCH_2)Mn(CO)_5$ (3.46 g, 1.21 mmol) were dissolved in a mixture of *n*-heptane (5 mL) and toluene (10 mL). The mixture was refluxed for 10 h and the solution was cooled to −20 °C overnight. Then the supernatant was removed and the solid residue was washed three times with 20 mL of diethyl ether and twice with 20 mL of pentane and dried under vacuum. Yield: 2.0 g (81%). $C_{18}H_6Mn_2N_2O_8$ (488.1): calcd. C 44.29, H 1.24, N 5.74; found C 44.49, H 1.15, N 5.60. IR (CH_2Cl_2): ṽ = 2072 w, 1997 vs, 1981 s, 1938 m cm^{-1}. ^{1}H NMR (400 MHz, [D$_6$]acetone): δ = 8.98 (d, ^3J =

 © 2004 Wiley-VCH Verlag GmbH & Co. KGaA, Weinheim

5.4 Hz, 2 H), 7.53 (d, ^3J = 4.9 Hz, 2 H), 7.34 (t, ^3J = 5.5 Hz, 1 H), 7.21 (t, ^3J = 7.3 Hz, 1 H) ppm.

2-[2′,6′-Bis(dibenzocymantren-1′′-yl)phenyl]pyrimidine (12a): From **12** (0.3 g, 0.62 mmol), toluene (10 mL) and a solution of **1c** (0.47 g, 2.46 mmol) in toluene (3 mL). Addition 25 min, stirring for an additional 35 min. Chromatography on SiO_2 (5 °C), **12a** was eluted with dichloromethane/*n*-hexane (80:20). Yellow powder. Yield: 0.28 g (61%). $C_{42}H_{22}Mn_2N_2O_6{\cdot}1/3CH_2Cl_2$ (516.4): calcd. C 64.48, H 2.90, N 3.55; found C 64.38, H 2.97, N 3.61. IR (CH_2Cl_2): $\tilde{\nu}$ = 2018 s, 1934 s cm^{-1}. ^{1}H NMR (500 MHz, $CDCl_3$, 263 K): δ = 8.52 (d, ^3J = 7.8 Hz, 2 H), 8.03 (t, ^3J = 7.7 Hz, 1 H), 7.98 (d, ^3J = 8.6 Hz, 4 H), 7.56 (d, ^3J = 4.9 Hz, 2 H), 7.29 (d, ^3J = 8.7 Hz, 4 H), 7.10 (t, ^3J = 7.6 Hz, 4 H), 7.05 (t, ^3J = 7.6 Hz, 4 H), 6.15 (t, ^3J = 4.9 Hz, 1 H) ppm. ^{13}C NMR (125 MHz, $CDCl_3$, 263 K): δ = 225.3 (3 CO), 166.0, 155.3, 142.4, 136.2, 132.2, 130.1, 127.6, 124.6, 124.5, 123.9, 117.5, 107.3, 92.6, 84.6 ppm.

1,4-Diacetyl-2,5-bis(dibenzocymantren-1′-yl)benzene (13a): From **13** (0.22 mmol), *n*-hexane (7 mL) and a solution of **1c** (0.88 mmol) in toluene (5 mL). Addition 30 min, stirring for an additional 60 min. Compound **13a** precipitated as a yellow solid. Due to its insolubility in most polar solvents (THF, DMSO) it could not be further purified. This precipitate was washed several times with *n*-hexane and acetone and dried under reduced pressure. M.p. 233−240 °C. IR (KBr): $\tilde{\nu}$ = 2013 vs, 1926 s, 1694 w cm^{-1}. FAB-MS+: *m*/*z* = 767 [M + H]$^+$, 682 [M − 3 CO + H]$^+$, 613 [4 matrix + H]$^+$, 599 [M − $Mn(CO)_3$ − 3 CO + H]$^+$, 488 [M − 2 $Mn(CO)_3$]$^+$, 460 [3 matrix + H]$^+$.

2-{2′-(9-Fluorenyl)phenyl}-3-methylpyridine (14): Compound **2b** (0.2 g, 0.5 mmol) was dissolved in a mixture of diethyl ether (5 mL) and methanol (10 mL). The sealed Schlenk tube containing the solution was then irradiated with the aid of a medium-pressure Hg lamp. A slight precipitation of brownish air-sensitive solid was noticed shortly after the beginning of the UV irradiation. The organic product **14** was purified by chromatography on SiO_2 and recovered as an off-white solid. Yield: 0.1 g (71%). HRMS (FAB+): calcd. for $C_{25}H_{20}N$ [MH$^+$] 334.159565; found 334.159575. ^{1}H NMR (300 MHz, $CDCl_3$): δ = 8.59 (m, 1 H), 7.85 (d, ^3J = 7.5 Hz, 2 H), 7.77 (d, ^3J = 7.5 Hz, 1 H), 7.45 (m, 1 H), 7.34 (m, 6 H), 7.24 (t, ^3J = 7.4 Hz, 2 H), 7.14 (t, ^3J = 7.4 Hz, 1 H), 6.42 (d, ^3J = 6.7 Hz, 1 H), 4.88 (s, 1 H), 2.41 (s, 3 H) ppm. ^{13}C NMR (75 MHz, [D_6]acetone): δ = 160.1, 149.7, 147.7, 142.4, 141.1, 138.9, 132.6, 129.9, 129.1, 128.7, 128.2, 128.1, 127.2, 126.5 (2 C), 123.5, 120.6, 51.2, 19.8 ppm.

Experimental Procedure for the X-ray Diffraction Analysis of Compounds 4a, 5a, 6a, 7a, 8a, 9a, 9b, 11a and 12a: Acquisition and processing parameters are displayed in Tables 5 and 6. Reflections were collected with a Nonius KappaCCD diffractometer using Mo-K_α graphite-monochromated radiation (λ = 0.71073 Å). The structures were solved by direct methods and were refined against |*F*| with the Nonius OpenMoleN package.[35] Hydrogen atoms were introduced as fixed contributors. Flack's *x* parameter for **9a** was determined to be *x* = 0.36(2). CCDC-220450 to -220458 contain the supplementary crystallographic data for this paper. These data can be obtained free of charge at www.ccdc.cam.ac.uk/conts/retrieving.html [or from the Cambridge Crystallographic Data Centre, 12 Union Road, Cambridge CB2 1EZ, UK; Fax: (internat.) + 44-1223-336-033; E-mail: deposit@ccdc.cam.ac.uk].

Supporting Information: One- and two-dimensional (^{1}H-^{1}H COSY, ROESY and ^{1}H-^{13}C HETCORR) NMR spectra for compound **7b**

Table 5. Acquisition and refinement parameters for the X-ray diffraction analyses of complexes **4a−7a**

	4a	**5a**	**6a**	**7a**
Empirical formula	$C_{26}H_{16}MnNO_3$	$C_{40}H_{25}FeMnN_2O_3{\cdot}CH_2Cl_2$	$C_{26}H_{16}MnNO_5{\cdot}CH_2Cl_2$	$C_{20}H_{14}MnNO_3$
M	445.36	777.38	562.29	371.28
Crystal system	triclinic	monoclinic	triclinic	orthorhombic
Space group	$P\bar{1}$	$P2_1/c$	$P\bar{1}$	*Pbca*
a [Å]	8.3364(2)	16.3945(3)	10.1810(3)	12.4955(2)
b [Å]	11.6063(4)	13.8198(3)	11.1509(4)	13.1900(2)
c [Å]	12.1151(4)	14.9630(4)	11.5676(4)	20.4495(4)
α [°]	101.778(5)	90	75.737(5)	90
β [°]	106.174(5)	94.573(5)	84.768(5)	90
γ [°]	108.494(5)	90	70.853(5)	90
V [Å^3]	1011.11(5)	3379.4(1)	1202.27(7)	3370.4(1)
Z	2	4	2	8
Crystal dim. [mm]	0.10 × 0.06 × 0.06	0.14 × 0.14 × 0.10	0.20 × 0.16 × 0.16	0.16 × 0.14 × 0.08
D_c [g·cm^{-3}]	1.46	1.53	1.55	1.46
*F*000	456	1584	572	1520
μ [mm^{-1}]	0.682	1.005	0.812	0.801
Trans. min./max.	0.9107/1.0000	0.865/0.904	0.9479/1.0000	0.9596/1.1284
hkl limits	−11, 11/−16, 14/−17, 15	−21, 21/−19, 17/−23, 23	−13, 13/−10, 15/−13, 15	−17, 17/−18, 18/−28, 28
θ limits [°]	2.5/30.11	2.5/30.02	2.5/29.13	2.5/30.03
Data measd.	6862	16735	8501	9815
Data with $I > 3\sigma(I)$	3392	4404	3850	2613
Number of var.	280	451	325	226
R	0.040	0.037	0.037	0.030
Rw	0.049	0.044	0.047	0.039
GOF	1.008	1.039	1.048	1.049
Largest peak in final diff. [e·Å^{-3}]	0.351	0.787	0.410	0.266

 © 2004 Wiley-VCH Verlag GmbH & Co. KGaA, Weinheim

Table 6. Acquisition and refinement parameters for the X-ray diffraction analyses of complexes **8a**, **9a**, **9b**, **11a** and **12a**

	8a	*rac*-**9a**	(*rel*)-*u*-**9b**	**11a**	**12a**
Empirical formula	$C_{24}H_{15}MnO_4$	$C_{22}H_{12}CrMnNO_6{\cdot}CH_2Cl_2$	$C_{26}H_{14}CrMnNO_6$	$C_{48}H_{26}Mn_2N_2O_6{\cdot}2CH_2Cl_2$	$C_{42}H_{22}Mn_2N_2O_6$
M	422.32	578.21	543.34	1006.49	760.53
Crystal system	triclinic	orthorhombic	orthorhombic	monoclinic	orthorhombic
Space group	$P\bar{1}$	$P2_12_12_1$	*Pbcn*	$P2_1/n$	*Pbcn*
a [Å]	8.5271(2)	9.1959(2)	38.2715(1)	8.0794(1)	8.2243(2)
b [Å]	10.4016(2)	13.6927(3)	7.6620(2)	18.4324(2)	15.4115(4)
c [Å]	11.2111(3)	18.1864(5)	15.1092(5)	30.1912(4)	26.9270(7)
α [°]	103.243(5)	90	90	90	90
β [°]	99.995(5)	90	90	93.110(5)	90
γ [°]	93.117(5)	90	90	90	90
V [Å^3]	948.63(4)	2289.97(9)	4430.6(2)	4489.53(9)	3413.0(2)
Z	2	4	8	4	4
Crystal dim. [mm]	0.10 × 0.08 × 0.06	0.20 × 0.10 × 0.08	0.16 × 0.12 × 0.08	0.12 × 0.12 × 0.10	0.12 × 0.10 × 0.08
D_c [g·cm^{-3}]	1.48	1.68	1.63	1.49	1.48
*F*000	432	1160	2192	2040	1544
μ [mm^{-1}]	0.724	1.300	1.105	0.854	0.794
Trans. min./max.	0.9678/1.0000	0.768/0.901	0.835/0.925	0.9482/1.0000	0.907/0.938
hkl limits	−12, 12/−14, 14/−15, 15	−12, 12/−19, 19/−25, 25	−10, 10/−20, 20/−52, 52	−10, 10/−24, 22/−39, 39	0, 10/0, 20/0, 34
θ limits [°]	2.5/30.06	2.5/30.01	2.5/29.11	2.5/27.85	2.5/27.48
Data measd.	8741	6365	11275	19403	4424
Data with $I > 3\sigma(I)$	3557	2661	3535	6102	2360
Number of var.	262	307	316	577	237
R	0.034	0.035	0.032	0.049	0.035
Rw	0.042	0.043	0.044	0.072	0.049
GOF	1.075	1.041	1.058	1.277	1.052
Largest peak in final diff. [e·Å^{-3}]	0.312	0.470	0.366	1.301	0.580

in $CDCl_3$ at 243 K (see also footnote on the first page of this article).

Acknowledgments

The authors would like to thank the Centre National de la Recherche Scientifique and the Deutsche Forschungs Gemeinshaft for their financial contribution. One of us (J. P. D.) acknowledges also the financial support provided by the Alexander von Humboldt foundation. We thank Drs. Rolland Graff and Lionel Allouche (CNRS, Institut de Chimie de Strasbourg) for carrying out the multidimensional and low-temperature NMR experiments.

[1] [1a] C. Michon, J. P. Djukic, Z. Ratkovic, J. P. Collin, M. Pfeffer, A. de Cian, J. Fischer, D. Heiser, K. H. Dötz, M. Nieger, *Organometallics* **2002**, *21*, 3519−3535. [1b] J. P. Djukic, A. Maisse-François, M. Pfeffer, K. H. Dötz, A. de Cian, J. Fischer, *Organometallics* **2000**, *19*, 5484−5499.

[2] [2a] K. J. Reimer, A. Shaver, *J. Organomet. Chem.* **1975**, *93*, 239−252. [2b] W. A. Herrmann, B. Reiter, M. Huber, *J. Organomet. Chem.* **1977**, *139*, C4−C8. [2c] W. A. Herrmann, *Chem. Ber.* **1978**, *111*, 2458−2460.

[3] [3a] T. W. Spradau, J. A. Katzenellenbogen, *Organometallics* **1998**, *17*, 2009−2017. [3b] F. Minutolo, J. A. Katzenellenbogen, *J. Am. Chem. Soc.* **1998**, *120*, 4514−4515. [3c] F. Minutolo, J. A. Katzenellenbogen, *Organometallics* **1999**, *18*, 2519−2530. [3d] F. Minutolo, J. A. Katzenellenbogen, *Angew. Chem.* **1999**, *111*, 1730−1732; *Angew. Chem. Int. Ed.* **1999**, *38*, 1617−1620. [3e] R. R. Cesati, J. A. Katzenellenbogen, *J. Am. Chem. Soc.* **2001**, *123*, 4093−4094.

[4] [4a] J. R. Dilworth, S. J. Parrott, *Chem. Soc. Rev.* **1998**, *27*, 43−55. [4b] J. Bernard, K. Ortner, B. Spingler, H.-J. Pietzch, R. Alberto, *Inorg. Chem.* **2003**, *42*, 1014−1022.

[5] M. Salmain, M. Grunn, A. Gorfis, S. Top, G. Jaouen, *Bioconj. Chem.* **1993**, *4*, 425−433.

[6] Z. Wang, B. A. Roe, K. M. Nicholas, R. L. White, *J. Am. Chem. Soc.* **1993**, *115*, 4399−4400.

[7] G. Jaouen, S. Top, A. Veyssières, P. Pigeon, G. Leclercq, I. Laios, *Chem. Commun.* **2001**, 383−384.

[8] [8a] S. Kudis, G. Helmchen, *Angew. Chem.* **1998**, *110*, 3210−3212; *Angew. Chem. Int. Ed.* **1998**, *37*, 3047−3050. [8b] C. Bolm, M. Kesselgruber, N. Hermanns, J. P. Hildebrand, G. Raabe, *Angew. Chem. Int. Ed.* **2003**, *40*, 1488−1490. [8c] T. D. Weiß, G. Helmchen, U. Kazmaier, *Chem. Commun.* **2002**, 1270−1271. [8d] C. Bolm, L. Xiao, M. Kesselgruber, *Org. Biomol. Chem.* **2003**, *1*, 145−152. [8e] O. Delacroix, J. A. Gladysz, *Chem. Commun.* **2003**, 665−675.

[9] [9a] M. Enders, R. Rudolph, H. Pritzkow, *J. Organomet. Chem.* **1997**, *549*, 251−256. [9b] K. Theopold, *Eur. J. Inorg. Chem.* **1998**, 15−24. [9c] C. Müller, D. Vos, P. Jutzi, *J. Organomet. Chem.* **2000**, *600*, 127−143. [9d] U. Siemeling, *Chem. Rev.* **2000**, *100*, 1495−1526. [9e] M. Enders, G. Kohl, H. Pritzkow, *J. Organomet. Chem.* **2001**, *622*, 66−73. [9f] K. Kunz, G. Erker, S. Döring, R. Fröhlich, G. Kehr, *J. Am. Chem. Soc.* **2001**, *123*, 6181−6182. [9g] M. Enders, P. Fernandez, G. Ludwig, H. Pritzkow, *Organometallics* **2001**, *20*, 5005−5007. [9h] T. Dreier, R. Fröhlich, G. Erker, *J. Organomet. Chem.* **2001**, *621*, 197−206.

[10] [10a] S. J. Gould, N. Tamayo, C. R. Melville, M. C. Cone, *J. Am. Chem. Soc.* **1994**, *116*, 2207−2208. [10b] S. Mithani, G. Weeratunga, N. J. Taylor, G. I. Dmitrienko, *J. Am. Chem. Soc.* **1994**, *116*, 2209−2210. [10c] D. P. Arya, D. J. Jebaratnam, *J. Org. Chem.* **1995**, *60*, 3268−3269. [10d] W. Williams, X. Sun, D. Jebaratnam, *J. Org. Chem.* **1997**, *62*, 4364−4369. [10e] S. J. Gould, *Chem. Rev.* **1997**, *97*, 2499−2509. [10f] R. S. Laufer, G. I. Dmitrienko, *J. Am. Chem. Soc.* **2002**, *124*, 1854−1855.

[11] H. J. Eppley, S. M. lato, A. D. Ellington, J. M. Zaleski, *Chem. Commun.* **1999**, 2405−2406.

 © 2004 Wiley-VCH Verlag GmbH & Co. KGaA, Weinheim

[12] F. M. Mathooko, Y. Kubo, A. Inaba, R. Nakamura, *Postharvest Biol. Technol.* **1995**, *5*, 221−233.
[13] [13a] M. Regitz, G. Maas, in *Diazo Compounds, Properties and Synthesis*, Academic Press, Orlando, USA, **1986**. [13b] *The Chemistry of Diazonium and Diazo groups*, part I (Ed.: S. Patai), Wiley, Chichester, U.K., **1978**. [13c] B. Eistert, M. Regitz, G. Heck, H. Schwall, in *Methoden der Organischen Chemie*, 4th ed. (Ed.: E. U. Miller), Georg Thieme Verlag, Stuttgart, **1968**, vol. X/4, p. 473−893. [13d] M. Bösch, J. Fink, H. Heydt, O. Wagner, M. Regitz, in *Methoden der Organischen Chemie*, 6th ed. (Eds.: D. Klaman, H. Hagemann), Georg Thieme Verlag, New York, **1990**, vol. E14B, p. 996−1010. [13e]A. Albini, H. Kirsch, *Top. Curr. Chem.* **1976**, *65*, 105−145.
[14] [14a] H. Staudinger, O. Kupfer, *Ber. Dtsch. Chem. Ges.* **1911**, *44*, 2197−2212. [14b] P. S. R. Anjaneyulu, A. K. Lala, *FEBS Lett.* **1982**, *146*, 165−167.
[15] [15a] J. Pfeiffer, M. Nieger, K. H. Dötz, *Chem. Eur. J.* **1998**, *4*, 1843−1851. [15b] L. J. McDowell, M. M. Khodaei, D. Bethell, *Org. Biomol. Chem.* **2003**, *1*, 995−1003.
[16] T. Weil, M. Cais, *J. Org. Chem.* **1963**, *28*, 2472−2473.
[17] [17a] D. Rewicki, C. Tuchscherer, *Angew. Chem.* **1972**, *84*, 31−32. [17b] R. O. Duthaler, H. G. Förster, J. D. Roberts, *J. Am. Chem. Soc.* **1978**, *100*, 4974−4979. [17c] J. E. Baldwin, K. A. Black, *J. Am. Chem. Soc.* **1984**, *106*, 1029−1040.
[18] W. R. Bamford, T. S. Stevens, *J. Chem. Soc.* **1952**, 4735−4740.
[19] C. S. Marvel, C. W. Hinman, *J. Am. Chem. Soc.* **1954**, *76*, 5435−5437.
[20] [20a] S. Kapur, N. C. Mathur, K. McManus, A. L. Pincock, J. A. Pincock, *Can. J. Chem.* **1988**, *66*, 2888−2893. [20b] A. Marrochi, L. Minuti, A. Tatichi, H. W. Scheeren, *Tetrahedron* **2001**, *57*, 4959−4965.
[21] W. E. von Doering, C. H. DePuy, *J. Am. Chem. Soc.* **1953**, *75*, 5955−5957.
[22] M. Regitz, A. Liedhegener, *Tetrahedron* **1967**, *23*, 2701−2708.
[23] [23a] M. I. Bruce, M. Z. Iqbal, F. G. A. Stone, *J. Chem. Soc. A* **1970**, 3204−3209. [23b] R. L. Bennet, M. I. Bruce, I. Matsuda, R. J. Doedens, R. G. Little, J. T. Veal, *J. Organomet. Chem.* **1974**, *67*, C72−C74. [23c] G. J. Depree, N. D. Chiderhouse, B. K. Nicholson, *J. Organomet. Chem.* **1997**, *533*, 143−159.
[24] [24a] L. F. Veiros, *J. Organomet. Chem.* **1999**, *587*, 221−232. [24b] L. F. Veiros, *Organometallics* **2000**, *19*, 3127−3136. [24c] L. F. Veiros, *Organometallics* **2000**, *19*, 5549−5558. [24d] M. Stradiotto, M. J. McGlinchey, *Coord. Chem. Rev.* **2001**, *219−221*, 311−378.
[25] M. J. Calhorda, L. F. Veiros, *Coord. Chem. Rev.* **1999**, *185−186*, 37−51.
[26] A. G. Orpen, L. Brammer, F. H. Allen, O. Kennard, D. G. Watson, R. Taylor, *J. Chem. Soc., Dalton Trans.* **1989**, S1−S83.
[27] CSDB refcodes for: [27a] Cymantrenes: BEHGAW: V. G. Andrianov, Yu. T. Struchkov, P. V. Petrovskii, E. I. Fedin, D. N. Kursanov, S. P. Dolgova, V. N. Setkina, *J. Organomet. Chem.* **1981**, *221*, 183−191; BUWDEC: V. B. Ribakov, L. A. Aslanov, V. M. Ionov, S. A. Eremin, *Zh. Strukt. Khim.* **1983**, *24*, 74−82; CPMNCO01: P. J. Fitzpatrick, Y. Le Page, J. Sedman, I. S. Butler, *Inorg. Chem.* **1981**, *20*, 2852−2861; CPMNCO02: J. Cowie, E. J. M. Hamilton, J. C. V. Laurie, A. J. Welch, *J. Organomet. Chem.* **1990**, *394*, 1−13; CUMGUM: V. A. Milyukov, A. V. Zverev, S. M. Podlesnov, D. B. Krivolapov, I. A. Litvinov, A. T. Gubaidullin, O. N. Kataena, A. G. Ginzburg, O. G. Sinyashin, *Eur. J. Inorg. Chem.* **2000**, 225−228; DAJSOW: A. Tuozzi, C. L. Sterzo, A. Sperandio, G. Bocelli, *Tetrahedron* **1999**, *55*, 461−474; *E*TCYMT: N. M. Loim, Z. N. Parnes, V. G. Andrianov, Yu. T. Struchkov, D. N. Kursanov, *J. Organomet. Chem.* **1980**, *201*, 301−310; FAZXAF: V. A. Makskov, N. V. Podberezskaya, V. E. Zavodnik, I. V. Bragina, L. K. Kedrova, E. D. Korniets, V. K. Bel'skii, V. V. Bakakin, S. P. Gubin, *Koord. Khim.* **1986**, *12*, 1132−1140; HIGRIY: T. Bitterwolf, A. L. Rheingold, M. B. Allen, *private communication*, 1996; LASLOG: S. Pitter, G. Huttner, O. Walter, L. Zsolnai, *J. Organomet. Chem.* **1993**, *454*, 183−198; MIRSOV: J. C. Roder, F. Meyer, R. F. Winter, E. Kaifer, *J. Organomet. Chem.* **2002**, *641*, 113−120; NEZSUG: T. E. Bitterwolf, S. C. Everly, A. L. Rheingold, G. Yapp, *J. Organomet. Chem.* **1997**, *531*, 1−7; QIFBEM: M. A. O. Volland, S. Kudis, G. Helmchen, I. Hyla-Kryspin, F. Rominger, R. Gleiter, *Organometallics* **2001**, *20*, 227−230.; QODVEK: M. Enders, G. Kohl, H. Pritzkow, *J. Organomet. Chem.* **2001**, *622*, 66−73; *SENSOT*: M. D. Raush, W. C. Spink, B. G. Conway, R. D. Rogers, J. L. Atwood, *J. Organomet. Chem.* **1990**, *383*, 227−252; VAVHIJ: P. Harter, G. Boguth, E. Herdtweck, J. Riede, *Angew. Chem.* **1989**, *101*, 1058−1059; VIPGEG: S. Fortier, M. C. Baird, K. F. Preston, J. R. Morton, T. Ziegler, T. J. Jaeger, W. C. Watkins, J. H. McNeil, K. A. Watson, K. Hensel, Y. Le Page, J. P. Charland, A. J. Williams, *J. Am. Chem. Soc.* **1991**, *113*, 542−551; YIHMOR: V. D. Makhaev, M. Kh. Dzhafarov, N. K. Baranetskaya, V. D. Vil'chevskaya, A. S. Batsanov, A. I. Yanovsky, Yu. T. Struchkov, *Koord. Khim.* **1994**, *20*, 838−841; YUNGAP, YUNGET: K. Onotsuka, N. Hosokawa, T. Adachi, T. Yoshida, K. Sonogashira, *Chem. Lett.* **1994**, 2067−2070. [27b] Monobenzocymantrenes: BINCMN: N. B. Honan, J. L. Atwood, I. Bernal, W. A. Herrmann, *J. Organomet. Chem.* **1979**, *179*, 403−410; TURNID: C. Qian, J. Guo, J. Sun, J. Chen, P. Zheng, *Inorg. Chem.* **1997**, *36*, 1286−1295. [27c] Dibenzocymantrene: BAHFEW: A. de Cian, J. P. Djukic, J. Fischer, M. Pfeffer, K. H. Dötz, *Chem. Commun.* **2002**, 638−639; MIYXAT: A. Decken, A. J. Mackay, M. J. Brown, F. Bottomley, *Organometallics* **2002**, *21*, 2006−2009; ZUKLOG: A. I. Yarmolenko, S. V. Kukharenko, L. N. Novikova, N. A. Ustinyuk, F. M. Dlogushin, A. I. Yanovsky, Yu. T. Struchkov, T. G. Kaftaeva, Yu. F. Oprunenko, V. V. Strelets, *Izv. Akad. Nauk. SSSR, Ser. Khim.* **1996**, 199−203.
[28] The structures of η^1-fluorenyl complexes of $Mn(CO)_5$ and $Re(CO)_5$, respectively, are referenced by the CSDB as: MIYXEX: A. Decken, A. J. MacKay, M. J. Brown, F. Bottomley, *Organometallics* **2002**, *21*, 2006−2009; WENQOV: A. L. Mejdrich, T. W. Hanks, *Synth. React. Inorg. Met.-Org. Chem.* **1998**, *28*, 953−973.
[29] CSDB refcode ROMQIT: A. Decken, S. S. Rigby, L. Girard, A. D. Bain, M. J. McGlinchey, *Organometallics* **1997**, *16*, 1308−1315.
[30] S. Top, E. B. Kaloun, S. Toppi, A. Herrbach, M. J. McGlinchey, G. Jaouen, *Organometallics* **2001**, *20*, 4554−4561.
[31] T. Wang, I. S. Cloudsdale, *Synth. Commun.* **1997**, *27*, 2521−2526.
[32] H. Bredereck, R. Gompper, G. Morlock, *Chem. Ber.* **1957**, *90*, 942−952.
[33] [33a] C. Glidewell, S. Z. Ahmed, M. Gottfried, P. Lightfoot, B. J. L. Royles, J. P. Scott, J. Wonnemann, *J. Organomet. Chem.* **1997**, *530*, 177−185. [33b] P. Zanello, M. Fontani, S. Z. Ahmed, C. Glidewell, *Polyhedron* **1998**, *17*, 4155−4162.
[34] M. Pfeffer, E. Urriolabeitia, J. Fischer, *Inorg. Chem.* **1995**, *34*, 643−650.
[35] C. K. Fair in *MolEN. An Interactive Intelligent System for Crystal Structure Analysis*, Nonius, Delft, The Netherlands, **1990**.

Received November 19, 2003
Early View Article
Published Online April 6, 2004

 © 2004 Wiley-VCH Verlag GmbH & Co. KGaA, Weinheim

Reaction of $[In(NEt_2)_3]_2$ with $N(CH_2CH_2NSiMe_3H)_3$: Synthesis and Characterization of New Azaindatranes and Azaindocane

Pavel L. Shutov,[a] Sergey S. Karlov,*[b] Klaus Harms,[a] Andrei V. Churakov,[c] Jörg Lorberth,[a] and Galina S. Zaitseva[b]

Keywords: N ligands / Indium / Tripodal ligands / Amides

$[In(NEt_2)_3]_2$ and $N(CH_2CH_2NSiMe_3H)_3$ react to yield monomeric azaindatrane **1**, $N(CH_2CH_2NSiMe_3)_3In$, which is unstable without additional donor (e.g. pyridine), turning into dimeric azaindatrane **2**, $[N(CH_2CH_2NSiMe_3)_2(CH_2CH_2NH)In]_2$. An intermediate product of this transformation is oligomeric azaindocane **3**, $[N(CH_2CH_2NSiMe_3)_2In(CH_2CH_2NSiMe_3)]_3$. The composition and structures of new compounds have been established by ^1H and ^{13}C NMR spectroscopy. The crystal structures of **1**·Py, *trans*-**2**, and **3** have been determined by X-ray diffraction studies.
(© Wiley-VCH Verlag GmbH & Co. KGaA, 69451 Weinheim, Germany, 2004)

Introduction

The chemistry of indium amido compounds continues to be of interest due to their importance in preparing nitride ceramic materials and semiconductors.[1−3] During our studies of groups 13−15 metallatranes (**A**, Scheme 1, Y = O) and azametallatranes (**A**, Scheme 1, Y = NR)[4−8] we have reported the synthesis and X-ray investigation of the first azaindatrane − $[N(CH_2CH_2NMe)_3In]_2$.[8] This compound is dimeric both in the solid phase and in solution due to the formation of an $(In-N)_2$ core with a very unusual set of In−N distances.[8]

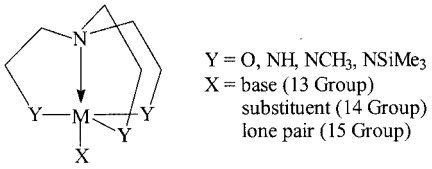

A

Scheme 1

Monomeric tris-amides of group 13 elements are a promising class of precursors of technologically important group 13 nitride semiconductors.[1−3] Bulky substituents R in the parent tetramine $N[CH_2CH_2NRH]_3$ are expected to stabilize the monomeric structure of azaindatranes. We report here the reactions of $[In(NEt_2)_3]_2$ and $InCl_3$ with $N[CH_2CH_2N(SiMe_3)H]_3$ (Me_3Si-tren) and the lithium salt of Me_3Si-tren $\{N[CH_2CH_2N(SiMe_3)Li]_3\}$, respectively. We aimed to prepare Me_3Si-containing azaindatranes and to estimate the influence of bulky Me_3Si groups on structure and stability of monomeric species.

We therefore synthesized four new indium tris-amides containing $[N(CH_2CH_2NSiMe_3)_3]^{3-}$ or $[N(CH_2CH_2NSiMe_3)_2(CH_2CH_2NH)]^{3-}$ moieties: $N(CH_2CH_2NSiMe_3)_3In$ (**1**), $N(CH_2CH_2NSiMe_3)_3In{\cdot}C_5H_5N$ (**1**·Py), dimeric derivative **2**, and oligomeric compound **3** (Scheme 2). The structures of compounds **1**·Py, *trans*-**2**, and **3** have been confirmed by X-ray diffraction studies.

Results and Discussion

Verkade et al. have carried out syntheses, NMR spectroscopy investigations and X-ray diffraction studies of closely related tris(*N*,*N*′′,*N*′′-trimethylsilyl)azaatranes of boron (**4**), aluminium (**5**), and gallium (**6**) (Scheme 3).[9−11] The reaction of $B(NMe_2)_3$ with Me_3Si-tren afforded **4** in low yield (6%),[9] which was explained by the preferred formation of polymeric products. However, the structure of these polymeric products was not established. Compounds of the type $N(CH_2CH_2NSiMe_3)_3M$ [M = Al (**5**), yield 18%;[9] Ga (**6**), yield 88%[11]] were synthesized also, via transamination of $M(NMe_2)_3$ with Me_3Si-tren. Dimeric aluminium azaatrane **7**, the structure of which is analogous to azaindatrane **2**, was obtained during attempts to grow single crystals of **5** from pentane solution.[10]

Our synthetic results are summarized in Scheme 4. Treatment of $[In(NEt_2)_3]_2$ with Me_3Si-tren in the presence of an

[a] Fachbereich Chemie, Philipps-Universität Marburg, Hans-Meerwein-Strasse, 35032 Marburg/Lahn, Germany
[b] Chemistry Department, Moscow State University, Leninskie Gory 1, str. 3, 119899 Moscow, Russia
E-mail: sergej@org.chem.msu.su
[c] Institute of General and Inorganic Chemistry, RAS, Leninsky Prospect 31, 119991 Moscow, Russia

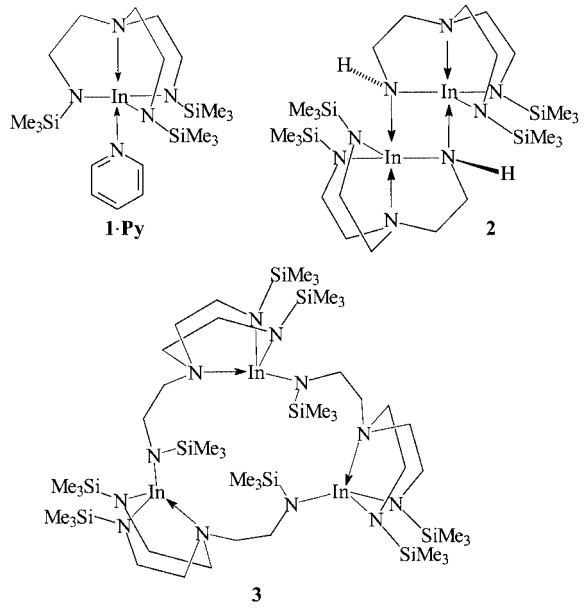

Scheme 2

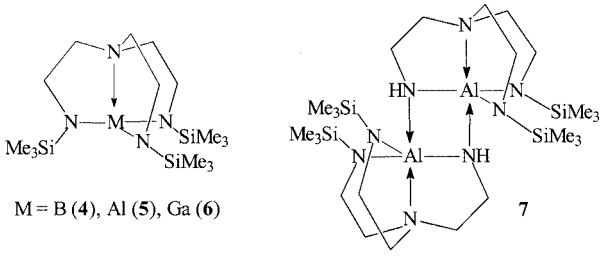

Scheme 3

excess of C_5H_5N led, after standard workup, to **1**·Py in good yield. Notably, carrying-out this reaction without pyridine led to complex **1** (NMR spectroscopic data). Unfortunately, **1** could not be obtained as a pure solid. According to NMR spectroscopic data this compound is an adduct of **1** with one molecule of $HNEt_2$ formed during transamination. However, no additional evidence of this structure was obtained by other methods. Compound **1** is unstable in toluene and in C_6D_6 and turns over 24 h into the oligomeric compound azaindocane **3**, which was obtained after recrystallization from pentane (−30 °C). This transformation might be explained by the lesser steric hindrances in **3** compared with monomeric complex **1**. To the best of our knowledge no similar reactions have been found in "atrane" chemistry.

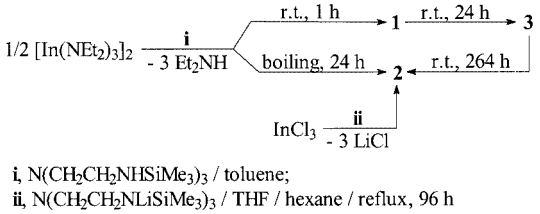

Scheme 4

Further standing of solutions of **3** at room temperature afforded dimeric azaindatrane **2**. The conversion (≈ 70%, ^{1}H NMR data) of the oligomeric ocane **3** into the dimer **2** was observed after 11 days. Formally, the bulky Me_3Si group is substituted by hydrogen during this reaction. However, the true nature of this transformation is unclear. An analogous dimerization passing through desilylation processes has been found for $(Me_3Si)_3$-azaalumatrane **6**[10] and related titanium derivatives (compounds **8** and **9**, Scheme 5).[12] A hydrolytic pathway in the first case, and the reaction of titanium complexes with solvent protons (THF), have been proposed as possible explanations for the formation of desilylated dimers. However, all attempts to prepare **7** by controlled hydrolysis of monomeric **6** failed.[10] The authors did not report the formation of any oligomeric products during both dimerization reactions.[10,12]

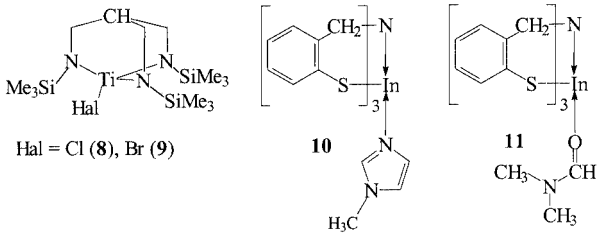

Scheme 5

Complex **1**·Py also turns into **2** at room temperature (40 days, 100%). However, the formation of **3** was undoubtedly detected by NMR spectroscopy in this reaction. Azaatrane **2** was obtained in moderate yield from the reaction of $[In(NEt_2)_3]_2$ with Me_3Si-tren at 95 °C (24 h) − no traces of **1** and **3** being detected in reaction mixture after heating. Compound **2** was the only product that contains an atrane framework in the reaction between $InCl_3$ and the Li_3-salt of Me_3Si-tren. The lithium salt was prepared in situ by treatment of tetramine (Me_3Si-tren) with three equivalents of *n*BuLi.

Compound **2** has a *trans* structure for the central $(In-NH)_2$ core, as confirmed by X-ray data (vide infra). However, the ^{13}C NMR spectra of all the reaction mixtures that lead to **2** contain signals (trace amounts) that may be assigned to *cis*-**2** (Scheme 6), but the *cis*-isomer was not isolated as a pure solid. Conversely, only the *cis*-isomer of **7** was formed in the dimerization of $N(CH_2CH_2NSiMe_3)_3Al$ (**6**).[10] Analogously, we recently found that only the *cis*-isomer of $[N(CH_2CH_2NMe)_3In]_2$ was formed in the reaction of $[In(NEt_2)_3]_2$ with Me-tren $[N(CH_2CH_2NMeH)_3]$, with no traces of *trans*-isomer.[8]

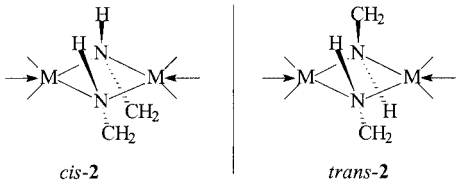

Scheme 6

 © 2004 Wiley-VCH Verlag GmbH & Co. KGaA, Weinheim

Thus, we conclude that the dimeric azaatrane **2** is the most thermodynamically stable product of the transamination reaction of $[In(NEt_2)_3]_2$ with Me_3Si-tren. Donor ligands (e.g. pyridine) partially stabilize the monomeric structure of azaindatrane (compound **1**·Py).

Both ^1H and ^{13}C NMR data agree with the suggested structures for **1**, **1**·Py, **2**, and **3**. In the ^1H NMR spectra of **1** and **1**·Py, signals of methylene protons of the azaindatrane skeleton appear as a set of two pseudo-triplets, forming an AA′MM′ spin system (J = 4.9−5.1 Hz). This pattern is a general feature of the "azaatrane" framework for various azametallatranes.[13] The δ_C signals of the azaatrane skeleton lie within the range typical of those in closely related monomeric derivatives of group 13 elements.[9−11] Thus, **1** and **1**·Py are monomeric in C_6D_6 solution.

In contrast, the ^1H and ^{13}C NMR spectra of **2** and **3** are more complicated. For **2** the data are consistent with a dimer. After purification, **2** was found in solution as one of two geometrical isomers (according to X-ray data − *trans*-**2**) of the In_2N_2 core (Scheme 6). This is documented by two singlets of the Me_3Si groups and twelve partially overlapping multiplets of six CH_2 groups in the ^1H NMR spectrum of **2**. Eight signals of the atrane skeleton carbon atoms appear in the ^{13}C NMR spectrum of **2**. The hydrogen atoms of six methylene groups and methylene carbon atoms as well as each Me_3Si group of one monomeric unit in **3** are also non-equivalent.

Notably, no molecular ions $[M^+]$ or heavy ions that contain at least one In atom were found in mass-spectra (EI, 70 eV) of studied compounds (**1**·Py, **2** and **3**).

Herein we report the crystal structures of azaindatranes **1**·Py and **2** and also of **3** [Figure 1 (one independent molecule), Figure 2 and Figure 3, respectively]. Important bond lengths and angles for **1**−**3** are summarized in Table 1.

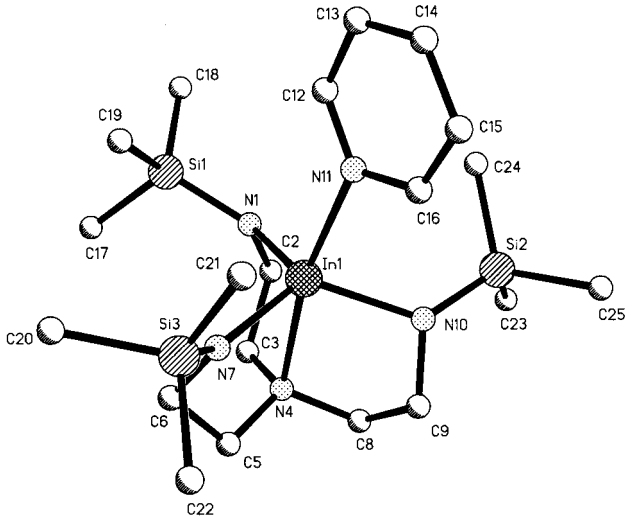

Figure 1. Molecular structure of **1**·Py (one independent molecule); hydrogen atoms omitted for clarity

'The coordination polyhedron of the In atom in complex **1**·Py represents a distorted trigonal bipyramid (TBP) with N(4) (N_{ax}) and N(11) (N^b_{ax}) (Scheme 7) occupying the axial

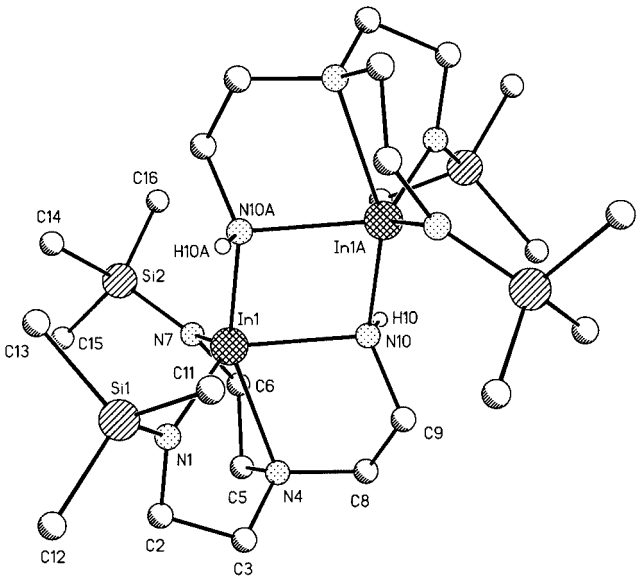

Figure 2. Molecular structure of **2**; hydrogen atoms (except H10 and H10A) omitted for clarity

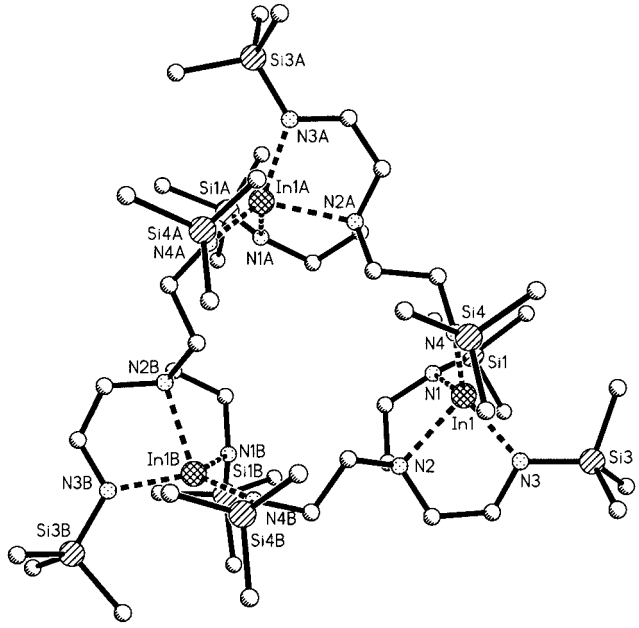

Figure 3. Molecular structure of **3**; hydrogen atoms and solvate cyclohexane molecule omitted for clarity

positions. Three other nitrogen atoms [N(1), N(7), and N(10)] lie in equatorial sites (N_{eq}); $N_{eq}-In-N_{eq}$ angles range between 112.3(1)° and 121.5(1)°, $N_{ax}-In-N_{eq}$ angles range between 78.4(1)° and 80.9(1)°, and $N^b_{ax}-In-N_{eq}$ angles range between 90.8(1)° and 107.3(1)° for **1**·Py. The N(4)−In−N(11) fragment is close to linear for both independent molecules of **1**·Py [169.3(1), 169.2(1)°]. These angles are smaller than those of closely related structures: 179.1(2)° for **10** and 178.4(4)° for **11** (Scheme 5).[14] However, they are greater than those in the dimer $[N(CH_2CH_2NMe)_3In]_2$: 150.3(1)−157.77(9)° for two independent molecules.[8] The latter proves that there is less

 © 2004 Wiley-VCH Verlag GmbH & Co. KGaA, Weinheim

Table 1. Selected bond lengths (Å) and angles (°) for **1**·Py (two independent molecules), **2**, and **3** ([a]: Displacement of In atom from the plane defined by the three N_{eq} atoms towards the N_{ax} atom; [b]: displacement of N_{ax} atom from the plane defined by the three carbon atoms towards the indium atom)

	1·Py		**2**	**3**
$N_{ax}\rightarrow In$	2.412(3)	2.427(1)	2.398(3)	2.294(4)
$N_{ax}\rightarrow In^b$	2.340(3)	2.206(1)	2.326(3)	–
$In-N_{eq}$	2.091(3)	2.076(1)	2.096(3)	2.066(5)
	2.100(3)	2.098(1)	2.107(3)	2.106(5)
	2.120(3)		2.123(3)	
$In-N_{eq}$* (**2**) or $In-N^b_{eq}$ (**3**)	–	2.249(1)	–	2.054(5)
ΔIn (to N_{ax})[a]	0.38	0.44	0.38	0.22
ΔN^b_{ax} (to In)	0.36	0.39	0.37	0.42
$N_{ax}-In-N_{ax}$ [b]	169.3(1)	153.89(5)	169.2(1)	–
$N_{eq}-In-N_{eq}$ (or N^b_{eq}, or N_{eq}*)	112.3(1)	119.43(6)	113.7(1)	126.3(2)
	121.5(1)	108.64(6)	116.5(1)	113.3(2)
	116.6(1)	119.19(5)	120.4(1)	117.0(2)
$N_{eq}-M-N^b_{ax}$	103.9(1)	119.59(6)	104.0(1)	–
	107.3(1)	102.87(5)	106.4(1)	
	90.6(1)	81.51(5)	90.8(1)	
$N_{eq}-M-N_{ax}$	80.1(1)	79.86(5)	80.9(1)	119.9(2)
	79.7(1)	78.70(5)	79.8(1)	83.3(2)
	79.0(1)	75.33(5)	78.4(1)	84.2(2)
$C-N_{ax}-C$	114.7(3)	112.7(1)	114.8(3)	115.9(5)
	114.2(3)	114.0(1)	112.4(3)	109.2(5)
	113.5(3)	113.4(1)	114.9(3)	111.0(5)

steric hindrance in **1**·Py than in dimeric $[N(CH_2CH_2NMe)_3In]_2$. Analogously to **1**·Py, the coordination environment at the In atom in **2** is formed by three covalently linked nitrogen atoms [N_{eq}: N(1), N(7); N^b_{eq}: N(10)] and two-coordinated nitrogen atoms – N_{ax}: N(4) and N^b_{ax}: N(10A) and may be regarded as TBP, which is more distorted than that in **1**·Py due to the steric influence of second azaatrane framework. For compound **2**, the central $(In-N)_2$ unit is planar, differing from that of closely related $[N(CH_2CH_2NMe)_3In]_2$ and **7** where central arrays form a puckered rectangle.[8,10]

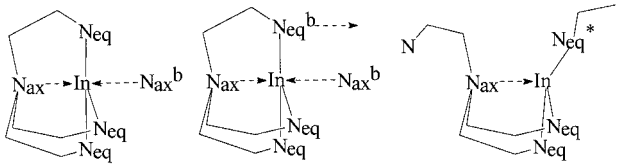

Scheme 7

For both **1**·Py and **2**, the indium atoms are displaced by 0.38 Å (**1**·Py, both independent molecules) and 0.44 Å (**2**) from the plane defined by the three equatorial nitrogen atoms toward pyridine ring (**1**·Py) or N(10A) (**2**). These values characterize the extent of TBP distortion (this displacement should be zero in an ideal TBP).

The transannular bond lengths $N_{ax}\rightarrow In$ [2.412(3), 2.398(3) Å for **1**·Py; 2.427(1) for **2**] and $N^b_{ax}\rightarrow In$ [2.340(3), 2.326(3) Å for **1**·Py; 2.206(1) Å for **2**] in both compounds lie within the typical range for similar indium–nitrogen interactions [2.099(2)–2.62 Å]. Interestingly, the considerable contraction of $N^b_{ax}\rightarrow In$ in **2**, compared with that in **1**·Py, does not noticeably influence the $N_{ax}\rightarrow In$ contact. To the best of our knowledge, the structures of only two tris(amido) indium species containing pyridine as additional ligand $[(C_6H_5)_2N]_3In\cdot Py$, $(2,6\text{-}iPr_2C_6H_3NH)_3In\cdot 2Py$] have previously been studied by X-ray diffractometry.[2,3] Notably, $N^b_{ax}\rightarrow In$ (Py→In) in **1**·Py [2.340(3), 2.206(1) Å, two independent molecules] are shorter than those in (2,6-$iPr_2C_6H_3NH)_3In\cdot 2Py$ [2.460(4), 2.421(4) Å] with a pentacoordinate In atom,[3] but similar to that in the complex $[(C_6H_5)_2N]_3In\cdot Py$ [2.264(4) Å] with a tetracoordinate indium atom.[2]

Compound **3** appears to be only the second ''azaindocane'', the first being the structurally characterized dimeric **12** (Scheme 8)[15]. In contrast to the type of In atom coordination environment found in **1**·Py and **2**, the coordination polyhedron of In atoms in trimeric compound **3** represents a strongly distorted trigonal monopyramid. Each indium atom in **3** is displaced by 0.22 Å from the plane defined by the two N_{eq} and one N_{eq}* atoms towards the N_{ax} atom (Scheme 7). The angles formed by the three equatorial nitrogen atoms and indium atom deviate by less than 7° from the ideal value of 120°, and both $N_{ax}-In-N_{eq}$ angles are close to 90°. However, the $N_{ax}-In-N_{eq}$* angle is noticeably greater than 90°. The lower In coordination number in **3** ($CN = 4$) compared with **1**·Py and **2** ($CN = 5$) leads to considerable shortening of $N_{ax}-In$ in **2** [2.294(4) Å] as against those in **1**·Py [2.412(3), 2.427(1) Å] and **2** [2.398(3) Å].

All five-membered rings of the atrane skeleton in **1**·Py and **2** as well as the ocane framework of **3** adopt an ''envelope''-like conformation (Scheme 8, **B**). All carbon atoms in β-positions to the N_{ax} atom in **1**·Py and **2** occupy ''flap'' sites, while C-α atoms form the base of the envelope plane.

 © 2004 Wiley-VCH Verlag GmbH & Co. KGaA, Weinheim

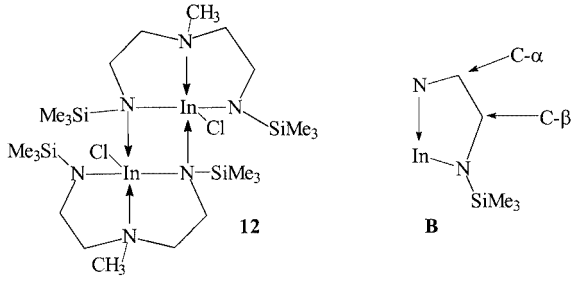

Scheme 8

This is contrary to conformations of ocane rings in **3** and those previously found for ''usual'' metallatranes (without C-β substituents).[16] However, as observed for azametallatranes, C-β as well as C-α atoms may occupy ''flap'' sites of the ''envelope''.[6,17]

Conclusion

Transamination of $[In(NEt_2)_3]_2$ and $N(CH_2CH_2NSiMe_3H)_3$ affords the monomeric azaindatrane **1**, which is converted into the dimeric azaindatrane **2** via the unexpected azaindocane **3**. The desilylated dimer **2** has also been obtained from the reaction of $InCl_3$ with $N(CH_2CH_2NSiMe_3Li)_3$. The structures of **2** and **3** as well as of the adduct **1**·Py have been confirmed by X-ray diffraction analyses.

Experimental Section

General Remarks: All manipulations were performed under dry, oxygen-free argon using standard Schlenk techniques. Solvents were dried by standard methods and distilled prior to use. $InCl_3$ (Aldrich) was used as supplied. The starting materials Me_3Si-tren[18] and $[In(NEt_2)_3]_2$ [19] were prepared according to the literature. C_6D_6 was obtained from Deutero GmbH and dried with sodium. ^1H and ^{13}C NMR spectra were recorded with Bruker AC200, AC300, AC500 spectrometers at 300 K. ^1H and ^{13}C chemical shifts are reported in ppm relative to Me_4Si as external standard. Elemental analyses were carried out by the Microanalytical Laboratory of the Fachbereich Chemie of the Philipps-University of Marburg (Heraeus Rapid Analyser). Mass spectra (EI-MS) were recorded with a Varian CH-7a device using electron impact ionization at 70 eV; mass spectra (FD-MS) were recorded with a HP-5989B device; all assignments were made with reference to the most abundant isotopes.

Azaindocane 3 (Reaction of $[In(NEt_2)_3]_2$ with Me_3Si-tren): A solution of Me_3Si-tren (0.85 g, 2.35 mmol) in toluene (15 mL) was added at room temperature to a solution of $[In(NEt_2)_3]_2$ (0.78 g, 1.18 mmol) in toluene (10 mL). The NMR spectrum of reaction mixture revealed the presence of **1**[20] after 1 h. The reaction mixture was then stirred for a further 24 h, and all volatiles were subsequently removed under reduced pressure. The resultant solid residue was recrystallized from *n*-pentane (10 mL) to give colorless crystals **3** (yield 0.95 g, 85%). All attempts to obtain an analytically pure sample failed, probably due to the presence of traces of dimeric **2** (analytical data below) as well as variable amounts of solvent, which could not completely be removed. Single crystals of **3** suitable for X-ray analysis were collected by recrystallizaton from cyclohexane.

Data for 1: ^1H NMR (C_6D_6, 300.130 MHz): δ = −0.26 (s, 27 H, $3SiMe_3$), 2.04 (t, $^3J_{H,H}$ = −5 Hz, 6 H, $N(CH_2)_3$], 3.02 (t, $^3J_{H,H}$ = −5 Hz, 6 H, $3SiNCH_2$) ppm. ^{13}C NMR (C_6D_6, 75.47 MHz): δ = −2.21 ($SiCH_3$), 45.61 ($SiNCH_2$), 58.06 [$N(CH_2)_3$] ppm.[21]

Data for 3: ^1H NMR (C_6D_6, 500.130 MHz): δ = −0.19 (s, 27 H, $3SiMe_3$), 0.32, 0.33 (2s, 54 H, $6SiMe_3$), 2.10−2.15 (m, 3 H), 2.30−2.32 (m, 6 H), 2.55−2.61 (m, 3 H), 2.83−2.89 (m, 3 H), 2.91−2.98 (m, 6 H), 3.15−3.17 (m, 3 H), 3.20 (br. s, 6 H), 3.27−3.33 (m, 3 H), 3.42−3.48 (m, 3 H) ($18CH_2$ groups) ppm. ^{13}C NMR (C_6D_6, 50.32 MHz): δ = −1.72 ($SiCH_3$), 1.77 ($SiCH_3$), 3.05 ($SiCH_3$), 40.79, 42.75, 44.82, 54.61, 57.28, 58.20 (CH_2 groups) ppm. EI-MS and FD-MS: [M^+] was not found. $C_{45}H_{117}In_3N_{12}Si_9$ (1423.73): calcd. C 37.96, H 8.28, N 11.81; found C 36.82, H 8.68, N 10.93.

Conversion of 3 into 2: After standing for 11 days at room temperature, a toluene solution of **3** was converted into dimeric **2** (70%), as detected by NMR spectroscopy.

***trans*-*N*,*N*′-Bis(trimethylsilyl)azaindatrane Dimer 2.**[22] **Method A (Reaction of $[In(NEt_2)_3]_2$ with Me_3Si-tren):** A solution of Me_3Si-tren (1.67 g, 4.62 mmol) in toluene (25 mL) at room temperature was added to a solution of $[In(NEt_2)_3]_2$ (1.53 g, 2.31 mmol) in toluene (15 mL). The reaction mixture was then boiled under reflux for 24 h, and then all volatiles were removed under reduced pressure. The so-obtained solid residue was recrystallized from *n*-pentane (10 mL) to give colorless crystals **2** (yield 1.45 g, 66%) after standing at −30 °C.

Method B (Reaction of $InCl_3$ with Li_3-Salt of Me_3Si-tren): A solution of trilithium salt, freshly prepared from Me_3Si-tren (3.8 g, 10.5 mmol) and *n*-butyllithium (1.6 M in *n*-hexane, 19.7 mL, 9.8 mmol), in THF (15 mL) at room temperature, with stirring, was added dropwise to a suspension of $InCl_3$ (2.32 g, 10.5 mmol) in THF (20 mL). The reaction mixture was then boiled under reflux for 96 h, and all volatiles were subsequently removed under reduced pressure. *n*-Pentane (40 mL) was then added to the residue, and insoluble substances were removed by filtration. The solution was then reduced in volume to 10 mL and stored at −30 °C for 3 days to obtain colorless crystals, which were separated by rapid decantation of the cold mother liquor to give **2** (yield 2.41 g, 57%). An analytically pure sample was obtained by recrystallization from pentane. ^1H NMR (C_6D_6, 500.130 MHz): δ = −0.28 (br. s, 36 H, $4SiMe_3$), 1.72−1.98 (m, 4 H), 2.08−2.29 (m, 8 H), 2.49−2.67 (m, 4 H), 2.80−3.11 (m, 8 H) ($12CH_2$ groups) ppm; the NH proton signals could not be located, probably due to overlap with CH_2 multiplets. ^{13}C NMR (C_6D_6, 75.47 MHz): δ = −2.24 ($SiCH_3$), 3.21 ($SiCH_3$), 42.62, 43.31, 43.82, 59.29, 60.55, 60.93 (CH_2 groups) ppm. EI-MS and FD-MS: [M^+] was not found. $C_{24}H_{62}In_2N_8Si_4$ (804.79): calcd. C 35.82, H 7.77, N 13.92; found C 35.05, H 8.04, N 13.09.

Adduct of *N*,*N*′*N*′′-Tris(trimethylsilyl)azaindatrane with Pyridine, 1·Py (Reaction of $[In(NEt_2)_3]_2$ with Me_3Si-tren in the Presence of Pyridine): Pyridine (5 mL) and then a solution of Me_3Si-tren (2.99 g, 8.25 mmol) in toluene (20 mL) were added at room temperature to a solution of $[In(NEt_2)_3]_2$ (2.73 g, 4.12 mmol) in toluene (10 mL). The reaction mixture was then stirred for 12 h, and all volatiles were subsequently removed under reduced pressure. The resultant solid residue was recrystallized from *n*-pentane (10 mL) to give colorless crystals **1**·Py (yield 3.59 g, 79%). Single crystals of **1**·Py suitable for X-ray analysis were collected by recrystallizaton from *n*-pentane (−30 °C, saturated solution). ^1H NMR (C_6D_6,

 © 2004 Wiley-VCH Verlag GmbH & Co. KGaA, Weinheim

Table 2. Crystal data, data collection, structure solution and refinement parameters for **1**·Py, **2**, and **3**

Compound	**1**·Py	**2**	**3**
Empirical formula	$C_{20}H_{44}In_1N_5Si_3$	$C_{24}H_{62}In_2N_8Si_4$	$C_{48}H_{123}In_3N_{12}Si_9$
Molecular mass	553.69	804.82	1465.85
Colour, habit	colourless prism	colourless prism	colourless plate
Crystal size (mm)	0.35 × 0.31 × 0.30	0.45 × 0.24 × 0.21	0.39 × 0.15 × 0.05
Crystal system	monoclinic	monoclinic	trigonal
Space group	$P2_1/c$	$P2_1/c$	R-3
Unit cell dimensions, a (Å)	19.426(1)	10.364(1)	22.485(1)
b (Å)	12.0030(4)	16.309(1)	
c (Å)	24.639(1)	11.797(1)	22.485(1)
β (°)	90.080(4)	107.886(7)	26.544(2)
Volume (Å^3)	5745.0(4)	1897.6(3)	11622(1)
Z	8	2	6
Density (calculated) [g·cm^{-3}]	1.280	1.409	1.257
Absorption coefficient [mm^{-1}]	0.963	1.367	1.061
F(000)	2320	832	4608
θ range (°)	1.34−25.89	2.20−26.18	1.30−24.98
Index ranges	$-23 \le h \le 23$ $-13 \le k \le 14$ $-30 \le l \le 30$	$-12 \le h \le 12$ $-20 \le k \le 20$ $-14 \le l \le 14$	$-26 \le h \le 26$ $-24 \le k \le 26$ $-31 \le l \le 31$
Reflections collected	55794	17852	20441
Independent reflections	11076 [R_{int} = 0.0394]	3754 [R_{int} = 0.0308]	4520 [R_{int} = 0.0764]
Data/restraints/parameters	11076/0/542	3754/0/183	4520/0/226
Goodness-of-fit on F^2	1.031	1.054	0.954
Final R indices [$I > 2\sigma(I)$]	R_1 = 0.0280, wR_2 = 0.0718	R_1 = 0.0172, wR_2 = 0.0422	R_1 = 0.0490, wR_2 = 0.1287
R indices (all data)	R_1 = 0.0332, wR_2 = 0.0733	R_1 = 0.0205, wR_2 = 0.0431	R_1 = 0.0727, wR_2 = 0.1374
Extinction coefficient	−	0.0003(4)	−
Largest diff. peak/hole [e·Å^{-3}]	0.521/−0.708	0.285/−0.263	0.938/−0.624

300.130 MHz): δ = −0.14 (s, 27 H, $3SiMe_3$), 2.30 [t, $^3J_{H,H}$ = −5 Hz, 6 H, $N(CH_2)_3$], 3.14 (t, $^3J_{H,H}$ = −5 Hz, 6 H, $3SiNCH_2$), 6.55−6.59 (m, 2 H, Py hydrogen atoms), 6.81−6.86 (m, 1 H, Py hydrogen), 8.80−8.83 (m, 2 H, Py hydrogen atoms) ppm. ^{13}C NMR (C_6D_6, 75.47 MHz): δ = −2.82 ($SiCH_3$), 44.51 ($SiNCH_2$), 61.76 [$N(CH_2)_3$], 124.24, 138.11, 150.12 (Py carbon atoms) ppm.[21] EI-MS: [M^+] not found. $C_{20}H_{44}InN_5Si_3$ (553.676): calcd. C 43.39, H 8.01, N 12.65; found C 42.99, H 7.70, N 11.92.

Conversion of 1·Py into 2: After standing at room temperature for 40 days, a toluene solution of **1**·Py was converted into dimer **2** (100%), as detected by NMR spectroscopy. According to ^1H NMR data the reaction mixture contained **1**·Py, **2**, and **3** (ratio 5:3:2) after 18 days.

X-ray Crystallographic Study: Crystal data, data collection, structure solution and refinement parameters for compounds **1**·Py, **2**, and **3** are presented in Table 2. Experimental intensities were measured with a Stoe IPDS diffractometer using graphite-monochromatized Mo-K_α radiation (λ = 0.71073 Å) at 193(2) K. The structures were solved by direct methods[23] and refined by full-matrix least-squares on F^2 [24] with anisotropic thermal parameters for all non-hydrogen atoms. All H atoms were placed in calculated positions and refined using a riding model.

CCDC-224379 (for **1**·Py), -224380 (for **2**), and -224381 (for **3**) contain the supplementary crystallographic data for this paper. These data can be obtained free of charge at www.ccdc.cam.ac.uk/conts/retrieving.html [or from the Cambridge Crystallographic Data Centre, 12 Union Road, Cambridge CB2 1EZ, UK; Fax: (internat.) +44-1223-336-033; E-mail: deposit@ccdc.cam.ac.uk].

Acknowledgments

This work was supported by the Philipps-University Marburg, Chemistry Department, with a grant for P. L. S.

[1] A. P. Purdy, *Inorg. Chem.* **1994**, *33*, 282−286.
[2] J. Kim, S. G. Bott, D. M. Hoffman, *Inorg. Chem.* **1998**, *37*, 3835−3841.
[3] J. S. Silverman, C. J. Carmalt, A. H. Cowley, R. D. Culp, R. A. Jones, B. G. McBurnett, *Inorg. Chem.* **1999**, *38*, 296−300.
[4] P. L. Shutov, S. S. Karlov, K. Harms, A. V. Churakov, J. A. K. Howard, J. Lorberth, G. S. Zaitseva, *Eur. J. Inorg. Chem.* **2002**, 2784−2788.
[5] P. L. Shutov, S. S. Karlov, K. Harms, D. A. Tyurin, A. V. Churakov, J. Lorberth, G. S. Zaitseva, *Inorg. Chem.* **2002**, *41*, 6147−6152.
[6] P. L. Shutov, D. A. Sorokin, S. S. Karlov, K. Harms, Yu. F. Oprunenko, A. V. Churakov, M. Yu. Antipin, G. S. Zaitseva, J. Lorberth, *Organometallics* **2003**, *22*, 516−522.
[7] E. V. Gauchenova, S. S. Karlov, A. A. Selina, E. S. Chernyshova, A. V. Churakov, J. A. K. Howard, N. A. Troitsky, S. N. Tandura, J. Lorberth, G. S. Zaitseva, *J. Organomet. Chem.* **2003**, *676*, 8−21.
[8] P. L. Shutov, S. S. Karlov, K. Harms, O. Kh. Poleshchuk, J. Lorberth, G. S. Zaitseva, *Eur. J. Inorg. Chem.* **2003**, 1507−1510.
[9] J. Pinkas, B. Gaul, J. G. Verkade, *J. Am. Chem. Soc.* **1993**, *115*, 3925−3931.
[10] J. Pinkas, T. Wang, R. A. Jacobson, J. G. Verkade, *Inorg. Chem.* **1994**, *33*, 4202−4210.

 © 2004 Wiley-VCH Verlag GmbH & Co. KGaA, Weinheim

[11] J. Pinkas, T. Wang, R. A. Jacobson, J. G. Verkade, *Inorg. Chem.* **1994**, *33*, 5244−5253.
[12] S. Friedrich, L. H. Gade, A. J. Edwards, M. McPartlin, *Chem. Ber.* **1993**, *126*, 1797−1805.
[13] J. G. Verkade, *Coord. Chem. Rev.* **1994**, *137*, 233−295.
[14] R. J. Motekaitis, A. E. Martell, S. A. Koch, J. Hwang, D. A. Quarless, M. J. Welch, *Inorg. Chem.* **1998**, *37*, 5902−5911.
[15] N. Emig, H. Nguyen, H. Krautscheid, R. Réau, J.-B. Cazaux, G. Bertrand, *Organometallics* **1998**, *17*, 3599−3608.
[16] G. S. Zaitseva, S. S. Karlov, B. A. Siggelkow, E. V. Avtomonov, A. V. Churakov, J. A. K. Howard, J. Lorberth, *Z. Naturforsch., Teil B* **1998**, *53*, 1247−1254.
[17] P. L. Shutov, S. S. Karlov, K. Harms, D. A. Tyurin, A. V. Churakov, J. A. K. Howard, J. Lorberth, G. S. Zaitseva, *J. Molec. Struct. J. Mol. Struct.* **2004**, *689* 261−268.
[18] G. S. Zaitseva, B. A. Siggelkow, S. S. Karlov, G. V. Pen'kovoy, J. Lorberth, *Z. Naturforsch., Teil B* **1998**, *53*, 1255−1258.
[19] G. Rossetto, N. Brianese, A. Camporese, M. Porchia, P. Zanella, R. Bertoncello, *Main Group Met. Chem.* **1991**, *14*, 113−122.
[20] 4,6,11-Tris(trimethylsilyl)-1,4,6,11-tetraaza-5-indatricylo-[3.3.3.$0^{1,5}$]undecane.
[21] Assignments of CH_2 signals agree with the data of Verkade et al. for $N(CH_2CH_2NSiMe_3)_3M$ (M = B, Al).[9]
[22] 4,6-Bis(trimethylsilyl)-1,4,6,11-tetraaza-5-indatricylo-[3.3.3.$0^{1,5}$]undecane dimer.
[23] G. M. Sheldrick, *Acta Crystallogr., Sect. A* **1990**, *46*, 467−473.
[24] G. M. Sheldrick, *SHELXL-97*. Program for the Refinement of Crystal Structures. University of Göttingen, Germany, **1997**.

Received November 26, 2003
Early View Article
Published Online April 6, 2004

 © 2004 Wiley-VCH Verlag GmbH & Co. KGaA, Weinheim

Synthesis and Characterisation of Two Supramolecular Polymers $[CuAg_4(CN)_6(tacn)]_n$ and $[CuAu_2(CN)_4(tacn)]_n$ Containing Metal−Metal Interactions

Wei Han,[a] Long Yi,[a] Zhan-Quan Liu,[a] Wen Gu,[a] Shi-Ping Yan,*[a,b] Peng Cheng,[a] Dai-Zheng Liao,[a] and Zong-Hui Jiang[a]

Keywords: Silver / Gold / Macrocyclic ligands / Metal−metal interactions

Two novel heterobimetallic supramolecular polymers, $[CuAg_4(CN)_6(tacn)]_n$ (**1**) and $[CuAu_2(CN)_4(tacn)]_n$ (**2**) (tacn = 1,4,7-triazacyclononane), have been synthesised from the building block $[Cu(tacn)]^{2+}$, together with $[Ag(CN)_2]^-$ (for **1**) and $[Au(CN)_2]^-$ (for **2**). The large difference in structural type between **1** and **2** is probably due to the fact that the Ag^I centre is three-coordinate and trigonal whereas the Au^I centre is linear. Metal–metal interactions play an important role in the formation of the supramolecular framework of **1** and the novel topology of **2**.
(© Wiley-VCH Verlag GmbH & Co. KGaA, 69451 Weinheim, Germany, 2004)

Introduction

The construction of supramolecular arrays by coordination has developed into a central theme of supramolecular chemistry.[1] Many novel supramolecular complexes have been produced with single metal centres linked by bi- or multifunctional ligands.[2] Cyanometalate anions, because of their ability to form strong bonds with transition metal cations, have been extensively used as building blocks in supramolecular coordination polymers.[3] Compared to the higher-coordination counterparts of various transition metals, there has been less investigation of two-coordinate, linear cyanometalate building blocks in the construction of coordination polymers.[3] Therefore, we chose the linear units $[Ag(CN)_2]^-$ and $[Au(CN)_2]^-$ in order to construct multi-dimensional structures and novel topologies. At the same time, investigations into the attractive interactions between closed-shell metal atoms and ions continue to generate much interest.[4] As well as being able to use their cyano groups as bridging ligands, $[Ag(CN)_2]^-$ and $[Au(CN)_2]^-$ can also produce polymeric structures through Ag···Ag and Au···Au interactions. It is now well-established that Ag^I and Au^I complexes aggregate with a metal−metal interaction that is shorter than the sum of their van der Waals radii (3.44 Å for Ag and 3.6 Å for Au).[4,5] Although crystal engineering of supramolecular structures by Ag···Ag and Au···Au interactions is well-documented,[6] most of the reported structures contain only gold or silver without other metals, and there are few reports on heterobimetallic M−Ag or M−Au supramolecular compounds.[7] Leznoff has reported some Cu−Ag and Cu−Au complexes with capping amine ligands,[7] however, to the best of our knowledge, the use of the tacn ligand in a such system has not been reported.

Our interest has focused especially on the field of the d^{10}-d^{10} interactions of Ag^I and Au^I complexes. The energy of these interactions is similar to that of hydrogen bonds,[7] and they have been employed in the construction of multi-dimensional structures and novel topologies. We would therefore like to report the structural properties of two novel supramolecular polymers **1** and **2**, containing the tacn ligand and the linear units $[Ag(CN)_2]^-$ (in **1**) and $[Au(CN)_2]^-$ (in **2**). The differences between the structural properties, novel topologies and metal−metal interactions of both complexes form the subject of this contribution.

Results and Discussion

The coordination environment of **1** is shown in Figure 1; selected bond lengths and angles are listed in Table 1. Each of the $[Cu(tacn)]^{2+}$ cations is connected to two cyano groups; each copper(II) ion is therefore five-coordinate. The copper centre adopts a distorted square-pyramidal coordination, such that one nitrogen atom of the tacn ligand is coordinated apically, and the four equatorial positions are occupied by the two nitrogen atoms of the tacn ligand and the two cyano groups. The apical Cu−N bond length [Cu1−N1 = 2.171(8) Å] is slightly shorter than those of the previously reported distorted copper complexes (apical

[a] Department of Chemistry, NanKai University, Tianjin 300071, P. R. China
E-mail: yansp@nankai.edu.cn
[b] State Key Laboratory of Chemistry and Application of Rare Earth Materials, Peking University, Beijing 100871, P. R. China

 © 2004 Wiley-VCH Verlag GmbH & Co. KGaA, Weinheim DOI: 10.1002/ejic.200300678

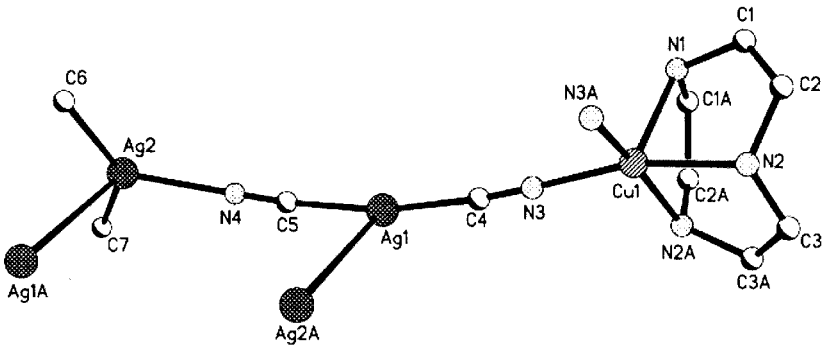

Figure 1. Perspective view of $[CuAg_4(CN)_6(tacn)]_n$ (**1**) showing the atom numbering; hydrogen atoms are omitted for clarity

Table 1. Selected bond lengths [Å] and angles [°] for complex **1**

Ag(1)−C(5)	2.062(7)	Cu(1)−N(3)	1.967(6)
Ag(1)−C(4)	2.066(8)	Cu(1)−N(2)	2.039(5)
Ag(1)−Ag(2)#1	3.2940(13)	Cu(1)−N(1)	2.171(8)
Ag(2)−C(7)	2.138(6)	Ag(2)−C(6)	2.112(6)
Ag(2)−N(4)	2.279(7)	N(2)−Cu(1)−N(2)#2	82.3(3)
C(5)−Ag(1)−C(4)	168.9(3)	N(3)−Cu(1)−N(1)	107.5(2)
C(5)−Ag(1)−Ag(2)#1	87.42(19)	N(2)−Cu(1)−N(1)	83.1(2)
C(4)−Ag(1)−Ag(2)#1	92.8(2)	C(1)−N(1)−Cu(1)	105.1(5)
C(6)−Ag(2)−C(7)	134.7(2)	C(3)−N(2)−Cu(1)	109.5(5)
C(6)−Ag(2)−N(4)	115.8(3)	C(2)−N(2)−Cu(1)	108.4(5)
C(7)−Ag(2)−N(4)	109.4(2)	C(4)−N(3)−Cu(1)	174.9(6)
C(6)−Ag(2)−Ag(1)#1	68.4(2)	N(3)−C(4)−Ag(1)	175.2(6)
C(7)−Ag(2)−Ag(1)#1	102.27(19)	C(5)−N(4)−Ag(2)	166.4(6)
N(4)−Ag(2)−Ag(1)#1	104.40(16)	N(4)−C(5)−Ag(1)	174.2(6)
N(3)−Cu(1)−N(3)#2	93.5(3)	N(5)#3−C(6)−Ag(2)	174.5(7)
N(3)−Cu(1)−N(2)	166.7(3)	N(6)#4−C(7)−Ag(2)	172.08(18)
N(3)#2−Cu(1)−N(2)	90.9(2)		

Symmetry transformations used to generate equivalent atoms: #1: $-x+3, -y+1, -z+1$; #2: $x, y, -z+1/2$; #3: $x, -y+3/2, -z+1$; #4: $x, y, -z+3/2$.

Cu−N bond length = 2.2−2.7 Å).[8] It should be noted that the coordination numbers of the Ag centres for Ag1 and Ag2 are 3 and 4, respectively.

The X-ray crystal analysis of **1** revealed a one-dimensional structure constructed from necklace-shaped rings. Each ring contains one copper, six silver and seven cyano groups, as shown in Figure 2. These necklaces-shaped rings are linked by shared edges up and down in the [011] direction. To the best of our knowledge, this structure is the first example of a necklace-shaped topology. The 1D structures in **1** are alternately linked via Ag···Ag interactions of 3.2940(13) Å [which is significantly less than the sum of the van der Waals radii of the two Ag(I) centres], and creates a 2D array in the *a* direction. Figure 3 shows the Ag···Ag metallic bonds that exist between the planes of the 2D array. As a result, the silver−silver interactions have increased the dimensionality of **1** from one to two, and can thus be viewed as a tool with which to increase structural dimensionality.[3]

The 2D arrays are connected into a weakly bonded supramolecule through further weak interactions between silver ladders (Figure 4). Within each silver ladder, there are

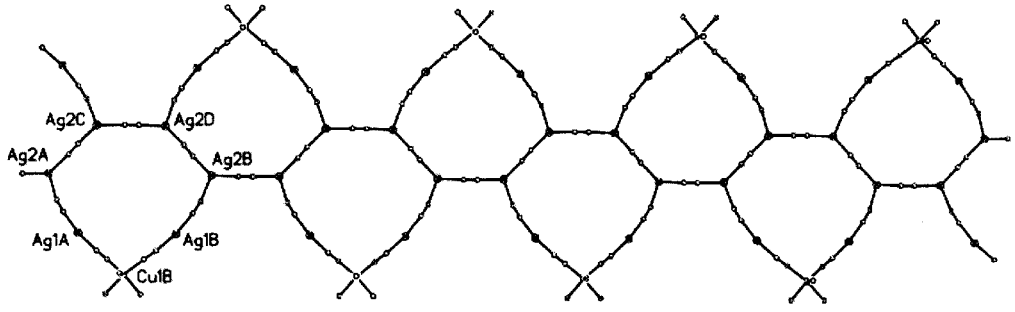

Figure 2. 1D structure of complex **1**; uncoordinated carbon atoms of the tacn ligands are omitted for clarity

 © 2004 Wiley-VCH Verlag GmbH & Co. KGaA, Weinheim

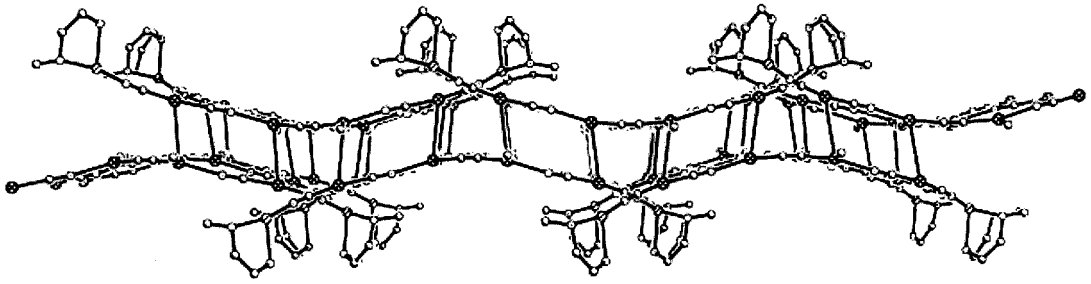

Figure 3. View of the double two-dimensional structure of **1**, showing metal−metal interactions between the two planes

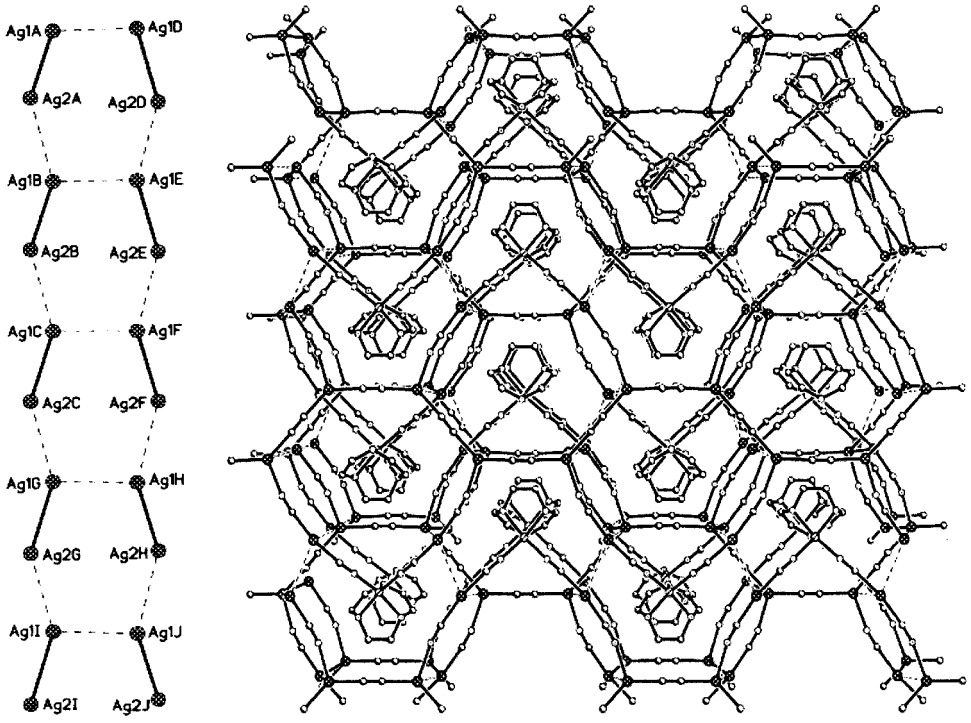

Figure 4. The silver ladder (left) and supramolecular structure (right) of complex **1**

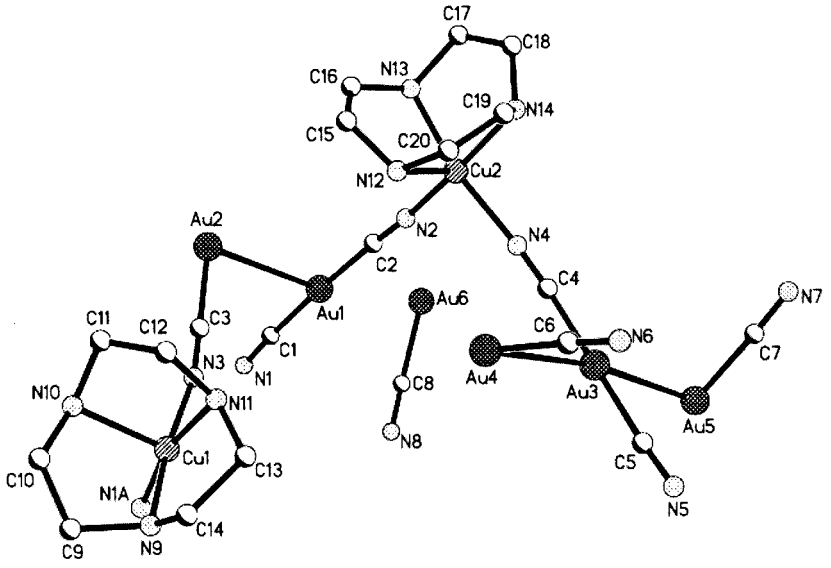

Figure 5. Perspective view of $[CuAu_2(CN)_4(tacn)]_n$ (**2**) showing the atom numbering; hydrogen atoms are omitted for clarity

 © 2004 Wiley-VCH Verlag GmbH & Co. KGaA, Weinheim

no significant silver−silver interactions. The sum of the van der Waals radii of the two Ag^I centres is 3.44 Å, and is thus at the upper limit of a distance for a viable aurophilic interaction.[5] The Ag1B···Ag1E distance of 3.486 Å is beyond this threshold, and the Ag1B···Ag2A distance of 3.748 Å is even larger. As shown in Figure 4, the frameworks of AgCN exhibit a hexagon-like supramolecular structure. The siting of copper ions within these hexagons is an example of a rather rare topology.

Complex **2** was obtained by repeating the same procedure as for the preparation of **1**, but by using $[Au(CN)_2]^-$ instead of $[Ag(CN)_2]^-$. The coordination environment of **2** is shown in Figure 5; selected bond lengths and angles are listed in Table 2. Each of the $[Cu(tacn)]^{2+}$ cations is five-coordinate and adopts a distorted square-pyramidal coordination, similar to the Cu^{II} ions of **1**. The apical Cu1−N10 and Cu2−N12 bond lengths are 2.176(13) Å and 2.159(15) Å, respectively.

The packing structure of **2** reveals that there are two kinds of gold chains (see Figure 6), and that the copper ions act as bridges to link these gold chains together to form a 3D polymer. The zigzag chain is formed from gold ions in four kinds of coordination environment, in an **ABCDABCD** pattern. The distances of Au3A···Au4A and Au3A···Au5A are 3.2295(12) and 3.2614(12) Å, respectively; much shorter than the van der Waals separation of Au···Au. Chain b shows two kinds of centrosymmetric trinuclear units and two kinds of free $[Au(CN)_2]^-$ units, which are connected alternately with Au1A···Au2A and Au1A···Au6A interactions of 3.1321(11) and 3.33(8) Å, respectively. The axis of these gold chains is in the *a* direction, and they alternate along the *b* direction. As in **1**, the copper centre is five-

Table 2. Selected bond lengths [Å] and angles [°] for complex **2**

Au(1)−C(2)	1.941(19)	Au(6)−C(8)	1.99(2)
Au(1)−C(1)	1.967(16)	Cu(1)−N(1)#5	1.950(14)
Au(1)−Au(2)	3.1321(11)	Cu(1)−N(3)	1.975(14)
Au(2)−C(3)	1.959(18)	Cu(1)−N(9)	2.016(13)
Au(2)−Au(1)#1	3.1321(11)	Cu(1)−N(11)	2.044(14)
Au(3)−C(5)	1.960(17)	Cu(1)−N(10)	2.176(13)
Au(3)−C(4)	1.964(16)	Cu(2)−N(2)	1.967(15)
Au(3)−Au(4)	3.2295(12)	Cu(2)−N(13)	1.973(17)
Au(3)−Au(5)	3.2614(12)	Cu(2)−N(14)	1.996(14)
Au(4)−C(6)	1.94(2)	Cu(2)−N(4)	1.999(16)
Au(4)−Au(3)#2	3.2295(12)	Cu(2)−N(12)	2.159(15)
Au(5)−C(7)	1.93(2)	N(1)−Cu(1)#5	1.950(14)
Au(5)−Au(3)#3	3.2614(12)		
C(2)−Au(1)−C(1)	177.0(7)	N(9)−Cu(1)−N(10)	83.0(6)
C(2)−Au(1)−Au(2)	87.8(5)	N(11)−Cu(1)−N(10)	83.9(6)
C(1)−Au(1)−Au(2)	94.0(5)	N(2)−Cu(2)−N(13)	90.5(8)
C(3)−Au(2)−C(3)#1	180.000(1)	N(2)−Cu(2)−N(14)	167.3(7)
C(3)−Au(2)−Au(1)#1	86.3(5)	N(13)−Cu(2)−N(14)	83.4(8)
C(3)−Au(2)−Au(1)	93.7(5)	N(2)−Cu(2)−N(4)	92.2(6)
Au(1)#1−Au(2)−Au(1)	180.000(3)	N(13)−Cu(2)−N(4)	172.0(7)
C(5)−Au(3)−C(4)	176.4(7)	N(14)−Cu(2)−N(4)	92.5(7)
C(5)−Au(3)−Au(4)	92.7(5)	N(2)−Cu(2)−N(12)	107.7(7)
C(4)−Au(3)−Au(4)	84.1(5)	N(13)−Cu(2)−N(12)	83.6(8)
C(5)−Au(3)−Au(5)	79.8(5)	N(14)−Cu(2)−N(12)	82.8(7)
C(4)−Au(3)−Au(5)	103.5(5)	N(4)−Cu(2)−N(12)	102.7(7)
Au(4)−Au(3)−Au(5)	171.49(2)	C(1)−N(1)−Cu(1)#5	166.4(14)
C(6)−Au(4)−C(6)#2	180.000(4)	C(2)−N(2)−Cu(2)	174.3(15)
C(6)−Au(4)−Au(3)#2	94.6(6)	C(3)−N(3)−Cu(1)	164.2(15)
C(6)−Au(4)−Au(3)	85.4(6)	C(4)−N(4)−Cu(2)	164.8(15)
Au(3)#2−Au(4)−Au(3)	180.0	C(14)−N(9)−Cu(1)	114.1(10)
C(7)−Au(5)−C(7)#3	180.000(3)	C(9)−N(9)−Cu(1)	103.6(11)
C(7)−Au(5)−Au(3)	90.8(5)	C(10)−N(10)−Cu(1)	107.8(10)
C(7)#3−Au(5)−Au(3)	89.2(5)	C(11)−N(10)−Cu(1)	100.8(10)
Au(3)−Au(5)−Au(3)#3	180.0	C(13)−N(11)−C(12)	114.7(16)
C(8)−Au(6)−C(8)#4	180.000(1)	C(13)−N(11)−Cu(1)	104.4(11)
N(1)#5−Cu(1)−N(3)	93.5(6)	C(12)−N(11)−Cu(1)	109.2(11)
N(1)#5−Cu(1)−N(9)	91.8(6)	N(1)−C(1)−Au(1)	176.9(16)
N(3)−Cu(1)−N(9)	172.2(6)	N(2)−C(2)−Au(1)	174.4(15)
N(1)#5−Cu(1)−N(11)	166.2(6)	N(3)−C(3)−Au(2)	175.4(16)
N(3)−Cu(1)−N(11)	90.8(6)	N(4)−C(4)−Au(3)	172.4(16)
N(9)−Cu(1)−N(11)	82.7(6)	N(5)−C(5)−Au(3)	175.5(17)
N(1)#5−Cu(1)−N(10)	108.1(6)	N(6)−C(6)−Au(4)	178(2)
N(3)−Cu(1)−N(10)	100.9(6)	N(8)−C(8)−Au(6	173.2(19)

Symmetry transformations used to generate equivalent atoms: #1: $-x+1, -y+1$, -z; #2: $-x+1, -y+1, -z+1$; #3: $-x+1, -y+2, -z+1$; #4: $-x+1, -y+2$, -z; #5: $-x+2, -y+1, -z$.

 © 2004 Wiley-VCH Verlag GmbH & Co. KGaA, Weinheim

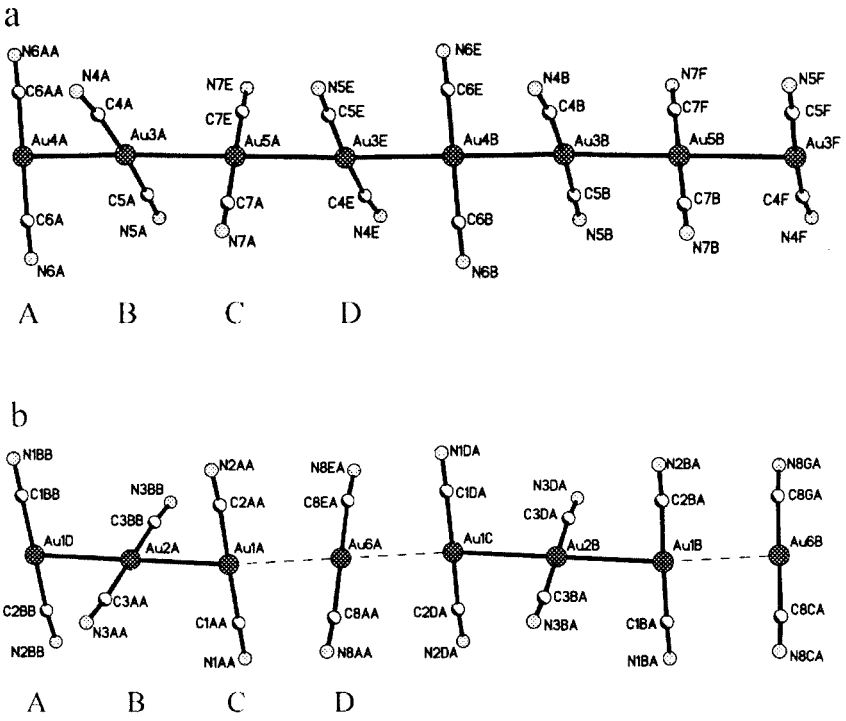

Figure 6. The two kinds of gold chains in complex **2**

coordinate with two sites occupied by nitrogen atoms of the cyano groups; thus the copper atoms function as bridges. In the *bc* plane, the copper ions linking two kinds of chains with single and double bridges form a 3D polymer of **2** (Figure 7). Leznoff has reported some Au−Cu complexes similar to **2**,[7] which also demonstrated the importance of Au···Au interactions in forming coordination polymers.

Complexes **1** and **2** exhibit different structures and topologies, which is probably mainly due to the different coordination numbers of Ag and Au (the Ag^I centre is three coordinate and trigonal, whereas the Au^I centre is linear). In addition, the different metallic radii of Ag and Au have led to the fact that silver−silver interactions have been reported and calculated to be weaker than gold−gold interactions,[3] which may also be the reason for the different structures of **1** and **2**. In the FT-IR spectra (KBr discs), there are three sharp ν_{CN} bands at 2174.4, 2136.2, and 2113.7 cm^{-1} for **1**, and at 2189.9, 2151.9, and 2138.5 cm^{-1} for **2**. The IR band at 2113.7 cm^{-1} is unusually low for an $[Ag(CN)_2]^-$-containing system (free $[Ag(CN)_2]^-$ is at 2139 cm^{-1}); this is somewhat hard to rationalise. It is noticeable that the vibration frequencies of the three bands in **1** are lower than those in **2**, which could be due to the slightly stronger coordination of the cyano group with Au than

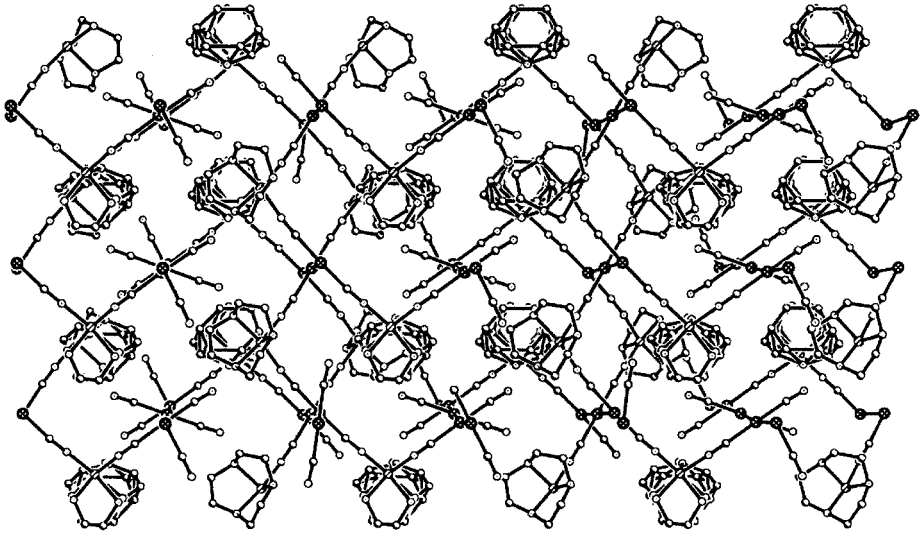

Figure 7. View of the three-dimensional polymeric structure of complex **2** along the *b* axis; hydrogen atoms are omitted for clarity

 © 2004 Wiley-VCH Verlag GmbH & Co. KGaA, Weinheim

with Ag. The UV/Vis spectra of both **1** and **2** in DMF solution (concentration 0.10 mol/L) have similar strong absorption bands in the 200−270 nm range; **2** also displays two weak peaks at 279 and 289 nm, which may be assigned to the lower-energy MLCT absorption bands ($^1\Pi_u$-1 and $^3\Pi_u$-1).[9] Although Patterson has reported the UV/Vis spectra of $[Ag(CN)_2]^-$ and $[Au(CN)_2]^-$, we get different results in our work because of the different solvents and the nature of our complexes. In the visible range, the peaks at 566 nm (for **1**) and at 643 nm (for **2**) can be attributed to the *d-d* bands of Cu^{II}.[10]

Experimental Section

Materials and Methods: All of the starting materials were of reagent grade and were used without further purification. The macrocycle ligand tacn was prepared according to the procedures previously described.[11,12] C, H, N elemental analyses were carried out with a Perkin−Elmer analyzer, model 240. Electronic spectra were recorded with a Shimadzu UV-2101PC spectrophotometer in the 200−2000 nm range at room temperature. The FT-IR spectra were recorded with KBr pellets in the range 4000−400 cm^{-1} with a Bio-Rad FTS 135 spectrometer.

Synthesis of $C_{12}H_{15}Ag_4CuN_9$ (1): A solution of $CuCl_2{\cdot}2H_2O$ (0.17 g, 1 mmol) in water (2.5 mL) was slowly added to a solution of tacn (0.13 g, 1 mmol) in methanol (2.5 mL) with stirring. The deep blue solution was stirred for 30 min and then filtered. The above-mentioned deep blue filtrate was introduced to one arm of an H-shaped tube and a solution of $K[Ag(CN)_2]$ (0.20 g, 1 mmol) in water (5 mL) was added to the other arm. After a few weeks, deep blue blocks of complex **1** (0.302 g, 68%, based on Ag salts) were obtained. $C_{12}H_{15}Ag_4CuN_9$: calcd. C 18.55, H 1.79, N 16.48; found C 18.46, H 1.92, N 16.14.

Synthesis of $C_{10}H_{15}Au_2CuN_7$ (2): This was synthesised according to the procedure described above (using similar reaction conditions), but using $K[Au(CN)_2]$ instead of $K[Ag(CN)_2]$, to provide deep blue needles of **2** (0.317 g, 46%, based on gold salts). $C_{10}H_{15}Au_2CuN_7$: calcd. C 17.15, H 2.31, N 14.26; found C 17.37, H 2.17, N 14.19.

X-ray Crystallographic Study: Single crystal X-ray diffraction measurements of the two complexes were carried out with a Bruker Smart 1000 CCD area detector using graphite-monochromated Mo-K_α radiation (λ = 0.71073 Å). Intensity data were measured at 293(2) K by the $\omega/2\theta$ technique. Semi-empirical absorption analysis was performed using the SADABS program. The structures were solved by direct-method successive Fourier difference analysis (SHELXS-97)[13] and refined by the full-matrix least-squares method on F^2 with anisotropic thermal parameters for all non-hydrogen atoms (SHELXS-97).[13] Hydrogen atoms were added theoretically and refined with riding model position parameters and fixed isotropic thermal parameters. The crystallographic data and processing parameters for structural analyses of complexes **1** and **2** are summarised in Table 3.

CCDC-219629 (for **1**) and -219957 (for **2**) contain the supplementary crystallographic data for this paper. These data can be obtained free of charge at www.ccdc.cam.ac.uk/conts/retrieving.html [or from the Cambridge Crystallographic Data Centre, 12 Union Road, Cambridge CB2 1EZ, UK; Fax: (internat.) +44-1223-336-033; E-mail: deposit@ccdc.cam.ac.uk].

Table 3. Crystal data and structure refinements for compounds **1** and **2**

Compound	**1**	**2**
Empirical formula	$C_{12}H_{15}Ag_4CuN_9$	$C_{10}H_{15}Au_2CuN_7$
M_w	445.91	690.76
Temperature [K]	293(2)	293(2)
Wavelength [Å]	0.71073	0.71073
Crystal system	orthorhombic	triclinic
Space group	Pbcm	$P\bar{1}$
a [Å]	6.640(2)	8.321(3)
b [Å]	16.270(5)	12.946(4)
c [Å]	18.073(5)	15.859(5)
α [Å]	90	82.284(6)
β [°]	90	88.419(5)
γ [°]	90	73.558(5)
V [Å^3]	1952.5(10)	1623.6(9)
Z	7	4
$D_{calcd.}$ [g·cm^{-3}]	2.655	2.826
Absorption coefficient [mm^{-1}]	5.028	19.325
Reflections collected	7493	7562
Unique data measured	1771	5358
Goodness-of-fit on F^2	1.028	1.031
R_1, wR_2 [$I > 2\sigma(I)$]	0.0402, 0.0758	0.0593, 0.1433
R_1, wR_2 (all data)	0.0703, 0.0854	0.0964, 0.1682

Acknowledgments

This work was supported by the National Science Foundation of China (Nos. 90101028, 20171026 and 50173011), the National Science Foundation of Tianjin (No. 013605811) and the TRAPOYT of MOE, China.

[1] [1a] B. J. Holliday, C. A. Mirkin, *Angew. Chem. Int. Ed.* **2001**, *40*, 2022. [1b] M. Munakata, L. P. Wu, T. Kuroda-Sowa, *Adv. Inorg. Chem.* **1999**, *46*, 173.
[2] For example: [2a] S. Leninger, B. Olenyuk, P. J. Stang, *Chem. Rev.* **2000**, *100*, 853. [2b] H. Zhang, X. M. Wang, K. C. Zhang, B. K. Teo, *Coord. Chem. Rev.* **1999**, *183*, 157. [2c] H. Zhang, X. M. Wang, H. Zhu, W. Xiao, B. K. Teo, *J. Am. Chem. Soc.* **1997**, *119*, 5463.
[3] [3a] R. L. White-Morris, M. Stender, D. S. Tinti, A. L. Balch, *Inorg. Chem.* **2003**, *42*, 3237. [3b] C. J. Shorrock, B. Y. Xue, P. B. Kim, R. J. Batchelor, B. O. Patrick, D. B. Leznoff, *Inorg. Chem.* **2002**, *41*, 6743.
[4] [4a] M. Gorol, N. C. M. Zanetti, H. W. Roesdy, M. Noltemeyer, H. G. Schmidt, *Chem. Commun.* **2003**, 46. [4b] E. J. Fernandez, J. M. L. de Luzuriaga, M. Monge, M. E. Olmos, J. Perez, A. Laguna, A. A. Mohamed, J. P. Fackler, *J. Am. Chem. Soc.* **2003**, *125*, 2022. [4c] R. E. Cramer, D. W. Smith, W. VanDoorne, *Inorg. Chem.* **1998**, *37*, 5895.
[5] [5a] H. Schmidbaur, *Nature* **2001**, *413*, 31. [5b] A. Hamel, N. W. Mitzel, H. Schmidbaur, *J. Am. Chem. Soc.* **2001**, *123*, 516. [5c] A. A. Mohamed, J. Chen, A. E. Bruce, M. R. M. Bruce, *Inorg. Chem.* **2003**, *42*, 2203. [5d] D. Sun, R. Cao, J. Weng, M. Hong, Y. Liang, *J. Chem. Soc., Dalton Trans.* **2002**, 291. [5e] Q. M. Wang, T. C. W. Mak, *Chem. Eur. J.* **2003**, *9*, 44.
[6] [6a] P. Pyykkö, *Chem. Rev.* **1997**, *97*, 597. [6b] P. M. Van Calcar, M. M. Olmstead, A. L. Balch, *J. Chem. Soc., Chem. Commun.* **1995**, 1773. [6c] M. J. Irwin, L. M. Muir, K. W. Muir, R. J.

 © 2004 Wiley-VCH Verlag GmbH & Co. KGaA, Weinheim

Puddephatt, D. S. Yufit, *Chem. Commun.* **1997**, 219. [6d] R. J. Puddephatt, *Chem. Commun.* **1998**, 1055. [6e] M. J. Irwin, G. Jia, N. C. Payne, R. J. Puddephatt, *Organometallics* **1996**, *15*, 51. [6f] M. Contel, J. Garrido, M. C. Gimeno, P. G. Jones, A. Laguna, M. Laguna, *Organometallics* **1996**, *15*, 4939. [6g] W. Schneider, A. Bauer, H. Schmidbaur, *Organometallics* **1996**, *15*, 5445. [6h] T. J. Mathieson, A. G. Langdon, N. B. Milestone, B. K. Nicholson, *J. Chem. Soc., Dalton Trans.* **1999**, 201. [6i] A. J. Amoroso, A. J. Blake, J. P. Danks, D. Fenske, M. Schröder, *New J. Chem.* **1999**, *23*, 345. [6j] C. W. Liu, I. J. Shang, C. M. Hung, J. C. Wang, T. C. Keng, *J. Chem. Soc., Dalton Trans.* **2002**, 1974. [6k] W. E. van Zyl, J. M. López-de-Luzuriaga, A. A. Mohamed, R. J. Staples, J. P. Fackler Jr., *Inorg. Chem.* **2002**, *41*, 4579. [6l] V. J. Catalano, M. A. Malwitz, *Inorg. Chem.* **2003**, *42*, 5483. [6m] K. M. Lee, H. M. J. Wang, I. J. B. Lin, *J. Chem. Soc., Dalton Trans.* **2002**, 2852. [6n] K. Nomiya, H. Yokoyama, *J. Chem. Soc., Dalton Trans.* **2002**, 2483. [6o] Q. M. Wang, T. C. W. Mak, *Inorg. Chem.* **2003**, *42*, 1637. [6p] H. Ehlich, A. Schier, H. Schmidbaur, *Inorg. Chem.* **2002**, *41*, 3721. [6q] Q. M. Wang, T. C. W. Mak, *Dalton Trans.* **2003**, 25. [6r] A. A. Mohamed, J. Chen, A. E. Bruce, M. R. M. Bruce, *Inorg. Chem.* **2003**, *42*, 2203.

[7] [7a] W. F. Yeung, W. T. Wong, J. L. Zuo, T. C. Lau, *J. Chem. Soc., Dalton Trans.* **2000**, 629. [7b] Z. D. B. Leznoff, B. Y. Xue, R. J. Batchelor, F. W. B. Einstein, B. O. Ratrick, *Inorg. Chem.* **2001**, *40*, 6026. [7c] C. J. Shorrock, B. Y. Xue, P. B. Kim, R. J. Batchelor, B. O. Patrick, D. B. Leznoff, *Inorg. Chem.* **2002**, *41*, 6743. [7d] M. I. Bruce, B. C. Hall, B. W. Skelton, M. E. Smith, A. H. White, *J. Chem. Soc., Dalton Trans.* **2002**, 995. [7e] T. Soma, T. Iwamoto, *Inorg. Chem.* **1996**, *35*, 1849. [7f] E. Colacio, F. Lloret, R. Kivekas, J. S. Varela, M. R. Sundberg, R. Uggla, *Inorg. Chem.* **2003**, *42*, 560. [7g] C. J. Shorrock, H. Jong, R. J. Batchelor, D. B. Leznoff, *Inorg. Chem.* **2003**, *42*, 3917.

[8] [8a] B. J. Hathaway, in *Comprehensive Coordination Chemistry* (Eds.: G. Wilkinson, R. D. Gillard, J. A. McCleverty), Pergamon: Oxford, **1987**; vol. 5, p. 533. [8b]H. Z. Kou, H. M. Wang, D. Z. Liao, P. Cheng, Z. H. Jiang, S. P. Yan, X. Y. Huang, G. L. Wang, *Aust. J. Chem.* **1998**, *51*, 661. [8c] H. Yuge, T. Iwamoto, *J. Chem. Soc., Dalton Trans.* **1994**, 1237.

[9] [9a] M. A. Rawashdeh-Omary, M. A. Omary, H. H. Patterson, *J. Am. Chem. Soc.* **2000**, *122*, 10371. [9b] M. A. Rawashdeh-Omary, M. A. Omary, H. H. Patterson, J. P. Fackler Jr., *J. Am. Chem. Soc.* **2001**, *123*, 11237.

[10] S. Sabbani, K. D. Samar, *Inorg. Chem. Commun.* **2003**, *6*, 10.

[11] J. E. Richman, T. J. Atkins, *J. Am. Chem. Soc.* **1974**, *96*, 2268.

[12] A. McAuley, P. R. Norman, O. Olubuyide, *Inorg. Chem.* **1984**, *23*, 1938.

[13] [13a] G. M. Sheldrick, SHELXS 97, Program for the Solution of Crystal Structures, University of Göttingen, **1997**. [13b] G. M. Sheldrick, SHELXL 97, Program for the Refinement of Crystal Structures, University of Göttingen, **1997**.

Received September 27, 2003
Early View Article
Published Online April 1, 2004

 © 2004 Wiley-VCH Verlag GmbH & Co. KGaA, Weinheim

Properties of Organometallic Sulfur-Rich Dithiolate Complexes $[M(L)(C_8H_4S_8)]$ (M = Rh^{III} and Ir^{III}; L = η^5-C_5H_5 and η^5-C_5Me_5) and Their Oxidation

Kazuhiro Kawabata,[a] Motohiro Nakano,[a] Hatsue Tamura,[a] and Gen-etsu Matsubayashi*[a]

Keywords: Electrical conductivity / EPR spectroscopy / Iridium / Oxidation / Rhodium / S ligands / X-ray diffraction

$[Rh(\eta^5\text{-}C_5H_5)(C_8H_4S_8)]$ and $[M(\eta^5\text{-}C_5Me_5)(C_8H_4S_8)]$ [M = Rh^{III} and Ir^{III}. $C_8H_4S_8^{2-}$ = 2-{(4,5-ethylenedithio)-1,3-dithiole-2-ylidene}-1,3-dithiole-4,5-dithiolate(2–)] were prepared by reactions of $[NMe_4]_2[C_8H_4S_8]$ with $[Rh(\eta^5\text{-}C_5H_5)Cl_2]_2$ or $[M(\eta^5\text{-}C_5Me_5)Cl_2]_2$ (M = Rh and Ir). They exhibit oxidation potentials of between +0.16 and +0.24 V (versus Ag/Ag^+) with oxidation of the dithiolate ligand. The geometries and electronic states of their one-electron-oxidized species $[M(L)(C_8H_4S_8)]^+$ and $[RhX(L)(C_8H_4S_8)]$ (M = Rh and Ir; X = Br and I; L = η^5-C_5H_5 and η^5-C_5Me_5), obtained by reactions of the above complexes with bromine, iodine, or the ferrocenium cation are discussed based on their ESR spectra. The oxidized η^5-C_5Me_5-metal complexes exhibit electrical conductivities of between 10^{-6} and 10^{-4} S cm^{-1}, while some oxidized η^5-C_5H_5-Rh complexes show conductivities of between 10^{-3} and 10^{-2} S cm^{-1} measured for compacted pellets at room temperature. The X-ray crystal structures of the two-electron-oxidized species $[MI(\eta^5\text{-}C_5Me_5)(C_8H_4S_8)](I_3)$ (M = Rh and Ir) were also clarified.

(© Wiley-VCH Verlag GmbH & Co. KGaA, 69451 Weinheim, Germany, 2004)

Introduction

Metal complexes with the sulfur-rich dithiolate ligands $C_3S_5^{2-}$ [4,5-disulfanyl-1,3-dithiole-2-thiolate(2−)] and $C_8H_4S_8^{2-}$ [2-{(4,5-ethylenedithio)-1,3-dithiole-2-ylidene}-1,3-dithiole-4,5-dithionate(2−)] have attracted much attention because the oxidized species exhibit unusual electrical and magnetic properties.[1−4] In particular, the oxidized $C_8H_4S_8$-metal complexes often form effective electron-conduction pathways through several sulfur-sulfur non-bonding contacts in the solid state, resulting in the formation of good electrical conductors. Although planar metal complexes are generally efficient for molecular packing in the solid state, non-planar $C_8H_4S_8$-metal complexes may also form a unique molecular packing with some sulfur-sulfur non-bonding contacts in the solid state and are expected to exhibit new physical properties.

From this standpoint, oxidized cyclopentadienyl- and pentamethylcyclopentadienyl-metal complexes with sulfur-rich dithiolate ligands as non-planar species are of much interest. In our previous studies we reported the related C_3S_5-Co^{III} [5] and -Rh^{III} complexes[6] and some non-planar cyclopentadienyl-metal complexes with the $C_8H_4S_8$ ligand exhibiting high electrical conductivities.[7−9]

This paper reports the preparation and properties of $[Rh(\eta^5\text{-}C_5H_5)(C_8H_4S_8)]$ and $[M(\eta^5\text{-}C_5Me_5)(C_8H_4S_8)]$ (M = Rh and Ir) and their oxidation. Furthermore, the geometries and electronic states of their one-electron-oxidized species $[M(L)(C_8H_4S_8)]^+$ and $[RhX(L)(C_8H_4S_8)]$ (M = Rh and Ir; X = Br and I; L = η^5-C_5H_5 and η^5-C_5Me_5), obtained by reaction of the above complexes with bromine, iodine, or the ferrocenium cation, are discussed based on their ESR spectra. The electrical conductivities of the one-electron- and further electron-oxidized species obtained, together with X-ray crystal structures of $[MI(\eta^5\text{-}C_5Me_5)(C_8H_4S_8)](I_3)$ [M = Rh^{III} and Ir^{III}], are also described.

Results and Discussion

Electrochemical Properties of $[Rh(\eta^5\text{-}C_5H_5)(C_8H_4S_8)]$ (1), $[Rh(\eta^5\text{-}C_5Me_5)(C_8H_4S_8)]$ (2) and $[Ir(\eta^5\text{-}C_5Me_5)(C_8H_4S_8)]$ (3)

Figure 1 shows the cyclic voltammogram of complex **2** measured in dichloromethane. The coupled oxidation/reduction peak potentials at +0.15/+0.05 V and at +0.55/+0.45 V (versus Ag/Ag^+) are ascribed to the almost reversible processes of the $[Rh(\eta^5\text{-}C_5Me_5)(C_8H_4S_8)]$/$[Rh(\eta^5\text{-}C_5Me_5)(C_8H_4S_8)]^+$ and $[Rh(\eta^5\text{-}C_5Me_5)(C_8H_4S_8)]^+$/$[Rh(\eta^5\text{-}C_5Me_5)(C_8H_4S_8)]^{2+}$ species, respectively. These oxidation peak potentials are lower than those (+0.55 and +0.66 V) of the corresponding complex $[Rh(\eta^5\text{-}C_5Me_5)(C_3S_5)]$,[6] since many $C_8H_4S_8$-metal complexes exhibit

[a] Department of Applied Chemistry and Frontier Research Center, Graduate School of Engineering, Osaka University
1−16, Machikaneyama, Toyonaka, Osaka 560−0043, Japan
E-mail: matsu@ch.wani.osaka-u.ac.jp

somewhat lower oxidation potentials than the corresponding C_3S_5-metal complexes.[4,7−11] The oxidation occurs essentially on the sulfur-rich dithiolate ligand, as observed for other metal complexes with $C_8H_4S_8^{2-}$ [4,7−9] or $C_6S_8R_2^{2-}$ (R = long alkyl chains) dithiolate ligands.[12]

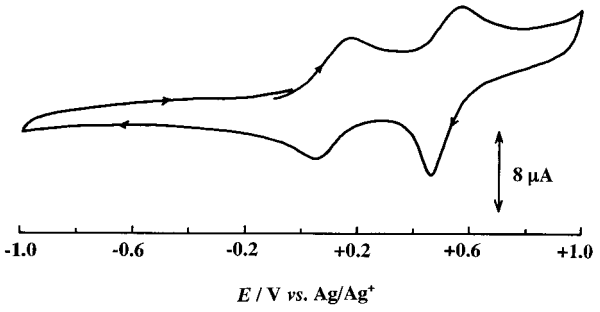

Figure 1. Cyclic voltammogram of complex **2** (1.0×10^{-3} mol·dm^{-3}) in dichloromethane; supporting electrolyte, 0.1 mol·dm^{-3} [N*n*Bu$_4$][ClO$_4$]; sweep rate 500 mV s^{-1}

Complex **1** exhibits somewhat higher oxidation potentials (+0.20 and +0.71 V versus Ag/Ag$^+$) than those of **2**. This finding is ascribed to the more electron-releasing property of the η^5-C_5Me_5 group, as observed for other η^5-C_5H_5- and η^5-C_5Me_5-metal complexes with the $C_8H_4S_8$ ligand [M = Co^{III},[7] Ti^{IV} and Zr^{IV} [8,9]].

The oxidation potentials (+0.44 and +0.65 V versus Ag/Ag$^+$) of the η^5-C_5Me_5-Ir^{III} complex **3** are somewhat higher than those of the corresponding η^5-C_5Me_5-Rh^{III} complex **2**, as has also been observed for the related C_3S_5-metal complexes: [Rh(η^5-C_5Me_5)(C_3S_5)], +0.45 and 0.73 V;[6] [Ir(η^5-C_5Me_5)(C_3S_5)], +0.54 and +0.78 V (versus Ag/Ag$^+$).[13]

Thus, complexes **1**−**3** can be oxidized by bromine, iodine and the ferrocenium ion.

Oxidation of Complexes 1−3

The electronic absorption spectra of complex **2** in dichloromethane in the presence of varying amounts of iodine as an oxidizing agent are shown in Figure 2. Addition of excess amounts of the oxidant gives the final spectrum of the two-electron-oxidized species [RhI(η^5-C_5Me_5)($C_8H_4S_8$)]$^+$, as described below. The band at 700 nm due to the intramolecular charge transfer (CT) transition from the η^5-C_5Me_5 group to the Rh^{III} ion/$C_8H_4S_8$ ligand moiety[7] is shifted to the region around 1100 nm. Upon addition of iodine a broad band ascribed to the one-electron-oxidized species appears initially at around 1200 nm and finally the strong band due to the two-electron-oxidized species appears at 1040 nm. Addition of bromine to **2** in dichloromethane also affords similar bands due to the oxidized species. For the oxidation of the Ir^{III} complex **3** similar bands due to the one- and two-electron-oxidized species occur at 1050−1200 nm.

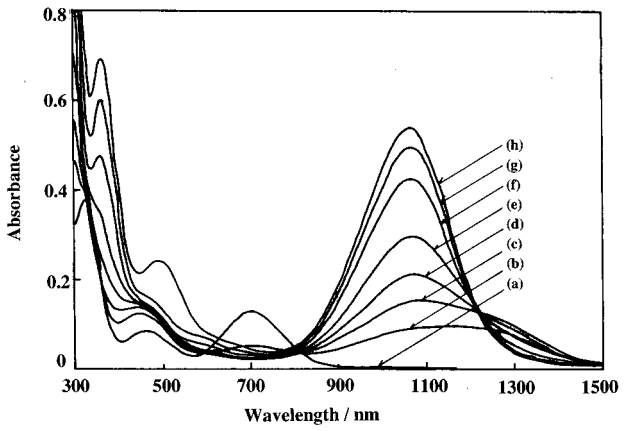

Figure 2. Electronic absorption spectra of complex **2** (2.0×10^{-5} mol·dm^{-3}) in dichloromethane in the presence of iodine; concentration of iodine (mol·dm^{-3}): (a) 0, (b) 0.6×10^{-5}, (c) 1.0×10^{-5}, (d) 1.4×10^{-5}, (e) 2.0×10^{-5}, (f) 3.0×10^{-5}. (g) 4.0×10^{-5}, (h) 2.0×10^{-4}

The reaction of **1** with bromine or iodine gives the one-electron-oxidized species [Rh(η^5-C_5H_5)($C_8H_4S_8$)](Br) (**4**), [Rh(η^5-C_5H_5)($C_8H_4S_8$)](I) (**6**) and [Rh(η^5-C_5H_5)($C_8H_4S_8$)]($I_{4.2}$) (**7**). The oxidized species **7** obtained by the reaction with an excess amount of iodine contains formally the $4.2I^-$ ion, actually made up from approximately equimolar amounts of both the I_3^- and I_5^- ions, as confirmed by the Raman spectrum, which exhibits bands at 114 and 166 cm^{-1} ascribed to the I_3^- and I_5^- ions, respectively.[14,15] Oxidation reactions of **2** with bromine, iodine or [Fe(η^5-C_5H_5)$_2$][PF$_6$] gave the one-electron-oxidized complexes [RhBr(η^5-C_5Me_5)($C_8H_4S_8$)] (**5**), [RhI(η^5-C_5Me_5)($C_8H_4S_8$)] (**9**), [Rh(η^5-C_5Me_5)($C_8H_4S_8$)][PF$_6$] (**13**), and the two-electron-oxidized species [RhI(η^5-C_5Me_5)($C_8H_4S_8$)](I_3) (**10**). Similarly, complex **3** was oxidized to afford the one-electron-oxidized species [IrBr(η^5-C_5Me_5)($C_8H_4S_8$)] (**6**), [IrI(η^5-C_5Me_5)($C_8H_4S_8$)] (**11**), [Ir(η^5-C_5Me_5)($C_8H_4S_8$)][PF$_6$] (**14**), and the two-electron-oxidized complex [IrI(η^5-C_5Me_5)($C_8H_4S_8$)](I_3) (**12**). The presence of M−X bonds (M = Rh and Ir; X = Br and I) in the oxidized complexes **5**, **6**, **9** and **11** was confirmed by the ESR spectra, as described below.

ESR Spectra of the Oxidized Species

Figure 3 shows the ESR spectra of the one-electron-oxidized species [RhBr(η^5-C_5Me_5)($C_8H_4S_8$)] (**5**) and [Rh(η^5-C_5Me_5)($C_8H_4S_8$)][PF$_6$] (**13**) dissolved in dichloromethane at room temperature. Complex **13** shows an intense, sharp isotropic signal at g = 2.009 (peak-to-peak line width, 0.51 mT). This is ascribed to the radical species of the oxidized $C_8H_4S_8$ ligand moiety, as observed for other oxidized $C_8H_4S_8$-metal [Co^{III},[7] Ti^{IV},[8] Pt^{II},[10] V^{IV} and Mo^{IV},[11] and Au^{III} [16]] complexes with a dithiolate ligand-centered oxidation. The one-electron-oxidized Ir^{III} analog **14** also exhibits a sharp ESR signal at g = 2.009 (peak-to-peak line width, 0.49 mT). Both these complexes in the solid state have shown a somewhat broad isotropic signal at g = 2.008 (peak-to-peak line width, 6.0−7.0 mT).

 © 2004 Wiley-VCH Verlag GmbH & Co. KGaA, Weinheim

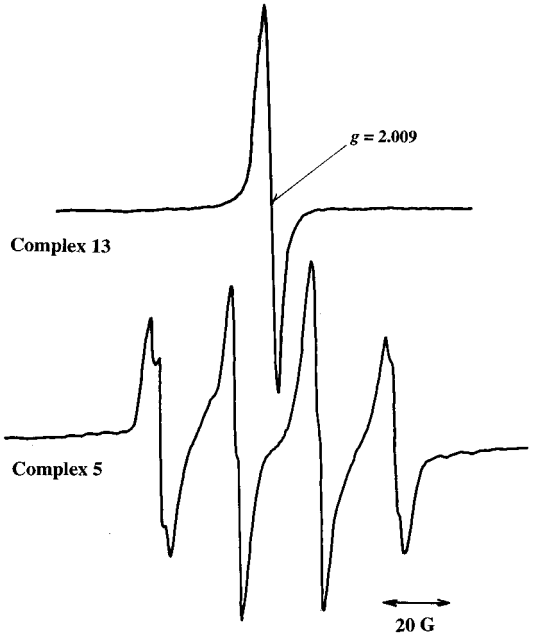

Figure 3. ESR spectra of one-electron-oxidized complexes **5** and **13** in dichloromethane at room temperature

Complex **5** shows an isotropic signal at $g = 2.007$ which consists of a doublet (^{103}Rh, $I = 1/2$) of quadruplets [^{79}Br (50.54%) and ^{81}Br (49.46%), $I = 3/2$]; the ^{103}Rh and $^{79/81}$Br hyperfine couplings are 0.27×10^{-3} and 2.1×10^{-3} cm^{-1}, respectively. This confirms the Rh−Br bond for the oxidized species in solution. These small hyperfine coupling values indicate much lower spin-densities on the metal and bromine atoms, which is very similar to the cases of [RhBr(η^5-C_5Me_5)(C_3S_5)][6] and [CoBr(η^5-C_5Me_5)(C_3S_5)].[5] For the present complex, a one-electron oxidation also occurs at the $C_8H_4S_8$ ligand moiety, as confirmed by the Mulliken spin densities calculated for [RhBr(η^5-C_5Me_5)(C_3S_5)][6] and [CoBr(η^5-C_5Me_5)(C_3S_5)].[5] The ^{103}Rh and $^{79/81}$Br hyperfine couplings for the present complex are appreciably smaller than those (0.47×10^{-3} and 3.0×10^{-3} cm^{-1}, respectively) of [RhBr(η^5-C_5Me_5)(C_3S_5)],[6] suggesting the delocalization of more spin density onto the $C_8H_4S_8$ ligand.

Figure 4 shows the ESR spectra of a dichloromethane solution of [Rh(η^5-C_5Me_5)($C_8H_4S_8$)] in the presence of varying amounts of iodine. [RhI(η^5-C_5Me_5)($C_8H_4S_8$)] is formed in solution (Figure 4a), as indicated by an isotropic signal coupled with the ^{127}I ($I = 5/2$) nucleus [hyperfine coupling, 3.3×10^{-3} cm^{-1}]. The spectrum of isolated [RhI(η^5-C_5Me_5)($C_8H_4S_8$)] (**9**) is the same as that shown in Figure 4a. Upon further addition of iodine to the solution (Figure 4b and 4c) the intensity of the signal is weakened, since the amount of the diamagnetic two-electron-oxidized species is increased. In the presence of an excess amount of iodine (Figure 4d), the signal essentially disappears, with the presence of a very small amount of the one-electron-oxidized species [Rh(η^5-C_5Me_5)($C_8H_4S_8$)]$^+$. The two-electron-oxidized species [RhI(η^5-C_5Me_5)($C_8H_4S_8$)](I_3) (**10**) was obtained by the reaction of **2** with excess amounts of iodine and its crystal structure determined, as discussed below.

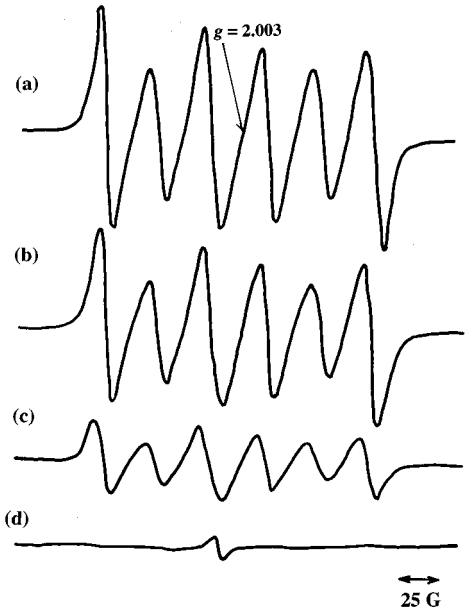

Figure 4. ESR spectra of complex **2** (5.0×10^{-4} mol·dm^{-3}) in dichloromethane in the presence of varying amounts of iodine; concentration of iodine (mol·dm^{-3}): (a) 2.5×10^{-4}, (b) 3.5×10^{-4}, (c) 5.0×10^{-4}, (d) 2.0×10^{-4}

Oxidation of the Ir^{III} analog **3** by the reaction with bromine or iodine yielded both [IrX(η^5-C_5Me_5)($C_8H_4S_8$)] (X = Br and I) and [Ir(η^5-C_5Me_5)($C_8H_4S_8$)]$^+$ as one-electron-oxidized species. Figure 5 shows the ESR spectra of the one-electron-oxidized complex [IrI(η^5-C_5Me_5)($C_8H_4S_8$)] (**11**) dissolved in dichloromethane and in the solid state. The spectrum in solution consists of a sharp signal of [Ir(η^5-C_5Me_5)($C_8H_4S_8$)]$^+$ and a sextet for [IrI(η^5-C_5Me_5)($C_8H_4S_8$)] due to coupling with the ^{127}I nucleus, indicating that the complex consists of both the oxidized species. The solid-state spectrum also shows signals due to both species.

Oxidation of [Rh(η^5-C_5H_5)($C_8H_4S_8$)] (**1**) with bromine or iodine affords essentially the oxidized species without Rh−Br and Rh−I bonds. The ESR spectra of these oxidized species **4**, **6** and **7** show a sharp isotropic signal at $g = 2.006-2.008$. They are one-electron-oxidized species with a $C_8H_4S_8$ ligand-centered oxidation.

X-ray Crystal Structures of [RhI(η^5-C_5Me_5)($C_8H_4S_8$)](I_3) (**10**) and [IrI(η^5-C_5Me_5)($C_8H_4S_8$)](I_3) (**12**)

The crystal structure of **10** consists of three independent molecules which have very similar geometries. This also occurs for **12**. The molecular structure of one of the three cation moieties of **10** is shown in Figure 6, together with the atom-labeling scheme. Selected bond lengths and angles relevant to the $C_8H_4S_8$-Rh moieties of **10**, as well as those of **12**, are listed in Table 1. The Rh(1) atom is bonded to one η^5-C_5Me_5 subunit with Rh−C distances of 2.180−2.218 Å [Rh(2)−C: 2.157−2.201; Rh(3)−C:

 © 2004 Wiley-VCH Verlag GmbH & Co. KGaA, Weinheim

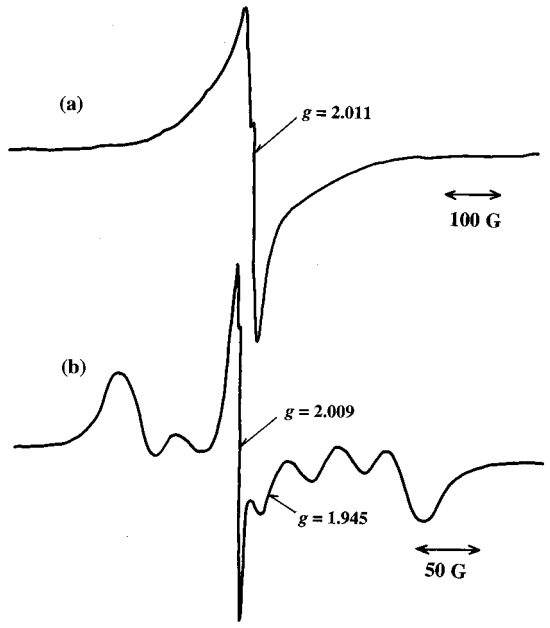

Figure 5. ESR spectra of complex **11** in the solid state (a) and in dichloromethane (b)

2.153−2.204 Å] and to the bidentate chelating dithiolate ligand with Rh(1)−S(1) and −S(8) bonds of 2.326(1) and 2.346(2) Å, respectively, [Rh(2)−S(9) and −S(16): 2.355(2) and 2.308(2) Å; Rh(3)−S(17) and −S(24): 2.328(2) and 2.300(2) Å], which, together with the Rh−I bond, give a formally hexacoordinate geometry. This is close to the geometry of [CoBr(η^5-C_5Me_5)(C_3S_5)].[5] The Rh−S distances are similar to those of related η^5-C_5Me_5-Rh^{III} dithiolate complexes, such as [Rh(η^5-C_5Me_5)(C_3S_5)]$_2$ (2.3571, 2.3774 Å),[6] [Rh(η^5-C_5Me_5){$S_2C_2(CN)_2$}] (2.345, 2.346 Å)[17] and [Rh(η^5-C_5Me_5){$S_2C_2(CN)_2$}]$_2$ (2.350, 2.351 A).[18] The Rh−I distances [2.6854(7), 2.6932(7), 2.7001(5) Å] are also close to that [2.709(1) Å] of [RhI(COEt)(PPh_3){$S_2C_2(CN)_2$}].[19] For the coordinating $C_8H_4S_8$ ligand, the dihedral angle between the Rh(1)−S(1)−S(8) plane and the S(1)−C(1)−C(8)−S(8) plane is 5.72°, and the $C_8H_4S_8$ moiety is almost planar (±0.07 Å). This is also the case for the Rh(2) and Rh(3) moieties. These findings are similar to those of other oxidized $C_8H_4S_8$-metal complexes with a $C_8H_4S_8$ ligand-centered oxidation — [Pt(bpy)($C_8H_4S_8$)][BF_4] (bpy = 2,2′-bipyridine)[20] and [Au(ppy)($C_8H_4S_8$)]$_2$[PF_6] [ppy^- = *C*-deprotonated-2-phenylpyridine(−)][21] — but are in great contrast to the characteristic folding of the TiS_2C_2 plane along the S(1)−S(8) axis, by 35.9°, observed for [Ti(η^5-C_5Me_5)$_2$($C_8H_4S_8$)].[8] The Ir−I, Ir−S and Ir−C bond lengths of **12** are also very close to those of the corresponding Rh−I, Rh−S and Rh−C bonds of **10**.

The crystal structure of **10** is illustrated in Figure 7. Between the three non-equivalent [RhI(η^5-C_5Me_5)($C_8H_4S_8$)]$^+$ cation moieties there are many S−S non-bonding contacts (< 3.7 Å; 3.518−3.662 Å) (19 S···S contacts in a unit cell), together with many other S···I contacts (< 4.0 Å;

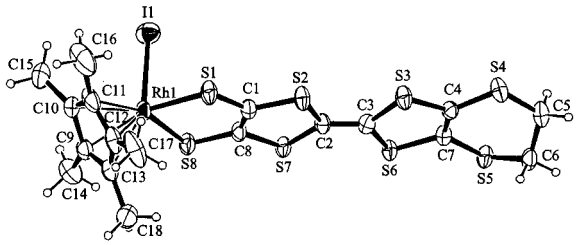

Figure 6. Molecular geometry of one of the cation moieties of complex **10** together with the atom-labeling scheme

Table 1. Relevant bond lengths (Å) and angles (°) for complexes **10** and **12**

	10 (M = Rh)	**12** (M = Ir)
M(1)−I(1)	2.6932(7)	2.703(1)
M(2)−I(2)	2.7001(5)	2.703(1)
M(3)−I(3)	2.6854(7)	2.690(1)
M(1)−S(1-1)	2.326(1)	2.312(3)
M(1)−S(8-1)	2.346(2)	2.325(3)
M(2)−S(1-2)	2.355(2)	2.338(3)
M(2)−S(8-2)	2.308(2)	2.297(3)
M(3)−S(1-3)	2.328(2)	2.319(3)
M(3)−S(8-3)	2.300(2)	2.296(3)
M(1)−C(C_5Me_5, mean)	2.190	2.20
M(2)−C(C_5Me_5, mean)	2.185	2.20
M(3)−C(C_5Me_5, mean)	2.186	2.19
S(1-1)−C(1-1)	1.683(6)	1.68(1)
S(1-2)−C(1-2)	1.684(6)	1.69(1)
S(1-3)−C(1-3)	1.675(6)	1.68(1)
S(8-1)−C(8-1)	1.678(5)	1.682(9)
S(8-2)−C(8-2)	1.684(5)	1.684(10)
S(8-3)−C(8-3)	1.687(5)	1.684(9)
C(1-1)−C(8-1)	1.411(8)	1.42(2)
C(1-2)−C(8-2)	1.417(9)	1.41(2)
C(1-3)−C(8-3)	1.413(9)	1.40(2)
C(2-1)−C(3-1)	1.373(8)	1.37(1)
C(2-2)−C(3-2)	1.378(7)	1.39(1)
C(2-3)−C(3-3)	1.384(7)	1.39(1)
I(1)−M(1)−S(1-1)	89.23(5)	88.45(8)
I(2)−M(2)−S(1-2)	92.04(5)	90.96(9)
I(3)−M(3)−S(1-3)	89.41(4)	88.77(7)
I(1)−M(1)−S(8-1)	88.59(5)	88.25(8)
I(2)−M(2)−S(8-2)	89.53(5)	89.06(9)
I(3)−M(3)−S(8-3)	87.00(4)	86.76(8)
S(1-1)−M(1)−S(8-1)	87.13(5)	86.89(9)
S(1-2)−M(2)−S(8-2)	87.20(6)	87.0(1)
S(1-3)−M(3)−S(8-3)	87.88(6)	87.5(1)
M(1)−S(1-1)−C(1-1)	104.0(2)	104.9(3)
M(2)−S(1-2)−C(1-2)	103.2(2)	103.9(4)
M(3)−S(1-3)−C(1-3)	102.8(2)	103.4(4)
M(1)−S(8-1)−C(8-1)	103.4(2)	104.3(4)
M(2)−S(8-2)−C(8-2)	104.8(2)	105.2(4)
M(3)−S(8-3)−C(8-3)	104.4(2)	104.6(4)
S(1-1)−C(1-1)−C(8-1)	122.3(4)	121.6(7)
S(1-2)−C(1-2)−C(8-2)	122.7(4)	121.9(7)
S(1-3)−C(1-3)−C(8-3)	123.7(4)	123.0(7)
S(8-1)−C(8-1)−C(1-1)	122.8(4)	121.9(7)
S(8-2)−C(8-2)−C(1-2)	121.8(4)	121.8(8)
S(8-3)−C(8-3)−C(1-3)	120.9(4)	121.2(8)

 © 2004 Wiley-VCH Verlag GmbH & Co. KGaA, Weinheim

3.648−3.989 Å) (27 S···I contacts in a unit cell) between the $C_8H_4S_8$ moieties and the I_3^- ions, which results in the formation of a two-dimensional molecular array along the *a* and *b* axes. These molecular arrays are separated by both the η^5-C_5Me_5 moieties and the I_3^- ions along the *c* axis. Complex **12** has essentially the same crystal structure as that of **10**.

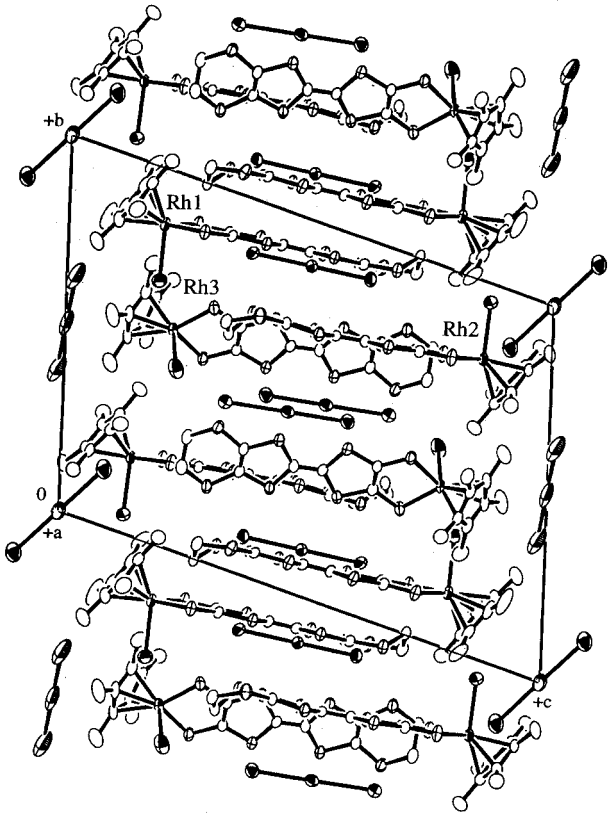

Figure 7. Packing diagram of complex **10**

Electrical Conductivities of the Oxidized Complexes

The electrical conductivities of the oxidized complexes measured for compacted pellets at room temperature are listed in Table 2.

Table 2. Electrical conductivities (σ) of the oxidized complexes[a]

Complex[a]	σ_{RT} (S cm^{-1})
[Rh(η^5-C_5H_5)($C_8H_4S_8$)](Br) (**4**)	6.5×10^{-3}
[Rh(η^5-C_5H_5)($C_8H_4S_8$)](I) (**7**)	2.5×10^{-2}
[Rh(η^5-C_5H_5)($C_8H_4S_8$)]($I_{4.2}$) (**8**)	7.6×10^{-5}
[RhBr(η^5-C_5Me_5)($C_8H_4S_8$)] (**5**)	6.1×10^{-6}
[RhI(η^5-C_5Me_5)($C_8H_4S_8$)] (**9**)	2.0×10^{-4}
[RhI(η^5-C_5Me_5)($C_8H_4S_8$)](I_3) (**10**)	1.2×10^{-5}
[RhI(η^5-C_5Me_5)($C_8H_4S_8$)][PF_6] (**13**)	2.4×10^{-6}
[IrBr(η^5-C_5Me_5)($C_8H_4S_8$)] (**6**)	3.0×10^{-6}
[IrI(η^5-C_5Me_5)($C_8H_4S_8$)] (**11**)	1.1×10^{-6}
[IrI(η^5-C_5Me_5)($C_8H_4S_8$)](I_3) (**12**)	5.0×10^{-6}
[IrI(η^5-C_5Me_5)($C_8H_4S_8$)][PF_6] (**14**)	$< 10^{-7}$

[a] Measured for compacted pellets at room temperature.

The conductivities of the one-electron-oxidized η^5-C_5Me_5-Rh^{III} and -Ir^{III} complexes are very low. This seems essentially to come from an inadequate molecular packing in the solid state, which results in ineffective S−S nonbonding interactions between the oxidized $C_8H_4S_8$ ligand moieties. On the other hand, the one-electron-oxidized η^5-C_5H_5-Rh^{III} species **4** and **7** exhibit considerably higher electrical conductivities. These species without Rh−X (X = Br and I) bonds seem to have a more effective molecular packing through S···S interactions. These packing modes may be similar to those of the [Co(η^5-C_5H_5)($C_8H_4S_8$)]$^+$ species, which also exhibits high electrical conductivity.[7] The present study also shows the effectiveness of the $C_8H_4S_8$ ligand for the construction of an electron conduction pathway even for non-planar metal complexes.

Experimental Section

Materials: [Rh(η^5-C_5H_5)Cl_2]$_2$,[22] [Rh(η^5-C_5Me_5)Cl_2]$_2$ [22,23] and $C_8H_4S_8(CH_2CH_2CN)_2$,[10,24,25] as a pro-ligand for the $C_8H_4S_8^{2-}$ dithiolate ligand, as well as [Fe(η^5-C_5Me_5)$_2$][PF_6],[26] were prepared according to the literature procedures.

Preparation of [Rh(η^5-C_5H_5)($C_8H_4S_8$)] (1), [Rh(η^5-C_5Me_5)($C_8H_4S_8$)] (2) and [Ir(η^5-C_5Me_5)($C_8H_4S_8$)] (3): All the following reactions were performed under an argon atmosphere. A methanol (0.48 mL) solution of NMe_4OH (120 mg, 1.3 mmol) was added with vigorous stirring to a tetrahydrofuran (50 mL) solution of $C_8H_4S_8(CH_2CH_2CN)_2$ (190 mg, 0.42 mmol) and the mixture was stirred for 15 min. The resulting red brown [NMe_4]$_2$[$C_8H_4S_8$] was filtered, and dissolved in ethanol (50 mL). A dichloromethane (20 mL) solution of [Rh(η^5-C_5H_5)Cl_2]$_2$ (100 mg, 0.21 mmol) was then added with stirring, and the mixture was stirred for 5 min at room temperature. The resulting black **1** was collected by filtration, washed with ethanol and hexane, and dried in vacuo (200 mg, 89%). $C_{13}H_9RhS_8$ (524.65): calcd. C 29.76, H 1.73; found C 29.60, H 1.89. ^{1}H NMR ([D_6]DMSO): δ = 3.41 (s, 5 H, CH_2), 5.97 (s, 5 H, C_5H_5) ppm.

Similarly, violet **2** was prepared by the reaction of an ethanol solution of [NMe_4]$_2$[$C_8H_4S_8$] with a dichloromethane solution of [Rh(η^5-C_5Me_5)Cl_2]$_2$ (94% yield). $C_{18}H_{19}RhS_8$ (594.79): calcd. C 36.34, H 3.51; found C 36.35, H, 3.22. ^{1}H NMR (CD_2Cl_2): δ = 2.01 (s, 15 H, C_5Me_5), 3.27 (s, 4 H, CH_2) ppm.

Complex **3** was also prepared by the reaction of [NMe_4]$_2$[$C_8H_4S_8$] with [Ir(η^5-C_5Me_5)Cl_2]$_2$ as a violet solid by the same procedure as described for **2** (94%). $C_{18}H_{19}IrS_8$ (684.10): calcd. C 31.60, H 2.80; found C 31.68, H 3.06. ^{1}H NMR (CD_2Cl_2): δ = 2.10 (s, 15 H, C_5Me_5), 3.28 (s, 4 H, CH_2) ppm.

Preparation of [Rh(η^5-C_5H_5)($C_8H_4S_8$)](Br) (4), [RhBr(η^5-C_5Me_5)($C_8H_4S_8$)] (5) and [IrBr(η^5-C_5Me_5)($C_8H_4S_8$)] (6): A dichloromethane (1.0 mL) solution of bromine [2.6 mm^3 (d = 3.1 g cm^{-3}), 0.050 mmol] was added with stirring to a dichloromethane (500 mL) solution of **1** (53 mg, 0.10 mmol), and the mixture was stirred for 15 h. The obtained black **4** was collected by filtration, washed with dichloromethane and hexane, and dried in vacuo (18 mg, 30%). $C_{13}H_9BrRhS_8$ (604.56): calcd. C 25.83, H 1.50; found C 25.26, H 1.76.

Similarly, the reaction of **2** (0.10 mmol) with bromine (0.05 mmol) in dichloromethane (100 mL) afforded black **5** (80%).

 © 2004 Wiley-VCH Verlag GmbH & Co. KGaA, Weinheim

$C_{18}H_{19}BrRhS_8$ (674.69): calcd. C 32.04, H 2.84; found C 32.17, H 2.92. The presence of the Rh−Br bond in **5** was confirmed by ESR spectroscopy, as described above.

Complex **6** was also obtained by the reaction of **3** with bromine in dichloromethane as a black solid according to the procedure described for **4** (81%). $C_{18}H_{19}BrIrS_8$ (764.00): calcd. C 28.30, H 2.51; found C 27.71, H 2.70. The presence of the Ir−Br bond of **6** was confirmed by ESR spectroscopy, as described above.

Preparation of [Rh(η⁵-C_5H_5)($C_8H_4S_8$)](I) (7) and [Rh(η⁵-C_5H_5)($C_8H_4S_8$)]($I_{4.2}$) (8): A dichloromethane (10 mL) solution of iodine (6.3 mg, 0.025 mmol) was added with stirring to a dichloromethane (500 mL) solution of **1** (53 mg, 0.10 mmol) and the solution was stirred for 15 h. The obtained black **7** was collected by filtration, washed with dichloromethane and hexane, and dried in vacuo (12 mg, 19%). $C_{13}H_9IRhS_8$ (651.55): calcd. C 23.96, H 1.39; found C 24.28, H 1.50.

Similarly, black **8** was obtained from the reaction of **1** with 10 molar equivalents of iodine in dichloromethane (57%). $C_{13}H_9I_{4.2}RhS_8$ (1331.98): calcd. C 14.76, H 0.86; found C 14.56, H 0.96. The Raman spectrum of **8** showed that it contains both the I_3^- and I_5^- ions [114 cm^{-1} $\nu(I_3^-)$, 166 cm^{-1} $\nu(I_5^-)$].[14,15]

Preparation of [RhI(η⁵-C_5Me_5)($C_8H_4S_8$)] (9), [RhI(η⁵-C_5Me_5)($C_8H_4S_8$)](I_3) (10), [IrI(η⁵-C_5Me_5)($C_8H_4S_8$)] (11) and [IrI(η⁵-C_5Me_5)($C_8H_4S_8$)](I_3) (12): A dichloromethane (100 mL) solution of **2** (60 mg, 0.10 mmol) was added with stirring to a dichloromethane (10 mL) solution of iodine (13 mg, 0.050 mmol) and the solution was stirred for 5 min. The volume of the solution was reduced to 50 mL under reduced pressure and hexane was added to the solution (500 mL) to afford black **9**. This was collected by filtration, washed with hexane, and dried in vacuo (60 mg, 83%). $C_{18}H_{19}IRhS_8$ (787.01): calcd. C 29.96, H 2.65; found C 29.19, H 2.66. The presence of the Rh−I bond of **9** was confirmed by ESR spectroscopy, as described below.

In a similar procedure, a dichloromethane (200 mL) solution of **2** (120 mg, 0.20 mmol) was added to a dichloromethane (40 mL) solution of iodine (100 mg, 0.40 mmol) to afford black **10** (170 mg, 77%). $C_{18}H_{19}I_4RhS_8$ (1363.67): calcd. C 19.61, H 1.74; found C 19.88, H 1.68. The presence of the I_3^- ion was confirmed by the Raman spectrum [112 cm^{-1} $\nu(I_3^-)$]. Black plates of **10** suitable for X-ray crystallography were obtained by recrystallization from a dichloromethane (20 mL) solution of **2** (0.020 mmol) and iodine (0.030 mmol) upon addition of hexane (40 mL).

Complexes **11** and **12** were also obtained by reaction of **3** with iodine according to the procedures described for **9** and **10**, respectively, as black solids (65 and 70%, respectively). For **11**. $C_{18}H_{19}IIrS_8$ (811.00): calcd. C 26.30, H 2.51; found C 26.29, H, 2.51. For **12**. $C_{18}H_{19}I_4IrS_8$ (1191.70): calcd. C 18.14, H 1.61; found C 18.18, H 1.79. The Raman spectrum of **12** showed the presence of both the I_3^- and I_5^- ions [109 and 166 cm^{-1}, respectively]. Black plates of **12** suitable for X-ray crystallography were obtained by recrystallization from a dichloromethane (30 mL) solution of **12** (0.010 mmol) upon further addition of hexane (60 mL).

Preparation of [Rh(η⁵-C_5Me_5)($C_8H_4S_8$)][PF_6] (13) and [Ir(η⁵-C_5Me_5)($C_8H_4S_8$)][PF_6] (14): A dichloromethane (100 mL) solution of [Fe(η⁵-C_5H_5)$_2$][PF_6] (33 mg, 0.10 mmol) was added with stirring to a dichloromethane (100 mL) solution of **2** (60 mg, 0.10 mmol). The volume of the solution was reduced to 50 mL under reduced pressure and then hexane (500 mL) was added, to yield black **13**. This was collected by filtration, washed with hexane, and dried in vacuo (60 mg, 81%). $C_{18}H_{19}F_6PRhS_8$ (739.75): calcd. C 29.23, H 2.59; found C 30.23, H 2.70.

By a similar procedure, a dichloromethane (200 mL) solution of **3** (68 mg, 0.10 mmol) was added to a dichloromethane (100 mL) solution of [Fe(η⁵-C_5H_5)$_2$][PF_6] (33 mg, 0.10 mmol) to give black **14** (69 mg, 83%). $C_{18}H_{19}F_6IrPS_8$ (829.06): calcd. C 26.08, H 2.33; found C 26.78, H 2.55.

Physical Measurements: IR, electronic absorption, ESR[27] and powder reflectance spectra[12] were recorded as described previously. ^1H NMR spectra were also measured as reported previously.[28] Raman spectra were measured using a Nippon-bunko NR-1800 laser-Raman spectrophotometer at the Graduate School of Science, Osaka University. Cyclic voltammograms of the complexes in dichloromethane were measured using [NBu_4][ClO_4] as an electrolyte.[29] The electrical resistivities of the oxidized complexes were measured at room temperature for compacted pellets by the conventional two-probe method.[29]

Crystal-Structure Determinations of [RhI(η⁵-C_5Me_5)($C_8H_4S_8$)](I_3) (10) and [IrI(η⁵-C_5Me_5)($C_8H_4S_8$)](I_3) (12): Diffraction data were collected up to $2\theta = 60.0°$ for **10** and 55.0° for **12** on a Rigaku RAXIS-RAPID imaging plate diffractometer equipped with a Rigaku low-temperature device (liquid nitrogen as the coolant) and graphite-monochromated Mo-K_α ($\lambda = 0.71069$ Å) radiation at the Graduate School of Engineering, Osaka University. Indexing was performed for reflections obtained from three oscillations exposed for 200 s. The final values of the cell parameters were obtained from least-squares refinement of the positions of 32780 observed reflections for **10** and of 39553 reflections for **12**. Equivalent reflections were merged by use of the PROCESS-AUTO program package. For **10**, 25640 reflections were unique ($R_{int} = 0.047$) from 50511, and for **12** 19335 reflections were unique ($R_{int} = 0.047$) from 37695. The data were corrected for absorption using the program ABSCOR[30] (transmission factors: 0.475−0.900 for **10** and 0.322−0.634 for **12**) and for Lorentz and polarization effects. Crystallographic data are summarized in Table 3.

Table 3. Crystallographic data for [IrI(η⁵-C_5Me_5)($C_8H_4S_8$)](I_3) (**10**) and [RhI(η⁵-C_5Me_5)($C_8H_4S_8$)](I_3) (**12**)

	10	**12**
Empirical formula	$C_{18}H_{19}I_4RhS_8$	$C_{18}H_{19}I_4IrS_8$
M	1102.35	1191.67
Crystal system	triclinic	triclinic
Space group	$P\bar{1}$	$P\bar{1}$
Unit cell dimensions		
a (Å)	11.1432(3)	11.1666(3)
b (Å)	18.4541(3)	18.5094(6)
c (Å)	24.4044(5)	24.426(1)
α (°)	103.4506(4)	103.639(2)
β (°)	102.5416(7)	102.570(2)
γ (°)	105.552(1)	105.628(1)
V (Å^3)	4488.0(2)	4506.5(3)
Z	6	6
$D_{calcd.}$ (g cm^{-3})	2.447	2.634
T (K)	223	233
μ (Mo-K_α) (mm^{-1})	5.27	9.13
Reflection collected	50511	37695
Independent reflections	25640	19306
R[a]	0.042	0.052
R_w [b] (all data)	0.122[c]	0.125[d]

[a] $R = \Sigma(F_o^2 - F_c^2)/\Sigma F_o^2$. [b] $R_w = \Sigma w(F_o^2 - F_c^2)^2$. [c] $w^{-1} = \sigma^2(F_o^2) + (0.0601P)^2 + 0.0000P$. [d] $w^{-1} = \sigma^2(F_o^2) + (0.1000P)^2 + 0.0000P$, where $P = (F_o^2 + 2F_c^2)/3$.

 © 2004 Wiley-VCH Verlag GmbH & Co. KGaA, Weinheim

The structure was solved by the Patterson method (PATTY),[31] expanded using Fourier techniques (DIRDIF94)[32] and refined on F^2 by the full-matrix least-squares method (SHELXL-97).[33] All the non-hydrogen atoms were refined anisotropically. The positions of all hydrogen atoms were calculated geometrically and refined with isotropic thermal parameters riding on those of the parent atoms. Atomic scattering factors were taken from the usual sources.[34] Figure 1 and 2 were drawn with ORTEP II.[35]
CCDC-219811 (for **10**) and -219812 (for **12**) contain the supplementary crystallographic data for this paper. These data can be obtained free of charge at www.ccdc.cam.au.uk/conts/retrieving.html [or from the Cambridge Crystallographic Data Centre, 12 Union Road, Cambridge CB2 1EZ, UK; Fax: (internat.) + 44-1223-336-033; E-mail: deposit@ccdc.cam.ac.uk].

Acknowledgments

We are grateful to Professor S. Suzuki (Graduate School of Science) for measurement of ESR spectra. This research was supported in part by grants-in-Aid for scientific research (nos. 14044056 and 15550049) from the Ministry of Education, Science, Sports and Culture, Japan, and by a Strategic Research Base Upbringing Special Coordination Fund for Promoting Science and Technology.

[1] P. Cassoux, L. Valade, K. Kobayashi, A. Kobayashi, R. A. Clark, A. E. Underhill, *Coord. Chem. Rev.* **1991**, *110*, 115−160.
[2] R.-M. Olk, B. Olk, W. Dietzsch, R. Kirmse, E. Hoyer, *Coord. Chem. Rev.* **1992**, *117*, 99−131.
[3] A. E. Pullen, R.-M. Olk, *Coord. Chem. Rev.* **1999**, *188*, 211−262.
[4] G. Matsubayashi, M. Nakano, H. Tamura, *Coord. Chem. Rev.* **2002**, *226*, 143−151.
[5] H. Mori, M. Nakano, H. Tamura, G. Matsubayashi, W. Mori, *Chem. Lett.* **1998**, 729−730.
[6] K. Kawabata, M. Nakano, H. Tamura, G. Matsubayashi, *J. Organomet. Chem.*, **2004**, *689*, 405−410.
[7] H. Mori, M. Nakano, H. Tamura, G. Matsubayashi, *J. Organomet. Chem.* **1999**, *574*, 77−85.
[8] K. Saito, M. Nakano, H. Tamura, G. Matsubayashi, *Inorg. Chem.* **2000**, *39*, 4815−4820.
[9] K. Saito, M. Nakano, H. Tamura, G. Matsubayashi, *J. Organomet. Chem.* **2001**, *625*, 7−17.
[10] M. Nakano, A. Kuroda, H. Tamura, R. Arakawa, G. Matsubayashi, *Inorg. Chim. Acta* **1998**, *279*, 165−171.
[11] G. Matsubayashi, M. Nakano, K. Saito, T. Yonamine, R. Arakawa, *J. Organomet. Chem.* **2000**, *611*, 364−369.
[12] T. Nakazono, M. Nakano, T. Tamura, G. Matsubayashi, *J. Mater. Chem.* **1999**, *9*, 2413−2417.
[13] K. Kawabata, M. Nakano, H. Tamura, G. Matsubayashi, manuscript to be published.
[14] M. Cowie, A. Gleizes, G. W. Grynkewich, D. W. Kalina, M. S. McClure, R. P. Scaringe, R. C. Teitelbaum, S. L. Ruby, J. A. Ibers, C. R. Kannewurf, T. J. Marks, *J. Am. Chem. Soc.* **1979**, *101*, 2921−2936.
[15] B. N. Diel, T. Inabe, J. W. Lyding, K. F. Schoch Jr., C. R. Kannewurf, T. J. Marks, *J. Am. Chem. Soc.* **1983**, *105*, 1551−1567.
[16] K. Kubo, M. Nakano, H. Tamura, G. Matsubayashi, M. Nakamoto, *J. Organomet. Chem.* **2003**, *669*, 141−148.
[17] R. Ziessel, M.-T. Youinou, F. Balegroune, D. Grandjean, *J. Organomet. Chem.* **1992**, *441*, 143−154.
[18] M.-J. Don, K. Yang, S. G. Bott, M. G. Richmond, *J. Organomet. Chem.* **1997**, *544*, 15−21.
[19] C.-H. Cheng, B. C. Spivack, R. Eisenberg, *J. Am. Chem. Soc.* **1977**, *99*, 3003−3011.
[20] K. Kubo, M. Nakano, H. Tamura, G. Matsubayashi, *Inorg. Chim. Acta* **2002**, *336*, 120− 124.
[21] K. Kubo, M. Nakano, H. Tamura, G. Matsubayashi, *Eur. J. Inorg. Chem.* **2003**, 4093−4098.
[22] J. W. Kang, K. Moseley, P. M. Maitlis, *J. Am. Chem. Soc.* **1969**, *91*, 5970−5977.
[23] "Jikken Kagaku Kouza (in Japanese)", Maruzen Co. Tokyo, Japan, **1991**, *18*, p. 344.
[24] N. Svenstrup, K. M. Rasmussen, T. K. Kansen, J. Becher, *Synthesis* **1994**, 809.
[25] L. Binet, J. M. Fabre, C. Montginoul, K. B. Simonsen, J. Becher, *J. Chem. Soc., Perkin Trans. 1* **1996**, 783−788.
[26] K. Akiba, G. Matsubayashi, T. Tanaka, *Inorg. Chim. Acta* **1989**, *165*, 245−248.
[27] K. Natsuaki, M. Nakano, G. Matsubayashi, *Inorg. Chim. Acta* **2000**, *299*, 112−117.
[28] G. Matsubayashi, T. Ryowa, H. Tamura, M. Nakano, R. Arakawa, *J. Organomet. Chem.* **2002**, *645*, 94−100.
[29] A. Nakahama, M. Nakano, G. Matsubayashi, *Inorg. Chim. Acta* **1999**, *284*, 55−60.
[30] T. Higashi, ABSCOR, a computer program for absorption correction, Rigaku Corporation, Tokyo, Japan, **1995**.
[31] PATTY: P. T. Beurskens, G. Admiraal, G. Beurskens, W. P. Bosman, R. de Gelder, R. Israel, J. M. M. Smits, DIRDIF94 program system, Technical report of the Crystallography laboratory, University of Nijmegen, The Netherlands, **1994**.
[32] P. T. Beurskens, G. Admiraal, G. Beurskens, W. P. Bosman, R. de Gelder, R. Israel, J. M. M. Smits, DIRDIF94 program system, Technical report of the Crystallography Laboratory, University of Nijmegen, The Netherlands, **1994**.
[33] G. M. Sheldrick, SHELXL 97, a computer program for the refinement of crystal structures, University of Göttingen, Germany, **1997**.
[34] *International Tables for X-ray Crystallography*, vol. 4, Kynoch Press, Birmingham, England, **1974**.
[35] C. K. Johnson, ORTEP-II, Report ORNL-5138, Oak Ridge National Laboratory, Oak Ridge, TN, **1976**.

Received October 23, 2003
Early View Article
Published Online April 1, 2004

 © 2004 Wiley-VCH Verlag GmbH & Co. KGaA, Weinheim

Self-Assembly of Novel Silver Polymers Based on Flexible Sulfonate Ligands

Daofeng Sun,[a] Rong Cao,*[a] Wenhua Bi,[a] Xiaoju Li,[a] Yanqin Wang,[a] and Maochun Hong[a]

Keywords: Self-assembly / Silver / Sulfonate / Polymers

Self-assembly reactions of sulfonates with $AgNO_3$ in the presence of secondary N- or P-containing ligands result in the formation of four new silver-sulfonate polymers, $[Ag(PIP)]_n \cdot [Ag(pesp)]_n \cdot 2nH_2O$ (**1**), $[Ag_2(pesp)(dabco)]_n \cdot 5nH_2O$ (**2**), $[\{Ag(pesp)_{1/2}(hmt)_{1/4}\} \cdot 0.5H_2O]_n$ (**3**) and $[Ag(PPh_3)\text{-}(pesp)_{1/2}]_n \cdot n$MeOH (**4**), whose structures change from one-dimensional chains to three-dimensional open frameworks based on the secondary ligands.
(© Wiley-VCH Verlag GmbH & Co. KGaA, 69451 Weinheim, Germany, 2004)

Introduction

In the past decades, much attention has been focused on the design and synthesis of metal-organic coordination networks (MOCNs)[1−3] based on coordination bonds and non-covalent interactions (such as hydrogen bonding, π-π−stacking and/or weak interactions between molecules),[4] due to their interesting molecular topologies and crystal-packing motifs, along with potential applications as functional materials.[5] In the construction of MOCNs, the stereo and interactive information stored in the ligand, as well as the coordination geometry of the metal ions, should be taken into account.[6] Previous studies have proved that careful selection of a suitable, polyfunctional, organic ligand containing certain features, such as, flexibility, versatile binding modes, and the ability to undergo hydrogen bonding, is helpful for constructing and tailoring the architectures of MOCNs.[7]

Recently, much effort has been devoted to the investigation of new synthetic strategies for constructing MOCNs possessing special architectures, such as, 1D helical-chain and 3D channel-like structures, with the use of rigid or flexible ligands containing oxygen or hybrid oxygen/nitrogen atoms, namely, multi-carboxylate, 4,4′-bipy or their derivatives.[8−12] Surprisingly, fewer examples containing sulfonate ligands have been reported, probably due to their weak coordination ability compared to N- or O-containing ligands.[13] However, the recent development of supramolecular chemistry has made it possible to rationally design and synthesize MOCNs by using ligands that in the past have been regarded as poorly coordinating anions, such as sulfonate ligands. Almost no systematic study in the field of sulfonate ligands has been reported. Only recently, the diversity of complexes, particularly transition-metal complexes, constructed by sulfonates has attracted much interest, not only because of the value of these compounds as inorganic synthons,[14] but also because of their important role in proteins.[13b] However, most of the studies reported are focused on aromatic sulfonates, for example when $-SO_3$ is directly connected to the aromatic ring,[15,16] and the studies on non-aromatic flexible sulfonates are almost neglected[17] because the coordination ability of the latter is much weaker than that of the former.

We have begun to study the reactions of flexible sulfonate ligands with silver(I) salts[18] by self-assembly with twofold aims: one is to obtain coordination information on such ligands and the other is to construct novel coordination polymers. Our strategy, in order to overcome the weak coordination ability of flexible sulfonate ligands, is to employ additional coordination sites in the ligand other than the $-SO_3$ group. Thus, we selected the dipotassium salt of piperazine-1,4-bis(2-ethanesulfonic acid) (K_2pesp) (see Scheme 1) as assembly ligand in view of the following characteristics: a) it contains a piperazine ring and the additional coordi-

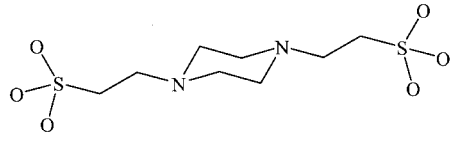

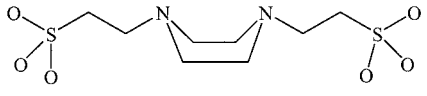

Scheme 1. The possible configuration of the piperazine ring in $pesp^{2-}$

[a] State Key Laboratory of Structural Chemistry, Fujian Institute of Research on the Structure of Matter, Chinese Academy of Sciences,
Fujian, Fuzhou, 350002, China
E-mail: rcao@ms.fjirsm.ac.cn

 © 2004 Wiley-VCH Verlag GmbH & Co. KGaA, Weinheim **DOI: 10.1002/ejic.200300813**

nation from the piperazine nitrogen may be useful for improving the coordination ability; b) it contains the flexible ethyl group that may allow the ligand to adapt to the geometric requirements of the metal ions;[19] c) it can act as a hydrogen-bond acceptor due to the sulfonate oxygen atoms and the nitrogen atoms of the piperazine ring, which may allow the formation of a high-dimensional supramolecular architecture.

A novel, one-dimensional silver polymer containing two different helical chains, $[Ag(PIP)]_n{\cdot}[Ag(pesp)]_n{\cdot}2n$H2O (**1**),[20] was obtained by the self-assembly reaction of the dipotassium salt of piperazine-1,4-bis(2-ethanesulfonic acid) (K_2pesp) with $AgNO_3$, in the presence of piperazine (PIP) in a mixed water/MeOH solution. To extend our work, we carried out systematic studies by introducing other secondary ligands, such as 1,4-diazabicyclo[2.2.2]octane (dabco), hexamethylenetetramine (hmt) and PPh_3, and three other interesting polymers were successfully synthesized. Herein, we describe the details of the preparation and characterization of the four novel silver(I) polymers: $[Ag(PIP)]_n{\cdot}[Ag(pesp)]_n{\cdot}2nH_2O$ (**1**), $[Ag_2(pesp)(dabco)]_n{\cdot}5nH_2O$ (**2**), $[\{Ag(pesp)_{1/2}(hmt)_{1/4}\}{\cdot}0.5H_2O]_n$ (**3**) and $[Ag(PPh_3)(pesp)_{1/2}]_n{\cdot}n$MeOH (**4**), based on mixed sulfonate and N- or P-containing ligands.

Results and Discussions

Syntheses

Previous studies have established the role of the secondary ligand in mixed ligand systems, for example, a bridging secondary ligand, such as 4,4′-bipy, generates extended frameworks,[21] whereas a terminal ligand, such as phen, often yields low-dimensional structures.[22] In order to obtain novel structural topologies based on secondary ligands, different N-containing secondary ligands, such as piperazine (PIP), 1,4-diazabicyclo[2.2.2]octane (dabco), hexamethylenetetramine (hmt) (see Scheme 2), were introduced in our study. It was found that increasing the coordination sites of the secondary ligand increased the dimensionality of the complex thus formed. When a terminal PPh_3 ligand was employed as a secondary ligand, complex **4**, which possesses a one-dimensional branch-like chain structure, was successfully isolated. The result is similar to previous observations.[21,22] Unfortunately, the effort to extend the study to diphosphane-bridging ligands, such as dppe [ethylenebis(diphenylphosphane)], failed and only a one-dimensional helical chain constructed by dppe was obtained,[23] indicating that the diphosphane-bridging ligands have higher coordination ability than $pesp^{2-}$.

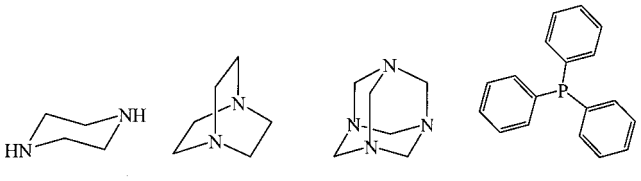

Scheme 2. The secondary ligands introduced in our work

An interesting reaction was observed during the preparation of complexes **1** and **2**. When the pH value was adjusted to 7 or 8 by $HClO_4$, a previously reported complex, $[Ag_2(\mu_2\text{-}OH_2)(pesp)]_n$, was obtained.[18] This result may arise from partial protonation of piperazine or 1,4-diazabicyclo[2.2.2]octane and then loss of their coordination ability. In complexes **1**−**4**, all the piperazine rings in $pesp^{2-}$, as well as in the PIP ligands, adopt the most stable "chair" configuration (see Scheme 1), as found in other Ag-PIP complexes.[24] The strong peaks at 1250−1150 cm^{-1} in the IR spectra correspond to the sulfonate groups in **1**−**4**.[13c] Complexes **1**−**4** are insoluble in water and other organic solutions such as MeOH, EtOH, and DMF. The coordination modes of $pesp^{2-}$ in **1**−**4** are given in Scheme 3.

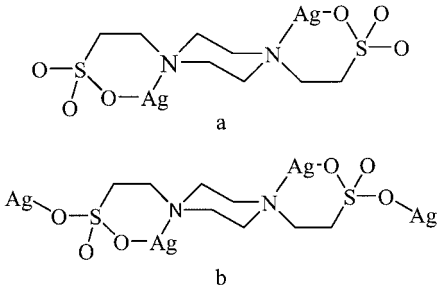

Scheme 3. The coordination modes of $pesp^{2-}$ in **2**−**4**

Structural Description

The structure of complex **1** has already been reported[20] and a detailed discussion will not be carried out here.

X-ray diffraction shows that complex **2** has a pseudo-two-dimensional layer structure, made up of a 1D zigzag chain containing a three-coordinate silver center. As shown in Figure 1(a), each silver ion is coordinated to one oxygen atom from the sulfonate group and to two nitrogen atoms from the $pesp^{2-}$ and dabco ligands, in a trigonal geometry. The coordination mode of $pesp^{2-}$ is similar to that seen in **1** as a μ_2-chelating ligand with the oxygen atom of the sulfonate group and the nitrogen atom of the piperazine ring (see a in Scheme 3). The average $Ag{-}N_{pesp}$ distance is 2.283(5) Å, which is shorter than that observed in **1** [2.334(9) Å],[20] presumably due to the coordination influence of the secondary ligand. Thus, each $pesp^{2-}$ ligand chelates two silver ions to form an $[Ag_2pesp]$ unit and such units are linked head-to-tail by dabco [the average $Ag{-}N_{dabco}$ distance is 2.237(6) Å] to form a 1D, infinite, zigzag chain structure (see Figure 1b). Although the coordination mode of $pesp^{2-}$ is the same in complexes **1** and **2**, the structures of the chains are quite different: in **1**, the helical chain is formed only by $pesp^{2-}$ and each $pesp^{2-}$ ligand links two silver ions and vice versa to form the 1D helical chain; whereas in **2**, the 1D polymer is formed by the mixed ligands, $pesp^{2-}$ and dabco, that alternate in the chain. Complex **2** can also be regarded as a variation of complex **1**, in which every second $pesp^{2-}$ ligand is replaced by dabco.

 © 2004 Wiley-VCH Verlag GmbH & Co. KGaA, Weinheim

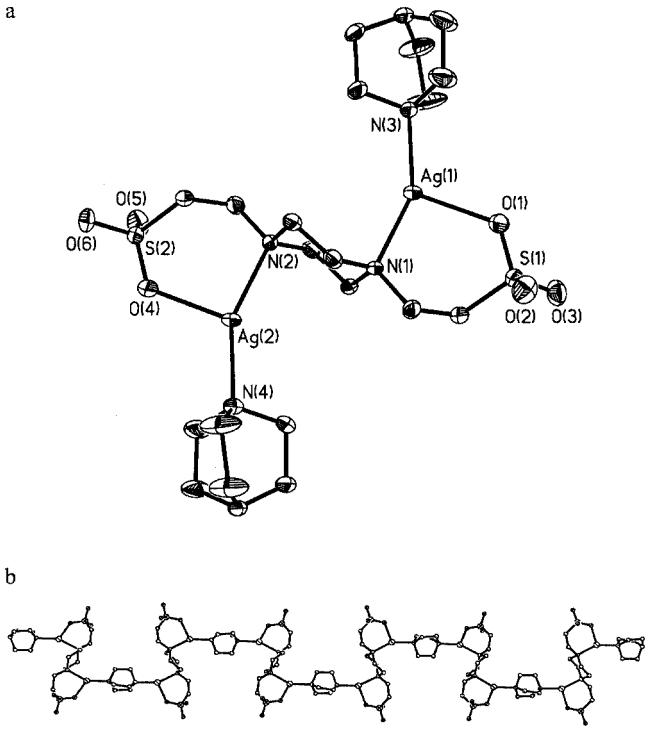

Figure 1. Coordination environment of the silver ion in **2** (a); the 1D chain structure of **2** (b)

There are weak interactions between the chains: the oxygen atom of the sulfonate group is weakly coordinated to the silver ion of the adjacent chain; the Ag−O distance is 2.665 Å (see Figure 2). These weak interactions make the complex a 2D brick-wall-like supramolecular structure [Figure 2 (top)], in which, if considering the weak Ag−O bond, the silver ion is four-coordinate, in a tetrahedral geometry, as in **1**. The free water molecules reside in the grids and form hydrogen bonds with the uncoordinated sulfonate oxygen atoms (O···O distances 2.790−2.987 Å). It should be noted that the 2D brick wall is one of the supramolecular isomers found in the self-assembly of T-shape modules.[25] Meanwhile, a 1D helical chain, $[Ag_2pesp]_n$, is generated by the weak Ag−O bonds [Figure 2 (bottom)]. Thus, the 2D layer can also be viewed as consisting of ladders sharing side pieces, which are formed by $[Ag_2pesp]_n$ helical chains and the rungs by dabco ligands, and **2** can be described as a pseudo-two-dimensional supramolecular architecture formed by weak coordinate bonds.

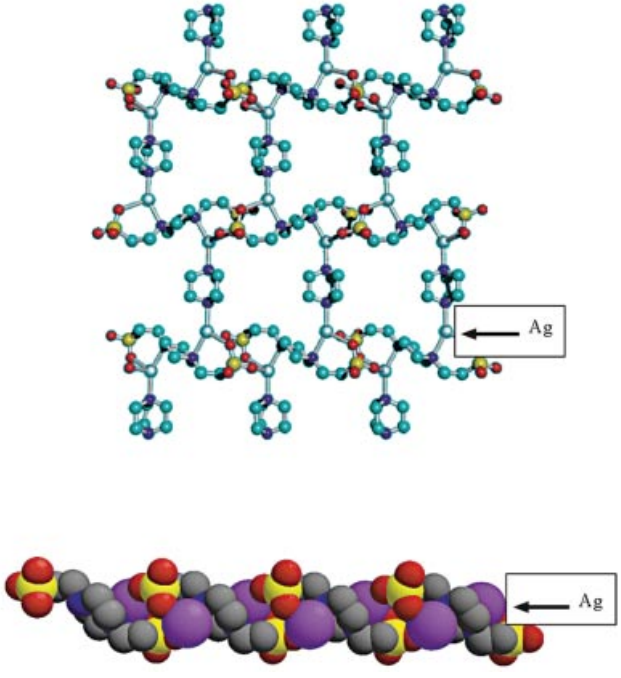

Figure 2. Two-dimensional layer structure (top) and one-dimensional helical chain (bottom) generated by the weak Ag−O bonds in **2**

In contrast with complexes **1** and **2**, X-ray diffraction shows that **3** is a three-dimensional polymer with open-square channels. The central silver ion is coordinated to two oxygen atoms from two different $pesp^{2-}$ ligands and to two nitrogen atoms from hmt and $pesp^{2-}$ in a tetrahedral geometry (see Figure 3); the average Ag−O and Ag−N distances are 2.395(9) and 2.346(7) Å, respectively. The Ag−N distance is longer than that observed in **1** and **2**, probably due to the influence of the secondary ligand. Each $pesp^{2-}$ adopts a chelating-bridging coordination mode to link four silver ions (see b in Scheme 3), which is not observed in **1** and **2**. The hmt ligand acts as a μ_4-bridge, which links four silver ions to four nitrogen atoms, as observed in $[Ag_2(\mu_4\text{-hmt})(SO_4)(H_2O)]\cdot 4H_2O$,[26] to form an $[Ag_4(hmt)]$ tetrahedral core, in which the four silver ions occupy the vertexes and hmt stands at the center (average Ag−Ag distance and Ag−Ag−Ag angle 6.262 Å and 60°, respectively). Each silver ion in the Ag_4 core is chelated by one oxygen of the $-SO_3$ group and the adjacent nitrogen of the piperazine ring of $pesp^{2-}$ (see b in Scheme 3) to form an $[Ag_4(hmt)(pesp)_4]$ unit that may be viewed as the basic building unit of the entire structure. The Ag_4 units are joined together by $pesp^{2-}$ ligands to form a 2D layer structure along the *ab*

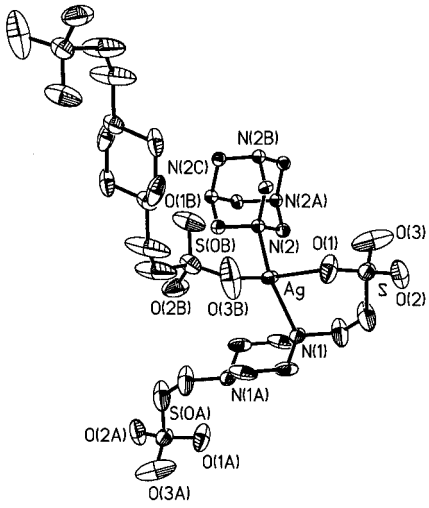

Figure 3. Coordination environment of the silver ion in **3**

 © 2004 Wiley-VCH Verlag GmbH & Co. KGaA, Weinheim

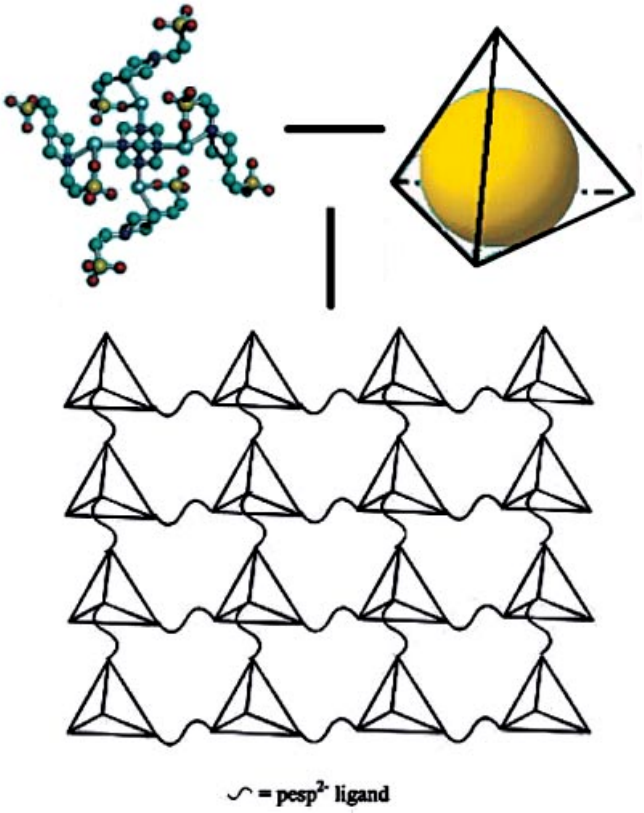

Figure 4. Two-dimensional diagram showing the connections between the Ag_4 cores that form the 2D layer in **3**

plane (see Figure 4). The adjacent layers are further connected by Ag−O bonds, provided by the remaining oxygen atoms of the sulfonate groups, to complete the tetrahedral coordination environments of the AgI ions, thereby generating a 3D open framework with square channels along the *a* axis, in which the free water molecules reside (see Figure 5). Hydrogen-bonding interactions between the uncoordinated sulfonate oxygen atoms and the free water molecules are present; the O···O distance is 2.965 Å.

X-ray diffraction analysis shows that **4** is a one-dimensional branch-like polymer containing a 1D helical backbone made up of an $[Ag_2(pesp)]$ unit and PPh_3 "leaves". As shown in Figure 6, the central silver ion is coordinated to two oxygen atoms and one nitrogen atom from two $pesp^{2-}$ ligands, and the remaining coordination site is occupied by the phosphorous atom of PPh_3 [the Ag−O, Ag−N and Ag−P distances are 2.431(8), 2.317(9) and 2.371(3) Å, respectively], in a tetrahedral geometry. The $pesp^{2-}$ ligand adopts the same coordination mode as in **3** (see b in Scheme 3), linking four silver ions. The dinuclear unit $[Ag_2(pesp)]$, formed by one chelating $pesp^{2-}$ ligand and two silver ions, may be viewed as the basic building block of the whole structure. Each Ag_2 unit is connected to another Ag_2 unit through Ag-O bonding to generate a one-dimensional branch-like chain structure (see Figure 7), in which every silver is coordinated to a PPh_3 "leaf" to prevent the framework from extending to a two- or three-dimensional architecture. It should be noted that the backbone of the polymer possesses a one-dimensional helical chain, namely $[Ag_2(pesp)]_n$, which is similar to that found in **2** except that the Ag-O interactions between the chains in **2** are weak. When considering the weak Ag−O bond in **2**, the coordination environments of the metal ion and $pesp^{2-}$ are the same in **2** and **4**. The solvent molecules are located at the two sides of the chain.

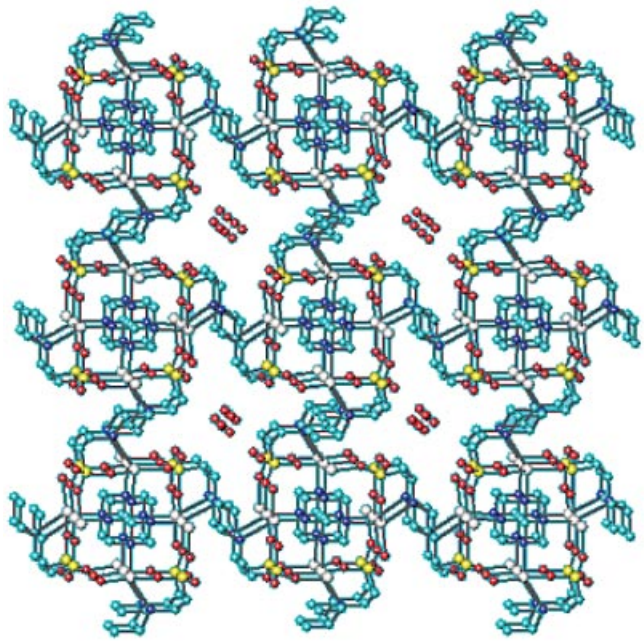

Figure 5. Three-dimensional open framework of **3** with square channels

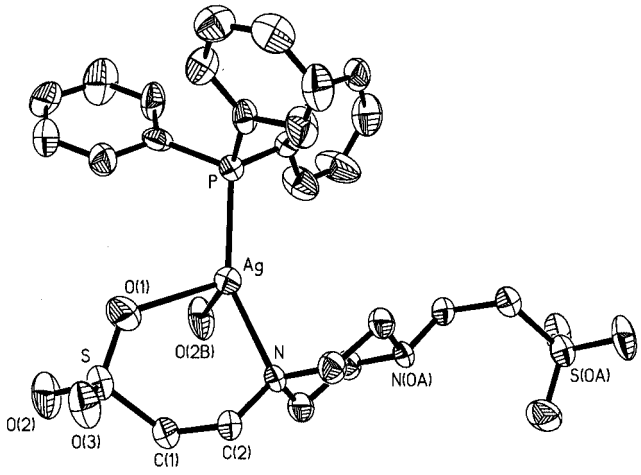

Figure 6. Coordination environment of the silver ion in **4**

Thermogravimetric Analysis for 3

Thermogravimetric analysis (TGA) for complex **3** shows that there is a weight loss of 2.85 % from 42 °C to 140 °C, which is equivalent to the loss of 0.5 uncoordinated water molecules (calcd. 2.97 %). At temperatures above 150 °C, complex **3** starts to decompose and the decomposition ends above 800 °C. In order to determine whether the backbone can be retained after removal of the guest water molecules,

 © 2004 Wiley-VCH Verlag GmbH & Co. KGaA, Weinheim

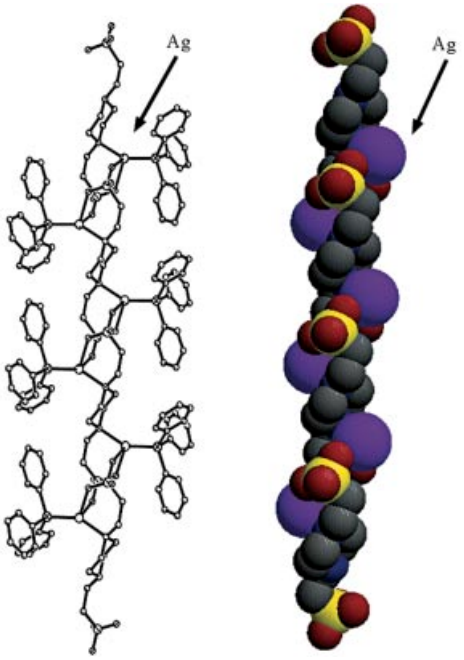

Figure 7. One-dimensional chain structure of **4**

heating-cooling and dehydrate-hydrate experiments were carried out according to the TGA results and monitored by X-ray powder diffraction (XRPD). When **3** was heated to 140 °C, part of the guest water molecules evolved from the sample and the samples were changed into powders; XRPD determination showed that most of the characteristic XRPD peaks had disappeared. After rehydrating the sample for 24 hours, the XRPD pattern showed that hardly any characteristic XRPD peaks were recovered. These results illustrate that the backbone collapses after removal of the water molecules, indicating that complex **3** possesses low thermal stability.

Conclusions

Four novel silver polymers possessing different architectures were synthesized by self-assembly reactions of flexible sulfonate ligands with silver salts, in the presence of secondary ligands, at room temperature, in mixed solvents (H_2O/DMF or H_2O/MeOH). Contrary to our previously reported complex, $[Ag_2(\mu_2\text{-}OH_2)(pesp)]_n$,[18] the flexible ligand $pesp^{2-}$ adopts bent configurations in the four complexes, acting as a μ_2-bridge in **1** and μ_4-bridges in **2**, **3** and **4** through bridging and/or chelating modes. The formation of the four complexes may be controlled by the secondary ligands,[27] and the dimensionality of the complexes increases when increasing the coordination sites of the secondary ligands (see Table 1). Our results indicate that the flexible ligand is more adjustable than the rigid one and can adopt various configurations and coordination modes to meet the different geometric requirements of the metal ions.[19] The architecture of the MOCNs can be tailored by changing the secondary ligands.

Table 1. Comparison of bond lengths and dimensionality in **1**, **2**, **3** and **4**

	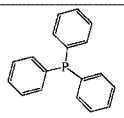 **4**	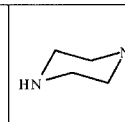 **1**	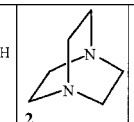 **2**	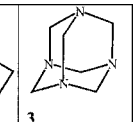 **3**
Ag-N/$P_{secondary}$	2.371 Å	2.197, 2.203 Å	2.222, 2.251 Å	2.335 Å
Dimensionality	1D branch-like chain	1D helical chain	2D layer	3D open framework

Experimental Section

Materials and Analyses: All chemicals were used are as purchased without further purification. IR spectra were recorded on a Magna 750 FT-IR spectrophotometer as KBr pellets. Elementary analyses were carried out in the elementary analysis group of this institute.

Synthesis of $[Ag_2(pesp)(dabco)]n\cdot 5nH_2O$ (2): K_2pesp (0.045 g, 0.125 mmol) and dabco (0.015 g, 0.125 mmol) were dissolved in water (5 mL) and placed on the bottom of a glass tube. A solution of $AgNO_3$ (0.043 g, 0.25 mmol) in MeOH (5 mL) was carefully layered on it through an H_2O/MeOH (5 mL) buffer. The tube was left standing in the dark for about two weeks and colorless prism-like crystals were obtained (0.054 g). Yield 30 %. $C_{14}H_{38}Ag_2N_4O_{11}S_2$ (718.33): calcd. C 23.41, H 5.33, N 7.80; found C 23.25, H 5.25, N 7.85. IR (KBr, cm^{-1}): 3450 (vs), 2966 (m), 2949 (m), 2825 (s), 1655 (m), 1462 (s), 1356 (s), 1315 (s), 1250 (s), 1213 (vs), 1196 (vs), 1167 (vs), 1055 (vs), 1039 (vs), 1009 (s), 781 (m), 652 (s), 586 (vs), 526 (s).

Synthesis of $[\{Ag(pesp)_{1/2}(hmt)_{1/4}\}\cdot 0.5H_2O]_n$ (3): K_2pesp (0.045 g, 0.125 mmol) and hmt (0.035 g, 0.25 mmol) were dissolved in water (5 mL) and placed on the bottom of a glass tube. A solution of $AgNO_3$ (0.043 g, 0.25 mmol) in DMF (5 mL) was carefully layered on it through an H_2O/DMF (5 mL) buffer. The tube was left standing in the dark for about two weeks and colorless, large prism-like crystals were obtained (0.042 g). Yield 55 %. $C_{5.5}H_{12}AgN_2O_{3.5}S$ (302.09): calcd. C 21.87, H 4.00, N 9.27; found C 21.88, H 4.10, N 9.25. IR (KBr, cm^{-1}): 3448 (vs), 2949 (s), 1655 (m), 1462 (m), 1356 (m), 1315 (s), 1248 (s), 1215 (vs), 1200 (vs), 1167 (vs), 1039 (vs), 1007 (vs), 816 (s), 688 (s), 588 (vs).

Synthesis of $[Ag(PPh_3)(pesp)_{1/2}]_n\cdot n$MeOH (4): K_2pesp (0.045 g, 0.125 mmol) was dissolved in a mixed H_2O/MeOH solution (v/v = 1:1; 4 mL) and placed on the bottom of a glass tube. A solution of $AgNO_3$ (0.043 g, 0.25 mmol) and PPh_3 (0.065 g, 0.25 mmol) in a mixed MeOH/EtOH solution (v/v = 1:1; 4 mL) was carefully layered on it through an H_2O/MeOH (5 mL) buffer. The tube was left standing in the dark for about three weeks and colorless well-formed prism-like crystals were obtained (0.055 g). Yield 40 %. $C_{23}H_{27}AgNO_4PS$ (552.37): calcd. C 50.01, H 4.93, N 2.54; found C 50.15, H 4.80, N 2.45. IR (KBr, cm^{-1}): 3450 (s), 3055 (s), 1585 (m), 1479 (s), 1437 (vs), 1398 (vs), 1385 (vs), 1296 (vs), 1095 (s), 1028 (m), 744 (vs), 694 (vs), 515 (vs).

Crystallographic Analyses: The intensity data of **1**−**4** were collected on a SIEMENTS SMART CCD diffractometer with graphite-monochromated Mo-K_α (λ = 0.71073 Å) radiation at room tem-

 © 2004 Wiley-VCH Verlag GmbH & Co. KGaA, Weinheim

Table 2. Crystallographic data for complexes **2**−**4**

Complex	**2**	**3**	**4**
Empirical formula	$C_{14}H_{38}Ag_2N_4O_{11}S_2$	$C_{5.5}H_{13}AgN_2O_4S$	$C_{23}H_{27}AgNO_4PS$
Formula mass	718.26	311.11	552.36
Space group	*Pna*2(1)	*I*4(1)/*a*	*P*21/*n*
T (°C)	293	293	293
a (Å)	20.5479(4)	23.1184(5)	9.4059(10)
b (Å)	9.34230(10)	23.1184(5)	17.3134(17)
c (Å)	12.8479(3)	6.7338(2)	15.1957(16)
β (deg)	90	90	104.316(2)
V (Å^3)	2466.34(8)	3598.95(15)	2397.7(4)
Z	4	16	4
$\rho_{calcd.}$ (g cm^{-3})	1.935	2.297	1.530
λ (Å)	0.71073	0.71073	0.71073
μ (mm^{-1})	1.817	2.460	1.023
Reflections collected	7677	5412	7908
Independent reflections	3586 [*R*(int) = 0.0206]	1574 [*R*(int) = 0.0399]	4213[*R*(int) = 0.0992]
Data/restraints/parameters	3586/1/298	1574/0/127	4213/0/289
Goodness of fit	1.094	1.079	1.205
$R_1[I > 2\sigma(I)]$	0.0330	0.0496	0.0914
wR_2	0.0768	0.1185	0.1392

Table 3. Selected bond lengths [Å] and angles [°] for **2**−**4**

2			
Ag(1)−N(3)	2.222(6)	Ag(2)−N(4)	2.251(6)
Ag(1)−N(1)	2.274(5)	Ag(2)−N(2)	2.291(5)
Ag(1)−O(1)	2.425(5)	Ag(2)−O(4)	2.482(5)
N(3)−Ag(1)−N(1)	150.41(18)	N(4)−Ag(2)−N(2)	52.13(18)
N(3)−Ag(1)−O(1)	114.04(18)	N(4)−Ag(2)−O(4)	113.58(18)
N(1)−Ag(1)−O(1)	92.08(18)	N(2)−Ag(2)−O(4)	93.19(17)
3			
Ag−N(2)	2.335(6)	Ag−O(1)	2.358(7)
Ag−N(1)	2.356(7)	Ag−O(3)[a]	2.431(9)
N(2)−Ag−N(1)	121.4(3)	N(2)−Ag−O(3)[a]	115.0(3)
N(2)−Ag−O(1)	112.7(3)	N(1)−Ag−O(3)[a]	120.2(4)
N(1)−Ag−O(1)	86.9(3)	O(1)−Ag−O(3)[a]	89.3(3)
4			
N−Ag	2.317(9)	Ag−O(1)	2.431(8)
P−Ag	2.371(3)	Ag−O(2)[b]	2.514(8)
N−Ag−P	150.2(2)	N−Ag−O(2)[b]	94.4(3)
N−Ag−O(1)	91.5(3)	P−Ag−O(2)[b]	104.2(2)
P−Ag−O(1)	109.7(2)		

[a] Symmetry transformations used to generate equivalent atoms: $y - 1/4, -x + 5/4, -z + 5/4$. [b] $-x + 2, -y - 1, -z$.

perature. All absorption corrections were performed with the SADABS program. The structures were solved by direct methods and refined on F^2 by full-matrix least-squares using the SHELXTL-97 program package on a legend computer. All non-hydrogen atoms were refined anisotropically. The organic hydrogen atoms were generated geometrically (C−H 0.96 Å). The crystallographic data of complexes **1**−**4** are listed in Table 2, selected bond lengths and angles in Table 3. Additional crystallographic details have been deposited at the Cambridge Crystallographic Data Center. CCDC-188274 (for **1***) and -200970 to -200972 (for **2**−**4**) contain the supplementary crystallographic data for this paper. These data can be obtained free of charge at www.ccdc.cam.ac.uk/conts/retrieving.html [or from the Cambridge Crystallographic Data Centre, 12 Union Road, Cambridge CB2 1EZ, UK; Fax: (internat.) + 44-1223-336-033; E-mail: deposit@ccdc.cam.ac.uk].

Acknowledgments

The authors thank the National Natural Science Foundation of China (90206040, 29901005), the Natural Science Foundation of the Fujian Province, the Key and the "One-hundred Talent" Projects from CAS for financial support.

[1] [1a] S. R. Batten, R. Robson, *Angew. Chem. Int. Ed.* **1998**, *37*, 1460−1494. [1b] P. J. Hagrman, D. Hagrman, J. Zubieta, *Angew. Chem. Int. Ed.* **1999**, *38*, 2638−2684. [1c] B. Moulton, M. J. Zaworotko, *Chem. Rev.* **2001**, *101*, 1629−1658. [1d] D. T. Vodak, M. E. Braun, J. Kim, M. Eddaoudi, O. M. Yaghi, *Chem. Commun.* **2001**, 2534−2535.

[2] [2a] H. J. Choi, M. P. Suh, *J. Am. Chem. Soc.* **1998**, *120*, 10622−10628. [2b] H. L. Li, C. E. Davis, T. L. Groy, D. G. Kelley, O. M. Yaghi, *J. Am. Chem. Soc.* **1998**, *120*, 2186−2187. [2c] S. M. Lo, S. S. Chui, L. Y. Shek, Z. Y. Lin, X. X. Zhang, G. H. Wen, I. D. Williams, *J. Am. Chem. Soc.* **2000**, *122*, 6293−6294.

[3] [3a] S. Masaoka, S. Furukawa, H. C. Chang, T. Mizutani, S. Kitagawa, *Angew. Chem. Int. Ed.* **2001**, *40*, 3817−3819. [3b] P. M. Forster, A. K. Cheetham, *Angew. Chem. Int. Ed.* **2002**, *41*, 457−459. [3c] Y. Cui, O. R. Evans, H. L. Ngo, P. S. White, W. B. Lin, *Angew. Chem. Int. Ed.* **2002**, *41*, 1159−1162.

[4] [4a] D. F. Sun, R. Cao, Y. Q. Sun, X. Li, W. H. Bi, M. C. Hong, Y. J. Zhao, *Eur. J. Inorg. Chem.* **2003**, 94−98. [4b] G. R. Desiraju, *Angew. Chem. Int. Ed. Engl.* **1995**, *35*, 2311−2313. [4c] C. Janiak, *J. Chem. Soc., Dalton Trans.* **2000**, 3885−3897. [4d] A. J. Blake, N. R. Champness, P. A. Cooke, J. E. B. Nicolson, C. Wilson, *J. Chem. Soc., Dalton Trans.* **2000**, 3811−3821. [4e] M. Nakash, Z. Clyde-Watson, N. Feeder, S. J. Teat, J. K. M. Sanders, *Chem. Eur. J.* **2000**, *6*, 2112−2119. [4f] C. Janiak, S. Deblon, H. P. Wu, M. J. Kolm, P. Klufers, H. Piotrowski, P. Mayer, *Eur. J. Inorg. Chem.* **1999**, 1507−1521.

[5] [5a] O. M. Yaghi, H. Li, C. Davis, D. Richardson, T. L. Groy, *Acc. Chem. Res.* **1998**, *31*, 474−484. [5b] A. J. Blake, N. R. Champness, P. Hubberstey, W. S. Li, M. A. Withersby, M. Schroer, *Coord. Chem. Rev.* **1999**, *183*, 117−138. [5c] O. Sato, T.

 © 2004 Wiley-VCH Verlag GmbH & Co. KGaA, Weinheim

Iyoda, A. Fujishima, K. Hashimoto, *Science* **1996**, *271*, 49−51. [5d] O. Kahn, C. Martinez, *Science* **1998**, *279*, 44−48. [5e] M. Fujita, Y. J. Kwon, S. Washizu, K. Ogura, *J. Am. Chem. Soc.* **1994**, *116*, 1151−1152.

[6] [6a] J. M. Lehn, *Supramolecular Chemistry: Concepts and Perspectives*, VCH, Weinheim, **1995**. [6b]M. C. Hong, W. P. Su, R. Cao, M. Fujita, J. X. Lu, *Chem. Eur. J.* **2000**, *6*, 427−431.

[7] [7a] Y. Suenaga, T. Kuroda-Sowa, M. Maekawa, M. Munakata, *J. Chem. Soc., Dalton Trans.* **2000**, 3620−3624. [7b] P. L. Caradoc-Davies, L. R. Hanton, *Chem. Commun.* **2001**, 1098−1099. [7c] I. Ino, L. P. Wu, M. Munakata, M. Maekawa, Y. Suenaga, T. Kuroda-Sowa, Y. Kitamori, *Inorg. Chem.* **2000**, *39*, 2146−2151.

[8] [8a] S. Konar, P. S. Mukherjee, E. Zangrando, F. Lioret, N. R. Chaudhun, *Angew. Chem. Int. Ed.* **2002**, *41*, 1561−1563. [8b] E. Lee, Y. Kim, D. Y. Jung, *Inorg. Chem.* **2002**, *41*, 501−506. [8c] M. Eddaoudi, J. Kim, M. O'Keeffe, O. M. Yaghi, *J. Am. Chem. Soc.* **2002**, *124*, 376−377. [8d] J. M. Rueff, S. Pillet, N. Claiser, G. Bonaventure, M. Souhassou, P. Rabu, *Eur. J. Inorg. Chem.* **2002**, 895−900.

[9] [9a] R. Cao, D. F. Sun, Y. C. Liang, M. C. Hong, K. Tatsumi, Q. Shi, *Inorg. Chem.* **2002**, *41*, 2087−2094. [9b] D. F. Sun, R. Cao, J. B. Weng, M. C. Hong, Y. C. Liang, *J. Chem. Soc., Dalton Trans.* **2002**, 291−293. [9c] R. G. Harrison, O. D. Fox, M. O. Meng, N. K. Dalley, L. J. Barbour, *Inorg. Chem.* **2002**, *41*, 838−843. [9d] C. Livage, N. Guillou, J. Marrot, G. Férey, *Chem. Mater.* **2001**, *13*, 4387−4392.

[10] [10a] J. J. Lu, A. Mondal, B. Moulton, M. J. Zaworotko, *Angew. Chem. Int. Ed.* **2001**, *40*, 2113−2116. [10b] L. Pan, B. S. Finkel, X. Y. Huang, J. Li, *Chem. Commun.* **2001**, 105−106. [10c] L. Pan, E. B. Woodlock, X. T. Wang, C. Zheng, *Inorg. Chem.* **2000**, *39*, 4174−4178.

[11] [11a] C. He, B. G. Zhang, C. Y. Duan, J. H. Li, Q. J. Meng, *Eur. J. Inorg. Chem.* **2000**, 2549−2554. [11b] L. Carlucci, G. Ciani, D. M. Proserpio, A. Sironi, *Angew. Chem. Int. Ed. Engl.* **1995**, *34*, 1895−1898. [11c] X. H. Bu, K. Biradha, T. Yamaguchi, M. Nishimura, T. Ito, K. Tanaka, M. Shionoya, *Chem. Commun.* **2000**, 1953−1954.

[12] [12a] K. Biradha, M. Fujita, *Chem. Commun.* **2001**, 15−16. [12b] K. A. Hirsch, S. R. Wilson, J. S. Moore, *Inorg. Chem.* **1997**, *36*, 2960−2968.

[13] [13a] G. K. H. Shimizu, G. D. Enright, C. I. Ratcliffe, K. F. Preston, J. L. Reid, J. A. Ripmeester, *Chem. Commun.* **1999**, 1485−1486. [13b] A. Onoda, Y. Yamada, M. Doi, T. Okamura, N. Ueyama, *Inorg. Chem.* **2001**, *40*, 516−521. [13c] Y. R. Xie, R. G. Xiong, X. Xue, X. T. Chen, Z. L. Xue, X. Z. You, *Inorg. Chem.* **2002**, *41*, 3323−3326.

[14] G. A. Lawrance, *Chem. Rev.* **1986**, *86*, 17−33 and references cited therein.

[15] [15a] V. A. Russell, M. C. Etter, M. D. Ward, *J. Am. Chem. Soc.* **1994**, *116*, 1941−1952. [15b] G. Smith, D. E. Lynch, C. H. L. Kennard, *Inorg. Chem.* **1996**, *35*, 2711−2712. [15c] G. K. H. Shimizu, G. D. Enright, C. I. Ratchiffe, G. S. Rego, J. L. Reid, J. A. Ripmeester, *Chem. Mater.* **1998**, *10*, 3282−3283. [15d] G. Smith, B. A. Cloutt, D. E. Lynch, K. A. Byriel, C. H. L. Kennard, *Inorg. Chem.* **1998**, *37*, 3236−3242. [15e] G. K. H. Shimizu, G. D. Enright, G. S. Rego, J. A. Ripmeester, *Can. J. Chem.* **1999**, *77*, 313−318. [15f] G. K. H. Shimizu, G. D. Enright, C. I. Ratcliffe, J. A. Ripmeester, *Chem. Commun.* **1999**, 461−462.

[16] [16a] J. W. Cai, C. H. Chen, C. Z. Liao, J. H. Yao, X. P. Hu, X. M. Chen, *J. Chem. Soc., Dalton Trans.* **2001**, 1137−1142. [16b] J. W. Cai, C. H. Chen, X. L. Feng, C. Z. Liao, X. M. Chen, *J. Chem. Soc., Dalton Trans.* **2001**, 2370−2375. [16c] B. J. Gunderman, P. J. Squattrito, *Inorg. Chem.* **1994**, *33*, 2924−2931. [16d] B. J. Gunderman, P. J. Squattrito, *Inorg. Chem.* **1995**, *34*, 2399−2406. [16e] S. k. Mäkinen, N. J. Melcer, M. Parvez, G. K. H. Shimizu, *Chem. Eur. J.* **2001**, *7*, 5176−5182.

[17] S. A. Dalrymply, M. Parvez, G. K. H. Shimizu, *Inorg. Chem.* **2002**, *41*, 6986−6996.

[18] D. F. Sun, R. Cao, Y. C. Liang, M. C. Hong, *Chem. Lett.* **2002**, 198−199.

[19] [19a] P. K. Bowyer, K. A. Porter, A. D. Rae, A. C. Willis, S. B. Wild, *Chem. Commun.* **1998**, 1153−1154. [19b] B. L. Fei, W. Y. Sun, T. Okamura, W. X. Tang, N. Ueyama, *New J. Chem.* **2001**, *25*, 210−212.

[20] D. F. Sun, R. Cao, Y. Q. Sun, W. H. Bi, X. Li, M. C. Hong, Y. J. Zhao, *Eur. J. Inorg. Chem.* **2003**, 38−41.

[21] [21a] P. Lightfoot, A. Snedden, *J. Chem. Soc., Dalton Trans.* **1999**, 3549−3556. [21b] S. M.-F. Lo, S. S.-Y. Chui, L. Y. Shek, Z. Y. Lin, X. X. Zhang, G. H. Wen, I. D. Williams, *J. Am. Chem. Soc.* **2000**, *122*, 6293−6294.

[22] [22a] D. F. Sun, R. Cao, Y. C. Liang, M. C. Hong, W. P. Su, J. B. Weng, *Acta Crystallogr. Sect. C* **2000**, *56*, 240−241. [22b] J. Cano, G. De Munno, J. L. Sanz, R. Ruiz, J. Faus, F. Lloret, M. Julve, A. Caneschi, *J. Chem. Soc., Dalton Trans.* **1997**, 1915−1921. [22c] X. M. Chen, G. F. Liu, *Chem. Eur. J.* **2002**, *8*, 4811−4818.

[23] Crystal data: C30H32AgNO4P2, triclinic, space group $P\bar{1}$, a = 11.3360, b = 12.1783, c = 13.1311 Å, α = 108.350°, β = 108.863°, γ = 106.766°, V = 1466.49, unpublished results.

[24] [24a] L. Carlucci, G. Ciani, D. M. Proserpio, A. Sironi, *Inorg. Chem.* **1995**, *34*, 5698−5700. [24b] T. Soma, T. K. Miyamoto, T. Iwamoto, *Chem. Lett.* **1997**, 319−320.

[25] H. Gudbjartson, K. Biradha, K. M. Poirier, M. J. Zaworotko, *J. Am. Chem. Soc.* **1999**, *121*, 2599−2600.

[26] M. L. Tong, S. L. Zheng, X. M. Chen, *Chem. Commun.* **1999**, 561−562.

[27] C. J. Kepert, T. J. Prior, M. J. Rosseinsky, *J. Am. Chem. Soc.* **2000**, *122*, 5158−5168.

Received November 5, 2003
Early View Article
Published Online April 1, 2004

 © 2004 Wiley-VCH Verlag GmbH & Co. KGaA, Weinheim

Ruthenium(II) Complexes Bearing Carboxylato and 2-Oxocarboxylato Ligands

Rainer Müller,[a] Eike Hübner,[a] and Nicolai Burzlaff*[a]

Keywords: Scorpionate ligands / Ruthenium / Bioinorganic chemistry / Tripodal ligands

The syntheses of ruthenium(II) acetato and benzoato complexes [Ru(bdmpza)(O_2CCH_3)(PPh_3)] (**6**) and [Ru(bdmpza)(O_2CPh)(PPh_3)] (**7**) [bdmpza = bis(3,5-dimethylpyrazol-1-yl)-acetate] are reported. The complexes **6** and **7** are synthesized in high yield from [Ru(bdmpza)Cl(PPh_3)$_2$] (**1**) and thallium acetate (**2**) or thallium benzoate (**3**). In a similar substitution reaction a benzoylformate complex [Ru(bdmpza){$O_2CC(O)Ph$}(PPh_3)] (**8**) is obtained from **1** and thallium benzoylformate (**4**). Reaction of **6** or **7** with benzoylformic acid also yields **8**. In analogous reactions several 2-oxocarboxylato ruthenium(II) complexes [Ru(bdmpza){$O_2CC(O)R$}(PPh_3)] (**9**: R = $CH_2CH_2CO_2H$, **10**: R = Me, **11**: R = Et) can be obtained. The low-spin ruthenium(II) complexes **8** to **11** exhibit a purple or brownish-red colour caused by MLCT transitions and thus a HOMO–LUMO gap which is almost identical to that of high-spin 2-oxoglutarate dependent iron oxygenases. **6** crystallises as a water adduct, **6**·H_2O and **8** forms an acetonitrile adduct **12**. Crystal structures of the water adduct **6**·H_2O and **8** were obtained.

(© Wiley-VCH Verlag GmbH & Co. KGaA, 69451 Weinheim, Germany, 2004)

Introduction

In recent years the 2-His-1-carboxylate facial triad, an iron binding motif that is found in the active sites of mononuclear non-heme iron(II) and iron(III) dependent enzymes, has attracted increasing interest.[1] The class of 2-oxoglutarate (α-ketoglutarate) dependent iron(II) enzymes, especially, are representative examples of such enzymes. Two iron binding histidines and one aspartate are conserved throughout many of these enzymes.[2] Several protein structures of 2-oxoglutarate (2-OG) dependent iron(II) enzymes have been solved in the last decade, such as deacetoxycephalosporin C synthase (DAOCS),[3] clavaminic acid synthase (CAS),[4] proline hydroxylase,[5] taurine dioxygenase (TauD) (Figure 1)[6] or anthocyanidin synthase (ANS).[7]

Pseudo-kinetic X-ray diffraction experiments on the related enzyme isopenicillin N synthase (IPNS)[2] showed several changes in the electron density close to the substrate but no changes to the 2-His-1-carboxylate facial triad throughout the catalytic cycle.[8] This fixed geometry of the three iron binding amino acids renders them perfect targets for structural model complexes. Especially bulky hydridotris-(pyrazol-1-yl)borato (Tp) and tris(2-pyridylmethyl)amine (TPA) have been used to mimic the active sites of these enzymes.[9,10] Iron benzoylformate complexes with Tp, TPA or TPA-related ligands have been investigated as structural models for more than ten years.[11,12] Recently, we reported on the bis(3,5-dimethylpyrazol-1-yl)acetato ligand

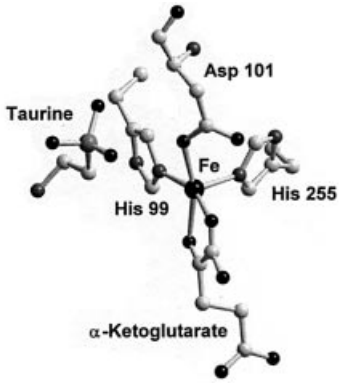

Figure 1. Active site of taurine dioxygenase TauD with 2-oxoglutarate bound to iron(II) and taurine substrate (PDB-Code: 1GY9)[6]

(bdmpza) and its application in ferrous and ferric iron complexes [Fe(bdmpza)$_2$] and [NEt_4][Fe(bdmpza)Cl_3].[13,14] The mono-anionic heteroscorpionate ligand proved, in these cases, to be a promising structural mimic for the facial 2-His-1-carboxylate triad. The O_2 adduct formation and oxygen-activation, key steps in the catalytic pathway of 2-oxoglutarate dependent enzymes, have also been studied upon oxygen-treatment of ruthenium(II) complexes with Tp or trispyridylalkoxymethane ligands.[15] Ruthenium(II) bis(pyrazol-1-yl)acetato complexes such as [Ru(bdmpza)Cl(PPh_3)$_2$] or enantiopure [Ru(bpa^{4cam})Cl(PPh_3)$_2$] and [Ru(bpa^{4menth})-Cl(PPh_3)$_2$] {bpa^{4cam}: bis[4,5,6,7-tetrahydro-7,8,8-trimethyl-(4*S*,7*R*)-methano-N^1,N^1-indazolyl]acetate; bpa^{4menth}: bis[4,5,6,7-tetrahydro-(4*R*)-methyl-(7*R*)-isopropyl-N^1,N^1-indazolyl]-acetate} have recently been described by us.[16,17] We now report on ruthenium(II) bis(3,5-dimethylpyrazol-1-yl)acet-

[a] Fachbereich Chemie der Universität Konstanz,
Universitätsstraße 10, Fach M728,
78457 Konstanz, Germany
Fax: (internat.) + 49-(0)7531-88-3136
E-mail: nicolai@chemie.uni-konstanz.de

ato complexes bearing carboxylato or 2-oxocarboxylato ligands.

Results and Discussion

Ferrous iron complexes with N,N,O ligands are often difficult to investigate, due to their paramagnetic high-spin constitution, and they are very sensitive to oxidation and ligand exchange. In contrast, ruthenium(II) complexes are low spin and thus suitable for NMR characterisation and are also easier to handle. In our attempt to find suitable models for the active site of 2-oxoglutarate dependent iron enzymes, we therefore focused on bis(3,5-dimethylpyrazol-1-yl)acetato ruthenium(II) complexes.

The complex [Ru(bdmpza)Cl(PPh_3)$_2$] (**1**) reacts slowly with thallium carboxylates Tl[O_2CR] (**2**: R = Me, **3**: R = Ph) to produce the $\kappa^2O^1,O^{1\prime}$-carboxylato complexes [Ru(bdmpza)(O_2CR)(PPh_3)] **6** and **7** through loss of one PPh_3 and the chloro ligand (Scheme 1).

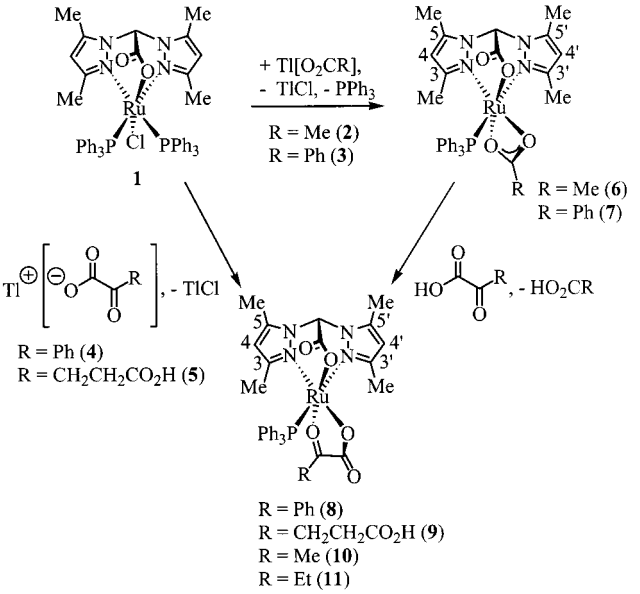

Scheme 1. Formation of carboxylato and 2-oxocarboxylato ruthenium(II) complexes

The thallium benzoate (**3**) and thallium 2-oxocarboxylates (see below) used in this work are easily available by the reaction of thallium acetate with benzoic acid or 2-oxocarboxylic acids [Equation (1)].

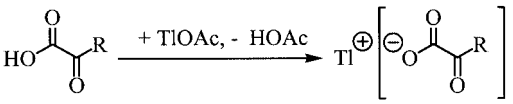

R = Ph (**4**)
R = $CH_2CH_2CO_2H$ (**5**) (1)

These syntheses take advantage of the lower pK_a values of these acids (benzoic acid: 4.22, benzoylformic acid: 1.2, 2-oxoglutaric acid: 2.31/5.14, pyruvic acid: 2.49) compared with acetic acid (4.76).[18] The free acetic acid is distilled off with water as an azeotrope and the thallium carboxylates are obtained in high purity.

Two sets of ^{1}H and ^{13}C signals are detected for the pyrazolyl groups of the bdmpza ligand. Therefore a chiral geometry with a PPh_3 *trans* to one of the pyrazolyl groups has to be assumed for **6** and **7**. A single ^{31}P NMR signal for each of the resulting ruthenium(II) complexes at δ = 62.0 ppm (**6**) and 60.2 ppm (**7**) proves the loss of one PPh_3. For **6** the ^{1}H NMR signal ($CDCl_3$) at δ = 1.00 ppm and the ^{13}C NMR signals (CD_2Cl_2) at δ = 23.6 ppm and 189.0 ppm are assigned to the acetato ligand. The benzoato ligand of **7** shows ^{13}C NMR signals ($CDCl_3$) at 127.1, 127.5, 131.1, 132.1 and 183.8 ppm. The ^{31}P NMR signals as well as the ^{13}C NMR signals correspond well with those of [Ru(Tp)(η^2-O_2CCHPh_2)(PPh_3)] [^{31}P: 63.7 ppm, ^{13}C(CO_2^-): 186.97 ppm].[19]

Admixing three equivalents of water to an NMR sample of **6** in CD_2Cl_2 causes an additional set of signals besides those of **6** which we assign to the formation of an adduct **6**·H_2O. In particular, a slight high-field shift of the acetate ^{13}C NMR signal (CO_2^-: 187.4 ppm) is indicative of this adduct, **6**·H_2O. The shift is in good agreement with the results recently reported by Alper et al. for the formation of [Ru(OAc)$_2$(H_2O)($Ph_2PProMe$)$_2$].[20] An NMR sample of sodium acetate and three equivalents of water in CD_2Cl_2 shows a ^{13}C NMR signal at δ = 181.6 ppm. Therefore, release of acetate and formation of [Ru(bdmpza)(H_2O)$_2$(PPh_3)][O_2CCH_3] can be excluded. After drying the sample in vacuo, only signals of **6** with no water can be detected. This proves that the formation of **6**·H_2O is fully reversible.

An X-ray structure determination of **6** revealed the water adduct of **6**·H_2O, with H_2O coordinated to ruthenium(II) and a monodentate κ*O*-acetato ligand (Figure 2, Table 1).

An intramolecular hydrogen bond between the water molecule and the non-coordinated oxygen atom of the acetate is indicated by the short distance *d*[O(4)···O(5)] = 2.720(6) Å. The presence of water can be explained by the fact that the crystals were grown under humid conditions and is proven by a CHN analysis of the crystals. Thus, $\kappa^2O^1,O^{1\prime}$-carboxylato ligands are hemilabile, chelating ligands. Once water is present, it can readily displace one of the oxygen atoms of the coordinating carboxylate. A very similar hydrogen bond was recently observed in a DAOCS protein structure presenting a DAOCS:Fe^{II}:CO_2:succinate:H_2O complex.[3b] The ring tension of the metalla-tetracycle is probably reduced by this water coordination.

The reaction of [Ru(bdmpza)Cl(PPh_3)$_2$] (**1**) with thallium 2-oxocarboxylates Tl[O_2CC(O)R] (**4**: R = Ph, **5**: R = $CH_2CH_2CO_2H$) produces κ^2O^1,O^2-2-oxocarboxylato complexes (Scheme 1). Single ^{31}P NMR signals at δ = 57.9 ppm (**8**) and 58.2 ppm (**9**) once again prove the loss of one PPh_3 ligand. Traces of a second structural isomer can be observed at δ = 57.1 ppm for **9**. The coordination of the 2-oxocarboxylates is backed by the [M^+] peaks in the FAB-

 © 2004 Wiley-VCH Verlag GmbH & Co. KGaA, Weinheim

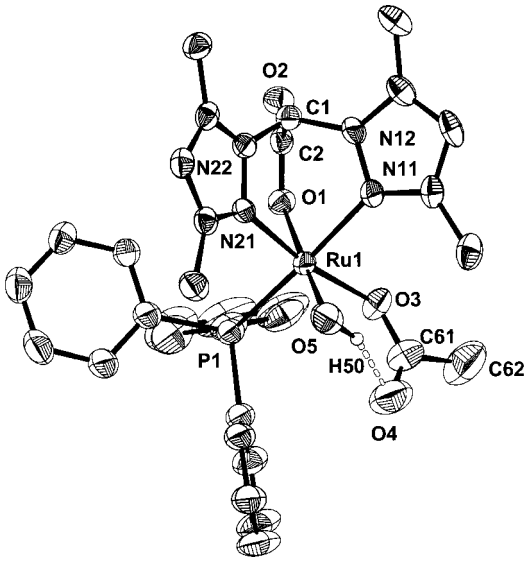

Figure 2. Molecular structure of [Ru(bdmpza)(H_2O)(O_2CCH_3)(PPh_3)] (**6**·H_2O); thermal ellipsoids are drawn at the 50% probability level

Table 1. Selected bond lengths (Å) and angles (°) of complex **6**·H_2O

Ru−N(11)	2.143(3)	C(1)−C(2)	1.547(6)
Ru−N(21)	2.081(4)	C(2)−O(1)	1.295(5)
Ru−O(1)	2.096(3)	C(2)−O(2)	1.231(5)
Ru−O(3)	2.087(3)	C(1)−N(12)	1.469(5)
Ru−O(5)	1.974(3)	C(1)−N(22)	1.446(5)
Ru−P(1)	2.3501(14)	O(3)−C(61)	1.255(6)
O(4)−O(5)	2.720(6)	O(4)−C(61)	1.220(7)
N(11)−Ru−N(21)	83.42(13)	N(11)−Ru−O(3)	86.85(14)
O(1)−Ru−N(11)	86.25(13)	N(11)−Ru−O(5)	91.77(14)
O(1)−Ru−N(21)	87.24(13)	N(21)−Ru−P(1)	98.73(10)
O(1)−Ru−P(1)	85.46(9)	N(21)−Ru−O(3)	170.24(13)
O(1)−Ru−O(3)	91.47(12)	N(21)−Ru−O(5)	91.65(16)
O(1)−Ru−O(5)	177.83(13)	O(3)−Ru−O(5)	89.31(15)
N(11)−Ru−P(1)	171.33(10)	O(3)−C(61)−O(4)	127.1(6)

MS and the ^{13}C NMR signals of the 2-oxo groups (**8**: 202.8 ppm, **9**: 215.5 ppm). Both complexes exhibit one (**8**) and two (**9**) additional CO_2^- signals in the ^{13}C NMR spectra. As to be expected for a chelate binding of the 2-oxocarboxylate, the complexes exhibit a chiral environment and therefore two sets of signals in the ^1H and ^{13}C NMR spectra for the pyrazolyl groups. Due to this chirality in **9**, an ABXY system in the ^1H NMR spectrum can be assigned to CH_2CH_2 of the 2-oxoglutarate. The X-ray structure determination of **8** establishes the chelate binding of the benzoylformate (Figure 3, Table 2).

The most striking feature of this structure is the position of the 2-oxo group *trans* to the carboxylate donor of the bdmpza ligand. This configuration agrees well with the coordination of the 2-oxoglutarate in the active site of 2-oxoglutarate dependent enzymes where the 2-oxo group is found *trans* to the iron binding aspartate (Figure 1).

As shown in Figure 3, the phenyl group of the benzoylformate ligand is almost parallel to one of the phenyl groups of PPh_3. Despite this parallel orientation the torsion

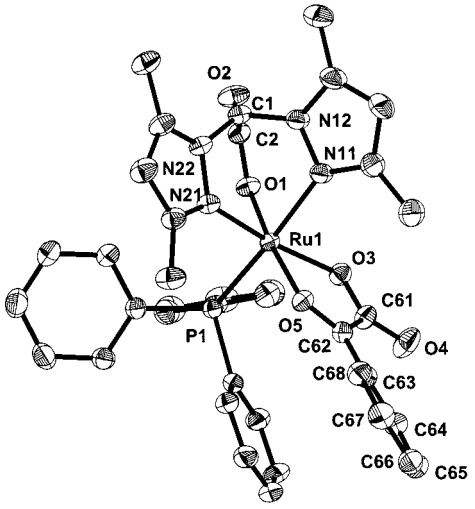

Figure 3. Molecular structure of [Ru(bdmpza){$O_2CC(O)Ph$}(PPh_3)] (**8**); thermal ellipsoids are drawn at the 50% probability level

Table 2. Selected bond lengths (Å) and angles (°) of complex **8**

Ru−N(11)	2.170(3)	C(2)−O(1)	1.292(4)
Ru−N(21)	2.074(3)	C(2)−O(2)	1.224(4)
Ru−O(1)	2.086(3)	C(1)−N(12)	1.466(4)
Ru−O(3)	2.095(2)	C(1)−N(22)	1.451(4)
Ru−O(5)	2.078(3)	O(3)−C(61)	1.282(4)
Ru−P(1)	2.322(2)	O(4)−C(61)	1.237(4)
C(1)−C(2)	1.551(4)	O(5)−C(62)	1.258(4)
N(11)−Ru−N(21)	81.95(11)	N(11)−Ru−O(3)	90.44(11)
O(1)−Ru−N(11)	86.71(11)	N(11)−Ru−O(5)	93.11(11)
O(1)−Ru−N(21)	88.79(11)	N(21)−Ru−P(1)	98.45(9)
O(1)−Ru−P(1)	86.59(9)	N(21)−Ru−O(3)	171.96(9)
O(1)−Ru−O(3)	93.36(11)	N(21)−Ru−O(5)	100.66(11)
O(1)−Ru−O(5)	170.44(8)	O(3)−Ru−O(5)	77.08(10)
N(11)−Ru−P(1)	173.28(7)	O(3)−C(61)−O(4)	125.0(3)

angle O(5)−C(62)−C(63)−C(68) of 20.4° indicates that there is still conjugation to the CO_2^- group via the 2-oxo group. The distances and angles of the [Ru(bdmpza)(PPh_3)] fragments in **6** and **8** agree well with those reported earlier for [Ru(bdmpza)Cl(PPh_3)$_2$] (**1**).[16]

The complexes **8** and **9** can also be obtained in high yield and high purity by reaction of benzoylformic acid and 2-oxoglutaric acid with the acetato complex **6** or the benzoato complex **7**. It is noteworthy, that this exchange of a carboxylato ligand by a 2-oxocarboxylato ligand is similar to the regeneration step of the biocatalytic pathway postulated for the 2-oxoglutarate dependent enzymes. In these enzymes an iron(II) bound succinate is replaced by 2-oxoglutarate to "reload" the active site of the enzyme after the hydroxylation of the substrate.[6]

It is even possible to combine the two synthetic steps: Reaction of the chloro complex **1** with thallium acetate and 2-oxocarboxylic acid affords the 2-oxocarboxylato ruthenium(II) complexes [Ru(bdmpza){$O_2CC(O)R$}(PPh_3)] (**8**: R = Ph, **9**: R = $CH_2CH_2CO_2H$, **10**: R = Me, **11**: R = Et) within 2 h (**8**, **10** and **11**) or 24 h (**9**). The ^{31}P NMR spectra of the complexes **10** and **11** exhibit a single signal

 © 2004 Wiley-VCH Verlag GmbH & Co. KGaA, Weinheim

each [δ = 58.1 ppm (**10**) and 58.5 ppm (**11**)]. The coordination of the 2-oxocarboxylates follows from the [M^+] peaks in the FAB MS, the ^{13}C NMR signals assigned to the 2-oxo carbonyl groups (**10**: δ = 215.8 ppm, **11**: δ = 217.9 ppm) and additional CO_2^- signals. Again the complexes are chiral and therefore two sets of signals appear in the ^1H and ^{13}CNMR spectra for the pyrazolyl groups. Complex **11** presents an ABX_3 system in the ^1H NMR spectrum that can be assigned to the CH_2CH_3 group. In some of the IR spectra of **8**−**11** two resonances occur around 1660 cm^{-1} which can be assigned to the two $\nu_{asym}(CO_2^-)$ of the bdmpza ligand and the 2-oxocarboxylate. It was not possible to assign unambiguously $\nu_{sym}(CO_2^-)$ of the complexes **6**−**11** to absorptions in the region of 1300 to 1500 cm^{-1}. This is due to the weakness of the signals and several overlapping absorptions of the PPh_3 ligand in that region.

In the case of **8**, **10** and **11** longer reaction times cause the occurrence of additional NMR signal sets, which are probably due to the formation of structural isomers. A mixture of the isomers was isolated for the 2-oxoglutarate complex **9**. We are currently investigating the character of these minor isomers, which most likely exhibit a geometry that involves the 2-oxo group being *trans* to a pyrazolyl group.

The formation of the 2-oxocarboxylato complexes is clearly indicated by a purple (**8**) or brownish-red (**9**−**11**) colour (Figure 4).

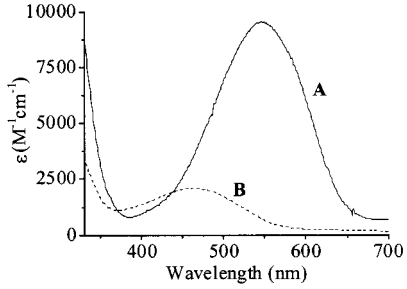

Figure 4. Electronic spectra of (A) [Ru(bdmpza){O_2CC(O)Ph}(PPh_3)] (**8**) (−) and (B) [Ru(bdmpza){O_2CC(O)CH_3}(PPh_3)] (**10**) (--) in CH_2Cl_2. Spectra of **9** and **11** are almost identical to **10**

Also, for the 2-oxoglutarate dependent enzymes, the addition of Fe^{II} and 2-oxoglutarate to the enzymes under anaerobic conditions results in a purple colour with a broad absorption band centred near 530 nm.[10c] The colour has been attributed to charge-transfer transitions from the metal centre to the coordinated 2-oxo group (MLCT absorption).[10c,11d,12c,21] Complexes **8**−**11** exhibit extinction coefficients at 546 nm (**8**) or 463 nm (**9**−**11**), which are almost 20-fold larger than those of the iron(II) models or enzymes {e.g. [Fe^{II}(Tp^{Ph2}){O_2CC(O)Ph}] ε (M^{-1}·cm^{-1}) = 540; [Fe^{II}TauD(2-OG)] ε (M^{-1}·cm^{-1}) = 140}.[10c] To verify this MLCT hypothesis for these ruthenium(II) complexes, extended Hückel[22] and DFT calculations were performed. The calculated HOMO−LUMO energy gaps of the DFT calculations are too small by a factor of about 2.5 compared with the measured, longest $\lambda_{max.}$. This is a well-known behaviour involving the gap between the HOMO−LUMO eigenvalues of DFT calculations, due to theoretical reasons.[23] According to the DFT calculations the band at the longest wavelength should shift to longer wavelengths by about 150 nm when the 2-oxocarboxylato complex **10** (R = Me) is replaced by **8** (R = Ph). Such a shift to longer wavelengths is indeed observed in the UV/Vis spectra, although to a smaller extent (Figure 4). The calculated results could be confirmed by the HOMO−LUMO energy gaps of the Hückel-calculation which also predicts this shift. Contour plots of the HOMO and LUMO for both complexes are shown in Figure 5.

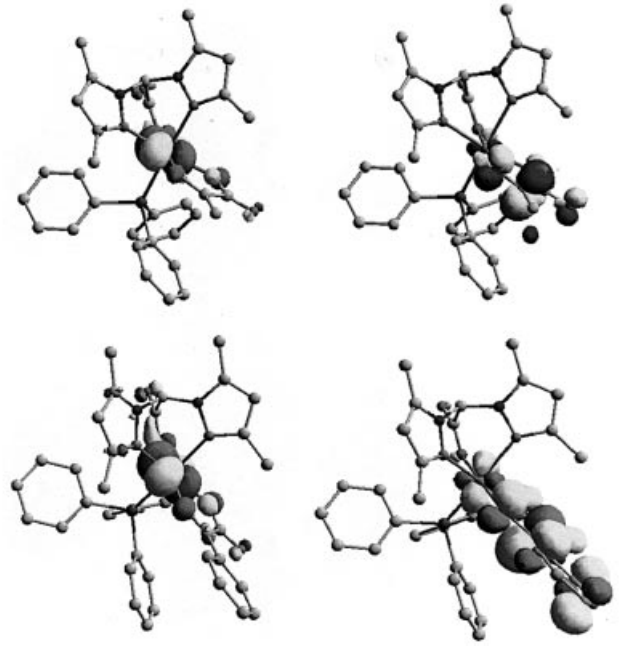

Figure 5. Contour plots of the delocalised HOMO (left) and LUMO (right) (DFT calculation) for **10** (top) and **8** (bottom)

The HOMO is clearly localised at the ruthenium(II) metal centre in **10** as well as in **8**. Two other MOs are only slightly lower in energy in both cases. Contour plots of these three orbitals exhibit geometries that are characteristic for d_{xy}, d_{xz} and d_{yz} orbitals. This is quite reasonable for a $4d^6$ low spin ruthenium(II) complex. Thus, all six d-electrons are available for a HOMO−LUMO transition. As a result of the good orientation of two of the HOMOs towards the LUMO, the HOMO−LUMO orbital overlap in the ruthenium(II) complexes should be better than in the iron complexes or iron enzymes. Moreover, this is true for ruthenium(II) 4d orbitals and not iron(II) 3d orbitals. These findings might explain why the extinction coefficients for the MLCT bands are almost 20-fold larger than those of the iron(II) models or enzymes.

The LUMOs in **8** and **10** are localised at the 2-oxocarboxylato ligands. They are composed of p_z density on the 2-oxo group with some conjugation to the carboxylate p_z. This is in good agreement with the π* LUMO of a coordinated pyruvate which was reported earlier by Solomon.[21] In **8** the LUMO is also delocalised into the aromatic substituent. The missing delocalisation into an aromatic system

 © 2004 Wiley-VCH Verlag GmbH & Co. KGaA, Weinheim

can explain the hypsochromic shift of the longest wavelength absorption of **10**. The structure of the LUMO is supported by the results of the Hückel calculations, which deliver a nearly identical electron density distribution.

Therefore, the calculations verify the metal-to-ligand charge transfer (MLCT). Although the ruthenium(II) complexes **8** and **10** have a low-spin t_{2g}^6 configuration they exhibit a HOMO−LUMO gap which is almost identical in size to that of the $t_{2g}^4e_g^2$ iron centres of the enzymes.

A solution of the benzoylformate complex **8** in acetonitrile changes its colour from purple to yellow upon heating. This can be explained by the formation of an adduct [Ru(bdmpza){$O_2CC(O)Ph$}($NCCH_3$)(PPh_3)] (**12**) with the solvent acetonitrile. A similar behaviour was reported earlier for 2-oxocarboxylato iron complexes.[11b,12] Besides the colour change the adduct formation is documented by IR and ^1H NMR spectroscopic data as well as an 802 [MH^+] peak in the FAB-MS. Due to the rather labile coordination of CH_3CN in **12** we were unable to obtain a correct CHN elemental analysis and ^{13}C NMR spectroscopic data.

Therefore, the 2-oxocarboxylates as well as the carboxylates are hemilabile ligands and should render the additional coordination of reactive species possible. Although **8** seems to be rather stable under aerobic conditions, a solution of **8** in 1,2-dichloroethane, when exposed to air, decomposed within two weeks to form red crystals of the ruthenium(III) complex [Ru(bdmpza)Cl_2(PPh_3)] (**13**), which we reported recently.[16] Further work will focus on these oxidation reactions.

Experimental Section

General Remarks: All operations were carried out under either nitrogen or argon by using conventional Schlenk techniques. Solvents were distilled from appropriate drying agents and degassed before use. The yields refer to analytically pure compounds and were not optimised. IR: Biorad FTS 60, CaF_2 cuvettes (0.5 mm). ^1H NMR and ^{13}C NMR: Bruker AC 250, Varian Inova-400, δ values relative to TMS. ^{31}P NMR: JEOL GX 400, Bruker DRX 600 Avance, δ values relative to an external standard from Wilmad (H_3PO_4 100%). 2D NMR experiments: Bruker DRX 600 Avance, Varian Inova-400. Mass spectra were recorded on a modified Finnigan MAT 312 using the FAB technique and 3-nitrobenzyl alcohol as matrix. Elemental analyses: Heraeus CHN−O-Rapid. UV/Vis: Hewlett−Packard Diode-Array spectrophotometer 8452A (silica cuvette; d = 1 cm). A modified Siemens P4 diffractometer was used for X-ray structure determination.

Thallium acetate (**2**), benzoic acid, pyruvic acid, 2-oxobutyric acid, benzoylformic acid and 2-oxoglutaric acid were used as purchased. Ruthenium(III) trichloride hydrate was a generous gift of the Degussa AG. The synthesis of [Ru(bdmpza)Cl(PPh_3)$_2$] (**1**) was reported recently.[16]

Method A. General Procedure for the Synthesis of Thallium Carboxylates: Equimolar amounts of thallium acetate (**2**) and the carboxylic acid were dissolved in water. The water/HOAc mixture was removed by azeotropic distillation and the procedure was repeated once. The remaining residue was washed with acetone and re-crystallised from acetone/water to yield thallium carboxylate suitable for further reactions.

Method B. General Procedure for the Synthesis of Carboxylato Ruthenium(II) Complexes: A solution of [Ru(bdmpza)Cl(PPh_3)$_2$] (**1**) and a slight excess of thallium carboxylate in CH_2Cl_2 was stirred at ambient temperature. The mixture was filtered through celite and dried in vacuo. Precipitation from CH_2Cl_2 solution with pentane yielded the carboxylato ruthenium(II) complex.

Method C. General Procedure for the Synthesis of Ruthenium(II) 2-Oxocarboxylato Complexes: A solution of [Ru(bdmpza)Cl(PPh_3)$_2$] (**1**), a slight excess of thallium acetate and an excess of a 2-oxocarboxylic acid were stirred in CH_2Cl_2 at ambient temperature. The mixture was filtered through celite and dried in vacuo. Precipitation from CH_2Cl_2 solution with pentane yielded the 2-oxocarboxylato ruthenium(II) complex.

Tl[O_2CPh] (3): Reaction of thallium acetate (**2**) (2.01 g, 7.63 mmol) and benzoic acid (0.933 g, 7.64 mmol) in water (2 × 100 mL) according to procedure A yielded **3** as a white microcrystalline powder. Yield 1.99 g (80%); m.p. > 300 °C. ^1H NMR (D_2O + 1% v/v [D_6]acetone, 250 MHz): δ = 7.30−7.41 (m, 3 H, *p*-Ph and *m*-Ph), 7.73 (m, 2 H, *o*-Ph) ppm. ^{13}C NMR (D_2O + 1% v/v [D_6]acetone, 62.9 MHz): δ = 129.7, 130.2, 132.7, 137.6 (Ph), 176.8 (CO_2^-) ppm. $C_7H_5O_2Tl$ (325.50): calcd. C 25.83, H 1.55; found C 26.00, H 1.68.

Tl[$O_2CC(O)Ph$] (4): Reaction of thallium acetate (**2**) (2.01 g, 7.63 mmol) and benzoylformic acid (1.22 g, 8.13 mmol) in water (2 × 50 mL) according to procedure A yielded **4** as a white microcrystalline powder. Yield 2.50 g (93%); m.p. 140 °C (dec.). ^1H NMR (D_2O +1% v/v [D_6]acetone, 250 MHz): δ = 7.45 (vt, 2 H, *m*-Ph), 7.61 (t, 1 H, *p*-Ph), 7.81 (d, 2 H, *o*-Ph) ppm. ^{13}C NMR (D_2O +1% v/v [D_6]acetone, 62.9 MHz): δ = 129.5, 130.0, 132.3, 135.5 (Ph), 173.0 (CO_2^-), 197.0 (CO) ppm. $C_8H_5O_3Tl$ (353.51): calcd. C 27.18, H 1.43; found C 27.36, H 1.31.

Tl[$O_2CC(O)CH_2CH_2CO_2H$] (5): Reaction of thallium acetate (**2**) (1.00 g, 3.80 mmol) and 2-oxoglutaric acid (555 mg, 3.80 mmol) in water (50 mL) according to procedure A yielded crude **5** after removing HOAc and H_2O at 55 °C and reduced pressure. Re-crystallisation from H_2O/Acetone yielded white microcrystalline powder. Yield 1.20 g (90%); m.p. 130 °C (dec.). ^1H NMR (D_2O + 1% v/v [D_6]acetone, 250 MHz): δ = 2.49 (t, $^3J_{H,H}$ = 6.6 Hz, 2 H, $CH_2CO_2^-$), 2.85 (t, $^3J_{H,H}$ = 6.6 Hz, 2 H, CH_2CO) ppm. ^{13}C NMR (D_2O + 1% v/v [D_6]acetone, 62.9 MHz): δ = 28.6 (CH_2CO), 34.6 ($CH_2CO_2^-$), 170.3 (CO_2^-), 178.6 (CO_2H) ppm. $C_5H_5O_5Tl$ (349.47): calcd. C 17.18, H 1.44; found C 16.82, H 1.40.

[Ru(bdmpza)(O_2CCH_3)(PPh_3)] (6): Reaction of [Ru(bdmpza)-Cl(PPh_3)$_2$] (**1**) (663 mg, 0.730 mmol) and thallium acetate **2** (235 mg, 0.892 mmol) in CH_2Cl_2 (50 mL) according to method B yielded product **6** as a yellow solid after 60 h. Yield 0.367 g (75%); m.p. 200 °C (dec.). ^1H NMR ($CDCl_3$, 250 MHz): δ = 1.00 (s, 3 H, Ac−CH_3), 1.77 (s, 3 H, C^3−CH_3), 2.41 (s, 3 H, $C^{3'}$−CH_3), 2.44 (s, 3 H, C^5−CH_3), 2.51 (s, 3 H, $C^{5'}$−CH_3), 5.68 (s, 1 H, H_{pz}), 6.11 (s, 1 H, $H_{pz'}$), 6.36 (s, 1 H, CH), 7.15−7.75 (m, 15 H, PPh_3) ppm. ^1H NMR (CD_2Cl_2, 400 MHz): δ = 0.93 (s, 3 H, Ac−CH_3), 1.66 (s, 3 H, C^3−CH_3), 2.31 (s, 3 H, $C^{3'}$−CH_3), 2.35 (s, 3 H, C^5−CH_3), 2.42 (s, 3 H, $C^{5'}$−CH_3), 5.62 (s, 1 H, H_{pz}), 6.06 (s, 1 H, $H_{pz'}$), 6.23 (s, 1 H, CH), 7.05−7.40 (m, 15 H, PPh_3) ppm. ^{13}C NMR ($CDCl_3$, 62.9 MHz): δ = 11.2 (C^5−CH_3), 11.5 ($C^{5'}$−CH_3), 12.5 ($C^{3'}$−CH_3), 14.6 (C^3−CH_3), 23.5 (Ac−CH_3), 68.8 (CH), 108.0 (C^4), 109.2 ($C^{4'}$), 127.8 (d, $^3J_{C,P}$ = 9.1 Hz, *m*-PPh_3), 129.1 (*p*-PPh_3), 134.3 (br., *o*-PPh_3), 140.9 ($C^{5'}$), 142.2 (C^5), 155.0 (C^3), 158.2 ($C^{3'}$), 168.2 (CO_2^-), 188.7 (CO_2^-) ppm. ^{13}C NMR (CD_2Cl_2, 100.5 MHz): δ = 11.2 (C^5−CH_3), 11.5 ($C^{5'}$−CH_3), 12.5 ($C^{3'}$−CH_3), 14.5 (C^3−CH_3), 23.6 (Ac−CH_3), 69.0 (CH), 108.2 (C^4), 109.3 (d, $^4J_{C,P}$ = 2.8 Hz, $C^{4'}$), 128.0 (d, $^3J_{C,P}$ = 9.2 Hz, *m*-PPh_3), 129.4 (*p*-PPh_3), 134.3 (br., *o*-

 © 2004 Wiley-VCH Verlag GmbH & Co. KGaA, Weinheim

PPh_3), 141.6 ($C^{5'}$), 143.1 (C^5), 155.2 (d, $^3J_{C,P}$ = 2.7 Hz, C^3), 158.3 ($C^{3'}$), 168.1 (CO_2^-), 189.0 (CO_2^-) ppm. ^{31}P NMR ($CDCl_3$, 161.8 MHz): δ = 62.0 ppm. IR (THF): $\tilde{\nu}$ = 1674 vs (CO_2^-), 1653 w, 1560 w (C=N), 1464 m, 1436 m, 1420 w cm^{-1}. IR (CH_2Cl_2): $\tilde{\nu}$ = 1661 vs (CO_2^-), 1563 w (C=N), 1483 w, 1463 m, 1435 m, 1418 w cm^{-1}. IR (KBr): $\tilde{\nu}$ = 1668 vs (CO_2^-), 1585 w, 1563 m (C=N), 1482 w, 1462 m, 1434 m, 1418 w cm^{-1}. UV/Vis (CH_2Cl_2): $\lambda_{max.}$ (log ε) = 233.0 (4.37) nm. EI-MS (70 eV, 370 °C): *m*/*z* (%) = 670 (3) [M^+], 626, (1) [$M^+ - CO_2$], 566 (3) [$M^+ - CO_2 - HOAc$]. FAB-MS (NBOH): *m*/*z* (%) = 748 (83) [$M^+ + H_2O + HOAc$], 670 (100) [M^+], 611 (39) [$M^+ - OAc$], 566 (44) [$M^+ - CO_2 - HOAc$]. $C_{32}H_{33}N_4O_4PRu$ (669.68): calcd. C 57.39, H 4.97, N 8.37; found C 56.88, H 5.34, N 8.36.

Reaction of 6 with H_2O. Formation of [Ru(bdmpza)(OAc)(H_2O)(PPh_3)] (6·H_2O): Three equivalents of water (6.00 μL, 0.336 mmol) were added to an NMR sample of [Ru(bdmpza)(OAc)(PPh_3)] (**6**) (75 mg, 0.112 mmol) in CD_2Cl_2 (0.7 mL). NMR spectra were immediately recorded, showing new signals besides those of **6**, due to the presence of **6**·H_2O. ^1H NMR (CD_2Cl_2, 400 MHz): δ = 1.50, 1.65, 2.06, 2.25, 2.45 (s, some signals are broad and covered, 5 × CH_3 and H_2O), 5.80 (s, 1 H, H_{pz} or $H_{pz'}$), 5.89 (s, 1 H, H_{pz} or $H_{pz'}$), 6.41 (s, 1 H, CH), 7.05−7.40 (m, 15 H, PPh_3) ppm. ^{13}C NMR (CD_2Cl_2, 100.5 MHz): δ = 10.9, 12.9, 13.0, 14.0 (4 × CH_3), 24.8 (Ac−CH_3), 69.5 (CH), 108.8, 109.2 (C^4 and $C^{4'}$), PPh_3 signals covered, 141.8, 143.7 (C^5 and $C^{5'}$), 154.5, 159.1 (C^3 and $C^{3'}$), 168.7 (CO_2^-), 187.4 (CO_2^-) ppm. ^{31}P NMR (CD_2Cl_2, 161.8 MHz): δ = 57.1 ppm. Crystallisation of **6** with CH_2Cl_2/hexane under humid conditions yielded yellow crystals of the adduct **6**·H_2O. M.p. 200−205 °C (dec.). FAB-MS (NBOH): *m*/*z* (%) = 748 (18) [$M^+ + H_2O + HOAc$], 670 (100) [M^+], 611 (31) [$M^+ - OAc$], 566 (37) [$M^+ - CO_2 - HOAc$]. Crystals: $C_{32}H_{33}N_4O_4PRu{\cdot}CH_2Cl_2{\cdot}H_2O$ (772.63): calcd. C 51.30, H 4.83, N 7.25; found C 51.56, H 4.54, N 7.30.

[Ru(bdmpza)(O_2CPh)(PPh_3)] (7): Reaction of [Ru(bdmpza)Cl(PPh_3)$_2$] (**1**) (493 mg, 0.543 mmol) with thallium benzoate (**3**) (212 mg, 0.651 mmol) in CH_2Cl_2 (40 mL) according to method B yielded product **7** as a pale yellow microcrystalline powder after 60 h. Yield 298 mg (75%); m.p. 130 °C (dec.). ^1H NMR ($CDCl_3$, 600 MHz): δ = 1.87 (s, 3 H, C^3-CH_3), 2.22 (s, 3 H, $C^{3'}-CH_3$), 2.45 (s, 3 H, C^5-CH_3), 2.50 (s, 3 H, $C^{5'}-CH_3$), 5.71 (s, 1 H, H_{pz}), 6.05 (s, 1 H, $H_{pz'}$), 6.38 (s, 1 H, CH), 7.13−7.51 (m, 20 H, Ph & PPh_3) ppm. ^{13}C NMR ($CDCl_3$, 150.9 MHz): δ = 11.2 (C^5-CH_3), 11.5 ($C^{5'}-CH_3$), 13.0 ($C^{3'}-CH_3$), 14.8 (C^3-CH_3), 68.9 (CH), 108.1 (C^4), 109.2 ($C^{4'}$), 127.1 (*m*-Ph), 127.5 (*o*-Ph), 127.7 (d, $^3J_{C,P}$ = 9.2 Hz, *m*-PPh_3), 129.0 (*p*-PPh_3), 131.1 (*p*-Ph), 132.1 (*i*-Ph), 134.2 (br., *o*-PPh_3), 140.8 (C^5), 142.2 ($C^{5'}$), 155.3 ($C^{3'}$), 158.3 (C^3), 168.2 (CO_2^-), 183.8 (CO_2^-) ppm. ^{31}P NMR ($CDCl_3$, 161.8 MHz): δ = 60.2 ppm. IR (CH_2Cl_2): $\tilde{\nu}$ = 1662 vs (CO_2^-), 1645 w, 1563 w (C=N), 1505 w, 1501 w, 1482 w, 1463 w, 1435 m, 1428 m, 1419 w cm^{-1}. IR (KBr): $\tilde{\nu}$ = 1671 vs (CO_2^-), 1561 w (C=N), 1499 w, 1482 w, 1460 w, 1431 m, 1421 sh cm^{-1}. UV/Vis (CH_2Cl_2): $\lambda_{max.}$ (log ε) = 235.0 (4.43), 316.0 (3.91) nm. FAB-MS (NBOH): *m*/*z* (%) = 732 (100) [M^+], 611 (41) [$M^+ - O_2CPh$], 566 (38) [$M^+ - CO_2 - HO_2CPh$]. $C_{37}H_{35}N_4O_4PRu{\cdot}H_2O$ (749.77): calcd. C 59.27, H 4.97, N 7.47; found C 59.30, H 5.30, N 7.46.

[Ru(bdmpza){$O_2CC(O)Ph$}(PPh_3)] (8): Reaction of [Ru(bdmpza)Cl(PPh_3)$_2$] (**1**) (333 mg, 0.367 mmol), thallium acetate (**2**) (115 mg, 0.437 mmol) and benzoylformic acid (69.0 mg, 0.460 mmol) in CH_2Cl_2 (30 mL) according to method C yielded product **8** as a dark purple microcrystalline powder after 2 h. Yield 253 mg (91%); m.p. 240 °C (dec.). ^1H NMR ($CDCl_3$, 600 MHz): δ = 1.88 (s, 3 H, $C^{3'}-CH_3$), 1.89 (s, 3 H, C^3-CH_3), 2.47 (s, 3 H, C^5-CH_3), 2.49 (s, 3 H, $C^{5'}-CH_3$), 5.80 (s, 1 H, $H_{pz'}$), 5.93 (s, 1 H, H_{pz}), 6.45 (s, 1 H, CH), 7.20 (m, 6 H, *m*-PPh_3), 7.26 (m, 3 H, *p*-PPh_3), 7.32 (m, 6 H, *o*-PPh_3), 7.33 (m, 2 H, *m*-Ph), 7.52 (t, 1 H, *p*-Ph), 8.33 (d, 2 H, *o*-Ph) ppm. ^{13}C NMR ($CDCl_3$, 150.9 MHz): δ = 11.1 (C^5-CH_3), 11.6 ($C^{5'}-CH_3$), 13.4 (C^3-CH_3), 14.3 ($C^{3'}-CH_3$), 69.0 (CH), 108.8 ($C^{4'}$), 109.2 (C^4), 128.2 (d, $^3J_{C,P}$ = 11.6 Hz, *m*-PPh_3), 128.3 (*m*-Ph), 129.6 (*p*-PPh_3), 130.4 (*o*-Ph), 133.5 (*i*-Ph), 134.1 (d, $^2J_{C,P}$ = 6.9 Hz, *o*-PPh_3), 134.4 (*p*-Ph), 140.9 (C^5), 142.9 ($C^{5'}$), 154.6 (C^3), 158.8 ($C^{3'}$), 168.0 (CO_2^-), 169.7 (CO_2^-), 202.8 (C=O) ppm. ^{31}P NMR ($CDCl_3$, 161.8 MHz): δ = 57.9 ppm. IR (CH_2Cl_2): $\tilde{\nu}$ = 1659 s, 1653 vs (CO_2^-), 1563 (C=N), 1483 w, 1463 w, 1446 w, 1435 w, 1418 w cm^{-1}. IR (KBr): $\tilde{\nu}$ = 1652 br (CO_2^-), 1563 w (C=N), 1482 w, 1461 w, 1446 w, 1434 w, 1418 w cm^{-1}. UV/Vis (CH_2Cl_2): $\lambda_{max.}$ (log ε) = 233.0 (4.68), 275.0 (4.38), 284.0 (4.38), 546.0 (3.98) nm. FAB-MS (NBOH): *m*/*z* (%) = 760 (100) [M^+], 611 (34) [$M^+ - O_2CC(O)Ph$]. $C_{38}H_{35}N_4O_5PRu$ (759.76): calcd. C 60.07, H 4.64, N 7.37; found C 60.04, H 4.90, N 7.57.

Complex **8** was also obtained in similar yield and purity either by reaction of the chloro complex **1** with thallium benzoylformate (**4**) or by reaction of benzoylformic acid with **6** or **7**. Crystals of **8** suitable for X-ray structure determination were obtained from a solution of 1,2-dichloroethane with traces of MeOH and H_2O (400:2:1, v/v/v).

[Ru(bdmpza){$O_2CC(O)CH_2CH_2CO_2H$}(PPh_3)] (9): Reaction of [Ru(bdmpza)Cl(PPh_3)$_2$] (**1**) (405 mg, 0.446 mmol), thallium acetate (**2**) (130 mg, 0.493 mmol) and 2-oxoglutaric acid (80.0 mg, 0.548 mmol) in CH_2Cl_2 (20 mL) according to method C yielded product **9** as brownish-red microcrystalline powder after 24 h. Yield 320 mg (95%); m.p. 150−160 °C (dec.). **1. Isomer:** ^1H NMR (CD_2Cl_2, 400 MHz): δ = 1.67 (s, 3 H, C^3-CH_3), 1.82 (s, 3 H, $C^{3'}-CH_3$), 2.05 (ddd, J_{AB} = 21.1, $^3J_{H,H}$ = 5.3, $^3J_{H,H}$ = 5.3 Hz, 1 H, CH_2-CO), 2.26 (ddd, J_{AB} = 17.6, $^3J_{H,H}$ = 5.3, $^3J_{H,H}$ = 5.3 Hz, 1 H, CH_2-COOH), 2.34 (s, 3 H, $C^{5'}-CH_3$), 2.37 (ddd, J_{AB} = 17.6, $^3J_{H,H}$ = 8.8, $^3J_{H,H}$ = 5.4 Hz, 1 H, CH_2-COOH), 2.40 (s, 3 H, C^5-CH_3), 2.95 (ddd, J_{AB} = 21.1, $^3J_{H,H}$ = 8.8, $^3J_{H,H}$ = 5.4 Hz, 1 H, CH_2-CO), 5.72 (s, 1 H, H_{pz}), 5.92 (s, 1 H, $H_{pz'}$), 6.51 (s, 1 H, CH), 7.08 (m, 6 H, *o*-Ph), 7.22 (m, 6 H, *m*-Ph), 7.32 (m, 3 H, *p*-Ph) ppm. ^{13}C NMR (CD_2Cl_2, 100.5 MHz): δ = 11.0 ($C^{5'}-CH_3$), 11.6 (C^5-CH_3), 13.0 ($C^{3'}-CH_3$), 13.9 (C^3-CH_3), 26.9 (CH_2-CO_2H), 34.5 (CH_2-CO), 68.6 (CH), 109.2 (C^4), 109.5 (d, $^4J_{C,P}$ = 2.7 Hz, $C^{4'}$), 128.6 (d, $^3J_{C,P}$ = 9.3 Hz, *m*-PPh_3), 130.1 (d, $^4J_{C,P}$ = 2.5 Hz, *p*-PPh_3,), 131.0 (d, $^1J_{C,P}$ = 40.7 Hz, *i*-PPh_3), 134.1 (d, $^2J_{C,P}$ = 10.1 Hz, *o*-PPh_3), 142.2 ($C^{5'}$), 144.4 (C^5), 155.0 (d, $^3J_{C,P}$ = 2.5 Hz, $C^{3'}$), 159.3 (C^3), 169.2 (CO_2^-), 169.3 (CO_2^-), 174.1 (CO_2H), 215.5 (C=O) ppm. ^{31}P NMR ($CDCl_3$, 161.8 MHz): δ = 58.2.

2. Isomer: ^1H NMR (CD_2Cl_2, 400 MHz): δ = 1.76 (s, 3 H, C^3-CH_3), 1.84 (s, 3 H, $C^{3'}-CH_3$), 2.36 (s, 3 H, $C^{5'}-CH_3$), 2.41 (s, 3 H, C^5-CH_3), 3H covered by the other isomer, 2.83 (ddd, J_{AB} = 21.7, $^3J_{H,H}$ = 8.5, $^3J_{H,H}$ = 6.2 Hz, 1 H, CH_2-CO), 5.74 (s, 1 H, H_{pz}), 5.91 (s, 1 H, $H_{pz'}$), 6.50 (s, 1 H, CH), 7.08 (m, 6 H, *o*-Ph), 7.22 (m, 6 H, *m*-Ph), 7.32 (m, 3 H, *p*-Ph) ppm. ^{13}C NMR (CD_2Cl_2, 100.5 MHz): δ = 11.0 ($C^{5'}-CH_3$), 11.6 (C^5-CH_3), 12.9 ($C^{3'}-CH_3$), 13.8 (C^3-CH_3), 26.8 (CH_2-CO_2H), 34.6 (CH_2-CO), 68.8 (CH), 108.9 (C^4), 109.5 (d, $^4J_{C,P}$ = 2.9 Hz, $C^{4'}$), 128.7 (d, $^3J_{C,P}$ = 12.2 Hz, *m*-PPh_3), 130.0 (*p*-PPh_3), 132.2 (d, $^3J_{C,P}$ = 10.0 Hz, *o*-PPh_3), 141.9 ($C^{5'}$), 143.6 (C^5), 155.2 (d, $^3J_{C,P}$ = 2.6 Hz, $C^{3'}$), 157.9 (C^3), 167.5 (CO_2^-), 168.6 (CO_2^-), 173.6 (CO_2H), 216.8 (C=O) ppm. ^{31}P NMR ($CDCl_3$, 161.8 MHz): δ = 57.1 ppm. IR (CH_2Cl_2): $\tilde{\nu}$ = 1657 vs (CO_2^-), 1563 w (C=N), 1483 w, 1463 w, 1435 m, 1417 w cm^{-1}. IR (KBr): $\tilde{\nu}$ = 1653 vs (CO_2^-), 1560 w (C=N), 1482 w, 1465 w, 1436 w, 1420 w cm^{-1}. UV/Vis (CH_2Cl_2): $\lambda_{max.}$

 © 2004 Wiley-VCH Verlag GmbH & Co. KGaA, Weinheim

(log ε) = 235.0 (4.38), 268.0 (3.84), 275.0 (3.85), 294.0 (3.84), 463.0 (3.36) nm. FAB-MS (NBOH): *m/z* (%) = 756 (100) [M^+], 611 (50) [$M^+ - O_2CC(O)CH_2CH_2CO_2H$], 566 (30) [$M^+ - CO_2 - HO_2CC(O)CH_2CH_2CO_2H$]. $C_{35}H_{35}N_4O_7PRu$ (755.73): calcd. C 55.63, H 4.67, N 7.41; found C 55.17, H 4.76, N 7.44.

Complex **9** was also obtained in similar yield and purity either by reaction of the chloro complex **1** with thallium 2-oxoglutarate (**5**) or by reaction of 2-oxoglutaric acid with **6** or **7**.

[Ru(bdmpza){$O_2CC(O)CH_3$}(PPh_3)] (10): Reaction of [Ru(bdmpza)Cl(PPh_3)$_2$] (**1**) (440 mg, 0.484 mmol), thallium acetate (**2**) (157 mg, 0.596 mmol) and pyruvic acid (145 mg, 1.65 mmol) in CH_2Cl_2 (40 mL) according to method C yielded product **10** as brownish-red microcrystalline powder after 2 h. Yield 323 mg (96%); m.p. 250 °C (dec.). ^{1}H NMR ($CDCl_3$, 250 MHz): δ = 1.78 (s, 3 H, C^3 or $C^{3'}-CH_3$), 1.91 (s, 3 H, C^3 or $C^{3'}-CH_3$), 2.07 [s, $C(O)CH_3$], 2.46 (s, 3 H, C^5 or $C^{5'}-CH_3$), 2.47 (s, 3 H, C^5 or $C^{5'}-CH_3$), 5.77 (s, 1 H, H_{pz} or $H_{pz'}$), 5.97 (s, 1 H, H_{pz} or $H_{pz'}$), 6.46 (s, 1 H, CH), 7.19−7.38 (m, 15 H, PPh_3) ppm. ^{13}C NMR ($CDCl_3$, 62.9 MHz): δ = 11.1 (C^5 or $C^{5'}-CH_3$), 11.6 (C^5 or $C^{5'}-CH_3$), 13.3 (C^3 or $C^{3'}-CH_3$), 14.1 (C^3 or $C^{3'}-CH_3$), 25.9 [$C(O)CH_3$], 69.0 (CH), 108.9 (C^4 or $C^{4'}$), 109.2 (C^4 or $C^{4'}$), 128.3 (d, $^3J_{C,P}$ = 9.8 Hz, *m*-PPh_3), 129.7 (*p*-PPh_3), 131.2 (d, $^1J_{C,P}$ = 42.3 Hz, *i*-PPh_3), 134.0 (d, $^2J_{C,P}$ = 8.9 Hz, *o*-PPh_3), 141.1 (C^5 or $C^{5'}$), 143.2 (C^5 or $C^{5'}$), 154.4 (C^3 or $C^{3'}$), 159.1 (C^3 or $C^{3'}$), 168.2 (CO_2^-), 169.3 (CO_2^-), 215.8 (C=O) ppm. ^{31}P NMR ($CDCl_3$, 161.8 MHz): δ = 58.1 ppm. IR (CH_2Cl_2): $\tilde{\nu}$ = 1656 vs (CO_2^-), 1563 w (C=N), 1483 w, 1463 w, 1435 w, 1418 w cm^{-1}. IR (KBr): $\tilde{\nu}$ = 1669 s, 1653 vs (CO_2^-), 1560 w (C=N), 1482 w, 1460 w, 1433 m, 1420 w cm^{-1}. UV/Vis (CH_2Cl_2): $\lambda_{max.}$ (log ε) = 241.0 (4.16), 291.0 (3.79), 463.0 (3.32) nm. FAB-MS (NBOH): *m/z* (%) = 698 (100) [M^+], 611 (48) [$M^+ - O_2CC(O)CH_3$], 566 (30) [$M^+ - CO_2 - HO_2CC(O)CH_3$]. $C_{33}H_{33}N_4O_5PRu$ (697.69): calcd. C 56.81, H 4.77, N 8.03; found C 56.32, H 4.78, N 7.74.

[Ru(bdmpza){$O_2CC(O)CH_2CH_3$}(PPh_3)] (11): Reaction of [Ru(bdmpza)Cl(PPh_3)$_2$] (**1**) (327 mg, 0.360 mmol), thallium acetate (**2**) (108 mg, 0.410 mmol) and 2-oxobutyric acid (47 mg, 0.460 mmol) in CH_2Cl_2 (30 mL) according to method C yielded product **11** as a brownish-red microcrystalline powder after 2 h. Yield 248 mg (97%); m.p. 220 °C (dec.). ^{1}H NMR ($CDCl_3$, 600 MHz): δ = 0.95 (t, $^3J_{H,H}$ = 7.0 Hz, 3 H, CH_2CH_3), 1.80 (s, 3 H, $C^{3'}-CH_3$), 1.89 (s, 3 H, C^3-CH_3), 2.09 (dq, J_{AB} = 21.1, $^3J_{H,H}$ = 7.0 Hz, 1 H, CH_2), 2.46 (s, 3 H, $C^{5'}-CH_3$), 2.46 (s, 3 H, C^5-CH_3), 2.66 (dq, J_{AB} = 21.1, $^3J_{H,H}$ = 7.0 Hz, 1 H, CH_2), 5.75 (s, 1 H, $H_{pz'}$), 5.96 (s, 1 H, H_{pz}), 6.45 (s, 1 H, CH), 7.18−7.40 (m, 15 H, PPh_3) ppm. ^{13}C NMR ($CDCl_3$, 62.9 MHz): δ = 6.9 (CH_2CH_3), 11.1 ($C^{5'}-CH_3$), 11.6 (C^5-CH_3), 13.3 (C^3-CH_3), 14.1 ($C^{3'}-CH_3$), 32.7 (CH_2), 68.9 (CH), 108.9 ($C^{4'}$), 109.3 (C^4), 128.4 (d, $^3J_{C,P}$ = 9.8 Hz, *m*-PPh_3), 129.8 (*p*-PPh_3), 131.1 (d, $^1J_{C,P}$ = 42.3 Hz, *i*-PPh_3), 134.0 (d, $^2J_{C,P}$ = 9.8 Hz, *o*-PPh_3), 141.2 ($C^{5'}$), 143.2 (C^5), 154.4 ($C^{3'}$), 159.1 (C^3), 168.5 (CO_2^-), 169.2 (CO_2^-), 217.9 (C=O) ppm. ^{31}P NMR ($CDCl_3$, 161.8 MHz): δ = 58.5 ppm. IR (CH_2Cl_2): $\tilde{\nu}$ = 1655 vs (CO_2^-), 1563 w (C=N), 1483 w, 1462 w, 1435 w, 1418 w cm^{-1}. IR (KBr): $\tilde{\nu}$ = 1670 s, 1658 vs (CO_2^-), 1560 w (C=N), 1482 w, 1460 w, 1435 m, 1420 w cm^{-1}. UV/Vis (CH_2Cl_2): $\lambda_{max.}$ (log ε) = 241.0 (4.10), 268.0 (3.81), 275.0 (3.82), 297.0 (3.83), 457.0 (3.38) nm. FAB-MS (NBOH): *m/z* (%) = 712 (100) [M^+], 611 (36) [$M^+ - O_2CC(O)CH_2CH_3$], 566 (18) [$M^+ - CO_2 - HO_2CC(O)CH_2CH_3$]. $C_{34}H_{35}N_4O_5PRu$ (711.72): calcd. C 57.38, H 4.96, N 7.87; found C 57.13, H 4.96, N 7.84.

[Ru(bdmpza){$O_2CC(O)Ph$}($NCCH_3$}(PPh_3)] (12): A dark purple suspension of [Ru(bdmpza){$O_2CC(O)Ph$}(PPh_3)] (**8**) (141 mg, 0.186 mmol) in acetonitrile (20 mL) was heated under reflux. Within 2 h the reaction mixture changed into a yellow solution. The solvent was reduced in vacuo and the product was precipitated with Et_2O and filtered off. The product **12** was obtained as a yellow microcrystalline powder. Yield 107 mg (72%); m.p. 85 °C (dec.). ^{1}H NMR (CD_3CN, 250 MHz): δ = 1.62 (s, 3 H, CH_3), 1.97 (s, 3 H, CH_3CN), 2.41 (s, 3 H, CH_3), 2.52 (s, 3 H, CH_3), 2.55 (s, 3 H, CH_3), 6.05 (s, 1 H, $H_{pz'}$ or H_{pz}), 6.24 (s, 1 H, $H_{pz'}$ or H_{pz}), 6.68 (s, 1 H, CH), 7.30−7.60 (m, 18 H, PPh_3 & Ph), 7.91 (m, 2 H, *o*-Ph) ppm. ^{31}P NMR (CD_3CN, 161.8 MHz): δ = 49.7 ppm. IR (KBr): $\tilde{\nu}$ = 2277 w (C≡N), 1669 vs (CO_2^-), 1605 s (CO), 1565 w (C=N), 1484 w, 1465 w, 1436 w, 1419 w cm^{-1}. UV/Vis (CH_2Cl_2): $\lambda_{max.}$ (log ε) = 239.0 (4.49), 341.0 nm (2.96). FAB-MS (NBOH): *m/z* (%) = 802 (3) [MH^+], 760 (31) [$M^+ - CH_3CN$], 652 (81) [$M^+ - O_2CC(O)Ph$], 611 (100) [$M^+ - O_2CC(O)Ph - CH_3CN$]. $C_{40}H_{38}N_5O_5PRu$ (800.82): calcd. C 59.99, H 4.78, N 8.75; CHN analysis not obtained due to loss of CH_3CN.

Calculations: DFT-calculations and full geometry optimisations were carried out by using Jaguar 5.0[24] running on Linux-2.4.18−3smp on three Athlon MP 2400+ dual-processor workstations (Beowulf-cluster) parallelised with MPICH 1.2.4. The crystal structure of the ruthenium(II) benzoylformate complex was used as starting geometry. Complete geometry optimisations were carried out on the implemented BP86/LACVP* basis set (using the 6−31G* basis set and Hay−Wadt effective core potentials on Ru). Extended Hückel MO calculations were performed with the program package Hyperchem[25] running on a single Athlon 1.3 GHz workstation with Windows NT 4.0. The HOMO−LUMO gap energies were calculated using standard parameters as given in the program from the optimised structures of the DFT-calculations. Orbital plots were obtained using Maestro 5.1, the graphical interface of Jaguar.[24]

X-ray Structure Determinations: Single crystals of **6** and **8** were mounted with Paratone-N on a glass fibre. A modified Siemens P4-Diffractometer was used for data collection (graphite monochromator, Mo-K_α radiation, λ = 0.71073 Å, scan rate 4−30°min^{-1} in ω). The structures were solved by using direct methods and refined with full-matrix least-squares against F^2 {Siemens SHELX-97}.[26] A weighting scheme was applied in the last steps of the refinement with $w = 1/[\sigma^2(F_o^2) + (aP)^2 + bP]$ and $P = [2F_c^2 + \max(F_o^2,0)]/3$. Hydrogen atoms were included in their calculated positions and refined in a riding model.

In the asymmetric unit of **6**·H_2O one molecule of dichloromethane was found and refined. The hydrogen atom of the coordinated water molecule bridging to O(4) of the acetato ligand was found. Restraints had to be applied to refine the water hydrogen atoms. About 100 different crystallisation experiments were necessary to obtain crystals of **8**. Finally a mixture of 1,2-dichloroethane with traces of methanol and H_2O (400:2:1, v/v/v) was successful. Using this mixture ten out of ten crystallisation experiments yielded suitable crystals of **8** for X-ray structure determination. **8** crystallised with one molecule of water and methanol each, and half a molecule of 1,2-dichloroethane. Restraints were used in the refinement of the 1,2-dichloroethane. The water molecule forms hydrogen bonds to the methanol and the 2-oxo O(5) atom of other asymmetric units. There is also a hydrogen bond between the methanol and a bdmpza O(1) atom of another asymmetric unit. All details and parameters

 © 2004 Wiley-VCH Verlag GmbH & Co. KGaA, Weinheim

Table 3. Structure determination details of compounds **6**·H_2O and **8**

	6·H_2O	**8**
Empirical formula	$C_{32}H_{35}N_4O_5PRu \times CH_2Cl_2$	$C_{38}H_{35}N_4O_5PRu \times {}^1/_2C_2H_4Cl_2 \times H_2O \times H_3COH$
Formula mass	772.61	859.27
Crystal colour/habit	orange block	violet block
Crystal system	triclinic	triclinic
Space group	$P\bar{1}$	$P\bar{1}$
a (Å)	10.877(6)	11.814(10)
b (Å)	12.253(6)	12.659(10)
c (Å)	15.085(7)	14.785(14)
α (°)	92.67(2)	91.95(6)
β (°)	108.52(3)	99.54(6)
γ (°)	113.55(3)	114.35(4)
V (Å^3)	1712.5(15)	1974(3)
θ (°)	2.11−26.00	2.14−27.00
h	−1 to 12	−14 to 14
k	−13 to 13	−16 to 14
l	−18 to 18	−18 to 18
F(000)	792	886
Z	2	2
μ(Mo-K_α) (mm^{-1})	0.707	0.559
Crystal size (mm)	0.25 × 0.2 × 0.1	0.6 × 0.5 × 0.4
$D_{calcd.}$ (gcm^{-3})	1.498	1.446
T (K)	188(2)	188(2)
Reflections collected	7680	9979
Independent reflections	6569	8513
Observed reflections [>2σ(I)]	5298	6977
Parameters	421	505
Weight parameter a	0.0532	0.0571
Weight parameter b	2.8749	1.5342
R_1 (obsd.)	0.0504	0.0431
R_1 (overall)	0.0679	0.0593
wR_2 (obsd.)	0.1159	0.1037
wR_2 (overall)	0.1257	0.1123
Diff. peak/hole (e/Å^3)	1.133/−1.190	0.946/−1.235

of the measurements are summarised in Table 3. The structure pictures were prepared with the program Diamond 2.1e.[27] CCDC-222723 (for **6**·H_2O) and -222724 (for **8**) contain the supplementary crystallographic data for this paper. These data can be obtained free of charge at www.ccdc.cam.ac.uk/conts/retrieving.html or from the Cambridge Crystallographic Data Centre, 12 Union Road, Cambridge CB2 1EZ, UK [Fax: (internat.) +44-1223-336-033; E-mail: deposit@ccdc.cam.ac.uk].

Acknowledgments

Generous financial support by the Fonds der Chemischen Industrie (Liebig-Stipendium granted to N. B.) and the European Commission (Copernicus 2 Program, Contract no° ICA2-CT-2000-10002) is gratefully acknowledged. Special thanks to Prof. Dr. H. Fischer for support and discussion. We are indebted to Mr Galetskiy for recording mass spectra, Ms Friemel for 2D NMR experiments and Mr. Haunz for ^{31}P NMR experiments. We acknowledge a generous gift of ruthenium(III) trichloride hydrate by the Degussa AG.

[1] [1a] E. L. Hegg, L. Que Jr., *Eur. J. Biochem.* **1997**, *250*, 625−629. [1b] S. J. Lange, L. Que Jr., *Curr. Opin. Chem. Biol.* **1998**, *2*, 159−172. [1c] L. Que Jr., *Nat. Struct. Biol.* **2000**, *7*, 182−184. [1d] E. I. Solomon, T. C. Brunold, M. I. Davis, J. N. Kemsley, S.-K. Lee, N. Lehnert, F. Neese, A. J. Skulan, Y.-S. Yang, J. Zhou, *Chem. Rev.* **2000**, *100*, 235−349. [1e] M. J. Ryle, R. P. Hausinger, *Curr. Opin. Chem. Biol.* **2002**, *6*, 193−201.

[2] [2a] P. L. Roach, I. J. Clifton, V. Fülöp, K. Harlos, G. J. Barton, J. Hajdu, I. Andersson, C. J. Schofield, J. E. Baldwin, *Nature* **1995**, *375*, 700−704. [2b] P. L. Roach, I. J. Clifton, C. M. H. Hensgens, N. Shibata, C. J. Schofield, J. Hajdu, J. E. Baldwin, *Nature* **1997**, *387*, 827−830.

[3] [3a] K. Valegård, A. C. Terwisscha van Scheltinga, M. D. Lloyd, T. Hara, S. Ramaswamy, A. Perrakis, A. Thompson, H.-J. Lee, J. E. Baldwin, C. J. Schofield, J. Hajdu, I. Andersson, *Nature* **1998**, *394*, 805−809. [3b] H.-J. Lee, M. D. Lloyd, K. Harlos, I. J. Clifton, J. E. Baldwin, C. J. Schofield, *J. Mol. Biol.* **2001**, *308*, 937−948.

[4] Z. Zhang, J. Ren, D. K. Stammers, J. E. Baldwin, K. Harlos, C. J. Schofield, *Nat. Struct. Biol.* **2000**, *7*, 127−133.

[5] I. J. Clifton, L.-C. Hsueh, J. E. Baldwin, K. Harlos, C. J. Schofield, *Eur. J. Biochem.* **2001**, *268*, 6625−6636.

[6] [6a] J. M. Elkins, M. J. Ryle, I. J. Clifton, J. C. Dunning Hotopp, J. S. Lloyd, N. I. Burzlaff, J. E. Baldwin, R. P. Hausinger, P. L. Roach, *Biochemistry* **2002**, *41*, 5185−5192. [6b] J. R. O'Brien, D. J. Schuller, V. S. Yang, B. D. Dillard, W. N. Lanzilotta, *Biochemistry* **2003**, *42*, 5547−5554.

[7] R. C. Wilmouth, J. J. Turnbull, R. W. D. Welford, I. J. Clifton, A. G. Prescott, C. J. Schofield, *Structure* **2002**, *10*, 93−103.

[8] [8a] N. I. Burzlaff, P. J. Rutledge, I. J. Clifton, C. M. H. Hensgens, M. Pickford, R. M. Adlington, P. L. Roach, J. E. Baldwin, *Nature* **1999**, *401*, 721−724. [8b] J. M. Ogle, I. J. Clifton, P. J. Rutledge, J. M. Elkins, N. I. Burzlaff, R. M. Adlington, P. L. Roach, J. E. Baldwin, *Chem. Biol.* **2001**, *8*, 1231−1237. [8c] J. M. Elkins, P. J. Rutledge, N. I. Burzlaff, I. J. Clifton, R. M. Adlington, P. L. Roach, J. E. Baldwin, *Org. Biomol. Chem.* **2003**, *1*, 1455−1460.

[9] [9a] N. Kitajima, H. Fukui, Y. Moro-oka, Y. Mizutani, T. Kitagawa, *J. Am. Chem. Soc.* **1990**, *112*, 6402−6403. [9b] I. B. Gorell, G. Parkin, *Inorg. Chem.* **1990**, *29*, 2452−2456. [9c] N. Kitajima, N. Tamura, H. Amagai, H. Fukui, Y. Moro-oka, Y. Mizutani, T. Kitagawa, R. Mathur, K. Heerwegh, C. A. Reed, C. R. Randall, L. Que Jr., K. Tatsumi, *J. Am. Chem. Soc.* **1994**, *116*, 9071−9085. [9d] C. R. Randall, L. Shu, Y.-M. Chiou, S. Hagen, M. Ito, N. Kitajima, R. J. Lachicotte, Y. Zang, L. Que Jr., *Inorg. Chem.* **1995**, *34*, 1036−1039. [9e] M. Ito, H. Amagai, H. Fukui, N. Kitajima, Y. Moro-oka, *Bull. Chem. Soc. Jpn.* **1996**, *69*, 1937−1945. [9f] T. Ogihara, S. Hikichi, M. Akita, T. Uchida, T. Kitagawa, Y. Moro-oka, *Inorg. Chim. Acta* **2000**, *297*, 162−170.

[10] [10a] Y. Zang, L. Que Jr., *Inorg. Chem.* **1995**, *34*, 1030−1035. [10b] S. K. Mandal, L. Que Jr., *Inorg. Chem.* **1997**, *36*, 5424−5425. [10c] R. Y. N. Ho, M. P. Mehn, E. L. Hegg, A. Liu, M. J. Ryle, R. P. Hausinger, L. Que Jr., *J. Am. Chem. Soc.* **2001**, *123*, 5022−5029.

[11] [11a] E. H. Ha, R. Y. N. Ho, J. F. Kisiel, J. S. Valentine, *Inorg. Chem.* **1995**, *34*, 2265−2266. [11b] S. Hikichi, T. Ogihara, K. Fujisawa, N. Kitajima, M. Akita, Y. Moro-oka, *Inorg. Chem.* **1997**, *36*, 4539−4547. [11c] E. L. Hegg, R. Y. N. Ho, L. Que Jr., *J. Am. Chem. Soc.* **1999**, *121*, 1972−1973. [11d] M.-P. Mehn, K. Fujisawa, E. L. Hegg, L. Que Jr., *J. Am. Chem. Soc.* **2003**, *125*, 7828−7842.

[12] [12a] Y.-M. Chiou, L. Que Jr., *J. Am. Chem. Soc.* **1992**, *114*, 7567−7568. [12b] Y.-M. Chiou, L. Que Jr., *Inorg. Chem.* **1995**, *34*, 3270−3278. [12c] Y.-M. Chiou, L. Que Jr., *J. Am. Chem. Soc.* **1995**, *117*, 3999−4013.

[13] A. Beck, B. Weibert, N. Burzlaff, *Eur. J. Inorg. Chem.* **2001**, 521−527.

[14] A. Beck, A. Barth, E. Hübner, N. Burzlaff, *Inorg. Chem.* **2003**, *42*, 7182−7188.

[15] [15a] Y. Takahashi, S. Hikichi, M. Akita, Y. Moro-oka, *Chem. Commun.* **1999**, 1491−1492. [15b] M. Akita, Y. Takahashi, S. Hikichi, Y. Moro-oka, *Inorg. Chem.* **2001**, *40*, 169−172. [15c]

 © 2004 Wiley-VCH Verlag GmbH & Co. KGaA, Weinheim

M. H. V. Huynh, L. M. Witham, J. M. Lasker, M. Wetzler, B. Mort, D. L. Jameson, P. S. White, K. J. Takeuchi, *J. Am. Chem. Soc.* **2003**, *125*, 308−309.
[16] A. López-Hernández, R. Müller, H. Kopf, N. Burzlaff, *Eur. J. Inorg. Chem.* **2002**, 671−677.
[17] [17a] I. Hegelmann, N. Burzlaff, *Eur. J. Inorg. Chem.* **2003**, 409−411. [17b] L. Peters, N. Burzlaff, *Polyhedron* **2004**, *23*, 245−251.
[18] [18a] M. S. K. Niazi, *Bull. Chem. Soc. Jpn.* **1989**, *62*, 1253−1257. [18b] M. B. Fleury, J. C. Dufresne, *Bull. Soc. Chim. Fr.* **1972**, 844−850. [18c] K. V. Kŭnchev, Y. I. Tur'yan, Kh. A. Dinkov, *Russ. J. Gen. Chem.* **1992**, *62*, 311−315. [18d] K. J. Pedersen, *Acta Chem. Scand.* **1952**, *6*, 243−256. [18e] N. Kawabata, I. Higuchi, J.-I. Yoshida, *Bull. Chem. Soc. Jpn.* **1981**, *54*, 3253−3258.
[19] M. S. Sandford, M. R. Valdez, R. H. Grubbs, *Organometallics* **2001**, *20*, 5455−5463.
[20] V. F. Kuznetsov, G. P. A. Yap, H. Alper, *Organometallics* **2001**, *20*, 1300−1309.
[21] E. G. Pavel, J. Zhou, R. W. Busby, M. Gunsior, C. A. Townsend, E. I. Solomon, *J. Am. Chem. Soc.* **1998**, *120*, 743−753.
[22] R. Hoffman, *J. Chem. Phys.* **1963**, *39*, 1397−1412.
[23] R. Hoffmann, R. Stowasser, *J. Am. Chem. Soc.* **1999**, *121*, 3414−3420.
[24] Jaguar 5.0, Schrödinger, LLC, Portland, Oregon, **2002**.
[25] HyperChem(TM), Hypercube, Inc., 1115 NW 4th Street, Gainesville, Florida 32601, USA.
[26] G. M. Sheldrick, SHELX-97, Programs for Crystal Structure Analysis, University of Göttingen, Göttingen (Germany), **1997**.
[27] K. Brandenburg, M. Berndt, Diamond − Visual Crystal Structure Information System, Crystal Impact GbR, Bonn (Germany), **1999**; for Software Review see: W. T. Pennington, *J. Appl. Crystallogr.* **1999**, *32*, 1028−1029.

Received November 5, 2003
Early View Article
Published Online April 1, 2004

 © 2004 Wiley-VCH Verlag GmbH & Co. KGaA, Weinheim

Bis(phosphane oxide) Adducts of $Rh_2(MTPA)_4$ — Kinetics and Chirality Discrimination

Tamás Gáti,[a] András Simon,[a] Gábor Tóth,*[a] Anna Szmigielska,[b] Anna M. Maj,[b] K. Michał Pietrusiewicz,[b,c] Stefan Moeller,[d] Damian Magiera,[d] and Helmut Duddeck*[d]

Dedicated to the memory of Prof. Dr. Dr.h.c.(H) Günther Snatzke (1928−1992)[‡]

Keywords: Rhodium / Phosphane ligands / NMR spectroscopy / Complexation modes / Chiral discrimination

The symmetrical bis(phosphane oxide) **1** and its chiral derivatives **2** and **3** form a variety of adduct species with the dirhodium complex **[Rh–Rh]** which can be identified by low-temperature ^1H and ^{31}P NMR spectroscopy by using varying **[Rh–Rh]**:ligand ratios. The asymmetric bis(phosphane oxide) **3** shows a distinct preference for binding through the Ph_2P=O (P^a) as compared to the *t*Bu(Ph)P=O (P^b) functionality due to the bulky *tert*-butyl group. The chiral bis(phosphane oxides) **2** and **3** form complex mixtures of various adduct species. Nevertheless, it is possible to monitor enantiomeric compositions from various NMR signal duplications at 213 K and even at room temperature or slightly elevated temperatures.

(© Wiley-VCH Verlag GmbH & Co. KGaA, 69451 Weinheim, Germany, 2004)

Introduction

Dirhodium complexes as well as their phosphane adducts have been the focus of interest for many years.[1] They were first introduced as homogeneous catalysts in various reactions[2] and have even found medicinal applications.[3] We have shown that the enantiomers of chiral phosphane chalcogenides can easily be discriminated by adding an equimolar amount of the dirhodium complex $[Rh^{II}_2\{(R)\text{-}(+)\text{-MTPA}\}_4]$ (**[Rh−Rh]**, MTPA-H = methoxytrifluoromethylphenylacetic acid ≡ Mosher's acid; see Scheme 1) to their $CDCl_3$ solution and monitoring the diastereomeric dispersion Δν of their ^1H or ^{31}P NMR signals at room temperature ("dirhodium method" of chirality recognition).[4] However, we noticed that coalescence effects may broaden the NMR signals even at room temperature and that phosphane oxides seemed to have a different ligand behaviour from their sulfide and selenide analogues.[4c] Moreover, when we attempted to study some chiral bis(phosphane oxides) (Scheme 1) by variable-temperature NMR spectroscopy we found signals of complicated mixtures of free and ligated species.

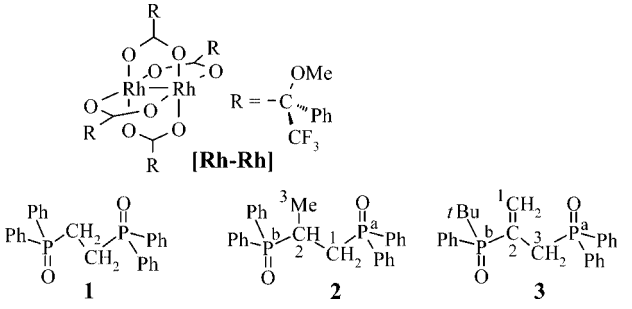

Scheme 1. Structures of the dirhodium complex and the phosphanyl chalcogenides studied

Recently, Deubel has communicated a theoretical study based on density-functional theory (DFT) calculations of donor-acceptor interactions contributing to the binding energy in the adducts of dirhodium(II) tetraformate and a representative choice of strong and weak ligands (e.g., methylene carbene vs. benzene).[5] As a result, attractive contri-

[a] Institute for General and Analytical Chemistry of the Budapest University of Technology and Economics,
Szent Gellért tér 4, 1111 Budapest, Hungary
Fax: (internat.) +36-1-463-3408
E-Mail: g-toth@tki.aak.bme.hu
[b] Maria Curie-Sklodowska University, Department of Organic Chemistry,
Lublin, Poland
Fax: (internat.) +48-81-524-2251
E-Mail: michal@hermes.umcs.lublin.pl
[c] Polish Academy of Sciences, Institute of Organic Chemistry,
ul. Kasprzaka 44/52, 01-224 Warsaw, Poland
Fax: (internat.) +48-22-632 6681
E-Mail: kmp@icho.edu.pl
[d] Hannover University, Institute of Organic Chemistry,
Schneiderberg 1B, 30167 Hannover, Germany
Fax: (internat.) +49-511-762-4616
E-mail: duddeck@mbox.oci.uni-hannover.de
[‡] On the occasion of what would have been his 75th birthday

 © 2004 Wiley-VCH Verlag GmbH & Co. KGaA, Weinheim **DOI: 10.1002/ejic.200300853**

butions were shown to be a blend of electrostatic and HOMO−LUMO interactions, the former always dominating.[5] In a comparative study of the ligand properties of the triphenylphosphane chalcogenides $Ph_3P{=}X$ (X = Se, S, and O), and of methyldiphenylphosphane oxide, $Ph_2(CH_3)P{=}O$, we have recently found that, in contrast to phosphane selenides and sulfides, phosphane oxides bind primarily by an electrostatic attraction, and orbital interactions can be neglected.[6] Moreover, this binding energy is strongly sensitive to steric crowding around the P=O group.[6] For $Ph_3P{=}O$, the binding constant *K* is only about 1 (weak donor). In contrast, *K* is larger than 100 for $Ph_2(CH_3)P{=}O$ (strong donor); no free ligand molecules can be detected in the presence of an excess of rhodium sites in the latter case, for example in an equimolar mixture of **[Rh−Rh]** and $Ph_2(CH_3)P{=}O$.[6] Since bis(phosphane oxides) are considered to be useful ligands in homogeneous catalysis, we extended this work to the bis(phosphane oxides) **1**−**3** in order to explore how bifunctional phosphane oxide ligands behave under "dirhodium method" experimental conditions and whether or not chirality recognition is still possible. In addition, we wanted to see whether there is a binding competition between the two P=O groups in each of the asymmetric compounds **2** and **3**.

Table 1. ^1H, ^{13}C and ^{31}P NMR chemical shifts as well as $^{31}P,^1H$ and $^{31}P,^{13}C$ coupling constants (*J* in Hz) of the free ligands **1**−**3**, recorded at room temperature[a]

			^1H	^{13}C	^{31}P	$^nJ(^{31}P,^1H)$	$^nJ(^{31}P,^{13}C)$
1		CH_2	2.52	21.6	33.8	n.d.[b]	
		ipso	−	131.9		−	
		ortho	7.70	130.7			
		meta	7.45	128.7		n.d.	
		para	7.51	132.0		n.d.	
2[c]		CH_3	1.20	13.6	P^a: 32.5	^3J = 16.9	^2J = 3.2
						$^4J \approx 0$	^3J = 0.9
		$>CH_2$: H^a	2.48	28.8	P^b: 39.0	n.d.	^1J = 69.2
							^2J = 1.7
		$>CH_2$: H^b	2.56			n.d.	
		CH	2.99	26.9		n.d.	^1J = 70.5
							^2J = 4.0
	P^a	*ipso*	−	131.1/131.0		n.d.	$^1J \approx$ 97/96
		ortho	7.68−7.76	131.1/131.0		n.d.	^2J = 9.6/9.6
		meta	7.37−7.47	129.3/129.2		n.d.	^3J = 11.3/11.7
		para	7.47−7.58	131.9/131.8		n.d.	^4J = 2.8/2.8
	P^b	*ipso*	−	133.4/132.6		n.d.	^1J = 98.3/99.5
		ortho	7.68−7.76	131.5/131.5		n.d.	^2J = 8.6/8.9
		meta	7.37−7.47	129.1/129.1		n.d.	^3J = 11.9/11.4
		para	7.47−7.58	131.9/131.9		n.d.	^4J = 3.1/3.1
3[c]		C-2	−	132.9	P^a: 32.7	−	^1J = 80.6
							^2J = 7.8
		C(*t*Bu)	−	34.0	P^b: 42.9	−	^1J = 69.2
		$>CH_2$: H^a	3.40			^2J = 15.5	
				31.0		^3J = 8.5	^1J = 66.7
							^2J = 7.5
		$>CH_2$: H^b	3.57			^2J = 12.5	
						^3J = 8.5	
		$=CH_2$:[d] H^a	6.80			^3J = 39.8	
				132.3		^4J = 1.6	$^2J \approx$ 7.5
							$^3J \approx$ 7.5
		$=CH_2$:[d] H^b	6.04			^3J = 17.2	
						$^4J \approx 0$	
		CH_3	1.16	25.2		^3J = 14.9	$^2J \approx 0$
	P^a	*ipso*	−	132.6/131.8		−	^1J = 100.3/101.6
		ortho	7.72/7.83	131.0/130.9		^3J = 11.7/ 11.6	^2J = 8.3/8.0
		meta	7.29/7.46	128.3/128.6		n.d./n.d.	^3J = 12.1/11.9
		para	7.35/7.50	131.5/131.8		n.d./n.d.	^4J = 2.7/2.9
	P^b	*ipso*	−	129.2		−	^1J = 89.1
		ortho	7.62	131.9		^3J = 9.5	^2J = 8.2
		meta	7.37	128.1		n.d.	^3J = 10.9
		para	7.46	131.6		n.d.	^4J = 2.9

[a] For both P atoms of **2** and for P^a of **3** two entries exist for each aromatic ^1H and ^{13}C nucleus because the phenyl groups are diastereotopic. The first entry belongs to one phenyl group and the second entry to the other; a stereochemical differentiation is not possible. [b] n.d.: not detectable. [c] Compound **2**: $^3J(^{31}P^a,^{31}P^b)$ = 49.4 Hz; compound **3**: $^3J(^{31}P^a,^{31}P^b)$ = 18.2 Hz. [d] The protons of the methylene group (=CH_2) can be differentiated because of their $^3J(^{31}P,^1H)$-values to P^b: H^a is *trans* to P^b (^3J = 39.8 Hz), and H^b is *cis* (^3J = 17.2 Hz).

 © 2004 Wiley-VCH Verlag GmbH & Co. KGaA, Weinheim

Results and Discussion

NMR Signal Assignment

The assignment of the NMR signals of the free ligands **1**−**3** (cf. Scheme 1) was straightforward in most cases when routine NMR methods such as DEPT, HMQC, HMBC and NOE techniques were applied. Thereby, all ^{1}H, ^{13}C and ^{31}P NMR signals could be identified; the unequivocal assignment of the ^{31}P signals of the two heterotopic phosphorus sites in **2** and **3** was achieved by $\{^{31}P\}$ ^{1}H-detected HMBC experiments correlating P^{b} with the methyl or the *tert*-butyl protons, respectively. In the case of **[Rh−Rh]** adducts the identification of the ligand signals was occasionally hampered by overlapping Mosher acid signals, particularly when aromatic signals were involved. All NMR signals of the free ligands **1**−**3**, as well their complexation shifts Δδ (in ppm), for 1:1 adducts at room temperature are collected in Table 1 and 2.

Table 2. Complexation shifts in **1**−**3** in 1:1 adducts (in ppm); recorded at room temperature[a]

			Δδ(^{1}H)	Δδ(^{13}C)	Δδ(^{31}P)
1		CH_2	+0.29	[b]	+3.9
		ipso	−		
		ortho	+0.13		
		meta	−0.20		
		para	−0.10		
2		CH_3	+0.26	−0.5/−0.6[c]	
		$>CH_2$: H^a	+0.29	+0.2/+0.1[c]	
		$>CH_2$: H^b	+0.32		
		CH	+0.45	+0.1/−0.1[c]	
	P^a	*ipso*	−/−	n.d./n.d.	+5.6
		ortho	+0.17/+0.25	−0.1/+0.1	
		meta	−0.28/−0.24	−0.8/−0.7	
		para	n.d./−0.14	n.d./−0.3	
	P^b	*ipso*	−/−	n.d./n.d.	+4.6
		ortho	−0.04 /+0.08	−0.5/−0.5	
		meta	−0.26/−0.31	−0.6/−0.6	
		para	n.d./−0.17	n.d./−0.2	
3		C-2	−	0.0	
		C(*t*Bu)	−	+0.4/+0.3[c]	
		$>CH_2$: H^a	+0.24	−0.5	
		$>CH_2$: H^b	+0.46		
		$=CH_2$: H^a	+0.40	+2.1	
		$=CH_2$: H^b	−0.10		
		CH_3	+0.03	0.0/−0.1[c]	
	P^a	*ipso*	−/−	n.d./n.d.	+4.4
		ortho	+0.16/+0.08	+0.5/+0.4	
		meta	−0.30/−0.32	−0.2/−0.7	
		para	−0.17/−0.20	−0.4/−0.2	
	P^b	*ipso*	−	n.d.	+3.1
		ortho	+0.11	+0.4	
		meta	−0.18	+0.3	
		para	−0.09	−0.2	

[a] For both P atoms of **2** and for P^a of **3** two entries exist for each aromatic ^{1}H and ^{13}C nucleus because the phenyl groups are diastereotopic. The first entry belongs to one phenyl group and the second entry to the other; a stereochemical differentiation is not possible. [b] No ^{13}C NMR spectroscopic data were recorded for the **[Rh−Rh]-1** mixture because precipitation of solid material from the solution occurred after a few hours. [c] Signal duplication due to dispersion effects (see text).

Identification of the Various Adduct Species

1,2-Bis(diphenylphosphinoyl)ethane (**1**) contains two chemically equivalent P=O residues; each is connected to two phenyl rings and to the ethylene chain. Thus, one can expect that its complexing properties are similar to those of triphenylphosphane oxide and methyldiphenylphosphane oxide.[6]

The low-temperature (213 K) ^{31}P NMR spectra of **1** at various molar ratios (Figure 1) allow the identification of the adduct species involved (Scheme 2). Spectrum **a** (0.5:1) was recorded for a solution with an excess of rhodium sites, spectrum **b** (1:1) for a solution with equimolar amounts of both **[Rh−Rh]** and **1**, and spectra **c** and **d** with an excess of P=O sites. The ratios were chosen in such a way that the molar amount of **1** relative to that of **[Rh−Rh]** is doubled when going from one spectrum to the next (**a** to **b**, **b** to **c**, and **c** to **d**) so that the P=O content increases strongly from bottom to top.

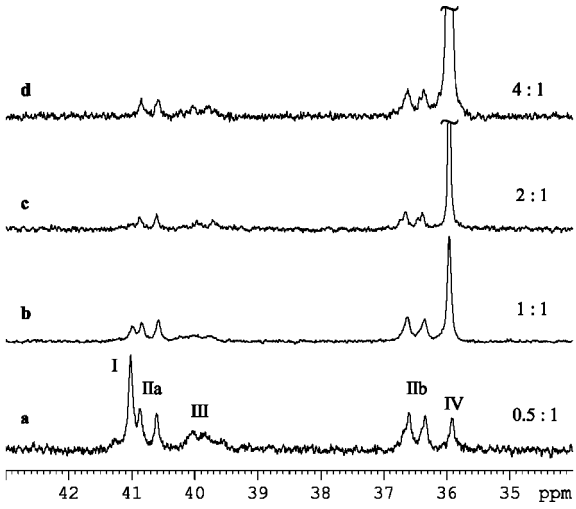

Figure 1. ^{31}P NMR spectra of **1** and **[Rh−Rh]**, recorded at 213 K; molar ratios are (a) 0.5:1, (b) 1:1, (c) 2:1 and (d) 4:1

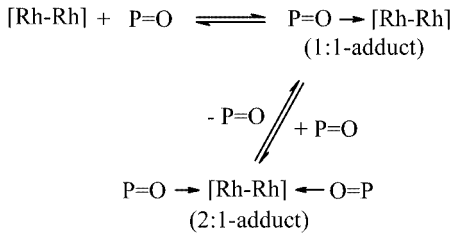

Scheme 2. Equilibria between free components and the adducts[a]
[a] "P=O" symbolizes phosphane oxide groups

By comparing the ^{31}P NMR signals and their relative intensities in Figure 1, the following assignments can be deduced. There are two different signal groupings: one at δ = 39.5−41.5 ppm for ligated P=O sites (Rh···O=P) and another at δ = 36−37 ppm for free P=O sites. The free ligand of **1** corresponds to the signal at δ = 36.1 ppm (**IV**; Scheme 3) as proven by its strong intensity increase upon further addition of **1** (spectra **b**, **c** and **d**). The signal at δ =

 © 2004 Wiley-VCH Verlag GmbH & Co. KGaA, Weinheim

41.2 ppm (singlet) belongs to a doubly complexed ligand molecule which is in a symmetrical environment and therefore does not show the typical doublet splitting due to the $^{31}P,^{31}P$ coupling in unsymmetric bis(phosphane oxides) or analogous adducts. Thus, this species is of type **I** (Scheme 3). The intensity of this peak is rather large in spectrum **a** (Rh site excess), low in spectrum **b** (1:1), and the signal vanishes totally in spectra **c** and **d** with their increasing P=O site excess.

I: Rh—Rh ← O=P-CH_2-CH_2-P=O → Rh—Rh

II: Rh—Rh ← O=P^a-CH_2-CH_2-P^b=O

III: ···CH_2-P=O → Rh—Rh ← O=P-CH_2-CH_2-P=O → Rh—Rh ← O=P-CH_2···

IV: O=P-CH_2-CH_2-P=O (free ligand)

Scheme 3. Adduct species of **1** and **[Rh−Rh]** identified by low-temperature ^{31}P NMR spectroscopy (see text and Figure 1); the Mosher acid residues in **[Rh−Rh]** and the phenyls at the phosphoryl groups have been omitted for clarity

The two doublets at δ = 40.7 and 36.5 ppm correspond to an unsymmetrically ligated molecule of type **II** (Scheme 3). The former doublet (signal **IIa**) is from the complexed end of **1** (P^a=O) and the latter (signal **IIb**) from the free one (P^b=O). The signal splitting is the vicinal $^3J_{^{31}P,^{31}P}$ coupling constant (53.5 Hz). Finally, there is a broad hump at δ = 39.7−40.5 ppm corresponding to Rh···O=P situations of type **III**; apparently, these are the ^{31}P NMR resonances of doubly complexed ligand molecules incorporated in oligomeric structures (Scheme 3).

This interpretation is supported by the ^1H NMR signals of the methoxy group of the Mosher acid residues of **[Rh−Rh]** at low-temperature, as displayed in Figure 2, taken from the same samples as used for Figure 1. Signal **A** (δ = 3.14 ppm) representing the free **[Rh−Rh]** complexes without any ligating **1** has an intensity of about 40% in the solution at 0.5:1 molar ratio, falling to about 25% at P=O site excess. The majority of dirhodium moieties (ca. 50%), however, are in the 1:1 adduct situation represented by signal **B** (δ = 3.03 ppm). There is hardly any change in the proportion of this adduct with increasing amounts of **1**. Finally, signal **C** (δ = 2.93 ppm) can be attributed primarily to a Mosher methoxy signal in the 2:1 adduct situation; its proportion varies from about 10% at a 0.5:1 ratio to about 20% at a 4:1 ratio. This proportion of the 2:1 adducts is surprisingly low, especially with high P=O site excess, and is a consequence of the low donor properties of **1** and the severe steric congestion around the P=O group, similar to Ph_3P=O.[6] Additionally, this small amount of 2:1 adducts may be associated with the observation that some insoluble material precipitated from the $CDCl_3$ solution after several hours. We suspect that this material is a copolymer of type **III** (Scheme 3).

It should be noted that the temperature dependence of the ^1H NMR spectrum proves that a small part of signal **C** in spectrum **a** belongs to the CH_2 signal, which is averaged

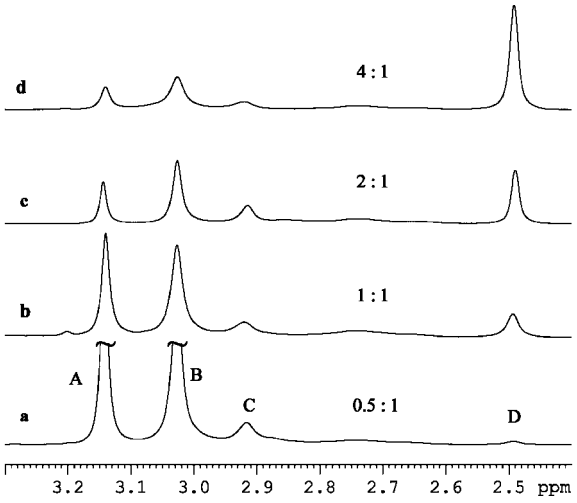

Figure 2. Sections of the ^1H NMR spectra of **1** and **[Rh−Rh]**, recorded at 213 K; molar ratios (a) 0.5:1, (b) 1:1, (c) 2:1 and (d) 4:1

at room temperature (δ = 2.77 ppm) but splits into two (δ = 2.93 and 2.52 ppm) at 213 K. The former part (δ = 2.93 ppm) belongs to Rh···O=P−CH_2 situations and the latter one (δ = 2.52 ppm) to free O=P−CH_2 groups (signal **D**); the relative proportion of signal **D** is strongly increased upon addition of larger amounts of **1** when going from spectrum **a** to spectrum **d** in Figure 2. The exchange barrier of the adduct formation can be estimated easily from the temperature dependence of the CH_2 and the methoxy protons ($\Delta G_c^{\ddagger}$ = 51.3 ± 1 kJ/mol). This value is somewhat higher than those of the monophosphane chalcogenides ($\Delta G_c^{\ddagger}$ = 46.4−48.0 ± 1 kJ/mol).[6]

All these spectra lead to the conclusion that the phosphane oxide group of **1** is only a weak donor; even under Rh site excess there is a substantial proportion of free P=O sites (P^b=O in **II** and **IV**; Scheme 3). Thus, the steric congestion in **1** must be higher than in $Me(Ph_2)P$=O and more similar to that of Ph_3P=O.[6] The majority of the molecules of **1** form adducts **II** and, eventually, oligomers **III** with their composition depending on the P=O site excess: oligomers become more and more dominant the higher the P=O content becomes.

In contrast to **1**, 1,2-bis(diphenylphosphinoyl)propane (**2**) is a *C*-chiral compound derived from **1** by formal methylation of one methylene carbon (cf. Scheme 1). Here, the two Ph_2P=O groups are heterotopic, and separate NMR signals are observable for each of them. In order to distinguish the two phosphoryl groups we use the superscript "a" for that Ph_2P=O group which is attached to CH_2 (C-1) and thereby structurally closest to **1**. The same procedure was applied to differentiate the two P=O groups in **3** (see below). The method of assigning the two phosphorus atoms to the two ^{31}P signals has already been described above.

The room-temperature ^{31}P NMR signals of **2** in the presence of **[Rh−Rh]** are broad humps showing averaged peaks. As can be seen in Figure 3, however, the low-temperature spectra (213 K) display a number of signals indicating the existence of several species, the concentrations of which de-

 © 2004 Wiley-VCH Verlag GmbH & Co. KGaA, Weinheim

pend on the molar ratio of the components **2** and **[Rh−Rh]**. The ratio producing the lower spectrum was 2:1 — it was recorded under P=O site excess — whereas that in the top spectrum was 0.5:1 — Rh site excess. It should be noted that further spectra were taken from samples with 1:1 and 4:1 molar ratios. These are not displayed in Figure 3 but support the following conclusions.

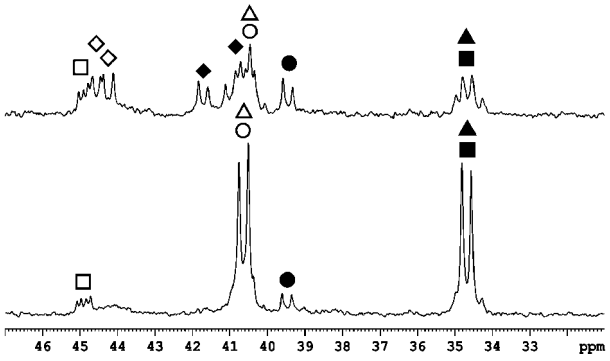

Figure 3. ^{31}P NMR spectra of **2** in the presence of various amounts of **[Rh−Rh]**, recorded at 213 K; top, molar ratio **2**:**[Rh−Rh]** 0.5:1, bottom 2:1; see Scheme 4 for the meaning of the symbols

The different ratio conditions enabled us to assign the peaks. Moreover, we recorded a ^{31}P,^{31}P COSY spectrum (not depicted) correlating the two heterotopic ^{31}P nuclei within each species. For sake of clarity we used the following icons for the ^{31}P signal assignment (Scheme 4): ▲/Δ for the free ligand OP^a∼P^{b}O, ●/○ for the adduct Rh···OP^a∼P^{b}O, ■/□ for the adduct OP^a∼P^{b}O···Rh and ◆/◇ for the adduct Rh···OP^a∼P^{b}O···Rh; filled icons refer to P^a and open ones to P^b (see also Scheme 4; "∼" depicts the carbon chain between the phosphorus atoms).

▲	OP^a ∼ P^{b}O	△
●	Rh → OP^a ∼ P^{b}O	○
■	OP^a ∼ P^{b}O ← Rh	□
◆	Rh → OP^a ∼ P^{b}O ← Rh	◇

Scheme 4. Assignment of the symbols to the phosphorus atoms in the Rh*-ligand species; filled icons refer to P^a and open ones to P^b, "∼" represents the carbon chain between the phosphorus atoms

It is obvious that the two doublet signals of the free ligand **2** (▲/Δ) are the largest ones in the bottom spectrum due to an excess of **2**. On the other hand, four small signals appear in the top spectrum that are not visible in the bottom spectrum; they were assigned to ″symmetrical″ adduct species (◆/◇). The fact that each of them appears twice can be attributed to the existence of two diastereomeric adducts (*R*)-**[Rh−Rh]**···[(*R*)-OP^a∼P^{b}O]···(*R*)-**[Rh−Rh]** and (*R*)-**[Rh−Rh]**···[(*S*)-OP^a∼P^{b}O]···(*R*)-**[Rh−Rh]**, an example of chirality recognition (**2** exists as a racemate). The signals of the "unsymmetrical" species (●/○ and ■/□) are visible in both spectra. Taking the relative intensities (●/○ vs. ■/□) into account and the fact that the signals of the free ligand **2** (▲/Δ) still exist under excess Rh site conditions, one can state that, like in **1**, both phosphoryl groups, P^a=O as well as P^b=O, of bis(phosphane oxide) **2** are weak donors, and that there is no significant selection between the two competing P=O groups.

This interpretation is supported by the low-temperature (213 K) ^{1}H NMR spectrum in the ligand methyl group region recorded under **2**:**[Rh−Rh]** = 0.5:1 molar ratio conditions (Rh site excess; Figure 4). It shows signals of the various species whereas at room temperature the averaged signal is a doublet of doublets due to the $^3J_{^1H,^1H}$ (7.0 Hz) and $^3J_{^{31}P,^1H}$ (16.8 Hz) couplings (not depicted). The assignment shown was proven unequivocally by a {^{31}P} ^{1}H-detected HMBC spectrum (not depicted) correlating the methyl protons with the P^b atoms in each species. The integration shows that only about 30% of all ligand molecules are complexed to rhodium on both sides (◇); the content of free ligand molecules (Δ) cannot be derived safely due to signal overlap but there is no doubt that a considerable amount of it exists. Moreover, the amount of the species with only one complexed phosphoryl (○ for Rh···OP^a∼P^{b}O and □ for OP^a∼P^{b}O···Rh) is roughly similar so that the complexation constants of both phosphoryl groups must be similar as well; the methyl group has, indeed, no significant directing effect for an adduct formation preference of P^a vs. P^b (or vice versa).

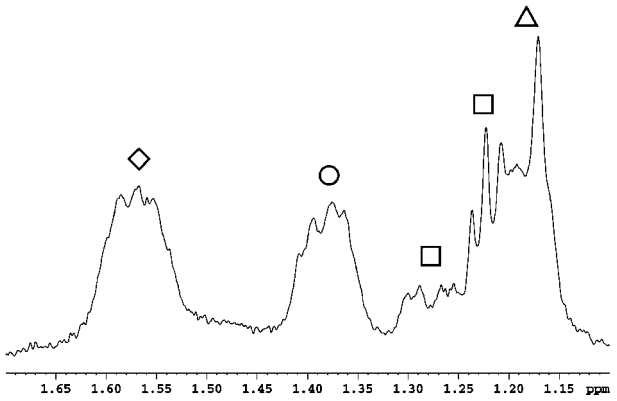

Figure 4. Methyl ^{1}H NMR signal of **2** in the presence of two molar equivalents of **[Rh−Rh]**, recorded at 213 K

Three factors make the ^{1}H NMR signals appear as broad multiplets instead of doublets of doublets: (a) the existence of different species regarding the 1:1 and 2:1 adduct situations of the Rh−Rh fragments, (b) high-order spin systems (ABX) because the methylene protons are diastereotopic, and (c) diastereomeric dispersion effects (compare the two signals marked by "□").

Whereas the bis(phosphane oxide) **2** has a chiral carbon center, 2-(*tert*-butylphenylphosphinoyl)-3-(diphenylphosphinoyl)propene (**3**) is *P*-chiral (P^b). In analogy to **2**, the two ^{31}P NMR signals of **3** were unambiguously assigned by a {^{31}P} ^{1}H-detected HMBC experiment at room temperature. Figure 5 shows the ^{31}P NMR spectra of **3** in the presence of three different molar equivalents of **[Rh−Rh]**, recorded at 213 K. The assignment of the various species was performed in analogy to those of **2** and is given in Figure 5 by icons similar to those used for **2** in Scheme 4. The signals

 © 2004 Wiley-VCH Verlag GmbH & Co. KGaA, Weinheim

of P^a appear at δ = 35−39 ppm (filled icons) and those of P^b at δ = 44−49.5 ppm (open icons).

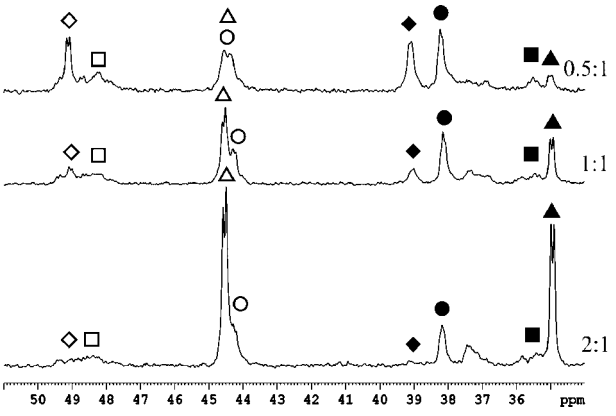

Figure 5. ^{31}P NMR spectrum of **3** in the presence of various amounts of **[Rh−Rh]**, recorded at 213 K; top: 0.5:1 molar ratio (**3**:**[Rh−Rh]**), middle: 1:1, bottom: 2:1; the icons used for the assignment of the various species of **3** have the same meaning as for **2** (see Scheme 4)

The basic difference in the complexing behaviour of the bis(phosphane oxides) **2** and **3** lies in the relative concentrations of the monoligated species Rh···OP^a∼P^bO (●/○) and OP^a∼P^bO···Rh (■/□). ^{31}P NMR signal integrations show that the ratio of the former relative to the latter is about 1.4 (**3**:**[Rh−Rh]** = 2:1, P=O site excess; Figure 5, bottom), about 1.7 (1:1; middle) and about 2.5 (0.5:1, Rh site excess; Figure 5, top). This clearly reflects the steric effects during complexation and reveals that the *tert*-butyl group at P^b creates a larger steric congestion during adduct formation and thereby repels approaching **[Rh−Rh]** molecules much more than the second phenyl group at P^a. Figure 6 shows the ^1H NMR signals of the *tert*-butyl group attached to P^b; some of these signals are multiplets for the same reasons as those described for the methyl protons of **2** (see above). The signal group at δ ≈ 1 ppm appears to be two overlapping doublets of the Rh···OP^a∼P^bO species, apparently another case of chirality recognition (see below).

The difference in adduct formation energies of the two P=O groups is also evident when comparing the intensities of the *tert*-butyl ^1H NMR signal (○ vs. □; Figure 6).

Chirality Recognition

Dispersion effects, Δν, due to the existence of diastereomeric adducts have been identified in some low-temperature ^1H NMR spectra (see previous section). They are difficult to detect at room temperature because most NMR signals are severely broadened by coalescence effects. However, some atoms in the aliphatic part of the two chiral bis(phosphane oxides) **2** and **3** offer the possibility of enantiomeric discrimination. In the case of the racemic **2**, the ^{13}C NMR signals are split: $\Delta\nu(CH_3)$ = 11.1 Hz, $\Delta\nu(CH_2)$ = 18.2 Hz and $\Delta\nu(CH)$ = 9.9 Hz. The time-averaged *tert*-butyl signal in the ^1H NMR spectrum of **3** (ratio **3**:**[Rh−Rh]** = 2:1) recorded at elevated temperature (330 K; Figure 7) displays a signal dispersion of 4.9 Hz (recorded at 11.74 T).

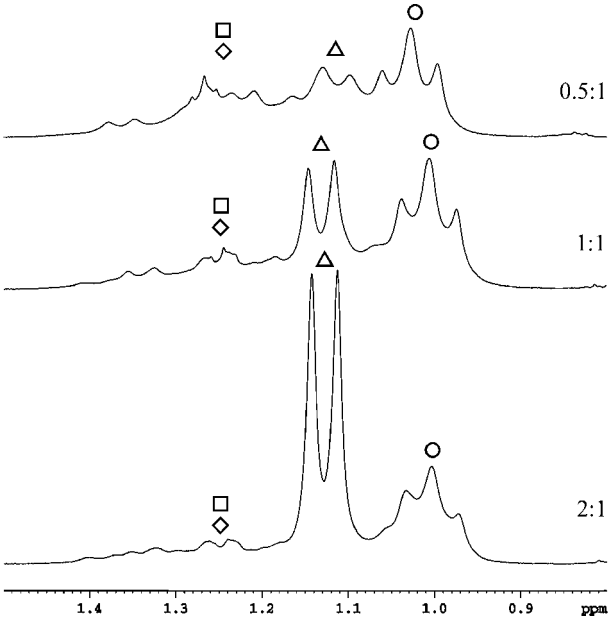

Figure 6. ^1H NMR signals of the *tert*-butyl group of **3**, recorded at 213 K; top: 1:2 molar ratio (**3**:**[Rh−Rh]**), middle: 1:1, bottom: 2:1; the icons used for the assignment of the various species of **3** have the same meaning as for **2** (see Scheme 4)

Moreover, the carbon signals of the *tert*-butyl group (recorded at 300 K) are duplicated as well: $\Delta\nu(CH_3)$ = 2.5 Hz and $\Delta\nu[C(t\text{Bu})]$ = 6.5 Hz. Interestingly, these diastereomeric dispersions occur preferably at the phosphane oxide group of **3** (P^b) that is clearly the weaker donor and, time-averaged, is further away from the Rh sites. Apparently, the branched structure of **3** guarantees that free P^b=O moieties cannot easily escape such interactions so that they come into closer spatial contact with the Mosher acid residues.

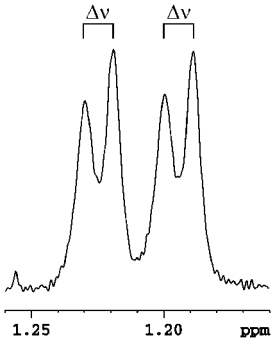

Figure 7. ^1H NMR signal of the *tert*-butyl group of **3** in the presence of an equimolar amount of **[Rh−Rh]**, recorded at 330 K, resolution enhanced; Δν = 4.9 Hz and $^3J_{^{31}P,^1H)}$ = 15.1 Hz

Conclusion

The bidentate 1,2-bis(diphenylphosphinoyl)ethane derivatives **1**−**3** are weak donors in adducts to the dirhodium complex **[Rh−Rh]**. Consequently, all conceivable species exist: free ligands, 1:1 adducts, 2:1 adducts and various iso-

 © 2004 Wiley-VCH Verlag GmbH & Co. KGaA, Weinheim

mers and oligomers thereof. Their relative concentrations strongly depend on the molar ratio of **[Rh−Rh]** and the ligands so that an identification by low-temperature ^{31}P NMR spectroscopy is possible. Enantiomers can easily be resolved in the case of chiral bidentate ligands **2** and **3**.

Experimental Section

Substances: The synthesis of **[Rh−Rh]** has been communicated by us previously.[7] 1,2-Bis(diphenylphosphinoyl)ethane (**1**)[8] was prepared from the respective commercially available bisphosphane by oxidation with H_2O_2 in water.

1,2-Bis(diphenylphosphinoyl)propane (2): Diphenylphosphane oxide (1.19 g, 5.9 mmol) and diphenyl(propadienyl)phosphane oxide[9] (1.43 g, 5.9 mmol) were dissolved in toluene (25 mL), and the resulting solution was heated to reflux for 3 days. Evaporation of the solvent and recrystallization of the solid residue from toluene/diethyl ether (10:1) gave 1.84 g of 2,3-bis(diphenylphosphinoyl)propene as white crystals. Yield 70%; m.p. 132−133 °C. IR (KBr): $\tilde{\nu}$ = 1482, 1437, 1397, 1261, 1199 cm^{-1}. ^1H NMR ($CDCl_3$): δ = 3.39 (br. d, J = 12.7 Hz, 1 H), 3.46 (br. d, J = 12.2 Hz, 1 H), 5.49 (dd, J = 20.5, 2.5 Hz, 1 H), 6.64 (dd, J = 41.6, 1.7 Hz), 7.21−7.89 (m, 20 H) ppm. ^{31}P NMR ($CDCl_3$): δ = 30.5 (d, J = 24 Hz), 32.6 (d, J = 24 Hz) ppm. $C_{27}H_{24}O_2P_2$ (442.4) calcd. C 72.96, H 5.84; found C 72.51, H 5.96.

Pd/C (20%; 0.096 g) was added to a solution of 2,3-bis(diphenylphosphinoyl)propene (0.2 g, 0.45 mmol) in 10 mL of methanol, and the resulting mixture was stirred at room temperature under a hydrogen atmosphere (balloon) for 2 days. The catalyst was then removed by filtering the reaction mixture through a thin bed of celite, and the methanol was evaporated to dryness. Recrystallization of the solid residue from toluene/hexane gave 0.175 g of **2**. Yield 87%; m.p. 128−131 °C. EI-HRMS: $C_{27}H_{26}O_2P_2$ [M^+] calcd. 444.1408; found 444.1399. See Table 2 for ^1H, ^{13}C and ^{31}P NMR spectroscopic data.

2-(*tert*-Butylphenylphosphinoyl)-3-(diphenylphosphinoyl)propene (3): *tert*-Butylphenylphosphane oxide (0.38 g, 2.1 mmol) was added to a solution of diphenyl(propadienyl)phosphane oxide[9] (0.51 g, 2.1 mmol) in 15 mL of toluene and the resulting solution was heated to 110 °C for 2 days. Evaporation of the solvent and recrystallization of the solid residue from diethyl ether/hexane (20:1) gave 0.51 g of **3**. Yield 57%; m.p. 84−86 °C. IR (KBr): $\tilde{\nu}$ = 1484, 1474, 1462, 1439, 1277, 1258, 1214, 1184 cm^{-1}. $C_{25}H_{28}O_2P_2$ (422.4) calcd. C 71.08, H 6.68; found C 70.71, H 6.80. See Table 2 for ^1H, ^{13}C and ^{31}P NMR spectroscopic data.

NMR Spectroscopy: Room-temperature ^1H (400.1 MHz), $^{13}C\{^1H\}$ (100.6 MHz), and $^{31}P\{^1H\}$ (161.9 MHz), NMR measurements were performed on a Bruker Avance DPX-400 spectrometer (9.4 T). Chemical shift standards were internal tetramethylsilane (δ = 0 ppm) for ^1H and ^{13}C, and external aqueous H_3PO_4 for ^{31}P (δ = 0 ppm). Signal assignments were assisted by NOE-difference, COSY, HMQC and HMBC (standard Bruker software) as well as by inspecting couplings to ^{31}P. Digital resolutions were 0.14 Hz/point in the ^1H, 0.24 Hz/point in the ^{13}C, and 0.22 Hz/point in the ^{31}P NMR spectra. One drop of [D_6]acetone was added to each NMR sample before measurement in order to increase the solubility of **[Rh−Rh]**.[10]

Variable-temperature ^1H (500.1 MHz) and $^{31}P\{^1H\}$ NMR (202.4 MHz) spectra were recorded in the presence of **[Rh−Rh]** on a Bruker Avance DRX-500 spectrometer (11.74 T). Temperatures varied from 213 to 330 K (333 K in the case of **1**) and were read from the instrument panel; no further measurements for more precise temperature determinations were taken.

$\{^{31}P\}$ ^1H-detected HMBC experiments were recorded at 213 K; relaxation delay 1.5 s, number of scans 32, delay optimized for long-range couplings (8 Hz); spectral width δ = 30−50 (^{31}P) and δ = 0−9 (^1H). Gradient-edited ^{31}P,^{31}P COSY spectra were recorded at 213 K; relaxation delay 4.0 s, number of scans 32, spectral width δ = 31−52 (^{31}P).

Acknowledgments

This work was performed within the project "Biologically Active Natural Products: Synthetic Diversity" (Department of Chemistry, Hannover University) and was supported by the Deutsche Forschungsgemeinschaft (Projects Du 98/22 436 UNG 113/148 and 436 POL 113/83), by the Hungarian Academy of Sciences (Project MTA/DFG 2002−2004) and the Hungarian National Research Foundation (OTKA No. T032180). A. S. thanks for Békésy and Varga/Rohr fellowships.

[1] [1a] E. B. Boyar, S. D. Robinson, *Coord. Chem. Rev.* **1983**, *50*, 109−208. [1b] *Multiple Bonds between Metal Atoms*, 2nd ed. (Eds.: F. A. Cotton, R. A. Walton), **1993**, Clarendon, Oxford.
[2] [2a] C. Mertis, M. Kravaritoy, M. Chorianopoulou, S. Koinis, N. Psaroudakis, *Top. Mol. Org. Engineer.* **1994**, *11*, 321−329. [2b] *Modern Catalytic Methods for Organic Synthesis with Diazo Compounds: From Cyclopropanes to Ylides* (Eds.: M. P. Doyle, M. A. McKervey, T. Ye), **1998**, John Wiley & Sons, New York. [2c]A. Endres, G. Maas, *Tetrahedron* **2002**, *58*, 3999−4005; and references cited therein.
[3] M. J. Clarke, F. Zhu, D. R. Frasca, *Chem. Rev.* **1999**, *99*, 2511−2533.
[4] [4a] S. Rockitt, H. Duddeck, J. Omelanczuk, *Chirality* **2001**, *13*, 214−223. [4b] S. Malik, H. Duddeck, J. Omelanczuk, M. I. Choudhary, *Chirality* **2002**, *14*, 407−411. [4c] D. Magiera, S. Moeller, Z. Drzazga, Z. Pakulski, K. M. Pietrusiewicz, H. Duddeck, *Chirality* **2003**, *15*, 391−399.
[5] D. V. Deubel, *Organometallics* **2002**, *21*, 4303−4305.
[6] T. Gáti, A. Simon, G. Tóth, D. Magiera, S. Moeller, H. Duddeck, *Magn. Reson. Chem.*, in print.
[7] K. Wypchlo, H. Duddeck, *Tetrahedron: Asymmetry* **1994**, *5*, 27−30.
[8] M. Quenard, V. Bonmarin, G. Gelbard, L. Krumenacker, *New J. Chem.* **1989**, *13*, 183−91.
[9] A. P. Boiselle, N. A. Meinhardt, *J. Org. Chem.* **1962**, *27*, 1828−1833.
[10] C. Meyer, H. Duddeck, *Magn. Reson. Chem.* **2000**, *38*, 29−32.

Received November 19, 2003
Early View Article
Published Online April 1, 2004

 © 2004 Wiley-VCH Verlag GmbH & Co. KGaA, Weinheim

Synthesis and Characterization of Homoleptic Lanthanide Guanidinate Complexes and Their Catalytic Activity for the Ring-Opening Polymerization of Trimethylene Carbonate

Liying Zhou,[a] Yingming Yao,[a] Yong Zhang,[a] Mingqiang Xue,[a] Jinglei Chen,[a] and Qi Shen*[a,b]

Keywords: Insertion / Lanthanides / N ligands / Polymerization

Two methods to synthesize homoleptic guanidinate lanthanide complex are described. The samarium guanidinate complex $[Sm\{Ph_2NC(NCy)_2\}_3]\cdot 2C_7H_8$ (**1**) can be synthesized by the metathesis reaction of lithium guanidinate with anhydrous samarium trichloride in a 3:1 molar ratio. The analogous complexes $[Ln\{Ph_2NC(NCy)_2\}_3]\cdot 2C_7H_8$ [Ln = Yb (**2**), Nd (**3**)] can also be synthesized by the insertion reaction of *N*,*N*′-dicyclohexylcarbodiimide into the Ln–N bond of $[(THF)_4Li][Ln(NPh_2)_4]$ in a 3:1 molar ratio in good yield. Complexes **1**–**3** were characterized by elemental analysis, IR and ^1H NMR spectroscopy. The molecular structures of complexes **1** and **3** were further determined by X-ray diffraction techniques. These complexes showed high activity for the ring-opening polymerization of trimethylene carbonate (TMC), giving polymers with M_w/M_n ranging from 1.41–1.73.

(© Wiley-VCH Verlag GmbH & Co. KGaA, 69451 Weinheim, Germany, 2004)

Introduction

Lanthanocene complexes exhibit a variety of catalytic abilities for the polymerization of olefins, polar monomers and for organic transformations, such as hydrogenation, cyclic hydroamination of both alkynes and alkenes and so on.[1] Although guanidinate ligands have been well established as a versatile and flexible ligand system that is a potential alternative to cyclopentadienyl-based systems, and its application in organolanthanide complexes has led to the synthesis of a number of guanidinate derivatives of lanthanides,[2−7] the catalytic behavior of these complexes was not investigated until quite recently, when it was first reported that a monoguanidinate derivative of lanthanum $[La\{CyNC[N(SiMe_3)_2]NCy\}(OC_6H_3tBu_2\text{-}2,6)_2]$ can catalyze the ring-opening polymerization of D,L-lactide.[6] Very recently, methyllanthanide bis(guanidinate) complexes were found to be effective catalysts not only for the polymerization of ε-caprolactone and MMA,[5] but also for the polymerization of styrene,[8] which is normally quite difficult to polymerize with organolanthanide complexes. These fascinating results prompted us to study the chemistry of lanthanide guanidinate complexes further.

In this paper we report the synthesis of the homoleptic guanidinate lanthanides $[Ln\{Ph_2NC(NCy)_2\}_3]\cdot 2C_7H_8$ (Ln = Sm, Yb, and Nd) by a metathesis reaction (Sm) or by the insertion of *N*,*N*′-dicyclohexylcarbodiimide into the Ln−N bond of $[(THF)_4Li][Ln(NPh_2)_4]$ (Yb and Nd). All these complexes show good catalytic activity for the ring-opening polymerization of trimethylene carbonate (TMC).

Results and Discussion

Synthesis and Characterization of the Lanthanide Guanidinate Complexes

The metathesis reaction is one of the most versatile methods for the synthesis of organolanthanide derivatives. Thus, the new complex $[Sm\{Ph_2NC(NCy)_2\}_3]$ was prepared in good yields by the metathesis reaction of anhydrous $SmCl_3$ with $Li[Ph_2NC(NCy)_2]$, freshly prepared by the reaction of $LiNPh_2$ with CyN=C=NCy in THF [Equation (1)].

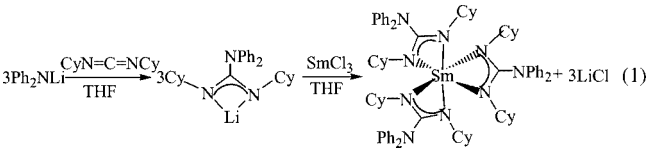

(1)

It has been reported that the insertion of one equivalent of the carbodiimide into the Ln−N bond of lanthanide amides leads to the formation of the corresponding lanthanide

[a] Department of Chemistry and Chemical Engineering, Suzhou University,
Suzhou 215006, China
Fax: (internat.) +86-512-6511-2371
E-mail: qshen@suda.edu.cn
[b] State Key Laboratory of Organometallic Chemistry, Shanghai Institute of Organic Chemistry, Chinese Academy of Sciences, Shanghai 200032, China

monoguanidinate derivatives,[6,7] so we wondered whether three molecules of the carbodiimide could insert into three Ln−N bonds of homoleptic lanthanide amides to give the corresponding homoleptic lanthanide guanidinate complexes. To answer this question, the reaction of *N*,*N*′-dicyclohexylcarbodiimide with $[(THF)_4Li][Ln(NPh_2)_4]$ in a 3:1 molar ratio was tried in THF. After workup, the homoleptic lanthanide guanidinate complexes $[Ln\{Ph_2NC(NCy)_2\}_3]\cdot 2C_7H_8$ [Ln = Yb (**2**), Ln = Nd (**3**)] were isolated in good yields. It is interesting that neither $LiLn[Ph_2NC(NCy)_2]_4$ nor $Li[Ph_2NC(NCy)_2]$ was obtained; the only Li product recovered was $LiNPh_2$ [Equation (2)]. This result indicates that the insertion of carbodiimide into the Ln−N bond is easier than into the Li−N bond.

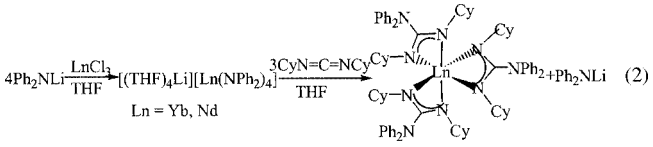

All these lanthanide complexes are air and moisture sensitive, and are soluble in toluene, THF, and diethyl ether. They were characterized by elemental analysis and IR spectroscopy. The IR spectra of these complexes exhibit strong absorptions in the range of 1600−1640 cm^{-1}, which are consistent with a partial C=N double-bond character, indicating that the π-electrons are delocalized within the double bond of the N−C−N linkage.

Crystal Structure Analyses

The molecular structures of **1** and **3** were further determined by X-ray diffraction. Crystals of **1** and **3** suitable for X-ray diffraction were grown from toluene solutions. The molecular structures of **1** and **3** are shown in Figure 1 and 2, respectively. Selected bond lengths and angles are given in Table 1.

As shown in Figure 1 and 2, complexes **1** and **3** have analogous solid-state structures: they are both monomeric with a six-coordinate lanthanide center ligated by six nitrogen atoms of three chelating bidentate guanidinate ligands. The coordination geometry around the lanthanide ion for each complex is best described as a distorted trigonal prism. The C−N distances within the chelating guanidinate ligands (see Table 1) are approximately equivalent and significantly shorter than C−N single bond lengths, indicating that the π-electrons in these complexes are delocalized within the N−C−N fragment. The Sm−N bond lengths in complex **1** range from 2.425(6) to 2.460(6) Å, giving an average of 2.442(6) Å. This value is similar to that in $[Sm\{CH(SiMe_3)_2\}\{CyNC[N(SiMe_3)_2]NCy\}_2]$ [av. 2.417(4) Å].[3] As expected, the coordinated guanidinate group and the lanthanide atom form essentially a planar four-membered ring [N(1)−Sm(1)−N(2) = 54.6(2)°, C(1)−N(1)−Sm(1) = 94.4(5)°, C(1)−N(2)−Sm(1) = 94.9(4)°, N(1)−C(1)−N(2) = 115.9(7)°; sum of angles: 359.8°]. The N(1)−Sm(1)−N(2), N(4)−Sm(1)−N(5), and N(7)−Sm(1)−N(8) bond angles are 54.6(2)°, 55.2(2)°, and 54.8(2)°, respectively, and are similar to the corresponding angles in $[Sm\{CH(SiMe_3)_2\}\{CyNC[N(SiMe_3)_2]NCy\}_2]$ [55.06(13)°, and 55.59(13)°][3] and $[Yb\{CyNC(Ph)NCy\}_3]\cdot 2THF$ [58.1(2)° and 57.98(17)°].[9]

The Nd−N bond lengths vary from 2.464(4) to 2.494(4) Å, similar to those in $[\{(Me_3Si)_2NC(NiPr)_2\}_2Nd(\mu\text{-}Me)_2Li(TMEDA)]$ [2.476(7) to 2.523(6)Å].[5] The guanidinate groups bind to Nd through two nitrogen atoms to yield a

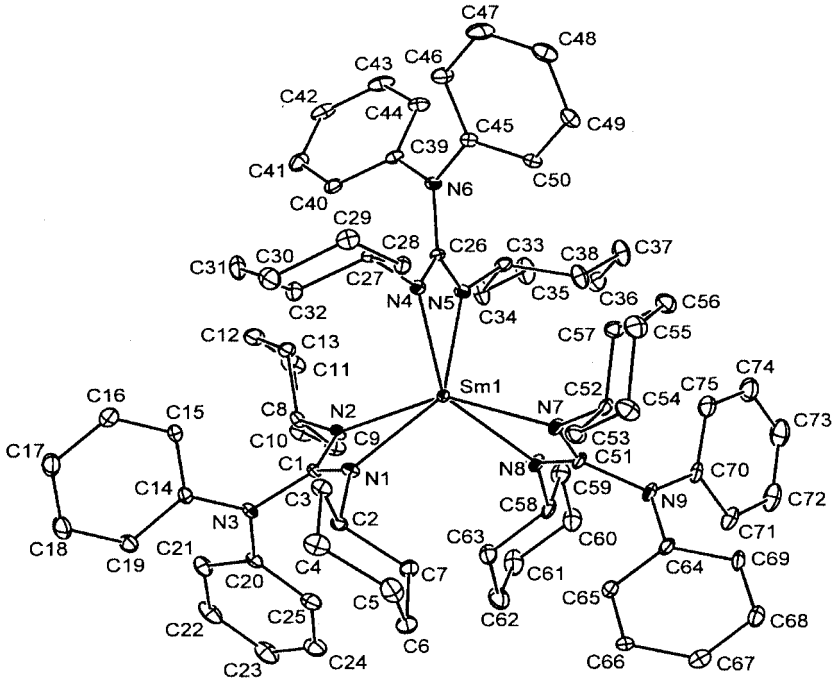

Figure 1. The molecular structure of complex **1**

 © 2004 Wiley-VCH Verlag GmbH & Co. KGaA, Weinheim

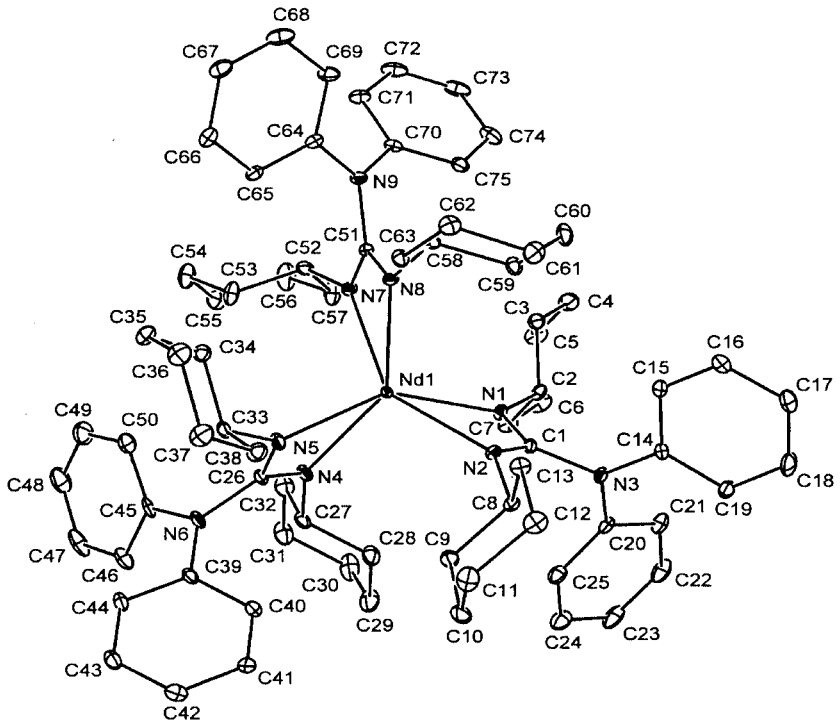

Figure 2. The molecular structure of complex **3**

Table 1. Selected bond lengths (Å) and angles (°) for **1** and **3**

Bond length (Å)	**1**	**3**	Bond length (Å)	**1**	**3**
Ln(1)−N(1)	2.442(7)	2.478(4)	Ln(1)−N(2)	2.435(6)	2.485(4)
Ln(1)−N(4)	2.448(4)	2.464(4)	Ln(1)−N(5)	2.440(4)	2.494(4)
Ln(1)−N(7)	2.460(6)	2.475(3)	Ln(1)−N(8)	2.425(6)	2.477(2)
Ln(1)−C(26)	2.863(4)	2.889(5)	Ln(1)−C(51)	2.858(8)	2.891(3)
N(1)−C(1)	1.32(1)	1.312(5)	N(3)−C(1)	1.46(1)	1.324(5)
N(2)−C(1)	1.316(9)	1.324(6)	N(5)−C(26)	1.332(7)	1.327(5)
N(4)−C(26)	1.326(8)	1.332(6)	N(7)−C(51)	1.309(8)	1.324(5)
N(6)−C(26)	1.431(6)	1.441(6)	N(9)−C(51)	1.44(1)	1.439(4)
N(8)−C(51)	1.33(1)	1.314(5)			
Angle (°)	**1**	**3**	**Angle (°)**	**1**	**3**
N(1)−Ln(1)−N(2)	54.6(2)	53.9(1)	C(51)−N(8)−Ln(1)	94.6(4)	94.4(2)
N(4)−Ln(1)−N(5)	55.2(2)	54.7(1)	N(1)−C(1)−N(2)	115.9(7)	117.0(4)
N(7)−Ln(1)−N(8)	54.8(2)	54.1(1)	N(4)−C(26)−N(5)	116.7(4)	117.8(4)
C(1)−N(1)−Ln(1)	94.4(5)	94.8(3)	N(7)−C(51)−N(8)	116.9(7)	117.2(3)
C(1)−N(2)−Ln(1)	94.9(4)	94.2(3)	C(26)−Ln(1)−C(51)	119.1(2)	118.4(1)
C(26)−N(4)−Ln(1)	93.9(3)	94.4(3)	Ln(1)−C(26)−N(6)	178.3(4)	178.8(3)
C(26)−N(5)−Ln(1)	94.1(3)	93.1(3)	Ln(1)−C(51)−N(9)	177.4(5)	177.9(3)
C(51)−N(7)−Ln(1)	93.6(4)	94.2(2)			

planar four-membered ring (sum of angles 359.9°) with bite angles of 53.9(1)°, 54.7(1)° and 54.7(1)°, respectively, which are similar to those in complex **1**, and $[\{(Me_3Si)_2NC(N\mathit{i}Pr)_2\}_2Nd(\mu\text{-}Me)_2Li(TMEDA)]$ [53.5(2)° and 54.0(2)°].[5]

Ring-Opening Polymerization of Trimethylene Carbonate (TMC)

Polycarbonate is a biomaterial with good biodegradability, biocompatibility, and low toxicity, and therefore the

 © 2004 Wiley-VCH Verlag GmbH & Co. KGaA, Weinheim

study of its preparation has attracted much attention. The ring-opening polymerization of a cyclic carbonate is an easy way to get a polycarbonate, and several Lewis acids are effective catalysts for this polymerization reaction. However, there are only a few papers dealing with the polymerization of cyclic carbonates catalyzed by organolanthanide complexes.[10−15] Evans et al. have found that a Sm^{II} complex can catalyze the copolymerization of ε-caprolactone (ε-CL) and ethylene carbonate, but cannot catalyze the homopolymerization of ethylene carbonate,[10] and Yasuda et al. have reported that Sm^{II} complexes show catalytic activity for the homopolymerization of trimethylene carbonate and the copolymerization of trimethylene carbonate with ε-CL.[11] Recently, Shen et al. have found that homoleptic lanthanide(III) aryloxides are effective initiators for the ring-opening polymerization of 2,2-dimethyltrimethylene carbonate.[12b] We therefore decided to examine the catalytic activity of the homoleptic guanidinate lanthanide complexes in the ring-opening polymerization of TMC (Scheme 1).

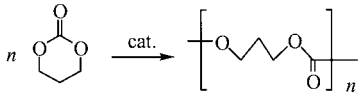

Scheme 1

The preliminary results are listed in Table 2, where it can be seen that all the complexes tested show high activity for the ring-opening polymerization of TMC. The monomer conversion is over 85% for all the polymerizations under the conditions of [M]/[I] = 500 (mole ratio) at 40 °C in 30 min (entries 1, 5, and 10). An effect of the central metal on the catalytic activity can also be observed. For example, the conversion reaches 95% in the case of [M]/[I] = 700 at 40 °C in 30 min using **2** as the initiator, while it is only 56% and 12% for complexes **1** and **3**, respectively (entries 2, 7 and 11). The conversion was still 89.5% even when the [M]/[I] ratio was increased to 1000 with **2** as the initiator (entry 8). Therefore, the activity order under the present polymerization conditions is Yb > Sm > Nd, which is opposite to the order of the ionic radii.

An effect of the polymerization temperature on the conversion can also be observed. The conversion increases with an increase of temperature from 20 to 60 °C with **1** or **3** as the initiator (entries 2, 3, 9, 10).

The catalytic activity of these tris(guanidinate) lanthanide complexes is similar to that of $La(OAr)_3$ (OAr = 2,6-di-*tert*-butyl-4-methyl phenolate) for the ring-opening polymerization of TMC,[12c] but is higher than that of $LnCl_3$ [12e] and $BX_3{\cdot}Et_2O$.[16] In comparison with the above catalysts, our lanthanide tris(guanidinate) complexes give polymers with a relatively narrow molecular-weight distribution.

Conclusion

In summary, homoleptic guanidinate lanthanide complexes can be easily prepared in good yield by the metathesis reaction of lithium guanidinate with anhydrous lanthanide trichlorides or by the insertion reaction of carbodiimide into the Ln−N bonds of $[(THF)_4Li][Ln(NPh_2)_4]$ in a 3:1 molar ratio. Their structural features have been determined by X-ray diffraction. These complexes show good catalytic activity for the ring-opening polymerization of trimethylene carbonate and the polymerization gives polymers with a relatively narrow molecular-weight distribution (M_w/M_n = 1.41−1.73).

Experimental Section

General Procedures: All manipulations were performed under pure Ar with rigorous exclusion of air and moisture using standard Schlenk techniques. Solvents were distilled from Na/benzophenone ketyl prior to use. Anhydrous $LnCl_3$,[17] $[Li(THF)_4][Ln(NPh_2)_4]$[18] and trimethylene carbonate (TMC)[19] were prepared according to the literature procedures. *N*,*N*′-Dicyclohexylcarbodiimide was purchased from Aldrich and used as received without further purification. Melting points were determined in sealed Ar-filled capillary tubes. Metal analyses were carried out by complexometric titration. Carbon, hydrogen and nitrogen analyses were performed by direct combustion on a Carlo−Erba EA = 1110 instrument. The IR spectra were recorded on a Magna-IR 550 spectrometer. Molecular weight and molecular weight distributions were determined against

Table 2. Polymerization of TMC initiated by homoleptic lanthanide guanidinate complexes[a]

Entry	Init	[M]/[I]	Temp (°C)	Time (min)	Yield[b] (%)	M_n ($\times 10^4$)	M_w/M_n [c]
1	**1**	500	20	30	86.4	1.15	1.70
2	**1**	700	40	30	56.11	0.87	1.69
3	**1**	700	60	30	100	1.47	1.75
4	**2**	500	20	30	94.9	2.08	1.73
5	**2**	500	40	30	92.0	2.65	1.64
6	**2**	500	60	30	94.4	2.95	1.56
7	**2**	700	40	30	95.7	1.79	1.62
8	**2**	1000	60	30	89.5	1.68	1.59
9	**3**	500	20	30	21.26	0.89	1.41
10	**3**	500	40	30	85.65	2.43	1.66
11	**3**	700	40	30	12.4	0.90	1.63

[a] Polymerization conditions: toluene, [TMC] = 1 mol/L. [b] Yield = weight of polymer obtained/weight of monomer used. [c] Measured by GPC (calibrated with standard polystyrene samples).

 © 2004 Wiley-VCH Verlag GmbH & Co. KGaA, Weinheim

a polystyrene standard by gel-permeation chromatography (GPC) on a waters 1515 apparatus with three HR columns (HR-1, HR-2 and HR-4); THF was used as an eluent at 30 °C. ^{1}H NMR spectra were measured on a Unity Inova-400 spectrometer.

Synthesis of [Sm{Ph$_2$NC(NCy)$_2$}$_3$]·2C$_7$H$_8$ (1): A Schlenk flask was charged with Ph_2NH (2.1 mL,15.0 mmol), THF (30 mL), and a stir bar. The solution was cooled to 0 °C, and *n*BuLi (9.6 mL, 15.0 mmol, 1.56 M in hexane) was added. It was then slowly warmed to room temperature and stirred for 1 h. *N*,*N*′-Dicyclohexylcarbodiimide (3.15 g, 15.3 mmol in 10 mL of THF) was then added to this solution at 0 °C. The solution was slowly warmed to room temperature, stirred for 1 h and then added slowly to a pale-gray slurry of $SmCl_3$ (1.28 g 5.11 mmol) in 20 mL of THF. The resulting solution was stirred for 1 h at 273 K and then stirred for 48 h at room temperature. The solvent was removed in vacuo and the residue was extracted with toluene and LiCl removed by centrifugation. After the extracts were concentrated, colorless crystals (5.50 g, 74%)were obtained at room temperature after a few days. M.p. 212 °C (dec.). ^{1}H NMR (400 MHz, C_6D_6, 25 °C): δ = 6.88−7.39 (m, 42 H, Ph), 3.62 (m, 6 H, unique H-Cy), 0.34−2.15 (br., 60 H, C_6H_{10}) ppm. $C_{89}H_{112}N_9Sm$ (1458.3): calcd. C 73.30, H 7.75, N 8.64, Sm 10.31; found C 73.24, H 7.20, N 8.63, Sm 9.85. IR (KBr pellet): $\tilde{\nu}$ = 3426 cm^{-1} (s), 2928 (m), 2855 (w), 1636 (s), 1590 (m), 1559 (w), 1493 (m), 1454 (w), 1400 (w), 1366 (w), 1235 (s), 1158 (s), 891 (w), 756 (w), 694 (w), 625 (w), 505 (m).

Synthesis of [Yb{Ph$_2$NC(NCy)$_2$}$_3$]·2C$_7$H$_8$ (2): A Schlenk flask was charged with a solution of [Li(THF)$_4$][Yb(NPh$_2$)$_4$] (4.56 g, 4.0 mmol) in 30 mL of THF and a stir bar. Then, a solution of *N*,*N*′-dicyclohexylcarbodiimide (2.47 g, 12.0 mmol) in 20 mL of THF was added slowly. The color of the solution slowly became yellow. The solution was then stirred for another 48 h and the solvents evaporated to dryness in vacuo. The residue was extracted with toluene and LiCl was removed by centrifugation. The solution was concentrated and stored at room temperature for crystallization. Complex **2** was obtained as yellow crystals (4.62 g, 78%). M.p. 287−289 °C (dec.). ^{1}H NMR (400 MHz, C_6D_6, 25 °C): δ = 6.88−7.40 (m, 42 H, Ph), 3.16−3.98 (m, 6 H, unique H-Cy), 0.34−2.15 (br., 60 H, C_6H_{10}) ppm. $C_{89}H_{112}N_9Yb$ (1481.0): calcd. C 72.18, H 7.62, N 8.51, Yb 11.69; found C 71.96, H 8.05, N 8.79, Yb 10.73. IR (KBr pellet): $\tilde{\nu}$ = 3430 cm^{-1} (s), 2928 (s), 2855 (m), 1640 (s), 1590 (m), 1493 (m), 1451 (w), 1308 (w), 1235 (w), 1154 (w), 1076 (w), 1030 (w), 891 (w), 752 (m), 694 (m).

Synthesis of [Nd{Ph$_2$NC(NCy)$_2$}$_3$]·2C$_7$H$_8$ (3): Following the procedure for the synthesis of **2**, the reaction of *N*,*N*′- dicyclohexylcarbodiimide (1.36 g, 6.6 mmol) in 20 mL of THF with [Li(THF)$_4$][Nd(NPh$_2$)$_4$] (2.45 g, 2.2 mmol) in 30 mL of THF afforded **3** as light-blue crystals (2.88 g, 65%). M.p. 131 °C. ^{1}H NMR (400 MHz, C_6D_6, 25 °C): δ = 6.87−7.40 (m, 42 H, Ph), 3.56−3.62 (m, 6 H, unique H-Cy), 0.34−2.15 (br., 60 H, C_6H_{10}) ppm. $C_{89}H_{112}N_9Nd$ (1452.2): calcd. C 73.61, H 7.77, N 8.68, Nd 9.94; found C 73.25, H 7.96, N 8.92, Nd 9.55. IR (KBr pellet): $\tilde{\nu}$ = 3442 cm^{-1} (s), 3280 (m), 3257 (m), 2964 (m), 1628 (m), 1405 (w), 1266 (m), 1088 (s), 1027 (s), 918 (w), 888 (w), 803 (s), 695 (w), 533 (w), 440 (w).

Typical Procedure for the Polymerization Reactions: A 50-mL Schlenk flask equipped with a magnetic stir bar was charged with a solution of TMC (0.3583 g, 3.51 mmol) in 2.8 mL of toluene. To this solution was added 0.7 mL of a solution of complex **2** in toluene (1.0×10^{-2} M, 7.00×10^{-3} mmol) with a syringe. The contents of the flask were then vigorously stirred for 30 min at 20 °C. The polymerization was quenched by adding a 5% solution of HCl in methanol,. The polymer precipitated from methanol and was dried under vacuum.

X-ray Structural Determination of 1 and 3: Suitable single crystals of complexes **1** and **3** were each sealed in a thin-walled glass capillary, and intensity data were collected on a Rigaku Mercury CCD equipped with graphite-monochromated Mo-K_α (λ = 0.71073 Å) radiation. Details of the intensity data collection and crystal data are given in Table 3. The crystal structures of these complexes were solved by direct methods and expanded by Fourier techniques. Atomic coordinates and thermal parameters were refined by full-matrix least-squares analysis on F^2. All non-hydrogen atoms were refined anisotropically. Hydrogen atoms were all generated geometrically with assigned appropriate isotropic thermal parameters. CCDC-224364 (for **1**) and -224365 (for **3**) contain the supplementary crystallographic data for this paper. These data can be obtained free of charge at www.ccdc.cam.ac.uk or from the Cambridge Crystallographic Data Center, 12 Union Road, Cambridge CB2 1EZ, UK [Fax: (internat.) + 44-1223-336-033; E-mail: deposit@ccdc.cam.ac.uk].

Table 3. Details of the crystallographic data collection and refinement for **1** and **3**

	1	**3**
Empirical formula	$C_{89}H_{112}N_9Sm$	$C_{89}H_{112}N_9Nd$
Molecular weight	1458.32	1452.16
Temperature (K)	193.1	193.1
Wavelength (Å)	0.7107	0.7107
Size (mm)	0.40 × 0.42 × 0.25	0.60 × 0.55 × 0.30
Crystal system	monoclinic	monoclinic
Space group	$P2_1$ (no. 4)	$P2_1$ (no. 4)
a (Å)	14.086(2)	14.1338(13)
b (Å)	21.782(2)	21.7685(13)
c (Å)	14.541(2)	14.5916(13)
α (°)	90	90
β (°)	117.843(5)	118.017(3)
γ (°)	90(5)	90
V (Å^3)	3945.0(8)	3963.3(6)
Z	2	2
$D_{calcd.}$ (g cm^{-3})	1.228	1.217
Absorption coefficient (mm^{-1})	0.796	0.705
F (000)	1542.00	1538.00
Theta range for collection (°)	3.0−27.5	3.2−27.5
Reflection collected	87950	79450
Independent reflections	17924	18014
Variables	918	918
R [$I > 3\sigma(I)$]	0.045	0.035
Rw	0.106	0.091
Goodness-of-fit on F^2	0.973	1.023

Acknowledgments

We are indebted to the Chinese National Natural Science Foundation for financial support.

[1] [1a] M. R. Gagne, C. L. Stern, T. J. Marks, *J. Am. Chem. Soc.* **1992**, *114*, 275. [1b] M. A. Giardello, Y. Yamamoto, L. Brard, T. J. Marks, *J. Am. Chem. Soc.* **1995**, *117*, 3276. [1c] G. Desurmont, Y. Li, H. Yasuda, *Organometallics* **2000**, *19*, 1811. [1d] X. G. Zhou, M. Zhu, *J. Organomet. Chem.* **2002**, *647*, 28. [1e] Z. M. Hou, Y. Wakatsuki, *J. Organomet. Chem.* **2002**, *647*, 61. [1f] Q. Shen, Y. M. Yao, *J. Organomet. Chem.* **2002**, *647*, 180.

 © 2004 Wiley-VCH Verlag GmbH & Co. KGaA, Weinheim

[2] P. J. Bailey, S. Pace, *Coord. Chem. Rev.* **2001**, *214*, 91.
[3] Y. L. Zhou, G. P. A. Yap, D. S. Richeson, *Organometallics* **1998**, *17*, 4387.
[4] Z. Lu, G. P. A. Yap, D. S. Richeson, *Organometallics* **2001**, *20*, 706.
[5] Y. J. Luo, Y. M. Yao, Q. Shen, K. B. Yu, L. H. Weng, *Eur. J. Inorg. Chem.* **2003**, 318.
[6] G. R. Giesbrecht, G. D. Whitener, J. Arnold, *J. Chem. Soc., Dalton Trans.* **2001**, 923.
[7] J. Zhang, R. F. Cai, L. H. Weng, X. G. Zhou, *J. Organomet. Chem.* **2003**, *672*, 94.
[8] Y. J. Luo, Y. M. Yao, Q. Shen, *Macromoleculars* **2002**, *35*, 8670.
[9] Y. J. Luo, Y. M. Yao, Q. Shen, *J. Organomet. Chem.* **2002**, *662*, 144.
[10] W. J. Evans, H. Katsumata, *Macromolecules* **1994**, *27*, 4011.
[11] H. Yasuda, M-S. Aludin, N. Kitamura, M. Tanebe, H. Sirahama, *Macromolecules* **1999**, *32*, 6047.
[12] [12a] J. Ling, Y. Zhang, Z. Shen, *Chin. Chem. Lett.* **2001**, *12*, 41. [12b] J. Ling, Z. Shen, Q. Huang, *Macromolecules* **2001**, *34*, 7613. [12c] J. Ling, Z. Shen, *Macromol. Chem. Phys.* **2002**, *203*, 735. [12d] Y. Q. Shen, Z. Q. Shen, Y. F. Zhang, *J. Appl. Polym. Sci.* **1997**, *64*, 2131. [12e] Y. Q. Shen, Z. Q. Shen, Y. F. Zhang, Q. H. Hang, *J. Polym. Sci., Part A: Polym. Chem.* **1997**, *35*, 1339.
[13] A. P. Pego, Z. Y. Zhong, P. J. Dijkstra, D. W. Grijpma, J. Feijen, *Macromol. Chem. Phys.* **2003**, *204*, 747.
[14] M. Schappacher, T. Fabre, A. F. Mingotaud, A. Soum, *Biomaterials* **2001**, *22*, 2849.
[15] V. Onfroy, M. Schappacher, A. Soum, *International Symposium on Ionic Polymerization*, Paris, France, **1997**, 246.
[16] H. R. Kricheldorf, B. Weegen-Schulz, *Macromolecules* **1993**, *26*, 5991.
[17] M. D. Taylor, C. P. Carter, *J. Inorg. Nucl. Chem.* **1962**, *24*, 387.
[18] X. H. Lu, *M. Sc. Thesis*, Suzhou University, 2001.
[19] S. Sarel, L. A. Pohoryles, *J. Am. Chem. Soc.* **1958**, *80*, 4596.

Received November 20, 2003
Early View Article
Published Online April 1, 2004

 © 2004 Wiley-VCH Verlag GmbH & Co. KGaA, Weinheim

Cobalt(II), Nickel(II), Copper(II), and Zinc(II) Complexes with a *p-tert*-Butylcalix[4]arene Fitted with Phosphinoyl Pendant Arms

Vladimira Videva,[a] Anne-Sophie Chauvin,[b] Sabi Varbanov,[c] Christophe Baux,[b] Rosario Scopelliti,[b] Mariana Mitewa,[a] and Jean-Claude G. Bünzli*[b]

Keywords: Calix[4]arene / Transition metals / Stability constants / X-ray diffraction / Polynuclear compounds

A series of complexes of $M^{II}X_2$ transition metal salts (X = ClO_4, M = Co, Ni, Cu, Zn; X = Cl, M = Cu, Zn) with a calix[4]arene substituted at the lower rim {L = 5,11,17,23-tetra-*tert*-butyl-25,26,27,28-tetrakis[(dimethylphosphinoyl)-methoxy]calix[4]arene} are isolated and characterized. Two different stoichiometries are evidenced, 1:1 for the Co^{II}, Ni^{II}, and Cu^{II} complexes, independently of the anion (Cl^- or ClO_4^-), as well as for the $Zn(ClO_4)_2$ complex, while a 2:1 metal/ligand ratio is found for the complex with $ZnCl_2$. The coordination mode and structure of the complexes are investigated by several spectroscopic and magnetochemical methods, both in the solid state and in solution. Coordination through the phosphoryl groups of the ligand is ascertained by X-ray diffraction and IR and NMR spectroscopic data. The crystal structure of the 2:1 Zn compound (triclinic, $P\bar{1}$, $Z = 2$) shows the presence of the tetrametallic species Zn_4L_2 with three different tetrahedral Zn environments, $ZnCl_2O_2$, $ZnCl_3O$, and $ZnClO_3$, the latter bridging two ligand molecules. Magnetic susceptibility, EPR data, and electronic spectra are indicative of a tetrahedral arrangement of the ligands in the Co^{II} (high-spin d^7) 1:1 complex, which is also most probably the ligand geometry in the Ni^{II} and Cu^{II} 1:1 complexes. In solution, the extent of the interaction between L and the M^{II} ions has been determined by UV/Vis spectrophotometric titrations. The resulting stability constants for 1:1 complexes are in the range $\log K_1 = 4.8–5.4$.
(© Wiley-VCH Verlag GmbH & Co. KGaA, 69451 Weinheim, Germany, 2004)

Introduction

During the last decade, a great deal of interest has been devoted to the design of functionalized calixarenes in view of their excellent coordination and extraction properties.[1−4] Phosphorus-containing calixarenes have proven particularly useful in the separation of lanthanides and actinides.[5] Moreover, transition metal complexes with calixarenes are good models for mimicking biological processes.[6] For example, Co^{II} or $Cu^{I/II}$ complexes can be used to transport and activate small molecules of biological interest, such as dioxygen, and/or for studying the catalytic effect of copper enzymes in non-aqueous solvents.[7a] Other applications lie in analytical chemistry, as recently reported for calixarene-based luminescent sensors for Cu^{II} [7b] and Zn^{II},[7c] for instance. In the recent past, we have reported the synthesis of narrower-rim substituted *p-tert*-butylcalix[*n*]arenes fitted with either ether−amide (n = 4,[8a] 6[8b]) or phosphinoyl groups [n = 4 (L),[8c] 6[4]]. In particular, the thermodynamic and photophysical properties of the 1:1 and 1:2 (metal/ligand) complexes of L (see scheme) with trivalent lanthanide ions (La^{III}, Eu^{III}, Tb^{III}) were studied in detail.[8c] The ligand itself adopts a flattened cone conformation and a Δ-enantiomeric form which should also be quite convenient for the binding of 3d transition metal ions forming tetracoordinated species. In this paper we therefore investigate the coordination ability of L towards Co^{II}, Ni^{II}, Cu^{II} and Zn^{II} perchlorates, as well as the structural properties of the resulting isolated complexes. Influence of the anion on the stoichiometry of the complexes is tested for Cu^{II} and Zn^{II} by replacing perchlorate with chloride.

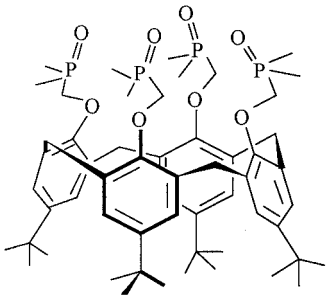

L

[a] University of Sofia, Department of Chemistry, 1126 Sofia, Bulgaria
[b] Laboratory of Lanthanide Supramolecular Chemistry, BCH 1402, Swiss Federal Institute of Technology, 1015 Lausanne, Switzerland
[c] Institute of Polymers, Bulgarian Academy of Sciences, 1113 Sofia, Bulgaria
Supporting information for this article is available on the WWW under http://www.eurjic.org or from the author.

Results and Discussion

Isolation of the Complexes and Solid-State Properties

The complexes were isolated from ethanolic solutions and elemental analyses are consistent with the formation of compounds with a 1:1 metal/ligand stoichiometry: $M(ClO_4)_2L{\cdot}2H_2O$ [M = Co (**1**), Ni (**2**), Zn (**5**); $Cu(ClO_4)_2L{\cdot}4H_2O$ (**3**), and $CuCl_2L{\cdot}4H_2O$ (**4**)], while a compound with a 2:1 (M/L) stoichiometric ratio was isolated with zinc chloride: Zn_2Cl_4L (**6**). IR spectroscopic data (Table S1, Figure S1, Supporting Information) are consistent with an interaction taking place through the P=O groups of the ligand. In the free ligand, the P=O stretching vibration appears as an intense split band with components at 1160 and 1171 cm^{-1}, pointing to inequivalent phosphoryl groups. In the chloride complexes (1:1, Cu^{II} and 2:1, Zn^{II}) this band undergoes a further splitting leading to the observation of **3** (Zn^{II}, 2:1 complex) and **4** (Cu^{II}, 1:1 complex) components, all of them being red-shifted with respect to those of the free ligand. That is, the P=O groups become more inequivalent in the complexes; as a matter of fact, the crystal structure of the Zn^{II} 2:1 complex (vide infra) shows three types of P=O groups, coordinated to monodentate $ZnCl_3^-$, bidentate bridging $ZnCl_2$ and tridentate bridging $ZnCl^+$ units. The shift of the more intense component with respect to the ligand, $\Delta\tilde{\nu} \approx 50$ cm^{-1}, is considerably larger than the one reported for $ZnCl_2(Ph_3PO)_2$[9] or for zinc halide adducts with (aminomethyl)dimethylphosphane oxide[10] (ca. 35 cm^{-1}), pointing to a stronger interaction with the metal ion, despite the fact that chloride ions remain coordinated. Analysis of the P=O vibrations for the 1:1 perchlorate complexes is not easy in view of the overlap with the perchlorate modes. The spectra of all complexes are relatively similar, with three components in the ranges 1104−1109, 1121−1123 and 1143−1144 cm^{-1} (the middle component is not seen in the spectrum of the Co^{II} complex). The shifts are difficult to determine since the more intense band does not correspond to the same components in the various spectra, but they range between 27 and 60 cm^{-1}, again indicating a substantial interaction between the phosphoryl groups and the metal ions. Several vibrations are seen in the 627−636 cm^{-1} range, so that the presence of non-ionic (possibly coordinated) perchlorate ions cannot be ruled out. For instance, in $[Co(ClO_4)(topo)_4]ClO_4$ (topo = trioctylphoshane oxide) in which perchlorate anions are coordinated, $\Delta\tilde{\nu}(P{=}O) \approx 30$ cm^{-1}.[11]

In order to obtain additional information about the geometrical arrangement of the ligating atoms in the paramagnetic complexes, susceptibility measurement and EPR spectra have been recorded for Co^{II}, Ni^{II} and Cu^{II} (Figure 1), as well as electronic spectra. The effective magnetic moment μ_{eff} of the Co^{II} complex amounts to 5.0 B.M. at room temperature and is temperature-dependent, which is typical of a high-spin d^7 complex with either octahedral or tetrahedral ligand arrangements. The relatively large value of μ_{eff} could be more consistent with an octahedral arrangement (reported values are in the range 4.7−5.2 B.M., while four-coordinate high-spin compounds have μ_{eff} in the range 4.2−4.9 B.M. [4.76 B.M. for $(Ph_3PO)_2CoCl_2$, for instance].[12] On the other hand, the intense blue color of the complex points to the latter being more likely tetrahedral.[13] Reasoning in terms of idealized symmetries, a tetrahedral arrangement generates three spin-allowed transitions, $^4A_2 \rightarrow {}^4T_2$, $^4T_1(F)$, $^4T_1(P)$; the latter is situated between 600 and 650 nm and is usually the more intense, while the other two transitions are in the NIR range (1−2 μm). Octahedral d^7 complexes also display three d-d transitions $^4T_{1g}(F) \rightarrow {}^4T_{1g}(P)$, $^4A_{2g}$, $^4T_{2g}$ the first being the more intense one and occurring between 500 and 600 nm; it often appears as being split because the $^4A_{2g}$ level is close to $^4T_{1g}(P)$; the transition to $^4T_{2g}$ occurs in the NIR region; generally speaking these transitions are about one order of magnitude less intense than the transitions of the tetrahedral complexes.[13] In our case, the reflectance spectrum displays two weak d-d transitions at 473 and 516 nm, a main component at 597 nm, and two additional broad and very weak bands at 916 and ca. 1450 nm. In CH_3CN solution (2.7×10^{-3} M, Figure 2), the corresponding bands appear at 454(86) (ε = 112 $M^{-1}{\cdot}cm^{-1}$), 515(11), 586(65), and 1407(55) nm. The relatively large values of the molar absorption coefficients are more in line with a tetrahedral arrangement of the ligands; the latter appears to be severely distorted, leading to a low symmetry, henceforth the observation of several transitions in the range 450−600 nm [splitting of the $^4T_1(P)$ level]. The effective magnetic moment of the Ni^{II} complex at room temperature is equal to 3.1 B.M. and is temperature-independent, down to about 30 K. For a hexacoordinate, octahedral complex, a value between 2.9 and 3.4 B.M. is expected, while tetrahedral complexes have μ_{eff} in the range

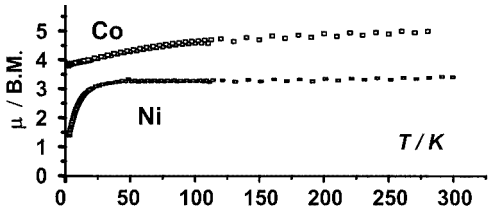

Figure 1. Temperature dependence of the effective magnetic moment of the Co^{II}, and Ni^{II} complexes

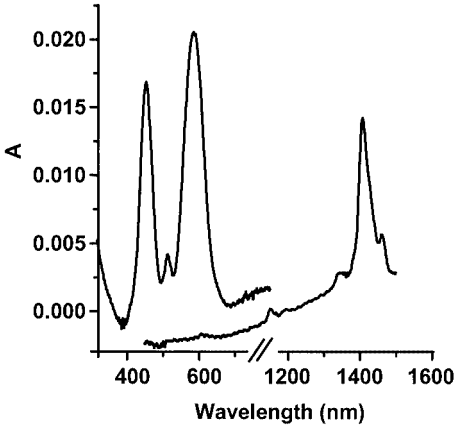

Figure 2. Parts of the electronic spectrum of $CoL(ClO_4)_2{\cdot}2H_2O$, 2.7×10^{-3} M in CH_3CN

 © 2004 Wiley-VCH Verlag GmbH & Co. KGaA, Weinheim

3.0−3.5, if they are severely distorted, or 3.5−4.0 B.M., if they are less distorted.[12,13] The value we find for the calixarene complex is therefore clearly compatible with either one of the first two situations. The reflectance spectrum displays a band at 446 nm, with two shoulders on the low energy side and a weak one at 905 nm and is therefore compatible with a tetrahedral coordination. While Co^{II} and Ni^{II} complexes are EPR-silent, the Cu^{II} chloride compound exhibits a single anisotropic line with $g = 2.13 \pm 0.01$, both at room and low (130 K) temperatures, again consistent with a distorted tetrahedral coordination geometry.

Crystals of complex **6** have been obtained by slow concentration of a methanolic solution of L and $ZnCl_2$ (each 10^{-3} M) and its solid-state structure has been elucidated by X-ray diffraction. The structure is comprised of discrete units encompassing two molecules of ligand linked to four Zn^{II} cations. The coordination of the metal ions is tetrahedral, even if the nature of the coordinating atoms differ (Figure 3): Zn1 is coordinated by one chloride anion and three oxygen atoms from phosphinoyl arms belonging to two calixarenes, thus creating a bridge between them; Zn2 and Zn4 are coordinated by two chloride anions and two oxygen atoms from neighboring phosphinoyl arms on the same ligand; Zn3 is coordinated by three chloride anions and only one oxygen atom from the last phosphinoyl arm. The mean P=O bond length, 1.51(1) Å, is in the range expected for P=O double bonds, although this distance is larger than the one observed in the free ligand (1.483 Å).[8c] The lengthening of the P=O bond upon coordination is consistent with the red-shift observed for the $\tilde{\nu}$(P=O) vibration. The Zn−Cl bond lengths are comparable for the four zinc atoms [2.237(6)Å], while the Zn−O distance ranges from 1.92(1) to 2.01(1) Å. The two different donor atoms around the Zn^{II} ions generate distorted tetrahedral coordination polyhedra, essentially with respect to the Ln−X distances; angles deviate less than 10° from the expected tetrahedral value (Table S2, Supporting Information). The two calixarenes adopt a typical flattened cone conformation (Table S3, Supporting Information) with two opposite phenolic units almost parallel to each other while the other two are approximately at right angles.

Solution Properties of the Complexes

The complexes have also been characterized in solution. Electrospray mass spectrometry (ES-MS) confirms that the metal:ligand ratios are maintained in solution (Table 1).

The corresponding spectra display peaks due to the free ligand as $[L]^+$, $[L + 2\ H]^{2+}$ species in addition to the expected cations $[L + Co]^{2+}$, $[L + Ni]^{2+}$, $[L + Cu]^{2+}$, $[L + Zn]^{2+}$. Hydrated ligand species are also seen in the case of **3**, **5** and **6**, but only the spectrum of **5** presents peaks attributable to a hydrated metal ion (Zn^{II}). For complexes **1**−**5**, dissociation of the complexes occurs according to Equations (1) and (2).

$$MLX_2 \rightarrow L + MX_2 \quad (1)$$

$$MLX_2 \rightarrow [ML]^{2+} + 2\,X^- \quad (2)$$

Spectra of the dimetallic Zn^{II} complex **6**, have been recorded in both positive and negative modes and the following species were unambiguously identified: $[ZnL]^{2+}$, $[ZnCl(L)]^+$, $[Zn_2Cl(L)]^{3+}$ and $[ZnCl_3]^-$. The presence of these species, particularly the negatively charged trichloride, leads to the hypothesis that the complex in solution may be formulated as $[ZnCl(L)][ZnCl_3]$. The dimetallic species is more difficult to account for. One may think that dissolution of the tetrametallic complex characterized by X-ray diffraction results in a reorganization of the Zn1 and Zn3 coordination sphere to give monomeric dimetallic complexes Zn_2Cl_4L with each metal ion coordinated to two chloride ions and two phosphoryl groups. However, spectrophotometric titrations (vide infra) point to the sole pres-

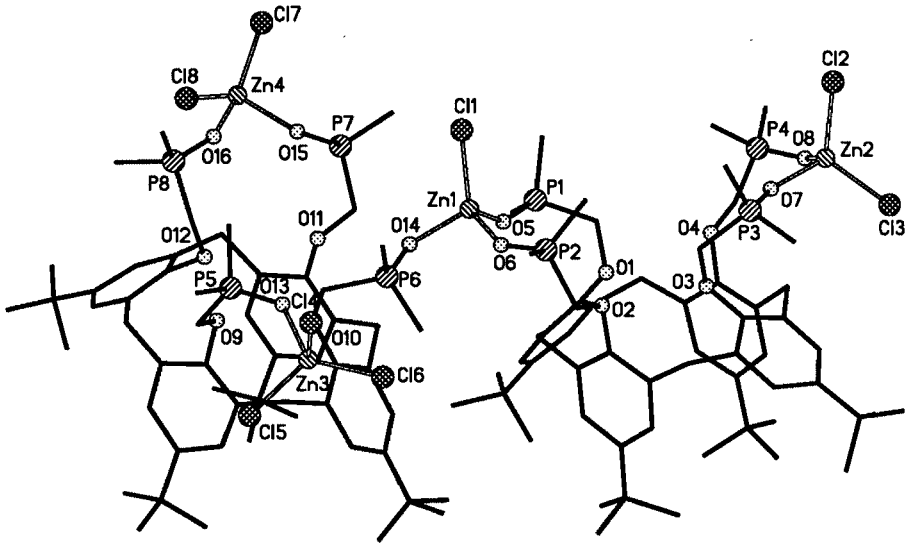

Figure 3. Ball-and-stick representation of the crystal structure of **6** showing the atom-numbering scheme for all atoms but carbon atoms (hydrogen atoms and external water molecules are not shown while the size of carbon atoms has been reduced to zero for the sake of clarity)

 © 2004 Wiley-VCH Verlag GmbH & Co. KGaA, Weinheim

Table 1. Molecular peaks and main fragments observed by ES-MS analysis (positive and negative modes) for the complexes of **L**

Compound (No.)	Mol. mass	Species	Obsd. *m*/*z*	Calcd. *m*/*z*
L	1009.17	$[L]^{+}$	1009.80	1009.17
$CoL(ClO_4)_2{\cdot}2H_2O$	1303.05	$[Co + 2\ L + 6\ H]^{8+}$	260.27	260.36
1		$[L + Co]^{2+}$	534.00	534.05
		$[L + 2\ H]^{2+}$	505.86	505.59
		$[L + H]^{+}$	1009.79	1010.17
$NiL(ClO_4)_2{\cdot}2H_2O$	1302.79	$[L + Ni + 3\ H + 4\ CH_3OH]^{5+}$	240.29	239.80
2		$[L + Ni + 3\ H + 7\ CH_3OH]^{5+}$	259.31	259.03
		$[L + Ni]^{2+}$	533.38	533.93
		$[L + Ni + CH_3CN]^{2+}$	554.36	554.45
		$[L + 2\ H]^{2+}$	505.86	505.58
		$[L + H]^{+}$	1009.86	1010.17
$CuL(ClO_4)_2{\cdot}4H_2O$	1303.05	$[L + 2\ H]^{2+}$	505.82	505.58
3		$[L + 2\ H + H_2O]^{2+}$	524.32	523.58
		$[L + Cu]^{2+}$	536.98	536.79
$CuLCl_2{\cdot}4H_2O$	1215.69	$[L + Cu]^{2+}$	536.22	536.36
4		$[L + 2\ H]^{2+}$	505.86	505.58
		$[L + H]^{+}$	1009.86	1010.17
$ZnL(ClO_4)_2{\cdot}2H_2O$	1309.48	$[L + 4\ H + H_2O]^{4+}$	257.25	257.79
5		$[2\ L + Zn + 2\ H + H_2O]^{4+}$	524.33	524.43
		$[L + Zn]^{2+}$	537.28	537.28
		$[L + H]^{+}$	1009.27	1010.27
Zn_2LCl_4	1281.76	$[L + Zn + 2\ H + CH_3CN]^{4+}$	279.38	279.40
6		$[L + 2\ Zn + Cl]^{3+}$	391.35	391.79
		$[L + 2\ H]^{2+}$	505.82	505.78
		$[L + 2\ H + 2\ H_2O]^{2+}$	524.32	523.58
		$[L + Zn]^{2+}$	536.32	537.28
		$[L + H]^{+}$	1009.86	1010.17
		$[L + Zn + Cl]^{+}$	1109.80	1110.00
		$[Zn + 3\ Cl]^{-}$	171.73	172.82
		$[L + 2\ Zn + 10\ Cl]^{6-}$	248.84	249.08

ence of 1:1 species in solution, so that the dimetallic species probably forms under the electrospray conditions, when the droplets evaporate.

The ^1H and $^{31}P\{^1H\}$ NMR spectroscopic data obtained for the free ligand and its Zn^{II} complex in $[D_6]$DMSO are reported in Table 2. Although the latter occurs within a fast exchange process, the coordination mode in solution through the phosphoryl groups is confirmed: both ^1H and $^{31}P\{^1H\}$ NMR shifts are affected by the complexation. The signal of the $CH_3P(O)$ protons is shifted by $\Delta\delta$ = 0.06−0.11 ppm. Large ^{31}P shifts are observed for the coordinated phosphoryl groups: $\Delta\delta$ = 4.27 ppm, from 36.81 for the free ligand to 41.08 ppm for $ZnL(ClO_4)_2{\cdot}2H_2O$, and $\Delta\delta$ = 7.98 ppm, to 44.79 ppm for the Zn_2LCl_4 complex **6**. Analogous ^{31}P chemical shifts are measured in CD_3OD: $\Delta\delta$ = 2.69 ppm for **5** and $\Delta\delta$ = 6.08 ppm for **6**.

On the other hand, the difference in chemical shifts between **5** and **6**, with $\Delta\delta(\mathbf{6}-\mathbf{5})$ = 3.71 ppm, strongly suggests that the species in solution are quite different. Addition of 1 equiv. of tetramethylammonium chloride or zinc chloride directly to the solution containing $ZnL(ClO_4)_2$, followed by heating of the NMR tube for 2 min, for solubility reasons, results in the observation of only one peak in the $^{31}P\{^1H\}$ spectrum, at δ = 44.30 ppm, meaning that complex **5** immediately evolves into **6** upon chloride addition. Despite that the ratio of Zn/L/Cl not being the same (1:1:1 upon addition of Me_4NCl and 2:1:2 upon addition of $ZnCl_2$), the same species forms.

Table 2. ^1H and $^{31}P\{^1H\}$ NMR spectroscopic data of $[ZnL](ClO_4)_2\ 2H_2O$ (**5**) and $[Zn_2L]Cl_4$ (**6**) in $[D_6]$DMSO

Compound[a]	$CH_3P(O)$		$CH_2P(O)$	$Ar-CH_2-Ar$		$Ar-H$	$C(CH_3)_3$	$P{=}O$	$P{=}O$[b]
	δ [ppm]	$J_{H,P}$ [Hz]	δ [ppm]	δ [ppm]	$^2J_{H,H}$ [Hz]	δ [ppm]	δ [ppm]	δ [ppm]/$\Delta\delta$ [ppm]	δ [ppm]/$\Delta\delta$ [ppm]
L	1.43(d)	12.80	4.53 (bs)	3.19(d), 4.72(d)	12.80, 12.80	6.80 (s)	1.04 (s)	+36.81(s)/−	+43.63(s)/−
5	1.49(d)	13.16	4.56 (bs)	3.24(d), 4.65(d)	12.80, 12.80	6.82 (s)	1.05 (s)	+41.08(s)/4.27	+46.32/2.69
6	1.54 (d)	13.16	4.59 (bs)	3.25(d), 4.65(d)	12.80, 12.80	6.84 (s)	1.05 (s)	+44.79(s)/7.98	+49.71(s)/6.08

[a] Key: bs: broad singlet; d: doublet; s: singlet. [b] In CD_3OD.

 © 2004 Wiley-VCH Verlag GmbH & Co. KGaA, Weinheim

Interaction of L with Co^{II}, Ni^{II}, Cu^{II} and Zn^{II} in Acetonitrile

To assess the strength of the calixarene−metal interaction, we have determined stability constants in acetonitrile or acetonitrile containing a small amount of dichloromethane by spectrophotometric titrations of dilute solutions of L by the metal perchlorates $M(ClO_4)_2 \cdot 6H_2O$ (M = Cu, Zn) and chlorides $MCl_2 \cdot nH_2O$ (M = Co, Ni, n = 6; M = Cu, n = 2; M = Zn, n =0), at 25 °C. For solubility reasons, no supporting electrolyte could be added. Figure 4 shows a typical example of such a titration. Data were analyzed by Specfit[14] and factor analysis gave only two absorbing species for all the systems studied while absorbance versus metal/ligand ratios R displayed breaks at R = 1 (Figure S2, Supporting Information), so that under the experimental conditions used, only 1:1 complexes are formed, in line with the NMR spectroscopic data discussed above. The results reported in Table 3 show that the thermodynamic stability of the complexes is moderate, log K_1 being in the range 4.2−5.4 and increasing slightly with increasing charge density of the metal ions. For zinc and copper complexes, stability constants were determined both with perchlorate and chloride salts to assess the influence of the anion. Only slight differences were obtained, which lie within experimental errors. The fact that perchlorate salts were hexahydrated (M = Cu, Zn) also has to be taken into account: the presence of water molecules can interfere with the formation of the $M(ClO_4)_2L$ complexes while analogous titrations with chloride salts were performed with less hydrated salts (Cu, Zn). In contrast, much larger stability constants are reported for the 1:1 and 1:2 complexes formed with lanthanum perchlorate, e.g. 11.4 ± 1.5 (log K_1) and 19.6 ± 1.8 ($\log\beta_2$),[8c] this much larger stability can be traced back to the larger positive charge borne by the lanthanide cations.

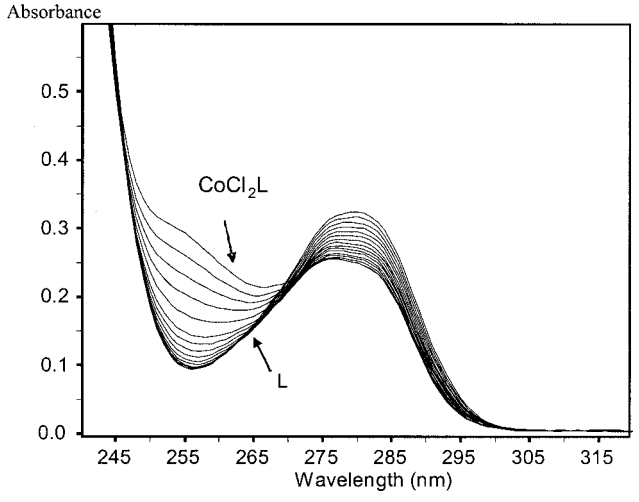

Figure 4. Variation of the absorption spectra observed during the spectrophotometric titration of [L] = 9.51 × 10^{-5} M with [$CoCl_2 \cdot 6H_2O$] = 1.01 × 10^{-3} M

Conclusion

The lower-rim phosphinoyl-substituted calix[4]arene L interacts with divalent 3d transition metal ions M^{II} (M = Co, Ni, Cu and Zn) to yield reasonably stable 1:1 complexes in ethanol. Isolated complexes also display 1:1 stoichiometry, except in the case of the Zn^{II} chloride system for which a tetrametallic species crystallizes, which could be characterized by X-ray crystallography. Both IR and ^{31}P NMR spectroscopic data show the coordination of phosphoryl groups through strong M^{II}−O=P bonds. Magnetochemical measurements and optical spectra cannot be interpreted unambiguously, but most of the reported features point to a tetrahedral arrangement of the ligands around Co^{II} (high-spin d^7), Ni^{II} and Cu^{II}. In view of the ligand conformation, tetrahedral coordination of the four phosphoryl groups can be ruled out, so that the coordination sphere of the metal ions probably contains either 1−2 water molecules and/or chloride or perchlorate ions. We note that magnetic susceptibility data are consistent with isolated and non-interacting magnetic centers, which means that if polymetallic species are also present in the isolated Co, or Ni complexes, such as those evidenced in $[Zn_2Cl_4L]_2$ (**6**), the metal−metal distances are large enough (cf. 7.8−11 Å in **6**) to prevent magnetic interaction.

Experimental Section

Solvent and Starting Materials: The ligand was obtained as described previously.[8c] The metal salts were analytically pure and purchased from Fluka AG and Aldrich. All reagents and solvents were research grade and were used without further purification.

Caution: Perchlorate salts combined with organic ligands are potentially explosive and should be handled in small quantities and with adequate precautions.[15]

Analytical and Physico-Chemical Measurements: Elemental analyses were performed by Dr H. Eder from the Microchemical Laboratory of the University of Geneva (for the determination of C and H) or by the Ilse Beetz Laboratory (96301 Kronach, Germany) for the determination of P and Cl. Atomic absorption (AAS) analyses were performed with a Perkin−Elmer 1100 B spectrometer. IR spectra were obtained from KBr pellets with a Perkin−Elmer Spectrum One FT-IR spectrometer. The ES-MS spectra were obtained with a Finnigan SSQ 710C spectrometer using a capillary tempera-

Table 3. Stability constants of the complexes of L with Co^{II}, Ni^{II}, Cu^{II} and Zn^{II} in CH_3CN; [L] = 10^{-4} M and [M] = 10^{-3} M

	$CoCl_2$	$NiCl_2$[a]	$Cu(ClO_4)_2$	$CuCl_2$	$Zn(ClO_4)_2$	$ZnCl_2$
log K_1	4.8 ± 0.1	4.9 ± 0.1	4.2 ± 0.7	5.0 ± 0.1	4.6 ± 0.3	5.4 ± 0.2

[a] In CH_3CN/CH_2Cl_2 (97.1:2.9, v/v).

 © 2004 Wiley-VCH Verlag GmbH & Co. KGaA, Weinheim

ture of 200 °C and acceleration potential of 4.5 kV. The $10^{-5}-10^{-4}$ M solutions of the free ligand or its complexes dissolved in methanol were infused in a mixture of $CH_3OH/H_2O/HCOOH$ (50:50:1, v/v) for the ligand, or pure CH_3CN for the complexes. ^1H and $^{31}P\{^1H\}$ NMR spectroscopic data ([D_6]DMSO or CD_3OD) were collected with a Bruker AVANCE 400-DRX spectrometer (400 MHz) while EPR spectra of powdered samples were measured with a Bruker B-ER 420 spectrometer. Magnetic susceptibility measurements were performed with a MPMS5 SQUID susceptometer (Quantum Design Inc.) operating at a magnetic field strength of 1 kOe. Corrections for diamagnetism were estimated from Pascal constants.[16] Effective magnetic moments were calculated as $\mu_{eff} = 2.828\ (\chi_{para}\cdot T)^{1/2}$ where χ_{para} is the molar paramagnetic susceptibility of the metal ion.

Spectrophotometric Titrations: For the titrations with chloride salts $MCl_2\cdot nH_2O$ (M = Co, Ni, n = 6; M = Cu, n = 2; M = Zn, n = 0), the electronic spectra in the UV/Vis range were recorded at 298 K with a Perkin−Elmer Lambda-7 connected to an external computer, using quartz cells of 0.100 cm path length. Solutions were prepared in a thermostatted vessel (Metrohm 6.1418.220) kept under Ar and the titrant solution was added with an automated burette from Metrohm (6.1569.150 or.210) fitted with an anti-diffusion device. In a typical experiment, 50 mL of L (10^{-4} M) was titrated with 10^{-3} M solutions of M^{II} salts. After each addition of 0.5 mL and a delay of 15 min to equilibrate the solution, the spectrum was measured and transferred to the computer. Alternatively, titrations with perchlorate salts $M(ClO_4)_2\cdot 6H_2O$ (M = Cu, Zn) were performed with a J&M diode array TIDAS II spectrometer using a thermostatted (20.0 ± 0.1 °C) glass-jacketed vessel filled with Ar. The starting volume was 25 mL and aliquots of the titrant (0.2 mL) were added using a Socorex® micropipette. The solvents used (CH_3CN, CH_2Cl_2) were of spectroscopic grade and purchased from Fluka AG (Buchs, Switzerland). Acetonitrile was dried with molecular sieves (3 Å) and the solutions were stored under argon. The metal-ion content was determined by AAS after decomposition of the samples in boiling 60% $HClO_4$, or, in the case of **5**, by complexometric titration with H_2edta^{2-} in the presence of xylenol orange and urotropine. The phosphorus content of some samples was determined spectrophotometrically using the phosphomolybdate method.[17]

Preparation of the Complexes

$CoL(ClO_4)_2\cdot 2H_2O$ (1): An ethanolic solution (1 mL) of $Co(ClO_4)_2\cdot 2H_2O$ (0.0292 g; 0.0798 mmol) was slowly added to 3 mL of a solution of L (0.1000 g; 0.0957 mmol) in EtOH (3 mL), at room temp. and under constant stirring. A light blue precipitate formed immediately. The reaction mixture was stirred for 8 h. and the precipitate was centrifuged, washed repeatedly with ethanol and dried under high vacuum over P_4O_{10} for 4 h. Yield 0.1029 g (99%). $C_{56}H_{84}Cl_2CoO_{16}P_4\cdot 2H_2O$ (1303.0): calcd. C 51.62, H 6.81, Cl 5.44, Co 4.52, P 9.51; found C 52.05, H 6.87, Cl 5.39, Co 4.59, P 9.74.

$NiL(ClO_4)_2\cdot 2\ H_2O$ (2): A solution of $Ni(ClO_4)_2\cdot 6H_2O$ (0.0292 g; 0.0797 mmol) in 1 mL of ethanol was added dropwise at constant stirring and ambient temperature to a solution of L (0.1000 g; 0.0957 mmol) in 2 mL ethanol. The reaction mixture was stirred for 10 h; the resulting, pale-yellow precipitate was centrifuged, washed repeatedly with ethanol and dried under high vacuum for 4 h. Yield 0.0888 g (85%). $C_{56}H_{84}Cl_2NiO_{16}P_4\cdot 2H_2O$ (1302.83): calcd. C 51.63, H 6.81, Cl 5.44, Ni 4.51, P 9.51; found C 51.60, H 6.80, Cl 5.59, Ni 4.18, P 9.48.

$CuL(ClO_4)_2\cdot 4H_2O$ (3): An ethanolic solution (1 mL) of $Cu(ClO_4)_2\cdot 7H_2O$ (0.0186 g; 0.0478 mmol) was slowly added to 1.5 mL of a solution of L (0.0500 g; 0.0478 mmol) in EtOH, at room temp. and under constant stirring. A lemon-yellow precipitate formed immediately. The reaction mixture was stirred for 8 h. The resulting precipitate was centrifuged, washed repeatedly with ethanol and dried under high vacuum over P_4O_{10} for 4 h. Yield 0.0513 g (82%). $C_{56}H_{84}Cl_2CuO_{16}P_4\cdot 4H_2O$ (1307.7): found C 50.06, H 6.90, Cl 5.33, P 9.25; calcd. C 49.88, H 6.55, Cl 5.28, P 9.22.

$CuLCl_2\cdot 4\ H_2O$ (4): An ethanolic solution of $CuCl_2\cdot 2H_2O$ (0.0272 g; 0.1595 mmol; 0.5 mL was added dropwise to 1 mL of an ethanolic solution of L (0.2000 g; 0.1914 mmol) at constant stirring and room temp. A few minutes after being mixed, an intensely yellow precipitate formed. The complex was centrifuged, washed repeatedly with ethanol and dried under high vacuum over P_4O_{10} for 4 h. Yield 0.1102 g (57%). $C_{56}H_{84}Cl_2CuO_8P_4\cdot 4H_2O$ (1215.7): found C 54.95, H 7.28, Cl 5.96, Cu 5.54, P 10.12; calcd. C 55.33, H 7.63, Cl 5.83, Cu 5.22, P 10.19.

$ZnL(ClO_4)_2\cdot 2H_2O$ (5): A solution of $Zn(ClO_4)_2\cdot 6H_2O$ (0.0323 g, 0.0869 mmol) in ethanol (1.2 mL) was added dropwise to a solution of L (0.1035 g, 0.0956 mmol) in ethanol (0.5 mL) at constant stirring and room temp. The prepared reaction mixture was stirred for 12 h. The white precipitate formed was separated by centrifugation and washed repeatedly with ethanol and dried under high vacuum at 60 °C for 15 h. Yield 0.1160 g (quantitative). $C_{56}H_{84}Cl_2O_{16}P_4Zn\cdot 2H_2O$ (1309.5): found C 51.67, H 6.78, Cl 5.44, P 9.46, Zn 5.05; calcd. C 51.36, H 6.77, Cl 5.44, P 9.46, Zn 4.99.

Zn_2LCl_4 (6): An ethanolic solution (1 mL) of $ZnCl_2$ (0.0237 g; 0.1739 mmol) was added dropwise to 2 mL of an ethanolic solution of L (0.2000 g; 0.1913 mmol), while stirring and the prepared mixture was stirred at room temp. for a further 10 h. The white precipitate obtained was centrifuged, washed repeatedly with ethanol and dried under high vacuum over P_4O_{10} for 30 h. Yield 0.1050 g (94%). $C_{56}H_{84}Cl_4O_8P_4Zn_2$ (1281.76): found C 52.53, H 6.77, Cl 11.16, P 9.95, Zn 10.24; calcd. C 52.48, H 6.60, Cl 11.06, P 9.66, Zn 10.20.

Crystal Structure of 6: Crystals have been obtained by slow concentration of a methanol solution of L and $ZnCl_2$ (each dissolved in 10^{-3} M). Data collection was performed at 140 K with a marresearch mar345 IPDS. Data reduction was carried out with CrysAlis RED, release 1.7.0.[18] An empirical absorption correction was applied to the data set.[19] Structure solution and refinement as well as molecular graphics and geometrical calculations were performed with the SHELXTL software package, release 5.1.[20] The structures were refined using the full-matrix least squares on F^2 with all non-H atoms anisotropically defined. H atoms were placed in calculated positions using the "riding model" (except those belonging to water molecules, which were not included in the final model) and fixing their U_{iso} to 0.08 Å^2. The crystals are triclinic, space group $P\bar{1}$, Z = 2, with a = 16.033(8) Å, b = 16.654(7) Å, c = 26.727(17) Å, α = 100.07(4)°, β = 93.18(5)°, γ = 95.07(4)°. CCDC-219688 contains the supplementary crystallographic data for this paper which can be obtained free of charge at www.ccdc.cam.ac.uk/conts/retrieving.html [or from the Cambridge Crystallographic Data Centre, 12 Union Road, Cambridge CB2 1EZ, UK; Fax: (internat.) + 44-1223-336-033; E-mail: deposit@ccdc.cam.ac.uk].

Acknowledgments

The authors thank Assoc. Prof. Dr. Elena Russeva for her help in the determination of the phosphorus contents, Dr. Lucia Bonomo and Dr. Geoffroy Guillemot for magnetic susceptibility measurements, Dr Vittorio Esposito for a gift of *p-tert*-butylcalix[4]arene, and Dr. Natacha Guérin for collecting some of the NMR spectro-

scopic data. This work was supported through a grant from the Swiss National Science Foundation (Project SCOPES 7BUPJ062293.00/1).

[1] *Calixarenes 2001* (Eds.: Z. Asfari, V. Böhmer, J. Harrowfield, J. Vicens), Kluwer Academic Publ., Dordrecht, **2001**.
[2] *Calixarenes for Separations* (Eds.: G. J. Lumetta, R. D. Rogers, A. Gopalan), ACS Symposium Series, American Chemical Society, Washington D. C., **2000**, vol. 757.
[3] M. P. O. Wolbers, F. C. J. M. Vanveggel, F. G. A. Peters, E. S. E. Vanbeelen, J. W. Hofstraat, F. J. Geurts, D. N. Reinhoudt, *Chem. Eur. J.* **1998**, *4*, 772−780.
[4] F. de M. Ramirez, S. Varbanov, C. Cécile, G. Muller, N. Fatin-Rouge, R. Scopelliti, J.-C. G. Bünzli, *J. Chem. Soc., Dalton Trans.* **2002**, 4505−4513.
[5] [5a] C. Wieser-Jeunesse, D. Matt, M. R. Yaftian, M. Burgard, J. M. Harrowfield, *C. R. Acad. Sci. Paris, Ser. IIC* **1998**, *1*, 479−502. [5b] S. Barboso, M. A. G. Carrera, S. E. Matthews, F. Arnau-Neu, V. Böhmer, J. F. Dozol, H. Rouquette, M. J. Schwing-Weill, *J. Chem. Soc., Perkin Trans. 2* **1999**, 719−723. [5c] A. Arduini, V. Böhmer, L. Delamu, J.-F. Desreux, J.-F. Dozol, M. A. G. Carrera, B. Lambert, C. Musigmann, A. Pochini, A. Shivanyuk, F. Ugozzoli, *Chem. Eur. J.* **2000**, 2135−2144. [5d] S. E. Matthews, P. Parzuchowski, A. Garcia-Carrera, C. Gruttner, J. F. Dozol, V. Böhmer, *Chem. Commun.* **2001**, 417−18. [5e] Yu. I. Rudzevich, A. B. Drapailo, V. L. Rudzevich, V. I. Miroshnichenko, V. I. Kalchenko, I. V. Smirnov, V. A. Babain, A. A. Varnek, G. Wipff, *Russ. J. Gen. Chem.* **2002**, *72*, 1736−1742.
[6] J. M. Harrowfield, "Metal Ions in Biological Systems" in *The Lanthanides and Their Interrelations With Biosystems* (Eds.: A. Sigel, H. Sigel), M. Dekker Inc., New York, **2003**, vol. 40, chapter 4.
[7] [7a] P. Molenved, J. F. J. Engbersen, D. N. Reinhoudt, *Chem. Soc. Rev.* **2000**, *29*, 75−86. [7b] H. Ma, Q. Ma, M. Su, L. Nie, H. Han, S. Xiong, B. Xin, G. Liu, *New. J. Chem.* **2002**, *26*, 1456−60. [7c] I. A. Bagatin, E. S. de Souza, A. S. Ito, H. E. Toma, *Inorg. Chem. Commun.* **2003**, *6*, 288−293.
[8] [8a] F. de M. Ramirez, L. J. Charbonnière, G. Muller, R. Scopelliti, J.-C. G. Bünzli, *J. Chem. Soc., Dalton Trans.* **2001**, 3205−3213. [8b] F. de M. Ramirez, L. J. Charbonnière, G. Muller, J.-C. G. Bünzli, *Eur. J. Inorg. Chem.*, in press. [8c]L. Le Saulnier, S. Varbanov, R. Scopelliti, M. Elhabiri, J.-C. G. Bünzli, *J. Chem. Soc., Dalton Trans.* **1999**, 3919−3925.
[9] G. B. Deacon, J. H. S. Green, *Spectrochim. Acta, Part A* **1968**, *24*, 845−852.
[10] G. Borisov, S. Varbanov, L. M. Venanzi, A. Albinati, F. Demartin, *Inorg. Chem.* **1994**, *33*, 5430−5437.
[11] C. M. Mikulski, L. L. Pytlewski, N. M. Karayannis, *Synth. React. Inorg. Met.-Org. Chem.* **1979**, *9*, 401−408.
[12] B. N. Figgis, J. Lewis, *Prog. Inorg. Chem.* **1964**, *6*, 37−222.
[13] F. A. Cotton, G. Wilkinson, *Advanced Inorganic Chemistry*, 5th ed., Wiley Interscience, New York, **1988**.
[14] H. Gampp, M. Maeder, C. J. Meyer, A. D. Zuberbühler, *Talanta* **1985**, *23*, 1133−1139.
[15] K. N. Raymond, *Chem. Eng. News* **1983**, *61*, 4.
[16] L. N. Mulay in *Theory and Applications of Molecular Paramagnetism* (Eds.: E. A. Boudreaux, L. N. Mulay), John Wiley & Sons, New York **1976**, p. 491−495.
[17] S. G. Varbanov, E. D. Russeva, N. N. Nikolov, *Bulg. Chem. Commun.* **1999**, *26*, 91−97.
[18] Oxford Diffraction Ltd., Abingdon, Oxfordshire, UK, **2003**.
[19] DELABS: N. Walker, D. Stuart, *Acta Crystallogr., Sect. A* **1983**, *39*, 158−166.
[20] G. M. Sheldrick, University of Göttingen, Germany, **1997**; Bruker AXS, Inc., Madison, Wisconsin 53719, USA, **1997**.

Received November 20, 2003
Early View Article
Published Online April 6, 2004

 © 2004 Wiley-VCH Verlag GmbH & Co. KGaA, Weinheim

Structure, Bonding, and Tyrosinase-Like Reactivity of Copper Complexes Coordinated by Mononucleating Tridentate N−O−N Type Ligands

Yen-Ting Cheng,[a] Hsiao-Lan Chen,[a] Shiou-Yuan Tsai,[a] Chan-Cheng Su,*[a] Huan-Sheng Tsang,[a] Ting-Shen Kuo,[a] Yi-Chou Tsai,[b] Fen-Ling Liao,[b] and Sue-Lein Wang[b]

Keywords: Enzyme models / N,O ligands / Copper / Oxidations

Copper complexes with mononucleating tridentate ligands of the N–O–N type, including 1,3-bis(benzimidazol-2-yl)-2-oxapropane (bbmo), 1,3-bis(*N*-methylbenzimidazol-2-yl)-2-oxapropane (bb^{Me}mo), 1,3-bis(*N*-*n*-propylbenzimidazol-2-yl)-2-oxapropane (bb^{Pr}mo), and 1,3-bis(pyrid-2-yl)-2-oxapropane (bpmo), were tested for the oxygenation of phenols. Mixed ligand copper complexes of [Cu(N–O–N)(N–N)](ClO$_4$)$_2$, where N–N denotes 2,2′-bipyridine (bipy), 1,10-phenanthroline (phen), ethylenediamine (en), and/or *N*,*N*,*N*′,*N*′-tetramethylethylenediammine (tmen), were prepared and characterized by elemental analyses, and electronic, vibrational, and epr spectroscopic measurements. The molecular structures of *fac*-[Cu(bb^{Me}mo)(bipy)(H$_2$O)](ClO$_4$)$_2$(H$_2$O) (**1a**), *fac*-[Cu(bb^{Me}mo)(phen)](ClO$_4$)$_2$(CH$_3$CN) (**4a**), *fac*-[Cu(bb^{Pr}mo)(phen)](ClO$_4$)$_2$ (**5a**), and *fac*-[Cu(bpmo)(bipy)(ClO$_4$)](ClO$_4$) (**7a**) were determined by X-ray diffraction methods. The structures of these complexes are square pyramids or elongated octahedra with the heterocycle nuclei forming the basal or equatorial planes. The terminal heterocycles of the facially coordinated tridentate ligands are nearly perpendicular to the basal or equatorial planes. Similar structures are proposed for the remaining complexes, based on spectroscopic data. Both stoichiometric and catalytic oxidation reactions of 2,4-di-*tert*-butylphenol and 2,4-di-*tert*-butylphenolate with dioxygen adducts of [Cu(bb^{Pr}mo)]$^+$ at room temperature afforded 3,3′,5,5′-tetra-*tert*-butyl-2,2′-biphenol and 3,5-di-*tert*-butyl-*o*-quinone. Similar reactions with the dioxygen adduct of [Cu(bpmo)]$^+$ yielded only 3,3′,5,5′-tetra-*tert*-butyl-2,2′-biphenol. In light of the tyrosinase-like reactivity, the possible intermediates, [(bb^{Pr}mo)$_2$Cu$_2$(μ-η^2:η^2-peroxo)]$^{2+}$, [(bb^{Pr}mo)$_2$Cu$_2$(μ-oxo)$_2$]$^{2+}$, and [(bpmo)$_2$Cu$_2$(μ-oxo)$_2$]$^{2+}$ are proposed.
(© Wiley-VCH Verlag GmbH & Co. KGaA, 69451 Weinheim, Germany, 2004)

Introduction

Tyrosinase and hemocyanins represent type 3 copper proteins that have been extensively characterized.[1−3] Their dicopper active sites bind dioxygen via the redox process, 2 Cu^{I} + O$_2$ → Cu^{II}(O$_2^{2-}$)Cu^{II}, to form (μ-η^2:η^2-peroxo)dicopper(II) units.[4] The formation of (μ-η^2:η^2-peroxo)dicopper(II) cores is likely governed by enclosure by the bulky protein residues and by the bonding capability of the three-coordinated imidazoles of the histidine residues to each copper. These peroxo units may be further involved in O$_2$ activation, via the *o*-hydroxylation of the phenol of tyrosine by tyrosinase, or take the reverse process, functioning as O$_2$ carriers in hemocyanins. To date some well-characterized peroxodicopper(II) complexes have been reported involving ligands with heterocycles other than imidazole,[5−8] or even without heterocycles.[9−14] Although these complexes are generally not stable at room temperature in contrast to their biological counterparts, they can be used as models to mimic the structures and/or functions of the active centers of the native systems. Among the three classes of synthetic peroxodicopper(II) complexes shown in Scheme 1,[15] μ-η^2:η^2-peroxodicopper(II) behaves differently from the other two and has a nonbasic or electrophilic reactivity.[16−18] Depending on the specific ligand, steric bulk, counterion, and solvent effects, μ-η^2:η^2-peroxodicopper(II) complexes have been shown to be in equilibrium with the isoelectronic bis(μ-oxo)dicopper(III) species.[11,19−23] Their substrate reactivities are different. The μ-η^2:η^2-peroxodicopper(II) favors oxygen atom transfer reactions,[18] while the bis(μ-oxo)dicopper(III) prefers hydrogen atom abstraction.[24] The oxidation reactions of phenolates with μ-η^2:η^2-peroxodicop-

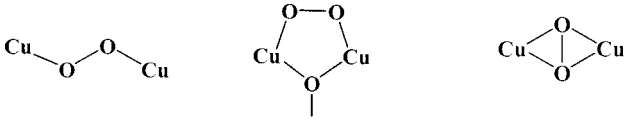

trans-μ-1,2-peroxo *cis*-1,2-peroxo μ-η^2 : η^2-peroxo

Scheme 1. Types of peroxodicopper(II) species

[a] Department of Chemistry, National Taiwan Normal University, Taipei 11718, Taiwan, ROC
Fax: (internat.) + 996-29324249
E-mail: chefv003@scc.ntnu.edu.tw
[b] Department of Chemistry, National Tsing Hua University, Hsinchu, Taiwan, ROC

 © 2004 Wiley-VCH Verlag GmbH & Co. KGaA, Weinheim DOI: 10.1002/ejic.200300636

per(II) mainly afford catechols and *o*-quinones,[25] whereas similar reactions of phenols with bis(μ-oxo)dicopper(III) give rise to biphenols.[26]

In this report we describe the structures and substrate reactivity of a class of copper complexes coordinated by mononucleating tridentate ligands of N−O−N type, including 1,3-bis(benzimidazol-2-yl)-2-oxapropane (bbmo), 1,3-bis(*N*-methylbenzimidazol-2-yl)-2-oxapropane ($bb^{Me}mo$), 1,3-bis(*N*-*n*-propylbenzimidazol-2-yl)-2-oxapropane ($bb^{Pr}mo$), and 1,3-bis(pyrid-2-yl)-2-oxapropane (bpmo). The oxidation reactions of 2,4-di-*tert*-butylphenol and 2,4-di-*tert*-butylphenolate with dioxygen in the presence of stoichiometric or catalytic amounts of $[Cu(bb^{Pr}mo)]^+$ or $[Cu(bpmo)]^+$ at room temperature resulted in the generation of 3,3′,5,5′-tetra-*tert*-butyl-2,2′-biphenol and/or 3,5-di-*tert*-butyl-*o*-quinone, inferring the formation of bis(μ-oxo)dicopper(III) and/or (μ-η^2:η^2-peroxo)dicopper(II) intermediates during the reactions. The purpose of this report is to elucidate the conformation and coordination properties of the N−O−N tridentate ligands in order to reveal their roles in the peroxodicopper(II)/bis(μ-oxo)dicopper(III) equilibrium and substrate reactivity.

Results and Discussion

Synthesis of Complexes

The mixed-ligand complexes, $[Cu(bbmo)(LL)]^{2+}$, $[Cu(bb^{Me}mo)(LL)]^{2+}$, $[Cu(bb^{Pr}mo)(LL)]^{2+}$, and $[Cu(bpmo)(LL)]^{2+}$ (LL = phen and/or bipy), were prepared by the addition of one equivalent of the bidentate ligand, phen or bipy, to a 1:1 mixture of Cu^{II} perchlorate and the tridentate ligand, bbmo, $bb^{Me}mo$, $bb^{Pr}mo$, or bpmo. Attempts to prepare the 1:1 complexes, $[Cu(N-O-N)]^{2+}$, by mixing equivalent amounts of the ligands and copper perchlorate were unsuccessful. Instead, the 1:2 complexes, $[Cu(N-O-N)_2]^{2+}$, were isolated. In the case of the en and tmen complexes, only $[Cu(bb^{Pr}mo)(en)](ClO_4)_2$ (**6**) and $[Cu(bpmo)(tmen)](ClO_4)_2$ (**9**) complexes were isolated in pure form. As evidenced from X-ray structure results (vide infra) and spectroscopic studies, the tridentate ligands bond to the central Cu^{II} ion in a facial conformation for all of the mixed ligand complexes, in agreement with the usual findings that the strong benzimidazole and pyridine donors tend to bind at the equatorial positions and the weak ether oxygen at the axial site for the Cu^{II} complexes.

X-ray Structures

fac-$[Cu(bb^{Me}mo)(bipy)(H_2O)](ClO_4)_2(H_2O)$ (1a), *fac*-$[Cu(bb^{Me}mo)(phen)](ClO_4)_2(CH_3CN)$ (4a), and *fac*-$[Cu(bb^{Pr}mo)(phen)](ClO_4)_2$ (5a)

The molecular structures of mixed ligand complexes **1a**, **4a**, and **5a** are shown in Figures 1, 2, and 3, respectively. Selected bond lengths and angles are listed in Table 1. These complexes are composed of discrete copper complex cations, perchlorate anions, and/or solvent molecules. In the case of complex **1a**, the copper cation binds a H_2O molecule at the axial site to complete an elongated octahedron, with the copper slightly above the equatorial plane, inclined toward the H_2O. The deviations from the best equatorial plane of CuN_4 are Cu(1) +0.1709 Å, N(1) −0.1320 Å, N(2) +0.0499 Å, N(3) −0.1298 Å, and N(5) +0.0411 Å. The structures of the complex cations of **4a** and **5a** are square pyramidal [τ = 0.162 (**4a**); τ = 0.017 (**5a**)], because the perchlorate ions are too far away from the central copper ions. The deviations from the best basal plane of CuN_4 are Cu(1) +0.0467 Å, N(1) −0.0358 Å, N(2) +0.0136 Å, N(3) −0.0351 Å, and N(5) +0.0106 Å for **4a**, Cu(1) +0.0101 Å, N(1) −0.0087 Å, N(2) +0.0039 Å, N(3) −0.0084 Å, and N(5) +0.0032 Å for **5a**. The complex cations contain a facial $bb^{Me}mo$ or $bb^{Pr}mo$, with an elongated axial Cu−O of 2.570(4) Å for **1a**, 2.520(3) Å for **4a**, and 2.527(4) Å for **5a**. The fact that these axial Cu−O distances are significantly shorter than the corresponding axial Cu−N of 2.597(6) Å for the *trans*-*fac*-$[Cu(bbmn)_2](ClO_4)_2(H_2O)_2$ complex[27] (bbmn = 1,3-bis(benzimidazol-2-yl)-2-azapropane) is unexpected. The mean Cu−N distances and the intraligand ∠N−Cu−N angles of the tridentate ligands are 1.984±0.004 Å and 91.6(2)° for **1a**, 1.981±0.004 Å and 89.8(1)° for **4a**, and 1.995±0.006 Å and 88.1(2)° for **5a**. The mean bite angles of the five-member chelates of the tridentate ligands are 73.3±0.3° for **1a**, 75.6±0.2° for **4a**, and 75.6±0.2° for **5a**. The benzimidazole nuclei of these complexes lie nearly perpendicular to the CuN_4 basal or equatorial plane, with dihedral angles of 94.6° and 111.7° for **1a**, 89.4° and 105.9° for **4a**, and 86.5° and 93.5° for **5a**. All these geometric figures are analogous to those reported for *trans*-*fac*-$[Cu(bbmn)_2](ClO_4)_2(H_2O)_2$[27] (mean Cu−N of 2.010±0.008 Å; intraligand ∠N−Cu−N of 88.1°; mean bite angle of the five-member chelates ∠N−Cu−N of 74.9±0.4°), suggesting that the coordination capabilities of

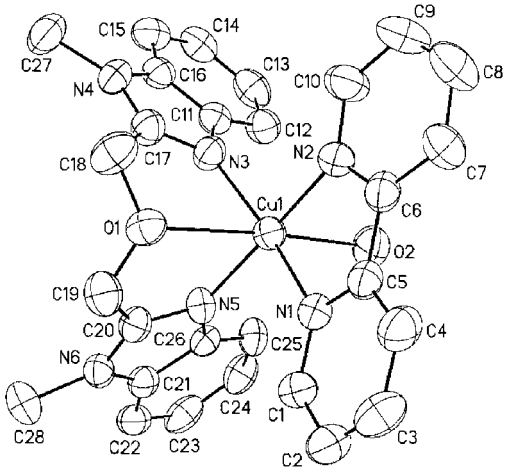

Figure 1. ORTEP diagram of *fac*-$[Cu(bb^{Me}mo)(bipy)(H_2O)](ClO_4)_2(H_2O)$ (**1a**); perchlorates, H_2O, and hydrogen atoms have been omitted for clarity

 © 2004 Wiley-VCH Verlag GmbH & Co. KGaA, Weinheim

the tridentate ligands of these mixed ligand complexes are similar.

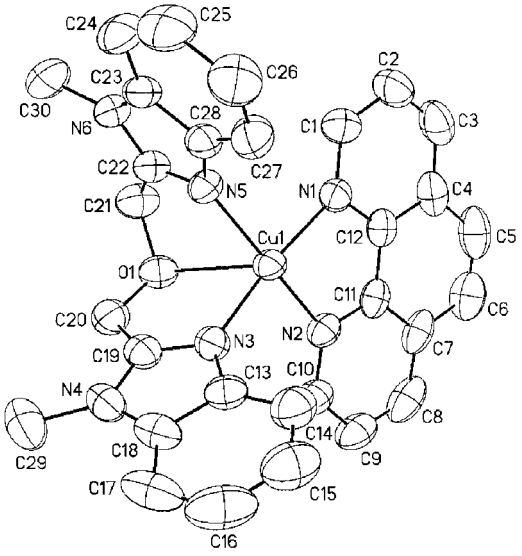

Figure 2. ORTEP diagram of *fac*-[Cu(bb^{Me}mo)(phen)]-$(ClO_4)_2(CH_3CN)$ (**4a**); perchlorates, CH_3CN, and hydrogen atoms have been omitted for clarity

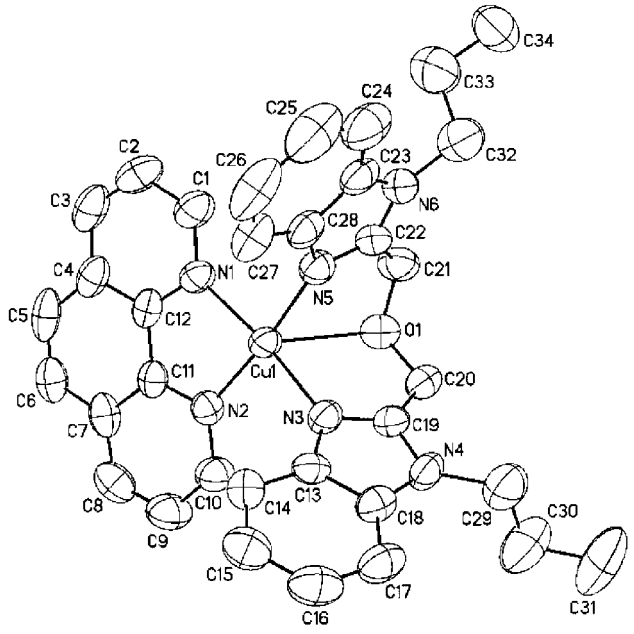

Figure 3. ORTEP diagram of *fac*-[Cu(bb^{Pr}mo)(phen)]$(ClO_4)_2$ (**5a**); perchlorates and hydrogen atoms have been omitted for clarity

It is interesting to note that the mean Cu−N bond lengths of 2.010±0.016 Å and the bite angles of 81.3±0.5° for the diimine ligands of these three complexes are also very similar, indicative of similar bonding abilities of the diimine ligands. Although the thermal vibrations are somewhat large for some oxygen atoms of the perchlorates, the bond lengths and angles of these complexes are in the normal ranges.[27−29] The largest difference peaks of 1.108 for **1a** and 1.281 for **5a** appear near the Cl(1) atom for **1a** and Cl(2) for **5a**, respectively.

Table 1. Selected bond lengths (Å) and angles (°) for complexes **1a**, **4a**, **5a**, and **7a**

fac-[Cu(bb^{Me}mo)(bipy)(H_2O)]$(ClO_4)_2(H_2O)$ (**1a**)

Cu(1)−N(1) 2.022(4)	Cu(1)−N(2) 2.013(4)
Cu(1)−N(3) 2.000(4)	Cu(1)−N(5) 1.989(4)
Cu(1)−O(1) 2.527(4)	Cu(1)−O(2) 2.368(4)
N(1)−Cu(1)−N(2) 80.8(2)	N(1)−Cu(1)−N(3) 162.3(2)
N(1)−Cu(1)−N(5) 94.7(2)	N(2)−Cu(1)−N(3) 94.3(2)
N(2)−Cu(1)−N(5) 172.0(2)	N(3)−Cu(1)−N(5) 88.1(2)
N(1)−Cu(1)−O(1) 88.0(2)	N(2)−Cu(1)−O(1) 97.7(2)
N(3)−Cu(1)−O(1) 75.8(2)	N(5)−Cu(1)−O(1) 75.4(2)
N(1)−Cu(1)−O(2) 91.4(2)	N(2)−Cu(1)−O(2) 86.5(2)
N(3)−Cu(1)−O(2) 105.3(2)	N(5)−Cu(1)−O(2) 100.3(2)
O(1)−Cu(1)−O(2) 175.5(2)	

fac-[Cu(bb^{Me}mo)(phen)]$(ClO_4)_2(CH_3CN)$ (**4a**)

Cu(1)−N(1) 2.020(4)	Cu(1)−N(2) 2.006(3)
Cu(1)−N(3) 1.979(3)	Cu(1)−N(5) 2.000(3)
Cu(1)−O(1) 2.529(3)	
N(1)−Cu(1)−N(2) 81.8(2)	N(1)−Cu(1)−N(3) 173.0(1)
N(1)−Cu(1)−N(5) 93.0(1)	N(2)−Cu(1)−N(3) 93.9(2)
N(2)−Cu(1)−N(5) 167.7(1)	N(3)−Cu(1)−N(5) 92.2(2)
N(1)−Cu(1)−O(1) 111.7(1)	N(2)−Cu(1)−O(1) 97.4(1)
N(3)−Cu(1)−O(1) 74.3(1)	N(5)−Cu(1)−O(1) 74.0(2)

fac-[Cu(bb^{Pr}mo)(phen)]$(ClO_4)_2$ (**5a**)

Cu(1)−N(1) 2.016(4)	Cu(1)−N(2) 2.005(4)
Cu(1)−N(3) 1.980(4)	Cu(1)−N(5) 1.987(4)
Cu(1)−O(1) 2.570(4)	
N(1)−Cu(1)−N(2) 81.4(2)	N(1)−Cu(1)−N(3) 173.3(2)
N(1)−Cu(1)−N(5) 93.2(2)	N(2)−Cu(1)−N(3) 93.7(2)
N(2)−Cu(1)−N(5) 174.3(2)	N(3)−Cu(1)−N(5) 91.6(2)
N(1)−Cu(1)−O(1) 112.5(2)	N(2)−Cu(1)−O(1) 110.7(2)
N(3)−Cu(1)−O(1) 73.5(2)	N(5)−Cu(1)−O(1) 73.0(2)

fac-[Cu(bpmo)(bipy)(ClO_4)](ClO_4) (**7a**)

Cu(1)−N(1) 2.031(4)	Cu(1)−N(2) 2.028(4)
Cu(1)−N(3) 2.003(4)	Cu(1)−N(4) 1.994(4)
Cu(1)−O(1) 2.323(4)	Cu(1)−O(2) 2.417(4)
N(1)−Cu(1)−N(2) 85.8(2)	N(1)−Cu(1)−N(3) 174.3(2)
N(1)−Cu(1)−N(4) 97.0(2)	N(2)−Cu(1)−N(3) 95.0(2)
N(2)−Cu(1)−N(4) 172.5(2)	N(3)−Cu(1)−N(4) 81.6(2)
N(1)−Cu(1)−O(1) 79.3(2)	N(2)−Cu(1)−O(1) 79.0(2)
N(3)−Cu(1)−O(1) 95.3(2)	N(4)−Cu(1)−O(1) 94.6(2)
N(1)−Cu(1)−O(2) 89.7(2)	N(2)−Cu(1)−O(2) 98.1(2)
N(3)−Cu(1)−O(2) 95.8(2)	N(4)−Cu(1)−O(2) 89.0(2)
O(1)−Cu(1)−O(2) 168.8(2)	

fac-[Cu(bpmo)(bipy)(ClO_4)](ClO_4) (7a)

The molecular structure of **7a** is shown in Figure 4. Selected bond lengths and angles are listed in Table 1. The discrete elongated octahedral copper(II) complex cation comprises a facial bpmo, an equatorial bipy, and a perchlorate anion at the axial site. The deviations from the best equatorial plane of CuN_4 are Cu(1) +0.088 Å, N(1) −0.012 Å, N(2) −0.033 Å, N(3) −0.010 Å, and N(4) −0.033 Å. The facial bpmo has a mean Cu−N distance of 2.030±0.002 Å,

 © 2004 Wiley-VCH Verlag GmbH & Co. KGaA, Weinheim

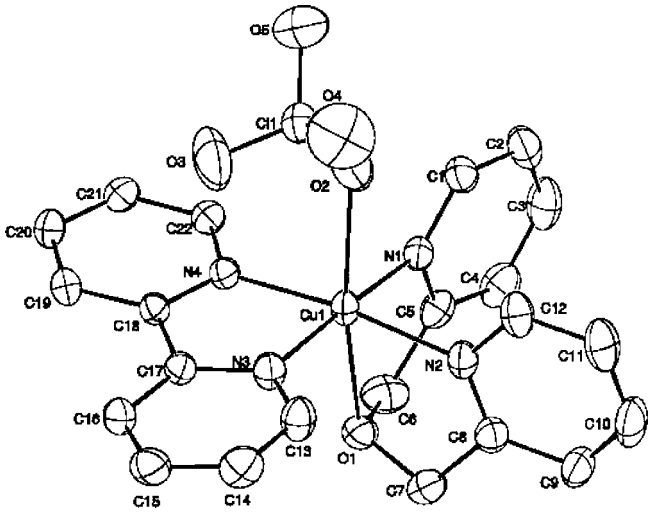

Figure 4. ORTEP diagram of *fac*-[Cu(bpmo)(bipy)(ClO_4)](ClO_4) (**7a**); one perchlorate and hydrogen atoms have been omitted for clarity

which is slightly longer than that of complex **1a** of 1.984±0.004 Å. However, the axial Cu−O of 2.323(4) Å of the bpmo is shorter than that of complex **1a** of 2.570(4) Å. It is likely that the bonding ability of the pyridine nucleus in bpmo is weaker than that of the benzimidazole nucleus.

Table 2. EPR spectroscopic data for bbmo, $bb^{Pr}mo$, $bb^{Me}mo$, and bpmo Cu^{II} complexes[a]

$g_{\|}$	$g_{\perp}$	$A_{\|}$(Cu)	$A_{\perp}$(Cu)	$A_{\perp}$(N)	$A_{\perp}$(N′)[b]	
[Cu($bb^{Pr}mo$)(en)](ClO_4)$_2$ (**6**)						
2.232	(2.052 2.013)[c]	197				Powder
2.269	2.086	184	17	17	16	dmf glass
[Cu(bpmo)(tmen)](ClO_4)$_2$ (**9**)						
2.216	2.066					Powder
2.259	2.082	182	17	17	14	dmf glass
[Cu($bb^{Me}mo$)(bipy)](ClO_4)$_2$ (**1**)						
2.214	2.060	190				Powder
2.289	2.084	184	17	17	16	dmf glass
[Cu($bb^{Pr}mo$)(bipy)](ClO_4)$_2$(H_2O) (**2**)						
2.260	(2.073 2.008)[c]					Powder
2.286	2.084	184	17	17	16	dmf glass
[Cu(bbmo)(bipy)](ClO_4)$_2$(CH_3CN)$_{0.5}$ (**3**)						
2.249	(2.166 2.067)[c]	181				Powder
2.288	2.085	184	17	17	14	dmf glass
[Cu(bpmo)(bipy)](ClO_4)$_2$(H_2O)$_{0.5}$ (**7**)						
[d]	2.070					Powder
2.277	2.085	182	18	17	14	dmf glass
[Cu($bb^{Me}mo$)(phen)](ClO_4)$_2$(H_2O)$_3$ (**4**)						
2.230	2.057	174				Powder
2.293	2.086	184	17	17	16	dmf glass
[Cu($bb^{Pr}mo$)(phen)](ClO_4)$_2$(H_2O)$_2$ (**5**)						
2.251	(2.073 2.008)[c]	166				Powder
2.291	2.085	184	17	17	15	dmf glass
[Cu(bpmo)(phen)](ClO_4)$_2$(H_2O)$_{0.5}$ (**8**)						
2.233	2.066	185				Powder
2.279	2.084	183	17	17	15	dmf glass

[a] X-band EPR spectra measured at room temperature for powder samples, and at 77 K for glass. Hyperfine coupling constants in 10^{-4} cm^{-1}. [b] N′ denotes the second nitrogen. [c] Rhombic powder spestrum with g_y and g_x. [d] Not observed.

The pyridine nuclei of the bpmo lie nearly perpendicular to the CuN_4 equatorial plane, with dihedral angles of 89.6° and 92.9°. A comparison of the mean Cu−N bond lengths of bipy of 1.999±0.005 Å for **7a** with that of 2.010±0.016 Å for complex **1a** suggests that the bonding capability of the bipy is nearly equal in these two complexes. The bond lengths and angles of complex **7a** are in the normal ranges.

Spectroscopic Studies

Selected i.r. data are listed in the Experimental section. In the 3500 cm^{-1} region, broad O−H stretching absorption peaks appear for some of the complexes, suggesting the presence of H_2O. Two characteristic N−H stretching peaks at 3345 and 3283 cm^{-1} indicate the en ligand in (**6**). There are some characteristic vibration absorptions for the heterocycle nuclei including the C=N and C=C stretching at ca.1600 to 1480 cm^{-1}, aromatic C−H bending at ca. 740 cm^{-1}, and ring deformation at ca. 430 cm^{-1}. It is generally useful to account for the coordination of the perchlorate by counting the number of very strong ν(Cl−O) at ca. 1100 cm^{-1}. However, care must be exercised in elucidating the complexes with N−O−N tridentate ligands, because of the interference by the strong ν(C−O) peaks in the same region. For some complexes, the Cu−N stretching peaks in the ca. 300 cm^{-1} region are tentatively assigned.

Table 2 lists e.p.r. spectroscopic data of the compounds. The powder e.p.r. spectra of the axial or axial rhombic types of these complexes are consistent with square pyramidal and tetragonal structures and indicative of a $d_{x^2-y^2}$ or d_{xy} ground state.[30−31] For the glass spectra in dmf, CH_3OH/CH_3CN, or CH_3CN matrices, characteristic superhyperfine splittings were observed for all of the complexes. The g_z values are larger in dmf glass than in CH_3OH/CH_3CN or CH_3CN matrices, while the reverse is true for the A_z values. It is likely that the coordination of the axial ether oxygen of the tridentate ligand is replaced by the dmf molecule, consistent with the UV/Vis spectroscopic data (vide infra), and that the basal or equatorial plane is also slightly distorted toward a tetrahedron.[32]

Electronic spectroscopic data for the tridentate complexes are shown in Table 3. The reflectance LF spectra of the mixed-ligand complexes exhibit similar envelopes with a main peak at ca. 524 nm to ca. 710 nm and a pronounced shoulder or small peak on the low energy side of ca. 900 nm extending to ca. 1200 nm. In CH_3OH/CH_3CN or CH_3CN solution, these complexes show a peak at ca. 560 nm to ca. 610 nm with a shoulder at ca. 900 nm extending to 1200 nm, suggesting that the structures of the dissolved complexes are either square pyramidal or tetragonal, as are their solid counter species. The LF band maxima suggest that the bonding strengths of the N-donor ligands are consistent with their σ-donating capabilities, namely, amines are stronger than imines. However, it is noteworthy that the d-d bands (reflectance and acetonitrile solution) appear in general at higher energy region for bpmo complexes than the corresponding $bb^{R}mo$ (R = Pr, Me, and H) complexes. Because pyridine and benzimidazole have comparable basicities, the differences in the ligand field spectra are attribu-

 © 2004 Wiley-VCH Verlag GmbH & Co. KGaA, Weinheim

Table 3. Electronic spectroscopic data for bbmo, bb^{Pr}mo, bb^{Me}mo, and bpmo Cu^{II} complexes

Compd.	Intraligand λ_{max} ($\varepsilon \times 10^3$), nm[a]	CT λ_{max} (ε), nm[a]	LF λ_{max} (ε), nm[a]
6/rflx.			570, 800 sh 1100 sh
6/MeOH[b]	252 (20.0), 257 (19.5), 273 (17.5), 279 (17.4), 285 sh (13.5)	337 (360)	570 (79)
6/dmf	273 (16.9), 279 (17.7), 287 (14.4)	322 sh (970)	586 (75)
9/rflx.			524, 623 sh
9/MeCN	259 (12.5)	300 sh (5700)	560 (76), 800 sh (16)
9/dmf			658 (87)
1/rflx.			638, 1100
1/MeCN[c]	244 (30.5), 274 (19.8), 281 (19.3), 302 (16.5), 312 (15.0)	363 sh (450)	605 (77), 950 (20)
1/dmf	275 (46.7), 288 (28.8), 300 sh (20)		640 (80), 950 sh (15)
2/rflx.			668 1100 sh
2/MeOH[b]	247 (32.8), 274 (25.0), 280 (24.7), 301 (17.8), 311 (16.0)	362 sh (530)	609 (78), 845 (24)
2/dmf	282 sh (29.2), 287 (29.8), 300 sh (21.5), 312 sh (17.3)		640 (87), 850 (31)
3/rflx.			670 1100
3/MeCN	240 (27.6), 273 (18.2), 280 (17.0), 302 (13.8), 312 (12.6)	364 sh (540)	600 (84), 987 sh (20)
3/dmf			623 (98)
7/rflx.			628
7/MeCN	231 sh (22.5), 256 (23.1), 273 sh (15.1), 301 (12.5), 312 (10.7)		605 (54), 850 sh (15)
7/dmf	300 (11.1), 312 (9.20)	382 sh (280)	645 (58), 900 sh (20)
4/rflx.			558, 630, 800 sh
4/MeCN[c]	235 sh (35.4), 250 sh (25.6), 273 (47.0), 295 sh (10.6)	368 sh (540)	605 (80), 900 sh (28)
4/dmf	282 (30.7), 288 (30.1), 300 sh	313 (11300), 417 (747)	663 (97), 950 sh (30)
5/rflx.			710 1100 sh
5/MeOH[b]	204 (132), 230 sh (48.6), 273 (61.3), 297 sh (14.6)	362 sh (550)	607 (75), 845 sh (14)
5/dmf	274 (54.5), 287 sh (32.5), 294 sh (18.2)	405 sh (410)	637 (83), 845 sh (25)
8/rflx.			633
8/MeCN	205 (47.3), 226 (40.5), 258 sh (36.5), 268 (36.9), 295 sh (9.93)		611 (53), 850 sh (14)
8/dmf	271 (36.0), 296 sh (10.9)	382 sh (292)	651 (57), 965 sh (14)
L1/MeOH	247 (13.5), 252 sh (13.3), 270 sh (12.1), 275 (15.8), 282 (14.5)		
L1/EtOH[d]	252 (13.8), 272 (17.0), 282 (15.1)		
L2/MeOH	253 sh (13.8), 258 (14.6), 272 sh (12.9), 278 (14.6), 287 (12.5)		
L3/MeOH	258 (17.4), 272 sh (14.9), 278 (16.3), 286 (13.4)		
L4/MeCN	256 sh (13.4), 260 (13.9), 266 sh (11.2)		

[a] ε in $M^{-1}cm^{-1}$. [b] MeOH/MeCN = 2:1. [c] Contains 10% MeOH. [d] Ref.[42]

table to the π-interactions between the copper d_π orbitals and the π orbitals of the heterocycles of the tridentate ligands.

The intraligand transitions for the N−O−N tridentate ligands are assigned in the ca. 245 nm to ca. 290 nm region. There are essentially no shifts of the π→π* transition peaks of the tridentate ligands for the en and tmen complexes as compared with those of the corresponding free ligand molecules. Despite some interference due to the diimine ligands, blue shifts of the π→π* transition peaks of the tridentate ligands were observed for the mixed-ligand bipy complexes, indicative of π interactions involved in the coordination bonds between the central copper and the heterocycles of the tridentate ligands.

While dissolving these complexes in dmf, the blue solution gradually turned green. The LF bands at ca. 600 nm were red-shifted by ca. 30 nm to ca. 40 nm, but not the low energy peak or shoulder. New CT bands were observed in the 300 nm region. These spectral changes indicate that the central ether oxygen atoms of the tridentate ligands are replaced by the dmf molecules, in agreement with the e.p.r. data (vide supra).

Oxidation of Phenols or Phenolates

The results of stoichiometric and catalytic oxidation reactions of DBP and phenolates, DBP−NEt_3, are summarized in Table 4. It is obvious that the N−O−N tridentate ligands are indispensable for the oxidation reactions, since no oxidized products were observed for the reactions of DBP with $[Cu(CH_3CN)_4]^+$ (entries 5 and 10).

In the stoichiometric reactions, both TBBP (3,3′,5,5′-tetra-*tert*-butyl-2,2′-biphenol) and DBQ (3,5-di-*tert*-butyl-*o*-quinone) were produced in nearly equal amounts for the reactions of DBP, and DBP−NEt_3 as well, with Cu(bb^{Pr}mo)−O_2 adduct in CH_2Cl_2 at 25 °C (entries 1 and 2). Although mechanistic studies[16−18] have indicated that the aromatic ligand hydroxylation involves an electrophilic attack on the arene ring by (μ-η^2:η^2-peroxo)dicopper(II) intermediate, most of the reported studies on the intermolecular oxidations of DBP with peroxo intermediate report TBBP as a major product.[15,23,33−35] Our results with high DBQ generation are in reasonably good agreement with the mechanistic studies, inferring the formation of (μ-η^2:η^2-peroxo)dicopper(II) and bis(μ-oxo)dicopper(III) intermediates supported by bb^{Pr}mo during the reactions. The reactions of DBP, and also DBP-NEt_3, with the Cu(bpmo)-O_2 adduct in CH_2Cl_2 at 25 °C (entries 3 and 4), however, generate only TBBP, implying the presence of a bis(μ-oxo)dicopper(III) intermediate. These reactions can also be carried out under catalytic conditions (entries 6−9). The catalytic reactions require a much longer reaction time (3 to 14 days), due to

 © 2004 Wiley-VCH Verlag GmbH & Co. KGaA, Weinheim

Table 4. Oxidation reactions of DBP with O_2 in the presence of $Cu^I(N-O-N)$ complexes[a]

Entry[a]	N−O−N/substrate[b]	TBBP[c] (%)	DBQ[d] (%)	DBP[e] (%)
I. Stoichiometric reactions[f]				
1	$bb^{pr}mo$/DBP	45	42	10
2	$bb^{pr}mo$/DBP-NEt_3	43	44	10
3	bpmo/DBP	43	0	47
4	bpmo/DBP-NEt_3	10	0	59
5	$[Cu(MeCN)_4]^+$/DBP	0	0	75
II. Catalytic reactions[g]				
6	$bb^{pr}mo$/DBP[h]	68	6	20
7	$bb^{pr}mo$/DBP-NEt_3[h]	55	0	9
8	bpmo/DBP[i]	56	0	37
9	bpmo/DBP-NEt_3[i]	37	0	59
10	$[Cu(MeCN)_4]^+$/DBP[i]	trace	0	[j]

[a] The dioxygen adducts for the stoichiometric reactions were prepared by the reaction of O_2 with a solution of equimolar Cu^I and N−O−N at room temperature for 24 h. [b] DBP = 2,4-di-*tert*-butylphenol. DBP−NEt_3 = DBP/NEt_3 (1:1). [c] Isolated yield. TBBP = 3,3′,5,5′-tetra-*tert*-butyl-2,2′-biphenol. [d] Isolated yield. DBQ = 3,5-di-*tert*-butyl-*o*-quinone. [e] Recovered DBP. [f] Molar ratio of Substrate/Cu(N−O−N) = 1:1. The reactions were carried out in CH_2Cl_2 at 25 °C for 24 h. [g] Molar ratio of Substrate/Cu(N−O−N) = 1:0.01. The reactions were carried out in CH_2Cl_2 at 25 °C. [h] 14 days. [i] 3 days. [j] Not measured.

the small amount (one hundredth) of the copper catalyst employed, and the turn over numbers are in the order of 10^3.

The oxygenation reactions of phenolates to catechols by $[(\mu\text{-}\eta^2\text{:}\eta^2\text{-}O_2)Cu_2(L\text{-}66)]$[36−39] {L-66 = α,α′-bis{bis[2-(1-methyl-2-benzimidazolyl)ethyl]amino}-*m*-xylene} and by $[(\mu\text{-}\eta^2\text{:}\eta^2\text{-}O_2)Cu_2(L^{Py2Bz})_2]$[40] {$L^{Py2Bz}$ = *N*,*N*-bis[2-(2-pyridyl)ethyl]-α,α-dideuteriobenzylamine} have been demonstrated. The oxidation of 4MP-Li (lithium 4-methylphenolate) with Cu($bb^{Pr}mo$)−O_2 adduct afforded 3,5-di-*tert*-butyl-1,2-catechol in 37% isolated yield further assuring that the adduct is mainly ($\mu\text{-}\eta^2\text{:}\eta^2$-peroxo)dicopper(II). It is noteworthy that the copper complex with the mononucleating ligand, L-6 {*N*,*N*-bis[2-(1-methyl-2-benzimidazolyl)-ethyl]amine},[37] is inactive in the monooxygenase reaction. The reactivity with respect to oxygenation can be attributed to the conformations of the coordinated tridentate ligands. The L-6 ligand tends to coordinate to copper(II) in a meridional fashion, while N−O−N ligands, bb^Rmo and bpmo, should assume a facial conformation. Accordingly, it would be proper for $[Cu(N-O-N)]^+$ to accommodate a side-on O_2, but not $[Cu(L\text{-}6)]^+$.

Conclusion

The oxygenation reactions of DBP (2,4-di-*tert*-butylphenol) and DBP−NEt_3 (2,4-di-*tert*-butylphenolate) with the Cu($bb^{Pr}mo$)−O_2 adduct give rise to the production of DBTQ (3,5-di-*tert*-butyl-*o*-quinone). The same reaction of 4MP-Li (lithium 4-methylphenolate) produces 4-methyl-1,2-catechol. These tyrosinase-like reactions infer strongly the presence of $\mu\text{-}\eta^2\text{:}\eta^2$-peroxodicopper(II) intermediate supported by $bb^{Pr}mo$. The intermediate coordinated by $bb^{Pr}mo$ having a facial conformation is likely stabilized by π-interactions of the two perpendicularly oriented terminal benzimidazole nuclei, and tends to become stable at room temperature. Further investigation on π-interactions is currently in progress.

Experimental Section

General Remarks: Electronic spectra were recorded on a Hitachi U-3501 spectrophotometer equipped with an integrating sphere for reflectance measurements. IR spectra were recorded as Nujol mulls on a BIO-RAD FTS-40 FTIR spectrometer and a JASCO FT/IR 700 spectrometer. Nuclear magnetic resonance (NMR) spectra were recorded with Varian Gemini 2000 (200 MHz) and Bruker AV-400 (400 MHz) spectrometers. EPR spectra were obtained by using a Bruker EMX 10 spectrometer. The EPR simulations were performed using WINEPR SimFonia program. Mass spectra were acquired on a Finnigan TSQ 700 spectrometer. Elemental analyses were carried out by the microanalysis laboratories of National Chung-Hsin University, Taichung, Taiwan.

Preparation of Ligands

bbmo (L1):[41] Diglycolic acid (6.05 g, 45 mmol) and *o*-phenylenediamine (9.75 g, 90 mmol) in 4 N HCl solution (250 mL) were refluxed for 14 h. After cooling to room temperature, the precipitates were filtered and then dissolved in hot H_2O. The aqueous solution was neutralized with conc. NH_4OH. The precipitates were filtered and dissolved in CH_3OH and treated with activated carbon to afford white products. Yield 72%. mp, 280 °C. MS (EI): *m*/*z* = 279 [M + 1] (100). ^1H NMR (200 MHz [D_6]DMSO): δ = 4.87 (s, 4 H, CH_2), 7.23−7.17 (m, 4 H, benzimidazolyl-5,6-*H*), 7.59−7.54 (m, 4 H, benzimidazolyl-4,7-*H*) ppm. {^1H NMR, ([D_6]DMSO): δ = 4.95 (s, 4 H), 7.3 (m, 4 H), 7.7 (m, 4 H) ppm[42]}; {^1H NMR (CD_3OD): δ = 4.95 (s, 4 H), 7.15 (m, 4 H), 7.7 (m, 4 H) ppm[41]}. IR (cm^{-1}): ν(C=C, C=N) 1623 mw, 1587 mw, 1533 mw, 1465 s, ν(C−O) 1102 s, 1039 m, δ(CH, bim) 768 m, 748 s, δ(bim) 434 mw.

$bb^{Me}mo$ (L2): This compound was prepared similarly as bbmo but using *N*-methyl-*o*-phenylenediamine. Yield 65%. mp, 174 °C. MS (FAB^+): *m*/*z* = 307 [M + 1] (40). ^1H NMR (400 MHz, $CDCl_3$): δ = 3.81 (s, 6 H, CH_3), 4.93 (s, 4 H, CH_2), 7.34−7.28 (m, 4 H, benzimidazolyl-5,6-*H*), 7.77−7.75 (m, 4 H, benzimidazolyl-4,7-*H*) ppm. IR (cm^{-1}): ν(C=C, C=N) 1615 mw, 1506 w, 1475 s, ν(C−O) 1081 s, 1021 m, δ(CH, bim) 771 ms, 756 s, 747 s, δ(bim) 411 w.

$bb^{Pr}mo$ (L3):[43] Powdered KOH (1.40 g, 25 mmol) was added to a stirred suspension of 1,3-bis(benzimidazol-2-yl)-2-oxapropane (1.39 g, 5 mmol) in acetone (10 mL). After 20 min, iodopropane (1.70 g, 10 mmol) of was added to the white cloudy reaction mixture. After stirring at room temperature for 2 h, the orange reaction mixture was transferred to a separating funnel containing benzene (100 mL). The organic layer was washed with water (1 × 20 mL) and saturated sodium chloride solution (20 mL) and was dried with $MgSO_4$ (5 g). The filtered organic solution was rotary evaporated and then added with diethyl ether to give white precipitates. Yield 70%. Mp, 79 °C. MS (FAB^+): *m*/*z* = 363 [M + 1] (100). ^1H NMR (400 MHz, [D_6]DMSO): δ = 0.79 (t, *J* = 7 Hz, 3 H, CH_3), 1.69 (h, *J* = 7 Hz, 2 H, CH_2), 4.20 (t, *J* = 7 Hz, 2 H, CH_2), 4.87 (s, 4 H, CH_2), 7.22−7.17 (m, 4 H, benzimidazolyl-5,6-*H*), 7.59−7.54 (m, 4 H, benzimidazolyl-4,7-*H*) ppm. IR (cm^{-1}): ν(C=C, C=N) 1667 s, 1614 s, 1515 ms, ν(C−O) 1089 s, 1007 s, δ(CH, bim) 743 s, δ(bim) 434 mw.

 © 2004 Wiley-VCH Verlag GmbH & Co. KGaA, Weinheim

bpmo (L4):[44] 2-(Hydroxymethyl)pyridine (2.89 g, 25.9 mmol) was added to a solution of NaH (60%, 2.10 g, 52.5 mmol) in DMF (75 mL). The solution was stirred at 40 °C for 2 h and then cooled to room temperature. 2-(Bromomethyl)pyridine hydrobromide (6.48 g, 25.6 mmol) was added to a DMF solution (50 mL) of NaH (60%, 1.35 g, 33.7 mmol), and stirred at room temperature for 2 h. The solutions were mixed, heated at 70 °C for 2 h, and then quenched by adding H_2O (10 mL). Both H_2O and DMF were removed by vacuum distillation. The residue was dissolved in H_2O (100 mL) and extracted with diethyl ether (2 × 100 mL). The organic extract was rotary evaporated to give yellow products. Yield 22%. MS (FAB^+): *m/z* = 201.06 [M + 1] (100). ^1H NMR (400 MHz, $CDCl_3$): δ = 4.81 (s, 4 H, C*H*$_2$), 7.22 (t, *J* = 7 Hz, 2 H, pyridyl-4-*H*), 7.55 (d, *J* = 8 Hz, 2 H, pyridyl-3-*H*), 7.74 (t, *J* = 7 Hz, 2 H, pyridyl-5-*H*), 8.58 (d, *J* = 4 Hz, 2 H, pyridyl-6-*H*) ppm. IR (cm^{-1}): ν(C=C, C=N) 1634 m, 1591 s, ν(C−O) 1117 s, δ(CH, py) 755 s, δ(py) 425 mw.

Preparation of Complexes

[Cu(bb^{Me}mo)(bipy)](ClO$_4$)$_2$ (1): To a stirred CH_3OH solution (5 mL) of $Cu(ClO_4)_2·6H_2O$ (741 mg, 2 mmol), a solution of bb^{Me}mo (612 mg, 2 mmol) in CH_3OH (10 mL) was added. After reaction at room temperature for 2 h, a solution of bipy (313 mg, 2 mmol) in CH_3OH (10 mL) was added dropwise to the cloudy green solution and the reaction solution was stirred for another 2 h. The blue products were filtered and dried under vacuum. Yield 90%. M.p. 246 °C (dec.); found C 46.71, H 3.37, N 11.20. $C_{28}H_{26}Cl_2CuN_6O_9$: calcd. C 46.39, H 3.61, N 11.59%. IR (cm^{-1}): ν(C=C, C=N) 1605 m, 1508 s, 1500 s, ν(ClO_4^-) 1094 vs br., 623 s, ν(C−O) 1048 s, 1033 s, δ(CH, bipy) 784 ms, δ(CH, bim) 772 ms, 763 ms, 753 ms, δ(bim) 432 w, ν(Cu−N) 345 w, 304 mw, 282 mw. The purple crystals, *fac*-[Cu(bb^{Me}mo)(bipy)(H_2O)](ClO$_4$)$_2$(H_2O) (**1a**), suitable for X-ray diffraction were obtained by slow diffusion of diethyl ether to a dmf solution.

[Cu(bb^{Pr}mo)(bipy)](ClO$_4$)$_2$(H_2O) (2): This blue complex was prepared similarly as the previous complex but using bb^{Pr}mo and was recrystallized from CH_3CN and diethyl ether. Yield 42%. M.p. 240 °C (dec.); found C 48.05, H 4.22, N 10.80. $C_{32}H_{36}Cl_2CuN_6O_{10}$: calcd. C 48.10, H 4.54, N 10.52%. IR (cm^{-1}): ν(O−H) 3562 m br., ν(C=C, C=N) 1610 s, 1605 s, 1567 m, 1503 s, 1495 s, ν(ClO_4^-) 1081 vs br., 623 s, δ(CH, bipy) 767 s br., δ(CH, bim) 730 s, δ(bim) 438 w, δ(bipy) 415w.

[Cu(bbmo)(bipy)](ClO$_4$)$_2$(CH_3CN)$_{0.5}$ (3): This blue complex was prepared similarly as the previous complex but using bbmo and was recrystallized from CH_3CN/CH_3OH (1:1) and diethyl ether. Yield 81%. M.p. 234 °C (dec.); found C 45.08, H 3.15, N 12.60. $C_{27}H_{23.5}Cl_2CuN_{6.5}O_9$: calcd. C 45.19, H 3.28, N 12.69% IR (cm^{-1}): ν(N−H) 3274 m br., ν(C=C, C=N) 1612 m, 1603 m, 1540 w, 1498 m, ν(ClO_4^-) 1093 vs br., 622 s, δ(CH, bipy) 770 ms, δ(CH, bim) 752 s, 743 s, δ(bim) 431 w, ν(Cu−N) 330 w, 304 w, 292 mw, 282 mw.

[Cu(bb^{Me}mo)(phen)](ClO$_4$)$_2$(H_2O)$_3$ (4): This blue complex was prepared similarly as the previous complex but using bb^{Me}mo and phen. Yield 90%. M.p. 232 °C (dec.); found C 45.17, H 3.87, N 10.42. $C_{30}H_{32}Cl_2CuN_6O_{12}$: calcd. C 44.87, H 4.01, N 10.46%. IR (cm^{-1}): ν(OH) 3625w br, 3400w br, ν(C=C, C=N) 1610 mw, 1591 mw, 1542 mw, 1508 m, ν(ClO_4^-) 1091 vs br., 624 s, ν(C−O) 1044 m sh, 1012 mw, δ(CH, phen) 852 ms, δ(CH, bim) 757 s, 750 ms, 745 ms, δ(bim) 432 mw, ν(Cu−N) 341 mw, 312 mw, 282 mw. The blue crystals, *fac*-[Cu(bb^{Me}mo)(phen)](ClO$_4$)$_2$(CH_3CN) (4**a**), suitable for X-ray diffraction were obtained by slow diffusion of diethyl ether to an acetonitrile solution.

[Cu(bb^{Pr}mo)(phen)](ClO$_4$)$_2$(H_2O)$_2$ (5): This green complex was prepared similarly as the previous complex but using bb^{Pr}mo. Yield 51%. M.p. 242 °C (dec.); found C 48.33, H 4.16, N 10.35. $C_{34}H_{38}Cl_2CuN_6O_{11}$: calcd. C 48.55, H 4.55, N 9.99%. IR (cm^{-1}): ν(OH) 3564 w br., ν(C=C, C=N) 1610 mw. 1590 mw. 1521 m. 1495 s, ν(ClO_4^-) 1101 vs br., 623 s, ν(C−O) 1040 m sh. 1005 mw, δ(CH, phen) 850 ms, δ(CH, bim) 763 s. 740 m. 720 s, δ(bim) 437 mw. The purple crystals, *fac*-[Cu(bb^{Pr}mo)(phen)](ClO$_4$)$_2$ (**5a**), suitable for X-ray diffraction were obtained by slow diffusion of diethyl ether to a dmf solution.

[Cu(bb^{Pr}mo)(en)](ClO$_4$)$_2$ (6): This purple complex was prepared similarly as the previous complex but using bb^{Pr}mo and en. Yield 55%. M.p. 226 °C (dec.); found C 42.04, H 5.02, N 11.95. $C_{24}H_{34}Cl_2CuN_6O_9$: calcd. C 42.08, H 5.00, N 12.27%. IR (cm^{-1}): ν(NH) 3345 ms, 3283 ms, ν(C=C, C=N) 1611 m, 1594 s, 1503 s, 1496 s, ν(ClO_4^-) 1107 vs br., 626 s, ν(C−O) 1035 s sh, 1050 s, δ(CH, bim) 800 m, 765 s, 705 m, δ(bim) 435 mw.

[Cu(bpmo)(bipy)](ClO$_4$)$_2$(H_2O)$_{0.5}$ (7): This blue complex was prepared similarly as the previous complex but using bpmo and bipy. Yield 75%. M.p. 206 °C (dec.); found C 41.76, H 2.99, N 8.96. $C_{22}H_{21}Cl_2CuN_4O_{9.5}$ calcd. C 42.09, H 3.37, N 8.92%. IR (cm^{-1}): ν(OH) 3442 ms br., ν(C=C, C=N) 1606 s, 1573 m, ν(ClO_4^-) 1098 vs br., 623 s, ν(C−O) 1030 s, 985 m, δ(CH, bipy) 775 s, δ(CH, py) 765 s sh, 730 s, δ(py) 420 mw. The blue crystals, *fac*-[Cu(bpmo)(bipy)(ClO$_4$)](ClO$_4$) (**7a**), suitable for X-ray diffraction were obtained by slow diffusion of diethyl ether to an acetonitrile solution.

[Cu(bpmo)(phen)](ClO$_4$)$_2$(H_2O)$_{0.5}$ (8): This blue complex was prepared similarly as the previous complex but using bpmo and phen. Yield 74%. M.p. 201 °C (dec.); found C 44.11, H 3.34, N 8.25. $C_{24}H_{21}Cl_2CuN_4O_{9.5}$ calcd. C 44.22, H 3.24, N 8.59%. IR (cm^{-1}): ν(OH) 3600 w br., 3445 w br., ν(C=C, C=N) 1633 m, 1608 ms, 1586 m, 1520 ms, ν(ClO_4^-) 1092 vs br., 623 s, ν(C−O) 1052 m, 1008 w, δ(CH, phen) 853 ms, δ(CH, py) 782 m, 762 ms, δ(py) 434 mw.

[Cu(bpmo)(tmen)](ClO$_4$)$_2$ (9): This purple complex was prepared similarly as the previous complex but using bpmo and tmen. Yield 38%. M.p. 78 °C; found C 37.70, H 5.03, N 10.13. $C_{18}H_{28}Cl_2CuN_4O_9Cl_2$: calcd. C 37.35, H 4.84, N 9.68%. IR (cm^{-1}): ν(C=C, C=N) 1609 m, 1573 w, ν(ClO_4^-) 1093 vs br., 623 s, ν(C−O) 1164 m, δ(CH, py) 770 s, δ(py) 424 w.

Oxidation of Phenol or Phenolate with Peroxodicopper(II) and/or Bis(μ-oxo)dicopper(III): The μ-η^2:η^2-peroxodicopper(II) and/or bis(μ-oxo)dicopper(III) intermediates were generated by the reaction of [Cu(CH_3CN)$_4$](ClO$_4$) (185 mg, 0.56 mmol) and tridentate ligand (0.56 mmol) in CH_2Cl_2/CH_3CN (8:2, 10 mL) with O_2 at room temperature overnight. After removal of excess O_2 by bubbling N_2 gas into the solution for 15 min, a solution of DBP (117 mg, 0.56 mmol) with or without NEt_3 (0.56 mmol) in CH_2Cl_2 (5 mL) was added into the solution by cannulation. The mixture was stirred under N_2 at room temperature for 24 h. After evaporation of the solvent, the residue formed was columned on silica gel (ethyl acetate/hexane, 1:8), affording 3,3′,5,5′-tetra-*tert*-butyl-2,2′-biphenol, 3,5-di-*tert*-butyl-*o*-quinone, and the starting 2,4-di-*tert*-butylphenol. The oxygenation of 4MP-Li (lithium 4-methylphenolate) was carried out similarly in acetone, yielding 4-methylcatechol.[40]

Catalytic Oxidation of 2,4-Di-*tert*-butylphenol (DBP) or 2,4-Di-*tert*-butylphenolate (DBP-NEt$_3$) in the Presence of Copper(I) Complexes of bb^{Pr}mo or bpmo: A CH_2Cl_2 solution (10 mL) of 2,4-di-*tert*-butylphenol (1.65 g, 7.98 mmol) with or without NEt_3 (7.98 mmol)

 © 2004 Wiley-VCH Verlag GmbH & Co. KGaA, Weinheim

Table 5. Crystallographic data for **1a**, **4a**, **5a**, and **7a**

	1a	**4a**	**5a**	**7a**
Emprical formula	$C_{28}H_{30}Cl_2CuN_6O_{11}$	$C_{32}H_{29}Cl_2CuN_7O_9$	$C_{34}H_{34}Cl_2CuN_6O_9$	$C_{22}H_{20}Cl_2CuN_4O_9$
Molecular mass	761.02	790.06	805.11	618.87
Crystal system	monoclinic	triclinic	triclinic	triclinic
Space group	$P2_1/c$	$P\bar{1}$	$P\bar{1}$	$P\bar{1}$
a (Å)	15.5495(7)	10.1156(5)	10.2008(14)	8.8186(1)
b (Å)	10.1854(4)	11.6347(6)	11.7156(15)	10.6142(2)
c (Å)	20.5931(9)	16.9338(9)	16.628(2)	15.0084(4)
α [°]	90	78.495(1)	72.383(2)	88.644(1)
β [°]	101.532(1)	76.100(1)	77.804(2)	75.102(1)
γ [°]	90	64.906(1)	70.921(2)	67.897(2)
V (Å^3)	3195.7(2)	1741.19(16)	1776.0(4)	1243.63(4)
Z	4	2	2	2
F(000)	1564	810	830	630
$D_{calcd.}$ [Mg·m^{-1}]	1.582	1.507	1.506	1.640
μ(Mo-K_α) [mm^{-1}]	0.920	0.844	0.829	1.14
Crystal size [mm]	0.10 × 0.08 × 0.05	0.40 × 0.25 × 0.20	0.25 × 0.18 × 0.10	0.40 × 0.35 × 0.15
Diffractometer	Siemens SMART CCD	Siemens SMART CCD	Siemens SMART CCD	Bruker Kappa CCD
θ range [°]	1.34−28.32	1.94−28.29	1.90−28.29	27.52
T_{max}, T_{min}	0.98078, 0.83846	0.95739, 0.80920	0.96645, 0.85317	0.746, 0.682
hkl range	$-20 \le h \le 20$, $-13 \le k \le 13$, $-27 \le l \le 23$	$-13 \le h \le 13$, $-15 \le k \le 15$, $-22 \le l \le 22$	$-13 \le h \le 13$, $-15 \le k \le 15$, $-21 \le l \le 22$	$-10 \le h \le 11$, $-13 \le k \le 13$, $-19 \le l \le 19$
No. of reflns. measd.	20477	18424	18936	12335
No. of unique reflns.	7763	8233	8415	5915
No. of reflns. obsd.	3514($I > 2\sigma$)	5172($I > 2\sigma$)	3868($I > 2\sigma$)	4564($I > 3\sigma$)
R_{int}	0.0658	0.0411	0.0623	0.036
No. of param./restraints	427/0	460/0	469/0	344/0
R, R_w	0.0649, 0.1765	0.0743, 0.1919	0.0754, 0.1764	0.047, 0.090
Max./min. Δρ [e·Å^{-3}]	1.281/-0.830	0.914/-0.488	1.108/-0.337	0.48/-0.54
Goodness-of-fit	0.928	1.023	0.930	1.155

was added to a mixture of $[Cu(CH_3CN)_4](ClO_4)$ (26.1 mg, 0.0798 mmol) and tridentate ligand (0.0798 mmol) in CH_2Cl_2/CH_3CN (8:2, 10 mL) under N_2. The reaction solution was stirred under an O_2 atmosphere at room temperature and was monitored by checking the UV/Vis absorption in the region of 300 nm to 800 nm. After the absorption peaks stopped growing, the reaction mixture was worked up as described above, yielding 3,3′,5,5′-tetra-*tert*-butyl-2,2′-biphenol, and/or 3,5-di-*tert*-butyl-*o*-quinone.

X-ray Crystallographic Study: Details of crystal data and intensity collection are summarized in Table 5, using Siemens Smart-CCD or Bruker−Kappa CCD diffractometers. Intensity data [θ/2θ scan] were collected at ca. 298 K and corrected for Lorentz and polarization effects and absorption. The structures were solved by direct methods using the SIR92 for (**7a**) and SHELXS-97 for the rest. The hydrogen atoms included in the refinement were located in succeeding difference Fourier syntheses or with ideal positions after the non-hydrogen atoms were refined anisotropically. CCDC-217573 to -217576 contains the supplementary crystallographic data for this paper. These data can be obtained free of charge at www.ccdc.cam.ac.uk/conts/retrieving.html [or from the Cambridge Crystallographic Data Centre, 12 Union Road, Cambridge CB2 1EZ, UK; Fax: (internat.) + 44-1223-336-033; E-mail: deposit@ccdc.cam.ac.uk].

Acknowledgments

Financial support form the National Science Council of the Republic of China (NSC89-2113-M-003-018) is gratefully acknowledged. Our gratitude also goes to the Academic Paper Editing Clinic, NTNU.

[1] K. A. Magnus, H. Ton-That, J. E. Carpenter, in: *Bioinorganic Chemistry of Copper* (Ed.: K. D. Karlin, Z. Tyeklar), Chapman & Hall, New York, **1993**, 143−150.
[2] K. A. Magnus, H. Ton-That, J. E. Carpenter, *Chem. Rev.* **1994**, *94*, 727−735.
[3] E. I. Solomon, M. J. Baldwin, M. D. Lowery, *Chem. Rev.* **1992**, *92*, 521−542.
[4] E. I. Solomon, U. M. Sundaram, T. E. Machonkin, *Chem. Rev.* **1996**, *96*, 2563−2605.
[5] N. Kitajima, K. Fujisawa, C. Fujimoto, Y. Moro-Oka, S. Hashimoto, T. Kitagawa, K. Toriumi, K. Tatsumi, A. Nakamura, *J. Am. Chem. Soc.* **1992**, *114*, 1277−1291.
[6] E. Pidcock, S. DeBeer, H. V. Obias, B. Hedman, K. O. Hodgson, K. D. Karlin, E. I. Solomon, *J. Am. Chem. Soc.* **1999**, *121*, 1870−1878.
[7] M. Kodera, K. Katayama, Y. Tachi, K. Kano, S. Hirota, S. Fujinami, M. Suzuki, *J. Am. Chem. Soc.* **1999**, *121*, 11006−11007.
[8] Z. Hu, G. N. George, S. M. Gorun, *Inorg. Chem.* **2001**, *40*, 4812−4813.
[9] S. Mahapatra, J. A. Halfen, E. C. Wilkinson, G. Pan, X. Wang, V. G. Young, Jr., C. J. Cramer, L. Que, Jr., W. B. Tolman, *J. Am. Chem. Soc.* **1996**, *118*, 11555−11574.
[10] J. A. Halfen, S. Mahapatra, E. C. Wilkinsin, S. Kaderli, V. G. Young, Jr., L. Que, Jr., A. D. Zuberbuhler, W. B. Tolman, *Science* **1996**, *271*, 1397−1400.
[11] S. Mahapatra, V. G. Young, Jr., S. Kaderli, A. D. Zuberbuhler,

 © 2004 Wiley-VCH Verlag GmbH & Co. KGaA, Weinheim

W. B. Tolman, *Angew. Chem.* **1997**, *109*, 125−127; *Angew. Chem. Int. Ed. Engl.* **1997**, *36*, 130−133.
[12] N. W. Aboelella, E. A. Lewis, A. M. Reynolds, W. W. Brennessel, C. J. Cramer, W. B. Tolman, *J. Am. Chem. Soc.* **2002**, *124*, 10660−10661.
[13] D. J. E. Spencer, A. M. Reynolds, P. L. Holland, B. A. Jazdzewski, C. Duboc-Toia, L. Le Pape, S. Yokota, Y. Tachi, S. Itoh, W. B. Tolman, *Inorg. Chem.* **2002**, *41*, 6307−6321.
[14] V. Mahadevan, Z. Hou, A. P. Cole, D. E. Root, T. K. Lal, E. I. Solomon, T. D. P. Stack, *J. Am. Chem. Soc.* **1997**, *119*, 11996−11997.
[15] P. P. Paul, Z. Tyeklar, R. R. Jacobson, K. D. Karlin, *J. Am. Chem. Soc.* **1991**, *113*, 5322−5332.
[16] M. S. Nasir, B. I. Cohen, K. D. Karlin, *J. Am. Chem. Soc.* **1992**, *114*, 2482−2494.
[17] K. D. Karlin, M. S. Nasir, B. I. Cohen, R. W. Cruse, S. Kaderli, A. D. Zuberbuhler, *J. Am. Chem. Soc.* **1994**, *116*, 1324−1336.
[18] E. Pidcock, H. V. Obias, C. X. Zhang, K. D. Karlin, E. I. Solomon, *J. Am. Chem. Soc.* **1998**, *120*, 7841−7847.
[19] W. B. Tolman, *Acc. Chem. Res.* **1997**, *30*, 227−237.
[20] J. Cahoy, P. L. Holland, W. B. Tolman, *Inorg. Chem.* **1999**, *38*, 2161−2168.
[21] L. Que, Jr., W. B. Tolman, *Angew. Chem.* **2002**, *114*, 1160−1185; *Angew. Chem. Int. Ed.* **2002**, *41*, 1114−1137.
[22] H.-C. Liang, C. X. Zhang, M. J. Henson, R. D. Sommer, K. R. Hatwell, S. Kaderli, A. D. Zuberbuehler, A. L. Rheingold, E. I. Solomon, K. D. Karlin, *J. Am. Chem. Soc.* **2002**, *124*, 4170−4171.
[23] V. Mahadevan, M. J. Henson, E. I. Solomon, T. D. P. Stack, *J. Am. Chem. Soc.* **2000**, *122*, 10249−10250.
[24] M. J. Henson, P. Mukherjee, D. E. Root, T. D. P. Stack, E. I. Solomon, *J. Am. Chem. Soc.* **1999**, *121*, 10332−10345.
[25] L. M. Mirica, M. Vance, D. J. Rudd, B. Hedman, K. O. Hodgson, E. I. Solomon, T. D. P. Stack, *J. Am. Chem. Soc.* **2002**, *124*, 9332−9333.
[26] V. Mahadevan, J. L. DuBois, B. Hedman, K. O. Hodgson, T. D. P. Stack, *J. Am. Chem. Soc.* **1999**, *121*, 5583−5584.
[27] M. Palaniandavar, T. Pandiyan, M. Lakshminarayanan, H. Manohar, *J. Chem. Soc., Dalton Trans.* **1995**, 455−461.
[28] L. Casella, O. Carugo, M. Gullotti, S. Doldi, M. Frassoni, *Inorg. Chem.* **1996**, *35*, 1101−1113.
[29] Y. Nishida, K. Takashi, *J. Chem. Soc., Dalton Trans.* **1988**, 691−699.
[30] B. J. Hathaway, in: *Comprehensive Coordination Chemistry* (Ed.: G. Wilkinson, R. D. Gillard, J. A. McCleverty), vol. 5, Pergamon Press, Oxford, **1987**, pp. 594−774.
[31] B. J. Hathaway, A. A. G. Tomlison, *Coord. Chem. Rev.* **1970**, *5*, 1−142.
[32] U. Sakaguchi, A. W. Addison, *J. Chem. Soc., Dalton Trans.* **1979**, 600−608.
[33] N. Kitajima, T. Koda, Y. Iwata, Y. Moro-oka, *J. Am. Chem. Soc.* **1990**, *112*, 8833−8839.
[34] H. V. Obias, Y. Lin, N. N. Murthy, E. Pidcock, E. I. Solomon, M. Ralle, N. J. Blackburn, Y.-M. Neuhold, A. D. Zuberbuhler, K. D. Karlin, *J. Am. Chem. Soc.* **1998**, *120*, 12960−12961.
[35] J. A. Halfen, V. G. Young, Jr., W. B. Tolman, *Inorg. Chem.* **1998**, *37*, 2102−2103.
[36] L. Casella, M. Gullotti, R. Radaelli, P. Di Gennaro, *J. Chem. Soc., Chem. Commun.* **1991**, 1611−1612.
[37] L. Casella, E. Monzani, M. Gullotti, D. Cavagnino, G. Cerina, L. Santagostini, R. Ugo, *Inorg. Chem.* **1996**, *35*, 7516−7525.
[38] E. Monzani, L. Quinti, A. Perotti, L. Casella, M. Gullotti, L. Randaccio, S. Geremia, G. Nardin, P. Faleschini, G. Tabbi, *Inorg. Chem.* **1998**, *37*, 553−562.
[39] L. Santagostini, M. Gullotti, E. Monzani, L. Casella, R. Dillinger, F. Tuczek, *Chem. Eur. J.* **2000**, *6*, 519−522.
[40] S. Itoh, H. Kumei, M. Taki, S. Nagatomo, T. Kitagawa, S. Fukuzumi, *J. Am. Chem. Soc.* **2001**, *123*, 6708−6709.
[41] H. P. Berends, D. W. Stephan, *Inorg. Chim. Acta* **1984**, *93*, 173−178.
[42] G. Batra, P. Mathur, *Inorg. Chem.* **1992**, *31*, 1575−1580.
[43] Y. Kikugawa, *Synthesis* **1981**, 124−125.
[44] D. Nanty, M. Laurent, M. A. Khan, M. T. Ashby, *Acta Crystallogr., Sect. C* **2000**, *56*, 35−36.

Received September 9, 2003
Early View Article
Published Online April 1, 2004

 © 2004 Wiley-VCH Verlag GmbH & Co. KGaA, Weinheim

EurJIC
European Journal of Inorganic Chemistry

Issue 11/2004

Pages 2189–2392

Papers available ahead of print in Early View at www.interscience.wiley.com

Earliest available Table of Contents:
Automatically, free of charge by e-mail through
www.interscience.wiley.com/alerts

COVER PICTURE

The cover picture shows the successful cooperation between biotechnology, main-group chemistry and organometallic chemistry to generate a highly enantioselective diphosphane ligand for homogeneous catalysis. The details are described in the article by W. Braun, A. Salzer et al. on p. 2235ff. The work was sponsored by the Deutsche Forschungsgemeinschaft (DFG) within the Collaborative Research Centre (SFB 380) "Asymmetric Syntheses with Chemical and Biological Methods". The authors are indebted to Mr. M. Stauten, Cologne, for his help concerning the artwork of the cover picture.

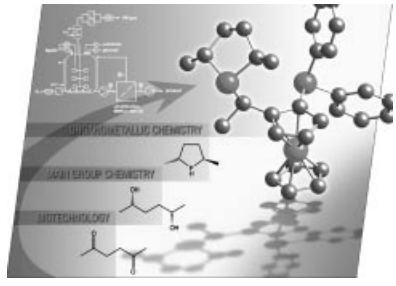

MICROREVIEW

Contents

2203 **R. Roncone, E. Monzani, S. Nicolis, L. Casella***

Engineering and Prosthetic-Group Modification of Myoglobin: Peroxidase Activity, Chemical Stability and Unfolding Properties

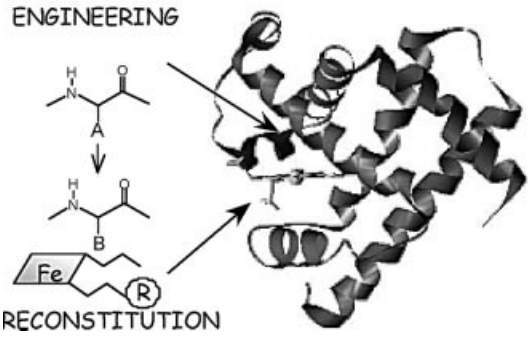

Keywords: Bioinorganic chemistry / Heme proteins / Enzyme models / Protein engineering / Structure-activity relationships / Myoglobin

 © 2004 Wiley-VCH Verlag GmbH & Co. KGaA, Weinheim

SHORT COMMUNICATIONS

2215 **Z. D. Tomić,* S. B. Novaković, S. D. Zarić***

Intermolecular Interactions between Chelate Rings and Phenyl Rings in Square-Planar Copper(II) Complexes

Keywords: Chelate rings / Delocalized π-bonds / Copper / Aromaticity / Stacking interactions

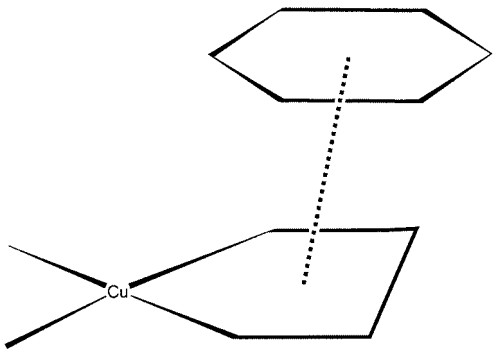

2219 **M. Moragues-Cánovas, M. Helliwell, L. Ricard, É. Rivière, W. Wernsdorfer, E. Brechin, T. Mallah***

An Ni_4 Single-Molecule Magnet: Synthesis, Structure and Low-Temperature Magnetic Behavior

Keywords: Nickel / Ferromagnetism / Single-molecule studies / Cubane complexes / Tripodal ligands

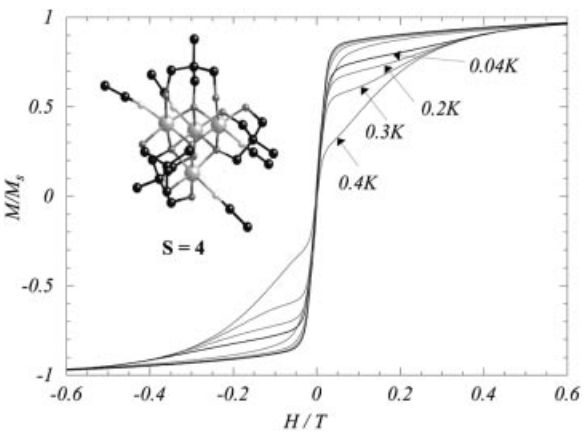

2223 **D.-L. Shieh, K.-B. Shiu, J.-L. Lin***

Scanning Tunneling Study of the Assembly of Octa- and Tetraruthenium Supermolecules on Graphite

Keywords: Supermolecular chemistry / Scanning tunneling microscopy / Graphite / Ruthenium

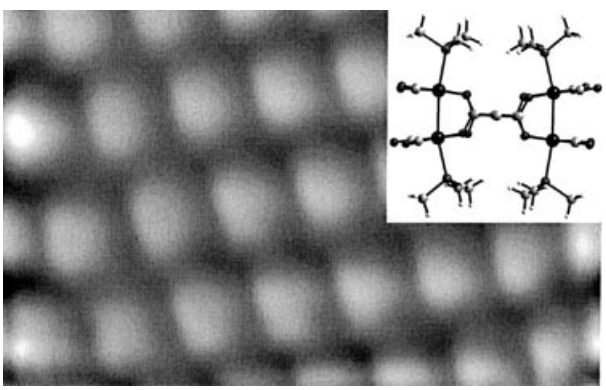

2228 **X. Li, R. Cao,* D. Sun, W. Bi, D. Yuan**

A Novel 3-D Self-Penetrating Topological Network Assembled by Mixed Bridging Ligands

Keywords: Mixed bridging ligands / Interlocking / Self-penetrating

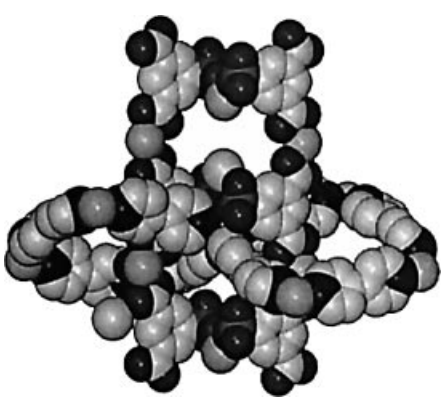

 © 2004 Wiley-VCH Verlag GmbH & Co. KGaA, Weinheim

2232 **S.-D. Li,* C.-Q. Miao, G.-M. Ren**

D_{5h} Cu_5H_5X: Pentagonal Hydrocopper Cu_5H_5 Containing Pentacoordinate Planar Nonmetal Centers (X = B, C, N, O)

Keywords: Ab initio calculations / Density functional calculations / Hydrocopper / Pentacoordinate planar carbon / Electronic structures

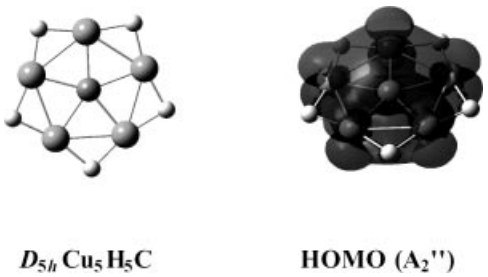

FULL PAPERS

2235 **W. Braun, B. Calmuschi, J. Haberland, W. Hummel, A. Liese, T. Nickel, O. Stelzer, A. Salzer***

Optically Active Phospholanes as Substituents on Ferrocene and Chromium-Arene Complexes

Keywords: Iron / Chromium / Sandwich complexes / P ligands / Asymmetric catalysis

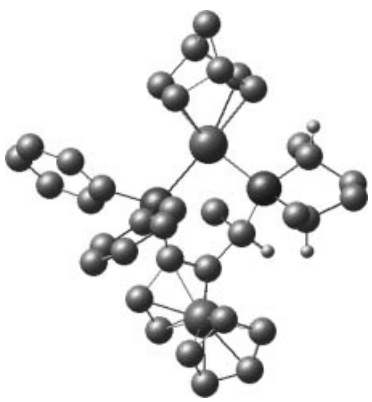

2244 **A. Doppiu, A. Salzer***

A New Route to Cationic Half-Sandwich Ruthenium(II) Complexes with Chiral Cyclopentadienylphosphane Ligands

Keywords: Asymmetric catalysis / Constrained geometry ligands / Cyclopentadienyl ligands / P ligands / Ruthenium

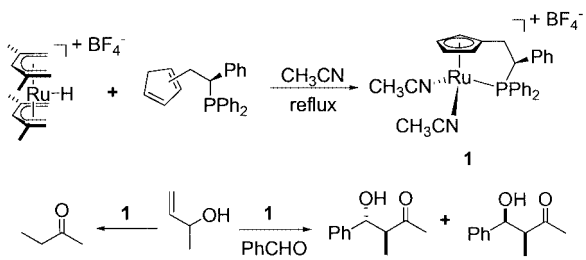

2253 **J. Kaizer, J. Pap, G. Speier,* L. Párkányi**

The Reaction of μ-η^2:η^2-Peroxo- and Bis(μ-oxo)-dicopper Complexes with Flavonol

Keywords: Quercetinase / Model compounds / Copper / Oxygen / Flavonol

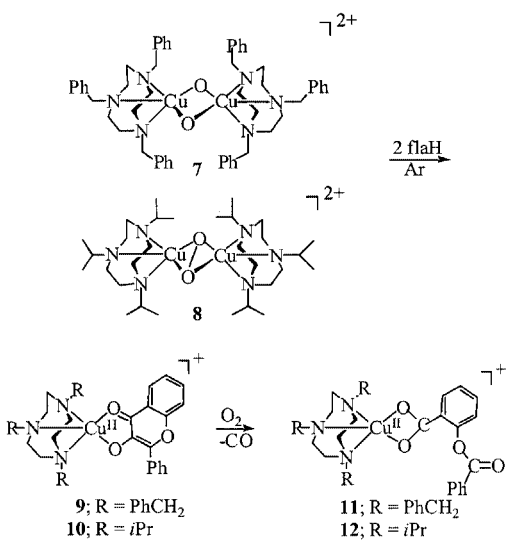

 © 2004 Wiley-VCH Verlag GmbH & Co. KGaA, Weinheim

2260 **J. Cano Sierra, S. G. Kehr, R. Fröhlich, G. Erker***

A Fulvene Route to Group 4 Metallocene Complexes Bearing 4,7-Bis(dimethylamino)-Substituted Indenyl Ligands

Keywords: Aminofulvenes / Cyclopentadienide / Zirconium / Ring-closure / Sandwich complexes

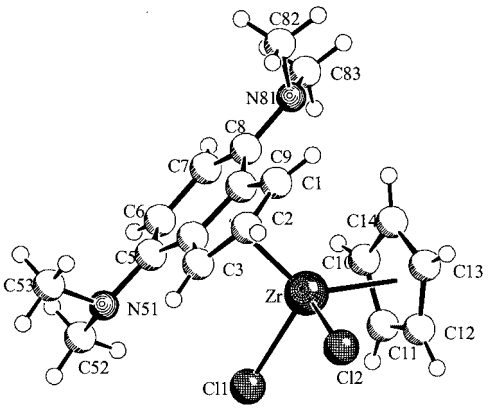

2266 **L.-Y. Wang, L.-C. Li, D.-Z. Liao, Z.-H. Jiang,* S.-P. Yan**

Synthesis, Crystal Structure and Magnetic Properties of A New Thiazolyl-Substituted Nitronyl Nitroxide and Its Copper(II) Complexes

Keywords: Thiazole radicals / Nitronyl nitroxide / Copper / Magnetic properties

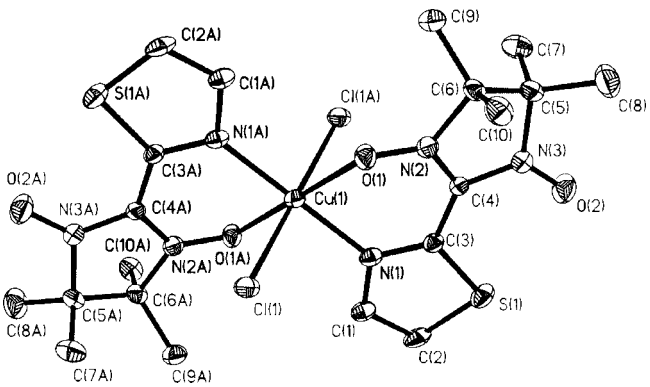

2272 **M. Ben Salah, S. Vilminot,* T. Mhiri, M. Kurmoo**

Synthesis, Crystal Structure, and Magnetic Properties of $Mn_2(OH)_2SO_4$: A Novel Layered Hydroxide

Keywords: Hydroxysulfate / Hydrothermal synthesis / Magnetic properties / Manganese

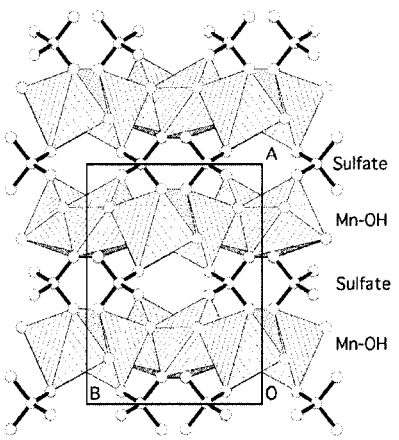

2277 **C.-W. Jiang**

Dimeric 2,2′-Bipyridylruthenium(II) Complexes Containing 2,2′-Bis(1,2,4-triazin-3-yl)-4,4′-bipyridine-Like Bridging Ligands: Syntheses, Characterization and DNA Binding

Keywords: Dinuclear complexes / Ruthenium / DNA binding modes / Enantioselectivity

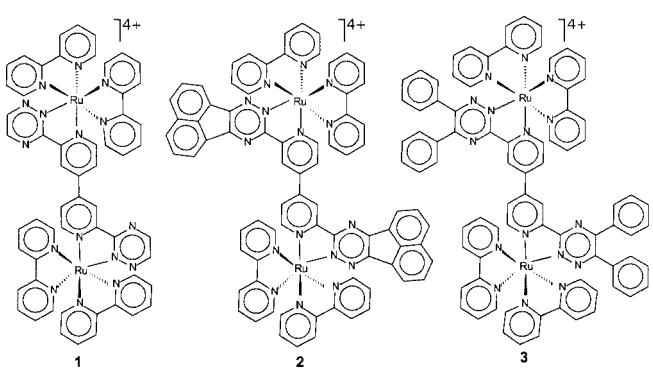

 © 2004 Wiley-VCH Verlag GmbH & Co. KGaA, Weinheim

2283 **N. Chaniotakis,* K. Jurkschat,* D. Müller, K. Perdikaki, G. Reeske**

Bis[di-*n*-alkyl(fluoro)stannyl]methanes, $(R_2FSn)_2$-CH_2 (R = *n*-octyl, *n*-dodecyl): Stable Fluoride-Selective Carriers

Keywords: Tin / Fluorine / Anion carrier / NMR spectroscopy

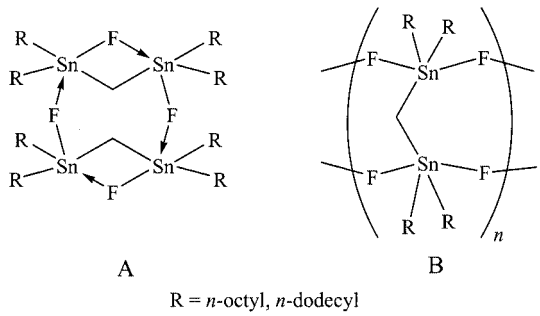

2289 **K. Miqueu, J.-M. Sotiropoulos, G. Pfister-Guillouzo,* V. L. Rudzevich, H. Gornitzka, V. Lavallo, V. D. Romanenko**

Syntheses, Structures, Bonding and Photoelectron Spectra of "Push-Pull"-Substituted *P*-[2,6-Bis(trifluoromethyl)phenyl]-$\sigma^2\lambda^3$-iminophosphanes

Keywords: Iminophosphanes / X-ray diffraction / Photoelectron spectroscopy / Density functional calculations / Ionization potentials

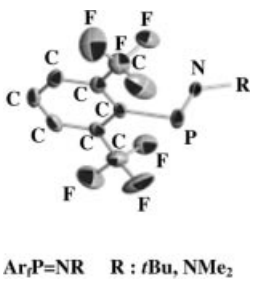

2301 **M. Wilhelm, S. Deeken, E. Berssen, W. Saak, A. Lützen, R. Koch, H. Strasdeit***

The First Structurally Authenticated Organomercury(1+) Thioether Complexes − Mercury−Carbon Bond Activation Related to the Mechanism of the Bacterial Enzyme Organomercurial Lyase

Keywords: Bioinorganic chemistry / Enzyme models / Ligand effects / Mercury / S ligands

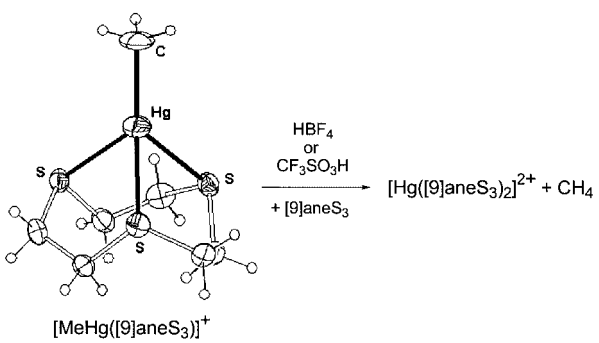

2313 **P. Kölle, R. Dronskowski***

Synthesis, Crystal Structures and Electrical Conductivities of the Ionic Liquid Compounds Butyldimethylimidazolium Tetrafluoroborate, Hexafluorophosphate and Hexafluoroantimonate

Keywords: Electrochemistry / Ionic liquids / Packing efficiency / X-ray diffraction

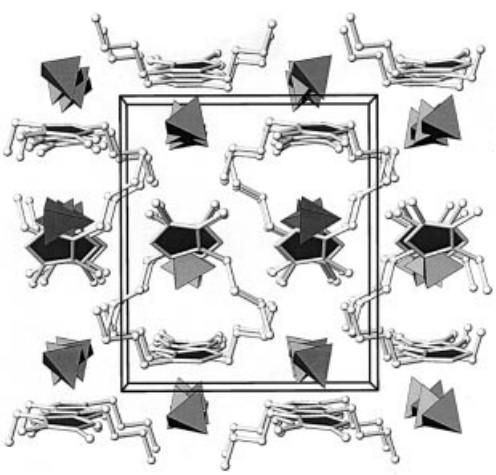

 © 2004 Wiley-VCH Verlag GmbH & Co. KGaA, Weinheim

2321 **D. Nikolova, C. von Hänisch,* A. Adolf**

Synthesis and Characterisation of Novel Main Group Element Clusters with Tin-Phosphorus, Tin-Arsenic, and Germanium-Phosphorus Skeletons

Keywords: Tin / Phosphorus / Arsenic / Germanium / Cluster compounds

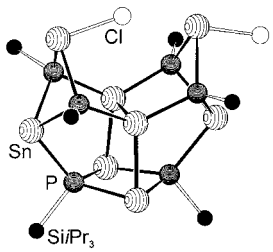

2326 **C. Bartolomé, P. Espinet,* J. M. Martín-Álvarez, F. Villafañe**

Bis(fluoromesityl) Palladium Complexes, Archetypes of Steric Crowding and Axial Protection by *ortho* Effect − Evidence for Dissociative Substitution Processes − Observation of $^{19}F-^{19}F$ Through-Space Couplings

Keywords: Palladium / Dissociative substitution / Fluorine / Bulky ligands / Steric crowding / Through-space coupling

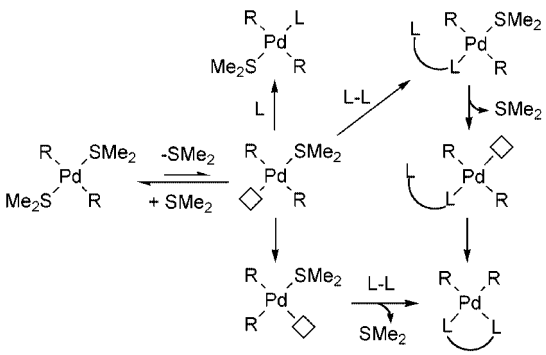

2338 **M. Carbó, L. R. Falvello, R. Navarro,* T. Soler, E. P. Urriolabeitia***

Different Coordination Modes of the Polyfunctional Ylide $Ph_3P{=}C(H)C(O)CH_2C(O)OEt$: *C*- vs. *O,O′*-Bonding in Pd^{II}, Pt^{II} and Au^{I} Complexes

Keywords: Palladium / Platinum / Gold / Ylides / Structure elucidation

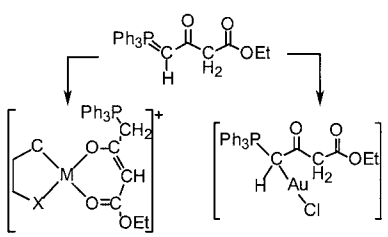

2348 **F. de M. Ramírez, L. Charbonnière, G. Muller, J.-C. G. Bünzli***

Tuning the Stoichiometry of Lanthanide Complexes with Calixarenes: Bimetallic Complexes with a Calix[6]arene Bearing Ether-Amide Pendant Arms

Keywords: Lanthanides / Calixarenes / Europium / Luminescence

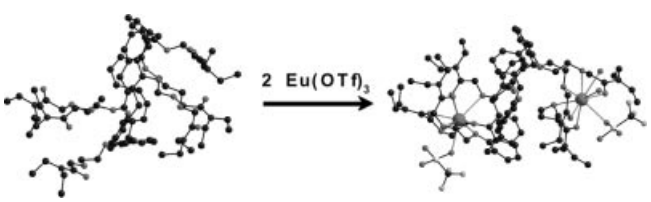

 © 2004 Wiley-VCH Verlag GmbH & Co. KGaA, Weinheim

2356 **T. Glaser,* T. Lügger, R.-D. Hoffmann**

Iron Complexes with the Alcoholato Donor-Rich Ligand 4-*tert*-Butyl-2,6-bis(hydroxymethyl)-phenol: Synthesis and Characterization of a Tetra-Anionic Fe_2 Complex and a Neutral $Fe_{10}Na_4$ Complex

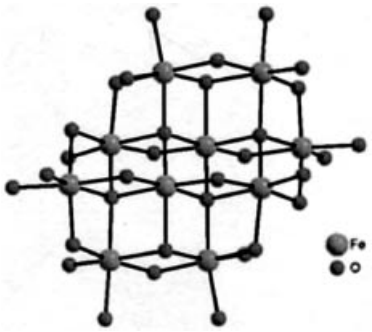

Keywords: Iron / O ligands / Oxo ligands / Bridging ligands / Hydrogen bonds

2363 **M. C. Aragoni, M. Arca, F. Demartin, F. A. Devillanova,* A. Garau, P. Grimaldi, F. Isaia, F. Lelj, V. Lippolis, G. Verani**

First ICN Adduct with a Selenium Donor (R = Se): Is It an Ionic $[RSeCN]^+I^-$ or a "T-Shaped" R(I)SeCN Hypervalent Compound?

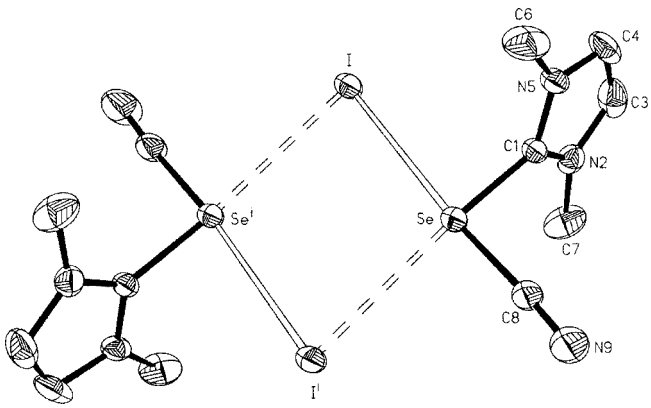

Keywords: Density functional calculations / Donor-acceptor systems / ICN / Hypervalent compounds / Se ligands

2369 **P. Cheng,* S.-P. Yan,* C.-Z. Xie, B. Zhao, X.-Y. Chen, X.-W. Liu, C.-H. Li, D.-Z. Liao, Z.-H. Jiang, G.-L. Wang**

Ferromagnetic and Antiferromagnetic Polymeric Complexes with the Macrocyclic Ligand 1,4,7-Triazacyclononane

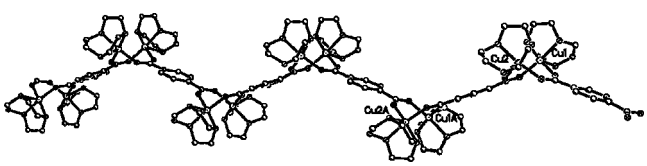

Keywords: Benzenedicarboxylic acids / Polymer chains / Magnetic properties / Copper

2379 **V. Patroniak, P. N. W. Baxter, J.-M. Lehn,* Z. Hnatejko, M. Kubicki**

Synthesis and Luminescence Properties of New Dinuclear Complexes of Lanthanide(III) Ions

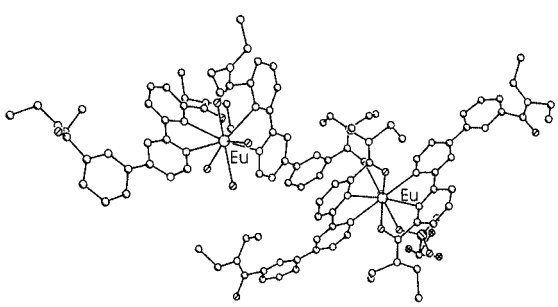

Keywords: Dinuclear complexes / Lanthanides / Bis(tridentate) ligands / Self-assembly

 © 2004 Wiley-VCH Verlag GmbH & Co. KGaA, Weinheim

2385 **P. H. M. Budzelaar,* A. N. J. Blok**

Mechanism of Oxidation of (olefin)Rh^{I} and -Ir^{I} Complexes by H_2O_2

Keywords: Density functional calculations / Iridium / Oxidation / Oxygenation / Rhodium

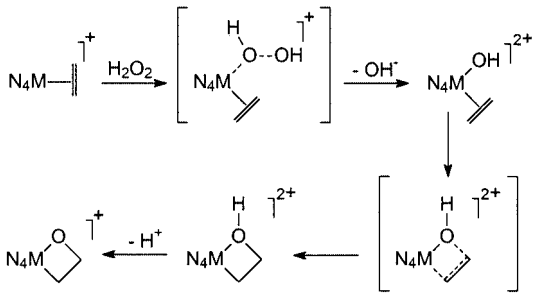

 © 2004 Wiley-VCH Verlag GmbH & Co. KGaA, Weinheim

Engineering and Prosthetic-Group Modification of Myoglobin: Peroxidase Activity, Chemical Stability and Unfolding Properties

Raffaella Roncone,[a] Enrico Monzani,[a] Stefania Nicolis,[a] and Luigi Casella*[a]

Keywords: Bioinorganic chemistry / Heme proteins / Enzyme models / Protein engineering / Structure-activity relationships / Myoglobin

The role of myoglobin (Mb) is not yet completely understood and recent evidence indicates it is involved in a variety of pseudo-enzymatic functions. Mb is also extensively used as a tool to redesign novel active-site features and introduce new activities into a protein. This review summarizes our approach to enhance the peroxidase-like activity of Mb toward phenolic compounds by combining two different strategies of protein modification, i.e. active-site engineering and cofactor replacement. The main objective of active-site engineering is to increase the rate of hydrogen peroxide activation upon reaction at the iron(III) center, while cofactor replacement facilitates substrate interaction at the protein active site, thereby increasing the efficiency of the catalytic process and stereoselective recognition of the substrate. The thermodynamic stability of the modified Mb derivatives has been evaluated through guanidinium chloride induced and thermal unfolding experiments. As expected, both protein mutation and cofactor replacement decrease the stability of the protein, the latter effect being somewhat more pronounced for the Mb derivatives studied here. For evaluating the catalytic efficiency of the protein in non-natural reactions, the chemical stability of the protein during catalysis is also important and therefore a new protocol was developed to evaluate the competitive degradation undergone by the protein upon substrate oxidation. It was found that autodegradation can occur through two different pathways involving oxidation of protein residues by the Mb active species or by a substrate-derived phenoxy radical. The peroxidase-like nitrating activity and the sulfoxidation reactions promoted by Mb, both involving the nitrite ion as a cosubstrate, have also been briefly described.

(© Wiley-VCH Verlag GmbH & Co. KGaA, 69451 Weinheim, Germany, 2004)

Introduction

Myoglobin (Mb), "the hydrogen atom of biology",[1] is a monomeric protein which gives muscles their red color. It has a globular structure consisting of eight α helices wrapping around a central hydrophobic pocket containing iron protoporphyrin IX as the prosthetic group. Since the early 19th century, Mb was believed to function in the storage of dioxygen and in facilitating its transport from the periphery of the cell to the mitochondria,[2] although, the situation has now changed and it appears that Mb may play additional roles. Four conserved cavities surrounding the heme group, termed xenon cavities because they can host Xe atoms, are lined with highly conserved hydrophobic residues and appear to be actively involved in the binding of small molecules like O_2, CO and NO.[3] This suggests that Mb is built like a miniature chemical reactor with the iron atom as active centers and the cavities as chambers in which reactants are concentrated and oriented. Since different molecules react at different sites of the protein, Mb could be considered as an allosteric enzyme.[1,3] In the case of NO, for example, binding of the ligand to the oxygenated form of Mb (oxyMb) is followed by rapid conversion into the nitrate.[4−6] Since NO is an inhibitor of cytochrome *c* oxidase, it has been suggested that the scavenging effect of Mb protects the cell from inhibition of cellular respiration.[3,7] Other recent observations support a multiple role for Mb. Studies using a gene disruption strategy to produce mice that lack Mb show that the protein acts as an important modulator of cardiac function.[8] In addition, in vitro Mb is active in oxidative phosphorylation, shows some peroxidase and P450-like catalytic activities,[9] and protects cells against oxidative damage.[10,11] In vivo Mb may be present up to a concentration of 0.2 mM within the cytosol of myocardial cells and exists prevalently as oxyMb. However, high concentrations of oxidants, such as those present under in-

[a] Dipartimento di Chimica Generale,
Via Taramelli 12, 27100 Pavia, Italy
Fax: (internat.) +39-0382-528544
E-mail: bioinorg@unipv.it

MICROREVIEWS: This feature introduces the readers to the author's research through a concise overview of the selected topic. Reference to important work from others in the field is included.

flammatory conditions, or acidic pH may induce autoxidation of the protein with formation of metMb. This is the state in which Mb can exhibit a peroxidase-like behavior.

The similarity that the Mb heme environment shares with other heme proteins, like cytochromes or peroxidases, makes Mb so widely employed for engineering novel metalloproteins by redesign of the existing metal-binding site.[12] Redesign of heme proteins gives insight into the factors governing structure and function within members of a closely related family and is invaluable for the developing area of de novo protein design. In this respect, Mb has several advantages because of its relatively small size, compact structure, and the extensively accumulated biochemical and biophysical characterization, including a large number of X-ray crystal structures available for both the native proteins from various sources and several mutants.[13] The current strategies for the modification of heme proteins follow four different approaches: i) rational design of heme enzymes; ii) directed evolution of heme enzymes; iii) exon shuffling of hemoglobin; and iv) replacement of the native heme prosthetic group (reconstitution).[14] For instance, the engineering of heme proteins is used as a strategy to develop new blood substitutes.[15,16] The availability of the expression system for recombinant Mb in *E. coli* and the relatively easy methods of site-directed mutagenesis make the engineering approach of extreme importance for investigating the role of critical residues and for introducing non-natural activities into the protein.[17,18] On the other hand, reconstitution of Mb with a modified prosthetic group (Figure 1) allows the introduction into the protein of a specific binding site for exogenous substrates or protein−protein interactions.[19,20] In this review, we summarize the results obtained in our group on the peroxidase-like activity of Mb upon modification of the protein by site-directed mutagenesis and by altering the prosthetic group. Combining the two approaches allowed us to develop a powerful method to enhance the reactivity and selectivity of Mb derivatives. Peroxidative processes mediated by Mb appear to be important in the oxidative degradation of lipid compounds in biological systems and foods.[21] Moreover, the transient protein radical, produced by the reaction between Mb and hydrogen peroxide, appears to be a key determinant of oxidative damage in ischemic heart.[10]

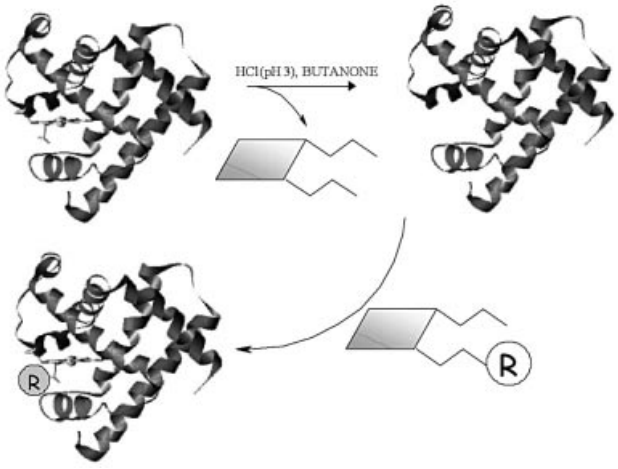

Figure 1. Two steps of the Mb reconstitution process: (i) extraction of the native heme with an organic solvent at acidic pH, and (ii) introduction of the chemically modified heme cofactor into apoMb

Characteristic Features of Peroxidases

Peroxidases are a class of ubiquitous heme enzymes that catalyze the oxidation of a wide range of substrates by hydrogen peroxide.[22,23] The stoichiometry of the reaction is normally as follows:

$$2\,SH + H_2O_2 \rightarrow 2\,S^{\cdot} + 2\,H_2O \quad (1)$$

Raffaella Roncone was born in Vigevano (Pv, Italy). She obtained her degree in Chemistry from the University of Pavia in 1999 and her Ph.D. degree in Chemistry in 2003 under the supervision of Prof. L. Casella. She was responsible for a Young Scientist Project with the title: "A Potential Nitric Oxide Dependent Toxicity: Reactive Nitrogen Species Generated by Metallo-Proteins" at the University of Pavia. Her current research interests focus on the chemistry of heme proteins and the study of protein modification induced by oxidative radical species.

Enrico Monzani was born in Locate Triulzi (Mi, Italy). He received his degree in Industrial Chemistry at the University of Milan in 1991 and his Ph.D. degree in Chemistry at the University of Pavia in 1994. He did his post-university training at the enzymology laboratory of the "Istituto di Ricerche Farmacologiche Mario Negri", Milan, Italy. From 1997 he obtained a permanent position as a Research Associate in Inorganic Chemistry at the University of Pavia. His research interest is in the field of Bioinorganic chemistry, in particular, on the structural and functional characterization of heme and copper proteins, covering both studies on the macromolecules and on the low molecular weight model systems.

Stefania Nicolis was born in Brescia in 1977. She obtained her degree in Chemistry from the University of Pavia in 2001. Since 2001 she is a Ph.D. student with Prof. L. Casella at the Faculty of Sciences at the University of Pavia.

Luigi Casella was born in Milano in 1947. He obtained his degree in Chemistry from the University of Milano in 1973. In the period between 1978-1979 he did his postdoc with J.A. Ibers at Northwestern University, Evanston (USA) with a CNR-NATO fellowship. Since 1990 he is a full professor of Inorganic Chemistry at the Faculty of Sciences at the University of Pavia. He is the Chairperson of the European COST Chemistry Action D21 "Metalloenzymes and chemical biomimetics". His scientific interest lies in the chemistry of metal enzymes containing heme or copper cofactors involved in oxidative processes. He is the author of more than 150 papers in international chemical and biochemical journals, and he has an international patent.

 © 2004 Wiley-VCH Verlag GmbH & Co. KGaA, Weinheim

which emphasizes that the typical activity of these enzymes involves the one-electron oxidation of two substrate molecules by hydrogen peroxide or other peroxides. In their catalytic cycle, the resting state Fe^{III} center of peroxidases is oxidized by H_2O_2 to generate an intermediate containing an $Fe^{IV}=O$ group with a porphyrin or protein cation radical, which is known as Compound I. In the presence of a suitable substrate Compound I is reduced to a second ferryl intermediate, known as Compound II, and subsequently to the resting state by two sequential one-electron oxidations of substrate molecules.[23,24] The reaction with H_2O_2 is facilitated by a "push−pull" mechanism, to which suitably positioned residues located in both the heme proximal and distal sites contribute.[25,26] The distal arginine and histidine residues favor O−O bond polarization of the Fe-bound hydroperoxide and proton transfer from the Fe-bound oxygen atom to the other to form, after cleavage of the O−O bond, the $Fe^{IV}=O$ species and a water molecule (Figure 2). The proximal aspartate participates in the weakening of the peroxide O−O bond by increasing the electron-donating character of the proximal histidine through a hydrogen bond to the imidazole NH group, which enhances back-donation from Fe into the peroxide π* orbitals[27] (Figure 2).

Typical low molecular weight substrates processed by peroxidases according to reaction 1 are electron-rich organic compounds such as phenols or aromatic amines.[28] These bind to the enzyme near the heme edge but cannot enter into the heme distal pocket, the access to which is controlled by several aromatic residues.[29−31] The disposition of the substrate at the heme edge allows an efficient transfer of electrons to the enzyme active species through the extended porphyrin π system.[32] In the past decades we have extensively studied the kinetics and mechanisms of these reactions using a variety of phenolic compounds and enzymes from various sources.[33−36] In particular, by using paramagnetic NMR spectroscopic and relaxation rate measurements we could gain an understanding of the selectivity and stereoselectivity effects observed in the enzymatic reactions in terms of the interaction between the enzymes and the substrates.

In addition to the classical peroxidase reaction, phenolic substrates can be efficiently nitrated on the aromatic ring by peroxidases in the presence of nitrite and hydrogen peroxide.[37,38] This reaction is important in vivo because nitration of tyrosine, to give 3-nitrotyrosine, has been associated with a wide range of human and animal diseases.[39,40] In fact, nitrite is a major product of nitrogen monoxide metabolism[41] and accumulates upon activation of NO synthases under inflammatory and other disease conditions. Interestingly, we have recently found that both peroxidases[42,43] and myoglobin[44] perform nitration of tyrosine derivatives through two distinct pathways which involve nitrogen dioxide or peroxynitrite, respectively, as nitrating agents depending on the conditions.

Reconstitution of Myoglobin with Chemically Modified Hemins and Site-Directed Mutagenesis

Mb, with peroxidases, shares the same heme cofactor and the same heme distal and proximal His residues (His64 and His93, respectively, in Mb). However, its globular shape, the different functional oxidation state of the iron atom, and the differences in heme environment and overall polarity of the active site, make the catalytic activity of Mb in peroxidase-type reactions markedly lower than that of the enzymes. In particular, Mb lacks the amino acid residues that are essential for the activation of hydrogen peroxide, i.e. a distal arginine and a proximal aspartate (Figure 2), and a specific cleft for substrate binding near the heme. The scope of our modifications of Mb basically aimed at introducing these characteristic features into the protein. In our initial attempts an Arg−Ala residue was covalently linked to one of the propionate side chains of protohemin and the resulting complex, HM−RA (Scheme 1), was inserted into horse heart apoMb.[45] Insertion of a modified hemin into Mb affects the pre-existing network of hydrogen bonds be-

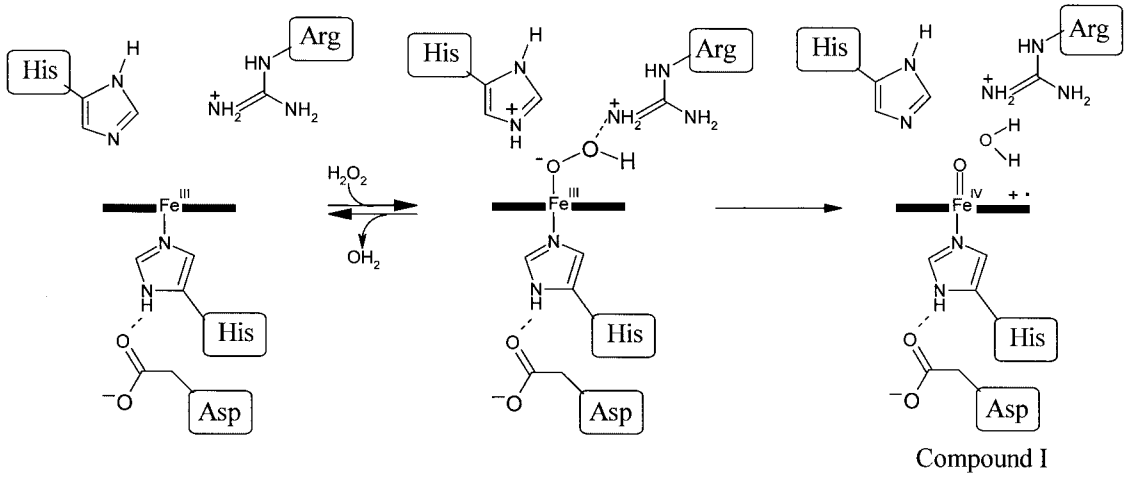

Figure 2. Mechanism of compound I formation in peroxidases promoted by general acid−base catalysis of polar residues in the active site

 © 2004 Wiley-VCH Verlag GmbH & Co. KGaA, Weinheim

tween the propionate groups of the cofactor and side chain residues of the protein. In the case of HM−RA, the polypeptide fragment Phe43−Lys47 of Mb acquired sufficient mobility to allow collapse of the distal helix and binding of distal His to the sixth coordination position of the iron.[45] The presence of distal His as the sixth ligand hindered the binding of hydrogen peroxide to the iron and reduced the activity of the reconstituted protein. On the contrary, when the heme cofactor was modified by attachment of a histidine residue, HM−H (Scheme 1), the reconstituted Mb contained a significant portion of high spin form, which reacted normally with hydrogen peroxide. Since the His imidazole group of the HM−H prosthetic group is partially protonated at physiological pH, it could play a role similar to that of distal arginine in peroxidases.

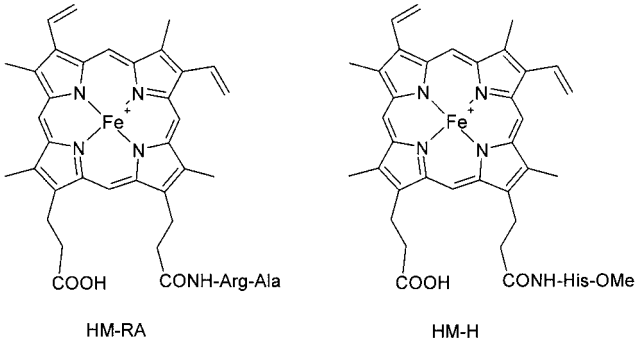

Scheme 1

Reconstitution of Mb with monosubstituted protohemins like HM−RA and HM−H unavoidably leads to a mixture of protein isomers. The hemin derivatives are in fact obtained as 1:1 mixtures of isomers containing the covalent modification at positions 6 or 7 of the porphyrin ring. Therefore, upon reconstitution of apoMb four protein isomers are obtained, depending on the type of substitution on the porphyrin and the mode of incorporation (“up” or “down”) of the prosthetic group into the protein (Scheme 2).[45] The ratio of these protein isomers is dictated by their relative stability and generally produces one major and one minor isomer for both 6- and 7-substituted HM−H derivatives, assessed by NMR spectroscopy.

The problem of Mb reconstitution isomers is reduced in the approach followed by Hayashi and Hisaeda, where Mb was reconstituted with synthetic protohemins bearing identical substituents at both the porphyrin propionates;[19,20] although, it is expected that the resulting protein derivatives will bear additional loss of stability because the interactions between the prosthetic group and the protein are further weakened.

In further developments we produced site-directed mutants of sperm whale Mb containing those amino acid residues critical for peroxide activation in peroxidases. In particular, we replaced the distal Thr67 with either Arg (T67R Mb)[46] or the more flexible Lys residue (T67 K Mb)[47] and obtained a double mutant where, in addition to the Thr67Arg mutation, the proximal Ser92 was substituted

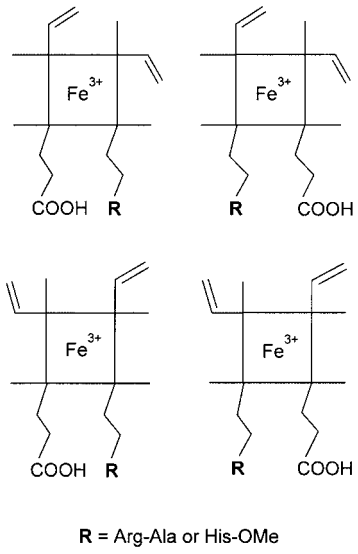

Scheme 2

with an Asp residue (T67R/S92D Mb) (Figure 3).[48] The mutants T67 K Mb and T67R/S92D Mb were also reconstituted with HM−H, while with T67R Mb we could not obtain a stable derivative. The reconstituted sperm whale Mb derivatives will be indicated as WT Mb−H, T67 K Mb−H and T67R/S92D Mb−H.

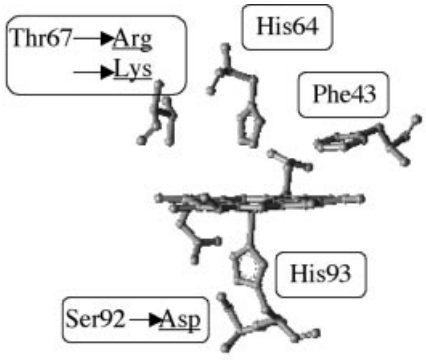

Figure 3. Engineering of the Mb active site: site-directed mutated residues are underlined

In general, point mutations do not appreciably affect the overall protein structure and only marginally perturb the heme environment.[46] The most significant change has been shown by the X-ray structure of T67R/S92D Mb to consist of an increase in the conformational mobility of the porphyrin propionate-7, which allows this group to span the heme proximal and distal sides through hydrogen-bonding interactions with water molecules.[46] The conformational mobility of propionate-7 is confirmed by marked shift of its signal in the ^{1}H NMR spectra of all Mb mutants with respect to the position of the signal in the spectrum of wild type Mb.[48] Reconstitution of Mb with synthetic hemins results in more substantial changes in the NMR spectra,

 © 2004 Wiley-VCH Verlag GmbH & Co. KGaA, Weinheim

but the problem of the existence of several protein isomers makes a detailed analysis of the NMR spectra impossible.

Ligand Binding Data, Peroxide Activation and Catalytic Activity

Two representative ligands of different charge and size, azide and imidazole, were used as probes to investigate the effect of Mb modification on the affinity and accessibility of the iron site to external donor molecules. The affinity for azide is systematically increased upon introduction of a positively charged Arg, Lys or His residue into Mb by either engineering or reconstitution of the protein with HM−H, whereas with the bulky imidazole ligand a significant increase in the binding affinity is generally obtained only with the reconstituted proteins, due to the higher protein mobility at the entrance of the distal pocket (Table 1). The enhanced azide binding affinity exhibited by the modified Mb derivatives is expected to similarly stabilize the binding of H_2O_2 to the iron as a hydroperoxide ligand. As with peroxidases, this binding step is rapidly followed by cleavage of the O−O bond in the Fe^{III}−O−OH complex to produce a ferryl Mb species and a protein radical ($^{\cdot}MbFe^{IV}$=O). The positively charged residue introduced into the modified Mbs is expected to favor the heterolytic cleavage of the bound hydroperoxide, even though it cannot be suitably positioned to produce such a strong polarization effect of the O−O bond as that promoted by distal Arg in peroxidases. The rate constants for the formation of the Fe^{IV}=O Mb radical species (k_1) indeed show an appreciable increase for the modified Mbs, from a value of 760 ± 10 M^{-1} s^{-1} for WT Mb to 2100 ± 40 M^{-1} s^{-1} for the T67R/S92D Mb mutant.[46−48] Regarding the location of the protein radical, several studies indicate that it is distributed among several residues, including tyrosine, tryptophan and histidine residues,[49−53] with tyrosine being largely preferred, leading to the formation of Tyr−Tyr cross-links and Mb dimerization.[54]

To investigate the peroxidase activity of the Mb derivatives we followed a similar approach as in our previous studies with peroxidases.[33−35] We therefore selected a group of phenolic substrates which are related to tyrosine and contain substituents on the aromatic ring that can be useful for investigating selectivity effects in the enzymatic reaction. During activity, the phenolic substrates undergo one-electron oxidation to phenoxy radicals by the Mb active species, according to a reaction scheme analogous to that of peroxidases, which can be summarized as follows.

$$MbFe^{3+} + H_2O_2 \xrightarrow{k_1} {}^{\cdot}MbFe^{IV}{=}O + H_2O \quad (2)$$

$$^{\cdot}MbFe^{IV}{=}O + PhOH \xrightarrow{k_2} MbFe^{IV}{=}O + PhO^{\cdot} + H^+ \quad (3)$$

$$MbFe^{IV}{=}O + PhOH + H^+ \xrightarrow{k_3} MbFe^{3+} + PhO^{\cdot} + H_2O \quad (4)$$

$$2\ PhO^{\cdot} \longrightarrow \text{Dimers} \quad \text{(fast)} \quad (5)$$

The phenoxy radicals evolve independently of the protein catalyst in solution, giving a fast coupling reaction to dimeric products,[46] which subsequently yield complex mixtures of oligomers, as in the peroxidase-catalyzed reactions.[36,55] As discussed above, the rate constant k_1 can be determined by the reaction between Mb and hydrogen peroxide. The rate of reduction of the first protein intermediate ($^{\cdot}MbFe^{IV}$=O) by the substrate (k_2) is difficult to determine because this intermediate has optical features similar to the second intermediate ($MbFe^{IV}$=O), but the process is probably fast. Considering that $^{\cdot}MbFe^{IV}$=O does not accumulate in solution, the catalytic scheme can be reduced to a bimolecular ping-pong mechanism.[33] A further simplification in the in vitro kinetic scheme can be obtained by operating under saturating H_2O_2 conditions because in this case the rate equation reduces to conventional Michaelis−Menten kinetics, rate = k_{cat}[substrate]/(K_M + [substrate]).[46] Under these conditions, the third step, reduction of $MbFe^{IV}$=O by substrate, is rate limiting, and we can assume that the rate constant k_3 coincides with the turnover rate constant (k_{cat}).

The kinetic parameters for the catalytic oxidation of (*p*-hydroxyphenyl)propionic acid obtained with the various Mb derivatives exemplify how the catalytic performance of Mb is enhanced in an additive fashion by engineering and cofactor reconstitution (Table 2). The k_{cat} parameter, in particular, measures the electron transfer rate from the substrate to the $MbFe^{IV}$=O center. For a given substrate, this parameter depends on (i) the redox potential of the ferryl species, which is likely to increase by introduction of positively charged residues into Mb, and (ii) the mode of substrate interaction with the protein, which allows a closer approach to the heme, especially in the case of the reconstituted proteins. This interpretation is confirmed by the selectivity effects observed in the catalytic reactions, which could

Table 1. Ligand binding constants (K_B) for azide and imidazole by the Mb derivatives, in 0.2 M phosphate buffer pH 6.0 at 25 °C

Protein	Azide, K_B (M^{-1})	Imidazole, K_B (M^{-1})	References
WT Mb	(5.0 ± 0.1) × 10^4	25 ± 1	[46]
WT Mb−H	(5.6 ± 0.1) × 10^4	38 ± 1	[47]
T67 K Mb	(9.8 ± 0.5) × 10^4	32 ± 1	[47]
T67 K Mb−H	(27.0 ± 0.1) × 10^4	60 ± 1	[47]
T67R Mb	(6.0 ± 0.5) × 10^4	12 ± 1	[46]
T67R/S92D Mb	(9.0 ± 0.1) × 10^4	47 ± 1	[48]
T67R/S92D Mb−H	(15.0 ± 0.1) × 10^4	89 ± 2	[48]

 © 2004 Wiley-VCH Verlag GmbH & Co. KGaA, Weinheim

Table 2. Kinetic parameters for the catalytic oxidation of (*p*-hydroxyphenyl)propionic acid by hydrogen peroxide in the presence of the Mb derivatives, measured in phosphate buffer pH 6.0 at 25 °C

Protein	k_{cat} (s^{-1})	K_M (mM)	k_{cat}/K_M (M^{-1} s^{-1})	References
WT Mb	1.0 ± 0.1	72 ± 5	14 ± 0.4	[46]
WT Mb−H[a]	−	−	−	[47]
T67 K Mb	2.3 ± 0.2	28 ± 5	83 ± 9	[47]
T67 K Mb−H	6.7 ± 0.4	26 ± 3	255 ± 18	[47]
T67R Mb	2.3 ± 0.1	12 ± 2	190 ± 25	[46]
T67R/S92D Mb	1.5 ± 0.6	20 ± 2	80 ± 6	[48]
T67R/S92D Mb−H	6.6 ± 0.3	20 ± 2	330 ± 20	[48]

[a] Biphasic kinetics.

be rationalized according to a structural model for the protein-substrate interaction deduced from paramagnetic ^1H NMR spectroscopic relaxation measurements. According to this technique it is possible to obtain an estimate of the distances between the protons of the bound substrate and the paramagnetic Fe center through the enhancement of the relaxation rate of the nuclei caused by the proximity of the paramagnetic, high-spin Fe center of the protein (Figure 4).[46,47]

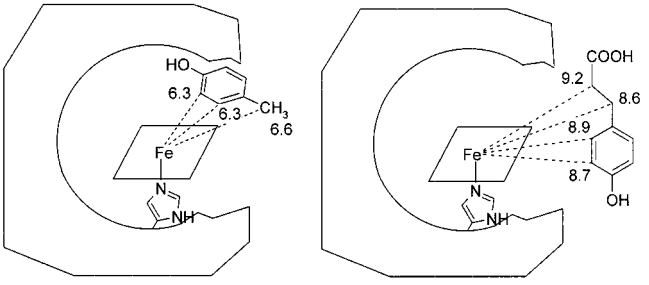

Figure 4. Distances (in Å), deduced by NMR spectroscopic relaxation measurements, between the paramagnetic Mb iron(III) center and the protons of protein-bound aromatic substrates: *p*-cresol (left) and (*p*-hydroxyphenyl)propionic acid (right)

(*p*-Hydroxyphenyl)propionic acid carries a side chain with a charge complementary to that of the residues introduced in the Mb heme environment and is therefore favored from the point of view of the protein-substrate interaction. Among the Mb derivatives, the highest catalytic activity (both in terms of k_{cat} and k_{cat}/K_M) is exhibited by T67 K Mb−H and T67R/S92D Mb−H (Table 2), because with these reconstituted proteins (*p*-hydroxyphenyl)propionic acid can reach closest to the Fe center and thus offer the most favorable arrangement for the electron transfer process.[47,48] The opposite trend holds for tyramine, which carries a positive charge in the side chain, while tyrosine is a very poor substrate for all Mb derivatives because it binds strongly to the protein but at a distance from the heme.[46−48]

The best performance by the Mb derivatives, in terms of k_{cat}/K_M, is obtained with *p*-cresol. The behavior of this substrate is unusual since its size is comparable with that of imidazole, and it can enter into the distal cavity of Mb, as shown by the short distance to the heme (Figure 4).[46] The reaction between *p*-cresol and the Mb active species is therefore unusually fast (almost similar to that of peroxidases),[46] and becomes limited by the reaction between the Fe^{3+} species and H_2O_2, making the comparison between the various Mb derivatives difficult.

Thermodynamic Stability and Stability of the Proteins during Catalysis

Many globular proteins can be reversibly unfolded in solution by addition of a denaturant, like urea or guanidinium chloride (Gdn−HCl), to the solution.[56,57] The stability of the protein, in terms of the unfolding free energy, can be determined by the analysis of a denaturant-induced unfolding curve as a function of the denaturant concentration. Unfolding of Mb has been studied intensively, and in the urea or Gdn−HCl denaturation experiments the behavior of the protein has been satisfactorily described by a two-state model (native/unfolded), without any defined intermediate state.[58−62] We obtained thermodynamic data on the stability of the various Mb derivatives through thermal and Gdn−HCl denaturation experiments, which were analyzed according to the two-state model.[62] The Gdn−HCl induced denaturation process was found to be completely reversible, indicating that the heme remains bound to the polypeptide chain even at high concentration of denaturant. On the contrary, the behavior of the proteins with temperature is different since they tend to precipitate at higher temperatures and the denaturation process becomes irreversible, possibly because, in this case, the heme is released by the protein. Nevertheless, the trend of thermal stabilities follows the same order as that found in the Gdn−HCl denaturation experiments.[47] As shown by the data reported in Table 3, both protein mutation and protein reconstitution decrease the stability of Mb, but in the latter case the effect is more pronounced. The observed trend can be accounted for in terms of the interactions involved in the binding of the heme to the protein, since heme binding gives the most prominent contribution to the stability of the holo protein. This contribution has been factored into that of the covalent bond between the iron atom and proximal His93 (25%), those of hydrophobic interactions between the heme and apolar residues in the pocket (50%), and those of specific interactions, which include hydrogen bonds and charge effects, between the protein and the propionate

 © 2004 Wiley-VCH Verlag GmbH & Co. KGaA, Weinheim

Table 3. Thermodynamic parameters for unfolding induced by Gdn−HCl (ΔG^0_{N-U} and $-m$) and Gdn−HCl concentration causing 50% denaturation of the Mb derivatives ($[Gdn-HCl]_0$), obtained in 0.2 M phosphate buffer pH 6.0 at 25 °C

Protein	ΔG^0_{N-U} (kcal mol^{-1})	$-m$ (kcal mol^{-1} M^{-1})	$[Gdn-HCl]_0$ (M)	References
WT Mb	4.95 ± 0.13	3.45 ± 0.09	1.46 ± 0.01	[47]
WT Mb−H	3.99 ± 0.08	3.64 ± 0.07	1.09 ± 0.01	[47]
T67 K Mb	4.71 ± 0.12	3.50 ± 0.09	1.36 ± 0.01	[47]
T67 K Mb−H	3.35 ± 0.07	3.97 ± 0.08	0.83 ± 0.01	[47]
T67R Mb	4.08 ± 0.11	3.44 ± 0.09	1.20 ± 0.01	this work
T67R/S92D Mb	4.48 ± 0.09	3.79 ± 0.08	1.16 ± 0.01	this work
T67R/S92D Mb−H	1.10 ± 0.06	1.35 ± 0.05	0.88 ± 0.03	this work

groups (25%).[63] The specific hydrogen-bonding and electrostatic interactions involving the propionates in sperm whale Mb are with Leu89, Ser92, His93 and His97 for propionate-7, and with His64 and Arg45 for propionate-6.[64][65] The decrease in stability of Mb upon mutation of the Thr67 residue can be attributed mainly to a change in conformation of the propionate-7 group, which is shown by the NMR spectra of the Mb mutants[46−48] and is confirmed by the X-ray structure of T67R/S92D Mb.[48] The loss of the hydrogen-bonding structure can be partially compensated by new interactions established by the mutated residue. This is suggested by the observation that the most stable Mb mutant, T67 K Mb, is the one that contains the engineered residue with most flexible side chain that can more easily establish interactions with other groups in the protein. The parameter $-m$ that is related to the protein−water interaction and the surface roughness of the protein is reported in Table 3. Surprisingly, this parameter is much smaller for T67R/S92D Mb−H than the other Mb derivatives. This may indicate a significant difference in the solvent-exposed surface area of the reconstituted Mb double mutant or, more likely, the existence of some intermediate state in the unfolding process. The decrease in stability observed for the reconstituted Mb derivatives is largely due to the loss of one of the hydrogen-bonding networks maintained by the two heme propionates in the native protein. This increases the protein mobility around the heme, facilitating the interaction with the denaturant. The lowest free energy of unfolding is observed for the engineered and reconstituted Mb−H derivatives; here, an additional repulsive interaction occurs between the positively charged Lys or Arg residues and the His residue present in the HM−H cofactor. Although the reconstitution isomers of each Mb−H derivative may have different stabilities, the fact that, in every case, the various protein isomers are formed in similar amounts indicates that such differences in stability are limited.

Of particular interest is the problem of protein stability during catalysis since this is an important aspect for the assessment of biological catalysts. The Mb active species formed during turnover are not only able to oxidize exogenous substrates but can competitively react with amino acid residues, which ultimately leads to loss of catalytic activity. When the Mb derivative reacts with hydrogen peroxide in the absence of a substrate, a fast inactivation process occurs, which is characterized by an autodegradation rate constant k_D. The inactivation depends on the formation of radical species, produced at various protein residues, as discussed above.[49−54] In the presence of substrate the catalytic reaction competes with protein degradation and the possible pathways are summarized in Scheme 3. In this scheme, I is the Mb active species, S the substrate, IS the complex substrate−Mb active species, and $Mb_{inactivated}$ the degradation product (e.g. the protein derivative resulting from autoxidation of amino acid residues or the porphyrin) which can be formed directly or through a process mediated by the bound substrate. The latter process is characterized by rate constant k'_D.

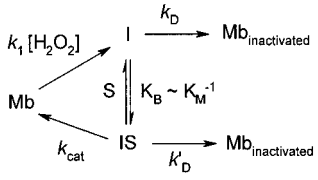

Scheme 3

The competition between the catalytic reaction and protein degradation depends on substrate concentration but, at least with the phenolic substrates, inactivation can never be completely neglected. In fact, the substrate-bound by Mb can also promote protein inactivation, and the relative importance of this process with respect to substrate oxidation is governed by the ratio between the rate constants k'_D/k_{cat}. Different situations can be envisaged according to whether $k_D \approx k'_D$, $k'_D > k_D$, or $k'_D < k_D$ (Table 4 and Figure 5). Protein autodegradation may not be affected by the presence of the substrate ($k'_D < k_D$), as in the case of T67R Mb and T67R/S92D Mb, or only marginally affected by the presence of the substrate ($k_D \approx k'_D$), as in the case of WT Mb, WT Mb−H and T67 K Mb. This situation occurs when the active site is relatively closed and the phenoxy radicals produced by the Mb active species rapidly diffuse in the solution, thus preventing the substrate-induced degradation of the protein. The protecting effect exerted by the protein accounts for the longer lifetime of these biocatalysts with respect to simple hemins or microperoxidases where the active site is quite open and allows for a close approach of the substrate to the heme, which strongly facilitates the substrate induced degradation process.[66−68] A

 © 2004 Wiley-VCH Verlag GmbH & Co. KGaA, Weinheim

Table 4. Protein autodegradation rate constants (k_D) and protein degradation rate constants in the presence of the substrate (*p*-hydroxyphenyl)propionic acid (k'_D) during catalysis for the Mb derivatives

Protein	k_D (s^{-1})	k'_D (s^{-1})	References
WT Mb	$1.93 \times 10^{-3} \pm 4 \times 10^{-5}$	1.9×10^{-3}	[47]
WT Mb−H	$8.31 \times 10^{-3} \pm 1 \times 10^{-5}$	8.3×10^{-3}	[47]
T67 K Mb	$0.94 \times 10^{-3} \pm 8 \times 10^{-5}$	0.9×10^{-3}	[47]
T67 K Mb−H	$2.40 \times 10^{-3} \pm 4 \times 10^{-4}$	6.1×10^{-3}	[47]
T67R Mb	$2.29 \times 10^{-2} \pm 3 \times 10^{-4}$	≈ 0	this work
T67R/S92D Mb	$8.16 \times 10^{-3} \pm 1 \times 10^{-4}$	1.9×10^{-3}	this work
T67R/S92D Mb−H	$1.18 \times 10^{-2} \pm 2 \times 10^{-4}$	1.2×10^{-2}	this work

similar situation is observed with T67 K Mb−H only, for which the inactivation process in the presence of substrate is faster than in the absence of substrate ($k'_D > k_D$). This is consistent with the already mentioned increased accessibility of the heme site of T67 K Mb−H to the substrate. In this case, the phenoxy radical produced by the Mb active species can attack the porphyrin before diffusing into the solution, thus causing protein inactivation. However, it is worth emphasizing that the closer binding of the substrate to the heme has the advantage of increasing the catalytic turnover, and we can see from the data in Table 2 and Table 4 that the increase in k_{cat} exhibited by T67 K Mb−H with respect to WT Mb is significantly larger than the increase in k'_D. An increase in the ratio k_{cat}/k'_D always improves the performance of the biological catalyst. In general, at least with phenolic substrates, the numerical values of the protein degradation rate constants k_D and k'_D are about two orders of magnitude smaller than the turnover rate constants (k_{cat}), indicating that all Mb derivatives perform a large number of catalytic turnovers before undergoing significant degradation.

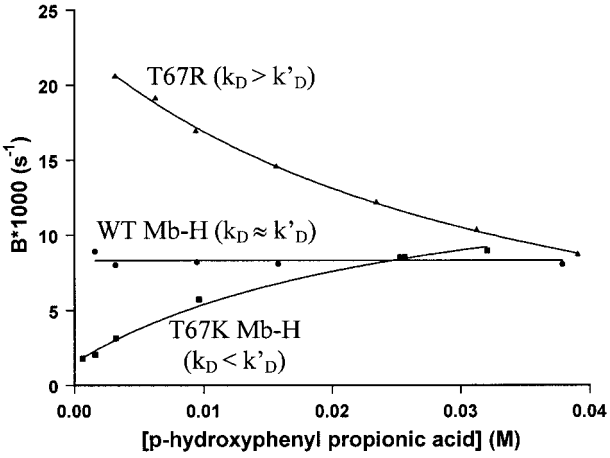

Figure 5. Types of behavior of Mb derivatives in the degradation processes undergone during catalysis; the dependence of parameter B [defined as $B = (k_D K_M + k'_D[S])/(K_M + [S])$][47] on (*p*-hydroxyphenyl)propionic acid concentration is shown under the various conditions that can affect the degradation process: $k_D \approx k'_D$, $k'_D < k_D$ or $k'_D > k_D$, depending on the way the substrate interacts with the protein; protein autodegradation may be only marginally affected ($k_D \approx k'_D$), unaffected ($k'_D < k_D$), or strongly affected ($k'_D > k_D$) by the presence of substrate

New Peroxidase-Like Reactions of Myoglobin Promoted by Nitrite Activation

Nitrite is a major product of nitrogen monoxide metabolism.[69,70] Although nitrite is considered a harmless metabolite, its accumulation is reported in some pathological conditions.[71] Actually, NO_2^- dramatically enhances hydrogen peroxide toxicity in the presence of heme proteins because these systems can generate powerful oxidizing and nitrating species.[39,40][72] We have recently demonstrated that enzymatic nitration of tyrosine derivatives[43] promoted by peroxidase/H_2O_2/NO_2^- proceeds through two distinct pathways which involve nitrogen dioxide or peroxynitrite, depending on the conditions, as nitrating agents. A similar behavior is exhibited by the metMb/NO_2^-/H_2O_2 system.[44] At low nitrite concentration Mb reacts through the classical peroxidase-like cycle, with two active intermediates which can either react with the phenolic substrate, according to reactions (2)−(4), or with nitrite to generate nitrogen dioxide in the competing reactions:

$$^{\cdot}MbFe^{IV}{=}O + NO_2^- \rightarrow MbFe^{IV}{=}O + NO_2^{\cdot} \quad (6)$$

$$MbFe^{IV}{=}O + NO_2^- \rightarrow MbFe^{3+} + NO_2^{\cdot} \quad (7)$$

The enzymatically produced phenoxy radical and $NO_2^{\cdot}$ can give then a fast recombination reaction producing the nitrophenol:

$$NO_2^{\cdot} + Ph{-}O^{\cdot} \rightarrow O_2N\text{-}Ph\text{-}OH \quad (8)$$

$$NO_2^{\cdot} + Ph{-}OH \rightarrow Ph{-}O^{\cdot} + NO_2^- \quad (9)$$

The phenoxy radical can also be produced by reaction of $NO_2^{\cdot}$ with phenol. At high nitrite levels this acts as a ligand for the iron center, and hydrogen peroxide reacts with the iron-bound nitrite producing an active species that we formulate as a protein-bound peroxynitrite, $MbFe^{3+}{-}N(O)OO^-$. This is capable of nitrating the phenol in a two-electron process:

 © 2004 Wiley-VCH Verlag GmbH & Co. KGaA, Weinheim

$$MbFe^{3+} + NO_2^- \rightleftarrows MbFe^{3+}-NO_2^- \quad (10)$$

$$MbFe^{3+}-NO_2^- + H_2O_2 \rightarrow MbFe^{3+}-N(O)OO^- + H_2O \quad (11)$$

$$MbFe^{3+}-N(O)OO^- + PhOH \rightarrow MbFe^{3+} + O_2N\text{-}PhOH \quad (12)$$

In the absence of an exogenous substrate Mb catalyzes its own nitration. Mb contains several amino acid residues that can be nitrated. Upon treatment of Mb with peroxynitrite Bourassa et al.[73] found that nitration occurs at the exposed Tyr103, while Herold et al.[74] found that nitration occurs at Tyr146. By reacting Mb with nitrite and hydrogen peroxide, we found that the first and most important nitration site is the heme (30% to 50% yield depending on the conditions), while a secondary protein nitration site has been identified as Tyr146 (about 5% yield).[44] This is a surprising result considering that Tyr146 is an inner residue lined to the Xe1 cavity of Mb and it is farther from the heme iron center than Tyr103 (the closest C atom of the phenol ring is 9.7 Å from the iron atom for Tyr146 and 3.3 Å for Tyr103).[3][75] Therefore, the nitrating agent responsible for the self nitration of Mb does not come from the outside of the protein but diffuses from the heme to the Xe1 cavity and reacts through an intramolecular reaction.

Heme peroxidases catalyze the oxidation of organic sulfides to sulfoxides with a certain degree of stereoselectivity.[28,76] This type of reaction is catalyzed much more efficiently by chloroperoxidase.[77–79] Through the engineering of Mb, the group of Watanabe obtained mutants that exhibit catalytic turnovers and interesting stereoselectivity effects in the sulfoxidation of thioanisole.[80–82] We have studied the effect of nitrite in the oxidation of aromatic sulfides catalyzed by various Mb derivatives. As shown before, in the presence of hydrogen peroxide nitrite produces nitrogen dioxide or peroxynitrite, which are both powerful nitrating and oxidizing species. The idea was that these species could participate in the sulfoxidation catalytic cycle of Mb and increase the efficiency and/or selectivity of the reaction. Indeed, nitrite caused a general improvement in the enantioselectivity in the produced sulfoxide (with *ee* up to about 50% for sulfoxidation of thioanisole).[83] By analogy with peroxidases,[79] the catalytic scheme we propose for the sulfoxidation by Mb is the following:

$$MbFe^{3+} + H_2O_2 \rightarrow {}^{\cdot}MbFe^{IV}=O + H_2O \quad (12)$$

$${}^{\cdot}MbFe^{IV}=O + S \rightarrow MbFe^{3+} + SO \quad (13)$$

$${}^{\cdot}MbFe^{IV}=O + S \rightarrow MbFe^{IV}=O + S^{\cdot+} \quad (14)$$

$$MbFe^{IV}=O + S \rightarrow MbFe^{3+} + S^{\cdot+} \text{ (slow)} \quad (15)$$

$$S^{\cdot+} + S^{\cdot+} + H_2O \rightarrow S + SO + 2\,H^+ \quad (16)$$

where S indicates the sulfide and SO the sulfoxide. The first protein intermediate, ${}^{\cdot}MbFe^{IV}=O$, can convert sulfide to sulfoxide by a direct *O*-transfer reaction [formally a two-electron process, reaction (13)], or to a sulfur cation radical by a one-electron oxidation according to reaction (14). The second protein intermediate, $MbFe^{IV}=O$, can only produce a sulfur cation radical. The former reaction gives the sulfoxide with a certain degree of enantioselectivity, while dismutation of sulfur cation radicals by reaction (16) gives racemic sulfoxide.[79,84–86] Therefore, the observed enantioselectivity depends on the fraction of Mb that reacts by reaction (13). Nitrite efficiently reduces intermediate $MbFe^{IV}=O$ to the native state[44] according to:

$$MbFe^{IV}=O + NO_2^- \rightarrow MbFe^{3+} + NO_2^{\cdot} \quad (17)$$

and this process is faster than reaction (15). Therefore, the effect of nitrite is to reduce the contribution of the pathway that produces the sulfoxide through the stereochemically unproductive coupling of sulfur cation radicals.

Concluding Remarks

In this review we summarized our contribution to the search for new catalytic activities of Mb by combining site-directed mutagenesis with prosthetic-group modification. We focused on peroxidase-type reactions promoted by the activation of hydrogen peroxide because this reagent transforms the iron center into an active species that can, in principle, perform controlled reactions on exogenous substrates. Due to similarities between the active sites of Mb and peroxidases, the changes that are introduced in the protein are insignificant relative to those that are necessary for the simulation of the activities of other enzymes using Mb. In general, the results obtained so far clearly indicate that the strategies of active-site engineering and cofactor modification are cumulative in enhancing the pseudo-peroxidase activity of Mb, and can be further elaborated to introduce more sophisticated substrate recognition sites into the protein. We have also introduced a new experimental method to evaluate the relative stability of the Mb catalysts under operational conditions and identified the pathways by which the protein undergoes competitive degradation. Although the investigated reactivities are not natural for Mb, both peroxide and nitrite activation by this protein may bear particular importance under pathological conditions where bursts of nitric oxide and hydrogen peroxide are produced by the immune defense system.[87] Manipulating protein activities by chemical or genetic methods is an intellectual challenge that will strongly affect the way chemists devise new approaches to synthetic methods and applications.

Acknowledgments

This work was supported by funds from PRIN (Progetto di Ricerca di Interesse Nazionale) of the Italian MIUR. The University of Pavia and the European COST D21 program are also gratefully

 © 2004 Wiley-VCH Verlag GmbH & Co. KGaA, Weinheim

acknowledged for support. R. Roncone is a recipient of a research fellowship from C.I.R.C.M.S.B.

[1] H. Frauenfelder, B. H. McMahon, P. W. Fenimore, *Proc. Natl. Acad. Sci. USA* **2003**, *100*, 8615−8617.
[2] J. B. Wittenberg, *Biol. Bull.* **1959**, *117*, 402−403.
[3] M. Brunori, Q. H. Gibson, *EMBO reports* **2001**, *2*, 674−679.
[4] S. Herold, M. Exner, T. Nauser, *Biochemistry* **2001**, *40*, 3385−3395.
[5] P. K. Witting, D. J. Douglas, A. G. Mauk, *J. Biol. Chem.* **2001**, *276*, 3991−3998.
[6] A. Gödecke, A. Molojavyi, J. Heger, U. Flögel, Z. Ding, C. Jacoby, J. Schrader, *J. Biol. Chem.* **2003**, *278*, 21761−21766.
[7] M. Brunori, *Trends. Biochem. Sci.* **2001**, *26*, 21−23.
[8] D. J. Garry, S. B. Kanatous, P. P. A. Mammen, *Trends. Cardiovasc. Med.* **2003**, *13*, 111−116.
[9] J. B. Wittenberg, B. Wittenberg, *Annu. Rev. Biophys. Biophys. Chem.* **1990**, *19*, 217−241.
[10] D. Galaris, E. Cadenas, P. Hochstein, *Arch. Biochem. Biophys.* **1989**, *273*, 497−504.
[11] M. Nakamura, S. Nakamura, *Biophys. Biochim. Acta* **1996**, *1289*, 329−335.
[12] Y. Lu, S. M. Berry, T. D. Pfister, *Chem. Rev.* **2001**, *101*, 3047−3080.
[13] H. M. Berman, J. Westbrook, Z. Feng, G. Gilliland, T. N. Bhat, H. Weissig, I. N. Shindyalov, P. E. Bourne, *Nucl. Acids. Res.* **2000**, *28*, 235−242.
[14] Y. Watanabe, *Curr. Opin. Chem. Biol.* **2002**, *6*, 1−9.
[15] S. K. Ritter, *Science* **1998**, 37−44.
[16] T. J. Redi, *Transfusion* **2003**, *43*, 280−287.
[17] S. Ozaki, M. P. Roach, T. Matsui, Y. Watanabe, *Acc. Chem. Res.* **2001**, *34*, 818−825.
[18] Y. Watanabe, T. Ueno, *Bull. Chem. Soc. Jpn.* **2003**, *76*, 1309−1322.
[19] T. Hayashi, Y. Hitomi, T. Ando, T. Mizutani, Y. Hisaeda, T. Kitagawa, H. Ogoshi, *J. Am. Chem. Soc.* **1999**, *121*, 7747−7750.
[20] T. Hayashi, Y. Hisaeda, *Acc. Chem. Res.* **2002**, *35*, 35−43.
[21] C. P. Baron, H. J. Andersen, *J. Agric. Food Chem.* **2002**, *50*, 3887−3897.
[22] J. Everse, K. E. Everse, M. B. Grisham, *Peroxidase in Chemistry and Biology*, CRC Press, Boca Raton, FL, **1991**, vols. I and II.
[23] H. B. Dunford, *Heme peroxidases*,Wiley, New York, **1999**, ch. 1−3.
[24] H. Anni, T. Yonetani, *Met. Ions Biol. Syst.* **1992**, *28*, 219−241.
[25] I. S. Isaac, J. H. Dawson, *Essays Biochem.* **1999**, *34*, 51−69.
[26] P. Anzenbacher, J. H. Dawson, T. Kitagawa, *J. Mol. Struct.* **1989**, *214*, 149−158.
[27] T. L. Poulos, J. Kraut, *J. Biol. Chem.* **1980**, *255*, 8199−8205.
[28] W. Adam, M. Lazarus, C. R. Saha-Moller, U. Weichold, D. Haring, P. Schreirer, *Advances in Biochemical Engineering/Biotechnology* (Ed.: Th. Sceper), Springer-Verlag, Berlin, **1999**, pp. 74−108.
[29] P. R. Ortiz de Montellano, *Annu. Rev. Pharmacol. Toxicol.* **1992**, *32*, 89−107.
[30] M. Gajhede, D. J. Schuller, A. Henriksen, A. T. Smith, T. L. Poulos, *Nature Struct. Biol.* **1997**, *4*, 1032−1038.
[31] L. Banci, *J. Biotechnol.* **1997**, *53*, 253−263.
[32] L. K. Folkes, L. P. Candeias, *FEBS Lett.* **1997**, *412*, 305−308.
[33] L. Casella, S. Poli, M. Gullotti, C. Selvaggini, T. Beringhelli, A. Marchesini, *Biochemistry* **1994**, *33*, 6377−6386.
[34] L. Casella, E. Monzani, M. Gullotti, E. Santelli, S. Poli, T. Beringhelli, *Gazz. Chim. Ital.* **1996**, *126*, 121−125.
[35] E. Monzani, A. L. Gatti, A. Profumo, L. Casella, M. Gullotti, *Biochemistry* **1997**, *36*, 1918−1926.
[36] A. De Riso, M. Gullotti, L. Casella, E. Monzani, A. Profumo, L. Gianelli, L. De Gioia, N. Gariji, S. Colonna, *J. Mol. Catal. A* **2003**, *204/205*, 390−400.
[37] A. van der Vliet, J. P. Eiserich, B. Halliwell, C. E. Cross, *J. Biol. Chem.* **1997**, *272*, 7617−7625.
[38] J. P. Eiserich, M. Hristova, C. E. Cross, A. D. Jones, B. A. Freeman, B. Halliwell, A. van der Vliet, *Nature* **1998**, *391*, 393−397.
[39] H. Ischiropoulos, *Arch. Biochem. Biophys.* **1998**, *356*, 1−11.
[40] I. V. Turko, F. Murad, *Pharmacol. Rev.* **2002**, *54*, 619−634.
[41] R. G. Knowles, S. Moncada, *Biochem. J.* **1994**, *298*, 249−258.
[42] L. Casella, E. Monzani, R. Roncone, S. Nicolis, A. Sala, A. De Riso, *Environ. Health Persp.* **2002**, *110*, 709−711.
[43] E. Monzani, R. Roncone, M. Galliano, W. H. Koppenol, L. Casella, *Eur. J. Biochem.* **2004**, *271*, 1−12.
[44] S. Nicolis, E. Monzani, R. Roncone, L. Gianelli, L. Casella, *Chem. Eur. J.* **2004**, in press.
[45] E. Monzani, G. Alzuet, L. Casella, C. Redaelli, C. Bassani, A. M. Sanangelantoni, M. Gullotti, L. De Gioia, L. Santagostini, F. Chillemi, *Biochemistry* **2000**, *39*, 9571−9582.
[46] C. Redaelli, E. Monzani, L. Santagostini, L. Casella, A. M. Sanangelantoni, R. Pierattelli, L. Banci, *ChemBioChem* **2002**, *3*, 226−233.
[47] R. Roncone, E. Monzani, S. Labò, A. M. Sanangelantoni, L. Casella, **2004**, submitted for publication.
[48] R. Roncone, E. Monzani, M. Murtas, G. Battaini, A. M. Sanangelantoni, S. Zuccotti, M. Bolognesi, L. Casella, *Biochem. J.* **2004**, *77*, 717−724.
[49] C. W. Fenwick, A. M. English, *J. Am. Chem. Soc.* **1996**, *118*, 12236−12237.
[50] J. A. Degray, M. R. Gunther, R. Tschirret-Guth, P. R. Ortiz de Montellano, *J. Biol. Chem.* **1997**, *272*, 2359−2362.
[51] K. Sugiyama, R. J. Highet, A. Woods, R. J. Cotter, Y. Osawa, *Proc. Natl. Acad. Sci. USA* **1997**, *94*, 796−801.
[52] M. R. Gunther, R. A. Tschirret-Guth, H. E. Witowska, Y. C. Fann, D. P. Barr, P. R. Ortiz de Montellano, R. P. Mason, *Biochem. J.* **1998**, *330*, 1293−1299.
[53] K. Tsukuhara, K. Kiguchi, M. Matsui, N. Kubota, R. Arakawa, T. Sakurai, *J. Biol. Inorg. Chem.* **2000**, *5*, 765−773.
[54] O. M. Lardinois, P. R. Ortiz de Montellano, *J. Biol. Chem.* **2003**, *278*, 36214−36226.
[55] R. A. Gross, A. Kumar, B. Klara, *Chem. Rev.* **2001**, *101*, 2097−2124.
[56] J. K. Myers, C. N. Pace, J. M. Scholtz, *Science* **1995**, *4*, 2138−2148.
[57] G. I. Makhatadze, P. L. Privalov, *Adv. Protein. Chem.* **1996**, *47*, 307−425.
[58] D. Barrick, R. L. Baldwin, *Biochemistry* **1993**, *32*, 3790−3796.
[59] D. Barrick, F. M. Hughson, R. L. Baldwin, *J. Mol. Biol.* **1994**, *237*, 588−601.
[60] M. S. Kay, R. L. Baldwin, *Biochemistry* **1998**, *37*, 7859−7868.
[61] J. Choi, M. Terazima, *J. Phys. Chem. B* **2002**, *106*, 6587−6593.
[62] M. M. Santoro, D. W. Bolen, *Biochemistry* **1988**, *27*, 8063−8068.
[63] M. S. Hargrove, J. S. Olson, *Biochemistry* **1996**, *35*, 11310−11318.
[64] M. S. Hargrove, D. Barrick, J. S. Olson, *Biochemistry* **1996**, *35*, 11293−11299.
[65] C. L. Hunter, E. Lloyd, L. D. Eltis, S. P. Rafferty, H. Lee, M. Smith, A. G. Mauk, *Biochemistry* **1997**, *36*, 1010−1017.
[66] I. D. Cunningham, J. L. Bachelor, J. M. Pratt, *J. Chem. Soc., Perkin Trans. 2* **1991**, 1839−1843.
[67] T. G. Traylor, W. A. Lee, D. V. Stynes, *Tetrahedron* **1984**, *40*, 553−568.
[68] L. Casella, L. De Gioia, G. Frontoso Silvestri, E. Monzani, C. Redaelli, R. Roncone, L. Santagostini, *J. Inorg. Biochem.* **2000**, *79*, 31−39.
[69] L. J. Ignarro, J. M. Fukuto, J. M. Griscavage, N. E. Rogers, R. E. Byrns, *Proc. Natl. Acad. Sci. USA* **1993**, *90*, 8103−8107.
[70] S. Pfeiffer, B. Mayer, B. Hemmens, *Angew. Chem. Int. Ed.* **1999**, *38*, 1714−1731.
[71] D. Torre, G. Ferrario, F. Speranza, A. Orani, G. P. Fiori, C. Zeroli, *J. Clin. Pathol. (Lond.)* **1996**, *49*, 574−576.

 © 2004 Wiley-VCH Verlag GmbH & Co. KGaA, Weinheim

[72] M.-L. Brennan, W. Wu, X. Fu, Z. Shen, W. Song, H. Frost, C. Vadseth, L. Narine, E. Lenkiewicz, M. T. Borchers, A. J. Lusis, J. J. Lee, N. A. Lee, H. M. Abu-Soud, H. Ischiropulos, S. L. Hazen, *J. Biol. Chem.* **2002**, *277*, 17415−17427.
[73] J. L. Bourassa, E. P. Ives, A. L. Marqueling, R. Shimanovich, J. T. Groves, *J. Am. Chem. Soc.* **2001**, *123*, 5142−5143.
[74] S. Herold, K. Shivashankar, M. Melh, *Biochemistry* **2002**, *41*, 13460−13472.
[75] H. Fraunfelder, B. H. McMahon, R. H. Austin, K. Chu, J. T. Groves, *Proc. Natl. Acad. Sci. USA* **2001**, *98*, 2370−2374.
[76] F. van de Velde, F. van Rantwijk, R. A. Sheldon, *Trends in Biotechnology* **2001**, *19*, 73−80.
[77] S. Colonna, N. Gaggero, A. Manfredi, L. Casella, M. Gullotti, G. Carrea, P. Pasta, *Biochemistry* **1990**, *29*, 10465−10468.
[78] S. Colonna, N. Gaggero, L. Casella, G. Carrea, P. Pasta, *Tetrahedron: Asymmetry* **1992**, *3*, 95−106.
[79] L. Casella, M. Gullotti, R. Ghezzi, S. Poli, T. Beringhelli, S. Colonna, G. Carrea, *Biochemistry* **1992**, *31*, 9451−9459.
[80] S. Ozaki, H. Yang, T. Matsui, Y. Goto, Y. Watanabe, *Tetrahedron: Asymmetry* **1999**, *10*, 183−192.
[81] S. Kato, H. Yang, T. Ueno, S. Ozaki, G. N. Philips, S. Fukuzumi, Y. Watanabe, *J. Am. Chem. Soc.* **2002**, *124*, 8506−8507.
[82] H. Yang, T. Matsui, S. Ozaki, S. Kato, T. Ueno, G. N. Phillips Jr., S. Fukuzumi, Y. Watanabe, *Biochemistry* **2003**, *42*, 10174−10181.
[83] S. Nicolis, E. Monzani, V. Pironti, S. Colonna, L. Casella, **2004**, to be submitted for publication.
[84] U. Perez, H. B. Dunford, *Biochim. Biophys. Acta* **1990**, *1038*, 98−104.
[85] U. Perez, H. B. Dunford, *Biochemistry* **1990**, *29*, 2757−2763.
[86] E. Baciocchi, O. Lanzalunga, S. Malandrucco, *J. Am. Chem. Soc.* **1996**, *118*, 8973−8974.
[87] J. K. Hurst, S. V. Lymar, *Acc. Chem. Res.* **1999**, *32*, 520−528.

Received February 16, 2004

 © 2004 Wiley-VCH Verlag GmbH & Co. KGaA, Weinheim

Intermolecular Interactions between Chelate Rings and Phenyl Rings in Square-Planar Copper(II) Complexes

Zoran D. Tomić,*[a] Sladjana B. Novaković,[a] and Snežana D. Zarić*[b]

Keywords: Chelate rings / Delocalized π-bonds / Copper / Aromaticity / Stacking interactions

Analysis of the geometrical parameters in crystal structures of square-planar copper(II) complexes from the CSD shows that the short noncovalent copper(II)–phenyl carbon distances are a consequence of the interaction between the phenyl ring and the chelate ring with delocalized π-bonds. The data show a correlation between the distances between the centers of the chelate and phenyl rings and the copper(II)–carbon distances, as well as a mutual slipped-parallel orientation of the phenyl and chelate rings.
(© Wiley-VCH Verlag GmbH & Co. KGaA, 69451 Weinheim, Germany, 2004)

Introduction

The investigation of noncovalent interactions is of continuing interest.[1−8] Noncovalent interactions involving metal atoms has gained particular attention with the recognition that metal atoms can bind to the phenyl ring; and this can be explained in terms of cation−π interactions.[9−14] Cationic metal complexes are involved in similar metal−ligand aromatic cation−π interactions[15−18] that can also be considered as a type of X−H···π hydrogen bond.[19−22] The importance of this interaction in protein structures has been shown previously.[15]

Recently, a few studies of noncovalent interactions of chelate rings with delocalized π-bonds have been published.[23−25] We have reported[24] the structure of the square-planar bis(acetone-1-naphthoylhydrazinato)copper(II) complex. In this structure the closest intermolecular distance between the copper(II) and aromatic carbon atom is 3.185(3) Å, which is below the sum of van der Waals radii (4.05 Å). Similar arrangements have been found previously,[26−28] and on the basis of geometrical characteristics it was proposed that phenyl carbon is part of the copper(II) coordination sphere. Besides providing linkages, these contacts may also serve as a path for exchange interactions. The EPR studies on the single-crystal samples of (L-tryptophanyl-glycinato)copper(II)[29] suggest that magnetic interactions are transmitted through cation−π contacts.

The observed mutual slipped-parallel (offset face to face) orientation of the chelate ring, with delocalized π-bonds, and the phenyl ring,[24] resemble the stacking orientation of two benzene molecules.[30] We assumed that chelate rings with delocalized π-bonds can be involved in noncovalent interactions in ways similar to aromatic organic molecules. A calculation of the partial atomic charges of the chelate and phenyl rings in the bis(acetone-1-naphthoylhydrazinato)copper(II) complex has been performed.[24] The distribution of charges in these two rings is very similar to that observed in complexes with the slipped-parallel interaction between two benzene rings, further supporting the stacking interaction between the phenyl and chelate rings.[24]

The role of the chelate ring in the position of the phenyl ring has also been discussed in the analysis of the crystal structure of aqua(2-benzylmalonato)(1,10-phenanthroline)-copper(II) trihydrate.[25]

The assumption that copper(II)−carbon contacts arise as a result of the interactions between the chelate and phenyl rings prompted us to investigate the chelate-ring to phenyl-ring interactions in the crystal structures of copper(II) complexes. We now report on a study based on analyzing the crystal structures in the Cambridge Structural Database (CSD), since by analysing crystal structures from databases it is possible to elucidate the facts about intermolecular and intramolecular interactions.[31−33] To the best of our knowledge this is the first systematic study of chelate-ring to phenyl-ring interactions.

Results and Discussion

For the investigated data set of 487 crystal structures we calculated the closest intermolecular distance between the copper(II) and phenyl carbon (D) atoms (Scheme 1). This distance has a range of 3.06−8.96 Å. In order to establish

[a] "Vinča" Institute of Nuclear Sciences, Laboratory of Theoretical Physics and Condensed Matter Physics, 11001, Belgrade, P. O. Box 522, Yugoslavia
Fax: (internat.) +381-11-8065829
E-mail: zorant@vin.bg.ac.yu
[b] Department of Chemistry, University of Belgrade, Studentski trg 16, 11000 Belgrade, Yugoslavia
Fax: (internat.) +381-11-638-785
E-mail: szaric@chem.bg.ac.yu

if the presence of the chelate ring has an influence on the copper(II)−carbon distance, the distribution for the copper(II)−carbon distances (D) were compared for complexes with and without a chelate ring (Figure 1).

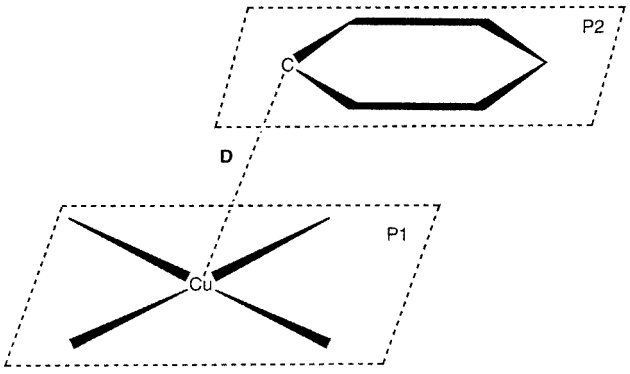

Scheme 1

In the complexes without a chelate ring the peak of distribution is in the region above the sum of the van der Waals radii (4.05 Å), while in the complexes with a chelate ring the peak of distribution is in the region below the sum of the van der Waals radii. Hence, in the presence of a chelate ring with delocalized π-bonds there is a close contact between the copper(II) atom and the carbon atom of the phenyl ring.

Another important difference between complexes with and without a chelate ring is seen when looking at the distribution of the dihedral angles θ, the angle between the mean plane of the phenyl ring (P2) and the mean coordination plane (P1) (plane consisting of copper and coordinated atoms). The planes are shown in Scheme 1. In the histogram for the structures with chelate rings, the peak of distribution is in the region of the small angle θ, where the phenyl ring is oriented in an approximately parallel manner to the mean coordinating plane (Figure 2). In the histogram for the structures without the chelate rings the peak of distribution is in the region of the large angle θ, where the phenyl ring is almost normal to the coordinating plane; there are no structures with a dihedral angle of less than 10° (Figure 2).

The data in Figure 1 and Figure 2, the short copper(II)−carbon distances, and the tendency for a parallel orientation of the phenyl ring in complexes with chelate rings, indicate possible phenyl-ring to chelate-ring stacking interactions.

In order to verify that the interaction between the chelate ring and the phenyl ring is really responsible for the shorter copper(II)−carbon distances observed in the complexes with chelate rings, the values of the distances between the centers of the chelate and phenyl rings (Ct) are plotted versus the copper(II)−carbon distance (D) (Figure 3). The plot shows that there is a correlation between the distance Ct and the distance D; the copper(II)−carbon distances are shorter when there is a short distance between the centers of the chelate and phenyl rings. This correlation can only exist if the chelate and phenyl rings tend to overlap each other. Hence, the interaction between the phenyl and chelate rings is responsible for the short copper(II)−carbon distances.

The positions of the phenyl rings with respect to the chelate rings, indicates that, in all cases with small θ angles, the two rings are in mutual slipped-parallel orientations (offset face to face). This is in agreement with the previously observed slipped-parallel orientation in the bis(acetone-1-naphthoylhydrazinato)copper(II) complex.[24] Additional support for the idea that the interaction between the chelate ring and the phenyl ring is similar to the interaction between two benzene molecules has been provided by the distribution of the calculated partial atomic charges[24] which are similar to those observed in complexes with stacking interactions between two benzene molecules.[30]

Conclusion

Our analyses of the geometrical parameters in the crystal structures of copper(II) square-planar complexes from the CSD show that in cases where a chelate ring with delocalized π-bonds is present, the peak of the distribution of the copper(II)−phenyl carbon distances is in the region be-

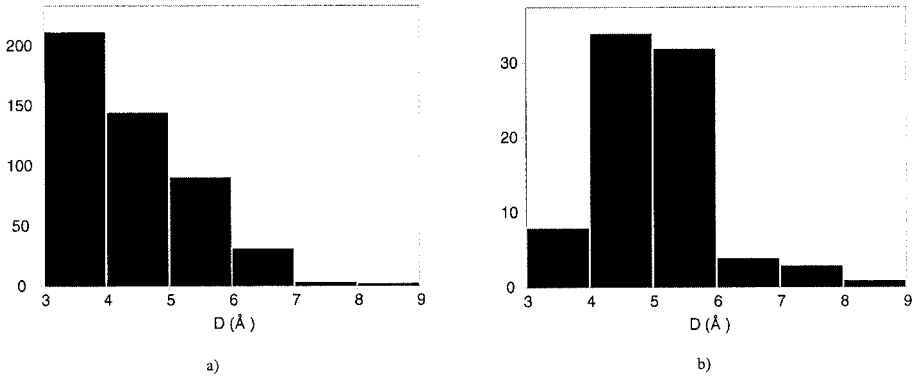

Figure 1. Histograms showing the distribution of the parameter *D*, copper(II)−carbon distance, in structures with (a) and without (b) chelate rings

 © 2004 Wiley-VCH Verlag GmbH & Co. KGaA, Weinheim

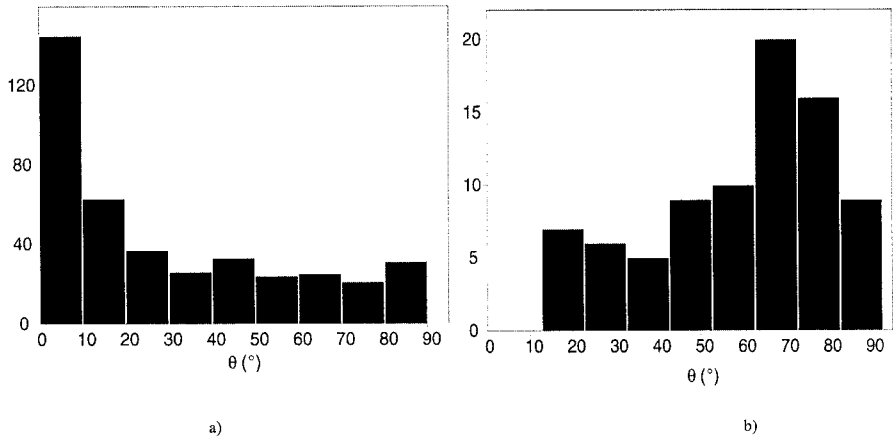

Figure 2. Histograms showing the distribution of the dihedral angle θ between the mean plane of the phenyl ring and the mean plane of copper(II) with coordinated atoms (Scheme 1); a) with chelate rings; b) without chelate rings

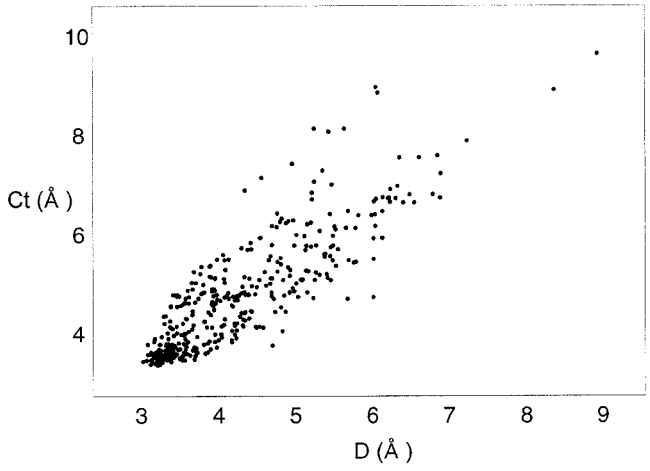

Figure 3. Plot of the distances between the centers of the chelate and phenyl rings (Ct) versus the copper(II)−carbon distance *D*

low the sum of van der Waals radii. The correlation between the copper(II)−carbon distances and the distances between the centers of the chelate and phenyl rings, as well as the mutual slipped-parallel orientation of the two rings, show that stacking interactions between phenyl and chelate rings are similar to the stacking interactions between two benzene rings.

Experimental Section

A Cambridge Structural Database (CSD)[34] search was performed for mononuclear copper(II) complexes having exactly four single bonds to atoms belonging to groups 5A, 6A or 7A. The oxidation state of copper was taken as those given by the authors. To exclude the possible influence of the constraints in the molecule we only looked at the intermolecular contacts between the copper(II) atom and the carbon atom of the phenyl ring. As a convenient choice for this investigation, we concentrated on square-planar copper(II) complexes due to the relative planarity of such molecules, and the absence of steric hindrance for the approach of other molecule into the axial position. To minimize the possible steric influence towards the approach of two molecules, the *trans* angles around the copper atom were constrained to lie between the 150 and 180°. To avoid problems which could possibly arise as a result of "structural inhomogeneity", we used structures that contain the phenyl ring as part of the complex molecule, and only those with one complex species in the asymmetric unit. Polymeric, disordered, and structures with $R > 0.10$ were excluded. This gave 487 entries. Among them 405 structures had five-membered or six-membered chelate rings. The bond lengths in the chelate rings indicate that in all the structures the chelate rings have delocalized π-bonds. When considering the influence of the chelate ring on the position of the phenyl ring, we took the distance between the centroids of the phenyl and chelate rings as a criteria. In cases with more than one chelate ring in the complex, we accepted the closest chelate ring as the one that is involved in the interaction with the phenyl ring.

Acknowledgments

The authors would like to thank Prof. E. W. Knapp and Prof. M. B. Hall for support. This work was supported by the ministry of science of the republic of serbia (grant I01795).

[1] G. A. Jeffrey, W. Saenger, *Hydrogen Bonding in Biological Structures*, Springer, Berlin, **1991**.
[2] G. R. Desiraju, T. Steiner, *The Weak Hydrogen Bonds in Structural Chemistry and Biology*, Oxford University Press, **1999**.
[3] E. V. Pletneva, A. T. Laederach, D. B. Fulton, N. M. Kostic, *J. Am. Chem. Soc.* **2001**, *123*, 6232.
[4] N. Juranic, M. C. Moncrieffe, V. A. Likic, F. G. Prendergast, S. Macura, *J. Am. Chem. Soc.* **2002**, *124*, 14221.
[5] S. Yanagisawa, K. Sato, M. Kikuchi, T. Kohzuma, C. Dennison, *Biochemistry* **2003**, *42*, 6853.
[6] E. A. Meyer, R. K. Castellano, F. Diederich, *Angew. Chem. Int. Ed.* **2003**, *42*, 1210.
[7] T. Steiner, *Angew. Chem. Int. Ed.* **2002**, *41*, 48.
[8] O. Yamauchi, A. Odani, M. Takani, *J. Chem. Soc., Dalton Trans.* **2002**, 3411.
[9] J. C. Ma, D. A. Dougherty, *Chem. Rev.* **1997**, *97*, 1303.
[10] W. Schmitt, C. E. Anson, J. P. Hill, A. K. Powell, *J. Am. Chem. Soc.* **2003**, *125*, 11142.
[11] R. Amunugama, M. T. Rodgers, *Int. J. Mass Spectrom.* **2003**, *227*, 339.
[12] T. Lovell, F. Himo, W. G. Han, L. Noodleman, *Coord. Chem. Rev.* **2003**, *238*, 211.
[13] W. L. Zhu, X. J. Tan, J. H. Shen, X. M. Luo, F. Cheng, P. C.

 © 2004 Wiley-VCH Verlag GmbH & Co. KGaA, Weinheim

Mok, R. Y. Ji, K. X. Chen, H. L. Jiang, *J. Phys. Chem. A* **2003**, *107*, 2296.
[14] D. Kim, S. Hu, P. Tarakeshwar, K. S. Kim, J. M. Lisy, *J. Phys. Chem. A* **2003**, *107*, 1228.
[15] S. D. Zaric, D. Popovic, E. W. Knapp, *Chem. Eur. J.* **2000**, *6*, 3935.
[16] S. D. Zaric, Chem. Phys. Lett. **1999**, *311*, 77; M. Milcic, S. D. Zaric, *Eur. J. Inorg. Chem.* **2001**, 2143.
[17] J. Sponer, J. E. Sponer, J. Leszczynski, *J. Biomol. Struct. Dyn.* **2000**, *17*, 1087.
[18] E. C. Magnuson, J. Koehler, G. Lamm, G. R. Pack, *Int. J. Quantum Chem.* **2002**, *88*, 236.
[19] S. D. Zaric, *Eur. J. Inorg. Chem.* **2003**, 2197.
[20] H. Suezawa, T. Yoshida, Y. Umezawa, S. Tsuboyama, M. Nishio, *Eur. J. Inorg. Chem.* **2002**, 3148.
[21] H. Kumita, T. Kato, K. Jitsukawa, H. Einaga, H. Masuda, *Inorg. Chem.* **2001**, *40*, 3936.
[22] D. U. Miodragovic, S. M. Milosavljevic, M. J. Malinar, M. B. Celap, N. Todorovic, N. Juranic, *Enantiomer* **2002**, *7*, 375.
[23] G. A. Bogdanovic, A. S. Bire, S. D. Zaric, *Eur. J. Inorg. Chem.* **2002**, 1599.
[24] Z. D. Tomic, V. M. Leovac, S. V. Pokorni, D. Zobel, S. D. Zaric, *Eur. J. Inorg. Chem.* **2003**, 1222.
[25] A. Castiñeiras, A. G. Sicilia-Zafra, J. M. González-Pérez, D. Choquesillo-Lazarte, J. Niclós-Gutiérrez, *Inorg. Chem.* **2002**, *41*, 6956.
[26] R. Fazlic, V. Divjakovic, V. M. Leovac, S. Y. Chundak, *Acta Crystallogr., Sect. C* **1991**, *47*, 714.
[27] H. Masuda, A. Odani, O. Yamauchi, *Inorg. Chem.* **1989**, *28*, 624.
[28] O. R. Nascimento, A. J. Costa-Filho, D. I. De Morais, J. Ellena, L. F. Delboni, *Inorg. Chim. Acta* **2001**, *312*, 133.
[29] A. J. Costa-Filho, O. R. Nascimento, L. Ghivelder, R. Calvo, *J. Phys. Chem. B* **2001**, *105*, 5039.
[30] S. Tsuzuki, K. Honda, T. Uchimaru, M. Mikami, K. Tanabe, *J. Am. Chem. Soc.* **2002**, *124*, 104.
[31] C. Janiak, *J. Chem. Soc., Dalton Trans.* **2000**, 3885.
[32] S. D. Zaric, D. Popovic, E. W. Knapp, *Biochemistry.* **2001**, *40*, 7914.
[33] T. Dudev, Y. I. Lin, M. Dudev, C. Lim, *J. Am. Chem. Soc.* **2003**, *125*, 3168.
[34] F. H. Allen, S. Bellard, M. D. Brice, B. A. Cartwright, A. Doubleday, H. Higgs, T. Hummelink, B. G. Hummelink-Peters, O. Kennard, W. D. S. Motherwell, J. R. Rodgers, D. G. Watson, *Acta Crystallogr., Sect. B* **1979**, *35*, 2331.

Received February 2, 2004

 © 2004 Wiley-VCH Verlag GmbH & Co. KGaA, Weinheim

An Ni_4 Single-Molecule Magnet: Synthesis, Structure and Low-Temperature Magnetic Behavior

María Moragues-Cánovas,[a] Madeleine Helliwell,[b] Louis Ricard,[c] Éric Rivière,[a] Wolfgang Wernsdorfer,[d] Euan Brechin,*[b] and Talal Mallah*[a]

Keywords: Nickel / Ferromagnetism / Single-molecule studies / Cubane complexes / Tripodal ligands

The reaction of $Ni(NO_3)_2 \cdot 6H_2O$ with H_3thme (trihydroxymethylethane) in the presence of NaOMe leads to a tetranuclear Ni_4 complex with a cubane-like structure. Intramolecular ferromagnetic interactions [$J = 10$ cm^{-1} based on $H = -J(S_1 \cdot S_2 + S_1 \cdot S_3 + S_1 \cdot S_4 + S_2 \cdot S_3 + S_2 \cdot S_4 + S_3 \cdot S_4)$] lead to an $S = 4$ ground state stabilized by 40 cm^{-1} from the first $S = 3$ excited state. Magnetization vs. field studies at different temperatures above 2 K suggest the presence of an axial magnetic anisotropy. Single-crystal magnetization measurements show a single-molecule-magnetic behavior below $T = 0.5$ K with fast relaxation of the magnetization due to resonant quantum tunneling.
(© Wiley-VCH Verlag GmbH & Co. KGaA, 69451 Weinheim, Germany, 2004)

Introduction

Cubane-like Ni_4 tetranuclear complexes have been extensively studied since the first report by Andrew and Blake in 1969 of a ferromagnetic interaction that lead to an $S = 4$ ground state.[1] The origin of the exchange interaction in such compounds is well-understood and is correlated to the Ni−O−Ni angle within the cubane;[1,2] ferromagnetic interaction is found when the Ni−O−Ni angle is lower than 98°.[1,3] The discovery of Single-Molecule Magnetism (SMM) in Ni(II) high spin molecular clusters[4] and particularly in cubane-like Ni_4 tetranuclear complexes[5] revived the interest in such compounds in order to study the correlation between the magnetic anisotropy of the high spin ground state and the relaxation of the magnetization at low temperature.

Here, we report on the preparation, crystal structure, and magnetic behavior of a new cubane-like Ni_4 tetranuclear complex with the general formula $[Ni_4(C_5H_{11}O_3)_4(CH_3CN)_4](NO_3)_4 \cdot 1.33\ NaNO_3$, obtained using 1,1,1-trihydroxymethylethane (H_3thme) as the bridging organic ligand.

Results and Discussion

The reaction between $Ni(NO_3)_2 \cdot 6H_2O$, H_3thme and $NaOCH_3$ in methanol affords, after evaporation of the solvent and extraction of the solid with acetonitrile, blue crystals suitable for structure determination (see Experimental Section). The organic ligand H_3thme has the ability to act as a terminal and/or bridging ligand depending on its degree of protonation. In the present case the single-crystal studies show that the ligand is a monoanion and the complex has a cubane-like structure. Each Ni atom of the cubane is surrounded by two protonated oxygen atoms of H_2thme$^-$ that act as terminal atoms and by the alkoxo-like oxygen atom that bridges three Ni atoms of the cubane core. The coordination sphere of Ni is completed with one acetonitrile molecule (Figure 1). The complex has four positive charges which are compensated by four NO_3^- ions. The crystal contains Na^+ and NO_3^- ions (see formula). The molecule has a principal C_2 axis parallel to the Ni−N bonds. The geometry around Ni is slightly distorted. The shortest Ni−O distances correspond to the oxygen atoms that belong to the cubane core (2.023 and 2.043 Å), and the remaining four Ni−X distances are slightly longer (around 2.056 Å). The main distortion is due to the O−Ni−O angle within the cubane which is equal to 82.01°, while the other X−Ni−X angles are around 92°. There are three different Ni−O−Ni angles; these are equal to 97.25° for the two opposite faces and to 97.04° and 97.95° for the remaining four faces.

[a] Laboratoire de Chimie Inorganique, UMR CNRS 8613, Université Paris-Sud,
91405 Orsay, France
E-mail: mallah@icmo.u-psud.fr
[b] Department of Chemistry, The University of Manchester, Oxford Road, Manchester, M13 9PL, UK
E-mail: mbdssekb@man.ac.uk
[c] Phosphore et Métaux de Transition, UMR CNRS 7653, École Polytechnique,
91128 Palaiseau, France
[d] Laboratoire Louis Néel − CNRS, 25, Avenue des Martyrs BP 166,
38042 Grenoble, Cedex 9, France

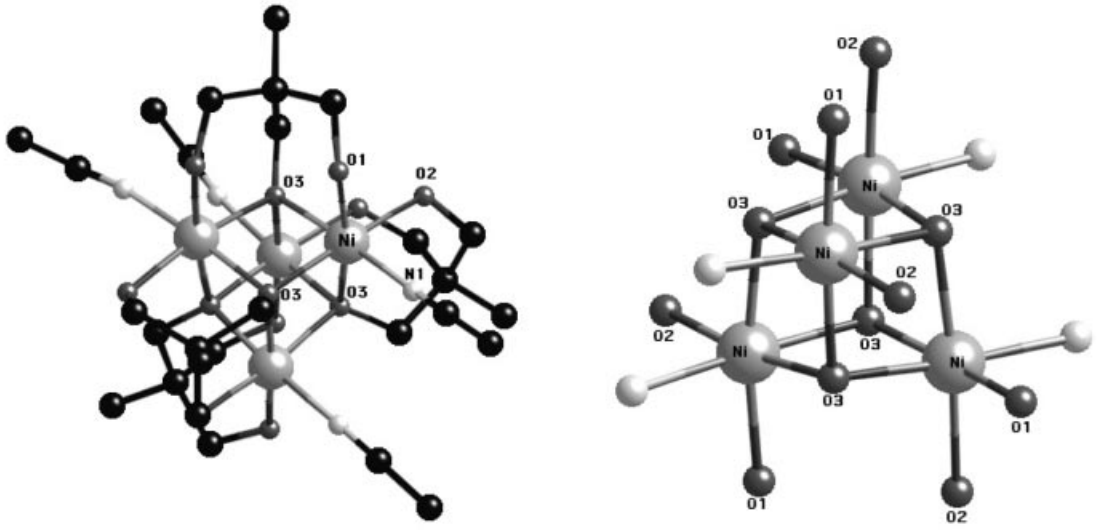

Figure 1. View of the molecular structure of Ni_4

The magnetic data which are presented in the form of $\chi_M T = f(T)$ show that the exchange interaction is ferromagnetic; the $\chi_M T$ product increases on cooling (Figure 2). The maximum $\chi_M T$ value at low temperature (11.85 $cm^3\ mol^{-1}\ K$ at $T = 9$ K) is in agreement with that expected for a $S = 4$ ground state with a g-value larger than 2. The decrease in $\chi_M T$ below 9 K is assumed to be due to zero-field splitting within the ground state, even though the presence of weak intermolecular interactions cannot be excluded. The data were fitted to the theoretical expression of the susceptibility derived from the above-mentioned spin Hamiltonian including the Zeeman term ($g\beta HS$ where S is the spin operator corresponding to the total spin and β the Bohr Magneton) and the zero-field splitting ($D[S_z^2 - S(S + 1)/3]$ where D is the axial zero-field splitting parameter within the $S = 4$ ground state) within the $S = 4$ ground state. Therefore, we first assumed only one exchange coupling parameter between the four Ni atoms. The fit gives the following parameters: $J = 10\ cm^{-1}$, $g = 2.18$, $|D| = 0.5\ cm^{-1}$, and an agreement factor $R = 1.5 \times 10^{-4}$. The magneto-structural correlations for Ni_4 cubane-like complexes lead to the conclusion that a change from ferromagnetic to antiferromagnetic exchange coupling corresponds to a Ni−O−Ni angle of about 98°.[3] For the present complex there are two different sets of Ni−O−Ni angles so that two exchange coupling parameters may be used corresponding to the spin Hamiltonian (Equation 1).

$$H = -J_1(S_1 \cdot S_2 + S_3 \cdot S_4) - J_2(S_1 \cdot S_3 + S_1 \cdot S_4 + S_2 \cdot S_3 + S_2 \cdot S_4) \quad (1)$$

The fit of the magnetic data assuming two exchange parameters leads to the following results: $J_1 = 15\ cm^{-1}$, $J_2 = 8\ cm^{-1}$, $g = 2.18$, $|D| = 0.5\ cm^{-1}$, and an agreement factor $R = 10^{-4}$. The larger ferromagnetic exchange coupling parameter (J_1) corresponds to the smaller Ni−O−Ni angles, as expected from magneto-structural correlations based on the idea that the overlap integral is weaker for angles closer to 90°. It must be stressed here that although two exchange parameters are used, the quality of the fit is not particularly improved. On the other hand, trying to fit the $\chi_M T = f(T)$ data by introducing intermolecular intercations does not lead to satisfactory results. The decrease in $\chi_M T$ at low temperature can thus be (at this level) ascribed mainly to zero-field splitting within the ground state even though the sign of D cannot usually be determined from susceptibility data on powder.

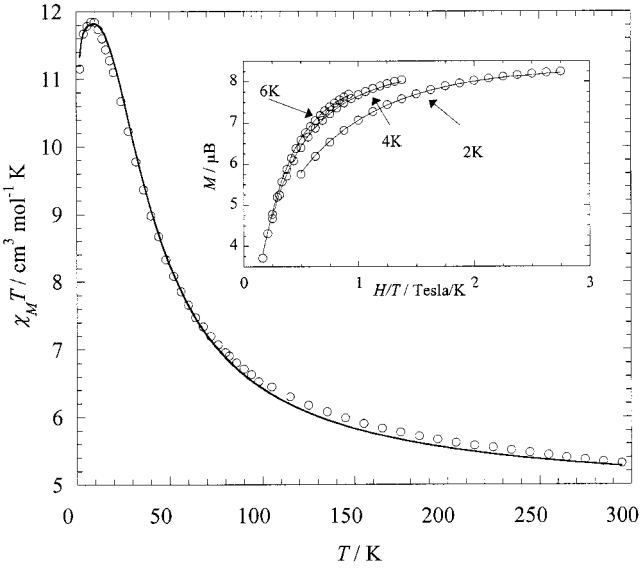

Figure 2 $\chi_M T = f(T)$ for Ni_4, the line corresponds to the best fit with $J = 10\ cm^{-1}$, $g = 2.18$ and $|D| = 0.5\ cm^{-1}$; inset: $M = f(H/T)$ for Ni_4 for $T = 2$, 4 and 6 K, the lines correspond to the best fit with $D = -0.43\ cm^{-1}$, $E/D = 0.04$ and $g = 2.22$

In order to have a better estimation of the zero-field splitting parameters, magnetization vs. field studies at $T = 2$, 4 and 6 K were carried out. The $M = f(H/T)$ plots for H between 1 and 5.5 Tesla (Figure 2 inset) are not superimposable and therefore indicate the presence of magnetic an-

 © 2004 Wiley-VCH Verlag GmbH & Co. KGaA, Weinheim

isotropy within the ground state. Since the $S = 3$ first excited state is separated by about 40 cm^{-1} from the ground state, we assume that only the ground state is responsible for the magnetization response. The magnetization data were fitted by diagonalizing the energy matrix for different orientations of the magnetic field. Two reasonable sets of parameters may be obtained depending on the starting values: $D = -0.43$ cm^{-1}, $E/D = 0.04$, $g = 2.22$, $R = 2 \times 10^{-5}$ and $D = -0.48$ cm^{-1}, $E/D = 0.23$, $g = 2.25$, $R = 6.6 \times 10^{-5}$. It is not unusual to find more than one set of parameters with very different E/D values since the E parameter has little influence on the shape of the $M = f(H)$ plots. However, the D values as found are generally very close and can be considered as very good estimates of the magnetic anisotropy of the ground state. The negative sign of D indicates that there is an easy magnetization axis. In such a case one may expect a blocking of the magnetization as a result of a long relaxation time at low temperature.[6] On the other hand, it is well-understood that the magnitude of the E parameter which defines the deviation from purely axial anisotropy is crucial for relaxation by a quantum tunneling process. For large E/D values it is expected that fast relaxation occurs at $H = 0$ and at low temperatures because of the relatively large mixing between the low-lying $M_S = +4$ and -4 sublevels. This may completely preclude the observation of a hysteresis loop in the magnetization plots. However, for weak rhombicity (E/D close to zero) relaxation by quantum tunneling may occur, but not fast enough such that hysteresis may still be present.[7]

In order to get insight into the behavior at very low temperatures, magnetization studies were carried out on a single-crystal using an array of micro-SQUIDs.[8] The measurements were performed with the magnetic field parallel to the easy axis of the crystal. The applied magnetic field was swept at different rates between -1 and 1 Tesla and then back to -1 Tesla at different temperatures between 0.4 and 0.04 K. The data obtained at a sweep rate of 0.14 Tesla/s show a hysteresis loop which includes two steps: a broad one at about 0.3 Tesla and the other very close to zero (Figure 3). The presence of a hysteresis loop indicates that below $T = 0.4$ K, the magnetization is blocked. However, the presence of two steps is the result of rapid relaxation of the magnetization at a given magnetic field where level crossing is avoided. As the temperature decreases, the number of molecules that undergo relaxation by thermal activation diminishes and those that undergo relaxation by tunneling increases. The result is a narrowing of the hysteresis loop with steeper steps. This observation is seen in the present Ni_4 complex. In order to confirm the quantum tunneling of the magnetization, measurements were performed at $T = 0.04$ K for different sweep rates of the magnetic field. The magnetic field was set at $H = -1$ Tesla and then swept towards $H = 1$ Tesla (Figure 4). At $H = -1$ Tesla, all the molecules are in the $M_S = +4$ state. When the magnetic field reaches zero, there is resonance between the $+4$ and the -4 M_S levels and part of the molecules tunnel to $M_S = -4$, while the remaining stay in the former state. This explains the observation of a step at $H = 0$. The height of the step indicates that the tunneling process is relatively fast and thus there is sufficient mixing of the low-lying $M_S = +4$ and -4 levels. On increasing the field above zero, one expects another step corresponding to the molecules tunneling from the $M_S = +4$ to the $M_S = -3$ sublevel. This should occur when H is very close to $D/g\beta$ (about $H = 0.41$ Tesla).[9] A step is actually observed, but at a field closer to 0.32 Tesla. Furthermore, the step is not very steep and this may be due to the presence of different tunneling processes that are not resolved. One possible explanation for such a shift is the presence of very weak intermolecular interactions (exchange or dipolar).[10,11] The tunnel probability de-

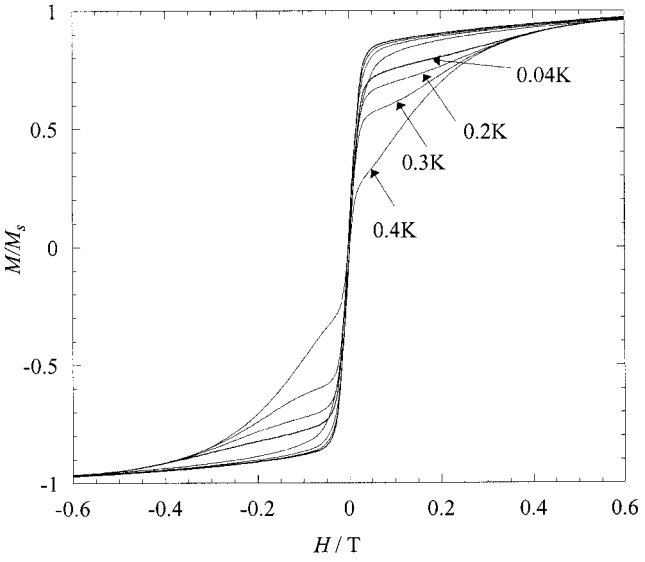

Figure 3. $M/M_S = f(H)$ for a single crystal of Ni_4 with H parallel to the easy axis at different temperatures

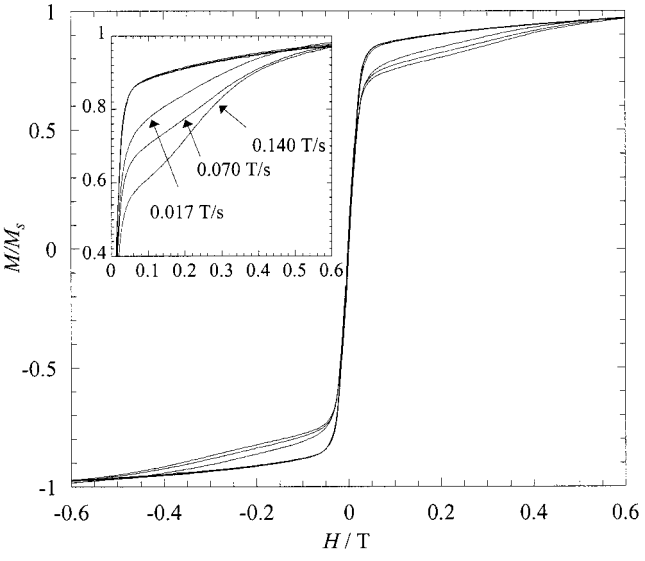

Figure 4. $M/M_S = f(H)$ for a single crystal of Ni_4 with H parallel to the easy axis at different sweep rates of H from -1 to 1 Tesla and back to -1 Tesla; inset: $M/M_S = f(H)$ for a single crystal of Ni_4 with H parallel to the easy axis at different sweep rates of H from 0 to 1 Tesla and back to 0 Tesla

 © 2004 Wiley-VCH Verlag GmbH & Co. KGaA, Weinheim

creases when the sweep rate is increased,[12] therefore, when the same experiment is carried out at higher sweep rates, the number of molecules tunneling at zero field is less important and the hysteresis loop is larger as shown in Figure 4.

The width of the hysteresis loop depends on the magnetic "history" i.e. the starting magnetic state before varying the magnetic field. Thus, when the field is swept from zero rather than from −1 Tesla (T = 0.04 K), the hysteresis is larger (Figure 4 inset). This can be understood by the fact that there are an almost equal number of molecules in the $M_S = -4$ and $M_S = +4$ states when starting at zero field. When the field is increased from zero, the number of molecules that stay in the $M_S = +4$ state is larger than when the field is swept from $H = -1$ Tesla, resulting in a larger hysteresis. This is true especially for systems with relatively fast relaxation by tunneling processes, as is the case for the present complex.

From the above studies, one may conclude that the Ni_4 complex presents a rich magnetic behavior at low temperature. The magnitude of the rhombicity is clearly weak and a value of E/D of about 0.04 seems more reasonable than 0.23. High-field high-frequency EPR studies are underway in order to accurately determine the spin Hamiltonian parameters D and E and confirm the magnitude of the transverse anisotropy term E responsible for the resonant tunneling at very low temperatures.

Experimental Section

Synthesis: Solid H_3thme (137 mg, 1.14 mmol) and $NaOCH_3$ (185 mg, 3.4 mmol) were added to a solution of $Ni(NO_3)_2 \cdot 6\,H_2O$ (1 g, 3.4 mmol) in methanol (25 mL). The mixture was stirred at room temperature for 24 h, affording a dark green solution which was evaporated to dryness. Extraction of the green powder with 15 mL of MeCN afforded blue crystals suitable for X-ray diffraction. $C_{28}H_{56}N_{9.33}Na_{1.33}Ni_4O_{28}$; M = 1236.98 g mol^{-1}; anal. calcd Na 1.90, Ni 19.43; ; found Na 1.20, Ni, 19.4.

General Remarks: Crystal data: $C_{28}H_{56}N_{9.33}Na_{1.33}Ni_4O_{28}$, M = 1236.98, cubic, a = 24.190(3) Å, U = 14155(3) Å^3, T = 100 K, space group I-43d, Z = 12, Mo-$K(\alpha 1)$ = 0.71069 Å, 16171 reflections measured, of which 2091 were unique (R_{int} = 0.1176). The structure was solved by direct methods (SHELXS-97) and refined with SHELXL-97.[13,14] The final conventional R-factor (based on F and 1876 data with $F > 4(F)$) was 0.0841.

CCDC-233996 contains the supplementary crystallographic data for this paper. These data can be obtained free of charge at www.ccdc.cam.ac.uk/conts/retrieving.html [or from the Cambridge Crystallographic Data Centre, 12 Union Road, Cambridge CB2 1EZ, UK; Fax: (internat.) +44-1223-336-033; E-mail: deposit@ccdc.cam.ac.uk].

Acknowledgments

The authors thank the ESF (Programme Molecular Magnets), the European Union (TMR network "Molecules as Nanomagnets" HPRN-CT-1999-00012) and the EPSRC(UK) for financial support.

[1] J. E. Andrew, A. B. Blake, *J. Chem. Soc. (A)* **1969**, 1456.
[2] J. A. Bertrand, J. A. P. Ginsberg, R. I. Kaplan, C. E. Kirkwood, R. L. Martin, R. C. Sherwood, *Inorg. Chem.* **1971**, *10*, 240.
[3] [3a] J. A. Barnes, W. E. Hatfield, *Inorg. Chem.* **1971**, *10*, 2355. [3b] W. L. Gladfelter, M. W. Lynch, W. P. Schaefer, D. N. Hendrickson, H. B. Gray, *Inorg. Chem.* **1981**, *20*, 2390. [3c] F. Paap, E. Bouwman, W. L. Driessen, R. A. G. Graaff, J. Reedijk, *J. Chem. Soc., Dalton Trans.* **1985**, 737. [3d] L. Ballester, E. Coronado, A. Gutiérrez, A. Monge, M. F. Perpiñan, E. Pinilla, T. Rico, *Inorg. Chem.* **1992**, *31*, 2053. [3e] A. J. Blake, E. K. Brechin, A. Codron, R. O. Gould, G. M. Grant, S. Parsons, J. M. Rawson, R. E. P. Winpenny, *J. Chem. Soc., Chem. Commun.* **1995**, 1983. [3f] M. A. Halcrow, J. -S. Sun, J. C. Huffman, G. Christou, *Inorg. Chem.* **1995**, *34*, 4167. [3g] M. S. E. Fallah, E. Rentschler, A. Caneschi, D. Gatteschi, *Inorganica Chimica Acta* **1996**, 231. [3h] A. Escuer, M. Font-Bardía, S. B. Kumar, X. Solans, R. Vicente, *Polyhedron* **1999**, *18*, 909. [3i] J. M. Clemente-Juan, B. Chansou, B. Donnadieu, J. -P. Tuchagues, *Inorg. Chem.* **2000**, *39*, 5515. [3j] N. Hoshino, T. Ito, M. Nihei, H. Oshio, *Chemistry letters* **2002**, 844. [3k] C. Boskovic, E. Rusanov, H. Stoeckli-Evans, H. U. Güdel, *Inorganic Chemistry Communications* **2002**, *5*, 881. [3l] S. Mukherjee, T. Weyhermüller, E. Bothe, K. Wieghardt, P. Chaudhuri, *Eur. J. Inorg. Chem.* **2003**, 863. [3m] T. K. Paine, E. Rentschler, T. Weyhermüller, P. Chaudhuri, *Eur. J. Inorg. Chem.* **2003**, 3167.
[4] [4a] C. Cadiou, M. Murrie, C. Paulsen, V. Villar, W. Wernsdorfer, R. E. P. Winpenny, *Chem. Commun.* **2001**, 2666. [4b] H. Andres, R. Basler, A. J. Blake, C. Cadiou, G. Chaboussant, G. M. Grant, H. U. Güdel, M. Murrie, S. Parsons, C. Paulsen, F. Semadini, V. Villar, W. Wernsdorfer, R. E. P. Winpenny, *Chem. Eur. J.* **2002**, *8*, 4867. [4c] S. T. Ochsenbein, M. Murrie, E. Rusanov, H. Stoeckli-Evans, C. Sekine, H. U. Güdel, *Inorg. Chem.* **2002**, *41*, 5133.
[5] E. C. Yang, W. Wersdorfer, S. Hill, R. S. Edwards, M. Nakano, S. Maccagnano, L. N. Zakharov, A. L. Rheingold, G. Christou, D. N. Hendrickson, *Polyhedron* **2003**, *22*, 1727.
[6] R. Sessoli, D. Gatteschi, A. Caneschi, M. A. Novak, *Nature* **1993**, *365*, 141.
[7] A. L. Barra, P. Debrunner, D. Gatteschi, Ch. E. Schulz, R. Sessoli, *Europhys. Lett.* **1996**, *35*, 133.
[8] W. Wernsdorfer, K. Hasselbach, A. Benoit, B. Barbara, D. Mailly, J. Tuaillon, J. P. Perez, V. Dupuis, J. P. Dupin, G. Giraud, A. Perex, *J. Appl. Phys.* **1995**, *78*, 7192.
[9] R. Sessoli, D. Gatteschi, *Angew. Chem. Int. Ed.* **2003**, *42*, 268; and references cited therein.
[10] W. Wernsdorfer, S. Bhaduri, R. Tiron, D. N. Hendrickson, G. Christou, *Phys. Rev. Lett.* **2002**, *89*, 197201.
[11] W. Wernsdorfer, N. Aliaga-Alcalde, D. N. Hendrickson, G. Christou, *Nature* **2002**, *416*, 406.
[12] W. Wernsdorfer, R. Sessoli, *Science* **1999**, *284*, 133.
[13] A. Altomare, G. Cascarano, C. Giacovazzo, A. Guagliardi, *J. Appl. Crystallogr.* **1993**, *26*, 343.
[14] G. M. Sheldrick, Institut für Anorganische Chemie der Universität, Tammannstraße 4, 3400 Göttingen, Germany, **1998**.

Received February 11, 2004

 © 2004 Wiley-VCH Verlag GmbH & Co. KGaA, Weinheim

Scanning Tunneling Study of the Assembly of Octa- and Tetraruthenium Supermolecules on Graphite

Dong-Lin Shieh,[a] Kom-Bei Shiu,[a] and Jong-Liang Lin*[a]

Keywords: Supermolecular chemistry / Scanning tunneling microscopy / Graphite / Ruthenium

Surface layer structures of $[\{Ru_2(CO)_4(PMe_3)_2\}(\mu\text{-}O_2CCO_2)]_4$ and $[\{Ru_2(CO)_4(PMe_3)_2\}(\mu\text{-}O_2CCH_2CO_2)]_2$ with $[Ru_2(CO)_4(PMe_3)_2]$ building blocks *cis*-ligated by either O_2CCO_2 or $O_2CCH_2CO_2$ on highly oriented pyrolytic graphite (HOPG) have been investigated by scanning tunneling microscopy and spectroscopy. STM images of well-ordered assemblies of these two molecules with molecular or submolecular resolution were obtained. These two molecules can adopt an orientation with their Ru–Ru bonds parallel or perpendicular to the substrate surface forming ordered 2D-arrays with different layer structures and tunneling spectra.

(© Wiley-VCH Verlag GmbH & Co. KGaA, 69451 Weinheim, Germany, 2004)

Introduction

The design and applications of unique molecular structures containing special functional units, such as rigid *cis*-bridge transition-metal macrocycles, are major subjects of supermolecular chemistry. An ordered arrangement of supermolecules with rigid macrocyclic structures on surfaces or in their film states is of interest in producing nanoscale devices. Thin-film materials based on tetrametallic squares have been preliminarily proven to show the properties of nanoscale porosity, size-selective transport, and molecular or ionic sensing.[1−3] As an example, it has been reported that the bridge-ligated Re/Pd square cationic complexes, prepared by the reaction of $Re(CO)_3Cl(4,4'\text{-bpy})_2$ and $Pd(dppp)(triflate)_2$, show photoluminescent characteristics which can be used for ClO_4^- anion sensing.[1] However, to date we know of no reported surface structure investigations of either a monolayer or a thin film of rigid superstructures of bridged transition metals.

In the present work we investigate the two dimensional (2D) structures of $[\{Ru_2(CO)_4(PMe_3)_2\}(\mu\text{-}O_2CCO_2)]_4$ (**1**) and $[\{Ru_2(CO)_4(PMe_3)_2\}(\mu\text{-}O_2CCH_2CO_2)]_2$ (**2**) as the first model for supermolecules based on dimetal building units coordinated by *cis*-bridging ligands on HOPG using scanning tunneling microscopy. Figure 1 shows the molecular structures of **1** and **2**. Molecule **1** has an octametallic square shape with four nominally equivalent corner components containing dimetal $[Ru_2(CO)_4(PMe_3)_2]$ building units. Molecule **2** is a molecular loop with two nominally equivalent building blocks. Their crystal structures have been well-characterized by X-ray crystallography.[4] The unique shapes and known dimensions of these molecules allow for the submolecular analysis of the measured STM images. Supermolecules based on dimetal building units can contain various organic ligands that control properties such as solubility, pore size, and electrochemical activity.[5] Furthermore, the spectroscopic and magnetic properties of the dimetal units can be varied for diversified applications.

[a] Department of Chemistry, National Cheng Kung University
1, Ta Hsueh Road, Tainan, Taiwan 701, Republic of China
Fax: (internat.) + 886-6-2740552
E-mail: jonglin@mail.ncku.edu.tw

Results and Discussion

Our scanning tunneling results of $[\{Ru_2(CO)_4(PMe_3)_2\}(\mu\text{-}O_2CCO_2)]_4$ are shown in Figures 2 and 3, and of $[\{Ru_2(CO)_4(PMe_3)_2\}(\mu\text{-}O_2CCH_2CO_2)]_2$ in Figures 4 and 5. Figure 2 (a) shows a 1000×1000 nm^2 STM image with a step separating two terraces after deposition of **1** on the HOPG. The tunneling image and spectrum obtained around point A in the lower area (the dark terrace) is similar to those of a clean graphite surface. Therefore, the dark terrace is attributed to an uncovered area of the graphite surface. Figure 2 (b) shows the STM image recorded at point B on the bright terrace. In this image, the bright lobes form an ordered array and have the same size and tunneling characteristics, suggesting that they are caused by the same molecular or submolecular groups. In Figure 2 (b), the rows of bright lobes along directions C and D have an included angle of $93 \pm 2°$. The distance between two neighboring lobes in both directions is 6.8 ± 0.2 Å. The geometric characteristics of the STM image corresponds to the angle of Ru4−Ru1−Ru8 (92.5°) and the Ru···Ru distance of Ru1−Ru4 or Ru1−Ru8 (6.9 Å) of **1** as shown in Figure 1.

As molecules of **1** are adsorbed with their 2.7 Å Ru−Ru bonds of $[Ru_2(CO)_4(PMe_3)_2]$ building units perpendicular to the HOPG surface, that is, with the PMe_3 groups pointing either toward or away from the HOPG surface; the adsorbed molecular orientation explains the observed

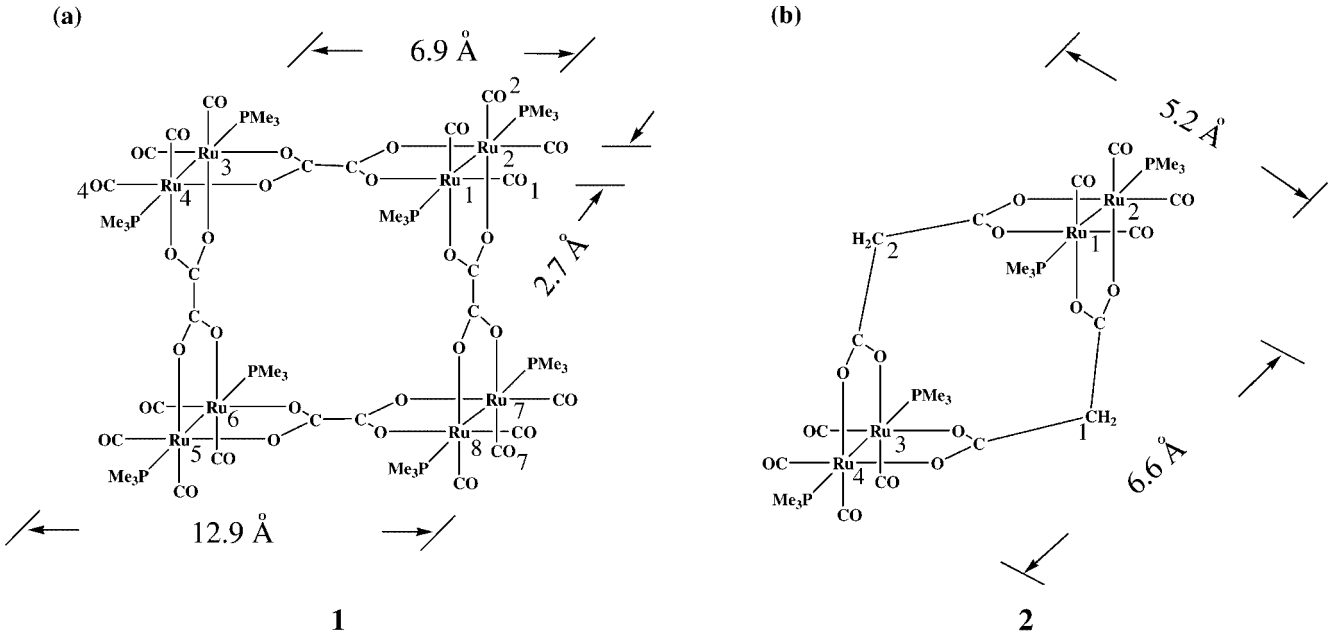

Figure 1. (a) Molecular structure of $[\{Ru_2(CO)_4(PMe_3)_2\}(\mu\text{-}O_2CCO_2)]_4$; the shape of this molecule is close to a square, with four approximately equivalent $[Ru_2(CO)_4(PMe_3)_2]$ corner components; (b) molecular structure of $[\{Ru_2(CO)_4(PMe_3)_2\}(\mu\text{-}O_2CCH_2CO_2)]_2$

distance and angle of the neighboring lobes exactly. The four lobes connected by the square shown in Figure 2 (b) corresponds to a molecule of **1**. Each lobe represents the submolecular image of one corner component, that is, one $[Ru_2(CO)_4(PMe_3)_2]$ unit of **1**. We were able to record a well-ordered 2D domain of approximately 35 × 35 nm^2 at submolecular resolution. Figure 2 (c) shows the proposed molecular adsorption orientation, as well as the 2D assembly of **1** that matches the observed STM image. This layer structure has a surface unit cell of 13.6 × 13.6 Å^2 with a 93° included angle. The size of the unit cell is slightly larger than that of a unit of **1** [O1−O4 = O2−O7 = 12.9 Å as shown in Figure 1 (a)]; that is, the surface molecules are closely packed together.

This packing characteristic has been observed in the previous STM investigation of the $(Co_4L_4)(AsF_6)_8$ layer on HOPG [L = 4,6-bis(2′,2′′-bipyridyl-6-yl)pyrimidine].[6,7] The monolayer has a periodicity of 25 × 24 Å^2, which corresponds to the size of the Co_4L_4 complex ion with a metal grid unit as well. Figure 2 (d) contains the line profiles taken along the directions of C and D shown in Figure 2 (b); the corrugation is approximately 2.2 Å in both cases. Figure 2 (e) compares the tunneling spectra recorded for the area covered by **1** (similar I-V curves are recorded when the tip is positioned on the peaks and valleys of the corrugation) and for a clean graphite surface. The close packing of the bright lobes [c.a. 6.8 Å between two neighboring lobes, Figure 2 (b)] for **1** excludes the possibility that the adsorbed molecules of **1** adopt an orientation where the Ru−Ru bonds (Ru1−Ru2, Ru3−Ru4, Ru5−Ru6, and Ru7−Ru8) are approximately parallel to the HOPG surface [see Figure 1 (a)], because the distance from the H atoms of a PMe_3 group to those of the opposite PMe_3 group in the same corner unit $[Ru_2(CO)_4(PMe_3)_2]$ is approximately 11.5 Å. Taking the van der Waals radius into account, if the adsorbed molecules of **1** on the HOPG have this orientation, the length between two neighboring bright lobes in either the C or D direction should be larger than 11.5 Å [Figure 2 (b)]. Interestingly, an adsorption orientation with the Ru−Ru bonds approximately parallel to the surface is also observed (Figure 3).

Figure 3 (a) shows another STM image (400 × 400 nm^2), with a step separating two terraces, after deposition of **1** on the HOPG. The dark terrace is attributed to the uncovered area of the graphite surface based on the tunneling images and spectra taken in this area. Figure 3 (b) shows the STM image recorded at point A on the bright terrace. In Figure 3 (b) the size of the bright lobes (c.a. 12.8 × 11.6 Å^2) is about four times that found in Figure 2 (b), and corresponds to the size of a molecule of **1** as shown in Figure 3 (c); implying that each bright lobe in Figure 3 (b) represents a molecule of **1**. In other words, this matched dimension implies that **1** adopts an orientation where the four Ru−Ru bonds are approximately parallel to the HOPG surface. Note that the molecular adsorption orientation in this case is perpendicular to that shown in Figure 2 (c). The ordered array of the bright lobes in Figure 3 (b) has a unit cell of 13.7 ± 0.2 × 14.7 ± 0.2 Å^2 with an included angle of 120 ± 2°. Figure 3 (d) shows the proposed molecular adsorption orientation and the 2D assembly of **1** that matches the observed STM image of Figure 3 (b) according to the size of the bright lobes and the unit cell. Although the included angle of 120 ± 2° [i.e. approximately hexagonal symmetry, Figure 3 (b)] may indicate the superperiodic pattern of a bare HOPG surface, other tunneling features are not consistent with this argument. First, in Figure 3 (b) the corru-

 © 2004 Wiley-VCH Verlag GmbH & Co. KGaA, Weinheim

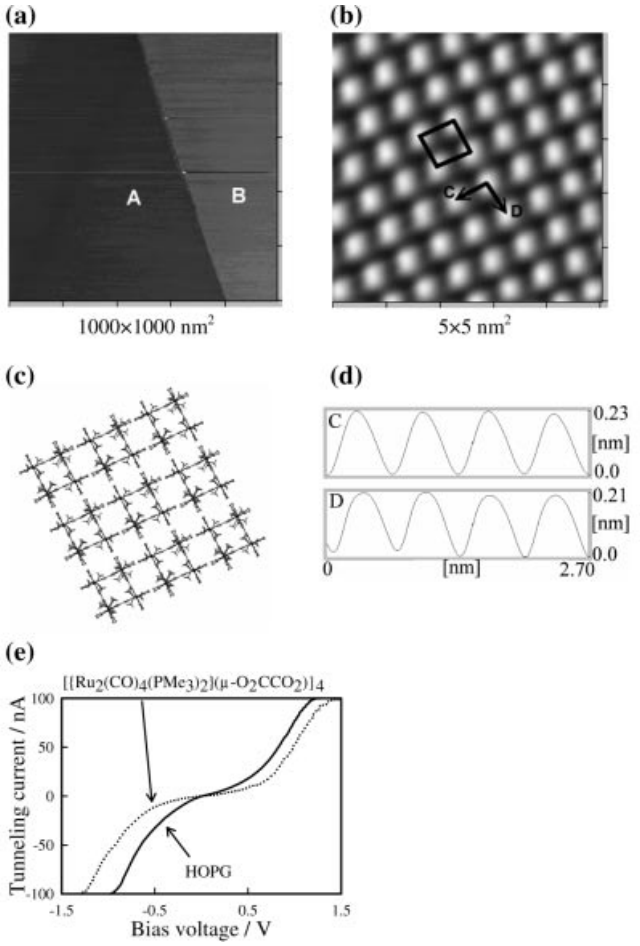

Figure 2. (a) STM image of 1000 × 1000 nm² with a step separating a bright terrace representing a $[\{Ru_2(CO)_4(PMe_3)_2\}(\mu\text{-}O_2CCO_2)]_4$-covered area and a dark terrace representing uncovered area of HOPG; (b) high-resolution STM image of the $[\{Ru_2(CO)_4(PMe_3)_2\}(\mu\text{-}O_2CCO_2)]_4$-covered area on HOPG; (c) proposed 2D array that matches the STM image; (d) line profiles in the directions of C and D; (e) comparison of tunneling spectra of the $[\{Ru_2(CO)_4(PMe_3)_2\}(\mu\text{-}O_2CCO_2)]_4$-covered surface and a bare HOPG surface. V = 0.1 V and I = 0.25 nA were used to record the STM images

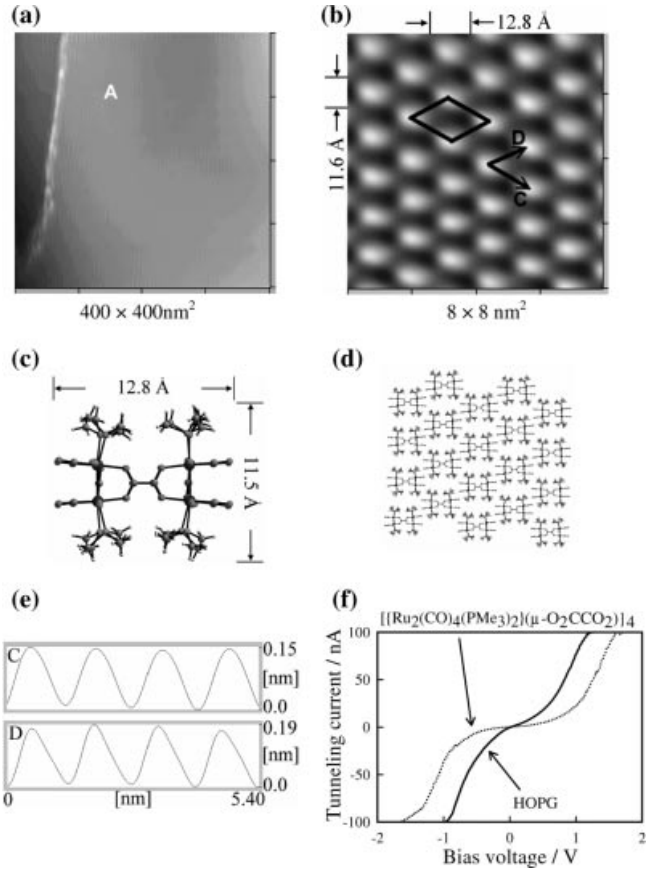

Figure 3. (a) STM image of 400 × 400 nm² with a step separating a bright terrace representing a $[\{Ru_2(CO)_4(PMe_3)_2\}(\mu\text{-}O_2CCO_2)]_4$-covered area and a dark terrace representing uncovered area of HOPG; (b) high-resolution STM image of the $[\{Ru_2(CO)_4(PMe_3)_2\}(\mu\text{-}O_2CCO_2)]_4$-covered area on HOPG; (c) $[\{Ru_2(CO)_4(PMe_3)_2\}(\mu\text{-}O_2CCO_2)]_4$ structure with the indicated dimensions similar to those of the bright lobes in the STM image; (d) proposed 2D array that matches the STM image; (e) line profiles in the directions of C and D; (f) comparison of tunneling spectra of the $[\{Ru_2(CO)_4(PMe_3)_2\}(\mu\text{-}O_2CCO_2)]_4$-covered surface and a bare HOPG surface; V = 0.1 V and I = 0.25 nA were used to record the STM images

gations in the C and D directions [these are approximately 0.17 nm, as shown in Figure 3 (e)] are much smaller than the approximate 1−1.5 nm reported for HOPG superlattices.[8,9] Second, no graphite atomic fringes were observed in Figure 3 (b), which were also observed in the STM images of HOPG superlattices.[8,9] Figure 3 (f) shows the tunneling spectrum of Figure 3 (b).

Figure 4 (a) shows the STM image of a covered area comprising molecules of **2** on the HOPG. The rows of bright lobes along directions C and D have an included angle of 110 ± 2°. The distance between two neighboring lobes in either direction is 6.8 ± 0.2 Å. This length corresponds to 6.6 Å between the equivalent parts of the $[Ru_2(CO)_4(PMe_3)_2]$ unit, as shown in Figure 1 (b), suggesting that the bright lobes in Figure 4 (a) are due to $[Ru_2(CO)_4(PMe_3)_2]$ units. Note that the distance between the two CH_2 groups of **2** is only 5.2 Å, which is approximately 1.6 Å less than the distance between two neighboring lobes in Figure 4 (a). Furthermore, the sizes of the bright lobes in Figure 2 (b) for **1** and in Figure 4 (a) for **2** are similar. Therefore, the bright lobes in Figure 4 (a) are not attributed to the CH_2 groups of **2**, but rather to the $[Ru_2(CO)_4(PMe_3)_2]$ units, and as a result, we propose that **2** is adsorbed in such a way that the PMe_3 groups of $[Ru_2(CO)_4(PMe_3)_2]$ point either toward or away from the HOPG surface. Because each bright lobe in Figure 4 (a) corresponds to a $[Ru_2(CO)_4(PMe_3)_2]$ unit, there are three possible 2D assemblies [as shown in Figure 4 (b)] that match the observed STM image. The three different 2D layer structures have surface unit cells of 12.1 × 15.8 Å² with an 87° included angle, 12.1 × 8.0 Å² with a 99° angle, and 13.5 × 8.0 Å² with an 124° angle. Note that the three different layer structures displayed next to each other in Figure 4 (b) do not mean that they co-exist in the STM sampling area of Figure 4 (a). Figure 4 (c) shows the line profiles in the directions of C and D of Figure 4 (a). Figure 4 (d) compares the tunneling spectra recorded for the layer of **2** and

 © 2004 Wiley-VCH Verlag GmbH & Co. KGaA, Weinheim

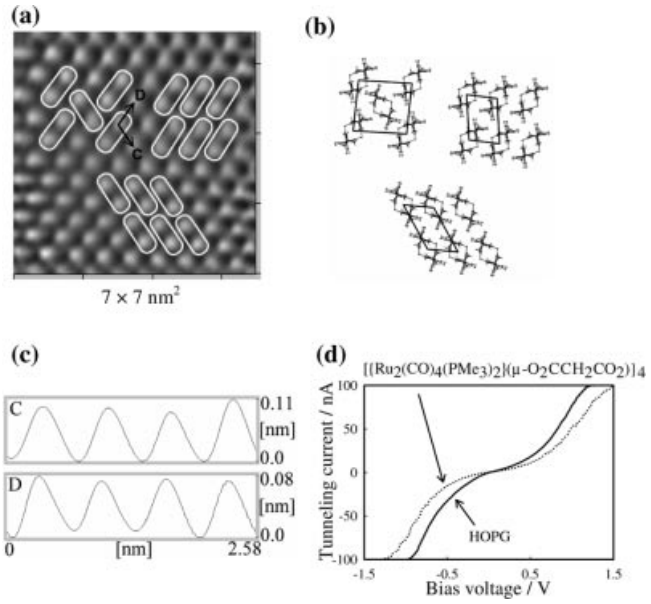

Figure 4. (a) STM image of a $[\{Ru_2(CO)_4(PMe_3)_2\}(\mu\text{-}O_2CCH_2CO_2)]_2$-covered area on HOPG; (b) proposed three possible 2D arrays that match the STM image; (c) line profiles in the directions of C and D; (d) comparison of tunneling spectra of the $[\{Ru_2(CO)_4(PMe_3)_2\}(\mu\text{-}O_2CCH_2CO_2)]_2$-covered surface and a bare HOPG surface; $V = 0.05$ V and $I = 0.34$ nA were used to record the STM image

a clean HOPG surface. Note that because the molecular adsorption orientations of **1** and **2** are similar [Figure 2 (c) and Figure 4 (b), respectively], that is, with the PMe_3 groups pointing either toward or away from the HOPG surface, the tunneling spectra of **1** and **2** are also similar [Figure 2 (e) and Figure 4 (d), respectively].

Figure 5 (a) shows another observed STM image of **2**, consisting of an ordered array of bright lobes with an approximate size of 11.5×10.2 Å^2. Similar dimensions of a molecule of **2** are shown in Figure 5 (b). This similarity suggests that each lobe in Figure 5 (a) corresponds to a molecule of **2** adsorbed with the two Ru−Ru bonds approximately parallel to the HOPG surface. Note that the orientation of the surface molecules in this case is perpendicular to that shown in Figure 4 (b). The ordered array of the bright lobes in Figure 5 (a) has a unit cell of $11.3 \pm 0.2 \times 13.8 \pm 0.2$ Å^2 with an included angle of $83 \pm 3°$. Figure 5 (c) shows the proposed molecular adsorption orientation and the 2D assembly of molecules of **2** that match the STM image of Figure 5 (a). Figure 5 (d) shows the line profiles in the directions of C and D of Figure 5 (a). Figure 5 (e) compares the tunneling spectra recorded for a layer of **2** with a clean HOPG surface.

Conclusion

In summary, we find that on the HOPG the studied octa- and tetraruthenium supermolecules can both adopt an orientation with their Ru−Ru bonds parallel or perpendicular to the substrate surface, forming ordered 2D arrays with different layer structures and tunneling spectra. We

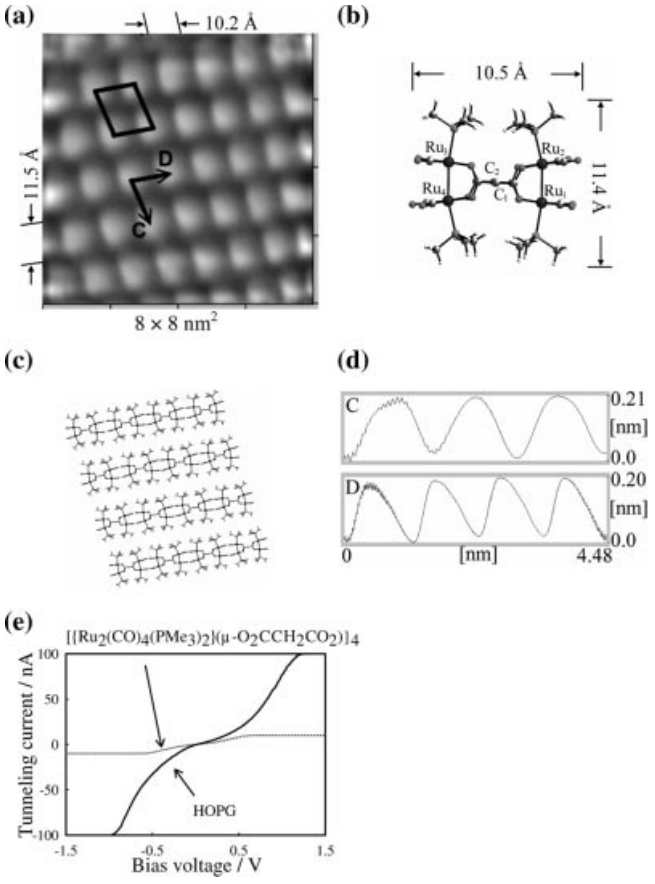

Figure 5. (a) STM image of a $[\{Ru_2(CO)_4(PMe_3)_2\}(\mu\text{-}O_2CCH_2CO_2)]_2$-covered area on HOPG; (b) $[\{Ru_2(CO)_4(PMe_3)_2\}(\mu\text{-}O_2CCH_2CO_2)]_2$ structure with the indicated dimensions similar to those of the bright lobes in the STM image; (c) proposed 2D array that matches the STM image; (d) line profiles in the directions of C and D; (e) comparison of tunneling spectra of the $[\{Ru_2(CO)_4(PMe_3)_2\}(\mu\text{-}O_2CCH_2CO_2)]_2$-covered surface and a bare HOPG surface. $V = 0.05$ V and $I = 0.34$ nA were used to record the STM image

compare, with the aid of the software *Diamond*, the observed 2D structures of the molecules of **1** and **2** on the HOPG to the crystallographic planes of 3D structures of **1** and **2** and find no similar cases that simultaneously have both the same dimensions of the unit cells and the same molecular orientations as those in Figure 2 (c), 3 (d), 4 (b), or 5 (c). This result indicates the influence of the HOPG surface on the 2D assemblies of molecules of **1** and **2**.

Experimental Section

General: $[\{Ru_2(CO)_4(PMe_3)_2\}(\mu\text{-}O_2CCO_2)]_4$ (**1**) and $[\{Ru_2(CO)_4(PMe_3)_2\}(\mu\text{-}O_2CCH_2CO_2)]_2$ (**2**) were synthesized through the reactions of freshly prepared $Ru_3(CO)_{12}$, oxalic acid, and PMe_3 in THF according to a procedure previously described.[5] In the preparation of adsorption films of **1** and **2** on HOPG, a droplet of **1** (0.01 M) or **2** (0.03 M) in CH_2Cl_2 was deposited onto a freshly cleaved surface of HOPG (ZYB quality). The CH_2Cl_2 was allowed to vaporize before STM images were recorded (Seiko Instruments, SPA 400) at constant current mode under ambient conditions. The film systems were stable, permitting repeated scans within several months of the

 © 2004 Wiley-VCH Verlag GmbH & Co. KGaA, Weinheim

investigation period. Electrochemically etched W tips were used for the STM study.

Acknowledgments

We gratefully acknowledge the support of the National Science Council of the Republic of China (NSC 92-2113-M-006-016).

[1] R. V. Slone, D. I. Yoon, R. M. Calhoun, J. T. Hupp, *J. Am. Chem. Soc.* **1995**, *117*, 11813−11814.
[2] R. V. Slone, K. D. Benkstein, S. B'elanger, J. T. Hupp, I. A. Guzei, A. L. Rheingold, *Coord. Chem. Rev.* **1998**, *171*, 221−243.
[3] S. B'elanger, J. T. Hupp, C. L. Stern, R. V. Slone, D. F. Watson, T. G. Carrell, *J. Am. Chem. Soc.* **1999**, *121*, 557−563.
[4] K.-B. Shiu, H.-C. Lee, G.-H. Lee, Y. Wang, *Organometallics* **2002**, *21*, 4013−4016.
[5] F. A. Cotton, C. Lin, C. A. Murillo, *Acc. Chem. Res.* **2001**, *34*, 759−771.
[6] A. Semenov, J. P. Spatz, M. Möller, J.-M. Lehn, B. Sell, D. Schubert, C. H. Weidl, U. S. Schubert, *Angew. Chem. Int. Ed.* **1999**, *38*, 2547−2550.
[7] A. Semenov, J. P. Spatz, J.-M. Lehn, C. H. Weidl, U. S. Schubert, M. Möller, *Appl. Surf. Sci.* **1999**, *144−145*, 456−460.
[8] M. Kuwabara, D. R. Clarke, D. A. Smith, *Appl. Phys. Lett.* **1990**, *56*, 2396−2398.
[9] J. Xhie, K. Sattler, M. Ge, N. Venkateswaran, *Phys. Rev. B* **1993**, *47*, 15835−15841.

Received November 24, 2003

 © 2004 Wiley-VCH Verlag GmbH & Co. KGaA, Weinheim

A Novel 3-D Self-Penetrating Topological Network Assembled by Mixed Bridging Ligands

Xing Li,[a] Rong Cao,*[a] Daofeng Sun,[a] Wenhua Bi,[a] and Daqiang Yuan[a]

Keywords: Mixed bridging ligands / Interlocking / Self-penetrating

The assembly of 5-sulfoisophthalic acid (H_3sipa) and 4,4′-bipyridine (bpy) with Cd^{2+} ions gave rise to a new polymeric complex $\{[Cd_3(sipa)_2(bpy)_4(H_2O)_2]\cdot 3H_2O\}_n$ (**1**). X-ray diffraction analysis reveals that complex **1** has a 3-D self-penetrating network formed by the interlocking and interweaving of two types of one-dimensional chains comprising two kinds of $Cd_4(sipa)_4$ and $Cd_4(bpy)_4$ units, respectively. The $sipa^{3-}$ ligand serves as the connector and the Cd^{2+} ion as the node. Thermogravimetric analysis (TGA) and the luminescence property of **1** are discussed.
(© Wiley-VCH Verlag GmbH & Co. KGaA, 69451 Weinheim, Germany, 2004)

The analyses and studies of diverse topological networks have recently received much attention.[1] In these reports a variety of fascinating types of entanglements of individual motifs observed are of special interest due to their important role in natural organic entities.[2] In the past decades, a number of new types of entanglements that are often described as interpenetrating networks,[3] have been constructed from organic building units. Among these entangled polymeric systems, some representative species such as catenanes(**I**), rotaxanes (**II**) or pseudocatenate/rotaxanes (**III**), have been reported (Scheme 1).[4−8] Based on studies on catenane and rotaxane molecules, the introduction of metal ions into polymeric frameworks greatly intrigued many chemists. Aside from unique topological features, these entangled metal-containing species are attractive for use in new functional materials, as well as for the development of molecular devices and studies on bionics.[9−11] The formation of different entanglements or interpenetrations may result from the presence of large free voids in a single network.[3b,7a] It has been shown that long bridging ligands can produce large voids, which may generate interpenetrating structures or large open cavities. For example, 1,3,5-benzenetricarboxylate (btc) which serves as a three-part connector that affords the (6,3) graphite-like sheet and terephthalate and 4,4′-bipyridine that generate the (4,4) sheet, were widely used to design and synthesize directed compounds with interpenetrating or large open cavity structures.[12] Our synthetic approach starts by focusing on the construction of new topological frameworks using different kinds of bridging ligands. Two long bridging ligands, 4,4′-bipyridine (bpy) and 5-sulfoisophthalic acid (H_3sipa), were used, together with Cd^{2+} ions. We hoped each of them could form independent structural units with large voids, and the interlocking or interpenetrating of the two kinds of units with each other could generate an entangled structure. In this communication, we report on a 3-D self-penetrating coordination polymer, $\{[Cd_3(sipa)_2(bpy)_4(H_2O)_2]\cdot 3H_2O\}_n$ (**1**), constructed by the interlocking and interconnecting of two types of metal-ligand rings $Cd_4(sipa)_4$ and $Cd_4(bpy)_4$.

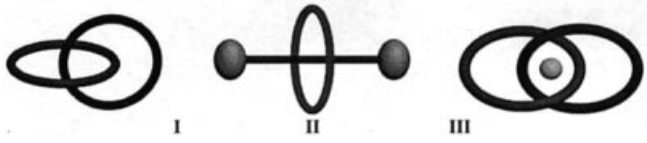

Scheme 1

The hydrothermal reaction of NaH_2sipa, $Cd(NO_3)_2\cdot 4H_2O$, 4,4′-bipyridine and water at 160 °C for 3 days resulted in the formation of light-yellow crystals of **1**. The element analysis and IR spectrum confirm the formula of **1**. Single-crystal X-ray diffraction reveals complex **1** has a 3-D self-penetrating framework constructed from Cd^{2+} ions, and the ligands $sipa^{3-}$ and bpy. There are two types of coordination environments around the Cd^{2+} ions in the crystal structure: Cd(1), which is at the center of a distorted octahedral geometry, is coordinated by two oxygen atoms from two $-SO_3$ groups of different $sipa^{3-}$ ligands and four nitrogen atoms from four bpy ligands; Cd(2) is coordinated by two nitrogen atoms from two bpy ligands, four oxygen atoms from a water molecule and two carboxylate groups, in a highly distorted octahedral geometry. Here, two coordination oxygen atoms from two $-SO_3$ groups on Cd(1) and two coordination nitrogen atoms from two bpy on Cd(2) are located in *cis*-positions with bond angles of 86.00 and

[a] State Key Laboratory of Structural Chemistry, Fujian Institute of Research on the Structure of Matter, Chinese Academy of Sciences,
Fuzhou, Fujian, China
Fax: (internat.) +86-591-371-4946
E-mail: rcao@ms.fjirsm.ac.cn

 © 2004 Wiley-VCH Verlag GmbH & Co. KGaA, Weinheim **DOI: 10.1002/ejic.200400044**

97.48° for O−Cd(1)−O and N−Cd(2)−N, respectively. Such *cis* positions that are sterically hindered have rarely been observed in reported studies,[13] and may induce the formation of the ring structures $Cd_4(sipa)_4$ and $Cd_4(bpy)_4$. The formation of open cavities or channels may be favored by the *trans* locations of the ligands.

In **1**, four cadmium ions and four bpy ligands form a $Cd_4(bpy)_4$ unit with a side length of 11.46 × 11.79 Å and diagonal measurement of 15.55 × 17.28 Å based on the metal−metal distances. Different metal−metal distances in the tetragonal sheet arise as a result of the different torsions and curves of the bpy ligands linking Cd(1) and Cd(2), respectively. The fully deprotonated $sipa^{3-}$ ligand acts as a tridentate ligand linking three cadmium ions by its monodentate sulfonic, monodentate carboxylate and chelating carboxylate groups. Four $sipa^{3-}$ ligands and four cadmium ions form a 32-membered ring unit, $Cd_4(sipa)_4$. The two kinds of units, $Cd_4(sipa)_4$ and $Cd_4(bpy)_4$, interlock and interconnect with each other to produce a self-penetrating structural unit (Figure 1),[2c,14] in which the $sipa^{3-}$ ligand penetrates through the $Cd_4(bpy)_4$ ring and strong face to face π-π stacking interactions involving the aromatic rings from the closest neighboring $sipa^{3-}$ and bpy ligands (with an average distance of about 3.50 Å) is observed. Each $Cd_4(bpy)_4$ unit interlocks two $Cd_4(sipa)_4$ units and each $Cd_4(sipa)_4$ unit interlocks two $Cd_4(bpy)_4$ units through cadmium ion nodes, yielding an interwoven structure that is extended in different directions forming a three-dimensional self-penetrating topological network.

In the $Cd_4(bpy)_4$ unit, four cadmium ions are coplanar, and two such adjacent planes have a dihedral angle of 57°. Therefore, through the sharing of the vertex cadmium ion knots, the $Cd_4(bpy)_4$ units are further extended into a one-dimensional twisted 8-like chain (see a in Figure 2). Through the sharing of the $sipa^{3-}$ sides, the $Cd_4(sipa)_4$ units propagate a one-dimensional ladder-like chain (see b in Figure 2), in which all the cadmium ions are coplanar and the $sipa^{3-}$ ligands are situated in the zygomorphic sites of the plane. The two types of one-dimensional chains interlock and interweave together to form a two-dimensional framework through the sharing of cadmium ions in the *ab* plane (see c in Figure 2). The 1-D ladder-like chains comprising $Cd_4(sipa)_4$ units possess an AB array (left, direction up; right, direction down) along the *a* axis and AA array along the *c* axis, while the 1-D twisted 8-like chains formed by the $Cd_4(bpy)_4$ units have an AA illustration down the *b* axis and ABC display along the *c* axis. The two-dimensional structure extend in different directions generating a 3-D packing network with micro channels that can accommodate free water molecules (Figure 3). It is worth noting that the structure of **1** reveals a new topological net: Cd1 acts as a "6-connected" center, Schäfli symbol (4^2; 6^4; 8^9); Cd2 as a "4-connected" center, Schäfli symbol (4; 6^4; 8); and $sipa^{3-}$ as a "3-connected" center, Schäfli symbol (6^2; 8). Considering the stoichiometry, the overall topology is $(Cd1)(Cd2)_2(sipa)_2$, Schäfli symbol (4^2; 6^4; 8^9)(4; 6^4; $8)_2$ (6^2; $8)_2$.

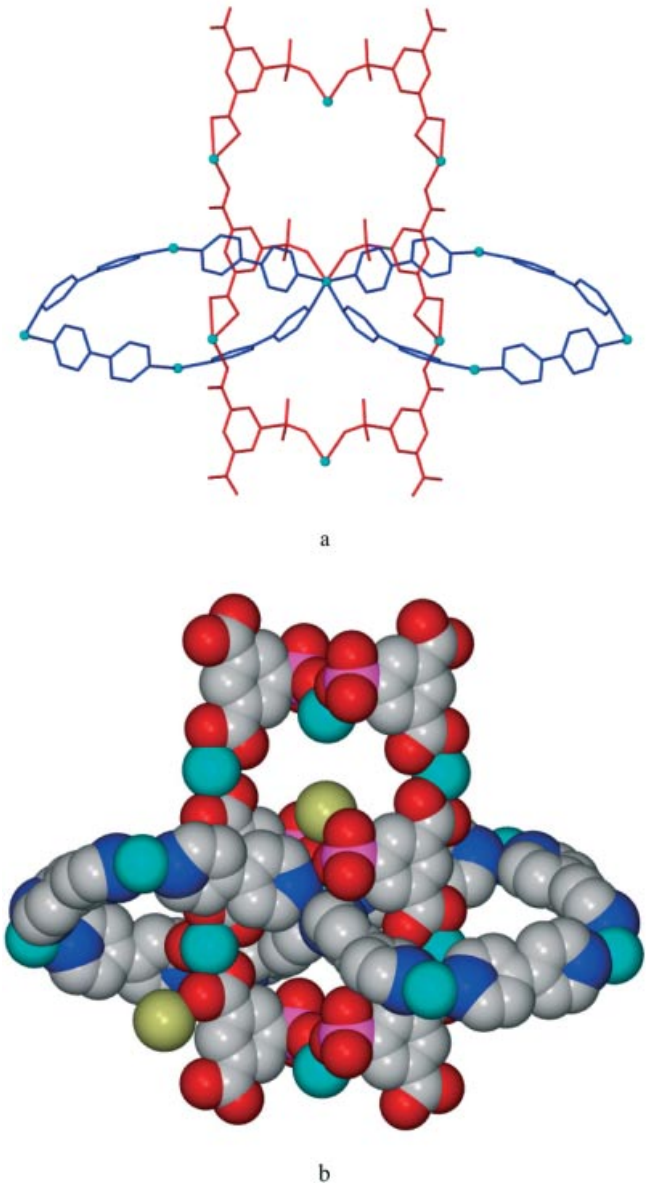

Figure 1. (a) The interlocking self-penetrating unit formed by $Cd_4(sipa)_4$ (red) and $Cd_4(bpy)_4$ (blue) units through sharing node Cd^{2+} ions; (b) space-filling diagram: turquoise sphere representing Cd^{2+} ion, brown-yellow: free water, scarlet red: oxygen, gray: carbon, blue: nitrogen, pink: sulfur

The thermogravimetric analysis (TGA) study shows that the first weight loss of 5.75% (calcd: 5.86%) observed from 63 to 144 °C corresponds to the loss of three free water and coordinated water molecules per formula unit ($5H_2O$/$\{[Cd_3(sipa)_2(bpy)_4(H_2O)_2]\cdot 3H_2O\}$), and the structural framework begins to collapse at 340 °C. Heating-cooling and dehydrate-hydrate experiments were carried out according to the TGA results, and monitored by X-ray powder diffraction. The crystalline sample of complex **1** is heated to 145 °C under autogenous pressure for 4 hours, the guest water molecules are lost from the sample and some characteristic XRPD peaks become weaker or disappear. However, when the resulting dehydrated products are immersed

 © 2004 Wiley-VCH Verlag GmbH & Co. KGaA, Weinheim

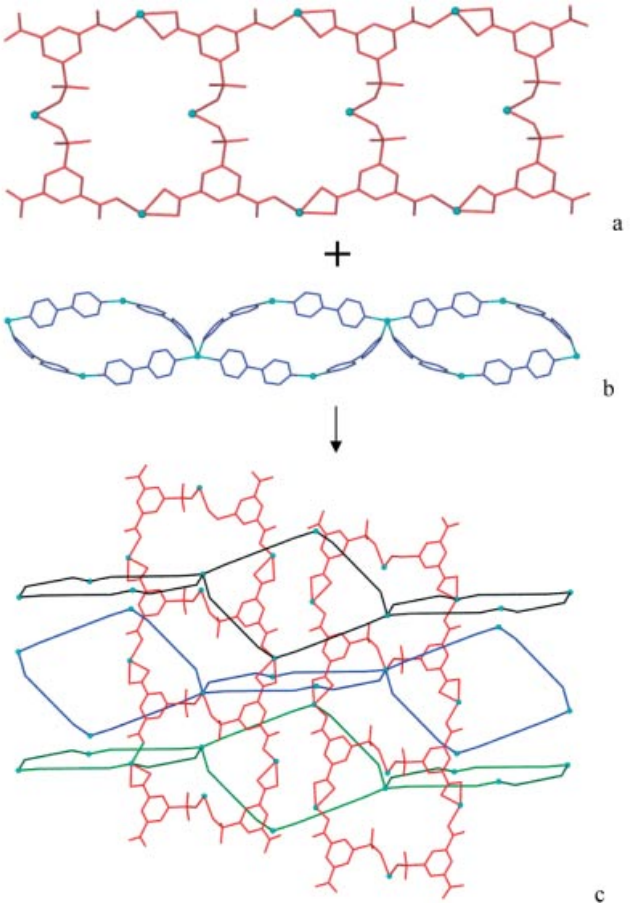

Figure 2. (a) 1-D ladder-like chains formed by $Cd_4(sipa)_4$ units(red); (b) 1-D twisted 8-like chains formed by $Cd_4(bpy)_4$ units (blue); (c) schematic presentation of 2-D framework in the *ab* plane

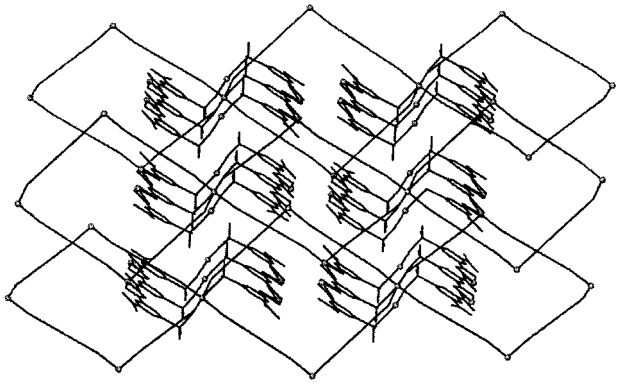

Figure 3. 3-D packing structure for **1** along the *b* axis, guest water molecules are omitted for clarity

in water for 12 hours, the XRPD pattern and infrared spectrum for the rehydrated sample are almost the same as those of the original sample, illustrating that the framework of **1** is retained on the removal of guest water molecules. The details of the XRPD analyses for **1** are provided as Supporting Information. The luminescence spectrum of **1** in the solid state at ambient temperature exhibits an intense broadband fluorescent emission at 453 nm on photo-excitation at 354 nm, suggesting that **1** may be suitable as a candidate for a stable and solvent-resistant blue fluorescent material due to its stability in air and insolubility in common solvents.[15]

In summary, a novel three-dimensional self-penetrating network constructed from two mixed bridging ligands has successfully been prepared; although many entangled structures have been reported, those constructed by mixed bridging ligands are rather few. The present work shows that a novel structure can be designed and assembled through the combination of the topology of organic ligand and the coordination geometry of metal ion. Further studies on this subject are still underway.

Experimental Section

Synthesis of 1: A mixture of NaH_2sipa (0.266 g, 1.0 mmol), $Cd(NO_3)_2{\cdot}4H_2O$ (0.231 g, 0.75 mmol), 4,4′-bipyridine dihydrate (0.192 g, 1.0 mmol) and water (10 mL) was placed in a 25 mL Teflon^R-lined stainless autoclave under autogenous pressure at 160 °C for 3 days after which it was cooled slowly to room temperature over a 24 hour period. The light yellow block-like crystals of **1** were separated from the reaction mixture in about a 23% yield (0.35 g). $C_{56}H_{48}Cd_3N_8O_{19}S_2$: calcd. C 43.72, H 3.14, N 7.28; found C 43.60, H 2.94, N 7.31%. IR (KBr (cm^{-1})): 1605 (vs), 1556 (s), 1491 (w), 1416 (m), 1363 (s), 1230 (s), 1198 (s), 1105 (w), 1043 (m), 806 (m), 719 (w), 629 (m), 582 (m), 492 (w), 432 (w).

X-ray Crystallography: $C_{56}H_{48}Cd_3N_8O_{19}S_2$, **1**, M_r = 1538.34, 0.28 × 0.22 × 0.18 mm^3, monoclinic, space group *C*2/*c*, *a* = 35.578(4), *b* = 10.232(1), *c* = 16.211(1) Å, β = 108.913(2)°, *V* = 5583.5(1) $Å^3$, *Z* = 4, D_c = 1.830 Mg/m^3, F_{000} = 3072, μ = 1.293 mm^{-1}, *T* = 298(2) K, $2\theta_{max}$ = 50.1°, 8252 reflections collected, 4836 unique (R_{int} = 0.0437). Final GooF = 1.077, R_1 = 0.0469, wR_2 = 0.0833 with $I > 2\sigma(I)$.

Data collection for **1** was performed on a Siemens SMART-CCD diffractometer equipped with a graphite-monochromated Mo-K_α radiation (λ = 0.71073 Å) at 293 K. All absorption corrections were applied using the SADABS program. The structures were solved by direct methods, the metal atoms were located from the E-maps, and other non-hydrogen atoms were derived from the successive difference Fourier syntheses. The hydrogen atoms were located from the difference map and refined isotropically. The structure was refined on F^2 by full-matrix least-squares using the SHELXTL-97 program package.

CCDC-221212 (for **1**) contains the supplementary crystallographic data for this paper. These data can be obtained free of charge at www.ccdc.cam.ac.uk/conts/retrieving.html [or from the Cambridge Crystallographic Data Center, 12 Union Road, Cambridge CB2 1EZ, UK; Fax: (internat.) +44-1223-336-033; E-mail: deposit@ccdc.cam.ac.uk].

Acknowledgments

The authors are grateful for the financial support from NNSF of China (90206040, 20325106, 20333070), NSF of Fujian Province (B9820003), and the key and the "One Hundred Talent" projects from CAS.

 © 2004 Wiley-VCH Verlag GmbH & Co. KGaA, Weinheim

[1] [1a] L. Carlucci, G. Ciani, D. M. Proserpio, *Coordin, Chem. Rev.* **2003**, *246*, 247−289. [1b] M. L. Tong, X. M. Chen, S. R. Batten, *J. Am. Chem. Soc.* **2003**, *125*, 16170−16171.
[2] [2a] L. M. Adleman, *Science* **1994**, *266*, 1021−1024. [2b] P. W. K. Rothemund, *Proc. Natl. Acad. Sci. U. S. A.* **2000**, *97*, 984−989. [2c] L. Carlucci, G. Ciani, D. M. Proserpio, *CrystEngCommun.* **2003**, *5*, 269−279.
[3] [3a] X. S. Wang, H. Zhao, Z. R. Qu, Q. Ye, J. Zhang, R. G. Xiong, X. Z. You, H. K. Fun, *Inorg. Chem.* **2003**, *42*, 5786−5788. [3b] S. R. Batten, R. Robson, *Angew. Chem. Int. Ed.* **1998**, *37*, 1461−1494.
[4] [4a] G. Schill, *Catenane, Rotaxanes, and Knots*, New York, **1971**. [4b]D. B. Amabilino, J. F. Stoddart, *Chem. Rev.* **1995**, *95*, 2722−2828. [4c] T. J. Hubin, A. G. Kolchinski, A. L. Vance, D. H. Busch, *Adv. Supramol. Chem.* **1999**, *5*, 237−257.
[5] [5a] C. A. Hunter, *J. Am. Chem. Soc.* **1992**, *114*, 5303−5311. [5b] C. Theresa, A. M. Heiss, S. J. Cantrill, M. C. T. Fyfe, A. R. Pease, S. J. Rowan, J. F. Stoddart, D. J. Williams, *Org. Lett.* **2000**, *2*, 2943−2946. [5c] V. Balzani, A. Credi, S. J. Langford, F. M. Raymo, J. F. Stoddart, M. Venturi, *J. Am. Chem. Soc.* **2000**, *122*, 3542−3543.
[6] [6a] S. J. Loeb, J. A. Wisner, *Chem. Commun.* **2000**, 845−846. [6b] H. Kawasaki, N. Kihara, T. Takata, *Chem. Lett.* **1999**, 1015−1016.
[7] [7a] G. F. Liu, B. H. Ye, Y. H. Ling, X. M. Chen, *Chem. Commun.* **2002**, 1442−1443. [7b] J.-P. Sauvage, *Acc. Chem. Res.* **1998**, *31*, 611−619. [7c] R. Ballardini, V. Balzani, A. Credi, M. T. Gandolfi, M. Venturi, *Acc. Chem. Res.* **2001**, *34*, 445−455.
[8] [8a] L. Carlucci, G. Ciani, M. Moret, D. M. Proserpio, S. Rizzato, *Angew. Chem. Int. Ed.* **2000**, *39*, 1506. [8b] B. Moulton, M. J. Zaworotko, *Chem. Rev.* **2001**, *101*, 1629−1658.
[9] [9a] J.-M. Lehn, *Angew. Chem. Int. Ed. Engl.* **1990**, *29*, 1304−1319. [9b] J.-M. Lehn, *Supramolecular Chemistry: Concepts and perspectives*, VCH, Weinheim, Germany, **1995**.
[10] [10a] C. P. Collier, G. Mattersteig, E. W. Wong, Y. Luo, K. Beverly, J. Sampaio, F. M. Raymo, J. F. Stoddart, J. R. Heath, *Science* **2000**, *289*, 1172−1175. [10b] G. W. Gokel, A. Mukhopadhyay, *Chem. Soc. Rev.* **2001**, *30*, 274−286.
[11] [11a] C. D. Mao, W. Q. Sun, N. C. Seeman, *Nature* **1997**, *386*, 137−138. [11b] V. Balzani, A. Credi, F. M. Raymo, J. F. Stoddart, *Angew. Chem. Int. Ed.* **2000**, *39*, 3349−3391.
[12] [12a] T. M. Reineke, M. Eddaoudi, D. Moler, M. O'Keeffe, O. M. Yaghi, *J. Am. Chem. Soc.* **2000**, *122*, 4843−4844. [12b] J. C. Dai, X. T. Wu, Z. Y. Fu, S. M. Hu, W. X. Du, C. P. Cui, L. M. Wu, H. H. Zhang, R. Q. Sun, *Chem. Commun.* **2000**, 12−13. [12c] J. Tao, M. L. Tong, X. M. Chen, *J. Chem. Soc., Dalton Trans.* **2000**, 3669−3674.
[13] [13a] S. Tanase, M. Andruh, A. Müller, M. Schmidtmann, C. Mathonière, G. Rombaut, *Chem. Commun.* **2001**, 1084−1085. [13b] M. L. Tong, H. Chen, X. M. Chen, *Inorg. Chem.* **2000**, *39*, 2235−2238.
[14] R. G. Scharein, Knotplot, http://www.pims.math.ca/knotplot/
[15] R. X. Yuan, R. G. Xiong, Y. L. Xie, X. Z. You, S. M. Peng, G. H. Lee, *Inorg. Chem. Commun.* **2001**, *4*, 384387.

Received January 18, 2004

 © 2004 Wiley-VCH Verlag GmbH & Co. KGaA, Weinheim

D_{5h} Cu_5H_5X: Pentagonal Hydrocopper Cu_5H_5 Containing Pentacoordinate Planar Nonmetal Centers (X = B, C, N, O)

Si-Dian Li,*[a] Chang-Qing Miao,[b] and Guang-Ming Ren[b]

Keywords: Ab initio calculations / Density functional calculations / Hydrocopper / Pentacoordinate planar carbon / Electronic structures

Pentacoordinate planar nonmetals (PPNs) centered in perfect pentagonal hydrocopper complexes Cu_5H_5X (X = B, C, N, O), as determined by density functional theory methods, are presented in this communication. The results obtained in this work complete the hypercoordinate planar carbon series with high symmetries (D_{4h}, D_{5h}, and D_{6h}), and may shed new insight in catalyst chemistry.
(© Wiley-VCH Verlag GmbH & Co. KGaA, 69451 Weinheim, Germany, 2004)

Introduction

Exploring the bonding nature of carbon beyond the tetrahedral concept in organic chemistry has attracted considerable attention since Hoffmann et al.[1] proposed the possibility of tetracoordinate planar carbon (TPC) thirty years ago. Recent experimental and theoretical investigations have confirmed the existence of TPCs in Al_4C^- with D_{4h} symmetry,[2] Al_3XC and Al_3XC^- with C_{2v} symmetry (X = Si, Ge),[3,4] and $[CAl_4]^{2-}$.[5] A similar observation was reported for tetracoordinate planar Si and Ge in MAl_4 and MAl_4^-.[6] Even more interesting, the possibility of pentacoordinate planar carbons (PPC) in $-C_3B_3-$, $-C_2B_4-$, and $-CB_5-$ subgroups and hexacoordinate planar carbons (HPCs) in B_6C^{2-} with D_{6h} symmetry was also explored by Schleyer et al.[7–9] recently at the density functional theory (DFT) level. In a very recent paper,[10] our group performed an ab initio investigation of tetracoordinate planar nonmetals (TPNs) centered in perfect square hydrometals M_4H_4 in D_{4h} M_4H_4X complexes (X = B, C, N and O; M = Cu and Ni), and extended the tetracoordinate planar centers from carbon to other first-row nonmetal elements and the ligands from *p*-block elements to transition metal atoms. However, unlike D_{4h} TPCs and D_{6h} HPCs observed in simple molecules, a PPC center with a high D_{5h} symmetry is still missing. Here, we present theoretical investigations of pentacoordinate planar nonmetals (PPNs) in Cu_5H_5X (X = B, C, N, O) complexes that contain D_{5h} X centers in a perfect pentagonal hydrocopper (Cu_5H_5) proposed by Tsipis et al.[11] To the best of our knowledge, there have been no investigations reported to date on D_{5h} PPCs or other TPNs centered in perfect pentagonal structures composed of transition metal ligands. The results obtained in this work complete the hypercoordinate planar carbon series with the high symmetries of D_{4h}, D_{5h}, and D_{6h}.

Initial structures obtained at DFT B3LYP/Lanl2d$_z$ were further optimized at DFT B3LYP/6-311+G(3df,p) and imaginary frequencies were checked at the same level of theory.

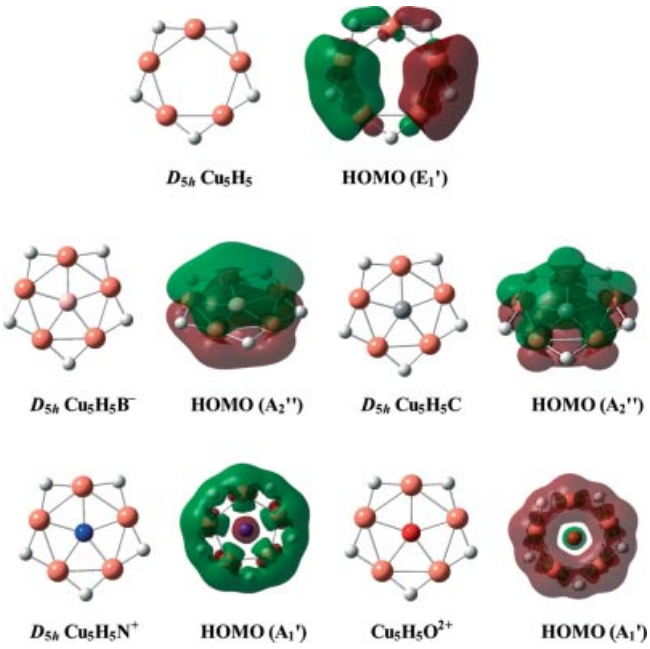

Figure 1. Optimized structures of D_{5h} Cu_5H_5X complexes (X = B, C, N, O) and their HOMO diagrams compared with that of hydrocopper D_{5h} Cu_5H_5 at the B3LYP/6-311+G(3df,p) level

[a] Institute of Materials Sciences and Department of Chemistry, Xinzhou Teachers' University,
Xinzhou 034000, Shanxi, P. R. China
Fax: (internat.) +86-0350-3031845
E-mail: lisidian@yahoo.com
[b] Institute of Materials sciences and Department of Chemistry, Xinzhou Teachers' University,
Xinzhou 034000, Shanxi, P. R. China

 © 2004 Wiley-VCH Verlag GmbH & Co. KGaA, Weinheim **DOI: 10.1002/ejic.200400223**

Table 1. Optimized DFT bond lengths R, lowest vibrational frequencies ν_{min} (cm^{-1}) and H NMR shielding tensors of D_{5h} Cu_5H_5X complexes (X = B, C, N, O); optimized bond lengths at MP2 are also listed for comparison

	Cu_5H_5		$Cu_5H_5B^-$		Cu_5H_5C		$Cu_5H_5N^+$		$Cu_5H_5O^{2+}$	
	B3LYP	MP2	B3LYP	MP2	B3LYP	MP2	B3LYP	MP2	B3LYP	MP2
R_{Cu-Cu} /Å	2.494	2.454	2.394	2.310	2.368	2.255	2.392	2.285	2.476	2.414
R_{Cu-H} /Å	1.605	1.561	1.651	1.580	1.625	1.576	1.605	1.577	1.597	1.584
R_{Cu-X} /Å			2.037	1.965	2.014	1.918	2.035	1.934	2.106	2.054
ν_{min} /cm^{-1}	63		57		52		49		52	
H NMR tensors /ppm	32.5		34.5		36.1		35.3		39.5	

The calculated binding energy ΔE = 255.7 kJ/mol for the reaction $Cu_5H_5C = Cu_5H_5 + C$ clearly demonstrates the stability of the D_{5h} Cu_5H_5C with respect to dissociation to the hydrocopper Cu_5H_5 and the free C atom. When refined at the MP2/6-311+G(d,p) level of theory, the DFT bond lengths are systematically shortened by about 2 to 5%. The NMR shielding tensors were calculated using the gauge-independent atomic orbital (GIAO) procedure[12] at the B3LYP/6-311+G(3df,p) level. The optimized DFT structures and corresponding highest occupied molecular orbital (HOMO) diagrams of the D_{5h} Cu_5H_5X series are depicted and compared with that of the pentagonal hydrocopper Cu_5H_5 at the same level of theory in Figure 1. The optimized bond parameters, lowest vibrational frequencies and NMR shielding tensors at DFT, and the bond lengths at MP2 are summarized in Table 1. All the calculations were performed using the Gaussian 03 suite of programs.[13]

Different from the squared Cu_4H_4X series,[10] all the isoelectronic Cu_5H_5X neutral and charged ions possess perfect planar pentagonal structures with the highest symmetry, D_{5h} (see Figure 1). As can be seen from Figure 1 of ref. 10,[10] the Cu_4H_4 square is too small to accommodate the B and C centers. However, the Cu_5H_5 pentagon studied here is shown to have the correct size such that the first-row nonmetal centers (from B, C, N to O) can be accommodated to form D_{5h} Cu_5H_5X complexes without imaginary frequencies (see Table 1). In addition, structures with initial C_{5v} symmetry and off-plane X atoms along the fivefold axis are found to be automatically converted into perfect planar pentagons during structural optimization, further confirming that these D_{5h} complexes are true minima on their potential energy surfaces. Various initial structures with lower symmetries have also been tested; however, optimized structures with lower energies are not obtained. These high symmetry D_{5h} geometries with the lowest energies obtained in this work possess high stabilities as discussed above for D_{5h} Cu_5H_5C and have no imaginary frequencies that lead to structural distortions. The Cu−Cu separations in the Cu_5H_5X complexes are systematically shorter than those in the parent Cu_5H_5, but these distances increase from $Cu_5H_5N^+$ to $Cu_5H_5O^{2+}$. The bonding characteristics of the HOMOs of the complex series are clearly demonstrated in the molecular orbital diagrams shown in Figure 1. The molecular orbital analyses indicate that for $Cu_5H_5B^-$ and Cu_5H_5C, the doubly occupied highest occupied molecular orbitals (HOMOs) are delocalized π bonds (A_1') mainly composed of the $2p_z$ orbitals of the central atoms (with a slight contribution from the 3d orbitals of the Cu ligands), while the HOMOs of $Cu_5H_5N^+$ and $Cu_5H_5O^{2+}$ are delocalized σ bonds (A_2'') with the largest contribution from the 4s and 3d orbitals of the Cu ligands and partial contribution from the 2s orbitals of the central atoms. The delocalized σ HOMOs obtained here for $Cu_5H_5N^+$ and $Cu_5H_5O^{2+}$ are similar to the σ HOMOs observed in D_{4h} $Cu_4H_4N^+$ and $Cu_4H_4O^{2+}$.[10]

Natural bond orbital (NBO) analyses give new insights into the understanding of the atomic charge distribution and electron configurations of these complexes. The NBO results indicate that in the Cu_5H_5X complexes the X atoms serve as the negatively charged nonmetal centers, the Cu atoms at the periphery form a positively charged ring, and the bridging H atoms carry negative charges to maintain the overall charge balance. For example, Cu_5H_5C has the atomic charges of C −1.91 |e|, Cu +0.79 |e|, and H −0.41 |e|, and the corresponding values for $Cu_5H_5B^-$ are B −2.36|e|, Cu +0.72|e|, and H −0.44|e|. Even in the positively charged $Cu_5H_5N^+$ and $Cu_5H_5O^{2+}$ structures, the N and O centers carry the negative charges of −1.54|e| and −1.19|e|, the Cu atoms possess the positive charges of +0.87|e| and +0.96|e|, and the H atoms have negative charges of −0.37|e| and −0.33 |e|, respectively. This "sandwich" charge distribution reflects the consequence of electron transfer from the Cu ligands to the nonmetal centers X and the bridging H atoms, and results in the nearly pure lone pairs of electrons in the $2p_z$ orbitals of the central atoms. The high occupancies of the $2p_z$ orbitals are clearly demonstrated in the atomic electron configurations of $B[He]2s^{1.75}2p_x^{0.82}2p_y^{0.82}2p_z^{1.88}$, $C[He]2s^{1.86}2p_x^{1.05}2p_y^{1.05}2p_z^{1.92}$, $N[He]2s^{1.93}2p_x^{1.30}2p_y^{1.30}2p_z^{1.95}$, and $O[He]\ 2s^{1.97}2p_x^{1.60}2p_y^{1.60}2p_z^{1.97}$ in the corresponding complexes. It is interesting to note that in $Cu_5H_5B^-$ and Cu_5H_5C the nearly doubly occupied $2p_z$ orbitals of the central atoms dominate the formation of the π-typed HOMOs, while in the positively charged $Cu_5H_5N^+$ and $Cu_5H_5O^{2+}$ structures, the $2p_z$ orbitals mainly participate in the formation of the molecular orbitals next to the HOMOs (HOMO−1), which are also π-typed orbitals (not shown in Figure 1). For all the D_{5h} TPNs studied in this work, the 2s, $2p_x$, and $2p_y$ valence orbitals of the central atom form sp^2 hybrids to form five equivalent partial bonds with the periphery copper ligands.

 © 2004 Wiley-VCH Verlag GmbH & Co. KGaA, Weinheim

The orbital hybridization pattern observed here for PPNs parallels those in the TPCs in planar D_{4h} CH_4 and Ni_4H_4C structures, where the C center with three sp^2 hybrids forms equivalent bonds with its four equivalent ligands.[1,10] These D_{4h} TPC and D_{5h} PPN structures are achieved by resonances between equivalent structures allowed by the hybridization patterns of the central atoms and the arrangements of the specific ligands around them, as discussed in the case of D_{4h} CH_4.[1]

In order to assess the aromaticity of Cu_5H_5X complexes we observe the variation of the NMR spectroscopic chemical shifts of the H atoms relative to the NMR shielding tensor of the H atoms in tetrahedral $Si(CH_3)_3$ (δ = 31.9 ppm), since the geometrical center of the Cu_5H_5 pentagon is occupied by a nonmetal center. For X = B, C, N and O the calculated δ_H = +2.6, +4.2, +3.4, and +7.6 ppm, respectively. These up-field chemical shifts calculated for the H atoms outside the Cu_5 ring clearly indicate that the ring current effects in Cu_5H_5[11] vanish because of the introduction of the X atoms at the ring centers, and therefore the Cu_5H_5X complexes studied here are nonaromatic in nature. This finding is in agreement with the results obtained for the M_4H_4X series.[10]

In this work we have presented ab initio evidence of PPCs and other PPNs centered in perfect pentagonal Cu_5H_5X complexes. Investigations on heteropentagonal systems $M_xM'_yH_5X$ ($x + y = 5$) containing PPNs are under progress. Dimerization or formation of even higher aggregates are also possible, similar to the systems containing double HPCs.[9] Hydrometal complexes centered with hypercoordinate planar nonmetals are important in fundamental research and could have important applications in catalyst chemistry.

Acknowledgments

This work was financially supported by The Shanxi Natural Science Foundation. S.-D. L. is grateful to Dr. Hai-Shun Wu, Xiao-Hong Xu, and Hai-Jun Jiao for inspiring discussions and suggestions.

[1] R. Hoffmann, R. W. Alder, C. F. Wilcox Jr., *J. Am. Chem. Soc.* **1970**, *92*, 4992.
[2] X. Li, L.-S. Wang, A. I. Boldyrev, J. Simons, *J. Am. Chem. Soc.* **1999**, *121*, 6033.
[3] L. S. Wang, A. I. Boldyrev, X. Li, J. Simons, *J. Am. Chem. Soc.* **2000**, *122*, 7681.
[4] X. Li, H.-J. Zhai, L.-S. Wang, *Chem. Phys. Lett.* **2002**, *357*, 415.
[5] X. Li, H.-F. Zhang, L.-S. Wang, G. D. Geske, A. I. Boldyrev, *Angew. Chem. Int. Ed.* **2000**, *39*, 3630.
[6] A. I. Boldyrev, X. Li, L.-S. Wang, *Angew. Chem. Int. Ed.* **2000**, *39*, 3307.
[7] Z.-X. Wang, P. v. R. Schleyer, *Science* **2001**, *292*, 2465.
[8] K. Exner, P. v. R. Schleyer, *Science* **2000**, *290*, 1937.
[9] Z.-X. Wang, P. v. R. Schleyer, *Angew. Chem. Int. Ed.* **2002**, *41*, 4082.
[10] S.-D. Li, G.-M. Ren, C.-Q. Miao, Z.-H. Jin, *Angew. Chem. Int. Ed.* **2004**, *43*, 1371.
[11] A. C. Tsipis, C. A. Tsipis, *J. Am. Chem. Soc.* **2003**, *125*, 1136.
[12] R. Ditchfield, *Mol. Phys.* **1974**, *27*, 789; K. Wolinski, J. F. Hilton, P. Pulay, *J. Am. Chem. Soc.* **1990**, *112*, 8251.
[13] Gaussian 03, Revision A.1, M. J. Frisch, G. W. Trucks, H. B. Schlegel, G. E. Scuseria, M. A. Robb, J. R. Cheeseman, J. A. Montgomery, Jr., T. Vreven, K. N. Kudin, J. C. Burant, J. M. Millam, S. S. Iyengar, J. Tomasi, V. Barone, B. Mennucci, M. Cossi, G. Scalmani, N. Rega, G. A. Petersson, H. Nakatsuji, M. Hada, M. Ehara, K. Toyota, R. Fukuda, J. Hasegawa, M. Ishida, T. Nakajima, Y. Honda, O. Kitao, H. Nakai, M. Klene, X. Li, J. E. Knox, H. P. Hratchian, J. B. Cross, C. Adamo, J. Jaramillo, R. Gomperts, R. E. Stratmann, O. Yazyev, A. J. Austin, R. Cammi, C. Pomelli, J. W. Ochterski, P. Y. Ayala, K. Morokuma, G. A. Voth, P. Salvador, J. J. Dannenberg, V. G. Zakrzewski, S. Dapprich, A. D. Daniels, M. C. Strain, O. Farkas, D. K. Malick, A. D. Rabuck, K. Raghavachari, J. B. Foresman, J. V. Ortiz, Q. Cui, A. G. Baboul, S. Clifford, J. Cioslowski, B. B. Stefanov, G. Liu, A. Liashenko, P. Piskorz, I. Komaromi, R. L. Martin, D. J. Fox, T. Keith, M. A. Al-Laham, C. Y. Peng, A. Nanayakkara, M. Challacombe, P. M. W. Gill, B. Johnson, W. Chen, M. W. Wong, C. Gonzalez, J. A. Pople, Gaussian Inc., Pittsburgh PA, **2003**.

Received March 20, 2004

 © 2004 Wiley-VCH Verlag GmbH & Co. KGaA, Weinheim

Optically Active Phospholanes as Substituents on Ferrocene and Chromium-Arene Complexes

Wolfgang Braun,[a] Beatrice Calmuschi,[a] Jürgen Haberland,[b] Werner Hummel,[c] Andreas Liese,[b] Thomas Nickel,[d] Othmar Stelzer,[d] and Albrecht Salzer*[a]

In memoriam Othmar Stelzer

Keywords: Iron / Chromium / Sandwich complexes / P ligands / Asymmetric catalysis

An improved synthesis of (*R*,*R*)- and (*S*,*S*)-hexane-2,5-diol is presented. The (*S*,*S*)-derivative was converted into a cyclic sulfate, which on treatment with $NaPH_2$ in liquid ammonia ultimately gave the secondary (*R*,*R*)-2,5-dimethylphospholane. This phospholane can be introduced into the side chain of chiral tricarbonylchromium and ferrocene derivatives to give new bidentate ligands of the Josiphos and Daniphos type. Both the ferrocene- and tricarbonylchromium-based diphosphanes have been characterized by X-ray diffraction analysis. A discussion of their structural features is included. The new ligands were successfully applied to the enantioselective hydrogenation of itaconic acid esters.
(© Wiley-VCH Verlag GmbH & Co. KGaA, 69451 Weinheim, Germany, 2004)

Introduction

Enantioselective homogeneous catalysis remains one of the most challenging topics in organic and organometallic chemistry. Continuous improvements are being made, largely due to the development of new families of ligands. The Nobel committee recognized this by awarding the 2001 Nobel Prizes in chemistry for achievements in this field.[1]

In the search for novel catalysts and ligands, chemists have used all types of organic backbones, natural as well as unnatural. Whereas earlier research focused on ligands derived from the "chiral pool", e.g. tartaric acid, terpenes, amino acids, and sugars, the emphasis has shifted somewhat towards other ligand systems not derived from natural sources. This is largely due to the enormous success of such ligand families as BINAP and its derivatives, the DUPHOS ligands,[2,3] as well as the "Josiphos" family of ligands.[4,5] It should be noted that these ligands contain unusual elements of chirality, such as planar and axial chirality. The Josiphos ligands are also special in that they incorporate a transition metal containing unit as the central core around which the ligand framework is constructed. This transition metal itself is not involved in the catalysis, but is part of the scaffold to which the ligand functions are attached. The function of the metal is to create a chiral environment, the spatial and dynamic properties of which could not be achieved by an organic framework alone.

We have recently described a similar class of metal complexes, known as "Daniphos" complexes, which are based on chiral arenetricarbonylchromium complexes.[6−10] In many aspects, these ligands are similar to the Josiphos ligands but differ both in steric as well as electronic properties. They also match the ferrocene ligands in enantioselectivity in a number of catalytic applications. The major advantage of the chromium systems is their easy availability in an optically active form without any need for resolution, because the organic ligand itself (phenylethylamine), is commercially available in both enantiomers and with a variety of functional derivatives. Furthermore, the simple and straightforward synthetic route to the Daniphos ligands allows the construction of these diphosphanes in a modular fashion, a concept that has attracted considerable attention in the last decade.[11]

We sought to combine the advantages of both the metal-containing chiral frameworks of ferrocene and chromium-arene derivatives with the chirality of the phospholane units used in DUPHOS ligands. A necessary prerequisite was the availability of the secondary chiral phospholane (*R*,*R*)-2,5-dimethylphospholane, which has been briefly mentioned in

[a] Institut für Anorganische Chemie, RWTH Aachen, 52074 Aachen, Germany
Fax: (internat.) +49-(0)241-8092288
E-mail: albrecht.salzer@ac.rwth-aachen.de
[b] Institut für Biotechnologie, Forschungszentrum Jülich, 52425 Jülich, Germany
[c] Institut für Enzymtechnologie, Forschungszentrum Jülich, 52426 Jülich, Germany
[d] Fachbereich Chemie, Bergische Universität GH Wuppertal, 42097 Wuppertal, Germany

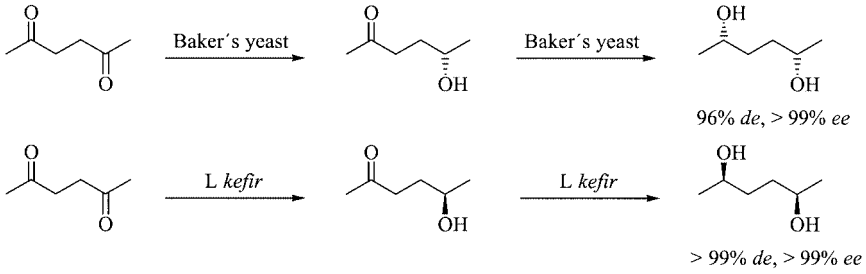

Scheme 1

the literature but was not isolated or fully characterized.[12] We therefore sought a route to prepare this phospholane directly from PH_3, and to incorporate it into both Josiphos and Daniphos ligands.

Results and Discussion

Optically active 2,5-hexanediol can be prepared by several routes, preferably by asymmetric homogeneous hydrogenation or enzymatic methods. Due to the commercial success of the DUPHOS ligands, larger quantities of this chemical in both the (*R*,*R*)- and (*S*,*S*)-forms are now in demand, and therefore we tried to scale the enzymatic route to allow the synthesis of kilogram amounts. The synthesis of both enantiomers could be achieved with quantitative conversion and with excellent diastereo- and enantioselectivities (> 96% *de*, > 99% *ee* for the (*R*,*R*)-isomer and 99% *de*, > 99% *ee* for the (*S*,*S*)-isomer) (Scheme 1).[13] Both enantiomers prepared by this route are now also commercially available.[13c]

The introduction of phospholane units into suitable organic frameworks remains a synthetic challenge even nowadays. The standard method employed today for the synthesis of the various DUPHOS ligands starts from a bis(primary)phosphane [e.g. the benzene derivative *o*-$C_6H_4(PH_2)_2$], which has to be synthesized by an elaborate route. This compound is then deprotonated and treated with the cyclic sulfate derived from hexanediol (Scheme 2).[3] A possible alternative is the reductive cleavage of a phenylphospholane with lithium metal, which then can be treated with organic halides.[14] Once again, however, this method is quite elaborate and (with larger substituents) can result in epimerization at C-2 and C-5. A third route has recently been described by Börner et al., in which *P*-(trimethylsilyl)phospholane, prepared from $P(TMS)_3$ in a two-step cyclization, undergoes nucleophilic addition to dichloromaleic anhydride.[15]

A fourth possible alternative is the use of a secondary phospholane, which proved to be difficult to isolate and characterize due to its volatility and extreme sensitivity. It was stabilized as a borane adduct, which however restricted its use to the synthesis of ligands with remote phospholane groups.[12]

Unfortunately, none of the above-mentioned reagents can be used for the introduction of phospholane units into the side-chain of Josiphos or Daniphos ligands. We therefore sought a route to prepare the secondary phospholane directly from PH_3. $NaPH_2$ was generated by deprotonation of PH_3 with sodium in liquid ammonia, and then treated with the cyclic sulfate of (*S*,*S*)-2,5-hexanediol. By following the reaction with ^{31}P and ^{1}H NMR spectroscopy, we were able to show that the ring-opening phosphination of the cyclic sulfate proceeded much faster than the second insertion step. The intermediate primary phosphane **1** (δ_P = −110.7 ppm) can be isolated and appears to be quite stable. By using two equivalents of $NaPH_2$, the reaction can be driven to completion, and after 48 h at −35 to −40 °C the secondary phospholane **2** (δ_P = −27.7 ppm) was isolated in the (*R*,*R*)-form with no evidence of epimerization, as the substitution proceeds cleanly by double inversion. The phospholane **2** can be purified by distillation, but due to its high volatility and pyrophoric nature, we were not able to obtain an elemental analysis. This compound can be stabilized as a BH_3 adduct **3**, as described earlier (Scheme 3).[12]

The standard method of introducing phosphanes onto the side chain of chiral (*R*,*R*)-1-[1-(dimethylamino)ethyl]-2-diphenylphosphanylferrocene is by refluxing this compound

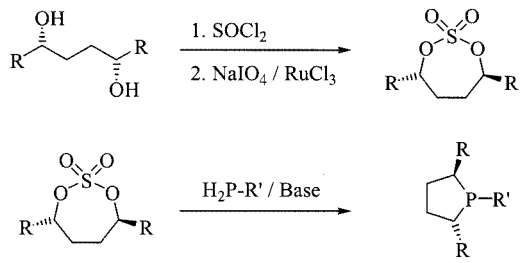

Scheme 2

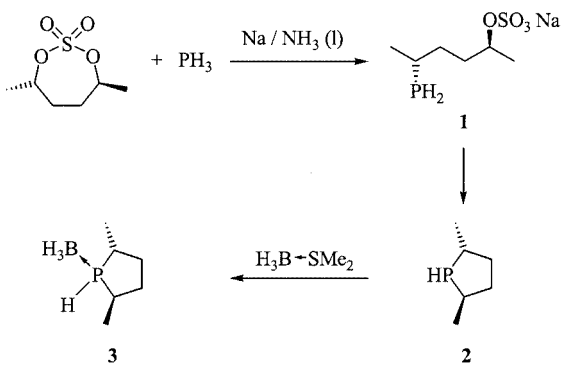

Scheme 3

 © 2004 Wiley-VCH Verlag GmbH & Co. KGaA, Weinheim

with a secondary phosphane in glacial acetic acid.[16] With the phospholane **2**, this reaction gave the desired diphosphane **4** in 55% yield. A somewhat different reaction path is necessary for the chromium complexes — an acetone solution of (*R*,*R*)-[1-(1-chloroethyl)-2-diphenylphosphanyl-η^6-benzene]chromium tricarbonyl was treated with **2**. An acetone solution of $TlPF_6$ was then slowly added to this mixture over one hour by an automatic syringe. The same reaction was also performed with the (*S*,*S*)-chromium com plex and the two diastereomeric products **5** and **6** were isolated in 80% and 96%, respectively (Scheme 4).

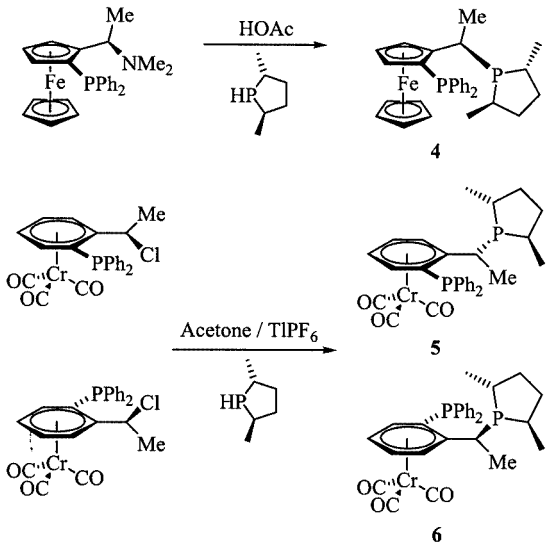

Scheme 4

Table 1. Comparison of characteristic torsion angles [°]

Torsion angle	4	7	10	9
	55.6(3)	74.1(3)	63.3(4)	179.1(4)	58.2(2)
	-113.3(3)	44.7(4)	33.9(6)	-69.9(5)	71.1(3)
	-60.2(4)	80.1(4)	74.6(6)	-28.2(9)	20.6(4)
	-149.1(3)	-134.9(3)	-148.4(4)	-69.1(4)	81.6(3)

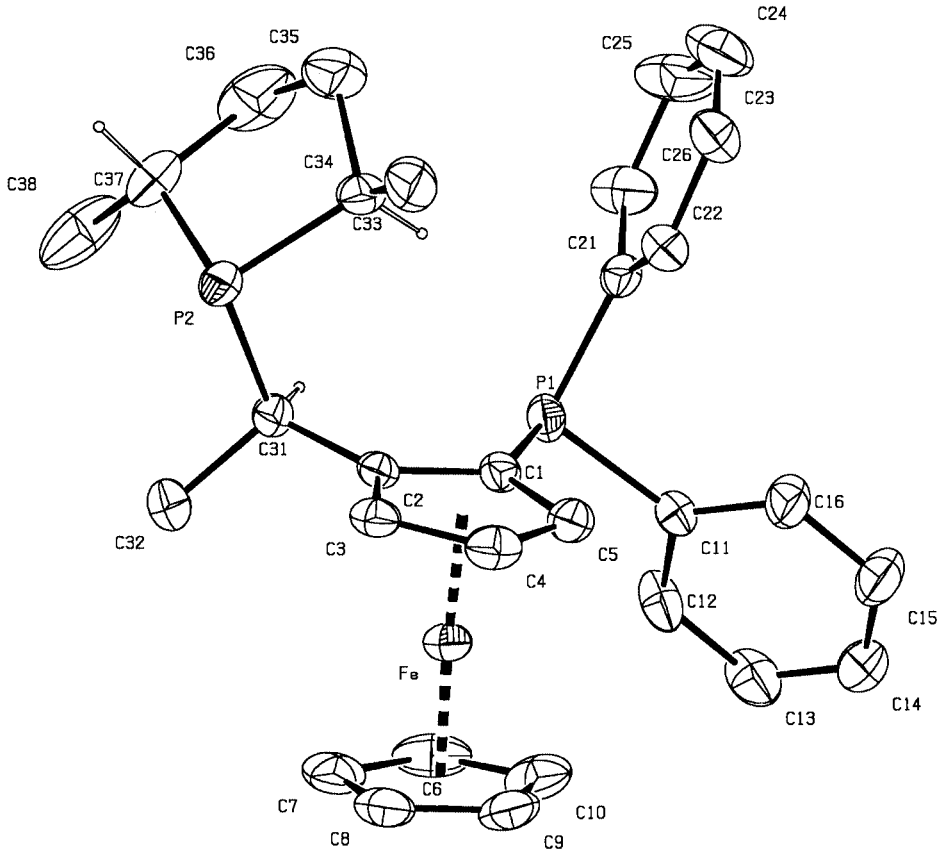

Figure 1. Displacement ellipsoids plot (PLATON[17]) of **4**; ellipsoids are at the 30% probability level; all H atoms except for those on the asymmetric carbon atoms have been omitted for clarity.

 © 2004 Wiley-VCH Verlag GmbH & Co. KGaA, Weinheim

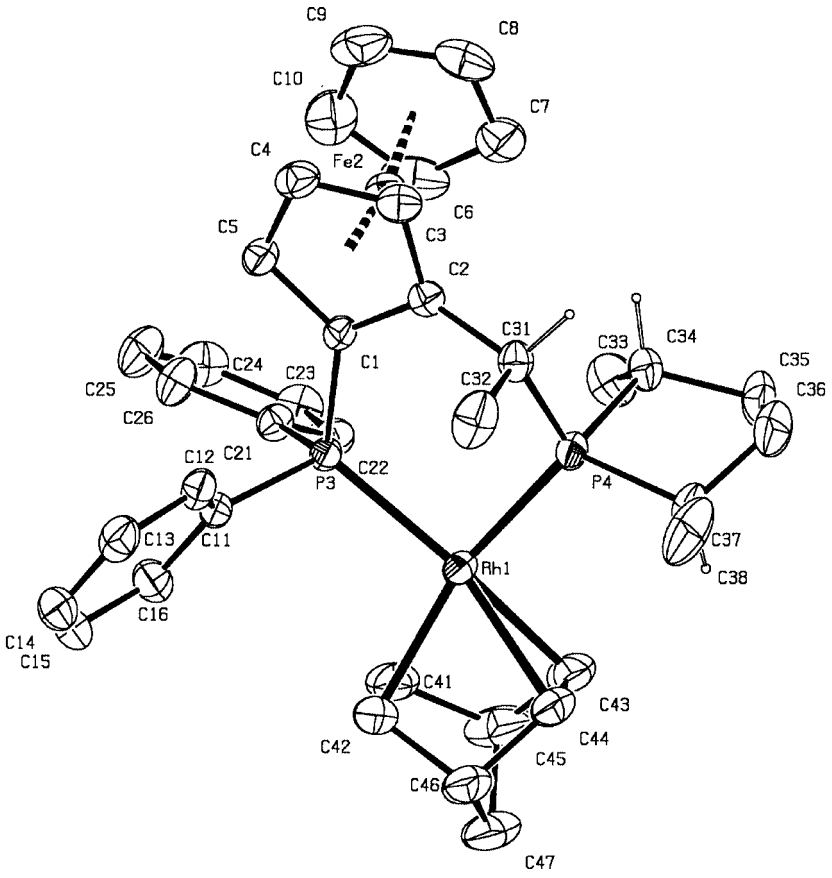

Figure 2. Displacement ellipsoids plot (PLATON[17]) of the cation of **7**; ellipsoids are at the 30% probability level; all H atoms except for those on the asymmetric carbon atoms have been omitted for clarity

We were able to grow single crystals of the ferrocene derivative **4** (Figure 1). Not surprisingly, **4** adopts a conformation in which the bulky phospholane is above the plane of the cyclopentadienyl ring. Some relevant dihedral angles are shown in Table 1.

For applications to catalysis, we also prepared the (norbornadiene)Rh complexes of both the iron and chromium compounds (**7**−**9**). Again, we were fortunate to obtain single crystals of the Fe−Rh complex **7** (Figure 2) and the Cr−Rh complex **9** (Figure 3). We also synthesized and structurally characterized the bis(ferrocene) rhodium complex **10** (Figure 4). Experimental crystallographic and crystal data are collected in Table 7.

As expected, the diphosphane **4**, on coordination to the square-planar environment of rhodium, has to undergo a considerable conformational change (Figures 1, 2 and 4). By comparing rhodium complexes of both Josiphos and Daniphos ligands, we were able to show that this conformational change is even more severe for the chromium complexes than for the iron complexes (Table 1), possibly due to the narrower bite angle of the benzene ring relative to the cyclopentadienyl ring.[9] Some selected bond lengths and angles for complexes **4**, **7**, **9** and **10** are summarized in Tables 2−5.

Table 2. Selected distances for **4**

Distances, Å			
P1−C1	1.814(3)	P2−C31	1.882(3)
P1−C11	1.841(3)	P2−C34	1.867(4)
P1−C21	1.845(4)	P2−C37	1.868(4)

Table 3. Selected distances and angles for **7**

Distances, Å			
Rh1−P3	2.3098(1)	Rh1−P4	2.3020(10)
Rh1−C41	2.214(5)	Rh1−C43	2.195(4)
Rh1−C42	2.226(4)	Rh1−C44	2.220(4)
P3−C1	1.801(3)	P4−C31	1.853(4)
P3−C11	1.832(3)	P4−C34	1.874(4)
P3−C21	1.832(3)	P4−C37	1.877(3)
Angles, deg			
P3−Rh1−P4	92.98(3)		
P3−Rh1−C41	97.90(13)	P4−Rh1−C43	98.75(16)
P3−Rh1−C42	100.34(11)	P4−Rh1−C44	97.39(13)
C42−Rh1−C44	64.75(17)	C41−Rh1−C43	65.8(2)

 © 2004 Wiley-VCH Verlag GmbH & Co. KGaA, Weinheim

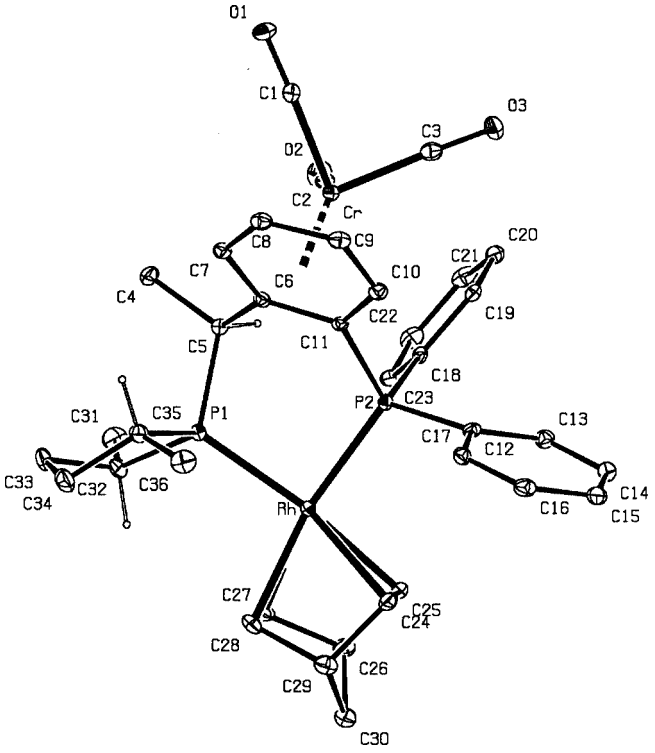

Figure 3. Displacement ellipsoids plot (PLATON[17]) of the cation of **9**; ellipsoids are at the 30% probability level; all H atoms except for those on the asymmetric carbon atoms have been omitted for clarity

Table 4. Selected distances and angles for **10**

Distances, Å			
Rh−P11	2.3281(12)	Rh−P21	2.3213(12)
Rh−P12	2.3056(11)	Rh−P22	2.4008(13)
P11−C101	1.811(5)	P21−C201	1.823(5)
P11−C111	1.840(5)	P21−C211	1.823(5)
P11−C121	1.847(5)	P21−C221	1.836(5)
P12−C132	1.865(5)	P22−C232	1.870(6)
P12−C134	1.843(5)	P22−C234	1.864(6)
P12−C137	1.887(5)	P22−C237	1.868(7)
Angles, deg			
P11−Rh−P12	89.21(4)	P12−Rh−P21	95.15(4)
P21−Rh- P22	89.71(4)	P11−Rh−P22	93.21(5)
P11−Rh−P21	156.83(5)	P12−Rh−P22	161.75(5)

The respective conformations of each ligand are also manifested by the P,P coupling constants in the ^{31}P NMR spectra. This is normally governed by the orientation of the lone pairs on the phosphorus atoms with respect to each other and the accompanying dihedral angle.[18] As can be seen from Figure 1, the phospholane moiety in compound **4** adopts a position away from the bulky diphenylphosphane group, so that the two phosphorus atoms are almost anti-periplanar. As a consequence, no P,P coupling constant can

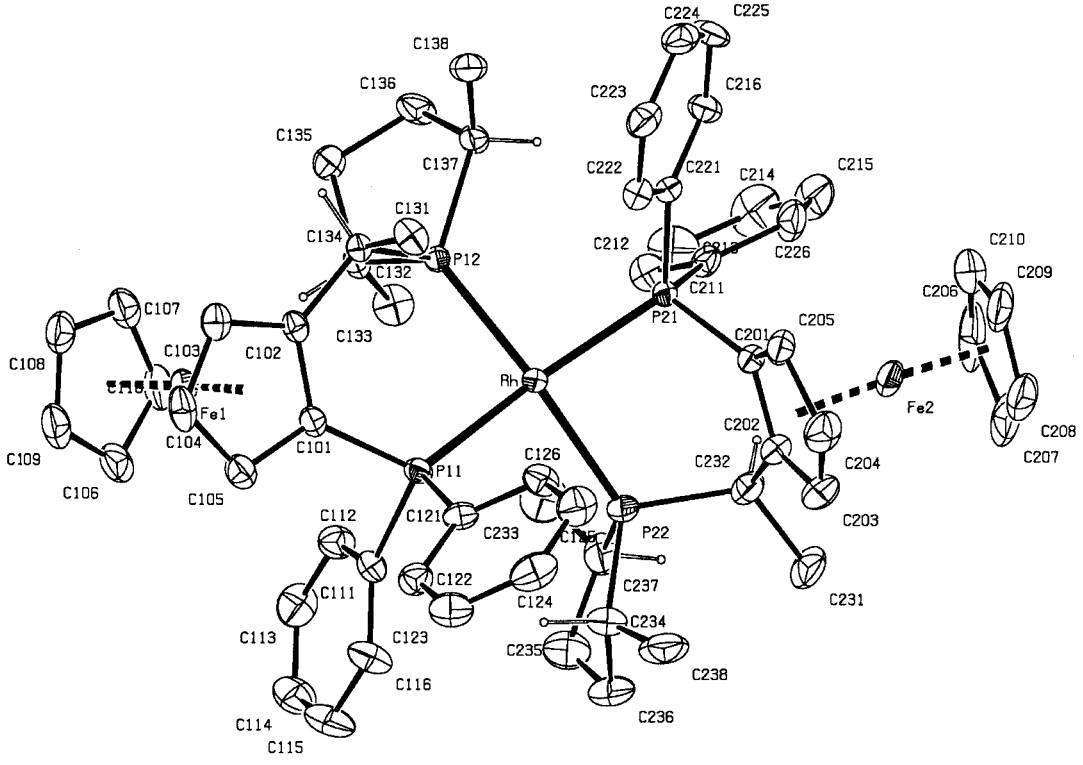

Figure 4. Displacement ellipsoids plot (PLATON[17]) of the cation of **10**; ellipsoids are at the 30% probability level; all H atoms except for those on the asymmetric carbon atoms have been omitted for clarity

 © 2004 Wiley-VCH Verlag GmbH & Co. KGaA, Weinheim

Table 5. Selected distances and angles for **9**

Distances, Å			
Rh−P1	2.2806(8)	Rh−P2	2.2794(8)
Rh−C27	2.215(3)	Rh−C24	2.210(3)
Rh−C28	2.218(3)	Rh−C25	2.220(3)
P1−C5	1.863(3)	P2−C11	1.839(3)
P1−C32	1.853(3)	P2−C12	1.818(3)
P1−C35	1.855(3)	P2−C18	1.814(3)
Angles, deg			
P1−Rh−P2	91.48(3)		
P1−Rh- C27	100.82(8)	P2−Rh−C24	99.58(9)
P1−Rh- C28	98.79(9)	P2−Rh−C25	97.57(8)
C25−Rh−C27	65.25(11)	C24−Rh−C26	53.25(12)

be observed in the ^{31}P NMR spectrum of **4**. In contrast, when the ligand is attached to rhodium, it has to undergo a severe conformational change (as mentioned above). The two phosphorus atoms are now synperiplanar, and consequently the NMR spectrum shows a clear set of two double doublets, revealing a P,P coupling constant of 45.8 Hz ($J_{P,Rh}$ = 150.2 Hz). The same can be said for the chromium ligands: whereas the (*R*,*R*)-diastereomer **5** as the free ligand shows only singlets, a set of two double doublets is observed for its rhodium complex **8**. In contrast, the (*S*,*S*)-diastereomer **6** shows "normal" behaviour in its uncomplexed form, with two doublets and a set of two double doublets in the rhodium complex **9**.

Hydrogenation of Dimethyl Itaconate

For an assessment of the catalytic performance of the ligands, some preliminary hydrogenations were carried out, using dimethyl itaconate as the substrate (Scheme 5). The results are summarized in Table 6.

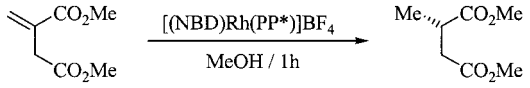

Scheme 5

Table 6. Results of the hydrogenation of itaconate (reaction time = 1 h)

Ligand	Conversion [%]	chemical yield [%]	*ee* [%][a]	Configuration	TOF [1/h]
4	100	100	> 99	*S*	200
5	12	12	25	*S*	24
6	53	53	86	*S*	106

[a] Determined by GC on a Lipodex *E* column at 100 °C.

It should be noted that the experiments were stopped after one hour in order to get an insight into the reaction rate of each ligand, which explains the incomplete conversions in some cases. Taking into account that a relatively high substrate-to-catalyst ratio of 200 was chosen, it can be concluded that the ferrocene ligand **4** is working quite efficiently, whereas its chromium analogues are somewhat slower. It also shows excellent enantioselectivity, whereas the enantiomeric excess is considerably lower for the chromium ligands. It is noteworthy that diastereomer **6** results in a much higher *ee* than diastereomer **5**. This exemplifies vividly that the stereochemical outcome of a catalysis is very sensitive to the steric as well as the electronic features of the employed ligand, because the ferrocene derivative **4** possesses the same stereochemical features as chromium ligand **5**, but a different backbone, whereas the stereochemistry in the backbone of **6** is reversed. (It should be noted that, due to its carbonyl ligands, the chromium tripod is strongly electron-withdrawing, whereas the ferrocene unit is a potent electron donor). In this context it seems desirable to have an analogous ferrocene diastereomer in hand for comparison.

In conclusion, it seems likely that the *ee* value of the product is not governed by the phospholane unit alone, but that the configuration (and nature) of the planar chiral backbone plays an important role as well. More detailed investigations in that respect are currently being carried out.

Conclusion

A novel method for preparing the secondary (*R*,*R*)-dimethylphospholane has been elaborated, making it available in moderate-to-good yields from enantiopure (*S*,*S*)-hexanediol, itself synthesized on a large scale by an improved enzymatic route. The phospholane has been successfully introduced onto ligand scaffolds both of the Daniphos and the Josiphos type. These have been structurally studied in detail by X-ray analyses. Preliminary catalytic studies on the hydrogenation of itaconic acid esters showed encouraging results. Further studies on catalysis employing these ligands are currently under investigation and are due to be published soon.

Experimental Section

General Remarks: All manipulations were carried out under nitrogen using standard Schlenk techniques. Solvents were dried and deoxygenated by standard procedures. Chromatography was carried out with Merck alumina 90. NMR spectra were recorded with Varian Mercury 200 (^1H: 200 MHz, ^{13}C: 50 MHz, ^{31}P: 81 MHz), Varian Unity 500 (^1H: 500 MHz, ^{13}C: 125 MHz, ^{31}P: 202 MHz), Bruker AC 250 (^1H: 250 MHz, ^{13}C: 63 MHz, ^{31}P: 101 MHz) and Bruker AMX 400 (^1H: 400 MHz, ^{13}C: 100 MHz, ^{31}P: 162 MHz) spectrometers at ambient temperature. IR spectra were recorded with a Perkin−Elmer FT-IR model 1720 X spectrometer. Mass spectra were obtained with a Finnigan MAT 95 spectrometer, using CI (with isobutane as the reactant gas) and SIMS recording techniques for the chromium and rhodium complexes, respectively.

(2*S*,5*S*)-Hexanediol and (2*R*,5*R*)-Hexanediol: In a thermostatted vessel (30 °C) glucose (169.2 g, 0.858 mol glucose) was dissolved in distilled water (1.5 L). Baker's yeast (*Saccharomyces cerevisiae*) (271.5 g) was then added portionwise. The pH was adjusted to 6

 © 2004 Wiley-VCH Verlag GmbH & Co. KGaA, Weinheim

with 4 N NaOH, and 2,5-hexanedione (4.63 mL, 25 mmol) added. Quantitative conversion was achieved after 24 h (96% *de*, > 99% *ee*). The biomass was separated by centrifugation (20 min, 5000 *g*). The resulting supernatant liquid was extracted with ethyl acetate (3 L) and the organic phase evaporated. (2*S*,5*S*)-hexanediol crystallized overnight at 4 °C and was recrystallized from 1-octanol (75% yield). For a detailed description of the synthesis of (2*R*,5*R*)-hexanediol see ref.[13]

(2*R*,5*R*)-Dimethylphospholane (2): Ammonia (300 mL) was condensed into a three-necked flask at −78 °C. Sodium (5.4 g, 234 mmol) was added in small portions. Using a slight pressure excess (0.1 bar), PH_3 was added until the solution was saturated (yellow colour). The cyclic sulfate of (2*S*,5*S*)-hexanediol (21.1 g, 117 mmol) was added. After complete evaporation of the ammonia, the residue was dissolved in Et_2O (300 mL) and stirred for two days. The sodium sulfate was then filtered off and washed with Et_2O (100 mL). The solvent was removed by distillation and the remaining residue distilled at ambient pressure. Yield 7.4 g (63.8 mmol, 55%). ^{1}H NMR (C_6D_6): δ = 2.75 (ddd, $J_{P,H}$ = 181.8, $J_{H,H}$ = 11.2, $J_{H,H}$ = 8.9 Hz, 1 H, PH), 2.55−2.45 (m, 1 H, CH), 1.92−1.82 (m, 1 H, CH), 2.05 −1.82 (m, 2 H, CH_2), 1.22−1.02 (m, 2 H, CH_2), 1.10 (dd, $J_{P,H}$ = 17.6, $J_{H,H}$ = 7.6 Hz, 3 H), 1.11 (dd, $J_{P,H}$ 11.4, $J_{H,H}$ = 6.3 Hz, 3 H) ppm. ^{13}C NMR (C_6D_6): δ = 40.75 (d, $J_{P,C}$ = 6.1 Hz, CH_2), 38.70 (d, $J_{P,C}$ = 3.1 Hz, CH_2), 32.46 (d, $J_{P,C}$ = 8.6 Hz, CH), 29.31 (d, $J_{P,C}$ = 6.6 Hz, CH), 21.65 (d, $J_{P,C}$ = 31.0 Hz, CH_3*cis*P(l.p.)], 19.43 (s, CH3*trans*P(l.p.)] ppm. ^{31}P NMR (C_6D_6): δ = −27.7 (d, $^1J_{P,H}$ = 181.1 Hz) ppm.

(2*R*,5*R*)-Dimethylphospholane−BH_3 Adduct: Equimolar amounts of the phospholane **2** and borane−dimethylsulfide complex (10.0 M solution in dimethyl sulfide) were stirred at room temperature for 4 h. All volatile components were then removed in vacuo to provide the adduct (quantitative conversion). ^{1}H NMR (C_6D_6): δ = 4.34 (m, $J_{P,H}$ = 349.3 Hz, PH), 2.71−2.56 (m, 1 H, CH_2−CH_2), 2.29−2.11 (m, 3 H, CH_2−CH_2), 1.48−1.32 (m, 2 H, CH), 1.27 (dd, $J_{P,H}$ = 15.5, $J_{H,H}$ = 6.9 Hz), 1.16 (dd, $J_{P,H}$ = 17.0, $J_{H,H}$ = 7.4 Hz), 0.49 (m, $J_{B,H}$ = 98.0 Hz) ppm. ^{13}C NMR (C_6D_6): δ = 37.04 (d, $J_{P,C}$ = 3.1 Hz, CH_2), 36.79 (s, CH_2), 33.77 (d, $J_{P,C}$ = 36.6 Hz, CH), 28.15 (d, $J_{P,C}$ = 34.6 Hz, CH), 17.52 (d, $J_{P,C}$ = 3.1 Hz, CH_3), 16.04 (d, $J_{P,C}$ = 5.1 Hz, CH_3) ppm. ^{31}P{^{1}H} NMR: δ = 24.0 (d, $J_{P,B}$ = 44.3 Hz) ppm. ^{31}P NMR: δ = 24.0 (d, $J_{P,H}$ = 349.3 Hz) ppm. $C_6H_{16}BP$ (129.97): calcd. C 55.34, H 12.39; found C 53.47, H 12.16.

For convenience, in the following experimental descriptions, the abbreviation "DMP" is used for the structural unit "2,5-dimethylphospholane".

(*R*,*R*)-[(C_5H_5)Fe{C_5H_3(CHMe{(*R*,*R*)-DMP})(PPh_2)}] (4): (*R*,*R*)-2,5-Dimethylphospholane (0.14 g, 1.20 mmol) was added to a stirred solution of (*R*,*R*)-[(C_5H_5)Fe{C_5H_3(CHMeNMe_2)(PPh_2)}] (0.53 g, 1.20 mmol) in glacial acetic acid (7 mL), and heated to 75 °C for 1 h. The solvent was removed in vacuo and the resulting solid was washed with ethanol twice. The pure product was obtained as an orange solid by recrystallization from ethanol. Yield 0.34 g (0.66 mmol, 55%). ^{1}H NMR (500 MHz, C_6D_6): δ = 7.72 (m, 2 H, arom. H), 7.55 (m, 2 H, arom. H), 7.03 (m, 6 H, arom. H), 4.40 (m, 1 H, Cp), 4.19 (m, 2 H, Cp), 3.83 (s, 5 H, Cp), 3.29 (m, 1 H, Fc-C*H*CH_3), 1.90 (m br., 1 H, PC*H*CH_3), 1.76 (dd, $J_{H,H}$ = 6.7, J_{PH} = 16.2 Hz, 3 H, Fc-CHCH_3), 1.44 (m br., 1 H, PC*H*CH_3), 1.40−0.80 (m br., 4 H, CH_2), 1.21 (t, $J_{H,H}$ = 8.1 Hz, 3 H, PCHCH_3), 0.96 (dd, $J_{H,H}$ = 7.0, $J_{P,H}$ = 17.1 Hz, 3 H, PCHCH_3) ppm. ^{13}C NMR (125 MHz, C_6D_6): δ = 135.68, 135.50, 133.49, 133.34, 129.14 (PPh_2), 70.21 (*Cp*), 69.64 (*Cp*), 69.12 (CpC_{ipso}), 36.63 (*Me*-Phospholane), 36.49 (*Me*-Phospholane), 34.85 (CH_2), 31.68 (CH_2), 25.43 [d, $J_{C,P}$ = 31.3 Hz, PCH(Me)CH_2], 24.27 [d, $J_{C,P}$ = 14.2 Hz, PCH(Me)CH_2], 21.13 (d, $J_{C,P}$ = 13.7 Hz, CHMe), 14.33 (CH*Me*) ppm. ^{31}P NMR (80 MHz, C_6D_6): δ = 20.22 (α-P), −30.49 (*ortho*-P) ppm. $C_{30}H_{34}FeP_2$ (512.4): calcd. C 70.32, H 6.69; found C 69.95, H 6.67.

General Procedure for the Synthesis of the Chromium Tricarbonyl Ligands 5 and 6: (*R*,*R*)-2,5-Dimethylphospholane (1 equiv.) was added to a stirred solution of the appropriate chloride-substituted chromium complex[8,10] (1 equiv.) in dry acetone (20 mL/mmol). Subsequently, $TlPF_6$ (1 equiv.), dissolved in 20 mL/mmol of acetone, was added dropwise over a period of one hour with an automatic syringe. The reaction mixture was stirred overnight at ambient temperature, quenched by adding NEt_3, filtered, evaporated and subjected to column chromatography (Al_2O_3, pentane followed by Et_2O).

[η^6-(*R*,*R*)-{[(*R*,*R*)-DMP]CHMe}$C_6H_4PPh_2$]Cr(CO)$_3$ (5'): Compound **5** was made from (*R*,*R*)-2,5-dimethylphospholane (0.25 g, 2.15 mmol), [η^6-(*R*,*R*)-{(Cl)CHMe}$C_6H_4PPh_2$]Cr(CO)$_3$ (0.99 g, 2.15 mmol) and $TlPF_6$ (0.71 g, 2.04 mmol) according to the general procedure described above. Yield: 0.93 g (1.72 mmol, 80%). ^{1}H NMR (500 MHz, C_6D_6): δ = 7.63−7.53 [m, 2 H, $H_{ar.}$(PPh_2)], 7.43−7.34 [m, 2 H, $H_{ar.}$ (PPh_2)], 7.14−6.99 [m, 6 H, $H_{ar.}$(PPh_2)], 5.17 (ddt, $J_{H,H}$ = 6.5, $J_{H,P}$ = 3.2, $J_{H,H}$ = 1.1 Hz, 1 H, $H_{ar.}$), 4.69 (dt, *J* = 6.1, *J* = 1.3 Hz, $H_{ar.}$), 4.52 (t, *J* = 6.5 Hz, $H_{ar.}$), 4.29 (td, *J* = 6.3, *J* = 1.1 Hz, $H_{ar.}$), 3.64 (sext, *J* = 6.7, *J* = 1.1 Hz, 1 H, C*H*Me), 1.77 [m, 1 H, PC*H*(Me)CH_2], 1.63 (dd, $J_{H,P}$ = 15.6, $J_{H,H}$ = 6.8 Hz, 3 H, CH*Me*), 1.42−1.34 (m br., 2 H, CH_2), 1.20 [m, 1 H, PC*H*(Me)CH_2], 0.95 [dt, *J* = 8.1, *J* = 1.5 Hz, 3 H, PCH(*Me*)CH_2], 0.77 (d, *J* = 7.0 Hz, *J* = 17.0 Hz, 3 H, PCH(*Me*)CH_2], 0.58 (m, 1 H, CH_2), 0.48 (m, 1 H, CH_2) ppm. ^{13}C NMR (125 MHz, C_6D_6): δ = 233.18 (*C*O), 135.24−127.12 [12 C, $C_{ar.}$(PPh_2)], 127.54 (d, *J* = 21.1 Hz, $C_{ipso,ar.}$), 104.53 (d, *J* = 20.1 Hz, $C_{ipso,ar.}$), 96.32 (d, *J* = 2.0 Hz, $C_{ar.}$), 92.95 (dd, $^2J_{C,P}$ = 15.4, $^4J_{C,P}$ = 3.8 Hz, $C_{ar.}$), 92.55 ($C_{ar.}$), 91.55 ($C_{ar.}$), 37.49 (d, *J* = 2.9 Hz, CH_2), 36.44 (s, CH_2), 36.28 (d, *J* = 17.2 Hz, *Me*-phospholane), 34.26 (d, *J* = 12.4 Hz, *Me*-phospholane), 24.85 [d, *J* = 28.8 Hz, PC*H*(Me)CH_2], 20.82 [d, *J* = 36.1 Hz, PC*H*(Me)CH_2], 15.19 (*C*HMe), 5.67 (CH*Me*) ppm. ^{31}P NMR (80 MHz, C_6D_6): δ = 29.16 (s, α-P), −20.63 (s, *ortho*-P) ppm. IR (C_6D_6): ν_{CO} = 1967, 1893 cm^{-1}. $C_{29}H_{30}CrO_3P_2$ (540.5): calcd. C 64.44, H 5.59; found C 64.22, H 5.69.

[η^6-(*S*,*S*)-{[(*R*,*R*)-DMP]CHMe}$C_6H_4PPh_2$]Cr(CO)$_3$ (6): Compound **6** was made from (*R*,*R*)-2,5-dimethylphospholane (0.227 g, 1.953 mmol), [η^6-(*S*,*S*)-{(Cl)CHMe}$C_6H_4PPh_2$]Cr(CO)$_3$ (0.90 g, 1.953 mmol) and $TlPF_6$ (0.648 g, 1.855 mmol) according to the general procedure described above. Yield: 1.01 g (1.77 mmol, 96%). ^{1}H NMR (500 MHz, C_6D_6): δ = 7.64 [m, 2 H, $H_{ar.}$ (PPh_2)], 7.42 [m, 2 H, $H_{ar.}$ (PPh_2)], 7.15−7.05 [m, 6 H, $H_{ar.}$ (PPh_2)], 4.87 (dt, *J* = 6.1, *J* = 1.2 Hz, $H_{ar.}$), 4.63 (t, *J* = 6.4 Hz, $H_{ar.}$), 4.56 (m, 1 H, $H_{ar.}$), 4.26 (dt, *J* = 6.4, *J* = 0.9 Hz, $H_{ar.}$), 4.01 (q, *J* = 7.0 Hz, 1 H, C*H*Me), 1.91 [m, 1 H, PC*H*(Me)CH_2], 1.74 [m, 1 H, PC*H*(Me)CH_2], 1.62 (m, 1 H, CH_2), 1.50 (m, 1 H, CH_2), 1.41 (m, 1 H, CH_2), 1.33 (dd, *J* = 7.0, *J* = 4.0 Hz, 3 H, CH*Me*), 1.00 [PCH(*Me*)CH_2], 0.96 [PCH(*Me*)CH_2], 0.82 (m, 1 H, CH_2) ppm. ^{13}C NMR (125 MHz, C_6D_6): δ = 233.10 (*C*O), 136.58 [d, *J* = 6.5 Hz, $C_{ipso,ar.}$(PPh_2)], 136.36 [d, *J* = 13.7 Hz, $C_{ipso,ar.}$(PPh_2)], 135.26−125.30 (10 C, P*Ph*$_2$), 127.00 (d, *J* = 23.0 Hz, $C_{ipso,ar.}$), 103.62 (d, *J* = 17.5 Hz, $C_{ipso,ar.}$), 98.74 ($C_{ar.}$), 93.80 ($C_{ar.}$), 90.23 ($C_{ar.}$), 88.45 (dd, *J* = 6.9 Hz; *J* = 3.6 Hz, $C_{ar.}$), 37.80 (d, *J* = 3.8 Hz, CH_2), 36.95 (s, CH_2), 35.65 [d, *J* = 18.1 Hz, PC*H*(Me)CH_2], 30.65 [d, *J* = 18.7 Hz, PC*H*(Me)CH_2], 21.50 [PCH(*Me*)CH_2], 21.23 [PCH(*Me*)CH_2], 18.18 (*C*HMe), 14.78 (CH*Me*) ppm. ^{31}P NMR

 © 2004 Wiley-VCH Verlag GmbH & Co. KGaA, Weinheim

(80 MHz, C_6D_6): δ = 19.96 (d, $J_{P,P}$ = 20.1 Hz, α-P), −18.99 (d, $J_{P,P}$ = 20.1 Hz, *ortho*-P) ppm. IR (C_6D_6): $\tilde{\nu}_{CO}$ = 1968, 1898 cm^{-1}. $C_{29}H_{30}CrO_3P_2$ (540.5): calcd. C 64.44, H 5.59; found C 64.25, H 5.71.

General Procedure for the Synthesis of the Rhodium Complexes: $[NBDRhCl]_2$ (1 equiv.) and $AgBF_4$ (2 equiv.) were dissolved in THF (10 mL) in a Schlenk flask and the solution was stirred vigorously for 30 minutes at ambient temperature. The clear solution was removed from the precipitated AgCl by a syringe equipped with a filter needle, and dripped into a solution of the diphosphane (2 equiv.) in THF (5 mL). After stirring for 10 minutes, the product [(diene)Rh(PP*)]BF_4 was precipitated by adding Et_2O. The ethereal solution was discarded and the solid dried in vacuo.

[(NBD)Rh{(*R*,*R*)-(C_5H_5)Fe[C_5H_3(CHMe{(*R*,*R*)-DMP})(PPh_2)]}]-BF_4 (7): Compound **7** was obtained by treating complex **4** (44 mg, 0.085 mmol) with $[NBDRhCl]_2$ (20 mg, 0.043 mmol) and $AgBF_4$ (17 mg, 0.085 mmol), according to the general procedure described above. Yield: 50 mg (0.063 mmol, 74%). ^{31}P NMR (200 MHz, $CDCl_3$): δ = 61.03 (dd, $J_{P,P}$ = 45.8, $J_{P,Rh}$ = 150.2 Hz, α-P), 20.08 (dd, $J_{P,P}$ = 45.8, $J_{P,Rh}$ = 150.2 Hz, *ortho*-P) ppm. MS (SIMS): *m*/*z* (rel. int.) = 86.8 (100) $[BF_4]^-$, 707.5 (3.2) [(NBD)-Rh{(*R*,*R*)-(C_5H_5)Fe[C_5H_3(CHMe{(*R*,*R*)-DMP})(PPh_2)]}]$^+$.

[(NBD)Rh{[η^6-(*R*,*R*)-{[(*R*,*R*)-DMP]CHMe}$C_6H_4PPh_2$]Cr($CO)_3$}]-BF_4 (8): Compound **8** was obtained by treating complex **5** (125 mg, 0.232 mmol) with $[NBDRhCl]_2$ (53 mg, 0.116 mmol) and $AgBF_4$ (45 mg, 0.232 mmol), according to the general procedure described above. Yield: 122 mg (0.150 mmol, 64%). ^{31}P NMR (200 MHz, $CDCl_3$): δ = 68.92 (dd, $J_{P,P}$ = 38.5, $J_{P,Rh}$ = 130.0 Hz, α-P), 30.87 (dd, $J_{P,P}$ = 38.5, $J_{P,Rh}$ = 130.0 Hz, *ortho*-P) ppm. MS (SIMS): *m*/*z* (rel. int.) = 86.9 (100) $[BF_4]^-$, 734.8 (8.0) [(NBD)Rh{[η^6-(*R*,*R*)-{[(*R*,*R*)-DMP]CHMe}$C_6H_4PPh_2$]Cr($CO)_3$}]$^+$.

[(NBD)Rh{[η^6-(*S*,*S*)-{[(*R*,*R*)-DMP]CHMe}$C_6H_4PPh_2$]Cr($CO)_3$}]-BF_4 (9): Compound **9** was obtained by treating complex **6** (140 mg, 0.260 mmol) with $[NBDRhCl]_2$ (60 mg, 0.130 mmol) and $AgBF_4$ (51 mg, 0.260 mmol), according to the general procedure described above. Yield: 130 mg (0.160 mmol, 61%). ^{31}P NMR (200 MHz, $CDCl_3$): δ = 61.07 (dd, $J_{P,P}$ = 43.0, $J_{P,Rh}$ = 156.6 Hz, α-P), 28.66 (dd, $J_{P,P}$ = 43.0, $J_{P,Rh}$ = 156.6 Hz, *ortho*-P) ppm. MS (SIMS): *m*/*z* (rel. int.) = 87.0 (100) $[BF_4]^-$, 734.8 (20) [(NBD)Rh{[η^6-(*S*,*S*)-{[(*R*,*R*)-DMP]CHMe}$C_6H_4PPh_2$]Cr($CO)_3$}]$^+$.

{(*R*,*R*)-[C_5H_5]Fe[C_5H_3(CHMe{(*R*,*R*)-DMP})(PPh_2)]}$_2BF_4$ (10): Compound **10** was obtained by treating complex **4** (30.0 mg, 0.0586 mmol) with $[(NBD)_2Rh]BF_4$ (11.0 mg, 0.0293), according to the general procedure described above. Recrystallization from MeOH afforded single crystals suitable for X-ray diffraction.

Hydrogenation of Dimethyl Itaconate: Hydrogenations were carried out by putting a weighed amount of the [(NBD)Rh(PP*)]BF_4 complex (approx. 3 mg) in a glass vial and adding (under argon) the appropriate amount of a stock solution of the substrate in methanol (0.25 mmol/mL), in order to give a substrate-to-catalyst ratio of 200. After purging with hydrogen three times, the reaction was left to run for one hour.

X-ray Crystallographic Study: Single crystals suitable for X-ray analyses were grown from dry methanol. Crystal data and details of the structure determination are listed in Table 7. Data set for **4** was collected with an Enraf Nonius CAD4 diffractometer (Mo-K_α radiation, λ = 0.71073 Å, graphite monochromator). The unit cell parameters were obtained by the least-squares refinement of 25 re-

Table 7. Crystallographic data for compounds **4**, **7**, **9** and **10**

Compound	**4**	**7**	**10**	**9**
Empirical formula	$C_{30}H_{34}P_2Fe$	$[C_{37}H_{42}P_2FeRh]BF_4$	$[C_{60}H_{68}Fe_2P_4Rh]BF_4$	$[C_{36}H_{38}O_3P_2CrRh]$ BF_4·CH_3OH
Formula mass	512.36	794.22	1214.44	854.37
Crystal habit, color	blocks, orange	blocks, red	blocks, red	rods, cognac
Crystal dimensions (mm)	0.4 × 0.32 × 0.2	0.51 × 0.32 × 0.16	0.32 × 0.23 × 0.2	0.41 × 0.1 × 0.04
Crystal system	monoclinic	monoclinic	orthorhombic	orthorhombic
Space Group	$P2_1$	$P2_1$	$P2_12_12_1$	$P2_12_12_1$
a (Å)	8.594(3)	9.614(3)	15.1856(19)	10.7121(10)
b (Å)	10.830(3)	17.084(4)	15.692(2)	12.6034(12)
c (Å)	14.631(4)	10.950(3)	25.684(3)	26.471(2)
β [°]	102.78(2)	104.545(8)	90.00	90.00
V (Å^3)	1328.1(7)	1740.8(8)	6120.4(13)	3573.9(6)
Z	2	2	4	4
D [g·cm^{-1}]	1.281	1.515	1.318	1.588
*F*000	540	812	2504	1744
μ (Mo-K_α) [cm^{-1}]	0.704	1.030	0.886	0.916
Diffractometer	Enraf−Nonius CAD4	Bruker−Smart CCD	Bruker−Smart CCD	Bruker−Smart CCD
T [K]	221(2)	293(2)	293(2)	110(2)
θ range	2.36−26.90	2.19−28.27	2.05−28.46	1.79−28.37
Reflections collected	7812	23873	85295	49337
Unique reflections	5773	8499	15370	8912
R_{int}	0.0284	0.0226	0.0715	0.0662
Reflections used	4429	8202	14441	8912
Parameters refined	301	418	655	459
R_1	0.0451	0.0347	0.0615	0.0339
wR_2	0.0910	0.0868	0.1546	0.0744
Flack's parameter	−0.008(16)	−0.012(15)	0.04(2)	0.001(17)
GooF	1.003	1.105	1.258	1.013
Diff. peak/ hole [e/Å^3]	0.29/−0.20	0.69/−0.40	1.35/−0.70	0.79/−0.34

 © 2004 Wiley-VCH Verlag GmbH & Co. KGaA, Weinheim

flections. The data collection for **7**, **9** and **10** was performed with a Bruker Smart CCD (Mo-K_α radiation, λ= 0.71073 Å, graphite monochromator) area detector. The unit cell parameters were obtained by the least-squares refinement of 8096 reflections. All structures were solved by direct methods (SHELXS-97)[19] and refined by full-matrix least-squares procedures based on F^2 with all measured reflections (SHELXL-97.[19] The SADABS[20] program was used for absorption correction of the structures **7**, **9** and **10**. All non-hydrogen atoms were refined anisotropically. All H atom positions were introduced at their idealized positions (d_{C-H} = 0.96 Å) and were refined using a riding model. The absolute configuration was confirmed by evaluation of the Flack[21] parameter. CCDC-217865, -217866, -217867 and -21786 contain the supplementary crystallographic data for this paper. These data can be obtained free of charge at www.ccdc.cam.ac.uk/conts/retrieving.html [or from the Cambridge Crystallographic Data Centre, 12 Union Road, Cambridge CB2 1EZ, UK; Fax: (internat.) + 44-1223-336-033; E-mail: deposit@ccdc.cam.ac.uk].

Acknowledgments

The authors wish to gratefully acknowledge financial support by the Deutsche Forschungsgemeinschaft DFG within the Collaborative Research Centre (SFB, 380) "Asymmetric Synthesis with Chemical and Biological Methods" and by the "Fonds der Chemischen Industrie". We thank Dr. Felix Spindler of Solvias for his help with the catalytic experiments. B. C. is grateful to the Graduiertenkolleg: "Methods of Asymmetric Synthesis" for a scholarship.

[1] W. S. Knowles, *Adv. Synth. Catal.* **2003**, *345*, 3; R. Noyori, *Adv. Synth. Catal.* **2003**, *345*, 15; W. S. Knowles, *Angew. Chem. Int. Ed.* **2002**, *41*, 1998; R. Noyori, *Angew. Chem. Int. Ed.* **2002**, *41*, 2008; K. B. Sharpless, *Angew. Chem. Int. Ed.* **2002**, *41*, 2024.
[2] M. J. Burk, in *Handbook of Chiral Ligands*, Marcel Dekker, New York, **1999**, 339.
[3] M. J. Burk, *Acc. Chem. Res.* **2000**, *33*, 363.
[4] H. U. Blaser, *Adv. Synth. Catal.* **2002**, *344*, 17.
[5] H. U. Blaser, W. Brieden, B. Pugin, F. Spindler, M. Studer, A. Togni, *Top. Catal.* **2002**, *19*, 3.
[6] U. Englert, A. Salzer, D. Vasen, *Tetrahedron: Asymmetry* **1998**, *9*, 1867.
[7] U. Englert, R. Haerter, D. Vasen, A. Salzer, E. B. Eggeling, D. Vogt, *Organometallics* **1999**, *18*, 4390.
[8] D. Vasen, A. Salzer, F. Gerhards, H. J. Gais, R. Stürmer, N. H. Bieler, A. Togni, *Organometallics* **2000**, *19*, 539.
[9] A. Salzer, *Coord. Chem. Rev.* **2003**, *242*, 59.
[10] W. Braun, A. Salzer, H.-J. Drexler, A. Spannenberg, D. Heller, *J. Chem. Soc., Dalton Trans.* **2003**, 1606.
[11] For recent examples see: [11a] L. Dahlenburg, *Eur. J. Inorg. Chem.* **2003**, *15*, 2733. [11b] M. Dieguez, A. Ruiz, C. Claver, *J. Chem. Soc., Dalton Transactions* **2003**, *15*, 2957. [11c] M. P. Sibi, R. Zhang, S. Manyem, *J. Am. Chem. Soc.* **2003**, *125*, 9306. [11d] S. Ferrer, M. Pasto, B. Rodriguez, A. Riera, M. A. Pericas, *Tetrahedron: Asymmetry* **2003**, *14*, 1747. [11e] J. I. van der Vlugt, J. M. Bonet, A. M. Mills, A. L. Spek, D. Vogt, *Tetrahedron Lett.* **2003**, *4*, 4389. [11f] C. Jimeno, M. Pasto, A. Riera, M. Pericas, *J. Org. Chem.* **2003**, *68*, 3130. [11g] J. F. Jensen, I. Sotofte, H. O. Sorensen, M. Johannsen, *J. Org. Chem.* **2003**, *68*, 1258. [11h] L. J. Goossen, *Angew. Chem. Int. Ed.* **2002**, *41*, 3775. [11i] V. Cesar, S. Bellemin-Laponnaz, L. H. Gade, *Organometallics* **2002**, *21*, 5204. [11j] F. Blume, S. Zemolka, T. Fey, R. Kranich, H.-G. Schmalz, *Adv. Synth. Cat.* **2002**, *344(8)*, 868. [11k] M. C. Perry, X. Cui, K. Burgess, *Tetrahedron: Asymmetry* **2002**, *13*, 1969. [11l] S. Bellemin-Laponnaz, L. H. Gade, *Angew. Chem. Int. Ed.* **2002**, *41*, 3473. [11m] M. A. Pericas, C. Puigjaner, A. Riera, A. Vidal-Ferran, M. Gomez, F. Jimenez, G. Muller, M. Rocamora, *Chem. Eur. J.* **2002**, *8*, 4164. [11n] I. M. Pastor, P. Vaestilae, H. Adolfsson, *Chem. Commun.* **2002**, *18*, 2046. [11o] M. Pasto, A. Riera, M. A. Pericas, *Eur. J. Org. Chem.* **2002**, *14*, 2337. [11p] I. J. S. Fairlamb, *Synlett* **2002**, *7*, 1176. [11q] M. Dieguez, A. Ruiz, C. Claver, *J. Org. Chem.* **2002**, *67*, 3796. [11r] M. Dieguez, O. Pamies, A. Ruiz, C. Claver, *Tetrahedron: Asymmetry* **2002**, *13*, 83. [11s] P. I. Dalko, L. Moisan, J. Cossy, *Angew. Chem. Int. Ed.* **2002**, *41*, 625. [11t] I. M. Pastor, H. Adolfsson, *Tetrahedron Lett.* **2002**, *43*, 1743. [11u] J. Blankenstein, A. Pfaltz, *Angew. Chem. Int. Ed.* **2001**, *40*, 4445.
[12] M. J. Burk, A. Pizzano, J. A. Martin, L. M. Liable-Sands, A. L. Rheingold, *Organometalics* **2000**, *19*, 250.
[13] [13a] J. Haberland, W. Hummel, T. Daussmann, A. Liese, *Org. Process. Res. Dev.* **2002**, *6*, 458. [13b] J. Haberland, A. Kriegesmann, E. Wolfram, W. Hummel, A. Liese, *Appl. Microbiol. Biotechnol.* **2002**, *58*, 595. [13c] Jülich Fine Chemicals GmbH, Rudolf-Schulten-Straße 5, 52428 Jülich, Germany; www.juelich-chemicals.de.
[14] [14a] M. J. Burk, J. E. Feaster, R. L. Harlow, *Organometallics* **1990**, *9*, 2653. [14b] M. J. Burk, J. E. Feaster, R. L. Harlow, *Tetrahedron: Asymmetry* **1991**, *2*, 569.
[15] J. Holz, A. Monsees, H. Jiao, J. You, I. Kamarov, C. Fischer, K. Drauz, A. Börner, *J. Org. Chem.* **2003**, *68*, 1701.
[16] A. Togni, C. Breutel, A. Schnyder, F. Spindler, H. Landert, A. Tijani, *J. Am. Chem. Soc.* **1994**, *116*, 4062.
[17] A. L. Spek, *Acta Crystallogr., Sect. A* **1990**, *46*, C-34.
[18] [18a] R. H. Contreras, J. E. Peralta, *Prog. Nucl. Magn. Reson. Spectrosc.* **2000**, *37*, 321. [18b] J. Hahn in *Phosphorus-31 NMR Spectroscopy in Stereochemical Analysis* (Ed.: J. G. Verkade, L. D. Quinn), VCH Publishers Inc., Deerfield Beach, **1987**, 331. [18c] L. D. Quinn in ref.[18b], pp. 417.
[19] G. M. Sheldrick, SHELXS-97 and SHELXL-97, University of Göttingen, Germany.
[20] G. M. Sheldrick, SADABS, **1996**, University of Göttingen, Germany.
[21] H. D. Flack, *Acta Crystallogr., Sect. A* **1983**, *39*, 876−881.

Received September 30, 2003
Early View Article
Published Online April 1, 2004

 © 2004 Wiley-VCH Verlag GmbH & Co. KGaA, Weinheim

A New Route to Cationic Half-Sandwich Ruthenium(II) Complexes with Chiral Cyclopentadienylphosphane Ligands

Angelino Doppiu[a] and Albrecht Salzer*[a]

Keywords: Asymmetric catalysis / Constrained geometry ligands / Cyclopentadienyl ligands / P ligands / Ruthenium

Optically active cyclopentadienyl-linked phosphane ligands L_n of general formula $C_5H_5CH_2CH(R)PR'_2$ (R = Ph, R′ = Ph, L_1; R = Ph, R′ = Cy, L_2; R = mesityl, R′ = Ph, L_3) and $C_5H_5CH(R)CH_2PPh_2$ (R = Cy, L_4; R = Bzl, L_5) are synthesised by ring-opening reactions of 1-R-spiro[2.4]hepta-4,6-dienes (R = Ph, Cy, mesityl, benzyl), with lithium phosphides $LiPR'_2$ (Ar = Ph, Cy). Reaction of the ligands L_n with $[RuH(\eta^5\text{-}C_7H_{11})_2][BF_4]$ in acetonitrile at reflux affords the bis(acetonitrile) ruthenium(II) complexes $[Ru(\eta^5\text{-}C_5H_4(C_2H_3R)PR'_2\text{-}\kappa P)(CH_3CN)_2][BF_4]$, in which the ligands are coordinated to the metal through the cyclopentadienyl and the phosphane moieties forming a chelate, in almost quantitative yields. The complexes are active catalysts in the redox isomerisation of geraniol affording chiral citronellal but with low enantioselectivity. They also catalyze an aldol-type C–C coupling reaction between 3-buten-2-ol and benzaldehyde affording almost racemic 4-hydroxy-3-methyl-4-phenyl-2-butanone with good diastereoselectivity (*syn*/*anti* ratio up to 77:23).
(© Wiley-VCH Verlag GmbH & Co. KGaA, 69451 Weinheim, Germany, 2004)

Introduction

Organometallic ruthenium complexes are becoming increasingly important in homogeneous catalyses such as reduction, oxidation, isomerisation, and carbon−carbon bond-formation.[1] The preparation of the necessary ruthenium catalysts most often starts from $RuCl_3{\cdot}nH_2O$, $[Ru(H_2O)_6]^{2+}$, $[RuCl_2(PPh_3)_3]$, $[RuCl_2(COD)]_n$, or $[RuCl_2(cymene)]_n$.[2] Analogously, the chemistry of cyclopentadienylruthenium complexes is based on few starting materials, mainly on the readily available precursors $[Ru(Cp)Cl(PPh_3)_2]$ and $[Ru(Cp)Cl(CO)_2]$.[2] However, the selective replacement of either PPh_3 or CO has proved difficult, limiting the synthetic utility. Coordinatively unsaturated complexes and complexes with labile ligands are the most promising candidates for catalytic applications, since the availability of a vacant coordination site is a prerequisite for both stoichiometric and catalytic organic transformations at the transition metal centre. Therefore, more labile systems, including $[Ru(Cp)(CH_3CN)_3]^+$,[3] and [Ru(Cp)Cl(COD)],[4] have been developed. In particular, the cationic complex $[Ru(Cp)(CH_3CN)_3]^+$ is a promising versatile intermediate since the acetonitrile ligands (AN) are substitutionally labile and can be replaced by other ligands.[5,6] This complex can be regarded as a source of the highly active coordinatively unsaturated fragment $[Ru(Cp)]^+$, which may well have interesting potential in catalysis. Indeed, several C−C bond-forming reactions catalysed by this compound have been reported by Trost.[7] Kirchner has shown that substitution of one acetonitrile ligand in $[Ru(Cp)(AN)_3]^+$ for tertiary phosphanes PR_3 $[Ru(Cp)(AN)_2(PR_3)]^+$ [8a] also gave a very active catalyst for the redox isomerisation of allylic alcohols,[8b] and C−C bond-formation.[8c−8l] Various attempts have been made to link the Cp and phosphorus moieties in such compounds through a spacer. In almost all cases, these complexes contain a PPh_3 ligand, as the synthesis, starting from $[RuCl_2(PPh_3)_3]$, gives no alternate choice.[9] Only in one case could bis(acetonitrile) complexes be isolated by Takahashi in which the linker connects through an ester group at the cyclopentadienyl ligand.[10] These complexes were tested in catalytic allylic amination and alkylation with excellent results.[11] Prompted by the results of Kirchner and Takahashi, we endeavoured to develop a synthetic route to $[Ru(Cp{-}P)(AN)_2]^+$-type chiral complexes containing a phosphane ligand tethered onto the cyclopentadienyl ring via a two-carbon linker (Cp−P). We have recently reported a route to such complexes,[12] and we have shown, in collaboration with Kirchner, that they react with alkynes displaying unusual reactivity.[13] Here we report on an improved method that affords the desired optically active ruthenium(II) complexes in almost quantitative yields, as well as a preliminary account of their application in catalytic organic transformations.

Results and Discussion

Synthesis of the Ligands

When we started our research, there was a dearth of general procedures to prepare chiral Cp−P ligands by a

[a] Institut für Anorganische Chemie der RWTH Aachen, Professor Pirlet Strasse 1, 52056, Aachen, Germany
Fax: (internat.) +49-(0)241/809-2288
E-mail: albrecht.salzer@ac.rwth-aachen.de

 © 2004 Wiley-VCH Verlag GmbH & Co. KGaA, Weinheim DOI: 10.1002/ejic.200300934

method that allows their modular construction by independent variation of the three components, namely the cyclopentadienyl, the linker, and the phosphane.[9] We have developed such a route by adapting the method first reported by Kauffmann,[14] which is based on the ring-opening reactions of spiro[2.4]hepta-4,6-dienes.[15] Traditionally, the spiro compounds have been synthesised by bis-alkylation of cyclopentadiene with the corresponding dibromoalkane in the presence of sodium amide or sodium hydride.[16] However, a more convenient approach to introduce chirality into these spiroannulated precursors is the use of the corresponding bis(mesylate)s or bis(tosylate)s as alkylating reagents. Rieger has used this route to synthesise ethyl-bridged bis(cyclopentadienyl) ligands starting from styrene epoxide.[17] The same approach was recently adopted by Whitby for the synthesis of chiral indenyl-linked phosphane ligands.[18] Our synthetic strategy is based on the use of chiral vicinal diols as starting materials, as depicted in Scheme 1. The chiral diols can be obtained in high enantiomeric purity by several methods, for example Sharpless asymmetric dihydroxylation,[19] Jacobsen hydrolytic kinetic resolution of epoxides,[20] and biological means. They are easily converted into the bis(methanesulfonate) esters in almost quantitative yield by reaction with methanesulfonyl chloride. Displacement of the methanesulfonate groups by excess cyclopentadiene/sodium amide affords the spiroannulated dienes in excellent yields (79−95%). The formation of the spiro compound involves first a nucleophilic substitution of one mesylate group by the cyclopentadienyl anion, followed by a fast deprotonation of the resulting substituted cyclopentadiene, and finally a second nucleophilic substitution of the other mesylate group and ring closure. The nucleophilic substitution at the chiral carbon is entirely stereoselective and proceeds with complete inversion of configuration at the stereogenic centre.[15] The chiral spiro compounds that have been synthesised by this methodology are shown in Scheme 2.

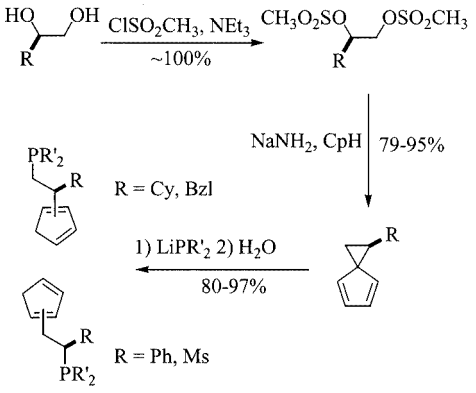

Scheme 1

The ring-opening reaction of (*S*)-1-R-spiro[2.4]hepta-4,6-dienes (R = phenyl, mesityl) with lithium diphenylphosphide or lithium dicyclohexylphosphide proceeds with complete regiospecificity by attack of the nucleophile at the activated benzylic position of the cyclopropane ring affording the ligands L_{1-3}. Interestingly, this regioselectivity is the opposite to that found for the nucleophilic opening of phenyl epoxide and phenyl episulfide with lithium phosphides; in that context, the attack of the nucleophile proceeds regioselectively at the less-hindered site.[21] The ring-opening reaction proceeds with complete inversion of the configuration at the stereogenic centre, as is demonstrated by X-ray crystal structure determinations of some derived metal complexes.[12,15] The opposite regioselectivity is observed in the ring-opening reaction of (*R*)-1-benzylspiro[2.4]hepta-4,6-diene and (*S*)-1-cyclohexylspiro[2.4]hepta-4,6-diene, which lack the activated benzylic position in the cyclopropane ring. In this case, the nucleophilic attack with lithium diphenylphosphide occurs on the unsubstituted carbon atom of the cyclopropane ring, affording the ligands L_4 and L_5.[22] The same regioselectivity has been observed in the ring-opening of 2-cyclohexylspiro(cyclopropane-1,1′-indene).[18] For convenience of storage, the lithium salts of the ligands can be reacted with H_2O to afford the cyclopentadienyl(alkyl)phosphanes as a mixture of two positional isomers depending on to which olefinic carbon atom of the Cp the linker is attached. The ligands are shown in Scheme 3. The overall yields for three steps (starting from the diols) are excellent (63 to 88%).

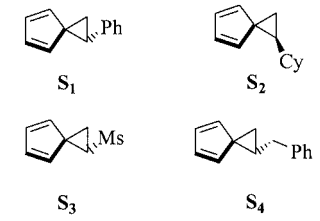

Scheme 2

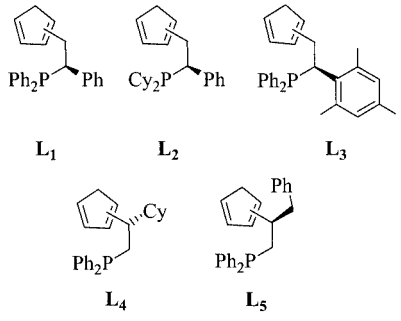

Scheme 3

Synthesis of the Ruthenium Complexes

We have recently reported that reaction of $[RuCl_2(\eta^3{:}\eta^3\text{-}C_{10}H_{16})]_2$ with the Cp-linked phosphane ligand L_1 in a 1:2 ratio in a mixture of acetonitrile and ethanol at room temperature, in the presence of Li_2CO_3 and KPF_6, affords the cationic complex $[Ru(\eta^5\text{-}C_5H_4CH_2CH(Ph)PPh_2\text{-}\kappa P)(AN)_2][PF_6]$ in 70−75% yield.[12] However, apart from the desired compound, side products were also formed that have not been identified yet. The purification of the desired

 © 2004 Wiley-VCH Verlag GmbH & Co. KGaA, Weinheim

complex was accomplished by a cumbersome crystallisation step. Therefore, we sought for a better synthetic route. A paper from Cox and Roulet provided inspiration for a new method.[23] The paper reports: "Dissolution of complex **1** in deoxygenated acetonitrile leads to rapid displacement of one molar equiv. of 2,4-dimethylpenta-1,3-diene and formation of the cation $[Ru(\eta^5\text{-}C_7H_{11})(AN)_3]^+$". [Bis($\eta^5$-2,4-dimethylpentadienyl)hydridoruthenium] tetrafluoroborate (**1**) is known to show a fluxional behaviour, as the hydrido ligand is involved in three-centre Ru−H−C agostic interactions with all terminal methylene groups of the dimethylpentadienyl ligands (Scheme 4).[24]

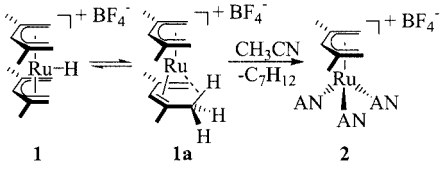

Scheme 4

The species **1a**, which is in equilibrium with **1**, is highly reactive towards two-electron ligands, and the η^4-C_7H_{12} ligand is substitutionally labile, as it is easily replaced by acetonitrile. We performed the reaction between L_1 and $[Ru(\eta^5\text{-}C_7H_{11})_2H][BF_4]$, and we were delighted to obtain the pure bis(acetonitrile) complex **Ru$_1$** in almost quantitative yield (Scheme 5).

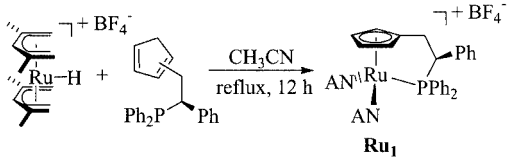

Scheme 5

A possible reaction mechanism that accounts for the formation of **Ru$_1$** is presented in Scheme 6. At first, **2** may be formed, with subsequent coordination of phosphorus to afford **3**. The reaction has been followed by means of a ^{31}P NMR experiment, revealing the formation of intermediate species with ^{31}P resonances at about $\delta = 30$ ppm. The coordination of the phosphorus atom seems to be very fast, as no signals of the free ligands could be observed ($\delta = 0.4$ and 0.9 ppm). No other intermediates could be detected, and the species convert into the final complex, which shows a singlet at $\delta = 88.7$ ppm. The evolution of **3** to **4** involves the intramolecular coordination of the cyclopentadiene group, which is favoured on thermodynamic grounds by the formation of a chelate species. At this stage, an intramolecular H-transfer between the cyclopentadiene and the dimethylpentadienyl group may be postulated. It may occur with participation of the metal through a hydrido species. The species **5** thus formed contains the labile η^4-dimethylpentadiene ligand that is replaced by acetonitrile affording the desired compound in a straightforward way. When the reaction is carried out on a gram scale, the evolution of the mixture can easily be followed by the colour changes of the solution. Initially, the mixture is brown-yellow and becomes immediately yellow upon addition of the ligand. Upon refluxing, a red-orange colour appears and lasts for a few minutes, eventually converting to an orange-yellow colour.

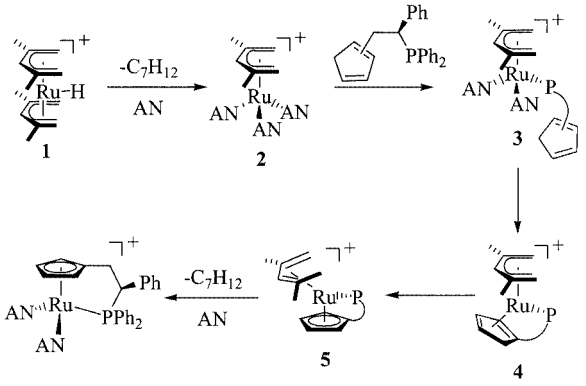

Scheme 6

According to this synthetic procedure, the ruthenium complexes depicted in Scheme 7 could be obtained in almost quantitative yields. They were characterised by analytical and spectroscopic methods. The phosphorus resonates at low field in **Ru$_{1-3}$** ($\delta \approx 88$ ppm); the same signal appears at higher field in **Ru$_4$** and **Ru$_5$** ($\delta \approx 52$ ppm). In the free ligands, the phosphorus shows two signals in the ^{31}P NMR spectrum due to the two regioisomers at about $\delta = 0.5$ (L_1), 18 (L_2), −6 (L_3), −18 (L_4), and −20 ppm (L_5). The large downfield shift upon coordination is characteristic of the formation of a five-membered chelate ring.[25] In the ^1H NMR spectra, the signals of the C−H hydrogen of the linker are low-field shifted in **Ru$_{1-3}$** ($\delta = 4.66$, 4.19, and 5.42 ppm respectively); for comparison, the hydrogen resonates at $\delta = 1.94$ and 2.55 ppm for **Ru$_4$** and **Ru$_5$** respectively. The coordinated acetonitrile ligands give rise to two doublets with a long range coupling (^5J) with phosphorus of about 1 Hz. Easy replacement of the acetonitrile ligands with CD_3CN was confirmed by means of ^1H NMR spectroscopy, suggesting that they are substitutionally labile.

Catalytic Applications

With several chiral complexes in hand, we began a preliminary screening of their catalytic activity in organic transformations. Kirchner has reported that $[Ru(Cp)(AN)_2(PPh_3)]^+$, in which the phosphane is not connected to the Cp, is a highly active catalyst at 57 °C for the redox isomerisation of allylic alcohols to give the corresponding carbonyl compounds.[8b] We tested **Ru$_1$** in this reaction and, in line with his report, we found that it catalyses the isomerisation of allylic alcohols (R = H, Me, Ph) at room temperature [Equation (1)]; details are given in the Exp. Sect.

 © 2004 Wiley-VCH Verlag GmbH & Co. KGaA, Weinheim

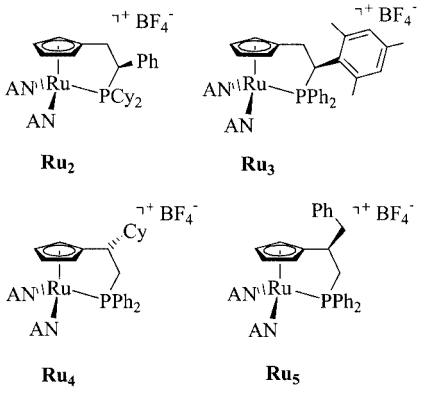

Scheme 7

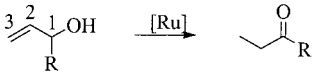

(1)

Kirchner also found that C^1-substituted allylic alcohols react much more quickly than those featuring substituents at the C^3 carbon; heating was required to effect the conversion of 2,3-disubstituted alcohols, while C^1- and C^3-disubstituted alcohols were not converted. To test the reactivity of our optically active complexes in the redox isomerisation of pro-chiral allylic alcohols, we chose geraniol and nerol as substrates. Isomerisation of diethylgeranylamine for the production of practically optically pure (+)-citronellal catalysed by a Rh^+/BINAP complex is a very important industrial process leading to key intermediates for the fragrance and flavour industry.[26] Comparable success has not been achieved for the corresponding isomerisation of readily available geraniol or nerol. To the best of our knowledge, the hitherto best catalyst system reported is based on a Rh^+/BINAP complex, and affords citronellal with 60% *ee*.[27] Initially, the reaction was performed in CH_2Cl_2 at room temperature and at reflux but only modest or no conversion into citronellal was obtained, corroborating the finding of Kirchner that C^3-disubstituted alcohols are not prone to undergo the redox isomerisation. However, when we performed the reaction in THF at reflux, we were pleased to observe conversion of the alcohol to citronellal [Equation (2)]. The results are summarised in Table 1.

Table 1. Redox isomerisation of geraniol and nerol[a]

Catalyst	Substrate	Product	Conversion	ee
Ru_1	geraniol	(+)-citronellal	73%	19%
Ru_1	nerol	citronellal	18%	*nd*
Ru_2	geraniol	−	0%	−
Ru_3	geraniol	(−)-citronellal	71%	8%
Ru_4	geraniol	(+)-citronellal	97%	17%
Ru_4	nerol	(−)-citronellal	35%	*nd*
Ru_5	geraniol	(+)-citronellal	32%	13%

[a] The values given in the table are the average of at least two runs. See the Exp. Sect. for more details.

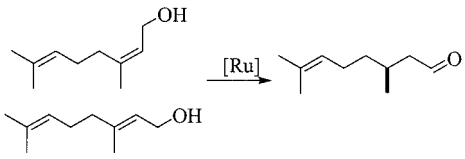

(2)

The conversion depends strongly on the complex used, the best results being found for **Ru_1** and **Ru_4** for the conversion of geraniol. The poor conversion of nerol has already been observed in other catalytic systems.[27] **Ru_2** is not active under these conditions; this fact may be ascribed to the steric bulkiness or the high Lewis basicity of the PCy_2 fragment. Unfortunately, the complexes are not able to induce high enantioselectivity. Further studies are necessary to determine if this catalytic system could be improved. Nevertheless, the results obtained with our complexes, although moderate, represent the first application of a ruthenium catalyst in the isomerisation of geraniol to optically enriched citronellal.[28]

The mechanistic rationale for the ruthenium-catalysed redox isomerisation of allylic alcohols postulates the formation of a ruthenium-enolate complex.[29] We envisioned that the formed enolate could be trapped by an electrophile, and indeed we found that an aldol-type product was formed via a ruthenium-catalysed cross-coupling of 3-buten-2-ol and benzaldehyde [Equation (3)].

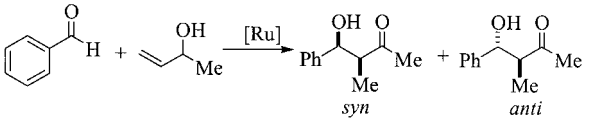

(3)

It has recently been reported that $[RuCl_2(PPh_3)_3]$ catalyses this reaction.[30] The results obtained with our complexes are detailed in Table 2. The yields are not satisfactory due to the concurrent isomerisation of the allylic alcohol to

Table 2. Aldol reaction between benzaldehyde and 3-buten-2-ol[a]

Catalyst	Loading (mol %)	Solvent	Yield (%)	*syn*/*anti*
Ru_1	5	CH_2Cl_2	31	69:31
	1		25	74:26
	0.1		26	67:33
	5	THF	57	76:24
	1		80	77:23
	0.1		51	77:23
Ru_2	1	THF	49	71:29
Ru_3	1	THF	47	62:38
Ru_4	1	THF	49	60:40
Ru_5	1	THF	53	63:37

[a] Reactions carried out at room temperature until complete consumption of the allylic alcohol. Isolated yields based on benzaldehyde are reported. The diastereoselectivity was based on ^1H NMR analysis of the crude product. The values given in the table are the average of at least two runs.

 © 2004 Wiley-VCH Verlag GmbH & Co. KGaA, Weinheim

butan-2-one; this may also explain the non-linear dependence of product yield on catalyst loading. The enantioselectivity is also disappointing, and a maximum of 5% *ee* has been obtained. However, the diastereoselectivity is appreciable, favouring the *syn* diastereomer. A substantial improvement in both yield and diastereoselectivity could be obtained upon switching from CH_2Cl_2 to THF, and it is noteworthy that the catalysts are quite active even at low loading. Further studies to improve the catalyst performance are intended.

Conclusion

A novel synthetic method has been developed that allows the one-pot synthesis of optically active cationic bis(acetonitrile)ruthenium(II) complexes of chiral cyclopentadienyl-linked phosphane ligands in very high yields. The method is general and allows the use of ligands bearing phosphanes with variable steric and electronic features. Moreover, the linker, which connects the cyclopentadienyl unit to the phosphane, can be straightforwardly modified. Considering the labile nature of the acetonitrile ligands, these complexes are potential candidates for catalytic implementation. Indeed, a preliminary study on their reactivity revealed that the complexes catalyse the isomerisation of geraniol to citronellal, as well as an aldol-type cross-coupling reaction between 3-buten-2-ol and benzaldehyde. Although the *ee* values obtained are rather low, the method is of interest for preparing other complexes that may find various applications in asymmetric catalysis.

Experimental Section

General Remarks: All reactions were carried out under nitrogen using standard Schlenk techniques. Solvents were dried and deoxygenated by standard methods. NMR spectra were recorded on a Varian Unity 500 spectrometer (500 MHz, ^{1}H; 125 MHz, ^{13}C; 202 MHz, ^{31}P) at room temperature. Chemical shifts are given in ppm relative to the solvent signal (^{1}H and ^{13}C) or to external H_3PO_4 (^{31}P). ^{1}H and ^{13}C{^{1}H} signal assignments were confirmed by ^{1}H,^{1}H-COSY, APT, ^{1}H,^{13}C-HETCOR, and NOE-difference experiments. (*R*)-1-Phenylethane-1,2-diol was obtained by reduction of (*R*)-mandelic acid with LAH.[31] (*S*)-1-Cyclohexylethane-1,2-diol was obtained by initial reduction of the arene ring of (*S*)-mandelic acid with hydrogen using 5% Rh on alumina as catalyst, followed by reduction of the carboxylic group with LAH.[32] (*R*)-3-Phenylpropane-1,2-diol was obtained by reduction of the corresponding acid with LAH. (*R*)-1-(2,4,6-Trimethylphenyl)ethane-1,2-diol was obtained by Sharpless asymmetric dihydroxylation of the corresponding olefin.[33] $[Ru(\eta^5\text{-}C_7H_{11})_2H][BF_4]$[34] was prepared according to a published procedure. All other chemicals were purchased and used without further purification.

Preparation of the Bis(methanesulfonate) Esters: NEt_3 (2.4 equiv.) was added to a solution of the diol in CH_2Cl_2 (ca. 10 mL/g). The solution was cooled in an ice-water bath and methanesulfonyl chloride (2.2 equiv.) in CH_2Cl_2 (5 mL/mL) was added dropwise over 1 h. The mixture was stirred for 1 h at 0 °C and then for 2 h at room temp. The mixture was poured into 1 M HCl. The layers were separated and the aqueous phase was washed with CH_2Cl_2 (3 × 50 mL). The combined organic extracts were washed successively with 1 M HCl, saturated $NaHCO_3$ and brine, and dried over $MgSO_4$. The solution was then filtered, and the solvent was removed under reduced pressure. The bis(methanesulfonate) esters were obtained in almost quantitative yield and they were used without further purification for the preparation of the spiro compounds.

Preparation of the Spiro Compounds: Freshly cracked cyclopentadiene (2 equiv.) was added dropwise to a suspension of $NaNH_2$ (2.5 equiv.) in THF (ca. 25 mL/g). The addition of CpH was adjusted so as to maintain a gentle reflux. Upon complete addition, the mixture was stirred for 1/2 h and subsequently, a solution of the bis(methanesulfonate) in THF (ca. 15 mL/g) was added dropwise. The addition was accompanied by considerable heat evolution. The reaction mixture was stirred at room temperature overnight. MeOH and H_2O were carefully added, the mixture was diluted with Et_2O and the layers separated. The aqueous phase was washed with Et_2O (3 × 50 mL). The combined organic extracts were washed with brine, dried over $MgSO_4$, and treated with decolourising charcoal. The solution was finally filtered, and the solvent removed under reduced pressure. The oil obtained was purified by filtration through a short column of basic alumina (activity I) with hexane as eluent. Reproducible elemental analyses could not be obtained, as the solvent could not be removed completely from the oily compounds.

Preparation of the Ligands by Ring Opening of the Spiro Compounds with Lithium Phosphides: The lithium phosphide was prepared by treating a solution of the secondary phosphane in THF (ca. 10 mL/g) with *n*BuLi (1.1 equiv.) at −78 °C. The deep-orange solution formed was stirred for 15 minutes at room temperature and then cooled again to −78 °C. At this temperature, the spiro compound (1.1 equiv.) dissolved in THF (1 mL/g) was added to the solution and the reaction mixture was allowed to reach room temperature overnight. The solvent was removed under reduced pressure and the oil left was washed several times with hexane until precipitation of the lithium salt of the ligand. This was dissolved in THF and degassed H_2O was added. After several extractions with CH_2Cl_2, the combined organic phases were dried over $MgSO_4$ and treated with decolourising charcoal. The solution was filtered through a short column of basic alumina (activity I), and the solvent removed under reduced pressure affording the pure ligand as an air-sensitive oil or solid as a one to one mixture of two regioisomers. The signals in the ^{1}H NMR spectra are highly overlapped and could not be attributed. Accordingly, only selected ^{13}C NMR data and the ^{31}P resonances are given. The ligands were characterised as their derived ruthenium complexes.

Synthesis of the Ruthenium Complexes: A flask was charged with the ligand and **1** in equimolar amounts. CH_3CN (ca. 20 mL/g) was added and the solution refluxed overnight. Then, the solution was filtered through a short pad of deactivated alumina (activity V) and the solvents evaporated to dryness. The solid obtained was washed several times with Et_2O and dried under high vacuum.

(*S*)-1-Phenylspiro[2.4]hepta-4,6-diene (S_1): The title compound was prepared, according to the representative procedure, from 10.0 g of (*R*)-phenyl-1,2-bis(methanesulfonyloxy)ethane as a colourless or pale-yellow oil. Yield: 4.64 g (81%). $[\alpha]_D^{20} = +229$ (c = 1, $CHCl_3$). ^{1}H NMR ($CDCl_3$): δ = 2.06 (dd, $^2J_{H,H}$ = 4.58, $^3J_{H,H}$ = 8.85 Hz, 1 H, CH_2), 2.32 (dd, $^2J_{H,H}$ = 4.58, $^3J_{H,H}$ = 7.93 Hz, 1 H, CH_2), 3.32 (t, $^3J_{H,H}$ = 8.24 Hz, 1 H, C*H*Ph), 5.92 (m, 1 H, C*H*), 6.21 (m, 1 H, C*H*), 6.45 (m, 1 H, C*H*), 6.50 (m, 1 H, C*H*), 7.18−7.30 (m,

 © 2004 Wiley-VCH Verlag GmbH & Co. KGaA, Weinheim

5 H, Ph) ppm. ^{13}C NMR ($CDCl_3$): δ = 17.05 (*C*H$_2$), 30.85 (*C*HPh), 45.55 (*C*$_{spiro}$), 126.37 (*C*H, Ph), 127.93 (*C*H, Ph), 128.05 (*C*H, Ph), 128.57 (*C*H), 130.21 (*C*H), 135.73 (*C*H), 138.77 (*C*H), 139.28 (*C*, Ph) ppm. HRMS [M$^+$]: calcd. 168.09390; found 168.09335.

(*S*)-1-Cyclohexylspiro[2.4]hepta-4,6-diene (S$_2$): The title compound was prepared, according to the representative procedure, from 20.0 g of (*S*)-cyclohexyl-1,2-bis(methanesulfonyloxy)ethane as a colourless or pale-yellow oil. Yield: 9.15 g (79%). $[\alpha]_D^{20}$ = −36 (*c* = 1, $CHCl_3$). ^{1}H NMR ($CDCl_3$): δ = 0.90−2.0 (m, 11 H, Cy), 1.60 (dd, $^2J_{H,H}$ = 3.96, $^3J_{H,H}$ = 7.32 Hz, 1 H, C*H*$_2$), 1.79 (dd, $^2J_{H,H}$ = 3.96, $^3J_{H,H}$ = 8.55 Hz, 1 H, C*H*$_2$), 1.90 (m, 1 H, C*H*, Cy), 6.09 (m, 1 H, C*H*), 6.29 (m, 1 H, C*H*), 6.49 (m, 1 H, C*H*), 6.59 (m, 1 H, C*H*) ppm. ^{13}C NMR ($CDCl_3$): δ = 19.18 (*C*H$_2$, Cy), 26.00 (*C*H$_2$, Cy), 26.22 (*C*H$_2$), 26.38 (*C*H$_2$, Cy), 32.91 (*C*H$_2$, Cy), 33.29 (*C*H$_2$, Cy), 35.23 (*C*HCy), 42.09 (*C*H, Cy), 42.77 (*C*$_{spiro}$), 127.50 (*C*H), 129.95 (*C*H), 135.67 (*C*H), 139.77 (*C*H) ppm. HRMS [M$^+$]: calcd. 174.14085; found 174.14067.

(*S*)-1-(2,4,6-Trimethylphenyl)spiro[2.4]hepta-4,6-diene (S$_3$): The title compound was prepared, according to the representative procedure, from 12.5 g of (*R*)-(2,4,6-trimethylphenyl)-1,2-bis(methanesulfonyloxy)ethane as a pale-yellow oil. Yield: 6.80 g (87%). $[\alpha]_D^{20}$ = +2 (*c* = 1, $CHCl_3$). ^{1}H NMR ($CDCl_3$): δ = 2.17 (dd, $^2J_{H,H}$ = 4.27, $^3J_{H,H}$ = 8.55 Hz, 1 H, C*H*$_2$), 2.23 (dd, $^2J_{H,H}$ = 4.27, $^3J_{H,H}$ = 9.16 Hz, 1 H, C*H*$_2$), 2.29 (s, 9 H, C*H*$_3$), 3.14 (t, $^3J_{H,H}$ = 8.85 Hz, 1 H, C*H*Ms), 5.85 (m, 1 H, C*H*), 6.34 (m, 1 H, C*H*), 6.50 (m, 1 H, C*H*), 6.58 (m, 1 H, C*H*), 6.83 (s, 2 H, Ms) ppm. ^{13}C NMR ($CDCl_3$): δ = 20.23 (*C*H$_2$), 20.80 (*C*H$_3$), 28.61 (*C*HMs), 45.03 (*C*$_{spiro}$), 128.55 (*C*H, Ms), 129.11 (*C*H), 130.04 (*C*H), 133.19 (*C*, Ms), 135.94 (*C*, Ms), 137.52 (*C*H), 139.19 (*C*H) ppm. HRMS [M$^+$]: calcd. 210.14085; found 210.14114.

(*R*)-1-Benzylspiro[2.4]hepta-4,6-diene (S$_4$): The title compound was prepared, according to the representative procedure, from 25.4 g of (*S*)-benzyl-1,2-bis(methanesulfonyloxy)ethane as a pale-yellow oil. Yield: 14.3 g (95%). $[\alpha]_D^{20}$ = −11 (*c* = 1, $CHCl_3$). ^{1}H NMR ($CDCl_3$): δ = 1.71 (dd, $^2J_{H,H}$ = 4.27, $^3J_{H,H}$ = 7.32 Hz, 1 H, C*H*$_2$), 1.85 (dd, $^2J_{H,H}$ = 4.27, $^3J_{H,H}$ = 8.55 Hz, 1 H, C*H*$_2$), 2.30 (m, 1 H, C*H*Bzl), 2.94 (d, $^3J_{H,H}$ = 7.02 Hz, 2 H, C*H*$_2$Ph), 6.10 (m, 1 H, C*H*), 6.33 (m, 1 H, C*H*), 6.49 (m, 1 H, C*H*), 6.58 (m, 1 H, C*H*), 7.1−7.3 (m, 5 H, Ph) ppm. ^{13}C NMR ($CDCl_3$): δ = 19.46 (*C*H$_2$), 28.29 (*C*HBzl), 38.32 (*C*H$_2$Ph), 43.20 (*C*$_{spiro}$), 126.10 (*C*H, Ph), 127.95 (*C*H, Ph), 128.29 (*C*H, Ph), 128.29 (*C*H), 130.68 (*C*H), 135.41 (*C*H), 139.64 (*C*H) 140.74 (*C*) ppm. HRMS [M$^+$]: calcd. 182.10955; found 182.10938.

(*S*)-[2-(Cyclopenta-1,4-dienyl)-1-phenylethyl]diphenylphosphane and (*S*)-[2-(Cyclopenta-1,3-dienyl)-1-phenylethyl]diphenylphosphane (L$_1$): The title compound was prepared as an equal mixture of two regioisomers according to the representative procedure from 5.0 g of S$_1$ and 5.0 g of $HPPh_2$ as a colourless solid. Yield: 9.2 g (97%). ^{13}C NMR ($CDCl_3$, selected data): δ = 33.67 (d, $^2J_{C,P}$ = 23.1 Hz, *C*H$_2$), 34.29 (d, $^2J_{C,P}$ = 23.0 Hz, *C*H$_2$), 41.07 (s, *C*H$_2$, Cp), 43.70 (s, *C*H$_2$, Cp), 45.28 (d, $^1J_{C,P}$ = 13.4 Hz, *C*HPh), 46.17 (d, $^1J_{C,P}$ = 14.4 Hz, *C*HPh), 140.83 (s, *C*, Cp), 140.90 (s, *C*, Cp), 144.69 (d, $^2J_{C,P}$ = 13.5 Hz, *C*, Ph), 147.20 (d, $^2J_{C,P}$ = 13.4 Hz, *C*, Ph) ppm. ^{31}P NMR ($CDCl_3$): δ = 0.458 (s), 0.886 (s) ppm. HRMS [M$^+$]: calcd. 354.15374; found 354.15323.

(*S*)-Dicyclohexyl[2-(cyclopenta-1,4-dienyl)-1-phenylethyl]phosphane and (*S*)-Dicyclohexyl[2-(cyclopenta-1,3-dienyl)-1-phenylethyl]phosphane (L$_2$): The title compounds were prepared as an equimolar mixture of two regioisomers, according to the representative procedure, from 4.7 g of **S$_1$** and 5.0 g of $HPCy_2$ as a colourless solid. Yield: 8.6 g (93%). ^{13}C NMR ($CDCl_3$, selected data): δ = 32.83 (d, $^1J_{C,P}$ = 9.6 Hz, *C*H, Cy), 32.98 (d, $^1J_{C,P}$ = 8.6 Hz, *C*H, Cy), 33.24 (d, $^1J_{C,P}$ = 2.9 Hz, *C*H, Cy), 33.7 (d, $^1J_{C,P}$ = 2.9 Hz, *C*H, Cy), 34.79 (d, $^2J_{C,P}$ = 22.1 Hz, *C*H$_2$), 35.48 (d, $^2J_{C,P}$ = 23.0 Hz, *C*H$_2$), 39.37 (d, $^1J_{C,P}$ = 19.2 Hz, *C*HPh), 40.37 (d, $^1J_{C,P}$ = 20.1 Hz, *C*HPh), 40.93 (s, *C*H$_2$, Cp), 43.61 (s, *C*H$_2$, Cp), 142.50 (s, *C*, Cp), 142.53 (s, *C*, Cp), 145.03 (d, $^2J_{C,P}$ = 12.4 Hz, *C*, Ph), 147.60 (d, $^2J_{C,P}$ = 13.5 Hz, *C*, Ph) ppm. ^{31}P NMR ($CDCl_3$): δ = 18.08 (s), 18.75 (s) ppm. HRMS [M$^+$]: calcd. 366.24764; found 366.24738.

(*S*)-[2-(Cyclopenta-1,3-dienyl)-1-(2,4,6-trimethylphenyl)ethyl]diphenylphosphane and (*S*)-[2-(Cyclopenta-1,4-dienyl)-1-(2,4,6-trimethylphenyl)ethyl]diphenylphosphane (L$_3$): The title compounds were prepared as an equimolar mixture of two regioisomers, according to the representative procedure, from 3.1 g of **S$_3$** and 2.5 g of $HPPh_2$ as a colourless oil. Yield: 5.0 g (93%). ^{13}C NMR ($CDCl_3$, selected data): δ = 20.74 (*C*H$_3$), 21.36 (*C*H$_3$), 22.49 (*C*H$_3$), 22.65 (*C*H$_3$), 31.47 (d, $^2J_{C,P}$ = 20.1 Hz, *C*H$_2$), 32.12 (d, $^2J_{C,P}$ = 21.1 Hz, *C*H$_2$), 39.87 (d, $^1J_{C,P}$ = 17.2 Hz, *C*HMs), 40.85 (d, $^1J_{C,P}$ = 18.2 Hz, *C*HMs), 41.03 (s, *C*H$_2$, Cp), 43.56 (s, *C*H$_2$, Cp) ppm. ^{31}P NMR ($CDCl_3$): δ = −6.53 (s), −6.26 (s) ppm. HRMS [M$^+$]: calcd. 397.20852; found 397.20828.

(*R*)-[2-Cyclohexyl-2-(cyclopenta-1,3-dienyl)ethyl]diphenylphosphane and (*R*)-[2-Cyclohexyl-2-(cyclopenta-1,4-dienyl)ethyl]diphenylphosphane (L$_4$): The title compound was prepared as an equimolar mixture of two regioisomers, according to the representative procedure, from 2.1 g of **S$_2$** and 2.0 g of $HPPh_2$ as a colourless solid. Yield: 3.1 g (80%). ^{13}C NMR ($CDCl_3$, selected data): δ = 29.99 (d, $^1J_{C,P}$ = 15.3 Hz, *C*H$_2$), 31.37 (d, $^1J_{C,P}$ = 10.55 Hz, *C*H$_2$), 39.73 (s, *C*H$_2$, Cp), 40.81 (s, *C*H$_2$, Cp), 41.76 (d, $^3J_{C,P}$ = 8.54 Hz, *C*H, Cy), 42.16 (d, $^2J_{C,P}$ = 13.4 Hz, *C*HCy), 42.89 (d, $^2J_{C,P}$ = 13.4 Hz, *C*HCy), 43.03 (d, $^3J_{C,P}$ = 7.79 Hz, *C*H, Cy), 137.78 (d, $J_{C,P}$ = 14.4 Hz, *C*), 138.92 (d, $J_{C,P}$ = 13.4 Hz, *C*), 139.22 (d, $J_{C,P}$ = 14.4 Hz, *C*), 147.19 (d, $J_{C,P}$ = 3.8 Hz, *C*), 149.85 (d, $J_{C,P}$ = 4.8 Hz, *C*) ppm. ^{31}P NMR ($CDCl_3$): δ = −18.89 (s), −18.19 (s) ppm. HRMS [M$^+$]: calcd. 360.20069; found 360.20039.

(*S*)-[2-Benzyl-2-(cyclopenta-1,3-dienyl)ethyl]diphenylphosphane and (*S*)-[2-Benzyl-2-(cyclopenta-1,4-dienyl)ethyl]diphenylphosphane (L$_5$): The title compound was prepared as an equal mixture of two regioisomers according to the representative procedure from 6.5 g of **S$_4$** and 6.0 g of $HPPh_2$. Yield: colourless solid, 11.0 g (93%). ^{13}C NMR ($CDCl_3$, selected data): δ = 33.11 (d, $^1J_{C,P}$ = 12.4 Hz, *C*H$_2$), 34.41 (d, $^1J_{C,P}$ = 12.4 Hz, *C*H$_2$), 39.20 (d, $^2J_{C,P}$ = 15.45 Hz, *C*HBzl), 39.96 (d, $^1J_{C,P}$ = 15.3 Hz, *C*HBzl), 40.91 (s, *C*H$_2$, Cp), 41.32 (s, *C*H$_2$, Cp), 42.42 (d, $^3J_{C,P}$ = 8.54 Hz, *C*H$_2$Ph), 43.98 (d, $^3J_{C,P}$ = 9.55 Hz, *C*H$_2$Ph) ppm. ^{31}P NMR ($CDCl_3$): δ = −20.56 (s), −20.47 (s) ppm. HRMS [M$^+$]: calcd. 368.16939; found 368.16937.

(*S*)-Bis(acetonitrile)[(η^5-2-cyclopentadienyl-1-phenylethyl)diphenylphosphane-κ*P*] ruthenium(II) Tetrafluoroborate (Ru$_1$). This compound was prepared, according to the representative procedure, from 2.8 g of **L$_1$** and 3.0 g of **1** as yellow crystals. The NMR spectroscopic data are identical to those already reported for [Ru{η^5-$C_5H_4CH_2CH(Ph)PPh_2$-κ*P*}$(CH_3CN)_2$][PF_6].[12] Yield: 4.73 g (96%). M.p.: 165−170 °C. $[\alpha]_D^{20}$ = +8.7 (*c* = 1, $CHCl_3$). IR (KBr): $\tilde{\nu}$ = 2274 cm^{-1}, 1600, 1581, 1058, 704. MS (FAB): *m*/*z* = 536 [M$^+$], 495 [M$^+$ − CH_3CN], 454 [M$^+$ − 2CH_3CN]. $C_{29}H_{28}BF_4N_2PRu$ (623.38): calcd. C 55.87, H 4.53, N 4.49; found C 55.73, H 4.62, N 4.35.

(*S*)-Bis(acetonitrile)[dicyclohexyl(η^5-2-cyclopentadienyl-1-phenylethyl)phosphane-κ*P*]ruthenium(II) Tetrafluoroborate (Ru$_2$): This compound was prepared, according to the representative procedure, from 1.1 g of **L$_2$** and 1.13 g of **1** as a yellow solid. Yield: 1.9 g (100%). M.p.: 195−200 °C. $[\alpha]_D^{20}$= +97.5 (*c* = 1, CH_3CN).

 © 2004 Wiley-VCH Verlag GmbH & Co. KGaA, Weinheim

^{1}H NMR (CD_2Cl_2): δ = 0.52 (m, 1 H, *Cy*), 1.0−2.21 (m, 21 H, *Cy*), 2.41 (d, $^5J_{H,P}$ = 0.91 Hz, 3 H, CH_3CN), 2.44 (d, $^5J_{H,P}$ = 0.92 Hz, 3 H, CH_3CN), 2.47−2.67 (m, 2 H, CH_2), 3.95 (m, 1 H, Cp), 4.19 (m, 1 H, C*H*Ph), 4.25 (m, 1 H, Cp), 5.05 (m, 1 H, Cp), 5.13 (m, 1 H, Cp), 7.26−7.41 (m, 5 H, Ph) ppm. ^{13}C NMR (CD_2Cl_2): δ = 4.45 (*C*H$_3$, *C*H$_3$CN), 4.67 (*C*H$_3$, *C*H$_3$CN), 26.83 (*C*H$_2$, *Cy*), 27.16 (*C*H$_2$, *Cy*), 27.40 (*C*H$_2$, *Cy*), 27.70 (d, $J_{C,P}$ = 13.4 Hz, *C*H$_2$, *Cy*), 28.48 (d, $^2J_{C,P}$ = 12.44 Hz, *C*H$_2$), 28.65 (*C*H$_2$, *Cy*), 30.92 (d, $J_{C,P}$ = 5.78 Hz, *C*H$_2$, *Cy*), 33.08 (d, $^1J_{C,P}$ = 17.34 Hz, *C*H, *Cy*), 36.06 (d, $^1J_{C,P}$ = 13.32 Hz, *C*H, *Cy*), 56.54 (d, $^1J_{C,P}$ = 18.22 Hz, *C*HPh), 57.62 (*C*H, Cp), 68.80 (*C*H, Cp), 77.86 (d, $J_{C,P}$ = 7.66 Hz, *C*H, Cp), 90.97 (d, $J_{C,P}$ = 3.89 Hz, *C*H, Cp), 102.88 (d, $J_{C,P}$ = 3.77 Hz, C_{ipso}, Cp), 127.44 (*C*, *C*N), 127.82 (*C*H), 128.21 (d, $J_{C,P}$ = 2.89 Hz, *C*H), 128.48 (*C*, *C*N), 129.21 (*C*H), 138.47 (d, $J_{C,P}$ = 8.67 Hz, *C*) ppm. ^{31}P NMR (CD_2Cl_2): δ = 88.78 (s, *P*Cy$_2$) ppm. IR (KBr): $\tilde{\nu}$ = 2274 cm^{-1}, 1600, 1058, 704. MS (FAB): *m*/*z* (%) = 549 (15) [M$^+$ + 1], 508 (85) [M$^+$ − CH$_3$CN], 466 (100) [M$^+$ − 2CH$_3$CN], 87 (100) [BF_4^-]. $C_{29}H_{40}BF_4N_2PRu$ (635.47): calcd. C 54.80, H 6.36, N 4.41; found C 55.18, H 6.60, N 3.91.

(*S*)-Bis(acetonitrile){[η^5-2-cyclopentadienyl-1-(2,4,6-trimethylphenyl)ethyl]diphenylphosphane-κ*P*}ruthenium(II) Tetrafluoroborate (Ru$_3$): This compound was prepared, according to the representative procedure, from 1.4 g of **L$_3$** and 1.33 g of **1** as a yellow solid. Yield: 2.3 g (99%). M.p.: 160−165 °C. $[\alpha]_D^{20}$= −12.4 (*c* = 1, CH_3CN). ^{1}H NMR (CD_2Cl_2): δ = 1.40 (s, 3 H, CH_3), 1.76 (d, $^5J_{H,P}$ = 1.22 Hz, 3 H, CH_3CN), 2.15 (s, 3 H, CH_3), 2.20 (s, 3 H, CH_3), 2.37 (d, $^5J_{H,P}$ = 0.92 Hz, 3 H, CH_3CN), 2.42−2.79 (m, 2 H, CH_2), 4.30 (m, 1 H, Cp), 4.45 (m, 1 H, Cp), 5.18 (m, 1 H, Cp), 5.31 (m, 1 H, Cp), 5.42 (m, 1 H, C*H*Ms), 6.48 (s, 1 H, *Ms*), 6.76 (s, 1 H, *Ms*), 7.20−7.50 (m, 10 H, Ph) ppm. ^{13}C NMR (CD_2Cl_2): δ = 3.29 (*C*H$_3$, *C*H$_3$CN), 4.48 (*C*H$_3$, *C*H$_3$CN), 20.80 (*C*H$_3$), 22.22 (*C*H$_3$), 22.63 (*C*H$_3$), 30.16 (d, $^2J_{C,P}$ = 10.55 Hz, *C*H$_2$), 60.71 (*C*H, Cp), 64.28 (d, $^1J_{C,P}$ = 23.12 Hz, *C*HMs), 65.37 (*C*H, Cp), 82.82 (d, $J_{C,P}$ = 7.66 Hz, *C*H, Cp), 87.19 (d, $J_{C,P}$ = 5.78 Hz, *C*H, Cp), 107.97 (d, $J_{C,P}$ = 4.77 Hz, C_{ipso}, Cp), 126.04 (*C*, *C*N), 127.63 (*C*, *C*N), 128.70 (d, $J_{C,P}$ = 9.55 Hz, *C*H), 128.48 (d, $J_{C,P}$ = 8.67 Hz, *C*H), 129.57 (*C*H), 129.82 (*C*H), 130.90 (*C*), 131.16 (*C*H), 131.43 (*C*H), 132.29 (d, $J_{C,P}$ = 8.67 Hz, *C*), 132.91 (d, $J_{C,P}$ = 9.67 Hz, *C*H), 135.50 (*C*), 136.14 (*C*), 136.57 (d, $J_{C,P}$ = 11.56 Hz, *C*H), 137.25 (*C*), 138.98 (*C*) ppm. ^{31}P NMR (CD_2Cl_2): δ = 86.78 (s, *P*Ph$_2$) ppm. IR (KBr): $\tilde{\nu}$ = 2274 cm^{-1}, 1629, 1600, 1581, 1058, 704. MS (FAB): *m*/*z* (%) = 579 (20) [M$^+$ + 1], 538 (60) [M$^+$ − CH$_3$CN + 1], 497 (100) [M$^+$ − 2CH$_3$CN + 1], 87 (100%) [BF_4^-]. $C_{32}H_{34}BF_4N_2PRu$ (665.45): calcd. C 57.75, H 5.15, N 4.21; found C 57.70, H 5.38, N 4.29.

(*S*)-Bis(acetonitrile)[(2-cyclohexyl-η^5-2-cyclopentadienylethyl)diphenylphosphane-κ*P*]ruthenium(II) Tetrafluoroborate (Ru$_4$): The title compound was prepared, according to the representative procedure, from 1.1 g of **L$_4$** and 1.15 g of **1** as a yellow solid. Yield: 1.8 g (95%). M.p.: 142−145 °C. $[\alpha]_D^{20}$= +4 (*c* = 1, CH_3CN). ^{1}H NMR (CD_2Cl_2): δ = 0.80−1.86 (m, 11 H, *Cy*), 1.94 (m, 1 H, C*H*Cy), 1.97 (d, $^5J_{H,P}$ = 0.91 Hz, 3 H, CH_3CN), 2.21 (d, $^5J_{H,P}$ = 1.22 Hz, 3 H, CH_3CN), 2.92 (td, $J_{H,P}$ = 13.42, $J_{H,H}$ = 6.10 Hz, 1 H, CH_2), 3.18 (td, $J_{H,P}$ = 13.12, $J_{H,H}$ = 4.88 Hz, 1 H, CH_2), 4.02 (m, 1 H, Cp), 4.27 (m, 1 H, Cp), 5.12 (m, 1 H, Cp), 5.24 (m, 1 H, Cp), 7.39−7.56 (m, 10 H, Ph) ppm. ^{13}C NMR (CD_2Cl_2): δ = 3.69 (*C*H$_3$, *C*H$_3$CN), 4.12 (*C*H$_3$, *C*H$_3$CN), 26.37 (*C*H$_2$, *Cy*), 31.54 (*C*H$_2$, *Cy*), 33.44 (*C*H$_2$, *Cy*), 42.57 (d, $^2J_{C,P}$ = 20.10 Hz, *C*HCy), 42.72 (d, $^3J_{C,P}$ = 4.77 Hz, *C*H, *Cy*), 47.94 (d, $^1J_{C,P}$ = 33.54 Hz, *C*H$_2$), 57.48 (*C*H, Cp), 68.61 (*C*H, Cp), 79.98 (d, $J_{C,P}$ = 7.79 Hz, *C*H, Cp), 88.62 (d, $J_{C,P}$ = 5.65 Hz, *C*H, Cp), 112.82 (d, $J_{C,P}$ = 4.77 Hz, C_{ipso}, Cp), 126.56 (*C*, *C*N), 127.28 (*C*, *C*N), 129.05 (d, $J_{C,P}$ = 4.90 Hz, *C*H), 129.13 (d, $J_{C,P}$ = 4.77 Hz, *C*H), 130.38 (*C*H), 130.76 (*C*H), 132.05 (d, $J_{C,P}$ = 10.55 Hz, *C*H), 133.29 (d, $J_{C,P}$ = 11.56 Hz, *C*H), 133.53 (*C*), 133.82 (*C*) ppm. ^{31}P NMR (CD_2Cl_2): δ = 52.14 (s, *P*Ph$_2$) ppm. IR (KBr): $\tilde{\nu}$ = 2274 cm^{-1}, 1629, 1600, 1581, 1058, 704. MS (FAB): *m*/*z* (%) = 502 (60) [M$^+$ − CH$_3$CN + 1], 461 (100) [M$^+$ −2CH$_3$CN + 1], 87 (100) [BF_4^-]. $C_{29}H_{34}BF_4N_2PRu$ (629.42): calcd. C 55.33, H 5.44, N 4.45; found C 54.93, H 5.69, N 4.08.

(*S*)-Bis(acetonitrile)[(2-benzyl-η^5-2-cyclopentadienylethyl)diphenylphosphane-κ*P*]ruthenium(II) Tetrafluoroborate (Ru$_5$): The title compound was prepared, according to the representative procedure, from 2.69 g of **L$_5$** and 2.75 g of **1** as a yellow solid. Yield: 4.65 g (100%). $[\alpha]_D^{20}$= −10.7 (*c* = 1, CH_3CN). M.p.: 141−144 °C. ^{1}H NMR (CD_2Cl_2): δ = 1.99 (d, $^5J_{H,P}$ = 1.22 Hz, 3 H, CH_3CN), 2.18 (d, $^5J_{H,P}$ = 1.53 Hz, 3 H, CH_3CN), 2.55 (m, 1 H, C*H*Bzl), 2.82 (dd, $^2J_{H,H}$ = 13.43, $^3J_{H,H}$ = 8.24 Hz, 1 H, CH_2Ph), 2.95 (dd, $^2J_{H,H}$ = 13.43, $^3J_{H,H}$ = 6.72 Hz, 1 H, CH_2Ph), 3.02−3.18 (m, 2 H, CH_2), 4.12 (m, 1 H, Cp), 4.14 (m, 1 H, Cp), 5.06 (m, 1 H, Cp), 5.25 (m, 1 H, Cp), 7.01−7.74 (m, 15 H, Ph) ppm. ^{13}C NMR (CD_2Cl_2): δ = 3.78 (*C*H$_3$, *C*H$_3$CN), 4.16 (*C*H$_3$, *C*H$_3$CN), 38.60 (d, $^2J_{C,P}$ = 6.66 Hz, *C*HBzl), 41.12 (d, $^3J_{C,P}$ = 21.11 Hz, *C*H$_2$Ph), 50.36 (d, $^1J_{C,P}$ = 33.54 Hz, *C*H$_2$), 57.87 (*C*H, Cp), 67.78 (*C*H, Cp), 80.47 (d, $J_{C,P}$ = 8.67 Hz, *C*H, Cp), 88.39 (d, $J_{C,P}$ = 5.78 Hz, *C*H, Cp), 112.42 (d, $J_{C,P}$ = 4.77 Hz, C_{ipso}, Cp), 126.69 (*C*, *C*N), 126.86 (*C*H), 127.26 (*C*, *C*N), 128.76 *C*H), 129.13 (*C*H), 129.21 (*C*H), 129.33 (*C*H), 129.40 (*C*H), 130.56 (d, $J_{C,P}$ = 5.78 Hz, *C*H), 130.83 (d, $J_{C,P}$ = 1.88 Hz, *C*H), 132.18 (d, $J_{C,P}$ = 9.67 Hz, *C*H), 132.99 (*C*), 133.26 (d, $J_{C,P}$ = 11.43 Hz, *C*H), 133.62 (*C*), 139.77 (*C*) ppm. ^{31}P NMR (CD_2Cl_2): δ = 52.87 (s, *P*Ph$_2$) ppm. IR (KBr): $\tilde{\nu}$ = 2277 cm^{-1}, 1630, 1602, 1058, 744, 699. MS (FAB): *m*/*z* = 510 (30) [M$^+$ − CH$_3$CN + 1], 469 (100) [M$^+$ − 2CH$_3$CN + 1], 87 (100) [BF_4^-]. $C_{30}H_{30}BF_4N_2PRu$ (637.40): calcd. C 56.53, H 4.74, N 4.40; found C 56.65, H 4.67, N 4.31.

Procedure for the Isomerisation of Allylic Alcohols: In a representative experiment, an NMR tube was charged under nitrogen with the catalyst (1 mol %), CD_2Cl_2 was added (0.5 mL), followed by the allylic alcohol (prop-2-en-1-ol, but-3-en-2-ol, or 1-phenylprop-2-en-1-ol). The tube was capped and vigorously shaken. The reaction was monitored by ^{1}H and ^{13}C{^{1}H} NMR spectroscopy. Typically, the reaction was completed (no olefinic protons were detected) after three hours at room temperature affording exclusively the carbonyl compounds with only traces of unidentified side-products.

Procedure for the Isomerisation of Geraniol and Nerol: A flask was charged with a catalytic amount of the ruthenium complex (5 mol %) and THF (10 mL) and the allylic alcohol (2 mL) were then added. The reaction mixture was refluxed for 24 hours. The solvent was then removed under reduced pressure and the residue was filtered through a short pad of silica gel eluting with Et_2O. The oil left after evaporation of the solvent was bulb-to-bulb distilled (100−110 °C/10 mbar) affording pure citronellal. The conversion was determined on the crude reaction product by ^{1}H NMR spectroscopy. The *ee* was determined by comparison of the optical rotation (neat) with that reported in the literature.[27]

Procedure for the Catalytic Aldol Reaction: A flask was charged with a catalytic amount of the ruthenium complex (5 to 0.1 mol %). The solvent was added (5 or 10 mL), followed by benzaldehyde (5 or 10 mmol) and then 3-buten-2-ol (10 or 20 mmol). The reaction mixture was stirred at room temperature until complete consumption of the allylic alcohol (checked by TLC). The solvent was then removed under reduced pressure and the residue was purified by

 © 2004 Wiley-VCH Verlag GmbH & Co. KGaA, Weinheim

flash column chromatography (hexane/ethyl acetate, 7:3). The *syn*/*anti* ratio was determined by ^{1}H NMR spectroscopy. The enantioselectivities were determined by HPLC analysis with a Chiralpak AS column (eluent: hexane/2-propanol, 95:5; flow rate: 0.8 mL/min; column temperature: 30 °C; retention times for the *syn* diastereoisomer: 15 min and 22 min).

Acknowledgments

The generous financial support by the Deutsche Forschungsgemeinschaft DFG within the Collaborative Research Centre (SFB, 380) "Asymmetric Syntheses by Chemical and Biological Means" and by the "Fonds der Chemischen Industrie" is gratefully acknowledged. We thank Prof. Carsten Bolm for a generous gift of (*R*)-1-(2,4,6-trimethylphenyl)ethane-1,2-diol.

[1] [1a] S.-I. Murahashi, T. Naota, *J. Synth. Org. Chem. Jpn.* **1988**, *46*, 930−956. [1b] T. Naota, H. Takaya, S.-I. Murahashi, *Chem. Rev.* **1998**, *98*, 2599−2660. [1c] B. M. Trost, F. D. Toste, A. B. Pinkerton, *Chem. Rev.* **2001**, *101*, 2067−2096. [1d] B. M. Trost, *Acc. Chem. Res.* **2002**, *35*, 695−705. [1e] V. Ritleng, C. Sirlin, M. Pfeffer, *Chem. Rev.* **2002**, *102*, 1731−1769.

[2] [2a] M. I. Bruce, M. A. Bennett, T. W. Matheson, *Comprehensive Organometallic Chemistry* (Eds.: G. Wilkinson, F. G. A. Stone, E. W. Abel), Pergamon Press: Oxford, **1982**. [2b] M. I Bruce, M. A. Bennett, A. F. Hill, *Comprehensive Organometallic Chemistry II* (Eds.: G. Wilkinson, F. G. A. Stone, E. W. Abel), Pergamon Press: Oxford, **1995**. [2c] U. Kölle, *Encyclopedia of Inorganic Chemistry* (Ed.: R. King), Wiley Chichester, **1994**, *7*, 3533−3545.

[3] [3a] T. P. Gill, K. R. Mann, *Organometallics* **1982**, *1*, 485−488. [3b] B. M. Trost, C. M. Older, *Organometallics* **2002**, *21*, 2544−2547.

[4] M. O. Albers, D. J. Robinson, A. Shaver, E. Singleton, *Organometallics* **1986**, *5*, 2199−2205.

[5] C. Slugov, E. Rüba, R. Schmid, K. Kirchner, K. Mereiter, *Monatsh. Chem.* **2000**, *131*, 1241−1248.

[6] W. Luginbühl, P. Zbinden, P. A. Pittet, T. Armbruster, H. B. Bürgi, A. E. Merbach, A. Ludi, *Inorg. Chem.* **1991**, *30*, 2350−2355.

[7] [7a] B. M. Trost, P. L. Fraisse, Z. T. Ball, *Angew. Chem.* **2002**, *114*, 1101−1103; *Angew. Chem. Int. Ed.* **2002**, *41*, 1059−1162. [7b] B. M. Trost, H. C. Shen, *Angew. Chem.* **2001**, *113*, 2375−2378; *Angew. Chem. Int. Ed.* **2001**, *40*, 2313−2317. [7c] B. M. Trost, J.-P. Surivet, *Angew. Chem.* **2001**, *113*, 1516−1519; *Angew. Chem. Int. Ed.* **2001**, *40*, 1468−1472. [7d] B. M. Trost, A. B. Pinkerton, *Angew. Chem.* **2000**, *112*, 368−370; *Angew. Chem. Int. Ed.* **2000**, *39*, 360−362. [7e] B. M. Trost, A. B. Pinkerton, M. Seidel, *J. Am. Chem. Soc.* **2001**, *123*, 12466−12476. [7f] B. M. Trost, A. B. Pinkerton, F. D. Toste, M. Sperrle, *J. Am. Chem. Soc.* **2001**, *123*, 12504−12509. [7g] B. M. Trost, M. T. Rudd, *J. Am. Chem. Soc.* **2002**, *124*, 4178−4179. [7h] B. M. Trost, A. B. Pinkerton, *J. Am. Chem. Soc.* **1999**, *121*, 10842−10843. [7i] B. M. Trost, F. D. Toste, *J. Am. Chem. Soc.* **1999**, *121*, 9728−9729. [7l] B. M. Trost, R. E. Brown, F. D. Toste, *J. Am. Chem. Soc.* **2000**, *122*, 5877−5878. [7m] B. M. Trost, F. D. Toste, H. Sheng, *J. Am. Chem. Soc.* **2000**, *122*, 2379−2380. [7n] B. M. Trost, F. D. Toste, *J. Am. Chem. Soc.* **2000**, *122*, 714−715. [7o] B. M. Trost, A. B. Pinkerton, *J. Am. Chem. Soc.* **2000**, *122*, 8081−8082. [7p] B. M. Trost, A. B. Pinkerton, D. Kremzow, *J. Am. Chem. Soc.* **2000**, *122*, 12007−12008. [7q] B. M. Trost, J.-P. Surivet, F. D. Toste, *J. Am. Chem. Soc.* **2001**, *123*, 2897−2898. [7r] B. M. Trost, M. Machacek, M. J. Schnaderbeck, *Org. Lett.* **2000**, *2*, 1761−1764. [7s] B. M. Trost, H. C. Shen, *Org. Lett.* **2000**, *2*, 2523−2525. [7t] B. M. Trost, F. D. Toste, *Tetrahedron Lett.* **1999**, *40*, 7739−7743.

[8] [8a] E. Rüba, W. Simanko, K. Mauthner, K. M. Soldouzi, C. Slugovc, K. Mereiter, R. Schmid, K. Kirchner, *Organometallics* **1999**, *18*, 3843−3850. [8b] C. Slugovc, E. Rüba, R. Schimd, K. Kirchner, *Organometallics* **1999**, *18*, 4230−4233. [8c] C. M. Standfest-Hauser, K. Mereiter, R. Schmid, K. Kirchner, *Dalton Trans.* **2003**, *11*, 2329−2334. [8d] C. M. Standfest-Hauser, K. Mereiter, R. Schmid, K. Kirchner, *Organometallics* **2002**, *21*, 4891−4893. [8e] E. Rüba, K. Mereiter, R. Schmid, V. N. Sapunov, K. Kirchner, H. Schottenberger, M. J. Calhorda, L. F. Veiros, *Chem. Eur. J.* **2002**, *8*, 3948−3961. [8f] E. Rüba, K. Mereiter, R. Schmid, K. Kirchner, E. Bustelo, M. C. Puerta, P. Valerga, *Organometallics* **2002**, *21*, 2912−2920. [8g] E. Becker, C. Slugovc, E. Rüba, C. Standfest-Hauser, K. Mereiter, R. Schmid, K. Kirchner, *J. Organomet. Chem.* **2002**, *649*, 55−63. [8h] E. Rüba, K. Mereiter, R. Schmid, K. Kirchner, H. Schottenberger, *J. Organomet. Chem.* **2001**, *637−639*, 70−74. [8i] E. Rüba, K. Mereiter, R. Schmid, K. Kirchner, *Chem. Commun.* **2001**, *19*, 1996−1997. [8l] K. Mauthner, K. M. Soldouzi, K. Mereiter, R. Schmid, K. Kirchner, *Organometallics* **1999**, *18*, 4681−4683.

[9] H. Butenschön, *Chem. Rev.* **2000**, *100*, 1527−1564.

[10] [10a] N. Dodo, Y. Matsushima, M. Uno, K. Onitsuka, S. Takahashi, *J. Chem. Soc., Dalton Trans.* **2000**, 35−41. [10b] Y. Matsushima, N. Komatsuzaki, Y. Ajioka, M. Yamamoto, H. Kikuchi, Y. Takata, N. Dodo, K. Onitsuka, M. Uno, S. Takahashi, *Bull. Chem. Soc. Jpn.* **2001**, *74*, 527−537.

[11] Y. Matsushima, K. Onitsuka, T. Kondo, T. Mitsudo, S. Takahashi, *J. Am. Chem. Soc.* **2001**, *123*, 10405−10406.

[12] A. Doppiu, U. Englert, A. Salzer, *Inorg. Chim. Acta* **2003**, *350*, 435−441.

[13] E. Becker, K. Mereiter, M. Puchberger, R. Schmid, K. Kirchner, A. Doppiu, A. Salzer, *Organometallics* **2003**, *22*, 3164−3170.

[14] [14a] T. Kauffmann, J. Ennen, H. Lhotak, A. Rensing, F. Steinseifer, A. Woltermann, *Angew. Chem.* **1980**, *92*, 328−329; *Angew. Chem. Int. Ed. Engl.* **1980**, *19*, 301−302. [14b] T. Kauffmann, K. Berghus, A. Rensing, *Chem. Ber.* **1985**, *118*, 4507−4516.

[15] [15a] S. Ciruelos, U. Englert, A. Salzer, C. Bolm, A. Maischak, *Organometallics* **2000**, *19*, 2240−2242. [15b] S. Ciruelos, A. Doppiu, U. Englert, A. Salzer, *J. Organomet. Chem.* **2002**, *663*, 183−191.

[16] [16a] C. F. Wilcox, R. R. Craig, *J. Am. Chem. Soc.* **1961**, *83*, 3866−3871. [16b] A. I. D'yachenko, L. G. Menchikov, O. M. Nefedov, *Bull. Acad. Sci. USSR, Div. Chem. Sci. (Engl. Transl.)* **1985**, 649−651.

[17] [17a] B. Rieger, G. Jany, R. Fawzi, M. Steimann, *Organometallics* **1994**, *13*, 647−653. [17b] B. Rieger, G. Jany, M. Steimann, R. Fawzi, *Z. Naturforsch., Teil B* **1994**, *49*, 451−458.

[18] D. C. Brookings, S. A. Harrison, R. J. Whitby, B. Crombie, R. V. H. Jones, *Organometallics* **2001**, *20*, 4574−4583.

[19] H. C. Kolb, M. S. Van Nieuwenhze, K. B. Sharpless, *Chem. Rev.* **1994**, *94*, 2483−2547.

[20] S. E. Schaus, B. D. Brandes, J. F. Larrow, M. Tokunaga, K. B. Hansen, A. E. Gould, M. E. Furrow, E. N. Jacobsen, *J. Am. Chem. Soc.* **2002**, *124*, 1307−1315.

[21] [21a] E. N. Tsvetkov, N. A. Bondarenko, I. G. Malakhova, M. I. Kabachnik, *Synthesis* **1986**, 198−205. [21b] H. B. Kagan, M. Tahar, J.-C. Fiaud, *Tetrahedron Lett.* **1991**, *32*, 5959−5962. [21c] P. Pellon, *Tetrahedron Lett.* **1992**, *33*, 4451−4452. [21d] E. Hauptmann, P. J. Fagan, W. Marshall, *Organometallics* **1999**, *18*, 2061−2073.

[22] In addition to NMR spectroscopic data, the regio- and stereochemistry in the ring opening of (*S*)-1-cyclohexylspiro[2.4]hepta-4,6-diene has also been confirmed by an X-ray structural determination of a metal complex with the derived cyclopentadienylphosphane ligand: U. Englert, personal communication.

[23] T. Lumini, D. N. Cox, R. Roulet, K. Schenk, *J. Organomet. Chem.* **1992**, *434*, 363−385.

[24] D. N. Cox, R. Roulet, *J. Chem. Soc., Chem. Commun.* **1989**, 175−176.

 © 2004 Wiley-VCH Verlag GmbH & Co. KGaA, Weinheim

[25] I. Lee, F. Dahan, A. Maisonnat, R. Poilblanc, *Organometallics* **1994**, *13*, 2743−2750.
[26] [26a] S. Otsuka, K. Tani, *Synthesis* **1991**, 665−680. [26b] R. Noyori, *Asymmetric Catalysis in Organic Synthesis, Chapter 3*, J. Wiley & Sons, New York, **1994**. [26c] S. Akutagawa, K. Tani, *Catalytic Asymmetric Synthesis, Chapter 3* (Ed.: I. Ojima), Wiley-VCH, New York, **2000**.
[27] C. Chapuis, M. Barthe, J.-Y. de Saint Laumer, *Helv. Chim. Acta* **2001**, *84*, 230−242.
[28] For a discussion of the difficulties encountered in catalyzing the isomerisation of allylic alcohols, see: [28a] C. Bianchini, A. Meli, W. Oberhauser, *New J. Chem.* **2001**, *25*, 11−12. [28b] R. Uma, C. Crévisy, R. Grée, *Chem. Rev.* **2003**, *103*, 27−52.
[29] [29a] R. C. van der Drift, E. Bouwman, E. Drent, *J. Organomet. Chem.* **2002**, *650*, 1−24. [29b] B. M. Trost, R. J. Kulawiec, *J. Am. Chem. Soc.* **1993**, *115*, 2027−2036.
[30] [30a] M. Wang, C.-J. Li, *Tetrahedron Lett.* **2002**, *43*, 3589−3591. [30b] X.-F. Yang, M. Wang, R. S. Varma, C.-J. Li, *Org. Lett.* **2003**, *5*, 657−660. [30c] M. Wang, X.-F. Yang, C.-J. Li, *Eur. J. Org. Chem.* **2003**, 998−1003.
[31] J. M. Brown, B. A. Murrer, *J. Chem. Soc., Perkin Trans. 2* **1982**, 489−497.
[32] D. P. Riley, R. E. Shumate, *J. Org. Chem.* **1980**, *45*, 5187−5193.
[33] G. Miao, B. E. Rossiter, *J. Org. Chem.* **1995**, *60*, 8424−8427.
[34] [34a] A. Bauer, U. Englert, S. Geyser, F. Podewils, A. Salzer, *Organometallics* **2000**, *19*, 5471−5476. [34b] A. Salzer, M. Käser, A. Hosang, A. Bauer, U. Effertz, E. Klinkhammer, F. Podewils, *Synthetic Methods of Organometallic and Inorganic Chemistry* (Eds.: W. A. Herrmann, G. Brauer), Georg Thieme Verlag: Stuttgart, **2000**; *9*, 45−58. [34c]A. Salzer, A. Bauer, S. Geyser, F. Podewils, *Inorg. Synth.* **2003**, *34*, in press. [34d] A. Salzer, F. Podewils, S. Geyser, *Eur. Patent. Appl.* 110429.8, *Int. Patent. Appl.* PCT/IB01/00784.

Received December 15, 2003
Early View Article
Published Online April 7, 2004

 © 2004 Wiley-VCH Verlag GmbH & Co. KGaA, Weinheim

The Reaction of μ-η²:η²-Peroxo- and Bis(μ-oxo)dicopper Complexes with Flavonol

József Kaizer,[a] József Pap,[b] Gábor Speier,*[a] and László Párkányi[c]

Keywords: Quercetinase / Model compounds / Copper / Oxygen / Flavonol

The $[Cu_2(\mu\text{-}O)_2]^{2+}$ and $[Cu_2(\mu\text{-}\eta^2\text{:}\eta^2\text{-}O)_2]^{2+}$ motifs with coordinated *N,N,N*-tribenzyl-1,4,7-triazacyclononane and *N,N,N*-triisopropyl-1,4,7-triazacyclononane auxiliary ligands in their reaction with flavonol do not lead to ring scission products of the heterocycle, but the formation of the corresponding (flavonolato)copper(II) complexes $[Cu(fla)(Bz\text{-}TAC)]ClO_4$ and $[Cu(fla)(i\text{Pr-}TAC)]ClO_4$. The subsequent oxygenolysis of the coordinated flavonolate ligand leads to *O*-benzoylsalicylate at elevated temperature, resulting in the enzyme mimicking products $[Cu(O\text{-bs})(Bz\text{-}TAC)]ClO_4$, $[Cu(O\text{-bs})(i\text{Pr-}TAC)]ClO_4$) as well as carbon monoxide. The X-ray structures of $[Cu(fla)(Bz\text{-}TAC)]ClO_4$, $[Cu(O\text{-bs})(Bz\text{-}TAC)]ClO_4$, and $[Cu(O\text{-bs})(i\text{Pr-}TAC)]ClO_4$) are presented.

(© Wiley-VCH Verlag GmbH & Co. KGaA, 69451 Weinheim, Germany, 2004)

Introduction

Biological oxygenations catalyzed by oxygenases are very important processes in nature for the metabolism of various organic substances.[1−5] To date, four prokaryotic dioxygenases are known, which catalyze an oxidative C−C bond cleavage with incorporation of two O-atoms into, and release of CO from the substrates quercetin (**1**) (flavonol 2,4-dioxygenase),[6−13] 3-hydroxy-4-oxo-1*H*-quinaldine (**3**) (3-hydroxy-4-oxo-1*H*-quinaldine 2,4-dioxygenase), 3-hydroxy-4-oxo-1*H*-quinoline (**4**) (3-hydroxy-4-oxo-1*H*-quinoline 2,4-dioxygenase),[14,15] and (*S*)-1,2-dihydroxy-3-oxo-5-(methylthio)pentene anion (**5**) [(*S*)-1,2-dihydroxy-3-oxo-5-(methylthio)pentene anion 1,3-dioxygenase].[16,17] Flavonol 2,4-dioxygenase ("quercetinase"), which catalyzes the cleavage of quercetin to carbon monoxide and phenolic carboxylic acid ester was produced by the species *Aspergillus flavus* and *Pullularia* (Scheme 1).[18]

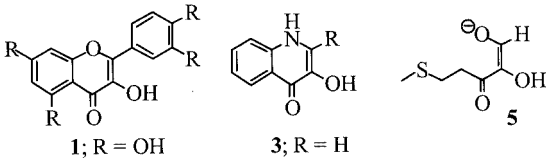

1; R = OH
2; R = H
3; R = H
4; R = Me
5

[a] Research Group for Petrochemistry, Hungarian Academy of Sciences,
8201 Veszprém, Hungary
[b] Department of Organic Chemistry, University of Veszprém,
8201 Veszprém, Wartha V. u. 1, Hungary
Fax: (internat.) + 36-88427492
E-mail: speier@almos.vein.hu
[c] Hungarian Academy of Sciences, Institute of Chemistry, Chemical Research Center,
1525 Budapest, Hungary

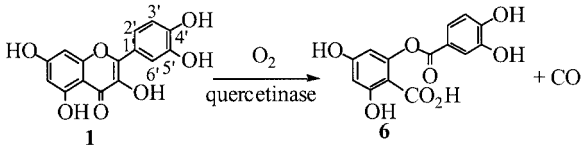

1 **6**

Scheme 1

Quercetinase has been reported to contain two Cu^{II} centers per molecule.[19,20] Recent diffraction studies on single crystals of quercetin 2,3-dioxygenase obtained from *Aspergillus japonicus*, at a resolution of 1.8 Å, showed that the enzyme forms homodimers, which are stabilized by an *N*-linked heptasaccharide at the dimer interface.[21] Each unit is mononuclear, with a type 2 copper center displaying two distinct geometries: a distorted tetrahedral coordination with three histidine units and one water molecules, and a distorted trigonal bipyramidal environment with an additional carboxylate. Substrate docking studies hinted to the eventual catalytic importance of the different geometries. In general, the process of oxygenase catalyzed reactions may be divided into three steps in an organic chemical sense. The first step is the activation of molecular oxygen and/or a substrate. The second step is the formation of a reactive intermediate, which would be a peroxidic compound in the case of dioxygenases,[22] and an oxygenated compound such as an arene oxide in the case of monooxygenases.[2,5,23] The third step involves the transformation of such an intermediate into the final product. From our earlier results obtained with redox[24−32] and non-redox[33,35] metal-containing model systems we concluded, that the oxygenolysis of the coordinated flavonolate ligand in aprotic solvents takes place mainly *via* an endoperoxide intermediate resulting in *O*-benzoylsalicylate as an enzyme-like

product,[36] and to a lesser extent through a 1,2-dioxethane intermediate.[37] Apart from these mechanisms, and despite recent suggestions in the literature,[38] the oxygenation of flavonol to enzyme-like products can also be postulated with the primary formation of copper-dioxygen species as the key reaction step. Earlier studies assumed coordination of quercetin to the copper(II) site through its 3-OH and 4-C=O groups.[39–41] Model studies have reinforced this hypothesis, and a fair number of copper complexes of flavonolate ligands have been isolated and structurally characterized.[24,25,28–30,42] It has also been postulated, that monodentate coordination of quercetin may be responsible for the substrate activation.[21,38,43] Since we have found in our model studies, that the oxygenation of flavonolate coordinated either to copper(I) or copper(II) requires higher reaction temperatures (around 100 °C) it cannot be excluded, that the first step in the catalytic cycle is the activation of dioxygen. In order to gain experimental support for this possibility we have directly evaluated the feasibility of this transformation by examining the reaction of flavonol with (μ-η^2:η^2-peroxo)- and bis(μ-oxo)dicopper complexes.[44–47] Herein we report that $[Cu_2(\mu\text{-}O)_2]^{2+}$ and $[Cu_2(\mu\text{-}\eta^2\text{:}\eta^2\text{-}O)_2]^{2+}$ cores coordinated to *N*-trisubstituted triazacyclononanes do not promote the ring cleavage reaction of the heterocycle but react with two equivalents of flavonol yielding (flavonolato)copper(II) complexes. Subsequent oxygenation of the (flavonolato)copper(II) complexes by dioxygen at elevated temperatures results in (*O*-benzoylsalicylato)copper(II) complexes and CO.

Results and Discussion

Addition of two equivalents of flavonol (**2**; flaH) to a solution of $[\{Cu(Bz\text{-}TAC)\}_2(\mu\text{-}O)_2](ClO_4)_2$ or $[\{Cu(i\text{Pr-}TAC)\}_2(\mu\text{-}\eta^2\text{:}\eta^2\text{-}O)_2](ClO_4)_2$ in CH_2Cl_2 at −80 °C caused bleaching of their respective optical absorption features (Bz-TAC = *N*,*N*,*N*-tribenzyl-1,4,7-triazacyclononane, *i*Pr-TAC = *N*,*N*,*N*-triisopropyl-1,4,7-triazacyclononane). Upon subsequent warming and workup, the green complexes $[Cu(fla)(Bz\text{-}TAC)]ClO_4$ (**9**) or $[Cu(fla)(i\text{Pr-}TAC)]ClO_4$ (**10**) (fla = flavonolate) were isolated as crystalline solids in yields of 95 and 90%, respectively (Scheme 2). The reaction products were identified on the basis of spectroscopic comparisons with previously reported examples, magnetic properties, and X-ray crystallography. Tests for the concomitant formation of H_2O_2 did not give convincing results irrespective of whether there was a selectivity in terms of forming either H_2O_2 or H_2O from the peroxo or oxo copper complexes.

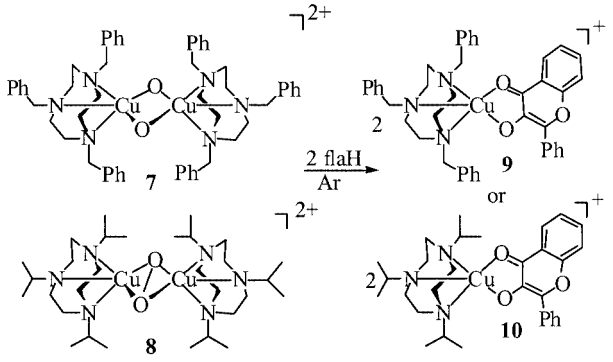

Scheme 2

The IR spectra of the complexes $[Cu(fla)(Bz\text{-}TAC)]ClO_4$ and $[Cu(fla)(i\text{Pr-}TAC)]ClO_4$ show principal bands corresponding to coordinated flavonolate at 1545 and 1554 cm^{-1}, respectively. Decreases of approximately 50 cm^{-1} in the ν(CO) bands compared with that of flavonol [ν(CO) = 1602 cm^{-1}] are due to chelation and formation of stable five-membered rings.[48] The charge transfer region in the electronic spectra of the complexes $[Cu(fla)(Bz\text{-}TAC)]ClO_4$ and $[Cu(fla)(i\text{Pr-}TAC)]ClO_4$ exhibit bands of the coordinated flavonolate ligand at 432 and 434 nm. Bands at 615 and 653 nm are associated with d-d transitions of the complexes.

The molecular structure together with selected bond lengths and angles of $[Cu(fla)(Bz\text{-}TAC)]ClO_4$ are shown in Figure 1. The molecule is monomeric in the solid state. The copper(II) center is in a distorted square-pyramidal environment as judged by the method of Allison and co-workers (τ = 0.12)[49] with basal planes defined by two nitrogen atoms derived from the tridentate *N*,*N*,*N*-tribenzyl-1,4,7-triazacyclononane ligand [Cu−N19, 2.040(3); Cu−N22, 2.027(3) Å], and two oxygen atoms of the flavonolate [Cu−O1, 1.917(3); Cu−O8, 2.012(3) Å]. The third nitrogen atom of the *N*,*N*,*N*-tribenzyl-1,4,7-triazacyclononane ligand [Cu−N25, 2.231(3) Å] is in the apical position. The Cu−O8 bond is 0.095 Å longer than the Cu−O1 bond. The C2−O1 distance is shorter while the C7−O8 distance is longer than those in the uncoordinated flavonol [1.357(3) and 1.232(3) Å].[50] Due to coordination to the copper ion there are also

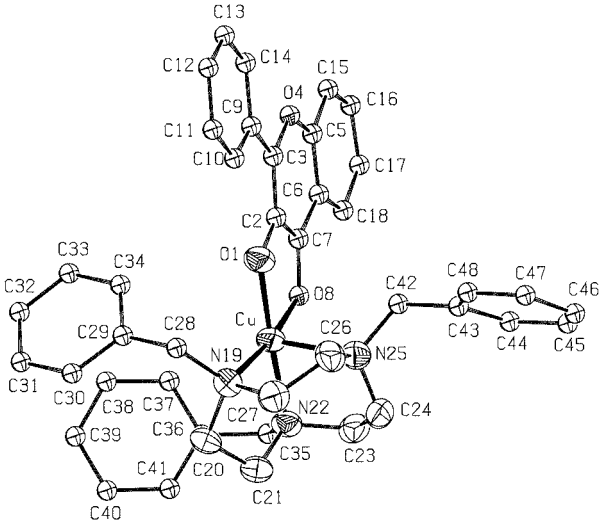

Figure 1. View showing the structure of $[Cu(fla)(Bz\text{-}TAC)]ClO_4$ (**9**); selected bond lengths (Å) and angles (deg): Cu−O1 1.917(3), Cu−O8 2.012(3), Cu−N22 2.027(3), Cu−N19 2.040(3), Cu−N25 2.231(3), O1−C2 1.339(4), O8−C7 1.273(4), C2−C3, 1.381(5), C2−C7 1.401(5); O1−Cu−N22 177.60(12), O8−Cu−N19 170.25(12), N19−Cu−N25 85.94(12), C2−O1−Cu 111.5(2), C7−O8−Cu 109.9(2)

 © 2004 Wiley-VCH Verlag GmbH & Co. KGaA, Weinheim

changes in the bond lengths of the pyranone ring. The O4−C3 [1.362(4) Å] and C5−C6 [1.381(5) Å] bond lengths become longer, and the C2−C7 bond length [1.401(5) Å] is somewhat shorter, which may be assigned to delocalization of the π-system over the whole molecule. Similar reactions of peroxo- and bis(μ-oxo)dicopper complexes bearing the *N*,*N*,*N*-trisubstituted 1,4,7-triazacyclononane ligands with catechols resulted in the corresponding copper(II) semiquinone complexes.[51] Since the amine macrocyclic ligands are hard, and prefer copper(II), the copper ion remained in this oxidation state. It was not specified, however, whether H_2O or H_2O_2 was formed as the reduction product from O_2.

Treatment of the (flavonolato)copper complexes [Cu(fla)(Bz-TAC)]ClO_4 or [Cu(fla)(*i*Pr-TAC)]ClO_4 with dioxygen in DMF solution at elevated temperatures leads to the corresponding (*O*-benzoylsalicylato)copper complexes [Cu(*O*-bs)(Bz-TAC)]ClO_4 (**11**) and [Cu(*O*-bs)(*i*Pr-TAC)]-ClO_4 (**12**) (Scheme 3). The IR spectra of the complexes [Cu(*O*-bs)(Bz-TAC)]ClO_4 and [Cu(*O*-bs)(*i*Pr-TAC)]ClO_4 show principal bands corresponding to ν(CO) at 1741 and 1747 cm^{-1}, respectively. Bands corresponding to ν(CO_2) for the two complexes appear at 1586 and 1432, and 1584 and 1428 cm^{-1}, respectively.

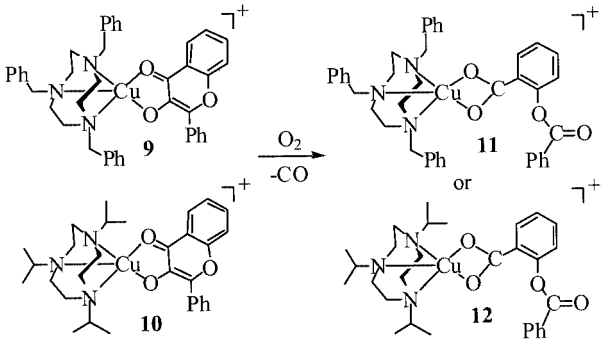

Scheme 3

The molecular structure together with selected bond lengths and angles of [Cu(*O*-bs)(Bz-TAC)]ClO_4 are shown in Figure 2. The copper(II) center is in a distorted square pyramidal environment ($\tau = 0.16$)[49] with basal planes defined by two nitrogen atoms derived from the tridentate *N*,*N*,*N*-tribenzyl-1,4,7-triazacyclononane ligand, and two oxygen atoms of the bidentate carboxylate group. The apical position is occupied by the other nitrogen atom of the *N*,*N*,*N*-tribenzyl-1,4,7-triazacyclononane ligand. The copper−nitrogen bond lengths [Cu−N1 2.000(2), Cu−N4 2.010(2), and Cu−N7 2.182(2) Å] are similar to values obtained for [Cu(fla)(Bz-TAC)]ClO_4. The Cu−O bond lengths are shorter than those in [Cu(*O*-bs)(idpaH)]ClO_4 [1.995(5) and 2.344(6) Å].[30]

Crystallographic characterization has shown that in [Cu(*O*-bs)(*i*Pr-TAC)]ClO_4 (**12**, Figure 3), the copper(II) ion has a distorted square pyramidal arrangement ($\tau = 0.10$)[49] with basal planes defined by two nitrogen atoms derived from the tridentate *N*,*N*,*N*-triisopropyl-1,4,7-triazacyclo-

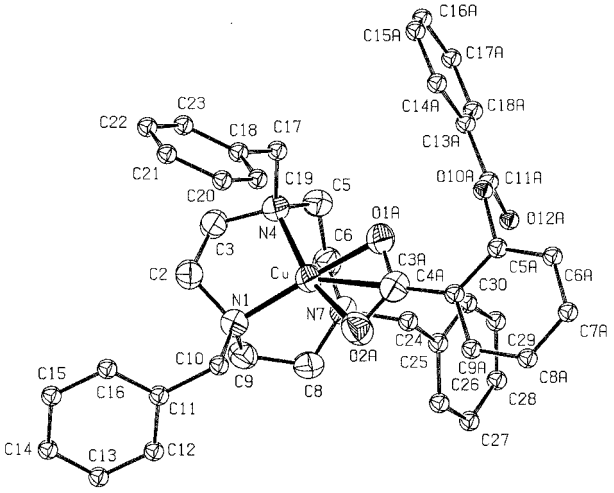

Figure 2. View showing the structure of [Cu(*O*-bs)(Bz-TAC)]ClO_4 (**11**); selected bond lengths (Å) and angles (deg): Cu−O1A 1.9772(17), Cu−O2A 2.0685(19), Cu−N1 2.000(2), Cu−N4 2.010(2), Cu−N7 2.182(2) O1A−C3A, 1.273(3) O2A−C3A, 1.256(3); O1A−Cu−N1 171.19(8), O1A−Cu−O2A 64.87(7), N4−Cu−O2A 161.55(8), N4−O1−N7 86.94(8)

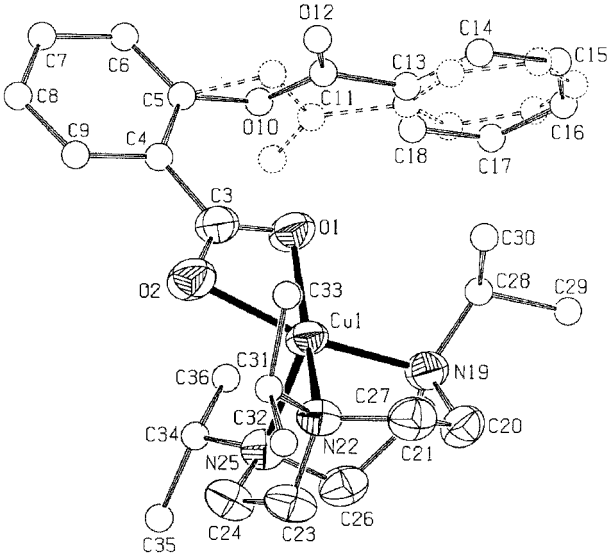

Figure 3. View showing the structure of [Cu(*O*-bs)(*i*Pr-TAC]ClO_4 (**12**); selected bond lengths (Å) and angles (deg): Cu1−O1 1.981(6), Cu1−O2 2.020(7), Cu1−N19 2.020(7), Cu1−N22 2.033(6), Cu1−N25 2.208(7), O1−C3 1.261(10), O2−C3 1.268(10); O1−Cu1−N22 159.8(3), O1−Cu1−O2 64.8(2), N19−Cu1−O2 165.6(2), N22−Cu1−N25 87.7(3)

nonane ligand, and two oxygen atoms of the bidentate carboxylate group. The apical position is occupied by the other nitrogen atom of the *N*,*N*,*N*- triisopropyl-1,4,7-triazacyclononane ligand. A view of the coordination geometry as well as selected bond lengths and angles are given in Figure 2. The copper−nitrogen bond lengths [Cu1−N19 2.020(7), Cu1−N22 2.033(6), Cu1−N25,= 2.208(7) Å] are similar to values obtained for [Cu(*O*-bs)(Bz-TAC)]ClO_4. The value of (Cu1−O2) − (Cu1−O1) (0.039 Å) is somewhat shorter than that found in the complex [Cu(*O*-bs)(Bz-TAC)]ClO_4 (0.0913 Å), which may be assigned to the higher degree of delocalization in the carboxylate group.

 © 2004 Wiley-VCH Verlag GmbH & Co. KGaA, Weinheim

Oxygenation reactions of [Cu(fla)(Bz-TAC)]ClO_4 and [Cu(fla)(*i*Pr-TAC)]ClO_4 complexes were followed by UV-Vis spectroscopy. Plots of log[Cu(fla)(Bz-TAC)]ClO_4 and log[Cu(fla)(*i*Pr-TAC)]ClO_4 versus time showed linear dependences under pseudo-first-order conditions (constant dioxygen pressure) in agreement with a rate equation of first-order dependence with respect to [Cu(fla)(Bz-TAC)]-ClO_4 and [Cu(fla)(*i*Pr-TAC)]ClO_4, respectively. Experiments performed at different dioxygen concentrations showed that both of the reactions are also first order with respect to dioxygen concentration. According to the kinetic data obtained, the oxygenation reactions obey an overall second-order rate equation, from which the mean values of the kinetic constants k_{obs} of 3.31 ± 0.01 × 10^{-3} ([Cu(fla)(Bz-TAC)]ClO_4) and 1.51 ± 0.01 × 10^{-3} mol^{-1}·dm^3 s^{-1} ([Cu(fla)(*i*Pr-TAC)]ClO_4) at 120 °C were obtained. The calculated rate constant is, in the case of [Cu(fla)(Bz-TAC)]-ClO_4, almost two times larger than that for [Cu(fla)(*i*Pr-TAC)]ClO_4. Oxidative cleavage of the C2−C3 double bond of the pyranone ring of the coordinated flavonolato ligand in both cases takes place in a similar fashion as in the enzymatic reaction. Stoichiometric oxygenation reactions can be interpreted as shown in Scheme 4. We are inclined to assume a redox role for the copper(II). Due to the valence isomerism of the copper(II) flavonolate complexes, copper(I) flavonoxy radical species are also formed, as suggested earlier.[37] Similar electromeric effects between metal catecholate and metal semiquinone complexes have been demonstrated.[52,53] They have two redoxactive sites, the flavonoxy radical ligand and the Cu^I center, which can react with dioxygen in a slow step to form the endoperoxide intermediates. These then break down rapidly to the corresponding (*O*-benzoylsalicylato)copper(II) complexes and CO.

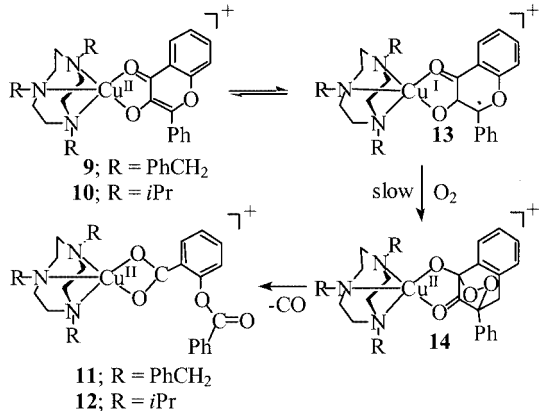

Scheme 4

Conclusion

In conclusion, we have found that $Cu_2^{III}(\mu\text{-}O)_2$ and $Cu_2^{II}(\mu\text{-}\eta^2\text{:}\eta^2\text{-}O)_2$ complexes with triazacyclononane auxiliary ligands are not able to cleave the C2−C3 double bond in flavonol under mild reaction conditions. Instead, the corresponding (flavonolato)copper(II) complexes are formed. The latter complexes, however, undergo ring scission in their reaction with dioxygen under more forcing conditions resulting in the (*O*-benzoylsalicylato)copper(II) complexes and carbon monoxide. These results enable us to conclude, that in the enzyme catalyzed reaction, the activation of the substrate flavonol through its coordination to the copper(II) center probably takes place, and its oxygenation and subsequent reaction of the copper-dioxygen species with flavonol is the real catalytic situation.

Experimental Section

General Remarks: All reagents and solvents were purchased from commercial sources and were of reagent quality unless otherwise stated. All air-sensitive compounds were handled under argon using standard Schlenk techniques.[54]

Caution! *Perchlorate salts of metal complexes with organic ligands are potentially explosive. Only small amounts of material should be prepared, and these should be handled with great care.*

Synthesis of [Cu(fla)(Bz-TAC)]ClO_4 (9): A solution of [{Cu(Bz-TAC)}$_2$(μ-O)$_2$]$(ClO_4)_2$ in CH_2Cl_2 (15 mL) at −80 °C was prepared as described previously (0.164 g, 0.5 mmol scale of Cu^I precursor).[46,47] After removal of excess dioxygen by purging with argon at −80 °C for 10 min, a solution of flavonol (0.119 g, 0.5 mmol) in CH_2Cl_2 (5 mL) was added, resulting in an instantaneous color change from red-brown to intense green. The reaction mixture was stirred at −80 °C for 1 h, and then warmed to room temperature. After concentrating the solution by evaporation under vacuum, Et_2O was added to induce precipitation of a green solid which was collected by filtration, washed with Et_2O, and air-dried (95%, m.p. 224−226 °C). The crude product was recrystallized from CH_3CN. $C_{42}H_{42}ClCuN_3O_7$ (799.80): calcd. C 63.1, H 5.3, N 5.3; found C 62.9, H 5.5, N 5.5. UV-Vis (DMF): $\lambda_{max.}$ (log ε) = 269 (4.23) 432 (2.23), 615 (2.90), 1040 (1.73) nm. IR (KBr, cm^{-1}): $\tilde{\nu}$ = 1097 (vs, νClO_4^-), 634 (s, νClO_4^-), 1545 (s, νCO). EPR (MeCN): g = 2.115, A = 66.0 G. μ_{eff} = 1.93 BM.

Synthesis of [Cu(fla)(*i*Pr-TAC)]ClO_4 (10): This compound was prepared analogously to [Cu(fla)(Bz-TAC)]ClO_4 but by treating [{Cu(*i*Pr-TPA)}$_2$(μ-η^2:η^2-O)$_2$]$(ClO_4)_2$ [44] with flavonol (90%, m.p. 235−237 °C). The crude product was recrystallized from CH_3CN. $C_{30}H_{42}ClCuN_3O_7$ (655.7): calcd. C 55.0, H 6.5, N 6.4; found C 54.8, H 6.3, N 6.5. UV-Vis (DMF): $\lambda_{max.}$ (log ε) = 274 (3.54) 434 (3.52), 653 (2.15), 1065 (1.89) nm. IR (KBr, cm^{-1}): $\tilde{\nu}$ = 1097 (vs, νClO_4^-), 628 (s, νClO_4^-), 1554 (s, νCO). EPR (MeCN): g = 2.116, A = 66.4 G. μ_{eff} = 1.89 BM.

Oxygenation of [Cu(fla)(R-TAC)]ClO_4 (R = Bz, *i*Pr): [Cu(fla)(Bz-TAC)]ClO_4 or [Cu(fla)(*i*Pr-TAC)]ClO_4) (0.25 mmol) was dissolved in DMF (5 mL) and stirred at 120 °C under dioxygen for 12 h. The formation of [Cu(*O*-bs)(Bz-TAC)]ClO_4 or [Cu(*O*-bs)(*i*Pr-TAC)]-ClO_4 from [Cu(fla)(Bz-TAC)]ClO_4 or [Cu(fla)(*i*Pr-TAC)]ClO_4 requires dioxygen but no apparent uptake was observed because the absorption of dioxygen, and the liberation of carbon monoxide compensate each other. Dilute NH_3 solution (0.5 mL) was added to a portion of the reaction mixture (1 mL) at room temperature, and the organic phase was extracted with diethyl ether. Diazomethane solution (1 mL) was then added and the conversion to the coordinated flavonolate (78 and 57%) was determined by GC.

 © 2004 Wiley-VCH Verlag GmbH & Co. KGaA, Weinheim

Synthesis of [Cu(*O*-bs)(Bz-TAC)]ClO_4 (11): To a solution of $[Cu(CH_3CN)_4]ClO_4$ (0.119 g, 0.5 mmol) and Bz-TAC (0.13 g, 0.5 mmol) in CH_3CN (10 mL) was added *O*-benzoylsalycilic acid (0.121 g, 0.5 mmol) in CH_3CN (10 mL), and the solution was heated to reflux for 5 h under O_2. After concentrating the solution by evaporation under vacuum, Et_2O was added to induce precipitation of a blue solid, which was collected by filtration, washed with Et_2O, and air-dried (92%, m.p. 198−200 °C). X-ray quality crystals were obtained by slow evaporation of a CH_3CN solution. $C_{41}H_{42}ClCuN_3O_8$ (803.8): calcd. C 61.3, H 5.3, N 5.2; found C 60.8, H 5.1, N 5.0. UV-Vis (DMF): $\lambda_{max.}$ (log ε) = 276 (3.81), 650 (1.96), 1035 (1.62) nm. IR (KBr, cm^{-1}): $\tilde{\nu}$ = 1097 (vs, νClO_4^-), 628 (s, νClO_4^-), 1741 (s, νCO), 1586 (s, $\nu_{as}CO_2$). 1432 (s, ν_sCO_2). EPR (MeCN): g = 2.120, A = 62.0 G. μ_{eff} = 1.99 BM.

Synthesis of [Cu(*O*-bs)(*i*Pr-TAC)]ClO_4 (12): This compound was prepared analogously to [Cu(*O*-bs)(Bz-TAC)]ClO_4 but using the *i*Pr-TAC ligand instead (90%, m.p. 235−237 °C). X-ray quality crystals were obtained by slow evaporation of a CH_3CN solution. $C_{29}H_{42}ClCuN_3O_8$: calcd. C 52.8, H 6.4, N 6.4; found C 52.4, H 6.2, N 6.6. UV-Vis (DMF): $\lambda_{max.}$ (log ε) = 278 (3.23), 670 (1.43), 1060 (1.73) nm. IR (KBr, cm^{-1}): $\tilde{\nu}$ = 1095 (vs, νClO_4^-), 627 (s, νClO_4^-), 1747 (s, νCO), 1584 (s, $\nu_{as}CO_2$). 1428 (s, ν_sCO_2). EPR (MeCN): g = 2.121, A = 60.3 G. μ_{eff} = 1.97 BM.

Kinetic Measurements: Reactions of [Cu(fla)(Bz-TAC)]ClO_4 and [Cu(fla)(*i*Pr-TAC)]ClO_4 with dioxygen were performed in DMF solutions. In a typical experiment [Cu(fla)(Bz-TAC)]ClO_4 or [Cu(fla)(*i*Pr-TAC)]ClO_4 was dissolved under argon in a thermostatically controlled reaction vessel with an inlet for taking samples with a syringe, and connected to a mercury manometer to maintain a constant pressure. The solution was then heated to the appropriate temperature. A sample was then taken by syringe and the initial concentration of [Cu(fla)(Bz-TAC)]ClO_4 or [Cu(fla)(*i*Pr-TAC)]ClO_4 was determined by UV-Vis spectroscopy measuring the absorbance of the reaction mixture at 432 nm or 434 nm {$\lambda_{max.}$ of a typical band of [Cu(fla)(Bz-TAC)]ClO_4 or [Cu(fla)(*i*Pr-TAC)]ClO_4]}, respectively. The argon was then replaced by dioxygen and consumption of the latter was periodically monitored. The rate of oxygenation was independent of the stirring rate, excluding

Table 1. Crystal data, data collection, and structural refinement details

	9	**12**	**11**
Empirical formula	$C_{84}H_{84}Cl_2Cu_2N_6O_{14}$	$C_{29}H_{42}ClCuN_3O_8$	$C_{41}H_{42}ClCuN_3O_8$
Molecular mass	1599.55	659.65	803.77
Temperature	293(2) K		
Radiation and wavelength	Mo-K_α, λ = 0.71073 Å		
Crystal system	triclinic	triclinic	monoclinic
Space group	$P\bar{1}$	$P\bar{1}$	$P2_1/c$
Unit cell dimensions			
a (Å)	9.831(3)	10.756(1)	19.373(3)
b (Å)	12.065(2)	12.589(1)	11.683(3)
c (Å)	16.512(3)	12.787(2)	19.355(2)
α (°)	87.33(2)	79.47(1)	90
β (°)	83.26(1)	73.31(1)	117.82(1)
γ (°)	76.07(2)	75.13(1)	90
Volume (Å^3)	1887.4(7)	1591.8(3)	3874.4(12)
Z	1	2	4
Density (calcd.) (Mg·m^{-3})	1.41	1.38	1.38
Absorption coeff., μ (mm^{-1})	0.71	0.82	0.69
F(000)	834	694	1676
Crystal color	grayish green	dark green	bluish green
Crystal description	plate	block	plate
Crystal size (mm)	0.60 × 0.15 × 0.05	0.40 × 0.35 × 0.25	0.50 × 0.30 × 0.25
Absorption correction	psi-scan		
Transmission, max. and min.	0.9811 and 0.8005	0.9854 and 0.7605	0.9817 and 0.9781
θ Range [°]	2.42 ≤ θ ≤ 26.97	2.28 ≤ θ ≤ 29.96	2.38 ≤ θ ≤ 27.97
Index ranges	−12 ≤ h ≤ 12	−15 ≤ h ≤ 15	−25 ≤ h ≤ 22
−15 ≤ k ≤ 15	−17 ≤ k ≤ 17	0 ≤ k ≤ 15	
−21 ≤ l ≤ 21	−17 ≤ l ≤ 17	0 ≤ l ≤ 25	
Reflections collected	17820	19419	9786
Completeness to 2θ	0.992	0.986	0.994
Number of standard reflections	3		
Decay	0%	1%	4%
Independent reflections	8152 [R(int) = 0.0422]	9112 [R(int) = 0.0265]	9280 [R(int) = 0.0142]
Reflections I>2σ(I)	3692	5140	4537
Refinement method	full-matrix least-squares on F^2		
Data/restraints/parameters	8152 /47/497	9112 /34 /463	9280 /93 /530
Goodness-of-fit on F^2	0.856	0.902	0.867
Final R indices I>2σ(I)	$R1$ = 0.0544, $wR2$ = 0.1257	$R1$ = 0.0559, $wR2$ = 0.1446	$R1$ = 0.0427, $wR2$ = 0.0970
R indices (all data)	$R1$ = 0.1411, $wR2$ = 0.1478	$R1$ = 0.1026, $wR2$ = 0.1621	$R1$ = 0.1171, $wR2$ = 0.1098
Max. and mean shift/esd.	0.001; 0.000	0.067; 0.002	2.637; 0.112
Largest diff. peak and hole (e·Å^{-3})	0.749 and −0.456	1.000 and −0.689	0.363 and −0.312

 © 2004 Wiley-VCH Verlag GmbH & Co. KGaA, Weinheim

eventual diffusion control effects. The dioxygen concentration was calculated from literature data (as 6.96×10^{-3} M)[55] taking into account the partial pressure of DMF,[56] and assuming the validity of Dalton's law.

X-ray Crystallographic Studies: Intensity data were collected on an Enraf−Nonius CAD4 diffractometer (graphite monochromator; Mo-K_α radiation, $\lambda = 0.71073$ Å) at 293(2) K using $\omega/2\theta$ scans. The intensities of three standard reflections were monitored regularly (every 60 min). Psi-scan absorption corrections were applied to the data.[57]

The structures were solved by direct methods (and subsequent difference syntheses),[58] and refined by anisotropic full-matrix least-squares on F^2 for all non-hydrogen atoms.[59] Hydrogen atomic positions were calculated from assumed geometries. Hydrogen atoms were included in structure factor calculations but they were not refined. The isotropic displacement parameters of the hydrogen atoms were approximated from the U_{eq} value of the atom to which they were bonded. Crystal data, data collection, and refinement details are shown in Table 1. The ClO_4^- anions are disordered in all three structures. In **11** the perchlorate O1c atom is ordered and the remaining three oxygens split into seven partially occupied positions. The sum of these occupation factors were bound to give three. The high maximum and mean shift/esd is due to the site occupation factor of O3c. In **12** (Figure 3) only one perchlorate oxygen atom splits but the O10···C18 (Ph−COO) moiety is, however, disordered with 2/3:1/3 occupancies. For the presentation of the molecular structures, the molecular graphics program PLATON was used.[60]

CCDC-201803 (for **9**), -201804 (for **11**), and -201805 (for **12**) contain the supplementary crystallographic data for this paper. These data can be obtained free of charge at ww.ccdc.cam.ac.uk/conts/retrieving.html or from Cambridge Crystallographic Data Center, 12, Union Road, Cambridge CB2 1EZ, UK [Fax: (internat.) +44-1223/336-033; E-mail: deposit@ccdc.cam.ac.uk].

Acknowledgments

We thank the Hungarian Research Fund (OTKA T-030400 and T-043414) for financial support.

[1] B. G. Fox, J. D. Lipscomb in *Biological Oxidation Systems* (Eds.: C. Reddy, G. A. Hamilton), Academic Press, New York, **1990**, p. 367.
[2] *Bioinorganic Chemistry of Copper* (Eds.: K. D. Karlin, Z. Tyeklár), Chapman & Hall, New York, **1992**.
[3] E. I. Solomon, M. J. Baldwin, M. D. Lowery, *Chem. Rev.* **1992**, *92*, 521.
[4] K. D. Karlin, *Science* **1993**, *261*, 701.
[5] *Catalysis by Metal Complexes, Oxygenases and Model Systems* (Ed.: T. Funabiki), Kluwer Academic Press, Dordrecht, The Netherlands, **1997**.
[6] S. Hattori, I. Noguchi, *Nature* **1959**, *184*, 1145.
[7] H. K. Hund, J. Breuer, F. Lingens, J. Hüttermann, R. Kappl, S. Fetzner, *Eur. J. Biochem.* **1999**, *263*, 871.
[8] W. Barz, *Arch. Mikrobiol.* **1971**, *78*, 341.
[9] D. W. S. Westlake, G. Talbot, E. R. Blakley, F. J. Simpson, *Can. J. Microbiol.* **1959**, *5*, 621.
[10] D. W. S. Westlake, J. M. Roxburgh, G. Talbot, *Nature* **1961**, *189*, 510.
[11] T. Oka, F. J. Simpson, *J. Biochem. Biophys. Res. Commun.* **1971**, *43*, 1.
[12] H. G. Krishnamurty, F. J. Simpson, *J. Biol. Chem.* **1970**, *245*, 1467.
[13] T. Oka, F. J. Simpson, H. G. Krishnamurty, *Can. J. Microbiol.* **1972**, *18*, 493.
[14] I. Bauer, A. de Beyer, B. Tshisuaka, S. Fetzner, F. Lingens, *FEMS Microbiol. Lett.* **1994**, *117*, 299.
[15] I. Bauer, N. Max, S. Fetzner, F. Lingens, *Eur. J. Biochem.* **1996**, *240*, 576.
[16] J. W. Wray, R. H. Abeles, *J. Biol. Chem.* **1993**, *268*, 24785.
[17] J. W. Wray, R. H. Abeles, *J. Biol. Chem.* **1995**, *270*, 3147.
[18] T. Matsuura, *Tetrahedron* **1977**, *33*, 2869.
[19] T. Oka, F. J. Simpson, J. J. Child, S. C. Mills, *Can. J. Microbiol.* **1971**, *17*, 111.
[20] T. Oka, H. G. Krishnamurty, F. J. Simpson, *Can. J. Microbiol.* **1972**, *18*, 893.
[21] F. Fusetti, K. H. Schröter, R. A. Steiner, P. I. van Noort, T. Pijning, H. J. Rozeboom, K. H. Kalk, M. R. Egmond, B. W. Dijkstra, *Structure* **2002**, *10*, 259.
[22] C. W. Jefford, P. A. Cadby, *Prog. Chem. Nat. Prod.* **1981**, *40*, 191.
[23] *Catalytic Activation of Dioxygen by Metal Complexes; Catalysis by Metal Complexes Series*, (Ed.: Simándi, L. I.), Kluwer Academic Publishers, Dordrecht, **1992**, vol. 13, 185.
[24] G. Speier, V. Fülöp, L. Párkányi, *J. Chem. Soc., Chem. Commun.* **1990**, 512.
[25] É. Balogh-Hergovich, G. Speier, G. Argay, *J. Chem. Soc., Chem. Commun.* **1991**, 551.
[26] É. Balogh-Hergovich, J. Kaizer, G. Speier, *Inorg. Chim. Acta* **1997**, *256*, 9.
[27] I. Lippai, G. Speier, G. Huttner, L. Zsolnai, *Chem. Commun.* **1997**, 741.
[28] É. Balogh-Hergovich, J. Kaizer, G. Speier, G. Argay, L. Párkányi, *J. Chem. Soc., Dalton Trans.* **1999**, 3847.
[29] É. Balogh-Hergovich, J. Kaizer, G. Speier, V. Fülöp, L. Párkányi, *Inorg. Chem.* **1999**, *38*, 3787.
[30] É. Balogh-Hergovich, J. Kaizer, G. Speier, G. Huttner, L. Zsolnai, *Inorg. Chim. Acta* **2000**, *304*, 72.
[31] É. Balogh-Hergovich, J. Kaizer, G. Speier, G. Huttner, A. Jacobi, *Inorg. Chem.* **2000**, *39*, 4224.
[32] É. Balogh-Hergovich, J. Kaizer, G. Speier, *J. Mol. Catal. A: Chem.* **2000**, *159*, 215.
[33] L. Barhács, J. Kaizer, G. Speier, *J. Org. Chem.* **2000**, *65*, 3449.
[34] L. Barhács, J. Kaizer, G. Speier, *J. Mol. Catal. A: Chem.* **2001**, *172*, 117.
[35] J. Kaizer, J. Pap, G. Speier, L. Párkányi, L. Korecz, A. Rockenbauer, *J. Inorg. Biochem.* **2002**, *91*, 190.
[36] L. Barhács, J. Kaizer, J. Pap, G. Speier, *Inorg. Chim. Acta* **2001**, *320*, 83.
[37] É. Balogh-Hergovich, J. Kaizer, J. Pap, G. Speier, G. Huttner, L. Zsolnai, *Eur. J. Inorg. Chem.* **2002**, 2287.
[38] R. A. Steiner, K. H. Kalk, B. W. Dijkstra, *Proc. Nat. Acad. Sci.* **2002**, *99*, 16625.
[39] E. Makasheva, N. T. Golovkina, *Zh. Obsch. Khim.* **1973**, *43*, 1640.
[40] M. Thomson, C. R. Williams, *Anal. Chim. Acta* **1976**, *85*, 375.
[41] K. Takamura, M. Ito, *Chem. Pharm. Bull.* **1977**, *25*, 3218.
[42] I. Lippai, G. Speier, L. Zsolnai, G. Huttner, *Acta Crystallogr., Sect. C* **1997**, *53*, 1547.
[43] É. Balogh-Hergovich, J. Kaizer, G. Speier, *J. Mol. Catal. A: Chem.* **2003**, *206*, 83.
[44] W. B. Tolman, *Acc. Chem. Res.* **1997**, *30*, 227.
[45] S. Mahapatra, J. A. Halfen, E. C. Wilkinson, L. Que Jr., W. B. Tolman, *J. Am. Chem. Soc.* **1994**, *116*, 9785.
[46] J. A. Halfen, S. Mahapatra, E. C. Wilkinson, S. Kaderli, V. G. Young Jr., L. Que Jr., A. Zuberbühler, W. B. Tolman, *Science* **1996**, *271*, 1397.
[47] S. Mahapatra, J. A. Halfen, E. C. Wilkinson, G. Pan, X. Wang, V. G. Young Jr., C. J. Cramer, L. Que Jr., W. B. Tolman, *J. Am. Chem. Soc.* **1996**, *118*, 11555.
[48] L. M. Bellamy, in *Ultrarot-Spectrum und Chemische Konstitution*, Dr. Dietrich Steinkopff Verlag, Darmstadt, **1966**, 12.

 © 2004 Wiley-VCH Verlag GmbH & Co. KGaA, Weinheim

[49] A. W. Addison, T. N. Rao, J. Reedijk, J. van Rijn, G. C. Verschoor, *J. Chem. Soc., Dalton Trans.* **1984**, 1349.

[50] M. C. Etter, Z. Urbanczyk-Lipkowska, S. Baer, P. F. Barbara, *J. Mol. Struct.* **1986**, *144*, 155.

[51] L. M. Berreau, S. Mahapatra, J. A. Halfen, R. P. Houser, V. G. Young Jr., W. B. Tolman, *Angew. Chem. Int. Ed.* **1999**, *38*, 207.

[52] C. G. Pierpont, W. C. Lange, *Progr. Inorg. Chem.* **1994**, *41*, 331.

[53] G. Speier, Z. Tyeklár, P. Tóth, E. Speier, S. Tisza, A. Rockenbauer, A. M. Whalen, N. Alkire, *Inorg. Chem.* **2001**, *40*, 5653.

[54] D. F. Shriver, M. A. Drezdzon, in *The Manipulation of Air-Sensitive Compounds*, John Wiley & Sons, New York, **1986**.

[55] A. Kruis, in *Landolt-Börstein*, Springer Verlag, Berlin, **1976**,vol. 4, part 4, 269.

[56] G. Ram, A. R. Sharaf, *J. Ind. Chem. Soc.* **1968**, *45*, 13.

[57] A. C. North, D. C. Philips, F. Mathews, *Acta Crystallogr., Sect. A* **1968**, *24*, 350.

[58] G. M. Sheldrick, *SHELXS-97 Program for Crystal Structure Solution*, University of Göttingen, Germany, **1997**.

[59] G. M. Sheldrick, *SHELXL-97 Program for Crystal Structure Refinement*, University of Göttingen, Germany, **1997**.

[60] Molecular Graphics: PLATON, A. L. Spek, *Acta Crystallogr., Sect. A* **1990**, *46*, C34.

Received August 26, 2003
Early View Article
Published Online April 7, 2004

 © 2004 Wiley-VCH Verlag GmbH & Co. KGaA, Weinheim

A Fulvene Route to Group 4 Metallocene Complexes Bearing 4,7-Bis(dimethylamino)-Substituted Indenyl Ligands

Jesus Cano Sierra,[a] Sierra Gerald Kehr,[a] Roland Fröhlich,[a][‡] and Gerhard Erker*[a]

Keywords: Aminofulvenes / Cyclopentadienide / Zirconium / Ring-closure / Sandwich complexes

N,*N*,*N*′,*N*′-Tetramethylsuccinamide (**15**) was selectively converted into the functionalized aminofulvene **16**. Subsequent treatment with reagent **17**, $[ZrCl_2(NMe_2)_2(L)_2]$ (L = THF or 0.5 DME), resulted in the formation of the cyclization product 4,7-bis(dimethylamino)indene (**21**). Deprotonation with *n*-butyllithium, followed by the reaction of the resulting substituted indenyllithium reagent **22** with $ZrCl_4$, gave the metallocene [4,7-bis(dimethylamino)indenyl]$_2ZrCl_2$ (**23**). The reaction of **22** with $ZrCl_3Cp$ furnished the complex [4,7-bis(dimethylamino)indenyl]$CpZrCl_2$ (**24**). Fulvene **16**, as well as the metallocene dichlorides **23** and **24**, were characterized by X-ray diffraction.
(© Wiley-VCH Verlag GmbH & Co. KGaA, 69451 Weinheim, Germany, 2004)

Introduction

Fulvenes are often used as precursors for the preparation of cyclopentadienyl ligands and related systems. Most of these syntheses make use of the electrophilicity of the fulvene C6 carbon center, which allows the formation of substituted cyclopentadienides by means of nucleophilic addition (a) or deprotonation (b) (see Scheme 1).[1−3]

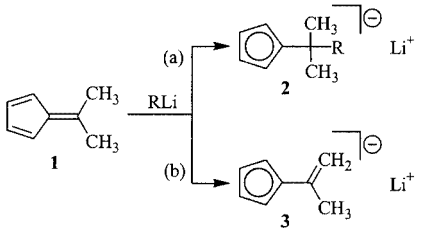

Scheme 1

We have already synthesized substituted indenyl ligands by a series of related reactions. The reaction of 2,5-hexanedione (**4**) with cyclopentadienide under "Thiele conditions"[4] (pathway [a] in Scheme 2) gave the ring-closed 4,7-dimethylindene product **5**,[5] whereas the related reaction under "Stone/Little conditions" ([b] in Scheme 2)[6] furnished the respective bis(fulvene) **6**, which was subsequently used as a starting material for the preparation of the ligand system **7** and of *ansa*-metallocenes derived thereof.[7]

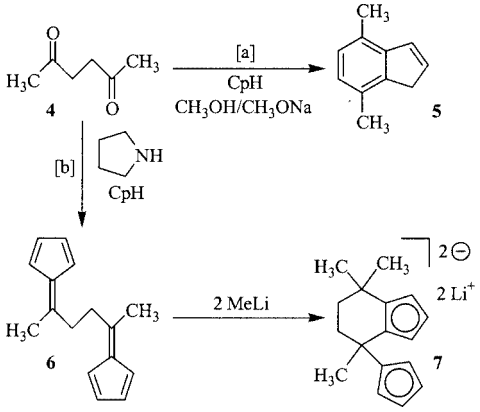

Scheme 2

The unsymmetrical 1,4-diketone **8** allowed the selective preparation of the mono(fulvene) **9** (see Scheme 3). Its treatment with a cuprate nucleophile yielded the substituted tetrahydroindenyl ligand precursor **10**.[8] Similarly, the mono(fulvene) **12** was derived from **11**. In this case the subsequent nucleophilic attack did not result in a related ring-

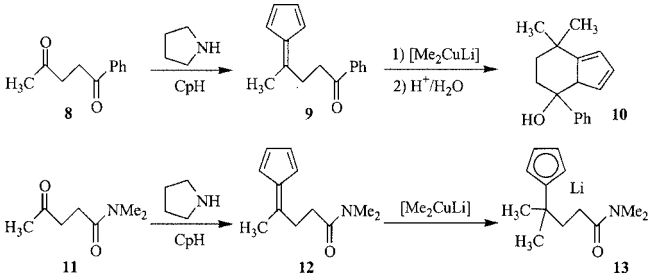

Scheme 3

[a] Organisch-Chemisches Institut der Universität Münster
Corrensstr. 40, 48149 Münster, Germany
Fax: (internat.) + 49-251-83-36503
E-mail: erker@uni-muenster.de
[‡] X-ray crystal-structure analyses.

 © 2004 Wiley-VCH Verlag GmbH & Co. KGaA, Weinheim **DOI: 10.1002/ejic.200300799**

closure reaction but led to the clean formation of the functionalized Cp derivative **13** instead, which was used in the metallocene synthesis.[9]

We now used succinamide **15** as the starting material for a series of related reactions, based on the initial formation of a substituted 6-(dimethylamino)fulvene. In this case we observed a clean ring-closure reaction to yield the corresponding 4,7-bis(dimethylamino)indene product **21** upon treatment with a mild Lewis acid (see Scheme 4). Details of this reaction series, which complements the family of fulvene-to-indene conversions summarized above, are described in this account.

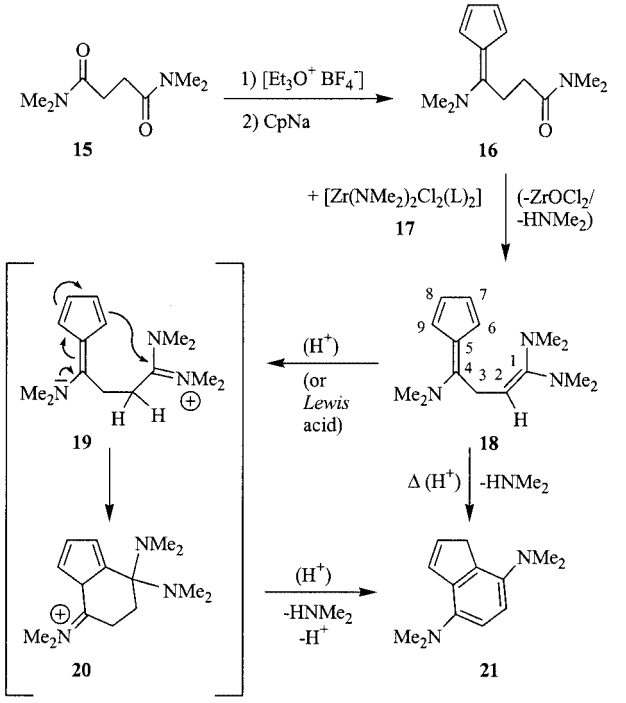

Scheme 4

Results and Discussion

Our synthetic scheme started from succinyl dichloride (**14**), which was treated with dimethylamine to yield the corresponding diamide **15**. The bifunctional carboxylic acid derivative **15** was then selectively converted into its mono(fulvene) derivative **16**. For this purpose, we applied a method that was developed by Hafner et al. for the synthesis of amino-substituted pentafulvenes.[10] The succinamide **15** was mono-*O*-alkylated by treatment with Meerwein's reagent, $[Et_3O^+][BF_4^-]$, and the resulting, stabilized carbenium ion reacted with sodium cyclopentadienide to selectively yield the aminopentafulvene **16**, which bears a residual $-CONMe_2$ functional group (92 % isolated). The fulvene system **16** was characterized by X-ray diffraction (see Figure 1). It shows the typical features of an aminopentafulvene moiety with alternating double and single bonds (see Figure 1) and a trigonal-planar carbon center, C6. The C6−N1 bond length amounts to 1.337(2) Å, which is slightly shorter than the C9−N2 distance [1.349(2) Å] of the delocalized pendent $-CONMe_2$ functional group [C9−O 1.222(2) Å]. In the crystal, compound **16** attains a conformation that is characterized by the antiperiplanar central section of the substituent chain [dihedral angle θ(C6−C7−C8−C9) = −173.1(2)°] with a gauche arrangement at the junction with the fulvene nucleus [θ(C1−C6−C7−C8) = 89.8(2)°].

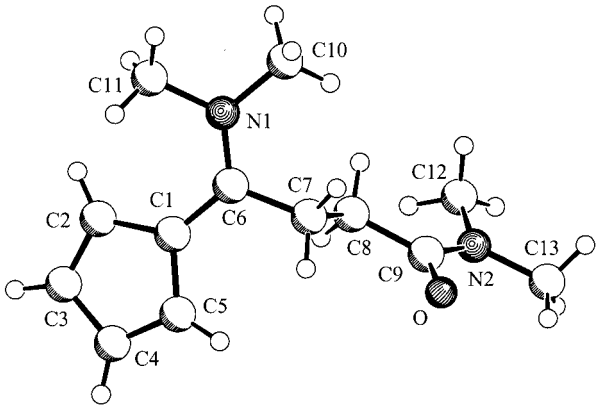

Figure 1. View of the carboxamide-functionalized aminopentafulvene system **16**; selected bond lengths [Å] and angles [°]: C1−C2 1.450(2), C2−C3 1.355(3), C3−C4 1.421(3), C4−C5 1.357(3), C5−C1 1.438(3), C1−C6 1.399(2), C6−N1 1.337(2), C6−C7 1.511(2), C7−C8 1.527(2), C8−C9 1.515(2), C9−O 1.222(2), C9−N2 1.349(2); C2−C1−C5 105.1(2), C2−C1−C6 130.1(2), C5−C1−C6 124.7(2), C1−C6−N1 124.9(2), C1−C6−N7 118.3(2), N1−C6−C7 116.8(2), C6−C7−C8 112.1(1), C7−C8−C9 111.5(1), C8−C9−O 120.9(1), C8−C9−N2 117.0(2), O−C9−N2 122.1(2)

Fulvene **16** was treated with 1 mol-equiv. of $[ZrCl_2(NMe_2)_2{\cdot}DME]$[11] (**17a**) in toluene at reflux temperatures for 3 h. Workup and extraction with pentane furnished the metal-free organic product 4,7-bis(dimethylamino)indene (**21**) as a pale yellow liquid in close to 90 % yield. The product is characterized by a pair of ^1H NMR $(NCH_3)_2$ singlets (δ = 2.60 and 2.65 ppm), each representing six hydrogen atoms. We monitored a set of four indene methine-proton resonances (δ = 6.31, 6.77, 6.83, and 7.21 ppm) and the indene CH_2 ^1H NMR signal at δ = 3.31 (2 H) ppm.

Weingarten et al. have shown that ketene aminals are formed upon treatment of suitably substituted carboxamide starting materials with, for example, $Zr(NMe_2)_4$.[12] It seems that the here observed reaction sequence of the transformation **16** → **21** is initiated by a similar conversion of the *N*,*N*-dimethylcarboxamide functional group. We observed that treatment of **16** with a stoichiometric quantity of the reagent $[ZrCl_2(NMe_2)_2{\cdot}2THF]$[11b] (**17b**) in toluene at room temperature gives the corresponding ketene aminal system **18**. The intermediate **18** was not isolated in a pure form, but was obtained, after washing with pentane, as a solid that was probably still admixed with the zirconium-containing reaction product (perhaps $ZrOCl_2$ or a derivative thereof). Subsequent heating of this mixture in toluene eventually gave rise to the formation of **21**.

 © 2004 Wiley-VCH Verlag GmbH & Co. KGaA, Weinheim

The intermediate **18** was characterized spectroscopically. Its ^{1}H NMR spectrum shows four clearly separated fulvene methine-hydrogen resonances at δ = 7.09, 6.97, 6.86 and 6.79 ppm (in [D_6]benzene) in addition to the typical ketene aminal ^{1}H NMR resonance at δ = 3.62 (t, ^3J = 6 Hz, 1 H) ppm. The adjacent CH_2 group gives rise to a ^{1}H NMR doublet (^3J = 6 Hz) at δ = 3.38 ppm. Compound **18** gives rise of three different NMe_2 ^{1}H NMR singlets at δ = 2.68 (6 H, "fulvene"-NMe_2) and δ = 2.48/2.12 [each 6 H, (*Z*)- and (*E*)-ketene aminal-NMe_2] ppm. The fulvene carbon center (C4−NMe_2) gives rise to a ^{13}C NMR feature at δ = 161.2 ppm, whereas the carbon atoms of the −CH=$C(NMe_2)_2$ ketene aminal show ^{13}C NMR resonances at δ = 156.2 (C1) and 88.4 (C2, $^1J_{C,H}$ = 157 Hz) ppm; the C3 resonance was found at δ = 32.6 ppm with $^1J_{C,H}$ = 133 Hz.

We assume that the observed ring-closure reaction that eventually yields the indene derivative **21** is initiated by activation of the ketene aminal intermediate **18** by protonation or addition of a zirconium-based Lewis-acid catalyst at the C2 carbon atom (see Scheme 4). Intramolecular nucleophilic addition of the Me_2N-activated cyclopentadienide ring at the strongly electrophilic incipient amidinium moiety would then give the product framework. Removal of the H^+ (or $ZrOCl_2$ Lewis acid) catalyst with concomitant dimethylamine elimination and tautomerization would directly lead to the observed product **21**.

Treatment of **21** with *n*-butyllithium results in deprotonation and formation of the substituted indenyllithium reagent **22**, which exhibits the expected ^{1}H NMR features of a C_{2v}-symmetry averaged structure in [D_6]benzene/[D_8]THF (10:1) solution at ambient temperature [δ = 6.80 (t, 1 H, 2-H), 6.42 (d, 2 H, 1-H and 3-H), 6.32 (s, 2 H, 5-H and 6-H), 2.94 (s, 12 H, NMe_2) ppm; see Scheme 5].

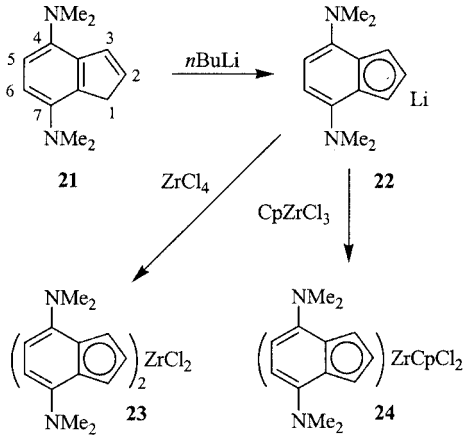

Scheme 5

Reagent **22** was used for the preparation of two zirconocene complexes. Treatment of $ZrCl_4$ with **22** in a toluene suspension gave bis[4,7-bis(dimethylamino)indenyl]$ZrCl_2$ (**23**). Similarly, the reaction of reagent **22** with $CpZrCl_3$[13] gave the mixed indenyl/Cp-zirconium complex **24** (isolated in ca. 70 % yield).

Both **23** and **24** were characterized by X-ray crystal structure analyses. Complex **23** is C_2-symmetric in the crystal. The symmetry-equivalent indenyl ligands are η^5-bound to the zirconium atom through their five-membered rings, although in a rather unsymmetrical way: the bonds between the zirconium atom and the "external" CH centers are short [Zr−C1 2.467(3), Zr−C2 2.484(3), Zr−C3 2.540(3) Å], whereas the Zr−C linkages to the internal indenyl carbon atoms are markedly longer [see Figure 2; Zr−C4 2.639(3), Zr−C9 2.579(3) Å]. The Zr−Cl bond length in complex **23** amounts to 2.417(1) Å.

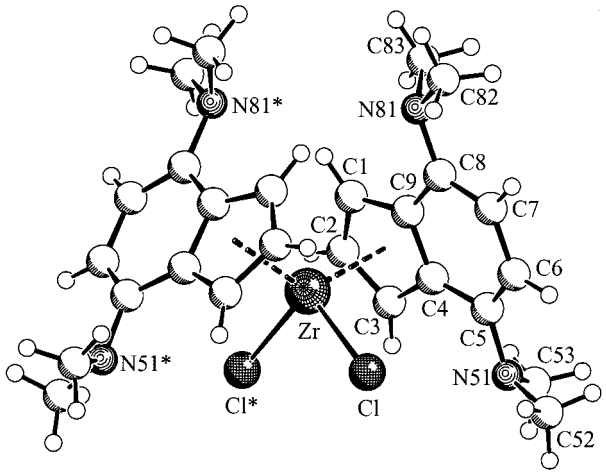

Figure 2. View of the molecular structure of complex **23** (with unsystematic atom-numbering scheme); selected bond lengths [Å] and angles [°]: Zr−Cl 2.417(1), Zr−C1 2.467(3), Zr−C2 2.484(3), Zr−C3 2.540(3), Zr−C4 2.639(3), Zr−C9 2.579(3), C1−C2 1.393(5), C1−C9 1.439(4), C2−C3 1.398(5), C3−C4 1.427(5), C4−C9 1.444(4), C8−C9 1.436(4), C4−C5 1.422(4), C8−N81 1.422(4), C5−N51 1.417(4); Cl−Zr−Cl* 98.80(5), C1−C2−C3 109.9(3), C2−C1−C9 107.6(3), C2−C3−C4 108.3(3), C1−C9−C8 132.9(3), C3−C4−C5 132.0(3), C9−C8−N81 119.0(3), C4−C5−N51 118.0(3)

In the crystal, complex **23** features a chiral metallocene conformation, in which the indenyl six-membered rings point to different lateral sides of the bent metallocene wedge. This leads to a spatial differentiation of the $-NMe_2$ substituents at each of the indenyl ligands: the Me_2N51 group points toward the open-front side and the Me_2N81 substituent is oriented toward the narrow back side of the bent metallocene wedge (see Figure 2). In solution this differentiation is not observed: here rapid rotation about the zirconium−Cp(centroid) vector leads to symmetry-averaged NMR spectra (for details see the Exp. Sect.).

Complex **24** shows an η^5-Cp ligand that is rather uniformly coordinated to the zirconium atom [with Zr−C(Cp) bond lengths ranging from 2.483(2) to 2.537(2) Å]. The bonding features of the substituted indenyl ligand are very similar to those found in the related complex **23** (see above and Figure 3). The single η^5-bis(4,7-dimethylamino)indenyl ligand in complex **24** has a similar conformational orientation to that of the ligands in **23**. In **24** the indenyl ligand has its substituted phenylene moiety oriented towards the lateral side of the bent metallocene wedge.

 © 2004 Wiley-VCH Verlag GmbH & Co. KGaA, Weinheim

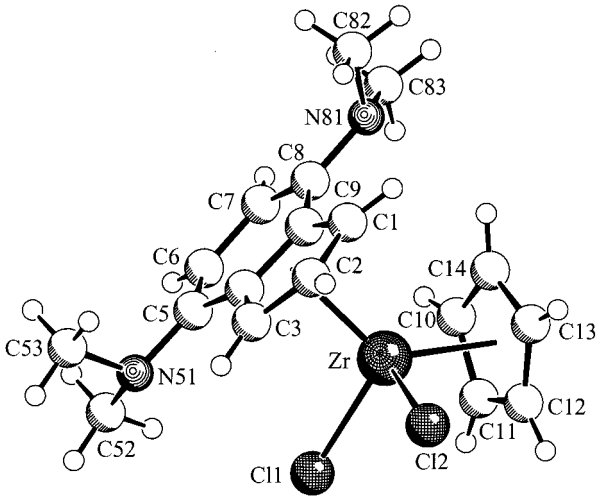

Figure 3. Molecular structure of complex **24**; selected bond lengths [Å] and angles [°]: Zr−Cl1 2.440(1), Zr−Cl2 2.441(1), Zr−C1 2.477(2), Zr−C2 2.508(2), Zr−C3 2.527(2), Zr−C4 2.601(2), Zr−C9 2.577(2), Zr−C10 2.494(2), Zr−C11 2.537(2), Zr−C12 2.514(2), Zr−C13 2.483(2), Zr−C14 2.492(2), C1−C2 1.404(3), C1−C9 1.440(3), C2−C3 1.403(3), C3−C4 1.439(3), C4−C9 1.438(3), C8−C9 1.433(3), C4−C5 1.427(3), C8−N81 1.411(3), C5−N51 1.421(3); Cl1−Zr−Cl2 96.98(2), C1−C2−C3 109.9(2), C2−C1−C9 107.5(2), C2−C3−C4 107.6(2), C1−C9−C8 132.4(2), C3−C4−C5 131.5(2), C9−C8−N81 118.7(2), C4−C5−N51 118.1(2)

Conclusion

We conclude that treatment of the functionalized fulvene system **16** with the zirconium reagent **17** provides a very convenient and selective synthetic pathway to 4,7-bis(dialkylamino)indene systems. We have also shown that these can be easily attached at electrophilic transition-metal centers to yield the respective metallocene systems. The specific influence of the nucleophilic $-NR_2$ substituents on the properties of such organometallic compounds will be investigated in the future.

Experimental Section

General Remarks: All reactions were carried out under dry argon in Schlenk-type glassware or in a glove box. Solvents, including deuterated solvents used for NMR spectroscopy, were dried and distilled prior to use. For additional general conditions, including a list of instruments used for physical characterization of the compounds, see reference.[9]

Preparation of $C_2H_4(CONMe_2)$ (15): Succinyl dichloride (14.7 g, 94 mmol) was added dropwise to a solution of NMe_2H (24 g, 520 mmol) in diethyl ether at −78 °C. The mixture was allowed to warm to room temperature, stirred for 15 min, and filtered to separate the ammonium salt. The residue was extracted with THF (2 × 200 mL) and the solvent was removed under vacuum. The resulted solid was recrystallized from diethyl ether (5 mL) and cooled to −35 °C to give **15** as a light white crystalline solid. Suitable crystals for X-ray crystal-structure analysis[14] were obtained from a concentrated solution in diethyl ether (14.8 g, 91 %). ^{1}H NMR ($CDCl_3$): δ = 3.03 (s, 6 H, NMe), 2.92 (s, 6 H, NMe), 2.64 (s, 4 H, CH_2) ppm. $^{13}C\{^1H\}$ NMR ($CDCl_3$): δ = 172.1 (CO), 36.9 (NMe), 35.3 (NMe), 28.1 (CH_2). $C_8H_{16}N_2O_2$ (172.22): calcd. C 55.79, H 9.36, N 16.27; found C 55.65, H 9.38, N 15.84.

Preparation of Fulvene 16: A CH_2Cl_2 solution of $[Et_3O^+][BF_4^-]$ (14.71 g, 77.4 mmol) was added to a CH_2Cl_2 solution of **15** (13.31 g, 77.4 mmol) at −30 °C. The orange solution was allowed to warm to room temperature and stirred for 2 h. The solvent was removed under vacuum, leading to an oily product. The brown oil was frozen with liquid nitrogen, a solution of NaCp (6.81 g, 77.4 mmol) in THF, cooled to −40 °C, was immediately added and the solution was stirred overnight. The THF was evaporated to dryness and the residue extracted and recrystallized with diethyl ether to yield **16**, as a crystalline solid. Suitable crystals for X-ray crystal-structure analysis were obtained from a concentrated solution in diethyl ether (15.7 g, 92 %). ^{1}H NMR ($CDCl_3$): δ = 6.60, 6.56, 6.43, 6.31 (each broad, each 1 H, fulvene), 3.35 (s, 6 H, 4-NMe), 3.18 (m, 2 H, CH_2), 2.96, 2.95 (each s, each 3 H, 1-NMe), 2.63 (m, 2 H, CH_2) ppm. $^{13}C\{^1H\}$ NMR ($CDCl_3$): δ = 170.8 (C1), 161.3 (C4), 122.3, 119.9, 119.7, 117.0 (fulvene), 117.1 (C5), 43.7 (4-NMe), 37.0, 35.5 (1-NMe), 33.8 (C2), 28.6 (C3) ppm. $C_{13}H_{20}N_2O$ (220.31): calcd. C 70.87, H 9.15, N 12.72; found C 70.56, H 9.27, N 12.49.

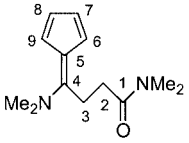

X-ray Crystal-Structure Analysis of 16: Empirical formula $C_{13}H_{20}N_2O$, M = 220.31, yellow-orange crystal 0.20 × 0.15 × 0.10 mm, a = 10.390(1), b = 13.607(1), c = 8.946(1) Å, β = 90.54(1)°, V = 1264.7(2) Å^3, $D_{calcd.}$ = 1.157 g cm^{-3}, μ = 5.79 cm^{-1}, no absorption correction ($0.893 \le T \le 0.944$), Z = 4, monoclinic, space group $P2_1/c$ (No. 14), λ = 1.54178 Å, T = 223 K, ω/2θ scans, 2731 reflections collected ($\pm h$, $-k$, $-l$), [(sinθ)/λ] = 0.62 Å^{-1}, 2562 independent ($R_{int.}$ = 0.035) and 1763 observed reflections [$I \ge 2\sigma(I)$], 150 refined parameters, R = 0.047, wR^2 = 0.133, max. residual electron density 0.18 (−0.16) e·Å^{-3}, hydrogen atoms calculated and refined as riding atoms.

Formation of the Ketene Aminal Intermediate 18: Toluene (100 mL) was added to a Schlenk flask containing **16** (0.28 g, 1.3 mmol) and $[Zr(NMe_2)_2Cl_2{\cdot}THF_2]$ (**17b**) (0.51 g, 1.3 mmol). The resulting solution was stirred at room temperature for 1 h, concentrated to dryness and washed with pentane to give **18** as a light brown solid (0.59 g). ^{1}H NMR (C_6D_6): δ = 7.09 (m, 1 H, 6-H), 6.97 (m, 1 H, 8-H), 6.86 (m, 1 H, 7-H), 6.79 (m, 1 H, 9-H), 3.62 (t, $J_{H,H}$ = 6.3 Hz, 1 H, 2-H), 3.39 (d, $J_{H,H}$ = 6.3 Hz, 2 H, 3-H), 2.68 (s, 6 H, 4-NMe), 2.48 [s, 3 H, 1-$NMe_{(Z)}$], 2.12 [s, 6 H, 1-$NMe_{(E)}$] ppm. $^{13}C\{^1H\}$ NMR (C_6D_6): δ = 161.2 (C4), 156.2 (C1), 123.3 (C8), 121.4 (C6), 120.3 (C7), 119.0 (C5), 118.1 (C9), 88.4 (C2, $^1J_{C,H}$ = 157 Hz), 42.8 (NMe-4), 40.6 [$NMe_{(Z)}$], 40.6 [$NMe_{(E)}$], 32.6 (C3) ppm. ^{1}H-^{13}C GHSQC (C_6D_6): δ(^{13}C)/δ(^{1}H) = 123.3/6.97 (8-CH), 121.4/7.09 (6-CH), 120.3/6.86 (7-CH), 118.1/6.79 (9-CH), 88.4/3.62 (2-CH), 42.8/2.68 (4-NMe), 40.6/2.48 [1-$NMe_{(Z)}$], 40.6/2.12 [1-$NMe_{(E)}$], 32.6/3.39 (3-CH_2). ^{1}H-^{13}C GHMBC (C_6D_6): δ(^{13}C)/δ(^{1}H) = 161.2/3.39, 2.68 (C4/3-H, 4-NMe), 156.2/3.39, 2.48, 2.12 [C1/3-H, 1-$NMe_{(Z)}$, 1-$NMe_{(E)}$], 119.0/3.39 (C5/3-H). ^{1}D TOCSY (C_6D_6): δ($^1H_{irr}$)/δ($^1H_{res}$) = 7.09/6.97, 6.86, 6.79 (6-H/8-H, 7-H, 9-H), 3.62/3.39 (2-

 © 2004 Wiley-VCH Verlag GmbH & Co. KGaA, Weinheim

H/3-H). NOE (C_6D_6): δ($^1H_{irr}$)/δ($^1H_{res}$) = 2.12/2.48, 3.62 [1-NMe$_{(E)}$/1-NMe$_{(Z)}$, 2-H]; 2.48/2.12, 3.39 [1-NMe$_{(Z)}$/1-NMe$_{(E)}$, 3-H]; 2.68/3.39, 3.62, 6.79 (4-NMe/3-H, 2-H, 9-H); 3.39/2.48, 2.68, 3.62, 7.09 [3-H/1-NMe$_{(Z)}$, 4-NMe, 2-H, 6-H]; 3.62/2.12, 3.39 [2-H/1-NMe$_{(E)}$, 3-H].

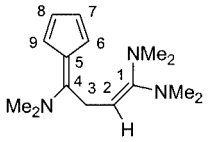

Preparation of the Substituted Indene 21: Toluene (100 mL) was added to a Schlenk flask containing **16** (1.06 g, 4.6 mmol) and [Zr(NMe$_2$)$_2$Cl$_2$·DME] (**17a**) (2.10 g, 4.6 mmol) and the mixture vigorously stirred at room temperature for 3 h. The resulting red solution was filtered, the solvent removed under vacuum and the residue extracted with pentane to yield **19** as a yellow liquid (0.82 g, 88 %). ^1H NMR (C_6D_6): δ = 7.21, 6.31 (each dt, $J_{H,H}$ = 5.6, 1.9 Hz,·each 1 H, 2,3-H), 6.83, 6.77 (AB $J_{H,H}$ = 8.7 Hz,·each 1 H, 5,6-H), 3.31 (t, $J_{H,H}$ = 1.9 Hz, 2 H, CH$_2$), 2.65, 2.60 (each s, each 6 H, NMe) ppm. $^{13}C\{^1H\}$ NMR (C_6D_6): δ = 145.1, 143.1 (C4,7), 139.5, 137.1 (C3a,7a), 132.3, 130.9 (C2,3), 116.0, 114.9 (C5,6), 44.6, 43.6 (NMe$_2$), 39.3 (CH$_2$) ppm. $C_{13}H_{18}N_2$ (202.29): calcd. C 77.18, H 8.97, N 13.85; found C 76.73, H 9.20, N 13.86.

Preparation of the Indenyllithium Reagent 22: BuLi (1.6 M) was added to a solution of **19** (0.56 g, 2.77 mmol) in pentane (150 mL), cooled to −78 °C. The white suspension formed was warmed slowly to room temperature and stirred for 12 h. Filtration and removal of the solvent at reduced pressure gave **22** as a white solid (0.55 g, 95 %). ^1H NMR (C_6D_6, TDF): δ = 6.80 (t, $J_{H,H}$ = 3.4 Hz, 1 H, 2-H), 6.42 (d, $J_{H,H}$ = 3.4 Hz, 2 H, 1,3-H), 6.32 (s, 2 H, 5,6-H), 2.94 (s, 12 H, NMe) ppm. $^{13}C\{^1H\}$ NMR (C_6D_6, TDF): δ = 142.1 (C4,7), 122.9 (C3a,7a), 112.7 (C2), 101.8 (C5,6), 92.2 (C1,3), 44.0 (NMe) ppm.

Preparation of the Zirconium Complex 23: $ZrCl_4$ (0.156 g, 0.67 mmol) was added to a suspension of **22** (0.28 g, 1.34 mmol) in toluene (100 mL) at −40 °C. The cooling bath was removed and the reaction mixture stirred at room temperature for 12 h. After filtration, the solvent was removed under vacuum and the residue washed with pentane (2 × 50 mL) to give **23** as a red crystalline solid (0.21 g, 57 %). ^1H NMR (CD_2Cl_2): δ = 6.77 (d, $J_{H,H}$ = 3.0 Hz, 2 H, 1,3-H), 6.50 (s, 2 H, 5,6-H), 6.08 (t, $J_{H,H}$ = 3.0 Hz, 1 H, 2-H), 2.90 (s,·12 H, NMe) ppm. $^{13}C\{^1H\}$ NMR (CD_2Cl_2): δ = 143.2 (C4,7), 123.4 (C3a,7a), 118.8 (C2), 111.9 (C5,6), 104.3 (C1,3), 43.3 (NMe) ppm. $C_{26}H_{34}Cl_2N_4Zr$ (564.70): calcd. C 55.30, H 6.07, N 9.92; found C 55.15, H 6.14, N 9.72.

X-ray Crystal-Structure Analysis of 23: Empirical formula $C_{26}H_{34}Cl_2N_4Zr$, M = 564.69, red crystal 0.15 × 0.05 × 0.03 mm, a = 41.733(1), b = 7.036(1), c = 17.528(1) Å, V = 5146.8(8) Å^3, $D_{calcd.}$ = 1.458 g cm^{-3}, μ = 6.57 cm^{-1}, empirical absorption correction with SORTAV (0.908 ≤ T ≤ 0.981), Z = 8, orthorhombic, space group $Fdd2$ (No. 43), λ = 0.71073 Å, T = 198 K, ω and φ scans, 9228 reflections collected (±h, ±k, ±l), [(sinθ)/λ] = 0.66 Å^{-1}, 3023 independent (R_{int} = 0.053) and 2492 observed reflections [$I \geq 2\sigma(I)$], 154 refined parameters, R = 0.038, wR^2 = 0.068, max. residual electron density 0.36 (−0.59) e·Å^{-3}, Flack −0.04(5), hydrogen atoms calculated and refined as riding atoms.

Preparation of the Zirconium Complex 24: $CpZrCl_3$ was added to a suspension of **22** in toluene (100 mL) at −40 °C. The cooling bath was removed and the reaction mixture was stirred at room temperature for 12 h. After filtration, the solvent was removed under vacuum and the residue was washed with pentane (2 × 50 mL) to give **24** as a red crystalline solid (0.61 g, 71 %). ^1H NMR (CD_2Cl_2): δ = 6.73 (t, $J_{H,H}$ = 3.2 Hz, 1 H, 2-H), 6.71 (d, $J_{H,H}$ = 3.2 Hz, 2 H, 1,3-H), 6.52 (s, 2 H, 5,6-H), 6.24 (s, 5 H, Cp), 2.92 (s, 6 H, NMe) ppm. $^{13}C\{^1H\}$ NMR (CD_2Cl_2): δ = 145.0 (C4,7), 123.9 (C3a,7a), 123.5 (C2), 118.7 (Cp), 113.3 (C5,6), 105.2 (C1,3), 44.8 (NMe) ppm. $C_{18}H_{22}Cl_2N_2Zr$ (428.50): calcd. C 50.45, H 5.17, N 6.54; found C 50.67, H 5.37, N 6.48.

X-ray Crystal-Structure Analysis of 24: Formula $C_{18}H_{22}Cl_2N_2Zr$, M = 428.50, red crystal 0.15 × 0.15 × 0.05 mm, a = 7.919(1), b = 13.135(1), c = 17.552(1) Å, V = 1825.7(3) Å^3, $D_{calcd.}$ = 1.559 g cm^{-3}, μ = 8.95 cm^{-1}, empirical absorption correction with SORTAV (0.877 ≤ T ≤ 0.957), Z = 4, orthorhombic, space group $P2_12_12_1$ (No. 19), λ = 0.71073 Å, T = 198 K, ω and φ scans, 12933 reflections collected (±h, ±k, ±l), [(sinθ)/λ] = 0.65 Å^{-1}, 4158 independent (R_{int} = 0.034) and 3879 observed reflections [$I \geq 2\sigma(I)$], 213 refined parameters, R = 0.024, wR^2 = 0.052, max. residual electron density 0.24 (−0.57) e·Å^{-3}, refined as a racemic twin with a ratio of 0.67(3):0.33, hydrogen atoms calculated and refined as riding atoms.

X-ray Crystallographic Study: Data sets were collected with Enraf−Nonius CAD4 and Nonius KappaCCD diffractometers; the latter was equipped with a rotating anode generator, Nonius FR591. Programs used: data collection EXPRESS (Nonius B. V., **1994**) and COLLECT (Nonius B. V., **1998**), data reduction MolEN (K. Fair, Enraf−Nonius B. V., **1990**) and Denzo-SMN (Z. Otwinowski, W. Minor, *Methods Enzymol.* **1997**, *276*, 307−326), absorption correction for CCD data SORTAV (R. H. Blessing, *Acta Crystallogr., Sect. A* **1995**, *51*, 33−37; R. H. Blessing, *J. Appl. Crystallogr.* **1997**, *30*, 421−426), structure solution SHELXS-97 (G. M. Sheldrick, *Acta Crystallogr., Sect. A* **1990**, *46*, 467−473), structure refinement SHELXL-97 (G. M. Sheldrick, Universität Göttingen, **1997**), graphics SCHAKAL (E. Keller, Universität Freiburg, **1997**). CCDC-220797, -220798 and -220799 contain the supplementary crystallographic data for this paper. These data can be obtained free of charge at www.ccdc.cam.ac.uk/conts/retrieving.html [or from the Cambridge Crystallographic Data Centre, 12 Union Road, Cambridge CB2 1EZ, UK; Fax: (internat.) + 44-1223/336-033; E-mail: deposit@ccdc.cam.ac.uk].

Acknowledgments

Financial support from the Fonds der Chemischen Industrie and the Deutsche Forschungsgemeinschaft is gratefully acknowledged. J. C. S. thanks the Alexander-von-Humboldt-Stiftung for a fellowship.

[1] [1a] K. Ziegler, W. Schäfer, *Justus Liebigs Ann. Chem.* **1934**, *511*, 101−109. [1b] K. Ziegler, H.-G. Gellert, H. Martin, K. Nagel, J. Schneider, *Justus Liebigs Ann. Chem.* **1954**, *589*, 91−121. [1c] M. F. Sullivan, W. F. Little, *J. Organomet. Chem.* **1967**, *8*, 277−285.

[2] [2a] P. Renaut, G. Tainturier, B. Gautheron, *J. Organomet. Chem.* **1978**, *148*, 35−42. [2b] G. Erker, R. Nolte, R. Aul, S. Wilker, C. Krüger, R. Noe, *J. Am. Chem. Soc.* **1991**, *113*, 7594−7602.

[3] [3a] G. Erker, R. Aul, *Chem. Ber.* **1991**, *124*, 1301−1310. [3b] G. Erker, S. Wilker, C. Krüger, R. Goddard, *J. Am. Chem. Soc.* **1992**, *114*, 10983−10984. [3c] G. Erker, S. Wilker, C. Krüger, M. Nolte, *Organometallics* **1993**, *12*, 2140−2151. [3d] L. Duda, G.

 © 2004 Wiley-VCH Verlag GmbH & Co. KGaA, Weinheim

Erker, R. Fröhlich, F. Zippel, *Eur. J. Inorg. Chem.* **1998**, 1153−1162. [3e] W.-L. Nie, G. Erker, G. Kehr, R. Fröhlich, *Angew. Chem.,* in press.

[4] [4a] J. Thiele, *Ber. Dtsch. Chem. Ges.* **1900**, *33*, 666−673. [4b] J. Thiele, H. Balhorn, *Justus Liebigs Ann. Chem.* **1906**, *348*, 1−15.

[5] [5a] A. Weiß, doctoral dissertation, Univ. Münster, **1993**. [5b] J. W. Coe, M. G. Vetelino, D. S. Kemp, *Tetrahedron Lett.* **1994**, *35*, 6627−6630. For remotely related ligand systems see, for example: [5c] P. Foster, M. D. Rausch, J. C. W. Chien, *J. Organomet. Chem.* **1997**, *527*, 71−74. [5d] J. de Armas, S. P. Kolis, A. H. Hoveyda, *J. Am. Chem. Soc.* **2000**, *122*, 5977−5983.

[6] K. J. Stone, R. D. Little, *J. Org. Chem.* **1984**, *49*, 1849−1853.

[7] [7a] K. Hafner, *Angew. Chem.* **1958**, *70*, 419−430. [7b] G. Büchi, D. Berthet, R. Decorzant, A. Grieder, A. Hauser, *J. Org. Chem.* **1976**, *41*, 3208−3209. [7c] M. Neuenschwander, P. Kronig, S. Schönholzer, M. Slongo, B. Uebersax, C. Rentsch, *Croat. Chem. Acta* **1981**, *53*, 625−636. [7d] P. Kronig, M. Slongo, M. Neuenschwander, *Makromol. Chem.* **1982**, *163*, 359−375. [7e] G. Erker, C. Psiorz, C. Krüger, M. Nolte, *Chem. Ber.* **1994**, *127*, 1551−1553. [7f] G. Erker, C. Psiorz, R. Fröhlich, M. Grehl, C. Krüger, R. Noe, M. Nolte, *Tetrahedron* **1995**, *51*, 4347−4358.

[8] M. Könemann, G. Erker, R. Fröhlich, S. Kotila, *Organometallics* **1997**, *16*, 2900−2908.

[9] D. Hüerländer, R. Fröhlich, G. Erker, *J. Chem. Soc., Dalton Trans.* **2002**, 1513−1520.

[10] [10a] K. Hafner, G. Schulz, K. Wagner, *Justus Liebigs Ann. Chem.* **1964**, *678*, 39−53. [10b] K. Hafner, K. H. Völpel, G. Ploss, C. König, *Org. Synth.* **1967**, *47*, 52−54. [10c] K. Kunz, J. Pflug, A. Bertuleit, R. Fröhlich, E. Wegelius, G. Erker, E.-U. Würthwein, *Organometallics* **2000**, *19*, 4208−4216.

[11] [11a] T. H. Warren, G. Erker, R. Fröhlich, B. Wibbeling, *Organometallics* **2000**, *19*, 127−134. [11b] S. Brenner, R. Kempe, P. Arndt, *Z. Anorg. Allg. Chem.* **1995**, *621*, 2121−2124.

[12] H. Weingarten, W. A. White, *J. Am. Chem. Soc.* **1966**, *88*, 850, *J. Org. Chem.* **1966**, *31*, 2874−2875.

[13] [13a] G. Erker, K. Berg, L. Treschanke, K. Engel, *Inorg. Chem.* **1982**, *21*, 1277−1278. [13b] G. Erker, K. Berg, C. Sarter, *Organometallic Syntheses* (Eds. R. B. King, J. J. Eisch), Elsevier, Amsterdam **1986**, vol. 3, p. 29.

[14] B. M. Rapko, B. K. McNamara, R. D. Rogers, G. J. Lumetta, B. P. Hay, *Inorg. Chem.* **1999**, *38*, 4585−4592.

Received October 30, 2003
Early View Article
Published Online April 7, 2004

 © 2004 Wiley-VCH Verlag GmbH & Co. KGaA, Weinheim

Synthesis, Crystal Structure and Magnetic Properties of A New Thiazolyl-Substituted Nitronyl Nitroxide and Its Copper(II) Complexes

Li-Ya Wang,[a,b] Li-Cun Li,[c] Dai-Zheng Liao,[a] Zong-Hui Jiang,*[a] and Shi-Ping Yan[a]

Keywords: Thiazole radicals / Nitronyl nitroxide / Copper / Magnetic properties

A new building block for molecule-based magnetic materials — thiazole-substituted nitronyl nitroxide NIT2-thz [**1**, NIT2-thz = 4,4,5,5-tetramethyl-2-(2′- thiazolyl)imidazolin-1-oxyl 3-oxide] and its copper(II) complexes [Cu(NIT2-thz)$_2$(N$_3$)$_2$] (**2**) and [CuCl$_2$(NIT2-thz)$_2$] (**3**) — have been synthesized and characterized structurally and magnetically. Compound **1** is found to contain two crystallographically independent molecules; the shortest contact between nitroxide groups is 4.900 Å. Both **2** and **3** are mononuclear complexes, in which the copper(II) centers are hexacoordinate. In complex **2**, the copper(II) ion has an elongated octahedral geometry, but complex **3** has a rare compressed-octahedral coordination sphere. Magnetic susceptibility data for compounds **1**–**3** have been measured in the range 5–300 K. There are ferromagnetic interactions (J = 10.13 cm^{-1}) between the Cu^{II} ions and the radicals of **2**, and antiferromagnetic interactions (J = –8.17 cm^{-1}) between the Cu^{II} ions and the radicals of **3**. The magnetic properties of complexes **2** and **3** are discussed in connection with their crystal structures.

(© Wiley-VCH Verlag GmbH & Co. KGaA, 69451 Weinheim, Germany, 2004)

Introduction

In the preparation of molecular magnetic materials, transition metal complexes with organic nitronyl nitroxide radical ligands have attracted widespread interest in recent years.[1−5] However, the weakly basic character of nitronyl nitroxide strongly limits their coordination ability. This has led to the development of functionalized nitronyl nitroxide radicals, in which a strong co-ligand is incorporated. Research has focused on nitronyl nitroxide radicals with electron-donating substituents such as 2-pyridyl,[6,7] imidazolyl,[8,9] 2,2′-bipyridinyl,[10] and 1,2,4-triazolyl.[11] Among them, the 2-pyridyl- and imidazolyl-substituted nitroxides have the advantage of forming stable chelated complexes with the support of the auxiliary substituent groups. The thiazolyl substituent too has a strong chelating ability for complexes with metal ions. This prompted us to synthesize a new thiazole-substituted nitronyl nitroxide radical and a group of metal compounds containing this radical ligand. In this contribution, we wish to report the synthesis, crystal structure and magnetic properties of the radical NIT2-thz [**1**, NIT2-thz = 4,4,5,5-tetramethyl-2-(2′- thiazolyl)imidazolin-1-oxyl 3-oxide] (Scheme 1) and its complexes [Cu(NIT2-thz)$_2$(N$_3$)$_2$] (**2**) and [CuCl$_2$(NIT2-thz)$_2$] (**3**).

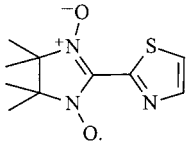

Scheme 1

Results and Discussion

Crystal Structure of 1

Compound **1** (Figure 1) is found to contain two crystallographically independent molecules, but these two structures are not significantly different from each other. The N−O bond lengths of 1.284(4) Å [O(1)−N(3)] and 1.278(4) Å [O(2)−N(2)], respectively, are in agreement with those in radicals synthesized by other groups.[12,13] The two S−C bond lengths of 1.729(4) Å [S(1)−C(3)] and 1.692(5) Å [S(1)−C(1)], respectively, are longer than other three bond lengths of 1.305(5) Å [N(1)−C(3)], 1.366(5) Å [N(1)−C(2)] and 1.319(6) Å [C(1)−C(2)] in the thiazole ring. The dihedral angles between the nitronyl nitroxide fragment and the thiazole ring are 7.1(5)° and 3.6(4)°, respectively. The shortest contact between nitroxide groups is 4.900 Å [O(4)···O(4), (x, 1 − y, 1/2 + z)].

[a] Department of Chemistry, Nankai University, Tianjin 300071, P. R. China
[b] Department of Chemistry, Luoyang Teachers College, Luoyang 471022, P. R. China
[c] State Key Laboratory of Structural Chemistry, Fujian Institute of Research on the Structure of Matter, Chinese Academy of Sciences, Fuzhou 350002, P. R. China

 © 2004 Wiley-VCH Verlag GmbH & Co. KGaA, Weinheim **DOI: 10.1002/ejic.200300885**

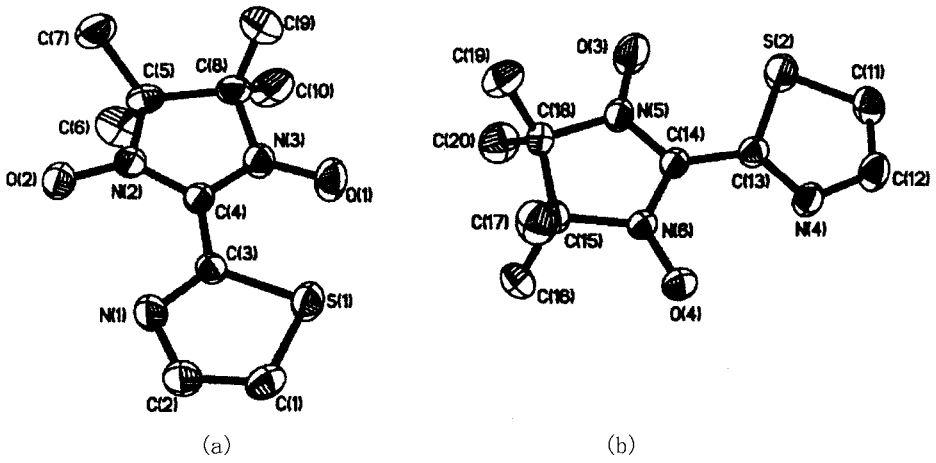

Figure 1. ORTEP drawing of compound **1**

Crystal Structures of 2 and 3

The structures of **2** (Figure 2) and **3** (Figure 3) are centrosymmetric, and the copper(II) ions have a distorted octahedral environment. In both complexes, two NIT2-thz radicals, acting as bidentate chelating ligands, coordinate the copper(II) ion through the N−O unit and the nitrogen atom of the thiazole ring. However, the geometries of complexes **2** and **3** are different.

In complex **2**, the two nitrogen atoms [N(4), N(4A)) of the azide groups and the two nitrogen atoms [N(1), N(1A)) of the radical ligands are coordinated at the equatorial positions. The Cu−N bond lengths are 1.995(3) Å [Cu(1)−N(4)] and 2.024(2) Å [Cu(1)−N(1)], respectively. The two oxygen atoms [O(2), O(2A)] on the NO groups of the radical ligands are bonded at the axial positions, with a Cu−O distance of 2.364(2) Å, which is longer than for those coordinated at the equatorial positions. The copper(II) ion has, as expected, an elongated octahedral geometry.

In complex **3**, the basal plane is formed by the two oxygen atoms [O(1), O(1A)] of the NO groups [with a Cu−O bond length of 2.370(5) Å], and two chloride anions [with a Cu−Cl bond length of 2.348(2) Å]. The axial positions are occupied by the two nitrogen atoms [N(1), N(1A)) of the thiazole rings, with a Cu−N distance 2.001(6) Å, which is significantly shorter than for those coordinated at the equatorial positions. Thus the copper(II) ion has a rare compressed-octahedral coordination sphere.

The uncoordinated N−O bond lengths of 1.278(3) Å (for **2**) and 1.280(7) Å (for **3**), and the coordinated N−O bond lengths of 1.276(3) Å (for **2**) and 1.293(7) Å (for **3**), are close to those of the free radical NIT2-thz [corresponding N−O bond lengths 1.284(4) Å and 1.278(4) Å]. The dihedral angle between the nitronyl nitroxide fragment and the thiazole ring is 5.4(4)° (for **2**) and 16.7(11)° (for **3**). The shortest distances between the nitroxide groups are 4.728 Å (for **2**) and 4.521 Å (for **3**).

Magnetic Properties

The magnetic susceptibilities of compounds **1**, **2** and **3** were measured in the range 5−300 K at a magnetic field of 1 T.

For compound **1**, the variation of $\chi_M T$ vs. T is plotted in Figure 4. The $\chi_M T$ value is close to 0.357 $cm^3 \cdot K \cdot mol^{-1}$ in the range 30−300 K, and corresponds to the expected value

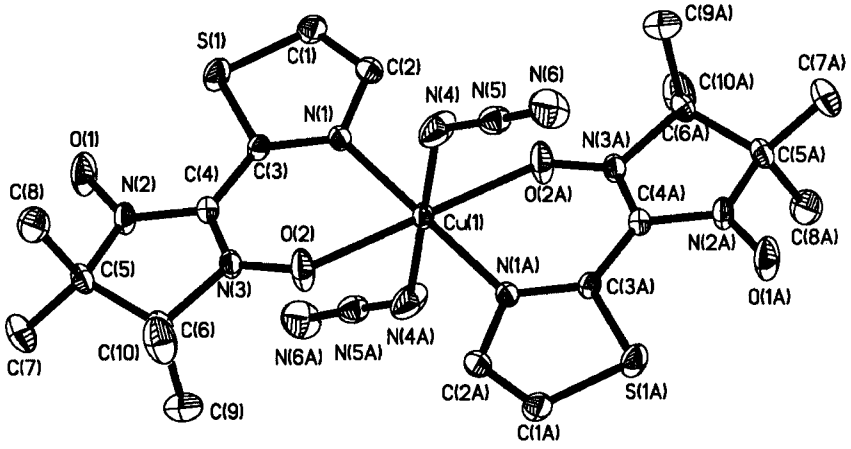

Figure 2. ORTEP drawing of complex **2**

 © 2004 Wiley-VCH Verlag GmbH & Co. KGaA, Weinheim

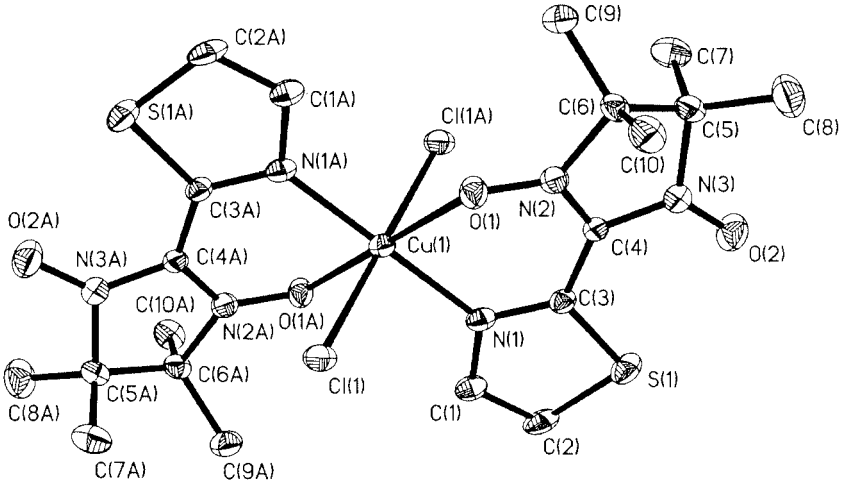

Figure 3. ORTEP drawing of complex **3**

(0.374 $cm^3 \cdot K \cdot mol^{-1}$) for a non-correlated $S = 1/2$ spin. As the temperature is lowered from about 30 K to 5 K, $\chi_M T$ decreases rapidly. Below 30 K, the magnetic susceptibility data obeys a Curie−Weiss law $\chi = C/(T - \theta)$, with the Weiss constant $\theta = -1.46$ K and $C = 0.364$ (inset in Figure 4). This behaviour is characteristic of weak intermolecular antiferromagnetic interactions.

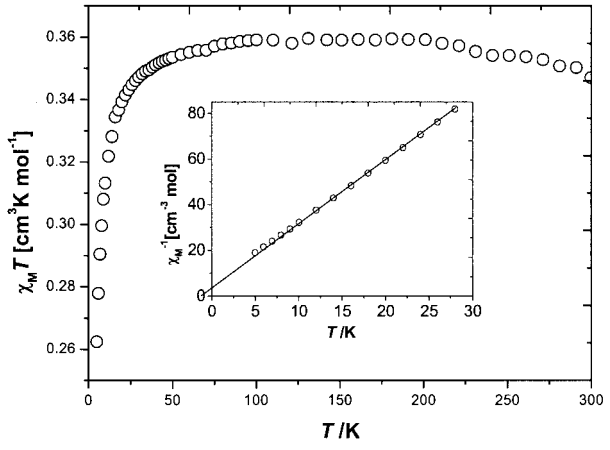

Figure 4. Plot of $\chi_M T$ vs. T for compound **1**. Inset: plot of $\chi_M{}^{-1}$ vs. T

For complex **2**, the plots of $\chi_M T$ and χ_M vs. T are shown in Figure 5. At 300 K, the $\chi_M T$ value is equal to 1.17 $cm^3 \cdot K \cdot mol^{-1}$, which is slightly higher than that expected for a non-interacting $S = 1/2$ spin for Cu^{II} and two $S = 1/2$ spins for the radicals (spin-only value 1.13 $cm^3 \cdot K \cdot mol^{-1}$). As the temperature decreases from about 300 to 5 K, $\chi_M T$ gradually increases and reaches a maximum of 1.475 $cm^3 \cdot K \cdot mol^{-1}$ at 7.0 K, from where it decreases down to a temperature of 4.91 K. This indicates that there are ferromagnetic interactions between the nitroxide radical and the copper(II) ion.

The magnetic data for **2** were treated by the theoretical expression[14] derived through the spin Hamiltonian $H = -J(S_{R1}S_{Cu} + S_{R2}S_{Cu})$, where J represents the exchange interaction between the Cu^{II} ion and the thiazole radical. Considering the magnetic coupling between the molecules, we used the mean-field approximation (zJ').[15] The best fitting for the data gives $J = 10.13 cm^{-1}$, $zJ' = -0.46$ cm^{-1}, $g_{cu} = 2.13$, $g_{rad} = 2.0$ (fixed), and an agreement factor [defined as $R = (\chi_M)_{obsd.} - (\chi_M)^2_{calcd.}/(\chi_M)^2_{obsd.}$] of 3.34×10^{-4}. These results indicate a weak ferromagnetic exchange interaction between the Cu^{II} ion and the radical.

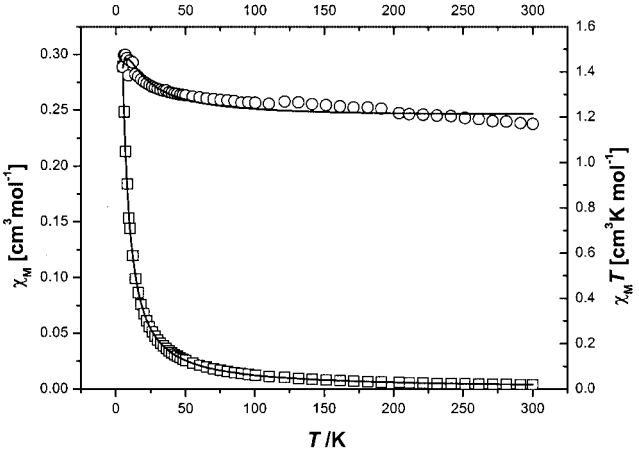

Figure 5. Plots of $\chi_M T$ vs. T and χ_M vs. T of complex **2**. The solid line represents the fitting values

The plots of $\chi_M T$ and χ_M vs. T for **3** are shown in Figure 6. At 300 K, $\chi_M T$ is 1.12 $cm^3 \cdot K \cdot mol^{-1}$, which is consistent with that expected for one non-interacting $S_{Cu} = 1/2$ spin and two $S_{rad} = 1/2$ spins (1.13 $cm^3 \cdot K \cdot mol^{-1}$). Starting from a temperature of 300 K, $\chi_M T$ decreases smoothly down to 50 K, then rapidly decreases to 0.43 $cm^3 \cdot K \cdot mol^{-1}$ at 5 K. This magnetic behavior is clearly indicative of antiferromagnetic interactions.

The magnetic data for **3** were treated with a similar theoretical expression to that used for **2**; J characterizes the exchange interaction between the Cu^{II} ion and the thiazole radical.

 © 2004 Wiley-VCH Verlag GmbH & Co. KGaA, Weinheim

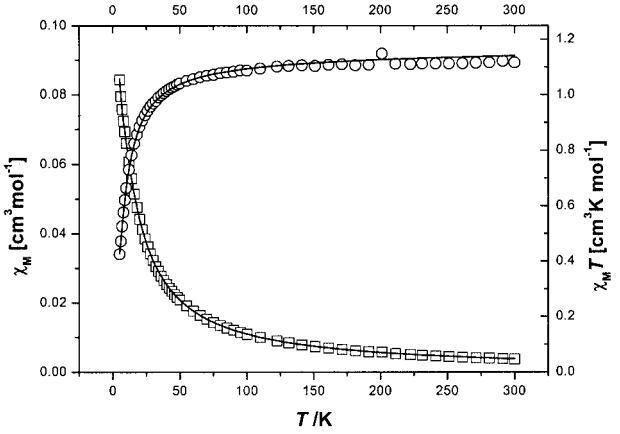

Figure 6. Plots of $\chi_M T$ vs. T and χ_M vs. T for complex **3**. The solid line represents the fitting values

The best fitting for the data gives $J = -8.17\text{cm}^{-1}$, $zJ' = -0.36\ \text{cm}^{-1}$, $g_{cu} = 2.04$, $g_{rad} = 2.0$ (fixed), with an agreement factor [defined as $R = [(\chi_M)_{obsd.} - (\chi_M)_{calcd.}]^2/[(\chi_M)_{obsd.}]^2$] of 5.41×10^{-6}. The results indicate a weak antiferromagnetic exchange interaction between the Cu^{II} ion and the radical.[11]

The geometrical parameters of the binding of the radical to the metal are of great importance for the understanding of the magnetic properties of the complexes **2** and **3**. In our two complexes, the magnetic orbital of the nitronyl nitroxide radical is a π* orbital, with its axis lying perpendicular to the O−*N*−C−*N*−O plane.[16] The magnetic orbital of the copper(II) ion with an octahedral coordination environment is $d_{z^2-y^2}$ or d_{z^2}. Following the Kahn−Briat rules,[17] the extent of overlap between metal and radical magnetic orbitals is responsible for the appearance of antiferromagnetic interactions, whereas orthogonality of the same orbitals induces ferromagnetic contributions. With these ideas in mind, it is possible to correlate the metal-radical coupling to the crystal structures of the complexes. Complex **2** has an elongated-octahedral geometry, with the two nitroxide groups bound in an axial position. It is generally accepted that the interaction between a copper(II) centers and an axially bound nitroxide radical is ferromagnetic because, in this geometry, the π* radical orbital is strictly orthogonal to the $d_{x^2-y^2}$ orbital of the copper(II) ion.[18] Thus, the positive value of the copper(II) nitroxide coupling constant ($J_{Cu,rad} = 10.13\ \text{cm}^{-1}$) has been ascribed to the interaction between the copper(II) ion and the radicals located in axial positions. The relatively low value observed arises from the fact that the Cu−O distances are fairly long [Cu(1)−O(2) = 2.364(2) Å].

For compound **3**, two nitroxide groups coordinate in equatorial positions. In general, this results in a strong antiferromagnetic coupling between copper and radical.[19] However, in this case, a weak antiferromagnetic interaction is observed ($J_{Cu,rad} = -8.17\ \text{cm}^{-1}$). In complex **3**, the copper(II) ion has a compressed octahedral coordination geometry and the magnetic orbital of the copper(II) ion is d_{z^2}. This geometry will induce a weak antiferromagnetic coupling between the copper(II) ion and the radical due to the poor magnetic orbital overlap.

Conclusions

In summary, the novel thiazole-substituted nitronyl nitroxide radical **1** and the complexes **2** and **3** (the first examples of a new family of complexes) have been synthesized. In complex **3**, the copper(II) ion has a rare compressed-octahedral coordination sphere. This geometry results in a weak antiferromagnetic interaction between the copper(II) ion and the radical, even though the radical is coordinated in the equatorial plane.

Experimental Section

General: All reagents were purchased from commercial sources and used as received. Solvents were purified and dried by standard methods. Elemental analyses for C, H, and N were carried out with a Perkin−Elmer 240 elemental analyzer. The infrared spectra were recorded in KBr pellets in the range 4000−600 cm^{-1} with a SHIMADZU-408 IR spectrometer. EPR spectra were recorded as a solution of the compound in CH_2Cl_2 with a JESFEIXG EPR spectrometer. Variable-temperature magnetic susceptibilities were measured with a MPMS-7 SQUID magnetometer. Diamagnetic corrections were made using Pascal's constants for all the constituent atoms.

X-ray diffractions were measured with a RAXIS-IV area detector for **2** and **3** and with a Bruker−Smart 1000 diffractometer for **1**. The structures were solved by direct methods using the SHELXS-97[20] program. H atoms were assigned with common isotropic displacement factors and included in the final refinement by use of geometrical restraints. A full-matrix least-squares refinement on F^2 was carried out using SHELXL 97.[21] Crystal data are summarized in Table 1, selected structural parameters in Table 2−4.

Preparation of Nitronyl Nitroxide Radical NIT2-thz: Prepared from 2-thiazolecarboxaldehyde by the literature method.[22,23] The dark green crystals of **1** were recrystallized from cyclohexane/ethyl acetate (5:1) in 55% yield. $C_{10}H_{14}N_3O_2S$: calcd. C 49.94, H 5.87, N 17.48; found C 49.89, H 5.85, N 17.40. IR: $\tilde{\nu}_{thz}$ = 1418, 1185, 1140 cm^{-1}; $\tilde{\nu}_{N\text{-}O}$ = 1375 cm^{-1}. ESR (299 K, CH_2Cl_2): five lines; g = 2.00; a_N = 7.8 G.

Preparation of [Cu(NIT2-thz)$_2$(N$_3$)$_2$] (2): $Cu(ClO_4)_2 \cdot 6H_2O$ (0.093 g, 0.25 mmol) and NaN_3 (0.033 g, 0.5 mmol) were added with stirring to a solution of **1** (0.120 g, 0.5 mmol) in dry methanol (30 mL), and the mixture was then filtered to remove a small amount of precipitate. The dark brown solution was allowed to stand at room temperature in the dark for two weeks. Black crystals were obtained in 43% yield. $C_{20}H_{28}CuN_{12}O_4S_2$: calcd. C 38.24, H 4.49, N 26.74; found C 38.30, H 4.44, N 26.76. IR: $\tilde{\nu}_{thz}$ = 1420, 1190, 1136 cm^{-1}; $\tilde{\nu}_{N\text{-}O}$ = 1375 cm^{-1}.

Preparation of [CuCl$_2$(NIT2-thz)$_2$] (3): $CuCl_2 \cdot 2H_2O$ (0.086 g, 0.5 mmol) was added with stirring to a solution of **1** (0.120 g, 0.5 mmol) in dry ethanol (30 mL), and the mixture was then filtered to remove a small amount of precipitate. The dark brown solution was allowed to stand at room temperature in the dark for three weeks. Dark blue crystals were obtained in 45% yield. $C_{20}H_{28}Cl_2CuN_6O_4S_2$: calcd. C 39.06, H 4.59, N 13.66; found C

 © 2004 Wiley-VCH Verlag GmbH & Co. KGaA, Weinheim

Table 1. Crystallographic data for **1**, **2** and **3**

	1	**2**	**3**
Empirical formula	$C_{10}H_{14}N_3O_2S$	$C_{20}H_{28}CuN_{12}O_4S_2$	$C_{20}H_{28}Cl_2CuN_6O_4S_2$
Molecular mass	240.30	628.20	615.04
Temperature (K)	293 (2)	291(2)	291(2)
Wavelength (Å)	0.71073	0.71073	0.71073
Crystal system	monoclinic	monoclinic	triclinic
Space group	*C*2/*c*	$P2_1/c$	$P\bar{1}$
a (Å)	23.257(11)	10.171(2)	9.061(2)
b (Å)	23.447(10)	12.018(2)	9.856(2)
c (Å)	9.136(4)	11.180(2)	7.6988(15)
α (°)	90	90	97.25(3)
β (°)	96.458(9)	103.91(3)	94.89(3)
γ (°)	90	90	75.43(3)
V (Å^3)	4950(4)	1326.5(5)	659.1(2)
Z, calculated density (g·cm^{-3})	16, 1.290	2, 1.573	1, 1.550
Absorption coefficient (mm^{-1})	0.252	1.034	1.341
F(000)	2032	650	317
Crystal size/mm	0.25×0.20×0.10	0.26×0.20×0.20	0.25×0.21×0.20
θ range for data collection (°)	1.24 to 23.24	2.06 to 27.55	2.15 to 24
Reflections collected/unique	8365/3543 [*R*(int) = 0.0417]	4167/2279 [*R*(int) = 0.0209]	1714/1714 [*R*(int) = 0.0000]
Data/restraints/parameters	3543/2/297	3543/2/297	1709/ 0/161
Goodness-of-fit on F^2	1.052	1.096	1.038
R 1 [$I>2\sigma(I)$]	0.0536	0.0360	0.0776
wR	0.1461	0.0844	0.1923
R 1 (all data)	0.0931	0.0465	0.0886
wR	0.1701	0.0869	0.2098

Table 2. Selected bond lengths (Å) and angles (°) for **1**

S(1)−C(1)	1.692(5)	N(1)−C(2)	1.366(5)
S(1)−C(3)	1.729(4)	N(2)−C(4)	1.348(5)
S(2)−C(11)	1.676(5)	N(2)−C(5)	1.515(5)
S(2)−C(13)	1.735(4)	N(3)−C(4)	1.341(5)
O(1)−N(3)	1.284(4)	N(3)−C(8)	1.505(5)
O(2)−N(2)	1.278(4)	N(4)−C(13)	1.290(5)
O(3)−N(5)	1.285(5)	N(4)−C(12)	1.367(5)
O(4)−N(6)	1.278(4)	N(5)−C(14)	1.329(5)
N(1)−C(3)	1.305(5)	N(5)−C(18)	1.489(5)
N(6)−C(15)	1.509(4)	N(6)−C(14)	1.363(5)
C(1)−C(2)	1.319(6)	C(11)−C(12)	1.335(6)
C(1)−S(1)−C(3)	89.4(2)	C(13)−N(4)−C(12)	110.4(3)
C(11)−S(2)−C(13)	89.5(2)	O(3)−N(5)−C(14)	122.8(3)
C(3)−N(1)−C(2)	109.4(3)	O(3)−N(5)−C(18)	122.0(3)
O(2)−N(2)−C(4)	126.2(3)	C(14)−N(5)−C(18)	115.2(3)
O(2)−N(2)−C(5)	122.1(3)	O(4)−N(6)−C(14)	126.2(3)
C(4)−N(2)−C(5)	111.6(3)	O(4)−N(6)−C(15)	121.4(3)
O(1)−N(3)−C(4)	125.1(3)	C(14)−N(6)−C(15)	112.4(3)
O(1)−N(3)−C(8)	122.0(3)	C(4)−N(3)−C(8)	112.7(3)

Table 3. Selected bond lengths (Å) and angles (°) for **2**

Cu(1)−N(4)	1.995(3)	N(2)−O(1)	1.278(3)
Cu(1)−N(1)	2.024(2)	N(2)−C(4)	1.343(3)
Cu(1)−O(2)	2.364(2)	N(2)−C(5)	1.503(4)
N(3)−O(2)	1.276(3)	N(3)−C(4)	1.340(4)
S(1)−C(1)	1.699(3)	N(4)−N(5)	1.180(4)
S(1)−C(3)	1.721(3)	N(5)−N(6)	1.144(4)
N(1)−C(3)	1.325(3)	N(3)−C(6	1.508(3)
N(1)−C(2)	1.364(3)	C(1)−C(2)	1.346(4)
N(4)#1−Cu(1)−N(1)	91.92(10)	N(4)#1−Cu(1)−O(2)	89.87(13)
N(4)−Cu(1)−N(1)	88.08(10)	N(4)−Cu(1)−O(2)	90.13(13)
N(4)#1−Cu(1)−N(4)	180.0	N(1)#1−Cu(1)−O(2)	96.23(8)
N(1)−Cu(1)−O(2)	83.77(8)	O(2) #1−Cu(1)−O(2)	180.0
C(3)−N(1)−C(2)	111.2(2)	N(5)−N(4)−Cu(1)	128.6(2)
C(3)−N(1)−Cu(1)	129.69(18)	N(6)−N(5)−N(4)	177.6(3)
C(2)−N(1)−Cu(1)	118.49(17)	N(3)−O(2)−Cu(1)	120.38(17)

Symmetry transformations used to generate equivalent atoms (#1): $-x+1, -y+1, -z$

Table 4. Selected bond lengths (Å) and angles (°) for **3**

Cu (1)−N(1)	2.001(6)	N(1)−C(3)	1.328(9)
Cu (1)−Cl(1)	2.348(2)	N(1)−C(1)	1.363(9)
Cu (1)−Ol(1)	2.370(5)	N(2)−O(1)	1.293(7)
S(1)−C(2)	1.710(9)	N(2)−C(4)	1.330(8)
S(1)−C(3)	1.715(7)	N(2)−C(6)	1.498(8)
N(3)−C(5)	1.512(9)	N(3)−O(2)	1.280(7)
N(1)−Cu(1)−Cl(1)	89.0(2)	N(1)−Cu(1)−N(1)#1	180.0
N(1)#1−Cu(1)−Cl(1)	91.0(2)	Cl(1)#1−Cu(1)−O(1)#1	93.22(13)
Cl(1)−Cu(1)−Cl(1)#1	180.0	O(1)−Cu(1)−O(1)#1	180.0
N(1)−Cu(1)−O(1)	84.1(2)	C(2) −S(1)−C(3)	90.1(3)
N(1)#1−Cu(1)−O(1)	95.9(2)	C(3)−N(1)−C(1)	111.0(6)
Cl(1)−Cu(1)−O(1)	93.22(13)	C(3)−N(1)−Cu(1)	126.2(5)
Cl(1)#1−Cu(1)−O(1)	86.78(13)	C(1)−N(1)−Cu(1)	122.1(5)

Symmetry transformations used to generate equivalent atoms (#1): -x, $-y+1, -z+1$

 © 2004 Wiley-VCH Verlag GmbH & Co. KGaA, Weinheim

38.97, H 4.56, N 13.59. IR: $\tilde{\nu}_{thz}$ = 1418, 1189, 1137 cm^{-1}; $\tilde{\nu}_{N\text{-}O}$ = 1380 cm^{-1}.

CCDC-209220, -210729 and -210736 contain the supplementary crystallographic data for this paper. These data can be obtained free of charge at www.ccdc.cam.ac.uk/conts/retrieving.html [or from the Cambridge Crystallographic Data Centre, 12 Union Road, Cambridge CB2 1EZ, UK; Fax: (internat.) +44-1223-336-033; E-mail: deposit@ccdc.cam.ac.uk].

Acknowledgments

This work was supported by the Natural Science Foundation of China (Nos. 20171025, 20331010, and 90101028) and Tianji Natural Science Foundation (No. 033602011).

[1] J. Omata, T. Ishida, D. Hashizume, F. Iwasaki, T. Nogam, *Inorg. Chem.* **2001**, *40*, 3954−3958.
[2] K. E. Vostrikova, D. Luneau, W. Wernsdorfer, P. Rey, M. Verdaguer, *J. Am. Chem. Soc.* **2000**, *122*, 718−719.
[3] M. Fettouhi, M. Khaled, A. Waheed, S. Golhen, L. Ouahab, J. P. Sutter, O. Kahn, *Inorg. Chem.* **1999**, *38*, 3967−3971.
[4] Y. Yamamoto, T. Suzuki, S. Kaizaki, *J. Chem. Soc., Dalton Trans.* **2001**, 2943−2950.
[5] M. Kahn, J. Sutter, S. Golhen, P. Guionneau, L. Ouahab, O. Kahn, D. Chasseau, *J. Am. Chem. Soc.* **2000**, *122*, 3413−3421.
[6] D. Luneau, G. Risoan, P. Rey, A. Grand, A. Caneschi, D. Gatteschi, J. Laugier, *Inorg. Chem.* **1993**, *32*, 5616−5622.
[7] Y. Yamamoto, T. Yoshida, T. Suzuki, S. Kaizahi, *Inorg. Chim. Acta* **2001**, *325*, 187−192.
[8] K. Fegy, D. Luneau, E. Belorizky, M. Novak, J. L. Tholence, C. Paulsen, T. Ohm, P. Rey, *Inorg. Chem.* **1998**, *37*, 4524−4532.
[9] K. Fegy, D. Luneau, T. Ohm, C. Paulsen, P. Rey, *Angew. Chem. Int. Ed.* **1998**, *37*, 1270−1273.
[10] D. Luneau, F. M. Romeero, R. Ziessel, *Inorg. Chem.* **1998**, *37*, 5078−5087.
[11] J. P. Sutter, M. L. Kahn, S. Golhen, L. Ouahab, O. Kahn, *Chem. Eur. J.* **1998**, 4, 571−577.
[12] A. Caneschi, D. Gatteschi, P. Rey, *Prog. Inorg. Chem.* **1991**, *39*, 331−429.
[13] C. Rancurel, J. P. Sutter, O. Kahn, *New J. Chem.* **1997**, *21*, 275−277.
[14] O. Kahn, *Molecular Magnetism*, Wiley-VCH, Weinheim, **1993**, P214.
[15] A. P. Ginsberg, M. E. Lines, *Inorg. Chem.* **1972**, *11*, 2289−2291.
[16] A. Zheludev, V. Barone, M. Bonnet, B. Delly, A. Grand, E. Ressouche, P. Rey, R. Subra, J. Schweizer, *J. Am. Chem. Soc.* **1994**, *116*, 2019−2027.
[17] O. Kahn, B. Briat, *J. Chem. Soc., Faraday Trans. 2* **1976**, *72*, 268−281.
[18] A. Caneschi, D. Gatteschi, A. Grand, J. Laugier, P. Rey, L. Pardi, *Inorg. Chem.* **1988**, *27*, 1031−1035.
[19] H. Oshio, *Inorg. Chim. Acta* **2001**, *324*, 188−193.
[20] G. M. Sheldrick, SHELXS-97: Program for the Solution of Crystal Structures; University of Göttingen, Germany, **1997**.
[21] G. M. Sheldrick, SHELXL-97: Program for the refinement of Crystal Structures; University of Göttingen, Germany, **1997**.
[22] E. F. L. Call, *J. Org. Chem.* **1970**, *35*, 3623−3631.
[23] E. F. Ullman, J. H. Osiecki, D. G. B. Boocovk, R. Darcy, *J. Am. Chem. Soc.* **1972**, *94*, 7049−7059.

Received December 1, 2003
Early View Article
Published Online April 7, 2004

 © 2004 Wiley-VCH Verlag GmbH & Co. KGaA, Weinheim

Synthesis, Crystal Structure, and Magnetic Properties of $Mn_2(OH)_2SO_4$: A Novel Layered Hydroxide

Mohsen Ben Salah,[a] Serge Vilminot,*[a] Tahar Mhiri,[b] and Mohamedally Kurmoo[a]

Keywords: Hydroxysulfate / Hydrothermal synthesis / Magnetic properties / Manganese

$Mn_2(OH)_2SO_4$, obtained as pink prismatic crystals by the hydrothermal reaction of $MnSO_4 \cdot H_2O$ and NaOH at 240 °C for 24 h, consists of layers of Mn hydroxide connected to each other through μ^6-sulfate ions. Each layer exhibits vacancies, and each vacant space is capped at the top and bottom by the sulfate groups. The compound is paramagnetic above 50 K (C = 4.36 emu K mol^{-1}, μ_{eff} = 5.91 μ_B, Θ = −100 K). Below 45 K, the magnetization increases slightly, indicating canted-antiferromagnetic ($T_{Néel}$ = 42±1 K) behavior consistent with the linear dependence of the magnetization as a function of the field at 2 K, which reaches only 0.4 μ_B at 50 kOe, and the lack of any imaginary component of the ac-susceptibilities (ac = alternating current).

(© Wiley-VCH Verlag GmbH & Co. KGaA, 69451 Weinheim, Germany, 2004)

Introduction

Layered compounds have attracted continuing interest in many different fields of research.[1] The principal interest, in the early days, was due to their applications resulting from their sorption properties and, therefore, for selective separation, ion exchange chromatography, and as electrodes. These applications developed to include catalysis, since they have quite large surface areas, and also photopolymerization.[2] More recently, these materials have been of interest as a result of their magnetism, especially as models for low dimensional behavior in antiferromagnets but also for understanding the exchange mechanism through space when the layers are separated by non-magnetic intercalants.[3,4]

From a synthetic chemistry point of view, the layered compounds are very difficult to obtain as single crystals, and in cases where crystals of a few tens of nanometers in size have been obtained, resolution of the crystal structures was hampered by several dislocations and stacking faults, for example turbostratic faults.[5] Using hydrothermal techniques it has been possible to obtain a few compounds as single crystals.[6,7] Consequently, for those with crystal sizes large enough, their crystal structures were determined. In a few cases, the structures have been determined by Rietveld refinement of high-quality powder diffraction data.[8,9] Furthermore, certain disorders were fully characterized in some cases.[7,10]

Amongst the hydroxides of the divalent cations, the layer topology can be quite variable. The simplest case is that of brucite, which is adopted by the transition metal hydroxides $M(OH)_2$.[11−12] Variants of these are formed by replacing some of the hydroxides by other anions, such as $Cu_2(OH)_3NO_3$.[13] In the literature, these have been classified as β- and α-phases, respectively. A further modification of the layer topology can be achieved by periodically replacing some of the octahedra within the brucite layer, and capping the vacant sites by tetrahedrally coordinated MO_4 units. Examples of these are $Zn_5(OH)_8(H_2O)_2(NO_3)_2$,[14] $Zn_5(OH)_8Cl_2 \cdot H_2O$,[15] $Co_5(OH)_8(C_8H_{10}O_4) \cdot 4H_2O$,[7] and $Co_8(OH)_{12}(SO_4)_2(\text{pillar}) \cdot xH_2O$ {pillar = 1,2-diaminoethane or 4,4′-diazabicyclo[2.2.2]octane (dabco); x = 3 or 1}.[10] These structures are only observed for Zn and Co since both metals adopt a four-coordinate geometry. A more exotic layer topology can be found for $Co_2(OH)_2$(terephthalate),[9] which adopts a topology similar to the 110 planes of normal rutile, i.e. consisting of edge-sharing chains of octahedra connected to similar chains through the apices of the octahedra with the layers being interleaved by the bridging dianionic terephthalate. A further variant was found for $M_2(OH)_2(C_2O_4)$ (M = Co or Mn), which consists of dimers of edge-sharing octahedra connected to one another by their apices thus forming corrugated layers. These layers are then connected by the oxalate ions.[16] $Mn(OH)(OAc)_2 \cdot HOAc$ is an interesting layered compound employing both coordination and hydrogen bonds.[17]

In this paper we present the synthesis, crystal structure, and characterization by IR spectroscopy and DT-TGA of $Mn_2(OH)_2SO_4$. It displays a novel layered topology and be-

[a] Groupe des Matériaux Inorganiques, IPCMS, UMR 7504 (ULP-CNRS),
23 rue du Loess, B. P. 43, 67034 Strasbourg Cedex 2, France
E-mail: vilminot@ipcms.u-strasbg.fr
[b] Laboratoire de l'État Solide, Faculté des Sciences,
3038 Sfax, Tunisia

Supporting information for this article is available on the WWW under http://www.eurjic.org or from the author.

 © 2004 Wiley-VCH Verlag GmbH & Co. KGaA, Weinheim DOI: 10.1002/ejic.200300909

haves as a paramagnet above 50 K with a long-range Néel transition at 42 K, and the appearance of a weak magnetization due to a very small canting.

Results and Discussion

X-ray Diffraction

X-ray powder diffraction data collected on the pink crystals confirmed the formation of a new phase. The diffraction lines were indexed from the unit cell parameters measured on a single crystal using the pattern-matching mode of FULLPROF.[20] All lines were then indexed confirming, that the sample was a single phase. Figure S1 (see Supporting Information) gives the corresponding diffractogram.

Thermal Analysis

The TGA trace (Figure S2, Supporting Information) revealed that the decomposition takes place in three steps. The first step between 300 and 500 °C associated with an endothermic effect on the DTA trace, whose maximum is at 497 °C, can be attributed to the loss of hydroxy groups as water. The second step between 780 and 870 °C (endothermic effect at 862 °C) is related to the decomposition of the sulfate groups to SO_3. In the final step, weight loss at around 910 °C (endothermic at 912 °C) corresponds to the reduction of the manganese oxide previously formed at lower temperatures. Starting from an Mn^{II} compound, it is well known that the corresponding MnO oxide is not stable and will be transformed into Mn_2O_3. The corresponding oxidation reaction is well identified by the weight increase between 600 and 700 °C, and by the weight loss value between 780 and 870 °C, which is lower than predicted if MnO were to be stable. The experimental Mn content, 44.9 wt%, is in good agreement with the expected value of 45.8 wt%.

Structure Description

The structure is built up of a succession of layers parallel to the *bc* plane, alternating between layers containing MnO_6 octahedra, and layers containing SO_4 tetrahedra (Figure 1). Each tetrahedron shares its four corners with six different octahedra, three on each adjacent layer. Inside an $(MnO_6)_n$ layer, each octahedron shares its edges with three neighboring octahedra, and is further corner-shared with one octahedron. This results in a layer with apparent porosity (Figure 2). In the brucite layers, each octahedron is surrounded by six octahedra resulting in a full occupation of the layer space. The MnO_6 octahedra are distorted with three Mn−OH distances between 2.113 and 2.169 Å, and three Mn−O(sulfate) distances between 2.258 and 2.318 Å. Moreover, the interatomic angles also differ from the values expected for a regular octahedron, with values as low as 152° instead of 180°, and 117° instead of 90°. On the other hand, the sulfate tetrahedra are almost regular. OH and O(2) oxygen atoms are of the μ^3-type, OH being bonded to three Mn ions, and O(2) to two Mn centers and one S atom, whereas O(1) is a μ^2-oxo group, and is bonded to one Mn and one S atom. The O−H bond length of 0.77 Å is in agreement with the distances usually found from X-ray diffraction data. The H atom participates in a very weak hydrogen bond with O(1) with an H···O(1) distance of 2.12 Å. Bond valence calculations using the model of Brown and Altermatt[21] reveal, that values (Table 1) close to those expected are obtained for S, Mn and O2. For O1 and OH, the observed deviations are probably related to the uncertainty of the O−H and H···O(1) bond lengths.

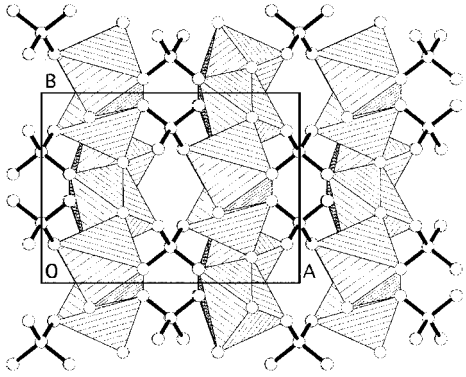

Figure 1. Projection of the structure along the *c* axis (perpendicular to the stacking axis) showing the connections between the layers by the sulfate ions; manganese atoms are presented as polyhedra and the sulfates as spheres and sticks

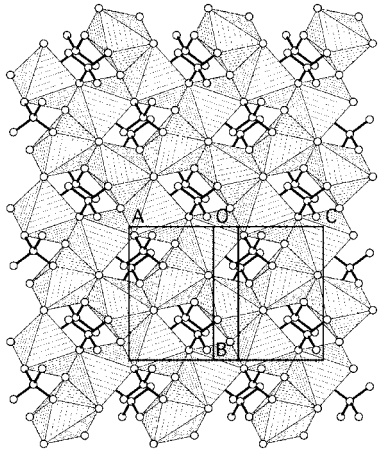

Figure 2. Projection of the structure perpendicular to the layers showing the vacancies, which are coordinated at the top and bottom by the sulfate ions

The required number of Mn−O bonds per formula unit is 12. This requirement is satisfied by the presence of three bonds from each hydroxide ion, and six bonds from the sulfate group. This is similar to that observed for $M_2(OH)_2C_2O_4$ (M = Mn or Co), and for $Co_2(OH)_2$(terephthalate) where, in both cases, the hydroxide ions are both μ^3-bridging and the carboxylate ion forms six bonds with

 © 2004 Wiley-VCH Verlag GmbH & Co. KGaA, Weinheim

Table 1. Bond valence calculations

	O(1)	O(2)	OH	OH	OH	H	S	Mn	Σs[a]
S	1.512	1.440							5.904
	1.512	1.440							
Mn	0.282	0.262	0.418	0.397	0.359				1.958
		0.240							
O(1)						0.035	1.512	0.282	1.829
O(2)							1.440	0.262	1.942
								0.240	
OH						1.354		0.418	2.528
								0.397	
								0.359	
H	0.035		1.354						1.389

[a] $s = \exp[(r_0 - r)/B]$ with $r_0(S) = 1.624$, $r_0(\mathrm{Mn}) = 1.790$, $r_0(\mathrm{H}) = 0.882$, $B = 0.37$ from ref.[21]

the surrounding metal atoms.[9,16] Such a μ^6-coordination for the sulfate is rare (Figure 3), it is commonly found as an independent anion, or displaying single-, μ^2-, μ^3- or μ^4-coordination.

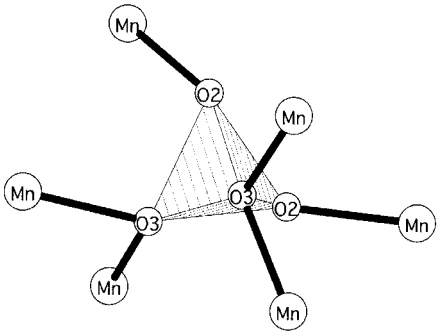

Figure 3. The six-fold coordination of the sulfate group

Infrared Spectroscopy

The infrared spectrum recorded between 500 and 4000 cm^{-1} (Figure S3, Supporting Information) exhibits vibrational bands related to the O−H and S−O bonds. The first ones are near 3500 cm^{-1} as well as in the 900−650 cm^{-1} region, whereas the second ones are near 1100 and 600 cm^{-1}.[22] The sharp band with its maximum at 3498 cm^{-1} can be attributed to the O−H stretching mode of the OH group. Its sharpness is related to the presence of an OH group not involved in hydrogen bonding as revealed by the structural data. The ν_3 and ν_4 vibrational bands of the sulfate group appear as doublets at 1153−1105 cm^{-1} and 617−603 cm^{-1}, respectively. The presence of two bands is related to the local symmetry of the tetrahedron.

Magnetic Susceptibility

In the paramagnetic region, the magnetic susceptibility measured on a randomly oriented sample, consisting of few selected washed crystals, follows the Curie−Weiss law, $\chi = C/(T - \theta) = 8.72/(T + 100)$ emu mol^{-1}, where the Curie and Weiss constants were obtained by fitting the $1/\chi$ experimental data in the temperature range 150−300 K (Figure 4). The negative θ value indicates that the dominant nearest neighbor exchange interactions within the layer are antiferromagnetic. From the Curie constant, $C = Ng^2\mu_B{}^2s(s + 1)/3k$, of 4.36 emu K per Mn and $s = 5/2$, we deduced a value of the Landé g factor of 1.997, in good agreement with a ^{6}A ground state ion. The effective moment $(8C)^{1/2}$ of 5.907 μ_B is close to the expected value of 5.92 μ_B, calculated with the spin-only formula.[23] It appears that the severe distortion of the MnO_6 octahedron has little effect on the moment. On lowering the temperature, χ exhibits a sharp increase starting around 45 K before reaching a plateau down to the lowest temperature. On the χT curve, a maximum can be detected at the previously mentioned temperature of 42 K before decreasing to a value close to zero at 4 K. This behavior has been attributed to the presence of a 3D-antiferromagnetic ordering below the Néel temperature $T_N = 42$ K. The sharp increase at 45 K may be due to a small canting of the sub-lattice. To verify that this anomaly is not due to a small amount of impurity, we performed the experiment on a clean single crystal and observed the same transition (Figure S4, Supporting Information). If we assume that the magnetic unit cell is the same as the nuclear one, that is with a propagation vector k (0,0,0),[24] we may therefore expect an antiferromagnetic ordering due to the presence of the center of symmetry. The isothermal magnetization at 2 K (Figure 5) shows a linear dependence and reaches 0.4 μ_B in a field of 50 kOe. Such behavior is consistent with long-range antiferromagnetic ordering. However, the near-zero residual magnetization indicates the canting angle is immeasurably small. A broad maximum in the real component of the ac-susceptibility (Figure 6) is consistent with the antiferromagnetic coupling, and long-range antiferromagnetism. Due to the very small canting angle, there is no imaginary component in the ac-susceptibility as a function of temperature. Using the moment (M_{2K}) at 2 K in an applied field of 100 Oe, we estimated the canting angle, $\sin^{-1}(M_{2K}/M_s) = \sin^{-1}(6.7/2 \times 5 \times 5585)$, to be $7{\cdot}10^{-3}$ °.

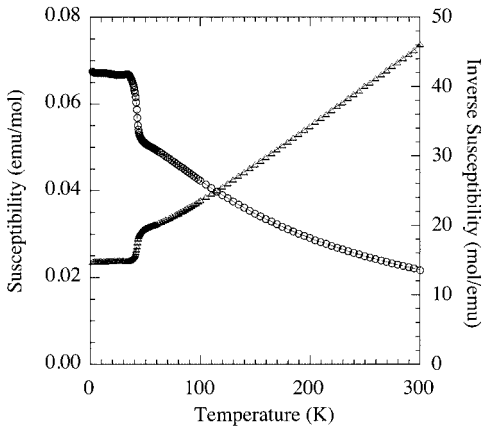

Figure 4. Temperature dependence of the dc-susceptibility (circles), and the inverse dc-susceptibility (triangles) of a polycrystalline sample measured in an applied field of 100 Oe

 © 2004 Wiley-VCH Verlag GmbH & Co. KGaA, Weinheim

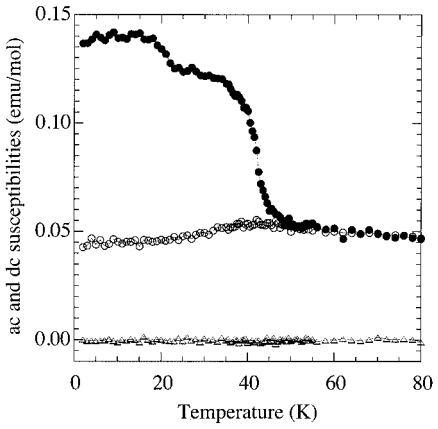

Figure 5. dc-Susceptibility (filled circles) on cooling in an applied dc-magnetic field of 2 Oe, and ac-susceptibilities (circles for the real, and triangles for the imaginary component) in an applied ac-field of 1 Oe oscillating at 17 Hz

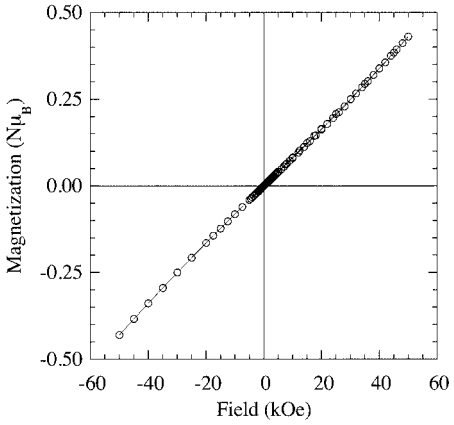

Figure 6. Isothermal magnetization at 2 K of a polycrystalline sample

Conclusion

High-quality crystals of $Mn_2(OH)_2SO_4$ were prepared as a minority phase by the hydrothermal reaction of $MnSO_4{\cdot}H_2O$ and NaOH. It displays a novel layered topology, and a canted-antiferromagnetic state below the Néel temperature of 42 K.

Experimental Section

Synthesis: $Mn_2(OH)_2SO_4$ was obtained by a hydrothermal synthesis. $MnSO_4{\cdot}H_2O$ (2.5 g, 14.8 mmol) and sodium hydroxide (0.7 g, 17.5 mmol) were separately dissolved in boiling distilled water (20 mL), and the two solutions were quickly mixed while still hot. The resultant suspension was immediately poured into the autoclave, which was then sealed and heated at 240 °C for 24 h under autogenous pressure. Under these conditions, a mixture of $Mn_3(OH)_2(SO_4)_2(H_2O)_2$[18] and $Mn_2(OH)_2SO_4$ was obtained. Several attempts to promote the formation of a single phase by varying the starting Mn/Na proportions, and the conditions of the hydrothermal synthesis (temperature, time, dilution) were unsuccessful. Fortunately, the crystal habits and colors of the two phases are quite different. It was therefore possible to separate the phases using an optical microscope. Whereas $Mn_3(OH)_2(SO_4)_2(H_2O)_2$ crystallizes as pale beige platelets, $Mn_2(OH)_2SO_4$ appears as larger pink prismatic crystals, which were easily separated. Following separation, the crystals were washed with acetone in an ultrasonic bath to remove small traces of the other phase and finally dried in air.

Characterization: The thermal analysis was performed with a TA-STD-Q600 apparatus, at a 3 °C/min heating rate, under air. Infrared spectra were recorded with an ATI Mattson spectrometer by transmission through KBr pellets containing 1% of the crystals. Powder X-ray diffraction patterns were recorded using a D5000 Siemens diffractometer equipped with a back monochromator (Cu-$K_{\alpha 1}$, 1.5406 Å). For X-ray data collection, a single crystal was selected and mounted on a glass fiber. A single set of 180 frames, 20 s/frame, scan of 1°/frame (each frame measured twice), crystal−detector distance = 30 mm, θ = 0°, κ = 0°, was collected at room temperature with a Nonius Kappa CCD diffractometer at the Service Commun de Rayons X, Université Louis Pasteur, Strasbourg. The structure was solved by means of a three-dimensional Patterson function allowing location of the positions of the manganese atoms. Subsequent parameter refinement cycles and three-dimensional difference Fourier maps using SHELXS-93[19] yielded the positions of all the other atoms. The final refinement included anisotropic displacement parameters, and a secondary extinction correction. The atomic coordinates of hydrogen atoms were isotropically refined. Additional experimental details are given in Table 2 and in the Supporting Information. Table 3 gives the final atomic positions and Table 4 the corresponding bond lengths and angles. The oxygen atoms of the sulfate and hydroxy groups have been labeled as O and OH, respectively. Further details of the crystal-structure investigation may be obtained from the Fachinformationszentrum Karlsruhe, 76344 Eggenstein-Leopoldshafen, Ger-

Table 2. Summary of the single-crystal X-ray data collection and structural refinement of $Mn_2(OH)_2SO_4$

a [Å]	11.2358(5)	μ [mm^{-1}]	5.58
b [Å]	7.4822(4)	hkl range	$-15 < h < 16$
c [Å]	6.1572(3)		$-9 < k < 10$
			$-8 < l < 8$
		θ range [°]	1−31
β [°]	115.061(3)	Total number of reflections	1229
V [Å^3]	468.90(8)	Unique reflections	738
Z	4	Unique $\lvert I_o\rvert > 2\sigma(I_o)$	655
Space group	$C2/c$ (no. 15)	R_{int} [%]	2.9
F (000)	448.0	R_F (all data) [%]	3.46
$D_{calcd.}$ [g·cm^{-3}]	3.399	$wR2(F_o^2)$ (all data) [%]	7.4
Radiation λ [Å]	0.71703	GoF [%]	1.105

Table 3. Fractional atomic coordinates for $Mn_2(OH)_2SO_4$ obtained from X-ray data at 295 K

Atom	x/a	y/b	z/c
Mn	0.25127(3)	0.09849(5)	0.18252(6)
S	0	0.31357(12)	0.25
OH	0.3147(2)	0.3689(3)	0.2011(3)
O1	0.0490(2)	0.2023(3)	0.1084(3)
O2	0.1087(2)	0.4293(3)	0.4143(3)
H	0.390(5)	0.359(5)	0.275(8)

 © 2004 Wiley-VCH Verlag GmbH & Co. KGaA, Weinheim

Table 4. Interatomic distances [Å] and angles [°] from the X-ray structure determination

S−O1	1.471(2) × 2	O1−S−O1	111.0(3)	O2−S−O2	108.9(2)
S−O2	1.489(2) × 2	O1−S−O2	109.1(3) × 2	<O−S−O>	109.5
<S−O>	1.480	O1−S−O2	109.4(3) × 2		
Mn−OH	2.113(2)	OH−Mn−OH	155.61(4)	OH−Mn−O2	88.16(7)
Mn−OH	2.132(2)	OH−Mn−OH	116.99(7)	OH−Mn−O1	83.73(7)
Mn−OH	2.169(2)	OH−Mn−O1	83.13(7)	OH−Mn−O2	74.58(7)
Mn−O1	2.258(2)	OH−Mn−O2	90.99(7)	OH−Mn−O2	160.11(4)
Mn−O2	2.286(2)	OH−Mn−O2	74.94(8)	O1−Mn−O2	151.96(7)
Mn−O2	2.318(2)	OH−Mn−OH	84.47(7)	O1−Mn−O2	114.56(7)
<Mn−O>	2.213	OH−Mn−O1	88.26(7)	O2−Mn−O2	89.99(7)
		OH−Mn−O2	106.73(7)		
OH−H	0.77(5)	H···O1	2.12(5)	OH−H···O1	148

many, on quoting the depository number CSD-413556 (they can be requested from Crysdata@FIZ-Karlsruhe.de).

[1] [1a] R. Schollhorn, *Intercalation Compounds*, Academic Press, London, **1984**. [1b]A. Clearfield, *Chem. Rev.* **1988**, *88*, 125. [1c] A. J. Jacobsen, *Intercalation Reactions of Layered Compounds* in *Solid State Chemistry: Compounds* (Eds.: P. Day and A. Cheetham), Oxford University Press, Oxford, **1992**. [1d] D. O'Hare, *Inorganic Intercalation Chemistry* in *Inorganic Materials* (Eds.: D. W. Bruce and D. O'Hare), Wiley, London, **1993**. [1e]A. Clearfield, *Curr. Opin. Solid State Chem.* **1996**, *1*, 268. [1f] A. Clearfield, *Inorganic Ion Exchange Materials* (Ed.: A. Clearfield), CRC Press Inc., Boca Raton, Florida, **1991**.

[2] [2a] T. Pinnavaia, *Science* **1983**, *220*, 365. [2b] T. Shichi, K. Takagi, Y. Sawaki, *Chem. Commun.* **1996**, 2027.

[3] *Magnetic Properties of Layered Transition Metal Compounds* (Ed.: L. J. De Jongh), Kluwer Academic Publishers, Dordrecht, **1990**.

[4] M. Kurmoo, *Phil. Trans. R. Soc., Lond.* **1999**, *357*, 3041; M. Kurmoo, *Chem. Mater.* **1999**, *11*, 3370; M. Kurmoo, *J. Mater. Chem.* **1999**, *9*, 2595; M. Kurmoo, P. Day, A. Derory, C. Estournes, R. Poinsot, M. J. Stead, C. J. Kepert, *J. Solid State Chem.* **1999**, *145*, 452.

[5] [5a] I. V. Mitchell, *Pillared Layered Structures; Current Trends and Applications*, Elsevier, London, **1990**. [5b]S. Carlino, *Solid State Ionics* **1997**, *98*, 73.

[6] A. Rabenau, *Angew. Chem. Int. Ed. Engl.* **1985**, *24*, 1026.

[7] M. Kurmoo, H. Kumagai, S. M. Hughes, C. J. Kepert, *Inorg. Chem.* **2003**, *42*, 6709.

[8] H. M. Rietveld, *J. Appl. Crystallogr.* **1969**, *2*, 65−71.

[9] M. Kurmoo, H. Kumagai, M. A. Green, B. W. Lovett, S. J. Blundell, A. Ardavan, J. Singleton, *J. Solid State Chem.* **2001**, *159*, 343.

[10] A. Rujiwatra, C. J. Kepert, J. B. Claridge, M. J. Rosseinsky, H. Kumagai, M. Kurmoo, *J. Am. Chem. Soc.* **2001**, *123*, 10584.

[11] H. R. Oswald, R. Asper in *Preparation and Crystal Growth of Materials with Layer Structures* (Ed.: R. M. A. Leith), Reidel, Dordrecht, **1977**, p. 71.

[12] C. Mockenhaupt, T. Zeiske, H. D. Lutz, *J. Mol. Struct.* **1998**, *443*, 191.

[13] [13a] H. L. Wells, S. L. Penfeld, *Am. J. Sci.* **1885**, *30*, 50. [13b] B. Bovio, S. Locchi, *J. Crystallogr. Spectr. Res.* **1982**, *12*, 507. [13c] H. Effenberger, *Z. Kristallogr.* **1983**, *165*, 127.

[14] W. Stahlin, H. R. Oswald, *Acta Crystallogr., Sect. B* **1970**, *26*, 860.

[15] R. Allmann, *Z. Kristallogr.* **1968**, *126*, 417.

[16] [16a] D. Price, F. Lionti, R. Ballou, P. T. Wood, A. K. Powell, *Phil. Trans. R. Soc., Lond.* **1999**, *A357*, 3099. [16b] Z. A. D. Lethbridge, A. F. Congreve, E. Esslemont, A. M. Z. Slawin, P. Lightfoot, *J. Solid State Chem.* **2003**, *172*, 212.

[17] D. J. Price, S. R. Batten, B. Moubaraki, K. S. Murray, *Polyhedron* **2003**, *22*, 2161.

[18] [18a] M. Ben Salah, S. Vilminot, G. André, M. Richard-Plouet, F. Bourée-Vigneron, T. Mhiri, M. Kurmoo, *Chem. Eur. J.*, in press. [18b]S. Vilminot, M. Richard-Plouet, G. André, D. Swierczynski, F. Bourée-Vigneron, M. Kurmoo, *Inorg. Chem.* **2003**, *42*, 6859.

[19] G. M. Sheldrick, *SHELXL*-93, *Program for the Refinement of Crystal Structures*, University of Göttingen, Germany, **1993**.

[20] J. Rodriguez-Carvajal, *FULLPROF: Rietveld, Profile Matching and Integrated Intensity Refinement of X-ray andlor Neutron Data*, ver. 3.5d, Léon-Brillouin Laboratory, CEA Saclay, France, **1998**.

[21] I. D. Brown, D. Altermatt, *Acta Crystallogr., Sect. B* **1985**, *41*, 244−247.

[22] K. Nakamoto, *Infrared and Raman Spectra of Inorganic and Coordination Compounds*, John Wiley, New York, **1986**.

[23] A. Herpin, *Theorie du Magnetisme*, Presse Universitaire de France, Paris, **1968**.

[24] E. F. Bertaut, *Acta Crystallogr., Sect. A* **1968**, *24*, 217.

Received December 8, 2003
Early View Article
Published Online April 7, 2004

 © 2004 Wiley-VCH Verlag GmbH & Co. KGaA, Weinheim

Dimeric 2,2′-Bipyridylruthenium(II) Complexes Containing 2,2′-Bis(1,2,4-triazin-3-yl)-4,4′-bipyridine-Like Bridging Ligands: Syntheses, Characterization and DNA Binding

Cai-Wu Jiang[a]

Keywords: Dinuclear complexes / Ruthenium / DNA binding modes / Enantioselectivity

Three new bridging ligands 2,2′-bis(1,2,4-triazin-3-yl)-4,4′-bipyridine (btb), 2,2′-bis(1,2,4-triazino[5,6-f]acenaphthylen-3-yl)-4,4′-bipyridine (btapb), 2,2′-bis(5,6-diphenyl-1,2,4-triazin-3-yl)-4,4′-bipyridine (bdptb) and their dimeric 2,2′-bipyridylruthenium(II) complexes $[Ru(bpy)_2(btb)Ru(bpy)_2]^{4+}$ (**1**), $[Ru(bpy)_2(btapb)Ru(bpy)_2]^{4+}$ (**2**), $[Ru(bpy)_2(bdptb)Ru(bpy)_2]^{4+}$ (**3**) have been synthesized and characterized by elemental analysis, fast atom bombardment (FAB) mass spectrometry or electrospray mass spectrometry (ES-MS), ^1H NMR and UV/Visible spectroscopy. The binding behavior of these dimeric complexes with calf thymus DNA (CT-DNA) was investigated by electronic absorption spectroscopy, viscosity measurements, and equilibrium dialysis experiments. The hypochromism of the metal-ligand charge transfer (MLCT) band in the electronic absorption spectra of the dinuclear complexes **1**, **2**, and **3** is 8.7%, 19% and 33%, respectively, with bathochromic shifts of 5, 5 and 14 nm, respectively. The binding constants are 7.5×10^4 M^{-1}, 4.8×10^5 M^{-1} and 7.6×10^5 M^{-1}, respectively. Increasing the size of the plane of the bridging ligand increases the hydrophobicity of their complexes, leading to stronger binding by the complexes to calf thymus DNA. The effect of increasing concentrations of these novel dimeric ruthenium(II) complexes on the relative viscosities of CT-DNA is less notable than that of well-known intercalators such as $[Ru(bpy)_2(dppz)]^{2+}$. The equilibrium experiments showed that ΛΛ–**3** binding is stronger than ΔΔ–**3** binding to CT-DNA. This is the first example of a dinuclear complex binding enantioselectively to CT-DNA measured by equilibrium dialysis. The experiments suggest that the three complexes may be DNA groove binders.
(© Wiley-VCH Verlag GmbH & Co. KGaA, 69451 Weinheim, Germany, 2004)

Introduction

The design of molecules that target particular DNA sequences is one of the major challenges in the field of molecular recognition. The potential application of ruthenium complexes with polypyridyl ligands in the design and development of photophysical and stereoselective probes of nucleic acid structure has been explored extensively in recent years.[1−6] However, this work has focused primarily on mononuclear complexes, with di- or polynuclear complexes attracting limited attention. Dimeric ruthenium(II) complexes have some advantages over other complexes as photo- and stereochemical probes for nucleic acids, such as greater variations in size and shape. Additionally, the incorporation of two chiral centers into a single dimeric complex may enable amplification of the chiral discrimination. More recently, non-intercalating dinuclear ruthenium(II) complexes have been synthesized as probes of DNA structure.[7−10]

In a previous communication, we reported a novel dimeric ruthenium(II) complex $[Ru(bpy)_2(bdptb)Ru(bpy)_2]^{4+}$ [**3**; bdptb = 2,2′-bis(5,6-diphenyl-1,2,4-triazin-3-yl)-4,4′-bipyridine] that displays enantiopreferential DNA-binding behavior after equilibrium dialysis.[10] We describe here the synthesis of the three new bridging ligands 2,2′-bis(1,2,4-triazin-3-yl)-4,4′-bipyridine (btb), 2,2′-bis(1,2,4-triazino[5,6-*f*]acenaphthylen-3-yl)-4,4′-bipyridine (btapb), bdptb and their dimeric 2,2′-bipyridylruthenium(II) complexes $[Ru(bpy)_2(btb)Ru(bpy)_2]^{4+}$ (**1**), $[Ru(bpy)_2(btapb)Ru(bpy)_2]^{4+}$ (**2**) and **3**. The binding behavior of these compounds with calf thymus DNA (CT-DNA) is also presented.

[a] Guangxi Traditional Chinese Medical University,
Nanning 530001, P. R. China
Fax: (internat.) +86-771-313-7377
E-mail: cwjiang@gxtcmu.edu.cn

Results and Discussion

1. Syntheses and Characterization

The synthetic routes to the bidentate bridging ligands and their complexes with bpy diruthenium(II) are summarized in Scheme 1. The synthesis of the bridging ligands was based on the method for the 1,2,4-triazine ring preparation established by Case.[11,12] The condensation of bahmb with glyoxal, acenaphthenequinone or benzil produced btb, btapb and bdptb, respectively, in 78%, 72% and 75% yields. Their identities were confirmed by elemental analysis, fast atom bombardment (FAB) mass spectrometry and NMR

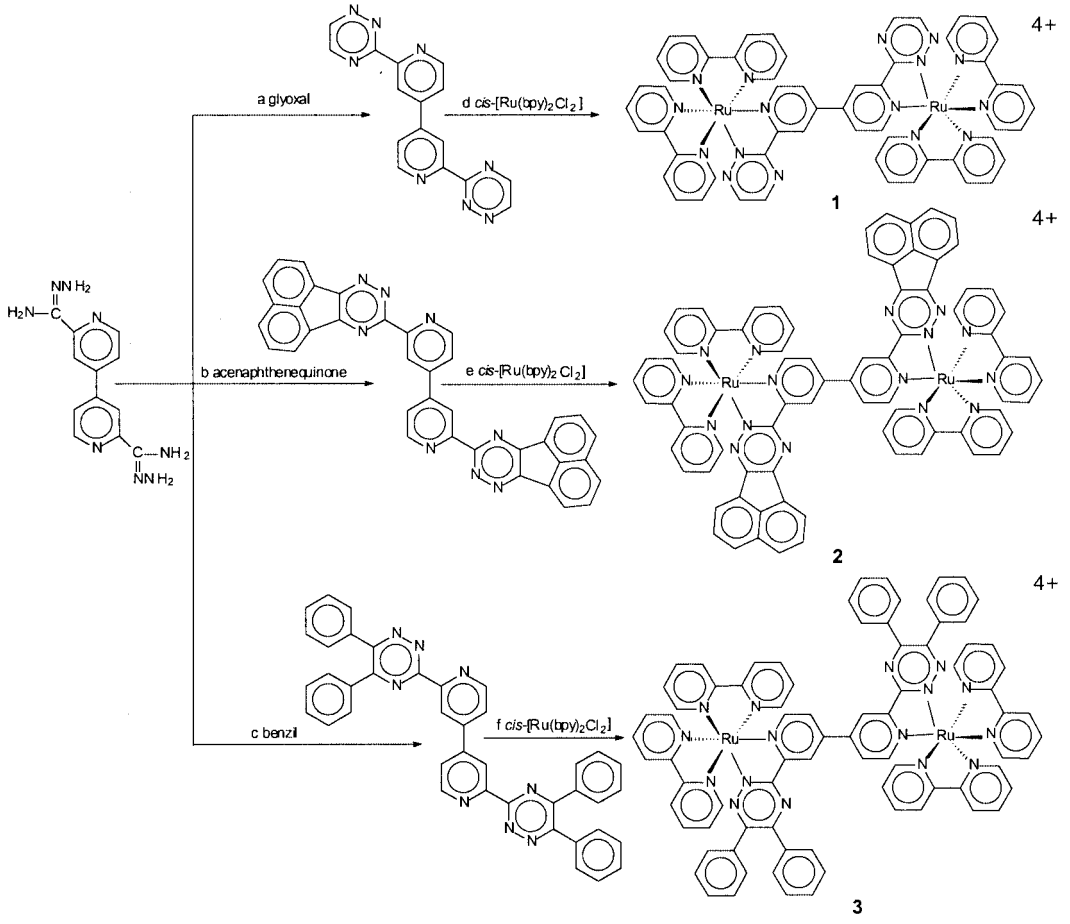

Scheme 1. The synthetic routes to the bidentate bridging ligands and bpy diruthenium(II) complexes

spectroscopy. Their complexes were also synthesized and characterized by elemental analysis and spectroscopic methods. The bridging ligands and their dimeric complexes give highly resolved ^{1}H NMR spectra in [D$_6$]DMSO and all proton resonance signals could be assigned by ^{1}H-^{1}H COSY experiments. The ^{1}H NMR spectral data of the dimeric complexes are listed in the Exp. Sect. The ^{1}H-^{1}H COSY NMR spectrum of the dimeric complex **2** is given in Figure 1 as an example.

Electrospray mass spectrometry (ES-MS) has recently been shown to be a powerful tool for measuring the molecular mass of nonvolatile, thermally unstable compounds.[13] In the ES-MS spectra for the diruthenium(II) complexes, intense signals for $[M - 2ClO_4]^{2+}$, $[M - 3ClO_4]^{3+}$ and $[M - 4ClO_4]^{4+}$ were observed. The ES-MS results are given in the Exp. Sect. The observed molecular weights are consistent with the expected values.

The electronic absorption spectra of the new bridging ligands and their dimeric complexes were recorded in chloroform and acetonitrile, respectively. The absorption data are shown in Table 1. The lowest energy absorption bands at 502, 532 and 506 nm for the dimeric complexes are assigned to the metal-ligand charge transfer (MLCT) transition. The high energy absorption bands are attributed to the intense intraligand π-π* transition by comparison with the spectra of the uncoordinated bridging ligand.[14]

2. DNA-Binding Studies

Electronic Absorption Titrations

The interaction of the diruthenium(II) complexes with DNA was investigated by electronic absorption spectroscopy. The absorption spectra of complexes **1**, **2** and **3** in the absence and presence of CT-DNA (with the same concentrations of the complexes) are given in Figure 2. The absorption spectrum of complex **3** has been reported previously.[10] These results are summarized in Table 2.

As the concentration of DNA is increased, the MLCT transition bands of the complexes **1**, **2** and **3** at 483, 523 and 492 nm, respectively, exhibit hypsochromic shifts of about 8.7%, 19% and 33%, and a bathochromism of 5, 5 and 14 nm, respectively. These spectral characteristics suggest that the complexes exhibit a high affinity for DNA.

In order to compare quantitatively the binding strength of the diruthenium(II) complexes, the intrinsic binding constants K_b of the complexes **1**, **2** and **3** with calf thymus DNA were determined from the decrease of the absorbance

 © 2004 Wiley-VCH Verlag GmbH & Co. KGaA, Weinheim

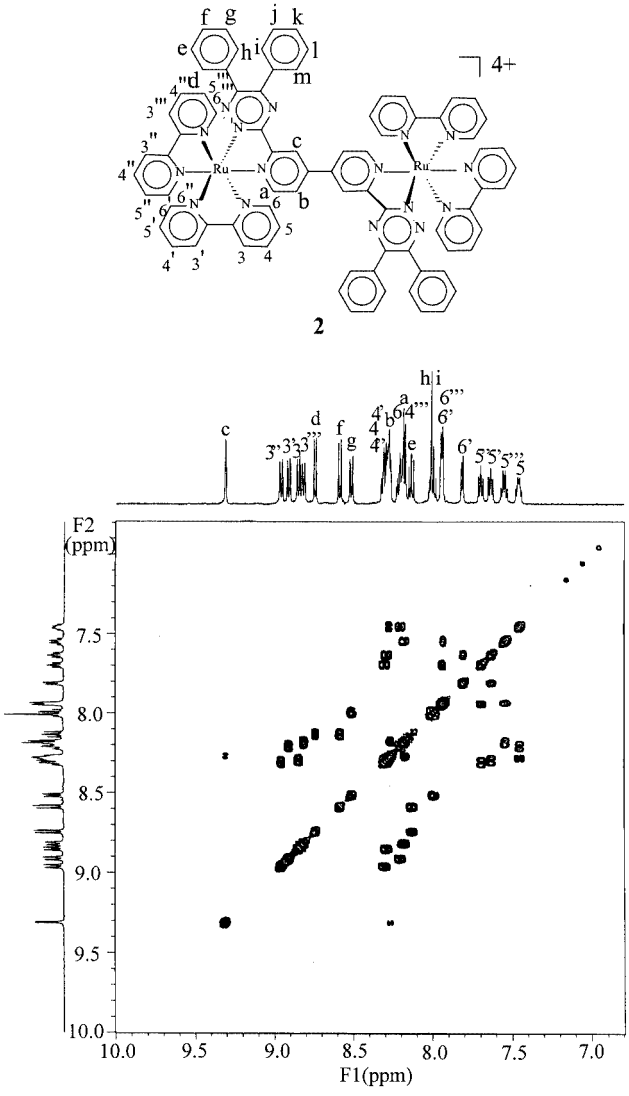

Figure 1. ^{1}H-^{1}H COSY spectra of $[Ru(bpy)_2(btapb)Ru(bpy)_2]]^{4+}$

Table 1. Electronic absorption spectroscopic data of the ligands and complexes

Compound	λ_{max}/nm(ε_{max}/M^{-1}·cm^{-1})
btb[a]	284.6(6540) 242(9630)
btapb[a]	316.6(11031) 235.8(10901)
bdptb[a]	304.4(7733) 240.8(10898)
1 [b]	502(23847) 421(27100) 284(109494) 244(69100)
2 [b]	532(24553) 434(26883) 386(41176) 284(101211)
3 [b]	506(32406) 425(32964) 284(119788) 245(64400)

[a] The solvent is chloroform for the ligands. [b] The solvent is acetonitrile for the complexes.

monitored, for the complexes **1**, **2** and **3**, at 483, 523 and 492 nm, respectively. The intrinsic binding constant K_b of the complex with CT-DNA was determined from the equation:[14] $[DNA]/(\varepsilon_a - \varepsilon_f) = [DNA]/(\varepsilon_b - \varepsilon_f) + 1/K_b \cdot (\varepsilon_b - \varepsilon_f)$ by a plot of $[DNA]/(\varepsilon_a - \varepsilon_f)$ versus [DNA], where [DNA] is the concentration of DNA as base pairs. The ap-

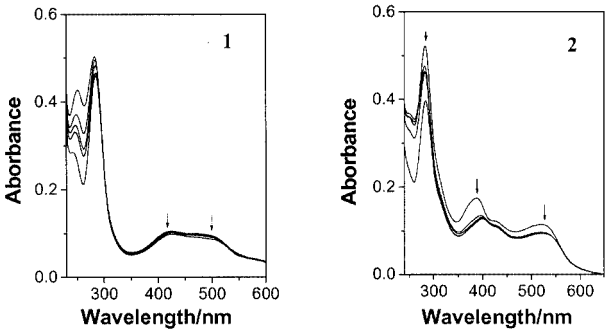

Figure 2. Absorption spectra of complexes **1** and **2** in Tris-HCl buffer upon addition of calf thymus DNA; [Ru] = 4 μM, [DNA] = (0−60) μM; the arrow shows the absorbance change upon increasing DNA concentrations

Table 2. Electronic absorption spectral changes upon addition of CT-DNA

Complexes	λ_{max}/nm free	bound	Bathochromism $\Delta\lambda$/ nm	Hypochromism %	K_b/M^{-1}
1	483	488	5	8.7	7.5×10^4
	422	426	4	8.2	
	284	274	−10	12	
2	523	528	5	19	4.8×10^5
	388	402	4	28.2	
	283	285	2	24	
3	492	506	14	33	7.6×10^5
	426	427	1	26	
	280	282	2	31	

parent absorption coefficients ε_a, ε_f and ε_b correspond to A_{obsd}/[Ru], the extinction coefficient for the free ruthenium complex and the extinction coefficient for the ruthenium complex in the fully bound form, respectively. The slope and *y* intercept of the linear fit of $[DNA]/(\varepsilon_a - \varepsilon_f)$ versus [DNA] give $1/(\varepsilon_b - \varepsilon_f)$ and $1/K_b \cdot (\varepsilon_b - \varepsilon_f)$, respectively. The intrinsic binding constant K_b can be obtained from the ratio of the slope and the *y* intercept. The intrinsic binding constants K_b of complexes **1**, **2** and **3** were calculated from the decrease of the absorbance to be 7.5×10^4, 4.8×10^5 and 7.6×10^5 M^{-1}, respectively. The K_b's of complexes **1**, **2** and **3** are smaller than that observed for $[Ru(bpy)_2(dppz)]^{2+}$ ($>10^6$ M^{-1}),[15] but larger than that observed for Δ-$[Ru(phen)_3]^{2+}$ (6.2×10^3 M^{-1}).[15] The experiments suggest that the three complexes may be bound to DNA by groove binding and that increasing the size of the plane of the bridging ligand increases the hydrophobicity of their complexes, leading to stronger binding by the complexes to calf thymus DNA.

Enantioselectivity of DNA-Binding

Equilibrium dialysis experiments offer the opportunity to examine the enantioselectivities of DNA-binding by the complexes. Figure 3 shows the UV region of the CD spectra for the dimeric ruthenium complexes **1**, **2** and **3** after their

 © 2004 Wiley-VCH Verlag GmbH & Co. KGaA, Weinheim

racemic solutions had been dialyzed against calf thymus DNA with stirring for 48 h. An interesting phenomenon was observed in the equilibrium dialysis of the complexes. After dialysis against calf thymus DNA with stirring for 48 h, the dialyzate of complex **3** shows two strong CD signals, with a positive peak at 263 nm and a negative peak at 289.5 nm, which are the CD signals of the ΔΔ-enantiomer of complex **3** assigned by comparison with the CD spectrum of the chiral complex **3.**[16] The presence of these signals indicates enrichment of the isomer which is less likely to bind DNA, indicating that the ΛΛ-enantiomer binds DNA more strongly than the ΔΔ-enantiomer. The other complexes, **1** and **2**, don't show strong CD signals for their enantiomers indicating that complexes **1** and **2** do not bind DNA stereoselectively. The results indicate that complex **3** is an enantioselective binder of DNA while complexes **1** and **2** are not, which may be explained by the differences in the bridging ligand of the complexes: the plane of the bridging ligand for **3** is the largest of the three complexes. To the best of our knowledge, complex **3** is the first example of a dinuclear ruthenium(II) complex binding enantioselectively to CT-DNA measured by equilibrium dialysis. Furthermore, it is interesting to observe that the ΛΛ-bpy complex was found to bind DNA more strongly than the ΔΔ-bpy complex, as indicated by the presence of CD signals. This contrasts with previous reports in which the ΔΔ-diruthenium(II) complexes show preferential DNA binding.[10]

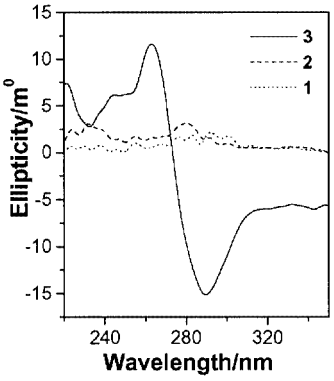

Figure 3. CD spectrum of complexes **1**, **2**,and **3** after 48 h of dialysis against calf thymus DNA with stirring of the solution

The equilibrium dialysis results indicate that complex **3** is a good candidate as an enantioselective binder of DNA.

Viscosity Measurements

In order to further clarify the interaction of the complexes **1**, **2** and **3** with DNA, viscosity measurements were carried out. Optical probes provide essential, but insufficient, evidence to support a binding model. Hydrodynamic measurements, which are sensitive to changes in molecular length (i.e. viscosity and sedimentation), are regarded as the least ambiguous and the most critical tests of a binding model in solution in the absence of crystallographic data.[17] A classical intercalation model demands that the DNA helix must lengthen as base pairs are separated to accommodate the binding ligand, leading to an increase in DNA viscosity. In contrast, a partial and/or non-classical intercalating ligand could bend (or kink) the DNA helix, reducing its effective length and, concomitantly, its viscosity.[18] The effects of complexes **1**, **2** and **3** on the viscosity of rod-like DNA are shown in Figure 4 together with the corresponding data for ethidium bromide (EB) and $[Ru(bpy)_3]^{2+}$.

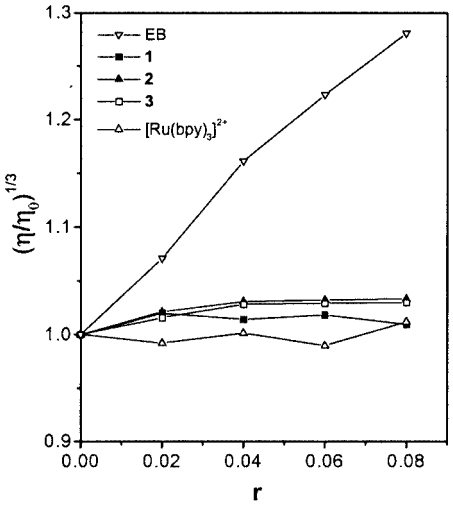

Figure 4. Effect of increasing amounts of complexes **1**, **2**, **3**, ethidium bromide (EB) and the parent complex $[Ru(bpy)_3]^{2+}$ on the relative viscosities of CT-DNA at 28.0 (± 0.1) °C, [DNA]= 0.5 mM and r = [Ru]/[DNA]

The experiments suggest that the dimeric ruthenium(II) complexes bind to the polyanionic DNA via a non-intercalating mode and may be bound to DNA by groove binding.

Conclusion

Three new asymmetric binuclear ligands 2,2′-bis(1,2,4-triazin-3-yl)-4,4′-bipyridine (btb), 2,2′-bis(1,2,4-triazino-[5,6-*f*]acenaphthylen-3-yl)-4,4′-bipyridine (btapb), 2,2′-bis(5,6-diphenyl-1,2,4-triazin-3-yl)-4,4′-bipyridine (bdptb) and their binuclear bpy complexes $[Ru(bpy)_2(btb)Ru(bpy)_2](ClO_4)_4$ (**1**), $[Ru(bpy)_2(btapb)Ru(bpy)_2](ClO_4)_4$ (**2**), $[Ru(bpy)_2(bdptb)Ru(bpy)_2](ClO_4)_4$ (**3**) were synthesized and characterized. Binding behavior of these dimeric complexes with calf thymus DNA was investigated by electronic absorption spectroscopy, viscosity measurements and equilibrium dialysis experiments. The results indicate that the three complexes bind to polyanionic DNA in a non-intercalating mode and may be bound to DNA by groove binding, and that complex **3** is a good candidate as an enantioselective binder of DNA.

 © 2004 Wiley-VCH Verlag GmbH & Co. KGaA, Weinheim

Experimental Section

Materials: All reagents and solvents were purchased commercially and used without further purification unless otherwise noted. Solutions of calf thymus DNA in 50 mM NaCl/5 mM Tris-HCl (pH 7.2) gave a ratio of UV absorbance at 260 and 280 nm of 1.8−1.9:1, indicating that the DNA was sufficiently free of protein.[19] The DNA concentration per nucleotide was determined by electronic absorption spectroscopy using the molar absorption coefficient (6600 $M^{-1}\cdot cm^{-1}$) at 260 nm.[20] Doubly distilled water was used to prepare buffers.

Physical Measurements: Microanalysis (C, H, and N) was carried out with a Perkin−Elmer 240Q elemental analyzer. Fast atom bombardment mass spectra were recorded on a VG ZAB-HS spectrometer using 3-nitrobenzyl alcohol as the matrix. Electrospray mass spectra were recorded on an LCQ system (Finnigan MAT, USA) using methanol as the mobile phase. The spray voltage, tube lens offset, capillary voltage and capillary temperature were set at 4.50 kV, 30.00 V, 23.00 V and 200 °C, respectively, and the quoted *m*/*z* values are for the major peak in the isotope distribution. ^{1}H NMR spectra were recorded on a Varian-500 spectrometer. All chemical shifts are relative to tetramethylsilane (TMS). UV/Vis spectra were recorded on a Shimadzu UV-3101PC or Agilent 8453 spectrophotometer. Emission spectra were recorded at room temperature on a Shimadzu RF-5000 luminescence spectrometer.

Viscosity measurements were carried out using an Ubbelodhe viscometer maintained at a constant temperature of 28.0 ± 0.1 °C in a thermostatted water bath. DNA samples of approximately 200 base pairs average length were prepared by sonication in order to minimize complexities arising from DNA flexibility.[21] Flow time was measured with a digital stopwatch. Each sample was measured three times and an average flow time was calculated. Data are presented as $(\eta/\eta^\circ)^{1/3}$ versus binding ratio,[22] where η is the viscosity of DNA in the presence of complex and η^0 is the viscosity of DNA alone.

Equilibrium dialyses were conducted at room temperature with 5 mL of CT-DNA (1.0 mM) sealed in a dialysis bag and 10 mL of the dinuclear rac complexes (10 μM) outside the bag. The solution containing the dialysis bag was stirred for 48 h.

Syntheses of Complexes

2,2′-Bis[amino(hydrazono)methyl]-4,4′-bipyridine (bahmb),[16] *cis*-$Ru(bpy)_2Cl_2$[23] were prepared as described previously.

2,2′-Bis(1,2,4-triazin-3-yl)-4,4′-bipyridine (btb): A mixture of bahmb (0.27 g, 1 mmol), 30% aqueous glyoxal (5 mL), and ethanol (20 mL) was refluxed with stirring for 2 h. After cooling to room temperature, the yellow precipitate was collected by filtration, washed with ethanol (3×5 cm^3), then dried at 50 °C in vacuo. Yield: 78%. $C_{16}H_{10}N_8$ (314.3): calcd. C 61.1, H 3.2, N 35.7; found C 59.8, H 2.9, N 36.2. FAB-MS: *m*/*z* = 315 ($C_{16}H_{10}N_8$ requires 314). ^{1}H NMR ([D$_6$]DMSO): 9.55 (d, *J* = 2.5 Hz, 2 H), 9.08 (d, *J* = 2.5 Hz, 2 H), 9.03 (dd, 2 H, *J* = 2.5, J_1 = 1, J_2 = 5.5 Hz), 8.90 (dd, J_1 = 0.5, J_2 = 1.5 Hz, 2 H), 8.19 (s, 2 H) ppm.

2,2′-Bis(1,2,4-triazino[5,6-*f*]acenaphthylen-3-yl)-4,4′-bipyridine (btapb): A mixture of bahmb (0.27 g, 1 mmol), acenaphthenequinone (0.346 g, 1.9 mmol) and ethanol (40 mL) was refluxed with stirring for 4 h. The resulting yellow precipitate was collected by filtration while hot, washed with ethanol (3×5 mL), then dried at 50 °C in vacuo. Yield: 72%. $C_{36}H_{18}N_8$ (562.6): calcd. C 76.9, H 3.2, N 19.9; found C 77.3, H 3.6, N 20.2. FAB-MS: *m*/*z* = 564 ($C_{36}H_{18}N_8$ requires 563). ^{1}H NMR ($CDCl_3$): 9.29 (d, *J* = 7.5 Hz, 2 H), 9.17 (d, *J* = 5 Hz, 2 H), 8.65 (dd, 2 H, J_1 = 5.5, J_2 =12 Hz), 8.31 (d, *J* = 8.5 Hz, 2 H), 8.24 (d, *J* = 8 Hz, 2 H), 8.18 (d, 2 H, J_1 = 2.5, J_2 = 9 Hz), 8.04 (d, *J* = 8 Hz, 2 H), 7.82 (t, *J* = 8 Hz, 2 H), 7.70 (t, *J* = 8 Hz, 2 H) ppm.

2,2′-Bis(5,6-diphenyl-1,2,4-triazin-3-yl)-4,4′-bipyridine (bdptb): A mixture of bahmb (0.27 g, 1.0 mmol), benzil (0.4 g, 1.9 mmol), and ethanol (40 cm^3) was refluxed with stirring for 4 h. The resulting yellow precipitate was collected by filtration while hot, washed with ethanol (3×5 mL), then dried at 50 °C in vacuo. Yield: 75%. $C_{40}H_{26}N_8$ (618.7): calcd. C 77.6, H 4.2, N 18.1; found C 78.0, H 3.9, N 18.2. FAB-MS: *m*/*z* = 619 ($C_{40}H_{26}N_8$ requires 618). ^{1}H NMR ($CDCl_3$): 9.13 (d, *J* = 2.5 Hz, 2 H), 9.11 (d, 2 H, *J* = 5 Hz), 7.9 (dd, 2 H, J_1 = 2, J_2 =5 Hz), 7.72 (dd, 4 H, J_1 = 1, J_2 = 8.5 Hz), 7.66 (dd, 4 H, J_1 = 1, J_2 = 8 Hz), 7.47 (t, *J* = 8 Hz, 4 H), 7.41 (t, *J* = 8 Hz, 4 H), 7.39 (t, *J* = 7 Hz, 4 H) ppm.

$[Ru(bpy)_2(btb)Ru(bpy)_2](ClO_4)_4$ (1): *cis*-$[Ru(bpy)_2Cl_2]\cdot 2H_2O$ (1 mmol, 0.432 g), btb (0.5 mmol, 0.157 g) and ethylene glycol (20 cm^3) were refluxed under argon for 6 h. The solution was cooled to room temperature, and H_2O (50 cm^3) was added. After filtration, a dark red precipitate was obtained by dropwise addition of aqueous $NaClO_4$ solution. The product was purified by column chromatography on alumina using acetonitrile/ethanol, 2:1 (v/v) as eluent and then dried in vacuo. Yield: 66%. $C_{56}H_{42}N_{16}Cl_4O_{16}Ru_2\cdot 2H_2O$ (1570.0): calcd. C 42.7, H 2.9, N 14.2%; found C 42.3, H 3.3, N 14.1%. ES-MS [CH_3OH, *m*/*z*]: 670.6 $[M - 2ClO_4]^{2+}$, 413.4 $[M - 3ClO_4]^{3+}$, 285.6 $[M - 4ClO_4]^{4+}$. ^{1}H NMR ([D$_6$]DMSO): δ = 9.33 (d, *J* = 6 Hz, 2 H), 9.18 (s, *J* = 6 Hz, 2 H), 9.16 (d, *J* = 6 Hz, 2 H), 8.91 (d, *J* = 10.5 Hz, 2 H), 8.88 (d, *J* = 7.5 Hz, 2 H), 8.85 (d, *J* = 12.5 Hz, 2 H), 8.81 (d, *J* = 8 Hz, 2 H), 8.27 (t, *J* = 8 Hz, 2 H), 8.24−8.19 (m, 6 H), 8.17 (d, *J* = 4 Hz, 2 H), 8.12 (d, *J* = 8 Hz, 4 H), 7.85 (d, *J* = 8 Hz, 4 H), 7.64 (t, *J* = 1 Hz, 4 H), 7.35 (dd, 4 H, J_1 = 7.5, J_2 =12 Hz) ppm.

$[Ru(bpy)_2(btapb)Ru(bpy)_2](ClO_4)_4$ (2): This complex (dark red) was synthesized in a similar manner to that described for complex **1**, with btapb (0.5 mmol, 0.286 g) in place of btb. Yield: 65%. $C_{76}H_{50}Cl_4N_{16}O_{16}Ru_2\cdot 3H_2O$ (840.0): calcd. C 49.6, H 3.1, N 12.2; found C 50.0, H 2.9, N 12.4. ES-MS [CH_3OH, *m*/*z*]: 793.4 $[M - 2ClO_4]^{2+}$, 496.5 $[M - 3ClO_4]^{3+}$, 347.7 $[M - 4ClO_4]^{4+}$. ^{1}H NMR ([D$_6$]DMSO): δ = 9.31 (s, 2 H), 8.98 (d, *J* = 8.5 Hz, 2 H), 8.93 (d, *J* = 8.5 Hz, 2 H), 8.87 (d, *J* = 7.5 Hz, 2 H), 8.83 (d, *J* = 8.5 Hz, 2 H), 8.75 (d, *J* = 7 Hz, 2 H), 8.59 (d, *J* = 8.5 Hz, 2 H), 8.52 (d, *J* = 8.5 Hz, 2 H), 8.33−8.27 (m, 8 H), 8.19 (dd, 6 H, J_1 = 7.5, J_2 = 19.5 Hz), 8.14 (t, *J* = 8 Hz, 2 H), 8.00 (dd, 4 H, J_1 = 6.5, J_2 =14 Hz), 7.94 (t, *J* = 5 Hz, 4 H), 7.82 (d, *J* = 5 Hz, 2 H), 7.70 (t, *J* = 7 Hz, 2 H), 7.64 (t, *J* = 7 Hz, 2 H), 7.56 (dd, 2 H, *J* = 7 Hz), 7.46 (dd, 2 H, J_1 = 6, J_2 = 11.5 Hz) ppm.

$[Ru(bpy)_2(bdptb)Ru(bpy)_2](ClO_4)_4$ (3): This complex (dark red) was synthesized in a similar manner to that described for complex **1**, with bdptb (0.5 mmol, 0.307 g) in place of btb. Yield: 68%. $C_{80}H_{58}Cl_4N_{16}O_{16}Ru_2\cdot H_2O$ (1856.1): calcd. C 51.6, H 3.3, N 12.0%; found C 51.8, H 3.6, N 12.3%. ES-MS [CH_3OH, *m*/*z*]: 821.6 $[M - 2ClO_4]^{2+}$, 516 $[M - 3ClO_4]^{3+}$, 361.7 $[M - 4ClO_4]^{4+}$. ^{1}H NMR ([D$_6$]DMSO): δ = 9.17 (s, *J* = 2 Hz, 2 H), 8.93 (d, *J* = 8 Hz, 2 H), 8.88 (d, *J* = 8 Hz, 2 H), 8.78 (t, *J* = 8 Hz, 4 H), 8.29 (dd, 6 H, J_1 = 7.5, J_2 = 9 Hz), 8.14 (dd, 2 H, J_1 = 1, J_2 = 5.5 Hz), 7.94 (t, *J* = 9 Hz, 2 H), 7.88 (d, *J* = 5.5 Hz, 2 H), 7.75 (t, *J* = 5.5 Hz, 6 H), 7.67 (t, *J* = 5.5 Hz, 2 H), 7.60−7.52 (m, 8 H), 7.48−7.40 (m, 6 H), 7.11 (d, *J* = 7.5 Hz, 4 H) ppm.

 © 2004 Wiley-VCH Verlag GmbH & Co. KGaA, Weinheim

Acknowledgments

The author is grateful to Guangxi Traditional Chinese Medical University for financial support, and would like to thank Dr. H. Chao and Prof. L.-N. Ji for their guidance.

[1] B. Norden, P. Lincoln, B. Akerman, E. Tuite In, *Met. Ions. Biol. Syst.* (Eds.: A. Sigel, H. Sigel), vol. 33, Dekker, New York, **1996**, p. 177−252.
[2] J. K. Barton, *Science* **1986**, *233*, 727−734.
[3] A. E. Friedman, J. C. Chambron, J. P. Sauvage, N. J. Turro, J. K. Barton, *J. Am. Chem. Soc.* **1990**, *112*, 4960−4962.
[4] W. J. Mei, J. Liu, K. C. Zheng, L. J. Lin, H. Chao, A. X. Li, F. C. Yun, L. N. Ji, *J. Chem. Soc., Dalton Trans.* **2003**, 1352−1359.
[5] X. H. Zou, B. H. Ye, H. Li, Q. L. Zhang, H. Chao, J. G. Liu, L. N. Ji, X. Y. Li, *J. Bio Inorg. Chem.* **2001**, *6*, 143−150.
[6] C. W. Jiang, H. Chao, H. Li, L. N. Ji, *J. Inorg. Biochem.* **2003**, *93*, 247−255.
[7] X. H. Zou, B. H. Ye, J. G. Liu, Y. Xiong, L. N. Ji, *J. Chem. Soc., Dalton Trans.* **1999**, 1423−1428.
[8] P. Lincoln, B. Norden, *J. Chem. Soc., Chem. Commun.* **1996**, 2145−2146.
[9] F. M. Foley, F. R. Keene, J. G. Collins, *J. Chem. Soc., Dalton Trans.* **2001**, 2968−2974.
[10] C. W. Jiang, H. Chao, X. L. Hong, W. J. Mei, H. Li, L. N. Ji, *Inorg. Chem. Commun.* **2003**, *6*, 773−775.
[11] F. H. Case, *J. Heterocycl. Chem.* **1968**, *5*, 223−225.
[12] F. H. Case, *J. Org. Chem.* **1965**, *30*, 931−933.
[13] W. Henderson, C. Evans, *Inorg. Chim. Acta* **1999**, *294*, 183−192.
[14] R. Wang, J. G. Vos, R. H. Schehl, R. Hage, *J. Am. Chem. Soc.* **1992**, *114*, 1964−1970.
[15] X. M. Xiao, M. A. Hage, T. Matsumura-lnoue, Y. Ru, W. A. Anthony, K. Kano, *J. Chem. Soc., Dalton Trans.* **1993**, 2477−2483.
[16] C. W. Jiang, *J. Inorg. Biochem.* **2004**, *98*, 497−501.
[17] S. Satyanarayana, J. C. Dabrowiak, J. B. Chaires, *Biochemistry* **1992**, *31*, 9319−9324.
[18] S. Satyanarayana, J. C. Dabrowiak, J. B. Chaires, *Biochemistry* **1993**, *32*, 2573−2584.
[19] J. Marmur, *J. Mol. Biol.* **1961**, *3*, 208−214.
[20] M. E. Reichmann, S. A. Rice, C. A. Thomas, P. Doty, *J. Am. Chem. Soc.* **1954**, *76*, 3047−3053.
[21] J. B. Chaires, N. Dattagupta, D. M. Crothers, *Biochemistry* **1982**, *21*, 3933−3940.
[22] G. Cohen, H. Eisenberg, *Biopolymers* **1969**, *8*, 45−51.
[23] B. P. Sullivan, D. J. Salmon, T. J. Meyer, *Inorg. Chem.* **1978**, *17*, 3334−3341.

Received October 8, 2003
Early View Article
Published Online April 7, 2004

 © 2004 Wiley-VCH Verlag GmbH & Co. KGaA, Weinheim

Bis[di-*n*-alkyl(fluoro)stannyl]methanes, $(R_2FSn)_2CH_2$ (R = *n*-octyl, *n*-dodecyl): Stable Fluoride-Selective Carriers

Nikolas Chaniotakis,*[a] Klaus Jurkschat,*[b] Dirk Müller,[c] Katerina Perdikaki,[a] and Gregor Reeske[b]

Keywords: Tin / Fluorine / Anion carrier / NMR spectroscopy

The synthesis of bis[di-*n*-alkyl(fluoro)stannyl]methanes, $[(R_2)FSn]_2CH_2$, (**3**, R = *n*-octyl; **4**, R = *n*-dodecyl), is reported and their unprecedented dimeric structure in solution with pentacoordinate tin atoms is rationalized on the basis of ^{19}F and ^{119}Sn NMR spectroscopy, osmometric molecular mass determination and electrospray mass spectrometry (ESMS). ^{19}F and ^{119}Sn MAS NMR and Mössbauer spectroscopy also indicate pentacoordinate tin atoms for the solid state. The ability of compounds **3** and **4** to bind fluoride ion selectively and reversibly is evaluated through potentiometric measurements. Compared with the previously reported organotin(IV)-based fluoride ionophore $[Cl(Ph_2)Sn]_2CH_2$, **3** and **4** exhibit a drastically improved lifetime, while retaining their high preference for fluoride over all other lipophilic anions evaluated. (© Wiley-VCH Verlag GmbH & Co. KGaA, 69451 Weinheim, Germany, 2004)

Introduction

Various recent publications deal with the anion recognition properties of organotin compounds. As shown, mainly by variable-temperature NMR spectroscopy and single-crystal X-ray diffraction analysis, open-chain as well as cyclic bis(haloorganostannyl)alkanes function as bicentric Lewis acids towards Lewis bases such as fluoride and chloride ions[1−7]. The methylene-, dimethylene- and *o*-phenylene-bridged ditin derivatives $[Ph_2(X)Sn]_2CH_2$,[3] $Ph_2XSnCH_2CH_2SnXPh_2$,[4] and *o*-$C_6H_4(SnXMe_2)_2$ [1] (X = F, Cl), respectively, preferably chelate fluoride over chloride ions. Moreover, bis[chloro(diphenyl)stannyl]methane, $[Cl(Ph_2)Sn]_2CH_2$, and bis[dichloro(phenyl)stannyl]methane, $[Cl_2(Ph)Sn]_2CH_2$, when incorporated into polymeric-membrane ion-selective electrodes, are highly selective carriers for fluoride[8] and phosphate ions,[9] respectively. When these carriers are used to develop chemical sensors, the observed signal is unstable over prolonged periods, while repeated use influences both the sensitivity (the slope of the calibration curve expressed in mV per −log[anion] units) and detection limit of the sensor. This signal drift could be due to carrier decomposition, ligand exchange, or poisoning due to the very strong binding to the primary ion[10]. Such signal drift is the only obstacle to the application and commercialization of these ionophores in chemical sensors. The origin of the carrier instability in the sensor membrane is not completely understood, but is postulated to be hydrolysis for $[Cl_2(Ph)Sn]_2CH_2$. Furthermore, with both $[Cl_2(Ph)Sn]_2CH_2$ and $[Cl(Ph_2)Sn]_2CH_2$, chloride exchange with other anions present in the solution to be analyzed could occur. Additionally, the stability problem might originate from anion-induced organic group migration[11] and also from too low a lipophilicity of the carriers. Low carrier lipophilicity facilitates leaching from the organic phase, drastically influencing membrane characteristics.[12] We present here the synthesis and structure of bis[di-*n*-alkyl(fluoro)stannyl]methanes $[F(R_2)Sn]_2CH_2$ (**3**, R = *n*-octyl; **4**, R = *n*-dodecyl)) designed to overcome the above-mentioned problems. Their higher lipophilicity, in combination with an improved membrane composition, gives an optimal fluoride-selective electrode.

[a] Laboratory of Analytical Chemistry, Department of Chemistry University of Crete,
Crete, Greece
Fax: (internat.) + 30-81-393601
E-mail: nchan@chemistry.uch.gr
[b] Lehrstuhl für Anorganische Chemie II der Universität Dortmund
44221 Dortmund, Germany
Fax: (internat.) + 49-(0)231-7555048
E-mail: kjur@platon.chemie.uni-dortmund.de
klaus.jurkschat@uni-dortmund.de
[c] Institut für Angewandte Chemie Berlin-Adlershof e.V.
Richard-Willstätter Straße 12, 12489 Berlin, Germany
Fax: (internat.) + 49-(0)30-63924165
E-mail: mueller_dirk@aca-Berlin.de

Results and Discussion

Synthesis of the Title Compound and Its Structure in Solution and in the Solid State

Bis[dibromo(phenyl)stannyl]methane, $[Br_2(Ph)Sn]_2CH_2$,[13] and four equivalents of *n*-octylMgBr react to give bis[di-*n*-

octyl(phenyl)stannyl]methane, [*n*-octyl$_2$(Ph)Sn]$_2$CH$_2$ (**1**) which was subsequently treated with iodine to provide bis-[iodo(di-*n*-octyl)stannyl]methane, [I(*n*-octyl)$_2$Sn]$_2$CH$_2$ (**2**). Reaction of the latter with excess of potassium fluoride then gave bis[fluoro(di-*n*-octyl)stannyl]methane, [F(*n*-octyl)$_2$Sn]$_2$-CH$_2$ (**3**) (Scheme 1). Bis[di-*n*-dodecyl(fluoro)stannyl]-methane, [(*n*-dodecyl)$_2$FSn]$_2$CH$_2$, (**4**), was prepared analogously.

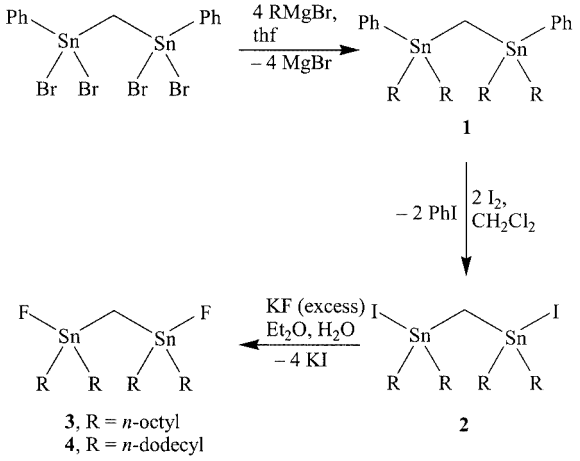

Scheme 1. Synthesis of bis[fluoro(di-*n*-octyl)stannyl]methane (**3**) and bis[di-*n*-dodecyl(fluoro)stannyl]methane (**4**)

Compounds **3** and **4** were obtained as colorless amorphous materials that are sparingly soluble in common organic solvents such as CH_2Cl_2 and $CHCl_3$. The ^{119}Sn NMR spectrum at ambient temperature ($CH_2Cl_2/D_2O_{capillary}$) of compound **3** reveals a doublet of doublet of doublets at δ = 38.8 ppm [$^1J(^{119}Sn-^{19}F)$ 690, 1468, $^3J(^{119}Sn-^{19}F)$ 107 Hz]. The essentially concentration-independent ^{19}F NMR spectrum ($CDCl_3$) shows two triplet resonances of equal integral ratio at −112.9 ppm [$^1J(^{19}F-^{119/117}Sn)$ = 683, $^2J(^{19}F-^{19}F)$ = 71 Hz] and −157.2 ppm [$^1J(^{19}F-^{119/117}Sn)$ = 1474, $^2J(^{19}F-^{19}F)$ = 69 Hz]. The satellite-to-signal-to-satellite integral ratio (15:70:15) for both resonances indicates that each fluorine atom couples with two ^{117}Sn and two ^{119}Sn nuclei. Based on these spectroscopic data and osmometric molecular weight determinations in chloroform (1336 g/mol) and *n*-hexane (1493 g/mol) compound **3** probably adopts the dimeric structure (A) (Figure 1) in solution. This is supported by the electrospray mass spectrometric studies reported below.

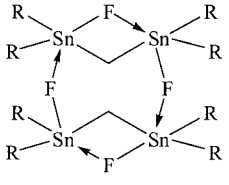

(A)
R = *n*-octyl, *n*-dodecyl

Figure 1. Dimeric structure of **3** in solution

The ^{19}F and ^{119}Sn NMR spectra of compound **4** are similar (see Exp. Sect.).

The ^{119}Sn MAS NMR spectrum of **3** is dominated by anisotropy of chemical shift interaction. The isotropic peak shows a triplet at δ = 2.4 ppm [$\nu_{1/2}$ 325, $J(^{119}Sn-^{19}F)$ = 1270 Hz]. From the intensities of the corresponding triplet-shaped spinning side bands the main components of the shielding tensor were estimated to be δ = 261.9, −113.0 and −141.7 ppm, respectively. The solid-state ^{19}F NMR spectrum recorded at a spinning rate of 30 kHz exhibits a singlet at δ = −142.1 ppm ($\nu_{1/2}$ 150 Hz) with unresolved $J(^{19}F-^{117/119}Sn)$ satellites of 1272 Hz (satellite-to-signal-to-satellite ratio 12.6:74:13.4). These spectroscopic data are reasonably consistent with the polymeric structure (B) shown in Figure 2, with, at least on the ^{19}F and ^{119}Sn time scales, symmetric Sn−F−Sn bridges. This view is further supported by the Mössbauer spectrum (I.S. 1.34 mm/s, Q.S. 3.69 mm/s), which unambiguously indicates pentacoordinate tin atoms. Similar spectroscopic data have been reported for dimethylphenyltin fluoride[14]

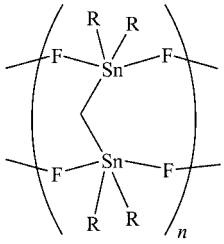

(B)
R = *n*-octyl, *n*-dodecyl

Figure 2. Polymeric structure of **3** in the solid state

The ^{119}Sn NMR spectrum of **3** at room temperature in CD_2Cl_2 solution to which had been added one molar equivalent of $Bu_4NF{\cdot}2H_2O$ shows a complex resonance (four lines with different half widths) centered at δ = −38 ppm, which upon cooling to −80°C turns into a doublet of doublet of doublets at δ = −32 ppm [$^1J(^{119}Sn-^{19}F)$ 648, 1946, $^3J(^{119}Sn-^{19}F)$ 121 Hz]. These findings are consistent with the formation of the organostannate complex **5** [Equation (1)].

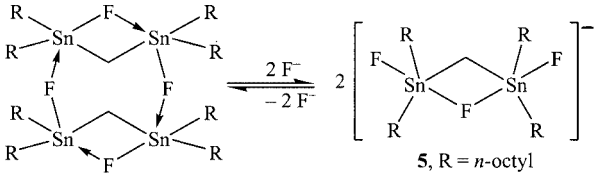

(1)

The ^{119}Sn NMR spectrum was unchanged upon addition of a second molar equivalent of $Bu_4NF{\cdot}2H_2O$. Compound **4** behaves analogously upon addition of one molar equivalent of $Bu_4NF{\cdot}2H_2O$ [δ (^{119}Sn) = −40 ppm at room temperature in CD_2Cl_2 solution, complex pattern with four lines].

 © 2004 Wiley-VCH Verlag GmbH & Co. KGaA, Weinheim

Chloride ions can break the fluoride bridges in the A-type dimer. Thus, the ^{119}Sn NMR spectrum of **3** at room temperature in CD_2Cl_2 solution to which had been added one molar equivalent Ph_4PCl shows a broad resonance at $\delta = -19$ ppm that upon cooling to -20 °C turns into a complex pattern centered at $\delta = -20$, which was not analyzed further.

The ESMS spectrum (negative mode) of a solution of **3** and Ph_4PCl in acetonitrile shows the following mass clusters with the expected isotopic patterns: {[F(*n*-octyl)$_2$Sn]$_2$CH$_2$·F}$^-$ (761.6), {[F(*n*-octyl)$_2$Sn]$_2$CH$_2$·Cl}$^-$ (777.5), {[Cl(*n*-octyl)$_2$Sn]$_2$CH$_2$·F}$^-$ (793.6), [{[F(*n*-octyl)$_2$Sn]$_2$CH$_2$}$_2$·F]$^-$ (1502.7), and [{[F(*n*-octyl)$_2$Sn]$_2$CH$_2$}$_2$·Cl]$^-$ (1520.3). The latter two support the dimeric structure (A) (Figure 1) of compound **3** in solution (see above).

Potentiometric Studies

Bis[fluoro(di-*n*-octyl)stannyl]methane, [F(*n*-octyl)$_2$Sn]$_2$CH$_2$, (**3**), and bis[di-*n*-dodecyl(fluoro)stannyl]methane, [(*n*-dodecyl)$_2$FSn]$_2$CH$_2$, (**4**), were used to develop a solvent polymeric membrane electrode that was examined for its selectivity and sensitivity (slope) to fluoride. The results are compared with previously obtained potentiometric data based on bis[chloro(diphenyl)stannyl]methane, [Cl(Ph$_2$)Sn]$_2$CH$_2$.[8] Compounds **3** and **4** are more lipophilic than [Cl(Ph$_2$)Sn]$_2$CH$_2$ and do not favor halide exchange. Therefore, they are expected not only to preserve the excellent fluoride selectivity obtained with the [Cl(Ph$_2$)Sn]$_2$CH$_2$-based system, but also to exhibit a considerably longer lifetime within the organic membrane layer.

Potentiometric Response

The potentiometric response of a liquid polymeric membrane doped with an ion carrier provides direct evidence of the interaction of the carrier with the ions in solution. Based on these data, one can determine the selectivity, the binding constant in the organic phase, the reversibility and the stability of the ionophore−anion complex. Thus, the overall potentiometric response (ΔE), the calibration curve, and the base line return and stability of the electrodes based on carriers **3** and **4**, were monitored and analyzed. Figure 3 shows the potential changes observed and the resulting calibration curve of the ion-selective electrodes (ISEs).

Figure 3 shows that the two sensors have different analytical characteristics. The slope of the calibration curves for the ISEs based on carriers **3** and **4** are -87.8 and -68.2 mV/$-$log[F$^-$], respectively. Carrier **3** with the octyl substituents shows a higher sensitivity to fluoride anion, indicating that the organic substituents R have little influence on the coordination of the carrier to fluoride. The slope to fluoride of both carriers is higher than can be explained by the Nernst theory, according to which the sensitivity for monovalent anions such as fluoride is -59.16 mV/$-$log[anion]. The high sensitivity of organometallic carriers to anions observed previously [15−17] is suggested to be connected with a less than one-to-one complex formed between the carrier and the primary ion in the polymeric membrane phase of the sensor.[18,19] This stoichiometry was not observed in the NMR titrations performed in CD_2Cl_2.

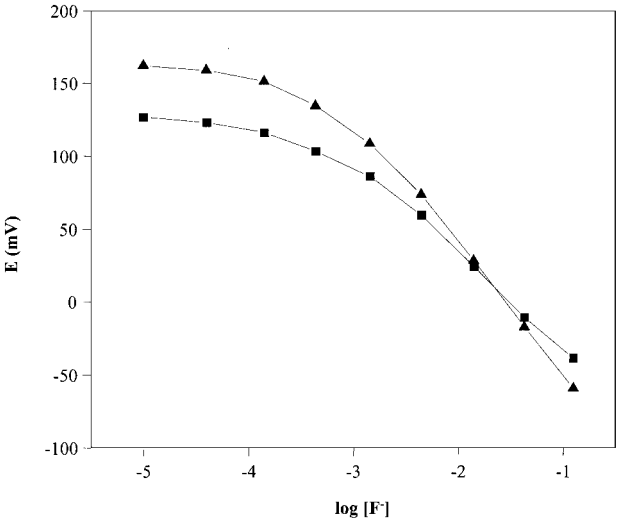

Figure 3. Calibration curves of the ISEs based on compounds **3** (solid triangle) and **4** (solid square) in aqueous solutions buffered with MES to pH 5.5

Ionophore Stability Studies: A very important characteristic of an ionophore is its stability (chemical and structural) over time under operational conditions, which can be very well studied using potentiometry. The interfacial potential generated due to the ability of the carrier to complex the ion under investigation is directly related to the state of the ionophore. Any signal drift, loss in sensitivity or selectivity is thus a measure of the ionophore's instability. Therefore, the sensitivity of ISEs based on carriers **3** and **4** was monitored for a period of 40 days. Figure 4 shows that the sensitivity of the membrane to fluoride remained practically unchanged for over 20 days of continuous use, the slope remaining above 50 mV/$-$log[F$^-$].

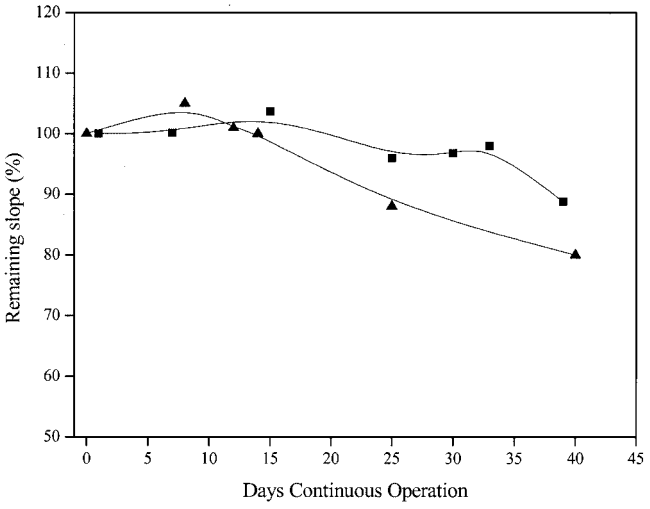

Figure 4. Stability of the ISE1 and ISE2 sensors, based on carriers **3** (solid triangle) and **4** (solid square), respectively, according to the sensitivity of the sensor over time under continuous monitoring in MES (buffered to pH 5.5)

 © 2004 Wiley-VCH Verlag GmbH & Co. KGaA, Weinheim

The effect is even more obvious when the more lipophilic dodecyl-substituted carrier (carrier **4**) is used. This is a large improvement when compared with the previously reported carrier [$(ClPh_2Sn)_2CH_2$] which showed a lifetime of not longer than 4 days.

Ionophore Selectivity: The selectivity of the ionophore was studied using the overall potentiometric response of the membrane between a solution of plain buffer, and that containing 0.01 M of the salt under study. Figure 5 shows the overall potentiometric response (in ΔE) of sensors based on carriers **3** and **4**. Based on these data, the logarithms of the potentiometric selectivity coefficients log $K^{pot}_{F,J}$ were determined according to the Nikolskii−Eisenman equation (Equation 2) (Table 1 and 2).

$$E_M = E^0 + \frac{RT}{zF}\ln(a_i + K_{ij}^{pot} a_j^{\frac{zi}{zj}}) \quad (2)$$

E_M is the membrane potential in mV, a_i the activity (concentration) of the primary ion, a_j the activity of the interfering ion and z_i and z_j the charge of the primary and interfering ions, respectively. Negative potentiometric selectivity coefficients $K^{pot}_{F,J}$ indicate that the ISE is more selective to the primary ion (fluoride in this study), whereas positive values indicate that the ISE is more selective to the interfering ion. The selectivity order based on the overall potentiometric response in a MES-buffered solution at pH 5.5 for both ISEs is similar, $F^- \approx SCN^- > I^- > ClO_4^- > Cl^- > NO_3$. For comparison, the classical Hofmeister selectivity order for a quaternary ammonium ion-based sensor is $ClO_4^- > SCN^- > I^- > NO_3^- > Cl^- > F^-$.

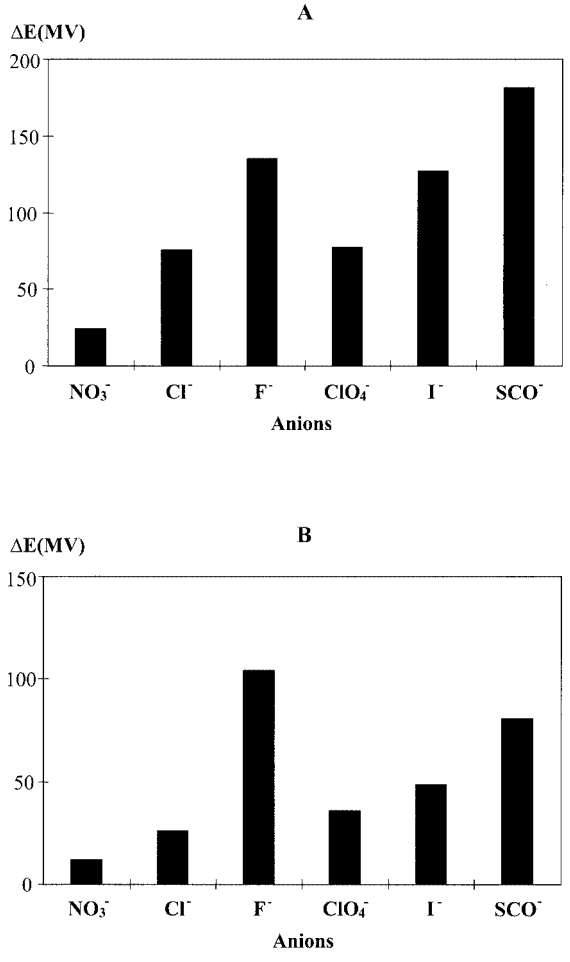

Figure 5. Overall potentiometric response of the ISEs based on carriers **3** (**A**) and **4** (**B**) towards several anions at pH 5.5 (MES, 0.001 M)

Table 1. Potentiometric selectivity coefficients $K^{pot}_{F,J}$ of the ISE based on carrier **3**.

Anion	log K^{pot}
NO_3^-	−1.9
Cl^-	−1.0
F^-	0.0
ClO_4^-	−1
I^-	−0.1
SCN^-	0.8

Table 2. Potentiometric selectivity coefficients $K^{pot}_{F,J}$ of the ISE based on carrier **4**

Anion	log K^{pot}
NO_3^-	−1.6
Cl^-	−1.3
F^-	0.0
ClO_4^-	−1.2
I^-	−0.9
SCN^-	−0.4

Evidently, from the overall potentiometric response and the calculated selectivity coefficients, the fluoride ion is preferred over several other more lipophilic ions, such as perchlorate, nitrate, and iodide. The anti-Hofmeister selectivity sequence obtained for **3** and **4** is closely related to that obtained for the less stable ionophore $[Cl(Ph_2)Sn]_2CH_2$.[8]

These results clearly show that, even though the sensor based on ionophore **3** has a good sensitivity and selectivity for fluoride, an improved sensor in terms of selectivity and stability over time is produced when the membrane is doped with ionophore **4**.

Conclusion

The stability of previously evaluated highly selective fluoride carriers can be drastically improved by the use of lipophilic organic substituents. The closely related carriers $(FR_2Sn)_2CH_2$ (**3**, R = *n*-octyl; **4**, R = *n*-dodecyl) and the previously reported $[Cl(Ph_2)Sn]_2CH_2$ are compared for their fluoride selectivity and their ability to develop stable fluoride-selective electrodes. Based on spectroscopic studies, in organic phases these carriers form a reversible one-to-one complex with fluoride anions. Furthermore, the stability of the sensors depends on the lipophilicity of the carrier, which in turn can be controlled by the organic substituents attached to the tin atoms. However, the selectivity is not influ-

 © 2004 Wiley-VCH Verlag GmbH & Co. KGaA, Weinheim

enced drastically, allowing the development of a robust and highly selective liquid polymeric fluoride-selective electrode. This result will be useful in improving the stability and lifetime of other ionophores that are highly selective for anions such as phosphate and chloride.

Experimental Section

General Remarks: All manipulations were performed under nitrogen using standard Schlenk and vacuum line techniques. Solvents were distilled from the appropriate desiccants prior to use. Literature procedures were used to prepare bis[dibromo(phenyl)stannyl]-methane, $[Br_2(Ph)Sn]_2CH_2$.[13] NMR spectra were recorded in $CDCl_3$ using a spectrometer at 500.13 (^{1}H), 100.63 (^{13}C) 182.36 (^{19}F), 111.92 and 149.21 (^{119}Sn) MHz. Chemical shifts (δ ppm) were referenced to Me_4Sn (^{119}Sn), $CFCl_3$ (^{19}F) and Me_4Si (^{13}C, ^{1}H). ^{119}Sn MAS NMR spectra were recorded with a Varian Unityplus 500 spectrometer at 186.40 MHz using a Doty supersonic CP/MAS probe (rotor diameter 5 mm) with a 10 kHz spinning rate. The corresponding ^{19}F MAS NMR spectra were recorded with a Bruker Avance 400 spectrometer at 376.52 MHz using rotors of 2.5 mm diameter with spinning rates of up to 32 kHz. Elemental analyses were performed with an instrument from Carlo Erba Instrumentation (model 1106). Molecular weight determinations were carried out with a Knauer Dampfdruck-Osmometer K-7000. The calibration standard was Polystyrene 2000 (Fluka) with *n*-hexane and chloroform as solvents.

Electrochemical Studies: Instrumentation: Potentiometric measurements were performed with a XENON CI-317 8-channel electrometer (Halandri, Athens, Greece) versus an Orion Research (Beverly, MA, USA) 900200 double junction reference electrode. Data were collected with a personal computer program written in BASIC for storage and further analysis.

Reagents: High purity potassium salts (p.a. Fluka, p.a. Merck) were used for the preparation of electrolyte solutions. 2-Morpholinoethanesulfonic acid (MES) (Merck) was used as the pH buffer. The membranes were constructed from poly(vinyl chloride) (PVC) (high molecular weight, Selectophore, Fluka), as membrane matrix, bis(2-ethylhexyl) sebacate (DOS) (Selectophore, Fluka) as plasticizer, and tetrahydrofuran (THF) (p.a. Merck), doubly distilled before use, as membrane solvent.

Membrane preparation: All the membranes examined had the following composition: 2% carrier, 33% PVC and 65% DOS. The mixture of components (100 mg) was dissolved in THF (ca. 1.5 mL), and the resultant solution was poured into a glass ring (i.d. 17 mm), the latter being placed on a glass plate. Membranes were formed after solvent evaporation. Circular pieces (diameter 7 mm) of the membranes were cut off and mounted for testing on type IS 561 Phillips electrode bodies (from Willi Möller AG, Glasbläserei, Zürich, Switzerland). The internal solution of the electrode was 0.01 M KCl.

Selectivity measurements and calibration curves: All electrodes were tested without prior pretreatment, except when specifically mentioned. All electrolyte solutions were 10^{-2}, and buffered with MES 10^{-3} M (pH = 5.5). The potential was monitored and the potential difference recorded when the readings were stable in either the calibrating or test solutions. The selectivity coefficients were determined by the separate solution method (SSM)[20], assuming that the electrode shows a theoretical slope of −59.16 mV for monovalent anions.

Synthesis of Bis[di-*n*-octyl(phenyl)stannyl]methane, $[(n\text{-octyl})_2(Ph)Sn]_2CH_2$ (1): A solution of *n*-octylmagnesium bromide prepared from *n*-octyl bromide (5.01 g, 25.9 mmol) and magnesium (0.63 g, 25.9 mmol) in THF (50 mL) was added to a solution of bis[dibromo(phenyl)stannyl]methane[13] (4.70 g, 6.48 mmol) in THF (150 mL). After stirring at room temperature (4 h) the resulting mixture was hydrolyzed with water (50 mL). The organic layer was then separated, dried with Na_2SO_4 and filtered. Evaporation of the solvent gave 3.9 g (70% yield) of bis[di-*n*-octyl(phenyl)-stannyl]methane (**1**) as a colorless oil. ^{1}H NMR (500.13 MHz, $CDCl_3$, 300 K): δ = 0.12 [s, $^2J(^1H\text{-}^{119}Sn)$ = 57.4 Hz, 2 H, Sn−CH_2−Sn], 0.92 [t, $^2J(^1H\text{-}^1H)$ = 7 Hz, 12 H, −CH_3], 0.99−1.63 [m, *J* = 56 Hz, −CH_2−], 7.26−7.55 [m, 10 H, Sn−Ph] ppm. $^{13}C\{^1H\}$ NMR (125.77 MHz, $CDCl_3$ 300 K): δ = −19.5 [$^1J(^{13}C\text{-}^{117}Sn)$ = 226.9, $^1J(^{13}C\text{-}^{119}Sn)$ = 236.7 Hz, Sn−CH_2−Sn], 11.67 [$^1J(^{13}C\text{-}^{117}Sn)$ = 337.2, $^1J(^{13}C\text{-}^{119}Sn)$ = 253.3 Hz, C-1], 14.12 (C-8), 22.71 (C-7), 26.82 [$^2J(^{13}C\text{-}^{117/119}Sn)$ = 20.1 Hz, C-2], 29.18−29.73 (C-4, C-5), 31.96 (C-6), 34.44 [$^3J(^{13}C\text{-}^{117/119}Sn)$ = 59.4 Hz, C-3], 127.93 [$^3J(^{13}C\text{-}^{117/119}Sn)$ = 41.8 Hz, C_m], 12810 [C_p], 136.24 [$^2J(^{13}C\text{-}^{117/119}Sn)$ = 32.7 Hz, C_o], 142.92 [C_i] ppm. $^{119}Sn\{^1H\}$ NMR (149.21 MHz, $CDCl_3$): δ = −16.5 [$^2J^{117}Sn\text{-}^{119}Sn$) = 239 Hz] ppm. $C_{45}H_{80}Sn_2$ (858.5): calcd. C 63.0, H 9.4; found C 63.7, H 9.9.

Synthesis of Bis[iodo(di-*n*-octyl)stannyl]methane, $[I(n\text{-octyl})_2Sn]_2CH_2$ (2): Iodine (3.61 g, 10.22 mmol) was added in small portions under ice-cooling to a stirred solution of **1** (6.10 g, 7.11 mmol) in CH_2Cl_2 (50 mL). The reaction mixture was then stirred overnight, after which the solvent and the iodobenzene were removed in vacuo. Addition of CH_2Cl_2 (20 mL), filtration and evaporation of the solvent then afforded 6.4 g (94% yield) bis[iodo(di-*n*-octyl)-stannyl]methane **(2)** as a light yellow oil. ^{1}H NMR (500.13 MHz, $CDCl_3$, 300 K): δ = 0.87 [t, $^2J(^1H\text{-}^1H)$ = 7 Hz, 12 H, −CH_3], 1.19−1.65 (m, 56 H, −CH_2−] ppm. $^{13}C\{^1H\}$ NMR (125.77 MHz, $CDCl_3$ 300 K): δ = −3.01 [Sn−CH_2−Sn], 14.09 (C-8), 19.45 [$^1J(^{13}C\text{-}^{117}Sn)$ = 334.0, $^1J(^{13}C\text{-}^{119}Sn)$ = 349.3 Hz, C-1], 22.63 (C-7), 26.83 [$^2J(^{13}C\text{-}^{117/119}Sn)$ = 25.9 Hz, C-2], 28.90−29.18 [C-4−C-5], 31.84 (C-6), 33.44 [$^3J(^{13}C\text{-}^{117/119}Sn)$ = 70.1 Hz, C-3] ppm. $^{119}Sn\{^1H\}$ NMR (111.92 MHz, $CDCl_3$): δ = 87.3 ppm. $C_{33}H_{70}I_2Sn_2$ (958.14): calcd. C 41.4, H 7.4; found C 42.0, H 7.5.

Synthesis of Bis[fluoro(di-*n*-octyl)stannyl]methane, $[F(n\text{-octyl})_2Sn]_2CH_2$ (3): A solution of bis[iodo(di-*n*-octyl)stannyl]methane (5 g, 5.23 mmol) in diethyl ether (50 mL) was poured into a solution of potassium fluoride (2.98 g, 52.2 mmol) in water (50 mL). The resultant mixture was stirred for 24 h, and then the organic layer was separated, washed with water (2 × 50 mL), filtered and dried with sodium sulfate. After removing the solvent, the remaining residue was washed with dichloromethane (20 mL), filtered and dried in vacuo to give 2.3 g (60%) of compound **3**. ^{1}H NMR (400.13 MHz, $CDCl_3$): δ = 0.87 [t, $^2J(^1H\text{-}^1H)$ = 7 Hz, 24 H, −CH_3], 1.05−1.65 [m, 14 H, −CH_2−] ppm. $^{13}C\{^1H\}$ NMR (100.62 MHz, $CDCl_3$): δ = 14.12 (C-8), 20.23 (t, C-1), 22.72 (C-7), 25.53 [$^2J(^{13}C\text{-}^{117/119}Sn)$ = 26.2 Hz, C-2], 29.32−29.44 (C-4, C-5), 31.99 (C-6), 34.14 [$^3J(^{13}C\text{-}^{117/119}Sn)$ = 80.7 Hz, C-3] ppm. $^{19}F\{^1H\}$ NMR (282.36 MHz, $CDCl_3$): δ = −115.1 [t, $^2J(^{19}F\text{-}^{19}F)$ = 71.2, $^1J(^{19}F\text{-}^{119}Sn)$ = 686.6 Hz], −159.3 [$^2J(^{19}F\text{-}^{19}F)$ = 68.9, $^1J(^{19}F\text{-}^{119}Sn)$ = 1472.0 Hz] ppm. $^{119}Sn\{^1H\}$ NMR (149.21 MHz, CH_2Cl_2, $D_2O_{capillary}$): δ = 38.1 [ddd, $^1J(^{19}F\text{-}^{119}Sn)$ = 1468, $^1J(^{19}F\text{-}^{119}Sn)$ =

 © 2004 Wiley-VCH Verlag GmbH & Co. KGaA, Weinheim

690, $^3J(^{19}F\text{-}^{119}Sn)$ = 107 Hz] ppm. $C_{33}H_{70}F_2Sn_2$ (742.33): calcd. C 53.4, H 9.5; found C 53.2, H 9.6.

Synthesis of Bis[di-*n*-dodecyl(fluoro)stannyl]methane, [(*n*-dodecyl)$_2$FSn]$_2$CH$_2$ (4): Compound **4** was prepared by a procedure analogous to that for **3**. Thus, bis[dibromo(phenyl)stannyl]methane (9.4 g, 13.0 mmol) was reacted with the Grignard reagent made from 1-dodecyl bromide (1.34 g, 56.0 mmol) and magnesium turnings to give bis[di-*n*-dodecyl(phenyl)stannyl]methane (7.4 g, 53%) as a viscous oil ($^{119}Sn\{^1H\}$ NMR (111.92 MHz, $CDCl_3$): δ = −15.1), which was used for the subsequent reaction without further purification. Treatment of bis[di-*n*-dodecyl(phenyl)stannyl]methane (6.40 g, 5.9 mmol) with iodine (3.00 g, 11.8 mmol) gave bis[iodo(di-*n*-dodecyl)stannyl]methane (6.9 g, 93%) as a slightly yellow oil ($^{119}Sn\{^1H\}$ NMR (111.92 MHz, $CDCl_3$): δ = 85.8 ppm) that was used without further purification for the subsequent reaction.

A solution of bis[iodo(di-*n*-dodecyl)stannyl]methane (1.67, 1.4 mmol) in diethyl ether (30 mL) was added to a solution of potassium fluoride (0.82, 14.1 mmol) in water (20 mL). The mixture was then stirred for 24 h followed by the workup procedure described for compound **3** to give bis[di-*n*-dodecyl(fluoro)stannyl]methane (1.07 g, 79%) as a colorless amorphous solid. ^1H NMR (400.13 MHz, $CDCl_3$): δ = 0.86 [t, $^2J(^1H\text{-}^1H)$ = 6 Hz, 12 H, $-CH_3$], 1.05−1.65 [m, 84 H, $-CH_2-$] ppm. $^{13}C\{^1H\}$ NMR (100.62 MHz, $CDCl_3$): δ = 14.12 (C-12), 20.26 (t, C-1), 22.72 (C-11), 25.54 [$^2J(^{13}C\text{-}^{117/119}Sn)$ = 26.2 Hz, C-2], 29.36−29.45 (C-4−C-9), 31.97 (C-10), 34.15 [$^3J(^{13}C\text{-}^{117/119}Sn)$ = 80.2 Hz, C-3] ppm. $^{19}F\{^1H\}$ NMR (282.36 MHz, $CDCl_3$): δ = −115.0 [t, $^2J(^{19}F\text{-}^{19}F)$ = 68.8, $^1J(^{19}F\text{-}^{119}Sn)$ = 686.6 Hz], −159.3 [t, $^2J(^{19}F\text{-}^{19}F)$ = 66.6, $^1J(^{19}F\text{-}^{119}Sn)$ = 1479.1 Hz] ppm. $^{119}Sn\{^1H\}$ NMR (149.21 MHz, CH_2Cl_2, $D_2O_{capillary}$) δ = 38.2 [ddd, $^1J(^{19}F\text{-}^{119}Sn)$ = 1466, $^1J(^{19}F\text{-}^{119}Sn)$ = 688, $^3J(^{19}F\text{-}^{119}Sn)$ = 105 Hz]. $C_{49}H_{102}F_2Sn_2$ (965.9): calcd. C 59.9, H 10.5; found C 59.5, H 10.6.

Acknowledgments

K. J., G. R., and D. M. thank the Deutsche Forschungsgemeinschaft for financial support. N. C. and K. P. thank Professor Euripides Stefanou for the coordination of the program YPER '97 and the States Scholarship Foundation of Greece (97 YPER 174) for financial support. We are grateful to Dr. B. Mahieu, Louvain-la-Neuve, Belgium, for recording the Mössbauer spectrum of compound **3** and to Dr. D. Heidemann, Humboldt-Universität Berlin, for recording the ^{19}F MAS NMR spectrum. This work includes parts of the intended Ph.D. thesis of G. Reeske.

[1] R. Altmann, K. Jurkschat, M. Schürmann, D. Dakternieks, A. Duthie, *Organometallics* **1998**, *17*, 5858−5866.
[2] R. Altmann, O. Gausset, D. Horn, K. Jurkschat, M. Schürmann, M. Fontani, P. Zanello, *Organometallics* **2000**, *17*, 430−443.
[3] D. Dakternieks, K. Jurkschat, H. Zhu, T. Tiekink, *Organometallics* **1995**, *14*, 2512−2521.
[4] K. Jurkschat, F. Hesselbarth, M. Dargatz, J. Lehmann, E. Kleinpeter, A. Tzschach, J. Meunier-Piret, *J. Org. Chem.* **1990**, *381*, 259−271.
[5] K. Jurkschat, H. G. Kuivila, S. Liu, J. A. Zubieta, *Organometallics* **1989**, *8*, 2755−2759.
[6] K. Jurkschat, A. Rühlemann, A. Tzschach, *J. Organomet. Chem.* **1990**, *381*, C53−C56.
[7] M. Schulte, M. Schürmann, K. Jurkschat, *Chem. Eur. J.* **2001**, *7*, 347−355.
[8] K. Perdikaki, I. Tsagatakis, N. A. Chaniotakis, R. Altmann, K. Jurkschat, G. Reeske, *Anal. Chim. Acta* **2002**, *467*, 197−204.
[9] J. K. Tsagatakis, N. A. Chaniotakis, K. Jurkschat, *Helv. Chim. Acta* **1994**, *77*, 2191−2196.
[10] I. Tsagatakis, N. A. Chaniotakis, R. Altmann, K. Jurkschat, R. Willem, J. C. Martins, Y. Quin, E. Bakker, *Helv. Chim. Acta* **2001**, *84*, 1952−1961.
[11] D. Dakternieks, H. J. Zhu, *Organometallics* **1992**, *11*, 3820−3825.
[12] O. Dinten, U. E. Spichiger, N. A. Chaniotakis, P. Gehrig, B. Rusterholz, W. E. Morf, W. Simon, *Anal. Chem.* **1991**, *63*, 596−603.
[13] M. Gielen, K. Jurkschat, *J. Organomet. Chem.* **1984**, *273*, 303−312.
[14] J. Beckmann, D. Horn, K. Jurkschat, F. Rosche, M. Schürmann, U. Zachwieja, D. Dakternieks, A. Duthie, A. E. K. Lim, *Eur. J. Inorg. Chem.* **2003**, 164−174.
[15] K. Perdikaki, J. K. Tsagatakis, N. A. Chaniotakis, *Mikrochim. Acta* **2001**, *136*, 217−221.
[16] U. Wuthier, H. V. Pham, E. Pretsch, D. Ammann, A. K. Beck, D. Seebach, W. Simon, *Helv. Chim. Acta* **1985**, *68*, 1822−1826.
[17] M. L. Lehaire, R. Scopelliti, H. Piotrowski, K. Severin, *Angew. Chem. Int. Ed.* **2002**, *41*, 1419−1422.
[18] U. Schaller, E. Bakker, U. E. Spichiger, E. Pretsch, *Anal. Chem.* **1994**, *66*, 391−398.
[19] S. Amemiya, P. Bühlmann, E. Pretsch, B. Rusterholz, Y. Umezawa, *Anal. Chem.* **2000**, *72*, 1618−1631.
[20] G. G. Guilbault, R. A. Durst, M. S. Frant, H. Freiser, E. H. Hansen, T. S. Light, E. Pungor, G. Rechnitz, N. M. Rice, T. J. Rom, W. Simon, J. D. R. Thomas, *Pure Appl. Chem.* **1976**, *48*, 127−131.

Received October 24, 2003
Early View Article
Published Online April 7, 2004

 © 2004 Wiley-VCH Verlag GmbH & Co. KGaA, Weinheim

Syntheses, Structures, Bonding and Photoelectron Spectra of "Push-Pull"-Substituted *P*-[2,6-Bis(trifluoromethyl)phenyl]-$\sigma^2\lambda^3$-iminophosphanes[‡]

Karinne Miqueu,[a] Jean-Marc Sotiropoulos,[a] Genevieve Pfister-Guillouzo,*[a] Valentyn L. Rudzevich,[b] Heinz Gornitzka,[c] Vincent Lavallo,[d] and Vadim D. Romanenko[e]

Keywords: Iminophosphanes / X-ray diffraction / Photoelectron spectroscopy / Density functional calculations / Ionization potentials

$\sigma^2\lambda^3$-"Push-pull" iminophosphanes Ar_f–P=N–R, bearing an electron-acceptor substituent at phosphorus [Ar_f = 2,6-bis(trifluoromethyl)phenyl] and a donor group at nitrogen (R = *t*Bu, NMe_2), have been synthesized and characterized by NMR spectroscopy and X-ray analysis. Density functional calculations [B3LYP/6-311G(d,p)] have been carried out on different iminophosphanes: HP=NH (**1**), Ar_fP=NH (**2**), Ar_fP=$NSiMe_3$ (**3**), Ar_fP=N*t*Bu (**4**), HP=$NNMe_2$ (**5**) and Ar_fP=$NNMe_2$ (**6**) in order to determine the electronic effect of the Ar_f substituent and the influence of the donor group R on the stability of the monomeric species. A comparison of the theoretical results and UV photoelectron spectroscopy data for the iminophosphanes **4** and **6** is presented. Theoretical and experimental data suggest that for all iminophosphanes under investigation the π-system of the Ar_f group is almost orthogonal to the $\pi_{P=N}$ system, preventing any stabilizing interaction between the $\pi_{P=N}$ and the $\pi^*_{b1(aryl)}$ orbitals previously observed for the Ar_fPH^- anion. Here, the Ar_f substituent effect is mainly steric.

(© Wiley-VCH Verlag GmbH & Co. KGaA, 69451 Weinheim, Germany, 2004)

Introduction

$\sigma^2\lambda^3$-Iminophosphanes, XP=NR, have been the subject of enthusiastic study for the last two decades because they constitute a bridge between the classical chemistry of C-C unsaturated systems and unconventional pπ-bonded compounds of heavy main group elements.[1] Consequently, a plethora of structures have been reported and characterized, including several short-lived species.[2,3] In general, because of the inherent "electronegativity" of the P-N double bond, most of the known iminophosphanes feature π-donors (R_2N, RO, R_2P) or electron-rich alkyl/aryl substituents (*t*Bu, Mes, Mes*) at the dicoordinated phosphorus atom.[3–5] Compared with the rich chemistry of iminophosphanes having electron-donating substituents, little is known about iminophosphanes containing electron-accepting groups. Notable exceptions are the heteroatom-substituted iminophosphanes Cl–P=NMes* and TfO–P=NMes*. In these examples the X–P bond tends to become ionic due to the large difference in electronegativity between phosphorus, chlorine and oxygen. This large difference in electronegativity promotes the formation of a close ion-pair $[X]^-[PNMes^*]^+$.[6–9] Theoretical studies of iminophosphanes, using simple models, have demonstrated that replacement of the hydrogen atom at phosphorus in HP=NH by more electronegative substituents (π-acceptors) results in an appreciable strengthening of the double bond. At the same time the *Z*-configuration becomes more stable with respect to the *E*-configuration. Exactly opposite effects have been predicted for the influence of the corresponding substituents at nitrogen.[10,11] This concept is strongly operative in *P*-halo- and *P*-oxy-iminophosphanes, but its application to highly sterically crowded *P*-carbosubstituted species has evident limitations. We expected iminophosphanes bearing electron-acceptor carbon substituents at the phosphorus

[‡] Application of Photoelectron Spectroscopy to molecular properties, 67. Part 68: K. Miqueu, J.-M. Sotiropoulos, P. Baylère, S. Joantéguy, G. Pfister-Guillouzo, H. Ranaivonjatovo, J. Escudié, M. Bouslikhane, *J. Mol. Struct.* **2004**, *690*, 53–61.

[a] Laboratoire de Chimie Théorique et Physico-Chimie Moléculaire, CNRS UMR 5624, Université de Pau et des Pays de l'Adour Avenue de l'Université,
BP 1155, 64013 Pau Cedex, France
Fax: (internat.) + 33-5-59407588
E-mail: genevieve.pfister@univ-pau.fr
[b] Institute of Organic Chemistry, National Academy of Sciences of Ukraine,
Murmanskaya St. 5, Kiev, 02094, Ukraine
[c] Laboratoire d'Hétérochimie Fondamentale et Appliquée du CNRS (UMR, 5069), Université Paul Sabatier 118,
Route de Narbonne, 31062 Toulouse Cedex 04, France
[d] Department of Chemistry, University of California Riverside, CA 92521-0403, USA
[e] Institute of Bioorganic Chemistry and Petrochemistry, National Academy of Sciences of Ukraine,
Murmanskaya St. 1, Kiev, 02094, Ukraine

atom would be interesting, since the presence of an electron-acceptor substituent at the phosphorus atom should considerably increase the polarity of the P=N double bond. Moreover, the combination of substituents with acceptor and donor properties at the P=N bond ("push-pull" substitution) should lead to unusually stable XP=NR species.

Recently, molecular design utilizing the highly electronegative 2,6-bis(trifluoromethyl)phenyl group[12] allowed us to prepare the first phosphanide salt, $[K([15]\text{-crown-}5)_2]^+[Ar_fPH]^-$, featuring a "naked" dicoordinated phosphorus anion.[13] Our observations indicate that the planar structure is a privileged form of the anion, due to a strong interaction between the p^π phosphorus lone-pair and the $\pi^*_{b1(aryl)}$ orbital (localized on the C1 and C4 atoms of the aryl ring).Thus, the Ar_f group behaves like a π-electron acceptor and contributes considerably to the observed structure of the Ar_fPH^- anion. Along these lines, desiring to study the *P*-carbosubstituted iminophosphanes bearing electron-withdrawing substituents, we turned our attention to *P*-[2,6-bis(trifluoromethyl)phenyl-$\sigma^2\lambda^3$-iminophosphanes. Two different stabilizing interactions may be envisioned in these compounds because of energetically closely spaced π (P=N) and σ (combination of lone-pair at P and N) frontier orbitals: (i) n^+ (*trans*) or n^- (*cis*) → $\pi^*_{b1(aryl)}$ [π system of Ar_f orthogonal to the $\pi_{P=N}$ system, as observed for the carbene $(iPr_2N)_2PCAr_f$][14] or (ii) $\pi_{P=N} \rightarrow \pi^*_{b1(aryl)}$ (π system of Ar_f coplanar to $\pi_{P=N}$ system, as previously observed for Ar_fPH^-).[13] The latter type of stabilizing interaction is related to electronic effects previously observed for the Ar_fPH^- anion and would be especially pronounced in the case of "push-pull" substitution.

This paper deals with the preparation and characterization of a series of iminophosphanes Ar_f–P=NR. Along with our exploration into the synthesis of new and highly reactive PN multiple-bond systems, we performed a theoretical analysis of their structures to study the effect of the Ar_f group and the variation of the donor group R. The following iminophosphanes were studied theoretically: HP=NH (**1**), Ar_fP=NH (**2**), Ar_fP=$NSiMe_3$ (**3**), Ar_fP=N*t*Bu (**4**), HP=$NNMe_2$ (**5**) and Ar_fP=$NNMe_2$ (**6**). Full characterization of the iminophosphanes **4** and **6** included an investigation by NMR spectroscopy and X-ray analysis. A comparison of the results of our theoretical calculations [B3LYP/6-311G(d,p)] and UV/PE studies is also reported.

Results and Discussion

Iminophosphanes containing a CP=N skeleton are rare. These compounds are usually unstable due to their dimerization or oligomerization and can only be isolated in the presence of bulky substituents. Very effective in this sense is the 2,4,6-tri-*tert*-butylphenyl group (Mes*), which provides access to a series of stable R–P=NMes* compounds upon condensation of phosphorus chlorides $RPCl_2$ with the silylamide [LiN($SiMe_3$)Mes*] followed by a 1,2-elimination reaction.[15] Iminophosphanes Mes*P=NR are not accessible by this route since the reaction of the sterically crowded dichlorophosphane Mes*PCl_2 with silylamides [LiN($SiMe_3$)R] leads exclusively to the diphosphene Mes*P=PMes*.[3] We found that the interaction of Ar_fPCl_2 with silylamides [LiN($SiMe_3$)R] proceeds by the "normal" way, allowing the isolation of amino(chloro)phosphanes $Ar_fP(Cl)N(SiMe_3)R$. Thus, treatment of Ar_fPCl_2 with an equimolar quantity of [LiN($SiMe_3$)$_2$] in THF solution at −78 °C afforded the corresponding amino(chloro)phosphane in virtually quantitative yield (Scheme 1). However, elimination of Me_3SiCl from $Ar_fP(Cl)N(SiMe_3)_2$ occurs only at high temperatures (>180 °C) and leads to 1,3,2,4-diazadiphosphetidine **3′** instead of the expected monomeric iminophosphane **3**. The ^{19}F NMR spectrum of **3′** exhibits doublets at δ = 23.0 ppm ($^4J_{F,P}$ = 72.3 Hz) and δ = 27.4 ppm ($^4J_{F,P}$ = 134.7 Hz), corresponding to the resonances of two magnetically non-equivalent *ortho*-CF_3 groups on the Ar_f substituent. The ^{31}P resonance is observed as a multiplet at δ = 277.3 ppm.

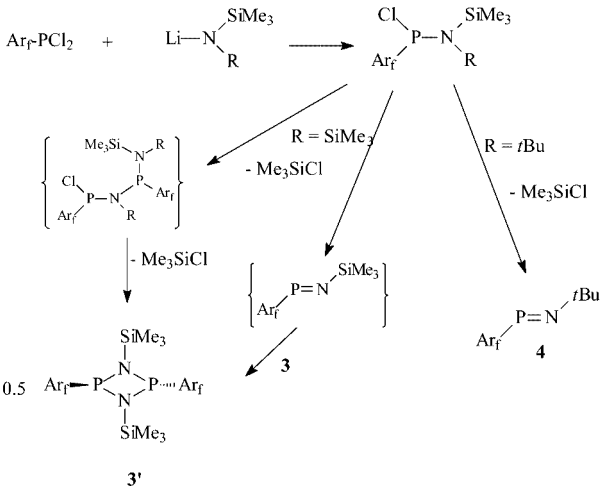

Scheme 1

The molecular structure of **3′** is presented in Figure 1. The four-membered P_2N_2 cycle is planar, as observed in most other *trans*-1,3,2,4-diazadiphosphetidines.[16] The Ar_f rings form a twist angle of 39.3°. The geometry around the nitrogen atoms is trigonal planar. The average P–N bond length is about 1.722 Å and the PNP and NPN bond angles are 95.73° and 84.27°, respectively.

In contrast to *N*,*N*-disilyl analogues, thermolysis of $Ar_fP(Cl)N(SiMe_3)$*t*Bu (120 °C, 80 h) afforded the monomeric iminophosphane **4**. The latter was characterized by mass spectrometry and NMR spectroscopy. The ^{31}P NMR spectrum shows a septet at δ = 412.4 ppm ($^4J_{F,P}$ = 28 Hz), in a region characteristic of the CP=N backbone.[2] The X-ray crystal structure of **4** is shown in Figure 2. Molecules of **4** adopt a *trans* geometry and the P=N bond length of 1.537 Å is consistent with a bond order of two; it is 0.019 Å shorter than that in *trans* Mes*-P=N-*t*Bu.[17] The P–C bond length (1.866 Å) falls in the normal range for a single bond. The aromatic ring is in an orthogonal orientation to the CPN plane (the corresponding dihedral angle is 99.8°).

 © 2004 Wiley-VCH Verlag GmbH & Co. KGaA, Weinheim

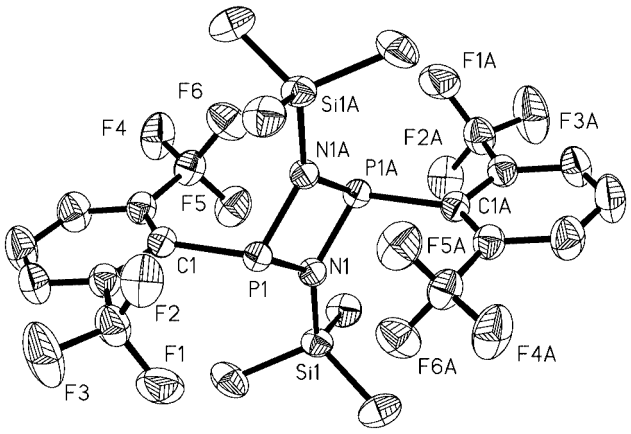

Figure 1. Crystal structure of $(Ar_fPNSiMe_3)_2$ (**3′**); hydrogen atoms are omitted for clarity; selected bond lengths (Å) and bond angles (deg): P1−N1(A) 1.713(2), P1(A)−N1(A) 1.714(2), P1−C1 1.935(2); P1−N1−P1(A) 95.73(1), N1−P1−N1(A) 84.27(1)

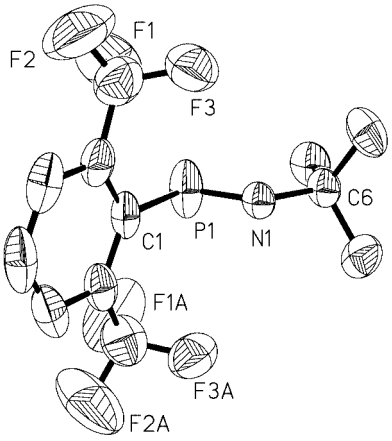

Figure 2. Crystal structure of $Ar_fP{=}NtBu$ (**4**); hydrogen atoms are omitted for clarity; selected bond lengths (Å) and bond angles (deg): P1−N1 1.537(3), P1−C1 1.866(4), N1−C6 1.489(4); C1−P1−N1 99.73(1), C6−N1−P1 123.82(0)

The C1P1N1 and C6N1P1 angles are 99.73° and 123.82°, respectively. In the related iminophosphane $R_fP{=}NR_f$ [R_f = 2,4,6-$(CF_3)_3C_6H_2$] the angle around the phosphorus is 99.81°, while the angle at nitrogen is more opened (130.22°).[18]

The strategy for the preparation of **4** was successfully extended to the synthesis of iminophosphanes **6** containing the π-donor NMe_2 group at the nitrogen atom (Scheme 2). Compared to $Ar_fP(Cl)-N(SiMe_3)R$ (R = Me_3Si, *t*Bu), the corresponding dimethylhydrazino derivative splits off Me_3SiCl under considerably milder conditions (0.05 Torr, < 100 °C). However, attempts to isolate **6** in pure form by vacuum distillation failed. In contrast to the quite thermally stable compound **4**, compound **6**, which is stable for extended periods of time in pure form and in solution, easily disproportionates on heating to form the diphosphene $Ar_fP{=}PAr_f$ (δ_P = 478 ppm).[19] This property is without precedent in iminophosphane chemistry and suggests that the P=N bond strength is dramatically reduced by "push-pull" substitution. Interestingly, the iminophosphane **7** (δ_P = 173.1 ppm), which can be obtained by a similar route starting from iPr_2NPCl_2 and $Me_2NN(SiMe_3)Li$, undergoes dimerization to form *trans*-$[iPr_2NPNNMe_2]_2$ (δ_P = 74.2 ppm) instead of disproportionation. We found, however, that chloroform as solvent promotes Me_3SiCl elimination reaction from $P(Cl)-N(SiMe_3)R$ moiety. Thus, when $Ar_fP(Cl)-N(SiMe_3)_2NMe_2$ was treated with anhydrous $CHCl_3$ (25 °C, 14 h), Me_3SiCl elimination with formation of **6** takes place quantitatively. In **6** the signal for the two-coordinate phosphorus atom is shifted drastically up field (δ_P = 224.3 ppm) in comparison to that of **4** (δ_P = 412.4 ppm).

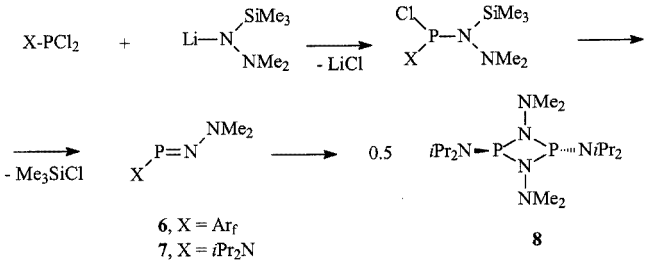

Scheme 2

Bright-yellow crystals of **6** were grown from a saturated toluene solution. The molecular structure of the compound is shown in Figure 3. Essentially, the molecule adopts a *trans*-configuration and the aromatic ring system is almost orthogonal to the CPN system (the corresponding dihedral angle is 110°). The planar-coordinated N atoms of the hy-

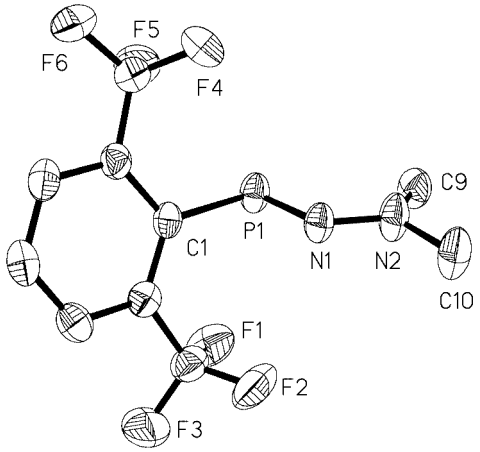

Figure 3. Crystal structure of $Ar_fP{=}NNMe_2$ (**6**); hydrogen atoms are omitted for clarity; selected bond lengths (Å) and bond angles (deg): P1−N1 1.629(1), P1−C1 1.863(5), N1−N2 1.319(2); C1−P1−N1 95.31(7), P1−N1−N2 121.13 (1)

 © 2004 Wiley-VCH Verlag GmbH & Co. KGaA, Weinheim

drazine moiety and the P atom of the double-bond system are located in one plane (three-center, four π-electron system). The P−N bond in **6** is the longest (1.629 Å) ever found for iminophosphanes.[20,21] The opposite effect is observed for the N−N single bond (1.319 Å). Thus, the tendency of the iminophosphane **6** to disproportionate at high temperatures can be inferred from the remarkably long P−N bond, which is evident in the X-ray structure analysis of the molecule.

Theoretical and PE Spectroscopic Studies

HP=NH (1), Ar_fP=NH (2) and Ar_fP=NSiMe_3 (3)

In order to estimate the effect of the Ar_f substituent on the CP=N part we compared the HP=NH (**1**) and Ar_fP=NH (**2**) model molecules. The geometrical parameters of these species are summarized in Table 1. Two minima were found on the potential-energy surface corresponding to the *cis* and *trans* isomers. For **2**, the π-system of the aryl substituent in both isomers is almost orthogonal to the $\pi_{P=N}$ system (the dihedral angles for *cis* and *trans* structures are 116.6° and 115.6° respectively). The P−N bond lengths in *cis*- and *trans*-**2** are slightly shorter than those in **1**. The *cis*-**2** isomer is more stable than *trans*-**2** by 1.42 kcal/mol. This is in agreement with an opening of the P and N bond angles on passing from *trans*-**2** to *cis*-**2**. Unlike **1** and **2** only the *cis*-**3** isomer was found on the potential energy surface, as was previously observed for ClP=NSiMe_3 and ClAs=NSiMe_3.[22] The aromatic ring in **3** is almost orthogonal to the plane of the CPN skeleton (dihedral angle is 89.6°). Such a conformation excludes any interaction between the π-system of the P=N bond and the π^*_{b1}(aryl) orbital of the aromatic ring. As a consequence, the P−C (1.957 Å) and P−N (1.539 Å) bond lengths correspond to a single and double bond, respectively. The latter is longer than the experimental value for the P−N bond of *cis*-ClP=NMes* (1.495 Å).[6] The silyl group at the nitrogen atom leads to a shortening of the P=N bond [1.574 Å (*cis*-**1**), 1.562 Å (*cis*-**2**), 1.539 Å (*cis*-**3**)] and an opening of the bond angle at nitrogen, as was previously observed for FP=NSiH_3.[23] Moreover, we observed a lengthening of the P−C bond.

For the *cis* isomers of **1**, **2** and **3** the energetic positions of the n^+, π and n^- orbitals as well as the plot[24] of the MO are displayed in Figure 4. For *cis*-**2**, the antibonding combination of lone pairs (n^-) is mixed with the σ_{PC} orbital while the bonding combination of lone pairs (n^+) is mixed with the $\pi_{b1(aryl)}$ orbital of the Ar_f ring. For *trans*-**2**, the bonding combination of lone pairs (n^+) is mixed with the σ_{PC} orbital while the antibonding combination of lone pairs (n^-) is mixed with the σ_{PC} and the $\pi_{b1(aryl)}$ orbitals (Figure 5).

Thus, in this case, the stabilizing effect of the CF_3 groups is attenuated or counterbalanced by destabilizing interactions with the σ_{PC} orbital and the $\pi_{b1(aryl)}$ orbital, respectively (see Figure 4 and Figure 5). For **2**, the energetic position of the n^- orbital is weakly modified when going from **1** to **2**. At the same time the n^+ orbital is destabilized.

Table 1. Bond angles (°) and bond lengths (Å) for the minima (mini: Ar_f almost orthogonal to the PNR moiety) and transition states (ts: Ar_f coplanar to the PNR moiety) of HP=NH (**1**), Ar_fP=NH (**2**), Ar_fP=NSiMe_3 (**3**), Ar_fP=N*t*Bu (**4**), HP=NNMe_2 (**5**), Ar_fP=NNMe_2 (**6**); corresponding energies in ua (E_{elec} for electronic energy and E_{rep} for repulsive energy)

Parameter	*cis*	*trans* (mini)	*trans* (ts)
	HP=NH (**1**)		
P=N	1.574 (1.539)[10] (1.611)[b][38]	1.588 (1.578)[a][10] (1.618)[b] [38]	/
PNH	118.52 (120.0)[10] (113.7)[b] [37]	109.79 (112.3)[10] (107.6)[b] [37]	/
HPN	105.95 (104.8)[10]	98.77 (99.9)[10]	/
E_{elec}	-446.929393	-446.859285	
E_{rep}	49.626276	49.555519	
	Ar_fP=NH (**2**)		
P=N	1.562	1.576	1.571
P−C_{Arf}	1.920	1.890	1.893
PNH	120.91	110.66	105.59
C_{Arf}PN	108.23	100.14	110.53
E_{elec}	-2624.280808	-2624.457073	-2618.133251
E_{rep}	1321.595174	1321.774013	1315.457185
	Ar_fP=NSiMe_3 (**3**)		
P=N	1.539	–	–
P−C_{Arf}	1.957	–	–
PNSi	154.63	–	–
C_{Arf}PN	107.29	–	–
E_{elec}	−3764.610290		
E_{rep}	2053.155544		
	Ar_fP=N*t*Bu (**4**)		
P=N	1.546	1.576	1.567
P-C_{Arf}	1.962	1.895	1.902
PNC_{tBu}	146.14	99.34	126.17
C_{Arf}PN	111.86	124.68	104.85
E_{elec}	−3378.517746	−3347.618957	−3338.250879
E_{rep}	1918.535908	1887.636238	1878.275201
	HP=NNMe_2 (**5**)		
P=N	1.629	1.655	–
N−N	1.301	1.303	–
PNN	131.82	122.58	–
HPN	102.98	93.38	–
E_{elec}	−758.689409	−759.664804	
E_{rep}	227.388860	228.363706	
	Ar_fP=NNMe_2 (**6**)		
P=N	1.600	1.637	1.629
P−C_{Arf}	1.937	1.878	1.875
N−N	1.300	1.304	1.296
PNN	142.12	123.93	124.54
C_{Arf}PN	110.28	96.70	102.24
E_{elec}	−3202.638297	−3173.831281	−3168.455747
E_{rep}	1765.966288	1737.156040	1731.785927

[a] SCF double zeta basis set. [b] QCISD/LanL2DZdp.

 © 2004 Wiley-VCH Verlag GmbH & Co. KGaA, Weinheim

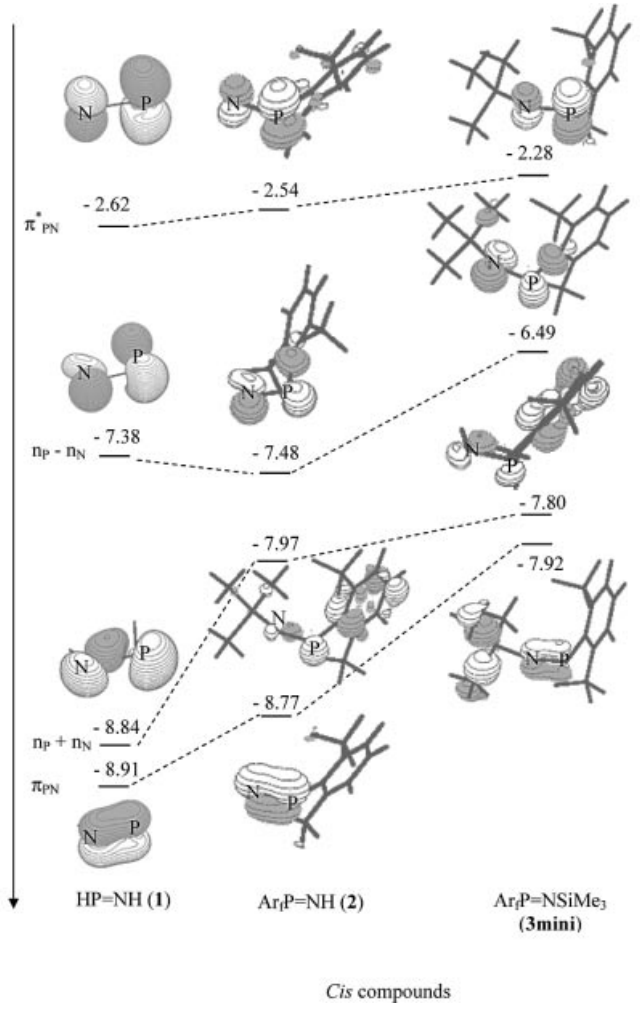

Figure 4. Kohn−Sham energies in eV and Kohn−Sham orbitals calculated with the B3LYP functional hybrid and the 6-311G(d,p) basis set for the *cis* isomers of HP=NH (**1**) and Ar_fP=NR [R = H (**2**), $SiMe_3$ (**3**); π_{CC}(Arf) almost perpendicular to $\pi_{P=N}$]

The H/$SiMe_3$ substitution promotes destabilization of the n^+, n^- and π orbitals. The destabilization of the n^- orbital is more important than that of the n^+ orbital because of the strong p character of the nitrogen lone pair in the n^- orbital. In fact, for the previous system only the push effect is observed.

Ar_fP=NtBu (4)

In addition to X-ray analysis, compound **4** was studied by coupling the Ultraviolet Photoelectron Spectroscopy in the gas phase (UV-PES) and calculations. The UV-PE spectrum of **4** presents a first ionization at 8.5 eV, a second band at 10.0 eV with a broad shoulder at 9.8 eV and then a broad signal with different shoulders at 11.0 and 11.8 eV (Figure 6, a).

In contrast to **3**, the *trans* isomer of **4** is slightly more stable than the *cis* isomer (0.72 kcal/mol). The energetically privileged form *trans*-**4mini** features an aromatic ring almost perpendicular to the CPN plane (dihedral angle is 116.1°), in agreement with the X-ray structure.

We studied the rotation process of the aryl group theoretically. One transition state has been found on the potential energy surface. It corresponds to a structure where the π-system of the aromatic ring is coplanar with the $\pi_{P=N}$ system (**4ts**). The latter is energetically very close to the minimum (4.38 kcal/mol). Thus, taking into account this weak energetic difference, a free rotation of the Ar_f group can occur in the gas phase. The geometric parameters of **4mini** and **4ts** are summarized in Table 1. It is noteworthy to mention that the geometric parameters for both rotamers are similar in spite of the different positions of the aromatic ring. Moreover, the P=N (1.576 Å for **4mini**; 1.567 Å for **4 ts**) and P−C (1.895 Å for **4mini**; 1.902 Å for **4 ts**) bonds are slightly longer than the experimental ones (1.537 Å and 1.866 Å, correspondingly). In the same way, the calculated Kohn−Sham energies (Figure 5) are energetically close ($n_P + n_N$, σ_{PC}: − 6.44 eV for **4mini** and − 6.33 eV for **4ts**; $\pi_{P=N}$: −7.64 eV for **4mini** and −7.49 eV for **4ts**). All these observations show that the orientation of the aromatic ring seems to have a negligible effect on the geometric and electronic structures of Ar_fP=N*t*Bu. In contrast to the coplanar structure of the $[Ar_fPH]^-$ anion where only the interaction between $n^{\pi}_P \rightarrow \pi^*_{b1(aryl)}$ occurs (9.4 kcal/mol),[13] for **4ts** the stabilizing $\pi_{P=N} \rightarrow \pi^*_{b1(aryl)}$ interaction [4.8 kcal/mol (NBO calculation)] is added to the destabilizing interaction $\pi_{P=N} \rightarrow \pi_{b1(aryl)}$ (the plot of the molecular orbital in Figure 7 visualizes these interactions). On the contrary, for **4mini** the stabilizing ($n_P \rightarrow \pi^*_{b1(aryl)}$) interaction is not observed.

Considering the free P−C rotation in the gas phase, the UV-PE spectrum (Figure 6, a) corresponds to the superposition of all the rotamers' spectra close to **4mini** and **4ts**. Thus, taking into account this observation as well as the nature of the molecular orbital, the ΔSCF values for the first ionic state (**4 mini**: $n_P + n_N + \sigma_{PC}$: 8.25 eV; **4 ts**: $n_P + n_N + \sigma_{PC}$: 8.10 eV) and the energetic position of the Kohn−Sham orbitals for **4mini** and **4ts** (Table 2), we assigned the first band in the PE spectrum (8.5 eV) to the removal of an electron from the $n_P + n_N$ orbitals mixed with the σ_{PC} orbital. The second band (centered at 10 eV), which is more intense and broader than the first band, is associated with the ionization of the $\pi_{P=N} - \pi_{b1(aryl)}$ and $\pi_{P=N} + \pi_{b1(aryl)}$ orbitals as well as the π_{a2} ionizations of the aromatic ring. Finally, the ionization at 11.0 eV was assigned to the removal of an electron from the $n_P - n_N$ orbitals (in interaction with the σ_{PC} orbital).

Surprisingly, the energetic positions of the n^+ and π ionizations of **4** were found to be close to the spectroscopic findings for *t*BuP=N*t*Bu. Indeed, the HeI PE spectrum of the latter presents two first ionizations at 8.11 and 9.70 eV, which have been assigned to the n^+ and π_{PN} orbitals, respectively.[25] The close energetic position of the π_{PN} orbital for **4** and *t*BuP=N*t*Bu (9.8 eV and 9.7 eV, respectively) means that the Ar_f group has a destabilizing effect on the π-system close to the *t*Bu group.

As for the σ-bond system, one could expect an important gap between the n^+ orbitals of **4** (σ-attractor effect of Ar_f) and *t*BuP=N*t*Bu (σ-donor effect of *t*Bu), whereas the gap

 © 2004 Wiley-VCH Verlag GmbH & Co. KGaA, Weinheim

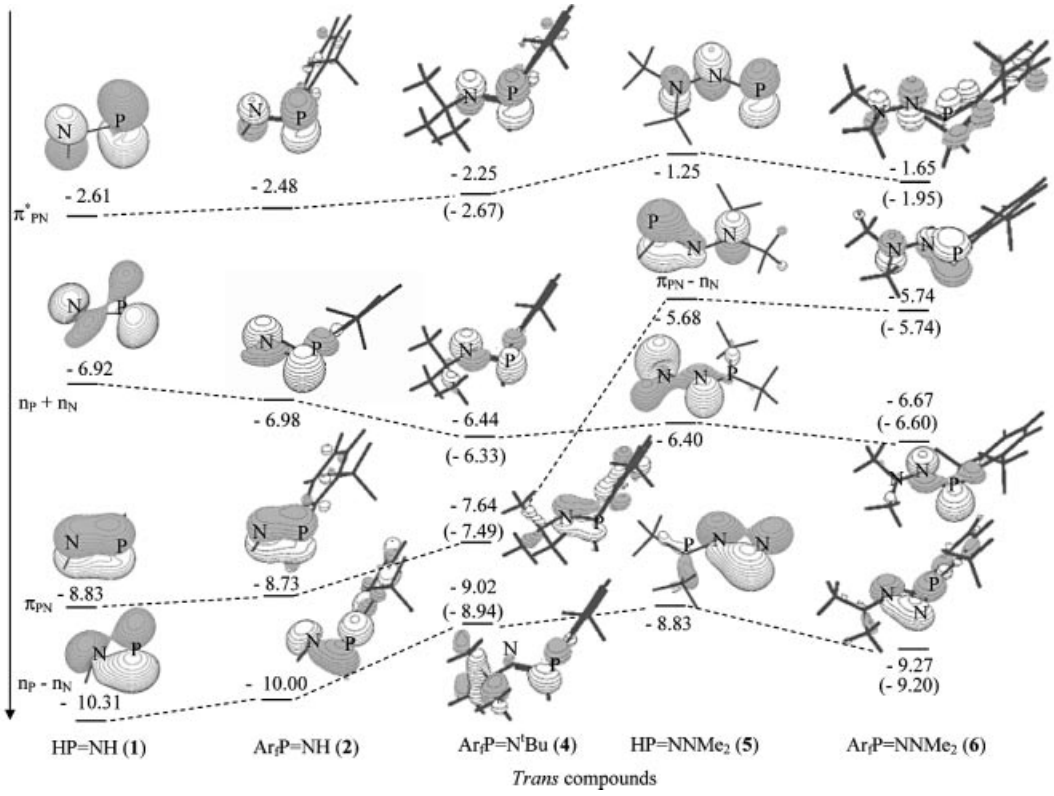

Figure 5. Kohn−Sham energies in eV and Kohn−Sham orbitals calculated with the B3LYP functional hybrid and the 6-311G(d,p) basis set for the *trans* isomers of HP=NH (**1**), HP=NNMe$_2$ (**5**) and Ar_fP=NR [R = H **2mini**; R = *t*Bu **4mini**; R = NMe$_2$ **6mini**; Ar_f almost orthogonal to the PNR moiety]; Kohn−Sham energies in brackets for the transition state (Ar_f planar to the PNR moiety)

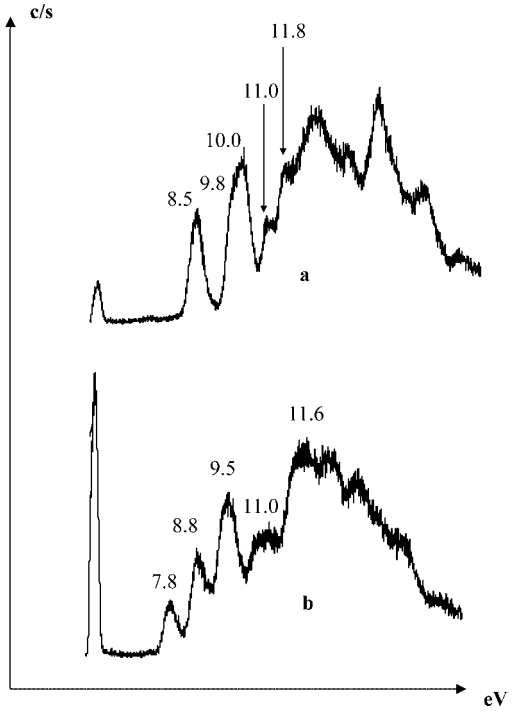

Figure 6. HeI photoelectronic spectra of a) Ar_fP=N*t*Bu (**4**) and b) Ar_fP=NNMe$_2$ (**6**)

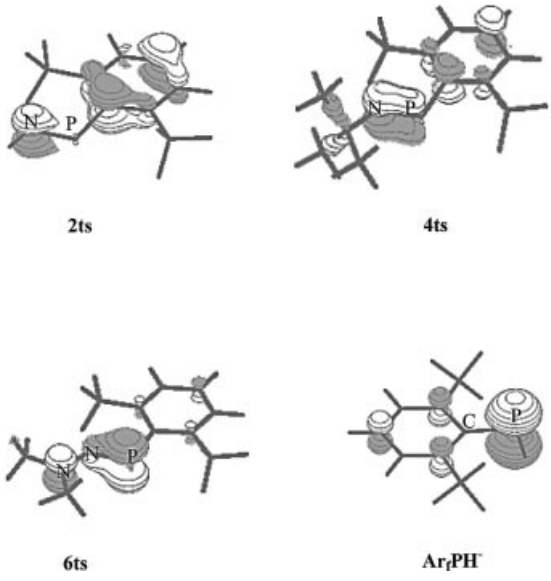

Figure 7. Plot of the $\pi_{P=N} - \pi_{b1(aryl)}$ (+ $\pi^*_{b1(aryl)}$) orbital for the transition state (Ar_f coplanar to the PNR moiety) of Ar_fP=NH (**2 ts**), Ar_fP=N*t*Bu (**4 ts**) and Ar_fP=NNMe$_2$ (**6 ts**); plot of the $n_P - \pi^*_{b1(aryl)}$ for the minimum of Ar_fPH^-

was actually found to be relatively weak (0.4 eV). This is consistent with the previous theoretical conclusion: the strong stabilizing effect of the fluorinated aryl group is balanced by the destabilizing interaction between the bonding or antibonding combination of lone pairs and the σ_{PC} orbital. The expected stabilizing effect of the Ar_f group is not really observed either on the σ- or the π-systems. Indeed, *t*BuP=N*t*Bu and Ar_fP=N*t*Bu present close electronic

 © 2004 Wiley-VCH Verlag GmbH & Co. KGaA, Weinheim

Table 2. Kohn−Sham energies in eV and Kohn−Shan orbitals for the minimum (mini) and transition state (ts) of $Ar_fP{=}NSiMe_3$ (**3**), $Ar_fP{=}NtBu$ (**4**) and $Ar_fP{=}NNMe_2$ (**6**); ΔSCF values (in eV) in brackets

3		**4**		**6**		
Theor.	Theor.		Exp.	Theor.		Exp.
3mini	**4mini**[a]	**4ts**	**4**	**6mini**[a]	**6ts**	**6**
−6.49 $n_P - n_N$	−6.44 *(8.25)* $n_P + n_N + \sigma_{PC}$	−6.33 *(8.10)* $n_P + n_N + \sigma_{PC}$	band at 8.5 eV	−5.74 *(7.51)* $\pi_{P=N} - n_{Namino}$	−5.74 *(7.44)* $\pi_{P=N} - n_{Namino}$	band at 7.8 eV
−7.80 $\pi_{b1(aryl)}$ $(-n^+)$	−7.64 $\pi_{P=N}$ $(-\pi_{b1(aryl)})$	−7.49 $\pi_{P=N} - \pi_{b1(aryl)}$		−6.67 $n_P + n_N + \sigma_{PC}$	−6.60 $n_P + n_N + \sigma_{PC}$	band at 8.8 eV
−7.92 $\pi_{P=N} - \pi_{SiC}$	−8.05 π_{a2}	−8.09 π_{a2}	band centred at 10.0 eV	−7.73 $\pi_{b1(aryl)}$ [b]	−7.74 $\pi_{a2(aryl)}$ [c]	band at 9.5 eV
−8.19 π_{a2}	−8.11 $\pi_{P=N}$ $(+\pi_{b1(aryl)})$	−8.58 $\pi_{P=N} + \pi_{b1(aryl)}$		−7.78 $\pi_{a2(aryl)}$	−7.91 $\pi_{b1(aryl)}$	
−8.24 σ_{SiC}	−9.02 $n_P - n_N + \sigma_{PC}$	−8.94 $n_P - n_N + \sigma_{PC,\ CC}$	band at 11.0 eV	−9.27 $n_P - n_N + \sigma_{PC}$	−9.20 $n_P - n_N + \sigma_{PC}$	band at 11.0 eV
−9.13 $\pi_{P=N} + \pi_{SiC}$	−9.50 σ_{CC}	−9.49 $n_P - n_N + \sigma_{NC,\ CC}$	band at 11.8 eV	−9.71 "$\pi_{N=N}$"	−9.92 "$\pi_{N=N}$"	band at 11.6 eV

[a] $\pi_{CC(Arf)}$ almost orthogonal to the $\pi_{P=N}$ system. [b] Symmetrical orbital against the C_1C_4 axis of the aryl group. [c] Anti-symmetrical orbital against the C_1C_4 axis of the aryl group.

properties [π: 9.7 eV (**4**) and 9.8 eV (*t*BuP=N*t*Bu); n: 8.5 eV (**4**) and 8.11 eV (*t*BuP=N*t*Bu)]. Thus, Ar_f seems to exert a kinetic rather than a stabilizing electronic effect on the −P=N*t*Bu system bonds. In passing, we note that the **3** → **3′** dimerization process cannot be explained either by the nature of the energetic position of the π and π* orbitals or the polarity of the P=N bond. In fact, for **3** and **4**, the gap between the $\pi_{P=N}$ and the $\pi_{P=N}$ orbitals is relatively large and more pronounced in the case of the silyl derivative (5.64 eV vs. 5.39 eV: see Figure 4 and 5). Moreover, the polarity of the P=N double bonds are also close, although slightly higher for **3** (Figure 8). On this basis, it seems that the reason for the higher stability of **4** in comparison with **3** is that $SiMe_3$ is a less-bulky protecting group than *t*Bu. Indeed, the Si−C bond is longer than the C−C bond and the bond angle at Si is more open than the bond angle at C. Consequently the dimerization is easier with $SiMe_3$.

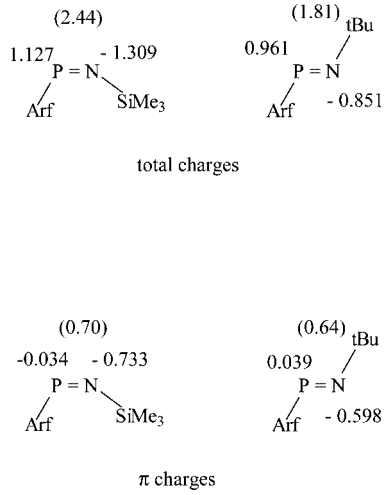

Figure 8. NBO charges (total and π) for $Ar_fP{=}NSiMe_3$ (**3**) and $Ar_fP{=}NtBu$ (**4**); polarity of the PN bond in brackets

$Ar_fP{=}NNMe_2$ (6)

In order to determine the role of the Ar_f group on the $-P{=}N{-}NMe_2$ moiety, a theoretical study of the model molecule $HP{=}NNMe_2$ (**5**) was undertaken. The isomer *trans*-**5** was found to be slightly more stable than the *cis* isomer (0.22 kcal/mol). This corresponds to the form where the electronic energy is more important (see Table 1). The geometrical parameters of the *cis* and *trans* forms are described in Table 1. In contrast to the previously studied iminophosphanes Tmp-P=N−$N(SiMe_3)_2$,[26] (Tmp = 2,2,6,6-tetramethylpiperidino) and $tBu_2P{-}P{=}N{-}N(SiMe_3)_2$,[20] the NMe_2 group in **6** is coplanar with the $C_{Ar_f}PN$ moiety. This orientation involves the presence of an important stabilizing interaction between the amino nitrogen lone-pair and the $\pi^*_{P=N}$ orbital [$n_N \rightarrow \pi^*_{P=N}$ = 77 kcal/mol (*cis*); $n_N \rightarrow \pi^*_{P=N}$ = 76.5 kcal/mol (*trans*)]. The *trans* form features a P−N bond (1.653 Å) that is significantly longer than the corresponding distance in **1** (1.588 Å). The N−N bond (1.302 Å) is intermediate between a single (1.450 Å) and a double bond (1.250 Å). As can be seen in Figure 5, the replacement of H by an NMe_2 group at the nitrogen atom destabilizes the $\pi_{P=N}$ orbital by 3.15 eV (Figure 5). The NMe_2 group also has an important influence on the energetic position of the antibonding combination of lone pairs mainly localized on nitrogen. On the other hand, the bonding combination of lone pairs is less affected by this sub-

 © 2004 Wiley-VCH Verlag GmbH & Co. KGaA, Weinheim

stituent (the difference in the energies is 1.48 eV and 0.52 eV, respectively).

Next we carried out calculations on compound **6**. Two minima corresponding to the *trans* and *cis* isomers were found on the potential energy surface. In both isomers, the amino nitrogen atom is sp^2 hybridized and the NMe_2 group is coplanar with the CPN moiety, thus establishing a three-center, four-electron system. The *trans* form **6mini** (energetic minimum) is more stable than the *cis* form by 2.07 kcal/mol because of less steric hindrance (see Table 1, E_{rep}). For **6mini** the dihedral angle between the Ar_f group and the CPN system is 126.4°. The substitution of H by Ar_f in **5** has only a weak influence on the geometrical parameters of the CPN system (Table 1). The P−C bond length (1.878 Å) remains characteristic of a single bond. These theoretical results are in agreement with the RX structure (Figure 3). As previously observed, the structure with the Ar_f group coplanar with the PNN moiety (**6ts**) corresponds to a transition state. It is energetically very close to the minimum (3.3 kcal/mol) and should involve a free rotation of the aromatic group in the gas phase. For **6ts**, the P−N, P−C and N−N bond lengths are slightly shorter than in **6mini**.

The calculated NBO charges of the $Ar_fP{=}N{-}R$ (R: *t*Bu **4**, NMe_2 **6**) system show that the phosphorus charge is about 0.961 au for **4** and 0.638 au for **6**. This modification affects the ^{31}P NMR chemical shift (**4**: δ = 412.4 ppm; **6**: δ = 224.2 ppm). The peak due to the NMe_2-substituted phosphorus atom appears at higher field than the *t*Bu-substituted phosphorus atom. This result is in agreement with those previously reported by Yoshifuji et al.[1b] on the −P=P− part.

The weak geometrical changes between the forms **5**, **6mini** and **6ts** lead to negligible modifications of their electronic structure. Figure 9 summarizes the energetic positions of the n^+, n^- and $\pi_{P=N}$ orbitals for these compounds. The inductive σ-attractor effect of Ar_f exerts a weak stabilizing influence on the n^+ and n^- orbitals (0.2−0.3 eV for n^+ and 0.37−0.44 eV for n^-); this stabilization is more pronounced for the n^- orbital since it is mainly localized on phosphorus. The plots of the combination of lone pairs show a destabilizing interaction with the σ_{PC} orbital (as previously observed for **3** and **4**), which reduces the stabilizing inductive effect of the CF_3 groups. This is the reason why the energetic positions of the n^+ and n^- orbitals in **5** and **6** are not strongly modified. In the same way, whatever the orientation of the fluorinated aromatic group, the substitution on phosphorus by Ar_f group seems to have no effect on the energetic position of the $\pi_{P=N}$ orbital. Indeed, the Kohn−Sham energies are similar for these three compounds [−5.68 (**5**), −5.74 (**6mini**), −5.74 eV (**6ts**)]. For **6ts**, taking into account the orientation of the aryl group, we might expect an interaction between the $\pi_{b1(aryl)}$ orbital of Ar_f and the $\pi_{P=N}$ system. In fact, the presence of a planar amino group coplanar with the PNN moiety involves a destabilization of the $\pi_{P=N}$ orbital (interaction $n_N \rightarrow \pi_{P=N}$). Consequently, the energy gaps $\pi_{P=N}/\pi^*_{b1(aryl)}$ and $\pi_{P=N}/\pi_{b1(aryl)}$ are decreased and increased, respectively. In the particular case of **6ts**, the strong destabilizing $\pi_{P=N} \rightarrow \pi_{b1(aryl)}$ interaction is counterbalanced by the stabilizing $\pi_{P=N} \rightarrow \pi^*_{b1(aryl)}$ interaction (see MO plots Figure 7). However, it should be noted that even when the aromatic group is coplanar with the PNN system the $\pi_{P=N} \rightarrow \pi^*_{b1(aryl)}$ interaction is not important enough to allow a strong delocalization of the $\pi_{P=N}$ system. Perhaps, the presence of strong σ-donor groups on the amino nitrogen would allow the stabilizing $\pi_{P=N} \rightarrow \pi^*_{b1(aryl)}$ interaction to be more important than the destabilizing $\pi_{P=N} \rightarrow \pi_{b1(aryl)}$ interaction. In this case a structure close to the Ar_fPH^- anion structure would be observed.

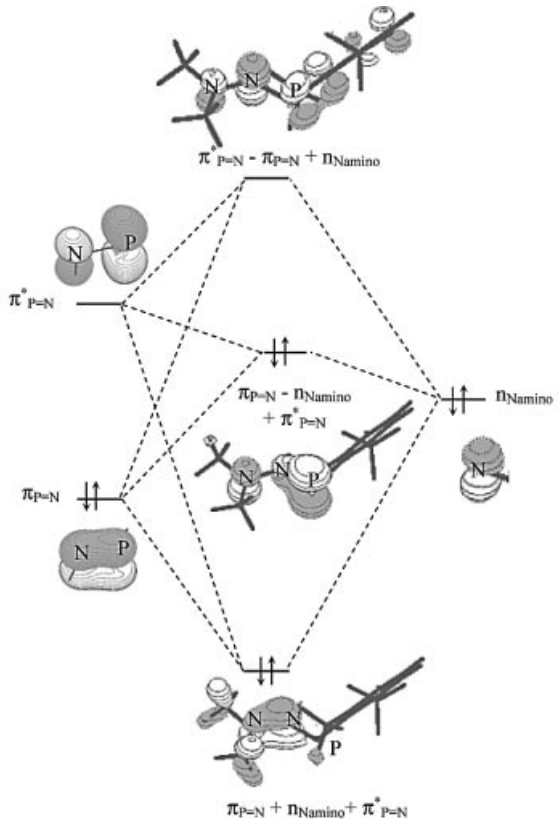

Figure 9. Plot of the molecular orbitals for the minimum of $Ar_fP{=}NNMe_2$ (**6mini**)

We have recorded the He^I PE spectrum of **6** in order to confirm the modifications of the electronic structure of the CP=N part on going from **4** to **7** (Figure 6b). It presents three first-ionization bands at 7.8, 8.8 and 9.5 eV which are lower in energy than the first ionizations of $Ar_fP{=}Nt$Bu (8.5, 10.0 and 11.0 eV). The ΔSCF values (**6mini**: $\pi_{P=N} - n_{Namino}$ = 7.51 eV; **6ts**: $\pi_{P=N} - n_{Namino}$ = 7.44 eV) as well as the Kohn−Sham energy orbitals allowed us to assign the first band at 7.8 eV to the removal of an electron from the ($\pi_{P=N} - n_{Namino} - \pi^*_{P=N}$) orbital of all rotamers around **6mini** and **6ts** (see Figure 9); the second band at 8.8 eV was assigned to the phosphorus and nitrogen bonding combination of lone pairs ($n_P + n_N$) for the different rotamers. The experimental gap (1 eV) between the first two orbitals is theoretically well represented (0.86−0.93 eV). The third ionization at 9.5 eV corresponds to the removal of an elec-

 © 2004 Wiley-VCH Verlag GmbH & Co. KGaA, Weinheim

tron from the π_{a2} orbitals of the aromatic ring. We can note an inversion of the first two orbitals. Compared to **4** (n^+, $\pi_{P=N}$ for **4** and $\pi_{P=N}$, n^+ for **6**), the $\pi_{P=N}$ orbital is being destabilized because of the interaction with the nitrogen lone pair of the amino group. The following bands at 11.0 and 11.6 eV are assigned to the ionization from the ($n_P - n_N$) orbital and the ($\pi_{P=N} + n_{Namino} + \pi^*_{P=N)}$ orbitals, respectively. In fact, the plot of this latter looks like the plot of a $\pi_{N=N}$ orbital, since the interaction between the $\pi_{P=N}$ and $\pi^*_{P=N}$ orbitals cancels the weight on the phosphorus atom (Figure 9).

In summary, previous works on the effect of the Ar_f group on the stabilization of the reactive part of the molecule have shown that this latter could act as a spectator group or a π-acceptor group. For instance, for the two following compounds: the carbene $Ar_fCP(NiPr_2)_2$ [14] and the anion Ar_fPH^-, [13] a delocalization of the carbene lone pair (carbene) or the π phosphorus lone pair (anion) in the Ar_f group was observed, respectively. The $C_{carb}-C_{aryl}$ (1.390 Å) or $P-C_{aryl}$ (1.794 Å) bonds are short and the $C_{A(aryl)}-C_{B(aryl)}$ or $C_{A(aryl)}-C_{B'(aryl)}$ bonds [$C_{A(aryl)}$: carbon linked to the carbon center or phosphorus, $C_{B(aryl)}$ and $C_{B'(aryl)}$: carbon in α position to $C_{A(aryl)}$] of the Ar_f groups are longer than the other bonds of the ring (1.43−1.44 Å compared to 1.37−1.39 Å), indicating a delocalization of the carbene lone pair or the negative charge (phosphanide anion) over the ring. In this case, the Ar_f group behaves like a π-electron acceptor by the $\pi^*_{b1(aryl)}$ orbitals of the aryl group.

A recent publication[27] has shown that the potentially π-acceptor Ar_f group can also act as a spectator group. Indeed, for the amino(aryl)carbene $Ar_fCN(Me)tBu$, it has been shown that the $C_{carb}-C_{aryl}$ bond is long (1.453 Å), the carbene bond angle acute and the C−C bonds of the aryl group quite similar (1.37−1.42 Å), which indicates that the Ar_f group does not interact with the carbene lone pair and is therefore a spectator.

In our case [iminophosphanes $Ar_fP{=}NtBu$ (**4**) and $Ar_fP{=}NNMe_2$ (**6**)], all the C−C bonds of the aryl group are almost similar (1.38−1.41 Å) and the $P-C_{aryl}$ bond quite long (single bonds: 1.866 Å for **4** and 1.863 Å for **6**). We did not observe a shortening of the $P-C_{aryl}$ bond or a lengthening of the $C_{A(aryl)}-C_{B(aryl)}$ or $C_{A(aryl)}-C_{B'(aryl)}$ bonds. These geometrical data can be compared to the previous ones and allow us to conclude that the Ar_f substituent effect is mainly steric.

Conclusion

The experimental (NMR, X-rays and UV Photoelectron Spectroscopy data) and theoretical studies on the iminophosphanes $Ar_f-P{=}NR$ (R: *t*Bu, NMe_2) show that the Ar_f group is orthogonal to the PNR moiety. This orientation could have allowed an interaction between the phosphorus lone pair and the $\pi^*_{b1(aryl)}$ orbital of the Ar_f group, as previously observed for $(iPr_2N)_2PCAr_f$ (p character of the carbon σ lone pair, short $C_{carb}-C_{aryl}$ bond). However, taking into account the strong s character of the phosphorus lone pair (phosphorus angle shrunk), this interaction is not efficient. In fact, in these compounds the Ar_f group acts mainly as a sterically protective ligand. The stabilizing effect of Ar_f is not efficient in the σ system because it is attenuated by a destabilizing interaction between the phosphorus and nitrogen combination of lone pairs and the σ_{PC} orbital. Moreover, in spite of a different electronic effect between $SiMe_3$ and *t*Bu, the isolation of the monomer in the latter case can only be explained by a smaller protecting effect of the $SiMe_3$ substituent compared to *t*Bu.

In addition, all these results show that the Ar_f group only stabilizes a system which presents a weakly nucleophilic lone pair with a strong p character. In this case, it can behave like an acceptor group with the $\pi^*_{b1(aryl)}$ orbital. Thus, it seems interesting to use Ar_f in order to stabilize anionic species with a heteroatom. This substituent could allow us to stabilize the singlet state of phosphinidenes and homologues.

Experimental Section

General Remarks: All reactions and manipulations were carried out under argon using standard Schlenk techniques. Solvents were dried according to the appropriate method: dichloromethane and chloroform with P_4O_{10}, pentane and hexane with calcium hydride, toluene, xylene, tetrahydrofuran and diethyl ether with sodium/benzophenone.

NMR spectra were recorded on Bruker AC200, and WM250 spectrometers. ^1H and ^{13}C chemical shifts are reported in ppm relative to tetramethylsilane as an external reference. ^{19}F and ^{31}P NMR downfield chemical shifts are expressed with a positive sign relative to external CF_3COOH and 85% H_3PO_4, respectively. Mass spectra were obtained on a Nermag R 10−10 instrument. The photoelectron spectra were recorded on a Helectros 0078 instrument equipped with a 127° cylindrical analyser and monitored by a micro-computer supplemented with a digital analogic converter. The spectra were calibrated with the known auto-ionization of helium at 4.98 eV [HeII(He)] and nitrogen ionization at 15.59 eV.

$Ar_fP(Cl)-N(SiMe_3)_2$: A 1.6 M solution of *n*BuLi in hexane (6.92 mmol) was added to a solution of $HN(SiMe_3)_2$ (1.12 g, 6.92 mmol) in THF (8 mL) at −50 °C. The mixture was then warmed to ambient temperature and stirred for 1 h. This solution of $LiN(SiMe_3)_2$ was added dropwise to a solution of Ar_fPCl_2 (2.18 g, 6.92 mmol) in THF (5 mL) at −80 °C. The reaction mixture was slowly warmed to ambient temperature, stirred for 1 h and the solvents evaporated. Pentane was added to the residue and the precipitated LiCl was filtered off. Removal of solvent and volatiles in vacuo yielded $Ar_fP(Cl)N(SiMe_3)_2$ as a yellow oil. Yield 86% (95% pure by NMR). ^1H NMR ($CDCl_3$): δ = 0.02 (s, 9 H, $SiMe_3$), 6.59 (t, $^3J_{H,H}$ = 7 Hz, 1 H, *p*-H_{arom}), 7.82 (d, $^3J_{H,H}$ = 7 Hz, 2 H, *m*-H_{arom}) ppm. ^{13}C NMR ($CDCl_3$): δ = 4.1 (d, $^3J_{P,C}$ = 7.4 Hz, $SiMe_3$), 124.1 (dq, $^3J_{P,C}$ = 5.6, $^1J_{P,C}$ = 275.6 Hz, CF_3), 129.3 (d, $^4J_{P,C}$ = 2.8 Hz, *p*-C_{arom}), 130.7 (m, *m*-C_{arom}), 134.7 (dq, $^2J_{P,C}$ = 11.1, $^2J_{C,F}$ = 32.4 Hz, *o*-C_{arom}), 149.0 (d, $^1J_{P,C}$ = 110.9 Hz, *ipso*-C_{arom}) ppm. ^{19}F NMR ($CDCl_3$): δ = 24.45 (d, $^4J_{F,P}$ = 39 Hz) ppm. $^{31}P\{^1H\}$ NMR ($CDCl_3$): δ = 143.9 (sept, $^4J_{F,P}$ = 39 Hz) ppm.

$[Ar_fPNSiMe_3]_2$ (3′): A solution of $Ar_fP(Cl)N(SiMe_3)_2$ (1.20 g, 2.73 mmol) in 1,2,4-trichlorobenzene (5 mL) was heated at 150 °C

 © 2004 Wiley-VCH Verlag GmbH & Co. KGaA, Weinheim

for 40 h. The solvent was evaporated in vacuo (60 °C, 0.1 Torr) and the crude **3′** was purified by washing with hexane (5 mL). This procedure gave 0.81 g (90% yield) of pure product. ^{1}H NMR (CD_2Cl_2): δ = −0.28 (s, 18 H, $SiMe_3$), 7.73 (t, $^3J_{H,H}$ = 8 Hz, 2 H, *p*-H_{arom}), 8.11 (two d, $^3J_{H,H}$ = 8 Hz, 4 H, *m*-H_{arom}) ppm. ^{13}C NMR (CD_2Cl_2): δ = −1.1 (s, $SiMe_3$), 124.1 (q, $^1J_{F,C}$ = 275.3 Hz, CF_3), 124.6 (q, $^1J_{F,C}$ = 276.7 Hz, CF_3), 130.7 (s, *p*-C_{arom}), 131.3 (q, $^3J_{F,C}$ = 32.1 Hz, *m*-C_{arom}), 139.6 (dq, $^2J_{C,P}$ = 36.1, $^2J_{F,C}$ = 29.4 Hz, *o*-C_{arom}), 151.4 (d, $^1J_{C,P}$ = 132.3 Hz, *ipso*-C_{arom}) ppm. ^{19}F NMR (CD_2Cl_2): δ = 23.04 (d, $^4J_{F,P}$ = 72.3 Hz) and 27.39 (d, $^4J_{F,P}$ = 134.7 Hz) ppm. ^{31}P{^{1}H} NMR (CD_2Cl_2): δ = 277.3 (m) ppm. $C_{22}H_{24}F_{12}N_2P_2Si_2$ (662.54): calcd. C 39.88, H 3.65; found C 39.65, H 3.89.

$Ar_fP(Cl)-N(SiMe_3)tBu$: A solution of [$LiN(SiMe_3)t$Bu] in THF (12 mL), prepared from $HNtBu(SiMe_3)$ (1.44 g, 9.89 mmol) and an equimolar amount of a 1.6 M solution of *n*BuLi in hexane at −30 °C, was added dropwise to a solution of Ar_fPCl_2 (3.12 g, 9.89 mmol) in THF (7 mL) at −80 °C. The reaction mixture was slowly warmed to ambient temperature, stirred for 1 h and the solvents evaporated. Pentane was added to the residue and the precipitated LiCl was filtered off. Removal of the solvent and volatiles in vacuo yielded 3.4 g (81%) of product. ^{1}H NMR ($CDCl_3$): δ = 0.03 (s, 9 H, $SiMe_3$), 1.54 (s, 9 H, *t*Bu), 7.56 (t, $^3J_{H,H}$ = 7.4 Hz, 1 H, *p*-H_{arom}), 7.79 (d, $^3J_{H,H}$ = 7.4 Hz, 2 H, *m*-H_{arom}) ppm. ^{13}C NMR ($CDCl_3$): δ = 6.4 (s, Me_3Si), 32.7 (d, $^3J_{P,C}$ = 13.9 Hz, C*Me*$_3$), 61.5 (d, $^2J_{C,P}$ = 29.6 Hz, *C*Me_3), 123.9 (dq, $^1J_{F,C}$ = 242.3, $^4J_{C,P}$ = 5.5 Hz, CF_3), 129.0 (d, $^4J_{C,P}$ = 3.7 Hz, *p*-C_{arom}), 129.9 and 131.6 (m, *m*-C_{arom}), 134.9 (m, *o*-C_{arom}), 148.4 (d, $^1J_{P,C}$ = 98.0 Hz, *ipso*-C_{arom}) ppm. ^{19}F NMR ($CDCl_3$): δ = 24.89 (*pseudo* t, $^4J_{F,P}$ = 37 Hz) ppm. ^{31}P{^{1}H} NMR ($CDCl_3$): δ = 145.0 (sept, $^4J_{F,P}$ = 36 Hz) ppm.

$Ar_fP{=}NtBu$ (4): A solution of $Ar_fP(Cl)N(SiMe_3)t$Bu (1.95 g, 4.61 mmol) in xylene (4 mL) was heated at 120 °C for 80 h, then the solvent was evaporated. Distillation in vacuo afforded 0.80 g (55%) of **4**; b.p. 56−60 °C at 0.05 Torr. ^{1}H NMR ($CDCl_3$): δ = 1.49 (d, $^4J_{H,P}$ = 1.8 Hz, 9 H, *t*Bu), 7.63 (t, $^3J_{H,H}$ = 7.8 Hz, 1 H, *p*-H_{arom}), 7.89 (d, $^3J_{H,H}$ = 7.8 Hz, 2 H, *m*-H_{arom}) ppm. ^{13}C NMR ($CDCl_3$): δ = 32.5 (d, $^3J_{C,P}$ = 15.7 Hz, C*Me*$_3$), 64.6 (d, $^2J_{C,P}$ = 10.2 Hz, *C*Me_3), 124.1 (dq, $^1J_{F,C}$ = 275.6, $^3J_{C,P}$ = 1.9 Hz, CF_3), 129.8 (s, *p*-C_{arom}), 129.9 (q, $^3J_{F,C}$ = 5.6 Hz, *m*-C_{arom}), 133.2 (dq, $^2J_{C,P}$ = 4.6, $^2J_{F,C}$ = 31.5 Hz, *o*-C_{arom}), 147.0 (d, $^1J_{C,P}$ = 84.2 Hz, *ipso*-C_{arom}) ppm. ^{19}F NMR ($CDCl_3$): δ = 21.65 (d, $^4J_{F,P}$ = 28 Hz) ppm. ^{31}P{^{1}H} NMR ($CDCl_3$): δ = 412.4 (sept, $^4J_{F,P}$ = 28 Hz) ppm. $C_{12}H_{12}F_6NP$ (315.19): calcd. C 45.73, H 3.84; found C 45.40, H 3.55.

$Ar_fP(Cl)-N(SiMe_3)NMe_2$: A 1.6 M solution of *n*BuLi in hexane (10.38 mmol) was added to a solution of $HN(SiMe_3)(NMe_2)$ (1.37 g, 10.38 mmol) in THF (15 mL) at −30 °C. The mixture was then warmed to ambient temperature and stirred for 1 h. This solution of lithium hydrazide was added dropwise to a solution of Ar_fPCl_2 (3.27 g, 10.38 mmol) in THF (7 mL) at −80 °C. The reaction mixture was slowly warmed to ambient temperature, stirred for 1 h and the solvents evaporated. Pentane was added to the residue and the precipitated LiCl was filtered off. Solvent and volatile compounds were removed in vacuo. The resulting solid contained the chlorophosphane $Ar_fP(Cl)N(SiMe_3)NMe_2$ and about 20% of the diphosphene $Ar_fP{=}PAr_f$. Recrystallization from diethyl ether afforded the pure product as dark yellow crystals. Yield 2.1 g (49%). ^{1}H NMR (C_6D_6): δ = 0.02 (s, 9 H, $SiMe_3$), 2.51 (br. s, 6 H, Me_2N), 6.71 (t, $^3J_{H,H}$ = 7.8 Hz, 1 H, *p*-H_{arom}), 7.38 (d, $^3J_{H,H}$ = 7.8 Hz, 2 H, *m*-H_{arom}) ppm.^{13}C NMR (C_6D_6): δ = 1.9 (d, $^3J_{P,C}$ = 2.8 Hz, Me_3Si), 47.1 (d, $^3J_{P,C}$ = 103.6 Hz, Me_2N), 124.6 (q, $^1J_{F,C}$ = 275.6 Hz, F_3C), 130.8 (s, *p*-C_{arom}), 130.9 (br. m, *m*-C_{arom}), 135.6 (dq, $^2J_{P,C}$ = 19.4, $^2J_{C,F}$ = 31.4 Hz, *o*-C_{arom}), 138.2 (d, $^1J_{P,C}$ = 83.23 Hz, *ipso*-C_{arom}) ppm. ^{19}F NMR (C_6D_6): δ = 22.50 (d, $^4J_{F,P}$ = 46 Hz) ppm. ^{31}P{^{1}H} NMR (C_6D_6): δ = 122.5 (sept, $^4J_{F,P}$ = 46 Hz) ppm. MS (70 eV): *m*/*z* (%) = 375 (100) [M − Cl]$^+$. $C_{13}H_{18}ClF_6N_2PSi$ (410.80): calcd. C 38.01, H 4.42; found C 38.19, H 4.22.

$Ar_fP{=}N{-}NMe_2$ (6): A solution of $Ar_fP(Cl)N(SiMe_3)NMe_2$ (1.96 g, 4.78 mmol) in xylene (4 mL) was heated at 120 °C for 2 h, then the solvent was evaporated. Distillation in vacuo (60−70 °C, 0.05 Torr) afforded **6** in ca. 50% yield and, according to the NMR spectra, $Ar_fP{=}PAr_f$ (δ_P = 478 ppm) as a side product (ca. 10%). Pure **6** was isolated after stirring a solution of the amido(chloro)-phosphane (1.52 g, 3.70 mmol) in $CHCl_3$ (2 mL) at 25 °C for 14 h. Yield 95%; b.p. 65−70 °C at 0.5 Torr. ^{1}H NMR ($CDCl_3$): δ = 3.34 (d, $^4J_{H,P}$ = 7.4 Hz, 6 H, Me_2N), 7.55 (t, $^3J_{H,H}$ = 8 Hz, 1 H, *p*-H_{arom}), 7.89 (d, $^3J_{H,H}$ = 8 Hz, 2 H, *m*-H_{arom}) ppm. ^{13}C NMR ($CDCl_3$): δ = 47.9 (d, $^3J_{C,P}$ = 12.95 Hz, Me_2N), 124.1 (q, $^1J_{F,C}$ = 275.6 Hz, CF_3), 128.6 (s, *p*-C_{arom}), 129.6 (q, $^3J_{F,C}$ = 5.5 Hz, *m*-C_{arom}), 135.3 (dq, $^2J_{C,P}$ = 4.6, $^2J_{F,C}$ = 29.6 Hz, *o*-C_{arom}), 144.0 (d, $^1J_{C,P}$ = 71.2 Hz, *ipso*-C_{arom}) ppm. ^{19}F NMR ($CDCl_3$): δ = 20.92 (d, $^4J_{F,P}$ = 23.5 Hz) ppm. ^{31}P NMR ($CDCl_3$): δ = 224.3 (br.s) ppm. $C_{10}H_9F_6N_2P$ (302.16): calcd. C 39.75, H 3.00; found C 40.10, H 3.38.

***i*$Pr_2NP(Cl)-N(SiMe_3)NMe_2$:** A 1.6 M solution of *n*BuLi in hexane (6.36 mmol) was added to a solution of $HN(SiMe_3)(NMe_2)$ (0.84 g, 6.36 mmol) in THF (10 mL) at −30 °C. This solution of lithium hydrazide was added dropwise to a solution of *i*Pr_2NPCl_2 (1.27 g, 6.36 mmol) in THF (5 mL) at −80 °C. The reaction mixture was slowly warmed to ambient temperature, stirred for 1 h and the solvents evaporated. Pentane (20 mL) was added to the residue and the precipitated LiCl was filtered off. The solution was evaporated to yield colorless crystals of the product (89%). M.p. 32−34 °C. ^{1}H NMR (C_6D_6): δ = 0.39 (s, 9 H, $SiMe_3$), 1.08 and 1.28 (d, $^3J_{H,H}$ = 6.8 Hz, 12 H, $CH(CH_3)_2$], 2.52 and 2.61 (s, 6 H, NMe_2), 3.71 [m, 2 H, $CH(CH_3)_2$] ppm. ^{13}C NMR: δ = 3.2 (d, $^3J_{P,C}$ = 3.7 Hz, Me_3Si), 23.2 [d, $^3J_{P,C}$ = 12.95 Hz, $CH(CH_3)_2$], 23.9 [d, $^3J_{P,C}$ = 4.62 Hz, $CH(CH_3)_2$], 46.7 [d, $^3J_{P,C}$ = 10.2 Hz, $N(CH_3)_2$], 47.4 [d, $^2J_{P,C}$ = 44.4 Hz, $CH(CH_3)_2$], 47, 6 [d, $^2J_{P,C}$ = 39.8 Hz, $CH(CH_3)_2$] ppm. ^{31}P NMR ($CDCl_3$): δ = 129.3 (s) ppm. $C_{13}H_{18}ClF_6N_2PSi$ (410.80): calcd. C 38.01, H 4.42; found C 38.19, H 4.22.

***i*$Pr_2NP{=}NNMe_2$ (7):** A solution of *i*$Pr_2NP(Cl)N(SiMe_3)NMe_2$ (1.43 g, 4.80 mmol) in toluene (10 mL) was heated at 100 °C for 10 h. Solvent was removed in vacuo to afford iminophosphane **7** contaminated by a small amount (<10%) of the dimer [*i*$Pr_2NPNNMe_2$]$_2$.

7: ^{1}H NMR (C_6D_6): δ = 1.19 and 1.44 [br. s, 12 H, $CH(CH_3)_2$], 2.58 (s, 6 H, NMe_2), 3.32 and 4.10 [br. s, 2 H, $CH(CH_3)_2$] ppm. ^{13}C NMR (C_6D_6): δ = 22.2 and 27.6 [br. s, $CH(CH_3)_2$], 44.8 [s, $N(CH_3)_2$], 49.3 [*pseudo* t, $^2J_{P,C}$ = 5.55 Hz, $CH(CH_3)_2$] ppm. ^{31}P NMR (C_6D_6): δ = 173.13 (s) ppm. MS (70 eV): *m*/*z* (%) = 189 (15) [M$^+$]. $C_8H_{20}N_3P$ (189.24).

Iminophosphane **7** slowly dimerizes at room temperature to give 1,3,2,4-diazadiphosphetidine [*i*$Pr_2NPNNMe_2$]$_2$ according to X-ray analysis. ^{1}H NMR ($CDCl_3$): δ = 1.24 [d, $^3J_{H,H}$ = 6.8 Hz, 12 H, $CH(CH_3)_2$], 2.69 (s, 6 H, NMe_2), 3.84 [br. s, 2 H, $CH(CH_3)_2$]; ppm. ^{13}C NMR ($CDCl_3$): δ = 24.6 [br. s, $NCH(CH_3)_2$], 43.6 (t, $^3J_{P,C}$ = 4.6 Hz, NMe_2), 49.1 (t, $^2J_{P,C}$ = 5.6 Hz, $CH(CH_3)_2$] ppm. ^{31}P NMR ($CDCl_3$): δ = 74.2 (s) ppm. MS (70 eV): *m*/*z* (%) = 378 (17) [M$^+$]. $C_8H_{20}N_3P$ (189.24): calcd. C 50.77, H 10.65, N 22.20; found C 50.86, H 10.84, N 22. 08. $C_{16}H_{40}N_6P_2$ (378.48): calcd. C 50.77, H 10.65, N 22.20; found C 50.55, H 10.49, N 22.13.

 © 2004 Wiley-VCH Verlag GmbH & Co. KGaA, Weinheim

Table 3. Crystallographic data for **3′**, **4** and **6**

	3′	**4**	**6**
Empirical formula	$C_{11}H_{12}F_6NPSi$	$C_{12}H_{12}F_6NP$	$C_{10}H_9F_6N_2P$
Molecular mass	331.28	315.20	302.16
Temp. (K)	223(2)	193(2)	193(2)
Wavelength (Å)	0.71073	0.71073	0.71073
Crystal system	monoclinic	orthorhombic	triclinic
Space group	$P2_1/c$	Pnma	$P\bar{1}$
a (Å)	10.378(2)	7.031(1)	7.160(1)
b (Å)	17.730(3)	13.348(1)	9.245(1)
c (Å)	15.790(4)	15.263(2)	10.565(1)
α (°)	–	–	67.164(2)
β (°)	93.75(2)	–	78.394(2)
γ (°)	–	–	85.958(2)
V (Å^3)	2899.3(9)	1432.4(3)	631.4(1)
Z	8	4	2
θ range for data collection (°)	1.73 to 28.28	2.03 to 24.71	2.13 to 29.46
No. of rflns collected	21424	6955	4296
No. of indep rflns.	7171 [R(int) = 0.0246]	1278 [R(int) = 0.0452]	3074 [R(int) = 0.0231]
No. of parameters	385	102	174
Goodness of fit on F^2	1.021	1.043	1.026
$R1$ [$I > 2\sigma(I)$]	0.0504	0.0537	0.0476
$wR2$ (all data)	0.1572	0.1471	0.1387
Largest diff peak, hole (e·Å^{-3})	1.158 and −0.283	0.357 and −0.311	0.342 and −0.297

Computational Details: Calculations were performed with the Gaussian 98 program[28,29] using the Density Functional theory method.[30] The various structures were fully optimized at the B3LYP level.[31] This functional is built with Becke's three-parameter exchange functional[31a] and the Lee−Yang−Parr correlation functional.[31c] The 6-311G(d,p) basis set was used. All atoms were augmented with a single set of polarization functions. The second derivatives were calculated in order to determine if a minimum or a transition state (one negative eigenvalue) existed for the resulting geometry.

All total energies have been zero-point energy (ZPE) and temperature corrected using unscaled density functional frequencies.

NBO analysis population[32] was performed in order to determine the presence of stabilizing interactions between a filled orbital and an empty orbital. Ionization energies were determined as the difference between the cation and the neutral molecule energies (IE = $E_{cation} - E_{molecule}$; ΔSCF method). For the large molecules, an association between the ionization potential and Kohn−Sham (KS) energies calculated with common functionals (Koopmans' theorem-like) has been discussed in depth. Arduengo and co-workers[33] first used DFT calculations at the nonlocal level to assign their photoelectron spectra. They applied a uniform shift to the orbital energies considering the difference between the calculated and experimental molecular ionization potentials. The aim was to directly compare the KS energies to the experimental energies. Moreover, Werstiuk and Rademacher[34] have developed and successfully applied a routine for the interpretation of PE spectra based on B3LYP theory. This routine requires the calculation of the molecule's first vertical ionization potential IP_v. Calculated orbital energies $-\varepsilon$ are then shifted uniformly so that the HOMO energy equals that of the IP_v, giving the higher IPs. More recently, Hoffmann[35] has underlined that the KS orbitals are a good basis for qualitative interpretation of molecular orbital. He concluded that if one wants to go a step beyond a qualitative interpretation and look at orbital energies as rough ionization potentials, and if the DFT calculations are done with commonly used potentials, then one must take the absolute constant and linear orbital energy shift into account by applying a suitable (ax + b) scaling. In the case of large molecules, the ordering of levels found by using the DFT calculations seems to be qualitatively as well translated as by using HF methods. This fact, despite the evident limits of correlation, gives a good basis for discussion about the ionizations assignments which cannot be reached by a direct calculation.

X-ray Crystallographic Study: Crystal data for **3′**, **4** and **6** are presented in Table 3. All data were collected at low temperature (−50 °C for **3′** and −80 °C for **4** and **6**) on a Bruker-AXS CCD 1000 diffractometer with Mo-K_α radiation (λ = 0.71073 Å). The structures were solved by direct methods by means of SHELXS-97[36] and refined with all data on F^2 by means of SHELXL-97.[37] All non-hydrogen atoms were refined anisotropically.
CCDC 223052−223054 (for **3′**, **4** and **6** respectively) contain the supplementary crystallographic data for this paper. These data can be obtained free of charge at www.ccdc.cam.ac.uk/conts/retrieving.html [or from the Cambridge Crystallographic Data Centre, 12 Union Road, Cambridge CB2 1EZ, UK; fax: (internat.) +44-1223/336-033; E-mail: deposit@ccdc.cam.ac.uk].

Acknowledgments

Financial support of this work by the CNRS (France) is gratefully acknowledged. We also thank the Institut du Developpement de Ressources en Informatique Scientifique (IDRIS, Orsay, France), administered by the CNRS, for the calculation facilities, and Dr. Gijs Schaftenaar for allowing us to use his graphic program.[24]

[1] [1a] E. Niecke, in *Multiple Bonding and Low Coordination in Phosphorus Chemistry* (Eds.: M. Regitz, O. J. Scherer), Thieme Verlag, Stuttgart, **1990**, 293−320. See also the following references for captodative or push-pull diphosphenes: [1b]M. Abe, K. Toyota, M. Yoshifuji, *Chem. Lett.* **1992**, 2349−2352; M. Abe, K. Toyota, M. Yoshifuji, *Bull. Chem. Soc. Jpn.* **1993**, *66*, 3831−3833.
[2] E. Niecke, D. Gudat, *Angew. Chem.* **1991**, *103*, 251−270; *Angew. Chem. Int. Ed. Engl.* **1991**, *30*, 217−236.

 © 2004 Wiley-VCH Verlag GmbH & Co. KGaA, Weinheim

[3] [3a] L. N. Markovskii, V. D. Romanenko, A. V. Ruban, *The Chemistry of Acyclic Twofold Coordinated Phosphorus Compounds*, Naukova Dumka, Kiev, **1988**, 123−198. [3b]M. Yoshifuji, N. Inamoto, K. Hirotsu, *J. Am. Chem. Soc.* **1981**, *103*, 4587−4589; M. Yoshifuji, N. Inamoto, K. Hirotsu, *J. Am. Chem. Soc.* **1982**, *104*, 6167.
[4] E. Niecke, M. Nieger, C. Gaertner-Winkhaus, B. Kramer, *Chem. Ber.* **1990**, *123*, 477−479.
[5] L. N. Markovskii, V. D. Romanenko, A. V. Ruban, A. B. Drapailo, G. V. Reitel, A. N. Chernega, M. I. Povolotskii, *Zh. Obshch. Khim.* **1990**, *60*, 2453−2462.
[6] E. Niecke, M. Nieger, F. Reichert, *Angew. Chem.* **1988**, *100*, 1781−1784; *Angew. Chem. Int. Ed. Engl.* **1988**, *27*, 1715−1718.
[7] A. N. Chernega, A. A. Korkin, N. E. Aksinenko, A. V. Ruban, V. D. Romanenko, *Zh. Obshch. Khim.* **1990**, *60*, 2462−2469.
[8] V. D. Romanenko, G. Reitel, A. N. Chernega, O. V. Kirichenko, A. V. Ruban, M. Sanchez, R. Wolf, M. R. Mazieres, *Heteroatom Chem.* **1992**, *3*, 453−458.
[9] E. Niecke, R. Detsch, M. Nieger, F. Reichert, W. W. Schoeller, *Bull. Chem. Soc. Fr.* **1993**, *130*, 25−31.
[10] W. W. Schoeller, T. Busch, E. Niecke, *Chem. Ber.* **1990**, *123*, 1653−1654.
[11] G. David, V. von der Gonna, E. Niecke, T. Busch, W. W. Schoeller, P. Rademacher, *J. Chem. Soc., Faraday Trans.* **1994**, *90*, 2611−2616.
[12] The electronic and steric properties of the related 2,4,6-tris(trifluoromethylphenyl) group have been reviewed: F. T. Edelman, *Comments Inorg. Chem.* **1992**, *12*, 259−284.
[13] V.-L. Rudzevich, H. Gornitzka, K. Miqueu, J.-M. Sotiropoulos, G. Pfister-Guillouzo, V.-D. Romanenko, G. Bertrand, *Angew. Chem. Int. Ed.* **2002**, *114*, 1241−1243; *Angew. Chem. Int. Ed.* **2002**, *41*, 1193−1195.
[14] C. Buron, H. Gornitzka, V.-D. Romanenko, G. Bertrand, *Science* **2000**, *288*, 834−836.
[15] L. N. Markovskii, V. D. Romanenko, A. B. Drapailo, A. V. Ruban, *Zh. Obshch. Khim.* **1986**, *56*, 2231−2242.
[16] T. Lübben, H. W. Roesky, H. Gornitzka, A. Steiner, D. Stalke, *Eur. J. Solid State Inorg. Chem.* **1995**, *32*, 121−130.
[17] A. N. Chernega, M. Yu. Antipin, Yu. T. Struchkov, A. V. Ruban, V. D. Romanenko, *Zh. Struct. Khim.* **1987**, *28*, 105−110.
[18] J.-T. Ahlemann, H. W. Roesky, R. Murugavel, E. Parisini, M. Noltemeyer, H.-G. Schmidt, O. Müller, R. Herbst-Irmer, L. N. Markovskii, Y. G. Shermolovich, *Chem. Ber./Recueil* **1997**, *130*, 1113−1121.
[19] J. Escudie, C. Couret, H. Ranaivonjatovo, M. Lazraq, J. Satge, *Phosphorus, Sulfur Rel. Elem.* **1987**, *31*, 27−31.
[20] U. Dressler, E. Niecke, S. Pohl, W. Saak, W. W. Schoeller, H.-G. Schaefer, *J. Chem. Soc., Chem. Commun.* **1986**, 1086−1087.
[21] O. Altmeyer, E. Niecke, M. Nieger, T. Busch, W. W. Schoeller, D. Stalke, *Heteroatom Chem.* **1990**, *1*, 191−194.
[22] K. Miqueu, J.-M. Sotiropoulos, G. Pfister-Guillouzo, V.-D. Romanenko, *New J. Chem.* **2001**, 930−938.
[23] W. W. Schoeller, T. Busch, E. Niecke, *Chem. Ber.* **1990**, 1653−1654.
[24] G. Schaftenaar, J. H. Noordik, *J. Comput. -Aided Mol. Des.* **2000**, *14*, 123−134.
[25] S. Elbel, A. Ellis, E. Niecke, H. Egsgaard, L. Carlsen, *J. Chem. Soc., Dalton Trans.* **1985**, 879−884.
[26] U. Dressler, E. Niecke, S. Pohl, W. Saak, W. W. Schoeller, H. G. Schäfer, *J. Chem. Soc., Chem. Commun.* **1986**, 1086−1087.
[27] S. Solé, H. Gornitzka, W. W. Schoeller, D. Bourissou, G. Bertrand, *Science* **2001**, *292*, 1901−1903.
[28] Gaussian 98, M. J. Frisch, G. W. Trucks, H. B. Schlegel, G. E. Scuseria, M. A. Robb, J. R. Cheeseman, V. G. Zakrzewski, J. A. Montgomery, R. E. Stratman J. C. Burant S. Dapprich, J. M. Millam, A. D. Daniels, K. N. Kudin, M. C. Strain, O. Farkas, J. Tomasi, V. Barone, M. Cossi, R. Cammi, B. Mennucci, C. Pomelli, C. Adamo, S. Clifford, J. Ochterski, G. A. Petersson, P. Y. Ayala, Q. Cui, K. Morokuma, D. K. Malick, A. D. K. Rabuck, Raghavachari, J. B. Foresman, J. Cioslowswi, J. V. Ortiz, A. G. Baboul, B. B. Stefanov, G. Liu, A. Liashenko, P. Piskorz, I. Komaromi, R. Gomperts, R. Martin, D. J. Fox, T. Keith, M. A. Al-Laham, C. Y. Peng, A. Nanayakkara, C. Gonzalez, M. Challacombe, P. M. W. Gill, B. Jonhson, W. Chen, M. W. Wong, J. L. Andres, M. Head-Gordon, E. S. Replogle, J. A. Pople, Gaussian 98, Revision A.7, Gaussian Inc., Pittsburgh PA, **1998**.
[29] W. J. Hehre, L. Radom, P. v. R. Schleyer, J. A. Pople, *Ab Initio Molecular Orbital Theory*, John Wiley & Sons: New York, **1986**.
[30] R. G. Parr, W. Yang, *Functional Theory of Atoms and Molecules* (Eds.: R. Breslow, J. B. Goodenough), Oxford University Press: New York, **1989**.
[31] [31a] A. D. Becke, *Phys. Rev.* **1988**, *A38*, 3098−3100. [31b] A. D. Becke, *J. Chem. Phys.* **1993**, *98*, 5648−5652. [31c] C. Lee, W. Yang, R. G. Parr, *Phys. Rev.* **1988**, *B37*, 785−789.
[32] [32a] A. E. Reed, L. A. Curtiss, F. Weinhold, *Chem. Rev.* **1988**, *88*, 899−926. [32b] J. P. Foster, F. Weinhold, *J. Am. Chem. Soc.* **1980**, *102*, 7211−7218.
[33] A. J. Arduengo III, H. Bock, H. Chen, M. Denk, D. A. Dixon, J. C. Green, W. A. Hermann, N. L. Jones, M. Wagner, R. West, *J. Am. Chem. Soc.* **1994**, *116*, 6641−6649.
[34] [34a] H. M. Muchall, P. Rademacher, *J. Mol. Struct.* **1997**, *435*, 157−167. [34b] H. M. Muchall, P. Rademacher, *J. Mol. Struct.* **1998**, *471*, 189−194. [34c] H. M. Muchall, N. H. Werstiuk, B. Choudhurry, *Can. J. Chem.* **1998**, *76*, 221−227. [34d] H. M. Muchall, N. H. Werstiuk, B. Choudhurry, J. Ma, J. Warkentin, J. P. Pezacki, *Can. J. Chem.* **1998**, *76*, 238−240.
[35] R. Stowasser, R. Hoffmann, *J. Am. Chem. Soc.* **1999**, *121*, 3414−3420.
[36] G. M. Sheldrick, *Acta Crystallogr., Sect. A* **1990**, *46*, 467−473.
[37] G. M. Sheldrick SHELXL-97, *Program for Crystal Structure Refinement*, University of Göttingen, Germany, **1997**.
[38] C.-H. Lai, M.-D. Su, S.-Y. Chu, *J. Phys. Chem. A.* **2003**, *107*, 2700−2710.

Received November 5, 2003
Early View Article
Published Online April 7, 2004

 © 2004 Wiley-VCH Verlag GmbH & Co. KGaA, Weinheim

The First Structurally Authenticated Organomercury(1+) Thioether Complexes − Mercury−Carbon Bond Activation Related to the Mechanism of the Bacterial Enzyme Organomercurial Lyase

Michaela Wilhelm,[a][‡] Stefan Deeken,[a] Eva Berssen,[a] Wolfgang Saak,[a] Arne Lützen,[a] Rainer Koch,[a] and Henry Strasdeit*[b]

Keywords: Bioinorganic chemistry / Enzyme models / Ligand effects / Mercury / S ligands

The new compounds [MeHg([9]aneS$_3$)](BF$_4$) (**1**), [MeHg([12]aneS$_3$)](BF$_4$) (**2**), and [(MeHg)$_2$([14]aneS$_4$)](BF$_4$)$_2$ (**3**) have been prepared and their crystal structures determined. In **1**, the thioether acts as a tridentate ligand [Hg–S 2.611(2)–2.768(2) Å] and thus the metal atom is tetrahedrally coordinated, which is rare in organomercury chemistry. Temperature-dependent ^{1}H and ^{13}C NMR spectra showed that this coordination is retained in acetonitrile solution. In crystalline **2** and **3**, linear-coordinated Hg^{II} occurs with Hg–S bond lengths of 2.441(4) and 2.425(2) Å. [MeHg([9]aneS$_3$)]$^+$ was found to be stable towards ligand substitution by $CF_3SO_3^-$ in dimethyl sulfoxide, whereas the thioether was partly displaced by $CF_3CO_2^-$ and completely by $CH_3CO_2^-$. Protonolysis by the very strong Brønsted acid CF_3SO_3H in [D$_3$]nitromethane transformed the methanido ligand into methane. The degree of Hg–C bond cleavage was ca. 25% for the four-coordinate [MeHg([9]aneS$_3$)]$^+$ after 1 h, whereas no reaction was observed for two-coordinate [MeHg(SEt$_2$)]$^+$ or MeHgCl under similar conditions even after 24 h. The product Hg^{2+} was trapped as [Hg([9]aneS$_3$)$_2$]$^{2+}$, which is a six-coordinate complex, as shown by a crystal structure analysis of [Hg([9]aneS$_3$)$_2$](BF$_4$)$_2$·2 CH$_3$CN. Quantum chemical calculations [MP2/SDD + SDD ECP Hg, 6-31+G(d,p) other elements] confirmed that hydrogen transfer activation barriers are significantly lower for "high"-coordinate (CN > 2) complexes. Hg–C bond activation by the enzyme organomercurial lyase is possibly also based on multiple (cysteinyl) sulfur ligation. We propose a hypothetical reaction mechanism that involves an OH-containing amino acid side chain or a water molecule simultaneously serving as a proton acceptor (from Cys–SH) and donor (to R$^-$ of RHg$^+$). This mechanism is supported by quantum chemical calculations on a model system.

(© Wiley-VCH Verlag GmbH & Co. KGaA, 69451 Weinheim, Germany, 2004)

Introduction

The high toxicity of various mercury compounds is a constant issue of environmental and public health concern. Consequently, the global cycle of mercury, including the considerable effects of anthropogenic activities, has been intensely studied.[1−6] It was found that in the marine environment, the reduction of inorganic mercury (Hg^{2+}) to the elemental form (Hg^0), and the biomethylation of Hg^{2+} to methylmercury ($MeHg^+$) and dimethylmercury ($HgMe_2$) are major reactions. While Hg^0 is released into the atmosphere where it represents the dominant transport form of mercury, methylmercury is partly incorporated by plankton species and accumulates in the food chain, especially in predatory fish.[7,8] Methylmercury is known to be an extreme neurotoxin.[9−16] A recent study estimates that in the USA alone, over 60,000 children are born each year at risk of neurological problems caused by in utero exposure to methylmercury.[9,17]

One of the main factors responsible for the facile biomagnification of methylmercury in the food chain is the relatively high stability of the Hg−CH_3 bond under physiological conditions.[18,19] It is therefore interesting that the bacterial enzyme organomercurial lyase or MerB (gene: *merB*) is capable of accelerating the protonolytic cleavage of methylmercury and other RHg^+ cations by a factor of 10^6-10^7.[20] The products of the enzymatic reaction are the hydrocarbon RH and Hg^{2+} which is eventually complexed by exogenous thiolates. Organomercurial lyase is part of a broad-spectrum mercury resistance system in which a second enzyme, termed mercuric reductase or MerA (gene: *merA*), catalyzes the reduction of Hg^{2+} to Hg^0 with the latter finally diffusing out of the bacterial cell.[21−26] The

[a] Institut für Reine und Angewandte Chemie der Universität Oldenburg
Carl-von-Ossietzky-Str. 9−11, 26129 Oldenburg, Germany
Fax: (internat.) + 49-(0)441-798-3329
[b] Institut für Chemie der Universität Hohenheim
Garbenstr. 30, 70593 Stuttgart, Germany
Fax: (internat.) + 49-(0)711-459-3950
E-mail: h-strasd@uni-hohenheim.de
[‡] Present address: Universität Bremen FB 4/IW3, Keramische Werkstoffe und Bauteile
Am Biologischen Garten 2, 28359 Bremen, Germany

three-dimensional structure and the enzymatic mechanism of organomercurial lyase are still unknown. However, a general mechanistic hypothesis proposed by Walsh and coworkers is available.[20,27] One of its key features is the coordination of the substrate RHg^+ to one or two cysteinyl-S^- groups, enhancing the polarity of the Hg−C bond. A Brønsted-acidic group of the enzyme, possibly a cysteinyl-SH, is thought to be the proton donor in the subsequent protonolysis step (for further details see Results and Discussion). In model studies, Barbaro et al. have demonstrated that a high "primary" coordination number of mercury can contribute to the activation of Hg−C bonds. They found that the tetrahedral phosphane complexes $[RHg\{N(CH_2CH_2PPh_2)_3\}]^+$ (R = Me, Ph) were unusually susceptible to protonolytic Hg−C bond cleavage.[28,29] Results of a theoretical study, comparing Hg−C bond cleavage in $[MeHg(PH_3)]^+$ and $[MeHg(PH_3)_3]^+$, agreed with the experimental observations.[30] Metal ion coordination by phosphanes, however, is "non-physiological". Synthetic analogues that more closely mimic the proposed substrate binding by organomercurial lyase are lacking.

In this paper we describe methylmercury(1+) thioether complexes with properties relevant to the suggested mechanism of organomercurial lyase. Our experimental and theoretical study addresses, among other things, the question of Hg−C bond activation by multiple sulfur ligation. Perhaps surprisingly, $MeHg^+$−thioether complexes have low thermodynamic stabilities with typical log *K* values for the formation of 1:1 complexes falling in the range −1 to 2.[31,32] In marked contrast, the stability constants of thioether complexes of Hg^{2+} are by about ten orders of magnitude larger (log *K* = 8−12).[33] This difference may be attributed to "anti-symbiosis" which means that the soft methanido ligand reduces the affinity of mercury(II) for another soft ligand in the *trans* position.[34] So far, only a few organomercury(1+) thioether complexes have been isolated[35] and, to the best of our knowledge, no crystal structures have been determined.[36] In the following, we report the syntheses and X-ray crystal structures of three new $MeHg^+$ complexes with meso- and macrocyclic thioether ligands. Part of this work has been communicated previously.[37]

Results and Discussion

Syntheses of the Methylmercury Complexes

A suitable methylmercury starting compound was obtained by treating methylmercury hydroxide with a slight excess of tetrafluoroboric acid in aqueous solution. After removal of the solvent, a colorless oil remained. It is known that in strongly acidic aqueous solutions $[MeHg(OH_2)]^+$ is by far the main $MeHg^+$ species.[38] It therefore seemed safe to assume that the obtained product was $[MeHg(OH_2)](BF_4)\cdot xH_2O$. The complex $[MeHg(OH_2)]^+$ should have a similar structure to $[MeHg(DMSO)]^+$, which contains *O*-coordinated dimethyl sulfoxide in solution as well as in the solid state.[39]

In tetrahydrofuran or acetonitrile/diethyl ether, the thioethers [9]aneS$_3$, [12]aneS$_3$, and [14]aneS$_4$ are capable of displacing the aqua ligand from $[MeHg(OH_2)]^+$ {Equation (1); L = [9]aneS$_3$ or [12]aneS$_3$: *n* = 1; L = [14]aneS$_4$: *n* = 2}.

$$n\,[MeHg(OH_2)](BF_4) + L \rightarrow [(MeHg)_nL](BF_4)_n + n\,H_2O \qquad (1)$$

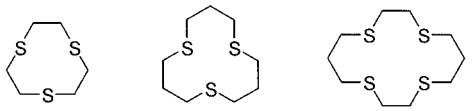

[9]aneS$_3$ [12]aneS$_3$ [14]aneS$_4$

By this route, we prepared the new coordination compounds $[MeHg([9]aneS_3)](BF_4)$ (**1**), $[MeHg([12]aneS_3)](BF_4)$ (**2**), and $[(MeHg)_2([14]aneS_4)](BF_4)_2$ (**3**). They were isolated as analytically pure, crystalline solids in yields of 85% (**1**), 68% (**2**), and 92% (**3**), respectively. We did not succeed in preparing complexes with different numbers of $MeHg^+$ cations per ligand molecule by variation of the starting material ratios. NMR experiments showed, however, that [12]aneS$_3$ can probably bind more than one $MeHg^+$ group (see below). Compounds **1**−**3** are air-stable and soluble in strongly polar organic solvents such as acetonitrile, nitromethane, and dimethyl sulfoxide.

Crystal Structures of Compounds 1−3

Crystals of $[MeHg([9]aneS_3)](BF_4)$ (**1**) consist of discrete $[MeHg([9]aneS_3)]^+$ cations and BF_4^- anions. The compound crystallizes with two formula units in the asymmetric unit. The two symmetry-independent $[MeHg([9]aneS_3)]^+$ complexes have essentially the same structure (Figure 1). Each of the Hg atoms is in a distorted tetrahedral coordination environment formed by a methanido and a tridentate thioether ligand.[29] One Hg−S bond is shorter than the other two. Nevertheless, all three are "primary" bonds. The shortest Hg−S bond is involved in the largest S−Hg−C angle [complex **1**: 142.7(4)°; complex **2**: 136.4(4)°], demonstrating a slight distortion towards the linear coordination usually preferred in RHg^+ complexes. As expected, the mean Hg−S bond length of the four-coordinate complexes in **1** (2.71 Å) is considerably larger than the Hg−S bond lengths of the two-coordinate complexes in **2** [2.441(4) Å] and **3** [2.425(2) Å]. The Hg−C bond lengths are, however, not significantly different [**1**: 2.080(8), 2.075(8) Å; **2**: 2.11(2) Å; **3**: 2.068(7) Å] and correspond well with the average value of 2.07 Å that was derived from a large number of $MeHg^+$ compounds.[29b] As in the free form,[40] the ligand [9]aneS$_3$ in **1** adopts the [333] conformation.[41,42] Coordination to the $MeHg^+$ group resulted in a small increase of the mean transannular S···S distance from 3.451(2) to 3.489 Å and a decrease of the mean S−C−C−S torsion angle from 58.5 to 56.0°. The maximum change of an individual torsion angle was −4.4° at a C−C bond and +4.6° at an S−C bond.

 © 2004 Wiley-VCH Verlag GmbH & Co. KGaA, Weinheim

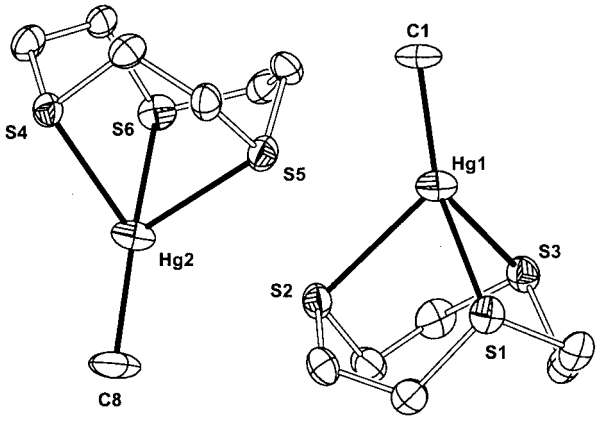

Figure 1. Ellipsoid plot (50% probability level) of the two symmetry-independent $[MeHg([9]aneS_3)]^+$ complexes in **1** showing their mutual orientation in the crystal (hydrogen atoms are omitted); bond lengths [Å] and angles [°]: Hg1−S1 2.611(2), Hg1−S2 2.768(2), Hg1−S3 2.760(2), Hg1−C1 2.080(8), Hg2−S4 2.720(2), Hg2−S5 2.732(2), Hg2−S6 2.677(2), Hg2−C8 2.075(8); S1−Hg1−S2 81.1(1), S1−Hg1−S3 79.6(1), S2−Hg1−S3 79.0(1), S1−Hg1−C1 142.7(4), S2−Hg1−C1 124.9(3), S3−Hg1−C1 127.3(4), S4−Hg2−S5 79.9(1), S4−Hg2−S6 80.4(1), S5−Hg2−S6 80.4(1), S4−Hg2−C8 132.2(3), S5−Hg2−C8 126.6(4), S6−Hg2−C8 136.4(4)

In contrast to the rare tetrahedral coordination observed in **1**, the much more common diagonal coordination of the Hg atom[29] occurs in $[MeHg([12]aneS_3)](BF_4)$ (**2**) and $[(MeHg)_2([14]aneS_4)](BF_4)_2$ (**3**). In addition to the Hg−S and Hg−C "primary" bonds, however, intermolecular "secondary" bonds to the S and F atoms exist in crystals of **2** and **3** (Figures 2 and 3). The sum of the van der Waals radii (R_{vdW}) of the participating atoms usually serves as reference point for establishing the presence of such weak metal−ligand bonds. The R_{vdW} values of Hg^{II} (1.75 Å),[43] S (1.60−2.03 Å), and F (1.30−1.38 Å)[44] give Hg···S and Hg···F van der Waals distances of 3.35−3.78 Å and 3.05−3.13 Å, respectively. The three intermolecular contacts in **2** i.e. two Hg···S and one Hg···F, are below the lower ends of these ranges. In **3**, two Hg···F contacts are at least 0.10 Å shorter than the minimum van der Waals distance. The respective S−Hg···X and C−Hg···X angles (X = S, F) fall within a range reasonable for Hg···X bonding interactions [76.6(4)−101.4(6)°]. Small distortions from linearity of the S−Hg−C angles [**2**: 168.1(6)°; **3**: 174.7(2)°] may be attributed to the influence of the "secondary" bonds. Compared with the free ligand molecules,[45,46] the basic conformations of $[12]aneS_3$ and $[14]aneS_4$ ([3333] and [3434], respectively)[41] are retained in the $MeHg^+$ complexes. The maximum change of a torsion angle between the free and the coordinated forms amounts to ±6−7° both for $[12]aneS_3$ (at S−C) and $[14]aneS_4$ (at S−C and C−C).[47] $[14]aneS_4$ in **3**, as in the free form, possesses a crystallographically imposed center of symmetry.

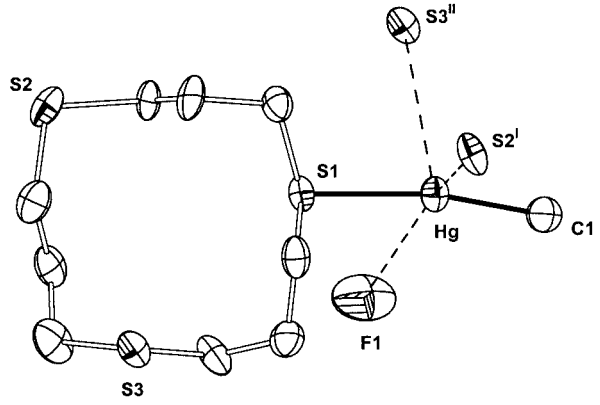

Figure 2. Ellipsoid plot (50% probability level) of the $[MeHg([12]aneS_3)]^+$ complex in crystals of **2** (hydrogen atoms are omitted); bond lengths [Å] and angles [°]: Hg−S1 2.441(4), Hg−C1 2.11(2), Hg···S2^{I} 3.176(4), Hg···S3^{II} 3.256(4), Hg···F1 2.97(1); S1−Hg−C1 168.1(6); symmetry transformations: ^{I}: 0.5 + *x*, 0.5 − *y*, 0.5 + *z*; ^{II}: 0.5 + *x*, 0.5 + *y*, *z*

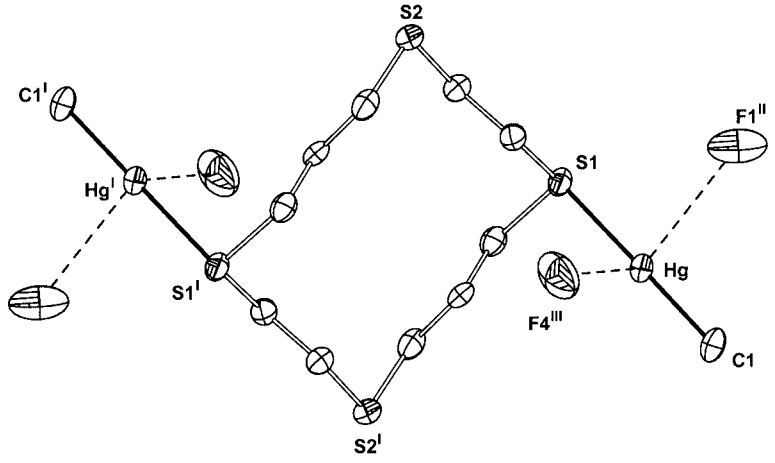

Figure 3. Ellipsoid plot (50% probability level) of the $[(MeHg)_2([14]aneS_4)]^{2+}$ complex in crystals of **3** (hydrogen atoms are omitted); bond lengths [Å] and angles [°]: Hg−S1 2.425(2), Hg−C1 2.068(7), Hg···F1^{II} 2.947(5), Hg···F4^{III} 2.946(5); S1−Hg−C1 174.7(2); symmetry transformations: ^{I}: − *x*, 2 − *y*, 2 − *z*; ^{II}: −0.5 + *x*, 1.5 − *y*, −0.5 + *z*; ^{III}: 0.5 − *x*, 0.5 + *y*, 1.5 − *z*

 © 2004 Wiley-VCH Verlag GmbH & Co. KGaA, Weinheim

Properties in Solution and Behavior Towards Competing Ligands

At room temperature, **1**−**3** showed rapid ligand exchange resulting in averaged NMR signals for coordinated and free thioether ligands. In suitable solvents, the $[MeHg([9]aneS_3)]^+$ complex of **1** is rather stable against solvolysis. This was demonstrated by an NMR experiment in which increasing amounts of $[MeHg(OH_2)](BF_4)\cdot xH_2O$ were added to a 0.06 M solution of $[9]aneS_3$ in CD_3CN. The $^2J(^1H,^{199}Hg)$ value was found to be independent of the $MeHg^+/[9]aneS_3$ molar ratio in the range of 0.5−0.95:1 and identical to the coupling constant measured for solutions of **1** in CD_3CN. At ratios > 1:1, the carbon atoms of the thioether showed a constant chemical shift identical to that observed for **1**. The two NMR quantities $^2J(^1H,^{199}Hg)$ and $\delta_C(CH_2)$ differ clearly between **1** (237.4 Hz; 30.4 ppm) and the "free" components ($[MeHg(OH_2)]^+$: ca. 260 Hz; $[9]aneS_3$: 35.4 ppm). A marked dissociation equilibrium would be sensitive to an excess of either of the two starting materials, resulting in non-constant values of the NMR parameters. The experimental results thus enabled us to conclude that $[MeHg([9]aneS_3)]^+$ does not strongly dissociate in CD_3CN.

An analogous experiment with $[12]aneS_3$ showed that the $[MeHg([12]aneS_3)]^+$ complex in **2** is markedly dissociated in CD_3CN. At a $MeHg^+/[12]aneS_3$ molar ratio of 0.5:1 the $^2J(^1H,^{199}Hg)$ coupling constant was 221.9 Hz (**2**: 224.2 Hz), indicating a more complete complexation of methylmercury due to the excess of thioether. When the ratio was increased from 1:1 to 4.5:1, a continuous increase in the $^2J(^1H,^{199}Hg)$ value resulted. However, this increase was significantly smaller than expected from the contribution of $[MeHg(OH_2)]^+$ or $[MeHg(NCCD_3)]^+$. This discrepancy can be explained by the binding of more than one methylmercury group per thioether molecule. From the $\delta_C(MeHg)$ values {8.9 ppm at $MeHg^+/[12]aneS_3$ = 1:1; 4.5 ppm at 4.5:1; $[MeHg(OH_2)]^+$: ca. 0.0 ppm} one can easily estimate that at the highest $MeHg^+/[12]aneS_3$ ratio (4.5:1) each thioether ligand binds, on average, slightly more than two $MeHg^+$ cations. Consistent with this picture, the $\delta_C(SCH_2)$ value of the ligand continuously increased from 30.3 ppm (at 1:1) to 32.6 ppm (at 4.5:1). The value for free $[12]aneS_3$ is 28.9 ppm.

Some years ago, Rabenstein suggested that the $^2J(^1H,^{199}Hg)$ coupling constant of the methylmercury group may be utilized as a general indicator of the presence of chelating ligands.[48] Indeed, it has been reported that complexes of potentially chelating ligands of the 2,2′-bipyridyl and 1,10-phenanthroline type have higher values (235.1−239.8 Hz) than those of monodentate pyridine derivatives (225.2−229.6 Hz).[49] A comparison of $[MeHg\{N(CH_2CH_2PPh_2)_3\}]^+$ (174 Hz, CN 4)[28] with $[MeHg(PR_3)]^+$ complexes (167−173 Hz, CN 2)[50] shows the same trend, albeit less pronounced. Accordingly, we observed a higher ^2J value for the tetrahedral complex $[MeHg([9]aneS_3)]^+$ (237.4 Hz) than for the two-coordinate $[MeHg([12]aneS_3)]^+$ species (224.2 Hz). The latter value compares well with coupling constants found for other two-coordinate thioether complexes, e.g. $[MeHg(SMe_2)]^+$ (220.7 Hz),[35b] [MeHg(methionineH)]$^{2+}$ (223 Hz),[32] and $[MeHg(SEt_2)]^+$ (218 Hz; see Exp. Sect.). Surprisingly, $[(MeHg)_2([14]aneS_4)]^{2+}$, which exhibits primary two-coordination in crystals of **3** (see above), has a relatively large coupling constant (231.1 Hz) which is strongly temperature-dependent. Raising the temperature from −30 to +60 °C resulted in an increase by 9.7 Hz (**1**: 1.9 Hz; **2**: 2.6 Hz). One possible explanation is that **3** is more strongly dissociated than, for example, **2**. In this case, the contribution of the dissociation product $[MeHg(NCCD_3)]^+$ would increase the observed (average) ^2J value. Another explanation is supported by the observation that the Hg−C bonds are activated towards protonolytic cleavage in $[(MeHg)_2([14]aneS_4)]^{2+}$ but not in $[MeHg(SEt_2)]^+$ (see below). It is conceivable that in solution, three-coordinate isomers of the former complex exist where the $[14]aneS_4$ ligand forms five-membered HgS_2C_2 chelate rings. This binding situation has a precedent in the complex $[(HgCl_2)_2([14]aneS_4)]$, in which the thioether is simultaneously coordinated to two $HgCl_2$ moieties.[51] Higher temperatures may favor the accompanying ligand conformations which are probably energetically less favored than the one observed in crystalline **3**.

The ^1H NMR spectrum of **1** at −30 °C shows that the tetrahedral structure observed in the solid state is retained in solution. The signal of the CH_2 groups forms a characteristic AA′BB′ (or AA′XX′) pattern[52] in accordance with the presence of three five-membered chelate rings which rapidly alternate between the λ and δ conformations (Scheme 1).

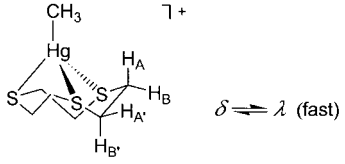

Scheme 1

Upon raising the temperature, this pattern collapses into a broad and finally, at 60 °C, a sharp singlet, obviously because of fast exchange of the thioether ligand. Between −30 °C and room temperature, $^2J(^1H,^{199}Hg)$ (see above) and the coordination-induced chemical shifts of **1** are practically temperature-independent. For example, the relative shift of the CH_2 groups $\Delta\delta_C = \delta_C(\text{coordinated}) - \delta_C(\text{free ligand})$ has a constant value of −5.0 ppm in CD_3CN. It can therefore be concluded that the tetrahedral structure is also present at room temperature. In the room temperature ^1H and ^{13}C NMR spectra of **2** and **3**, the number of observed resonances is less than would be expected from the solid-state structures. This can be explained either by fast thioether ligand exchange as in the case of **1**, fast intramolecular migration of the $MeHg^+$ group(s) at the macrocycle via intermediate chelates, or both. At −30 °C, the number and multiplicity of the signals remain unchanged. Thus, at this

 © 2004 Wiley-VCH Verlag GmbH & Co. KGaA, Weinheim

temperature, at least one of these processes cannot be "frozen" as opposed to the ligand exchange in **1**.

The relative stability of $[MeHg([9]aneS_3)]^+$ towards a number of neutral or monoanionic potential ligands, $L^{(-)}$, was studied by NMR spectroscopy. In this study, fast ligand exchange at room temperature proved beneficial because it resulted in only one ^{13}C NMR signal for mixtures of coordinated and released $[9]aneS_3$. The position of this signal between the two extremes, δ_C(coordinated) = 29.5 ppm and δ_C(free ligand) = 33.9 ppm, gave a qualitative indication of the position of equilibrium [Equation (2)].

$$[MeHg([9]aneS_3)]^+ + L^{(-)} \leftrightarrows [MeHgL]^{(+)} + [9]aneS_3 \quad (2)$$

The δ_C values are given for solutions in $[D_6]$DMSO, which was used for solubility reasons. The solutions were initially 50 mM in each of the two components **1** and $L^{(-)}$. L^- anions were introduced as their Et_4N^+ salts. It appeared that the position of the equilibrium according to Equation (2) was far to the left side when L^- was an oxo anion with a largely delocalized charge such as $CF_3SO_3^-$, *p*-$CH_3C_6H_4SO_3^-$ or NO_3^-. With $L^{(-)} = CH_3CO_2^-$, F^-, Cl^-, Br^-, I^- or PPh_3, however, complete substitution of the thioether ligand was observed. An intermediate situation occurred with $L^{(-)} = CF_3CO_2^-$ or NEt_3 where the equilibrium concentrations of $[MeHg([9]aneS_3)]^+$ and $[MeHgL]^{(+)}$ were of the same order of magnitude. As expected, the monodentate ligand $[12]aneS_3$ cannot displace the tridentate $[9]aneS_3$ (experiment conducted in CD_3CN). In summary, it can be concluded that $[9]aneS_3$ is an unusually strong ligand for $MeHg^+$ when compared with other thioethers, but still a rather weak ligand on an absolute scale, comparable for example with trifluoroacetate.

Hypothetical Reaction Mechanism of Organomercurial Lyase

The bacterial enzyme organomercurial lyase catalyzes the simple reaction shown in Equation (3) (R = alkyl, aryl). A model for the reaction mechanism of this enzyme was proposed some years ago[20,27] (see Introduction) and has very recently been refined.[53] It consists of at least four steps (Scheme 2).

$$RHg^+ + H^+ \rightarrow Hg^{2+} + RH \quad (3)$$

Step 1: Enz(-SH)$_2$ + RHg(SR') ⇌ HS-Enz-SHgR + R'SH

Step 2: HS-Enz-SHgR ⟶ Enz-S$_2$Hg + RH

Step 3: Enz-S$_2$Hg + R'SH ⇌ HS-Enz-SHg(SR')

Step 4: HS-Enz-SHg(SR') + R'SH ⇌ Enz(-SH)$_2$ + Hg(SR')$_2$

Scheme 2. Reaction steps in the mechanism of organomercurial lyase (Enz = enzyme)

In the first step, a cysteinyl-SH group of the enzyme protonates and displaces an exogenous thiolate, such as the anion of cysteine or glutathione (R′SH), thereby binding the RHg^+ cation at the active site. There the key step follows, namely the protonolytic Hg−C bond cleavage, in which a second SH group of the enzyme is involved (step 2). In the last two steps, exogenous thiolates coordinate to the product Hg^{2+} and finally remove it from the enzyme. Pitts and Summers proposed that Cys159[54] could be the primary ligand for the substrate RHg^+ (step 1), while Cys96 donates the proton in step 2.[53] They also pointed out that further amino acid residues, for example Tyr93 and Cys117, are possible candidates as ligands and/or proton donors. The latter is also one of three highly conserved cysteines, besides Cys96 and Cys159. However, there are indications that Cys117 may have no catalytic function.

From the viewpoint of coordination chemistry, step 2 is the most intriguing one. It raises the question of how the Hg−C bond is activated for protonolysis. From model studies on phosphane[28] and thioether complexes (this work), it seems less likely that sufficient activation of the Hg−C bond is possible in the binding situation depicted in Scheme 3 (A). Here, Cys96 can only act as a weak thiol donor and has a spatial orientation typical of secondary ligands. Scheme 3 (B) shows the original proposal[20,27] extended by recent biochemical results.[53] The mercury atom is three-coordinate, and therefore an enhanced polarity and a significant activation of the Hg−C bond may be expected. In Scheme 3 (C) we suggest a model that carries features of both previous ones and takes into account the occurrence of several conserved OH-containing amino acid residues in the enzymes. In this model, activation and protonation depend on the participation of Y−OH, which represents an alcoholic or a phenolic amino acid residue. Alternatively Y−OH could be a water molecule, which may be involved in hydrogen bonding to an OH-containing side chain. The oxygen atom of Y−OH simultaneously serves as proton acceptor (from Cys96−SH) and donor (to R^-). Proton withdrawal from Cys96−SH imposes thiolate character on the sulfur atom. This, together with the overall spatial arrangement, would allow the formation of a second primary Hg−S bond. Candidates for Y−OH include the conserved residues Thr77, Thr81, Tyr93, Ser115, and Thr120. In addition, the ligand AA−X^- (shown in Scheme 3, B) could also be present here. The model in Scheme 3 (C) is purely hypothetical but it is supported by results of quantum chemical calculations, which are presented below. It might be tested experimentally on suitable site-directed mutants.

Protonolysis of Hg−C Bonds in Methylmercury Thioether Complexes

The four-coordinate complex $[MeHg([9]aneS_3)]^+$ offered the opportunity of studying, for the first time, the effect of multiple sulfur ligation on the reactivity of the Hg−C bond. The very strong Brønsted acid CF_3SO_3H in $[D_3]$nitromethane was used as proton donor.[55] An additional equivalent of $[9]aneS_3$ was employed in order to trap the reaction product Hg^{2+} as $[Hg([9]aneS_3)_2]^{2+}$. After the protonolysis step, the thioether is thus functionally similar to the exogenous thiols in the mechanism of organomercurial lyase

 © 2004 Wiley-VCH Verlag GmbH & Co. KGaA, Weinheim

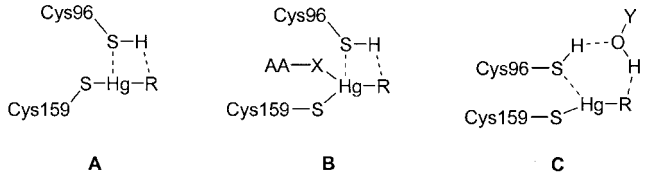

Scheme 3. Proposals for the key step of the reaction mechanism of organomercurial lyase; A: with only Cys96 and Cys159 being involved; B: with a further primary ligand $AA-X^-$, for example Tyr93 (X = O) or Cys117 (X = S); C: with participation of an additional amino acid (or water) Y–OH as a simultaneous proton donor and acceptor

(steps 3 and 4). The overall reaction can be expressed by Equation (4).

$$[MeHg([9]aneS_3)]^+ + CF_3SO_3H + [9]aneS_3 \rightarrow [Hg([9]aneS_3)_2]^{2+} + CF_3SO_3^- + CH_4 \quad (4)$$

Methane was identified as one of the reaction products by using deuterated acid. In the CF_3SO_3D-containing system, a mixture of CH_3D and CH_4 formed due to the presence of traces of H_2O (see below). For CH_3D we measured $^2J(H,D) = 1.9$ Hz and a deuterium isotope effect $\delta_H(CH_3D) - \delta_H(CH_4) = -15.3$ ppb in [D$_3$]nitromethane. These results are in good agreement with very accurately measured values in different solvents, for example in [D$_6$]-acetone: 1.9361 ± 0.0008 Hz and −15.555 ± 0.002 ppb.[56] The reaction product $[Hg([9]aneS_3)_2]^{2+}$ could be isolated as crystalline $[Hg([9]aneS_3)_2](BF_4)_2 \cdot 2\,CH_3CN$ (**4**) when the reaction was carried out in acetonitrile with HBF_4 instead of CF_3SO_3H [Equation (5)].

$$[MeHg([9]aneS_3)](BF_4) + HBF_4 + [9]aneS_3 \xrightarrow{CH_3CN} [Hg([9]aneS_3)_2](BF_4)_2 \cdot 2CH_3CN + CH_4 \quad (5)$$

Compound **4** was obtained in 72% yield. Its identity was confirmed by comparison with a sample that had been prepared independently from $HgPh_2$, HBF_4, and [9]aneS$_3$. Compound **4** was characterized, inter alia, by an X-ray structural analysis. In the crystals, the $[Hg([9]aneS_3)_2]^{2+}$ cation is located on a crystallographic center of inversion. The six sulfur atoms form a distorted octahedral coordination environment around the metal atom (see Figure 4). The molecular structure will not be further discussed here, since it is similar to those of other $[Hg([9]aneS_3)_2]^{2+}$ salts whose structures have already been described in the literature.[57]

The progress of the reaction according to Equation (4) was monitored by NMR spectroscopy, but attempts to determine kinetic data were unsuccessful because the measurements were impaired by unavoidable traces of water (ca. 0.3 equiv.). The effect of water could be demonstrated by intentionally adding 1 equiv., which almost entirely suppressed the protonolysis reaction. However, as the water content was the same in all experiments, it was possible to obtain semi-quantitative values to compare the relative reactivities of different $MeHg^+$ complexes. We found for example, that under the conditions described in the Exp. Sect., the degree of protonolysis reached ca. 25% for both **1** and **3** after 1 h. In contrast, $[MeHg(SEt_2)]^+$ and MeHgCl showed no detectable reaction even after 24 h. MeHgCl is known to be resistant towards strong acids; concentrated hydrochloric acid, for example, causes less than 1% protonolysis after 100 min.[58] This is despite the fact that chloride forms a stronger 1:1 $MeHg^+$ complex than [9]aneS$_3$, as our competition experiments have shown (see above). It therefore seems very likely that the higher coordination number in $[MeHg([9]aneS_3)]^+$ compared with MeHgCl is the most crucial factor in Hg–C bond activation. The large difference in reactivity between $[(MeHg)_2([14]aneS_4)]^{2+}$, which is two-coordinate in crystals of **3**, and $[MeHg(SEt_2)]^+$ appears to contradict this conjecture. However, the $^2J(^1H,^{199}Hg)$ value indicates that in solutions of **3**, the coordination number of mercury may exceed 2, as already discussed. In order to better understand the role of the coordination number, quantum chemical calculations were carried out.

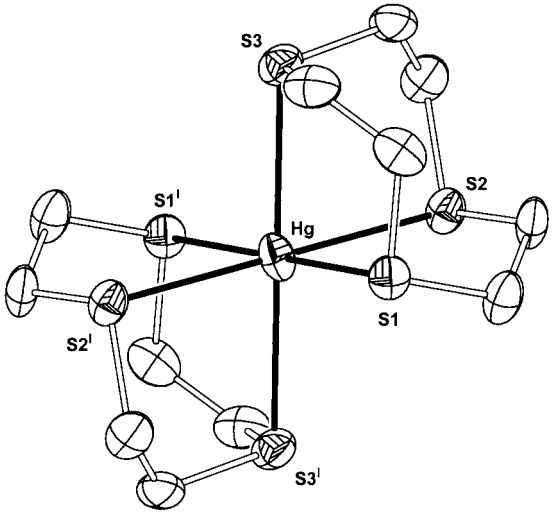

Figure 4. Ellipsoid plot (50% probability level) of the $[Hg([9]aneS_3)_2]^{2+}$ complex in crystals of **4** (hydrogen atoms are omitted); bond lengths [Å] and angles [°]: Hg–S1 2.677(1), Hg–S2 2.660(1), Hg–S3 2.711(1); S1–Hg–S2 83.69(3), S1–Hg–S3 82.49(3), S1–Hg–S1^I 180.0, S1–Hg–S2^I 96.31(3), S1–Hg–S3^I 97.51(3), S2–Hg–S3 83.14(3), S2–Hg–S2^I 180.0, S2–Hg–S3^I 96.86(3), S3–Hg–S3^I 180.0; symmetry transformation: ^{I}: $-x, 1-y, -z$

Results of Quantum Chemical Calculations

In the following, structural properties[59] such as metrical data as well as NMR chemical shifts and mechanistic pathways for Hg–C bond activation[60] have been examined. In order to obtain reliable data, for example on coordination-induced chemical shifts, it is of the utmost importance to find a method/basis set combination that allows the accurate description of the molecules studied herein. In a first attempt, we therefore employed several ab initio and density functional theoretical approaches to reproduce the structure of the $[MeHg([9]aneS_3)]^+$ cation of **1**, the main focus

 © 2004 Wiley-VCH Verlag GmbH & Co. KGaA, Weinheim

Table 1. Metal−ligand bond lengths [Å] in the complex $[MeHg([9]aneS_3)]^+$, determined at different levels of theory, compared with the experimental values

Method	Hg−C	Hg−S
X-ray diffraction	2.075(8), 2.080(8)	2.611(2)−2.768(2) (mean: 2.711)
AM1	2.057	2.738−2.752
PM3	2.076	2.590
B3LYP/LANL2DZ	2.237	2.986−2.997
B3LYP/SDD + SDD ECP Hg	2.143	2.886−2.912
B3LYP/SDD + SDD ECP Hg, 6-31G(d) C,H,S	2.138	2.856−2.864
BP86/SDD + SDD ECP Hg, 6-31G(d) C,H,S	2.134	2.839−2.844
B3LYP/SDD + SDD ECP Hg, SDD + 6-31G(d) C,H,S	2.137	2.858−2.870
B3LYP/SDD + SDD ECP Hg, SDD + 6-31+G(d,p) C,H,S	2.136	2.856−2.866
MP2/SDD + SDD ECP Hg, 6-31G(d) C,H,S	2.110	2.771−2.776
MP2/SDD + SDD ECP Hg, 6-31+G(d,p) C,H,S [a]	2.111	2.768−2.774

[a] In the discussion this level of theory is denoted MP2/I.

being on the Hg−C and Hg−S bond lengths. Table 1 summarizes the results. In each case, the basic structural feature of the complex, i.e. the tetrahedral coordination of mercury, is reproduced. The necessity of including a large basis set as well as an effective core potential can be clearly seen from the DFT calculations.[61] However, the Hg−S bonds were still much too long. Only the treatment at the correlated level[62] gave good agreement for these distances. Therefore the last method from Table 1 was used for the subsequent NMR calculation. Interestingly, the bond lengths were also well reproduced by the AM1 method. However, despite the good semiempirical description of the experimental structure, all evaluated ab initio calculations of NMR chemical shifts based on both AM1 and PM3 geometries failed to give satisfactory results.

As mentioned before, a reliable structure is indispensable for the evaluation of NMR chemical shifts in general,[63] and for organomercury compounds in particular.[64] The approach used herein applied the MP2-GIAO method[65] together with the SDD basis set and an ECP on mercury,[66] and the 6-31+G(d,p) basis set[67] on the remaining atoms based on the MP2-optimized geometries of $[MeHg([9]aneS_3)]^+$ and $[9]aneS_3$. Experimentally, a coordination-induced shift of −5.0 ppm (from 35.4 to 30.4 ppm) was observed for the CH_2 carbon atoms of the thioether ligand (see above). Such a high-field shift is perhaps counter-intuitive. However, it was reproduced quite accurately by our theoretical model: the averaged ^{13}C NMR shift changed by −7.4 ppm (from 38.9 to 31.5 ppm) when $[9]aneS_3$ underwent coordination. The ^{13}C NMR signal position of the methanido ligand of $[MeHg([9]aneS_3)]^+$, which has been found experimentally at 0.7 ppm, was also satisfactorily reproduced by theory (at $\delta = -3.1$ ppm).

The protonolytic cleavage of $Hg-CH_3$ bonds by trifluoromethanesulfonic acid has been investigated at several levels of theory (for pertinent experimental results see above). This includes the transition state for the proton transfer from CF_3SO_3H to methylmercury complexes of the type $[MeHgL]^{+\text{ or }0}$ leading to methane and, initially,

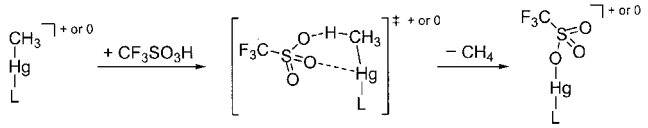

Scheme 4. Pathway of the reaction between $[MeHgL]^{+\text{ or }0}$ and trifluoromethanesulfonic acid (L = Cl^-, SEt_2, $MeSCH_2CH_2SMe$, or $[9]aneS_3$)

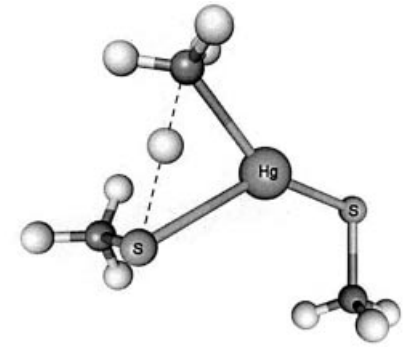

TS1

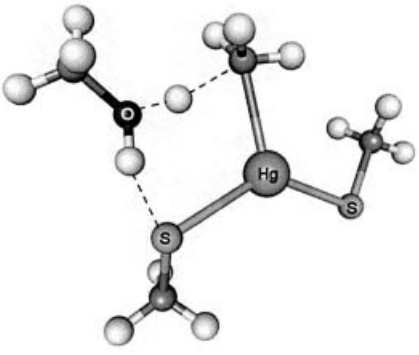

TS2

Figure 5. MP2/I-calculated transition states for the protonolytic Hg−C bond cleavage in MeHg(SMe) by methanethiol with (TS2), and without (TS1) assistance by methanol

 © 2004 Wiley-VCH Verlag GmbH & Co. KGaA, Weinheim

$[(CF_3SO_3)HgL]^{+\text{ or }0}$ (Scheme 4). The latter can further react with another L to yield $[HgL_2]^{2+\text{ or }0}$.

The results of the MP2/I calculations (see Table 1 for basis set explanation) show that the hydrogen transfer activation barriers for the two complexes with digonal mercury coordination are similar, namely 23 kcal·mol^{-1} for MeHgCl and 20 kcal·mol^{-1} for $[MeHg(SEt_2)]^+$. Significantly lower activation barriers were found for the complexes with higher coordination numbers of mercury: 14 kcal·mol^{-1} for $[MeHg(MeSCH_2CH_2SMe)]^+$ (CN 3) and 12 kcal·mol^{-1} for $[MeHg([9]aneS_3)]^+$ (CN 4). This confirms the above described experimental finding that multiple sulfur ligation activates Hg−CH_3 bonds towards protonolytic cleavage. The possible relevance for the enzymatic reaction mechanism is obvious.

Finally, we sought an answer for the possible involvement of OH-containing amino acid residues in the enzymatic reaction mechanism. The model investigated consists of methylmercury methanethiolate i.e. MeHg(SMe), to which a proton is transferred from methanethiol, either directly or by assistance from methanol. Our model corresponds to the situations depicted in Scheme 3 (A and C). Optimization of the two proton transfer transition states at the MP2/I level of theory (Figure 5) demonstrates a clear preference of 14 kcal·mol^{-1} for the six-membered transition structure TS2 which involves the additional hydroxy group. The activation energies for the two pathways are 39 and 25 kcal·mol^{-1}, respectively. Although these values are still high for an enzymatic reaction this model shows, that the involvement of OH groups can significantly lower the activation barrier for protonolytic Hg−C bond cleavage, and should therefore be considered when discussing possible reaction mechanisms of organomercurial lyase.

Conclusions

The following are the principal results and conclusions of this work: (i) Complexes between the methylmercury(1+) cation and the cyclic thioethers [9]aneS_3, [12]aneS_3, and [14]aneS_4 are isolable as crystalline tetrafluoroborates $[MeHg([9]aneS_3)](BF_4)$ (**1**), $[MeHg([12]aneS_3)](BF_4)$ (**2**), and $[(MeHg)_2([14]aneS_4)](BF_4)_2$ (**3**), respectively, in good yields. In **2** and **3**, Hg^{II} has an unexceptional linear coordination. In **1**, however, the thioether acts as a tridentate ligand. The resultant tetrahedral metal coordination is rarely found in organomercury compounds. (ii) The unusual coordination has a distinct influence on the reactivity of $[MeHg([9]aneS_3)]^+$. This complex is significantly more stable to substitution of its sulfur ligand than other $MeHg^+$−thioether complexes. Besides, its Hg−C bond is much more susceptible to cleavage by a strong Brønsted acid than the Hg−C bonds in linear coordinated $[MeHg(SEt_2)]^+$ or MeHgCl. Quantum chemical calculations confirm that the coordination number is an important factor in Hg−C bond activation. (iii) Our experimental and theoretical findings strengthen the hypothesis that multiple sulfur coordination, in this case by cysteinyl S atoms, plays a key role in the mechanism of organomercurial lyase. Assistance by an OH group, for example from an amino acid side chain, could further facilitate the protonolytic Hg−C bond cleavage in the enzyme's active site.

Experimental Section

Safety Precautions: Soluble mercury(II) compounds are highly toxic. In addition to the precautions routinely taken when toxic metal species are handled, further protection measures are necessary when working with methylmercury ($MeHg^+$).[10,11,68] In particular, laminate gloves that are specially designed for chemical resistance (Silver Shield) should be worn under neoprene or nitrile gloves. Disposable latex gloves are not sufficient! Medical surveillance of the mercury concentration in the blood should be considered for those repeatedly working with methylmercury compounds. Methylmercury-containing wastes can be treated with strong oxidants, for example aqua regia, to give inorganic mercury (Hg^{2+}). Using the "supertoxic" compound dimethylmercury as an Hg NMR standard is not to be recommended (see below).

Instrumentation: ^1H and $^{13}C\{^1H\}$ NMR spectra were recorded at 300 K with a Bruker DPX 300 or a DRX 500 instrument. Chemical shifts are given relative to TMS (δ = 0 ppm). $^{199}Hg\{^1H\}$ NMR spectra were recorded with the DRX 500 spectrometer at 290 K. A 0.10 M solution of $Hg(ClO_4)_2$ in 0.10 M perchloric acid in D_2O served as an external standard.[69,70] The standard was prepared as follows: in a 1-mL volumetric flask, D_2O was added to yellow HgO (21.7 mg, 0.100 mmol) and $DClO_4$ (26.4 μL of a 68% solution in D_2O, ρ = 1.694 g·cm^{-3}, 0.300 mmol); after ca. 30 min, the HgO had completely dissolved, and the flask was filled to the mark. ^{199}Hg chemical shifts were referenced to neat $HgMe_2$ (δ_{Hg} = 0 ppm) with this solution (δ_{Hg} = −2250 ppm on the $HgMe_2$ scale). IR spectra (KBr pellets) were obtained with a Bio-Rad FTS 7PC spectrometer. Mass spectra were measured with a Finnigan MAT 212 instrument. Melting points were determined in unsealed glass capillaries. Elemental analyses were performed by the Mikroanalytisches Labor Pascher, Remagen (Germany).

Starting Materials: The ligand 1,5,9-trithiacyclododecane ([12]aneS_3) was prepared according to a literature method starting from bis(3-hydroxypropyl) sulfide.[45] The other starting materials, including methylmercury hydroxide (1 M aqueous solution, Alfa Aesar), were purchased from commercial sources and used as received. The solvents were of reagent grade.

Preparation of $[MeHg([9]aneS_3)](BF_4)$ (1): HBF_4 (150 μL of a 50% aqueous solution, ρ = 1.38 g·cm^{-3}, 1.2 mmol) was added to MeHgOH (1.00 mL of a 1 M aqueous solution, 1.0 mmol). After 12 h, the solution was concentrated in vacuo to give a colorless oil, which was redissolved in tetrahydrofuran (2 mL). A solution of [9]aneS_3 (180 mg, 1.00 mmol) in tetrahydrofuran (5 mL) was added dropwise whilst stirring. A white, microcrystalline solid formed immediately. After stirring for 12 h, the reaction was complete, and the solid was collected on a glass filter, washed with tetrahydrofuran and dried under vacuum. Yield: 412 mg (85%). M.p. ca. 190 °C (dec.). ^1H NMR (300 MHz, CD_3CN, 40 mM): δ = 1.09 [s with satellites, $^2J(^1H,^{199}Hg)$ = 237.4 Hz, 3 H; $HgCH_3$], 3.09 (br. s, 12 H, CH_2) ppm. ^{13}C NMR (75.5 MHz, CD_3CN, 40 mM): δ = 0.7 ($HgCH_3$, superposed by solvent signal[71]), 30.4 (CH_2) ppm. ^{199}Hg NMR (89.6 MHz, CD_3CN, 40 mM): δ = −194 ppm. IR: $\tilde{\nu}$ = 2920 (w), 1449 (m), 1410 (m), 1287 (m), 1161 (w), 1144 (w), 1047 (s, br), 1036 (s, br), 926 (m), 889 (m), 816 (m), 783 (m), 521 cm^{-1} (m). MS

 © 2004 Wiley-VCH Verlag GmbH & Co. KGaA, Weinheim

(CI, isobutane): *m/z* (%) = 397 (2) $[MeHg([9]aneS_3)]^+$, 181 (100) $[[9]aneS_3 + H]^+$. $C_7H_{15}BF_4HgS_3$ (482.8): calcd. C 17.41, H 3.13, Hg 41.55, S 19.93; found C 17.35, H 3.03, Hg 41.2, S 19.8.

Preparation of $[MeHg([12]aneS_3)](BF_4)$ (2): HBF_4 (75 μL of a 50% aqueous solution, ρ = 1.38 g·cm^{-3}, 0.6 mmol) was added to MeHgOH (0.50 mL of a 1 M aqueous solution, 0.5 mmol). After 12 h, the solution was concentrated in vacuo to give a colorless oil, to which $[12]aneS_3$ (111 mg, 0.50 mmol), dissolved in acetonitrile (5 mL), was added. The reaction flask was connected to another flask that contained diethyl ether. During the next 7 d the diethyl ether was allowed to diffuse into the reaction mixture through the gas phase. A colorless, crystalline solid formed, which was collected on a glass filter, washed with tetrahydrofuran and dried under vacuum. Yield: 179 mg (68%). M.p. ca. 166 °C (dec.). ^{1}H NMR (300 MHz, CD_3CN): δ = 1.11 [s with satellites, $^2J(^1H,^{199}Hg)$ = 224.2 Hz, 3 H, $HgCH_3$], 1.99 (quint, $^3J_{H,H}$ = 6.6 Hz, 6 H, $CH_2CH_2CH_2$), 2.93 (t, $^3J_{H,H}$ = 6.6 Hz, 12 H, SCH_2) ppm. ^{13}C NMR (75.5 MHz, CD_3CN): δ = 8.9 ($HgCH_3$), 27.0 ($CH_2CH_2CH_2$), 30.3 (SCH_2) ppm. ^{199}Hg NMR (89.6 MHz, CD_3CN, 40 mM): δ = −886 ppm. IR: ṽ = 2926 (w), 1449 (m), 1431 (m), 1416 (m), 1300 (w), 1260 (m), 1250 (m), 1177 (w), 1049 (s, br), 1030 (s, br), 793 (m), 756 (m), 519 cm^{-1} (m). MS (CI, isobutane): *m/z* (%) = 439 (4) $[MeHg([12]aneS_3)]^+$, 223 (100) $[[12]aneS_3 + H]^+$. $C_{10}H_{21}BF_4HgS_3$ (524.9): calcd. C 22.88, H 4.03, Hg 38.22, S 18.33; found C 22.88, H 3.90, Hg 38.4, S 18.3.

Preparation of $[(MeHg)_2([14]aneS_4)](BF_4)_2$ (3): HBF_4 (150 μL of a 50% aqueous solution, ρ = 1.38 g·cm^{-3}, 1.2 mmol) was added to MeHgOH (1.00 mL of a 1 M aqueous solution, 1.0 mmol). After 12 h, the solution was concentrated in vacuo to give a colorless oil, to which $[14]aneS_4$ (134 mg, 0.50 mmol), dissolved in acetonitrile (5 mL), was added. The reaction flask was connected to another flask that contained diethyl ether. During the next 4 d the diethyl ether was allowed to diffuse into the reaction mixture through the gas phase. Small, plate-like crystals formed, which were collected on a glass filter, washed with a small amount of tetrahydrofuran and dried under vacuum. Yield: 403 mg (92%). M.p. ca. 129 °C (dec.). ^{1}H NMR (500 MHz, CD_3CN): δ = 1.16 [s with satellites, $^2J(^1H,^{199}Hg)$ = 231.1 Hz, 6 H, $HgCH_3$], 2.10 (quint, $^3J_{H,H}$ = 7.3 Hz, 4 H, $CH_2CH_2CH_2$), 3.05 (t, $^3J_{H,H}$ = 7.3 Hz, 8 H, $CH_2CH_2CH_2$), 3.26 (s, 8 H, SCH_2CH_2S) ppm. ^{13}C NMR (125.8 MHz, CD_3CN): δ = 7.6 ($HgCH_3$), 30.2 ($CH_2CH_2CH_2$), 32.7 ($CH_2CH_2CH_2$), 33.3 (SCH_2CH_2S) ppm. IR: ṽ = 2942 (w, br), 1445 (m), 1287 (w), 1215 (w), 1182 (m), 1084 (s, br), 1051 (s, br), 1036 (s, br), 789 (m), 521 cm^{-1} (m). MS (CI, isobutane): *m/z* (%) = 485 (2) $[MeHg([14]aneS_4)]^+$, 351 (6) $[MeHg([7]aneS_2)]^+$,[72] 107 (100) $[C_3H_6S_2$ (dithiolane) + $H]^+$. $C_{12}H_{26}B_2F_8Hg_2S_4$ (873.4): calcd. C 16.50, H 3.00, Hg 45.93, S 14.69; found C 16.75, H 3.00, Hg 45.7, S 14.7.

Preparation of $[Hg([9]aneS_3)_2](BF_4)_2 \cdot 2\ CH_3CN$ (4). Method A: Diphenylmercury (177 mg, 0.50 mmol) and $[9]aneS_3$ (180 mg, 1.00 mmol) were dissolved in tetrahydrofuran (10 mL). Addition of HBF_4 (152 μL of a 54% solution in diethyl ether, ρ = 1.19 g·cm^{-3}, 1.1 mmol) resulted in the immediate precipitation of a white, microcrystalline solid. After 6 h, the solid was collected on a glass filter, washed with tetrahydrofuran and redissolved in acetonitrile (20 mL) in a flask, which then was connected to another flask containing diethyl ether. During the next 5 d the diethyl ether was allowed to diffuse into the solution through the gas phase. Colorless, elongated tabular crystals formed, which were collected on a glass filter, washed with tetrahydrofuran and briefly dried under vacuum. Yield: 358 mg (88%). M.p. ca. 189 °C (dec.). ^{1}H NMR (300 MHz, CD_3CN): δ = 1.96 (s, ca. 6 H, CH_3CN), 2.9−3.3 (m, 24 H, SCH_2) ppm. ^{13}C NMR (75.5 MHz, CD_3CN): δ = 28.3 (SCH_2) ppm. ^{199}Hg NMR (89.6 MHz, CD_3CN, 40 mM): δ = −305 ppm. IR: ṽ = 2911 (w), 2899 (w), 2249 (w), 1443 (m), 1408 (m), 1300 (sh), 1285 (m), 1059 (s, br), 1036 (s, br), 920 (m), 883 (m), 822 (m), 534 (m), 521 (m), 424 cm^{-1} (m). MS (CI, isobutane): *m/z* (%) = 181 (100) $[[9]aneS_3 + H]^+$, 121 (97) $[C_4H_8S_2$ (dithiane) + $H]^+$. $C_{16}H_{30}B_2F_8HgN_2S_6$ (817.0): calcd. C 23.52, H 3.70, Hg 24.55, N 3.43, S 23.55; found C 23.58, H 3.57, Hg 25.0, N 3.15, S 23.9. **Method B:** HBF_4 (136 μL of a 54% solution in diethyl ether, ρ = 1.19 g·cm^{-3}, 1.0 mmol) was added whilst stirring to a solution of **1** (96 mg, 0.20 mmol) and $[9]aneS_3$ (36 mg, 0.20 mmol) in acetonitrile (5 mL). After stirring for ca. 30 min, the reaction mixture was stored at ca. 0 °C. After 24 h, colorless crystals of **4** had formed, which were collected on a glass filter, washed with a small amount of an ice-cold acetonitrile/diethyl ether mixture (1:1, v/v) and briefly dried under vacuum. Yield: 117 mg (72%). The ^{1}H and ^{13}C NMR spectra and the IR spectrum were identical to those of the material prepared by Method A.

Estimation of the Rates of Protonolysis: Solutions for the NMR measurements were prepared in a stream of dry nitrogen as a protection against atmospheric moisture. A typical experiment was conducted as follows. **1** (48.3 mg, 100 μmol) and $[9]aneS_3$ (18.0 mg, 100 μmol) were weighed out in a 1-mL volumetric flask, which had been flushed with dry nitrogen. Hexamethylbenzene (300 μL of a 50 mM stock solution in $[D_3]$nitromethane, 15.0 μmol) was then added, which served as a reference standard for determining the concentration change of methylmercury. After addition of $[D_3]$nitromethane (ca. 0.3 mL), the flask was shaken until a clear solution was obtained. Trifluoromethanesulfonic acid (98 μL of a 1.02 M stock solution in $[D_3]$nitromethane, 100 μmol) was then added. After briefly shaking, the flask was filled to the mark with $[D_3]$nitromethane. After shaking again, most of the solution was immediately transferred to an NMR tube, which had been flushed with dry nitrogen. The tube was sealed with a standard cap and parafilm. The initial ^{1}H NMR spectrum was measured typically 8 min after addition of the acid. Subsequent spectra were recorded every 3 min during the first 30 min, and later at increasingly longer time intervals. The temperature was kept at 20 °C. NMR spectroscopic data were collected over a period of ca. 6 h. The ^{1}H NMR spectra were analyzed by measuring the change of the integral intensity of the $MeHg^+$ signal (at δ = 1.10 ppm) relative to the signal of hexamethylbenzene (at δ = 2.19 ppm). For **3**, MeHgCl, and $[MeHg(SEt_2)]^+$ the sample preparations and measuring conditions were similar to those described above. However, the concentrations were adjusted less rigorously, and much longer time intervals between successive measurements were chosen because the main purpose was to establish whether the reaction had occurred at all. Between measurements, the NMR samples were stored at 20 °C. In the case of **3** (0.04 M solution), two moles of trifluoromethanesulfonic acid per mole of complex were applied and no hexamethylbenzene was added. Instead, the intensity of the $CH_2CH_2CH_2$ ligand signal served as a reference. It occurred at δ ≈ 2.45 ppm and, later, split to give an additional signal at δ = 2.36 ppm, which was assigned to the product complex(es) that formed as a result of the protonolysis. The MeHgCl solution was 0.07 M, and contained a known concentration (0.02 M) of hexamethylbenzene. $[MeHg(SEt_2)]^+$ was prepared in situ. To this end, aqueous solutions of MeHgOH (0.30 mmol) and HBF_4 (0.36 mol) were mixed. After 1 h, the reaction solvents were evaporated in vacuo. The residue was dissolved in nitromethane (ca. 0.7 mL), and the resultant solution was concentrated again. This procedure was repeated four times in order to remove water and excess HBF_4. The residue was then dissolved in $[D_3]$nitromethane (1.0 mL). Addition of 1 equiv.

 © 2004 Wiley-VCH Verlag GmbH & Co. KGaA, Weinheim

of diethyl sulfide resulted in a sharp decrease in the $^2J(^1H,^{199}Hg)$ coupling constant from 251 to 218 Hz, indicating the formation of $[MeHg(SEt_2)]^+$ {^{1}H NMR (300 MHz, [D$_3$]nitromethane): δ = 1.17 [s with satellites, $^2J(^1H,^{199}Hg)$ = 218 Hz, 3 H, $HgCH_3$], 1.55 (t, $^3J_{H,H}$ = 7.3 Hz, 6 H, CH_2CH_3), 3.49 (q, $^3J_{H,H}$ = 7.3 Hz, 4 H; SCH_2)}. Finally, 1 equiv. of trifluoromethanesulfonic acid was added. The intensity of the SCH_2 signal of the thioether served as a reference.

X-ray Crystallography: Crystal data and details of the data collections and structural refinements are summarized in Table 2. The crystals were embedded in perfluoropolyalkyl ether (viscosity 1600 cSt., m.p. −20 °C; ABCR, Karlsruhe, Germany) and placed into glass capillaries. The capillaries were sealed and transferred into the cold gas stream of a STOE IPDS area detector diffractometer. Mo-K_α radiation (λ = 0.71073 Å) was used for intensity data collection. The measuring temperature was 193 K. Numerical absorption corrections were applied to the data. The structures were solved by direct methods and refined on F^2 values. Anisotropic displacement parameters were refined for the non-hydrogen atoms, except for the C atom of the $MeHg^+$ group of compound **2**, which gave unreasonable values on anisotropic refinement. All hydrogen atoms were included in idealized positions by use of riding models. Programs used were those of the SHELX-97 software package[73] and DIAMOND for the graphical representations.[74] **1:** Single crystals were grown by diffusion of diethyl ether through the gas phase into a solution of **1** in acetonitrile. The four largest peaks in the final difference map are located at distances < 0.9 Å from the Hg atoms. The remaining difference peaks are smaller than 0.7 e·Å^{-3}. **2:** A method similar to that described above for this compound yielded suitable single-crystals. The structure was successfully refined in the non-centrosymmetric space group *Cc*. The absolute structure parameter was −0.05(2) for the final model. **3:** Suitable single crystals were obtained using a procedure similar to that described above for this compound, however with use of a 1:1 ratio of the starting materials $[MeHg(OH_2)](BF_4)\cdot xH_2O$ and [14]aneS$_4$. **4:** Suitable single crystals were obtained by slow diffusion of diethyl ether through the gas phase into a solution of $[PhHg([9]aneS_3)](BF_4)$ in acetonitrile. Under these conditions, symmetrization of the $PhHg^+$ compound to **4** and $HgPh_2$ occurred.[37a] The BF_4^- anion is disordered; its F atoms were refined on two positions with an occupancy ratio of 2:1. CCDC-207378 (**1**), -207379 (**2**), -207380 (**3**), and -207381 (**4**) contain the supplementary crystallographic data for this paper. These data can be obtained free of charge at www.ccdc.cam.ac.uk/conts/retrieving.html [or from the Cambridge Crystallographic Data Center, 12 Union Road, Cambridge CB2 1EZ, UK; Fax: (internat.) + 44-1223/336-033; Email: deposit@ccdc.cam.ac.uk].

Computational Methods: The semiempirical calculations (AM1[75] and PM3[76]) employed the program package MOPAC 2002,[77] while the ab initio and DFT calculations were performed with Gaussian 98.[78] With the exception of a single B3LYP/LANL2DZ[79] optimization, all calculations at the correlated MP2 or the DFT BP86,[80] and the hybrid functional B3LYP[81][82] levels of theory used the Stuttgart/Dresden SDD basis set and the effective core potential for Hg.[66] The remaining atoms were described with the 6-31G(d) or 6-31+G(d,p) basis sets.[67] In two cases the SDD basis sets were added to these Pople bases. Local minima and transition states were verified by determination of the number of imaginary frequencies. Details of the NMR chemical shift calculations are given in the Results and Discussion section.

Acknowledgments

We thank Prof. Anne O. Summers and Dr. Irene Wagner-Döbler for providing information about structural and mechanistic details of organomercurial lyase. We also thank Prof. Martin Kaupp for helpful discussions on the computation of chemical shifts in Hg-containing systems. Financial support from the Deutsche Forschungsgemeinschaft and generous allocation of computer time at

Table 2. Crystallographic data and details of the data collection and structure refinement for compounds **1**−**4**

	1	**2**	**3**	**4**
Empirical formula	$C_7H_{15}BF_4HgS_3$	$C_{10}H_{21}BF_4HgS_3$	$C_{12}H_{26}B_2F_8Hg_2S_4$	$C_{16}H_{30}B_2F_8HgN_2S_6$
M_r	482.8	524.9	873.4	817.0
Crystal system	monoclinic	monoclinic	monoclinic	orthorhombic
Space group	$P2_1/c$	*Cc*	$P2_1/n$	*Pbca*
a [Å]	7.7802(4)	10.306(1)	8.6904(6)	8.8396(3)
b [Å]	42.319(2)	12.449(1)	13.951(1)	21.463(1)
c [Å]	8.6996(5)	12.590(1)	9.8959(9)	15.137(1)
β [°]	109.098(6)	92.067(10)	102.86(1)	90
V [Å^3]	2706.7(2)	1614.2(2)	1169.7(2)	2871.9(3)
Z	8	4	2	4
$\rho_{calcd.}$ [g cm^{-3}]	2.369	2.160	2.480	1.890
μ(Mo-K_α) [mm^{-1}]	11.852	9.946	13.526	5.858
Crystal size [mm]	0.40 × 0.33 × 0.21	0.70 × 0.16 × 0.06	0.36 × 0.17 × 0.12	0.44 × 0.27 × 0.18
Exposures	259	139	136	200
Oscillation angle for each exposure [°]	0.7	1.4	1.4	1.0
$2\Theta_{max.}$ [°]	52.06	51.56	51.54	51.96
Completeness to $2\Theta_{max.}$ [%]	95.0	94.7	93.5	94.5
Reflections collected	19449	5868	8270	21248
Independent reflections (R_{int})	5087 (0.1899)	2872 (0.0891)	2095 (0.0651)	2662 (0.1139)
Data/restraints/parameters	5087/0/289	2872/2/167	2095/0/128	2662/0/197
*R*1 [$I > 2\sigma(I)$]	0.0448	0.0499	0.0258	0.0232
*wR*2 (all data)	0.0907	0.1323	0.0597	0.0553
Goodness-of-fit on F^2	0.983	1.024	0.940	0.922
Largest difference peak/hole [e·Å^{-3}]	+2.06/−2.35	+1.16/−1.53	+1.05/−0.84	+0.31/−0.53

 © 2004 Wiley-VCH Verlag GmbH & Co. KGaA, Weinheim

HLRN, Hannover (Germany), and APAC, Canberra (Australia), are gratefully acknowledged.

[1] C. H. Lamborg, W. F. Fitzgerald, J. O'Donnell, T. Torgersen, *Geochim. Cosmochim. Acta* **2002**, *66*, 1105−1118.

[2] United States Environmental Protection Agency, *Mercury Study Report to Congress*, vol. 3 ("Fate and Transport of Mercury in the Environment") to be found under http://www.epa.gov/oar/mercury.html, **1997**.

[3] W. F. Fitzgerald, R. P. Mason, in *Metal Ions in Biological Systems*, vol. 34 (Eds.: A. Sigel, H. Sigel), Dekker, New York, **1997**, pp. 53−111.

[4] R. P. Mason, W. F. Fitzgerald, F. M. M. Morel, *Geochim. Cosmochim. Acta* **1994**, *58*, 3191−3198.

[5] J. O. Nriagu, *Nature* **1989**, *338*, 47−49.

[6] J. O. Nriagu, J. M. Pacyna, *Nature* **1988**, *333*, 134−139.

[7] R. A. Bodaly, V. L. St. Louis, M. J. Paterson, R. J. P. Fudge, B. D. Hall, D. M. Rosenberg, J. W. M. Rudd, in *Metal Ions in Biological Systems*, vol. 34 (Eds.: A. Sigel, H. Sigel), Dekker, New York, **1997**, pp. 259−287.

[8] A. Boudou, F. Ribeyre, in *Metal Ions in Biological Systems*, vol. 34 (Eds.: A. Sigel, H. Sigel), Dekker, New York, **1997**, pp. 289−319.

[9] Committee on the Toxicological Effects of Methylmercury, National Research Council, *Toxicological Effects of Methylmercury*, National Academy Press, Washington, DC, **2000**; also to be found under http://www.nap.edu/books/0309071402/html/.

[10] D. W. Nierenberg, R. E. Nordgren, M. B. Chang, R. W. Siegler, M. B. Blayney, F. Hochberg, T. Y. Toribara, E. Cernichiari, T. Clarkson, *New Engl. J. Med.* **1998**, *338*, 1672−1676.

[11] H. Strasdeit, *Nachr. Chem. Tech. Lab.* **1998**, *46*, 846−848.

[12] United States Environmental Protection Agency, *Mercury Study Report to Congress*, vol. 5 ("Health Effects of Mercury and Mercury Compounds"), to be found under http://www.epa.gov/oar/mercury.html, **1997**.

[13] N. K. Mottet, M. E. Vahter, J. S. Charleston, L. T. Friberg, in *Metal Ions in Biological Systems*, vol. 34 (Eds.: A. Sigel, H. Sigel), Dekker, New York, **1997**, pp. 371−403.

[14] R. Hamada, K. Arimura, M. Osame, in *Metal Ions in Biological Systems*, vol. 34 (Eds.: A. Sigel, H. Sigel), Dekker, New York, **1997**, pp. 405−420.

[15] R. Hamada, M. Osame, in *Toxicology of Metals* (Ed.: L. W. Chang), CRC, Boca Raton, FL, **1996**, pp. 337−351.

[16] *The Toxicity of Methyl Mercury* (Eds.: C. U. Eccles, Z. Annau), Johns Hopkins University Press, Baltimore, **1987**.

[17] M. Schrope, *Nature* **2001**, *409*, 124.

[18] H. Strasdeit, A. von Döllen, W. Saak, M. Wilhelm, *Angew. Chem.* **2000**, *112*, 803−805; *Angew. Chem. Int. Ed.* **2000**, *39*, 784−786.

[19] L. Magos, in *Metal Ions in Biological Systems*, vol. 34 (Eds.: A. Sigel, H. Sigel), Dekker, New York, **1997**, p. 327.

[20] M. J. Moore, M. D. Distefano, L. D. Zydowsky, R. T. Cummings, C. T. Walsh, *Acc. Chem. Res.* **1990**, *23*, 301−308.

[21] In the absence of organomercurial lyase, mercury resistance is restricted to Hg^{2+} ("narrow-spectrum" resistance).

[22] S. M. Miller, in *Essays in Biochemistry*, vol. 34 (Ed.: D. P. Ballou), Portland Press, London, **1999**, pp. 17−30.

[23] A. M. Osborn, K. D. Bruce, P. Strike, D. A. Ritchie, *FEMS Microbiol. Rev.* **1997**, *19*, 239−262.

[24] J. L. Hobman, N. L. Brown, in *Metal Ions in Biological Systems*, vol. 34 (Eds.: A. Sigel, H. Sigel), Dekker, New York, **1997**, pp. 527−568.

[25] A. O. Summers, *Annu. Rev. Microbiol.* **1986**, *40*, 607−634.

[26] Transgenic plants engineered to express *merB* seem promising for the degradation of methylmercury at polluted sites; see for example: [26a] S. P. Bizily, C. L. Rugh, R. B. Meagher, *Nat. Biotechnol.* **2000**, *18*, 213−217. [26b] S. P. Bizily, C. L. Rugh, A. O. Summers, R. B. Meagher, *Proc. Natl. Acad. Sci. USA* **1999**, *96*, 6808−6813.

[27] T. P. Begley, A. E. Walts, C. T. Walsh, *Biochemistry* **1986**, *25*, 7192−7200.

[28] P. Barbaro, F. Cecconi, C. A. Ghilardi, S. Midollini, A. Orlandini, A. Vacca, *Inorg. Chem.* **1994**, *33*, 6163−6170.

[29] Tetrahedral coordination is very rare in organomercury chemistry. Instead, RHg^+ cations strongly prefer linear coordination of the Hg atom. Additional coordinate bonds occur frequently, but usually they are weak, "secondary" bonds: [29a] J. S. Casas, M. S. García-Tasende, J. Sordo, *Coord. Chem. Rev.* **1999**, *193−195*, 283−359. [29b] C. E. Holloway, M. Melník, *J. Organomet. Chem.* **1995**, *495*, 1−31.

[30] V. Barone, A. Bencini, F. Totti, M. G. Uytterhoeven, *J. Phys. Chem.* **1995**, *99*, 12743−12750.

[31] R. D. Bach, H. B. Vardhan, *J. Org. Chem.* **1986**, *51*, 1609−1610.

[32] M. T. Fairhurst, D. L. Rabenstein, *Inorg. Chem.* **1975**, *14*, 1413−1415.

[33] T. E. Jones, L. S. W. L. Sokol, D. B. Rorabacher, M. D. Glick, *J. Chem. Soc., Chem. Commun.* **1979**, 140−141.

[34] R. G. Pearson, *Inorg. Chem.* **1973**, *12*, 712−713.

[35] See for example: [35a] V. A. Nikanorov, V. I. Rozenberg, G. V. Gavrilova, O. A. Reutov, *Dokl. Akad. Nauk SSSR* **1982**, *262*, 108−113; English translation: *Dokl. Chem.* **1982**, *262*, 4−7. [35b] P. L. Goggin, R. J. Goodfellow, S. R. Haddock, J. G. Eary, *J. Chem. Soc., Dalton Trans.* **1972**, 647−653.

[36] [36a] *Cambridge Structural Database (CSD)*, version 5.24 (November 2002, 272066 entries) and updates (February−July 2003, 24361 entries). [36b] F. H. Allen, *Acta Crystallogr., Sect. B* **2002**, *58*, 380−388.

[37] [37a] M. Wilhelm, Doctoral Dissertation, University of Oldenburg, Germany, **2001**; also to be found under http://docserver.bis.uni-oldenburg.de/publikationen/dissertation/2001/wilneu01/wilneu01.html. [37b] H. Strasdeit, S. Deeken, W. Saak, M. Wilhelm, *GDCh-Jahrestagung Chemie 2001*, Würzburg, Germany, September 23−29, **2001**, Abstract WÖHLER-044. [37c] H. Strasdeit, M. Wilhelm, S. Deeken, E. Berssen, R. Koch, *35th Int. Conf. Coord. Chem.* Heidelberg, Germany, July 21−26, **2002**, Abstract P1.128.

[38] [38a] A. De Robertis, C. Foti, G. Patanè, S. Sammartano, *J. Chem. Eng. Data* **1998**, *43*, 957−960. [38b] D. L. Rabenstein, C. A. Evans, M. C. Tourangeau, M. T. Fairhurst, *Anal. Chem.* **1975**, *47*, 338−341. [38c] G. Schwarzenbach, M. Schellenberg, *Helv. Chim. Acta* **1965**, *48*, 28−46.

[39] [39a] C. A. Barradell, H. G. M. Edwards, D. N. Smith, *J. Organomet. Chem.* **1991**, *421*, 137−146. [39b] H. Schmidbaur, H.-J. Öller, S. Gamper, G. Müller, *J. Organomet. Chem.* **1990**, *394*, 757−764.

[40] R. S. Glass, G. S. Wilson, W. N. Setzer, *J. Am. Chem. Soc.* **1980**, *102*, 5068−5069.

[41] For a definition of the conformational nomenclature see: J. Dale, *Acta Chem. Scand.* **1973**, *27*, 1115−1129.

[42] A detailed conformational study of [9]aneS_3 in metal complexes is available: J. Beech, P. J. Cragg, M. G. B. Drew, *J. Chem. Soc., Dalton Trans.* **1994**, 719−729.

[43] [43a] P. Pyykkö, M. Straka, *Phys. Chem. Chem. Phys.* **2000**, *2*, 2489−2493. [43b] A. J. Canty, G. B. Deacon, *Inorg. Chim. Acta* **1980**, *45*, L225−L227. [43c] The possibility of a larger R_{vdW} value of Hg^{II} (around 2.0 Å) has been discussed, see for example: K. R. Flower, V. J. Howard, S. Naguthney, R. G. Pritchard, J. E. Warren, A. T. McGown, *Inorg. Chem.* **2002**, *41*, 1907−1912; S. S. Batsanov, *J. Chem. Soc., Dalton Trans.* **1998**, 1541−1545.

[44] Because van der Waals radii of sulfur and fluorine have been found to be anisotropic, ranges are used here instead of single values: S. C. Nyburg, C. H. Faerman, *Acta Crystallogr., Sect. B* **1985**, *41*, 274−279.

[45] S. C. Rawle, G. A. Admans, S. R. Cooper, *J. Chem. Soc., Dalton Trans.* **1988**, 93−96.

[46] R. E. DeSimone, M. D. Glick, *J. Am. Chem. Soc.* **1976**, *98*, 762−767.

 © 2004 Wiley-VCH Verlag GmbH & Co. KGaA, Weinheim

[47] Only the non-disordered α and β_1 molecules of free [14]aneS$_4$ were used for comparison, see ref.[46]
[48] D. L. Rabenstein, *Acc. Chem. Res.* **1978**, *11*, 100−107.
[49] A. J. Canty, A. Marker, *Inorg. Chem.* **1976**, *15*, 425−430.
[50] [50a] P. L. Goggin, R. J. Goodfellow, D. M. McEwan, A. J. Griffiths, K. Kessler, *J. Chem. Res. (S)* **1979**, 194−195; *J. Chem. Res. (M)* **1979**, 2315−2343. [50b] K. Stanley, J. Martin, J. Schnittker, R. Smith, M. C. Baird, *Inorg. Chim. Acta* **1978**, *27*, L111−L113. [50c] H. Schmidbaur, K.-H. Räthlein, *Chem. Ber.* **1973**, *106*, 2491−2507.
[51] N. W. Alcock, N. Herron, P. Moore, *J. Chem. Soc., Dalton Trans.* **1978**, 394−399.
[52] See for example: H. Friebolin, *Basic One- and Two-Dimensional NMR Spectroscopy*, 3rd ed., Wiley-VCH, Weinheim, **1998**, p. 124f.
[53] K. E. Pitts, A. O. Summers, *Biochemistry* **2002**, *41*, 10287−10296.
[54] The numbering of the amino acid residues refers to the organomercurial lyase that is encoded by plasmid R831b, see ref.[53]
[55] T. Fujinaga, I. Sakamoto, *J. Electroanal. Chem.* **1977**, *85*, 185−201.
[56] F. A. L. Anet, D. J. O'Leary, *Tetrahedron Lett.* **1989**, *30*, 2755−2758.
[57] [57a] J. Pickardt, J. Shen, *Z. Naturforsch., Teil B* **1993**, *48*, 969−972. [57b] W. N. Setzer, Q. Guo, G. J. Grant, J. L. Hubbard, R. S. Glass, D. G. VanDerveer, *Heteroat. Chem.* **1990**, *1*, 317−325. [57c] A. J. Blake, A. J. Holder, T. I. Hyde, G. Reid, M. Schröder, *Polyhedron* **1989**, *8*, 2041−2045.
[58] C. Walsh, T. Begley, A. Walts, *Pure Appl. Chem.* **1987**, *59*, 295−298.
[59] For theoretical studies on mercury-second-row element complexes see: [59a] Ref.[30][59b]T. Rambusch, K. Hollmann-Gloe, K. Gloe, *J. Prakt. Chem.* **1999**, *341*, 202−217.
[60] For theoretical studies on Hg−C bond cleavage see: [60a] V. Barone, A. Bencini, F. Totti, M. G. Uytterhoeven, *Organometallics* **1996**, *15*, 1465−1469. [60b] V. Barone, A. Bencini, F. Totti, M. G. Uytterhoeven, *Int. J. Quantum Chem.* **1997**, *61*, 361−367. [60c] J. A. Tossell, *J. Phys. Chem. A* **1998**, *102*, 3587−3591.
[61] [61a] J. A. Altmann, N. C. Handy, V. E. Ingamells, *Int. J. Quantum Chem.* **1996**, *57*, 533−542. [61b] J. A. Altmann, N. C. Handy, *Phys. Chem. Chem. Phys.* **1999**, *1*, 5529−5536.
[62] M. Kaupp, *Chem. Ber.* **1996**, *129*, 535−544.
[63] G. Schreckenbach, T. Ziegler, *Theor. Chem. Acc.* **1998**, *99*, 71−82.
[64] [64a] M. Kaupp, O. L. Malkina, *J. Chem. Phys.* **1998**, *108*, 3648−3659. [64b] J. Vaara, O. L. Malkina, H. Stoll, V. G. Malkin, M. Kaupp, *J. Chem. Phys.* **2001**, *114*, 61−71.
[65] Review: J. Gauss, J. F. Stanton, *Adv. Chem. Phys.* **2002**, *123*, 355−422, and references cited therein.
[66] W. Kuechle, M. Dolg, H. Stoll, H. Preuss, *Mol. Phys.* **1991**, *74*, 1245−1263.
[67] [67a] P. C. Hariharan, J. A. Pople, *Mol. Phys.* **1974**, *27*, 209−214. [67b] M. M. Francl, W. J. Pietro, W. J. Hehre, J. S. Binkley, M. S. Gordon, D. J. DeFrees, J. A. Pople, *J. Chem. Phys.* **1982**, *77*, 3654−3665.
[68] M. B. Blayney, J. S. Winn, D. W. Nierenberg, *Chem. Eng. News* **1997**, *75*, 7.
[69] B. Wrackmeyer, R. Contreras, *Annu. Rep. NMR Spectrosc.* **1992**, *24*, 267−329.
[70] T. V. O'Halloran, C. P. Singer, *^{199}Hg NMR Standards*, to be found under http://www.chem.nwu.edu/~ohallo/HgNMRStandards/index.html, **1998**.
[71] The signal position was inferred from the proton-coupled ^{13}C NMR spectrum in which the CH_3 quadruplet is only partly superposed. The $^1J(^{13}C,^1H)$ values are 138.5 Hz ($HgCH_3$) and 143.9 Hz (CH_2).
[72] The isotopic pattern unambiguously showed that this signal was not due to $[(MeHg)_2([14]aneS_4)]^{2+}$.
[73] G. M. Sheldrick, *SHELX-97*, Universität Göttingen, Göttingen, Germany, **1997**.
[74] *DIAMOND−−Visual Crystal Structure Information System*, version 2.1, Crystal Impact, Bonn, Germany, **1999**.
[75] [75a] M. J. S. Dewar, E. G. Zoebisch, E. F. Healy, J. J. P. Stewart, *J. Am. Chem. Soc.* **1985**, *107*, 3902−3909. [75b] M. J. S. Dewar, Y. C. Yuan, *Inorg. Chem.* **1990**, *29*, 3881−3890. [75c] M. J. S. Dewar, C. Jie, *Organometallics* **1989**, *8*, 1547−1549.
[76] [76a] J. J. P. Stewart, *J. Comput. Chem.* **1989**, *10*, 209−220. [76b] J. J. P. Stewart, *J. Comput. Chem.* **1991**, *12*, 320−341.
[77] J. J. P. Stewart, *MOPAC 2002*, Fujitsu Limited, Tokyo, Japan, **2002**.
[78] M. J. Frisch, G. W. Trucks, H. B. Schlegel, G. E. Scuseria, M. A. Robb, J. R. Cheeseman, V. G. Zakrzewski, J. A. Montgomery, R. E. Stratmann, J. C. Burant, S. Dapprich, J. M. Millam, A. D. Daniels, K. N. Kudin, M. C. Strain, O. Farkas, J. Tomasi, V. Barone, M. Cossi, R. Cammi, B. Mennucci, C. Pomelli, C. Adamo, S. Clifford, J. Ochterski, G. A. Petersson, P. Y. Ayala, Q. Cui, K. Morokuma, D. K. Malick, A. D. Rabuck, K. Raghavachari, J. B. Foresman, J. Cioslowski, J. V. Ortiz, B. B. Stefanov, G. Liu, A. Liashenko, P. Piskorz, I. Komaromi, R. Gomperts, R. L. Martin, D. J. Fox, T. Keith, M. A. Al-Laham, C. Y. Peng, A. Nanayakkara, C. Gonzalez, M. Challacombe, P. M. W. Gill, B. G. Johnson, W. Chen, M. W. Wong, J. L. Andres, M. Head-Gordon, E. S. Replogle, J. A. Pople, *GAUSSIAN*, Gaussian, Inc., Pittsburgh, PA, USA, **1998**.
[79] [79a] T. H. Dunning, Jr., P. J. Hay in *Modern Theoretical Chemistry*, vol. 3 ("Methods of Electronic Structure Theory") (Ed.: H. F. Schaefer, III), Plenum, New York, **1977**, p. 1−27. [79b]P. J. Hay, W. R. Wadt, *J. Chem. Phys.* **1985**, *82*, 270−283.
[80] [80a] A. D. Becke, *Phys. Rev. A* **1988**, *38*, 3098−3100. [80b] J. Perdew, *Phys. Rev. B* **1986**, *33*, 8822−8824. [80c] J. Perdew, *Phys. Rev. B* **1986**, *34*, 7406.
[81] C. Lee, W. Yang, R. G. Parr, *Phys. Rev. B* **1988**, *37*, 785−789.
[82] A. D. Becke, *J. Chem. Phys.* **1993**, *98*, 5648−5652.

Received December 5, 2003
Early View Article
Published Online April 7, 2004

 © 2004 Wiley-VCH Verlag GmbH & Co. KGaA, Weinheim

Synthesis, Crystal Structures and Electrical Conductivities of the Ionic Liquid Compounds Butyldimethylimidazolium Tetrafluoroborate, Hexafluorophosphate and Hexafluoroantimonate

Philipp Kölle[a] and Richard Dronskowski*[a]

Keywords: Electrochemistry / Ionic liquids / Packing efficiency / X-ray diffraction

The crystal structures of three very low-melting ionic liquid (IL) salts containing the 1-butyl-2,3-dimethylimidazolium cation and the fluoro anions BF_4^-, PF_6^- and SbF_6^- are reported. These are considered model compounds for ambient temperature ionic liquids, which are currently being explored as solvents for various types of synthetic reactions. All three compounds adopt significantly different structures in the solid state, highlighting the influence of counterion size in a series comprising a common cation. The crystal structures are discussed with respect to the possible existence of polar and non-polar domains, which are considered to be involved with the solvation of polar and non-polar substrates. The melting points of all three compounds are within the range 40–45 °C. A comparative measurement of conductivities of the molten salts in the vicinity of 20–50 °C has been made, including the new IL 1-allyl-2,3-dimethylimidazolium tetrafluoroborate and the widely applied 1-butyl-3-methylimidazolium tetrafluoroborate (BMIMBF_4).
(© Wiley-VCH Verlag GmbH & Co. KGaA, 69451 Weinheim, Germany, 2004)

Introduction

The solvent properties of ionic liquids (IL) have attracted a lot of interest with respect to applications as reaction media for both polar and non-polar solvates.[1a−1f] Homogeneous catalysis using organometallic or coordination compound catalysts is one prominent example where ILs based on 1,3-substituted imidazolium cations in particular have been employed, not only because of their non-volatility, but also due to their variability with respect to the possible adjustment of solvent properties.[1g] The degree of polarity can be varied by adapting the length of the 1-alkyl chain and the counterion to the desired reaction conditions. The investigation of structural properties in the liquid state requires considerable experimental effort (as for example in X-ray absorption spectroscopy[2]), and little information can be gained if heavy elements are missing. Model compounds that are crystalline at ambient temperature have therefore been used for structural investigations. It has been known for some time that salts C_nMeImX incorporating a common anion X^- will usually exhibit low melting points with medium-length alkyl chains ($n = 4-9$),[3] as in these cases crystal packing forces are not strong enough to raise melting points above 300 K. Lower chain-length salts are often readily crystallized, and structural studies have mainly focused on 1-ethyl-3-methylimidazolium (EMIM) salts with various counterions. The EMIM cation, which is asymmetric but rather small, is readily crystallized not only with high charge-density anions such as chloride, but even with hexafluorophosphate, a typical counterion for the liquid-state salts. The crystal structure of EMIMPF_6 (melting point 331 K) has been reported by Fuller et al.[4] EMIMBF_4, on the other hand, which is liquid at ambient temperature, may serve as an example for the influence of counterion size, since the higher charge density of BF_4^- vs. PF_6^- is expected to increase the Coulombic part of the lattice energy and therefore the melting point. An example of a long chain-length salt has been reported by Seddon et al. who solved the crystal structure of C_{12}MIMPF_6.[5]

Long-chain IL salts have attracted some interest due to their liquid crystalline (LC) properties. The origin for these can be found in the formation of domains, "Coulombic" layers where the ionic head-groups interact with the counterions, and "van der Waals" layers built from (anti)parallel stacking of the alkyl chains. Hexafluorophosphate salts with cations up to C_{20}MIM have been investigated by differential thermal analysis (DTA) and show one or more LC transitions. Melting to isotropic liquids occurs at rather high temperatures (>100 °C) .[5] The phase behavior of long chain-length imidazolium and pyridinium chlorides, tetrachlorocobaltates and tetrachloronickelates showing LC properties has also been reported.[6]

Larsen et al. have reported the synthesis and crystal structures of several EMIM, ethyldimethylIM, octylMIM and BDMIM alkylboranes, and the authors rationalized trends in melting points according to the packing efficiency of the asymmetrically substituted cation.[7] More recently, Dupont et al. investigated C−H-π interactions in the solid

[a] Institut für Anorganische Chemie, Rheinisch-Westfälische Technische Hochschule
52056 Aachen, Germany
E-mail: drons@HAL9000.ac.rwth-aachen.de

state and in solution of BMIM tetraphenylborate,[8] and van den Broeke et al. introduced substituents at the phenyl rings of this salt and reported their influence on the structural and physical properties.[9]

A thorough investigation into the electrochemical and rheological properties of various substituted imidazolium/anion combinations by Bonhôte et al.[10] revealed some general trends for melting/glass transition points. One of the most notable findings in this respect was that methylation at the 2-position of the heteroaromatic ring generally raised melting points by more than 50 K. This was observed even with anions which were expected to be strong hydrogen-bond acceptors for the "acidic" hydrogen at C(2) and for which the opposite effect might have been expected. The influence of ion size and viscosity of IL melts on their electric conductivity is also reported by these authors and was more recently investigated by McEwen et al.[11] Increasing the volume of either cation or anion has generally been found to result in lower absolute values and higher activation energies for conductivity.

The present work is focused on the influence of counterion size on the solid-state structures and liquid-state mobilities of IL compounds comprising the medium chain-length cation 1-butyl-2,3-dimethylimidazolium (BDMIM).

Results and Discussion

All IL compounds reported in this work contain the cation 1-butyl-2,3-dimethylimidazolium (BDMIM). The cation adopts slightly different conformations in the different compounds with respect to the butyl chain, which is kinked from the plane of the imidazolium ring in all cases studied here.

The two crystallographically independent BF_4^- ions in the structure of BDMIMBF_4 **I** were both found to be disordered. The type of disorder was investigated by means of three-dimensional Fourier maps, and is depicted in Figure 1. For BF_4^-(1), the two different orientations are related by a (non-crystallographic) mirror plane and for BF_4^-(2) by a (non-crystallographic) threefold axis, which corresponds to the B(2)−F(9) bond. For both BF_4^- sites, the type of disorder appears to be maintained at 298 K as suggested by the corresponding Fourier maps. Disorder is not observed with the cations, thus apparent disorder originating from the use of twinned data can be excluded.

The title compound **I** is the first IL tetrafluoroborate to be structurally characterized. The structure can be described as being composed of two different types of double layers extending in the crystallographic (0 1 0) plane (Figure 2). The anionic parts of these two layers are very similar, showing the tetrahedral ions in two different orientations with shortest center-to-center distances of 690 pm within the layers. The cationic part composed of the two crystallographically independent imidazolium cations is, however, markedly different for the two double layers, leading to different environments for the BF_4^- sites. The butyl chains extend roughly in the direction of the *b* axis, away from the charged centers of the layers. Pairwise shortest contacts of 402 and 409 pm between the outer methyl/methylene groups of the butyl chain are found along the *b* axis, which roughly correspond to the sum of the van der Waals radii.

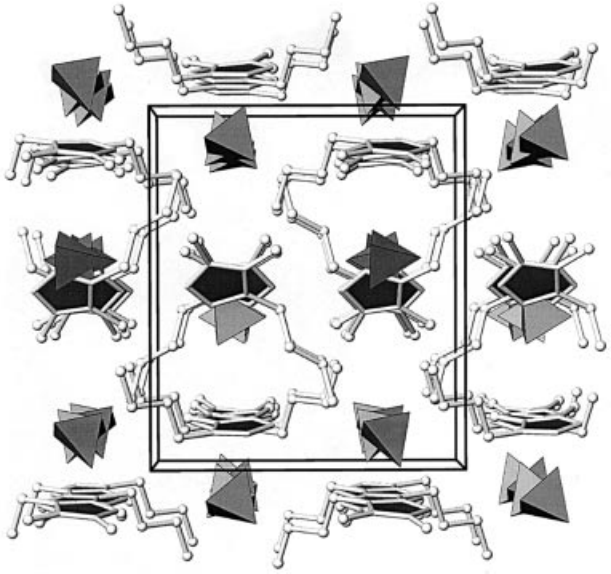

Figure 2. View of the crystal structure of BDMIMBF_4 along the crystallographic *c*-axis; BF_4^- ions are shown as grey tetrahedra; all hydrogen atoms of the imidazolium cation have been omitted for clarity; anions and cations in the central double layer are crystallographically equivalent, a second set of crystallographically equivalent molecules can be distinguished above and below

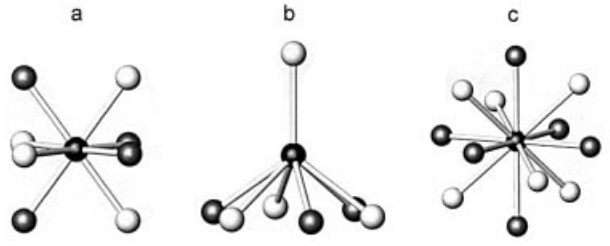

Figure 1. Disorder observed for the BF_4^- ions in BDMIMBF_4 at 213 K (a, b) and for the PF_6^- ions at 298 K in BDMIM PF_6 (c), as observed from difference Fourier syntheses; the two disorder components are shown with different shadings

Pronounced anisotropy as found in **I** has been observed in crystal structures of ionic liquid salts before. Relatively high-melting EMIM halides exhibit hydrogen-bonded 3-D networks.[12] The formation of layered structures recently reported for BMIMCl is, however, promoted by strong hydrogen bonds between cation and anion.[13,14] Intermolecular H···F interactions are considered to be very weak in compounds of the type reported here as indicated by the crystallographic disorder observed for BF_4^- and PF_6^-. This issue is discussed further below. Consequently, arrangements of the BDMIM cation and the low charge-density fluoro

 © 2004 Wiley-VCH Verlag GmbH & Co. KGaA, Weinheim

anions result from a balance of weak Coulombic and dispersive interactions, whereas hydrogen bonding in IL chlorides is always strong, as indicated by their much higher melting points. Compound **I** exhibits channels between the cationic layers where the anions are accommodated, similar to those observed in BMIMCl. In the former case, the "structure-directing principle" (close packing of the molecules maximizing non-directional interactions) leads to flat layers which, on the other hand, are corrugated in the BMIMCl structure, driven by maximizing the strongly directional C−H···Cl H-bonds.

The coordination environments of the BF_4^- ions are depicted in Figure 3. Closest distances between fluoride and C/N atoms of the ring are summarized in Table 1. Carbon/nitrogen-fluorine distances of 300−350 pm roughly correspond to the sum of the van der Waals radii $r_F + r_{C/N}$ (147, 175 and 155 pm respectively[15,16]). Four of these contacts are found for BF_4^-(1), whereas there are only three, slightly larger ones for BF_4^-(2). This is probably the reason why the disorder found for BF_4(2) is more pronounced than for BF_4(1).

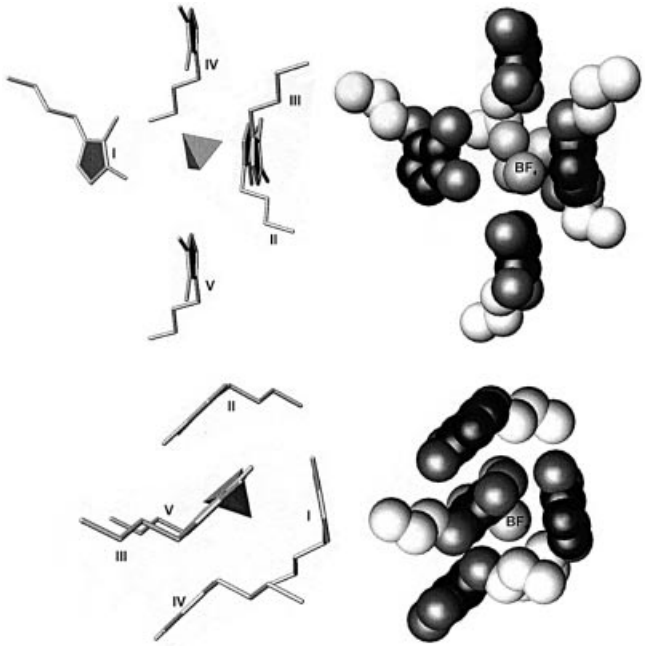

Figure 3. Coordination environments of the BF_4^- ions in BDMIMBF_4; cations are numbered sequentially with increasing center-to-center distances to the BF_4^- ion; the closest contacts between ring atoms and BF_4^- fluorides are summarized in Table 1; in the space-filling models, atoms are shown with different shadings, according to parts of the molecule of increasing polarity (ring C,N atoms as black spheres, methyl/methylene directly bound to the ring as grey spheres, the three outer butyl carbons as white spheres)

Table 1. Closest contacts (pm) between EF_x^- (E = B, P, Sb; x = 4, 6) fluorines and ring atoms of the cations in BDMIMEF_x, as shown for the BF_4^- ions in Figure 3

	BF_4(1)	BF_4(2)	PF_6	SbF_6
I	308 (C−F)	348 (N−F)	310 (C−F)	345 (C−F)
II	305 (C−F)	318 (C−F)	319 (N−F)	325 (C−F)
III	315 (C−F)	407 (N−F)	323 (C−F)	356 (C−F)
IV	329 (C−F)	334 (C−F)	356 (C−F)	342 (C−F)
V	454 (C−F)	423 (C−F)	451 (C−F)	447 (N−F)
VI			446 (C−F)	475 (N−F)

Due to the pronounced asymmetry of the cation, a naive analysis of intermolecular distances is probably not justified here. None of the C(4)−H, C(5)−H ring hydrogen atoms, however, shows an orientation which would suggest hydrogen bonding to the fluorines of BF_4^-.

The crystals of BDMIM PF_6 **II** were obtained from the melt as described in the Exp. Sect. They were typically 0.5−1 mm in diameter; twinning was never observed. The compound adopts an acentric monoclinic structure in space group *Cc* with four formula units per unit cell. The hexafluorophosphate ion is entirely ordered at 213 K while disorder, as in the case of the BF_4^- compound, is observed only at 298 K. The two orientations of the disordered ion are related to each other by a 60° rotation around the threefold axis of the octahedron (Figure 1). The crystal structure of **II** is composed of alternating layers of cations and anions extending in the crystallographic (0 1 1) plane, with all imidazolium ring planes coplanar (roughly perpendicular to the *a* axis) and all butyl chains aligned in one direction, roughly parallel to the *a* axis, as can be seen from Figure 4. As there are only translational symmetry elements (a single glide plane and centering translations), the structure is noncentrosymmetric and no double layers as in the case of **I** are formed. Shortest contacts of 432 pm between the butyl chains are found among adjacent rows of cations in direction of the *c* axis. The hexafluorophosphate ion is surrounded by six cations with the centers forming a distorted trigonal prism.

The PF_6^- group with its surrounding imidazolium ions is depicted in Figure 5. Cations **I**−**IV** all make contacts to fluorine atoms within distances of 310 to 356 pm, summarized in Table 1. The contacts with the two remaining cations are considerably longer (451 and 446 pm). As in the structure of **I**, the butyl chains are kinked from the ring planes, and a closer approach of cations and anions along the *a*

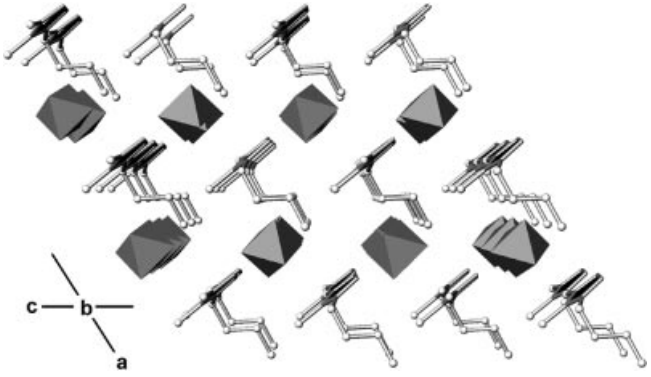

Figure 4. View of the crystal structure of BDMIMPF_6 along the crystallographic *b*-axis; PF_6^- ions are shown as grey octahedra; all hydrogen atoms of the imidazolium ring have been omitted for clarity

 © 2004 Wiley-VCH Verlag GmbH & Co. KGaA, Weinheim

axis is obviously restricted by the butyl chains. The distance between the terminal methyl carbon and the ring plane of the adjacent layer in the direction of the *a* axis is only 355 pm such that a tighter surrounding of the anion is prevented. Although C−H···F contacts involving the ring hydrogens can be found which adopt a close to linear arrangement, generally considered a prerequisite for hydrogen bonding, the distances involved are rather long: C−F distances of 337 and 355 pm and H···F distances of 248 and 267 pm, with both angles being virtually 160°. However, these distances are within the sum of the van der Waals radii for H and F (125 + 147 pm), and weak hydrogen bonding could well be present according to the definition of Taylor and Kennard.[16] Very similar H···F distances have also been found in the structure of EMIMPF_6,[4] but hydrogen bonding was suggested to be extremely weak or absent, due to the absence of red shifts of the ν_{CH} bands in the IR spectrum. Evidence from the present structure is entirely consistent with this observation. Comparing the structure of **II** with that of EMIMPF_6 is instructive. Whereas the former compound exhibits a pronounced layer structure, the latter shows cations in a pairwise arrangement and a much less discerned hydrophobic region resulting from the shorter ethyl chains. Although the acentric cation arrangement in **II** is not expected to exist in the melt, the greater tendency to separate into non-polar (very often referred to as hydrophobic, although this is not adequate in pure ILs) and ionic domains as compared to EMIMPF_6 is obvious.

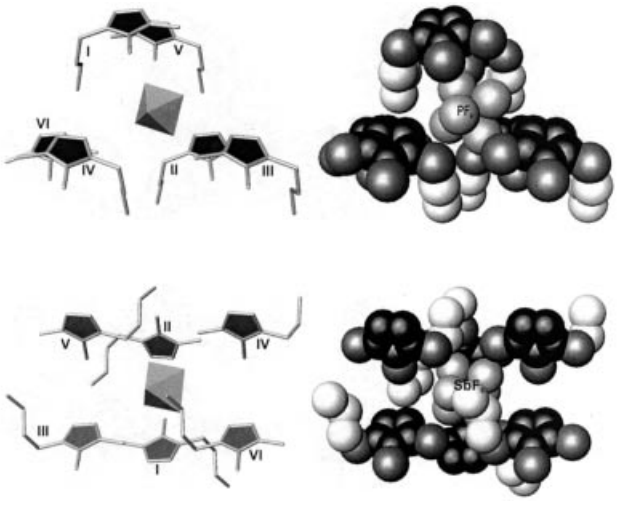

Figure 5. Coordination environments of the hexafluorophosphate ion in BDMIMPF_6 (top) and the hexafluoroantimonate ion in BDMIMSbF_6 (bottom); cations are numbered sequentially with increasing center-to-center distances; closest contacts between ring atoms are summarized in Table 1; shading of the ring atoms is analogous to the scheme adopted in Figure 3

No disorder is observed for the hexafluoroantimonate ion in the structure of BDMIMSbF_6 **III** even at ambient temperature. The crystal lattice is again distinctly different from the two previous compounds; a view of the structure along the *a* axis is depicted in Figure 6. There is no more orientational preference in the cation sub-lattice. The imidazolium moieties are in fact oriented with ring planes parallel to the (0 1 1), (0 $\bar{1}$ $\bar{1}$), (0 1 $\bar{1}$) and (0 $\bar{1}$ 1) crystallographic planes. The packing of cations and anions can be described as being reminiscent of the NiAs structure type, with the SbF_6^- octahedra surrounded by six nearest neighbor cations in a distorted trigonal prismatic coordination, and the cations being surrounded by six SbF_6^- ions in a distorted octahedral arrangement. The NiAs structure type may of course only serve as a schematic rationale for the true structure, as can be judged from large differences in the center-to-center distances between cations and anions. There are no short contacts between carbon atoms of the butyl chains, and thus short-range repulsive interactions between the cations are further diminished with respect to the hexafluorophosphate compound.

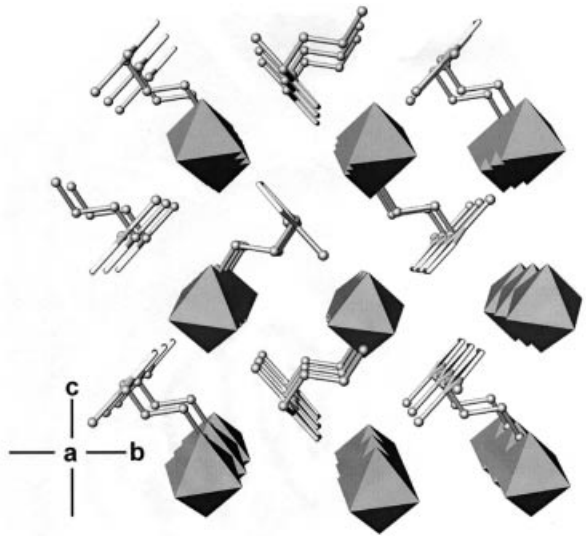

Figure 6. View of the structure of BDMIMSbF_6 along the crystallographic *a*-axis; SbF_6-ions are shown as grey octahedra; all hydrogen atoms of the imidazolium cation have been omitted for clarity; the SbF_6^- ions make a close to hexagonal packing with the imidazolium ions located in the "octahedral holes"

The existence of polar and non-polar domains in liquid BMIMBF_4 has been proposed from diffusion studies of ions and neutral molecules by Schröder et al.[17] The accelerated diffusion of $Fe(CN)_6^{4-}$ as well as the diffusion of neutral molecules was attributed to formation of a "nanostructure" of polar (ionic) and non-polar domains which became even more pronounced upon the addition of water to the IL phase. The formation of polar and non-polar domains, as found in the long chain-length IL compounds, can be recognized, at least to some extent, in the double-layer structure of **I** and the structure of **II**, whereas no such domains can be distinguished in the structure of **III**. This is due to the difference in packing modes, determined by anion size in the present series. The influence of anion size in these non hydrogen-bonded IL compounds can be rationalized by comparing the two compounds **II** and **III** with the BDMIM carborane compounds reported by Larsen et al. Packing in the structure of **I** is obviously determined by the arrange-

 © 2004 Wiley-VCH Verlag GmbH & Co. KGaA, Weinheim

ment in the cation sub-lattice, the influence of which prevails for the structure of **II**. By further increasing the size of the anion as in **III**, vacancies in the anion sub-lattice expand such as to accommodate the cations in a way that cation−cation contacts are no longer observed, despite their asymmetry. With even larger anions such as the carboranes, packing will be entirely dominated by the anions, such that close-packing of cations is prevented and disorder of the latter becomes frequent.

The presence of hydrogen bonding in solid IL salts incorporating weakly coordinating anions has been a cause for debate for some time because shifts of the corresponding IR bands indicative of H-bonding are weak or absent within experimental error. Whereas there is no doubt as to the existence of strong H-bonding in IL halides and weaker H-bonding in EMIMNO_3,[18] for example, it has been considered absent in haloaluminates,[19] and the results for anions like BF_4^- and PF_6^- are inconclusive. The closest H···F bond in EMIMPF_6 is reported as being 256 pm, clearly below the sum of the van der Waals radii. Several investigations of liquid EMIMBF_4, BMIMBF_4 and BMIMPF_6 [20−22] by NMR spectroscopy (including intermolecular ^{1}H-^{19}F NOE) established a close proximity between the hydrogens of the heteroaromatic core and the fluorines of the anion. The hydrogen-bonding interaction can be extended to include rather weak contacts as was recently shown by Seddon and co-workers for the C−H···Cl bond.[23] The absence of *significant* hydrogen bonding in all compounds of the present series is supported by infrared spectroscopy. Although the charge density of the anion varies considerably in the series, the wavenumbers of the two principal absorption bands of the aromatic hydrogens remain virtually constant. The three compounds exhibit a common pattern in this region, with a strong band at 3156 cm^{-1} and an associated weak band at 3187 cm^{-1}. Further support of this interpretation is lent by the low melting points of the present compounds as compared to truly H-bonded structures.[24]

The molecular volumes of the fluoro-anions EF_x^- have been calculated assuming a spherical geometry. Volumes are calculated as $V = 4/3\pi(d_{EF} + r_F)^3$, where d_{EF} is the interatomic distance and r_F is the "packing radius" of fluorine, as derived by Gavezzotti.[25] The bias introduced by this arbitrary choice of atomic radii is considered to be tolerable, as comparison is made only between the members of the present series of compounds. The molecular volumes of the BDMIM cation in the crystal were then calculated from the difference of the cell volumes and the respective anion volumes according to Equation (1).

$$V_{BDMIM} = V_{cell}/Z - V_{EF_x^-} \quad (1)$$

The molecular volumes V_{BDMIM} are found to be very similar, namely 230, 225 and 232 Å^3 for **I**, **II** and **III** respectively. This suggests a similar "packing coefficient" k for the three structures, as defined in Equation (2).[26]

$$k = ZV_{mol}/V_{cell} \quad (2)$$

All three structures can therefore be regarded as being fairly close-packed, a notion that is further supported by the absence of cation disorder, contrary to the carboranes reported by Larsen et al., where disorder of the cations was observed in most of the crystal structures.

The melting points and the temperature-dependent electrical conductivities of the melts were measured for compounds **I**−**III**. The melting points of the three BDMIM salts are found within a narrow range around 315 K, about 100 K above the glass-transition points reported for the respective BMIM compounds (Table 2).

Table 2. Melting points (K) of BDMIMEF_x salts determined in this work as compared to those of respective EMIM salts taken from ref.[4] and glass transition (T_g) points of the respective BMIM salts taken from ref.[20]

	BF_4^-	PF_6^-	SbF_6^-
BDMIM	312.8(5)	313.0(5)	317.5(5)
EMIM	288	331	
BMIM	192 (T_g)	212 (T_g)	

The conductivities of the low-melting IL salts BDMIMX (X = BF_4^-, PF_6^-, SbF_6^-), some of which have been reported previously,[27] were measured using a conventional conductivity cell as described below. In order to elucidate the influence of viscosity and the substitution pattern at the imidazolium ring, conductivities of BMIMBF_4 and the new ionic liquid 1-allyl-2,3-dimethylimidazolium tetrafluoroborate (ADMIMBF_4) were measured as well. The temperatures were chosen such that a range of about 10 K above and below the respective melting points was covered, except for the latter two compounds which are far above their glass-transition points at ambient temperature. Conductivities were found to follow linear $\ln(\sigma)$ vs. $1/T$ behavior in the narrow temperature range covered here, whereas the Vogel−Tamman−Fulcher equation has been previously found to describe the temperature-dependent conductivity of several ionic liquids in a wider temperature range.[11] The conductivities are depicted in Figure 7 and summarized in Table 3.

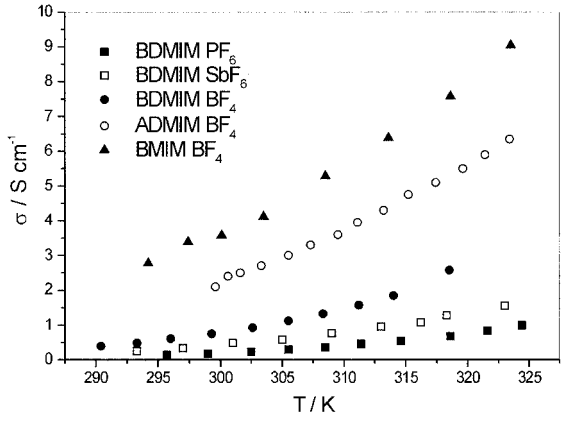

Figure 7. Plot of conductivity vs. temperature of the molten salts; the BDMIM compounds of BF_4^- and PF_6^- and of SbF_6^- are in the supercooled state below 313 and 318 K respectively

 © 2004 Wiley-VCH Verlag GmbH & Co. KGaA, Weinheim

Table 3. Conductivities σ (S cm^{-1}) of the molten salts at 298 K depicted in Figure 7, and activation energies E_A (kJ/mol) obtained from the corresponding Arrhenius plots

	σ	E_A
BMIMBF_4	3.4	31.6(7)
ADMIMBF_4	2.1	36.0(8)
BDMIMBF_4	0.7	50.1(6)
BDMIMSbF_6	0.4	47(1)
BDMIMPF_6	0.2	54.1(9)

A comparison of the conductivities was first made among the three BDMIM compounds. Since the viscosities could not be determined, only the effect of ion size can be taken into account. Compound **I** has the highest conductivity and the lowest is observed for **II**, although the difference between **II** and **III** is not large. The conductivities of the latter two compounds are reversed as to what would be expected from their anion size and melting points. It has been shown previously that large anions can produce melts of low viscosity if they have low charge-density and if hydrogen bonding is absent.[10] The slightly lower conductivity of the PF_6^- salt as compared to that of SbF_6^- could still be due to the latter effect as discussed above. An unusually low conductivity of EMIMPF_6 as compared to the much larger EMIM bis(trifluoromethylsulfonyl)imide has been previously reported by McEwen et al.[11] The values obtained in this work for **I** and **II** are similar, although reversed in order with respect to those reported by Sutto et al., determined using the complex impedance method.[27]

The activation energies for conductivity decrease in the order $PF_6^- > BF_4^- > SbF_6^-$, with absolute values consistent with that reported for the similar compound dimethylpropylimidazolium hexafluorophosphate (DMPIPF_6).[11]

The second series compared are the BF_4^- salts of BMIM, BDMIM and ADMIM. The ADMIM compound was synthesized in order to verify whether trisubstituted imidazolium salts with this types of anion are generally solid at ambient temperature. ADMIMBF_4 turned out to be a liquid of rather low viscosity even at approx. 260 K, thus methylation in the 2-position cannot be exclusively responsible for the large increase of melting points. Conductivities of the BF_4^- salts increase in the order BMIM > ADMIM > BDMIM. This order could otherwise be described as: a) exchange of an allyl for a butyl group at the nitrogen plus methylation in the 2-position, resulting in lower mobility of the cation, and b) reverse exchange of butyl for allyl, decreasing the mobility even further. The large effect produced by the second step (cf. Figure 7) is a particularly unexpected result, and is probably explained by weaker van der Waals bonding with the allyl group as compared to butyl, rather than a large increase in the overall size of the cation.

Conclusion

From the present work we conclude that packing inefficiency as a prerequisite for the low melting points of ionic liquid salts, reflected by frequent crystallographic disorder, can be ruled out for the present compounds, contrary to the IL carboranes reported by Larsen et al. Instead, the low-melting compounds containing the BDMIM cation and fluoro anions suggest a certain degree of cation−cation repulsive interaction for compounds with smaller anions (BF_4^- and PF_6^-) which is no longer influential in the case of SbF_6^- owing to lattice expansion. The existence of polar and non-polar domains, believed to be associated with the unique "amphiphilic" solvent properties of ILs, are found in the structures of the BF_4^- and PF_6^- salts. A similar trend as with melting points is observed with ionic mobilities in the respective molten salts, inferred from measurements of electric conductivities. However, since the charge densities of the conducting species are low and dispersive interactions make up an important part of the adhesive forces in these melts, factors other than ion size, especially polarizability, have to be taken into account. Introducing unsaturated side chains at the imidazolium ring (possibly perfluorinated ones in order to reduce reactivity) might be a worthwhile issue with respect to the design of low viscosity melts, as suggested by the new IL ADMIMBF_4.

Experimental Section

Preparations: BMIMCl and BDMIMCl were obtained from *n*-chlorobutane and 1,2-dimethylimidazole (Aldrich 98%) as reported previously.[18] The BF_4^-, PF_6^- and SbF_6^- salts were prepared by a modified procedure according to Suarez et al.[20] The imidazolium chloride was stirred with a 1.1-fold excess of $NaBF_4$, KPF_6 or $NaSbF_6$ in dry acetone at ambient temperature for 48 hours. Sodium chloride was then filtered from the solution, and most of the acetone was removed under reduced pressure. Dichloromethane was then added in order to precipitate the remaining sodium salts, and the mixture was kept at −10 °C for 24 hours. The precipitates were filtered from the solution and the organic solvents were removed under reduced pressure. The resulting ionic liquid was then heated at 70 °C/10^{-2} bar for 12 hours to remove any remaining volatiles. Purity was checked by NMR spectroscopy and elemental analysis; chloride impurities were generally below the detection limit with silver ions. Some of these ionic liquid salts are now commercially available.[28] 1-Allyl-3-methylimidazolium bromide was synthesized from allyl bromide and 1,2-dimethylimidazole and bromide ions were exchanged for tetrafluoroborate as described above.

Crystal Growth: Suitable crystals for X-ray single crystal diffraction of BDMIMBF_4 (**I**) and BDMIMPF_6 (**II**) could only be obtained from the molten salts. Crystals of BDMIMSbF_6 (**III**) were obtained from solution. The crystal growth of the imidazolium salts from the melt was performed in Schlenk tubes (approx. 10 cm in length and 1 cm in diameter) equipped with a septum through which a wire ending in a loop with seed crystals was immersed into the melt. The tubes were kept in a water bath maintained about 1 °C below the melting point. Crystals started growing at the loop and were separated from the melt typically after a couple of hours by slowly lifting the wire out of the liquid. Crystals of **III** were obtained from mixtures of MeCN/Et_2O typically within less than 24 hours.

Conductivity Measurements: AC conductivities of the molten salts were measured using a conventional conductivity cell equipped with 1 cm^2 platinum electrodes with a nominal cell constant of 0.7

 © 2004 Wiley-VCH Verlag GmbH & Co. KGaA, Weinheim

Table 4. Crystallographic data of BDMIMBF_4, BDMIMPF_6 and BDMIMSbF_6

	$C_9H_{17}BF_4N_2$	$C_9H_{17}F_6N_2P$	$C_9H_{17}F_6N_2Sb$
a (Å)	13.080(3)	15.389(3)	9.100(2)
b (Å)	11.270(2)	8.604(2)	12.510(2)
c (Å)	16.930(3)	11.730(2)	13.000(3)
β (°)	93.14(4)	122.46(3)	100.14(3)
V (Å^3)	2491.79(8)	1310.4(5)	1457.27(5)
T (K)	213(1)	213(1)	293(3)
Molecular weight (g/mol)	240.05	298.21	371.86
Space group	$P2_1/c$ (No. 14)	Cc (No. 10)	$P2_1/n$ (No. 14)
Z	8	4	4
λ (Å)	0.71069	0.71069	0.71069
$\rho_{calcd.}$ (g/cm^3)	1.307	1.512	1.773
$R1$	0.080	0.062	0.040
$wR2$ (all data)	0.230	0.175	*0.107*

cm^{-1}. The cell was calibrated with a 0.01 M aqueous solution of KCl and connected to a WTF conductivity analyzer model LF 410, operating at 4 MHz ac current. The temperature of the cell was maintained constant within 0.5 °C using a thermostatted water bath. The compounds were cautiously dried at 70 °C under reduced pressure before measurement and transferred to the cell inside an argon-filled glove box.

NMR and Infrared Spectra: Both NMR spectra in CD_2Cl_2 solution, recorded on a Varian Mercury 200 spectrometer (200 MHz), as well as IR spectra of solid samples run as KBr pellets with a Nicolet FTIR spectrometer (model Avatar), are virtually identical for the three BDMIM compounds. NMR and IR spectroscopic data for **III** and for the new compound ADMIMBr are summarized below. Compounds **I**−**III** and ADMIMBr were also submitted to elemental analysis.

1-Butyl-2,3-dimethylimidazolium Hexafluoroantimonate (III): ^{1}H NMR: δ = 1.0 [t, C(11)H3], 1.3 [tt, C(10)H2], 1.7 [tt, C(9)H2], 2.5 [s, C(8)H3], 3.7 [s, C(7)H3], 4.0 [t, C(6)H2], 7.2 [dd, C(4)H, C(5)H] ppm. ^{13}C NMR: δ = 10.0 (C-8), 14.0 (C-11), 20.0 (C-10), 32.0 (C-9), 35.0 (C-7), 49.0 (C-6), 121.0 (C-4), 123.0 (C-5), 144.0 (C-2) ppm. IR (600−4000 cm^{-1}, KBr pellets): $\tilde{\nu}$ = 3186, 3153 aromatic ν(C−H); 2968−2881 aliph. ν_s(C−H); 1608−1469 ν_s(C=C/C=N ring); 1426−1080 aliph. δ_{as}(C−H), ν_s(ring), δ(C−H ring); 950 δ(in plane ring C−H); 750 δ_{as}(out of plane ring). $C_9H_{17}N_2F_6Sb$ (388.91): calcd. C 27.8, H 4.4, N 7.2; found C 27.5, H 4.7, N 6.8.
I: $C_9H_{17}N_2F_4B$ (239.91): calcd. C 45.0, H 7.1, N 11.7; found C 44.8, H 8.0, N 11.2.
II: $C_9H_{17}N_2F_6P$ (298.11): calcd. C 36.2, H 5.7, N 9.4; found C 36.2, H 6.0, N 9.1.

1-Allyl-2,3-dimethylimidazolium Bromide: ^{1}H NMR: δ = 2.58 [s, C(7)H3], 3.79 [s, C(6)H3], 4.95 [dt, C(8)H2], 5.28 [d/m, C(10)H-*E*], 5.38 [d/m, C(10)H-*Z*], 5.98 [m, C(9)H], 7.61 [d, C(4)H], 7.73 [d, C(5)H] ppm. ^{13}C NMR: δ = 11.08 (C-7), 27.69 (C-8), 36.30 (C-6), 120.65 (C-9), 120.65 (C-5), 121.77 (C-4), 123.22 (C-10), 130.4 (C-9), 144.66 (C-2) ppm. IR (600−4000 cm^{-1}, KBr pellets): $\tilde{\nu}$ = 3169 (w), 3106 (m), 3056 (3014) (s) aromatic/allyl ν(C−H); 2929−2860 aliph. ν_s(C−H); 1586−1461 ν_s(C=C/C=N ring/allyl); 1410−1170 aliph. δ_{as}(C−H), ν_s(ring), δ(C−H) ring; 950 δ(in plane ring C−H); 750 δ_{as}(out of plane ring). $C_8H_{13}N_2Br$ (216.99): calcd. C 44.2, H 6.4, N 12.9; found C 44.6, H 6.2, N 12.9.

X-ray Structure Determinations: Single crystal diffraction was performed with a Bruker diffractometer equipped with graphite monochromator and a Smart-Apex CCD detector (Siemens) using Mo-K_α radiation. A complete hemisphere was recorded in 600, 435 and 230 frames, at φ angles of 0°, 90° and 180°, respectively. A scan width of 0.3° was used. Indexing was done using the program SMART, frame integration and data reduction using the SAINTPLUS suite. Absorption correction was performed using the program SADABS (all ©Bruker AXS). Sample crystals were placed into glass capillaries and sealed under argon atmosphere. Recording temperatures and crystallographic parameters for compounds **I**−**III** are summarized in Table 4. Crystals of **I** were obtained as two-component twins in all cases. The crystals, however, were large and of excellent quality, thus a sufficient number of non-overlapping reflections could be collected to allow for separation of contributions from the two components, structure solution and batch scaling of the data according to the degree of overlap during least-squares refinement. Diffraction data were collected at 213 K and indexed with a monoclinic unit cell containing eight formula units, which had previously been obtained from a powder diffraction pattern where twinning is not of concern.
CCDC-221752 (for BDMIMBF_4), -221753 (for BDMIMPF_6) and -221754 (for BDMIMSbF_6) contain the supplementary crystallographic data for this paper. These data can be obtained free of charge at www.ccdc.cam.ac.uk/conts/retrieving.html [or from the Cambridge Crystallographic Data Centre, 12, Union Road, Cambridge CB2 1EZ, UK; Fax: (internat.) +44-1223-336-033; E-mail: deposit@ccdc.cam.ac.uk].

Acknowledgments

Support by the Fonds der Chemischen Industrie is gratefully acknowledged.

[1] [1a] P. Wasserscheid, W. Keim, *Angew. Chem. Int. Ed.* **2000**, *39*, 3772. [1b] R. Sheldon, *Chem. Commun.* **2001**, 2399. [1c] C. M. Gordon, *Appl. Catal. A* **2001**, *222*, 101. [1d] P. Dyson, *Trans. Metal Chem.* **2001**, *27*, 353. [1e] J. Dupont, R. F. de Souza, P. A. Z. Suarez, *Chem. Rev.* **2002**, *102*, 3667. [1f] C. Baudequin, J. Baudoux, J. Levillain, D. Cahard, A.-C. Gaumont, J.-C. Plaquevent, *Tetrahedron Asymmetry* **2003**, *14*, 3081. [1g] Y. Chauvin, L. Mußmann, H. Olivier, *Angew. Chem. Int. Ed. Engl.* **1995**, *34*, 2698.
[2] A. J. Dent, K. R. Seddon, T. Welton, *J. Chem. Soc., Chem. Commun.* **1990**, 315.
[3] J. D. Holbrey, K. R. Seddon, *J. Chem. Soc., Dalton Trans.* **1999**, 2133.

 © 2004 Wiley-VCH Verlag GmbH & Co. KGaA, Weinheim

[4] J. Fuller, R. T. Carlin, H. C. D. Long, D. Haworth, *J. Chem. Soc., Chem. Commun.* **1994**, 299.
[5] C. M. Gordon, J. D. Holbrey, A. R. Kennedy, K. R. Seddon, *J. Mater. Chem.* **1998**, *8*, 2627.
[6] C. J. Bowlas, D. W. Bruce, K. R. Seddon, *Chem. Commun.* **1996**, 1625.
[7] A. S. Larsen, J. D. Holbrey, F. S. Tham, C. A. Reed, *J. Am. Chem. Soc.* **2000**, *122*, 7246.
[8] J. Dupont, P. A. Z. Suarez, R. F. De Souza, R. A. Burrow, J.-P. Kintzinger, *Chem. Eur. J.* **2000**, *6*, 2377.
[9] J. van den Broeke, M. Stam, M. Lutz, H. Kooijman, A. L. Spek, B.-J. Deelman, G. van Koten, *Eur. J. Inorg. Chem.* **2003**, 2798.
[10] P. Bonhôte, A.-P. Dias, N. Papageorgiou, K. Kalyanasundaram, M. Graetzel, *Inorg. Chem.* **1996**, *35*, 1168.
[11] A. B. McEwen, H. L. Ngo, K. LeCompte, J. L. Goldman, *J. Electrochem Soc.* **1999**, *146*, 1687.
[12] A. Elaiwi, P. B. Hitchcock, K. R. Seddon, N. Srinivasan, Y.-M. Tan, T. Welton, J. A. Zora, *J. Chem. Soc., Dalton Trans.* **1995**, 3467.
[13] S. Saha, S. Hayashi, A. Kobayashi, H. Hamaguchi, *Chem. Lett.* **2003**, *32*, 740.
[14] J. D. Holbrey, W. M. Reichert, M. Nieuwenhuyzen, S. Johnston, K. R. Seddon, R. Rogers, *Chem. Commun.* **2003**, 1636.
[15] A. Bondi, *J. Phys. Chem.* **1964**, *68*, 461.
[16] R. Taylor, O. Kennard, *J. Am. Chem. Soc.* **1982**, *104*, 5063.
[17] U. Schröder, J. D. Wadhawan, R. G. Compton, F. Marken, P. A. Z. Suarez, C. S. Consorti, R. F. de Souza, J. Dupont, *New J. Chem.* **2000**, *24*, 1009.
[18] J. S. Wilkes, M. Zaworotko, *J. Chem. Soc., Chem. Commun.* **1992**, 965.
[19] P. B. Hitchcock, K. R. Seddon, T. Welton, *J. Chem. Soc., Dalton Trans.* **1993**, 2639.
[20] S. E. P. A. Z. Suarez, J. E. Dullius, R. F. de Souza, J. Dupont, *J. Chim. Phys.* **1998**, *95*, 1626.
[21] J.-F. Huang, P.-Y. Chen, I.-W. Sun, S. P. Wang, *Inorg. Chim. Acta* **2001**, *320*, 7.
[22] A. Mele, C. D. Tran, S. H. De Paoli Lacerda, *Angew. Chem. Int. Ed.* **2003**, *36*, 4364.
[23] C. B. Aakeröy, T. A. Evans, K. R. Seddon, I. Palinko, *N. J. Chem.* **1999**, 145.
[24] P. Kölle, R. Dronskowski, *Inorg. Chem.*, in press.
[25] A. Gavezzotti, in *Structure Correlation Vol. 2* (Eds.: H. B. Bürgi, J. D. Dunitz), VCH: Weinheim, **1994**.
[26] A. I. Kitaigorodski, *Molecular Crystals and Molecules*, Academic Press: New York **1973**.
[27] T. E. Sutto, H. L. De Long, P. C. Trulove, *Progress in Molten Salt Chemistry 1* (Eds.: R. W. Berg, H. A. Hjuler), Elsevier: Paris, **2000**, 511.
[28] Solvent Innovation GmbH, Köln (www.solvent-innovation.com).

Received December 16, 2003
Early View Article
Published Online April 7, 2004

 © 2004 Wiley-VCH Verlag GmbH & Co. KGaA, Weinheim

Synthesis and Characterisation of Novel Main Group Element Clusters with Tin-Phosphorus, Tin-Arsenic, and Germanium-Phosphorus Skeletons

Donna Nikolova,[a] Carsten von Hänisch,*[a] and Ariane Adolf[a]

Keywords: Tin / Phosphorus / Arsenic / Germanium / Cluster compounds

The reaction of iPr$_3$SiPLi$_2$ with SnCl$_2$ in the mol ratio 1:1 leads to the formation of [Sn$_7$(PSiiPr$_3$)$_7$] (**1**). The cluster [Sn$_8$(PSiiPr$_3$)$_6$Cl$_2$] (**3**) is obtained, if the same reaction is carried out with a slight excess of the metal salt. Similar lithium chloride elimination reactions between SnCl$_2$ and iPr$_3$SiAsLi$_2$ in the mol ratio 1:1 and 2:3, however, yield [Sn$_7$(AsSiiPr$_3$)$_7$] (**2**) and [Sn$_4$(AsSiiPr$_3$)$_6$Li$_4$(Et$_2$O)$_2$] (**4**), respectively. The metal salt GeCl$_2$(diox)$_2$ (diox = 1,4-dioxane) reacts with iPr$_3$SiPLi$_2$ to give [Ge$_6$(PSiiPr$_3$)$_6$] (**5**). Compounds **1**–**5** were characterised by NMR and IR spectroscopic techniques as well as elemental analysis. The crystal structures were identified by X-ray diffraction analysis, which confirmed that the heptameric skeletons of **1** and **2** are structurally analogous. The Sn/P cluster **3** contains subvalent tin atoms, while **4** forms a Sn$_4$As$_6$Li$_4$ rhombododecahedron and **5** a slightly distorted hexagonal prism.
(© Wiley-VCH Verlag GmbH & Co. KGaA, 69451 Weinheim, Germany, 2004)

Introduction

A survey of coordination chemistry literature reveals that besides investigations into the formation of polynuclear complexes with the participation of transition metals,[1−3] an increasing number of studies are currently devoted to problems of synthesis and characterisation of cluster compounds containing elements from the main groups.[4] For a better understanding of the correlation between size, structure and properties of binary semiconductor compounds, the availability of clusters of different size and structure is of considerable interest. However, the knowledge on 14/15 cluster compounds is still relatively scarce. For the systems Sn/P and Sn/As there are only a few cyclic and cage compounds reported to date.[5,6] Even fewer examples are known for Ge/P compounds.[7]

Different types of starting materials and synthetic methods have been described for the synthesis of tin phosphorus and germanium phosphorus compounds. A convenient method for the formation of Sn−P bonds is the metalation of primary phosphanes RPH$_2$ (R = iPr$_3$Si, tBu$_3$Si) with Sn[N(SiMe$_3$)$_2$]$_2$, leading to [Sn$_4$(PSitBu$_3$)$_4$] and [Sn$_6$(PSiiPr$_3$)$_6$] species.[5b,5c] Salt elimination reactions between NaAsH$_2$ and Sn^{IV} compounds such as tBu$_2$SnCl$_2$ have been used for the synthesis of Sn/As compounds.[6a][6c] Recently Fenske and co-workers reported the catalytic transformation of P(SnMe$_3$)$_3$ into the Sn/P-cage compound [P$_4$(SnMe$_2$)$_6$].[5a]

[a] Institut für Nanotechnologie, Forschungszentrum Karlsruhe, Postfach 3640, 76021 Karlsruhe
Fax: (internat.) +49-(0)7247-82-6368
E-Mail: carsten.vonhaenisch@int.fzk.de

Herein we report on the successful synthesis of new 14/15 compounds with unknown structural motifs. Simple lithium chloride elimination reaction of iPr$_3$SiELi$_2$ (E = P, As) with the metal salts SnCl$_2$ and GeCl$_2$(diox)$_2$ (diox = 1,4-dioxane) was used in these reactions.[8]

Results and Discussion

The reaction of iPr$_3$SiPLi$_2$ with SnCl$_2$ in the mol ratio 1:1 in Et$_2$O yields [Sn$_7$(PSiiPr$_3$)$_7$] (**1**) which can be obtained as red crystals by cooling the reaction mixture to 0 °C. The X-ray analysis revealed that the compound consists of seven Sn atoms and seven PSiiPr$_3$ fragments. **1** crystallises in the trigonal space group $R\bar{3}$.

The cluster can be described as follows: The tin and phosphorus atoms Sn1, Sn1′, Sn1′′ and P1, P2, P2′, P2′′ form a heterocubane, however, the fourth Sn atom is missing. Instead of it the three P atoms P2, P2′, P2′′ are connected to the corresponding Sn atoms (Sn2, Sn2′, Sn2"") which also form an incomplete heterocubane together with P3, P3′, P3′′ and Sn3. The Sn−P bonds in **1** are 264.5 pm on average. This value is within the range of lengths typically observed for most of the already known Sn^{II}/P compounds.[5] All of the P centres are coordinated to three tin atoms and one triisopropylsilyl group, forming a very distorted tetrahedral environment. The tin atoms possess no exocyclic ligands and consequently only have a coordination number of three.

The compound [Sn$_7$(AsSiiPr$_3$)$_7$] (**2**) is formed by the reaction of iPr$_3$SiAsLi$_2$ with SnCl$_2$ (1:1) in diethyl ether as a solvent. The compound crystallises isotypically into **1** (see Figure 1). Therefore its structure will not be discussed in

detail. The average Sn−As bond lengths are 272.8 pm. The As−Si bond lengths are in the range of 234.5 to 238.7 pm. All values are in the usual range for single bonds between these elements.[6,10]

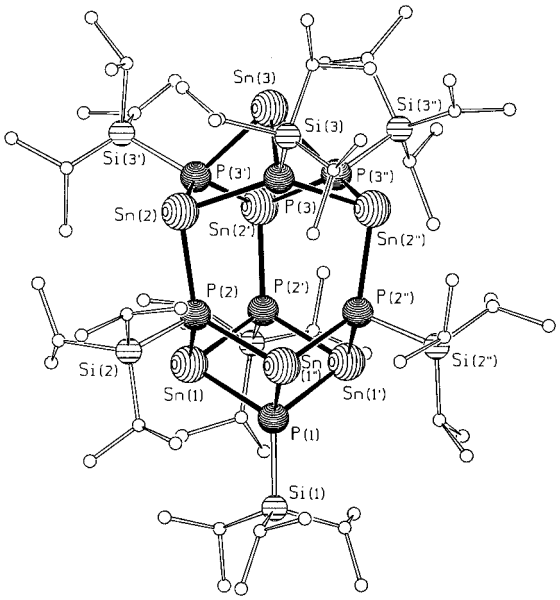

Figure 1. Molecular structure of **1**, selected bond lengths (pm) and angles (°): Sn−P 262.3(3)−265.8(3), Si−P 225.2(6)−228.1(4); Sn−P(1)−Sn 96.2(1), Sn(1)−P(2)−Sn(1′) 96.3(1), Sn(1)/Sn(1′)−P(2)−Sn(2) 123.3(1)−223.9(1), Sn(2)−P(3)−Sn(2′) 133.5(1), Sn(2)/Sn(2′)−P(3)−Sn(3) 90.4(1)−90.6(1), P(1)−Sn(1)−P(2)/P(2′) 83.6(1)−83.8(1), P(2)−Sn(1)−P(2′) 100.6(1), P(2)−Sn(2)−P(3)/P(3′) 101.0(1)−101.3(1), P(3)−Sn(2)−P(3′) 84.5(1), P−Sn(3)−P 83.4(1)

Similar heptameric structures have been found for the related imidoalanes, imidogallanes and phosphinidene-alanes $[RMER']_7$ (M = Al: E = N, P; M = Ga: E = N).[9]

Surprisingly, when the corresponding reaction between $Li_2PSi\textit{i}Pr_3$ and $SnCl_2$ is carried out with a slight excess of the metal salt, the compound $[Sn_8(PSi\textit{i}Pr_3)_6Cl_2]$ (**3**) is obtained.

In contrast to **1**, **3** contains an excess of Sn relative to $PSi\textit{i}Pr_3$ groups and possesses two chloride ligands. **3** crystallizes in the monoclinic space group $P2_1/c$. A formal charge of −2 can be assigned to each of the six $PSi\textit{i}Pr_3$ fragments, the two Cl ions contribute one negative charge each. Therefore the total formal negative charge to be compensated amounts to −14. Consequently, the molecule must consist of two types of Sn atoms due to the neutrality of the molecule. The outer Sn atoms (Sn1, Sn2, Sn3, Sn4) are in the +2 oxidation state and account for +8 of the total formal positive charge. The remaining four tin centres (Sn5, Sn6, Sn7, Sn8) compensate with a formal charge of +6, indicating that a reduction process must have taken place. These tin atoms form the structural core and exhibit three Sn−Sn bonds. The middle bond between Sn5 and Sn6 (283.4 pm) is slightly shorter than the adjacent two Sn−Sn bonds (Sn5−Sn7 288.8 pm, Sn6−Sn8 288.0 pm). However they are still in the range of normal tin-tin bonds as found in grey tin (280 pm) or in the tin-phosphorus compound $[P_2(Sn_2Me_4)_3]$ (279 pm).[5g] Two of the tin atoms (Sn5 and Sn6) of this four-membered tin fragment are tetrahedrally surrounded by two P and two Sn atoms. Two phosphorus and one tin atom coordinate the other two Sn atoms (Sn7 and Sn8). The outer Sn centres (Sn1, Sn2, Sn3, Sn4) are also three-coordinate due to the coordination of either three phosphorus atoms (Sn3 and Sn4) or two phosphorus atoms and one chloride ligand (Sn1 and Sn2). These Cl ligands are most likely oriented in this asymmetric manner as a result of the sterically demanding $\textit{i}Pr_3Si$ moieties and weak bonding interactions between Cl1 and Sn2 (Cl1···Sn2 distance: 303.0 pm). Assuming that the tetrahedrally surrounded Sn atoms (Sn5 and Sn6) contribute four electrons to the cluster framework, the core structure possesses 42 valence electrons for 21 bonds (dark lines in Figure 2) and therefore the cluster is electron precise.

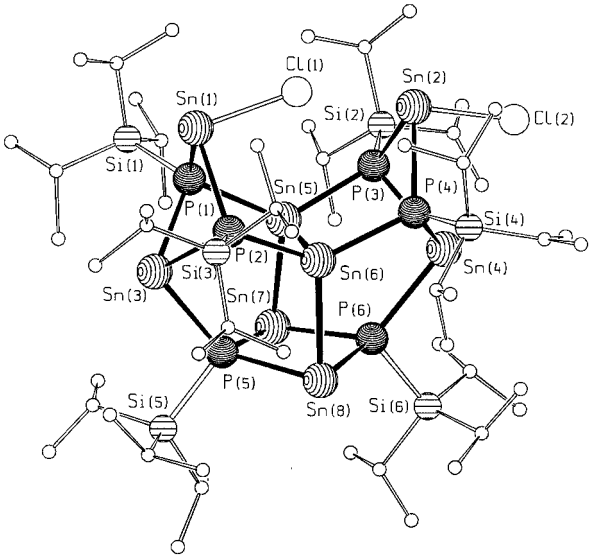

Figure 2. Molecular structure of **3**, selected bond lengths (pm) and angles (°): Sn(5)−Sn(6) 283.4(1), Sn(5)−Sn(7) 288.8(2), Sn(6)−Sn(8) 288.0(2), Sn(1)−Cl(1) 257.2(6), Sn(2)−Cl(2) 255.3(6), Sn−P 253.8(5)−272.8(5), Si−P 226.7(5)−228.3(5); Sn(5)−Sn(6)−Sn(8) 100.10(4), Sn(6)−Sn(5)−Sn(7) 99.05(4)

The rhombododecahedron $[Sn_4(AsSi\textit{i}Pr_3)_6Li_4(Et_2O)_2]$ (**4**, Figure 3) can be isolated if the reaction of $SnCl_2$ with $\textit{i}Pr_3SiAsLi_2$ is carried out in the ratio 2:3.

Two four-membered Sn_2As_2 rings are observed in the molecule. The Sn atoms are three-coordinate. The As atoms reveal a coordination number of five. These rings are bridged by the As centres As3 and As3′. The resulting Sn_4As_6 skeleton carries a formal charge of −4, which is compensated by four Li counterions. Each Li ion binds to one As atom of the two Sn_2As_2 rings and to one of the bridging As centres. Li1 and Li1′ are further coordinated by one diethyl ether molecule each. The Sn^{II}−As bonds in **4** are 274.1 pm on average and are therefore longer than the representative Sn^{IV}−As bonds (263.1−261.5 pm) in the ring compounds $(\textit{t}Bu_2SnAsH)_2$ and $(\textit{t}Bu_2SnAsSiMe_3)_2$.[6a,6c] A Sn−As bond length of 270−277 pm, how-

 © 2004 Wiley-VCH Verlag GmbH & Co. KGaA, Weinheim

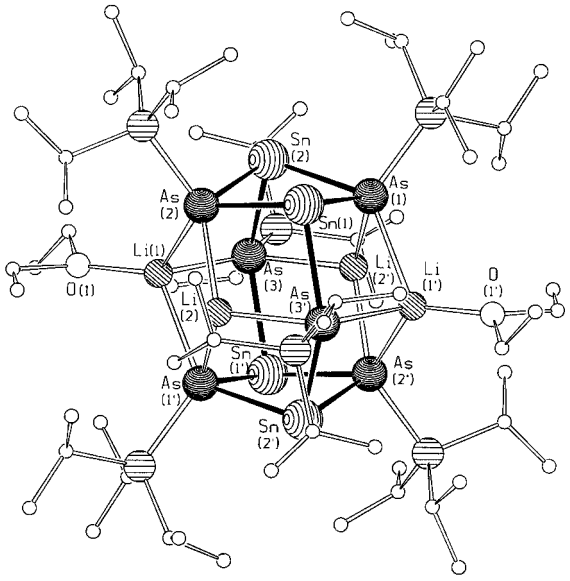

Figure 3. Molecular structure of **4**, selected bond lengths (pm) and angles (°): Sn−As 272.0(4)−278.8(2), As−Si 234.6(3)−236.7(4), As−Li 257(2)−279(2); Sn(1)−As(1)−Sn(2) 85.37(4), Sn(1)−As(2)−Sn(2) 85.44(4) Sn(1′)−As(3)−Sn(2) 137.49(4), As(1)−Sn(1)−As(2) 91.34(4), As(1)−Sn(1)−As(3′) 90.64(5), As(2)−Sn(1)−As(3′) 98.25(4), As(1)−Sn(2)−As(2) 91.86(4), As(1)−Sn(2)−As(3) 99.41(4), As(2)−Sn(2)−As(3) 91.87(4)

ever, can be observed in the cyclic arsanylstannylene $[Sn\{As(SiMe_3)_2\}_2]_2$ and $[Sn(As\mathit{t}Bu_2)Cl]_2$ [6d,6e] as well as in **2**. A similar rhombododecahedral structure is observed for the related tin-phosphorus compound $[Sn_4(PCy)_6\{Li(THF)\}_4]$ and the aluminium-arsenic compound $[(HAl)_4(AsSi\mathit{i}Pr_3)_6Li_4(Et_2O)_2]$.[11]

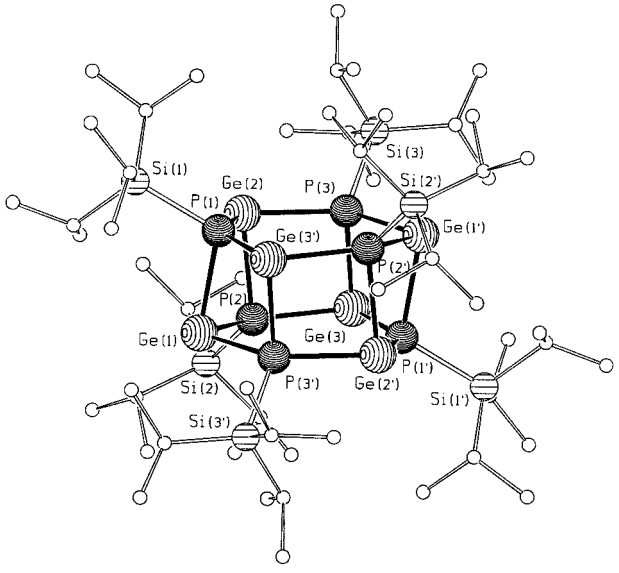

Figure 4. Molecular structure of **5**, selected bond lengths (pm) and angles (°): Ge−P 241.6(2)−248.7(2), P−Si 226.6(3)−227.9(2); Ge−P−Ge(four-membered ring): 90.78(5)−92.69(4), Ge−P−Ge(six-membered ring): 135.14(7)−137.67(9), P−Ge−P(four-membered ring): 85.84(6)−88.83(7), P−Ge−P(six-membered ring): 10071(6)−103.48(6)

$[Ge_6(PSi\mathit{i}Pr_3)_6]$ (**5**, Figure 4) is obtained from the reaction of $\mathit{i}Pr_3SiPLi_2$ with $GeCl_2(diox)_2$. The compound crystallises in the triclinic space group $P\bar{1}$ with two independent inversion symmetric molecules in the elementary cell. They differ insignificantly; therefore only one of them will be discussed.

The Ge and P atoms form a distorted hexagonal prism, in which all of the Ge centres are coordinated trigonal-pyramidally by three P atoms. The P atoms are surrounded by one triisopropylsilyl group and three Ge atoms. The average Ge−P distances within each Ge_3P_3 plane (242.5 pm) are slightly shorter than the corresponding Ge−P distances between the Ge_3P_3 rings (247.7 pm). These values are larger than the corresponding Ge^{IV}−P distances in $[\mathit{t}BuMesGePH]_2$ (234.6 pm) but shorter than the Ge^{II}−P bonds in $[Ge(P\mathit{t}Bu_2)Cl]_2$ (248.8−249.3 pm).[7] The molecular structure of **5** is analogous to the tin compounds $[Sn_6(ESi\mathit{i}Pr_3)_6]$ (E = P, As) and the lead arsenic compound $[Pb_6(AsSi\mathit{i}Pr_3)_6]$.[5c,6b,12]

Experimental Section

All manipulations were carried out under rigorous exclusion of oxygen and moisture, using a Schlenk line and nitrogen atmosphere. All solvents were dried and freshly distilled before usage. The starting materials $\mathit{i}Pr_3SiPH_2$, $\mathit{i}Pr_3SiAsH_2$, $GeCl_2(diox)_2$ were prepared according to the relevant instructions found in the literature.[13] $SnCl_2$ was obtained from Aldrich and used as received. The ^1H and ^{31}P NMR spectra were recorded with a Bruker AC 250 spectrometer. All isolated compounds gave C,H analyses consistent with their formulas. In the IR spectra the typical peaks of the $\mathit{i}Pr_3Si$ groups are observed.

1: A butyllithium solution (1.25 mL, 1.6 M; 2 mmol) was added to a solution of $\mathit{i}Pr_3SiPH_2$ (0.19 g, 1 mmol) in Et_2O (10 mL) at 0 °C. After stirring for 10 min, this solution was added to a suspension of $SnCl_2$ (0.19 g, 1 mmol) in Et_2O (15 mL) at 0 °C. The reaction mixture was allowed to warm up to ambient temperature and then stirred for an additional 16 hours. The resulting red solution was filtered to remove the precipitated LiCl and cooled to 0 °C. Red crystals of **1** formed over a period of 5 days. Yield: 0.1 g (32%). $C_{63}H_{147}P_7Si_7Sn_7$ (2149.11): calcd. C 35.21, H 6.89; found C 34.63, H 6.60. ^1H NMR ([D$_8$]toluene): δ = 1.0−1.5 (m, *i*Pr) ppm. $^{31}P\{^1H\}$ NMR ([D$_8$]toluene): δ = −243.9 (s), −294.9 (s), −373.0 (s) ppm.

2: BuLi (1.63 mL, 1.6) was added at 0 °C to a solution of $\mathit{i}Pr_3SiAsH_2$ (0.31 g, 1.3 mmol) in Et_2O (10 mL). This solution was added at 0 °C to a suspension of $SnCl_2$ (0.25 g, 1.3 mmol) in Et_2O (10 mL). The purple red mixture was stirred for an additional 18 . The resulting red solution was filtered to remove the precipitated LiCl and cooled to 0 °C. Red crystals of **2** formed over a period of 5 days. Yield: 0.13 g (28.5%). $C_{63}H_{147}As_7Si_7Sn_7$ (2457.74): calcd. C 30.80, H 6.03; found C 30.11, H 5.99. ^1H NMR (C_6D_6): δ = 1.0−1.5 (m, *i*Pr) ppm.

3: A butyllithium solution (1.19 mL, 1.6 M) was added to a solution of $\mathit{i}Pr_3SiPH_2$ (0.18 g, 0.95 mmol) in Et_2O (5 mL) at 0 °C. After warming to room temperature, the solution of $\mathit{i}Pr_3SiPLi_2$ was added to a suspension of $SnCl_2$ (0.22 g, 1.16 mmol) in Et_2O (20 mL) at 0 °C. Subsequently, the red mixture was warmed to ambient temperature while stirring and then agitated overnight. The resulting red solution was filtered to remove the precipitated LiCl and cooled to 0 °C. Red crystals of **3** formed over a period of 5

 © 2004 Wiley-VCH Verlag GmbH & Co. KGaA, Weinheim

Table 1. Crystallographic data of **1**−**5**[8]

Compound	**1**	**2**	**3**	**4**	**5**
Formula	$C_{63}H_{147}P_7Si_7Sn_7$	$C_{63}H_{147}As_7Si_7Sn_7$	$C_{54}H_{126}Cl_2P_6Si_6Sn_8$	$C_{62}H_{146}As_6Li_4O_2Si_6Sn_4$	$C_{54}H_{126}Ge_6P_6Si_6$
Space group	$R\bar{3}$	$R\bar{3}$	$P2_1/c$	$P2_1/n$	$P\bar{1}$
Z	6	6	4	2	2
Temperature	200 K	200 K	200 K	200 K	200 K
Lattice constants	a = 2058.3(3) pm	a = 2068.9(3) pm	a = 2258.9(5) pm	a = 1440.9(3) pm	a = 1402.8(3) pm
	b = 2058.3(3) pm	b = 2068.9(3) pm	b = 1376.4(3) pm	b = 2296.7(5) pm	b = 1497.1(3) pm
	c = 4000.0(8) pm	c = 4067.6(8) pm	c = 2782.4(6) pm	c = 1453.0(3) pm	c = 1927.9(4) pm
	α = 90°	α = 90°	α = 90°	α = 90°	α = 80.02(3)°
	β = 90°	β = 90°	β = 100.56(3)°	β = 109.53(3)°	β = 80.74(3)°
	γ = 120°	γ = 120°	γ = 90°	γ = 90°	γ = 76.80(3)°
Volume	14676(4) Å^3	15078(4) Å^3	8504(3) Å^3	4532(2) Å^3	3851(1) Å^3
Density	1.459 g/cm^3	1.623 g/cm^3	1.679 g/cm^3	1.498 g/cm^3	1.350 g/cm^3
2Θ range	2.5−50°	2.5−44°	3−48°	3.5−45°	3−48°
Reflections measured	13564	15285	23804	16732	17306
Independent reflections	5676 (R_{int} = 0.0423)	4082 (R_{int} = 0.0313)	12372 (R_{int} = 0.0695)	5743 (R_{int} = 0.1451)	11709 (R_{int} = 0.0551)
Ind. reflections with $F_o > 4\sigma(F_o)$	3993	3490	6210	4176	7019
Parameter	253	244	685	354	649
μ(Mo-K_α)	1.988 mm^{-1}	4.107 mm^{-1}	2.599 mm^{-1}	3.375 mm^{-1}	2.560 mm^{-1}
$R1$	0.0593	0.0460	0.0556	0.0630	0.0458
$wR2$ (all data)	0.1975	0.1557	0.1349	0.1699	0.1081
Residual electron density	2.164 e/Å^3	1.357 e/Å^3	2.201 e/Å^3	0.952 e/Å^3	0.953 e/Å^3

days. Yield: 0.1 g (30%). $C_{54}H_{126}Cl_2P_6Si_6Sn_8$ (2150.4): calcd. C 30.16, H 5.92; found C 30.89, H 6.43. ^{1}H NMR ([D$_8$]toluene): δ = 1.2−1.4 (m, *i*Pr) ppm. ^{31}P{^{1}H} NMR ([D$_8$]toluene): δ = −372.3 (s) ppm.

4: BuLi (1.23 mL, 1.6 M) was added dropwise to a solution of iPr$_3$SiAsH$_2$ (0.23 g, 0.98 mmol) in Et$_2$O (10 mL) at 0 °C. The resulting yellow solution was added at 0 °C to a suspension of SnCl$_2$ (0.12 g, 0.65 mmol) in Et$_2$O (15 mL).The purple red mixture was stirred for an additional 16 h and then filtered. After cooling of the solution to 0 °C **4** was obtained as violet crystals. Yield: 0.09 g (27%). Elemental analysis after drying in vacuo. $C_{54}H_{126}As_6Li_4Si_6Sn_4$ (1896.16): calcd. C 34.21, H 6.70; found C 34.17, H 6.853. ^{1}H NMR (C$_6$D$_6$): δ = 0.8−1.4 (m, *i*Pr) ppm.

5: BuLi (0.99 mL 1.6 M) was added at 0 °C to a solution of iPr$_3$SiPH$_2$ (0.15 g, 0.79 mmol)in Et$_2$O (5 mL). This solution was added at 0 °C to a suspension of GeCl$_2$(diox)$_2$ (0.25 g, 0.79 mmol) in Et$_2$O (20 mL). The orange mixture was stirred overnight and than filtered. After cooling of the solution to 0 °C **5** was obtained as orange crystals. Yield: 0.05 g (24%). $C_{54}H_{126}Ge_6P_6Si_6$ (1565.49): calcd. C 41.43, H 8.11; found C 40.56, H 7.81. ^{31}P(^{1}H) (C$_6$D$_6$): δ = −323.3 (s) ppm. ^{1}H(C$_6$D$_6$): δ = 1.42 [d, $^3J_{H,H}$ = 7.5 Hz, CH(CH_3)$_2$], 1.82 [sept, $^3J_{H,H}$ = 7.5 Hz, CH(CH$_3$)$_2$] ppm.

Acknowledgments

The authors thank Dr. P. Kramkowski for his valuable help with the manuscript and Prof. Dr. D. Fenske for helpful discussions and for providing excellent working conditions.

[1] [1a] S. Dehnen, A. Eichhöfer, D. Fenske, *Eur. J. Inorg. Chem.* **2002**, 279−317. [1b] O. Fuhr, A. Meredith, D. Fenske, *J. Chem. Soc., Dalton Trans.* **2002**, 4091−4094. [1c] V. N. Soloviev, A. Eichhöfer, D. Fenske, U. Banin, *J. Am. Chem. Soc.* **2001**, *123*, 2354−2364.

[2] N. T. Tran, D. R. Powell, L. F. Dahl, *Angew. Chem.* **2000**, *112*, 4287−4291; *Angew. Chem. Int. Ed.* **2000**, *39*, 4121−4125.

[3] J. Bai, A. V. Virovets, M. Scheer, *Science* **2003**, *300*, 781−783.

[4] [4a] M. Driess, *Adv. Inorg. Chem.* **2000**, *50*, 235−284. [4b] M. A. Paver, C. A. Russell, D. S. Wright, *Angew. Chem.* **1995**, *107*, 1679−1688; *Angew. Chem. Int. Ed. Engl.* **1995**, *34*, 1545−1554.

[5] [5a] O. Fuhr, D. Fenske, *Z. Anorg. Allg. Chem.* **2004**, *630*, 244−246. [5b] M. Westerhausen, M. Krofta, N. Wiberg, H. Noth, A. Pfitzner, *Z. Naturforsch., Teil B* **1998**, *53*, 1489−1493. [5c] M. Driess, S. Martin, K. Merz, V. Pintchouk, H. Pritzkow, H. Grützmacher, M. Kaupp, *Angew. Chem.* **1997**, *109*, 1982−1985; *Angew. Chem. Int. Ed. Engl.* **1997**, *36*, 1894−1897. [5d] D. Hänssgen, A. Dörr, H. Hens, R. Jeske, *J. Organomet. Chem.* **1995**, *487*, 17−21. [5e] D. Hänssgen, H. Aldenhoven, *Chem. Ber.* **1990**, *123*, 1833−1835. [5f] D. Hänssgen, H. Aldenhoven, M. Nieger, *Chem. Ber.* **1990**, *123*, 1837−1839. [5g] M. Dräger, B. Mathiasch, *Angew. Chem.* **1981**, *93*, 1079−1080; *Angew. Chem. Int. Ed. Engl.* **1981**, *20*, 1029−1030.

[6] [6a] D. Hanssgen, R. Jeske, M. Nieger, W. Roos, *Z. Anorg. Allg. Chem.* **2000**, *626*, 687−691. [6b] M. Westerhausen, N. Makropoulos, H. Piotrowski, M. Warchhold, H. Noth, *J. Organomet. Chem.* **2000**, *614*, 70−73. [6c] D. Hanssgen, R. Jeske, N. Korber, C. Mohr, M. Nieger, *Z. Anorg. Allg. Chem.* **1998**, *624*, 1202−1206. [6d] M. Westerhausen, M. M. Enzelberger, W. Schwarz, *J. Organomet. Chem.* **1995**, *491*, 83−90. [6e] A. H. Cowley, D. M. Giolando, R. A. Jones, C. M. Nunn, J. M. Power, *Polyhedron* **1988**, *7*, 1317−1319.

[7] [7a] C. Druckenbrodt, W.-W. du Mont, F. Ruthe, P. G. Jones, *Z. Anorg. Allg. Chem.* **1998**, *624*, 590−594. [7b] M. Driess, H. Pritzkow, U. Winkler, *Chem. Ber.* **1992**, *125*, 1541−1546. [7c] A. R. Dahl, A. D. Norman, H. Shenav, R. Schaeffer, *J. Am. Chem. Soc.* **1975**, 6364−6370.

[8] STOE-IPDS2 (Mo-K_α radiation, λ = 0.71073 Å). The structures were solved by direct methods and refined by full-matrix least-squares techniques against F^2 (Sn, Ge, As, P, Si, C refined anisotropically, H atoms were calculated at ideal positions). For compound **2** the C atoms of one iPr$_3$Si group were refined isotropically, no H atoms were calculated. The solvent molecules of compound **4** were refined isotropically, no H atoms were calculated at these C atoms. CCDC-219412 (for **1**),

-219414 (for **2**), -219413 (for **3**), -219415 (for **4**) and -219416 (for **5**) contains the supplementary crystallographic data for this paper. These data can be obtained free of charge from www.ccdc.cam.ac.uk/conts/retrieving.html (or from Cambridge Crystallographic Data Centre, 12 Union Road, Cambridge CB21EZ, UK; Fax: +44-1223-336-033; E-mail: deposit@ccdc.cam.ac.uk).

[9] [9a] B. Luo, W. L. Gladfelter, *Inorg. Chem.* **2002**, *41*, 590−597. [9b] M. Driess, S. Kuntz, C. Monse, K. Merz, *Chem. Eur. J.* **2000**, 4343−4347. [9c] B. P. Hitchcock, J. D. Smith, K. M. Thomas, *J. Chem. Soc., Dalton Trans.* **1976**, 1433−1437.

[10] C. von Hänisch, *Z. Anorg. Allg. Chem.* **2001**, *627*, 1414 −1416.

[11] [11a] M. Driess, S. Kuntz, K. Merz, H. Pritzkow, *Chem. Eur. J.* **1998**, *4*, 1628−1632. [11b] R. E. Allen, M. A. Beswick, N. L. Cromhout, M. A. Paver, P. R. Raithby, M. Trevithick, D. S. Wright, *Chem. Commun.* **1996**, 1501−1502.

[12] C. von Hänisch, D. Nikolova, *Z. Anorg. Allg. Chem.* **2004**, *630*, 345−346.

[13] [13a] M. Westerhausen, M. Wieneke, W. Schwarz, *J. Organomet. Chem.* **1999**, *572*, 249−257. [13b] M. Westerhausen, R. Löw, W. Schwarz, *J. Organomet. Chem.* **1996**, *513*, 213−229.

Received October 17, 2003
Early View Article
Published Online April 7, 2004

 © 2004 Wiley-VCH Verlag GmbH & Co. KGaA, Weinheim

Bis(fluoromesityl) Palladium Complexes, Archetypes of Steric Crowding and Axial Protection by *ortho* Effect − Evidence for Dissociative Substitution Processes − Observation of $^{19}F-^{19}F$ Through-Space Couplings

Camino Bartolomé,[a] Pablo Espinet,*[a] Jose M. Martín-Álvarez,[a] and Fernando Villafañe[a]

Keywords: Palladium / Dissociative substitution / Fluorine / Bulky ligands / Steric crowding / Through-space coupling

Bisarylated complexes *trans*-[Pd(Fmes)$_2$(SR$_2$)$_2$] [Fmes = 2,4,6-tris(trifluoromethyl)phenyl (fluoromesityl); SR$_2$ = SMe$_2$, tht; tht = tetrahydrothiophene] are precursors for various bisarylated fluoromesityl palladium(II) complexes by ligand-substitution reactions. Boiling under reflux in acetonitrile gives the mixed complexes *trans*-[Pd(Fmes)$_2$(NCMe)(SR$_2$)], whereas boiling under reflux in toluene leads to *trans*-[PdCl$_2$L$_2$] (L = PMe$_3$, *t*BuNC, *p*Tol-NC, 4-MePy), in the presence of neutral monodentate ligands, or to (N*n*Bu$_4$)[*trans*-Pd(Fmes)$_2$I(SR$_2$)] when treated with (N*n*Bu$_4$)I. *trans*-[Pd(Fmes)$_2$(SMe$_2$)$_2$] reacts with bidentate ligands, also boiling under reflux in toluene, to give [Pd(Fmes)$_2$(L–L)] [L–L = Me$_2$bipy, 2,2′-biquinolyl, κ^2N,N'-OCPy$_2$, dppm (Ph$_2$PCH$_2$PPh$_2$), dppe (Ph$_2$PCH$_2$CH$_2$PPh$_2$), pte (PhSCH$_2$CH$_2$SPh), κ^2S,N-SPPh$_2$Py, κ^2O,N-OPPhPy$_2$], or the bimetallic complex [Pd(Fmes)$_2$(μ-1κ*N*:1,2κ*O*:2κ*N*-Py$_2$MeCO)Pd(Fmes)(SMe$_2$)] (characterized by X-ray diffractometry) when treated with (OH)(CH$_3$)CPy$_2$. The crowding associated with two Fmes groups produces several interesting features: (1) trans complexes are preferred over cis complexes, against the expected electronic preferences; (2) the low-temperature NMR spectra of several complexes, or the X-ray diffraction structure of [Pd(Fmes)$_2$(2,2′-biquinolyl)], reveal significant structural distortions associated with steric crowding; (3) the need for boiling under reflux in the synthesis suggests a dissociative substitution mechanism, which is unknown so far for Pd; (4) some of the complexes show $^{19}F-^{19}F$ through-space couplings.
(© Wiley-VCH Verlag GmbH & Co. KGaA, 69451 Weinheim, Germany, 2004)

Introduction

2,4,6-Tris(trifluoromethyl)phenyl (nonafluoromesityl or Fmes) is an interesting ligand for main group and transition metals.[1,2] It combines steric bulk with a certain electron-withdrawing character, and lacks hydrogens susceptible to H-elimination. The latter two features may facilitate the preparation of stable derivatives where the consequences (structural or otherwise) of steric crowding can be tested. However, its bulkiness limits direct arylation as a method of obtaining organometallics that contain more than one Fmes group. Our initial studies on the coordination of Fmes in palladium(II) complexes by arylation indicated that bisarylated complexes are only accessible for small ancillary ligands.[2a] After the first arylation (Scheme 1), the coordinated Fmes exerts a high axial protection (*ortho* effect) against subsequent nucleophilic attack, which can progress reasonably well only when the spatial requirements of the ancillary ligands are small, so that the initially coordinated Fmes can tilt and facilitate the approach of the entering Fmes$^-$ nucleophile. In kinetic terms, the activation enthalpy

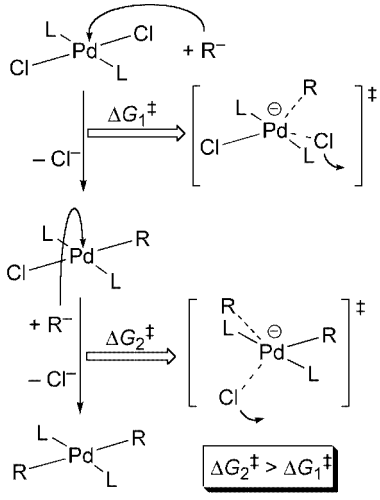

Scheme 1. Associative mechanism for an arylation reaction

for the second arylation ($\Delta G_2^{\ddagger}$) is noticeably higher than $\Delta G^{\ddagger}$, its value increasing as the hindrance of the ancillary ligands to the tilting of the coordinated Fmes increases.

However, ligand substitution on bisarylated complexes obtained by arylation might allow the synthesis of a wider range of bisarylated species. Here we describe the synthesis and characterization of different bisarylated Fmes pal-

[a] Departamento de Química Inorgánica, Facultad de Ciencias, Universidad de Valladolid,
47005 Valladolid, Spain
E-mail: espinet@qi.uva.es

 © 2004 Wiley-VCH Verlag GmbH & Co. KGaA, Weinheim **DOI: 10.1002/ejic.200300756**

ladium(II) complexes obtained by treating *trans*-$[Pd(Fmes)_2(SR_2)_2]$ (SR_2 = SMe_2, tht; tht = tetrahydrothiophene) with monodentate or bidentate ligands. The reactions must be carried out in either toluene or acetonitrile boiling under reflux, suggesting a dissociative ligand substitution mechanism, which is unusual for Pd. Some of the *cis*-bisarylated complexes obtained show interesting structural features associated with their steric crowding. Several complexes exhibit $^{19}F-^{19}F$ through-space couplings between both Fmes. References on such couplings in organometallic compounds are scarce,[3] even though many *cis*-bisarylated fluoroaryl complexes are known.[4]

Results

Syntheses of Bisarylated Complexes

The complex *trans*-$[Pd(Fmes)_2(SMe_2)_2]$ (**1a**) was obtained by arylation of *trans*-$[PdCl_2(SMe_2)_2]$ with Li(Fmes), as described previously for *trans*-$[Pd(Fmes)_2(tht)_2]$ (**1b**).[2a] This complex is a better precursor for the preparation of other bisarylated complexes (Scheme 2) as SMe_2 has a higher volatility (b.p. 38 °C) than tht (b.p. 119 °C). Although in related Pd complexes (e.g. *trans*-$[Pd(C_6F_5)_2(SMe_2)_2]$, or *trans*-$[Pd(C_6F_5)_2(tht)_2]$) SMe_2 or tht are easily displaced by other ligands at room temperature,[4a] in these bis-Fmes derivatives they resist displacement, even in the presence of a large excess of the entering ligand. Displacement is achieved only when the mixture is submitted to reflux in high-boiling temperature solvents such as toluene or MeCN.

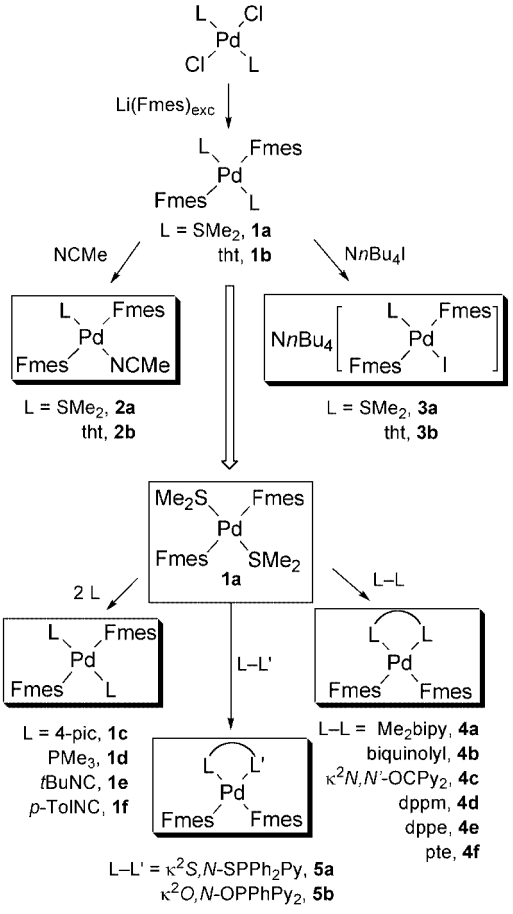

Scheme 2. Synthesis of the complexes

Thus, neutral monodentate ligands L replace SMe_2 from **1a**, in refluxing toluene, to give the corresponding neutral mononuclear complexes *trans*-$[Pd(Fmes)_2L_2]$ (L = 4-pic, **1c**; PMe_3, **1d**; *t*BuNC, **1e**, *p*Tol-NC, **1f**). The reactions do not proceed under milder conditions. Boiling under reflux **1a** or **1b** in NCMe produced *trans*-$[Pd(Fmes)_2(NCMe)(SMe_2)]$ (**2a**).

Treatment of **1a** or **1b** with excess ($NnBu_4$)I did not lead to the substitution of both thioether ligands by iodide, but to the formation of the monoanionic ($NnBu_4$)[*trans*-$Pd(Fmes)_2I(SMe_2)]$ (**3a**) or ($NnBu_4$)[*trans*-$Pd(Fmes)_2I(tht)]$ (**3b**), respectively.

Boiling under reflux in toluene was also required to replace the thioether ligands when **1a** was treated with neutral bidentate ligands L-L. This produced $[Pd(Fmes)_2(L\text{-}L)]$ (L-L = Me_2bipy (4,4′-Me_2-2,2′-bipyridine), **4a**; biquinolyl, **4b**; κ^2N,N'-$OCPy_2$ (Py = 2-pyridyl), **4c**; dppm ($Ph_2PCH_2PPh_2$), **4d**; dppe ($Ph_2PCH_2CH_2PPh_2$), **4e**; pte ($PhSCH_2CH_2SPh$), **4f**).

Bisarylated complexes containing chemically non-equivalent Fmes groups were obtained with bidentate ligands containing two different donor atoms (L-L′). Thus the S,N-donor ligand $SPPh_2Py$ gave $[Pd(Fmes)_2(\kappa^2S,N\text{-}SPPh_2Py)]$ (**5a**). Remarkably, equimolar amounts of **1a** and $OPPhPy_2$, which usually coordinates as κ^2N,N-donor to Pd^{II},[5] gave $[Pd(Fmes)_2(\kappa^2O,N\text{-}OPPhPy_2)]$ (**5b**). The treatment of $(OH)(CH_3)CPy_2$ with *trans*-$[Pd(Fmes)_2(SMe_2)_2]$ (**1a**) did not afford the expected *cis* bisarylated complex, but gave instead the binuclear complex $[Pd(Fmes)_2(\mu\text{-}1\kappa N{:}1,2\kappa O{:}2\kappa N\text{-}Py_2MeCO)Pd(Fmes)(SMe)_2]$ (**6**) (Scheme 3).

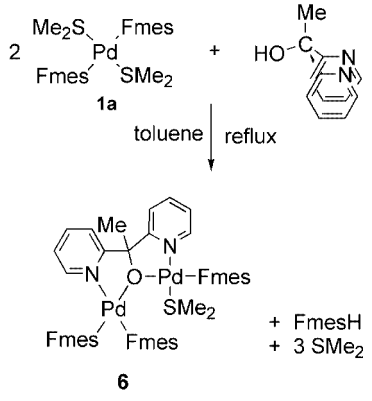

Scheme 3. Preparation of **6**

Characterization of Bisarylated Complexes

Solid-state IR spectra of all the bisarylated complexes show characteristic absorptions for the Fmes group.[6] Absorption in the region 710−670 cm^{-1} for several polyfluorophenyl has been associated with the R−M fragment and can be structurally informative: the *cis* isomers exhibit two

 © 2004 Wiley-VCH Verlag GmbH & Co. KGaA, Weinheim

medium-to-strong bands in this range, whereas the *trans* isomers show only one.[4a,7] This feature is also observed at 690−680 cm^{-1} for the Fmes complexes, which supports their structural assignments. No additional evidence is provided by the IR data of **1a** (although the *trans* isomer was found in the structural determination of **1b**, previously reported),[2a] and **1c**. The *trans* geometry for **1e** and **1f** is further supported by the presence of only one ν(C≡N) absorption for the coordinated isocyanides.

trans-[Pd(Fmes)$_2$(*p*Tol-NC)$_2$] (**1f**) was characterized by solid-state X-ray diffractometry, as an example of a complex with a ligand with minimal steric requirements in the vicinity of the coordination sites. The molecular structure of **1f** (Figure 1) and selected distances and angles (Table 1) are given here.

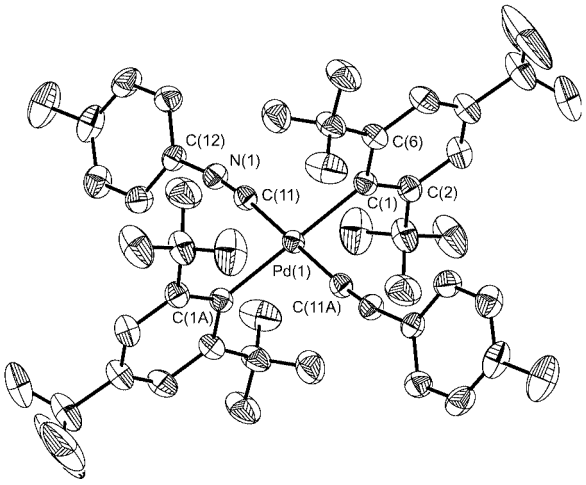

Figure 1. Molecular structure of *trans*-[Pd(Fmes)$_2$(*p*Tol-NC)$_2$] (**1f**). All hydrogen atoms omitted for clarity

Table 1. Selected bond lengths (Å) and angles (°) for *trans*-[Pd(Fmes)$_2$(*p*Tol-NC)$_2$] (**1f**); #1: $-x+1, -y+1, -z+1$; #2: $-x, -y, -z$

Pd(1)−C(1)	2.102(4)	C(11)−Pd(1)−C(1)	92.80(14)
Pd(1)−C(11)	1.960(4)	C(11)−Pd(1)−C(1)#1	87.20(13)
C(11)−N(1)	1.152(5)	C(6)−C(1)−C(2)	114.4(3)
N(1)−C(12)	1.405(5)	C(22)−C(21)−C(26)	115.0(3)
Pd(2)−C(21)	2.098(4)	C(11)−N(1)−C(12)	171.5(4)
Pd(2)−C(31)	1.959(5)	C(31)−N(2)−C(32)	174.5(4)
C(31)−N(2)	1.152(5)	C(31)−Pd(2)−C(21)	91.93(15)
N(2)−C(32)	1.407(6)	C(31)#2−Pd(2)−C(21)	88.07(15)

There are two independent molecules of **1f** in the unit cell, but only one-half of each molecule is included in the asymmetric unit. The molecules show a square-planar coordination for Pd, with the two isocyanide ligands in *trans* disposition (related by an inversion centre) and the isocyanide and the Fmes group forming an angle C(11)−Pd(1)−C(1) = 92.80(14)° in one molecule and C(31)−Pd(2)−C(21) = 91.93(15)° in the other. The two Fmes groups are coplanar and nearly perpendicular to the coordination plane, one showing the two Fmes groups tilted only 5.8(4)° and the other 2.2(4)° to the coordination plane. The Pd−C_{ipso} distances [Pd(1)−C(1), 2.102(4) Å; Pd(2)−C(21), 2.098(4) Å] are similar to those found in *trans*-[Pd(Fmes)$_2$(tht)$_2$],[2a] and somewhat longer than those in other complexes where the ligand *trans* to the Fmes is harder (see, for instance, other structures in this paper and in ref. 2). As usually observed in Fmes palladium complexes, the C−C−C angles at the *ipso* carbon are significantly less than 120° and those at the *ortho* carbon atoms are rather larger than 120° due to the electronic effects of the electropositive metal and electronegative CF_3 substituents at these positions.[8] The C−N−C angle of the two isocyanide groups is < 180°, a common feature for isocyanides coordinated to transition metals.[9] The structure suggests that there are no important repulsive interactions between neighbouring CF_3 groups, otherwise the rings would tilt to scatter these as much as possible. The elongation of the Pd−CF_3 distance compared with other complexes (and similar to *trans*-[Pd(Fmes)$_2$(tht)$_2$]) is then attributed mostly to a high *trans* influence of the Fmes group. Presumably, with these Pd−Fmes distances, there is little steric repulsion between facing CF_3 groups in a *trans*-[Pd(Fmes)$_2$L$_2$] complex.

The ^{19}F NMR spectra of all the *trans* complexes **1** display two singlets with 2:1 intensities, except for **1d** where a triplet is observed for the *ortho*-CF_3 due to coupling with two equivalent phosphorus atoms. The *trans* geometry of complexes **2** and **3** is confirmed by the chemical equivalence of both Fmes groups.

The *cis* complexes **4** exhibit only one singlet for *para* CF_3 groups (which is consistent with the equivalence of the two Fmes groups), and another signal for the equivalent *ortho*-CF_3 groups. However, with biquinolyl **4b** and pte **4f** the latter signal is very broad, which is interpreted as owing to a slow concerted tilting of both Fmes groups, as observed for related systems.[2a] The ^1H NMR spectra show that the two halves of the chelate ligands are equivalent through a C_2 axis.

To explore the expected distortions when more sterically demanding ligands are used, **4b** (L-L = 2,2′-biquinolyl) was characterized by solid-state X-ray diffractometry (Figure 2); Table 2 gives relevant distances and angles. The two Fmes ligands are coordinated in a *cis* arrangement, and the two N atoms of the biquinolyl ligand occupy the other coordination sites. The biquinolyl ligand is not planar, with the two halves forming an angle of 25.0(5)°. Moreover, the average plane of the biquinolyl ligand forms a dihedral angle of 35.8(5)° with the average coordination plane. This makes the nitrogen atoms pyramidal, as found in [Pd(biquinolyl)(allyl)]$^+$ complexes.[10] The square-planar geometry of Pd is severely distorted towards tetrahedral with the C_{ipso} atoms of the two Fmes situated 0.42 and 0.98 Å above and below, respectively, the N−Pd−N plane. For comparison, the related complex [Pd(Fmes)$_2$(bipy)], which is also tetrahedrally distorted,[2a] shows a smaller distortion with the C_{ipso} atoms 0.40 Å above and below the N−Pd−N plane. Tetrahedral distortion is associated with angles that differ greatly from those expected for a square-planar geo-

 © 2004 Wiley-VCH Verlag GmbH & Co. KGaA, Weinheim

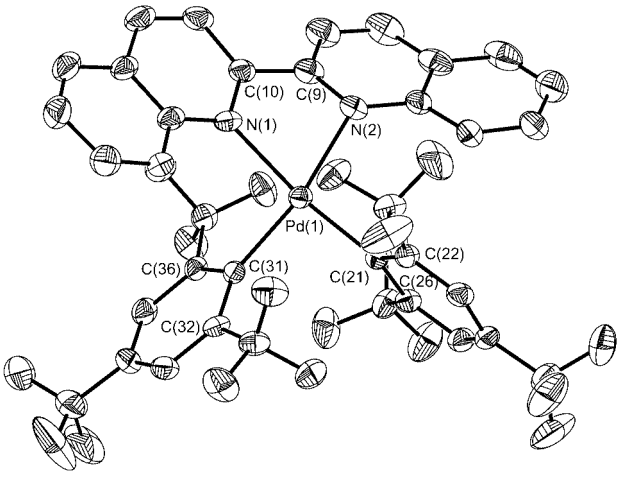

Figure 2. Molecular structure of [Pd(Fmes)$_2$(biquinolyl)] (**4b**)

Table 2. Selected bond lengths (Å) and angles (°) for [Pd(Fmes)$_2$-(biquinolyl)] (**4b**)

Pd(1)−C(21)	2.014(6)	C(21)−Pd(1)−C(31)	93.9(2)
Pd(1)−C(31)	2.056(5)	C(21)−Pd(1)−N(2)	100.46(19)
Pd(1)−N(1)	2.136(5)	C(31)−Pd(1)−N(1)	94.83(19)
Pd(1)−N(2)	2.248(4)	N(1)−Pd(1)−N(2)	75.88(18)
		C(26)−C(21)−C(22)	113.8(5)
		C(36)−C(31)−C(32)	113.5(5)

metry: C(21)−Pd(1)−C(31) 93.9(2)°; C(21)−Pd(1)−N(2) 100.46(19)°; C(31)−Pd(1)−N(1) 94.83(19)°. The N(1)−Pd(1)−N(2) angle is 75.88(18)°, a normal value for this small-bite chelating ligand. Despite these distortions the Pd−C and Pd−N distances are not affected noticeably, remaining very similar to those of the square-planar [Pd-(bipy)(Fmes)$_2$].[2a]

κ^2O,N-Coordination of OPPhPy$_2$ in **5b** is supported by the phosphorus chemical shift in the $^{31}P\{^1H\}$ NMR spectrum, which clearly differs from those shifts when OPPhPy$_2$ acts as κ^2N,N-donor (Table 3), and is closer to those of the κ^2O,N-chelate OPPh$_2$Py.[2c,5,11] The difference with the latter can be accounted for by the higher shielding effect on P of Py compared with Ph. The P−O stretching absorptions are usually useful in differentiating κ^2O,N- and κ^2N,N-coordination modes of OPPhPy$_2$ [12] but this band is not detected in the IR spectrum of **5b** due to other intense absorptions in the same range.

Unequivocal characterization of [Pd(Fmes)$_2$(μ-1κ*N*:1,2κ*O*:2κ*N*-Py$_2$MeCO)Pd(Fmes)(SMe$_2$)] (**6**) required an X-ray diffraction study. A perspective view of the molecular structure is given in Figure 3, and selected distances and angles are listed in Table 4.

The complex is binuclear and the two Pd coordination planes make a dihedral angle of 72.1(4)° (Figure 3). The molecule contains three non-equivalent Fmes groups, two

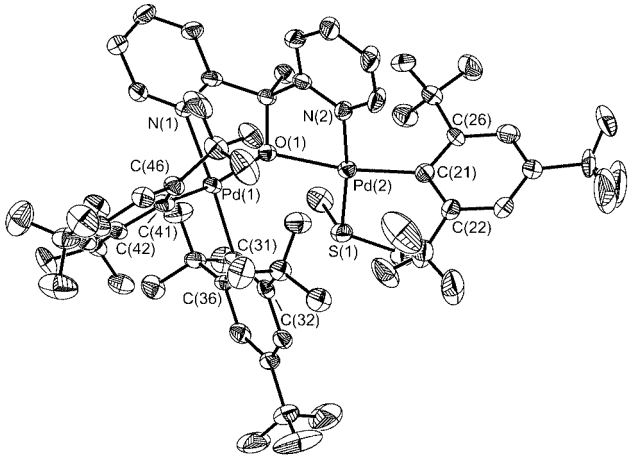

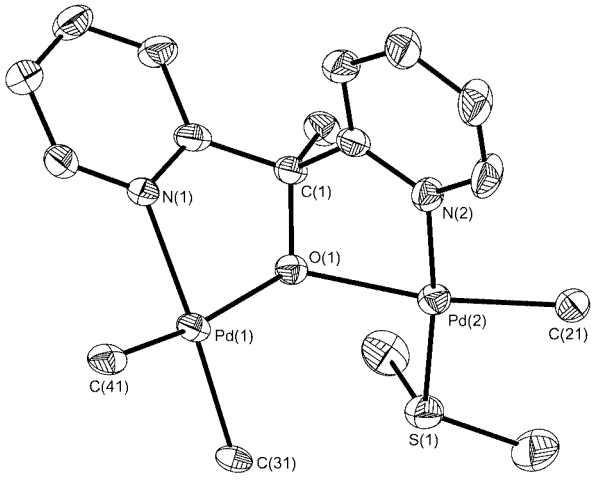

Figure 3. (top) Molecular structure of [Pd(Fmes)$_2$(μ-1κ*N*:1,2κ*O*:2κ*N*-Py$_2$MeCO)Pd(Fmes)(SMe$_2$)] (**6**); (bottom) view of the skeleton showing the mode of coordination of the [O(CH$_3$)CPy$_2$]$^-$ ligand

Table 3. ^{31}P NMR chemical shifts of 2-pyridylphosphane oxide and bis(2-pyridyl)phosphane oxide palladium complexes, at room temperature in CDCl$_3$

Complexes	Coordination mode	δ[ppm]	Ref.
[Pd(Fmes)$_2$(OPPhPy$_2$)] (**5b**)	κ^2O,N	39.01	this work
[Pd(C$_6$F$_5$)$_2$(OPPh$_2$Py)]	κ^2O,N	49.8	[5]
[Pd(C$_6$F$_5$)Br(OPPh$_2$Py)]	κ^2O,N	49.9	[5]
[Pd(Fmes)(NCMe)(OPPhPy$_2$)]BF$_4$	κ^2N,N	21.1	[11]
[PdCl(Fmes)(OPPhPy$_2$)]	κ^2N,N	20.4	[2c]
[Pd(C$_6$F$_5$)X(OPPhPy$_2$)]	κ^2N,N	20.7−21.0	[5]
[Pd(C$_6$F$_5$)$_2$(OPPhPy$_2$)]	κ^2N,N	20.7	[5]

 © 2004 Wiley-VCH Verlag GmbH & Co. KGaA, Weinheim

Table 4. Selected bond lengths (Å) and angles (°) for [Pd(Fmes)$_2$(μ-1κ*N*:1,2κ*O*:2κ*N*-Py$_2$MeCO)Pd(Fmes)(SMe$_2$)](C$_6$H$_5$CH$_3$)$_{0.5}$ (**6**·0.5 toluene)

Pd(1)−C(41)	2.011(13)	C(31)−Pd(1)−N(1)	167.3(4)
Pd(1)−C(31)	2.027(10)	C(41)−Pd(1)−O(1)	168.4(4)
Pd(1)−N(1)	2.101(8)	C(21)−Pd(2)−N(2)	92.4(4)
Pd(1)−O(1)	2.147(6)	N(2)−Pd(2)−O(1)	79.5(3)
Pd(2)−C(21)	2.005(11)	C(21)−Pd(2)−S(1)	94.2(3)
Pd(2)−N(2)	2.049(10)	O(1)−Pd(2)−S(1)	93.9(2)
Pd(2)−O(1)	2.122(7)	N(2)−Pd(2)−S(1)	173.3(3)
Pd(2)−S(1)	2.290(4)	C(21)−Pd(2)−O(1)	170.7(3)
C(41)−Pd(1)−C(31)	95.6(4)	C(26)−C(21)−C(22)	115.5(12)
C(41)−Pd(1)−N(1)	91.8(4)	C(36)−C(31)−C(32)	113.7(10)
C(31)−Pd(1)−O(1)	93.6(3)	C(46)−C(41)−C(42)	111.8(11)
N(1)−Pd(1)−O(1)	80.4(3)		

of them *cis* coordinated to one of the metal centres, Pd(1). Each pyridyl group of the [O(CH$_3$)CPy$_2$]$^-$ ligand is coordinated to a different palladium atom, whereas the oxygen atom bridges the two metal centres. The SMe$_2$ ligand occupies the fourth coordination site in the monoarylated Pd atom.

The Pd−C distances are all very similar [Pd(1)−C(41) 2.011(13), Pd(1)−C(31) 2.027(10), Pd(2)−C(21) 2.005(11) Å], lying in the range of other *cis* bisarylated or monoarylated Fmes Pd complexes.[2a−2e] The distances and angles of the [O(CH$_3$)CPy$_2$]$^-$ ligand are similar to those found in In^{III} [13] and Cu^{II} [14] complexes, where it is also coordinated as a bridging ligand.

Whereas the geometry of the monoarylated palladium centre is nearly square planar, that of the bisarylated palladium centre is very distorted, since N(1) is 0.574(15) Å out of the plane defined by O(1)−C(41)−Pd(1)−C(31). The N(1)−Pd(1)−O(1) and N(2)−Pd(2)−O(1) angles are significantly lower than 90° [80.4(3)° and 79.5(3)°], which is compensated for by the C(31)−Pd(1)−O(1) and O(1)−Pd(2)−S(1) angles [93.6(3)° and 93.9(2)°, respectively]. The *cis* angle involving the carbon atoms of the Fmes ligands is larger than 90° [95.6(4)°], presumably as a result of steric constraints.

The Fmes groups are not perpendicular to the coordination plane, but tilted in the same sense by 70.4° [C(41)], 64.6° [C(31)] and 78.6° [C(21)]. This tilting, observed for other *cis* bis(Fmes) palladium complexes,[2a] seems to help in minimizing the repulsions between the *ortho*-CF$_3$ substituents of *cis* Fmes groups.

^{19}F NMR spectra of complexes **5a**, **5b**, and **6** reveal ^{19}F−^{19}F through-space coupling (see below).

Discussion

For square-planar aryl complexes, although the C−M bonding interaction is little affected by the dihedral angle between the aryl and the coordination plane, the aryl groups tend to lie perpendicular to the coordination plane to minimize steric repulsions.[15] Conversely, ligand-substitution reactions on 16e palladium(II) complexes follow an associative mechanism via 18e pentacoordinate transition states, rather than the alternative dissociative pathway via 14e three-coordinate intermediates.[16] We know of no exception to this rule for palladium, although several dissociative ligand substitution have been found in bis(aryl) derivatives of platinum.[17] The aryl complexes reported here show dramatic deviations from the normal behaviour of Pd^{II} complexes due to the steric crowding produced by the four *ortho*-CF$_3$ groups competing for the same axial space over the coordination plane. It is convenient to discuss first their structural features to better understand their reactivity. Fortunately, many results for these bis(Fmes) complexes can be directly compared with those in the literature for C$_6$F$_5$ complexes, and with the mono(Fmes) complexes recently reported.[2c]

Structures in the Solid State and in Solution

(A) Complexes *trans*-[Pd(Fmes)$_2$L$_2$] (L = monodentate ligand): X-ray structures of the complexes with L = tht,[2a] *p*Tol-NC show an essentially square-planar geometry, with the Fmes rings almost coplanar and perpendicular to the coordination plane. The same arrangement has been found in the square planar *trans*-[Au(Fmes)$_2$I$_2$]$^-$.[1f] However, in the linear complex [Au(Fmes)$_2$]$^-$ the aryl planes of the two Fmes groups make an angle of 27.2°. For comparison, the complex [Au(C$_6$F$_5$)$_2$]$^-$ shows coplanar rings.[18] Thus, two *trans* Fmes groups are better stabilized as coplanar and lay perpendicular to the coordination plane when the other two positions in the square-planar geometry are occupied. When there are no ancillary ligands present, as in [Au(Fmes)$_2$]$^-$, the Fmes groups scatter by rotation, giving rise to a pseudohelicoidal geometry and relieving the repulsion between the facing *ortho*-CF$_3$ groups. Such behaviour suggests that the steric repulsion between two *trans* Fmes groups is perceptible but very moderate.

(B) Complexes *cis*-[Pd(Fmes)$_2$(L-L′)] [L-L = bipy;[2a] biquinolyl (4b), or the *cis*-bisarylated moiety of 6]: These square-planar geometries are clearly more distorted towards tetrahedral than those of *trans* bisarylated complexes. The distortion increases with the size of the ancillary ligands. The Pd−C distances are shorter than for the *trans* bisarylated complexes (the *trans* effect of the ancillary ligands is lower than that of Fmes), and slightly longer than those in monoarylated Fmes Pd complexes (the latter are usually below 2.0 Å).[2c] The Fmes groups are not perpendicular to the coordination plane, as is usual in common aryl derivatives, but tilted in the same sense by ca. 20° from the perpendicular. Since the steric crowding in a *cis* bisarylated moiety is clearly higher than in *trans* bisarylated complexes, so must be the corresponding repulsions. This concerted tilt appears to be the best distortion to minimize repulsions between the *ortho*-CF$_3$ of the two contiguous Fmes ligands, even if it increases the repulsions with the ancillary ligands. This distortion should make chemically non-equivalent the *exo* and *endo* (relative to the C−Pd−C angle) *ortho*-CF$_3$ groups. In solution all the *cis* bisarylated complexes reported here are stereochemically dynamic, and a concerted tilting of the two Fmes ligands gives rise to an

 © 2004 Wiley-VCH Verlag GmbH & Co. KGaA, Weinheim

averaged geometry in which the Fmes groups would be perpendicular to the coordination plane. The barrier to this *endo*−*exo* exchange is low, but a broadening of the *ortho*-CF_3 signals is observed in the low-temperature ^{19}F NMR spectra of some of the *cis* bisarylated complexes. The tilting has been frozen out in the recently reported related Ni complex [Ni(Fmes)$_2$(1,2-dimethoxyethane)$_2$],[19] where the smaller metal atom leads to greater crowding.

No spectroscopic evidence was found in solution for the tetrahedral distortion observed in the solid-state structures of some of the complexes. For instance, the ^{19}F NMR of **4b** should give four *ortho*-CF_3 signals if the solid-state structure were "frozen" in solution, but only one signal is observed. This indicates that the barriers for the process averaging the coordination plane and that for the concerted tilting are low, and that the processes are fast even at low temperatures.

(C) Complexes *cis*-[Pd(Fmes)$_2$(L-L′)] with Other Chelating Ligands. $^{19}F-^{19}F$ Through-Space Couplings: Complexes **5a**, **5b**, and **6** have less symmetric structures and their spectra reveal $^{19}F-^{19}F$ through-space couplings between close non-equivalent *ortho*-CF_3 groups. The *para*-CF_3 groups are too far away to show through-space coupling.

In [Pd(Fmes)$_2$(SPPh$_2$Py)] (**5a**) the ligand SPPh$_2$Py coordinates to the bisarylated fragment as a κ^2S,N-donor in an averaged planar chelate ring (Scheme 4). The fast envelope-shift movement of the five-membered chelate rings has a very low activation energy, allowing us to consider the five-membered metallacycle as planar.[20] Accordingly, the ^{19}F NMR spectrum of **5a** shows two high-field singlets due to the two non-equivalent *para*-CF_3, whereas the *ortho*-CF_3 groups form a $X_3A_3A'_3X'_3$ system, which affords two quadruplets, with $J = 9.3$ Hz. This value may be ascribed to through-space coupling between the fluorine atoms on the same side of the coordination plane (Scheme 4), as there are too many bonds between the inequivalent atoms to permit significant scalar coupling, and the coupling constant is similar to those detected in some fluoroaryl complexes described by our group.[3] No diagonal coupling is detected between CF_3 groups of different Fmes groups, nor between different CF_3 groups at opposite sides of the coordination plane.

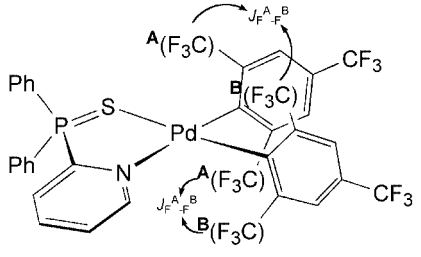

Scheme 4. $^{19}F-^{19}F$ through-space couplings in **5a**

In [Pd(Fmes)$_2$(κ^2O,N-OPPhPy$_2$)] (**5b**) the ligand OPPhPy$_2$ coordinates to the bisarylated moiety as κ^2O,N-donor (Scheme 6). As for **5a**, the inequivalent *para*-CF_3 give rise to two high-field singlets, whereas the *ortho*-CF_3 groups now constitute an $A_3K_3M_3X_3$ system, giving rise to four quadruplets. The coupling constants (7.5, 6.0 Hz) are similar to those of **5a**, indicating that the observed through-space coupling occurs between *ortho*-CF_3 groups in different Fmes rings, but at the same side of the coordination plane. As before, no other couplings are detected.

For [Pd(Fmes)$_2$(μ-1κ*N*:1,2κ*O*:2κ*N*-Py$_2$MeCO)Pd(Fmes)(SMe$_2$)] (**6**) the ^{19}F NMR spectrum shows three singlets in the *para*-CF_3 region, confirming the presence of three non-equivalent Fmes groups. Six signals (one singlet and five multiplets) are detected in the *ortho*-CF_3 region (Figure 4), indicating that they are all non-equivalent. Homonuclear decoupling experiments allowed us to assign which nuclei are involved in each coupling (Figure 4), assuming that all the coupling constants observed are due to through-space coupling between fluorine atoms on the same side of the coordination planes, as observed for **5a** and **5b**. While $F_3C(29)$ appears as non-coupled because it is far from the rest of fluoromethyl groups, $F_3C(37)$ is coupled with $F_3C(49)$ (both on the same metal) and with $F_3C(27)$ (which is on the other Pd atom). The coupling constants are 10 and 8.5 Hz, respectively. The other two fluoromethyl groups showing couplings are $F_3C(47)$ and $F_3C(39)$, with $J = 8$ Hz. These through-space coupling constants give an estimation of the distance between the fluoromethyl groups;[21] the higher coupling the shorter distance, regardless of whether the fluoromethyl groups belong to Fmes coordinated to the same or to different metal centres.

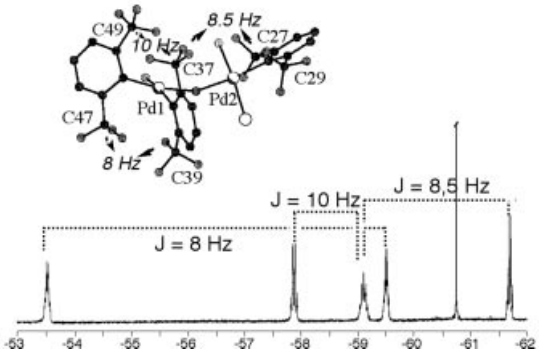

Figure 4. ^{19}F NMR of [Pd(Fmes)$_2$(μ-1κ*N*:1,2κ*O*:2κ*N*-Py$_2$MeCO)Pd(Fmes)(SMe$_2$)] (**6**) (*ortho*-CF_3) in $CDCl_3$ at 298 K, showing the through-space couplings observed

Complex **6** shows a slow dynamic process in solution that involves the SMe_2 group. Its ^1H and ^{19}F spectra in $CDCl_3$ at room temperature accord with the solid-state structure, but the two signals for the methyl groups of the SMe_2 are broad at room temperature, and coalesce at 333 K. This equivalence can be achieved by a process requiring both inversion of the sulfur atom and rotation about the Pd−S bond. The high steric crowding could be responsible for the very slow exchange at room temperature. However, a process involving SMe_2 dissociation and reassociation occurs

 © 2004 Wiley-VCH Verlag GmbH & Co. KGaA, Weinheim

for other isomerizations in complexes with this weakly bound ligand[3b] and can not be discounted here.

Mechanisms of the Syntheses of Bisarylated Complexes

In contrast with the reaction features of ligand substitution in [PdCl(Fmes)L_2] complexes, which suggest an associative mechanism,[2c] the harsh conditions required for ligand substitution in the bis-Fmes complexes suggest a dissociative mechanism, implying a positive activation entropy, which is favoured at high temperature.[22] Although associative ligand substitutions dominate palladium(II) chemistry (so far they are the only type observed), dissociative mechanisms could become competitive (faster) as the associative are disfavoured. Dissociative ligand substitution could be favoured by (i) PdR_2 substrates where R is a good σ-donor;[23] (ii) complexes with bulky ligands;[17e,22] and (c) substrates with labile leaving ligands. These three requirements are met by **1a**. An associative mechanism through a five-coordinate transition state should be disfavoured in our system for electronic reasons (the palladium centre in bisarylated substrates is electron rich), and even more so for steric reasons: as the *z* axis is occupied above and below the metal coordination plane by the *ortho*-CF_3 of the two Fmes groups, the attack of even a small nucleophile looks to be extremely difficult (*ortho* effect).

This leads us to propose the mechanism depicted in Scheme 5 for the substitution reactions. The formation of only *trans* bis-Fmes complexes from the reactions of *trans*-[Pd(Fmes)$_2$(SMe_2)$_2$] with monodentate ligands contrasts with previous observations for reactions on *trans*-[Pd(C_6F_5)$_2$(tht)$_2$], where *cis* complexes are formed in preference.[22b] This means that *trans*-[Pd(Fmes)$_2$$L_2$] and *cis*-[Pd($C_6F_5$)$_2$$L_2$] are the thermodynamic products, respectively, for these two aryls. Formation of the *trans* isomer with Fmes complexes occurs against the antisymbiotic effect (or transphobia),[24] indicating that the relief of steric crowding in the *trans* complex compensates for the higher electronic destabilization associated with two *trans* Fmes groups.

Boiling under reflux complexes **1** in NCMe furnishes *trans*-[Pd(Fmes)$_2$(NCMe)(SR_2)] (**2**) complexes. The bis(acetonitrile) complex [Pd(Fmes)$_2$(NCMe)$_2$] has not been detected, suggesting that the first substitution of SMe_2 by the poorer donor NCMe makes the complex less electron rich, and the dissociation of a second SR_2 becomes disfavoured.

The formation of the monosubstituted products, (N*n*Bu_4)[*trans*-Pd(Fmes)$_2$I(SR_2)] (**3**), after the reactions of *trans*-[Pd(Fmes)$_2$(SR_2)$_2$] (**1**) with (N*n*Bu_4)I can be considered normal. The formation of (N*n*Bu_4)$_2$[Pd(Fmes)$_2$$X_2$] is, apparently, counter-thermodynamic; similar results have been found for non-crowded bisarylated complexes. For instance, no [Pd(C_6F_5)$_2$$X_2$]$^{2-}$ complexes have been reported, despite many studies on (pentafluorophenyl)palladium complexes.[25]

The formation of complexes **4** and **5** involves a *trans*-to-*cis* isomerization from the starting material to the final product. Thus, a topomerization of the *trans* to the corresponding *cis* three-coordinate intermediate is needed

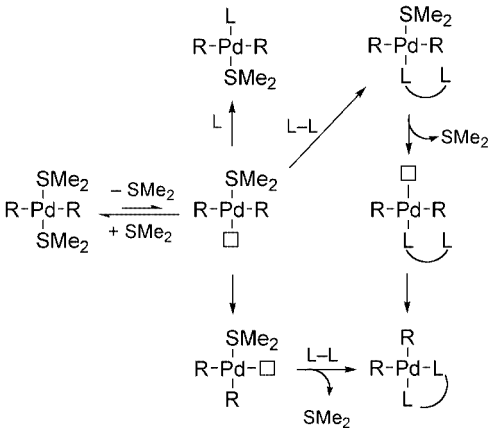

Scheme 5. Dissociative mechanism of the substitution processes

(Scheme 5). Thermodynamically, the "chelate effect", and in most cases the use of a stronger ligand, contribute to compensate the destabilization caused by the higher repulsion between two *cis* Fmes groups. In addition, the first dissociative substitution by a better σ-donor with a higher *trans* influence (except for the ligand pte, where the change is *S*-donor for *S*-donor), favors, kinetically, the dissociation of the second SR_2 ligand.

The κ^2*O*,*N*-coordination of $OPPhPy_2$ found in **5b** was unknown for square-planar palladium(II), although it occurs in pseudo-octahedral molybdenum(II) derivatives.[26] κ^2*N*,*N*-Coordination usually observed in Pd^{II} complexes is probably disfavoured in our case by the high degree of steric crowding due to the presence of two *cis* Fmes groups, quite similarly to its prevention in octahedral complexes. The κ^2*O*,*N*-coordination takes the substituents of the phosphorus away from the axial positions, minimizing the steric congestion. Interestingly, monoarylated complexes [PdCl(Fmes)(κ^2*N*,*N*-$OPPhPy_2$)] and [Pd(Fmes)(NCMe)-(κ^2*N*,*N*-$OPPhPy_2$)]BF_4 have been isolated and characterized.[2c,11] Therefore, one Fmes group is compatible with an axial disposition of the phenyl group in κ^2*N*,*N*-coordination, but two Fmes groups (here) or an octahedral metal centre (Mo complex cited above) force κ^2*O*,*N*-coordination. This highlights the very different "axial" encumbrance produced in monoarylated and bisarylated Fmes complexes. In monoarylated derivatives the Fmes group is probably tilted to accommodate the phenyl group (Scheme 6). The ability

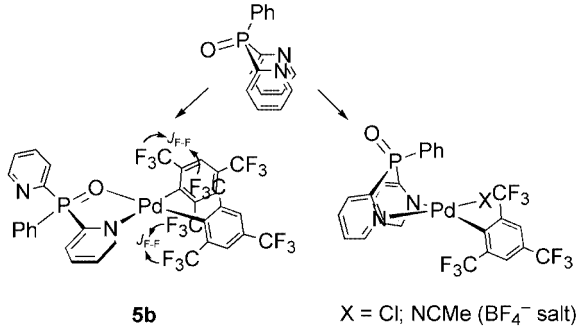

Scheme 6. Bisarylated (indicating detected $^{19}F-^{19}F$ through-space coupling) and monoarylated $OPPhPy_2$ complexes

 © 2004 Wiley-VCH Verlag GmbH & Co. KGaA, Weinheim

of Fmes to tilt and make the space in the *z* direction accessible to attack by nucleophiles explains why the reactions involving monoarylated substrates can proceed by associative mechanisms,[2c] while those reported here seem to require ligand dissociation.

We used a ligand with smaller substituents, $(OH)(CH_3)CPy_2$, to check whether κ^2N,N-coordination occurred, but this yielded, unexpectedly, [Pd(Fmes)$_2$(μ-1κ*N*:1,2κ*O*:2κ*N*-Py_2MeCO)Pd(Fmes)(SMe_2)] (**6**), and HFmes as by-product (Scheme 3). The alcoholic hydrogen has been previously reported to be acidic when the ligand is coordinated to other metals, such as In^{III}.[13] However, no deprotonation occurred during the reactions of $(OH)(CH_3)CPy_2$ with the monoarylated complexes *trans*-[PdClFmes(SMe_2)$_2$] or [Pd(Fmes)($NCMe)_3$]BF_4, which lead to [PdClFmes(κ^2N,N'-$(OH)(CH_3)CPy_2$)][2c] and [Pd(Fmes)-{κ^2N,N'-$(OH)(CH_3)CPy_2$}(NCMe)]BF_4, respectively.[11] This suggests that acidic activation of the O−H bond might require previous *O*-coordination to a putative three-coordinate palladium intermediate. This might occur in the dissociative mechanism for bisarylated complexes but not in the associative substitution operating for monoarylated species.[2c]

Conclusion

Substitution and isomerization processes in bisarylated Fmes palladium complexes seem to occur by dissociative mechanisms, forced by the extreme axial protection produced by the *ortho* CF_3 substituents (*ortho* effect). Consequently, harsh reaction conditions are required, unlike the mild substitution by associative mechanisms found for the related monoarylated Fmes complexes,[2c] or for the analogous bisarylated C_6F_5 complexes.[5]

The lesser steric repulsion of two bulky Fmes mutually *trans*-stabilizes better the *trans* isomers, which should not be the thermodynamic products on the basis of only electronic effects ("antisymbiotic effect" or transphobia); *cis* isomers are obtained only for bidentate ancillary ligands, due to the chelate effect.

The $^{19}F-^{19}F$ couplings observed have no significant scalar contribution, and are due to through-space coupling that depends on the distance between the interacting nuclei. This is clearly so as the magnitude of the coupling does not depend on whether the fluoromethyl groups are on Fmes coordinated to the same metal or on Fmes coordinated to different metals in a binuclear complex.

Experimental Section

General Remarks: All reactions were carried out under dry N_2. Solvents were purified according to standard procedures.[27] The complexes *trans*-[$PdCl_2$(tht)$_2$],[28] *trans*-[$PdCl_2(SMe_2)_2$],[28] *trans*-[Pd(Fmes)$_2$(tht)$_2$] (**1b**)[2a] and the ligands $OPPhPy_2$,[29] $SPPh_2Py$,[30] and $(OH)(CH_3)CPy_2$,[31] were prepared according to literature procedures. *p*Tol-NC was synthesized as reported[32] using triphosgene as dehydrating agent.[33] 1,3,5-$C_6H_3(CF_3)_3$ (FmesH) from Fluorochem was used as received, and Li(Fmes) was prepared in situ as described in the literature.[34] The rest of the reactants were purchased from commercial suppliers and used as received.

Infrared spectra were recorded with a Perkin−Elmer 883 apparatus as Nujol mulls between polystyrene films from 4000 to 200 cm^{-1}. NMR spectra were recorded with Bruker AC-300 or ARX-300 instruments. ^1H, $^{31}P\{^1H\}$ and ^{19}F NMR spectra are referenced to TMS, 85% aqueous H_3PO_4, and $CFCl_3$, respectively. Elemental analyses were performed with a Perkin−Elmer 2400B microanalyzer.

***trans*-[Pd(Fmes)$_2$(SMe_2)$_2$] (1a):** *trans*-[$PdCl_2(SMe_2)_2$] (0.604 g, 2 mmol) was added to a freshly prepared solution of Li(Fmes) (7.95 mmol) in Et_2O (40 mL). The reaction mixture was maintained at 40 °C for 24 h, and then two drops of water were added to hydrolyse the excess organolithium reagent. The volatiles were pumped off, and the residue was extracted with toluene and filtered through silica gel. The solvent was then evaporated and the resultant pale brown residue was recrystallized from dichloromethane/hexane at −20 °C to give pale yellow crystals that were decanted, washed with hexane and vacuum-dried. Yield 0.801 g (51%). IR: $\tilde{\nu}$ = 687 s cm^{-1}. ^{19}F NMR: δ = −63.18 (s, 6 F, *para*-CF_3), −60.41 (s, 12 F, *ortho*-CF_3) ppm. ^1H NMR: δ = 1.66 [s, 12 H, $S(CH_3)_2$], 7.92 [s, 4 H, $C_6H_2(CF_3)_3$] ppm. $C_{22}H_{16}F_{18}PdS_2$ (792.86): calcd. C 33.33, H 2.03; found C 33.16, H 2.03.

***trans*-[Pd(Fmes)$_2$(4-pic)$_2$] (1c):** 4-pic (21.4 μL, 0.021 g, 0.22 mmol) was added to a solution of **1a** (0.080 g, 0.1 mmol) in toluene (10 mL) and boiled under reflux for 3 h. The so-obtained solution was filtered through dry Celite, the volatiles were pumped off, and the resultant white solid was washed with hexane and vacuum dried [yield 0.055 g (65%)]. Recrystallization from dichloromethane/hexane gave colourless crystals. IR: $\tilde{\nu}$ = 688 m cm^{-1}. ^{19}F NMR: δ = −63.12 (s, 6 F, *para*-CF_3), −59.73 (s, 12 F, *ortho*-CF_3) ppm. ^1H NMR: δ = 2.22 [s, 6 H, $NC_5H_4(CH_3)$], 6.76 [d, *J* = 6.5 Hz, 4 H, $NC_5H_4(CH_3)$], 7.82 [s, 4 H, $C_6H_2(CF_3)_3$], 7.92 [d, *J* = 6.5 Hz, 4 H, $NC_5H_4(CH_3)$] ppm. $C_{30}H_{18}F_{18}N_2Pd$ (854.86): calcd. C 42.15, H 2.12, N 3.28; found C 42.27, H 2.38, N 3.50.

***trans*-[Pd(Fmes)$_2$(PMe_3)$_2$] (1d):** In a Young-valve-fitted Schlenk flask, PMe_3 (200 μL of 1 M in THF, 0.2 mmol) was added to a solution of **1a** (0.080 g, 0.1 mmol) in toluene (10 mL) and heated to 110 °C for 7 h. Work up as for **1c** then yielded 0.028 g (34%) of material. Recrystallization from dichloromethane/hexane gave colourless crystals. IR: $\tilde{\nu}$ = 688 s cm^{-1}. ^{19}F NMR: δ = −63.13 (s, 6 F, *para*-CF_3), −59.51 (t, *J* = 5.5 Hz, 12 F, *ortho*-CF_3) ppm. $^{31}P\{^1H\}$ NMR: δ = −20.12 (sept, *J* = 5.5 Hz) ppm. ^1H NMR: δ = 0.83 [$A_9XX'A_9'$ syst., *J* = 7 Hz, 18 H, $P(CH_3)_3$], 7.89 [s, 4 H, $C_6H_2(CF_3)_3$] ppm. $C_{24}H_{22}F_{18}P_2Pd$ (820.76): calcd. C 35.12, H 2.7, found C 34.86, H 2.59.

***trans*-[Pd(Fmes)$_2$(*t*BuNC)$_2$] (1e):** *t*BuNC (225 μL, 0.165 g, 2 mmol) was added to a solution of **1a** (0.080 g, 0.1 mmol) in toluene (10 mL) and boiled under reflux for 5 h. Work up as for **1c** subsequently yielded 0.070 g (83%) of material. Recrystallization from dichloromethane/hexane gave colourless crystals. IR: $\tilde{\nu}$ = 686 s cm^{-1}. ^{19}F NMR: δ = −63.00 (s, 6 F, *para*-CF_3), −61.74 (s, 12 F, *ortho*-CF_3) ppm. ^1H NMR: δ = 1.16 (s, 18 H, CNC_4H_9), 7.92 [s, 4 H, $C_6H_2(CF_3)_3$] ppm. $C_{28}H_{22}F_{18}N_2Pd$ (834.87): calcd. C 40.28, H 2.66, N 3.36; found C 40.27, H 2.61, N 3.21.

***trans*-[Pd(Fmes)$_2$(*p*Tol-NC)$_2$] (1f):** *p*Tol-NC (0.100 g, 0.85 mmol) was added to a solution of **1a** (0.160 g, 0.2 mmol) in toluene (15 mL) and boiled under reflux for 8 h. Subsequent work up as for **1c** yielded 0.045 g (28%) of material. Recrystallization from di-

 © 2004 Wiley-VCH Verlag GmbH & Co. KGaA, Weinheim

chloromethane/ethanol gave colourless crystals. IR: $\tilde{\nu}$ = 2197 s (ν CN), 688 s cm^{-1}. ^{19}F NMR: δ = −63.07 (s, 6 F, *para*-CF_3), −61.64 (s, 12 F, *ortho*-CF_3) ppm. ^1H NMR: δ = 2.31 (s, 18 H, CNC_4H_9), 7.01 (part B of AB system, *J* = 8.4 Hz, 4 H), 7.10 (part A, *J* = 8.4 Hz, 4 H), 7.96 [s, 4 H, $C_6H_2(CF_3)_3$] ppm. $C_{34}H_{18}F_{18}N_2Pd$ (902.91): calcd. C 45.23, H 2.01, N 3.10; found C 44.93, H 2.18, N 3.21.

***trans*-[Pd(Fmes)$_2$(NCMe)(SMe$_2$)] (2a): 1a** (0.080 g, 0.1 mmol) was dissolved in acetonitrile (15 mL) and boiled under reflux for 7 h. Work up as for **1c** yielded then afforded 0.042 g (54%) of material. Recrystallization from dichloromethane/hexane gave pale yellow crystals. IR: $\tilde{\nu}$ = 686 m cm^{-1}. ^{19}F NMR: δ = −63.08 (s, 6 F, *para*-CF_3), −60.51 (s, 12 F, *ortho*-CF_3) ppm. ^1H NMR: δ = 1.61 [s, 6 H, $S(CH_3)_2$], 1.99 (s, 3 H, $NCCH_3$), 7.90 [s, 4 H, $C_6H_2(CF_3)_3$] ppm. $C_{22}H_{13}F_{18}NPdS$ (771.79): calcd. C 34.24, H 1.70, N 1.81; found C 34.17, H 1.85, N 1.85.

***trans*-[Pd(Fmes)$_2$(NCMe)(tht)] (2b): 1b** (0.127 g, 0.15 mmol) was dissolved in acetonitrile (15 mL) and boiled under reflux for 24 h. Subsequent work up as for **1c** yielded 0.042 g (35%) and recrystallization from dichloromethane/hexane gave yellow crystals. IR: $\tilde{\nu}$ = 688 m cm^{-1}. ^{19}F NMR: δ = −63.06 (s, 6 F, *para*-CF_3), −60.21 (s, 12 F, *ortho*-CF_3) ppm. ^1H NMR: δ = 1.70 (m, 4 H, H^{β}, SC_4H_8), 1.99 (s, 3 H, $NCCH_3$), 2.21 (m, 4 H, H^{α}, SC_4H_8), 7.89 [s, 4 H, $C_6H_2(CF_3)_3$] ppm. $C_{24}H_{16}F_{18}NPdS$ (798.83): calcd. C 36.13, H 1.90, N 1.76; found C 36.07, H 1.94, N 2.10.

N*n*Bu$_4$[*trans*-Pd(Fmes)$_2$I(SMe$_2$)] (3a): N*n*Bu$_4$I (0.037 g, 0.1 mmol) was added to a solution of **1a** (0.080 g, 0.1 mmol) in toluene (10 mL) and boiled under reflux for 2 h. Work up as for **1c** yielded 0.047 g (43%), and subsequent recrystallization from dichloromethane/hexane gave orange crystals. IR: $\tilde{\nu}$ = 687 s, 666 w cm^{-1}. ^{19}F NMR: δ = −62.74 (s, 6 F, *para*-CF_3), −58.33 (s, 12 F, *ortho*-CF_3) ppm. ^1H NMR: δ = 0.93 [m, 12 H, N*n*$(C_4H_9)_4$], 1.31 [m, 8 H, N*n*$(C_4H_9)_4$], 1.51 [m, 8 H, N*n*$(C_4H_9)_4$], 1.64 [s, 6 H, $S(CH_3)_2$], 3.03 [m, 8 H, N*n*$(C_4H_9)_4$], 7.77 [s, 4 H, $C_6H_2(CF_3)_3$] ppm. $C_{36}H_{46}F_{18}INPdS$ (1100.110): calcd. C 39.31, H 4.21, N 1.27; found C 39.52, H 4.18, N 1.52.

N*n*Bu$_4$[*trans*-Pd(Fmes)$_2$I(tht)] (3b): N*n*Bu$_4$I (0.037 g, 0.1 mmol) was added to a solution of **1b** (0.084 g, 0.1 mmol) in toluene (10 mL) and boiled under reflux for 6 h. Work up as for **1c** then yielded 0.036 g (32%), and subsequent recrystallization from dichloromethane/hexane gave orange crystals. IR: $\tilde{\nu}$ = 687 s, 663 vw. ^{19}F NMR: δ = −62.73 (s, 6 F, *para*-CF_3), −58.01 (s, 12 F, *ortho*-CF_3) ppm. ^1H NMR: δ = 0.92 [m, 12 H, N*n*$(C_4H_9)_4$], 1.28 [m, 8 H, N*n*$(C_4H_9)_4$], 1.48 [m, 8 H, N*n*$(C_4H_9)_4$], 1.70 [m, 4 H, N*n*$(C_4H_9)_4$], 2.28 [m, 4 H, SCH_2], 3.03 [m, 8 H, N*n*$(C_4H_9)_4$], 7.76 [s, 4 H, $C_6H_2(CF_3)_3$] ppm. $C_{38}H_{48}F_{18}INPdS$ (1126.15): calcd. C 40.53, H 4.30, N 1.24; found C 40.38, H 4.11, N 1.27.

[Pd(Fmes)$_2$(Me$_2$bipy)] (4a): Me_2bipy (0.022 g, 0.12 mmol) was added to a solution of **1a** (0.080 g, 0.1 mmol) in toluene (10 mL) and boiled under reflux for 7 h. Work up as for **1c** then yielded 0.067 g (79%) of material. Recrystallization from acetone/hexane then afforded yellow crystals. IR: $\tilde{\nu}$ = 692 s, 685 s cm^{-1}. ^{19}F NMR: δ = −63.10 (s, 6 F, *para*-CF_3), −57.73 (s, 12 F, *ortho*-CF_3) ppm. ^1H NMR: δ = 2.51 [s, 6 H, $\{NC_5H_3(CH_3)\}_2$], 7.11 [d, *J* = 5.4 Hz, 2 H, $\{NC_5H_3(CH_3)\}_2$], 7.44 [d, *J* = 5.4 Hz, 2 H, $\{NC_5H_3(CH_3)\}_2$], 7.77 [s, 4 H, $C_6H_2(CF_3)_3$], 7.88 [s, 2 H, H^3, $\{NC_5H_3(CH_3)\}_2$] ppm. $C_{30}H_{16}F_{18}N_2Pd$ (852.85): calcd. C 42.25, H 1.89, N 3.28; found C 41.56, H 2.16, N 3.20.

[Pd(Fmes)$_2$(biquinolyl)] (4b): 2,2′-Biquinoline (0.026 g, 0.1 mmol) was added to a solution of **1a** (0.080 g, 0.1 mmol) in toluene (10 mL) and boiled under reflux for 15 h; work up as for **1c** then yielded 0.053 g (57%). Subsequent recrystallization from toluene/hexane then gave yellow crystals. IR: $\tilde{\nu}$ = 686 m, 669 m cm^{-1}. ^{19}F NMR: δ = −63.23 (s, 6 F, *para*-CF_3), −57.99 (br., 12 F, *ortho*-CF_3) ppm. ^1H NMR: δ = 7.29 [t, *J* = 7 Hz, 2 H, $(NC_9H_6)_2$], 7.53 [t, *J* = 7 Hz, 2 H, $(NC_9H_6)_2$], 7.66 [s, 4 H, $C_6H_2(CF_3)_3$], 7.82 [d, *J* = 8.5 Hz, 2 H, $(NC_9H_6)_2$], 7.87 [d, *J* = 8.5 Hz, 2 H, $(NC_9H_6)_2$], 8.30 [d, *J* = 8.5 Hz, 2 H, $(NC_9H_6)_2$], 8.58 [d, *J* = 8.5 Hz, 2 H, $(NC_9H_6)_2$] ppm. ^{19}F NMR (CD_2Cl_2, 183 K): δ = −62.43 (s,, 6 F *para*-CF_3), −59.10 (br., 6 F, *ortho*-CF_3), −55.89 (br., 6 F, *ortho*-CF_3) ppm. ^1H NMR (CD_2Cl_2, 183 K): δ = 7.31 [t, *J* = 7 Hz, 2 H, $(NC_9H_6)_2$], 7.49 [t, 2 H, *J* = 7 Hz, $(NC_9H_6)_2$], 7.66 [m, 8 H, $C_6H_2(CF_3)_3$ and $N_2C_{18}H_{12}$], 8.24 [d, 2 H, *J* = 7 Hz, $(NC_9H_6)_2$], 8.44 [d, *J* = 8 Hz, 2 H, $(NC_9H_6)_2$] ppm. $C_{36}H_{16}F_{18}N_2Pd$ (924.91): calcd. C 46.75, H 1.74, N 3.03; found C 46.45, H 1.87, N 2.96.

[Pd(Fmes)$_2$(κ^2*N*,*N*′-OCPy$_2$)] (4c): $OCPy_2$ (0.018 g, 1 mmol) was added to a solution of **1a** (0.080 g, 0.1 mmol) in toluene (10 mL) and boiled under reflux for 3 h. Subsequent work up as for **1c** yielded 0.020 g (47%), and recrystallization from toluene/hexane then gave yellow crystals. IR: $\tilde{\nu}$ = 693 m, 686 s cm^{-1}. ^{19}F NMR: δ = −63.28 (s, 6 F, *para*-CF_3), −57.70 (s, 12 F, *ortho*-CF_3) ppm. ^1H NMR: δ = 7.41 [m, 2 H, $OC(NC_5H_4)_2$], 7.69 [s, 4 H, $C_6H_2(CF_3)_3$], 8.04 [m, 2 H, $OC(NC_5H_4)_2$], 8.22 [m, 4 H, $OC(NC_5H_4)_2$] ppm. $C_{29}H_{12}F_{18}N_2OPd$ (852.80): calcd. C 40.84, H 1.42, N 3.28; found C 40.95, H 1.60, N 3.48.

[Pd(Fmes)$_2$(dppm)] (4d): The ligand dppm (0.046 g, 0.12 mmol) was added to a solution of **1a** (0.080 g, 0.1 mmol) in toluene (10 mL) and boiled under reflux for 7 h. Work up as for **1c** then yielded 0.063 g (60%), and subsequent recrystallization from toluene/hexane gave yellow crystals. IR: $\tilde{\nu}$ = 693 s, 664 w cm^{-1}. ^{19}F NMR: δ = −63.19 (s, 6 F, *para*-CF_3), −57.25 ($X_6AA'X_6'$ syst., N = J_{AX} + $J_{AX'}$ = 11.9 Hz, 12 F, *ortho*-CF_3) ppm. $^{31}P\{^1H\}$ NMR: δ = −36.85 (m) ppm. ^1H NMR: δ = 4.18 [t, *J* = 9.5 Hz, 2 H, $\{(C_6H_5)_2P\}_2CH_2$], 7.20 [m, 15 H, $\{(C_6H_5)_2P\}_2CH_2$], 7.38 [m, 5 H, $\{(C_6H_5)_2P\}_2CH_2$], 7.64 [s, 4 H, $C_6H_2(CF_3)_3$] ppm. $C_{43}H_{26}F_{18}P_2Pd$ (1053.01): calcd. C 49.05, H 2.49; found C 49.59, H 2.69.

[Pd(Fmes)$_2$(dppe)] (4e): The ligand dppe (0.044 g, 0.11 mmol) was added to a solution of **1a** (0.080 g, 0.1 mmol) in toluene (10 mL) and boiled under reflux for 3 h. Subsequent work up as for **1c** afforded 0.080 g (75%), and recrystallization from toluene/hexane then gave colourless crystals. IR: $\tilde{\nu}$ = 689 s, 665 m cm^{-1}. ^{19}F NMR: δ = −63.26 (s, 6 F, *para*-CF_3), −56.90 ($X_6AA'X_6'$ syst., N = J_{AX} + $J_{AX'}$ = 11.2 Hz, 12 F, *ortho*-CF_3) ppm. $^{31}P\{^1H\}$ NMR: δ = 35.62 (m) ppm. ^1H NMR: δ = 2.54 ($X_2AA'X_2'$ syst., N = J_{AX} + $J_{AX'}$ = 18.4 Hz, CH_2, 4 H), 7.35 (m, C_6H_5, 5 H), 7.24 (m, C_6H_5, 15 H), 7.52 [s, $C_6H_2(CF_3)_3$, 4 H], 7.35 (m, C_6H_5, 5 H) ppm. $C_{44}H_{28}F_{18}P_2Pd$ (1067.03): calcd. C 49.53, H 2.64; found C 49.90, H 2.85.

[Pd(Fmes)$_2$(pte)] (4f): The ligand pte (0.016 g, 0.065 mmol) was added to a solution of **1a** (0.040 g, 0.05 mmol) in toluene (10 mL) and boiled under reflux for 5 h. The usual work up, as for **1c**, then yielded 0.015 g (33%), and subsequent recrystallization from toluene/hexane gave yellow crystals. IR: $\tilde{\nu}$ = 685 s, 664 m cm^{-1}. ^{19}F NMR: δ = −63.38 (s, 6 F, *para*-CF_3), −56.23 (br., 12 F, *ortho*-CF_3) ppm. ^1H NMR: δ = 3.42 (s, 4 H, CH_2), 7.35 (m, 10 H, C_6H_5), 7.65 (br., 4 H, C_6H_5) ppm. ^{19}F NMR (213 K): δ = −62.86 (s, 6 F, *para*-CF_3), −59.50 (br., 6 F, *ortho*-CF_3), −52.50 (br., 6 F, *ortho*-CF_3) ppm. ^1H NMR (213 K): δ = 3.38 (s, 4 H, CH_2), 7.37 (m, 10 H, C_6H_5), 7.56 [br., 2 H, $C_6H_2(CF_3)_3$], 7.78 [br., 2 H, $C_6H_2(CF_3)_3$] ppm. $C_{32}H_{18}F_{18}PdS_2$ (914.99): calcd. C 42.01, H 1.98; found C 41.81, H 2.16.

 © 2004 Wiley-VCH Verlag GmbH & Co. KGaA, Weinheim

[Pd(Fmes)$_2$(κ^2*S*,*N*-SPPh$_2$Py)] (5a): $SPPh_2Py$ (0.033 g, 0.11 mmol) was added to a solution of **1a** (0.080 g, 0.1 mmol) in toluene (10 mL) and boiled under reflux for 4 h. The usual work up, as for **1c**, then yielded 0.069 g (72%), and recrystallization from toluene/hexane then gave yellow crystals. IR: $\tilde{\nu}$ = 688 s, 664 vw cm^{-1}. ^{19}F NMR: δ = −63.18 (s, 3 F, *para*-CF_3), −63.12 (s, 3 F, *para*-CF_3), −58.11 (q, $J_{F,F}$ = 9.3 Hz, 6 F, *ortho*-CF_3), −56.34 (q, $J_{F,F}$ = 9.3 Hz, 6 F, *ortho*-CF_3) ppm. ^{31}P{^{1}H} NMR: δ = 57.05 (s) ppm. ^{1}H NMR: δ = 7.35 [m, 2 H, SP(C_6H_5)$_2$(NC_5H_4)], 7.67 [s, 2 H, $C_6H_2(CF_3)_3$], 7.68 [s, 2 H, $C_6H_2(CF_3)_3$], 7.70 [m, 10 H, SP(C_6H_5)$_2$(NC_5H_4)], 7.87 [m, 1 H, SP(C_6H_5)$_2$(NC_5H_4)], 7.99 [m, 1 H, SP(C_6H_5)$_2$(NC_5H_4)] ppm. $C_{35}H_{18}F_{18}NPPdS$ (963.95): calcd. C 43.61, H 1.88, N 1.45; found C 43.53, H 1.94, N 1.40.

[Pd(Fmes)$_2$(κ^2*O*,*N*-OPPhPy$_2$)] (5b): $OPPhPy_2$ (0.031 g, 0.11 mmol) was added to a solution of **1a** (0.080 g, 0.1 mmol) in toluene (10 mL) and boiled under reflux for 2 h. The usual work up, as for **1c**, yielded 0.056 g (59%) of material. Subsequent recrystallization from toluene/hexane then gave yellow crystals. IR: $\tilde{\nu}$ = 685 s, 665 w cm^{-1}. ^{19}F NMR: δ = −63.17 (s, 3 F, *para*-CF_3), −63.16 (s, 3 F, *para*-CF_3), −58.23 (q, $J_{F,F}$ = 7.5 Hz, 3 F, *ortho*-CF_3), −57.55 (q, $J_{F,F}$ = 6 Hz, 3 F, *ortho*-CF_3), −57.28 (q, $J_{F,F}$ = 6 Hz, 3 F, *ortho*-CF_3), −56.28 (q, $J_{F,F}$ = 7.5 Hz, 3 F, *ortho*-CF_3) ppm. ^{31}P{^{1}H} NMR: δ = 39.02 (s) ppm. ^{1}H NMR: δ = 7.34 [m, 1 H, OP(C_6H_5)(NC_5H_4)$_2$], 7.58 [m, 4 H, OP(C_6H_5)(NC_5H_4)$_2$], 7.68 [m, 1 H, OP(C_6H_5)(NC_5H_4)$_2$], 7.70 [s, 1 H, $C_6H_2(CF_3)_3$], 7.72 [s, 1 H, $C_6H_2(CF_3)_3$], 7.76 [s, 1 H, $C_6H_2(CF_3)_3$], 7.79 [s, 1 H, $C_6H_2(CF_3)_3$], 7.91 [m, 1 H, OP(C_6H_5)(NC_5H_4)$_2$], 8.00 [m, 1 H, OP(C_6H_5)(NC_5H_4)$_2$], 8.11 [m, 3 H, OP(C_6H_5)(NC_5H_4)$_2$], 8.37 [t, *J* = 7 Hz, 1 H, OP(C_6H_5)(NC_5H_4)$_2$], 8.88 [d, *J* = 4.7 Hz, 1 H, OP(C_6H_5)(NC_5H_4)$_2$] ppm. $C_{34}H_{17}F_{18}N_2OPPd$ (948.87): calcd. C 43.03, H 1.81, N 2.95; found C 43.42, H 1.98, N 2.96.

[Pd(Fmes)$_2$(μ-1κ*N*:1,2κ*O*:2κ*N*-Py$_2$MeCO)Pd(Fmes)(SMe$_2$)] (6): $(OH)(CH_3)Cpy_2$ (225 μL, 0.010 g, 0.05 mmol) was added to a solution of **1a** (0.080 g, 0.1 mmol) in toluene (10 mL) and boiled under reflux for 11 h. The usual work up, as for **1c**, then yielded 0.022 g (33%), and subsequent recrystallization from toluene gave yellow crystals. IR: $\tilde{\nu}$ = 694 s, 685 s cm^{-1}. ^{19}F NMR: δ = −63.21 (s, 3 F, *para*-CF_3), −63.11 (s, 3 F, *para*-CF_3), −63.07 (s, 3 F, *para*-CF_3), −61.70 (q, *J* = 8.8 Hz, 3 F, *ortho*-CF_3), −60.75 (s, 3 F, *ortho*-CF_3), −59.52 (q, *J* = 8.0 Hz, 3 F, *ortho*-CF_3), −59.12 (qq, *J* = 8.5, 10.0 Hz, 3 F, *ortho*-CF_3), −57.88 (q, *J* = 10.0 Hz, 3 F, *ortho*-CF_3), −53.53 (q, *J* = 8.0 Hz, 3 F, *ortho*-CF_3) ppm. ^{1}H NMR: δ = 1.09 [br., 3 H, S(CH_3)$_2$], 2.36 [br., 3 H, S(CH_3)$_2$], 2.53 (s, 3 H, CH_3), 6.62 (d, *J* = 8.0 Hz, 1 H, C_5H_4N), 7.09 (t, *J* = 6.0 Hz, 1 , C_5H_4NH), 7.17 (t, *J* = 6.0 Hz, 1 H, C_5H_4N), 7.29 (d, *J* = 5.2 Hz, 1 H, C_5H_4N), 7.61 [s, 1 H, $C_6H_2(CF_3)_3$], 7.63 [s, 1 H, $C_6H_2(CF_3)_3$], 7.67 [m, 2 H, $C_6H_2(CF_3)_3$, C_5H_4N], 7.71 [s, 1 H, $C_6H_2(CF_3)_3$], 7.85 [s, 1 H, $C_6H_2(CF_3)_3$], 7.94 [m, 2 H, $C_6H_2(CF_3)_3$ and C_5H_4N] ppm. $C_{41}H_{23}F_{27}N_2Pd_2OS$ (1317.47): calcd. C 37.38, H 1.76, N 2.17; found C 37.67, H 1.89, N 2.17.

X-ray Crystallographic Study: Suitable crystals of **1f** and **4b** were grown by slow diffusion of a concentrated dichloromethane solution of the complex into diethyl ether (**1f**) or n-hexane (**4b**) at −20 °C. For **6**·0.5 toluene, crystals were grown by slow evaporation of a concentrated toluene solution of the complex at 8 °C. X-ray measurements were made using a Bruker SMART CCD area-detector diffractometer with Mo-K_α radiation (λ = 0.71073 Å).[35] Intensities were integrated from several series of exposures,[36] each exposure covering 0.3° in ω, the total data set being a hemisphere. Absorption corrections were applied, based on multiple and symmetry-equivalent measurements.[37] The structure was solved by direct methods and refined by least-squares on weighted F^2 values for

Table 5. Crystal data and structure refinement for *trans*-[Pd(Fmes)$_2$(*p*Tol-NC)$_2$] (**1f**), [Pd(Fmes)$_2$(biquinolyl)] (**4b**), and [Pd(Fmes)$_2$(μ-1κ*N*:1,2κ*O*:2κ*N*-Py$_2$MeCO)Pd(Fmes)(SMe$_2$)]($C_6H_5CH_3$)$_{0.5}$ (**6**·0.5 toluene)

	1f	**4b**	**6**·0.5 toluene
Empirical formula	$C_{34}H_{18}F_{18}N_2Pd$	$C_{36}H_{16}F_{18}N_2Pd$	$C_{44.5}H_{27}F_{27}N_2OPd_2S$
Molecular mass	902.90	924.91	1363.54
Temperature	298(2) K	293(2) K	293(2)
Wavelength (Å)	0.71073	0.71073	0.71073
Crystal system	triclinic	triclinic	triclinic
Space group	$P\bar{1}$	$P\bar{1}$	$P\bar{1}$
a (Å)	9.262(5)	11.5004(13)	15.400(4)
b (Å)	12.424(6)	11.9885(14)	18.748(5)
c (Å)	16.720(8)	13.7943(15)	20.396(5)
α (deg)	95.169(10)	77.804(3)	62.940(5)
β (deg)	102.807(10)	67.306(2)	79.447(6)
γ (deg)	105.098(9)	75.890(2)	81.438(7)
V (Å^3)	1788.9(15)	1687.0(3)	5141(2)
Z	2	2	4
$D_{calcd.}$ (g cm^{-3})	1.676	1.821	1.762
Absorption coefficient (mm^{-1})	0.640	0.682	0.875
F(000)	888	908	2668
Crystal size (mm)	0.29 × 0.16 × 0.15	0.12 × 0.12 × 0.06	0.39 × 0.12 × 0.05
Theta range for data collection	1.26 to 23.28°	1.61 to 23.29°	1.13 to 23.32°
Reflections collected	8283	7906	24237
Independent reflections	5091 (R_{int} = 0.0180)	4838 (R_{int} = 0.0400)	14733 (R_{int} = 0.0531)
Absorption correction	SADABS	SADABS	SADABS
Maximum and minimum transmission factor	1.000000, 0.876647	1.000000, 0.652705	1.000000, 0.631134
Data/restraints/parameters	5091/0/501	4838/0/514	14733/0/1353
Goodness-of-fit on F^2	1.050	1.006	1.015
R_1 [$I > 2\sigma(I)$]	0.0363	0.0474	0.0611
wR_2 (all data)	0.1074	0.1040	0.1926

 © 2004 Wiley-VCH Verlag GmbH & Co. KGaA, Weinheim

all reflections (Table 5).[38] All non-hydrogen atoms were assigned anisotropic displacement parameters and refined without positional constraints, except that the carbon atoms of the toluene molecule in **6**·0.5 toluene were refined isotropically. Hydrogen atoms were constrained to ideal geometries and refined with fixed isotropic displacement parameters. Refinement proceeded smoothly to give the residuals shown in Table 5. Complex neutral-atom scattering factors were used.[39] CCDC-221232 (for **1f**), -221233 (for **4b**) and -221234 (for **6**·0.5 toluene) contain the supplementary crystallographic data for this paper. These data can be obtained free of charge at www.ccdc.cam.ac.uk/conts/retrieving.html [or from the Cambridge Crystallographic Data Centre, 12 Union Road, Cambridge CB2 1EZ, UK; Fax: (internat.) +44-1223-336-033; E-mail: deposit@ccdc.cam.ac.uk].

Acknowledgments

The authors thank the DGI (BQU2001−2015) and the JCyL (VA058/03) for financial support.

[1] See, for example: [1a] F. T. Edelmann, *Comments, Inorg. Chem.* **1992**, *12*, 259−284, and references cited therein. [1b] A. S. Batsanov, K. B. Dillon, V. C. Gibson, J. A. K. Howard, L. J. Sequeira, J. W. Yao, *J. Organomet. Chem.* **2001**, *631*, 181−187. [1c] K. B. Dillon, V. C. Gibson, J. A. K. Howard, L. J. Sequeira, J. W. Yao, *J. Organomet. Chem.* **1997**, *528*, 179−183. [1d] V. C. Gibson, C. Redshaw, L. J. Sequeira, K. B. Dillon, W. Clegg, J. M. R. Elsegood, *Chem. Commun.* **1996**, 2151−2152. [1e] R. D. Schluter, A. H. Cowley, D. A. Atwood, R. A. Jones, M. R. Bond, C. J. Carrano, *J. Am. Chem. Soc.* **1993**, *115*, 2070−2071. [1f] P. Espinet, S. Martín-Barrios, F. Villafañe, P. G. Jones, A. K. Fischer, *Organometallics* **2000**, *19*, 290−295.

[2] [2a] C. Bartolomé, P. Espinet, F. Villafañe, S. Giesa, A. Martín, A. G. Orpen, *Organometallics* **1996**, *15*, 2019−2028. [2b] C. Bartolomé, R. de Blas, P. Espinet, J. M. Martín-Alvarez, F. Villafañe, *Angew. Chem. Int. Ed.* **2001**, *40*, 2521−2524. [2c] C. Bartolomé, P. Espinet, J. M. Martín-Alvarez, F. Villafañe, *Eur. J. Inorg. Chem.* **2003**, 3127−3138. [2d] C. Bartolomé, P. Espinet, J. M. Martín-Alvarez, F. Villafañe, *Inorg. Chim. Acta* **2003**, *347*, 49−52. [2e] C. Bartolomé, P. Espinet, L. Vicente, F. Villafañe, J. P. H. Charmant, A. G. Orpen, *Organometallics* **2002**, *21*, 3536−3543.

[3] [3a] A. C. Albéniz, A. L. Casado, P. Espinet, *Organometallics* **1997**, *16*, 5416−5423. [3b] A. C. Albéniz, A. L. Casado, P. Espinet, *Inorganic Chemistry* **1999**, *38*, 2510−2515. [3c] M. A. Alonso, J. A. Casares, P. Espinet, J. M. Martínez-Ilarduya, C. Pérez-Briso, *Eur. J. Inorg. Chem.* **1998**, 1745−1753.

[4] [4a] R. Usón, J. Forniés, *Adv. Organomet. Chem.* **1988**, *28*, 219−297. [4b] M. P. García, M. V. Jiménez, F. S. Lahoz, L. A. Oro, *Inorg. Chem.* **1995**, *34*, 2153−2159. [4c] J. M. Casas, F. A. Cotton, L. R. Falvello, J. Forniés, A. Martín, M. Tomás, R. Usón, *J. Am. Chem. Soc.* **1994**, *116*, 7160−7165. [4d] L. R. Falvello, J. Forniés, C. Fortuño, F. Martínez, *Inorg. Chem.* **1994**, *33*, 6242−6246. [4e] J. Casabó, G. García, G. López, C. Miratvitlles, E. Molins, J. Ruiz, C. Vicente, *Inorg. Chem.* **1991**, *30*, 2605−2610. [4f] G. B. Deacon, K. T. Nelson-Reed, *J. Organomet. Chem.* **1987**, *322*, 257−268. [4g] R. Usón, A. Laguna, *Coord. Chem. Rev.* **1986**, *70*, 1−50.

[5] J. A. Casares, P. Espinet, J. M. Martínez-Ilarduya, Y. S. Lin, *Organometallics* **1997**, *16*, 770−779.

[6] F. T. Edelmann, M. Belay, *J. Fluorine Chem.* **1997**, *84*, 29−33.

[7] [7a] P. Espinet, J. M. Martínez-Ilarduya, C. Pérez-Briso, A. L. Casado, M. A. Alonso, *J. Organomet. Chem.* **1998**, *551*, 9−20. [7b] G. López, G. García, M. D. Santana, G. Sánchez, J. Ruiz, J. A. Hermoso, A. Vegas, M. Martínez-Ripoll, *J. Chem. Soc., Dalton Trans.* **1990**, 1621−1626.

[8] [8a] P. G. Jones, *J. Organomet. Chem.* **1988**, *345*, 405−411. [8b] A. Domenicano, A. Vaciago, C. A. Coulson, *Acta Crystallogr., Sect. B* **1975**, *31*, 221−234. [8c] A. Domenicano, P. Murray-Rust, A. Vaciago, *Acta Crystallogr., Sect. B* **1983**, *39*, 457−468 and references cited therein.[8d] R. Norrestam, L. Schepper, *Acta Chem. Scand., Ser. A.* **1981**, *35*, 91−103. [8e] A. Domenicano, P. Mazzeo, A. Vaciago, *Tetrahedron Lett.* **1976**, 1029−1032.

[9] [9a] S. Coco, P. Espinet, F. Mayor, X. Solans, *J. Chem. Soc., Dalton Trans.* **1991**, 2503−2509. [9b] P. Leoni, E. Vichi, S. Lencioni, M. Pasquali, E. Chiarentin, A. Albinati, *Organometallics* **2000**, *19*, 3062−3068. [9c] S. Cristofani, P. Leoni, M. Pasquali, F. Eisentraeger, A. Albinati, *Organometallics* **2000**, *19*, 4589−4595.

[10] [10a] A. J. Deeming, I. P. Rothwell, *J. Chem. Soc., Chem. Commun.* **1979**, 670−672. [10b] A. Albinati, C. Ammann, P. S. Pregosin, H. Rüegger, *Organometallics* **1990**, *9*, 1826−1833.

[11] C. Bartolomé, R. de Blas, P. Espinet, F. Villafañe, manuscript in preparation.

[12] [12a] K. Nakamoto, *Infrared and Raman Spectra of Inorganic and Coordination Compounds*, 3rd ed. John Wiley & Sons, New York, **1978**. [12b]T. S. Lobana, *Prog. Inorg. Chem.* **1989**, *37*, 495.

[13] A. J. Canty, L. A. Titcombe, B. W. Skelton, A. H. White, *J. Chem. Soc., Dalton Trans.* **1988**, 35−45.

[14] A. Basu, S. Bhaduri, N. Y. Sapre, P. G. Jones, *J. Chem. Soc., Chem. Commun.* **1987**, 1724−1725.

[15] See, for example: M. A. Bennett, G. B. Robertson, A. Rokicki, W. A. Wickramasinghe, *J. Am. Chem. Soc.* **1988**, *110*, 7098−7105, and references cited therein.

[16] R. J. Cross, *Adv. Inorg. Chem.* **1989**, *34*, 219−291.

[17] [17a] U. Frey, L. Helm, A. E. Merbach, R. Romeo, *J. Am. Chem. Soc.* **1989**, *111*, 8161−8165, and references cited therein. [17b] S. Lanza, D. Minniti, P. Moore, J. Sachindis, R. Romeo, M. Tobe, *Inorg. Chem.* **1984**, *23*, 4428−4433. [17c] R. Romeo, A. Grassi, L. M. Scolaro, *Inorg. Chem.* **1992**, *31*, 4383−4390. [17d] G. Alibrandi, L. M. Scolaro, R. Romeo, *Inorg. Chem.* **1991**, *30*, 4007−4013, and references cited therein. [17e] R. Romeo, *Comments, Inorg. Chem.* **1990**, *11*, 21−57 and references cited therein.

[18] [18a] R. Usón, A. Laguna, J. Vicente, J. García, P. G. Jones, G. M. Sheldrick, *J. Chem. Soc., Dalton Trans.* **1981**, 655−657. [18b] P. G. Jones, *Naturforsch., B* **1982**, *37*, 937−940.

[19] G. M. Benedikt, B. L. Goodall, S. Iyer, L. H. McIntosh III, R. Mimna, L. F. Rhodes, C. S. Day, V. W. Day, *Organometallics* **2001**, *20*, 2565−2569.

[20] J. A. Casares, S. Coco, P. Espinet, Y. S. Lin, *Organometallics* **1995**, *14*, 3058−3067.

[21] L. Ernst, K. Ibrom, *Angew. Chem. Int. Ed. Engl.* **1995**, *34*, 1881−1882.

[22] [22a] D. Minniti, *Inorg. Chem.* **1994**, *33*, 2631−2634. [22b] A. L. Casado, J. A. Casares, P. Espinet, *Inorg. Chem.* **1998**, *37*, 4154−4156.

[23] [23a] R. H. Crabtree, *The Organometallic Chemistry of the Transition Elements*, 2nd ed., John Wiley & Sons, New York, **1994**. [23b] A. Yamamoto, *Organotransition Metal Chemistry. Fundamental Concepts and Applications*, John Wiley & Sons, New York, **1986**.

[24] [24a] J. Vicente, A. Arcas, D. Bautista, *Organometallics* **1997**, *16*, 2127−2138. [24b] J. Vicente, J. A. Abad, A. D. Frankland, M. C. Ramírez de Arellano, *Chem. Eur. J.* **1999**, *5*, 3066−3075. [24c] J. Vicente, J. A. Abad, E. Martinez-Viviente, P. G. Jones, *Organometallics* **2002**, *21*, 4454−4467. [24d] J. Vicente, A. Arcas, D. Bautista, M. C. Ramírez de Arellano, *J. Organomet. Chem.* **2002**, *663*, 164−172.

[25] R. Usón, J. Forniés, F. Martínez, M. Tomás, I. Reoyo, *Organometallics* **1983**, *2*, 1386−1390.

[26] P. Espinet, R. Hernando, G. Iturbe, A. G. Orpen, I. Pascual, F. Villafañe, *Eur. J. Inorg. Chem.* **2000**, 1031−1038.

[27] D. D. Perrin, W. L. F. Armarego, *Purification of Laboratory Chemicals*, 3rd ed.; Pergamon Press: Oxford, U. K., **1988**.

 © 2004 Wiley-VCH Verlag GmbH & Co. KGaA, Weinheim

[28] R. Usón, J. Forniés, F. Martínez, M. Tomás, *J. Chem. Soc., Dalton Trans.* **1980**, 888−894.
[29] G. R. Newkome, D. C. Hager, *J. Org. Chem.* **1978**, *43*, 947−949.
[30] F. G. Mann, J. Watson, *J. Org. Chem.* **1948**, *13*, 502−531.
[31] Treatment of $OCPy_2$ with LiMe and further hydrolysis affords $(OH)(CH_3)CPy_2$, which can be recrystallized from dichloromethane/hexane. Spectroscopic data agree with those previously reported: S. Bhaduri, N. Y. Sapre, P. G. Jones, *J. Chem. Soc., Dalton Trans.* **1991**, 2539−2543.
[32] I. Ugi, R. Meyr, *Chem. Ber.* **1960**, *93*, 239−248.
[33] H. Eckert, B. Forster, *Angew. Chem. Int. Ed. Engl.* **1987**, *26*, 894−895.
[34] [34a] G. E. Carr, R. D. Chambers, T. F. Holmes, D. G. Parker, *J. Organomet. Chem.* **1987**, *325*, 13−23. [34b] M. Scholz, H. W. Roesky, D. Stalke, K. Keller, F. T. Edelmann, *J. Organomet. Chem.* **1989**, *366*, 73−85.
[35] SMART V5.051 diffractometer control software, Bruker Analytical X-ray Instruments Inc., Madison, WI, **1998**.
[36] SAINT V6.02 integration software, Siemens Analytical X-ray Instruments Inc., Madison, WI, **1999**.
[37] G. M. Sheldrick. *SADABS: A program for absorption correction with the Siemens SMART system*; University of Göttingen: Germany, **1996**.
[38] *SHELXTL program system version 5.1*; Bruker Analytical X-ray Instruments Inc., Madison, WI **1998**.
[39] *International Tables for Crystallography*, Kluwer, Dordrecht, **1992**, vol. C.

Received October 20, 2003
Early View Article
Published Online April 7, 2004

 © 2004 Wiley-VCH Verlag GmbH & Co. KGaA, Weinheim

Different Coordination Modes of the Polyfunctional Ylide Ph_3P=C(H)C(O)CH_2C(O)OEt: *C*- vs. *O*,*O*′-Bonding in Pd^{II}, Pt^{II} and Au^{I} Complexes

Marta Carbó,[a] Larry R. Falvello,[a] Rafael Navarro,*[a] Tatiana Soler,[a] and Esteban P. Urriolabeitia*[a]

Keywords: Palladium / Platinum / Gold / Ylides / Structure elucidation

Treatment of the polyfunctional ylide Ph_3P=C(H)C(O)CH_2-COOEt (**1**) with the solvated complexes [M(C^X)$(THF)_2$]ClO_4 gave the *O*,*O*′ derivatives [M(C^X)($Ph_3PCH_2C(O)$=C(H)–C(=*O*)OEt-κ-*O*,*O*′]ClO_4 [M(C^X) = Pd($C_6H_4CH_2NMe_2$) (**2**), Pd($CH_2C_9H_6N$) (**3**), Pd(NC_5H_4-2-C_6H_4) (**4**), Pd($NC_{13}H_8$) (**5**), Pd[(*S*)–$C_6H_4C(H)MeNMe_2$] (**6**), Pt[*o*-$CH_2C_6H_4P$(*o*-tol)$_2$] (**7**), Pd[*o*-$CH_2C_6H_4P$(*o*-tol)$_2$] (**8**), and Pd(C_6F_5)(SC_4H_8) (**9**)]. During the reaction, one proton of the methylene unit is transferred to the ylidic carbon, which is transformed into a phosphonium group generating the zwitterion [$Ph_3PCH_2C(O)$=C(H)–C(=*O*)OEt], which coordinates to the metal center as an *O*,*O*′-chelating ligand. Treatment of **1** with [AuCl(SC_4H_8)] or [Au(PPh_3)($OCMe_2$)]ClO_4 gave [AuCl{C(H)(PPh_3)C(O)-CH_2COOEt}] (**10**) or [Au{C(H)(PPh_3)C(O)CH_2COOEt}-(PPh_3)]ClO_4 (**11**), in which the ylide is *C*-bonded. The X-ray crystal structures of complexes **2a**, **9** and **10** have been determined.

(© Wiley-VCH Verlag GmbH & Co. KGaA, 69451 Weinheim, Germany, 2004)

Introduction

We have recently shown that the keto-stabilized ylides [Ph_3P=C(H)C(O)R] (R = Me, OMe, Ph) can behave as ambidentate ligands towards Pd^{II} complexes, since they can coordinate either through the soft ylidic C_α atom or through the hard carbonyl oxygen depending on the vacant coordination site at the palladium precursor. This coordination occurs with notable selectivity, which has been explained in terms of the anti-symbiotic effect and the nature of the donor atoms bonded to the Pd^{II} center.[1] In all cases studied, the ylide bonds to the metal center using only one donor atom. Further introduction of new functional groups at the molecular skeleton of the ylide should result in an expansion of its bonding abilities and in the transformation of the aforementioned ambidenticity to polydenticity. We are currently pursuing the study of the coordinating properties of polydentate ylides, and how the presence of new functionalities alters the bonding patterns observed in ambidentate ylides.

Here we describe the complete characterization of ethyl 3-oxo-4-(triphenylphosphoranylidene)butanoate [Ph_3P=C(H)C(O)CH_2COOEt] (**1**) and its reactivity towards complexes of Pd^{II}, Pt^{II} and Au^{I}, in order to determine its coordinating ability. The ylide **1** could behave, at first sight, as a C-donor ligand (through the C_α atom), as an O-donor ligand (through three different O atoms) or as a polydentate ligand (using combinations of the four possible donor atoms). The synthesis of **1** was reported four decades ago[2] but, with the exception of applications in purely synthetic organic processes,[3] its bonding properties have remained unexplored. We have found quite different patterns of reactivity of this ylide as a function of the metallic precursor: *C*-bonding in Au^{I} complexes (leaving the β-keto ester functionality unchanged) and *O*,*O*′-coordination in Pd^{II} and Pt^{II} derivatives (which generates a phosphonium functionality). This paper describes the results obtained, and synthetic possibilities are also discussed.

[a] Departamento de Química Inorgánica, Instituto de Ciencia de Materiales de Aragón, Universidad de Zaragoza-CSIC, 50009 Zaragoza, Spain
E-mail: esteban@unizar.es

Results and Discussion

1. Palladium(II) and Platinum(II) Complexes

The ylide **1** was prepared following the method described by Serratosa and Solé,[2b] and has been characterized through its analytical and spectroscopic data. Here we also report the ^1H and $^{13}C\{^1H\}$ NMR spectroscopic parameters, since they were not provided in the original[2] or subsequent works[3f] (see Exp. Sect.). In order to check the chelating ability of **1**, its reactivity towards the bis(solvated) derivatives [M(C^X)$(THF)_2$]ClO_4 was examined (see Scheme 1). These bis(solvate) complexes were prepared by treatment of the corresponding dinuclear μ-halide complexes [M(C^X)(μ-Cl)]$_2$ with $AgClO_4$ (1:2 molar ratio) in THF, followed by removal of AgCl by filtration. The freshly prepared solutions of [M(C^X)$(THF)_2$]ClO_4 were treated with the stoichiometric amount of **1**. After the initial dissolution of **1**, complexes **2**–**9** precipitated as yellow solids from the

 © 2004 Wiley-VCH Verlag GmbH & Co. KGaA, Weinheim DOI: 10.1002/ejic.200300801

respective reaction solutions. The process is represented in Scheme 1.

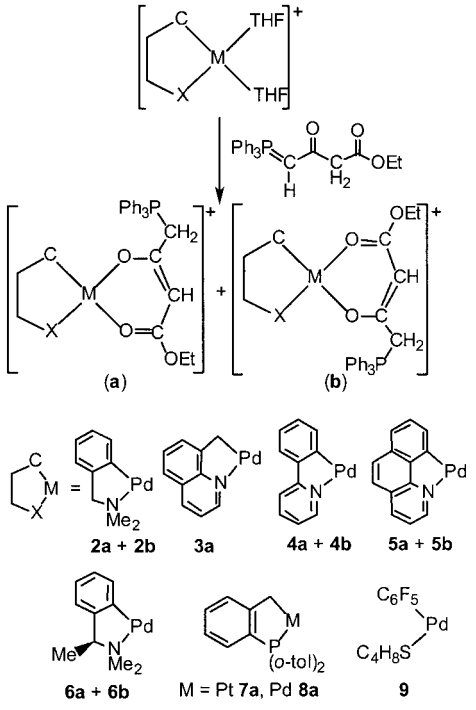

Scheme 1

Complexes **2**−**9** gave elemental analyses in good agreement with the stoichiometries depicted in Scheme 1, and the mass spectra in all cases show the presence of the cationic molecular peak $[M - ClO_4]^+$ with the correct isotopic distribution. The IR spectra of **2**−**9** clearly show two strong absorptions in the 1500−1630 cm^{-1} region: one at approximately 1614−1628 cm^{-1} (attributed to the ν_{COO} stretch) and the other one at around 1502−1525 cm^{-1}, assigned to the ν_{CO} stretch of the carbonyl group adjacent to the ylide unit. A comparison of these values with those obtained for the free ylide **1** (1717 and 1546 cm^{-1}, respectively)[2b] shows that both absorptions have been shifted to lower energies. This fact strongly suggests that both carbonyl groups are bonded to the metal center, since it has been well established that *C*-coordination of the keto-stabilized ylides produces a high energy shift of the ν_{CO} stretch (with respect to the free ylide)[1] and, thus, a shift of the absorption at 1546 cm^{-1} to higher wavenumbers should be observed for *C*-bonding of **1**.

The NMR spectra of complex **2** provide valuable structural information. Firstly, all NMR spectra (^1H, $^{13}C\{^1H\}$ and $^{31}P\{^1H\}$) display two identical sets of signals (ratio 4.5:1), showing the presence of two isomers (a) and (b) in solution. Due to the asymmetric nature of **1** and its *O*,*O*′-bonding mode, two geometric isomers can be envisaged. In addition, the ^1H NMR spectrum of **2** shows three notable features: (i) the signals due to the CH_2N and NMe_2 protons appear as singlets, indicating that the molecular plane is a symmetry plane; (ii) signals which could result from the methylene protons or the ylidic proton $P{=}C_\alpha(H)$ were not observed; (iii) instead, two singlets appear at δ = 4.5−5 ppm (δ = 4.81 ppm, major isomer; 4.86 ppm, minor isomer) and two doublets at about 4.15 ppm (δ = 4.13 ppm, J_{PH} = 13.8 Hz, major isomer, 4.16 ppm, J_{PH} = 13.8 Hz, minor isomer), with a relative intensity ratio singlet/doublet = 1:2. These observations strongly suggest that the methylene-ylide skeleton [$-CH_2-C(O)-C(H){=}P$] in **1** has been transformed into the phosphonium-enolate functionality [$-C(H){=}C(O)-CH_2P$] in **2**, by the transfer of one H atom from the methylene group to the ylidic carbon C_α (see Scheme 2). The signals in the range 4.5−5 ppm can then be attributed to the $=C(H)-$ proton (shifted slightly to high-field with respect to the usual position in β-diketonate ligands)[4] and the signals at about 4.15 ppm can be assigned to the CH_2P protons.[5] The resultant structure of the coordinated ligand in **2** is shown in Scheme 1.

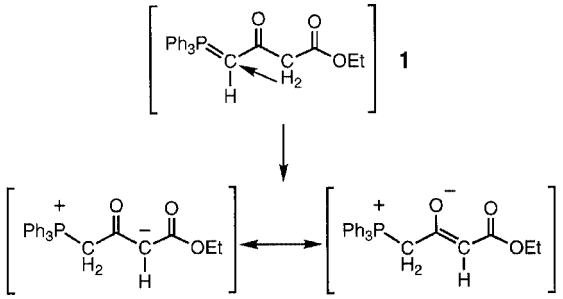

Scheme 2. Proton transfer in **1** and resonance forms of the zwitterion [$Ph_3PCH_2-C(O){=}C(H)C(=O)OEt$]

The structures depicted in Scheme 1 also account for the observation, in the $^{31}P\{^1H\}$ NMR spectrum of **2**, of two resonances at approximately 22 ppm, typical for phosphonium groups.[5] In addition, the $^{13}C\{^1H\}$ NMR spectrum (acquired as APT) of **2** also shows signals characteristic of the generated phosphonium-enolate moiety: (i) two doublets at about 36 ppm ($^1J_{P,C} \approx 53$ Hz) with negative phase can be attributed to the CH_2P carbon atoms, and (ii) two doublets at about 90 ppm ($^3J_{P,C} \approx 7$ Hz) with positive phase can be assigned to the $=C(H)$ carbon atoms. Finally, the question of whether structure (a) or (b) in Scheme 1 corresponds to the major isomer must be addressed. The assignment of structure (a) to the major isomer can easily be inferred from the ^1H NMR spectrum in which the signals assigned to the protons of the metallated C_6H_4 group, for the major isomer, appear well spread in the range δ = 7.0−5.8 ppm, with the signal due to the H^6 proton (*ortho* to the metallated position) at δ = 5.89 ppm. This signal is clearly shifted to high field with respect to its position in the starting dinuclear derivative $[Pd(\mu\text{-}Cl)(C_6H_4CH_2NMe_2)]_2$ (δ ≈ 7.0 ppm), and this high-field shift must be due to the anisotropic shielding[6] produced by a phenyl ring of the PPh_3 group. This fact implies a *cis* arrangement of the C_6H_4 fragment of the metallated ligand and the PPh_3 unit of the phosphonium-enolate ligand, which occurs in structure (a). Moreover, this anisotropic shielding should not be produced in the other isomer (which possesses an OEt group in a position remote from the H^6 proton) and, in fact, the

 © 2004 Wiley-VCH Verlag GmbH & Co. KGaA, Weinheim

aromatic resonances of the metallated C_6H_4 ring in the minor isomer all appear around 7.0 ppm. We can thus conclude, on the basis of the NMR spectroscopic data, that the major isomer is that represented in Scheme 1 by structure (a) and the minor isomer by structure (b).

The IR data of complexes **2**−**9**, and their comparison with those for the free ylide **1** show that, in all cases, the bonding mode of the ylide to the metal center should be the same (*O*,*O*′-chelate), since the same shifts of the carbonyl absorptions were observed.

Moreover, the NMR spectroscopic data of complexes **2**−**9** show two relevant facts: (i) in all cases the coordinated ylide has undergone a proton transfer and, hence, the actual *O*,*O*′-bonded ligand is the zwitterionic tautomer of **1** [$Ph_3(P^+)-CH_2-C(O^-)=C(H)C(O)OEt$] (Scheme 2); (ii) complexes **3**, **7**, **8**, and **9** were obtained as single isomers, within the limit of detection of the technique, while complexes **2**, **4**, **5** and **6** were obtained as a mixture of the geometric isomers (a) and (b) depicted in Scheme 1.

For complexes **4**, **5**, and **6**, the assignment of structure (a) to the major isomers can be inferred, as for complex **2**, from their ^1H NMR spectra. In the case of **4**, the resonance assigned to the $H^{6'}$ proton (*ortho* to the metallated position) in the major isomer appears shifted to high field (δ = 6.07 ppm), and the same shift was observed in complex **5** (δ =6.05 ppm). In complex **6**, the signal due to the H^6 proton appears at δ = 5.88 ppm, virtually the same chemical shift as that observed for **2**. Thus, we can assign structure (a) for the major isomers of **4**, **5** and **6**.

The assignment of structure (a) to complex **3** rests on the similarity of the chemical shifts of the carbonyl C atoms in the $^{13}C\{^1H\}$ NMR spectrum with those in **2a** and **4a**−**6a**. These chemical shifts appear in a very narrow range of frequencies [δ_{CO} = 173.44 (**3**), 173.67 (**2a**), 173.89 (**4a**), 173.90 (**5a**), 173.78 (**6a**) ppm; δ_{COO} = 171.33 (**3**), 171.21 (**2a**), 171.57 (**4a**), 171.51 (**5a**), 171.21 (**6a**) ppm], suggesting quite similar chemical environments and a very similar structural arrangement. In comparison, the corresponding resonances of the minor isomers (b) appear, systematically, at lower field. Moreover, the resemblance of the ancillary *C*,*N*-cyclometallated ligands in **3** with those in **2**, **4**, **5** or **6** (they do not show notable structural differences and similar behavior should be expected) also supports this assignment. These extrapolations cannot be performed for complexes **7** and **8**. Here, changes in the donor atom (N replaced by P) induce a change in the electronic requirements at the *trans* position, and the substituents at the donor atom also change (the P atom contains two bulky *ortho*-tolyl groups) so that the steric requirements at the *cis* position are different. However, the assignment of structure (a) for **7** and **8** can be inferred from the $^{13}C\{^1H\}$ NMR spectra, since the signal of the methylene carbon CH_2P appears as a doublet of doublets through coupling with the adjacent phosphonium P atom and with the *trans* P atom of the cyclometallated ligand [$^4J_{P,C}$ = 5.9 Hz for **7** and $^4J_{P,C}$ = 5.1 Hz for **8**]. Moreover, the remote *trans* location of the two bulkiest fragments of the molecule, $-CH_2PPh_3$ and $P(o\text{-tol})_2$, should be energetically more stable, since it minimizes intramolecular steric repulsions.

In the case of complex **9** we have also observed the formation of a single isomer, although we do not have direct spectroscopic evidence in favor of a given structure for this complex. Throughout the description of the structures of **2**−**8** it is possible to detect a repetitive arrangement of the ligands, which places the carbonyl oxygen of the C(O)OEt unit *trans* to the metallated carbon atom, and the oxygen of the enolate group *trans* to the heteroatom. Since we also have a metallated carbon atom (C_6F_5 ligand) and a neutral heteroatom (the S atom of the SC_4H_8 ligand) in **9**, we propose a similar stereochemistry for **9** and, thus, the structure (a) as depicted in Scheme 1. This hypothesis has been corroborated through the determination of the X-ray structure (see below).

In summary, the interaction of the ylide **1** with Pd^{II} and Pt^{II} complexes promotes the generation of the phosphonium-enolate [$Ph_3(P^+)-CH_2-C(O^-)=C(H)C(O)OEt$] ligand in all cases. It is remarkable to observe the presence of a free phosphonium unit in a ligand strongly anchored to the metal center. This phosphonium moiety could be the clue for further functionalization of the ligand, since its deprotonation would generate a new ylide unit, which could be involved in a variety of new processes (e.g. synthesis of polynuclear complexes, Wittig reactions, etc.) which are not possible starting from the free ligand **1**.

2. Gold(I) Complexes

As we have seen in the preceding discussion, the reactivity of **1** towards cationic bis(solvate) complexes of Pd^{II} and Pt^{II} does not result in the expected *C*-coordination. In an attempt to involve the ylidic C_α atom in bonding to a transition metal, we have focused our attention to gold(I) compounds, taking into account the exceptional stability of Au^I complexes with *C*-bonded α-stabilized P-ylides,[7] and also that the *O*-coordination of keto-stabilized P-ylides to Au^I remains unknown.

Treatment of [$AuCl(SC_4H_8)$] with **1** (1:1 molar ratio) in CH_2Cl_2 at room temperature occurs with displacement of the labile ligand SC_4H_8 and *C*-bonding of the ylide, giving the neutral derivative [$AuCl\{C(H)(PPh_3)C(O)CH_2C(O)OEt\}$] (**10**). In addition, treatment of the solvated complex [$Au(OCMe_2)(PPh_3)]ClO_4$ (obtained by treatment of [$AuCl(PPh_3)$] with $AgClO_4$ in acetone, see details in Exp. Sect.) with **1** (1:1 molar ratio) results in the formation of [$Au\{C(H)(PPh_3)COCH_2COOEt\}(PPh_3)]ClO_4$ (**11**), which also contains the *C*-coordinated ylide. These two processes are presented in Scheme 3.

Both complexes gave elemental analyses and mass spectra in good agreement with the proposed structures. The C-bonding of the ylide **1** in compounds **10** and **11** can be inferred from the IR spectra, since the absorptions assigned to the C=O stretch appear at 1731 cm^{-1} (ν_{COO}) and 1666 cm^{-1} (ν_{CO}) in **10**, and at 1724 and 1657 cm^{-1} for the respective absorptions in **11**. A comparison of these values with those reported for the free ylide (1717 and 1546 cm^{-1})[2b] shows that the absorption of the carboxylate

 © 2004 Wiley-VCH Verlag GmbH & Co. KGaA, Weinheim

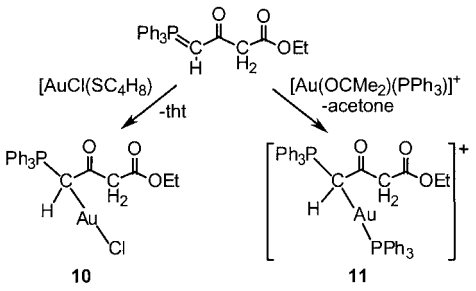

Scheme 3

group undergoes very small shifts, suggesting that it does not interact with the metal center, whereas that due to the carbonyl adjacent to the ylide group appears shifted to high energy by up to 120 cm^{-1}. This latter shift implies a higher participation of the keto-form in the description of the bonded ylide, and it is a clear indicator of the presence of a *C*-coordinated ylide.[1]

Additional evidence for the *C*-coordination of the ylide, and for the concomitant hybridization change ($sp^2 \rightarrow sp^3$), comes from the analysis of the NMR spectroscopic data. Key features of the NMR spectra of **10** and **11** are: (i) the ylidic proton $PC_\alpha(H)$ appears at about 4.8 ppm as a singlet in **10** or as a doublet in **11**, with a small coupling constant $^2J_{PH}$ (9 Hz); (ii) the methylene protons appear diastereotopic, showing the absence of a symmetry plane; (iii) the P atom $PC_\alpha(H)$ appears in the $^{31}P\{^1H\}$ NMR spectrum as a singlet (**10**) or as a doublet (**11**), shifted to low field (24.84 ppm for **10**, 26.15 ppm for **11**) with respect to the free ylide (δ =15.50 ppm); (iv) the ylidic carbon atom $PC_\alpha(H)$ appears in the $^{13}C\{^1H\}$ NMR spectrum (acquired as APT) as a doublet with positive phase, with a $^1J_{P,C}$ coupling constant (55.7 Hz for **10**, 58.6 Hz for **11**) smaller than that observed in **1** (108.3 Hz), and shifted to high field with respect to the corresponding signal in **1**. All these changes are in good agreement with the presence of a *C*-bonded ylide.[1]

As expected, the chemical behavior in this case is quite different from that observed in Pd^{II} and Pt^{II} complexes. The *C*-bonding of the ylide **1** blocks further reactivity at the C_α atom, but leaves the β-keto ester moiety unchanged. It seems likely then, that any further reactivity of the gold complexes could be directed selectively to the methylene group. This is not possible in the free ligand **1**, in which most of its reactivity occurs at the C_α center after deprotonation of the CH_2 unit.

Crystal Structure of $[Pd(C_6H_4CH_2NMe_2)(Ph_3PCH_2C(O)=C(H)C(=O)OEt\text{-}\kappa\text{-}O,O')]ClO_4$ (2a)

A solution of a mixture of **2a**/**2b** in CH_2Cl_2 was slowly evaporated to dryness at room temperature. During this process very regular yellow crystals were formed, which should be a mixture of the complexes **2a** and **2b** in the same molar ratio as that of the crude complex, and from this mixture of crystals, a yellow block was selected. The structure corresponds to that of complex **2a**, already established by spectroscopic methods.

A drawing of the cationic organometallic fragment is shown in Figure 1. The parameters concerning the data collection and refinement are given in Table 1, and selected bond lengths and angles are collected in Table 2. The Pd atom is located in a slightly distorted square-planar environment, surrounded by the *ortho*-metallated carbon atom C(25), the aminic N atom N(1), and the two oxygen atoms, O(1) and O(2), of the phosphonium-enolate [$Ph_3PCH_2C(O)=CH-C(O)OEt$] ligand, which coordinates as an *O*,*O*′-chelate. The structural parameters of the *ortho*-

Table 1: Crystal data and structure refinement for complexes **2a**, **9** and **10**

	2a	**9**	**10**
Empirical formula	$C_{33}H_{35}ClNO_7PPd$	$C_{34}H_{31}ClF_5O_7PPdS$	$C_{24}H_{23}AuClO_3P$
Mol mass	730.44	851.47	622.81
Crystal system	triclinic	triclinic	monoclinic
Space group	$P\bar{1}$	$P\bar{1}$	$P21/n$
a (Å)	11.3130(6)	11.7925(8)	12.2186(11)
b (Å)	12.2269(6)	11.8733(8)	14.5885(13)
c (Å)	14.2943(7)	13.2719(9)	12.9320(12)
α (°)	94.123(1)	77.936(1)	
β (°)	112.790(1)	87.107(1)	96.1960(10)
γ (°)	116.409(1)	79.959(1)	
V (Å^3)	1559.61(14)	1789.2(2)	2291.7(4)
Z	2	2	4
$D_{calcd.}$ (Mg·m^{-3})	1.555	1.580	1.805
μ (mm^{-1})	0.782	0.769	6.628
Reflections collected	9964	9962	13973
Unique reflections	6729, R_{int} = 0.0103	6237, R_{int} = 0.0183	5157, R_{int} = 0.0264
Data/restraints/parameters	6729/0/400	6237/0/452	5157/0/272
*R*1 [$I > 2\sigma(I)$]	0.0220	0.0590	0.0248
*wR*2 [$I > 2\sigma(I)$]	0.0556	0.1450	0.0620
Goodness of fit	1.087	1.045	1.041
T/K	100(2)	291(2)	100(2)
λ(Mo-K_α)/Å	0.71073	0.71073	0.71073

 © 2004 Wiley-VCH Verlag GmbH & Co. KGaA, Weinheim

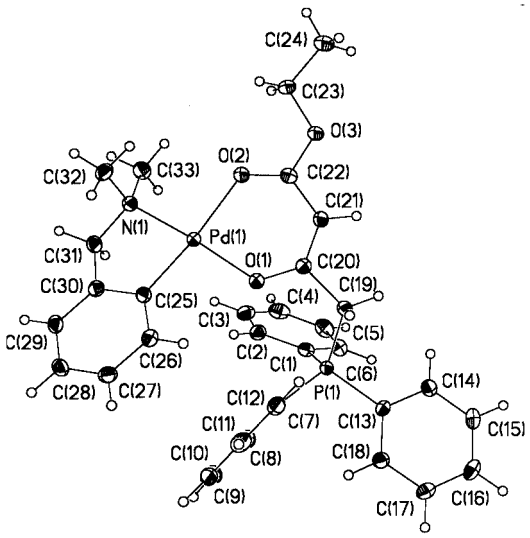

Figure 1. Thermal ellipsoid plot of the cationic fragment of **2a**. Non-hydrogen atoms are drawn at the 50% probability level

Table 2. Selected bond lengths (Å) and angles (°) for **2a**

Pd(1)−C(25)	1.9619(16)	Pd(1)−O(1)	2.0390(11)
Pd(1)−N(1)	2.0511(14)	Pd(1)−O(2)	2.1265(11)
P(1)−C(7)	1.7840(16)	P(1)−C(1)	1.7930(17)
P(1)−C(13)	1.7941(16)	P(1)−C(19)	1.8129(16)
C(19)−C(20)	1.521(2)	C(20)−O(1)	1.2876(19)
C(20)−C(21)	1.372(2)	C(21)−C(22)	1.426(2)
C(22)−O(2)	1.240(2)	C(22)−O(3)	1.3376(19)
O(3)−C(23)	1.4546(19)	C(23)−C(24)	1.504(2)
C(25)−C(26)	1.394(2)	C(25)−C(30)	1.398(2)
C(26)−C(27)	1.396(2)	C(27)−C(28)	1.385(3)
C(28)−C(29)	1.390(3)	C(30)−C(31)	1.498(2)
C(31)−N(1)	1.497(2)	N(1)−C(33)	1.481(2)
N(1)−C(32)	1.487(2)		
C(25)−Pd(1)−O(1)	93.73(6)	C(25)−Pd(1) −N(1)	82.39(6)
O(1)−Pd(1)−N(1)	175.490(5)	C(25)−Pd(1)−O(2)	174.25(6)
O(1)−Pd(1)−O(2)	90.91(4)	N(1)−Pd(1)−O(2)	93.11(5)
C(7)−P(1)−C(1)	111.86(8)	C(7)−P(1)−C(13)	105.77(7)
C(1)−P(1)−C(13)	112.50(8)	C(7)−P(1)−C(19)	112.28(8)
C(1)−P(1)−C(19)	107.54(7)	C(13)−P(1)−C(19)	106.85(7)
C(20)−C(19)−P(1)	111.41(11)	O(1)−C(20)−C(21)	129.57(15)
O(1)−C(20)−C(19)	113.40(13)	C(21)−C(20)−C(19)	117.02(14)
C(20)−C(21)−C(22)	124.69(15)	O(2)−C(22)−O(3)	127.33(15)
O(3)−C(22)−C(21)	112.75(14)		

metallated $C_6H_4CH_2NMe_2$ ligand are similar to those reported in related complexes and they do not show special features.[8] The two Pd−O bond lengths are different [Pd(1)−O(1) = 2.0390(11) Å; Pd(1)−O(2) = 2.1265(11) Å] probably due to two concurrent facts, namely (i) the different nature of the two oxygen atoms involved, since the C(22)−O(2) bond shows a higher double bond character [1.240(2) Å] than the C(20)−O(1) bond [1.2876(19) Å] (see Scheme 2), and (ii) the different *trans* influences of the C- and N-donor atoms of the $C_6H_4CH_2NMe_2$ ligand. A comparison of these distances with those of related complexes shows that the Pd(1)−O(1) bond length falls in the range usually reported for *O,O′*-acetylacetonate derivatives of Pd^{II} (range 2.007−2.073 Å),[9] while the Pd(1)−O(2) bond length is only slightly shorter than those found in other *O*-bonded α-stabilized keto-ylides [2.154(2) Å].[8b] These facts are in good agreement with a higher keto character for the C(22)−O(2) bond and a higher enolic character for the C(20)−O(1) bond. Moreover, the C−C bond lengths in the chelate ring are also quite different. The C(21)−C(22) bond length [1.426(2) Å] shows a small double bond component, since it is intermediate between a single σ(C−C) bond and a double C=C bond,[10] while the C(20)−C(21) bond length [1.372(2) Å] clearly shows double bond character. Outside the ring, the C(19)−C(20) bond length [1.521(2) Å] implies a single σ(C−C) bond, and all P−C bond lengths are also in the range found for single bonds.[10]

The geometry around the carbon atoms C(20) and C(22) is strictly planar [sum of the bond angles = 359.99(15)° in both cases] and the bond angle C(20)−C(21)−C(22) [124.69(15)°] also reflects its sp^2 character. The environments around the atoms C(19) and P(1) are tetrahedral. Furthermore, the intramolecular distance P(1)−O(1) [3.001(2) Å] is shorter than the sum of the van der Waals radii (3.32 Å),[11] suggesting an intramolecular interaction between the positively charged phosphonium atom P(1) and the formally anionic atom O(1). This type of 1,4-interaction has recently been described by us for keto-stabilized P-ylides.[12] However, this intramolecular interaction should be weaker than those described in P-ylides, as can be deduced from the value of the torsion angle P(1)−C(19)−C(20)−O(1) (51.2°), which is considerably different from the value obtained in the more stable *cisoid* forms of the ylides (nearly 0°).[12] Finally, the H atom H(26) [bonded to C(26)] points to the phenyl ring C(7)−C(12), the distance between H(26) and the best least-squares plane defined by the C atoms of the Ph ring being 2.74 Å. It is reasonable to assume that this short intramolecular distance could explain the strong anisotropic shielding exhibited by this proton in the ^1H NMR spectrum of **2a**.

Crystal Structure of [Pd(C_6F_5)(SC_4H_8)($Ph_3PCH_2C(O)$=C(H)C(=O)OEt-κ-*O,O′*)]ClO_4 (9)

A solution of **9** in CH_2Cl_2 was very slowly evaporated to dryness at room temperature. During this process yellow crystals were formed. A drawing of the cationic organometallic fragment is shown in Figure 2. The parameters concerning the data collection and refinement are summarized in Table 1, and selected bond lengths and angles are given in Table 3. The Pd atom is located in a distorted square-planar environment, surrounded by the *ipso* carbon atom C(1) of the C_6F_5 ligand, the S(1) atom of the tht ligand, and the two oxygen atoms, O(1) and O(2), of the phosphonium-enolate [$Ph_3PCH_2C(O)$=CH−C(O)OEt] ligand. The structural arrangement confirms that the enolate oxygen O(2) is *trans* to the sulfur atom S(1) and, hence, that the carbonylic oxygen O(1) is *trans* to the *ipso* carbon atom C(1) of the C_6F_5 group, as we proposed previously. The Pd(1)−C(1) bond length [1.987(5) Å] is typical for C_6F_5 groups *trans* to O-donor ligands,[4b] and the Pd(1)−S(1) bond length [2.2772(17) Å] also falls in the usual range of distances found in the literature for this type of bond.[9] The two

 © 2004 Wiley-VCH Verlag GmbH & Co. KGaA, Weinheim

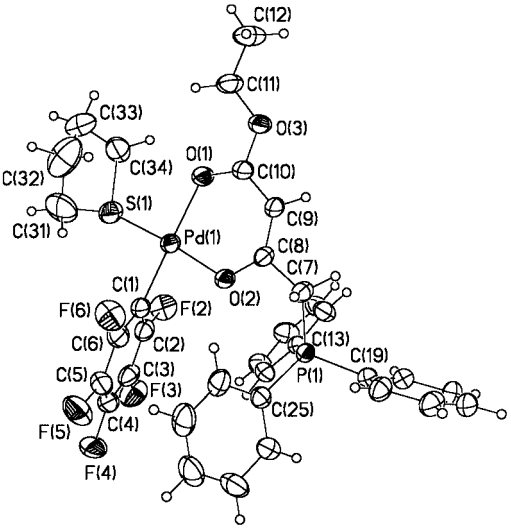

Figure 2. Thermal ellipsoid plot of the cationic fragment of **9**. Non-hydrogen atoms are drawn at the 50% probability level

Table 3. Selected bond lengths (Å) and angles (°) for **9**

Pd(1)−C(1)	1.987(5)	Pd(1)−O(1)	2.066(4)
Pd(1)−S(1)	2.2772(17)	Pd(1)−O(2)	2.028(3)
P(1)−C(25)	1.794(6)	P(1)−C(19)	1.797(5)
P(1)−C(13)	1.799(5)	P(1)−C(7)	1.804(5)
O(1)−C(10)	1.250(6)	O(2)−C(8)	1.283(6)
O(3)−C(10)	1.324(6)	O(3)−C(11)	1.453(7)
C(7)−C(8)	1.523(7)	C(8)−C(9)	1.351(7)
C(9)−C(10)	1.414(7)	C(11)−C(12)	1.473(9)
C(1)−Pd(1)−O(2)	86.94(18)	C(1)−Pd(1)−O(1)	178.47(18)
O(2)−Pd(1)−O(1)	91.57(14)	C(1)−Pd(1)−S(1)	87.76(15)
O(2)−Pd(1)−S(1)	173.97(11)	O(1)−Pd(1)−S(1)	93.74(11)
C(25)−P(1)−C(19)	107.1(3)	C(25)−P(1)−C(13)	111.2(2)
C(19)−P(1)−C(13)	110.9(3)	C(25)−P(1)−C(7)	111.9(3)
C(19)−P(1)−C(7)	105.0(2)	C(13)−P(1)−C(7)	110.5(3)
C(10)−O(1)−Pd(1)	123.7(3)	C(8)−O(2)−Pd(1)	122.9(3)
C(10)−O(3)−C(11)	118.4(4)	C(8)−C(7)−P(1)	114.6(4)
O(2)−C(8)−C(9)	129.2(5)	O(2)−C(8)−C(7)	113.6(4)
C(9)−C(8)−C(7)	117.1(5)	C(8)−C(9)−C(10)	125.3(5)
O(1)−C(10)−O(3)	118.9(5)	O(1)−C(10)−C(9)	127.1(5)
O(3)−C(10)−C(9)	114.0(5)	O(3)−C(11)−C(12)	108.0(5)

Pd−O bond lengths are different [Pd(1)−O(1) = 2.066(4) Å and Pd(1)−O(2) = 2.028(3) Å], as we have described for **2a**, reflecting the different *trans* influences of the *trans* donor atoms, although in **9** the differences between them are less pronounced than in **2a** [2.1265(11) Å and 2.0390(11) Å]. The internal bond lengths and angles of the phosphonium-enolate ligand are identical, within experimental error, to those described for complex **2a**, and thus the same structural conclusions can be derived here. Finally, the similarity between the structures of complexes **2a** and **9** is also reflected in the presence of short intramolecular P···O contacts[12] [P(1)−O(2) = 2.950(7) Å], although in this case the value of the torsion angle P(1)−C(7)−C(8)−O(2) (35.5°) is clearly narrower than that reported for **2a**.

Crystal Structure of [AuCl{C(H)(PPh_3)C(O)CH_2C(O)OEt}] (10)

Crystals of complex **10** were grown by slow vapor diffusion of Et_2O into a CH_2Cl_2 solution of the crude complex at room temperature. A drawing of the molecular structure of **10** is shown in Figure 3. The parameters concerning the data collection and refinement are presented in Table 1, and selected bond lengths and angles are collected in Table 4. Complex **10** crystallizes in the monoclinic space group $P2_1/c$. Since this space group is centrosymmetric, and although the complex is chiral, the crystal as a whole is racemic. The structure shown in Figure 3 corresponds to an absolute configuration (*S*) for the ylidic carbon C_α, following the system of priorities of Cahn, Ingold and Prelog.[13] The gold atom lies in a nearly linear environment, since the bond angle C(19)−Au(1)−Cl(1) is 176.48(9)°. The bond lengths Au(1)−C(19) [2.079(3) Å] and Au(1)−Cl(1) [2.2928(9) Å] are similar to those found in the literature for related structural arrangements.[14] The bond lengths C(20)−O(1) [1.214(4) Å] and C(22)−O(3) [1.199(4) Å] are typical[8,9] for carbonyl groups which are not delocalized through adjacent functional groups (e.g. the ylide function), while the bond length C(19)−C(20) is identical (within ex-

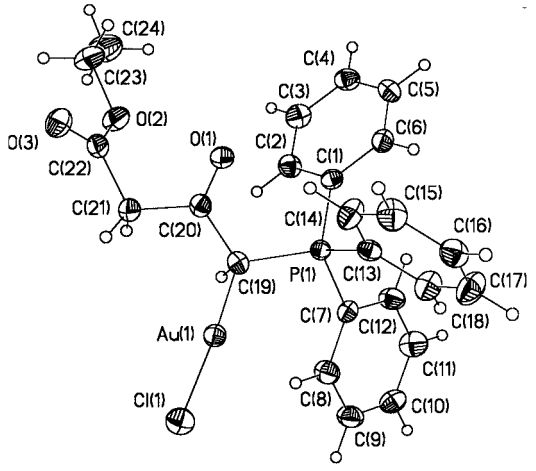

Figure 3. Thermal ellipsoid plot of **10**. Non-hydrogen atoms are drawn at the 50% probability level

Table 4. Selected bond lengths (Å) and angles (°) for **10**

Au(1)−C(19)	2.079(3)	Au(1)−C1(1)	2.2928(9)
P(1)−C(19)	1.780(3)	P(1)−C(7)	1.799(3)
P(1)−C(13)	1.800(3)	P(1)−C(1)	1.801(3)
C(19)−C(20)	1.487(5)	C(20)−O(1)	1.214(4)
C(20)−C(21)	1.529(4)	C(21)−C(22)	1.499(5)
C(22)−O(3)	1.199(4)	C(22)−O(2)	1.330(4)
C(23)−C(24)	1.501(6)		
C(19)−P(1)−C(13)	114.20(16)	C(7)−P(1)−C(13)	107.48(15)
C(19)−P(1)−C(1)	109.98(15)	C(7)−P(1)−C(1)	107.40(16)
C(13)−P(1)−C(1)	110.00(15)	C(20)−C(19)−P(1)	115.1(2)
C(20)−C(19)−Au(1)	104.9(2)	P(1)−C(19)−Au(1)	113.53(17)
O(1)−C(20)−C(19)	125.2(3)	O(1)−C(20)−C(21)	120.4(3)
C(19)−C(20)−C(21)	114.3(3)	C(3)−C(22)−O(2)	124.5(3)
O(3)−C(22)−C(21)	125.2(3)	C(19)−Au(1)−Cl(1)	176.48(9)
O(2)−C(22)−C(21)	110.2(3)	C(19)−P(1)−C(7)	107.50(16)

 © 2004 Wiley-VCH Verlag GmbH & Co. KGaA, Weinheim

perimental error) to that found in other *C*-bonded keto-stabilized ylides.[8a] The P(1)−C(19) bond length [1.780(3) Å] is slightly shorter than the other P−C(Ph) bond lengths and, in turn, is similar to those found in other *C*-coordinated stabilized ylides.[8a] Typical single bond σ(C−C) distances are found for C(20)−C(21) [1.529(4) Å] and C(21)−C(22) [1.499(5) Å]. Finally, the environments around P(1) and C(19) are tetrahedral, while those around the carbonyl atoms C(20) and C(22) are strictly planar.

Conclusion

The polyfunctional ylide $[Ph_3P{=}C(H)C(O)CH_2C(O)OEt]$ (**1**) shows versatile reactivity towards different transition metals, giving very different structural motifs as a function of the metal center. Towards cationic Pd^{II} and Pt^{II} complexes with two available coordination sites, **1** undergoes a proton transfer giving the zwitterionic phosphonium-enolate $[Ph_3(P^+)CH_2C(O^-){=}CH{-}C(O)OEt]$ ligand, which coordinates as an *O,O′*-chelate. The presence of a phosphonium group, which can be easily deprotonated, could open new pathways of reactivity towards polynuclear complexes with a great variety of structural arrangements. On the other hand, the reactivity of **1** towards Au^I derivatives gives complexes with the ylide *C*-bonded, leaving the β-keto ester unit −C(O)CH$_2$C(O)OEt unchanged. This fact also opens new pathways of reactivity. This rich coordination chemistry is unprecedented for α-stabilized ylide ligands and the fine tuning of the reactivity allows us to suggest that new and more interesting results may await discovery.

Experimental Section

CAUTION: Perchlorate salts of metal complexes with organic ligands are potentially explosive. Only small amounts of these materials should be prepared and handled with great caution.[15]

General Methods: Solvents were dried and distilled under argon using standard procedures. Elemental analyses were carried out with a Perkin−Elmer 2400-B machine. Infrared spectra (4000−200 cm^{-1}) were recorded with a Perkin−Elmer 883 infrared spectrometer from nujol mulls between polyethylene sheets. Mass spectra (positive ion FAB) were recorded from CH_2Cl_2 solutions with a V. G. Autospec spectrometer. ^{1}H (300.13 MHz), $^{13}C\{^1H\}$ (75.47 MHz), ^{19}F (282.40 MHz), and $^{31}P\{^1H\}$ (121.49 MHz) NMR spectra were recorded in $CDCl_3$ or CD_2Cl_2 solutions at room temperature with a Bruker ARX-300 spectrometer. The ^{1}H and $^{13}C\{^1H\}$ NMR spectra were referenced using the residual solvent signal as the internal standard, whereas the $^{31}P\{^1H\}$ NMR spectra were referenced to external H_3PO_4 (85%). The ^{19}F NMR spectra were referenced to $CFCl_3$. The starting compounds were prepared following published methods: **1**,[2b] $[Pd(\mu\text{-}Cl)\{(C_6H_4CH_2NMe_2\text{-}(C^2,N)\}]_2$,[16] $[Pd(\mu\text{-}Cl)\{(S)\text{-}C_6H_4C(H)MeNMe_2(C^2,N)\}]_2$,[16] $[Pd(\mu\text{-}Cl)\{NC_{13}H_8(C^8,N)\}]_2$,[17] $[Pd(\mu\text{-}Cl)\{CH_2NC_9H_6(C^8,N)\}]_2$,[6,18] $[Pd(\mu\text{-}Cl)\{NC_5H_4\text{-}2\text{-}C_6H_4(C^2,N)\}]_2$,[19] $[Pd(\mu\text{-}Cl)(tht)(C_6F_5)]_2$,[20] $[M(\mu\text{-}Cl)\{o\text{-}CH_2C_6H_4P(o\text{-}tol_2)(C,P)\}]_2$ (M = Pd,[21] Pt[22]), [AuCl(tht)],[23] and $[AuCl(PPh_3)]$.[23]

$[Ph_3P{=}C(H){-}C(O){-}CH_2{-}COOEt]$ (1): The ylide **1** was prepared following the method reported by F. Serratosa and E. Solé.[2b] The analytical and IR data were in good agreement with those previously published. Here we present the MS and NMR spectroscopic data for **1**, which have not been reported previously. MS (FAB+): *m/z* (%) = 391 (100) [M$^+$]. ^{1}H NMR (CD_2Cl_2): δ = 1.26 (t, $^3J_{H,H}$ = 7.2 Hz, 3 H, CH_3), 3.29 (d, $^4J_{PH}$ = 1.5 Hz, 2 H, CH_2), 3.77 (d, $^2J_{PH}$ = 24.9 Hz, 1 H, P=CH), 4.16 (q, 2 H, OCH_2), 7.46−7.70 (m, 15 H, PPh_3) ppm. $^{13}C\{^1H\}$ NMR (CD_2Cl_2): δ = 14.53 (CH_3), 48.63 (d, CH_2, $^3J_{P,C}$ = 15.5 Hz), 52.18 (d, $^1J_{P,C}$ = 108.3 Hz, P=C$_\alpha$), 60.81 (OCH_2), 127.13 (d, $^1J_{P,C}$ = 90.8 Hz, C$_{ipso}$, PPh_3), 129.28 (d, $^2J_{P,C}$ = 12.2 Hz, C$_{ortho}$, PPh_3), 132.66 (d, $^4J_{P,C}$ = 2.8 Hz, C$_{para}$, PPh_3), 133.50 (d, $^3J_{P,C}$ = 10.2 Hz, C$_{meta}$, PPh_3), 170.79 (s, COO), 184.22 (d, $^2J_{P,C}$ = 2.9 Hz, C=*O*) ppm. $^{31}P\{^1H\}$ NMR (CD_2Cl_2): δ = 15.50 ppm.

Complex 2: To a suspension of $[Pd(\mu\text{-}Cl)(C_6H_4CH_2NMe_2)]_2$ (0.0755 g, 0.137 mmol) in THF (20 mL) under argon, was added $AgClO_4$ (0.0567 g, 0.273 mmol). The resultant mixture was stirred at room temperature for 20 min with exclusion of light, then filtered through a Celite pad. The freshly prepared solution of the bis(solvate) was treated with **1** (0.107 g, 0.273 mmol) giving a yellow solution, which was stirred for an additional 30 min. During this time, **2** precipitated as a yellow solid, which was filtered, washed with Et_2O (10 mL) and air dried. Yield: 0.100 g (50%). Complex **2** was characterized by NMR spectroscopy as a mixture of the isomers **2a/2b** in molar ratio **2a/2b** = 4.5:1. $C_{33}H_{35}ClNO_7PPd$ (730.47): calcd. C 54.26, H 4.83, N 1.92; found C 54.26, H 4.83, N 1.93. MS (FAB+): *m/z* (%) = 630 (100) [M − ClO_4]$^+$. IR: $\tilde{\nu}$ = 1628 (ν_{COO}), 1525 (ν_{CO}) cm^{-1}. ^{1}H NMR (CD_2Cl_2): δ = 1.23 (t, $^3J_{H,H}$ = 7.2 Hz, CH_3, **2a**), 1.27 (t, $^3J_{H,H}$ = 6.9 Hz, CH_3, **2b**), 2.24 (s, NMe_2, **2b**), 2.75 (s, NMe_2, **2a**), 3.76 (s, CH_2N, **2b**), 3.86 (s, CH_2N, **2a**), 4.06 (q, OCH_2, **2a**), 4.13 (d, $^2J_{PH}$ = 13.8 Hz, CH_2P, **2a**), 4.16 (d, $^2J_{PH}$ = 13.8 Hz, CH_2P, **2b**), 4.18 (q, OCH_2, **2b**), 4.81 (d, $^4J_{PH}$ = 0.6 Hz, = CH, **2a**), 4.86 (s, =CH, **2b**), 5.89 (dd, $^3J_{H^6H^5}$ = 8.1, $^4J_{H^6H^4}$ = 0.9 Hz, H^6, C_6H_4, **2a**), 6.43 (td, $^3J_{H^5H^6}$ = $^3J_{H^5H^4}$ = 8.1, $^4J_{H^5H^3}$ = 2.4 Hz, H^5, C_6H_4, **2a**), 6.83−7.01 [m, H^3 + H^4 (**2a**) + C_6H_4 (**2b**)], 7.66−7.87 (m, PPh_3, **2a** + **2b**) ppm. $^{13}C\{^1H\}$ NMR (CD_2Cl_2): δ = 14.49 (Me, **2a** + **2b**), 36.36 (d, $^1J_{P,C}$ = 52.5 Hz, CH_2P, **2a**), 36.47 (d, $^1J_{P,C}$ = 54.2 Hz, CH_2P, **2b**), 52.36 (NMe_2, **2a** + **2b**), 61.26 (OCH_2, **2a**), 61.75 (OCH_2, **2b**), 73.20 (CH_2N, **2a**), 73.78 (CH_2N, **2b**), 88.91 (d, $^3J_{P,C}$ = 7.4 Hz, =CH, **2b**), 90.43 (d, $^3J_{P,C}$ = 7.0 Hz, =CH, **2a**), 118.50 (d, $^1J_{P,C}$ = 87.8 Hz, C$_{ipso}$, PPh_3, **2a**), 118.88 (d, C$_{ipso}$, PPh_3, **2b**, $^1J_{P,C}$ = 88.1 Hz), 121.67 (2 C), 124.74 (2 C), 143.33 (C^2), 147.53 (C^1) (C_6H_4, **2a**), 124.98 (2 C), 125.09 (2 C), 144.23 (C^2), 147.75 (C^1), (C_6H_4, **2b**), 130.72 (d, $^2J_{P,C}$ = 12.7 Hz, C$_{ortho}$, **2a** + **2b**), 134.11(C$_{para}$, **2b**), 134.34 (d, $^3J_{P,C}$ = 10.0 Hz, C$_{meta}$, **2a** + **2b**), 135.64 (C$_{para}$, **2a**, PPh_3), 171.21 (CO_2, **2a**), 172.48 (CO_2, **2b**), 173.67 (d, $^2J_{P,C}$ = 7.2 Hz, CO, **2a**), 175.18 (d, $^2J_{P,C}$ = 7.1 Hz, CO, **2b**) ppm. $^{31}P\{^1H\}$ NMR (CD_2Cl_2): δ = 22.11 (**2b**), 22.71 (**2a**) ppm.

Complex 3: Complex **3** was prepared following a synthetic procedure similar to that reported for **2**. Thus, $[Pd(\mu\text{-}Cl)(CH_2C_9H_6N)]_2$ (0.192 g, 0.338 mmol) reacted, in THF (20 mL), with $AgClO_4$ (0.140 g, 0.676 mmol) and **1** (0.264 g, 0.676 mmol) to give **3** as a yellow solid. Yield: 0.344 g (69%). $C_{34}H_{31}ClNO_7PPd$ (738.45): calcd. C 55.30, H 4.23, N 1.89; found C 55.38, H 4.37, N 1.83. MS (FAB+): *m/z* (%) = 638 (100) [M − ClO_4]$^+$. IR: $\tilde{\nu}$ = 1624 (ν_{COO}), 1521 (ν_{CO}) cm^{-1}. ^{1}H NMR (CD_2Cl_2): δ = 1.31 (t, $^3J_{H,H}$ = 7.2 Hz, 3 H, CH_3), 3.02 (s, 2 H, CH_2Pd), 4.19 (d, $^2J_{PH}$ = 13.5 Hz, 2 H, CH_2P), 4.22 (q, 2 H, OCH_2), 4.92 (s, 1 H, =CH), 7.40−7.52 (m, 2 H, C_9H_6N), 7.62−7.76 (m, 15 H, PPh_3), 7.82−7.87 (m, 2 H, C_9H_6N), 8.31 (dd, $^3J_{H^4H^3}$ = 8.4, $^4J_{H^4H^2}$ = 1.5 Hz, 1 H, H^4, C_9H_6N),

 © 2004 Wiley-VCH Verlag GmbH & Co. KGaA, Weinheim

8.58 (dd, $^3J_{H^2H^3}$ = 5.1, $^4J_{H^2H^4}$ = 1.5 Hz, 1 H, H^2, C_9H_6N) ppm. $^{13}C\{^1H\}$ NMR (CD_2Cl_2): δ = 14.54 (CH_3), 22.48 (CH_2Pd), 37.08 (d, $^1J_{P,C}$ = 57.6 Hz, CH_2P), 61.15 (OCH_2), 89.32 (d, $^3J_{P,C}$ = 7.9 Hz, =CH), 119.34 (d, $^1J_{P,C}$ = 88.4 Hz, C_{ipso}, PPh_3), 121.93, 124.23, 128.65, 128.81, 129.47, 138.37, 147.85, 148.33, 153.61 (C_9H_6N), 130.52 (d, $^2J_{P,C}$ = 13 Hz, C_{ortho}), 134.25 (d, $^3J_{P,C}$ = 10.3 Hz, C_{meta}), 135.38 (d, $^4J_{P,C}$ = 3 Hz, C_{para}) (PPh_3), 171.33 (COO), 173.44 (d, $^2J_{P,C}$ = 7.2 Hz, CO) ppm. $^{31}P\{^1H\}$ NMR (CD_2Cl_2): δ = 23.15 ppm.

Complex 4: Complex **4** was prepared following a synthetic procedure similar to that reported for **2**. Thus, $[Pd(\mu\text{-}Cl)(NC_5H_4\text{-}2\text{-}C_6H_4)]_2$ (0.118 g, 0.20 mmol) reacted, in THF (20 mL), with $AgClO_4$ (0.083 g, 0.40 mmol) and **1** (0.156 g, 0.40 mmol) to give **4** as a yellow solid. Yield: 0.227 g (75.8%). Complex **4** was characterized by NMR as a mixture of the isomers **4a/4b** in molar ratio **4a/4b** = 3.2:1. $C_{35}H_{31}ClNO_7PPd$ (750.46): calcd. C 56.02, H 4.16, N 1.87; found C 55.69, H 4.49, N 1.67. MS (FAB+): *m/z* (%) = 650 (100) $[M - ClO_4]^+$. IR: $\tilde{\nu}$ = 1620 (ν_{COO}), 1515 (ν_{CO}) cm^{-1}. ^1H NMR (CD_2Cl_2): δ = 1.28 (t, $^3J_{H,H}$ = 7.2 Hz, CH_3, **4a**), 1.30 (t, $^3J_{H,H}$ = 7.2 Hz, CH_3, **4b**), 4.16 (q, OCH_2, **4a**), 4.18 (d, $^2J_{PH}$ = 14 Hz, CH_2P, **4b**), 4.20 (d, $^2J_{PH}$ = 16 Hz, CH_2P, **4a**), 4.24 (q, OCH_2, **4b**), 4.87 (d, $^4J_{PH}$ = 1 Hz, =CH, **4a**), 4.90 (s, =CH, **4b**), 6.07 (dd, $^3J_{H,H}$ = 7.8, $^4J_{H,H}$ = 1.2 Hz, $NC_5H_4\text{-}2\text{-}C_6H_4$, **4a**), 6.58 (td, $^3J_{H,H}$ = 7.9, $^4J_{H,H}$ = 1.2 Hz, $NC_5H_4\text{-}2\text{-}C_6H_4$, **4a**), 6.68 (td, $^3J_{H,H}$ = 7.2, $^4J_{H,H}$ = 1.2 Hz, $NC_5H_4\text{-}2\text{-}C_6H_4$, **4b**), 7.01 (td, $^3J_{H,H}$ = 7.5, $^4J_{H,H}$ = 1 Hz, $NC_5H_4\text{-}2\text{-}C_6H_4$, **4a**), 7.16 (m, $NC_5H_4\text{-}2\text{-}C_6H_4$, **4a**), 7.33 (dd, $^3J_{H,H}$ = 7.9, $^4J_{H,H}$ = 1.2 Hz, $NC_5H_4\text{-}2\text{-}C_6H_4$, **4a**), 7.88−7.57 (m, PPh_3 + $NC_5H_4\text{-}2\text{-}C_6H_4$), 8.35 (dd, $^3J_{H,H}$ = 5.7, $^4J_{H,H}$ = 1 Hz, $NC_5H_4\text{-}2\text{-}C_6H_4$, **4a**) ppm. The assignment of resonances for the $NC_5H_4\text{-}2\text{-}C_6H_4$ ligand could be performed unequivocally only for the major isomer **4a**, due to extensive overlapping of the signals of the minor isomer **4b** with those of the major isomer and with the PPh_3 group. $^{13}C\{^1H\}$ NMR (CD_2Cl_2): δ = 14.43 (CH_3, **4a** + **4b**), 36.23 (d, $^1J_{P,C}$ = 52.1 Hz, CH_2P, **4a** + **4b**), 61.56 (OCH_2, **4a**), 62.03 (OCH_2, **4b**), 89.89 (d, $^3J_{P,C}$ = 7.3 Hz, =CH, **4b**), 91.07 (d, $^3J_{P,C}$ = 6.7 Hz, =CH, **4a**), 118.37 (d, $^1J_{P,C}$ = 87.7 Hz, C_{ipso}, PPh_3, **4a**), 118.58 (d, $^1J_{P,C}$ = 86.0 Hz, C_{ipso}, PPh_3, **4b**), 119.15, 122.79, 123.49, 125.18, 129.16, 131.30, 139.57, 145.24, 148.45, 151.47, 165.51 ($NC_5H_4\text{-}2\text{-}C_6H_4$, **4a**), 119.20, 122.58, 123.49, 125.48, 129.41, 131.31, 139.58, 145.32, 148.41, 152.67, 165.91 ($NC_5H_4\text{-}2\text{-}C_6H_4$, **4b**), 130.76 (d, $^2J_{P,C}$ = 12.4 Hz, C_{ortho}, PPh_3), 134.35 (d, $^3J_{P,C}$ = 9.1 Hz, C_{meta}, PPh_3), 135.69 (s, C_{para}, PPh_3, both isomers), 171.57 (COO, **4a**), 172.69 (COO, **4b**), 173.89 (d, $^2J_{P,C}$ = 7.3 Hz, CO, **4a**), 175.23 (d, $^2J_{P,C}$ = 6.6 Hz, CO, **4b**) ppm. $^{31}P\{^1H\}$ NMR (CD_2Cl_2): δ = 22.57 (**4b**), 22.84 (**4a**) ppm.

Complex 5: Complex **5** was prepared following a synthetic procedure similar to that reported for **2**. Thus, $[Pd(\mu\text{-}Cl)(C_{13}H_8N)]_2$ (0.101 g, 0.158 mmol) reacted, in THF (20 mL), with $AgClO_4$ (0.065 g, 0.32 mmol) and **1** (0.123 g, 0.316 mmol) to give **5** as a yellow solid. Yield: 0.0622 g (25.5%). Complex **5** was characterized by NMR as a mixture of the isomers **5a/5b** in molar ratio **5a/5b** = 3.6:1. $C_{37}H_{31}ClNO_7PPd$ (774.48): calcd. C 57.38, H 4.03, N 1.81; found C 56.90, H 4.05, N 1.79. MS (FAB+): *m/z* (%) = 674 (100) $[M - ClO_4]^+$. IR: $\tilde{\nu}$ = 1616 (ν_{COO}), 1512 (ν_{CO}) cm^{-1}. ^1H NMR (CD_2Cl_2): δ = 1.33 (t, $^3J_{H,H}$ = 7.2 Hz, CH_3, **5a**), 1.35 (t, $^3J_{H,H}$ = 6.3 Hz, CH_3, **5b**), 4.21 (q, OCH_2, **5a**), 4.21 (d, $^2J_{PH}$ = 13.8 Hz, CH_2P, **5b**), 4.28 (d, $^2J_{PH}$ = 13.8 Hz, CH_2P, **5a**), 4.30 (q, OCH_2, **5b**), 4.93 (s, =CH, **5b**), 4.94 (s, =CH, **5a**), 6.05 (dd, $^3J_{H,H}$ = 7.5, $^4J_{H,H}$ = 0.6 Hz, $C_{13}H_8N$, **5a**), 6.94 (t, $^3J_{H,H}$ = 7.5 Hz, $C_{13}H_8N$, **5a**), 6.97 (dd, $^3J_{H,H}$ = 8.1, $^3J_{H,H}$ = 5.1 Hz, $C_{13}H_8N$, **5b**), 7.18 (dd, $^3J_{H,H}$ = 5.1, $^4J_{H,H}$ = 1.2 Hz, $C_{13}H_8N$, **5b**), 7.30 (dd, $^3J_{H,H}$ = 8.1, $^3J_{H,H}$ = 5.1 Hz, $C_{13}H_8N$, **5a**), 7.30 (dd, $^3J_{H,H}$ = 6.0, $^4J_{H,H}$ = 0.9 Hz, $C_{13}H_8N$, **5b**), 7.39 (t, $^3J_{H,H}$ = 7.5 Hz, $C_{13}H_8N$, **5b**), 7.47 (d, $^3J_{H,H}$ = 7.5 Hz, $C_{13}H_8N$, **5a**), 7.51 (d, $^3J_{H,H}$ = 8.7 Hz, $C_{13}H_8N$, **5a**), 7.55 (dd, $^3J_{H,H}$ = 7.5, $^4J_{H,H}$ = 0.6 Hz, $C_{13}H_8N$, **5b**), 7.85−7.63 (m, PPh_3 + $C_{13}H_8N$, **5a** + **5b**), 8.16 (dd, $^3J_{H,H}$ = 8.1, $^4J_{H,H}$ = 1.2 Hz, $C_{13}H_8N$, **5a**), 8.20 (dd, $^3J_{H,H}$ = 8.1, $^4J_{H,H}$ = 1.2 Hz, $C_{13}H_8N$, **5b**), 8.31 (dd, $^3J_{H,H}$ = 5.1, $^4J_{H,H}$ = 1.2 Hz, $C_{13}H_8N$, **5a**) ppm. $^{13}C\{^1H\}$ NMR (CD_2Cl_2): δ (signals due to **5b** in the low field region were not observed) = 14.50 (CH_3, **5a** + **5b**), 36.26 (d, $^1J_{P,C}$ = 52.3 Hz CH_2P, **5a** + **5b**), 61.63 (OCH_2, **5a**), 62.12 (OCH_2, **5b**), 88.92 (d, $^3J_{P,C}$ = 5.9 Hz, =CH, **5b**), 91.12 (d, $^3J_{P,C}$ = 6.7 Hz, =CH, **5a**), 118.47 (d, $^1J_{P,C}$ = 87.8 Hz, C_{ipso}, PPh_3, **5a**), 118.63 (d, $^1J_{P,C}$ = 87.8 Hz, C_{ipso}, PPh_3, **5b**), 121.66, 122.92, 123.65, 128.37, 128.74, 129.15, 133.44, 137.55, 141.03, 147.26, 148.43, 154.83 ($C_{13}H_8N$, **5a**, one of the quaternary carbon atoms was not observed), 130.76 (d, PPh_3, $^2J_{P,C}$ = 12.8 Hz, C_{ortho}), 134.40 (d, $^3J_{P,C}$ = 9.4 Hz, C_{meta}, PPh_3), 135.63 (C_{para}, PPh_3), 171.51 (COO, **5a**), 173.90 (d, $^2J_{P,C}$ = 6.9 Hz, CO, **5a**) ppm. $^{31}P\{^1H\}$ NMR (CD_2Cl_2): δ = 23.08 (**5a**), 22.74 (**5b**) ppm.

Complex 6: Complex **6** was prepared following a synthetic procedure similar to that reported for **2**. Thus, $[Pd(\mu\text{-}Cl)\{(S)\text{-}C_6H_4C(H)MeNMe_2\}]_2$ (0.105 g, 0.181 mmol) reacted, in THF (20 mL), with $AgClO_4$ (0.075 g, 0.362 mmol) and **1** (0.142 g, 0.36 mmol) to give **6** as a yellow solid. Yield: 0.2627 g (97.5%). Complex **6** was characterized by NMR spectroscopy as a mixture of the isomers **6a/6b** in molar ratio **6a/6b** = 4.3:1. $C_{34}H_{37}ClNO_7PPd$ (744.50): calcd. C 54.85, H 5.01, N 1.88; found: C 55.19, H 4.73, N 1.89. MS (FAB+): *m/z* (%) = 644 (65) $[M - ClO_4]^+$. IR: $\tilde{\nu}$ = 1622 (ν_{COO}), 1505 (ν_{CO}) cm^{-1}. ^1H NMR (CD_2Cl_2): δ = 1.23 (t, $^3J_{H,H}$ = 7.2 Hz, CH_3, **6a**), 1.26 (t, $^3J_{H,H}$ = 7.2 Hz, CH_3, **6b**), 1.35 [d, $^3J_{H,H}$ = 6.9 Hz, CH(*Me*), **6b**], 1.48 [d, $^3J_{H,H}$ = 6.6 Hz, CH(*Me*), **6a**], 2.03 (s, NMe_2, **6b**), 2.31 (s, NMe_2, **6b**), 2.55 (s, NMe_2, **6a**), 2.81 (s, NMe_2, **6a**), 3.86 [q, C*H*(Me), **6a**], 4.06 (q, OCH_2, **6a**), 4.12−4.25 [m, OCH_2 (**6b**) + C*H*(Me) (**6b**) + CH_2P (**6a**) + CH_2P (**6b**)], 4.83 (s, =CH, **6a**), 4.88 (s, =CH, **6b**), 5.88 (dd, $^3J_{H,H}$ = 7.5, $^4J_{H,H}$ = 1.2 Hz, H^6, C_6H_4, **6a**), 6.42 (td, $^3J_{H,H}$ = 7.5, $^4J_{H,H}$ = 1.5 Hz, H^5, C_6H_4, **6a**), 6.77 (d, $^3J_{H,H}$ = 7 Hz, C_6H_4, **6a**), 6.90 (td, $^3J_{H,H}$ = 7.5, $^4J_{H,H}$ = 1.2 Hz, C_6H_4, **6a**), 6.92 (td, $^3J_{H,H}$ = 4.0, $^4J_{H,H}$ = 1.2 Hz, C_6H_4, **6b**), 6.97−7.02 (m, C_6H_4, **6b**), 7.65−7.84 (m, PPh_3, **6a** + **6b**) ppm. $^{13}C\{^1H\}$ NMR (CD_2Cl_2): δ = 14.51 (CH_3, **6a**), 17.38 (CH_3, **6b**), 18.28 (CH*Me*), **6a**), 30.53 (CH*Me*), **6b**), 36.30 (d, $^1J_{P,C}$ = 52.8 Hz, CH_2P, **6a**), 36.51 (d, CH_2P, **6b**, $^1J_{P,C}$ = 54.2 Hz), 46.12 (NMe_2, **6b**), 46.34 (NMe_2, **6a**), 51.58 (NMe_2, **6b**), 51.87 (NMe_2, **6a**), 61.23 (OCH_2, **6a**), 61.67 (OCH_2, **6b**), 75.30 [*C*H(Me), **6a**], 75.72 [*C*H(Me), **6b**], 88.88 (d, $^3J_{P,C}$ = 6.6 Hz, =CH, **6b**), 90.30 (d, $^3J_{P,C}$ = 6.8 Hz, =CH, **6a**), 118.59 (d, $^1J_{P,C}$ = 87.8 Hz, C_{ipso}, PPh_3, **6a**), 118.94 (d, $^1J_{P,C}$ = 88.1 Hz, C_{ipso}, PPh_3, **6b**), 122.16 (2 C, C_6H_4, **6a**), 124.71 (2 C, C_6H_4, **6a**), 122.32, 124.98, 125.08, 125.21 (C_6H_4, **6b**), 130.69 (d, $^2J_{P,C}$ = 11.5 Hz, C_{ortho}, PPh_3, **6a** + **6b**), 134.35 (d, $^3J_{P,C}$ = 10.0 Hz, C_{meta}, PPh_3, **6a** + **6b**), 135.60 (C_{para}, PPh_3, **6a** + **6b**), 143.87 (C_6H_4, **6a**), 144.91 (C_6H_4, **6b**), 152.77 (C_6H_4, **6b**), 152.80 (C_6H_4, **6a**), 171.21 (COO, **6a**), 172.48 (COO, **6b**), 173.78 (d, CO, **6a**, $^2J_{P,C}$ = 7.2 Hz), 175.26 (d, $^2J_{P,C}$ = 6.9 Hz, CO, **6b**) ppm. $^{31}P\{^1H\}$ NMR (CD_2Cl_2): δ = 22.74 (**6a**), 22.10 (**6b**) ppm.

Complex 7: Complex **7** was prepared following a synthetic procedure similar to that reported for **2**. Thus, $[Pt(\mu\text{-}Cl)\{o\text{-}CH_2C_6H_4P(o\text{-}tol)_2\}]_2$ (0.135 g, 0.126 mmol) reacted, in THF (20 mL), with $AgClO_4$ (0.052 g, 0.25 mmol) and **1** (0.103 g, 0.264 mmol) to give **7** as a pale yellow solid. Yield: 0.222 g (88.6%). $C_{45}H_{43}ClO_7P_2Pt$ (988.32): calcd. C 54.69, H 4.38; found C 54.52, H 4.08. MS (FAB+): *m/z* (%) = 888 (45) $[M - ClO_4]^+$. IR: $\tilde{\nu}$ = 1614 (ν_{COO}), 1520 (ν_{CO}) cm^{-1}. ^1H NMR (CD_2Cl_2): δ = 1.18 (t,

 © 2004 Wiley-VCH Verlag GmbH & Co. KGaA, Weinheim

$^3J_{H,H}$ = 7.2 Hz, 3 H, CH_3), 2.40 (s, 3 H, Me tolyl), 2.64 (s, 3 H, Me tolyl), 2.98 (s broad, 2 H, CH_2Pt), 3.61 (q, 2 H, OCH_2), 4.27 (d, $^2J_{PH}$ = 13.5 Hz, 2 H, CH_2P), 5.08 (s, 1 H, =CH), 6.78−7.74 (m, 27 H, PPh_3 + C_6H_4) ppm. $^{13}C\{^1H\}$ NMR ($CDCl_3$): δ = 7.77 ($PtCH_2$), 13.98 (CH_3), 22.19 (CH_3 tolyl), 30.31 (CH_3 tolyl), 36.21 (dd, $^1J_{P,C}$ = 55.4, $^4J_{P,C}$ = 5.9 Hz, CH_2P), 60.97 (OCH_2), 90.41 (d, $^3J_{P,C}$ = 7.5 Hz, =CH), 118.86 (d, $^1J_{P,C}$ = 88.02 Hz, C_{ipso}, PPh_3), 125.66 (d, $J_{P,C}$ = 9.1 Hz, C_6H_4, tolyl), 127.09 (d, $J_{P,C}$ = 15.9 Hz, C_6H_4, tolyl), 130.07 (d, $^2J_{P,C}$ = 13.0 Hz, C_{ortho}, PPh_3), 130.40−132.62 (m, C_6H_4, tolyl), 133.90 (d, $^3J_{P,C}$ = 10.3 Hz, C_{meta}, PPh_3), 134.61 (C^1, C_6H_4, tolyl), 134.80 (d, $^4J_{P,C}$ = 2.5 Hz, C_{para}, PPh_3), 158.51 (d, $^2J_{P,C}$ = 24.7 Hz, C^2, C_6H_4, tolyl), 169.26 (s, COO), 172.22 (d, $^2J_{P,C}$ = 7.3 Hz, CO) ppm. $^{31}P\{^1H\}$ NMR ($CDCl_3$): δ = 23.27 (s, PPh_3), 10.72 [s, $^1J_{Pt,P}$ = 4739 Hz, Pt(C^P)] ppm.

Complex 8: Complex **8** was prepared following a synthetic procedure similar to that reported for (**2**). Thus, [Pd(μ-Cl){*o*-$CH_2C_6H_4P(o\text{-tol})_2$}]$_2$ (0.129 g, 0.145 mmol) reacted, in THF (20 mL), with $AgClO_4$ (0.060 g, 0.29 mmol) and **1** (0.113 g, 0.290 mmol) to give **8** as a pale yellow solid. Yield: 0.190 g (72.8%). $C_{45}H_{43}ClO_7P_2Pd$ (899.63): calcd. C 60.08, H 4.82; found C 60.25, H 4.46. MS (FAB+): *m*/*z* (%) = 799 (100) $[M - ClO_4]^+$. IR: $\tilde{\nu}$ = 1619 (ν_{COO}), 1512 (ν_{CO}) cm^{-1}. ^1H NMR (CD_2Cl_2): δ = 1.18 (t, $^3J_{H,H}$ = 6.9 Hz, 3 H, CH_3), 2.40 (s, 3 H, CH_3 tolyl), 2.52 (d, $^2J_{H,H}$ = 11.0 Hz, 1 H, CH_2Pd), 2.63 (s, 3 H, CH_3 tolyl), 2.91 (d, 1 H, CH_2Pd), 3.56 (q, 2 H, OCH_2), 4.24 (d, $^2J_{PH}$ = 13.2 Hz, 2 H, CH_2P), 4.92 (s, 1 H, =CH), 6.67−7.74 (m, 27 H, C_6H_4 + PPh_3) ppm. $^{13}C\{^1H\}$ NMR ($CDCl_3$): δ = 14.34 (CH_3), 22.73 (d, $^3J_{P,C}$ = 9.8 Hz, CH_3 tolyl), 28.72 ($PdCH_2$), 30.51 (CH_3 tolyl), 37.53 (dd, $^1J_{P,C}$ = 56, $^4J_{P,C}$ = 5.1 Hz, CH_2P), 60.72 (OCH_2), 88.68 (d, $^3J_{P,C}$ = 7.1 Hz, =CH), 119.45 (d, $^1J_{P,C}$ = 88.2 Hz, C_{ipso}, PPh_3), 125.83 (C_6H_4, tolyl), 126.58 (d, $J_{P,C}$ = 8.2 Hz, C_6H_4, tolyl), 127.51 (d, $J_{P,C}$ = 10.5 Hz, C_6H_4, tolyl), 127.88 (C_6H_4, tolyl), 130.47 (d, $^2J_{P,C}$ = 12.8 Hz, C_{ortho}, PPh_3), 131.43−133.66 (m, C_6H_4, tolyl), 134.28 (d, $^3J_{P,C}$ = 9.9 Hz, C_{meta}, PPh_3), 135.35 (s, C_{para}, PPh_3), 142.44 (d, $^2J_{P,C}$ = 13.0 Hz, C^2, C_6H_4, tolyl), 156.82 (d, $^1J_{P,C}$ = 29.1 Hz, C^1, C_6H_4, tolyl), 171.26 (s, COO), 173.78 (d, $^2J_{P,C}$ = 7.1 Hz, CO) ppm. $^{31}P\{^1H\}$ NMR (CD_2Cl_2): δ = 34.83 [s, Pd(C^P)], 23.43 (s, PPh_3) ppm.

Complex 9: Complex **9** was prepared following a synthetic procedure similar to that reported for **2**. Thus, [Pd(μ-Cl)(C_6F_5)(tht)]$_2$ (0.1164 g, 0.146 mmol) reacted, in THF (20 mL), with $AgClO_4$ (0.061 g, 0.29 mmol) and **1** (0.115 g, 0.292 mmol) to give **9** as a deep yellow solid. Yield: 0.189 g (75.7%). $C_{34}H_{31}ClF_5O_7PPdS$ (851.50): calcd. C 47.96, H 3.67; found C 47.89, H 3.36. MS (FAB+): *m*/*z* (%) = 752 (47) $[M - ClO_4]^+$. IR: $\tilde{\nu}$ = 1603 (ν_{COO}), 1502 (ν_{CO}), 1283 (tht), 959, 798 (C_6F_5) cm^{-1}. ^1H NMR (CD_2Cl_2): δ = 1.26 (t, $^3J_{H,H}$ = 7.2 Hz, 3 H, CH_3), 2.06 (s, 4 H, H_β, tht), 2.64 (s, 2 H, H_α, tht), 3.12 (s, 2 H, H_α, tht), 4.07 (q, $^3J_{H,H}$ = 7.2 Hz, 2 H, OCH_2), 4.23 (d, $^2J_{PH}$ = 13.5 Hz, 2 H, $-CH_2P$), 5.07 (s, 1 H, =CH), 7.43−7.81 (m, 15 H, PPh_3) ppm. $^{13}C\{^1H\}$ NMR (CD_2Cl_2): δ = 14.40 (CH_3), 30.39 (C_β, SC_4H_8), 35.49 (d, $^1J_{P,C}$ = 57.2 Hz, CH_2P), 37.01 (C_α, SC_4H_8), 62.20 (OCH_2), 89.39 (d, $^3J_{P,C}$ = 8.1 Hz, =CH), 118.88 (d, $^1J_{P,C}$ = 88.7 Hz, C_{ipso}, PPh_3), 130.33 (d, $^2J_{P,C}$ = 12.7 Hz, C_{ortho}, PPh_3), 133.80 (d, $^3J_{P,C}$ = 10.0 Hz, C_{meta}, PPh_3), 135.21 (C_{para}, PPh_3), 137.13 (m, C_6F_5), 140.12 (m, C_6F_5), 146.29 (m, C_6F_5), 149.36 (m, C_6F_5), 171.84 (d, $^4J_{P,C}$ = 1.3 Hz, COO), 174.26 (d, $^2J_{P,C}$ = 7.1 Hz, CO) ppm. ^{19}F NMR (CD_2Cl_2): δ = −120.89 (d, $^3J_{F,F}$ = 22 Hz, 2 F, F_{ortho}), −159.33 (t, $^3J_{F,F}$ = 22 Hz, 1 F, F_{para}), −162.41 (t, 2 F, F_{meta}) ppm. $^{31}P\{^1H\}$ NMR (CD_2Cl_2): δ = 22.61 ppm.

Complex 10: To a solution of **1** (0.110 g, 0.281 mmol) in CH_2Cl_2 (15 mL) was added [AuCl(tht)] (0.090 g, 0.28 mmol) at room temperature, and the resultant solution was stirred for 30 min. The solvent was then evaporated to dryness and the white residue treated with Et_2O (30 mL), giving **10** as a white solid, which was filtered, washed with additional Et_2O (10 mL) and air dried. Yield: 0.170 g (96.9%). $C_{24}H_{23}AuClO_3P$ (622.84): calcd. C 46.28, H 3.72; found C 46.21, H 3.71. MS (FAB+): *m*/*z* (%) = 623 (9) $[M + H]^+$, 587 (15) $[M - Cl]^+$. IR: $\tilde{\nu}$ = 1731 (ν_{COO}), 1666 (ν_{CO}) cm^{-1}. ^1H NMR (CD_2Cl_2): δ = 1.24 (t, $^3J_{H,H}$ = 7.2 Hz, 3 H, CH_3), 3.48 (dd, $^2J_{H,H}$ = 15.3, $^4J_{PH}$ = 2.7 Hz, 1 H, CH_2), 3.93 (dd, $^2J_{H,H}$ = 15.3, $^4J_{PH}$ = 1.5 Hz, 1 H, CH_2), 4.15 (q, 2 H, OCH_2), 4.73 (s, 1 H, AuCHP), 7.53−7.83 (m, 15 H, PPh_3) ppm. $^{13}C\{^1H\}$ NMR (CD_2Cl_2): δ = 14.34 (CH_3), 38.08 (d, $^1J_{P,C}$ = 55.7 Hz, AuCHP), 49.17 (d, $^3J_{P,C}$ = 10.3 Hz, CH_2), 61.82 (OCH_2), 123.89 (d, $^1J_{P,C}$ = 88.17 Hz, C_{ipso}, PPh_3), 129.84 (d, $^2J_{P,C}$ = 12.5 Hz, C_{ortho}, PPh_3), 134.07 (d, $^4J_{P,C}$ = 2.7 Hz, C_{para}), 134.24 (d, $^3J_{P,C}$ = 10 Hz, C_{meta}), 196.28 (d, $^2J_{P,C}$ = 4.5 Hz, CO) ppm. $^{31}P\{^1H\}$ NMR (CD_2Cl_2): δ = 24.84 ppm.

Complex 11: To a solution of [Au(Cl)PPh_3] (0.104 g, 0.210 mmol) in acetone (30 mL), was added $AgClO_4$ (0.0436 g, 0.210 mmol). The resultant suspension was stirred in the dark for 30 min at room temperature and then filtered through a Celite pad. To the freshly prepared solution of [Au($OCMe_2$)PPh_3]ClO_4 (0.210 mmol) was added the ylide **1** (0.0821 g, 0.210 mmol), and the resultant solution stirred for 15 min. The solvent was evaporated to dryness, and the oily residue treated with Et_2O (25 mL), giving complex **11** as a white solid. Yield: 0.131 g (65.6%). $C_{42}H_{38}AuClO_7P_2$ (949.13): calcd. C 53.15, H 4.04; found C 53.28, H 4.15. MS (FAB+): *m*/*z* (%) = 849 (15) $[M - ClO_4]^+$. IR: $\tilde{\nu}$ = 1724 (ν_{COO}), 1657 (ν_{CO}) cm^{-1}. ^1H NMR (CD_2Cl_2): δ = 1.18 (t, $^3J_{H,H}$ = 7.2 Hz, 3 H, CH_3), 3.65 (dd, $^2J_{H,H}$ = 15.3, $^4J_{PH}$ = 2.4 Hz, 1 H, CH_2), 3.93 (dd, $^2J_{H,H}$ = 15.3, $^4J_{PH}$ = 1.8 Hz, 1 H, CH_2), 4.10 (q, 2 H, OCH_2), 4.83 (d, $^2J_{PH}$ = 9 Hz, 1 H, AuCHP), 7.18−7.76 (m, 30 H, PPh_3) ppm. $^{13}C\{^1H\}$ NMR ($CDCl_3$): δ = 14.09 (CH_3), 49.33 (d, $^3J_{P,C}$ = 10.4 Hz, CH_2), 50.83 (dd, $^1J_{P,C}$ = 58.6, $^2J_{P,C}$ = 54.6 Hz, AuCHP), 61.35 (OCH_2), 123.02 (d, $^1J_{P,C}$ = 88.6 Hz, C_{ipso}, $CPPh_3$), 127.90 (d, $^1J_{P,C}$ = 58.6 Hz, C_{ipso}, $AuPPh_3$), 129.55 (d, $^2J_{P,C}$ = 11.8 Hz, C_{ortho}, $CPPh_3$), 129.78 (d, $^2J_{P,C}$ = 12.7 Hz, C_{ortho}, $AuPPh_3$), 132.27 (d, $^4J_{P,C}$ = 2.2 Hz, C_{para}, $AuPPh_3$), 133.64 (d, $^3J_{P,C}$ = 10.1 Hz, C_{meta}, $AuPPh_3$), 133.83 (d, $^3J_{P,C}$ = 9.6 Hz, C_{meta}, $CPPh_3$), 134.01 (C_{para}, $CPPh_3$), 167.94 (COO), 196.69 (t, $^2J_{P,C} \approx {}^3J_{P,C}$ = 4.9 Hz, CO) ppm. $^{31}P\{^1H\}$ NMR (CD_2Cl_2): δ = 39.89 (d, $^3J_{P,P}$ = 11.2 Hz, $AuPPh_3$), 26.15 (d, $CHPPh_3$) ppm.

Crystallography

Data Collection: Crystals of complexes **2a** and **9** of adequate quality for X-ray purposes were obtained by slow evaporation of solutions of either the crude mixture of complexes **2a**/**2b**, or the crude complex **9** in CH_2Cl_2. In contrast, crystals of **10** were grown by slow vapor diffusion of Et_2O into a CH_2Cl_2 solution of the crude complex at room temperature. A crystal of dimensions 0.36 × 0.34 × 0.22 mm (**2a**), 0.39 × 0.25 × 0.043 mm (**9**) or 0.49 × 0.30 × 0.19 mm (**10**) was mounted onto a quartz fiber in a random orientation and covered with epoxy. Data collection was performed at 100 K (**2a**, **10**) or at room temperature (**9**) with a Bruker Smart Apex CCD diffractometer using graphite-monochromated Mo-K_α radiation (λ = 0.71073 Å). In all cases, a hemisphere of data was collected based on three ω-scan runs. For each of these runs, frames (606, 435, and 230, respectively) were collected at 0.3° intervals and 10 s per frame. In all cases, the diffraction frames were integrated using the program SAINT[24] and the integrated intensities were corrected for systematic errors with SADABS.[25]

 © 2004 Wiley-VCH Verlag GmbH & Co. KGaA, Weinheim

Structure Solution and Refinement: The structures were solved by Patterson and Fourier methods.[26] All non-hydrogen atoms were refined with anisotropic displacement parameters. The hydrogen atoms were placed at idealized positions and treated as riding atoms, except for those of the methyl groups, which were first located in a local slant − Fourier calculation and then refined as riding atoms with the torsion angles about the O−C(methyl) or N−C(methyl) bonds treated as variables. Each hydrogen atom was assigned an isotropic displacement parameter equal to 1.2 times the equivalent isotropic displacement parameter of its parent atom. The structures were refined to F_o^2, and all reflections were used in the least-squares calculations.[27]

The final difference Fourier map for **9** showed two peaks with densities of 1.88 and 1.16 e/Å^3, which delimit a vector roughly parallel to the Pd(1)−S(1) bond and displaced less than 1 Å from it, suggesting a possible minor disorder component for these two atoms. Detailed analysis of these peaks and their environment confirmed the possibility of an accompanying disorder of the tht moiety, and also indicated that such a disorder could exist without causing any important changes to the remainder of the structure. We refined a disordered model for Pd(1) and S(1), obtaining a population of 0.083(3) for the second component. However, no difference peaks appeared in the area of the tht, where the carbon atoms of a putative minor disorder component would be located. As a further diagnostic for the source of the difference peaks, we conducted a twin analysis using the program ROTAX.[28,29] No plausible twin model was obtained. We report here the results of the refinement without disorder. Results of a refinement including the minor congeners for Pd(1) and S(1), which did not involve observable changes in the geometric parameters of the principal component, are available from the authors.

CCDC-222324 (for **2a**), -222325 (for **9**), and -222326 (for **10**) contain the supplementary crystallographic data for this paper. These data can be obtained free of charge at www.ccdc.cam.ac.uk/conts/retrieving.html [or from the Cambridge Crystallographic Data Center, 12 Union Road, Cambridge CB2 1EZ, UK; Fax: (internat.) +44-1223-336-033; E-mail: deposit@ccdc.cam.ac.uk].

Acknowledgments

Funding by the Dirección General de Investigación Científica y Técnica (DGICYT) (Spain, Projects BQU2002−0510 and BQU2002−00554) is gratefully acknowledged. T. S. thanks the MECD (Spain) for a postdoctoral fellowship.

[1] R. Navarro, E. P. Urriolabeitia, *J. Chem. Soc., Dalton Trans.* **1999**, 4111 and references given therein.
[2] [2a] H. Muxfeldt, G. Grethe, K. Uhlig, H. Zeugner, *Chem. Ber.* **1963**, *96*, 2943. [2b] F. Serratosa, E. Solé, *An. R. Soc., Esp. Fis. Quim. Ser. B* **1966**, *62*, 431.
[3] [3a] C. M. Moorhof, D. F. Schneider, D. Winkler, *J. Chem. Res. (S)* **1998**, 763. [3b] C. M. Moorhoff, *J. Chem. Soc., Perkin Trans. 1* **1997**, 1987 and references cited therein. [3c] S. G. Hegde, R. D. Bryant, *Synth. Commun.* **1993**, *23*, 2753. [3d] C. M. Moorhof, D. F. Schneider, *Tetrahedron Lett.* **1987**, *28*, 4721. [3e] K. M. Pietrusiewicz, J. Monkiewicz, *Tetrahedron Lett.* **1986**, *27*, 739. [3f] K. M. Pietrusiewicz, J. Monkiewicz, R. Bodalski, *J. Org. Chem.* **1983**, *48*, 788.
[4] [4a] J. Forniés, F. Martínez, R. Navarro, E. P. Urriolabeitia, *J. Organomet. Chem.* **1995**, *495*, 185. [4b] J. Forniés, R. Navarro, M. Tomás, E. P. Urriolabeitia, *Organometallics* **1993**, *12*, 940. [4c] J. Forniés, F. Martínez, R. Navarro, E. P. Urriolabeitia, *Organometallics* **1996**, *15*, 1813.
[5] [5a] L. R. Falvello, S. Fernández, R. Navarro, A. Rueda, E. P. Urriolabeitia, *Organometallics* **1998**, *17*, 5887. [5b] L. R. Falvello, S. Fernández, R. Navarro, E. P. Urriolabeitia, *Inorg. Chem.* **1999**, *38*, 2445.
[6] A. J. Deeming, I. P. Rothwell, M. B. Hursthouse, L. New, *J. Chem. Soc., Dalton Trans.* **1978**, 1490.
[7] [7a] J. Vicente, M. T. Chicote, *Coord. Chem. Rev.* **1999**, 193−195, 1143 and references cited therein. [7b] J. Vicente, M. T. Chicote, M. C. Lagunas, *Helv. Chim. Acta* **1999**, *82*, 1202.
[8] [8a] L. R. Falvello, S. Fernández, R. Navarro, I. Pascual, E. P. Urriolabeitia, *J. Chem. Soc., Dalton Trans.* **1997**, 763. [8b] L. R. Falvello, S. Fernández, R. Navarro, E. P. Urriolabeitia, *Inorg. Chem.* **1996**, *35*, 3064.
[9] A. G. Orpen, L. Brammer, F. H. Allen, D. Kennard, D. G. Watson, R. Taylor, *J. Chem. Soc., Dalton Trans.* **1989**, S1−S83.
[10] F. H. Allen, O. Kennard, D. G. Watson, L. Brammer, A. G. Orpen, R. Taylor, *J. Chem. Soc., Perkin Trans. 2* **1987**, 685−S1−S19).
[11] A. Bondi, *J. Phys. Chem.* **1964**, *68*, 441.
[12] A. Lledós, J. J. Carbó, E. P. Urriolabeitia, *Inorg. Chem.* **2001**, *40*, 4913.
[13] R. S. Cahn, C. Ingold, V. Prelog, *Angew. Chem. Int. Ed. Engl.* **1966**, *5*, 385.
[14] [14a] J. P. Fackler, B. Trzcinska-Bancroft, *Organometallics* **1985**, *4*, 1891. [14b] L. C. Porter, H. Knachel, J. P. Fackler, *Acta Crystallogr., Sect. C* **1987**, *43*, 1833.
[15] W. C. Wolsey, *J. Chem. Educ.* **1973**, *50*, A335.
[16] A. C. Cope, E. C. Friedrich, *J. Am. Chem. Soc.* **1968**, *90*, 909.
[17] [17a] A. Kasara, *Bull. Chem. Soc. Jpn.* **1968**, *41*, 1272. [17b] B. N. Cockburn, D. V. Howe, T. Keating, B. F. G. Johnson, J. Lewis, *J. Chem. Soc., Dalton Trans.* **1973**, 404.
[18] G. E. Hartwell, R. V. Lawrence, M. J. Smas, *J. Chem. Soc., Chem. Commun.* **1970**, 912.
[19] M. A. Gutiérrez, G. R. Newkome, J. Selbin, *J. Organomet. Chem.* **1980**, *202*, 341.
[20] R. Usón, J. Forniés, P. Espinet, G. Alfranca, *Synth. Inorg. Metal-Org. Chem.* **1980**, *10*, 579.
[21] W. A. Herrmann, C. Brossman, K. Öfele, C. Reisinger, T. Priermeier, M. Beller, H. Fischer, *Angew. Chem. Int. Ed. Engl.* **1995**, *34*, 1844.
[22] J. Forniés, A. Martín, R. Navarro, V. Sicilia, P. Villarroya, *Organometallics* **1996**, *15*, 1826.
[23] R. Usón, A. Laguna, M. Laguna, *Inorg. Synth.* **1989**, *26*, 85.
[24] SAINT Version 5.0; Bruker Analytical X-ray Systems, Madison, WI, **1995**.
[25] G. M. Sheldrick, SADABS: Empirical absorption correction program; University Göttingen, **1996**.
[26] SHELXS-86, G. M. Sheldrick, *Acta Crystallogr., Sect. A* **1990**, *46*, 467.
[27] G. M. Sheldrick, SHELXL-97: FORTRAN program for the refinement of crystal structures from diffraction data; University of Göttingen, **1997**. Molecular graphics were done using the commercial package SHELXTL-PLUS, Release 5.05/V; Siemens Analytical X-ray Instruments, Inc.: Madison, WI, **1996**.
[28] S. Parsons, R. O. Gould, ROTAX, a program to test for possible twin laws for merohedral and non-merohedral twins indexed on a single orientation matrix.
[29] R. I. Cooper, R. O. Gould, S. Parsons, D. J. Watkin, *J. Appl. Cryst.* **2002**, *35*, 168.

Received October 30, 2003
Early View Article
Published Online April 7, 2004

 © 2004 Wiley-VCH Verlag GmbH & Co. KGaA, Weinheim

Tuning the Stoichiometry of Lanthanide Complexes with Calixarenes: Bimetallic Complexes with a Calix[6]arene Bearing Ether-Amide Pendant Arms

Flor de María Ramírez,[a,b] Loïc Charbonnière,[c] Gilles Muller,[a,d] and Jean-Claude G. Bünzli*[a]

Keywords: Lanthanides / Calixarenes / Europium / Luminescence

A de-*tert*-butylated calix[6]arene (A_6L^6) fitted with six ether-amide pendant arms was synthesized and characterized in solution. NMR spectroscopic data point to the six phenoxide units adopting an average D_{6h} conformation on the NMR time scale. According to MM3 molecular mechanics, and MOPAC quantum mechanical calculations, A_6L^6 is a ditopic ligand featuring two nonadentate coordination sites, each built from three pendant arms, and extending in opposite directions with one above, and the other under the main ring. A_6L^6 reacts with Ln^{III} ions (Ln = La, Eu) in acetonitrile to successively form 1:1 and 2:1 complexes. The isolated Eu^{III} 2:1 complex is luminescent (quantum yield: 2.5% in acetonitrile, upon ligand excitation). In the solid state, the luminescence decay is bi-exponential, with lifetimes equal to 1.66 and 0.46 ms (upon direct metal excitation), pointing to the presence of two differently coordinated metal ions, one with essentially no bound water molecules, and the other one with two ligated water molecules. According to molecular mechanics calculations, the more stable isomer is indeed asymmetric with two nine-coordinated metal ions. Both Eu^{III} ions are bound to three bidentate arms, and one monodentate triflate anion, but one metal ion completes its coordination sphere with two phenoxide oxygen atoms, and the other one with two water molecules, consistent with IR spectroscopic and luminescence data. In acetonitrile solution, the two metal ion sites become equivalent, and the relatively long lifetime (1.35 ms) is indicative of a coordination environment free of water molecules. This work demonstrates, that the stoichiometry of lanthanide complexes with calixarenes can be tuned by a suitable choice of the narrow and/or wide rim substituents.
(© Wiley-VCH Verlag GmbH & Co. KGaA, 69451 Weinheim, Germany, 2004)

Introduction

Calixarenes act as versatile building blocks in supramolecular and coordination chemistry, since both their lower and upper rims may be derivatized to induce specific functionalities.[1,2] They are currently being used in the design of chemical sensors,[3] catalysts,[4] and selective ligands for the complexation of d[5] and f[6,7] metal ions, as well as for the self-assembly, through π-stacking, H-bonding or coordination interactions, of elaborate supramolecular structures.[8,9] As a consequence, many studies have aimed at using calixarenes for the development of separation processes,[10] and the nuclear industry is particularly interested in these ligands for the separation of highly radioactive actinides from non-radioactive lanthanides before nuclear waste confinement.[11−13]

In recent years, we have been developing model calixarene molecules for the study of energy migration mechanisms in luminescent lanthanide-containing compounds, and of magnetic 4f−4f interactions.[7] We have also been interested in calixarenes having 4f−5f separation capabilities. This leads to the formation of luminescent 4f-species which can be easily analyzed during the extraction process. With this in mind, we have focused on two series of branched calixarenes, one bearing ether-amide pendant arms A, and the other having phosphanylyl groups B (see Scheme 1). The ether-amide substituent was designed so that it can act as a bidentate ligand forming a five-membered cycle upon coordination of its ether and amide functions to trivalent lanthanide ions Ln^{III}. We have shown that A_4bL^4 acts as an inorganic-organic receptor, encapsulating both a lanthanide ion and a solvent molecule. In addition, the crystal structure of the Lu^{III} 1:1 complex shows the coordination cavity predisposed to further accommodate one

[a] Institute of Molecular and Biological Chemistry, Swiss Federal Institute of Technology,
BCH 1402, 1015 Lausanne, Switzerland
E-mail: jean-claude.bunzli@epfl.ch
[b] Instituto Nacional de Investigaciones Nucleares, Departamento de Química,
Km 36.5 Carretera México-Toluca, Apartado Postal 111, Lerma, Edo. de México, C.P. 52045, Mexico
[c] École de Chimie, Polymères et Matériaux, Laboratoire de Chimie Moléculaire, UMR 7008 CNRS,
25 rue Becquerel, 67087 Strasbourg Cedex 2, France
[d] Department of Chemistry, University of Minnesota Duluth, MN 55812-3020, USA
Supporting information for this article is available on the WWW under http://www.eurjic.org or from the author.

 © 2004 Wiley-VCH Verlag GmbH & Co. KGaA, Weinheim **DOI: 10.1002/ejic.200300824**

water molecule hydrogen-bonded to the oxygen atoms of the phenol units, which rigidifies the induced cavity, and binds the metal ion.[14] The phosphanylyl-substituted calixarenes B_nbL^n (n = 4, 6) form complexes with 1:1 and 1:2 Ln^{III} ligand ratios having significant stability in acetonitrile,[15,16] and interesting luminescent[15,16] and 4f−5f separation[17] properties. Several derivatized calix[6]arenes have been tested in extraction studies[18−20] and, in our case, B_6bL^6 proved to be a better extracting agent than B_4bL^4.[17] Despite that calix[6]arene complexes with lanthanide ions have also been proposed as luminescent probes,[21,22] little is known about the interaction between calix[6]arenes and Ln^{III} ions. The reaction of europium nitrate with *p-tert*-butylcalix[6]arene leads to the formation of a 1:2 (Eu^{III}/L) compound in which only one calix[6]arene molecule is bound to the 8-coordinate metal ion through a single phenoxide unit, as shown by its X-ray structure.[23] Replacing nitrate with trifluoromethanesulfonate (triflate) results in the formation of bimetallic 2:1 species (Ln = La, Sm, Yb) in which the two metal cations are anchored on both sides of the macrocycle in the 1,2,3-alternate conformation, which acts as a bidentate ligand, while the coordination sphere of the 7-coordinate Ln^{III} ions (Ln = Sm, Yb) is completed by one monodentate triflate and one nitrogen donor atom from the pyridine and/or terpyridine.[24]

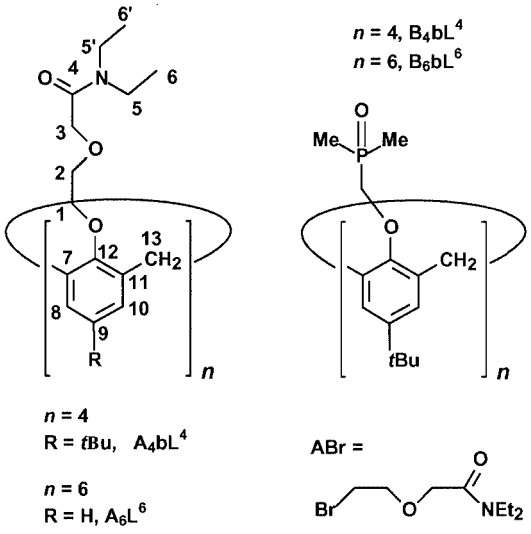

Scheme 1

In this paper, we discuss how the removal of the *p-tert*-butyl groups influences the conformation of the calix[6]-arene derivatized with pendant arms A and, consequently, the stoichiometry of the Ln^{III} complexes. Removal of the *tert*-butyl groups should result in easier conformational interconversion, and a relief in steric hindrance is expected to favor the formation of the 2:1 complexes, contrary to what has been observed for B_6bL^6, which forms 1:2 complexes. The calixarene A_6L^6, with *tert*-butyl groups removed, was therefore synthesized, and characterized both in the solid state and in solution, as well as its 2:1 complex with Eu^{III}. Molecular mechanics and quantum mechanical calculations were performed to help understand the structures of both the free ligand and the complex.

Results and Discussion

Synthesis and Characterization of the Substituted Calixarene A_6L^6

The branched calix[6]arene A_6L^6 (Scheme 1) was obtained in two steps via a Williamson reaction (Scheme 2) from the brominated pendant arm **ABr**, synthesised as described previously,[14] and the calix[6]arene H_6L^6. The hexasodium derivative of calix[6]arene was prepared in toluene, demonstrating that this salt can be formed in a non-polar solvent despite the high fluxionality of calix[6]arene, provided adequate experimental conditions are used i.e. heating, vigorous stirring, and a nitrogen atmosphere to avoid oxidation and protonation of the phenoxide groups. The macrocycle is soluble in CH_2Cl_2, $CHCl_3$, CH_3CN, toluene, methanol, and ethanol. Its IR spectrum displays an intense band at 1639 cm^{-1} typical of the carbonyl groups in an *N,N′*-disubstituted amide (1646 cm^{-1} in **ABr**). The absorption band associated with contributions from the aliphatic ether groups appears at 1126 cm^{-1} (1119 cm^{-1} in **ABr**), medium bands at 1218 and 1045 cm^{-1} are typical of the phenoxide groups, while the three neighboring aromatic C−H groups generate a characteristic symmetric out-of-plane bending at 765 cm^{-1}. In the UV/Vis spectrum, the structured band at 270 nm (37040 cm^{-1}) with a shoulder at 278 nm (35970 cm^{-1}) indicates complete functionalization of the phenoxide groups. This structured absorption band is associated with π→π* transitions involving orbitals mainly located on the phenyl rings. A band corresponding to transitions primarily located on the carbonyl groups can be seen at 223 nm (44840 cm^{-1}) in the diffuse reflectance spectrum.

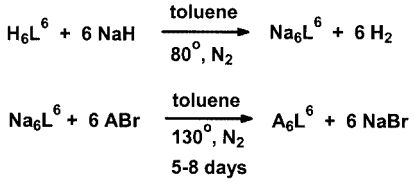

Scheme 2

The ^1H NMR spectrum of A_6L^6 in CD_3CN at room temperature is shown in Figure 1 together with its complete assignment (see Scheme 1 for atomic numbering). The limited number of signals points to a high average symmetry on the NMR time scale. This may be interpreted as a consequence either of fast interconversion processes between the different conformers on the NMR timescale, or of the presence of a single species of high symmetry, such as the 1,3,5 alternate conformation belonging to the S_6 point group. While the introduction of long complexing arms on the *p-tert*-butylcalix[6]arene moiety may be expected to freeze the oxygen-through-the-annulus rotation,[25,26] removal of the

 © 2004 Wiley-VCH Verlag GmbH & Co. KGaA, Weinheim

bulky *tert*-butyl groups favors the aromatic-through-the-annulus rotation. Since the latter mechanism has been observed with *O*-substituted *p-tert*-butylcalix[6]arenes,[26] it is reasonable to assume that the lack of substitution on the phenol groups allows for rapid aromatic-through-the-annulus rotation and, hence, the apparent high symmetry observed is the result of fast interconversion between the different conformers.

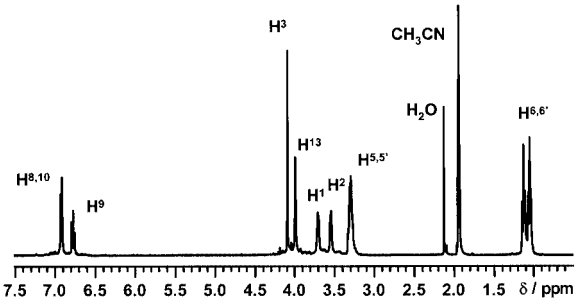

Figure 1. ^{1}H NMR spectrum of A_6L^6 10^{-3} M in CD_3CN at 295 K

A detailed comparison of the chemical shifts of the proton atoms of the complexing arms in A_6L^6 and A_4bL^4 further enlightens an unusual point. While the ethyl groups of the amide functions are found essentially at the same chemical shifts in both ligands, signals corresponding to the H^1 and H^2 protons are shifted significantly upfield (more than 0.4 ppm) in A_6L^6 compared with A_4bL^4.[14] ^{1}H NMR spectroscopic data of A_4bL^4 indeed showed the compound adopting a cone conformation in solution, in which the four complexing arms are held together in closed proximity, thereby providing a suitable octadentate coordination site for lanthanide cations.[14] The X-ray crystal structure of the lutetium complex further showed that a water molecule was encapsulated in the cavity formed by the four dioxo-ethylene bridges (O−C1−C2−O), with H-bonding interactions between this water molecule and the oxygen atoms. Interestingly, an elemental analysis of free A_4bL^4 revealed the presence of one water molecule, even after the drying process. It was suspected, that the H-bonding interactions with the water molecule are also present in the free ligand in solution, leading to a decrease of the electronic density on the ethylene bridges, and a concomitant upfield shift of the corresponding signals in the ^{1}H NMR spectrum. For the larger and more flexible calix[6]arene, NMR spectroscopic data indicate that the cone conformation is not the most favorable conformation, leading to chemical shifts similar to those found in the brominated **ABr** molecule or its hydroxy precursor. The same reasoning can be applied to the corresponding carbon atoms (C1 and C2), one of which is shifted upfield by 1.1 ppm in A_4bL^4 compared with A_6L^6.

$^{13}C\{^1H\}$ NMR spectra in both $CDCl_3$ and CD_3CN confirm the fast exchange hypothesis (see Figure S1 in the Supporting Information; see also the footnote on the first page of this article) since $\delta(C^{13}) = 30.95$ ppm points to a *syn* orientation of adjacent phenol rings,[27] thus excluding the hypothetical 1,3,5-alternate conformation in which adjacent rings are in an *anti* conformation. Only four signals are observed for the aromatic carbon atoms, indicating the equivalence of the six aromatic rings on the NMR time scale, and an average hexagonal (D_{6h}) symmetry for the calixarene core. All the carbon atoms of the pendant arms also give rise to one signal, except those of the ethyl groups which are split into two components pointing to a somewhat restricted rotation around the amide function.

To substantiate the interpretation of the NMR spectra, we turned to molecular mechanics calculations, and evaluated the A_6L^6 structure using a MOPAC PM3 procedure, taking into account solvent effects (water). The conformer with the lowest energy is shown in Figure 2. It displays a pinched "chair" conformation of the 1,2,3-alternate type. Three consecutive phenol groups are positioned in such a way, that the pendant arms form two cavities predisposed towards metal ion coordination, each built up of three pendant arms, and extending on opposite sides of the macrocycle.

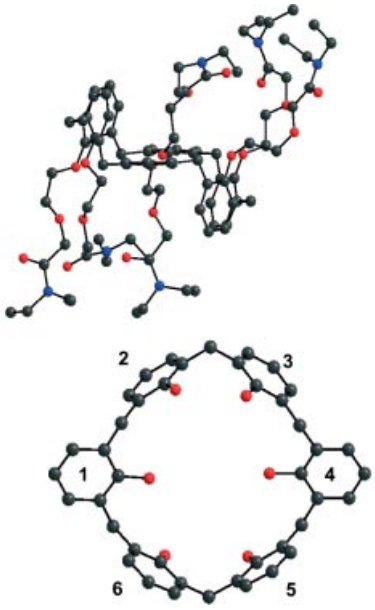

Figure 2. (Top) optimized geometry of A_6L^6 as determined by MOPAC PM3 calculations taking into account the solvent effect (water); (bottom) View of the calixarene core only

Interaction of A_6L^6 with La^{III} and Eu^{III} in Acetonitrile

To gain information on the interaction between lanthanide ions and the calixarene A_6L^6, solutions of the latter (typically 10^{-3} M) were titrated with solutions of lanthanide triflates $Ln(OTf)_3{\cdot}6H_2O$ (typically 10^{-3} M, Ln = La, Eu) for ratios $R = [Ln^{III}]_t/[A_6L^6]_t$ varying from 0 to 3. The spectra are shown in Figure 3 (S2, and S3, see Supporting Information). In all cases, the spectra display broad overlapping signals, probably as a result of fast exchange reactions of the complexed species. This prevented a quantitative treatment. For $R < 1$, the free ligand and a complex species coexist in solution. For $R = 1$, a distinct AB spin system can be observed (Ln = La) with two doublets at 4.45 and

 © 2004 Wiley-VCH Verlag GmbH & Co. KGaA, Weinheim

3.60 ppm for the methylene proton atoms bridging two phenolic units. This strongly suggests an average cone-like conformation for the 1:1 LnA_6L^6 complex. The broadness of the peaks corresponding to the protons of the arms may be attributed to exchange processes, possibly between forms in which these arms are complexed or not complexed to the metal cation. For $R > 1$, the peaks of the non-coordinated ligand disappear, and signals corresponding to at least two species with different LnA_6L^6 stoichiometries can be identified. Since the spectra do not change further when R is increased from 2 to 3, we conclude that two species form successively in solution, with 1:1 and 2:1 metal-to-ligand ratios. This is in line with the calculated structure of A_6L^6 which shows two sets of three pendant arms extending on opposite sides of the calixarene (cf. Figure 2). Attempts to establish a more quantitative speciation by ES-MS failed due to hydrolysis at high dilution in the capillary during the analysis (T = 200 °C). As a result, only monometallic species were detected for R values in the range 1−3, in addition to free A_6L^6 (Table 1).

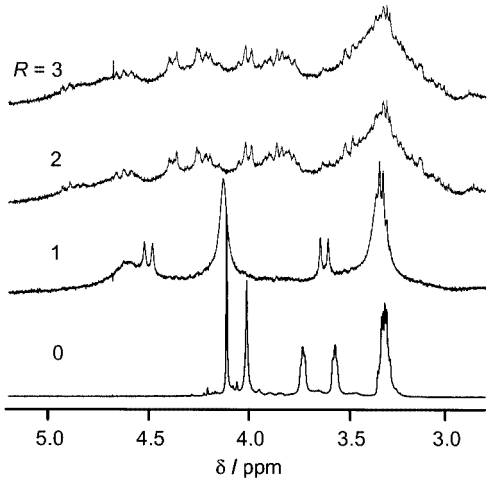

Figure 3. Part of the ^{1}H NMR spectra obtained during the titration of A_6L^6 by $La(OTf)_3{\cdot}6H_2O$ in CD_3CN at room temperature; $R = [La]_t/[A_6L^6]_t$

Isolation and Characterization of the 2:1 Eu^{III} Complex

The complex can be isolated in good yield from stoichiometric mixtures of A_6L^6 and europium triflate in acetonitrile. The elemental analysis is consistent with the formula $Eu_2(OTf)_6(A_6L^6){\cdot}9H_2O$. Coordination of the carbonyl groups of the pendant arms can be ascertained from the IR data (obtained after drying the pellet at 118 °C), the $\nu_{C=O}$ vibration being red-shifted by 25 cm^{-1} compared with the ligand, pointing to a strong metal-to-ligand interaction. Moreover, the intensity of the band arising from the aliphatic ether functions of the arm is strongly reduced, in line with the coordination of these moieties to the metal ion. The vibration involving contribution from the aromatic ether could not be identified, probably being masked by another band, contrary to what we reported for the $[Ln(A_4bL^4)]^{3+}$ complexes, for which (i) this band is little affected by the complexation, and (ii) the crystal structure of $[Lu(A_4bL^4)(H_2O)](OTf)_3{\cdot}2Et_2O$ does not show evidence of any coordination of aromatic ethers.[14] In our case, this suggests some change in the ligand conformation upon complexation and, possibly, coordination of these groups to the metal ion. Other ligand vibrations, for instance the bending CH_2 mode (1450 cm^{-1}), and the out-of-plane ring bending mode (760 cm^{-1}), experience small, but characteristic changes upon complexation. In addition, two strong bands at 1030 and 638 cm^{-1} can be assigned to the $\nu_s(SO_2)$ and $\nu_{as}(SO_3)$ modes of coordinated triflate,[28] while the band at 1321 cm^{-1} is evidence for ionic triflate. Finally, water coordination can be deduced from a sharp band near 520 cm^{-1}.[29] Attempts to grow single-crystals by slow vapor diffusion of diethyl ether or diisopropyl ether in acetonitrile, THF or MeOH, were unsuccessful.

^{1}H NMR spectra obtained during the titration of A_6L^6 with europium triflate (Figure S3, see Supporting Information) revealed that complexation induces freezing of the ligand conformation, resulting in a very complex pattern, which is difficult to interpret. Variable temperature NMR spectra of a $Eu_2(OTf)_6(A_6L^6){\cdot}9H_2O$ solution in CD_3CN were recorded up to 75 °C. Although the overall pattern becomes somewhat simplified, the spectrum remains complex. Higher temperatures could not be reached, because the complex experiences de-metallation in DMSO, a solvent in which, for instance, B_6bL^6 undergoes complete interconversion of its isomers on the NMR time scale at 132 °C.[16]

Photophysical Properties of A_6L^6 and Its 2:1 Eu^{III} Complex

The photophysical properties of A_6L^6, and of the 2:1 Eu^{III} complex have been determined both for solid state samples (295 and 77 K), and for frozen acetonitrile solutions (77 K). The excitation spectrum of the ligand is similar to the absorption and reflectance spectra discussed above. Excitation of a solid sample of A_6L^6 at 275 nm

Table 1. Main species observed in the ES-MS spectra of solutions containing A_6L^6 and $Eu(Otf)_6{\cdot}6H_2O$ in various proportions (see text)

Species	Obsd. *m/z*	Rel. Int.	Calcd. *m/z*
$[Eu(OH)_3(A_6L^6)(H_2O)_5 + H]^+$	1873.4	< 15%	1873.9
$[Eu(OH)(CF_3SO_3)(A_6L^6)(CH_3CN)]^+$	1940.3	< 15%	1939.1
$[Eu(OH)(CF_3SO_3)(A_6L^6)(H_2O)(CH_3CN)]^+$	1958.4	15−20%	1957.1
$[Eu(OH)(CF_3SO_3)(A_6L^6)(H_2O)_3(CH_3CN)]^+$	1993.8	25−50%	1993.2
$[A_6L^6 + H]^+$	1580.8	100%	1581.0

 © 2004 Wiley-VCH Verlag GmbH & Co. KGaA, Weinheim

(36360 cm^{-1}) and 77 K yields two emission bands centered at 305 nm (32790 cm^{-1}), which can be assigned as arising from the $^1\pi\pi^*$ state, and at 446 nm (22420 cm^{-1}), attributed to the $^3\pi\pi^*$ state, as ascertained by the lifetime, which amounts to 104 ± 8 ms in frozen acetonitrile solution (2×10^{-3} M). This can be compared with 83 ± 4 ms for B_6bL^6 under the same experimental conditions.[16]

The absorption spectrum of the 2:1 complex in acetonitrile (4.74×10^{-5} M) displays three bands at 268 nm (37310 cm^{-1}, ε = 9490 $mol^{-1}\cdot cm^{-1}$), 276 nm (36230 cm^{-1}, ε = 8650 $mol^{-1}\cdot cm^{-1}$), and 293 nm (34130 cm^{-1}, ε = 3380 $mol^{-1}\cdot cm^{-1}$). The first two bands are blue-shifted 265 cm^{-1} compared with those in the uncomplexed ligand. The third band is only present in the complex. The excitation spectrum of the complex, obtained at 10 K with concomitant monitoring of the $^5D_0 \rightarrow {}^7F_2$ transition, reveals the usual f-f transitions as well as a broad band in the range of 320−450 nm with a maximum at 372 nm (26880 cm^{-1}), which could possibly be associated with a ligand-to-metal charge transfer (LMCT) band. Excitation in the ligand levels yields a luminescence spectrum displaying both ligand-centered and metal-centered $^5D_0 \rightarrow {}^7F_J$ emission bands, pointing to incomplete ligand-to-metal energy transfer. The high-resolution laser-excited excitation spectrum in the range of the $^5D_0 \leftarrow {}^7F_0$ transition, monitored via the $^5D_0 \rightarrow {}^7F_2$ transition, results in a single, broad component at 17267 cm^{-1} at 10 K (full width at half height fwhh = 37 cm^{-1}), and 17280 cm^{-1} at 295 K (fwhh = 24 cm^{-1}), indicative of a sample with several slightly different chemical environments for the Eu^{III} ion, possibly arising from different conformations of the macrocycle and associated pendant arms.[30] Excitation in either the $^5D_0 \leftarrow {}^7F_0$ or $^5L_6 \leftarrow {}^7F_0$ transitions yields relatively broad emission spectra dominated by the hypersensitive $^5D_0 \rightarrow {}^7F_2$ transition, which are characteristic of a chemical environment with low symmetry (Figure S4, Supp. Inf.). The relative and corrected intensities of the $^5D_0 \rightarrow {}^7F_J$ transitions are 1.0, 7.4, 0.1, and 1.9 (10 K) and 1.0, 7.2, 0.2, and 2.0 (295 K) for J = 1, 2, 3, and 4, respectively.

The lifetimes of the excited $^5D_0$ level were measured at 10, 77, and 295 K both upon ligand and direct metal excitation (Table 2). The luminescence decays of the solid state sample are bi-exponential and temperature dependent, decreasing roughly by a factor of two between 10 K and room temperature. This is indicative of vibrational and/or electronic radiationless de-activation mechanisms. Here, both processes are probably operating in view of the fluxional nature of the calixarene, and of the LMCT band apparent in the excitation spectrum. Lifetimes measured upon ligand excitation are longer than those obtained through direct excitation of the $^5D_0$ level, pointing to a feeding level with a long lifetime, namely the triplet state. High energy vibrations such as those generated by O−H groups are known to efficiently de-excite Ln^{III} excited levels,[31] and phenomenological equations have been proposed to relate $\Delta k_{obsd.} = 1/\tau_{obsd.} - 1/\tau_{ref}$ where τ_{ref} is the lifetime measured on the corresponding deuterated sample or in deuterated water, and the number of water molecules q directly bound to the Ln^{III} ion, either in the solid state[32] or in solution.[33] Interpreting our lifetime data along these lines, we note that one lifetime, τ_1, is long. It decreases, under direct excitation, from 1.66 ms (10 K) to 0.86 ms (295 K). Such a lifetime, at least at low temperature, is consistent with the inner coordination sphere containing no water molecules. The other lifetime, τ_2, is much shorter, decreasing from 0.46 ms (10 K) to 0.28 ms (295 K), under direct excitation of the Eu^{III} ion. Taking $\tau_1 = \tau_{ref}$ as a first approximation, and $q = 1.05\ \Delta k_{obsd.}$,[32] we calculate, that the number of bound water molecules lies between 1.6 (10 K) and 2.5 (77 and 295 K). The apparent increase in q with increasing temperature could be simply due to outer sphere water molecules hydrogen-bonded to the complex, which become more labile when the temperature increases, or to other vibrational temperature-dependent deactivation processes affecting the de-excitation of the two metal ions differently.

Table 2. Lifetimes (ms) of the $^5D_0$(Eu) level in a solid state sample of $Eu_2(OTf)_6(A_6L^6)\cdot 9H_2O$ under various experimental conditions

T (K)	$\tilde{\nu}_{ex}$ (cm^{-1})	τ_1 (ms)	τ_2 (ms)
10	32468	2.01 ± 0.05	0.97 ± 0.04
77	32468	1.71 ± 0.03	0.48 ± 0.01
295	32468	1.09 ± 0.02	0.36 ± 0.01
10	17268	1.66 ± 0.01	0.46 ± 0.02
77	17268	1.19 ± 0.04	0.31 ± 0.01
295	17280	0.86 ± 0.02	0.28 ± 0.01
295[a]	25445	−	1.38 ± 0.02

[a] Acetonitrile solution 2×10^{-3} M; single exponential.

In solution, the $^5D_0$ luminescence decay becomes a single exponential, with a value (1.38 ms) compatible with the absence of OH oscillators directly bound to Eu^{III}. Dissolution of the complex results, therefore, in a change in the coordination environment of the Eu^{III} ions, since the lifetime is now larger than those observed for the two different sites in the solid state. The quantum yield measured in acetonitrile upon ligand excitation Q^L_{Eu} amounts to 2.5%, a value similar to that found for $[Eu(B_6bL^6)_2]^{3+}$.

Optimized Structure of the Eu^{III} 2:1 Complex

In order to confirm the feasibility of our interpretation, we resorted to molecular mechanics calculations to evaluate a potential structure for the 2:1 complex. Several systems were tested, taking into account the experimental data, which suggested that the isolated compound has coordinated triflate anions and water molecules (IR), and two different metal ion sites with $q \approx 0$ and 2 (luminescence lifetimes). It turned out, that the conformer with the lowest energy, as calculated by the MM3 and Conflex procedures, and shown in Figure 4 (see also Table S1 in the Supporting Information), has indeed an asymmetric structure with two 9-coordinate Eu^{III} ions. One ion (site I) is bound to two phenolic oxygen atoms, three bidentate arms, and one monodentate triflate anion. The coordination environment of

 © 2004 Wiley-VCH Verlag GmbH & Co. KGaA, Weinheim

the second ion (site II) is somewhat different, with two water molecules replacing the bonding to the phenolic ether atoms. Therefore, the suggested formulation of the 2:1 complex is $[Eu_2(OTf)_2(A_6L^6)(H_2O)_2]^{4+}$. Generally speaking, the Ln−O distances are too long compared with the expected ones for 9-coordinate Eu^{III}, which lie in the range 2.45−2.60 Å[34] [averages: 2.72(17) Å for site I and 2.83(18) Å for site II]. Relative distances, however, can be discussed. The coordination in site I is comprised of six short bonds (three carbonyl groups, one ether function, and the two phenoxide moieties), and three longer bonds (in 13%) involving two ether functions and the triflate anion. The situation for site II is somewhat different in that it features only three short bonds (carbonyl groups) identical to those of Site I, all the other distances being 13% longer. It is noteworthy, that site I builds a more protective cavity around the metal ion than site II does. Moreover, contrary to what was inferred from the ligand design, the phenoxide groups participate more than expected in the bonding (Site I), with Ln−O distances similar to those with carbonyl functions.

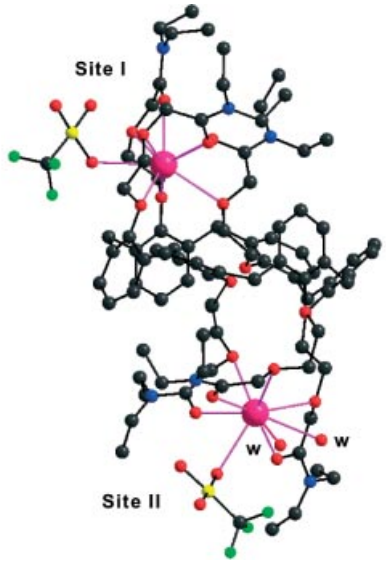

Figure 4. Optimized geometry of the Eu^{III} 2:1 complex with A_6L^6 as determined by MM3 Augmented and Conflex CAChe procedures

Conclusion

The calix[6]arene A_6L^6 exhibits a 1,2,3-alternate conformation in which two sets of three arms extend on opposite sides of the phenoxide framework, henceforth leading to a ditopic ligand able to bind to two metal ions. Complexes with a 2:1 (Ln/A_6L^6) stoichiometry could effectively be observed in solution by ^1H and ^{13}C NMR spectroscopy, and the Eu^{III} complex was isolated. The calculated structure of this complex confirms the results of the luminescence study, and resembles those found experimentally for the 2:1 complexes with *p-tert*-butylcalix[6]arene H_6bL^6 (Ln = Sm, Yb).[24] The absence of substituents on the narrower rim of H_6L^6 allows easy interconversion between different conformers, through either one of the "*tert*-butyl through the annulus" or "narrower rim through the annulus" pathways,[35] facilitating the formation of the 2:1 complexes. On the other hand, *p-tert*-butyl-substituted B_6bL^6 displays a less labile alternate *in-out* conformation in which the six phosphanylyl pendant arms are located on the same side of the molecule, and no 2:1 complexes are obtained with this receptor but, instead, compounds with 1:1 and 1:2 stoichiometries can be isolated.[16] This demonstrates once again the versatility of the calixarene frameworks, since a conformation favoring a given stoichiometry of the Ln^{III} complexes can be induced by modifying either the wider or the narrower rim of the ligand, a property which should prove useful in the development of convenient extraction systems.

Experimental Section

Solvents and Starting Materials: Tetrahydrofuran and toluene were distilled from Na, and acetonitrile was distilled from CaH_2.[36] Diglycolic anhydride, $BH_3{\cdot}Me_2S$ (2 M solution in THF), Et_2NH, Et_3N, formalin (36% solution), butylphenol, KOH, $AlCl_3$ phenol, chloroform, acetone, and $SOBr_2$ were purchased from Fluka AG (Buchs, Switzerland) or Merck, and used without further purification.

Syntheses

Preparation of the Pendant Arm: The brominated ether-amide arm **ABr** was synthesized as described previously (see Scheme 1).[14] It was dried for 3 h over 4-Å molecular sieves, which had been previously dried at 240 °C under high vacuum (24 h, 10^{-5} Torr).

Calix[6]arene H_6L^6: *p-tert*-Butylcalix[6]arene (H_6bL^6) was synthesized according to the procedure reported by Gutsche et al.,[37] and its purity checked by TLC analysis: $R_f = 0.65$ in CH_2Cl_2/petroleum ether (1:1, v/v), $R_f = 0.36$ in acetone/petroleum ether (1:9, v/v). The compound was further characterized by IR, ^1H, and ^{13}C NMR spectroscopy, and EI mass spectrometry. The *tert*-butyl groups were then removed following an $AlCl_3$ catalyzed retro-Friedel−Crafts reaction in the presence of phenol.[38] TLC analysis yielded $R_f = 0.61$ in CH_2Cl_2/petroleum ether (1:1, v/v), and $R_f = 0.31$ in acetone/petroleum ether (1:9, v/v). It was further characterized by IR, ^1H, and ^{13}C NMR and EI mass spectrometry.

Functionalization of Calix[6]arene: All operations were performed under strictly anhydrous conditions under nitrogen. Dried calix[6]arene (135 mg, 0.21 mmol) and NaH (60% in mineral oil, 149 mg, 3.73 mmol) were placed into a 100-mL round-bottomed flask fitted with a nitrogen inlet and a condenser, and dried toluene (60 mL) was added. The turbid mixture was heated with stirring, becoming almost transparent at 70 °C. The temperature increased spontaneously to 76 °C, hydrogen evolved, and a white emulsion formed. The temperature was slowly increased to 90 °C, and the mixture maintained at this temperature until no fluorescent UV spot corresponding to H_6L^6 was observed on the TLC plate (approximately 1 h). The hot emulsion was quickly poured into a 100-mL three-necked round-bottomed flask containing a solution of dried brominated arm **ABr** (808 mg, 3.4 mmol) in dry toluene (5 mL), which had been previously heated with stirring at 115 °C for 2 h. More toluene was added (10 mL), and the temperature was increased to 130 °C. As the reaction progressed the solution became

 © 2004 Wiley-VCH Verlag GmbH & Co. KGaA, Weinheim

turbid and its color changed from brownish-orange to reddish-orange. The reaction was stopped after 6 days. The solid was separated at room temp. by vacuum filtration, and washed with warm toluene until the filtrate became colorless. The filtered organic solution was washed several times with doubly distilled water until the pH of the latter remained unchanged, and no AgBr formed upon addition of 2% $AgNO_3$ to the aqueous phase. During the washing, a white emulsified intermediate phase formed, which disappeared quickly. The organic phase was dried with anhydrous magnesium sulfate, filtered, concentrated at 40 °C, and finally evaporated under vacuum (10^{-2} Torr) at 60−70 °C. A deep orange glassy-solid was obtained (ca. 150 mg) which was ground up. *n*-Hexane (20 mL) was added, the mixture was stirred and heated to 45 °C for 30 min, and the yellow solution was separated. This step was repeated until the solution became colorless. The bulk of the solvent was separated, the remaining solvent removed under vacuum (10^{-2} Torr), and the orange waxy solid dried at 70 °C under high vacuum (10^{-5} Torr) for 1 day. It was then re-dissolved in a minimum amount of methanol, and diisopropyl ether was added until cloudiness was observed. This mixture was left in the refrigerator overnight to induce precipitation. Small and slightly yellow, brilliant glassy crystals formed after 2 days, which were collected and dried at 100 °C under high vacuum (10^{-5} Torr) for 48 h. The final deliquescent compound (66 mg, 0.042 mmol, 20% yield) was then characterized, $C_{90}H_{126}N_6O_{18}$ (Mol wt. 1580.02). IR (KBr, cm^{-1}): $\tilde{\nu}$ = 1639 ($\nu_{C=O}$), 1249 (ν_{C-O-C}), 1126 (ν_{O-CH_2}), 1218 and 1045 (ν_{Ar-O}), 765 (ν_{C-H}). UV/Vis (dried and degassed spectroscopic grade CH_3CN): λ = 270, 278 nm. Diffuse reflectance (5% in MgO): 44840 (C=O) and 36630 (phenyl) cm^{-1}. ES-MS (10^{-4} M, CH_3CN): *m/z* = 1580.82 ($[M + H]^+$, calcd. 1581.03), 1602.86 ($[M + Na]^+$ calcd. 1603.02). ^1H NMR (10^{-3} M, CD_3CN, 400 MHz): δ = 6.94 (d, ^2J = 7.44 Hz, 12 H, H^8, H^{10}), 6.79 (t, ^3J = 7.44 Hz, 6 H, H^9), 4.11 (s, 12 H, H^3), 4.00 (s, 12 H, H^{13}), 3.72 (broad, 12 H, H^1), 3.56 (broad, 12 H, H^2), 3.35−3.25 (m, 24 H, H^5, $H^{5'}$), 2.14 (s, 4 H, $2H_2O$), 1.14 (t, ^3J = 7.1 Hz, 18 H, H^6, $H^{6'}$), 1.07 (t, ^3J = 7.1 Hz, 18 H, H^6, $H^{6'}$) ppm. $^{13}C\{^1H\}$ NMR (1×10^{-3} M, CD_3CN, 50 MHz): δ = 168.9 (C^4), 155.8 (C^{12}), 135.7 (C^7, C^{11}), 129.8 (C^9), 124.8 (C^8, C^{10}), 73.1, 71.3 (C^1, C^2), 71.0 (C^3), 41.9, 40.5 (C^5, $C^{5'}$), 31.0 (C^{13}), 14.7, 13.3 (C^6, $C^{6'}$) ppm.

Synthesis of the Complex: $Eu(CF_3SO_3)_3 \cdot 6H_2O$ (21 mg, 0.026 mmol) was dissolved in dry MeCN (2 mL) at 36 °C with stirring under N_2, and A_6L^6 (20.5 mg, 0.013 mmol) in dry MeCN (4 mL) was added dropwise. The resultant mixture was stirred for 1 h, cooled to room temp., and stirred for a further 4 h. The solvent was partially evaporated under vacuum, and diisopropyl ether was added dropwise until cloudiness appeared. The mixture was left overnight at −20 °C. The precipitate was centrifuged, washed with diisopropyl ether (2 mL), and dried under vacuum (10^{-2} Torr) at room temp., and then at 80 °C for 24 h under high vacuum (10^{-5} Torr), yielding a pale pink hygroscopic compound (34 mg, yield 82%). $Eu_2(CF_3SO_3)_6 \cdot A_6L^6 \cdot 9H_2O$, $C_{96}H_{144}Eu_2F_{18}N_6O_{45}S_6$ (2940.51): calcd. C 39.2, H 4.8, N 2.9; found C 38.8, H 4.9, N 2.8. IR (KBr, dried at 118 °C, cm^{-1}): $\tilde{\nu}$ = 1614 ($\nu_{C=O}$), 1321 ($\nu_{s(SO_3)}$ion), 1237 ($\nu_{s(C-O-C)}$), 1030 ($\nu_{s(SO_2)}$), 760 (ν_{C-H}), 638 ($\delta_{as(SO_3)}$), 520 (ν_{H_2O}). Diffuse reflectance (5% in MgO): 37310, 36230, 34130 cm^{-1}.

Spectroscopic and Analytical Measurements: IR spectra were measured with a Mattson Alpha Centauri FT spectrometer as KBr pellets for solid samples, and films on AgCl for oily samples. ES-MS spectra were measured with a Finnigan SSQ 710C spectrometer driven by a Digital Personal station 5000/25 using 10^{-4} M solutions in methanol or dry acetonitrile, and a $MeOH/HCO_2H$ mixture as eluent. NMR spectra were recorded with Bruker AM-360 (360 MHz) or DRX Advance 400 (400 MHz) spectrometers; chemical shifts δ are given with respect to TMS or CD_3CN. Low resolution luminescence spectra of solid state samples (295 and 77 K) were recorded with a Perkin−Elmer LS-50B spectrofluorimeter. Lifetimes of solutions (data reported are averages of at least five determinations), and quantum yields were measured with the same instrument. The quantum yield of the metal-centered luminescence was determined in degassed and anhydrous CH_3CN at room temperature with respect to $[Eu(L)]^{3+}$ 3×10^{-5} M in acetonitrile (Q_{abs} = 23% [39]) where L is a cyclen derivative {1,3,7,10-tetrakis[*N*-(4-phenylacetyl)carbamoylmethyl]-1,4,7,10-tetraazacyclododecane} using the following formula:

$$Q_x/Q_r = [A_r(\lambda)/A_x(\lambda)] \cdot [D_x/D_r] \cdot [n_x^2/n_r^2]$$

where the subscript *r* stands for the reference, and *x* for the sample. *A* is the absorbance at the excitation wavelength λ, *n* the refractive index (1.344 for solution in CH_3CN and 1.333 for the solution in water), and *D* the integrated luminescence intensity. The same excitation wavelength (279 nm) and absorbance (0.27) were used for the sample and the reference, and a bandpass filter (350 nm or 390 nm) was inserted to eliminate both the Rayleigh diffusion band and second order spectra. High resolution laser excited luminescence spectra were recorded using published procedures.[40] Lifetime data for solid samples were measured at different temperatures under pulsed excitation provided by a FL-3001 dye laser from Lambda Physik coupled to an excimer XeCl laser EMG-101-MSC from Lambda Physik. Elemental analyses were performed by Dr H. Eder (Microchemical Laboratory, University of Geneva).

Semi-Empirical Calculations: The optimized structures and energy minima of the free ligand, and of the 2:1 complex were calculated by using MM3 augmented and CONFLEX procedures, respectively, from the CAChe Pro 5.02 or 5.04 program package for Windows® (Fujitsu Ltd., 2000−2002). The structure of A_6L^6 was further optimized with respect to its enthalpy of formation by MOPAC PM3 molecular orbital calculations using the same program package. The effect of solvent (water) was taken into account using the COSMO procedure built into CAChe Pro. Experimental data for both the free ligand and the Eu^{III} complex (IR, NMR, luminescence) were taken into account for optimizing the calculations.

Acknowledgments

This work was supported through grants from the Swiss National Science Foundation, and by Conacyt (México), project Nr. 36689-E. We thank Véronique Foiret for her help in gathering the luminescence data.

[1] C. D. Gutsche, *Calixarenes Revisited*, Monographs in Supramolecular Chemistry (Ed.: J. F. Stoddart), The Royal Society of Chemistry, Cambridge, **1998**.
[2] Z. Asfari, V. Böhmer, J. M. Harrowfield, J. Vicens, *Calixarenes 2001*, Kluwer Academic Publishers, Dordrecht, **2001**.
[3] F. Cadogan, K. Nolan, D. Diamond, in *Calixarenes 2001* (Eds.: Z. Asfari, V. Böhmer, J. M. Harrowfield), Kluwer Academic Publishers, Dordrecht, **2001**, chapter 34, 627−641.
[4] C. Dieleman, S. Steyer, C. Jeunesse, D. Matt, *J. Chem. Soc., Dalton Trans.* **2001**, 2508−2517.
[5] D. M. Roundhill, *Prog. Inorg. Chem.* **1995**, *43*, 533−592.
[6] P. Thuery, M. Nierlich, J. M. Harrowfield, M. Ogden, in *Calixarenes 2001* (Eds.: Z. Asfari, V. Böhmer, J. M. Harrowfield, J. Vicens), Kluwer Academic Publishers, Dordrecht, **2001**, chapter 30, 561−582.
[7] J.-C. G. Bünzli, F. Besançon, F. Ihringer, *Calixarenes for Separ-*

 © 2004 Wiley-VCH Verlag GmbH & Co. KGaA, Weinheim

ations (Eds.: G. J. Lumetta, R. D. Rogers, A. Gopalan), American Chemical Society, Washington D. C., **2000**, *ACS Symposium Series*, vol. 757, chapter 14, 179−194.
[8] J. Rebek, *Chem. Commun.* **2000**, 637−643.
[9] J. L. Atwood, L. J. Barbour, M. J. Hardie, C. L. Raston, *Coord. Chem. Rev.* **2001**, *222*, 3−32.
[10] *Calixarenes for Separations*, ACS Symposium Series (Eds.: G. J. Lumetta, R. D. Rogers, A. Gopalan), American Chemical Society, Washington D. C., **2000**, *ACS Symposium Series*, vol. 757.
[11] J. F. Dozol, V. Lamare, N. Simon, R. Ungaro, A. Casnati, *Calixarenes for Separations* (Eds.: G. J. Lumetta, R. D. Rogers, A. Gopalan), American Chemical Society, Washington D. C., **2000**, *ACS Symposium Series*, vol. 757, chapter 2, 12−25.
[12] F. Arnaud-Neu, M.-J. Schwing-Weill, F. Dozol, *Calixarenes 2001* (Eds.: Z. Asfari, V. Böhmer, J. M. Harrowfield, J. Vicens), Kluwer Academic Publishers, Dordrecht, **2001**, chapter 35, 642−662.
[13] P. D. Beer, G. D. Brindley, D. B. Fox, A. Grieve, M. I. Ogden, F. Szemes, M. G. B. Drew, *Dalton Trans.* **2002**, 3101−3111.
[14] F. de M. Ramirez, L. J. Charbonnière, G. Muller, R. Scopelliti, J.-C. G. Bünzli, *J. Chem. Soc., Dalton Trans.* **2001**, 3205−3213.
[15] L. Le Saulnier, S. Varbanov, R. Scopelliti, M. Elhabiri, J.-C. G. Bünzli, *J. Chem. Soc., Dalton Trans.* **1999**, 3919−3925.
[16] F. de M. Ramirez, S. Varbanov, C. Cécile, G. Muller, N. Fatin-Rouge, R. Scopelliti, J.-C. G. Bünzli, *Dalton Trans.* **2002**, 4505−4513.
[17] F. de M. Ramirez, S. Varbanov, J.-C. G. Bünzli, unpublished work, **2003**.
[18] R. Ludwig, K. Inoue, T. Yamato, *Solv. Extr. Ion Exch.* **1993**, *11*, 311−330.
[19] R. Ludwig, D. Lentz, T. K. D. Nguyen, *Radiochim. Acta* **2000**, *88*, 335−343.
[20] T. Oshima, T. Yamamoto, K. Ohto, M. Goto, F. Nakashio, S. Furusaki, *Solvent Extr. Res. Develop. (Japan)* **2001**, *8*, 194−204.
[21] E. M. Georgiev, J. Clymire, G. L. McPherson, D. M. Roundhill, *Inorg. Chim. Acta* **1994**, *227*, 293−296.
[22] N. Sato, I. Yoshida, S. Shinkai, *Chem. Lett.* **1993**, 1261−1264.
[23] L. M. Engelhardt, B. M. Furphy, J. M. Harrowfield, D. L. Kepert, A. H. White, F. R. Wilner, *Aust. J. Chem.* **1988**, *41*, 1465−1476.
[24] P. C. Leverd, D. Rinaldo, M. Nierlich, *Eur. J. Inorg. Chem.* **2001**, 2021−2025.
[25] A. Casnati, P. Minari, A. Pochini, R. Ungaro, *J. Chem. Soc., Chem. Commun.* **1991**, 1413−1414.
[26] K. Araki, N. Hashimoto, H. Otsuka, T. Nagasaki, S. Shinkai, *Chem. Lett.* **1993**, 829−832.
[27] C. Jaime, J. De Mendoza, P. Prados, P. M. Nieto, C. Sanchez, *J. Org. Chem.* **1991**, *56*, 3372−3376.
[28] M. E. M. Hamidi, J.-L. Pascal, *Polyhedron* **1994**, *13*, 1787−1792.
[29] K. Nakamoto, *Infrared and Raman Spectra of Inorganic and Coordination Compounds. Part A. Theory and Applications in Inorganic Chemistry*, Wiley Interscience, New York, **1997**.
[30] F. Nicolo, D. Plancherel, G. Chapuis, J.-C. G. Bünzli, *Inorg. Chem.* **1988**, *27*, 3518−3526.
[31] J.-C. G. Bünzli, *Spectroscopic Properties of Rare Earths in Optical Materials* (Eds.: G. K. Liu, B. Jacquier), Springer Verlag, Berlin, **2004**, chapter 11, in press.
[32] W. de W. Horrocks Jr., D. R. Sudnick, *J. Am. Chem. Soc.* **1979**, *101*, 334−340.
[33] R. M. Supkowski, W. de W. Horrocks Jr., *Inorg. Chim. Acta* **2002**, *340*, 44−48.
[34] J.-C. G. Bünzli, in *Rare Earths* (Eds.: R. Saez Puche, P. Caro), Editorial Complutense, Madrid, **1998**, 223−259.
[35] W. P. van Hoorn, F. C. J. M. van Veggel, D. N. Reinhoudt, *J. Phys. Chem.* **1998**, *102*, 6676−6681.
[36] D. D. Perrin, W. L. F. Armarego, *Purification of Laboratory Chemicals*, Pergamon Press, Oxford, **1988**.
[37] C. D. Gutsche, B. Dhawan, M. Leonis, D. Stewart, *Org. Synth.* **1990**, *68*, 238−242.
[38] C. D. Gutsche, L. G. Lin, *Tetrahedron* **1986**, *42*, 1633−1640.
[39] G. Zucchi, A.-C. Ferrand, R. Scopelliti, J.-C. G. Bünzli, *Inorg. Chem.* **2002**, *41*, 2459−2465.
[40] J.-C. G. Bünzli, A. Milicic-Tang, *Inorg. Chim. Acta* **1996**, *252*, 221−228.

Received November 7, 2003
Early View Article
Published Online April 7, 2004

 © 2004 Wiley-VCH Verlag GmbH & Co. KGaA, Weinheim

Iron Complexes with the Alcoholato Donor-Rich Ligand 4-*tert*-Butyl-2,6-bis(hydroxymethyl)phenol: Synthesis and Characterization of a Tetra-Anionic Fe_2 Complex and a Neutral $Fe_{10}Na_4$ Complex

Thorsten Glaser,*[a] Thomas Lügger,[a] and Rolf-Dieter Hoffmann[a]

Keywords: Iron / O ligands / Oxo ligands / Bridging ligands / Hydrogen bonds

The reaction of 4-*tert*-butyl-2,6-bis(hydroxymethyl)phenol (H_3L) with Fe^{III} ions in methanol in the presence of an excess of NaOH afforded the tetra-anionic dinuclear complex $Na_4[(HL)_4Fe^{III}_2(CO_3)]\cdot 11MeOH\cdot 3H_2O$ (**1**). Changing the solvent to an ethanol/dme (dme = 1,2-dimethoxyethane) mixture led to the formation of the decanuclear complex $[(HL)_{12}Fe^{III}_{10}Na_4(\mu_4\text{-}O)_4(\mu_3\text{-}OH)_2(dme)_2(EtOH)_2]\cdot 2dme\cdot 8EtOH$ (**2**). The Mössbauer spectra of **1′** and **2** at 80 K are consistent with high spin Fe^{III} sites in distorted octahedral O_6 coordination environments. Compound **1** consists of a tetra-anionic dinuclear iron complex with the unprecedented $[Fe^{III}(\mu_2\text{-}OBz)_2(\mu_2\text{-}CO_3)Fe^{III}]^{2+}$ core. Compound **2** contains a core of hydrous ferric oxide produced by a modified hydrolysis of Fe^{III} ions in the presence of the ligand. Eight benzyl alcohol groups are located on the surface of **2** leading to a 2D network structure by intermolecular hydrogen bonding. The temperature dependence of the magnetic susceptibilities of **1′** and **2** indicates antiferromagnetic interactions between the ferric ions. The data for **1′** were fitted with $J = -4.4$ cm^{-1} and $g = 1.98$, $H = -2J\mathbf{S}_1\mathbf{S}_2$.
(© Wiley-VCH Verlag GmbH & Co. KGaA, 69451 Weinheim, Germany, 2004)

Introduction

Polynuclear oxo-, hydroxo-, and alcoholato-bridged iron complexes have received a great deal of attention in the fields of bioinorganic chemistry and molecular magnetic materials. In the former, they have been discussed as models for the high-nuclearity hydrous ferric oxide core of the iron storage protein ferritin.[1] Additionally, high-nuclearity iron complexes with high spin ground states and large negative magnetic anisotropy can behave as single-molecule magnets (SMMs).[2] A number of polynuclear complexes with a non-wheel-like structure comprised of up to 19 iron centers are known.[3] Joining together such aggregates into 1D, 2D, or 3D assemblies can yield materials with interesting magnetic properties.[4]

In this respect, we have been exploring the coordination chemistry of ligands based on 2,6-bis(hydroxymethyl)-phenol **A** (Scheme 1) and the sulfur-substituted derivatives, which are of particular interest due to the number of possible binding modes that they may display. Although the coordination chemistry of the corresponding ligand types 2,6-bis(aminomethyl)phenol **B** and 2,6-bis(iminomethyl)-phenol **C** (dinucleating ligands or Robson type ligands)[5] is well established, neither the coordination chemistry of the benzyl alcohol ligand **A**,[6] nor the coordination chemistry of benzyl alcohol ligands in general is well established. One important property of alcoholato ligands is their strong basicity, mainly due to the lack of resonance stabilization of the corresponding anion. This leads to their pronounced tendency to bridge metal centers[7] rather than to bind to one metal center in a terminal fashion, which is the usual coordination mode of amine and imine nitrogen donors. The coordination chemistry of ligand types **B** and **C** is, therefore, dominated by dinuclear metal complexes whereas ligand type **A** is well suited for the preparation of a variety of high-nuclearity complexes with differing coordination modes.[8] The related ligand 2,6-bis(hydroxymethyl)pyridine has been used for the synthesis of polynuclear manganese complexes, which exhibit single-molecule magnetic behavior.[9]

Recently, we reported that the reaction of 4-*tert*-butyl-2,6-bis(hydroxymethyl)phenol (H_3L) with $[Fe^{III}(acac)_3]$ in CH_3CN in the presence of Et_3N yields the tetranuclear complex $(Et_3NH)_2[(HL)_6Fe^{III}_4(acac)_2]$ (**3**) with a core of two face-sharing cuboidal $[Fe_3O_4]$ fragments.[6a] The central phenolato donor (OPh^-) in each of the three crystallographically independent ligand molecules coordinates in a terminal fashion to one Fe ion. The two benzyl alcohol groups of each ligand are distinguishable. One benzyl alcohol group of each ligand is deprotonated (OBz^-) while the other one is not (BzOH). The deprotonated benzyl alcoholato donors coordinate either in a μ_2- or in a μ_3-bridging mode. The protonated, non-coordinating benzyl alcohol groups form intra- as well as intermolecular hydrogen

[a] Institut für Anorganische und Analytische Chemie, Westfälische Wilhelms-Universität Münster
Wilhelm-Klemm-Straße 8, 48149 Münster, Germany
Fax: (internat) +49-(0)251 833 3108
E-mail: tglaser@uni-muenster.de
Supporting information for this article is available on the WWW under http://www.eurjic.org or from the author.

 © 2004 Wiley-VCH Verlag GmbH & Co. KGaA, Weinheim **DOI: 10.1002/ejic.200300575**

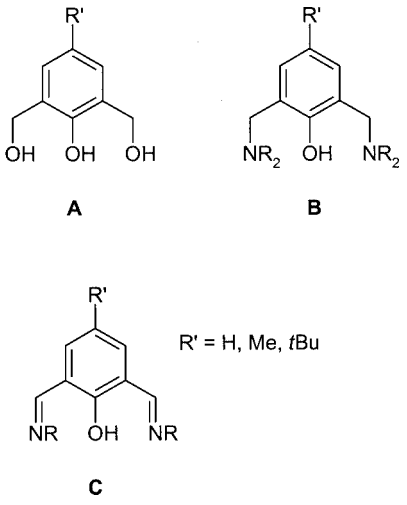

Scheme 1

bonds. In this way, the zero-dimensional paramagnetic building block was arranged into a 1D array by hydrogen bonding. Here, we report on the reaction between H_3L and $Fe^{III}(ClO_4)_3 \cdot 10H_2O$ in the presence of NaOH in protic solvents. Using MeOH as the solvent led to a tetra-anionic dinuclear iron complex and using an EtOH/dme mixture (dme = 1,2-dimethoxyethane) led to a decanuclear complex which forms a 2D network structure in the solid state by intermolecular hydrogen bonds.

Results and Analysis

Synthesis and Structural Characterization

The reaction between H_3L and $Fe^{III}(ClO_4)_3 \cdot 10H_2O$ in a 2:1 molar ratio in methanol in the presence of excess NaOH per ligand yielded large red crystals of **1** which were isolated by filtration. The FTIR spectrum exhibits bands at 2954, 2868, 1480, 1392 and 1363 cm^{-1} that are characteristic of the *tert*-butylbenzene section of the ligand H_3L. The C−O stretching frequencies of the phenolic C−O bonds are at 1307, 1276, and 1219 cm^{-1} compared with 1219 cm^{-1} in the free ligand H_3L.[6a,10] The broad band of the benzylic C−O bond at 1015 cm^{-1} in the free ligand splits into two sharp bands at 1039 and 1021 cm^{-1} in **1**. A broad flat absorption in the range of 2500−3500 cm^{-1} indicates the occurrence of hydrogen bonds. Red crystals of **1** were investigated by means of a single-crystal X-ray diffraction study and a composition of $Na_4[(HL)_4Fe_2(CO_3)] \cdot 11MeOH \cdot 3H_2O$ was obtained. Samples used for magnetic measurements were dried under high vacuum and analysis revealed a composition of $Na_4[(HL)_4Fe_2(CO_3)] \cdot 8MeOH \cdot 2H_2O$ (**1′**) indicating the loss of 3 MeOH molecules and one H_2O molecule. Tetra-anionic dinuclear complexes $[(HL)_4Fe_2(CO_3)]^{4-}$ (Figure 1) are bridged in one direction by a complicated and disordered network of sodium cations, methanol and water molecules. Although the dinuclear complex could be refined well, the heavily disordered Na^+ cations and methanol and water molecules (≈ 35% of total scattering power) have precluded complete refinement. Therefore, we have used the results from the X-ray diffraction analysis as proof only of atomic connectivity.[11]

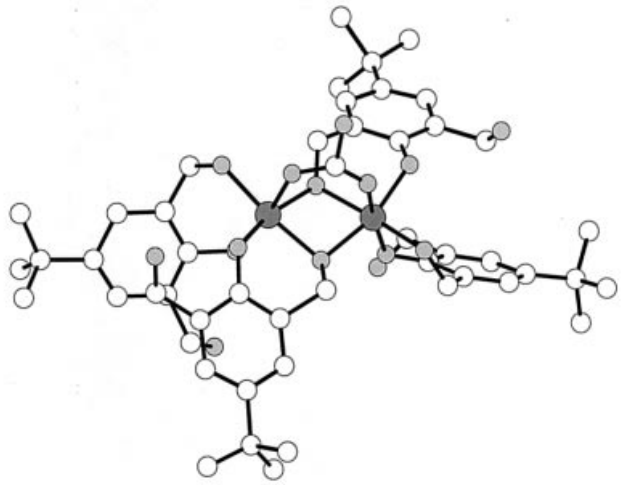

Figure 1. Atomic connectivity in the dinuclear complex $[(LH)_4Fe_2(CO_3)]^{4-}$ in **1**; dark grey circles: Fe; light grey circles: O; empty circles: C

Due to the lack of added carbonate, CO_3^{2-}, or hydrogen carbonate, HCO_3^-, the incorporated carbonato ligand has to originate from atmospheric CO_2. To test this hypothesis, we performed the same reaction under an argon atmosphere and no pure product was obtained. In other attempts to obtain **1** in a more controlled fashion Na_2CO_3, a typical precursor for the preparation of iron-carbonato complexes,[12] was added to the reaction mixture. However, no pure product was obtained. Although the controlled reaction for the preparation of **1** proved not to be straightforward, the reaction under a normal atmosphere was repeated several times and large red crystals were obtained in each case. It is interesting to note that analogous reactions using LiOH, KOH, CsOH, or even *t*BuOK and Et_3N as bases did not yield the tetra-anion of **1**. It might be speculated, therefore, that there is a synergistic effect of CO_2 incorporation and the incorporation of Na^+ ions in the solid state. Fixation of CO_2 under the highly basic conditions used in our preparations is not surprising, and this has been studied in detail by Kitajima et al.[13]

The potentially tridentate ligand is only doubly deprotonated i.e. HL^{2-}. In two ligand molecules, the phenolato group acts as a terminal donor, whereas the deprotonated benzyl alcoholato donor acts as a μ_2-bridge between the iron ions. The non-deprotonated benzyl alcohol functions form hydrogen bonds with the coordinated phenolato oxygens and with methanol molecules. In the other two ligands, the phenolato oxygen atom and the deprotonated benzyl alcohol oxygen atom chelate an iron atom whereas the non-deprotonated benzyl alcohol group binds to two sodium ions. The dinuclear complex is composed of a central $[Fe^{III}(\mu_2\text{-}OBz)_2Fe^{III}]^{4+}$ core which represents a fundamental unit in iron-oxygen donor chemistry of metallo-pro-

 © 2004 Wiley-VCH Verlag GmbH & Co. KGaA, Weinheim

teins and of biomimetic model compounds.[14] Several examples of complexes with the $[Fe^{III}(\mu_2\text{-}OR)_2(\mu_2\text{-}OOCR')Fe^{III}]^{3+}$ core have been reported.[15] Whereas $[Fe^{III}(\mu_2\text{-}O)(\mu_2\text{-}CO_3)Fe^{III}]^{2+}$ is known[12,13], however, complex **1** is to the best of our knowledge the first evidence of a $[Fe^{III}(\mu_2\text{-}OR)_2(\mu_2\text{-}CO_3)Fe^{III}]^{2+}$ core.

The reaction of H_3L and $Fe^{III}(ClO_4)_3\cdot 10H_2O$ in a molar ratio of 2:1 in ethanol in the presence of excess NaOH and dme yielded dark red crystals of **2**. The FTIR spectrum shows the bands of the *tert*-butylbenzene part of the ligand H_3L at 2954, 2867, 1480, 1393, and 1363 cm^{-1}. The absorptions at 1306, 1275, and 1220 cm^{-1} can be assigned to C−O stretching modes of the phenolic C−O bonds, and those at 1038 and 1022 cm^{-1} to the C−O stretching modes of the benzylic C−O bonds. The intensity patterns of these C−O vibrations differ from those observed in the FTIR spectrum of **1**. A broad flat absorption in the 3400−2500 cm^{-1} range is indicative of hydrogen bonding. Structural characterization by single-crystal X-ray diffraction gave the formulation as $[(HL)_{12}Fe^{III}_{10}Na_4(\mu_4\text{-}O)_4(\mu_3\text{-}OH)_2(dme)_2(EtOH)_2]\cdot 2dme\cdot 8EtOH$ (**2**).

The molecular structure of the decanuclear complex in crystals of **2** is shown in Figure 2 (a). The decanuclear iron unit including the bridging oxygen atoms is shown in Figure (b). Selected bond lengths and bond angles are given in Table 1. The asymmetric unit consists of one half of the complex with the other half generated by a crystallographic center of inversion. All iron atoms are in distorted octahedral FeO_6 environments and are bridged by four $\mu_4\text{-}O^{2-}$ (O1, O1′, O3, O3′), two $\mu_3\text{-}OH^-$ (O3, O3′), and twelve $\mu_2\text{-}OBz^-$ ligands (O2a, O2a′, O2b, O2b′, O2c, O2c′, O2d, O2d′, O2e, O2e′, O2f, O2f′). The coordination of the iron ions is completed by OPh^- ligands and two EtOH ligands (coordinated to Fe3 and Fe3′). The assignment of O2 (and O2′) to an OH^- instead of an O^{2-} ligand is not only based on charge considerations. The three Fe−O bond lengths to O2 (mean value 2.09 Å) are significantly longer than the four bond lengths to O1 (2.02 Å) and O3 (2.05 Å). For O2 being a $\mu_3\text{-}O^{2-}$, it must have shorter bonds compared with a $\mu_4\text{-}O^{2-}$. Additionally, one oxygen of dme adopts the fourth position of an idealized tetrahedron around O2 at a distance of 2.77 Å, consistent with a hydrogen bond (see Figure S1 in the Supporting Information, for Supporting Information see also the footnote on the first page of this article). The Fe−O bond lengths span a range from 1.95 Å to 2.12 Å. A comparison of the bridging ligands shows that the $\mu_2\text{-}OBz^-$ ligands have shorter bonds (mean value 2.00 Å) compared with the $\mu_4\text{-}O^{2-}$ (mean value 2.03 Å) and the $\mu_3\text{-}OH^-$ ligands (mean value 2.09 Å). The Fe···Fe distances can be divided into two categories: a short distance was found for Fe1−Fe1′, Fe1−Fe2′, and Fe2−Fe1′ at 3.00−3.02 Å and a significantly longer distance range of 3.10−3.22 Å for all other Fe···Fe separations.

The iron-oxygen core can be regarded as a part of a hydrous ferric oxide phase. The oxygen atoms of the bridging $\mu_4\text{-}O^{2-}$, $\mu_3\text{-}OH^-$, $\mu_2\text{-}OBz^-$, and the terminal OPh^- and EtOH may be considered to form an idealized cubic close packed structure with the iron atoms in octahedral voids (A B C A B stacking sequence, see Figure S2 in the Supporting Information). In this respect, the iron-oxygen core in **2** may be regarded as a small part of γ-Fe·O·OH or lepidocrocite stabilized by an organic shell. Two Fe_{10} complexes with a similar iron-oxygen core were reported, namely $[Fe_{10}O_4(OCH_3)_{16}(dbm)_6]\cdot x CHCl_3$ (Hdbm = 1,3-diphenyl-1,3-propanedione)[3e] and $[Fe_{10}O_4Cl_8(OCH_3)_{14}(CH_3OH)_6]\cdot 2CH_3OH$.[3f] This indicates a high stability of the iron-oxygen core based on the different kind of outer shell ligands used for the preparation of the three compounds.

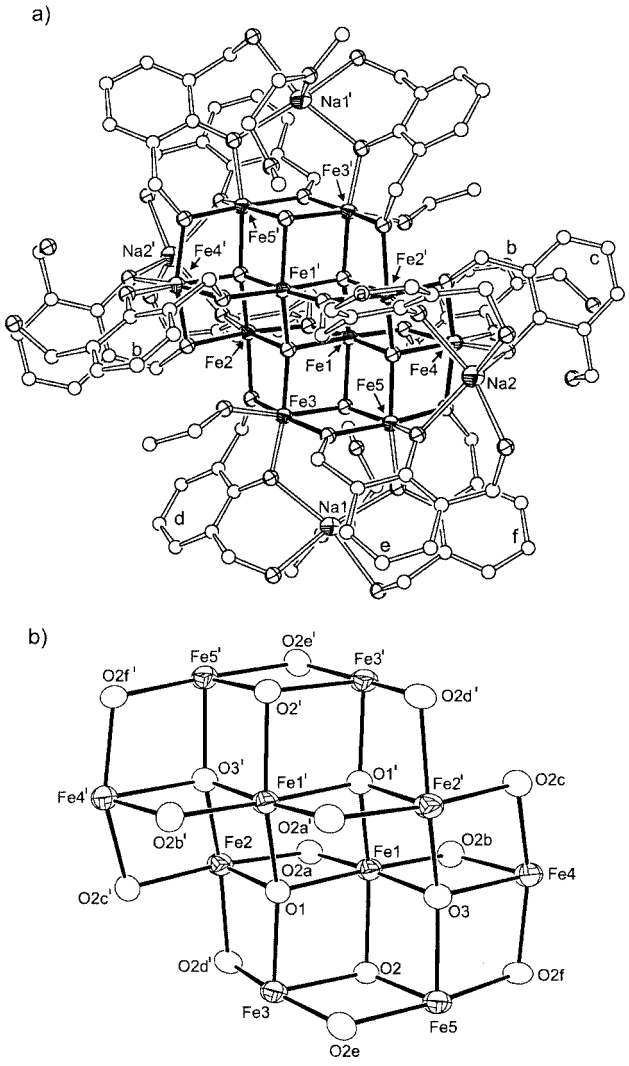

Figure 2. a) Molecular structure of $[(HL)_{12}Fe^{III}_{10}Na_4(\mu_4\text{-}O)_4(\mu_3\text{-}OH)_2(dme)_2(EtOH)_2]$ in crystals of **2**; hydrogen atoms and *tert*-butyl groups are omitted for clarity. The six independent ligand molecules are labeled a−f; b) ORTEP plot of the central Fe_{10} core including the bridging oxygen atoms; thermal ellipsoids are shown at the 50% probability level

The potentially tridentate ligand H_3L appears in all six independent ligand molecules (labeled a−f in Figure 2, a) as only doubly deprotonated HL^{2-}. One of the BzOH groups of each ligand is not deprotonated (O3a−O3f). The six ligand molecules coordinate in two different binding modes. Ligand b (O1b, O2b, O3b) and ligand c (O1c, O2c,

 © 2004 Wiley-VCH Verlag GmbH & Co. KGaA, Weinheim

Table 1. Selected interatomic distances (Å) and bond angles (°) for **2**

Fe1−O1 (μ_4-O)	2.062(4)	Fe1−Fe3	3.131(1)
Fe1−O1′ (μ_4-O)	1.950(4)	Fe1−Fe4	3.165(2)
Fe1−O3 (μ_4-O)	2.066(4)	Fe1−Fe5	3.161(1)
Fe1−O2 (μ_3-OH)	2.083(4)	Fe2−Fe1′	2.993(2)
Fe1−O2a (μ_2-OBz)	1.974(4)	Fe2−Fe3	3.098(2)
Fe1−O2b (μ_2-OBz)	1.944(4)	Fe2−Fe4′	3.153(1)
Fe2−O1 (μ_4-O)	2.089(4)	Fe3−Fe5	3.214(2)
Fe2−O3′ (μ_4-O)	1.964(4)	Fe4−Fe2′	3.153(1)
Fe2−O2a (μ_2-OBz)	2.029(4)	Fe4−Fe5	3.170(2)
Fe2−O2c′ (μ_2-OBz)	2.108(4)	Fe1−O1(μ_4-O)−Fe1′	97.6(2)
Fe2−O2d (μ_2-OBz)	2.013(4)	Fe1−O1′(μ_4-O)−Fe1′	97.6(2)
Fe2−O1a (μ_2-OPh)	1.909(4)	Fe1−O1(μ_4-O)−Fe2	97.2(2)
Fe3−O1 (μ_4-O)	1.972(4)	Fe1−O2a(μ_2-OBz)−Fe2	102.2(2)
Fe3−O2 (μ_3-OH)	2.083(4)	Fe1−O1′(μ_4-O)−Fe2′	95.6(2)
Fe3−O2d (μ_2-OBz)	1.978(4)	Fe1−O3(μ_4-O)−Fe2′	95.9(2)
Fe3−O2e (μ_2-OBz)	1.975(4)	Fe1−O1(μ_4-O)−Fe3	101.8(2)
Fe3−O1d (μ_2-OPh)	1.919(4)	Fe1−O2(μ_3-OH)−Fe3	97.5(2)
Fe3−O30 (HOEt)	2.095(4)	Fe1−O2b(μ_2-OBz)−Fe4	104.2(2)
Fe4−O3 (μ_4-O)	2.137(4)	Fe1−O3(μ_4-O)−Fe4	97.7(2)
Fe4−O2b (μ_2-OBz)	2.065(4)	Fe1−O2(μ_3-OH)−Fe5	97.7(2)
Fe4−O2c (μ_2-OBz)	2.009(4)	Fe1−O3(μ_4-O)−Fe5	101.1(2)
Fe4−O2f (μ_2-OBz)	1.946(4)	Fe2−O1(μ_4-O)−Fe1′	95.6(2)
Fe4−O1b (OPh)	1.970(4)	Fe2−O3′(μ_4-O)−Fe1′	95.9(2)
Fe4−O1c (OPh)	1.973(5)	Fe2−O1(μ_4-O)−Fe3	99.4(2)
Fe5−O3 (μ_4-O)	2.029(4)	Fe2−O2d(μ_2-OBz)−Fe3	101.8(2)
Fe5−O2 (μ_3-OH)	2.113(4)	Fe2−O2c′(μ_2-OBz)−Fe4′	100.0(2)
Fe5−O2e (μ_2-OBz)	2.003(4)	Fe2−O3′(μ_4-O)−Fe4′	100.4(2)
Fe5−O2f (μ_2-OBz)	1.989(4)	Fe3−O2(μ_3-OH)−Fe5	100.0(2)
Fe5−O1e (μ_2-OPh)	1.945(5)	Fe3−O2e(μ_2-OBz)−Fe5	107.7(2)
Fe5−O1f (μ_2-OPh)	2.020(4)	Fe4−O2c(μ_2-OBz)−Fe2′	100.0(2)
Fe1−Fe1′	3.020(2)	Fe4−O3(μ_4-O)−Fe2′	100.4(2)
Fe1−Fe2	3.115(2)	Fe4−O2f(μ_2-OBz)−Fe5	107.3(2)
Fe1−Fe2′	2.993(2)	Fe4−O3(μ_4-O)−Fe5	99.1(2)

O3c) bind only in a chelating fashion to the iron centers via the OPh^- (O1b, O1c) and OBz^- (O2b, O2c) groups, and OBz^- bridges two iron centers. The second non-deprotonated BzOH (O3b, O3c) of these two ligands is not coordinated to a metal center. Ligands a, d, e, f chelate additionally to a Na^+ ion via the OPh^- group and the non-deprotonated BzOH. Furthermore, the non-deprotonated BzOH groups are involved in intra- and intermolecular hydrogen bonding. O3b and O3c (O3b′ and O3c′) form an intramolecular hydrogen bond with a distance of 2.79 Å. Intermolecular hydrogen bonds between O3f and O3b (2.68 Å) and between O3c and O3d (2.76 Å) lead to a hydrogen bonded 2D network structure in the *bc*-plane (Figure 3).

Spectroscopic Characterization

The ^{57}Fe Mössbauer spectrum of **1′** at 80 K shows a quadrupole doublet with an isomer shift $\delta = 0.47\ mm{\cdot}s^{-1}$ and a quadrupole splitting $|\Delta E_Q| = 0.69\ mm{\cdot}s^{-1}$. The isomer shift is typical for high-spin ferric ions ($S_i = 5/2$) ligated by oxygen donors. The quadrupole splitting of $0.69\ mm{\cdot}s^{-1}$ is consistent with a moderate distortion from octahedral symmetry since the valence-electron contribution to ΔE_Q is negligible for a high-spin Fe^{III} ion. The effective magnetic moment (μ_{eff}, calculated per iron dimer unit) of **1′** decreases with decreasing temperature which is indicative of antiferromagnetic coupling (Figure 4). The data could be easily fitted using the spin-Hamiltonian for an Fe^{III} ($S_i = 5/2$) dimer

$$H = -2J\mathbf{S}_1\mathbf{S}_2 + \sum_{i=1}^{2}[\mu_B g_i \mathbf{S}_i \mathbf{B}]$$

using a full-matrix diagonalization approach with $J = -4.4\ cm^{-1}$ and an isotropic g value of 1.98 including a paramagnetic impurity ($S = 5/2$) of 4.1%.[16]

The Mössbauer spectrum of **2** at 80 K exhibits a well resolved doublet with $\delta = 0.51\ mm{\cdot}s^{-1}$ and $|\Delta E_Q| = 0.73\ mm{\cdot}s^{-1}$ typical for high-spin ferric ions. The subspectra originating from the five distinctive iron ions in **2** were not resolved. The temperature dependence of μ_{eff} indicates antiferromagnetic interactions between the Fe^{III} ions. At low temperatures, the μ_{eff} values appear to be sample-dependent. This may be due to different amounts of paramagnetic impurities (presumably mononuclear Fe^{III} species) or to sample inhomogeneities. Crystals rapidly loose solvent leading to different mixtures of crystalline ($Fe_{10}Na_4{\cdot}2dme{\cdot}8EtOH$) and amorphous parts ($Fe_{10}Na_4{\cdot}x dme{\cdot}x EtOH$) with loss of the regular hydrogen bonding pattern as observed in crystals of $Fe_{10}Na_4{\cdot}2dme{\cdot}8EtOH$. The change in the chemical environment of the formerly hydrogen bonded BzOH groups may have a direct effect on the bridges between the iron centers and thus on the exchange interactions leading to the observed differences in the magnetic measurements.

Discussion

The reaction of H_3L with $Fe^{III}(ClO_4)_3{\cdot}10H_2O$ in the presence of NaOH resulted in the formation of **1** using MeOH as the solvent, and **2** using an EtOH/dme mixture as the solvent. Complex **1** has an $[Fe^{III}(\mu_2\text{-}OBz)_2(\mu_2\text{-}CO_3)Fe^{III}]^{2+}$ core which, to the best of our knowledge, is the first example of an Fe_2O_2 unit bridged by a carbonato ligand. The exchange coupling constant was found to be $J = -4.4\ cm^{-1}$. Analogous complexes with a carboxylato instead of the carbonato bridge, i.e. $[Fe^{III}(\mu_2\text{-}OR)_2(\mu_2\text{-}O_2CR)Fe^{III}]^{3+}$, were reported to have J values in the range of -3.9 to $-10.5\ cm^{-1}$.[15c,15d,15e]

Uncoordinated benzyl alcohol groups, coordinated phenolato groups, and the uncoordinated oxygen atom of the coordinated carbonato ligand in **1** create an oxygen donor rich, negatively charged environment around the central $[(HL)_4Fe_2(CO_3)]^{4-}$ unit. These uncompensated charges and hydrogen bond donors lead to a disordered network of Na^+ ions as well as MeOH and H_2O molecules along the *b* axis. It is interesting to compare this arrangement with the iron binding site of the metalloprotein lactoferrin, which is known to reversibly bind two Fe^{III} ions concomitantly with two CO_3^{2-} groups by two equal mononuclear binding sites.[17] A synergistic relationship between cation- and anion-binding has been established. The carbonate anion coordinated to the Fe^{III} ion is tightly fixed by five hydrogen bonds from the protein backbone. In this respect, the stabilization of CO_3^{2-} in **1** by hydrogen bonds and Na^+ ions indicates that the oxygen rich environment of the dinuclear

 © 2004 Wiley-VCH Verlag GmbH & Co. KGaA, Weinheim

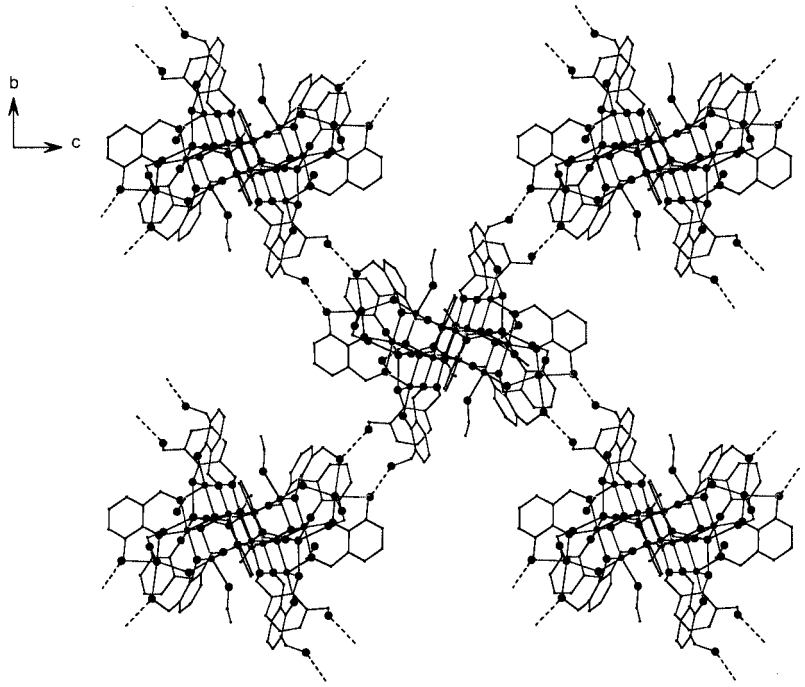

Figure 3. Projection down the *bc*-plane of the 2D network formed from interconnected $Fe_{10}Na_4$ complexes by intermolecular hydrogen bonds in crystals of **2**

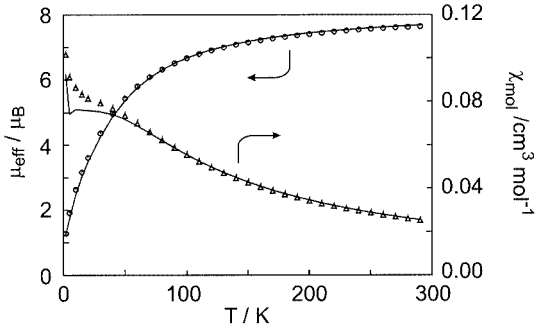

Figure 4. Temperature dependence of the effective magnetic moment, μ_{eff}, of **1′** at 1 T; the solid line is a fit of the experimental data using the spin-Hamiltonian given in the text with $J = -4.4$ cm^{-1}, $g = 1.98$, and a paramagnetic impurity of same molecular mass of 4.1% ($S = 5/2$)

iron unit corroborated by the Na^+/MeOH/H_2O network is perfectly suited for CO_3^{2-} binding. It may be speculated that this is the reason why, by use of MeOH as the solvent, **1** is formed rather than a high-nuclearity iron complex analogous to **2**.

Complex **2** possesses a central iron-oxygen core which may be regarded as a small fraction of the hydrous ferric oxide mineral lepidocrocite. This iron-oxygen core is surrounded by 12 HL^{2-} ligands. In the case of **2**, the uncompensated negative charges of the oxygen donors are saturated by incorporation of four Na^+ ions to give the neutral $Fe_{10}Na_4$ complex. The packing of **2** in the solid state is not governed by van der Waals forces. The presence of eight BzOH functions grouped in four pairs on the surface of **2** leads to a regular hydrogen bonding pattern in a 2D array in the *bc*-plane. The only weakly bound solvent molecules evaporate very rapidly when the crystals are extracted from the mother liquor.

In summary, the coordination chemistry of the ligand 4-*tert*-butyl-2,6-bis(hydroxymethyl)phenol (H_3L) is different from its 2,6-bis(amino) and 2,6-bis(imino) derivatives. Several different coordination modes of H_3L were observed in compounds **1**, **2**, and **3**. The tendency of the OBz^- functions to bridge between metal centers and the availability of BzOH for hydrogen bonds leads to high nuclearity complexes and/or to intermolecular interactions in the solid state. The preparation of manganese complexes of H_3L with the possibility of interesting magnetic properties is currently under way.

Experimental Section

Syntheses: All manipulations were performed under aerobic conditions, using materials as received. 4-*tert*-butyl-2,6-bis(hydroxymethyl)phenol (H_3L) was prepared as described previously[6a]

Safety Note: *Although we have not encountered any problems, it has been noted that the reaction between perchlorate salts and organic ligands may lead to potentially explosive materials and must be performed with great care and appropriate precautions.*

$Na_4[(HL)_4Fe^{III}_2(CO_3)]\cdot 8MeOH\cdot 2H_2O$ (1′): A stirred solution of 4-*tert*-butyl-2,6-bis(hydroxymethyl)phenol (400 mg, 1.90 mmol) in methanol (30 mL) was treated with $Fe^{III}(ClO_4)_3\cdot 10H_2O$ (508 mg, 0.95 mmol) resulting in a deep blue solution. Addition of NaOH (380 mg, 9.51 mmol) caused a color change to dark red. The solu-

 © 2004 Wiley-VCH Verlag GmbH & Co. KGaA, Weinheim

tion was heated at reflux for 4 h during which the color became light red, cooled to room temperature, and filtered. Slow evaporation of the solvent produced red crystals which were vacuum dried. Yield: 420 mg (63%). IR (KBr): $\tilde{\nu}$ = 3538, 2954, 2904, 2868, 1605, 1480, 1392, 1363, 1307, 1276, 1219, 1124, 1039, 1021 878, 832, 757, 690, 549 cm^{-1}.$C_{57}H_{100}Fe_2Na_4O_{25}$ (1389.06): calcd. C 49.29, H 7.26; found C 49.31, H 6.98.

$[(HL)_{12}Fe^{III}{}_{10}Na_4(\mu_4\text{-}O)_4(\mu_3\text{-}OH)_2(dme)_2(EtOH)_2]\cdot 2dme\cdot 8EtOH$ (2): A stirred solution of 4-*tert*-butyl-2,6-bis(hydroxymethyl)phenol (300 mg, 1.43 mmol) in ethanol (10 mL) was treated with $Fe^{III}(ClO_4)_3\cdot 10H_2O$ (389 mg, 0.73 mmol) resulting in the formation of a deep blue color. Addition of a solution of NaOH (214 mg, 5.35 mmol) in ethanol (10 mL) caused a color change to dark red. After stirring for 30 min, dme (3 mL) was added and the solution was filtered. Slow evaporation of the solvent produced red crystals which were vacuum dried. Yield: 160 mg (63%). IR (KBr): $\tilde{\nu}$ = 3424, 2954, 2867, 1624, 1606, 1540, 1480, 1393, 1363, 1306, 1275, 1220, 1122, 1038, 1022, 878, 833, 759, 617, 555 cm^{-1}. $C_{156}H_{226}Fe_{10}Na_4O_{48}$ (3519.91): calcd. C 53.23, H 6.47; found C 53.12, H 6.14.

Crystal Structure Determination: Data were collected with a Bruker AXS APEX diffractometer equipped with a rotating anode using Mo-K_α radiation (λ = 0.71073 Å). An empirical absorption correction was applied for **2** using SADABS.[18] The structure was solved with SHELXS[19] using direct methods and refined with SHELXL.[20]

Single crystals of **2** rapidly desolvate when extracted from the mother liquor indicating the presence of weakly bound solvent molecules. The structure solution shows the well defined complex $[(HL)_{12}Fe^{III}{}_{10}Na_4(\mu_4\text{-}O)_4(\mu_3\text{-}OH)_2(dme)_2(EtOH)_2]$ which could be refined unrestrained using anisotropic thermal parameters. These molecules are separated by solvent layers. Due to heavy disorder, the solvent positions are only poorly resolved and are estimated to consist of eight ethanol and two dme molecules per $Fe_{10}Na_4$ complex. Hydrogen atoms were added in calculated positions and no hydrogen positions were calculated for solvent molecules. Additional data collection and refinement details are listed in Table 2. CCDC-170255 contains the supplementary crystallographic data for compound **2**. These data can be obtained free of charge via www.ccdc.cam.ac.uk/conts/retrieving.html [or from the CCDC, 12 Union Road, Cambridge CB2 1EZ, UK; Fax: (internat.) +44 1223 336033; E-mail: deposit@ccdc.cam.ac.uk].

Other Measurements: Infrared spectra (400−4000 cm^{-1}) of solid samples were recorded with a Bruker Vector 22 spectrometer as KBr disks. Temperature-dependent magnetic susceptibilities of powdered samples in gelatin capsules were measured using a SQUID magnetometer (Quantum Design) at 1.0 T (2.0−300 K). For calculations of the molar magnetic susceptibility, χ_M, the measured susceptibilities were corrected for the diamagnetism of the sample holder and for the underlying diamagnetism of the sample by using tabulated Pascal's constants (**1′**: $\chi_{dia} = -813 \times 10^{-6}$ $cm^3\cdot mol^{-1}$; **2**: $\chi_{dia} = -1997 \times 10^{-6}$ $cm^3\cdot mol^{-1}$). ^{57}Fe Mössbauer spectra were recorded with an alternating constant-acceleration spectrometer. The minimal line-width was 0.24 $mm\cdot s^{-1}$ full-width at half-height. The sample temperature was maintained in an Oxford Instruments Variox Cryostat. ^{57}Co/Rh was used as the radiation source. Isomer shifts were determined relative to α-iron at 300 K.

Electronic Supporting Information Available (see also footnote on the first page of this article): Graphical representations of the hydrogen bond between O2 and O11 in **2** and the packing of the iron-oxygen core in **2** have been deposited.

Table 2. Crystallographic data for **2**

	2
Habit	orange plates
Crystal size (mm)	0.45 × 0.14 × 0.06
Empirical formula	$C_{180}H_{294}Fe_{10}Na_4O_{60}$
Molecular mass (amu)	4068.61
a (Å)	17.9317(4)
b (Å)	23.5919(4)
c (Å)	26.7758(5)
β (deg)	91.028(1)
V (Å^3)	11325.5(4)
Space group	$P2_1/c$
Z	2
μ (mm^{-1})	0.699
Absorption correction	multi-scan (SADABS)
$T_{min.}/T_{max.}$	0.744/0.956
2Θ Range (deg)	2.3−45
T (K)	153(2)
Measured data	49353
Unique data	14752
Observed [$I > 2\sigma(I)$]	9881
R (observed) (%)	7.71, R_w = 24.10
R (all) (%)	10.88, R_w = 26.88
GOF	1.044
Number of variables	1062
Number of restrains	0
Res. electron density ($e\cdot Å^{-3}$)	−0.783/1.316

Acknowledgments

We thank Dr. E. Bill (Max-Planck-Institut für Bioanorganische Chemie, Mülheim) for susceptibility and Mössbauer measurements and valuable discussions. Prof. A. K. Powell (University Karlsruhe) is thanked for helpful discussions. T. G. gratefully acknowledges Professor F. E. Hahn for his generous support. This work was supported by the Fonds der Chemischen Industrie (Liebig-Stipendium for T. G.), the BMBF (Kooperationsbereich Neue Materialien), the Deutsche Forschungsgemeinschaft (Priority Program "Molecular Magnetism"), and the Dr. Otto Röhm Gedächtnisstiftung.

[1] A. K. Powell, *Structure and Bonding* **1997**, *88*, 1−38 and references cited therein.
[2] [2a] A.-L. Barra, P. Debrunner, D. Gatteschi, Ch. E. Schulz, R. Sessoli, *Europhys. Lett.* **1996**, *35*, 133−138. [2b] H. Oshio, N. Hoshino, T. Ito, *J. Am. Chem. Soc.* **2000**, *122*, 12602−12603. [2c] A. L. Barra, A. Caneschi, A. Cornia, F. Fabrizi de Biani, D. Gatteschi, C. Sangregorio, R. Sessoli, L. Sorace, *J. Am. Chem. Soc.* **1999**, *121*, 5302−5310.
[3] [3a] Fe_{19}/Fe_{17}: A. K. Powell, S. L. Heath, D. Gatteschi, L. Pardi, R. Sessoli, G. Spina, F. Del Giallo, F. Pieralli, *J. Am. Chem. Soc.* **1995**, *117*, 2491−2502. [3b] Fe_{14}: J. Burger, P. Klüfers, *Angew. Chem.* **1997**, *109*, 801−804; *Angew. Chem. Int. Ed. Engl.* **1997**, *36*, 776−779. [3c] Fe_{13}: A. Bino, M. Ardon, D. Lee, B. Springler, S. J. Lippard, *J. Am. Chem. Soc.* **2002**, *124*, 4578−4579. [3d] Fe_{11}: S. M. Gorun, G. C. Papaefthymiou, R. B. Frankel, S. J. Lippard, *J. Am. Chem. Soc.* **1987**, *109*, 3337−3348. [3e] Fe_{10}: A. Caneschi, A. Cornia, A. C. Fabretti, D. Gatteschi, *Angew. Chem.* **1995**, *107*, 2862−2864; *Angew.*

 © 2004 Wiley-VCH Verlag GmbH & Co. KGaA, Weinheim

Chem. Int. Ed. Engl. **1995**, *34*, 2862−2864. [3f] Fe_{10}': S. Asirvatham, M. A. Khan, K. M. Nicholas, *Inorg. Chem.* **2000**, *39*, 2006−2007. [3g] Fe_9: A. Bino, I. Shweky, S. Cohen, E. R. Bauminger, S. J. Lippard, *Inorg. Chem.* **1998**, *37*, 5168−5172. [3h] Fe_8: C. Delfs, D. Gatteschi, R. Sessoli, K. Wieghardt, D. Hanke, *Inorg. Chem.* **1993**, *32*, 3099−3103. [3i] Fe_8': V. S. Nair, K. S. Hagen, *Inorg. Chem.* **1994**, *33*, 185−186. [3j] Fe_8'': I. Gautier-Luneau, C. Fouquard, C. Merle, J.-L. Pierre, D. Luneau, *J. Chem. Soc., Dalton Transactions* **2001**, 2127−2131.

[4] M. Murugesu, C. E. Anson, A. K. Powell, *Chem. Commun.* **2002**, 1054−1055.

[5] [5a] R. Robson, *Inorg. Nucl. Chem. Lett.* **1970**, *6*, 125−128. [5b] R. Robson, *Aust. J. Chem.* **1970**, *23*, 2217−2224. [5c] H. Okawa, S. Kida, *Bull. Chem. Soc. Jpn.* **1971**, *44*, 1172. [5d] A. J. Atkins, D. Black, R. L. Flinn, A. Martin-Becerra, A. J. Blake, L. Ruiz-Ramirez, W.-S. Li, M. Schröder, *Dalton Trans.* **2003**, 1730−1737 and references cited therein.

[6] [6a] T. Glaser, T. Lügger, *Inorg. Chim. Acta* **2002**, *337*, 103−112. [6b] A. Rammel, F. Brisach, M. Henry, *J. Am. Chem. Soc.* **2001**, *123*, 5612−5613.

[7] [7a] K. Hegetschweiler, H. Schmalle, H. M. Streit, W. Schneider, *Inorg. Chem.* **1990**, *29*, 3625−3627. [7b] A. Cornia, D. Gatteschi, K. Hegetschweiler, L. Hausherr-Primo, V. Gramlich, *Inorg. Chem.* **1996**, *35*, 4414−4419. [7c] R. W. Saalfrank, I. Bernt, E. Uller, F. Hampel, *Angew. Chem.* **1997**, *109*, 2596−2599; *Angew. Chem. Int. Ed. Engl.* **1997**, *36*, 2482−2485. [7d] O. Waldmann, R. Koch, S. Schromm, J. Schülein, P. Müller, I. Bernt, R. W. Saalfrank, R. Hampel, E. Balthes, *Inorg. Chem.* **2001**, *40*, 2986−2996. [7e] R. W. Saalfrank, I. Bernt, M. M. Chowdhry, F. Hampel, G. B. M. Vaughan, *Chem. Eur. J.* **2001**, *7*, 2765−2769.

[8] [8a] R. E. P. Winpenny, *Adv. Inorg. Chem.* **2001**, *52*, 1−111. [8b] R. E. P. Winpenny, *Dalton Trans.* **2002**, 1−10.

[9] [9a] E. K. Brechin, J. Yoo, M. Nakano, J. C. Huffmann, D. N. Hendrickson, G. Christou, *Chem. Commun.* **1999**, 783−784. [9b] C. Boskovic, W. Wernsdorfer, K. Folting, J. C. Huffmann, D. N. Hendrickson, G. Christou, *Inorg. Chem.* **2002**, *41*, 5107−5118.

[10] [10a] B. P. Gaber, V. Miskowski, T. G. Spiro, *J. Am. Chem. Soc.* **1974**, *96*, 6868−6873. [10b] D. C.-T. Siu, A. M. Orville, J. D. Lipscomb, D. H. Ohlendorf, L. Que Jr., *Biochemistry* **1992**, *31*, 10443−10448. [10c] A. Mukherjee, M. McGlashen, T. G. Spiro, *J. Phys. Chem.* **1995**, *99*, 4912−4917.

[11] **1**: Triclinic, $P\bar{1}$, a = 13.204(2), b = 9.924(2), c = 30.102(2) Å, α = 90.0°, β = 112.098(2)°, γ = 90.0°, V = 3654.4(3) Å^3, T = 123(2) K, Z = 2. The dinuclear complex (65% of total scattering power) obeys monoclinic symmetry (*P*2/*c*) with regards to the given cell constants. The Na^+/MeOH/H_2O network (35% of total scattering power) forces a symmetry reduction (*P*2/*c* → $P\bar{1}$; *translationengleiche* symmetry reduction of index *t*2). Although the dinuclear complex refines well in $P\bar{1}$ in combination with the twin law

$$\begin{pmatrix} \bar{1} & 0 & 0 \\ 0 & 1 & 0 \\ 0 & 0 & \bar{1} \end{pmatrix},$$

the Na^+/MeOH/H_2O network still exhibits disorder which precludes complete refinement.

[12] [12a] D. L. Jameson, C.-J. Xie, D. N. Hendrickson, J. A. Potenza, H. J. Schugar, *J. Am. Chem. Soc.* **1987**, *109*, 740−746. [12b] S. Drueke, K. Wieghardt, B. Nuber, J. Weiss, *Inorg. Chem.* **1989**, *28*, 1414−1417. [12c] N. Arulsamy, D. J. Hodgson, J. Glerup, *Inorg. Chim. Acta* **1993**, *209*, 61−69. [12d] N. Arulsamy, P. A. Goodson, D. J. Hodgson, J. Glerup, K. Michelsen, *Inorg. Chim. Acta* **1994**, *216*, 21−29. [12e] J. Glerup, K. Michelsen, N. Arulsamy, D. J. Hodgson, *Inorg. Chim. Acta* **1998**, *274*, 155−166. [12f] R. E. Norman, R. C. Holz, S. Menage, C. J. O'Connor, J. H. Zhang, L. Que Jr., *Inorg. Chem.* **1990**, *29*, 4629−4637. [12g] A. Nishida, A. Goto, T. Akamatsu, S. Ohba, T. Fujita, T. Toki, S. Okada, *Chem. Lett.* **1994**, 641−644. [12h] R. Hazell, K. B. Jensen, C. J. McKenzie, H. Toftlund, *J. Chem. Soc., Dalton Trans.* **1995**, 707−717.

[13] N. Kitajima, S. Hikichi, M. Tanaka, Y. Moro-oka, *J. Am. Chem. Soc.* **1993**, *115*, 5496−5508.

[14] [14a] A. L. Feig, S. J. Lippard, *Chem. Rev.* **1994**, *94*, 759−805. [14b] L. Que Jr., Y. Dong, *Acc. Chem. Res.* **1996**, *29*, 190−196. [14c] L. Que Jr., *J. Chem. Soc., Dalton Trans.* **1997**, 3933−3940.

[15] [15a] B. F. Anderson, D. A. Buckingham, G. B. Robertson, J. Webb, K. S. Murray, P. E. Clark, *Nature* **1976**, *262*, 722−724. [15b] G. M. Grant, M. J. Knapp, J. C. Huffman, D. N. Hendrickson, G. Christou, *Chem. Commun.* **1998**, 1753−1754. [15c] G. M. Grant, M. J. Knapp, W. E. Streib, J. C. Huffman, D. N. Hendrickson, G. Christou, *Inorg. Chem.* **1998**, *37*, 6065−6070. [15d] A. Horn Jr., A. Neves, I. Vencato, V. Drago, C. Zucco, R. Werner, W. Haase, *J. Braz. Chem. Soc.* **2000**, *11*, 7−10. [15e] M. Scarpellini, A. Neves, A. J. Bortoluzzi, I. Vencato, V. Drago, W. Ortiz, C. Zucco, *J. Chem. Soc., Dalton Trans.* **2001**, 2616−2623.

[16] The JULIUS routine was used for spin Hamiltonian simulations of the data (C. Krebs, E. Bill, F. Birkelbach, V. Staemmler, unpublished results). For the calculation of the magnetic susceptibiliy of the paramagnetic impurity JULIUS uses the molar mass of the main component. Thus the obtained value of 4.1% for the paramagnetic impurity is far overestimated if a mononuclear Fe^{III} species is anticipated.

[17] [17a] E. N. Baker, S. V. Rumball, B. F. Anderson, *Trends Biochem. Sci.* **1987**, *12*, 350−354. [17b] E. N. Baker, *Adv. Inorg. Chem.* **1994**, *41*, 389−463.

[18] SMART, Bruker AXS, **2000**.

[19] SHELXS-97, G. M. Sheldrick, *Acta Crystallogr., Sect. A* **1990**, *46*, 467−473.

[20] SHELXL-97, G. M. Sheldrick, University of Göttingen, **1997**.

Received August 18, 2003
Early View Article
Published Online April 7, 2004

 © 2004 Wiley-VCH Verlag GmbH & Co. KGaA, Weinheim

First ICN Adduct with a Selenium Donor (R = Se): Is It an Ionic $[RSeCN]^+I^-$ or a "T-Shaped" R(I)SeCN Hypervalent Compound?

M. Carla Aragoni,[a] Massimiliano Arca,[a] Francesco Demartin,[b] Francesco A. Devillanova,*[a] Alessandra Garau,[a] Patrizio Grimaldi,[c] Francesco Isaia,[a] Francesco Lelj,[c] Vito Lippolis,[a] and Gaetano Verani[a]

Keywords: Density functional calculations / Donor-acceptor systems / ICN / Hypervalent compounds / Se ligands

The reaction between 1,3-dimethyl-4-imidazoline-2-selone (**2**) and ICN gave the adduct **2**·ICN, whose crystal structure features dimers made up of two $[\mathbf{2}\cdot CN]^+$ and two I^- which strongly interact. Hybrid DFT calculations on the adduct **2**·ICN, on the cation $[\mathbf{2}\cdot CN]^+$, and on the dimer $(\mathbf{2}\cdot ICN)_2$ account for a partially hypervalent selenium atom in **2**·ICN and for the observed structural features.

(© Wiley-VCH Verlag GmbH & Co. KGaA, 69451 Weinheim, Germany, 2004)

Introduction

Hypervalent chalcogen compounds featuring a linear X−E−X moiety (X = Cl, Br, I; E = S, Se) can be considered to derive from the oxidative addition of an X_2 molecule to a donor molecule containing the chalcogen atom. With donors containing thio- or seleno-carbonyl groups, the "T-shaped" nature of the corresponding adducts is well explained by the VSEPR model,[1] according to which the geometry at the chalcogen atom is a pseudo-trigonal bipyramid (tbp) with the halogens occupying the apical positions. These compounds are commonly reported as 10−E−3 systems,[2] indicating that the chalcogen atom E is formally associated with five electron pairs (10 electrons), only 3 of which are bond pairs. As with a tri-halide, the chemical bond in the linear X−E−X fragment has also been described as a three-center−four-electron (3c-4e) system, whose simplified MO diagram can be built by combining the p_z atomic orbitals of the central chalcogen and those of the two terminal halogen atoms.[3] Four electrons occupy only the bonding and non-bonding orbitals, thus determining a total bond order of 1 (0.5 for each E−X bond). This description agrees with the qualitative observation[4,5] that on increasing the electronegativity difference between the halogen and the chalcogen, hypervalent chalcogen adducts are formed more easily than charge-transfer (CT) adducts bearing the E−X−X linear group (10−X−2 hypervalent halogen compounds).[2] Indeed, the number of hypervalent sulfur and selenium compounds structurally characterized decreases on passing from chlorine to iodine, and hypervalent sulfur compounds with di-iodine are unknown.[6] In addition, the first hypervalent selenium compounds with iodine were only reported in 1994,[7,8] and the first hypervalent sulfur compound with bromine appeared in 1977,[9] and the second in 1999.[10]

For the oxidative addition of inter-halogens (ICl, IBr), only two examples of "T-shaped" adducts have been reported, i.e. **1**·IBr,[9] which is very unstable, and **3**·2IBr.[11] In addition, **1**·BrCN (characterized by X-ray diffraction)[9] and **1**·ClCN (characterized only by IR spectroscopy)[9] are the only reported examples of S- or Se-adducts with pseudo-halogens (ICN, BrCN, and ClCN). Therefore, the synthesis of new such adducts is an important step towards understanding not only the nature of the chemical bond in these systems, but also the possible role of hypervalent chalcogen compounds as intermediates in the formation of the many classes of compounds obtained by reacting chalcogen donors with halogens and inter-halogens.[6,12,13]

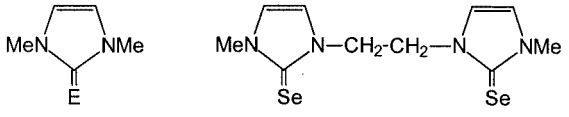

E = S (**1**)
E = Se (**2**)

3

[a] Dipartimento di Chimica Inorganica ed Analitica, Università di Cagliari, Cittadella Universitaria,
09042 Monserrato-Cagliari, Italy
Fax: (internat.) + 39-070-6754456
E-mail:devilla@unica.it
[b] Dipartimento di Chimica Strutturale e Stereochimica Inorganica e Centro CNR, Università di Milano,
Via G. Venezian 21, 20133 Milano, Italy
[c] LAMI Dipartimento di Chimica and LASCAMM-INSTM Sezione Basilicata, Università della Basilicata,
Via N. Sauro, 85100 Potenza, Italy

This paper contributes to this chemistry by reporting both the crystal structure of the first selenium adduct with the pseudo-halogen ICN and the DFT calculations that have been of great help in ascertaining the nature of the chemical bond in the ISeCN fragment.

Results and Discussion

Synthesis and Structural Characterization: The reaction of **2** with one equivalent of ICN in CH_2Cl_2 gave well-shaped crystals by slow evaporation of the solvent. X-Ray diffraction analysis showed that the asymmetric unit is formed by the adduct 2·ICN bearing the I···Se−CN linear group [I···Se−C(8) 174.8(2)°] almost perpendicular to the imidazolidine ring, with a very long Se···I distance [3.300(1) Å] and a short Se−CN bond [1.885(5) Å]. Two 2·ICN units are arranged about a crystallographic inversion center to form dimers via Se···I contacts that are only 0.117 Å longer than the Se···I distance within the asymmetric unit (Figure 1), so that the two selenium and two iodine atoms are located on the opposite corners of an almost regular rhombus. The very long Se···I distances suggest the isolated compound has an ionic nature.

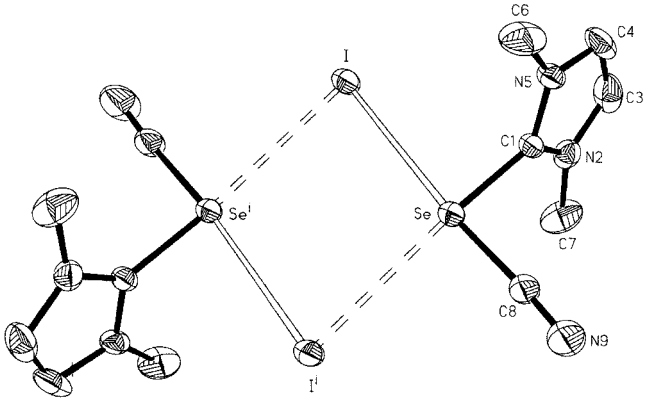

Figure 1. Molecular structure and atom labelling scheme for the adduct **2**·ICN; selected bond lengths and angles: Se···I 3.300(1), Se···I^i 3.417(1), C(1)−Se 1.913(4), C(8)−Se 1.885(5)Å, C(1)−Se−C(8) 93.2(2), I···Se−C(8) 174.8(2), Se···I···Se^i 80.24(1), I···Se···I^i 99.76(1), N(2)−C(1)−Se−C(8) 83.2(4)°; i = $-x$, $1-y$, $1-z$

The structural features of **2**·ICN can usefully be compared with those of **1**·BrCN, the only other reported adduct between an S- or Se-donor and a pseudo-halogen.[9] According to the very long S···Br bond length, the authors described **1**·BrCN as an ion pair [**1**·CN]$^+$ Br$^-$. However, a dimeric arrangement similar to that observed for **2**·ICN can also be envisaged for **1**·BrCN, with two significantly different S···Br distances (3.270 and 3.587 Å). The S···Br involving the Br atom *trans* to the cyano group is the longest, contrary to what is observed in the dimer (**2**·ICN)$_2$. Intriguingly, the S···Br and Se···I distances *trans* to the cyano group in the two compounds are very similar, although the involved atoms are S and Br in **1**·BrCN and their heavier congeners, Se and I, in **2**·ICN. Thus, **2**·ICN might not be a pure ionic compound, and a partial selenium−iodine covalent character should be considered to fully explain the compound's structural features.

DFT Calculations: A partial covalent character for the Se···I bond in **2**·ICN would agree with a description for it as a strongly polarized hypervalent-selenium compound. Actually, the linearity of the I···Se−CN group supports this view, although this is not direct evidence for hypervalency of the selenium atom. Recently, we reported the crystal structure of **3**·2IBr, which was the first example of a hypervalent selenium compound with IBr. In **3**·2IBr, the two I−Se···Br systems were strongly polarized, both Se···Br bonds having, therefore, a partial ionic character.[11]

DFT calculations have greatly enabled deeper insight into the nature of the chemical bond in some CT and tbp adducts between halogens or inter-halogens and some S- or Se-donors, including **2**.[11,12] In particular, for **2**·I_2,[12] **2**·Br_2,[12] and **2**·IBr,[11] the calculated geometries of the organic frameworks are in very good agreement with the experimental data for **2**·I_2,[7] **3**·2I_2,[7] **3**·2Br_2,[14] and **3**·2IBr,[11] though in general the Se−X bond lengths were slightly overestimated. Hence, we performed calculations at the same level of theory on **2**·ICN (both in the tbp and in the CT type arrangements), on the dimer (**2**·ICN)$_2$ and on the [**2**·CN]$^+$ cation. Interestingly, the optimized geometry for the tbp **2**·ICN adduct agrees fairly well with the structural data (Figure 2) with the exception of the Se···I length, which is underestimated (3.233 Å) as compared with the experimental value [3.300(1) Å]. The structural features of the organic framework for the optimized geometry of (**2**·ICN)$_2$ are very similar to those of the calculated geometry of **2**·ICN (Figure 2). The Se···I distances are calculated to be slightly dissimilar (3.448 and 3.422 Å, respectively) as ex-

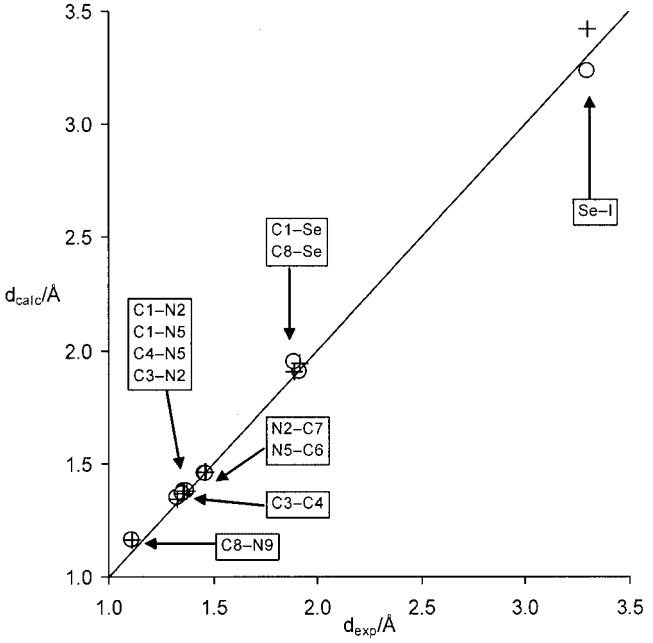

Figure 2. Correlation between the experimental (d_{exp}) bond lengths for **2**·ICN and the optimized (d_{calc}) ones for **2**·ICN (O) and (**2**·ICN)$_2$ (+)

 © 2004 Wiley-VCH Verlag GmbH & Co. KGaA, Weinheim

perimentally found, but overestimated with respect to the experimental data [Se···I^{i}, 3.417(1); Se···I, 3.300(1) Å, Figure 1].

Previously,[11,12] we proved by DFT calculations that the complete removal of one of the two halogen atoms as a halide from an X−Se−X (X = I, Br) hypervalent system (the two extremes being the covalent and completely ionic bonds) causes the carbon−selenium−halogen angle to open from lower than 90° towards values closer that expected for a tetrahedral environment around the chalcogen atom. For example, the calculated C−Se−X (X = I, Br) angles pass from 84.3° for the "T-shaped" **2**·Br_2 adduct to 97.2° for the cation [**2**·Br]$^+$, and from 85.4° for the analogous **2**·I_2 adduct to 98.3° for [**2**·I]$^+$.[11,12] The widening of the C−Se−X angle represents the most significant change observed in the optimized structural parameters upon lengthening of one Se−X bond of the hypervalent system towards the formation of the [>C−Se−X]$^+$ cation; all the other structural features are only slightly changed. In the present case, the calculated C−Se−CN angle shows a very small variation (91.8° in **2**·ICN; 94.7° in [**2**·CN]$^+$; Table 1). This small variation is justified as the optimized geometry for the "T-shaped" **2**·ICN adduct already shows a very strong polarization of the Se···I bond determined by the very different electronic effects of the I and CN groups bonded to the Se atom. This is also indicated by the calculated NBO[15,16] charges on the iodine atom, which are −0.665 and −0.718e for **2**·ICN and (**2**·ICN)$_2$ respectively. Therefore, the increase in the negative charge on the iodine atom up to the limit case of −1 in [**2**·CN]$^+$ does not change significantly the structural features of the organic framework including the C−Se−CN angle. Interestingly, the experimental C−Se−CN angle [93.2(2)°] is exactly in between those calculated for the tbp **2**·ICN adduct and the cation [**2**·CN]$^+$. A similar situation is observed for **1**·BrCN:[9] the experimental C−S−CN angle of 96.3° is slightly lower than the 98.5° calculated for the cation [**1**·CN]$^+$ (footnote [c] in Table 1) and very close to the 96.5° calculated for the tbp **1**·BrCN adduct.

In any event, the greater the difference in the electron-withdrawing features of the two groups interacting with the chalcogen atom, the lower is the covalency of the system X−Se−Y, which tends to become more polarized and ionic in nature.

In fact, the C−Se−I angle calculated for the tbp **2**·IBr adduct and the cation [**2**·I]$^+$ are 86.5 and 98.3°, respectively;[11] the same angles observed for the two I−Se−Br units in the crystal structure of **3**·2IBr are 95.6(3)° and 90.6(3)°, in agreement with the different degree of covalency and hypervalency in the two systems.[11]

Partial hypervalency of the selenium atom in **2**·ICN is also supported by analysis of the LUMO and the LUMO+1 calculated for both cations [**1**·CN]$^+$ and [**2**·CN]$^+$. In fact, they are σ* and π* in nature with respect to the Se−C−N vector and very close in energy and symmetry-allowed to accept charge density either from donor halides *trans* to the cyano group (LUMO) or *trans* to the imidazoline ring (LUMO+1) (Figure 3). Thus, the formation of (**2**·ICN)$_2$ could be described as a charge-transfer interaction between the HOMOs of two I$^-$ and the LUMO and LUMO+1 of two cations [**2**·CN]$^+$. The closeness in energy of LUMO and LUMO+1 tends to make the interactions in the two directions equally likely, and solid-state

Table 1. Selected bond lengths, angles, and NBO charges for the optimized geometries of "T-shaped" adducts between **2** and XY (X = Y = Cl, Br, I; X = I and Y = Cl, Br, CN), calculated at the DFT level

X Y	Cl[a] Cl	Br[b] Br	I[a] I	I[a] Br	I[a] Cl	I[a][c] CN	I[a,c] CN dimer
d(C−Se)/Å	1.894	1.870	1.890	1.891	1.891	1.905	1.910
d(Se−X)/Å	2.588	2.602	2.983	2.964	2.953	3.233	3.422
d(Se−Y)/Å	2.588	2.602	2.983	2.794	2.619	1.952	1.945
X−Se−C/deg	84.8	84.3	85.4	86.5	87.2	71.8	71.2
Y−Se−C/deg	84.8	84.3	85.4	83.8	82.8	91.8	90.7
Q_X/e	−0.488	−0.449	−0.393	−0.387	−0.392	−0.665	−0.718
Q_Y/e	−0.488	−0.449	−0.393	−0.447	−0.486	−0.378	−0.342
Q_{Se}/e	0.403	0.354	0.212	0.259	0.305	0.472	0.488
Q_C/e	0.280	0.220	0.271	0.275	0.276	0.271	0.280

[a] LANL2DZ basis set for halogen atoms. [b] 6−31 g** Basis set for halogen atoms. [c] Values for the [**2**·CN]$^+$ cation: *d*(C−Se) 1.918, *d*(Se−CN) 1.861 Å, ∠C−Se−CN 94.7°, Q_{Se} +0.532, Q_{CN} −0.251 e; for [**1**·CN]$^+$, *d*(C−S) 1.768, *d*(S−CN) 1.712 Å, ∠C−S−CN 98.5°, Q_S +0.366, Q_{CN} −0.177 e.

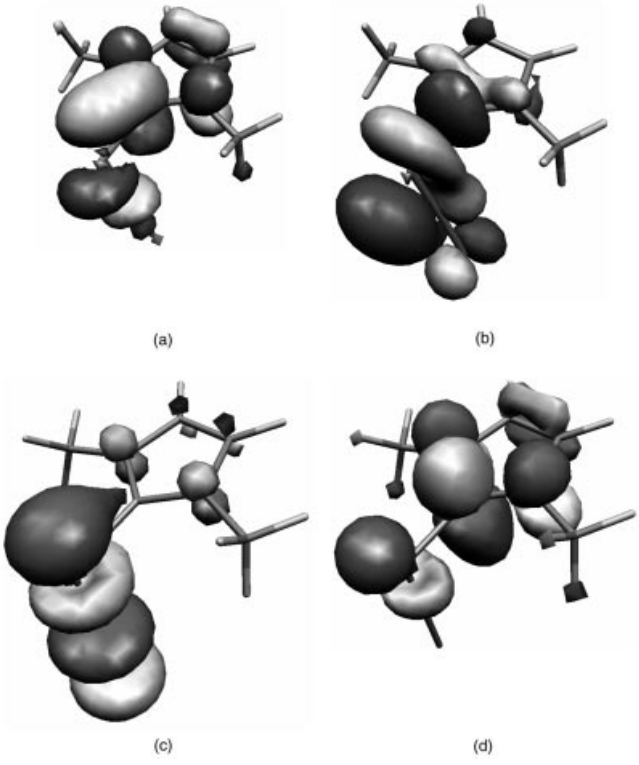

Figure 3. DFT LUMOs and (LUMO+1)s calculated for [**2**·CN]$^+$ (a and b, respectively) and [**2**·I]$^+$ (c and d, respectively); the calculated KS-orbital energies are −0.2222 (a), −0.1969 (b), −0.2902 (c), and −0.1853 (d) hartree; the corresponding molecular orbitals calculated for [**2**·Br]$^+$, [**1**·CN]$^+$, and [**1**·I]$^+$ show similar compositions

 © 2004 Wiley-VCH Verlag GmbH & Co. KGaA, Weinheim

effects might presumably be crucial in determining the balance between the entities of the two interactions. NBO population analysis shows that the two generated hybrid atomic orbitals of I^- (1.89 and 1.83e) have a direction suitable to put electron charge on LUMO and LUMO+1. The NBO population suggests that the amount of electron transfer is very low, but it should be important to determine the geometrical arrangement of the two **2**·ICN units in $(\mathbf{2}\cdot ICN)_2$. Conversely, for the hypervalent adducts with halogens and interhalogens, analysis of the LUMOs and (LUMO+1)s of the cations $[\mathbf{2}\cdot X]^+$ (X = I, Br; Figure 3) shows that both orbitals are σ* in nature with respect to the Se−X vector and considerably separated in energy. Therefore, the donor−acceptor interaction between the lone pair of a halide Y^- (Y = I, Br) and the LUMO of the cation $[\mathbf{2}\cdot X]^+$ is the only one possible, giving a linear X−Se−Y moiety. This explains why, in hypervalent-chalcogen compounds with halogens,[6,12] the chalcogen−halogen bonds within the hypervalent systems are always considerably shorter than the chalcogen···halogen intermolecular contacts between adjacent adduct molecules. Thus, the topological analysis of the LUMO and LUMO+1 and the charge distribution seem to give both a decisive proof that the description of **2**·ICN as a polarized hypervalent-selenium compound is realistic and a good explanation for the different arrangements of the adduct units found in **1**·BrCN and **2**·ICN with respect to those observed for hypervalent-chalcogen systems with halogens and interhalogens.

Notably, a partial hypervalent nature of the Se atom in **2**·ICN does not imply a description of the Se···I bond as covalent, since DFT calculations indicate that this bond is strongly polarized and therefore appreciably ionic. However, comparison of the Se···I distances calculated both for **2**·ICN and $(\mathbf{2}\cdot ICN)_2$ with those of hypervalent adducts of **2**

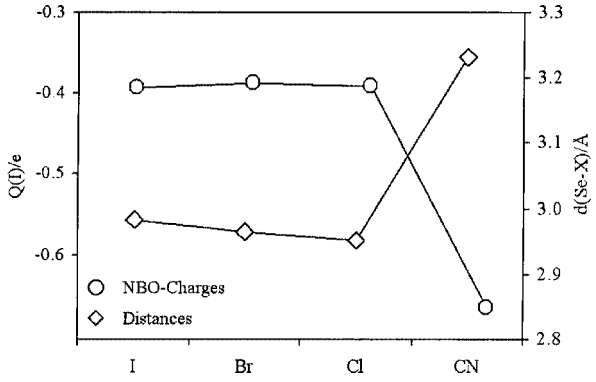

Figure 4. Trends of Se−I bond lengths and calculated NBO charge on the iodine atom for the I−Se−X system in **2**·IX T-shaped adducts (X = I, Br, Cl, CN)

containing the Se−I bond (Table 1) and the trend of the calculated NBO[15,16] charge on the iodine atom of the I−Se−X system on passing from X = I to Br, Cl, and CN (Figure 4; Table 1) shows that **2**·ICN and $(\mathbf{2}\cdot ICN)_2$ are different from the other systems. The considerably long Se−I distances and the strongly negative charge on iodine [−0.665 and −0.718e in **2**·ICN and $(\mathbf{2}\cdot ICN)_2$ respectively][16] agree with the strongly polarized character of the Se···I bond in the present compound.

We have also examined the relative energy of $(\mathbf{2}\cdot ICN)_2$ with respect to **2**·ICN and the starting reagents **2** and ICN. DFT-calculated energies show that, neglecting solvation effects and BSSE corrections, the **2**·ICN adducts of both the CT and the T-shaped types are unstable by 1.95 and 4.39 kcal mol^{-1}, respectively, compared with the free components **2** and ICN (Figure 5). Though slightly unstable with respect to **2** and ICN, $(\mathbf{2}\cdot ICN)_2$ is more stable than the CT and tbp **2**·ICN adducts by 1.20 and 3.64 kcal mol^{-1}, respectively. Contrarily, in all the hypervalent compounds of **2**

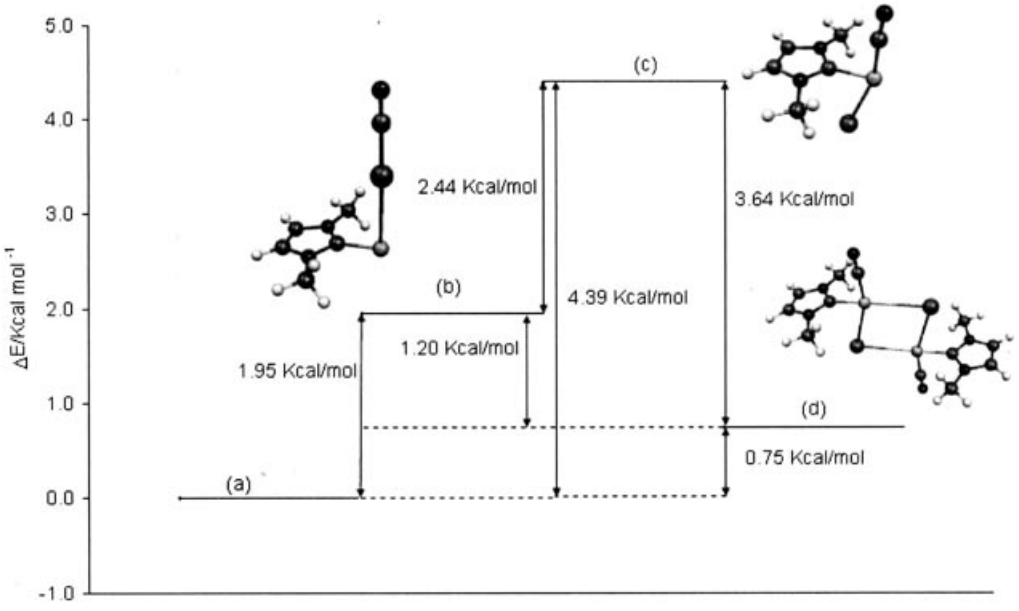

Figure 5. Relative DFT energies between CT and tbp adducts of **2** and ICN with respect to the free components: (a) ΔE[**2**+ICN]; (b) ΔE[**2**·ICN (CT)]; (c) ΔE[**2**·ICN (tbp)]; (d) 1/2 ΔE[$(\mathbf{2}\cdot ICN)_2$]

 © 2004 Wiley-VCH Verlag GmbH & Co. KGaA, Weinheim

with halogens and inter-halogens, the T-shaped adduct formation always occurs with a stabilization energy >10.25 kcal mol^{-1}, which is the value calculated for **2**·I_2 (see values for all considered systems in the Theoretical Calculations section).

In this respect, we note that although very small changes are calculated in the I−Se−X system on passing from X = I to Br, and Cl, hypervalent selenium compounds with ICl are unknown. Thus, it should also be possible to prepare S- and Se-hypervalent tbp adducts with ICl, which are still unknown, despite numerous attempts to synthesize them. In fact, the Se-hypervalent system with ICl is expected to be very similar to that observed with IBr, as shown in Figure 4 by the regular trend and small variations in calculated Se−I distances and NBO charges on the iodine atom of I−Se−X systems (X = Cl, Br, I). This is strongly supported by the stabilization energy of the tbp **2**·ICl adduct, which is calculated as 16.70 kcal mol^{-1} with respect to the starting reagents **2** and ICl.

In conclusion, we report the first adduct between a selenium donor and ICN characterized by X-ray diffraction analysis. DFT calculations account for the strong polarity of the Se−I bond with the Se atom in a partial hypervalent state. **2**·ICN could also be described as the product of a donor−acceptor interaction between I^- and the selenium atom of the organic cation [**2**·CN]$^+$. DFT calculations clarify the ability of the organic cation [**2**·CN]$^+$ to interact with I^- donors in the two directions predetermined by the compositions of LUMO and LUMO+1, thus explaining the dimeric nature of **2**·ICN. The two different views lead to exactly the same final product: in the first case we consider the selenium partially hypervalent and a strong polarization of the Se···I bond (charge separation of 0.665e between the two fragments in **2**·ICN); in the second case, the ions approach until 0.335 electrons are reversed from I^- into the LUMO of the cation.

Experimental Section

Materials and Methods: All solvents and reagents were purchased from Aldrich and used as received. Elemental analysis and FT-Raman spectra were carried out as described previously.[12]

Synthesis of 2·ICN: Compound **2**·ICN was obtained as brown crystals (60% yield) by slow evaporation in air at room temperature of a mixture of 1,3-dimethyl-4-imidazoline-2-selone (**2**) (50 mg, 0.286 mmol) and ICN in a 1:1 molar ratio in CH_2Cl_2. $C_6H_8IN_3Se$: calcd. C 21.97, H 2.46, N 12.81; found C 22.10, H 2.56, N 12.98. FT-IR (2500−500 cm^{-1}): $\tilde{\nu}$ = 2078 w, 1561 m, 1493 ms, 1417 mw, 1391 w, 1338 w, 1240 vs, 1159 m, 1091 m, 1023 m, 858 m, 771 s, 760 vs, 734 s, 649 s, 612 w. FT-Raman (500−100 cm^{-1}; relative intensities in parentheses related to the highest peak taken equal to 10): $\tilde{\nu}$ = 278(0.9), 258(2.6), 221(10), 195(8), 143(0.3).

X-ray Crystal Structure Determination of 2·ICN: 1834 diffraction data were collected on a Nonius CAD-4 diffractometer with graphite-monochromated Mo-K_α (λ = 0.71073 Å) radiation. The structure was solved by Patterson and Fourier methods and refined on F^2 using SHELXL-97.[17] Non-hydrogen atoms were refined with anisotropic thermal parameters. Hydrogen atoms were experimentally observed and allowed to ride on the pertinent atoms. $C_6H_8IN_3Se$, M = 328.01, triclinic, space group $P\bar{1}$ (No. 2), a = 6.946(1), b = 8.567(2), c = 8.907(2) Å; α = 98.54(1), β = 95.52(1), γ = 91.18(1)°; U = 521.4(1) Å^3, Z = 2, $d_{calcd.}$ = 2.089 g·cm^{-3}, T = 293(2) K, μ(Mo-K_α) = 6.511 mm^{-1}, wR_2 = 0.077, R = 0.030 for 1593 observed reflections [$I > 2\sigma(I)$]. CCDC-205962 contains the supplementary crystallographic data for this paper. These data can be obtained free of charge at www.ccdc.cam.ac.uk/conts/retrieving.html [or from the Cambridge Crystallographic Data Centre, 12 Union Road, Cambridge CB2 1EZ, UK; Fax: (internat.) + 44-1223/336-033; E-mail: deposit@ccdc.cam.ac.uk].

Theoretical Calculations: Using the commercially available suite of programs in the Gaussian 98 package,[18] quantum-mechanical DFT-calculations on **2**, **2**·Br_2, **2**·I_2, **2**·IBr, [**2**·Br]$^+$, and [**2**·I]$^+$ have been reported.[11,12] For the present work, DFT-calculations were carried out on Cl_2, Br_2, I_2, IBr, ICl, ICN, **1**·BrCN, **2**·Cl_2, **2**·ICl, **2**·ICN (both CT and T-shaped), (**2**·ICN)$_2$, and [**2**·CN]$^+$ at the same level of theory as the previous calculations, i.e. using the hybrid Becke3LYP functional,[19] the Schäfer, Horn and Ahlrichs pVDZ[20] basis sets for C, H, N, O, S, and Se, and the LANL2DZ basis sets, together with effective core potentials (ECP)[21] for halogen atoms. For **2**·Br_2, the 6−31 g** basis set was used as described previously.[11] For comparison, the calculations on [**2**·CN]$^+$ were extended to the sulfured analogue [**1**·CN]$^+$. Numerical integration was performed using the FineGrid option, which indicates that a total of 7500 points are used for each atom, and the optimized structure was verified by normal-mode harmonic frequency analysis obtained using the second derivatives of the DFT energy, and computed by differentiation of the DFT energy gradients. For all compounds, zero-point energy corrections were applied to calculate the relative total energies. NBO calculations[15] were performed for each molecule using the converged density matrix corresponding to the equilibrium geometries. For all calculations, no basis set superposition error (BSSE) correction was applied. The results of the calculations were analyzed with the MOLEKEL 4.3[22] and Molden 3.9[23] programs. The ZPE corrected total energies of the selenium hypervalent adducts compared with the free components are: ΔE(**2**·Cl_2) = −33.01; ΔE(**2**·Br_2) = −28.95; ΔE(**2**·I_2) = −10.25; ΔE (**2**·ICl) = −16.70; ΔE (**2**·IBr) = −13.89; ΔE (**2**·ICN)$_{CT}$ = +1.95; ΔE (**2**·ICN)$_{tbp}$ = +4.39; 1/2ΔE[(**2**·ICN)$_2$] = +0.75 kcal·mol^{-1}. Calculations were performed on a SGI Origin 3800 with 128 RISC 14000 processor elements running at 500 MHz equipped with 128 Gb of DRAM.

Further Information: Optimized geometries in the form of Cartesian orthogonal coordinates, frontier orbital composition, NBO charges, and harmonic frequencies for each mentioned compound are available from the authors on request.

Acknowledgments

CINECA (Consorzio Interuniversitario per il Calcolo Automatico dell′Italia Nord Orientale) is gratefully acknowledged for computational facilities.

[1] R. J. Gillespie, I. Hargittai, *The VSEPR Model of Molecular Geometry*, Allyn and Bacon, **1991**, Boston, Massachusetts, USA.
[2] C. W. Perkins, J. C. Martin, A. J. Arduengo, W. Law, A. Alegria, J. K. Kochi, *J. Am. Chem. Soc.* **1980**, *102*, 7753−7759.
[3] Ky Akiba, *Chemistry of Hypervalent Compounds*, Wiley-VCH, **1999**, New York, USA.
[4] N. C. Baenziger, R. E. Buckles, R. J. Maner, T. D. Simpson, *J. Am. Chem. Soc.* **1969**, *91*, 5749−5755.

 © 2004 Wiley-VCH Verlag GmbH & Co. KGaA, Weinheim

[5] W. Nakanishi, S. Hayashi, H. Tukada, H. Iwamura, *J. Phys. Org. Chem.* **1990**, *3*, 358−368.
[6] M. C. Aragoni, M. Arca, F. Demartin, F. A. Devillanova, A. Garau, F. Isaia, V. Lippolis, G. Verani, *Trends, Inorg. Chem.* **1999**, *6*, 1−18.
[7] F. Bigoli, A. M. Pellinghelli, P. Deplano, F. A. Devillanova, V. Lippolis, M. L. Mercuri, E. F. Trogu, *Gazz. Chim. It.* **1994**, *124*, 445−454.
[8] N. Kuhn, T. Kratz, G. Henkel, *Chem. Ber.* **1994**, *127*, 849−851.
[9] A. J. Arduengo, E. M. Burgess, *J. Am. Chem. Soc.* **1977**, *99*, 2376−2378.
[10] N. Bricklebank, P. J. Skabara, D. E. Hibbs, M. B. Hursthouse, K. M. Abdul Malik, *J. Chem. Soc., Dalton Trans.* **1999**, 3007−3014.
[11] M. C. Aragoni, M. Arca, A. J. Blake, F. A. Devillanova, W.-W. du Mont, A. Garau, F. Isaia, V. Lippolis, G. Verani, C. Wilson, *Angew. Chem. Int. Ed.* **2001**, *40*, 4229−4232.
[12] M. C. Aragoni, M. Arca, F. Demartin, F. A. Devillanova, A. Garau, F. Isaia, F. Lelj, V. Lippolis, G. Verani, *Chem. Eur. J.* **2001**, *7*, 3122−3133 and references cited therein.
[13] M. D. Rudd, S. V. Lindeman, S. Husebye, *Acta Chem. Scand.* **1997**, *51*, 689−708.
[14] F. Bigoli, P. Deplano, F. A. Devillanova, V. Lippolis, M. L. Mercuri, M. A. Pellinghelli, E. F. Trogu, *Eur. J. Inorg. Chem.* **1998**, 137.
[15] A. E. Reed, L. A. Curtiss, F. Weinhold, *Chem. Rev.* **1988**, *88*, 899−926.
[16] NBO charges on [**2**·ICN] and [**2**·ICN]$_2$: C1 0.271, 0.280; N2/N3 −0.394, −0.394; C3/C4 −0.016, −0.019; Se 0.472, 0.488; I −0.665, −0.718; C8 −0.027, 0.005; N9 −0.351, −0.346. Mulliken charges on [**2**·ICN] and [**2**·ICN]$_2$: C1 −0.278, −0.260; N2/N3 −0.142, −0.149; C3/C4 0.086, 0.085; Se 0.771, 0.810; I −0.560, −0.624; C8 −0.442, −0.429; N9 −0.117, −0.104 e.
[17] G. M. Sheldrick, SHELXL-97, University of Göttingen, **1997**.
[18] Gaussian 98, Revision A.7, M. J. Frisch, G. W. Trucks, H. B. Schlegel, G. E. Scuseria, M. A. Robb, J. R. Cheeseman, V. G. Zakrzewski, J. A. Montgomery, Jr., R. E. Stratmann, J. C. Burant, S. Dapprich, J. M. Millam, A. D. Daniels, K. N. Kudin, M. C. Strain, O. Farkas, J. Tomasi, V. Barone, M. Cossi, R. Cammi, B. Mennucci, C. Pomelli, C. Adamo, S. Clifford, J. Ochterski, G. A. Petersson, P. Y. Ayala, Q. Cui, K. Morokuma, D. K. Malick, A. D. Rabuck, K. Raghavachari, J. B. Foresman, J. Cioslowski, J. V. Ortiz, A. G. Baboul, B. B. Stefanov, G. Liu, A. Liashenko, P. Piskorz, I. Komaromi, R. Gomperts, R. L. Martin, D. J. Fox, T. Keith, M. A. Al-Laham, C. Y. Peng, A. Nanayakkara, C. Gonzalez, M. Challacombe, P. M. W. Gill, B. Johnson, W. Chen, M. W. Wong, J. L. Andres, C. Gonzalez, M. Head-Gordon, E. S. Replogle, J. A. Pople, Gaussian, Inc., Pittsburgh PA, **1998**.
[19] [19a] A. D. Becke, *J. Chem. Phys.* **1993**, *98*, 1372−1377; *J. Chem. Phys.* **1993**, *98*, 5648−5652. [19b] C. Lee, W. Yang, R. G. Parr, *Phys. Rev. B* **1988**, *37*, 785−789.
[20] A. Schäfer, H. Horn, R. Ahlrichs, *J. Chem. Phys.* **1992**, *97*, 2571−2577.
[21] P. J. Hay, W. R. Wadt, *J. Chem. Phys.* **1985**, *82*, 270−283.
[22] MOLEKEL 4.3, P. Flükiger, H. P. Lüthi, S. Portmann, and J. Weber, Swiss Center for Scientific Computing, Manno (Switzerland), **2000**.
[23] G. Schaftenaar, J. H. Noordik, *J. Comput.-Aided Mol. Design* **2000**, *14*, 123−134.

Received October 21, 2003
Early View Article
Published Online April 7, 2004

 © 2004 Wiley-VCH Verlag GmbH & Co. KGaA, Weinheim

Ferromagnetic and Antiferromagnetic Polymeric Complexes with the Macrocyclic Ligand 1,4,7-Triazacyclononane

Peng Cheng,*[a] Shi-Ping Yan,*[a] Cheng-Zhi Xie,[a] Bin Zhao,[a] Xiao-Yan Chen,[a] Xuan-Wen Liu,[a] Chun-Hui Li,[a] Dai-Zheng Liao,[a] Zong-Hui Jiang,[a] and Geng-Lin Wang[a]

Keywords: Benzenedicarboxylic acids / Polymer chains / Magnetic properties / Copper

Three novel copper polymers, $\{[Cu_4(tacn)_4(o\text{-bda})_2](ClO_4)_4(H_2O)_2\}_n$ (**1**), $\{[Cu(tacn)(m\text{-bda})](CH_3OH)_{0.5}(H_2O)_{0.5}\}_n$ (**2**), and $\{[Cu_2(tacn)_2(p\text{-bda})](ClO_4)_2\}_n$ (**3**) (tacn = 1,4,7-triazacyclononane, bda = benzenedicarboxylic acid) have been synthesized and structurally characterized. Compound **1** belongs to the monoclinic space group *C*2, while **2** and **3** crystallize in the orthorhombic space group *Pmc*2(1) and the monoclinic space group $P2_1/n$, respectively. They are all 1D zigzag polymers, which can be considered as $Cu(tacn)^{2+}$ building units linked by isomers of benzenedicarboxylic acid. The variable-temperature (2–300 K) magnetic behavior revealed the existence of ferromagnetic interactions in **1** and **2**. The best fittings of the experimental magnetic susceptibilities gave $J = 4.0$ cm^{-1} and $g = 2.04$ for **1**, $J = 1.2$ cm^{-1}, $zJ' = -0.18$ cm^{-1} and $g = 2.07$ for **2**, whereas the exchange coupling between Cu^{II} ions in **3** is antiferromagnetic with $J = -13.1$ cm^{-1} and $g = 2.05$. The transformation of interactions between copper ions from ferromagnetic to antiferromagnetic is closely related to the variations in the isomeric benzenedicarboxylic acids.

(© Wiley-VCH Verlag GmbH & Co. KGaA, 69451 Weinheim, Germany, 2004)

Introduction

The development of metal-based coordination polymers constructed by self-assembly processes has developed at a tremendous rate recently.[1−7] This expansion, which has been driven by potential magnetic, optical, electronic and catalytic applications,[8−11] may ultimately lead to new functional materials. Although the design and construction of coordination polymers is still a great challenge due to the difficulties in selecting proper metal ions and polydentate ligands,[12] many such coordination polymers with novel topological structures and fascinating properties constructed from polycarboxylic acids have been described.[13−16] Surprisingly, however, 1D or multi-dimensional polymers with tacn (tacn = 1,4,7-triazacyclononane) as the terminal ligand have seldom been reported so far, which can probably be attributed to the fact that tacn is such a strong tridentate chelating 6-electron donor, that it can effectively prevent building blocks from forming an effectively infinite aggregation. In principle, half-sandwich complexes containing tacn can be extended into infinite structures through proper bridging ligands, but controlling the ratio of reagents and the selection of bridging ligands is critical to the formation of polymers. With this goal in mind, we have investigated the bridging bda (bda = benzenedicarboxylic acid) ligands and employed the strategy of an equal stoichiometry of reagents. We report herein, the preparation of three novel copper polymers, $\{[Cu_4(tacn)_4(o\text{-bda})_2](ClO_4)_4(H_2O)_2\}_n$ (**1**), $\{[Cu(tacn)(m\text{-bda})](CH_3OH)_{0.5}(H_2O)_{0.5}\}_n$ (**2**), and $\{[Cu_2(tacn)_2(p\text{-bda})](ClO_4)_2\}_n$ (**3**).

In order to design and synthesize complexes with expected magnetic behavior, it is extremely important to probe the essential magneto-structural relationship. Hoffmann et al.[17] and Kahn et al.[18] have described investigations of the effects on magnetic exchange interactions of the metal−ligand−metal bridge angle, the bridging atom electronegativity, and the geometrical environment around the central metal ion. In contrast, and to the best of our knowledge, systematic studies of the influence of various isomers of some dicarboxylic acids on magnetic properties have not been reported to date. In this study we have used three isomers of bda as bridging ligands to obtain complexes **1**−**3**. Furthermore, we have investigated the relationship between their structures and magnetic properties.

Results and Discussion

X-ray crystal structure analyses revealed 1D zigzag polymeric structures for **1**, **2** and **3**. The ORTEP diagrams are shown in Figures 1−3, respectively. Notably, in these polymers, the copper(II) ions are all five-coordinate: three nitrogen atoms of tacn and two oxygen atoms of the bda ligand

[a] Department of Chemistry, Nankai University
Tianjin 300071, P. R. China
Fax: (internat.) + 86-22-23502458
E-mail: pcheng@nankai.edu.cn

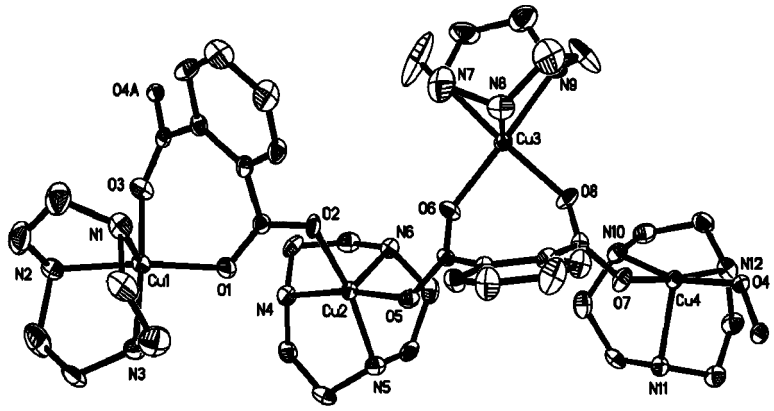

Figure 1. ORTEP diagram of **1**; H atoms, perchloric acid anions and solvent molecules are omitted for clarity

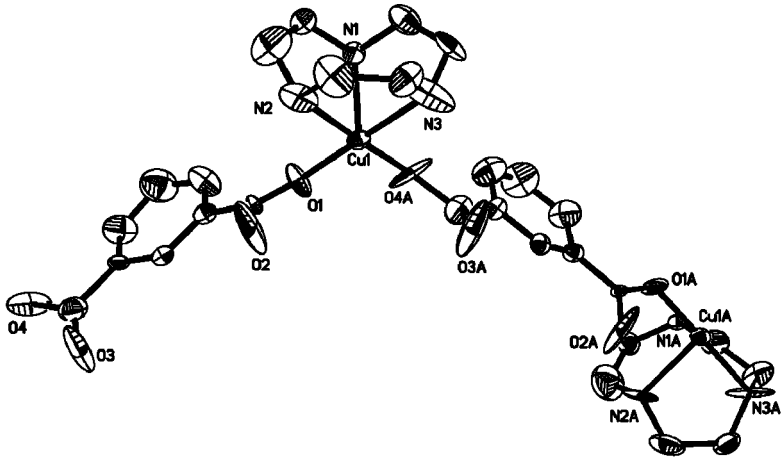

Figure 2. ORTEP diagram of **2**; H atoms and solvent molecules are omitted for clarity

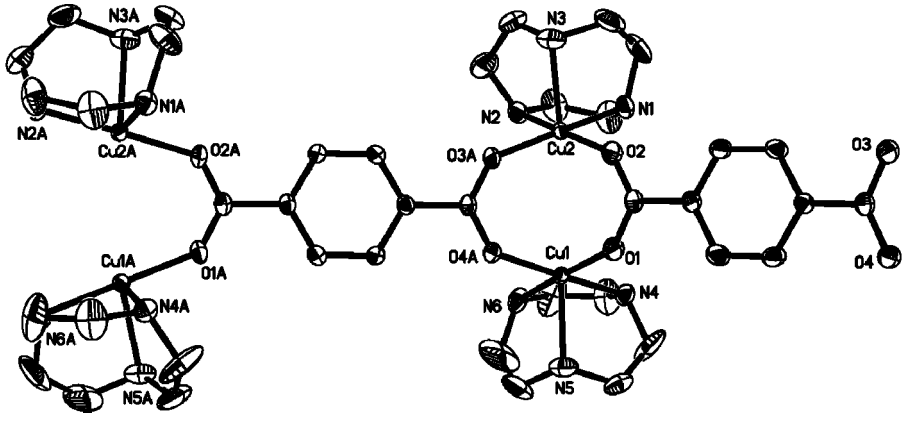

Figure 3. ORTEP diagram of **3**; H atoms and perchloric acid anions are omitted for clarity

complete the square-based pyramidal coordination geometry.

Crystal Structure of $\{[Cu_4(tacn)_4(o\text{-}bda)_2](ClO_4)_4(H_2O)_2\}_n$ (1)

The structure of **1** contains the cation $[Cu_4(tacn)_4(o\text{-}bda)_2]^{4+}$, the anion ClO_4^- as well as solvated water molecules. The cation exhibits a zigzag chain-like structure as shown in Figure 1. The copper atom is in a distorted square-pyramidal environment. Interestingly, there are two types of copper atoms according to the copper−oxygen coordination modes, namely chelating (Cu1) and bridging (Cu2). Two carboxylate oxygen atoms from the same *o*-bda ligand are chelated to Cu1 [Cu1−O1 1.974(6), Cu1−O3 1.955(7) Å], and three nitrogen atoms of the tacn ligand complete the configuration. The apical site of the distorted square pyramid is occupied by N1. The axial

 © 2004 Wiley-VCH Verlag GmbH & Co. KGaA, Weinheim

copper−nitrogen bond [Cu1−N1 2.322(6) Å] is somewhat longer than the equatorial ones [Cu1−N2 2.022(8), Cu1−N3 2.013(9) Å]. The largest deviation from the mean N2N3O1O3 basal plane is 0.132(5) Å for N2. The Cu1 atom is displaced toward the apical site by 0.097(2) Å. The angles O1−Cu1−N2 and O3−Cu1−N3 are 170.5(3) and 173.7(3)°, respectively. For Cu2, there are two carboxylate oxygen atoms from two *o*-bda ligands as well as three coordinated nitrogen atoms from tacn. The basal plane consists of N4N5O2O5 with the largest deviation of 0.087(5) Å for N5. The Cu2 atom is displaced toward the apical site by 0.162(8) Å. The average Cu2−O bond length is slightly longer than that of Cu1−O, whereas the average Cu2−N bond length is shorter than that of Cu1−N. Similar differences were also observed for the N−Cu−N and N−Cu−O angles. These features may result from the Cu2−O2(O5) bridging coordination mode. The dihedral angle between the mean coordination planes of Cu1 and Cu2 is 85.0°. These two types of copper centers are alternately arrayed in **1**, which leads to the zigzag chain-like structure (Figure 4, a). The shortest Cu−Cu distance is 5.010 Å along the chain.

In **1**, all Cu−N bond lengths ranging from 2.013(9) to 2.322(6) Å, are similar to those in other (tacn)Cu^{II} complexes.[19,20] The Cu−O distances, ranging from 1.954(6) to 1.990(6) Å, are also in line with the corresponding values in phthalato complexes.[21] It is noteworthy that the coordination geometry of *o*-bda bridged complexes largely relies on the terminal ligands. In our published report,[22] the cyclic tetranuclear complex $[Mn_4(\mu\text{-}o\text{-bda})_2(bpy)_8](ClO_4)_2{\cdot}3H_2O$ was constructed from an *o*-bda bridge, the metal center is six-coordinate with four nitrogen atoms and two oxygen atoms. Once the terminal ligand is replaced by tridentate tacn, complex **1** was obtained as a 1D coordination polymer.

$\{[Cu(tacn)(m\text{-bda})](CH_3OH)_{0.5}(H_2O)_{0.5}\}_n$ (2)

In **2** (Figure 2), the apical site of the distorted square pyramid is occupied by N1 [Cu1−N1 2.184(8) Å]. The Cu−N bond lengths vary slightly from 2.124(8) to 2.184(8) Å. Compared with those in the *m*-bda bridged complexes, the Cu−O bonds (Cu1−O1 1.906(9) Å, Cu1−O4A 1.870(14) Å] are somewhat shorter,[23,24] which may be due to the distorted square-pyramidal structure caused by the

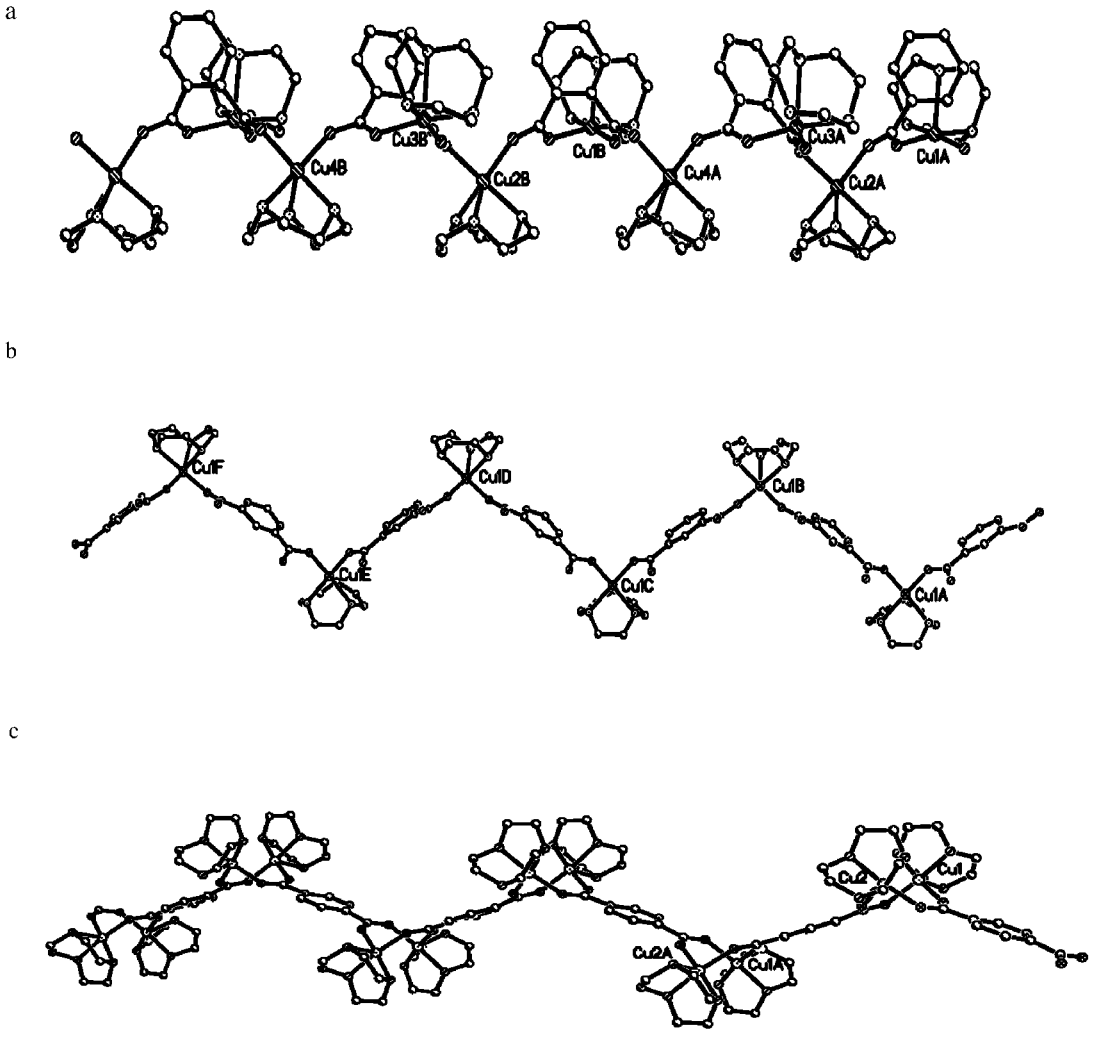

Figure 4. Zigzag chain structure for **1** (a), **2** (b), and **3** (c)

 © 2004 Wiley-VCH Verlag GmbH & Co. KGaA, Weinheim

coordination of the rigid tridentate tacn ligand. The best equatorial plane can be defined by N2, N3, O1 and O4A. The largest deviation from the mean plane is 0.0641(7) Å for O4A and the Cu1 atom is 0.0276(4) Å from this plane. The dihedral angle between the benzene ring of the *m*-bda ligand and the equatorial plane of the Cu1 square pyramid is 72.7(5)°.

The *m*-bda group acts as a bis(monodentate) ligand, which bridges copper(II) ions to form a 1D zigzag chain-like motif as shown in Figure 4 (b). The distance between the copper(II) ions along the chain is 10.783 Å, which is much longer than the shortest distance between copper centers (7.171 Å) in neighboring chains. It is worth noting that examples of structurally characterized polymers with bridging *m*-bda groups[25] are relatively rare.

$\{[Cu_2(tacn)_2(p\text{-bda})](ClO_4)_2\}_n$ (3)

The polymeric cationic $[Cu_2(p\text{-bda})(tacn)_2]^{2+}$ unit of **3** is shown in Figure 3. The carboxylic groups of *p*-bda make it behave as a tetrakis(monodentate) ligand, which is bound on each side to two copper(II) ions through the oxygen atoms of the carboxylic groups in a *syn-syn* conformation[26] yielding a zigzag chain, which runs parallel to the *z* axis (Figure 4, c). The copper environments are distorted square-pyramidal. The equatorial plane includes O1 and O4A from the carboxylic groups as well as N4 and N6 from one of the tacn ligands. N5 of tacn occupies the apical position [Cu−N 2.011(4)−2.235(4), Cu−O 1.954(3)−1.961(3) Å; all angles of the square pyramid range from 83.36(17) to 100.55(15)°]. The Cu−O bond lengths are in the normal range.[27−29] The largest deviation from the mean plane is 0.0517(8) Å for N4, and the Cu1 atom is 0.0525(4) Å from this plane. Two copper(II) ions linked by two carboxylic groups form an eight-membered ring, $Cu_2C_2O_4$, and the crystallographic inversion center is located at the center of the eight-membered ring.

Recent reports of *p*-bda-bridged Cu^{II} centers include descriptions of seven kinds of coordination modes of *p*-bda, which are listed in Scheme 1.[27−32] Materials containing both short and long bridges have been reported based on *p*-bda-bridged Mn^{II} and Cu^{II} complexes.[29,33] Long *p*-bda bridges typically produce M···M separations of about 11 Å. With respect to the *p*-bda ligand, the most remarkable structural feature of **3** is its rare tetrakis(monodentate) coordinating character used in the assembly of its chain-like structure. In the complex its eight carbon atoms are strictly coplanar. The shortest Cu1···Cu2 separation is 3.486 Å. The intra-chain separations are 10.496 and 11.044 Å for Cu1···Cu1A and Cu1···Cu2A, respectively.

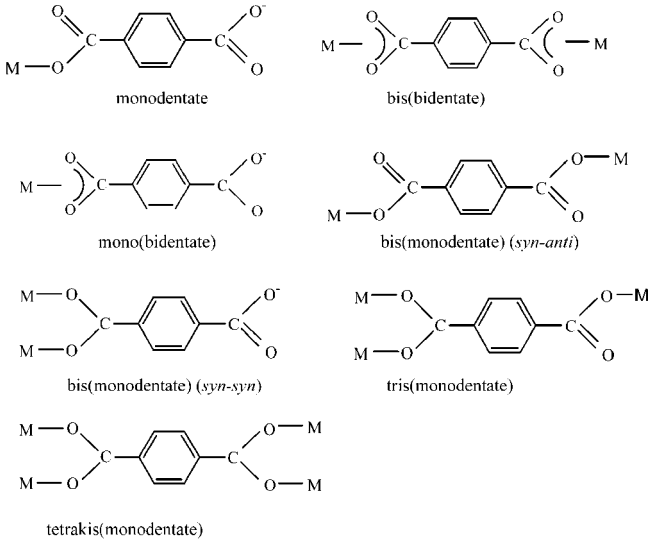

Scheme 1

Comparing the crystal structures of **1**, **2**, and **3**, the distortion of the square pyramid decreases on varying the bridging ligand from *o*-bda to *p*-bda. The differences in the bond angles and bond lengths decrease upon changing the bridging ligand. A summary of the main structural features of **1**, **2**, and **3** is listed in Table 1.

Magnetic Properties

The molar magnetic susceptibilities χ_M of **1**, **2**, and **3** were measured in the temperature range of 2−300 K in a field of 5 KOe. The plots of χ_M and μ_{eff} versus *T* for **1**−**3** are shown in Figures 5−7, respectively.

The bridging modes of bda and the chain structures of **1**, **2**, and **3** exhibit subtle differences, however, which lead to significantly different magnetic interactions between copper(II) ions. Initial magnetic studies of the three coordination polymers indicate interesting magnetic behavior.

The effective magnetic moment of **1** is 1.766 μ_B at 300 K. This is smaller than the spin-only value for the isolated cop-

Table 1. Summary of structural features of **1**, **2** and **3**

Compound	**1**	**2**	**3**
Length of chain motif	11.709 Å	16.175 Å	15.744 Å
Coordination mode of bridgng ligand (bda)	mono(bidentate), bis(monodentate) (*syn-anti*)	bis(monodentate) (*syn-anti*)	tetrakis(monodentate)
Ratio metal ion/bridging ligand/terminal ligand	4:2:4	1:1:1	2:1:2
Coordination number	5	5	5
Metal ion numbers coordinated to bridging ligand	3	2	4
Square pyramid angles	82.3(3)−108.0(3)°	79.9(5)−101.3(5)°	83.36(17)−100.55(15)°
Average bond length difference	0.368 Å	0.314 Å	0.281 Å
Shortest Cu···Cu distance	5.010 Å	7.171 Å	3.486 Å

 © 2004 Wiley-VCH Verlag GmbH & Co. KGaA, Weinheim

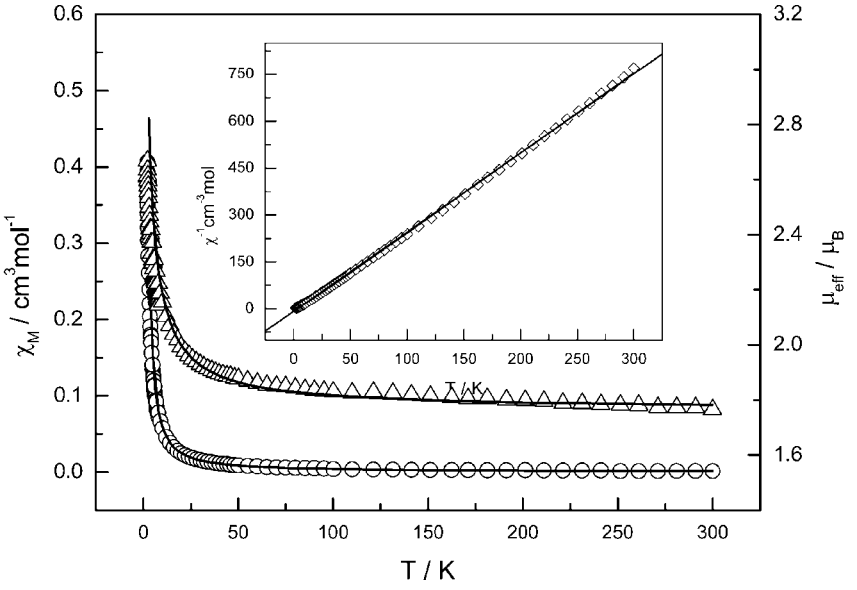

Figure 5. Plots of χ_M vs. T (open circles) and μ_{eff} vs. T (open triangles) and χ_M^{-1} vs. T (open squares) (inset) for **1**; the solid line represents the theoretical curve with the best fit parameters

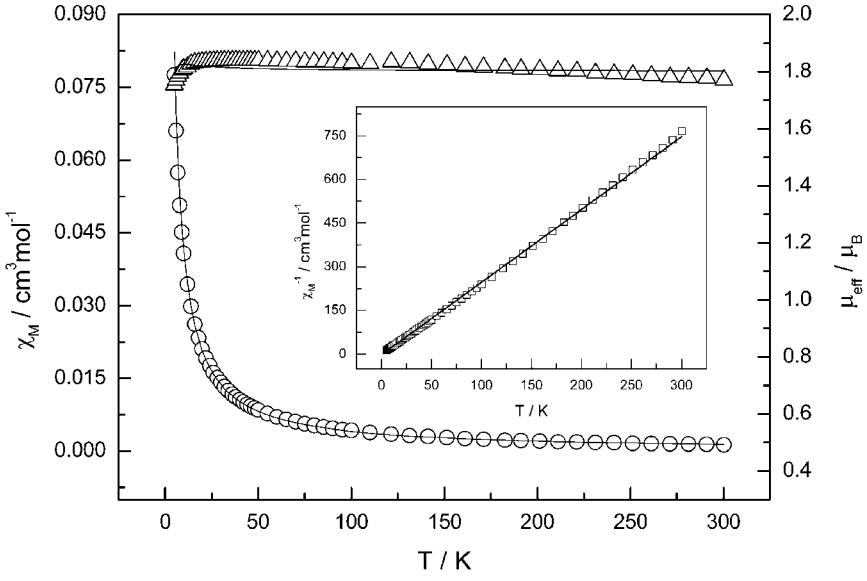

Figure 6. Plots of χ_M vs. T (open circles) and μ_{eff} vs. T (open triangles) for **2** and χ_M^{-1} vs. T (open squares) (inset); the solid line represents the theoretical curve with the best fit parameters

per(II) ion (1.73 μ_B, g = 2.0). With decreasing temperature, the μ_{eff} value for **1** increases smoothly down to ca. 20 K, and then sharply reaches a maximum value of 2.67 μ_B at 2.2 K (as shown in Figure 5). This behavior suggests the existence of a ferromagnetic interaction between the metal centers, and we know that the bridging group *o*-bda usually transmits a ferromagnetic exchange interaction between copper(II) ions.[23] The χ^{-1} data for **2** obey the Curie−Weiss law with a Curie−Weiss temperature θ = 3.18 K, and a Curie constant C = 0.39 emu K·mol^{-1} (inset of Figure 5). The Curie constant is close to the expected value for one uncoupled Cu^{2+} spin (S = 1/2, $C_{theor.}$ = 0.375 emu·K·mol^{-1}). The positive sign of the Weiss constant suggests ferromagnetic interactions between copper centers. Upon examining the crystal structure of **1**, we found that the neighboring Cu···Cu distances are almost equal, and only one kind of exchange pathway is available, namely Cu−O−C−O−Cu. The magnetic susceptibility data were, therefore, fitted by Equation (1) incorporating ferromagnetic chain properties with S = 1/2[34] and $H = -2JS_1S_2$

 © 2004 Wiley-VCH Verlag GmbH & Co. KGaA, Weinheim

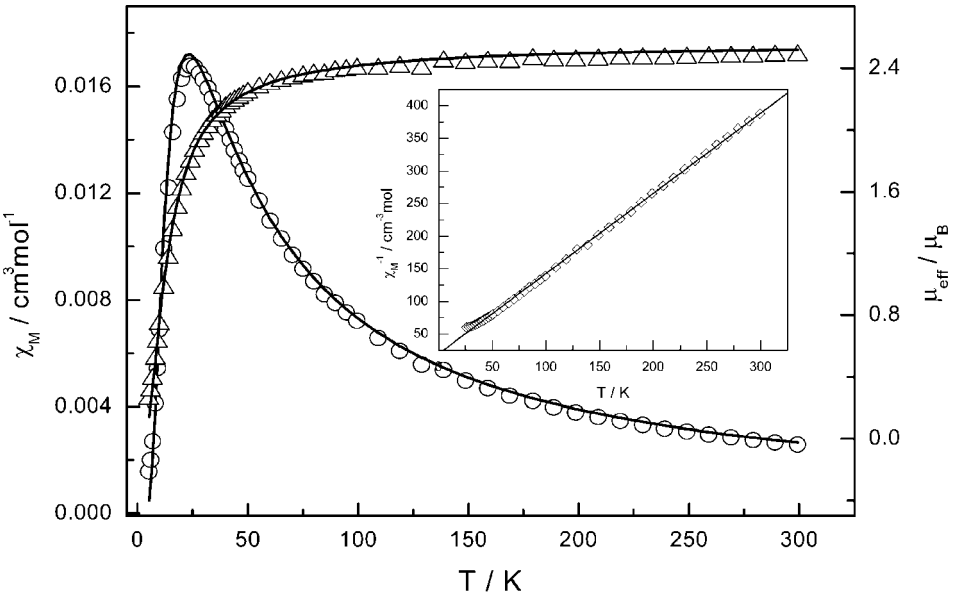

Figure 7. Plots of χ_M vs. T (open circles) and μ_{eff} vs. T (open triangles) for **3** and χ_M^{-1} vs. T (open squares) (inset); the solid line represents the theoretical curve fitted by Equation (3)

in which $A = 5.7979916$, $B = 16.902653$, $C = 29.376885$, $D = 29.832959$, $E = 14.036918$, $A' = 2.7979916$, $B' = 7.0086780$, $C' = 8.6538644$, $D' = 4.5743114$, and $x = J/2kT$.

$$\chi_{chain} = \frac{Ng^2\beta^2}{4kT}\left[\frac{1+Ax+Bx^2+Cx^3+Dx^4+Ex^5}{1+A'x+B'x^2+C'x^3+D'x^4}\right]^{2/3} + N\alpha \quad (1)$$

A temperature-independent susceptibility term ($N\alpha$) was also included, and was set as 60×10^{-6} cm^3·mol^{-1}. Other symbols have their usual meanings. The best fit of the magnetic susceptibility data yielded $J = 4.0$ cm^{-1}, $g = 2.04$, and $R = 3.2 \times 10^{-3}$ [agreement factor, defined as $\Sigma(\chi_M^{obsd.} - \chi_M^{calcd.})^2/\Sigma(\chi_M^{obsd.})^2$]. These results confirm the ferromagnetic coupling between adjacent copper(II) ions through the bridging *o*-bda ligand.

For compound **2** the effective magnetic moment is 1.77 μ_B at room temperature. This value is close to that of the isolated Cu^{II} ion (1.73 μ_B). As the temperature is lowered, μ_{eff} of **2** smoothly increases to a maxmium value of 1.84 μ_B at 36 K, and then decreases to 1.75 μ_B at 2 K. The increase in μ_{eff} is due to the intra-chain ferromagnetic coupling, while the inter-chain antiferromagnetic coupling results in a decrease of μ_{eff} below 36 K. We used the same theoretical susceptibility equation for **1** to obtain a fit of the data. As a consequence of the decrease of μ_{eff} below 36 K, a molecular field correction was applied [Equation (2)].

$$\chi_M = \chi_{chain}/(1 - zJ'\chi_{chain}/Ng^2\beta^2) \quad (2)$$

The fit (as shown in Figure 6) was obtained with values of $J = 1.2$ cm^{-1}, $zJ' = -0.18$ cm^{-1}, $g = 2.07$, and $R = 1.6 \times 10^{-3}$. The fitting parameters indicate the weak ferromagnetic coupling between adjacent copper ions along the chain, while $zJ' < 0$ indicates the weak antiferromagnetic interaction between the chains. The χ^{-1} data for **2** obey the Curie–Weiss law with a Curie–Weiss temperature $\theta = 2.54$ K and a Curie constant $C = 0.395$ emu·K·mol^{-1} (inset of Figure 6). The Curie constant is close to the expected value for one uncoupled Cu^{2+} spin ($S = 1/2$, $C_{theor.} = 0.375$ emu·K·mol^{-1}). The positive sign of the Weiss constant suggests that ferromagnetic interactions are dominant.

For **3**, μ_{eff} is 2.48 μ_B at 299 K. This is similar to the spin-only value of 2.45 μ_B for two uncoupled copper(II) ions (Figure 7). The value of μ_{eff} decreases gradually as the temperature decreases, indicating the presence of antiferromagnetic interactions. The occurrence of a sharp susceptibility maximum around 24 K is characteristic of an antiferromagnetic interaction with a singlet ground state. The χ^{-1} data for **3** obey the Curie–Weiss law above 24 K with a Curie–Weiss temperature $\theta = -16.0$ K and a Curie constant $C = 0.81$ emu·K·mol^{-1} (inset of Figure 7). The negative sign of the Weiss constant suggests antiferromagnetic interactions between the copper centers.

The magnetic parameters were estimated from a least-squares fitting of the susceptibility data by the equation given in the literature for dinuclear Cu^{II} complexes [Equation (3)].[35]

$$\chi_M = \frac{2Ng^2\beta^2}{kT}\left[3 + \exp(-2J/kT)\right]^{-1} + N\alpha \quad (3)$$

 © 2004 Wiley-VCH Verlag GmbH & Co. KGaA, Weinheim

Table 2. Selected structural and magnetic parameters of terephthalato-bridged dinuclear and 1D copper(II) complexes

Complex[a]	Bridged mode	Shortest Cu···Cu separation [Å]	d_{inter} [Å]	J [cm^{-1}]	Ref.
$[Cu_2(bipy)_4(p\text{-bda})](ClO_4)_2$	bis(monodentate) *syn-anti*	7.638	11.004	−2.20	[30]
$[Cu_2(terpy)_2(H_2O)_2(p\text{-bda})](ClO_4)_2$	bis(monodentate) *syn-anti*	7.272	10.913	−0.01	[30]
$[Cu_2(SalNEt_2)_2(p\text{-bda})](H_2O)(CH_3OH)$	bis(monodentate) *syn-anti*	8.8179	11.0348	+0.6	[32]
$[\{Cu(pmedien)(H_2O)\}_2(p\text{-bda})]$	bis(monodentate) *syn-anti*	7.840	11.129	−2.70	[36]
$[\{Cu(petdien)(H_2O)\}_2(p\text{-bda})](ClO_4)_2(H_2O)$	bis(bidentate)	8.215, 8.140	10.710	0	[36]
$[Cu_2(dien)_2(p\text{-bda})](ClO_4)_2$	bis(monodentate) *syn-anti*	4.179	11.006	−3.66	[37]
$[Cu(en)(H_2O)_2(p\text{-bda})]_n$	bis(monodentate) *syn-anti*	5.7263	11.1673	+4[b]	[37]
$[Cu(p\text{-bda})(H_2O)_2](H_2O)$	bis(monodentate) *syn-syn*	3.150	12.002	−12.72	[27]
$\{[CuL(\mu_2\text{-}p\text{-bda})](CH_3OH)_2\}_n$	bis(monodentate) *syn-anti*	6.034	11.284	0.02	[38]
$[Cu_2(p\text{-bda})(tacn)_2](ClO_4)_2$	tetrakis(monodentate)	3.486	10.496, 11.044	−13.1	this work
$[L'_2Cu_2(H_2O)_2(p\text{-bda})](ClO_4)_2$	bis(monodentate) *syn-anti*	7.587	11.252	−140	[39]

[a] *p*-bda = terephthalato, bipy = 2,2′-bipyridine, terpy = 2,2′:6′,2″-terpyridine, $SalNEt_2$ = *N*-[2-(diethylamino)ethylsalicylidenaminate], pmdien = *N*,*N*,*N*′,*N*″,*N*″-pentamethyldiethylenetriamine, pedien = *N*,*N*,*N*′,*N*″,*N*″-pentaethyldiethylenetriamine, dien = diethylenetriamine, en = ethylenediamine, L = *N*,*N*-dimethyl-*N*′-(pyrid-2-ylmethyl)ethylenediamine, L′ = 1,4,7-trimethyl-1,4,7-triazacyclononane. [b] The intra-chain exchange interaction was ferromagnetic with $J = +4$ cm^{-1} and the inter-chain exchange interaction was antiferromagnetic with $zJ = -7$ cm^{-1}.

A temperature-independent susceptibility term ($N\alpha$) was also included and was set as 1.2×10^{-4} cm^3·mol^{-1}. The best fit was obtained for $J = -13.1$ cm^{-1}, $g = 2.05$, and $R = 6.5 \times 10^{-4}$. The above results confirmed the antiferromagnetic coupling between copper atoms in the dinuclear unit.

The relatively strong antiferromagnetic interactions in **3** can be explained by the short bridge, via one carboxylate end, between two copper atoms. Due to the special tetrakis(monodentate) coordination mode of *p*-bda, longer bridges through the benzene ring exist at the same time, but they are too weak to be taken into account. Some related (*p*-bda)Cu complexes are listed in Table 2 together with selected magneto-structural data. The *J* values of the complexes listed in Table 2 do not follow a simple trend. In spite of the large variation of the nearest metal−metal separation (from 3.150 to 8.818 Å), the values of *J* are insensitive to this. It can be seen that the magnetic interaction is very weak except in the last example. The weak coupling observed is not surprising in the light of the large intramolecular metal−metal separation. The *J* value reported for the last compound is anomalously large in comparison with the others. Bürger et al. attributed this strong antiferromagnetic coupling to the formation of an intramolecular O−H···O hydrogen bond between the H_2O molecule and the carbonyl oxygen atom of the coordinated carboxylate. In Table 2, the *J* value of $[Cu(p\text{-bda})(H_2O)_2](H_2O)$ is similar to that of **3**. For the former, the coordination mode of *p*-bda [bis(monodentate), as shown in Scheme 1], and the H_2O bridges result in the close intramolecular Cu···Cu separation, which leads to the correspondingly large antiferromagnetic coupling. In our work, however, the effective antiferromagnetic exchange pathway was achieved by the unusual tetrakis(monodentate) coordination mode of *p*-bda. From Table 2 we can see, that (*p*-bda)Cu complexes with the tetrakis(monodentate) coordination mode have rarely been reported. Samuel et. al prepared $[Cu_4(p\text{-bda})_3(4,4'\text{-bipy})_2]_n$, containing tetrakis(monodentate) coordinated *p*-bda, by a hydrothermal synthesis,[40] but they did not further investigate its magnetic properties. Our study provides some useful structural and magnetic information about this type of complex.

The transformation of interactions between copper ions from ferromagnetic to antiferromagnetic is closely related to changes in the bridging ligands. In compound **2**, the Cu···Cu distance is somewhat longer than that in **1**, and the exchange pathway passes across the benzene ring, which greatly weakens the ferromagnetic interactions. In consideration of the comparatively large antiferromagnetic interactions in the dinuclear unit of **3**, the weak interaction through the benzene ring can be ignored.

Conclusion

Three novel zigzag chain copper coordination polymers containing the tacn ligand were successfully constructed by deliberate selection of the bridging bda ligand. Among the previously reported complexes with tacn, coordination polymers with infinite structures are rather rare. Systematic investigations of the structures and magnetic properties of coordination polymers with a series of isomers of dicarboxylic bridging ligands have not been reported so far. Most importantly, the structural differences caused by the bridging ligands lead to unexpected magnetic behavior including changes from ferromagnetic to antiferromagnetic coupling. The present work provides another possible direction for exploring the magneto-structural relationship.

Experimental Section

Physical Measurements: C, H, and N analyses were obtained at the Institute of Elemental Organic Chemistry, Nankai University.

 © 2004 Wiley-VCH Verlag GmbH & Co. KGaA, Weinheim

Variable-temperature magnetic susceptibilities were measured with a Quantum Design MPMS-7 SQUID magnetometer. Diamagnetic corrections were made with Pascal's constants for all the constituent atoms.

Preparation of $\{[Cu_4(tacn)_4(o\text{-bda})_2](ClO_4)_4(H_2O)_2\}_n$ (1): A methanol solution (30 mL) of *o*-bda (0.4 mmol, 66.45 mg), and freshly prepared $Cu(OH)_2$ (0.4 mmol, 39.0 mg) was heated to reflux for 2 h, then filtered; tacn (0.4 mmol, 51.6 mg), dissolved in methanol (10 mL), and an aqueous solution of $NaClO_4$ (0.4 mmol, 49.0 mg) were added to the filtrate. The resultant mixture was heated to reflux for 2 h, and then filtered. Several weeks later, blue crystals were obtained by concentration of the filtrate at room temperature. Yield: 76.7 mg (50%). $C_{40}H_{72}Cl_4Cu_4N_{12}O_{26}$ (1533.06): calcd. C 31.3, H 4.63, N 11.0; found C 31.7, H 4.88, N 10.8.

$\{[Cu(tacn)(m\text{-bda})](CH_3OH)_{0.5}(H_2O)_{0.5}\}_n$ (2): An acetonitrile/methanol (1:1) mixture (30 mL) was added to a mixture of *m*-bda (0.4 mmol, 66.45 mg), and freshly prepared $Cu(OH)_2$ (0.4 mmol, 39.0 mg). After heating to reflux for 1 h, methanol (10 mL), tacn (0.4 mmol, 51.6 mg), and water (1 mL) were added. The resultant mixture was heated to reflux for a further 2 h, and then filtered. The filtrate was concentrated slowly at room temperature. Blue crystals were obtained after one month. Yield: 106.9 mg (70%). $C_{14.5}H_{22}CuN_3O_5$ (381.89): calcd. C 45.6, H 5.76, N 11.0; found C 45.9, H 5.89, N 10.7.

$\{[Cu_2(tacn)_2(p\text{-bda})](ClO_4)_2\}_n$ (3): Ligand *p*-bda (42 mg, 0.25 mmol) and a few drops of piperidine were added to an aqueous solution (30 mL) of $Cu(ClO_4)_2{\cdot}6H_2O$ (0.186 g, 0.5 mmol), and tacn (0.065 g, 0.5 mmol). The resultant mixture was stirred at room temperature for 15 h. The solution was then filtered, and the filtrate was allowed to stand for several days resulting in the formation of well-formed light blue crystals. Yield: 104.8 mg (56%). $C_{20}H_{34}Cl_2Cu_2N_6O_{12}$ (748.51): calcd. C 32.06, H 4.54, N 11.22; found C 31.79, H 4.88, N 10.71.

Crystallographic Studies: Crystals, having the approximate dimensions 0.30 mm × 0.25 mm × 0.20 mm for **1** and **2**, and 0.35 mm × 0.30 mm × 0.20 mm for **3**, were mounted on glass fibers. Determination of the unit cells and data collection were performed with Mo-K_α radiation (λ = 0.71073 Å) with a Bruker Smart 1000 diffractometer equipped with a CCD camera. Cell parameters were determined from least-squares refinements on the setting angles in the range $0.99° < \theta < 25.03°$ (**1**), $2.29° < \theta < 25.03°$ (**2**), and $1.66° < \theta < 26.40°$ (**3**) at 293(2) K. The ω-2θ scan technique was employed. Crystal parameters and structural refinements for **1**, **2**, and **3** are summarized in Table 3; selected bond lengths and angles are listed in Table 4. The structures were solved primarily by direct methods and secondly by Fourier difference techniques, and refined by the full-matrix least-squares method. The computations were performed with the SHELXL-97 program.[41,42] All non-hydrogen atoms were refined anisotropically. The hydrogen atoms were set in calculated positions and refined as riding atoms with a common fixed isotropic thermal parameter. CCDC-196813 to -196815 (**1**−**3**) contain the supplementary crystallographic data for this paper. These data can be obtained free of charge via www.ccdc.cam.ac.uk/conts/retrieving.html [or from the Cambridge Crystallographic Data Center, 12 Union Road, Cambridge CB2 1EZ, UK; Fax: (internat.) + 44-1223-336-033; or E-mail: deposit@ccdc.cam.ac.uk].

Acknowledgments

This work was supported by the National Natural Science Foundation of China (No. 90101028, 50173011) and the Teaching and Research Award Program for Outstanding Young Teachers in Higher Education Institutions of MOE, P. R. C.

Table 3. Data collection and processing parameters for **1**, **2**, and **3**

	1	**2**	**3**
Empirical formula	$C_{40}H_{72}Cl_4Cu_4N_{12}O_{26}$	$C_{14.5}H_{22}CuN_3O_5$	$C_{20}H_{34}Cl_2Cu_2N_6O_{12}$
Formula mass	1533.06	381.89	748.51
T [K]	293(2)	293(2)	293(2)
Space group	$C2$	$Pmc2(1)$	$P2_1/n$
a [Å]	41.327(19)	7.1711(14)	11.1165(7)
b [Å]	9.984(5)	7.5961(15)	24.5625(17)
c [Å]	14.460(7)	17.751(4)	11.4332(8)
β [°]	96.217(9)	90.10(3)	111.6840(10)
V [Å^3]	5931(5)	967.0(3)	2900.9(3)
Z	4	2	4
ρ [g·cm^{-3}]	1.717	1.312	1.714
μ [mm^{-1}]	1.687	1.154	1.720
θ [°]	0.99−25.03	2.29−25.03	1.66−26.40
Index ranges	$-48 \le h \le 49$	$-7 \le h \le 8$	$-13 \le h \le 13$
	$-11 \le k \le 8$	$-9 \le k \le 5$	$-30 \le k \le 30$
	$-17 \le l \le 16$	$-20 \le l \le 21$	$-14 \le l \le 7$
Refl. collected	12419	3343	13519
Independent refl.	7713 (R_{int} = 0.0403)	2839 (R_{int} = 0.0865)	5940 (R_{int} = 0.0270)
Max./min. transmission	0.7290/0.6315	0.8020/0.7233	0.9664/0.5843
Data/restraints/parameter	7713/13/787	2839/20/227	5940/8/412
Goodness-of-fit on F^2	0.908	0.972	1.035
R_1, wR_2 [$I > 2\sigma(I)$]	0.0486, 0.1218	0.0820, 0.1658	0.0492, 0.1342
R_1, wR_2 (all data)	0.0664, 0.1332	0.1478, 0.1919	0.0672, 0.1477
Largest diff. peak/hole [e·Å^{-3}]	0.894/−0.435	0.573/−0.488	1.070/−0.436

 © 2004 Wiley-VCH Verlag GmbH & Co. KGaA, Weinheim

Table 4. Selected bond lengths [Å] and angles [°] for **1**, **2**, and **3**

Complex **1**			
Cu1−O3	1.955(7)	Cu1−O1	1.974(6)
Cu1−N2	2.022(8)	Cu1−N3	2.013(9)
Cu1−N1	2.322(6)	Cu2−O5	1.974(6)
Cu2−O2	1.990(6)	Cu2−N4	2.021(7)
Cu2−N5	2.046(8)	Cu2−N6	2.202(8)
Cu3−O6	1.954(6)	Cu3−O8	1.959(6)
Cu4−O7	1.964(6)	Cu4−O4	1.970(5)
O3−Cu1−O1	89.5(3)	O3−Cu1−N2	91.6(3)
O3−Cu1−O1	89.5(3)	O3−Cu1−N2	91.6(3)
O1−Cu1−N2	170.5(3)	O3−Cu1−N3	173.7(3)
O1−Cu1−N3	93.1(3)	N2−Cu1−N3	84.9(4)
O3−Cu1−N1	103.7(3)	O1−Cu1−N1	106.5(3)
N2−Cu1−N1	82.3(3)	N3−Cu1−N1	81.0(3)
O5−Cu2−O2	88.4(2)	O5−Cu2−N4	170.1(3)
O2−Cu2−N4	93.5(3)	O5−Cu2−N5	91.5(3)
O2−Cu2−N5	168.1(3)	N4−Cu2−N5	84.7(3)
O5−Cu2−N6	104.7(3)	O2−Cu2−N6	108.0(3)
N4−Cu2−N6	83.9(3)	N5−Cu2−N6	83.6(3)
Complex **2**[a]			
Cu1−O3	1.955(7)	Cu1−O1	1.974(6)
Cu1−O4#1	1.870(14)	Cu1−O1	1.906(9)
Cu1−N2	2.124(8)	Cu1−N3	2.129(9)
Cu1−N1	2.184(8)		
O4#1−Cu1−O1	88.9(5)	O4#1−Cu1−N2	176.9(6)
O1−Cu1−N2	94.2(5)	O4#1−Cu1−N3	92.8(7)
O1−Cu1−N3	177.7(4)	N2−Cu1−N3	84.1(5)
O4#1−Cu1−N1	98.0(5)	O1−Cu1−N1	101.3(5)
N2−Cu1−N1	81.1(4)	N3−Cu1−N1	79.9(5)
C1−O1−Cu1	135.6(9)		
Complex **3**[b]			
Cu1−O1	1.954(3)	Cu1−O4#1	1.961(3)
Cu1−N6	2.011(4)	Cu1−N4	2.014(4)
Cu1−N5	2.230(4)	Cu2−O3#1	1.957(3)
Cu2−O2	1.959(3)	Cu2−N1	2.012(4)
Cu2−N2	2.018(4)	Cu2−N3	2.235(4)
O1−Cu1−O4#1	95.05(14)	O1−Cu1−N6	172.65(17)
O4#1−Cu1−N6	91.56(15)	O1−Cu1−N4	89.26(15)
O4#1−Cu1−N4	173.69(15)	N6−Cu1−N4	83.90(17)
O1−Cu1−N5	97.74(17)	O4#1−Cu1−N5	100.55(15)
N6−Cu1−N5	84.18(19)	N4−Cu1−N5	83.38(16)
O3#1−Cu2−O2	95.15(13)	O3#1−Cu2−N1	174.15(15)
O2−Cu2−N1	89.42(15)	O3#1−Cu2−N2	90.74(15)
O2−Cu2−N2	172.76(16)	N1−Cu2−N2	84.43(16)
O3#1−Cu2−N3	98.72(15)	O2−Cu2−N3	99.84(16)
N1−Cu2−N3	84.04(17)	N2−Cu2−N3	83.36(17)
C1−O1−Cu1	136.7(3)	C1−O2−Cu2	130.6(3)

[a] # 1: $x, -y + 1, z + 1/2$. [b] #1: $x + 1/2, -y + 1/2, z - 1/2$.

[1] M. Eddaoudi, J. Kim, N. Rosi, D. Vodak, J. Wachter, M. O'Keeffe, O. M. Yaghi, *Science* **2002**, *295*, 469.
[2] B. Zhao, P. Cheng, Y. Dai, C. Cheng, D. Z. Liao, S. P. Yan, Z. H. Jiang, G. L. Wang, *Angew. Chem. Int. Ed.* **2003**, *42*, 934.
[3] B. L. Chen, M. Eddaoudi, S. T. Hyde, M. O'Keeffe, O. M. Yaghi, *Science* **2001**, *291*, 1021.
[4] J. S. Seo, D. Whang, H. Lee, S. I. Jun, J. Oh, Y. J. Jeon, K. Kim, *Nature* **2000**, *404*, 982.
[5] H. Li, M. Eddaoudi, M. O'Keeffe, O. M. Yaghi, *Nature* **1999**, *402*, 276.
[6] M. Aoyagi, K. Biradha, M. Fujita, *J. Am. Chem. Soc.* **1999**, *121*, 7457.
[7] M. Fujita, S. Y. Yu, T. Kusukawa, H. Funaki, K. Ogura, K. Yamaguchi, *Angew. Chem. Int. Ed.* **1998**, *37*, 2082.
[8] D. Gatteschi, *Adv. Mater.* **1994**, *6*, 635.
[9] C. Janiak, *Angew. Chem. Int. Ed. Engl.* **1997**, *36*, 1431; S. R. Batten, R. Robson, *Angew. Chem. Int. Ed.* **1998**, *37*, 1461; A. K. Cheetham, G. Ferey, T. Loiseau, *Angew. Chem. Int. Ed.* **1999**, *38*, 3269.
[10] M. J. Zaworotko, *Chem. Soc. Rev.* **1994**, 283.
[11] G. B. Gardner, D. Venkataraman, J. S. Moore, S. Lee, *Nature* **1995**, *374*, 792.
[12] B. J. Holliday, C. A. Mirkin, *Angew. Chem. Int. Ed.* **2001**, *40*, 2022.
[13] S. S.-Y. Chui, S. M.-F. Lo, J. P. H. Charmant, A. G. Orpen, I. D. Williams, *Science* **1999**, *283*, 1148.
[14] L. Pan, X. Y. Huang, J. Li, Y. G. Wu, N. W. Zheng, *Angew. Chem. Int. Ed.* **2000**, *39*, 527.
[15] O. M. Yaghi, C. E. Davis, G. Li, H. Li, *J. Am. Chem. Soc.* **1997**, *119*, 2861; H. J. Choi, M. P. Suh, *J. Am. Chem. Soc.* **1998**, *120*, 10622.
[16] O. M. Yaghi, H. L. Li, C. Davis, D. Richardson, T. L. Groy, *Acc. Chem. Res.* **1998**, *31*, 474.
[17] P. J. Hay, J. C. Thibeault, R. Hoffmann, *J. Am. Chem. Soc.* **1975**, *97*, 4884.
[18] J. J. Girerd, Y. Journeaux, O. Kahn, *Chem. Phys. Lett.* **1981**, *82*, 534.
[19] A. C. Benniston, D. Ellis, L. J. Farrugia, R. Kennedy, R. D. Peacock, S. Walker, *Polyhedron* **2002**, *21*, 333.
[20] X. Y. Chen, P. Cheng, X. W. Liu, S. P. Yan, W. M. Bu, D. Z. Liao, Z. H. Jiang, *Chem. Lett.* **2003**, *32*, 118.
[21] S. K. Shakhatreh, E. G. Bakalbassis, I. Brüdgam, H. Hartl, J. Mrozinski, C. A. Tsipis, *Inorg. Chem.* **1991**, *30*, 2801.
[22] Z.-H. Jiang, S.-L. Ma, D.-Z. Liao, S.-P. Yan, G.-L. Wang, X.-K. Yao, R.-J. Wang, *J. Chem. Soc., Chem. Commun.* **1993**, 745.
[23] X. M. Chen, G. F. Liu, *Chem. Eur. J.* **2002**, *8*, 4811.
[24] H. X. Zhang, B. S. Kang, A. W. Xu, Z. N. Chen, Z. Y. Zhou, A. S. C. Chan, K. B. Yu, C. Ren, *J. Chem. Soc., Dalton Trans.* **2001**, 2559.
[25] X.-S. Tan, J. Sun, D.-F. Xiang, W.-X. Tang, *Inorg. Chim. Acta* **1997**, *255*, 157.
[26] J. Cano, G. De Munno, J. Sanz, R. Ruiz, F. Lloret, J. Faus, M. Julve, *J. Chem. Soc., Dalton Trans.* **1994**, 3465.
[27] L. Deakin, A. M. Arif, J. S. Miller, *Inorg. Chem.* **1999**, *38*, 5072.
[28] E. Bakalbassis, P. Bergerat, O. Kahn, S. Jeannin, Y. Jeannin, Y. Dromzee, M. Guillot, *Inorg. Chem.* **1992**, *31*, 625.
[29] L. Yang, F. Bian, S. P. Yan, D. Z. Liao, P. Cheng, Z. H. Jiang, *Inorg. Chem. Commun.* **2003**, *6*, 1188.
[30] J. Cano, G. DeMunno, J. L. Sanz, R. Ruiz, J. Faus, F. Lloret, M. Julve, A. Caneschi, *J. Chem. Soc., Dalton Trans.* **1997**, 1915; E. G. Bakalbassis, J. Mrozinski, C. A. Tsipis, *Inorg. Chem.* **1986**, *25*, 3684.
[31] P. Chaudhuri, K. Oder, K. Wieghardt, S. Gehring, W. Haase, B. Nuber, J. Weiss, *J. Am. Chem. Soc.* **1988**, *110*, 3657.
[32] C. E. Xanthopoulos, M. P. Sigalas, G. A. Katsoulos, C. A. Tsipis, A. Terzis, M. Mentzafos, A. Hountas, *Inorg. Chem.* **1993**, *32*, 5433; Z. L. Deng, J. Shi, Z. H. Jiang, D. Z. Liao, S. P. Yan, G. L. Wang, H. G. Wang, R. J. Wang, *Polyhedron* **1992**, *11*, 885.
[33] C. S. Hong, Y. Do, *Inorg. Chem.* **1997**, *36*, 5684.
[34] D. D. Swank, C. P. Landee, R. D. Willet, *Phys. Rev.* **1979**, *B20*, 2154; B. E. Myers, L. Berger, S. A. Friedberg, *J. Appl. Phys.* **1968**, *40*, 1149.
[35] O. Kahn, *Molecular Magnetism*, Wiley-VCH, New York, **1993**.
[36] M. Verdaguer, J. Gouteron, S. Jeannin, Y. Jeannin, O. Kahn, *Inorg. Chem.* **1984**, *23*, 4291.
[37] E. Bakalbassis, C. Tsipis, A. Bozopoulos, W. Dreissig, H. Hartl, J. Mrozinski, *Inorg. Chim. Acta* **1991**, *186*, 113; E. G. Bakalbassis, A. P. Bozopoulos, J. Mrozinski, P. J. Rentzeperis, C. A. Tsipis, *Inorg. Chem.* **1988**, *27*, 529.

 © 2004 Wiley-VCH Verlag GmbH & Co. KGaA, Weinheim

[38] H. D. Bian, J. Y. Xu, W. Gu, S. P. Yan, D. Z. Liao, Z. H. Jiang, P. Cheng, *Inorg. Chem. Commun.* **2003**, *6*, 573.
[39] K. S. Bürger, P. Chaudhuri, K. Wieghardt, B. Nuber, *Chem. Eur. J.* **1995**, *1*, 583.
[40] S. M.-F. Lo, S. S.-Y. Chui, L. Y. Shek, Z. Y. Lin, X. X. Zhang, G. H. Wen, I. D. Williams, *J. Am. Chem. Soc.* **2000**, *122*, 6293.
[41] G. M. Sheldrick, *SHELXS 97, Program for the Solution of Crystal Structures*, University of Göttingen, Germany, **1997**.
[42] G. M. Sheldrick, *SHELXL 97, Program for the Refinement of Crystal Structures*, University of Göttingen, Germany, **1997**.

Received October 28, 2003
Early View Article
Published Online April 7, 2004

 © 2004 Wiley-VCH Verlag GmbH & Co. KGaA, Weinheim

Synthesis and Luminescence Properties of New Dinuclear Complexes of Lanthanide(III) Ions

Violetta Patroniak,[a,b] Paul N. W. Baxter,[a,c] Jean-Marie Lehn,*[a] Zbigniew Hnatejko,[b] and Maciej Kubicki[b]

Dedicated to the memory of Professor Marian Elbanowski

Keywords: Dinuclear complexes / Lanthanides / Bis(tridentate) ligands / Self-assembly

As a result of coordination of the ligand **L**, containing two tridentate binding units, to samarium(III), europium(III), terbium(III), and dysprosium(III) ions, new dinuclear architectures containing two ions with coordination number 9 were formed. The structures of the complexes have been assigned on the basis of their solution spectroscopic and microanalytical data, and confirmed by X-ray crystallography in the case of the europium(III) complex **2**. The structural analysis of the dinuclear complex **2** showed the presence of two europium centers [Eu(1) and Eu(2)] and four ligands **L**. Each europium ion is coordinated by 9 donor atoms with typical Eu–N and Eu–O distances.
(© Wiley-VCH Verlag GmbH & Co. KGaA, 69451 Weinheim, Germany, 2004)

Introduction

The coordination chemistry of lanthanides has become increasingly significant in the last few years due to the wide variety of potential applications of their complexes in many important areas of inorganic chemistry,[1] biology,[2] and medicine.[2c,3] The complexes of lanthanides also play a role as accelerators of hydrolytic cleavage of RNA model compounds,[4] and their applications as MRI contrast agents are very popular, especially complexes of Gd^{III}.[5] Lanthanide complexes are well known to undergo luminescence in the visible and near-IR wavelength regions,[1a,6] and have found widespread applications as fluorescence bio-markers.[2c,7] The design and synthesis of dinuclear complexes of lanthanides constitute a special area of study in bioinorganic chemistry, in particular because of their uses as spectroscopic probes for active sites in metalloproteins.[8]

During the course of our studies on the self-assembly and properties of supramolecular grid-type metal complexes, ligand **L** was shown to successfully form tetranuclear [2 × 2]G architectures upon correct stoichiometric combination with a range of first row transition metal ions.[9] In the resultant grid complexes, the metal ions are octahedrally coordinated by two N,N,O ligand donor sets. Grid complexes of this type may be expected to exhibit interesting photophysics and redox chemistry.

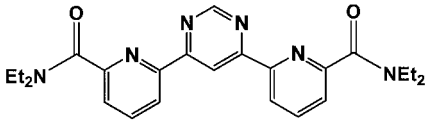

Figure 1. Structure of ligand **L**

In view of the fact that lanthanide ions prefer to be coordinated by relatively hard oxygen donor ligands, it was anticipated that ligand **L** would be able to form stable coordination architectures upon appropriate stoichiometric combination with specific lanthanide salts. However, ligand **L** possesses an insufficient number of donor sites to satisfy the coordination requirement of lanthanide(III) ions. The reaction between **L** and lanthanide ions may, therefore, be expected to result in a variety of possible outcomes depending on factors such as the M:L ratio, solvent, counterions etc.

In this report we describe our initial investigations into the lanthanide coordination chemistry of **L**, and demonstrate that this ligand is able to form structurally novel multinuclear lanthanide complexes of 2:4 M:**L** stoichiometry with Sm^{3+}(**1**), Eu^{3+}(**2**), Tb^{3+}(**3**), and Dy^{3+}(**4**).

The lanthanide complexes with **L** were characterized on the basis of ESI-MS, microanalysis and, in the case of the Eu^{3+} complex **2**, X-ray crystallography. Of particular significance is the fact, that the complexes are luminescent upon irradiation with UV light. A detailed investigation

[a] ISIS-Université Louis Pasteur, CNRS UMR 7006,
8 Allée Gaspard Monge, BP 70028, 67083 Strasbourg, France
E-mail: lehn@isis.u-strasbg.fr
[b] Faculty of Chemistry, Adam Mickiewicz University,
Grunwaldzka 6, 60780 Poznań, Poland
[c] Current address: Institut Charles Sadron,
6 Rue Boussingault, 67083 Strasbourg, France

into the luminescence properties of the lanthanide complexes was therefore also undertaken in order to obtain the photophysical properties characteristic of the $[M_2L_4]^{6+}$ {M = lanthanide(III)} system.

Results and Discussion

Initial investigations into the lanthanide complexation by **L** focussed upon the reaction between 1:1 stoichiometric combinations of M^{III}/**L** [M^{III} = Sm^{III} (**1a**), Eu^{III} (**2a**), Tb^{III} (**3a**), and Dy^{III} (**4a**)] in the hope of obtaining $[M_4L_4]^{12+}$ grid-type products. Evidence for the existence of $[M_4L_4]^{12+}$ species for the lanthanide ion systems, which may be of a grid-type structure, was obtained using ESI-MS. The ESI-MS data indicate, that many kinds of multinuclear structures co-exist in solution, which may be formulated as grids or helicates. Since we could not obtain crystals suitable for X-ray analysis, thereby confirming the structural identities of the components in the mixture, we decided to change the molar ratio of M^{III}/**L** to 2:3, and we obtained, unexpectedly, new dinuclear complexes of Sm^{III} (**1**), Eu^{III} (**2**), Tb^{III} (**3**), and Dy^{III} (**4**). The dinuclear nature of these species was confirmed by the X-ray crystal structure of the Eu^{III} complex **2**.

The ESI-MS investigations of all complexes were performed on acetonitrile solutions at concentrations of approximately 10^{-4} mol·L^{-1}. For example, the ESI mass spectrum of **1** showed peaks corresponding to multiply charged species containing the $[Sm_2L_4]^{6+}$ unit. These data confirmed the presence of dinuclear complex **1** in solution.

Photophysical Properties

The luminescence lifetimes of Eu^{III} excited states were measured with the use of a detection system consisting of a nitrogen laser-pumped dye laser. Excitation spectra assigned to the $^7F_0-{}^5D_0$ transition of the Eu^{III} ion were obtained with the same pulsed dye laser. The laser was continuously scanned from 578 to 581.5 nm while monitoring the $^5D_0-{}^7F_2$ emission at 618 nm. Details of the instrumentation, and procedures used for determining emission lifetimes of europium complexes have been described elsewhere.[10] The electronic absorption spectra for a 10^{-5} mol·L^{-1} acetonitrile solution of complex **2** and **L** are shown in Figure 2.

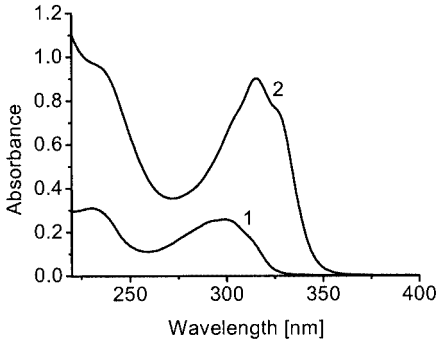

Figure 2. Electronic absorption spectra for acetonitrile solutions of ligand **L** (1.2×10^{-5} mol·L^{-1}), and of the Eu^{III} complex **2** (1.07×10^{-5} mol·L^{-1})

Two absorption maxima are present, which correspond to π-π* transition bands of the ligand. The absorption maxima, molar extinction coefficients (ε) for the free ligand, and its complexes with lanthanide(III) ions in acetonitrile are listed in Table 1. All the studied complexes show bathochromic shifts of the absorption maxima (ca. 18 nm) indicating ligand-lanthanide interaction. Similar bathochromic shifts have been reported for lanthanide complexes with other azaaryl ligands.[1a,11]

The luminescence properties of Sm^{III}, Eu^{III}, Tb^{III}, and Dy^{III} complexes have been studied in acetonitrile solution at room temperature. The emission spectra of the lanthanide(III) complexes, excited into the lowest energy LC absorption band, showed the well-known structured luminescence of the lanthanide ions.

The excitation spectrum for complex **2** consists of a broad curve with a maximum at ca. 330 nm, assigned to the π-π* transition of the ligand. For a given ligand, the Ln^{III} complexes displayed similar excitation spectra with identical excitation maxima. The emission from the lowest luminescent level to the ground state manifold, i.e. $^4G_{5/2}-{}^6H_{7/2}$ (598 nm) for Sm^{III}, $^5D_0-{}^7F_2$ (618 nm) for Eu^{III}, $^5D_4-{}^7F_5$ (547 nm) for Tb^{III}, and $^4F_{9/2}-{}^6H_{15/2}$ (576 nm) for Dy^{III} was measured. Strong red (Figure 3) and strong green emissions were observed for the Eu^{III} and Tb^{III} complexes, whereas the emissions of the Sm^{III} and Dy^{III} complexes were weak (Table 1).

The close agreement between the absorption and excitation spectra (see Figures 2 and 3) shows, that the excitation of Ln^{III} ions is caused by an indirect process, i.e. a ligand-to-metal energy transfer, the ligand units acting as an antenna.[1a]

The Eu^{III} ion is unique in that both the ground state $^7F_0$, and excited emissive state $^5D_0$ are non-degenerate. Since the $^7F_0-{}^5D_0$ transition occurs between non-degenerate energy levels, neither of which can be split by a ligand field, a single environment gives rise to only a single transition. If more than one Eu^{III} environment is present, each will have its own characteristic transition energy. The lifetime of the $^5D_0$ level of Eu^{III} is also a sensitive probe of local structure, particularly in the case of Eu^{III} ions in the presence of OH-oscillators.[12]

The excitation spectrum of complex **2** in the solid state showed two compounds with the $^7F_0-{}^5D_0$ transition (Figure 4).

The peak maxima of the $^7F_0-{}^5D_0$ excitation spectrum were found at 579.77 and 580.33 nm. The two compounds indicated by the analysis of the excitation spectrum of complex **2** suggest, that the Eu^{III} ions interact with two different types of binding sites, each with a different number of residual Eu hydration.

The lifetimes of the $^5D_0$ excited state for solid complex **2** were obtained by measuring the luminescence decays at wavelengths of 579.77 and 580.33 nm. The lifetime values were calculated using the mono-exponential decay method.

 © 2004 Wiley-VCH Verlag GmbH & Co. KGaA, Weinheim

Table 1. Absorption and luminescence data of the ligand **L** and complexes **1**−**4** in acetonitrile solution

Compound	Absorption		Fluorescence			Lum. quant.yield
	$\lambda_{max.}$ [nm]	$\varepsilon \times 10^4$ [L·mol^{-1}·cm^{-1}]	λ_{ex} [nm]	λ_{em} [nm]	I_{lum} [a.u.]	Φ[a]
L	299.4	2.15	–	–	–	–
1	317.0	8.56	328	598	448	0.0016
2	316.5	8.79	328	618	36800	0.059
3	316.0	9.35	328	547	32100	0.049
4	317.0	9.63	328	576	1880	0.0033

[a] Excitation at 328 nm; $Ru(bpy)_3^{2+}$ (Φ = 0.028 in water) was used as a standard for all Ln^{III} complexes; experimental error ca. 30%.

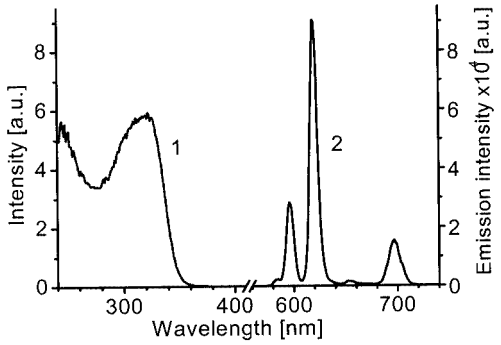

Figure 3. Excitation (1) and emission (2) spectra of complex **2** in acetonitrile solution, [Eu^{III}] = 1.07 × 10^{-5} mol·L^{-1}

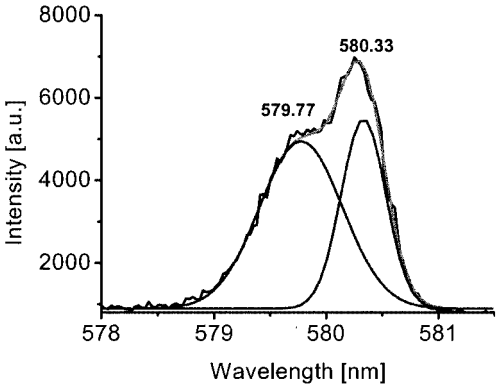

Figure 4. The $^7F_0-{}^5D_0$ selective excitation spectra of complex **2** in the solid state, obtained by analyzing at 618 nm ($^5D_0-{}^7F_2$ transition), and its deconvolution using a Gaussian-type function. Experimental data (dark line), calculated data (light line)

Two separate lifetime values of 280 and 511 μs were obtained, respectively. The hydration numbers of the Eu^{III} ions in complex **2** were found directly from the lifetime measurements using the equation: $n_{H2O} = 1.05k_{obsd.}$ (ms^{-1}) −0.7, where $k_{obsd.}$ is the reciprocal of the excited state lifetime.[13]

The numbers of water molecules bound in the inner coordination sphere of the Eu^{III} ions were determined as 3 and 1. The presence of the two species was found on the excitation spectrum of complex **2** (Figure 4). The peak at the shorter excitation wavelength (579.77 nm) can be assigned to the Eu complex with three molecules of H_2O in the inner coordination sphere, and the peak at the longer wavelength (580.33 nm) to the Eu complex with one molecule of H_2O. The presence of one and three-coordinated H_2O molecules in complex **2** is in agreement with crystallographic data.

Crystallographic Characterization of Complex 2

Single crystals of complex **2** were obtained by slow diffusion of *tert*-butyl methyl ether into a solution of the complex in acetonitrile, and its structure was determined by X-ray crystallography. The structure of the Eu^{III} complex is shown in Figure 5.

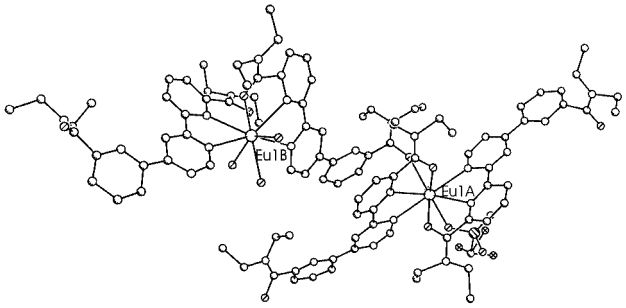

Figure 5. Molecular structure of complex **2** in the crystal. $Eu_2(C_{24}H_{28}N_6O_2)_4(CF_3SO_3)_6{\cdot}6H_2O$

In the crystal structure the complex exists as a binuclear compound. The europium(III) ions are nine-coordinate, and the geometry around the central ions can be described as distorted, tri-capped trigonal prismatic. Both ions are coordinated (almost symmetrically) by two ligands, that utilize three centers each: two aromatic ring nitrogen atoms, and one carbonyl oxygen atom, all from the same half of the molecule. Only one out of four ligands (D) joins two europium ions, and effectively acts as a tetradentate ligand. The coordination of Eu1A is completed by one of the triflate counterions and one water molecule, while Eu1B has three water molecules at the coordination sites.

One Eu^{III} ion is coordinated by six donor atoms from two molecules of the ligand **L** [each ligand comprises bis(tridentate) N,N,O (carbonyl) donor sets], and three remaining positions are occupied by oxygen atoms of water molecules. The second Eu^{III} ion is also nine-coordinate, but its coordination environment is filled by six donor atoms from two molecules of the ligand **L**. The seventh position is occupied by the oxygen atom of a triflate ion, the eighth

 © 2004 Wiley-VCH Verlag GmbH & Co. KGaA, Weinheim

site contains the oxygen atom of a water molecule, and in the ninth site there is an oxygen carbonyl atom of ligand **L** (D), which is coordinated to the first Eu^{III} ion, and plays a role as bridge between two metal ions. To the best of our knowledge, only six complexes with Eu^{III}-triflate bonds are known.[4e,14]

Two binuclear complexes **2**, related by a center of symmetry at (1/2, 1/2, 1/2), form a dimer connected via two water molecules, and two triflate molecules by means of hydrogen bonds (Figure 6).

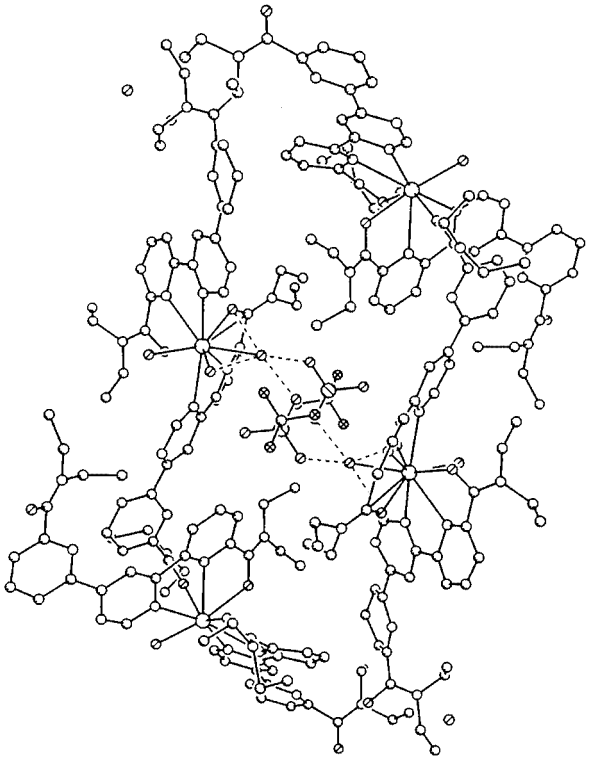

Figure 6. Hydrogen-bonded centrosymmetric dimer (see text)

These dimers, in turn, are connected by O(water)···O(carbonyl) hydrogen bonds, and make infinite chains along the *y* direction. In the crystal structure, the water molecules, which can both donate and accept hydrogen bonds act as a kind of "glue", which connects the molecules in the crystal structure. This structure is additionally strengthened by a number of weak C−H···O hydrogen bonds.

The Eu−O and Eu−N distances are well within typical ranges. The mean values are as follows (in parentheses are the mean values from the December 2002 version of the Cambridge Structural Database[15]): Eu(1A)−O(water): 2.45(2) [2.45(6)], Eu−O(carbonyl): 2.43(2) [2.40(6)], and Eu−N(aromatic): 2.60(2) [2.62(8)]. The conformation of the ligand molecules can be described by the values of the dihedral angles between the least-squares planes of the pyridine rings. Three ligands, which are bound to a single Eu ion, have quite similar values for these twist angles (15°−23°), while the ligand D, which binds two Eu ions, is significantly more twisted, the dihedral angle being 46(1)°.

Conclusion

We have described four new photoactive lanthanide complexes. Ligand **L**, containing two N,N,O tridentate binding sites for complexation, is a good Eu^{III} and Tb^{III} sensitizer. The europium complex **2** shows excellent luminescence properties with a high quantum yield, and effective intramolecular energy transfer from the ligand to the Eu^{III} ions. These factors, along with the stability of this complex in solution, make these compounds good candidates as luminescence and laser materials. ES-MSI and luminescence indicate, that the structure found in the crystal is essentially maintained in solution.

In conclusion, the investigated complexes may be of use in several fields of lanthanide coordination chemistry or as luminescent supramolecular nano-devices.

Experimental Section

General Remarks: CH_3CN was freshly distilled under argon from CaH_2. Ligand **L** was prepared according to the literature.[9] The lanthanide triflates were used without further purification from Aldrich. ESI-mass spectra were determined in acetonitrile using a Waters Micromass ZQ apparatus. Microanalyses were obtained using an Elementor Vario El III microanalyzer.

All absorption spectra, in acetonitrile or aqueous solution, were recorded with a Shimadzu UVPC 2001 spectrophotometer, between 200 and 400 nm, in 10 × 10 mm quartz cells. The concentration of Ln^{III} ions was $1-2 \times 10^{-5}$ mol·L^{-1} in all experiments. Excitation and emission spectra were measured at room temperature on a Perkin−Elmer MPF3 spectrofluorimeter with excitation and emission slits at 5 nm.

The quantum yields of the metal-centered luminescence were determined using published procedures, with $Ru(bpy)_3^{2+}$ as a standard,[16] in CH_3CN at room temperature. The refractive indexes were 1.346 for solutions in CH_3CN, and 1.333 for solutions in water. The excitation wavelength was 326 or 328 nm for all lanthanide ions.

Sm^{III} Complex 1: A mixture of $Sm(CF_3SO_3)_3$ (9.1 mg, 15 μmol) and ligand **L** (9.9 mg, 23 μmol) in CH_3CN (5 mL) was stirred at room temperature for 24 h. The solvent was evaporated under reduced pressure to yield a white powder in quantitative yield. ESI-MS: *m*/*z* (%) = 1314 (8) $\{[Sm_2(\mathbf{L})_4](CF_3SO_3)_4\}^{2+}$, 827 (3) $\{[Sm_2(\mathbf{L})_4](CF_3SO_3)_3\}^{3+}$, 583 (100) $\{[Sm_2(\mathbf{L})_4](CF_3SO_3)_2\}^{4+}$, 437 (20) $\{[Sm_2(\mathbf{L})_4](CF_3SO_3)\}^{5+}$, 339 (5) $\{[Sm_2(\mathbf{L})_4]\}^{6+}$. $Sm_2\mathbf{L}_4(CF_3SO_3)_6{\cdot}6H_2O$ (3033.31): calcd. C 40.39, H 4.12, N 11.08, S 6.34; found C 40.45, H 3.92, N 10.35, S 6.80.

Sm^{III} Complex 1a: A solution of ligand **L** (10.4 mg, 24 μmol) and $Sm(CF_3SO_3)_3$ (14.5 mg, 24 μmol) in CH_3CN (5 mL) was stirred at room temperature for 19 h. The white complex was isolated in quantitative yield by evaporation of the solvent. ESI-MS: *m*/*z* (%) = 1910.2 (3) $\{[Sm_4(\mathbf{L})_4](CF_3SO_3)_{10}\}^{+2}$, 1316.4 (7) $\{[Sm(\mathbf{L})_2](CF_3SO_3)_2\}^{+}$, 1180.1 (7) $\{[Sm_3(\mathbf{L})_2](CF_3SO_3)_7\}^{2+}$, 1096.9 (10) $\{[Sm_2(\mathbf{L})_3](CF_3SO_3)_4\}^{2+}$, 881.9 (100) $\{[Sm_4(\mathbf{L})_4](CF_3SO_3)_8\}^{4+}$, 736.3 (18) $\{[Sm_3(\mathbf{L})_2](CF_3SO_3)_6\}^{3+}$, 681.9 (2) $\{[Sm_2(\mathbf{L})_3]$-

 © 2004 Wiley-VCH Verlag GmbH & Co. KGaA, Weinheim

$(CF_3SO_3)_3\}^{3+}$, 515.9 (2) $\{[Sm_3(\mathbf{L})_2](CF_3SO_3)_5\}^{4+}$, 365.5 $\{[Sm_4(\mathbf{L})_4](CF_3SO_3)_4\}^{8+}$. $Sm_4\mathbf{L}_4(CF_3SO_3)_{12}$ (4120.3): calcd. C 31.48, H 2.74, N 8.16, S 9.34; found C 30.06, H 2.56, N 9.01, S 7.85. Excitation, λ = 326 nm. Luminescence spectrum (MeCN, 2×10^{-5} M, at 20 °C): λ_{em} = 566 nm ($^4G_{5/2} \rightarrow {}^6H_{5/2}$), 597 nm ($^4G_{5/2} \rightarrow {}^6H_{7/2}$), 647 nm ($^4G_{5/2} \rightarrow {}^6H_{9/2}$).

Eu^{III} Complex 2: A solution of ligand **L** (11.9 mg, 28 μmol) and $Eu(CF_3SO_3)_3$ (11.0 mg, 18 μmol) in CH_3CN (5 mL) was stirred at room temperature for 24 h. The white complex was isolated in quantitative yield by evaporation of the solvent. ESI-MS: *m*/*z* (%) = 1316 (30) $\{[Eu_2(\mathbf{L})_4](CF_3SO_3)_4\}^{2+}$, 827 (7) $\{[Eu_2(\mathbf{L})_4](CF_3SO_3)_3\}^{3+}$, 583 (100) $\{[Eu_2(\mathbf{L})_4](CF_3SO_3)_2\}^{4+}$, 436 (100) $\{[Eu_2(\mathbf{L})_4](CF_3SO_3)\}^{5+}$, 340 (10) $\{[Eu_2(\mathbf{L})_4]\}^{6+}$. $Eu_2\mathbf{L}_4(CF_3SO_3)_6 \cdot 6H_2O$ (3036.59): calcd. C 40.35, H 4.12, N 11.07, S 6.34; found C 39.23, H 4.03, N 10.67, S 6.02.

Eu^{III} Complex 2a: An equimolar mixture of $Eu(CF_3SO_3)_3$ (7.5 mg, 17 μmol) and ligand **L** (10.4 mg, 17 μmol) in CH_3CN (5 mL) was stirred at room temp. for 16 h. The solvent was evaporated under reduced pressure to yield a yellowish powder. ESI-MS: *m*/*z* (%) = 1914.5 (3) $\{[Eu_4(\mathbf{L})_4](CF_3SO_3)_{10}\}^{2+}$, 1314.9 (10) $\{[Eu_2(\mathbf{L})_4](CF_3SO_3)_4\}^{2+}$, 1226.0 (10) $\{[Eu_4(\mathbf{L})_4](CF_3SO_3)_9\}^{3+}$, 1181.5 (3) $\{[Eu_3(\mathbf{L})_2](CF_3SO_3)_7\}^{2+}$, 1097.9 (23) $\{[Eu_2(\mathbf{L})_3](CF_3SO_3)_4\}^{2+}$, 881.9 (100) $\{[Eu_4(\mathbf{L})_4](CF_3SO_3)_8\}^{4+}$, 827.4 (5) $\{[Eu_2(\mathbf{L})_4](CF_3SO_3)_3\}^{3+}$, 738.1 (14) $\{[Eu_3(\mathbf{L})_2](CF_3SO_3)_6\}^{3+}$, 682.5 (20) $\{[Eu_2(\mathbf{L})_3](CF_3SO_3)_3\}^{3+}$, 673.8 (10) $\{[Eu_4(\mathbf{L})_4](CF_3SO_3)_7\}^{5+}$, 582.8 (15) $\{[Eu_2(\mathbf{L})_4](CF_3SO_3)_2\}^{4+}$, 538.3 (25) $\{[Eu_4(\mathbf{L})_4](CF_3SO_3)_6\}^{6+}$, 435.2 (10) $\{[Eu_2(\mathbf{L})_4](CF_3SO_3)\}^{5+}$, 366.9 (10) $\{[Eu_4(\mathbf{L})_4](CF_3SO_3)_4\}^{8+}$, 350.0 (3) $\{[Eu_2(\mathbf{L})_3](CF_3SO_3)\}^{5+}$. $Eu_4\mathbf{L}_4(CF_3SO_3)_{12}$ (4126.77): calcd. C 31.43, H 2.75, N 8.15, S 9.32; found C 30.16, H 2.55, N 7.97, S 8.53. UV/Vis ($c = 1.8 \times 10^{-5}$ M): λ = 303 nm, 314 nm, 326 nm. Excitation λ = 326 nm. Luminescence spectrum (MeCN, at 20 °C): λ_{em} = 590 nm ($^5D_0 \rightarrow {}^7F_1$), 615 nm ($^5D_0 \rightarrow {}^7F_2$), 648 nm ($^5D_0 \rightarrow {}^7F_3$), 691 nm ($^5D_0 \rightarrow {}^7F_4$).

Tb^{III} Complex 3: A mixture of $Tb(CF_3SO_3)_3$ (6.7 mg, 11 μmol) and ligand **L** (7.2 mg, 17 μmol) in CH_3CN (5 mL) was stirred at room temperature for 24 h. The solvent was evaporated under reduced pressure to yield a white product in quantitative yield. ESI-MS: *m*/*z* (%) = 1322 (15) $\{[Tb_2(\mathbf{L})_4](CF_3SO_3)_4\}^{2+}$, 586 (100) $\{[Tb_2(\mathbf{L})_4](CF_3SO_3)_2\}^{4+}$, 341 (8) $\{[Tb_2(\mathbf{L})_4]\}^{6+}$. $Tb_2\mathbf{L}_4(CF_3SO_3)_6 \cdot 8H_2O$ (3074.37): calcd. C 39.85, H 4.16, N 10.93, S 6.26; found C 37.14, H 4.11, N 10.20, S 6.42.

Tb^{III} Complex 3a: A solution of ligand **L** (7.0 mg, 16 μmol) and $Tb(CF_3SO_3)_3$ (9.8 mg, 16 μmol) in CH_3CN (5 mL) was stirred at room temperature for 21 h. The white complex was isolated in quantitative yield by evaporation of the solvent. ESI-MS: *m*/*z* (%) = 2360.4 (1) $\{[Tb_2(\mathbf{L})_3](CF_3SO_3)_5\}^{+}$, 1927.2 (2) $\{[Tb_4(\mathbf{L})_4](CF_3SO_3)_{10}\}^{2+}$, 1236.4 (2) $\{[Tb_4(\mathbf{L})_4](CF_3SO_3)_9\}^{3+}$, 1192.1 (1) $\{[Tb_3(\mathbf{L})_2](CF_3SO_3)_7\}^{2+}$, 1105.4 (80) $\{[Tb_2(\mathbf{L})_3](CF_3SO_3)_4\}^{2+}$, 889.2 (37) $\{[Tb_4(\mathbf{L})_4](CF_3SO_3)_8\}^{4+}$, 687.4 (92) $\{[Tb_2(\mathbf{L})_3](CF_3SO_3)_3\}^{3+}$, 543.2 (15) $\{[Tb_4(\mathbf{L})_4](CF_3SO_3)_6\}^{6+}$, 370.1 (12) $\{[Tb_4(\mathbf{L})_4](CF_3SO_3)_4\}^{8+}$. $Tb_4\mathbf{L}_4(CF_3SO_3)_{12}$ (4154.6): calcd. C 31.22, H 2.72, N 8.09, S 9.26; found C 30.98, H 2.82, N 8.23, S 8.22. Excitation λ = 326 nm. Luminescence spectrum (MeCN, 2×10^{-5} M at 20 °C): λ_{em} = 494 nm ($^5D_4 \rightarrow {}^7F_6$), 549 nm ($^5D_4 \rightarrow {}^7F_5$), 588 nm ($^5D_4 \rightarrow {}^7F_4$), 621 nm ($^5D_4 \rightarrow {}^7F_3$).

Dy^{III} Complex 4: A mixture of $Dy(CF_3SO_3)_3$ (8.3 mg, 14 μmol) and ligand **L** (8.8 mg, 20 μmol) in CH_3CN (4 mL) was stirred at room temperature for 24 h. The solvent was evaporated under reduced pressure to yield a white powder in quantitative yield. ESI-MS: *m*/*z* (%) = 1326 (10) $\{[Dy_2(\mathbf{L})_4](CF_3SO_3)_4\}^{2+}$, 589 (100) $\{[Dy_2(\mathbf{L})_4](CF_3SO_3)_2\}^{4+}$, 441 (20) $\{[Dy_2(\mathbf{L})_4](CF_3SO_3)\}^{5+}$, 342 (10) $\{[Dy_2(\mathbf{L})_4]\}^{6+}$. $Dy_2\mathbf{L}_4(CF_3SO_3)_6 \cdot 8H_2O$ (3093.62): calcd. C 39.57, H 4.14, N 10.87, S 6.21; found C 36.53, H 4.07, N 10.09, S 6.25.

Dy^{III} Complex 4a: A solution of ligand **L** (8.2 mg, 19 μmol) and $Dy(CF_3SO_3)_3$ (11.5 mg, 19 μmol) in CH_3CN (5 mL) was stirred at room temperature for 21 h. The white complex was isolated in quantitative yield by evaporation of the solvent. ESI-MS: *m*/*z* (%) = 1325 (10) $\{[Dy_2(\mathbf{L})_4](CF_3SO_3)_4\}^{+2}$, 1108 (2) $\{[Dy_2(\mathbf{L})_3](CF_3SO_3)_4\}^{2+}$, 893 (10) $\{[Dy_4(\mathbf{L})_4](CF_3SO_3)_8\}^{4+}$, 546 (3) $\{[Dy_4(\mathbf{L})_4](CF_3SO_3)_6\}^{6+}$, 481 (5) $\{[Dy_2(\mathbf{L})_3](CF_3SO_3)_2\}^{4+}$, 447 (5) $\{[Dy_4(\mathbf{L})_4](CF_3SO_3)_5\}^{7+}$, 433 (100) [**L** + H]), 393 (5) $\{[Dy_3(\mathbf{L})_2](CF_3SO_3)_4\}^{5+}$, 150 (5) $[Dy_3(\mathbf{L})_2]^{9+}$. $Dy_4\mathbf{L}_4(CF_3SO_3)_{12}$ (4168.9): calcd. C 31.12, H 2.71, N 8.06, S9.23; found C 30.22, H 2.89, N 8.23, S 9.50. Excitation, λ = 326 nm. Luminescence spectrum (MeCN, $c = 2 \times 10^{-5}$ M, at 20 °C): λ_{em} = 483 nm ($^4F_{9/2} \rightarrow {}^6H_{13/2}$), 577 nm ($^4F_{9/2} \rightarrow {}^6H_{15/2}$).

X-ray Crystallographic Study: Data were collected using the ω-scan technique in the θ range 2−25° with a KUMA KM4CCD[17] four-circle diffractometer with a CCD detector, using graphite-monochromated Mo-K_α radiation (λ = 0.71073 Å). Accurate cell parameters were determined by a least-squares fit of the 5250 reflections of highest intensity, chosen from the whole experiment. Data were corrected for Lorentz-polarization[18] and absorption effects.[19] Due to the long *b* parameter of the unit cell, the potential overlapping of reflections was also taken into account. The structure was solved by direct methods with SHELXS-97,[20] and refined with SHELXL-97.[21] Non-hydrogen atoms were refined anisotropically, hydrogen atoms were located in calculated positions, and refined using the "riding model" with their isotropic thermal parameters set at 1.2 times the U_{eq} value of the appropriate carrier atom. The final model involves some disorder in the crystal structure ($N-Et_2$ groups and two triflates). Weak constraints to the thermal parameters of chosen atoms were applied. Crystallographic data for complex **2** are listed in Table 2.

Table 2. Crystallographic data for the structural analyses of the complex **2**

Empirical formula	$Eu_2(C_{24}H_{28}N_6O_2)_4(CF_3SO_3)_6 \cdot 6H_2O$
Molecular mass	3036.59
a (Å)	12.254(2)
b (Å)	41.250(4)
c (Å)	25.654(2)
α (°)	90
β (°)	94.03(1)
γ (°)	90
V (Å^3)	12936(2)
Z	4
Space group	$P2_1/n$
$D_{calcd.}$ (g·cm^{-3})	1.56
μ(Mo-K_α) (mm^{-1})	1.17
$R(F)$ [$F^2 > 2\sigma(F^2)$][a]	0.084
$R_w(F^2)$ [all data][b]	0.180

[a] $R(F) = \Sigma||F_o| - |F_c||/\Sigma|F_o|$ [b] $Rw(F2) = (\Sigma[w(F_o^2 - F_c^2)^2/\Sigma w(F_o^2)^2])^{1/2}$.

CCDC-210662 contains the supplementary crystallographic data for this paper. These data can be obtained free of charge at www.ccdc.cam.ac.uk/conts/retrieving.html [or from the Cambridge Crystallographic Data Center, 12 Union Road, Cambridge CB2 1EZ, UK; Fax: (internat.) +44-1223/336-033; E-mail: deposit@ccdc.cam.ac.uk].

 © 2004 Wiley-VCH Verlag GmbH & Co. KGaA, Weinheim

Acknowledgments

This work was partially supported by grant No. 4 T09A 049 24 from the Polish State Committee for Scientific Research and NATO for a post-doctoral fellowship (V. P.).

[1] [1a] N. Sabbatini, M. Guardigli, J.-M. Lehn, *Coord. Chem. Rev.* **1993**, *123*, 201−228. [1b] Ch.-D. Wu, C.-Z. Lu, W.-B. Yang, S.-F. Lu, H.-H. Zhuang, J.-S. Huang, *Eur. J. Inorg. Chem.* **2002**, 797−800. [1c] Y. Bretonnière, M. Mazzanti, J. Pécaut, M. M. Olmstead, *J. Am. Chem. Soc.* **2002**, *124*, 9012−9013. [1d] S. Nishihara, T. Akutagawa, T. Hasegawa, T. Nakamura, *Inorg. Chem.* **2003**, *42*, 2480−2482.

[2] [2a] P. Caravan, J. J. Ellison, T. J. McMurry, R. B. Lauffer, *Chem. Rev.* **1999**, *99*, 2293−2352. [2b] D. Parker, *Coord. Chem. Rev.* **2000**, *205*, 109−130. [2c] G. Mathis, *Clinical Chem.* **1993**, *39*, 1953−1959.

[3] [3a] L. Thunus, R. Lejeune, *Coord. Chem. Rev.* **1999**, *184*, 125−155. [3b] K. Wang, R. Li, Y. Chen, B. Zhu, *Coord. Chem. Rev.* **1999**, *190−192*, 297−308. [3c] M. Woods, Z. Kovacs, A. D. Sherry, *J. Supramolecular Chem.* **2002**, *2*, 1−15.

[4] [4a] K. Matsumara, M. Endo, M. Komiyama, *J. Chem. Soc., Chem. Commun.* **1994**, 2019−2020. [4b] D. Magda, R. A. Miller, J. L. Sessler, B. L. Iverson, *J. Am. Chem. Soc.* **1994**, *116*, 7439−7440. [4c] B. F. Baker, H. Khalili, N. Wei, J. R. Morrow, *J. Am. Chem. Soc.* **1997**, *119*, 8749−8755. [4d] R. Häner, J. Hall, *Antisense Nucleic Acid.* **1997**, *7*, 423−430. [4e] T. Gunnlaugsson, R. J. H. Davies, M. Nieuwenhuyzen, C. S. Stevenson, R. Viguier, S. Mulready, *Chem. Commun.* **2002**, 2136−2137.

[5] [5a] M. Botta, *Eur. J. Inorg. Chem.* **2000**, 399−407. [5b] F. A. Dunand, R. S. Dickins, D. Parker, A. E. Merbach, *Chem. Eur. J.* **2001**, 5160−5167. [5c] S. Aime, L. Frullano, S. Geninatti Crich, *Angew. Chem. Int. Ed.* **2002**, *41*, 1017−1019. [5d] K. Kimpe, T. N. Parac-Vogt, S. Laurent, C. Piérart, L. Vander Elst, R. N. Muller, K. Binnemans, *Eur. J. Inorg. Chem.* **2003**, 3021−3027.

[6] [6a] A. Beeby, R. S. Dickins, S. FitzGerald, L. J. Govelock, Ch. L. Maupin, D. Parker, J. P. Riehl, G. Siligardi, J. A. G. Williams, *Chem. Commun.* **2000**, 1183−1184. [6b] T. Gunnlaugsson, D. A. Mac Dónaill, D. Parker, *J. Am. Chem. Soc.* **2001**, *123*, 12866−12876.

[7] L. M. Vallarino, *J. Alloys Comp.* **1997**, *249*, 69−75.

[8] [8a] M. F. Tweedle, in *Lanthanide Probes in Life*, Chemical and Earth Sciences (Eds.: J.-C. Bünzli, G. R. Choppin), Elsevier, Amsterdam, **1989**, chapt. 5. [8b] C. H. Evans, in *Biochemistry of Lanthanides* (Ed.: E. Frieden), Plenum Press, New York, **1990**, Chapt. 9.

[9] V. Patroniak, P. N. W. Baxter, J.-M. Lehn, M. Kubicki, M. Nissinen, K. Rissanen, *Eur. J. Inorg. Chem.* **2003**, 4001−4009.

[10] S. Lis, Z. Hnatejko, Z. Stryła, *Opt. Appl.* **2001**, *31*, 643−648.

[11] C. Galaup, J. Azema, P. Tisnes, C. Picard, P. Ramos, O. Juanes, E. Brunet, J. C. Rodriguez-Ubis, *Helv. Chim. Acta* **2002**, *85*, 1613−1625.

[12] [12a] W. D. Horrocks, D. R. Sudnick, *J. Am. Chem. Soc.* **1979**, *101*, 334−340. [12b] W. D. Horrocks, D. R. Sudnick, *Acc. Chem. Res.* **1981**, *14*, 384−392. [12c] M. Albin, W. D. Horrocks, *Inorg. Chem.* **1985**, *24*, 895−900. [12d] Z. Hnatejko, S. Lis, M. Elbanowski, *J. Alloys Comp.* **2000**, *300−301*, 38−44.

[13] P. P. Barthelemy, G. R. Chopin, *Inorg. Chem.* **1989**, *28*, 3354−3357.

[14] [14a] F. Renaud, C. Piguet, G. Bernardinelli, J.-C. Bünzli, G. Hopfgartner, *Chem. Eur. J.* **1997**, *3*, 1660−1667. [14b] N. Martin, J.-C. Bünzli, V. McKee, C. Piguet, G. Hopfgartner, *Inorg. Chem.* **1998**, *37*, 577−589. [14c] C. Husson, P. Delangle, J. Pecaut, P. J. A. Vottero, *Inorg. Chem.* **1999**, *38*, 2012−2019. [14d] P. Gawryszewska, L. Jerzykiewicz, M. Pietraszkiewicz, J. Legiendziewicz, J. P. Riehl, *Inorg. Chem.* **2000**, *39*, 5365−5372. [14e] S. Batsanov, J. I. Bruce, T. Ganesh, P. J. Low, R. Kataky, H. Puschmann, P. G. Steel, *J. Chem. Soc., Perkin Trans. 1* **2002**, 932−937.

[15] F. H. Allen, *Acta Crystallogr., Sect. B* **2002**, *58*, 380−388.

[16] [16a] Y. Haas, G. Stein, *J. Phys. Chem.* **1971**, *75*, 3668−3677, [16b] K. Nakamaru, *Bull. Chem. Soc. Jpn.* **1982**, *55*, 2697−2705. [16c] J.-M. Lehn, M. Pietraszkiewicz, J. Karpiuk, *Helv. Chim. Acta* **1990**, *73*, 106−111. [16d] V. Balzani, E. Berghmans, J.-M. Lehn, N. Sabbatini, R. Terorde, R. Ziessel, *Helv. Chim. Acta* **1990**, *73*, 2083−2089.

[17] CrysAlisCCD, User Guide vers. 168, Kuma Diffraction, Wrocław, Poland, **1999**.

[18] CrysAlisRed, Program for Reduction of the Data from Kuma CCD Diffractometer, Kuma Diffraction, Wrocław, Poland, **1999**.

[19] R. H. Blessing, *J. Appl. Crystallogr.* **1989**, *22*, 396−397.

[20] G. M. Sheldrick, *Acta Crystallogr., Sect. A* **1990**, *46*, 467−473.

[21] G. M. Sheldrick, SHELXL-97, Program for the Refinement of Crystal Structures, University of Göttingen, Göttingen (Germany), **1997**.

Received November 26, 2003
Early View Article
Published Online April 7, 2004

 © 2004 Wiley-VCH Verlag GmbH & Co. KGaA, Weinheim

Mechanism of Oxidation of (olefin)Rh^I and -Ir^I Complexes by H_2O_2

Peter H. M. Budzelaar*[a] and Arno N. J. Blok[a]

Keywords: Density functional calculations / Iridium / Oxidation / Oxygenation / Rhodium

A DFT study of the oxidation of (tpa)$M^I(C_2H_4)^+$ and (dpa-R)M^I(cod)$^+$ complexes (M = Rh, Ir) by H_2O_2 indicates that the reaction starts with heterolytic cleavage of the peroxide O–O bond, leading to M^{III}(olefin)$(OH)^{2+}$ species. These can then undergo cyclisation, followed by deprotonation to oxetanes. In the oxidation of COD complexes, further cyclisation to internal ethers has a modest barrier, and the observed products (ethers for Rh, oxetanes for Ir) are suggested to be the thermodynamic ones.

(© Wiley-VCH Verlag GmbH & Co. KGaA, 69451 Weinheim, Germany, 2004)

Introduction

The oxidation of hydrocarbons at transition metal centres comprises a class of important yet poorly understood reactions. In addition to the more traditional organometallic reaction types, single-electron transfer steps and radical intermediates have to be considered. Moreover, oxidations are highly exothermic and often involve a cascade of elementary steps. These complications make the rational design and control of such reactions difficult and point to the need for a more detailed mechanistic understanding.

Still, not all oxidation reactions need necessarily be very complicated. Several years ago, De Bruin discovered the first clean example of the oxidation of a rhodium-coordinated ethene to an oxetane by H_2O_2 (Scheme 1).[1]

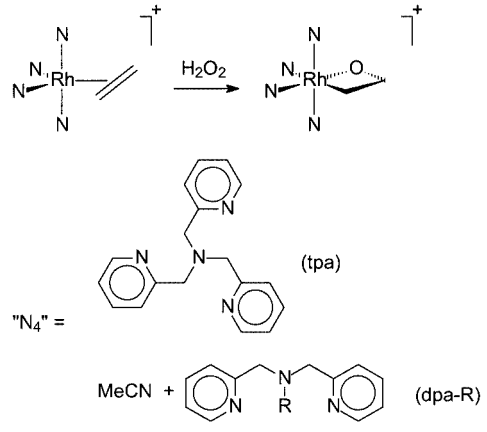

Scheme 1. Oxetane formation from ethene complexes and H_2O_2

Since then, this chemistry has been extended to cover also a few Ir examples, a few other N-donor ligands, propene and cyclooctadiene (COD).[2–5] In addition, the initial oxetane products have been converted into amido-substituted alkyl compounds, formylmethyl groups or acetaldehyde (Scheme 2).[6–8]

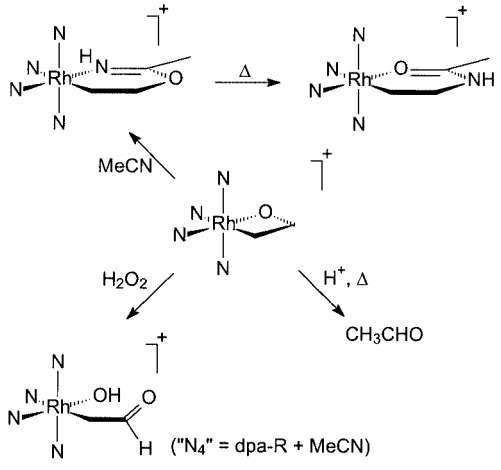

Scheme 2. Reactivity of oxarhodetanes

For COD the chemistry is somewhat more complex, since the second double bond can also participate in the oxygenation reaction, leading to internal ethers (Scheme 3). Depending on the metal, various isomeric ethers (Rh) or oxetanes (Ir) have been observed; in some cases, similar products have been observed in the oxidation of COD complexes by dioxygen (O_2).[3,9–11] It is not yet clear whether the observed isomers represent thermodynamic or kinetic products. In any case, they eventually rearrange to hydroxy-enediyl complexes.[2–4,9]

[a] Metal-Organic Chemistry, University of Nijmegen, Toernooiveld 1, 6525 ED Nijmegen, The Netherlands
Fax: (internat.) + 31-24-355-3450
E-mail: budz@sci.kun.nl

Supporting information for this article is available on the WWW under http://www.eurjic.org or from the author.

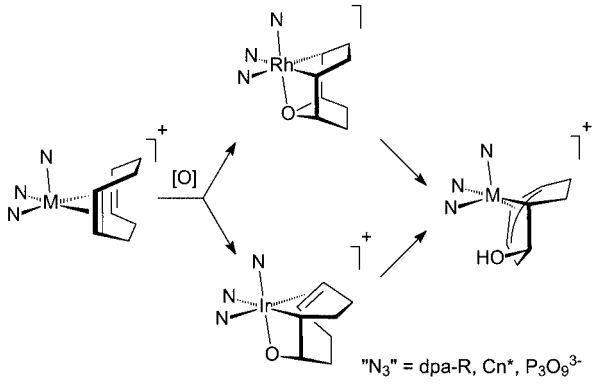

Scheme 3. Oxygenation of COD complexes

We have now studied the oxidation by H_2O_2 using DFT methods. For the initial oxidation step, three alternatives were considered, as summarised in Scheme 4: (*a*) concerted O−O bond breaking and Rh−O/C−O bond formation, followed by elimination of water; (*b*) heterolytic O−O cleavage, and then either (*b1*) deprotonation to an oxo complex, followed by cyclisation to an oxetane, or (*b2*) cyclisation to a protonated oxetane, followed by loss of the proton.

These reactions were studied for (tpa)M$(C_2H_4)^+$ complexes (M = Rh, Ir) as well as (dpa)M$(cod)^+$, (dpa-Me)M$(cod)^+$ (dpa-Me being a generic model for *N*-alkyl-substituted dpa ligands) and (tpa)M$(cod)^+$ (to explicitly include the possibility of a dangling picolyl group participating in the chemistry). For the COD complexes, interconversions between the various isomeric oxetane and ether products were investigated as well.

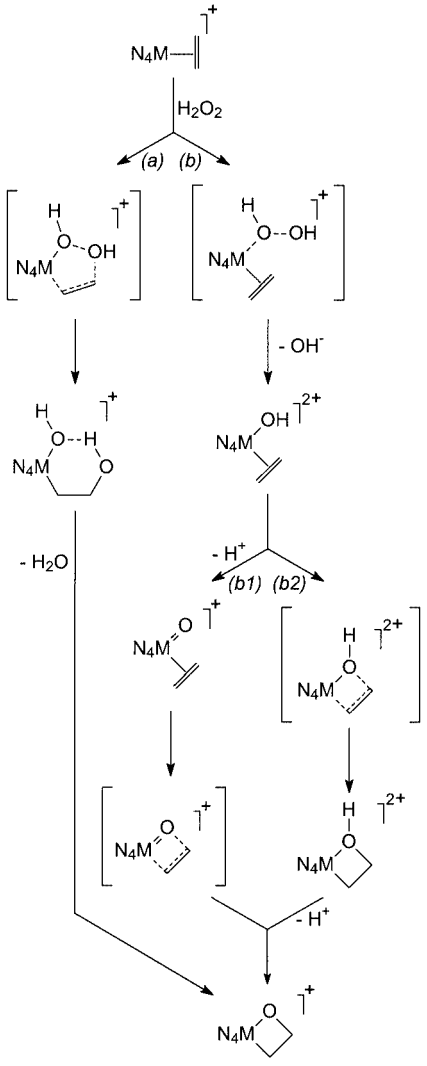

Scheme 4. Alternative mechanisms (*a*, *b1*, *b2*) for H_2O_2 oxidation of olefin complexes

Results and Discussion

Initial Attack of H_2O_2

Figure 1 shows the energy profiles for approach of H_2O_2 and $H_2O_2{\cdot}H_2O$ to (tpa)Rh$(C_2H_4)^+$ *cis* to the amine group [similar curves have been calculated for the *trans* approach and the corresponding reactions of (dpa)Rh$(cod)^+$ and (dpa-Me)Rh$(cod)^+$; see Supporting Information]. Starting from a weakly bound complex, the initial approach of the oxygen atom to the metal centre is slowly uphill in all cases. This is unsurprising, given the coordinatively saturated (18 e) nature of the metal centre. If only an isolated H_2O_2 molecule is used (Figure 1, diamonds), the approach stays repulsive up until fairly short M−O distances. The energy then goes down suddenly,[12] but the path does not lead to a protonated oxetane and separate OH^-, which would be too high in energy. Instead, a neighbouring acidic proton is immediately abstracted by the nascent OH^- group. Depending on the system, this can be the NH proton of dpa, a picolyl CH_2 proton of dpa or tpa, or the proton left on the OH group that was transferred to the metal atom. If a molecule of water is added, it hydrogen-bonds to H_2O_2. Now, on approach of an H_2O_2 oxygen atom to the metal atom the energy starts to go down already at longer M−O distances (Figure 1, squares), resulting in a marginally lower barrier.[12] For approach of both H_2O_2 and $H_2O_2{\cdot}H_2O$, the first step of the reaction appears to be heterolytic O−O cleavage, to form an OH^- ion (strongly stabilized by water if present) and an oxidized M^{III}(olefin)$(OH)^{2+}$ species. In practice, the H_2O_2 oxidation reactions always involve water and excess H_2O_2 able to sta-

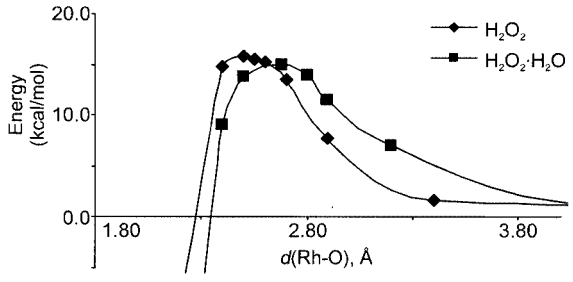

Figure 1. Potential-energy curve [kcal/mol] for approach of H_2O_2 or $H_2O_2{\cdot}H_2O$ to (tpa)Rh$(C_2H_4)^+$, *cis* to the amine nitrogen atom

 © 2004 Wiley-VCH Verlag GmbH & Co. KGaA, Weinheim

bilize this nascent OH^-,[1−5] so easy heterolytic cleavage, assisted by hydrogen bonding, would be expected.

The calculated transition state (Figure 2) appears to be early, since the Rh−O distance (2.680 Å) is quite long. The barrier is mainly caused by the lateral movement of the coordinated ethene and the lengthening of the two in-plane Rh−N bonds, i.e. H_2O_2 displaces a nitrogen donor ligand and the Rh centre avoids a 20-electron surrounding. However, at the transition state the O−O bond is already elongated significantly relative to free $H_2O_2{\cdot}H_2O$ (1.465 Å). The barrier of about 15 kcal/mol (25 kcal/mol relative to the separated reactants) corresponds to a reaction that would be fast at room temperature. The results for Ir and for (dpa)M(cod)$^+$ and (dpa-Me)M(cod)$^+$ are very similar.

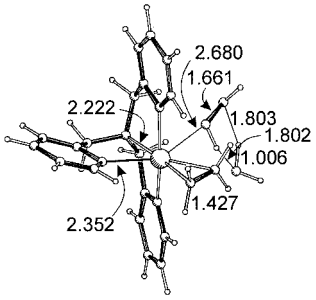

Figure 2. Calculated transition state for attack of $H_2O_2{\cdot}H_2O$ on (tpa)Rh$(C_2H_4)^+$ *cis* to the amine nitrogen atom; bond lengths in Å

The above constitutes the first step of variations (*b1*)and (*b2*) of Scheme 4. We have also considered variation (*a*) in which the nascent OH^- immediately attacks the olefin in a concerted manner. Despite extensive searches, no transition state for such an approach could be located; we conclude that no direct single-step reaction path exists. It remains possible that OH^- would first be lost and then attacks the olefin in a separate step. However, in that case approach to the olefin would be expected *trans* to the metal atom, and this would not lead to the COD oxidation products observed experimentally. In any case, it is not clear why, if route (*a*) were followed, the initially formed $M^{III}(OH)(CH_2CH_2OH)^{2+}$ complex would quickly rearrange to the (strained) oxetane observed experimentally. For these reasons, possibility (*a*) was not considered further.

Stereochemistry of H_2O_2 Attack

We assume that, once an M−O bond has been formed, the coordination chemistry around the metal atom is "frozen". This seems reasonable, since from that point on the complexes are octahedral ML_6 d^6 species and hence rather inert. Therefore, the final product distribution should reflect the stereochemistry of the initial H_2O_2 attack.

For oxidation of (tpa)Rh$(C_2H_4)^+$ by $H_2O_2{\cdot}H_2O$, we calculate a marginal preference (0.2 kcal/mol) for attack *cis* to the amine group. This agrees qualitatively with the stereochemistry observed experimentally, although the absence of any observable *trans* product[7] suggests that the real stereo preference is significantly higher than we calculate.

For oxidation of (dpa-Me)Rh(cod)$^+$ by $H_2O_2{\cdot}H_2O$, we calculate a similarly small preference (0.6 kcal/mol) for attack *cis* to the amine group, which corresponds to an expected *cis*/*trans* ratio of 3:1 at 0 °C. Experimentally, De Bruin observed a ratio of ca. 5:1 at room temperature and "selective" *cis* attack at −10 °C, which can be taken as reasonable agreement. The calculated *cis* preference is much larger (2.6 kcal/mol) for the oxidation of (dpa)Rh(cod)$^+$, where an additional hydrogen bond is formed between the auxiliary water molecule and the ligand NH group in the *cis*-attack transition state. It is not clear whether this is relevant to the "real" oxidation reaction, since there more water molecules would be present and the NH group would be involved in hydrogen bonding for *both* stereochemistries. In any case, the experimentally observed stereochemistry is indeed almost quantitatively *cis* to amine group for dpa-type ligands without a substituent at the amine nitrogen atom.

Formation of the First C−O Bond

Of the remaining variations (*b1* and *b2*), our results make the former one rather unlikely. The oxo intermediate in this mechanism is very high in energy. Its formation from the [(olefin)M^{I}]$^+$ complex and H_2O_2 is virtually thermoneutral, whereas the presumed intermediate hydroxo complex is about 40 kcal/mol lower in energy. The low stability of the oxo species is due to its lack of M−O π-bonding.[13] Thus, it is better represented by the zwitterionic M^+-O^- structure. Such an oxo complex is a very strong base, about 40 kcal/mol stronger than the final oxetane product. If it were formed at all, it would quickly cyclize to the oxetane; the calculated barrier for olefin insertion is negligible (1−2 kcal/mol).

In the second variation (*b2*), intramolecular nucleophilic attack of the OH group on the coordinated olefin has a modest barrier in all cases (5−15 kcal/mol). Thus, this represents a reasonable path for C−O bond formation. Subsequent loss of H^+ should also be easy, given the +2 charge of the complex. Therefore, we believe this path to be the more reasonable one, although, given the rough nature of our "solvation correction" (see Exp. Sect.) (*b1*) cannot be ruled out. Figure 3 shows the ring-closure transition state

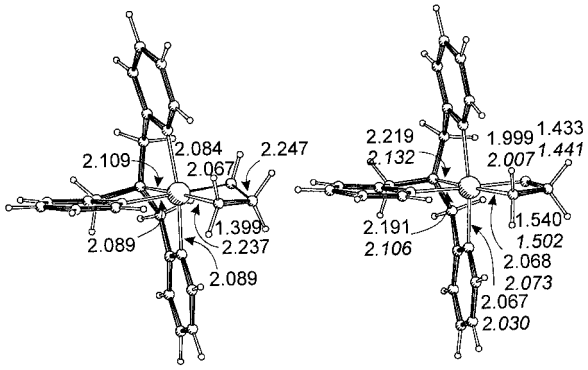

Figure 3. Calculated OH attack transition state and oxetane final product (after deprotonation) for *cis* attack on (tpa)Rh$(C_2H_4)^+$; calculated bond lengths in Å [observed values for (Me-tpa)Rh$(C_2H_4)^+$ [7] in *italics*]

 © 2004 Wiley-VCH Verlag GmbH & Co. KGaA, Weinheim

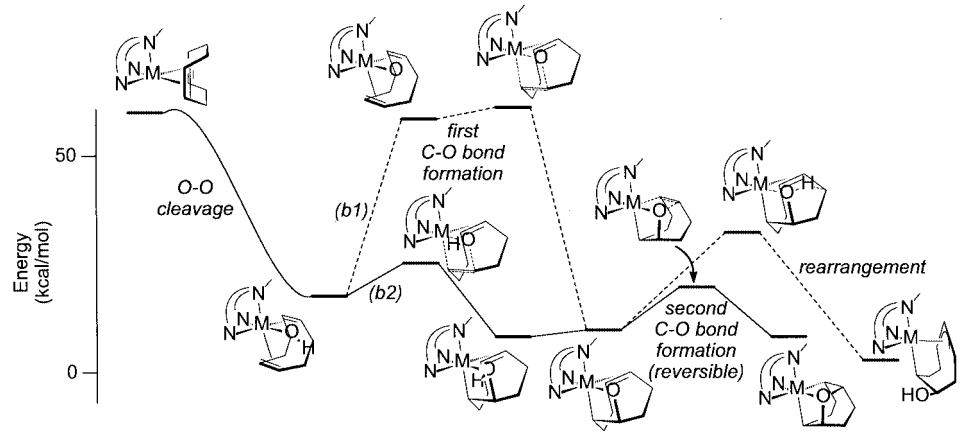

Figure 4. Calculated energy profile [kcal/mol] for *asym* attack at (tpa)Rh(cod)$^+$

and the oxetane final product for the preferred *cis*-to-amine attack on (tpa)Rh$(C_2H_4)^+$.

Figure 4 shows the complete calculated energy profile, including the steps discussed in the following sections, for *asym* (*cis* to the amine group) attack at (tpa)Rh(cod)$^+$.

COD-Derived Oxetanes and Ethers

For COD, the experimentally observed products of the oxidation can be either oxetanes (for M = Ir) or ethers (for M = Rh). We have calculated both types of isomeric products, as well as the transition states for their interconversion, using the *fac*-κ^3-coordinated tpa ligand. We chose this ligand because, depending on the disposition of the nitrogen donor groups around the metal atom, it can displace the remaining C=C bond of the oxetane product, as discussed below.

The results are summarised in Scheme 5. The barriers for ether formation are about 10 kcal/mol for Rh; they represent reactions that would rapidly reach equilibrium at room temperature. The barriers for Ir are slightly larger, as expected. The calculations predict the ether products (***s2***, ***a3***) to be more stable than their oxetane isomers for Rh, whereas for Ir the oxetanes (***s1***, ***a2***) are more stable, in agreement with experiment.

If a tetradentate ligand (tpa) is used in this reaction, it initially has a dangling picolyl group (structures ***s1−2***, ***a1−3***). Depending on the disposition around the metal atom, this can, in some cases, displace the remaining C=C bond of the oxetane product (***s3***, ***a4***). Indeed, for Rh Krom observed displacement in the *sym* isomer but not in the *asym* isomer, whereas for Ir experiment suggests the C=C bond remains coordinated in both isomers.[5] Our calcu-

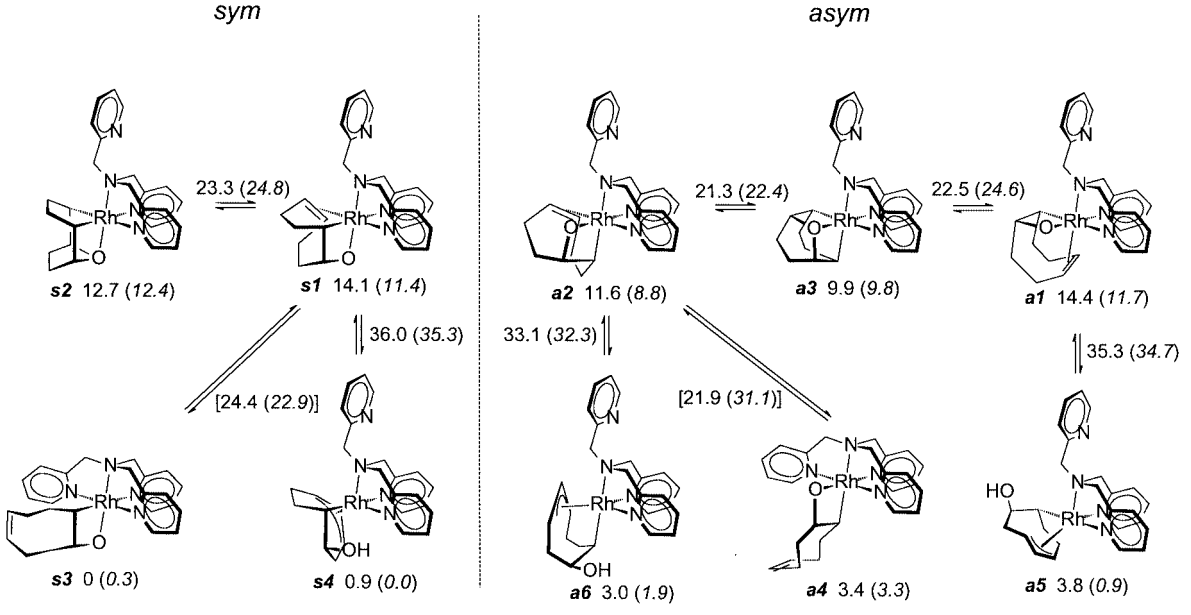

Scheme 5. Calculated relative energies of minima and transition states [kcal/mol] for Rh oxidation products[14] (values for Ir in *italics*)

 © 2004 Wiley-VCH Verlag GmbH & Co. KGaA, Weinheim

lations do not agree with this and predict C=C displacement by the dangling Py group to be favourable in all cases. We do not at present have a satisfactory explanation for this discrepancy. It is unlikely to be due to kinetic factors, since even intermediates having both C=C and Py groups detached are predicted to be accessible.[14]

Decomposition of COD-Derived Oxetanes

Experimentally, the oxetane and ether products derived from COD slowly rearrange to hydroxy-enediyl derivatives. This reaction appears to be accelerated by acid, at least for Rh.[3] Here, we have studied the uncatalysed rearrangement, which involves intramolecular transfer of an allylic proton to the oxetane oxygen atom. The calculated barriers (20−25 kcal/mol) are significant but not prohibitive, suggesting that uncatalysed rearrangement would certainly be possible. For Rh in the *asym* series, the path leading to isomer ***a6*** is predicted to be marginally more favourable than that leading to isomer ***a5***; experimentally, isomer ***a5*** is formed exclusively with the dpa ligand. For Ir, the route leading to ***a6*** also has a slightly lower calculated barrier, yet for Me-dpa an isomer of type ***a5*** is still observed experimentally.[4] Obviously, there is no a priori reason why any catalysed rearrangement should have the same selectivity as the uncatalysed reaction.

A Comparison with Ti^{IV}- and Mo^{VI}-Catalysed Epoxidation

It is interesting to contrast the sequence of steps described here to that occurring in olefin epoxidation by H_2O_2 (or ROOH) catalysed by the early transition metals Ti^{IV} [15] and Mo^{VI} (Scheme 6).[16] There, the hydrogen peroxide forms a metal hydroperoxide, from which an oxygen atom is transferred to an olefin without direct metal−olefin coordination. The metal atom activates the OOR group through η^2-coordination, making the OR group a good leaving group,[17] but the metal atom itself is redox-inactive. In the present late-transition-metal case, H_2O_2 oxidizes M^{I} to M^{III}, and this in turn oxidizes the olefin through intramolecular Wacker-type chemistry.[18]

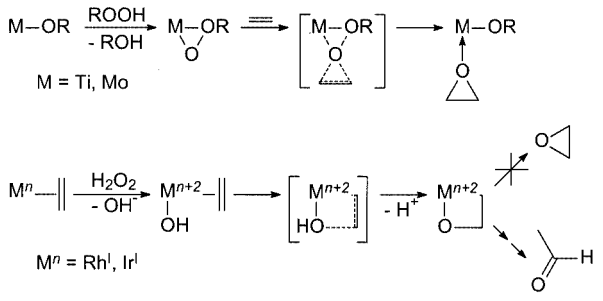

Scheme 6. Comparison of olefin oxidation by peroxides at early and late transition metal atoms

These different mechanisms explain the differences in product types. In Ti^{IV} and Mo^{VI} reactions, the epoxide is the initial product, and unless it is opened in the reaction medium by electrophilic or nucleophilic attack, it will also be the final product. In the type of metal-mediated oxidation chemistry studied here, the initial product is a (protonated) metallaoxetane, from which reductive elimination to the highly strained epoxide would only be expected if the metal atom is in an unusually high oxidation state. That is not the case for Rh^{III} or Ir^{III}, so decomposition to an aldehyde or ketone by β-hydrogen elimination is a more likely outcome.

Conclusions

Calculations have provided a consistent and reasonable picture of the oxidation of $[N_x(olefin)Rh^{I}]^+$ complexes by H_2O_2. The initial step is proposed to be heterolytic O−O cleavage, possibly assisted by hydrogen bonding of, for example, water to the nascent OH^- ion. The next step is probably intramolecular attack of coordinated OH^- on coordinated olefin, followed by loss of a proton. For COD complexes, the oxetanes formed in this way can undergo reversible intramolecular attack of the alkoxide oxygen atom on the remaining C=C bond, leading to ether products. The calculated stabilities and barriers suggest that the products observed experimentally are the thermodynamic ones. For Ir, oxetanes are calculated to be slightly more stable than their ether isomers, but apart from that the differences between Rh and Ir appear to be small.

Table 1. Relative energies [kcal/mol] for oxidation of $(tpa)M(C_2H_4)^+$

	Rh		Ir	
	cis[a]	*trans*[a]	*cis*[a]	*trans*[a]
$(tpa)M(C_2H_4)^+$	66.9		70.2	
H_2O_2 complex	79.6	79.8	82.2	82.3
O−O cleavage TS	93.0	92.8	97.8	95.6
$H_2O_2{\cdot}H_2O$ complex	77.2	80.0	80.6	82.8
O−O cleavage TS	92.1	92.3	96.4	96.6
$(tpa)M(C_2H_4)(OH)^{2+}$[b]	12.9	12.7	7.5	8.4
C_2H_4 insertion TS[b]	17.2	16.7	17.0	16.8
$(tpa)M(CH_2CH_2OH)^{2+}$ [b]	1.9	0.0	1.3	0.0
$(tpa)M(C_2H_4)(O)^+$	55.6	55.3	50.1	52.9
C_2H_4 insertion TS	57.0	55.7	56.7	56.2
$(tpa)M(CH_2CH_2O)^+$	8.3	6.9	8.1	7.3

[a] Position of O attack relative to the amine nitrogen atom. [b] Correction for energies for dicationic species: see Exp. Sect.

Table 2. Relative energies [kcal/mol] for initial step of oxidation of $(dpa)M(cod)^+$ and $(dpa\text{-}Me)M(cod)^+$ by $H_2O_2{\cdot}H_2O$

	Rh		Ir	
	cis[a]	*trans*[a]	*cis*[a]	*trans*[a]
$(dpa)M(cod)^+$	0.0		0.0	
$H_2O_2{\cdot}H_2O$ complex	11.7	10.1	11.1	10.0
O−O cleavage TS	25.6	28.3	25.1	28.5
$(dpa\text{-}Me)M(cod)^+$	0.0		0.0	
$H_2O_2{\cdot}H_2O$ complex	10.9	9.4	11.4	10.3
O−O cleavage TS	24.2	24.8	25.5	25.4

[a] Position of O attack relative to the amine nitrogen atom.

 © 2004 Wiley-VCH Verlag GmbH & Co. KGaA, Weinheim

Table 3. Relative energies [kcal/mol] for oxidation of (tpa)M(cod)$^+$

	Rh			Ir		
	cis1[a]	*cis2*[a]	*trans*[a]	*cis1*[a]	*cis2*[a]	*trans*[a]
(κ^3-tpa)M(cod)$^+$		59.6			59.7	
(κ^3-tpa)M(cod)(OH)$^{2+}$[b]	19.0		25.4	11.5		17.5
cod insertion TS[b]	30.7	26.3	31.5	26.8	23.2	27.8
(κ^3-tpa)M(cod-oxetaneH)$^{2+}$ [b]	15.2	10.2	15.5	13.1	6.5	13.1
(κ^3-tpa)M(cod)(O)$^+$	58.0		57.9	49.9		50.6
cod insertion TS	60.7	60.5	58.8	57.2	57.9	56.5
(κ^3-tpa)M(cod-oxetane)$^+$	14.4	11.6	14.4	11.7	8.8	11.4
oxetane-ether TS	22.5	21.3	23.3	24.6	22.4	24.8
(κ^3-tpa)M(cod-ether)$^+$	9.9		12.7	9.8		12.4
H shifts TS	35.3	33.1	36.0	34.7	32.3	35.3
(κ^3-tpa)M(hydroxy-enediyl)$^+$	3.8	3.0	0.9	0.9	1.9	0.0
(κ^3-tpa)M(κ^2-cod-oxetane)$^+$		21.9	24.4		31.1	22.9
(κ^4-tpa)M(κ^2-cod-oxetane)$^+$		3.4	0.0		3.3	0.3

[a] Position of O attack relative to the amine nitrogen atom. *cis1* (*cis2*) has the M−C bond *cis* (*trans*) to the amine nitrogen atom. [b] Correction for energies for dicationic species: see Exp. Sect.

Experimental Section

General Methods: All calculations were carried out with the Turbomole program[19a] coupled to the PQS Baker optimiser.[20] Geometries were fully optimised as minima or transition states at the bp86[21]/RIDFT[22] level using the Turbomole SV(P) basis set[19c][19d] on all atoms (small-core pseudopotential[19c][19e] on Rh and Ir); the nature of each stationary point was then checked by a numerical frequency analysis. Improved energies were obtained from single-point calculations at the b3-lyp level[23] using the TZVP basis[19c][19f] (small-core pseudopotential[19c][19e] on Rh and Ir) and a fine ("m4") integration grid. Solvent corrections were calculated at the b3-lyp/TZVP level using the COSMO solvation model[24] with a dielectric constant of 36.67 (acetonitrile). The final energies cited in the text and figures are free energies obtained by combining these solvation-corrected TZVP results with zero-point energy (ZPE) and thermal corrections (enthalpy and entropy, 273 K, 1 bar) calculated from the bp86/RIDFT frequency analyses. All species were put on common energy scales by adding H_2O_2, H_2O, OH^- etc. where appropriate. Tables 1−3 list the relative free energies for species discussed in the text. Complete listings of total energies are given as Supporting Information (Tables S1−S4).

Relative Energies of Mono- and Dicationic Species: Even with the inclusion of COSMO solvation corrections, the present level of calculation fails to provide realistic *relative* energies for species of different charges, such as occur in our heterolytic cleavage reactions of H_2O_2. This must at least in part be due to the neglect of strong *specific* solute−solvent interactions (e.g., hydrogen bonding) in the solvation model. The error made in the specific case of ionisation of water can be estimated from Equation (1), where $\varepsilon_{H_3O^+}$, ε_{OH^-}, and ε_{H_2O} are calculated at the COSMO/TZVP/b3-lyp level using the dielectric constant of water (80.37).

$$\Delta\varepsilon = \varepsilon_{H_3O^+} + \varepsilon_{OH^-} - 2\varepsilon_{H_2O} - RT\ln K_{H_2O}$$
$$K_{H_2O} = \frac{[H_3O^+][OH^-]}{[H_2O]^2} \approx (18)^2\,10^{-20} \quad (1)$$

As a very rough correction for the charge-separation problem, we subtracted this "fudge factor" from all calculated energies of dicationic species. This probably results in over-stabilisation of the dicationic species, since H_3O^+ is likely to have stronger specific solvent interactions than most other solutes, but at present we do not have a method that is guaranteed to produce more realistic relative energies for charge-separated species.

Acknowledgments

We are grateful to Prof. P. Burger (Hamburg) for providing the coupling module between Turbomole and the PQS optimiser, and to Sabic EPC for financial assistance.

[1] B. de Bruin, M. J. Boerakker, J. J. J. M. Donners, B. E. C. Christiaans, P. P. J. Schlebos, R. de Gelder, J. M. M. Smits, A. L. Spek, A. W. Gal, *Angew. Chem. Int. Ed. Engl.* **1997**, *36*, 2064.
[2] T. C. Flood, M. Iimura, J. M. Perotti, A. L. Rheingold, T. E. Concolino, *Chem. Commun.* **2000**, 1681.
[3] B. de Bruin, J. A. Brands, J. J. J. M. Donners, M. P. J. Donners, R. de Gelder, J. M. M. Smits, A. W. Gal, A. L. Spek, *Chem. Eur. J.* **1999**, *5*, 2921.
[4] R. J. N. A. M. Kicken, PhD Thesis, Nijmegen, **2001**.
[5] M. Krom, PhD Thesis, Nijmegen, **2003**.
[6] B. de Bruin, M. J. Boerakker, R. de Gelder, J. M. M. Smits, A. W. Gal, *Angew. Chem. Int. Ed.* **1999**, *38*, 219.
[7] B. de Bruin, M. J. Boerakker, J. A. W. Verhagen, R. de Gelder, J. M. M. Smits, A. W. Gal, *Chem. Eur. J.* **2000**, *6*, 298.
[8] B. de Bruin, J. A. W. Verhagen, C. H. J. Schouten, A. W. Gal, D. Feichtinger, D. A. Plattner, *Chem. Eur. J.* **2001**, *7*, 416.
[9] V. W. Day, W. G. Klemperer, S. P. Lockledge, D. J. Main, *J. Am. Chem. Soc.* **1990**, *112*, 2033.
[10] (olefin)Rh and -Ir complexes can react with oxygen to form peroxo complexes (see, for example, ref.[2]), which can hydrolyze to hydrogen peroxide. Therefore, many O_2 oxygenations may well involve H_2O_2 as the actual oxidant of the olefin complex (as suggested in ref.[11]).
[11] B. de Bruin, T. P. J. Peters, J. B. M. Wilting, S. Thewissen, J. M. M. Smits, A. W. Gal, *Eur. J. Inorg. Chem.* **2002**, 2671.
[12] We could not always locate transition states for the "sudden-collapse" paths involving only H_2O_2. For the smoother paths using $H_2O_2{\cdot}H_2O$, all relevant transition states were found.
[13] See, for example: T. Cundari, *Chem. Rev.* **2000**, *100*, 807 and references cited therein.
[14] The "transition state energies" given in Scheme 5 for displacement of a COD C=C bond by a picolyl group represent the energies of hypothetical 16e intermediates having *both* the picolyl group and the C=C bond detached from the metal atom.
[15] See, for example: [15a] Y.-D. Wu, D. K. W. Lai, *J. Org. Chem.*

 © 2004 Wiley-VCH Verlag GmbH & Co. KGaA, Weinheim

1995, *60*, 673. [15b] Y.-D. Wu, D. K. W. Lai, *J. Am. Chem. Soc.* **1995**, *117*, 11327. [15c] I. V. Yudanov, P. Gisdakis, C. di Valentin, N. Rösch, *Eur. J. Inorg. Chem.* **1999**, 2135.

[16] See, for example: [16a] I. V. Yudanov, C. di Valentin, P. Gisdakis, N. Rösch, *J. Mol. Catal.* **2000**, *A158*, 189. [16b] D. V. Deubel, J. Sundermeyer, G. Frenking, *J. Am. Chem. Soc.* **2000**, *122*, 10101. [16c] D. V. Deubel, J. Sundermeyer, G. Frenking, *Inorg. Chem.* **2000**, *39*, 2314. [16d] D. V. Deubel, J. Sundermeyer, G. Frenking, *Eur. J. Inorg. Chem.* **2001**, 1819.

[17] Assistance by hydrogen-bond formation has also been suggested for Ti^{IV}-catalysed epoxidation: [17a] D. Tantanak, M. A. Vincent, I. H. Hillier, *Chem. Commun.* **1998**, 1031. However, a later solvation study did not show any specific effect of hydrogen bonding on the ease of oxygen transfer: [17b] R. R. Sever, T. W. Root, *J. Phys. Chem.* **2003**, *B107*, 4090.

[18] See also: B. de Bruin, P. H. M. Budzelaar, A. W. Gal, *Angew. Chem.,* accepted.

[19] [19a] R. Ahlrichs, M. Bär, H.-P. Baron, R. Bauernschmitt, S. Böcker, M. Ehrig, K. Eichkorn, S. Elliott, F. Furche, F. Haase, M. Häser, C. Hättig, H. Horn, C. Huber, U. Huniar, M. Kattannek, A. Köhn, C. Kölmel, M. Kollwitz, K. May, C. Ochsenfeld, H. Öhm, A. Schäfer, U. Schneider, O. Treutler, K. Tsereteli, B. Unterreiner, M. von Arnim, F. Weigend, P. Weis, H. Weiss, *Turbomole*, version 5, Theoretical Chemistry Group, University of Karlsruhe, January **2002**. [19b]O. Treutler, R. Ahlrichs, *J. Chem. Phys.* **1995**, *102*, 346. [19c] Turbomole basis set library, *Turbomole*, version 5, see ref.[12a][19d]A. Schäfer, H. Horn, R. Ahlrichs, *J. Chem. Phys.* **1992**, *97*, 2571. [19e] D. Andrae, U. Haeussermann, M. Dolg, H. Stoll, H. Preuss, *Theor. Chim. Acta* **1990**, *77*, 123. [19f] A. Schäfer, C. Huber, R. Ahlrichs, *J. Chem. Phys.* **1994**, *100*, 5829.

[20] [20a] *PQS*, version 2.4, Parallel Quantum Solutions, Fayetteville, Arkansas, USA, **2001** (the Baker optimiser is available separately from PQS upon request). [20b]J. Baker, *J. Comput. Chem.* **1986**, *7*, 385.

[21] [21a] A. D. Becke, *Phys. Rev. A* **1988**, *38*, 3089. [21b] J. P. Perdew, *Phys. Rev. B* **1986**, *33*, 8822.

[22] K. Eichkorn, F. Weigend, O. Treutler, R. Ahlrichs, *Theor. Chem. Acc.* **1997**, *97*, 119.

[23] [23a] C. Lee, W. Yang, R. G. Parr, *Phys. Rev. B* **1988**, *37*, 785. [23b] A. D. Becke, *J. Chem. Phys.* **1993**, *98*, 1372. [23c] A. D. Becke, *J. Chem. Phys.* **1993**, *98*, 5648. [23d] All calculations were performed using the Turbomole functional "b3-lyp", which is not the same as the Gaussian "B3LYP" functional.

[24] A. Klamt, G. Schüürmann, *J. Chem. Soc., Perkin Trans. 2* **1993**, 799.

Received August 7, 2003
Early View Article
Published Online April 7, 2004

 © 2004 Wiley-VCH Verlag GmbH & Co. KGaA, Weinheim

EurJIC
European Journal of Inorganic Chemistry

Issue 12/2004

Pages 2393–2594

Papers available ahead of print in Early View at www.interscience.wiley.com

Earliest available Table of Contents:
Automatically, free of charge by e-mail through
www.interscience.wiley.com/alerts

COVER PICTURE

The cover picture shows the half-open way from well-known (arene)ruthenium complexes to π-conjugated materials. This work illustrates the transition from molecular catalysts to molecular building blocks for conducting polymers and nonlinear optics. Details are discussed in the Short Communication by F. Chérioux et al. on p. 2405 ff. The authors are grateful to the Swiss National Science Foundation for financial support.

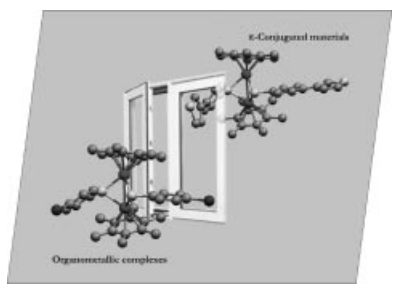

SHORT COMMUNICATION

Contents

2405 **M. J.-L. Tschan, F. Chérioux,* B. Therrien, G. Süss-Fink**

Subsequent Hydride Substitution in (Arene)trihydridodiruthenium Complexes: Synthesis and Structure of Thiolato-Bridged Diruthenium Cations of the Type $[H_2(arene)_2Ru_2(p\text{-}X{-}C_6H_4{-}S)]^+$ and $[H(arene)_2Ru_2(p\text{-}X{-}C_6H_4{-}S)_2]^+$

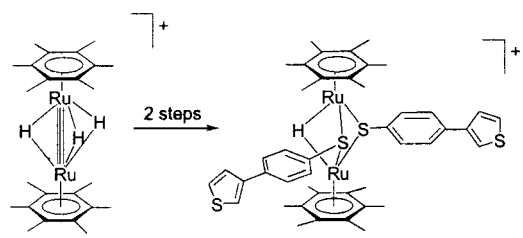

Keywords: Ruthenium / Sulfur / Hydrides / Complexes / Cross-coupling

 © 2004 Wiley-VCH Verlag GmbH & Co. KGaA, Weinheim

2413 **G. Leibeling, S. Demeshko, B. Bauer-Siebenlist, F. Meyer,* H. Pritzkow**

Polynuclear and Extended Coordination Compounds from Preorganized Bimetallic Components: Tuning the Magnetic Properties of Dinickel(II) Building Blocks

Keywords: Molecular magnetism / Nickel / Dinuclear complexes / Tetranuclear complexes / Magnetic properties / Azides

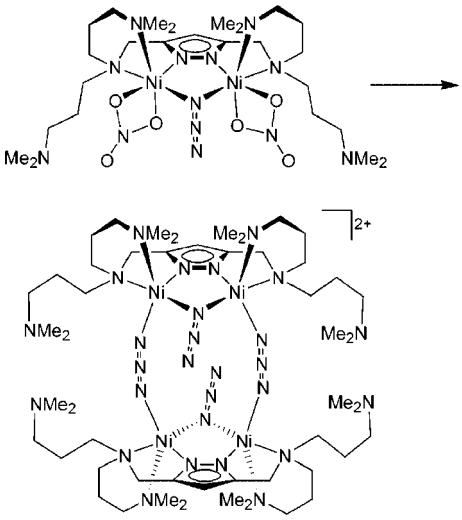

2421 **I. L. Fedushkin,* A. N. Lukoyanov, S. Dechert, H. Schumann***

Synthesis and Molecular Structure of Calcium Difluoranthenide, $[Ca(THF)_6][C_{16}H_{10}]_2 \cdot 2C_{16}H_{10}$

Keywords: Calcium / Fluoranthene / Radical-anion / Structure elucidation

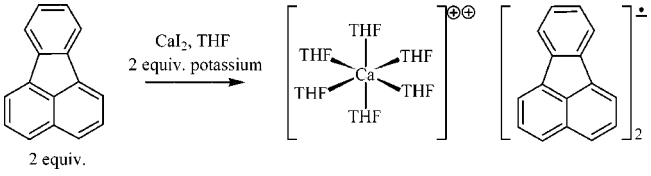

2425 **Y. Nie, H. Pritzkow, W. Siebert***

Reactivity Studies on 2,3,4,5-Tetraethyl-1,6-diiodo-2,3,4,5-tetracarba-*nido*-hexaborane(6): Synthesis and Structures of New C_4B_2 *nido*-Carborane Derivatives

Keywords: Boron / Carboranes / Nucleophilic substitution / Iron / Cobalt

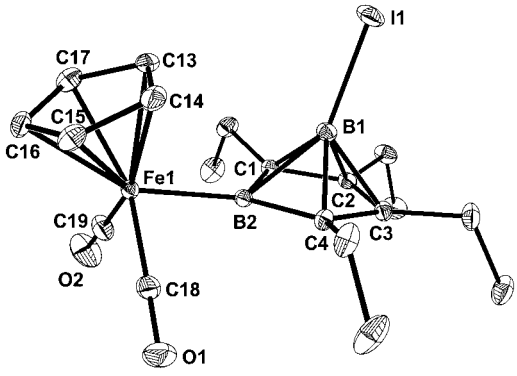

2434 **T. A. Vanderah,* T. Siegrist, R. S. Roth, A. P. Ramirez, R. G. Geyer**

Crystal Structure and Properties of $Ba_{11}FeTi_{27}O_{66.5}$

Keywords: Mixed metal oxides / X-ray diffraction / Magnetic susceptibility / Dielectric constants / Dielectric loss tangent

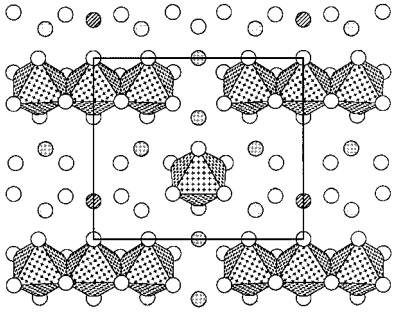

 © 2004 Wiley-VCH Verlag GmbH & Co. KGaA, Weinheim

2442 **B. van Oort, E. Tangen, A. Ghosh***

Electronic Structure of Transition Metal−Isocorrole Complexes: A First Quantum Chemical Study

Keywords: Calculations / Corrole / Isocorrole / Non-innocent ligands / Radicals / Transition metals

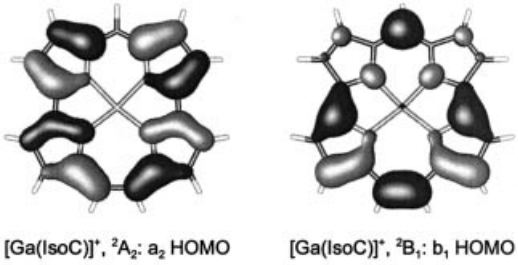

2446 **C. Knapp, E. Lork, R. Mews,* A. V. Zibarev***

Inclusion Complexes of the Bicyclic Aryl-Substituted Sulfur-Nitrogen Compounds Ar−CN_5S_3 with Fluorocarbon and Hydrocarbon Aromatics

Keywords: Polyfluoroaromatic compounds / Inclusion compounds / π-Stacking interactions / Molecular recognition / Crystal engineering

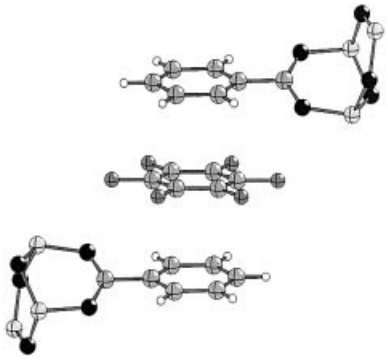

2452 **T. Borrmann, E. Lork, R. Mews,* M. M. Shakirov, A. V. Zibarev***

Preparation and Structural Characterization of $[K(18\text{-crown-6})]^+$ Salts of $[RNSN]^-$ Anions and the $[NSN]^{2-}$ Dianion

Keywords: Sulfur / Nitrogen / X-ray diffraction / NMR spectroscopy

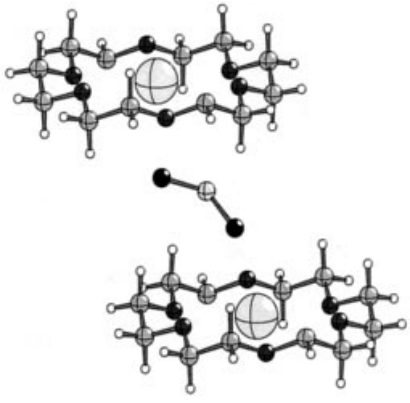

2459 **R.-M. Sebastián, L. Griffe, C.-O. Turrin, B. Donnadieu, A.-M. Caminade, J.-P. Majoral***

Synthesis and Core and Surface Reactivity of Phosphorus-Based Dendrons

Keywords: Azides / Dendrimers / Dendrons / N,P ligands / Phosphorus

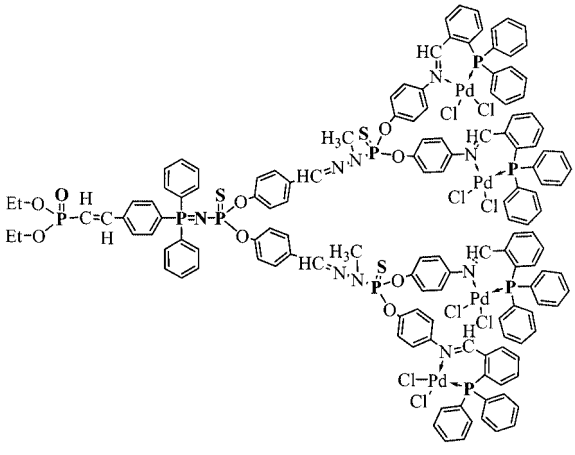

 © 2004 Wiley-VCH Verlag GmbH & Co. KGaA, Weinheim

2467 **F. Borbone, U. Caruso, R. Centore,* A. De Maria, A. Fort, M. Fusco, B. Panunzi, A. Roviello,* A. Tuzi**

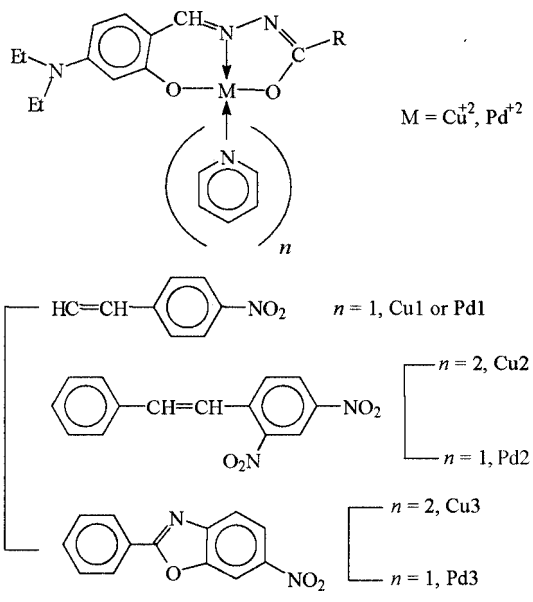

Second Order Optical Nonlinearities of Copper(II) and Palladium(II) Complexes with *N*-Salicylidene-*N*′-aroylhydrazine Tridentate Ligands

Keywords: Tridentate ligands / Nonlinear optics / Polymers / Copper / Palladium

2477 **C. Schlünken, M. A. Esteruelas, F. J. Lahoz, L. A. Oro, H. Werner***

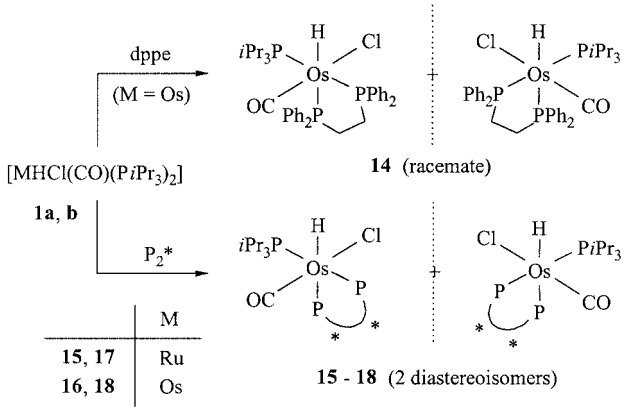

Synthesis, Molecular Structure and Catalytic Activity of Six-Coordinate Chloro(hydrido)- and Dihydridoruthenium(II) and -osmium(II) Complexes with the Chiral Ligands P*i*Pr$_2$NH(Me)Ph, (*S*,*S*)-Chiraphos and (*S*,*S*)-Diop

Keywords: Chirality / Hydrido complexes / Osmium / Phosphane complexes / Ruthenium

2488 **R. Wilberger, C. Krinninger, H. Piotrowski, P. Mayer, I.-P. Lorenz***

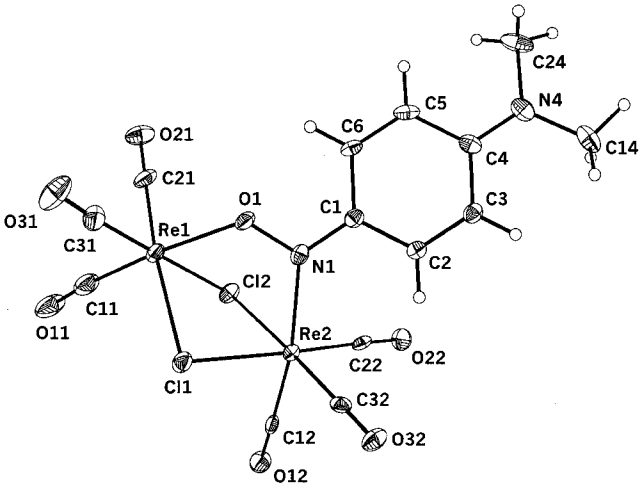

A New Dichroic, Nitroso-Bridged Complex of Rhenium: Di-μ_2-chloro[μ_2-(η^2-*N*,*O*)-*N*,*N*-dimethyl-4-nitrosoaniline]bis[tricarbonylrhenium(I)]

Keywords: Rhenium / C,N ligand / N,O bridge / Dichroism

 © 2004 Wiley-VCH Verlag GmbH & Co. KGaA, Weinheim

2493 **K. Melánová, L. Beneš,* V. Zima, M. Trchová, J. Dybal**

Vanadyl Phosphate Intercalated with Diethyl Ether

Keywords: Intercalation / Vibrational spectroscopy / X-ray diffraction / Ab initio calculations / Semiempirical calculations

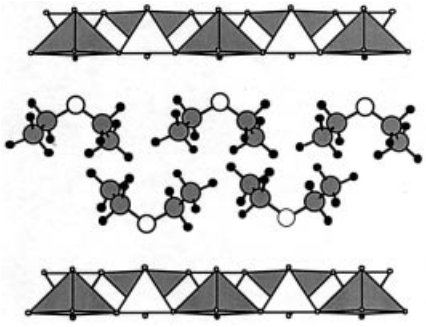

2498 **P. L. Shutov, S. S. Karlov,* K. Harms, D. A. Tyurin, J. Sundermeyer, J. Lorberth, G. S. Zaitseva**

Intramolecular Nucleophilic Substitution in a C_6F_5 Moiety Assisted by Antimony

Keywords: Antimony / Amides / Density functional calculations / Fluorinated ligands / Nucleophilic substitution

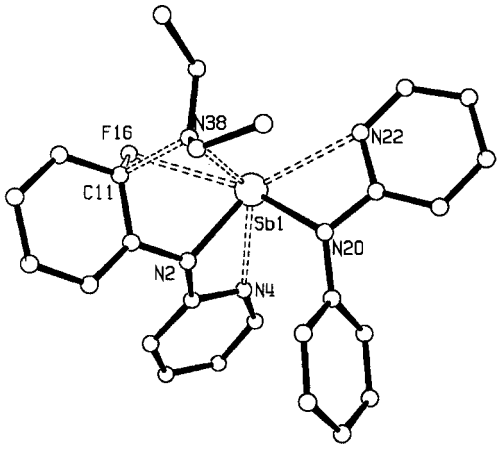

2504 **X. L. Lu, W. K. Leong, L. Y. Goh,* A. T. S. Hor***

Supramolecular Structures in [Ag(dppf)] Complexes [dppf = 1,1′-Bis(diphenylphosphanyl)-ferrocene] Stabilized by Coordinatively Versatile Trifluoroacetate (TFA) Ligands

Keywords: Silver / Trifluoroacetate / Coordination polymer / Supramolecular chemistry / Hydrogen bonding

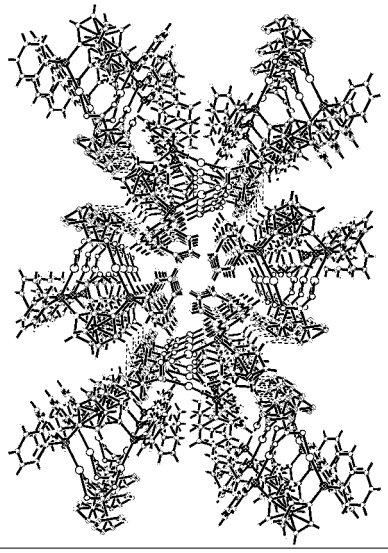

2514 **N. Psychogios, J.-B. Regnouf-de-Vains,* H. M. Stoeckli-Evans**

A Water-Soluble Calix[4]arene-Based Podand Incorporating 4,4′-Dicarboxy-2,2′-bipyridine Chelating Units − Synthesis and Complexation Properties towards Copper Ions

Keywords: Calix[4]arene / Bipyridine / Podand / Copper / Zinc

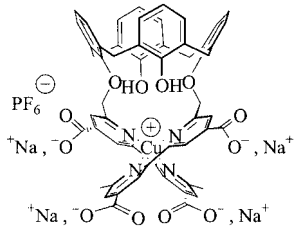

 © 2004 Wiley-VCH Verlag GmbH & Co. KGaA, Weinheim

2524 **V. Di Marco, M. Kilyen, T. Jakusch, P. Forgó, G. Dombi, T. Kiss***

Complexation Properties of Ethylenediaminetetramethylenephosphonic Acid (EDTMP) with Al^{III} and $V^{IV}O$

Keywords: Aluminum / Aminophosphonates / Bioinorganic chemistry / Speciation / Vanadium

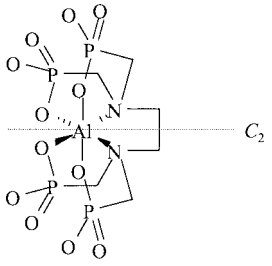

2533 **S. Banerjee, J. Gangopadhyay, C.-Z. Lu, J.-T. Chen, A. Ghosh***

Nickel(II) Complexes Incorporating Pyridyl, Imine and Amino Chelate Ligands: Synthesis, Structure, Isomer Preference, Structural Transformation and Reactivity Towards Nickel(III) Derivatives

Keywords: Coordination modes / Isomer specificity / N ligands / Nickel / Structural transformation

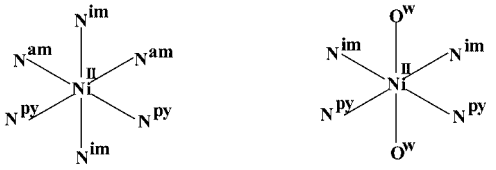

1 2

2542 **G. Espino, F. A. Jalón, M. Maestro, B. R. Manzano,* M. Pérez-Manrique, A. C. Bacigalupe**

Synthesis and Structure of New (Polyphosphane)-ruthenium Complexes with the Hemilabile Ligand 2-(Diphenylphosphanyl)-1-methyl-1*H*-imidazole − An Unexpected Rearrangement of $[RuCl_2(PN)(PPh_3)_2]$

Keywords: Ruthenium / Hemilabile ligands / Hydride ligands / Phosphanes / N,P ligands

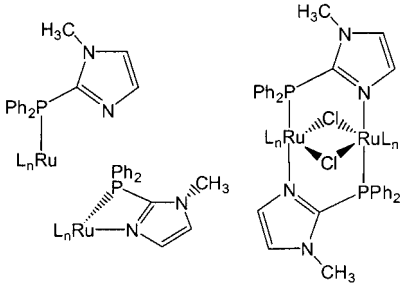

2553 **R. Kiebach, F. Studt, C. Näther, W. Bensch***

$[Ni(C_4H_{13}N_3)_2]_3(Sb_3S_6)_2$: The First Structure Containing Isolated Heterocyclic $[Sb_3S_6]^{3-}$ Anions

Keywords: Thioantimonates / Heterocycles / Hydrothermal synthesis / Antimony / Sulfur

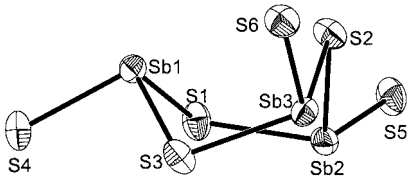

2557 **L. Flamigni,* A. M. Talarico, B. Ventura, G. Marconi, C. Sooambar, N. Solladié***

Conformational Effects on the Photoinduced Energy Transfer in a Star-Shaped Pentaporphyrin with Nucleosidic Linkers

Keywords: Circular dichroism / Energy transfer / Porphyrinoids / Photochemistry / Supramolecular chemistry

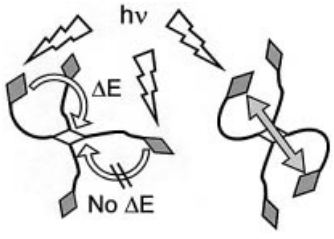

 © 2004 Wiley-VCH Verlag GmbH & Co. KGaA, Weinheim

2570 **T. K. Ronson, J. Nelson,* G. B. Jameson, J. C. Jeffery, S. Brooker***

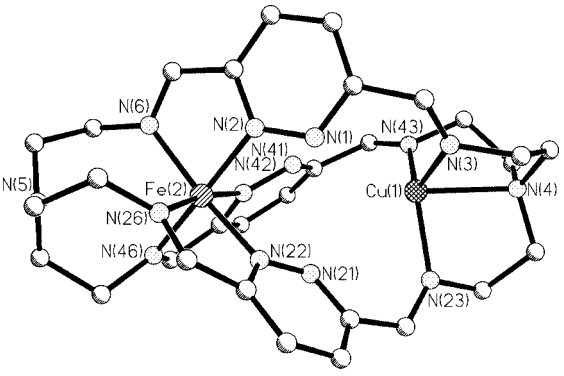

Controlled Access to Mixed-Metal Pyridazine-Linked Cryptates

Keywords: Cryptates / Cyclic voltammetry / Heterometallic complexes / N ligands / Structure elucidation

2585 **D. B. Werz, J. H. Schulte, B. J. Rausch, R. Gleiter,* F. Rominger**

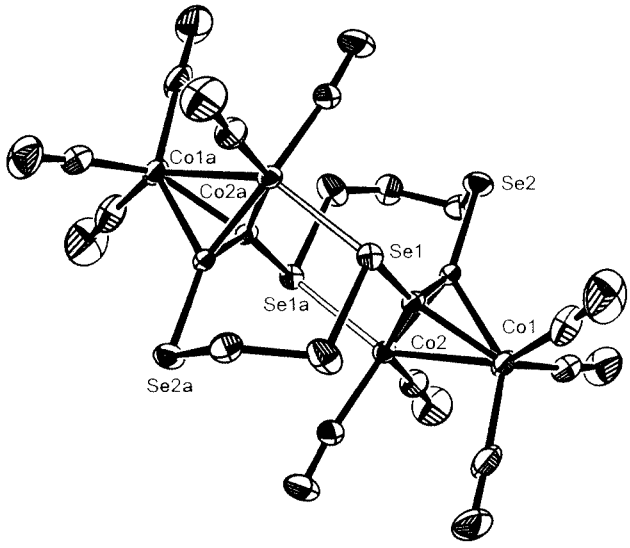

Structural Properties of Bis(hexacarbonyldicobalt) Complexes with Heteroatoms Next to the Former Triple Bonds − A Contribution to the Mechanism of the Pauson−Khand Reaction

Keywords: Alkynes / Chalcogens / Cobalt / Pauson−Khand reaction

 © 2004 Wiley-VCH Verlag GmbH & Co. KGaA, Weinheim

Subsequent Hydride Substitution in (Arene)trihydridodiruthenium Complexes: Synthesis and Structure of Thiolato-Bridged Diruthenium Cations of the Type $[H_2(arene)_2Ru_2(p\text{-}X-C_6H_4-S)]^+$ and $[H(arene)_2Ru_2(p\text{-}X-C_6H_4-S)_2]^+$

Mathieu J.-L. Tschan,[a] Frédéric Chérioux,*[a,b] Bruno Therrien,[a] and Georg Süss-Fink[a]

Dedicated to Professor Jean-Marie Lehn on the occasion of his 65th birthday

Keywords: Ruthenium / Sulfur / Hydrides / Complexes / Cross-coupling

The cationic complexes $[HRu_2(\eta^6\text{-arene})_2\{\mu_2\text{-}(p\text{-}X\text{–}C_6H_4)\text{–}S\}_2]^+$ and $[H_2Ru_2(\eta^6\text{-arene})_2\{\mu_2\text{-}(p\text{-}X\text{–}C_6H_4)\text{–}S\}]^+$ (arene = 1,2,4,5-$Me_4C_6H_2$ or C_6Me_6; X = Br and Me) are accessible in good yields from p-X–C_6H_4–SH with $[H_3Ru_2(1,2,4,5\text{-}Me_4C_6H_2)_2][BF_4]$ and $[H_3Ru_2(C_6Me_6)_2][BF_4]$, respectively. The dibromo derivative $[HRu_2(C_6Me_6)_2(p\text{-}Br\text{–}C_6H_4\text{–}S)_2]^+$ is found to undergo double Suzuki coupling reactions with 3-thiophene boronic acid to give $[HRu_2(C_6Me_6)_2(p\text{-}C_4H_3S\text{–}C_6H_4\text{–}S)_2]^+$. This dibromo complex is a potential precursor for the insertion of dinuclear hydrido organometallic entities in the main chain of conjugated molecules.

(© Wiley-VCH Verlag GmbH & Co. KGaA, 69451 Weinheim, Germany, 2004)

Introduction

The field of π-conjugated molecules and polymers containing metal centers has attracted continuous attention over the past two decades because of their electronic, magnetic, or catalytic properties,[1−4] and more recently, for the development of sensors.[5,6] To the best of our knowledge, except for a very recent work by Kim et al. who synthesized a dinuclear organomolybdenum sulfide complex,[7] all relevant molecules are built around mononuclear building blocks that are coordinated with different types of organic ligands. Therefore, there are still challenges to develop versatile and selective strategies, with the view of creating new molecular designs and bridging ligands for the formation of oligomers and polymers which contain metal centers.

In recent studies,[8−10] we have shown that dinuclear dichloro complexes $[Ru(\eta^6\text{-arene})Cl_2]_2$ and $[Rh(\eta^5\text{-}C_5Me_5)Cl_2]_2$ react in ethanol with p-bromothiophenol to give the cationic complexes $[Ru_2(\eta^6\text{-arene})_2\{\mu_2\text{-}(p\text{-}Br-C_6H_4)-S\}_3]^+$ and $[Rh_2(\eta^5\text{-}C_5Me_5)_2\{\mu_2\text{-}(p\text{-}Br-C_6H_4)-S\}_3]^+$, respectively, which could be isolated as the chloride salts in quantitative yield. We have also synthesized the first star-shaped π-conjugated oligomers built around dinuclear organometallic complexes.[11] The presence of bromo functions at the periphery of $[Ru_2(\eta^6\text{-arene})_2\{\mu_2\text{-}(p\text{-}Br-C_6H_4)-S\}_3]^+$ and $[Rh_2(\eta^5\text{-}C_5Me_5)_2\{\mu_2\text{-}(p\text{-}Br-C_6H_4)-S\}_3]^+$ was judiciously exploited to insert thiophene derivatives by standard Suzuki cross-coupling reactions.[12] However, despite the successful synthesis of conjugated oligomers (i.e. coupling with monoboronic acids), we were unable to characterize the corresponding polymers (i.e. coupling with diboronic acids). This can be explained by a large degree of reticulation due to the presence of three bromine atoms in the starting complexes. Consequently, the challenge consists of finding new complexes that contain only one or two bromine atoms (instead of three) at their periphery, therefore allowing a better control for the synthesis of conjugated polymers.

In this paper, we report the first example of dinuclear organometallic conjugated molecules in a "zig-zag"-like arrangement with mono- and disulfur connectivities, $[H_2Ru_2(\eta^6\text{-arene})_2\{\mu_2\text{-}(p\text{-}X-C_6H_4)-S\}]^+$ and $[HRu_2(\eta^6\text{-arene})_2\{\mu_2\text{-}(p\text{-}X-C_6H_4)-S\}_2]^+$, respectively, and give one example of extending their conjugation by Suzuki cross-coupling reactions with 3-thiophene boronic acid.

Results and Discussion

In order to overcome the reticulation problem which arises as a result of the three bromine atoms at the periphery of dinuclear precursors, we first focussed our attention on two different strategies to synthesize mono- and difunctional dinuclear complexes (see Scheme 1): in route A, dif-

[a] Institut de Chimie, Université de Neuchâtel,
Avenue de Bellevaux, 51 2000, Switzerland
Fax: (internat.) +41-327-182-511
E-mail: frederic.cherioux@unine.ch
[b] Département LPMO, Institut FEMTO-ST, CNRS UMR 6174,
32 Avenue de l'Observatoire, 25044 Besançon cedex, France
Fax: (internat.) +33-381-853-998
E-mail: frederic.cherioux@lpmo.edu

ferent *para*-substituted thiophenols are mixed together, leading to a mixture of all possible substitution compounds in a stoichiometric ratio, as observed by NMR (^{1}H and ^{13}C{^{1}H}) and mass spectrometry. In route B, an excess of the dinuclear dichloro complex is used to favor the formation of mono- and di-μ_2-thiolato complexes.

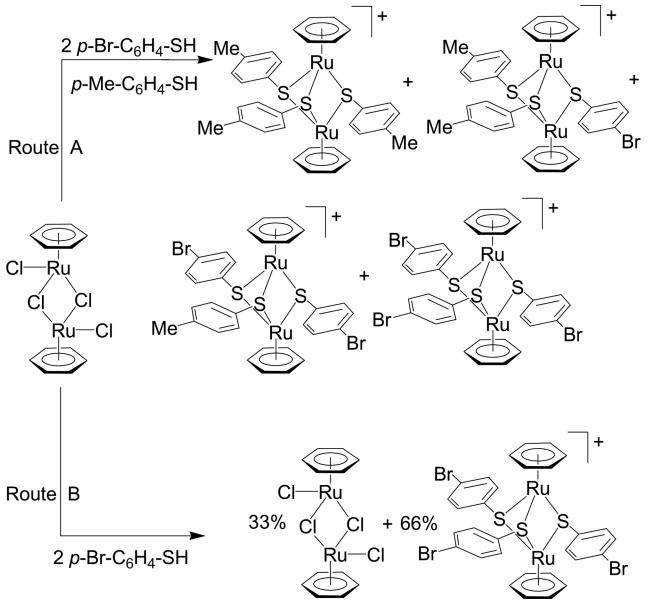

Scheme 1. Strategies for the synthesis of mono- or difunctional dinuclear complexes

Unfortunately, the different compounds obtained as a mixture from route A could not be separated by standard chromatographic techniques, whereas route B only afforded tri-μ_2-thiolato complexes, despite a strict 1:2 ratio of the reagents.

Consequently, we reasoned that strategy B would, in principle, be the most promising method to synthesize of difunctional dinuclear complexes; however, the dinuclear dichloro complexes [Ru(η^6-arene)Cl$_2$]$_2$ were too reactive to stop at the formation of the di-μ_2-thiolato derivatives. In order to overcome this problem, we used the trihydrido complexes [H$_3$Ru$_2$(η^6-arene)$_2$]$^+$, which are accessible from the reaction of the dinuclear dichloro complexes [Ru(η^6-arene)Cl$_2$]$_2$ (arene: C$_6$Me$_6$, 1,2,4,5-Me$_4$C$_6$H$_2$) with NaBH$_4$,[13−15] instead of the dichloro complexes themselves.

The dinuclear trihydrido complex [H$_3$Ru$_2$(C$_6$Me$_6$)$_2$]$^+$ was found to react with one equivalent of *p*-X−C$_6$H$_4$−SH (X = Me or Br) in ethanol to give a mixture of the cationic complexes [H$_2$Ru$_2$(C$_6$Me$_6$)$_2$(*p*-X−C$_6$H$_4$−S)]$^+$ (**1a**−**b**) and [HRu$_2$(C$_6$Me$_6$)$_2$(*p*-X−C$_6$H$_4$−S)$_2$]$^+$ (**2a**−**b**) in a 3:1 ratio. These cationic complexes can be isolated in good yields as the tetrafluoroborate salts. In the case of the durene analogue [H$_3$Ru$_2$(1,2,4,5-Me$_4$C$_6$H$_2$)$_2$]$^+$, the reaction with one equivalent of *p*-X−C$_6$H$_4$−SH (X = Me or Br) in ethanol yields the cationic complexes [H$_2$Ru$_2$(1,2,4,5-Me$_4$C$_6$H$_2$)$_2$(*p*-X−C$_6$H$_4$−S)]$^+$ (**1c**−**d**) and [HRu$_2$(1,2,4,5-Me$_4$C$_6$H$_2$)$_2$(*p*-X−C$_6$H$_4$−S)$_2$]$^+$ (**2c**−**d**), in a 1:4 ratio (see Scheme 2).

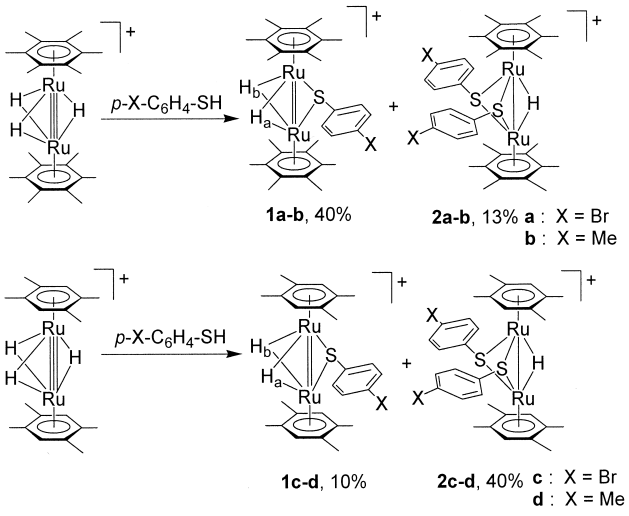

Scheme 2. Reaction of [H$_3$Ru$_2$(η^6-arene)$_2$]$^+$ with one equivalent of *para*-substituted thiophenol

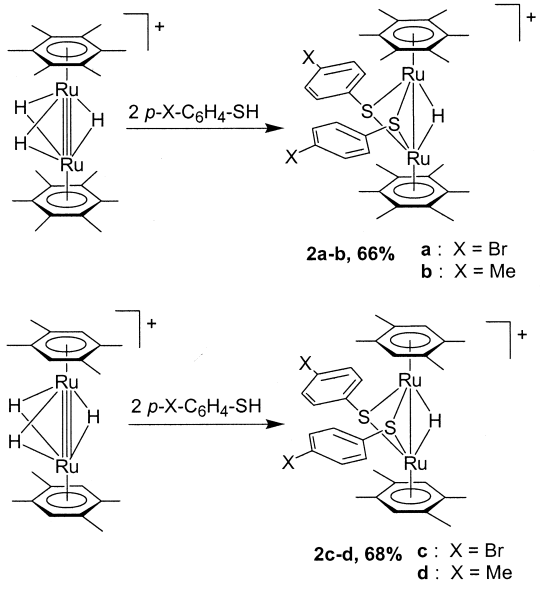

Scheme 3. Reaction of [H$_3$Ru$_2$(η^6-arene)$_2$]$^+$ with two or more equivalents of *para*-substituted thiophenol

Surprisingly, if two (or more) equivalents of *p*-X−C$_6$H$_4$−SH were used with [H$_3$Ru$_2$(η^6-arene)$_2$][BF$_4$], the reaction led exclusively to the formation of the cationic complexes [HRu$_2$(C$_6$Me$_6$)$_2$(*p*-X−C$_6$H$_4$−S)$_2$]$^+$ (**2a**−**b**) and [HRu$_2$(1,2,4,5-Me$_4$C$_6$H$_2$)$_2$(*p*-X−C$_6$H$_4$−S)$_2$]$^+$ (**2c**−**d**, see Scheme 3), and no trace of the mono- or tri-μ_2-thiolato complexes was detected by mass spectrometry.

Both cations **1** and **2** were unambiguously characterized as the tetrafluoroborate salts (see Exp. Sect.). These ionic compounds are highly soluble in alcohols, acetone and chlorinated solvents. The molecular structures of selected complexes **1a**, **2a**, **2c** and **2d** were confirmed by single-crystal X-ray structure analysis of the tetrafluoroborate salts. These cationic species consist of a trigonal bipyramidal

 © 2004 Wiley-VCH Verlag GmbH & Co. KGaA, Weinheim

H_2Ru_2S or HRu_2S_2 core, each ruthenium atom being coordinated to an η^6-C_6Me_6 or an η^6-1,2,4,5-$Me_4C_6H_2$ ligand, and each sulfur atom carrying a *p*-substituted phenyl group. The molecular structures of **1a** and **2a** are shown in Figure 1, and those of **2c** and **2d** are shown in Figure 2.

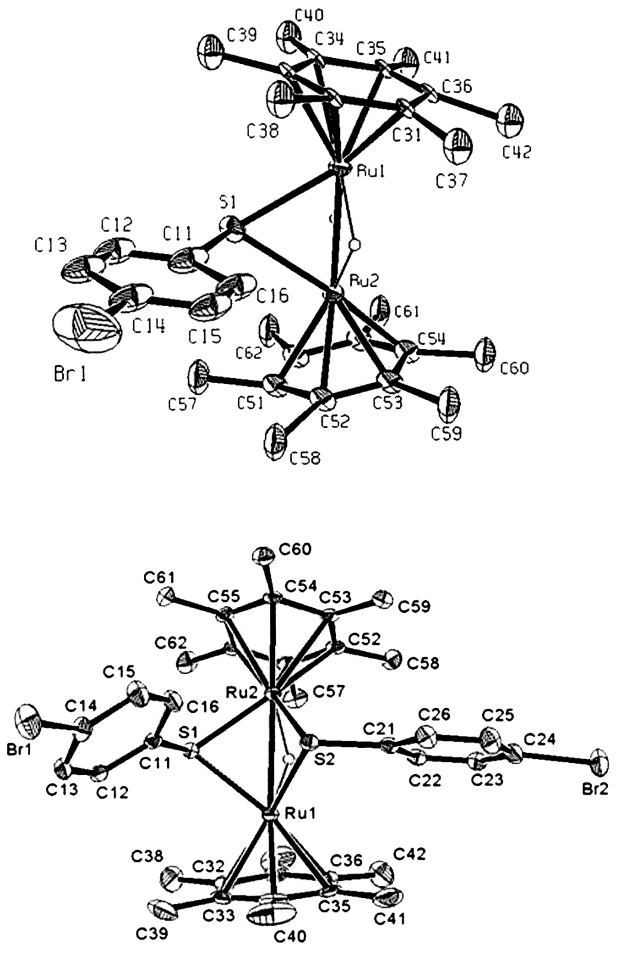

Figure 1. Molecular structures of [**1a**][BF_4] (top) and [**2a**][BF_4] (bottom); tetrafluoroborate anions, solvent molecules and H atoms have been omitted for clarity; displacement ellipsoids are drawn at the 25 and 35% probability level, respectively; selected bond lengths (Å) and angles (°) are listed in Table 1

The metal backbone of **1a** and **2a** consists of two ruthenium atoms, the Ru−Ru distances being in accordance with a metal−metal double bond [**1a**: Ru−Ru = 2.624(2) Å] or single bond [**2a**: Ru−Ru = 2.8112(6) Å]. The presence of one or two thiolato bridging ligands forces the arene−Ru−Ru−arene moieties to adopt a distorted geometry. The two C_6Me_6 arene ligands are not parallel to each other, and the angles between the C_6Me_6 planes are 21.2° in **1a** and 37.4° in **2a**.

The single-crystal X-ray structure analysis of [**1a**]BF_4 explains the large difference in the chemical shifts observed in ^{1}H NMR spectrum of this complex between the two hydrido ligands (−12.88 and −16.75 ppm), as well as that observed for the other dihydrido complexes **1b**−**d** (see Exp. Sect.). The angle defined by the μ_2-(*p*-X−C_6H_4)−S bridging ligand and the ruthenium atoms is close to 110°, thus

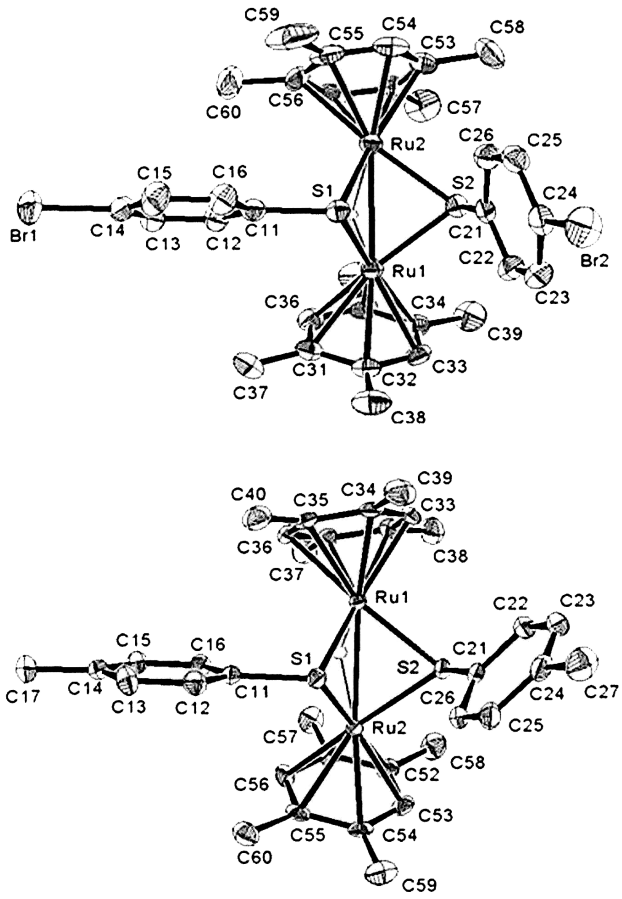

Figure 2. Molecular structures of [**2c**][BF_4] (top) and [**2d**][BF_4] (bottom); tetrafluoroborate anions and H atoms have been omitted for clarity; displacement ellipsoids are drawn at the 35 and 50% probability level, respectively; selected bond lengths (Å) and angles (°) are listed in Table 1

leading to a strongly distorted structure. Consequently, the two hydrido ligands are nonequivalent, because one of them, H_a (see Scheme 2), is closer to the *p*-X−C_6H_4−S moiety than the other (H_b). Moreover, H_a is in the plane of deshielding of the *para*-substituted thiophenyl group (see Figure 1). This phenomenon leads to a large difference in the chemical shift of H_a (−12.88 ppm) and H_b (−16.75 ppm), as observed in ^{1}H NMR spectrum of **1a**. As far as complexes **2** are concerned, the chemical shifts assigned to the hydrido ligands are found between −11 and −12 ppm. As the molecular structures of **2a**, **2c** and **2d** (see Figure 1 and Figure 2) reveal, the hydrido ligand of these complexes is also in the plane of deshielding of the thiophenyl moiety, leading to chemical shifts similar to those observed for the most deshielded hydrido ligands in complexes **1**.

The reactivities of the dinuclear trihydrido complexes $[H_3Ru_2(\eta^6\text{-arene})_2]^+$ are completely different from that of the $[Ru(\eta^6\text{-arene})Cl_2]_2$ complexes. In the case of the chloro-bridged complexes, only the trisubstituted products are formed, whereas the hydrido-bridged complexes exclusively give rise to mono- and dithiolato derivatives. This is probably due to the lower reactivity of the μ_2-hydrido ligand, relative to that of the μ_2-chloro ligand, which implies no

 © 2004 Wiley-VCH Verlag GmbH & Co. KGaA, Weinheim

modification of the metal−metal bond during the replacement with a μ_2-thiolato ligand, as is the case for the substitution of a μ_2-hydrido bridge.

As only the disubstituted complexes $[HRu_2(\eta^6\text{-arene})_2\{\mu_2\text{-}(p\text{-}X{-}C_6H_4){-}S\}_2]^+$ (**2**) are accessible from the reaction of $[H_3Ru_2(\eta^6\text{-arene})_2]^+$ or $[H_2Ru_2(\eta^6\text{-arene})_2\{\mu_2\text{-}(p\text{-}X{-}C_6H_4){-}S\}_2]^+$ (**1**) with an excess of $p\text{-}X{-}C_6H_4{-}SH$, the introduction of a third *para*-substituted thiophenyl group seems impossible. In fact, the molecular structures of **2a**, **2c** and **2d** show an important constraint on the two arene ligands due to steric repulsion with the *para*-substituted thiophenyl groups already incorporated (see Figure 1 and Figure 2, selected bond lengths and angles are listed in Table 1), which prevents substitution of the last hydrido ligand by a third thiolato ligand. In addition, the steric hindrance provided by the arene moieties also controls the reactivity of $[H_3Ru_2(\eta^6\text{-arene})_2]^+$ with one equivalent of the *para*-substituted thiophenol. In this case, the ratio of complexes **1** and **2** formed is reversed by making the arene ligands more bulky: 1:4 for $1,2,4,5\text{-}Me_4C_6H_2$ in contrast to 3:1 for C_6Me_6 (see Scheme 1). Similar effects of arene ligands have not been observed so far in the case of $[Ru(\eta^6\text{-arene})Cl_2]_2$ complexes.[10,11] As a consequence, it can be stated that: i) $[Ru(\eta^6\text{-arene})Cl_2]_2$ complexes give only trisubstituted compounds ($[Ru_2(\eta^6\text{-arene})_2\{\mu_2\text{-}(p\text{-}X{-}C_6H_4){-}S\}_3]^+$), while the lower reactivity of $[H_3Ru_2(\eta^6\text{-arene})_2]^+$ leads to the mono- and disubstituted compounds, $[HRu_2(C_6Me_6)_2(p\text{-}X{-}C_6H_4{-}S)_2]^+$ and $[H_2Ru_2(C_6Me_6)_2(p\text{-}X{-}C_6H_4{-}S)]^+$; ii) the ratio between mono- and disubstituted complexes can be tuned by the steric hindrance of the arene substituents in the starting trihydrido complexes. This can be used for the synthesis of multifunctional complexes containing the desired number of functionalized ligands at the periphery.

In order to develop well-defined conjugated polymers possessing dinuclear organometallic entities, we investigated the ability of complex **2a** (substituted by two bromine atoms at its periphery) to react with boronic acid by a Suzuki cross-coupling reaction, as depicted in Scheme 3.

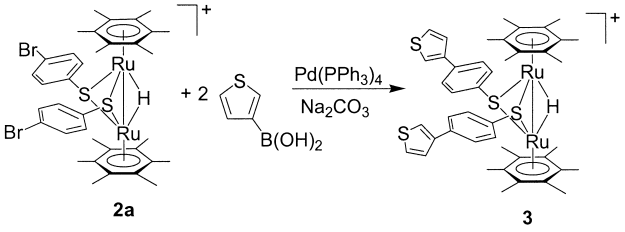

2a 3

Scheme 4. Suzuki cross-coupling reaction of 3-thiophene boronic acid with dibromo complex **2a**

Cation **2a** was found to react with 3-thiophene boronic acid in ethanol in the presence of $Pd(PPh_3)_4$ as a catalyst to give the conjugated complex $[HRu_2(C_6Me_6)_2(p\text{-}C_4H_3S{-}C_6H_4{-}S)_2]^+$ (**3**) with yields ranging from 10 to 15%. We observed the formation of the difunctionalized compounds only. Cation **3** was unambiguously characterized by standard methods (See Experimental Section). This cationic complex, as the tetrafluoroborate salt, is highly soluble in alcohols, acetone and chlorinated solvents. The molecular structure of **3** was confirmed by a single-crystal X-ray structure analysis of the BF_4 salt: the cation maintains the trigonal-bipyramidal HRu_2S_2 framework of its precursor, as shown in Figure 3.

New materials with unique properties should be accessible by this method, because standard organic dibromo reagents (for example 2,5-dibromothiophene, 2,7-dibromofluorene etc.) can be replaced by these organometallic entities. This original approach could lead to the development of

Table 1. Selected bond lengths (Å) and angles (°) for [**1a**][BF_4], [**2a**][BF_4], [**2c**][BF_4], [**2d**][BF_4], and [**3**][BF_4]

	[**1a**][BF_4]	[**2a**][BF_4]	[**2c**][BF_4]	[**2d**][BF_4]	[**3**][BF_4]
Interatomic distances					
Ru(1)−S(1)	2.420(9)	2.3642(10)	2.3740(11)	2.3635(8)	2.369(3)
Ru(1)−S(2)		2.3669(10)	2.3578(12)	2.3676(9)	2.340(3)
Ru(2)−S(1)	2.440(8)	2.3426(10)	2.3724(11)	2.3577(7)	2.374(3)
Ru(2)−S(2)		2.3744(10)	2.3594(11)	2.3548(7)	2.396(3)
Ru(1)−Ru(2)	2.624(2)	2.8112(6)	2.7845(5)	2.7963(5)	2.7884(12)
S(1)−C(11)	2.06(2)	1.787(4)	1.783(4)	1.794(3)	1.806(12)
S(2)−C(21)		1.779(4)	1.789(4)	1.789(3)	1.785(11)
C(14)−Br(1)	1.67(2)	1.894(4)	1.899(5)		
C(24)−Br(2)		1.904(4)	1.905(5)		
C(14)−C(17)				1.507(4)	1.441(15)
C(24)−C(27)				1.514(4)	1.516(15)
Angles					
Ru(1)−S(1)−Ru(2)	65.35(14)	73.35(3)	71.84(3)	72.64(2)	72.01(8)
Ru(1)−S(2)−Ru(2)		72.73(3)	72.35(3)	72.62(2)	72.13(9)
Ru(1)−S(1)−C(11)	110.9(7)	113.86(12)	112.33(15)	108.59(10)	111.5(3)
Ru(1)−S(2)−C(21)		108.17(13)	110.48(14)	108.12(10)	113.9(4)
Ru(2)−S(1)−C(11)	112.4(7)	116.34(12)	110.17(14)	109.87(9)	113.9(4)
Ru(2)−S(2)−C(21)		109.43(14)	111.67(14)	117.52(9)	117.0(4)

 © 2004 Wiley-VCH Verlag GmbH & Co. KGaA, Weinheim

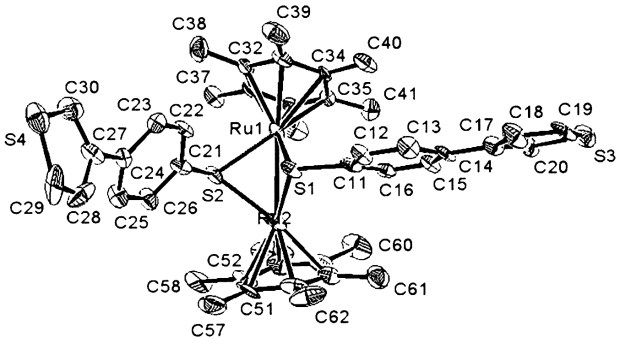

Figure 3. Molecular structure of [**3**][BF_4]; the tetrafluoroborate anion, solvent molecule, and H atoms have been omitted for clarity; displacement ellipsoids are drawn at the 25% probability level; selected bond lengths (Å) and angles (°) are listed in Table 1

promising materials based on the "zig-zag" design as a result of the disulfur connectivities of the type observed in $[HRu_2(C_6Me_6)_2(p\text{-}Br{-}C_6H_4{-}S)_2][BF_4]$.

Conclusion

In conclusion, we reported the synthesis of dinuclear organometallic entities, based on trigonal-bipyramidal HRu_2S_2 and H_2Ru_2S frameworks. We demonstrated that it is possible to control the functionalization (i.e. insertion of one or two *para*-substituted thiophenyl ligands) by the use of dinuclear trihydrido complexes $[H_3Ru_2(\eta^6\text{-arene})_2]^+$. The dibromo-substituted derivative $[HRu_2(C_6Me_6)_2(p\text{-}Br{-}C_6H_4{-}S)_2]^+$ reacts with 3-thiophene boronic acid by Suzuki cross-couplings to form the conjugated complex $[HRu_2(C_6Me_6)_2(p\text{-}C_4H_3S{-}C_6H_4{-}S)_2]^+$. The development of original and promising conjugated polymers from the dinuclear complexes possessing two bromine substituents at their periphery is currently under investigation.

Experimental Section

General Remarks: All reactions were carried out under a nitrogen atmosphere, by using standard Schlenk techniques, and the solvents were degassed prior to use. The dinuclear trihydrido complexes $[H_3Ru_2(\eta^6\text{-arene})_2]^+$ (arene: C_6Me_6, 1,2,4,5-$Me_4C_6H_2$) were synthesized by previously described methods.[16−18] All other reagents were purchased (Fluka, Acros) and used as received. NMR spectra were recorded on a Varian−Gemini 200 BB instrument and referenced to the signals of the residual protons in the deuterated solvents. The mass spectra were recorded at the University of Fribourg (Switzerland) by Prof. Titus Jenny. Microanalyses were carried out by the Laboratory of Pharmaceutical Chemistry, University of Geneva (Switzerland).

Preparation of $[H_2Ru_2(C_6Me_6)_2(p\text{-}X{-}C_6H_4{-}S)][BF_4]$: The dinuclear trihydrido salt $[H_3Ru_2(C_6Me_6)_2][BF_4]$ (50 mg, 81 μmol) and *p*-bromothiophenol (19 mg, 101 μmol) or *p*-thiocresol (12.5 mg, 101 μmol) were dissolved in degassed technical grade ethanol (60 mL) and heated under reflux for 16 hours. After cooling to room temperature, the purple solution was filtered, and the solvent was evaporated to dryness under reduced pressure. The purple solid was washed with diethyl ether (3 × 20 mL), dissolved in dichloromethane, and isolated by preparative thin-layer chromatography on silica (eluent: acetone/hexane, 1:1, followed by acetone/dichloromethane, 1:50). The purple fraction was recovered to give the product.

$[H_2Ru_2(C_6Me_6)_2(p\text{-}Br{-}C_6H_4{-}S)][BF_4]$ ([1a][BF_4]): Yield: 40%, 26 mg, 32 μmol. Crystals were obtained by diffusion of diethyl ether in a saturated solution of dichloromethane. ^{1}H NMR (200 MHz, [D_6]acetone, 21 °C): δ = −16.69 (d, ^2J = 3 Hz, 1 H, hydride), −13.07 (d, ^2J = 3 Hz, 1 H, hydride), 2.28 (s, 36 H, $C_6(CH_3)_6$], 7.19 (d, ^3J = 8 Hz, 2 H, *H*-Ar), 7.50 (d, ^3J = 8 Hz, 2 H, *H*-Ar) ppm. ^{13}C{^{1}H} NMR (50 MHz, [D6]acetone, 21 °C): δ = 17.3 (Ru−C−CH_3), 95.6 (Ru−*C*−CH_3), 120.8 (*C*−Br), 131.2 (*C*−H Ar), 135.5 (*C*−H Ar), 141.1 (*C*−S) ppm. MS (ESI): *m*/*z* = 717 [M^+ + H]. $C_{30}H_{42}BBrF_4Ru_2S$ (803.57): calcd. C 43.14, H 5.43; found C 43.60, H 5.71.

$[H_2Ru_2(C_6Me_6)_2(p\text{-}Me{-}C_6H_4{-}S)][BF_4]$ ([1b][BF_4]): Yield: 43%, 26 mg, 35 μmol. ^{1}H NMR (200 MHz, [D_6]acetone, 21 °C): δ = −16.75 (d, ^2J = 3.4 Hz, 1H, hydride), −12.88 (d, ^2J = 3.4 Hz, 1H. hydride), 2.26 [s, 36 H, $C_6(CH_3)_6$], 7.09 (d, ^3J = 8.6 Hz, 2 H, *H*-Ar), 7.15 (d, ^3J = 8.6 Hz, 2 H, *H*-Ar) ppm. ^{13}C{^{1}H} NMR (50 MHz, [D_6]acetone, 21 °C): δ = 17.2 (Ru−C−CH_3), 20.4 (S−C_6H_4−CH_3), 95.4 (Ru−*C*−CH_3), 129.0 (*C*-Ar), 133.5 (*C*-Ar), 137.1 (*C*-Ar), 137.6 (*C*−S) ppm. MS (ESI): *m*/*z* = 652 [M^+ + H]. $C_{31}H_{45}BF_4Ru_2S$ (738.7): calcd. C 50.40, H 6.14; found C 50.62, H 6.25.

Preparation of $[H_2Ru_2(1,2,4,5\text{-}Me_4C_6H_2)_2(p\text{-}X{-}C_6H_4{-}S)][BF_4]$: The dinuclear trihydrido salt $[H_3Ru_2(1,2,4,5\text{-}Me_4C_6H_2)_2][BF_4]$ (40 mg, 71 μmol) and *p*-bromothiophenol (14.55 mg, 77 μmol) or *p*-thiocresol (9.56 mg, 77 μmol) were dissolved in degassed technical grade dichloromethane (60 mL) and heated at 50 °C for 16 hours. After cooling to room temperature, the red solution was filtered, and the solvent was evaporated to dryness under reduced pressure. The red solid was washed with diethyl ether (3 × 20 mL), dissolved in dichloromethane, and isolated by preparative thin-layer chromatography on silica (eluent: acetone/hexane 1:1, followed by acetone/dichloromethane, 1:50). The purple fraction was recovered to give the product.

$[H_2Ru_2(1,2,4,5\text{-}Me_4C_6H_2)_2(p\text{-}Br{-}C_6H_4{-}S)][BF_4]$ ([1c][BF_4]): Yield: 6%, 3.2 mg, 4 μmol. ^{1}H NMR (200 MHz, [D_6]acetone, 21 °C): δ = −16.20 (d, ^2J = 2.9 Hz, 1 H, hydride), −12.38 (d, ^2J = 2.9 Hz, 1 H, hydride), 2.13 (s, 12H, ($C_6H_2(CH_3)_4$], 2.35 (s, 12H, ($C_6H_2(CH_3)_4$], 5.93 (s, 4H, *H*-Ar), 7.33 (d, ^3J = 8.5 Hz, 2H, *H*-Ar), 7.45 (d, ^3J = 8.5 Hz, 2H, *H*-Ar) ppm. MS (ESI): *m*/*z* = 661 [M^+ + H]. $C_{26}H_{34}BBrF_4Ru_2S$ (747.46): calcd. C 41.78, H 4.58; found C 41.62, H 4.67.

$[H_2Ru_2(1,2,4,5\text{-}Me_4C_6H_2)_2(p\text{-}Me{-}C_6H_4{-}S)][BF_4]$ ([1d][BF_4]): Yield: 6%, 3 mg, 4 μmol. ^{1}H NMR (200 MHz, [D_6]acetone, 21 °C): δ = −16.35 (d, ^2J = 3.4 Hz, 1 H, hydride), −12.25 (d, ^2J = 3.4 Hz, 1 H, hydride), 2.08 (s, 12H, $C_6H_4(CH_3)_4$], 2.31 (s, 3 H, Ar-CH_3), 2.33 (s, 12H, $C_6H_2(CH_3)_4$], 5.87 (s, 4 H, *H*-Ar), 7.10 (d, ^3J = 7.8 Hz, 2 H, *H*-Ar), 7.21 (d, ^3J = 7.8 Hz, 2 H, *H*-Ar) ppm. MS (ESI): *m*/*z* = 596 [M^+ + H]. $C_{27}H_{37}BF_4Ru_2S$ (682.6): calcd. C 47.51, H 5.46; found C 47.37, H 5.39.

Preparation of $[HRu_2(C_6Me_6)_2(p\text{-}X{-}C_6H_4{-}S)_2][BF_4]$: The dinuclear trihydrido salt $[H_3Ru_2(C_6Me_6)_2][BF_4]$ (60 mg, 97 μmol) and *p*-bromothiophenol (37 mg, 196 μmol) or *p*-thiocresol (24 mg, 196 μmol) were dissolved in degassed technical grade ethanol (60 mL) and heated under reflux for 16 hours. After cooling to room temperature, the red solution was filtered, and the solvent was evaporated to dryness under reduced pressure. The red solid obtained

 © 2004 Wiley-VCH Verlag GmbH & Co. KGaA, Weinheim

was washed with diethyl ether (3 × 20 mL), dissolved in dichloromethane, and isolated by preparative thin-layer chromatography on silica (eluent: acetone/hexane 1:1, followed by acetone/dichloromethane 1:50). The red fraction was recovered to give the product.

[$HRu_2(C_6Me_6)_2$(*p*-Br−C_6H_4−S)$_2$][BF_4] ([2a][BF_4]): Yield: 67%, 64 mg, 65 μmol. Crystals were obtained by diffusion of diethyl ether in a saturated solution of dichloromethane. ^{1}H NMR (200 MHz, [D$_6$]acetone, 21 °C): δ = −11.97 (s, 1H, hydride), 2.22 (s, 36H, $C_6(CH_3)_6$], 7.6−7.1 (m, 4 H, *H*-Ar); ^{13}C{^{1}H} NMR (50 MHz, [D$_6$]acetone, 21 °C): δ = 16.7 (Ru−C−CH_3), 98.1 (Ru−*C*−CH_3), 121.5 (*C*−Br), 131.5 (*C*-Ar), 135.2 (*C*-Ar), 137.7 (*C*−S) ppm. MS (ESI): *m*/*z* = 903 [M$^+$ + H]. $C_{36}H_{45}BBr_2F_4Ru_2S_2$ (990.6): calcd. C 45.11, H 4.73; found C 45.52, H 4.81.

[$HRu_2(C_6Me_6)_2$(*p*-Me−C_6H_4−S)$_2$][BF_4] ([2b][BF_4]): Yield: 65%, 54 mg, 63 μmol. ^{1}H NMR (200 MHz, [D$_6$]acetone, 21 °C): δ = −11.97 (s, 1 H, hydride), 2.17 (s, 36 H, $C_6(CH_3)_6$], 2.31 (s, 6 H, Ar-CH_3), 7.4−7.0 (m, 4 H, *H*-Ar); ^{13}C{^{1}H} NMR (50 MHz, [D$_6$]acetone, 21 °C): δ = 16.5 (Ar-*C*H$_3$), 16.8 (Ru−C−*C*H$_3$), 97.7 (Ru−*C*−H), 129.3 (*C*-Ar), 133.5 (*C*-Ar), 137.4 (*C*−S) ppm. MS (ESI): *m*/*z* = 774 [M$^+$ + H]. $C_{38}H_{51}BF_4Ru_2S_2$ (860.89): calcd. C 53.02, H 5.97; found C 52.88, H 6.11.

Preparation of [HRu_2(1,2,4,5-$Me_4C_6H_2$)$_2$(*p*-X−C_6H_4−S)$_2$][BF_4]: The dinuclear trihydrido salt [H_3Ru_2(1,2,4,5-$Me_4C_6H_2$)$_2$][BF_4] (40 mg, 71 μmol) and *p*-bromothiophenol (30 mg, 160 μmol) or *p*-thiocresol (20 mg, 160 μmol) were dissolved in dichloromethane (40 mL) and heated under reflux for 16 hours. After cooling to room temperature, the red solution was filtered, and the solvent was evaporated to dryness under reduced pressure. The red solid was washed with diethyl ether (3 × 20 mL), dissolved in dichloromethane, and isolated by preparative thin-layer chromatography on silica (eluent: acetone/hexane, 1:1, followed by acetone/dichloromethane, 1:50). The red fraction was recovered to give the product.

[HRu_2(1,2,4,5-$Me_4C_6H_2$)$_2$(*p*-Br−C_6H_4−S)$_2$][BF_4] ([2c][BF_4]): Yield: 67%, 45 mg, 48 μmol. Crystals were obtained by diffusion of diethyl ether into a saturated solution of dichloromethane. ^{1}H NMR (200 MHz, [D$_6$]DMSO, 21 °C): δ = −11.24 (s, 1H, hydride), 1.72 (s, 12 H, $C_6H_2(CH_3)_4$], 2.25 (s, 12 H, $C_6H_2(CH_3)_4$], 6.01 (s, 4 H, $C_6H_2(CH_3)_4$], 7.6−7.2 (m, 8 H, *H*-Ar) ppm. ^{13}C{^{1}H} NMR (50 MHz, [D$_6$]DMSO, 21 °C): δ = 17.4 (Ru−C−*C*H$_3$), 18.8 (Ru−C−*C*H$_3$), 89.7 (Ru−*C*−CH$_3$), 99.3 (Ru−*C*−CH$_3$), 100.9 (Ru−*C*−H), 131.5 (*C*−Br), 131.9 (*C*−Br), 134.3 (*C*-Ar), 134.9 (*C*-Ar), 135.9 (*C*-Ar), 136.5 (*C*−S), 139.8 (*C*−S) ppm. MS (ESI): *m*/*z* = 848 [M$^+$ + H]. $C_{32}H_{37}BBr_2F_4Ru_2S_2$ (934.52): calcd. C 41.12, H 3.99; found C 41.84, H 4.19.

[HRu_2(1,2,4,5-$Me_4C_6H_2$)$_2$(*p*-Me−C_6H_4−S)$_2$][BF_4] ([2d][BF_4]): Yield: 70%, 40 mg, 50 μmol. Crystals were obtained by diffusion of diethyl ether into a saturated solution of dichloromethane. ^{1}H NMR (200 MHz, [D$_6$]acetone, 21 °C): δ = −11.12 (s, 1 H, hydride), 1.85 (s, 12 H, $C_6H_2(CH_3)_4$], 2.28 (s, 3 H, Ar-C*H*$_3$), 2.33 (s, 3 H, Ar-C*H*$_3$), 2.38 (s, 12 H, $C_6H_2(CH_3)_4$], 5.95 (s, 4 H, $C_6H_2(CH_3)_4$], 7.10 (d, ^3J = 8.2 Hz, 2 H, *H*-Ar), 7.11 (d, ^3J = 8.2 Hz, 2 H, *H*-Ar), 7.29 (d, ^3J = 8.2 Hz, 2H, *H*-Ar), 7.46 (d, ^3J = 8.2 Hz, 2 H, *H*-Ar) ppm. ^{13}C{^{1}H} NMR (50 MHz, [D$_6$]DMSO, 21 °C): δ = 16.6 (Ru−C−*C*H$_3$), 17.9 (Ru−C−*C*H$_3$), 20.5 (Ar-*C*H$_3$), 20.6 (Ar-*C*H$_3$), 89.6 (Ru−*C*−CH$_3$), 91.7 (Ru−*C*−H), 98.5 (Ru−*C*−H), 99.2 (Ru−*C*−H), 100.3 (Ru−*C*−H), 129.0 (*C*-Ar), 129.3 (*C*-Ar), 129.6 (*C*-Ar), 130.6 (*C*-Ar), 132.9 (*C*-Ar), 133.3 (*C*-Ar), 134.1 (*C*-Ar), 136.9 (*C*−S), 138.2 (*C*−S) ppm. MS (ESI): *m*/*z* = 848 [M$^+$ + H]. $C_{32}H_{37}BBr_2F_4Ru_2S_2$ (934.52): calcd. C 41.12, H 3.99; found C 41.84, H 4.19.

Preparation of [$HRu_2(C_6Me_6)_2$(*p*-C_4H_3S−C_6H_4−S)$_2$][BF_4] ([3][BF_4]): The dinuclear hydrido salt [$HRu_2(C_6Me_6)_2$(*p*-S−C_6H_4−Br)$_2$][BF_4] (50 mg, 56 μmol) and 3-thiophene boronic acid (20.5 mg, 160 μmol) were dissolved in distilled ethanol

Table 2. Crystallographic and selected experimental data of [**1a**][BF_4], [**2a**][BF_4], [**2c**][BF_4], [**2d**][BF_4], and [**3**][BF_4]

	[**1a**][BF_4]·C_6H_6	[**2a**][BF_4]·$CO(CH_3)_2$	[**2c**][BF_4]	[**2d**][BF_4]	[**3**][BF_4]·CH_2Cl_2
Chemical formula	$C_{36}H_{48}BBrF_4Ru_2S$	$C_{39}H_{51}BBr_2F_4ORu_2S_2$	$C_{32}H_{37}BBr_2F_4Ru_2S_2$	$C_{34}H_{43}BF_4Ru_2S_2$	$C_{45}H_{53}BCl_2F_4Ru_2S_4$
Molecular mass	881.66	1048.69	934.51	804.75	1081.96
Crystal system	monoclinic	triclinic	monoclinic	triclinic	triclinc
Space group	*Cc*	$P\bar{1}$	$P2_1/n$	$P\bar{1}$	$P\bar{1}$
Color and shape	red plate	red rod	red block	red block	orange plate
Crystal size	0.40 × 0.08 × 0.04	0.28 × 0.08 × 0.08	0.25 × 0.25 × 0.15	0.32 × 0.26 × 0.24	0.48 × 0.25 × 0.05
a (Å)	16.144(1)	11.906(1)	11.3006(6)	11.775(2)	10.731(1)
b (Å)	15.021(1)	13.600(1)	16.872(1)	11.796(1)	14.166(2)
c (Å)	15.856(1)	14.603(1)	18.383(1)	12.374(2)	16.975(3)
α (°)	90	72.62(1)	90	93.00(2)	87.39(2)
β (°)	111.400(9)	81.35(1)	90.700(7)	94.01(1)	73.87(1)
γ (°)	90	84.41(1)	90	101.19(2)	70.03(1)
V (Å^3)	3580.1(6)	2227.3(4)	3504.5(4)	1678.1(4)	2326.1(6)
Z	4	2	4	2	2
T (K)	153(2)	153(2)	293(2)	153(2)	153(2)
D_c (g·cm^{-3})	1.636	1.564	1.771	1.593	1.545
μ (mm^{-1})	2.063	2.610	3.304	1.070	0.991
Scan range (°)	3.84 < 2θ < 52.88	4.26 < 2θ < 51.92	4.20 < 2θ < 51.90	4.48 < 2θ < 52.16	4.06 < 2θ < 51.90
Unique reflections	6537	8111	6816	6163	8373
Reflections used [$I > 2\sigma(I)$]	3505	5997	4443	4834	2936
R_{int}	0.0832	0.0294	0.0528	0.0337	0.1198
Final *R* indices[$I > 2\sigma(I)$]	0.1203, wR_2 0.3025	0.0327, wR_2 0.0769	0.0339, wR_2 0.0723	0.0264, wR_2 0.0626	0.0704, wR_2 0.1496
R indices (all data)	0.1878, wR_2 0.3499	0.0501, wR_2 0.0846	0.0633, wR_2 0.0779	0.0376, wR_2 0.0666	0.1725, wR_2 0.1726
Goodness-of-fit	1.089	0.918	0.857	0.939	0.735
Max, Min Δρ/e (Å^{-3})	4.264, -2.093	1.079, −0.870	1.007, −0.606	0.495, −1.082	0.773, −0.651

 © 2004 Wiley-VCH Verlag GmbH & Co. KGaA, Weinheim

(15 mL). Sodium carbonate (17 mg, 160 μmol) and tetrakis(triphenylphosphane)palladium (12 mg, 16 μmol) were then added to the solution, which was heated under reflux for four days. After cooling to room temperature, the red-brown solution was filtered, and the solvent was evaporated to dryness under reduced pressure. The red solid was dissolved in dichloromethane and purified by preparative thin-layer chromatography on silica (eluent: acetone/hexane, 1:1, acetone/dichloromethane, 1:50). The red fraction containing the desired product was collected. Yield: 14%, 8 mg, 8 μmol. Crystals were obtained by diffusion of diethyl ether into a saturated solution of dichloromethane. The MS (ESI) spectra shows the molecular peak [M^+ + H] m/z = 910 and two other peaks corresponding to the loss of one and two thienyl groups (m/z = 827, m/z = 744). ^{1}H NMR (200 MHz, [D6]acetone, 21 °C): δ = −11.89 (s, 1 H, hydride), 2.23 [s, 36 H, $C_6(CH_3)_6$], 7.93−7.24 (m, 14 H, S−C_6H_4−C_4H_3S) ppm. for $C_{44}H_{51}BF_4Ru_2S_4$ (997.1): calcd. C 53.00, H 5.16; found C 49.87, H 5.19.

X-ray Crystallographic Study: The data were measured on a Stoe Image Plate Diffraction system equipped with a φ circle, using Mo-K_α graphite-monochromated radiation (λ = 0.71073 Å) with φ range 0−200°, increment ranging from 1.0−1.8°, 2θ range from 2.0−26°, $D_{max}-D_{min}$ = 12.45−0.81 Å. The structures were solved by direct methods with the program SHELXS-97.[19] The refinement and all further calculations were carried out using SHELXL-97.[20] The H-atoms were included in calculated positions and treated as riding atoms with the SHELXL default parameters. The non-H atoms were refined anisotropically, using weighted full-matrix least-square on F^2. Figures were drawn with ORTEP.[21] All crystallographic data are collected in Table 2. CCDC-220959 for [**1a**][BF_4], -220962 for [**2a**][BF_4], -220961 for [**2c**][BF_4], -220960 for [**2d**][BF_4], and -220963 for [**3**][BF_4] contain the supplementary crystallographic data. These data can be obtained free of charge at www.ccdc.cam.ac.uk/conts/retrieving.html [or from the Cambridge Crystallographic Data Centre, 12 Union Road, Cambridge CB2 1EZ, UK; Fax: (internat.) + 44-1223-336-033; E-mail: deposit@ccdc.cam.ac.uk]

Acknowledgments

Financial support of the Fond National Suisse de la Recherche Scientifique is gratefully acknowledged. The authors are also indebted to the Johnson Mathey Technology Centre for a loan of ruthenium trichloride hydrate.

[1] J.-M. Lehn, *Supramolecular Chemistry, Concepts and Perspectives*, VCH, Weinheim, **1995**.
[2] R. Ziessel, L. Charbonnière, M. Cesario, T. Prangé, H. Nierengarten, *Angew. Chem. Int. Ed.* **2002**, *41*, 975−979.
[3] K. Sénéchal, O. Maury, H. le Bozec, I. Ledoux, J. Zyss, *J. Am. Chem. Soc.* **2002**, *124*, 4560−4561.
[4] U. S. Schubert, C. Eschbaumer, *Angew. Chem. Int. Ed.* **2002**, *41*, 2892−2926 and references cited therein.
[5] K. K.-W. Lo, W.-K. Hui, D. C.-M. Ng, *J. Am. Chem. Soc.* **2002**, *124*, 9344−9345.
[6] D. T. MacQuade, A. E. Pullen, T. M. Swager, *Chem. Rev.* **2000**, *100*, 2537−2574.
[7] D. H. Kim, J.-H. Kim, T. H. Kim, D. M. Kang, Y. H. Kim, Y.-B. Shim, S. C. Shin, *Chem. Mater.* **2003**, *15*, 825−827.
[8] F. Chérioux, C. M. Thomas, B. Therrien, G. Süss-Fink, *Chem. Eur. J.* **2002**, *8*, 4377−4382.
[9] F. Chérioux, C. M. Thomas, T. Monnier, G. Süss-Fink, *Polyhedron* **2003**, *22*, 543−548.
[10] F. Chérioux, B. Therrien, G. Süss-Fink, *Inorg. Chim. Acta* **2004**, *357*, 834−838.
[11] F. Chérioux, B. Therrien, G. Süss-Fink, *Eur. J. Inorg. Chem.* **2003**, 1043−1047.
[12] N. Miyaura, A. Suzuki, *Chem. Rev.* **1995**, *95*, 2457−2483.
[13] M. A. Bennett, T.-N. Huang, T. W. Matheson, A. K. Smith, *Inorg. Syntheses* **1982**, *21*, 74.
[14] M. Jahncke, G. Meister, G. Rheinwald, H. Stoeckli-Evans, G. Süss-Fink, *Organometallics* **1997**, *16*, 1137−1143.
[15] L. Vieille-Petit, B. Therrien, G. Süss-Fink, *Inorg. Chim. Acta* in press.
[16] R. A. Zelonka, M. C. Baird, *Can. J. Chem.* **1972**, *50*, 3063−3068.
[17] J. W. Wang, K. Moseley, P. M. Maitlis, *J. Am. Chem. Soc.* **1969**, 5970−5977.
[18] M. A. Bennett, A. K. Smith, *J. Chem. Soc., Dalton Trans.* **1974**, 233−241.
[19] G. M. Sheldrick, *Acta Crystallogr., Sect. A* **1990**, *46*, 467.
[20] G. M. Sheldrick, SHELXL-97, University of Göttingen, Göttingen, Germany, **1999**.
[21] L. J. Farrugia, *J. Appl. Crystallogr.* **1997**, *30*, 565.

Received January 9, 2004
Early View Article
Published Online May 13, 2004

 © 2004 Wiley-VCH Verlag GmbH & Co. KGaA, Weinheim

Polynuclear and Extended Coordination Compounds from Preorganized Bimetallic Components: Tuning the Magnetic Properties of Dinickel(II) Building Blocks

Guido Leibeling,[a] Serhiy Demeshko,[a] Bernhard Bauer-Siebenlist,[a] Franc Meyer,*[a] and Hans Pritzkow[b]

Keywords: Molecular magnetism / Nickel / Dinuclear complexes / Tetranuclear complexes / Magnetic properties / Azides

Various dinucleating pyrazole ligands with chelating side arms in the 3- and 5-positions of the heterocycle have been shown to form Ni^{II}/azido complexes, where the metal ions are spanned by the pyrazolate, and an azido bridge. Four new complexes have been characterized by X-ray crystallography and variable-temperature magnetic susceptibility studies. The Ni···Ni distance, and hence the intra-dimer coordination mode of the azide (μ-1,1 or μ-1,3), is determined by the chelate arm length, such that the magnetic properties of the bimetallic units can be controlled. The intramolecular coupling between the Ni^{II} (S = 1) ions was found to be ferromagnetic (J = +4.0 ± 0.5 cm^{-1}) in the case of $[L^1Ni_2(N_3)(NO_3)_2]$ (**1**) with a μ-1,1 azide, but antiferromagnetic (J = −25.7 ± 0.3 cm^{-1}) for $[L^2Ni_2(N_3)](ClO_4)_2$ (**2**) with a μ-1,3 azide. Such bimetallic units can serve as building blocks for the construction of high-nuclearity Ni^{II}/azide compounds, as demonstrated for the tetranuclear complexes $[L^1_2Ni_4(\mu\text{-}1,1\text{-}N_3)_2(\mu\text{-}1,3\text{-}N_3)_2](BPh_4)_2$ (**3**), and $[L^3Ni_2(N_3)_3]_2$ (**4**). Complex **3** was obtained by the replacement of the labile nitrates in **1** by additional azido ligands, that bridge the two $[L^1Ni_2(N_3)]^{2+}$ subunits in the μ-1,3 mode. Complex **4** incorporates two additional azides, and two of its azido linkages were found in the rare μ-1,1,3 binding mode (albeit with relatively long Ni–N bond lengths). The magnetic properties of the tetranuclear species were as predicted from the building blocks and the respective azide binding, with ferromagnetic intra-dimer and antiferromagnetic inter-dimer exchanges, yielded an overall S = 0 ground state.
(© Wiley-VCH Verlag GmbH & Co. KGaA, 69451 Weinheim, Germany, 2004)

Introduction

Recent years have seen extensive studies of the magnetic properties of polynuclear metal complexes with exchange coupled magnetic centers.[1,2] With the objective of obtaining nanoscale molecular magnets, current activities focus on increasing the nuclearity of single-molecule clusters, that have ground electronic states with a large spin[3] and enhancing the anisotropy of single-molecule type systems.[4] In relation to the latter, nickel(II) is a preferred spin carrier due to its large single-ion zero-field splitting. Also, the flexidentate azido ligand is frequently being used as a bridging ligand, since it provides coordination compounds with great structural variety and efficiently mediates different kinds of magnetic exchange depending on its mode of coordination.[5] The favorable combination of nickel(II) ions and azide ligands has indeed provided a variety of molecular architectures in which the azide normally adopts one of its common bridging modes.[6] These are the μ-1,1 mode (*end-on*, Figure 1), which usually results in ferromagnetic coupling, and the μ-1,3 mode (*end-to-end*), which in most cases gives rise to antiferromagnetic behavior. Other triply or quadruply bridging azide coordination modes such as μ_3-1,1,1, μ_3-1,1,3, μ_4-1,1,1,1 or μ_4-1,1,3,3 have remained relatively scarce,[7−9] although these are of particular interest with respect to the construction of high-nuclearity complexes or polymeric systems.

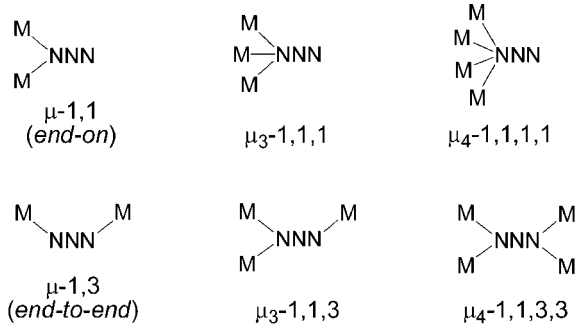

Figure 1. Azide bridging modes

A major task in the rational design of nickel/azide-based coordination compounds with predictable magnetic properties is the control of the azide bridging mode and, even

[a] Institut für Anorganische Chemie, Georg-August-Universität, Tammannstrasse 4, 37077 Göttingen, Germany
Fax: (internat.) + 49-(0)551-393063
E-mail: franc.meyer@chemie.uni.goettingen.de
[b] Anorganisch-Chemisches Institut der Universität Heidelberg, Im Neuenheimer Feld 270, 69120 Heidelberg, Germany

more demanding, the direct assembly of larger complexes with a desired nuclearity and topology. It is not so long ago, however, that a review article started it would be impossible to synthetically determine which coordination mode of the azide linkage would be adopted.[6] The aim of the present work here is twofold. Firstly, it is demonstrated that the azide binding mode in the bimetallic pocket of a preorganized dinickel(II) array, and hence the magnetic properties of the dinuclear compound, can be selectively altered by appropriate changes to the dinucleating ligand scaffold. Secondly, it is shown that such bimetallic units can serve as building blocks for the targeted construction of tetranuclear species with significant magnetic coupling.

Results and Discussion

Synthesis and Characterization of Complexes

A set of compartmental pyrazolate-based ligands HL^1, HL^2, and HL^3 was chosen as dinucleating scaffolds for this work (Figure 2). These three ligands differ in the number of N-donor sites in their chelate side arms (HL^1 versus HL^3), as well as by the side arm chain length (HL^1 versus HL^2). The latter was previously shown to determine the metal-metal separation in the resultant bimetallic complexes. Whereas the longer ligand side arms in HL^1 allow the metal ions to approach relatively close to distances of about 3.5 Å, the shorter side arms in HL^2 pull the metal ions back and apart, thereby enforcing metal-metal distances above 4 Å.[10] This has drastic consequences for an azide co-ligand accommodated within the bimetallic pocket, since the larger metal-metal separation will necessarily lead to an *end-to-end* coordination, whereas the shorter metal-metal separation should only be suitable for an *end-on* bound azide. Dinickel(II) complexes of the related ligand HL^4 have previously proved valuable as building blocks for the controlled synthesis of structurally alternating 1D chains (*J*-alternating chains),[11,12] with the expected μ-1,3 azide coordination within the bimetallic entities.[12]

These considerations were confirmed by the X-ray crystallographic findings for complexes $[L^1Ni_2(N_3)(NO_3)_2]$ (**1**) and $[L^2Ni_2(N_3)](ClO_4)_2$ (**2**), both of which were obtained in a straightforward manner from the respective ligand, one equivalent of base, one equivalent of NaN_3, and two equivalents of a nickel salt such as $Ni(NO_3)_2{\cdot}6H_2O$ or $Ni(ClO_4)_2{\cdot}6H_2O$. The molecular structures of **1** and of the cation of **2** are depicted in Figure 3 and 4, respectively, along with selected bond distances and angles.

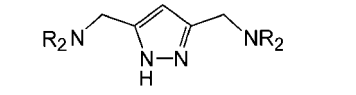

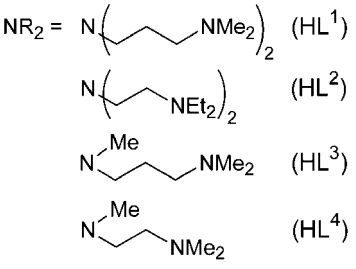

Figure 2. Ligands used in this work

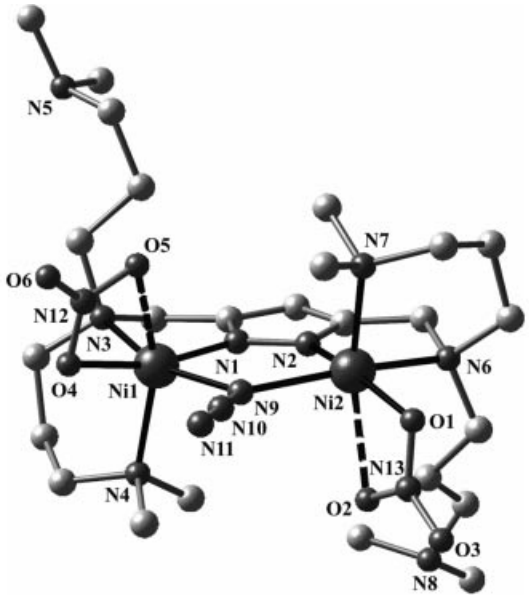

Figure 3. View of the molecular structure of **1**. In the interests of clarity all hydrogen atoms have been omitted. Selected bond distances (Å) and angles (°): Ni1−N1 1.928(1), Ni1−O4 2.070(1), Ni1−N4 2.102(1), Ni1−N9 2.162(1), Ni1−N3 2.222(1), Ni1−O5 2.298(1), Ni2−N2 1.943(1), Ni2−O1 2.061(1), Ni2−N7 2.094(1), Ni2−N9 2.151(2), Ni2−N6 2.235(1), Ni2−O2 2.350(2), Ni1···Ni2 3.660(2), N9−N10 1.212(2), N10−N11 1.150(2); Ni1−N9−Ni2 116.12(6), Ni1−N9−N10 118.22(12), Ni2−N9−N10 124.83(12)

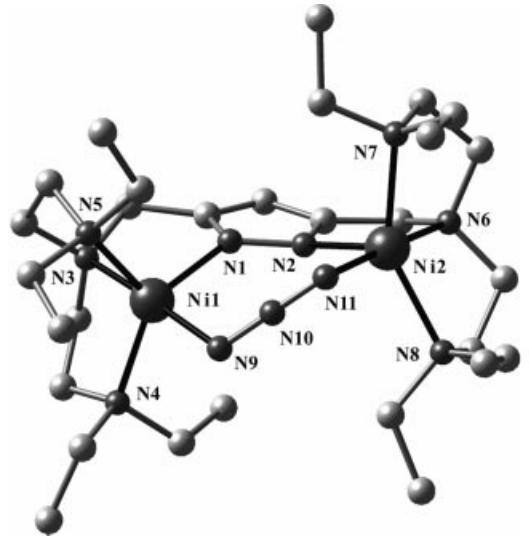

Figure 4. View of the molecular structure of the cation of **2**. In the interests of clarity all hydrogen atoms have been omitted. Selected bond distances (Å) and angles (°): Ni1−N1 2.013(2), Ni1−N9 2.065(2), Ni1−N3 2.087(2), Ni1−N4 2.105(4), Ni1−N5 2.123(2), Ni2−N2 2.007(2), Ni2−N11 2.059(2), Ni2−N6 2.095(2), Ni2−N7 2.121(2), Ni2−N8 2.155(2), Ni1···Ni2 4.421(2), N9−N10 1.178(2), N10−N11 1.179(2); Ni1−N9−N10 114.81(13), Ni2−N11−N10 113.75(13)

 © 2004 Wiley-VCH Verlag GmbH & Co. KGaA, Weinheim

In complex **2**, both nickel ions are nested within their respective coordination compartments, and are five-coordinate (intermediate between TBP-5 and SP-5: τ = 0.60/0.52)[13] with the azide bound in the anticipated *end-to-end* fashion within the bimetallic pocket. While certainly too large to allow for μ-1,1 azide binding, the Ni···Ni distance of 4.421 Å in **2** is still relatively short for a μ-1,3 azide linkage and thus causes the linear azide to tilt severely with respect to the pyrazolate plane. At the same time, the metal ions are forced out of that plane in order to allow for reasonable Ni1−N9−N10 and Ni2−N11−N10 bond angles of 114.8(5)° and 113.8(5)°, respectively. In the absence of geometric constraints by a dinucleating ligand framework, much wider Ni−N−N_{azide} angles are usually observed (>120°). These particular geometric constraints of the [L^2Ni_2] scaffold have previously led to the identification of an extremely bent cyanide coordination within its bimetallic pocket.[14]

In contrast to **2**, the longer ligand side arms in **1** give rise to a much shorter Ni···Ni distance of 3.660 Å. This induces incorporation of the azide in a μ-1,1 mode and a rather relaxed binding situation, as judged from the fact that both nickel ions as well as the azide-N9 centers are located roughly within the plane of the pyrazolate heterocycle. The almost linear azide makes an angle of ≈ 7° with that plane. While the N_3 unit is symmetric in **2** [*d*(N−N) = 1.178(2)/1.179(2) Å], it is distinctly asymmetric in **1** [*d*(N9−N10) = 1.212(2) Å, *d*(N10−N11) = 1.150(2) Å]. Interestingly, the lower stability of the six-membered chelate rings in **1** allows the nitrate anions to displace one side arm donor at each nickel, which is left uncoordinated and dangling. The nitrates are found semi-chelating with one short [2.061(1)/2.070(1) Å], and one much longer [2.350(2)/2.298(1) Å] N−O bond. Unfortunately, we have not been able to grow single crystals of a $[L^1Ni_2(N_3)]^{2+}$ complex with weakly coordinating counterions such as ClO_4^- or BPh_4^-.

Despite the different binding modes of the azide ligands in **1** and **2**, their $\nu_{as}(N_3)$ stretches are similar (Table 1). Binding of the azide and the nitrates in **1** is apparently of comparable strength, since both $[L^1Ni_2(N_3)(NO_3)]^+$ and $[L^1Ni_2(NO_3)_2]^+$ are found as dominant ions in the FAB mass spectrum of the complex. It was thus tempting to provide additional potentially bridging azide ions instead of the nitrates, in order to assemble two (or even more) dinuclear units $[L^1Ni_2(\mu\text{-}1,1\text{-}N_3)]^{2+}$ into larger nickel/azido complexes. A similar strategy has recently been reported to provide tetranuclear nickel(II) complexes from coordinatively unsaturated thiophenolate-based dinickel(II) building blocks or some pyrazolate-based tetranickel(II) complexes with novel azide binding.[9,15] This procedure also proved successful in the present case, since treatment of $[L^1]^-$ with two equivalents of Ni^{2+} and two equivalents NaN_3 gave the tetranuclear species **3**, which could be crystallized as its BPh_4^--salt. The molecular structure of the cation is displayed in Figure 5, along with selected metric parameters.

Table 1. Selected IR absorptions of complexes **1**−**4**, in cm^{-1}

Complex	$\nu_{as}(N_3)$
1	2058 (s)
2	2067 (s)
3	2129 (s), 2064 (m)
4	2103 (s), 2055 (s), 2037 (s)

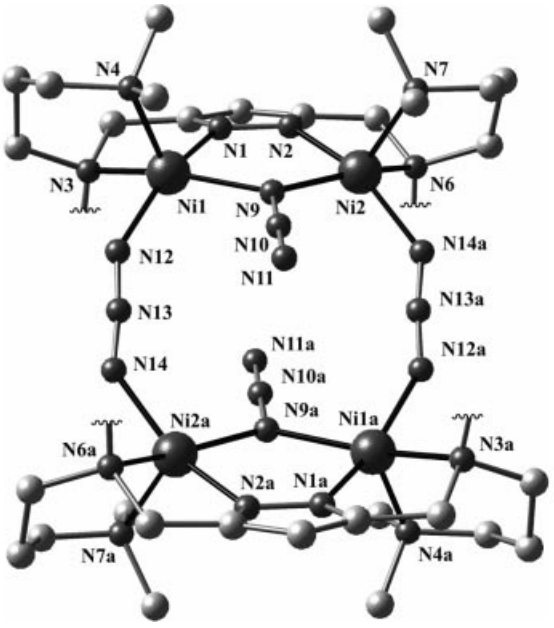

Figure 5. View of the molecular structure of the cation of **3**. In the interests of clarity all hydrogen atoms and the dangling ligand side arms attached to N3 and N6 have been omitted. Selected atom distances (Å) and angles (°): Ni1−N1 1.946(1), Ni1−N12 2.037(2), Ni1−N4 2.064(2), Ni1−N9 2.119(2), Ni1−N3 2.165(2), Ni2−N2 1.945(2), Ni2−N14 2.026(2), Ni2−N7 2.074(2), Ni2−N9 2.120(2), Ni2−N6 2.174(2), Ni1···Ni2 3.639(2), Ni1···Ni2a 5.788(2), Ni1···Ni1a 6.719(2), N9−N10 1.196(2), N10−N11 1.143(2), N12−N13 1.158(2), N13−N14 1.166(2); Ni1−N9−Ni2 118.31(7), N12−N13−N14 174.5(2)

In **3**, two dinuclear $[L^1Ni_2(\mu\text{-}1,1\text{-}N_3)]^{2+}$ entities are linked through two μ-1,3 azide ions to give a rectangular tetranuclear species with crystallographic C_i symmetry. Complex **3** is formally derived from the aggregation of two complexes **1** via replacement of the semi-chelating nitrates by the μ-1,3 bridging azides. Indeed, each pyrazolate-based bimetallic subunit of **3** is basically similar to the dinuclear complex **1** and exhibits a similar Ni···Ni distance [3.639(2) Å], although in this case the nickel and μ-1,1 azide ions are somewhat more displaced out of the plane of the pyrazolate heterocycle and the two dangling side arms are found on the same side of the dinuclear component. The separation of the nickel ions spanned by the μ-1,3-N_3 is 5.788(2) Å. While the μ-1,1 azide is again highly asymmetric [*d*(N9−N10) = 1.196(2) Å versus *d*(N10−N11) = 1.143(2) Å], the μ-1,3 azide is almost symmetric [*d*(N12−N13) = 1.158(2) Å versus *d*(N13−N14) = 1.166(2) Å].

Since one side arm of each ligand coordination compartment remains uncoordinated in **3**, it seemed appropriate to also attempt to employ the related bis(tridentate) ligand

 © 2004 Wiley-VCH Verlag GmbH & Co. KGaA, Weinheim

$[L^3]^-$ for the preparation of similar polynuclear complexes. To this end, a tetranickel(II) complex was obtained from the reaction of $[L^3]^-$ with $Ni(ClO_4)_2 \cdot 6H_2O$ and NaN_3. However, in this case the product $[L^3Ni_2(N_3)_3]_2$ (**4**) is neutral due to the coordination of additional azide ions. The structure of **4** was elucidated by X-ray crystallography, and is depicted in Figure 6 together with selected bond distances and bond angles.

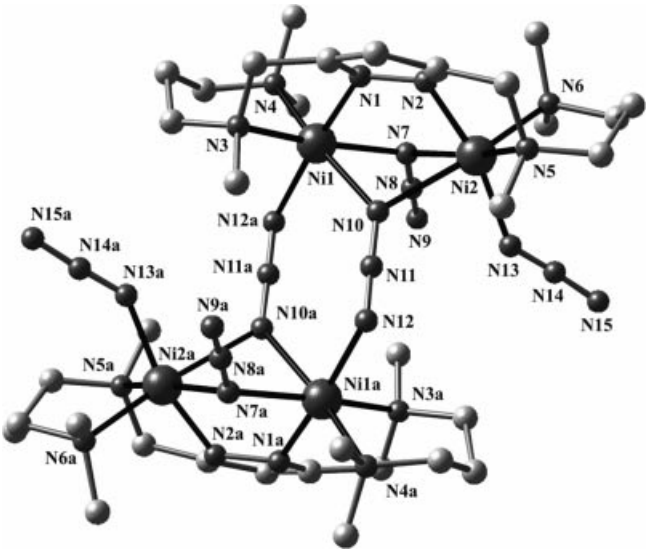

Figure 6. View of the molecular structure of **4**. In the interests of clarity all hydrogen atoms have been omitted. Selected atom distances (Å) and angles (°): Ni1−N1 1.995(3), Ni1−N12a 2.066(3), Ni1−N4 2.141(3), Ni1−N7 2.147(3), Ni1−N3 2.179(3), Ni1−N10 2.310(3), Ni2−N2 2.004(3), Ni2−N13 2.028(3), Ni2−N6 2.128(3), Ni2−N7 2.148(3), Ni2−N5 2.178(3), Ni2−N10 2.443(3), Ni1···Ni2 3.350(3), Ni1···Ni1a 5.358(3), Ni1···Ni2a 5.913(3), N7−N8 1.207(4), N8−N9 1.153(4), N10−N11 1.176(4), N11−N12 1.168(4), N13−N14 1.134(4), N14−N15 1.163(5); Ni1−N7−Ni2 102.49(12), Ni1−N10−Ni2 89.57(10)

Again, complex **4** is composed of two pyrazolate-based dinuclear components $[L^3Ni_2(\mu\text{-}1,1\text{-}N_3)]^{2+}$, that are linked by two further azides. Due to the presence of a fifth and sixth azide, which bind terminally to Ni2, however, the N_3^- group linking the bimetallic subunits is shifted from the μ-1,3 position in **3** to a μ_3-1,1,3 position in **4**. All metal centers are thus six-coordinate in **4** but five-coordinate in **3**. Triply bridging μ_3-1,1,3 azide ions are scarce, and in most cases exhibit two rather long $N_{azide}-M$ bonds,[9,16] as can also be observed in **4** [*d*(Ni1−N10) = 2.310(3) Å and *d*(Ni2−N10) = 2.433(3) Å, in contrast to *d*(Ni1−N12a) = 2.066(3) Å]. Complex **4** enables a comparison to be made of the metric parameters for three different types of N_3^- ligands in a single compound. N−N bond lengths are clearly elongated for the μ-1,1 and μ_3-1,1,3 bridges compared with the terminal N_3^-, and the asymmetry is least pronounced in the μ_3-1,1,3 azide [1.168(4)/1.178(4) Å versus 1.153(4)/1.207(4) Å in the μ-1,1 azide and 1.134(4)/1.163(5) Å for the terminal azide]. It seems reasonable to assign the high-energy IR bands for $\nu_{as}(N_3)$ at 2129 (**3**) and 2103 cm^{-1} (**4**) to the μ-1,1 and μ-1,1,3 azido ligands, respectively (Table 1).

Magnetic Properties

For all complexes, the magnetic susceptibility measurements were carried out at two different magnetic fields in a temperature range from 2.0 K to 295 K (300 K). No significant field dependence was observed for any of the complexes.

The temperature dependence of the magnetic susceptibility χ_M, and of the product $\chi_M T$ for the dinuclear complexes **1** and **2** are shown in Figure 7 and 8, respectively. As would be expected from the different binding modes of the azide bridge, the magnetic properties of the two compounds differ fundamentally. In the case of **1**, the observed $\chi_M T$ value of 2.66 $cm^3 \cdot K \cdot mol^{-1}$ (4.62 μ_B) at room temperature remains nearly constant down to 100 K. Below this temperature $\chi_M T$ gradually increases, reaching a maximum of 3.13 $cm^3 \cdot K \cdot mol^{-1}$ (corresponding to a μ_{eff} value of 5.01 μ_B) at 12 K, indicating ferromagnetic exchange. At even lower temperatures, $\chi_M T$ drops rapidly, which may be due to the effects of zero-field splitting or intermolecular antiferromagnetic interactions.

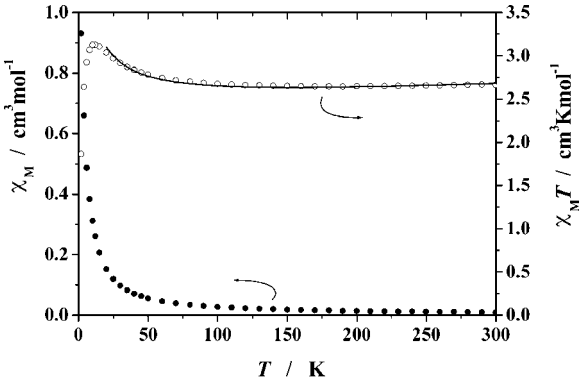

Figure 7. Plot of χ_M (solid circles) and $\chi_M T$ (open circles) vs. *T* for **1** at 2000 G. The solid line represents the calculated curve fit (see text)

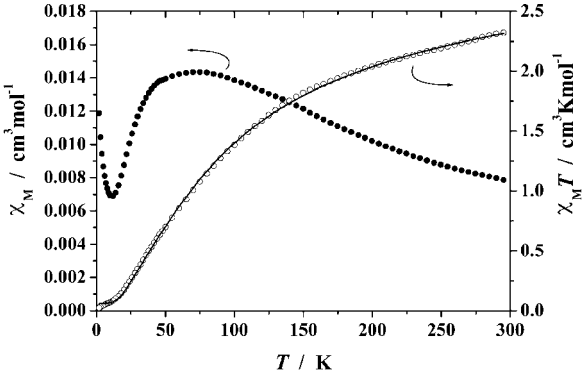

Figure 8. Plot of χ_M (solid circles) and $\chi_M T$ (open circles) vs. *T* for **2** at 2000 G. The solid line represents the calculated curve fit (see text)

The experimental data for **1** were modeled in the range from 300 K to 20 K using Equation (1)[1b] deduced from the Hamiltonian $H = -2JS_1S_2$, with additional terms accounting for small amounts of paramagnetic impurities (ρ), and

 © 2004 Wiley-VCH Verlag GmbH & Co. KGaA, Weinheim

for the temperature independent paramagnetism (*TIP*). A satisfactory fit was obtained with the parameters $g = 2.25 \pm 0.01$ and $J = +4.0 \pm 0.5$ cm^{-1} ($\rho = 2\%$, $TIP = 6.0 \times 10^{-4}$ cm^3·mol^{-1}), confirming moderate ferromagnetic coupling. Owing to the likely occurrence of zero-field splitting at low temperatures, however, the magnitude of J should be interpreted with caution.

$$\chi_M = \frac{Ng^2\mu_B{}^2}{kT}\frac{2e^{2(J/kT)} + 10e^{6(J/kT)}}{1 + 3e^{2(J/kT)} + 5e^{6(J/kT)}}(1-\rho) + \frac{2Ng^2\mu_B{}^2}{3kT}\rho + TIP \quad (1)$$

For complex **2** the observed $\chi_M T$ value at 295 K is 2.32 cm^3·K·mol^{-1} (4.31 μ_B). It drops steadily with decreasing temperature, and finally tends to zero, indicating an $S = 0$ ground state. This behavior is typical for dinuclear complexes with intramolecular antiferromagnetic coupling. The experimental magnetic data for **2** were modeled in the range from 295 K to 2 K using Equation (1),[1b] which gives the fit parameters $g = 2.28 \pm 0.02$, $J = -25.7 \pm 0.3$ cm^{-1}, $\rho = 5.7 \pm 0.1\%$, and $TIP = 7.9 \times 10^{-4}$ cm^3·mol^{-1}.

A number of dinuclear nickel(II) complexes with only a single μ-1,3 azido bridge have been characterized magnetically.[17] Two geometric parameters, the angles Ni−N−N and the dihedral angle φ along the azide ligand, are often considered for magnetostructural correlations.[6] For a Ni−N_3−Ni torsion angle of φ = 180°, the antiferromagnetic coupling can be predicted to have a maximum at Ni−N−N angles around 108°, and to decrease at larger angles. On the other hand, for all Ni−N−N angles, the maximum coupling would be expected for a torsion angle of 180°. However, the effect of torsion should be less pronounced than the effect of the bond angle. In the absence of any constraining ligand scaffold, Ni−N−N angles tend to lie in the range 130°−145° with φ = 180°, resulting in J values in the range of −8 to −22 cm^{-1}.[6,18] In view of the very acute Ni−N−N angles (114.8° and 113.7°), and the fact that φ = 55.4° for **2**, a J value even more negative than the lower limit of the above range was thus expected, in good agreement with experimental findings. Although some contribution from the pyrazolate is certainly present, the azide appears to provide the dominant pathway for the antiferromagnetic exchange coupling.

Dinuclear nickel(II) complexes with two *end-on* azido bridges and a {Ni(μ−1,1−N_3)$_2$Ni} central core generally feature Ni−N−Ni angles θ in the narrow range 101−105°, and J values between +13 and +37 cm^{-1}.[6,18] DFT calculations have suggested a clear correlation between the exchange coupling and θ, with the interaction predicted to be ferromagnetic for all the range of θ angles explored.[19] For the {Ni(μ-1,1-N_3)$_2$Ni} core, a maximum is expected when θ ≈ 104°. On the other hand, the out-of-plane displacement of the azide should only have a minor influence. The Ni1−N9−Ni2 angle induced by the dinucleating ligand scaffold in **1** is unusually large [116.12(6)°], and a small J value could thus be expected for the single μ-1,1 azide, in accordance with experimental results. Despite this, and despite a likely antiferromagnetic contribution from the pyrazolate bridge, however, the exchange in **1** is still clearly ferromagnetic.

Complex **3** features a $\chi_M T$-value of 3.89 cm^3·K·mol^{-1} (5.58 μ_B) at 295 K, which is close to the spin-only value expected for four uncoupled $S = 1$ ions (4.00 cm^3·K·mol^{-1} 5.66 μ_B, respectively). Figure 9 shows the temperature dependence of the magnetic susceptibility χ_M and the $\chi_M T$ value at a field of 2000 G. By lowering the temperature $\chi_M T$ decreases, indicating an overall antiferromagnetic coupling between the Ni centers. From the molecular structure we can expect two principal magnetic exchange pathways, one intra-dimer coupling via the pyrazolate and the μ-1,1 azide and an inter-dimer coupling between the subunits, which is mediated by the μ-1,3 azide. The experimental data were analyzed by means of the program MAGMUN[20] in a model based on the isotropic exchange Hamiltonian $H = -2J_1(S_2S_3 + S_1S_4) - 2J_2(S_1S_2 + S_3S_4)$ (**A** in Figure 10). The solid line in Figure 9 represents the best fit with $g = 2.01 \pm 0.01$, $J_1 = -16.2 \pm 0.2$ cm^{-1}, $J_2 = +2.0$ cm^{-1}, $\rho = 2.5\%$, $\Theta = 3.5$ K, and $TIP = 2.0 \times 10^{-4}$ cm^3·mol^{-1}.

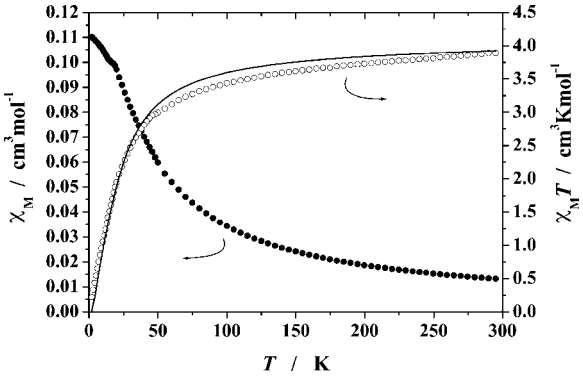

Figure 9. Plot of χ_M (solid circles) and $\chi_M T$ (open circles) vs. T for **3** at 2000 G. The solid line represents the calculated curve fit (see text)

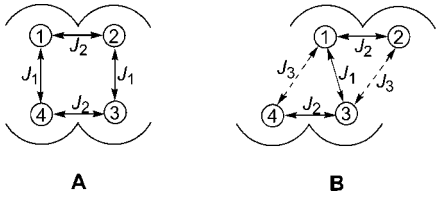

Figure 10. Coupling schemes for **3** (**A**) and **4** (**B**)

In view of the ferromagnetic behavior observed for **1**, it is reasonable to assign J_2 to the coupling within the bimetallic constituents of **3**, and J_1 to the antiferromagnetic inter-dimer exchange mediated by the μ-1,3-N_3 linkages. The intra-dimer coupling is determined by the azide binding mode within the bimetallic pocket and is ferromagnetic as anticipated, its value being of the same order of magnitude as the coupling constant in **1**. Small differences may reflect subtle geometric differences between **1** and the μ-1,1 azido

 © 2004 Wiley-VCH Verlag GmbH & Co. KGaA, Weinheim

bridged building blocks of **3**, in particular the even larger Ni1−N9−Ni2 angle [θ = 118.31(7)°], which is predicted to reduce the ferromagnetic contribution, and the more distinct out-of-plane displacement of the N_3^- ligand in the case of **3**. It should also be noted, that coordination numbers and coordination geometries are quite different for the two dinickel(II) arrays. The inter-dimer antiferromagnetic exchange is in the range expected for a μ-1,3 azide with comparatively wide Ni−N−N angles [141.7(2) and 148.1(2)°] and a torsion of φ = 36.1°.

The $\chi_M T$ value observed for **4** at 295 K is 5.15 $cm^3 \cdot K \cdot mol^{-1}$ (6.42 μ_B). Figure 11 depicts a plot of the temperature dependence of χ_M and $\chi_M T$ at 2000 G. With respect to the topology of **4**, a three-*J* coupling scheme sketched in Figure 10 (**B**) applies. Considering the very long Ni2−N10 bond lengths for the central μ-1,1,3 azido linkages, however, it is reasonable to approximate J_3 as negligible, and that a two-*J* model is adequate for a qualitative analysis of the data. Fitting was carried out with the program MAGMUN[20] based on the isotropic exchange Hamiltonian $H = -2J_1(S_1S_3) - 2J_2(S_1S_2 + S_3S_4)$ (corresponding to **B** and $J_3 = 0$, Figure 10) to give $g = 2.29 \pm 0.02$, $J_1 = -19.7 \pm 0.8$ cm^{-1}, $J_2 = +6.0$ cm^{-1} $\rho = 3.0\%$, $\Theta = 1.8$ K, and $TIP = 3.6 \times 10^{-4}$ $cm^3 \cdot mol^{-1}$ (solid line in Figure 8).

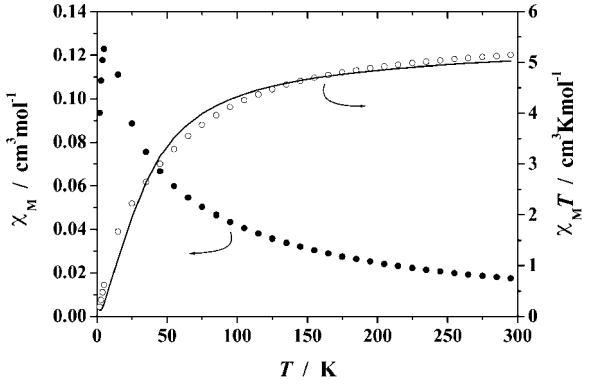

Figure 11. Plot of χ_M (solid circles) and $\chi_M T$ (open circles) vs. *T* for **4** at 2000 G. The solid line represents the calculated curve fit (see text)

Similar to the case of **3**, it would seem appropriate to assign J_2 to the intra-dimer exchange, which is expected to be ferromagnetic, while J_1 should reflect the antiferromagnetic interaction between the two pyrazolate-based subunits. The J_1 value is a little more negative than in the case of **3**, in accordance with the somewhat more acute Ni−N−N angles [Ni1a−N12−N11: 127.4(2)°; Ni1−N10−N11: 133.9(2)°], which are assumed to be the most relevant magnetostructural parameters for a μ-1,3 azido bridge.[6] Likewise, the larger ferromagnetic intra-dimer exchange in **4** may be traced to the much more acute Ni−N−Ni angle for the μ-1,1 azide [Ni1−N7−Ni2: 102.5(1) in **4**].

Conclusion

The present study has established well defined pyrazolate-based dinickel(II) azido complexes as building blocks for the construction of high nuclearity nickel/azido systems. A particular advantage of these compounds is the possibility of tuning the magnetic properties of the bimetallic components, since their spin ground state ($S = 0$ or $S = 2$) is determined by the intra-dimer azide bridging mode, which can be controlled by suitable modifications of the ligand scaffold. Some tetranuclear complexes that arise from the assembly of two Ni_2 subunits are reported in this work as examples. The magnetic exchange within the Ni_2 subunits of the new Ni_4 species is as anticipated and is basically governed by the choice of the building blocks (i.e. ferromagnetic exchange in **1** as well as in **3** and **4**). However, the magnitude of the coupling may differ somewhat, since subtle geometric changes in the subunits occur upon linking the Ni_2 species to give high-nuclearity $\{Ni_2\}_n$ compounds, which represents a general limitation to the prediction of magnetic properties of polynuclear complexes from the magnetic properties of their constituents. Future work will focus on, inter alia, increasing the rigidity of the bimetallic entities and strategies to more efficiently control the linking of the building blocks. In view of the great variety of available dinucleating pyrazolate ligands, we expect a wide range of new oligonuclear and 1D-chain nickel(II) azido systems to be accessible via this precursor based approach.

Experimental Section

Caution! *Although no problems were encountered in this work, transition metal perchlorate and azide complexes are potentially explosive, and should be handled with proper precautions.*

General: Ligands HL^1, HL^2, and HL^3 were prepared as described previously.[10a,21] HPLC grade methanol (CHROMASOLV) was obtained from Riedel-de-Haen. Solvents were dried by established processes. All other chemicals were purchased from commercial sources and used as received. Microanalyses were performed by the Analytisches Labor des Anorganisch-Chemischen Instituts der Universität Göttingen. IR spectra: Digilab Excalibur, recorded as KBr pellets. Mass spectra: Finnigan MAT 95 (FAB-MS). The susceptibility measurements were carried out with a Quantum-Design MPMS-5S SQUID magnetometer equipped with a 5 Tesla magnet in the range of 2 to 300 K. The powdered samples were contained in a gel bucket and fixed in a non-magnetic sample holder. Each raw data file for the measured magnetic moment was corrected for the diamagnetic contribution of the sample holder and the gel bucket. The molar susceptibilities were corrected using the Pascal constant and the increment method according to Haberditzl.[22]

Synthesis of $[L^1Ni_2(\mu\text{-}1,1\text{-}N_3)(NO_3)_2]$ (1): A solution of HL^1 (190 mg, 0.41 mmol) in MeOH (70 mL) was treated with one equivalent of KO*t*Bu (45.7 mg, 0.41 mmol), two equivalents of $Ni(NO_3)2{\cdot}6H_2O$ (236.8 mg, 0.81 mmol), and one equivalent of sodium azide (26.5 mg, 0.41 mmol), and the reaction mixture was stirred at room temperature for 12 h. All volatile materials were then evaporated under reduced pressure and the residue taken up in acetone (60 mL). After filtration, the solution was layered with

 © 2004 Wiley-VCH Verlag GmbH & Co. KGaA, Weinheim

light petroleum to yield green crystals (194 mg, 63%) of the product **1**. MS (FAB+): *m/z* (rel. intensity) = 705 (25) $[L^1Ni_2(NO_3)_2]^+$, 685 (60) $[L^1Ni_2(N_3)(NO_3)]^+$, 665 (25) $[L^1Ni_2(N_3)_2]^+$, 623 (15) $[L^1Ni_2(N_3)]^+$. IR (KBr): $\tilde{\nu}$ = 2939 (w), 2860 (w), 2819 (w), 2767 (w), 2058 (s), 1479 (m), 1385 (vs), 1284 (m), 1234 (w), 1188(w), 1040 (w), 1021(w), 981 (w), 832 (w) cm^{-1}. $C_{25}H_{53}N_{13}Ni_2O_6$ (749.2): calcd. C 40.08, H 7.13, N 24.31; found C 40.28, H 7.23, N 24.78.

Synthesis of $[L^2Ni_2(\mu\text{-}1,3\text{-}N_3)](ClO_4)_2$ (2): A solution of HL^2 (149 mg, 0.285 mmol) in MeOH (70 mL) was treated with one equivalent of KO*t*Bu (32.0 mg, 0.285 mmol), two equivalents of $Ni(ClO_4)2{\cdot}6H_2O$ (208.4 mg, 0.570 mmol), and one equivalent of sodium azide (18.5 mg, 0.285 mmol), and the reaction mixture was stirred at room temperature for 12 h. All volatile materials were then evaporated under reduced pressure and the residue taken up in acetone (50 mL). After filtration the solution was layered with light petroleum to yield green crystals (216 mg, 86%) of the product **2**. MS (FAB+): *m/z* (rel. intensity) = 778 (25) $[L^2Ni_2(N_3)(ClO_4)]^+$, 679 (50) $[L^2Ni_2(N_3)]^+$. IR (KBr): $\tilde{\nu}$ = 2984 (w), 2946 (w), 2884 (w), 2067 (s), 1459 (w), 1388 (w), 1315 (w), 1263 (w), 1092 (vs), 914 (w), 797 (w), 736 (w), 624 (m) cm^{-1}. $C_{29}H_{61}Cl_2N_{11}Ni_2O_8$ (880.2): calcd. C 39.57, H 6.99, N 17.51; found C 39.65, H 7.10, N 17.51.

Synthesis of $[L^1_2Ni_4(\mu\text{-}1,1\text{-}N_3)_2(\mu\text{-}1,3\text{-}N_3)_2](BPh_4)_2{\cdot}2C_3H_6O$ (3·2C_3H_6O): A solution of HL^1 (180 mg, 0.386 mmol) in MeOH (70 mL) was treated with one equivalent of KO*t*Bu (43.3 mg, 0.386 mmol), two equivalents of $Ni(ClO_4)_2{\cdot}6H_2O$ (282.1 mg, 0.771 mmol) and two equivalents of sodium azide (50.2 mg, 0.771 mmol) and was stirred at room temperature for 12 h. All volatile materials were then evaporated under reduced pressure, the residue taken up in ethanol (100 mL), and sodium tetraphenylborate (264 mg, 0.771 mmol) was added. The resultant precipitate was separated by filtration and taken up in acetone (60 mL). The solution was again filtered, and then layered with light petroleum to gradually yield some green crystals (76 mg, 20%) of the product **3**. MS (FAB+): *m/z* (rel. intensity) = 1649 (5) $[L^1_2Ni_4(N_3)_4(BPh_4)]^+$, 665 (100) $[L^1Ni_2(N_3)_2]^+$, 623 (35) $[L^1Ni_2(N_3)]^+$. IR (KBr): $\tilde{\nu}$ = 2964 (m), 2923 (m), 2859 (w), 2129 (s), 2064 (m), 1460 (m), 1384 (s), 1261 (s), 1097 (s), 1032 (s), 803 (s), 732 (w), 703 (w), 612 (w) cm^{-1}. $C_{104}H_{158}B_2N_{28}Ni_4O_2$ (2089.0): calcd. C 59.80, H 7.62, N 18.77; found C 56.42, H 7.18, N 17.68.

Synthesis of $[L^3Ni_2(N_3)_3]_2{\cdot}2CH_2Cl_2$ (4·2CH_2Cl_2): A solution of HL^3 (255 mg, 0.786 mmol) in MeOH (20 mL) was treated with one equivalent of KO*t*Bu (92.7 mg, 0.786 mmol) and two equivalents of $Ni(ClO_4)_2{\cdot}6H_2O$ (580.7 mg, 1.572 mmol). After stirring the mixture for 30 min at room temperature the solution was evaporated to dryness and the residue was taken up in acetone (25 mL). NaN_3 (154.8 mg, 2.358 mmol) was added, and the reaction mixture was stirred for a further 24 h. The green precipitate was separated by filtration then dissolved in dichloromethane (25 mL). Layering the solution with light petroleum (boiling range 40−60 °C, 75 mL) afforded green crystals of the product **4** (148 mg, 29%). MS (FAB+): *m/z* (rel. intensity) = 1088 (16) $[L^3_2Ni_4(N_3)_5]^+$, 523 (100) $[L^3Ni_2(N_3)_2]^+$, 423 (12) $[L^3Ni(N_3)]^+$. IR (KBr): $\tilde{\nu}$ = 3011 (w), 2967 (w), 2909 (w), 2864 (w), 2103 (vs), 2055 (vs), 2037 (vs), 1650 (w), 1472 (m), 1458 (m), 1030 (m), 1009 (w), 826 (w), 669 (w) cm^{-1}. $C_{36}H_{74}Cl_4N_{30}Ni_4$ (1303.8): calcd. C 33.17, H 5.72, N 32.23; found C 33.59, H 5.78, N 32.50.

X-ray Crystallographic Studies: Data collection was carried out with a Bruker AXS CCD diffractometer using graphite-monochromated Mo-K_α radiation (λ = 0.71073 Å). Structures were solved by direct methods (SHELXS-97) and refined by full-matrix least-

Table 2. Crystal data and refinement details for complexes **1**, **2**, **3**, and **4**

	$[L^1Ni_2(\mu\text{-}1,1\text{-}N_3)(NO_3)_2]$ **1**	$[L^2Ni_2(\mu\text{-}1,3\text{-}N_3)](ClO_4)_2$ **2**	$[L^1_2Ni_4(\mu\text{-}1,1\text{-}N_3)_2(\mu\text{-}1,3\text{-}N_3)_2](BPh_4)_2$ **3**	$[L^3Ni_2(N_3)_3]_2$ **4**
Empirical formula	$C_{25}H_{53}N_{13}Ni_2O_6$	$C_{29}H_{61}Cl_2N_{11}Ni_2O_8{\cdot}0.5H_2O$	$C_{98}H_{146}B_2N_{28}Ni_4{\cdot}2C_3H_6O$	$C_{34}H_{70}N_{30}Ni_4{\cdot}2CH_2Cl_2$
Molecular mass (g/mol)	749.22	888.21	2089.04	1303.89
Crystal size (mm)	0.50 × 0.45 × 0.15	0.37 × 0.25 × 0.25	0.40 × 0.23 × 0.20	0.22 × 0.13 × 0.03
Crystal system	monoclinic	monoclinic	triclinic	monoclinic
Space group	$P2_1/n$	$P2_1/n$	$P\bar{1}$	$P2_1/n$
a (Å)	10.3639(5)	11.3834(5)	14.0149(7)	9.8084(5)
b (Å)	33.708(2)	27.6474(2)	14.4822(7)	23.4284(2)
c (Å)	10.6517(6)	12.8429(6)	14.8493(7)	12.3392(7)
α (°)	90	90	97.759(1)	90
β (°)	110.851(1)	99.731(1)	106.411(1)	103.965(1)
γ (°)	90	90	102.041(1)	90
Volume ($Å^3$)	3477.4(3)	3983.8(3)	2766.4(2)	2751.7(3)
$\rho_{calcd.}$ (g/cm^3)	1.431	1.481	1.254	1.574
Z	4	4	1	2
F(000)	1592	1880	1116	1360
Temperature (K)	103(2)	103(2)	297(2)	103(2)
hkl Range	−15 to 14, 0 to 50, 0 to 15	−16 to 16, 0 to 41, 0 to 18	−20 to 18, −20 to 20, 0 to 21	−14 to 14, 0 to 34, 0 to 18
2θ Range (deg)	4.26 to 64.04	4.36 to 64.02	3.14 to 61.02	3.48 to 64.06
Measured reflections	58577	47464	45514	26628
Unique reflections	11942 [*R*(int) = 0.0302]	13577 [*R*(int) = 0.0374]	16829 [*R*(int) = 0.0384]	9476 [*R*(int) = 0.0560]
Obsd. reflections [$I > 2\sigma(I)$]	10821	10666	11612	6267
Refinined params	627	771	925	482
Residual electron density (e $Å^{-3}$)	0.580 and −0.994	1.083 and −0.606	0.516 and −0.339	0.964 and −1.933
*R*1 [$I > 2\sigma(I)$]	0.0397	0.0426	0.0420	0.0531
*wR*2 (all data)	0.0909	0.1074	0.1099	0.1439
Goodness-of-fit	1.222	1.046	1.015	1.065

 © 2004 Wiley-VCH Verlag GmbH & Co. KGaA, Weinheim

squares techniques based on F^2 (SHELXL-97).[23] Atomic coordinates and thermal parameters of the non-hydrogen atoms were refined in fully anisotropic models. Hydrogen atoms were either located in the difference Fourier map or included using the riding model with U_{iso} tied to U_{iso} of the parent atoms. Crystal data and refinement details are listed in Table 2. CCDC-223071 (for **1**), -223072 (for **2**), -223073 (for **3**), and -223074 (for **4**) contain the supplementary crystallographic data for this paper. These data can be obtained free of charge at www.ccdc.cam.ac.uk/conts/retrieving.html or from the Cambridge Crystallographic Data Center, 12 Union Road, Cambridge CB2 1EZ, UK [Fax: (internat.) +44-1223-336-033; E-mail: deposit@ccdc.cam.ac.uk].

Acknowledgments

We sincerely thank the DFG (priority program 1137 "Molecular Magnetism") and the Fonds der Chemischen Industrie for support of this work.

[1] [1a] O. Kahn, *Angew. Chem.* **1985**, *97*, 837−853; *Angew. Chem. Int. Ed. Engl.* **1985**, *24*, 834−850. [1b] O. Kahn, *Molecular Magnetism*, VCH Publishers Inc., New York, **1993**. [1c] J. S. Miller, A. J. Epstein, *Angew. Chem.* **1994**, *106*, 399−432; *Angew. Chem. Int. Ed. Engl.* **1994**, *33*, 385−415. [1d] *Molecule-Based Magnetic Materials* (Eds.: M. M. Turnbull, T. Sugimoto, L. K. Thompson), ACS Symposium Series 644, Washington, **1996**.

[2] *Magnetism: Molecules to Materials* (Eds.: J. S. Miller, M. Drillon), Wiley-VCH, Weinheim, **2001**.

[3] [3a] R. Sessoli, H.-L. Tsai, A. N. Schake, S. Wang, J. B. Vincent, K. Folting, D. Gatteschi, G. Christou, D. N. Hendrickson, *J. Am. Chem. Soc.* **1993**, *115*, 1804−1816. [3b] A. K. Powell, S. L. Heath, D. Gatteschi, L. Pardi, R. Sessoli, G. Spina, F. Del Giallo, F. Pieralli, *J. Am. Chem. Soc.* **1995**, *117*, 2491−2502. [3c] A. Müller, F. Peters, M. T. Pope, D. Gatteschi, *Chem. Rev.* **1998**, *98*, 239−271. [3d] D. Gatteschi, R. Sessoli, A. Cornia, *Chem. Commun.* **2000**, 725−732. [3e] J. Larionova, M. Gross, M. Pilkington, H. Andres, H. Stoeckli-Evans, H. U. Güdel, S. Decurtins, *Angew. Chem.* **2000**, *112*, 1667−1672; *Angew. Chem. Int. Ed.* **2000**, *39*, 1605−1609.

[4] [4a] O. Kahn, *Metal-Organic and Organic Molecular Magnets*, Spec. Publ. 252, Royal Society of Chemistry, **2000**, 150−168. [4b] O. Kahn, J. Larionova, L. Ouahab, *Chem. Commun.* **1999**, 945−952. [4c] A. Caneschi, D. Gatteschi, C. Sangregorio, R. Sessoli, L. Sorace, A. Cornia, M. A. Novak, C. Paulsen, W. Wernsdorfer, *J. Magn. Magn. Mater.* **1999**, *200*, 182−201.

[5] [5a] M.-F. Charlot, O. Kahn, M. Chaillet, C. Larrieu, *J. Am. Chem. Soc.* **1986**, *108*, 2574−2581. [5b] L. K. Thompson, S. S. Tandon, *Comments, Inorg. Chem.* **1996**, *18*, 125−144.

[6] J. Ribas, A. Escuer, M. Monfort, R. Vicente, R. Cortés, L. Lezama, T. Rojo, *Coord. Chem. Rev.* **1999**, *193−195*, 1027−1068.

[7] [7a] M. A. Halcrow, J. C. Huffman, G. Christou, *Angew. Chem.* **1995**, *107*, 971−973; *Angew. Chem. Int. Ed. Engl.* **1995**, *34*, 889−891. [7b] M. A. Halcrow, J.-S. Sun, J. C. Huffman, G. Christou, *Inorg. Chem.* **1995**, *34*, 4167−4177. [7c] M. W. Wemple, D. M. Adams, K. S. Hagen, K. Folting, D. N. Hendrickson, G. Christou, *J. Chem. Soc., Chem. Commun.* **1995**, 1591−1593. [7d] D. Ma, S. Hikichi, M. Akita, Y. Moro-oka, *J. Chem. Soc., Dalton Trans.* **2000**, 1123−1134. [7e] M. A. S. Goher, J. Cano, Y. Journaux, M. A. M. Abu-Youssef, F. A. Mautner, A. Escuer, R. Vicente, *Chem. Eur. J.* **2000**, *6*, 778−784.

[8] G. S. Papaefstathiou, S. P. Perlepes, A. Escuer, R. Vicente, M. Font-Bardia, X. Solans, *Angew. Chem.* **2001**, *113*, 908−910; *Angew. Chem. Int. Ed.* **2001**, *40*, 884−886.

[9] F. Meyer, P. Kircher, H. Pritzkow, *Chem. Commun.* **2003**, 774−775.

[10] [10a] F. Meyer, S. Beyreuther, K. Heinze, L. Zsolnai, *Chem. Ber./Recueil* **1997**, *130*, 605−613. [10b] F. Meyer, K. Heinze, B. Nuber, L. Zsolnai, *J. Chem. Soc., Dalton Trans.* **1998**, 207−213. [10c] F. Meyer, P. Rutsch, *Chem. Commun.* **1998**, 1037−1038. [10d] F. Meyer, E. Kaifer, P. Kircher, K. Heinze, H. Pritzkow, *Chem. Eur. J.* **1999**, *5*, 1617−1630. [10e] J. Ackermann, F. Meyer, E. Kaifer, H. Pritzkow, *Chem. Eur. J.* **2002**, *8*, 247−258.

[11] F. Meyer, U. Ruschewitz, P. Schober, B. Antelmann, L. Zsolnai, *J. Chem. Soc., Dalton Trans.* **1998**, 1181−1186.

[12] F. Meyer, H. Pritzkow, *Inorg. Chem. Commun.* **2001**, *4*, 305−307.

[13] The angular structural parameter τ is defined as $\tau = (\beta - \alpha)/60$, where α and β represent two basal angles with $\beta > \alpha$. It is a measure of the degree of trigonality: A perfect TB-5 structure is associated with $\tau = 1$, while $\tau = 0$ is expected for an idealized SPY-5 geometry; A. W. Addison, T. N. Rao, J. Reedijk, J. van Rijn, G. C. Verschoor, *J. Chem. Soc., Dalton Trans.* **1984**, 1349−1356.

[14] F. Meyer, R. F. Winter, E. Kaifer, *Inorg. Chem.* **2001**, *40*, 4597−4603.

[15] B. Kersting, G. Steinfeld, D. Siebert, *Chem. Eur. J.* **2001**, *7*, 4253−4258.

[16] [16a] M. Montfort, J. Ribas, X. Solans, *J. Chem. Soc., Chem. Commun.* **1993**, 350. [16b] J. Ribas, M. Montfort, X. Solans, M. Drillon, *Inorg. Chem.* **1994**, *33*, 742. [16c] I. Agrell, *Acta Chem. Scand.* **1967**, *21*, 2647. [16d] M. A. S. Goher, A. Escuer, M. A. M. Abu-Youssef, F. A. Mautner, *Polyhedron* **1998**, *17*, 4265.

[17] [17a] C. G. Pierpont, D. N. Hendrickson, D. M. Duggan, F. Wagner, E. K. Barefield, *Inorg. Chem.* **1975**, *14*, 604−610. [17b] F. Wagner, M. T. Mocella, M. J. J. D′Aniello, A. H. J. Wang, E. K. Barefield, *J. Am. Chem. Soc.* **1974**, *96*, 2625−2627. [17c] G. A. McLachlan, G. D. Fallon, R. L. Martin, B. Moubaraki, K. S. Murray, L. Spiccia, *Inorg. Chem.* **1994**, *33*, 4663−4668. [17d] L. Fabbrizzi, P. Pallavicini, L. Parodi, A. Perotti, N. Sardone, A. Taglietti, *Inorg. Chim. Acta* **1996**, *244*, 7−9. [17e] A. Escuer, C. J. Harding, Y. Dussart, J. Nelson, V. McKee, R. Vicente, *J. Chem. Soc., Dalton Trans.* **1999**, 223−228. [17f] Z.-H. Zhang, X.-H. Bu, Z.-H. Ma, W.-M. Bu, Y. Tang, Q.-H. Zaho, *Polyhedron* **2000**, *19*, 1559−1566.

[18] F. Meyer, H. Kozlowski, in *Comprehensive Coordination Chemistry II* (Eds.: J. A. McCleverty, T. J. Meyer), Pergamon, **2004**, vol. 6, 247−554.

[19] E. Ruiz, J. Cano, S. Alvarez, P. Alemany, *J. Am. Chem. Soc.* **1998**, *120*, 11122−11129.

[20] The fits for the tetranuclear complexes **3** and **4** were performed by the program MAGMUN. This program has been developed by Dr. Z. Xu in collaboration with Prof. L. K. Thompson and Dr. O. Waldmann. The program is available free of charge from the authors. See also: L. K. Thompson, O. Waldmann, Z. Xu, in *Magnetism: Molecules to Materials IV* (Eds.: J. S. Miller, M. Drillon), Wiley-VCH, Weinheim, **2002**, p. 173−202.

[21] J. C. Röder, F. Meyer, M. Konrad, S. Sandhöfner, E. Kaifer, H Pritzkow, *Eur. J. Org. Chem.* **2001**, 4479−4487.

[22] [22a] W. Haberditzel, *Angew. Chem.* **1966**, *78*, 277−288; *Angew. Chem. Int. Ed. Engl.* **1966**, *5*, 288−299. [22b] W. Haberditzel, *Magnetochemie*, Akademie-Verlag, Berlin, **1968**.

[23] G. M. Sheldrick, SHELXS-97, *Program for Crystal Structure Solution*, University of Göttingen, **1997**; G. M. Sheldrick, SHELXL-97, *Program for Crystal Structure Refinement*, University of Göttingen, **1997**.

Received November 10, 2003
Early View Article
Published Online April 26, 2004

 © 2004 Wiley-VCH Verlag GmbH & Co. KGaA, Weinheim

Synthesis and Molecular Structure of Calcium Difluoranthenide, $[Ca(THF)_6][C_{16}H_{10}]_2 \cdot 2C_{16}H_{10}$

Igor L. Fedushkin,*[a] Anton N. Lukoyanov,[a] Sebastian Dechert,[b] and Herbert Schumann*[b]

Dedicated to Prof. Mikhail N. Bochkarev on the occasion of his 65th birthday

Keywords: Calcium / Fluoranthene / Radical-anion / Structure elucidation

The treatment of $CaI_2(THF)_2$ with potassium and fluoranthene (mole ratio 1:2:2) in THF affords $[Ca(THF)_6][C_{16}H_{10}]_2 \cdot 2C_{16}H_{10}$ (**1**). The X-ray structure analysis of **1** shows that the compound consists of separate $[Ca(THF)_6]^{2+}$ cations, $[C_{16}H_{10}]^{\cdot-}$ radical anions and neutral fluoranthene molecules. The neutral and radical-anionic fluoranthene species can be distinguished by the differences in the skeleton C–C bond lengths. The presence of fluoranthene radical anions in THF solutions of **1** is proved by ESR spectroscopy and is further supported by the ^1H NMR spectrum of **1**, which does not give any indication of radical coupling.
(© Wiley-VCH Verlag GmbH & Co. KGaA, 69451 Weinheim, Germany, 2004)

Introduction

ansa-Metallocenes are an important class of organometallic compounds, which serve as versatile reagents for a number of organic-substrate transformations, especially for the polymerization of α-olefins.[1] In 2001, we reported on *ansa*-metallocenes of the type $(\eta^5{:}\eta^5\text{-}C_{24}H_{16})M(THF)_2$ (where M = Yb,[2] Sm,[2] Ca[3]), formed by reduction of acenaphthylene with the respective metals or their naphthalenides, $[C_{10}H_8]M(THF)_2$. The calcium derivative can also be prepared by treating $CaI_2(THF)_2$ with potassium and acenaphthylene,[4] and, quite recently, we succeeded in the preparation of the *ansa*-calcocene $(\eta^5{:}\eta^5\text{-}C_{15}H_{18})_2Ca(THF)_2$ from $CaI_2(THF)_2$, potassium, and guaiazulene.[5] (Acenaphthylene)lanthanide(III) complexes $(\eta^5{:}\eta^5\text{-}C_{24}H_{16})LnI(THF)$ (where Ln = Dy, Er, Tm, Lu) were prepared by treating $LnI_3(THF)_3$ with 2 equiv. of potassium and 2 equiv. of acenaphthylene in THF.[4] These results show that the radical anions of the nonalternating hydrocarbons (acenaphthylene and guaiazulene), initially formed in these reactions, combine diastereoselectively to give C_2-symmetric *ansa*-ligands (see Scheme 1).

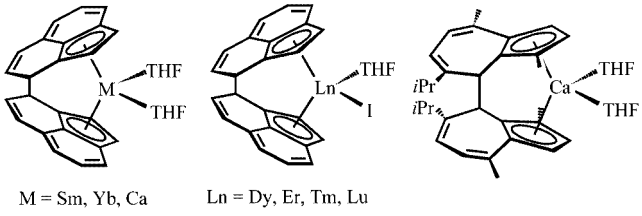

M = Sm, Yb, Ca Ln = Dy, Er, Tm, Lu

Scheme 1

Since the first and the second reduction potentials of fluoranthene (−1.77 and −2.18 V), a nonalternating hydrocarbon, compare well with those of acenaphthylene (−1.63 and −1.85 V) and guaiazulene (−1.65 and −2.45 V),[6] we investigated the reaction of $CaI_2(THF)_2$ with potassium and fluoranthene, in order to find out whether the hydrocarbons would be reduced to mono-valent radical anions and whether the latter would combine to form a two-valent *ansa*-ligand, coordinating the calcium ion.

Results and Discussion

Synthesis

The one-pot reaction of calcium diiodide with potassium and fluoranthene in a mole ratio of 1:2:2 in THF proceeds smoothly and within two hours produces a dark red-brown suspension. The compound $[Ca(THF)_6][C_{16}H_{10}]_2 \cdot 2C_{16}H_{10}$ (**1**) was isolated in 87 % yield [calculated for Ca on the basis

[a] G. A. Razuvaev Institute of Organometallic Chemistry of Russian Academy of Sciences
Tropinina 49, 603950 Nizhny Novgorod GSP-445, Russia
Fax: (internat) +7-8312-127497
E-mail: igorfed@imoc.sinn.ru
[b] Institut für Chemie der Technischen Universität Berlin
Straße des 17. Juni 135, 10623 Berlin, Germany
Fax: (internat.) +49-30-31422168
E-mail: schumann@chem.tu-berlin.de

of the stoichiometry of Equation (1)] from the solution obtained after separation of the potassium iodide and of a dark coloured solid formed in the reaction. The deep red, almost black crystals of **1** melt with decomposition at 148 °C. The formulation of **1** as calcium difluoranthenide containing separate, THF-coordinated calcium cations and fluoranthene radical anions is justified by the spectroscopic and structural properties of **1**, described below. Considering the composition of **1** on the one hand and the stoichiometry of the reagents used for its synthesis on the other hand, one is lead to suggest that, in the course of the reaction, a partial disproportionation of the fluoranthene radical anions into neutral fluoranthene and fluoranthene dianions also take place and we assume that the dark coloured solid precipitating from the reaction mixture, along with the potassium iodide, is probably the calcium fluoranthenide $[Ca(THF)_x][C_{16}H_{10}]$ [see Equation (1)]. Similar observations have been made in the reactions of radical anions of naphthalene with calcium diiodide or lanthanide halides.[4,7] However, in these reactions the disproportionation to naphthalene and naphthalene dianions was almost complete and no calcium or lanthanide compounds containing naphthalene radical anions were isolated.

$$3\ CaI_2(THF)_2 + 6\ K + 6\ C_{16}H_{10} \xrightarrow[-\ 6\ KI]{THF} \underset{\mathbf{1}}{[Ca(THF)_6][C_{16}H_{10}]_2 \cdot 2\ C_{16}H_{10}} + 2\ [Ca(THF)_x][C_{16}H_{10}] \quad (1)$$

The IR spectrum of **1** shows absorptions at 1015 and 865 cm^{-1}, indicating the presence of coordinated THF molecules. The most intense absorptions appear at 785 and 730 cm^{-1} and can be assigned to the aromatic C−H stretching vibrations of the fluoranthene radical anions. The corresponding vibrations of neutral fluoranthene appear at 775 and 735 cm^{-1}.

The ^1H NMR spectrum of **1** shows only the broadened signals of THF. However, the ^1H NMR spectrum of the *ansa*-acenaphthylene complex, $(\eta^5{:}\eta^5\text{-}C_{24}H_{16})Ca(THF)_2$,[4] shows along with the THF signals, the expected eight signals for the ring protons of the *ansa*-ligand.

The assumption that compound **1** is paramagnetic, due to the presence of uni-negative fluoranthene radical anions is confirmed by the ESR spectrum. The spectrum of a solution of **1** in THF shows an ESR signal [g = 2.0029; A_H = 0.008 (2H), 0.017 (2H), 0.121 (2H), 0.390 (2H) and 0.520 (2H) mT], which corresponds to the signal reported by Gerson et al.[8] for the fluoranthene radical anion. Solutions of the above-mentioned *ansa*-acenaphthylene complex $(\eta^5{:}\eta^5\text{-}C_{24}H_{16})Ca(THF)_2$ in THF also show an ESR signal, although a very weak one, due to partial dissociation of the *ansa*-ligand into radical anions. However, the presence of such small amounts of paramagnetic radical anions does not seem to affect the ^1H NMR spectroscopy behaviour of this complex.

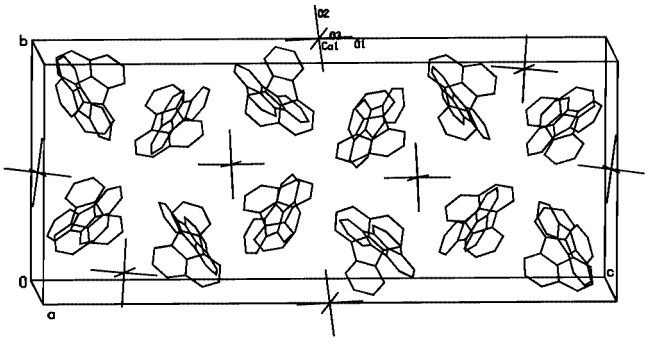

Figure 1. Crystal packing in **1**

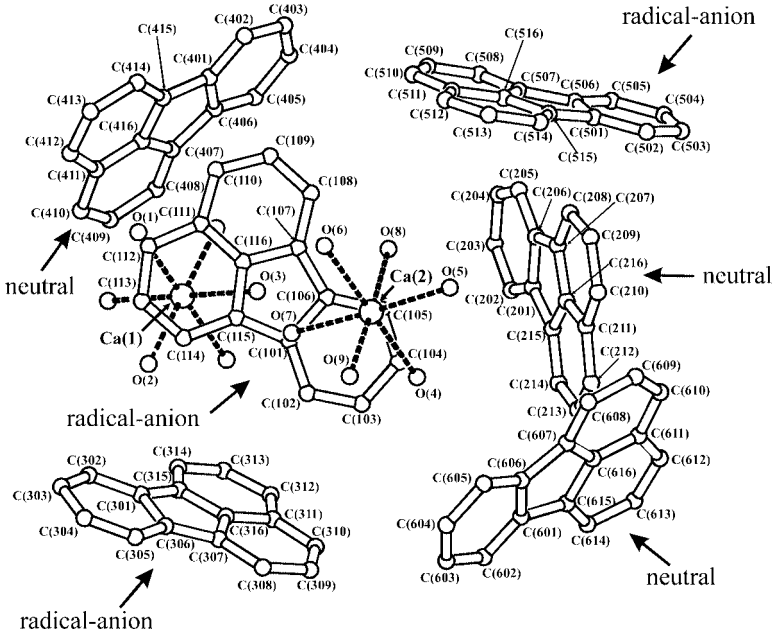

Figure 2. Molecular structure of **1**; the hydrogen atoms as well as the carbon atoms of THF are omitted for clarity

 © 2004 Wiley-VCH Verlag GmbH & Co. KGaA, Weinheim

Thus, the spectroscopic data of **1** clearly demonstrate that, in contrast to our initial expectation, the radical anions of fluoranthene formed in the reduction reaction do not couple to give the corresponding *ansa*-ligand.

Molecular Structure

To determine the "non-metallocene" structure of **1**, the X-ray structure analysis of a crystal grown from THF was carried out. Compound **1** crystallizes in the monoclinic space group $P2_1/n$. Figure 1 shows the crystal packing. The asymmetric unit of **1** (see Figure 2) consists of 1.5 solvated $[Ca(THF)_6]^{2+}$ cations, three radical-anionic, and three neutral fluoranthene species. One cation occupies only general positions, whereas the metal atom of the second cation resides on a centre of inversion. Each calcium atom is surrounded by six coordinating THF molecules in an almost regular, octahedral fashion with virtually identical $Ca-O_{THF}$ distances, which range from 2.325(3) to 2.341(3) Å.

To decide which of the six fluoranthene molecules in the asymmetric unit are the radical anions, an accurate analysis of their skeleton C−C bond lengths, with respect to the symmetry of the ligand boundary molecular orbitals, was carried out (see Figure 3). The C(6)−C(7) and C(1)−C(15) bonds of three molecules show the most significant differences. Since the HOMO of the radical anion is of bonding character, it seems reasonable to assign the fluoranthene molecules with the shortest C(6)−C(7) and C(1)−C(15) bonds as the radical anions. The shorter C(1)−C(6) bond lengths of the other three molecules thus declared the neutral fluoranthene molecules [1.406(7), 1.409(7) and 1.428(7) Å], agree quite well with the length of the corresponding bond in the free ligand (1.40 Å) and in the silver complex $[Ag_3(C_{16}H_{10})(ClO_4)_3]$ (1.40 Å).[9]

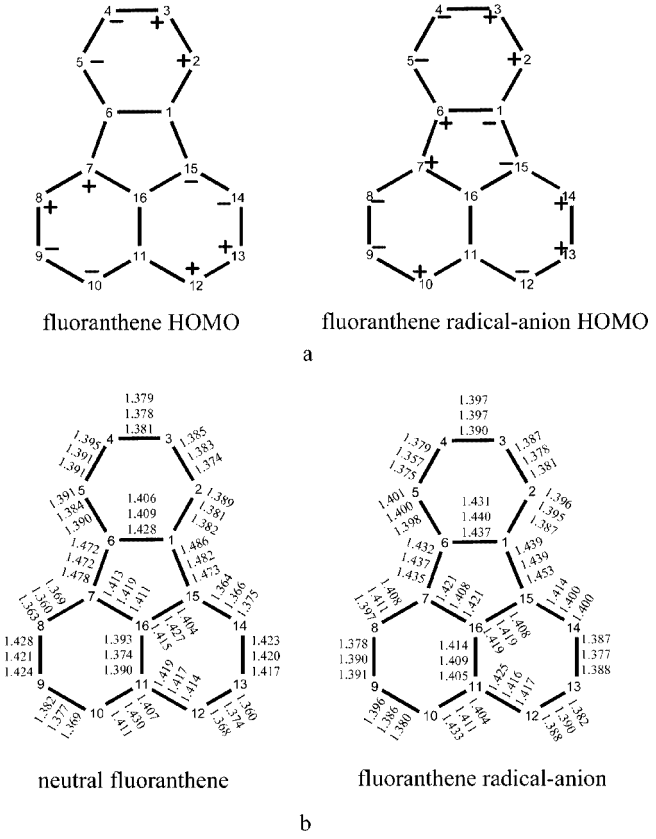

Figure 3. Molecular symmetry of the HOMO of fluoranthene and of its radical anion (a); C−C bond lengths of the fluoranthene moieties in the asymmetric unit of **1** (b)

Conclusion

In contrast to the radical anions of acenaphthylene and guaiazulene, the radical anions of fluoranthene do not dimerize to form twofold negatively charged *ansa*-ligands, under the same reaction conditions. This behaviour can be attributed to the fact that the negative charge is not strongly localized on the five-membered ring unit of the fluoranthene radical anion, thus preventing the formation of a metal-coordinating cyclopentadienyl-like π-system. On the contrary, the negative charge is delocalized over the whole ring system of the radical anion. Furthermore, in contrast to the dimerizing radical anions of acenaphthylene and guaiazulene, the radical anions of fluoranthene tend to disproportionate into neutral ligands and dianionic species.

Experimental Section

General Remarks: All manipulations were carried out under vacuum using Schlenk ampoules. The solvent THF was distilled from sodium benzophenone prior to use. Fluoranthene was purchased from Aldrich and used without further purification. The melting point of **1** was measured in a sealed capillary. IR spectra were recorded on a Specord M80 spectrometer, ESR spectra on a Bruker ER 200D-SRC spectrometer equipped with the low-temperature controller ER 4111 VT. The ESR signal was referenced to the signal of diphenylpycrylhydrazil (DPPH, $g = 2.0037$).

$[Ca(THF)_6][C_{16}H_{10}]_2 \cdot 2C_{16}H_{10}$ (1): A mixture of $CaI_2(THF)_2$ (3.65 g, 8.3 mmol), potassium (0.65 g, 16.6 mmol), and fluoranthene (3.36 g, 16.6 mmol) in THF (40 mL) was stirred for 2 hours. Within this time frame, the potassium had dissolved completely and the mixture had turned dark red-brown with the precipitation of potassium iodide and of a dark coloured solid. After separation of the solids by filtration, the THF was removed in vacuo and the residue was dried in vacuo at ambient temperature for 30 min. Then THF (40 mL) was added to the dried solid and the insoluble parts were filtered off. Reduction of the solution volume, by partial evaporation of the solvent in vacuo, caused precipitation of crystals, which were redissolved by heating the mixture to 60 °C. After standing the solution at room temperature for 24 hours, large black crystals of **1** separated. Yield 3.1 g (87 %). M.p. 148 °C(dec). IR (Nujol): 1505 m, 1430 s, 1380 m, 1445 w, 1290 s, 1215 m, 1165 s, 1130 m, 1080 m, 1115 vs, 1015 vs, 915 w, 865 vs, 830 m, 785 vs, 730 vs, 670 w, 615 m cm^{-1}. The extremely high air sensitivity of **1** prevented its analytical characterization.

Single-Crystal X-ray Structure Determination of 1: The crystal data and details of data collection are given in Table 1. The data were collected on a SMART CCD diffractometer (graphite-monochromated Mo-K_α radiation, ω-scan technique, $\lambda = 0.71073$ Å) at −100 °C. The structure was solved by direct methods using SHELXS-

 © 2004 Wiley-VCH Verlag GmbH & Co. KGaA, Weinheim

Table 1. Crystal data and structure refinement for **1**

Empirical formula	$C_{88}H_{88}CaO_6$
Molecular mass	1281.66
Temperature [K]	173(2)
Wavelength [Å]	0.71073
Crystal system	monoclinic
Space group	$P2_1/n$
Unit cell dimensions	
a [Å]	15.7291(2)
b [Å]	16.5059(3)
c [Å]	39.4418(6)
α [°]	90
β [°]	92.567(1)
γ [°]	90
V [Å^3]	10229.7(3)
Z	6
Density (calcd.) [Mg/m^3]	1.248
Absorption coefficient [mm^{-1}]	0.150
F(000)	4104
Crystal size [mm^3]	0.42 × 0.42 × 0.18
θ range for data collection [°]	1.03 to 25.00
Index ranges	$-18 \le h \le 17$, $-15 \le k \le 19$, $-46 \le l \le 39$
Reflections collected	49363
Independent reflections	17925 [R(int) = 0.1191]
Completeness to θ = 25.00°	99.4 %
Absorption correction	Empirical
Max. and min. transmission	0.955248 and 0.546909
Refinement method	Full-matrix least-squares on F^2
Data/restraints/parameters	17925/0/1417
Goodness-of-fit on F^2	0.903
Final R indices [$I > 2\sigma(I)$]	$R_1 = 0.0717$, $wR_2 = 0.1120$
R indices (all data)	$R_1 = 0.1823$, $wR_2 = 0.1451$
Largest diff. peak and hole [e × Å^{-3}]	0.260 and −0.402

97[10] and was refined on F^2 with SHELXL-97[11] using all reflections. All non-hydrogen atoms were refined anisotropically and the hydrogen atoms were placed in calculated positions and assigned to an isotropic displacement parameter of 0.08 Å^2. SADABS[12] was used to perform area-detector scaling and absorption corrections. The geometrical aspects of the structure were analyzed by using the PLATON program.[13] CCDC-223839 contains the supplementary crystallographic data, which can be obtained free of charge at www.ccdc.cam.ac.uk/conts/retrieving.html or from the Cambridge Crystallographic Data Centre, 12 Union Road, Cambridge CB2 1EZ, UK; Fax: (internat.) + 44-1223-336-033; E-mail: deposit@ccdc.cam.ac.uk.

Acknowledgments

This work was supported by the Russian Foundation for Basic Research (Grant No. 03-03-32246a), the Grant of President of Russian Federation (No. 58.2003.03), the Alexander von Humboldt Stiftung (ILF), the Fonds der Chemischen Industrie, and the Deutsche Forschungsgemeinschaft (Graduiertenkolleg "Synthetische, mechanistische und reaktionstechnische Aspekte von Metallkatalysatoren").

[1] [1a] H. H. Brintzinger, D. Fischer, R. Mülhaupt, B. Rieger, R. M. Waymouth, *Angew. Chem.* **1995**, *107*, 1255−1283; *Angew. Chem. Int. Ed. Engl.* **1995**, *34*, 1143−1170. [1b] K. Angermund, G. Fink, V. R. Jensen, R. Kleinschmidt, *Chem. Rev.* **2000**, *100*, 1457−1470. [1c] G. G. Hlatky, *Coord. Chem. Rev.* **2000**, *199*, 235−329.

[2] I. L. Fedushkin, S. Dechert, H. Schumann, *Angew. Chem.* **2001**, *113*, 584−586; *Angew. Chem. Int. Ed.* **2001**, *40*, 561−563.

[3] I. L. Fedushkin, T. V. Petrovskaya, M. N. Bochkarev, S. Dechert, H. Schumann, *Angew. Chem.* **2001**, *113*, 2540−2543; *Angew. Chem. Int. Ed.* **2001**, *40*, 2474−2477.

[4] I. L. Fedushkin, Y. A. Kurskii, V. I. Nevodchikov, M. N. Bochkarev, S. Muehle, H. Schumann, *Russ. Chem. Bull., Int. Ed.* **2002**, *51*, 160−169.

[5] I. L. Fedushkin, Y. A. Kurskii, T. V. Balashova, M. N. Bochkarev, S. Dechert, S. Mühle, H. Schumann, *Russ. Chem. Bull., Int. Ed.* **2003**, *52*, 1363−1371.

[6] E. de Boer, *Adv. Organomet. Chem.* **1964**, *2*, 115−155.

[7] [7a] A. V. Protchenko, L. N. Zakharov, M. N. Bochkarev, Yu. T. Struchkov, *J. Organomet. Chem.* **1993**, *447*, 209−212. [7b] I. L. Fedushkin, M. N. Bochkarev, H. Schumann, L. Esser, G. Kociok-Kohn, *J. Organomet. Chem.* **1995**, *489*, 145−151. [7c] M. N. Bochkarev, I. L. Fedushkin, R. B. Larichev, *Russ. Chem. Bull. Int. Ed.* **1996**, *45*, 2443−2444. [7d] M. N. Bochkarev, I. L. Fedushkin, A. A. Fagin, H. Schumann, J. Demtschuk, *Chem. Commun.* **1997**, 1783−1784.

[8] F. Gerson, *High Resolution ESR spectroscopy*, John Wiley & Sons, Verlag Chemie, **1970**.

[9] M. Munakata, L. P. Wu, G. L. Ning, T. Kuroda-Sowa, M. Maekawa, Y. Suenaga, N. Maeno, *J. Am. Chem. Soc.* **1999**, *121*, 4968−4976.

[10] G. M. Sheldrick, *SHELXS-97 Program for the Solution of Crystal Structures*; University of Göttingen, **1990**.

[11] G. M. Sheldrick, *SHELXL-97 Program for the Refinement of Crystal Structures*; University of Göttingen, **1997**.

[12] G. M. Sheldrick, *SADABS Program for Empirical Absorption Correction of Area Detector Data*; University of Göttingen, **1996**.

[13] A. L. Spek, *PLATON A Multipurpose Crystallographic Tool*, University of Utrecht, **2000**.

Received December 11, 2003
Early View Article
Published Online April 20, 2004

 © 2004 Wiley-VCH Verlag GmbH & Co. KGaA, Weinheim

Reactivity Studies on 2,3,4,5-Tetraethyl-1,6-diiodo-2,3,4,5-tetracarba-*nido*-hexaborane(6): Synthesis and Structures of New C_4B_2 *nido*-Carborane Derivatives

Yong Nie,[a] Hans Pritzkow,[a] and Walter Siebert*[a]

Dedicated to Professor Manfred T. Reetz on the occasion of his 60th birthday

Keywords: Boron / Carboranes / Nucleophilic substitution / Iron / Cobalt

The reactivity of the title compound 2,3,4,5-tetraethyl-1,6-diiodo-2,3,4,5-tetracarba-*nido*-hexaborane(6) (**1**) towards a variety of nucleophiles is reported. When **1** is treated with RC_2Li (R = Ph, *t*Bu, $SiMe_3$, *p*-tolyl) and Ph_2PLi, the corresponding new C_4B_2 *nido*-carborane derivatives **2a**–**d** and **3**, respectively, are obtained by selective substitution at the basal B–I group, whereas the apical B–I bond remains inert. The reaction of **1** with $K[(\eta^5\text{-}C_5H_5)Fe(CO)_2]$ affords the novel species **4**, which contains a $CpFe(CO)_2$ fragment σ-bonded to the basal boron atom of the C_4B_2 cluster. Attempts to isolate **4** by chromatography on silica gel led to cleavage of the Fe–B bond and formation of compound **5**, containing a basal BH vertex, which can be separately prepared by the reaction of **1** and $LiBEt_3H$. In the reactions of **1** with PhLi and Me_3SnLi, respectively, **6a** and **7a** are formed as the predominant B6-substituted carborane products. In addition, trace amounts of 1,6-disubstituted species **6b** and **7b** are also detected. The substitution at the apical B–I group in **2a** with an alkynyl group is effected by a Pd^0-catalyzed Negishi-type cross-coupling reaction to give compound **8**. The reaction of **1** and monolithio-*o*-carborane affords the C_4B_2–C_2B_{10} carborane **10**, while the reaction of **2a** and $Co_2(CO)_8$ furnishes the double cluster **9** (C_4B_2–C_2Co_2). In both **9** and **10** two different types of clusters are directly connected by a B–C bond. Compound **1** reacts with $ClZnC_6H_4C_6H_4ZnCl$ in the presence of the catalyst $Pd(PPh_3)_4$ to give **11**, in which two C_4B_2 clusters are linked by a $C_6H_4C_6H_4$ unit. The constitutions of the products follow from spectroscopic data, and X-ray diffraction analyses for **2a**, **2d**, **4**, **8**, **9**, and **10**.

(© Wiley-VCH Verlag GmbH & Co. KGaA, 69451 Weinheim, Germany, 2004)

Introduction

Although peralkylated 2,3,4,5-tetracarba-*nido*-hexaboranes(6)[1] are more stable than the parent compound $C_4B_2H_6$,[2] and are readily available by a variety of methods, their reactivity has only recently been studied.[3,4] To investigate substitution reactions in C_4B_2 *nido*-carboranes, functional groups at the boron atom(s) other than alkyl groups are needed. Wrackmeyer et al. were able to obtain 1,6-dibromo-2,3,4,5-tetracarba-*nido*-hexaboranes(6)[3a] by treating 1,4,6,9-tetraalkyl-3,8-diethyl-2,7-bis(diethylboryl)-5-stannaspiro[4.4]nona-1,3,6,8-tetraenes with BBr_3. They also studied the reaction between peralkylated 2,3,4,5-tetracarba-*nido*-hexaboranes(6) and an excess of BBr_3, whereby the corresponding B6-bromo-substituted carboranes were formed.[3b] Nucleophiles were found to replace the basal B6-bromo atom to give the corresponding carboranes with organyl,[3c] stannyl,[3d] diphenylphosphanyl[3e] as well as the *N*-bonded $(\mu\text{-NS})Fe_2(CO)_6$ [3f] group. In the 1,6-dibromo case, substitution with the *N*-bonded $(\mu\text{-NS})Fe_2(CO)_6$ cluster took place at the basal B−Br bond, an excess of the nucleophile did not induce additional substitution at the 1-position.[3f]

Berndt et al.[4] have reported that the reduction of *nido*-$(Me_3SiC)_2(CH)_2(BtBu)_2$ with Li in tetrahydrofuran affords a novel 1,3-diborabenzene anion, which could in turn be oxidized to give the starting carborane in refluxing 1,2-dibromoethane. As part of reactivity studies, we have reported transition metal derivatives of a benzo-C_4B_2 *nido*-carborane compound[5a] with metal complex fragments coordinated to the benzene ring.[5b] Very recently we have developed a convenient one-pot synthesis of 2,3,4,5-tetraalkyl-1,6-diiodo-2,3,4,5-tetracarba-*nido*-hexaborane(6) derivatives,[6] involving disubstituted alkynes, BI_3 and $NaK_{2.8}$. In this paper, we report the reactivity of the title compound **1** towards a variety of nucleophiles, and characterization of the resulting new carboranes.

[a] Anorganisch-Chemisches Institut der Universität Heidelberg
Im Neuenheimer Feld 270, 69120 Heidelberg, Germany
Fax: (internat.) + 49-6221-545-609
E-mail: walter.siebert@urz.uni-heidelberg.de

Results and Discussion

Regiospecific Substitution at the Basal Boron Atom

Nucleophilic substitution reactions of **1** with RC_2Li (R = Ph, *t*Bu, $SiMe_3$, *p*-tolyl) proceed smoothly, and the corresponding basal-boron-substituted carborane derivatives **2a**–**d** were produced in high yields (Scheme 1). The *nido*-C_4B_2 framework is retained, as little differences have been found in the ^1H and ^{13}C NMR spectra when compared with that of **1**. In the ^{11}B NMR spectra, the basal boron atoms give rise to signals at δ = 9.8–10.9 ppm, which are only slightly shifted downfield from that of **1** (δ = 5.5 ppm), while the shifts of the signals for the apical boron atoms are the same as that for **1** (δ = −52.5 ppm).

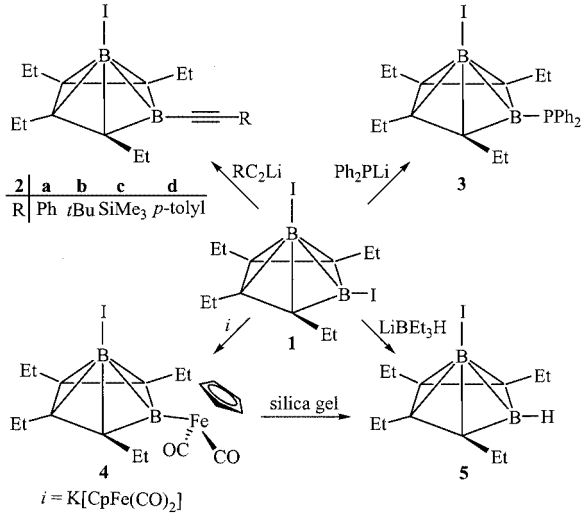

Scheme 1

X-ray structure analyses of **2a** and **2d** confirm the spectroscopic results. In agreement with Herberhold, Wrackmeyer et al.,[3f] an excess of lithium acetylide did not effect additional substitution at the apical boron atoms. Similar results are observed in the reactions of **1** with Ph_2PLi and $K[(\eta^5\text{-}C_5H_5)Fe(CO)_2]$ to give **3** and **4**, respectively, with regiospecific substitution at the basal position. In the ^{11}B NMR spectrum of **3**, the signal of the basal boron atom is shifted downfield by about 9 ppm, while the apical boron atom is unaffected. In the case of **4**, the basal boron atom of the C_4B_2 *nido*-cluster is significantly deshielded (δ = 28.6 ppm), and the signal of the apical boron is slightly shifted to δ = −49.6 ppm. This reveals that the $CpFe(CO)_2$ fragment is directly bonded to the basal boron atom by an Fe–B σ-bond, which is confirmed by an X-ray diffraction study (vide infra). Thus, **4** is the first transition metal derivative of the C_4B_2 *nido*-carborane with direct metal–boron bonding. A few iron derivatives[7] with other carborane or polyborane frameworks of this type have been reported with Fe–B or Fe–C bonding. Cooling of the solution of the crude product in hexane resulted in yellow crystals of **4**, along with an unknown paramagnetic impurity, which makes the NMR spectra not so satisfactory.

The initial isolation of **4** by column chromatography on silica gel led to cleavage of the Fe–B bond to give **5** and paramagnetic impurities. The designed synthesis of **5** is achieved by the separate reaction of **1** with $LiBEt_3H$. No redox reaction between **1** and $(MeS)_2$ takes place, indicating the B–I bonds in **1** are dissimilar to the classical B–I bond of sp^2-hybridized boron atoms, which reacts to give the corresponding B–SMe products.[8]

Reactions Involving Substitution at Both Boron Atoms

In the reactions of **1** with more than 2 equiv. of PhLi and Me_3SnLi, respectively (Scheme 2), the B6-substituted products **6a** and **7a** are formed, together with trace amounts of the disubstituted species **6b** and **7b**, as detected by mass spectrometry. For **6a** and **7a**, the ^{11}B NMR signals of the basal boron atoms are shifted downfield to δ = 17.9 and 16.1 ppm, respectively, while the signals of the apical boron atoms are unchanged.

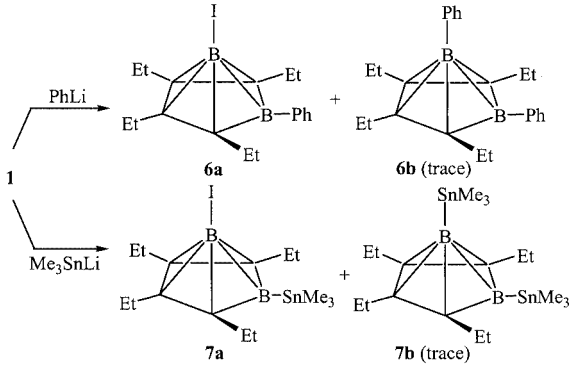

Scheme 2

In most of the cases the apical B–I bonds are found to be inert, although its substitution by an alkynyl group has been realized by a Pd^0-catalyzed Negishi-type cross-coupling reaction of **2a** and Me_3SiC_2ZnCl in THF (Scheme 3). Heating of the reaction mixture for 10 d leads to yellow **8**. Interestingly, the ^{11}B NMR signal of the substituted apical boron atom is only slightly shifted downfield to δ = −50.7 ppm. Its structure was established by an X-ray diffraction analysis (see below). The mechanism of such Pd-catalyzed coupling reactions involving B–I bonds[9a] is expected to be similar to that of carbon–carbon cross coupling, however the very first step in the catalytic cycle — the oxidative addition of the B–I bond leading to a B–Pd–I species — has not yet been verified. Stirring of a mixture of **2a** and $Pd(PPh_3)_4$ in THF leads to a brown solution, whose ^{31}P NMR spectrum shows a signal at δ = 22.4 ppm, which is in the expected region {$[PdIPh(PPh_3)_2]$: δ = 22.3 ppm}.[9b] Its ^{11}B NMR spectrum shows a signal at δ = −36 ppm, which might be due to the formation of the (σ-carboranyl)palladium iodide complex. Shore et al.[10] have studied the reaction of $Pd(PPh_3)_4$ with the iodoborane clus-

 © 2004 Wiley-VCH Verlag GmbH & Co. KGaA, Weinheim

ter 9-I-1,7-$(SMe_2)_2B_{12}H_9$ and they observed similar results (δ^{31}_P = 24.2/24.0 ppm).

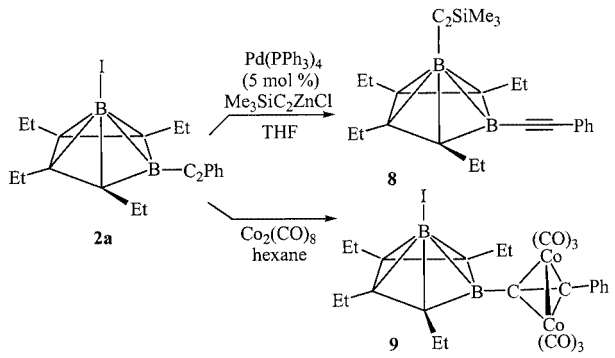

Scheme 3

Cluster Linkages

Nucleophilic substitution of *B*-functionalized C_4B_2 *nido*-carboranes by an anionic cluster $(\mu\text{-NS})Fe_2(CO)_6^-$ [3f] has been shown to be an effective way to linked clusters. The reaction of **2a** with $Co_2(CO)_8$, shown in Scheme 3, leads to the deep-brown product **9**, in which the *nido*-C_4B_2 and the C_2Co_2 tetrahedrane cluster are directly joined by a B−C bond at the basal position. In the ^{11}B NMR spectrum, the signal for the basal boron atom is shifted downfield by 6.5 ppm relative to that of **2a**, while the signal for the apical boron atom is only slightly shifted downfield by about 1.5 ppm. The molecular structure of **9** was confirmed by an X-ray diffraction analysis (see below). There are only a few acetylene−$Co_2(CO)_6$ complexes with boron groups attached to the acetylene unit,[11] and two[11b,11c] structurally characterized examples carry B−cat groups (cat = catechol). The C_4B_2−C_2B_{10} linked cluster **10** (Scheme 4) is produced by the reaction of **1** with monolithio-*o*-carborane, in which the C_4B_2 cluster is directly connected to the icosahedral *o*-carborane by a B6−C bond, as confirmed by X-ray diffraction analysis.

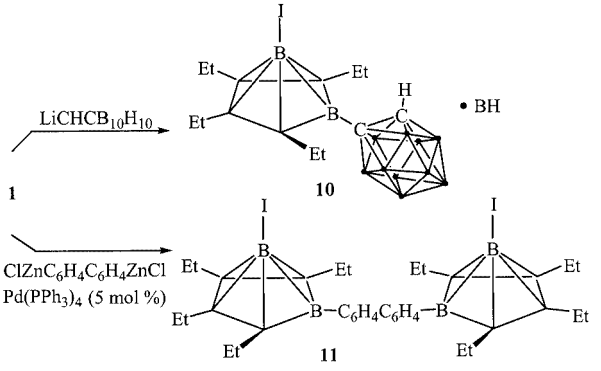

Scheme 4

Compound **11** with two C_4B_2 clusters connected by a $C_6H_4C_6H_4$ unit (Scheme 4) is obtained from the reaction of **1** with $ClZnC_6H_4C_6H_4ZnCl$ in the presence of a catalytic amount of $Pd(PPh_3)_4$. It should be noted that the reaction leading to **11** is performed in toluene because the basal B−I bond in **1** is sensitive to THF, resulting first in a yellow and then a deep-green solution. This is significantly different to the bromo derivatives of *nido*-C_4B_2, which have been studied in THF solution.[3d−3f] In compounds **10** and **11** the ^{11}B NMR signals of the basal boron atoms are shifted downfield to δ = 13.9 and 22.0 ppm, respectively, while the apical boron atom is essentially unaffected (δ = −53.4 ppm for **10** and δ = −52.4 ppm for **11**). The MS spectra exhibit the respective molecular ion peaks with the correct isotopic patterns.

The reaction of **1** with $LiC_6H_4C_6H_4Li$ did not yield the expected product **11**, instead the oxygen-bridged species **12** was detected, formed by the hydrolysis of **1**. In the Et_3N/H_2O reaction (Scheme 5), the formed by-product ammonium salt $[Et_3NH]I$, was identified by FAB-MS. Compound **12** was characterized by ^{11}B NMR spectroscopy (δ = 22.1 and −51.9 ppm) and HR-MS which exhibits the molecular ion peak with the correct isotopic pattern.

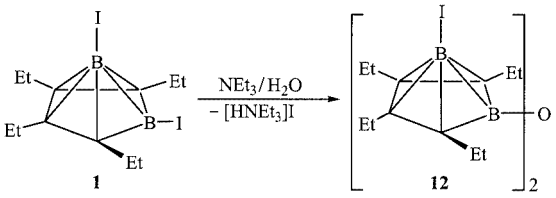

Scheme 5

X-ray Structure Analyses of 2a, 2d, 4, 8, 9 and 10

The molecular structures of **2a**, **4**, **8**, **9** and **10** are shown in Figures 1, 2, 3, 4, and 5, respectively. As the structure of **2d** (at room temperature) is very similar to that of **2a**, it will not be shown here. In the structures, the C_4B_2 *nido*-carborane frameworks are essentially the same as that of the start-

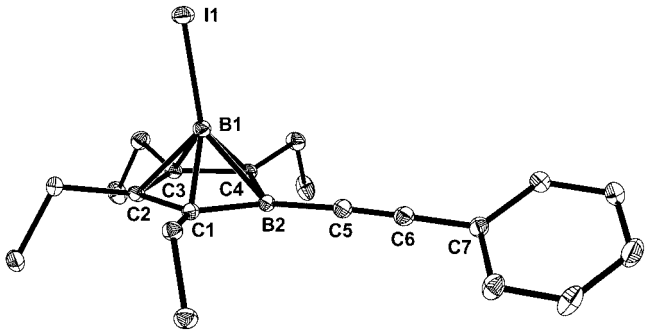

Figure 1. Molecular structure of **2a**; hydrogen atoms omitted for clarity; thermal ellipsoids are shown at 40% probability; selected bond lengths [Å] and angles [°]: I(1)−B(1) 2.139(2), B(1)−C(1) 1.714(3), B(1)−C(2) 1.722(3), B(1)−C(3) 1.714(3), B(1)−C(4) 1.706(3), B(1)−B(2) 1.825(3), B(2)−C(1) 1.537(3), B(2)−C(4) 1.532(3), C(1)−C(2) 1.453(3), C(2)−C(3) 1.446(2), C(3)−C(4) 1.459(3), B(2)−C(5) 1.529(3), C(5)−C(6) 1.211(3), C(6)−C(7) 1.435(3); B(2)−B(1)−I(1) 143.3(1), C(5)−B(2)−B(1) 131.2(2), C(6)−C(5)−B(2) 177.0(2), C(5)−C(6)−C(7) 178.3(2)

 © 2004 Wiley-VCH Verlag GmbH & Co. KGaA, Weinheim

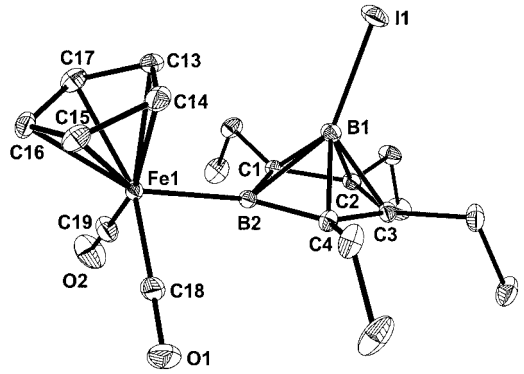

Figure 2. Molecular structure of **4**; hydrogen atoms omitted for clarity; thermal ellipsoids are shown at 40% probability; selected bond lengths [Å] and angles [°]: I(1)−B(1) 2.135(2), B(1)−C(1) 1.692(2), B(1)−C(2) 1.711(2), B(1)−C(3) 1.709(2), B(1)−C(4) 1.689(3), B(1)−B(2) 1.841(3), B(2)−C(1) 1.547(2), B(2)−C(4) 1.547(2), C(1)−C(2) 1.460(2), C(2)−C(3) 1.431(2), C(3)−C(4) 1.468(2), Fe(1)−B(2) 2.069(2), Fe(1)−C(19) 1.739(2), Fe(1)−C(18) 1.742(2), Fe(1)−C_{Cp} 2.094−2.116(2), O(1)−C(18) 1.150(2), O(2)−C(19) 1.151(2); B(2)−B(1)−I(1) 142.91(11), B(1)−B(2)−Fe(1) 133.48(11), C(19)−Fe(1)−C(18) 92.59(10), C(19)−Fe(1)−B(2) 86.26(8), C(18)−Fe(1)−B(2) 85.03(8), O(1)−C(18)−Fe(1) 178.7(2), O(2)−C(19)−Fe(1) 178.6(2)

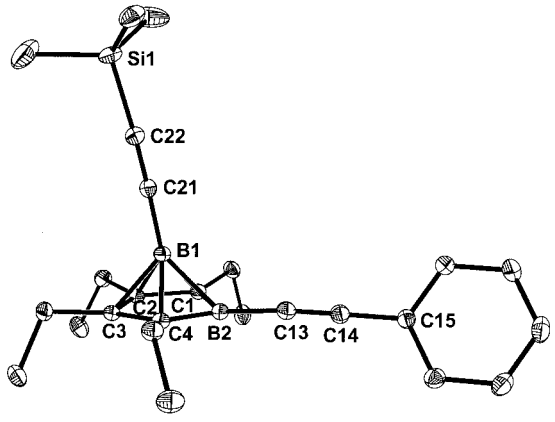

Figure 3. Molecular structure of **8**; hydrogen atoms omitted for clarity; thermal ellipsoids are shown at 40% probability; selected bond lengths [Å] and angles [°]: B(1)−C(1) 1.723(2), B(1)−C(2) 1.735(2), B(1)−C(3) 1.734(2), B(1)−C(4) 1.731(2), B(1)−B(2) 1.833(2), B(2)−C(1) 1.532(2), B(2)−C(4) 1.532(2), C(1)−C(2) 1.455(2), C(2)−C(3) 1.440(2), C(3)−C(4) 1.452(2), B(2)−C(13) 1.536(2), C(13)−C(14) 1.207(2), C(14)−C(15) 1.438(2), B(1)−C(21) 1.522(2), C(21)−C(22) 1.205(2); C(21)−B(1)−B(2) 142.49(10), C(13)−B(2)−B(1) 132.30(10), C(14)−C(13)−B(2) 175.39(13), C(13)−C(14)−C(15) 178.79(13), C(22)−C(21)−B(1) 177.62(12) C(21)−C(22)−Si(1) 175.45(12)

ing carborane **1**.[6] The B−I bond lengths in **2a** (2.139 Å), **2d** (2.119 Å), **4** (2.135 Å), **9** (2.121 Å) and **10** (2.125 Å) are very similar to the corresponding value (2.126 Å) in **1** despite the B6-substitution. In the alkynyl-substituted compounds **2a**, **2d** and **8**, the B−C−C moieties are almost linear, and the corresponding B−C−C bond angles are 177.0° for **2a**, 173.2° for **2d**, and 177.6° (apical)/175.4° (basal) for **8**. The B−C and C≡C bond lengths in **2a** (1.529, 1.211 Å), **2d** (1.530, 1.197 Å), and **8** (1.522, 1.205 Å) are similar to each other, and are also in agreement with the reported values for borylacetylenes.[11c,12] In **2a**, **2d**, **4**, **8**, **9** and **10**, the apical substituents are bent away from the B_{basal} group, the

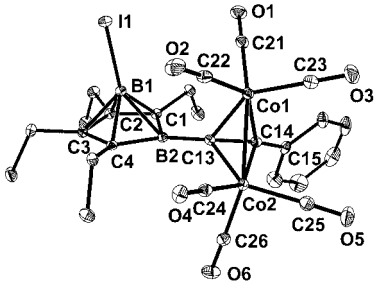

Figure 4. Molecular structure of **9**; hydrogen atoms omitted for clarity; thermal ellipsoids are shown at 40% probability; selected bond lengths [Å] and angles [°]: I(1)−B(1) 2.121(2), B(1)−C(1) 1.712(3), B(1)−C(2) 1.712(3), B(1)−C(3) 1.718(3), B(1)−C(4) 1.705(3), B(1)−B(2) 1.826(3), B(2)−C(1) 1.537(3), B(2)−C(4) 1.537(3), C(1)−C(2) 1.458(3), C(2)−C(3) 1.443(3), C(3)−C(4) 1.456(3), B(2)−C(13) 1.554(3), C(13)−C(14) 1.348(3), C(14)−C(15) 1.465(3), Co(1)−Co(2) 2.483(4), Co(1)−C(13) 1.999(2), Co(1)−C(14) 1.952(2), Co(2)−C(13) 1.990(2), Co(2)−C(14) 1.976(2); B(2)−B(1)−I(1) 140.7(2), C(13)−B(2)−B(1) 130.5(2), C(14)−C(13)−B(2) 141.1(2), C(13)−C(14)−C(15) 140.1(2)

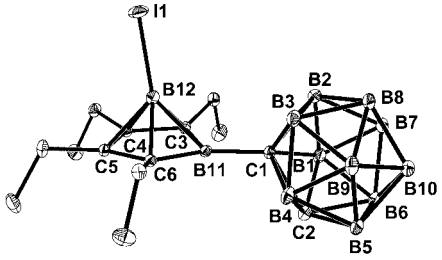

Figure 5. Molecular structure of **10**; hydrogen atoms omitted for clarity; thermal ellipsoids are shown at 40% probability; selected bond lengths [Å] and angles [°]: I(1)−B(12) 2.125(2), B(12)−C(3) 1.708(2), B(12)−C(4) 1.731(2), B(12)−C(5) 1.731(2), B(12)−C(6) 1.710(2), B(11)−B(12) 1.817(2), B(11)−C(3) 1.543(2), B(11)−C(6) 1.541(2), B(11)−C(1) 1.595(2), C(1)−C(2) 1.687(2), B(11)−B(12)−I(1) 141.46(10), C(1)−B(11)−B(12) 132.04(12)

B2−B1−X angle being 143.3(3)°, 141.3(3)°, 141.9(1)°, 142.5(1)°, 140.7(2)° and 141.5(1)°, respectively (in **1** the corresponding angle is 140.06°).

In **4**, a $CpFe(CO)_2$ fragment is directly σ-bonded to the basal boron atom, the Fe−B bond length is 2.069 Å, which is significantly longer than the corresponding values for iron−boryl complexes, [1.959(6)−2.034(3) Å,[13a,13b] 1.964(8)−2.027(5) Å[13c,13d]] and iron−borylene complexes [2.010(3) Å[13e]], but in the range of the reported values for ferracarboranes (1.968−2.161 Å[13f]). This long Fe−B distance is also consistent with the easy decomposition of **4** with the cleavage of the Fe−B bond on silica gel. The iron center achieves an 18-electron configuration through coordination to two CO ligands (2e donor), the cyclopentadienyl group (5e donor), and the Fe−B interaction (1e donor).

In the structure of **9** (Figure 4), the almost linear B−C≡C−Cmoiety in **2a** has been altered by the complexation of the $Co_2(CO)_6$ fragment, with the angles decreasing to 141.07° (B2−C13−C14) and 140.1° (C13−C14−C15). The Co1−Co2 and C13−C14 bond lengths of 2.483 and 1.348 Å, respectively, are similar to the corresponding values in similar complexes carrying B−cat groups.[11b,11c]

 © 2004 Wiley-VCH Verlag GmbH & Co. KGaA, Weinheim

The structure of **10** (Figure 5) contains the small C_4B_2 *nido*-cluster connected to the large *closo*-*o*-carboranyl cluster. Interestingly, in the asymmetric unit two cocrystallized free *o*-carborane molecules have been found, and surprisingly there is no significant intermolecular interaction among the three molecules. The B11−C1 bond length of 1.595 Å is typical of a C−B single bond. In the *o*-carboranyl fragment the C1−C2 bond length is 1.687 Å, which is significantly longer than that in *o*-carborane [1.630(6) Å].[14] The B−B bond lengths [av. distance 1.776(2) Å, ranging from 1.744(2) to 1.793(2) Å] and the C−B bond lengths [av. distance 1.720(2) Å, ranging from 1.703(2) to 1.731(2) Å] are close to the expected values.

Conclusion

The reactivity of compound **1** towards various nucleophiles has been investigated. In most of the cases, the substitution with hydride, alkynyl, diphenylphosphanyl, trimethylstannyl, $CpFe(CO)_2$, and even the bulky *o*-carboranyl group, takes place regiospecifically at the basal boron atom of the *nido*-C_4B_2 frameworks, while the "inert" apical B−I bond can be substituted by a Pd^0-catalyzed Negishi-type cross-coupling reaction, as demonstrated in the synthesis of compound **8**. A new strategy for cluster linkages has been developed, and compounds with different types of cluster linkages have been prepared, either by direct B−C bonding ($C_4B_2-C_2B_{10}$ and $C_4B_2-C_2Co_2$), or by a linking $C_6H_4C_6H_4$ unit, at the basal boron atom of the *nido*-C_4B_2 skeletons. The reactivity of the basal B−I bond of **1** is further shown by its sensitivity to THF as solvent and by the formation of the oxygen-bridged species **12**.

Experimental Section

General: All reactions and manipulations were performed in dry glassware under argon or nitrogen using standard Schlenk techniques. Solvents were dried, distilled, and saturated with nitrogen. NMR spectra were recorded with a Bruker DRX 200 spectrometer (^{1}H: 200.13 MHz, ^{11}B: 64.21 MHz, ^{13}C: 50.32 MHz) in $CDCl_3$ as the solvent. $Et_2O{\cdot}BF_3$ was used as the external standard for ^{11}B NMR spectroscopy, and as internal references for ^{1}H and ^{13}C NMR spectroscopy the signals of the deuterated solvents were used and calculated relative to TMS. MS: ZAB-2F VH Micromass CTD spectrometer, and a JEOL MS Station JMS 700 spectrometer both using the EI or FAB ionization techniques. Melting points (uncorrected) were measured with a Büchi apparatus, using capillaries which were filled under nitrogen and sealed. $K[(\eta^5-C_5H_5)Fe(CO)_2]$[15] and Me_3SnLi[16] were prepared according to literature procedures.

2,3,4,5-Tetraethyl-1-iodo-6-(phenylethynyl)-2,3,4,5-tetracarba-*nido*-hexaborane(6) (2a): *n*BuLi (2.5 M in hexanes, 2 mL) was added at −50 °C to a solution of phenlyacetylene (507 mg, 5 mmol) in hexane (30 mL), the mixture was stirred for 30 min, and then warmed up to room temp. The resulting white suspension was cooled to −60 °C, and added with a syringe to a solution of **1** (900 mg, 2.05 mmol) in hexane (30 mL). The mixture was warmed to room temperature and stirred for 2 d. Filtration (G4 frit) gave a light-yellow filtrate, which was dried in vacuo to give **2a** as a yellow powder (746 mg, 88%), m.p. 74 °C. Crystals suitable for X-ray diffraction analysis were grown from a toluene/hexane solution at −28 °C. ^{1}H NMR: δ = 1.25 (t, $^3J_{H,H}$ = 7.6 Hz, 6 H, CH_3), 1.33 (t, $^3J_{H,H}$ = 7.6 Hz, 6 H, CH_3), 2.0 (m), 2.38 (m) (8 H, CH_2), 7.27−7.48 (m, Ph) ppm. ^{11}B NMR: δ = 10.3 (s, B_{basal}), −52.6 (s, B_{apical}) ppm. ^{13}C NMR: δ = 13.4, 14.3 (CH_3), 18.4, 19.8 (CH_2), 104.4 (br., *B*-bound basal C atoms), 113.0 (skeletal C atoms non-adjacent to the basal B atom), 124.6, 127.6, 128.1, 131.7 (Ph) ppm; signals of alkynyl C atoms not observed. EI-MS: *m*/*z* (%) = 414 (100) [M^+], 287 (14.6) [M^+ − I]. HR-MS (EI): *m*/*z* = 414.1224 [M^+]; calcd. for $^{12}C_{20}{}^1H_{25}{}^{11}B_2{}^{127}I$ 414.1187 (Δ*m* = 3.7 mmu).

6-(*tert*-Butylethynyl)-2,3,4,5-tetraethyl-1-iodo-2,3,4,5-tetracarba-*nido*-hexaborane(6) (2b): Prepared in a similar manner to **2a** from *t*BuC≡CLi (750 mg, 8.5 mmol) and **1** (528 mg, 1.2 mmol) in hexane (50 mL). Compound **2b** (450 mg, 95%) was obtained as a yellow oil. ^{1}H NMR: δ = 1.2 (br., 6 H, CH_3), 1.25 (br., 6 H, CH_3), 1.25 (s, 9 H, *t*Bu-H), 1.91 (m), 2.28 (m) (8 H, CH_2) ppm. ^{11}B NMR: δ = 10.8 (s, B_{basal}), −52.6 (s, B_{apical}) ppm. ^{13}C NMR: δ = 13.4, 14.0 (CH_3), 18.3, 19.6 (CH_2), 30.8 [$C(CH_3)_3$], 31.2 [$C(CH_3)_3$], signals of *B*-bound basal C atoms not observed, 112.3 (skeletal C atoms non-adjacent to the basal B atom) ppm; signals of alkynyl C atoms not observed. EI-MS: *m*/*z* (%) = 394 (100) [M^+], 267 (10.8) [M^+ − I]. HR-MS (EI): *m*/*z* = 394.1517 [M^+]; calcd. for $^{12}C_{18}{}^1H_{29}{}^{11}B_2{}^{127}I$ 394.1500 (Δ*m* = 1.7 mmu).

2,3,4,5-Tetraethyl-1-iodo-6-(trimethylsilylethynyl)-2,3,4,5-tetracarba-*nido*-hexaborane(6) (2c): Prepared in a similar manner to **2a** from $Me_3SiC{\equiv}CH$ (310 mg, 3.16 mmol), *n*BuLi (2.5 M in hexanes, 3 mmol) and **1** (634 mg, 1.44 mmol) in hexane (50 mL). Compound **2c** (536 mg, 91%) was obtained as a yellow oil. ^{1}H NMR: δ = 0.18 (s, $SiMe_3$), 1.21 (t, $^3J_{H,H}$ = 7.6 Hz, 6 H, CH_3), 1.26 (t, $^3J_{H,H}$ = 7.6 Hz, 6 H, CH_3), 1.94 (m), 2.29 (m) (8 H, CH_2) ppm. ^{11}B NMR: δ = 9.8 (s, B_{basal}), −52.8 (s, B_{apical}) ppm. ^{13}C NMR: δ = 0.18 ($SiMe_3$), 13.3, 14.1 (CH_3), 18.3, 19.7 (CH_2), 105.2 (*B*-bound basal C atoms), 112.8 (skeletal C atoms non-adjacent to the basal B atom) ppm; signals of alkynyl C atoms not observed. ^{29}Si NMR ($CDCl_3$, 39.7 MHz): δ = −19.8 ppm. EI-MS: *m*/*z* (%) = 410 (100) [M^+], 283 (13.5) [M^+ − I]. HR-MS (EI): *m*/*z* = 410.1265 [M^+]; calcd. for $^{12}C_{17}{}^1H_{29}{}^{11}B_2{}^{127}I$ 410.1269 (Δ*m* = −0.4 mmu).

2,3,4,5-Tetraethyl-1-iodo-6-(*p*-tolylethynyl)-2,3,4,5-tetracarba-*nido*-hexaborane(6) (2d): Prepared in a similar manner to **2a** from *p*-tolylacetylene (431 mg, 3.72 mmol) and **1** (264 mg, 0.6 mmol) in hexane (50 mL). Compound **2d** (247 mg, 96%) was obtained as a yellow solid, m.p. 81 °C. Crystals suitable for X-ray analysis were grown from a toluene solution at −28 °C. ^{1}H NMR: δ = 1.24 (t, $^3J_{H,H}$ = 7.6 Hz, 6 H, CH_3), 1.31 (t, $^3J_{H,H}$ = 7.6 Hz, 6 H, CH_3), 1.97 (m), 2.29 (m) (8 H, CH_2), 2.32 (s, 3 H, *p*-tolyl-CH_3), 7.08 (d, $^3J_{H,H}$ = 7.94 Hz, C_6H_4), 7.38 (d, $^3J_{H,H}$ = 7.94 Hz, C_6H_4) ppm. ^{11}B NMR: δ = 10.9 (B_{basal}), −52.6 (s, B_{apical}) ppm. ^{13}C NMR: δ = 13.3, 14.2 (CH_3), 18.4, 19.7 (CH_2), 21.4 (*p*-tolyl-CH_3), signals of *B*-bound basal C atoms not observed, 112.9 (skeletal C atoms non-adjacent to the basal B atom), 121.6, 128.8, 131.6, 137.6 (C_6H_4) ppm; signals of alkynyl C atoms not observed. EI-MS: *m*/*z* (%) = 428 (100) [M^+], 301 (13.6) [M^+ − I]. HR-MS (EI): *m*/*z* = 428.1360 [M^+]; calcd. for $^{12}C_{21}{}^1H_{27}{}^{11}B_2{}^{127}I$ 428.1344 (Δ*m* = 1.6 mmu).

2,3,4,5-Tetraethyl-1-iodo-6-(diphenylphosphanyl)-2,3,4,5-tetracarba-*nido*-hexaborane(6) (3): A suspension of Ph_2PLi (170 mg, 0.88 mmol, prepared in situ from $HPPh_2$ and *n*BuLi in hexane) in hexane (5 mL) was cooled to −60 °C and added to a solution of **1** (194 mg, 0.44 mmol) in hexane (10 mL). The mixture was allowed to warm to room temp., stirred overnight and filtered. The yellow

 © 2004 Wiley-VCH Verlag GmbH & Co. KGaA, Weinheim

filtrate was dried in vacuo to give **3** (158 mg, 72%) as a yellow oil. ^{1}H NMR: δ = 0.99 (t, $^3J_{H,H}$ = 7.6 Hz, 6 H, CH_3), 1.37 (t, $^3J_{H,H}$ = 7.6 Hz, 6 H, CH_3), 1.94 (m), 2.36 (m) (8 H, CH_2), 7.37−7.56 (m, 10 H, aromatic H) ppm. ^{11}B NMR: δ = 14.8 (br., B_{basal}), −52.8 (s, B_{apical}) ppm. ^{13}C NMR: δ = 13.7, 15.1 (CH_3), 18.8, 19.2 (CH_2), signals of *B*-bound basal C atoms not observed, 116.1 (skeletal C atoms non-adjacent to the basal B atom), 127.2, 128.5, 134.4, 138.2 (aromatic C) ppm; signals of alkynyl C atoms not observed. ^{31}P{^{1}H} NMR ($CDCl_3$, 80.92 MHz): δ = −40.1 ppm. EI-MS: *m*/*z* (%) = 498 (59.1) [M^+], 371 (9.8) [M^+ − I], 186 (100) [$HPPh_2$]. HR-MS (EI): *m*/*z* = 498.1307 [M^+]; calcd. for $^{12}C_{24}{}^1H_{30}{}^{11}B_2{}^{127}I{}^{31}P$ 498.1316 (Δ*m* = −0.9 mmu).

6-[Dicarbonyl(η^5-cyclopentadienyl)iron]-2,3,4,5-tetraethyl-1-iodo-2,3,4,5-tetracarba-*nido*-hexaborane(6) (4): A solution of **1** (317 mg, 0.72 mmol) in hexane (10 mL) was added to a suspension of K[(η^5-C_5H_5)Fe(CO)$_2$] (395 mg, 1.8 mmol) in toluene (30 mL) at room temp. The mixture was stirred for 4 d and then filtered. The deep-red filtrate was concentrated and cooled to −28 °C; yellow crystals were formed after one week (258 mg, 73%), m.p. 132 °C. ^{1}H NMR: δ = 1.2 (br., 6 H, CH_3) , 1.3 (br., 6 H, CH_3), 1.93 (m), 2.22 (m) (8 H, CH_2), 4.8 (s, Cp) ppm. ^{11}B NMR: δ = 28.6 (br., B_{basal}), −49.6 (s, B_{apical}) ppm. ^{13}C NMR: δ = 13.6, 14.1 (CH_3), 19.3, 21.7 (CH_2), 88.1 (Cp), 106.5 (*B*-bound basal C atoms), 117.9 (skeletal C atoms non-adjacent to the basal B atom), 217.2 (CO) ppm; signals of alkynyl C atoms not observed. IR (hexane): ν_{co}: 1998.1 (s), 1942.4 (s) cm^{-1}. EI-MS: *m*/*z* (%) = 490 (4.2) [M^+], 462 (24.1) [M^+ − CO], 434 (100) [M^+ − 2 CO], 405 (7.3) [M^+ − 2 CO − Et], 307 (22.9) [M^+ − 2 CO − I]. HR-MS (EI): *m*/*z* = 490.0431 [M^+]; calcd. for $^{12}C_{19}{}^1H_{25}O_2{}^{11}B_2Fe^{127}I$ 490.0435 (Δ*m* = −0.4 mmu).

2,3,4,5-Tetraethyl-6-hydrido-1-iodo-2,3,4,5-tetracarba-*nido*-hexaborane(6) (5). a) By Decomposition of 4: In an attempt to separate **4** by column chromatography on silica gel, the crude product was eluted with hexane; only decomposition was observed. Compound **5** and paramagnetic impurities were formed, as indicated by the NMR spectroscopy. **b) By Reaction of 1 with LiBEt$_3$H:** A solution of LiBEt$_3$H (1.0 M in THF, 0.4 mmol) was added dropwise at −65 °C to a solution of **1** (194 mg, 0.44 mmol) in hexane (5 mL). A white precipitate was formed, the mixture was allowed to warm to room temp. and filtered. The colorless filtrate was dried in vacuo to give **5** (123 mg, 89%) as a colorless oil. ^{1}H NMR: δ = 1.2 (br., 6 H, CH_3), 1.2 (br., 6 H, CH_3), 2.04 (m), 2.21 (m) (8 H, CH_2) ppm. ^{11}B NMR: δ = 11.5 (d, $J_{B,H}$ = 148.3 Hz, B_{basal}), −53.8 (s, B_{apical}) ppm. ^{13}C NMR: δ = 13.1, 14.3 (CH_3), 18.5, 20.1 (CH_2), 106.3 (*B*-bound basal C atoms), 114.8 (skeletal C atoms non-adjacent to the basal B atom) ppm. EI-MS: *m*/*z* (%) = 314 (100) [M^+], 187 (10) [M^+ − I]. HR-MS (EI): *m*/*z* = 314.0893 [M^+]; calcd. for $^{12}C_{12}{}^1H_{21}{}^{11}B_2{}^{127}I$ 314.0874 (Δ*m* = 1.9 mmu).

2,3,4,5-Tetraethyl-1-iodo-6-phenyl-2,3,4,5-tetracarba-*nido*-hexaborane(6) (6a): A suspension of PhLi [obtained upon solvent removal from a solution (1.6 M) in diethyl ether/cyclohexane, 1 mmol] in hexane (5 mL) was cooled to −60 °C and added to a solution of **1** (194 mg, 0.44 mmol) in hexane (10 mL). The mixture was allowed to warm to room temp., stirred overnight and filtered. The light-yellow filtrate was dried in vacuo to give **6a** (150 mg, 87%) as a colorless oil, and trace amount of **6b**. ^{1}H NMR: δ = 1.19 (t, $^3J_{H,H}$ = 7.6 Hz, 6 H, CH_3), 1.4 (t, $^3J_{H,H}$ = 7.6 Hz, 6 H, CH_3), 2.08 (m), 2.36 (m) (8 H, CH_2), 7.40−7.55 (m, Ph) ppm. ^{11}B NMR: δ = 17.9 (s, B_{basal}), −52.4 (s, B_{apical}) ppm. ^{13}C NMR: δ = 13.7, 14.2 (CH_3), 18.5, 19.0 (CH_2), 103.4 (br., *B*-bound basal C atoms), 112.9 (skeletal C atoms non-adjacent to the basal B atom), 126.8, 127.2, 128.8, 133.2, 141.3 (Ph) ppm. EI-MS: *m*/*z* (%) = 390 (100) [M^+], 361 (10.8) [M^+ − Et], 263 (5.9) [M^+ − I]. HR-MS (EI): *m*/*z* = 390.1188 [M^+]; calcd. for $^{12}C_{18}{}^1H_{25}{}^{11}B_2{}^{127}I$ 390.1187 (Δ*m* = 0.1 mmu); *m*/*z* = 340.2532 (**6b**)$^+$; calcd. for $^{12}C_{24}{}^1H_{30}{}^{11}B_2$ 340.2534 (Δ*m* = −0.2 mmu).

2,3,4,5-Tetraethyl-1-iodo-6-(trimethylstannyl)-2,3,4,5-tetracarba-*nido*-hexaborane(6) (7a): A solution of **1** (194 mg, 0.44 mmol) in hexane (10 mL) was added to a suspension of Me_3SnLi (1 mmol) in hexane (20 mL) at −60 °C. The mixture was allowed to warm to room temp., stirred for 3 d and then filtered. The light-yellow filtrate was dried in vacuo to give **7a** (170 mg, 81%) as a yellow oil, and a trace amount of **7b**. ^{1}H NMR: δ = 0.3 (s, 9 H, $SnMe_3$), 1.2 (br., 6 H, CH_3), 1.3 (br., 6 H, CH_3), 2.11 (m), 2.24 (m) (8 H, CH_2) ppm. ^{11}B NMR: δ = 16.1 (br., B_{basal}), −52.6 (s, B_{apical}) ppm. ^{13}C NMR: δ = −6.0 ($SnMe_3$), 13.5, 14.1 (CH_3), 19.2, 22.2 (CH_2), signals of *B*-bound basal C atoms not observed, 118.6 (skeletal C atoms non-adjacent to the basal B atom) ppm. ^{119}Sn NMR ($CDCl_3$, 74.5 MHz): δ = −97.9 ppm. EI-MS: *m*/*z* (%) = 463 (100) [M^+ − CH_3], 499 (68.5) [**7b**$^+$ − CH_3]. HR-MS (EI): *m*/*z* = 463.0254 [M^+ − CH_3]; calcd. for $^{12}C_{14}{}^1H_{26}{}^{11}B_2{}^{127}I{}^{120}Sn$ 463.0288 (Δ*m* = −3.4 mmu); *m*/*z* = 501.0996 [**7b**$^+$ − CH_3]; calcd. for $^{12}C_{17}{}^1H_{35}{}^{11}B_2{}^{120}Sn_2$ 501.0968 (Δ*m* = 2.8 mmu).

2,3,4,5-Tetraethyl-6-(phenylethynyl)-1-(trimethylsilylethynyl)-2,3,4,5-tetracarba-*nido*-hexaborane(6) (8): A portion of lithium trimethylsilylacetylide (138 mg, 1.33 mmol) was dissolved in THF (15 mL) at room temp. and $ZnCl_2$ (180 mg, 1.33 mmol) was added. The mixture was stirred for 3 h and was then added to a mixture of **2a** (146 mg, 0.35 mmol) and Pd(PPh$_3$)$_4$ (20 mg, 0.017 mmol). The resulting yellow mixture was stirred for 3 d and then heated at reflux for 10 d. The solvent was removed, the black residue was extracted with hexane (2 × 20 mL) and filtered. The yellow filtrate was dried in vacuo to give a yellow viscous oil. A minimum amount of hexane was added and, on cooling to −28 °C, yellow crystals of **8** (115 mg, 85%) grew, m.p. 72 °C. ^{1}H NMR: δ = 0.08 ($SiMe_3$), 1.22 (t, $^3J_{H,H}$ = 7.6 Hz, 6 H, CH_3), 1.30 (t, $^3J_{H,H}$ = 7.6 Hz, 6 H, CH_3), 2.22 (m), 2.35 (m) (8 H, CH_2), 7.27−7.50 (m, 5 H, Ph) ppm. ^{11}B NMR: δ = 9.8 (s, B_{basal}), −50.7 (s, B_{apical}) ppm. ^{13}C NMR: δ = 0.01 ($SiMe_3$), 13.6, 14.7 (CH_3), 17.4, 19.1 (CH_2), 104.4 (*B*-bound basal C atoms), 112.4 (skeletal C atoms non-adjacent to the basal B atom), 125.0, 127.4, 128.0, 131.7 (Ph) ppm; signals of alkynyl C atoms not observed. ^{29}Si NMR ($CDCl_3$, 39.7 MHz): δ = −19.4 ppm. EI-MS: *m*/*z* (%) = 384 (100) [M^+]. HR-MS (EI): *m*/*z* = 384.2621 [M^+]; calcd. for $^{12}C_{25}{}^1H_{34}{}^{11}B_2{}^{28}Si$ 384.2616 (Δ*m* = 0.5 mmu).

3-Carboranyl-4-phenyl-1,2-bis(tricarbonylcobalta)tetrahedrane (9): A solution of **2a** (193 mg, 0.47 mmol) in hexane (15 mL) was added to a solution of $Co_2(CO)_8$ (178 mg, 0.52 mmol) in hexane (15 mL) at −40 °C. The mixture was allowed to warm to room temp. and stirred for 4 d until the reaction was complete. The solvent was removed in vacuo and the black residue was extracted with dichloromethane (2 mL) and separated by column chromatography (Florisil®) with hexane as eluent. After a small amount of unchanged $Co_2(CO)_8$, a deep-brown band was eluted. The solution was concentrated and cooled to −28 °C to give black crystals of **9** (170 mg, 52%), m.p. 140−141 °C (decomp.). ^{1}H NMR: δ = 1.09 (br., 6 H, CH_3), 1.35 (br., 6 H, CH_3), 1.84 (br.), 2.28 (br.) (8 H, CH_2), 7.26−7.51 (m, 5 H, Ph) ppm. ^{11}B NMR: δ = 16.3 (br., B_{basal}), −51.1 (s, B_{apical}) ppm. ^{13}C NMR: δ = 13.6, 14.1 (CH_3), 18.6, 19.0 (CH_2), 102.6 (*B*-bound basal C atoms), 114.0 (skeletal C atoms non-adjacent to the basal B atom), 127.2, 128.4, 129.7 (Ph), 200.4 (CO) ppm. EI-MS: *m*/*z* (%) = 672 (13.0) [M^+ − CO], 644 (12.1) [M^+ − 2 CO], 616 (19.0) [M^+ − 3 CO], 588 (28.2) [M^+ − 4 CO], 560 (11.7) [M^+ − 5 CO], 532 (100) [M^+ − 6 CO], 473 (20.6) [M^+ − 6 CO − 2 Et]. HR-MS (EI): *m*/*z* = 671.9595 [M^+ − CO];

 © 2004 Wiley-VCH Verlag GmbH & Co. KGaA, Weinheim

calcd. for $^{12}C_{25}{}^{1}H_{25}O_5{}^{11}B_2Co_2{}^{127}I$ 671.9596 (Δm = −0.1 mmu). $C_{26}H_{25}B_2Co_2IO_6$ (699.9): calcd. C 44.62, H 3.60; found C 44.08, H 3.98.

6-(*o*-Carboranyl)-2,3,4,5-tetraethyl-1-iodo-2,3,4,5-tetracarba-*nido*-hexaborane(6) (10): *n*BuLi (2.5 M in hexanes, 0.4 mL, 1 mmol) was added at −65 °C to a solution of *o*-carborane (126 mg, 0.875 mmol) in toluene (15 mL). The colorless mixture was allowed to warm to room temp. and stirred overnight. The resulting white suspension was cooled to −65 °C and a solution of **1** (264 mg, 0.58 mmol) in hexane (7 mL) was added. The mixture was warmed to room temp., heated at reflux overnight, and filtered. The colorless filtrate was dried in vacuo to give a solid. A minimum amount of $CDCl_3$ was added and, on cooling to −28 °C, colorless crystals of **10** (200 mg, 76%) were obtained, m.p. 108 °C. ^{1}H NMR: δ = 1.20 (t, $^3J_{H,H}$ = 7.6 Hz, 6 H, CH_3), 1.28 (t, $^3J_{H,H}$ = 7.6 Hz, 6 H, CH_3), 1.93 (m), 2.25 (m) (8 H, CH_2), 3.3−3.8 (m, *o*-carborane) ppm. ^{11}B{^{1}H} NMR: δ = 13.9 (s, B_{basal}), −2.4 (2 B), −9.2 (2 B), −13.6 (4 B), −14.8 (2 B), −53.4 (s, B_{apical}) ppm. ^{13}C NMR: δ = 13.6, 14.7 (CH_3), 17.4, 19.1 (CH_2), 59.6 (C_{cage}), 102.3 (br., *B*-bound basal C atoms), 114.5 (skeletal C atoms non-adjacent to the basal B atom) ppm. EI-MS: *m*/*z* (%) = 456 (100) [M$^+$]. HR-MS (EI): *m*/*z* = 458.2604 [M$^+$]; calcd. for $^{12}C_{14}{}^{1}H_{31}{}^{11}B_{12}{}^{127}I$ 458.2587 (Δm = 1.7 mmu).

The $C_6H_4C_6H_4$-Connected Carborane 11: *n*BuLi (2.5 M in hexanes, 0.6 mL, 1.5 mmol) was added to a solution of 4,4′-dibromobiphenyl (164 mg, 0.53 mmol) in THF (15 mL) at −65 °C, and stirred at that temp. for 2 h. $ZnCl_2$ (150 mg, 1.1 mmol) was added in one portion to the resulting white suspension. The mixture was allowed to warm to room temp. to form a cloudy mixture, which was dried, and dry toluene (25 mL), **1** (200 mg, 0.45 mmol, in 5 mL of hexane) and $Pd(PPh_3)_4$ (60 mg, 0.052 mmol) were added to the solid. The resulting yellow mixture was stirred at room temp. for 3 d and filtered. The light-yellow filtrate was dried in vacuo, the residue was extracted with hexane (2 × 20 mL) and filtered. The colorless filtrate was dried in vacuo to give **11** as an oil (90 mg, 50%). ^{1}H NMR: δ = 1.2 (br., 6 H, CH_3), 1.3 (br., 6 H, CH_3), 2.10 (m), 2.32 (m) (8 H, CH_2), 7.41 (d, *J* = 8 Hz, 4 H), 7.48 (d, *J* = 8 Hz, 4 H, $C_6H_4C_6H_4$) ppm. ^{11}B NMR: δ = 22.0 (br., 2 B, B_{basal}), −52.4 (s, 2 B, B_{apical}) ppm. ^{13}C NMR: δ = 13.4, 14.3 (CH_3), 18.4, 19.8 (CH_2), 104.4 (*B*-bound basal C atoms), 113.0 (skeletal C atoms non-adjacent to the basal B atom), 124.6, 127.6, 128.1, 131.7 ($C_6H_4C_6H_4$) ppm. FAB-MS: *m*/*z* (%) = 778 (100) [M$^+$]. HR-MS (FAB): *m*/*z* = 778.2294 [M$^+$]; calcd. for $^{12}C_{36}{}^{1}H_{48}{}^{11}B_4{}^{127}I_2$ 778.2217 (Δm = 7.7 mmu).

The Oxygen-Bridged Carborane 12: Wet Et_3N (92 mg) was added to a solution of **1** (198 mg, 0.45 mmol) in hexane (5 mL) at − 60 °C. The mixture was allowed to warm to room temp. and stirred overnight. The colorless filtrate and the white precipitate were then separated by filtration. The filtrate was dried in vacuo to give **12** as an oil (100 mg, 69%). ^{11}B NMR: δ = 22.1 (br., 2 B, B_{basal}), −51.9 (s, 2 B, B_{apical}) ppm. EI-MS: *m*/*z* (%) = 642 (100) [M$^+$], 613 (61.2) [M$^+$ − Et], 515 (48.6) [M$^+$ − I]. HR-MS (EI): *m*/*z* = 642.1533 (100) [M$^+$]; calcd. for $^{12}C_{24}{}^{1}H_{40}{}^{11}B_4{}^{127}I_2{}^{16}O$ 642.1541 (Δm = −0.8 mmu). Negative FAB-MS of the white precipitate exhibited peaks at *m*/*z* = 356 $[Et_3NH]I_2^-$, 483 $[Et_3NH]I_3^-$, 584.9 $[Et_3NH]_2I_3^-$, indicating its identity as $[Et_3NH]I$.

X-ray Structure Determinations: Crystal data and details of the structure determinations are listed in Tables 1 and 2. The intensity data for **2a**, **4**, **8**, **9**, and **10** were collected with a Bruker AXS Smart CCD diffractometer at 103(2) K, and for **2d** at 298 K (Mo-K_α radiation, λ = 0.71073 Å, graphite monochromator, ω-scans). Data were corrected for Lorentz polarization and absorption effects (semiempirical, SADABS[17]). The structures were solved by direct methods (SHELXS-86)[18] and refined by least-squares methods

Table 1. Crystal data and structure refinement for **2a**, **2d**, **4**

	2a	**2d**	**4**
Empirical formula	$C_{20}H_{25}B_2I$	$C_{21}H_{27}B_2I$	$C_{19}H_{25}B_2FeIO_2$
Formula mass	413.92	427.95	489.76
Crystal system	triclinic	triclinic	monoclinic
Space group	$P\bar{1}$	$P\bar{1}$	$P2_1/c$
a [Å]	7.3783(6)	7.8362(4)	9.5495(5)
b [Å]	10.4260(8)	8.3469(4)	24.2877(11)
c [Å]	12.5718(9)	18.2876(10)	8.9340(4)
α [°]	86.083(1)	80.286 (1)	90
β [°]	86.301(1)	85.038(1)	99.480(1)
γ [°]	85.441(2)	64.989(1)	90
V [Å^3]	960.09(13)	1068.29(9)	2043.8(2)
Z	2	2	4
$D_{calcd.}$ [g cm^{-3}]	1.432	1.330	1.592
μ(Mo-K_α) [mm^{-1}]	1.664	1.498	2.257
F(000)	416	432	976
Crystal size [mm]	0.35 × 0.09 × 0.04	0.45 × 0.32 × 0.27	0.32 × 0.25 × 0.20
Θ_{max} [°]	32.0	26.3	32.0
Index ranges	−10/10, −15/15, −0/18	−9/9, −10/10, 0/22	−14/14, 0/36, 0/13
Reflections collected	16837	13336	27347
Independent (R_{int})	6504 (0.0387)	4370(0.0210)	7027(0.0239)
No. of parameters	308	319	326
GooF	1.071	1.064	1.215
*R*1 ($I > 2\sigma I$)	0.0304	0.0404	0.0290
*wR*2 (all reflections)	0.077	0.1092	0.0670
Resid. electron dens. [e·Å^{-3}]	1.322/−1.248	0.973/−0.623	1.292/−0.713

 © 2004 Wiley-VCH Verlag GmbH & Co. KGaA, Weinheim

Table 2. Crystal data and structure refinement for **8**, **9** and **10**

	8	**9**	**10**
Empirical formula	$C_{25}H_{34}B_2Si$	$C_{26}H_{25}B_2Co_2IO_6$	$C_{14}H_{31}B_{12}I{\cdot}2(C_2H_{12}B_{10})$
Formula mass	384.23	699.84	744.44
Crystal system	monoclinic	monoclinic	monoclinic
Space group	$P2_1$	$P2_1/c$	$P2/c$
a [Å]	7.3346(4)	16.7233(9)	26.1136(12)
b [Å]	8.9453(4)	12.4541(7)	6.8725(3)
c [Å]	19.1092(10)	13.5390(8)	24.6178(12)
α [°]	90	90	90
β [°9	91.254(1)	93.599(1)	115.469(1)
γ [°]	90	90	90
V [Å^3]	1253.46(11)	2814.3(3)	3988.7(3)
Z	2	4	4
$D_{calcd.}$ [g cm^{-3}]	1.018	1.652	1.240
μ(Mo-K_α) [mm^{-1}]	0.101	2.313	0.821
F(000)	416	1384	1504
Crystal size [mm]	0.15 × 0.24 × 0.36	0.33 × 0.10 × 0.06	0.55 × 0.30 × 0.23
Θ_{max} [°]	32.01	32.0	32.0
Index ranges	−10/10, −10/13, −0/28	−24/24, 0/18, 0/20	−38/35, 0/10, 0/36
Reflections collected	11997	37985	53142
Independent (R_{int})	6728 (0.0247)	9662(0.0429)	13706(0.0342)
No. of parameters	389	434	680
GooF	1.066	1.050	1.114
$R1$ ($I > 2\sigma I$)	0.0385	0.0318	0.0348
$wR2$ (all reflections)	0.1018	0.0780	0.0819
Resid. electron dens. (e·Å^{-3})	0.393/−0.180	1.002/−0.522	1.197/−1.009

based on F^2 with all measured reflections (SHELXL-97).[18] All non-hydrogen atoms were refined anisotropically. CCDC-221474 (**2a**), -221475 (**2d**), -221476 (**4**), -221477 (**8**), -221478 (**9**) and -221479 (**10**) contain the supplementary crystallographic data for this paper. These data can be obtained free of charge at www.ccdc.cam.ac.uk/conts/retrieving.html [or from the Cambridge Crystallographic Data Centre, 12 Union Road, Cambridge CB2 1EZ, UK; Fax: (internat.) + 44-1223-336-033; E-mail: deposit@ccdc.cam.ac.uk].

Acknowledgments

We thank the Deutsche Forschungsgemeinschaft (DFG, Schwerpunktprogramm Polyeder) and the Fonds der Chemischen Industrie for financial support of this work.

[1] [1a] P. Binger, *Tetrahedron Lett.* **1966**, 2675−2680. [1b] P. Binger, *Angew. Chem.* **1968**, *80*, 288−289; *Angew. Chem. Int. Ed. Engl.* **1968**, *7*, 286. [1c] R. Köster, M. A. Grassberger, *Angew. Chem.* **1967**, *79*, 197−252; *Angew. Chem. Int. Ed. Engl.* **1967**, *6*, 218. [1d] L. Killian, B. Wrackmeyer, *J. Organomet. Chem.* **1977**, *132*, 213−221. [1e] H. O. Berger, H. Nöth, B. Wrackmeyer, *Chem. Ber.* **1979**, *112*, 2884−2893.

[2] [2a] T. P. Onak, G. T. F. Wong, *J. Am. Chem. Soc.* **1970**, *92*, 5226−5226. [2b] V. R. Miller, R. N. Grimes, *Inorg. Chem.* **1972**, *11*, 862−865.

[3] [3a] B. Wrackmeyer, G. Kehr, *J. Organomet. Chem.* **1995**, *501*, 87−93. [3b] B. Wrackmeyer, A. Glöckle, *Z. Naturforsch., Teil B* **1996**, *51*, 859−864. [3c] B. Wrackmeyer, G. Kehr, unpublished results, cited in ref.[3b] [3d] B. Wrackmeyer, A. Glöckle, *Main Group Met. Chem.* **1997**, *20*, 181−189. [3e] B. Wrackmeyer, G. Kehr, A. Glöckle, *Phosphorus, Sulfur Silicon* **1997**, *131*, 25−35. [3f] M. Herberhold, U. Bertholdt, W. Milius, A. Glöckle, B. Wrackmeyer, *Chem. Commun.* **1996**, 1219−1220.

[4] C. Balzereit, H. J. Winkler, W. Massa, A. Berndt, *Angew. Chem.* **1994**, *106*, 2394−2396; *Angew. Chem. Int. Ed. Engl.* **1994**, *33*, 2306.

[5] [5a] H. Michel, D. Steiner, S. Wocadlo, J. Allwohn, N. Stamatis, W. Massa, A. Berndt, *Angew. Chem.* **1992**, *104*, 629−632; *Angew. Chem. Int. Ed. Engl.* **1992**, *31*, 607. [5b] B. Deobald, J. Hauss, H. Pritzkow, D. Steiner, A. Berndt, W. Siebert, *J. Organomet. Chem.* **1994**, *481*, 205−210.

[6] Y. Nie, S. Schwiegk, H. Pritzkow, W. Siebert, *Eur. J. Inorg. Chem.*, in press.

[7] [7a] L. I. Zakharkin, L. V. Orlova, B. V. Lokshin, L. A. Fedorov, *J. Organomet. Chem.* **1972**, *40*, 15−28. and references cited therein. [7b] F. Sato, T. Yamamoto, J. R. Wilkinson, L. J. Todd, *J. Organomet. Chem.* **1975**, *86*, 243−251. [7c] M. B. Fischer, D. F. Gaines, J. A. Ulman, *J. Organomet. Chem.* **1982**, *231*, 55−62.

[8] W. Siebert, R. Full, J. Edwin, K. Kinberger, *Chem. Ber.* **1978**, *111*, 823−831.

[9] [9a] T. Peymann, C. B. Knobler, M. F. Hawthorne, *Inorg. Chem.* **1998**, *37*, 1544−1548. [9b] W. J. Marshall, R. J. Young Jr., V. V. Grushin, *Organometallics* **2001**, *20*, 523−533.

[10] R. G. Kultyshev, S. Liu, H. T. Leung, J. Liu, S. G. Shore, *Inorg. Chem.* **2003**, *42*, 3199−3207.

[11] [11a] P. Galow, A. Sebald, B. Wrackmeyer, *J. Organomet. Chem.* **1983**, *259*, 253−268. [11b] Ch. Ester, A. Maderna, H. Pritzkow, W. Siebert, *Eur. J. Inorg. Chem.* **2000**, 1177−1184. [11c] Y. Gu, H. Pritzkow, W. Siebert, *Eur. J. Inorg. Chem.* **2001**, 373−379. [11d] H. Yao, M. Sabat, R. N. Grimes, P. Zanello, F. Fabrizi de Biani, *Organometallics* **2003**, *22*, 2581−2593.

[12] H. Schulz, G. Gabert, H. Pritzkow, W. Siebert, *Chem. Ber.* **1993**, *126*, 1593−831.

[13] [13a] J. F. Hartwig, S. Huber, *J. Am. Chem. Soc.* **1993**, *115*, 4908−4909. [13b] X. He, J. F. Hartwig, *Organometallics* **1996**, *15*, 400−407. [13c] H. Brauschweig, C. Kollann, U. Englert, *Eur. J. Inorg. Chem.* **1998**, 465−468. [13d] H. Brauschweig, M. Colling, C. Kollann, U. Englert, *J. Chem. Soc., Dalton Trans.* **2002**,

 © 2004 Wiley-VCH Verlag GmbH & Co. KGaA, Weinheim

2289−2296. [13e] A. Cowley, *J. Am. Chem. Soc.* **1998**, *120*, 6401−6402. [13f] J. Spencer, *Inorg. Chem.* **1992**, *31*, 1731−1733.
[14] M. G. Davidson, T. G. Hibbert, J. A. K. Howard, A. Mackinnon, K. Wade, *Chem. Commun.* **1996**, 2285−2286.
[15] J. E. Ellis, E. A. Flom, *J. Organomet. Chem.* **1975**, *99*, 263−268.
[16] C. Tamborski, F. E. Ford, E. J. Soloski, *J. Org. Chem.* **1963**, *28*, 237−239.
[17] G. M. Sheldrick, *SADABS*, Univ. Göttingen, **1999**.
[18] G. M. Sheldrick, *SHELXS-86*, Univ. Göttingen, **1986**; G. M. Sheldrick, *SHELXL-97*, Univ. Göttingen, **1997**.

Received December 16, 2003
Early View Article
Published Online April 20, 2004

 © 2004 Wiley-VCH Verlag GmbH & Co. KGaA, Weinheim

Crystal Structure and Properties of $Ba_{11}FeTi_{27}O_{66.5}$

Terrell A. Vanderah,*[a] Theo Siegrist,[b] Robert S. Roth,[a] Arthur P. Ramirez,[b] and Richard G. Geyer[c]

Keywords: Mixed metal oxides / X-ray diffraction / Magnetic susceptibility / Dielectric constants / Dielectric loss tangent

The crystal structure of $Ba_{11}FeTi_{27}O_{66.5}$ was determined using single-crystal and powder X-ray diffraction methods. This phase crystallizes in the monoclinic space group *C*2/*m* (No. 12) (*a* = 23.324(1) Å, *b* = 11.388(1) Å, *c* = 9.8499(3) Å, β = 90.104(3)°; *Z* = 2; $\rho_{calcd.}$ = 4.98 g/cm^3), and exhibits a 10-layer structure built from close-packed [O,(Ba,O)] layers with a stacking sequence $(cchhc)_2$. Octahedral sites are occupied by a mixture of Fe^{3+} and Ti^{4+}, with some preferential ordering suggested by analysis of bond valence sums. The structure features vertex-, edge-, and face-sharing of the [Ti(Fe)O_6] octahedra. Indexed X-ray powder diffraction data for a polycrystalline specimen are given. $Ba_{11}FeTi_{27}O_{66.5}$ and the 8-layer phase $Ba_4Fe_2Ti_{10}O_{27}$ are built from the same types of polyhedral layers, some of which feature vacant sites between two Ba ions, which substitute for three oxygens in a row. The single-crystal results suggest that the basic structural formula of the phase is $A_{11}B_{28}O_{66+x}$, with the value of x (and hence the Fe/Ti ratio) determined by partial occupancy of one of these vacant sites. Variation of this occupancy factor with synthesis temperature may account for apparent slight differences in the stoichiometry of this phase in polycrystalline and single-crystal form. However, solid solution formation was not observed for polycrystalline specimens. A comparison of the crystal structure obtained for $Ba_{11}FeTi_{27}O_{66.5}$ with that previously proposed for "Zr^{4+}-stabilized $Ba_2Ti_5O_{12}$" indicates that the phase "$Ba_2Ti_5O_{12}$" is actually a ternary compound which forms upon addition (either deliberately or inadvertently) of a trivalent ion such as Fe^{3+} or Al^{3+}. The specimens $Ba_{11}Al_2Ti_{26}O_{66}$, $Ba_{11}Al_2Ti_{24}Sn_2O_{66}$, and $Ba_{11}Al_2Ti_{24}Zr_2O_{66}$ were also prepared and were found to form the $A_{11}B_{28}O_{66+x}$-type phase. $Ba_{11}FeTi_{27}O_{66.5}$ exhibits paramagnetic behavior that deviates somewhat from the Curie–Weiss Law below 75 K. Application of this formalism to the $1/\chi$ vs. *T* data above 75 K yields an effective moment consistent with the presence of high-spin Fe^{3+} (*S* = 5/2), and a negative Weiss constant (about –25 K) indicating weak cooperative magnetic interactions that are overall antiferromagnetic. The relative permittivity and dielectric loss tangent of a sintered polycrystalline disk were measured at 5.33 GHz, yielding values (corrected for theoretical density) of 55 and 7.7(±0.3) × 10^{-4}, respectively.

(© Wiley-VCH Verlag GmbH & Co. KGaA, 69451 Weinheim, Germany, 2004)

Introduction

Ceramic magnetic oxides serve important functions in a wide variety of electronic applications, including wireless communications. For example, circulators and isolators contain ceramic magnets that provide a static magnetic field to interact with the propagating microwave, thus steering and conditioning the signal. The properties required for such ceramics include large saturation magnetization, low dielectric loss, and a high dielectric constant. Materials currently in use include various garnets, spinels, and hexaferrites,[1,2] which exhibit relatively low relative permittivities (about 15). New materials with larger permittivities would permit miniaturization of these components. To this end, the $BaO:Fe_2O_3:TiO_2$ phase diagram has been systematically investigated[3] to elucidate compounds forming between the high-dielectric-constant polytitanates (e.g. $Ba_2Ti_9O_{19}$ and $BaTi_4O_9$), and strongly magnetic compounds such as barium hexaferrite ($BaFe_{12}O_{19}$). The phase diagram study confirmed the formation of a number of ternary phases with new structural types, including the title compound, denoted previously as phase "G"[3] with a stoichiometry close to "$Ba_{14}Fe_2Ti_{35}O_{87}$" (= 0.28:0.02:0.70 $BaO:Fe_2O_3:TiO_2$), as estimated by the disappearing phase method. The present report describes the crystal structure and more precise stoichiometry of this compound, as determined by single-crystal and X-ray powder diffraction methods, and characterization of its dielectric and magnetic properties. In addition, the relationship between this ternary phase and the compound reported as "$Ba_2Ti_5O_{12}$" is described.

[a] National Institute of Standards and Technology, Materials Science and Engineering Laboratory
Gaithersburg, MD 20899, USA
[b] Bell Laboratories, Lucent Technologies
600 Mountain Ave, Murray Hill, NJ 07974, USA
[c] National Institute of Standards and Technology, Electronics and Electrical Engineering Laboratory
Boulder, CO 80305, USA

Results and Discussion

Description of the Crystal Structure and Stoichiometry

The results of the single-crystal structure determination are given in Table 1. Selected bond lengths and bond-val-

ence sums are collected in Table 2, and indexed experimental X-ray powder diffraction data for a polycrystalline specimen are given in Table 3. As seen in Table 1, electron density was observed at the O22 site indicating a partial occupancy factor of 0.24(7), resulting in an overall stoichiometry of $Ba_{11}FeTi_{27}O_{66.5}$ ($BaO:Fe_2O_3:TiO_2$ = 0.2857:0.0130:0.7013) (Z = 2). With site O22 empty, the overall stoichiometry would be $Ba_{11}Fe_2Ti_{26}O_{66}$ (= 0.2895:0.0263:0.6842 $BaO:Fe_2O_3:TiO_2$). The basic structural formula for this phase is therefore $A_{11}B_{28}O_{66+x}$, where A = Ba^{2+} and B = Ti^{4+}, substituted with a small amount (<10 atom%) of a trivalent metal which determines the value of x. The subsolidus study[3] of the system at 1260 °C suggested little, if any, solid solution formation for this phase, and several closely spaced specimens indicated that the phase forms near the stoichiometry 0.28:0.02:0.70 $BaO:Fe_2O_3:TiO_2$, which is closer to the first formula with less Fe and a higher oxygen content. However, two polycrystalline specimens subsequently prepared precisely at $Ba_{11}FeTi_{27}O_{66.5}$ and $Ba_{11}Fe_2Ti_{26}O_{66}$ were not single-phase, despite repeatedly heating for hundreds of hours. The former composition contained small amounts (several %) of $BaTi_2O_5$ and $Ba_6Ti_{17}O_{40}$, while the latter contained an appreciable amount (>10%) of $Ba_4Fe_2Ti_{10}O_{27}$. According to the subsolidus phase diagram,[3] this suggests that at 1260° the compound forms with a composition between $Ba_{11}FeTi_{27}O_{66.5}$ and $Ba_{11}Fe_2Ti_{26}O_{66}$, with a lower O22 site occupancy factor than that determined for crystals grown by cooling from 1390 °C. As discussed below, these slight variations in Fe/Ti/O stoichiometry (note, however, that the A-cation/B-cation ratios remain constant) are readily accommodated by the crystal structure, and have been observed for other compounds occurring in the $BaO:Fe_2O_3:TiO_2$ system.[3–5] For convenience, the compound in the present study is referred to as $Ba_{11}FeTi_{27}O_{66.5}$, according to Table 1. The X-ray powder pattern, calculated using the single-crystal results (Table 1) and the refined unit cell (Table 3), is in excellent agreement with the pattern observed for a polycrystalline sample (0.28:0.02:0.70 $BaO:Fe_2O_3:TiO_2$) of this phase, as shown in Figure 1.

The structure of $Ba_{11}FeTi_{27}O_{66.5}$ may be described as a 10-layer (*10L*) close-packed (*cp*) arrangement built from [O] and [Ba,O] layers, stacked along the *a*-axis, with the transition metals occupying octahedral interstices. The connectivity of the structure includes vertex-, edge-, and face-sharing of [$(Ti^{4+}/Fe^{3+})O_6$] octahedra. The *a*-parameter of the unit cell indicates an average *cp* layer thickness of 2.362 Å, which is similar to that observed for other close-packed structures in this chemical system.[6,7] The arrangement is illustrated in Figure 2, as viewed along the ⟨011⟩ direction to reveal the stacking pattern of the cubic (*ccp*), and hexagonal (*hcp*) close-packed layers. The stacking sequence is $(cchhc)_2$ (*c* denotes a cubic close-packed layer and *h* denotes a hexagonally close-packed layer), where octahedral interstices share faces across *hcp* layers. In pairs of face-sharing octahedra that are occupied, the cations are displaced away from each other resulting in cation-cation distances of the order of 2.7 Å to 2.8 Å.

Table 1. Structural Parameters obtained for $Ba_{11}FeTi_{27}O_{66.5}$, M = $Ti^{4+}(Fe^{3+})$

Atom	Site	x	*y*	*z*	$100*U_{iso}$	occ.
Ba 1	2a	0	0	0	1.58(12)	
Ba 2	4h	1/2	0.22715(23)	1/2	1.61(8)	
Ba 3	4i	0.89468(9)	0	0.67147(22)	1.01(7)	
Ba 4	8j	0.60238(7)	0.22859(16)	0.83942(16)	1.51(6)	
Ba 5	4i	0.78713(10)	0	0.33795(24)	1.46(8)	
M 1	8j	0.34924(21)	0.1378(5)	0.7628(5)	1.48(15)	
M 2	8j	0.45461(18)	0.2624(4)	0.8370(4)	1.03(13)	
M 3	4i	0.0494(3)	0	0.6582(7)	0.94(20)	
M 4	4i	0.3580(3)	0	0.4872(7)	1.36(23)	
M 5	8j	0.74963(19)	0.1340(5)	0.7190(5)	1.37(15)	
M 6	4i	0.1401(3)	0	0.9918(7)	1.01(21)	
M 7	4i	0.2617(3)	0	0.0032(7)	1.10(21)	
M 8	8j	0.14852(20)	0.7558(4)	0.5063(5)	1.13(15)	
M 9	4f	1/4	3/4	0	1.50(24)	
M10	4i	0.5373(3)	0	0.1630(8)	2.1(3)	
O1	4i	0.6040(10)	0	0.3246(23)	0.66(6)	
O2	8j	0.5024(7)	0.1329(15)	0.2383(16)	0.66(6)	
O3	4g	0	0.2386(21)	0	0.66(6)	
O4	2c	0	0	1/2	0.66(6)	
O5	4i	0.8988(10)	0	0.1725(23)	0.66(6)	
O6	8j	−0.0025(7)	0.1224(14)	0.2513(16)	0.66(6)	
O7	8j	0.3988(7)	0.1292(15)	0.4214(16)	0.66(6)	
O8	8j	0.1013(7)	0.2441(15)	0.3195(16)	0.66(6)	
O9	8j	0.9019(7)	0.1310(15)	0.4211(16)	0.66(6)	
O10	8j	0.1986(7)	0.1326(15)	0.4192(16)	0.66(6)	
O11	8j	0.2100(7)	0.2511(15)	0.1709(16)	0.66(6)	
O12	8j	0.5962(7)	0.1267(14)	0.0957(16)	0.66(6)	
O13	8j	0.2979(7)	0.1300(15)	0.0900(16)	0.66(6)	
O14	8j	0.0970(7)	0.1203(15)	0.0786(16)	0.66(6)	
O15	8j	0.6889(7)	0.1256(14)	0.4118(16)	0.66(6)	
O16	4i	0.2937(10)	0	0.3369(23)	0.66(6)	
O17	4i	0.6973(10)	0	0.1673(23)	0.66(6)	
O18	8j	0.3044(7)	0.2488(15)	0.3389(16)	0.66(6)	
O19	4i	0.2099(10)	0	0.1806(23)	0.66(6)	
O20	8j	0.7998(7)	0.1130 (15)	0.0609(16)	0.66(6)	
O21	2b	1/2	0	0	0.66(6)	
O22	4i	0.401(4)	0	0.210(10)	0.66(6)	0.24(7)

The polyhedral arrangements within each of the ten layers in the $Ba_{11}FeTi_{27}O_{66.5}$ structure are shown in Figure 3. This compound and $Ba_4Fe_2Ti_{10}O_{27}$ [6] (isostructural with $Ba_4Al_2Ti_{10}O_{27}$ [8]) are built from the same three types of layers: the first type contains strings of three edge-sharing octahedra plus isolated octahedra (layers 1,5,6,10), the second contains groups of five edge-sharing octahedra plus isolated octahedra (layers 2,4,7,9), and a third type contains continuous zigzag strips of edge-sharing octahedra (layers 3,8). The *8L* phase $Ba_4Fe_2Ti_{10}O_{27}$ [6] is built from two layers of the first type, four layers of the second type, and two layers of the third type (Figure 3 of ref.[6]). Not surprisingly, these two phases occur in equilibrium with one another.[3] The similarity of the two structures suggests that intergrowths between them may form easily, and could be the source of the relatively high residual in the structure refinement.

An interesting crystal-chemical feature, reminiscent of the barium polytitanates,[9] is the occurrence of vacancies in the oxygen/barium *cp* layers. As seen in Figure 3, and shown in detail in Figure 4, the vacancies occur in the first

 © 2004 Wiley-VCH Verlag GmbH & Co. KGaA, Weinheim

Table 2. Selected bond lengths and cation bond valence sums (BVS)* for $Ba_{11}FeTi_{27}O_{66.5}$; * calculated using the formalism and parameters (B = 0.37; r_0 values 2.285, 1.815, 1.759 for Ba^{2+}, Ti^{4+}, Fe^{3+}, respectively) from ref.[23]

Ba 1	−O3	2.718 (24) Å	(2 ×)	M 3	−O4	1.939 (16) Å	
	−O5	2.912 (23) Å	(2 ×)		−O5	2.060 (24) Å	
	−O6	2.844 (16) Å	(4 ×)		−O6	1.985 (17) Å	(2 ×)
	−O14	2.757 (16) Å	(4 ×)		−O9	2.032 (17) Å	(2 ×)
	BVS	*3.00*			*BVS(Ti^{4+})*	*3.62*	
Ba 2	−O2	2.795 (16) Å	(2 ×)		BVS(Fe^{3+})	*3.11*	
	−O4	3.108 (16) Å		M 4	−O1	2.056 (24) Å	
	−O6	2.992 (16) Å	(2 ×)		−O7	1.870 (17) Å	(2 ×)
	−O7	2.723 (16) Å	(2 ×)		−O15	2.059 (17) Å	(2 ×)
	−O8	2.979 (16) Å	(2 ×)		−O16	2.109 (24) Å	
	−O9	2.908 (16) Å	(2 ×)		*BVS(Ti^{4+})*	*3.75*	
	BVS	*2.21*			*BVS(Fe^{3+})*	*3.33*	
Ba 3	−O4	2.985 (16) Å		M 5	−O10	1.822 (17) Å	
	−O6	2.976 (16) Å	(2 ×)		−O11	1.959 (17) Å	
	−O8	2.784 (16) Å	(2 ×)		−O13	2.187 (17) Å	
	−O9	2.890 (16) Å	(2 ×)		−O16	1.911 (16) Å	
	−O10	2.796 (16) Å	(2 ×)		−O18	1.904 (17) Å	
	−O14	2.826 (16) Å	(2 ×)		−O19	2.050 (17) Å	
	−O19	2.844 (23) Å			*BVS(Ti^{4+})*	*4.12*	
	BVS	*2.57*			*BVS(Fe^{3+})*	*3.54*	
Ba 4	−O2	2.780 (16) Å		M 6	−O5	1.858 (24) Å	
	−O3	2.892 (16) Å			−O14	1.904 (17) Å	(2 ×)
	−O5	3.094 (16) Å			−O19	2.472 (24) Å	
	−O6	3.019 (16) Å			−O20	1.973 (17) Å	(2 ×)
	−O7	2.810 (16) Å			*BVS(Ti^{4+})*	*3.95*	
	−O9	3.027 (16) Å			*BVS(Fe^{3+})*	*3.40*	
	−O12	2.785 (16) Å					
	−O13	2.675 (16) Å			−O13	1.908 (17) Å	(2 ×)
	−O14	2.922 (16) Å			−O17	1.935 (24) Å	
	−O18	2.809 (16)Å			−O19	2.128 (24) Å	
	−O20	3.070 (16) Å			−O20	2.029 (17) Å	(2 ×)
	−O22	2.650 (16) Å			*BVS(Ti^{4+})*	*3.85*	
	BVS	*2.61*			*BVS(Fe^{3+})*	*3.31*	
Ba 5	−O5	3.076 (22) Å		M 8	−O7	1.953 (17) Å	
	−O9	3.174 (16) Å	(2 ×)		−O8	2.146 (17) Å	
	−O10	2.851 (16) Å	(2 ×)		−O9	1.887 (17) Å	
	−O15	2.799 (16) Å	(2 ×)		−O10	1.928 (17) Å	
	−O17	2.686 (16) Å			−O15	1.990 (17) Å	
	−O18	2.889 (16) Å	(2 ×)		−O18	1.882 (17) Å	
	−O20	3.034 (16) Å	(2 ×)		*BVS(Ti^{4+})*	*4.13*	
	BVS	*2.23*			*BVS(Fe^{3+})*	*3.55*	
				M 9	−O11	1.927 (16) Å	(2 ×)
M 1	−O1	2.098 (16) Å			−O13	1.977 (17) Å	(2 ×)
	−O8	1.949 (16) Å			−O20	2.037 (17) Å	(2 ×)
	−O11	1.986 (16) Å			*BVS(Ti^{4+})*	*3.88*	
	−O12	1.893 (16) Å			*BVS(Fe^{3+})*	*3.34*	
	−O15	1.943 (16) Å					
	−O17	2.031 (16) Å		M10	−O1	2.226 (24) Å	
	BVS(Ti^{4+})	*3.88*			−O2	1.879 (17) Å	(2 ×)
	BVS(Fe^{3+})	*3.34*			−O12	2.100 (17) Å	(2 ×)
					−O21	1.827 (13) Å	
M 2	−O2	1.923 (16) Å			*BVS(Ti^{4+})*	*3.94*	
	−O3	1.924 (16) Å			*BVS(Fe^{3+})*	*3.39*	
	−O6	1.932 (16) Å					
	−O8	2.021 (17) Å					
	−O12	2.058 (17) Å					
	−O14	1.982 (17) Å					
	BVS(Ti^{4+})	*3.94*					
	BVS(Fe^{3+})	*3.39*					

 © 2004 Wiley-VCH Verlag GmbH & Co. KGaA, Weinheim

Table 3. X-ray powder diffraction data for $Ba_{11}FeTi_{27}O_{66.5}$; *C2/m*; $a = 23.324(1)$ Å, $b = 11.388(1)$ Å, $c = 9.8499(3)$ Å, $\beta = 90.104(3)°$

h	*k*	*l*	$2\theta_{obs}$	I_{obs}	$2\theta_{calcd.}$	$\Delta 2\theta$	$d_{obs.}$
1	1	0	8.633	4	8.634	−0.001	10.23
−1	1	1	12.460	<1	12.458	0.002	7.098
0	2	0	15.569	1	15.550	0.019	5.686
2	2	0	17.332	6	17.317	0.015	5.112
−4	0	1	17.637	2	17.647	−0.010	5.024
2	2	1	19.548	17	19.541	0.007	4.537
4	2	0	21.800	1	21.798	0.002	4.0735
5	1	1	22.481	<1	22.483	−0.002	3.9516
3	1	2	22.751	4	22.753	−0.002	3.9053
4	2	1	23.622	25	23.625	−0.003	3.7632
6	0	1	24.603	9	24.615	−0.012	3.6153
2	2	2	25.082	5	25.086	−0.004	3.5474
1	3	1	25.414	3	25.416	−0.002	3.5018
3	3	0	26.120	2	26.102	0.018	3.4087
5	1	2	27.460	<1	27.476	−0.016	3.2453
3	3	1	27.668	5	27.659	0.009	3.2214
7	1	0	27.867	<1	27.875	−0.008	3.1989
2	0	3	28.216	19	28.227	−0.011	3.1601
1	1	3	28.537	27	28.534	0.003	3.1253
6	2	1	29.249	100	29.246	0.003	3.0508
8	0	0	30.640	13	30.639	0.001	2.9154
0	2	3	31.429	84	31.426	0.003	2.8440
−5	3	1	31.688	25	31.682	0.006	2.8213
3	3	2	31.911	36	31.900	0.011	2.8021
−2	2	3	32.369	10	32.360	0.009	2.7635
−7	1	2	33.352	7	33.353	−0.001	2.6842
−2	4	1	33.623	2	33.626	−0.003	2.6632
5	1	3	34.300	2	34.315	−0.015	2.6122
8	2	0	34.526	1	34.534	−0.008	2.5956
−4	2	3	35.051	1	35.051	0.000	2.5579
−5	3	2	35.477	9	35.474	0.003	2.5282
8	2	1	35.753	20	35.766	−0.013	2.5093
−4	4	1	36.244	6	36.241	0.003	2.4764
−1	3	3	36.347	6	36.347	0.000	2.4696
−7	3	1	36.997	3	36.998	−0.001	2.4277
−2	0	4	37.273	7	37.276	−0.003	2.4104
−3	3	3	37.996	2	37.992	0.004	2.3662
10	0	0	38.570	12	38.568	0.002	2.3323
3	1	4	39.167	8	39.168	−0.001	2.2981
4	4	2	39.686	49	39.681	0.005	2.2692
−9	1	2	40.036	3	40.042	−0.006	2.2502
6	4	1	40.293	8	40.295	−0.002	2.2364
−2	2	4	40.618	<1	40.613	0.005	2.2193
−5	3	3	41.130	2	41.122	0.008	2.1928
3	5	0	41.252	1	41.270	−0.018	2.1866
9	3	0	42.191	9	42.187	0.004	2.1401
−3	5	1	42.308	13	42.317	−0.009	2.1344
2	4	3	42.737	8	42.720	0.017	2.1140
−10	2	1	42.840	7	42.843	−0.003	2.1091
4	2	4	42.925	6	42.904	0.021	2.1052
6	4	−2	43.426	87	43.418	0.008	2.0820
−1	5	2	43.926	<1	43.932	−0.006	2.0595
−8	2	3	44.432	6	44.425	0.007	2.0372
8	2	3	44.519	4	44.499	0.020	2.0334
4	4	3	44.892	1	44.896	−0.004	2.0174
5	5	1	45.227	11	45.221	0.006	2.0032
−3	3	4	45.378	14	45.369	0.009	1.9969
−6	2	4	46.387	2	46.400	−0.013	1.9558
7	1	4	46.525	3	46.548	−0.023	1.9503
12	0	0	46.692	1	46.694	−0.002	1.9437
−11	1	2	47.295	<1	47.281	0.014	1.9203
8	4	−2	48.296	47	48.290	0.006	1.8828
8	0	4	48.395	41	48.387	0.008	1.8792
−1	5	3	48.775	15	48.774	0.001	1.8655
7	5	1	49.302	9	49.308	−0.006	1.8468
2	6	1	49.490	11	49.490	0.000	1.8402
11	3	1	50.121	1	50.113	0.008	1.8185
12	2	1	50.437	24	50.444	−0.007	1.8078
−10	2	3	50.526	22	50.524	0.002	1.8048
−5	1	5	50.892	3	50.876	0.016	1.7927
4	2	5	51.510	4	51.513	−0.003	1.7727
7	3	4	52.082	6	52.082	0.000	1.7545
2	6	2	52.224	4	52.204	0.020	1.7501
−13	1	1	52.394	6	52.394	0.000	1.7448
11	3	2	52.811	2	52.816	−0.005	1.7320
4	6	2	54.082	18	54.084	−0.002	1.6943
−6	2	5	54.580	35	54.574	0.006	1.6800
1	5	4	55.032	1	55.021	0.011	1.6672
14	0	1	55.947	19	55.946	0.001	1.6421
2	6	3	56.530	2	56.519	0.011	1.6266
1	7	0	56.683	3	56.671	0.012	1.6225
−9	5	2	56.890	3	56.910	−0.020	1.6171
9	3	4	57.011	3	57.004	0.007	1.6140
12	4	0	57.342	1	57.352	−0.010	1.6054
−1	7	1	57.505	1	57.505	0.000	1.6013
3	1	6	57.954	1	57.957	−0.003	1.5899
−14	2	1	58.408	11	58.406	0.002	1.5787
−5	5	4	58.580	9	58.575	0.005	1.5744
−8	6	1	58.735	8	58.742	−0.007	1.5706
−13	1	3	59.132	3	59.145	−0.013	1.5610
−7	3	5	59.620	1	59.626	−0.006	1.5494
−13	3	2	59.961	1	59.962	−0.001	1.5414
−12	4	2	60.597	24	60.593	0.004	1.5268
−4	2	6	60.758	18	60.750	0.008	1.5231
−5	7	1	60.992	12	60.991	0.001	1.5178
−3	7	2	61.106	12	61.107	−0.001	1.5153
6	0	6	61.262	4	61.284	−0.022	1.5118
−1	3	6	61.612	2	61.624	−0.012	1.5040
−7	5	4	62.001	2	62.019	−0.018	1.4955
−11	3	4	62.688	1	62.688	0.000	1.4808
−15	1	2	63.139	<1	63.148	−0.009	1.4713
−5	7	2	63.361	2	63.362	−0.001	1.4666
3	5	5	63.535	3	63.542	−0.007	1.4631
7	1	6	63.717	1	63.714	0.003	1.4593
4	6	4	63.915	1	63.917	−0.002	1.4553
7	7	1	64.391	<1	64.382	0.009	1.4457
13	1	4	64.806	1	64.815	−0.009	1.4374
−8	6	3	65.072	2	65.080	−0.008	1.4322
8	0	6	65.234	6	65.218	0.016	1.4290
0	4	6	65.570	48	65.590	−0.020	1.4225
8	4	5	65.937	6	65.955	−0.018	1.4155
11	5	3	66.647	6	66.634	0.013	1.4021
2	8	1	66.838	9	66.836	0.002	1.3985
−15	1	3	66.986	6	66.994	−0.008	1.3958
−8	2	6	67.420	<1	67.395	0.025	1.3879
15	3	2	67.848	17	67.829	0.019	1.3802
9	7	0	67.966	14	67.980	−0.014	1.3780
−3	1	7	68.145	5	68.144	0.001	1.3749
−4	8	1	68.428	1	68.450	−0.022	1.3699
−7	5	5	68.923	5	68.947	−0.024	1.3612
−2	6	5	69.140	5	69.129	0.011	1.3575
13	3	4	69.386	1	69.370	0.016	1.3533
−12	4	4	69.818	8	69.837	−0.019	1.3460
12	2	5	69.972	11	69.978	−0.006	1.3434

Table 3. *(Continued)*

 © 2004 Wiley-VCH Verlag GmbH & Co. KGaA, Weinheim

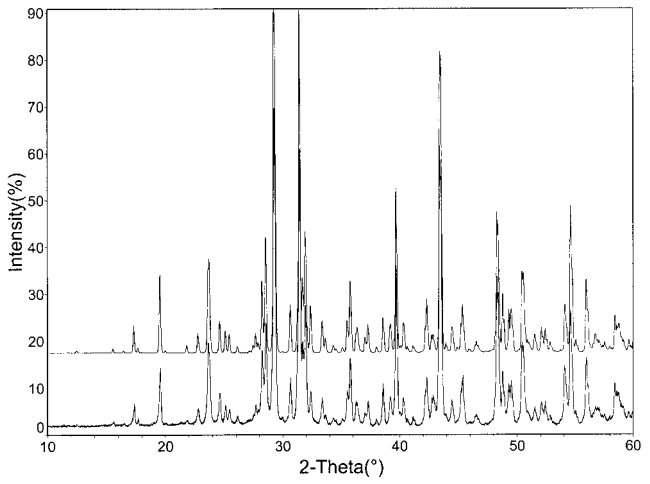

Figure 1. The X-ray powder diffraction pattern for $Ba_{11}FeTi_{27}O_{66.5}$ calculated from the single-crystal results (*top*) is in excellent agreement with the observed pattern (*bottom*) for a polycrystalline sample ($BaO:Fe_2O_3:TiO_2$ = 0.28:0.02:0.70); the stoichiometry of this phase in polycrystalline form (prepared at 1260°) apparently differs slightly from that of the single crystals (grown by cooling from 1390°), suggesting slightly different occupancy factors for the oxygen site O22 (Table 2); charge-balance is maintained by a corresponding change in the Fe/Ti ratio; in both cases, however, the A-cation/B-cation ratio remains the same (11:28)

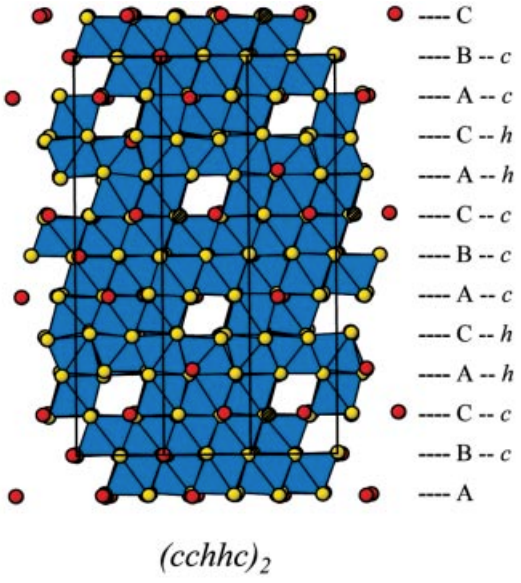

Figure 2. The crystal structure of *10L* $Ba_{11}FeTi_{27}O_{66.5}$ (*C2/m*; *a* = 23.324(1), *b* = 11.388(1), *c* = 9.8499(3) Å; β = 90.104(3)°] viewed approximately parallel to the close-packed (*cp*) [O,(Ba,O)] layers; the 10-layer stacking sequence is $(cchhc)_2$; the octahedra are occupied by Ti^{4+}/Fe^{3+}, with some preferential ordering suggested by analysis of bond valence sums; red spheres represent Ba^{2+}, yellow spheres represent oxygen with the hatched yellow spheres indicating the partially occupied O22 site (Table 2)

and second types of layers, where two Ba ions replace three oxygens in a row, reducing their coordination number from twelve to eleven. For $Ba_{11}FeTi_{27}O_{66.5}$, this results in a coordination number of 11 and a relatively low bond-valence sum for Ba2 (Table 2, Figure 4). The partially occupied site

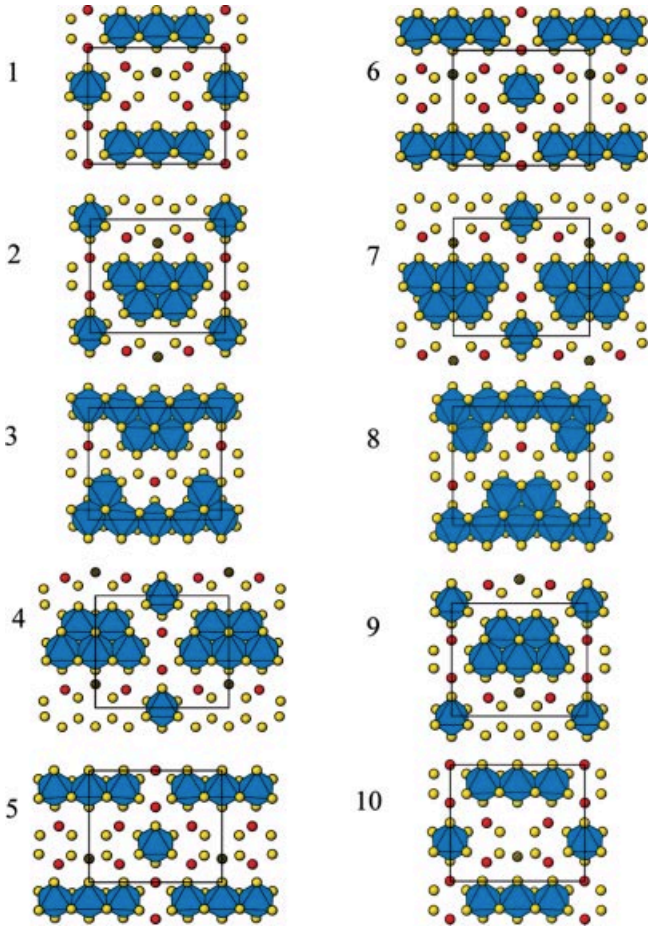

Figure 3. The structural arrangements within each of the ten layers of the close-packed structure of $Ba_{11}FeTi_{27}O_{66.5}$, viewed perpendicular to the layers; the representations are the same as in Figure 1; as seen here, the structure is built from three types of layers (*type 1* = layers 1,5,6,10; *type 2* = layers 2,4,7,9; *type 3* = layers 3,8); the same types of layers occur in the *8L* structure of $Ba_4Fe_2Ti_{10}O_{27}$; as observed for the barium polytitanate phases, the *cp* layers (types 1 and 2) are characterized by the occurrence of vacancies, wherein two Ba ions substitute for three oxygen positions in a row; the partially occupied O22 site (hatched yellow spheres) corresponds to one of these vacancies between two Ba ions

O22 corresponds to one of these *cp* vacancies, and occurs within bonding distance of Ba4 (Table 2, Figure 4). The occupancy factor of 0.24(7) for O22 obtained in the single-crystal study therefore suggests that 25% of the Ba4 sites are 12-coordinated and 75% are 11-coordinated.

The bond-valence sums about the M sites (Table 2) were calculated separately using the r_0 parameters for Ti^{4+} and Fe^{3+}, and are generally consistent with the high Ti-content of this phase. However, site M3 was observed to have slightly longer bond lengths than the other sites, and returns a bond-valence sum suggesting preferential occupation by the slightly larger trivalent Fe ion (Table 3). The M3 sites occur in pairs of vertex-linked octahedra in adjacent layers of the first type described above (Figure 3, layers 1,5,6,107). Interestingly, the coordination sphere about M3 has no next-nearest neighbors within 3.5 Å, whereas the other M sites have from 3 to 9, with an average of 7, next-

 © 2004 Wiley-VCH Verlag GmbH & Co. KGaA, Weinheim

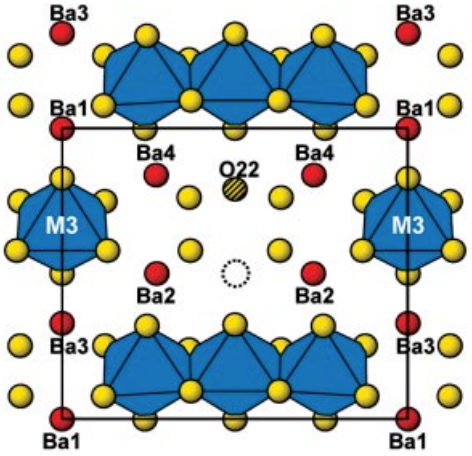

Figure 4. Magnified view of layer 1 in the structure of $Ba_{11}FeTi_{27}O_{66.5}$ (representations as in Figure 1), labeled to clarify the positions of the vacancies in the *cp* layers (dotted circle and hatched yellow O22 site); using the ligands on the upper and lower faces of the octahedra as a guide, the Ba2 sites are seen to occur in the lower *cp* layer, with the vacancy (dotted sphere) between them, thereby reducing their coordination number to eleven (Table 3); similarly, the Ba4 sites are seen to occur in the upper *cp* layer, but in this case the vacant site between them appears to be partially occupied (O22, Table 2), according to the electron density observed in the single-crystal study; note the marked displacement of O22 out of the *cp* row towards the interior of the unit cell; sites M3 occur in vertex-linked pairs of octahedra in adjacent layers, and exhibit bond-valence sums suggestive of preferential occupation by the somewhat larger Fe^{3+} ion

nearest neighbors within this distance. The M3 sites are therefore unusually isolated in the structure, which may facilitate accommodation of a larger cation.

Relationship to "$Ba_2Ti_5O_{12}$" (A Ternary Compound)

The synthesis, stability, and crystal chemistry of the phase referred to as "$Ba_2Ti_5O_{12}$" has long been of interest to researchers concerned with the phases occurring between $BaTiO_3$ and TiO_2, the so-called "barium polytitanates", which have technically important dielectric properties. The existence of $Ba_2Ti_5O_{12}$ was first reported by Jonker and Kwestroo[10] during the course of phase equilibria studies of the ternary systems with either ZrO_2 or SnO_2. They reported considerable solid solution of both oxides in the phase labeled $Ba_2Ti_5O_{12}$. However, many studies of the pure BaO-TiO_2 system failed to confirm the formation of this binary phase.[11–14] A subsequent study[15] found that "$Ba_2Ti_5O_{12}$" did not form in the ternary system with SnO_2, in contrast to the earlier report.[10] The phase did form, however, upon addition of ZrO_2. Small single crystals were grown and found to adopt a pseudo-orthorhombic unit cell with $a = 9.941$, $b = 11.482$, and $c = 23.528$ Å.[15] A later preliminary structural refinement of these crystals[16] suggested that the actual composition was $Ba_{11}(Ti,Zr)_{28}O_{66}O$, with the 67th oxygen in a position not located.[9] Subsequent chemical analyses of these crystals using an ion-microprobe[12] found about 0.25 wt% Al_2O_3 in addition to the expected amounts of BaO, TiO_2, and ZrO_2, although no alumina had been intentionally added. A comparison of the pseudo-orthorhombic unit cell for these crystals as well as the proposed crystal structure (Figure 10 in ref.[9]) reveals that they are essentially identical to those for $Ba_{11}FeTi_{27}O_{66.5}$ reported here (Table 1, Figure 3). Apparently, the phase "$Ba_2Ti_5O_{12}$" is actually a ternary compound stabilized by a relatively small content of a trivalent metal such as Fe^{3+} or Al^{3+}. Note that the A:B:O A-cation:B-cation:oxygen ratios are very similar for all of these compositions. As previously noted,[10] Jonker and Kwestroo[4] "wet-milled" their specimens twice, once before and once after calcination, and this process is notorious for the introduction of impurities from the ceramic spheres used for milling. To confirm this, specimens with compositions $Ba_{11}Al_2Ti_{26}O_{66}$, $Ba_{11}Al_2Ti_{24}Sn_2O_{66}$, and $Ba_{11}Al_2Ti_{24}Zr_2O_{66}$ were synthesized (1250 °C, 1275 °C, and 1275 °C, respectively), and were all found to contain the $A_{11}B_{28}O_{66+x}$-type phase as the major product (>95%) [the phase was not observed to form in compositions with Mg^{2+} or Zn^{2+} (i.e. $Ba_{11}MgTi_{27}O_{66}$ or $Ba_{11}ZnTi_{27}O_{66}$)].

Magnetic and Dielectric Properties of $Ba_{11}FeTi_{27}O_{66.5}$

The inverse magnetic susceptibility vs. temperature measured for $Ba_{11}FeTi_{27}O_{66.5}$ is shown in Figure 5. The behavior is paramagnetic, with highly dilute magnetic species, and follows the Curie–Weiss law above about 75 K. The slight curvature below 75 K and the extrapolated temperature intercept of −25 K indicate weak cooperative interactions between Fe spins that are, overall, antiferromagnetic in nature. Application of the Curie–Weiss formalism to the near-linear data above 75 K yields an effective moment of 5.2 μ_β/Fe, which is similar to the free-ion spin-only moment for high-spin Fe^{3+} ($S = 5/2$; 5.9 μ_β/Fe).

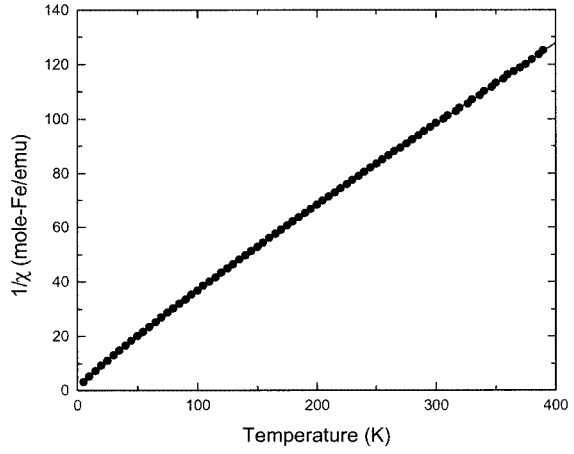

Figure 5. Inverse magnetic susceptibility vs. temperature for $Ba_{11}FeTi_{27}O_{66.5}$; the slight curvature below 75 K and the extrapolated temperature intercept of −25 K indicate weak cooperative interactions among the magnetic species that are overall antiferromagnetic in nature; the effective magnetic moment calculated from the essentially linear data above 75 K is consistent with the presence of high-spin Fe^{3+}

 © 2004 Wiley-VCH Verlag GmbH & Co. KGaA, Weinheim

A corrected relative permittivity of 55, and a dielectric loss tangent, tanδ, of 7.7(±0.3) × 10^{-4} were obtained for $Ba_{11}FeTi_{27}O_{66.5}$. Both values were essentially independent of frequency between 5.0 and 5.5 GHz. Using Shannon's values for atomic polarizabilities and the Clausius−Mosotti theory,[18] a dielectric constant of 45 was estimated for this compound, a value in fair agreement with the experimental results given the uncertainty of the porosity measurement.

Conclusions

The crystal structure of the new ternary oxide $Ba_{11}FeTi_{27}O_{66.5}$ has been characterized by single-crystal and powder X-ray diffraction methods. The compound adopts a monoclinic *10L* structure built from close-packed (*cp*) [O,(Ba,O)] layers with a stacking sequence $(cchhc)_2$. Octahedral sites are occupied by Fe^{3+} and Ti^{4+}. The structure features vertex-, edge-, and face-sharing of the [Ti(Fe)O_6] octahedra. $Ba_{11}FeTi_{27}O_{66.5}$ is built from the same three types of layers as the neighboring *8L* compound $Ba_4Fe_2Ti_{10}O_{27}$. As observed for the binary barium polytitanates, some of the *cp* layers also feature vacant sites between two Ba ions which substitute for three oxygens in a row. The single-crystal structural results for $Ba_{11}FeTi_{27}O_{66.5}$ indicate that one of these sites is partially occupied, and that the basic structural formula for this phase is $A_{11}B_{28}O_{66+x}$, where A = Ba^{2+} and B = Ti^{4+} substituted with a small amount (<10 atom%) of a trivalent metal, which determines the value of x. The stoichiometry, or x-value, of the phase prepared in polycrystalline form at 1260 °C is slightly different from that of the crystals grown by cooling from 1390 °C, and occurs between the compositions $Ba_{11}FeTi_{27}O_{66.5}$ and $Ba_{11}Fe_2Ti_{26}O_{66}$. This variation in oxygen content and Fe/Ti ratio suggests that the partial occupancy site factor depends on the synthesis temperature. Interestingly, the phase apparently forms as a point compound in the subsolidus, with little or no solid solution formation. Analysis of the structural details using the bond valence method revealed one unusual B site, which was relatively expanded and isolated within the structure. This site is probably preferentially occupied by the larger, lower-valent Fe^{3+} cations. The crystal structure obtained here for $Ba_{11}FeTi_{27}O_{66.5}$ is essentially identical to that proposed earlier for "Zr^{4+}-stabilized $Ba_2Ti_5O_{12}$"[9,15] crystals. The phase originally reported as "$Ba_2Ti_5O_{12}$"[10] is actually a ternary compound, which forms upon addition (either deliberately or inadvertently via, e.g., ball-milling) of a trivalent ion such as Fe^{3+} or Al^{3+}. The specimens $Ba_{11}Al_2Ti_{26}O_{66}$ $Ba_{11}Al_2Ti_{24}Sn_2O_{66}$, and $Ba_{11}Al_2Ti_{24}Zr_2O_{66}$ were also prepared, and were found to form the $A_{11}B_{28}O_{66+x}$-type phase.

$Ba_{11}FeTi_{27}O_{66.5}$ was found to exhibit paramagnetic behavior above about 75 K. Application of the Curie−Weiss formalism to the $1/\chi$ vs. T data above 75 K yielded an effective moment consistent with the presence of high-spin Fe^{3+}, and a negative Weiss constant (about −25 K) indicating weak cooperative magnetic interactions that are overall antiferromagnetic. The relative permittivity and dielectric loss tangent of a sintered polycrystalline disk were measured at 5.33 GHz, yielding values (corrected for theoretical density) of 55 and 7.7(±0.3) × 10^{-4}, respectively.

Experimental Section

Dark reddish-brown polycrystalline $Ba_{11}FeTi_{27}O_{66.5}$ was prepared by solid-state reaction of reagent-grade $BaCO_3$, Fe_2O_3, and phosphate-free TiO_2 in air in the molar ratio $BaO:Fe_2O_3:TiO_2$ = 0.28:0.02:0.70. Prior to each heating, the sample was ground for 15−20 min with an agate pestle and mortar, pressed into pellets, and placed on sacrificial powder of the same composition in an alumina combustion boat. After an initial overnight calcine at 1000 °C, four one-week heatings at 1260 °C resulted in a well crystallized, nearly single-phase* sample (10-g scale) [* the pattern contains two weak peaks (I_{rel} < 0.8%), which can be attributed to $Ba_6Ti_{17}O_{40}$. Detection of small amounts of the phase $Ba_4Fe_2Ti_{10}O_{27}$ was precluded by peak overlap with the title phase]. Dark red platelet-like single crystals were obtained by slowly cooling (1 °C/h) a slightly non-stoichiometric liquid ($BaO:Fe_2O_3:TiO_2$ = 0.28:0.02:0.70) from 1390 °C to 1260 °C, followed by step-cooling to 800 °C, and then air-quenching. Samples were contained in platinum capsules (2.6 mm i.d.) open to the air. Crystals were harvested from dark prismatic chunks obtained by breaking the crystallized reaction mass, and were then characterized by the precession camera method (Zr-filtered Mo-K_α radiation) to assess quality, approximate cell parameters, and space group.

Single-crystal X-ray diffraction data were obtained with an Enraf−Nonius CAD-4 diffractometer (certain commercial equipment is identified in order to adequately specify the experimental procedure; recommendation or endorsement by the National Institute of Standards and Technology is not therein implied) using graphite-monochromated Mo-K_α radiation. A Gaussian integration absorption correction was applied to all measured intensities. Calculations were carried out using the NRCVAX[19] suite of programs. The structure was solved using Patterson and Fourier methods. Octahedral sites were assumed to be randomly occupied by Ti^{4+} and a small amount (< 10 atom%) of Fe^{3+}. Since the contrast between Fe and Ti by X-ray diffraction is small, no attempt was made to directly refine their relative occupancies, and the scattering factor for Ti was used for atoms occupying the octahedral sites. The overall stoichiometry of the phase reported here was then deduced by simultaneous consideration of the following: 1) the disappearing phase method,[3] 2) charge balance in the presence of trivalent iron and tetravalent titanium, and 3) the degree of site occupancy of oxygen as indicated by the single-crystal X-ray diffraction data.

X-ray powder diffraction data were collected using a Philips diffractometer equipped with incident soller slits, theta-compensating slits, a 0.2 mm receiving slit, a graphite monochromator, and a scintillation detector. Data were collected at ambient temperature using Cu-K_α radiation with a 0.01° 2θ step size, and a 2 s count time. The sample was mounted in a welled glass slide. Intensity data, measured as relative peak heights above the background of hand-picked peaks, were obtained using the Jade 6 program suite. The observed 2θ line positions reported here were corrected using SRM 660, LaB_6,[20] as an external calibrating agent. The unit cell was refined from the corrected powder diffraction data (2θ values; Cu-$K_{\alpha 1}$ = 1.540593 Å) using the least-squares program CELLSVD.[21] During the refinement, the indices of selected peaks were fixed in

 © 2004 Wiley-VCH Verlag GmbH & Co. KGaA, Weinheim

accordance with the powder pattern calculated using the results of the single-crystal X-ray study and the Jade program jPOWD.

The conditions used for the single-crystal structure determination are given in Table 4. Further details of the crystal-structure investigation may be obtained from the Fachinformationszentrum Karlsruhe, 76344 Eggenstein-Leopoldshafen, Germany, on quoting depository number CSD-413889.

Table 4. Experimental details for the single-crystal X-ray diffraction study of $Ba_{11}FeTi_{27}O_{66.5}$

Crystal system	Monoclinic
Space group	*C 2/m*
Cell parameters	a = 23.321(2) Å b = 11.384(1) Å c= 9.847(1) Å β = 90.09(1) ° V = 2614.2(8) Å^3
Z	2
$\rho_{calcd.}$ [g cm^{-3}]	4.98
Crystal dimensions [mm]	0.1 × 0.1 × 0.03
μ [mm^{-1}]	12.22
2θ (max)	60°
Scan mode	T-scan
Reflections measured	15759
Unique reflections	3954
Reflections observed	1656
Transmission factors	0.15−0.31
Number of parameters	157
R_F	0.088
wR_F	0.065

Magnetization was measured using a Quantum Design SQUID (Superconducting Quantum Interference Device) magnetometer. Measurements were made on a polycrystalline sample in a field of 0.5 Tesla between 400 K and 5 K. Magnetization measurements were carried out in fields up to 4 Tesla.

Permittivity and dielectric loss tangent measurements were performed at 5.33 GHz under ambient conditions using a sintered polycrystalline disk, approximately 11 mm in diameter and 87% dense. As described previously,[6,7] a dielectric resonator technique utilizing higher-order $TE_{0\gamma\nu}$ modes was used that allows the measurement of dielectric properties of a single sample at several contiguous frequency sub-bands. Corrections to the crystallographic density were incorporated by estimating the pore volume of the sample (from size and mass), and applying the Bruggeman effective medium formulation[22] for a two-phase composite. Uncertainties in the measurement of pore volume suggest a realistic accuracy limit for the permittivity values of ±10%, confirmed by measurements of similarly dense test samples such as $LaAlO_3$,[6] for which reliable single-crystal data are available.

[1] G. Geiger, *Bull. Am. Ceram. Soc.* **1994**, *73*, 57−61.
[2] T. Abraham, *Bull. Am. Ceram. Soc.* **1994**, *73*, 62−65.
[3] T. A. Vanderah, J. M. Loezos, R. S. Roth, *J. Solid State Chem.* **1996**, *121*, 38−50.
[4] I. E. Grey, C. Li, L. M. D. Cranswick, R. S. Roth, T. A. Vanderah, *J. Solid State Chem.* **1998**, *135*, 312−321.
[5] T. A. Vanderah, W. Wong-Ng, B. H. Toby, V. M. Browning, R. G. Geyer, R. D. Shull, R. S. Roth, *J. Solid State Chem.* **1999**, *143*, 182−197.
[6] T. A. Vanderah, W. Wong-Ng, Q. Huang, R. S. Roth, R. G. Geyer, R. B. Goldfarb, *J. Phys. Chem. Solids* **1997**, *58*, 1403−1415.
[7] T. Siegrist, T. A. Vanderah, A. P. Ramirez, R. G. Geyer, R. S. Roth, *J. Alloys and Comp.* **1998**, *274*, 169−178.
[8] J. Schmachtel, H. Mueller-Buschbaum, *Z. Anorg. Allg. Chem.* **1981**, *472*, 89−94.
[9] R. S. Roth, C. J. Rawn, C. G. Lindsay, W. Wong-Ng, *J. Solid State Chem.* **1993**, *104*, 99−118.
[10] G. H. Jonker, W. Kwestroo, *J. Am. Ceram. Soc.* **1958**, *41*, 390−397.
[11] T. Negas, R. S. Roth, H. S. Parker, D. B. Minor, *J. Solid State Chem.* **1974**, *9*, 297−307.
[12] H. M. O'Bryan Jr., J. Thomson, *J. Am. Ceram. Soc.* **1974**, *57*, 522−526.
[13] J. J. Ritter, R. S. Roth, J. E. Blendell, *J. Am. Ceram. Soc.* **1986**, *69*, 155−162.
[14] K. W. Kirby, B. A. Wechsler, *J. Am. Ceram. Soc.* **1991**, *74*, 1841−1847.
[15] R. S. Roth, J. H. Ritter, H. S. Parker, D. B. Minor, *J. Am. Ceram. Soc.* **1986**, *69*, 858−862.
[16] B. G. Gatehouse, G. Fallon, and R. S. Roth, unpublished results, **1986**.
[17] B. G. Gatehouse, private correspondence to R. S. Roth, Dec. 11, **1987**.
[18] R. D. Shannon, *J. Appl. Phys.* **1993**, *73*, 348−366.
[19] E. J. Gabe, Y. LePage, J.-P. Charland, F. L. Lee, P. S. White, *J. Appl. Crystallogr.* **1989**, *22*, 384−387.
[20] C. R. Hubbard, Y. Zhang, R. L. McKenzie, Certificate of Analysis, SRM 660, National Institute of Standards and Technology, Gaithersburg, MD, 20899 (**1989**).
[21] Program CELLSVD by C. K. Lowe-Ma, Naval Air Warfare Center Weapons Division Technical Publication 8128, September **1993**.
[22] R. G. Geyer, J. Mantese, J. Baker-Jarvis, *NIST Tech. Note 1371* (**1994**).
[23] N. E. Brese, M. O'Keeffe, *Acta Crystallogr., Sect. B* **1991**, *47*, 192−197; with updated r_0 parameters from http://www.ccp14.ac.uk/ccp/web-mirrors/i_d_brown/bond_valence_param/

Received December 17, 2003
Early View Article
Published Online May 5, 2004

 © 2004 Wiley-VCH Verlag GmbH & Co. KGaA, Weinheim

Electronic Structure of Transition Metal−Isocorrole Complexes: A First Quantum Chemical Study

Bart van Oort,[a] Espen Tangen,[a] and Abhik Ghosh*[a]

Keywords: Calculations / Corrole / Isocorrole / Non-innocent ligands / Radicals / Transition metals

DFT calculations indicate that the broad electronic-structural features of metalloisocorroles are rather similar to those of analogous metallocorroles. Thus, like their corrole analogues, many metalloisocorroles feature substantially non-innocent ligands. Another key point is that both corroles and isocorroles can exhibit at least two kinds of radical character, a_2 and b_1. However, corrole and isocorrole derivatives also differ significantly in a few ways: for example, the $S = 1/2$ CoPh complexes of corrole and isocorrole exhibit ground states of different symmetries ($^2A''$ and $^2A'$, respectively, in C_s notation), reflecting different interplays of metal(d_π)–ligand(p_π) interactions in corrole versus isocorrole derivatives. The ligand non-innocence phenomena encountered in this study are broadly reminiscent of similar phenomena in peroxidase compound I intermediates and their synthetic models. It seems reasonable, therefore, to adopt the view that this study, along with related studies on corrole derivatives, provides a broader chemical context for appreciating the electronic structures of high-valent heme protein intermediates.
(© Wiley-VCH Verlag GmbH & Co. KGaA, 69451 Weinheim, Germany, 2004)

Compared with the current explosion of research on corrole derivatives,[1] the chemistry of isocorrole derivatives has remained essentially unexplored since their initial synthesis and characterization by Vogel and co-workers in 1997.[2] In this context, we chose to map out the broad electronic-structural features of prototype isocorrole first-row transition-metal complexes, using density functional theory (PW91/TZP) calculations as the key tool.[3−7] While chiefly of interest to porphyrin chemists, we were gratified to find that the results impinge on a range of issues of broader interest. For example, we believe that the findings deepen our understanding of the electron distributions of high-valent transition-metal complexes and of the phenomenon of ligand non-innocence. Indirectly, the results also help place the electronic structures of high-valent heme protein intermediates in a broader chemical context.[8−12]

Our results on Sc(IsoC), Ga(IsoC), Ni(IsoC), and Cu(IsoC) (IsoC = isocorrolato) as well as analogous results on the corresponding corrole[13] complexes provide a good starting point for our discussion. Table 1 presents selected adiabatic[14] ionization potentials and excitation energies for these complexes. The results show that the two lowest ionized states of Sc(IsoC) and Ga(IsoC) are almost degenerate, as they are for the analogous corrole derivatives,[13] which is clearly reminiscent of the behavior of porphyrin A_{1u} and A_{2u} radicals.[15] Figure 1 depicts the open-shell orbitals of the $^2A_2$ and $^2B_1$ π-cation radical states of [Ga(IsoC)]$^+$ and of [Ga(Cor)]$^+$ and it is worth noting that the a_2 and b_1 orbitals crudely resemble the porphyrin a_{1u} and a_{2u} HOMOs in shape, respectively.[13] Another point worth noting is that the corrole and isocorrole ionization potentials (*IP*s) are significantly lower than those of analogous metalloporphyrins, that is, metallocorroles and metalloisocorroles are significantly easier to oxidize than the analogous metalloporphyrins.[13]

As in the case of Ni(Cor),[13] two Ni^{II} π-cation radical states compete as ground states for Ni(IsoC), the high-valent Ni^{III} state being more than 1 eV higher in energy. In contrast, high-valent Cu^{III} ground states are predicted for Cu(IsoC), with low-lying Cu^{II} π-cation radical states, which again parallels the situation with Cu−corroles.[13] However, a careful examination of Table 1 reveals an interesting twist in the Cu−isocorrole case. In the case of Cu−corroles, temperature-dependent NMR spectroscopy strongly suggests the presence of thermally accessible paramagnetic excited states, consistent with the DFT results.[16−18] In contrast, for Cu(IsoC), the Cu^{II} π-cation radical states are not as low in energy, relative to the ground state, as they are for Cu(Cor), suggesting that, unlike Cu−corroles, Cu−isocorroles may not exhibit significantly temperature-dependent NMR spectra.

Table 2 presents some key structural parameters of the optimized geometries of the molecules studied in this work. All the isocorrole derivatives exhibit slightly but consistently shorter metal−nitrogen distances than the corresponding corrole derivatives. In particular, the

[a] Department of Chemistry, University of Tromsø, 9037 Tromsø, Norway
Supporting information for this article is available on the WWW under http://www.eurjic.org or from the author.

 © 2004 Wiley-VCH Verlag GmbH & Co. KGaA, Weinheim **DOI: 10.1002/ejic.200300949**

Table 1. Relative energies [eV] of different electronic states of metalloisocorroles and metallocorroles

Species studied[a][b]	State	*E* [eV] Isocorrole	Corrole
$Sc^{III}(L)$	$^1A_1$	0.0000	0.0000
$[Sc^{III}(L)]^+$	$^2B_1$	6.5730	6.3644
$[Sc^{III}(L)]^+$	$^2A_2$	6.6641	6.7080
$[Sc^{III}(L)]^-$	$^2B_1$	−1.5260	−1.1558
$Ni^{III}(L)$	$^2A_1$	1.3075	1.2705
$Ni^{II}(L^{\cdot})$	$^2B_1$	0.0000	0.0174
$Ni^{II}(L^{\cdot})$	$^2A_2$	0.1373	0.0000
$Cu^{III}(L)$	$^1A_1$	0.0000	0.0000
$Cu^{II}(L^{\cdot})$	$(x^2-y^2)^1a_2^1$ ($^3B_1$)	0.4084	0.3551
$Cu^{II}(L^{\cdot})$	$(x^2-y^2)^1b_1^1$ ($^3A_2$)	0.3033	0.1618
$Ga^{III}(L)$	$^1A_1$	0.0000	0.0000
$[Ga^{III}(L)]^+$	$^2B_1$	6.6658	6.6270
$[Ga^{III}(L)]^+$	$^2A_2$	6.7152	6.7007
$[Ga^{III}(L)]^-$	$^2B_1$	−1.5522	−0.8830

[a] L = corrolato or isocorrolato. [b] Note that although the electron affinities of Sc(L) and Ga(L) have been computed, they are not explicitly commented upon in this paper.

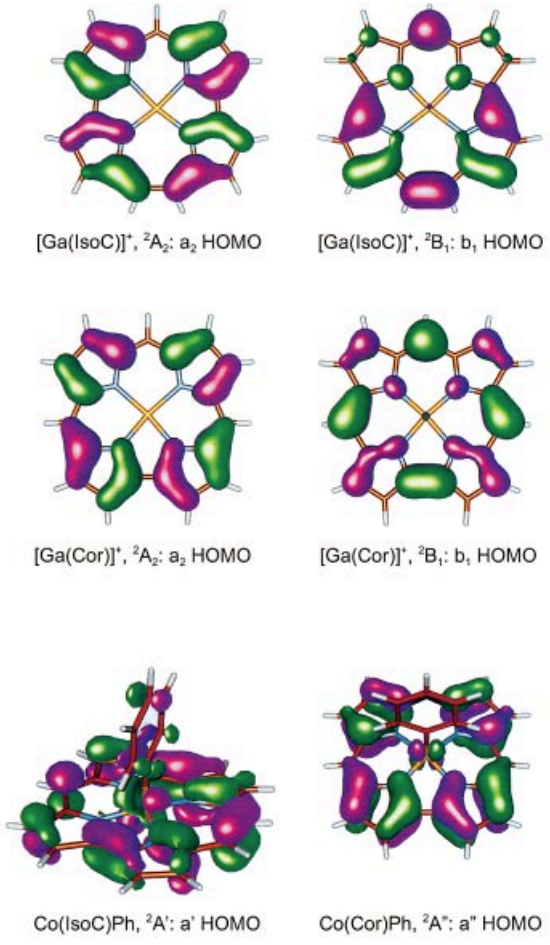

Figure 1. Majority-spin HOMOs of $[Ga(IsoC)]^+$ and $[Ga(Cor)]^+$, Co(IsoC)Ph and Co(Cor)Ph

metal−nitrogen distances in Cu(IsoC) are 0.02−0.03 Å shorter than those in Cu(Cor). This may well explain the greater stability of the d^8 Cu^{III} state, relative to Cu^{II} π-cation radical states, in the isocorrole case than in the corrole case.[13]

We are now in a position to discuss some of the intricacies of the electron distributions of corrole and isocorrole middle transition metal derivatives.[19−24] Figure 2 depicts the Mulliken spin populations of different M(IsoC)X complexes (M = Mn, Fe; X = Cl, Ph), along with those of the $^2A_2$ and $^2B_1$ π-cation radical states of $[Ga(IsoC)]^+$, for comparison. The notable point here is that the isocorrole macrocycle in the case of the M(IsoC)Cl (M = Mn, Fe) complexes carries significant minority spin-density distributed roughly in the form of the isocorrole b_1 HOMO. In other words, the electronic structures of these complexes may be viewed in terms of an $S = 2$ Mn^{III} or an $S = 3/2$ Fe^{III} center antiferromagnetically coupled to an isocorrole b_1 radical. In contrast, the isocorrole ligand in the case of M(IsoC)Ph (M = Mn, Fe) carries little spin-density and the metal center in these species is best viewed as "truly" high-valent, i.e. Mn^{IV} and Fe^{IV}. These findings closely parallel similar findings on corrole−Mn and −Fe derivatives.[25]

The electronic structures of Co(IsoC)Ph and Co(Cor)Ph appear to be of particular interest.[26,27] First, the electron spin-density profiles (Figure 2) are qualitatively different from those found in the Mn and Fe complexes. Thus, the corrole[27] or isocorrole ligand in the cobalt complexes carries large amounts of majority spin; indeed, the single unpaired electron spin appears to be roughly evenly distributed between the Co center and the macrocycle in these complexes as a result of a Co(d_π)−macrocycle(π) orbital interaction. Figure 1 depicts the majority-spin HOMOs of Co(IsoC)Ph and Co(Cor)Ph. The shapes of these MOs resemble the spin-density profiles of the two compounds, which reveals an interesting point: while the corrole a_2 HOMO (a″ in C_s) is largely responsible for ligand radical character in Co(Cor)Ph, the isocorrole b_1 (a′ in C_s) HOMO plays that role in Co(IsoC)Ph.

Overall, the broad electronic-structural features of metalloisocorroles are rather similar to those of the analogous metallocorroles. Thus, like their corrole analogues, many metalloisocorroles feature substantially non-innocent ligands. Another significant point is that both corroles and isocorroles can exhibit at least two kinds of radical character: a_2 and b_1. Having emphasized the similarities, we need to note that corrole and isocorrole derivatives also differ significantly in a few ways. For example, as mentioned above, the $S = 1/2$ CoPh complexes of corrole and isocorrole exhibit ground states of different symmetries ($^2A''$ and $^2A'$, respectively, in C_s notation), reflecting different interplays of metal(d_π)−ligand(p_π) interactions in corroles versus isocorrole derivatives. We believe that these results broaden our understanding of high-valent transition-metal complexes and of ligand non-innocence. The ligand non-innocence phenomena encountered in this study are broadly reminiscent of similar phenomena in peroxidase

 © 2004 Wiley-VCH Verlag GmbH & Co. KGaA, Weinheim

Table 2. Comparison of selected optimized geometrical parameters [Å] of the Ga, Sc, Cu, Mn, Fe and Co complexes of isocorrole and corrole

Central atom[a]	$d(M-N_1)$[b] (IsoC)	(Cor)	$d(M-N_2)$[b] (IsoC)	(Cor)	Mean $d(M-N)$[c] (IsoC)	(Cor)	$d(M-N_4)$[c] (IsoC)	(Cor)
Ga	1.906	1.911	1.905	1.924	1.906	1.918	0.000	0.000
Sc	1.823	1.943	1.873	2.049	1.848	2.016	0.000	0.000
Cu (Cu^{III})	1.839	1.887	1.874	1.864	1.857	1.876	0.000	0.000
Cu (Cu^{II} a_2 radical)	1.896	1.926	1.916	1.923	1.906	1.925	0.000	0.000
Cu (Cu^{II} b_1 radical)	1.900	1.915	1.909	1.913	1.905	1.914	0.000	0.000
MnPh (I)	1.894	1.918	1.917	1.922	1.901	1.920	0.353	0.344
MnPh (II)	1.893	1.916	1.913	1.925	1.903	1.921	0.329	0.347
FePh (I)	1.853	1.879	1.892	1.903	1.873	1.891	0.303	0.316
FePh (II)	1.851	1.882	1.893	1.930	1.872	1.906	0.282	0.340
CoPh (I)	1.832	1.858	1.884	1.888	1.858	1.873	0.194	0.211
CoPh (II)	1.830	1.860	1.883	1.890	1.857	1.875	0.165	0.224
MnCl	1.903	1.926	1.937	1.939	1.920	1.933	0.461	0.431
FeCl	1.837	1.893	1.920	1.926	1.894	1.910	0.426	0.407

[a] For the C_s metal-phenyl complexes, the axial phenyl group is perpendicular to the molecular symmetry plane for conformation I and lies in the molecular symmetry plane in conformation II. [b] The nitrogens referred to as N_1 belong to the pyrrole rings that are directly linked to the *meso*-carbon lying on a molecular symmetry plane, the other set of nitrogens being referred to as N_2. [c] "Mean $d(M-N)$" refers to the mean metal-nitrogen distance, while $d(M-N_4)$ refers to the out-of-plane displacement of the metal relative to the N_4 plane.

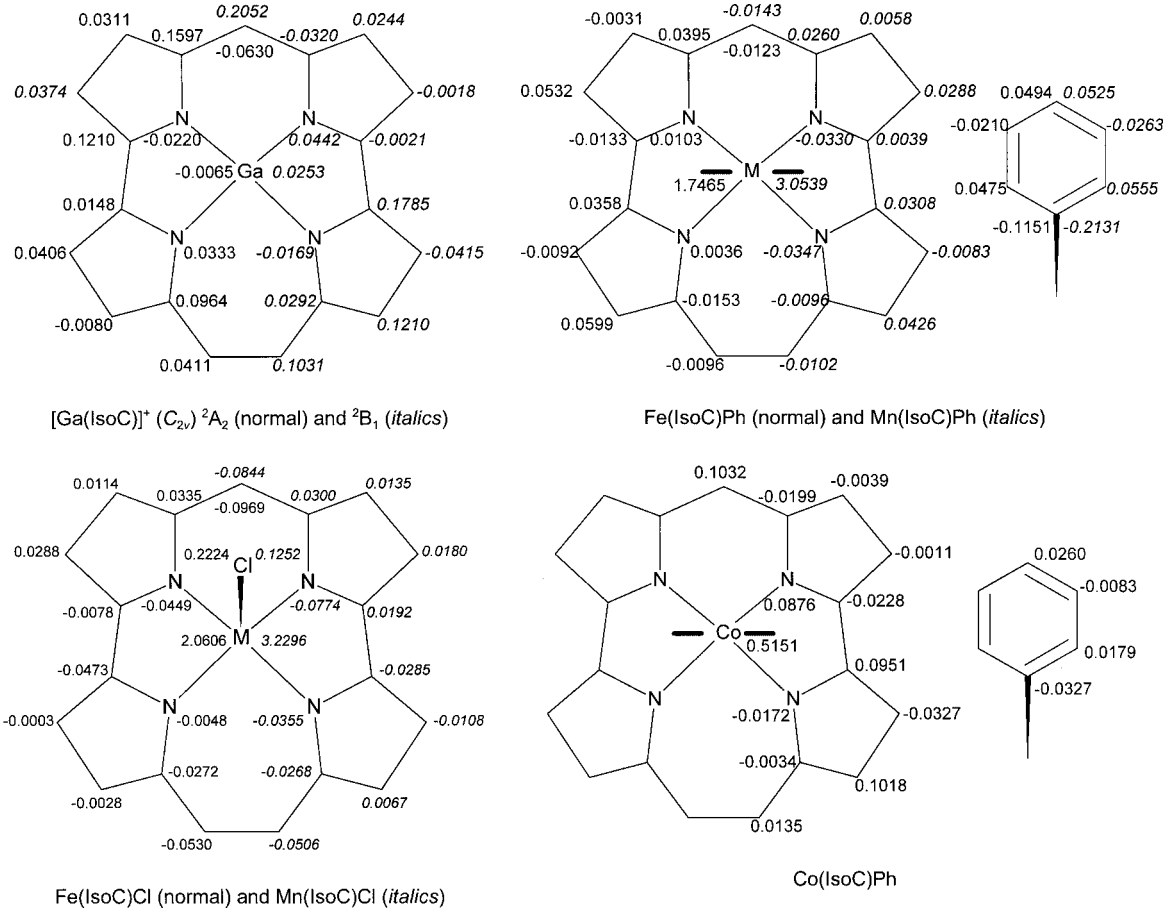

Figure 2. Gross atomic spin populations for selected molecules; note that certain atoms carry a significant minority spin population

compound I intermediates and their synthetic models. It seems reasonable to adopt the view, therefore, that this study, along with related studies on corrole derivatives, provides a broader chemical context for appreciating the electronic structures of high-valent heme protein intermediates.[28,29]

Supporting Information: Optimized Cartesian coordinates of the compounds studied. PW91/TZP atomic spin populations for relevant metallocorroles (see also footnote on the first page of this article).

Acknowledgments

This work was supported by the Norwegian Research Council and the VISTA program of Statoil and of the Norwegian Academy of the Sciences and Letters.

[1] [1a] For a review of recent, relevant synthetic developments, see: A. Ghosh, *Angew. Chem. Int. Ed.* **2004**, *43*, 1918; *Angew. Chem.* **2004**, *116*, 1952. [1b] C. Erben, S. Will, K. M. Kadish, in *The Porphyrin Handbook* (Eds.: K. M. Kadish, K. M. Smith, R. Guilard), Academic Press, San Diego, **2000**, chapter 11, p. 233−300.

[2] E. Vogel, B. Binsack, Y. Hellwig, C. Erben, A. Heger, J. Lex, Y.-D. Wu, *Angew. Chem. Int. Ed. Engl.* **1997**, *36*, 2612.

[3] All DFT calculations were carried out with the ADF program system using the gradient-corrected PW91 exchange-correlation functional, a spin-unrestricted formalism, Slater-type TZP basis sets, a fine mesh for numerical integration of matrix elements, and full geometry optimizations with tight convergence criteria. The theoretical methods used in ADF are discussed in: [3a] G. T. Velde, F. M. Bickelhaupt, E. J. Baerends, C. F. Guerra, S. J. A. Van Gisbergen, J. G. Snijders, T. Ziegler, *J. Comput. Chem.* **2001**, *22*, 931. [3b] S. J. A. Van Gisbergen, J. G. Snijders, E. J. Baerends, *Comput. Phys. Commun.* **1999**, *118*, 119. The ADF program system was obtained from Scientific Computing and Modeling, Department of Theoretical Chemistry, Vrije Universiteit, 1081 HV Amsterdam, The Netherlands.

[4] For a comparison of DFT (PW91 and B3LYP), CASPT2, and CCSD(T) studies on prototype transition metal complexes of bioinorganic relevance, see: A. Ghosh, P. R. Taylor, *Curr. Opin. Chem. Biol.* **2003**, *7*, 113.

[5] For an "early" review of DFT calculations on porphyrins, see: A. Ghosh, *Acc. Chem. Res.* **1998**, *31*, 189.

[6] Another review of DFT calculations on porphyrins: A. Ghosh, in *The Porphyrin Handbook* (Eds.: K. M. Kadish, K. M. Smith, R. Guilard), Academic Press, **2000**, vol. 7, pp. 1−38.

[7] For a recent review on DFT calculations on high-valent metalloporphyrins, see: A. Ghosh, E. Steene, *J. Biol. Inorg. Chem.* **2001**, *6*, 739.

[8] R. J. Deeth, *J. Am. Chem. Soc.* **1999**, *121*, 6074.

[9] Green has made a series of important contributions to this subject. See his latest contribution and references cited therein: M. T. Green, *J. Am. Chem. Soc.* **2001**, *123*, 9218.

[10] F. Ogliaro, S. P. de Visser, J. T. Groves, S. Shaik, *Angew. Chem. Int. Ed.* **2001**, *40*, 2874. For a correction, see: *Angew. Chem. Int. Ed.* **2001**, *40*, 3503.

[11] F. Ogliaro, S. Cohen, M. Filatov, N. Harris, S. Shaik, *Angew. Chem. Int. Ed.* **2001**, *40*, 647.

[12] For a comment on ref.[8], see: T. Vangberg, A. Ghosh, *J. Am. Chem. Soc.* **1999**, *121*, 12154.

[13] A. Ghosh, T. Wondimagen, A. B. J. Parusel, *J. Am. Chem. Soc.* **2000**, *122*, 5100.

[14] Some of the energetics data given in Table 1 differ slightly from those given in ref.[13] because, whereas here we report adiabatic *IP*s and excitation energies, vertical values are reported in ref.[13]

[15] For a recent study, see: T. Vangberg, A. Ghosh, *J. Am. Chem. Soc.* **2002**, *124*, 8122.

[16] S. Will, J. Lex, E. Vogel, H. Schmickler, J.-P. Gisselbrecht, C. Haubtmann, M. Bernard, M. Gross, *Angew. Chem. Int. Ed. Engl.* **1997**, *36*, 357.

[17] I. H. Wasbotten, T. Wondimagegn, A. Ghosh, *J. Am. Chem. Soc.* **2002**, *124*, 8104.

[18] C. Brückner, C. A. Barta, R. P. Brinas, J. A. K. Bauer, *Inorg. Chem.* **2003**, *42*, 1673.

[19] E. Vogel, S. Will, A. Schulze Tilling, L. Neumann, J. Lex, E. Bill, A. X. Trautwein, K. Wieghardt, *Angew. Chem. Int. Ed. Engl.* **1994**, *106*, 771.

[20] S. Cai, F. A. Walker, S. Licoccia, *Inorg. Chem.* **2000**, *39*, 3466.

[21] E. Steene, T. Wondimagegn, A. Ghosh, *J. Phys. Chem. B* **2001**, *105*, 11406. Addition/correction: *J. Phys. Chem. B* **2002**, *106*, 5312.

[22] A. Ghosh, E. Steene, *J. Inorg. Biochem.* **2002**, *91*, 423.

[23] O. Zakharieva, V. Schunemann, M. Gerdan, S. Licoccia, S. Cai, F. A. Walker, A. X. Trautwein, *J. Am. Chem. Soc.* **2002**, *124*, 6636.

[24] E. Steene, A. Dey, A. Ghosh, *J. Am. Chem. Soc.* **2003**, *125*, 16300.

[25] Atomic spin populations for selected metallocorrole derivatives are shown in Figure S1 in the Supporting Information.

[26] S. Will, J. Lex, E. Vogel, V. A. Adamian, E. Van Caemelbecke, K. M. Kadish, *Inorg. Chem.* **1996**, *35*, 5577.

[27] J. Harmer, S. Van Doorslaer, I. Gromov, M. Bröring, G. Jeschke, A. Schweiger, *J. Phys. Chem. B* **2002**, *106*, 2801.

[28] For a recent, pertinent study, see: J. Conradie, A. Ghosh, *J. Phys. Chem. B.* **2003**, *107*, 6486.

[29] For a recent, pertinent study, see: J. Conradie, J. Swarts, A. Ghosh, *J. Phys. Chem. B.* **2004**, *108*, 452.

Received December 17, 2003
Early View Article
Published Online April 20, 2004

 © 2004 Wiley-VCH Verlag GmbH & Co. KGaA, Weinheim

Inclusion Complexes of the Bicyclic Aryl-Substituted Sulfur-Nitrogen Compounds Ar−CN_5S_3 with Fluorocarbon and Hydrocarbon Aromatics

Carsten Knapp,[a] Enno Lork,[a] Rüdiger Mews,*[a] and Andrey V. Zibarev*[b]

Keywords: Polyfluoroaromatic compounds / Inclusion compounds / π-Stacking interactions / Molecular recognition / Crystal engineering

Inclusion compounds with a stoichiometry of 2:1 were prepared from 7-Ar-1λ⁴,3λ⁴,5λ⁴-trithia-2,4,6,8,9-pentaazabicyclo[3.3.1]nona-1(9),2,3,5,7-pentaenes Ar–CN_5S_3 and hexafluorobenzene (Ar = C_6H_5, 4-$CH_3C_6H_4$, 4-$C_6H_5C_6H_4$ and 2,6-$F_2C_6H_3$) and toluene (Ar = C_6F_5), by crystallization of the bicycles from the corresponding aromatics. Similar to the pure host compounds, the bicycles in the inclusion compounds form centrosymmetric dimers. The packing of the dimers in the pure host compounds is dominated by the interaction of the substituents at the aryl groups, and in the inclusion compounds by the interaction of the host and guest. The parallel-displaced arrangement of the aromatic rings of the host and guest is typical of non-covalent π-stacking interactions of the arene-polyfluroarene type. The inability of benzene (in contrast to hexafluorobenzene) to form an inclusion compound with the title bicycle (Ar = C_6H_5) indicates that inclusion is driven by π-stacking interactions of the arene-polyfluoroarene type. Crystallization of the title bicycle (Ar = C_6H_5) from a 1:1 molar mixture of benzene and hexafluorobenzene gave the same inclusion compound as the crystallization from pure hexafluorobenzene. This can be considered as molecular recognition based on π-stacking interactions. The compounds prepared provide the first example of aromatic units bearing extremely sterically demanding polyheteroatom bicyclic substituents involved in non-covalent arene-polyfluoroarene π-stacking interactions. Attempts to prepare inclusion compounds with octafluoronaphthalene and decafluorobiphenyl, as well as co-crystals of *para*-tolyl- and pentafluorophenyl-substituted bicycles, failed. The origin of the 2:1 stoichiometry and the lack of inclusion in the case of $C_{12}F_{10}$ and $C_{10}F_8$ are discussed.

(© Wiley-VCH Verlag GmbH & Co. KGaA, 69451 Weinheim, Germany, 2004)

Introduction

Non-covalent interactions[1] between aromatic groups,[2−5] including those between hydrocarbon and fluorocarbon counterparts featuring π-stacked arrangement (refs.[5−7] and references cited therein), are recognized to be one of the most general supramolecular motifs. The arene-polyfluoroarene π-stacking interactions are important not only in fundamental research but also in the design and synthesis of advanced functional materials (for example, nematic[8] and discotic[9] liquid crystals, J aggregates,[10] photochromic crystals,[11] etc.).

Recently, we described 1:1 molecular complexes between octafluoronaphthalene and acyclic (Ar−N=S=N−Ar, Ar−N=S=N−$SiMe_3$) and heterocyclic (7-methyl-2,1-benzisothiazole) sulfur-nitrogen compounds featuring π-stacking interactions of the arene-polyfluoroarene type.[6,7] It follows from the results obtained that geometrical matching of the components of the complexes can be considered a less significant structural requirement.

In the context of crystal engineering, it is of obvious interest to investigate how broad the molecular diversity of aryl-substituted sulfur-nitrogen compounds involved in the arene-polyfluoroarene π-stacking interactions can be, with special emphasis on derivatives with enlarged spatial demand.

The present work deals with the preparation and X-ray structural characterization of the molecular complexes of the aryl-substituted sulfur-nitrogen derivatives Ar−CN_5S_3 (7-aryl-1λ⁴,3λ⁴,5λ⁴-trithia-2,4,6,8,9-pentaazabicyclo[3.3.1]-nona-1(9),2,3,5,7-pentaenes) with aromatic compounds in both the fluorocarbon and hydrocarbon series.

Results and Discussion

The target complexes of the Ar−CN_5S_3 derivatives **1**−**4** (Ar = C_6H_5, 4-$CH_3C_6H_4$, 4-$C_6H_5C_6H_4$ and 2,6-$F_2C_6H_3$, respectively) with hexafluorobenzene were prepared (Scheme 1) as single crystals suitable for X-ray crystallography by crystallization of the compounds **1**−**4** from hexa-

[a] Institute for Inorganic and Physical Chemistry, University of Bremen,
28334 Bremen, Germany
Fax: (internat.) + 49-421/218-4267
E-mail: mews@chemie.uni-bremen.de
[b] Institute of Organic Chemistry, Russian Academy of Sciences, 630090 Novosibirsk, Russia
Fax: (internat.) + 7-3832/344-752
E-mail: zibarev@nioch.nsc.ru

 © 2004 Wiley-VCH Verlag GmbH & Co. KGaA, Weinheim **DOI: 10.1002/ejic.200300951**

fluorobenzene. All attempts to prepare similar complexes of decafluorobiphenyl and octafluoronaphthalene by co-crystallization of the components from organic solvents (cf. ref.[6]), including *n*-hexane, $CHCl_3$, THF and MeCN, failed.

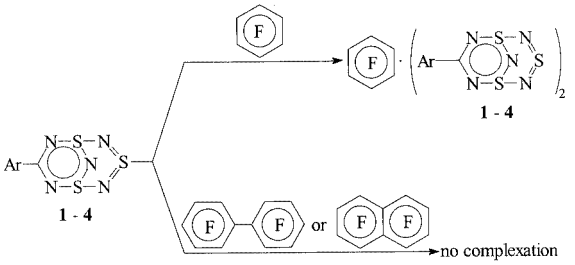

Ar = C_6H_5 (**1**), 4-$H_3CC_6H_4$ (**2**), 4-$C_6H_5C_6H_4$ (**3**), 2,6-$F_2C_6H_3$ (**4**)

Scheme 1. The circle in the dithiatriazine cycle of the bicycles means delocalization, not aromaticity

Single crystals, suitable for X-ray diffraction, of the complex of $C_6F_5-CN_5S_3$ (**5**) with toluene were obtained (Scheme 2) by low-temperature co-crystallization of the components from *n*-hexane. An attempt to co-crystallize compound **5** with compound **2** (which can be considered a toluene derivative) from THF was unsuccessful.

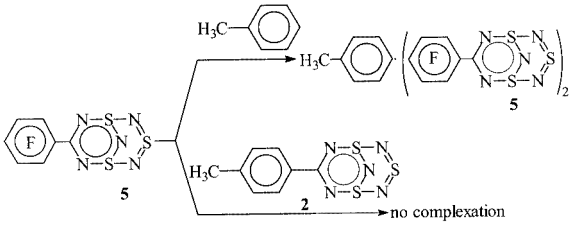

Scheme 2

According to the results from X-ray crystallography, all complexes of the Ar−CN_5S_3 derivatives with aromatic compounds prepared (both fluorocarbon and hydrocarbon) possess a 2:1 stoichiometry rather than the usual 1:1 stoichiometry (refs.[5−14] and references cited therein), despite the fact that the corresponding aromatics were used in the preparation as solvents, i.e. in a large molar excess. The detailed analysis of their crystal packing (see below) confirms the inclusion nature of the co-crystals. It was found that benzene, in contrast to hexafluorobenzene, under the same conditions, does not form an inclusion compound with **1**. This indicates directly the critical importance of the π-stacking interactions of the arene-polyfluoroarene type for the discussed inclusion compounds. Significantly, crystallization of compound **1** from a 1:1 molar mixture of benzene and hexafluorobenzene leads to the same C_6F_6·(**1**)$_2$ inclusion compound as the crystallization from pure hexafluorobenzene. This can be considered as molecular recognition based on π-stacking interactions (Scheme 3).

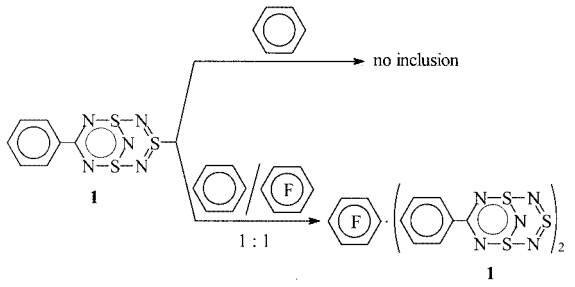

Scheme 3

Table 1 presents the crystal data and details of the structure refinements for the compounds C_6F_6·(**1**)$_2$, C_6F_6·(**2**)$_2$, C_6F_6·(**3**)$_2$, C_6F_6·(**4**)$_2$ and $CH_3C_6H_5$·(**5**)$_2$. For comparison, the structures of the pure host compounds **1** and **4** are given in Figure 1 and Figure 2**,** Figure 3−5 present the crystal packing of the inclusion compounds. The interactions of the π-systems in the crystals of C_6F_6·(**1**)$_2$ and $CH_3C_6H_5$·(**5**)$_2$ are shown in Figure 6 and Figure 7. Relevant bond lengths and bond angles are listed only for C_6F_6·(**3**)$_2$ and $CH_3C_6H_5$·(**5**)$_2$, because the structures of the parent host compounds 4-$C_6H_5C_6H_4-CN_5S_3$ (**3**) and $C_6F_5-CN_5S_3$ (**5**) are not reported in the literature. Compared to the pure host compounds **1**, **2**, and **4** the geometries of the aryl-substituted bicycles remain nearly unchanged in the inclusion compounds.

For compound **1** ($C_6H_5-CN_5S_3$)[15,16] and its derivatives Ar−CN_5S_3,[17] two dominant modes of molecular packing are known (for an in-depth discussion, see ref.[17]). They are described as "stacking" (the sulfur-nitrogen rings of neighboring molecules fit into one another like stacked crates; short N···C and N···S contacts are found), and "dimerization" (two molecules are arranged with their heterocyclic heads facing each other centrosymmetrically; only short S···N contacts are observed). Both packing patterns can be rationalized by Coulombic interactions between the CN_5S_3 units as shown by the mapped electrostatic potential.[17] Most of the Ar−CN_5S_3 bicycles including **1**, **2** and **4** form centrosymmetric dimers. The interaction between the dimers is influenced by the geometry of the monomers (e.g. Figure 1 and Figure 2) and the interaction of the substituents at the aryl groups.

Despite the differences in the packing of the individual host compounds, the crystal packing of the C_6F_6·Ar−CN_5S_3 complexes and also of the inverse complex $CH_3C_6H_5$·$Ar_F-CN_5S_3$, are very similar (Figure 3−5). A closer look shows that complex formation does not influence the geometry of the monomeric Ar−CN_5S_3 species, the formation of the dimer is also not affected, but the interaction between the dimers is dominated by π-stacking. Small differences in the π-stacking arise from the geometry and the charge distribution in the aryl substituents. π-Stacking H···F contacts (considered as supramolecular synthons)[18] seem to be important for the arrangement in the solid state (a representative example is given in Figure 3). The inclusion nature of the synthesized compounds ex-

 © 2004 Wiley-VCH Verlag GmbH & Co. KGaA, Weinheim

Table 1. Crystal data and structure refinement for $C_6F_6 \cdot (\mathbf{1})_2$, $C_6F_6 \cdot (\mathbf{2})_2$, $C_6F_6 \cdot (\mathbf{3})_2$, $C_6F_6 \cdot (\mathbf{4})_2$ and $CH_3C_6H_5 \cdot (\mathbf{5})_2$

Compound	$C_6F_6 \cdot (\mathbf{1})_2$	$C_6F_6 \cdot (\mathbf{2})_2$	$C_6F_6 \cdot (\mathbf{3})_2$	$C_6F_6 \cdot (\mathbf{4})_2$	$CH_3C_6H_5 \cdot (\mathbf{5})_2$
Empirical formula	$C_7H_5N_5S_3 \cdot 0.5\ (C_6F_6)$	$C_8H_7N_5S_3 \cdot 0.5\ (C_6F_6)$	$C_{13}H_9N_5S_3 \cdot 0.5\ (C_6F_6)$	$C_6H_3F_2N_5S_3 \cdot 0.5\ (C_6F_6)$	$C_7F_5N_5S_3 \cdot 0.5\ (C_7H_8)$
Molecular mass	348.37	362.40	424.46	384.35	391.37
Temperature, K	173(2)	173(2)	173(2)	173(2)	173(2)
Wavelength, pm	71.073	71.073	71.073	71.073	71.073
Crystal system	triclinic	triclinic	triclinic	triclinic	triclinic
Space group	$P\bar{1}$	$P\bar{1}$	$P\bar{1}$	$P\bar{1}$	$P\bar{1}$
a, pm	601.0(2)	600.90(12)	602.90(10)	760.90(10)	612.40(12)
b, pm	747.00(10)	750.80(15)	751.70(10)	879.1(2)	789.70(16)
c, pm	1462.9(2)	1561.1(3)	1939.9(3)	1127.1(2)	1520.0(3)
α (°)	87.400(10)	81.38(3)	85.010(10)	110.610(10)	92.44(3)
β (°)	87.49(2)	87.97(3)	84.080(10)	94.520(10)	90.94(3)
γ (°)	72.58(2)	74.26(3)	70.720(10)	103.790(10)	109.18(3)
Volume, nm^3	0.6257(2)	0.6702(2)	0.8241(2)	0.6743(2)	0.6933(2)
Z	2	2	2	2	2
$D_{calcd.}$, $Mg \cdot m^{-3}$	1.849	1.796	1.711	1.893	1.875
Absorption coefficient (mm^{-1})	0.629	0.591	0.495	0.614	0.599
Crystal size (mm^3)	0.90 × 0.50 × 0.10	0.50 × 0.40 × 0.10	0.60 × 0.40 × 0.10	0.60 × 0.50 × 0.50	0.40 × 0.40 × 0.30
θ range for data collection (°)	2.79−27.50	2.64−26.08	2.11−27.50	2.58−27.50	2.68−26.06
Reflections collected	3740	9442	4946	3771	9783
Independent reflections	2868 [*R*(int) = 0.0219]	2423 [*R*(int) = 0.0532]	3795 [*R*(int) = 0.0303]	3022 [*R*(int) = 0.0151]	2513 [*R*(int) = 0.0528]
Completeness to θ,% (θ,°)	99.8 (27.50)	91.0 (26.08)	99.9 (27.50)	97.6 (27.50)	91.3 (26.06)
Data/restrains/ parameters	2868/0/192	2423/0/202	3795/0/245	3022/0/210	2513/0/247
Goodness-of-fit on F^2	1.049	1.009	1.033	1.096	1.016
Final *R* indices [$I > 2\sigma(I)$]	*R*1 = 0.0310, *wR*2 = 0.0822	*R*1 = 0.0361, *wR*2 = 0.0942	*R*1 = 0.0372, *wR*2 = 0.0906	*R*1 = 0.0311, *wR*2 = 0.0877	*R*1 = 0.322, *wR*2 = 0.0853
R indices (all data)	*R*1 = 0.0383, *wR*2 = 0.0865	*R*1 = 0.0472, *wR*2 = 0.0993	*R*1 = 0.0490, *wR*2 = 0.0965	*R*1 = 0.0322, *wR*2 = 0.0887	*R*1 = 0.0399, *wR*2 = 0.0888
Largest diff. peak and hole, eA^{-3}	0.440, −0.320	0.497, −0.254	0.355, −0.364	0.363, −0.328	0.388, −0.255

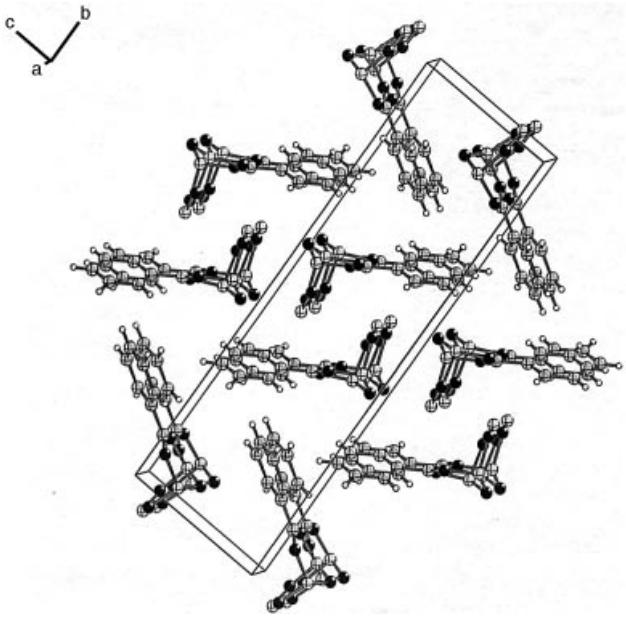

Figure 1. Crystal packing diagram of **1**[15,16]

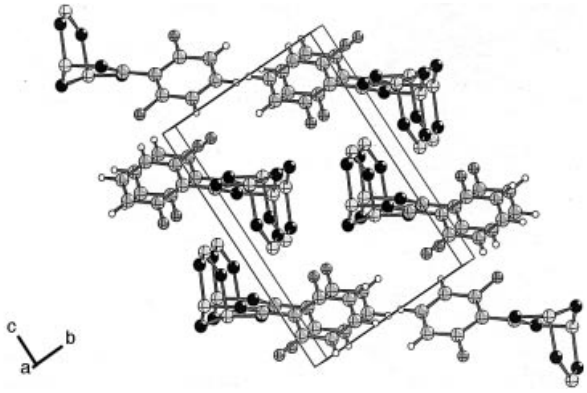

Figure 2. Crystal packing diagram of **4**[17]

plains the aforementioned unsuccessful co-crystallization with decafluorobiphenyl or octafluoronaphthalene since only the relatively small hexafluorobenzene and toluene molecules fit into the van der Waals holes in the co-crystals with **1**−**5**.

The 2:1 stoichiometry observed in the $(Ar-CN_5S_3)_2 \cdot C_6F_6$ and $(Ar_F-CN_5S_3)_2 \cdot C_6H_5CH_3$ compounds results from the non-equivalence of the two sides of the aryl ring planes in the bicycles. In the co-crystals, both the hexafluorobenzene and toluene groups interact with the side of the aryl ring of the $Ar-CN_5S_3$ species that is opposite to the N=S=N fragment (Figure 3−5). In the case of **3,** which possesses two non-equivalent aromatic rings, only the monosubstituted ring is involved in the inter-

 © 2004 Wiley-VCH Verlag GmbH & Co. KGaA, Weinheim

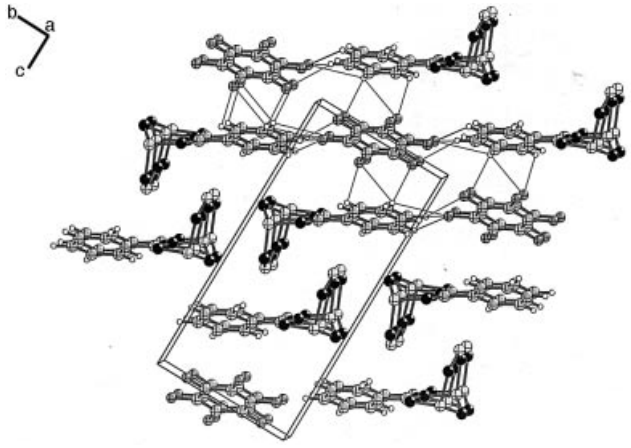

Figure 3. Crystal packing diagram of $C_6F_6{\cdot}(\mathbf{1})_2$ (molecular geometry of $\mathbf{1}$[15,16])

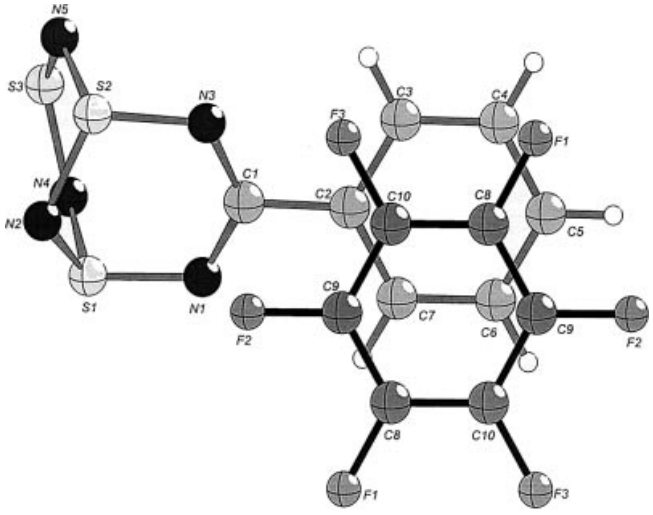

Figure 6. Arene-perfluoroarene overlap in $C_6F_6{\cdot}(\mathbf{1})_2$

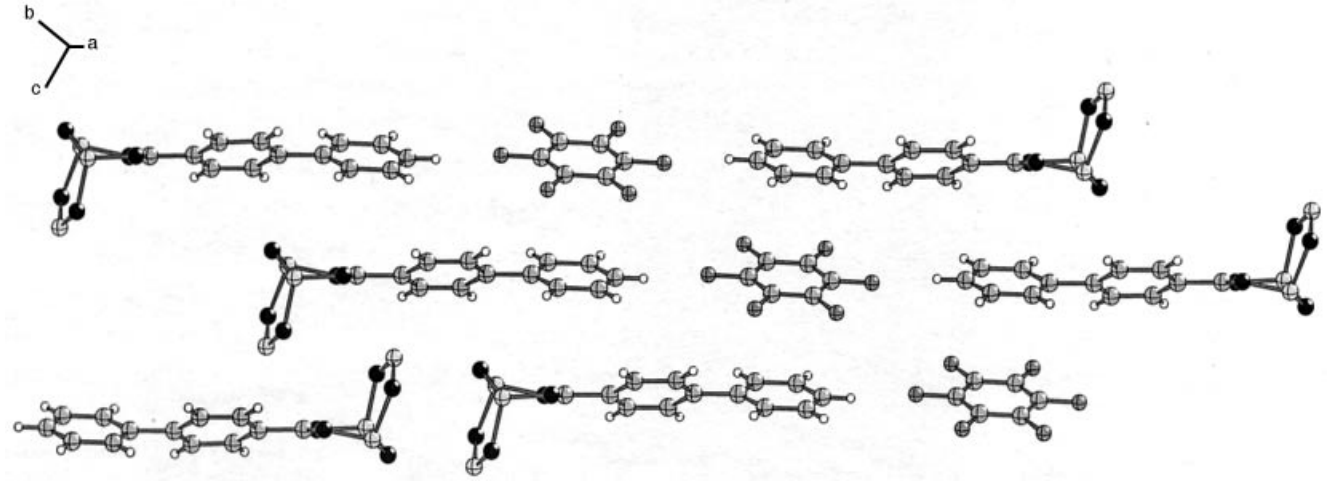

Figure 4. Crystal packing diagram of $C_6F_6{\cdot}(\mathbf{3})_2$; selected bond lengths (pm), bond and dihedral angles (°) of **3** (for atom numbering, see Figure 6): C(1)−N(1) 134.1(2), C(1)−N(3) 133.9(2), C(1)−C(2) 148.9(3), N(3)−S(2) 162.70(17), S(1)−N(1) 162.37(17), S(1)−N(2) 163.21(17), S(1)−N(4) 173.29(19), N(2)−S(2) 163.38(17), S(2)−N(5) 173.29(18), N(4)−S(3) 154.94(18), S(3)−N(5) 155.46(18); N(1)−C(1)−N(3) 130.06(18), N(3)−C(1)−C(2) 114.26(17), N(1)−C(1)−C(2) 115.67(17), C(1)−N(3)−S(2) 120.82(14), N(1)−S(1)−N(2) 108.63(9), N(1)−S(1)−N(4) 103.19(9), N(2)−S(1)−N(4) 106.05(9), S(1)−N(2)−S(2) 111.66(10), N(3)−S(2)−N(2) 110.06(9), N(3)−S(2)−N(5) 101.69(9), N(2)−S(2)−N(5) 105.57(9), C(1)−N(1)−S(1) 117.22(14), S(3)−N(4)−S(1) 122.55(11), N(4)−S(3)−N(5) 119.09(10), S(3)−N(5)−S(2) 117.76(10); *dihedral angle* between aromatic rings 39.7

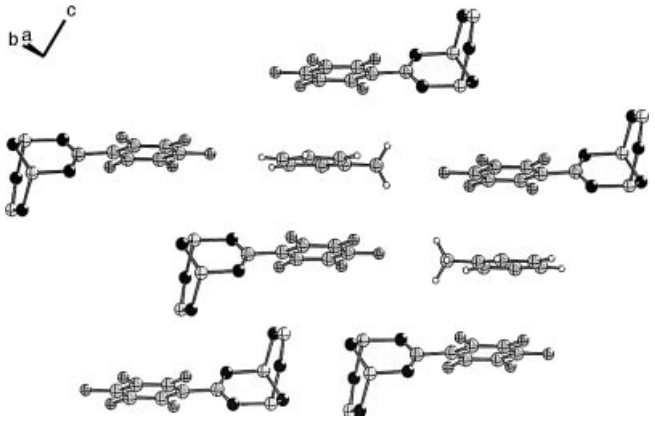

Figure 5. Crystal packing diagram of $CH_3C_6H_5{\cdot}(\mathbf{5})_2$

actions (Figure 4). All co-crystals demonstrate a parallel-displaced arrangement of the aromatics, i.e. face-to-face π-stacking of the aromatic rings of the bicycles with a ring of a second partner showing some offset of the interacting rings (Figure 6 and Figure 7). In $CH_3C_6H_5{\cdot}(\mathbf{5})_2$ the toluene molecules are highly disordered.

The dihedral angle between the planes of the cofacial hydrocarbon and fluorocarbon rings (the tilt) is 6.8, 8.6, 6.0, 12.7, and 5.8° for $C_6F_6{\cdot}(\mathbf{1})_2$, $C_6F_6{\cdot}(\mathbf{2})_2$, $C_6F_6{\cdot}(\mathbf{3})_2$, $C_6F_6{\cdot}(\mathbf{4})_2$ and $CH_3C_6H_5{\cdot}(\mathbf{5})_2$, respectively. The arene-polyfluoroarene separation within the stacks varies between 352.0−381.6 (366.4), 347.5−403.6 (373.9), 353.8−378.9 (366.4), 346.8−403.5 (374.6) and 360.1−389.6 (378.3) pm, respectively (in brackets: distance between the centers of the rings which is not equal to the separation due to the offset and tilt). For comparison, this separation is 377 pm[12] for the lowest-temperature phase of the benzene-hexafluoroben-

 © 2004 Wiley-VCH Verlag GmbH & Co. KGaA, Weinheim

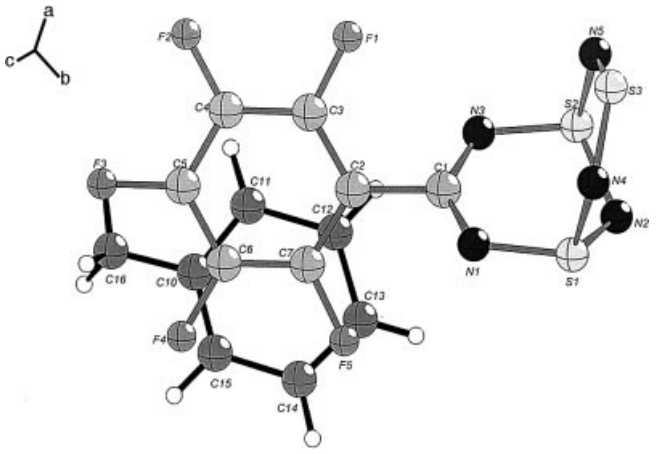

Figure 7. Arene-perfluoroarene overlap in $CH_3C_6H_5 \cdot (\mathbf{5})_2$; selected bond lengths (pm) and bond angles (°) of **5**: C(1)−N(1) 133.0(3), C(1)−N(3) 133.5(3), C(1)−C(2) 149.3(3), N(1)−S(1) 163.80(18), S(1)−N(2) 162.8(2), S(1)−N(4) 173.27(18), N(2)−S(2) 163.46(17), S(2)−N(3) 162.2(2), S(2)−N(5) 173.91(18), N(4)−S(3) 155.16(18), S(3)−N(5) 154.84(19), av. C−F 134.0; N(1)−C(1)−N(3) 131.88(19), N(1)−C(1)−C(2) 114.46(18), N(3)−C(1)−C(2) 113.64(17), C(1)−N(1)−S(1) 118.93(15), N(2)−S(1)−N(1) 110.44(9), N(2)−S(1)−N(4) 105.46(9), N(1)−S(1)−N(4) 101.37(9), S(1)−N(2)−S(2) 112.33(10), N(3)−S(2)−N(2) 109.76(9), N(3)−S(2)−N(5) 103.07(10), N(2)−S(2)−N(5) 105.17(9), C(1)−N(3)−S(2) 118.78(14), S(3)−N(4)−S(1) 119.99(11), N(5)−S(3)−N(4) 119.36(9), S(3)−N(5)−S(2) 120.81(10).

zene co-crystals, and 333−354 pm for the naphthalene−octafluoronaphthalene co-crystals at room temperature[13] and 327−352 pm for the low-temperature structure.[14] Such a parallel-displaced arrangement is typical for this type of interaction since it diminishes the repulsive π-electron interactions, which are roughly proportional to the π-overlapping area. Thus, the compounds obtained possess all the typical characteristics of the stacking of six-membered aromatic rings in crystals.[19]

On the other hand, the stoichiometry of 2:1 arises from the stability of the packing motifs observed in the crystals of $Ar-CN_5S_3$ towards the incorporation of hexafluorobenzene or toluene molecules into their crystal lattices.

From this point of view, these compounds should be classified as inclusion compounds. It is well-known that the formation of inclusion compounds is possible even in the absence of attractive forces between host and guest. During crystal growth from solution, solvent molecules may be caught and held in intermolecular cavities as guests also through repulsive forces.[20] However, for the compounds discussed, inclusion is definitely driven by attractive[2,5] π-stacking interactions of the arene-polyfluoroarene type, as proved by the ability of the crystal lattice of compound **1** to recognize and discriminate benzene and hexafluorobenzene molecules.

It also follows from the data obtained that the molecular geometries of compounds **1**, **2** and **4** (known previously[15−17]) are practically not affected by the interaction with C_6F_6 (cf. similar observations were made for complexes of $C_{10}F_8$ [6]). In some cases (for example, compounds **3** and **5**), the co-crystals are much better suited for X-ray crystallography than crystals of the individual compounds of interest (including situations when one component is a liquid in its pure state; for example see refs.[6,7]); a methodology could be developed which uses these types of co-crystals for the structural characterization of aromatic compounds (including liquids) for which good quality single crystals are not available.

Conclusion

Inclusion compounds of aryl-substituted sulfur-nitrogen bicycles $Ar-CN_5S_3$ with fluorocarbon and hydrocarbon aromatics with 2:1 stoichiometry have been prepared for the first time. Their crystal structures demonstrate a parallel-displaced arrangement of the aromatic rings of the host and the guest typical of non-covalent π-stacking interactions of the arene-polyfluoroarene type. Thus, the compounds provide the first example of aromatic units bearing extremely sterically demanding polyheteroatom bicyclic substituents involved in non-covalent arene-polyfluoroarene π-stacking interactions. This confirms our earlier conclusion that the geometrical matching of the components of the complexes can be considered a less significant structural requirement and thus provides new and interesting prospects to crystal engineering based on the arene-polyfluoroarene π-stacking interactions. Molecular recognition and discrimination are also possible with the arene-polyfluoroarene π-stacking interactions in the $Ar-CN_5S_3$/arene/polyfluoroarene systems. Based on these findings, it seems possible that the π-stacking interactions of the arene-polyfluoroarene type might be used in solving some serious challenges of contemporary materials science. In particular, significant progress has been made during the last decade in the field of organic molecular magnets, especially those based on aryl-substituted thiazyl radicals such as 4-aryl-1,2,3,5-dithiadiazolyls, 1,2,3- and 1,3,2-benzodithiazolyls, including fluoro-containing derivatives. However, in the solid state, these radicals reveal a general tendency to form diamagnetic dimers by means of out-of-plane π*-π* interactions, leading to shortened intermolecular S···S and S···N contacts. The inhibition of the dimerization process is very important for further developments in the field.[21] One might try to overcome the dimerization process by utilizing π-stacking interactions of the arene-polyfluoroarene type in the solid state between aryl-substituted thiazyl radicals and suitable polyfluoroaromatics, and this can be a direction for further investigations in the field.

Experimental Section

Materials and Methods: The bicycles **1**−**5** were prepared by published methods.[15,17,22] Their inclusion compounds with the corresponding aromatics were prepared in an argon atmosphere. The melting points were taken on a Gallencamp Melting Point Apparatus in sealed capillaries. For all complexes, melting is accompanied by decomposition with gas evolution.

Preparation of $C_6F_6 \cdot (1)_2$, $C_6F_6 \cdot (2)_2$, and $C_6F_6 \cdot (3)_2$: Compounds **1**−**3** (0.5 mmol) were dissolved in 5 mL of boiling hexafluorobenzene.

 © 2004 Wiley-VCH Verlag GmbH & Co. KGaA, Weinheim

The solution was filtered hot and gradually cooled in a thermostat to 20 °C. During the cooling, orange-yellow crystals formed which were separated by filtration.

Complex $C_6F_6\cdot(\mathbf{1})_2$ formed transparent orange-yellow plates (0.15 g, 86%), m.p. 125−126 °C.

Complex $C_6F_6\cdot(\mathbf{2})_2$ formed transparent orange-yellow elongated thin plates (0.15 g, 83%), m.p. 143−144 °C.

Complex $C_6F_6\cdot(\mathbf{3})_2$ formed transparent orange-yellow needles (0.20 g, 94%), m.p. 149−150 °C.

Preparation of $C_6F_6\cdot(\mathbf{4})_2$: Compound **4** (0.15 g, 0.5 mmol) was dissolved in 2 mL of hot hexafluorobenzene. At 20 °C, 2 mL of *n*-hexane was added to this solution forming a two-layered system. After 2 days, after the diffusion of solvents had ceased, the crystals formed were filtered. Complex $C_6F_6\cdot(\mathbf{4})_2$ formed transparent orange prisms (0.12 g, 65%), m.p. 104−105 °C.

Preparation of $CH_3C_6H_5\cdot(\mathbf{5})_2$: Compound **5** (0.17 g, 0.5 mmol) was dissolved in 2 mL of hot toluene. At 20 °C, 2 mL of *n*-hexane was added to this solution forming a two-layered system, which was placed into a cryostat at −30 °C. After 2 weeks, the crystals formed were filtered. Complex $CH_3C_6H_5\cdot(\mathbf{5})_2$ formed large transparent orange-yellow needles (0.10 g, 50%) m.p. 123−124 °C.

Preparation of $C_6F_6\cdot(\mathbf{1})_2$ from C_6H_6/C_6F_6: Compound **1** (0.13 g, 0.5 mmol) was dissolved in 3 mL of a 1:1 molar mixture of boiling benzene and hexafluorobenzene. The solution was filtered while still hot and gradually cooled in a thermostat to 30 °C (i.e. above the reported m.p. of the $C_6H_6\cdot C_6F_6$ complex, 24 °C[23]). The crystals formed were filtered. The complex $C_6F_6\cdot(\mathbf{1})_2$ (0.16 g, 92%) isolated by this procedure was identical (unit cell parameters, m.p.) to that obtained by crystallization of **1** from pure hexafluorobenzene.

The crystallization of **1** from benzene did not lead to an inclusion compound. Only **1** was recovered.

X-ray Crystallographic Study: The crystallographic data were collected on a Siemens P4 diffractometer [$C_6F_6\cdot(\mathbf{1})_2$, $C_6F_6\cdot(\mathbf{3})_2$, $C_6F_6\cdot(\mathbf{4})_2$] or on a Stoe IPDS [$C_6F_6\cdot(\mathbf{2})_2$, $CH_3C_6H_5\cdot(\mathbf{5})_2$] using Mo-$K_\alpha$ (0.71073 Å) radiation with a graphite monochromator. Refinement was based on F^2; $R1 = \|F_o| - |F_c\|/|F_o|$; $wR2 = \{[w(F_o^2 - F_c^2)^2]/[w(F_o^2)^2]\}^{1/2}$. Programs used: SHELX-97[24] and DIAMOND.[25]

The single crystals of the inclusion compounds were prepared as described above. They were mounted on a thin glass fiber using KEL-F oil. The structures were solved by direct methods (SHELXS[24]). Subsequent least-squares refinements (SHELXL-97−2[24]) located the positions of the remaining atoms in the electron density maps. All non-H atoms were refined anisotropically.

CCDC-226030 [for $C_6F_6\cdot(\mathbf{1})_2$], -226031 [for $C_6F_6\cdot(\mathbf{2})_2$], -226032 [for $C_6F_6\cdot(\mathbf{3})_2$], -226033 [for $C_6F_6\cdot(\mathbf{4})_2$], and -226034 [for $CH_3C_6H_5\cdot(\mathbf{5})_2$] contain the supplementary crystallographic data for this paper. These data can be obtained free of charge at www.ccdc.cam.ac.uk/conts/retrieving.html [or from the Cambridge Crystallographic Data Centre, 12 Union Road, Cambridge CB2 1EZ, UK; Fax: (internat.) +44-1223/336-033; E-mail: deposit@ccdc.cam.ac.uk].

Acknowledgments

The authors are grateful to Mr. Peter Brackmann for technical assistance, and to the DFG, Germany (Project 436 RUS 113/486/0−2 R), and RFBR, Russia (Project 02−03−04001), for joint financial support of the work. Financial support by the FNK, University of Bremen, is also gratefully acknowledged.

[1] K. Müller-Dethlefs, P. Hobza, *Chem. Rev.* **2000**, *100*, 143−167.
[2] S. Tsuzuki, K. Honda, T. Uchimaru, M. Mikami, K. Tanabe, *J. Am. Chem. Soc.* **2002**, *124*, 104−112.
[3] C. A. Hunter, K. R. Lawson, J. Perkins, C. J. Urch, *J. Chem. Soc., Perkin Trans. 2* **2001**, 651−669.
[4] H. Adams, J.-L. Jimenez Blanco, G. Chessari, C. A. Hunter, C. M. R. Low, J. M. Sanderson, J. G. Vinter, *Chem. Eur. J.* **2001**, *7*, 3494−3503.
[5] S. Lorenzo, G. R. Lewis, I. Dance, *New J. Chem.* **2000**, *24*, 295−304.
[6] I. Yu. Bagryanskaya, Yu. V. Gatilov, E. Lork, R. Mews, M. M. Shakirov, P. G. Watson, A. V. Zibarev, *J. Fluorine Chem.* **2002**, *116*, 149−156.
[7] E. Lork, R. Mews, M. M. Shakirov, P. G. Watson, A. V. Zibarev, *Eur. J. Inorg. Chem.* **2001**, 2123−2134.
[8] C. Dai, P. Nguyen, T. B. Marder, A. J. Scott, W. Clegg, C. Viney, *Chem. Commun.* **1999**, 2493−2494.
[9] M. Weck, A. R. Dunn, K. Matsumoto, G. W. Coates, E. B. Lobkovsky, R. H. Grubbs, *Angew. Chem. Int. Ed.* **1999**, *38*, 2741−2745.
[10] W. J. Feast, P. W. Loevenich, H. Puschmann, C. Taliani, *Chem. Commun.* **2001**, 505−506.
[11] M. Morimoto, S. Kobatake, M. Irie, *Cryst. Growth Des.* **2003**, *3*, 847−854.
[12] J. H. Williams, J. K. Cockroft, A. N. Fitch, *Angew. Chem. Int. Ed. Engl.* **1992**, *31*, 1655− 1657.
[13] J. Potenza, D. Mastropaolo, *Acta Crystallogr., Sect. B* **1975**, *31*, 2527−2529 (room-temperature structure).
[14] E. Lork, R. Mews, A. V. Zibarev, *unpublished results* **2002** (163 K structure).
[15] R. T. Boere, A. W. Cordes, R. T. Oakley, *J. Chem. Soc., Chem. Commun.* **1985**, 929− 930.
[16] A. W. Cordes, R. T. Oakley, R. T. Boere, *Acta Crystallogr., Sect. C* **1985**, *41*, 1833−1834.
[17] C. Knapp, E. Lork, T. Borrmann, W.-D. Stohrer, R. Mews, *Eur. J. Inorg. Chem.* **2003**, 3211−3220.
[18] V. R. Thalladi, H. C. Weiss, D. Bläser, R. Boese, A. Nangia, G. R. Desiraju, *J. Am. Chem. Soc.* **1998**, *120*, 8702−8710.
[19] M. L. Glowka, D. Martynowsky, K. Kozlowska, *J. Mol. Struct.* **1999**, *474*, 81−89.
[20] J. D. Dunitz, A. Gavezzotti, *Acc. Chem. Res.* **1999**, *32*, 677−684.
[21] J. M. Rawson, F. Palacio, *Struct. Bonding* **2001**, *100*, 93−128.
[22] R. T. Boere, J. Fait, K. Larsen, J. Yip, *Inorg. Chem.* **1992**, *31*, 1417−1423.
[23] C. R. Patrick, G. S. Prasser, *Nature* **1960**, *187*, 1021−1021.
[24] G. M. Sheldrick, *SHELX-97 Programs for Crystal Structure Analysis (Release 97−2)*, Institute for Inorganic Chemistry, University of Göttingen, Göttingen, Germany, **1997**.
[25] *DIAMOND − Visual Structure Information System*, Crystal Impact, Bonn, Germany.

Received December 18, 2003
Early View Article
Published Online April 7, 2004

 © 2004 Wiley-VCH Verlag GmbH & Co. KGaA, Weinheim

Preparation and Structural Characterization of $[K(18\text{-crown-6})]^+$ Salts of $[RNSN]^-$ Anions and the $[NSN]^{2-}$ Dianion

Tobias Borrmann,[a] Enno Lork,[b] Rüdiger Mews,*[b] Makhmut M. Shakirov,[c] and Andrey V. Zibarev*[c]

Keywords: Sulfur / Nitrogen / X-ray diffraction / NMR spectroscopy

$[K(18\text{-crown-6})]^+$ salts of the $[RNSN]^-$ anions (R = Alk, Ar) and the $[NSN]^{2-}$ dianion, which are thermally stable and very soluble in aprotic organic solvents, were prepared from $[K(18\text{-crown-6})]^+[t\text{BuO}]^-$ and the corresponding R–N=S=N–$SiMe_3$ and $(Me_3Si–N=)_2S$, respectively. The salts are characterized by multinuclear (^1H, ^{13}C, ^{14}N, ^{19}F, ^{29}Si and ^{39}K) NMR spectroscopy in solution and by X-ray diffraction in the solid state. The experimentally determined bond lengths confirm that the $[RNSN]^-$ anions are thiazylamides, $R–N^––S{\equiv}N$ rather than sulfur diimides, $R–N=S=N^–$. Relative to O=S=O, in the $[NSN]^{2-}$ dianion, which is the genuine aza-analogue of sulfur dioxide, the bond lengths are elongated and the bond angle is widened. This might reflect electrostatic repulsion between the negatively charged N atoms. The experimental results are in agreement with theoretical calculations (RHF, B3LYP, MP2). In the nitrogen NMR spectra, when going from $[AlkNSN]^-$ to $[ArNSN]^-$, the low-field signal of the terminal (unsubstituted) N atom reveals further deshielding, whereas the high-field signal of the internal (substituted) N atom displays further shielding. The ^{14}N NMR resonance for the $[NSN]^{2-}$ dianion is practically insensitive to the counterion.
(© Wiley-VCH Verlag GmbH & Co. KGaA, 69451 Weinheim, Germany, 2004)

Introduction

Although known for more than 50 years, the sulfur-nitrogen triple bond still belongs to the less studied multiple bonds. Only relatively few thiazyne derivatives, $R-S{\equiv}N$ and $R_3S{\equiv}N$, are unambiguously characterized, either because of their thermal instability or because of the lack of generally applicable synthetic routes.[1–5]

Recently, it was shown by low-temperature X-ray crystallography and non-empirical calculations at the MP2 and B3LYP levels of theory that $[RNSN]^-$ anions (R = Alk, Ar), which are easily accessible by the fluoride ion-induced desilylation of $R-N=S=N-SiMe_3$ precursors (Scheme 1), should be regarded as thiazylamides $R-N^–-S{\equiv}N$ rather than the expected sulfur diimides $R-N=S=N^–$.[6–8]

Besides their theoretical importance, the $[RNSN]^-$ anions and the related $[NSN]^{2-}$ dianion are also of practical interest for synthetic chemistry as key intermediates for various inter- and intramolecular condensations[9–19] They can also be used as ligands for coordination compounds.[20] The anions are also useful for the solving of some problems of molecular physics related to intramolecular electron-transfer processes,[21] and are worthy of investigation as potential components of molecular conductors based on radical-ion salts.[22]

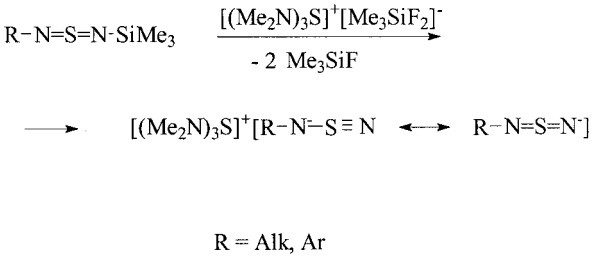

Scheme 1

Previously, the $[RNSN]^-$ anions were isolated and structurally characterized in the form of air-sensitive and thermally unstable salts of the tris(dimethylamino)sulfonium (TAS^+) cation (Scheme 1),[6–8] which decompose above about −20 °C, especially when R = Ar. Such instability seriously complicates further investigations and applications of the $[RNSN]^-$ anions.

On the other hand, the potassium salts of the $[RNSN]^-$ anions (where R = *t*Bu, Me_3Si) and of the $[NSN]^{2-}$ di

[a] Institute of Organic Chemistry, NW2 C, University of Bremen, 28334 Bremen, Germany
[b] Institute for Inorganic and Physical Chemistry, NW2 C, University of Bremen,
28334 Bremen, Germany
Fax: (internat.) + 49-421-218-4267
E-mail: mews@chemie.uni-bremen.de
[c] Institute of Organic Chemistry, Russian Academy of Sciences, 630090 Novosibirsk, Russia
Fax: (internat.) + 7-3832-344-752
E-mail: zibarev@nioch.nsc.ru

 © 2004 Wiley-VCH Verlag GmbH & Co. KGaA, Weinheim **DOI: 10.1002/ejic.200300954**

anion, in particular those prepared by the N−Si bond cleavage of the corresponding R−N=S=N−$SiMe_3$ precursors with *t*BuOK, are thermally very stable. They are almost insoluble in common aprotic solvents due to strong anion−cation interaction.[17,23,24] As a consequence, these salts have never been structurally characterized because they were not obtained as single crystals suitable for X-ray crystallography.

This article describes the preparation and isolation of the thermally stable [K(18-crown-6)]$^+$ salts of the [RNSN]$^-$ anions (R = Alk, Ar) and of the [NSN]$^{2-}$ dianion, which are readily soluble in organic solvents. The salts have been characterized by X-ray diffraction and by multinuclear (^{1}H, ^{13}C, ^{14}N, ^{19}F, ^{29}Si and ^{39}K) NMR spectroscopy in solution.

Results and Discussion

As mentioned above, K^+ salts of the [RNSN]$^-$ anions (R = *t*Bu, Me_3Si) and the [NSN]$^{2-}$ dianion were obtained previously by the action of *t*BuOK (and also KNH_2) on the R−N=S=N−$SiMe_3$ or $(Me_3SiN=)_2S$ sulfur diimides, respectively.[17,23,24] However, for these salts strong anion−cation interaction resulted in extremely low volatility (not sublimable) and solubility in organic solvents (not crystallizable), which complicated their further purification and unambiguous structural characterization.

The reaction of the R−N=S=N−$SiMe_3$ (R = Alk, Ar) and $(Me_3SiN=)_2S$ precursors with [K(18-crown-6)]$^+$ [*t*BuO]$^-$ under very mild conditions (at −30 °C in THF) has been used as a nearly quantitative general approach to the organic solvent-soluble salts **1**−**6** with the [RNSN]$^-$ anions and the [NSN]$^{2-}$ dianion (Scheme 2). The *t*Bu−O−$SiMe_3$ by-product (liquid, b. p. 102−103 °C) is inert under these reaction conditions and does not interfere with the isolation of the target salts.

$$R-N{=}S{=}N-SiMe_3 + [K(18\text{-crown-}6)]^+[t\text{BuO}]^- \longrightarrow [K(18\text{-crown-}6)]^+[RNSN]^- + t\text{BuOSiMe}_3$$

R = 1-Ad (**1**), *t*Bu (**2**), Me_3Si (**3**), Ph (**4**), 4-FC_6H_4 (**5**)

$$Me_3Si-N{=}S{=}N-SiMe_3 + 2[K(18\text{-crown-}6)]^+[t\text{BuO}]^- \longrightarrow \{[K(18\text{-crown-}6)]^+\}_2[NSN]^{2-} + 2\ t\text{BuOSiMe}_3$$

6

Scheme 2

The salts **1**−**6** (Scheme 2) are thermally very stable. They decompose (depending on R) in the range of approximately 100 °C (**5**) to approximately 150 °C (**2**, **6**) (see Exp. Sect. for details).

Importantly, by using this approach, it was possible to obtain the salts of interest in the form of single crystals suitable for X-ray crystallography using low-temperature crystallization from organic solvents. The solid-state structures of the salts **1** and **3**−**6** are shown in Figure 1 and Figures 2−5, respectively, and the details of the structure

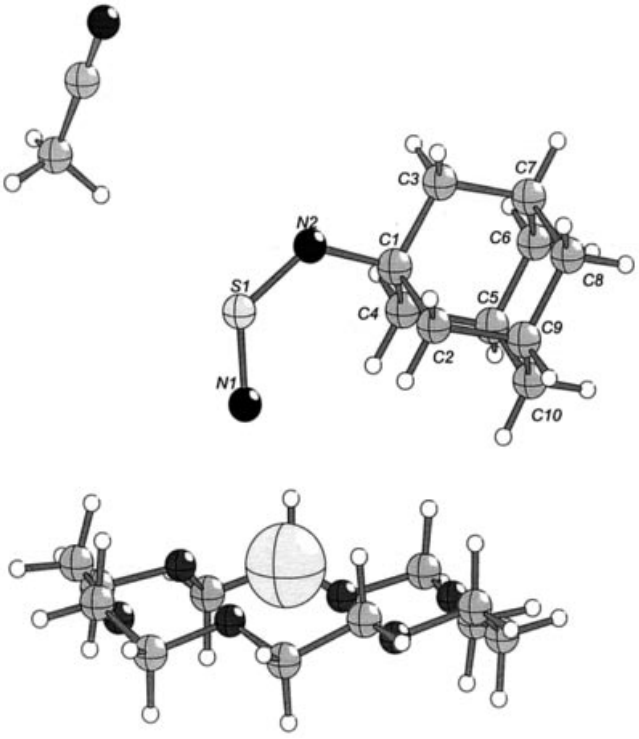

Figure 1. X-ray structure of [K(18-crown-6)]$^+$[1-AdNSN]$^-$·MeCN (**1**)

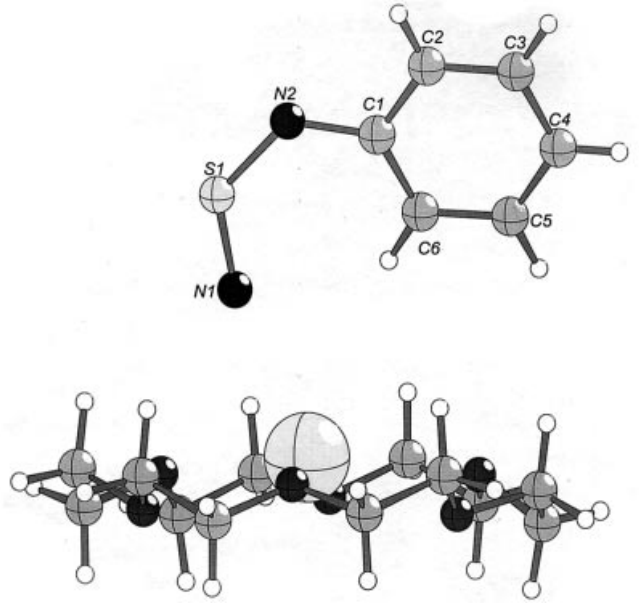

Figure 2. X-ray structure of [K(18-crown-6)]$^+$[PhNSN]$^-$ (**4**)

 © 2004 Wiley-VCH Verlag GmbH & Co. KGaA, Weinheim

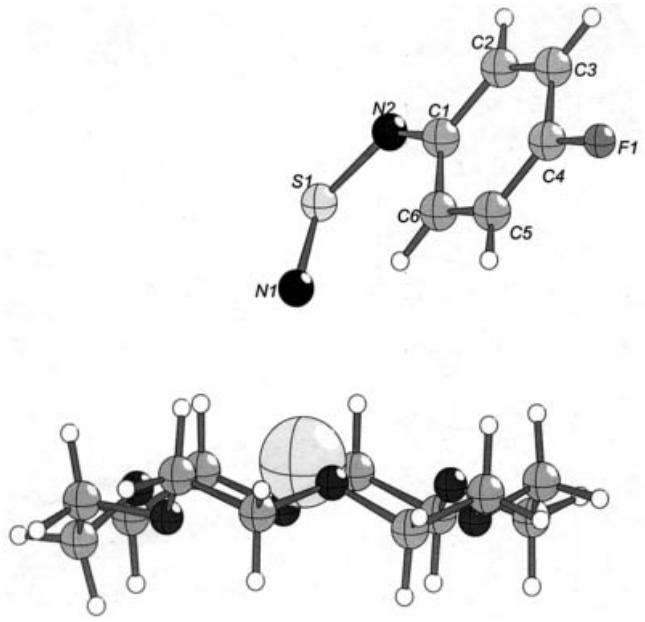

Figure 3. X-ray structure of $[K(18\text{-crown-6})]^+[4\text{-}FC_6H_4NSN]^-$ (**5**)

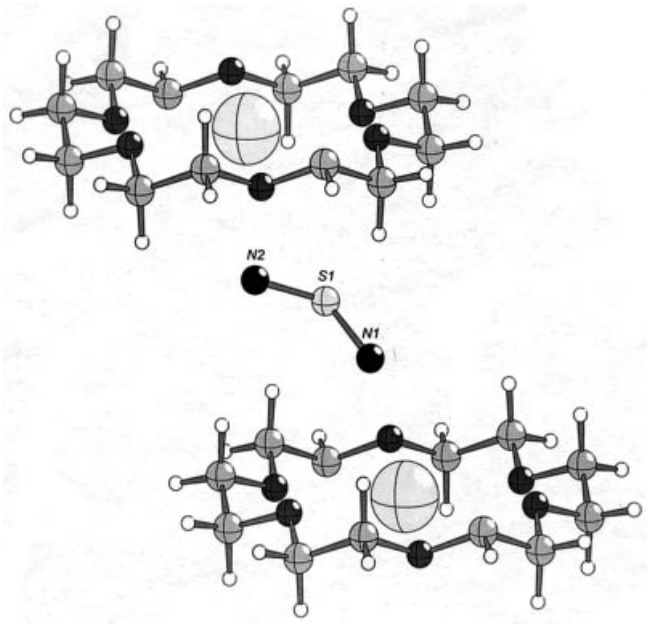

Figure 5. X-ray structure of $\{[K(18\text{-crown-6})]^+\}_2[NSN]^{2-}$ (**6**)

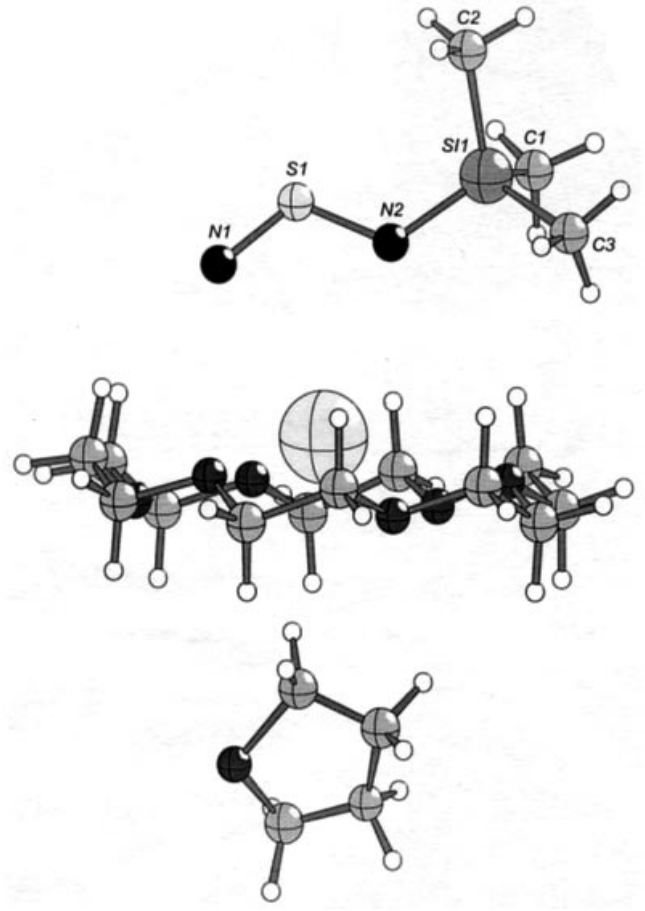

Figure 4. X-ray structure of $[K(18\text{-crown-6})]^+[Me_3SiNSN]^-$ (**3**)

determinations are listed in Table 1. Selected bond lengths and bond angles are given in Table 2. The structures of the $[PhNSN]^-$ anion (salt **4**), the parent anion of the $[ArNSN]^-$ family,[6,8] and the $[NSN]^{2-}$ dianion (salt **6**) are described for the first time. The X-ray structure of salt **2** was not solved due to strong disorder of both cation and anion, but this salt was unambiguously characterized in solution by multinuclear NMR spectroscopy (see below).

In the solid state, all $[RNSN]^-$ anions with R = 1-Ad, Ph, $4\text{-}FC_6H_4$ (salts **1**, **4**, **5**) exhibit the expected *Z*-configuration (Figure 1, Figure 2, Figure 3), whereas the $[Me_3SiNSN]^-$ anion (salt **3**) demonstrates the stereoelectronically unfavorable *E*-configuration (Figure 4), previously also observed for its TAS^+ salt (for the in-depth discussion of the *Z*- and *E*-configurations and the bonding properties of the $[RNSN]^-$ anions, see refs.[7,8]). In the salts with the anions in the *Z*-configuration, the K^+ counterion (encapsulated in the crown ether) is coordinated only by the terminal nitrogen atom (Figure 1, Figure 2, Figure 3), whereas the K^+ cation interacts with the anion in the *E*-configuration symmetrically with both the terminal and the internal N atoms (Figure 4). Due to this coordination the N−S−N bond angle in the $[Me_3SiNSN]^-$ anion is significantly narrower than in the other $[RNSN]^-$ anions (Table 2). In all cases, the N···K^+ separation in these salts (Table 2) is shorter than the sum of van der Waals radius of the N atom (150 pm) and the ionic radius of K^+ (157 and 164 pm for coordination numbers 8 and 12, respectively),[25] which implies relatively strong anion−cation interaction. Interestingly, for salt **3** the S···K^+ distance (Table 2) is rather close to the sum of the van der Waals radius of S (185 pm) and ionic radius of K^+.

Experimentally determined bond lengths (Table 2) confirm that the $[RNSN]^-$ anions should be described as thiazyl anions R−N^-−S≡N rather than sulfur diimide anions R−N=S=N^-. In the anions studied (Table 2), both the sulfur−nitrogen bonds are very different. While the terminal sulfur−nitrogen bond length falls into the range established for the S^{IV}≡N triple bond (146−148 pm), the internal sulfur−nitrogen bond is 9−13 pm longer (Table 2). Comparing the TAS^+ and $[K(18\text{-crown-6})]^+$ salts of the

 © 2004 Wiley-VCH Verlag GmbH & Co. KGaA, Weinheim

Table 1. Crystal data and structure refinement for the salts **1** and **3**−**6**

Salt	**1**	**3**	**4**	**5**	**6**
Empirical formula	$C_{22}H_{39}KN_2O_6S{\cdot}C_2H_3N$	$C_{15}H_{33}KN_2O_6SSi{\cdot}C_4H_8O$	$C_{18}H_{29}KN_2O_6S$	$C_{18}H_{28}FKN_2O_6S$	$C_{12}H_{24}KN_2O_6S$
Molecular mass	539.77	508.79	440.59	458.58	363.49
Temperature, K	173(2)	173(2)	173(2)	173(2)	173(2)
Wavelength, pm	71.073	71.073	71.073	71.073	71.073
Crystal system	orthorhombic	orthorhombic	triclinic	triclinic	monoclinic
Space group	*P*na2$_1$	$P2_12_12_1$	*P*1	$P\bar{1}$	$P2_1/c$
a, pm	1706.5(3)	943.85(19)	848.79(17)	989.5(2)	780.2(2)
b, pm	1519.6(3)	1408.8(3)	854.42(17)	991.1(2)	1490.9(2)
c, pm	1105.3(2)	2103.6(4)	881.42(18)	1398.1(3)	773.0(2)
α (°)	90	90	74.65(3)	94.20(3)	90
β (°)	90	90	69.36(3)	109.11(3)	99.85(2)
γ (°)	90	90	70.72(3)	114.95(3)	90
Volume, nm^3	2.8662(10)	2.7972(10)	0.55663(19)	1.1382(4)	0.8859(3)
Z	4	4	1	2	2
$D_{calcd.}$, Mg·m^{-3}	1.251	1.208	1.314	1.338	1.363
Absorption coefficient (mm^{-1})	0.298	0.344	0.367	0.368	0.445
Crystal size (mm^3)	0.50 × 0.40 × 0.40	0.50 × 0.40 × 0.30	0.50 × 0.40 × 0.40	0.40 × 0.25 × 0.20	0.70 × 0.50 × 0.40
θ range for data collection (°)	2.39−26.00	2.42−26.12	2.56−26.09	2.34−21.50	2.65−27.50
Reflections collected	39201	39199	7867	6246	8000
Independent reflections	5563 [*R*(int) = 0.0676]	5508 [*R*(int) = 0.0740]	4019 [*R*(int) = 0.0338]	2498 [*R*(int) = 0.0942]	2023 [*R*(int) = 0.0625]
Completeness to θ, % (θ°)	98.9 (26.00)	98.9 (26.12)	91.0 (26.09)	95.6 (21.50)	100.0 (27.50)
Data/restraints/parameters	5563/1/321	5508/0/286	4019/3/256	2498/0/264	2023/1/199
Goodness-of-fit on F^2	0.946	0.975	1.006	0.703	1.093
Final *R* indices [$I > 2\sigma(I)$]	*R*1 = 0.0395, *wR*2 = 0.0923	*R*1 = 0.0480, *wR*2 = 0.1225	*R*1 = 0.0308, *wR*2 = 0.0732	*R*1 = 0.0411, *wR*2 = 0.0571	*R*1 = 0.0345. *wR*2 = 0.0878
R indices (all data)	*R*1 = 0.0521, *wR*2 = 0.0963	*R*1 = 0.0617, *wR*2 = 0.1304	*R*1 = 0.0337, *wR*2 = 0.0742	*R*1 = 0.1092, *wR*2 = 0.0693	*R*1 = 0.0443, *wR*2 = 0.0933
Largest diff. peak and hole, eA^{-3}	0.376, −0.210	0.523, −0.315	0.291, −0.194	0.205, −0.196	0.326, −0.246

Table 2. Selected bond lengths (pm), bond angles (°) and N···K$^+$ separation (pm) in salts **1**, **3**−**6** (for atom numbering see Figure 1−5); for comparison, the data of the corresponding TAS$^+$ salts of **2**,[7] **3**,[7] and **5**[8] are included

Salt	R−N2	N2−S1	S1−N1	R−N2−S1	N2−S1−N1	N1···K$^+$
1	147.4(3)	156.5(2)	147.2(2)	125.70(17)	126.55(12)	270.3(2)
2(TAS$^+$)[7]	147.4(2)	157.6(1)	149.0(1)	123.81(10)	125.82(7)	−
3	172.1(3)	154.9(3)	146.4(3)	123.99(19)	118.80(17)	292.0(3)[a]
3(TAS$^+$)[7]	171.7(3)	156.4(3)	146.7(2)	124.5(2)	121.3(2)	−
4	140.3(3)	159.1(2)	145.8(2)	126.31(15)	125.45(11)	272.6(2)
5	141.9(6)	157.0(4)	146.1(4)	127.2(4)	125.3(2)	270.7(5)
5(TAS$^+$)[8]	138.8(7)	160.3(5)	146.9(5)	126.0(4)	124.5(3)	−
6	−	148.4(3)	148.4(3)	−	129.9(2)	295.0(4)/293.9(4)

[a] N2···K$^+$ 295.6(3), S1···K$^+$ 339.81(12) pm.

same [RNSN]$^-$ anions, it can be seen that exchange of the cation affects the bond lengths and bond angles in the anion to some extent; however the differences are relatively small (Table 2).

The reason for the reorganization of the chemical bonding on going from the R−N=S=N−SiMe$_3$ precursors to the corresponding R−N$^-$−S≡N anions is not entirely clear.[7,8] It follows from a preliminary analysis of the calculations at the MP2/6-31+G* level of theory that this reorganization is driven to some extent by the reduction of the local symmetry at the S atom.[25,26]

The [NSN]$^{2-}$ dianion (salt **6**) is the genuine aza-analogue of sulfur dioxide O=S=O (and isoelectronic with ozone, O$_3$). As mentioned above, no structural characterization using X-ray crystallography has been reported in the literature. On the basis of vibrational spectra,[23] its C_{2v} symmetry was determined and confirmed independently by quantum chemical calculations at the RHF level of theory.[27]

In the gas phase, the structure of the O=S=O molecule was determined by microwave spectroscopy with sulfur−oxygen bond lengths of 143.1 pm and a OSO bond

 © 2004 Wiley-VCH Verlag GmbH & Co. KGaA, Weinheim

angle of 119.3°.[28] Recently, the solid-state structure was also reported from a low temperature X-ray study [sulfur−oxygen bond length 142.97 (4) pm and OSO angle 117.5(1)°].[29]

In the crystal structure, the sulfur atom of the $[NSN]^{2-}$ dianion is situated very close to a crystallographic center of inversion and therefore the anion is disordered over two positions. The two independent S−N distances were refined with one common value and the calculations converged at 148.4(3) pm with a N−S−N angle of 129.9(2)°. Our theoretical calculations (Table 3) agree reasonably well with our experimental results.

Table 3. Bond lengths (pm) and bond angles (°) of the $[NSN]^{2-}$ anion from quantum chemical calculations

	RHF[a]	MP2[a]	B3LYP[a]	Exp.
(*d* S−N)	149.9	155.8	154.4	148.4(3)
(< N−S−N)	129.8	134.0	131.4	129.9(2)

[a] Basis set: 6−311+G*; for all methods NIMAG = 0.

Relative to O=S=O, in the $[NSN]^{2-}$ dianion, the bond lengths [148.4(3) pm] are elongated by ca. 5 pm and the bond angle [129.9(2)°] is widened by ca. 12 degrees (Table 2). This might reflect the electrostatic repulsion between the negatively charged N atoms. To the best of our knowledge, high level quantum chemical calculations on $[NSN]^{2-}$ are not reported in the literature. Earlier MNDO and HFS calculations,[27] not surprisingly, do not reproduce the experimentally observed geometry.

Previously, the $[RNSN]^-$ anions (R = *t*Bu, Me_3Si) and the $[NSN]^{2-}$ dianion (with Me_4N^+, nBu_4N^+ and TAS^+ as counterions) were characterized by multinuclear NMR spectroscopy (including nitrogen) in solution and in the solid state[7,30,31] (nitrogen NMR spectroscopy of binary sulfur-nitrogen anions, see ref.[32−34]). For $[RNSN]^-$, the high-field signal in the nitrogen (^{14}N and ^{15}N) NMR spectra can always be assigned to the internal (substituted) N atom and the low-field signal to the terminal (unsubstituted) N atom.

Table 4. Multinuclear NMR spectroscopic data (δ, ppm) for the salts **1**−**6**

R	^1H	^{13}C	^{14}N	^{39}K
1	3.55, 2.11, 1.93, 1.64	70.4, 57.5, 44.8, 37.6, 30.9	477, 310	−5.6
2	3.55, 1.20	70.5, 58.8, 31.1	485, 308	−5.3
3[a][b]	3.54, −0.16	70.5, 3.1	550, 286	−5.3
4	7.56, 7.10, 6.26, 3.54	150.9, 128.9, 123.1, 120.7, 71.0	512, 290	−6.1
5[c]	7.67, 6.82, 3.50	157.2, 147.3, 123.8, 114.7, 70.7	506.2[d], 285.1[d]	−5.4
6[e]	3.53	70.7	382	−4.0

[a] $\delta^{29}Si = -15.2$. [b] cf. Me_4N^+ salt: $\delta^1H = 3.24$ (Me_4N^+), −0.01; $\delta^{13}C = 56.0$ (Me_4N^+), 3.3; $\delta^{29}Si = -13.4$; $\delta^{14}N = 542, 294, 46$ (Me_4N^+). The salt was obtained from a 1:1 reaction of $(Me_3Si-N=)_2S$ with Me_4NF as large transparent orange-yellow scales (85%), m.p. (from MeCN) 140−141 °C (decomposition with gas evolution).[29] [c] $\delta^{19}F = 38.0$. [d] $\delta^{15}N$ ($\delta^{14}N = 507, 283$). [e] Me_4N^+ salt: $\delta^1H = 3.20$ (Me_4N^+); $\delta^{13}C = 55.9$ (Me_4N^+); $\delta^{14}N = 383, 46$ (Me_4N^+). The salt was obtained from a 1:2 reaction of $(Me_3Si-N=)_2S$ with Me_4NF as well-shaped orange-red prisms (90%), m.p. (from MeCN) 161−162 °C (decomposition with gas evolution).[29]

The multinuclear (^1H, ^{13}C, ^{14}N, ^{19}F, ^{29}Si, ^{39}K) NMR spectroscopic data for solutions of the salts **1**−**6** in acetonitrile are presented in Table 4. It follows from the Table 3 that on going from $[AlkNSN]^-$ (Alk = *t*Bu, 1-Ad) to $[ArNSN]^-$ (Ar = Ph, 4-FC_6H_4) (all four are in the *Z* configuration), the signal for the internal N atom shifts further high field, whereas the signal for the terminal N atom shifts in the opposite direction further low field. As a result, the $\Delta\delta^{14}N$ difference between magnetic shielding of the internal and terminal N atoms is larger in the $[ArNSN]^-$ than in the $[AlkNSN]^-$ anions.

The single ^{14}N NMR resonance for the $[NSN]^{2-}$ dianion is found between those of the terminal and the internal N atoms of the $[RNSN]^-$ anions (Table 3). The chemical shift is practically independent of the counterion (Me_4N^+, nBu_4N^+, TAS^+, $[K(18\text{-crown-6})]^+$).

Conclusion

$[K(18\text{-crown-6})]^+$ salts of the $[RNSN]^-$ anions (R = Alk, Ar), including that with R = Ph (the parent compound of the $[ArNSN]^-$ family), as well as of the $[NSN]^{2-}$ dianion, were prepared for the first time and structurally characterized by X-ray diffraction in the solid state and by multinuclear NMR spectroscopy (including nitrogen) in solution. The experimentally determined bond lengths confirm that the $[RNSN]^-$ anions are thiazylamides $R-N^--S\equiv N$ rather than sulfur diimides $R-N=S=N^-$. As observed for the corresponding TAS-salts, TAS^+RNSN^-, the substituent R occupies the electronically unfavorable E-position only in the Me_3Si derivative.[6−8] The present investigation shows that even bulky substituents and strong anion−cation interactions do not influence the preference of the alkyl and aryl substituents for the *Z*-position.

Relative to O=S=O, in the $[NSN]^{2-}$ dianion, which is the genuine aza-analogue of sulfur dioxide, the bond lengths are elongated and the bond angle is widened; this might reflect Coulombic repulsion between the N atoms. In the nitrogen NMR spectra, when going from $[AlkNSN]^-$ to $[ArNSN]^-$ the low-field signal of the terminal N atoms reveals further deshielding, whereas the high-field signal of internal N atoms display further shielding. The single ^{14}N NMR resonance for the $[NSN]^{2-}$ dianion is not influenced by the counterion.

Due to anion−cation interactions, the salts prepared are thermally very stable. Their stability and their good solubility in aprotic organic solvents (THF, MeCN) facilitates their use in synthetic chemistry as key intermediates for various inter- and intramolecular condensations. They can also be used as ligands for coordination compounds.

 © 2004 Wiley-VCH Verlag GmbH & Co. KGaA, Weinheim

Experimental Section

Materials and Methods: The starting $R-N=S=N-SiMe_3$ and $(Me_3Si-N=)_2S$ compounds were synthesized as described previously.[11,13,35] *t*BuOK (Janssen Chimica) was sublimed in vacuo, 18-crown-6 (Aldrich) was used as received. Absolute MeCN, THF, Et_2O and *n*-pentane were prepared by standard methods. The multinuclear NMR spectra were measured using a Bruker DRX-500 spectrometer at frequencies of 500.13 (^{1}H), 125.76 (^{13}C), 36.13 (^{14}N), 50.68 (^{15}N), 470.59 (^{19}F), 99.36 (^{29}Si), and 23.34 (^{39}K) MHz for solutions in CD_3CN; the chemical shifts (Table 2) are referred to TMS (^{1}H, ^{13}C, ^{29}Si), NH_3 (l) (^{14}N, ^{15}N), C_6F_6 (^{19}F) and KCl (aq.) (^{39}K). The melting points were measured using a Gallencamp Melting Point Apparatus in sealed capillaries. For all salts melting was accompanied by decomposition with gas evolution.

Preparation of $[K(18\text{-crown-6})]^+[RNSN]^-$ (R = Ad (1), *t*Bu (2), Ph (4), 4-FC_6H_4 (5): Under dry argon, at −40 °C, a solution of the corresponding $R-N=S=N-SiMe_3$ (5 mmol) in THF (5 mL) was added dropwise to a stirred solution of $[K(18\text{-crown-6})]^+[t\text{BuO}]^-$ (1.88 g, 5 mmol) in THF (20 mL) (prepared from *t*BuOK (0.56 g, 5 mmol) and 18-crown-6 (1.32 g, 5 mmol) at −20 °C). After an additional 2 h at the same temperature, the solvent was removed under high vacuum. MeCN (20 mL) was redistilled onto the solid residue via a vacuum line at −196 °C. On warming to −40 °C, the red solution formed was filtered through a sintered glass frit, cooled again to −196 °C, and Et_2O (20 mL) was condensed onto it. The reaction vessel was placed into a cryostat at −35 °C for crystal growth. After 2 weeks, when mutual diffusion of the solvents ceased, the mother liquor was removed with a syringe under dry argon at −40 °C. The crystalline residue was washed with Et_2O and dried in vacuo at ambient temperature.

$[K(18\text{-crown-6})]^+[1\text{-AdNSN}]^-\cdot$MeCN (1): Large transparent orange-yellow prisms, 2.30 g (85%), m.p. 106−108 °C.

$[K(18\text{-crown-6})]^+[t\text{BuNSN}]^-$ (2): Large transparent orange-yellow crystals, 1.90 g (90%), m.p. 149−150 °C.

$[K(18\text{-crown-6})]^+[\text{PhNSN}]^-$ (4): Orange-red crystals, 1.58 g (72%), m.p. 110−112 °C.

$[K(18\text{-crown-6})]^+[4\text{-}FC_6H_4NSN]^-$ (5): Orange-brown crystals, 1.28 g (56%), m.p. 98−100 °C.

Preparation of $[K(18\text{-crown-6})]^+[Me_3SiNSN]^-$ (3) (a) and $\{[K(18\text{-crown-6})]^+\}_2[NSN]^{2-}$ (6) (b): Under dry argon, at −40 °C, a solution of $(Me_3Si-N=)_2S$ (1.03 g, 5 mmol) (a) or (0.50 g, 2.5 mmol) (b) in THF (5 mL) was added dropwise to a stirred solution of $[K(18\text{-crown-6})]^+[t\text{BuO}]^-$ (1.88 g, 5 mmol) inTHF (20 mL), prepared as described above. After an additional 2 h at the same temperature, the reaction solution was filtered through a sintered glass frit and *n*-pentane (20 mL) was condensed onto it via a vacuum line at −196 °C. For crystal growth, the reaction vessel was placed into a cryostat at −35 °C (a) or kept at 20 °C (b). After 2 weeks, the solvents were removed as described above, and the crystalline residue was washed with Et_2O and dried in vacuo at ambient temperature.

$[K(18\text{-crown-6})]^+[Me_3SiNSN]^-\cdot$THF (3): Orange-yellow crystals, 2.09 g (82%), m.p. 106−108 °C.

$\{[K(18\text{-crown-6})]^+\}_2[NSN]^{2-}$ (6): Large bronze-brown crystals (orange-yellow when freshly prepared; dark orange in transmitting light), 1.50 g (90%), m.p. 152−154 °C.

X-ray Crystallographic Study: The single-crystal X-ray structure determinations (Table 1) were carried out on a Stoe IPDS for **1**, **3**, **4**, and on a Siemens P4 diffractometer for **5** and **6**, using Mo-K_α (0.71073 Å) radiation with a graphite monochromator. Refinement based on F^2; $R1 = \|F_o| - |F_c\|/|F_o|$; $wR2 = \{[w(F_o^2 - F_c^2)^2/[w(F_o^2)^2]\}^{1/2}$. Programs used: SHELX-97[36] and DIAMOND.[37] The structures of **1** and **4** were refined as racemic twins. In the crystal packing of **6**, the anion and cation are both disordered. The single crystals were mounted on a thin glass fiber using KEL-F oil. The structures were solved by direct methods (SHELXS[36]). Subsequent least-squares refinements (SHELXL-97-2[36]) located the positions of the remaining atoms in the electron density maps. All non-H atoms were refined anisotropically.
CCDC-227222 (for **1**), -227223 (for **2**), -227224 (for **4**), -227225 (for **5**), -227226 (for **6**) contain the supplementary crystallographic data for this paper. These data can be obtained free of charge at www.ccdc.cam.ac.uk/conts/retrieving.html [or from the Cambridge Crystallographic Data Centre, 12 Union Road, Cambridge CB2 1EZ, UK; Fax: (internat.) + 44-1223-336-033; E-mail: deposit@ccdc.cam.ac.uk].

Quantum Chemical Calculations: Quantum chemical calculations were performed with the Gaussian 98 set of programs.[38]

Acknowledgments

The authors are grateful to Dr. Paul G. Watson for NMR spectroscopic measurements on the Me_4N^+ salts, and to Mr. Peter Brackmann for technical assistance with the X-ray diffraction measurements. The joint financial support of this work by the DFG, Germany (Project 436 RUS 113/486/0−2 R), and the RFBR, Russia (Project 02−03−04001), is gratefully acknowledged. A.Z. is also grateful to the RFBR for financial support within Project 02−03−32794.

[1] O. Glemser, R. Mews, *Angew. Chem. Int. Ed. Engl.* **1980**, *19*, 883−899.
[2] G. Hartmann, R. Mews, G. M. Sheldrick, R. Anderskewitz, M. Niemeyer, H. J. Emeleus, H. Oberhammer, *J. Fluorine Chem.* **1986**, *34*, 46−58.
[3] R. Maggiulli, E. Lork, U. Behrens, K. Burger, R. Mews, *J. Fluorine Chem.* **2000**, *102*, 337−343.
[4] T. Yoshimura, *Rev. Heteroatom Chem.* **2000**, *22*, 101−120.
[5] T. Fujii, A. Itoh, K. Hamata, T. Yoshimura, *Tetrahedron Lett.* **2001**, *42*, 5041−5043.
[6] A. V. Zibarev, E. Lork, R. Mews, *Chem. Commun.* **1998**, 991−992.
[7] T. Borrmann, A. V. Zibarev, E. Lork, G. Knitter, S.-J. Chen, P. G. Watson, E. Cutin, M. M. Shakirov, W.-D. Stohrer, R. Mews, *Inorg. Chem.* **2000**, *39*, 3999−4005.
[8] T. Borrmann, E. Lork, R. Mews, W.-D. Stohrer, P. G. Watson, A. V. Zibarev, *Chem. Eur. J.* **2001**, *7*, 3504−3510.
[9] A. V. Zibarev, A. O. Miller, *J. Fluorine Chem.* **1990**, *50*, 359−363.
[10] A. V. Zibarev, Y. V. Gatilov, A. O. Miller, *Polyhedron* **1992**, *11*, 1137−1141.
[11] I. Y Bagryanskaya, Y. V. Gatilov, A. O. Miller, M. M. Shakirov, A. V. Zibarev, *Heteroatom Chem.* **1994**, *5*, 561−565.
[12] E. Lork, R. Mews, M. M. Shakirov, P. G. Watson, A. V. Zibarev, *Eur. J. Inorg. Chem.* **2001**, 2123−2134.
[13] E. Lork, R. Mews, M. M. Shakirov, P. G. Watson, A. V. Zibarev, *J. Fluorine Chem.* **2002**, *115*, 165−168.
[14] A. Y. Makarov, I. Y. Bagryanskaya, F. Blockhuys, C. Van Alsenoy, Y. V. Gatilov, V. V. Knyazev, A. M. Maksimov, T. V. Mikhalina, V. E. Platonov, M. M. Shakirov, A. V. Zibarev, *Eur. J. Inorg. Chem.* **2003**, 77−88.

 © 2004 Wiley-VCH Verlag GmbH & Co. KGaA, Weinheim

[15] M. Herberhold, S. Gerstmann, B. Wrackmeyer, *Phosphorus Sulfur Silicon Relat. Elem.* **1992**, *66*, 273−283.
[16] M. Herberhold, S. Gerstmann, B. Wrackmeyer, *Phosphorus Sulfur Silicon Relat. Elem.* **1996**, *113*, 89−106 (and references cited therein).
[17] D. Haenssgen, R. Boss, *Z. Anorg. Allg. Chem.* **1981**, *437*, 80−84.
[18] M. Herberhold, W. Ehrenreich, K. Guldner, *Chem. Ber.* **1984**, *117*, 1999−2005.
[19] A. Gieren, H. Betz, T. Huebner, V. Lamm, M. Herberhold, K. Guldner, *Z. Anorg. Allg. Chem.* **1984**, *513*, 160−174.
[20] N. P. C. Walker, M. B. Hursthouse, C. P. Warrens, J. D. Woollins, *J. Chem. Soc., Chem. Commun.* **1985**, 227−228.
[21] A. Modelli, V. Venuti, F. Scagnolari, D. Jones, *Chem. Phys. Lett.* **2001**, *346*, 492−496.
[22] O. A. Dyachenko, O. N. Kazheva, personal communication **2001**.
[23] M. Herberhold, W. Ehrenreich, *Angew. Chem.* **1982**, *94*, 637−638; *Angew. Chem. Int. Ed. Engl.* **1982**, *21*, 633−63: *Angew. Chem. Suppl.* **1982**, 1346.
[24] M. Herberhold, W. Ehrenreich, W. Buehlmeyer, K. Guldner, *Chem. Ber.* **1986**, *119*, 1424−1428.
[25] L. N. Shchegoleva, personal communication, **2002**.
[26] Y V. Gatilov, R. Mews, L. N. Shchegoleva, A. V. Zibarev, work in progress.
[27] M. Conti, M. Trsic, W. G. Laidlaw, *Inorg. Chem.* **1986**, *25*, 254−256.
[28] Y. Morino, M. Tanimoto, S. Saito, *Acta Chim. Scand., Ser. A* **1988**, *42*, 346−351.
[29] J. Buschmann, W. Steudel, personal communication.
[30] B. Wrackmeyer, S. Gerstmann, M. Herberhold, G. A. Webb, H. Kirosu, *Magn. Reson. Chem.* **1994**, *32*, 492−495.
[31] E. Lork, R. Mews, P. G. Watson, A. V. Zibarev, unpublished results, **2000**.
[32] T. Chivers, K. J. Schmidt, *Can. J. Chem.* **1992**, *70*, 710−718.
[33] T. Chivers, D. D. McIntyre, K. J. Schmidt, H. J. Vogel, *J. Chem. Soc., Chem. Commun.* **1990**, 1341−1342.
[34] T. Chivers, K. J. Schmidt, *J. Chem. Soc., Chem. Commun.* **1990**, 1342−1344.
[35] A. V. Zibarev, A. O. Miller, Y. V. Gatilov, G. G. Furin, *Heteroatom Chem.* **1990**, *1*, 443−453.
[36] G. M. Sheldrick, *SHELX-97 − Programs for Crystal Structure Analysis (Release 97−2)*, Institute for Inorganic Chemistry, University of Göttingen, Göttingen, Germany, **1997**.
[37] *DIAMOND − Visual Structure Information System*, Crystal Impact, Bonn, Germany.
[38] M. J. Frisch, G. W. Trucks, H. B. Schlegel, G. E. Scuseria, M. A. Robb, J. R. Cheeseman, V. G. Zakrzewski, J. A. Montgomery, Jr., R. E. Stratmann, J. C. Burant, S. Dapprich, J. M. Millam, A. D. Daniels, K. N. Kudin, M. C. Strain, O. Farkas, J. Tomasi, V. Barone, M. Cossi, R. Cammi, B. Mennucci, C. Pomelli, C. Adamo, S. Clifford, J. Ochterski, G. A. Petersson, P. Y. Ayala, Q. Cui, K. Morokuma, D. K. Malick, A. D. Rabuck, K. Raghavachari, J. B. Foresman, J. Cioslowski, J. V. Ortiz, A. G. Baboul, B. B. Stefanov, G. Liu, A. Liashenko, P. Piskorz, I. Komaromi, R. Gomperts, R. L. Martin, D. J. Fox, T. Keith, M. A. Al-Laham, C. Y. Peng, A. Nanayakkara, C. Gonzalez, M. Challacombe, P. M. W. Gill, B. Johnson, W. Chen, M. W. Wong, J. L. Andres, C. Gonzalez, M. Head-Gordon, E. S. Replogle, J. A. Pople, *Gaussian 98, Revision A.7*, Gaussian Inc., Pittsburgh PA, **1998**.

Received December 19, 2003
Early View Article
Published Online April 26, 2004

 © 2004 Wiley-VCH Verlag GmbH & Co. KGaA, Weinheim

Synthesis and Core and Surface Reactivity of Phosphorus-Based Dendrons

Rosa-María Sebastián,[a] Laurent Griffe,[a] Cédric-Olivier Turrin,[a] Bruno Donnadieu,[a] Anne-Marie Caminade,*[a] and Jean-Pierre Majoral*[a]

Keywords: Azides / Dendrimers / Dendrons / N,P ligands / Phosphorus

A series of phosphorus-containing dendrons is synthesized starting from a unique precursor $(EtO)_2P(O)CH{=}CHC_6H_4PPh_2$ (**3-G$_0$**), whose X-ray crystal structure shows an extended planarity between both phosphorus. Staudinger reactions with functionalized azides on the phosphino group are the first step for the growth of the dendrons, which is continued using a divergent method. Several types of reactions are performed on dendrons of several sizes, either at the level of the core or of the surface. The specific addition of methyl triflate to P=S and trimethylsilyl triflate to P=O at the level of the core affords a dicationic species. A ^{13}C NMR spectroscopic study indicates to what extent the charges are delocalized. Phosphanes are grafted on the surface of a second-generation dendron, and used for the complexation of $PdCl_2$. Both compounds possess five different types of phosphorus atoms, which helps in characterizing them by ^{31}P NMR spectroscopy.

(© Wiley-VCH Verlag GmbH & Co. KGaA, 69451 Weinheim, Germany, 2004)

Introduction

Dendrons[1] are dendritic wedges that differ from classical dendrimers[2] by the presence of a functional group at the level of the core. Such compounds can be built using either a convergent[3] or a divergent[4] process, and they have found applications as building blocks for the rapid synthesis of dendrimers[5] or for the coating of the surface of various materials, for example.[6] The nature of the function located at the core is of crucial importance when synthesizing dendrons, particularly if a divergent process is used. Indeed, this function is present from the beginning of the synthesis and hence it must be compatible with the whole synthetic process while remaining available for further reactions after the growth of the dendron. Due to the wide range of uses and applications of phosphonates in organic synthesis, biology and materials chemistry,[7] we decided to graft a phosphonate at the core, linked through a potentially conjugated linkage, which may act as a probe for sensing further reactivity.

We have already reported the divergent synthesis of phosphorus-containing dendrons[4,8,9] and dendrimers,[10] and shown that ^{31}P NMR spectroscopy is an extraordinarily useful tool for characterizing such compounds. However, when the chemical structure is similar at each layer, a partial overlap of signals may occur.[11] We and others have shown that using two[12] or three[13,14] types of chemical environment around the phosphorus atoms allows an easier characterization. We report in this paper the synthesis and characterization of a series of dendrons having a phosphonate at the core and up to five different types of phosphorus atoms in the structure; these are clearly distinguishable by ^{31}P NMR spectroscopy. Furthermore, these compounds possess a versatile reactivity at every step of the synthesis, as will be illustrated by three very different examples.

[a] Laboratoire de Chimie de Coordination CNRS
205, Route de Narbonne, 31077 Toulouse Cedex 4, France
Fax: +33-(0)5-61553003
E-mail: caminade@lcc-toulouse.fr
majoral@lcc-toulouse.fr

Results and Discussion

The method used for grafting the phosphonate at the core consists of the Horner−Wadsworth−Emmons reaction[15] of tetraethylmethylene *gem*-diphosphonate **1** with diphenylphosphino benzaldehyde **2** in the presence of NaH that we have already applied to the surface of dendrimers[16] (Scheme 1). The reaction creates a C=C bond connecting the phosphonate to the aryl group. The resulting vinyl phosphonate derivative **3-G$_0$** was isolated in quantitative yield. The expected *E*-configuration of the alkene bond is shown in the ^1H NMR spectrum by the large value of the $^3J_{H,H}$ coupling constant (17.2 Hz). Single crystals of **3-G$_0$** were obtained by slow evaporation of a solution in CH_2Cl_2 and allowed the determination of its structure by X-ray diffrac-

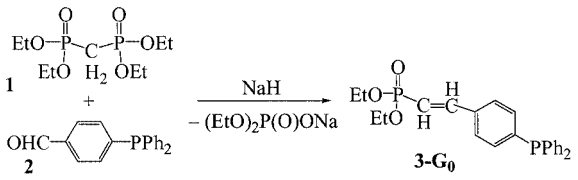

Scheme 1

tion. The ORTEP drawing is shown in Figure 1 and confirms the *E*-configuration of the C=C bond. All atoms from P2 to O3 are in a plane (Rms deviation 0.0685), indicating an extended conjugation of 11 atoms.

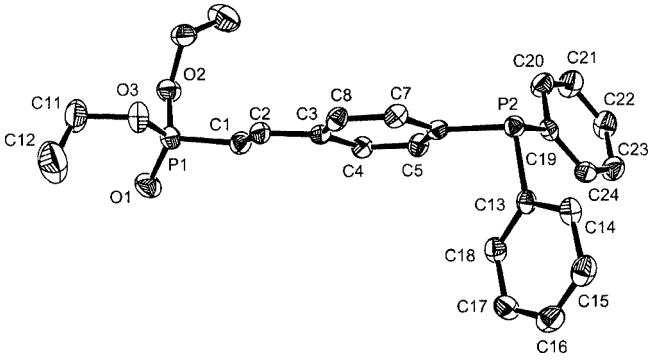

Figure 1. ORTEP drawing of **3-G$_0$**; selected bond lengths (Å) and angles (°): P1−O1 1.4605(16), P1−O2 1.5754(15), P1−O3 1.5794(16), P1−C1 1.775(2), C1−C2 1.322(3), P2−C6 1.8328(19), P2−C13 1.839(2), P2−C19 1.8421(19); P1−C1−C2 125.04(17), C1−C2−C3 126.25(19)

Compound **3-G$_0$** is the starting material for the synthesis of various dendrons. Indeed, the presence of a phosphane allows it to undergo Staudinger reactions with functionalized azides such as compound **4**, which affords the first generation dendron **3-G$_1$** (Scheme 2). As expected,[17] the P=N−P=S linkage created by the reaction is characterized in the ^{31}P NMR spectrum by two doublets at δ = 14.4 (P=N) and 50.2 (P=S) ppm with $^{2}J_{P,P}$ = 31 Hz. In the ^{13}C NMR spectrum a dramatic shielding of the signals corresponding to the carbons linked to the phosphorus that undergoes the reaction is observed ($\Delta\delta$ = −9.31 ppm for $C_{ipso}PPh_2$; $\Delta\delta$ = −10.65 ppm for $C_{ipso}PC_6H_4$) together with a very important increase of the $^{1}J_{C,P}$ coupling constant. More interestingly, the Staudinger reaction also induces changes for the vinyl linkage, where the signal corresponding to the =CH linked to C_6H_4 is shielded, whereas the signal corresponding to (O)P-CH= is deshielded ($\Delta\delta$ = +3.44 ppm), confirming a conjugation through the aromatic and vinyl linkages (Figure 2).

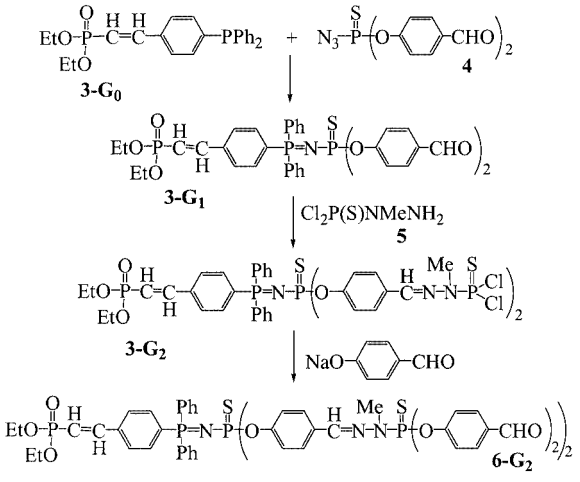

Scheme 2

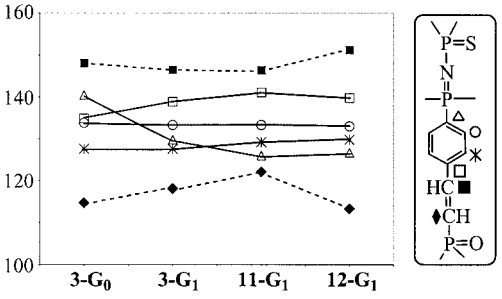

Figure 2. Variation of the chemical shifts (^{13}C NMR) for all carbon atoms located from P(O) to P for four compounds (**3-G$_0$**, **3-G$_1$**, **11-G$_1$**, and **12-G$_1$**)

To continue the growth of the dendron, our classical method of synthesis of dendrimers[18,19] was applied starting from the aldehydes of **3-G$_1$**, and using the phosphorhydrazide **5** to generate dendron **3-G$_2$**. Then, the nucleophilic substitution of Cl with hydroxybenzaldehyde sodium salt afforded compound **6-G$_2$**. It is noteworthy that none of these reactions has an influence on the vinylphosphonate group located at the core, as shown by ^{31}P NMR spectroscopy, with the presence of the singlet of the P=O group (δ = 18.2 ppm) together with the singlet of the P=S end groups (δ = 60.7 ppm) and both doublets corresponding to the P=N−P=S linkage (δ = 13.7 and 51.8 ppm, respectively).

Thus, the growth of the dendron could have been pursued to higher generations, as we have already shown with dendrons containing other types of functions at the core,[4,8,9,20] but we prefer to show the versatility and adaptability of this method of synthesis at every step, including starting from **3-G$_0$**. Indeed, other types of functionalized azides can be used, as shown by the reaction with compound **7** affording **8-G$_1$** (Scheme 3). Here also, the Staudinger reaction induces the appearance of two doublets in the ^{31}P NMR spectrum at δ = 12.8 (P=N) and 71.2 (P=S) ppm with $^{2}J_{P,P}$ = 17.2 Hz. Obviously, the presence of NH_2 groups opens the way to a tremendous number of reactions, in particular condensations with functionalized aldehydes. As an illustration, the carbohydrate derivative **9** (helicin) was condensed with **8-G$_1$**. The condensation induces an important shielding in the ^{31}P NMR spectrum for the signal corresponding to the P=S group, from δ = 71.2 ppm for **8-G$_1$** to δ = 62.5 ppm for **10-G$_1$**. A careful examination of the ^{1}H and ^{13}C NMR spectra of **10-G$_1$** shows that several signals corresponding to the helicin and hydrazone moieties are split into two series of signals in a 1:1 ratio; for example, the NCH_3 groups give two doublets at δ = 33.89 and 34.04 ppm. Such splitting might be ascribed to *E* and *Z* isomers of the hydrazone bond (C=N) with one *E* and one *Z* bond for each molecule of **10-G$_1$**. Phosphorhydrazone bonds are generally in the *E* configuration, thus the formation of a *Z* isomer might be due to the occurrence of hydrogen bonds, which forces one hydrazone linkage to be in the *Z* form, as previously noticed on the surface of dendrimers.[21] Due to the carbohydrate moieties, **10-G$_1$** is soluble in water, whereas all the other dendrons described in this paper are not.

 © 2004 Wiley-VCH Verlag GmbH & Co. KGaA, Weinheim

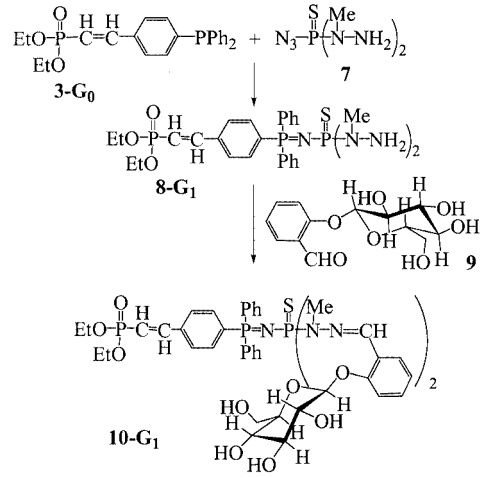

Scheme 3

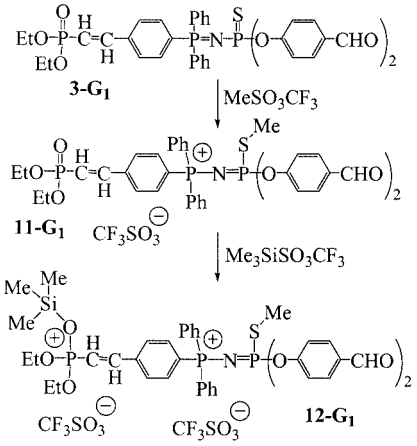

Scheme 4

We also tested another type of reactivity with compound **3-G$_1$** — alkylation reactions — with the aim of detecting to what extent the positive charge could be delocalized.[22] One equivalent of the strong alkylating reagent methyl trifluoromethanesulfonate was added to **3-G$_1$** (Scheme 4). We have already shown that this reagent is able to alkylate the sulfur atom included in a P=N−P=S linkage,[13,17,23] but such a reaction has never been performed in the presence of a phosphonate group, although we have reported the specific alkylation of P=S in macrocycles bearing phosphane oxide groups.[24] The ^{31}P NMR spectrum of the resulting compound **11-G$_1$** shows without any ambiguity that the alkylation occurs exclusively at the P=S group. Indeed, a $\Delta\delta$ value of −27 ppm was measured for the signal corresponding to P=S, whereas it is only −1 ppm for the P=O group, on going from **3-G$_1$** to **11-G$_1$**. Both signals corresponding to P=N (δ = 22.2 ppm) and P=S (δ = 23.1 ppm) are close; the assignment of the chemical shift was made by proton-coupled ^{31}P NMR spectroscopy, which gives a coupling constant of 18.2 Hz for the signal at δ = 23.1 ppm (P−S−Me). The positive charge is delocalized to some extent onto the adjacent P=N group ($\Delta\delta$ = +8 ppm). In view of the extended planarity seen in the X-ray structure of **3-G$_0$**, and the modification of the ^{13}C NMR spectra on going from **3-G$_0$** to **3-G$_1$**, the charge might even be delocalized all the way along the chain up to the phosphonate group. The ^{13}C NMR spectrum shows a deshielding of the signal corresponding to (O)P-*C*H=, which should correspond to a partial positive charge on this atom (Figure 2, rhombuses). However, the absence of a variation of the chemical shift corresponding to P=O seems to preclude an extension of the delocalization up to it, and is in agreement with the structure of **3-G$_0$** obtained by X-ray diffraction in which the oxygen of P=O lies outside the main plane.

This assumption was reinforced by checking the reactivity of trimethylsilyl trifluoromethanesulfonate with **11-G$_1$**, since we have already shown that it is able to react with phosphane oxides.[25] Indeed, the presence of a positive charge on P=O should hamper further addition of cations to this group. The reaction monitored by ^{31}P NMR spectroscopy shows a deshielding of the signal corresponding to the P=O group ($\Delta\delta$ = 4 ppm) whereas no change is observed for the other signals. The dicationic species **12-G$_1$** was obtained quantitatively. The ^{13}C NMR spectrum of **12-G$_1$** shows only modifications for the vinyl group, with a shielding of the carbon linked to phosphorus ($\Delta\delta$ = −9 ppm) and a deshielding of the other carbon ($\Delta\delta$ = 5 ppm) (Figure 2). Thus, the delocalization of the second positive charge only has an influence on the (O)P−CH=CH linkage.

The last example illustrating the versatile reactivity of this series of dendrons concerns **3-G$_2$**. Its P(S)Cl$_2$ end-groups can be reacted with various functionalized phenols such as **13**, which affords dendron **14-G$_2$** (Scheme 5). These phosphanyl end-groups are used because they are potential N,P ligands. Indeed, we have shown previously that the corresponding Pd complexes linked to the surface of dendrimers efficiently catalyze Stille coupling reactions.[26] The palladium complex **15-G$_2$** is readily obtained by reaction with [PdCl$_2$(COD)]. Here again the ^{31}P NMR spectrum gives very informative data for the characterization. Fig-

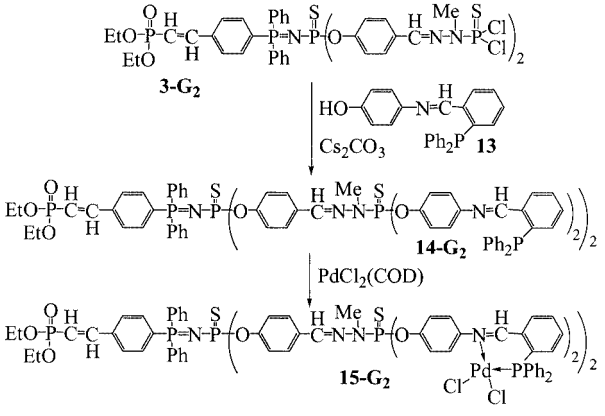

Scheme 5

 © 2004 Wiley-VCH Verlag GmbH & Co. KGaA, Weinheim

ure 3 shows the spectrum of **15-G$_2$**, with five different types of phosphorus atoms clearly distinguishable, and in the expected ratio.

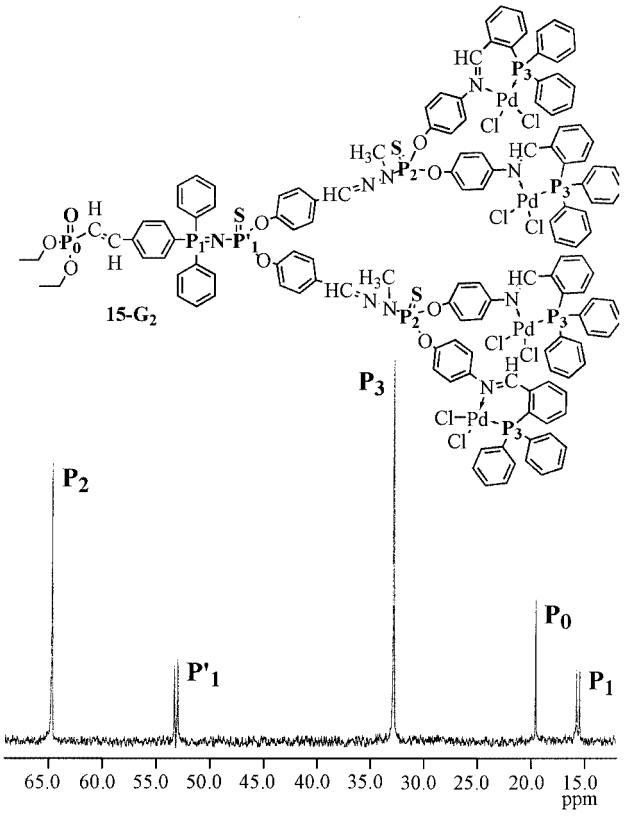

Figure 3. ^{31}P NMR spectrum and chemical structure of **15-G$_2$**

Conclusion

We have shown in this paper that compound **3-G$_0$** is a multifunctional diphosphorus derivative, readily usable as the core of various dendrons. These dendrons contain up to five different types of phosphorus groups, which act as sensitive labels that are able to detect subtle and remote chemical modification, as shown by ^{31}P NMR spectroscopy. These dendrons also possess a versatile reactivity both at the level of the core and of the end groups that is adaptable depending on the type of use desired. As an illustration, we have given three very different examples concerning modification of the solubility, alkylation with delocalization of the charges, and grafting of N,P ligands as end-groups, along with a preliminary study of their complexation properties. Obviously, many other examples of reactions can be envisaged, in particular concerning the use of phosphonates for the grafting of dendrons on the surface of various materials. Indeed, it is known that phosphonates are able to react, for instance, with alumina[27] and titania particles.[28] Thus, compound **15-G$_2$** could be used as precursor of heterogeneous catalysts.

Experimental Section

General Remarks: All manipulations were carried out with standard high vacuum and dry-argon techniques. The solvents were freshly dried and distilled (THF and diethyl ether over sodium/benzophenone; pentane and CH_2Cl_2 over phosphorus pentoxide; toluene over sodium); they were degassed prior to use in the case of experiments using trivalent phosphorus derivatives. ^{1}H, ^{13}C and ^{31}P NMR spectra were recorded with Bruker AC 200, AC 250, DPX 300 or AMX 400 spectrometers. References for NMR chemical shifts are 85% H_3PO_4 for ^{31}P NMR and $SiMe_4$ for ^{1}H and ^{13}C NMR spectroscopy. The attribution of the ^{13}C NMR signals was performed by using J_{mod}, two dimensional HMBC, and HMQC, Broad Band or CW ^{31}P decoupling experiments when necessary. The numbering used for the NMR assignments is depicted in Figure 4. Compounds **2**,[29] **4**,[30] **7**,[30] and **13**[26] were synthesized as reported previously.

Phosphane 3-G$_0$: A solution of $(EtO)_2P(O)CH_2P(O)(OEt)_2$ (0.500 g, 1.680 mmol) in THF (5 mL) was added to a suspension of NaH (0.043 g, 1.680 mmol) in THF (15 mL). After stirring for 10 min a clear solution was obtained. A solution of $CHOC_6H_4PPh_2$ (0.490 g, 1.68 mmol) in THF (5 mL) was then added dropwise. The resulting mixture was stirred overnight, then H_2O (10 mL) was added. The resulting mixture was concentrated under vacuum to eliminate THF, then CH_2Cl_2 (10 mL) was added. The organic phase was recovered, and the water phase was washed twice with CH_2Cl_2. The organic layers were combined and the solvents evaporated to dryness to afford a pale yellow powder. **3-G$_0$** was purified by column chromatography on silica gel (eluent: ethyl acetate) to afford a white powder in 99% yield (0.700 g). Translucent crystals suitable for X-ray diffraction were obtained after a slow evaporation of a solution in CH_2Cl_2. ^{1}H NMR ($CDCl_3$): δ = 1.30 (t, $^3J_{H,H}$ = 7.1 Hz, 6 H, CH_3), 4.09 (dt, $^3J_{H,H}$ = 7.1, $^3J_{H,P}$ = 14.3 Hz, 4 H, CH_2), 6.25 (t, $^3J_{H,H}$ = $^2J_{H,P}$ = 17.5 Hz, 1 H, =CH-P$_0$), 7.21−7.46 (m, 14 H, H_{Arom}), 7.51 (d, $^3J_{H,H}$ = 17.5 Hz, 1 H, C*H*=CH-P$_0$) ppm. ^{13}C{^{1}H}

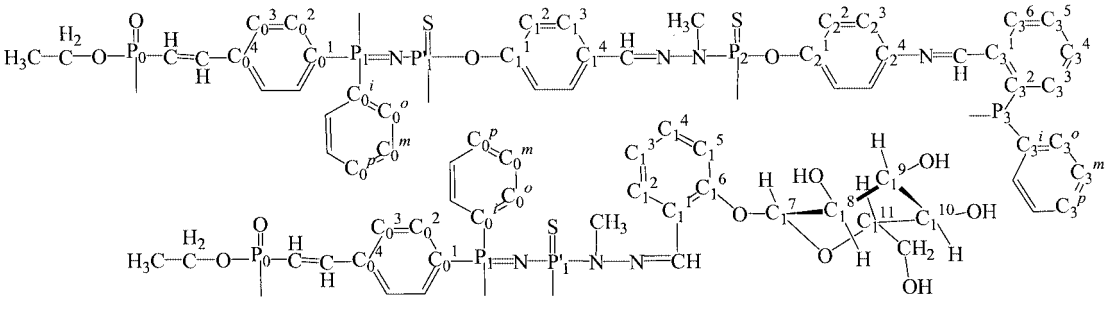

Figure 4. Numbering used for NMR spectroscopy

 © 2004 Wiley-VCH Verlag GmbH & Co. KGaA, Weinheim

NMR ($CDCl_3$): δ = 16.42 (d, $^3J_{C,P}$ = 6.0 Hz, CH_3), 61.84 (d, $^2J_{C,P}$ = 5.7 Hz, CH_2), 114.68 (d, $^1J_{C,P}$ = 191.2 Hz, =CH-P_0), 127.60 (d, $^3J_{C,P}$ = 7.3 Hz, C_0^3), 128.62 (d, $^3J_{C,P}$ = 6.0 Hz, C_0^m), 128.98 (s, C_0^p), 133.79 (d, $^2J_{C,P}$ = 21.2 Hz, C_0^o), 133.83 (d, $^2J_{C,P}$ = 16.3 Hz, C_0^2), 134.93 (d, $^3J_{C,P}$ = 23.4 Hz, C_0^4), 136.50 (d, $^1J_{C,P}$ = 10.1 Hz, C_0^i), 140.50 (d, $^1J_{C,P}$ = 13.5 Hz, C_0^1), 148.07 (d, $^1J_{C,P}$ = 7.6 Hz, *C*H=CH-P_0) ppm. $^{31}P\{^1H\}$ NMR ($CDCl_3$): δ = −5.2 (s, P_1), 19.5 (s, P_0) ppm. $C_{24}H_{26}O_3P_2$ (424.41): calcd. C 67.92, H 6.17; found C 67.96, H 6.19.

Dendron 3-G_1: CH_2Cl_2 (10 mL) was added to a powdered mixture of **3-G_0** (0.302 g, 0.712 mmol) and the azide $N_3P(S)(OC_6H_4CHO)_2$ (0.247 g, 0.712 mmol). A rapid evolution of nitrogen was observed. The solution was stirred overnight then evaporated to dryness to afford **3-G_1** as a pale yellow powder in 98% yield (0.520 g). A strict 1:1 ratio must be respected between **3-G_0** and the azide, because numerous washings of **3-G_1** did not allow the elimination of the unreacted starting materials. ^1H NMR ($CDCl_3$): δ = 1.30 (t, $^3J_{H,H}$ = 7.1 Hz, 6 H, CH_3), 4.09 (dt, $^3J_{H,H}$ = 7.1, $^3J_{H,P}$ = 14.6 Hz, 4 H, CH_2), 6.35 (t, $^3J_{H,H}$ = $^2J_{H,P}$ = 17.2 Hz, 1 H, =CH-P_0), 7.26 (d, $^3J_{H,H}$ = 8.0 Hz, 4 H, H-C_1^2), 7.37−7.66 (m, 14 H, H_{Arom}), 7.55 (d, $^3J_{H,H}$ = 17.2 Hz, 1 H, C*H*=CH-P_0), 7.73 (d, $^3J_{H,H}$ = 8.0 Hz, 4 H, H-C_1^3), 9.86 (s, 2 H, CHO). $^{13}C\{^1H\}$ NMR ($CDCl_3$): δ = 16.39 (d, $^3J_{C,P}$ = 5.9 Hz, CH_3), 62.07 (d, $^2J_{C,P}$ = 5.9 Hz, CH_2), 118.12 (d, $^1J_{C,P}$ = 189.6 Hz, =CH-P_0), 122.03 (d, $^3J_{C,P}$ = 4.1 Hz, C_1^2), 127.19 (dd, $^1J_{C,P}$ = 106.0, $^3J_{C,P}$ = 3.8 Hz, C_0^i), 127.63 (d, $^3J_{C,P}$ = 13.5 Hz, C_0^3), 128.84 (d, $^3J_{C,P}$ = 13.7 Hz, C_0^m), 129.85 (dd, $^1J_{C,P}$ = 113.0, $^3J_{C,P}$ = 3.5 Hz, C_0^1), 131.16 (s, C_1^3), 132.60 (s, C_1^4), 132.64 (d, $^2J_{C,P}$ = 11.7 Hz, C_0^o), 133.01 (s, C_0^p), 133.27 (d, $^2J_{C,P}$ = 11.6 Hz, C_0^2), 138.95 (d, $^3J_{C,P}$ = 24.3 Hz, C_0^4), 146.49 (d, $^2J_{C,P}$ = 6.6 Hz, *C*H=CH-P_0), 156.79 (d, $^2J_{C,P}$ = 9.4 Hz, C_1^1), 190.96 (s, CHO) ppm. $^{31}P\{^1H\}$ NMR ($CDCl_3$): δ = 14.4 (d, $^2J_{P,P}$ = 31.0 Hz, P_1), 18.0 (s, P_0), 50.2 (d, $^2J_{P,P}$ = 31.0 Hz, P'_1) ppm. $C_{38}H_{36}NO_7P_3S$ (743.69): calcd. C 61.37, H 4.88, N 1.88; found C 61.56, H 4.91, N 1.79.

Dendron 3-G_2: A solution of $H_2NNMeP(S)Cl_2$ in $CHCl_3$ (1.12 mL, 0.260 mmol) was added to a solution of **3-G_1** (0.088 g, 0.118 mmol) in THF (10 mL). The resulting solution was stirred for 4 hours then evaporated to dryness to afford an oil. This oil was washed three times with CH_2Cl_2/pentane then evaporated to dryness to afford **3-G_2** as a pale yellow powder in 81% yield (0.102 g). ^1H NMR ($CDCl_3$): δ = 1.34 (t, $^3J_{H,H}$ = 6.9 Hz, 6 H, CH_2−C*H*$_3$), 3.46 (d, $^3J_{H,P}$ = 7.0 Hz, 6 H, N-CH_3), 4.13 (dt, $^3J_{H,H}$ = 6.9, $^3J_{H,P}$ = 14.2 Hz, 4 H, CH_2), 6.35 (t, $^3J_{H,H}$ = $^2J_{H,P}$ = 17.2 Hz, 1 H, =CH-P_0), 7.21 (d, $^3J_{H,H}$ = 7.8 Hz, 4 H, H-C_1^2), 7.58 (d, $^3J_{H,H}$ = 7.8 Hz, 4 H, H-C_1^3), 7.44−7.65 (m, 17 H, H_{Arom}, CH=N, CH=CH) ppm. $^{13}C\{^1H\}$ NMR ($CDCl_3$): δ = 16.26 (d, $^3J_{C,P}$ = 6.4 Hz, CH_2−*C*H_3), 31.68 (d, $^2J_{C,P}$ = 13.9 Hz, N-CH_3), 62.09 (d, $^2J_{C,P}$ = 5.8 Hz, CH_2), 117.28 (d, $^1J_{C,P}$ = 190.7 Hz, =CH-P_0), 121.89 (d, $^3J_{C,P}$ = 5.0 Hz, C_1^2), 127.49 (d, $^3J_{C,P}$ = 13.6 Hz, C_0^3), 128.00 (dd, $^1J_{C,P}$ = 107.0, $^3J_{C,P}$ = 4.0 Hz, C_0^i), 128.24 (s, C_1^3), 128.61 (d, $^3J_{C,P}$ = 13.1 Hz, C_0^m), 130.09 (s, C_1^4), 130.15 (dd, $^1J_{C,P}$ = 110.0, $^3J_{C,P}$ = 4.0 Hz, C_0^1), 132.56 (d, $^2J_{C,P}$ = 10.4 Hz, C_0^o), 132.67 (s, C_0^p), 133.18 (d, $^2J_{C,P}$ = 11.4 Hz, C_0^2), 138.44 (dd, $^3J_{C,P}$ = 23.3, $^4J_{C,P}$ = 2.9 Hz, C_0^4), 141.08 (d, $^3J_{C,P}$ = 18.7 Hz, CH=N-N), 146.76 (d, $^2J_{C,P}$ = 5.5 Hz, *C*H=CH-P_0), 153.35 (d, $^2J_{C,P}$ = 14.8 Hz, C_1^1) ppm. $^{31}P\{^1H\}$ NMR ($CDCl_3$): δ = 13.5 (d, $^2J_{P,P}$ = 30.5 Hz, P_1), 18.3 (s, P_0), 51.6 (d, $^2J_{P,P}$ = 30.5 Hz, P'_1), 63.4 (s, P_2) ppm. $C_{40}H_{42}Cl_4N_5O_5P_5S_3$ (1065.7): calcd. C 45.08, H 3.97, N 6.57; found C 44.89, H 3.91, N 6.51.

Dendron 6-G_2: Powdered hydroxybenzaldehyde sodium salt (0.043 g, 0.301 mmol, an excess) was added to a solution of **3-G_2** (0.073 g, 0.069 mmol) in THF (5 mL). The resulting mixture was stirred overnight at room temperature. This solution was centrifuged then evaporated to dryness. The resulting powder was washed with THF/pentane (1:10) to afford **6-G_2** as a white powder in 90% yield (0.087 g). ^1H NMR ($CDCl_3$): δ = 1.32 (t, $^3J_{H,H}$ = 7.1 Hz, 6 H, CH_2-C*H*$_3$), 3.38 (d, $^3J_{H,P}$ = 11.0 Hz, 6 H, N-CH_3), 4.11 (dt, $^3J_{H,H}$ = 7.1, $^3J_{H,P}$ = 15.0 Hz, 4 H, CH_2), 6.35 (t, $^3J_{H,H}$ = $^2J_{H,P}$ = 17.2 Hz, 1 H, =CH-P_0), 7.19 (dd, $^3J_{H,H}$ = 8.7, $^4J_{H,P}$ = 1.4 Hz, 4 H, H-C_1^2), 7.37 (dd, $^3J_{H,H}$ = 8.5, $^4J_{H,P}$ = 1.4 Hz, 8 H, H-C_2^2), 7.57 (d, $^3J_{H,H}$ = 8.7 Hz, 4 H, H-C_1^3), 7.85 (d, $^3J_{H,H}$ = 8.5 Hz, 8 H, H-C_2^3), 7.40−7.74 (m, 17 H, H_{Arom}, CH=N, CH=CH), 9.92 (s, 4 H, CHO) ppm. $^{13}C\{^1H\}$ NMR ($CDCl_3$): δ = 16.27 (d, $^3J_{C,P}$ = 6.1 Hz, CH_2−*C*H_3), 32.56 (d, $^2J_{C,P}$ = 13.1 Hz, N-CH_3), 62.05 (d, $^2J_{C,P}$ = 5.7 Hz, CH_2), 117.48 (d, $^1J_{C,P}$ = 190.2 Hz, =CH-P_0), 122.01 (br. d, $^3J_{C,P}$ = 4.0 Hz, C_1^2, C_2^2), 127.28 (d, $^3J_{C,P}$ = 13.5 Hz, C_0^3), 127.98 (s, C_1^3), 128.01 (dd, $^1J_{C,P}$ = 106.5, $^3J_{C,P}$ = 5.0 Hz, C_0^i), 128.49 (d, $^3J_{C,P}$ = 14.0 Hz, C_0^m), 130.15 (dd, $^1J_{C,P}$ = 108.0, $^3J_{C,P}$ = 3.9 Hz, C_0^1), 130.40 (s, C_1^4), 131.26 (s, C_2^3), 132.65 (s, C_2^4), 132.68 (d, $^2J_{C,P}$ = 11.0 Hz, C_0^o), 132.72 (s, C_0^p), 133.20 (d, $^2J_{C,P}$ = 15.0 Hz, C_0^2), 138.51 (d, $^3J_{C,P}$ = 21.0 Hz, C_0^4), 140.08 (d, $^3J_{C,P}$ = 16.0 Hz, CH=N-N), 146.72 (d, $^2J_{C,P}$ = 6.0 Hz, *C*H=CH-P_0), 153.12 (d, $^2J_{C,P}$ = 10.2 Hz, C_1^1), 156.85 (d, $^2J_{C,P}$ = 9.8 Hz, C_2^1), 190.92 (s, CHO) ppm. $^{31}P\{^1H\}$ NMR ($CDCl_3$): δ = 13.7 (d, $^2J_{P,P}$ = 29.2 Hz, P_1), 18.2 (s, P_0), 51.8 (d, $^2J_{P,P}$ = 29.2 Hz, P'_1), 60.7 (s, P_2) ppm. $C_{68}H_{62}N_5O_{13}P_5S_3$ (1408.3): calcd. C 57.99, H 4.44, N 4.97; found C 58.11, H 4.47, N 4.94.

Dendron 8-G_1: Dichloromethane (1 mL) was added to a mixture of powdered **3-G_0** (0.100 g, 0.236 mmol) and azide **7** (0.046 g, 0.236 mmol), to dissolve both reagents. The resulting solution was stirred for three days at room temperature. The solvent was evaporated to afford **8-G_1** in quantitative yield as a white powder (0.140 g). ^1H NMR ($CDCl_3$): δ = 1.28 (t, $^3J_{H,H}$ = 7.0 Hz, 6 H, CH_2−C*H*$_3$), 2.66 (d, $^3J_{H,P}$ = 11.9 Hz, 6 H, N-CH_3), 3.56 (br. s, 4 H, NH_2), 4.06 (dt, $^3J_{H,H}$ = 7.0, $^3J_{H,P}$ = 14.5 Hz, 4 H, CH_2), 6.31 (t, $^3J_{H,H}$ = $^2J_{H,P}$ = 17.2 Hz, 1 H, =CH-P_0), 7.36−7.84 (m, 15 H, H_{Arom}, C*H*=CH-P_0) ppm. $^{13}C\{^1H\}$ NMR ($CDCl_3$): δ = 16.36 (d, $^3J_{C,P}$ = 5.9 Hz, CH_2−*C*H_3), 39.37 (d, $^2J_{C,P}$ = 6.0 Hz, N-CH_3), 62.00 (d, $^2J_{C,P}$ = 5.7 Hz, CH_2), 117.50 (d, $^1J_{C,P}$ = 190.5 Hz, =CH-P_0), 127.53 (d, $^3J_{C,P}$ = 13.1 Hz, C_0^3), 128.70 (d, $^3J_{C,P}$ = 12.2 Hz, C_0^m), 129.40 (br. d, $^1J_{C,P}$ = 110.0 Hz, C_0^i), 129.90 (d, $^1J_{C,P}$ = 110.0 Hz, C_0^1), 132.54 (s, C_0^p), 132.62 (d, $^2J_{C,P}$ = 10.2 Hz, C_0^o), 133.30 (d, $^2J_{C,P}$ = 11.5 Hz, C_0^2), 138.46 (d, $^3J_{C,P}$ = 23.7 Hz, C_0^4), 146.85 (d, $^2J_{C,P}$ = 6.7 Hz, *C*H=CH-P_0) ppm. $^{31}P\{^1H\}$ NMR ($CDCl_3$): δ = 12.8 (d, $^2J_{P,P}$ = 17.2 Hz, P_1), 18.2 (s, P_0), 71.2 (d, $^2J_{P,P}$ = 17.2 Hz, P'_1) ppm. $C_{26}H_{36}N_5O_3P_3S$ (591.59): calcd. C 52.79, H 6.13, N 11.84; found C 52.85, H 6.19, N 11.75.

Dendron 10-G_1: DMF (2 mL) was added to a mixture of powdered **8-G_1** (0.130 g, 0.219 mmol) and helicin **9** (0.125 g, 0.439 mmol). The resulting solution was stirred overnight then evaporated to dryness. **10-G_1** was isolated as an oil in quantitative yield (0.250 g). A strict stoichiometric amount of reagents must be used since it is difficult to eliminate the unreacted helicin. ^1H NMR ([D_8]THF): δ = 1.40 (t, $^3J_{H,H}$ = 7.0 Hz, 6 H, CH_2−C*H*$_3$), 3.28 (d, $^3J_{H,P}$ = 8.7 Hz, 3 H, N-CH_3), 3.30 (d, $^3J_{H,P}$ = 8.7 Hz, 3 H, N-CH_3), 3.41−3.92 (m, 12 H, CH_2 and CH helicin), 4.19 (dt, $^3J_{H,H}$ = 7.0, $^3J_{H,P}$ = 15.0 Hz, 4 H, CH_2OP), 4.74−5.11 (m, 10 H, OH, HC_1^7), 6.64 (t, $^3J_{H,H}$ = $^2J_{H,P}$ = 17.2 Hz, 1 H, =CH-P_0), 6.88 (m, 2 H, HC_1^3), 7.22 (m, 4 H, HC_1^4, HC_1^5), 7.56−8.11 (m, 19 H, H_{Arom}, C*H*=CH-P_0) ppm. $^{13}C\{^1H\}$ NMR ([D_8]THF): δ = 17.80 (d, $^3J_{C,P}$ = 5.9 Hz, CH_2−*C*H_3), 33.89 (d, $^2J_{C,P}$ = 9.8 Hz, N-CH_3), 34.04 (d, $^2J_{C,P}$ = 9.8 Hz, N-CH_3), 63.41 (d, $^2J_{C,P}$ = 5.7 Hz, CH_2OP), 63.72 (s, CH_2OH), 72.20 (s, C_1^{1o}), 75.87 (s, C_1^8), 79.01 (s, C_1^9 or C_1^{11}), 79.42 (s, C_1^{11} or C_1^9), 104.28 (s, C_1^7), 104.70 (s, C_1^7),

 © 2004 Wiley-VCH Verlag GmbH & Co. KGaA, Weinheim

119.24 (s, C_1^5), 119.61 (d, $^1J_{C,P}$ = 188.8 Hz, =CH-P_0), 119.74 (s, C_1^5), 124.13 (s, C_1^3), 124.30 (s, C_1^3), 127.43 (s, C_1^2), 129.21 (d, $^3J_{C,P}$ = 13.2 Hz, C_0^3), 129.42 (s, C_1^1), 129.86 (s, C_1^4), 130.20 (d, $^3J_{C,P}$ = 12.5 Hz, C_0^m), 132.18 (br. d, $^1J_{C,P}$ = 108.3 Hz, C_0^i), 132.24 (d, $^3J_{C,P}$ = 14.2 Hz, CH=N), 132.44 (d, $^1J_{C,P}$ = 110.0 Hz, C_0^1), 133.94 (s, C_0^p), 134.98 (d, $^2J_{C,P}$ = 10.8 Hz, C_0^o), 133.50 (d, $^2J_{C,P}$ = 10.6 Hz, C_0^2), 140.47 (d, $^3J_{C,P}$ = 23.6 Hz, C_0^4), 148.86 (d, $^2J_{C,P}$ = 6.7 Hz, *C*H=CH-P_0), 157.37 (s, C_1^6), 157.52 (s, C_1^6) ppm. $^{31}P\{^1H\}$ NMR ([D_8]THF): δ = 14.6 (d, $^2J_{P,P}$ = 26.6 Hz, P_1), 24.0 (s, P_0), 62.5 (d, $^2J_{P,P}$ = 26.6 Hz, P'_1) ppm. $C_{52}H_{64}N_5O_{15}P_3S$ (1124.08): calcd. C 55.56, H 5.74, N 6.23; found C 55.47, H 5.71, N 6.31.

Cationic Dendron 11-G_1: Methyl trifluoromethanesulfonate (50 μL, 0.470 mmol) was added dropwise to a solution of **3-G_1** (0.350 g, 0.470 mmol) in CH_2Cl_2 (10 mL) at 0 °C. The reaction mixture was stirred for 10 minutes at 0 °C and 20 minutes at room temperature and then evaporated to dryness. The crude residue was washed with pentane to afford **11-G_1** as a sticky yellow oil in 95% yield (0.405 g). ^1H NMR (CD_2Cl_2): δ = 1.30 (t, $^3J_{H,H}$ = 7.0 Hz, 6 H, CH_3), 2.63 (d, $^3J_{H,P}$ = 18.2 Hz, 3 H, P_1-S-CH_3), 4.16 (dt, $^3J_{H,H}$ = 7.2, $^3J_{H,P}$ = 14.5 Hz, 4 H, CH_2), 6.55 (t, $^3J_{H,H}$ = $^2J_{H,P}$ = 17.0 Hz, 1 H, =CH-P_0), 7.24−8.07 (m, 23 H, H_{Arom}, C*H*=CH-P_0), 9.95 (s, 2 H, CHO) ppm. $^{13}C\{^1H\}$ NMR (CD_2Cl_2): δ = 14.23 (d, $^2J_{C,P}$ = 5.3 Hz, S-CH_3), 16.62 (d, $^2J_{C,P}$ = 5.8 Hz, CH_3), 63.20 (br. s, CH_2), 121.28 (q, $^1J_{C,F}$ = 323.5 Hz, CF_3), 121.81 (d, $^3J_{C,P}$ = 4.9 Hz, C_1^2), 122.15 (d, $^1J_{C,P}$ = 186.2 Hz, =CH-P_0), 124.17 (dd, $^1J_{C,P}$ = 107.4, $^3J_{C,P}$ = 4.4 Hz, C_0^i), 126.03 (dd, $^1J_{C,P}$ = 101.7, $^3J_{C,P}$ = 5.8 Hz, C_0^1), 129.18 (d, $^3J_{C,P}$ = 12.8 Hz, C_0^3), 130.31 (d, $^3J_{C,P}$ = 13.5 Hz, C_0^m), 132.39 (s, C_1^3), 132.62 (d, $^2J_{C,P}$ = 11.7 Hz, C_0^o), 133.32 (d, $^2J_{C,P}$ = 12.0 Hz, C_0^2), 135.24 (d, $^4J_{C,P}$ = 2.9 Hz, C_0^p), 135.46 (s, C_1^4), 141.07 (d, $^3J_{C,P}$ = 26.4 Hz, C_0^4), 146.42 (br. s, *C*H=CH-P_0), 153.55 (d, $^2J_{C,P}$ = 10.9 Hz, C_1^1), 190.82 (s, CHO) ppm. $^{31}P\{^1H\}$ NMR (CD_2Cl_2): δ = 16.9 (s, P_0), 22.2 (d, $^2J_{P,P}$ = 20.5 Hz, P_1), 23.1 (d, $^2J_{P,P}$ = 20.5 Hz, P'_1) ppm. $C_{40}H_{39}F_3NO_{10}P_3S_2$ (907.79): calcd. C 52.92, H 4.33, N 1.54; found C 53.21, H 4.42, N 1.48.

Dicationic Dendron (12-G_1): Trimethylsilyl trifluoromethanesulfonate (85 μL, 0.470 mmol) was added dropwise to a solution of **11-G_1** (0.420 g, 0.470 mmol) in CH_2Cl_2 (10 mL) at 0 °C. The reaction mixture was stirred for 10 minutes at 0 °C and 30 minutes at room temperature and then evaporated to dryness. The crude residue was washed with pentane to afford **12-G_1** as a sticky yellow oil in 89% yield (0.473 g). ^1H NMR (CD_2Cl_2): δ = 0.10 (s, 9 H, $SiMe_3$), 1.47 (t, $^3J_{H,H}$ = 7.0 Hz, 6 H, CH_3), 2.62 (d, $^3J_{H,P}$ = 18.2 Hz, 3 H, P_1-S-CH_3), 4.40 (dt, $^3J_{H,H}$ = 7.2, $^3J_{H,P}$ = 14.6 Hz, 4 H, CH_2), 6.73 (t, $^3J_{H,H}$ = $^2J_{H,P}$ = 17.0 Hz, 1 H, =CH-P_0), 7.24−8.07 (m, 23 H, H_{Arom} and C*H*=CH-P_0), 10.03 (s, 2 H, CHO) ppm. $^{13}C\{^1H\}$ NMR (CD_2Cl_2): δ = 1.93 (s, $SiMe_3$), 14.21 (d, $^2J_{C,P}$ = 5.3 Hz, S-CH_3), 16.19 (d, $^2J_{C,P}$ = 5.8 Hz, CH_3), 66.97 (d, $^2J_{C,P}$ = 5.4 Hz, CH_2), 113.32 (d, $^1J_{C,P}$ = 194.2 Hz, =CH-P_0), 120.58 (q, $^1J_{C,F}$ = 323 Hz, CF_3), 121.77 (d, $^3J_{C,P}$ = 4.8 Hz, C_1^2), 123.56 (dd, $^1J_{C,P}$ = 106.9, $^3J_{C,P}$ = 4.1 Hz, C_0^i), 126.67 (dd, $^1J_{C,P}$ = 107.5, $^3J_{C,P}$ = 4.0 Hz, C_0^1), 129.85 (d, $^3J_{C,P}$ = 13.8 Hz, C_0^3), 130.33 (d, $^3J_{C,P}$ = 13.6 Hz, C_0^m), 132.41 (s, C_1^3), 132.62 (d, $^2J_{C,P}$ = 11.9 Hz, C_0^o), 133.26 (d, $^2J_{C,P}$ = 12.0 Hz, C_0^2), 135.31 (d, $^4J_{C,P}$ = 3.0 Hz, C_0^p), 135.52 (s, C_1^4), 139.78 (d, $^3J_{C,P}$ = 28.6 Hz, C_0^4), 151.19 (d, $^2J_{C,P}$ = 8.9 Hz, *C*H=CH-P_0), 153.52 (d, $^2J_{C,P}$ = 10.9 Hz, C_1^1), 190.83 (s, CHO) ppm. $^{31}P\{^1H\}$ NMR (CD_2Cl_2): δ = 22.0 (d, $^2J_{P,P}$ = 20.7 Hz, P_1), 23.2 (d, $^2J_{P,P}$ = 20.7 Hz, P'_1), 23.6 (s, P_0) ppm. $C_{44}H_{48}F_6NO_{13}P_3S_3Si$ (1130.1): calcd. C 46.77, H 4.28, N 1.24; found C 46.94, H 4.32, N 1.15.

Dendron 14-G_2: THF (8 mL) was added to a powdered mixture of **3-G_2** (0.055 g, 0.0516 mmol), compound **13** (0.086 g, 0.227 mmol, slight excess) and Cs_2CO_3 (0.150 g, 0.454 mmol, excess). The resulting mixture was stirred overnight then centrifuged, and the solution was evaporated to dryness. The resulting powder was washed with THF/pentane to eliminate unreacted **7**. Compound **14-G_2** was obtained as a white powder in 63% yield (0.081 g). ^1H NMR ($CDCl_3$): δ = 1.33 (t, $^3J_{H,H}$ = 7.1 Hz, 6 H, CH_2-CH_3), 3.33 (d, $^3J_{H,P}$ = 10.5 Hz, 6 H, N-CH_3), 4.12 (dt, $^3J_{H,H}$ = 7.1, $^3J_{H,P}$ = 14.8 Hz, 4 H, CH_2), 6.37 (t, $^3J_{H,H}$ = $^2J_{H,P}$ = 17.1 Hz, 1 H, =CH-P_0), 6.86 (d, $^3J_{H,H}$ = 8.1 Hz, 8 H, H-C_2^3), 6.92 (m, 4 H, H-C_3^3), 7.15 (d, $^3J_{H,H}$ = 8.1 Hz, 8 H, H-C_2^2), 7.23−7.78 (m, 73 H, H_{Arom}, CH=N, CH=CH), 8.15 (br. dd, $^3J_{H,H}$ = 6.9, $^4J_{H,P}$ = 4.1 Hz, 4 H, H-C_3^6), 9.02 (d, $^4J_{H,P}$ = 5.1 Hz, 1 H, CH=N-C) ppm. $^{13}C\{^1H\}$ NMR ($CDCl_3$): δ = 16.28 (d, $^3J_{C,P}$ = 6.0 Hz, CH_2-CH_3), 32.96 (d, $^2J_{C,P}$ = 13.1 Hz, N-CH_3), 61.94 (d, $^2J_{C,P}$ = 5.5 Hz, CH_2), 117.53 (d, $^1J_{C,P}$ = 189.0 Hz, =CH-P_0), 121.84 (br. s, C_1^2, C_2^2, C_2^3), 127.18 (d, $^3J_{C,P}$ = 13.3 Hz, C_0^3), 127.85 (s, C_1^3), 127.99 (d, $^3J_{C,P}$ = 14.2 Hz, C_0^m), 128.01 (dd, $^1J_{C,P}$ = 106.0, $^3J_{C,P}$ = 6.0 Hz, C_0^i), 128.17 (d, $^3J_{C,P}$ = 3.9 Hz, C_3^6), 128.52 (d, $^3J_{C,P}$ = 7.1 Hz, C_3^m), 128.79 (br. s, C_3^5, C_3^p), 130.10 (dd, $^1J_{C,P}$ = 108.0, $^3J_{C,P}$ = 3.6 Hz, C_0^1), 130.77 (s, C_3^4), 130.90 (s, C_1^4), 132.58 (d, $^2J_{C,P}$ = 11.0 Hz, C_0^o), 132.70 (s, C_0^p), 133.30 (d, $^2J_{C,P}$ = 15.3 Hz, C_0^2), 133.44 (s, C_3^3), 133.88 (d, $^2J_{C,P}$ = 19.9 Hz, C_3^o), 136.24 (d, $^1J_{C,P}$ = 8.7 Hz, C_3^i), 138.46 (d, $^2J_{C,P}$ = 20.4 Hz, C_3^1), 138.53 (d, $^3J_{C,P}$ = 21.0 Hz, C_0^4), 138.84 (d, $^1J_{C,P}$ = 17.3 Hz, C_3^2), 139.07 (br. d, $^3J_{C,P}$ = 13.5 Hz, CH=N-N), 146.68 (d, $^2J_{C,P}$ = 6.5 Hz, *C*H=CH-P_0), 148.54 (d, $^2J_{C,P}$ = 5.9 Hz, C_2^1), 148.55 (s, C_2^4), 152.92 (d, $^2J_{C,P}$ = 10.2 Hz, C_1^1), 158.62 (d, $^3J_{C,P}$ = 20.9 Hz, *C*H=N-C) ppm. $^{31}P\{^1H\}$ NMR ($CDCl_3$): δ = −13.1 (s, P_3), 13.5 (d, $^2J_{P,P}$ = 30.5 Hz, P_1), 18.3 (s, P_0), 51.8 (d, $^2J_{P,P}$ = 30.5 Hz, P'_1), 63.5 (s, P_2) ppm. $C_{140}H_{118}N_9O_9P_9S_3$ (2445.5): calcd. C 68.76, H 4.86, N 5.16; found C 68.64, H 4.82, N 5.11.

Complexed Dendron (15-G_2): A solution of **14-G_2** (0.200 g, 0.082 mmol) in CH_2Cl_2 (25 mL) was added slowly dropwise during 2 hours to a solution of [$PdCl_2$(COD)] (0.093 g, 0.327 mmol) in CH_2Cl_2 (25 mL). The resulting solution was stirred for 3 hours more then evaporated to dryness. The residue was washed with THF/pentane (1:10) to afford **15-G_2** as a pale yellow powder in 85% yield (0.219 g). ^1H NMR (CD_2Cl_2): δ = 1.30 (t, $^3J_{H,H}$ = 7.0 Hz, 6 H, CH_2-CH_3), 3.31 (d, $^3J_{H,P}$ = 10.7 Hz, 6 H, N-CH_3), 4.07 (m, 4 H, CH_2), 6.41 (t, $^3J_{H,H}$ = $^2J_{H,P}$ = 17.2 Hz, 1 H, =CH-P_0), 7.07 (m, 4 H, H-C_3^3), 7.16 (d, $^3J_{H,H}$ = 8.8 Hz, 8 H, H-C_2^3), 7.28 (d, $^3J_{H,H}$ = 8.8 Hz, 8 H, H-C_2^2), 7.40−7.80 (m, 73 H, H_{Arom}, CH=N, CH=CH), 7.93 (m, 4 H, H-C_3^6), 8.21 (d, $^4J_{H,P}$ = 5.1 Hz, 1 H, CH=N-C) ppm. $^{13}C\{^1H\}$ NMR (CD_2Cl_2): δ = 16.79 (d, $^3J_{C,P}$ = 5.9 Hz, CH_2-CH_3), 33.58 (d, $^2J_{C,P}$ = 13.1 Hz, N-CH_3), 62.59 (d, $^2J_{C,P}$ = 6.0 Hz, CH_2), 118.58 (d, $^1J_{C,P}$ = 189.1 Hz, =CH-P_0), 121.94 (d, $^2J_{C,P}$ = 3.8 Hz, C_2^2), 122.45 (d, $^2J_{C,P}$ = 5.3 Hz, C_1^2), 122.23 (d, $^1J_{C,P}$ = 49.4 Hz, C_3^2), 125.09 (s, C_2^3), 125.69 (d, $^1J_{C,P}$ = 61.1 Hz, C_3^i), 128.20 (d, $^3J_{C,P}$ = 13.7 Hz, C_0^3, C_0^m), 128.64 (br. s, C_1^3, C_3^6), 128.72 (dd, $^1J_{C,P}$ = 106.0, $^3J_{C,P}$ = 3.5 Hz, C_0^i), 129.26 (s, C_3^5), 129.58 (d, $^3J_{C,P}$ = 13.0 Hz, C_3^m), 131.50 (dd, $^1J_{C,P}$ = 106.0, $^3J_{C,P}$ = 4.0 Hz, C_0^1), 131.63 (s, C_1^4), 133.12 (d, $^4J_{C,P}$ = 5.5 Hz, C_3^p), 133.32 (s, C_3^4), 133.69 (d, $^2J_{C,P}$ = 13.2 Hz, C_0^o), 133.79 (s, C_0^p), 134.00 (d, $^2J_{C,P}$ = 16.0 Hz, C_0^2), 134.40 (s, C_3^3), 134.68 (d, $^2J_{C,P}$ = 10.9 Hz, C_3^o), 137.14 (d, $^2J_{C,P}$ = 15.9 Hz, C_3^1), 139.23 (d, $^3J_{C,P}$ = 21.0 Hz, C_0^4), 140.83 (d, $^3J_{C,P}$ = 12.8 Hz, CH=N-N), 146.99 (d, $^2J_{C,P}$ = 6.4 Hz, *C*H=CH-P_0), 149.77 (s, C_2^4), 150.34 (d, $^2J_{C,P}$ = 5.9 Hz, C_2^1), 153.59 (d, $^2J_{C,P}$ = 9.8 Hz, C_1^1), 166.7 (d, $^3J_{C,P}$ = 9.1 Hz, *C*H=N-C) ppm. $^{31}P\{^1H\}$ NMR (CD_2Cl_2): δ = 15.6 (d, $^2J_{P,P}$ = 29.1 Hz, P_1), 19.7 (s, P_0), 33.0 (s, P_3), 53.2 (d, $^2J_{P,P}$ = 29.1 Hz, P'_1), 64.8 (s, P_2) ppm. $C_{140}H_{118}Cl_8N_9O_9P_9Pd_4S_3$ (3154.8): calcd. C 53.30, H 3.77, N 4.00; found C 53.38, H 3.82, N 4.02.

X-ray Crystallographic Study: Data collection was performed on a Stoe Imaging Plate Diffraction System (IPDS), equipped with an

 © 2004 Wiley-VCH Verlag GmbH & Co. KGaA, Weinheim

Oxford Cryosystems Cryostream Cooler. Device and using a graphite-monochromated Mo-K_α radiation (λ = 0.71073Å), at T = 160 K. Further details are provided in Table 1. Final unit-cell parameters were obtained by means of a least-squares refinement of a set of 8000 well-measured reflections, and crystal decay was monitored during the data collection by measuring 200 reflections by exposure. No significant fluctuations of the intensities were observed during measurement.

Table 1. Crystal data, data collection and structure refinement

Empirical formula	$C_{24}H_{26}O_3P_2$
Molecular mass	424.39
Wavelength	0.71073Å
Crystal system, space group	triclinic, $P\bar{1}$
Unit cell dimensions	a = 15.435(2) Å b = 8.6930(11) Å c = 16.326(3) Å α = 90.179(17)° β = 92.141(18)° γ = 90.067(16)°
Volume	2189.1(5) Å^3
Z, calculated density	4, 1.288 mg/m^3
Absorption coefficient	0.221 mm^{-1}
F(000)	896
Crystal size	0.42 × 0.17 × 0.08 mm
Crystal colour and form	colourless plate
Tube power	1.50 kW
Tube voltage	50 kV
Tube current	30 mA
Collimator size	0.8 mm
Detector distance	70.0 mm
2θ range	3.3−52.1°
d(hkl) range	12.453−0.809 Å
φ movement mode	rotation
φ start	0.0°
φ end	200.2°
φ increment	1.1°
Number of exposures	182
Irradiation/exposure	2.00 min
Measurement duration	19 h
θ range for data collection	2.64−23.26°
Index ranges	$-17 \le h \le 17$ $-9 \le k \le 9$ $-18 \le l \le 18$
Reflections collected/unique	12240/3099 [R(int) = 0.0592]
Completeness to 2θ = 46.52	98.2%
Refinement method	Full-matrix least-squares on F^2
Data/restraints/parameters	3099/0/272
Goodness-of-fit on F^2	1.032
Weighting scheme	$1/[\sigma^2(F_o^2) + (0.0509P)^2 + 1.396P]$ where $P = (F_o^2 + 2F_c^2)/3$
Final R indices [$I > 2\sigma(I)$]	$R1$ = 0.0377, $wR2$ = 0.0979
R indices (all data)	$R1$ = 0.0413, $wR2$ = 0.1011
Largest diff. peak and hole	(0.705 and −0.364) e·Å^{-3}

The structure was solved by means of direct methods using the program SIR92[31] and subsequent difference Fourier maps, then refined by least-squares procedures on F^2 by using the program SHELXL-97.[32] Atomic scattering factors were taken from the International Tables for X-ray Crystallography.[33]

All hydrogen atoms were located in difference Fourier maps, but introduced in the refinement as fixed contributors by using a riding model with an isotropic thermal parameter fixed at 20% higher than those of the C_{sp^2} atoms and 50% for the C_{sp^3} atoms to which they are connected, excepted hydrogens atoms labelled H(1) and H(2) attached to the C(1) and C(2) carbons atoms, respectively, which were refined isotropically. Methyl groups were refined with the torsion angle as a free variable. All non-hydrogen atoms were refined anisotropically, and in the last cycles of refinement weighting schemes were used. The weights were calculated from the following formula: $W = 1/[\sigma^2(F_o^2) + (aP)^2 + bP]$ where $P = (F_o^2 + 2F_c^2)/3$. Criteria for a satisfactory complete analysis were the ratios of root-mean-square shift standard deviation being less than 0.1 and no significant features in the final difference Fourier maps. Drawings of the molecules were produced with the program ORTEP3[34] with 50% probability displacement ellipsoids for non-hydrogen atoms.

CCDC-228136 contains the supplementary crystallographic data for this paper. These data can be obtained free of charge at www.ccdc.cam.ac.uk/conts/retrieving.html [or from the Cambridge Crystallographic Data Centre, 12 Union Road, Cambridge CB2 1EZ, UK; Fax: (internat.) + 44-1223-336-033; E-mail: deposit@ccdc.cam.ac.uk].

[1] G. R. Newkome, C. N. Moorefield, F. Vögtle, *Dendrimers and Dendrons*, Wiley-VCH, Weinheim (Germany), **2001**.
[2] J. M. J. Fréchet, D. A. Tomalia, *Dendrimers and other Dendritic Polymers*, Wiley Europe, Chichester, **2001**.
[3] C. J. Hawker, J. M. J. Fréchet, *J. Am. Chem. Soc.* **1990**, *112*, 7638−7647.
[4] V. Maraval, R. Laurent, B. Donnadieu, M. Mauzac, A. M. Caminade, J. P. Majoral, *J. Am. Chem. Soc.* **2000**, *122*, 2499−2511.
[5] K. L. Wooley, C. J. Hawker, J. M. J. Fréchet, *J. Am. Chem. Soc.* **1991**, *113*, 4252−4261.
[6] D. C. Tully, J. M. J. Fréchet, *Chem. Commun.* **2001**, 1229−1239.
[7] P. Savignac, B. Iorga, *Modern Phosphonate Chemistry*, CRC Press, **2003**.
[8] V. Maraval, D. Prévôté-Pinet, R. Laurent, A. M. Caminade, J. P. Majoral, *New J. Chem.* **2000**, *24*, 561−566.
[9] V. Maraval, R. M. Sebastian, F. Ben, R. Laurent, A. M. Caminade, J. P. Majoral, *Eur. J. Inorg. Chem.* **2001**, 1681−1691.
[10] J. P. Majoral, A. M. Caminade, *Chem. Rev.* **1999**, *99*, 845−880.
[11] M. L. Lartigue, B. Donnadieu, C. Galliot, A. M. Caminade, J. P. Majoral, J. P. Fayet, *Macromolecules* **1997**, *30*, 7335−7337.
[12] M. L. Lartigue, N. Launay, B. Donnadieu, A. M. Caminade, J. P. Majoral, *Bull. Soc. Chim. Fr.* **1997**, *134*, 981−988.
[13] C. Galliot, C. Larré, A. M. Caminade, J. P. Majoral, *Science* **1997**, *277*, 1981−1984.
[14] G. M. Salamonczyk, M. Kuznikowski, E. Poniatowska, *Tetrahedron Lett.* **2002**, *43*, 1747−1749.
[15] B. E. Maryanoff, A. B. Reitz, *Chem. Rev.* **1989**, *89*, 863−927.
[16] D. Prévôté, S. Le Roy-Gourvennec, A. M. Caminade, S. Masson, J. P. Majoral, *Synthesis* **1997**, 1199−1207.
[17] C. Larré, A. M. Caminade, J. P. Majoral, *Angew. Chem.* **1997**, *109*, 614−617; *Angew. Chem. Int. Ed. Engl.* **1997**, *36*, 596−599.
[18] N. Launay, A. M. Caminade, R. Lahana, J. P. Majoral, *Angew. Chem.* **1994**, *106*, 1682−1684; *Angew. Chem. Int. Ed. Engl.* **1994**, *33*, 1589−1592.
[19] N. Launay, A. M. Caminade, J. P. Majoral, *J. Am. Chem. Soc.* **1995**, *117*, 3282−3283.
[20] V. Maraval, R. Laurent, S. Merino, A. M. Caminade, J. P. Majoral, *Eur. J. Org. Chem.* **2000**, 3555−3568.
[21] R. M. Sebastian, G. Magro, A. M. Caminade, J. P. Majoral, *Tetrahedron* **2000**, *56*, 6269−6277.
[22] G. Magro, B. Donnadieu, A. M. Caminade, J. P. Majoral, *Chem. Eur. J.* **2003**, *9*, 2151−2159.
[23] C. Larré, B. Donnadieu, A. M. Caminade, J. P. Majoral, *J. Am.*

 © 2004 Wiley-VCH Verlag GmbH & Co. KGaA, Weinheim

Chem. Soc. **1998**, *120*, 4029−4030.
[24] F. Gonce, A. M. Caminade, J. P. Majoral, *Tetrahedron Lett.* **1991**, *32*, 203−206.
[25] J. P. Majoral, M. Badri, A. M. Caminade, M. Delmas, A. Gaset, *Inorg. Chem.* **1991**, *30*, 344−346.
[26] M. Koprowski, R. M. Sebastian, V. Maraval, M. Zablocka, V. Cadierno-Menendez, B. Donnadieu, A. Igau, A. M. Caminade, J. P. Majoral, *Organometallics* **2002**, *21*, 4680−4687.
[27] G. Guerrero, P. H. Mutin, A. Vioux, *J. Mater. Chem.* **2001**, *11*, 3161−3165.
[28] G. Guerrero, P. H. Mutin, A. Vioux, *Chem. Mater.* **2001**, *13*, 4367−4373.
[29] G. P. Schiemenz, H. Kaack, *Justus Liebigs Ann. Chem.* **1973**, *9*, 1480−1493.
[30] J. Mitjaville, A. M. Caminade, R. Mathieu, J. P. Majoral, *J. Am. Chem. Soc.* **1994**, *116*, 5007−5008.
[31] A. Altomare, G. Cascarano, C. Giacovazzo, A. Guagliardi, *J. Appl. Crystallogr.* **1993**, *26*, 343−350.
[32] G. M. Sheldrick, *SHELX97 − Programs for Crystal Structure Analysis* (Release 97-2). Institut für Anorganische Chemie der Universität, Tammannstrasse 4, 3400 Göttingen, Germany, **1998**.
[33] *International Tables for X-ray Crystallography*, Vol IV, Kynoch press, Birmingham, England, **1974**.
[34] L. J. Farrugia, *J. Appl. Crystallogr.* **1997**, *30*, 565.

Received January 10, 2004
Early View Article
Published Online April 26, 2004

 © 2004 Wiley-VCH Verlag GmbH & Co. KGaA, Weinheim

Second Order Optical Nonlinearities of Copper(II) and Palladium(II) Complexes with *N*-Salicylidene-*N*′-aroylhydrazine Tridentate Ligands

Fabio Borbone,[a] Ugo Caruso,[a] Roberto Centore,*[a] Antonella De Maria,[a] Alain Fort,[b] Michela Fusco,[a] Barbara Panunzi,[c] Antonio Roviello,*[a] and Angela Tuzi[a]

Dedicated to Prof. A. Sirigu on the occasion of his 65th birthday

Keywords: Tridentate ligands / Nonlinear optics / Polymers / Copper / Palladium

Three new *N*-salicylidene-*N*′-aroylhydrazines tridentate ligands have been prepared: *N*-4-diethylaminosalicylidene-*N*′-(4-nitrocinnamoylhydrazine (L^1), *N*-4-diethylaminosalicylidene-*N*′-4-(2,4-dinitrophenylethylidene)benzoylhydrazine (L^2), *N*-4-diethylaminosalicylidene-*N*′-4-(6-nitro-2-benzoxazolyl)benzoylhydrazine (L^3). From these ligands, mononuclear acentric complexes of Copper(II) and Palladium(II), with pyridine as further ligand, have been prepared and characterized, also by single-crystal X-ray analysis. These complexes show high second order nonlinear optical activity (EFISH, $|\mu\beta|$ up to $3000 \cdot 10^{-48}$ esu, incident wavelength 1.907 μm). The properties of metallorganic polymers obtained by grafting commercial poly(4-vinylpyridine) with ML^1 fragment (M = Cu^{II} or Pd^{II}) are also reported.
(© Wiley-VCH Verlag GmbH & Co. KGaA, 69451 Weinheim, Germany, 2004)

Introduction

The design of dipolar metallorganic chromophores with second order optical nonlinearities has been carried out till now according to two chemical architectures: organometallic fragments as electron donor-acceptor groups at the end of a π conjugated system[1] or metals as constituents of the conjugation bridge between the donor and acceptor groups.[1c,2]

A nonlinear optically (NLO) active polymer material is obtained from the chromophore following two approaches widely used in the case of purely organic compounds:[3] noncovalent incorporation of active molecules (guest) in an organic polymeric matrix (host) or covalent incorporation of chromophores into a polymer chain or in a three dimensional network. In both cases a noncentrosymmetric polar alignment of the NLO active fragments (''poling'') must be achieved (generally by applying a strong electric field while the polymer is kept above its glass transition temperature) which is a necessary condition for bulk second order NLO activity. Drawbacks of the first approach are in the low time stability of the noncentrosymmetric polar order and in the low solubility of the chromophore in the polymer matrix (the latter effect is probably enhanced in the case of metallorganic NLO-phores); in the second approach, on the other hand, the chemical synthesis of the organometallic chromophore must include steps for its functionalization as monomer for polymerization reactions (e.g. as diol or methacrylate ester).

We have recently proposed a new approach to metal-coordinated second order NLO active polymer materials, based on the use of tridentate ligands of the *N*-salicylidene-*N*′-aroylhydrazine type.[4] The use of such ligands, properly functionalized with strong electron donor-acceptor groups, is based on two factors (see Scheme 1). First, upon coordination, the ligand changes from the cheto (amide) to the enolic form with extension of π conjugation along the whole structure; second, the formed complex is electrically neutral but the metal (Cu^{II}, Pd^{II}) is coordinatively unsaturated.

In the absence of other ligands the coordination sphere of the metal is completed by centrosymmetric coupling and dimers are formed (see Scheme 2); however, if other ligands are present, acentric monomeric complexes may be formed, as witnessed by the strong tendency of dimers to form monomeric adducts by reaction with neutral molecules containing N donor atoms (e.g. pyridine, imidazole, etc.).[4,5]

This feature is of relevant interest inasmuch as it allows the anchorage of NLO active metallorganic fragments to a suitable preformed polymer chain [e.g. poly(4-vinylpyri-

[a] Dipartimento di Chimica, Università di Napoli "Federico II", Via Cinthia, 80126 Napoli, Italy
E-mail: centore@chemistry.unina.it
roviello@chemistry.unina.it
[b] IPCMS-CNRS, Groupe d'Optique Nonlinéaire et d'Optoelélectronique,
23 Rue du Loess, 67037 Strasbourg Cedex, France
[c] Dipartimento di Scienza degli Alimenti, Università degli Studi di Napoli "Federico II",
Via Università 100, 80055 Napoli, Italy

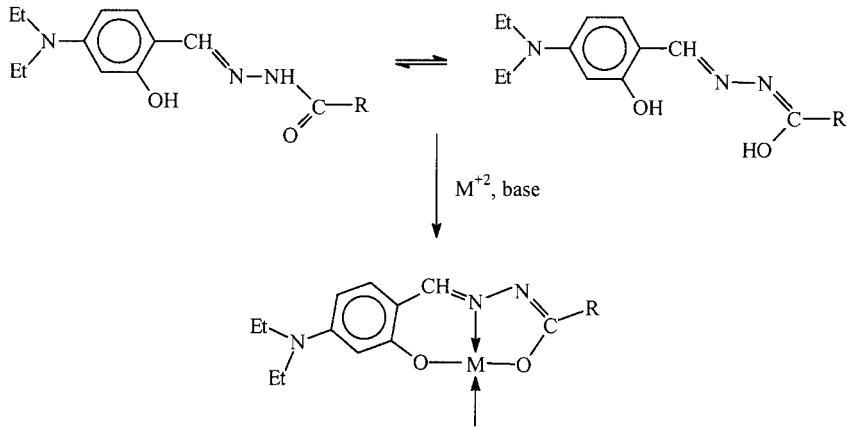

Scheme 1

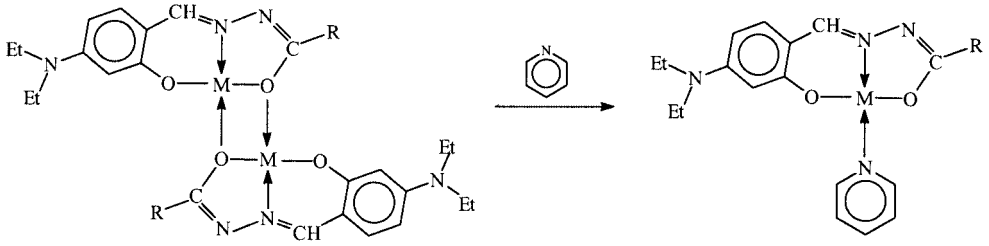

Scheme 2

dine)] through a coordination bond.[4b] The advantages of this approach are evident. Among others, we stress that the chemical synthesis of the chromophore and of the polymer can be worked out in a substantially independent way, no functionalization of the organic ligand is required and commercially available polymers can be used.

In this paper we report the synthesis and characterization of new monomeric complexes of this type exhibiting high NLO activity, whose formulae are shown in Scheme 3.

In addition we will also demonstrate the anchorage of one NLO active metallorganic fragment to commercial poly(4-vinylpyridine), according to Scheme 4, so that our complexes can be considered as rare examples of highly NLO active metallorganic chromophores from which polymers are successfully obtained. A full account of the properties of various commercial polymers grafted with all the above reported organometallic fragments will be given in a forthcoming publication from our laboratory.

Results and Discussion

Drawings of the crystallographic independent units of Cu1, Cu2, Pd2, and Cu3 are reported in Figures 1, 2, 3, and 4; selected bond lengths, bond angles, and torsion angles are reported in Table 1.

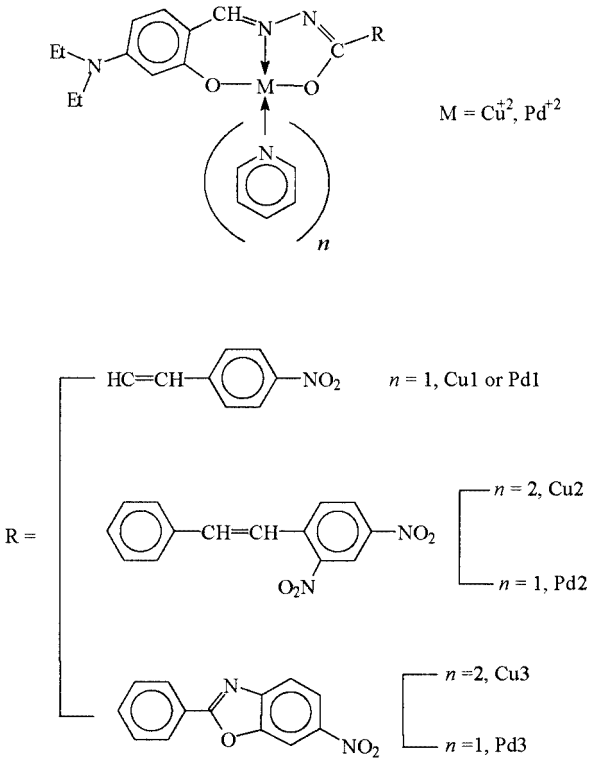

Scheme 3

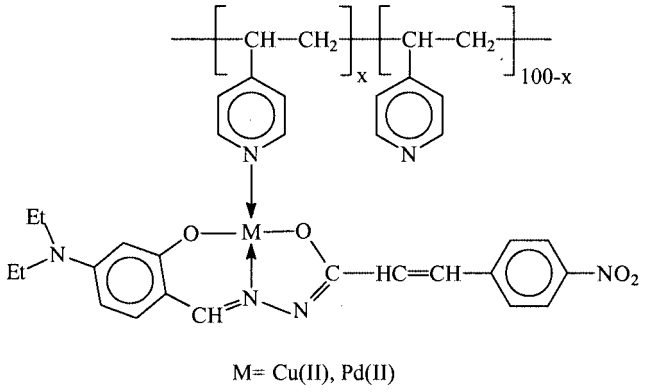

Scheme 4

In all the reported structures the tridentate ligand is in the enolic form. In fact, bond lengths C12−O2 [ranging from 1.286(5) to 1.306(5) Å] and C12−N3 [ranging from 1.298(7) to 1.320(5) Å] are respectively longer and shorter as compared with the values expected for an amide group.[6] On the other hand, IR spectra of free ligands in the solid state clearly show bands typical of the amide group. The structural change of the ligands upon coordination is also confirmed by the UV/Vis absorption patterns. In fact, as it is shown for L^1 in Figure 5, a significant red-shift of λ_{max} is observed upon coordination, with the λ_{max} of the coordinated ligand being substantially unchanged in the dimer, monomer, and grafted polymer.

The conformation of the ligands is close to be planar in all cases. In the complexes containing the ligand L^2 the nitro group in *para* position to the vinylene group is substantially coplanar with the phenyl, while the *ortho* nitro group is significantly twisted by torsion around the bond C26−N5 (Table 1). This is probably due to the close intramolecular contact between O6 and H atom bonded to C20 (the distance O6···C20 is 2.83 Å in Cu2 and 2.86 Å in Pd2). This contact could be relaxed also by torsion around the

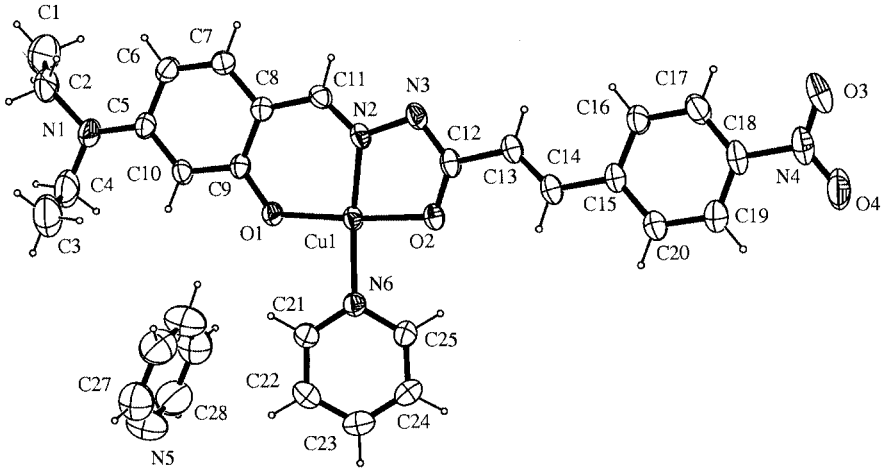

Figure 1. ORTEP view of Cu1; thermal ellipsoids are at 30% probability level; only one position of the non-coordinated pyridine molecule is shown

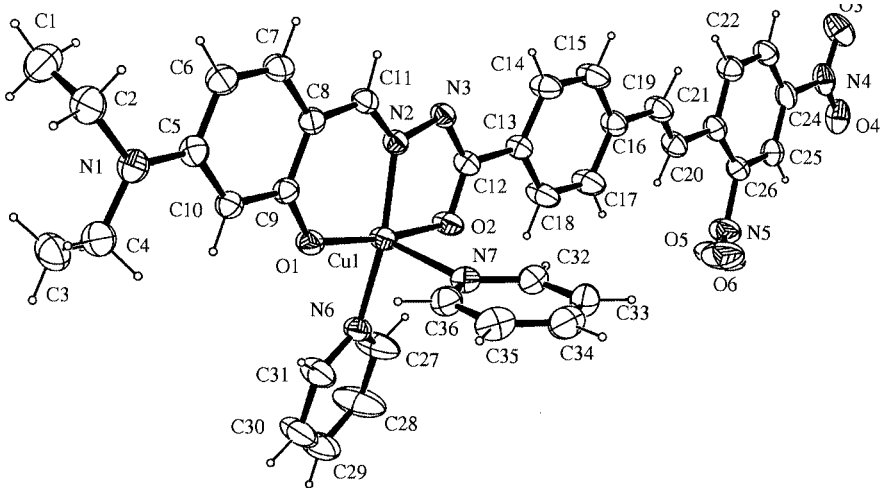

Figure 2. ORTEP view of Cu2; thermal ellipsoids are at 30% probability level

 © 2004 Wiley-VCH Verlag GmbH & Co. KGaA, Weinheim

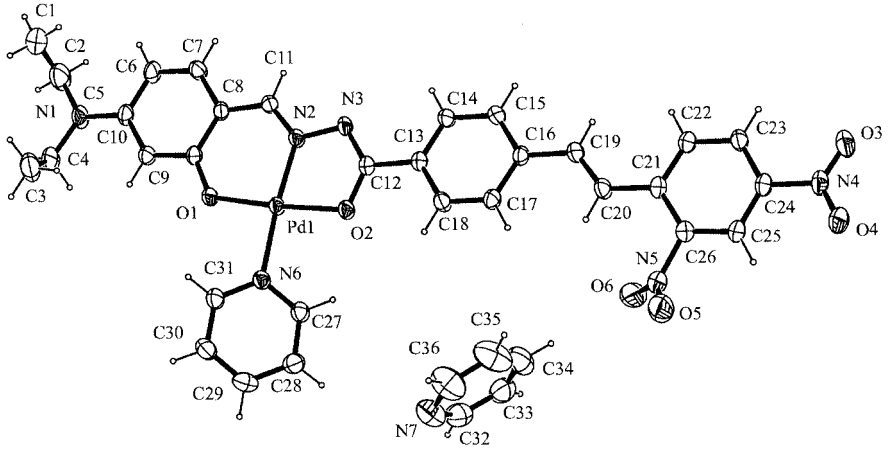

Figure 3. ORTEP view of Pd2; thermal ellipsoids are at 30% probability level

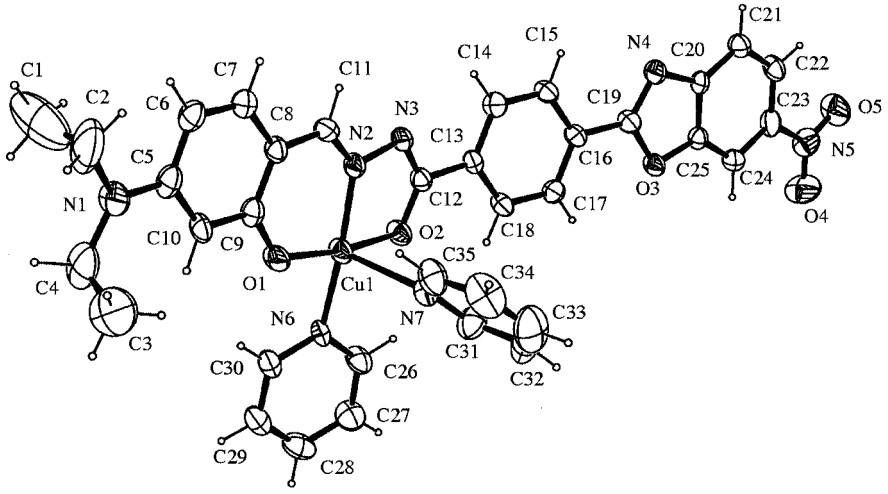

Figure 4. ORTEP view of Cu3; thermal ellipsoids are at 30% probability level

bond C20−C21, i.e. at cost of planarity of the ligand. The fact that this possibility is not adopted (it occurs instead in *trans*-stilbene which is twisted in the gas phase essentially for a similar reason[7]) seems to indicate a higher torsional potential around the bond C20−C21, probably resulting from charge transfer (CT) contributions to the ground state.

A coordination variability has been observed in the complexes of Cu^{II}. In fact, Cu1 is tetracoordinate (square planar) while Cu2 and Cu3 are pentacoordinate (square pyramidal with the metal atom lying substantially in the basal plane) and an additional pyridine molecule is bonded to the metal. For Pd^{II}, on the other hand, we have observed square-planar coordination with the same ligand giving a pentacoordinate copper complex; furthermore, the additional pyridine molecule present in the independent unit of crystals of Pd2 is not coordinated to the metal (Figure 3). This difference between Cu^{II} and Pd^{II} complexes is consistent with our previous results[4a] and is an evidence of the general tendency of Pd^{II} to give preferentially 16-electron complexes.

In the complexes reported here and in the similar complexes already reported by us[4a] the tendency of Cu^{II} to the pentacoordination appears to be favored by longer ligands. Since pentacoordination implies deviations from a flat molecular shape, may be that packing forces have a role in driving this behavior.

Both in tetracoordinate and in pentacoordinate complexes the ligand pyridine molecule in the basal plane is not coplanar with this plane but torsions around the M−N6 bond are observed (up to ca. 20°).

In the pentacoordinate complexes Cu2 and Cu3 the two ligand pyridine molecules are bonded to the metal with different strength, as it may be inferred by the corresponding bond lengths (Table 1). The more weakly bonded pyridine (i.e. the one-coordinated in apical position) is more easily lost as it is shown for example in the thermogravimetric analysis of Figure 6, while the second pyridine is lost at a much higher temperature.

This behavior is fairly reproducible so that loss of the apical pyridine is accomplished in all complexes in a tem-

 © 2004 Wiley-VCH Verlag GmbH & Co. KGaA, Weinheim

Table 1. Selected bond lengths (Å), bond angles (°), and torsion angles (°) for Cu1, Cu2, Pd2, Cu3

	Cu1	Cu2	Pd2	Cu3
M−O1	1.906(7)	1.908(2)	1.966(3)	1.912(4)
M−O2	1.946(8)	1.953(2)	1.994(3)	1.954(4)
M−N2	1.910(4)	1.931(2)	1.927(4)	1.910(5)
M−N6	1.992(4)	2.035(2)	2.051(4)	2.014(5)
M−N7		2.299(2)		2.409(6)
O2−C12	1.286(5)	1.289(3)	1.306(5)	1.295(6)
N1−C5	1.370(7)	1.379(3)	1.376(5)	1.379(8)
N2−C11	1.286(5)	1.281(3)	1.290(5)	1.280(7)
N2−N3	1.395(7)	1.396(2)	1.406(5)	1.402(6)
N3−C12	1.320(5)	1.306(3)	1.299(5)	1.298(7)
O1−M−N2	93.8(2)	93.63(8)	95.3(1)	93.0(2)
N2−M−O2	81.3(2)	80.28(8)	80.4(1)	80.7(2)
O1−M−N6	92.4(2)	91.72(8)	89.5(1)	92.2(2)
O2−M−N6	92.6(2)	92.40(8)	94.9(1)	93.2(2)
N2−M−N6	173.8(1)	161.84(8)	175.2(1)	168.0(2)
N2−M−N7		100.64(8)		96.7(2)
N6−M−N7		96.39(9)		93.6(2)
C11−N2−N3−C12	175.9(3)	179.6(2)	−180.0(4)	−177.4(5)
C7−C8−C11−N2	179.7(4)	−178.2(2)	−179.6(4)	−175.9(6)
N3−C12−C13−C18		−179.2(3)	172.7(4)	167.1(5)
O6−N5−C26−C21		−37.7(4)	48.0(7)	
C17−C16−C19−N4				−178.5(6)
C15−C16−C19−C20		−169.7(3)	−179.5(5)	
C19−C20−C21−C26		167.3(3)	−175.1(5)	
O1−M−N6−C25	168.9(3)			
O1−M−N6−C26				−164.4(5)
O1−M−N6−C27		161.1(3)	159.7(3)	

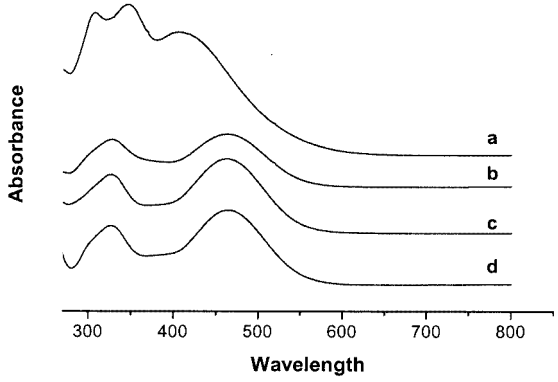

Figure 5. UV/Vis absorption spectra for: L^1 (curve a), $(PdL^1)_2$ (curve b), Pd1 (curve c), Pd35 (curve d)

perature interval ranging from 115 °C to 130 °C, while the basal pyridine is lost between 180 °C and 200 °C. The only relevant exception is given by Pd3 in which the pyridine ligand is lost around 276 °C (we have not succeeded in growing suitable single crystals of Pd3). In all cases, losing of all pyridine ligands restores $(ML^N)_2$ dimers as it is suggested by the decomposition temperatures which are identical.

Starting from commercial poly(4-vinylpyridine) we have prepared grafted polymers with a $(ML^1)_2$ content (by weight) of 35% and 60% both for Cu^{II} and Pd^{II}. The resulting polymers have good solubility in NMP, tetrachloroethane and DMF. Some thermal and analytical data of the

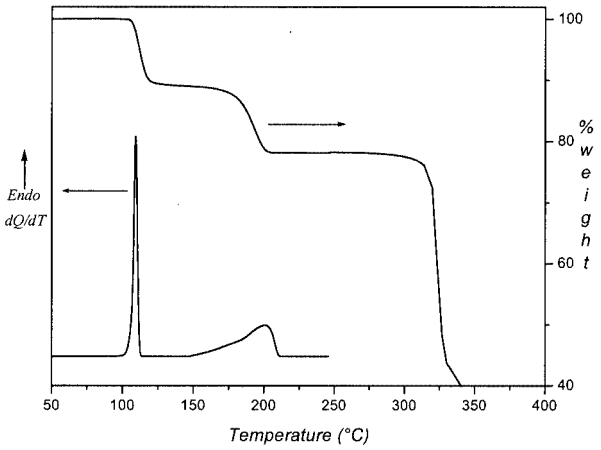

Figure 6. TGA/DTA curves of Cu2

Table 2. Relevant analytical data of grafted polymers MW

W = % $(ML^1)_2$ grafted (by weight)	Cu			Pd		
	T_g (°C)	η_{inh} (dL/g)[a]	x[b]	T_g (°C)	η_{inh} (dL/g)[a]	x[b]
0	147	0.28	0	147	0.28	0
35	192	0.12	0.130	191	0.27	0.118
60	217	0.09	0.360	227	0.18	0.328

[a] Inherent viscosity measured in DMF at 25 °C in 0.05 g/dL solutions (for Cu60 the measurement was performed at 60 °C). [b] Molar ratio of coordinated and uncoordinated pyridine units in the polymer.

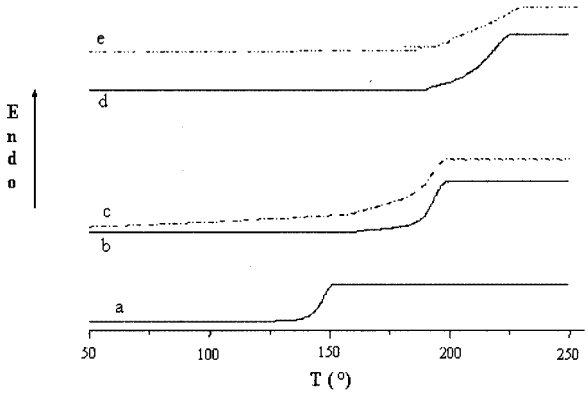

Figure 7. DSC thermograms, poly(2-vinylpyridine) (curve a); Pd35 (curve b); Cu35 (curve c); Pd60 (curve d); Cu60 (curve e)

polymers are reported in Table 2. In Figure 7 are reported the DSC thermograms.

The inflection corresponding to the glass transition is the only signal present in the curves. A regular increase of the glass transition temperature is observed upon grafting, with T_g's almost independent from the nature of the metal (Pd^{II} or Cu^{II}). The lack of any other inflection at temperatures lower than the T_g of the ungrafted polymer is an evidence of the absence of uncoordinated complex acting as a plasticizing agent; a further evidence, at least in the case of Pd containing polymers, is given by ^1H NMR analysis. In fact, in the spectra of Pd polymers, recorded in $[D_2]$dichlorome-

 © 2004 Wiley-VCH Verlag GmbH & Co. KGaA, Weinheim

thane, only broad peaks of resonance are present, which are typical of polymer samples, and no sharp signal pertaining to free low molecular weight compounds is observed.[4b]

All polymers are amorphous, as confirmed by DSC and X-ray diffraction experiments. From concentrated solutions of polymers in NMP (ca. 0.10 g/mL) we have obtained clear, transparent films of optical quality by spin coating. The decomposition temperatures of the grafted polymers, which are around 300 °C, are well above the glass transition temperature, which, in any case, can be modulated by varying the extent of grafting, and this allows poling procedures to be safely done on the films. We think that these grafted polymers can show advantages as compared to all organic polymers tailored for second order NLO applications, particularly for what concerns the poling procedure. In fact, the peculiar nature of the bond between the NLO active fragment and the polymer chain (a coordinative bond) and the large molar excess of pyridine ligand groups, should allow some mobility of ML^N fragment (through complexation-decomplexation equilibria) and, therefore, a high degree of orientation in the poling at high temperature ($> T_g$), with the mobility reduced (and the polar order frozen) at low temperature.

Second order optical nonlinearities of the complexes Cu*N* and Pd*N* are reported in Table 3. The discussion of their NLO properties can be usefully done at a comparative level with the similar complexes we have already studied.[4a]

Table 3. EFISH Results for the studied complexes

Complex	$\lvert\mu_g\cdot\beta_{vec}\rvert$[a]
Cu1	1100
Pd1	1500
Cu2	1300
Pd2	1100
Pd3	3000

[a] Estimated errors are: ±10% for Cu1, Pd1, Cu2, Pd2 and ±20% for Pd3.

The NLO activity of Cu1 and Pd1 is considerably higher as compared with Cu1 and Pd1 complexes of ref.[4a] whose ligand only differs by lack of the vinylene group.[8] Actually, introduction of the vinylene group produces a fairly long polyene-like chain between the donor and acceptor groups (see Scheme 5) and it is well-known that push-pull polyenes are highly NLO active chromophores.[9]

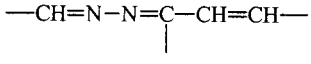

Scheme 5

The NLO activity of Cu2 and Pd2 is not significantly different as compared with Cu2 and Pd2 complexes of ref.[4a] whose ligand lacks the *ortho* nitro group. This finding may be explained on the basis of the crystallographic results; in fact, we have found that the *ortho* nitro group is significantly twisted with respect to the phenyl ring which is attached to (cf. Table 1) and so it gives a little contribution, if any, to the charge transfer.

The datum measured for Pd3 is consistent with the expected increase of nonlinear activity following the replacement of phenyl rings by low aromaticity heterocycles.[10] The high activity of this complex, which is among the highest reported to date for metallorganic chromophores,[1] coupled with the known features of high thermochemical and photochemical stability of the benzoxazole group,[11] make

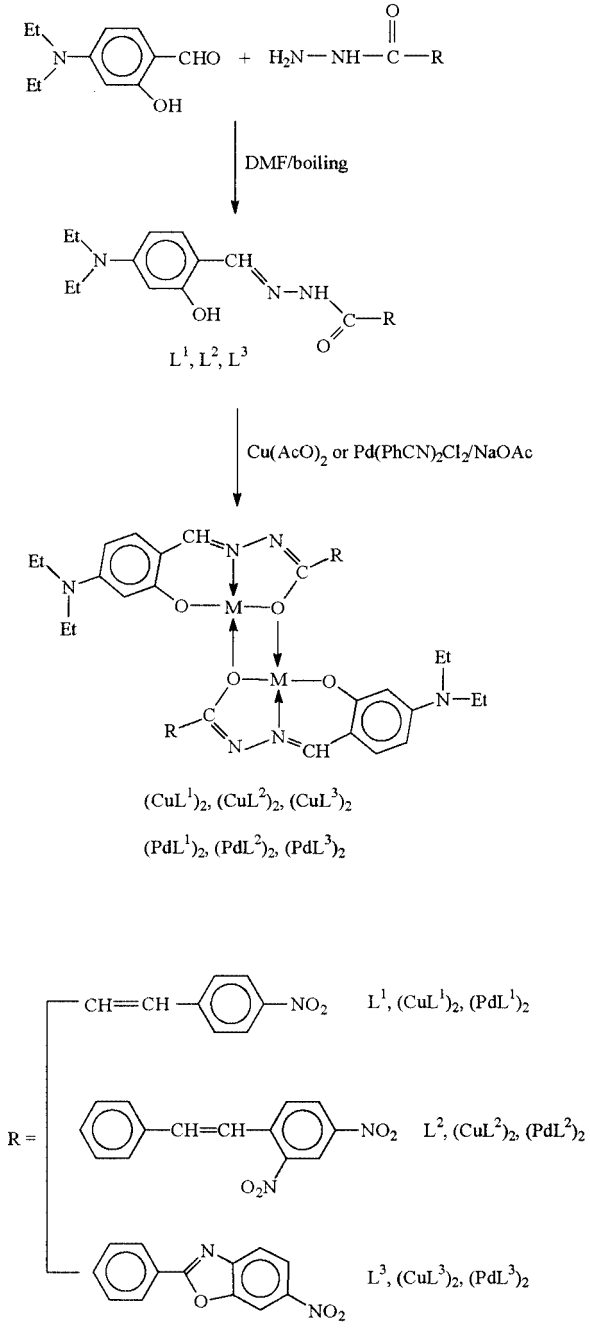

Scheme 6

 © 2004 Wiley-VCH Verlag GmbH & Co. KGaA, Weinheim

it a promising candidate for further developments of our research.

Experimental Section

Synthesis: Complexes Cu*N* and Pd*N* (*N* = 1, 2, 3) were synthesized according to the general procedure outlined in the scheme below (Scheme 6) which starts with the synthesis of the organic ligands L^N (*N* = 1, 2, 3), followed by the synthesis of dinuclear complexes $(ML^N)_2$ and, from these, of the final mononuclear complexes M*N*, according to Scheme 2.

4-Nitrocinnamohydrazide: 4-Nitrocinnamoyl chloride (obtained from the acid refluxed in $SOCl_2$) is dissolved in boiling ethanol to obtain the ethyl ester. 4-Nitrocinnamic acid ethyl ester (5.00 g, 22.6 mmol) is dissolved in THF (50 mL). The solution is poured into a mixture of water (25 mL), ethanol (50 mL), hydrazine (18 mL) and it is stirred for 1.5 h at room temperature. Finally the mixture is poured into water (100 mL) and cooled in a freezer for 12 h. An orange solid is recovered by vacuum filtration. Yield 30%. M.p. 214 °C. ^{1}H NMR (200 MHz, [D$_6$]DMSO, 25 °C): δ = 4.52 ppm (s, 2 H), 6.80 (d, *J* = 16.2 Hz, 1 H), 7.53 (d, *J* = 16.2 Hz, 1 H), 7.77 (d, *J* = 8.7 Hz, 2 H), 8.22 (d, *J* = 8.3 Hz, 2 H), 9.50 (s, 1 H).

***N*-4-Diethylaminosalicylidene-*N*′-(4-nitrocinnamoyl)hydrazine (L^1):** 4-Nitrocinnamohydrazide (4.50 g, 21.7 mmol) and 4-*N*,*N*-diethylamino-2-hydroxybenzaldehyde (4.60 g, 23.8 mmol) are dissolved in boiling DMF (80 mL). After 15 minutes the solution is cooled and then poured into water (400 mL) containing concentrated sulfuric acid (5 mL). The red solid obtained is recovered by filtration, washed several times with water, dried, and recrystallized from DMF. Yield 6.06 g (73%). M.p. 223 °C. ^{1}H NMR (200 MHz, [D$_6$]DMSO, 25 °C): δ = 1.08 ppm (t, *J* = 6.8 Hz, 6 H), 3.33 (m, 4 H), 6.10 (s, 1 H), 6.25 (d, *J* = 8.6 Hz, 1 H), 6.83 (d, *J* = 15.6 Hz, 1 H), 7.22 (d, *J* = 8.8 Hz, 1 H), 7.70 (d, *J* = 8.8 Hz, 1 H), 7.87 (d, *J* = 8.8 Hz, 2 H), 8.24 (s, 1 H), 8.26 (d, *J* = 8.8 Hz, 2 H), 11.23 (s, 1 H), 11.71 (s, 1 H). IR (KBr): $\tilde{\nu}$ = 3409 cm^{-1} (m), 3206 (m, N−H str.), 2978 (m), 2933 (w), 1632 (vs, C=O str.), 1592 (vs, N−H bend), 1520 (vs), 1355 (s), 1339 (s), 1247 (m), 1134 (m). UV/Vis: λ_{max} (nm), ε_{max} (dm^{3}mol^{-1}cm^{-1}): 406, 2.2·10^4.

Synthesis of $(CuL^1)_2$: L^1 (1.00 g, 2.61 mmol) and copper(II) acetate (0.521 g, 2.61 mmol) are dissolved in DMF (35 mL). The solution is heated to boiling and stirred for 15 minutes, then it is cooled and poured into water (100 mL) containing sodium acetate (0.700 g, 8.53 mmol). A red-brown solid is recovered by filtration, washed repeatedly with water, and recrystallized from DMF. Yield 91%. M.p. 312 °C dec. $C_{40}H_{40}N_8O_8Cu_2$: calcd. C 54.11, H 4.51, N 12.63, Cu 14.31; found C 54.22, H 4.64, N 12.57, Cu 13.91%. UV/Vis: λ_{max} (nm), ε_{max} (dm^{3}mol^{-1}cm^{-1}): 469, 4.5·10^4.

Synthesis of $(PdL^1)_2$: L^1 (1.00 g, 2.61 mmol) is dissolved in boiling THF (20 mL). The solution is added with THF (20 mL) containing bis(benzonitrile) Pd^{II} dichloride (1.00 g, 2.61 mmol). After 15 minutes of stirring, a solution of sodium acetate (1.00 g, 12.2 mmol) in water (20 mL) is added. The pH is raised to about 8−9 by adding a 10 wt.% solution of KOH. After some minutes, the addition of 100 mL of water affords the precipitation of a dark red solid, which is filtered off, washed repeatedly with water, dried and finally washed with boiling heptane. Yield 91%. M.p. 311 °C dec. $C_{40}H_{40}N_8O_8Pd_2$: calcd. C 49.34, H 4.11, N 11.51, Pd 21.90; found C 49.66, H 4.27, N 11.51, Pd 22.30%. ^{1}H NMR (200 MHz, [D$_6$]DMSO, 25 °C): δ = 1.09 ppm (m, 12 H), 3.45 (m,8 H), 6.16 (s, 2 H), 6.26 (d, 2 H), 7.08 (d, 2 H), 7.33 (d, 2 H), 7.46 (d, 2 H), 7.90 (d, 4 H), 8.19 (d, 6 H). UV/Vis: λ_{max} (nm), ε_{max} (dm^{3}mol^{-1}cm^{-1}): 459, 6.6·10^4.

4-(2,4-Dinitrophenylethylidene)benzoic Acid: 4-Formylbenzoic acid (10.0 g, 66.6 mmol) is dissolved in pyridine (50 mL) and piperidine (2 mL) and refluxed. 2,4-Dinitrophenylacetic acid (15.0 g, 66.6 mmol) is added in fractions of 3 g every 15 minutes. After 3 h the solution is concentrated to 30 mL and cooled. A yellow crystalline solid precipitates, then it is filtered off and washed with ethanol. Yield 72%. M.p. 263 °C. ^{1}H NMR (200 MHz, [D$_6$]DMSO, 25 °C): δ = 7.61 ppm (s, 2 H), 7.75 (d, *J* = 8.2 Hz, 2 H), 7.96 (d, *J* = 8.2 Hz, 2 H), 8.23 (d, *J* = 8.8 Hz, 1 H), 8.50 (d, *J* = 8.8 Hz, 1 H), 8.72 (d, *J* = 2.2 Hz, 1 H).

4-(2,4-Dinitrophenylethylidene)benzohydrazide: 4-(2,4-Dinitrophenylethylidene)benzoyl chloride (0.941 g, 2.83 mmol, obtained from the corresponding acid by reaction with thionyl chloride according to standard methods) is dissolved in hot anhydrous dioxane (20 mL). The solution is cooled and poured into a mixture of hydrazine (2.8 mL), dioxane (10 mL) and water (5 mL) whilst stirring. The reaction is rapid and after some minutes the mixture is poured in water (50 mL), affording the precipitation of a yellow solid, recovered by filtration, and washed repeatedly with water. Yield 86%. M.p. 234 °C. ^{1}H NMR (200 MHz, [D$_6$]DMSO, 25 °C): δ = 4.53 ppm (s, 2 H), 7.59 (s, 2 H), 7.72 (d, *J* = 7.8 Hz, 2 H), 7.87 (d, *J* = 7.8 Hz, 2 H), 8.23 (d, *J* = 8.8 Hz, 1 H), 8.51 (d, *J* = 8.6 Hz, 1 H), 8.74 (s, 1 H).9.83 (s, 1 H).

***N*-4-Diethylaminosalicylidene-*N*′-4-(2,4-dinitrophenylethylidene)-benzoylhydrazine (L^2):** 4-(2,4-dinitrophenylethylidene)benzohydrazide (3.55 g, 10.8 mmol) and 4-*N*,*N*-diethylamino-2-hydroxyibenzaldehyde (2.20 g, 11.4 mmol) are dissolved in boiling DMF (50 mL). After 15 minutes the solution is cooled and then poured into water (100 mL) containing concentrated sulfuric acid (2 mL). The brown solid obtained is recovered by filtration, washed several times with water, dried and recrystallized from DMF/water. Yield 5.06 g (93%). M.p. 276 °C. ^{1}H NMR (200 MHz, [D$_6$]DMSO, 25 °C): δ = 1.09 ppm (t, *J* = 6.8 Hz, 6 H), 3.33 (m, 4 H), 6.10 (s, 1 H), 6.23 (d, *J* = 8.8 Hz, 1 H), 7.17 (d, *J* = 8.8 Hz, 1 H), 7.62 (s, 2 H), 7.79 (d, *J* = 7.6 Hz, 2 H), 7.95 (d, *J* = 7.6 Hz, 2 H), 8.23 (d, *J* = 8.8 Hz, 1 H), 8.41 (s, 1 H), 8.50 (d, *J* = 8.6 Hz, 1 H), 8.73 (s, 1 H), 11.43 (s, 1 H), 11.82 (s, 1 H). IR (KBr): $\tilde{\nu}$ = 3334 cm^{-1} (m), 3208 (w, N−H str.), 2977 (m), 2933 (w), 1630 (vs, C=O str.), 1595 (vs, N−H bend), 1520 (vs), 1355 (s), 1334 (s), 1246 (m), 1133 (m). UV/Vis: λ_{max} (nm), ε_{max} (dm^{3}mol^{-1}cm^{-1}): 370, 5.6·10^4.

Synthesis of $(CuL^2)_2$: L^2 (1.00 g, 1.99 mmol) and copper(II) acetate (0.397 g, 1.99 mmol) are dissolved in DMF (35 mL). The solution is heated to boiling and stirred for 15 minutes, then it is cooled and poured into water (100 mL) containing sodium acetate (0.700 g, 8.53 mmol). A dark brown solid is recovered by filtration, washed repeatedly with water, and recrystallized from DMF. Yield 90%. M.p. 308 °C dec. $C_{52}H_{46}N_{10}O_{12}Cu_2$: Cu 11.25, C 55.27, H 4.10, N 12.39; found Cu 10.92, C 54.98, H 4.02, N 12.11%. UV/Vis: λ_{max} (nm), ε_{max} (dm^{3}mol^{-1}cm^{-1}): 400, 5.8·10^4.

Synthesis of $(PdL^2)_2$: L^2 (1.00 g, 1.99 mmol) is dissolved in boiling THF (15 mL). The solution is added with THF (10 mL) containing bis(benzonitrile)Pd^{II} dichloride (0.763 g, 1.99 mmol). A solution of sodium acetate (1.00 g, 12.2 mmol) in water (20 mL) is added. The pH is raised to 8−9 by adding a solution of 0.300 g of KOH in 100 mL of water. On heating, a dark red-brown solid coagulates, then filtered off, washed repeatedly with water, dried, and washed with boiling heptane. Yield 85%. M.p. 291 °C dec.

 © 2004 Wiley-VCH Verlag GmbH & Co. KGaA, Weinheim

$C_{52}H_{46}N_{10}O_{12}Pd_2$: Pd 17.50, C 51.37, H 3.81, N 11.52%; found Pd 17.21, C 51.08, H 3.65, N 11.24%. ^{1}H NMR (200 MHz, [D$_6$]DMSO, 25 °C): δ = 1.09 ppm (t, 12 H), 3.33 (m, 8 H), 6.15 (s, 2 H), 6.25 (d, 2 H), 7.32 (d, 2 H), 7.59 (s, 4 H), 7.66 (d, 4 H), 7.97 (d, 4 H), 8.25 (d, 2 H), 8.41 (s, 2 H), 8.48 (d, 2 H), 8.72 (s, 2 H). UV/Vis: λ_{max} (nm), ε_{max} (dm^{3}mol^{-1}cm^{-1}): 369, 5.2·10^4.

***N*-(4-Carboxybenzylidene)-2-hydroxy-4-nitroaniline:** 4-Formylbenzoic acid (5.00 g, 33.3 mmol) is suspended in boiling absolute ethanol (60 mL). Successively a solution of 2-hydroxy-4-nitroaniline (5.00 g, 32.4 mmol) in ethanol (60 mL) is added. After boiling 30 min the solution is cooled, obtaining a pure yellow solid, then filtered off. Yield 54%. M.p. 246 °C. ^{1}H NMR (200 MHz, [D$_6$]DMSO, 25 °C): δ = 7.35 ppm (d, J = 6.3 Hz, 1 H), 7.76 (d, J = 1.8 Hz, 1 H), 7.78 (dd, J_1 = 1.8, J_2 = 6.3 Hz, 1 H), 8.05 (d, J = 6.3 Hz, 2 H), 8.17 (d, J = 6.3 Hz, 2 H), 8.80 (s, 1 H), 13.32 (s, 1 H).

4-(6-Nitro-2-benzoxazolyl)benzoic Acid: *N*-(4-Carboxybenzylidene)-2-hydroxy-4-nitroaniline (5.20 g, 18.2 mmol) is suspended in glacial acetic acid (100 mL). Lead(IV) acetate (9.68 g, 21.8 mmol) is added slowly under strong stirring. The reaction takes 2 h. The product is filtered off, washed with acetic acid, and recrystallized from DMF. Yield 31%. M.p. 319 °C. ^{1}H NMR (200 MHz, [D$_6$]DMSO, 25 °C): δ = 7.90 ppm (d, J = 5.8 Hz, 1 H), 8.25 (d, J = 5.2 Hz, 2 H), 8.37 (d, J = 5.8 Hz, 1 H), 8.39 (d, J = 5.2 Hz, 2 H), 8.54 (s, 1 H).

4-(6-Nitro-2-benzoxazolyl)benzohydrazide: 4-(6-Nitro-2-benzoxazolyl)benzoyl chloride (3.00 g, 9.91 mmol, obtained from the corresponding acid by reaction with thionyl chloride according to standard methods) is dissolved in hot anhydrous dioxane (60 mL). The solution is cooled and poured into a mixture of ethanol (50 mL) and hydrazine monohydrate (5 mL) whilst stirring. The product is a yellow solid which is recrystallized from DMF. Yield 57%. M.p. 280 °C. ^{1}H NMR (200 MHz, [D$_6$]DMSO, 25 °C): δ = 4.67 ppm (s, 2 H), 8.06 (d, J = 8.4 Hz, 1 H), 8.18 (d, J = 8.4 Hz, 1 H), 8.30 (d, J = 8.6 Hz, 2 H), 8.39 (d, J = 8.4 Hz, 2 H), 8.76 (s, 1 H), 10.02 (s, 1 H).

***N*-4-Diethylaminosalicylidene-*N*′-4-(6-nitro-2-benzoxazolyl)benzoylhydrazine (L^3):** 4-(6-Nitro-2-benzoxazolyl)benzohydrazide (1.67 g, 5.60 mmol) and 4-*N*,*N*-diethylamino-2-hydroxyibenzaldehyde (1.14 g, 5.90 mmol) are dissolved in boiling DMF (30 mL). After 15 minutes the solution is cooled and then poured into water (100 mL) containing concentrated sulfuric acid (1 mL). The product is recovered by filtration, washed several times with water, dried, and recrystallized from DMF. Yield 2.39 g (90%). M.p. 257 °C. ^{1}H NMR (200 MHz, [D$_6$]DMSO, 25 °C): δ = 1.13 ppm (t, J = 6.6 Hz, 6 H), 3.37 (m, 4 H), 6.13 (s, 1 H), 6.27 (d, J = 6.9 Hz, 1 H), 7.21 (d, J = 8.7 Hz, 2 H), 8.05 (d, J = 8.4 Hz, 2 H), 8.16 (d, J = 8.4 Hz, 2 H), 8.23 (m, 2 H), 8.45 (s, 1 H), 8.73 (s, 1 H), 11.40 (s, 1 H), 11.99 (s, 1 H). IR (KBr): $\tilde{\nu}$ = 3474 cm^{-1} (w), 3201 (m, N−H str.), 2979 (m), 1654 (vs), 1628 (vs, C=O str.), 1593 (vs, N−H bend), 1520 (vs), 1360 (s), 1342 (s), 1248 (m), 1135 (m). UV/Vis: λ_{max} (nm), ε_{max} (dm^{3}mol^{-1}cm^{-1}): 343, 2.8·10^4.

Synthesis of $(CuL^3)_2$: L^3 (1.00 g, 2.11 mmol) and copper(II) acetate (0.422 g, 2.11 mmol) are solved in DMF (35 mL). The solution is heated to boiling and stirred for 15 minutes, then it is cooled and poured into water (100 mL) containing sodium acetate (0.700 g, 8.53 mmol). A dark orange solid is recovered by filtration, washed repeatedly with water, and recrystallized from DMF. Yield 89%. M.p. 327 °C dec. $C_{50}H_{42}N_{10}O_{10}Cu_2$: Cu 11.88, C 56.12, H 3.96, N 13.09 ; found Cu 12.30, C 55.96, H 3.77, N 12.86%. UV/Vis: λ_{max} (nm), ε_{max} (dm^{3}mol^{-1}cm^{-1}): 435, 5.2·10^4.

Synthesis of $(PdL^3)_2$: L^3 (1.00 g, 2.11 mmol) is suspended in 20 mL of boiling THF. The solution is added with THF (10 mL) containing bis(benzonitrile)Pd^{II} dichloride (0.809 g, 2.11 mmol), obtaining a yellow heterogeneous mixture which becomes a dark red solution by adding 20 mL of water containing sodium acetate (1.00 g, 12.2 mmol). The pH is raised to 8−9 with a solution of 0.300 g of KOH in 100 mL of water and a brown solid coagulates, which is filtered off, washed repeatedly with water, dried, and washed with boiling heptane. Yield 85%. M.p. 298 °C dec. $C_{50}H_{42}N_{10}O_{10}Pd_2$: Pd 18.41, C 51.96, H 3.66, N 12.12%; found Pd 18.35, C 51.85, H 3.55, N 12.01%. UV/Vis: λ_{max} (nm), ε_{max} (dm^{3}mol^{-1}cm^{-1}): 446, 6.0·10^4.

Synthesis of CuN and PdN: The corresponding dinuclear precursor is dissolved in pyridine at room temperature, then the solvent is allowed to evaporate from the solution leaving crystals of the mononuclear complex.

Cu1: $C_{25}H_{25}N_5O_4Cu{\cdot}1/2C_5H_5N$: calcd. C 58.71, H 4.93, N 13.69; found C 58.41, H 4.96, N 13.42. UV/Vis: λ_{max} (nm), ε_{max} (dm^{3}mol^{-1}cm^{-1}): 471, 2.8·10^4.

Pd1: $C_{30}H_{30}N_6O_4Pd$: calcd. C 55.86, H 4.69, N 13.03; found C 55.33, H 4.68, N 12.86. UV/Vis: λ_{max} (nm), ε_{max} (dm^{3}mol^{-1}cm^{-1}): 463, 3.3·10^4.

Cu2: $C_{36}H_{33}N_7O_6Cu$: calcd. C 59.79, H 4.60, N 13.56; found 59.51, H 4.70, N 13.36. UV/Vis: λ_{max} (nm), ε_{max} (dm^{3}mol^{-1}cm^{-1}): 400, 2.9·10^4.

Pd2: $C_{36}H_{33}N_7O_6Pd$: calcd. C 56.44, H 4.34, N 12.80; found C 56.05, H 4.45, N 12.69. UV/Vis: λ_{max} (nm), ε_{max} (dm^{3}mol^{-1}cm^{-1}): 361, 2.4·10^4.

Cu3: $C_{35}H_{31}N_7O_5Cu$: calcd. C 60.64, H 4.51, N 14.14; found C 59.21, H 4.40, N 13.80. UV/Vis: λ_{max} (nm), ε_{max} (dm^{3}mol^{-1}cm^{-1}): 460, 2.8·10^4.

Pd3: $C_{30}H_{26}N_6O_5Pd$: calcd. C 54.85, H 3.99, N 12.18; found C 54.71, H 4.12, N 12.53. UV/Vis: λ_{max} (nm), ε_{max} (dm^{3}mol^{-1}cm^{-1}): 450, 2.9·10^4.

Synthesis of Grafted Polymers: Commercial poly(4-vinylpyridine) (Aldrich, $M_{av} \approx$ 60000 D, T_g= 147 °C) was used as the starting material after drying at 120 °C in oven for 16 h. Grafted polymers were prepared according to a standard procedure. The polymer and the dinuclear complex $(ML^1)_2$ (total amount 1.0 g) in the proper weight ratio are solved in DMF (10 mL) at 90 °C. After stirring for 15′ at 90 °C, the mixture is poured in water (100 mL) containing 2% sodium acetate (by weight). The precipitated polymer is recovered by filtration (90% yield), washed repeatedly with water and dried in oven at 130 °C. Grafted polymers are indicated as MW, where M stands for Cu or Pd and W is the weight percent ratio of $(ML^1)_2$ to polymer. Grafted polymers Cu35, Pd35, Cu60, and Pd60 were prepared. Analytical data: Cu35: %Cu calcd. 5.01; found 5.08. Cu60: %Cu calcd. 8.59; found 8.47. Pd35: %Pd calcd. 7.67; found 7.67. Pd60: %Pd calcd. 13.13; found 13.21.

Physical Measurements: The thermal behavior of compounds was studied by differential scanning calorimetry (Perkin−Elmer Pyris, N_2 atmosphere, scanning rate 10 K/min), temperature controlled polarizing microscopy (Zeiss microscope, Mettler hot stage) and TGA-DTA analysis (TA Instruments SDT 2960, air atmosphere, scanning rate 10 K/min). Proton NMR spectra were recorded on a Varian XL 200 spectrometer. UV/Vis (DMF solution) and FT-IR (KBr) spectra were recorded with JASCO spectrometers. Films of the grafted polymers were obtained by the spin coating technique

 © 2004 Wiley-VCH Verlag GmbH & Co. KGaA, Weinheim

Table 4. Crystal, collection and refinement data for Cu1, Cu2, Pd2, Cu3

	Cu1	Cu2	Pd2	Cu3
Chemical formula	$2(C_{25}H_{25}N_5O_4Cu)\cdot C_5H_5N$	$C_{36}H_{33}N_7O_6Cu$	$C_{31}H_{28}N_6O_6Pd\cdot C_5H_5N$	$C_{35}H_{31}N_7O_5Cu$
Molecular mass	1125.20	723.23	766.09	693.21
T [K]	293	293	293	293
Crystal system	monoclinic	triclinic	monoclinic	monoclinic
Space group	$P2_1/c$	$P\bar{1}$	$C2/c$	$P2_1/c$
a [Å]	15.85(5)	9.224(4)	36.84(1)	16.029(7)
b [Å]	19.10(1)	10.793(2)	8.605(2)	12.924(9)
c [Å]	16.12(4)	18.132(7)	27.73(1)	16.59(1)
α [°]	90	101.71(3)	90	90
β [°]	146.9(1)	100.74(5)	129.9(1)	109.03(6)
γ [°]	90	98.69(2)	90	90
V [Å^3]	2660(10)	1703(1)	6744(3)	3249(3)
Z, D_x [g/cm^3]	2, 1.402	2, 1.411	8, 1.509	4, 1.417
μ [mm^{-1}]	0.863	0.698	0.608	0.727
Theta range	1.71°−27.97°	1.18°−27.97°	1.44°−27.97°	1.35°−27.97°
Data/parameters	6284/343	8198/451	8084/451	7759/433
$R1$, $wR2$ [$I > 2\sigma(I)$]	0.0515, 0.1281	0.0419, 0.1090	0.0507, 0.1095	0.0662, 0.1307
$R1$, $wR2$ (all data)	0.1416, 0.1562	0.0792, 0.1231	0.1285, 0.1319	0.3336, 0.1924

$$R1 = \frac{\sum \| F_0 | - | F_c \|}{\sum |F_0|}\ ; \quad wR2 = \left\{ \frac{\sum \left[w\left(F_o^2 - F_c^2\right)^2 \right]}{\sum \left[w\left(F_o^2\right)^2 \right]} \right\}^{1/2}$$

(NMP solutions, SCS P6700 spincoater operating at 800−1000 rounds/min). Residual solvent was removed by keeping the films in oven at 120 C for 12 h.

X-ray Analysis: Single crystals of Cu1, Cu2, Pd2, and Cu3 suitable for X-ray analysis were obtained by slow evaporation of pyridine solutions at ambient temperature. Cell parameters were obtained through a least-squares fit[12] to the θ angles of 25 accurately centered strong reflections in the ranges 12.173°≤ θ ≤ 13.480° for Cu1, 15.907°≤ θ ≤ 17.512° for Cu2, 12.009°≤ θ ≤ 13.551° for Pd2 and 9.140°≤ θ ≤ 12.147° for Cu3 on an Enraf−Nonius MACH 3 automated single crystal diffractometer, using graphite monochromated Mo-K_α radiation (λ= 0.71069 Å). Data collection was performed on the same apparatus. Semiempirical absorption correction (ψ scans) was applied in all cases. The structures were solved by direct methods (SIR92 program[13]), completed by difference Fourier methods and refined by the full-matrix least-squares method (SHELXL program of SHELX 97 package[14]). Refinement was on F^2 against all independent measured reflections; sigma weights were introduced in the last refinement cycles. The largest peaks and holes in the last Fourier difference were (e·Å^{-3}): 0.689 and −0.514 for Cu1, 0.379 and −0.235 for Cu2, 0.691 and −0.498 for Pd2, and 0.448 and −0.498 for Cu3. In all structures C, N, O and metal atoms were given anisotropic displacement parameters. H atoms were placed in calculated positions and refined by the riding model with U_{iso} equal to U_{eq} of the carrier atoms. In the crystals of Cu1 the pyridine molecule not coordinated to the metal is located on a crystallographic inversion center and therefore is statistically disordered (two centrosymmetrically related sites with 0.5 occupation factor). Some crystal, collection and refinement data are reported in Table 4. CCDC-221599 (for Cu1), -221600 (for Cu2), -221601 (for Pd2), and -221602 (for Cu3) contain the supplementary crystallographic data for this paper. These data can be obtained free of charge at www.ccdc.cam.ac.uk/conts/retrieving.html [or from the Cambridge Crystallographic Data Centre, 12 Union Road, Cambridge CB2 1EZ, UK; Fax: (internat.) +44-1223-336-033; E-mail: deposit@ccdc.cam.ac.uk].

NLO Measurements: Second order optical nonlinearities of chromophores, in the form of $\mu_g\beta$ products (μ_g is the ground state permanent dipole moment and β the quadratic hyperpolarizability of the molecules), were measured by the EFISH (Electric Field Induced Second Harmonic generation) technique.[15] Measurements were carried out in DMSO solutions at a fundamental wavelength of 1.907 μm, using a Q-switched, mode locked Nd3:YAG laser, whose 1.064 μm initial wavelength was shifted by stimulated Raman scattering in a high-pressure hydrogen cell.

Acknowledgments

We thank the CIMCF of the Università di Napoli "Federico II" for permission to use the Nonius MACH3 diffractometer and NMR spectrometers. Financial support of MIUR of Italy (PRIN 2002) is also acknowledged.

[1] [1a] N. J. Long, *Angew. Chem. Int. Ed. Engl.* **1995**, *34*, 21−38; *Angew. Chem.* **1995**, *107*, 37. [1b] I. R. Whittall, A. M. McDonagh, M. G. Humphrey, M. Samoc, *Adv. Organomet. Chem.* **1998**, *42*, 291−361. [1c] S. Di Bella, *Chem. Soc. Rev.* **2001**, *30*, 355−366.

[2] [2a] B. J. Coe, J. A. Harris, L. J. Harrington, J. C. Jeffery, L. H. Rees, S. Houbrechts, A. Persoons, *Inorg. Chem.* **1998**, *37*, 3391−3399. [2b] J. Buey, S. Coco, L. Diez, P. Espinet, L. M. Martin-Alvarez, J. A. Miguel, S. Garcia-Granda, A. Tesouro, I. Ledoux, J. Zyss, *Organometallics* **1998**, *17*, 1750−1755. [2c] R. Centore, B. Panunzi, A. Roviello, A. Tuzi, *Acta Crystallogr., Sect. C* **2002**, *58*, m26−m28. [2d] C. Fave, M. Hissler, K. Senechal, I. Ledoux, J. Zyss, R. Reau, *Chem. Commun.* **2002**, 1674−1675.

[3] L. Dalton, *Adv. Polymer Sci.* **2002**, *158*, 1−86.

 © 2004 Wiley-VCH Verlag GmbH & Co. KGaA, Weinheim

[4] [4a] F. Cariati, U. Caruso, R. Centore, W. Marcolli, A. De Maria, B. Panunzi, A. Roviello, A. Tuzi, *Inorg. Chem.* **2002**, *41*, 6597−6603. [4b] U. Caruso, A. De Maria, B. Panunzi, A. Roviello, *J. Polymer Sci., Part A: Polym. Chem.* **2002**, *40*, 2987−2992.
[5] [5a] M. F. Iskander, A. M. El-Aggan, L. S. Refaat, L. El Sayed, *Inorg. Chim. Acta* **1975**, *14*, 167−172. [5b] J. Jezierska, A. Jezierski, B. Jezowska-Trzebiatowska, A. Ozarowsky, *Inorg. Chim. Acta* **1983**, *68*, 7−13.
[6] F. H. Allen, O. Kennard, D. G. Watson, L. Brammer, A. Guy Orpen, R. Taylor, *J. Chem. Soc., Perkin Trans. 2* **1987**, S1−S19.
[7] M. Traetteberg, E. B. Frantsen, F. C. Mijlhoff, A. Hoekstra, *J. Mol. Struc.* **1975**, *26*, 57−68.
[8] From preliminary results of dipole moment measurement with the Guggenheim method, a μ value of 5 D may be estimated for Pd1, from which $\beta \approx 300 \cdot 10^{-30}$ esu is deduced.
[9] [9a] S. R. Marder, J. W. Perry, B. G. Tiemann, C. B. Gorman, S. Gilmour, S. L. Biddle, G. Bourhill, *J. Am. Chem. Soc.* **1993**, *115*, 2524−2526. [9b] S. R. Marder, C. B. Gorman, B. G. Tiemann, L.-T. Cheng, *J. Am. Chem. Soc.* **1993**, *115*, 3006−3007.
[10] [10a] V. P. Rao, A. K.-Y. Jen, J. Chandrasekhar, I. N. N. Namboothiri, A. Rathna, *J. Am. Chem. Soc.* **1996**, *118*, 12443−12448. [10b] I. D. L. Albert, T. J. Marks, M. A. Ratner, *J. Am. Chem. Soc.* **1997**, *119*, 6575−6582. [10c] A. Abbotto, S. Bradamante, A. Facchetti, G. A. Pagani, *J. Org. Chem.* **1997**, *62(17)*, 5755−5765. [10d] M. He, T. M. Leslie, J. A. Sinicropi, *Chem. Mater.* **2002**, *14*, 4662−4668.
[11] [11a] C. Arnold, *J. Polymer Sci., Macromol. Rev.* **1979**, *14*, 265. [11b] L. J. Mathias, S. U. Ahmed, P. D. Livant, *Macromolecules* **1985**, *18*, 616. [11c] P. M. Hergenrother, J. W. Connell, J. W. Labadie, J. L. Hedrick, *Adv. Polymer Sci.* **1994**, *117*, 67−110.
[12] R. Centore, *CELLFIT*; Università di Napoli "Federico II": Naples, Italy, **2002**.
[13] A. Altomare, G. Cascarano, C. Giacovazzo, A. Guagliardi, *J. Appl. Crystallogr.* **1993**, *26*, 343−350.
[14] G. M. Sheldrick, *SHELX-97*; University of Göttingen: Göttingen, Germany, **1997**.
[15] T. Thami, P. Bassoul, M. A. Petit, J. Simon, A. Fort, M. Barzoukas, A. Villaeys, *J. Am. Chem. Soc.* **1992**, *114*, 915−921.

Received October 15, 2003
Early View Article
Published Online April 20, 2004

 © 2004 Wiley-VCH Verlag GmbH & Co. KGaA, Weinheim

Synthesis, Molecular Structure and Catalytic Activity of Six-Coordinate Chloro(hydrido)- and Dihydridoruthenium(II) and -osmium(II) Complexes with the Chiral Ligands P*i*Pr$_2$NH(Me)Ph, (*S*,*S*)-Chiraphos and (*S*,*S*,)-Diop

Christoph Schlünken,[a] Miguel A. Esteruelas,[b] Fernando J. Lahoz,[b] Luis A. Oro,[b] and Helmut Werner*[a]

Dedicated to Professor Albrecht Salzer on the occasion of his 60th birthday

Keywords: Chirality / Hydrido complexes / Osmium / Phosphane complexes / Ruthenium

The five-coordinate compounds [MHCl(CO)(P*i*Pr$_3$)$_2$] (where **1a**: M = Ru; **1b**: M = Os) react with P*i*Pr$_2$R* [where R* = CH(Me)Ph] to give the octahedral complexes *mer*-[MHCl(CO)(P*i*Pr$_2$R*)$_3$] (**6** and **7**). The lability of the phosphane *trans* to the hydride is illustrated by the replacement reactions with CO, P(OMe)$_3$ and C$_2$(CO$_2$Me)$_2$, which afford the substitution products [MHCl(CO)(L)(P*i*Pr$_2$R*)$_2$] (**8**–**12**) in high yields. The reactions of **1a** and **1b** with (*S*,*S*)-Chiraphos and (*S*,*S*)-Diop lead to one or two diastereoisomers of the chelate complexes [MHCl(CO)(P*i*Pr$_3$)(Chiraphos)] (**15**, **16**) and [MHCl(CO)(P*i*Pr$_3$)(Diop)] (**17**, **18**); the ratio of the diastereoisomers is dependent on the metal, the bidentate ligand and the reaction conditions. The racemate of [OsHCl(CO)(P*i*Pr$_3$)(dppe)] (**14**) was obtained from **1b** and 1,2-C$_2$H$_4$(PPh$_2$)$_2$ (dppe). The hydrido(tetrahydroboranato) compounds [MH(κ^2-H$_2$BH$_2$)(CO)(P*i*Pr$_3$)$_2$] (where **2a**: M = Ru; **2b**: M = Os) also react with (*S*,*S*)-Chiraphos and (*S*,*S*)-Diop to give either the mononuclear, octahedral, chelate complexes **19**–**21** or, for M = Os and (*S*,*S*)-Diop, the dinuclear compound [{OsH$_2$(CO)(P*i*Pr$_3$)$_2$}$_2$(μ-Diop)] (**22**). The molecular structure of **22** was determined crystallographically. Treatment of [OsH$_2$Cl$_2$(P*i*Pr$_3$)$_2$] (**23**) with two equivalents of (*S*,*S*)-Chiraphos afforded stepwise [OsH$_2$Cl$_2$(P*i*Pr$_3$)(Chiraphos)] (**25**) and, after reductive elimination of HCl and displacement of P*i*Pr$_3$, *trans*-[OsHCl(Chiraphos)$_2$] (**24**). Both **24** and [OsH$_2$-(Chiraphos)$_2$] (**27**), which was prepared from **24** and NaBH$_4$/MeOH, were transformed with HBF$_4$ in diethyl ether into the dihydrogen complexes [OsCl(H$_2$)(Chiraphos)$_2$]BF$_4$ (**28**) and [OsH(H$_2$)(Chiraphos)$_2$]BF$_4$ (**29**) in excellent yields. The catalytic activity of the chloro(hydrido)- and dihydridometal derivatives in the asymmetric transfer hydrogenation of acetophenone with 2-propanol was investigated.
(© Wiley-VCH Verlag GmbH & Co. KGaA, 69451 Weinheim, Germany, 2004)

Introduction

In the context of our studies on the chemistry of the five-coordinate (hydrido)ruthenium(II) and (hydrido)osmium(II) complexes [MHCl(CO)(P*i*Pr$_3$)$_2$] (where **1a**: M = Ru; **1b**: M = Os),[1] we reported that the osmium compound **1b**, under hydrogen, catalyzes the reduction of cyclohexene, 1,3- and 1,4-cyclohexadiene, styrene, and diphenyl- and phenylacetylene.[2,3] Furthermore, in the presence of NaBH$_4$, it also serves as a catalyst for hydrogen transfer from 2-propanol to cyclohexanone, acetophenone, benzylidenacetone, etc.[4] It was shown that both **1a** and **1b** react with NaBH$_4$ to give the tetrahydroboranato compounds **2a** and **2b** (see Scheme 1), of which **2b**, upon treatment with 2-propanol, decomposes to the tetrahydride **3**.[5] Kinetic investigations suggest that in the hydrogen-transfer process catalyzed by **1b** and NaBH$_4$, the coordinatively unsaturated dihydride [OsH$_2$(CO)(P*i*Pr$_3$)$_2$], which is generated from **3** by loss of H$_2$, is the active catalytic species.[6]

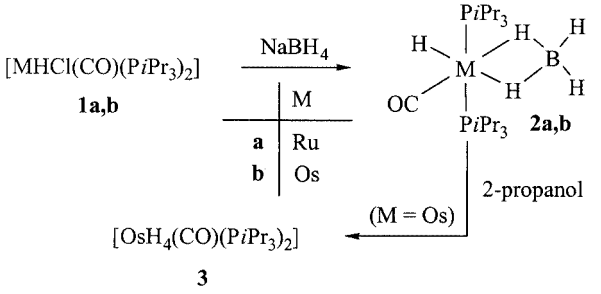

Scheme 1

As a continuation of our work on the reactivity of chloro(hydrido)-, hydrido(boranato)- and (dihydrido)ruthenium

[a] Institut for Anorganische Chemie, Universität Würzburg
Am Hubland, 97074 Würzburg, Germany
Fax: (internat.) +49-(0)931-888-4623
E-mail: helmut.werner@mail.uni-wuerzburg.de
[b] Departamento de Química Inorgánica, Universidad de Zaragoza − CSIC
50009 Zaragoza, Spain

and -osmium complexes we have now attempted to modify the coordination sphere by linking chiral mono- and bisphosphanes to the metal center. In this paper we describe the preparation and molecular structure of the compounds obtained and report some preliminary results concerning their catalytic activity in the asymmetric reduction of acetophenone by 2-propanol.

Results and Discussion

The preparation of the chiral aminophosphanes **4** and **5** (see Scheme 2) follows the route which was developed for the diphenylphosphanyl counterpart (*S*)-Ph_2PNHR^* [R* = CH(Me)Ph] by Brunner et al.[7] The reason for using isopropyl and *tert*-butyl substituents instead of phenyl at the phosphorus atom was that we wanted to make the phosphane comparable in size to P*i*Pr$_3$ and P*t*Bu$_2$Me, respectively. The reactions of R_2PCl and R^*NH_2 were carried out in diethyl ether and gave, after removal of ammonium chloride, the chiral products in 64−72 % isolated yield. Both **4** and **5** are colorless, extremely air-sensitive liquids, the composition of which was confirmed by elemental analysis and mass spectrometry. The ^{1}H NMR spectrum of **5** displays two resonances for the *tert*-butyl protons, which is a consequence of a chiral center next to the phosphorus atom. For the same reason four signals, which are pairwise equivalent, appear in the ^{1}H NMR spectrum of **4** for the methyl protons of the isopropyl groups. They are doublets of doublets and become doublets with $^3J_{H,H}$ = 6.4, 6.9 Hz in off resonance.

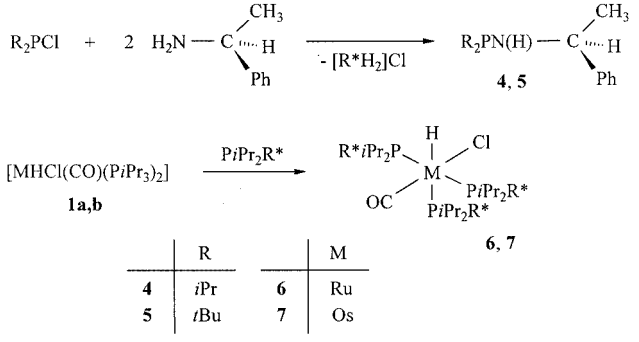

Scheme 2. [R* = NHCH(Me)Ph]

Attempts to prepare the five-coordinate complexes, $[MHCl(CO)(PiPr_2R^*)_2]$, (where M = Ru, Os) from ruthenium- and osmium trichloride, using the same methodology as that applied for the synthesis of **1a** and **1b**,[1] failed. Under the reaction conditions (stirring the reaction mixtures of $MCl_3 \cdot 3H_2O$ and **4** or **5** in methanol or 2-propanol under reflux) partial cleavage of the P−N bond of the aminophosphane and decomposition of possibly formed metal-containing intermediates occurred.

The reactions of **1a** and **1b** with an excess of the less sterically demanding phosphane, **4**, proceeded by ligand exchange as well as by addition of a third phosphane molecule to the metal center. After recrystallization from benzene/methanol, the six-coordinate compounds **6** and **7** were isolated as white, moderately air-stable solids in 67−71 % yield (see Scheme 2). The starting materials are inert toward **5** which is reminiscent to the behavior of other (phosphane)ruthenium and -osmium complexes, such as $[MCl_2(PPh_3)_3]$ (M = Ru, Os) toward P*t*Bu$_3$.[8] The most typical spectroscopic features of **6** and **7** are the two ^{31}P NMR signals at δ = 89.4 and 75.4 ppm for **6** and at δ = 57.2 and 48.5 ppm for **7**, which, together with the splitting pattern, indicate that two of the aminophosphane ligands are stereochemically equivalent while the third is not. Thus, a *mer* configuration for the octahedral compounds can be assigned. In agreement with this proposal, the ^{1}H NMR spectrum of **7** displays a high-field resonance at δ = −8.77 ppm for the Os−H proton, which appears as a doublet of triplets due to P−H coupling with different ^{31}P nuclei.

The results regarding the reactivity of **6** and **7** toward Lewis bases are summarized in Scheme 3. According to the strong *trans* influence of the hydride, the M−P bond in *trans* disposition was assumed to be rather labile and this was substantiated by the reactions of **6** and **7** with CO, $P(OMe)_3$ and $C_2(CO_2Me)_2$. Passing a slow stream of CO through a solution of **6** or **7** in benzene, after a short period of time, leads to a ligand exchange and affords the dicarbonyl complexes **8** and **9** in high yields. The white solids are thermally stable and for a few minutes can be handled in air. The IR spectra display two ν(CO)-stretching modes at 1970 and 1905 cm^{-1} (for **8**) and 1970 and 1910 cm^{-1} (for **9**), indicating that the two CO ligands are not stereochemically equivalent. The ^{1}H NMR spectra show a hydride signal at δ = −5.47 ppm (for **8**) and δ = −4.68 ppm (for **9**), which is split into a triplet due to P−H coupling.

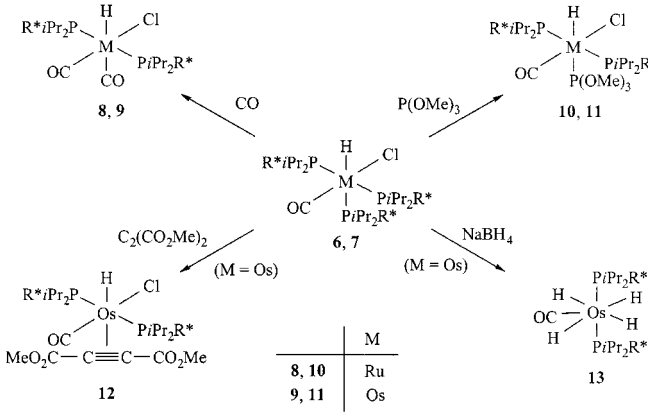

Scheme 3. [R* = NHCH(Me)Ph]

The preparation of the phosphite and alkyne derivatives **10**−**12** takes place under similar conditions (hexane, room temperature) as those used for the dicarbonyl complexes **8** and **9**. After evaporation of the solvent, compounds **10**−**12** were isolated as white, moderately air-stable solids, which readily dissolved in most common organic solvents (with the exception of methanol and hexane). The proposed

 © 2004 Wiley-VCH Verlag GmbH & Co. KGaA, Weinheim

structure for **10**–**12** with the phosphite or alkyne ligand *trans* to the hydride is supported by the mass spectra in which, besides the peak for the molecular M^+ ion, a second peak corresponding to $M^+ - P(OMe)_3$ or $M^+ - C_2(CO_2Me)_2$ appears. Thus, the hydride ligand presumably labilizes the M–P*i*Pr$_2$R* as well as the M–P(OMe)$_3$ and M$^+$–C$_2$(CO$_2$Me)$_2$ bonds in the *trans* position. The ^{31}P NMR spectra of the phosphite complexes **10** and **11** are noteworthy insofar as they show the pattern of an ABX system, which means that the two aminophosphane ligands are magnetically nonequivalent. Since the metal atom in the octahedral complexes **10** and **11** is a prochiral center, the two phosphane units are diastereotopic and thus give rise to two resonances in the ^{31}P NMR spectra. Accordingly, the ^{31}P NMR spectrum of the alkyne compound **12** displays the pattern of an AB spin system with $\delta_{PA} = 65.7$ ppm and $\delta_{PB} = 61.8$ ppm. There are also two signals for the NH and two for the NCHC*H*$_3$ protons of the P*i*Pr$_2$R* ligands in the ^{1}H NMR spectrum of **12**, which is consistent with the proposed stereochemistry. We note that even under forcing conditions no insertion of the alkyne into the Os–H bond occurs, which is in contrast to the behavior of the bis(triisopropylphosphane) analogue [OsHCl(CO){C$_2$(CO$_2$Me)$_2$}(P*i*Pr$_3$)$_2$] that rearranges in chloroform to give a product with a chelating vinyl ligand.[3]

The reaction of **7** with NaBH$_4$ in benzene/methanol proceeds similarly to that of **1b** with the same reagents.[4] We assume that in the initial step (see below the formation of **26**) the tetrahydroboranato compound, [OsH(κ^2-H$_2$BH$_2$)(CO)(P*i*Pr$_2$R*)$_2$], is generated and rapidly reacts with methanol to give **13** (see Scheme 3). The (tetrahydrido)osmium(IV) complex, **13**, is a light yellow, extremely air-sensitive solid, the IR spectrum of which shows a strong ν(CO) band at 1890 cm^{-1}. The ^{31}P NMR spectrum of **13** displays a singlet at $\delta = 87.4$ ppm which is converted into a symmetrical quintet in off resonance. Since the ^{1}H NMR spectrum shows a sharp triplet at $\delta = -8.76$ ppm, we assume that, similarly to the P*i*Pr$_3$ counterpart, the seven-coordinate molecule, **13**, also possesses a fluxional structure at room temperature, which leads to the equivalence of the hydrido ligands on the NMR time scale. The $^2J_{P,H}$ coupling constants for the hydride signal of **13** and [OsH$_4$(CO)(P*i*Pr$_3$)$_2$] are nearly the same.

To compare the catalytic activity of the ruthenium and osmium complexes with two monodentate P*i*Pr$_2$R* units on one side and a chiral bidentate bisphosphane on the other, the starting materials **1a** and **1b** were also treated with (*S*,*S*)-Chiraphos and (*S*,*S*)-Diop. As a test, prior to the reaction with the chiral bisphosphanes, the reaction of **1b** with 1,2-C$_2$H$_4$(PPh$_2$)$_2$ (dppe) was carried out and afforded the racemate of compound **14** in 80 % yield (see Scheme 4). Similarly to that of **10** and **11**, the ^{31}P NMR spectrum of **14** shows an ABX spin pattern which can be clearly resolved and was simulated with the program Laocoon. Typical features are the large coupling constant $^2J_{PA,PB}$ (250.6 Hz) for the *trans*-disposed ^{31}P nuclei and the small coupling constants $^2J_{PA,PX}$ (6.7 Hz) and $^2J_{PB,PX}$ (13.8 Hz) for the ^{31}P nuclei in *cis*-position.

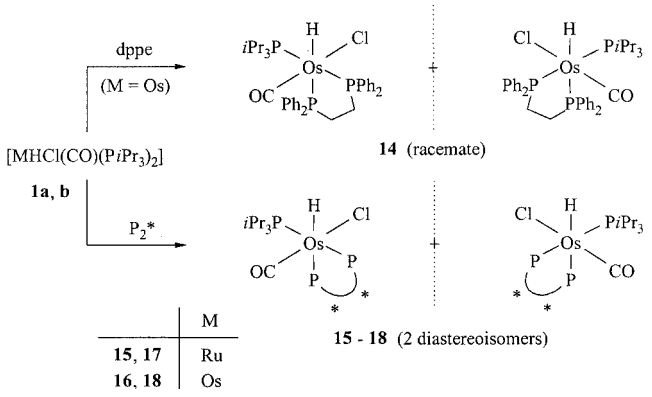

Scheme 4. [**15**, **16**: P$_2$* = (*S*,*S*)-Chiraphos; **17**, **18**: P$_2$* = (*S*,*S*)-Diop]

The chiral bisphosphanes (*S*,*S*)-Chiraphos and (*S*,*S*)-Diop behave analogously to dppe and under similar conditions (hexane, 24 h, reflux) give the chelate complexes **15**–**18** as white, moderately air-stable solids in 79–89 % isolated yield. Due to the presence of chiral centers at the metal and the chelating ligands, the formation of diastereoisomers should be expected and was confirmed for the Diop derivatives **17** and **18**. In contrast, the NMR spectra of the Chiraphos compounds **15** and **16** display only one set of signals, which probably means that only one diastereoisomer was generated. The high-field region of the ^{1}H NMR spectra of **15** and **16** consists of a sharp doublet of doublets of doublets at $\delta = -6.61$ ppm (for **15**) and $\delta = -6.69$ ppm (for **16**) with two small and one large $^2J_{P,H}$ coupling constant. Owing to these numbers, there is no doubt that one of the phosphorus atoms is *trans* to the hydride. Although the ^{31}P NMR spectra of **15** and **16** are in agreement with an ABX spin system, they differ from the spectrum of **14** insofar as the outer lines of the AB part were not observed and, therefore, the values for δ_{PA}, δ_{PB} and $^2J_{PA,PB}$ could not be determined. With regard to the structure of **15** and **16**, we assume that the five-membered chelate ring possesses the δ-conformation, which for steric arguments should be preferred.[9] We were unable to substantiate this by X-ray crystallography since all attempts to grow single crystals of **15** or **16** failed.

The reactions of **1a** and **1b** with (*S*,*S*)-Diop lead to two diastereoisomers, the ratio of which depends on the reaction conditions. For example, by refluxing a solution of **1b** and (*S*,*S*)-Diop in hexane for 24 h the two diastereoisomers **A** and **B** of compound **18** were obtained in a ratio of 3:2, whereas stirring the same mixture for five days gave the two species **A** and **B** in equal amounts. In the ruthenium case, an **A**/**B** ratio of 7:1 was found after refluxing the reaction mixture in hexane for 24 h, whereas only **A** was generated by carrying out the reaction at room temperature.

In contrast to the ^{1}H NMR spectra of **15** and **16**, those of **17** and **18** are rather complicated and therefore no exact assignment for the resonances (for $\delta = 0-9$) could be made. For each of the diastereoisomers **A** and **B** the hydride signal is a doublet of doublets of doublets with similar coupling constants as observed for **15** and **16**. The ^{31}P NMR spectra

 © 2004 Wiley-VCH Verlag GmbH & Co. KGaA, Weinheim

of **17** and **18** display the expected number of lines for ABX spin systems and thus the chemical shifts for the signals corresponding to P_A ($PiPr_3$), P_B and P_X (each PPh_2) could be exactly determined. The presence of the two diastereoisomers of **18** is also indicated by the IR spectrum, which shows two ν(CO) absorptions at 1905 and 1895 cm^{-1} with comparable intensities. We note that at room temperature, the diastereoisomers **A** and **B** of both **17** and **18** are stable and do not interconvert.

The preparation of the (dihydrido)ruthenium(II) and -osmium(II) complexes **19−22** followed the route that we already used to obtain compounds of the general composition $[MH_2(CO)(L)(PiPr_3)_2]$ (L = PMe_3, $P(OMe)_3$].[4] Treatment of **2a** and **2b** with (*S*,*S*)-Chiraphos and of **2a** with (*S*,*S*)-Diop in methanol under reflux conditions affords, after recrystallization from CH_2Cl_2/methanol, the chelate complexes **19−21** in 76−83 % isolated yield (see Scheme 5). In contrast to related dihydrido derivatives such as $[RuH_2(PMe_3)_4]$ or $[OsH_2(PMe_3)_4]$,[10] compounds **19−21** are only slightly air sensitive and, apart from hexane and methanol, readily soluble in common organic solvents. While the ^{31}P NMR spectrum of **19** clearly indicates that only one diastereoisomer is formed, the spectrum of **20** displays two sets of resonances for two diastereoisomers, **A** and **B**, in an approximate ratio of 10:1. For both **19** and the dominating isomer of **20**, the pattern corresponding to an ABX spin system is observed with values for the coupling constants $^2J_{PA,PB}$, $^2J_{PA,PX}$ and $^2J_{PB,PX}$ that are similar to those of **15** and **16**. For compound **21**, a mixture of two diastereoisomers in a 3:2 ratio was obtained; they are configurationally stable at room temperature and do not interconvert. The ^1H NMR spectra of **19** and **20** confirm the nonequivalence of the hydrido ligands and display two doublets of doublets of doublets of doublets at δ = −8.16 and −8.76 ppm (for **19**) and δ = −9.32 and −10.04 ppm (for **20**). In agreement with the size of the coupling constants, the signal for the lower chemical shift belongs to the hydride *trans* to CO and that for the higher chemical shift to the hydride *trans* to one of the PPh_2 groups. For the Diop compound, **21**, the two signals overlap and thus no correct δ values can be given.

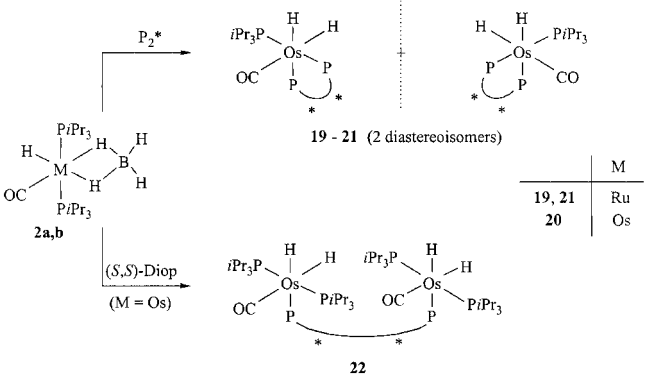

Scheme 5. [**19**, **20**: P_2* = (*S*,*S*)-Chiraphos; **21**, **22**: P_2* = (*S*,*S*)-Diop]

Quite surprisingly, the reaction of **2b** with (*S*,*S*)-Diop affords, under the same conditions as those used for the preparation of **19−21**, the dinuclear complex **22**, instead of a mononuclear one (see Scheme 5) in 81 % yield. The result is reminiscent of the formation of the catalytically active ruthenium compound $[\{RuCl_2(Diop)\}_2(\mu\text{-Diop})]$, obtained by James et al. from $[RuCl_2(PPh_3)_3]$ and a 2.5-fold excess of Diop.[11] Similarly to the ^1H NMR spectra of **19** and **20**, the ^1H NMR spectrum of **22** also shows two high-field signals at δ = −9.34 and −11.56 ppm, which appear both as doublets of doublets of triplets, due to two different P−H and to one H−H coupling. For the hydride *trans* to the PPh_2 unit, two significantly different $^2J_{P,H}$ coupling constants result. The ^{31}P NMR spectrum of **22** is more simple than the spectra of **19−21** and displays one doublet for the ^{31}P nuclei of the two $PiPr_3$ ligands and one triplet for the ^{31}P nuclei of Diop.

The X-ray crystal structure analysis of **22** (see Figure 1) confirms the proposed structure, including the presence of the bridging Diop unit. The high quality of data allowed the location of the hydrides in the Fourier maps and their isotropic refinement. Taken the positions of these ligands into consideration, the coordination geometry around both metal centers is best described as distorted octahedral with bond angles that in some cases deviate significantly from the ideal 90° value. The most remarkable feature is the size of the angles P(4)−Os−P(5) and P(3)−Os−P(6) [148.90(6)° and 145.65(5)°], which is unusual and probably explained by steric hindrance between the isopropyl and phenyl groups. The chirality (*S*,*S*) of the Diop ligand was maintained. The bond lengths between osmium and the phos-

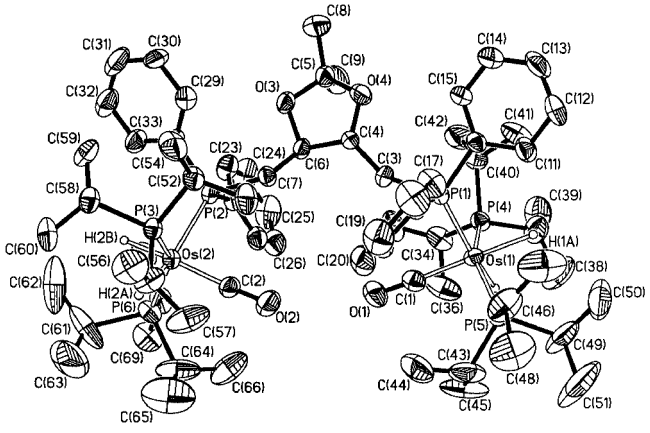

Figure 1. Molecular structure of compound **22**; selected bond lengths (Å) and angles (°): Os(1)−P(1) 2.3725(13), Os(2)−P(2) 2.3711(4), Os(2)−P(3) 2.3431(16), Os(1)−P(4) 2.3412(15), Os(1)−P(5) 2.3457(15), Os(2)−P(6) 2.3640(15), Os(1)−C(1) 1.873(7), Os(2)−C(2) 1.852(6), C(1)−O(1) 1.197(7), C(2)−O(2) 1.191(7); P(1)−Os(1)−P(4) 101.27(5), P(1)−Os(1)−P(5) 106.24(6), P(1)−Os(1)−C(1) 88.51(19), P(4)−Os(1)−P(5) 148.90(6), P(4)−Os(1)−C(1) 97.9(2), P(5)−Os(1)−C(1) 97.0(2), P(2)−Os(2)−P(3) 101.59(5), P(2)−Os(2)−P(6) 109.33(5), P(2)−Os(2)−C(2) 91.31(18), P(3)−Os(2)−P(6) 145.65(5), P(3)−Os(2)−C(2) 96.42(18), P(6)−Os(2)−C(2) 97.44(18), P(1)−C(3)−C(4) 126.2(4), P(2)−C(7)−C(6) 120.2(4), C(3)−C(4)−C(6) 110.7(4), C(7)−C(6)−C(4) 114.4(4), C(3)−C(4)−O(4) 113.1(5), C(7)−C(6)−O(3) 111.6(4), C(4)−O(4)−C(5) 111.4(4), C(6)−O(3)−C(5) 106.4(4).

 © 2004 Wiley-VCH Verlag GmbH & Co. KGaA, Weinheim

phorus atoms of the P*i*Pr$_3$ units are slightly shorter than in the five-coordinate vinyl complex [OsCl(CH=CHPh)(CO)(P*i*Pr$_3$)$_2$],[12] but somewhat longer than in the bis(triisopropylphosphane)osmium(IV) compound, [OsH$_2$Cl$_2$(P*i*Pr$_3$)$_2$] (**23**) (see below).[5] There is also a small difference in the distances Os−P*i*Pr$_3$ and Os−PPh$_2$X, which might be due to the different donor strength of the trialkylphosphane and alkyldiarylphosphane moieties.

The above-mentioned osmium(IV) compound, **23**, was also used as starting material for the reactions with (*S*,*S*)-Chiraphos (see Scheme 6). It was already known that the dichloro(dihydrido) complex reacts with CO and PMe$_3$ to give [OsCl$_2$(CO)$_2$(P*i*Pr$_3$)$_2$] and [OsCl$_2$(PMe$_3$)$_4$] by reductive elimination of H$_2$.[5]

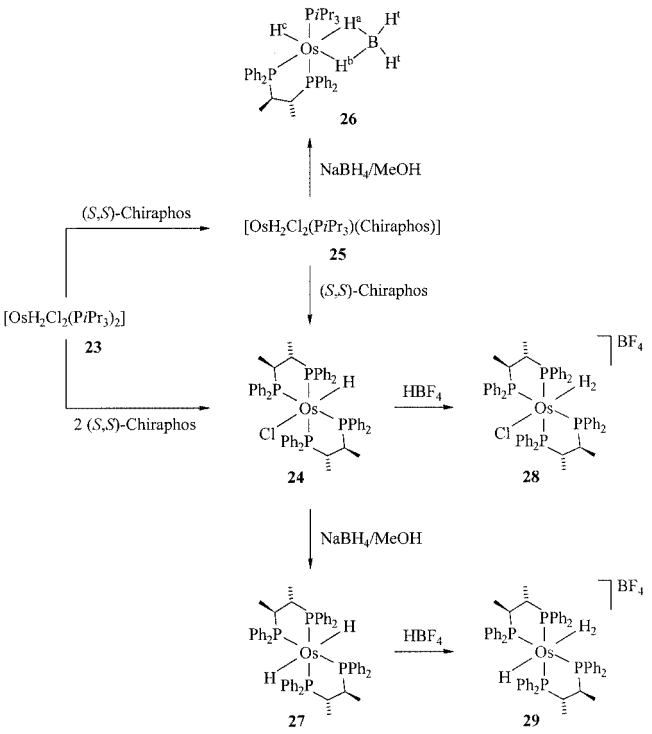

Scheme 6

The reaction of **23** with two equivalents of (*S*,*S*)-Chiraphos, however, does not lead to the elimination of H$_2$ but of HCl and affords the chloro(hydrido)osmium(II) compound **24** in 89 % isolated yield. If equimolar amounts of **23** and (*S*,*S*)-Chiraphos are reacted in hexane under reflux, a white, extremely air-sensitive solid, **25**, can be isolated and it slowly decomposes at room temperature, even under argon. The assumption that **25** is the substitution product of **23** is supported by the elemental analysis and, in particular, by the ^{31}P NMR spectrum, which displays the pattern of an ABX spin system. The ^{1}H NMR spectrum of **25** shows a broadened doublet of doublets of doublets in the high-field region, indicating that under these conditions the two hydrido ligands are magnetically equivalent on the NMR time scale. Since the three coupling constants $^2J_{P,H}$ are virtually the same, it is conceivable that the seven-coordinate molecule is fluxional in solution, as has also been observed for the osmium tetrahydrides [OsH$_4$(PPh$_3$)$_3$] and [OsH$_4$(PMe$_2$Ph)$_3$].[13] Since, by lowering the temperature, the high-field resonance in the ^{1}H NMR spectrum of **25** becomes broader and the coupling constants become smaller, the possibility of an equilibrium between a classical OsH$_2$ and a nonclassical Os(H$_2$) species was taken into consideration. Therefore, T_1 measurements were carried out at +20 °C, −20 °C and −50 °C resulting in T_1 values of 170, 110 and 100 ms, respectively. Since the T_1 minimum has not been found (for comparison see compounds **28** and **29**), the question that remains is whether a nonclassical octahedral osmium(II) complex, [OsCl$_2$(H$_2$)(P*i*Pr$_3$)(Chiraphos)], exists. If treated in 1,2-dichloroethane under reflux, compound **25** reacts with one equivalent of (*S*,*S*)-Chiraphos to give the bis(chelate) complex **24** in nearly quantitative yield. The ^{1}H NMR spectrum of **24** displays a complicated symmetrical multiplet for the hydrido ligand at $\delta = -20.27$ ppm; the chemical shift is similar to that of related chloro(hydrido)-metal derivatives with two chelating moieties.[14]

The reaction of **25** with an excess of NaBH$_4$ in toluene/methanol does not lead to the (tetrahydrido)osmium(IV) complex [OsH$_4$(P*i*Pr$_3$)(Chiraphos)] (the counterpart of compound **3**) but gives the hydrido(tetrahydroboranato)osmium(II) derivative **26** instead. A mixture of two diastereoisomers **A** and **B**, formed in about equal quantities, is obtained. The white solid is exceedingly air-sensitive and thermally not very stable; slow decomposition occurs even in toluene solution. The ^{1}H NMR spectrum of **26** shows two sharp doublets of doublets of doublets in the high-field region which are assigned to the metal-bonded proton H^c (see Scheme 6) of the two diastereoisomers. Apart from these sharp signals four rather broadened resonances appear at $\delta = -7.81$, −8.55, −9.42 and −10.10 ppm which probably belong to the bridging hydrides H^a and H^b. The broadening could be a consequence of the linkage of H^a and H^b to the boron nuclei. Since the spectrum does not change between −20 °C and +30 °C, we assume that, in contrast to [OsH(κ^2-H$_2$BH$_2$)(CO)(P*i*Pr$_3$)$_2$], the fragment Os(κ^2-H$_2$BH$_2$) of **26** is rigid in this temperature region and no exchange between the bridging and terminal hydrogens of the BH$_4$ moiety occurs. The situation is similar to that of the structurally related ruthenium compounds [RuH(κ^2-H$_2$BH$_2$)(PR$_3$)$_3$] (PR$_3$ = PMePh$_2$, PMe$_2$Ph), for which a rigid structure has also been proposed.[15,16]

The reaction of the chloro(hydrido) complex, **24**, with NaBH$_4$ and methanol in toluene does not yield a hydrido(tetrahydroboranato) derivative such as **26** but leads to the formation of the dihydridoosmium(II) compound **27** in good yield. Since the ^{31}P NMR spectrum of **27** displays only a singlet at $\delta = 50.9$ ppm, there is no doubt that the four PPh$_2$ units are chemically and spectroscopically equivalent. Due to this fact, the two hydrides must be in *trans* disposition. This stereochemistry is also supported by the IR spectrum that shows a ν(OsH) band at relatively low wavenumbers (1730 cm^{-1}). In the IR spectrum of the related complex *trans*-[OsH$_2$(dppe)$_2$], the ν(OsH) stretching mode is observed at 1721 cm^{-1}.[15] The ^{1}H NMR spectrum

 © 2004 Wiley-VCH Verlag GmbH & Co. KGaA, Weinheim

of **27** displays a quintet in the high-field region at $\delta = -10.70$ ppm, which equally suggests that the phosphido moieties are equivalent.

To further modify the reactivity of the osmium(II) compounds with Chiraphos as ligands, **24** and **27** were transformed into the cationic $OsCl(H_2)$ and $OsH(H_2)$ derivatives **28** and **29**, respectively (see Scheme 6). The preparation took place with HBF_4 in diethyl ether at room temperature (for **28**) or at −78 °C (for **29**) and gave the products as white solids in 71−83 % yield. Both **28** and **29** are air sensitive but can be stored under argon for days; they do not eliminate H_2 in THF, acetone or chloroform solutions. In the presence of N_2, no ligand exchange to afford $[OsX(N_2)(Chiraphos)_2]BF_4$ (X = Cl, H) occurs. The ^{31}P NMR spectra of **28** and **29** display in each case two triplets for the ^{31}P nuclei of the pairwise equivalent PPh_2 units with $^2J_{P,P}$ coupling constants that are similar to those of **24**. The ^1H NMR spectrum of **29** shows a broadened signal at $\delta = -6.45$ ppm and a sharp multiplet at $\delta = -8.63$ ppm with the relative intensities of 2:1. By decreasing the temperature, the broadened signal is shifted to the lower-field region, where free dihydrogen resonates. T_1 measurements of the broadened signal resulted in values of 70 ms at 20 °C, 60 ms at 0 °C, 50 ms at −20 °C and 40 ms at −50 °C. Although the minimum could not be exactly located in the given range of temperatures, a non-classical $Os(H_2)$ structure can be assumed. The T_1(min) value for the well-characterized complex $[OsH(H_2)(dppe)_2]^+$ is 18 ms at −85 °C.[17] In contrast to this species, which is dynamic and where an equilibration between the OsH and the $Os(H_2)$ protons occurs at room temperature, a similar process could not be observed for **29**. Whether this difference is a result of steric effects, that is, of the larger size of (*S*,*S*)-Chiraphos compared with dppe, is open to speculation.

Since the preparation of optically active alcohols by catalytic asymmetric transfer hydrogenation of ketones is an important process in organic synthesis,[18] we were prompted to explore the catalytic activity of some of the chiral ruthenium and osmium complexes prepared in this study. For this purpose, the reduction of acetophenone with 2-propanol was carried out in a mixture of 2-propanol/toluene (2:1) at 85 °C under an argon atmosphere. The results are listed in Table 1. In analogous studies, where rhodium, iridium and ruthenium compounds containing chiral phosphane,[19] amine,[20] and Schiff-base ligands were used,[21] the presence of KOH was necessary for the substitution of the halide by a coordinated isopropoxide group; the latter afforded a hydride-metal intermediate by β-elimination. However, for the Chiraphos and Diop complexes **15**−**18** the presence of KOH is not necessary; it does not lead to any significant improvement either in the rate of conversion or in the *ee* values. Although the *ee*'s in general are not very high, the chloro(hydrido) complexes **15** and **16** with Chiraphos as the chelating ligand are more active than the Diop counterparts **17** and **18** and, moreover, than the dihydrido compounds **19**−**22**. The (dihydrido)osmium(II) derivative **20** is not active at all. We note that for **16** and **17** the presence of KOH as cocatalyst changes the chirality of the product, which is not unexpected and in agreement with the general rule.[22]

Table 1. Asymmetric hydrogen transfer from 2-propanol to acetophenone, catalyzed by (hydrido)ruthenium and -osmium complexes

Catalyst	Time	Conversion (%)	*ee* (%)	Configuration
7	16 h	70	3.5	*R*-(+)
15	23 h	91	22.6	*S*-(−)
15/KOH	22 h	85	25.3	*S*-(−)
16	7 days	85	20	*S*-(−)
16/KOH	22 h	62	17.4	*R*-(+)
17	7 h	92	15.4	*R*-(+)
17/KOH	6 h	85	10.4	*S*-(−)
18	18 h	94	3.5	*R*-(+)
18/KOH	40 h	35	1.2	*S*-(−)
19	16 h	92	6.3	*S*-(−)
20	not active			
21	24 h	75	3.8	*R*-(+)
22	45 h	63	1.4	*R*-(+)
24	not active			
27	not active			
29	not active			

Conclusions

The work presented in this paper has shown that in five-coordinate ruthenium(II) and osmium(II) compounds $[MHCl(CO)(PiPr_3)_2]$ (**1a** and **1b**) either one or both triisopropylphosphane ligands can be replaced by an optically active monophosphane, such as $PiPr_2R^*$, or by a chiral chelating bisphosphane such as (*S*,*S*)-Chiraphos or (*S*,*S*)-Diop. In the isolated octahedral complexes $[MHCl(CO)(PiPr_2R^*)_3]$ (**6**, **7**), the M−P bond *trans* to the hydride is quite labile and thus substitution products $[MHCl(CO)(L)(PiPr_2R^*)_2]$ with L = CO, $P(OMe)_3$ and $C_2(CO_2Me)_2$ are readily obtained. The reactions of **1a** and **1b** and of the tetrahydroboranato derivatives **2a** and **2b** with (*S*,*S*)-Chiraphos and (*S*,*S*)-Diop afford a mixture of two diastereoisomers, the ratio of which depends on the metal, the chiral bisphosphane and the reaction conditions. For the Chiraphos complexes **15**, **16** and **19**, the formation of only one diastereoisomer was observed. With the osmium(IV) compound $[OsH_2Cl_2(PiPr_3)_2]$ (**23**) and (*S*,*S*)-Chiraphos as starting materials, chloro(hydrido)- and (dihydrido)osmium(II) complexes can be prepared and, by treatment with HBF_4 in diethyl ether, transformed into the cationic dihydrogen derivatives **28** and **29**, respectively. Regarding the catalytic potential in the asymmetric transfer hydrogenation of acetophenone with 2-propanol as a hydrogen source, the osmium(II) complexes with two Chiraphos ligands are completely inactive. The catalytic activity of the related ruthenium(II) and osmium(II) compounds **15**−**21** with one chiral chelating ligand is also not very pronounced and could be due to the fact that they are coordinatively saturated, that is, they have an 18-electron count. Although the *trans* influence of the hydride ligand is rather strong, it is probably not strong enough to open the *trans*-disposed co-

 © 2004 Wiley-VCH Verlag GmbH & Co. KGaA, Weinheim

ordination site by maintaining the chirality at the metal center. The introduction of optically active tridentate chelating ligands could possibly improve the optical yield but this has to be confirmed by further investigations.

Experimental Section

All operations were carried out under argon using Schlenk techniques. The starting materials **1a**, **1b**,[1] **2a**, **2b**,[4] and **23**[5] were prepared as described in the literature. The chlorophosphanes R_2PCl, the optically pure amine (*S*)-$H_2NCH(Me)Ph$ and the chelating phosphanes are commercially available. NMR: Bruker AC 200 and Jeol FX 90 Q. IR: Perkin−Elmer 397 and 1320. Mass spectra: Varian CH 7 MAT (70 eV). Melting points determined by DTA. Abbreviations used: R* = (*S*)-NHCH(Me)Ph; s, singlet; d, doublet; t, triplet; q, quadruplet; quint, quintet; m, multiplet; vt, virtual triplet; br, broadened signal; $N = {}^3J_{P,H} + {}^5J_{P,H}$.

Preparation of (*S*)-*i*Pr_2PNHCH(Me)Ph (4): A solution of *i*Pr_2PCl (6.1 mL, 40.0 mmol) in diethyl ether (50 mL) was added dropwise to a solution of (*S*)-$H_2NCH(Me)Ph$ (12.7 mL, 100.0 mmol) in diethyl ether (400 mL) at room temperature. The reaction mixture was stirred for 3 h at 25 °C and then filtered. The separated solid was washed three times with 20 mL portions of diethyl ether, and the combined filtrates were concentrated to about 15 mL in vacuo. The solution was poured into a column (height 5 cm) filled with finely divided SiO_2 and the product was eluted with 200 mL of diethyl ether. The solvent was evaporated in vacuo (20 mbar) and the residue maintained under high vacuum (0.01 mbar) at 70 °C to remove traces of the amine. A clear air-sensitive liquid was obtained; yield 6.8 g (72 %). MS: *m*/*z* (I_r) = 237 (10) [M^+]. IR: $\tilde{\nu}$ = 3370 ν(NH) cm^{-1}. ^1H NMR (90 MHz, $CDCl_3$): δ = 7.17 (m, 5 H, C_6H_5), 4.01 (ddq, $^3J_{H,H} = {}^3J_{H,H} = {}^3J_{P,H}$ = 6.6 Hz, 1 H, NCH), 1.51 (m, 2 H, PC*H*CH_3), 1.35 (d, $^3J_{H,H}$ = 6.6 Hz, 3 H, NCHCH_3), 1.05, 1.04 (both m, 3 H each PCHCH_3; both d in off resonance, $^3J_{H,H}$ = 6.4 Hz), 0.91, 0.88 (both m, 3 H each, PCHCH_3, both d in off resonance, $^3J_{H,H}$ = 6.9 Hz) ppm; signal of NH proton not exactly located. ^{31}P NMR (36.2 MHz, $CDCl_3$): δ = 60.3 (s) ppm. $C_{14}H_{24}NP$ (237.3): calcd. C 70.85, H 10.19, N 5.90; found C 69.93, H 10.09, N 5.71.

Preparation of (*S*)-*t*Bu_2PNHCH(Me)Ph (5): This compound was prepared as described for **4**, with *t*Bu_2PCl (4.5 mL, 25.0 mmol) and (*S*)-$H_2NCH(Me)Ph$ (8.0 mL, 63.0 mmol) as starting materials. The reaction mixture was refluxed for 10 h and, after cooling to room temperature, worked up as described for **4**. Colorless air-sensitive liquid; yield 4.2 g (64 %). MS: *m*/*z* (I_r) = 265 (7; M^+). IR: $\tilde{\nu}$ = 3380 ν(NH) cm^{-1}. ^1H NMR (90 MHz, $CDCl_3$): δ = 7.29 (m, 5 H, C_6H_5), 4.10 (ddq, $^3J_{H,H} = {}^3J_{H,H} = {}^3J_{P,H}$ = 6.6 Hz, 1 H, NCH), 1.45 (d, $^3J_{H,H}$ = 6.6 Hz, 3 H, NCHCH_3), 1.13, 0.96 (both d, $^3J_{P,H}$ = 14.6 Hz, 9 H each, $PCCH_3$) ppm, signal of the NH proton not exactly located. ^{31}P NMR (36.2 MHz, $CDCl_3$): δ = 71.9 (s) ppm. $C_{16}H_{28}NP$ (265.4): calcd. C 72.42, H 10.63, N 5.28; found C 71.33, H 10.13, N 5.61.

Preparation of *mer*-[RuHCl(CO)(P*i*Pr_2R*)$_3$] (6): A solution of **1a** (500 mg, 1.05 mmol) in benzene (30 mL) was treated dropwise with **4** (1.20 g, 5.05 mmol) and stirred for 2 h at room temperature. The solution was then concentrated to ca. 2 mL in vacuo and methanol (10 mL) was added. The volatile materials were evaporated in vacuo and a white solid precipitated. The solid was filtered, washed three times with 5 mL portions of methanol and dried; yield 617 mg (67 %); m.p. 86 °C (decomp). MS: *m*/*z* (I_r) = 612 (1; M^+ − CO−**4**). IR (KBr): $\tilde{\nu}$ = 3345, 3285, 3230 ν(NH), 1985 ν(RuH), 1890 ν(CO) cm^{-1}. ^1H NMR (90 MHz, C_6D_6): δ = 7.26 (m, 15 H, C_6H_5), 4.19 (m, 3 H, NCH), 2.30 (m, 6 H, PC*H*CH_3), 1.21 (br m, 45 H, NCHCH_3 and PCHCH_3) ppm; signals for RuH and NH protons not exactly located. ^{31}P NMR (36.2 MHz, C_6D_6): δ = 89.4 (d, $^2J_{P,P}$ = 13.2 Hz, two P*i*Pr_2R* in equatorial position), 75.4 (br, P*i*Pr_2R* in axial position) ppm. $C_{43}H_{73}ClN_3OP_3Ru$ (877.5): calcd. C 58.86, H 8.39, N 4.79; found C 59.03, H 8.42, N 4.61.

Preparation of *mer*-[OsHCl(CO)(P*i*Pr_2R*)$_3$] (7): A solution of **1b** (200 mg, 0.35 mmol) in benzene (30 mL) was treated dropwise with **4** (410 mg, 1.73 mmol) and stirred at room temperature until the color of the starting materials disappeared. The solution was then concentrated to ca. 2 mL in vacuo and methanol (10 mL) was added. A white microcrystalline solid precipitated and was filtered, washed three times with 5 mL portions of methanol and dried; yield 240 mg (71 %); m.p. 101 °C (decomp). MS: *m*/*z* (I_r) = 730 (1; M^+ − **4**). IR (KBr): $\tilde{\nu}$ = 3345, 3290, 3245 ν(NH), 2075 ν(OsH), 1885 ν(CO) cm^{-1}. ^1H NMR (90 MHz, C_6D_6): δ = 7.23 (m, 15 H, C_6H_5), 4.30 (m, 3 H, NCH), 2.49 (m, 6 H, PC*H*CH_3), 1.25 (br m, 45 H, NCHCH_3 and PCHCH_3), −8.77 (dt, $^2J_{P,H\,cis}$ = 28.5, $^2J_{P,H\,trans}$ = 88.6 Hz, 1 H, OsH) ppm; signal for NH proton not exactly located. ^{31}P NMR (36.2 MHz, C_6D_6): δ = 57.2 (d, $^2J_{P,P}$ = 13.9 Hz, two P*i*Pr_2R* in equatorial position), 48.5 (t, $^2J_{P,P}$ = 13.9 Hz, P*i*Pr_2R* in axial position) ppm. $C_{43}H_{73}ClN_3OOsP_3$ (966.7): calcd. C 53.43, H 6.61, N 4.35; found C 53.15, H 7.44, N 4.18.

Preparation of [RuHCl(CO)$_2$(P*i*Pr_2R*)$_2$] (8): A slow stream of carbon monoxide was passed for 2 min through a solution of **6** (200 mg, 0.23 mmol) in benzene (10 mL) at room temperature. After the solution was stirred for 30 min at 25 °C, the solvent was evaporated in vacuo, the oily residue was suspended in 5 mL of methanol and the suspension stored at −78 °C. A white solid precipitated and was filtered, washed twice with 3 mL portions of methanol (0 °C) and dried; yield 121 mg (78 %); m.p. 133 °C (decomp). MS: *m*/*z* (I_r) = 639 (1; M^+ − CO), 611 (1; M^+ − 2 CO). IR (KBr): $\tilde{\nu}$ = 3365, 3290 ν(NH), 1970, 1905 ν(CO) cm^{-1}. ^1H NMR (90 MHz, C_6D_6): δ = 7.14 (m, 10 H, C_6H_5), 4.16 (m, 2 H, NCH), 2.10 (m, 4 H, PC*H*CH_3), 1.09 (br m, 30 H, NCHCH_3 and PCHCH_3), −5.47 (t, $^2J_{P,H}$ = 20.3 Hz, 1 H, RuH) ppm; signal for NH proton not exactly located. ^{31}P NMR (36.2 MHz, C_6D_6): δ = 94.6 (s; d in off resonance) ppm. $C_{30}H_{49}ClN_2O_2P_2Ru$ (668.2): calcd. C 53.93, H 7.39, N 4.19; found 53.80, H 7.40, N 3.94.

Preparation of [OsHCl(CO)$_2$(P*i*Pr_2R*)$_2$] (9): This compound was prepared as described for **8**, using **7** (250 mg, 0.26 mmol) and CO as starting materials. White solid; yield 196 mg (83 %), m.p. 132 °C (decomp). MS: *m*/*z* (I_r) = 757 (1; M^+), 729 (1; M^+ − CO). IR (KBr): $\tilde{\nu}$ = 3380, 3290 ν(NH), 2040 ν(OsH), 1970, 1915 ν(CO) cm^{-1}. ^1H NMR (90 MHz, C_6D_6): δ = 7.18 (m, 10 H, C_6H_5), 4.02 (m, 2 H, NCH), 2.16 (m, 4 H, PC*H*CH_3), 1.35 (br m, 30 H, NCHCH_3 and PCHCH_3), −4.68 (t, $^2J_{P,H}$ = 20.7 Hz, 1 H, RuH) ppm; signal for NH proton not exactly located. ^{31}P NMR (36.2 MHz, C_6D_6): δ = 62.5 (s; d in off resonance) ppm. $C_{30}H_{49}ClN_2O_2OsP_2$ (757.3): calcd. C 47.59, H 6.52, N 3.69; found C 48.06, H 6.88, N 3.66.

Preparation of [RuHCl(CO){P(OMe)$_3$}(P*i*Pr_2R*)$_2$] (10): A solution of **6** (220 mg, 0.25 mmol) in hexane (10 mL) was treated with trimethylphosphite (60 μL, 0.51 mmol) and stirred for 30 min at room temperature. The solvent was evaporated in vacuo and a white solid began to precipitate. After the solution was stored at −20 °C for 6 h, the white solid was filtered, washed three times with 3 mL portions of hexane (−20 °C) and dried; yield 130 mg (69 %); m.p. 108

 © 2004 Wiley-VCH Verlag GmbH & Co. KGaA, Weinheim

°C (decomp). MS: *m*/*z* (I_r) = 764 (1) [M^+], 640 (4; $M^+ - P(OMe)_3$]. IR (KBr): $\tilde{\nu}$ = 3340, 3290 ν(NH), 2000 ν(RuH), 1910 ν(CO) cm^{-1}. ^1H NMR (90 MHz, C_6D_6): δ = 7.28 (m, 10 H, C_6H_5), 4.03 (m, 2 H, NCH), 3.61 [d, $^3J_{P,H}$ = 9.6 Hz, 9 H, $P(OMe)_3$], 2.29 (m, 4 H, PC*H*CH_3), 1.19 (br m, 30 H, NCHC*H*$_3$ and PCHC*H*$_3$), −6.86 (dt, $^2J_{P,Hcis}$ = 25.3, $^2J_{P,Htrans}$ = 193.1 Hz, 1 H, RuH) ppm; signal for NH proton not exactly located. ^{31}P NMR (36.2 MHz, C_6D_6): ABX spin system; AB part consists of four signals at δ = 93.5, 93.3, 92.7, 92.5 ppm and corresponds to two P*i*Pr_2R* ligands; X part consists of three signals at δ = 133.3, 132.7, 132.0 ppm and corresponds to the $P(OMe)_3$ ligand. $C_{32}H_{58}ClN_2O_4P_3Ru$ (764.3): calcd. C 40.29, H 7.65, N 3.67; found C 50.53, H 7.91, N 3.43.

Preparation of [OsHCl(CO){P(OMe)$_3$}(P*i*Pr$_2$R*)$_2$] (11): This compound was prepared as described for **10**, with **7** (250 mg, 0.26 mmol) and trimethylphosphite (62 μL, 0.52 mmol) as starting materials. White solid; yield 160 mg (72 %); m.p. 111 °C (decomp). MS: *m*/*z* (I_r) = 854 (1; M^+), 730 [5; $M^+ - P(OMe)_3$]. IR (KBr): $\tilde{\nu}$ = 3345, 3270 ν(NH), 2080 ν(OsH),1890 ν(CO) cm^{-1}. ^1H NMR (90 MHz, C_6D_6): δ = 7.30 (m, 10 H, C_6H_5), 4.20 (m, 2 H, NCH), 3.59 [d, $^3J_{P,H}$ = 10.0 Hz, 9 H, $P(OMe)_3$], 2.41 (m, 4 H, PC*H*CH_3), 1.17 (br m, 30 H, NCHC*H*$_3$ and PCHC*H*$_3$), −6.89 (dt, $^2J_{P,Hcis}$ = 25.1, $^2J_{P,Htrans}$ = 151.7 Hz, 1 H, RuH) ppm; signal for NH proton not exactly located. ^{31}P NMR (36.2 MHz, C_6D_6): ABX spin system; AB part consists of four signals at δ = 61.6, 61.5, 61.4, 60.9 ppm and corresponds to two P*i*Pr_2R* ligands; X part consists of three signals at δ = 101.6, 101.0, 100.4 ppm and corresponds to the $P(OMe)_3$ ligand. $C_{32}H_{58}ClN_2O_4OsP_3$ (853.4): calcd. C 45.04, H 6.85, N 3.28; found C 45.19, H 6.88, N 3.33.

Preparation of [OsHCl(CO){C$_2$(CO$_2$Me)$_2$}(P*i*Pr$_2$R*)$_2$] (12): This compound was prepared as described for **10**, with **7** (200 mg, 0.21 mmol) and $C_2(CO_2Me)_2$ (30 μL, 0.25 mmol) as starting materials. White solid; yield 145 mg (80 %); m.p. 76 °C (decomp). MS: *m*/*z* (I_r) = 872 (1; M^+), 730 [7; $M^+ - C_2(CO_2Me)_2$]. IR (KBr): $\tilde{\nu}$ = 3270 ν(NH), 2100 ν(OsH), 1930 ν(CO), 1790 ν(C≡C), 1695 ν(C=O) cm^{-1}. ^1H NMR (90 MHz, C_6D_6): δ = 7.29 (m, 10 H, C_6H_5), 5.02 (dd, $^2J_{P,H}$ = $^2J_{H,H}$ = 9.2 Hz, 1 H, NH), 4.72 (dd, $^2J_{P,H}$ = $^2J_{H,H}$ = 10.6 Hz, 1 H, NH), 4.25 (m, 2 H, NCH), 3.58 (s, 6 H, CO_2CH_3), 2.59 (m, 4 H, PC*H*CH_3), 1.56, 1.49 (both d, $^2J_{H,H}$ = 6.8 Hz, 3 H, each, NCHC*H*$_3$), 1.01 (m, 24 H, PCHC*H*$_3$), −3.49 (t, $^2J_{P,H}$ = 31.8 Hz, 1 H, OsH) ppm. ^{31}P NMR (36.2 MHz, C_6D_6): AB spin system; δ_{PA} = 65.7, δ_{PB} = 61.8 ppm, $^2J_{PA,PB}$ = 132.2 Hz; d in off resonance. $C_{35}H_{55}ClN_2O_5OsP_2$ (871.4): calcd. C 48.24, H 6.36, N 3.21; found C 48.63, H 6.51, N 3.08.

Preparation of [OsH$_4$(CO)(P*i*Pr$_2$R*)$_2$] (13): A solution of **7** (300 mg, 0.31 mmol) in benzene (10 mL) was first treated with $NaBH_4$ (150 mg, 3.95 mmol) and subsequently dropwise with methanol (1 mL). The solution was filtered and the filtrate concentrated to ca. 0.5 mL in vacuo. The residue was extracted twice with 8 mL portions of hexane and the combined extracts were dried in vacuo. The oily residue was suspended in 6 mL of methanol and the suspension stored for 12 h at −78 °C. A light yellow, extremely air-sensitive solid precipitated and was filtered, washed twice with 3 mL portions of methanol (−20 °C) and dried; yield 108 mg (51 %). IR (C_6H_6): $\tilde{\nu}$ = 3250 ν(NH), 2030, 1965 ν(OsH), 1890 ν(CO) cm^{-1}. ^1H NMR (90 MHz, C_6D_6): δ = 7.20 (m, 10 H, C_6H_5), 4.46 (m, 2 H, NCH), 1.50 (m, 4 H, PC*H*CH_3), 1.19 (d, $^2J_{H,H}$ = 6.8 Hz, 6 H, NCHC*H*$_3$), 0.82 (m, 24 H, PCHC*H*$_3$), −8.76 (t, $^2J_{P,H}$ = 9.8 Hz, 4 H, OsH_4) ppm; the signal for the NH protons not exactly located. ^{31}P NMR (36.2 MHz, C_6D_6): δ = 87.4 (s; quint in off resonance) ppm.

Preparation of [OsHCl(CO)(P*i*Pr$_3$)(dppe)] (14): A solution of **1b** (125 mg, 0.22 mmol) in hexane (15 mL) was treated with dppe (95 mg, 0.24 mmol) and stirred for 24 h under reflux. A white solid precipitated and once the reaction mixture was cooled to room temperature, it was filtered and then washed three times with 8 mL portions of hexane. Recrystallization from benzene/hexane (1:3) gave white air-stable crystals; yield 143 mg (80 %). IR (Nujol): $\tilde{\nu}$ = 2065ν(OsH), 1895 ν(CO) cm^{-1}. ^1H NMR (90 MHz, C_6D_6): δ = 7.47 (m, 10 H, C_6H_5), 3.01 (m, 4 H, PCH_2), 2.53 (m, 3 H, PC*H*CH_3), 1.21, 0.99 (both dvt, *N* = 12.0, $^3J_{H,H}$ = 7.1 Hz, 9 H each, PCHC*H*$_3$), −6.93 (ddd, 2 × $^2J_{P,Hcis}$ = 17.3, $^2J_{P,Htrans}$ = 93.2 Hz, 1 H, OsH) ppm. ^{31}P NMR (36.2 MHz, C_6D_6): ABX spin system; δ_{PA} = 39.6 ppm, δ_{PB} = 29.4 ppm, $^2J_{PA,PB}$ = 250.6 Hz; δ_{PX} = 13.8 ppm, $^2J_{PA,PX}$ = 6.7 Hz, $^2J_{PB,PX}$ = 13.8 Hz. $C_{36}H_{46}ClOOsP_3$ (813.3): calcd. C 53.16, H 5.70; found C 52.91, H 5.61.

Preparation of [RuHCl(CO)(P*i*Pr$_3$)(Chiraphos)] (15): This compound was prepared as described for **14**, with **1a** (150 mg, 0.31 mmol) and (*S*,*S*)-Chiraphos (135 mg, 0.32 mmol) as starting materials. White solid; yield 233 mg (79 %); m.p. 150 °C (decomp). IR (Nujol): $\tilde{\nu}$ = 1920 ν(CO) cm^{-1}. ^1H NMR (90 MHz, C_6D_6): δ = 7.71 (m, 20 H, C_6H_5), 3.91, 2.13 (both m, 1 H each, Ph_2PCH), 2.43 (m, 3 H, PC*H*CH_3), 1.18, 0.91 (both m, 9 H each, PCHC*H*$_3$; both d in off resonance, $^3J_{H,H}$ = 7.1 Hz), −6.61 (ddd, $^2J_{P,Hcis}$ = 17.9 and 22.2, $^2J_{P,Htrans}$ = 113.1 Hz, 1 H, RuH) ppm; signals for Ph_2CHCH_3 protons partly covered by signals of PCHC*H*$_3$ protons. ^{31}P NMR (36.2 MHz, C_6D_6): ABX spin system; AB part consists of four signals at δ = 54.5, 54.0, 53.8, 53.5 ppm and corresponds to the ^{31}P nuclei of Chiraphos; X part also consists of four signals at δ = 42.6, 42.3, 42.2, 41.9 ppm and corresponds to the ^{31}P nuclei of the P*i*Pr_3 ligand. $C_{38}H_{50}ClOP_3Ru$ (752.3): calcd. C 60.67, H 7.00; found C 60.45, H 6.70.

Preparation of [OsHCl(CO)(P*i*Pr$_3$)(Chiraphos)] (16): This compound was prepared as described for **14**, with **1b** (150 mg, 0.26 mmol) and (*S*,*S*)-Chiraphos (115 mg, 0.27 mmol) as starting materials. White solid; yield 180 mg (82 %); m.p. 197 °C (decomp). IR (Nujol): $\tilde{\nu}$ = 2030 ν(OsH), 1920 ν(CO) cm^{-1}. ^1H NMR (90 MHz, C_6D_6): δ = 7.78 (m, 20 H, C_6H_5), 3.67, 2.11 (both m, 1 H each, Ph_2PCH), 2.43 (m, 3 H, PC*H*CH_3), 1.14, 0.94 (both m, 9 H each, PCHC*H*$_3$, both d in off resonance, $^3J_{H,H}$ = 6.8 Hz), −6.69 (ddd, 2 × $^2J_{P,Hcis}$ = 19.1, $^2J_{P,Htrans}$ = 113.3 Hz, 1 H, OsH) ppm; signals for Ph_2CHCH_3 protons partly covered by signals of PCHC*H*$_3$ protons. ^{31}P NMR (36.2 MHz, C_6D_6): ABX spin system; AB part consists of three signals at δ = 24.4, 24.2, 24.1 ppm and corresponds to the ^{31}P nuclei of Chiraphos; X part consists of four signals at δ = 20.4, 20.3, 20.2, 20.0 ppm and corresponds to the ^{31}P nuclei of the P*i*Pr_3 ligand. $C_{38}H_{50}ClOOsP_3$ (841.4): calcd. C 54.25, H 5.99; found C 54.14, H 5.93.

Preparation of [RuHCl(CO)(P*i*Pr$_3$)(Diop)] (17): (a) A solution of **1a** (125 mg, 0.26 mmol) in hexane (15 mL) was treated with (*S*,*S*)-Diop (140 mg, 0.28 mmol) and stirred for 24 h under reflux. After the reaction mixture was cooled to room temperature, the white solid was filtered, washed three times with 8 mL portions of hexane, then with 5 mL of methanol and dried; yield 174 mg (81 %). Owing to the NMR spectra, two diastereoisomers **A** and **B** in the ratio of 7:1 were formed and could not be separated by fractional crystallization or column chromatography. (b) Analogously **1a** (180 mg, 0.37 mmol) was reacted with (*S*,*S*)-Diop (190 mg, 0.38 mmol) in hexane (15 mL) for 5 days under reflux. Under these conditions, only diastereoisomer **A** was obtained as a white solid; yield 250 mg (82 %); m.p. 143 °C (decomp). IR (Nujol): $\tilde{\nu}$ = 2000 ν(RuH), 1920 ν(CO) cm^{-1}. ^1H NMR (90 MHz, C_6D_6) diastereomer **A**: δ = −6.14 (ddd, $^2J_{P,Hcis}$ = 16.3 and 27.1, $^2J_{P,Htrans}$ = 109.1 Hz, 1 H, RuH) ppm; diastereomer **B**: δ = −6.71 (ddd,

 © 2004 Wiley-VCH Verlag GmbH & Co. KGaA, Weinheim

$^2J_{P,Hcis}$ = 17.7 and 26.1, $^2J_{P,Htrans}$ = 116.1 Hz, 1 H, RuH) ppm; all other signals for δ = 0−9 ppm overlap and cannot be exactly assigned. ^{31}P NMR (36.2 MHz, C_6D_6) diastereomer **A**: ABX spin system; δ_{PA} = 50.2, δ_{PB} = 21.2 ppm, $^2J_{PA,PB}$ = 267.2 Hz; δ_{PX} = 7.1 ppm, $^2J_{PA,PX}$ = 18.0, $^2J_{PB,PX}$ = 11.2 Hz; diastereomer **B**: ABX spin system; δ_{PA} = 52.8, δ_{PB} = 23.1 ppm, $^2J_{PA,PB}$ = 267.4 Hz; δ_{PX} = −3.5, $^2J_{PA,PX}$ = 17.6, $^2J_{PB,PX}$ = 11.6 Hz. $C_{41}H_{54}ClO_3P_3Ru$ (824.3): calcd. C 59.74, H 6.60; found C 59.91, H 6.79.

Preparation of [OsHCl(CO)(P*i*Pr$_3$)(Diop)] (18): This compound was prepared as described for **17**, with (a) **1b** (130 mg, 0.23 mmol) and (*S*,*S*)-Diop (123 mg, 0.25 mmol) or (b) **1b** (215 mg, 0.37 mmol) and (*S*,*S*)-Diop (195 mg, 0.39 mmol) as starting materials. White solid; yield 187 mg (89 %) for (a) and 307 mg (91 %) for (b). Owing to the NMR spectra, following route "a" the ratio of the two diastereomers **A** and **B** was 3:2 and following route "b" the ratio was 1:1. IR (Nujol): $\tilde{\nu}$ = 2055 ν(OsH), 1905 and 1895 ν(CO) cm^{-1}. ^{1}H NMR (90 MHz, C_6D_6) diastereomer **A**: δ = −6.09 (ddd, $^2J_{P,Hcis}$ = 18.4 and 24.1, $^2J_{P,Htrans}$ = 88.3 Hz, 1 H, OsH) ppm; diastereomer **B**: δ = −6.74 (ddd, $^2J_{P,Hcis}$ = 19.9 and 28.2, $^2J_{P,Htrans}$ = 96.2 Hz, 1 H, OsH) ppm; all other signals for δ = 0−9 ppm strongly overlap and cannot be assigned to one of the diastereomers. ^{31}P NMR (36.2 MHz, C_6D_6) diastereomer **A**: ABX spin system; δ_{PA} = 17.8, δ_{PB} = −12.3 ppm, $^2J_{PA,PB}$ = 243.2 Hz; δ_{PX} = −18.9 ppm, $^2J_{PA,PX}$ = 15.2, $^2J_{PB,PX}$ = 3.8 Hz; diastereomer **B**: ABX spin system; δ_{PA} = 19.6, δ_{PB} = −9.0 ppm, $^2J_{PA,PB}$ = 242.1 Hz; δ_{PX} = −29.2 ppm, $^2J_{PA,PX}$ = 17.5, $^2J_{PB,PX}$ = 4.1 Hz. $C_{41}H_{54}ClO_3OsP_3$ (913.5): calcd. C 53.91, H 6.02; found C 53.99, H 6.18.

Preparation of [RuH$_2$(CO)(P*i*Pr$_3$)(Chiraphos)] (19): A solution of **2a** (145 mg, 0.31 mmol) in methanol (15 mL) was treated with (*S*,*S*)-Chiraphos (140 mg, 0.33 mmol) and stirred for 24 h under reflux. After the solution was cooled to room temperature, it was concentrated to ca. 5 mL in vacuo. A white solid precipitated and was filtered, washed three times with 5 mL portions of methanol and dried. Recrystallization from dichloromethane/methanol (1:3) gave white, moderately air-sensitive crystals; yield 170 mg (76 %). IR (Nujol): $\tilde{\nu}$ = 1940 ν(RuH), 1930 ν(CO) cm^{-1}. ^{1}H NMR (200 MHz, C_6D_6): δ = 7.68 (m, 20 H, C_6H_5), 2.20, 1.83 (both m, 1 H each, Ph_2PCH), 1.79 (m, 3 H, $PCHCH_3$), 1.28 (dd, $^3J_{P,H}$ = 13.5, $^3J_{H,H}$ = 7.0 Hz, 9 H, $PCHCH_3$), 0.98 (dd, $^3J_{P,H}$ = 11.6, $^3J_{H,H}$ = 7.0 Hz, 9 H, $PCHCH_3$), −8.15 (dddd, 2 × $^2J_{P,Hcis}$ = 20.2, 1 × $^2J_{P,Hcis}$ = 30.4, $^2J_{H,H}$ = 4.1 Hz, 1 H, RuH *trans* to CO), −8.76 (dddd, 2 × $^2J_{P,Hcis}$ = 18.9, $^2J_{P,Htrans}$ = 77.4, $^2J_{H,H}$ = 4.1 Hz, 1 H, RuH *trans* to PPh_2) ppm; signals for Ph_2PCHCH_3 protons partly covered by signals for P*i*Pr$_3$ protons. ^{31}P NMR (81.0 MHz, C_6D_6): ABX spin system; δ_{PA} = 84.3, δ_{PB} = 77.7 ppm, $^2J_{PA,PB}$ = 217.2 Hz; δ_{PX} = 68.1 ppm, $^2J_{PA,PX}$ = 13.4, $^2J_{PB,PX}$ = 17.4 Hz. $C_{38}H_{51}OP_3Ru$ (717.8): calcd. C 63.58, H 7.16; found C 63.62, H 7.48.

Preparation of [OsH$_2$(CO)(P*i*Pr$_3$)(Chiraphos)] (20): This compound was prepared as described for **19**, with **2b** (150 mg, 0.27 mmol) and (*S*,*S*)-Chiraphos (125 mg, 0.29 mmol) as starting materials. White solid; yield 181 mg (83 %). Owing to the NMR spectra, one diastereomer was mainly obtained. The amount of the second isomer (data not given) was less than 10 %. IR (Nujol): $\tilde{\nu}$ = 1950 br ν(OsH), 1860 ν(CO) cm^{-1}. ^{1}H NMR (200 MHz, C_6D_6): δ = 7.64 (m, 20 H, C_6H_5), 2.25, 1.95 (both m, 1 H each, Ph_2PCH), 2.43 (m, 3 H, $PCHCH_3$), 1.26 (dd, $^3J_{P,H}$ = 13.4, $^3J_{H,H}$ = 6.9 Hz, 9 H, $PCHCH_3$), 0.95 (dd, $^3J_{P,H}$ = 11.5, $^3J_{H,H}$ = 6.9 Hz, 9 H, $PCHCH_3$), −9.32 (dddd, 3 × $^2J_{P,Hcis}$ = 21.4, $^2J_{H,H}$ = 4.2 Hz, 1 H, OsH *trans* to CO), −10.04 (dddd, 2 × $^2J_{P,Hcis}$ = 21.4, $^2J_{P,Htrans}$ = 62.1, $^2J_{H,H}$ = 4.2 Hz, 1 H, OsH *trans* to PPh_2) ppm; signals for Ph_2PCHCH_3 protons partly covered by signals for P*i*Pr$_3$ protons. ^{31}P NMR (81.0 MHz, C_6D_6): ABX spin system; δ_{PA} = 48.5, δ_{PB} = 40.9 ppm, $^2J_{PA,PB}$ = 207.0 Hz; δ_{PX} = 35.9 (br) ppm, $^2J_{PB,PX}$ = 13.9 Hz. $C_{38}H_{51}OOsP_3$ (807.0): calcd. C 56.56, H 6.37; found C 57.19, H 6.84.

Preparation of [RuH$_2$(CO)(P*i*Pr$_3$)(Diop)] (21): This compound was prepared as described for **19**, with **2a** (130 mg, 0.28 mmol) and (*S*,*S*)-Diop (150 mg, 0.30 mmol) as starting materials. White solid; yield 170 mg (77 %). Owing to the ^{31}P NMR spectrum, two diastereomers **A** and **B** in the ratio of 3:2 were obtained. IR (Nujol): $\tilde{\nu}$ = 1945 br ν(RuH), 1860 ν(CO) cm^{-1}. ^{31}P NMR (81.0 MHz, C_6D_6) diastereomer **A**: ABX spin system; δ_{PA} = 73.9, δ_{PB} = 42.4 ppm, $^2J_{PA,PB}$ = 212.1 Hz; δ_{PX} = 27.5 (br) ppm, $^2J_{PA,PX}$ = 18.0, $^2J_{PB,PX}$ = −15.6 Hz; diastereomer **B**: ABX spin system; δ_{PA} = 72.0, δ_{PB} = 44.2 ppm, $^2J_{PA,PB}$ = 209.8 Hz; δ_{PX} = 22.7 (br) ppm, $^2J_{PA,PX}$ = −6.1, $^2J_{PB,PX}$ = 39.1 Hz. $C_{41}H_{55}OP_3Ru$ (789.9): calcd. C 62.35, H 7.02; found C 62.20, H 7.13.

Preparation of [{OsH$_2$(CO)(P*i*Pr$_3$)}$_2$(μ-Diop)] (22): This compound was prepared as described for **19**, with **2b** (155 mg, 0.28 mmol) and (*S*,*S*)-Diop (160 mg, 0.32 mmol) as starting materials. White solid; yield 183 mg (81 %). IR (Nujol): $\tilde{\nu}$ = 1930 br ν(OsH), 1835 ν(CO) cm^{-1}. ^{1}H NMR (200 MHz, C_6D_6): δ = −9.34 (ddt, 2 × $^2J_{P,Hcis}$ = 24.3, $^3J_{H,H}$ = 5.0 Hz, 2 H, OsH *trans* to CO), −11.56 (ddt, 2 × $^2J_{P,Hcis}$ = 30.4, $^2J_{P,Htrans}$ = 61.8, $^2J_{H,H}$ = 5.0 Hz, 2 H, OsH *trans* to PPh_2) ppm; all other signals for δ = 0−9 ppm strongly overlap and cannot be assigned. ^{31}P NMR (36.2 MHz, C_6D_6): δ = 30.4 (d, $^2J_{P,P}$ = 11.2 Hz, P*i*Pr$_3$), −2.8 (t, $^2J_{P,P}$ = 11.2 Hz, Diop) ppm. $C_{69}H_{120}O_4Os_2P_6$ (1580.0): calcd. C 52.45, H 7.65; found C 51.91, H 7.13.

Preparation of *trans*-[OsHCl(Chiraphos)$_2$] (24): A solution of **23** (300 mg, 0.51 mmol) in dichloromethane (20 mL) was treated with (*S*,*S*)-Chiraphos (470 mg, 1.10 mmol) and stirred for 24 h under reflux. After the solution was cooled to room temperature, the solvent was evaporated in vacuo and the oily residue suspended in methanol (10 mL). The suspension was stored for 2 h and led to the precipitation of a pale yellow solid. This was separated from the mother liquor, washed twice with 5 mL portions of methanol and 5 mL portions of hexane and dried; yield 490 mg (89 %) IR (Nujol): $\tilde{\nu}$ = 2085 ν(OsH) cm^{-1}. ^{1}H NMR (200 MHz, C_6D_6): δ = 7.36 (m, 40 H, C_6H_5), 3.31, 1.85 (both m, 2 H each, Ph_2PCH), 0.88, 0.52 (both dvt, N = 12.0, $^3J_{H,H}$ = 6.1 Hz, 6 H each, Ph_2CHCH_3), −20.27 (m, 1 H, OsH) ppm. ^{31}P NMR (81.0 MHz, C_6D_6): δ = 42.3, 16.8 (both t, $^2J_{P,P}$ = 21.0 Hz) ppm. $C_{56}H_{57}ClOsP_4$ (1079.6): calcd. C 62.30, H 5.32; found C 62.35, H 5.75.

Preparation of [OsH$_2$Cl$_2$(P*i*Pr$_3$)(Chiraphos)] (25): A suspension of **23** (160 mg, 0.27 mmol) in hexane (20 mL) was treated with (*S*,*S*)-Chiraphos (117 mg, 0.27 mmol) and stirred for 10 h under reflux. After the solution was cooled to room temparature, the yellow-brown solid was filtered, washed twice with 5 mL portions of hexane and recrystallized from benzene/hexane (1:3); yield 174 mg (76 %). ^{1}H NMR (200 MHz, C_6D_6): δ = 7.50 (m, 20 H, C_6H_5), 4.02, 2.47 (both m, 5 H, PCH), 1.08 (br m, 24 H, $PCHCH_3$ and Ph_2PCHCH_3), −10.28 (ddd, 3 × $^2J_{P,H}$ = 15.1 Hz, 2 H, OsH_2) ppm; T_1 = 170 ms (20 °C), 110 ms (−20 °C), 100 ms (−50 °C). ^{31}P NMR (36.2 MHz, C_6D_6): ABX spin system; δ_{PA} = 1.4, δ_{PB} = 12.3 ppm, $^2J_{PA,PB}$ = 288.7 Hz; δ_{PX} = 31.2 ppm, $^2J_{PA,PX}$ = 6.2, $^2J_{PB,PX}$ = 17.2 Hz. $C_{37}H_{51}Cl_2OsP_3$ (848.9): calcd. C 52.26, H 6.05; found C 52.26, H 5.97.

Preparation of [OsH(κ^2-H$_2$BH$_2$)(P*i*Pr$_3$)(Chiraphos)] (26): A solution of **25** (150 mg, 0.18 mmol) in toluene (10 mL) was first treated with $NaBH_4$ (65 mg, 1.70 mmol) and then dropwise with 1 mL of methanol. After the evaporation of gas (H_2) had stopped, the solution was stirred for 15 min at room temperature and then filtered.

 © 2004 Wiley-VCH Verlag GmbH & Co. KGaA, Weinheim

The filtrate was concentrated to ca. 5 mL in vacuo and methanol (8 mL) was added. A white solid precipitated and was filtered, washed twice with 2 mL portions of methanol (0 °C) and dried; yield 97 mg (68 %). Owing to the NMR spectroscopic data, a mixture of the two diastereoisomers in about equal amounts was obtained. Attempts to separate the two diastereoisomers by fractional crystallization from benzene/methanol failed. IR (Nujol): $\tilde{\nu}$ = 2450, 2380 br ν(BH), 2070 ν(OsH) cm^{-1}. ^1H NMR (200 MHz, C_6D_6): δ = −7.81, −8.55 (both br, 1 H each, H^a of isomer **A** or **B**), −9.42, −10.10 (both br, 1 H each, H^b of isomer **A** or **B**), −16.71 (ddd, 2 × $^2J_{P,Hcis}$ = 16.0, 1 × $^2J_{P,Hcis}$ = 31.0 Hz, 1 H, H^c of isomer **A** or **B**), −17.40 (ddd, 3 × $^2J_{P,Hcis}$ = 23.0 Hz, 1 H, H^c of isomer **A** or **B**) ppm; signal of H^t not observed; all other signals for δ = 0−9 ppm overlap and cannot be assigned; for assignment of H^a, H^b, H^c, H^t see Scheme 6. $C_{37}H_{54}BOsP_3$ (792.8): calcd. C 56.06, H 6.87; found C 56.39, H 7.38.

Preparation of *trans*-[OsH_2(Chiraphos)$_2$] (27): This compound was prepared as described for **26**, with **24** (180 mg, 0.17 mmol), $NaBH_4$ (65 mg, 1.70 mmol) and methanol (1 mL) as starting materials. White solid; yield 109 mg (61 %). IR (Nujol): $\tilde{\nu}$ = 1730 br ν(OsH) cm^{-1}. ^1H NMR (200 MHz, C_6D_6): δ = 7.73 (m, 40 H, C_6H_5), 2.25 (br, 4 H, Ph_2PCH), 0.96 (br, 12 H, Ph_2PCHCH_3), −10.70 (quint, $^2J_{P,H}$ = 16.2 Hz, 2 H, OsH_2) ppm. ^{31}P NMR (81.0 MHz, C_6D_6): δ = 50.9 (s) ppm. $C_{56}H_{58}OsP_4$ (1045.2) calcd. C 64.35, H 5.56; found C 63.95, H 5.62.

Preparation of *trans*-[$OsCl(H_2)$(Chiraphos)$_2$]BF_4 (28): A suspension of **24** (90 mg, 0.08 mmol) in diethyl ether (10 mL) was treated with a solution of HBF_4 in diethyl ether (15 μL, 0.11 mmol) and stirred for 20 min at room temperature. The mother liquor was decanted, the precipitate was dissolved in dichloromethane (5 mL) and the solution was filtered. The filtrate was concentrated to ca. 1 mL in vacuo and diethyl ether (10 mL) was added. A white solid precipitated and was filtered, washed twice with 5 mL portions of diethyl ether (0 °C) and dried; yield 80 mg (83 %). ^1H NMR (200 MHz, $CDCl_3$): δ = 7.25 (m, 40 H, C_6H_5), 3.09, 1.81 (both m, 2 H each, Ph_2PCH), 0.89, 0.37 (both dvt, N = 12.0, $^3J_{H,H}$ = 6.1 Hz, 6 H each, Ph_2PCHCH_3), −11.62, (br, 2 H, OsH_2) ppm; T_1 = 110 ms (20 °C). ^{31}P NMR (81.0 MHz, $CDCl_3$): δ = 34.9, 2.0 (both t, $^2J_{P,P}$ = 17.3 Hz) ppm. $C_{56}H_{58}BClF_4OsP_4$ (1167.4): calcd. C 57.62, H 5.01; found C 57.24, H 5.16.

Preparation of *trans*-[$OsH(H_2)$(Chiraphos)$_2$]BF_4 (29): A solution of HBF_4 in diethyl ether (25 μL, 0.18 mmol)was added dropwise to a suspension of **27** (140 mg, 0.13 mmol) in diethyl ether (10 mL) under an H_2 atmosphere at −78 °C. After the solution was warmed to room temperature, it was stirred for 10 min and then filtered. The white solid was washed twice with 2 mL portions of diethyl ether (0 °C) and then recrystallized from dichloromethane/diethyl ether (1:5); yield 107 mg (71 %). IR (Nujol): $\tilde{\nu}$ = 2010 ν(OsH) cm^{-1}. ^1H NMR (200 MHz, $CDCl_3$): δ = 7.63 (m, 40 H, C_6H_5), 2.24, 2.13 (both m, 2 H each, Ph_2PCH), 0.98 (br m, 12 H, Ph_2PCHCH_3), −6.45, (br, 2 H, OsH_2), −8.63 (m, 1 H, OsH) ppm; T_1 = 70 ms (20 °C), 60 ms (0 °C), 50 ms (−20 °C), 40 ms (−50 °C). ^{31}P NMR (81.0 MHz, $CDCl_3$): δ = 42.0, 36.0 (both t, $^2J_{P,P}$ = 19.0 Hz). $C_{56}H_{59}BF_4OsP_4$ (1133.0): calcd. C 59.37, H 5.25; found C 59.33, H 5.15.

Hydrogen-Transfer Reactions: The catalytic reactions were carried out under an argon atmosphere in a mixture of 2-propanol/toluene (2:1), with magnetic stirring, in a 50 mL round-bottomed flask fitted with a condenser and provided with a serum cap. In a typical procedure, a solution of the catalyst (0.1 mmol) in 12.5 mL of toluene and 12.5 mL of 2-propanol was stirred for 1 h at 85 °C, and then a solution of acetophenone (10 mmol) in 12.5 mL of 2-propanol was injected. The progress of the reaction was monitored by a Perkin−Elmer 8900 gas chromatograph with a flame ionization detector and an FFAP on Chromosorb GHP 80/100 mesh column (3.6 × 1/8 in.) at 160 °C. The solvents were evaporated in vacuo, and the remaining mixture (alcohol and ketone) was isolated by distillation at reduced pressure. The *ee* was calculated from its optical rotation in ethanol solution, using a value of $[\alpha]_D^{19}$ = +42.9 (undil.)[23] for the (*R*)-(+)-1-phenylethanol isomer, and corrected to the composition of the distillate. Optical rotations were measured with a Perkin−Elmer 241 polarimeter. For reactions carried out in the presence of KOH as cocatalyst, a 0.1 M solution of KOH (3 mL) in 2-propanol was added to the solution of the catalyst.

X-ray Structure Determination of Compound 22: Single crystals of **22** were grown by slow diffusion of hexane into a solution of **22** in 1,2-dichloroethane at room temperature. Crystal data (from 62 reflections, 2.4° < θ < 18.36°): monoclinic, space group $P2_1$ (No. 4); a = 11.2952(6), b = 29.521(3), c = 11.7201(6) Å, β = 106.771(5)°; V = 3741.8 $Å^3$, Z = 2; $D_{calcd.}$ = 1.402 g cm^{-3}; μ(Mo-K_α) = 3.563 mm^{-1}; crystal size 0.42 × 0.35 × 0.31 mm; Siemens-Stoe AED-2 diffractometer, Mo-K_α radiation (0.71073 Å), graphite monochromator; T = 293(2) K; ω/2θ-scan, max. 2θ = 44.96°; 10271 reflections measured, 9707 independent (R_{int} = 0.016), 9461 with $I > 2\sigma(I)$. Intensity data were corrected for Lorentz, polarization and absorption effects.[24] The structure was solved by direct methods (SHELXS-97).[25] Atomic coordinates and anisotropic thermal parameters of the non-hydrogen atoms were refined by full-matrix least-square methods using SHELXL-97.[26] The hydride ligands H(1A), H(1B), H(2A) and H(2B) were found after proper refinement of the whole structure including a weighting scheme. They were included in the refinement as free isotropic atoms with a common thermal parameter. The positions of all other hydrogen atoms were calculated according to ideal geometry and refined by the riding method. Conventional R = 0.0208 [for 9461 reflections with $I > 2\sigma(I)$], and weighted wR_2 = 0.0508 for all 9707 located reflections; reflection/parameter ratio 12.6; absolute structure Flack parameter −0.017(4); residual electron density +0.487/−0.487 e·$Å^{-3}$.

CCDC-225188 contains the supplementary crystallographic data for this paper. These data can be obtained free of charge at www.ccdc.cam.ac.uk/conts/retrieving.html [or from the Cambridge Crystallographic Data Centre, 12, Union Road, Cambridge CB2 1EZ, UK; Fax: (internat.) +44-1223/336-033; E-mail: deposit@ccdc.cam.ac.uk].

Acknowledgments

This work was supported by the Deutsche Forschungsgemeinschaft (SFB, 347), the BASF AG, the Fonds der Chemischen Industrie and MCYT (BQU2000−1170 and BQU2002−1729). We thank Mrs. R. Schedl and Mr. C. P. Kneis for elemental analyses and DTA measurements, and Dr. G. Lange and Mr. F. Dadrich for mass spectra.

[1] M. A. Esteruelas, H. Werner, *J. Organomet. Chem.* **1986**, *303*, 221−231.
[2] M. A. Esteruelas, E. Sola, L. A. Oro, U. Meyer, H. Werner, *Angew. Chem.* **1988**, *100*, 1621−1622; *Angew. Chem. Int. Ed. Engl.* **1988**, *27*, 1563−1564.
[3] A. Andriollo, M. A. Esteruelas, U. Meyer, L. A. Oro, R. A. Sanchez-Delgado, E. Sola, C. Valero, H. Werner, *J. Am. Chem. Soc.* **1989**, *111*, 7431−7437.

[4] [4a] M. A. Esteruelas, E. Sola, L. A. Oro, H. Werner, U. Meyer, *J. Mol. Catal.* **1988**, *45*, 1−5. [4b] M. A. Esteruelas, E. Sola, L. A. Oro, H. Werner, U. Meyer, *J. Mol. Catal.* **1989**, *53*, 43−52. [4c] H. Werner, U. Meyer, M. A. Esteruelas, E. Sola, L. A. Oro, *J. Organomet. Chem.* **1989**, *366*, 187−196.
[5] H. Werner, M. A. Esteruelas, U. Meyer, B. Wrackmeyer, *Chem. Ber.* **1987**, *120*, 11−15.
[6] M. Aracama, M. A. Esteruelas, F. J. Lahoz, J. A. Lopez, U. Meyer, L. A. Oro, H. Werner, *Inorg. Chem.* **1991**, *30*, 288−293.
[7] H. Brunner, J. Doppelberger, *Chem. Ber.* **1978**, *111*, 673−691.
[8] J. Gotzig, unpublished results.
[9] H. Brunner, *Angew. Chem.* **1983**, *95*, 921−931; *Angew. Chem. Int. Ed. Engl.* **1983**, *22*, 897−907.
[10] H. Werner, J. Gotzig, *Organometallics* **1983**, *2*, 547−549.
[11] B. R. James, D. K. W. Wang, R. F. Voigt, *J. Chem. Soc., Chem. Commun.* **1975**, 574−575.
[12] H. Werner, M. A. Esteruelas, H. Otto, *Organometallics* **1986**, *5*, 2295−2299.
[13] [13a] N. Ahmad, J. J. Levison, S. D. Robinson, M. F. Uttley, *Inorg. Synth.* **1974**, *15*, 45−58. [13b] D. W. Hart, R. Bau, T. F. Koetzle, *J. Am. Chem. Soc.* **1989**, *111*, 7431−7437.
[14] [14a] J. Chatt, R. G. Hayter, *J. Chem. Soc.* **1961**, 2605−2611. [14b] J. Chatt, R. G. Hayter, *J. Chem. Soc.* **1961**, 5507−5511.
[15] R. H. Crabtree, A. J. Pearman, *J. Organomet. Chem.* **1978**, *157*, 335−344.
[16] J. W. Bruno, J. C. Huffman, K. G. Caulton, *Inorg. Chim. Acta* **1984**, *89*, 167−173.
[17] K. A. Earl, G. Jia, P. M. Maltby, R. H. Morris, *J. Am. Chem. Soc.* **1991**, *113*, 3027−3039.
[18] G. Mestroni, A. Camus, G. Zassinovich, *Aspects of Homogeneous Catalysis* (Ed.: R. Ugo), D. Reidel, Boston, **1981**, Vol. 4, p. 71−89.
[19] [19a] R. Spogliarich, G. Zassinovich, J. Kaspar, M. Graziani, *J. Mol. Catal.* **1982**, *16*, 359−361. [19b] M. Bianchi, U. Matteoli, P. Frediani, G. Menchi, F. Piacenti, *J. Organomet. Chem.* **1982**, *236*, 375−380. [19c] P. Kvintovics, J. Bakos, B. Heil, *J. Mol. Catal.* **1985**, *32*, 111−114. [19d] R. Spogliarich, J. Gaspar, M. Graziani, F. Morandini, *J. Organomet. Chem.* **1986**, *306*, 407−412. [19e] H. W. Krause, A. K. Bhatnagar, *J. Organomet. Chem.* **1986**, *302*, 265−267. [19f] R. Spogliarich, E. Farnetti, J. Kaspar, M. Graziani, E. Cesarotti, *J. Mol. Catal.* **1989**, *50*, 19−29. [19g] R. Chauvin, *J. Mol. Catal.* **1990**, *62*, 147−156.
[20] [20a] C. Botteghi, G. Chelussi, G. Chessa, G. Delugo, S. Gladiali, F. Soccolini, *J. Organomet. Chem.* **1986**, *304*, 217−225. [20b] P. Kvintovics, B. Heil, *J. Organomet. Chem.* **1989**, *361*, 117−122.
[21] [21a] G. Zassinovich, F. Grisoni, *J. Organomet. Chem.* **1983**, *247*, 24−26. [21b] G. Zassinovich, R. Betella, G. Mestroni, N. Bresciani-Pahor, S. Geremia, L. Randaccio, *J. Organomet. Chem.* **1989**, *370*, 187−202. [21c] S. De Martin, G. Zassinovich, G. Mestroni, *Inorg. Chim. Acta* **1990**, *174*, 9−11.
[22] H. Brunner, W. Zettlmeier, *Handbook of Enantioselective Catalysis*, VCH, Weinheim, **1993**.
[23] *Handbook of Chemistry and Physics* (Ed.: R. C. West), CRC Press, Boca Raton, FL, **1988**.
[24] N. Walker, D. Stuart, *Acta Crystallogr., Sect. A* **1983**, *39*, 158−166.
[25] G. M. Sheldrick, *Acta Crystallogr., Sect. A* **1990**, *46*, 467−473.
[26] G. M. Sheldrick, *SHELXL-97*, University of Göttingen, Göttingen, Germany, **1997**.

Received December 4, 2003
Early View Article
Published Online April 26, 2004

 © 2004 Wiley-VCH Verlag GmbH & Co. KGaA, Weinheim

A New Dichroic, Nitroso-Bridged Complex of Rhenium: Di-μ_2-chloro[μ_2-(η^2-*N*,*O*)-*N*,*N*-dimethyl-4-nitrosoaniline]bis[tricarbonylrhenium(I)]

Roland Wilberger,[a] Christoph Krinninger,[a] Holger Piotrowski,[a] Peter Mayer,[a] and Ingo-Peter Lorenz*[a]

Keywords: Rhenium / C,N ligand / N,O bridge / Dichroism

The dimeric μ_2-amino-phenoxy complexes of rhenium $[(CO)_3Re(\mu_2\text{-}O^{\frown}NH_2)]_2$ (**1**) do not react with the *C*-nitroso compounds R–C_6H_4NO [R = NMe_2 (**2**), H (**2′**)] in the presence of $AlCl_3$ by a condensation reaction to give the desired azo dye complexes $[(CO)_3Re(\mu_2\text{-}O^{\frown}N{=}NC_6H_4R)]_2$. Instead, they react to give the novel neutral η^2-*N*,*O*-bridged *C*-nitroso complexes $[\{(CO)_3ReCl\}_2ONC_6H_4R]$ (**3**, **3′**) by means of a substitution reaction. Both complexes yield golden gleaming crystals, and their solutions are deeply blue (**3**) or violet (**3′**) due to the broad UV/Vis absorption at λ = 617 (**3**) and 505 nm (**3′**). Single crystals of **3**, **3′** show nonlinear optical properties, they are dichroic and have a red and blue (**3**) or violet and green (**3′**) side. The molecular structures of **3**, **3′** have been determined by single-crystal X-ray analyses. Both compounds contain two face-joined octahedra, with two chloro and the NO ligands as bridges. The *C*-nitroso groups together with the NC_2 moiety of NMe_2 (**3**) lie almost exactly within the symmetry plane of the molecules. Both the N atoms of **3** have a trigonal-planar geometry. **3** and **3′** are the first single, neutral and dinuclear *C*-nitroso complexes with the rare non-assisted μ-(η^2-*N*,*O*) bridge and only single atoms as additional bridges.
(© Wiley-VCH Verlag GmbH & Co. KGaA, 69451 Weinheim, Germany, 2004)

Introduction

Recently we reported on the syntheses and structures of several dimeric μ_2-O amino-phenoxy complexes of rhenium of the type $[(CO)_3Re(\mu_2\text{-}O^{\frown}NH_2)]_2$ as well as on their condensation reactions with acetone to give the corresponding Schiff base products $[(CO)_3Re(\mu_2\text{-}O^{\frown}N{=}CMe_2)]_2$ in almost quantitative yields.[1] Because of the high reactivity and good selectivity of the complexes $[(CO)_3Re(\mu_2\text{-}O^{\frown}NH_2)_2]$ towards organic carbonyl compounds, the analogous condensation reaction with *C*-nitroso compounds should also be possible and should yield an N=N bond and hence the directed synthesis of azo dyes in the coordination sphere of a transition metal atom. The starting materials, however, did not react, and refluxing them for more than 2 h led to their decomposition. Attempts to catalyze the desired reaction by addition of some $AlCl_3$ for activating the nitroso compound immediately changed the situation. After a few minutes, the solution turned deep blue, and finally an almost black solid was separated, though in bad yield. Its characterization proved it to be the novel, neutral η^2-*N*,*O*-bridged nitroso complex $\{(CO)_3ReCl\}_2ONC_6H_4N(CH_3)_2$ (**3**).

There are three types of R_xNO-containing complexes (x = 0, 1). The first one (x = 0) is the large and well-known group of nitrosyl complexes.[2,3] They show the terminal linear (η^1-NO, 3e-donor), bent (η^1-NO, 1e-donor) or bridging μ_n-NO ligand function (n = 2–4). Even in the NO-containing triply bridged rhenium dimer, which is similar to **3**, the NO ligand is to be found in the terminal position.[4] Recently, metastable states of $[(CN)_5FeNO]^{2-}$ were detected with side-on-bound NO (η^2-NO) and η^1-ON ligands (isonitrosyl).[5]

The next family are RNO$^{\cdot}$ nitroxyl radicals, which normally coordinate through the oxygen atom.[6] Jaitner et al., however, reported on the η^2-*N*,*O* coordination of the special 2,2,6,6-tetramethylpiperidine-1-oxyl (= TEMPO).[7]

The coordination chemistry of organic RNO nitroso compounds has also been investigated,[8] their different ligand functions are summarized in Scheme 1. The terminal η^2-*N*,*O* ligand function (**I**) dominates,[9] the η^1-*N*,*O* linkage through the nitrogen atom (**II**) has also been well documented,[10,11] whereas that through the oxygen atom (**III**) has rarely been found.[12] The *C*-nitroso group may also bridge two metal centers in an η^1-*N* (**IV**),[11] an η^1- and η^2-fashion [μ-(η^1:η^2-*N*,*O*), **V**][13] or as an η^2-*N*,*O* moiety [μ-(η^1:η^1-*N*,*O*), **VI**]. The latter simply as a bridging ligand is less common;[11,14,15] most examples are known with supporting second coordination by a further donor system forming in addition a five- (**VII**)[16] or six-membered ring (**VIII**).[17] Only a few examples are known for bridging two metal atoms [μ_2-(η^2:η^2-*N*,*O*), **IX**][18] or four metal atoms

[a] Ludwig-Maximilians Universität München, Department of Chemistry,
Butenandtstraße 5–13, 81377 München, Germany
Fax: (internat.) + 49-(0)89-2180-77867
E-mail: ipl@cup.uni-muenchen.de

 © 2004 Wiley-VCH Verlag GmbH & Co. KGaA, Weinheim **DOI: 10.1002/ejic.200300928**

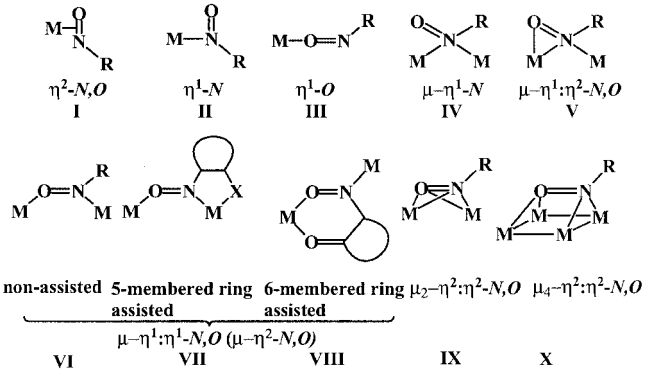

Scheme 1. Coordination modes of *C*-nitroso ligands

[μ_4-(η^2:η^2-*N*,*O*), **X**].[19] To the best of our knowledge type **VI** is only realized, besides a special case[11] in cationic dimers, with two further μ_2-thiolato bridges.[14]

Results and Discussion

The bad yield mentioned above and the chloro bridges of **3** led us to repeat the reaction not catalytically, but stoichiometrically. The reaction of **1**, **2** and $AlCl_3$ in the molar ratio 1:1:2 in boiling toluene for 5−10 min resulted in the formation of neutral di-μ_2-chloro[μ_2-(η^2-*N*,*O*)-*N*,*N*-dimethyl-4-nitrosoaniline]bis[tricarbonylrhenium(I)] (**3**; Scheme 2), and, indeed, the yield rose to about 70%. The same reaction was repeated with **1**, **2′** (nitrosobenzene) and $AlCl_3$, and the analogous nitroso complex **3′** was obtained. Many nitroso complexes have been synthesized by reduction of organic nitro compounds, which may proceed through an intermediate nitroso compound,[8] or by a nitrosyl migration reaction.[8]

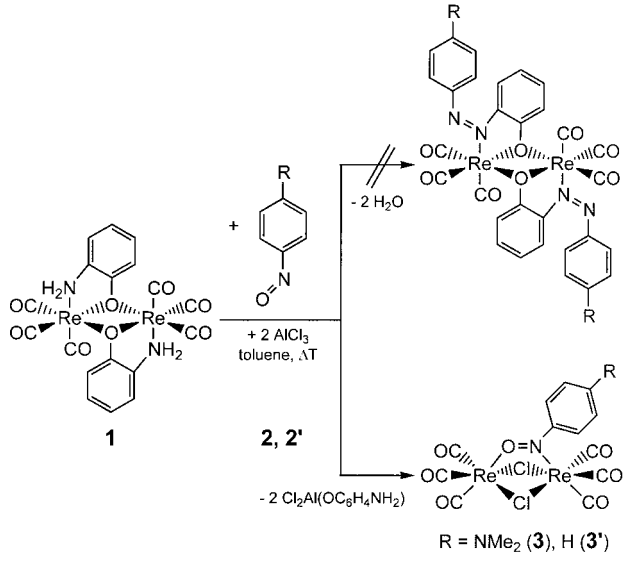

Scheme 2. Synthesis of **3**, **3′**

Compounds **3** and **3′** are obtained as golden gleaming crystals, which are stable towards air. They are soluble in THF, toluene, ketones and CH_2Cl_2 and even in pentane (**3′**). Compound **3** is not soluble in pentane. Solutions of **3** and **3′** in $CHCl_3$, CH_2Cl_2, THF or toluene are deep blue or violet, respectively. In the UV/Vis spectrum ($CHCl_3$) one very broad absorption at λ = 617 (**3**) and 505 nm (**3′**) due to a ligand-to-metal CT band [NO−Re(I)] is observed, which is shifted to lower frequency than the corresponding electronic transition ($\pi-\pi^*$ NO) of the ligands **2** (λ = 419 nm) and **2′** (λ = 306 nm). Single crystals of **3** and **3′** show non-linear optical properties; they are dichroic and viewed by transmitted light; they have a red and a blue (**3**) or violet and green side (**3′**), respectively. The absorption maxima of **3** are found at λ = 495 and 575 nm, those of **3′** have not yet been measured because of technical problems.

The IR spectra of **3**, **3′** in CH_2Cl_2 show four ν(CO) absorptions. As the NO group coordinates to one rhenium center with the nitrogen atom and to the other with the oxygen atom, the electronic situation at both rhenium centers is different. Therefore, there are two different $Re(CO)_3$ fragments, each with C_{3v} local symmetry, and we observe two separated patterns of ν(CO) (A_1 + E). Resulting from electronic reasons, the two absorptions at higher wavenumbers are assigned to the {$(CO)_3Re-N$} fragment [$\tilde{\nu}$ = 2041 (A_1), 1946 (E) cm^{-1}], whereas the two at $\tilde{\nu}$ = 2024 (A_1) and 1917 (E) cm^{-1} belong to the {$(CO)_3Re-O$} fragment as in **3**. The ν(NO) of **3** absorbs significantly lower at $\tilde{\nu}$ = 1605 cm^{-1}.

The ^1H NMR spectrum of **3** (in [D_8]THF) shows two singlets at δ = 3.54 and 3.55 ppm for the *N*-methyl protons, and the four double-doublets for the different pairs of *o*- and *m*-phenyl protons (see Exp. Sect.), that of **3′** (in CD_2Cl_2) exhibits only the multiplet at δ = 7.34−7.65 ppm for the phenyl protons. In the $^{13}C\{^1H\}$ NMR spectrum of **3** (in [D_8]THF) each carbon atom of the NMe_2 group and of the phenyl ring is found by separated signals between δ = 30 and 160 ppm; the signals of the CO ligands appear at δ = 190−200 ppm. The signals of the carbon atoms of **3′** are observed at δ = 129.1−131.3 ppm (phenyl) and δ = 188 ppm (CO) (in $CDCl_2$).

In the mass spectra of **3**, the parent peak as well as all signals of fragments resulting from the loss of up to six carbonyl groups are observed.

The composition and structure of complex **3** was confirmed by X-ray structure analysis; single crystals were obtained by diffusion of pentane into a solution of **3** in $CHCl_3$. The molecular structure and selected bond lengths and angles are given in Figure 1,[20] which shows two face-joined octahedra with two chloro and the NO ligands as bridges. The distance N(1)−O(1) is 1.319(8) Å and clearly longer than the N−O distance in the free *N*,*N*-dimethyl-4-nitrosoaniline (1.212 Å[21]). The bond Re(1)−O(1) [2.131(6)] is shorter than the Re(2)−N(1) [2.208(7)], whereas all Re−Cl bonds in the bridge are exactly the same [Re(1)−Cl*n* = 2.49 Å, Re(2)−Cl*n* = 2.49 Å). The dihedral angles Re(1)−O(1)−N(1)−Re(2) and O(1)−N(1)−C(1)−C(6) are 6.54° or 12.00°, respectively; that is, the NO group

 © 2004 Wiley-VCH Verlag GmbH & Co. KGaA, Weinheim

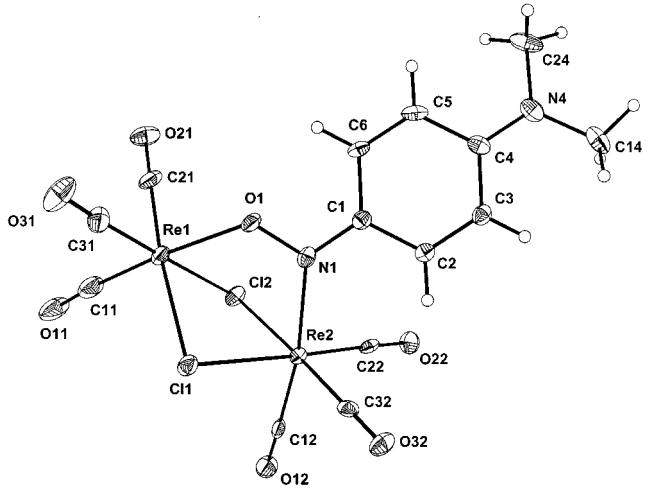

Figure 1. Molecular structure of **3**; selected bond lengths [Å] and angles [°]: Re(1)−C(11) 1.882(11), Re(1)−C(21) 1.887(10), Re(1)−C(31) 1.913(11), Re(1)−O(1) 2.131(6), Re(1)−Cl(2) 2.492(2), Re(1)−Cl(1) 2.497(2), C(11)−O(11) 1.175(13), C(21)−O(21) 1.161(11), C(31)−O(31) 1.132(11), Re(2)−C(22) 1.889(9), Re(2)−C(32) 1.891(9), Re(2)−C(12) 1.922(10), Re(2)−N(1) 2.208(7), Re(2)−Cl(2) 2.490(2), Re(2)−Cl(1) 2.493(2), C(12)−O(12) 1.145(10), C(22)−O(22) 1.170(10), C(32)−O(32) 1.169(10), O(1)−N(1) 1.319(8); C(21)−Re(1)−Cl(2) 95.6(3), Cl(2)−Re(1)−Cl(1) 80.69(7), O(1)−N(1)−C(1) 113.4(7), Re(2)−Cl(1)−Re(1) 90.36(7), Re(2)−Cl(2)−Re(1) 90.53(6)

lies almost within the symmetry plane of the molecule, whereas the phenyl ring is larger and turned out of this plane. It is noteworthy that both the nitrogen atoms are exactly trigonal planar in geometry [sum of angles for N(1) = 359°, for N(4) = 360°], consistent with their sp^2 nature. The analogous molecular structure was also found for **3′**, and is given in Figure 2.[20] In both compounds there

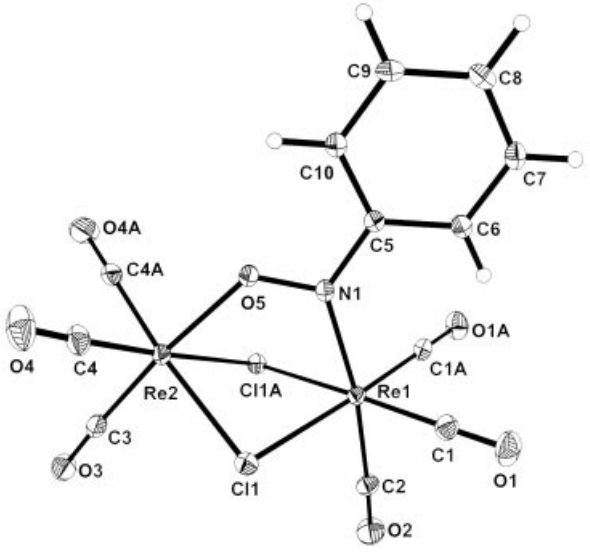

Figure 2. Molecular structure of **3′**; selected bond lengths [Å] and angles [°]: Re(1)−C(1) 1.906 (5), Re(1)−C(2) 1.976 (6), Re(1)−Cl(1) 2.4829 (12), Re(1)−N(1) 2.092 (5), Re(2)−C(3) 1.930 (8), Re(2)−C(4) 1.904 (6), Re(2)−Cl(1) 2.4829 (12), Re(2)−O(5) 2.106 (4), O(5)−N(1) 1.282 (7), N(1)−C(5) 1.440 (8), C(1)−O(1) 1.145 (6), C(2)−O(2) 1.124 (8), C(3)−O(3) 1.151 (9), C(4)−O(4) 1.144 (7); C(1)−Re(1)−Cl(1) 94.92 (14), O(5)−N(1)−C(5) 110.5 (5), Re(1)−Cl(1)−Re(2) 88.41 (4).

is no Re−Re interaction [Re(1)−Re(2) 3.540 Å (**3**), 3.463 Å (**3′**)].

Compounds **3** and **3′** are the first simple, neutral and dinuclear *C*-nitroso complexes which have the very rare non-assisted μ-(η^2-*N*,*O*) bridge (**VI**) and only single atoms as additional bridges, and which have been synthesized directly by means of nitroso compounds as starting materials. Their observed dichroism may be derived from the special ligand function of the nitroso compound and of its placement exactly in the plane of symmetry of **3** and **3′**. In a recent paper[22] a very similar structure of dialkylnitrosoamine complexes (*N*-nitroso ligand) of Cu^{II} with the same μ-(η^2-*N*,*O*) coordination and with the NO group roughly parallel to the Cu−Cu direction. Their single crystals, however, do not exhibit the dichroic effect.

First attempts using AlX_3 (X = Br, I) instead of $AlCl_3$ resulted in the formation of the corresponding bromo- and iodo-bridged dinuclear complexes. The μ_2-*O*-bridged precursor **1** apparently serves as a source for $Re(CO)_3$ fragments. Therefore, it might be assumed that $[Re(CO)_5Cl]$ can be used instead of **1**. First attempts with $[Re(CO)_5Cl]$ and **2** show that **3** is indeed formed.

Experimental Section

General: To remove oxygen, all operations were carried out under Ar in dry and Ar-saturated solvents.[23] $[(CO)_3Re(\mu_2\text{-}O\cap NH_2)]_2$ (**1**) was prepared according to a literature procedure.[1] *N*,*N*-Dimethyl-4-nitrosoaniline (**2**), nitrosobenzene (**2′**) and $AlCl_3$ were used as purchased. NMR spectra were recorded with a Jeol EX 400 spectrometer (^{1}H: 399.78 MHz; ^{13}C: 100.54 MHz) in [D$_8$]THF or CD_2Cl_2. Mass spectra were obtained with a Jeol MStation JMS 700. IR and UV/Vis spectra were measured with a Perkin−Elmer Spectrum One FT-IR or Perkin−Elmer UV Lambda 16 spectrometer, respectively. Elemental analyses were performed with a Heraeus Elementar Vario EL.

3: 1 (388.2 mg, 0.513 mmol), **2** (118.2 mg, 0.787 mmol) and $AlCl_3$ (173.2 mg, 1.035 mmol) were dissolved in toluene (100 mL) and refluxed for 10 min, whereby the solution turned deep blue. The solvent was evaporated, the shiny blue, almost black, residue was dissolved in CH_2Cl_2 and the compound purified by column chromatography. Yield: 258 mg (0.338 mmol, 66%), blue-red dichroic crystals; m.p. 189−191 °C (dec.). ^{1}H NMR (399.78 MHz, [D$_8$]THF): δ = 3.54 [s, 3 H, N(CH_3)$_2$], 3.55 [s, 3 H, N(CH_3)$_2$], 7.24 (dd, ^3J = 10.16, ^4J = 2.64 Hz, 1 H, *o*-Ar-*H*), 7.41 (dd, ^3J = 10.27, ^4J = 2.75 Hz, 1 H, *o*-Ar-*H*), 8.02 (dd, ^3J = 10.22, ^4J = 2.64 Hz, 1 H, *m*-Ar-*H*), 8.51 (dd, ^3J = 10.22, ^4J = 2.64 Hz, 1 H, *m*-Ar-*H*) ppm. ^{13}C{^{1}H} NMR (100.53 MHz, [D$_8$]THF): δ = 30.6 (*C*H$_3$NCH$_3$), 43.1 (CH$_3$N*C*H$_3$), 118.0 (*o*-Ar-*C*), 119.2 (*o*-Ar-*C*), 128.2 (*m*-Ar-*C*), 139.4 (*m*-Ar-*C*), 160.9 (Me$_2$NAr-C_q), 161.6 (ONAr-C_q), 191.8 (*C*O), 192.0 (*C*O), 195.3 (*C*O), 198.4 (*C*O) ppm. IR (KBr): $\tilde{\nu}$ = 3099.1 w [ν(Ar−H)], 2938.0 w [ν(CH$_2$)], 2857.4 w [ν(CH$_2$)], 2732.9 w, 2039.8 vs [ν(CO), A$_1$], 2021.4 vs [ν(CO), A$_1$], 1904.3 vs [ν(CO), E], 1604.4 s [ν(NO)], 1393.5 s [δ(CH$_3$)], 1331.1 s, 1170.7 vs, 1129.8 m, 930.9 w, 879.3 w, 833.7 m [γ(Ar)], 741.3 s, 644.3 w, 565.7 w, 518.2 w, 493.5 w, 465.8 w, 398.5 w cm^{-1}. IR (CH_2Cl_2): $\tilde{\nu}$ = 2041.4 s [ν(CO), A$_1$], 2024.0 vs [ν(CO), A$_1$], 1946.0 m [ν(CO), E], 1916.9 s [ν(CO), E], 1605.1 m [ν(NO)] cm^{-1}. UV/Vis ($CHCl_3$): λ (*A*) = 265 (0.3234), 364 (0.1048), 617 (0.9901) nm. $C_{14}H_{10}Cl_2N_2O_7Re_2$ (761.54): calcd. C 22.08, H 1.32, N 3.68; found

 © 2004 Wiley-VCH Verlag GmbH & Co. KGaA, Weinheim

Table 1. X-ray structure analysis of **3**[20]

	3	**3′**
Empirical formula	$C_{14}H_{10}Cl_2N_2O_7Re_2$	$C_{12}H_5Cl_2NO_7Re_2$
Formula mass [g mol^{-1}]	761.54	718.49
Crystal size [mm]	0.10 × 0.05 × 0.004	0.16 × 0.24 × 0.30
Crystal colour, habit	red platelet	black block
Crystal system	triclinic	monoclinic
Space group	$P\bar{1}$	$C2/m$
a [Å]	6.4246(2)	19.0607(7)
b [Å]	9.5409(3)	7.1842(3)
c [Å]	16.6048(4)	13.0451(4)
α [°]	83.7500(13)	90
β [°]	83.0888(13)	112.005(2)
γ [°]	70.9047(12)	90
Volume [Å^3]	952.20(5)	1656.21(11)
Z	2	4
Density calcd. [g cm^{-3}]	2.65620(14)	2.88151(17)
Absorption coefficient [mm^{-1}]	13.020	14.960
F(000)	696	1296
Index ranges	$-7 \le h \le 7$ $-11 \le k \le 11$ $-19 \le l \le 19$	$-24 \le h \le 24$ $-9 \le k \le 9$ $-16 \le l \le 16$
θ range [°]	3.41−25.00	3.28−27.48
Reflections collected	14429	9317
Independent reflections	3364	2026
Observed reflections	2737	1864
Parameter/restrains	246/0	130/0
$R1/wR2$ (all data)	0.0471/0.0731	0.0292/0.0560
$R1/wR2$ (final)	0.0331/0.0694	0.0242/0.0547
Goodness of fit	1.112	1.137
Min./max. ρ_e [e Å^3]	−1.125/1.321	−1.279/0.876
Temperature [K]	200(2)	200(2)
Diffractometer used	Nonius Kappa CCD	Nonius Kappa CCD
Scan type	area detection	area detection
Solution	SHELXS-97	SHELXS-97
Refinement	SHELXL-97	SHELXL-97

C 22.85, H 1.49, N 3.63. MS (DEI): *m/z* (%) = 762.5 (56) [M$^+$], 678.4 (9) [M$^+$ − 3 CO], 650.4 (62) [M$^+$ − 4 CO], 622.4 (35) [M$^+$ − 5 CO], 594.4 (29) [M$^+$ − 6 CO].

3′: Analogous procedure as for **3**, with **1** (83.9 mg, 0.111 mmol), **2′** (23.7 mg) and $AlCl_3$ (29.6 mg, 0.222 mmol) in toluene (20 mL), and stirring for 16 h, yield: 56.6 mg (0.079 mmol, 71%), violet-green dichroic crystals; m.p. 175−181 °C (dec.). ^{1}H NMR (399.78 MHz, CD_2Cl_2): δ = 7.34−7.65 (m, 5 H, Ar-*H*) ppm. ^{13}C{^{1}H} NMR (100.53 MHz, CD_2Cl_2): δ = 129.1 (Ar-*C*), 129.4 (Ar-*C*), 129.9 (Ar-*C*), 131.3 (Ar-*C*), 188.0 (*C*O). IR (KBr): $\tilde{\nu}$ = 2062.8 vs [ν(CO), A_1], 2029.1 vs [ν(CO), A_1], 1992.7 vs [ν(CO), E], 1916.2 vs [ν(CO), E], 1579.9 m [ν(NO)], 1262.3 s, 1190.7 w, 1141.1 s, 1099.3 s, 1023.4 s, 955.1 w, 887.6 w, 802.9 s, 703.4 w, 666.0 m, 628.1 w, 640.7 w, 490.8 w, 455.5 w, 437.4 w, 408.2 w cm^{-1}. IR (CH_2Cl_2): $\tilde{\nu}$ = 2066.8 m [ν(CO), A_1], 2023.8 vs [ν(CO), A_1], 1987.8 m [ν(CO), E], 1944.6 s [ν(CO), E] cm^{-1}. UV/Vis ($CHCl_3$): λ (*A*) = 255 (0.670), 322 (0.275), 505 (0.623), 709 (0.267) nm. $C_{12}H_5Cl_2NO_7Re_2$ (718.49): calcd. C 20.06, H 0.70, N 1.95; found C 20.18; H 0.65, N 1.91. MS (DEI): *m/z* (%) = 718.7 (75) [M$^+$], 634.8 (97) [M$^+$ − 3 CO], 578.8 (63) [M$^+$ − 5 CO], 550.8 (100) [M$^+$ − 6 CO].

Acknowledgments

We thank Sabine Otto and Christiane Kofink for their experimental support and Dr. Gregor Jung for his UV/Vis spectroscopic measurements.

[1] R. Wilberger, H. Piotrowski, P. Mayer, I..-P. Lorenz, *Inorg. Chem. Commun.* **2002**, *5*, 897−902.
[2] [2a] D. M. P. Mingos, D. J. Sherman, *Adv. Inorg. Chem.* **1989**, *34*, 293−377. [2b] B. F. G. Johnson, B. L. Haymore, J. R. Dilworth, *Comprehensive Coordination Chemistry*, Pergamon Press, Oxford, **1987**, vol. 2, p. 99−118. [2c]J. H. Enemark, R. D. Feltham, *Coord. Chem. Rev.* **1974**, *13*, 339−406. [2d] K. G. Caulton, *Coord. Chem. Rev.* **1975**, *14*, 317−355.
[3] [3a] A. K. Patra, R. Afshar, M. N. Olmstead, P. K. Mascharek, *Angew. Chem.* **2002**, *114*, 2622−2625; *Angew. Chem. Int. Ed.* **2002**, *41*, 2512−2515. [3b] D. Gusev, A. Llamazares, G. Artus, H. Jacobsen, H. Berke, *Organometallics* **1999**, *18*, 75−89. [3c] M. Schweiger, W. Beck, *Z. Anorg. Allg. Chem.* **1991**, *595*, 203−210. [3d] D. Veghini, S. E. Nefedov, H. Schmalle, H. Berke, *J. Organomet. Chem.* **1996**, *526*, 117−134.
[4] J. R. Norton, G. Dolcetti, *Inorg. Chem.* **1973**, *12*, 485−487.
[5] H. Paulsen, V. Rusanov, R. Benda, C. Herta, V. Scheinemann, C. Janiak, T. Dorn, A. I. Churmakov, H. Winkler, A. X. Trautwein, *J. Am. Chem. Soc.* **2002**, *124*, 3007−3011.
[6] [6a] N. Soh, T. Imato, K. Kawamura, M. Maeda, Y. Katayama, *Chem. Commun.* **2002**, 2650−2651. [6b] J. J. Watkins, A. L. Balch, *Inorg. Chem.* **1975**, *14*, 2720−2723.
[7] [7a] P. Jaitner, J. Veciana, C. Sporer, H. Kopacka, K. Wurst, D. Ruiz-Molina, *Organometallics* **2001**, *20*, 568−571. [7b] P. Jaitner, K. Jäger, A. Dorfer, K.-E. Schwarzhans, *J. Organomet. Chem.* **2001**, *621*, 173−176.
[8] M. Cameron, B. G. Gowenlock, G. Vasapollo, *Chem. Soc. Rev.* **1990**, *19*, 355−379.
[9] [9a] S. Otsuka, Y. Aotani, Y. Tatsuno, T. Yoshida, *Inorg. Chem.*

 © 2004 Wiley-VCH Verlag GmbH & Co. KGaA, Weinheim

1976, *15*, 656−660. [9b] L. S. Liebeskind, K. B. Sharpless, R. D. Wilson, J. A. Ibers, *J. Am. Chem. Soc.* **1978**, *100*, 7061−7063. [9c] D. A. Muccigrosso, S. E. Jacobson, P. A. Apgar, F. Mares, *J. Am. Chem. Soc.* **1978**, *100*, 7063−7065. [9d] C. J. Jones, J. A. McCleverty, A. S. Rothin, *J. Chem. Soc., Dalton Trans.* **1985**, 401−403. [9e] M. Pizzotti, F. Porta, S. Cenini, F. Demartin, N. Masciocchi, *J. Organomet. Chem.* **1987**, *330*, 265−278. [9f] C. Crotti, C. Sishta, A. Pacheco, B. R. James, *Inorg. Chim. Acta* **1988**, *141*, 13−15. [9g] M. Herberhold, A. F. Hill, *J. Organomet. Chem.* **1989**, *363*, 371−376. [9h] S. J. Skoog, J. P. Campbell, W. L. Gladfelter, *Organometallics* **1994**, *13*, 4137−4139. [9i] S. J. Skoog, W. L. Gladfelter, *J. Am. Chem. Soc.* **1997**, *119*, 11049−11060.

[10] [10a] R. G. Little, R. J. Doedens, *Inorg. Chem.* **1973**, *12*, 537−540. [10b] W. L. Bowden, W. F. Little, T. J. Meyer, *J. Am. Chem. Soc.* **1974**, *96*, 5605−5609. [10c] W. L. Bowden, W. F. Little, T. J. Meyer, *J. Am. Chem. Soc.* **1976**, *98*, 444−448. [10d] D. Mansuy, M. Dreme, J.-C. Chottard, J. Guilhem, *J. Organomet. Chem.* **1978**, *161*, 207−220. [10e] D. Mansuy, P. Battioni, J.-C. Chottard, C. Riche, A. Chiaroni, *J. Am. Chem. Soc.* **1983**, *105*, 455−463. [10f] C. J. Jones, J. A. McCleverty, A. S. Rothin, *J. Chem. Soc., Dalton Trans.* **1985**, 401−403. [10g] C. Crotti, C. Sishta, A. Pacheco, B. R. James, *Inorg. Chim. Acta* **1988**, *141*, 13−15. [10h] J. Chang, M. D. Seidler, R. G. Bergman, *J. Am. Chem. Soc.* **1989**, *111*, 3258−3271. [10i] R. S. Pilato, C. McGettigan, G. L. Geoffro, A. L. Rheingold, S. J. Geib, *Organometallics* **1990**, *9*, 312−317. [10j] W. H. Chin, K.-K. Cheung, C.-M. Che, *J. Chem. Soc., Chem. Commun.* **1995**, 441−442. [10k] J.-L. Liang, J.-S. Huang, Z.-Y. Zhon, K.-K. Cheung, C.-M. Che, *Chem. Eur. J.* **2001**, *7*, 2306−2317.

[11] D. L. Packett, W. C. Trogler, A. L. Rheingold, *Inorg. Chem.* **1987**, *26*, 4308−4309.

[12] [12a] G. Matsubayashi, K. Nakatsu, *Inorg. Chim. Acta* **1982**, *64*, L163−L164. [12b] S. Hu, D. M. Thompson, P. Ikekwere, R. J. Barton, K. E. Johnson, B. E. Robertson, *Inorg. Chem.* **1989**, *28*, 4552−4554.

[13] [13a] M. Calligaris, T. Yoshida, S. Otsuka, *Inorg. Chim. Acta* **1974**, *11*, L15−L16. [13b] P. R. Sharp, D. W. Hoard, C. L. Barnes, *J. Am. Chem. Soc.* **1990**, *112*, 2024−2026. [13c] D. W. Hoard, P.-R. Sharp, *Inorg. Chem.* **1993**, *32*, 612−620. [13d] H. G. Ang, W. L. Kwik, K. K. Ong, *J. Fluorine Chem.* **1993**, *60*, 43−48.

[14] T. Iwasa, H. Shimada, A. Takami, H. Matsuzaka, Y. Ishii, M. Hidai, *Inorg. Chem.* **1999**, *38*, 2851−2859.

[15] The recently reported Pt−Ge complex $(Et_3P)_2PtN(Ph)OGe\{N(SiMe_3)_2\}_2$(*Pt−Ge*) must be viewed as a special case obtained by cycloaddition of the corresponding germylene complex and nitrosobenzene, and having, therefore, a very long N−O bond: K. E. Litz, J. W. Kampf, M. M. B. Holl, *J. Am. Chem. Soc.* **1998**, *120*, 7484−7492.

[16] [16a] E. Colacio, J. M. Dominguez-Vera, A. Escuer, R. Kivekas, A. Romerosa, *Inorg. Chem.* **1994**, *33*, 3914−3924. [16b] E. Colacio, J. M. Dominguez-Vera, E. Escuer, M. Klinga, R. Kivekas, A. Romerosa, *J. Chem. Soc., Dalton Trans.* **1995**, 343−348. [16c] E. Colacio, J. M. Dominguez-Vera, A. Escuer, R. Kivekas, M. Klinga, J.-M. Moreno, A. Romerosa, *J. Chem. Soc., Dalton Trans.* **1997**, 1685−1689. [16d] K. K.-H. Lee, W.-T. Wong, *J. Chem. Soc., Dalton Trans.* **1997**, 2987−2995.

[17] [17a] E. Colacio, J. M. Dominguez-Vera, A. Romerosa, R. Kivekas, M. Klinga, A. Escuer, *Inorg. Chim. Acta* **1995**, *234*, 61−65. [17b] E. Colacio, C. Lopez-Magana, V. McKee, A. Romerosa, *J. Chem. Soc., Dalton Trans.* **1999**, 2923−2926.

[18] M. J. Scott, S. J. Lippard, *Organometallics* **1998**, *17*, 466−474.

[19] G. Gervasio, R. Rossetti, P. L. Stanghellini, *Chem. Commun.* **1997**, 387−388.

[20] CCDC-229256 (**3**) and -229255 (**3′**) contain the supplementary crystallographic data for this paper. These data can be obtained free of charge at www.ccdc.cam.ac.uk/conts/retrieving.html [or from the Cambridge Crystallographic Data Centre, 12 Union Road, Cambridge CB2 1EZ, UK; Fax: (internat.) + 44-1223-336-033; E-mail: deposit@ccdc.cam.ac.uk].

[21] C. Romming, H. J. Talberg, *Acta Chem. Scand.* **1973**, *27*, 2246−2248.

[22] A. Schmidpeter, H. Nöth, *Inorg. Chim. Acta* **1998**, *269*, 7−12.

[23] *Trocknen im Labor*, brochure from the series "Reagenzien", Merck, Darmstadt.

Received December 9, 2003
Early View Article
Published Online April 7, 2004

 © 2004 Wiley-VCH Verlag GmbH & Co. KGaA, Weinheim

Vanadyl Phosphate Intercalated with Diethyl Ether

Klára Melánová,[a] Ludvík Beneš,*[a] Vítězslav Zima,[a] Miroslava Trchová,[b] and Jiří Dybal[b]

Keywords: Intercalation / Vibrational spectroscopy / X-ray diffraction / Ab initio calculations / Semiempirical calculations

Vanadyl phosphate intercalated with diethyl ether has been prepared by replacing 2-propanol molecules in the corresponding $VOPO_4$ intercalate with diethyl ether. The intercalate contains one diethyl ether molecule per formula unit. The guest molecules are anchored to the host layers by an O–V donor–acceptor bond. The local structure and interactions in the intercalate have been suggested on the basis of quantum chemical calculations. The intercalate is thermally stable. Its diffractogram does not change up to 100 °C. A new phase with lower basal spacing appears at 130 °C. The intercalate is very moisture-sensitive; the diethyl ether molecules are easily replaced by water molecules. The replacement of diethyl ether in the vanadyl phosphate intercalate by the water molecules has been monitored by infrared spectroscopy.
(© Wiley-VCH Verlag GmbH & Co. KGaA, 69451 Weinheim, Germany, 2004)

Introduction

The ability of vanadyl phosphate dihydrate $VOPO_4{\cdot}2H_2O$ and other isostructural layered compounds to accommodate organic molecules having the character of Lewis bases in the interlayer space has been reviewed.[1] Compounds with functional groups containing oxygen atoms, i.e. alcohols, ketones, carboxylic acids and ethers, form a large group of such compounds. Intercalations of etheric oxygen-containing glycols[2] and cyclic ethers[3,4] have been described recently.

With glycols, diethylene glycol (DEG), triethylene glycol, and poly(ethylene glycol)s (PEG 200, 400, and 1000) have been intercalated into vanadyl phosphate. Depending on the reaction temperature, two phases are formed: a low-temperature phase, with guest chains arranged parallel to the host layer in a bimolecular way, and a high-temperature phase, where the chains are arranged monomolecularly. All these intercalates are stable in a dry environment but decompose slowly in humid air.[2] The structure of the DEG intercalated vanadyl phosphate, $VOPO_4{\cdot}HO(CH_2)_2O(CH_2)_2OH$, has been determined using a combination of synchrotron powder diffraction and molecular modeling.[5] The crystal system was determined to be tetragonal, space group *P*4/*n*, with the DEG molecules anchored to the vanadium atoms of the host layers through their etheric oxygen atoms.

The cyclic ethers tetrahydrofuran, tetrahydropyran,[3] dioxane, trioxane, and 18-crown-6[4] have been intercalated into vanadyl phosphate. All these guest molecules are anchored to the host layers by a donor−acceptor bond between an oxygen atom of the guest and a vanadium atom. These intercalates are stable at ambient conditions, and some are surprisingly thermally stable (the tetrahydrofuran intercalate is stable up to 160 °C). The structure of tetrahydrofuran intercalate has been determined using a combination of synchrotron powder diffraction and molecular modeling.[5] We report here on a diethyl ether intercalated vanadyl phosphate.

Results and Discussion

Diethyl ether cannot be intercalated directly in anhydrous vanadyl phosphate, and the replacement of water in $VOPO_4{\cdot}2H_2O$ does not lead to an intercalation. Consequently, the intercalate was prepared by replacing 2-propanol in the corresponding $VOPO_4$ intercalate with diethyl ether, to give a yellow crystalline solid, indicating that the vanadium(v) atom had not been significantly reduced. We did not succeed in intercalating dipropyl ether, dibutyl ether, or diisopropyl ether.

The diffractogram of the diethyl ether intercalate indicates that the tetragonal structure of the $VOPO_4$ host layer is retained. Three sharp (00*l*) and one weak (200) reflections appear in the pattern (Figure 1, a). The tetragonal lattice parameters a = 6.208 Å, c = 11.664 Å were determined from these lines. The absence of (*hkl*) lines is characteristic of a turbostratic structure in which the original tetragonal

[a] Joint Laboratory of Solid State Chemistry of Institute of Macromolecular Chemistry of Academy of Sciences and University of Pardubice,
Studentská 84, 53210 Pardubice, Czech Republic
Fax: (internat.) + 420-466036011
E-mail: ludvik.benes@upce.cz
[b] Institute of Macromolecular Chemistry, Academy of Sciences of the Czech Republic
Heyrovský Sq. 2, 16206 Prague 6, Czech Republic

layers of the host are retained but shifted in the directions of the *x* and/or *y* axes. The intercalate is very moisture-sensitive − the diethyl ether molecules are easily replaced by water. At a relative humidity (r.h.) of 25% the intercalate is stable, and only a small broad (001) reflection of vanadyl phosphate dihydrate is observed in the diffractogram after 1 h of exposure (Figure 1, b). At ambient conditions (r.h. = 55%), however, the intercalate rapidly decomposes, and only a small (001) reflection of the intercalate is present, together with a strong (001) line of the dihydrate, in the diffractogram measured immediately after exposure to ambient air (Figure 1, c). After 16 min, the sample is completely converted into vanadyl phosphate dihydrate (Figure 1, d).

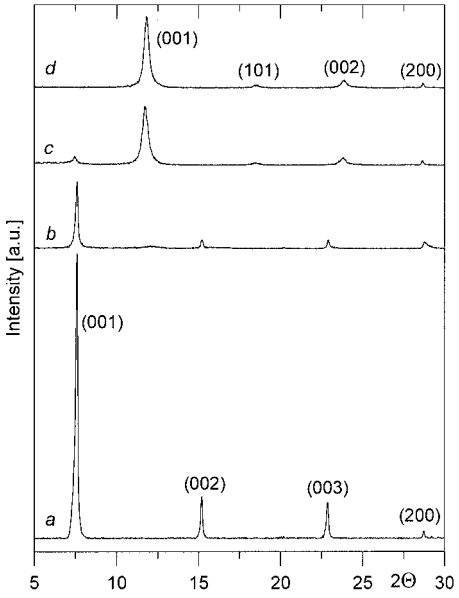

Figure 1. Diffractograms of samples of vanadyl phosphate intercalated with diethyl ether: (a) with excess diethyl ether; (b) after 1 h at r.h. =25%; (c) immediately after exposure to r.h. = 55%; (d) after 16 min exposure to r.h. = 55%

The thermal behavior of the intercalate was monitored by TG-DTA and X-ray diffraction. TG-DTA curves are given in Figure 2. The total weight loss (31%) corresponds to the formula $VOPO_4 \cdot C_2H_5OC_2H_5$ (theoretical weight loss 31.4%). As with intercalates of cyclic ethers, the diethyl ether intercalate is thermally stable. About half of diethyl ether is liberated in the first endothermic step up to 115 °C. The rest is released in two steps: the first up to 212 °C (the exothermic peak of the DTA curve is caused by the burning of diethyl ether) and the second, very slow, up to 550 °C. A small increase in weight between 550 and 750 °C is probably caused by oxidation of vanadium(IV). The basal spacing of the diethyl ether intercalate has been monitored as a function of temperature (Figure 3); it increases slightly up to 120 °C. The intensity of the (001) diffraction line does not change up to 100 °C and then decreases. A new phase with a basal spacing of about 8.2 Å appears at 130 °C and is present up to 170 °C. Above this temperature, the sample becomes green and amorphous. The new phase is probably caused by the loss of half of the guest molecules and by a change in arrangement of the guest molecules from bimolecular to monomolecular. Diethylene glycol intercalated $VOPO_4$ shows similar behavior during heating.[2]

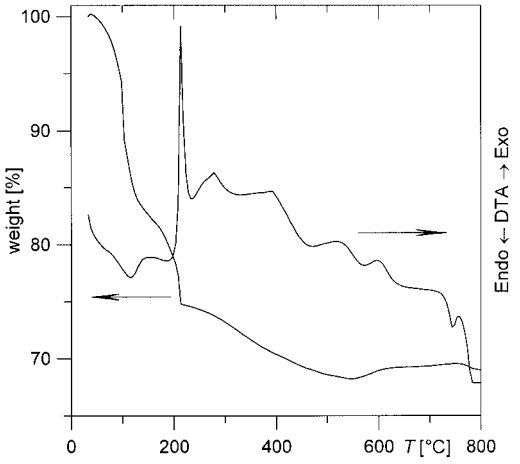

Figure 2. TG-DTA curves of vanadyl phosphate intercalated with diethyl ether

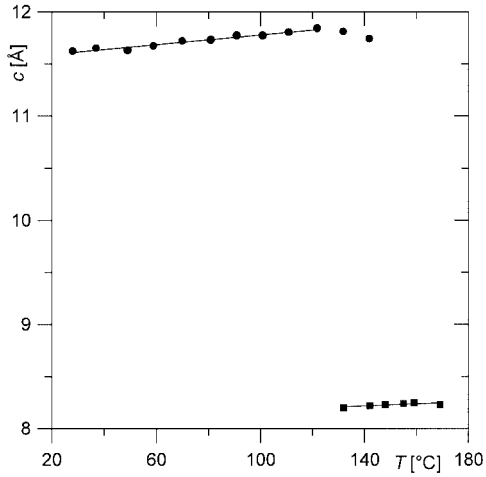

Figure 3. Basal spacing as a function of temperature during thermal decomposition of vanadyl phosphate intercalated with diethyl ether; circles represent basal spacings of the low-temperature phase, squares correspond to the high-temperature phase; errors of the basal spacings are within the dimensions of the data symbols

For infrared measurements, a sample of vanadyl phosphate intercalated with diethyl ether was placed in a purged sample compartment of the spectrometer (r.h. = 5%) for 5 min and for 7 and 22 h without removing the sample from the crystal between subsequent spectral measurements. Another sample was exposed to ambient conditions (r.h. = 60%) for 22 h and for 6, 10, 14 and 17 d. Such conditions allow a progressive replacement of the diethyl ether molecules in the vanadyl phosphate intercalate by atmospheric water. The infrared spectra of the intercalate at various stages of the deintercalation process under ambient conditions were compared with that of vanadyl phosphate dihydrate and with the spectrum of pure diethyl ether [Fig-

 © 2004 Wiley-VCH Verlag GmbH & Co. KGaA, Weinheim

ure 4 (2000 to 600 cm^{-1}) and Figure 5 (4000 to 2500 cm^{-1})].

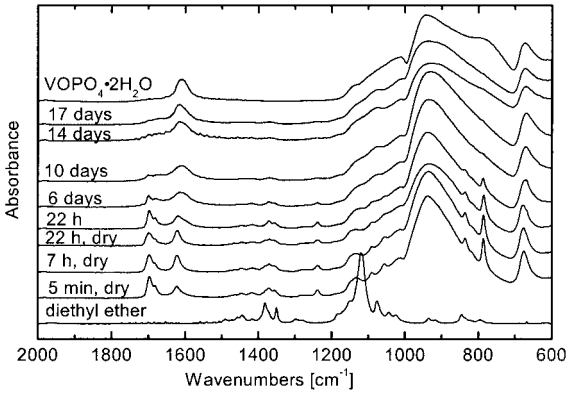

Figure 4. FTIR spectra (2000 to 600 cm^{-1}) of vanadyl phosphate dihydrate, of pure diethyl ether and of vanadyl phosphate intercalated with diethyl ether after 5 min, 7 h and 22 h in a purged spectrometer (r.h. = 5%), and after 22 h and 6, 10, 14 and 17 d under ambient conditions (r.h. = 60%)

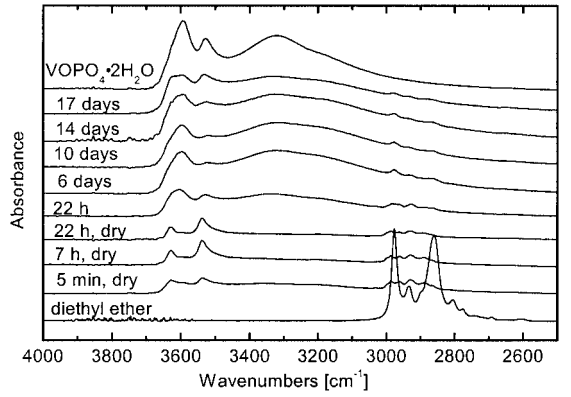

Figure 5. FTIR spectra (4000 to 2500 cm^{-1}) of vanadyl phosphate dihydrate, of pure diethyl ether and of vanadyl phosphate intercalated with diethyl ether after 5 min, 7 h and 22 h in a purged spectrometer (r.h. = 5%), and after 22 h and 6, 10, 14 and 17 d under ambient conditions (r.h. 60%)

The Raman spectra (3500−600 cm^{-1}) of vanadyl phosphate dihydrate, vanadyl phosphate intercalated with diethyl ether and pure diethyl ether are shown in Figure 6. Unfortunately, it was not possible to measure the kinetics of the replacement process of diethyl ether by Raman spectroscopy because of a partial escape of the diethyl ether molecules due to the laser beam during measurements.

Vibrational bands of the PO_4 tetrahedron, the vanadyl group V=O, and the P−O−V group can be identified in all spectra. The intense band at 945 cm^{-1} in the spectrum of vanadyl phosphate dihydrate (Figure 6) corresponds to the symmetric $\nu(PO_4)$ stretching vibration of the phosphate tetrahedron in $(VOPO_4)_\infty$. This band is shifted to 940 cm^{-1} in vanadyl phosphate intercalated with diethyl ether. The sharp band at 995 cm^{-1} in the vanadyl phosphate dihydrate spectrum is due to a vanadyl V=O stretching vibration. Its

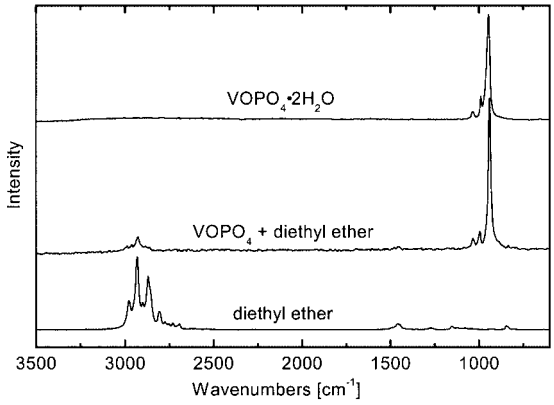

Figure 6. Raman spectra (3500−600 cm^{-1}) of vanadyl phosphate dihydrate, of vanadyl phosphate dihydrate intercalated with diethyl ether and of pure diethyl ether

position corresponds to the coordination of the oxygen atom of the water molecules in the VO_6 octahedron. The vanadyl stretching band appears to be especially sensitive to atoms coordinated to the vanadium atom within an octahedral arrangement in the host lattice structure. During the intercalation of water molecules into $VOPO_4$ its position at 1035 cm^{-1} in the anhydrous form changes to that typical for mono- and dihydrate (995 cm^{-1}).[6] In the Raman spectrum of the intercalate with diethyl ether the band at 994 cm^{-1} corresponds most probably to the coordination of the oxygen atom of diethyl ether to the vanadium atom, and the band at 1033 cm^{-1} to the anhydrous form of the host compounds. With the help of the Raman spectrum, we can assign the band with the maximum at 945 cm^{-1} in the IR spectrum (Figure 4) of vanadyl phosphate dihydrate to the symmetric $\nu(PO_4)$ stretching vibration, which is infrared-active due to distortion of the phosphate tetrahedron in the intercalate. The shoulder at 1011 cm^{-1} in the IR spectrum is most probably the V=O stretching band of the vanadyl group, while the band at 1135 cm^{-1} in the IR spectrum of the host is the asymmetric $\nu(PO_4)$ stretching vibration of the phosphate tetrahedron. The positions of the main spectral bands of the host structure differ only slightly from those of anhydrous vanadyl phosphate or its hydrated form.[6] This confirms that the structure of the original $VOPO_4$ layers remains unchanged after the intercalation reaction.

Conversely, bands due to pure diethyl ether are shifted in the spectrum of the intercalate; some bands disappear and some new bands appear (Figures 4 and 5). The C−H stretching vibration at 2978 cm^{-1} splits into 2985 and 2964 cm^{-1}, the bands at 2934, 2891 and 2862 cm^{-1} retain their positions but change in relative intensity. The C−H deformation vibration bands at 1490, 1448, 1383, 1351 and 1295 cm^{-1} shift to lower wavenumbers and a new band appears at 1238 cm^{-1} in the spectrum of the intercalate. The asymmetric COC stretching mode at 1120 cm^{-1} in the spectrum of pure diethyl ether is at about 1134 cm^{-1} in the spectrum of the intercalate. The bands at 1076 and 1025 cm^{-1} are overlapped by the symmetric $\nu(PO_4)$ stretching vibrational

 © 2004 Wiley-VCH Verlag GmbH & Co. KGaA, Weinheim

band and are observed as shoulders at 1089 and 1057 cm^{-1}. The symmetric COC mode at 935 cm^{-1} is completely overlapped and the bands at 846 and 796 cm^{-1} are shifted to 838 and 787 cm^{-1}. The diethyl ether bands reduce in intensity during exposure to the external conditions.

Most surprising are two sharp bands with maximum at about 3627 and 3530 cm^{-1} and a broad band with two maxima at 3354 and 3182 cm^{-1} seen during the first 5 min after removing the sample from the ampoule and placing it in the purged sample compartment of the spectrometer (r.h. = 5%). At the same time we observed a band at 1699 cm^{-1} with a shoulder at 1682 cm^{-1} and a band at 1624 cm^{-1}. When the sample is not removed from the purged sample spectrometer compartment, these bands remain unchanged and the broad band with two maxima at 3354 and 3182 cm^{-1} disappears in the spectrum measured after 22 h. In the spectra of the sample measured at ambient conditions (r.h. = 60%) the two sharp bands are shifted to 3594 and 3530 cm^{-1}, and the band at 1624 cm^{-1} is shifted to 1612 cm^{-1}. These new positions correspond to the spectrum of vanadyl phosphate dihydrate. The shoulder at 3627 cm^{-1} and the band at 1699 cm^{-1} disappear when the sample is kept under ambient conditions. The last spectrum of the intercalate, measured after 17 d, is very similar to that of $VOPO_4 \cdot 2H_2O$.[6]

We suppose that the new bands in the spectrum of the very fresh sample taken in the purged sample compartment of the spectrometer (r.h. = 5%) correspond to adsorbed water on the surface of the sample. As attenuated total reflection (ATR) is a very surface-sensitive method, we observed relatively strong bands of water in the spectra. In the spectra of samples taken under ambient conditions (r.h. = 60%), the positions of the bands of water correspond to bulk water molecules, and the spectra correspond to those of vanadyl phosphate dihydrate.

The character of the bonding between the guest molecules and the host layer in the diethyl ether intercalate was investigated by quantum mechanical calculations and modeling. Figure 7 shows the DFT-optimized structure of the molecular segment representing local interactions of vanadyl phosphate with diethyl ether, using the B3LYP functional and 6-31G(d) basis set. Calculations with the LanL2DZ basis set give an analogous geometry with slight differences in bond lengths (Figure 7). To keep the overall planar structure of the segment during full geometry optimizations, and to make the electronic structure in the segment close to the conditions appearing in the intercalates, an oxygen atom was inserted between two neighboring PO_4 groups and terminal oxygen atoms were substituted by OH groups.[7] The total charge of the model compound was set to +3. All geometry optimizations with various starting orientations of diethyl ether with respect to the vanadyl group lead to the structure displayed in Figure 7, indicating the formation of the C−O(−C)→V bond in the intercalates. The diethyl ether molecule exhibits central symmetry with respect to the oxygen atom and a gauche conformation around both C−O bonds (calculated dihedral angle C−C−O−C 71.4°).

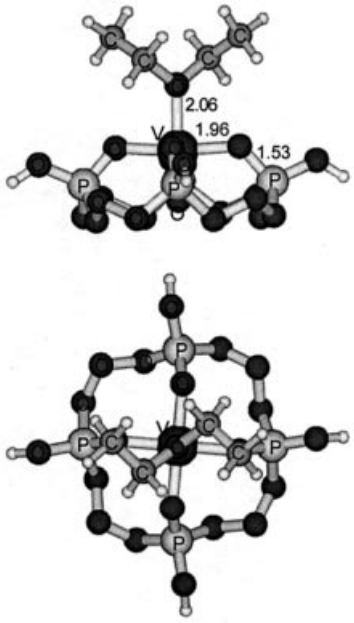

Figure 7. Optimized B3LYP/6-31G(d) structure of the molecular segment modeling the vanadyl phosphate−diethyl ether interaction, with indicated bond lengths [Å]

Simulations of larger local intercalate structures including two $VOPO_4$ layers were performed using the semiempirical quantum-chemical methods PM3 and AM1. The adequacy of the semiempirical methods for vanadyl phosphate intercalates has been illustrated in a previous study of intercalates with benzonitrile and tolunitrile, in which the results of modeling are in a very good agreement with experimental data obtained by X-ray, IR and Raman spectroscopy.[8] When the model structure shown in Figure 7 was reoptimized with the PM3 and AM1 methods, only slight changes in parameters were found in comparison with the DFT method. Optimized geometries of the molecular segment representing two layers of $VOPO_4$ and five molecules of diethyl ether intercalated between the two layers are shown in Figure 8. Terminal oxygen atoms were replaced by OH groups and the total charge of the model compounds set to −2. Coordinations of the vanadium atoms to the diethyl ether molecules in adjacent host interlayer spaces were simulated by coordinations with dimethyl ether molecules (not shown in Figure 8). The initial bond lengths and angles for the $VOPO_4$ layers were taken from the previous study of vanadyl phosphate intercalates with benzonitrile,[8] the initial basal spacing was set to the above given value of the lattice parameter c = 11.664 Å, determined by the X-ray diffraction, and the structure and bonding of diethyl ether were taken from the DFT calculations (Figure 7). In a series of geometry optimizations with various symmetry constraints and the parameter c fixed, the initial molecular and lattice parameters were refined to values suitable for the final overall energy minimization. All the variables defining the positions of the atoms both in the host and guest layers were fully optimized with the excep-

 © 2004 Wiley-VCH Verlag GmbH & Co. KGaA, Weinheim

tion of the constraints exposed by the symmetry conditions defining polyhedra in the $VOPO_4$ layers and relative orientations of the guest molecules in the interlayer with respect to the $VOPO_4$ layer. The basal spacings calculated with the PM3 and AM1 methods are 11.28 and 11.07 Å, respectively. In agreement with X-ray results, the mutual positions of the successive layers exhibit a shift characterized by a vector with calculated components of 0.02 and 0.53 Å by the PM3 method and of 0.99 and 1.29 Å with the AM1 method.

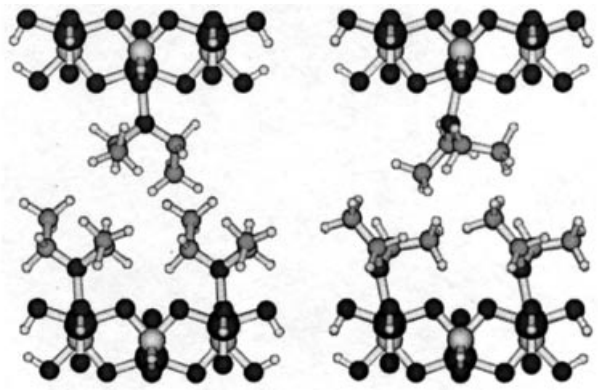

Figure 8. Side views of the PM3-optimized geometry of the molecular segment modeling the arrangement of diethyl ether molecules between the $VOPO_4$ layers

Experimental Section

Preparation: The 2-propanol intercalate was prepared by suspending microcrystalline $VOPO_4{\cdot}2H_2O$ in dry 2-propanol with subsequent short exposure to a microwave field. The intercalation compound was obtained by replacing 2-propanol in $VOPO_4{\cdot}2C_3H_7OH$ with diethyl ether. The 2-propanol intercalate (0.5 g) was dispersed in diethyl ether (15 mL) and exposed to a microwave field for 5 min. Samples used for XRD measurements contained small amounts of free diethyl ether. Dry samples for the TG and spectroscopic measurements were prepared by evaporation of diethyl ether at 25 °C in an evacuated ampoule.

X-ray: Powder data were obtained with a D8-Advance diffractometer (Bruker AXE, Germany) using Cu-K_α radiation with a secondary graphite monochromator. Diffraction angles were measured from 7 to 80° (2θ). The temperature measurements (22−200 °C) were carried out on the heated corundum plate with a thermocouple.[9] Each diffractogram was measured at constant temperature and a cycle of heating and measuring lasted about 30 min. The sample was covered with a foil for protection.

TG: TG analyses, using a Netzsch STA 449C instrument, were carried out in air between 30 and 800 °C at a heating rate of 5 °C·min^{-1}.

IR: Infrared measurements (400−4000 cm^{-1}) were carried out with a fully computerized Bruker IFS 55 EQUINOX FTIR spectrometer with a DLATGS detector (256 scans per spectrum at 4 cm^{-1} resolution). Spectra of the intercalates were recorded ex situ by an ATR technique using the Golden Gate™ Heated Diamond ATR Top-Plate (Specac Ltd.) at ambient temperature. The spectrum of the corresponding liquid diethyl ether was measured by an ATR technique with a ZnSe crystal. Spectra were corrected for the H_2O and CO_2 content of the optical path.

Raman: FT Raman spectra were collected using a Bruker IFS 55 EQUINOX FTIR spectrometer equipped with an FT Raman module FRA 106/S with a diode-pumped, temperature-stabilized Nd YAG laser, and an InGaAs detector [128 interferograms were coadded per one spectrum in the range 4000−(−1000) cm^{-1} at 4 cm^{-1} resolution].

Calculations: Quantum chemical calculations were carried out at the ab initio and semiempirical levels of theory employing GAUSSIAN 98[10] and MOPAC 2002[11] program packages, respectively. Local interactions and structures in the intercalates of vanadyl phosphate with diethyl ether were studied at the DFT level using a functional B3LYP with the basis sets 6-31G(d) and LanL2DZ. Geometrical optimizations of larger structures including two vanadyl phosphate layers were performed at a semiempirical level using PM3 and AM1 methods.

Acknowledgments

This study was supported by the Grant Agency of the Czech Republic (Grant No. 202/01/0520). The help of the Ministry of Education, Youth and Sports of the Czech Republic (VZ113200002) and the Academy of Sciences of the Czech Republic (AVOZ4050913) is also appreciated.

[1] J. Kalousová, J. Votinský, L. Beneš, K. Melánová, V. Zima, *Collect. Czech. Chem. Commun.* **1998**, *63*, 1−19.
[2] K. Melánová, L. Beneš, V. Zima, R. Vahalová, M. Kilián, *Chem. Mater.* **1999**, *11*, 2173−2178.
[3] V. Zima, K. Melánová, L. Beneš, P. Čapková, M. Trchová, P. Matějka, *Chem. Eur. J.* **2002**, *8*, 1703−1709.
[4] L. Beneš, V. Zima, K. Melánová, M. Trchová, P. Čapková, B. Koudelka, P. Matějka, *Chem. Mater.* **2002**, *14*, 2788−2795.
[5] K. Goubitz, P. Čapková, K. Melánová, W. Molleman, H. Schenk, *Acta Crystallogr., Sect. B* **2001**, *57*, 178−183.
[6] M. Trchová, P. Čapková, P. Matějka, K. Melánová, L. Beneš, *J. Solid State Chem.* **1999**, *148*, 197−204.
[7] V. Zima, K. Melánová, L. Beneš, M. Trchová, J. Dybal, *Eur. J. Inorg. Chem.* **2004**, 570−574.
[8] L. Beneš, V. Zima, K. Melánová, J. Dybal, M. Trchová, P. Matějka, *Eur. J. Inorg. Chem.* **2003**, 3662−3667.
[9] L. Beneš, *Sci. Pap. Univ. Pardubice Ser. A* **1996**, *2*, 151−155.
[10] M. J. Frisch, G. W. Trucks, H. B. Schlegel, G. E. Scuseria, M. A. Robb, J. R. Cheeseman, V. G. Zakrzewski, J. A. Montgomery, Jr., R. E. Stratmann, J. C. Burant, S. Dapprich, J. M. Millam, A. D. Daniels, K. N. Kudin, M. C. Strain, O. Farkas, J. Tomasi, V. Barone, M. Cossi, R. Cammi, B. Mennucci, C. Pomelli, C. Adamo, S. Clifford, J. Ochterski, G. A. Petersson, P. Y. Ayala, Q. Cui, K. Morokuma, D. K. Malick, A. D. Rabuck, K. Raghavachari, J. B. Foresman, J. Cioslowski, J. V. Ortiz, A. G. Baboul, B. B. Stefanov, G. Liu, A. Liashenko, P. Piskorz, I. Komaromi, R. Gomperts, R. L. Martin, D. J. Fox, T. Keith, M. A. Al-Laham, C. Y. Peng, A. Nanayakkara, C. Gonzalez, M. Challacombe, P. M. W. Gill, B. Johnson, W. Chen, M. W. Wong, J. L. Andres, C. Gonzalez, M. Head-Gordon, E. S. Replogle, J. A. Pople, *GAUSSIAN 98, Revision A.9*, Gaussian, Inc., Pittsburgh PA, **1998**.
[11] *MOPAC 2002*, Fujitsu Limited, Tokyo, Japan **1999**.

Received December 16, 2003
Early View Article
Published Online April 20, 2004

 © 2004 Wiley-VCH Verlag GmbH & Co. KGaA, Weinheim

Intramolecular Nucleophilic Substitution in a C_6F_5 Moiety Assisted by Antimony

Pavel L. Shutov,[a] Sergey S. Karlov,*[b] Klaus Harms,[a] Daniil A. Tyurin,[b] Jörg Sundermeyer,[a] Jörg Lorberth,[a] and Galina S. Zaitseva[b]

Keywords: Antimony / Amides / Density functional calculations / Fluorinated ligands / Nucleophilic substitution

Antimony tris-amides — $(Et_2N)_{3-n}Sb[N(C_6F_5)(2\text{-}C_5H_4N)]_n$ [n = 1 (**3**), 2 (**4**) or 3 (**5**)] — have been prepared by treatment of $Sb(NEt_2)_3$ (**1**) with stoichiometric amounts of (2-$C_5H_4N)(C_6F_5)NH$ (**2**). In contrast to amide **5**, compounds **3** and **4** are unexpectedly unstable and react further to give the bis-amido antimony fluorides [(2-Et_2N-C_6F_4)(2-C_5H_4N)N]-Sb(F)[$N(C_2H_5)_2$] (**6**) and [(2-Et_2N-C_6F_4)(2-C_5H_4N)N]Sb(F)-[$N(C_6F_5)$(2-C_5H_4N)] (**7**). The structure of **7** was confirmed by X-ray diffraction studies. DFT calculations, which reproduce the principal features of compound **7**'s geometry, have been used to explain the possible reaction pathway of this *ortho*-directed metathetical fluoride-amide exchange.
(© Wiley-VCH Verlag GmbH & Co. KGaA, 69451 Weinheim, Germany, 2004)

Introduction

During the past 50 years there has been a continuing interest in the chemistry of polyfluoro aromatic compounds. The main reason for this is that the unique properties of these derivatives suggest their possible use in various technological fields.[1,2] One of the most urgent aims of organofluorine chemistry is the preparation of polyfluorinated compounds with desired structures. As is well-known, organofluorine ligands have found widespread application in recent years for the stabilization of low-valent transition metal or main group species or for achieving unusual molecular geometries.[1,2] There is also a strong interest in activation of the C−F bond in polyfluoro organic compounds due to the possible utilization of these activation processes in organic synthesis.[3] A variety of methods for activating C−F bonds with transition metal centers have been published in the last two decades. Several catalytic systems based on transition metals have been used for the replacement of an F atom in polyfluoro aryl moieties, mostly by oxidative addition reactions.[3−5] Although only a few examples of early transition metal complexes (TMCs) useful for C−F bond activation have been found, most of the reported processes involving TMCs occur with late transition metals. As a common example of *intramolecular* oxidative addition of a C−F bond to a transition-metal center the reaction of C_6F_5−CH=N−(C_6H_4-*o*-NH_2) or similar Schiff bases with different TMCs [$W(CO)_3(PrCN)_3$, $Ni(COD)_2$ (COD = 1,5-cyclooctadiene) etc.], which give stable products of metal insertion into a C−F bond, should be noted.[4,6,7] Two different mechanisms have been suggested by Roundhill and co-workers for aromatic nucleophilic substitution of the *ortho*-F atom in *trans*-[PtMe(THF)($PPh_2C_6F_5$)$_2$] by hydroxide or alkoxide ion, one of which is an intramolecular process.[8]

Nucleophilic substitution reactions of an aryl carbon-fluorine bond assisted by main group element compounds (alkali, alkaline earth metals and silicon derivatives) have been investigated to a considerable extent.[3,4,9−11] However, to the best of our knowledge, most of the mechanistically studied examples have been ascribed to *intermolecular* processes, although suppositions about *intramolecular* origins have been made for exclusively *ortho*-directed fluorine-atom substitution for C_6F_5X species (X containing carbon or sulfur multiple bonds to oxygen or nitrogen atoms) in reactions with Li or Mg reagents, such as ArLi, AlkMgHal, ArMgHal or ArN(R)MgHal.[11,12]

As part of our program to investigate the structure and the chemical behavior of hypervalent main-group-element compounds with intramolecular transannular interactions[13−15] we herein report the reaction of $Sb(NEt_2)_3$ (**1**) with C_6F_5NH(2-C_5H_4N) (**2**, LH), which leads to the antimony tris-amides **3**−**5** with one, two or three C_6F_5-(2-pyridyl)-amine groups, respectively. Compounds **3** and **4** are unexpectedly unstable and they react further to give bis-amido antimony fluorides **6** and **7**, respectively, after 21 days in almost quantitative yield. To the best of our knowledge no such intramolecular rearrangements have been reported previously. Schrock et al. have found that a

[a] Fachbereich Chemie, Philipps-Universität Marburg,
Hans-Meerwein-Strasse, 35032 Marburg/Lahn, Germany
Fax: (internat.) +49-(0)6421-28-28917
E-mail: jsu@chemie.uni-marburg.de
[b] Chemistry Department Moscow State University,
B-234 Leninskie Gory, 119899 Moscow, Russia
Fax: (internat.) +7-095-932-8846
E-mail: sergej@org.chem.msu.su

 © 2004 Wiley-VCH Verlag GmbH & Co. KGaA, Weinheim **DOI: 10.1002/ejic.200400074**

similar nucleophilic substitution product formed (23% yield) in the reaction of $Mo(NMe_2)_4$ with $(C_6F_5NHCH_2CH_2)_2NMe$. However, they were unable to determine whether this was due to an intra- or intermolecular process.[16] The structure of **7** was confirmed by X-ray diffraction studies. DFT calculations, which reproduce the principal features of the geometry of compound **7**, have been used to distinguish possible reaction pathways.

Results and Discussion

Treatment of $Sb(NEt_2)_3$ (**1**) with two or three equivalents of ligand LH (**2**) in toluene afforded amides **4** or **5**, respectively (Scheme 1). Compound **4** is unstable in toluene solution as well as in C_6D_6 solution and reacts further to give fluoride **7** after 21 days at room temperature. The reaction of **1** with one equivalent of LH led to reaction mixture **A**, consisting of **3** (as a major component) and **4** as well as starting material **1**, after 12 hours. Unfortunately, it was impossible to prepare compound **3** in a pure form. However, NMR spectroscopy data unambiguously confirm its structure. As for **4**, compound **3** (reaction mixture **A**) is unstable in solution and reacts further to give fluoride **6** after 21 days at room temperature. After recrystallization in order to remove traces of compound **7** partially formed from **4**, fluoride **6** was obtained as a pure solid. At the same time only compound **5** has been found in the reaction of **1** with three equivalents of LH (**2**) and no traces of fluorides **6** or **7** have been detected during this process. Hydrolysis of **6** after standard workup led, with moderate yield, to free amine **8**, which is difficult to access by other methods.

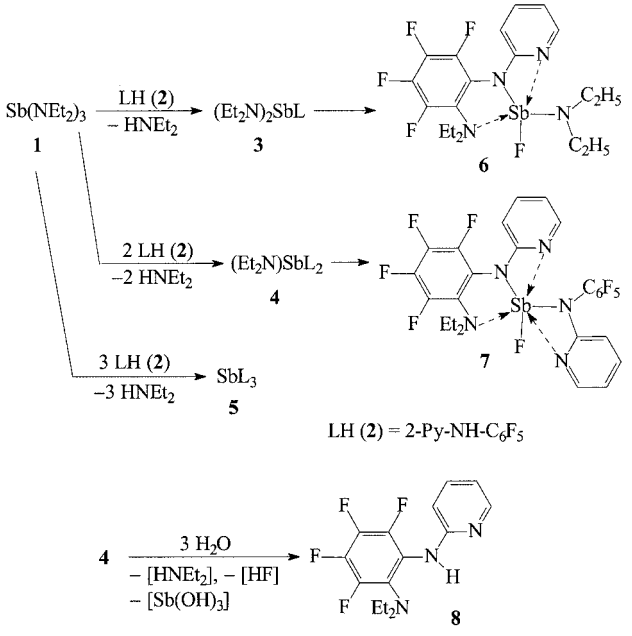

Scheme 1

The ^1H, ^{13}C, and ^{19}F NMR spectra of **3**–**8** are consistent with the proposed structural formula. In particular, the presence of the NEt_2 group, which is probably coordinated to the Sb atom, adjacent to the C_6F_4 ring in fluorides **6** and **7** stops the rotation of the $C_6F_4NEt_2$ group and the Py group of this ligand about the C–N bonds in C_6D_6 solution. This immobility results in the presence of two different signals for the $N(CH_2)_2$ carbon atoms of the NEt_2 group adjacent to the C_6F_4 ring (marked with an asterisk below) in the ^{13}C NMR spectra of **6** and **7**, a broadening of the $N(CH_2)_2$ signal in the ^1H NMR spectra of **6** and **7** (broad singlet instead of a quadruplet) as well as the presence of two different signals for the protons and carbons of CH_2''.

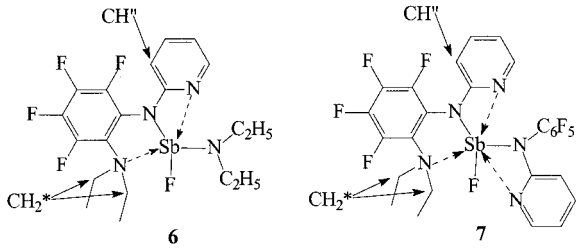

Single crystals of **7** were obtained as a toluene solvate from toluene solution (–30 °C). The molecular structure is presented in Figure 1; selected bond length and angles are summarized in Table 1. The primary coordination environment of the Sb atom is formed by the nitrogen atoms N(1) and N(14) and the F(1) atom, and may be treated as a trigonal pyramid. The $Sb-N_{cov}$ distances [2.103(2), 2.089(2) Å] are similar to those found for the closely related diamide $ClSb[N(SiMe_3)\{2\text{-}(6\text{-}Mepy)\}]_2$ (6-MepyH = 6-methylpyridine) [2.074(3)–2.127(8) Å][17] and somewhat shorter than in the tris-amide $Sb[N(SiMe_3)\{2\text{-}(6\text{-}Mepy)\}]_3$ [2.159(3)–2.167(3) Å].[18] The Sb(1)–F(1) distance [1.931(1) Å] is slightly shorter than those in the monofluoride $FSb(1,2\text{-}O_2C_6H_4)\cdot$1,10-phenanthroline [1.965(7) Å][19] and the difluoride $F_2Sb[OC(OCH_3)(2\text{-pyridyl})_2]$ [1.967(4) Å],[20] but slightly longer than those in $[SbF_3\cdot\{3\text{-}NH_2C(O)\text{-pyridine}\}_2]$ [1.911(8), 1.986(6) Å].[21] Internal coordination of both $N_{Pyridine}$ atoms and the N atom of the Et_2N group to antimony leads to a six-coordinate antimony in a

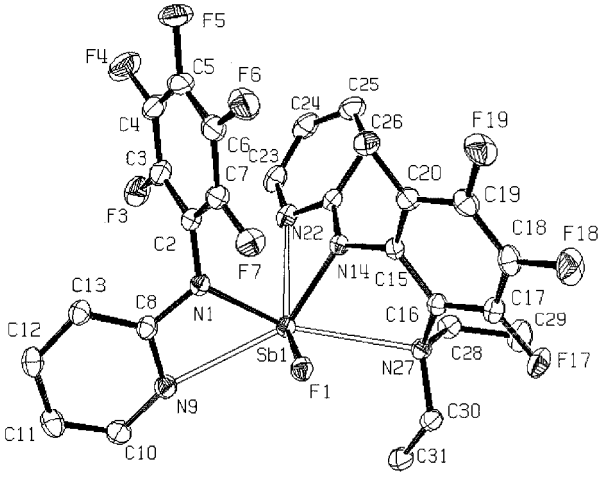

Figure 1. Molecular structure of **7**; hydrogen atoms and solvate toluene molecule are omitted for clarity

 © 2004 Wiley-VCH Verlag GmbH & Co. KGaA, Weinheim

Table 1. Most important bond lengths (Å) for **7** (X-ray data) and for **4**, **ts** and **7** (calculated data)

Compound	N(1)−Sb(1)	N(9)−Sb(1)	N(14)−Sb(1)	N(22)−Sb(1)	N(27)−Sb(1)	F(1)−Sb(1)	N(27)−C(16)	F(1)−C(16)
7 (X-ray data)	2.103(2)	2.780	2.089(2)	2.664	2.848	1.931(1)	1.429(2)	3.006
	N(20)−Sb(1)	N(22)−Sb(1)	N(2)−Sb(1)	N(4)−Sb(1)	N(38)−Sb(1)	F(16)−Sb(1)	N(38)−C(11)	F(16)−C(11)
4 (calcd. data)	2.163	2.679	2.172	2.647	3.070	1.984	1.428	3.135
ts (calcd. data)	2.160	2.768	2.126	2.563	2.326	2.802	1.714	1.560
7 (calcd. data)	2.197	2.763	2.201	2.685	2.057	3.364	3.290	1.349

strongly distorted octahedral environment, with the N(22) and F(1) atoms in axial positions and the four nitrogen atoms N(1), N(9), N(14), and N(27) in equatorial sites. It should be noted that the axial transannular Sb(1)−N(22) bond is considerably shorter than the equatorial transannular N(27)−Sb(1) and N(9)−Sb(1) bonds. The $Sb-N_{Pyridyl}$ bond lengths [Sb(1)−N(22), N(9)−Sb(1)] are similar to the values reported for an Sb compound contained pyridine moieties (2.371−2.837 Å).[22,23] The $Sb-NEt_2$ transannular bond length is similar to analogous $Sb-NMe_2$ contacts reported previously [2.766(4)−3.04(2) Å][24−26] and shorter than those in the hexacoordinate complex [Sb(2-$Me_2NCH_2C_6H_4)_3$] [3.03(2)−3.04(2) Å].[26] Finally, there is no short intramolecular contact between Sb and any of the F atoms (the sum of the van der Waals radii of Sb and F is 3.66 Å).[27]

In order to get a better understanding of the driving forces of this unusual *ortho*-directed methatetic fluoride-amide rearrangement of **4** to **7** (Figure 2−4) we carried out DFT calculations on compounds **4** and **7** up to the PBE level of theory. The most important calculated geometric parameters of these compounds are listed in Table 1. Taking into consideration that no X-ray derived structure of **4** is available, the calculated geometric data for this molecule are of particular interest. The primary coordination environment of the Sb atom in **4** may be treated as a trigonal pyramid. The $Sb-N_{Py}$ distances are significantly smaller than the sum of the van der Waals radii of antimony and nitrogen (3.74 Å).[27] Consequently, the Sb atom can be regarded as [3+2]-coordinated in **4**; the presence of an additional short contact between the Sb atom and one fluorine atom of the C_6F_5 group (3.36 Å) should be noted. Such steric proximity may be one of reasons for the easy rearrangement.

The DFT calculations predict that the geometry of **7** is significantly more stable (30.25 kcal mol^{-1}) than that of **4**. The relative energies and reaction barriers calculated at various computational levels are listed in Table 2. Taking into consideration the calculated structure of compound **4** (steric proximity of Sb atom and one fluorine atom of the C_6F_5 group) and the absence of *meta*- or *para*-substitution products a concerted reaction pathway may be proposed for the nucleophilic process. We have calculated the transition-state geometry (**ts**) of this process (Figure 3). A considerable shortening of the Et_2N-C distances accompanied by an elongation of the C−F bond was found in **ts** in comparison with that in **4**. An analogous alteration is observed for the Sb−F and $Sb-NEt_2$ distances. The considerable shift of the F atom from the plane of the phenyl ring in the **ts** geometry should be noted. The computed barrier of gas-phase interconversion of **4** into **7** is low (27.70 kcal mol^{-1}). According to the literature the calculated activation barrier of insertion reactions of $Pd(PH_3)_2$ into the C−F bond of different fluoroarenes ($F-C_6H_3XY$, X,Y = H, CN, NO_2) lies within the range 21.8−41.2 kcal mol^{-1} (RB3LYP/DZVP level of theory).[28] The use of the COSMO solvation model does not drastically change these results. The computational investigation of a single-step mechanism for the

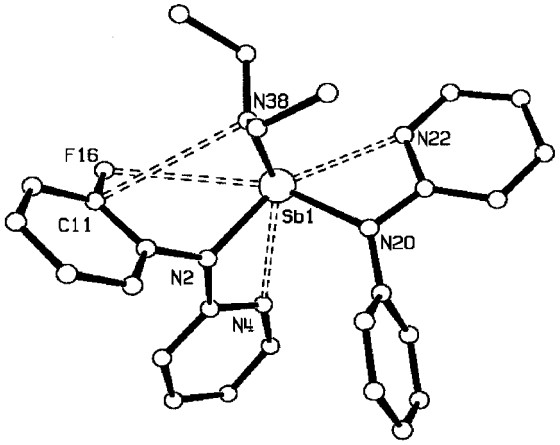

Figure 2. DFT calculated structure of **4**; hydrogen and fluorine atoms (except F16) are omitted for clarity

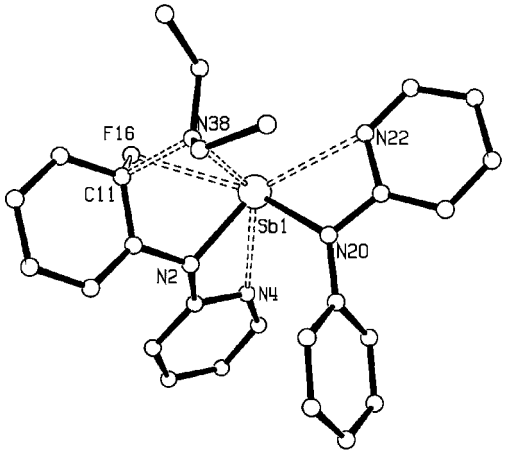

Figure 3. DFT calculated structure of **ts**; hydrogen and fluorine atoms (except F16) are omitted for clarity

 © 2004 Wiley-VCH Verlag GmbH & Co. KGaA, Weinheim

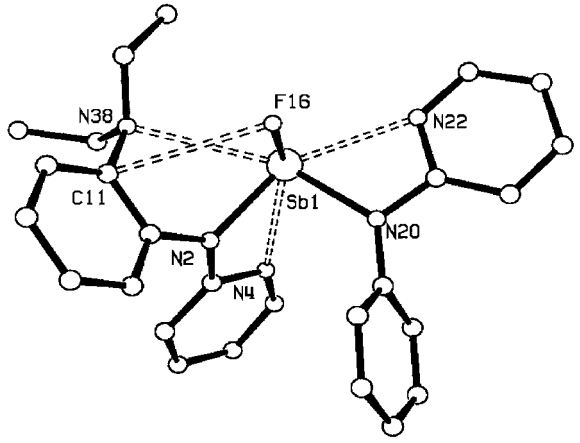

Figure 4. DFT calculated structure of **7**; hydrogen and fluorine atoms (except F16) are omitted for clarity

aromatic nucleophilic substitution of halobenzenes and halonitrobenzenes with halide anions for the reaction $C_6H_5X + X^- \rightarrow C_6H_5X + X^-$ (X = Cl, Br, I) gave similar values for the activation barrier (24.0−24.5 kcal mol^{-1}) at the MP2/6-31+G(d) + ZPE(HF/6-31+G(d) level.[29]

Table 2. Relative energies (kcal·mol^{-1}) of compounds **4** and **7** as well as the transition state (**ts**) of the rearrangement **4** → **7** (activation barrier in square brackets) calculated at various computational levels

	PBE	PBE-ZPE	RI-MP2//PBE
4	30.25	29.26	29.78
ts	57.95 [27.70]	57.18 [27.92]	62.37 [32.59]
7	0	0	0

Conclusion

This paper reports the syntheses of antimony tris-amides $(Et_2N)_{3-n}Sb[N(C_6F_5)(2\text{-}C_5H_4N)]_n$ [n = 1 (**3**), 2 (**4**) or 3 (**5**)] upon reaction of antimony tris-diethylamide (**1**) with stoichiometric amounts of $HN(C_6F_5)(2\text{-}C_5H_4N)$ (**2**). Compounds **3** and **4** are unstable in solution and rearrange to the corresponding fluorides $[(2\text{-}Et_2N\text{-}C_6F_4)(2\text{-}C_5H_4N)N]Sb(F)[N(C_2H_5)_2]$ (**6**) and $[(2\text{-}Et_2N\text{-}C_6F_4)(2\text{-}C_5H_4N)N]Sb(F)[N(C_6F_5)(2\text{-}C_5H_4N)]$ (**7**). A concerted mechanism of nucleophilic substitution has been proposed for this rearrangement according to density functional calculations. Hydrolysis of **6** provides a new entry to the tridentate amine $[(2\text{-}Et_2N\text{-}C_6F_4)(2\text{-}C_5H_4N)NH$.

Experimental Section

General Remarks: All manipulations were performed under a dry, oxygen-free argon atmosphere using standard Schlenk techniques. Solvents were dried by standard methods and distilled prior to use. Starting materials $Sb(NEt_2)_3$ [30] and $C_6F_5NH(2\text{-}C_5H_4N)$[31] were prepared according to the literature. C_6D_6 was obtained from Deutero GmbH and dried over sodium. ^1H, ^{13}C, and ^{19}F NMR spectra were recorded on a Bruker AC200 FT NMR and Bruker AC300 FT NMR spectrometers (in C_6D_6 at 23 °C). Chemical shifts in the ^1H and ^{13}C NMR spectra are given in ppm relative to internal $SiMe_4$; ^{19}F NMR experiments are referenced to $CFCl_3$ as an external standard. Mass spectra (EI-MS) were recorded on a Varian CH-7a device using electron-impact ionization at 70 eV; mass spectra (FD-MS) were recorded on an HP-5989B device; all assignments were made with reference to the most abundant isotopes. Elemental analyses were carried out by the Fachbereich Chemie of the Philipps University Marburg (Heraeus Rapid Analyzer). In this work, the nonempirical generalized gradient approximation (GGA) for the exchange-correlation functional of Perdew et al. (PBE) was employed and single point RI-MP2//PBE calculations were used.[32−36] All calculations were performed using the program "PRIRODA" developed by Laikov, which implements an economical computational procedure.[37] The all-electron large orbital basis sets of contracted Gaussian-type functions of the size (5s1p):[3s1p] for H, (11s6p2d):[4s3p2d] for C, (11s6p2d):[4s3p2d] for N, (11s6p2d):[4s3p2d] for F and (22s19p12d):[7s6p4d] for Sb were used for DFT-PBE. The all-electron basis set of contracted Gaussian-type functions of the size Sb {17,18,19,20,21,22/13,14,15,16,17/9,10,11}, N {8,9,10/5,6/2}, C {8,9,10/5,6/2}, H {5,6/2}, F {8,9,10/5,6/2} were used for RI-MP2. The frozen-core approximation was used in the RI-MP2 calculations. Full geometry optimization was performed by DFT-PBE for a number of structures followed by vibrational-frequency calculation using analytical first and second derivatives. Each structure was characterized by the vibrational analysis. The transition state has only one imaginary normal mode and equilibrium geometry states have only real normal modes. An IRC (intrinsic reaction coordinate) calculation was run starting from the transition-state geometry in both directions and verified the initial and final structures linked to the transition state. Transition-state normal modes were animated using MOLDEN.[38] Coordinates and normal modes for **1**, **2**, and **ts** in MOLDEN format are available from the author upon request. The present theoretical method has previously given very useful results in antimony chemistry.[8]

Diethylaminobis[*N*-pentafluorophenyl-*N*-(2-pyridyl)amino]stibane, $[Et_2NSb\{N(C_6F_5)(2\text{-}C_5H_4N)\}_2]$ (4): A solution of amine **2** (1.09 g, 4.2 mmol) in toluene (20 mL) was added dropwise at −78 °C to a stirred solution of the stibane **1** (0.70 g, 2.1 mmol) in toluene (15 mL). The reaction mixture was stirred for 12 h at room temperature and all volatiles were removed under reduced pressure to give **4** as a yellow oil (yield 1.43 g, 97%). ^1H NMR (C_6D_6, 300.130 MHz): δ = 0.74 (t, 6 H, CH_3), 2.98 (q, 4 H, NCH_2), 5.69 (m, 2 H), 6.18 (m, 2 H), 6.85 (m, 2 H), 7.73 (m, 2 H) (hydrogen atoms of pyridyl group) ppm. ^{13}C NMR (C_6D_6, 75.47 MHz): δ = 15.22 (CH_3), 43.82 (NCH_2), 107.00, 114.11, 138.93, 145.79, 160.76 (carbon atoms of pyridyl groups) ppm; the signals of the carbon atoms of C_6F_5 were not detected. ^{19}F NMR (C_6D_6, 200.13 MHz): δ = −164.45 (br. t, 4 F), −159.58 (br. t, 2 F), −143.95 (br. d, 4 F) ppm. FD-MS: *m*/*z* (%) = 711 (100) [M^+].

Bis(diethylamino)[*N*-pentafluorophenyl-*N*-(2-pyridyl)amino]stibane, $[(Et_2N)_2Sb\{N(C_6F_5)(2\text{-}C_5H_4N)\}]$ (3): Following the same experimental procedure as for **4** using **1** (0.67 g, 2.0 mmol), **2** (0.52 g, 2.0 mmol), and toluene (20 mL). Isolated as a yellow oil (reaction mixture **A**, 1.01 g; according to ^1H NMR spectroscopy the ratio **1**:**3**:**4** was approximately 1:2:1). Data for **3**: ^1H NMR (C_6D_6, 200.130 MHz): δ = 0.92 (t, 12 H, CH_3), 3.00 (q, 8 H, CH_2), 5.80

 © 2004 Wiley-VCH Verlag GmbH & Co. KGaA, Weinheim

(m, 1 H), 6.30 (m, 1 H), 7.00 (m, 1 H), 7.91 (m, 1 H) (hydrogen atoms of pyridyl group) ppm. ^{13}C NMR (C_6D_6, 50.32 MHz): δ = 16.23 (CH_3), 42.91 (CH_2), 106.79, 114.10, 138.54, 147.05, 161.00 (carbon atoms of pyridyl groups) ppm; the signals of the carbon atoms of C_6F_5 were not detected. ^{19}F NMR (C_6D_6, 188.28 MHz): δ = −164.04 (br. t, 2 F), −159.12 (t, 1 F), −145.46 (br. d, 2 F) ppm. FD-MS: *m*/*z* (%) = 524 (3) [M^+].

Tris[*N*-pentafluorophenyl-*N*-(2-pyridyl)amino]stibane, [Sb{N-(C_6F_5)(2-C_5H_4N)}$_3$] (5): Following the same experimental procedure as for **4** using **1** (0.56 g, 1.7 mmol), **2** (1.29 g, 5.0 mmol), and toluene (20 mL); yellow crystals (1.27 g, 83%) were obtained. ^{1}H NMR (C_6D_6, 200.13 MHz): δ = 5.56 (m, 3 H), 6.04 (m, 3 H), 6.77 (m, 3 H), 7.68 (m, 3 H) (hydrogen atoms of pyridyl group) ppm. ^{13}C NMR (C_6D_6, 50.32 MHz): δ = 107.05, 113.92, 139.53, 145.46, 160.42 (carbon atoms of pyridyl groups) ppm; the signals of the carbon atoms of C_6F_5 were not detected. ^{19}F NMR (C_6D_6, 188.28 MHz): δ = −164.53 (br. s, 6 F), −160.83 (br. t, 3 F), 144.51 (br. s, 6 F) ppm. EI-MS: *m*/*z* (%) = 898 (52) [M^+], 639 (39) [M^+ − N(C_5H_4N)(C_6F_5)]. $C_{33}H_{12}F_{15}N_6Sb$ (899.25): calcd. C 44.08, H 1.35, N 9.35; found C 43.87, H 1.31, N 9.15.

Diethylamino[*N*-(2-diethylamino-3,4,5,6-tetrafluorophenyl)-*N*-(2-pyridyl)amino]fluorostibane, [(Et_2N)Sb(F){N(C_6F_5)(2-C_5H_4N)}] (6): A solution of amide **3** (from reaction mixture **A**, 0.55 g, 1.1 mmol) in toluene (5 mL) was stirred for 21 days at room temperature and all volatiles were then removed under reduced pressure. Recrystallization of the residue from toluene/*n*-pentane (−30 °C) gave colorless crystals of **6** (yield 0.36 g, 66%). ^{1}H NMR (C_6D_6, 200.13 MHz): δ = 0.83 (br. s, 6 H, CH_3 of *o*-$Et_2NC_6F_4$ group), 1.03 (t, 6 H, CH_3 of Et_2NSb group), 2.95 (br. s, 4 H, CH_2 of *o*-$Et_2NC_6F_4$ group), 3.23 (q, 4 H, CH_2 of $SbNCH_2$), 5.79 and 5.80 (2 m, 1 H, CH′′), 6.17 (m, 1 H,), 6.96 (m, 1 H), 7.62 (m, 1 H) (hydrogen atoms of pyridyl group) ppm. ^{13}C NMR (C_6D_6, 50.32 MHz): δ = 12.13 (CH_3 of *o*-$Et_2NC_6F_4$ group), 16.38 (CH_3 of Et_2NSb group), 43.56 ($SbNCH_2$), 46.19 and 46.25 (CH_2 of *o*-$Et_2NC_6F_4$ group), 106.55 and 106.58 (CH′′), 112.96, 139.45, 145.42, 167.72 (carbon atoms of pyridyl groups) ppm; the signals of the carbon atoms of C_6F_5 were not detected. ^{19}F NMR (C_6D_6, 188.28 MHz): δ = −162.04 (br. t, 1 F), −161.42 (br. t, 1 F), −160.04 (br. s, 1 F, F−Sb), −148.02 (br. d, 1 F), −146.01 (br. d, 1 F) ppm. FD-MS: *m*/*z* (%) = 524 (13) [M^+], 505 (23) [M^+ − F], 452 [M^+ − NEt_2]. $C_{19}H_{24}F_5N_4Sb$ (525.17): calcd. C 43.45, H 4.61, N 10.67; found C 42.63, H 4.74, N 10.29.

[*N*-(2-Diethylamino-3,4,5,6-tetrafluorophenyl)-*N*-(2-pyridyl)amino]-[*N*-(pentafluorophenyl)-*N*-(2-pyridyl)amino]fluorostibane, [{(2-Et_2N-C_6F_4)(2-C_5H_4N)N}Sb(F){N(C_6F_5)(2-C_5H_4N)}] (7): A solution of amide **4** (1.23 g, 1.7 mmol) in toluene (5 mL) was stirred for 21 days at room temperature. Storage at −30 °C overnight resulted in colorless crystals of **7** (yield 0.87 g, 71%). ^{1}H NMR (C_6D_6, 300.130 MHz): δ = 0.74 (br. t, 6 H, CH_3), 2.82 (br. s, 4 H, NCH_2), 5.60 and 5.62 (2 m, 1 H, CH′′), 5.77 (m, 1 H), 6.02 (m, 1 H), 6.31 (m, 1 H), 6.77 (m, 1 H), 6.99 (m, 1 H), 7.66 (m, 1 H), 7.99 (m, 1 H) (hydrogen atoms of pyridyl group) ppm. ^{13}C NMR (C_6D_6, 75.47 MHz): δ = 11.61 (CH_3), 46.20 and 46.30 (NCH_2), 106.26 and 106.35 (CH′′), 106.81, 113.66, 114.16, 139.11, 139.97, 144.56, 146.43, 160.73, 161.23 (carbon atoms of pyridyl groups) ppm; the signals of the carbon atoms of C_6F_5 were not detected. ^{19}F NMR (C_6D_6, 188.28 MHz): δ = −164.45 (br. s, 2 F), −160.64 (br. t, 1 F), −160.07 (br. t, 1 F), −159.18 (br. t, 1 F), −154.72 (br. s, 1 F, F−Sb), −147.20 (br. d, 1 F), −146.85 (br. d, 1 F), −143.96 (br. t, 2 F) ppm. FD-MS: *m*/*z* (%) = 711 (45) [M^+]. $C_{26}H_{18}F_{10}N_5Sb$ (712.20): calcd. C 43.85, H 2.55, N 9.83; found C 43.47, H 2.64, N, 9.08.

***N*-(2-Diethylamino-3,4,5,6-tetrafluorophenyl)-*N*-(2-pyridyl)amine, HN(C_6F_5)(2-C_5H_4N) (8):** Water (2 mL) was added to a solution of stibane **6** (0.55 g, 1.1 mmol) in toluene (10 mL). The organic layer was separated, dried over Na_2SO_4 and all volatiles were removed under reduced pressure. Recrystallization of the residue from *n*-heptane gave colorless crystals of **8** (yield 0.10 g, 61%). ^{1}H NMR (C_6D_6, 200.13 MHz): δ = 0.65 (t, 6 H, CH_3), 2.66 and 2.67 (2 q, 4 H, NCH_2), 5.25 (br. s, 1 H, NH), 6.25 and 6.27 (2 m, 1 H), 6.39 (m, 1 H), 7.03 (m, 1 H), 8.14 (m, 1 H) (hydrogen atoms of pyridyl group) ppm. ^{19}F NMR (C_6D_6, 188.28 MHz): δ = −166.09 (br. t, 1 F), −160.77 (br. t, 1 F), −148.91 (br. d, 1 F), −141.88 (br. d, 1 F) ppm. $C_{15}H_{15}F_4N_3$ (313.29): calcd. C 57.51, H 4.83, N 13.41; found C 57.23, H 4.69, N 12.94.

X-ray Crystallographic Study. Crystal Data for 2: $C_{33}H_{26}F_{10}N_5Sb$, M_r = 804.34, triclinic, *a* = 8.5318(5), *b* = 11.6819(7), *c* = 16.680(1) Å, *α* = 83.687(5), *β* = 77.456(5), *γ* = 83.518(5)°, *V* = 1606.2(2) Å^3, space group $P\bar{1}$, *Z* = 2, D_c = 1.663 g·cm^{-3}, *F*(000) = 800, *μ*(Mo-K_α) = 0.950 mm^{-1}. Colourless crystal of approximate dimensions 0.45 × 0.27 × 0.18 mm^3 was used for data collection. Total of 23604 reflections (6418 unique, R_{int} = 0.0366) were measured on a Stoe IPDS-2 diffractometer (graphite-monochromatized Mo-K_α radiation, *λ* = 0.71073 Å) at 193(2) K. Data were collected in the range 1.76 < *θ* < 26.19° (−10 ≤ *h* ≤ 10, −14 ≤ *k* ≤ 14, −20 ≤ *l* ≤ 20). Absorption correction based on measurements of equivalent reflections resulted in transmission factors 0.6607/0.9884. The structure was solved by direct methods (SHELXS-86)[39] and refined by full-matrix least-squares on F^2 (SHELXL-97)[40] with anisotropic thermal parameters for all non-hydrogen atoms. All H atoms (except methyl hydrogens of solvate toluene) were refined isotropically. All other H atoms were refined by using a riding model. The final residuals were: R_1 = 0.0232 for 5935 reflections with $I > 2\sigma(I)$ and wR_2 = 0.0619 for all data with 535 parameters. Goof = 1.030, max. Δ*ρ* = 0.370 e·Å^{-3}.
CCDC-225205 (for **2**) contains the supplementary crystallographic data for this paper. These data can be obtained free of charge at www.ccdc.cam.ac.uk/conts/retrieving.html [or from the Cambridge Crystallographic Data Centre, 12 Union Road, Cambridge CB2 1EZ, UK; Fax: (internat.) +44-1223-336-033; E-mail: deposit@ccdc.cam.ac.uk].

Acknowledgments

We thank Dr. A. V. Churakov for helpful discussions and Dr. D. N. Laikov for placing at our disposal the program "PRIRODA". We thank also the Research Computing Center of the Moscow State University for computational time.

[1] *Organofluorine Chemistry: Principles and Commercial Applications* (Eds.: R. E. Banks, B. E. Smart, J. C. Tatlow), Plenum, New York, **1994**.
[2] T. Hiyama, *Organofluorine Compounds*, Springer, Berlin, **2000**.
[3] U. Mazurek, H. Schwarz, *Chem. Commun.* **2003**, 1321−1326.
[4] J. L. Kiplinger, T. G. Richmond, C. E. Osterberg, *Chem. Rev.* **1994**, *94*, 373−431.
[5] T. Braun, S. P. Foxon, R. N. Perutz, P. H. Walton, *Angew. Chem. Int. Ed.* **1999**, *38*, 3326−3329.
[6] T. G. Richmond, C. E. Osterberg, A. M. Arif, *J. Am. Chem. Soc.* **1987**, *109*, 8091−8092.
[7] T. G. Richmond, C. E. Osterberg, *Inorganic Fluorine Chemistry*, ACS Symposium Series **1994**, *555*, 392−404.
[8] S. Park, M. Pontier-Johnson, D. M. Roundhill, *J. Am. Chem. Soc.* **1989**, *111*, 3101−3103.
[9] J. Burdeniuc, B. Jedlicka, R. H. Crabtree, *Chem. Ber./Recueil* **1997**, *130*, 145−154.

 © 2004 Wiley-VCH Verlag GmbH & Co. KGaA, Weinheim

[10] M. Hudlicky, *Chemistry of Organic Fluorine Compounds*, 2nd ed., Ellis Horwood, Prentice Hall, **1992**.
[11] G. M. Brooke, *J. Fluorine Chem.* **1997**, *86*, 1−76.
[12] T. N. Gerasimova, N. A. Orlova, *J. Fluorine Chem.* **1985**, *28*, 361−380.
[13] P. L. Shutov, D. A. Sorokin, S. S. Karlov, K. Harms, Yu. F. Oprunenko, A. V. Churakov, M. Yu. Antipin, G. S. Zaitseva, J. Lorberth, *Organometallics* **2003**, *22*, 516−522.
[14] P. L. Shutov, S. S. Karlov, K. Harms, D. A. Tyurin, A. V. Churakov, J. Lorberth, G. S. Zaitseva, *Inorg. Chem.* **2002**, *41*, 6147−6152.
[15] P. L. Shutov, S. S. Karlov, K. Harms, O. Kh. Poleshchuk, J. Lorberth, G. S. Zaitseva, *Eur. J. Inorg. Chem.* **2003**, 1507−1510.
[16] F. V Cochran, P. J. Bonitatebus, R. R. Schrock, *Organometallics* **2000**, *19*, 2414−2416.
[17] C. L. Raston, B. W. Skelton, V.-A. Tolhurst, A. H. White, *Polyhedron* **1998**, *17*, 935−942.
[18] C. L. Raston, B. W. Skelton, V.-A. Tolhurst, A. H. White, *J. Chem. Soc., Dalton Trans.* **1987**, 1279−1285.
[19] H. Preut, F. Huber, G. Alonzo, N. Bertazzi, *Acta Crystallogr., Sect. B* **1982**, *38*, 935−937.
[20] G. Alonzo, N. Bertazzi, G. Bombieri, G. Bruno, *J. Chem. Soc., Dalton Trans.* **1987**, 2337−2340.
[21] P. L. Davidovich, V. V. Tkachev, L. O. Atovmyan, *Koord. Khim. (Russ.)(Coord. Chem.)* **1995**, *21*, 20−22.
[22] C. Jones, L. M. Engelhardt, P. C. Junk, D. S. Hutchings, W. C. Patalinghug, W. L. Raston, A. H. White, *J. Chem. Soc., Chem. Commun.* **1991**, 1560−1562.
[23] E. Block, G. Ofori-Okai, H. Kang, J. Wu, J. Zubieta, *Inorg. Chem.* **1991**, *30*, 4784−4788.
[24] T. Tokunaga, H. Seki, S. Yasuike, M. Ikoma, J. Kurita, K. Yamaguchi, *Tetrahedron* **2000**, *56*, 8833−8839.
[25] S. Okajima, S. Yasnike, N. Kakusawa, A. Osada, K. Yamaguchi, H. Seki, J. Kurita, *J. Organomet. Chem.* **2002**, *656*, 234−242.
[26] S. Kamepalli, C. J. Carmalt, R. D. Culp, A. H. Cowley, R. A. Jones, N. C. Norman, *Inorg. Chem.* **1996**, *35*, 6179−6183.
[27] J. Emsley, *The Elements*, 3rd ed. Clarendon Press, Oxford, U.K., **1998**.
[28] M. Jakt, L. Johannissen, H. S. Rzepa, D. A. Widdowson, R. Wilhelm, *J. Chem. Soc., Perkin Trans. 2* **2002**, 576−581.
[29] M. N. Glukhovtsev, R. D. Bach, S. Laiter, *J. Org. Chem.* **1997**, *62*, 4036−4046.
[30] A. Kiennemann, G. Levy, F. Schué, C. Taniélian, *J. Organomet. Chem.* **1972**, *35*, 143−148.
[31] R. Koppang, *J. Organomet. Chem.* **1972**, *46*, 193−200.
[32] J. P. Perdew, K. Burke, M. Ernzerhof, *Phys. Rev. Lett.* **1996**, *77*, 3865−3868.
[33] M. Ernzerhof, G. E. Scuseria, *J. Chem. Phys.* **1999**, *110*, 5029−5036.
[34] M. Feyereisen, G. Fitzgerald, A. Komornicki, *Chem. Phys. Lett.* **1993**, *208*, 359−363.
[35] O. Vahtras, J. Almlöf, M. W. Feyereisen, *Chem. Phys. Lett.* **1993**, *213*, 514−518.
[36] D. E. Bernholdt, R. J. Harrison, *Chem. Phys. Lett.* **1996**, *250*, 477−484.
[37] D. N. Laikov, *Chem. Phys. Lett.* **1997**, *281*, 151−156.
[38] G. Schaftenaar, J. H. Noordik, *J. Comput.-Aided Mol. Des.* **2000**, *14*, 123−134.
[39] G. M. Sheldrick, *Acta Crystallogr., Sect. A* **1990**, *46*, 467−473.
[40] G. M. Sheldrick, *SHELXL-97, Program for the Refinement of Crystal Structures*, University of Göttingen, Germany, **1997**.

Received January 29, 2004
Early View Article
Published Online April 26, 2004

 © 2004 Wiley-VCH Verlag GmbH & Co. KGaA, Weinheim

Supramolecular Structures in [Ag(dppf)] Complexes [dppf = 1,1′-Bis(diphenylphosphanyl)ferrocene] Stabilized by Coordinatively Versatile Trifluoroacetate (TFA) Ligands

Xiu Lian Lu,[a] Weng Kee Leong,[a] Lai Yoong Goh,*[a] and Andy T. S. Hor*[a]

Keywords: Silver / Trifluoroacetate / Coordination polymer / Supramolecular chemistry / Hydrogen bonding

The interaction of silver(I) trifluoroacetate and dppf in different molar equivalents has led to the isolation of dinuclear complexes $[Ag_2(\mu\text{-}O_2CCF_3)_2(\mu\text{-dppf})]$ (**1**) and $[Ag_2(\eta^1\text{-}O_2CCF_3)_2(dppf)_2]$ (**2**). Treatment of **1** with excess dppf gave a coordination polymeric compound $[Ag(\eta^2\text{-}O_2CCF_3)(dppf)]_n$ (**3**). Reaction of **1** with PMe_2Ph in MeOH in the presence of NH_4PF_6 led to displacement of trifluoroacetate, forming the mononuclear compound $[Ag(PMe_2Ph)_2(\eta^2\text{-dppf})]PF_6$ (**4**). All compounds have been characterized by microanalytical and spectroscopic analyses [IR, MS and NMR (^1H, ^{19}F and $^{31}P\{^1H\}$)] as well as X-ray diffraction studies. Molecular structures of the solvates of **1**, viz. **1A** (**1**·0.5THF) and **1B** (**1**·0.5CH_2Cl_2), **2** and **3** show that they contain trifluoroacetate in bridging, monodentate and bidentate bonding modes, respectively, with dppf as a bridging co-ligand. Compound **3** is an infinite linear [–dppf–Ag–dppf–Ag–dppf–Ag–]$_n$ coordination polymer. Interestingly, **1A** and **1B** form two different supramolecular network structures through C–H···F and C–H···O hydrogen-bonding interactions. Such secondary bonding interactions also lead to the formation of a 3D supramolecular structure in **3**.

(© Wiley-VCH Verlag GmbH & Co. KGaA, 69451 Weinheim, Germany, 2004)

Introduction

Transition-metal-mediated self-assembly is emerging as a new and pragmatic strategy for the design of nanostructures, supramolecular two- or three-dimensional network structures and coordination polymers.[1] Nitrogen-donor ligands have dominated these molecular designs.[1b−1d,1f,1h,2] Among the metals, the use of silver in this line of crystal engineering has escalated in the last decade[2,3] due to its rich structural diversity, which may be further tuned by numerous factors such as metal-to-ligand stoichiometry, counterions, ligand conformation, intra- and intermolecular H-bonding and solvents. Surprisingly, phosphanes have rarely been used in such assemblies until very recently, when some helices, rings, cages and polymers began to emerge in silver(I) systems containing (2-furyl)phosphane[3a] and some diphosphanes.[3b,3d] In particular, the role of the metallodiphosphane 1,1′-bis(diphenylphosphanyl)ferrocene (dppf) in supramolecular assemblies has not been investigated. We expect that the variable conformation modes of dppf in combination with coordinatively flexible ligands, such as acetate or nitrate as ancillary ligands,[4] will give a multitude of molecular and crystal structural possibilities with a metal like silver, which can adopt variable geometries, especially when assisted by intermolecular forces such as H-bonding. We describe here the results of such a study.

[a] Department of Chemistry, National University of Singapore, Kent Ridge, Singapore 117543
Fax: (internat.) + 65-6779-1691
E-mail: chmgohly@nus.edu.sg
andyhor@nus.edu.sg

Results and Discussion

Synthesis

Treatment of $Ag(O_2CCF_3)$ with dppf (2:1 molar ratio) in THF/MeOH for 8 h afforded an air-stable, non-light-sensitive yellow crystalline solid of a THF solvate of the disilver complex $[Ag_2(O_2CCF_3)_2(dppf)]$ (**1**) in 34% yield. Workup of the supernatant of **1** in CH_2Cl_2/ether gave the solvate **1**·0.5CH_2Cl_2 (30% yield). This solvate was obtained in 90% yield directly from a 6 h reaction in CH_2Cl_2. Recrystallization of **1** from THF/MeOH gave diffraction-quality crystals of **1**·0.5THF (**1A**) after 1 d at ambient temperature, while the same process in CH_2Cl_2/diethyl ether gave diffraction-quality crystals of **1**·0.5CH_2Cl_2 (**1B**). Treatment of $Ag(O_2CCF_3)$ with 1 mol-equiv. of dppf in CH_2Cl_2 for 3 h at room temperature yielded a yellow solid of the dinuclear complex $[Ag_2(O_2CCF_3)_2(dppf)_2]$ (**2**) in 87% yield. The reaction of **1** with 1 mol-equiv. of dppf in CH_2Cl_2 for 3.5 h afforded orange solids of the polymeric complex $[Ag(O_2CCF_3)(dppf)]_n$ (**3**) in 88% yield. These reactions are shown in Scheme 1. When monitored in an NMR tube in $CDCl_3$, the latter reaction showed no evidence of **2** (see Exp. Sect.); **2** is, though, very stable in $CDCl_3$. Reaction of **1** with PMe_2Ph in MeOH in the presence of NH_4PF_6 led to displacement of the O_2CCF_3 ligand and isolation of the

mononuclear complex $[Ag(dppf)(PMe_2Ph)_2]PF_6$ (**4**) in 48% yield (Scheme 2).

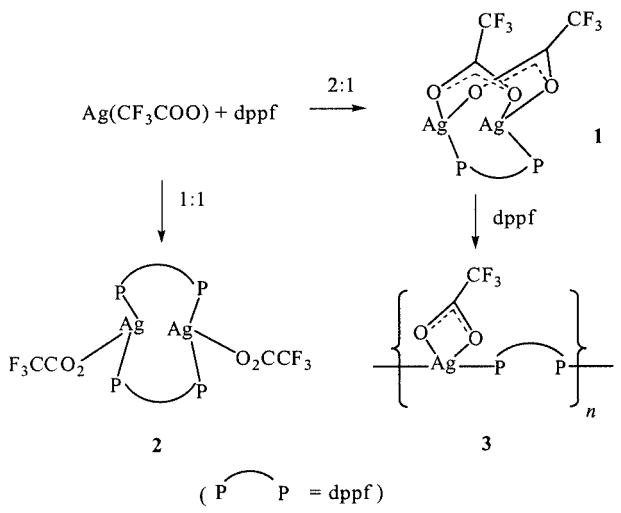

Scheme 1

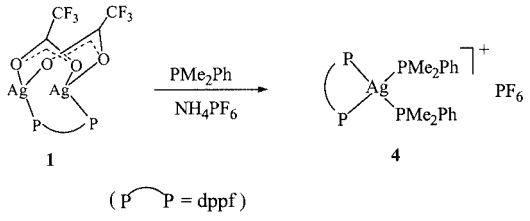

Scheme 2

Structural Studies

[Ag$_2$(μ-O$_2$CCF$_3$)$_2$(μ-dppf)] (1)

The solvate molecules **1**·0.5C_4H_8O (**1A**) and **1**·0.5CH_2Cl_2 (**1B**) are isostructural; two views of the molecular structure of **1A** are illustrated in Figure 1. The structure consists of a dinuclear Ag_2 core bridged by two trifluoroacetate groups and a dppf ligand, similar to the structure of [Ag_2($O_2CR)_2$(dppf)] (R = H, CH_3, Ph).[4] The Ag···Ag distances [3.156(2) Å in **1A** and 3.2434(4) Å in **1B**] agree with reported non-bond distances of 3.104(1) Å in [Ag_2($O_2CCH_3)_2$(dppf)] and 3.346(4) Å in [Ag_2($O_2CPh)_2$(dppf)].[4b] With three bridging ligands and no formal M−M bond, we can view this as two macrocycles hinged at the two Ag^I centers. A twofold axis passes through the mid-point of the Ag(1)···Ag(1A) axis and the Fe(2) atom of the dppf ligand in **1A**. Selected bond parameters (Table 1) show that the equivalent bond lengths of **1A** and **1B** are very similar, but their bond angles deviate significantly, viz. the O−Ag−O, O−Ag−Ag, O−Ag−P, P−Ag−Ag and O−C−O angles.

The crystal packing of **1A** and **1B** shows weak C−H···O and C−H···F hydrogen-bonding interactions, resulting in H···O distances of 2.62−2.63 Å in **1A** and 2.48−2.63 Å in **1B**, H···F distances of 2.50−2.54 Å in **1A** and 2.37−2.69 Å in **1B** (Table 2). The H···O and C···O distances, and C−H−O angles, fall within the reported ranges, viz. 2.52−2.70 Å, 3.32−3.60 Å and 128−155°, respectively, found in a CpFe half-sandwich and related carbonyl complexes of first-row transition metals, reported by Desiraju and co-workers. Likewise, the H···F distances and C−H−F angles are found in the range reported for in $C_6H_{6-x}F_x$ (x = 1−5), viz. 2.41 −2.87 Å and 120−174°, respectively.[5] Packing diagrams of the supramolecular networks in **1A** and **1B** viewed from the z and x axis, respectively, are illustrated in Figures 2 and 3. In **1A**, there is close packing of four molecules through two types of hydrogen bonds: C−H(Ph)···O and C−H(Cp)···F−C. The Figure shows four Ag_2 units clustering around a "central" region, which is effectively surrounded by four phenyl rings, one from each Ag_2 unit; molecules of THF are discernible in the lattice. In **1B**, the elementary prototype shows four molecular units connected by four types of H-bonds, viz. C−H(Cp)···O, C−H(Ph)···O, C−H(Cp)···F−C and C−H(Ph)···F−C. Figure 3 shows the relative orientation of three pairs of Ag_2 units; considering the dppf ligand as the "head" end of the unit and the bridging TFA ligands as the "tail" end, there is one pair pointing "head-to-head" towards each other such that their Cp rings come close to the two CH_2Cl_2 molecules in the central portion of the molecule, while the other

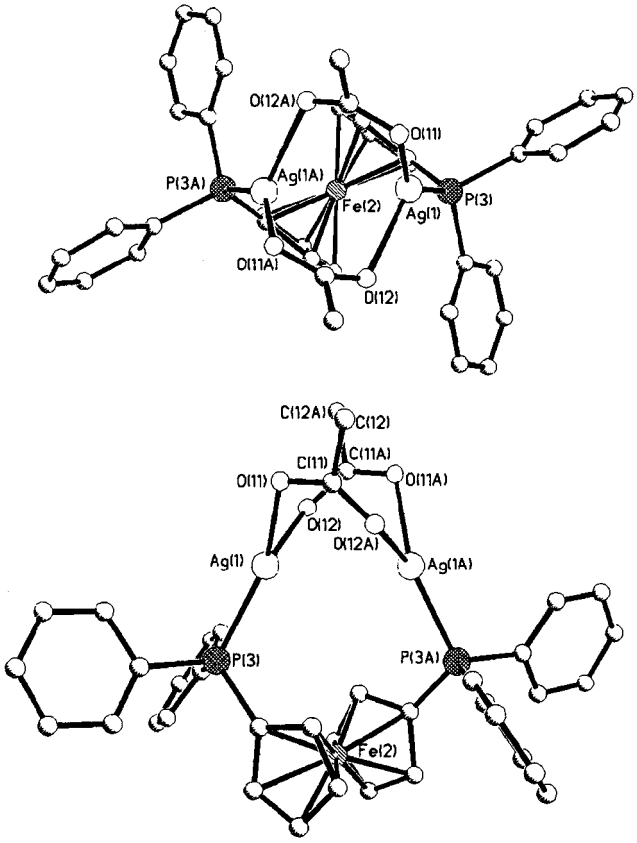

Figure 1. Two views of the molecular structure of [$Ag_2(O_2CCF_3)_2$(dppf)]·0.5THF (**1A**); hydrogen and fluorine atoms omitted for clarity

 © 2004 Wiley-VCH Verlag GmbH & Co. KGaA, Weinheim

Table 1. Selected bond lengths [Å] and bond angles [°] for solvates of $Ag_2(O_2CCF_3)_2(dppf)$ (**1**); symmetry transformations used to generate the "A" atoms: $x + 0, -y + 1.5, -z + 0.25$

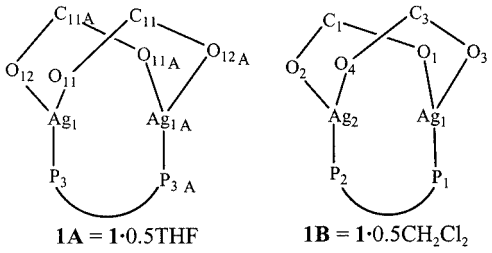

Equivalent bond lengths [Å] in the two molecules	**1A**	**1B**		**1A**	**1B**
Ag1−P3/Ag1−P1	2.358(3)	2.3539(8)	Ag1−Ag1A/Ag1−Ag2	3.156(2)	3.2434(4)
Ag2−P2	−	2.3459(9)	Ag1−O11/Ag1−O1	2.248(9)	2.315(3)
Ag1−O12/Ag1−O3	2.407(11)	2.222(3)	Ag2−O2	−	2.309(4)
Ag2−O4	−	2.204(3)	C11−O11/C1−O1	1.219(16)	1.209(5)
C11A−O(12)/C1−O2	1.219(15)	1.221(6)	C11−O12A/C3−O3	1.219(15)	1.204(5)
C11−O11/C3−O4	1.219(15)	1.237(5)			

Equivalent bond angles [°] in the two molecules	**1A**		**1B**	
O11−Ag1−O12	87.6(4)		O4−Ag2−O2	98.99(18)
O11−Ag1−P3	146.7(3)		O4−Ag2−P2	138.43(12)
P3−Ag1−O12	124.4(3)		P2−Ag2−O2	121.11(12)
O11−Ag1−Ag1A	83.2(2)		O4−Ag2−Ag1	76.29(9)
P3−Ag1−Ag1A	116.33(8)		P2−Ag2−Ag1	123.19(2)
O12−Ag1−Ag1A	65.9(3)		O2−Ag2−Ag1	72.86(9)
O11−C11−O12A	129.9(14)		O4−C3−O3	131.1(4)
O11A−C11A−O12	113.0(10)		O1−C1−O2	129.6(4)

two pairs orientate tail-to-tail towards each other, such that their CF_3 groups radiate towards the CH_2Cl_2 molecules. Adjacent molecules are linked into a 2D layer network by H-bonding (C−H···F and C−H···O), and these layers are linked into a 3D network through interlayer H-bond interactions.

The different crystal packing encountered in these two solvates of **1** must be associated with their different bond parameters, as well as the presence and location of the solvent molecules in the crystal lattice, factors that influence the nature and strength of hydrogen bonds supporting the network.

Table 2. Hydrogen bond lengths [Å] and bond angles [°] for **1A** and **1B**

D−H	D−H [Å]	A	H···A [Å]	D−A [Å]	∠DHA	Symmetry
1A:						
C326−H326	0.94	O11	2.63	3.441(19)	146	$1 - y, x, -z$
C315−H315	0.94	O12	2.62	3.399(19)	141	$1 - y, x, -z$
C2−H2	0.93	F11	2.54	3.094(24)	119	$1 - y, x, -z$
C2−H2	0.93	F13	2.50	3.251(6)	138	$1 - y, x, -z$
1B:						
C4A−H4A	0.94	F1	2.61	3.344(6)	136	$2 - x, 1 - y, 2 - z$
C3C−H3C	0.94	F1	2.69	3.420(8)	135	$x - 1, y, z$
C13−H13	0.99	F3	2.68	3.250(5)	117	$2 - x, y - 0.5, 1.5 - z$
C11−H11	0.99	F4	2.48	3.079(7)	119	$x, 1.5 - y, -0.5 + z$
C11−H11	0.99	F4A	2.67	3.182(10)	113	$x, 1.5 - y, -0.5 + z$
C12−H12	0.99	F5A	2.37	3.071(11)	127	$1 - x, y - 0.5, 1.5 - z$
C6C−H6C	0.94	F6A	2.64	3.225(15)	121	$x, 1.5 - y, -0.5 + z$
C3D−H3D	0.94	O1	2.54	3.205(6)	128	$x, 1.5 - y, -0.5 + z$
C3B−H3B	0.94	O2	2.63	3.403(6)	139	$2 - x, y - 0.5, 1.5 - z$
C7−H7	0.99	O4	2.48	3.468(6)	178	$1 - x, y - 0.5, 1.5 - z$

 © 2004 Wiley-VCH Verlag GmbH & Co. KGaA, Weinheim

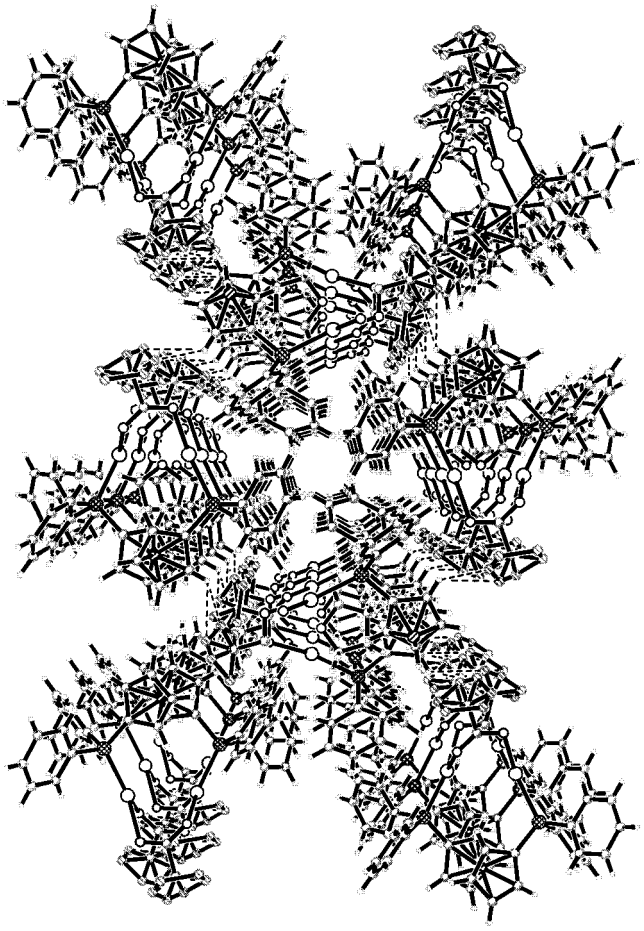

Figure 2. Packing diagram of the supramolecular network in **1A** viewed from the *z* axis, showing C−H(Ph)···O and C−H(Cp)···F−C hydrogen bonds; the four THF molecules in each layer are visible

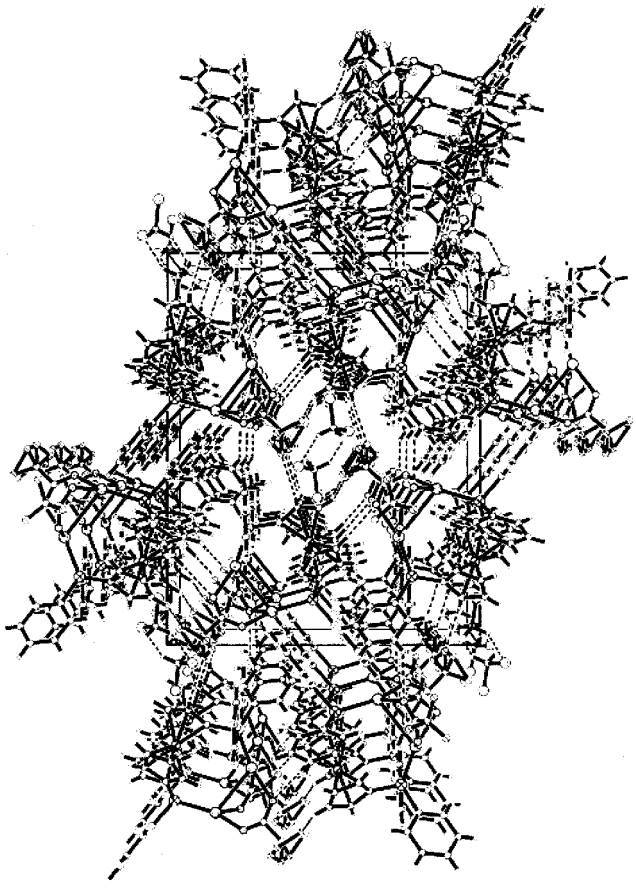

Figure 3. Packing diagram of the supramolecular network in $[Ag_2(O_2CCF_3)_2(dppf)]\cdot 0.5CH_2Cl_2$ (**1B**) viewed from the *x* axis; four types of H-bonds are illustrated: C−H(Cp)···O, C−H(Ph)···O, C−H(Cp)···F−C and C−H(Ph)···F−C

[Ag$_2$(O$_2$CCF$_3$)$_2$(dppf)$_2$] (2)

$[Ag_2(O_2CCF_3)_2(dppf)_2]$ (**2**) (Figure 4) contains two three-coordinate silver atoms doubly bridged by two dppf ligands; being η^1-coordinated to an oxygen atom of trifluoroacetate anions, each Ag atom achieves a 16e configuration. Selected bond parameters of **2** are given in Table 3. Similar structures have been reported for $[Ag_2(NO_3)_2(dpm)_2]$ and $[Ag_2(dpm)_2(O_2CCH_2Ph)_2]$ (dpm = $Ph_2PCH_2PPh_2$) with monodentate nitrate and carboxylate ligands, respectively,[6a,6b] which possess Ag···Ag distances of 3.085(1) and 3.080(1) Å, respectively; however, there is no metal−metal interaction in **2** (Ag···Ag = 3.781 Å), as with $Ag_2(NO_3)_2(dppf)_2$ [Ag···Ag = 3.936(2) Å].[4b] The Ag−P distances are also very close to those reported for $Ag_2(NO_3)_2(dppf)_2$.[4b] Except for a H-bond between the $CHCl_3$ solvent molecule and an oxygen atom of TFA, viz. C1−H1S($CHCl_3$)···O2 (2.12 Å), there are no secondary bonding interactions of the types observed in **1A**, **1B** and **3**.

The structures of **1** and **2** illustrate a preference of the 16e Ag^I center in these dinuclear species for a trigonal-planar configuration, with the diphosphane adopting a bridging coordination mode, while the weakly coordinating carboxylate group adapts as a bridging or monodentate ligand, forming an $[Ag_2(dppf)_2]$ ring structure in the latter situation, as was found in $Ag_2(NO_3)_2(dpm)_2$ and $[Ag_2(dpm)_2(O_2CCH_2Ph)_2]$.[6a,6b]

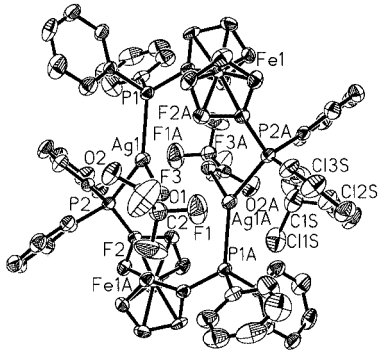

Figure 4. Molecular structure of **2**; hydrogen atoms omitted for clarity; thermal ellipsoids drawn to 50% probability

[Ag(O$_2$CCF$_3$)(dppf)]$_n$ (3)

The structure of **3** consists of a polymeric chain made up of repeating units of $[-PAg(\eta^2\text{-}O_2CCF_3)P-]_n$ where P−P = dppf (Figure 5). Each silver atom is four-coordi-

 © 2004 Wiley-VCH Verlag GmbH & Co. KGaA, Weinheim

Table 3. Selected bond lengths [Å] and bond angles [°] for **2**

Ag1−O1	2.471(4)	Ag1−P2	2.4775(15)
Ag1−P1	2.4776(15)	C1−O1	1.239(7)
C1−O2	1.226(7)		
O1−Ag1−P2	103.23(9)	O1−Ag1−P1	117.42(9)
P2−Ag1−P1	136.45(5)	C11−P1−Ag1	121.82(18)
C111−P1−Ag1	114.31(18)	C121−P1−Ag1	110.66(19)
C1−O1−Ag1	119.3(4)	O2−C1−O1	127.0(6)
O2−C1−C2	116.3(5)	O1−C1−C2	116.7(5)

nate, being bonded to a chelating trifluoroacetate ligand and two phosphorus atoms of two different dppf ligands, thus forming a one-dimensional infinite chain, which is further reinforced by intra-chain hydrogen-bond interactions [C−H(Cp)···O 2.47 Å, 155°]. A plane of symmetry passes through the Ag atom and bisects the AgOCO ring. Notably, the chelating mode of the carboxylate ligand in Ag^{I} complexes is rarely encountered,[7] in contrast to the commonly reported monodentate and μ-bridging modes.[8] Selected bond parameters and hydrogen bond parameters are given in Table 4. The Ag−P distance [Ag(1)−P(1) 2.4270(16) Å] is intermediate between those encountered in the other Ag(dppf) complexes in this study (2.34−2.57 Å). The Ag(1)−O(1) bond is longer [2.527(7) Å] than those in **1A** and **1B** (2.21, 2.31 Å), in which TFA bridges two Ag atoms, and in **2** (2.47 Å), in which TFA is monodentate. While no inter-chain hydrogen-bonding interactions are found between adjacent polymeric chains viewed from the *x* axis, they do exist between adjacent chains viewed from the *y* axis (Table 5 and packing diagram in Figure 6).

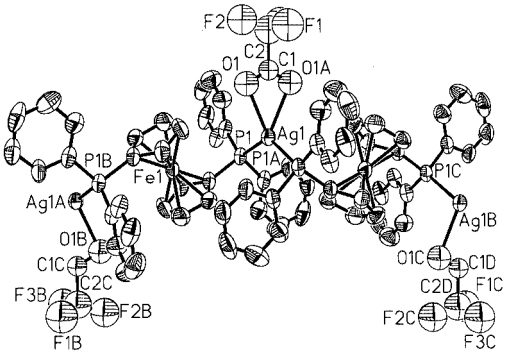

Figure 5. Section of the polymeric chain of **3**; hydrogen atoms omitted for clarity; thermal ellipsoids drawn to 50% probability

In the above complexes the participation of weak hydrogen bonding between C−H(Cp/Ph) bonds to O and/or F−C of coordinated ligands stabilizes supramolecular structures, the nature of which is further influenced by the presence of solvent molecules in the crystal lattice, as in **1A** and **1B**. The role of such weak hydrogen-bonding interactions in such phenomena has been reported frequently in recent years in organic systems[5,9] and coordination compounds[2g,10−12] though less frequently in organometallic complexes,[12−15] e.g. in the bonding of C−H(arene) to O(carbonyl) in a chromium complex,[12] of C−H(arene) to F of the anions, BF_4^- [13] or PF_6^- [16] and of C−F of C_6F_5 to O(carbonyl) in complexes of Fe, Co, Mn and Re.[15]

[Ag(PMe$_2$Ph)$_2$(dppf)]PF$_6$ (4)

This molecule possesses a mononuclear structure in which the silver atom assumes a distorted tetrahedral geometry with coordination to a chelating dppf and two monodentate dimethyl(phenyl)phosphane ligands (Figure 7). Selected bond parameters are given in Table 6. The bite angle of the dppf ligand, P(1)−Ag(1)−P(2) 105.96(4)°, is similar to that in $[Ag(dppf)_2]ClO_4$ [105.71(4)°]; the other angles at Ag [P(3)−Ag(1)−P(4) 105.87(5)°, P(3)−Ag(1)−P(1) 113.80(4)°, P(4)−Ag(1)−P(2) 107.58(4)°] show small deviations from those in $[Ag(dppf)_2]ClO_4$ [98.39(4)°, 113.15(4)°, 114.54(4)°].[17]

Spectral Characteristics

VT-^{1}H NMR Spectral Features

At 328 K the ^{1}H NMR spectrum of **1** in $CDCl_3$ shows two singlets at δ = 3.96 and 4.45 ppm for the α- and β-protons of the Cp rings of dppf and a multiplet at δ = 7.39−7.54 ppm (unresolved δ = 7.39, 7.41, 7.44, 7.47, 7.50, 7.52 and 7.54 ppm) for the Ph protons of dppf. These features vary little upon lowering the temperature to 243 K − there is mainly a loss of resolution in the Ph multiplet and slight broadening of the β-CpH signal (δ = 4.39 ppm) with concurrent greater broadening of the α-CpH signal (δ = 3.85 ppm); below 243 K both α and β signals undergo extensive broadening.

The ^{1}H NMR spectrum of **2** in $(CD_3)_2CO$ at 300 K and above shows only one peak, at δ = 4.44 ppm, for the Cp protons of dppf and two multiples, δ = 7.45−7.50 and 7.68−7.70 ppm, for the Ph protons of dppf. Below 273 K, the Cp singlet transforms into a broad unresolved multiplet,

Table 4. Selected bond lengths [Å] and bond angles [°] for complex **3**; symmetry transformations used to generate the "A" atoms: $-x$, y, $-z + 0.5$

Ag1−P1	2.4267(17)	Ag1−O1	2.518(8)	Ag1−P1A	2.4267(17)
Ag1−O1A	2.518(8)	C1−O1	1.190(9)	C1−C2	1.67(3)
C1−O1A	1.190(9)				
P1−Ag1−P1A	129.58(9)	P1−Ag1−O1A	115.47(18)	P1A−Ag1−O1A	110.07(18)
P1−Ag1−O1	110.07(18)	P1A−Ag1−O1	115.47(18)	O1A−Ag1−O1	49.6(3)
C1−O1−Ag1	92.6(8)	O1−C1−C2	117.4(7)	O1−C1−O1A	125.2(14)

 © 2004 Wiley-VCH Verlag GmbH & Co. KGaA, Weinheim

Table 5. Hydrogen-bond lengths [Å] and bond angles [°] for **3**

D−H	D−H [Å]	A	H···A [Å]	D−A [Å]	∠DHA [°]	Symmetry
C4A−H4A	0.94	F2	2.63	3.479(19)	149	$0.5 - x, 0.5 - y, 1 - z$
C5−H5	0.94	O1	2.47	3.351(10)	155	$-x, 1 - y, 1 - z$

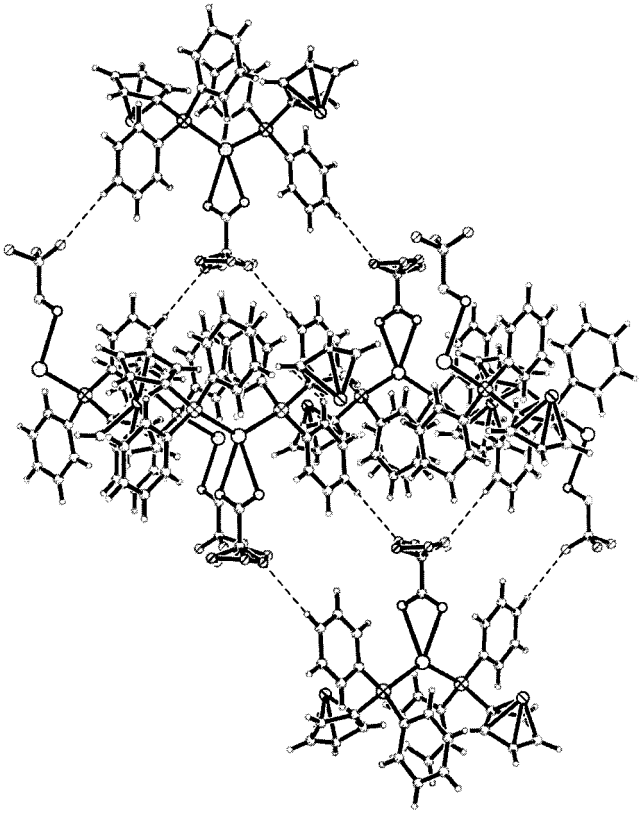

Figure 6. Packing diagram of **3** viewed from the *y* axis, showing two layers in the central chain, and inter-chain [C−H(Ph)···F−C] hydrogen-bonding interactions

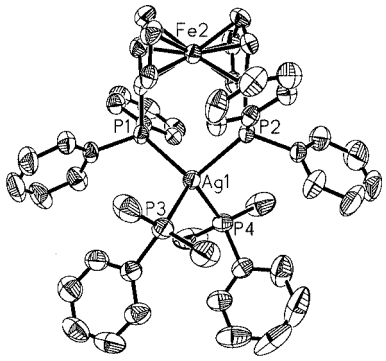

Figure 7. Molecular structure of cationic **4**; hydrogen atoms omitted for clarity; thermal ellipsoids drawn to 50% probability

which at 223 K, is centered at δ = 4.50 ppm, while the multiplicity of the phenyl protons is also drastically changed.

In $CDCl_3$ at 300 K, the Ph protons of **3** are seen as a broad peak at δ = 7.52 ppm and a multiplet centered at δ = 7.37 ppm, and the Cp signals as two broad singlets at δ = 4.34 and 4.25 ppm; at lower temperatures these were transformed into several unassignable broad peaks at δ = 2.5−6.3 ppm.

Table 6. Selected bond lengths [Å] and bond angles [°] for complex **4**

Ag(1)−P(1)	2.5474(12)	Ag(1)−P(2)	2.5700(12)
Ag(1)−P(3)	2.5371(13)	Ag(1)−P(4)	2.5212(13)
P(1)−C(101)	1.08(5)	P(2)−C(201)	1.808(5)
P(3)−C(301)	1.820(5)	P(4)−C(401)	1.816(5)
P(3)−C(31)	1.821(5)	P(3)−C(32)	1.829(5)
P(4)−C(41)	1.812(5)	P(4)−C(42)	1.817(6)
P(1)−Ag(1)−P(2)	105.96(4)	P(3)−Ag(1)−P(4)	105.87(5)
P(4)−Ag(1)−P(1)	112.47(4)	P(3)−Ag(1)−P(1)	113.80(4)
P(4)−Ag(1)−P(2)	107.5(4)	P(3)−Ag(1)−P(2)	111.07(4)

VT-^{19}F NMR Spectral Features

The sharp ^{19}F signal of **1** in $CDCl_3$ varies slightly, from δ = 1.6 ppm at 300 K to δ = 1.7 ppm at 223 K, while that of complex **2** in $(CD_3)_2CO$ undergoes a greater downfield shift, from δ = 2.4 ppm at 323 K to δ = 2.7 ppm at 223 K, with increasing line-width broadening. Below this, the peak transformed into two broad overlapping peaks, which at 183 K are seen at δ = 3.1 and 2.8 ppm (relative intensity ca. 1:2); these overlapping peaks indicate the presence of trifluoroacetate ligands in different coordination environments, most probably caused by different denticities of the ligands. This is accompanied by complex variations in the ^{1}H and ^{31}P{^{1}H} NMR spectra.

The VT-^{19}F NMR spectrum of **3** in $CDCl_3$ shows only one sharp peak (δ = 1.2 ppm) in the range 300−223 K, while at 213 K a minor peak (ca. 10%) emerges at δ = 1.7 ppm, indicating two types of coordinated trifluoroacetate ligands, as in **2** above.

VT-^{31}P{^{1}H} NMR Spectral Features

The variations of **1** in $CDCl_3$ are shown in Figure 8. A broad peak at δ = 6.6 ppm ($\nu_{1/2}$ = 405 Hz) at 328 K broadens further at 313 K (δ = 6.5 ppm, $\nu_{1/2}$ = 607 Hz). At 296 K, three overlapping broad peaks appear at δ = 10.1, 7.4 and 4.2 ppm ($\nu_{1/2}$ = 146, 255 and 146 Hz, with relative intensity ca. 1:2:1); these gradually transform into two pairs of sharp doublets at 223 K, being centered at δ = 7.6 ppm ($J^{107/109}$Ag−P = 695 and 805 Hz), indicative of coordination of one P atom to an Ag atom,[18] which is in agreement with its solid-state structure. These VT features can be rationalized in terms of ^{31}P−^{107}Ag/^{109}Ag inter- and intramolecular exchange processes first observed by Dean

 © 2004 Wiley-VCH Verlag GmbH & Co. KGaA, Weinheim

and co-workers in dinuclear Ag complexes containing bridging diphosphanes.[19]

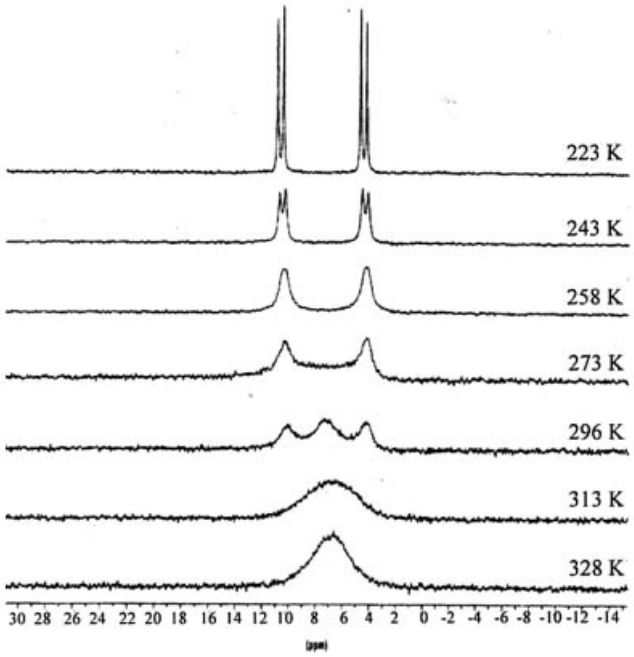

Figure 8. VT $^{31}P\{^{1}H\}$ NMR spectra of **1** in $CDCl_3$

^{31}P NMR spectra in $(CD_3)_2CO$ of **2** show a very broad peak at $\delta = -1.2$ ppm ($\nu_{1/2} \approx 300$ Hz) at 300 K. As the temperature is lowered to 183 K, a combination of broad bands and $^{107/109}Ag$-coupled doublets appear. With **3**, a decrease of temperature causes the broad ambient-temperature signal [$\delta = -1.5$ ppm ($\nu_{1/2} = 600$ Hz)] to transform into a very complex pattern, consisting of several broad "humps", which can not be rationalized. The only distinctive feature is a doublet at $\delta = -3.45$ ppm , which is observable at 223 K and below with $J^{107/109}Ag-P$ couplings of 418 and 482 Hz, indicative of coordination of two P atoms per Ag atom, which is consistent with its solid-state linear polymeric structure.

Mass Spectra

FAB^+-MS spectra of **1A/1B** and **2** do not show the parent ion fragment [M^+], but fragments arising from the consecutive loss of an O_2CCF_3 ligand and an $Ag(O_2CCF_3)$ moiety, leading to $m/z = 661$ [Ag + dppf] as the most intense fragment. The FAB^+-MS spectrum of **3** is identical to that of **2**. The highest mass fragment in the ESI^+-MS spectrum of **4** arises from the addition of 1 equiv. of PMe_2Ph to the parent ion at $m/z = 1216$ [$M^+ + PMe_2Ph$], followed by fragments showing consecutive losses of PMe_2Ph to yield $m/z = 661$ as the strongest peak. The FAB^+-MS spectrum of **5** only shows the most intense peak at $m/z = 662$.

Infrared Spectra

IR spectra of **1A/1B** show the bridging O_2CCF_3 vibration frequencies at $\tilde{\nu} = 1684$ (asymm.), 1437 (symm.), 1207 and 1133, with $\Delta\tilde{\nu}$(asymm. − symm.) = 247 cm^{-1} − outside the range (88−200 cm^{-1}) reported for bridging trifluoroacetate complexes.[20] The $\Delta\tilde{\nu}$(asymm. − symm.) = 231 cm^{-1} of **2** for monodentate trifluoroacetates is similar to 232 cm^{-1} in $PhHg(O_2CMe)$ containing monodentate carboxylate groups.[20] The IR stretching frequencies of **3** are close to those of **2**, with a $\Delta\tilde{\nu}$(asymm. − symm.) of 227 cm^{-1}, very close to that in **2**, even though, unlike **2**, its acetate ligand is in a chelating mode. Notably, $\Delta\tilde{\nu}$(asymm. − symm.) for the trifluoroacetate ligand in **3** far exceeds those of most chelating acetate ligands (65−175 cm^{-1}), except for those of $Sn(O_2CMe)_4$ (320, 440 cm^{-1}).[20] C−H stretches of the Cp and Ph rings of dppf in **2** are observed as two weak unresolved peaks at $\tilde{\nu} = 3077$ and 3058 cm^{-1}, while **1A/1B** and **3** also show two C−H stretches in the same frequency range, but in addition exhibit three other very weak peaks between $\tilde{\nu} = 2960$ and 2853 cm^{-1}. Presumably, these lower-frequency stretches pertain to C−H hydrogen-bonded to O or F of TFA, as shown in their crystal structures.

Conclusion

Facile interactions between silver trifluoroacetate and dppf afford a coordination polymer or dinuclear species possessing TFA in different bonding modes, depending on the stoichiometry of the reactants. Weak hydrogen-bonding interactions (C−H···F and C−H···O) in the dinuclear compounds yield 2D supramolecular structures, the nature of which varies with solvent molecules in the crystal lattice.

Experimental Section

General: $Ag(O_2CCF_3)$, PMe_2Ph and NH_4PF_6 were purchased from Aldrich, and dppf from STREM, and used as supplied. All reactions were performed under dry nitrogen using Schlenk techniques. Solvents were freshly distilled from standard drying agents. NMR spectra were recorded with a Bruker ACF300 FT NMR spectrometer (^1H at 300.13 MHz; $^{31}P\{^1H\}$ at 121.50 MHz and ^{19}F at 282.38 MHz), with chemical shifts referenced to residual non-deuterated solvent, external H_3PO_4 and external CF_3COOH, respectively. Infrared spectra were measured in KBr pellets in the range of 400−4000 cm^{-1} with a Perkin-Elmer 1600 FT-IR spectrometer. FAB and ESI mass spectra were obtained with Finnigan MAT95XL-T and MATLCQ spectrometers, respectively. All elemental analyses were carried out in-house.

Syntheses

Reactions of $Ag(O_2CCF_3)$ with dppf. Using Ag^+/dppf (2:1) in THF/MeOH. Synthesis of $[Ag_2(O_2CCF_3)_2(dppf)]$ (1): Ligand dppf (0.111 g, 0.20 mmol) in THF (10 mL) was added to a solution of $Ag(O_2CCF_3)$ (0.094 g, 0.43 mmol) in MeOH (10 mL) and the resultant solution stirred for 8 h. The so-obtained orange suspension was filtered through Celite, and the orange filtrate was concentrated to ca. 2 mL. Addition of diethyl ether (5 mL) and cooling at 0−5 °C for 3 h gave yellow air-stable, non-light-sensitive crystals of a THF solvate of $[Ag_2(O_2CCF_3)_2(dppf)]$ (**1**) (0.073 g, 0.07 mmol, 34%). $C_{38}H_{28}Ag_2F_6FeO_4P_2 \cdot 0.6C_4H_8O$ (1039.4): calcd. C 46.6, H 3.2, P 6.0; found C 45.9, H 2.7, P 6.0. ^1H NMR ($CDCl_3$, 300 K): $\delta = 7.39-7.55$ (m, 20 H, Ph), 4.44 and 3.92 (each s, 4 H, C_5H_4)

 © 2004 Wiley-VCH Verlag GmbH & Co. KGaA, Weinheim

ppm. $^{31}P\{^1H\}$ NMR: δ = 10.1, 7.4 and 4.2 ppm ($\nu_{1/2}$ = 146, 255 and 146 Hz, with relative intensity ca. 1:2:1). ^{19}F NMR: δ = 1.6 ppm. FAB$^+$-MS: *m*/*z* = 883 [M − O_2CCF_3]$^+$, 661 [M − Ag − 2 (O_2CCF_3)]$^+$, 1437 [M + dppf]$^+$. IR (KBr cm^{-1}): ν_{CO_2}: 1684, 1437, 1207, 1133; ν_{others}: 3071 w, 3050 w, 2960 vwbr, 2923 vw, 2852 vwbr, 1508 w, 1021 m, 838 m, 803 s, 724 vs, 696 s, 518 w, 456 w. Concentration of the mother liquor to dryness, redissolution in CH_2Cl_2, followed by addition of diethyl ether (3 mL) then gave an orange solid of **1**·0.5CH_2Cl_2 (0.065 g, 30% yield). $C_{38}H_{28}Ag_2F_6FeO_4P_2$·0.5$CH_2Cl_2$ (1038.6): calcd. C 44.5, H 2.8; found C 44.8, H 2.9. ^1H NMR ($CDCl_3$): As above with additional δ = 5.30 ppm (CH_2Cl_2). ^{19}F NMR: As above. $^{31}P\{^1H\}$ NMR: With slight variations: δ = 10.4, 7.4, 4.3 ppm ($\nu_{1/2}$ = 54, 121 and 54 Hz, relative intensity 1:2:1). A similar reaction of Ag(O_2CCF_3) (0.404 g, 1.83 mmol) and dppf (0.507 g, 0.92 mmol) in CH_2Cl_2 (20 mL) for 6 h furnished a yellow solid of **1**·CH_2Cl_2 (0.811 g, 90%). Crystallization of **1** in THF/MeOH and CH_2Cl_2/diethyl ether gave orange diffraction-quality crystals of **1**·0.5THF ≡ **1A** and **1**·0.5CH_2Cl_2 ≡ **1B**, respectively, after 1 d at ambient temperature.

Using Ag$^+$/dppf (1:1) in CH_2Cl_2. Synthesis of [Ag_2(O_2CCF_3)$_2$(dppf)$_2$] (2): Ligand dppf (1.014 g, 1.83 mmol) was added to a suspension of Ag(O_2CCF_3) (0.404 g, 1.83 mmol) in CH_2Cl_2 (15 mL) and the mixture stirred at room temperature for 3 h. The resultant orange homogeneous solution was concentrated to ca. 2 ml; the subsequent addition of hexane (2 mL) gave yellow solids of [Ag_2(O_2CCF_3)$_2$(dppf)$_2$] (**2**)·0.25CH_2Cl_2 (1.23 g, 86%). $C_{72}H_{56}Ag_2F_6Fe_2O_4P_4$·0.25$CH_2Cl_2$ (1571.8): calcd. C 55.2, H 3.6; found C 55.2, H 3.95. ^1H NMR [$(CD_3)_2CO$, 300 K]: δ = 7.69, 7.48 (each centered m, 8-H and 12-H, respectively, Ph), 4.44 (s, 8 H, C_5H_4) ppm. $^{31}P\{^1H\}$ NMR: δ = −1.2 ppm ($\nu_{1/2}$ ≈ 300 Hz). ^{19}F NMR: δ = 2.4 ppm. ^1H NMR ($CDCl_3$, 300 K): δ = 7.41, 7.33 (each centered m, 12-H and 8-H, respectively, Ph), 4.51 and 4.05 (each s, 4 H, C_5H_4) ppm. $^{31}P\{^1H\}$ NMR: δ = −1.0 ppm ($\nu_{1/2}$ ≈ 300 Hz). ^{19}F NMR: δ = −0.1 ppm. FAB$^+$-MS: *m*/*z* = 1437 [M − O_2CCF_3] $^+$, 1216 [M − Ag − 2 (O_2CCF_3)]$^+$, 661 [M − Ag − 2 (O_2CCF_3) − dppf]$^+$. IR (KBr, cm^{-1}): ν_{CO_2}: 1664 s, 1433 m, 1199 s, 1131 s; ν_{others}: 3077 wsh, 3058 wbr, 1480 w, 1313 vw, 1175 ssh, 1031 w, 837 m, 764 m, 697 s, 484 mbr. Diffraction-quality single crystals of **2** were obtained from a solution in $CHCl_3$ layered with hexane after 1 d at room temperature.

Reactions of [Ag_2(O_2CCF_3)$_2$(dppf)] (1). Reaction with dppf. Synthesis of [Ag(O_2CCF_3)(dppf)]$_n$ (3): Ligand dppf (0.03 mL, 0.05 mmol) was added to a solution of **1** (0.050 g, 0.05 mmol) in CH_2Cl_2 (15 mL) and the mixture stirred for 3.5 h. The homogeneous product solution was then concentrated to ca. 1 mL, followed by addition of hexane (1.5 mL), whereupon an orange solid of [Ag(O_2CCF_3)(dppf)]$_n$ (**3**) (0.034 g, 88%) separated. $C_{72}H_{56}Ag_2F_6Fe_2O_4P_4$ (1550.6): calcd. C 55.8, H 3.6; found C 55.2, H 3.95. ^1H NMR ($CDCl_3$, 300 K): δ = 7.52 ($\nu_{1/2}$ ≈ 20 Hz, 8 H, Ph), 7.37 (centered m, 12 H, Ph), 4.34 and 4.25 (each s, $\nu_{1/2}$ ≈ 15 Hz, 4 H, C_5H_4) ppm. $^{31}P\{^1H\}$ NMR: δ = −1.5 ppm with sh at −3.0 (combined $\nu_{1/2}$ ≈ 600 Hz). ^{19}F NMR: δ = 1.2 ppm. FAB$^+$-MS: As in **2**. IR (KBr, cm^{-1}): ν_{CO_2}: 1662 s, 1435 m, 1200 vs, 1133 s; ν_{others}: 3081 wsh, 3051 w, 2960 w, 2923 w, 2863 vw, 1480 w, 1098 m, 1031 w, 836 w, 798 vw, 745 m, 722 vw, 696 s, 513 ssh, 487 sbr. Diffraction-quality crystals were obtained from CH_2Cl_2, layered with hexane, after 1 d at ambient temperature. The reaction was also monitored in an NMR tube in $CDCl_3$ at intervals up to 5.5 h. After 15 min, the proton spectrum showed two broad overlapping Cp signals centered at δ = 4.35 and 4.22 ppm, with a combined halfwidth of ca. 75 Hz. These sharpened with time and after 3.5 h were at δ = 4.34 and 4.25 ppm; these then remained unchanged up to 5 h. The ^{31}P signals varied from δ = −1.4 to −1.0 ppm (ca. 400 Hz), while the F signals were seen as overlapping singlets of equal intensity at δ = 1.3 and 0.9 ppm. These resonances did not appear in the region of those in the spectrum of **2**.

Reaction with PMe_2Ph: Ligand PMe_2Ph (0.04 mL, 0.26 mmol) was added to a solution of **1** (0.05 g, 0.05 mmol) in MeOH (15 mL). After stirring for 1 h, NH_4PF_6 (0.035 g, 0.21 mmol) was added. A bright yellow precipitate then began to separate, and the mixture was stirred for a further 30 min. The precipitate was filtered off and recrystallized from CH_2Cl_2/diethyl ether to give air-stable, non-light-sensitive yellow crystals of [Ag(dppf)(PMe_2Ph)$_2$]PF_6 (**4**) (25.8 mg, 48%). $C_{50}H_{50}AgF_6FeP_5$·H_2O (1101.6): calcd. C 54.5, H 4.8; found C 54.2, H 4.8. ^1H NMR ($CDCl_3$): δ = 7.60−7.81 (Ph), 4.68, 4.56, 4.03 (C_5H_4), 1.82 (d, *J* = 13 Hz, P*Me*$_2$Ph) ppm. $^{31}P\{^1H\}$ NMR: δ = 39.8 and 3.9 (dppf), −5.5 (PMe_2Ph), −144 (sept) ppm. ESI$^+$-MS: *m*/*z* = 1216 [M + PMe_2Ph]$^+$, 798 [M − PMe_2Ph]$^+$, 661 [M − 2 PMe_2Ph]$^+$. IR (Nujol, cm^{-1}): ν_{PF_6}: 840 and 556. Single diffraction-quality crystals were obtained by recrystallization in MeOH/diethyl ether (1:4) after 1 d at −30 °C.

Variable-Temperature (VT) NMR Spectra: ^1H, $^{31}P\{^1H\}$ and ^{19}F VT NMR spectra obtained for complexes **1**−**3** are described in the Results and Discussion section.

Crystal Structure Determinations: Crystals were mounted on quartz fibers. X-ray data were collected with a Bruker AXS SMART CCD diffractometer, using Mo-K_α radiation (λ = 0.71073 Å) at 223 K (for **1**−**3**) or 293 K (for **4**) (Table 7).The program SMART[21] was used to collect the intensity data, indexing and determination of lattice parameters, SAINT[22] was used to integrate the intensity of reflections and scaling, SADABS[21] was used for absorption correction and SHELXTL[23] for space group and structure determination and least-squares refinements against F^2. The structure was solved by direct methods to locate the heavy atoms, followed by difference maps for the light, non-hydrogen atoms. Cp and Ph hydrogen atoms were placed in calculated positions. For **1A**, the crystal was modeled as a racemic twin. The CF_3 groups were treated as disordered over two alternative sites with equal occupancies; the two sites were symmetry-related. C−F and F···F distances were restrained to be equal, and the F atoms were given individual isotropic thermal parameters. There was a half molecule of THF disordered about a twofold axis. This was modeled over two alternative sites of equal occupancies with the oxygen and two carbon atoms common; all the carbon atoms were given a common isotropic thermal parameter, with that for the oxygen at 1.1 times that of the carbon atoms. Appropriate restraints were placed to keep the geometry reasonable. For **2**, the $CHCl_3$ solvent molecule was modeled as disordered over two sites; occupancies were refined and summed to unity. C−Cl and Cl···Cl distances were restrained to be equal. Anisotropic thermal parameters for each Cl atom were paired with that of the alternative site. For **3**, the CF_3 groups were treated as disordered over two alternative sites with equal occupancies; the two sites were symmetry-related. C−F and F···F distances were restrained to be equal, and atoms were given isotropic thermal parameters. Crystal data and refinement parameters are given in Table 7. Selected bond lengths and angles for **1A/1B**, **2**, **3** and **4** are in Tables 1, 3, 4 and 6, respectively. Hydrogen bonds and angles of **1A/1B** and **3** are in Tables 2 and 5, respectively. CCDC-193074 to -193076 and -215390 to -215391 for complexes **1B**, **3**, **1A**, **2** and **4**, respectively contain the supplementary crystallographic data for this paper. These data can be obtained free of charge at www.ccdc.cam.ac.uk/conts/retrieving.html [or from the Cambridge Crystallographic Data Centre, 12 Union Road, Cam-

 © 2004 Wiley-VCH Verlag GmbH & Co. KGaA, Weinheim

Table 7. Crystal data and parameters related to the structure determination and refinement for **1**−**4**

	1A (**1**·0.5C_4H_8O)	**1B** (**1**·0.5CH_2Cl_2)	**2**·$CHCl_3$	**3**	**4**
Empirical formula	$C_{40}H_{32}Ag_2F_6FeO_{4.50}P_2$	$C_{38.5}H_{29}Ag_2ClF_6FeO_4P_2$	$C_{37}H_{29}AgCl_3F_3FeO_2P_2$	$C_{36}H_{28}AgF_3FeO_2P_2$	$C_{50}H_{50}AgF_6FeP_5$
Formula mass	1032.19	1038.60	894.61	775.24	1083.47
Temperature [K]	223(2)	223(2)	223(2)	223(2)	293(2)
Crystal system	tetragonal	monoclinic	triclinic	monoclinic	monoclinic
Space group	*I*-42*d*	$P2_1/c$	$P\bar{1}$	*C*2/*c*	$P2_1/n$
Crystal size [mm]	0.32 × 0.22 × 0.16	0.40 × 0.40 × 0.38	0.22 × 0.08 × 0.04	0.30 × 0.25 × 0.15	0.30 × 0.16 × 0.09
a [Å]	28.3502(5)	10.2862(6)	12.1521(11)	12.790(2)	14.2739(2)
b [Å]	28.3502(5)	17.6488(9)	13.1192(12)	24.101(4)	20.9706(2)
c [Å]	10.6842(2)	22.0971(12)	13.7594(12)	16.495(3)	17.0519(2)
α [°]	90	90	118.007(2)	90	90
β [°]	90	90.6710(10)	103.871(2)	110.304(4)	106.9810(10)
γ [°]	90	90	95.312(2)	90	90
V [Å^3]	8587.3(3)	4011.2(4)	1825.6(3)	4768.7(15)	4881.65(10)
Z	8	4	2	4	4
$D_{calcd.}$ [Mg·m^{-3}]	1.597	1.720	1.627	1.080	1.474
Absorption coefficient	1.376	1.536	1.289	0.817	0.919
F(000)	4096	2052	896	1560	2208
Θ range for data collection [°]	2.03−24.71	1.84−25.00	2.07−26.37	2.14−26.37	2.21−29.41
Index ranges	$-23 \le h \le 23$	$-9 \le h \le 12$	$-15 \le h \le 14$	$-15 \le h \le 14$	$-19 \le h \le 17$
	$0 \le k \le 33$	$-19 \le k \le 20$	$-16 \le k \le 14$	$0 \le k \le 30$	$0 \le k \le 28$
	$0 \le l \le 12$	$-24 \le l \le 26$	$0 \le l \le 17$	$0 \le l \le 20$	$0 \le l \le 23$
Reflection collected	55438	22913	24654	19161	31993
Independent reflections	3619	7057	7445	4873	12074
Transmission, max./min.	0.8099/0.6673	0.5929/0.5785	0.9502/0.7646	0.8875/0.7920	0.9280 & 0.7639
Data/restraints/parameters	3619/32/243	7057/78/528	7445/30/452	4873/6/195	12074/0/568
Goodness-of-fit on F^2	1.254	1.037	1.082	1.132	1.027
Final *R* indices [$I > 2\sigma(I)$]	*R*1 = 0.0784	*R*1 = 0.0389	*R*1 = 0.0677	*R*1 = 0.0711	*R*1= 0.0612
	*wR*2 = 0.1827	*wR*2 = 0.1117	*wR*2 = 0.1449	*wR*2 = 0.2267	*wR*2= 0.1005
R indices (all data)	*R*1 = 0.0925	*R*1 = 0.0422,	*R*1 = 0.0891	*R*1 = 0.0989	*R*1= 0.1412
	*wR*2 = 0.1937	*wR*2 = 0.1144	*wR*2 = 0.1559	*wR*2 = 0.2384	*wR*2= 0.1284
Largest diff. peak/hole	0.923/−0.441	1.198/−1.055	1.865/−0.976	1.277/−0.492	0.621/−0.496

$R = (\Sigma F_o - F_c)\Sigma F_o$. $R_w = [(\Sigma\omega F_o - F_c)^2/\Sigma\omega F_o^2]^{1/2}$. GoF = $[(\Sigma\omega F_o - F_c)^2/(N_{obsd.} - N_{param.})]^{1/2}$.

bridge CB2 1EZ, UK; Fax: (internat.) + 44-1223-336-033; E-mail: deposit@ccdc.cam.ac.uk].

Acknowledgments

Support from the National University of Singapore as Grant No. RP14300077112 to L. Y. G., and a research scholarship to X. L. L., is gratefully acknowledged. We also thank Professors Philip A. W. Dean (University of Western Ontario, Canada) and William Henderson (University of Waikato, NZ) for helpful discussions, and Ms. G. K. Tan, Dr. Koh and Dr. B. W. Sun for technical assistance.

[1] See below and references cited therein: [1a] M. Eddaoudi, D. B. Moler, J. Li, B. Chen, T. M. Reineke, M. O'Keeffe, O. M. Yaghi, *Acc. Chem. Res.* **2001**, *34*, 319. [1b] S. Leininger, B. Olenyuk, P. J. Stang, *Chem. Rev.* **2000**, *100*, 853. [1c] P. J. Hagrman, D. Hagrman, J. Zubieta, *Angew. Chem. Int. Ed.* **1999**, *38*, 2638. [1d] A. J. Blake, N. R. Champness, P. Hubberstey, W.-S. Li, M. A. Withersby, M. Schröder, *Coord. Chem. Rev.* **1999**, *183*, 117. [1e] S. R. Batten, R. Robson, *Angew. Chem. Int. Ed.* **1998**, *37*, 1460. [1f] P. J. Stang, *Chem. Eur. J.* **1998**, *4*, 19. [1g] P. J. Stang, B. Olenyuk, *Acc. Chem. Res.* **1997**, *30*, 502. [1h] J. C. Noveron, M. S. Lah, R. E. Del Sesto, A. M. Arif, J. S. Miller, P. J. Stang, *J. Am. Chem. Soc.* **2002**, *124*, 6613. [1i] G. M. Whitesides, J. P. Mathias, C. T. Seto, *Science* **1991**, *254*, 1312.

[2] See for instance the following and references cited therein: [2a] L. Carlucci, G. Ciani, D. M. Proserpio, A. Sironi, *J. Am. Chem. Soc.* **1995**, *117*, 4562. [2b] W. Su, M. Hong, J. Weng, R. Cao, S. Lu, *Angew. Chem. Int. Ed.* **2000**, *39*, 2911. [2c] Y. Kang, S. S. Lee, K.-M. Park, S. H. Lee, S. O. Kang, J. Ko, *Inorg. Chem.* **2001**, *40*, 7027. [2d] D. M. L. Goodgame, D. A. Grachvogel, D. J. Williams, *J. Chem. Soc., Dalton Trans.* **2002**, 2259. [2e] C. B. Aakeroy, A. M. Beatty, *Chem. Commun.* **1998**, 1067. [2f] G. K. Patra, I. Goldberg, *J. Chem. Soc., Dalton Trans.* **2002**, 1051. [2g] S.-L. Zheng, M.-L. Tong, X.-L. Yu, X.-M. Chen, *J. Chem. Soc., Dalton Trans.* **2001**, 586.

[3] [3a] F. Bachechi, A. Burini, R. Galassi, B. R. Pietroni, D. Tesei, *Eur. J. Inorg. Chem.* **2002**, 2086. [3b] E. Lozano, M. Nieuwenhuyzen, S. L. James, *Chem. Eur. J.* **2001**, *7*, 2644. [3c] M.-C. Brandys, R. J. Puddephatt, *Chem. Commun.* **2001**, 1508. [3d] M.-C. Brandys, R. J. Puddephatt, *J. Am. Chem. Soc.* **2002**, *124*, 3946.

[4] [4a] S.-P. Neo, T. S. A. Hor, Z.-Y. Zhou, T. C. W. Mak, *J. Organomet. Chem.* **1994**, *464*, 113. [4b] T. S. A. Hor, S. P. Neo, C. S. Tan, T. C. W. Mak, K. V. P. Leung, R. J. Wang, *Inorg. Chem.* **1992**, *31*, 4510.

[5] [5a] G. R. Desiraju, *Acc. Chem. Res.* **1991**, *24*, 290. [5b] G. R. Desiraju, *Angew. Chem. Int. Ed. Engl.* **1995**, *34*, 2311 and references cited therein. [5c] D. Braga, F. Grepioni, K. Biradha, V. R. Pedireddi, G. R. Desiraju, *J. Am. Chem. Soc.* **1995**, *117*, 3156. [5d] V. R. Thalladi, H.-C. Weiss, D. Bläser, R. Boese, A. Nangia, G. R. Desiraju, *J. Am. Chem. Soc.* **1998**, *120*, 8702 and references cited therein. [5e] F. Grepioni, G. Cojazzi, S. M. Draper, N. Scully, D. Braga, *Organometallics* **1998**, *17*, 296.

 © 2004 Wiley-VCH Verlag GmbH & Co. KGaA, Weinheim

[6] [6a] D. M. Ho, R. Bau, *Inorg. Chem.* **1983**, *22*, 4073. [6b] M. Hong, D. Wu, H. Liu, T. C. W. Mak, Z. Zhou, D. Wu, S. Li, *Polyhedron* **1997**, *16*, 1957.
[7] S.-L. Zheng, M.-L. Tong, X.-L. Yu, X.-M. Chen, *J. Chem. Soc., Dalton Trans.* **2001**, 586.
[8] [8a] X.-M. Chen, T. C. W. Mak, *J. Chem. Soc., Dalton Trans.* **1991**, 1219. [8b] X.-M. Chen, T. C. W. Mak, *Polyhedron* **1991**, *10*, 1723. [8c] W.-Y. Huang, L. Lu, X.-M. Chen, T. C. W. Mak, *Polyhedron* **1991**, *10*, 2687. [8d] X.-M. Chen, T. C. W. Mak, *J. Chem. Soc., Dalton Trans.* **1991**, 3253. [8e] X.-M. Chen, T. C. W. Mak, *Aust. J. Chem.* **1991**, *44*, 1783. [8f] T. C. W. Mak, W. H. Yip, X.-M. Chen, *Inorg. Chim. Acta* **1993**, *203*, 97.
[9] V. R. Vangala, A. Nangia, V. M. Lynch, *Chem. Commun.* **2002**, 1304 and references cited therein.
[10] T. Spaniel, H. Gorls, J. Scholz, *Angew. Chem. Int. Ed.* **1998**, *37*, 1862.
[11] W. Huang, S. Gou, D. Hu, S. Chantrapromma, H.-K. Fun, Q. Meng, *Inorg. Chem.* **2002**, *41*, 864.
[12] L. Brammer, J. C. M. Rivas, R. Atencio, S. Fang, F. C. Pigge, *J. Chem. Soc., Dalton Trans.* **2000**, 3855.
[13] D. L. Reger, R. F. Semeniuc, M. D. Smith, *J. Chem. Soc., Dalton Trans.* **2002**, 476.
[14] D. Braga, L. Maini, F. Grepioni, *Angew. Chem. Int. Ed.* **1998**, *37*, 2240.
[15] M. P. Thornberry, C. Slebodnick, P. A. Deck, F. R. Fronczek, *Organometallics* **2000**, *19*, 5352.
[16] F. Grepioni, G. Cojazzi, S. M. Draper, N. Scully, D. Braga, *Organometallics* **1998**, *17*, 296.
[17] M. C. Gimeno, P. G. Jones, A. Laguna, C. Sarroca, *J. Chem. Soc., Dalton Trans.* **1995**, 1473.
[18] [18a] E. L. Muetterties, C. W. Alegranti, *J. Am. Chem. Soc.* **1972**, *84*, 6386. [18b] R. G. Goel, P. Pilon, *Inorg. Chem.* **1978**, *17*, 2876.
[19] P. A. W. Dean, J. J. Vittal, R. S. Srivastava, *Can. J. Chem.* **1987**, *65*, 2638.
[20] G. D. Deacon, R. J. Philips, *Coord. Chem. Rev.* **1980**, *33*, 227.
[21] *SMART & SAINT, Software Reference Manuals*, version 5.0, Bruker AXS Inc., Madison, WI, **1998**.
[22] G. M. Sheldrick, *SADABS, software for empirical absorption correction*, University of Göttingen, Germany, **2000**.
[23] *SHELXTL, Reference Manual*, version 5.1, Bruker AXS Inc., Madison, WI, **1998**.

Received September 30, 2003
Early View Article
Published Online April 7, 2004

 © 2004 Wiley-VCH Verlag GmbH & Co. KGaA, Weinheim

A Water-Soluble Calix[4]arene-Based Podand Incorporating 4,4′-Dicarboxy-2,2′-bipyridine Chelating Units − Synthesis and Complexation Properties towards Copper Ions

Nicolas Psychogios,[a] Jean-Bernard Regnouf-de-Vains,*[a] and Helen M. Stoeckli-Evans[b]

Keywords: Calix[4]arene / Bipyridine / Podand / Copper / Zinc

A water-soluble calix[4]arene-based podand has been prepared by incorporation, at the lower rim, of two 4,4′-dicarboxy-2,2′-bipyridine units in opposite positions. The association between its coordination and hydrophilic properties were beneficial to the complexation and solubilization of copper(I) in water, even in the presence of bovine serum albumin. The ligand and its corresponding Cu^{I} complex have been fully characterized, but attempts to crystallize them have been unsuccessful so far. For this reason, the dinuclear $ZnCl_2$ complex of the organic solvent soluble tetraester intermediate has been crystallized, and subjected to X-ray diffraction analysis, confirming the expected podand-like structure of the ligand.

(© Wiley-VCH Verlag GmbH & Co. KGaA, 69451 Weinheim, Germany, 2004)

Introduction

The transition from organic to aqueous solubility of the calixarenes, and their corresponding properties, is gaining attention as demonstrated by a rapid on-line survey on *water-soluble calixarenes*, and recent review literature.[1] The introduction of carboxylic acid functionalities at the lower[2] and upper rims,[3,4] or sulfonyl,[5,6] phosphonate,[7] and alkylamino groups[8] at the upper rim have been the main routes for making calixarenes water soluble. Many structural modifications have been carried out on these water-soluble structures, leading to new ligands for various metal cations.

With the aim of conducting, in water, some complexation experiments, that we have previously developed with lipophilic calixarene-based heterocyclic podands,[9−17] and in anticipation of future biological investigations, we attempted to synthesize a hydrophilic ligand able to complex the relatively unstable Cu^{I} cation in this medium. A number of very rare examples of water-soluble copper(I) coordination complexes have been described involving a sulfonated phosphane ligand,[18] or calix[6]-[19] and calix[4]arene[20−22] heterocyclic derivatives illustrating, in part, the difficulty of protecting this cation from disproportionation in water, and thus limiting investigations on its properties in aqueous media. The fact that the copper(I) complexes are diamagnetic and colored (metal-to-ligand charge transfer band at ca. 450 nm) should allow a convenient analysis of the complexation processes by NMR and UV spectroscopy.

In this report, we describe (a) the multi-step synthesis of the water-soluble calix[4]arene-based heterocyclic podand **6** in which the 2,2′-bipyridine arms exhibit both chelating and hydrophilic behavior, (b) its complexation properties towards Cu^{I} and Cu^{II} ions in water, and (c) the synthesis and characterization of the copper(I) complex **7**. Attempts to obtain crystals of **6** and **7** suitable for X-ray analysis did not succeed, but were successful for the dinuclear $ZnCl_2$ complex of the organic-solvent soluble tetraester intermediate **4**, allowing a preliminary structural investigation.

Results and Discussion

Ligand Syntheses

The calixarene podand species **4**−**7** were prepared according to Scheme 1. The starting calix[4]arenetetrol was synthesized as described previously.[23−26]

The bipyridine arms were introduced to the calixarene platform via the bromomethyl intermediate **3**, which was prepared according to Scheme 2 The starting bipyridine **1** was prepared following the Ni^{0}-mediated procedure of Alpha et al.,[27] from methyl 2-methyl-6-[(*p*-tolylsulfonyl)oxy]-pyridine-4-carboxylate. For the latter, the toxic and expensive pyridine generally used as base and solvent for the tosylation reaction was replaced by triethylamine and

[a] GEVSM, UMR 7565 CNRS-Université Henri Poincaré, Faculté de Pharmacie,
5, rue Albert Lebrun, BP 403, 54001 Nancy Cedex, France
Fax: (internat.) +33-3-83682345
E-mail: jean-bernard.regnouf@pharma.uhp-nancy.fr
[b] Laboratoire de Cristallographie, Institut de Chimie, Université de Neuchâtel,
51, C.P. 2, 2007 Neuchâtel, Switzerland
Fax: (internat.) +41-32-7182511
E-mail: Helen.Stoeckli-Evans@unine.ch

 © 2004 Wiley-VCH Verlag GmbH & Co. KGaA, Weinheim DOI: 10.1002/ejic.200300690

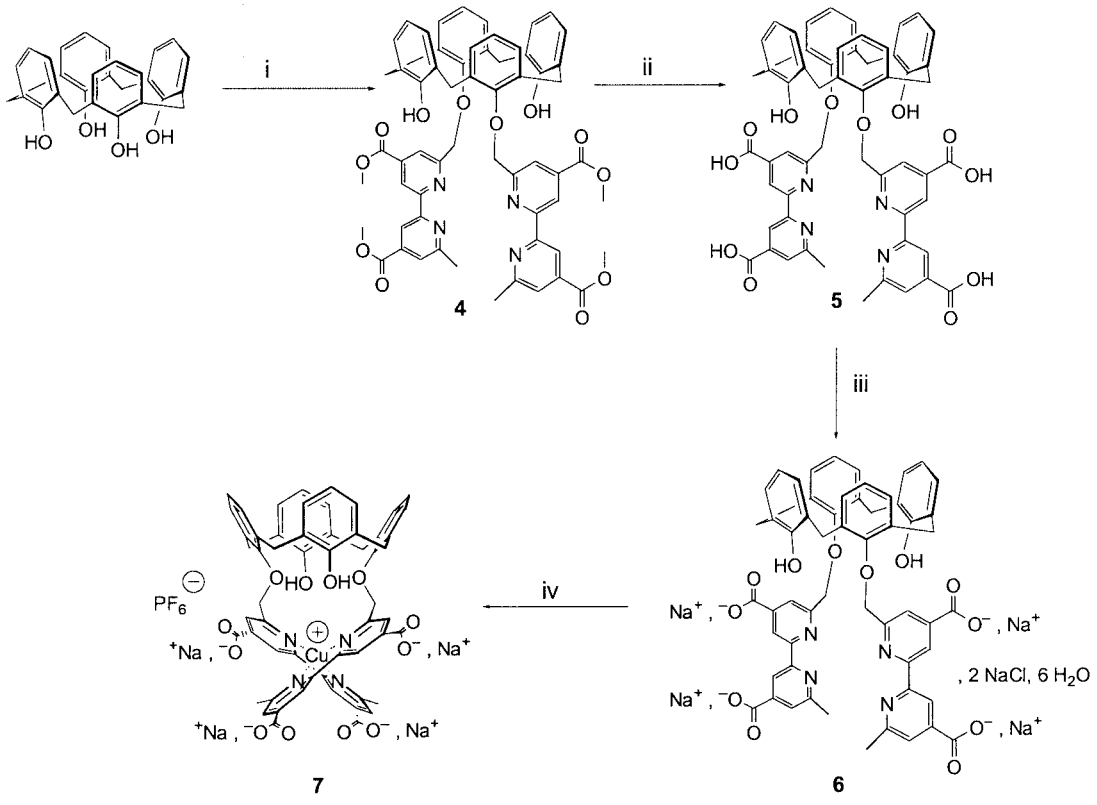

Scheme 1. i) **3**, MeCN, K_2CO_3, reflux, 83%; ii) a) NaOH, H_2O, EtOH, reflux; b) HCl, pH 3−4, 80%; iii) NaOH, H_2O, pH 7, 100%; iv) $Cu(MeCN)_4PF_6$, MeCN, H_2O

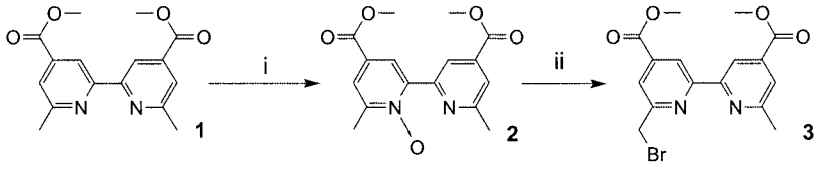

Scheme 2. i) *m*CPBA, CH_2Cl_2, 90%; ii) a) $(CF_3CO)_2O$; b) LiBr, THF, DMF, 55%

CH_2Cl_2.[28] This safe and economical procedure afforded the tosyl derivative in a yield of 90%.

The introduction of a single active bromomethyl functionality at the 6-position of **1** was performed via a three step process including a controlled *N*-oxidation, a Boeckelheide rearrangement, and a *pseudo*-halogen exchange. Compound **1** was initially treated in CH_2Cl_2 with 1 equiv. of *m*CPBA at 0 °C, then at room temperature to afford the mono-*N*-oxide **2**, mixed with ca. 5% of the corresponding di-*N*-oxide, and ca. 5% of unchanged bipyridine **1**. An analytical sample of **2** was obtained by chromatography on Al_2O_3 (CH_2Cl_2) but, unstable on this support, and in order to avoid dismutation, the above-mentioned raw mixture was frozen or directly transformed.

The second step was a modified Boekelheide rearrangement. This process initially described with picoline *N*-oxides[29−30] allows the functionalization, by an active carbonyl compound via a radical or ionic mechanism, of the methyl group in the α-position of the *N*-oxide function. With acetic anhydride, this leads to an acetate-protected hydroxymethyl functionality, a key compound for further transformations. This reaction was employed successfully to prepare more sophisticated activated heterocyclic systems, notably with 6,6′-dimethyl-2,2′-bipyridine and its analogues.[27,31−35]

The presence of the two ester functions in **1**, both of which are prone to hydrolysis, led us to employ a more sensitive pathway involving a labile trifluoroacetate derivative, which exhibits, in the alkyl[36] and arylalkyl series,[32,34] the interesting characteristic of being directly substituted by bromine in polar aprotic solvent, and at room temperature via a pseudo-halogen exchange with LiBr.

Thus, the raw mono-*N*-oxide **2** was heated to reflux in CH_2Cl_2 in the presence of an excess of trifluoroacetic anhydride. After evaporation of the solvent the solid residue, which contains the dimethyl 6-trifluoroacetyl-6′-methyl-2,2′-bipyridine-4,4′-dicarboxylate, was dissolved in dry DMF and dry THF in the presence of an excess of anhy-

 © 2004 Wiley-VCH Verlag GmbH & Co. KGaA, Weinheim

drous LiBr, itself dried under vacuum at 150 °C. The resultant monobromide **3** was obtained pure in a yield of 55%. The dibromomethyl analogue[27] was also isolated in a yield of 12%, and the bipyridine **1** (ca. 15%) was recovered. Their formation was explained by the partial dismutation of **2** under the given conditions of the reaction.[35]

A similar but longer process involving the consecutive formation of the trifluoroacetate, the alcohol, the mesylate, and then the bromide was also described for the *tert*-butyl ester analogue of **3**,[37] as well as another procedure involving a radical bromination.[38]

Following the procedure previously reported by Beer et al.[39] for the unsubstituted bipyridine, the monobromide **3**, calix[4]arenetetrol, and K_2CO_3 were heated to reflux in MeCN to give the podand **4** in a yield of 83% after chromatography (SiO_2, CH_2Cl_2). The four ester functions of **4** were saponified in an aqueous alcoholic NaOH solution at reflux. Acidification to pH 3−4 resulted in the precipitation of the tetraacid **5**, which was recovered in a yield of 80%. A controlled neutralization of **5** with NaOH afforded the tetrasodium carboxylate **6** in almost quantitative yield (Scheme 1).

Complexation Studies

The formation of the copper(I) complex **7** was initially studied by UV-visible spectroscopy in water (Figure 1). The addition of $[Cu(MeCN)_4]PF_6$ to a solution of **6** resulted in the immediate appearance of the expected MLCT band at 470 nm (red color), characteristic of tetrahedral copper(I) complexes. The evolution of this band, as well as the new ligand-centered band at ca. 300 nm, was complete upon addition of 1 equiv. of metal, confirming the formation of a mononuclear complex.

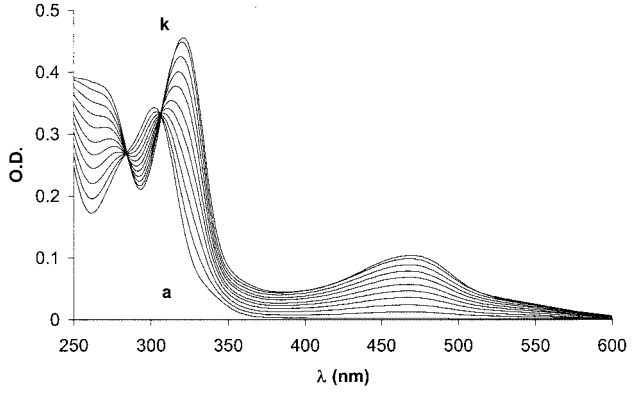

Figure 1. UV-visible titration of **6** with $[Cu(MeCN)_4]PF_6$: a) **6**, [2 mL; 1.71×10^{-5} M in H_2O]; from b) to k): addition of 1 equiv. of $[Cu(MeCN)_4]PF_6$ [$10 \times 4\mu L$; 9.98×10^{-4} M in MeCN]

The air-stable red complex **7** was prepared quantitatively by addition of 1 equiv. of $[Cu(MeCN)_4]PF_6$ in acetonitrile to an aqueous solution of **6**, followed by evaporation to dryness. Attempts to crystallize **7** for an X-ray structural analysis were unsuccessful.

Since the redox properties of copper are favorable for the doubly charged species, we have followed the complexation of $CuCl_2$ by UV-visible spectroscopy in water (Figure 2). The presence of two isosbestic points at 304 nm (0 to 1 equiv.) and 316 nm (1 to 2 equiv.) revealed the formation of two consecutive complex species, namely [$CuCl_2$/**6**] and [$(CuCl_2)_2$/**6**]. In order to prepare a sample of the corresponding final complex, the addition of 2 equiv. of $CuCl_2$ in water to an aqueous solution of **6** resulted in a brown-green coloration, nevertheless immediately followed by formation of a gel then precipitation. The solvent was removed by filtration and the residue was dried under high vacuum to give **8** as a green-brown powder. Surprisingly, the solid thus obtained remained insoluble in common solvents, even in DMSO. This behavior led us to believe that the water solubilizing carboxylate groups were in fact engaged in a chelating interaction with copper(II), giving oligomeric or polymeric chelate species resulting in loss of solubility of the material. No relevant mass analysis has been obtained.

An elemental analysis of the copper(II) complex **8** was consistent with the formula $C_{56}H_{40}ClCu_2N_4NaO_{12}\cdot 4.5H_2O$, corresponding to the loss of 3 equiv. of NaCl thus suggesting an ionic interaction between copper and the carboxylate groups. Such an interaction should involve a bridging mode of the copper ions between two calixarene moieties, in a linear polymeric network. Nevertheless, IR spectroscopy (KBr) did not show relevant modifications in the carbonyl region with regards to the ligand **6**. Attempts to improve this structure are under current investigation.

The bimetallic copper(II) complex [$(CuCl_2)_2 \subset$ **6**] formed during the UV titration experiment was subjected to reduction by ascorbate (Figure 3). The complex was fully reduced after the addition of 0.5 equiv. of ascorbate, as deduced by the appearance of the expected MLCT band at 470 nm, characterized by an ε value of 5500 $mol\cdot L^{-1}\cdot cm^{-1}$, similar to that of complex **7**. The addition of more ascorbate did not result in any further change in the absorption pattern.

In order to make a biological assessment of the complex **7**, competition experiments with bovine serum albumin were monitored by UV-visible spectroscopy (Figure 4). The results show that the presence of 1 equiv. or 10 equiv. of BSA relative to **7** did not change the absorption profile of the latter, the MLCT band being conserved even after 24 or 48 hours. Under the same conditions, the copper(I) complex of the corresponding free bipyridine decomposed. In parallel, we have verified that no absorption band of the MLCT type was generated by the interaction between BSA and $[Cu(MeCN)_4]PF_6$. This confirmed that the copper(I) ion is strongly maintained in a tetrahedral coordination by **6** under these conditions.

In contrast to, a similar test carried out with [$(CuCl_2)_2 \subset$ **6**] (Figure 5) resulted in the loss of the ligand-centered band at 322 nm, which was concomitant with the appearance of a new band at 312 nm (1 equiv. BSA), the latter being found again as a shoulder with 10 equiv. of BSA. After 1 day, the absorption pattern was found to be similar to the free ligand **6** ($\lambda_{max.}$ = 304 nm). No specific absorption bands were observed during the reaction between BSA and $CuCl_2$.

 © 2004 Wiley-VCH Verlag GmbH & Co. KGaA, Weinheim

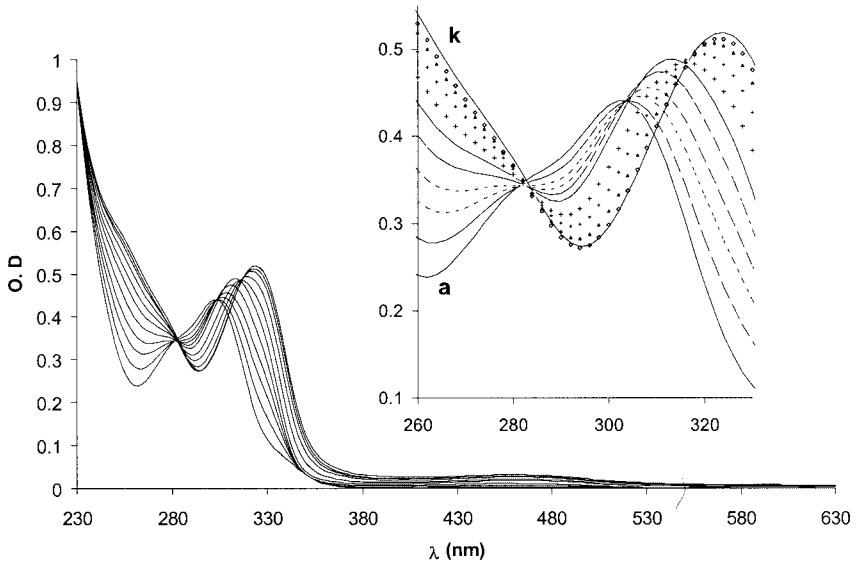

Figure 2. UV-visible titration of **6** by $CuCl_2{\cdot}2H_2O$: a) **6**, [2 mL; 2.0×10^{-5} M in H_2O]; from b) to k): addition of 2 equiv. of $CuCl_2{\cdot}2H_2O$ [10×8 μL; 1.00×10^{-3} M in H_2O]

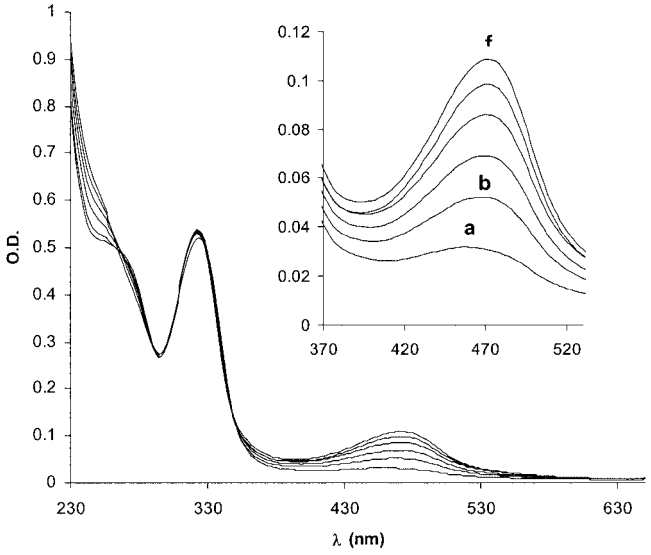

Figure 3. UV-visible titration of [$(CuCl_2)_2 \subset$ **6**] by ascorbic acid: a) [$(CuCl_2)_2 \subset$ **6**], [2 mL; 2.0×10^{-5} M in H_2O]; from b) to f): addition of 0.5 equiv. of ascorbic acid [5×4μL; 1.00×10^{-3} M in H_2O]

Compounds **2**−**7** gave satisfactory elemental, IR, MS and NMR analyses.

In particular, a preliminary elemental analysis performed on **6** dried with P_2O_5 showed the presence of 2 molecules of NaCl and 3 molecules of H_2O, but the instability of the mass during the weighing process suggested logically that **6** was hygroscopic. After equilibration under ambient conditions, the analysis of **6** was consistent with the presence of 2 molecules of NaCl and 6 molecules of H_2O. Argon plasma emission spectrophotometric analyses were consistent with the presence of 5 sodium ions for one ligand **6**, 5 sodium, and 1 copper ion for one complex **7**. Dialysis experiments performed with cellulose ester membranes (cut-off mol. wt. = 100) on aqueous solutions of **6** and **7** did not result in satisfactory removal of sodium chloride, the residual solutions giving precipitates of silver chloride upon addition of silver nitrate. Attempts to evaluate the water content in **6** and **7** by mass-coupled thermogravimetric analysis were not successful, the loss of water being observed over a wide range of temperatures (20−250 °C). Nevertheless, **6** showed a clean loss of four CO_2 molecules between 420 and 540 °C.

NMR Analyses

According to de Mendoza et al,[40,41] ^{13}C NMR spectroscopic analyses showed that **4**, **5** and **6** exist in the cone conformation.

The cone conformation of **6** was also demonstrated by ^1H NMR spectroscopy in D_2O, with the Ar-CH_2-Ar AB system located at δ = 3.18−3.96 ppm (J_{AB} = 15 Hz). 2D-COSY experiments allowed the full assignment of resonance signals. In the aromatic region, the ligand exhibits four perfectly well resolved bipyridyl singlets together with two doublets and two triplets for the calixarene moiety, which confirmed the expected structure. The terminal methyl groups and the methoxy linkers appear as singlets at δ = 2.53 and 5.33 ppm, respectively.

The ^1H NMR spectrum of the copper(I) complex **7** in D_2O (Figure 6) exhibits broad resonance signals in all the relevant frequency domains, except for the aromatic calixarene protons, which appear as well resolved doublets and triplets. The presence of more than the four expected bipyridyl resonance signals is in accordance with the probable presence of more than one species under these conditions. Addition of [D_6]DMSO to the aqueous solution resulted in the increasing of one of the signals, and a general sharpening of all signals. At the concentration used in the NMR experiments, it is possible to suggest that oligomeric or

 © 2004 Wiley-VCH Verlag GmbH & Co. KGaA, Weinheim

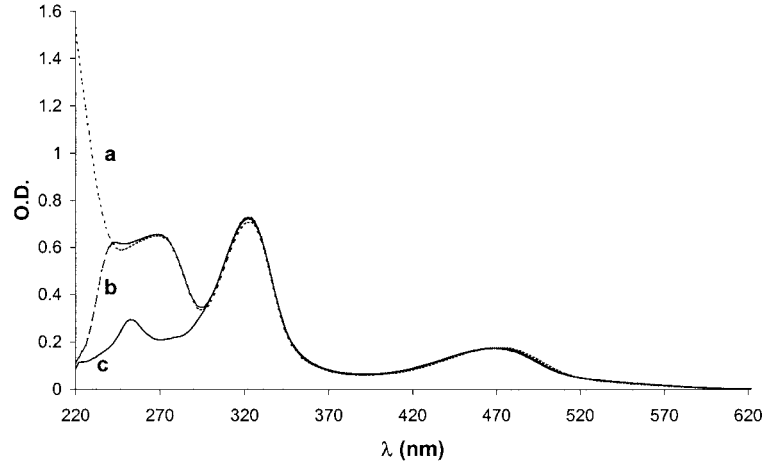

Figure 4. UV-visible analysis of **7** in the presence of bovine serum albumin: a) **7**, [1.6×10^{-5} M in H_2O]; b) 1 equiv. of BSA; c) 10 equiv. of BSA

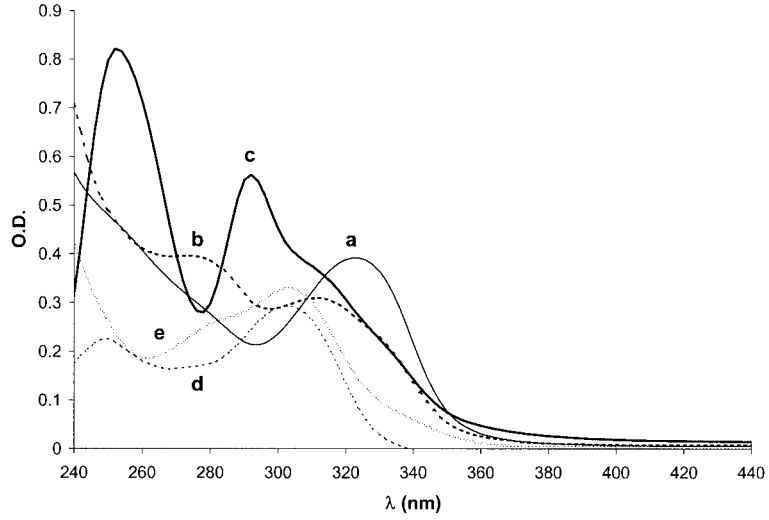

Figure 5. UV-visible analysis of [$(CuCl_2)_2 \subset$ **6**] in the presence of bovine serum albumin: a) [$(CuCl_2)_2 \subset$ **6**], [1.6×10^{-5} M in H_2O]; b) 1 equiv. of BSA; c) 10 equiv. of BSA; d) 10 equiv. of BSA, one day; e) **6** [1.6×10^{-5} M in H_2O]

polymeric complex species can be formed involving, due to the lack of steric hindrance at the upper rim, conic or non-conic calixarene platforms, that could correspond to the presence of multiple signals. The addition of DMSO may modify the solvation of these flexible species, resulting in the recovery of a conic conformer. Finally, pure [D_6]DMSO gave a well resolved NMR spectrum resulting in the presence of the expected cone conformer as the major compound with, notably, the presence of the four bipyridyl singlets, the aromatic succession of calixarene doublets and triplets, and the appearance of two AB systems at $\delta = 3.27$ and 4.24 ppm ($J_{AB} = 12$ Hz), and 5.31 and 6.27 ppm ($J_{AB} = 11$ Hz), which can be attributed to the Ar-CH_2-Ar and OCH_2-bpy spin systems, respectively. According to the results obtained with parent hydrophobic complexes ,[11,13] the presence of the Ar-CH_2-Ar AB system confirmed the cone conformation, and the OCH_2-bpy AB system confirmed the complexation of copper(I) in a prohelicoidal tetrahedral mode.

Mass Spectrometry

The mass analyses of ligand **6** and complex **7** were performed with the electrospray technique in the positive or negative mode. In the positive mode, **6** exhibited the mono-(sodium) and the doubly charged bis(sodium) derivatives at 1076.0 and 549.3 a.m.u. (base peak), respectively, accompanied by other entities, which were not well analyzed. Conversely, the negative mode analysis resulted in the exhibition of three groups of doubly charged (481.2, 492.2 and 503.2 a.m.u.), triply charged (327.8 and 320.5 a.m.u.), and tetra-charged (240.0 a.m.u.) species resulting from the loss of 2, 3 or 4 sodium ions compensated, when necessary, by replacement with 1 or 2 protons. The base peak appearing

 © 2004 Wiley-VCH Verlag GmbH & Co. KGaA, Weinheim

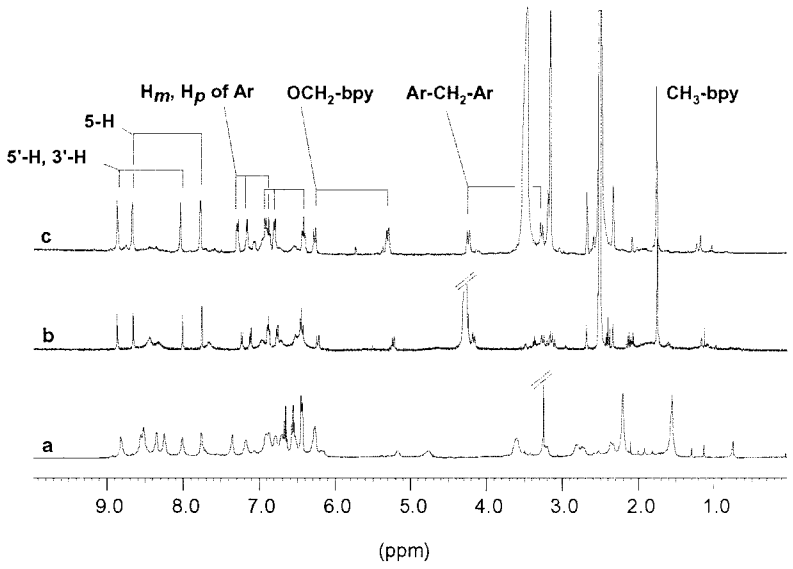

Figure 6. ^{1}H NMR spectrum of the copper(I) complex **7** (a: D_2O, b: D_2O + [D_6]DMSO, c: [D_6]DMSO; 400 MHz, room temp.)

in this case at 320.5 a.m.u. was attributed to the triply charged species [**6**−4Na^+ + H^+]$^{3-/3}$.

The copper(I) complex **7** gave no relevant information in the positive mode. In the negative mode, three groups of signals were observed. As for the ligand, the loss of 1, 3, and 4 sodium ions compensated by addition of protons when necessary, resulted in doubly charged species located at 544.1, 523.2, and 512.2 a.m.u. The loss of 4 sodium ions resulted in a triply charged species located at 341.3 a.m.u. Finally, the hexafluorophosphate anion appeared as a pure entity at 144.9 a.m.u. (base peak), and as an adduct with $NaPF_6$ at 312.9 a.m.u.

X-ray Crystallography

Attempts to obtain single crystals of the ligand **6**, its Cu^I complex **7**, and other transition metal complexes of **6** suitable for X-ray diffraction analyses were unsuccessful. In order to ascertain the podand structure, and considering that on the basis of NMR results, the general structure of **6** should not be different from the organic-solvent soluble tetraester intermediate **4**, we tried to prepare various metal complexes of the latter and good results were obtained with zinc(II). In particular, the reaction of **4** with $ZnCl_2$ gave the conic complex **9** which was characterized by 1D and 2D ^{1}H NMR spectroscopic experiments, mass spectrometry, and elemental analysis. Crystals of **9** suitable for X-ray diffraction analysis were obtained as yellow plates by slow diffusion of hexane into a dichloromethane solution of the complex.

Compound **9** crystallizes with 2 independent molecules, C and D, per asymmetric unit, hence the molecular formula is [Cl_2Zn**6**ZnCl_2]·2.25CH_2Cl_2.

The molecular structure without the solvent is illustrated in the PLATON[42] drawing (Figure 7) along with a partial crystallographic numbering scheme.

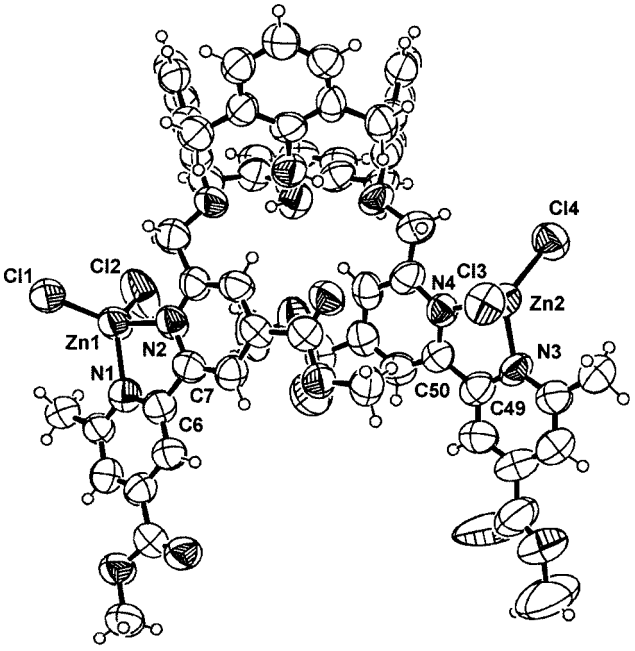

Figure 7. ORTEP side-view of complex **9**, molecule C

As expected, the calixarene subunit of **9** is in the cone conformation and substituted in alternate positions of the lower rim by two dimethyl 6-methyl-2,2′-bipyridyl-4,4′-dicarboxylate arms tethered to the platform by a 6′-methyleneoxy linker. Each bipyridyl unit coordinates via its nitrogen atoms to a tetrahedral Zn^{II} cation, with the two remaining coordination positions occupied by two chloride anions, as already observed.[43]

In the two independent molecules C and D, the [bpyZnCl_2] units are opposed to each other, facing outward

 © 2004 Wiley-VCH Verlag GmbH & Co. KGaA, Weinheim

Table 1. Selected torsion angles [°] around the zinc center in complex **9**

N2−Zn1−N1−C6	1.5(5)	N4−Zn2−N3−C50	−10.8(5)
N1−Zn1−N2−C7	2.1(5)	N3−Zn2−N4−C49	+8.0(5)
N1−C6−C7−N2	6.4(10)	N3−C50−C49−N4	−4.9(10)
N22−Zn21−N21−C66	4.5(8)	N24−Zn22−N23−C111	−7.9(6)
N21−Zn21−N22−C67	−1.0(8)	N23−Zn22−N24−C110	7.7(6)
N21−C66−C67−N22	6.5(17)	N24−C110−C111−N23	−0.3(12)

Table 2. Selected bond lengths [Å] and angles [°] around the zinc center in complex **9**

Zn1−N1	2.059(7)	N1−Zn1−N2	80.5(3)	N3−Zn2−N4	80.3(3)
Zn1−N2	2.083(7)	N1−Zn1−Cl2	116.2(2)	N3−Zn2−Cl4	119.0(2)
Zn1−Cl2	2.197(3)	N2−Zn1−Cl2	108.07(18)	N4−Zn2−Cl4	114.00(19)
Zn1−Cl1	2.204(3)	N1−Zn1−Cl1	114.61(19)	N3−Zn2−Cl3	108.8(2)
Zn2−N3	2.048(7)	N2−Zn1−Cl1	113.4(2)	N4−Zn2−Cl3	110.02(18)
Zn2−N4	2.074(6)	Cl2−Zn1−Cl1	117.88(13)	Cl4−Zn2−Cl3	118.47(10)
Zn2−Cl4	2.196(2)				
Zn2−Cl3	2.201(2)				
Zn21−N21	2.065(12)	N21−Zn21−N22	81.4(6)	N23−Zn22−N24	79.8(4)
Zn21−N22	2.134(16)	N21−Zn21−Cl21	114.5(3)	N23−Zn22−Cl23	115.0(3)
Zn21−Cl21	2.174(3)	N22−Zn21−Cl21	113.0(4)	N24−Zn22−Cl23	114.8(3)
Zn21−Cl22	2.190(4)	N21−Zn21−Cl22	110.5(3)	N23−Zn22−Cl24	110.0(2)
Zn22−N23	2.036(7)	N22−Zn21−Cl22	106.1(3)	N24−Zn22−Cl24	108.9(2)
Zn22−N24	2.100(9)	Cl21−Zn21−Cl22	123.32(16)	Cl23−Zn22−Cl24	120.9(2)
Zn22−Cl23	2.179(3)				
Zn22−Cl24	2.214(4)				

from the calixarene main axis, and orienting the chlorine atoms in the direction of the calixarene platform. A rotation of 90 ° around the C_2 axis shows that these two units are quasi parallel.

Looking more precisely at the complex subunits of molecules C and D, shows that the bipyridine units are planar, with N−C−C−N torsion angles between −4.9 and 6.5 ° (Table 1). The zinc(II) centers are in strongly distorted tetrahedral coordination environments, with N−Zn−N angles of ca. 80 °, Cl−Zn−Cl angles of ca. 120 °, and N−Zn−Cl between 106 and 119° (Table 2).

The Zn−N and ZnCl distances (Table 2) are consistent with those measured in a non-carboxylated analogue,[43] suggesting a poor influence of the electroactive ester substituents on the complex geometry.

Conclusion

A new water-soluble calix[4]arene-based bipyridyl podand **6** has been synthesized and subjected to complexation studies with copper(I) and copper(II) species in water. The copper(I) complex **7** exhibits considerable stability, even in the presence of bovine serum albumin, promising interesting behavior in biological media. It was fully characterized as a mononuclear species, involving probably a pro-helicoidal pseudo-tetrahedral complexation mode between the chelating bipyridines and the metallic center, as already observed for organic-solvent soluble analogues. No crystals of either water-soluble ligand **6** or the copper(I) complex **7** could be obtained, but the lipophilic tetra methyl ester intermediate **4** reacted with zinc(II) chloride to give a monocrystalline dinuclear complex **9** which was characterized by X-ray diffraction, thus confirming the expected podand-like structure of the ligand. The evaluation of the complexing ability of **6** with various transition metal cations in water and biological media, as well as their potent antimicrobial activities are under current investigation.

Experimental Section

General Remarks: Melting points (°C, uncorrected) were determined with an Electrothermal 9200 Capillary apparatus. ^{1}H, ^{13}C and ^{15n} NMR spectra were recorded with a Bruker DRX 400 (chemical shifts in ppm) instrument. Mass spectra (electronic ionization − EI, and electrospray − ES) were recorded with a Nermag R-1010C apparatus or a Micromass Platform II apparatus, respectively, at the Service Commun de Spectrométrie de Masse Organique, Nancy. Infrared spectroscopy was performed with a Mattson 5000 FT apparatus (KBr, $\tilde{\nu}$ in cm^{-1}) and UV spectra were recorded using a SAFAS UV mc^2 apparatus, $\lambda_{max.}$ in nm, ε in $dm^3 \cdot mol^{-1} \cdot cm^{-1}$. Elemental analyses were performed at the Service de Microanalyse, Nancy. Merck TLC plates were used for chromatographic analyses (SiO_2, ref 1.05554; Al_2O_3, ref 1.05581). Sodium and copper concentrations were determined by argon plasma emission spectrophotometry on a Spectrascan 7 Spectrametrics apparatus. Mass-coupled thermogravimetric analyses were performed with a Netzch STA 409 C apparatus.

All commercially available products were used without further purification unless otherwise specified.

***N*-Oxide 2:** To a solution of dimethyl 6,6′-dimethyl-2,2′-bipyridine-4,4′-dicarboxylate (**1**) (1 g, 3.30 mmol) in CH_2Cl_2 (20 mL) at 0 °C under argon, was added dropwise a solution of *m*-chloroperbenzoic acid (0.685 g, 3.96 mmol; from 0.975 g of 70% commercial

 © 2004 Wiley-VCH Verlag GmbH & Co. KGaA, Weinheim

*m*CPBA) in CH_2Cl_2 (10 mL). The mixture was then stirred at room temp. for 2.5 h (TLC monitoring; Al_2O_3, CH_2Cl_2/hexane, 90:10). The solvent was evaporated to dryness at 25 °C, and the residue was triturated with Et_2O to remove *m*CBA and unchanged *m*CPBA. The resultant solid, which contained 90% of the mono *N*-oxide, traces of di-*N*-oxide, and unchanged bipyridine was retained at −20 °C. (1.025 g). A small analytical sample of **2** was obtained by rapid chromatography (Al_2O_3; CH_2Cl_2). ^{1}H NMR ($CDCl_3$): δ = 2.62 (s, 3 H, *Me*bpy), 2.74 (s, 3 H, *Me*bpy), 3.98 (s, 3 H, COO*Me*), 3.99 (s, 3 H, COO*Me*), 7.82 (s, 1 H), 7.94 (d, *J* = 2.7 Hz, 1 H), 8.61 (d, *J* = 2.7 Hz, 1 H), 9.05 (s, 1 H) (3-H, 3′-H, 5-H, 5′-H) ppm. ^{13}C NMR ($CDCl_3$): δ = 18.80 (*Me*bpy), 24.99 (*Me*bpy), 53.22 (−O*Me*), 122.00, 123.75, 126.00, 126.38 (C3, C3′, C5, C5′), 125.74, 138.45, 147.61, 150.53, 150.77, 159.82 (C2, C2′, C4, C4′, C6, C6′), 164.96, 166.11 (*C*OOMe) ppm. $C_{16}H_{16}N_2O_5$·0.1H_2O (318.11): calcd. C 60.41, H 5.13, N 8.80; found C 60.17, H 4.98, N 8.57.

Bromide 3: Compound **2** (1 g, 5.0 mmol) was dissolved at room temp. in dry CH_2Cl_2 (10 mL), and trifluoroacetic anhydride (10 mL) was added. The solution was brought to reflux under argon over 1.5 h, during which time it became orange. The solvents were then evaporated to dryness. The raw material containing the trifluoroacetic ester was dissolved at room temp. in a 1:1 mixture of dry DMF and dry THF (15 mL), then anhydrous LiBr (2 g, 23 mmol, dried at 180 °C over 1 h) was added. The resultant yellow mixture was stirred under argon for 4 h (TLC monitoring, SiO_2, CH_2Cl_2), and the solvents were evaporated to dryness (2 torr, 70 °C). The residue was washed with water (3 × 20 mL) then chromatographed (SiO_2, CH_2Cl_2) to give the monobromide **3** (1 g, 55%), the dibromide (0.25 g, 12%), and unchanged **1**. White powder, m.p. 160−162 °C. IR: ṽ = 1565.8 (C=N), 1731.3 (COOMe). UV-vis (CH_2Cl_2): λ = 310 nm (16700). ^{1}H NMR ($CDCl_3$): δ = 2.75 (s, 3 H, *Me*bpy), 4.02 (s, 3 H, COO*Me*), 4.03 (s, 3 H, COO*Me*), 4.72 (s, 2 H, C*H*$_2$Br), 7.79 (d, *J* = 0.5 Hz, 1 H), 8.06 (d, *J* = 1.1 Hz, 1 H), 8.79 (d, *J* = 0.5 Hz, 1 H), 8.91 (d, *J* = 1.3 Hz, 1 H, 3-H, 3′-H, 5-H, 5′-H) ppm. ^{13}C NMR ($CDCl_3$): δ = 24.99 (*Me*bpy), 33.78 (Br*C*H$_2$), 53.12, 53.25 (O*Me*), 118.25, 120.32, 123.37, 123.46 (C3, C3′, C5, C5′), 139.16, 140.63, 155.83, 157.02, 157.97, 159.75 (C2, C2′, C4, C4′, C6, C6′), 165.79, 166.38 (*C*OOMe) ppm. MS (EI): *m*/*z* = 380−378 [**3**]$^+$, 322−320 [**3** − COOMe]$^+$; 299 [**3** − Br]$^+$. $C_{16}H_{15}BrN_2O_4$·0.1CH_2Cl_2 (387.7): calcd. C 49.88, H 3.95, N 7.23; found C 50.00, H 3.95, N 7.23.

Calixarene Tetraester 4: A suspension of calix[4]arene (1 g; 2.35 mmol) and K_2CO_3 (0.305 g; 2.35 mmol) in anhydrous CH_3CN (50 mL) was heated to reflux under argon for 30 min. The bromide **3** (1.88 g; 4.95 mmol) was then added and reflux was continued for 4 h (TLC monitoring; SiO_2, CH_2Cl_2/MeOH, 95:5). The solvent was evaporated to dryness, and the residue was washed with Et_2O and water before being chromatographed (SiO_2, CH_2Cl_2) to give **4** (2 g; 83%). White powder, m.p. 268−270 °C (dec.). IR: ṽ = 1567.9 (C=N), 1732.1 (COOMe). UV (CH_2Cl_2): λ = 310 nm (23200). ^{1}H NMR ($CDCl_3$): δ = 2.77 (s, 6 H, *Me*bpy), 3.48−4.43 ("q", AB, J_{AB} = 13 Hz, 8 H, Ar-C*H*$_2$-Ar), 3.55 (s, 6 H, −O*Me*), 3.99 (s, 6 H, −O*Me*), 5.47 (s, 4 H, −OC*H*$_2$bpy), 6.71 (t, *J* = 7.4 Hz, 2 H, 4-H of Ar-OH), 6.86 (t, *J* = 7.8 Hz, 2 H, 4-H of Ar), 7.00 (d, *J* = 7.6 Hz, 4 H, 3-H and 5-H of Ar), 7.12 (d, *J* = 7.4 Hz, 4 H, 3-H and 5-H of Ar-OH), 7.77 (d, *J* = 1 Hz, 2 H, 3′-H or 5′-H of bpy), 8.18 (s, 2 H, ArO*H*), 8.71 (d, *J* = 1.0 Hz, 2 H, 5′-H or 3′-H of bpy), 8.84 (d, *J* = 1.1 Hz, 2 H, 3-H or 5-H of bpy), 9.12 (d, *J* = 1 Hz, 2 H, 5-H or 3-H of bpy) ppm. ^{13}C NMR ($CDCl_3$): δ = 25.04 (*Me*bpy), 31.98 (Ar-*C*H$_2$-Ar), 52.63 (−O*Me*), 53.05 (−O*Me*), 78.77 (−O*C*H$_2$bpy), 117.95, 119.50, 120.11, 121.98, 123.28, 126.24 (C3, C3′, C5, C5′ of bpy, C_p of Ar), 128.98, 129.69 (C_m of Ar), 128.12, 133.52, 139.06, 139.82, 152.26, 153.88, 156.18, 156.25, 158.73, 159.82 (C2, C2′, C4, C4′, C6, C6′ of bpy; $C_{i,o,p}$ of Ar), 165.58, 166.43 (*C*OOMe) ppm. MS (ES, positive mode): *m*/*z* = 1020 [**4**]$^+$, 703 [**4** − OCH$_2$Bpy(COOMe)$_2$]$^+$. $C_{60}H_{52}N_4O_{12}$ (1021.07): calcd. C 70.58, H 5.13, N 5.49; found C 70.48, H 5.45, N 5.34.

Calixarene Tetraacid 5 and Calixarene Tetraacid Sodium Salt 6: A suspension of **4** (1 g; 0.98 mmol) in a solution of NaOH (0.4 g; 10 mmol) in MeOH (110 mL) and H_2O (90 mL) was heated to reflux under argon for 24 h. After cooling to room temp., the solution was acidified to pH 3−4 with 1 M HCl. The resultant precipitate of tetraacid **5** was filtered, washed with H_2O (4 × 30 mL), then dispersed in H_2O (50 mL) and dissolved by careful addition of 1 M NaOH up to pH 7.0. The resultant solution was evaporated to dryness to give **6** (0.97 g; 80%). **6:** White powder, m.p. 270−280 °C (dec.). IR: ṽ = 1555.8 (C=N), 1604.3 (COONa). UV (H_2O): λ = 302 nm (21600). ^{1}H NMR (D_2O): δ = 2.54 (s, 6 H, *Me*bpy), 3.18−3.96 ("q", J_{AB} = 15 Hz, 8 H, Ar-C*H*$_2$-Ar), 5.34 (s, 4 H, −OC*H*$_2$bpy), 6.41 (t, *J* = 7.5 Hz, 2 H, 4-H of Ar1), 6.63 (d, *J* = 7.4 Hz, 4 H, 3-H and 5-H of Ar1), 6.66 (t, *J* = 7.4 Hz, 2 H, 4-H of Ar2), 7.03 (d, *J* = 7.7 Hz, 4 H, 3-H and 5-H of Ar2), 7.53 (s, 2 H, 3′-H or 5′-H of bpy), 7.65 (s, 2 H, 5′-H or 3′-H of bpy), 7.96 (s, 2 H, 3-H or 5-H of bpy), 8.22 (s, 2 H, 5-H or 3-H of bpy) ppm. ^{13}C NMR (D_2O): δ = 23.29 (*Me*bpy), 30.79 (Ar-*C*H$_2$-Ar), 78.25 (−O*C*H$_2$), 119.24, 120.59, 121.68, 123.32, 124.07, 126.18 (C3, C3′, C5, C5′ of bpy; C_p of Ar), 128.46, 133.71 ($C_o$of Ar), 129.40 ($C_m$of Ar), 147.49, 147.64, 150.87, 152.09, 155.42, 156.00, 156.38, 159.68 (C2, C2′, C4, C4′, C6, C6′ of bpy; C_p of Ar), 172.93, 173.60 (COO^-) ppm. ES-MS: (positive mode, 30 V): *m*/*z* = 1075.98 [**6** + Na^+]$^+$, 549.27 [**6** + 2 Na^+]$^{2+/2}$; (negative mode, 20 V): *m*/*z* = 503.24 [**6** − 2 Na^+]$^{2-/2}$, 492.23 [**6** − 3 Na^+ + H^+]$^{2-/2}$, 481.22 [**6** − 4 Na^+ + 2 H^+]$^{2-/2}$, 327.87 [**6** − 3 Na^+]$^{3-/3}$, 320.53 [**6** − 4 Na^+ + H^+]$^{3-/3}$, 240.04 [**6** − 4 Na^+]$^{4-/4}$. $C_{56}H_{40}N_4Na_4O_{12}$·2NaCl·6$H_2O$ (1277.87): calcd. C 52.63, H 4.10, N 4.38; found C 52.88, H 3.82, N 4.24.

A solution of **6** (0.925 g, 0.724 mmol) in water (50 mL) (pH = 7.38) was carefully acidified to pH = 3.11 with 1 M HCl. The resultant yellow suspension was washed with CH_2Cl_2 (4 × 30 mL) before the residual organic solvent was removed under vacuum. The yellow precipitate was filtered off, washed with H_2O, CH_3OH and CH_2Cl_2, then dried under vacuum. (**5**; 0.65 g, 93%). M.p. 235 °C (dec.). IR: ṽ = 1568.1 (C=N), 1720.6 (COOH). ^{1}H NMR ([D$_6$]DMSO): δ = 2.67 (s, 6 H, *Me*bpy), 3.48−4.27 ("q", J_{AB} = 13 Hz, 8 H, Ar-C*H*$_2$-Ar), 5.41 (s, 4 H, C*H*$_2$O), 6.61 (t, *J* = 7.5 Hz, 2 H, H_p of Ar), 6.86 (t, *J* = 7.5 Hz, 2 H, H_p of Ar), 7.09 (d, *J* = 7.6 Hz, 4 H, $H_m$of Ar), 7.17 (d, *J* = 7.6 Hz, 4 H, $H_m$of Ar), 7.73 (d, *J* = 1 Hz, 2 H), 8.47 (s, 2 H), 8.62 (s, 4 H), 8.93 (s, 2 H, 3-H, 3′-H, 5-H, 5′-H of bpy and ArO*H*) ppm. ^{13}C NMR ([D$_6$]DMSO): δ = 25.03 (*Me*bpy), 31.59 (Ar-*C*H$_2$-Ar), 78.78 (−O*C*H$_2$), 118.02, 119.64, 119.81, 122.61, 123.74, 126.50 (C3, C3′, C5, C5′ of bpy, C_p of Ar), 128.13, 134.43 (C_o of Ar), 129.46, 129.99 (C_m of Ar), 140.49, 140.91, 152.75, 153.87, 155.77, 155.86, 158.79, 159.89 (C2, C2′, C4, C4′, C6, C6′ of bpy; C_{ipso} of Ar), 166.65, 167.19 (COOH) ppm. ES-Ms (pos. mode): *m*/*z* = 965.35 [**5** + H^+]$^+$, 483.30 [**5** + 2 H^+]$^{2+/2}$. $C_{56}H_{44}N_4O_{12}$·2.5H_2O (1010.01): calcd. C 66.59, H 4.89, N 5.55; found C 66.89, H 4.83, N 5.10.

Copper(I) Complex 7: A solution of [Cu(MeCN)$_4$]PF_6 (0.076 g, 0.205 mmol) in MeCN was added to a solution of **6** (0.3 g, 0.204 mmol) in H_2O (10 mL). The resultant deep red solution was stirred at room temp. for 10 min, and the solvents were evaporated to dryness to give **7** as a brown-red powder. (0.34 g, 100%). IR: ṽ = 855 (PF_6^-), 1555.4 (C=N), 1608.7 (COO^-). UV: λ = 320 (22780), 470 nm (5210; MLCT). ^{1}H NMR ([D$_6$]DMSO): δ = 1.76

 © 2004 Wiley-VCH Verlag GmbH & Co. KGaA, Weinheim

(s, 6 H, *Me*bpy), 3.27−4.24 ("q", J_{AB} = 12 Hz, 4 H, Ar-CH_2-Ar), 5.31−6.27 ("q", J_{AB} = 11.0 Hz, 4 H, CH_2O), 6.42 (t, J = 7.0 Hz, 2 H, H_p of Ar1), 6.80 (d, J = 7.4 Hz, 2 H, H_m of Ar1), 6.87 (t, J = 7.0 Hz, 2 H, H_p of Ar2), 6.92 (d, J = 7.6 Hz, 2 H, H_m of Ar1), 7.16 (d, J = 7.0 Hz, 2 H, H_m of Ar2), 7.28 (d, J= 7.0 Hz, 4 H, H_m of Ar2), 7.78 (s, 2 H, 5-H or 3-H bpy), 8.04 (s, 2 H, 5′-H or 3′-H bpy), 8.67 (s, 2 H, 3-H or 5-H bpy), 8.87 (s, 2 H, 3′-H or 5′-H bpy) ppm. ES-MS (neg. mode, 30 V): m/z = 544.4 [**6** + Cu^+ − Na^+ − 2 H^+]$^{2-/2}$, 523.20 [**6** + Cu^+ − 3 Na^+]$^{2-/2}$, 512.19 [**6** + Cu^+ − 4 Na^+ + H^+]$^{2-/2}$, 341.25 [**6** + Cu^+ − 4 Na^+]$^{3-/3}$, 312.83 [$NaPF_6$ + PF_6^-]$^-$, 144.87 [PF_6^-]$^-$. $C_{56}H_{40}N_4Na_4O_{12}$·$CuPF_6$·NaCl·4$H_2O$ (1391.91): calcd. C 48.32, H 3.48, N 4.03; found C 48.18, H 3.71, N 4.00.

Copper(ii) Complex 8: A solution of ligand **6** (0.1 g; 0.0783 mmol) in H_2O (3 mL) was mixed with a solution of $CuCl_2(H_2O)_2$ (0.0267 g; 0.156 mmoles) in H_2O (2 mL) at room temp., resulting in the immediate formation of a green-brown gelatinous precipitate. The solvent was evaporated to dryness under high vacuum without heating. The resultant solid was then triturated with H_2O (3 × 2 mL) and filtered to give **8**. (0.094 g; 98%). Deep-brown solid. IR: $\tilde{\nu}$ = 1559.20 (C=N), 1611.12 (COO^-). $C_{56}H_{40}Cu_2ClN_4NaO_{12}$·4.5$H_2O$ (1227.54): calcd. C 54.79, H 4.02, N 4.56; found C 54.70, H 3.83, N 4.65.

Zinc(ii) Complex 9: A solution of ligand **4** (0.05 g; 0.045 mmol) in CH_2Cl_2 (5 mL) was mixed with $ZnCl_2$ (0.06 g; 0.44 mmol) at room temp. under Ar. The resultant solvents were evaporated to dryness, twice dissolved in CH_2Cl_2 and filtered then evaporated to dryness. The residue was dissolved in CH_2Cl_2 (5 mL) and precipitated in an excess of Et_2O to give **9** as a light yellow powder (0.056 g; 95%). UV: λ = 338 nm (34650). ^{1}H NMR (CD_2Cl_2): δ = 3.11 (s, 6 H, *Me*bpy), 3.57 (s, 6 H, COO*Me*), 3.67, 4.36 (AB, J_{AB} = 13.5 Hz, 8 H, Ar-CH_2-Ar), 4.14 (s, 6 H, COO*Me*), 5.83 (s, 4 H, OCH_2bpy), 6.77 (t, J = 7.4 Hz, 2 H, H_p of Ar1), 6.99 (t, J = 7.4 Hz, 2 H, H_p of Ar2), 7.12 (d, J = 7.6 Hz, 4 H, H_m of Ar2), 7.20 (d, J = 7.6 Hz, 4 H, H_m of Ar1), 7.90 (s, 2 H, O*H*), 8.24 (s, 2 H, 3-H or 5-H of Mepy), 8.77 (s, 2 H, 3-H or 5-H of OCH_2py), 8.89 (s, 2 H, 3-H or 5-H of CH_3py), 9.90 (s, 2 H, 3-H or 5-H of OCH_2py) ppm. ES-MS (pos. mode, 100 V): m/z = 1315.3 [**4** + 2 $ZnCl_2$ + Na^+]$^+$, 1257.3 [**4** + $ZnCl_2$ + ZnCl]$^+$, 1179.4 [**4** + $ZnCl_2$ + Na^+]$^+$, 1043.4 [**4** + Na^+]$^+$, base peak. $C_{60}H_{52}Cl_2N_4O_{12}Zn_2$ (1293.63): calcd. C 55.71, H 4.05, N 4.39; found C 55.76, H 4.08, N 4.37.

X-ray Crystallographic Study: The intensity data were collected at 153 K (−120 °C) with a Stoe Mark II-Image Plate Diffraction System[44] equipped with a two-circle goniometer using Mo-K_α graphite-monochromated radiation. Image plate distance 100 mm, ω rotation scans 0−180° at φ 0°, and 0−21° at φ 90°, step Δω = 1.2°, 2θ range 2.29−59.53°, $d_{max.} - d_{min.}$ = 17.799−0.716 Å.

The structure was solved by direct methods using the program SHELXS-97.[45] The refinement and all further calculations were carried out using SHELXL-97.[46] The H-atoms were either located from Fourier difference maps and refined isotropically or included in calculated positions, and treated as riding atoms using SHELXL default parameters. The non-H atoms were refined anisotropically, using weighted full-matrix least-squares on F^2.

An empirical absorption correction was applied using the DIFABS routine in PLATON.[42] Transmission factors $T_{min.}/T_{max.}$ were 0.091 and 0.550, respectively. A considerable amount of disordered solvent was present and the SQUEEZE routine in PLATON revealed the presence of 380 electrons for a volume of 1559 Å^3. This could be equated to 9 molecules of CH_2Cl_2 per unit cell and the *hkl* file was modified accordingly.

Details for the experimental conditions, cell data, structure, and refinement data are given in Table 3.

Table 3. Crystal data and structural refinement of **9**

Empirical formula	$C_{62.25}H_{56.5}Cl_{8.5}N_4O_{12}Zn_2$ [$C_{14}Zn_2(C_{60}H_{52}N_4O_{12})$]·2.25($CH_2Cl_2$)]
Formula mass	1484.68
Temperature	153(2) K
Crystal system, Space group	triclinic, $P\bar{1}$
Unit cell dimensions	
a [Å]	11.6265(9)
b [Å]	16.3888(13)
c [Å]	36.039(3)
α [°]	80.222(6)
β [°]	89.128(6)
γ [°]	84.924(6)
V [Å^3]	6740.7(9)
Z	4
$D_{calcd.}$ [g·cm^{-3}]	1.463
Linear absorption coefficient [mm^{-1}]	1.110
F(000)	2656
Crystal size [mm]	0.50 × 0.24 × 0.10
θ Range for data collection [°]	1.15 to 24.10
Limiting indices	$-12 \le h \le 13$ $-18 \le k \le 18$ $-41 \le l \le 41$
Reflections collected/unique	43707/20350
Number of observed reflections	8602
Max./min. transmission	0.550 and 0.091
Data/restraints/parameters	20350/0/1468
Goodness-of-fit on F^2	1.022
Final R indices [$I > 2\sigma(I)$]	$R1$ = 0.0854, $wR2$ = 0.2138
R indices (all data)	$R1$ = 0.1575, $wR2$ = 0.2493
Densities (max./min.) [e·Å^3]	0.465/−0.865

CCDC-213363 contains the supplementary crystallographic data for this paper. These data can be obtained free of charge at www.ccdc.cam.ac.uk/conts/retrieving.html [or from the Cambridge Crystallographic Data Center, 12 Union Road, Cambridge CB2 1EZ, UK; Fax: (internat.) +44-1223/336-033; E-mail: deposit@ccdc.cam.ac.uk].

Acknowledgments

We are grateful to the MRES and CNRS for financial support, and to SAFAS (Monaco) for UV spectroscopy facilities. N. P. is grateful to the Fondation pour la Recherche Médicale, Paris, for a Fin de Thèse grant. The authors thank Mr. J.-M. Ziegler and Mrs. E. Eppiger for mass spectrometry, and NMR spectrometric measurements, respectively.

[1] A. Casnati, D. Sciotto, G. Arena, in *Calixarene 2001* (Eds.: Z. Asfari, V. Böhmer, J. Harrowfield, J. Vicens), Kluwer, Dordrecht, The Netherlands, **2001**, pp. 440−456.
[2] A. Arduini, A. Pochini, S. Reverberi, R. Ungaro, *J. Chem. Soc., Chem. Commun.* **1984**, 981.
[3] C. D. Gutsche, P. F. Pagoria, *J. Org. Chem.* **1985**, *50*, 5795.
[4] C. D. Gutsche, I. Alam, *Tetrahedron* **1988**, 4689.
[5] S. Shinkai, S. Mori, T. Tsukabi, T. Sone, O. Manabe, *Tetrahedron Lett.* **1984**, *25*, 5315.
[6] S. Shinkai, K. Araki, T. Tsubaki, T. Arimura, O. Manabe, *J. Chem. Soc., Perkin Trans. 1* **1987**, 2297.

 © 2004 Wiley-VCH Verlag GmbH & Co. KGaA, Weinheim

[7] M. Almi, A. Arduini, A. Casnati, A. Pochini, R. Ungaro, *Tetrahedron* **1989**, *45*, 2177.
[8] D. Gutsche, K. C. Nam, *J. Am. Chem. Soc.* **1988**, *110*, 6153.
[9] J.-B. Regnouf-de-Vains, R. Lamartine, *Helv. Chim. Acta* **1994**, *77*, 1817.
[10] J.-B. Regnouf-de-Vains, S. Pellet-Rostaing, R. Lamartine, *Tetrahedron Lett.* **1995**, *36*, 5745.
[11] J.-B. Regnouf-de-Vains, R. Lamartine, B. Fenet, C. Bavoux, A. Thozet, M. Perrin, *Helv. Chim. Acta* **1995**, *78*, 1607.
[12] S. Pellet-Rostaing, J.-B. Regnouf-de-Vains, R. Lamartine, *Tetrahedron Lett.* **1996**, *37*, 5889.
[13] S. Pellet-Rostaing, J.-B. Regnouf-de-Vains, R. Lamartine, P. Meallier, S. Guittonneau, B. Fenet, *Helv. Chim. Acta* **1997**, *80*, 1229.
[14] J.-B. Regnouf-de-Vains, R. Lamartine, B. Fenet, *Helv. Chim. Acta* **1998**, *81*, 661.
[15] S. Pellet-Rostaing, J.-B. Regnouf-de-Vains, R. Lamartine, B. Fenet, *Inorg. Chem. Commun.* **1999**, *2*, 4.
[16] Y. Molard, C. Bureau, H. Parrot-Lopez, R. Lamartine, J.-B. Regnouf-de-Vains, *Tetrahedron Lett.* **1999**, *40*, 6383.
[17] J.-O. Dalbavie, J.-B. Regnouf-de-Vains, R. Lamartine, S. Lecocq, M. Perrin, *Eur. J. of Inorg. Chem.* **2000**, *4*, 683.
[18] F. Tisato, F. Refosco, G. Bandoli, G. Pilloni, B. Corain, *Inorg. Chem.* **2001**, *40*, 1394.
[19] Y. Rondelez, G. Bertho, O. Reinaud, *Angew. Chem. Int. Ed.* **2002**, *41*, 1044.
[20] N. Psychogios, J.-B. Regnouf-de-Vains, *Tetrahedron Lett.* **2001**, *42*, 2799.
[21] N. Psychogios, J.-B. Regnouf-de-Vains, *Tetrahedron Lett.* **2002**, *43*, 77.
[22] N. Psychogios, J.-B. Regnouf-de-Vains, *Tetrahedron Lett.* **2002**, *43*, 7691.
[23] C. D. Gutsche, J. A. Levine, *J. Am. Chem. Soc.* **1982**, *104*, 2652.
[24] C. D. Gutsche, J. A. Levine, P. K. Sujeeth, *J. Org. Chem.* **1985**, *50*, 5802.
[25] H. M. Chawla, K. Srinivas, *Indian J. Chem.* **1993**, *32B*, 1162.
[26] B. Yao, J. Bassus, R. Lamartine, *An. Quim.* **1997**, *93*, 165.
[27] B. Alpha, E. Anklam, R. Deschenaux, J.-M. Lehn, M. Pietraskiewicz, *Helv. Chim. Acta* **1988**, *71*, 1042.
[28] L. Motta, J.-B. Regnouf de Vains, C. Bavoux, M. Perrin, *J. Chem. Crystallogr.* **1995**, *25*, 401.
[29] V. Boekelheide, D. L. Harrington, *Chem. Ind.* **1955**, 1423.
[30] V. J. Traynelis, R. F. Martello, *J. Am. Chem. Soc.* **1958**, *80*, 6590.
[31] G. R. Newkome, W. E. Puckett, G. E. Kiefer, V. K. Gupta, Y. Xia, M. Coreil, M. A. Hackney, *J. Org. Chem.* **1982**, *47*, 4116.
[32] J.-M. Lehn, J.-B. Regnouf de Vains, *Tetrahedron Lett.* **1989**, *30*, 2209.
[33] G. R. Newkome, K. J. Theriot, V. K. Gupta, F. R. Fronczek, G. R. Baker, *J. Org. Chem.* **1989**, *54*, 1766.
[34] J.-M. Lehn, J.-B. Regnouf de Vains, *Helv. Chim. Acta* **1992**, *75*, 1221.
[35] J.-B. Regnouf de Vains, A.-L. Papet, A. Marsura, *J. Heterocyclic Chem.* **1994**, *31*, 1069.
[36] F. Camps, V. Gasol, A. Guerrero, *Synthesis* **1987**, *5*, 511.
[37] M. Harding, U. Koert, J.-M. Lehn, A. Marquis-Rigault, C. Piguet, J. Siegel, *Helv. Chim. Acta* **1991**, *74*, 594.
[38] R. Ziessel, J.-M. Lehn, *Helv. Chim. Acta* **1990**, *73*, 1149.
[39] P.-D. Beer, J.-P. Martin, M. G. B. Drew, *Tetrahedron* **1992**, *48*, 9917.
[40] C. Jaime, J. de Mendoza, P. Prados, P. M. Nieto, C. Sanchez, *J. Org. Chem.* **1991**, *56*, 3372.
[41] J. O. Magrans, J. de Mendoza, M. Pons, P. Prados, *J. Org. Chem.* **1997**, *62*, 4518.
[42] "PLATON/PLUTON version Jan. 1999", A. L. Spek, *Acta Crystallogr., Sect. A* **1990**, *46*, C-34.
[43] J.-O. Dalbavie, J.-B. Regnouf-de-Vains, R. Lamartine, M. Perrin, S. Lecocq, B. Fenet, *Eur. J. Inorg. Chem.* **2002**, 901.
[44] Stoe & Cie, *X-Area V1.17 & X-RED32 V1.04 Software*, Stoe & Cie GmbH, Darmstadt, Germany, **2002**.
[45] G. M. Sheldrick, "SHELXS-97 Program for Crystal Structure Determination", *Acta Crystallogr., Sect. A* **1990**, *46*, 467.
[46] G. M. Sheldrick, "SHELXL-97", University Göttingen, Germany, **1999**.

Received September 30, 2003
Early View Article
Published Online April 20, 2004

 © 2004 Wiley-VCH Verlag GmbH & Co. KGaA, Weinheim

Complexation Properties of Ethylenediaminetetramethylenephosphonic Acid (EDTMP) with Al^{III} and $V^{IV}O$

Valerio Di Marco,[a] Melinda Kilyen,[b] Tamás Jakusch,[b] Péter Forgó,[c] György Dombi,[d] and Tamás Kiss*[b,e]

Keywords: Aluminum / Aminophosphonates / Bioinorganic chemistry / Speciation / Vanadium

The complexation properties (including stoichiometries and stability constants of the complexes formed) of ethylenediaminetetramethylenephosphonic acid with Al^{III} and $V^{IV}O$ were studied in aqueous solution at an ionic strength of 0.2 M KCl, at 25 °C by means of pH potentiometry. For Al^{III} both mononuclear ($AlLH_n$) and dinuclear (Al_2LH_n) species were found in solution, whereas for $V^{IV}O$ only mononuclear complexes were detected. For each metal ion, a solid complex was isolated at acidic pH and was characterized stoichiometrically. ^1H and ^{31}P NMR (for Al^{III}), UV/Vis and EPR (for $V^{IV}O$) spectra were used to confirm the potentiometric results and to suggest the most probable binding mode of the complexes formed in solution.

(© Wiley-VCH Verlag GmbH & Co. KGaA, 69451 Weinheim, Germany, 2004)

Introduction

Al^{III} is a toxic metal ion for living organisms. In many cases, the biological mechanism of its toxicity is well documented and includes enzyme inhibition, nucleotide destruction and mineral formation.[1] These effects are the results of a complicated chain of reactions involving the relatively unexplored chemical interactions of the metal ion with the relevant biomolecules.

Vanadium is a trace element and is beneficial for living organisms. Its most important oxidation states are +4 and +5, and some vanadium compounds have promising insulin-mimetic properties both in vitro and in vivo.[2,3] As for aluminium, the molecular action of vanadium is still not well known.

The complexation properties of ethylenediaminetetramethylenephosphonic acid (EDTMP, Figure 1) with metal ions allow its use as a valuable model for an understanding of their interactions with more complicated biomolecules containing the same amino and phosphonate moieties. EDTMP complexes with a number of metal ions have been studied;[4–13] almost exclusively divalent metal ions were considered: Mg^{II}, Ca^{II}, Sr^{II}, Ba^{II}, Mn^{II}, Fe^{II}, Co^{II}, Ni^{II}, Zn^{II}, Cd^{II}, Cu^{II} and Pb^{II}. In a few cases, trivalent cations were also studied (e.g. Sm^{III} and Ho^{III} by Jarvis et al.[11]) because of the use of EDTMP–lanthanide complexes as therapeutic radiopharmaceuticals. Fe^{III}–EDTMP complexes have been investigated by Westerback et al.,[7] Motekaitis et al.[9] and Oakes et al.,[14] but only in a qualitative way, with no reports of any definite data. In a recent paper, Popov et al.[15] reported a critical evaluation of the proton- and metal-complexation stability constants to be found in the literature up to 2000 for various aminophosphonic acids.

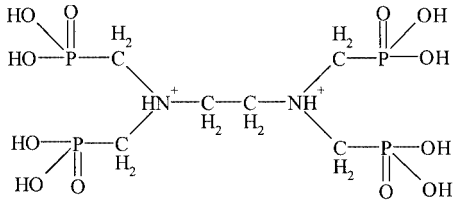

Figure 1. EDTMP in its fully protonated form ($H_{10}L^{2+}$)

In the present paper, Al^{III}–EDTMP and $V^{IV}O$–EDTMP interactions were examined by means of pH-potentiometric titrations and independent spectroscopic techniques.

[a] Department of Inorganic, Organometallic and Analytical Chemistry, University of Padova, Marzolo 1, 35131 Padova, Italy
[b] Biocoordination Chemistry Research Group of the Hungarian Academy of Sciences, University of Szeged, P. O. Box 440, 6701 Szeged, Hungary
[c] Department of Organic Chemistry, University of Szeged, Dóm tér 8, 6720 Szeged, Hungary
[d] Department of Pharmaceutical Analysis, University of Szeged, Somogyi B. u. 4, 6720 Szeged, Hungary
[e] Department of Inorganic and Analytical Chemistry, University of Szeged, P. O. Box 440, 6701, Hungary
Fax: (internat.) + 36-62/420-505
E-mail: tkiss@chem.u-szeged.hu
Supporting information for this article is available on the WWW under http://www.eurjic.org or from the author.

 © 2004 Wiley-VCH Verlag GmbH & Co. KGaA, Weinheim **DOI: 10.1002/ejic.200300693**

Results and Discussion

Acidity Constants of EDTMP

In principle EDTMP is a decaprotic acid (see Figure 1). Ichikawa et al. proposed the following deprotonation sequence for the fully protonated cation $H_{10}L^{2+}$: seven phosphonic protons, the first ammonium proton, the eighth phosphonic proton and the second ammonium proton.[16] Table 1 summarizes the pK_a values obtained from our potentiometric titrations. The pK_a for the species H_nL refer to the equilibrium $H_nL^{n-8} \rightleftarrows H_{n-1}L^{n-9} + H^+$. Under the experimental conditions used in our study, six of the possible ten proton dissociations could be detected. The first three pK_a values could not be measured in water because they are too low, while the last pK_a could not be measured because it is too high.[15]

Table 1. Acidity constants (pK_a ± 3 standard deviations) for EDTMP at 25 °C and I = 0.2 M KCl

Species	pK_a
H_7L^-	(1.16 ± 0.12)
H_6L^{2-}	2.80 ± 0.05
H_5L^{3-}	5.00 ± 0.03
H_4L^{4-}	6.24 ± 0.02
H_3L^{5-}	7.72 ± 0.02
H_2L^{6-}	9.64 ± 0.02
No. of points:	345
Fitting parameter:[a]	7.38×10^{-3}

[a] Goodness of the fit between the experimental and the calculated titration curves expressed in mL of the titrant.

Our results are in reasonable agreement with most of the data obtained in previous studies, as listed in Table 2. The only important difference was that in all the previous papers a pK_a value for HL^{7-} was also given, even if sometimes with very high uncertainty. The recent IUPAC critical compilation[15] suggests a provisional value for this protonation process, pK(HL) = 13.8 (see Table 2). We attempted to refine our data in light of these results, but it was not possible to obtain a reliable value for this very high pK_a. To achieve this, the ligand should be applied in a high concentration at pC = pK_w − pK_a + 0.5.[20] However, in this case the ionic strength could not be kept constant in the sample during the titration, and thus the pK_a value could be determined only with a rather high uncertainty. It is likely that an insufficient ligand concentration was the reason for our previous reporting of a pK_a value of 12.04.[17] Accordingly, we disregarded this last proton-dissociation process and considered HL^{7-} as the complex-forming species in the formation equilibrium $pM + qHL + rH \rightleftarrows M_pL_qH_{r+q}$. In this way, more accurate formation constants could be obtained, although their numerical values differed by the value of the last pK_a from those calculated in the usual way for the equilibrium $p\ M + q\ L + r\ H \rightleftarrows M_pL_qH_r$.

Al^{III} Complexes

The stability constants for the Al^{III}−EDTMP complexes, determined by potentiometric titration, are listed in Table 3.

Table 3. Stability constants (log β ± 3 standard deviations) for the Al^{III}−EDTMP complexes at 25 °C and I = 0.2 M KCl [the constants are calculated for the equilibrium: $p\ M + q\ HL + r\ H \rightleftarrows M_pL_qH_{r+q}$ (see text)]

Species	p	q	r	log β
$[Al_2LH_3]^+$	2	1	2	36.01 ± 0.08
$[Al_2LH_2]$	2	1	1	32.61 ± 0.09
$[Al_2LH]^-$	2	1	0	28.85 ± 0.07
$[AlLH]^{4-}$	1	1	0	17.21 ± 0.04
$[AlL]^{5-}$	1	1	−1	10.95 ± 0.03
$[AlLH_{-1}]^{6-}$	1	1	−2	0.40 ± 0.08
No. of points:				731
Fitting parameter:[a]				1.11×10^{-2}

[a] Goodness of the fit between the experimental and the calculated titration curves expressed in mL of the titrant.

A typical distribution diagram of the various metal−ligand species as a function of pH is shown in Fig-

Table 2. Acidity constants (pK_a) of EDTMP reported in the literature (if not specified, data are at 25 °C)

Conditions	H_8L	H_7L^-	H_6L^{2-}	H_5L^{3-}	H_4L^{4-}	H_3L^{5-}	H_2L^{6-}	HL^{7-}	Ref.
KCl (0.2 M)	−	(1.16)	2.80	5.00	6.24	7.72	9.64	−	this work
KCl (0.2 M)	−	1.34	2.75	5.00	6.28	7.80	9.70	12.04	[17]
KNO_3 (0.1 M)	2.43	2.73	3.80	5.63	7.39	9.27	10.48	10.60	[4]
KNO_3 (0.1 M)	−	(1.37)	3.15	5.26	6.57	8.13	10.01	(13.14)	[9]
KNO_3 (0.1 M)	−	1.33	3.02	5.17	6.42	7.94	9.78	12.99	[10]
KNO_3 (0.1 M)	−	−	2.96	5.12	6.40	7.87	9.85	13.0	[16]
K^+ (0.1 M)	−	1.3	3.00	5.12	6.40	7.90	9.82	13.8[a]	[15]
(I = 0.1 M)	1.46	2.72	5.05	6.18	6.63	7.43	9.22	10.95	[7]
KNO_3 (3 M)	−	1.24	2.98	4.86	6.05	7.60	9.36	12.36	[9]
KNO_3 (3 M)	−	1.24	2.82	4.77	5.88	7.42	9.02	12.01	[10]
NaCl (0.15 M, 37 °C)	−	1.24	2.83	5.08	6.31	7.63	9.47	10.67	[11]
NaCl (3 M)	−	2.03	3.79	5.32	6.65	8.22	10.51	14.0	[18]
−	−	−	3.00	5.23	6.54	8.08	10.18	12.10	[19]

[a] I = 3.5 M (Me_4N^+).

 © 2004 Wiley-VCH Verlag GmbH & Co. KGaA, Weinheim

ure 2. The accepted speciation model includes both mononuclear and dinuclear complexes, which predominated in the different pH ranges. In the pH range 11−7, only mononuclear species exist in solution: $[Al(OH)_4]^-$, $[AlLH_{-1}]^{6-}$, $[AlL]^{5-}$ and $[AlLH]^{4-}$. The most important Al^{III} complex is $[AlL]^{5-}$. It was initially expected that, at pH values lower than 6.5, other mononuclear species are formed. However, the best speciation model obtained with the assumption of mononuclear species only — $[AlLH_5]$, $[AlLH_4]^-$, $[AlLH_3]^{2-}$, $[AlLH_2]^{3-}$, $[AlLH]^{4-}$, $[AlL]^{5-}$ and $[AlLH_{-1}]^{6-}$ — had to be rejected because the fitting parameter was more than 70% poorer than the one reported in Table 3, obtained with the assumption of parallel-formed dinuclear complexes. The species detected at a pH below 6.5 are probably the dinuclear complexes $[Al_2LH]^-$, $[Al_2LH_2]$ and $[Al_2LH_3]^+$, although other oligonuclear complexes cannot be excluded. Although usually only mononuclear metal−EDTMP complexes have been detected so far,[4−13] it is noteworthy that dinuclear species have been recently reported for the Fe^{III}−EDTMP system.[16] The high affinity of Al^{III} towards phosphonic acid groups and the electrostatic repulsion between the negatively charged phosphonate arms of the ligand may explain the formation of some dinuclear complexes.[15]

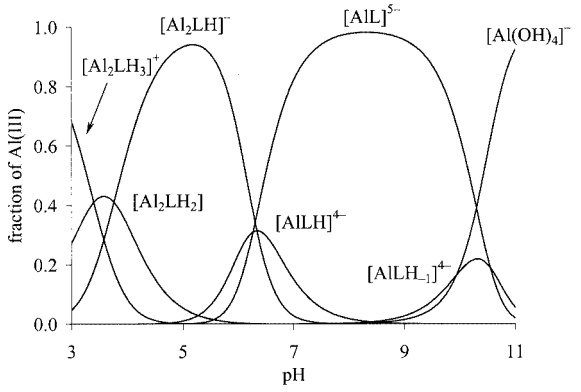

Figure 2. Distribution diagram (mol fraction of Al^{III} as a function of pH) for the Al^{III}−EDTMP system; $c_{Al^{III}} = c_{EDTMP} = 0.001$ M

It is known that Al^{III} readily forms dihydroxo-bridged dinuclear species. Accordingly, it would be reasonable to assume the formation of a complex $[Al_2L_2]^{10-}$ {or more precisely $[Al_2(HL)_2(OH)_2]^{10-}$} in which one of the amino groups is in a protonated form and two OH^- groups link the Al(HL) units together. However, when this species was assumed instead of the mononuclear complex $[AlL]^{5-}$ the fit was poorer by about 30%; when both species were included in the speciation model and were refined simultaneously, the dinuclear species was always rejected by the computer program. Furthermore, the ^1H and ^{31}P NMR results (at the pH value where $[AlL]^{5-}$ forms, vide infra) do not seem to support formation of the dinuclear species, either.

As mentioned in the Exp. Sect., the back-titrations (from the basic to the acidic pH range) had to be stopped at pH ≈ 3 because a solid compound precipitated (the species distribution diagram shown in Figure 2 is limited to this pH value). The elemental and ICP analyses of this solid compound gave the stoichiometry $Al_{1.00}C_{5.86}N_{2.04}$, which is in close agreement with the theoretic AlC_6N_2 stoichiometry of a 1:1 aluminium/ligand compound. The only neutral 1:1 species is $[AlLH_5]$. Therefore, this should be the stoichiometry of the compound that precipitates. The hydrogen content (vide infra) is in agreement with this formula, assuming between four and five coordinated water molecules, which are necessary to fill the hexacoordination sphere of the metal ion. The 1:1 stoichiometry of the solid suggests that mononuclear species actually exist in solution at acidic pH values, together with dinuclear species, which are formed, however, in negligible concentrations. In particular, $[AlLH_5]$ could not be detected during the potentiometric titrations due to its low solubility, which was found experimentally to be below 5×10^{-4} M. In the solid state Al^{III} forms poorly soluble, often layered, chain-polyphosphates[21] which may occur also in acidic solutions at higher Al^{III} concentrations.[15] The dinuclear species $[Al_2LH_x]$ (x = 1, 2, 3) assumed in this paper may be the precursors of these polyphosphates. The solid complex precipitated and characterised by the composition $[AlLH_5]$ is probably a mononuclear species, which exists at such low Al^{III} concentrations, although an oligonuclear structure cannot be fully excluded, either.

The ^1H and ^{31}P NMR spectra of the ligand alone are shown in Figure 3. Due to its symmetry, the free ligand has only two proton signals (a singlet and a doublet, assigned to the NCH_2 and PCH_2 moieties, respectively) and only one phosphorus signal. Signals of a small amount of P-containing impurities can be observed in the NMR spectra (see Exp. Sect.). It has been reported in the literature that the chemical shifts of these signals vary with the pH in a quite irregular manner[6,16] due to the parallel deprotonations and because these may be accompanied by the formation or disruption of intramolecular hydrogen bonding. Our measurements verified this reported pH dependence (data not shown here).

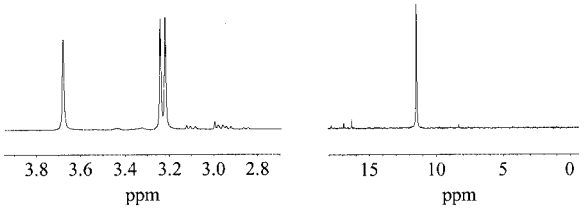

Figure 3. ^1H (left) and proton-decoupled ^{31}P (right) NMR spectra of an aqueous EDTMP solution at pH = 8.38; $c_{EDTMP} = 0.0249$ M

Selected ^1H and ^{31}P NMR spectra of solutions containing both Al^{III} and the ligand in a 0.8:1 ratio are shown in Figure 4. The speciation curves at this higher concentration are shown in Figure 5. At pH = 12.1 only the signals of the free ligand (denoted "lig.") are present, in agreement with the potentiometric data, which confirms negligible metal−ligand complexation at this pH value. Although complex formation between Al^{III} and phosphonates is very

 © 2004 Wiley-VCH Verlag GmbH & Co. KGaA, Weinheim

strong [displacement of the last dissociable proton of the ligand ($pK_a \approx 13.8$) and coordination of this donor group starts at pH ≈ 6], the affinity of Al^{III} to form the tetrahydroxo species $[Al(OH)_4]^-$ is even higher, and at pH > 12 the ligand is completely displaced by OH^- ions. At lower pH values (10.8, 8.3 and 6.3) new signals of the Al^{III}–EDTMP complexes appear in the spectra. For example, at pH = 8.3 two phosphorus signals (denoted "P" and "Q") and six groups of proton signals (denoted "A", …, "F") can be seen. The couplings in the ^1H NMR spectrum at pH = 8.3 were assessed by means of a COSY spectrum (Figure 1 in the Supporting Information; see footnote on the first page of this article): "A" couples with "E", "B" with "F" and "C" with "D". There are also weak couplings between "A" and "B" and between "B" and "C". Accordingly, signals "A" and "E" can be assigned to the methylene protons of the NCH_2CH_2N moiety: they are the simplest signals because they are those of the only protons which cannot couple with ^{31}P. Only the homonuclear coupling splits the signal, resulting in a "doublet-like structure" (AB quadruplet). The rest of the signals of different multiplicity should belong to the methylene protons of the four $CH_2PO_3^{2-}$ arms. Other assignments are less obvious and therefore have not been made. However, the spectra obtained are in agreement with the proposed structure of the complex $[AlL]^{5-}$, shown in Figure 6, which, according to the potentiometric data, is the most important aluminium species in the pH range 10.5–6.5. In this species, the fully deprotonated ligand chelates the metal ion in a hexadentate fashion. A similar hexadentate coordination mode was assumed for the carboxylate analogue EDTA in its $[AlL]^-$ complex.[22,24] This structure is rather rigid, accounting for the narrow peaks in the NMR spectra obtained, and has a C_2 symmetry axis so that the phosphorus atoms and the protons are equivalent in a pairwise manner. The $CH_2PO_3^{2-}$ arms bound to the same N atom are not equivalent; for this reason two ^{31}P signals of equal intensity are observed. A slight distortion of the structure may account for some asymmetry observed, especially in the ^1H NMR spectrum. The other assumption that only one N is involved in the coordination (the ligand is in the HL form) and an OH^- ion saturates the coordination sphere of each metal ion in a dinuclear dihydroxo-bridged species $[Al_2(HL)_2(OH)_2]^{10-}$ (vide supra) is not compatible with the relatively simple ^{31}P and complicated ^1H NMR spectra. In the case of a rigid dimer, at least three different P resonances should occur in the spectra: (i) the P atoms of the two $CH_2PO_3^{2-}$ arms at the coordinating side of the molecule, (ii) the coordinated P of the partially bound side of the molecule, and (iii) the P of the non-coordinating $CH_2PO_3^{2-}$ arm of this side. On the other hand, in the case of a flexible dimer the methylene protons in the N-attached phosphonate arms should become equivalent resulting in the appearance of a high-intensity doublet in the ^1H NMR spectra, which is not observed, instead rather complicated spectra are obtained (see Figure 4). It is noteworthy that identical structures for ML-type EDTMP complexes with other trivalent metal ions, such as Fe^{III}, Sm^{III} and Ho^{III}, were suggested by Westerback et al.[7] and by Motekaitis et al.,[10] and partly confirmed by Jarvis et al.[11]

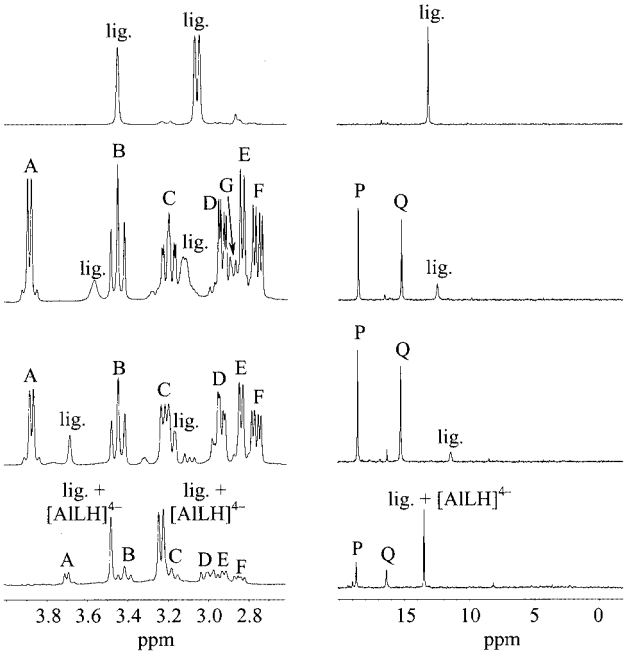

Figure 4. ^1H (left) and proton-decoupled ^{31}P (right) NMR spectra of solutions containing 0.020 M Al^{III} and 0.0252 M EDTMP; pH = 12.06, 10.81, 8.31 and 6.34 (from top to bottom)

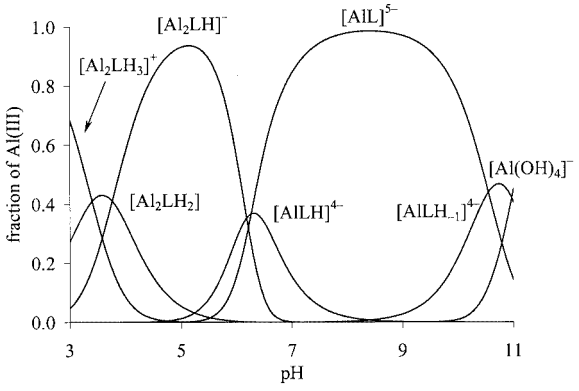

Figure 5. Distribution diagram (mol fraction of Al^{III} as a function of pH) for the Al^{III}–EDTMP system; $c_{Al^{III}}$ = 0.020 M, c_{EDTMP} = 0.025 M

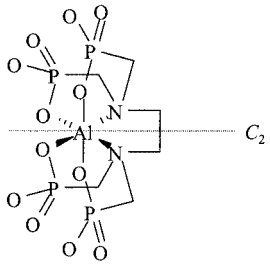

Figure 6. Proposed structure of $[AlL]^{5-}$; the symmetry axis is shown

The spectra at pH = 10.81, where the species $[AlL]^{5-}$ and $[AlLH_{-1}]^{6-}$ should coexist in solution, are very similar

 © 2004 Wiley-VCH Verlag GmbH & Co. KGaA, Weinheim

to those at pH = 8.31: the phosphorus signals are only slightly shifted, whereas in the ^{1}H NMR spectrum only a change in the shape of signals "C" and the appearance of a new signal, "G", can be observed. These suggest that $[AlLH_{-1}]^{6-}$ should have a similar structure to that of $[AlL]^{5-}$, apart from the fact that at least one coordinating site of the metal atom is no longer coordinated by the ligand, but by an OH^- ligand; in addition, it is suggested that the coordinated ligand arms rapidly exchange with the free ligand arm, so that the general symmetry of the complex is maintained and only a small shift of the signals can be observed. This binding mode is in accordance with the rather low value of the deprotonation constant of the species $[AlL]^{5-}$ (pK_{AlL} = 10.55).

In contrast, in the spectra at pH = 6.34, where the species $[AlL]^{5-}$ and $[AlLH]^{4-}$ coexist, the sharp signals of $[AlL]^{5-}$ tend to vanish without apparently being replaced by other well-separated metal−ligand peaks. To explain this finding, we may assume that EDTMP no longer chelates to the metal atom in a hexadentate way in $[AlLH]^{4-}$, as one of the amino groups is now protonated. Al^{III} coordinates mostly to the phosphonate functions, and the intramolecular exchange rate of the coordinated or free phosphonate moieties is high, as was found in previous studies for other Al^{III}−phosphonato complexes.[23,24] Due to this fast internal motion in the complex, no different ^{31}P or ^{1}H signals of the free and Al^{III}-bound phosphonate arms are observed, but the signals are merged and slightly shifted with pH. An amino group as the first protonated function has been reported for the Al^{III} complexes of other hexadentate aminophosphonates and aminocarboxylates.[22,24]

The pK_a calculated from the data in Table 3 for the deprotonation of $[AlLH]^{4-}$ to produce $[AlL]^{5-}$ is 6.26, significantly lower than the pK_a of the free ligand with the same number of protons, HL ($pK_a \approx 13$; see Table 2). This considerable decrease in the pK_a of the HL^{7-} proton due to the coordination of Al^{III} indicates the high stability of the hexadentate coordinated complex $[AlL]^{5-}$.

As seen in Figures 2 and 5, dinuclear complexes are formed at pH < 6. The NMR spectra of the equimolar Al^{III}−EDTMP solutions at acidic pH (not shown) are dominated by the signals of the free ligand, due to the low extent of formation of the dinuclear complexes under these conditions. In order to observe the signals of the Al^{III}-bound ligands, samples with an excess of metal ion were prepared and measured by NMR spectroscopy. These spectra are shown in Figure 7. At pH = 6.1, four new signals (denoted "R", "S", "T" and "U") could be observed at δ = 2−5 ppm in the ^{31}P NMR spectrum. The ^{1}H NMR spectrum is also significantly different from those obtained at higher pH values. The peaks are not well resolved, and only four signals (denoted "I", "J", "K" and "L") can be clearly distinguished in the chemical shift range δ = 3.6−4.1 ppm. From the integration values, it is evident that each of the signals "I", "J", "K" and "L" is due to a single proton of the Al^{III}-bound ligand. A new proton signal is observed at δ ≈ 10 ppm, which may belong to the amino or phosphonic protons. This low-field signal could not be detected in any of the other spectra, either in the absence or in the presence of Al^{III}. According to the speciation data (see Figure 5), the species $[Al_2LH]^-$ is the dominating complex at pH = 6.1. The NMR spectra suggest that $[Al_2LH]^-$ should be a rigid compound, and the four P and the two Al atoms must be chemically inequivalent. In Figure 8, a hypothetical structure is shown for $[Al_2LH]^-$. In this species two phosphonate arms behave as bridging moieties. Only one of the two amino-N atoms is coordinated, and the other may be involved in hydrogen bonding to a water molecule in the coordination sphere of the Al^{III} atom. This binding mode explains the appearance of the extra peak at δ ≈ 10 ppm, which belongs to the N-bound proton. Surprisingly, this amino (or phosphonic) proton does not undergo fast exchange with the bulk water protons on the NMR timescale. The slow kinetics of these processes is also suggested by the fairly long pH-equilibration time observed during the potentiometric titrations (see Exp. Sect.). Another possible explanation of this NMR feature is that besides the dinuclear complex, other oligonuclear complexes are formed at the higher concentrations used for the NMR measurements.

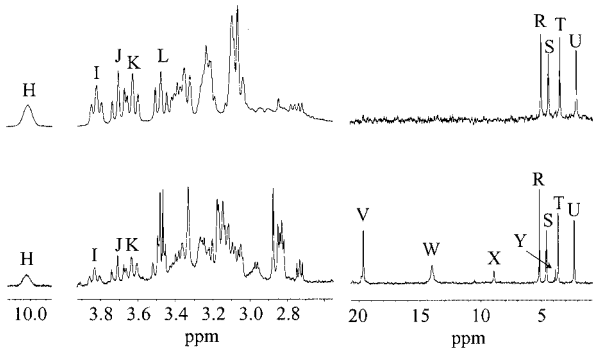

Figure 7. Top: ^{1}H (left) and proton-decoupled ^{31}P (right) NMR spectra of a solution containing 0.0471 M Al^{III} and 0.0251 M EDTMP at pH = 6.1; bottom: ^{1}H (left) and proton-decoupled ^{31}P (right) NMR spectra of a solution containing 0.0415 M Al^{III} and 0.0225 M EDTMP at pH = 3.9

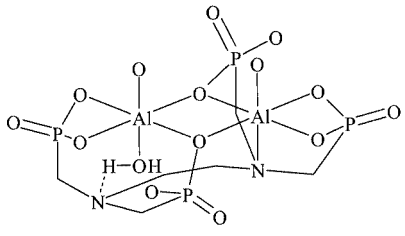

Figure 8. Proposed binding modes for $[Al_2LH]^-$

The NMR spectra measured at pH = 3.9 for the sample with an excess of Al^{III} are in agreement with the potentiometric data, predicting the presence of protonated dinuclear species $[Al_2LH]^-$ and $[Al_2LH_2]$. In the ^{31}P NMR spectrum (Figure 7), four new phosphorus signals appear ("V", "W", "X" and "Y") in addition to those ("R", "S", "T" and "U") belonging to the species $[Al_2LH]^-$. The assignation of these new signals is rather ambiguous, and they may belong

 © 2004 Wiley-VCH Verlag GmbH & Co. KGaA, Weinheim

to various binding isomers and/or to distinct species of different stoichiometry or protonation state. In the ^{1}H NMR spectrum the pattern is more complicated, but new signals can again be seen in the range $\delta = 3.7-2.8$ ppm, together with those also detected at pH = 6.1. These new signals are attributed to the neutral complex $[Al_2LH_2]$, which is probably not a single dinuclear species but a mixture of various (neutral) oligonuclear complexes (substituted by the single species $[Al_2LH_2]$ in the potentiometric speciation calculation). This may explain the rather complicated ^{1}H and ^{31}P NMR features of the Al^{III}−ligand system observed at this pH value (see Figure 7). Again, the proton signal at $\delta \approx 10$ ppm is observed, although with lower intensity than before. This allows us to assign this signal exclusively to the complex $[Al_2LH]^-$. Both $[Al_2LH]^-$ and $[Al_2LH_2]$ (or other oligonuclear species) are asymmetric molecules (Figure 8), in accordance with their NMR behaviour.

$V^{IV}O$ Complexes

The stability constants for the $V^{IV}O$−EDTMP complexes, determined by potentiometric titration, are listed in Table 4.

Table 4. Stability constants (log β ± 3 standard deviations) for the $V^{IV}O$−EDTMP complexes at 25 °C and $I = 0.2$ M KCl (the constants are calculated for the equilibrium: p M + q HL + r H $\rightleftarrows$ $M_pL_qH_{r+q}$)

Species	p	q	r	log β
$[VOLH_4]^{2-}$	1	1	3	29.72 ± 0.08
$[VOLH_3]^{3-}$	1	1	2	26.70 ± 0.07
$[VOLH_2]^{4-}$	1	1	1	22.85 ± 0.07
$[VOLH]^{5-}$	1	1	0	16.29 ± 0.06
$[VOL]^{6-}$	1	1	−1	8.63 ± 0.06
$[VOLH_{-1}]^{7-}$	1	1	−2	−2.07 ± 0.09
No of points:				305
Fitting parameter:[a]				-1.03×10^{-2}

[a] Goodness of the fit between the experimental and the calculated titration curves expressed in mL of the titrant.

A typical speciation diagram of the complexes as a function of pH is shown in Figure 9. The speciation model accepted for the $V^{IV}O$−EDTMP system includes only mononuclear complexes. A slight improvement in the fitting was obtained when alternative speciation was considered for the experimental data: the fitting parameter was about 5% lower when the species $[(VO)_2L_2H_{-2}]^{14-}$ was assumed instead of $[VOLH_{-1}]^{7-}$ in the speciation model. However, we chose the model reported in Table 4 in view of the EPR results (vide infra).

The EPR and UV/Vis spectroscopic data for the $V^{IV}O$−EDTMP system at different pH values, together with the most probable equatorial donor atom arrangements around the metal ion, are reported in Table 5. No EPR parameters for species formed in the acidic pH range could be determined because of the low intensity of the spectra (due to precipitation).

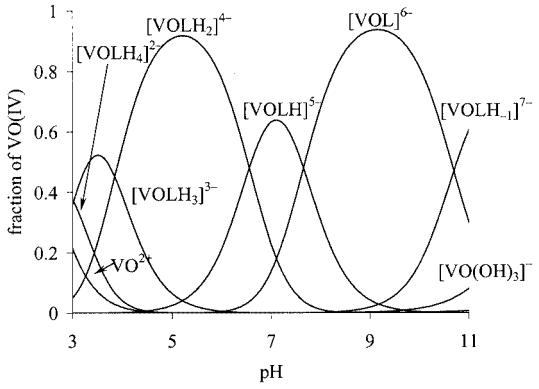

Figure 9. Distribution diagram (mol fraction of $V^{IV}O$ as a function of pH) for the $V^{IV}O$−EDTMP system; $c_{V^{IV}O} = c_{EDTMP} = 0.001$ M

As regards the EPR spectra, at pH = 12 a single species with $g_\parallel = 1.942$ and $A_\parallel = 166.4 \times 10^{-4}$ cm^{-1} is observed. Since these parameters are different than those of $[VO(OH)_3]^-$ ($g_\parallel = 1.957$ and $A_\parallel = 161.4 \times 10^{-4}$ cm^{-1}), this peak is attributed to $[VOLH_{-1}]^{7-}$. When this $A_\parallel$ value is compared with the estimated values obtained from the Chasteen additivity rule[25] it may correspond to either a species with two N [$A_\parallel^{est}$(N, N, PO_3^{2-}, PO_3^{2-}) = 165.2 or $A_\parallel^{est}$(N, N, PO_3^{2-}, OH^-) = 161.4] or with one N [$A_\parallel^{est}$(N, PO_3^{2-}, PO_3^{2-}, PO_3^{2-}) = 167.6 or $A_\parallel^{est}$(N, PO_3^{2-}, PO_3^{2-}, OH^-) = 163.8] in the equatorial plane. The metal ion must also be coordinated to an OH^- moiety, probably in the axial position, so this species should be $[VOL(OH)]^{7-}$, with a binding mode (N, N, PO_3^{2-}, PO_3^{2-})$_{eq}$(OH^-)$_{ax}$. The alternative dihydroxo-bridged, and thus EPR-silent, dimeric species $[(VO)_2L_2H_{-2}]^{14-}$ assumed from the pH-metric measurements in place of the mononuclear species $[VOLH_{-1}]^{7-}$ (vide supra) was rejected as no decrease in intensity of the EPR signal was observed in the formation pH range (pH > 10) of this species. At pH ≈ 9, where the potentiometric data indicates the predominant formation of $[VOL]^{6-}$, a single EPR signal could be detected, with parameters $g_\parallel = 1.936$ and $A_\parallel = 172.1 \times 10^{-4}$ cm^{-1}. The corresponding species is likely to have only one amino group in the equatorial plane of the metal centre (the other N may occupy the axial position or may be in the protonated noncoordinating form), because the half-field splitting constant is closer to the estimated value ($A_\parallel^{est} = 167.6 \times 10^{-4}$ cm^{-1}), and very similar to the half-field splitting constants of the analogous complexes of other aminooligophosphonic acids with the same binding mode.[26] The potentiometric data suggest that three species should coexist in the pH range 8.4−5.7: $[VOL]^{6-}$, $[VOLH]^{5-}$ and $[VOLH_2]^{4-}$. The EPR and potentiometric results correspond to one another. Namely, the stepwise protonation of species $[VOLH_{-1}]^{7-}$ → $[VOL]^{6-}$ → $[VOLH]^{5-}$ → $[VOLH_2]^{4-}$ should involve the axial OH^- group, one of the amino groups and one PO_3^{2-} group. These reactions may proceed in a parallel, overlapping way. What seems to be certain, though, is that only one N atom is in the equatorial plane. Under these conditions, $[VOL]^{6-}$, $[VOLH]^{5-}$ and $[VOLH_2]^{4-}$ have practically the

 © 2004 Wiley-VCH Verlag GmbH & Co. KGaA, Weinheim

Table 5. Spectral (EPR and UV/Vis) data and the most probable binding set of the $V^{IV}O-EDTMP$ complexes

Complex	$g_{\parallel}$	$10^4 \times A_{\parallel}$ (^{51}V) [cm^{-1}]	Equatorial donor set	λ_{max} [nm]
$VOLH_4^{2-}$	–	–	(PO_3^{2-}, 2 × HPO_3^-)	–
$VOLH_3^{3-}$	–	–	(2 × PO_3^{2-}, HPO_3^-)	–
$VOLH_2^{4-}$	1.936	172.1	(N, 2 × PO_3^{2-}, HPO_3^-)	860, 636
$VOLH^{5-}$	1.936	172.1	(N, 3 × PO_3^{2-})	864, 632
VOL^{6-}	1.936	172.1	(N, 3 × PO_3^{2-})	874, 642
$VOLH_{-1}^{7-}$	1.942	166.4	(2 × N, 2 × PO_3^{2-})[a]	878, 636

[a] See text.

same coordination geometry and donor sets in the equatorial plane, and therefore give the same EPR signals (see Table 5). At more acidic pH values the second nitrogen atom is also protonated and the EPR signals display the typical features of the exclusive coordination of phosphonate functions, as expected.

The main feature of the UV/Vis spectra is a blue-shift of the band at ca. 870 nm upon passing from $[VOLH_{-1}]^{7-}$ to $[VOLH_2]^{4-}$. This band may be attributed to the $d_{xy} \rightarrow d_{xz}$, d_{yz} transition.[27] Since the d_{xz} and d_{yz} orbitals are involved in π-bonds with the oxo ligand, the shift of the band indicates a stronger V=O ligand strength. This may be attributed to the structural and electronic rearrangements following the loss of the second nitrogen coordination and the stepwise protonations of the phosphonic arms.

As for Al^{III}, a solid compound was formed in the $V^{IV}O-EDTMP$ system at pH ≈ 3, and the pH-metric back-titrations had to be stopped at this point. The elemental and ICP analyses of the solid complex **2** gave the stoichiometry $(VO)_{1.80}C_{6.00}N_{2.14}$, (the average for the two solids isolated), which is between the theoretical 1:1 vanadium/ligand stoichiometry $[VOLH_6]$ and the 2:1 vanadium/ligand stoichiometry $[(VO)_2LH_4]$ (both are neutral). Therefore, it is reasonable to suggest that both these compounds may precipitate. The 2:1 stoichiometry of the solid appears a little surprising because no dinuclear species could be detected in solution. It may be supposed that $[(VO)_2LH_4]$ is an ionic compound formed by $[VO]^{2+}$ interacting with $[VOLH_4]^{2-}$.[28] However, the non-simple stoichiometry may more strongly suggest a chain-like oligomeric structure for the solid compound through simultaneous metal ion coordination to the (PO_3^{2-}, PO_3H^-) donor sets at both ends of the molecule, resulting in a similar stoichiometry $(VO)_n[(VOLH_4)_n]$ (see Figure 10). The negatively charged chain oligomers $[VOLH_4]_n^{2n-}$ may be partially neutralized by H^+ instead of $[VO]^{2+}$, leading to an $H_{2n}[(VOLH_4)_n]$ stoichiometry. The empty apical coordination sites of the $V^{IV}O$ centres and the free coordination sites of the terminal $V^{IV}O$ ions may be occupied by water molecules. Accordingly, the water content is not strictly defined; it may be around three or four, or even more. These facts are probably responsible for the moderate agreement between the found and calculated elemental analysis data (see Exp. Sect.). The NIR spectrum of the solid compound as compared with that of the ligand alone displays broad, poorly resolved signals, with little information about the binding mode of the complex. The intensity decrease in the ν[P(O)−H] stretching frequency range indicates at least partial deprotonation of the phosphonic groups, which is in accordance with the coordination of $V^{IV}O$ to these functions. The vibration occurring at $\tilde{\nu}$ = 980 cm^{-1} confirms the presence of $V^{IV}O$ in the solid compound.

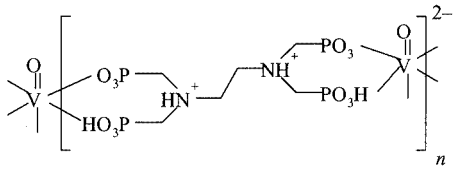

Figure 10. Schematic structure of the oligonuclear solid $V^{IV}O$ complex **2**

Conclusion

Potentiometric titrations of the $Al^{III}-EDTMP$ and $V^{IV}O-EDTMP$ systems revealed for both metal ions that even in equimolar solution the complexes formed are sufficiently stable to avoid the precipitation of $Al(OH)_3$ or $VO(OH)_2$ and the oxidation of $V^{IV}O$, respectively, in the neutral and basic pH range. In the predominant ML species formed in this pH range, the ligand seems to be coordinated to the metal ions through all six donors. In the more basic pH range, at pH > 10, mixed hydroxo species result, while in the acidic pH range partially protonated complexes are formed.

Besides these mononuclear 1:1 species, dinuclear complexes (and probably polynuclear species at higher concentrations) are also formed through the simultaneous coordination of metal ions at both ends of the ligand molecule. The solubilities of these complexes are different, due to the different charges of the metal ions. This may result in precipitation of the neutral complex $VO_n[VOLH_4]_n$ in the $V^{IV}O-EDTMP$ system and the mononuclear species $[AlLH_5]$ in the $Al^{III}-EDTMP$ system in the acidic pH range.

Experimental Section

Reagents: The ligand EDTMP was kindly provided by Monsanto,[29] and was used as received. The purity of the ligand was

checked by potentiometry. The solid EDTMP sample was assessed to be 94.5% pure, the impurity being mainly neutral compounds and water.[30] The P-containing impurities were less than 2%, obtained from peak integration of the NMR spectrum. A stock solution of Al^{3+} was prepared from $AlCl_3 \cdot 6H_2O$ (Fluka); the metal-ion concentration was determined gravimetrically from its oxinate. The stock solution of VO^{2+} was prepared as described previously[31] and standardized for metal-ion concentration by cerimetric titration. To prevent hydrolysis, both metal-ion stock solutions contained ca. 0.1 M HCl. All other chemicals were Fluka (KHphthalate) or Reanal (HCl, KOH and KCl) products.

pH-Metric Measurements: The potentiometric titrations on 25-mL or 50-mL samples were performed in aqueous solution at 25 ± 0.1 °C under argon. The titrations were recorded with an Orion pH-meter equipped with a Metrohm 6.0234.100 combined glass electrode and a Metrohm Dosimat automatic burette. The electrode system was calibrated for hydrogen-ion concentration according to Irving et al.[32] The value obtained for pK_w was 13.764 ± 0.005. EDTMP was standardized by KOH titration in the concentration range from 0.002 to 0.004 M. The data were processed with the computer program SUPERQUAD,[33] which allowed determination of the exact concentrations of the ligand solutions, and calculation of the protonation constants. Precipitation was observed when either Al^{III} or $V^{IV}O$ was added to acidic solutions containing the ligand, in agreement with previous findings on Fe^{III}–EDTMP complexes.[9,14] Accordingly, for determination of the metal–ligand complex-formation constants, back-titrations had to be performed: the starting solutions containing the ligand, the metal ion and excess KOH were titrated with an HCl solution of known concentration. Back-titrations were started at pH ≈ 11 and stopped when precipitation was observed (at pH = 2.5–3.5, depending on the composition of the samples). The volume of the titrant to reach the final pH value varied between 1.4 and 3.8 mL. Stable pH values were always reached within 1 min after addition of the titrant, except for the Al^{III} systems in the pH ranges 3.5–4 and 5.5–6, where the equilibration time was 5–6 min. Samples at different metal ion/ligand ratios were measured pH-potentiometrically. The composition of the samples varied between M/L ratios of 1:1 and 1:4, with Al^{III} concentrations ranging from 0.00080 M to 0.0036 M, and $V^{IV}O$ concentrations from 0.00052 M to 0.0020 M. Duplicate titrations were performed for both systems. For Al^{III}, titrations with excess metal ion were also planned in the pH range between 3 and 6. However, the precipitation of a solid compound (which seemed to be $AlLH_5$) could not be avoided, regardless of the procedure adopted for the addition of the metal-ion and the ligand solutions. Its dissolution at slightly acidic pH values is very slow (several hours), so that no accurate potentiometric titrations could be carried out under these conditions. The stability constants were calculated with the computer program PSEQUAD.[34] The following formation constants of the hydroxo complexes of Al^{III} and $V^{IV}O$ were taken from the literature, corrected to an ionic strength of 0.2 M by use of the Davies equation, and used during the data evaluation: $\log \beta(AlH_{-1}) = -5.41$, $\log \beta(AlH_{-2}) = -11.03$, $\log \beta(Al_3H_{-4}) = -13.09$, $\log \beta(Al_{13}H_{-32}) = -108.19$,[35] and $\log \beta(AlH_{-4}) = -23.44$;[36] $\log \beta[(VO)H_{-1}] = -5.94$, $\log \beta[(VO)_2H_{-2}] = -6.95$;[37] $\log \beta[(VO)H_{-3}] = -18.0$ and $\log \beta[(VO)_2H_{-5}] = -22.5$.[38]

NMR Experiments: ^1H and ^{31}P NMR spectra (the latter with ^1H decoupling) were recorded with a Bruker DMX 500 spectrometer at 298 K on solutions containing the ligand alone (0.025 M) and on solutions containing both the ligand and Al^{III}. Two metal/ligand ratios were explored: 0.8:1 and 1.9:1. Solutions were prepared in a 90:10 (v/v) mixture of H_2O and D_2O (Janssen, 98% D). The pH values were measured with a Metrohm glass electrode, previously calibrated in three buffer aqueous solutions (Sigma, pH = 4, 7 and 10, at 25 °C). The slight difference in composition of the solvents of the calibration and the sample solutions was ignored. A standard water pre-saturation technique was used to eliminate the intense water signal during the relaxation delay (2–3 s). The pH was adjusted by the addition of concentrated KOH and/or HCl solutions. In the samples containing an excess of metal ion, a small amount of solid was present (vide supra). NMR spectra were recorded on the supernatant.

EPR Experiments: Anisotropic X-band EPR spectra (9.15 GHz) were recorded at 120–140 K on aqueous solutions with a Varian E-9 spectrometer. As usual, a few drops of DMSO were added to the samples to ensure good glass formation in frozen solutions. Solutions containing 8×10^{-3} M EDTMP and 4×10^{-3} M $V^{IV}O$ at different pH values were analysed. The EPR spectra may be of further help in elucidating the binding modes of the complexes formed. For the $V^{IV}O$ systems, Chasteen[25] has introduced an additivity rule to estimate the hyperfine coupling constants $A_{\parallel}^{est}$ ($A_{\parallel}^{est} = \Sigma A_{\parallel i}$), based on the contributions $A_{\parallel i}$ of each of the four equatorial donor groups, its estimated uncertainty being $\pm 3 \times 10^{-4}$ cm^{-1}. The parameters $A_{\parallel i}$ of the individual coordinating groups were presented by Chasteen[25] and more recently by Smith et al.[39]

UV/Vis Experiments: Spectra were recorded with a Hewlett-Packard 8452 diode-array spectrometer. Solutions containing 2.4×10^{-2} M EDTMP and 2.4×10^{-2} M $V^{IV}O$ at different pH values were analysed in the wavelength range 300–900 nm.

Solid-State Preparation and Analysis

$Al(LH_5) \cdot 4H_2O$ (1): 10 mL of a 0.0316 M aqueous solution of the free acid H_6L (0.32 mmol) and 10 mL of 0.0320 M $AlCl_3$ (0.32 mmol) were mixed. The pH of the resulting solution was ca. 2. The sample was centrifuged and the supernatant was discarded. The white solid material was treated with 2 mL of 0.02 M HCl solution, stirred in an ultrasonic bath for about 30 min and left to stand overnight at room temperature. The same treatment was repeated three times, on the last occasion with the addition of 2 mL of water instead of HCl. Finally, the solid sample was lyophilized overnight and submitted to elemental analysis. The metal content was measured by ICP-AES. Yield: 130 mg (76%). $C_6H_{17}AlN_2O_{12}P_4 \cdot 4H_2O$ (532): calcd. C 13.53, H 4.70, Al 5.08, N 5.26; found C 13.33, H 4.70, Al 5.01, N 5.40.

$(VO)_x(LH_4)_y \cdot zH_2O$ (2): The complex was prepared in the same way as the Al^{III} complex, but the aqueous solution of the ligand EDTMP was mixed with 10 mL of a 0.0320 M $VOCl_2$ solution (0.32 mM). The solid obtained was a light-blue powder. Yield: 135 mg (78%). The best agreement with the experimental elemental analysis data was obtained with $x = 1.8$, $y = 1$ and $z = 4$. $C_6H_{16}N_2O_{12}P_4(VO)_{1.8} \cdot 4H_2O$ (541): calcd. C 11.78, H 4.09, N 4.58, V 15.02; found C 12.13, H 4.16, N 4.98, V 15.2. This indicates that the solid is probably not a compound with well-defined stoichiometry, but a mixture of the mononuclear metal complex $[VOLH_6]$ and various oligonuclear $VO(L-VO)_n$-type species with an average stoichiometric ratio of VO/L = 1.8 (see Results and Discussion).

Acknowledgments

The work was supported by the bilateral cooperation scheme of the Hungarian Academy of Sciences and CNR of Italy (MTA I108) and by the National Scientific Research Fund (OTKA T31896 and

 © 2004 Wiley-VCH Verlag GmbH & Co. KGaA, Weinheim

T37385). The authors thank Dr. D. Sanna (University of Sassari, Italy) for the preliminary EPR measurements, and Dr. G. Galbács and Mrs I. Varga for the elemental analyses of the compounds.

[1] T. Kiss, P. Zatta, B. Corain, *Coord. Chem. Rev.* **1996**, *149*, 329−346 and references cited therein.
[2] C. E. Heylinger, A. G. Tahiliani, J. H. McNeill, *Science* **1985**, *227*, 1474−1477.
[3] D. Rehder, *BioMetals* **1992**, *5*, 3−12.
[4] E. N. Rizkalla, M. T. M. Zaki, *Talanta* **1979**, *26*, 507−510.
[5] E. N. Rizkalla, M. T. M. Zaki, *Talanta* **1980**, *27*, 769−770.
[6] E. N. Rizkalla, G. R. Choppin, *Inorg. Chem.* **1983**, *22*, 1478−1482.
[7] G. Westerback, A. E. Martell, *Nature* **1956**, *178*, 321−322.
[8] K. Sawada, T. Miyagawa, T. Sakaguchi, K. Doi, *J. Chem. Soc., Dalton Trans.* **1993**, 3777−3784.
[9] R. J. Motekaitis, I. Murase, E. Martell, *Inorg. Nucl. Chem. Lett.* **1971**, *7*, 1103−1107.
[10] R. J. Motekaitis, I. Murase, E. Martell, *Inorg. Chem.* **1976**, *15*, 2303−2306.
[11] N. V. Jarvis, J. M. Wagener, G. E. Jackson, *J. Chem. Soc., Dalton Trans.* **1995**, 1411−1415.
[12] N. Palta, B. V. Rao, S. N. Dubey, D. M. Puri, *Polyhedron* **1984**, *3*, 527−534.
[13] I. N. Marov, G. I. Tsysin, A. A. Formanovsky, V. K. Belyaeva, G. A. Evtikova, D. P. Sokolov, Yu. A. Zolotov, *Proc. Conf. Coord. Chem.* **1991**, 167−170.
[14] J. Oakes, E. G. Smith, *J. Chem. Soc., Dalton Trans.* **1983**, 601−605.
[15] K. Popov, H. Rönkkömaki, H. J. L. Lajunen, *Pure Appl. Chem.* **2001**, *73*, 1641−1677.
[16] T. Ichikawa, K. Sawada, *Bull. Chem. Soc., Jpn.* **1997**, *70*, 829−835.
[17] J. Nagy, Msc Thesis, University of Szeged, Hungary, **1999**.
[18] N. A. Kostromina, *Teor. Eksp. Khim.* **1971**, *7*, 115−119.
[19] M. I. Kabachnik, R. P. Lastovskii, T. Ya. Medved, V. V. Mediyntsev, I. D. Kolpakova, N. M. Dyatlova, *Proc. Acad. Sci. USSR* **1967**, *175*, 351−354.
[20] M. T. Beck, I. Nagypál, *Chemistry of Complex Equilibria*, Akadémiai Kiadó, Budapest, **1990**, p. 198.
[21] N. N. Greenwood, A. Earnshaw, *Chemistry of the Elements*, 2nd ed., Butterworth-Henemann, Oxford, **1997**, p. 526.
[22] R. K. Iyer, S. B. Karweer, V. K. Jain, *Magn. Reson. Chem.* **1989**, *27*, 328−334.
[23] D. Champmartin, P. Rubini, A. Lakatos, T. Kiss, *J. Inorg. Biochem.* **2001**, *84*, 13−21.
[24] M. Kilyén, A. Lakatos, R. Latajka, I. Labádi, A. Salifoglou, C. P. Raptopoulou, H. Kozlowski, T. Kiss, *J. Chem. Soc., Dalton Trans.* **2002**, 3578−3586.
[25] N. D. Chasteen in *Biological Magnetic Resonance* (Eds.: J. Lawrence, L. J. Berliner, J. Reuben), Plenum, New York, **1981**, vol. 3, p. 53.
[26] D. Sanna, I. Bódi, S. Boushina, G. Micera, T. Kiss, *J. Chem. Soc., Dalton Trans.* **1999**, 3275−3282.
[27] C. J. Ballhausen, H. B. Gray, *Inorg. Chem.* **1962**, *1*, 111−116.
[28] According to this assumption, an apparent solubility product is estimated, from the stability constants listed in Table 4, by calculating the actual concentrations of the reacting species at the pH values where the solid starts to precipitate: $pK_s = -\log([VO^{2+}][VOLH_4^{2-}]) = 7.31 \pm 0.03$ (mean value obtained from three titrations).
[29] Monsanto Europe S. A., Brussels, Belgium.
[30] Monsanto Europe S. A., Technical Bulletin **1986**, 53−42 (E) ME-2 (1/1990).
[31] I. Nagypál, I. Fábián, *Inorg. Chim. Acta* **1982**, *61*, 109−114.
[32] H. M. Irving, M. G. Miles, L. D. Pettit, *Anal. Chim. Acta* **1967**, *38*, 475−481.
[33] A. Sabatini, A. Vacca, P. Gans, *Coord. Chem. Rev.* **1992**, *120*, 389−405.
[34] L. Zékány, I. Nagypál, G. Peintler, *PSEQUAD for Chemical Equilibria*, Technical Software Distribution, Baltimore, **1991**.
[35] S. Simpson, S. Sjöberg, K. Powell, *J. Chem. Soc., Dalton Trans.* **1995**, 1799−1804.
[36] L. O. Öhman, S. Sjöberg, *Acta Chem. Scand., Ser. A* **1982**, *36*, 47−53.
[37] R. P. Henry, P. C. H. Mitchell, J. E. Prue, *J. Chem. Soc., Dalton Trans.* **1973**, 1156−1159.
[38] A. Komura, M. Hayashi, H. Imanaga, *Bull. Chem. Soc. Jpn.* **1977**, *50*, 2927−2931.
[39] T. S. Smith II, R. LoBrutto, V. L. Pecoraro, *Coord. Chem. Rev.* **2002**, *228*, 1−18.

Received October 1, 2003
Early View Article
Published Online April 7, 2004

 © 2004 Wiley-VCH Verlag GmbH & Co. KGaA, Weinheim

Nickel(II) Complexes Incorporating Pyridyl, Imine and Amino Chelate Ligands: Synthesis, Structure, Isomer Preference, Structural Transformation and Reactivity Towards Nickel(III) Derivatives

Suparna Banerjee,[a] Jaydip Gangopadhyay,[b] Can-Zhong Lu,[c] Jiu-Tong Chen,[c] and Ashutosh Ghosh*[a]

Keywords: Coordination modes / Isomer specificity / N ligands / Nickel / Structural transformation

Facile condensation of 2-acetylpyridine with ethylenediamine in a 1:1 or 2:1 molar ratio yielded two neutral ligands with different denticity: 1-amino-4-(2-pyridyl)-3-azapent-3-ene (tridentate, L^1) and 2,7-bis(2-pyridyl)-3,6-diazaocta-2,6-diene (tetradentate, L^3), respectively. Replacing the ketone with 2-pyridinecarboxaldehyde gave a similar set of condensates (L^2 and L^4). The tridentate mono-Schiff bases (L^1 and L^2) react smoothly with $Ni(ClO_4)_2{\cdot}6H_2O$ furnishing the brown bis-chelate complexes (**1a** and **1b**) with an NiN_6 coordination sphere, while the tetradentate bis-Schiff bases (L^3 and L^4) form green pseudo-octahedral complexes (**2a** and **2b**) in which Ni^{II} is present in an N_4O_2 coordination environment. The isomer specificity for both types of complexes is conspicuous from the representative X-ray structures of **1a** and **2a**. *cis-trans-cis* and *cis-cis-trans* isomers are found exclusively for **1** and **2**, respectively. The crystal structure of **2a** reveals O–H···O hydrogen bond interactions assembling alternating cations and anions in an infinite chain-like array. Cyclic voltammetric measurements of **1** and **2** in MeCN solution show a quasi-reversible one-electron oxidation near 0.95 and 0.87 V (vs. SCE), respectively, attributed to a Ni^{III}-Ni^{II} redox couple. Another irreversible Ni^{IV}-Ni^{III} redox response was observed at higher potential near 1.70 and 1.80 V (vs. SCE) for **1** and **2**, respectively. Complexes **1** and **2** display a weak, broad d-d transition band along with a charge-transfer transition. Magnetic susceptibility measurements (at 298 K) confirmed that the spin states of the Ni^{II} centres in **1** and **2** are same, $S = 1$, in agreement with an octahedral configuration. Complexes **1** form stable reddish-brown Ni^{III} complexes (**3**) under exhaustive constant-potential electrolysis treatment. The Ni^{III} complexes display axial EPR spectra both at 298 K and 77 K with $g_\perp > g_\parallel$ indicating the presence of an unpaired electron primarily on the metal centre. Complexes of type **1** and **3** exhibit virtually superimposable cyclic voltammograms in a reverse electrode scan study which confirms no change in the coordination sphere on going from **1** to **3**. The effective magnetic moment values (ca. 2.10 μ_B) of **3** suggest a significant orbital contribution to the paramagnetism, consistent with a tetragonally distorted low spin $3d^7$ system. A colour change phenomenon has been observed for type **2** complexes.

(© Wiley-VCH Verlag GmbH & Co. KGaA, 69451 Weinheim, Germany, 2004)

Introduction

Over the last few decades considerable attention has been paid to rationalizing the underlying chemical aspects regarding the stabilizing and destabilizing factors of Ni^{III} species derived from Ni^{II} precursors in various coordination environments.[1,2]

We report here the synthesis and structural features of new NiN_6 and NiN_4O_2 coordination spheres derived from neutral mono-Schiff bases and bis-Schiff bases respectively, as ligands. The electrochemical behaviour of all the members of the two families was investigated with the aim of determining the relative stability of progressively higher oxidation states (+II, +III and +IV) and possible transformations thereof.[2–4] The NiN_6 complexes smoothly undergo electrochemical one-electron oxidation at ambient temperature to give Ni^{III} complexes with identical coordination environments. Hence this type of bis-chelate complex can be modelled to trigger the reversible electron-transfer reactions that are essential for biological[5] as well as catalytic[6] processes. The molecular packing of a representative of the NiN_4O_2 family (**2a**) has revealed two sterically uncongested ONN triangular faces forming O···O hydrogen-bond interactions with counter perchlorate anions. Under the appropriate conditions these open faces can be utilised to accommodate small guest molecules, an area that has been much less explored than the more common crown ethers,[7] imine

[a] Department of Chemistry, University College of Science and Technology, University of Calcutta,
92, A.P. C. Road, Kolkata 700 009, India
[b] Department of Inorganic Chemistry, Indian Association for the Cultivation of Science,
Kolkata 700 032, India
[c] The State Key Laboratory of Structural Chemistry, Fujian Institute of Research on the Structure of Matter, The Chinese Academy of Sciences,
Fuzhou, Fujian 350002, P. R. China

Schiff-base macrocycles[8] and cryptands.[9] A thermogravimetric experiment followed by spectroscopic characterisation showed a change from a six-coordinate octahedral geometry to a four-coordinate distorted square planar form by releasing two *trans* water co-ligands. The observed colour change (green→ red) is associated with this structural change, as is common for other Ni^{II} complexes in different coordination environments.[10]

Results and Discussion

Synthesis of the Complexes

The tridentate and tetradentate Schiff bases 1-amino-4-(2-pyridyl)-3-azapent-3-ene and 2,7-bis(2-pyridyl)-3,6-diazaocta-2,6-diene (general abbreviation, L) have been employed as chelating ligand in the present work. The analogous 2-pyridylcarboxaldimine ligands have also been used for a comparative study. The four complexes reported in this context belong to two different types **1** and **2**.

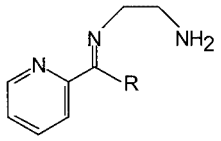

L^1 (R = CH_3)

L^2 (R = H)

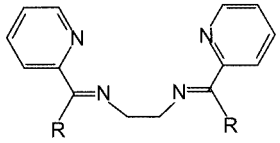

L^3 (R = CH_3)

L^4 (R = H)

The brown bis-chelate complexes **1** are formed in excellent yield upon reacting $Ni(ClO_4)_2{\cdot}6H_2O$ with L^1 or L^2 in a 1:2.2 molar ratio in aqueous methanol under reflux (Scheme 1).

$Ni(ClO_4)_2{\cdot}6H_2O$ reacts smoothly with either L^3 or L^4 in a 1:1.2 molar ratio in aqueous methanol under reflux to give the green complexes **2** in high yield (Scheme 2). Complexes **2** undergo an interesting dehydration-rehydration process, which is influenced by temperature and pressure. At ambient temperature and normal pressure the complexes are stable; the effect of heating on the dehydration process will be examined later.

Attempts to perform a template synthesis by condensation of the appropriate aldehyde or ketone with ethylenediamine followed by complexation with the metal ion in situ, maintaining the 2:2:1 and 2:1:1 molar ratio necessary for the formation of complexes **1** and **2** gave the exclusive formation of **1** due to the chelate effect.

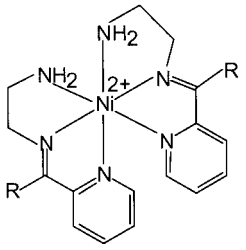

1a (R = CH_3)

1 (R = H)

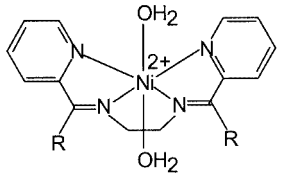

2a (R = CH_3)

2b (R = H)

The perchlorate salts act as 1:2 electrolytes in acetonitrile solution (Λ = 245−255 $\Omega^{-1}{\cdot}cm^2{\cdot}mol^{-1}$). Complexes of type **1** give the stable oxidised derivatives **3** under constant electrolysis treatment, whereas type **2** complexes are inherently unstable towards electrolytic treatment.

The *cis-trans-cis* and *cis-cis-trans* disposition of the N^pN^p-N^iN^i-N^aN^a (in type **1** complexes) and N^pN^p-N^aN^a-O^wO^w (in type **2** complexes) donor sets (N^p is pyridyl nitrogen, N^i is imine nitrogen, N^a is amino nitrogen and O^w is oxygen of water) are the striking features of these complexes.

Geometrical Preference and Structural Features

[Ni(L^1)$_2$](ClO$_4$)$_2$

This complex has a distorted octahedral geometry. The ligand encapsulates the divalent metal ion through six ligating nitrogen atoms from two pyridyl [N(1) and N(4)], two imine [N(2) and N(5)] and two amino [N(3) and N(6)] groups (Figure 1, Table 1). Several isomers are theoretically possible considering the relative arrangement of three types of coordinated nitrogen atoms around the metal centre, although the only one encountered here has the pyridine ni-

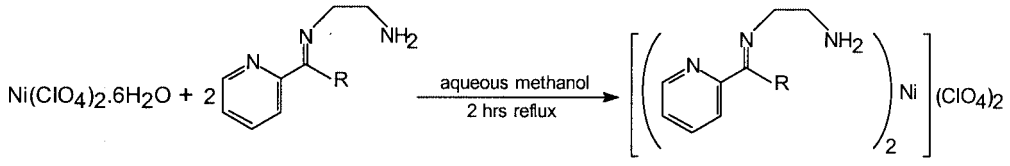

Scheme 1

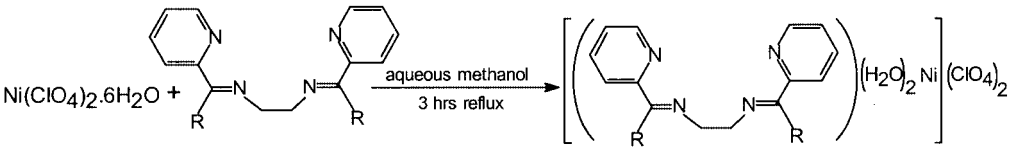

Scheme 2

 © 2004 Wiley-VCH Verlag GmbH & Co. KGaA, Weinheim

trogen atoms in the *cis* position and the imine nitrogen atoms in the *trans* positions, thereby leaving two *cis* positions available for the amino nitrogen donors. The *trans* disposition of two N^i donor sites in a *cis-trans-cis* geometry ensures competition between them for the same metal d-orbital, thus minimising the back-bonding stabilisation. This *cis-trans-cis* geometry (no NiN^i interaction) is sterically more favourable than any of the possible unobserved isomers (*cis-cis-trans, trans-cis-cis*) having a *cis* NiN^iN^i orientation (two NiN^i interactions). Evidently the steric relaxation completely offsets the back-bonding disadvantage in the case of the *cis-trans-cis* isomer and none of the other isomers are observed.

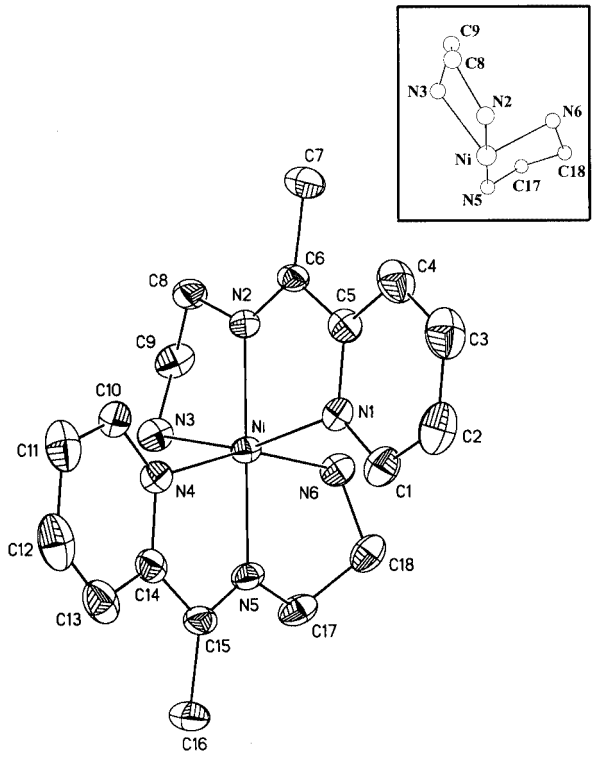

Figure 1. A perspective view and atom-labelling scheme of the complex cation of $[Ni(L^1)_2](ClO_4)_2$ (**1a**); all non-hydrogen atoms are represented by their 25% thermal probability ellipsoids; the inset shows the conformations of the dimethylene-bridged chelate rings

Table 1. Selected bond lengths (Å) and angles (°) for $[Ni(L^1)_2](ClO_4)_2$

Ni−N5	2.008(5)	Ni−N2	2.013(5)
Ni−N6	2.119(5)	Ni−N4	2.120(7)
Ni−N1	2.123(5)	Ni−N3	2.143(6)
N5−Ni−N2	179.4(2)	N5−Ni−N6	81.9(2)
N2−Ni−N6	97.5(2)	N5−Ni−N4	77.5(2)
N2−Ni−N4	103.1(2)	N6−Ni−N4	158.6(2)
N5−Ni−N1	102.5(2)	N2−Ni−N1	77.8(2)
N6−Ni−N1	91.7(2)	N4−Ni−N1	87.3(2)
N5−Ni−N3	99.0(2)	N2−Ni−N3	80.7(2)
N6−Ni−N3	94.4(3)	N4−Ni−N3	94.3(2)
N1−Ni−N3	158.2(2)		

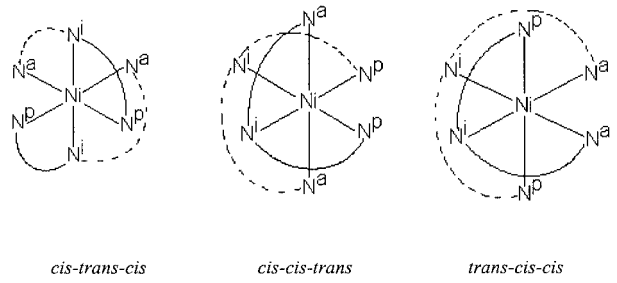

The N(1), N(3), N(4) and N(6) atoms define a severely distorted basal plane (mean deviation 0.39 Å). The five-membered chelate rings [Ni, N(1), C(5), C(6) and N(2)] and [Ni, N(4), C(14), C(15), and N(5)] along with the conjugated pyridyl moieties constitute satisfactory planes (mean deviation 0.06 Å and 0.07 Å respectively). The two remaining saturated five-membered metallo rings are out of plane (average mean deviation 0.16 Å) and the dimethylene bridges assume a twisted skew conformation (see inset, Figure 1). As a whole, two $Ni(L^1)$ fragments are not planar (average mean deviation 0.11 Å) essentially due to steric repulsion between the two dimethylene-bridged chelate rings. Two pyridylimine metallo rings enjoy extended π-electron delocalisation, inducing a more rigid nature and a decrease in the chelate bite angles (average 77.7°). On the contrary, the twisted dimethylene-bridged metallo rings are flexible with larger (closer to 90°) bite angles (average 81.3°). All metal-nitrogen bond lengths are consistent with literature values.[1,11−14] The $Ni-N^i$ bonds are shorter than the $Ni-N^p$ and $Ni-N^a$ bonds by about 0.11 Å. This $Ni-N^i$ bond-shortening stems from the better π-accepting ability of imine (C=N) functions than the N^p and N^a coordination sites.

[Ni(L³)(H₂O)₂] (ClO₄)₂

The *cis-cis-trans* geometry with respect to N^p, N^i and O^w donor sites is found exclusively rather than another possible *trans-cis-cis* isomer for complexes **2**. This isomer specificity primarily stems from the better degree of $Ni-N^i$ back-bonding in the *cis-cis-trans* isomer due mainly to the presence of a stronger *trans* σ-donor N^p atom (in the *trans-cis-cis* geometry a weaker O^w atom is *trans* to the $Ni-N^i$ bond) sharing the same metal d-orbital. Moreover the *cis-cis-trans* orientation (devoid of NiO^w interactions) is better in a steric sense than the unprecedented *trans-cis-cis* isomer with a *cis*-NiO^wO^w disposition (two destabilising NiO^w interactions). Therefore, we can rationalize the exclusive occurrence of the *cis-cis-trans* isomer in terms of both electronic and steric factors.

 © 2004 Wiley-VCH Verlag GmbH & Co. KGaA, Weinheim

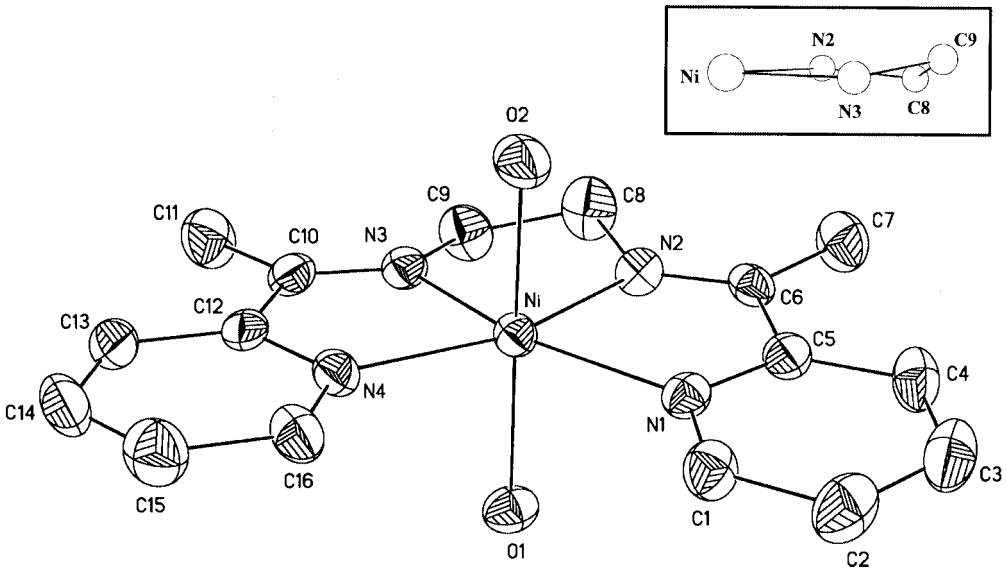

Figure 2. A perspective view and atom-labelling scheme of the complex cation of $[Ni(L^3)(H_2O)_2](ClO_4)_2$ (**2a**); all non-hydrogen atoms are represented by their 25% thermal probability ellipsoids; the inset shows the conformation of the dimethylene-bridged metallo ring

A molecular view of **2a** is presented in Figure 2, and selected bond parameters are listed in Table 2. The Ni^{II} ion sits in a reasonably planar equatorial plane (mean deviation 0.04 Å) defined by the N(1), N(2), N(3) and N(4) atoms.

Table 2. Selected bond lengths (Å) and angles (°) for $[Ni(L^3)(H_2O)_2](ClO_4)_2$

Ni−N2	1.997(6)	Ni−N3	2.002(6)
Ni−N4	2.071(6)	Ni−N1	2.088(6)
Ni−O2	2.100(6)	Ni−O1	2.118(5)
N2−Ni−N3	82.8(2)	N2−Ni−N4	161.5(3)
N3−Ni−N4	78.9(3)	N2−Ni−N1	78.5(2)
N3−Ni−N1	161.2(2)	N4−Ni−N1	119.9(2)
N2−Ni−O2	91.5(3)	N3−Ni−O2	95.0(2)
N4−Ni−O2	87.3(2)	N1−Ni−O2	88.0(2)
N2−Ni−O1	94.4(3)	N3−Ni−O1	92.4(2)
N4−Ni−O1	89.2(2)	N1−Ni−O1	86.6(2)
O2−Ni−O1	171.1(3)		

Hard donors, like oxygen atoms, coordinated along the axial direction force the metal ion to sit in the basal plane. Individual π-conjugated chelate rings are essentially completely planar (mean deviation 0.01 Å in both cases). The dimethylene-bridged chelate ring [Ni, N(2), C(8), C(9), N(3)] is only approximately planar (mean deviation 0.08 Å) as compared to the π-conjugated chelate fragments. The overall planarity of the $Ni(L^3)$ motif (mean deviation 0.08 Å) is disturbed because of the twisted dimethylene bridging segment (see inset, Figure 2). The chelate bite angles of N(4)−Ni−N(3) and N(1)−Ni−N(2) are 78.9(3) and 78.5(2)°, respectively, and are less than that observed for N(2)−Ni−N(3) [82.8(2)°]. Like **1a**, the difference in bite angles (>4°) is fully consistent with the varying degree of flexibility of the chelate rings. A comparison between the $Ni-N^p$ and $Ni-N^i$ distances clearly reveals a bond shortening of about 0.08 Å (on average) for the latter $Ni-N^i$ type, attributable to additional d(metal) → π*(C=N) back-bonding. Indeed this dative back-bonding is facilitated in presence of the *trans* N^p atom (strong σ-donor) sharing the same d orbital of the metal as the N^i donor. The average $Ni-N^p$ distance in **2a** is appreciably shorter (ca. 0.04 Å) than that observed for **1a**. The underlying reason presumably arises from the different relative orientations of the N^p and N^i donor atoms around the metal centres (*cis* for **2a** and *trans* for **1a**), inducing the pyridyl moiety to act as a better σ-donor in **2a**. The $Ni-O^w$ bonds are relatively weak[15,16] compared to other aquated Ni^{II} systems. The presence of intermolecular hydrogen-bonding accounts for the lengthening of the $Ni-O^w$ bonds, and is primarily an electronic effect. The effect of this unsymmetrical hydrogen bonding through two-coordinated water molecules is reflected in a bending of the O^w-Ni-O^w axis, making an angle of 171.1(3)°.

The uncoordinated perchlorate ions of **2a** form a hydrogen-bonded network with the two axially coordinated water molecules of the cationic part of the complex. Two water molecules of the Ni^{II} complex cation are engaged in three unsymmetrical O···O hydrogen-bond contacts with two open ONN triangular faces (average surface area, ≈4.1 $Å^2$) avoiding unwanted steric interactions. The molecular packing diagram reveals that the coordinated water molecules of a cation form hydrogen bonds with perchlorate ions belonging to two different asymmetric units. The relevant O···O contacts [O(1E)···O(8A): 2.850(6) Å, O(2E)···O(3C): 2.876(8) Å and O(2E)···O(10E): 2.722(8) Å] generate a chain-like cationic assembly in which alternating cations lie in an almost parallel fashion, as illustrated in Figure 3.

Electronic Spectra

The electronic spectra of the four complexes **1a**, **1b**, **2a** and **2b** were recorded both in the solid state (nujol mull)

 © 2004 Wiley-VCH Verlag GmbH & Co. KGaA, Weinheim

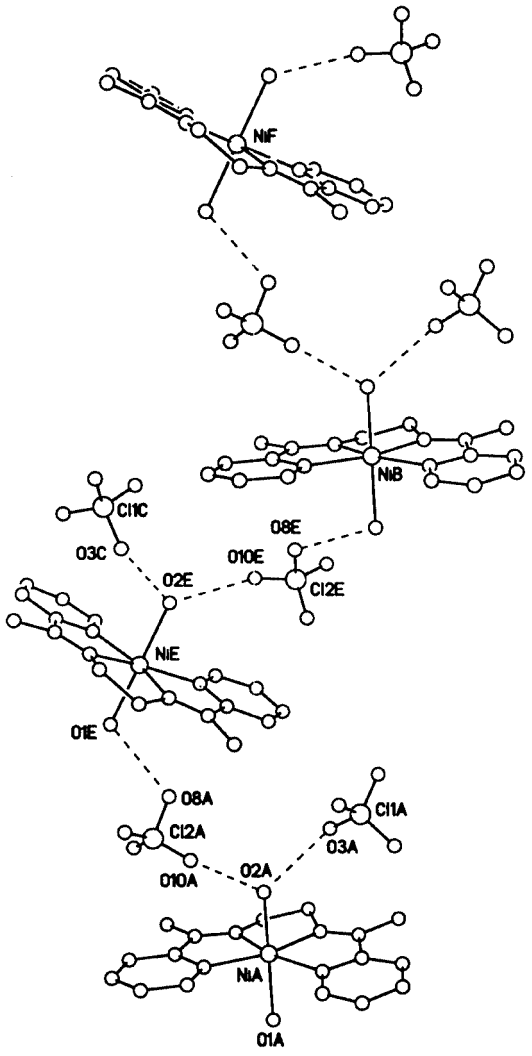

Figure 3. Molecular packing view of **2a** along the *x*-direction

and in acetonitrile solution. No significant differences were observed. A broad band is observed near 800 nm, well separated from the second transition at about 510 nm for both **1** and **2**. The third d-d band appears near 350 nm and is partly obscured by a strong charge-transfer transition. The three absorption peaks are assigned to transitions from the $^3A_{2g}$ ground state to $^3T_{2g}$, $^3T_{1g}(F)$ and $^3T_{1g}(P)$ excited states. In addition, a weak peak appears near 750 nm for complexes **2**, interpretable on the basis of a spin-forbidden $^3A_{2g} \rightarrow {}^1E_g$ transition. The calculated values of *Dq* lie in the range 1250−1260 cm^{-1} for all complexes, and are in agreement with literature values.[17,18] The reddish-brown Ni^{III} complexes **3** are characterised by an LMCT transition at about 425 nm with a shoulder near 645 nm.

Electrochemistry

With the aim of investigating the extent of stabilisation of nickel(II) species towards both oxidation and reduction, and thereby the possibility of accessing of variable valence states, cyclic voltammetry experiments were performed on **1** and **2** (Table 3).

Table 3. Electrochemical data for all divalent nickel complexes

Compound	$E_{1/2}$/V (ΔE_p/mV)[a]	
	Ni^{III}-Ni^{II} couple	Ni^{IV}-Ni^{III} couple
1a	0.95 (110)	1.69
1b	0.96 (110)	1.72
2a	0.85 (100)	1.78
2b	0.87 (100)	1.80

[a] ΔE_p = Peak-to-peak separation.

$[Ni(L^1)_2](ClO_4)_2$ and $[Ni(L^2)_2](ClO_4)_2$ are electroactive in acetonitrile solution (TEAP as supporting electrolyte) displaying two one-electron cyclic voltammetric responses with $E_{1/2}$ near +0.95 and +1.70 V vs. the saturated calomel electrode (SCE). Type **1** complexes undergo chemically reversible ($i_{pa}/i_{pc} \approx 1$) and electrochemically quasi-reversible (ΔE_p = 110 mV) one-electron oxidative responses due to the $[Ni^{III}(L^{1/2})_2]^{3+}/[Ni^{II}(L^{1/2})_2]^{2+}$ couple, near 0.95 V as observed for bis-pyridylazonaphthol-chelated complexes of Ni^{II}.[19] Appreciable reversibility is also inferred from the i_{pa},i_{pc} vs. $\nu^{1/2}$ plot, which is nearly constant for different scan rates (0.025, 0.05, 0.075 and 0.1 V/sec). The irreversible redox signal encountered near +1.70 V is attributed to the $Ni^{4+/3+}$ response. No voltammetric response consistent with a $Ni^{2+/1+}$ reduction is observed. Further, absence of a $Ni^0(s) \rightarrow Ni^{2+}$ stripping peak emphasises the reluctance of $[Ni^{II}(L^{1/2})_2]^{2+}$ to undergo a two-electron reduction. The relevant electron-transfer processes correlating metal valence span from +2 to +4 can be represented by Equation (1).

$$[Ni^{IV}(L^{1/2})_2]^{4+} \underset{-e^-}{\overset{+e^-}{\rightleftharpoons}} [Ni^{III}(L^{1/2})_2]^{3+} \underset{-e^-}{\overset{+e^-}{\rightleftharpoons}} [Ni^{II}(L^{1/2})_2]^{2+} \quad (1)$$

Such a relatively high $E_{1/2}$ value for the $Ni^{3+/2+}$ redox transformation is typical in complexes where nickel is in a mixed sulfur-nitrogen coordination environment.[20] Even higher $E_{1/2}$ values (ca. 1.6 V) have been reported for the $[Ni(bipy)_3]^{3+}/[Ni(bipy)_3]^{2+}$ couple.[21] The absence of any satellite response is fully consistent with the exclusive occurrence of one isomer (*cis-trans-cis*), in solution.

The redox behaviours of $[Ni(L^3)(H_2O)_2]$ $(ClO_4)_2$ and $[Ni(L^4)(H_2O)_2]$ $(ClO_4)_2$ follow a similar trend as **1a** and **1b**. Complex **2** in acetonitrile exhibits a quasi-reversible (ΔE_p = 100 mV) one-electron oxidation near 0.87 V consistent with the $[Ni^{III}(L^{3/4})(H_2O)_2]^{3+}/[Ni^{II}(L^{3/4})(H_2O)_2]^{2+}$ couple. The observed shift (in 0.08 V) of the $E_{1/2}$ value toward negative potential compared to the $E_{1/2}$ observed for $[Ni(L^{1/2})_2]^{3+/2+}$ accentuates the relative stabilisation of the Ni^{III} species derived from type **2** complexes. The *trans* disposition of the two imine donor motifs in $[Ni(L^{1/2})_2]^{2+}$ which becomes a *cis* orientation for $[Ni(L^{3/4})(H_2O)_2]^{2+}$ obviously facilitates greater delocalisation of the metal electron density, resulting in a higher potential barrier for the formation of Ni^{III} species from the latter complexes. This was observed experimentally from the irreversible peak near +1.80 V, ascribed to a

 © 2004 Wiley-VCH Verlag GmbH & Co. KGaA, Weinheim

$Ni^{4+/3+}$ redox process. This oxidative response is shifted to positive potential by 0.10 V in comparison with the $Ni^{4+/3+}$ couple for **1**. Like **1**, no $[Ni^{II}(L^{3/4})(H_2O)_2]^{2+}/[Ni^{I}(L^{3/4})(H_2O)_2]^{1+}$ redox couple is observed in acetonitrile solution.

In order to exclude any possibility of rapid isomerisation, cyclic voltammograms of **1** and **2** were run at various temperatures. Strong $Ni^{3+/2+}$ and $Ni^{4+/3+}$ responses for **1** and **2** were observed at 288 and 308 K at very nearly the same formal potential, and with similar current heights, as observed for the cyclic voltammograms recorded at 298 K (discussed earlier). Therefore, in this context the temperature effect upon the redox couples is not significant.

IR Spectra and Magnetism

The two primary NH_2 stretching modes are seen in type **1** complexes near 3340 and 3290 cm^{-1} as sharp bands (doublet) for the asymmetric and symmetric vibrations, respectively. The imine (C=N) stretch appears at about 1660 cm^{-1}, and the red shift of this C=N absorption of about 20 cm^{-1} on going from the free ligands (L^1, L^2) to the complexes indicates the weak π-accepting behaviour of the chelated ligands. The type **2** complexes exhibit a broad band in the range 3410−3440 cm^{-1}, assigned to the antisymmetric and symmetric O−H stretching vibrations of coordinated water molecules. ν_{Ni-O} appears near 450 cm^{-1} for **2**.[22] The diagnostic C=N stretch is observed near 1650 cm^{-1}, and is shifted to lower frequency by about 30 cm^{-1} relative to the free ligands. The difference in imine stretching frequencies of complexes **1** and **2** confirms the greater electron-withdrawing effect of the chelating bis-Schiff bases (L^3, L^4) in the latter. Broad structured ν_3 and sharp ν_4 vibrations of the perchlorate counteranion are observed near 1100 and 630 cm^{-1} for **1** and **2**, respectively.

The effective magnetic moment data of complexes **1** and **2** (polycrystalline state) clearly confirm the presence of two unpaired electrons ($t_2^6e^2$) in a pseudo-octahedral environment, in agreement with a high-spin configuration ($S = 1$). The magnetic moment values of 3.12, 3.15, 3.06 and 3.05μ_B at 298 K for **1a**, **1b**, **2a** and **2b**, respectively, suggest an appreciable orbital contribution to the spin-only moments.[23]

NMR Spectra

The ^1H NMR spectra of **1** (bulk material, in $[D_6]$DMSO) display paramagnetically shifted resolved signals of the aromatic, aliphatic and amino protons. The pyridyl and methylene proton resonances occur in the ranges $\delta = 6-12$ and $-12-45$ ppm, respectively. The methyl (**1a**) and aldimine (**1b**) hydrogen atom signals appear as singlets in the region $\delta = 2.5-3.5$ and 8−10 ppm, respectively. The amino protons resonate at lower field in the region $\delta = 75-95$ ppm. The absence of satellite peaks clearly confirms the exclusive occurrence of one isomer. The distinct spin-spin structures of the corresponding signals remove any scope for a rapid equilibrium between the possible isomers in solution. These results mean that the stereochemistry of **1** in the solid state is also retained in solution and no interconversion takes place as this would otherwise result in an averaging of nonequivalent protons.

Similarly in **2**, the pyridyl and methylene proton signals appear in the region $\delta = 7-14$ and $-7-30$ ppm respectively. The methyl (**2a**) and aldimine (**2b**) hydrogen resonances occur in similar regions to those of **1**. The aqua hydrogen resonances fall in the range $\delta = 60-85$ ppm. The large range of the NMR signals of **2** is consistent with its paramagnetic nature.

Thermal Analysis and Structural Transformation

Complexes **2a** and **2b** are both green and possess an octahedral geometry with axially coordinated water molecules. The TG curve reveals that upon heating both **2a** and **2b** undergo dehydration in the temperature range 50−95 °C and 60−100 °C, respectively, corresponding to the weight loss of two water molecules (observed: 6.96 and 7.01%; calculated: 6.43 and 6.77% for **2a** and **2b**, respectively). The anhydrous compounds begin to decompose at 275 and 270 °C, respectively, indicating their high thermal stability.

The colour of the samples changes from green to red during dehydration and this colour change is reversed on exposure to air for one day, suggesting a possible rehydration. To rationalize the observed colour change we performed magnetic susceptibility and spectral measurements of the red complexes. The magnetic study (300 K) revealed the diamagnetic nature of the dehydrated compounds, which is further supported by the solid-state electronic spectra (nujol mull), typical of square-planar Ni^{II} complexes (single peak at $\lambda_{max} \approx 480$ nm). Therefore the dehydration process is definitely accompanied by a structural transformation [octahedral (green) → square planar (red)] around the metal centre. It should be noted that this type of colour change associated with a structural transformation has been reported[10] for several bis-diamine complexes of Ni^{II}, but to the best of our knowledge is uncommon in complexes incorporating tetradentate bis-Schiff base ligands.

Electrosynthesis of $[Ni(L^{1/2})_2]^{3+}$: EPR and Magnetic Evidence

The search for trivalent analogues of **1** and **2** prompted us to carry out electrochemical oxidation (coulometrically) in dry acetonitrile solvent at 1.25 and 1.20 V respectively. The ratio of the observed coulomb count and the calculated coulomb count for the one-electron transfer is very close to unity (0.97 for **1a** and 0.98 for **1b**), suggesting an almost quantitative one-electron oxidation of Ni^{II} precursors to the Ni^{III} derivatives. The cyclic voltammograms of $[Ni(L^{1/2})_2]^{3+}$ (initial scan cathodic) are virtually superimposable with those of $[Ni(L^{1/2})_2]^{2+}$ (initial scan anodic). The observed redox behaviour of the oxidised Ni^{III} species confirms that the coulometric oxidation of $[Ni(L^{1/2})_2]^{2+}$ to $[Ni(L^{1/2})_2]^{3+}$ is accompanied by no major structural change. The uncontrolled decomposition of electrogenerated oxidised species of **2** in solution ruled out any possibility of isolation and further studies. They exist in solution only on the timescale of the voltammetry measurement, thus demonstrating the role of purely kinetic stabilisation[24] in trivalent nickel.

 © 2004 Wiley-VCH Verlag GmbH & Co. KGaA, Weinheim

The EPR spectroscopic data of the compounds are listed in Table 4. Polycrystalline samples of **3** at 298 K exhibit an axial spectrum[25] with $g_\perp$ and $g_\parallel$ values of 2.14 and 2.02 respectively (Figure 4). No superhyperfine structure of the $g_\parallel$ component attributed to σ-coupling with the two ^{14}N (imine) atoms coordinated in a mutual *trans* manner is observed. The bond-angle order N^i-Ni-N^i (ca. 179°) > N^p-Ni-N^a (ca. 158°) in the *cis-trans-cis* isomer of $[Ni(L^1)_2]^{2+}$ implies that both steric and electronic requirements will favour the orientation of a linear N^i-Ni-N^i moiety along the *z*-direction. Thus we can reasonably assume that this is also the case for **3** ($3d^7$). The observed *g* inequality ($g_\perp > g_\parallel$) is fully consistent with a tetragonally distorted octahedral geometry with elongation of the axial bond along the *z*-axis.[2,26,27] Hence a strong Jahn−Teller effect must be operative to lift the degeneracy of the e orbital set following the energy order $3d_{x^2-y^2} > 3d_{z^2}$. The spectra of **3** in a frozen (77 K) acetonitrile/toluene (2:1) glass also follow a similar axial pattern as observed for polycrystalline state, strongly indicating that the coordination environment is retained (in solid and solution). The axial spectra at 77 K are important as they suggest that the rhombic field is too weak to split the perpendicular absorption into individual g_{xx} and g_{yy} tensors. The *g* values for these complexes lie well above the spin-only value of a free electron (2.002). This excludes any possibility of the formation of Ni^{II} stabilised ligand radicals. Therefore, the observed EPR signals arise from one metal-centred unpaired electron, in agreement with the trivalent oxidation state.[28]

Table 4. EPR data for trivalent Ni^{III} species.

Compound	$g_\perp$	$g_\parallel$
3a	2.138,[a] 2.137[b]	2.018,[a] 2.018[b]
3b	2.139,[a] 2.139[b]	2.017,[a] 2.018[b]

[a] Polycrystalline state at 298 K. [a] In acetonitrile/toluene (2:1) glass at 77 K.

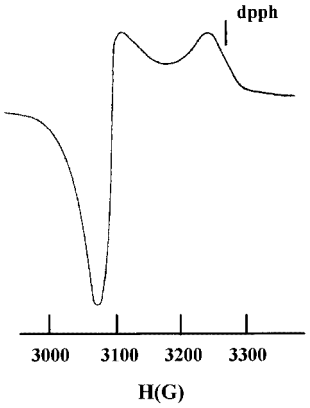

Figure 4. X-band EPR spectrum of $[Ni(L^1)_2]^{3+}$ (**3a**) in the polycrystalline solid state (298 K); instrument settings: power, 30 dB; frequency, 9.1 GHz; modulation, 100 KHz; scan time, 2 min; sweep centre, 3200 G

Further evidence for trivalent nickel complexes is provided by the magnetic moment data. The bulk magnetic moment for **3** at 298 K is consistent with a one-electron paramagnetic behaviour. The effective magnetic moment values of 2.12 and 2.09 μ_B for **3a** and **3b**, respectively, mean that the Ni^{III} complexes are present in a low spin ($t_2^6\ e^1$) configuration with $S = 1/2$. A large orbital contribution to the paramagnetism[24] is noticed, as expected. Unfortunately we were unable to grow single crystals of either **3a** or **3b**, although all the EPR and magnetic data unequivocally suggest the formation of trivalent nickel complexes.

Conclusion

The tridentate and tetradentate ligands presented here are characterised by their different nitrogen donor sites (pyridyl, imine and amino), and their different binding abilities towards a Ni^{II} centre provide us with NiN_6 and NiN_4O_2 types of coordination complexes. Bis-chelates were achieved without deprotonating the amino group. The *cis-trans-cis* isomer of **1** is the only isomer obtained due to steric relaxation, which completely offsets any electronic disadvantage, whereas the *cis-cis-trans* form of **2** is favoured by both steric and electronic factors. The effect of the low π-acidity of the ligands is clearly shown by the predominant localised nature of the bonding in the resulting complexes. Accessible cyclic voltammetric formal potentials of the Ni^{3+}/Ni^{2+} couple for **1** and **2** allowed us to synthesise the related Ni^{III} complexes electrochemically, although the complex formed from **2** is not particularly stable, unlike that formed from **1**.

Proper tuning of the coordination modes of tridentate ligands containing pyridyl, imine and amino donor atoms can afford stable trivalent nickel complexes. The design of such ligands with variable polymethylene spacers and the study of their efficacy to stabilize the higher oxidation states of different metals are in progress.

Experimental Section

Starting Materials: $Ni(ClO_4)_2{\cdot}6H_2O$, 2-acetylpyridine and 2-pyridinecarboxaldehyde were purchased from Aldrich and used as received. HPLC-grade acetonitrile was used for electrochemical, conductivity and UV/Vis work and all other chemicals and solvents were of reagent grade and were used as received.

CAUTION: *Perchlorate salts are hazardous and may explode.*

Physical Measurements: Spectral measurements were carried out using the following equipment: UV/Vis (both in acetonitrile solution and solid), Hitachi U-3501 spectrophotometer fitted with thermostatted cell compartments (sh is shoulder). IR (KBr disc), Perkin−Elmer RXI FT-IR spectrometer and Nicolet Magna IR 750 Series II. A Perkin−Elmer 2400 Series II elemental analyzer was used for microanalysis (C, H, N). EPR spectra was recorded at the X-band on a Varian E-109C spectrometer and calibrated with respect to diphenylpicrylhydrazyl (DPPH, $g = 2.0037$). Solution electrical conductivity was measured in acetonitrile with a Phillips PR 9500 bridge using a platinized electrode; solute concentration was approx. 10^{-3} M. ^1H NMR spectra were recorded on a

 © 2004 Wiley-VCH Verlag GmbH & Co. KGaA, Weinheim

Bruker FT 300 MHz spectrometer. The thermal analysis (TG-DTA) was carried out on a Metler Toledo TGA/SDTA 851 thermal analyzer under a dynamic atmosphere of dinitrogen (flow rate: 30 mL·min^{-1}). The sample was heated in an alumina crucible at a rate of 10 °C·min^{-1}. Magnetic susceptibilities were measured on a PAR 155 vibrating-sample magnetometer. Electrochemical measurements were performed under a dinitrogen atmosphere using a PAR model Versastat-2 electrochemical analyzer, with a platinum working electrode. The supporting electrolyte was tetraethylammonium perchlorate (TEAP), and the potentials are referenced to the saturated calomel electrode (SCE) without junction correction.

L^1: Ethylenediamine (0.9 g, 15 mmol) and 2-acetylpyridine (1.815 g, 15 mmol) were mixed in 20 mL of methanol and then refluxed for 3 h. The resulting solution was evaporated to 5 mL and cooled to room temperature. Upon cooling of the solution a yellow solid precipitated. The solid was collected by filtration and was recrystallised from hot methanol affording pale yellow cubes, which were dried in vacuo over fused $CaCl_2$. Yield: 2.11 g (85%). $C_9H_{13}N_3$: calcd. C 66.23, H 8.03, N 25.74; found C 66.17, H 8.07, N 25.81. IR: $\tilde{\nu}$ = 3345−3285 cm^{-1} (ν_{NH_2}), 2950−2850 (ν_{C-H}), 1678 ($\nu_{C=N}$), 1590 (δ_{N-H}), 1447−1302 ($\nu_{pyridine\ ring}$).

L^2: This ligand was prepared by a procedure similar to that for L^1, starting with ethylenediamine (0.9 g, 15 mmol) and 2-pyridinecarboxaldehyde (1.605 g, 15 mmol), to obtain a light-yellow semi-solid which, on recrystallisation from *n*-hexane, gave pale-yellow needles. Yield: 1.84 g (82%). $C_8H_{11}N_3$: calcd. C 64.40, H 7.43, N 28.17; found C 64.32, H 7.37, N 28.23. IR: $\tilde{\nu}$ = 3345−3281 cm^{-1} (ν_{NH_2}), 2952−2847 (ν_{C-H}), 1677 ($\nu_{C=N}$), 1591 (δ_{N-H}), 1450−1302 ($\nu_{pyridine\ ring}$).

L^3: Ethylenediamine (0.9 g, 15 mmol) and 2-acetylpyridine (3.630 g, 30 mmol) were mixed in 25 mL of methanol and then refluxed for 7 h. The resulting solution was evaporated to obtain a yellow semi-solid mass which, on recrystallisation from *n*-hexane, afforded light-yellow needles. The needles were dried in vacuo over fused $CaCl_2$. Yield: 2.44 g (61%). $C_{16}H_{18}N_4$: calcd. C 72.15, H 6.81, N 21.04; found C 72.22, H 6.75, N 21.09. IR: $\tilde{\nu}$ = 2990−2880 cm^{-1} (ν_{C-H}), 1680 ($\nu_{C=N}$), 1450−1307 ($\nu_{pyridine\ ring}$).

L^4: This ligand was prepared by a similar procedure to that employed for L^3, starting with ethylenediamine (0.9 g, 15 mmol) and 2-pyridinecarboxaldehyde (3.210 g, 30 mmol) to give light yellow microcrystals. Yield: 2.29 g (64%). $C_{14}H_{14}N_4$: calcd. C 70.57, H 5.92, N 23.51; found C 70.51, H 5.98, N 23.45. IR: $\tilde{\nu}$ = 2992−2877 cm^{-1} (ν_{C-H}), 1680 ($\nu_{C=N}$), 1451−1306 ($\nu_{pyridine\ ring}$).

$[Ni(L^1)_2](ClO_4)_2$ (1a): $Ni(ClO_4)_2·6H_2O$ (0.165 g, 0.45 mmol) dissolved in the minimum volume of water was added to a solution of L^1 (0.163 g, 0.99 mmol) in methanol (30 mL), and heated to reflux for 2 h to afford a brown solution. The resulting solution was cooled to room temperature and filtered. The filtrate was stripped of solvent under reduced pressure. The residue was washed twice (15 mL each) with hexane to remove the excess ligand and then dried in vacuo over fused $CaCl_2$. Yield: 242 mg (92%). $C_{18}H_{26}Cl_2N_6NiO_8$: calcd. C 37.02, H 4.49, N 14.39; found C 37.09, H 4.45, N 14.46. IR: $\tilde{\nu}$ = 3340, 3290 cm^{-1} (ν_{NH_2}), 2940−2862 (ν_{C-H}), 1658 ($\nu_{C=N}$), 1596 (δ_{N-H}), 1445−1305 ($\nu_{pyridine\ ring}$), 1089, 627 (ν_{ClO_4}).

$[Ni(L^2)_2](ClO_4)_2$ (1b): This complex was prepared by a similar procedure. Yield: 226 mg (90%). $C_{16}H_{22}Cl_2N_6NiO_8$: calcd. C 38.57, H 3.99, N 15.12; found C 38.53, H 4.05, N 15.07. IR: $\tilde{\nu}$ = 3341, 3288 cm^{-1} (ν_{NH_2}), 2942−2862 (ν_{C-H}), 1658 ($\nu_{C=N}$), 1594 (δ_{N-H}), 1441−1307 ($\nu_{pyridine\ ring}$), 1090, 628(ν_{ClO_4}).

$[Ni(L^3)(H_2O)_2](ClO_4)_2$ (2a): $Ni(ClO_4)_2·6H_2O$ (0.304 g, 0.83 mmol) dissolved in 10 mL of water was added to a solution of L^3 (0.266 g, 0.99 mmol) in methanol (40 mL), and heated to reflux for 3 h. The solution turned green. It was then filtered and the filtrate cooled to room temperature. Solvent removal from the filtrate under reduced pressure gave a green residue which was washed twice (10 mL each) with hexane to remove the excess ligand. The compound was then dried in vacuo over fused $CaCl_2$. Yield: 433 mg (93%). $C_{16}H_{22}Cl_2N_4NiO_{10}$: calcd. C 34.32, H 3.96, N 10.01; found C 34.26, H 4.01, N 10.04. IR: $\tilde{\nu}$ =3435−3413 cm^{-1} (ν_{O-H}), 2982−2885 (ν_{C-H}), 1647 ($\nu_{C=N}$), 1603 (δ_{O-H}), 1452−1307 ($\nu_{pyridine\ ring}$), 1096, 626(ν_{ClO_4}), 748 (ρ_r), 609 (ρ_w), 449 (ν_{Ni-O}).

$[Ni(L^4)(H_2O)_2](ClO_4)_2$ (2b): This complex was prepared by a similar procedure. Yield: 407 mg (92%). $C_{14}H_{18}Cl_2N_4NiO_{10}$: calcd. C 31.61, H 3.41, N 10.53; found C 31.55, H 3.48, N 10.50. IR: $\tilde{\nu}$ = 3437−3410 cm^{-1} (ν_{O-H}), 2981−2879 (ν_{C-H}), 1647 ($\nu_{C=N}$), 1604 (δ_{O-H}), 1449−1303 ($\nu_{pyridine\ ring}$), 1095, 625(ν_{ClO_4}), 747 (ρ_r), 610 (ρ_w), 449 (ν_{Ni-O}).

$[Ni(L^1)_2](ClO_4)_3$ (3a): This complex was prepared by an electrochemical technique. The complex $[Ni(L^1)_2](ClO_4)_2$ (0.146 g, 0.25 mmol) was dissolved in dry acetonitrile (30 mL) and TEAP was added as supporting electrolyte. The brown solution was then subjected to coulometric oxidation at 1.25 V vs. SCE under a dinitrogen atmosphere. The solution gradually turned reddish-brown and the oxidation was stopped when the Coulomb count corresponded to a one-electron oxidation. The solvent was then removed under reduced pressure to obtain a reddish-brown solid mixed with TEAP. The residue was dissolved in dichloromethane and TEAP was filtered off. Solvent removal from the filtrate afforded a reddish-brown compound which was then dried in vacuo over fused $CaCl_2$. Yield: 150 mg (88%). $C_{18}H_{26}Cl_3N_6NiO_{12}$: calcd. C 31.63, H 3.83, N 12.30; found C 31.58, H 3.80, N 12.34.

$[Ni(L^2)_2](ClO_4)_3$ (3b): This complex was synthesised by a similar electrochemical procedure in 89% yield. $C_{16}H_{22}Cl_3N_6NiO_{12}$: calcd. C 29.32, H 3.38, N 12.82; found C 29.36, H 3.33, N 12.76.

X-ray Crystallography: Brown or green single crystals of the complexes **1a** and **2a**, respectively, were grown by slow evaporation of solvent from a methanol solution. Data were collected on a Siemens SMART CCD diffractometer with graphite-monochromated Mo-K_α radiation (λ = 0.71073 Å) by the phi and omega scan technique in the range 3° ≤ 2θ ≤ 50° at 293 K. All the data were corrected for Lorentz-polarisation and absorption.[29] The structures were generated by direct methods followed by successive Fourier synthesis and refined by full-matrix least-squares based on F^2. All non-hydrogen atoms were made anisotropic. All the hydrogen atoms (barring water hydrogen atoms) for **2a** were added at the calculated positions. Hydrogen atoms apart from two amino groups (N3, N6) were added at the calculated positions for **1a**. Calculations were performed using the SHELXTAL™ v. 5.03 program package.[30] Significant crystal data are listed in Table 5.
CCDC-216308 (for **1a**) and -216309 (for **2a**) contain the supplementary crystallographic data for this paper. These data can be obtained free of charge at www.ccdc.cam.ac.uk/conts/retrieving.html [or from the Cambridge Crystallographic Data Centre, 12 Union Road, Cam-

 © 2004 Wiley-VCH Verlag GmbH & Co. KGaA, Weinheim

Table 5. Crystal data for complexes **1a** and **2a**

Complex	**1a**	**2a**
Formula	$C_{18}H_{26}Cl_2N_6NiO_8$	$C_{16}H_{22}Cl_2N_4NiO_{10}$
M	584.06	559.99
System	monoclinic	orthorhombic
Space group	$P2_1/c$	$P2_12_12_1$
a (Å)	15.5216(13)	11.3061(10)
b (Å)	10.1708(9)	12.9531(12)
c (Å)	15.7458(14)	15.803(2)
α (°)	90	90
β (°)	97.305(2)	90
γ (°)	90	90
V (Å^3)	2465.6(4)	2314.4
Z	4	4
D (mg m^{-3})	1.573	1.607
T (K)	293	293
μ (mm^{-1})	1.059	1.128
Independent reflections	4375	3639
R_{int}	0.0560	0.0347
Collected reflections $[I > 2\sigma(I)]$	10189	7779
$R1$, $wR2$	0.0685, 0.1452	0.0558, 0.1435

bridge CB2 1EZ, UK; Fax: (internat.) +44-1223/336-033; E-mail: deposit@ccdc.cam.ac.uk].

Acknowledgments

One of the authors (S. Banerjee) is thankful to the University Grants Commission (UGC), India, for awarding a Junior Research Fellowship (Sanction no. UGC/548/jr. Fellow Sc.2001/2002).

[1] L. Sacconi, F. Mani, A. Bencini, in *Comprehensive Coordination Chemistry* (Eds.: G. Wilkinson, R. D. Gillard and J. A. McCleverty), Pergamon Press, Oxford, **1987**, vol. 5, ch. 50, pp. 1−347.
[2] K. Nag, A. Chakravorty, *Coord. Chem. Rev.* **1980**, *33*, 87.
[3] L. Gomes, E. Pereira, B. Castro, *J. Chem. Soc., Dalton Trans.* **2000**, 1373.
[4] A. Chakravorty, *Isr. J. Chem.* **1985**, *25*, 99.
[5] [5a] *The Bioinorganic Chemistry of Nickel* (Ed.: J. R. Lancaster, Jr.), VCH, Deerfield Beach, FL, **1988.** [5b]S. M. Hecht, *Acc. Chem. Res.* **1986**, *19*, 383. [5c] Y. Sigura, T. Takita, H. Umezawa,, *Met. Ions Biol. Syst.* **1985**, *19*, 81.
[6] [6a] *Metal-Catalyzed Oxidations of Organic Compounds* (Eds.: R. A. Sheldon and J. K. Kochi), Academic Press: New York, **1981**, 359. [6b] *Catalytic Activation of Dioxygen by Metal Complexes* (Ed.: L. I. Simandi), Kluwer Academic Publishers: Dordrecht, **1992**, 318.
[7] M. T. Maede, D. H. Busch, in *Progress in Inorganic Chemistry* (Ed.: S. J. Lippard), Wiley Interscience: New York, **1985**, 33 and references cited therein.
[8] V. Alexander, *Chem. Rev.* **1995**, *95*, 273 and references cited therein.
[9] J. Lehn, *Pure Appl. Chem.* **1980**, *52*, 2441 and references cited therein.
[10] Y. Ihara, Y. Fukuda, K. Sone, *Inorg. Chem.* **1987**, *26*, 3745 and references cited therein.
[11] S. R. Cooper, *Acc. Chem. Res.* **1988**, *21*, 141.
[12] C. R. Lucas, S. Liu, *J. Chem. Soc., Dalton Trans.* **1994**, 185.
[13] D. Shellmann, H.-P. Neuner, F. Knoch, *Inorg. Chim. Acta* **1991**, *190*, 61.
[14] I. Castro, M. L. Calatayud, J. Sletten, F. Lloret, M. Julve, *J. Chem. Soc., Dalton Trans.* **1997**, 811.
[15] [15a] R. Soules, F. Dahan, J. P. Laurent, P. Castan, *J. Chem. Soc., Dalton Trans.* **1988**, 587. [15b] B. Q. Ma, S. Gao, H. L. Sun, G. X. Xu, *J. Chem. Soc., Dalton Trans.* **2001**, 130.
[16] J. A. C. van Ooijen, J. Reedijk, A. L. Spek, *Inorg. Chem.* **1979**, *18*, 1184.
[17] [17a] E. I. Baucom, R. S. Drago, *J. Am. Chem. Soc.* **1971**, *93*, 6469. [17b] P. Krumholtz, *Struct. Bonding* **1971**, *9*, 139.
[18] [18a] M. A. Robinson, J. D. Curry, D. H. Buch, *Inorg. Chem.* **1963**, *2*, 1178. [18b] H. M. Fischer, R. C. Stoufer, *Inorg. Chem.* **1966**, *5*, 1172.
[19] S. Mukhopadhyay, D. Ray, *J. Chem. Soc., Dalton Trans.* **1995**, 2265.
[20] E. M. Martin, R. D. Bereman, *Inorg. Chim. Acta* **1991**, *188*, 221.
[21] B. J. Henne, D. E. Bartak, *Inorg. Chem.* **1984**, *23*, 369.
[22] I. Nakagawa, T. Shimanouchi, *Spectrochim. Acta* **1964**, *20*, 429.
[23] R. S. Drago, in *Physical Methods in Chemistry*, Saunders: Philadelphia, **1977**, Chapter 11.
[24] L. Fabbrizzi, D. M. Proserpio, *J. Chem. Soc., Dalton Trans.* **1989**, 229.
[25] [25a] G. A. Foulds, *Coord. Chem. Rev.* **1990**, *98*, 1−122. [25b] M. Schroder, *Coord. Chem. Rev.* **1986**, *71*, 139−234.
[26] A. G. Lappin, A. McAuley, *Adv. Inorg. Chem.* **1988**, *32*, 241.
[27] R. I. Haines, A. McAuley, *Coord. Chem. Rev.* **1981**, *39*, 77.
[28] A. Abragam and B. Bleaney, *Electron Paramagnetic Resonance of Transition Metal Ions*, Clarendon, Oxford, UK, **1970**.
[29] G. M. Sheldrick, SADABS, Absorption Correction Program, University of Göttingen, Germany, **1996**.
[30] G. M. Sheldrick, SHELXTL™ v. 5.03, Bruker analytical X-ray systems, Madison, WI, **1994**.

Received November 25, 2003
Early View Article
Published Online April 20, 2004

 © 2004 Wiley-VCH Verlag GmbH & Co. KGaA, Weinheim

Synthesis and Structure of New (Polyphosphane)ruthenium Complexes with the Hemilabile Ligand 2-(Diphenylphosphanyl)-1-methyl-1*H*-imidazole − An Unexpected Rearrangement of $[RuCl_2(PN)(PPh_3)_2]$

Gustavo Espino,[a] Félix A. Jalón,[b] Miguel Maestro,[c] Blanca R. Manzano,*[b] Mercedes Pérez-Manrique,[a] and Ana C. Bacigalupe[a]

Keywords: Ruthenium / Hemilabile ligands / Hydride ligands / Phosphanes / N,P ligands

Several Ru^{II} complexes containing the potentially bidentate ligand 2-(diphenylphosphanyl)-1-methyl-1*H*-imidazole [PPh_2MeIm (PN)] have been synthesised and characterised. Reaction of the ligand with $[RuCl_2(PPh_3)_3]$ in different molar ratios led to the formation of the complexes *trans*,*mer*-$[RuCl_2(PPh_3)_2(\kappa^2\text{-}P,N\text{–}PPh_2MeIm)]$ (**1**), *fac*-$[RuCl(PPh_3)(\kappa^2\text{-}P,N\text{-}PPh_2MeIm)_2]Cl$ (**2a**), *mer*-$[RuCl(PPh_3)(\kappa^2\text{-}P,N\text{-}PPh_2MeIm)_2]Cl$ (**2b**), *fac*-$[RuCl(\kappa^1\text{-}P\text{-}PPh_2MeIm)(\kappa^2\text{-}P,N\text{-}PPh_2MeIm)_2]Cl$ (**3a**), and *mer*-$[RuCl(\kappa^1\text{-}P\text{-}PPh_2MeIm)(\kappa^2\text{-}PN\text{-}PPh_2MeIm)_2]Cl$ (**3b**). Complex **1** evolves in solution to **2a**, **2b** and the dinuclear species $[(PPh_3)(\kappa^1\text{-}P\text{-}PPh_2MeIm)ClRu(\mu\text{-}Cl)_2Ru(PPh_3)(\kappa^1\text{-}P\text{-}PPh_2MeIm)Cl]$ (**4a**), $[(PPh_3)ClRu(\mu\text{-}Cl)_2(\mu^2\text{-}P,N\text{-}PPh_2MeIm)_2Ru(PPh_3)Cl]$ (**4b**), and $[(PPh_3)(\kappa^2\text{-}P,N\text{-}PPh_2MeIm)ClRu(\mu\text{-}Cl)_2Ru(PPh_3)(\kappa^2\text{-}P,N\text{-}PPh_2MeIm)Cl]$ (**4c**). It is proposed that the formation of the dinuclear derivatives involves an Ru–N bond-breaking step that demonstrates the hemilabile behaviour of the ligand. When 2 equiv. of the PN ligand were added to $[RuCl_2(cod)(bpzm)]$ [cod = 1,5-cyclooctadiene, bpzm = bis(pyrazol-1-yl)methane], the complex *cis*-*P*-$[RuCl_2(\kappa^1\text{-}PPh_2MeIm)(\kappa^2\text{-}PPh_2MeIm)]$ (**5**) was formed as the only product. The derivatives $[Ru(\kappa^2\text{-}PPh_2MeIm)_3]X_2$ [(X = PF_6 (**6**), BF_4 (**7**)] were obtained upon treatment of $[RuCl_2(arene)]_2$ (arene = *p*-cymene, benzene) with 2 equiv. of the corresponding silver salts and the PN ligand. Both the *fac* (**6a**, **7a**) and *mer* (**6b**, **7b**) forms were obtained. Two new hydride complexes were also synthesised: *mer*-$[RuHClL_2(\kappa^2\text{-}PPh_2MeIm)]$ [L = PPh_3 (**8**) or κ^1-PN (**9**)] by reaction of the PN ligand with $[RuHCl(PPh_3)_3]$ or [RuHCl(cod)(bpzm)], respectively. The molecular structure of **4b** and *fac*-**7a** was solved by an X-ray diffraction study. Complex **4b** has a dinuclear structure with two chloride bridges and two head-to-tail PN bridges. The derivative *fac*-**7a** is mononuclear. Both enantiomers — Δ and Λ — were observed in the same unit cell.

(© Wiley-VCH Verlag GmbH & Co. KGaA, 69451 Weinheim, Germany, 2004)

Introduction

Ruthenium(II) derivatives containing tertiary phosphane ligands are important precursors in catalytic processes, particularly hydrogenation.[1] For example, complexes of formula $[RuCl_2L_n]$, $[RuClHL_n]$ (n = 3, 4), $[RuCl_2(CO)L_3]$ or $[RuClH(CO)L_3]$ are efficient catalysts in the hydrogenation of alkenes,[2] alkynes,[2,3] aromatic heterocycles[4] or hydrocarbons,[5] aldehydes and ketones.[6] In many of these catalytic processes, cycles involving the decoordination of phosphanes or chlorides are involved.[1,2] For instance, $[RuCl_2(PPh_3)_3]$ is a classical starting point to give an active catalyst through phosphane[7] or chloride[8] dissociation. This process allows the coordination of substrates such as hydrogen or molecules that act as a hydrogen source, such as alcohols.[9] A theoretical alternative to the complete decoordination of a tertiary phosphane is the partial decoordination of a bidentate and hemilabile phosphane that probably causes only a minor effect on the electronic stability of the catalyst. With this possibility in mind, we envisaged the reaction of typical precursors like $[RuCl_2(PPh_3)_3]$ or $[RuClH(PPh_3)_3]$ with 2-(diphenylphosphanyl)-1-methyl-1*H*-imidazol[10] (PPh_2MeIm; Scheme 1), in different molar ratios, to obtain potential catalyst precursors with different structures and nuclearities. In order to compare our results and obtain complexes that are free of triphenylphosphane, we also used as starting materials $[RuCl_2(cod)(bpzm)]$

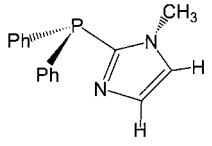

Scheme 1. PPh_2MeIm ligand

[a] Departamento de Química, Facultad de Ciencias, Universidad de Burgos,
Pza Misael Bañuelos s/n, 09001 Burgos, Spain
[b] Departamento de Química Inorgánica, Orgánica y Bioquímica, Universidad de Castilla-La Mancha,
13071 Ciudad Real, Spain
[c] Servicios Xerais de Apoio à Investigación, Universidade da Coruña,
Campus da Zapateira s/n, 15071 A Coruña, Spain

 © 2004 Wiley-VCH Verlag GmbH & Co. KGaA, Weinheim **DOI: 10.1002/ejic.200300892**

[cod = 1,5-cyclooctadiene, bpzm = bis(pyrazol-1-yl)methane] and $[RuCl_2(p\text{-cymene})]_2$ as halide precursors and [RuClH(cod)(bpzm)] as a hydride.[11] In contrast to the widely used phosphane 2-(diphenylphosphanyl)pyridine,[12] the use of PPh_2MeIm as a bidentate ligand offers a more strained bite angle. This situation can favour the partial decoordination of the phosphane group.

Results and Discussion

The following discussion concerns the synthesis and characterisation of the new Ru^{II} derivatives containing the hemilabile ligand PPh_2MeIm (PN). The discussion is divided according to the Ru species used as the starting material.

Reaction of PPh_2MeIm with $[RuCl_2(PPh_3)_3]$ − X-ray structure of $[(PPh_3)ClRu(\mu\text{-}Cl)_2(\mu^2\text{-}P,N\text{-}PPh_2MeIm)_2Ru(PPh_3)Cl]\cdot CH_2Cl_2$

The reaction of $[RuCl_2(PPh_3)_3]$ with the ligand PN was studied in different molar ratios and this led to the formation of different complexes containing either one, two or three ligands bonded to the ruthenium centre. When $[RuCl_2(PPh_3)_3]$ was heated under reflux with 1 equiv. of PN in CH_2Cl_2 the polyphosphane complex **1** was isolated in 89% yield [Equation (1)].

$$[RuCl_2(PPh_3)_3] + PN \rightarrow [RuCl_2(PPh_3)_2(\kappa^2\text{-}PN)]\,(\mathbf{1}) + PPh_3 \qquad (1)$$

The conductivity data indicate that **1** is a neutral molecule. The $^{31}P\{^1H\}$ NMR spectrum (in $CDCl_3$; see Table 1) of **1** consists of an AMX pattern with two *cis* ^2J ($^2J_{A,M}$ and $^2J_{A,X}$) and one *trans* ^2J ($^2J_{M,X}$) coupling constants. These data are in agreement with a *mer* disposition of the three P atoms. The high-field doublet of doublets [δ = −22.2 ppm (P_X)] is consistent with the formation of a four-membered chelate ring in the PN ligand.[13] The IR spectrum of complex **1** shows a single absorption band at 326 cm^{-1}, which is characteristic of ν(Ru−Cl) with mutual *trans*-chloride ions.[14,15] The FAB^+ mass spectrum is in complete agreement with the expected fragmentation pattern and contains a peak corresponding to the fragment $[RuCl(PPh_3)_2(PN)]^+$ at m/z = 927, which is the result of chloride loss from **1**. In subsequent steps, the loss of PPh_3 gives $[RuCl(PPh_3)(PN)]^+$ (m/z = 665), and $[RuCl(PN)]^+$ (m/z = 403). On the basis of these data, the structure of **1**, which must be present as a mixture of enantiomers, is believed to be that shown in Scheme 2.

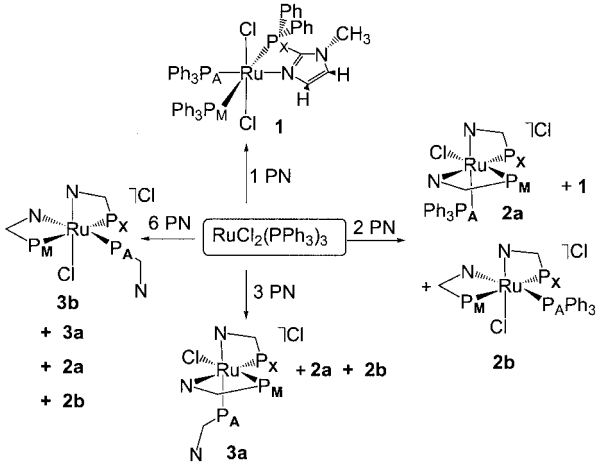

Scheme 2. Reaction scheme for the system $[RuCl_2(PPh_3)_3]/n$PN (n = 1, 2, 3, 6)

The reactions of $[RuCl_2(PPh_3)_3]$ with 2, 3 and 6 equiv. of the ligand PN were also investigated. These reactions led to the formation of four new complexes, as deduced from the corresponding $^{31}P\{^1H\}$ NMR spectra. The results can be summarised as follows (see Scheme 2): (i) When the Ru/PN ratio was 1:2, complex **1** was formed along with two new

Table 1. $^{31}P\{^1H\}$ NMR chemical shifts for the new complexes

Complex	Solvent	Spin system	δ [ppm]			J [Hz]		
			P_A	P_M or P_B	P_X	$^2J_{AM}$ or $^2J_{AB}$	$^2J_{AX}$	$^2J_{MX}$
mer-**1**	$CDCl_3$	AMX	43.70 dd	33.2 dd	−22.21 dd	29.00	32	322.15
fac-**2a**	$CDCl_3$	AMX	52.44 pt	7.55 pt	5.58 pt	36.01	28.2	27.51
mer-**2b**	$CDCl_3$	AMX	58.30 pt	−5.87 dd	−18.24 dd	31.73	26.3	304.02
fac-**3a**	$CDCl_3$	AMX	45.37 pt	15.91 pt	3.78 pt	32.02	33.6	32.03
mer-**3b**	$CDCl_3$	AMX	52.20 pt	−7.70 dd	−13.80 dd	31.31	28	312.81
4a	$CDCl_3$	AB	48.80 d	44.57 d	−	36.13	−	−
4b	$CDCl_3$	AM	68.09 d	19.43 d	−	36.63	−	−
4c	$CDCl_3$	AM	42.11 d	−1.12 d	−	25.32	−	−
5	$[D_6]$acetone[a]	AM	51.85 d	3.35 d	−	32.02	−	−
fac-**6a**[b]	$[D_6]$acetone	A_3	13.21 s	−	−	−	−	−
mer-**6b**[b]	$[D_6]$acetone	AMX	20.70 t	3.67[c] dd	−3.61[c] dd	26.93	26.91	290.52
fac-**7a**	$[D_6]$acetone	A_3	13.21 s	−	−	−	−	−
mer-**7b**	$[D_6]$acetone	AMX	20.70 t	3.67[c] dd	−3.61[c] dd	26.91	26.92	290.53
mer-**8**	C_6D_6	AMX	70.23 pt	53.82 dd	−14.90 dd	32.03	29.73	285.02
mer-**9**	C_6D_6	AMX	58.30 pt	40.49 dd	−10.00 dd	32.11	26.91	293.11

[a] At −90 °C. [b] The signal for the PF_6^- counteranion appears at δ = −143.2 (sept, $^1J_{F,P}$ = 708 Hz) ppm. [c] The assignment of P_M and P_X could be reversed.

 © 2004 Wiley-VCH Verlag GmbH & Co. KGaA, Weinheim

complexes (**2a** and **2b**). (ii) When the ratio was 1:3, complex **1** was not formed but **2a**, **2b** and a new complex (**3a**) were observed in the reaction medium. (iii) The reaction with a ratio of 1:6 led to the formation of **2a**, **2b**, **3a** and a new derivative (**3b**).

We were able to deduce the structures of the four new complexes with the help of information obtained from a $^{31}P,^{31}P$ COSY experiment in $CDCl_3$ on a sample of the material formed in the reaction with the 1:6 ratio, which contained the four new derivatives (see Figure 1). The conclusions reached can be summarised as follows: (i) The spin system of each derivative fits an AMX pattern. (ii) Compounds **2a** and **3a** exhibit a *fac-PPP* disposition. (iii) Compounds **2b** and **3b** exhibit a *mer-PPP* disposition. (iv) All of these new compounds have two four-membered chelate rings (PN ligand) and one monodentate phosphane ligand, as deduced from the existence of two high-field signals and a low-field resonance for each derivative.

From the point of view of stoichiometry, it seems reasonable that in the reaction with a 1:2 ratio, the replacement of two PPh_3 units by two PN ligands takes place with the concomitant loss of one chloride ligand from the ruthenium centre. In this case complexes **2a** and **2b** will be the *fac* and *mer* isomers with the stoichiometry $[RuCl(PPh_3)(\kappa^2\text{-}P,N\text{-}PPh_2MeIm)_2]Cl$. These compounds contain one PPh_3 group, which can be removed by another molecule of PN when larger amounts of the ligand are used. This change leads to complexes **3a** and **3b** and these are the corresponding *fac* and *mer* isomers of stoichiometry $[RuCl(\kappa^1\text{-}P\text{-}PPh_2MeIm)(\kappa^2\text{-}P,N\text{-}PPh_2MeIm)_2]Cl$. The structures of the new derivatives, which are consistent with the data obtained, are shown in Scheme 2.

Attempts were made to obtain crystals of **1** from a dichloromethane/hexane mixture (1:1) in order to carry out an X-ray structure determination. Unexpectedly, the crystals obtained corresponded to the dinuclear species $[(PPh_3)ClRu(\mu\text{-}Cl)_2(\mu^2\text{-}P,N\text{-}PPh_2MeIm)_2Ru(PPh_3)Cl]$ (**4b**) as a dichloromethane solvate. The ORTEP plot of **4b** is shown in Figure 2, a selection of bond lengths and angles are given in Table 2. Other crystallographic data are given in the Exp. Sect. The complex has a dinuclear structure with two chloride bridges and two other head-to-tail axial PN bridges. The two metal centres are in a slightly distorted octahedral geometry as a consequence of the bridge strain, which is exemplified by the N(1)−Ru(1)−Cl(1) (86.04°) and N(1)−Ru(1)−Cl(1A) (82.80°) angles. The two terminal positions for each of the ruthenium atoms are occupied by one Cl and one PPh_3 ligand.

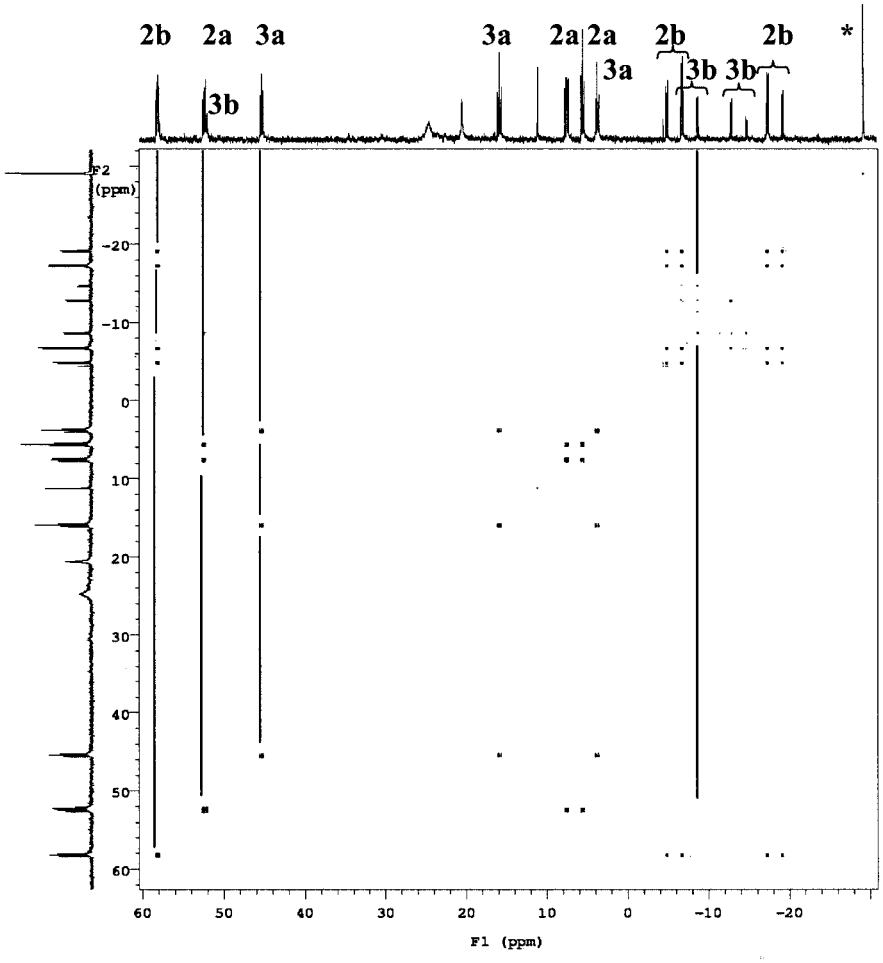

Figure 1. $^{31}P,^{31}P$ COSY spectrum (161.923 MHz) in $CDCl_3$ at room temperature for a sample of the reaction between $[RuCl_2(PPh_3)_3]$ and PMe_2MeIm in a 1:6 ratio; * indicates free PN

 © 2004 Wiley-VCH Verlag GmbH & Co. KGaA, Weinheim

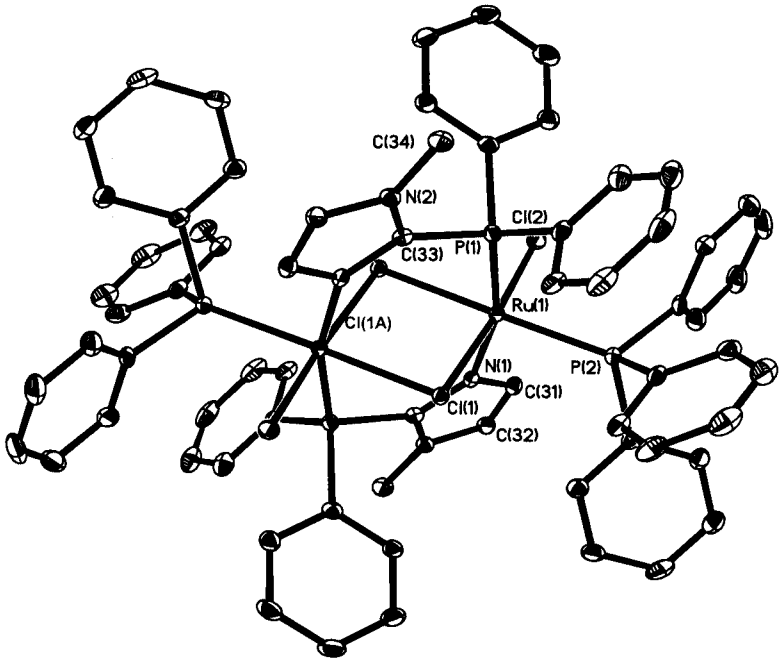

Figure 2. ORTEP plot of **4b**, showing atom labelling; hydrogen atoms have been omitted for clarity

Table 2. Selected bond lengths [Å] and angles [°] for **4b·CH_2Cl_2** and *fac*-**7a·$(CH_3)_2CO$** with estimated standard deviations in parentheses

4b·CH_2Cl_2			
Ru(1)−N(1)	2.146(3)	N(1)−Ru(1)−P(1)	164.83(7)
Ru(1)−P(1)	2.2929(9)	N(1)−Ru(1)−P(2)	93.92(7)
Ru(1)−P(2)	2.2967(9)	P(1)−Ru(1)−P(2)	100.81(3)
Ru(1)−Cl(1)	2.3878(8)	N(1)−Ru(1)−Cl(1)	86.04(7)
Ru(1)−Cl(2)	2.3987(8)	P(1)−Ru(1)−Cl(1)	89.47(3)
Ru(1)−Cl(1A)	2.4387(8)	P(2)−Ru(1)−Cl(1)	93.40(3)
P(1)−C(25)	1.832(3)	N(1)−Ru(1)−Cl(2)	87.43(7)
P(1)−C(19)	1.840(3)	P(1)−Ru(1)−Cl(2)	95.57(3)
P(1)−C(33)	1.861(3)	P(2)−Ru(1)−Cl(2)	92.04(3)
P(2)−C(13)	1.827(3)	Cl(1)−Ru(1)−Cl(2)	171.77(3)
P(2)−C(1)	1.848(3)	N(1)−Ru(1)−Cl(1A)	82.80(7)
P(2)−C(7)	1.852(3)	P(1)−Ru(1)−Cl(1A)	82.76(3)
		P(2)−Ru(1)−Cl(1A)	174.72(3)
		Cl(1)−Ru(1)−Cl(1A)	90.50(3)
		Cl(2)−Ru(1)−Cl(1A)	83.71(3)
		Ru(1)−Cl(1)−Ru(1A)	89.50(3)
fac-**7a·$(CH_3)_2CO$**			
Ru(1)−N(6)	2.140(2)	N(2)−Ru(1)−P(1)	68.74(6)
Ru(1)−N(4)	2.160(2)	N(4)−Ru(1)−P(2)	68.59(6)
Ru(1)−N(2)	2.173(2)	N(6)−Ru(1)−P(3)	69.04(7)
Ru(1)−P(1)	2.2954(8)	N(2)−C(13)−P(1)	105.50(18)
Ru(1)−P(3)	2.2990(9)	N(6)−C(45)−P(3)	104.58(18)
Ru(1)−P(2)	2.2995(8)	N(4)−C(29)−P(2)	105.28(18)

The Ru(1)−Ru(1A) distance is only 3.398 Å and is intermediate between those typically observed in complexes with $Ru^{II}(\mu\text{-}Cl)_2Ru^{II}$ bridges (but without an Ru−Ru bond, 3.68−3.91 Å)[11b,16] and those found in derivatives that do contain an Ru−Ru bond {e.g. 2.93 Å in $[RuCl_2(\mu^2\text{-}Cl_2)(\mu^2\text{-}dppm)RuCl_2]$}.[17] The presence of the two additional PCN bridges can lead to shortening of this distance, a situation that has been observed in other dinuclear Ru derivatives with additional short bridges.[18]

In addition, the distances between each of the chloride bridging ligands and each of the ruthenium atoms are asymmetric, with *d*[Ru(1)−Cl(1)] = 2.3878 Å and *d*[Ru(1A)−Cl(1)] = 2.4387 Å. This indicates a greater elongation of the μ-Cl−Ru bonds *trans* to PPh_3 in comparison to those *trans* to Cl^-. This situation is in keeping with the higher *trans* influence of a P-donor ligand than a chloride ligand.[18,19]

In order to understand the unexpected transformation of complex **1**, we monitored the evolution of a $CDCl_3$ solution of **1** during 3 d by $^{31}P\{^1H\}$ NMR spectroscopy. This experiment indicated that **1** undergoes a slow rearrangement in solution. The final $^{31}P\{^1H\}$ NMR spectrum is very complicated and shows the presence of several complexes (see Figure 3). A $^{31}P,^{31}P$ COSY experiment allowed each group of coupled signals to be correlated and indicated five independent spin systems and a singlet.

In this spectrum the resonances of **2a** and **2b** can be seen along with those of **4b**, which corresponds to an AM spin system (two doublets at δ = 19.43 and 68.09 ppm). The former of these signals can be assigned to a bridging coordination mode of the PN ligand on the basis of literature data.[20] The second doublet must correspond to coordinated PPh_3. Two additional spin systems can also be observed in the spectrum. Both of these have an AM pattern

 © 2004 Wiley-VCH Verlag GmbH & Co. KGaA, Weinheim

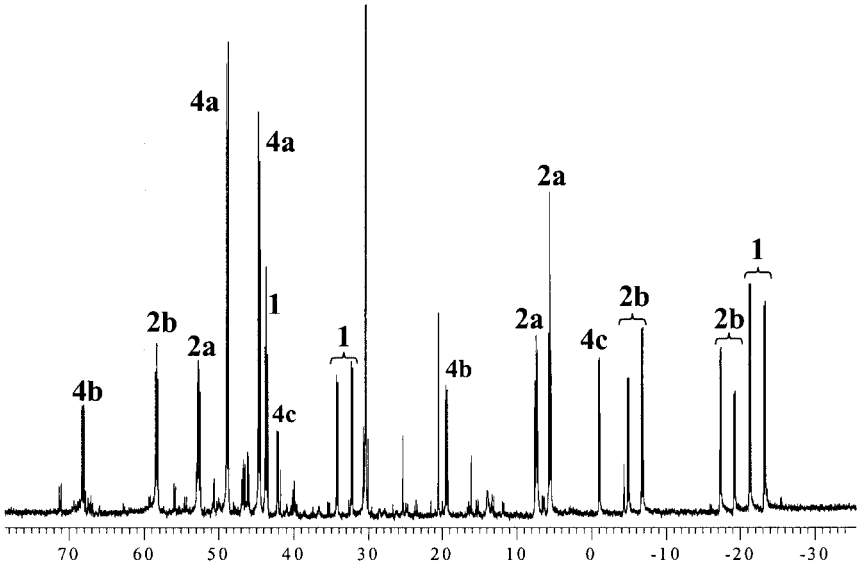

Figure 3. $^{31}P\{^{1}H\}$ NMR spectrum (161.923 MHz) in $CDCl_3$ at room temperature for a sample of **1** after 3 d in solution

with coupling constants typical of two P atoms in a *cis* disposition. The pair of signals for one complex, **4a**, have chemical shifts that do not correspond to either a chelating or bridging coordination of the PN ligand. Consequently, the PN ligand must exhibit monodentate coordination. One of the resonances of the other derivative, **4c**, indicates a chelating coordination. Considering this information we propose the structures indicated in Scheme 3 for complexes **4a** and **4c**. These structures are also reasonable in terms of the evolution of complex **1** after the loss of one PPh_3 ligand (see below). In the NMR spectrum there is also an intense singlet at $\delta = 30.3$ ppm, which can be assigned to $[RuCl_2(PPh_3)_3]$ — probably in equilibrium with free PPh_3.[21] According to the stoichiometry of the derivatives formed from **1**, both species must exist in the reaction medium (Scheme 3).

Although we do not have direct proof, we think that a reasonable mechanism for the dimerisation of **1** to **4a**, **4b** and **4c** is that shown in Scheme 4. This process would be favoured by the hemilabile character of the PN ligand and may involve the following steps: (i) Dissociation of one PPh_3 ligand. (ii) Partial dissociation of the PN ligand as a consequence of the strain in the four-membered ring and formation of two chloride bridges. Such a change leads to the formation of **4a**. The spontaneous dissociation of one PPh_3 group[22] and the consequent formation of chloride bridges[21b,23] has been reported for $[RuCl_2(PPh_3)_3]$. The coordination of the N atom to occupy the vacancy on each metal centre could take place in two ways, either to produce PN bridges between the two metal centres to give **4b**, or to regenerate a four-membered chelate ring on each metal atom to give **4c**.

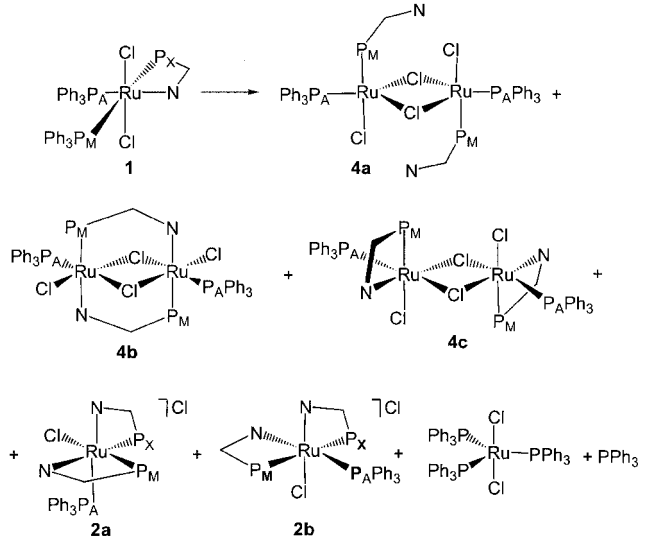

Scheme 3. Products formed after the evolution of **1** in solution

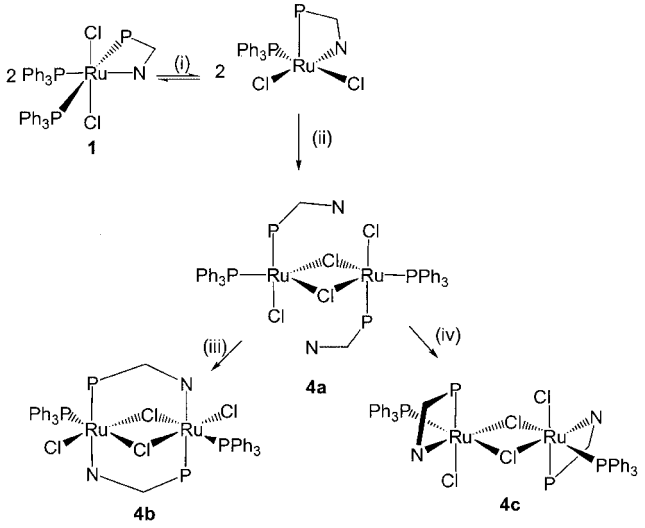

Scheme 4. Mechanism proposed for the dimerisation of **1**

 © 2004 Wiley-VCH Verlag GmbH & Co. KGaA, Weinheim

Reaction of PPh_2MeIm with $[RuCl_2(cod)(bpzm)]$

In the previous reactions between the PN ligand and $[RuCl_2(PPh_3)_3]$ we obtained a rich variety of products that included not only mononuclear species with different amounts of the PN ligand but also dinuclear derivatives. It is clear from these results that competition between the incoming ligand and PPh_3 is always present and frequently leads to the formation of product mixtures. Even when 6 equiv. of the PN ligand were used, the products that do not contain PPh_3 (**3a**, **3b**) were formed along with those containing 1 equiv. of the phosphane (**2a**, **2b**). Given these findings, we decided to use a starting material that did not contain the phosphane ligand and incorporated weakly coordinating ligands — $[RuCl_2(cod)(bpzm)]$ [cod = 1,5-cyclooctadiene, bpzm = bis(pyrazol-1-yl)methane]. It has been shown that both cod and bpzpm ligands are prone to replacement by PN donor ligands.[11a] When 2 equiv. of PPh_2MeIm were added to a suspension of this compound and the mixture heated under reflux in THF, the complex *cis*-*P*-$[RuCl_2(\kappa^1$-*P*-$PPh_2MeIm)(\kappa^2$-*P*,*N*-$PPh_2MeIm)]$ (**5**) was obtained as the only product [Equation (2)].

$$[RuCl_2(cod)(bpzm)] + 2\,PN \rightarrow cis\text{-}P\text{-}[RuCl_2(\kappa^1\text{-}PN)(\kappa^2\text{-}PN)]\,(\mathbf{5}) + cod + bpzm \quad (2)$$

The ^1H NMR spectrum at low temperature does not show any evidence of the presence of bpzm or cod ligands and signals for only two kinds of PN ligand were observed. The corresponding $^{31}P\{^1H\}$ NMR spectrum ([D_6]acetone) at room temperature contains two broad signals that must be due to some kind of fluxional process. In an attempt to obtain more information on the structure of the complex, a $^{31}P\{^1H\}$ NMR spectrum was recorded at low temperature (−90 °C) and an AM pattern was observed [δ = 3.35 (d) and 51.85 (d) ppm]. The high-field resonance can be assigned to a PN ligand with a chelating coordination mode while the lower-field signal belongs to a monodentate PN ligand. The $^2J_{P,P}$ value (32.02 Hz) is indicative of a *cis* disposition of the two atoms. Moreover, the FAB^+ mass spectrum shows a peak at *m*/*z* = 669 due to the cation $[RuCl(PN)_2]^+$, which is the result of the loss of one chloride ion from **5**. Two bands at 367 and 297 cm^{-1}, assigned to the stretching vibration modes of the $RuCl_2$ unit, were observed in the IR spectrum. It can be concluded from these data that the complex is a monomeric, pentacoordinate compound with one bidentate and one monodentate PN ligand in which the P atoms are in a *cis* disposition but can exchange their coordination modes at room temperature through a fast process.

Interestingly, the reaction of $[RuCl_2(cod)(bpzm)]$ with 3 equiv. of the ligand PN under reflux gave a precipitate that was identified as complex **3**, with no other compound being detected. Complex **3** was present as four diastereoisomers: the pair of enantiomers *fac*-**3a** and the pair *mer*-**3b** in a molar ratio of 4:1. As stated previously, these isomers were also obtained when $[RuCl_2(PPh_3)_3]$ was used as the starting material but always in a mixture with other derivatives (see Table 1 for the ^{31}P NMR spectroscopic data). The FAB^+ spectrum is consistent with the proposed formulation, as a peak corresponding to the cation of **3** is observed at *m*/*z* = 935. The rest of the peaks are in agreement with the loss of a chloride ion and two PN ligands in successive steps (see Exp. Sect.).

Reaction of PPh_2MeIm with $[RuCl_2(p\text{-cymene})]_2$ − X-ray Structure of *fac*-$[Ru(\kappa^2$-*P*,*N*-$PPh_2MeIm)_3](BF_4)_2\cdot(CH_3)_2CO$

Another goal of our study was the synthesis of derivatives of the type $[Ru(PN)_3]X_2$, with three chelate ligands. Such complexes would be expected to be chiral[24] and, considering the hemilabile character of the PN ligand, they could be interesting starting materials in catalytic or stoichiometric processes.[25] We succeeded in the synthesis of these compounds by using $[RuCl_2(arene)]_2$ (arene = *p*-cymene, benzene) as starting materials and adding silver salts to remove the chloride ions. In this way, the complexes $[Ru(\kappa^2$-*P*,*N*-$PPh_2MeIm)_3]X_2$ [X = PF_6 (**6**) and BF_4 (**7**)] were isolated after the addition of the ligand PPh_2MeIm to the solution obtained by treatment of a suspension of $[RuCl_2(arene)]_2$ in MeOH with $AgPF_6$ or $AgBF_4$, respectively, at room temperature [Equation (3)]. The same products were also formed upon treatment of $[RuCl_2(cod)(bpzm)]$ with the silver salt and the PN ligand, but in this case the reaction led to a mixture of derivatives. Consequently, the reaction outlined in Equation (3) is more convenient.

$$[RuCl_2(arene)]_2 + 4\,AgX + 6\,PN \rightarrow 2\,[Ru(\kappa^2\text{-}PN)_3]X_2 + 4\,AgCl \quad (3)$$

arene = *p*-cymene, X = PF_6 (**6**); arene = benzene, X = BF_4 (**7**)

In both cases the two pairs of stereoisomers, *fac* (**6a** and **7a**) and *mer* (**6b** and **7b**), were formed. The ^1H NMR spectra lack the characteristic signals of *p*-cymene or benzene. The $^{31}P\{^1H\}$ NMR spectrum of **6** exhibits the AM_6 pattern of the PF_6^- counteranion. Furthermore, a singlet for the *fac* stereoisomer (chemical shift of chelate coordination) and the AMX pattern of a *mer* stereoisomer are observed for both derivatives. Two signals at high field due to the *mer* form are typical of chelate coordination. However, the resonance at δ = 20.70 ppm could correspond to a chelating or bridging PN ligand, which means that the compound could be mono- or dinuclear in nature. In an effort to clarify this point, high-resolution mass spectra were obtained for **6** and **7**. Only the spectrum of compound **6** will be discussed as it is very similar to that of **7**. The spectrum displays a group of signals corresponding to the fragment $[\{Ru(PN)_3\}\{PF_6\}]^+$, whose most intense peak appears at *m*/*z* = 1045.2. In addition a signal at *m*/*z* = 450.13 was observed, which is consistent with the dicationic fragment $[\{Ru(PN)_3\}]^{2+}$, as deduced from the difference between the lines in this group of half a unit. The overall fragmentation pattern for this molecule is indicated in Scheme 5. No evidence for the existence of a dinuclear species was found in

 © 2004 Wiley-VCH Verlag GmbH & Co. KGaA, Weinheim

the mass spectrum. Consequently, all the data indicate a mononuclear structure for both derivatives (Scheme 6).

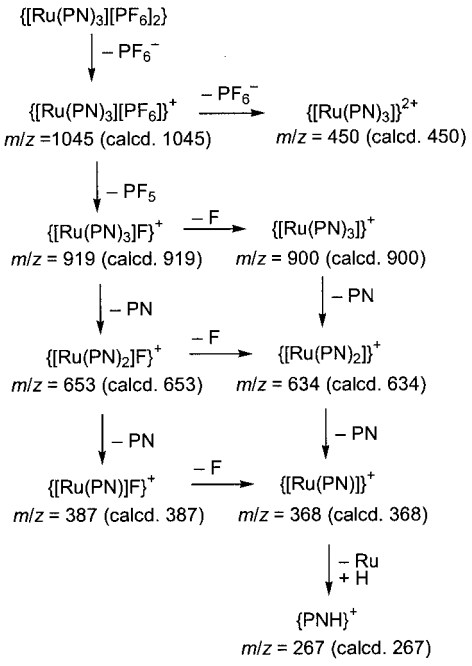

Scheme 5. Fragmentation pattern for **6**

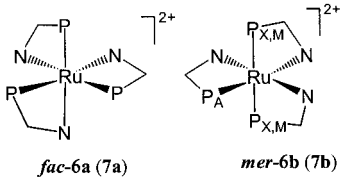

Scheme 6. Proposed structures for **6** and **7**

Finally, it was possible to crystallise the *fac* isomer of **7** (i.e. **7a**) as an acetone solvate and to determine its molecular structure by an X-ray diffraction study on a single crystal. The corresponding ORTEP plot is shown in Figure 4, selected bond lengths and angles are shown in Table 2 and crystallographic data are given in the Exp. Sect. The compound is mononuclear and exhibits a *fac* disposition of the three phosphorus atoms. Only the structure for the Δ isomer is shown in Figure 4a, although it should be noted that both the Δ and Λ enantiomers are present in the same unit cell (see Figure 4b).

At present, only one structure containing three four-membered PN chelate rings has been deposited with the CSD[26] and that corresponds to the complex [Ru(pyphos)$_3$](μ-Na$_2$)[Ru(pyphos)$_3$] in which each pseudo-octahedral ruthenium(II) centre has three PN chelating ligands [pyphos = 6-(diphenylphosphanyl)-2-pyridonate]. As in the case of **7a**, a *fac* disposition for the identical donor atoms was found.

A comparison between the free and the chelate-coordinated ligand in *fac*-**7a** reflects the fact that the P−C−N

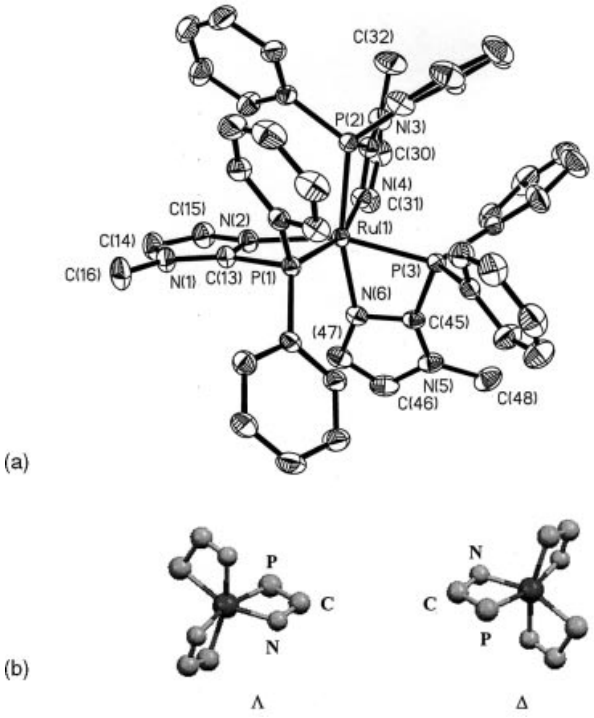

Figure 4. (a) ORTEP plot of the cation of the Δ enantiomer of *fac*-**7a**, showing the atom labelling; hydrogen atoms and phenyl groups have been omitted for clarity, as have counterions and solvent molecules; (b) ball-and-stick plots for *fac*-**7a**, showing both enantiomers

angle decreases with κ^2-*PN* coordination from 128.5(2)°[27] in the free ligand to about 105° in **7a**. Very similar angles (about 103°) are present in the previously mentioned [Ru(pyphos)$_3$] units. This situation can be seen as a consequence of the inherent strain associated with the four-membered chelate ring. Similarly, the Ru−N bonds are relatively long[28] and the bite angles of the PN donor ligands are small.

Hydride Complexes

We also tried to synthesise new hydride complexes containing the PPh_2MeIm ligand. In order to achieve this aim we used two types of hydride starting material, one containing PPh_3 and the other with more easily displaceable ligands — [RuHCl(PPh_3)$_3$] and [RuHCl(cod)(bpzm)].

When equivalent amounts of [RuHCl(PPh_3)$_3$] and PPh_2MeIm were mixed in toluene at 70 °C, *mer*-[RuHCl(PPh_3)$_2$(κ^2-*P,N*-PPh_2MeIm)] (**8**) was isolated in good yield [Equation (4)].

$$[RuHCl(PPh_3)_3] + PN \rightarrow mer\text{-}[RuHCl(PPh_3)_2(\kappa^2\text{-}PN)]\ (\mathbf{8}) + PPh_3 \quad (4)$$

The hydride region of the ^{1}H NMR (C_6D_6) spectrum of **8** shows a quadruplet at δ = −15.1 ppm ($^2J_{P,H}$ = 26.6, $^2J_{P,H}$ = 23.5, $^2J_{P,H}$ = 23.4 Hz) as the most characteristic signal. This relatively high-field chemical shift is typical for a hydride ion *trans* to an N atom, as reported in the litera-

 © 2004 Wiley-VCH Verlag GmbH & Co. KGaA, Weinheim

ture,[29] and is in contrast to the lower-field chemical shift observed for hydride ions *trans* to Cl ligands.[11,30] The values of the three coupling constants, determined separately by selective $^1H\{^{31}P\}$ NMR decoupling experiments, correspond to a *cis* disposition of the hydride ion with respect to the three P atoms, which also means a *mer-PPP* disposition. The $^{31}P\{^1H\}$ NMR (C_6D_6) spectrum of **8** confirms the stereochemistry of the complex, since it consists of an AMX pattern with one *trans*-PP coupling constant between a PPh_3 and a chelating PPh_2MeIm group. Consequently, the spectroscopic data indicate the presence of the *mer* stereoisomer in solution (see Scheme 7). Obviously, complex **8** is isolated as a racemic mixture.

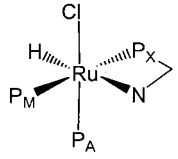

$P_A = P_M = PPh_3$, ***mer*-8**
$P_A = P_M = PPh_2MeIm$, ***mer*-9**

Scheme 7. Proposed structures of complexes **8** and **9**

An excess of the ligand PPh_2MeIm (6:1) was mixed with [RuHCl(cod)(bpzm)] in THF at −80 °C and the hydrido complex *mer*-[RuHCl(κ^1-*P*-PPh_2MeIm)$_2$(κ^2-*P*,*N*-PPh_2MeIm)] (**9**) was obtained [Equation (5)].

$$[RuHCl(cod)(bpzm)] + 6\,PN \rightarrow mer\text{-}[RuHCl(\kappa^1\text{-}PN)_2(\kappa^2\text{-}PN)]\,(\mathbf{9}) + cod + bpzm \quad (5)$$

The ^1H (C_6D_6) and $^{31}P\{^1H\}$ NMR (C_6D_6) spectra of **9** are completely analogous to those of **8**. Two of the phosphorus chemical shifts are typical of a monodentate coordination of the PN ligand while a resonance appearing at $\delta = -10$ ppm indicates the existence of a chelating PPh_2MeIm group. Consequently, the presence of the *mer* stereoisomer, as a racemic mixture, is again evident (see Scheme 7). The two PPh_3 ligands in compound **8** are monodentate PPh_3MeIm groups in **9**.

Conclusion

We have prepared new families of (polyphosphane)Ru complexes containing the ligand 2-(diphenylphosphanyl)-1-methyl-1*H*-imidazole. In the complexes described, three types of coordination modes for the N,P ligand have been found: *P*-monodentate, chelate and brigde. An unexpected rearrangement of [$RuCl_2$(Pn)(PPh_3)$_2$] that leads, among others, to the formation of dinuclear derivatives has been found. The formation of these species involves an Ru−N bond-breaking step that demonstrates the hemilabile behaviour of the ligand.

Experimental Section

General Comments: All manipulations were carried out under Ar using standard Schlenk techniques. Solvents (Merck) were dried and distilled under N_2 prior to use. [$RuCl_2(PPh_3)_3$],[31] [$RuHCl(PPh_3)_3$],[32] [$RuCl_2$(bpzm)(cod)],[33] [RuHCl(bpzm)-(cod)],[33] [$RuCl_2$(*p*-cymene)]$_2$,[34] [$RuCl_2(C_6H_6)$]$_2$ [34] and PPh_2MeIm[27] were prepared according to literature procedures. NMR spectra were recorded at room temperature (ca. 22 °C), unless otherwise stated, with a Varian Unity Inova-400 (400 MHz for ^1H; 161.9 MHz for ^{31}P; 100.6 MHz for ^{13}C) or with a Varian Unity-300 (300 MHz for ^1H; 121.4 MHz for ^{31}P; 75.4 MHz for ^{13}C) spectrometer. ^1H NMR shifts are referenced to the residual proton of the solvent as internal standard. All ^{31}P shifts were referenced internally to H_3PO_4. The ^{31}P,^{31}P COSY spectrum was acquired using a 30604 Hz spectral width; 24 transients were collected for each 240 increments. A 1 s relaxation delay, a 45° pulse width, and a 0.20 s acquisition time were used. IR spectra were recorded with a Nicolet Impact 410 spectrophotometer as KBr pellets or with a Perkin−Elmer 883 (4000−200 cm^{-1} range) as Nujol mulls. Conductivity measurements were made at 25 °C with freshly prepared 10^{-3} M solutions of the complex in acetone, using a CRISON 522 conductimeter. Molar conductivities (Λ_M) are given in units of $\Omega^{-1}\cdot mol^{-1}\cdot cm^2$. Elemental analyses were performed with a LECO CHNS932 microanalyser. FAB^+ mass spectra were recorded at the University of Zaragoza with a VG AutoSpec or at the University of Burgos with a Micromass Autospec by Liquid Secondary Ion Mass Spectrometry (LSMIS+) with Cs and NBA ions as the matrix.

***trans*,*mer*-[$RuCl_2(PPh_3)_2$(κ^2-*P*,*N*-PPh_2MeIm)] (1):** PPh_2MeIm (29.5 mg, 0.11 mmol) was added to a suspension of [$RuCl_2(PPh_3)_3$] (106 mg, 0.11 mmol) in 20 mL of CH_2Cl_2 (1:1). The resulting mixture was stirred and refluxed for 16 h. The original suspension became a red solution, which was concentrated to dryness. The orange solid obtained was washed with pentane (15 mL) and then with diethyl ether (3 × 15 mL) to remove any residual PPh_3. Finally, it was dried under vacuum. Yield: 89% (94.8 mg). The product is soluble in $CHCl_3$, CH_2Cl_2 and acetone. It decomposes in solution under air, giving rise to a green-brownish suspension after some minutes. However, it can be stored, as a solid, under nitrogen for months without appreciable decomposition. $C_{52}H_{45}Cl_2N_2P_3Ru$ (962.85): calcd. C 64.87, H 4.71, N 2.91; found C 65.11, H 4.80, N 2.83. FAB^+: *m*/*z* = 927 [M − Cl]$^+$, 665 [M − Cl − PPh_3]$^+$, 403 [M − Cl − 2PPh_3]$^+$.^1H NMR (400 MHz, $CDCl_3$, room temp.): δ = 7.9−6.7 (m, 40 H, 8 Ph), 6.6 (s, 1 H, H-Im), 5.56 (s, 1 H, H-Im), 3.0 (s, 3 H, Me-Im) ppm.$^{13}C\{^1H\}$ NMR (100.6 MHz, $CDCl_3$, room temp.): δ = 150−125 (m, 49 C, 8 Ph, C^2-Im), 130.7 (s, 1 C, *C*H-Im), 123.4 (s, 1 C, *C*H-Im), 34.2 (s, 1 C, Me-Im) ppm. $^{31}P\{^1H\}$ NMR: See Table 1. Λ_M (25 °C, acetone) = 10.35 $\Omega^{-1}\cdot mol^{-1}\cdot cm^2$. IR (nujol mull): $\tilde{\nu}$ = 326 cm^{-1} [ν(*trans*-$RuCl_2$)].

Reaction of [$RuCl_2(PPh_3)_3$] with PPh_2MeIm in a 1:2 Molar Ratio: The procedure is similar to that used for obtaining compound **1**. PPh_2MeIm (59 mg, 0.22 mmol) was added to a suspension of [$RuCl_2(PPh_3)_3$] (106 mg, 0.11 mmol) (2:1) in 20 mL of CH_2Cl_2. The resulting mixture was stirred and refluxed for 16 h. The original suspension became a red solution, which was concentrated to dryness. The orange solid obtained was washed with pentane (15 mL) and then with diethyl ether (3 × 10 mL) to remove any residual PPh_3 or PPh_2MeIm. Finally, it was dried under vacuum. The resulting mixture was studied by $^{31}P\{^1H\}$ NMR spectroscopy, and the following compounds were detected (see Table 1 for the $^{31}P\{^1H\}$ NMR spectroscopic data): **1**, *fac*-[RuCl(PPh_3)(κ^2-*P*,*N*-

 © 2004 Wiley-VCH Verlag GmbH & Co. KGaA, Weinheim

$PPh_2MeIm)_2$]Cl (**2a**) and *mer*-[RuCl(PPh_3)(κ^2-*P*,*N*-$PPh_2MeIm)_2$]Cl (**2b**).

Reaction of [$RuCl_2(PPh_3)_3$] with PPh_2MeIm in a 1:3 Molar Ratio: The procedure is similar to that described for the 1:2 molar ratio. Amounts are as follows: PPh_2MeIm (88.6 mg, 0.33 mmol), [$RuCl_2(PPh_3)_3$] (106 mg, 0.11 mmol) and 20 mL of CH_2Cl_2. The resulting mixture was studied by $^{31}P\{^1H\}$ NMR spectroscopy and the following compounds were detected (see Table 1 for the $^{31}P\{^1H\}$ NMR spectroscopic data): **2a**, **2b** and *fac*-[RuCl(κ^1-*P*-PPh_2MeIm)(κ^2-*P*,*N*-$PPh_2MeIm)_2$]Cl (**3a**).

Reaction of [$RuCl_2(PPh_3)_3$] with PPh_2MeIm in a 1:6 Molar Ratio: The procedure is similar to that described for the 1:2 molar ratio. Amounts are as follows: PPh_2MeIm (177 mg, 0.66 mmol), [$RuCl_2(PPh_3)_3$] (106 mg, 0.11 mmol) and 30 mL of CH_2Cl_2. The resulting mixture was studied by $^{31}P\{^1H\}$ NMR spectroscopy, and the following compounds were detected (see Table 1 for the $^{31}P\{^1H\}$ NMR spectroscopic data): **2a**, **2b**, **3a** and *mer*-[RuCl(κ^1-*P*-PPh_2MeIm)(κ^2-*P*,*N*-$PPh_2MeIm)_2$]Cl (**3b**).

[RuCl(κ^1-*P*-PPh_2MeIm)(κ^2-*P*,*N*-$PPh_2MeIm)_2$]Cl (3): PPh_2MeIm (139.9 mg, 0.526 mmol) was added to a suspension of [$RuCl_2$(cod)(bpzm)] (75 mg, 0.175 mmol) in THF (30 mL) (3:1). The resulting mixture was stirred and refluxed for 6 h. A yellow solid was obtained which, after filtering and washing with *n*-pentane (3 × 10 mL), was dried under vacuum. Yield: 72% (123 mg). The product is soluble in CH_2Cl_2 and $CHCl_3$. $C_{48}H_{45}Cl_2N_6P_3Ru$ (970.83): calcd. C 59.39, H 4.67, N 8.66; found C 59.22, H 4.81, N 8.57. FAB^+: *m*/*z* = 935 $[M]^+$, 900 $[M - Cl]^+$, 634 $[M - Cl - PN]^+$, 450 $[M - Cl^-]^{2+}$, 368 $[M - Cl - 2\ PN]^+$, 267 $[PN + H^+]^+$.

***fac*-[RuCl(κ^1-*P*-PPh_2MeIm)(κ^2-*P*,*N*-$PPh_2MeIm)_2$]Cl (3a):** ^1H NMR (400 MHz, $CDCl_3$, room temp.): δ = 9.0−6.2 (m, 36 H, 6 Ph, 3 CH-Im), 3.63 (s, 3 H, Me-Im), 3.22 (s, 3 H, Me-Im), 2.74 (s, 3 H, Me-Im) ppm.

***mer*-[RuCl(κ^1-*P*-PPh_2MeIm)(κ^2-*PN*-$PPh_2MeIm)_2$]Cl (3b):** ^1H NMR (400 MHz, $CDCl_3$, room temp.): δ = 9.0−6.2 (m, 36 H, 6 Ph, 3 CH-Im), 3.79 (s, 3 H, Me-Im), 3.26 (s, 3 H, Me-Im), 2.68 (s, 3 H, Me-Im) ppm. $^{31}P\{^1H\}$ NMR: See Table 1.

[(PPh_3)(κ^1-*P*-PPh_2MeIm)ClRu(μ-Cl)$_2$Ru(PPh_3)(κ^1-*P*-PPh_2MeIm)Cl] (4a): This compound was detected by $^{31}P\{^1H\}$ NMR spectroscopy in a solution of **1** in $CDCl_3$ after standing for 3 d at room temperature.

[(PPh_3)ClRu(μ-Cl)$_2$(μ^2-*P*,*N*-$PPh_2MeIm)_2$Ru(PPh_3)Cl] (4b): This compound was obtained as a crystalline solid from a solution of **1** in CH_2Cl_2/hexane under nitrogen and it was also detected by $^{31}P\{^1H\}$ NMR spectroscopy in a solution of **1** in $CDCl_3$ after standing at room temperature for 3 d.

[(PPh_3)(κ^2-*PN*-PPh_2MeIm)ClRu(μ-Cl)$_2$Ru(PPh_3)(κ^2-*PN*-PPh_2MeIm)Cl] (4c): This compound was detected by $^{31}P\{^1H\}$ NMR spectroscopy in a solution of **1** in $CDCl_3$ after standing at room temperature for 3 d.

***cis*-*P*-[$RuCl_2$(κ^1-*P*-PPh_2MeIm)(κ^2-*P*,*N*-PPh_2MeIm)] (5):** PPh_2-MeIm (66 mg, 0.24 mmol) was added to a suspension of [$RuCl_2$(cod)(bpzm)] (53.6 mg, 0.12 mmol) in 30 mL of THF (2:1). The resulting mixture was stirred and refluxed for 14 h, then filtered and the resulting solution concentrated to dryness. The pale-green solid obtained was washed with diethyl ether (2 × 10 mL) and finally dried under vacuum. Yield: 68% (60 mg). The compound is soluble in acetone and $CHCl_3$. $C_{32}H_{30}Cl_2N_4P_2Ru$ (704.55): calcd. C 54.55, H 4.29, N 7.95; found C 54.62, H 4.33, N 8.21. FAB^+: *m*/*z* = 669 $[M - Cl]^+$, 403 $[M - Cl - PN]^+$. ^1H NMR (300 MHz, [D_6]acetone, room temp.): δ = 8.0−6.8 (m, 24 H, 4 Ph, 4 CH-Im), 2.97 (s, 3 H, Me-Im) 2.81 (s, 3 H, Me-Im) ppm. $^{31}P\{^1H\}$ NMR: See Table 1. IR (Nujol mull): $\tilde{\nu}$ = 367, 297 cm^{-1} [ν(RuCl)].

[Ru(κ^2-*P*,*N*-$PPh_2MeIm)_3$][PF_6]$_2$ (6): $AgPF_6$ (253 mg, 1.00 mmol) was added to a suspension of [$RuCl_2$(*p*-cymene)]$_2$ (153 mg, 0.25 mmol) in 8 mL of MeOH at room temperature (4:1). The mixture was protected from light and stirred for 30 min. It was then filtered and the precipitated AgCl was removed. PPh_2MeIm (266.1 mg, 1.00 mmol) was then added to the previous orange solution, and the resulting mixture was stirred at room temperature for 3 h. The solvent was removed under vacuum and the obtained oil was transformed into a solid with pentane after stirring and scratching. The yellow solid was filtered and dried under vacuum. It is soluble in acetone. Yield: 87% relative to the ligand (344.7 mg). When the reaction was performed with 1.50 mmol of the PN ligand, other products besides **6** were formed. The compound was obtained as a mixture of four diastereoisomers: the pair of *fac* enantiomers **6a** and the *mer* pair **6b**. $C_{48}H_{45}F_{12}N_6P_5Ru$ (1189.9): calcd. C 48.45, H 3.81, N 7.06; found C 48.14, H 3.93, N 7.32. FAB^+ (see also Scheme 5): *m*/*z* = 1045 $[M - PF_6]^+$, 450 $[M - 2\ PF_6^-]^{2+}$, 919 $[M - PF_6^- - PF_5]^+$, 900 $[M - PF_6^- - PF_6]^+$, 653 $[M - PF_6^- - PF_5 - PN]^+$, 634 $[M - PF_6^- - PF_6 - PN]^+$, 387 $[M - PF_6^- - PF_5 - 2\ PN]^+$, 368 $[M - PF_6^- - PF_6 - 2\ PN]^+$, 267 $[PN + H^+]^+$.

6a: ^1H NMR (400 MHz, [D_6]acetone, room temp.): δ = 8.2−6.6 (m, 36 H, 6 Ph, 6 CH-Im), 3.72 (s, 3 H, Me-Im) 3.63 (s, 3 H, Me-Im) 3.57 (s, 3 H, Me-Im) ppm.

6b: ^1H NMR (400 MHz, [D_6]acetone, room temp.): δ = 8.2−6.6 (m, 36 H, 6 Ph, 6 CH-Im), 3.61 (s, 9 H, Me-Im) ppm. $^{31}P\{^1H\}$ NMR: See Table 1. IR (KBr): $\tilde{\nu}$ = 838 cm^{-1} [ν(P−F), PF_6^-].

[Ru(κ^2-*P*,*N*-$PPh_2MeIm)_3$][BF_4]$_2$ (7): $AgBF_4$ (389.4 mg, 2.00 mmol) was added to a suspension of [$RuCl_2$(benzene)]$_2$ (250 mg, 0.5 mmol) in 15 mL of MeOH at room temperature (4:1). The mixture was protected from light and stirred for 30 min. Then it was filtered and the precipitated AgCl was removed. PPh_2MeIm (532.2 mg, 2.00 mmol) was added to the previous orange solution, and the resulting mixture was stirred at room temperature for 3 h. The solvent was removed under vacuum and the obtained oil was transformed into a solid with pentane after stirring and scratching. The yellow solid was filtered and dried under vacuum. It is soluble in acetone. Yield: 76% relative to the ligand (535.8 mg). When the reaction was performed with 3.00 mmol of the PN ligand, other products besides **7** were formed. The compound was obtained as a mixture of four diastereoisomers: the pair of *fac* enantiomers **7a** and the *fac* pair **7b**. The *mer* enantiomers were crystallised from an Et_2O solution. $C_{48}H_{45}B_2F_8N_6P_3Ru$ (1073.5): calcd. C 53.70, H 4.23, N 7.83; found C 53.85, H 4.31, N 7.91. FAB^+: *m*/*z* = 987 $[M - BF_4^-]^+$, 450 $[M - 2\ BF_4^-]^{2+}$, 919 $[M - BF_4^- - BF_3]^+$), 900 $[M - BF_4^- - BF_4]^+$, 653$[M - BF_4^- - BF_3 - PN]^+$, 634 $[M - BF_4^- - BF_4 - PN]^+$, 387 $[M - BF_4^- - BF_3 - 2\ PN]^+$, 368 $[M - BF_4^- - BF_4 - 2\ PN]^+$, 267 $[PN + H^+]^+$. IR (KBr): $\tilde{\nu}$ = 1059 cm^{-1} [ν(B−F), BF_4^-], 544 [δ(FBF), BF_4^-].

7a: ^1H NMR (400 MHz, [D_6]acetone, room temp.): δ = 8.2−6.6 (m, 36 H, 6 Ph, 6 CH-Im), 3.72 (s, 3 H, Me-Im) 3.63 (s, 3 H, Me-Im) 3.57 (s, 3 H, Me-Im) ppm.

7b: ^1H NMR (400 MHz, [D_6]acetone, room temp.): δ = 8.2−6.6 (m, 36 H, 6 Ph, 6 CH-Im), 3.61 (s, 9 H, Me-Im) ppm. $^{31}P\{^1H\}$ NMR: See Table 1.

 © 2004 Wiley-VCH Verlag GmbH & Co. KGaA, Weinheim

***mer*-[RuHCl(PPh$_3$)$_2$(κ^2-*P*,*N*-PPh$_2$MeIm)] (8):** PPh$_2$MeIm (20.4 mg, 0.077 mmol) was added to a suspension of [RuHCl(PPh$_3$)$_3$] (61.4 mg, 0.07 mmol) in 20 mL of toluene (1.1:1). The resulting mixture was stirred and heated to 70 °C for 4 h. The original violet suspension became a dark green solution and was concentrated to dryness. The green solid obtained was washed with pentane (15 mL) and dried under vacuum. Yield: 85% (55 mg). It is very air-sensitive and soluble in toluene and benzene. $C_{52}H_{46}ClN_2P_3Ru$ (928.4): calcd. C 67.27, H 4.99, N 3.02; found C 67.21; H 5.02, N 3.14. ^{1}H NMR (400 MHz, C_6D_6, room temp.): δ = 8.2−6.6 (m, 41 H, 8 Ph, 1 CH-Im), 5.95 (s, 1 H, CH-Im), 3.5 (s, 3 H, Me-Im), −15.1 (q, $^2J_{P,H}$ = 26.6, $^2J_{P,H}$ = 23.5, $^2J_{P,H}$ = 23.4 Hz, 1 H, Ru−H) ppm. ^{31}P{^{1}H} NMR: See Table 1.

***mer*-[RuHCl(κ^1-*P*-PPh$_2$MeIm)$_2$(κ^2-*P*,*N*-PPh$_2$MeIm)] (9):** PPh$_2$-MeIm (351.6 mg, 1.32 mmol) was added to a suspension of [RuHCl(cod)(bpzm)] (86.6 mg, 0.22 mmol) in 20 mL of THF at −80 °C (6:1). The resulting mixture was stirred at this temperature for 45 min and at room temperature for furthe 30 min. The original suspension turned to a yellow solution with a small amount of solid in suspension. This mixture was concentrated to dryness and the yellow solid obtained was washed with diethyl ether (2 × 10 mL) to remove any bpzm, cod and unreacted ligand, and finally dried under vacuum. Yield: 73% (150 mg). The compound is very air-sensitive and soluble in C_6D_6, but it is insoluble in acetone. $C_{48}H_{46}ClN_6P_3Ru$ (936.39): calcd. C 61.57, H 4.95, N 8.97; found C 61.63, H 4.93, N 8.99. FAB$^+$: *m*/*z* = 935 [M − H$^-$]$^+$, 900 [M − H$^-$ − Cl]$^+$, 634 [M − H$^-$ − Cl − PN]$^+$, 450 [M − H$^-$ − Cl$^-$]$^{2+}$, 368 [M − H$^-$ − Cl − 2 PN]$^+$, 267 [PN + H$^+$]$^+$, 669 [M − H$^-$ − PN]$^+$, 403 [M − H$^-$ − 2 PN]$^+$.^{1}H NMR (400 MHz, C_6D_6, room temp.): δ = 8.4−6.4 (m, 36 H, 6 Ph, 6 CH-Im), 3.45 (s, 3 H, Me-Im), 2.97 (s, 3 H, Me-Im), 2.81 (s, 3 H, Me-Im), −14.8 (q, $^2J_{P,H}$ ≈ 25 Hz, 1 H, Ru-H) ppm. ^{31}P{^{1}H} NMR: See Table 1.

X-ray Diffraction: Suitable crystals of complexes **4b·CH$_2$Cl$_2$** (red block, dimensions 0.26 × 0.23 × 0.10 mm) and *fac*-**7a·(CH$_3$)$_2$CO** (yellowish prism, dimensions 0.50 × 0.30 × 0.30 mm) were used for the structure determination. X-ray data (Table 3) were collected using a Bruker SMART CCD area detector single-crystal diffractometer with graphite-monochromated Mo-K_α radiation (λ = 0.71073 Å) by the -ω scan method at 173(2) K (**4b**) or 296(2) (*fac*-**7a**). A total of 1271 frames of intensity data were collected for each compound. The first 50 frames were recollected at the end of data collection to monitor for decay. The crystals used for the diffraction studies showed a small amount of decomposition during data collection for **4b·CH$_2$Cl$_2$** (1.5%) and no decomposition for *fac*-**7a·(CH$_3$)$_2$CO**. The integration process yielded a total of 22750 reflections for **4b·CH$_2$Cl$_2$** and 28912 for *fac*-**7a·(CH$_3$)$_2$CO**, of which 7606 [*R*(int) = 0.0712] for **4b·CH$_2$Cl$_2$** and 11344 for *fac*-**7a·(CH$_3$)$_2$CO** were independent. Absorption corrections were applied using the SADABS[35] program (maximum and minimum transmission coefficients, 1.0000 and 0.809831 for **4b·CH$_2$Cl$_2$**). The structure was solved using the Bruker SHELXTL-PC[36] software by direct methods and refined by full-matrix least-squares methods on F^2. Hydrogen atoms were included in calculated positions and refined in the riding mode. For **4b·CH$_2$Cl$_2$** convergence was reached at a final $R1 = 0.0377$ [for $I > 2\sigma(I)$], $wR2 = 0.0789$ (for all data), 437 parameters, with allowance for the thermal anisotropy of all non-hydrogen atoms. The weighting scheme employed was $w = \{\sigma^2[F_o^2 + (0.0346P)^2]\}$, with $P = (|F_o|^2 + 2|F_c|^2)/3$ and the goodness of fit on F^2 was 0.923 for all observed reflections. For *fac*-**7b·(CH$_3$)$_2$CO** convergence was reached at a final $R1 = 0.0438$ [for $I > 2\sigma(I)$], $wR2 = 0.1221$ (for all data), 668 parameters, with allowance for the thermal anisotropy of all non-hydrogen atoms. The weighting scheme employed was $w = [\sigma^2(F_o)^2 + (0.0703P)^2 + (0.867P)]$, with $P = (|F_o|^2 + 2|F_c|^2)/3$ and the goodness of fit on F^2 was 1.080 for all observed reflections. CCDC-223473 (**4b·CH$_2$Cl$_2$**)

Table 3. Crystallographic data for **4b·CH$_2$Cl$_2$** and *fac*-**7a·(CH$_3$)$_2$CO**

	4b·CH$_2$Cl$_2$	*fac*-**7a·(CH$_3$)$_2$CO**
Empirical formula	$C_{36}H_{34}Cl_6N_2P_2Ru$	$C_{51}H_{51}B_2F_8N_6OP_3Ru$
Formula mass	870.36	1131.58
Temperature [K]	173(2)	296(2)
Wavelength [Å]	0.71073	0.71073
Crystal system	Monoclinic	Triclinic
Space group	$P2_1/n$	$P\bar{1}$
Unit cell dimensions	a = 15.756(3) Å	a = 12.296(3) Å
	b = 15.106(3) Å	b = 13.030(2) Å
	c = 15.771(3) Å	c = 18.068(4) Å
	α = 90°	α = 78.252(15)°
	β = 101.554(3)°	β = 88.132(18)°
	γ = 90°	γ = 67.028(17)°
Volume [Å^3]	3677.7(1)	2605.9(10)
Z	4	2
Density (calculated) [Mg/m^3]	1.572	1.442
Absorption coefficient [mm^{-1}]	0.979	0.465
F(000)	1760	1156
Crystal size [mm]	0.26 × 0.23 × 0.10	0.50 × 0.30 × 0.30
Index ranges	$-19 \le h \le 18$, $-18 \le k \le 15$, $-16 \le l \le 19$	$-15 \le h \le 16$, $-17 \le k \le 17$, $-23 \le l \le 23$
Reflections collected	22750	28912
Independent reflections	7606 [R(int) = 0.0712]	11344 [R(int) = 0.0300]
Data/restraints/parameters	7606/0/437	11344/0/668
Goodness-of-fit on F^2	0.923	1.080
Final R indices [$I > 2\sigma(I)$]	$R1$ = 0.0377, $wR2$ = 0.0715	$R1$ = 0.0438, $wR2$ = 0.1186
$\Delta\rho_{max/min}$ [e·Å^{-3}]	0.561/−0.709	0.843/−0.455

 © 2004 Wiley-VCH Verlag GmbH & Co. KGaA, Weinheim

and -223474 [*fac*-**7b**·$(CH_3)_2CO$] contain the supplementary crystallographic data for this paper. These data can be obtained free of charge at www.ccdc.cam.ac.uk/conts/retrieving.html [or from the Cambridge Crystallographic Data Centre, 12 Union Road, Cambridge CB2 1EZ, UK; Fax: (internat.) + 44-1223-336-033; E-mail: deposit@ccdc.cam.ac.uk].

Acknowledgments

We are grateful to the Spanish DGES/MCyT (Project N. BQU-2002-00286) and Consejería de Ciencia y Tecnología de la Junta de Comunidades de Castilla-La Mancha (PBI-02-002) for financial support. We also thank to J. J. Delgado and A. M. Arnáiz from SCAI, University of Burgos, Spain for carrying out elemental analyses and FAB^+ mass spectra.

[1] [1a] T. Naota, H. Takaya, S.-I. Murahashi, *Chem. Rev.* **1998**, *98*, 2599−2660. [1b] P. A. Chaloner, M. A. Esteruelas, F. Joó, L. A. Oro, *Homogeneous Hydrogenation*, Kluwer, London, **1994**. [1c]R. A. Sánchez-Delgado, M. Rosales, *Coord. Chem. Rev.* **2000**, *196*, 249−280. [1d] K. Nomura, *J. Mol. Catal. A, Chem.* **1998**, *130*, 1−28.

[2] F. H. Jardine, *Prog. Inorg. Chem.* **1984**, *32*, 265 and references cited therein.

[3] [3a] A. M. Stolzenberg, E. L. Muetterties, *Organometallics* **1985**, *4*, 1739−1742. [3b] B. R. James, L. D. Markham, D. K. W. Wang, *J. Chem. Soc., Chem. Commun.* **1974**, 439.

[4] [4a] R. H. Fish, A. D. Thormodsen, G. A. Cremer, *J. Am. Chem. Soc.* **1982**, *104*, 5234−5237. [4b] R. H. Fish, J. L. Tan, A. D. Thormodsen, *Organometallics* **1985**, *4*, 1743−1747.

[5] G. P. Pez, R. A. Grey, J. Corsi, *J. Am. Chem. Soc.* **1981**, *103*, 7528−7535.

[6] [6a] Y. Sasson, P. Albin, J. Blum, *Tetrahedron Lett.* **1974**, 833−836. [6b] J. Tsuji, H. Suzuki, *Chem. Lett.* **1977**, 1085. [6c] R. A. Sánchez-Delgado, O. L. de Ochoa, *J. Mol. Cat.* **1979**, *6*, 303−305. [6d] R. A. Sánchez-Delgado, O. L. de Ochoa, *J. Organomet. Chem.* **1980**, *202*, 427−434. [6e] R. A. Sánchez-Delgado, A. Andriollo, O. L. de Ochoa, T. Suárez, N. Valencia, *J. Organomet. Chem.* **1981**, *209*, 77−83.

[7] B. R. James, L. D. Markham, *Inorg. Chem.* **1974**, *13*, 97−100.

[8] P. W. Armit, A. S. F. Boyd, T. A. Stephenson, *J. Chem. Soc., Dalton Trans.* **1975**, 1663.

[9] [9a] Y. Sasson, G. L. Rempel, *Tetrahedron Lett.* **1974**, 3221−3224. [9b] Y. Sasson, J. Blum, *J. Org. Chem.* **1975**, *40*, 1887−1896. [9c] Y. Sasson, G. L. Rempel, *Tetrahedron Lett.* **1974**, 4133−4136. [9d] M. Dedieu, Y. L. Pascal, *J. Mol. Catal.* **1980**, *9*, 71−90.

[10] M. A. Jalil, T. Yamada, S. Fujinami, T. Honjo, H. Nishikawa, *Polyhedron* **2001**, *20*, 627−633.

[11] For the ability of these precursors to form Ru^{II} derivatives bearing P,N-donor ligands see: [11a] A. Caballero, F. A. Jalón, B. R. Manzano, *Chem. Commun.* **1998**, 1879−1880. [11b] P. Braunstein, F. Naud, A. Pfaltz, S. J. Rettig, *Organometallics* **2000**, *19*, 2676−2683.

[12] [12a] G. R. Newkome, *Chem. Rev.* **1993**, *93*, 2067−2089. [12b] P. Espinet, K. Soulantika, *Coord. Chem. Rev.* **1999**, *193−195*, 499−556.

[13] P. E. Garrou, *Chem. Rev.* **1981**, *81*, 229−266.

[14] G. E. Rodgers, W. R. Cullen, B. R. James, *Can. J. Chem.* **1983**, 1314.

[15] M. S. Lupin, B. L. Shaw, *J. Chem. Soc., A* **1968**, 741.

[16] [16a] A. V. Marchenko, J. C. Huffman, P. Valerga, M. J. Tenorio, M. C. Puerta, K. G. Caulton, *Inorg. Chem.* **2001**, *40*, 6444−6450. [16b] J. S. Kingsbury, J. P. A. Harrity, P. J. Bonitatebus Jr., A. H. Hoveyda, *J. Am. Chem. Soc.* **1999**, *121*, 791−799. [16c] B. Deschamps, F. Mathey, J. Fischer, J. H. Nelson, *Inorg. Chem.* **1984**, *23*, 3455−3462. [16d] F. A. Cotton, M. Matusz, R. C. Torralba, *Inorg. Chem.* **1989**, *28*, 1516−1620.

[17] A. R. Chakravarty, F. A. Cotton, M. P. Diebold, D. B. Lewis, W. J. Roth, *J. Am. Chem. Soc.* **1986**, *108*, 971−1976.

[18] S. Pal, S. Pal, *Inorg. Chem.* **2001**, *40*, 4807−4810.

[19] For other examples with asymmetric chloride bridges, see refs.[11b,16c,18]

[20] J. S. Field, R. J. Haines, C. J. Parry, *J. Chem. Soc., Dalton Trans.* **1997**, 2843−2848.

[21] [21a] K. G. Caulton, *J. Am. Chem. Soc.* **1974**, *96*, 3005−3006. [21b] P. R. Hoffmann, K. G. Caulton, *J. Am. Chem. Soc.* **1975**, *97*, 4221−4228.

[22] [22a] T. A. Stephenson, G. Wilkinson, *J. Inorg. Nucl. Chem.* **1966**, *28*, 945. [22b] B. R. James, L. D. Markham, *Inorg. Chem.* **1974**, *13*, 97−100.

[23] P. W. Armit, A. S. F. Boyd, T. A. Stephenson, *J. Chem. Soc., Dalton Trans.* **1975**, 1663.

[24] A. von Zelewsky. *Stereochemistry of Coordination Compounds*, Wiley, Chichester, **1996**.

[25] [25a] C. G. Arena, E. Rotondo, F. Faraone, M. Lanfranchi, A. Tiripicchio, *Organometallics* **1991**, *19*, 3877−3885. [25b] D. Drommi, C. G. Arena, F. Nicoló, G. Bruno, F. Faraone, *J. Organomet. Chem.* **1995**, *485*, 115−121. [25c] R. E. Rülke, V. E. Kaasjager, P. Wehman, C. J. Elsevier, P. W. N. M. van Leeuwen, K. Vrieze, J. Fraanje, K. Goubitz, A. L. Spek, *Organometallics* **1996**, *15*, 3022−3031. [25d] B. Therrien, T. R. Ward, *Angew. Chem. Int. Ed.* **1999**, *38*, 405−408; Angew. Chem. **1999**, *111*, 418−421. [25e] P. Braunstein, M. D. Fryzuk, F. Naud, S. J. Rettig, *J. Chem. Soc., Dalton Trans.* **1999**, 589−594.

[26] K. Mashina, Y. Kaneda, A. Fukumoto, M. Tanaka, K. Tani, H. Nakano, A. Nakumura, *Inorg. Chim. Acta* **1998**, *270*, 459.

[27] M. A. Jalil, T. Yamada, S. Fujinami, T. Honjo, H. Nishikawa, *Polyhedron* **2001**, *20*, 627−633.

[28] [28a] B. K. Keppler, W. Rupp, U. M. Juhl, H. Endres, R. Niebl, W. Balzer, *Inorg. Chem.* **1987**, *26*, 4366−4370. [28b] M. Tadokoro, H. Kanno, T. Kitajima, H. Shimada-Umemoto, N. Nakanishi, K. Isobe, K. Nakasuji, *Proc. Nat. Acad. Sci. USA* **2002**, *99*, 4950−4955.

[29] B. Moreno, S. Sabo-Etienne, B. Chaudret, A. Rodríguez, F. Jalón, S. Trofimenko, *J. Am. Chem. Soc.* **1995**, *117*, 7441−7451.

[30] [30a] M. L. Christ, S. Sabo-Etienne, G. Chung, B. Chaudret, *Inorg. Chem.* **1994**, *33*, 5316−5319. [30b] L. S. MacFarlane, A. M. Joshi, S. J. Rettig, B. R. James, *Chem. Commun.* **1997**, 1363−1364.

[31] P. S. Hallman, T. A. Stephenson, G. Wilkinson, *Inorg. Synth.* **1970**, *12*, 237−240.

[32] [32a] A. C. Skapski, P. G. H. Troughton, *J. Chem. Soc., Chem. Commun.* **1968**, 1230−1231. [32b] R. A. Schunn, E. R. Wonchoba, *Inorg Synth.* **1972**, *13*, 131−134.

[33] M. Fajardo, A. de la Hoz, E. Diéz-Barra, F. A. Jalón, A. Otero, A. Rodríguez, J. Tejeda, D. Belletti, M. Lanfranchi, M. A. Pellinghelli, *J. Chem. Soc., Dalton Trans.* **1993**, 1935−1939.

[34] [34a] M. A. Bennett, T. N. Huang, T. W. Matheson, A. K. Smith, *Inorg. Synth.* **1982**, *21*, 74−75. [34b] M. A. Bennett, A. K. Smith, *J. Chem. Soc., Dalton Trans.* **1974**, 233−241.

[35] G. M. Sheldrick, *SADABS, Program for absorption corrections using Bruker CCD data*, University of Göttingen, Germany, **1996**.

[36] PC version, Bruker Analytical X-ray Systems, Madison, WI, **1995**.

Received December 2, 2003
Early View Article
Published Online April 7, 2004

 © 2004 Wiley-VCH Verlag GmbH & Co. KGaA, Weinheim

$[Ni(C_4H_{13}N_3)_2]_3(Sb_3S_6)_2$: The First Structure Containing Isolated Heterocyclic $[Sb_3S_6]^{3-}$ Anions

Ragnar Kiebach,[a] Felix Studt,[a] Christian Näther,[a] and Wolfgang Bensch*[a]

Keywords: Thioantimonates / Heterocycles / Hydrothermal synthesis / Antimony / Sulfur

The novel thioantimonate(III) compound $[Ni(dien)_2]_3(Sb_3S_6)_2$, which was synthesised under solvothermal conditions, contains isolated $[Sb_3S_6]^{3-}$ anions. In the X-ray crystal structure, isolated cyclic $[Sb_3S_6]^{3-}$ anions occupy a boat-like conformation and two different isomeric $[Ni(dien)_2]^{2+}$ cations are arranged in separate stacks.
(© Wiley-VCH Verlag GmbH & Co. KGaA, 69451 Weinheim, Germany, 2004)

Introduction

In the structures of thioantimonates(III), the primary building units (PBU's) SbS_3, SbS_4 and the less common SbS_5 [1] or SbS_6 [1,2] PBU's are interconnected to form secondary building units (SBU's) such as the heterorings Sb_xS_x, with x ranging from 2 to 32. Rings with small values of x are very common in thioantimonate(III) structures whereas the larger rings are quite rare.[3,4] Very little is known about the processes occurring in the heterogeneous reaction mixtures, which result in the crystallisation of distinct thioantimonates(III). A few years ago, we isolated and characterised several antimony polysulfides such as $[Ph_4P]_2[Sb_2S_{15}]$,[5] $[Ph_4P]_3Sb_3S_{25}$ [6] and $[Ph_4P]_2[Sb_2S_{17}]$[7] which may play important roles as precursors in the syntheses. More recently, we synthesised and characterised $[Ni(dien)_2]_2Sb_4S_8$ [8] as well as $[Mn(C_3H_{10}N_2)_3]_2(Sb_4S_8)\cdot 2H_2O$[9] with the cyclic Sb_4S_4 heteroring as the main structural motif. The successful isolation of these compounds suggests that even these small heterocycles exist in solution. Using an upper limit of 3 Å for Sb−S bonds, the Sb_2S_2 ring can be found in $Ca_2Sb_2S_5$.[10] However, the Sb atoms of this ring have two additional S atoms at a distance less than 3.2 Å, in contrast to the Sb atoms of the Sb_4S_4 ring where no Sb···S contacts were observed below 4 Å. The small Sb_xS_x heteroring with $x = 3$ is commonly observed in extended thioantimonate(III) structures and two different conformations have been identified. In such structures, the Sb_3S_3 rings mostly occupy a chair-like conformation.[4,11−13] A special case of this chair-like conformation is an arrangement in which one endo-cyclic terminal sulfur atom is rotated by nearly 180° thus forming long bonds to the two other antimony atoms.[14,15] This arrangement has been classified as an Sb_3S_4 "semicube". We note that some authors also denote an Sb_3S_6 unit as a "semicube".[12] The boat-like conformation has also been identified in several thioantimonates.[16−18] During our continuing efforts in this area, we obtained the new compound $[Ni(dien)_2]_3(Sb_3S_6)_2$ which contains an isolated Sb_3S_3 heteroring as the main structural feature. This is the first compound containing this isolated Sb_3S_3 ring and it is only the third thioantimonate(III) compound reported with a small isolated thioantimonate(III) heteroring.

Results and Discussion

Crystal Structure

$[Ni(dien)_2]_3(Sb_3S_6)_2$ (dien = diethylenetriamine) crystallises in the triclinic space group $P\bar{1}$ with two formula units in the unit cell. In the crystal structure, there are two crystallographically independent $[Ni(dien)_2]^{2+}$ cations and one isolated heterocyclic $[Sb_3S_6]^{3-}$ anion (Figures 1−3). The $[Sb_3S_6]^{3-}$ anion and one of the two crystallographically independent $[Ni(dien)_2]^{2+}$ cations are located in general position whereas the second cation is located on a centre of inversion.

The Sb_3S_3 ring is formed by three vertex-linked SbS_3 trigonal pyramids (Figure 1). Each Sb atom of the Sb_3S_3 heteroring has a bond to a terminal S atom thus forming the final anion. The Sb−S distances in the Sb_3S_3 ring are similar to those reported for extended thioanti-

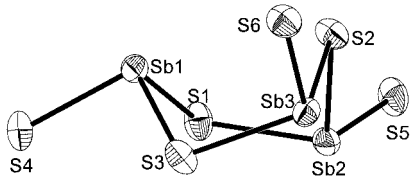

Figure 1. The $[Sb_3S_6]^{3-}$ anion in $[Ni(dien)_2]_3(Sb_3S_6)_2$ with labelling and displacement ellipsoids drawn at the 50% probability level

[a] Institut für Anorganische Chemie CAU Kiel
Olshausenstr. 40, 24098 Kiel, Germany
Fax: (internat.) +49-(0)431-880-1520
E-mail: wbensch@ac.uni-kiel.de

monates(III).[19−22] The Sb(1) and Sb(2) atoms each have one long intramolecular contact to an S atom [Sb(1)−S(2) 3.606 Å, Sb(2)−S(3) 3.891 Å]. No intermolecular Sb−S contacts shorter than 4.8 Å are present Table 1).

Table 1. Selected bond lengths (Å) and angles (°) for the $[Sb_3S_6]^{3-}$ anion in $[Ni(dien)_2]_3(Sb_3S_6)_2$

Sb(1)−S(4)	2.3310(9)	Sb(1)−S(3)	2.4756(10)
Sb(1)−S(1)	2.4838(9)	Sb(2)−S(5)	2.3333(9)
Sb(2)−S(2)	2.4617(9)	Sb(2)−S(1)	2.4623(9)
Sb(3)−S(6)	2.3216(9)	Sb(3)−S(3)	2.4702(9)
Sb(3)−S(2)	2.4774(9)		
S(4)−Sb(1)−S(3)	93.47(3)	S(4)−Sb(1)−S(1)	98.40(3)
S(3)−Sb(1)−S(1)	99.56(3)	S(5)−Sb(2)−S(2)	102.22(3)
S(5)−Sb(2)−S(1)	99.00(3)	S(2)−Sb(2)−S(1)	98.00(3)
S(6)−Sb(3)−S(3)	104.70(3)	S(6)−Sb(3)−S(2)	101.46(3)
S(3)−Sb(3)−S(2)	97.68(3)	Sb(2)−S(1)−Sb(1)	102.03(3)
Sb(2)−S(2)−Sb(3)	93.44(3)	Sb(3)−S(3)−Sb(1)	106.65(3)

The Ni^{2+} cations are in a distorted octahedral environment formed by six N atoms of two dien ligands with one unique $[Ni(dien)_2]^{2+}$ cation in the *u-fac* conformation [Ni(1)] and the other in the *s-fac* conformation (Figure 2). The Ni−N distances range between 2.100(3) and 2.145(3) Å, with N−Ni−N angles varying from 81.04(2) to 180.00(2)°. Angles and distances are similar to the corresponding literature values for $[Ni(dien)_2]^{2+}$ complexes (Table 2).[8,19,20]

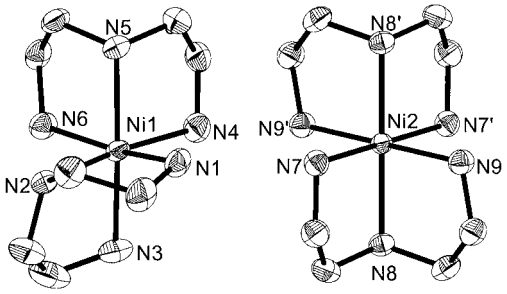

Figure 2. Coordination of the Ni cations in $[Ni(dien)_2]_3(Sb_3S_6)_2$ with labelling and displacement ellipsoids drawn at the 50% probability level (hydrogen atoms are omitted for clarity)

Cations and anions are packed in such a way that both form individual stacks parallel to the *a* axis (Figure 3). Four cations and two anions are arranged around a channel which is directed along the *a* axis. Disordered solvent molecules are located in this channel (see Exp. Sect.). A similar arrangement of cations and anions is also found in $[Ni(dien)_2]_3[SbS_4]_2$[20] and $[Ni(dien)_2]_2Sb_4S_8$.[8]

The three-dimensional arrangement of cations and anions is caused by N−H···S contacts. Every $[Sb_3S_6]^{3-}$ anion has fifteen such contacts with H···S distances between 2.440 and 2.903 Å and N−H···S angles ranging from 138.2 to 166.7°. The terminal S atoms have significantly more S···H contacts than the μ-S atoms (ratio: 2:1). The N−H atoms of the $[Ni(1)(dien)_2]^{2+}$ cation are involved in 10 and those of the second $[Ni(2)(dien)_2]^{2+}$ cation, in 5 H···S contacts.

Table 2. Selected bond lengths (Å) and angles (°) for the $[Ni(dien)_2]^{2+}$ cations in $[Ni(dien)_2]_3(Sb_3S_6)_2$

Ni(1)−N(4)	2.114(3)	Ni(1)−N(3)	2.114(3)
Ni(1)−N(1)	2.117(3)	Ni(1)−N(2)	2.127(3)
Ni(1)−N(5)	2.134(3)	Ni(1)−N(6)	2.145(3)
N(1)−C(1)	1.467(6)	C(1)−C(2)	1.522(6)
N(4)−Ni(1)−N(3)	94.70(14)	N(4)−Ni(1)−N(1)	93.88(13)
N(3)−Ni(1)−N(1)	95.88(13)	N(4)−Ni(1)−N(2)	173.65(12)
N(3)−Ni(1)−N(2)	81.48(13)	N(1)−Ni(1)−N(2)	81.52(12)
N(4)−Ni(1)−N(5)	82.52(12)	N(3)−Ni(1)−N(5)	172.95(12)
N(1)−Ni(1)−N(5)	90.79(11)	N(2)−Ni(1)−N(5)	101.85(11)
N(4)−Ni(1)−N(6)	94.99(13)	N(3)−Ni(1)−N(6)	92.79(12)
N(1)−Ni(1)−N(6)	167.04(12)	N(2)−Ni(1)−N(6)	90.28(12)
N(5)−Ni(1)−N(6)	81.04(11)		
Ni(2)−N(8)	2.100(3)	Ni(2)−N(9)	2.121(3)
Ni(2)−N(7)	2.130(3)		
N(8)−Ni(2)−N(9)	82.9(1)	N(8)−Ni(2)−N(9A)	97.2(1)
N(8A)−Ni(2)−N(7)	97.1(1)	N(8)−Ni(2)−N(7)	82.9(1)
N(9)−Ni(2)−N(7)	90.1(1)	N(9A)−Ni(2)−N(7)	89.9(1)

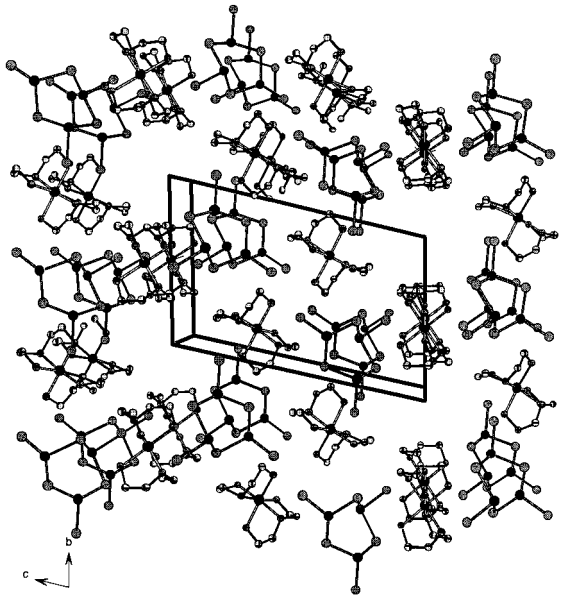

Figure 3. Crystal structure of $[Ni(dien)_2]_3(Sb_3S_6)_2$ viewed along the *a* axis (hydrogen atoms are omitted for clarity)

As mentioned above, the Sb_3S_3 unit usually occurs in a chair- or boat-like conformation, as in $[C_4H_{12}N_2]_{0.5}[CuSb_6S_{10}]$[18] or $[(CH_3NH_2)_{1.0}K_{2.97}][Sb_{12}S_{20}]\cdot 1.34H_2O$.[22] The latter is a rare example of the coexistence of two different conformations in one crystal. Interestingly, the Sb_3S_3 unit in the title compound also has a boat-like conformation. The geometry of this anion was optimised using GAUSSIAN98 indicating that the boat-like conformation is about 2 kcal/mol more stable than the chair-like conformation.

Thermal Investigations

Thermal stability of the complex was investigated using simultaneous differential thermal analysis and thermogravi-

 © 2004 Wiley-VCH Verlag GmbH & Co. KGaA, Weinheim

metry (DTA-TG). Heating single crystals of the title compound under helium in a thermobalance lead to decomposition in four steps with a total mass loss of 37.3% with all steps accompanied by endothermic peaks in the DTA curve ($T1_{peak}$ = 246 °C, Δm = 4.1%; $T2_{peak}$ = 260 °C, Δm = 24.4%; $T3_{peak}$ = 277 °C, Δm = 6.0%; and $T4_{peak}$ = 331 °C, Δm = 2.8%) (Figure 4).

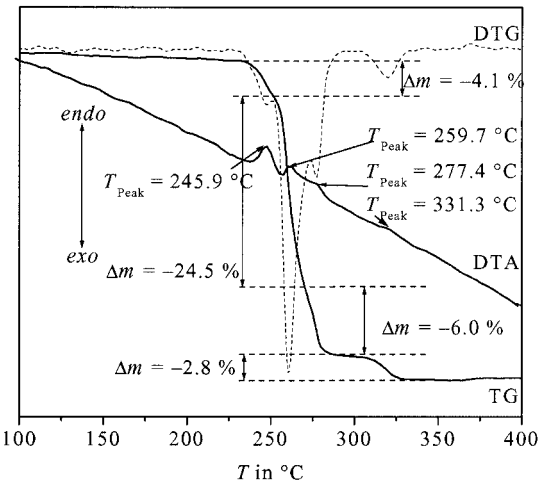

Figure 4. DTA, TG and DTG curves for $[Ni(dien)_2]_3(Sb_3S_6)_2$

Taking only the dien ligands into account, the expected mass loss is 31.4%, which is about 5.9% lower than the experimentally obtained value. This discrepancy may be due, in part, to the emission of H_2S and of solvent molecules (CH_3OH) which are located in the channels of the structure. Elemental analysis and mass spectroscopic investigations are in agreement with this. The elemental analysis gave a C,H and N content of 33.4% (C 16.2, H 4.4, N 12.8%), which is 2% larger than the theoretical content for the dien ligands alone. Mass spectra recorded simultaneously during decomposition showed a very intense signal for H_2S in the last step. Unfortunately, the content of CH_3OH could not be determined using mass spectrometry because of a substantial overlap of the different thermal processes and because of the experimental set-up of our instrument. The grey residue remaining after the thermal decomposition contained NiSbS (Ullmanit) and Sb_2S_3, both of which are frequently found after the thermal decomposition of thioantimonates containing nickel.[4,8,19–21]

Conclusion

The synthesis of thioantimonates was performed in basic solutions under solvothermal conditions. Little is known about the processes occurring in the heterogeneous reaction mixtures and which precursors determine the final structures that are formed under particular conditions. As mentioned above, in the extended structures of thioantimonates(III) many different secondary building units may be identified, which are formed by the condensation of the primary SbS_x (x = 3–6) units. After the successful isolation and characterisation of different antimony polysulfides and the $[Sb_4S_8]^{4-}$ anion containing the Sb_4S_4 heteroring, we were able to obtain the smallest known isolated thioantimonate anion $[Sb_3S_6]^{3-}$ containing the Sb_3S_3 ring as the main structural motif. However, the crystallisation of $[Sb_4S_8]^{4-}$ and $[Sb_3S_6]^{3-}$ does not necessarily mean that these species exist under solvothermal conditions. Further studies are necessary for a better understanding of the factors influencing product formation.

Experimental Section

Synthesis

$[Ni(dien)_2]_3(Sb_3S_6)_2$ (1): $[Ni(dien)_2]_3(Sb_3S_6)_2$ was synthesised from Sb (0.1217 g; 1 mmol), S (0.0962 g, 3 mmol), and $Ni(CH_3COO)_2{\cdot}4H_2O$ (0.2487 g; 1 mmol) dissolved in a mixture of dien (1 mL) and methanol (1 mL). The mixture was heated at 140 °C for 4 days in a Teflon^R-lined steel autoclave (volume ca. 20 mL) and was subsequently cooled to room temperature over a 3 h period. The brown crystalline product was filtered off, washed with water and acetone, cleaned in an ultrasonic bath and stored under vacuum. The compound is stable in air, water and acetone. The yield was approximately 30% based on Ni. $[Ni(dien)_2]Cl_2$ and $[Ni(dien)_2]_3(SbS_4)_2$ were identified as by-products.

X-ray Crystallography: The X-ray single-crystal data for **1** were collected at 293 K using a STOE Imaging Plate Diffraction System

Table 3. Crystal data and selected results for the structure refinement of $[Ni(dien)_2]_3(Sb_3S_6)_2$

Empirical formula	$C_{24}H_{78}N_{18}Ni_3Sb_6S_{12}$
Crystal colour	brown
Crystal habit	irregular
Molecular mass [g/mol]	1910.39
Crystal system	triclinic
Space group	$P\bar{1}$
a (Å)	7.1208(5)
b (Å)	12.3254(9)
c (Å)	19.165(2)
α (°)	76.169(8)
β (°)	84.462(9)
γ (°)	85.892(8)
V (Å^3)	1623.6(2)
Z	2
T [K]	293
λ(Mo-K_α) (Å)	0.71073
$d_{calcd.}$ [Mg·cm^{-3}]	1.945
μ(Mo-K_α) [mm^{-1}]	3.73
F(000)	930
2Θ range of data collection (°)	$6° \le 2\Theta \le 60°$
Index range	$-10 \le h \le 10$
	$-15 \le k \le 17$
	$-27 \le l \le 27$
Reflections collected	19706
Independent reflections	9342
Reflections with $F_o > 4\sigma(F_o)$	8114
$wR2$ for all reflections[a]	0.1014
$R1$ for reflections with $F_o > 4\sigma(F_o)$[b]	0.0354
Goodness of fit	1.028
Largest diff. peak/hole [e·Å^{-3}]	0.99/−1.61

[a] $wR2 = [\Sigma[w(F_o^2 - F_c^2)^2]/\Sigma[w(F_o^2)^2]]^{1/2}$ [b] $R1 = \Sigma||F_o| - |F_c||/\Sigma|F_o|$

 © 2004 Wiley-VCH Verlag GmbH & Co. KGaA, Weinheim

(IPDS). The intensities were corrected for Lorentz, polarisation and absorption effects. Structure solution was performed using SHELXS-97.[23] Refinement was done against F^2 by using the software SHELXL-97.[24] The non-hydrogen atoms were refined with anisotropic displacement parameters. The hydrogen atoms were positioned with idealised geometry and refined with isotropic displacement parameters using the riding model. The structure contains additional disordered solvent molecules in the channels for which no appropriate structure model could be found. Therefore, the data were treated with the SQUEEZE option for disordered solvent in PLATON.[25] In the first step, this program calculates the space which can be occupied by disordered solvent molecules starting from the refined structure model. In the next step the sum of electrons in this space is calculated and the measured data file is corrected in a way that these electrons are not considered. This calculation gives a volume of 182.2 Å^3/cell which can be used by disordered solvent. Selected crystal data and details of the structure determination are listed in Table 3.

CCDC-21630 contains the supplementary crystallographic data for this paper. These data can be obtained free of charge at www.ccdc.cam.ac.uk/conts/retrieving.html [or from the Cambridge Crystallographic Data Centre, 12 Union Road, Cambridge CB2 1EZ, UK; Fax: (internat.) +44-1223-336-033; E-mail: deposit@ccdc.cam.ac.uk].

DTA-TG-MS Investigations: DTA-TG-MS measurements were performed using a Netzsch STA-409. The sample (mass: 11.98 mg) was heated in a dynamic He atmosphere (flow rate 75 ml·min^{-1}) in an Al_2O_3 crucible with a heating rate of 4 K/min to 400 °C).

Density Functional Calculations: Spin-restricted DFT calculations using Becke's three parameter hybrid function with the correlation function of Lee, Yang and Parr (B3LYP)[26−28] were performed for the singlet ground state of $[Sb_3S_6]^{3-}$. The LanL2DZ basis set was used for the calculation. This applies Dunning/Huzinaga full double zeta (D95) basis functions[29] to the first row and Los Alamos effective core potentials plus DZ functions on all other atoms.[30,31] Convergence was reached when the relative change in the density matrix between subsequent iterations was less than $1\cdot10^{-8}$. All procedures were used as they are implemented in the GAUSSIAN 98 package.[32]

Acknowledgments

Financial support by the Deutsche Forschungsgemeinschaft and the State Schleswig-Holstein is gratefully acknowledged.

[1] J. Olivier-Fourcade, L. Izghouti, E. Philippot, *Rev. Chim. Miner.* **1981**, *18*, 207−217.
[2] W. S. Sheldrick, H.-J. Häusler, *Z. Anorg. Allgem. Chem.* **1988**, *561*, 149−156.
[3] J. B. Parise, *Science* **1991**, *251*, 293−294.
[4] R. Stähler, W. Bensch, *Z. Anorg. Allg. Chem.* **2002**, *628*, 1657−1662.
[5] H. Rijnberk, C. Näther, M. Schur, I. Jeß, W. Bensch, *Acta Crystallogr., Sect. C* **1998**, *54*, 920−923.
[6] M. Schur, W. Bensch, *Z. Anorg. Allg. Chem.* **1998**, *624*, 310−314.
[7] W. Bensch, M. Schur, *Z. Kristallogr.* **1997**, *212*, 305−307.
[8] W. Bensch, C. Näther, R. Stähler, *Chem. Commun.* **2001**, 477−478.
[9] L. Engelke, W. Bensch, *Acta Crystallogr., Sect. E* **2003**, *59*, 378−380.
[10] G. Cordier, H. Schäfer, *Rev. Chim. Miner.* **1981**, *18*, 218−223.
[11] H. A. Graf, H. Schäfer, *Z. Naturforsch., Teil B* **1972**, *27*, 735−739.
[12] A. V. Powell, S. Boissiere, A. M. Chippindale, *Chem. Mater.* **2000**, *12*, 182−187.
[13] G. Cordier, C. Schwidetzky, H. Schäfer, *J. Solid State Chem.* **1984**, *54*, 84−88.
[14] W. Bensch, M. Schur, *Z. Naturforsch., Teil B* **1997**, *52*, 405−409.
[15] G. Dittmar, H. Schäfer, *Z. Anorg. Allg. Chem.* **1977**, *437*, 183−187.
[16] B. Eisenmann, H. Schäfer, *Z. Naturforsch., Teil B* **1979**, *34*, 383−385.
[17] J. S. Swinnea, A. J. Tenorio, H. Steinfink, *American Mineralogist* **1985**, *70*, 1056−58.
[18] A. V. Powell, R. Paniagua, P. Vaquerio, A. M. Chippindale, *Chem. Mater.* **2002**, *14*, 1220−1224.
[19] R. Stähler, B.-D. Mosel, H. Eckert, W. Bensch, *Angew. Chem.* **2002**, *114*, 4671−4673; *Angew. Chem. Int. Ed.* **2002**, *41*, 4487−4489.
[20] R. Stähler, C. Näther, W. Bensch, *Acta Crystallogr., Sect. C* **2001**, *57*, 26−27.
[21] R. Stähler, W. Bensch, *Eur. J. Inorg. Chem.* **2001**, 3073−3078.
[22] X. Wang, A. J. Jacobson, F. Liebau, *J. Solid State Chem.* **1998**, *140*, 387−395.
[23] G. M. Sheldrick, *SHELXS-97*, University of Göttingen, **1992**.
[24] G. M. Sheldrick, *SHELXL-97*, University of Göttingen, **1997**.
[25] A. L. Spek, *PLATON, A Multipurpose Crystallographic Tool*, Utrecht University, Utrecht, The Netherlands, **2000**.
[26] A. D. Becke, *Phys. Rev. A* **1988**, *38*, 3098.
[27] A. D. Becke, *J. Chem. Phys.* **1993**, *98*, 1372.
[28] A. D. Becke, *J. Chem. Phys.* **1993**, *98*, 5648.
[29] T. H. Dunning, Jr., P. J. Hay in *Modern Theoretical Chemistry* (Ed.: H. F. Schaefer III), Plenum, New York, **1976**.
[30] P. J. Hay, W. R. Wadt, *J. Chem. Phys.* **1985**, *82*, 270 and 299.
[31] W. R. Wadt, P. J. Hay, *J. Chem. Phys.* **1985**, *82*, 284.
[32] M. J. Frisch, G. W. Trucks, H. B. Schlegel, G. E. Scuseria, M. A. Robb, J. R. Cheeseman, V. G. Zakrzewski, J. A. Montgomery, Jr., R. E. Stratmann, J. C. Burant, S. Dapprich, J. M. Millam, A. D. Daniels, K. N. Kudin, M. C. Strain, O. Farkas, J. Tomasi, V. Barone, M. Cossi, R. Cammi, B. Mennucci, C. Pomelli, C. Adamo, S. Clifford, J. Ochterski, G. A. Petersson, P. Y. Ayala, Q. Cui, K. Morokuma, P. Salvador, J. J. Dannenberg, D. K. Malick, A. D. Rabuck, K. Raghavachari, J. B. Foresman, J. Cioslowski, J. V. Ortiz, A. G. Baboul, B. B. Stefanov, G. Liu, A. Liashenko, P. Piskorz, I. Komaromi, R. Gomperts, R. L. Martin, D. J. Fox, T. Keith, M. A. Al-Laham, C. Y. Peng, A. Nanayakkara, M. Challacombe, P. M. W. Gill, B. Johnson, W. Chen, M. W. Wong, J. L. Andres, C. Gonzalez, M. Head-Gordon, E. S. Replogle, J. A. Pople, *GAUSSIAN98* Rev. A.11; Gaussian Inc., Pittsburgh, **2001**.

Received December 4, 2003
Early View Article
Published Online April 7, 2004

 © 2004 Wiley-VCH Verlag GmbH & Co. KGaA, Weinheim

Conformational Effects on the Photoinduced Energy Transfer in a Star-Shaped Pentaporphyrin with Nucleosidic Linkers

Lucia Flamigni,*[a] Anna Maria Talarico,[a] Barbara Ventura,[a] Giancarlo Marconi,[a] Chloé Sooambar,[b] and Nathalie Solladié*[b]

Keywords: Circular dichroism / Energy transfer / Porphyrinoids / Photochemistry / Supramolecular chemistry

The photophysical properties of a pentameric array (**FB-Zn$_4$**) containing peripheral Zn porphyrins and a free-base core, connected by nucleosidic linkers, have been determined and compared with the properties of the model dyad (**FB-Zn**) and of their individual components. The flexibility of the nucleosidic linkers allows the dyad to take two different conformations corresponding to a bent and an almost fully extended form of the linker, which are characterized by a chromophore separation of ca. 2 nm and ca. 3 nm, respectively. Energy transfer from the zinc porphyrin to the free-base porphyrin occurs, in the bent conformation, with a rate of 3.6×10^9 s^{-1}. Conversely, in the extended conformation, the Zn porphyrin decay is unperturbed, which is in good agreement with the expected dipole–dipole (Förster) energy transfer mechanism. In the pentameric array, the Zn porphyrin luminescence is quenched with a rate of 3.6×10^9 s^{-1} in 15% of the population, whilst the luminescence of the Zn porphyrin is unquenched for ca. 35% of the population. For comparison with the dyad, these two cases are assigned as arrays with a single linkage in a bent configuration and arrays with all linkages in the extended configuration, respectively. However, the most striking feature in the pentaporphyrin is that 50% of the Zn porphyrin excited state population exhibits a fast nonradiative deactivation (rate ca. 10^{10} s^{-1}) which also involves the free-base porphyrin core to some extent. This behavior is attributed to a strongly interacting conformation with the Zn porphyrins folded over the central free-base porphyrin. The proposed model is supported by CD spectroscopy, complexation experiments with bases, and the reactivity of the excited state towards external quenchers.
(© Wiley-VCH Verlag GmbH & Co. KGaA, 69451 Weinheim, Germany, 2004)

Introduction

Synthesis of multi-porphyrin architectures and determination of their photo properties is the object of intensive research activity.[1] These oligomeric arrays can mimic naturally occurring tetrapyrrolic aggregates that perform key processes in photosynthesis, i.e. light energy collection and charge separation.[2] The study of multi-porphyrin ensembles, in addition to providing basic knowledge in the fields of photochemistry, photophysics and photobiology, can be regarded as potentially informative in the construction of light-operated molecular-level information storage devices, [3] for the conversion of light energy into chemical or electrical energy,[1,4] and for the preparation of materials with novel properties.[5]

The present system, which consists of a pentaporphyrin containing a central free-base porphyrin and four peripheral zinc porphyrins connected via a flexible chiral nucleosidic linker,[6] was studied in order to determine its potential as an antenna system, capable of collecting light energy and conveying it to the energy sink at the central position. The peripheral zinc porphyrin chromophores can absorb light extensively over the full visible spectrum and the energy stored in the first excited singlet state (2.05 eV) could be conveyed to the central free-base porphyrin characterized by a lower lying excited singlet state (1.92 eV). The system can work effectively as an antenna if the absorbed light energy is efficiently conveyed to the central porphyrin and no competitive loss of the absorbed energy occurs. The study of convenient model compounds, **ZnU**, **FBS** and the dyad **FB-Zn**, whose structures are shown in Scheme 1, can help in the elucidation of the fundamental steps in the pentad system **FB-Zn$_4$**, where photophysical behavior could be strongly influenced by the existence of different conformations due to the flexible linkers. Steady state and time-resolved spectroscopic methods were used to quantify the energy transfer process which was postulated previously.[6]

[a] Istituto per la Sintesi Organica e Fotoreattivita' (ISOF), CNR, Via P. Gobetti 101, 40129 Bologna, Italy
E-mail: flamigni@isof.cnr.it
[b] Groupe de Synthèse de Systèmes Porphyriniques, Laboratoire d'Electrochimie et de Chimie Physique du Corps Solide, Université Louis Pasteur et CNRS (UMR 7512), Institut Le Bel,
4 rue Blaise Pascal, 67000 Strasbourg, France
E-mail: nsolladie@chimie.u-strasbg.fr

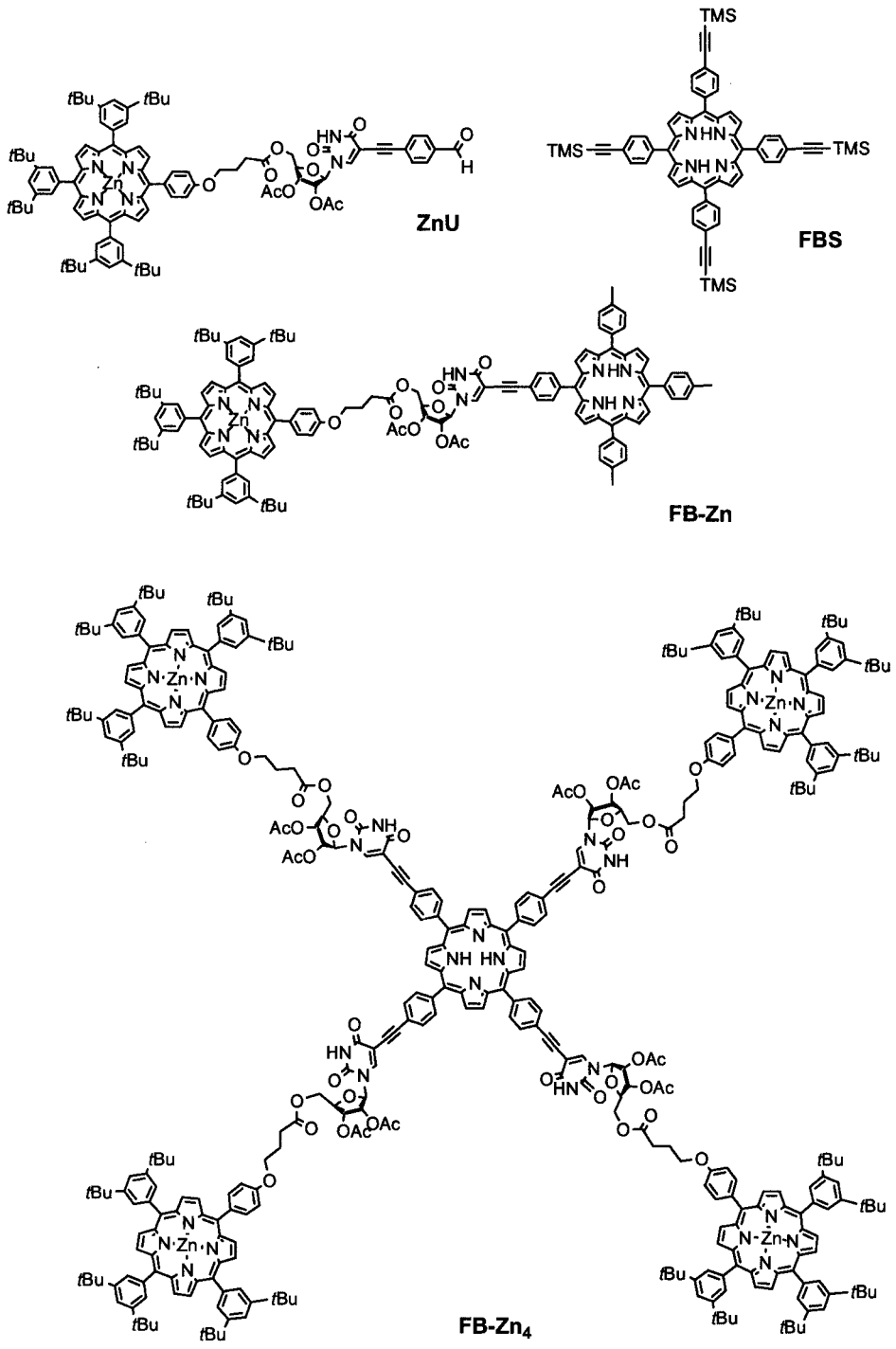

Scheme 1. The structures of the component models **ZnU** and **FBS**, the dyad **FB-Zn** and the pentad **FB-Zn$_4$**

Results and Discussion

Synthesis

The dyad was synthesized according to Lindsey's procedure for the construction of sterically hindered porphyrins.[7] One equivalent of aldehyde **ZnU**[6] and three equivalents of *p*-tolualdehyde were condensed, at room temperature and under an inert atmosphere, with four equivalents of pyrrole in chloroform in the presence of a catalytic amount of $BF_3{\cdot}OEt_2$. The resulting porphyrinogen was then oxidized by reflux with three equivalents of *p*-chloranil, for one and a half hours. After a tedious purification requiring many chromatographic separations over silica gel, the desired dyad was isolated in 10% yield. It was characterized by ^{1}H NMR and FAB mass spectrometry (m/z = 2104.5 $[M]^+$, calcd. 2104.9). The synthesis and characterization of the pentad has been reported previously.[6]

 © 2004 Wiley-VCH Verlag GmbH & Co. KGaA, Weinheim

Photoinduced Processes

The Dyad

The absorption spectrum of the dyad closely matches the superposition of its two components, as shown in Figure 1, where absorption spectra of both the component units, their sum and the absorption spectrum of the dyad are given. This indicates a very modest interaction between the components, as expected from the length and type of bridging ligand.

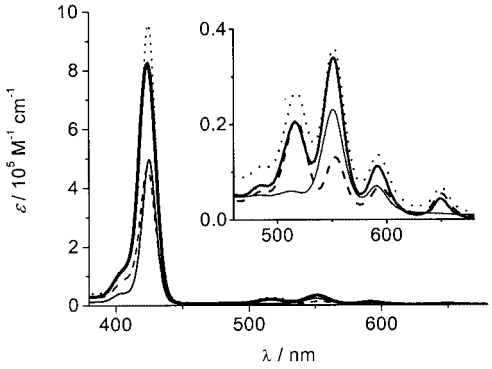

Figure 1. Molar absorption coefficients of the models **ZnU** (thin solid line) and **FBS** (dashed line), and of **FB-Zn** (thick solid line) in toluene solutions, the sum of the molar absorption coefficients of the models is also reported (dotted line)

The emission spectrum of the dyad, after excitation at a wavelength where only **FBS** absorbs, i.e. at $\lambda > 625$ nm, displays the emission spectrum of the **FBS** model, with an identical quantum yield within experimental error (Table 1). Selective excitation of the **ZnU** unit is not possible (see Figure 1) but excitation where both components absorb, yields an emission spectrum which shows the features of both the free base component ($\lambda_{max.}$ = 652 and 718 nm) and of the zinc component ($\lambda_{max.}$ = 598 nm and 646 nm). However, if the emission is compared to those of the component models absorbing the same number of photons as in the dyad (Figure 2), it is clear that, in the array, the emission of the zinc porphyrin unit is quenched whereas the emission of the free-base porphyrin moiety is increased, i.e. it is sensitized (Table 1).

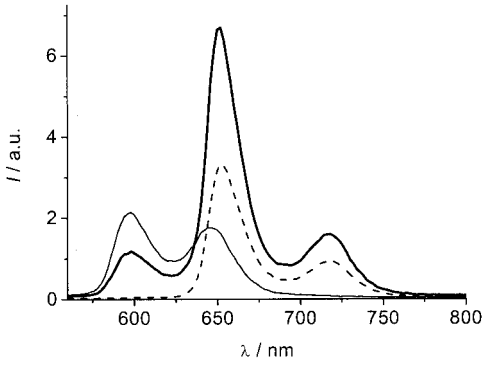

Figure 2. Emission spectra in toluene at 298 K of the models **ZnU** (thin solid line; A_{550nm} = 21.6%),**FBS** (dashed line; A_{550nm} = 11.7%), and the dyad **FB-Zn** (thick solid line; A_{550nm} = 33.4%, the partition of photons is A_{PZnU} = 21.6% and A_{FBS} = 11.7%) in toluene solutions; excitation at 550 nm

Time-resolved experiments with picosecond resolution (at λ = 600 nm, the maximum of the zinc porphyrin component emission) revealed a bi-exponential decay of the luminescence of the dyad, with lifetimes of 240 ps and 1.9 ns, accounting for ca. 30% and 70% of the total decay, respectively (Figure 3). Whilst the short lifetime could be due to the quenching of the luminescence of the zinc porphyrin component, the long lifetime is typical of the unquenched **ZnU** model (Table 1). The luminescence of the dyad at λ = 720 nm (Figure 3), where only the free base component emits, is characterized by a species with a lifetime of ca 240 ps, closely matching the fast decay of the zinc porphyrin component. A subsequent slower decay of 9.8 ns, typical of the emission of the model **FBS** (Table 1), was detected on a

Table 1. Luminescence properties and energy levels of the excited states of the models and arrays in toluene

		298 K				77 K	
	State	$\lambda_{max.}$ (nm)	φ_{fl} [a]	φ_{fl} [b]	τ (ns)[c] (% component)	$\lambda_{max.}$ (nm)	*E* (eV)[d]
FBS	^{1}FBS	652	0.18	0.18	9.5	646	1.92
ZnU	^{1}ZnU	598		0.073	1.9	604	2.05
FB-Zn	^{1}FB-Zn	652	0.19	0.33	0.240[e]; 9.8	647	1.92
	FB-^{1}Zn	598		0.042	0.240; 1.9 (30%); (70%)	604	2.05
FB-Zn$_4$	^{1}FB-Zn$_4$	652	0.13	–[f]	9.8	648	1.91
	FB-^{1}Zn$_4$	600		–[f]	0.110; 0.240; 1.9 (50%); (15%); (35%)	606	2.05

[a] Emission quantum yield. Selective excitation of the free-base porphyrin unit was at 650 nm. [b] Emission quantum yield. Excitation of both free-base and zinc porphyrin components was at 550 nm. The calculation is based on the photons absorbed directly by the moiety, as calculated by the molar absorption coefficients of the models **ZnU** and **FBS**. [c] Excitation was at 532 nm or at 337 nm for lifetimes > 2 ns. [d] Energy levels from the emission maxima at 77 K. [e] Lifetime of the rise. [f] In this array the interaction between components is strong (see text) and this prevents a reliable calculation of the partitions of photons between components. Consequently, it was impossible to measure the emission yields as done for the dyad (see above).

 © 2004 Wiley-VCH Verlag GmbH & Co. KGaA, Weinheim

longer time scale with a nanosecond time correlated single photon counting apparatus.

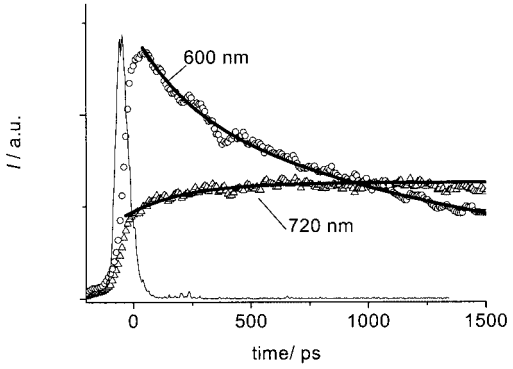

Figure 3. Time-resolved luminescence of **FB-Zn** in toluene solution after excitation at 532 nm; decay at 600 nm (open circles) and 720 nm (open triangles) with the bi-exponential fitting with lifetimes of 240 ps and 1.9 ns at 600 nm and of 240 ps and 9.8 ns at 720 nm; the exciting flash profile is also shown

The energy of the emission maxima, determined at 77 K, are conventionally assumed to correspond to the energy levels of the emitting states. From these, a value of 2.05 eV and 1.91 eV was derived for the energy of the singlet excited states localized on the zinc porphyrin and the free-base unit, respectively. The energy transfer from the zinc to the free-base porphyrin component is thermodynamically allowed and has a driving force of 0.14 eV. Therefore, the quenching of the zinc porphyrin donor and the sensitization of the free-base porphyrin acceptor are interpreted as being due to an energy transfer process. The rate constant can be calculated from the equation $k = 1/\tau - 1/\tau_0$, where τ and τ_0 are the lifetime of the quenched component (240 ps) and of the model compound (1.9 ns), respectively. The resulting rate constant is $k = 3.6 \times 10^9\ s^{-1}$. However, the bi-exponential nature of the decay indicates that only a fraction (30%) of the donor is quenched, whereas the main part (70%) is largely unaffected with respect to the model lifetime. This is indicative of the existence of two different conformers of the dyad (see below).

The occurrence of energy transfer from the zinc porphyrin unit to the free-base porphyrin unit is further supported by the excitation spectrum detected at 720 nm, where only the free-base porphyrin emits, which shows the contribution from the **ZnU** band at 550 nm, indicating that the emission of the free-base is sensitized by the absorption of the zinc component (Figure 4). The overlap between absorption spectrum and excitation spectrum of the dyad is not complete since the sensitization of free-base porphyrin by the zinc component only takes place in 30% of the excited conformation.

Energy transfer between singlet states can occur by two different mechanisms: the Förster mechanism (or dipole−dipole interaction)[8] or the Dexter mechanism (or electron exchange).[9] In case of energy transfer between singlet states with high absorbances and high emission quantum yields, the dipole−dipole mechanism usually prevails. For this mechanism, it is possible to calculate the rate k_{en}^F

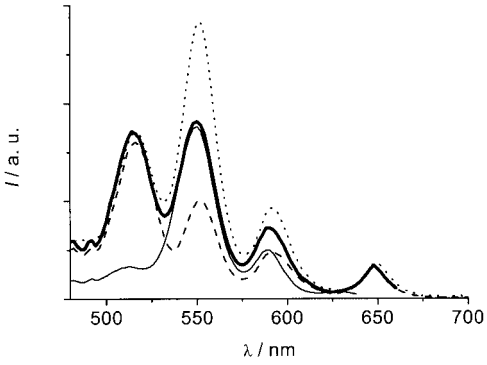

Figure 4. Excitation spectrum registered at $\lambda_{em} = 720$ nm (thick solid line) and an arbitrarily scaled absorption spectrum (dotted line) of **FB-Zn** in toluene solution; for comparative, purposes the excitation spectra of models **ZnU** at $\lambda_{em} = 646$ nm (thin solid line) and **FBS** at $\lambda_{em} = 720$ nm (dashed line) are also shown

by means of Equation (1),[8] in which Φ and τ are the emission quantum yield (0.073) and lifetime (1.9 ns) of the donor **ZnU**, respectively, d_{DA} is the donor−acceptor center-to-center distance, n is the refractive index of toluene and J^F is the overlap integral. κ^2, the orientation factor, takes into account the relative orientation of the transition dipole moments of the donor and the acceptor and in a pair of reactants freely diffusing in solution the value is statistical, i.e. 2/3, since they can randomly approach. In the present case, the statistical value 2/3 can be considered a good approximation because of the length and flexibility of the bond connecting the two components.

$$k_{en}^F = \frac{8.8\times10^{-25}\kappa^2\Phi}{n^4\tau d_{DA}^6}J^F \qquad (1)$$

The Förster overlap integral, J^F, is calculated from the overlap between the luminescence spectrum of the donor **ZnU**, $F(\bar{\nu})$ (cm^{-1} units) and the absorption spectrum $\varepsilon(\bar{\nu})$ of the acceptor **FBS** (cm^{-1} units), according to Equation (2).[8]

$$J^F = \frac{\int F(\bar{\upsilon})\varepsilon(\bar{\upsilon})/\bar{\upsilon}^4 d\bar{\upsilon}}{\int F(\bar{\upsilon})d\bar{\upsilon}} \qquad (2)$$

From the experimental emission and absorption spectra, an overlap integral J^F of $5.55 \times 10^{-14}\ cm^3\ M^{-1}$ was calculated, and from Equation (1) a critical transfer distance R_c of 28 Å was calculated. This is the distance at which the energy transfer rate equals the intrinsic deactivation rate of the donor and, given the sixth power dependence [see Equation (1)], for distances slightly larger, no energy transfer can occur because the intrinsic deactivation prevails. From Equation (1), the distance d_{DA}, at which the transfer occurs with the experimental rate of $3.6 \times 10^9\ s^{-1}$, can be calculated as being ca. 20 Å.

The presence of two different lifetimes in the decay of luminescence of the zinc donor component can be assigned to the presence of two different conformations of the dyad.

 © 2004 Wiley-VCH Verlag GmbH & Co. KGaA, Weinheim

In order to elucidate this point, a series of calculations based on the semiempirical AM1 hamiltonian[10] were carried out to describe a minimum conformation for this compound in vacuo. It was found that the most stable conformation corresponds to a bent structure, with a torsion angle of 67° defined by the C2′−C1′−N1−C6 atoms, and a heat of formation of 1174 kcal/mol. The C1′ and C2′ atoms are in the ribose unit and the N1 and C6 (C6 is the carbon atom involved in the double bond) are in the uracil nucleic base. In this conformation, the distance between the two chromophores Zn and FB is 23 Å, i.e. a distance in reasonable agreement with that calculated from the experimental energy transfer rate according to the Förster theory (ca. 20 Å, see above). However, we note that the molecule is quite free to rotate about the saturated bridges and that small variations of the torsion angle mentioned above lead to negligible variations in the overall energy of the compound. For example, a small increase in the twisting angle mentioned above, from 67° to 97°, leads to distances d−d greater than 28 Å, but the corresponding destabilization of the molecule is only 0.5 kcal/mol. It is quite possible that interaction of this molecule with a suitable solvent stabilizes an energy minimum corresponding to a donor−acceptor distance of at least 30 Å. Such a distance implies a reduced and, possibly, a no more competitive rate constant for the energy transfer process. The greatest distance achieved by rotation around the above twisting angle is ca. 32 Å.

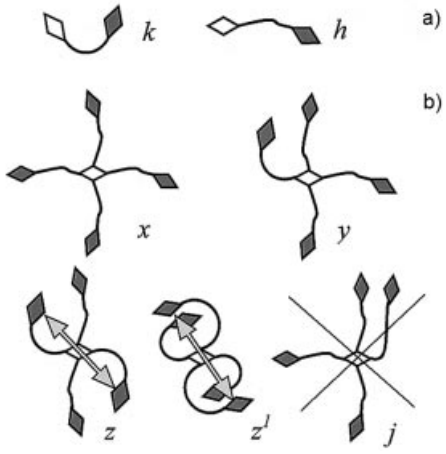

Scheme 2. Cartoon representation of the different conformations for **FB-Zn** (a) and **FB-Zn$_4$** (b); white diamonds represent the free-base porphyrin energy acceptor and gray diamonds the Zn porphyrin energy donor; the arrows indicate exciton interactions

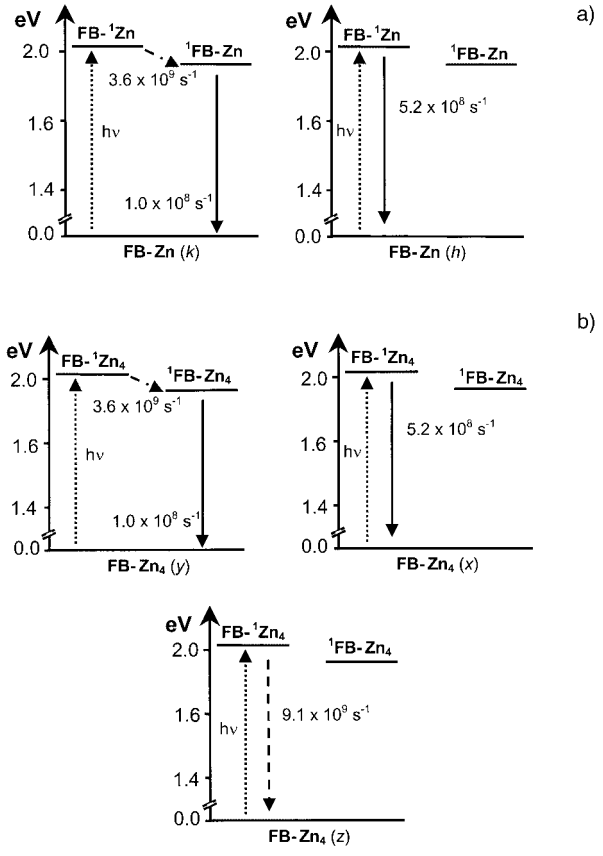

Scheme 3. Energy level scheme and photoinduced processes which can occur in the different conformations of **FB-Zn** (a) and **FB-Zn$_4$** (b); dotted lines represent light absorption, dashed lines represent non-radiative transitions, solid lines are radiative processes and dash-dot lines, energy transfer

On this basis, we interpret the results of the photoinduced processes in the dyad **FB-Zn** as follows. The dyad is composed of two populations of conformers which equilibrate on a long time scale compared to the photoinduced processes and therefore behave as independent species. Although the theoretical results in the gas phase indicate a folded structure as a shallow minimum conformer, the solution experimental results indicate that a more displaced conformation has been stabilized by solvent interactions and accounts for 70% of the population. A schematic illustration of the two conformers, whose structures are compatible with both the experimental findings and the theoretical results, is shown in Scheme 2 (a). Both conformers are in a bent configuration. However, in isomer *k* (Scheme 2, a) the two porphyrins are nearly overlapping, with a distance of the order of 20−23 Å between the donor−acceptor couple, which is sufficient to promote a dipole−dipole type energy transfer process. In the second open conformation, *h*, the planes containing the porphyrins are displaced and the center-to-center distance is increased to a value of ca. 32 Å, which does not allow Förster energy transfer to take place effectively.

Scheme 3 (a) shows schematic energy level diagrams illustrating the photoinduced processes occurring in both conformations of **FB-Zn**.

The Pentad

Unlike that found for the dyad, the absorption spectrum of the pentad **FB-Zn$_4$**, does not result from the simple superposition of the spectra of the component units. Figure 5 shows the absorption spectrum of the pentad compared with the sum of its components. Large effects on the Soret band, namely broadening, decrease in epsilon and a minor red shift are observed and, in addition, a rather important change in epsilon, a red shift and a change in spec-

 © 2004 Wiley-VCH Verlag GmbH & Co. KGaA, Weinheim

tral shape in the Q band region are also observed. Whenever porphyrins are connected to other species, some change in the Soret band region, which corresponds to the S_0-S_2 transition, is generally encountered. However, the effect on the Q band region, which corresponds to the S_0-S_1 transition, is rather unusual. This observation can be taken as indication of a rather important coupling between components. Since the type and length of the linker is not expected to couple the components substantially, a through-space interaction can be invoked to explain this observation. This must occur in a conformation where the components are in close contact and which can only be possible in **FB-Zn$_4$** and not in **FB-Zn**, since no such interaction was apparent in the latter.

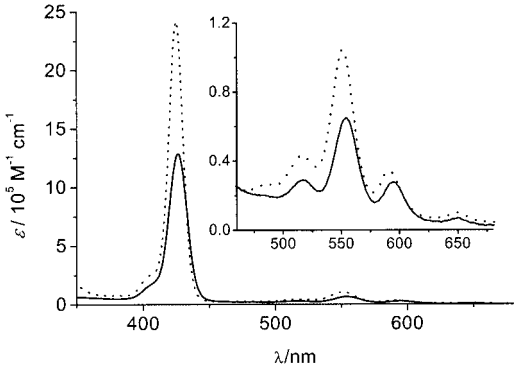

Figure 5. Molar absorption coefficient of **FB-Zn$_4$** in toluene solution (solid line); the sum of the molar absorption coefficients of the components, one **FBS** and four **ZnU** units, is also reported (dotted line)

Selective excitation of the free-base component at 650 nm results in a decrease of the emission quantum yield of this component compared to its model, from 0.18 to 0.13 (Table 1). This confirms the perturbation of the radiative and non-radiative parameters of the units when they are incorporated into the pentameric array. Under these strong coupling conditions, a quantitative consideration of the emission quantum yields of the individual components of the pentad as performed in Figure 2 for the dyad, is rather unreliable. In fact, that type of determination relies strongly on the fact that the properties of the components are not substantially modified when incorporated into the arrays. It is evident from both the ground state absorption spectrum (Figure 5) and from the free-base porphyrin emission yield (Table 1), which appears decreased in the pentad, that this is not the case. A qualitative experiment comparing the overall emission quantum yield of optically matched solutions of the dyad and the pentad is presented in Figure 6. This shows that the emission in the higher order array is strongly diminished for both the zinc porphyrin and the free-baseporphyrin. This cannot be attributed to an increased efficiency of the intramolecular energy transfer process, but rather to an overall increase in the non-radiative decay involving both components of the pentad, i.e. the free-base porphyrin and the Zn porphyrin.

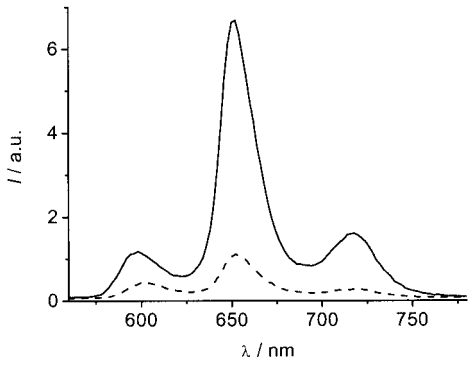

Figure 6. Emission detected from optically matched (A = 0.18) toluene solutions of **FB-Zn** (solid line) and **FB-Zn$_4$** (dashed line) after excitation at 550 nm

Upon excitation at 532 nm, the time-resolved luminescence of the pentad **FB-Zn$_4$** is reduced with respect to that of an optically matched **FB-Zn** dyad. The initial intensity at 600 nm is ca. 25% that of the dyad. A satisfactory fit of the decay at 600 nm, illustrated in Figure 7, was obtained using three exponentials of 110 ps (50%), 240 ps (15%) and 1.9 ns (35%). In this case, the band at 720 nm typical of the free-base porphyrin emission, is extremely low because of the numerical predominance of the zinc porphyrin chromophore, and no rise in the luminescence signal could be detected.

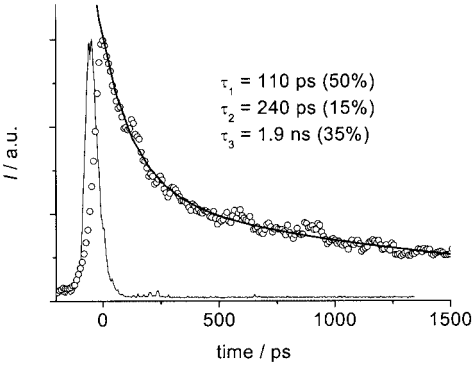

Figure 7. Time-resolved luminescence of **FB-Zn$_4$** in toluene solution after excitation at 532 nm; decay at 600 nm (O) and tri-exponential fitting with lifetimes of 110 ps, 240 ps and 1.9 ns. The exciting flash profile is also shown

The two longest lifetimes, 1.9 ns and 240 ps, are similar to those found in the dyad **FB-Zn**, and can be similarly assigned to unquenched conformations (1.9 ns), where the donor and acceptor are at the extremities of an extended linker and to quenched conformations (240 ps) with the donor and the acceptor at the extremities of a bent linker. The shortest (110 ps) and most important component in the luminescence decay, which accounts for ca. 50% of the intensity, is new and may be assigned to a different type of conformer which is only possible in the pentad. Multi-exponential decay of the zinc porphyrin luminescence is

 © 2004 Wiley-VCH Verlag GmbH & Co. KGaA, Weinheim

typical of flexible zinc porphyrin-based star compounds with a central free base porphyrin energy acceptor and has been frequently reported in the literature.[4k−4l]

In spite of the fact that the overall yield of the luminescence of the pentad is extremely low, sensitization of the free-base by the zinc component still occurs, as illustrated by the excitation spectrum registered at 720 nm, which is a wavelength normally indicative of free-base porphyrin emission (Figure 8). In this excitation spectrum, there is a clear contribution to the free-base emission from the zinc porphyrin donor band at 550 nm. Its extent is partial as in the dyad **FB-Zn**, and may be assigned to the fact that some conformations in **Fb-Zn$_4$** do not contribute to energy transfer. In spite of the fact that we could observe some sensitization of the free-base emission by the zinc porphyrin component (see Figure 8), the overall emission of the free-base porphyrin does not appear to increase in the pentad but rather to decrease, as shown in Figure 6. At the same time, we determined a quenching of the zinc porphyrin luminescence without detecting a corresponding sensitization in the free-base acceptor. A similar behavior was reported by Sanders et al. for a pentaporphyrin composed of a free base tetrapyridylporphyrin core coordinated via four axial bonds to a cyclic tetra-Zn porphyrin.[4s] The authors assigned the quenching of the luminescence of both components to an undefined photoinduced electron transfer process. In the present case, no photoinduced electron transfer can occur spontaneously since, according to their redox potentials,[6] the energy of the highest excited state (2.05 eV, Table 1) is insufficient to promote an electron transfer between the components. Therefore, in order to explain this observation, we have to assume that a remarkable loss of emission from the zinc porphyrin component, as well as from the free-base porphyrin unit, must take place through some non-radiative path.

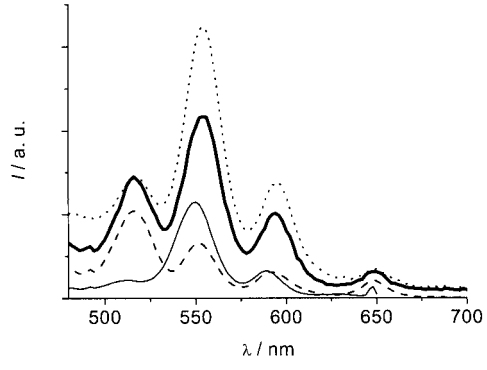

Figure 8. Excitation spectrum registered at λ_{em} = 720 nm (thick line) and absorption spectrum (dotted line) of **FB-Zn$_4$** in toluene solution; for comparative, purposes the excitation spectra of the models **ZnU** at λ_{em} = 646 nm (thin solid line) and **FBS** at λ_{em} = 720 nm (dashed line) are shown; the spectra are arbitrarily scaled

Some strong interacting conformer could account for the observed phenomena, namely non-additivity of absorption and a dramatic decrease in emission quantum yield of the pentad compared to the dyad as well as a new fast component (110 ps) in the quenching of the luminescence. This conformation must be precluded in the dyad, where the above effects were not observed. For the pentad, a series of different conformations can be envisaged, some of which are shown in Scheme 2 (b.) Conformation *x* (fully extended) and conformation *y* (partially bent) resemble the respective conformations of the dyad and should behave similarly. However, the conformations resulting from the concomitant bending of two (or more) Zn porphyrins over the free base component, denoted as *z* or *z'*, are unique to the pentad. Other types of conformations unique to the pentad, denoted as *j*, with the Zn porphyrins in a parallel arrangement, can be neglected. In fact, it seems unlikely that this type of conformation could affect the radiative parameters of the free-base component which is not involved in the interaction. Therefore, type *z* conformers are most likely responsible for the strong interaction observed in the pentad and this is supported by the data presented in the following sections.

A simplified interpretation of the data can be attempted as follows. The pentad is assumed to take (at least) three different types of conformations denoted as *x*, *y* and *z*. Conformations *x* and *y* behave "regularly" i.e. similarly to the corresponding bent or extended conformations in the dyad, as confirmed by the similar lifetimes detected in the luminescence quenching of the Zn porphyrin donor. The *z* type conformations may be responsible for the different behavior of the pentad array compared to the dyad. The short luminescence lifetime of the zinc porphyrin component (110 ps) is assigned to this type of conformation which, unlike the 240 ps component assigned to an energy transfer process in conformation *y*, has to be regarded as a fast, non-radiative decay of the excited state. In this type of conformation, an electronic, exciton type interaction also involving the free-base component, can occur. This induces a strong perturbation of the individual parameters of the components resulting in a greatly increased non-radiative decay. Since it accounts for about half of the excited state population, as calculated from the luminescence of the components, its behavior dominates the observed phenomena.

The ensemble Zn−FB−Zn in *z*, or Zn−Zn−FB−Zn−Zn in *z'*, typical of the pentad, is therefore deemed responsible for the new properties, caused by the strong electronic coupling between the components. Deactivation of the excited ensemble Zn−FB−Zn (or Zn−Zn−FB−Zn−Zn) proceeds rapidly, by non-radiative pathways, without producing any sensitization localized at the free-base. The free-base itself, when selectively excited, displays a decreased emission quantum yield in the pentad. This indicates that, irrespective of the excited component, the Zn−FB−Zn ensemble seems to follow non-radiative decay paths.

Further evidence supporting the importance of a conformation where the free-base porphyrin is somehow shielded from the exterior is given by the electrochemistry[6] and the triplet excited state lifetime data reported below.

A nanosecond flash photolysis experiment on the pentad **FB-Zn$_4$** in air free solution allows detection of the porphyrin triplet states of the zinc porphyrin donor and of the free-

 © 2004 Wiley-VCH Verlag GmbH & Co. KGaA, Weinheim

base porphyrin acceptor. The lifetime of the triplet state localized on the zinc porphyrin, FB-$^3Zn_4$, decays with a lifetime of 0.5 μs and sensitizes the lower energy triplet localized on the free-base porphyrin ^{3}FB-Zn_4, which has a lifetime of 500 μs, much higher than that measured in the model **FBS** and in the dyad **FB-Zn** which are, under the same conditions, 200 μs and 160 μs, respectively (Figure 9). This indicates that the reactive FB-$^3Zn_4$ excited state of the pentad is better shielded from trace impurities and oxygen contained in the solvent than in the models and the dyad, and supports the assignment of a rather compact structure which protects the central free-base porphyrin, as in the *z* conformations.

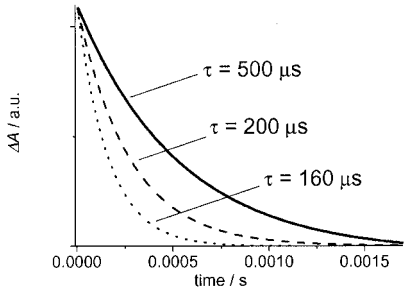

Figure 9. Normalized decay for absorption of the free-base triplet excited state in the model, ^{3}FBS (dashed line), in the dyad, ^{3}FB-Zn (dotted line), and in the pentad, ^{3}FB-Zn_4 (full line)

A similar indication comes from electrochemistry, which was reported previously.[6] The central free-base porphyrin behaves as an encapsulated electroactive molecule in pentaporphyrin **FB-Zn_4**, which is masked from electron transfer by the experimental conditions employed. The electrochemical studies make it clear that, in a flexible molecule such as pentaporphyrin **FB-Zn_4**, a substantial reduction of the electron transfer rate to the porphyrin core may be reasonably expected, i.e. the restricted accessibility to this core is probably assignable to conformational effects rather than to steric factors alone.

Scheme 3 shows the type of photoinduced processes which can occur in the arrays for extended (*x*), singly bent (*y*) or multiply bent (*z*) conformations.

Circular Dichroism Spectroscopy

In order to obtain further insight into the type and strength of interactions postulated in the different conformational cases, circular dichroism experiments were performed. The models **FBS** and **ZnU** display no optical activity when excited at the absorption bands of the porphyrin, while both **FB-Zn** and **FB-Zn_4** are optically active. Data from CD experiments for the dyad and the pentad in the Soret band region are shown in the upper panel of Figure 10 while the lower panel shows the electronic absorption bands for comparative purposes.

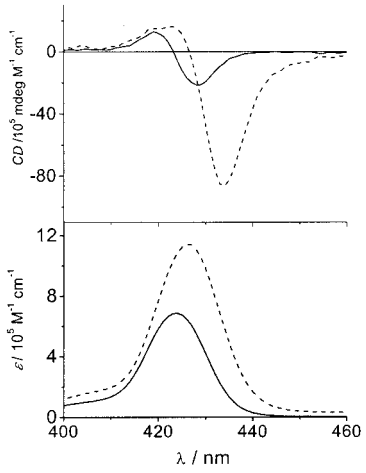

Figure 10. CD (upper panel) and UV (lower panel) spectra of **FB-Zn** (solid line) and **FB-Zn_4** (dashed line) in toluene solutions

The zero value of the CD signal at the wavelength of the maximum UV/Vis absorption band, together with the lack of signal for the separate units composing the pentad, indicates exciton coupling as the origin for the observed CD spectrum. In the simple case of the dyad, the CD spectrum arising from the exciton coupling between Zn and FB was calculated and the results obtained for the Soret band region are displayed in Figure 11. The molecular geometry used in the calculations was that obtained from the AM1 optimization, corresponding to the conformation *k* in Scheme 2 (a). The protocol described by Tinoco [11] for exciton coupling in the case of strongly allowed transitions was implemented by using energies and transition dipole moments calculated with the ZINDO/S program.[10]

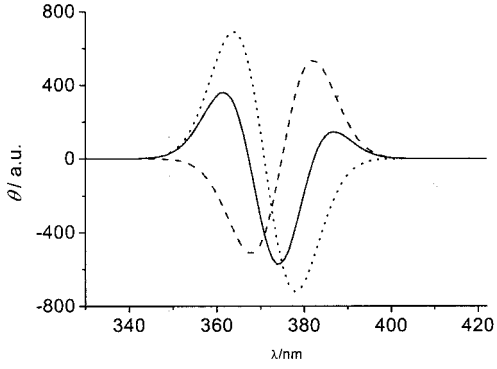

Figure 11. Calculated CD spectrum for the dyad **FB-Zn**; the solid line results from the sum of the exciton splitting of the parallel (dotted line) and perpendicular (dashed line) components of the Soret band

The calculations show that the crossed interactions between the two Soret states of **ZnU** and **FBS** give rise to two exciton bands of opposite sign (represented by the dotted and dashed curves in Figure 11), with a resulting component (solid line) presenting a dissymmetric pattern, the

 © 2004 Wiley-VCH Verlag GmbH & Co. KGaA, Weinheim

negative part being larger and at longer wavelength than the positive one. The other, smaller component calculated on the low energy side was not detected experimentally, and is derived from a direct inclusion of the two transition dipole components typical of the Soret band. In fact, usually just the parallel component of the band is included in the calculation, as the perpendicular one is partially deleted by the librational modes, as recently shown for similar compounds.[12] While the calculated energy appears, as usual, shifted to the blue when using the ZINDO/S program, the pattern and intensity of the signals appear consistent with experiment and, since the calculated CD spectrum appears very sensitive to the geometry adopted, these results corroborate the conformational hypotheses presented above.

Complexation

Zinc porphyrins are known to axially bind pyridine or pyridyl residues with association constants of the order of 10^4 M^{-1}. These constants have been found to increase dramatically up to ca. 10^8 M^{-1} when multiple bonds contribute to the complex formation (cooperative effect).

We have undertaken these experiments with both monodentate and bidentate pyridyl complexing agents in order to obtain information about the geometry of and the interactions between the zinc porphyrin chromophores. We have derived the association constants using different methods and additionally, we have monitored the effect of full complexation on several spectroscopic properties (i.e. luminescence and CD spectroscopy) with the aim of further understanding these systems.

Association of a pyridyl residue to Zn porphyrin induces a red shift, both on the Soret and Q absorption bands, and on the emission spectrum of the zinc porphyrins. A typical example is shown in Figure 12 for complexation of **ZnU** by pyridine (PYR). The spectral change, which is proportional to the concentration of complex, can be treated according to the equation below, which has been adapted and developed previously.[4j,13]

$$Obs = Obs_0 + \frac{\Delta Obs}{2S_0}\left\{K_d + X + S_0 - \left[(K_d + X + S_0)^2 - 4XS_0\right]^{1/2}\right\} \quad (3)$$

In this equation, the association constant K_{ass} is $1/K_d$, *Obs* is any observed signal intensity (i.e. absorbance or emission intensity), S_0 is the concentration of **ZnU**, or **FB-Zn** or **FB-Zn$_4$** (constant), X is the concentration of the complexing agent (variable), ΔObs is the maximum variation of the observed signal intensity under examination. The fitting of the absorbance data points of the maximum of the Soret band absorbance of the complexed form, at 431 nm, and the fitting of the emission intensity at $\lambda = 610$ nm are given in the insets of Figure 12.

Binding of the bidentate 1,4-diazabicyclo[2.2.2.]octane, DABCO, to Zn porphyrins to form a 1:2 complex has been reported to induce a shift in the UV-absorbance of the 1:1 complex by ca. 6 nm, caused by exciton coupling between the parallel porphyrin units.[14] Therefore, titration of the pentad with DABCO could give an indication of a simultaneous complexation of two porphyrins.[15] As illustrated in Figure 13, the complexation behavior of **FB-Zn$_4$** by DABCO is similar to that of **ZnU** by PYR. A single isosbestic point can be observed, indicating that only the uncomplexed and the 1:1 complex are present without any intermediate 2:1 (Zn porphyrin/DABCO) complex formation. This is indicative of the fact that in **FB-Zn$_4$** there are no couples of Zn porphyrins available for a cooperative binding. Further support for this observation comes from the comparison of the association constants derived by absorp-

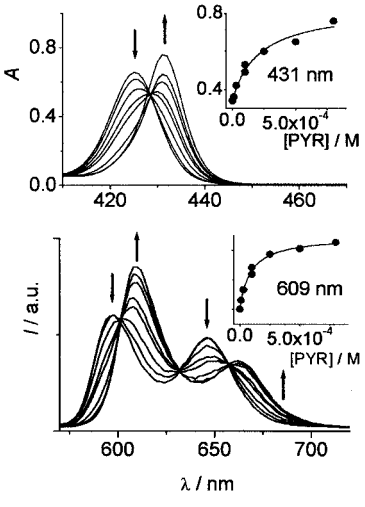

Figure 12. Electronic spectra of **ZnU** in toluene solution upon titration with increasing amounts of PYR; the upper panel shows the change of absorbance in the Soret band region and the inset shows the data points at 431 nm fitted according to Equation (3); in the lower panel, the change in emission intensity is shown and the inset shows the data points at 609 nm fitted according to Equation (3)

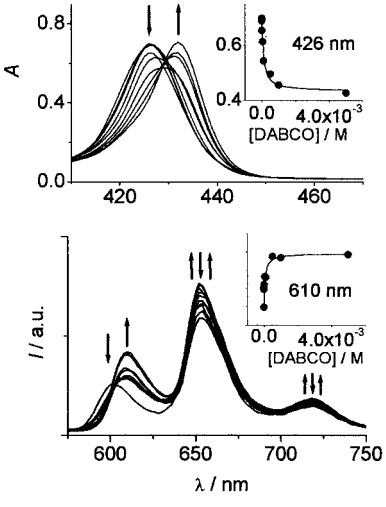

Figure 13. Electronic spectra of **FB-Zn$_4$** in toluene solution upon titration with increasing amounts of DABCO; change of absorbance in the Soret band region appears in the upper panel with the fitting of the data points at 426 nm according to Equation (3) shown in the inset; change in the emission intensity is reported in the lower panel with the fitting to data points at 610 nm according to Equation (3) shown in the inset

 © 2004 Wiley-VCH Verlag GmbH & Co. KGaA, Weinheim

Table 2. Association constants in toluene

	PYR		DABCO		BIPY	
	Abs[a] K_{ass} (M^{-1})	Em[b] K_{ass} (M^{-1})	Abs[a] K_{ass} (M^{-1})	Em[b] K_{ass} (M^{-1})	Abs[a] K_{ass} (M^{-1})	Em[b] K_{ass} (M^{-1})
ZnU	8×10^3	9×10^3	2×10^5	4×10^5	2×10^4	2×10^4
FB-Zn	5×10^4	9×10^4	5×10^4	5×10^4	2×10^4	5×10^4
FB-Zn$_4$	2×10^4	3×10^4	1×10^4	1×10^4	5×10^4	2×10^4

[a] Determined by spectrophotometric titration. The absorbance signal at $\lambda = 431 \pm 1$ was fitted to the equation given in the text. [b] Determined by spectrofluorimetric titrations upon excitation at the isosbestic of the absorption bands of uncomplexed and complexed forms, $\lambda = 428 \pm 1$. The emission signal at $\lambda = 610$ nm was fitted to the equation given in the text.

tion and emission methods. Table 2 shows these association constants determined for **ZnU**, **FB-Zn** and **FB-Zn$_4$** with PYR, DABCO and 4,4′ bipyridine (BIPY), respectively. The association constants of bidentate DABCO and BIPY with the dyad and pentad do not appear to differ substantially from the model **ZnU**. This indicates that the multiple binding sites of the pentad, compared to the model **ZnU** and the dyad **FB-Zn** are not detected by the bidentate complexing agent and confirms that the Zn porphyrin units in the pentad are not available for a cooperative binding, either because they are engaged in some different type of interaction, or because they cannot approach each other at an appropriate distance to complex at both ends of the bidentate units.

As a further experiment to help in the interpretation of the data, we observed the kind of changes in the emission and CD spectra brought about by complexation of the dyad and pentad with mono or bidentate bases. Figure 14 shows examples of the changes in the emission spectra occurring upon complexation of BIPY (concentration of complex > 95%) with the model **ZnU**, the dyad **FB-Zn** and the pentad **FB-Zn$_4$**. The results obtained using PYR and DABCO in place of BIPY (not reported) are essentially the same. In the axially bound model **ZnU**, maxima at 609 nm and 662 nm, compared to 598 nm and 646 nm in unbound **ZnU**, appear and an increased intensity of the first band (ratio 1.36) and a decrease in the intensity of the second band (ratio 0.7) with respect to unbound **ZnU** can be seen. Comparison of the emission spectra in Figure 14 confirms that the changes in the emission spectra of the dyad and the pentad can be ascribed only to the different luminescent properties of the axially coordinated zinc porphyrin. No other effect due to changes in the emission properties of the zinc porphyrin in the arrays can be detected.

An experiment similar to the one described for the emission experiment, was also carried out for the CD spectra. CD spectra of the dyad **FB-Zn** (middle panel) and the pentad **FB-Zn$_4$** (bottom panel) before and after complexation with BIPY (complex concentration > 95%), respectively, are shown in Figure 15. The spectrum for **ZnU**, where no signal was detected since it is not optically active, is given in the top panel for purposes of comparison. In **FB-Zn**, the CD signal was slightly shifted, similarly to the shift occurring in the absorption spectrum of the complexed **FB-Zn** as expected for an exciton coupling interaction. This indicates

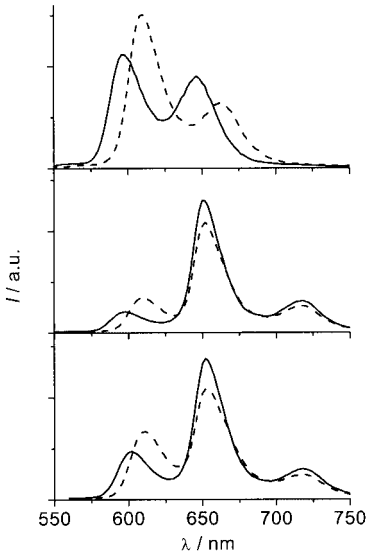

Figure 14. Emission spectra of **ZnU** (top panel), **FB-Zn** (middle panel) and **FB-Zn$_4$** (lower panel) in toluene solutions before (solid line) and after (dashed line) addition of BIPY (concentration of the complex > 95%)

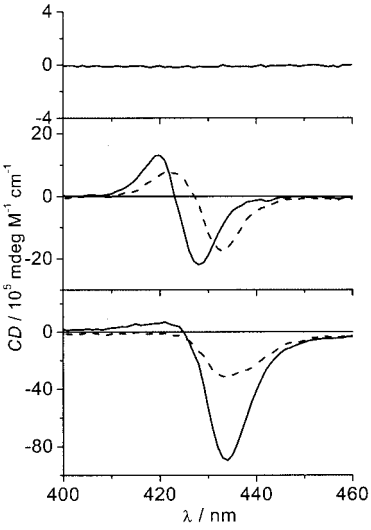

Figure 15. CD spectra of **FB-Zn** (middle panel) and **FB-Zn$_4$** (lower panel) in toluene solutions before (solid line) and after (dashed line) addition of BIPY (concentration of the complex > 95%); the top panel shows the signal obtained for the model **ZnU** for comparative purposes

 © 2004 Wiley-VCH Verlag GmbH & Co. KGaA, Weinheim

that the presence of BIPY does not alter the type of interaction in conformer *k*, which is responsible for the CD signal, as discussed in the previous section. Conversely, in the pentad **FB-Zn$_4$** axial binding to the zinc porphyrin unit by BIPY has a stronger effect on the signal. There was no shift, but a sizeable decrease of the CD band intensity was observed. The results obtained using DABCO or PYR are essentially the same.

An attempted interpretation of the results presented above follows. An increase in the luminescence would be expected if the postulated non-radiative decay responsible for the decrease in the luminescence yield of the pentad and for the rapid quenching assigned to non-radiative decay (110 ps) of the zinc porphyrin luminescence, is caused by a direct interaction between two zinc porphyrins. In that case, complexation by a bidentate BIPY should disrupt such an aggregate and re-establish the luminescence. The absence of this effect on the luminescence upon BIPY binding confirms that configuration *j* in Scheme 2 cannot be responsible for the detected decrease in luminescence yield.

If the CD spectra are considered, the behavior of **FB-Zn** is quite regular − upon complexation there is no disruption of the interaction responsible for exciton coupling, just a slight shift, which is in agreement with the change in the absorption spectrum of the complex form. This probably indicates that complexation of the Zn porphyrin in conformation *k*, occurs on the Zn porphyrin face remote from the free-base unit. In the case of the pentad, the situation is less straightforward. The complexing bases are unable to suppress the optical activity but modify it substantially. Whether this is indicative of the disruption of some exciton coupling in the pentad or just of a change in the parameters (distance, angles) caused by BIPY complexation, with a consequent cancellation of exciton contributions, is difficult to say. As a consequence, the existence of a conformer with more than two zinc porphyrins in a bent conformation over the central free-base, as in z^1, can not be excluded. In fact, in the latter case, complexation of the more internal Zn porphyrin would require some displacement or decoupling of the external Zn-porphyrin.

Conclusions

In conclusion, we have shown that the photoinduced processes in an **FB-Zn** dyad, covalently joined by a flexible nucleosidic linker, can be rationalized on the basis of the existence of two different conformers accounting, respectively, for ca. 30% and ca. 70% of the population. The major conformer is an extended one in which the distance between chromophores does not allow energy transfer to occur, while the minor conformer is a bent one where the shorter distance between chromophores allows energy transfer by a Förster mechanism with a rate of 3.6×10^9 s^{-1}. This latter bent isomer is assigned to the detected CD spectrum, which is deriving from the excitonic coupling of the electric transition dipole moments of the Soret band.

The corresponding pentad **FB-Zn$_4$** exhibits extremely complex behavior, which can only be explained by the existence of three different conformers. The two first identified conformers, which account for ca. 35% and 15% , respectively, correspond to one approximately extended conformation with a distance between chromophores which inhibits energy transfer, and one bent conformation with a distance that allows energy transfer toward the free-base porphyrin core to occur. These first two conformers are similar to those observed for the dyad **FB-Zn**. However, the most striking feature in this pentaporphyrin **FB-Zn$_4$** is the observed overall decrease in the luminescence quantum yield. This is attributed to the presence of a third conformer, which is only possible in the pentamer and accounts for ca. 50% of the population. In this conformer, a very fast, non-radiative decay of the excited state of the zinc porphyrin units (rate of ca. 10^{10} s^{-1}) is also associated with a decrease in the radiative rate constant of the central free-base porphyrin. On the basis of this evidence, a strongly interacting geometry, where Zn porphyrins are folded over the central free-base porphyrin, is assigned to this conformer. CD spectroscopy data, complexation experiments with mono and bidentate bases, electrochemistry results and reactivity of the excited states with external quenchers, all provide further support to the postulated model.

Experimental Section

Synthesis of the Dyad (FB-Zn): *p*-Tolualdehyde (49 mg, 0.41 mmol, 3 equiv.), the aldehyde **ZnU** (210 mg, 0.14 mmol, 1 equiv.) and pyrrole (36 mg, 37 μL, 0.55 mmol, 4 equiv.) were dissolved in chloroform, which had been dried with molecular sieves. $BF_3{\cdot}OEt_2$ (56 μL of a 3.2 M solution in chloroform) was then added. The solution turned red immediately. The reaction mixture was stirred at room temperature under argon for one and a half hours. *p*-Chloranil (100 mg, 0.41 mmol, 3 equiv.) was then added to oxidize the porphyrinogen formed during condensation and the mixture was refluxed for one and a half hours. The acidic solution was finally neutralized by addition of NEt_3 (25 μL) and the solvent was evaporated. The product was purified by column chromatography over silica gel (Φ = 3 cm, *h* = 23 cm, eluent: EtOAc/hexane, 50:50 to 60:40). The desired dyad **FB-Zn** was finally isolated in 10% yield (28 mg, 0.013 mmol).

FB-Zn: Purple glassy product. ^{1}H NMR ($CDCl_3$, 300 MHz): δ = 8.99 (s, 4 H, H_β), 8.96 (d, ^3J = 5.1 Hz, 2 H, H_β), 8.94 (d, ^3J = 5.1 Hz, 2 H, H_β), 8.87 (d, ^3J = 5.0 Hz, 2 H, H_β), 8.84 (d, ^3J = 4.6 Hz, 4 H, H_β), 8.81 (d, ^3J = 4.8 Hz, 2 H, H_β), 8.27 (d, ^3J = 8.3 Hz, 2 H, H_B), 8.10 (d, ^3J = 7.9 Hz, 2 H, H_o), 8.09 (d, ^4J = 1.7 Hz, 2 H, $H_{o''}$), 8.08 (d, 2 H, $H_{B'}$, hidden), 8.06 (d, ^4J = 1.7 Hz, 4 H, $H_{o'}$), 8.02 (d, 4 H, $H_{o'''}$, ^3J = 8.0 Hz), 7.99 (d, ^3J = 8.0 Hz, 2 H, H_A), 7.78 (t, ^4J = 1.6 Hz, 1 H, $H_{p''}$), 7.75 (t, ^4J = 1.7 Hz, 2 H, $H_{p'}$), 7.55 (d, ^3J = 7.9 Hz, 2 H, $H_{A'}$), 7.40 (d, ^3J = 6.1 Hz, 4 H, $H_{m'''}$), 7.28 (d, ^3J = 7.8 Hz, 2 H, H_m), 6.07 (d, ^3J = 4.6 Hz, 1 H, 1′-H), 5.50 (t, ^3J = 5.3 Hz, 1 H, 2′-H), 5.46 (t, ^3J = 5.1 Hz, 1 H, 3′-H), 4.51 (m, ^3J = 3.3 Hz, 2 H, 5′-H), 4.43 (t, ^3J = 3.6 Hz, 1 H, 4′-H), 4.37 (t, ^3J = 5.7 Hz, 2 H, $CH_2\gamma$), 2.99 (t, ^3J = 6.7 Hz, 2 H, $CH_2\alpha$,), 2.70 (s, 3 H, 7′-CH_3), 2.52 (s, 6 H, 7-CH_3), 2.41 (m, ^3J = 4.1 and 7.0 Hz, 2 H, $CH_2\beta$), 2.16 (s, 6 H, CH_3 2′,3′-OAc), 1.53 (s, 36 H, *t*Bu), 1.48 (s, 18 H, *t*Bu), −2.79 (s, 2 H, NH) ppm. MS (FAB$^+$): *m*/*z* = 2104.5 [M]$^+$, calcd. 2104.9.

 © 2004 Wiley-VCH Verlag GmbH & Co. KGaA, Weinheim

Spectroscopic and Photophysical Determinations: Toluene (spectroscopic grade, C. Erba) was used as received. Titration experiments for the determination of association constants were performed using a constant concentration of porphyrins and variable concentrations of PYR, DABCO and BIPY. Absorption spectra were recorded with a Perkin−Elmer Lambda 9 spectrophotometer. Emission spectra were measured using a Spex Fluorolog II spectrofluorimeter equipped with a Hamamatsu R928 photomultiplier and are uncorrected unless stated otherwise. Relative luminescence intensities were evaluated from the area (on an energy scale) of the luminescence spectra corrected for the photomultiplier response. Luminescence quantum yields φ for the components were obtained with reference to a standard zinc(II) porphyrin [Zn(II){5,10,15,20-tetrakis(4-*tert*-butylphenyl)porphyrin}] in toluene with φ = 0.08.[4h] Circular dichroism spectra were obtained with a Jasco J-710 dichrograph. Experiments at 77 K were done using quartz capillary tubes immersed in liquid nitrogen contained in a home-made quartz dewar.

Fluorescence lifetimes in the nanosecond range were determined using an IBH Time Correlated Single Photon Counting apparatus with excitation at 337 nm. Luminescence lifetimes shorter than one nanosecond were determined by an apparatus based on a Nd:YAG laser (Continuum PY62−10) with a 35 ps pulse duration, at 532 nm, 1 mJ/pulse and a Streak Camera. The luminescence signals from 1000 laser shots were averaged and the time profile was measured from the streak image in a wavelength range of ca. 20 nm about the selected wavelength. The fitting of the luminescence decays were performed by standard iterative non linear programs taking into consideration the instrumental response. Further details on the equipment can be found elsewhere.[16]

Transient absorbance in the nanosecond range made use of a laser flash photolysis apparatus based on a Nd:YAG laser (JK Lasers) delivering 532 nm pulses of 18 ns. Absorbance of the solutions at the exciting wavelength was ca 0.2 and an energy of 5 mJ/pulse was used for the determination of the spectra. In order to prevent undesired second-order T−T annihilation reactions, an energy of ca. 0.5 mJ/pulse was used for the triplet lifetime determination. Experiments were conducted in home-made, 10 mm optical path cuvettes, bubbled with argon for 5 min and sealed.

Computation of the integral overlap and of the rate for the energy transfer processes according to the Förster mechanism were performed with the use of Matlab 5.2.[17] Estimated errors are 10% on lifetimes, 20% on quantum yields and 30% on association constants. Working temperature, if not otherwise specified, was 295 ± 2 K.

The Hyperchem package [10] was used for both the conformational calculations (AM1 Hamiltonian) and the excited states properties calculations (ZNDO/S) of the free-base porphyrin and zinc porphyrin units necessary to perform the exciton coupling calculations.

Acknowledgments

Funding from the Italian CNR and Ministero dell'Istruzione, dell'Universita' e della Ricerca (FIRB, RBNE019H9 K) and financial support from the CNRS and the French Ministry of Research to N. S. (ACI Jeunes Chercheurs) are acknowledged. C. S. thanks the Région Guyane for a grant.

[1] [1a] V. Balzani, F. Scandola, *Supramolecular Photochemistry*, Ellis Horwood, Chichester, **1991**. [1b]M. R. Wasielewski, *Chem. Rev.* **1992**, *92*, 435−461. [1c] D. Gust, T. A. Moore, A. L. Moore, *Acc. Chem. Res.* **1993**, *26*, 198−205. [1d] H. Kurreck, M. Huber, *Angew. Chem.* **1995**, *107*, 992−946; *Angew. Chem. Int. Ed. Engl.* **1995**, *34*, 849−866. [1e] A. Harriman, J.-P. Sauvage, *Chem. Soc. Rev.* **1996**, 41−48. [1f] D. Gust, T. A. Moore, A. L. Moore, in *Electron Transfer in Chemistry* (Ed.: V. Balzani), Wiley-VCH, Weinheim, **2001**, vol. 3, part II, pp. 272−336. [1g]A. K. Burrell, D. L. Officer, P. G. Plieger, D. C. W. Reid, *Chem. Rev.* **2001**, *101*, 2751−2796.

[2] [2a] W. Kühlbrandt, D. N. Wang, Y. Fujiyoshi, *Nature* **1994**, *367*, 614−621. [2b] G. McDermott, S. M. Prince, A. A. Freer, A. M. Hawthornthwaite-Lawless, M. Z. Papiz, R. J. Cogdell, N. W. Isaacs, *Nature* **1995**, *374*, 517−521. [2c] T. Pullerits, V. Sundström, *Acc. Chem. Res.* **1996**, *29*, 381−389. [2d] J. Deisenhofer, H. Michel, *Angew. Chem.* **1989**, *101*, 872−890; *Angew. Chem. Int. Ed. Engl.* **1989**, *28*, 829−847. [2e] R. Huber, *Angew. Chem.* **1989**, *101*, 849− 870; *Angew. Chem. Int. Ed. Engl.* **1989**, *28*, 848−869.

[3] [3a] K. M. Roth, D. T. Gryko, C. Clausen, J. Li, J. S. Lindsey, W. G. Kuhr, D. F. Bocian, *J. Phys. Chem. B.* **2002**, *106*, 8639−8648. [3b] K. F. Cheng, C. M. Drain, K. Grohman, *Inorg. Chem.* **2003**, *42*, 2075−2083.

[4] [4a] G. Kodis, P. L. Lidell, L. de la Garza, P. C. Clausen, J. S. Lindsey, A. L. Moore, T. A. Moore, D. Gust, *J. Phys. Chem. A* **2002**, *106*, 2036−2048. [4b] H. Imahori, D. M. Guldi, K. Tamaki, Y. Yoshida, C. Luo, Y. Sakata, S. Fukuzumi, *J. Am. Chem. Soc.* **2001**, *123*, 6617−6628. [4c] R. A. Haycock, A. Yartsev, U. Michelsen, V. Sundström, C. A. Hunter, *Angew. Chem.* **2000**, *112*, 3762−3765; *Angew. Chem. Int. Ed.* **2000**, *39*, 3616−3619. [4d] H. S. Cho, H. Rhee, J. K. Song, C.-K. Min, M. Takase, N. Aratani, S. Cho, A. Osuka, T. Joo, D. Kim, *J. Am. Chem. Soc.* **2003**, *125*, 5849−5860. [4e] A. Nakano, A. Osuka, I. Yamazaki, T. Yamazaki, Y. Nishimura, *Angew. Chem.* **1998**, *110*, 3172−3176; *Angew. Chem. Int. Ed.* **1998**, *37*, 3023−3027. [4f] S. Hecht, T. Emrick, J. M. Fréchet, *Chem. Commun.* **2000**, 313−314. [4g] D. Holten, D. F. Bocian, J. S. Lindsey, *Acc. Chem. Res.* **2002**, *35*, 57−69. [4h] I. M. Dixon, J.-P. Collin, J-P. Sauvage, L. Flamigni, *Inorg. Chem.* **2001**, *40*, 5507−5517. [4i] L. Flamigni, M. R. Johnston, L. Giribabu, *Chem. Eur. J.* **2002**, *8*, 3938−3947. [4j] L. Flamigni, A. M. Talarico, F. Barigelletti, M. R. Johnston, *Photochem. Photobiol. Sci.* **2002**, *1*, 190−197. [4k] M-S. Choi, T. Aida, T. Yamazaki, I. Yamazaki, *Chem. Eur. J.* **2002**, *8*, 2668−2678. [4l] K. Kano, R. Nishiyabu, T. Yamazaki, I. Yamazaki, *J. Am. Chem. Soc.* **2003**, *125*, 10625−10634. [4m] T. Komatsu, M. Moritake, E. Tsuchida, *Chem. Eur. J.* **2003**, *9*, 4626−4633. [4n] M.-S. Choi, T. Aida, H. Luo, Y. Araki, O. Ito, *Angew. Chem. Int. Ed.* **2003**, *42*, 4060−4063. [4o] K. Kilså, J. Kajanus, A. Macpherson, J. Mårtensson, B. Albinsson, *J. Am. Chem. Soc.* **2001**, *123*, 3069−3080. [4p] E. Iengo, E. Zangrando, E. Alessio, J.-C. Chambron, V. Heitz, L. Flamigni, J.-P. Sauvage, *Chem. Eur. J.* **2003**, *9*, 5879−5887. [4q] E. K. L. Yeow, K. P. Ghiggino, J. N. H. Reek, M. J. Crossley, A. Bosman, A. P. H. J. Schenning, E. W. Meijer, *J. Phys. Chem. B* **2000**, *104*, 2596−2606. [4r] C. C. Mack, D. Pomeranc, M. Montalti, L. Prodi, J. K. M. Sanders, *Chem. Commun.* **1999**, 1083−1084. [4s] S. Anderson, H. L. Anderson, A. Bashall, M. McPartlin, J. K. M. Sanders, *Angew. Chem.* **1995**, *107*, 1196−1199; *Angew. Chem. Int. Ed. Engl.* **1995**, *34*, 1096−1099.

[5] [5a] H. L. Anderson, *Chem. Commun.* **1999**, 2323−2330. [5b] A. Tsuda, A. Osuka, *Science* **2001**, *293*, 79−82. [5c] I. V. Rubtsov, K. Susumu, G. I. Rubtsov, M. J. Therien, *J. Am. Chem. Soc.* **2003**, *125*, 2687−2696.

[6] N. Solladié, M. Gross, J.-P. Gisselbrecht, C. Sooambar, *Chem. Commun.* **2001**, 2206−2207.

[7] [7a] J. S. Lindsey, I. C. Schreiman, H. C. Hsu, P. C. Kearney, A. M. Marguerettaz, *J. Org. Chem.* **1987**, *52*, 827−836. [7b] J. S. Lindsey, R. W. Wagner, *J. Org. Chem.* **1989**, *54*, 828−836.

[8] Th. Förster, *Discuss. Faraday Soc.* **1959**, *27*, 7−17.

[9] D. L. Dexter, *J. Chem. Phys.* **1953**, *21*, 836−850.

[10] *Hyperchem version 6.02*, Hypercube Inc., Gainesville, Florida, **2000**.

[11] I. Tinoco Jr., *Adv. Chem. Phys.* **1962**, *4*, 113−160.

 © 2004 Wiley-VCH Verlag GmbH & Co. KGaA, Weinheim

[12] G. Pescitelli, S. Gabriel, Y. Wang, J. Fleischhauer, R. W. Woody, N. Berova, *J. Am. Chem. Soc.* **2003**, *125*, 7613−7628.
[13] L. Flamigni, A. M. Talarico, B. Ventura, *J. Porphyrins Phthalocyanines* **2003**, 7, 318−327.
[14] [14a] C. A. Hunter, M. N. Meah, J. K. M. Sanders, *J. Am. Chem. Soc.* **1990**, *122*, 5773−5780, [14b] C. C. Mak, N. Bampos, J. K. M. Sanders, *Angew. Chem.* **1998**, *110*, 3169−3172; *Angew. Chem. Int. Ed.* **1998**, *37*, 3020−3023.
[15] J. Brettar, J.-P. Gisselbrecht, M. Gross, N. Solladié, *Chem. Commun.* **2001**, 733−734.
[16] L. Flamigni, *J. Phys. Chem.* **1993**, *97*, 9566−9572.
[17] *Matlab 5.2.,* The MathWorks Inc., Natik Ma 01760, USA.

Received December 10, 2003
Early View Article
Published Online April 26, 2004

 © 2004 Wiley-VCH Verlag GmbH & Co. KGaA, Weinheim

Controlled Access to Mixed-Metal Pyridazine-Linked Cryptates

Tanya K. Ronson,[a] Jane Nelson,[b,c] Geoffrey B. Jameson,[d] John C. Jeffery,[e] and Sally Brooker*[a]

Keywords: Cryptates / Cyclic voltammetry / Heterometallic complexes / N ligands / Structure elucidation

The pyridazine-linked cryptand L [formed by the 3+2 condensation of 3,6-diformylpyridazine with tris(2-aminoethyl)amine (tren)] has been used to generate a series of heterodinuclear cryptates by a one-pot two-step method. The cryptates $[Mn^{II}Cu^{I}L](ClO_4)_2(BF_4)$, $[Fe^{II}Cu^{I}L](BF_4)_3{\cdot}CH_3CN$ and $[Ni^{II}Cu^{I}L](BF_4)_3{\cdot}H_2O$ have been structurally characterized, with elemental analyses and mass spectroscopic data providing further evidence of their heterodinuclear nature. The synthesis, structures and characterisation of the corresponding mononuclear cryptates $[M^{II}L](X)_2$ (M = Mn, Fe, Ni, X = BF_4^- or ClO_4^-) are also reported, along with the synthesis and characterisation of the homodinuclear dizinc(II) and disodium(I) cryptates, $[Zn_2L](ClO_4)_4$ and $[Na_2L](CF_3SO_3)_2$. Electrochemical studies on the heterodinuclear cryptates in CH_3CN indicate that the presence of the divalent cation influences the electrochemical potential and reversibility of the $Cu^{I} \rightarrow Cu^{II}$ oxidation with the redox potential of the Cu^{I}/Cu^{II} couple being inversely correlated with the distance between the two metal ions in the solid state as determined by X-ray crystallography. The previously synthesised $[Co^{II}Cu^{I}L](BF_4)_3$ is an exception to this trend, probably due to oxidation of the Co^{II} ion prior to that of the Cu^{I} ion.
(© Wiley-VCH Verlag GmbH & Co. KGaA, 69451 Weinheim, Germany, 2004)

Introduction

There are now a large number of cryptates reported and these have recently been reviewed.[1] However, very few mixed-metal cryptates have been prepared. Such heterodinuclear complexes are of interest as models for metalloenzyme active sites[2] and to study the mutual influences of the two metal centres on the electronic, magnetic and electrochemical properties of these systems.[3] Heterodinuclear cryptates synthesised to date include several structurally characterised transition metal-lanthanide cryptates of iminophenolate cryptands[4] and a $Fe^{II}Co^{II}$ cryptate of another iminophenolate cryptand,[5] although in this case the structural data are ambiguous.[6] An imidazolate-bridged $Zn^{II}Cu^{II}$ cryptate of an octa-amino cryptand has also been reported and is of interest as a model compound for the CuZn family of superoxide dismutases.[7]

Recently, we developed a system where we were able to isolate the mixed-valent complex $[Cu^{II}Cu^{I}L](BF_4)_3$ and the heterodinuclear complex $[Co^{II}Cu^{I}L](BF_4)_3$ [L is the cryptand formed by the 2+3 condensation of 3,6-diformylpyridazine with tris(2-aminoethyl)amine (tren), Figure 1].[8] In addition, we prepared the mononuclear cryptates $[Cu^{II}L](BF_4)_2$ and $[Co^{II}L](BF_4)_2$ of the same symmetrical cryptand.[9,10] This is possible because the binding of a single stereochemically demanding cation alters the conformation of the host in such a way as to prevent the formation of a homodinuclear complex. The resulting unsymmetrical mononuclear cryptates still have up to eight donor atoms available for coordination and so are able to bind a second non-stereochemically demanding cation such as copper(I)

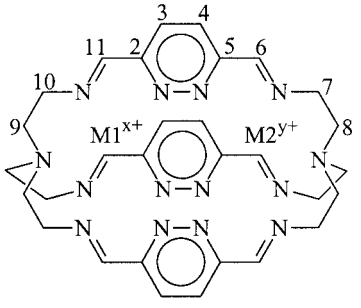

Figure 1. Schematic representation of the complex cations of the pyridazine containing cryptand L which have been prepared in this study, numbered as used in the NMR spectroscopic data assignments; note: M2^{y+} is (a) the same as M1^{x+} in the homodimetallic complexes, (b) absent in the monometallic complexes, (c) the Cu^{I} ion in the heterobimetallic complexes

[a] Department of Chemistry, University of Otago,
P. O. Box 56, Dunedin, New Zealand
Fax: (internat.) +64-3-479-7906
E-mail: sbrooker@alkali.otago.ac.nz
[b] School of Chemistry, Queens University of Belfast,
Belfast BT9 5AG, Northern Ireland
[c] Biomedical Sciences, University of Ulster,
Coleraine BT52 1SA, Northern Ireland
[d] Institute of Fundamental Sciences − Chemistry, Massey University,
P. O. Box 11222, Palmerston North, New Zealand
[e] School of Chemistry, University of Bristol,
Cantock's Close, Bristol BS8 ITS, United Kingdom
Supporting information for this article is available on the WWW under http://www.eurjic.org or from the author.

 © 2004 Wiley-VCH Verlag GmbH & Co. KGaA, Weinheim **DOI: 10.1002/ejic.200400068**

using four of these donor atoms, resulting in heterodinuclear complexes. Mixed metal complexes of symmetrical ligands are very unusual for acyclic systems and there are only a few examples for macrocyclic ligands.[4,5,7,11]

In this paper we report on the synthesis and characterisation of the heterodinuclear cryptates $[Mn^{II}Cu^{I}L](ClO_4)_2(BF_4)$, $[Fe^{II}Cu^{I}L](BF_4)_3{\cdot}CH_3CN$ and $[Ni^{II}Cu^{I}L](BF_4)_3{\cdot}H_2O$. We have completed a systematic study of the effect of the divalent cation on the copper(I) ion across the series $[M^{II}Cu^{I}L](X)_3$ (M = Mn, Fe, Co, Ni, Cu; X = BF_4^- or ClO_4^-), focussing on the electrochemical properties of these systems. In this context, it is useful to have a complex of a non-redox active cation; hence we have prepared $[Zn_2L](ClO_4)_4$. For completeness, the mononuclear cryptates $[Mn^{II}L](ClO_4)_2$, $[Fe^{II}L](BF_4)_2$ and $[Ni^{II}L](X)_2$ (X = BF_4^-, ClO_4^-) are also reported.

Results and Discussion

Synthesis and Characterisation of Mononuclear and Homodinuclear Cryptates

As we had previously observed that L readily forms the mononuclear cryptates $[Co^{II}L](BF_4)_2$ and $[Cu^{II}L](BF_4)_2$,[9,10] attempts were made to synthesise other mononuclear cryptates of first-row transition metals. The cryptates $[Mn^{II}L](ClO_4)_2$ and $[Ni^{II}L](X)_2$ (X = BF_4^-, ClO_4^-) were readily obtained in good purity and yield from the addition of one equivalent of the appropriate metal salt to L. The synthesis of $[Fe^{II}L](BF_4)_2$ proceeded in a lower yield and was sensitive to air and traces of solvent water.

Infrared spectra of the mononuclear cryptates confirmed that the L cryptand remains intact {imine at 1652 cm^{-1} for $[Mn^{II}L](ClO_4)_2$, 1638 cm^{-1} for $[Fe^{II}L](BF_4)_2$ and 1647 cm^{-1} for $[Ni^{II}L]^{2+}$} and confirms the presence of the expected anions {1116 and 1088 cm^{-1} for $[Mn^{II}L](ClO_4)_2$, 1052 and 1032 cm^{-1} for $[Fe^{II}L](BF_4)_2$, 1050 cm^{-1} for $[Ni^{II}L](BF_4)_2$ and 1083 cm^{-1} for $[Ni^{II}L](ClO_4)_2$}. In each case, the microanalyses support the proposed formula. The electrospray mass spectra show peaks for the successive loss of the two counterions. The molar conductivity values of 280 $mol^{-1}\,cm^2\,\Omega^{-1}$ for $[Mn^{II}L](ClO_4)_2$, 286 $mol^{-1}\,cm^2\,\Omega^{-1}$ for $[Fe^{II}L](BF_4)_2$ and 301 $mol^{-1}\,cm^2\,\Omega^{-1}$ for $[Ni^{II}L](BF_4)_2$ in acetonitrile indicate that all three cryptates behave as 2:1 electrolytes in solution.

The UV/Vis spectrum of yellow $[Mn^{II}L](ClO_4)_2$ in acetonitrile shows strong ligand-centred π-π* transitions at 208 nm (ε = 62100 $M^{-1}\,cm^{-1}$) and 250 nm (ε = 35100 $M^{-1}\,cm^{-1}$), with a lower intensity shoulder tailing off to longer wavelengths. The UV/Vis spectrum of $[Fe^{II}L](BF_4)_2$ in acetonitrile shows a band of at least four overlapping metal-to-ligand charge-transfer transitions with distinct peaks at 428 nm (ε = 4800 $M^{-1}\,cm^{-1}$) and 588 nm (ε = 8030 $M^{-1}\,cm^{-1}$) and shoulders at 370 nm and 540 nm. There are also transitions at 213 nm (ε = 64700 $M^{-1}\,cm^{-1}$) and a shoulder at about 250 nm which are probably due to ligand-centred π-π* transitions. The UV/Vis spectrum of $[Ni^{II}L](BF_4)_2$ in acetonitrile shows a band of overlapping weak d-d transitions (ε ≈ 30 $M^{-1}\,cm^{-1}$) with maxima at 825 and 908 nm. This is consistent with the presence of octahedral nickel(II). A second band at 211 nm (ε = 68700 $M^{-1}\,cm^{-1}$) with a shoulder at about 250 nm is assigned to ligand-centred π-π* transitions.

The ^1H NMR spectrum of $[Fe^{II}L](BF_4)_2$ at 243 K (Figure 2) is consistent with the existence of an unsymmetrical cryptate with the low spin iron(II) ion being located in one tren-derived cap site of the cryptand. The three strands are identical as expected. Each methylene group is differentiated into an axial triplet and equatorial doublet signal as a result of the accidental similarity of the geminal $^2J_{ax/eq}$ and vicinal $^3J_{ax/ax'}$ coupling constants of ca. 11−13 Hz (cf. 11−12 Hz for L).[9] Two-dimensional correlation NMR spectroscopic techniques were used to identify the signals for each end of the cryptand. The two ends of the cryptand were tentatively assigned by comparison with the $[ZnL](ClO_4)_2$ and $[Fe^{II}Cu^{I}L]^{3+}$ spectra and on the basis that the signals for the protons at end of the cryptand containing iron(II) are expected to be more deshielded due to the lower electron density in this half of the cryptand. It is worth noting that if this latter point is incorrect (and there are some inconsistencies in the carbon NMR spectrum), then the 'end' assignments would need to be reversed. At higher temperatures the ^1H NMR spectrum of $[Fe^{II}L](BF_4)_2$ shows significant changes, with the signals for the end of the cryptand which is believed to contain the iron(II) ion shifting, broadening or disappearing altogether as the

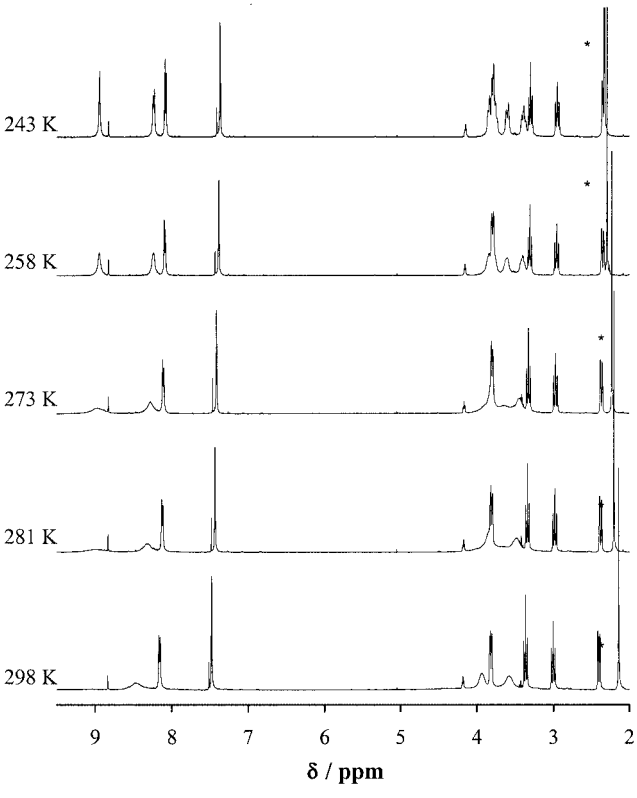

Figure 2. Variable temperature ^1H NMR spectra of $[Fe^{II}L](BF_4)_2$ in CD_3CN; the strong signal to the right hand side of the asterisk * is H_2O; note that the spectra at 273 K and 281 K were recorded on a different sample to the other spectra

 © 2004 Wiley-VCH Verlag GmbH & Co. KGaA, Weinheim

temperature is raised to 298 K (Figure 2). The signals for the other half of the cryptand remain sharp at all temperatures examined. This type of behaviour is characteristic of paramagnetic compounds, suggesting the existence of an equilibrium involving at least a small amount of high spin Fe^{II}. The broadening and shifting become more severe as the temperature is increased, in accordance with Curie-law behaviour. Another possibility that this temperature-dependent behaviour is simply due to fluxionality in the uncoordinated 'end' is believed to be unlikely on the basis that (a) the ^1H NMR spectrum of $[ZnL](ClO_4)_2$ is sharp at room temperature, (b) it would require the 'end' assignments to be reversed, and (c) whilst at first glance the H^{9a}/H^{9b} and H^{10a}/H^{10b} pairs of alkyl signals each appear to coalesce into two broad signals, for H^9 and H^{10}, respectively, at higher temperatures (δ = 3.94 and 3.59 ppm at 298 K), the position of these signals is not exactly at the averaged position (e.g. see relative positions of $H^{10a+10b}/H^{10}$ vs. H^{7b} as a function of temperature) and more seriously the integration is not correct as each broad signal integrates as equivalent to only one proton (not two). Finally, the H^{11} and H^3 signals shift as well as broaden.

The previous synthesis of $[Cu^I_2L](BF_4)_2$ and $[Ag^I_2L](ClO_4)_2$[9,10] suggested that it should be possible to synthesise homodinuclear cryptates of other non-stereochemically demanding metal ions.

The addition of two equivalents of zinc perchlorate to L in acetonitrile resulted in the dinuclear cryptate $[Zn_2L](ClO_4)_4$. The IR spectrum of $[Zn_2L](ClO_4)_4$ confirms that the cryptand is intact with an imine band at 1653 cm^{-1}. The bands for the ClO_4^- counterions, centred around 1121 cm^{-1} and 629 cm^{-1}, are both clearly split into three peaks indicating that there may be some interaction with the $[Zn_2L]^{4+}$ cation which lowers the symmetry of the ClO_4^- ion. The electrospray mass spectrum of $[Zn_2L](ClO_4)_4$ only shows peaks for the mononuclear species $[ZnL]^{2+}$ and $[ZnL](ClO_4)^+$. The elemental analysis, however, fits the dinuclear formulation. The UV/Vis spectrum of yellow $[Zn_2L](ClO_4)_4$ in acetonitrile shows transitions at 206 nm (ε = 51900 $M^{-1}\,cm^{-1}$) and 251 nm (ε = 30400 $M^{-1}\,cm^{-1}$) with lower intensity shoulders tailing to longer wavelengths.

The conductivity measurement of 359 $mol^{-1}\,cm^2\,\Omega^{-1}$ in acetonitrile is consistent with the complex being a 3:1 electrolyte (3:1, 340−420 $mol^{-1}\,cm^2\,\Omega^{-1}$)[12] instead of a 4:1 electrolyte as expected. The lower than expected conductivity value may well be a consequence of the reduced mobility often observed for large polycations,[12] although the 3:1 electrolyte cryptates described here have conductivity values within the expected ranges. Another, less likely, explanation is that it might be due to the symmetrical (see NMR spectrum later) coordination of one of the ClO_4^- counterions to the two zinc ions in solution. This would be consistent with the split ClO_4^- bands observed in the solid-state infrared spectrum (KBr disc), however, it would require a very different binding arrangement to those observed for all of the complexes of L studied to date, and such a bridging arrangement of the anion would also be unique for an imine, as opposed to amine, cryptand.[1] An X-ray structure determination would be required to test the latter hypothesis; however, the crystals of $[Zn_2L](ClO_4)_4$ obtained from acetonitrile were not of X-ray quality. Attempts to synthesise the BF_4^- analogue of $[Zn_2L](ClO_4)_4$ were unsuccessful, suggesting that the presence of ClO_4^- is necessary to form the dinuclear complex.

An attempted synthesis of $[Zn_2L](ClO_4)_4$ in methanol and a recrystallisation of $[Zn_2L](ClO_4)_4$ from dimethylformamide (DMF) both resulted in the mononuclear cryptate $[ZnL](ClO_4)_2$ in a slightly impure form. The NMR spectra of this mononuclear zinc complex in CD_3CN are sharp, in direct contrast to the broad and temperature-dependent ^1H NMR spectra obtained for $[Fe^{II}L](BF_4)_2$, and are consistent with an unsymmetrical cryptate in which the zinc(II) ion is located in one tren-derived cap site of the cryptand (see Exp. Sect. and Supporting Information). As expected, the ^1H NMR spectrum of the dinuclear zinc complex, $[Zn_2L](ClO_4)_4$, in CD_3CN is simple due to its high symmetry, with just one resonance for the imine protons and one for the aromatic protons, together with the expected two sets of axial and equatorial resonances for the tren-derived caps. This shows that in acetonitrile solution the dinuclear cryptate is stable with respect to the mononuclear analogue. Thus, the use of acetonitrile as the solvent also appears to be crucial for the stability of the dinuclear complex $[Zn_2L](ClO_4)_4$.

Further attempts to synthesise homodinuclear cryptates were carried out with the non-stereochemically demanding cations manganese(II) and sodium ions and resulted in $Mn^{II}_2LCl_4\cdot H_2O$ and $[Na_2L](CF_3SO_3)_2$, respectively, in the analytically pure form. Interestingly the conductivity value for $Mn^{II}_2LCl_4\cdot H_2O$ (224 $mol^{-1}\,cm^2\,\Omega^{-1}$ in methanol) is closest to that for a 2:1 electrolyte (ref. 2:1: 160−220 $mol^{-1}\,cm^2\,\Omega^{-1}$, 3:1: 290−350 $mol^{-1}\,cm^2\,\Omega^{-1}$)[12] rather than a 4:1 electrolyte initially expected. This suggests that either two of the chloride anions are coordinated to the manganese(II) ions in the dimanganese cryptate, either in a monodentate or bridging fashion, or that a monomanganese cryptate with a $[MnCl_4]^{2-}$ counterion has formed. The latter of these possibilities is not supported by negative ion mass spectrometry as this shows no evidence for the presence of $[MnCl_4]^{2-}$. Attempts to grow single crystals of $Mn^{II}_2LCl_4\cdot H_2O$ and $[Na_2L](CF_3SO_3)_2$, suitable for X-ray diffraction, were unsuccessful.

The addition of two equivalents of manganese(II) perchlorate to L resulted only in the mononuclear cryptate $[Mn^{II}L](ClO_4)_2$ (described above). Thus, although it appears to be possible to synthesise dinuclear cryptates of L with non-stereochemically demanding divalent cations, the choice of counterion and/or solvent appears to be crucial.

Synthesis and Characterisation of Heterodinuclear Cryptates

The previous synthesis of $[Co^{II}Cu^{I}L](BF_4)_3$ and $[Cu^{II}Cu^{I}L](BF_4)_3$[8] suggested that it should be possible to synthesise other heterodinuclear cryptates of L by the addition of a non-stereochemically demanding cation to the

 © 2004 Wiley-VCH Verlag GmbH & Co. KGaA, Weinheim

mononuclear cryptates $[M^{II}L](X)_2$ (M = Mn, Fe, Ni; X = BF_4^- or ClO_4^-). The heterodinuclear cryptates $[Mn^{II}Cu^{I}L](ClO_4)_2(BF_4)$, $[Fe^{II}Cu^{I}L](BF_4)_3{\cdot}CH_3CN$ and $[Ni^{II}Cu^{I}L](BF_4)_3{\cdot}H_2O$ were synthesised by the addition of one equivalent of an appropriate salt of the divalent cation followed by the addition of $Cu^{I}(CH_3CN)_4BF_4$. This one-pot approach is analogous to that used to synthesise the heterodinuclear cryptate $[Co^{II}Cu^{I}L](BF_4)_3$, except that acetonitrile was used as the solvent instead of methanol. The synthesis of $[Mn^{II}Cu^{I}L](ClO_4)_2(BF_4)$ required the addition of 1.1 equivalents of $Cu^{I}(CH_3CN)_4BF_4$ to avoid the formation of a yellow by-product proposed to be $[Mn^{II}L](ClO_4)_2$. The cryptates $[Mn^{II}Cu^{I}L](ClO_4)_2(BF_4)$ and $[Ni^{II}Cu^{I}L](BF_4)_3{\cdot}H_2O$ were isolated in good yield and purity by diethyl ether diffusion into the acetonitrile reaction mixtures. When this approach was used to isolate $[Fe^{II}Cu^{I}L](BF_4)_3{\cdot}CH_3CN$ a green crystalline by-product, apparently $[Cu^{II}L](BF_4)_2$, resulted. The production of this by-product was avoided by precipitating the product from the reaction mixture and recrystallising the crude product from acetonitrile by diethyl ether diffusion. The success of this strategy suggests that once formed there is no significant dissociation of the heterodinuclear cryptate in this case. The elemental analyses of all three complexes were consistent with their proposed formulae, with the metal analyses providing additional evidence of the presence of the two different metal ions.

Imine bands (and the absence of amine or carbonyl absorptions) in the infrared spectra of these heterodinuclear cryptates confirms that the L cryptand remains intact {1652 cm^{-1} for $[Mn^{II}Cu^{I}L](ClO_4)_2(BF_4)$, 1635 cm^{-1} for $[Fe^{II}Cu^{I}L](BF_4)_3{\cdot}CH_3CN$ and 1636 cm^{-1} for $[Ni^{II}Cu^{I}L](BF_4)_3{\cdot}H_2O$}. The infrared spectra of $[Fe^{II}Cu^{I}L](BF_4)_3{\cdot}CH_3CN$ and $[Ni^{II}Cu^{I}L](BF_4)_3{\cdot}H_2O$ show bands for the tetrafluoroborate counterions at 1083 cm^{-1}. The infrared spectrum of $[Mn^{II}Cu^{I}L](ClO_4)_2(BF_4)$ confirms the presence of both counterions with bands at 1117 cm^{-1} for ClO_4^- and 1083 cm^{-1} for BF_4^-.

The mass spectra of the three heterodinuclear cryptates confirm the presence of both metal ions with peaks observed for the mixed-metal clusters [MCuL] (M = Mn, Fe, Ni) in all cases. There is no evidence in any of the mass spectra for homodinuclear species of the type $[M_2L]$ or $[Cu_2L]$.

The conductivity values of 407 $mol^{-1}\,cm^2\,\Omega^{-1}$ for $[Mn^{II}Cu^{I}L](ClO_4)_2(BF_4)$, 393 $mol^{-1}cm^2\Omega^{-1}$ for $[Fe^{II}Cu^{I}L](BF_4)_3{\cdot}CH_3CN$ and 403 $mol^{-1}\,cm^2\,\Omega^{-1}$ for $[Ni^{II}Cu^{I}L](BF_4)_3{\cdot}H_2O$ indicate that all three cryptates behave as 3:1 electrolytes in acetonitrile solution.

The UV/Vis spectrum of $[Mn^{II}Cu^{I}L](ClO_4)_2(BF_4)$ has a band at 250 nm (ε = 33000 $M^{-1}\,cm^{-1}$) which is assigned to ligand-centred π-π^* transitions and is similar to that observed in the mononuclear cryptates and the free ligand L. This band has a broad shoulder at about 280 nm. No band corresponding to charge transfer transitions of the copper(I) ion can be clearly distinguished. The UV/Vis spectrum of $[Fe^{II}Cu^{I}L](BF_4)_3{\cdot}CH_3CN$ shows a group of at least four overlapping transitions with distinct peaks at 443 nm (ε = 10700 $M^{-1}\,cm^{-1}$) and 557 nm (ε = 10500 $M^{-1}\,cm^{-1}$) and shoulders at 390 nm and 540 nm. These transitions, which obscure any possible Cu^{I} MLCT band, are similar to those seen for $[Fe^{II}L](BF_4)_2$. There is also a strong π-π^* transition at 211 nm (ε = 75000 $M^{-1}\,cm^{-1}$) with a very broad shoulder extending out to 300 nm. The UV/Vis spectrum of $[Ni^{II}Cu^{I}L](BF_4)_3{\cdot}H_2O$ shows a band of weak d-d transitions ($\varepsilon \approx 20\ M^{-1}\,cm^{-1}$) with a peak at 806 nm. This is similar to the UV/Vis spectrum of $[Ni^{II}L](BF_4)_2$ and is consistent with the presence of octahedral nickel(II). There is also an additional band at 413 nm (ε = 2510 $M^{-1}\,cm^{-1}$) which is assigned to charge-transfer transitions of the copper(I) ion and is similar to that observed in $[Cu^{I}_2L](BF_4)_2$ (390 nm, ε = 3960 $M^{-1}\,cm^{-1}$).[10] Finally, a shoulder, due to ligand-centred π-π^* transitions, is observed at 250 nm.

The magnetic moments of 5.9 BM for $[Mn^{II}Cu^{I}L](ClO_4)_2(BF_4)$ and 3.1 BM for $[Ni^{II}Cu^{I}L](BF_4)_3{\cdot}H_2O$ are consistent with the presence of the spin-free paramagnetic divalent cation and the d^{10} copper(I) ion. The complex $[Fe^{II}Cu^{I}L](BF_4)_3{\cdot}CH_3CN$ was determined to be diamagnetic, which is consistent with the presence of low spin iron(II) and copper(I). The ^1H NMR spectrum of $[Fe^{II}Cu^{I}L](BF_4)_3{\cdot}CH_3CN$ (Figure 3) at 298 K shows sharp peaks, further confirming the diamagnetic nature of this complex. The spectrum is similar to that of $[ZnL](ClO_4)_2$ in that it is sharp and lacks end-to-end symmetry, and broadly similar to that of $[Fe^{II}L](BF_4)_2$, except that there is no broadening at room temperature and $^3J_{eq/eq}$ (ca. 4 Hz) coupling is observed. These observations, together with the absence of dissociation in solution noted earlier, indicate a regular octahedral site for the Fe^{II} ion in the $[Fe^{II}Cu^{I}L](BF_4)_3{\cdot}CH_3CN$ cryptate.

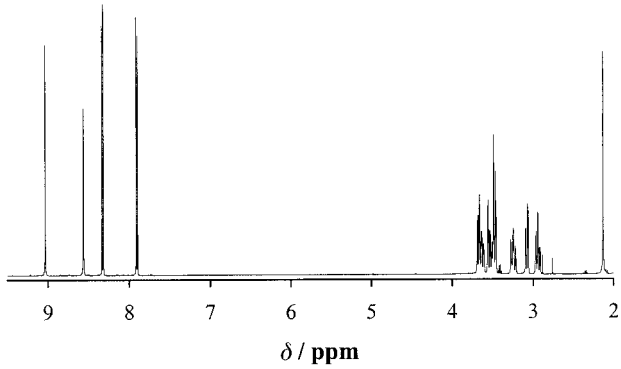

Figure 3. ^1H NMR spectrum of $[Fe^{II}Cu^{I}L](BF_4)_3{\cdot}CH_3CN$ at 298 K in CD_3CN

Crystal Structures of Mononuclear Cryptates

Single crystals of the mononuclear cryptates $[Mn^{II}L](ClO_4)_2$, $[Fe^{II}L](BF_4)_2$ and $[Ni^{II}L](ClO_4)_2$ were obtained by diethyl ether diffusion into dimethylformamide, acetonitrile and acetonitrile solutions of the cryptates, respectively, and the crystal structures were determined by X-ray diffraction techniques.

The d^5 manganese(II) ion in each of the two independent $[Mn^{II}L]^{2+}$ cryptates in the asymmetric unit is seven coordi-

 © 2004 Wiley-VCH Verlag GmbH & Co. KGaA, Weinheim

nate as a consequence of binding to three imine nitrogen atoms, three pyridazine nitrogen atoms and the bridgehead nitrogen atom (Figure 4, Table 1). However, the interaction with the bridgehead nitrogen atom is comparatively weak [av. $Mn-N_{imine}$ = 2.209 Å, av. $Mn-N_{pyridazine}$ = 2.384 Å, av. $Mn-N_{bridgehead}$ = 2.524 Å]. The $N_{bridgehead}\cdots N_{bridgehead}$ distance [N(4)···N(5) = 10.236(5) Å, N(54)···N(55) = 10.311(5) Å] is short in comparison with the free cryptand [10.443(7) Å].[9]

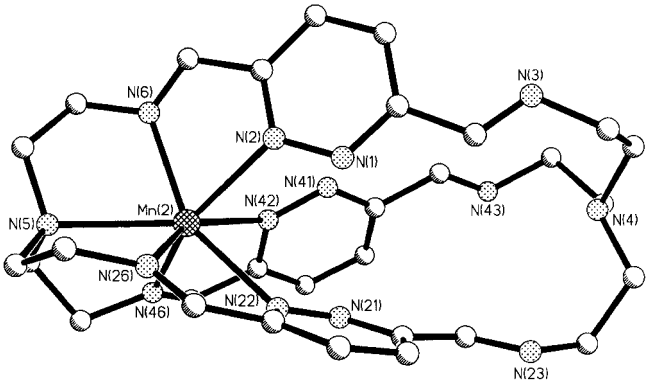

Figure 4. Perspective view of one of the two unique $[Mn^{II}L]^{2+}$ cations of $[Mn^{II}L](ClO_4)_2$; hydrogen atoms have been omitted for clarity

The structure of $[Ni^{II}L](ClO_4)_2$ is very similar to that of $[Co^{II}L]^{2+}$.[9] The nickel(II) ion in each of the two independent cryptates in the asymmetric unit is six coordinate as a consequence of binding to three imine nitrogen atoms and three pyridazine nitrogen atoms (Figure 5, Table 1). The twist angle (φ) of the nickel(II) ion [46.4° for Ni(2) and 47.0° for Ni(52)] indicates a distorted octahedral geometry (φ = 60° for octahedral and 0° for trigonal prismatic).[1] This is very similar to the twist angle of 46.9° seen for the cobalt(II) ion in $[Co^{II}L]^{2+}$.[9] The coordination of the nickel ion does not change the $N_{bridgehead}\cdots N_{bridgehead}$ distance of the cryptand by much [N(4)···N(5) = 10.519(9) Å, N(54)···N(55) = 10.421(9) Å; L 10.443(7) Å].

The structure of $[Fe^{II}L](BF_4)_2$ is similar to that of the above mononuclear cryptates, however, as the X-ray analysis is of poor quality, it is not discussed further (see Supporting Information).

The structures of $[M^{II}L]^{2+}$ (M = Mn, Fe, Co, Ni, Cu) indicate that L is able to accommodate a single, relatively stereochemically demanding, cation in geometries ranging from five to seven coordinate, although six coordination is the most common. In all of these mononuclear cryptates, all three of the strands of the organic host have all *trans* conformations. These strands would therefore have to change their conformations to all *cis* before a second metal cation could bind.

Crystal Structures of Heterodinuclear Cryptates

Single crystals of the heterodinuclear cryptates $[Mn^{II}Cu^{I}L](ClO_4)_2(BF_4)$, $[Fe^{II}Cu^{I}L](BF_4)_3{\cdot}2.5CH_3CN$ and $[Ni^{II}Cu^{I}L](BF_4)_3$ were obtained by the slow diffusion of diethyl ether vapour into acetonitrile solutions of the cryptates. A summary of key crystallographic information is given in Figures 6, 7, 8 and Tables 1−2. The structures of $[Mn^{II}Cu^{I}L]^{3+}$ and $[Ni^{II}Cu^{I}L]^{3+}$ are end-for-end disordered, as was the case in the previously determined structure of $[Co^{II}Cu^{I}L]^{3+}$ with the three strands of the cryptand also disordered in order to accommodate the differing coordination geometries of the two different metal cations.[8] Unless otherwise stated, only the major occupancy forms of each cryptate will be discussed. The structure of $[Fe^{II}Cu^{I}L]^{3+}$ is the first structure of a heterodinuclear cryptate of L that is not end-for-end disordered.

The structures of $[Mn^{II}Cu^{I}L]^{3+}$, $[Ni^{II}Cu^{I}L]^{3+}$ and $[Fe^{II}Cu^{I}L]^{3+}$ are similar to each other. In all cases, the divalent cation is six-coordinate and binds to three pyridazine and three imine nitrogen atoms. This is also observed in the previously reported heterodinuclear cryptate $[Co^{II}Cu^{I}L]^{3+}$ and the mixed-valent cryptate $[Cu^{II}Cu^{I}L]^{3+}$.[8]

Of all the $[M^{II}Cu^{I}L]^{3+}$ cryptates (M = Mn, Co, Fe, Ni, Cu), the geometry of the iron(II) ion in $[Fe^{II}Cu^{I}L]^{3+}$ is closest to a regular octahedron indicating that iron(II) is the most stereochemically demanding cation. Here the twist angle (φ) of the iron(II) ion within the N_6 donor set is 50.4°. In contrast, the twist angle of the manganese(II) ion in $[Mn^{II}Cu^{I}L]^{3+}$ [35.9° for Mn(2)] indicates that the geometry is intermediate between octahedral and trigonal prismatic. This is significantly different from the more octahedral geometries observed for the six-coordinate cryptates $[Co^{II}L]^{2+}$, $[Ni^{II}L]^{2+}$ and $[M^{II}Cu^{I}L]^{3+}$ (M = Fe, Co, Ni, Cu), where the twist angles range from 45.4−50.4° (Table 2). However, this is consistent with manganese(II) being less stereochemically demanding than the other divalent cations as a result of its d^5 configuration. The greater deviation from regular octahedral geometry for manganese(II) in $[Mn^{II}Cu^{I}L]^{3+}$ is also reflected in the wider range of *cis* N−M−N angles (71.5−105.4° for Mn(2) compared with 80.7−97.0° for Fe(2) in $[Fe^{II}Cu^{I}L]^{3+}$) (Table 2).

The non-stereochemically demanding copper(I) ion in $[Mn^{II}Cu^{I}L]^{3+}$, $[Ni^{II}Cu^{I}L]^{3+}$ and $[Fe^{II}Cu^{I}L]^{3+}$ has a distorted trigonal-pyramidal geometry and is coordinated by three imine nitrogen atoms and the bridgehead nitrogen atom. However, the interactions with the imine nitrogen atoms are stronger than those with the bridgehead nitrogen atoms [av. $Cu(1)-N_{imine}$ = 2.00 Å, $Cu(1)-N_{bridgehead}$ = 2.33 Å] (Table 2). The copper(I) ion is displaced from the mean plane of the three imine nitrogen donors towards the centre of the cavity by 0.24−0.31 Å (Table 2), that is, away from the bridgehead nitrogen atom. This is also seen in the structure of the dicopper(I) cryptate $[Cu^{I}_2L](BF_4)_2$, where the two copper(I) ions are displaced from their $(N_{imine})_3$ mean planes, away from the bridgehead nitrogen atoms, by 0.238 and 0.234 Å, respectively,[10] and in the structures of other tren-derived Schiff-base cryptates.[13] Thus, although the copper(I) ions are within bonding distance of the bridgehead nitrogen atom, this interaction is primarily due to their enforced proximity. The distances between Cu(1) and the pyridazine nitrogen atoms {for example, in $[Fe^{II}Cu^{I}L]^{3+}$, shortest $Cu-N_{pyridazine}$ distance is 3.007 Å,

 © 2004 Wiley-VCH Verlag GmbH & Co. KGaA, Weinheim

Table 1. Selected bond lengths [Å] and bond angles [°] for mononuclear and heterodinuclear cryptates of L

	$[Mn^{II}L]^{2+}$ [a]	$[Ni^{II}L]^{2+}$ [a]	$[Mn^{II}Cu^{I}L]^{3+}$ [b]	$[Fe^{II}Cu^{I}L]^{3+}$	$[Ni^{II}Cu^{I}L]^{3+}$ [c]
Cu(1)−N(3)			2.020(3)	2.002(3)	1.993(2)
Cu(1)−N(23)			2.068(3)	1.998(3)	2.003(2)
Cu(1)−N(43)			2.037(3)	2.010(3)	1.970(2)
Cu(1)−N(4)			2.298(3)	2.332(3)	2.365(3)
M(2)−N(46)	2.206(3)	2.116(5)	2.176(3)	1.966(3)	2.138(2)
M(2)−N(26)	2.205(3)	2.088(5)	2.251(3)	1.962(3)	2.136(2)
M(2)−N(6)	2.204(3)	2.108(5)	2.288(3)	1.971(3)	2.095(2)
M(2)−N(22)	2.405(3)	2.129(5)	2.315(4)	1.928(3)	2.067(3)
M(2)−N(42)	2.349(3)	2.103(5)	2.342(4)	1.937(3)	2.087(3)
M(2)−N(2)	2.369(3)	2.117(5)	2.360(4)	1.931(3)	2.070(3)
M(2)−N(5)	2.524(3)				
N(3)−Cu(1)−N(23)			117.62(12)	119.00(13)	116.95(10)
N(3)−Cu(1)−N(43)			121.69(12)	115.64(12)	115.83(10)
N(23)−Cu(1)−N(43)			114.38(12)	118.95(12)	119.59(10)
N(3)−Cu(1)−N(4)			82.47(10)	81.49(13)	80.71(9)
N(23)−Cu(1)−N(4)			81.20(11)	81.75(12)	80.11(9)
N(43)−Cu(1)−N(4)			81.09(11)	81.32(12)	81.39(10)
N(46)−M(2)−N(26)	111.21(11)	103.22(19)	105.44(12)	95.84(14)	100.13(9)
N(46)−M(2)−N(6)	110.35(11)	100.78(18)	103.86(11)	95.05(14)	96.72(9)
N(26)−M(2)−N(6)	111.41(11)	101.66(19)	100.11(11)	96.96(14)	102.20(9)
N(46)−M(2)−N(22)	94.85(10)	95.24(18)	103.60(13)	92.21(13)	93.93(10)
N(26)−M(2)−N(22)	70.39(10)	77.6(2)	73.12(13)	80.80(13)	76.65(10)
N(6)−M(2)−N(22)	150.80(10)	163.64(18)	152.54(14)	172.59(14)	169.31(10)
N(46)−M(2)−N(42)	71.02(11)	77.80(18)	72.68(13)	80.66(13)	77.63(10)
N(26)−M(2)−N(42)	150.78(11)	164.33(19)	156.82(16)	171.07(13)	167.49(10)
N(6)−M(2)−N(42)	93.74(11)	93.42(18)	102.76(14)	91.55(12)	90.30(10)
N(22)−M(2)−N(42)	80.40(10)	86.72(19)	84.74(16)	91.09(12)	91.16(11)
N(46)−M(2)−N(2)	151.09(11)	162.76(18)	157.08(16)	169.79(13)	163.90(10)
N(26)−M(2)−N(2)	93.74(10)	93.86(18)	97.48(14)	93.98(13)	95.84(10)
N(6)−M(2)−N(2)	71.26(10)	77.63(18)	71.54(12)	80.94(13)	77.80(10)
N(22)−M(2)−N(2)	79.55(10)	86.09(18)	82.81(15)	92.13(12)	91.70(11)
N(42)−M(2)−N(2)	80.07(10)	85.13(18)	86.25(16)	90.02(12)	87.19(11)
N(6)−M(2)−N(5)	71.99(10)				
N(26)−M(2)−N(5)	71.99(10)				
N(46)−M(2)−N(5)	72.31(10)				
N(42)−M(2)−N(5)	132.47(9)				
N(2)−M(2)−N(5)	131.74(10)				
N(22)−M(2)−N(5)	132.00(10)				

[a] Data for one of the two unique cations in the asymmetric unit. [b] Data for major occupancy cryptate. [c] Data for major occupancy cryptate of one of the two unique cations in the asymmetric unit.

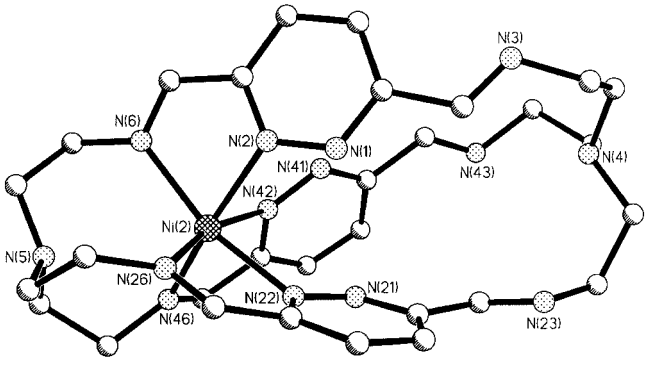

Figure 5. Perspective view of one of the two unique $[Ni^{II}L]^{2+}$ cations of $[Ni^{II}L](BF_4)_2$; hydrogen atoms have been omitted for clarity

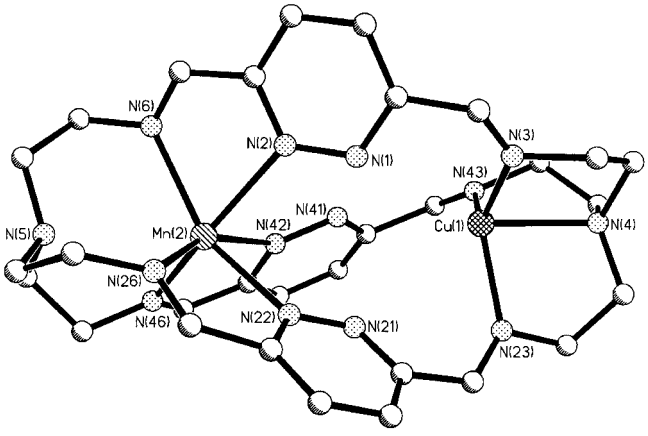

Figure 6. Perspective view of the major occupancy form of the $[Mn^{II}Cu^{I}L]^{3+}$ cation of $[Mn^{II}Cu^{I}L](ClO_4)_2(BF_4)$; hydrogen atoms have been omitted for clarity

 © 2004 Wiley-VCH Verlag GmbH & Co. KGaA, Weinheim

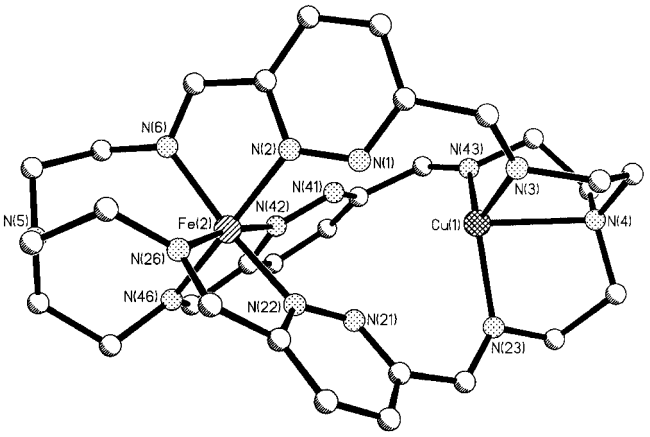

Figure 7. Perspective view of the cation $[Fe^{II}Cu^{I}L]^{3+}$ of $[Fe^{II}Cu^{I}L](BF_4)_3{\cdot}CH_3CN$; hydrogen atoms have been omitted for clarity

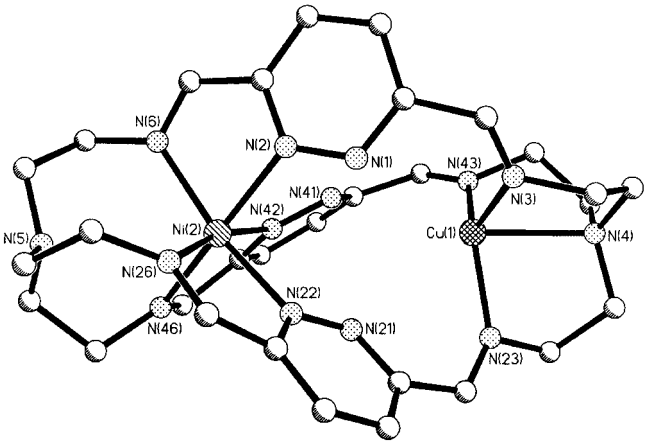

Figure 8. Perspective view of the major occupancy form of one of the two unique $[Ni^{II}Cu^{I}L]^{3+}$ cations of $[Ni^{II}Cu^{I}L](BF_4)_3{\cdot}H_2O$; hydrogen atoms have been omitted for clarity

for Cu(1)−N(41)} preclude further strong bonding interactions. In all cases, the geometry of the copper ion is consistent with the proposed +1 oxidation state.

In the series of heterodinuclear cryptates, the $M^{II}\cdots Cu^{I}$ interatomic distance follows the order Mn > Co > Cu > Ni > Fe (Table 2), decreasing with the decreasing ionic radius of the divalent cation.[14] This order is also weakly correlated to the trigonal prismatic twist angle φ, with Mn having the smallest (36°) and Fe the largest (50°) twist angle. The trend in $N_{bridgehead}\cdots N_{bridgehead}$ distances is less clear, although $[Fe^{II}Cu^{I}L]^{3+}$, which has the shortest $M^{II}\cdots Cu^{I}$ interatomic distance of 4.723(6) Å, also has the shortest $N_{bridgehead}\cdots N_{bridgehead}$ distance of 10.059(6) Å (Table 2). Conversely, the manganese cryptate $[Mn^{II}Cu^{I}L]^{3+}$ has the longest $M^{II}\cdots Cu^{I}$ interatomic distance of 5.231(10) Å and the longest $N_{bridgehead}\cdots N_{bridgehead}$ distance of 10.455(10) Å.

The structures of $[Mn^{II}Cu^{I}L]^{3+}$and $[Ni^{II}Cu^{I}L]^{3+}$ show both differences and similarities to the structures of the corresponding mononuclear cryptates $[Mn^{II}L]^{2+}$ and $[Ni^{II}L]^{2+}$. In both heterodinuclear cases, the L cryptand has adopted a conformation with mutually *cis* imino C=N functions in each strand in order to bind the copper(I) ions. This is in contrast to the mutually *trans* conformations seen in the corresponding mononuclear cryptates. For $[Mn^{II}Cu^{I}L]^{3+}$, the binding of copper(I) has also altered the coordination geometry of the manganese(II) ion, reducing its coordination number from seven to six as a result of a lengthening of the $Mn-N_{bridgehead}$ distance from 2.524(3) Å in $[Mn^{II}L]^{2+}$ to 2.931(6) Å in $[Mn^{II}Cu^{I}L]^{3+}$. Coordination of the copper(I) ion has also increased the overall length of the cryptand. The $N_{bridgehead}\cdots N_{bridgehead}$ distance is 10.455(10) Å for Mn(1) in $[Mn^{II}Cu^{I}L]^{3+}$ and 10.236(5) Å for $[Mn^{II}L]^{2+}$. The distorted octahedral geometry of the nickel(II) ion in $[Ni^{II}Cu^{I}L]^{3+}$ is similar to that seen in the mononuclear nickel(II) cryptate $[Ni^{II}L]^{2+}$. The twist angles of nickel(II) [47.2° for Ni(2) and 47.3° for Ni(3)] are very similar to that seen in $[Ni^{II}L]^{2+}$. The N···N bridgehead distances [10.309(6) and 10.413(6) Å for the two unique cations] are slightly shorter than those of $[Ni^{II}L]^{2+}$ [10.519(9) and 10.421(9) Å for the two unique cations].

The cryptate $[Fe^{II}Cu^{I}L]^{3+}$ is of some interest as a structural model for the oxygen binding site of cytochrome c oxidase. This dinuclear site consists of a heme a_3 iron and a copper ion (Cu_B) with an interatomic distance of 4.5−5.2 Å depending on the source of the enzyme.[15] The cation $[Fe^{II}Cu^{I}L]^{3+}$ has a similar Fe···Cu interatomic distance to cytochrome c oxidase with the same oxidation states present as in the fully reduced form of the enzyme. However, the iron(II) ion in $[Fe^{II}Cu^{I}L]^{3+}$ has more donor atoms than the

Table 2. Comparison of X-ray crystallographic data for heterodinuclear cryptates of L

Compound	φ(M^{2+}) [°]	Range of *cis* N−M−N angles [°]	$M^{II}\cdots Cu^{I}$ [Å]	Bridgehead distance [Å]	$Cu-N_{bridgehead}$ [Å]	Av. $Cu-N_{imine}$ [Å]	Cu displacement from $(N_{imine})_3$ plane [Å]
$[Mn^{II}Cu^{I}L]^{3+}$ [a]	35.9	71.5−105.4	5.231(10)	10.455(10)	2.298(3)	2.042	0.298
$[Fe^{II}Cu^{I}L]^{3+}$	50.4	80.7−97.0	4.723(6)	10.059(6)	2.332(3)	2.003	0.295
$[Co^{II}Cu^{I}L]^{3+}$ [b]	47	73.2−111.5	5.08(1)	10.159(14)	2.292(5)	1.996	0.324
$[Ni^{II}Cu^{I}L]^{3+}$ [c]	47.2	76.7−102.2	4.821(9)	10.309(6)	2.365(3)	1.989	0.320
	47.3	78.4−99.4	4.904(9)	10.413(6)	2.322(3)	1.949	0.242
$[Cu^{II}Cu^{I}L]^{3+}$ [b]	45.4	74.5−103.4	4.960(2)	10.306(8)	2.330(10)	2.001	0.27

[a] Data for the major occupancy cryptate. [b] Data from reference.[8] [c] Data for the major occupancy cryptates of the two unique cations in the asymmetric unit.

 © 2004 Wiley-VCH Verlag GmbH & Co. KGaA, Weinheim

Table 3. Summary of electrochemical data for cryptates of L

Compound	$E_{1/2}$ (ΔE)[a]									
$[Mn^{II}L]^{2+}$			−1.76 (0.08)	−1.49 (0.07)	−1.24 (0.08)			+1.03^{I}		
$[Fe^{II}L]^{2+}$			−1.87 (0.11)^{QR}	−1.42 (0.07)	−1.13 (0.07)	+0.78^{QR} [b]	+0.86^{QR} [b]			
$[Co^{II}L]^{2+}$ [c]			−1.71^{QR}	−1.56 (0.08)	−1.14 (0.07)	+0.29 (0.13)^{QR}	+0.95^{I}	+1.09^{I}	+1.34^{I}	+1.57^{I}
$[Ni^{II}L]^{2+}$			−1.88 (0.07)^{QR}	−1.34 [b]	−1.25[b]		+0.99^{I}	+1.05^{I}	+1.34^{I}	
$[Cu^{II}L]^{2+}$ [d],[e]				−1.75^{QR}	−1.37^{QR}	−0.38 (0.08)	+1.00^{I}	+1.16^{I}		
$[Mn^{II}Cu^{I}L]^{3+}$		−1.89^{QR} [b]	−1.77^{QR} [b]	−1.46 (0.09)	−1.25 (0.08)	−0.86^{I}	+0.25 (0.10)^{QR}	+0.81^{QR}	+1.07^{I}	
$[Fe^{II}Cu^{I}L]^{3+}$		−1.89^{QR}	−1.55 (0.07)	−1.27 (0.07)	−1.07 (0.09)		+0.49 (0.10)	+0.97^{I}	+1.11^{I}	
$[Co^{II}Cu^{I}L]^{3+}$		−1.55 (0.08)^{QR}	−1.41 (0.10)^{QR}	−1.15 (0.07)^{QR}	−0.88 (0.06)^{QR}	+0.08^{QR} [f]	+0.58^{QR} [f]	+1.07^{I}	+1.33^{I}	+1.63^{I}
$[Ni^{II}Cu^{I}L]^{3+}$		−1.89^{QR}	−1.53 (0.08)	−1.36^{QR}	−1.19 (0.12)		+0.46 (0.07)	+1.07^{I}	+1.34^{I}	
$[Cu^{II}Cu^{I}L]^{3+}$ [d]			−1.98^{QR}	−1.44^{QR}	−1.27^{QR}	−0.34 (0.08)	+0.33 (0.08)	+1.18^{I}		
$[Zn^{II}{}_2L]^{4+}$	−1.73^{QR}	−1.62^{QR}	−1.10 (0.07)	−0.95 (0.06)	−0.84 (0.06)			+1.30^{I}	+1.54^{I}	+1.78^{I}

[a] $E_{1/2}$ and $\triangle E$ in V. I = irreversible, hence value quoted is E_{pa}; QR = quasi-reversible; all other processes are reversible. Potentials for reversible processes are quoted from the cyclic voltammogram and potentials for quasi-reversible processes are quoted from the square wave voltammogram or the cyclic voltammogram. For quasi-reversible processes $\triangle E$ is only quoted where E_{pa} and E_{pc} are well defined. All potentials are vs. 0.01 mol L^{-1} $AgNO_3$/Ag. [b] Process overlaps with neighbouring process hence this is an estimated $E_{1/2}$ only. [c] As previously reported in reference.[9] [d] As previously reported in reference.[10] [e] When scanning out to −0.7 V an additional irreversible oxidation process is observed at +0.39 V which is associated with the reduction processes. [f] E_{pc} quoted (not $E_{1/2}$) since E_{pa} is poorly defined.

heme a_3 iron of cytochrome c oxidase and therefore seems less likely to bind exogenous ligands like oxygen, although the Cu^{I} ions will readily accept additional donor(s) on oxidation.

Electrochemical Studies on Mononuclear Cryptates

Unless otherwise stated, in this paper all potentials are quoted vs. 0.01 mol L^{-1} $AgNO_3$/Ag and all controlled potential experiments were carried out until the current reached 1% of the initial value.

The series of mononuclear cryptates show irreversible oxidation waves starting from about +1 V (Table 3) that are probably ligand-centred. In the case of iron(II) and cobalt(II), quasi-reversible oxidation waves at +0.78 and +0.29 V[9], respectively, which are likely to be attributable to metal-centred processes, are observed. For the copper(II) complex a reversible metal-centred reduction is observed at −0.38 V.[10]

The cyclic voltammogram of $[Mn^{II}L](ClO_4)_2$ (Figure 9, Table 3) reveals an irreversible oxidation process at +1.03 V. A coulometry experiment at +1.20 V resulted in no colour change and the transfer of 1.00 electron equivalents, indicating that this is a one-electron oxidation. Significant changes in the cyclic voltammogram of the complex after this oxidation indicated that this process is chemically irreversible. Further investigation would be required to determine whether the process at +1.03 V is metal- or ligand-centred. The absence of oxidation processes below +1.03 V indicates that the manganese(II) oxidation state is stabilised by the soft nitrogen donors and, more importantly, the seven coordinate geometry provided by L, as expected on the basis of the research of McKee and co-workers.[16] On scanning to negative potentials, three almost reversible, probably ligand-centred, processes are seen (Table 3). These are similar to the processes seen for $[Zn_2L](ClO_4)_4$ (see later), but are more spread out and occur at more negative potentials. Coulometry at −1.39 V resulted in the transfer of 1.80 electron equivalents and precipitation of the product. As all three reduction processes have similar peak heights and peak separations, it is likely that they are all two-electron processes. This provides further evidence that L is able to undergo two-electron reductions. However, it should be noted that the close proximity of these potentials diminishes confidence in the coulometric result.

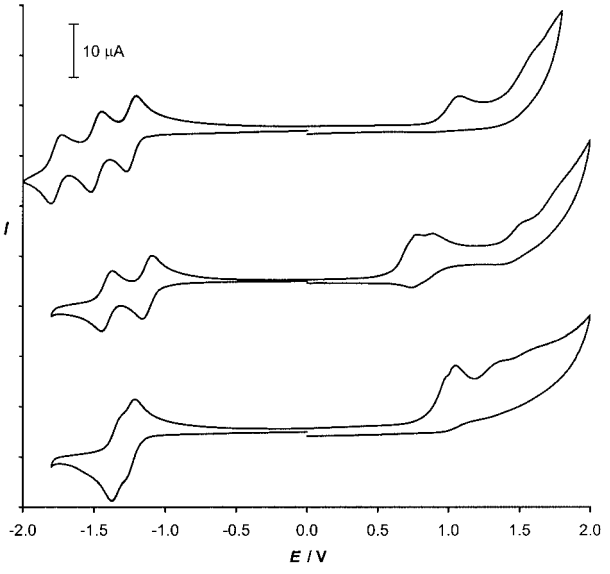

Figure 9. Full range cyclic voltammograms of the mononuclear cryptates $[Mn^{II}L](ClO_4)_2$ (top), $[Fe^{II}L](BF_4)_2$ (middle) and $[Ni^{II}L](BF_4)_2$ (bottom) in acetonitrile (200 mV s^{-1} vs. 0.01 mol L^{-1} $AgNO_3$/Ag); each scan starts at 0 V and initially scans to negative potentials

The cyclic voltammogram of the monoiron cryptate $[Fe^{II}L](BF_4)_2$ shows two almost reversible reductions (Figure 9, Table 3). A further quasi-reversible process is observed at −1.87 V (see Supporting Information). These processes are similar to the reduction processes observed for

 © 2004 Wiley-VCH Verlag GmbH & Co. KGaA, Weinheim

$[Mn^{II}L](ClO_4)_2$, but start at slightly less negative potentials and are more spread out. Coulometry at −1.26 V resulted in the transfer of 1.89 electrons suggesting that they are two-electron processes. This reduction resulted in decomposition of the complex as indicated by the cyclic voltammograms recorded after the coulometry experiment. On scanning to positive potentials two closely overlapping quasi-reversible oxidation processes are observed. As noted earlier, at least one of these processes is likely to be due to Fe^{II} to Fe^{III} oxidation.

The cyclic voltammogram of the nickel cryptate $[Ni^{II}L](BF_4)_2$ shows two closely overlapping reversible reduction processes (Figure 9, Table 3). Coulometry at −1.50 V resulted in the transfer of 1.97 electron equivalents and some precipitation. This suggests that both processes correspond to one-electron transfers, assuming that precipitation occurred after the second process rather than after the first. On scanning to more negative potentials a further quasi-reversible reduction process occurs. On scanning to positive potentials two overlapping irreversible oxidation processes are seen (Table 3). Although we are unable, in the absence of ESR experiments, to decide unambiguously whether any processes in these cyclic voltammograms are metal-centred, the fact that no oxidation processes of any sort occur below +0.99 V in this case demonstrates the stability of the nickel(II) oxidation state in the cryptand.[17]

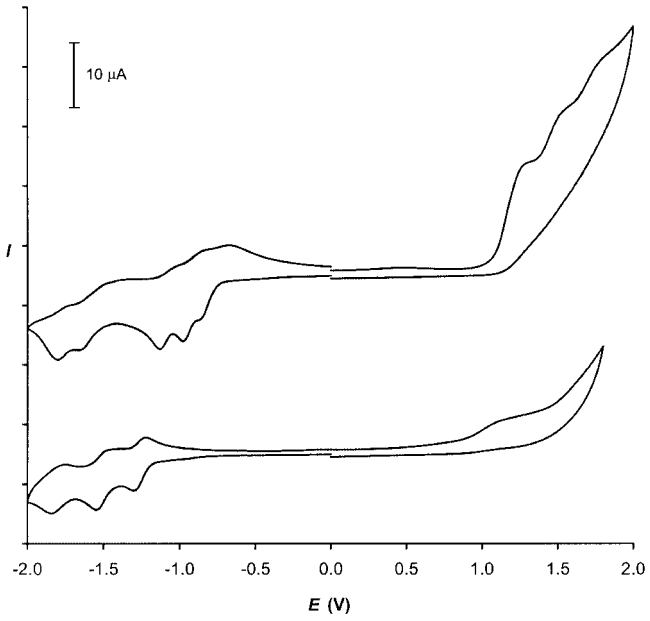

Figure 10. Full range cyclic voltammograms of $[Zn_2L](ClO_4)_4$ in acetonitrile before (top, two separate scans both starting from 0 V but one initially scanning to negative potentials and the other to positive potentials) and after (bottom, a single scan starting from 0 V and initially scanning to negative potentials) coulometry at −1.30 V (200 mV s^{-1} vs. 0.01 mol L^{-1} $AgNO_3$/Ag)

Electrochemical Studies on the Homodinuclear Zinc Cryptate

The electrochemistry of $[Zn_2L](ClO_4)_4$ was investigated in order to study the electrochemical processes of the L cryptand since the coordinated zinc ions are not expected to undergo reduction or oxidation in the potential range accessible in acetonitrile. The cyclic voltammogram of $[Zn_2L](ClO_4)_4$ shows three high-current irreversible oxidation processes as well as several reduction processes (Figure 10, Table 3). The oxidation processes had previously been observed in other cryptates of L,[10] and are also seen for some of the cryptates of L described here (Table 3), and are assigned to ligand oxidations. The first three overlapping reduction processes of $[Zn_2L](ClO_4)_4$ (Figure 11, Table 3) are almost reversible as indicated from a variable scan rate study. These processes are tentatively assigned to reduction of the three strands of the L cryptand. On scanning to more negative potentials two further quasi-reversible reduction processes are seen, which may correspond to further ligand reduction.

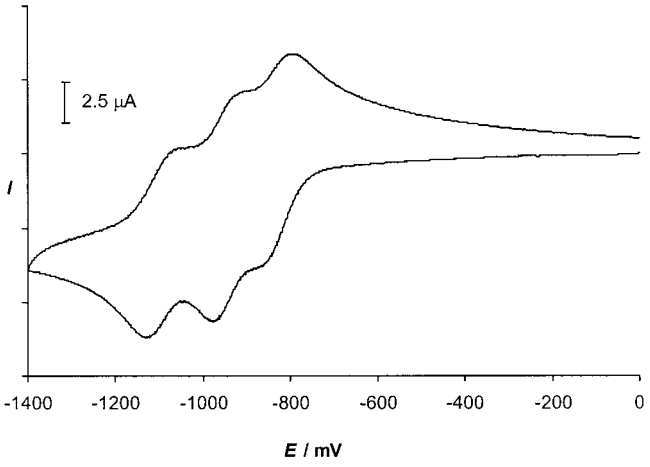

Figure 11. Cyclic voltammogram of $[Zn_2L](ClO_4)_4$ in acetonitrile showing the first three reversible reduction processes (200 mV s^{-1} vs. 0.01 mol L^{-1} $AgNO_3$/Ag). The scan starts at 0 V

The peak separations for the first two reduction processes in particular are smaller than expected for a one-electron process but larger than expected for a fully reversible two-electron process in our electrochemical cell. The closely overlapping nature of these processes made them difficult to study separately by coulometry. Coulometry at −1.30 V resulted in the transfer of just 2.00 electron equivalents, with coulometry at −1.05 V giving a similar result. During this two-electron reduction the pale yellow solution initially became an intense purple colour and then gradually became orange-yellow as the final two-electron reduction product formed. These colour changes could be accounted for by chemical reaction of an unstable radical product. Cyclic voltammograms measured after the two-electron reduction was complete demonstrate that the cryptate has indeed been altered: the behaviour at positive potentials has been affected (Figure 10), and whilst there are still three reduction processes at negative potentials, these are now at significantly more negative potentials and are more spread out (Figure 10 and 11). The processes, which now occur at $E_{1/2}$ = −1.26 V (ΔE = 0.07 V), −1.50 V (ΔE = 0.09 V) and −1.80 V (ΔE = 0.09 V), appear to be less reversible. These results indicate that the reduction of $[Zn_2L](ClO_4)_4$ is

 © 2004 Wiley-VCH Verlag GmbH & Co. KGaA, Weinheim

chemically irreversible and that the product of this reduction is harder to reduce than the original complex.

Electrochemical Studies on Heterodinuclear Cryptates

The electrochemical properties of the series of heterodinuclear cryptates $[M^{II}Cu^{I}L](X)_3$ (M = Mn, Fe, Co, Ni; X = BF_4^- or ClO_4^-) were investigated to study the effect of the divalent cation on the electrochemistry of the copper(I) ion and vice versa. In all cases, following the addition of the Cu^{I} ion, a reversible or quasi-reversible wave corresponding to the $Cu^{I} \rightleftarrows Cu^{II}$ couple is observed in the voltammograms. This wave is usually in the potential range which is inactive in the monometallic precursor complexes (exceptions include the $[Co^{II}Cu^{I}L]^{3+}$ and $[Cu^{II}Cu^{I}L]^{3+}$ complexes). In addition, a copper deposition and stripping peak is observed following the application of potentials below about −1 V for all except the $[Fe^{II}Cu^{I}L]^{3+}$ complex.

The cyclic voltammogram of the heterodinuclear cryptate $[Mn^{II}Cu^{I}L](ClO_4)_2(BF_4)$ (Figure 12, Table 3) shares several features with that of $[Mn^{II}L](ClO_4)_2$, as well as additional features due to the presence of copper(I). The reduction region contains two almost reversible processes at $E_{1/2}$ = −1.25 V (ΔE = 0.08 V) and −1.46 V (ΔE = 0.09 V). These processes are similar to the first two reduction processes for $[Mn^{II}L](ClO_4)_2$ and are probably ligand-centred. On scanning to more negative potentials there are two further overlapping quasi-reversible processes with $E_{1/2}$ approximately equal to −1.77 and −1.89 V which are probably also ligand-centred. There is also an irreversible reduction process at −0.86 V. This process is associated with a stripping wave at −0.54 V (resulting from deposition of copper on the electrode), which is present when scanning to potentials below about −0.8 V, and is assigned to the $Cu^{I} \rightarrow Cu^{0}$ process.

There is an irreversible oxidation process at +1.07 V. This is similar to the process seen at +1.03 V for $[Mn^{II}L](ClO_4)_2$ and may be metal or ligand-centred. There is also an additional quasi-reversible oxidation process at $E_{1/2}$ = +0.25 V (ΔE = 0.10 V) and an irreversible oxidation process at about +0.81 V. Coulometry at +0.50 V resulted in the transfer of 1.06 electron equivalents leading to the assignment of the process at $E_{1/2}$ = +0.25 V to $Cu^{I} \rightleftarrows Cu^{II}$. The colour change from orange-brown to green during this oxidation is consistent with this assignment. The cyclic voltammogram of the bulk oxidation product was unchanged from that of the original $[Mn^{II}Cu^{I}L]^{3+}$ cyclic voltammogram, apart from some reduction in the peak size of the processes at +0.25 V and +1.07 V which may indicate partial decomposition of the complex.

The cyclic voltammogram of $[Fe^{II}Cu^{I}L](BF_4)_3{\cdot}CH_3CN$ shows three reversible reduction processes (Figure 12, Table 3). These are similar to the ligand-centred processes seen for $[Fe^{II}L](BF_4)_2$ although they occur at less negative potentials and are closer together. Coulometry at −1.15 V resulted in the transfer of 2.05 electron equivalents (I_f, 2.5% of I_i) and some precipitation. This suggests that the process at −1.07 V is a two-electron reduction. There is also an almost reversible oxidation process at $E_{1/2}$ = +0.49 V (ΔE = 0.10 V). Coulometry at +0.60 V resulted in the transfer of 1.40 electron equivalents (I_f, 2% of I_i). Although it is not possible to conclude whether this is a one- or two-electron process from coulometry, comparison with the cyclic voltammograms of $[M^{II}Cu^{I}L]^{3+}$ (M = Mn, Ni, Cu) indicates that this is probably a one-electron oxidation corresponding to $Cu^{I} \rightleftarrows Cu^{II}$. The cyclic voltammogram was largely unchanged after this oxidation, although all processes appeared less reversible and a small copper stripping wave was present at −0.56 V. This indicates that the complex was at least partially intact after oxidation. On scanning to more positive potentials two further irreversible oxidation processes are seen; one of these is likely to be due to oxidation of Fe^{II}.

The cyclic voltammogram of the heterodinuclear cryptate $[Ni^{II}Cu^{I}L](BF_4)_3{\cdot}H_2O$ is complex showing at least four closely spaced processes in the reduction region, with $E_{1/2}$

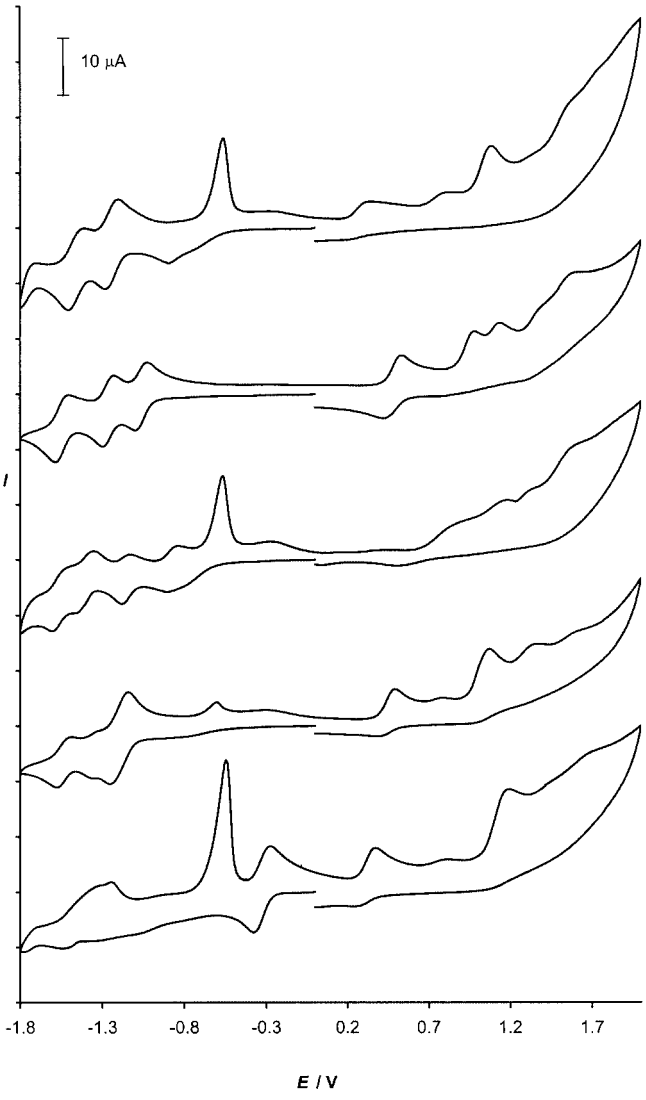

Figure 12. Full range cyclic voltammograms of the heterodinuclear cryptates in acetonitrile. From top to bottom: $[Mn^{II}Cu^{I}L](ClO_4)_2(BF_4)$, $[Fe^{II}Cu^{I}L](BF_4)_3{\cdot}CH_3CN$, $[Co^{II}Cu^{I}L](BF_4)_3$, $[Ni^{II}Cu^{I}L](BF_4)_3{\cdot}H_2O$ and $[Cu^{II}Cu^{I}L](BF_4)_3$ (200 mV s^{-1} vs. 0.01 mol L^{-1} $AgNO_3$/Ag); each scan starts at 0 V and initially scans to negative potentials

 © 2004 Wiley-VCH Verlag GmbH & Co. KGaA, Weinheim

approximately equal to −1.19, −1.36, −1.53 and −1.89 V (Figure 12 and Supporting Information, Table 3). The overlapping nature of the processes meant that coulometry experiments could not be carried out. A small stripping wave occurs at −0.59 V when scanning to potentials below −1.00 V, which is due to the formation of copper on the electrode.

On scanning to positive potentials a reversible oxidation process is seen at $E_{1/2}$ = +0.46 V. Coulometry at +0.70 V resulted in the transfer of 1.01 electron equivalents indicating that this is a one-electron process. This process is therefore assigned to $Cu^{I} \rightleftarrows Cu^{II}$. Furthermore, the colour changed during this oxidation from orange-brown to green, consistent with this assignment. The cyclic voltammogram of the oxidation product was unchanged immediately after the oxidation, indicating that the $[Ni^{II}Cu^{II}L]^{4+}$ product is stable under argon in dry acetonitrile. The cyclic voltammogram of $[Ni^{II}Cu^{I}L](BF_4)_3{\cdot}H_2O$ also shows an irreversible oxidation process at +1.07 V, which may correspond to the oxidation of nickel(II) to nickel(III)[17] or a ligand-centred process.

As shown in Figure 12, the cyclic voltammogram of $[Co^{II}Cu^{I}L](BF_4)_3$ is complex with many processes (Table 3). The reduction region shows a series of quasi-reversible processes, as well as a stripping wave at −0.54 V. These processes are probably a mixture of metal- and ligand-centred reductions.

The oxidation region shows several quasi-reversible and irreversible processes. Applying a potential of 0.00 V failed to generate current flow confirming that oxidation occurs at positive potentials vs. $AgNO_3$/Ag(s). On scanning to positive potentials, there are two quasi-reversible processes with poorly resolved oxidation peaks on the forward scan and reduction peaks at +0.58 and +0.08 V on the return scan. Coulometry at +1.00 V resulted in the transfer of 2.00 electron equivalents and caused the colour of the complex to change from orange to dark brown. Subsequent coulometry at +0.25 V resulted in the transfer of 0.95 electron equivalents. These results suggest that the two quasi-reversible processes are both one-electron oxidations. As the Co^{II} to Co^{III} oxidation in the mononuclear cryptate $[Co^{II}L](BF_4)_2$ occurs at the relatively low potential of $E_{1/2}$ = +0.29 V,[9] it is possible that the cobalt(II) (rather than Cu^{I}) centre is oxidised first, followed by conformational changes deriving from the appreciably smaller radius of the Co^{III} cation.

The electrochemical properties of the heterodinuclear cryptates $[M^{II}Cu^{I}L](X)_3$ (M = Mn, Fe, Co, Ni, Cu, X = BF_4^- or ClO_4^-) indicate that the divalent cation influences the potential and reversibility of the $Cu^{I} \rightleftarrows Cu^{II}$ process (Table 3, Figure 13). For the cryptates $[M^{II}Cu^{I}L]^{3+}$ (M = Mn, Fe, Ni, Cu) the $E_{1/2}$ for the $Cu^{I} \rightleftarrows Cu^{II}$ process in CH_3CN is inversely correlated with the solid-state $M^{II}\cdots Cu^{I}$ distance and follows the order: Fe (+0.49 V; 4.72 Å) > Ni (+0.46 V; 4.86 Å) > Cu (+0.33 V; 4.96 Å) > Mn (+0.25 V; 5.23 Å). Therefore the influence of the divalent cation on the electrochemistry of the copper(I) ion is predominantly electrostatic, with the copper(I) ion becoming harder to oxidise with closer proximity to the positively charged divalent cation. The copper(I) ion appears to be most stable towards reduction and towards any subsequent dissociation in $[Fe^{II}Cu^{I}L](BF_4)_3{\cdot}CH_3CN$ since no stripping wave is observed, even on scanning to −1.80 V.

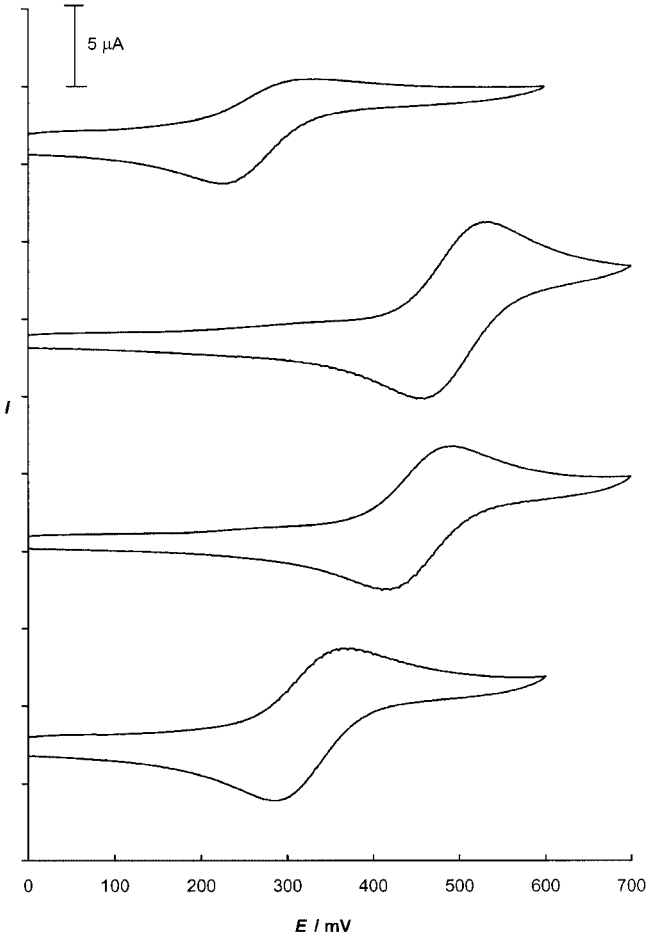

Figure 13. Cyclic voltammograms of heterodinuclear cryptates in acetonitrile showing the $Cu^{I} \rightleftarrows Cu^{II}$ process; from top to bottom: $[Mn^{II}Cu^{I}L](ClO_4)_2(BF_4)$, $[Fe^{II}Cu^{I}L](BF_4)_3{\cdot}CH_3CN$, $[Ni^{II}Cu^{I}L](BF_4)_3{\cdot}H_2O$ and $[Cu^{II}Cu^{I}L](BF_4)_3$ (200 mV s^{-1} vs. 0.01 mol L^{-1} $AgNO_3$/Ag); each scan starts at 0 V

Neither of the candidates for the $Cu^{I} \rightleftarrows Cu^{II}$ process for $[Co^{II}Cu^{I}L](BF_4)_3$, E_{pc} = +0.08 and +0.58 V ($M^{II}\cdots Cu^{I}$ 5.08 Å), fits into the above trend. This cryptate also shows the least reversible oxidation in this series of heterodinuclear cryptates. The anomalous behaviour of $[Co^{II}Cu^{I}L](BF_4)_3$ could be accounted for by the oxidation of the cobalt(II) ion (i.e. Co^{II} to Co^{III} at E_{pc} = +0.08 V) before the copper(I) ion (i.e. Cu^{I} to Cu^{II} at E_{pc} = +0.58 V). Oxidation of cobalt(II) to cobalt(III) may affect the M···Cu distance and would nevertheless enhance the positive charge (from +2 to +3) near the copper(I) ion, thus increasing its oxidation potential as observed.

It would be of interest to monitor the reciprocal effect of the copper(I) ion on the electrochemistry of the divalent cation in $[M^{II}Cu^{I}L](X)_3$ (M = Mn, Fe, Co, Ni, X = BF_4^- or ClO_4^-). However, this is ruled out due to the difficulty

 © 2004 Wiley-VCH Verlag GmbH & Co. KGaA, Weinheim

of differentiating such metal-centred processes from ligand-centred processes with the facilities available to us.

Conclusion

The symmetrical cryptand L readily forms mononuclear cryptates with first-row transition-metal ions with geometries ranging from five to seven coordinate. Addition of copper(I) to these unsymmetrical monometallic cryptates results in the controlled formation of the heterodinuclear cryptates $[M^{II}Cu^{I}L](X)_3$ (M = Mn, Fe, Co, Ni, X = BF_4^- or ClO_4^-). This is the first series of this kind to be reported.

The syntheses of $[Zn_2L](ClO_4)_4$ and $Mn_2LCl_4{\cdot}H_2O$ demonstrate that L can also form homodinuclear complexes with relatively non-stereochemically demanding divalent cations. However, the choice of counterion and/or solvent appears to be crucial for the formation of the dinuclear complexes, and there is evidence of interaction of the counterions with the divalent zinc or manganese ions. Electrochemical studies on $[Zn_2L](ClO_4)_4$ revealed that the L cryptand is able to undergo a series of reductions and oxidations, which were also observed in several other cryptates of L.

The series of heterodinuclear cryptates has been structurally characterised. In all cases, the divalent cation has a distorted octahedral geometry and the copper(I) ion has a distorted trigonal pyramidal geometry. The $M^{II}\cdots Cu^{I}$ distance in these cryptates decreases with decreasing ionic radius of the divalent cation.

Cyclic voltammetric studies on this series of heterodinuclear cryptates show that the $E_{1/2}$ of the Cu^{I}/Cu^{II} couple follows the order Fe > Ni > Cu > Mn and is inversely correlated to the $M^{II}\cdots Cu^{I}$ distance. The previously synthesised $[Co^{II}Cu^{I}L](BF_4)_3$ does not follow this trend, probably because the cobalt ion is in the +3 state at the time when Cu^{I} is oxidised.

Experimental Section

General: 3,6-Diformylpyridazine,[18] L[9] and $Cu^{I}(MeCN)_4X$ (X = BF_4^-)[19] were synthesised as described previously. For the electrochemical studies HPLC grade MeCN was distilled from CaH_2 immediately before use. Chloroform was extracted with the equivalent volume of water, four times, and dried over Na_2SO_4, before use. All other solvents and reagents were used as received. Physical measurements were carried out as described previously,[18,20] except for the following: the electrochemistry was carried out with 1 mmol L^{-1} dry acetonitrile solutions and 0.1 mol L^{-1} tetraethylammonium perchlorate or tetrabutylammonium hexafluorophosphate as the supporting electrolyte, on an EG&G Princeton Applied Research 273A potentiostat using a 0.01 mol L^{-1} $AgNO_3$/Ag reference electrode. As a further reference check, ferrocene was added at the conclusion of each experiment: the Fc/Fc^+ couple consistently occurred at $E_{1/2}$ = +0.07 ± 0.01 V with ΔE = 0.07 V. Magnetic measurements were carried using a Johnson−Matthey magnetic susceptibility balance MSB-MKI. All magnetic data were corrected for diamagnetic contributions using Pascal's constants.

Caution: *Whilst no problems were encountered in the course of this work perchlorate mixtures are potentially explosive and should therefore be handled with appropriate care.*

Preparation of $[Mn^{II}L](ClO_4)_2$: L (0.060 g, 0.1 mmol) was suspended in methanol (20 mL) and stirred. To this was added a methanol solution (10 mL) of $Mn(ClO_4)_2{\cdot}6H_2O$ (0.037 g, 0.1 mmol) which caused the cream suspension to turn bright yellow. After stirring overnight, the suspension was filtered yielding $[Mn^{II}L](ClO_4)_2$ as a yellow powder (0.066 g, 77%). Single crystals suitable for X-ray diffraction were obtained by recrystallisation of the product from DMF by vapour diffusion of diethyl ether. IR (KBr, inter alia): $\tilde{\nu}$ = 3415 (b, s), 1652 (m), 1144 (s), 1116 (s), 1088 (s), 625 cm^{-1} (m). UV/Vis (MeCN): λ_{max} (ε) = 208 (62100), 250 nm (35100 L $mol^{-1}cm^{-1}$), 290 (sh). MS (ESI): *m/z* (%) = 746 (34) $[MnC_{30}H_{36}N_{14}(ClO_4)^+]$, 324 (100) $[MnC_{30}H_{36}N_{14}^{2+}]$. μ = 6.3 BM (293 K); Λ_m(MeCN) = 280 $mol^{-1}\,cm^2\,\Omega^{-1}$ (2:1 = 220−300 $mol^{-1}\,cm^2\,\Omega^{-1}$).[12] $C_{30}H_{36}MnN_{14}(ClO_4)_2$ (846.6): calcd. C 42.56, H 4.29, N 23.16; found C 42.44, H 4.47, N 22.97.

Preparation of $[Fe^{II}L](BF_4)_2$: L (0.045 g, 0.08 mmol) was suspended in degassed acetonitrile (30 mL) and stirred under a nitrogen atmosphere. To this was added an acetonitrile solution (5 mL) of $Fe(BF_4)_2{\cdot}6H_2O$ (0.026 g, 0.08 mmol), which caused the suspension to clarify and become deep purple. After stirring under a nitrogen atmosphere for 4 h the volume of the solution was reduced to about 15 mL in vacuo. Diethyl ether diffusion into the resulting solution gave $[Fe^{II}L](BF_4)_2$ as a purple crystalline solid (0.032 g, 52%). ^1H NMR (500 MHz, solvent CD_3CN, reference CH_3CN, 243 K): δ = 8.94 (s, 1 H, H^{11}), 8.24 (d, 1 H, H^3), 8.08 (d, 1 H, H^4), 7.37 (s, 1 H, H^6), 3.71−3.88 (m, 3 H, H^{7b}, H^{10a}, H^{10b}), 3.61 (br, d, 1 H, H^{9b}), 3.39 (br, t, 1 H, H^{9a}), 3.30 (t, 1 H, H^{7a}), 2.95 (t, 1 H, H^{8a}), 2.36 (m, 1 H, H^{8b}); at 298 K: 8.49 (s, br), 8.16 (d), 7.48 (s), 3.94 (s, br), 3.82 (dt), 3.59 (s, br), 3.37 (t), 3.00 (t), 2.40 (dd). IR (KBr, inter alia): $\tilde{\nu}$ = 3414 (b, s), 1638 (m), 1617 (m), 1534 (w), 1437 (m), 1053 (s), 1032 (s), 521 cm^{-1} (w). UV/Vis (MeCN): λ_{max} (ε) = 213 (64700), 250 (sh), 370 (sh), 428 (4800), 540 (sh), 588 nm (8030 L $mol^{-1}\,cm^{-1}$). MS (ESI): *m/z* (%) = 735 (26) $[FeC_{30}H_{36}N_{14}(BF_4)^+]$, 648 (25) $[FeC_{30}H_{36}N_{14}^+]$, 615 (100) $[NaC_{30}H_{36}N_{14}^+]$, 324 (69) $[FeC_{30}H_{36}N_{14}^{2+}]$. Λ_m(MeCN) = 286 $mol^{-1}\,cm^2\,\Omega^{-1}$ (2:1 = 220−300 $mol^{-1}\,cm^2\,\Omega^{-1}$).[12] $C_{30}H_{36}FeN_{14}(BF_4)_2$ (822.2): calcd. C 43.83, H 4.41, N 23.85; found C 43.78, H 4.54, N 23.86.

Preparation of $[Ni^{II}L](BF_4)_2$: L (0.062 g, 0.1 mmol) was suspended in acetonitrile (40 mL) and stirred. To this was added an acetonitrile solution (10 mL) of $Ni(BF_4)_2{\cdot}6H_2O$ (0.036 g, 0.1 mmol), which caused the suspension to clarify and become pale greenish yellow. After stirring overnight, the volume was reduced to about 10 mL in vacuo. Diffusion of diethyl ether into the resulting solution gave brown crystals of $[Ni^{II}L](BF_4)_2$ (0.069 g, 80%). IR (KBr, inter alia): $\tilde{\nu}$ = 3419 (b, s), 1647 (m), 1440 (m), 1050 (s), 521 cm^{-1} (w). UV/Vis (MeCN): λ_{max} (ε) = 211 (68700), 250 (sh), 825 (30), 908 nm (30 L $mol^{-1}\,cm^{-1}$). MS (ESI): *m/z* (%) = 737 (52) $[NiC_{30}H_{36}N_{14}(BF_4)^+]$, 325 (100) $[NiC_{30}H_{36}N_{14}^{2+}]$. μ = 3.1 BM (293 K); Λ_m(MeCN) = 301 $mol^{-1}\,cm^2\,\Omega^{-1}$ (2:1 = 220−300 $mol^{-1}\,cm^2\,\Omega^{-1}$).[12] $C_{30}H_{36}N_{14}Ni(BF_4)_2$ (825.0): calcd. C 43.67, H 4.40, N 23.77; found C 43.86, H 4.42, N 23.57.

Preparation of $[Ni^{II}L](ClO_4)_2$: L (0.029 g, 0.05 mmol) was suspended in acetonitrile (10 mL) and stirred. To this was added an acetonitrile solution (8 mL) of $Ni(ClO_4)_2{\cdot}6H_2O$ (0.018 g, 0.05 mmol), which caused the suspension to clarify and become pale greenish yellow. After stirring overnight, the volume was reduced to about 5 mL in vacuo. Diffusion of diethyl ether into the

 © 2004 Wiley-VCH Verlag GmbH & Co. KGaA, Weinheim

resulting solution gave brown crystals of $[Ni^{II}L](ClO_4)_2$ (0.034 g, 81%). IR (KBr, inter alia): $\tilde{\nu}$ = 3414 (b, m), 2916 (m), 2849 (m), 1647 (m), 1442 (m), 1329 (m), 1083 (b, s), 622 cm^{-1} (s). $C_{30}H_{36}N_{14}Ni(ClO_4)_2$ (850.3): calcd. C 42.38, H 4.27, N 23.06; found C 42.55, H 4.18, N 23.19.

Preparation of $[Zn_2L](ClO_4)_4$: L (0.120 g, 0.2 mmol) was suspended in acetonitrile (50 mL) and stirred. To this was added an acetonitrile solution (5 mL) of $Zn(ClO_4)_2{\cdot}6H_2O$ (0.151 g, 0.4 mmol), which caused the cream suspension to clarify and become bright yellow. After stirring overnight, the volume was reduced to about 20 mL in vacuo. Diffusion of diethyl ether into the resulting solution gave $[Zn_2L](ClO_4)_4$ as a yellow crystalline solid (0.181 g, 80%). ^1H NMR (500 MHz, solvent CD_3CN, reference CH_3CN, 298 K): δ = 8.96 (s, 1 H, H^6), 8.34 (s, 1 H, H^3), 3.97 (br, t, 1 H, H^{7a}), 3.77 (dd, 1 H, H^{7b}), 3.24 (dd, 1 H, H^{8b}), 3.08 (td, 1 H, H^{8a}). ^{13}C NMR (126 MHz, solvent CD_3CN, reference CH_3CN, 298 K): δ = 166.1 (C^6), 153.7 (C^2), 135.1 (C^3), 58.8 (C^7), 54.0 (C^8). IR (KBr, inter alia): $\tilde{\nu}$ = 3417 (s, b), 1653 (m), 1437 (w), 1326 (w), 1147 (s), 1121 (s), 1077 (s), 637 (m), 629 (m), 624 cm^{-1} (m). UV/Vis (MeCN): λ_{max} (ε) = 206 (51900), 251 (30400 L mol^{-1} cm^{-1}), 290 (sh), 350 (sh) nm. MS (ESI): *m/z* (%) = 757 (73) $[ZnC_{30}H_{36}N_{14}(ClO_4)^+]$, 328 (100) $[ZnC_{30}H_{36}N_{14}{}^{2+}]$. Λ_m(MeCN) = 359 mol^{-1} cm^2 Ω^{-1} (3:1 = 340−420 mol^{-1} cm^2 Ω^{-1}).[12] $C_{30}H_{36}N_{14}Zn_2(ClO_4)_4$ (1121.3): calcd. C 32.13, H 3.24, N 17.49; found C 32.09, H 3.46, N 17.33. NMR spectroscopic data for the mononuclear zinc(II) complex $[ZnL](ClO_4)_2$: ^1H NMR (500 MHz, solvent CD_3CN, reference CH_3CN, 298 K): δ = 8.93 (d, 1 H, H^{11}), 8.35 (d, 1 H, H^3), 8.11 (d, 1 H, H^4), 7.38 (d, 1 H, H^6), 4.23 (tdd, 1 H, H^{10b}), 3.88 (dd, 1 H, H^{10a}), 3.83 (m, 1 H, H^{7b}), 3.32 (t, 1 H, H^{7a}), 3.17−3.29 (m, 2 H, H^{9a}, H^{9b}), 2.98 (td, 1 H, H^{8a}), 2.52 (dd, 1 H, H^{8b}). ^{13}C NMR (126 MHz, solvent CD_3CN, reference CH_3CN, 298 K): δ = 163.0 (C^{11}), 160.2 (C^5), 159.6 (C^6), 152.3 (C^2), 131.9 (C^4), 128.2 (C^3), 60.6 (C^7), 56.0 (C^1), 55.3 (C^8), 53.2 (C^9).

Preparation of $Mn^{II}_2LCl_4{\cdot}H_2O$: L (0.060 g, 0.10 mmol) was suspended in methanol (25 mL) and stirred. To this was added a methanol solution (5 mL) of $MnCl_2{\cdot}4H_2O$ (0.040 g, 0.20 mmol), which caused the cream suspension to turn bright yellow and clarify. After stirring overnight, the volume was reduced to about 10 mL in vacuo. Diffusion of diethyl ether into the resulting solution gave $Mn_2LCl_4.H_2O$ as a yellow crystalline solid (0.075 g, 88%). IR (KBr, inter alia): $\tilde{\nu}$ = 3445 (b, s), 1651 (s), 1433 (m), 1326 (m), 1035 (m), 927 (m), 581 cm^{-1} (w). UV/Vis (MeOH): λ_{max} (ε) = 250 nm (36300 L mol^{-1} cm^{-1}). MS (ESI): *m/z* (%) = 324 (100) $[MnC_{30}H_{36}N_{14}{}^{2+}]$, 216 (29) $[MnC_{30}H_{36}N_{14}H^{3+}]$. μ = 6.1 BM per Mn (293 K); Λ_m(MeOH) = 224 mol^{-1} cm^2 Ω^{-1} (2:1 = 160−220 mol^{-1} cm^2 Ω^{-1}).[12] $C_{30}H_{36}N_{14}Mn_2Cl_4{\cdot}H_2O$ (862.4): calcd. C 41.78, H 4.44, N 22.74, Cl 16.44; found C 42.79, H 4.13, N 22.46, Cl 16.44.

Preparation of $[Na_2L](CF_3SO_3)_2$: L (0.040 g, 0.07 mmol) was suspended in acetonitrile (20 mL) and stirred. To this was added an acetonitrile solution (10 mL) of $Na(CF_3SO_3)$ (0.024 g, 0.14 mmol), which caused the suspension to clarify slightly. After stirring overnight, the mixture was filtered to remove unreacted L. Diffusion of diethyl ether into the resulting solution gave the product as a white crystalline solid (0.021 g, 33% yield). ^1H NMR (500 MHz, solvent CD_3CN, reference CH_3CN, 298 K): δ = 8.56 (s, 1 H, H^6), 7.96 (s, 1 H, H^3), 3.86 (t, 2 H, H^7), 2.95 (t, 2 H, H^8). ^{13}C NMR (126 MHz, solvent CD_3CN, reference CH_3CN, 298 K): δ = 160.2 (C^6), 156.2 (C^2), 131.7 (C^3), 58.7 (C^7), 54.7 (C^8). IR (KBr, inter alia): $\tilde{\nu}$ = 3414 (m, b), 2850 (m), 2806 (m), 1654 (m), 1266 (s), 1223 (m), 1146 (s), 1033 (s), 639 (s), 516 cm^{-1} (m). UV/Vis (MeCN): λ_{max} (ε) = 247 nm (50400 L mol^{-1} cm^{-1}). MS (ESI): *m/z* (%) = 615 (100) $[NaC_{30}H_{36}N_{14}{}^+]$. $C_{30}H_{36}N_{14}Na_2(CF_3SO_3)_2$ (936.8): calcd. C 41.03, H 3.87, N 20.93; found C 41.07, H 3.95, N 21.09.

Preparation of $[M^{II}Cu^{I}L](X)_3$ (M = Mn, Fe, Ni, X = BF_4^- or ClO_4^-): L (0.06 g, 0.1 mmol) was suspended in acetonitrile (40 mL) and stirred under a nitrogen atmosphere. To this was added an acetonitrile solution (10 mL) of an appropriate salt of the divalent cation (0.1 mmol), which caused the suspension to clarify. After stirring for 30 min, solid $Cu^I(CH_3CN)_4BF_4$ (0.03 g, 0.1 mmol) was added to the solution causing it to change colour. After stirring overnight, the volume was reduced to about 20 mL in vacuo. Diffusion of diethyl ether into the resulting solution gave the products as crystalline solids.

$[Mn^{II}Cu^{I}L](ClO_4)_2(BF_4)$: Prepared as above, except that $Cu^I(CH_3CN)_4BF_4$ (0.035 g, 0.11 mmol) was added. Reddish brown crystals (0.088 g, 88% yield). IR (KBr, inter alia): $\tilde{\nu}$ = 3482 (b, s), 1652 (m), 1575 (w), 1440 (w), 1325 (w), 1143 (s), 1117 (s), 1083 (s), 1032 (m), 628 cm^{-1} (m). UV/Vis (MeCN): λ_{max} (ε) = 250 nm (33000 L mol^{-1} cm^{-1}), 280 (sh). MS (FAB): *m/z* (%) = 910 (17) $[MnCuC_{30}H_{36}N_{14}(ClO_4)_2]$, 809 (100) $[MnCuC_{30}H_{36}N_{14}(ClO_4)]$, 797 (26) $[MnCuC_{30}H_{36}N_{14}(BF_4)]$, 710 (48) $[MnCuC_{30}H_{36}N_{14}]$, 655 (77) $[CuC_{30}H_{36}N_{14}]$. μ = 5.9 BM (293 K); Λ_m(MeCN) = 407 $mol^{-1}cm^2\Omega^{-1}$ (3:1 = 340−420 mol^{-1} cm^2 Ω^{-1}).[12] $C_{30}H_{36}CuMnN_{14}(ClO_4)_2(BF_4)$ (996.9): calcd. C 36.15, H 3.64, N 19.67, Mn 5.51, Cu 6.37; found C 36.15, H 3.61, N 19.52, Mn 5.27, Cu 6.11.

$[Fe^{II}Cu^{I}L](BF_4)_3{\cdot}CH_3CN$: Prepared as above, except that the crude product was precipitated out by the addition of diethyl ether (approximately 50 mL) and then recrystallised from acetonitrile to give purple crystals (0.076 g, 75% yield). ^1H NMR (500 MHz, solvent CD_3CN, reference CH_3CN, 298 K): δ = 9.03 (s, 1 H, H^{11}), 8.56 (d, 1 H, H^6), 8.33 (d, 1 H, H^3), 7.90 (d, 1 H, H^4), 3.67 (dd, 1 H, H^{10b}), 3.62 (ddd, 1 H, H^{7a}), 3.54 (dd, 1 H, H^{7b}), 3.45−3.52 (m, 2 H, H^{10a}, H^{9b}), 3.25 (m, 1 H, H^{9a}), 3.08 (dd, 1 H, H^{8b}), 2.91 (td, 1 H, H^{8a}). ^{13}C NMR (126 MHz, solvent CD_3CN, reference CH_3CN, 298 K): δ = 170.8 (C^{11}), 161.6 (C^2), 158.9 (C^6), 157.5 (C^5), 131.6 (C^3), 128.1 (C^4), 61.1 (C^7), 60.6 (C^1), 54.6 (C^9), 52.3 (C^8). IR (KBr, inter alia): $\tilde{\nu}$ = 3424 (br), 1635 (m), 1532 (m), 1312 (m), 1123 (s), 1083 (s), 1034 (s), 533 (w), 521 cm^{-1} (w). UV/Vis (MeCN): λ_{max} (ε) = 211 (75000), 390 (sh), 441 (10700), 540 (sh), 580 nm (10500 L mol^{-1} cm^{-1}). MS (FAB): *m/z* (%) = 711 (100) $[FeCuC_{30}H_{36}N_{14}]$, 648 (86) $[FeC_{30}H_{36}N_{14}]$. μ = 0.0 BM (293 K); Λ_m(MeCN) = 393 mol^{-1} cm^2 Ω^{-1} (3:1 = 340−420 mol^{-1} cm^2 Ω^{-1}).[12] $C_{30}H_{36}CuFeN_{14}(BF_4)_3.CH_3CN$ (1013.6): calcd. C 37.92, H 3.88, N 20.73, Fe 5.51, Cu 6.27; found C 37.97, H 3.95, N 20.57, Fe 5.28, Cu 6.74.

$[Ni^{II}Cu^{I}L](BF_4)_3{\cdot}2H_2O$: Reddish brown crystals (0.076 g, 75% yield). IR (KBr, inter alia): $\tilde{\nu}$ = 3419 (b), 1636 (m), 1083 (s), 1035 (s), 533 (w), 521 cm^{-1} (w). UV/Vis (MeCN): λ_{max} (ε) = 250 (sh), 413 (2560), 806 nm (20 L mol^{-1} cm^{-1}). MS (ESI): *m/z* (%) = 737 (7) $[NiC_{30}H_{36}N_{14}BF_4{}^+]$, 400 (2) $[NiCuC_{30}H_{36}N_{14}BF_4{}^{2+}]$, 325 (100) $[NiC_{30}H_{36}N_{14}{}^{2+}]$, 238 (33) $[NiCuC_{30}H_{36}N_{14}{}^{3+}]$. μ = 3.1 BM (293 K); Λ_m(MeCN) = 410 mol^{-1} cm^2 Ω^{-1} (1:3 = 340−420 mol^{-1} cm^2 Ω^{-1}).[12] $C_{30}H_{36}CuNiN_{14}(BF_4)_3{\cdot}2H_2O$ (1011.4): calcd. C 35.63, H 3.99, N 19.39, Ni 5.80, Cu 6.28; found C 36.00, H 3.67, N 19.16, Ni 5.62, Cu 6.25.

X-ray Crystallography: Data were collected on Bruker SMART diffractometers (Universities of Canterbury, Auckland and Bristol), using graphite-monochromated Mo-K_α radiation (λ = 0.71013 Å). The data were corrected for Lorentz and polarisation effects and semi-empirical absorption corrections were applied. The structures were solved by direct methods (SHELXS-97)[21] and refined against all F^2 data. (SHELXL-97).[22] Hydrogen atoms were inserted at cal-

 © 2004 Wiley-VCH Verlag GmbH & Co. KGaA, Weinheim

Table 4. Crystallographic data for mononuclear and heterodinuclear cryptates of L

	$[Mn^{II}L](ClO_4)_2$	$[Ni^{II}L](ClO_4)_2$	$[Mn^{II}Cu^{I}L](ClO_4)_2(BF_4)$	$[Fe^{II}Cu^{I}L](BF_4)_3{\cdot}2.5CH_3CN$	$[Ni^{II}Cu^{I}L](BF_4)_3$
Formula	$C_{30}H_{36}Cl_2MnN_{14}O_8$	$C_{30}H_{36}Cl_2N_{14}NiO_8$	$C_{30}H_{36}CuMnN_{14}$[a]	$C_{35}H_{43.5}B_3CuF_{12}FeN_{16.5}$	$C_{30}H_{36}B_3CuF_{12}N_{14}NiO_{0.5}$
M_r	846.57	850.34	711.21[a]	1075.18	983.41
T [K]	173(2)	168(2)	168(2)	150(2)	150(2)
Crystal system	triclinic	triclinic	monoclinic	triclinic	triclinic
Space group	$P\bar{1}$	$P\bar{1}$	$P2_1/n$	$P\bar{1}$	$P\bar{1}$
a [Å]	9.6480(15)	9.738(4)	14.552(5)	9.84300(10)	12.67870(10)
b [Å]	13.316(3)	13.455(5)	15.406(5)	12.2499(2)	16.46700(10)
c [Å]	29.505(7)	29.674(11)	19.100(6)	20.03170(10)	21.2814(2)
α [°]	84.158(17)°	82.310(5)	90	82.4530(10)	96.1030(10)
β [°]	87.220(13)°	86.256(4)	110.982(4)	78.1380(10)	90.7510(10)
γ [°]	75.811(15)°	73.277(4)	90	74.1800(10)	90.5490(10)
V [Å^3]	3654.7(13)	3689(2)	3998(2)	2266.94(5)	4417.30(6)
Z	4	4	4	2	4
$\rho_{calcd.}$ [g/cm^3]	1.539	1.531	1.182[a]	1.575	1.479
μ [mm^{-1}]	0.578	0.740	0.885[a]	0.888	1.000
F(000)	1748	1760	1472[a]	1094	1992
Crystal size [mm]	0.50 × 0.50 × 0.49	0.61 × 0.56 × 0.40	0.55 × 0.45 × 0.07	0.28 × 0.18 × 0.08	0.48 × 0.40 × 0.24
θ range for data collection [°]	1.58 to 27.48	2.08 to 26.36	2.19 to 25.35	1.04 to 25.39	2.57 to 25.84
Reflections collected	38185	44887	46991	20354	40919
Independent reflections	16565	14572	7322	8270	16742
R(int)	0.0357	0.0381	0.0440	0.0267	0.0208
Max. and min. transmission	0.86 and 0.61	0.76 and 0.66	1.00 and 0.88	0.95 and 0.85	0.84 and 0.71
Data /parameters	16565/ 991	14572/991	7322/990	8270/660	16742/1206
Goof (F^2)	1.102	1.174	1.089	1.041	1.030
R_1 [$I > 2\sigma(I)$]	0.0540	0.0867	0.0499	0.0512	0.0506
wR_2 [all data]	0.1566	0.2052	0.1364	0.1387	0.1249

[a] Due to the use of SQUEEZE[23] these values refer only to the disordered cation.

culated positions (except where noted) and rode on the atoms to which they are attached (including isotropic thermal parameters which were equal to 1.2 times the equivalent isotropic displacement parameter for the attached non-hydrogen atom) and all non-hydrogen atoms were made anisotropic. CCDC 224698−224703 contain the supplementary crystallographic data for this paper. These data can be obtained free of charge via www.ccdc.cam.ac.uk/conts/retrieving.html [or from the Cambridge Crystallographic Data Centre, 12 Union Road, Cambridge CB2 1EZ, UK; Fax: (internat.) + 44-1223-336-033; E-mail: deposit@ccdc.cam.uk].

$[Mn^{II}Cu^{I}L_I](ClO_4)_2(BF_4)$: Notwithstanding several 0k0 reflections for which $I/\sigma(I) > 5$, we have solved this structure in $P2_1/n$. In space group Pn the pairs of cations are very clearly related by a centre of symmetry. The appearance of significant intensity for the 0k0 reflections is attributed to partial ordering of the anion species: in space group $P2_1/n$, each of the three anion sites is a composite of BF_4^- and ClO_4^- and in space group Pn ordering of the anions was not discernible. In view of the highly disordered anion sites, which together indicated an approximately 2:1 ratio ClO_4^-:BF_4^-, the structure was subjected to the SQUEEZE procedure of the PLATON suite.[23] A void volume of 968 Å^3 per cell containing 562 electrons was calculated. The electron count is very close to that calculated (568 electrons) for 8ClO_4^- and 4BF_4^- per cell. In contrast to poor convergence behaviour for refinements with disordered anion species, refinements on the SQUEEZEd structure converged quickly.

$[Fe^{II}Cu^{I}L_I](BF_4)_3{\cdot}2.5CH_3CN$: One of the BF_4^- anions was disordered over two sites with a common fluorine atom. One of the two acetonitrile molecules was disordered across a centre of inversion.

$[Ni^{II}Cu^{I}L_I](BF_4)_3$: The two complete cryptates in the asymmetric unit were both "end-for-end" disordered: in the first cryptate Cu(1) and Ni(2) are 0.76 occupancy [Cu(2) and Ni(1) minor occupancy] and in the second cryptate Cu(4) and Ni(3) are 0.65 occupancy [Cu(3) and Ni(4) minor occupancy]. Consequently the pyridazine rings of all strands are also disordered and this has been modelled. The SQUEEZE option of PLATON[23] was used to account better for the disordered anions and solvent molecules. This was found to be a reasonable approach as a total of 740 electrons in the void volume per cell was calculated, slightly greater than that of the best model, which comprised twelve BF_4^-, eight CH_3CN and four H_2O species for a total of 720 electrons per cell.

For crystal data see Table 4.

Supporting Information (see also footnote on the first page of this article): A table of the UV/Vis spectroscopic data, the ^{1}H NMR spectrum of $[ZnL](ClO_4)_2$, a summary of the X-ray structural parameters for $[Fe^{II}L](BF_4)_2$, and additional cyclic voltammograms of the cryptates described in this paper are provided.

Acknowledgments

This work was supported by grants from the University of Otago. We are grateful to Dr. J. Wikaira and Professor W. T. Robinson (University of Canterbury), and T. Groutso and Professors C. E. F. Rickard and P. D. W. Boyd (University of Auckland) for the X-ray data collections. We acknowledge the EPSRC Swansea FAB mass spectrometry service (Swansea) and B. M. Clark (University of Canterbury) for the mass spectra, Simon S. Iremonger (University of Otago) for re-running the UV/Vis spectrum of the dizinc(II) cryptate and a referee for helpful comments. SB thanks the Univer-

 © 2004 Wiley-VCH Verlag GmbH & Co. KGaA, Weinheim

sity of Otago for the granting of study leave and gratefully acknowledges her hosts Professor J. Nelson and the financial support of a Queens University Belfast Visiting Professorship and subsequently her hosts Dr. J. C. Jeffery, Professors M. D. Ward and J. McCleverty and the financial support of a Royal Society of Chemistry Journals Grant.

[1] J. Nelson, V. McKee, G. Morgan, *Prog. Inorg. Chem.* **1998**, *47*, 167−317.
[2] V. McKee, *Adv. Inorg. Chem.* **1993**, *40*, 323−399.
[3] O. Kahn, *Struct. Bond.* **1987**, *68*, 89−167.
[4] F. Avecilla, C. Platas-Iglesias, R. Rodríguez-Cortiñas, G. Guillemot, J.-C. G. Bünzli, C. D. Brondino, C. F. G. C. Geraldes, A. d. Blas, T. Rodríguez-Blas, *J. Chem. Soc., Dalton Trans.* **2002**, 4658−4665; R. Rodríguez-Cortiñas, F. Avecilla, C. Platas-Iglesias, D. Imbert, J.-C. G. Bünzli, A. de Blas, T. Rodríguez-Blas, *Inorg. Chem.* **2002**, *41*, 5336−5349; Q.-Y. Chen, Q.-H. Luo, Z.-L. Wang, J.-T. Chen, *Chem. Commun.* **2000**, 1033−1034; Q.-Y. Chen, Q.-H. Luo, D.-J. Fu, J.-T. Chen, *J. Chem. Soc., Dalton Trans.* **2002**, 2873−2878; Q.-Y. Chen, Q.-H. Luo, L.-M. Zheng, Z.-L. Wang, J.-T. Chen, *Inorg. Chem.* **2002**, *41*, 605−609; Q.-Y. Chen, Q.-H. Luo, X.-L. Hu, M.-C. Shen, J.-T. Chen, *Chem. Eur. J.* **2002**, *8*, 3984−3990.
[5] M. D. Timken, W. A. Marritt, D. N. Hendrickson, R. A. Gagné, E. Sinn, *Inorg. Chem.* **1985**, *24*, 4202−4208.
[6] R. E. Marsh, W. P. Schaefer, *Inorg. Chem.* **1986**, *25*, 3661−3662.
[7] J.-L. Pierre, P. Chantemps, S. M. Refaif, C. G. Beguin, A. El-Marzouki, G. Serratrice, P. Rey, J. Langier, *J. Chem. Soc., Chem. Commun.* **1994**, 1117−1118; J.-L. Pierre, P. Chantemps, S. M. Refaif, C. G. Beguin, A. El-Marzouki, G. Serratrice, E. Saint-Aman, P. Rey, *J. Am. Chem. Soc.* **1995**, *117*, 1965−1973.
[8] S. Brooker, J. D. Ewing, J. Nelson, J. C. Jeffery, *Inorg. Chim. Acta* **2002**, *337*, 463−466.
[9] S. Brooker, J. D. Ewing, J. Nelson, *Inorg. Chim. Acta* **2001**, *317*, 53−58.
[10] S. Brooker, J. D. Ewing, T. K. Ronson, C. J. Harding, J. Nelson, D. J. Speed, *Inorg. Chem.* **2003**, *42*, 2764−2773.
[11] S. Cromie, F. Launay, V. McKee, *Chem. Commun.* **2001**, 1918−1919.
[12] W. J. Geary, *Coord. Chem. Rev.* **1971**, *7*, 81−122.
[13] Q. Lu, J. M. Latour, C. J. Harding, N. Martin, D. J. Marrs, V. McKee, J. Nelson, *J. Chem. Soc., Dalton Trans.* **1994**, 1471−1478; D. J. Marrs, V. McKee, J. Nelson, Q. Lu, C. J. Harding, *Inorg. Chim. Acta* **1993**, *211*, 195−202.
[14] F. A. Cotton, G. Wilkinson, C. A. Murillo, M. Bochmann, *Advanced Inorganic Chemistry*, 6th ed., John Wiley & Sons, Inc., New York, **1999**.
[15] S. Iwata, C. Ostermeler, B. Ludwig, H. Michel, *Nature* **1995**, *376*, 660−669; T. Tsukihara, H. Aoyama, E. Yamashita, T. Tomizaki, H. Yamaguchi, K. Shinzawa-Itoh, R. Nakashima, R. Yaono, S. Yoshikawa, *Science* **1995**, *269*, 1069−1074.
[16] S. Brooker, V. McKee, *J. Chem. Soc., Dalton Trans.* **1990**, 2397−2401; J. McCrea, V. McKee, T. Metcalfe, S. S. Tandon, J. Wikaira, *Inorg. Chim. Acta* **2000**, *297*, 220−230.
[17] F. V. Lovecchio, E. S. Gore, D. H. Busch, *J. Am. Chem. Soc.* **1974**, *96*, 3109−3118; M. P. Suh, *Adv. Inorg. Chem.* **1997**, *44*, 93−146.
[18] S. Brooker, R. J. Kelly, *J. Chem. Soc., Dalton Trans.* **1996**, 2117−2122.
[19] G. J. Kubas, *Inorganic Syntheses, Vol. 28*, John Wiley and Sons, New York, **1990**, 68−70.
[20] S. Brooker, T. C. Davidson, S. J. Hay, R. J. Kelly, D. K. Kennepohl, P. G. Plieger, B. Moubaraki, K. S. Murray, E. Bill, E. Bothe, *Coord. Chem. Rev.* **2001**, *216−217*, 3−30.
[21] G. M. Sheldrick, *Acta Crystallogr., Sect. A* **1990**, *46*, 467−473; G. M. Sheldrick, *Methods Enzymol.* **1997**, *276*, 628−641.
[22] G. M. Sheldrick, T. R. Schneider, *Methods Enzymol.* **1997**, *277*, 319−343.
[23] P. van der Sluis, A. L. Spek, *Acta Crystallogr., Sect. A* **1990**, *46*, 194−201.

Received January 27, 2004
Early View Article
Published Online April 26, 2004

 © 2004 Wiley-VCH Verlag GmbH & Co. KGaA, Weinheim

Structural Properties of Bis(hexacarbonyldicobalt) Complexes with Heteroatoms Next to the Former Triple Bonds − A Contribution to the Mechanism of the Pauson−Khand Reaction

Daniel B. Werz,[a] J. Hilko Schulte,[a] Bernhard J. Rausch,[a] Rolf Gleiter,*[a] and Frank Rominger[a]

Keywords: Alkynes / Chalcogens / Cobalt / Pauson−Khand reaction

The bis(hexacarbonyldicobalt) complexes of cyclic diynes with sila-, thia- and selena-substituted acetylene units have been isolated. The structural features of these complexes have been elucidated by means of X-ray diffraction analyses on single crystals. In three cases (**24′**, **25′** and **29′**) the X-ray investigations show bis(pentacarbonyldicobalt) complexes instead of bis(hexacarbonyldicobalt) ones. Their empty coordination sites are each occupied by divalent chalcogen moieties from the opposite side of the molecule affording distorted C_2Co_2 cores. These results corroborate the possibility of intramolecular activation in Pauson–Khand reactions of chalcogen-containing substrates.
(© Wiley-VCH Verlag GmbH & Co. KGaA, 69451 Weinheim, Germany, 2004)

Introduction

The reaction of hexacarbonyldicobalt complexes of alkynes with olefins to yield cyclopentenones, first described by Pauson et al.,[1,2] has emerged as a frequently used procedure in chemistry.[3−6] Although this reaction has been known for more than 30 years, the mechanistic elucidation is still in progress. Some points which have been looked at more closely are the structural details of hexacarbonyldicobalt complexes[7,8] of various alkynes, and substituent[9] and solvent effects.[10] The energetics of reasonable intermediates along the possible pathway have also been calculated by computational chemistry.[11] One of the major questions in this field of chemistry is (besides the formation of stereoisomers)[12] the understanding of the formation of regioisomers and their control. The reaction of unsymmetrical alkynes with terminal olefins yields regioisomeric mixtures of cyclopentenones as shown in Scheme 1.

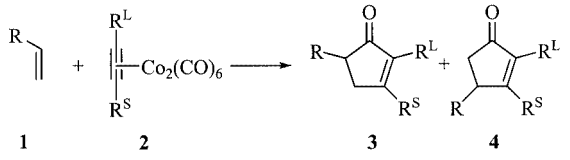

1 2 3 4

Scheme 1

Usually, the larger substituent (R^L) at the alkyne adopts the α-position to the CO group, whereas the substituent (R) at the olefin gives rise to the 1:1 mixture shown. To rationalize these results, an equilibrium between **5** and **6** was assumed before the insertion step.[3−6]

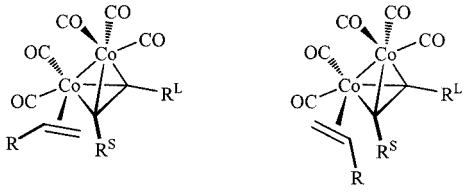

5 6

This assumption was further corroborated by a study in which heteroatoms were tethered to the olefin by a carbon chain. This led to the postulation that an intermediate such as **7** was involved,[13a] which would lead to a preference for **3**. Experiments with externally added sulfides confirmed this view.[13b]

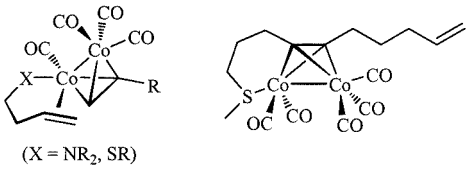

(X = NR_2, SR)

7 8

With respect to the role of heteroatom participation it is also of interest that the amine oxide promoted Pauson−Khand reaction is accelerated in the presence of heteroatoms such as sulfur, nitrogen and even oxygen in

[a] Organisch-Chemisches Institut der Universität Heidelberg, Im Neuenheimer Feld 270, 69120 Heidelberg, Germany
E-mail: rolf.gleiter@urz.uni-heidelberg.de

the homopropargylic position.[14] During these studies even intermediates such as **8** could be detected.[14]

Our interest in the effect of heteroatoms in the Pauson–Khand reaction, especially sulfur, arose when we studied the twofold Pauson–Khand reaction of cyclic diynes **9** and **10** with ethylene (Scheme 2).[9a,10c] We found a strong increase in the yield when **10** was used. Here the sulfur atom takes the homopropargylic position. To learn more about the effects of chalcogen atoms, even in other positions, we have synthesized a series of bis(hexacarbonyldicobalt) complexes of cyclic diynes with heteroatoms next to the $[C_2Co_2(CO)_6]$ core. In this paper we report on the syntheses and the structural investigations of these species. These studies allowed us to isolate three species in which a CO ligand is replaced by an intramolecular thio(seleno) ether ligand and to characterize them crystallographically.

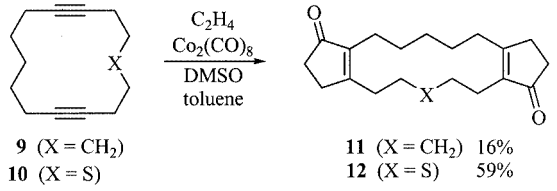

9 (X = CH_2)
10 (X = S)

11 (X = CH_2) 16%
12 (X = S) 59%

Scheme 2

Results and Discussion

We used the recently synthesized cyclic sila-, thia- and selenadiynes as starting materials. They were treated with octacarbonyldicobalt in dichloromethane to afford the corresponding complexes after crystallization or column chromatography. The resulting products, which could be obtained in 33–85% yield, are red to black solids, and several of them are sensitive to light. All new bis(hexacarbonyldicobalt) complexes and the isolated yields obtained for the syntheses of **13**–**30** are given in Table 1.

Most of the bis(hexacarbonyldicobalt) complexes show three characteristic absorptions in the IR spectrum in the range between 2000 and 2100 cm^{-1}. Group-theory considerations reveal that a $C_2Co_2(CO)_6$ core with a local C_{2v} symmetry should show five different IR-active vibrations in this range. The smaller number can be explained easily by the relatively low resolution of the spectrometer.

To study the structural data of these complexes, efforts were made to obtain single crystals suitable for X-ray crystallography. This was possible except for **17** and **18**. The crystallisation was performed either by solvent evaporation at room temperature or by crystallizing the complexes from the crude reaction mixture at −78 °C.

All the complexes are dominated by the bulky $C_2Co_2(CO)_6$ units (Figures 1 and 2). The tethers between

Table 1. Cyclic heterosubstituted $Co_2(CO)_6$ complexes **13**–**30** [Co_2 = $Co_2(CO)_6$]

Compound		Yield (%)	Compound		Yield (%)	Compound		Yield (%)
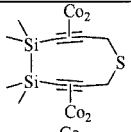	**13**	83	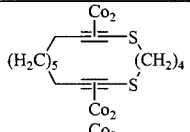	**19**	82	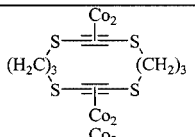	**25**	46
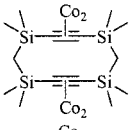	**14**	85	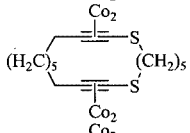	**20**	79	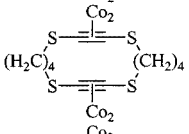	**26**	56
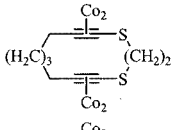	**15**	75	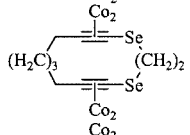	**21**	62	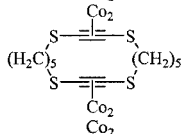	**27**	46
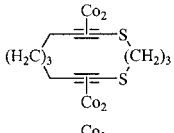	**16**	77	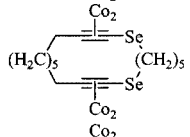	**22**	62	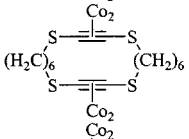	**28**	52
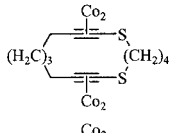	**17**	69	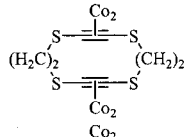	**23**	56	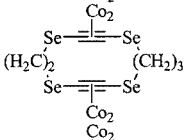	**29**	0[a]
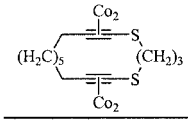	**18**	62	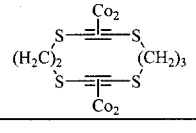	**24**	35	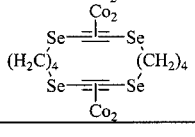	**30**	33

[a] Only the bis(pentacarbonyldicobalt) complex **29′** was isolated.

 © 2004 Wiley-VCH Verlag GmbH & Co. KGaA, Weinheim

these moieties often tend to adopt a zig-zag arrangement. However, the longer the tethers become, the more gauche conformations can be observed. Such conformations minimize the empty space between the coordinated triple bonds, as shown in Figure 2.

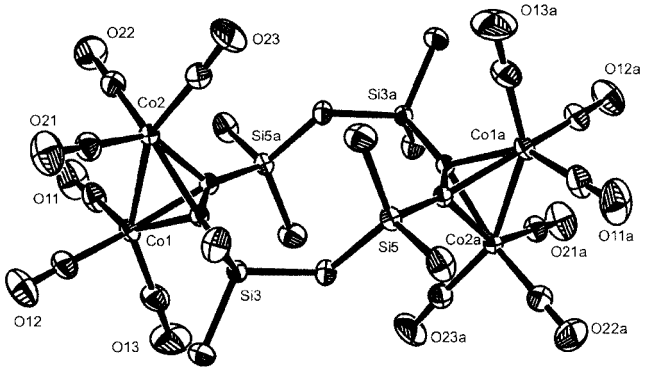

Figure 1. ORTEP plot (50% ellipsoid probability) of the molecular structure of **14**

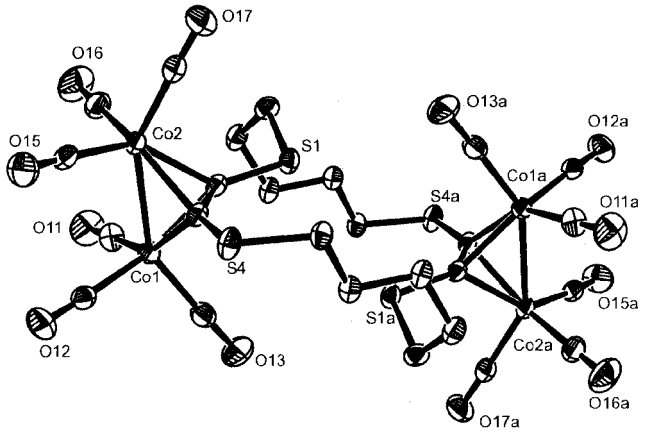

Figure 2. ORTEP plot (50% ellipsoid probability) of the molecular structure of **27**

Typical structural features of the heterosubstituted pseudo-tetrahedral Co_2C_2 cores are the planarity of the Co-coordinated fragments (the former triple bond and the adjacent heteroatoms or methylene groups lie in one plane), the elongation of the former triple bond due to its coordination (132−135 pm) and the bent geometry of the coordinated alkyne moieties (134−150°). The metal−carbonyl bond lengths vary between 177 and 185 pm. The longer distances are found *trans* to the acetylenic group, whereas the shorter ones are found in the *cis* position. These differences can be rationalized in terms of metal−ligand d → π* back-donation.[11a] The six CO ligands do not participate equally in the redistribution of electron density from the coordinated triple bond. As a result, different bond lengths are observed. Further structural data (except for **15**, which shows strong disorder) are given in Table 2; for the definition of the parameters see Figure 3.

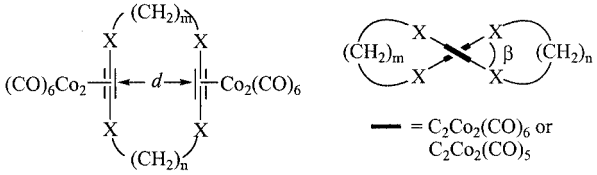

Figure 3. Definition of the transannular distance *d* and the torsion angle *β* in heterosubstituted cyclic bis(hexacarbonyldicobalt) and bis(pentacarbonyldicobalt) complexes

It is interesting to note that the bond lengths of the coordinated triple bonds in the chalcogen-substituted diyne complexes are somewhat larger than the values found in CH_2-substituted diyne complexes.[8l] This observation shows that the assumption of stronger bonding between the electron-rich triple bond of chalcogen-substituted acetylenes and the electron-poor $Co_2(CO)_6$ moiety is reasonable. Furthermore, a comparison of the Co−CC distances of the sila-substituted complexes **13** and **14** with the distances found in the chalcogen-substituted complexes reveals much

Table 2. Selected transannular distances between the former triple bonds, bond lengths and bond angles of the compounds **13**, **14**, **16**, **19**−**23**, **26**−**28** and **30**

Compd.	Distance *d* [a] Co_2C_2 [pm]	Torsion angle *β* [a] Co_2C_2 [°]	Bond lengths [pm]				Angles [°] X−C≡$C_{coord.}$ [b]
			C≡$C_{coord.}$	Co−CO	CoC≡O	Co−CC	
13	421.0	60.2	133.1−134.1	178.7−182.7	113.3−114.1	197.6−202.6	143.9−150.3
14	517.8	0	134.1	179.1−182.3	113.1−113.8	200.3−201.8	145.1−145.3
16	603.8	82.9	132.7−134.0	179.0−183.3	112.6−113.9	195.1−198.0	143.7−146.4
19	673.6	29.9	133.8−134.4	179.2−183.3	112.4−114.0	195.4−199.6	135.2−145.0
20	727.8	28.1	134.7−135.2	177.7−183.5	112.5−115.4	195.3−197.5	138.2−145.2
21	600.2	56.2	133.3−133.6	178.5−182.5	112.8−114.0	195.0−197.7	139.3−146.3
22	731.4	29.1	131.9	177.1−184.8	109.9−116.0	193.5−199.0	137.7−146.8
23	528.6	0	135.3	179.7−183.4	112.8−113.3	194.3−196.9	144.0−145.5
26	673.4	0	134.6	178.7−182.3	111.0−114.5	194.1−195.7	136.4−143.5
27	690.4	0	134.9	179.4−183.1	112.5−113.3	195.0−199.2	133.7−141.5
28	826.0	0	135.1	179.8−183.4	112.5−113.8	195.3−198.0	137.6−143.7
30	695.3	0	133.8	179.0−183.1	112.3−113.6	194.6−196.7	135.6−142.5

[a] See Figure 3 for definition of distance *d* and torsion angle *β*. [b] X = $Si(CH_3)_2$, S, Se or CH_2.

 © 2004 Wiley-VCH Verlag GmbH & Co. KGaA, Weinheim

longer distances for the slightly electron-poor sila-substituted alkyne, indicating a weaker coordination..

Crystallization experiments with **24**, **25** and **29** afforded crystals in which the molecules have lost two CO ligands (**24′**, **25′** and **29′**). The empty coordination sites are occupied by chalcogen donors placed at the opposite side of the molecule. A top and side view of structure **25′** is shown in Figure 4. Due to the C_1 symmetry of **24′**, and **29′**, and their low solubility in the usual solvents, it was not possible to get reliable NMR spectroscopic data for these compounds. The IR data show no significant differences to the corresponding bis(hexacarbonyldicobalt) complexes. Therefore, only the X-ray data of **24′**, **25′** and **29′** are discussed.

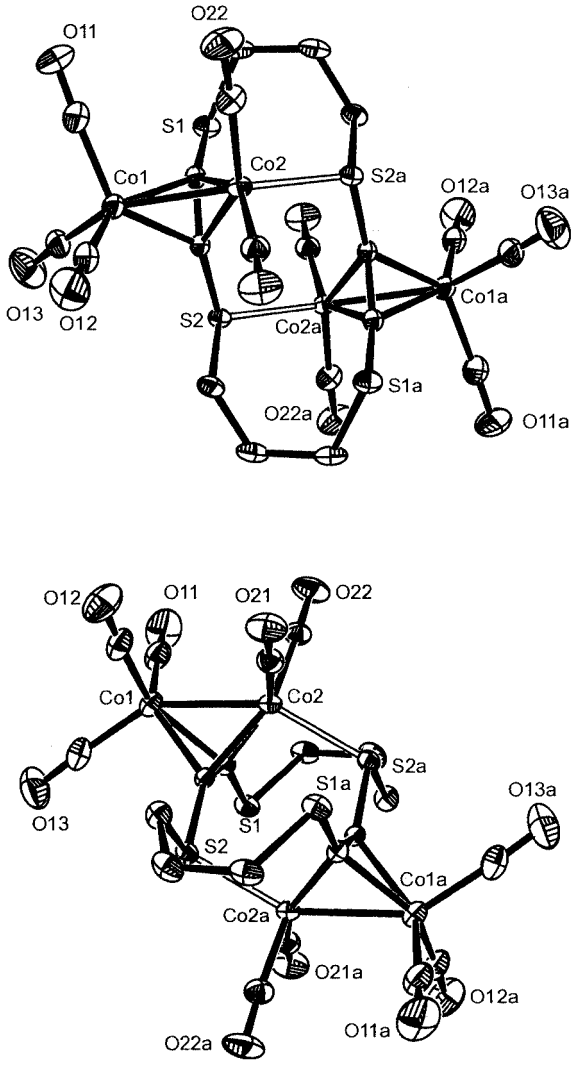

Figure 4. ORTEP plots (50% ellipsoid probability) of the bis(pentacarbonyldicobalt) complexe **25′** (top view and side view)

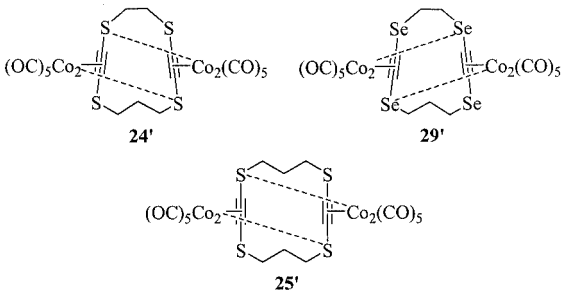

In Table 3 we present their most important structural features. From **24′** we obtained two different modifications (α and β). As Table 3 demonstrates, the C_2Co_2 core is much more distorted due to the chalcogen ligand — the Co−CC distances vary between 191 and 199 pm. The smaller $X-C{\equiv}C_{coord.}$ angles might be caused by the formation of a chelate complex. In Figure 5 the averaged structural parameters of a dithia-substituted $C_2Co_2(CO)_6$ core (type **A**) are compared with a dithia-substituted $C_2Co_2(CO)_5$ core with a further (pseudoaxial) sulfur ligand (type **B**). The averaged parameters are based on data of the four systems of type **A** and five systems of type **B**. Whereas the Co−CC distance in type **A** shows a value of 196 pm, the coordinating sulfur ligand strongly disfavors the former C_{2v} symmetry. As a result the Co−CC bond lengths vary between 192 and 198 pm. The changed electron density is also responsible for the different lengths of the OC−Co bonds indicating a significant change in metal−ligand d → π* backbonding. To the best of our knowledge, there is only one crystallographically characterized example in the literature showing a pentacarbonyldicobalt complex coordinated by a divalent sulfur atom in an intramolecular manner.[15] Selenium as a coordinating moiety and a doubly bridged bis(pentacarbonyldicobalt) complex were, until now, unknown.

Table 3. Selected transannular distances between the former triple bonds, bond lengths and bond angles of the compounds **24′α**, **24′β**, **25′** and **29′**

Compd.	Distance d [a] Co_2C_2 [pm]	Torsion angle β [a] Co_2C_2 [°]	Bond lengths [pm]					Angles [°] $X-C{\equiv}C_{coord.}$ [b]
			$C{\equiv}C_{coord.}$	Co−CO	CoC≡O	Co−CC	X−Co	
24′α [c]	361.1	0	135.8	180.0−182.6	113.3−114.7	190.9−199.2	224.6	135.2−139.6
	361.5	0.8	133.7−134.7	178.2−184.2	110.8−114.9	191.4−198.3	224.3−224.8	133.0−139.2
24′β	357.7	0	136.3	179.7−182.9	112.2−113.7	192.2−197.8	224.8	134.4−139.3
25′	365.4	0	135.7	178.9−183.3	112.6−113.4	192.9−199.2	225.1	135.4−139.9
29′	374.8	0	135.1	179.4−182.2	113.1−113.7	192.7−198.0	236.4	134.4−139.3

[a] See Figure 3 for definition of distance d and torsion angle β. [b] X = S or Se. [c] 1.5 independent molecules in the asymmetric unit.

 © 2004 Wiley-VCH Verlag GmbH & Co. KGaA, Weinheim

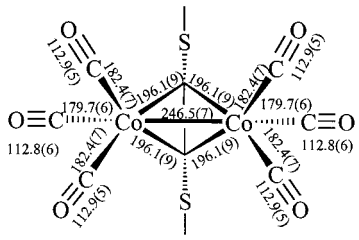

A

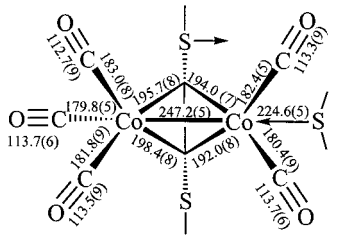

B

Figure 5. Comparison of the bond lengths (with standard deviation) in dithia-substituted hexacarbonyldicobalt complexes (type **A**) and pentacarbonyldicobalt complexes (type **B**); the averaged values refer to data of four systems of type **A** and five systems of type **B**

Conclusions

Our in-depth study of the structural features of sila-, thia- and selena-substituted bis(hexacarbonyldicobalt) complexes has revealed that the molecular solid-state structures of these complexes are the result of an interplay between the bulky $C_2Co_2(CO)_6$ moieties and the conformational needs of the tethers. In many cases the tethers adopt conformations that minimize the empty space between the bulky units. Our search to find evidence for cobalt−chalcogen interactions proved to be successful. Cobalt−heteroatom interactions, especially cobalt−sulfur interactions, are thought to play an important role in Pauson−Khand reactions. Two tetrathia- as well as one tetraselenacyclodiyne afforded bis(pentacarbonyldicobalt) complexes with coordinating divalent chalcogen atoms occupying the sixth coordination site of the C_2Co_2 core.

Experimental Section

General Methods: Moisture- and oxygen-sensitive reactions were conducted in oven-dried glassware under argon using dried solvents. Melting points are uncorrected. Due to the black color of several compounds some of the melting points (**23**−**25** and **28**) were determined by differential scanning calorimetry (DSC). Materials used for column chromatography: Neutral alumina (Merck), Celite (Fluka). ^{1}H NMR and ^{13}C NMR: Bruker Avance 300 (^{1}H at 300 MHz and ^{13}C at 75.47 MHz), Bruker Avance 500 (^{1}H at 500 MHz and ^{13}C at 125.77 MHz) using the residual solvent as internal standard. IR: Bruker Vector 22 FT-IR. UV/Vis: Hewlett Packard 8452 A spectrometer. MS (FAB+, EI+): High resolution: Jeol JMS-700. FD mass spectra refer to data from a Jeol JMS-700 instrument and were measured from dichloromethane solutions (c = 3−5 mg·mL^{-1}) of the corresponding complexes. For FD mass spectra no high resolution is possible. Elemental analyses were carried out by the Mikroanalytisches Laboratorium der Universität Heidelberg. The starting materials were prepared according to literature methods.[16−19]

General Procedure for the Preparation of the Bis(hexacarbonyldicobalt) Complexes from Cyclic Diynes: The cyclic diyne was dissolved in 30−50 mL of dichloromethane and the octacarbonyldicobalt was added in one portion. The reaction flask was wrapped with aluminium foil to exclude daylight. The resulting dark mixture was stirred at room temperature in the dark for 1−2 h. The crude mixture was filtered and stored at −78 °C overnight. In many cases crystals of the pure product could be obtained. In other cases, the crude product was absorbed on Celite and purified by column chromatography on neutral alumina (grade III), eluting with mixtures of light petroleum/diethyl ether.

(μ:μ-5,5,6,6-Tetramethyl-5,6-disila-1-thiacyclonona-3,7-diyne)bis(hexacarbonyldicobalt) (13): Starting materials: 5,5,6,6-tetramethyl-5,6-disila-1-thiacyclonona-3,7-diyne (250 mg, 1.10 mmol) and octacarbonyldicobalt (840 mg, 2.40 mmol). Yield: 727 mg (83%). Red solid, m.p. 104 °C (dec). ^{1}H NMR (500 MHz, C_6D_6): δ = 0.43 (br., 12 H, CH_3), 3.87 (br., 4 H, CH_2) ppm. ^{13}C NMR (125 MHz, C_6D_6): δ = 1.4 (CH_3), 40.1 (CH_2), 78.9 (C), 110.4 (C), 200.9 (CO) ppm. IR (KBr): $\tilde{\nu}$ = 2964, 2085, 2052, 2023, 1577, 1405 cm^{-1}. HRMS (FAB+): calcd. ($C_{22}H_{17}Co_4O_{12}SSi_2$) 796.7307; found 796.7300.

(μ:μ-1,1,3,3,6,6,8,8-Octamethyl-1,3,6,8-tetrasilacyclodeca-4,9-diyne)bis(hexacarbonyldicobalt) (14): Starting materials: 1,1,3,3,6,6,8,8-octamethyl-1,3,6,8-tetrasilacyclodeca-4,9-diyne (50 mg, 0.16 mmol) and octacarbonyldicobalt (220 mg, 0.65 mmol). Yield: 120 mg (85%). Dark red solid, m.p. 124 °C (dec). ^{1}H NMR (300 MHz, $CDCl_3$): δ = 0.38 (br., 28 H, CH_3/CH_2) ppm. ^{13}C NMR (75 MHz, $CDCl_3$): δ = 3.7 (CH_3), 5.8 (CH_2), 93.9 (C), 200.7 (CO) ppm. IR (KBr): $\tilde{\nu}$ = 2957, 2083, 2045, 2017, 1629, 1534, 1408 cm^{-1}. MS (FD+): m/z = 860 [M$^+$]. $C_{26}H_{28}Co_4O_{12}Si_4$ (880.6): calcd. C 35.46, H 3.21; found C 35.58, H 3.50.

(μ:μ-1,4-Dithiacyclotrideca-5,12-diyne)bis(hexacarbonyldicobalt) (15): Starting materials: 1,4-dithiacyclotrideca-5,12-diyne (210 mg, 1.00 mmol) and octacarbonyldicobalt (752 mg, 2.20 mmol). Yield: 590 mg (75%). Red solid, m.p. > 200 °C (dec). ^{1}H NMR (300 MHz, $CDCl_3$): δ = 1.72 (m, 4 H, CH_2), 3.10 (m, 10 H, CH_2) ppm. ^{13}C NMR (75 MHz, $CDCl_3$): δ = 27.1 (CH_2), 30.2 (CH_2), 33.9 (CH_2), 36.1 (CH_2), 91.6 (C), 100.4 (C), 199.0 (CO) ppm. IR (KBr): $\tilde{\nu}$ = 2936, 2089, 2050, 2023, 1625, 1432 cm^{-1}. UV/Vis (CH_2Cl_2): λ_{max} (log ε) = 266 nm (4.55), 292 (4.41), 314 (4.29), 360 (3.68), 374 (3.61), 408 (3.41). MS (FD+): m/z = 782 [M$^+$]. $C_{23}H_{14}Co_4O_{12}S_2$ (782.2): calcd. C 35.32, H 1.80, S 8.20; found C 35.20, H 1.95, S 8.08.

(μ:μ-1,5-Dithiacyclotetradeca-6,13-diyne)bis(hexacarbonyldicobalt) (16): Starting materials: 1,5-dithiacyclotetradeca-6,13-diyne (224 mg, 1.00 mmol) and octacarbonyldicobalt (752 mg, 2.20 mmol). Yield: 610 mg (77%). Red solid, m.p. 125 °C. ^{1}H NMR (300 MHz, $CDCl_3$): δ = 1.70 (m, 8 H, CH_2), 1.92 (m, 4 H, CH_2), 3.21 (m, 4 H, CH_2) ppm. ^{13}C NMR (75 MHz, $CDCl_3$): δ = 27.8 (CH_2), 32.0 (CH_2), 35.6 (CH_2), 35.8 (CH_2), 36.9 (CH_2), 94.2 (C), 102.3 (C), 199.2 (CO) ppm. IR (KBr): $\tilde{\nu}$ = 2936, 2088, 2050, 2022, 1625, 1432 cm^{-1}. UV/Vis (CH_2Cl_2): λ_{max} (log ε) = 286 nm (4.35), 318 (4.10), 352 (4.69). MS (FD+): m/z = 796 [M$^+$]. $C_{24}H_{16}Co_4O_{12}S_2 \cdot 0.5CH_2Cl_2$ (838.7): calcd. C 35.84, H 2.09; found C 35.68, H 2.14.

(μ:μ-1,6-Dithiacyclopentadeca-7,14-diyne)bis(hexacarbonyldicobalt) (17): Starting materials: 1,6-dithiacyclopentadeca-7,14-diyne

 © 2004 Wiley-VCH Verlag GmbH & Co. KGaA, Weinheim

(238 mg, 1.00 mmol) and octacarbonyldicobalt (752 mg, 2.20 mmol). Yield: 560 mg (69%). Red solid, m.p. 77 °C. ^{1}H NMR (300 MHz, $CDCl_3$): δ = 1.83 (m, 10 H, CH_2), 1.92 (m, 4 H, CH_2), 3.14 (m, 4 H, CH_2) ppm. ^{13}C NMR (75 MHz, $CDCl_3$): δ = 28.2 (CH_2), 28.8 (CH_2), 31.2 (CH_2), 33.2 (CH_2), 35.2 (CH_2), 94.7 (C), 101.7 (C), 199.4 (CO) ppm. IR (KBr): $\tilde{\nu}$ = 2929, 2086, 2047, 2019, 1628 cm^{-1}. UV/Vis (CH_2Cl_2): λ_{max} (log ε) = 294 nm (4.14), 324 (3.99). HRMS (EI+, 70 eV): calcd. ($C_{25}H_{18}Co_4O_{12}S_2$) 809.7568; found 809.7505.

(μ:μ-1,5-Dithiacyclohexadeca-6,15-diyne)bis(hexacarbonyldicobalt) (18): Starting materials: 1,5-dithiacyclohexadeca-6,15-diyne (190 mg, 0.75 mmol) and octacarbonyldicobalt (567 mg, 1.66 mmol). Yield: 380 mg (62%). Red solid, m.p. 87 °C. ^{1}H NMR (300 MHz, $CDCl_3$): δ = 1.70 (m, 12 H, CH_2), 2.10 (m, 4 H, CH_2), 3.14 (m, 4 H, CH_2) ppm. ^{13}C NMR (75 MHz, $CDCl_3$): δ = 25.7 (CH_2), 28.7 (CH_2), 29.4 (CH_2), 31.8 (CH_2), 35.8 (CH_2), 96.2 (C), 103.1 (C), 199.4 (CO) ppm. IR (KBr): $\tilde{\nu}$ = 2927, 2087, 2048, 2020, 1628 cm^{-1}. UV/Vis (CH_2Cl_2): λ_{max} (log ε) = 258 nm (4.53), 294 (4.37), 320 (4.24). HRMS (EI+, 70 eV): calcd. ($C_{26}H_{20}Co_4O_{12}S_2$) 823.7724; found 823.7687.

(μ:μ-1,6-Dithiacycloheptadeca-7,16-diyne)bis(hexacarbonyldicobalt) (19): Starting materials: 1,6-dithiacycloheptadeca-7,16-diyne (266 mg, 1.00 mmol) and octacarbonyldicobalt (752 mg, 2.20 mmol). Yield: 590 mg (82%). Red solid, m.p. 94 °C. ^{1}H NMR (300 MHz, $CDCl_3$): δ = 1.61 (m, 6 H, CH_2), 1.90 (m, 8 H, CH_2), 3.00 (m, 4 H, CH_2) ppm. ^{13}C NMR (75 MHz, $CDCl_3$): δ = 28.8 (CH_2), 29.0 (CH_2), 31.6 (CH_2), 31.8 (CH_2), 35.0 (CH_2), 37.6 (CH_2), 97.4 (C), 103.3 (C), 199.4 (CO) ppm. IR (KBr): $\tilde{\nu}$ = 2931, 2086, 2048, 2017, 1631 cm^{-1}. UV/Vis (CH_2Cl_2): λ_{max} (log ε) = 262 nm (4.36), 288 (4.24), 318 (4.12), 406 (3.30). HRMS (EI+, 70 eV): calcd. ($C_{27}H_{23}Co_4O_{12}S_2$) 838.7959; found 838.7913.

(μ:μ-1,7-Dithiacyclooctadeca-8,17-diyne)bis(hexacarbonyldicobalt) (20): Starting materials: 1,7-dithiacyclooctadeca-8,17-diyne (281 mg, 1.00 mmol) and octacarbonyldicobalt (752 mg, 2.20 mmol). Yield: 670 mg (79%). Red solid, m.p. 115 °C. ^{1}H NMR (300 MHz, $CDCl_3$): δ = 1.70 (m, 8 H, CH_2), 1.93 (m, 8 H, CH_2), 2.05 (m, 4 H, CH_2), 2.91 (m, 4 H, CH_2) ppm. ^{13}C NMR (75 MHz, $CDCl_3$): δ = 25.4 (CH_2), 27.3 (CH_2), 29.2 (CH_2), 29.6 (CH_2), 31.9 (CH_2), 32.3 (CH_2), 37.2 (CH_2), 99.0 (C), 103.7 (C), 200.2 (CO) ppm. IR (KBr): $\tilde{\nu}$ = 2932, 2086, 2046, 2018, 1628, 1338 cm^{-1}. UV/Vis (CH_2Cl_2): λ_{max} (log ε) = 262 nm (4.27), 294 (4.13), 324 (4.03). MS (FD+): *m*/*z* = 852 [M$^+$]. $C_{28}H_{24}Co_4O_{12}S_2$ (852.4): calcd. C 39.46, H 2.84, S 7.52; found C 39.53, H 3.00, S 7.55.

(μ:μ-1,4-Diselenacyclotrideca-5,12-diyne)bis(hexacarbonyldicobalt) (21): Starting materials: 1,4-diselenacyclotrideca-5,12-diyne (306 mg, 1.00 mmol) and octacarbonyldicobalt (752 mg, 2.20 mmol). Yield: 540 mg (62%). Red solid, m.p. > 230 °C (dec). ^{1}H NMR (300 MHz, $CDCl_3$): δ = 1.80 (m, 6 H, CH_2), 3.12 (m, 4 H, CH_2), 3.44 (m, 4 H, CH_2) ppm. ^{13}C NMR (75 MHz, $CDCl_3$): δ = 27.3 (CH_2), 28.5 (CH_2), 30.4 (CH_2), 34.2 (CH_2), 80.1 (C), 102.2 (C), 199.1 (CO) ppm. IR (KBr): $\tilde{\nu}$ = 2936, 2088, 2050, 2018, 1625, 1154 cm^{-1}. UV/Vis (CH_2Cl_2): λ_{max} (log ε) = 270 nm (4.49), 316 (4.26), 366 (3.52), 424 (3.16). MS (FD+): *m*/*z* = 876 [M$^+$]. $C_{23}H_{14}Co_4O_{12}Se_2$ (876.0): calcd. C 31.53, H 1.61; found C 31.64, H 1.74.

(μ:μ-1,7-Diselenacyclooctadeca-8,17-diyne)bis(hexacarbonyldicobalt) (22): Starting materials: 1,7-diselenacyclooctadeca-8,17-diyne (374 mg, 1.00 mmol) and octacarbonyldicobalt (752 mg, 2.20 mmol). Yield: 590 mg (62%). Red solid, m.p. 105 °C. ^{1}H NMR (500 MHz, $CDCl_3$): δ = 1.80 (m, 16 H, CH_2), 3.00 (m, 8 H, CH_2) ppm. ^{13}C NMR (125 MHz, $CDCl_3$): δ = 26.9 (CH_2), 28.3 (CH_2), 29.7 (CH_2), 29.8 (CH_2), 31.4 (CH_2), 32.0 (CH_2), 35.7 (CH_2), 86.5 (C), 104.6 (C), 199.8 (CO) ppm. IR (KBr): $\tilde{\nu}$ = 2932, 2086, 2047, 2019, 1628, 1430 cm^{-1}. UV/Vis (CH_2Cl_2): λ_{max} (log ε) = 260 nm (4.47), 302 (4.27), 324 (4.23). HRMS (EI+, 70 eV): calcd. ($C_{28}H_{24}Co_4O_{12}Se_2$) 946.6857; found 946.6910.

(μ:μ-1,4,7,10-Tetrathiacyclododeca-2,8-diyne)bis(hexacarbonyldicobalt) (23): Starting materials: 1,4,7,10-tetrathiacyclododeca-2,8-diyne (150 mg, 0.64 mmol) and octacarbonyldicobalt (438 mg, 1.28 mmol). Yield: 293 mg (56%). Black solid, m.p. 173 °C (dec). ^{1}H NMR (300 MHz, $CDCl_3$): δ = 3.26 (s, 8 H, CH_2) ppm. ^{13}C NMR (75 MHz, $CDCl_3$): δ = 38.3 (CH_2), 96.3 (C), 198.0 (CO) ppm. IR (KBr): $\tilde{\nu}$ = 2092, 2058, 2026, 1627, 1258, 875 cm^{-1}. UV/Vis (CH_2Cl_2): λ_{max} (log ε): = 264 nm (4.57), 426 (3.48). MS (FD+): *m*/*z* = 804 [M$^+$]. $C_{20}H_8Co_4O_{12}S_4$ (804.3): calcd. C 29.87, H 1.00, S 15.95; found C 29.82, H 1.15, S 15.68.

(μ:μ-1,4,7,10-Tetrathiacyclotrideca-2,8-diyne)bis(hexacarbonyldicobalt) (24): Starting materials: 1,4,7,10-tetrathiacyclotrideca-2,8-diyne (138 mg, 0.61 mmol) and octacarbonyldicobalt (400 mg, 1.17 mmol). Yield: 173 mg (35%). Black solid, m.p. 172 °C (dec). ^{1}H NMR (300 MHz, $CDCl_3$): δ = 2.20 (br., 2 H, CH_2), 3.17 (s, 8 H, CH_2) ppm. ^{13}C NMR (75 MHz, $CDCl_3$): δ = 26.3 (CH_2), 35.5 (CH_2), 36.6 (CH_2), 94.5 (C), 97.2 (C), 198.3 (CO) ppm. IR (KBr): $\tilde{\nu}$ = 2926, 2091, 2057, 2027, 1699, 1627, 1409, 874 cm^{-1}. UV/Vis (CH_2Cl_2): λ_{max} (log ε) = 266 nm (4.60), 318 (4.29), 436 (3.60). MS (FD+): *m*/*z* = 818 [M$^+$]. $C_{21}H_{10}Co_4O_{12}S_4$ (818.3): calcd. C 30.82, H 1.23; found C 30.41, H 1.54.

(μ:μ-1,4,8,11-Tetrathiacyclotetradeca-2,9-diyne)bis(hexacarbonyldicobalt) (25): Starting materials: 1,4,8,11-tetrathiacyclotetradeca-2,9-diyne (150 mg, 0.58 mmol) and octacarbonyldicobalt (400 mg, 1.16 mmol). Yield: 221 mg (46%). Black solid, m.p. 165 °C (dec). ^{1}H NMR (300 MHz, $CDCl_3$): δ = 2.31 (br., 4 H, CH_2), 3.15 (s, 8 H, CH_2) ppm. ^{13}C NMR (75 MHz, $CDCl_3$): δ = 29.1 (CH_2), 36.1 (CH_2), 97.2 (C), 198.5 (CO) ppm. IR (KBr): $\tilde{\nu}$ = 2920, 2091, 2054, 2027, 1628, 1437, 876 cm^{-1}. UV/Vis (CH_2Cl_2): λ_{max} (log ε) = 276 nm (4.48), 320 (4.30), 422 (3.62). MS (FD+): *m*/*z* = 832 [M$^+$], 804 (M$^+$ − CO), 776 [M$^+$ − 2CO]. $C_{22}H_{12}Co_4O_{12}S_4$ (832.3): calcd. C 31.75, H 1.45; found C 31.37, H 1.80.

(μ:μ-1,4,9,12-Tetrathiacyclohexadeca-2,10-diyne)bis(hexacarbonyldicobalt) (26): Starting materials: 1,4,9,12-tetrathiacyclohexadeca-2,10-diyne (180 mg, 0.62 mmol) and octacarbonyldicobalt (430 mg, 1.26 mmol). Yield: 299 mg (56%). Black solid, m.p. 153 °C (dec). ^{1}H NMR (300 MHz, CD_2Cl_2): δ = 1.98 (br., 8 H, CH_2), 2.92 (br., 8 H, CH_2) ppm. ^{13}C NMR (75 MHz, CD_2Cl_2): δ = 30.3 (CH_2), 37.6 (CH_2), 98.7 (C), 206.1 (CO) ppm. IR (KBr): $\tilde{\nu}$ = 2934, 2093, 2040, 2013, 1636, 1416, 876 cm^{-1}. UV/Vis (CH_2Cl_2): λ_{max} (log ε) = 274 nm (4.43), 314 (4.30), 326 (4.25), 474 (3.73). MS (FD+): *m*/*z* = 860 [M$^+$]. $C_{24}H_{16}Co_4O_{12}S_4$ (860.4): calcd. C 33.50, H 1.87, S 14.91; found C 33.26, H 2.05, S 14.81.

(μ:μ-1,4,10,13-Tetrathiacyclooctadeca-2,11-diyne)bis(hexacarbonyldicobalt) (27): Starting materials: 1,4,10,13-tetrathiacyclooctadeca-2,11-diyne (180 mg, 0.57 mmol) and octacarbonyldicobalt (430 mg, 1.26 mmol). Yield: 235 mg (46%). Dark red solid, m.p. 168 °C (dec). ^{1}H NMR (300 MHz, CD_2Cl_2): δ = 1.67 (m, 4 H, CH_2), 1.89 (m, 8 H, CH_2), 2.97 (m, 8 H, CH_2) ppm. ^{13}C NMR (75 MHz, CD_2Cl_2): δ = 27.7 (CH_2), 29.7 (CH_2), 37.8 (CH_2), 98.9 (C), 199.2 (CO) ppm. IR (KBr): $\tilde{\nu}$ = 2923, 2089, 2051, 2028, 1636, 1434, 869 cm^{-1}. UV/Vis (CH_2Cl_2): λ_{max} (log ε) = 278 nm (4.48), 322 (4.33), 474 (3.52). MS (FD+): *m*/*z* = 888 [M$^+$]. $C_{26}H_{20}Co_4O_{12}S_4$ (888.4): calcd. C 35.15, H 2.27, S 14.44; found C 34.84, H 2.52, S 14.44.

 © 2004 Wiley-VCH Verlag GmbH & Co. KGaA, Weinheim

Table 4. Crystallographic data and details of the refinement procedure for **13**−**16** and **19**−**20**

	13	**14**	**15**	**16**	**19**	**20**
Empirical formula	$C_{22}H_{16}Co_4O_{12}SSi_2$	$C_{26}H_{28}Co_4O_{12}Si_4$	$C_{23}H_{14}Co_4O_{12}S_2$	$C_{24}H_{16}Co_4O_{12}S_2$	$C_{27}H_{22}Co_4O_{12}S_2$	$C_{28}H_{24}Co_4O_{12}S_2$
Formula mass [g/mol]	796.31	880.56	782.18	796.21	838.29	852.31
Crystal size [mm]	0.36 × 0.18 × 0.04	0.36 × 0.24 × 0.18	0.33 × 0.18 × 0.10	0.34 × 0.18 × 0.05	0.26 × 0.24 × 0.24	0.37 × 0.30 × 0.11
Crystal colour	red	red	red	red	red	red
Crystal shape	polyhedron	polyhedron	polyhedron	polyhedron	polyhedron	irregular
Crystal system	monoclinic	monoclinic	monoclinic	orthorhombic	orthorhombic	monoclinic
Space group	*C*2/*c*	$P2_1/n$	*C*2/*c*	*P*bca	*P*bca	$P2_1/c$
a [Å]	24.6657(4)	10.0976(1)	15.5282(3)	15.9396(1)	23.2823(2)	12.3900(2)
b [Å]	8.1164(1)	17.7572(2)	14.5913(1)	13.6356(2)	10.3609(1)	10.5220(1)
c [Å]	31.8073(5)	10.4170(1)	14.9780(2)	27.6465(4)	27.3080(1)	26.7455(3)
α [°]	90	90	90	90	90	90
β [°]	102.97(1)	96.821(1)	118.154(1)	90	90	101.023(1)
γ [°]	90	90	90	90	90	90
V [Å^3]	6205.36(16)	1854.60(3)	2992.13(7)	6008.86(13)	6587.39(9)	3422.42(7)
$D_{calcd.}$ [g/cm^3]	1.71	1.58	1.74	1.76	1.69	1.65
Z	8	2	4	8	8	4
h_{min}/h_{max}	−29/29	−13/13	−20/20	−20/20	−30/29	−15/16
k_{min}/k_{max}	−9/9	−23/23	−18/18	−17/17	−13/13	−13/13
l_{min}/l_{max}	−36/38	−13/13	−19/19	−35/35	−35/35	−34/34
μ [mm^{-1}]	2.30	1.94	2.38	2.37	2.16	2.08
$T_{min.}/T_{max.}$	0.73/0.92	0.59/0.75	0.51/0.80	0.50/0.89	0.60/0.62	0.51/0.80
Refl. collected	22172	18838	15393	59728	64315	33775
Refl. unique	5371	4221	3431	6885	7552	7785
Refl. observed	4333	3822	2331	4101	5594	5871
Parameter	374	212	226	398	406	415
R(*F*)	0.028	0.021	0.039	0.037	0.027	0.090
$R_w(F^2)$	0.062	0.053	0.087	0.057	0.055	0.231
S (Gof) on F^2	1.16	1.06	1.03	0.99	1.04	1.20
$(\Delta\rho)_{max}$ [e·Å^{-3}]	0.41	0.35	0.59	0.47	0.34	1.91
$(\Delta\rho)_{min}$ [e·Å^{-3}]	−0.34	−0.39	−0.39	−0.53	−0.33	−1.02

Table 5. Crystallographic data and details of the refinement procedure for **21**−**25′**

	21	**22**	**23**	**24′α**	**24′β**	**25′**
Empirical formula	$C_{23}H_{14}O_{12}Se_2Co_4$	$C_{28.5}H_{25}O_{12}Se_2Co_4Cl$	$C_{20}H_8O_{12}S_4Co_4$	$C_{19}H_{10}O_{10}S_4Co_4$	$C_{19}H_{10}O_{10}S_4Co_4$	$C_{20}H_{12}O_{10}S_4Co_4$
Formula mass [g/mol]	875.98	988.57	804.26	762.27	762.27	776.30
Crystal size [mm]	0.37 × 0.34 × 0.29	0.24 × 0.13 × 0.02	0.11 × 0.10 × 0.04	0.08 × 0.07 × 0.05	0.24 × 0.06 × 0.02	0.40 × 0.22 × 0.01
Crystal colour	red	red	black	black	brown	black
Crystal shape	irregular	irregular	plate	irregular	plate	irregular
Crystal system	monoclinic	monoclinic	monoclinic	orthorhombic	monoclinic	orthorhombic
Space group	$P2_1/c$	*C*2/*c*	$P2_1/c$	*Pbca*	$P2_1/n$	*P*bca
a [Å]	14.9883(2)	57.887(8)	14.023(2)	13.3108(11)	7.485(1)	13.1604(3)
b [Å]	13.9693(2)	7.713(1)	7.8014(9)	12.9832(11)	14.779(2)	13.1567(3)
c [Å]	15.6865(1)	16.260(2)	13.218(2)	14.6488(13)	34.588(5)	15.1823(3)
α [°]	90	90	90	90	90	90
β [°]	111.454(1)	105.369(3)	105.006(2)	90	91.293(3)	90
γ [°]	90	90	90	90	90	90
V [Å^3]	3056.81(6)	7000(2)	1396.7(3)	2531.6(4)	3825.2(9)	2628.78(10)
$D_{calcd.}$ [g/cm^3]	1.90	1.88	1.91	2.00	1.99	1.96
Z	4	8	2	4	6	4
h_{min}/h_{max}	−19/19	−52/49	−17/18	−10/17	−9/9	−15/15
k_{min}/k_{max}	−18/18	−7/7	−7/10	−17/17	−19/11	−15/15
l_{min}/l_{max}	−20/20	−9/14	−17/17	−19/19	−46/42	−17/17
μ [mm^{-1}]	4.57	4.08	2.69	2.96	2.94	2.85
$T_{min.}/T_{max.}$	0.28/0.35	0.44/0.92	0.76/0.92	0.80/0.87	0.54/0.94	0.86/1.00
Refl. collected	30553	8346	9908	17625	26709	19496
Refl. unique	7008	2745	3471	3156	9468	2085
Refl. observed	5236	2202	3171	3009	4877	1545
Parameter	370	289	197	189	514	172
R(*F*)	0.032	0.057	0.034	0.054	0.054	0.026
$R_w(F^2)$	0.067	0.136	0.081	0.104	0.092	0.052
S (Gof) on F^2	1.01	1.04	1.09	1.34	0.86	1.02
$(\Delta\rho)_{max}$ [e·Å^{-3}]	1.55	0.84	1.13	0.62	1.13	0.33
$(\Delta\rho)_{min}$ [e·Å^{-3}]	−1.06	−0.73	−0.37	−0.68	−1.30	−0.31

 © 2004 Wiley-VCH Verlag GmbH & Co. KGaA, Weinheim

Table 6. Crystallographic data and details of the refinement procedure for **26**−**30**

	26	**27**	**28**	**29′**	**30**
Empirical formula	$C_{24}H_{16}O_{12}S_4Co_4$	$C_{26}H_{20}O_{12}S_4Co_4$	$C_{28}H_{24}O_{12}S_4Co_4$	$C_{19}H_{10}O_{10}Se_4Co_4$	$C_{24}H_{16}O_{12}Se_4Co_4$
Formula mass [g/mol]	860.37	888.42	916.48	949.85	1047.95
Crystal size [mm]	0.15 × 0.12 × 0.07	0.35 × 0.05 × 0.04	0.40 × 0.29 × 0.03	0.22 × 0.16 × 0.02	0.09 × 0.06 × 0.03
Crystal colour	black	black	black	black	dark red
Crystal shape	plate	polyhedron	plate	polyhedron	irregular
Crystal system	monoclinic	monoclinic	monoclinic	orthorhombic	monoclinic
Space group	$P2_1/c$	$P2_1/n$	$P2_1/c$	$Pbca$	$P2_1/n$
a [Å]	14.195(3)	7.9853(2)	11.6804(4)	13.3071(1)	14.08(1)
b [Å]	7.7600(2)	14.8038(3)	10.7416(4)	13.0699(2)	7.849(6)
c [Å]	15.668(3)	14.1503(3)	15.3996(6)	15.5527(1)	16.21(1)
α [°]	90	90	90	90	90
β [°]	109.752(4)	93.360(1)	111.015(1)	90	115.44(1)
γ [°]	90	90	90	90	90
V [Å^3]	1624.3(6)	1669.87(6)	1803.62(12)	2704.96(5)	1617(2)
$D_{calcd.}$ [g/cm^3]	1.76	1.77	1.69	2.33	2.15
Z	2	2	2	4	2
h_{min}/h_{max}	−18/18	−9/9	−15/15	−17/17	−18/17
k_{min}/k_{max}	−9/10	−18/18	−13/13	−16/16	−10/7
l_{min}/l_{max}	−20/18	−17/17	−19/19	−20/20	−21/17
μ [mm^{-1}]	2.32	2.26	2.10	7.84	6.58
$T_{max.}/T_{min.}$	0.72/0.85	0.51/0.92	0.49/0.94	0.58/1.00	0.59/0.83
Refl. collected	11295	15733	18132	26329	11595
Refl. unique	4054	3395	4133	3098	4036
Refl. observed	3377	2436	3116	2339	3054
Parameter	247	208	226	181	217
$R(F)$	0.053	0.033	0.028	0.032	0.045
$R_w(F^2)$	0.128	0.062	0.057	0.056	0.089
S (Gof) on F^2	1.08	1.01	1.03	1.12	1.07
$(\Delta\rho)_{max}$ [e·Å^{-3}]	0.73	0.37	0.38	0.75	1.12
$(\Delta\rho)_{min}$ [e·Å^{-3}]	−0.32	−0.36	−0.38	−0.76	−1.95

(μ:μ-1,4,11,14-Tetrathiacycloeicosa-2,12-diyne)bis(hexacarbonyldicobalt) (28): Starting materials: 1,4,11,14-tetrathiacycloeicosa-2,12-diyne (307 mg, 0.89 mmol) and octacarbonyldicobalt (610 mg, 1.78 mmol). Yield: 421 mg (52%). Black solid, m.p. 138 °C (dec). ^{1}H NMR (300 MHz, $CDCl_3$): δ = 1.55 (br., 8 H, CH_2), 1.86 (br., 8 H, CH_2), 2.95 (br., 8 H, CH_2) ppm. ^{13}C NMR (75 MHz, $CDCl_3$): δ = 28.1 (CH_2), 29.2 (CH_2), 37.6 (CH_2), 99.3 (C), 198.7 (CO) ppm. IR (KBr): $\tilde{\nu}$ = 2931, 2857, 2087, 2049, 2026, 1637, 1458, 870 cm^{-1}. UV/Vis (CH_2Cl_2): λ_{max} (log ε) = 280 nm (4.29), 318 (4.15), 472 (3.38), 556 (3.02). MS (FD+): m/z = 916 [M$^+$]. $C_{28}H_{24}Co_4O_{12}S_4$ (916.5): calcd. C 36.70, H 2.64, S 14.00; found C 36.51, H 2.94, S 13.99.

(μ:μ-1,4,7,10-Tetraselenacyclotrideca-2,8-diyne)bis(pentacarbonyldicobalt) (29′): Starting materials: 1,4,7,10-tetraselenacyclotrideca-2,8-diyne (102 mg, 0.24 mmol) and octacarbonyldicobalt (160 mg, 0.48 mmol). Yield: 143 mg (63%). Black solid, m.p. 144 °C (dec). ^{13}C NMR (75 MHz, $CDCl_3$): δ = 24.2 (CH_2), 27.3 (CH_2), 28.7 (CH_2), 31.2 (CH_2), 32.9 (CH_2), 208.1 (CO) ppm. IR (KBr): $\tilde{\nu}$ = 2924, 2056, 2016, 1621, 1404, 803 cm^{-1}. UV/Vis (CH_2Cl_2): λ_{max} [nm] (log ε): 304 (4.25), 348 (4.09), 448 (3.75), 490 (3.58). MS (FD+): m/z = 950 [M$^+$].

(μ:μ-1,4,9,12-Tetraselenacyclohexadeca-2,10-diyne)bis(hexacarbonyldicobalt) (30): Starting materials: 1,4,9,12-tetraselenacyclohexadeca-2,10-diyne (150 mg, 0.32 mmol) and octacarbonyldicobalt (219 mg, 0.64 mmol). Yield: 110 mg (33%). Black solid, m.p. 147 °C (dec). ^{1}H NMR (300 MHz, CD_2Cl_2): δ = 2.05 (br., 8 H, CH_2), 3.02 (br., 8 H, CH_2) ppm. ^{13}C NMR (75 MHz, CD_2Cl_2): δ = 31.0 (CH_2), 32.4 (CH_2), 105.1 (C), 206.7 (CO) ppm. IR (KBr): $\tilde{\nu}$ = 2929, 2090, 2053, 2037, 2011, 1637, 1413, 1200 cm^{-1}. UV/Vis (CH_2Cl_2): λ_{max} (log ε): 250 nm (4.25), 276 (3.91), 306 (4.04), 482 (3.44). MS (FD+): m/z = 1047 [M$^+$]. $C_{24}H_{16}Co_4O_{12}Se_4$ (1047.9): calcd. C 27.51, H 1.54; found C 26.95, H 1.68.

X-ray Diffraction Analyses: The reflections were collected with Bruker Smart CCD and Bruker APEX diffractometers (Mo-K_α radiation, graphite monochromator). Intensities were corrected for Lorentz and polarization effects. Numerical (face indexing for **23**) or empirical absorption corrections were applied using SADABS.[20] The structures were solved by direct methods. The structural parameters of the non-hydrogen atoms were refined anisotropically (except the carbon atoms of **22**) according to a full-matrix least-squares technique (F^2). The hydrogen atoms were calculated according to stereochemical aspects. In **15** we found disorder between the sulfur atoms and the methylene units by a C_2 axis. In **24′α**, **24′β** (two different modifications of **24′**) and **29′** we found disorder between the ethane and the propane chain by an inversion center. In **16**, **26**, **28** and **30** we found some disorder in the alkane chains, and the minor positions were refined as isotropic only. Structure solution and refinement were carried out with SHELXTL software package.[20] ORTEP drawings were obtained using the ORTEP-3 for Windows program by Farrugia.[21] Tables 4, 5 and 6 contain the crystallographic data and details of the data collection and the refinement procedure. CCDC-223985 to -224001 contain the supplementary crystallographic data for this paper. These data can be obtained free of charge at www.ccdc.cam.ac.uk/conts/retrieving.html [or from the Cambridge Crystallographic Data Centre, 12 Union Road, Cambridge CB2 1EZ, UK; Fax: (internat.) + 44-1223/336-033; E-mail: data.request@ccdc.cam.ac.uk].

Acknowledgments

We are grateful to the Deutsche Forschungsgemeinschaft (SFB 623), the Fonds der Chemischen Industrie and the BASF Aktienge-

sellschaft, Ludwigshafen, for financial support. D. B. W. and J. H. S. thank Michela Doria, Mathias Basler, Markus Seitz and Fanny Caroline Liu for preparative assistance. D. B. W. is grateful to the Studienstiftung des deutschen Volkes for a graduate fellowship. We thank Prof. W. Siebert for helpful discussions.

[1] I. U. Khand, G. R. Knox, P. L. Pauson, W. E. Watts, *J. Chem. Soc., Chem. Commun.* **1971**, 36.
[2] I. U. Khand, G. R. Knox, P. L. Pauson, W. E. Watts, *J. Chem. Soc., Perkin Trans. 1* **1973**, 975−977.
[3] P. L. Pauson, *Tetrahedron* **1985**, *41*, 5855−5860.
[4] [4a] O. Geis, H.-G. Schmalz, *Angew. Chem.* **1998**, *110*, 955−958; *Angew. Chem. Int. Ed.* **1998**, *37*, 911−915. [4b] A. J. Fletcher, S. D. R. Christie, *J. Chem. Soc., Perkin Trans. 1* **2000**, 1657−1668.
[5] [5a] K. M. Brummond, J. L. Kent, *Tetrahedron* **2000**, *56*, 3263−3283. [5b] T. Sugihara, M. Yamaguchi, M. Nishizawa, *Chem. Eur. J.* **2001**, *8*, 1589−1595.
[6] [6a] P. L. Pauson, in *Organometallics in Organic Synthesis* (Eds.: A. de Meijere, H. tom Dieck), Springer, Berlin **1988**, pp. 233−246. [6b] N. E. Schore, in *Comprehensive Organic Synthesis* (Ed.: B. M. Trost), Pergamon, Oxford **1991**, vol. 5, pp. 1037−1062. [6c]N. E. Schore, *Org. React.* **1991**, *40*, 1−90. [6d] N. E. Schore, in *Comprehensive Organometallic Chemistry II* (Eds.: E. W. Abel, F. G. A. Stone, G. Wilkinson), Pergamon, Oxford **1995**, vol. 12, pp. 703−739.
[7] [7a] F. A. Cotton, J. D. Jamerson, B. R. Stults, *J. Am. Chem. Soc.* **1976**, *98*, 1774−1779. [7b] F. Baert, A. Guelzim, J. M. Poblet, R. Wiest, J. Demuynck, M. Benard, *Inorg. Chem.* **1986**, *25*, 1830−1841. [7c] W. G. Sly, *J. Am. Chem. Soc.* **1959**, *81*, 18−20. [7d] N. A. Bailey, R. Mason, *J. Chem. Soc. (A)* **1968**, 1293−1299. [7e] D. Gregson, J. A. K. Howard, *Acta Crystallogr., Sect. C* **1983**, *39*, 1024−1027.
[8] [8a] M. Gruselle, B. Malezieux, J. Vaissermann, H. Amouri, *Organometallics* **1998**, *17*, 2337−2343. [8b] S. J. Doig, R. P. Hughes, R. E. Davis, S. M. Gadol, K. D. Holland, *Organometallics* **1984**, *3*, 1921−1922. [8c] M. Saha, S. Muchmore, D. van der Helm, K. M. Nicholas, *J. Org. Chem.* **1986**, *51*, 1960−1966. [8d] M. I. Bruce, B. C. Hall, B. D. Kelly, P. J. Low, B. W. Skelton, A. H. White, *J. Chem. Soc., Dalton Trans.* **1999**, 3719−3728. [8e] M. I. Bruce, B. D. Kelly, B. W. Skelton, A. H. White, *J. Organomet. Chem.* **2000**, *604*, 150−156. [8f] X. Verdaguer, A. Moyano, M. A. Pericàs, A. Riera, A. Alvarez-Larena, J.-F. Pinella, *Organometallics* **1999**, *18*, 4275−4285. [8g] M. A. Brook, J. Urschey, M. Stradiotto, *Organometallics* **1998**, *17*, 5342−5346. [8h] A. M. Montana, K. M. Nicholas, M. A. Khan, *J. Org. Chem.* **1988**, *53*, 5193−5201. [8i] J. Ju, B. R. Reddy, M. Khan, K. M. Nicholas, *J. Org. Chem.* **1989**, *54*, 5426−5428. [8j] A. Gelling, J. C. Jefferey, D. C. Povey, M. J. Went, *J. Chem. Soc., Chem. Commun.* **1991**, 349−351. [8k] B. Happ, T. Bartik, C. Zucchi, M. C. Rossi, F. Ghelfi, G. Palyi, G. Varadi, G. Szalontai, I. T. Horvath, A. Chiesi-Villa, C. Guastini, *Organometallics* **1995**, *14*, 809−819. [8l] B. J. Rausch, R. Gleiter, F. Rominger, *J. Chem. Soc., Dalton Trans.* **2002**, 2219−2226. [8m] J. H. Schulte, R. Gleiter, F. Rominger, *Org. Lett.* **2002**, *4*, 3301−3304. [8n] C. M. Gordon, M. Kiszka, I. R. Dunkin, W. J. Kerr, J. S. Scott, J. Gebicki, *J. Organomet. Chem.* **1998**, *554*, 147−154.
[9] [9a] B. J. Rausch, R. Gleiter, *Tetrahedron Lett.* **2001**, *42*, 1651−1653. [9b] F. Antras, M. Ahmar, B. Cazes, *Tetrahedron Lett.* **2001**, *42*, 8157−8160. [9c] M. E. Krafft, R. H. Romero, I. L. Scott, *Synlett* **1995**, 577−578. [9d] X. Verdaguer, J. Vázquez, G. Fuster, V. Bernardes-Génisson, A. E. Greene, A. Moyano, M. A. Pericàs, A. Riera, *J. Org. Chem.* **1998**, *63*, 7037−7052.
[10] [10a] J. G. Donkervoort, A. R. Gordon, C. Johnstone, W. J. Kerr, U. Lange, *Tetrahedron* **1996**, *52*, 7391−7420. [10b] N. Jeong, S. H. Hwang, *Angew. Chem.* **2000**, *112*, 650−652; *Angew. Chem. Int. Ed.* **2000**, *39*, 636−638. [10c] B. J. Rausch, H. Becker, R. Gleiter, F. Rominger, *Synlett* **2002**, 723−726.
[11] [11a] F. Robert, A. Milet, Y. Gimbert, D. Konya, A. E. Greene, *J. Am. Chem. Soc.* **2001**, *123*, 5396−5400. [11b] T. J. M. de Bruin, A. Milet, F. Robert, Y. Gimbert, A. E. Greene, *J. Am. Chem. Soc.* **2001**, *123*, 7184−7185. [11c] M. Yamanaka, E. Nakamura, *J. Am. Chem. Soc.* **2001**, *123*, 1703−1708.
[12] [12a] Y. K. Chung, *Coord. Chem. Rev.* **1999**, *188*, 297−341. [12b] K. M. Brummond, J. L. Kent, *Tetrahedron* **2000**, *56*, 3263−3283. [12c] I. Marchueta, E. Montenegro, D. Panov, M. Poch, X. Verdaguer, A. Moyano, M. A. Pericàs, A. Riera, *J. Org. Chem.* **2001**, *66*, 6400−6409. [12d] S. T. Ingate, J. Marco-Contelles, *Org. Prep. Proceed. Int.* **1998**, *30*, 121−143. [12e] M. A. Pericàs, J. Balsells, J. Castro, I. Marchueta, A. Moyano, A. Riera, J. Vázquez, X. Verdaguer, *Pure Appl. Chem.* **2002**, *74*, 167−174.
[13] [13a] M. E. Krafft, J. A. Juliano, I. L. Scott, C. Wright, M. D. McEachin, *J. Am. Chem. Soc.* **1991**, *113*, 1693−1703. [13b] T. Sugihara, M. Yamada, M. Yamaguchi, M. Nishizawa, *Synlett* **1999**, 771−773.
[14] M. E. Krafft, I. L. Scott, R. H. Romero, S. Feibelmannn, C. E. van Pelt, *J. Am. Chem. Soc.* **1993**, *115*, 7199−7207.
[15] J. E. Davies, L. J. Hope-Weeks, M. J. Mays, P. R. Raithby, *Chem. Commun.* **2000**, 1411−1412.
[16] [16a] E. Kloster-Jensen, G. Aamdal Eliassen, *Angew. Chem.* **1985**, *97*, 587−588; *Angew. Chem. Int. Ed. Engl.* **1985**, *24*, 565−566. [16b] R. Gleiter, J. Classen, B. J. Rausch, T. Oeser, F. Rominger, *J. Organomet. Chem.* **2002**, *641*, 3−8.
[17] C. Benisch, S. Bethke, R. Gleiter, T. Oeser, H. Pritzkow, F. Rominger, *Eur. J. Org. Chem.* **2000**, 2479−2488.
[18] D. B. Werz, R. Gleiter, F. Rominger, *J. Org. Chem.* **2002**, *67*, 4290−4297.
[19] J. H. Schulte, D. B. Werz, F. Rominger, R. Gleiter, *Org. Biomol. Chem.* **2003**, *1*, 2788−2794.
[20] G. M. Sheldrick, Bruker Analytical X-ray Division, Madison, WI, **1997**.
[21] ORTEP-3 for Windows: A Version of ORTEP-III with a Graphical User Interface (GUI): L. J. Farrugia, *J. Appl. Crystallogr.* **1997**, *30*, 565.

Received November 24, 2003
Early View Article
Published Online April 26, 2004

 © 2004 Wiley-VCH Verlag GmbH & Co. KGaA, Weinheim

EurJIC
European Journal of Inorganic Chemistry

Issue 13/2004

Pages 2595–2796

Papers available ahead of print in Early View at www.interscience.wiley.com

Earliest available Table of Contents:
Automatically, free of charge by e-mail through
www.interscience.wiley.com/alerts

COVER PICTURE

The cover picture shows the molecular structure of a (1,3-diboryl-2,4-diphenylcyclobutadiene)(cyclopentadienyl)cobalt complex obtained in an attempt to trimerize 1-(dithiocatecholboryl)-2-phenylacetylene with $CpCo(CO)_2$. Details are discussed in the article by W. Siebert et al. on p. 2635 ff.

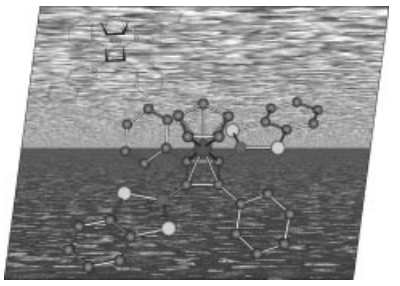

MICROREVIEW

Contents

2609 **R. Schmid, K. Kirchner***

Ruthenium-Mediated C–C Coupling Reactions of Alkynes – The Key Role of Ruthenacyclopentatriene Complexes

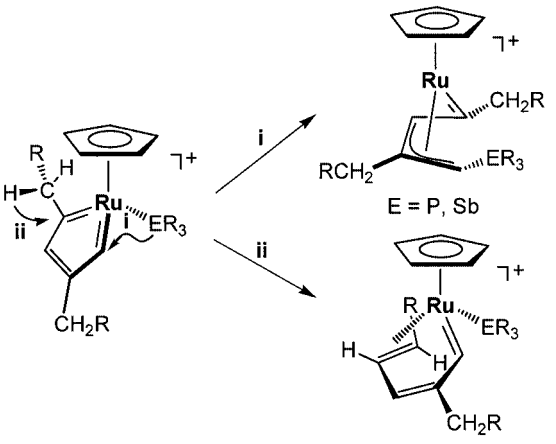

Keywords: Ruthenium / Cyclopentadienyl Ligands / Acetylenes / Oxidative coupling / Carbenes / Vinylidene ligands

 © 2004 Wiley-VCH Verlag GmbH & Co. KGaA, Weinheim

SHORT COMMUNICATIONS

2627 **M. Kontturi,* S. Peräniemi, J. J. Vepsäläinen, M. Ahlgrén**

A Structural Study of Bisphosphonate Metal Complexes − Three New Polymeric Structures of the Calcium Complex of Clodronic Acid

Keywords: Bisphosphonate / Clodronate / Calcium / Layered compounds / X-ray diffraction

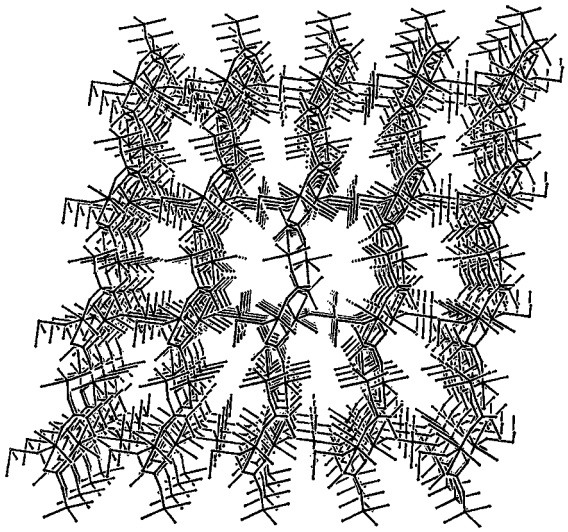

2632 **H. Suzuki, M. Hashimoto,* S. Okeya**

Synthesis and Crystal Structure of $Cs_2(CN_3H_6)_3$-$[(C_2H_5)_2NH_2][W_7O_{22}(O_2)_2]\cdot 3H_2O$

Keywords: Polyoxometallates / Peroxoisopolytungstates / Clathrates / Crystal structures

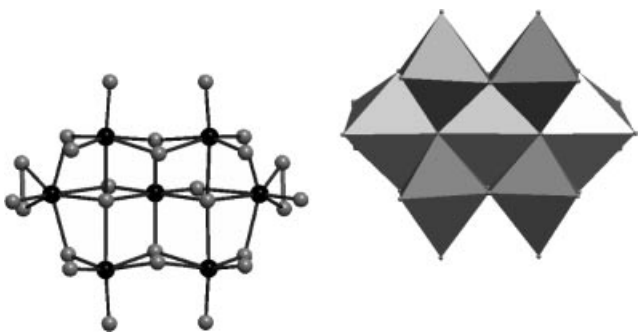

FULL PAPERS

2635 **A. Goswami, C.-J. Maier, H. Pritzkow, W. Siebert***

Cobalt-Mediated Cyclooligomerization Reactions of Borylacetylenes

Keywords: Boranes / Catalysts / (Cyclobutadiene)cobalt complexes / Mono(boryl)acetylenes / Triborylbenzenes

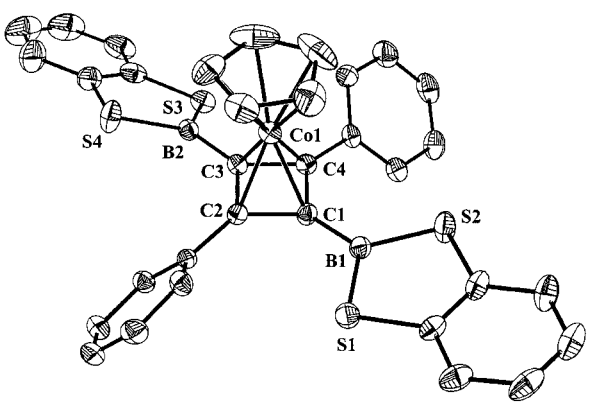

2646 **M. N. Jayaswal, H. N. Peindy, F. Guyon,* M. Knorr,* N. Avarvari, M. Fourmigué**

Novel Bonding Modes between Tetrathiafulvalenes (TTFs) and Transition Metal Centers: π-Bonding and Covalent $TTFSiMe_2-ML_n$ Coordination to Platinum

Keywords: Platinum / Tetrathiafulvalene / pi interactions / Si ligands / X-ray diffraction

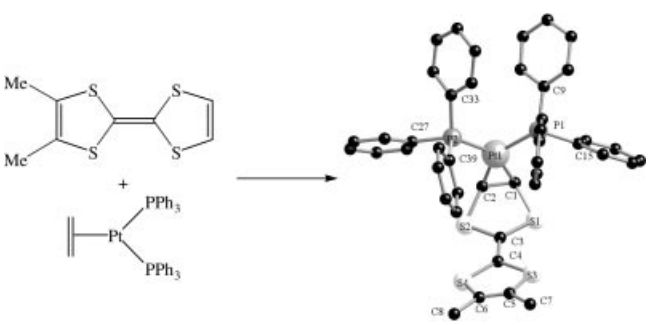

2652 **W. Zheng, M. J. Heeg, C. H. Winter***

Synthesis and Characterization of Potassium Complexes Containing Terminal η^2-Pyrazolato Ligands

Keywords: Hydrogen bonds / N ligands / Potassium / Pyrazolato ligands

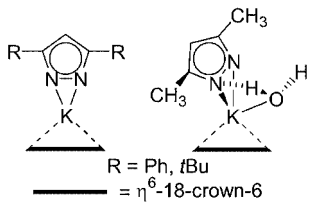

2658 **D. Sturmayr, U. Schubert***

DFT Calculations on the C−Cl/Si−H Exchange Catalyzed by *P*,*N*-Chelated Pt^{II} Complexes

Keywords: Chlorinated hydrocarbons / Hemilabile ligands / Oxidative addition / Reductive elimination / Silanes

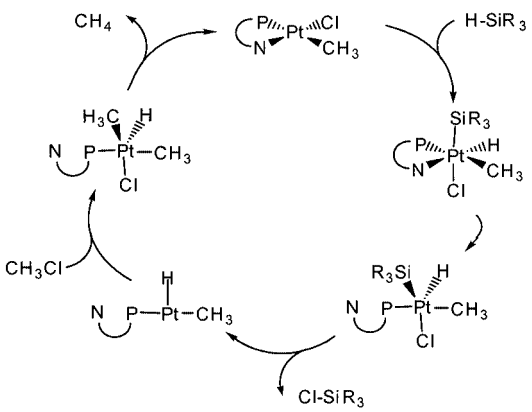

2662 **M. P. Coles,* P. B. Hitchcock**

Zinc Guanidinate Complexes and Their Application in Ring-Opening Polymerisation Catalysis

Keywords: Guanidinate / N ligands / O ligands / Ring-opening polymerisation / Zinc

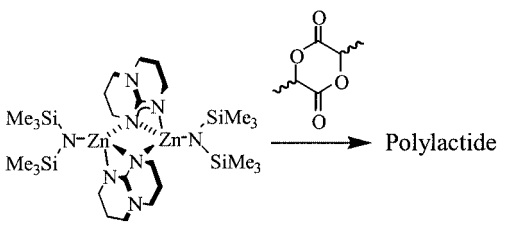

2673 **J. Chai, H. Zhu, Y. Peng, H. W. Roesky,* S. Singh, H.-G. Schmidt, M. Noltemeyer**

Synthesis and Structural Characterization of Monomeric Manganese(II) *N*-Heterocyclic Carbene Complexes $[MnX_2(C\{N(iPr)C(Me)\}_2)_2]$ (X = Cl, I, and MeCOO)

Keywords: Carbene ligands / Manganese / Halides / Acetate

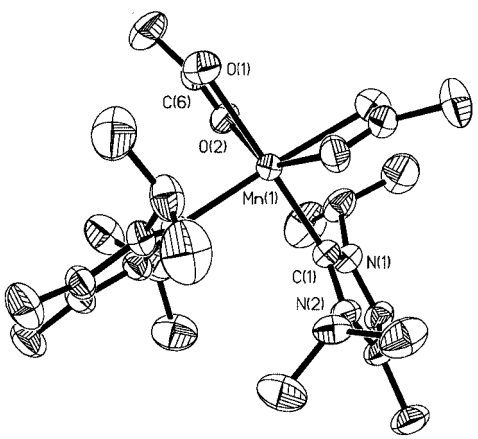

2678 **M. Gorol, N. C. Mösch-Zanetti, H. W. Roesky,* M. Noltemeyer, H.-G. Schmidt**

Synthesis of a Novel Organoiridium(I) Fluoro Complex

Keywords: Syntheses / Crystal structures / Iridium(I) / Fluoro complexes / Pentafluorosilicates

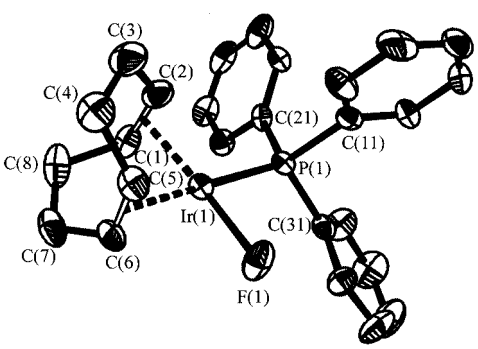

 © 2004 Wiley-VCH Verlag GmbH & Co. KGaA, Weinheim

2683 **T. Glaser,* I. Liratzis, T. Lügger, R. Fröhlich**

Synthesis and Characterization of Ti Complexes Using 4-*tert*-Butyl-2,6-bis(hydroxymethyl)phenol: X-ray Structures of a Confacial Bioctahedron with Terminal Nucleophilic Phenylmethoxide Ligands, and a Ti_4O_{16} Core Protected by Two Hydrophobic Binding Pockets

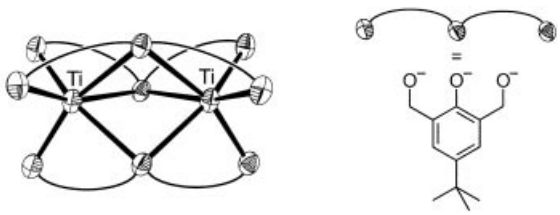

Keywords: Tridentate ligands / O ligands / Titanium

2690 **K. Burgemeister, D. Drewes, E. M. Limanski, I. Küper, B. Krebs***

Formation of Large Clusters in the Reaction of Lanthanide Cations with Heptamolybdate

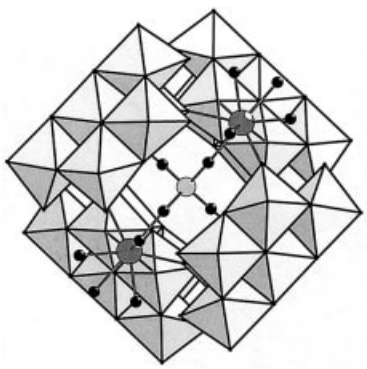

Keywords: Lanthanides / Molybdenum / Polyoxometalates / Structural analysis

2695 **B. Wu, D. Yuan, F. Jiang, R. Wang, L. Han, Y. Zhou, M. Hong***

Metal-Directed Self-Assembly: Two New Metal-Binicotinate Grid Polymeric Networks and Their Fluorescence Emission Tuned by Ligand Configuration

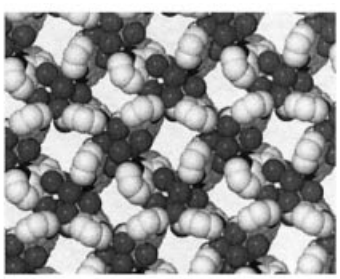

Keywords: Self-assembly / Binicotinic acid / Fluorescence / Coordination polymer / Chirality

2701 **S. Di Bella,* G. Consiglio, N. Leonardi, S. Failla,* P. Finocchiaro, I. Fragalà**

Film Polymerization − A New Route to the Synthesis of Insoluble Polyimides Containing Functional Nickel(II) Schiff Base Units in the Main Chain

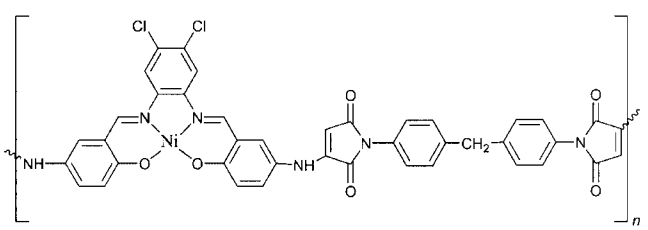

Keywords: Coordination polymer / Nickel / Film polymerization / Nonlinear optics

 © 2004 Wiley-VCH Verlag GmbH & Co. KGaA, Weinheim

2706 **J. L. Serrano,* I. J. S. Fairlamb,* G. Sánchez,* L. García, J. Pérez, J. Vives, G. López, C. M. Crawforth, R. J. K. Taylor**

Palladacyclopentadiene Complexes with Mono- and Didentate Imidato Ligands: Synthesis, Hemilabile Behaviour and Catalytic Application in the Stille Reaction

Keywords: Catalysis / Cross-coupling / N,O ligands / Palladium / Stille reactions

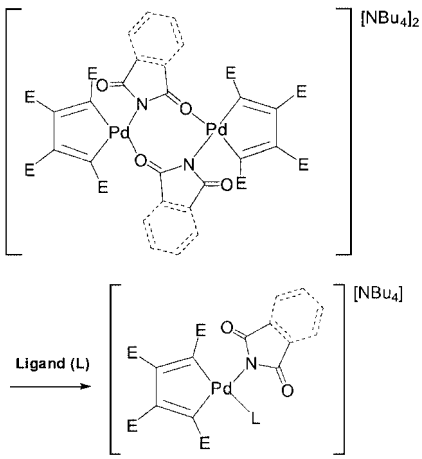

active catalysts for Stille cross-coupling of benzyl bromide with an organostannane

2716 **M. B. Meder, L. H. Gade***

Coordination Chemistry of 1,3-Bis(2-pyridylimino)- and 1,3-Bis(2-thiazolylimino)isoindole Copper Complexes: Investigation of Their Catalytic Behavior in Oxidation Reactions

Keywords: Copper / Allylic peroxylation / Coordination polymers / Radical reactions / Oxidation

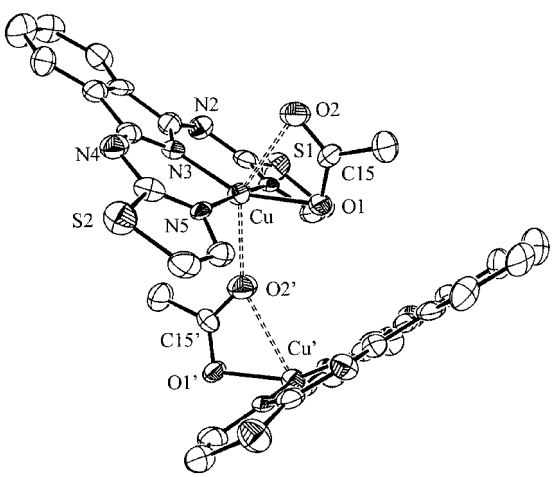

2723 **E. J. Padma Malar**

Can the *cyclo*-P_5 Ligand Introduce Basicity at the Transition Metal Center in Metallocenes? A Hybrid Density Functional Study on the *cyclo*-P_5 Analogues of Metallocenes of Fe, Ru and Os

Keywords: Basicity / Density functional calculations / Electronic structure / Metallocenes / Natural charge / Transition metals

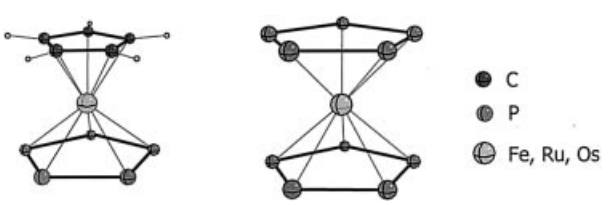

 © 2004 Wiley-VCH Verlag GmbH & Co. KGaA, Weinheim

2733 **F. Hussain, M. Reicke, U. Kortz***

The Hybrid Organic-Inorganic 2-D Material $(CsNa_2[\{Sn(CH_3)_2\}_3(H_2O)_4(\beta\text{-}XW_9O_{33})]\cdot 7H_2O)_\infty$ (X = As^{III}, Sb^{III}) and Its Solution Properties

Keywords: Hybrid materials / Organometallic compounds / Polyoxometalates / Self assembly / Tungsten

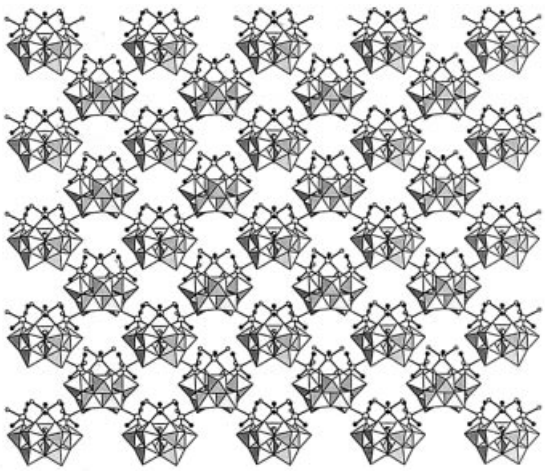

2739 **E. Vasca, G. Palladino, C. Manfredi, C. Fontanella, C. Sadun, R. Caminiti***

An Energy Dispersive X-ray Diffraction Study of Dioxouranium(VI) in 1 M Lithium Citrate

Keywords: X-ray Diffraction / Solution / Uranium / Lithium citrate

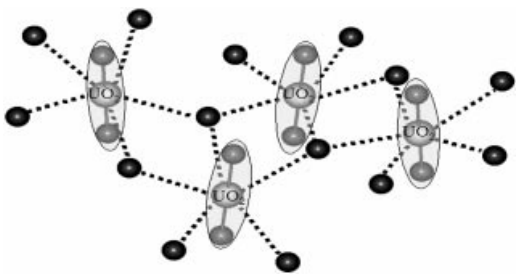

2747 **X. Li, Q. Shi, D. Sun, W. Bi, R. Cao***

Synthesis and Characterization of a Series of Lanthanide Complexes Constructed from Orotic Acid

Keywords: Lanthanides / O ligands / Polymers / Solvothermal synthesis

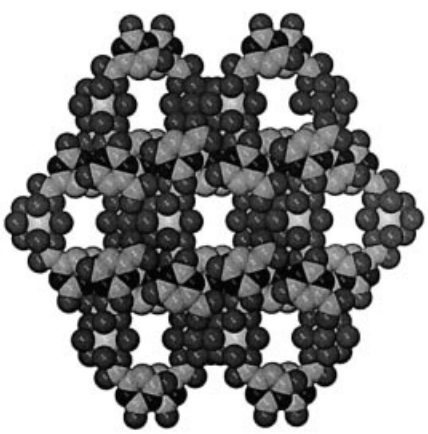

2754 **H. Zheng,* J. Zhou, M. F. Lappert, Y. Song, Y. Li, X. Xin**

Crystal Structure and Excited Optical Nonlinearity of a 1D Polymeric $[W_2O_2S_6Cu_4(NCMe)_4]_n$ Cluster

Keywords: Cluster compounds / Copper / Nonlinear optics / Polymers / Tungsten

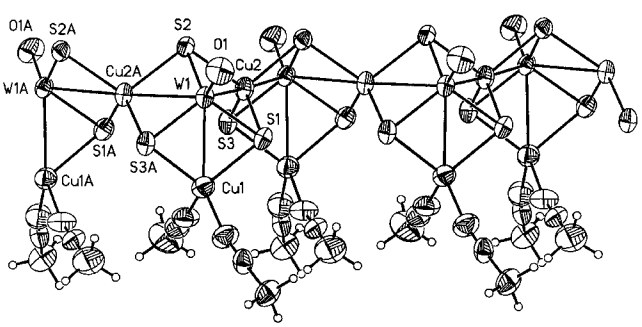

 © 2004 Wiley-VCH Verlag GmbH & Co. KGaA, Weinheim

2759 **F. A. Almeida Paz, F.-N. Shi, J. Klinowski, J. Rocha,* T. Trindade**

Synthesis and Characterisation of the First Three-Dimensional Mixed-Metal-Center Inorganic-Organic Hybrid Framework with *N*-(Phosphonomethyl)iminodiacetate

Keywords: Carboxylate ligands / Crystal engineering / Hydrothermal synthesis / N ligands / Organic-inorganic hybrid composites

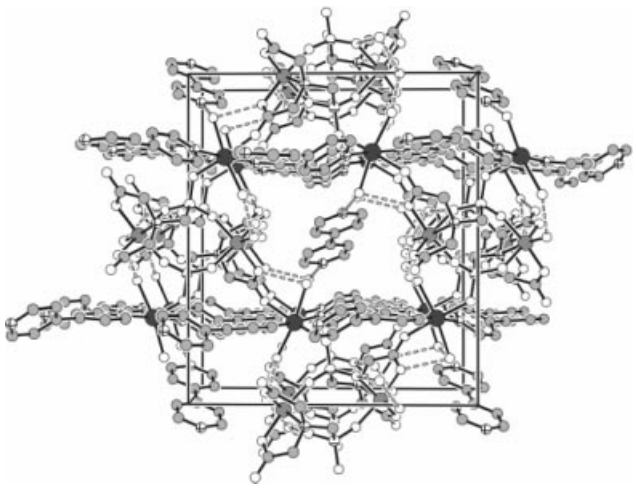

2769 **M. R. Bermejo,* M. I. Fernández, A. M. González-Noya, M. Maneiro, R. Pedrido, M. J. Rodríguez, M. Vázquez**

Chloride as Supramolecular Glue: Anion-Directed Assembly of a 2D Network of Mn^{III} Complexes

Keywords: Supramolecular chemistry / Manganese / Schiff bases / Hydrogen bond / Self-assembly

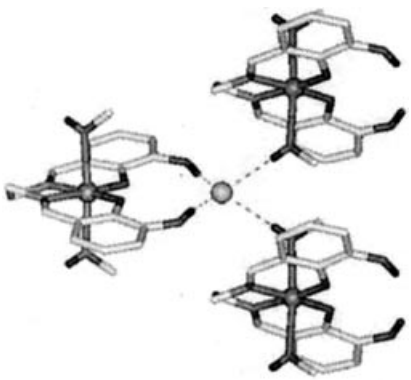

2775 **C. Ma,* J. Zhang, F. Li, R. Zhang**

Syntheses and Crystal Structures of Diorganotin Derivatives of 2,5-Dimercapto-1,3,4-thiadiazole

Keywords: Macrocyclic ligands / N ligands / Oxo ligands / S ligands / Tin

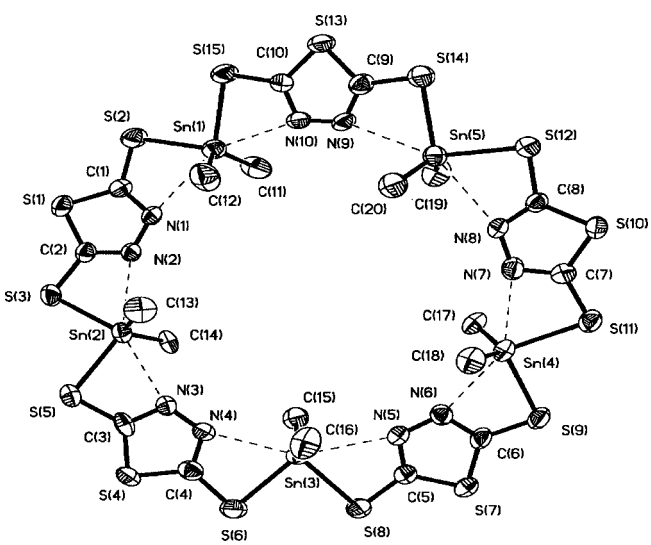

 © 2004 Wiley-VCH Verlag GmbH & Co. KGaA, Weinheim

2784 **A. Klein,* M. P. Feth,* M. Bertagnolli, S. Záliš**

On the Electronic Structure of Mesitylnickel Complexes of α-Diimines − Combining Structural Data, Spectroscopy and Calculations

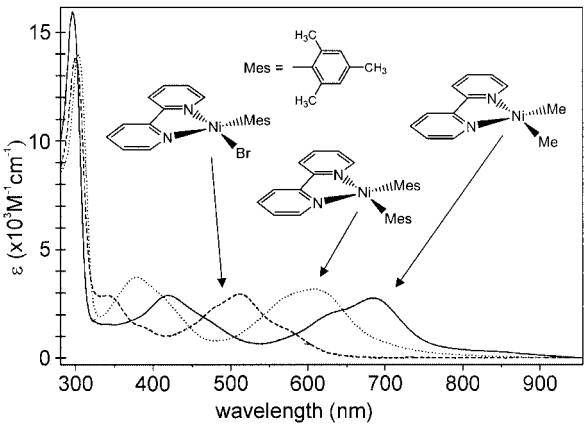

Keywords: Density functional calculations / Electronic structure / EXAFS / Nickel / Raman spectroscopy

 © 2004 Wiley-VCH Verlag GmbH & Co. KGaA, Weinheim

Ruthenium-Mediated C−C Coupling Reactions of Alkynes − The Key Role of Ruthenacyclopentatriene Complexes

Roland Schmid[a] and Karl Kirchner*[a]

Keywords: Ruthenium / Cyclopentadienyl Ligands / Acetylenes / Oxidative coupling / Carbenes / Vinylidene ligands

This review describes the highlights of the reactions of the substitutionally labile neutral pseudo 14VE complexes RuCp′(COD)Cl (Cp′ = Cp, Cp*; COD = 1,5-cyclooctadiene) and the cationic complexes $[CpRu(CH_3CN)_2L]^+$ and $[Ru(\eta^5\text{-}C_5H_4CH_2CH_2\text{-}\kappa^1P\text{-}PPh_2)]^+$ with alkynes. The ligand L is a co-ligand, whose nature turns out to be critical to the outcome of the reaction, and varies from halides to tertiary phosphanes, tertiary stibines, CO, and acetonitrile. Along these lines vast and diversified varieties of rearrangements within and between molecules ligated to the transition-metal center has been discovered. A crucial role in all reactions reported is the intermediacy of electrophilic ruthenacyclopentatriene complexes, an entity featuring a biscarbene functionality.

(© Wiley-VCH Verlag GmbH & Co. KGaA, 69451 Weinheim, Germany, 2004)

1. Introduction

Of the diverse elemental combinations, carbon−carbon bond-forming reactions have attracted great interest for their many applications in industrial and synthetic processes. This type of conversion is catalyzed mainly by transition-metal compounds. The basis of the catalytic action is the remarkable ability of transition-metal containing fragments to coordinate organic molecules. Besides the fascinating world of the structural chemistry of these complexes thus generated, a crucial consequence is the essential modification of the chemical behavior through ligation. In fact, some of the most powerful and selective methods for preparing organic molecules involve organometallic catalysis. Specifically of interest to our group are C−C and C−heteroatom bond-forming reactions involving alkynes, such as the cyclotrimerization of alkynes or the cyclocotrimerization of two alkynes with unsaturated organic compounds containing C=X bonds (X = C, O, S, N etc.) for obtaining carbocycle and heterocycle structures as exemplarily shown in Scheme 1.

The development of cyclization methods is a continuing challenge because of the ubiquitous occurrence of cyclic structures, especially among bioactive targets. For instance, the vast majority of pharmaceuticals in use today contain either one or two 5- or 6-membered rings. Among the wide range of transition-metal compounds that were found to actively catalyze cyclizations we have focused particularly on the ruthenium chemistry. Lying at the heart of the periodic table, ruthenium combines the valuable properties of both early- and late-transition-metal relatives. Thus, the

[a] Institute of Applied Synthetic Chemistry, Vienna University of Technology,
Getreidemarkt 9, 1060 Vienna, Austria

Roland Schmid (1945−2004) was a full professor of chemistry at the Vienna University of Technology, Vienna, and Head of the Organometallic Chemistry Division. He studied chemistry at the Vienna University of Technology, where he obtained his Ph.D. in 1971 with Prof. Viktor Gutmann. Since 1999 he was full Professor at the Institute of Applied Synthetic chemistry at the Vienna University of Technology. He has authored and co-authored over 140 research and review papers and the book "Non-formal Kinetics − in Search for Chemical Reaction Pathways". His research and teaching interests focused on general and inorganic chemistry, inorganic reaction mechanisms, solution chemistry, and chemistry for mechanical engineering.

Karl Kirchner (born in 1960 in Wiener Neustadt, Austria) obtained his Ph.D in 1987 at the Vienna University of Technology under the supervision of Prof. Roland Schmid. After a two-year postdoctoral stay at Washington State University with Prof. John P. Hunt and an additional postdoctoral year with Nobellaureate Prof. Henry Taube at Stanford University, he joined the research group of Prof. Roland Schmid. He became an associate Professor in 1994 at the Vienna University of Technology. He has authored and co-authored more than 110 research and review papers His research interests are in the fields of coordination chemistry, organometallic chemistry, and homogeneous catalysis.

MICROREVIEWS: This feature introduces the readers to the authors′ research through a concise overview of the selected topic. Reference to important work from others in the field is included.

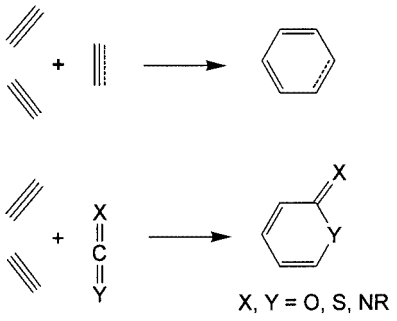

Scheme 1

high reactivity of elements to its left, and the less oxophilic and Lewis acidic nature of those to its right, results in a special array of desirable properties.[1] Accordingly, ruthenium is characterized by a high capacity of multiple metal bonding on the one hand and functional group tolerance on the other. For instance, even the formation of cyclic organosulfur compounds is mediated by appropriate ruthenium complexes,[2,3] while many other transition-metal centers are deactivated because of strong coordination to sulfur compounds.

The elucidation of the mechanistic aspects of homogeneous catalysis has been an ambitious scientific goal from the beginning of the interest in organometal catalysis. Unfortunately, kinetic studies in this field of research are scarce. One of the reasons is the fact that often the rates of the successive steps are too fast to be observed separately, and the diverse reaction intermediates are not stable enough to be characterized. Fortunately, due to the enormous progress in computational chemistry in the last several years, theoretical methods are playing an increasingly important role in identifying possible elementary reactions. These may be substitution, oxidative addition, reductive elimination, migratory insertion, hydrogen exchange, β-hydrogen transfer, σ-bond metathesis, and nucleophilic addition reactions.[4] Ultimately, one would like to understand these fundamental transformations to be able to monitor and tune changes in reactivity toward an obvious synthetic purpose. Thus it has become very useful for us to combine, whenever possible, experimental work with theoretical studies based on density functional theory (DFT) calculations.

In what follows we cover important results of our recent research in the context of work from others in the field. Specifically, we will describe the highlights of the reactions of the substitutionally labile neutral pseudo 14VE complexes RuCp′(COD)L (Cp′ = Cp, Cp*; COD = 1,5-cyclooctadiene; L = Cl, Br) and the cationic complexes $[CpRu(CH_3CN)_2L]^+$ and $[Ru(\eta^5\text{-}C_5H_4CH_2CH_2\text{-}\kappa^1P\text{-}PPh_2)(CH_3CN)_2]^+$ with various triple and double bonds. The ligand L is a co-ligand, whose nature turns out to be critical to the outcome of the reaction, and varies from halides to tertiary phosphanes, tertiary arsanes, tertiary stibines, CO, and acetonitrile (Scheme 2). Along these lines there are many diverse rearrangements within and between molecules ligated to the transition-metal center.

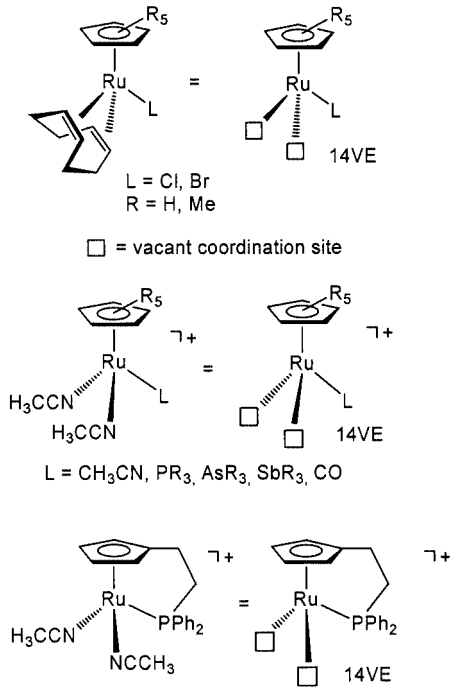

Scheme 2

2. The Cyclotrimerization of Alkynes Mediated by the Cp′RuCl Fragment

The thermal cyclotrimerization of acetylene to benzene is an intriguing process. Based on experimental heats of formation of benzene and acetylene, this trimerization is extremely exothermic ($\Delta H° = -143$ kcal/mol).[5] On the other hand, and contrary to the Hammond postulate, the activation energy is prohibitively high and is calculated to lie in the 60−80 kcal/mol region.[6] Such high barriers arise from the fact that some bonding orbitals of the reactants have to become antibonding orbitals in the product and vice versa. Therefore substantial distortions of the acetylenes have to occur so as to switch electron density from bonding regions in the reactants to bonding regions in the product.[6a] Another contribution to the high barrier stems from closed-shell repulsions between the filled π-orbitals (HOMO−HOMO interactions),[6b] despite some aromatic stabilization of the transition state.[7]

Noteworthy, the activation energy is diminished appreciably through the coordination of the alkynes to the transition-metal centers. Actually, since the pioneering work done in 1948 by Reppe,[8] who found that low-valent nickel complexes catalyze alkyne cyclooligomerization, the transition-metal mediated [2+2+2] cycloaddition of alkynes has developed as a very efficient method for synthesizing functionalized arene systems.[9] Subsequently, a wide array of transition-metal containing fragments were found to actively catalyze the reaction. Of these, derivatives of cobalt and ruthenium proved particularly efficient, while tolerating the presence of varied functionality of the alkyne. For the

 © 2004 Wiley-VCH Verlag GmbH & Co. KGaA, Weinheim

former, the $CpCoL_2$ (L = CO, PR_3, olefin) catalyst family was studied in great detail.[10,11] In recent years, the ruthenium complexes Cp′Ru(COD)L and Ru(η^5-C_9H_7)(COD)Cl were found to promote the cyclotrimerization of 1,6-diynes, as well as the cyclocotrimerization of 1,6-diynes with terminal alkynes,[12] olefins,[13] allylic ethers,[14] dicyanides,[15] nitriles,[16] tricarbonyl compounds,[17] isocyanates,[2] isothiocyanates, and CS_2.[3]

One problem that should be noted is that the reactions rarely proceed with high chemo- and regioselectivity. That is, when the method is to be applied to the preparation of substituted aromatic compounds from three different, unsymmetrical acetylenes, 38 homo- and cross-coupling products may possibly be produced.[18] Thus, the assembly of such acetylenes to form strictly one single aromatic compound is a formidable challenge. For this goal, a knowledge of the detailed mechanism of the catalytic cycles might be very helpful. The issues to be addressed are among others: which intermediate controls the selectivity of the overall cyclotrimerization process or what determines the size of the rings to be formed. Actually, in the development of cyclization methods, facilitating formation of unusual ring sizes represents a significant objective.[19]

There are three recent theoretical examinations of the mechanism of acetylene cyclotrimerization. One is based on $CpCo(L)_2$ complexes,[20] and the other two on the Cp′RuCl fragment.[21,22] The proposal derived from DFT/B3LYP calculations performed by our group is shown in Scheme 3 and reveals a few uncommon intermediates (see also Figure 1, Figure 2, and Figure 3). In the first step, the starting precatalyst Cp′Ru(COD)Cl undergoes two ligand-substitution reactions resulting in the formation of the bis-acetylene complex **A**. Subsequent oxidative coupling of the two acetylene ligands generates the metallapentatriene complex **B**. In the next step, **B** is readily able to coordinate a third acetylene to give the acetylene-coordinated ruthenacycle **C**. No less than three successive intermediates could be found for subsequent arene formation. The first, an unusual ruthenabicyclo[3.2.0]heptatriene **D** rearranges to a very unsymmetrical metallaheptatetraene **E**. Ultimately, an η^2-coordinated benzene ring appears in species **F** through a reductive elimination step. Completion of the cycle is achieved by an exothermic displacement of the arene by two acetylene molecules thereby regenerating **A**.

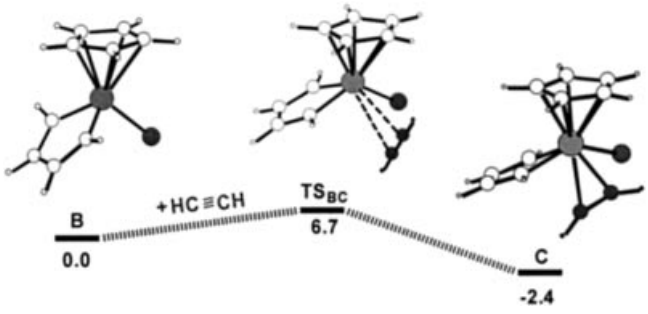

Figure 1. Energy profile for the cyclotrimerization of acetylene (energies in kcal mol^{-1}, relative to the bisacetylene complex **A**)

Some remarks about the key intermediates follows.

B: It is now safe to assume that all cyclization processes are initiated by a metallacycle as the first key intermediate. However, the bonding modes in **B** can vary with the metal fragment. While in the similar CpCo system the respective intermediate is better formulated as a metallacyclopentadiene (type **I**), in the RuCp′Cl case, **B** is clearly a metallacylopentatriene complex (type **II**) featuring a bis-carbene functionality. In recent years several ruthanacyclopentatriene complexes (and metallacylopentatriene complexes in general) have been isolated and unequivocally characterized by NMR spectroscopy and X-ray crystallography.[23] Two bi-

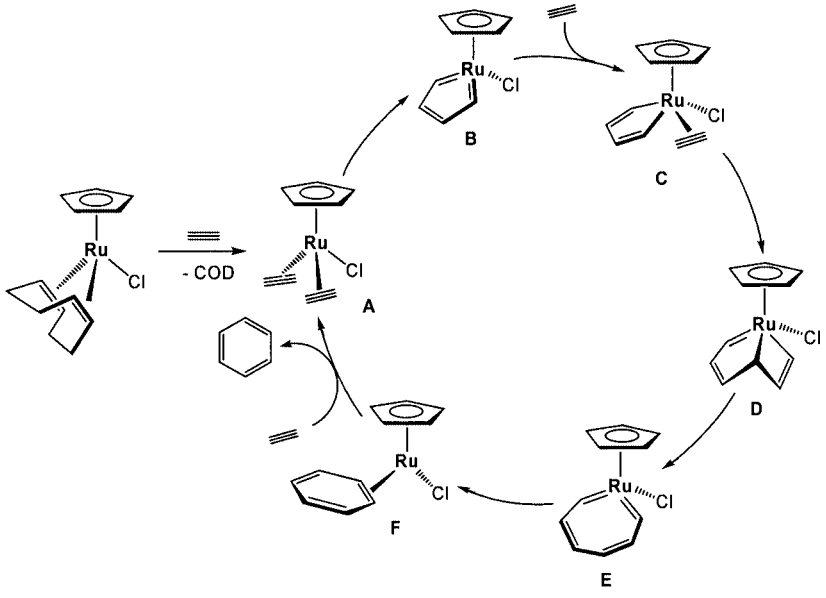

Scheme 3

 © 2004 Wiley-VCH Verlag GmbH & Co. KGaA, Weinheim

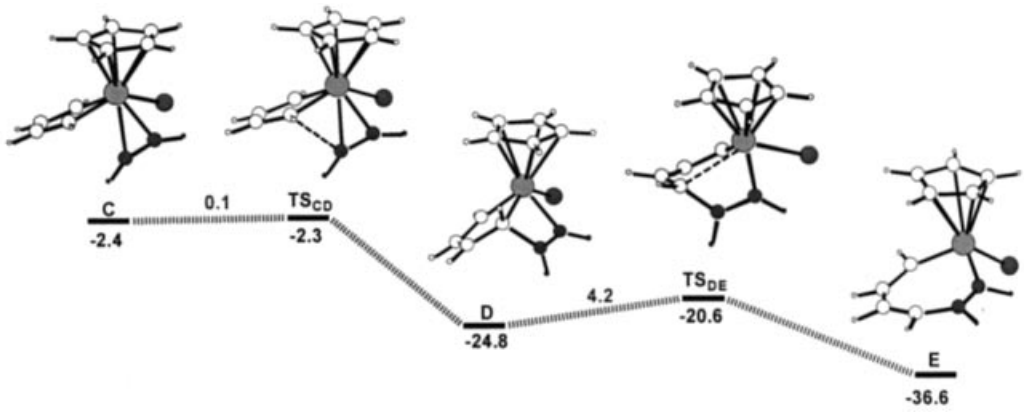

Figure 2. Energy profile for the cyclotrimerization of acetylene (energies in kcal mol^{-1}, relative to the bisacetylene complex **A**)

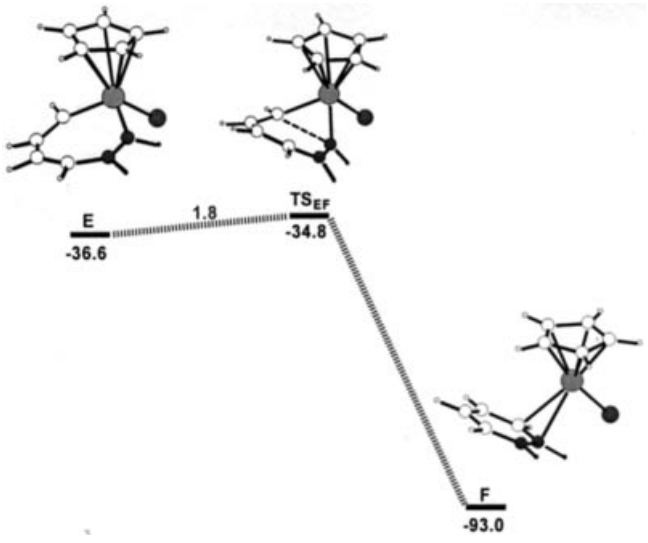

Figure 3. Energy profile for the cyclotrimerization of acetylene (energies in kcal mol^{-1}, relative to the bisacetylene complex **A**)

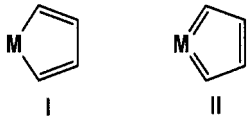

I II

cyclic analogues also have been isolated and characterized by X-ray crystallography.[24] In fact RuCp′(COD)L (L = Cl, Br) reacts with aryl acetylenes to give stable ruthenacyclopentatriene complexes (Scheme 4) that exhibit characteristic ^{13}C NMR resonances in the range of about 270−240 ppm. The oxidative coupling takes place regioselectively in a head-to-head fashion with the substituents ending up in the α and α′ position. It should be noted that ruthenacylopentatrienes serve as key intermediates in several catalytic reactions involving alkynes, for example, the double cyclopropanation of 1,6-diynes with strained cyclic olefins,[13a] the reaction of two alkyne molecules with carboxylic acids,[25] the cycloisomerization of alkynes and propargylic alcohols,[26] or the hydrative diyne cyclization.[27] The reactivity of **B** is guided by the possibility of an attack by another alkyne (or a nucleophile in general). It has been demonstrated that these species behave as masked, coordinatively unsaturated complexes and react readily with donor ligands such as tertiary phosphanes, phosphites, or amines to give "normal" metallacyclopentadiene complexes (Scheme 4).[23a,28] This is not a simple nucleophilic addition at the metal center but involves severe changes in the bonding mode. Addition of substrates to **B** becomes increasingly difficult in the case of a bulky co-ligand (see below), as well as bulky substituents in the 1- and 4-positions.

D: It may be noted that, very recently, such a structure could indeed be isolated for the first time, viz. a stable iridabicyclo[3.2.0]hepta-1,3,6-triene, which is reversibly transformed into an iridacycloheptatriene.[29] The crucial inter-

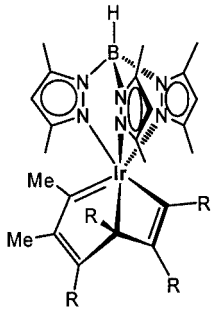

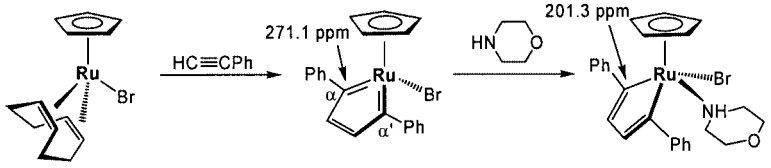

Scheme 4

 © 2004 Wiley-VCH Verlag GmbH & Co. KGaA, Weinheim

mediate **D** is shown in Figure 2 in order to emphasize the steric constraints between the hydrogen atom of the metallacycle (i.e. from the first two acetylene molecules) and that of the Cp ring. It is easy to see that this intermediate controls the selectivity of the overall cyclotrimerization process. Acetylene molecules carrying two bulky substituents will therefore experience considerable repulsion at this stage. In fact, cyclotrimerization is found to work well only when parent 1,6-diynes or unsymmetrical 1,6-diynes react with terminal alkynes.

E: This intermediate is most interesting as it reveals a notable asymmetry of the Cp-bonding or, in other words, ring slippage. The Cp ring can be considered as having a hapticity between η^3 and η^5, as is also found in other systems.[30] The asymmetry of **E** removes the symmetry-forbidden character from the final step.

F: This final complex is surprising when considering the 18e rule, because the benzene ring is η^2-bonded rather than η^4 as in the corresponding isoelectronic CpCo system. This becomes possible because of significant contraction of all of the five Ru−C(Cp) bonds. In this respect, the particular role played by the other co-ligand (in our case chloride) is worth emphasizing. If it were labile, the arene would be η^6-coordinated. The resulting stable and inert sandwich complexes would deactivate the catalyst and thus quench the catalytic cycle. This is exemplified when the complexes $[RuCp(CH_3CN)_3]^+$ or $[FeCp^*(CH_3CN)_3]^+$ are used as mediators for alkyne coupling reactions.[31,32]

3. The Cyclocotrimerization of Alkynes with Unsaturated Organic Molecules Mediated by the Cp′RuCl Fragment − Chemoselective Formation of Pyridine-2-one and Thiopyran-2-imine from Isocyanates and Thioisocyanates

As mentioned above, the cyclocotrimerization of two alkynes with unsaturated organic compounds containing C=X bonds (X = O, S, N etc.) is a synthetically useful and atom economic process for obtaining a variety of six-membered heterocyclic systems. Here we focus exemplarily on the particularly intriguing case of coupling of diynes with ambidentate molecules RN=C=X (X = O, S). Clearly, there are two different kinds of ring closures possible, which lead to either pyridine-2-ones and pyridine-2-thiones, or to pyran-2-imines and thiopyran-2-imines according to Scheme 1. Experimentally it was found that in the case of X = O, pyridine-2-ones, that is the nitrogen-heterocycle, are exclusively formed, whereas in the case of X = S, the chemoselectivity is reversed to give thiopyran-2-imines, that is the sulfur-heterocycle. Gratifyingly, the different chemoselectivities were reproduced well by the theoretical studies using DFT/B3LYP calculations performed in our laboratory.[33] The course of the reactions is characterized by two intermediates that are not so trivial in addition to the metallacyclopentatriene **B**, viz. the bicyclic carbene **C**, and the coordinatively unsaturated metallaheteronorbonene **D**, according to Scheme 5.

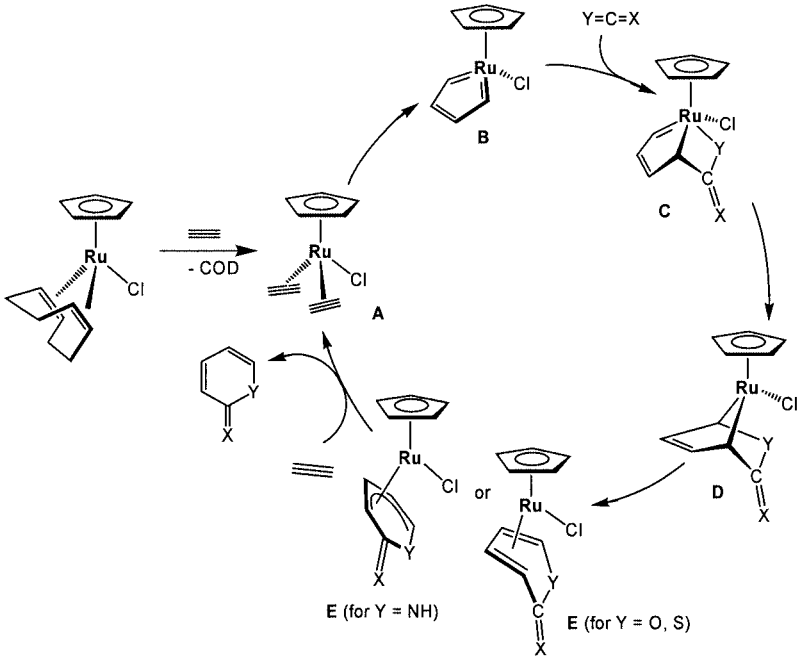

Scheme 5

 © 2004 Wiley-VCH Verlag GmbH & Co. KGaA, Weinheim

According to the proposed mechanism, the key reaction step is addition of a double bond to the metallacyclopentatriene to give a bicyclic carbene intermediate. This double-bond-addition is initiated by η^1 attack at the ruthenium center, and it is only the attacking atom that is finally incorporated in the cycle. Thus, the chemoselectivity arises from

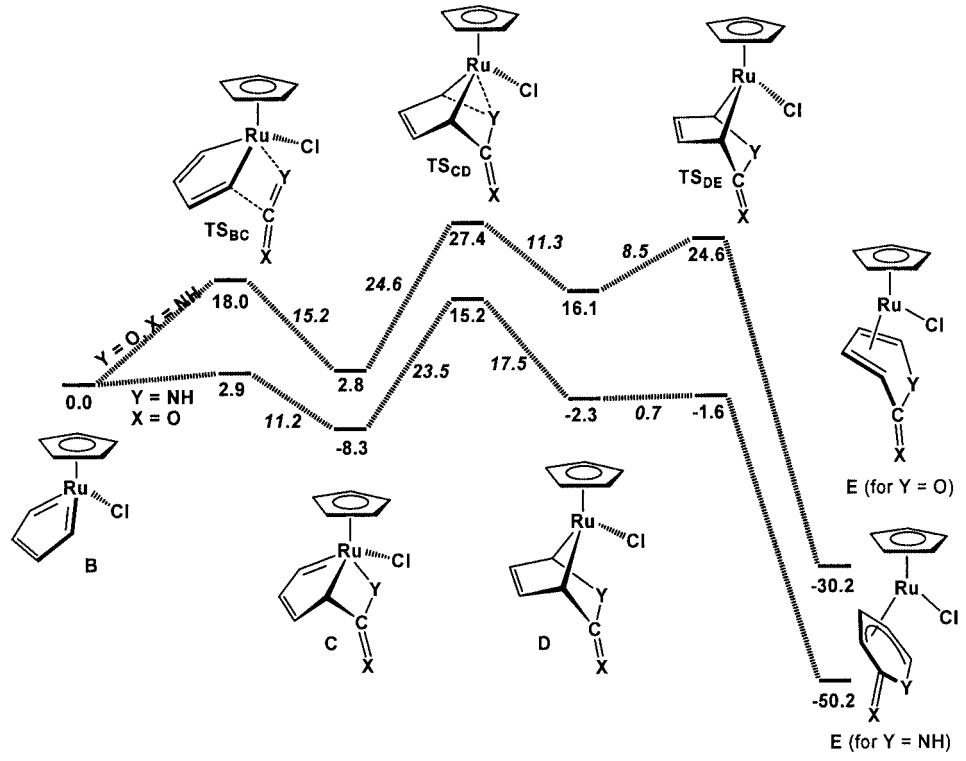

Scheme 6

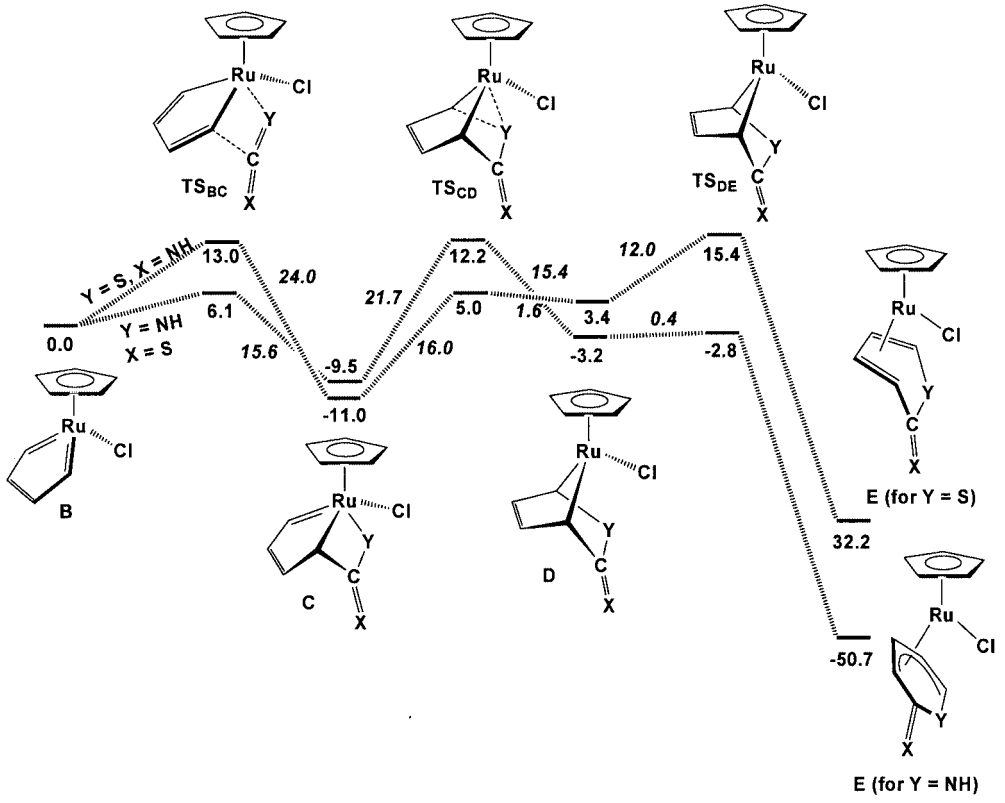

Scheme 7

 © 2004 Wiley-VCH Verlag GmbH & Co. KGaA, Weinheim

the fact that, for HNCO, N attack is preferred over O, but for HNCS, S attack is preferred over N. The energy profile for the two alternatives, viz. the orientation of N, O, and S towards the ruthenium center, is shown in Scheme 6 and Scheme 7.

4. Dramatic Changes seen upon Replacement of Cl in Cp′RuCl with ER_3 (P, Sb) and CO

At first glance, the 14-electron fragment $[RuCp(PR_3)]^+$ would seem a promising candidate for mediating cyclization reactions, since it is possible to vary the properties of the phosphane ligand through the substituents. In this way, the regioselectivity of the coupling process might be controlled. However, although this species is catalytically active in the isomerization of allyl alcohols[34] and is a catalyst for the transfer hydrogenation of acetophenone and cyclohexanone as well as the isomerization of allyl ethers,[35] the cyclotrimerization of alkynes is not initiated. Instead, a number of unusual and interesting products are obtained, depending on the structure of the alkyne and the substituent of the phosphane ligand.

In most reactions of the $[RuCp(PR_3)]^+$ fragment with alkynes the key intermediate is a cationic metallacyclopentatriene − in contrast to a metallacyclopentadiene − featuring two highly electrophilic carbene carbon atoms. In two cases, namely the reactions of $[RuCp(PCy_3)(CH_3CN)_2]^+$ and $[RuCp(SbPh_3)(CH_3CN)_2]^+$ with 2,8-decadiyne, such intermediates have been unequivocally identified by means of $^{13}C\{^1H\}$ NMR spectroscopy. The characteristic resonances in their $^{13}C\{^1H\}$ NMR spectra at $\delta = 325.6$ and 330.0 ppm, respectively, can be associated with the carbene ring carbon atoms. It is also very important to note that the initial oxidative coupling step with terminal alkynes takes place selectively in a head-to-tail rather than in head-to-head fashion as observed for the RuCp′Cl fragment. Thus, the substituents in the cationic metallacyclopentatriene intermediate are exclusively in the α- and β′-position (see Scheme 9). The electrophilicity of the two carbene carbon atoms gives rise to a wide array of inter-ligand transformations, preventing the attack of a third alkyne molecule. Among other structures, ruthenium allyl carbene (**I**), butadienyl carbene (**II**), and allenyl carbene complexes (**III**) are formed (Scheme 8).[36,37]

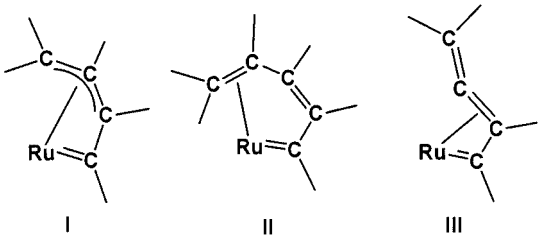

Scheme 8

4.1. Formation of Ruthenium Allyl Carbenes − Migration of a PR_3 Ligand

As shown in Scheme 9 (and in Scheme 10), the phosphane coligand migrates from Ru to C generating an allyl carbene. In the case of terminal alkynes, C−C coupling is highly selective in a head-to-tail fashion, with the result that the substituents are at the carbene carbon atom and the internal carbon atom of the allylic moiety, whereas with the diynes, the two internal sp carbon atoms are involved. In the allyl carbene systems formed in both cases, all four carbon atoms of the C_{1-4} chain are bonded to the RuCp fragment. This reaction proceeds very fast even if bulky phosphanes such as PCy_3 are used and substituents at the α-, α′-carbon atoms of the metallacycle are present. A structural view of $[CpRu(=CH\text{-}(\eta^3\text{-}CC(CH_2)_3CHPCy_3)]PF_6$ showing the migration of the bulky PCy_3 ligand is depicted in Figure 4.

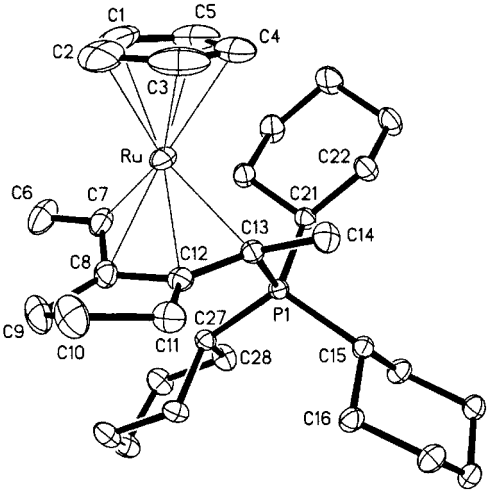

Figure 4. Structural view of $[CpRu(=CH\text{-}(\eta^3\text{-}CC(CH_2)_3CHPCy_3)]\text{-}PF_6$ (PF_6^- omitted for clarity)

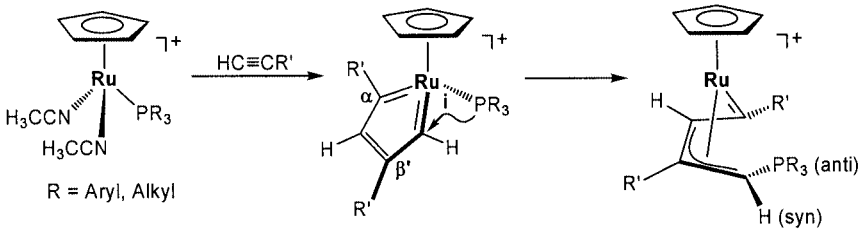

Scheme 9

 © 2004 Wiley-VCH Verlag GmbH & Co. KGaA, Weinheim

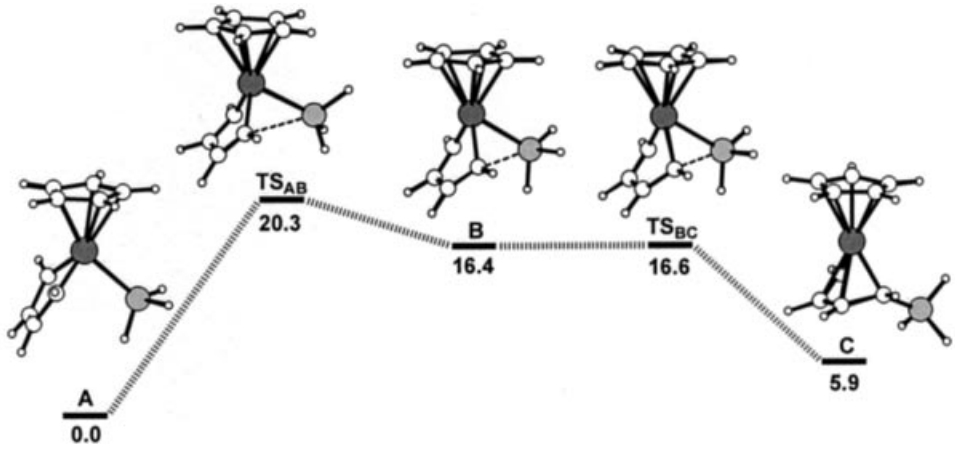

Figure 5. Energy profile of the B3LYP potential energy surfaces for the conversion of the ruthenacyclopentatriene complex **A** into the allyl carbene **C**

In the absence of kinetic data DFT/B3LYP calculations have been performed to shed light on the mechanism of this unusual phosphane migration process; the results are shown in Figure 5. The conversion of the metallacyclopentatriene **A** into the final allylcarbene complex **C** proceeds with relatively small activation barriers; the rate-limiting step is the initial distortion to produce the intermediate **B**. The metallacycle bends and approaches the C atoms in the β-position to the metal. Conversely, at the other side of the molecule, the Ru−C$_\alpha$ bond stretches and this carbon atom starts to form a new C$_\alpha$−P bond. This feature is already obvious in the transition state **TS$_{AB}$**, and the activation energy is 20.3 kcal mol^{-1}. **TS$_{AB}$** is much closer in energy to **B** than to **A**. The final transformation involves complete Ru−P bond breaking and formation of the C$_\alpha$−P bond, with simultaneous formation of the allylcarbene, and the adjustments of the carbon chain, which involve formation of the Ru−C$_\beta$ bonds.

4.2. Formation of Ruthenium Butadienyl Carbenes − Carbene to Olefin Interconversion through a 1,2-Hydrogen Shift

If the alkyne has an α-alkyl substituent, in some cases, a competitive intramolecular 1,2-hydrogen migration results in the formation of a butadienyl carbene (Scheme 10). A structural view of [CpRu(=C(CH$_3$)C(CH$_2$)$_4$C-η^2-CH=

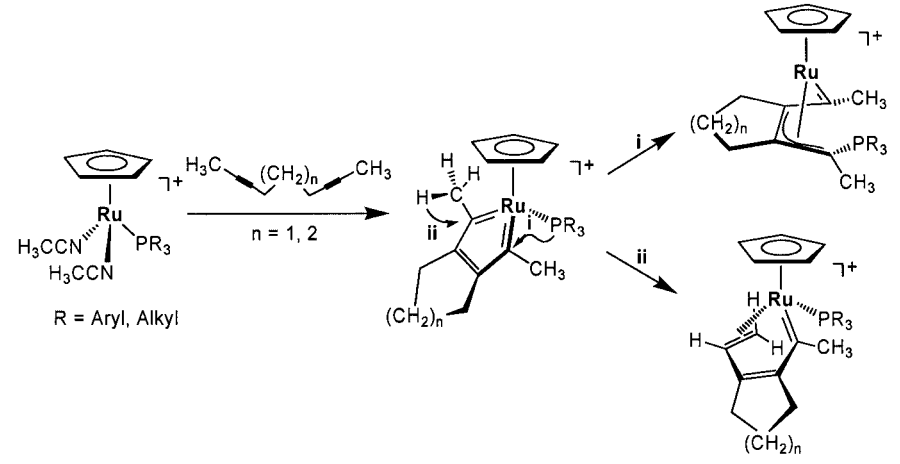

Scheme 10

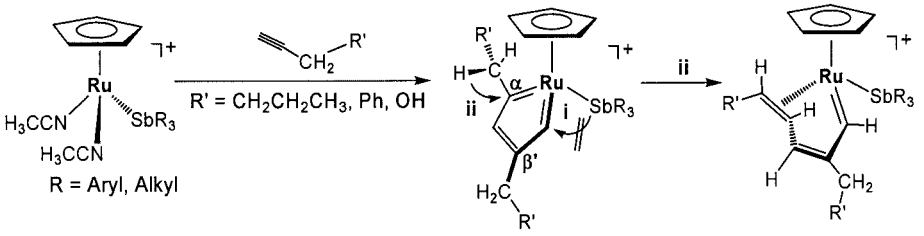

Scheme 11

 © 2004 Wiley-VCH Verlag GmbH & Co. KGaA, Weinheim

$CH_2)(PPh_3)]PF_6$ is given in Figure 6. When pathway (i) is preferred over (ii), the phosphane ligand is more nucleophilic. In this respect, the mechanistic change-over from (i) to (ii) is noted when phosphane is replaced by other group 15 ligands AsR_3 and SbR_3 (Scheme 11). Thus, arsane and stibine ligands have no tendency to migrate.[37] Under certain circumstances both allyl carbene and butadienyl carbene complexes can undergo further transformations as follows.

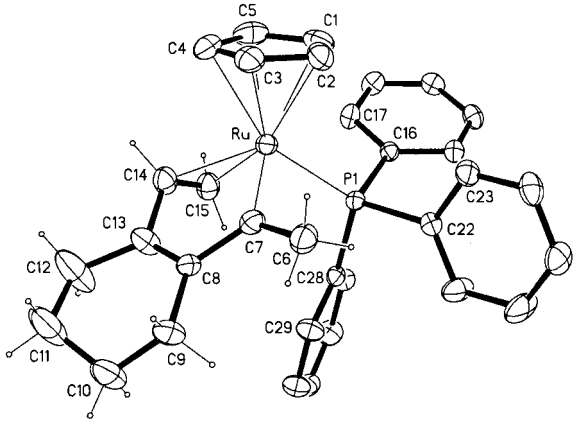

Figure 6. Structural view of $[CpRu(=C(CH_3)C(CH_2)_4C\text{-}\eta^2\text{-}CH=CH_2)(PPh_3)]PF_6$ (PF_6^- omitted for clarity)

4.3. Ruthenium Allyl Carbenes as Masked Coordinatively Unsaturated Complexes − Intramolecular C−H Bond Activation

Ruthenium η^3-allyl carbene complexes act as pseudo-16e species and are capable of activating C−H bonds of aryl and alkyl groups of the phosphane.[38] This occurs if the phosphanes are sufficiently bulky such as PPh_3 or PCy_3, whereas no such reaction is observed with PMe_3. Pertinent reactions are given in Scheme 12 to 14. The initially formed allyl carbene complexes are not stable and, in some cases, transform slowly at room temperature into novel η^4-butadiene complexes featuring an orthometallated arene ligand derived from PPh_3.

A somewhat different reaction takes place when the parent acetylene is used: the allyl carbene intermediate eventually rearranges into $[RuCp(\eta^3\text{-}CHCHCH-CH_2PPh_2\text{-}\eta^2\text{-}C_6H_4)]^+$, as shown in Scheme 12. The structure and bonding features of this complex are rather unusual. Firstly, an *ortho* C−H bond of the PPh_3 substituent is activated that results in C−C bond formation between the carbene carbon atom of the allyl carbene moiety and the *ortho* arene carbon atom. In the course of this process the *ortho* hydrogen atom is transferred to the terminal carbon of the allyl carbene unit; this involves carbon $sp^2 \rightarrow sp^3$ rehybridization. Furthermore, besides coordination to an η^3-allyl moiety, the metal center is η^2-coordinated to a double bond of a phenyl ring adjacent to the P-donor of the PPh_3 substituent. This bonding mode is very rare, and thus only a few examples

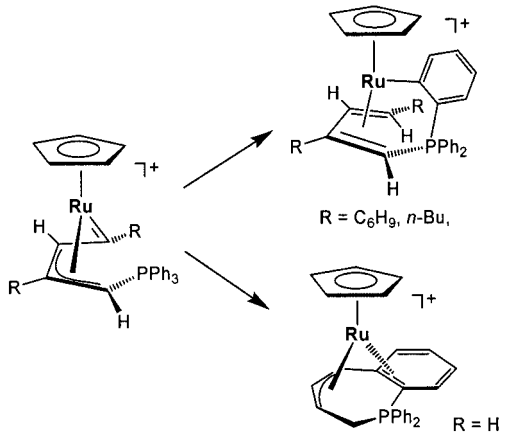

Scheme 12

have been reported recently.[39] Molecular structures of $[RuCp(\eta^4\text{-}CH(C_6H_9)CHC(C_6H_9)CH-PPh_2(\eta^1\text{-}C_6H_4))]PF_6$ and $[RuCp(\eta^3\text{-}CHCHCH-CH_2PPh_2\text{-}\eta^2\text{-}C_6H_4)]PF_6$ are shown in Figure 7 and Figure 8.

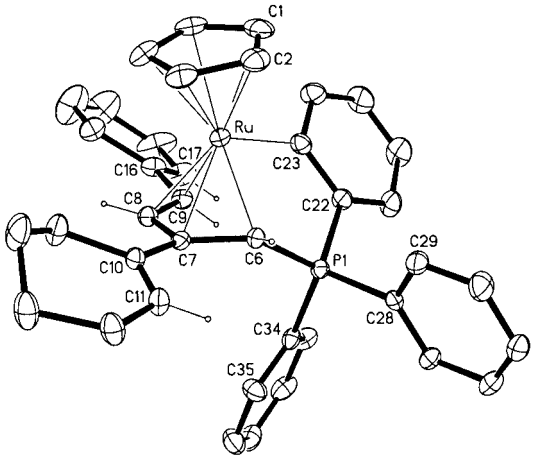

Figure 7. Structural view of $[RuCp(\eta^4\text{-}CH(C_6H_9)CHC(C_6H_9)CH-PPh_2(\eta^1\text{-}C_6H_4))]PF_6$ (PF_6^- omitted for clarity)

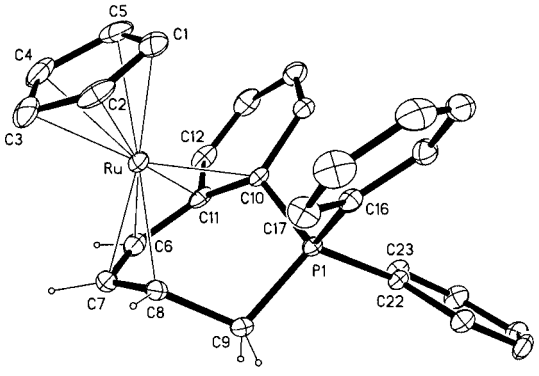

Figure 8. Structural view of $[RuCp(\eta^3\text{-}CHCHCH\text{-}CH_2PPh_2\text{-}\eta^2\text{-}C_6H_4)]PF_6$ (PF_6^- omitted for clarity)

Another example of facile intramolecular C−H bond activation initiated by allyl carbenes is shown in Scheme 13. Here one cyclohexyl substituent of the phosphane ligand is

 © 2004 Wiley-VCH Verlag GmbH & Co. KGaA, Weinheim

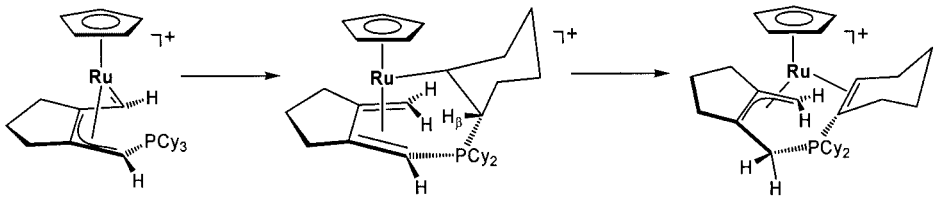

Scheme 13

converted into an η^2-coordinated cyclohexenyl ligand (Figure 9). The reaction does not stop after the oxidative addition step but β-elimination also takes place The overall transformation involves the transfer of two hydrogen atoms from a cyclohexyl ring of PCy_3 to the C4 chain of the allyl carbene moiety. Notably, related reactions have been reported recently, which in some cases require the addition of olefin as an external hydrogen acceptor.[40]

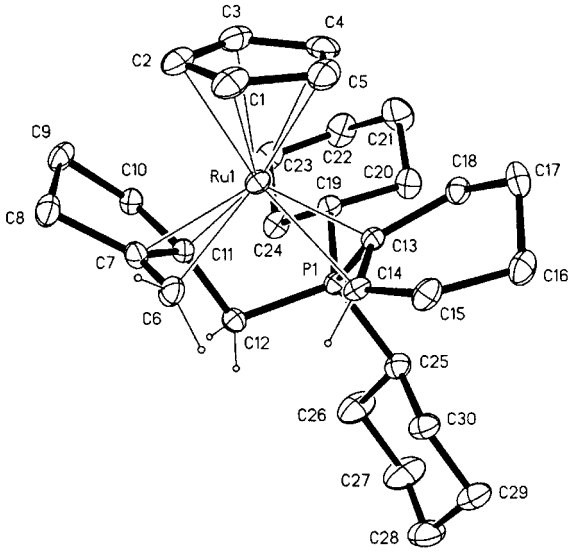

Figure 9. Molecular view of $[CpRu(\eta^3\text{-}CH_2C(CH_2)_3CCH_2PCy_2(\eta^2\text{-}C_6H_9)]PF_6$ (PF_6^- omitted for clarity)

In analogous fashion to RuCp complexes, reactions of acetylenes with the Cp* analogue $[RuCp^*(PEt_3)(CH_3CN)_2]^+$ have been performed. Scheme 14 summarizes the reactions of $[RuCp^*(PEt_3)(CH_3CN)_2]^+$ with the alkynes HC≡CR (R = COOMe, *n*Bu) and 1,6-heptadiyne. The η^3-allyl carbene complexes were obtained in high isolated yields. However, in contrast to the RuCp analog η^3-allyl carbene complexes, these compounds are unstable in solution and react slowly at room temperature to afford $[Ru(\eta^6\text{-}C_5Me_4CH_2)(\eta^4\text{-}CH(R)=CH-C(R)=CHPEt_3)]PF_6$ and $[Ru(\eta^6\text{-}C_5Me_4CH_2)(\eta^4\text{-}CH_2=C(CH_2)_3C=CH-PEt_3)]PF_6$, respectively. In both, one of the ring methyl C−H bonds

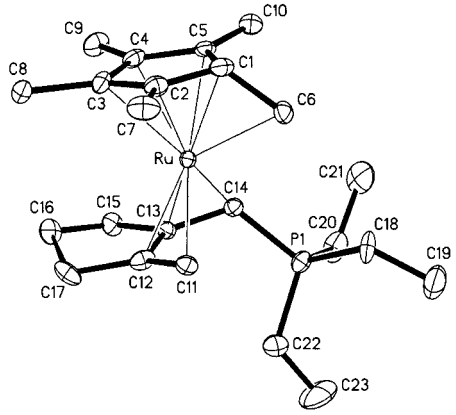

Figure 10. Structural view of $[Ru(\eta^6\text{-}C_5Me_4CH_2)(\eta^4\text{-}CH_2=C(CH_2)_3C=CHPEt_3)]PF_6$ (PF_6^- omitted for clarity)

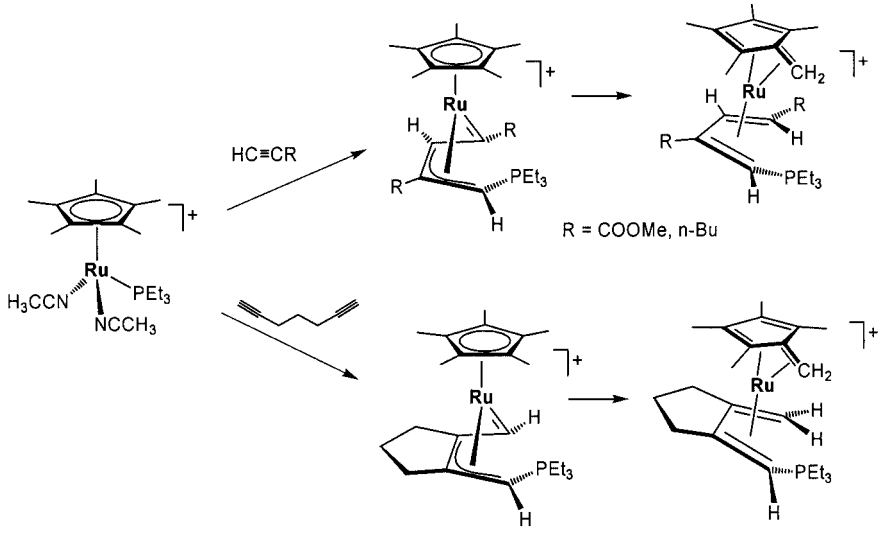

Scheme 14

 © 2004 Wiley-VCH Verlag GmbH & Co. KGaA, Weinheim

of the Cp* ligand has been cleaved (Scheme 14). In these transformations, the hydrogen atom is transferred to the carbene carbon atom at the inside face of the molecule to form an η^4-diene unit. Based on the NMR spectroscopic data, the newly formed η^6-$C_5Me_4CH_2$ ligand may be envisioned as a tetramethylfulvene rather than a tetramethylcyclopentadienyl-σ-alkyl ligand. The X-ray data are also consistent with a tetramethylfulvene rather than an η^1:η^5-$CH_2C_5Me_4$ (σ:η^5-$CH_2C_5Me_4$) description. A structural view of $[Ru(\eta^6\text{-}C_5Me_4CH_2)(\eta^4\text{-}CH_2{=}C(CH_2)_3\text{-}C{=}CHPEt_3)]PF_6$ is depicted in Figure 10. Related methyl C−H activation processes of transition-metal coordinated C_5Me_5 and C_6Me_6 ligands have been reported previously.[41,42]

4.4. Formation of Ruthenium Butadiene Amido Complexes

The above reactions of $[RuCp(PR_3)(CH_3CN)_2]PF_6$ with alkynes all involve phosphane migration and subsequent C−H bond activation at either the phosphane substituent or the Cp* ligand. In this respect it is interesting to switch over to the phosphanyl-amine ligand PPh_2NHPh from PR_3 in order to see whether migration appears at the P or the N site, and whether there will be N−H or C−H bond activation. Accordingly, the reaction of $[RuCp(PPh_2NHPh)(CH_3CN)_2]PF_6$ with HC=CR (R = Ph, *n*Bu, CH_2Ph), 1,6-heptadiyne, and 1,7-octadiyne results in the formation of the η^4-butadiene amido complexes $[RuCp(\eta^4\text{-}C_4H_3(R)_2\text{-}PPh_2\text{-}\kappa^1\text{-}(N)\text{-}NPh)]PF_6$, $[RuCp(\eta^4\text{-}C_4H_3(CH_2)_3\text{-}PPh_2\text{-}\kappa^1\text{-}(N)\text{-}NPh)]PF_6$, and $[RuCp(\eta^4\text{-}C_4H_3(CH_2)_4\text{-}PPh_2\text{-}\kappa^1\text{-}(N)\text{-}NPh)]PF_6$ in good yields (Scheme 15).[43] Thus, migration of the κ^1(P)-coordinated PPh_2NHPh ligand occurs through P rather than N in an analogous manner to that in the η^3-allyl carbene complexes already described. In contrast, however, instead of activation of a C−H bond involving the phenyl substituents of the PPh_2NHPh ligand, facile N−H activation of the NHPh-moiety occurs. In this way, RuCp η^4-butadiene amido complexes are afforded. This is noteworthy in view of the comparatively strained four-membered Ru-*N*−P−C ring system formed, in contrast to a five-membered Ru−C−C−P−C ring system in case of C−H bond activation.

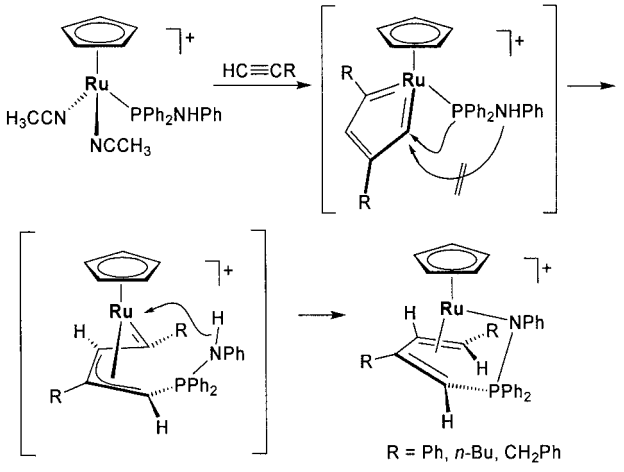

Scheme 15

4.5. Reactivity of Ruthenium Butadienyl Carbenes

In special cases, butadienyl carbene complexes undergo further rearrangement such as in the reaction of $[RuCp(SbR_3)(CH_3CN)_2]^+$ with $HC{\equiv}CCH_2Ph$,[37] to give an η^3-allyl-vinyl complex (Scheme 16). When $HC{\equiv}CCH_2OH$ is the alkyne, an η^3-allyl-acyl complex is obtained as illustrated in Scheme 17.

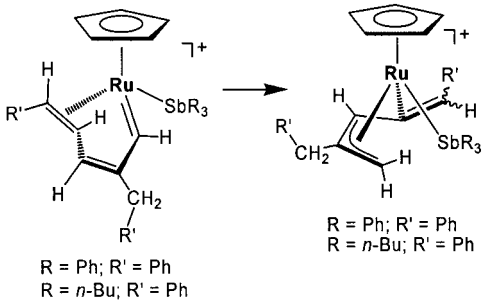

Scheme 16

The alkynes utilized above contain an α-alkyl substituent that is capable of facile 1,2-hydrogen shift. With alkynes lacking α-C−H bonds, namely $HC{\equiv}CC_6H_9$ and the propargylic alcohols $HC{\equiv}CC_6H_{10}OH$ and $HC{\equiv}CCMe_2OH$, η^3-butadienylvinyl complexes are formed as presented in Scheme 18.

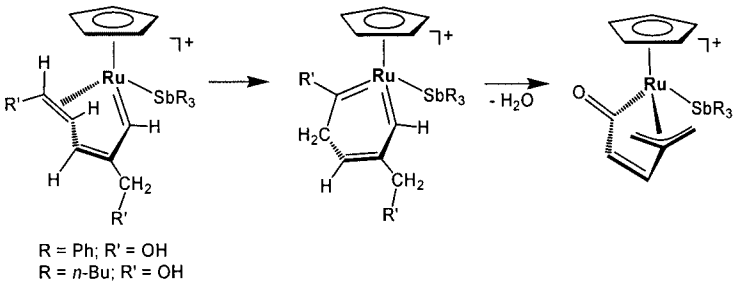

Scheme 17

 © 2004 Wiley-VCH Verlag GmbH & Co. KGaA, Weinheim

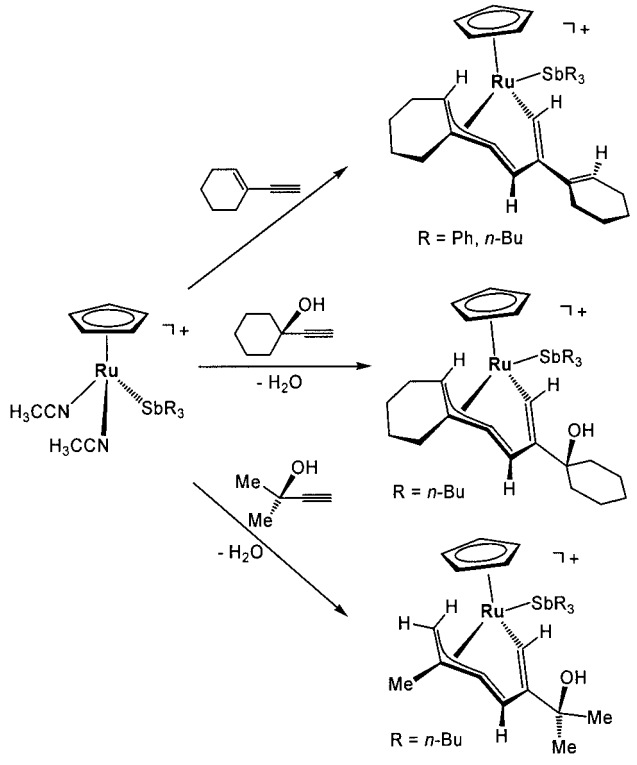

Scheme 18

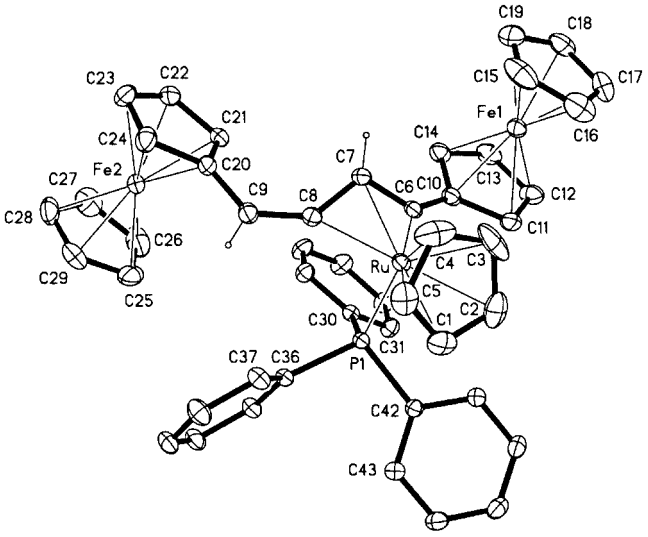

Figure 11. Structural view of [CpRu(=C(Fc)-η²-CH=C=CH-(Fc))(PR₃)]PF₆ (PF_6^- omitted for clarity)

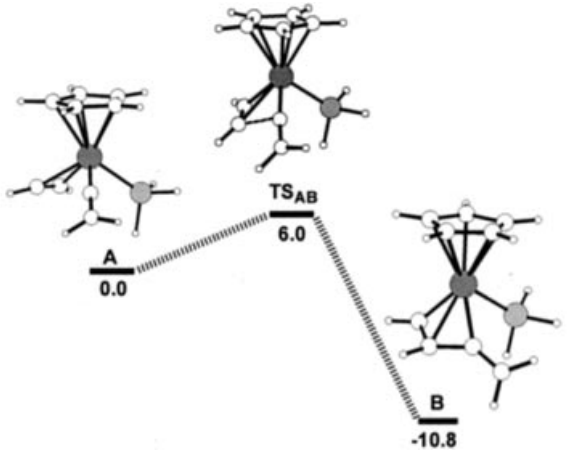

Figure 12. Energy profile of the B3LYP potential energy surface for the conversion of the vinylidene-acetylene complex **A** into the allenyl carbene **B**

4.6. Formation of Ruthenium Allenyl Carbenes

The formation of allenyl carbene complexes has also been observed in the reaction of $[RuCp(PR_3)(CH_3CN)_2]^+$ with a very atypical alkyne, viz. ferrocenyl and ruthenocenyl acetylene (see Scheme 19 and Figure 11).[36] This new type of C−C bond formation is affected by the strong electronic coupling between the ferrocenyl moiety and the conjugated

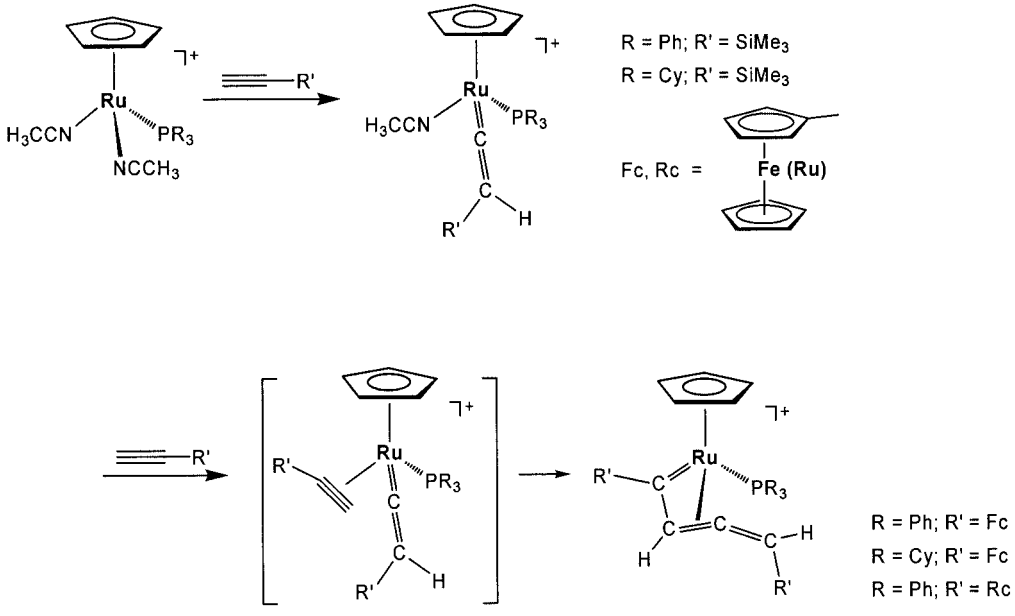

Scheme 19

 © 2004 Wiley-VCH Verlag GmbH & Co. KGaA, Weinheim

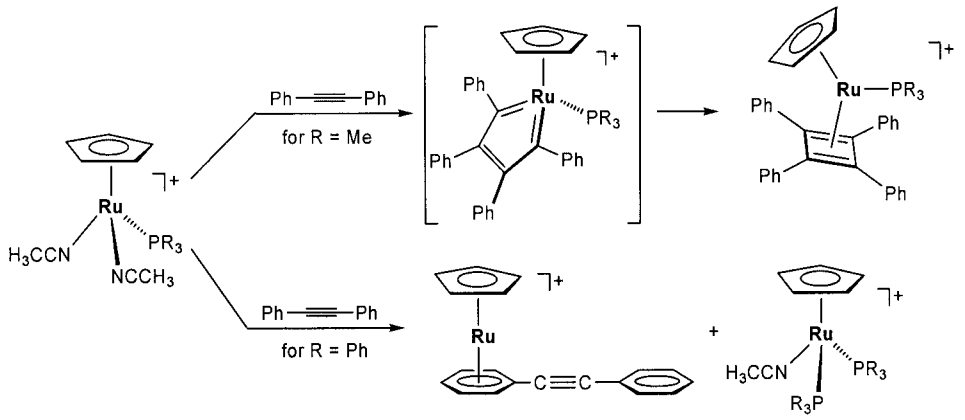

Scheme 20

allenyl carbene unit, which facilitates transient vinylidene formation with subsequent alkyne insertion into the Ru=C double bond. The strong electronic coupling is also apparent from the X-ray structures of the products. The alkyne-vinylidene coupling reaction is extremely facile requiring merely 6 kcal/mol according to recent DFT/B3LYP calculations performed with the model complexes $[RuCp(PH_3)(\eta^2\text{-}HC{\equiv}CH)(=CCH_2)]^+$ (Figure 12).

4.7. Formation of Ruthenium Cyclobutadiene Complexes

Under particular instances the metallacyclopentatriene can transform into an η^4-cyclobutadiene complex. This outcome has been observed in the reaction of $[RuCp(PMe_3)(CH_3CN)_2]^+$ with PhC≡CPh as shown in Scheme 20. Theoretical calculations reveal that this transformation is actually symmetry forbidden that involves HOMO/LUMO crossing. Thus, the kinetic barrier becomes prohibitively high, albeit the reaction appears to be energetically favorable. Any cyclobutadiene complexes known hitherto are derived from acetylenes with bulky substituents, such as phenyl or trimethylsilyl.[44,23b] There is obviously a subtle balance of factors that influence the availability of the cyclobutadiene pathway. In fact, in the above example, on switching from $[RuCp(PMe_3)(CH_3CN)_2]^+$ to $[RuCp(PPh_3)(CH_3CN)_2]^+$, a completely different reaction outcome is observed: sandwich complexes are formed. In a forthcoming paper we will investigate the detailed mechanism of the cyclobutadiene pathway, of which to date very little is known.

4.8. Formation of Ruthenium Cyclopentadienone Complexes

Similarly to tertiary phosphanes, in the present type of conversions, carbon monoxide is also not a spectator ligand, but instead functions as an active ligand. Thus the mono-carbonyl complex $[RuCp'(CO)(CH_3CN)_2]^+$ reacts with terminal and internal alkynes to afford ruthenium cyclopentadienone complexes (Scheme 21 and Scheme 22).[45]

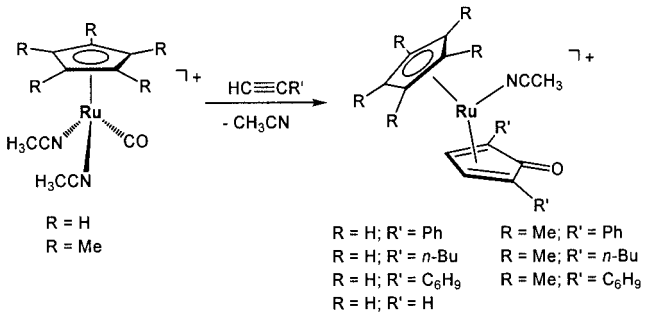

Scheme 21

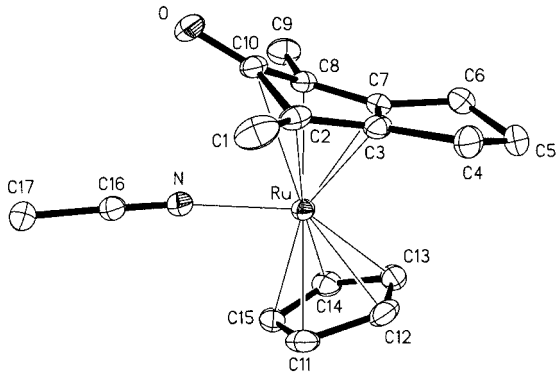

Figure 13. Molecular structure of $[RuCp(\eta^4\text{-}OC_5Me_2C_3H_6)(CH_3CN)]PF_6$ (PF_6^- omitted for clarity)

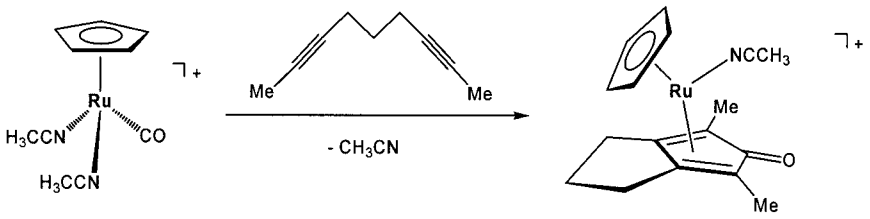

Scheme 22

 © 2004 Wiley-VCH Verlag GmbH & Co. KGaA, Weinheim

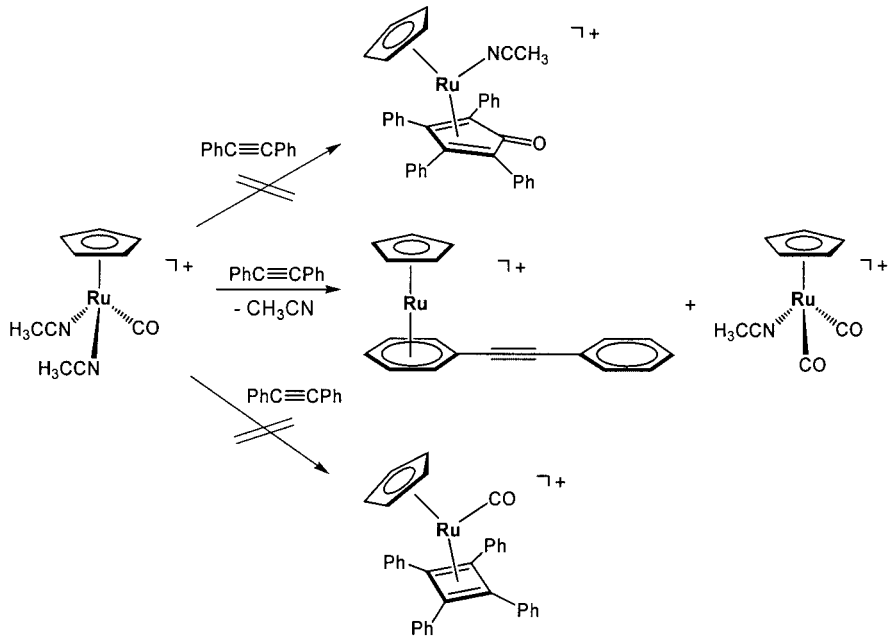

Scheme 23

A structural view of $[RuCp(\eta^4\text{-}OC_5Me_2C_3H_6)(CH_3CN)]PF_6$ is depicted in Figure 13.

These reactions are highly selective, yielding, in the case of terminal alkynes, only one regioisomer with the substituents exclusively in the α,α′-positions of the cyclopentadienone moiety. Further, in this case the substituent on the alkyne is of critical importance to the outcome of the reaction. Specifically, the reaction with PhC≡CPh does not yield the cyclopentadienone complex, but rather the sandwich complex $[RuCp(\eta^6\text{-}C_6H_5PhC{\equiv}CPh]^+$ and a biscarbonyl complex $[RuCp(CO)_2(CH_3CN)]^+$ in a 1:1 ratio (Scheme 23). Other reactions are also known in which

Table 1. Cyclotrimerization of alkynes mediated by $[RuCp(CH_3CN)_3]^+$

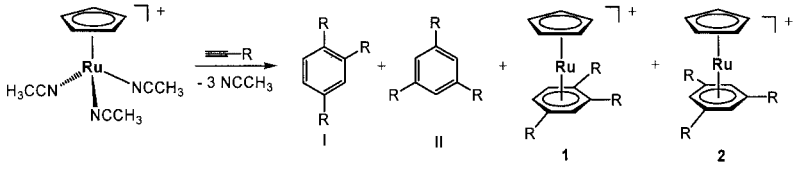

Alkynes	[2 + 2 + 2] Cycloadduct			Arene complexes		
	Conversion (%)[a]	I (%)	II (%)	Conversion (%)[b]	1 (%)	2 (%)
1-hexyne	45	75	25	88	75	25
3-phenylprop-1-yne	30	75	25	86	75	25
ethyl propiolate	85	75	25			
phenylacetylene				80	100	
1-ethynylcyclohexene				90	100	
1,6-heptadiyne	38	100[c]		83	100	
1,7-octadiyne	52	100[d]		89	100	

[a] With respect to substrate. [b] With respect to catalyst. [c] A mixture of dimers **III** and trimer **IV** by was obtained in ca. 38 and 52% yield, respectively:

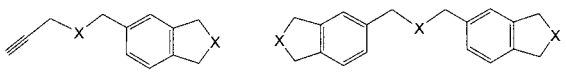

III X = CH_2, CH_2CH_2 **IV**

[d] A mixture of arene complexes with **III** and **IV** (X = CH_2CH_2) as ligands were formed in ca. 80% overall yield.

 © 2004 Wiley-VCH Verlag GmbH & Co. KGaA, Weinheim

cyclopentadienone complexes are formed from carbonyls and acetylenes. The first reported cyclopentadienone complex, $Fe(\eta^4\text{-}C_5H_4O)(CO)_3$, was obtained by treating $Fe(CO)_5$ with an excess of HC≡CH.[46] Other examples are complexes of the types $M(\eta^4\text{-}C_5H_4O)(CO)_3$ (M = Fe, Ru),[47] $MCp(\eta^4\text{-}C_5H_4O)$ (M = Co, Rh),[48] and $V(\eta^4\text{-}C_5H_4O)(CO)(PMe_3)$.[23f]

4.9. Formation of Arenes and Arene Complexes − Cyclotrimerization of Alkynes

In contrast to the above systems, if $[RuCp(L)(CH_3CN)_3]^+$ is used when L = CH_3CN, the catalytic cyclotrimerization of alkynes is promoted as shown in Table 1, although, this does not occur in a selective manner, and 1,2,4- as well as 1,3,5-trisubstituted arenes are formed in most cases.[31] However, in the course of the catalytic process, several pathways that form stable and inert sandwich complexes of the type $[RuCp(\eta^6\text{-arene})]^+$ become readily available. In this way the catalytically active intermediates are consumed and the catalytic cycle is gradually quenched. Therefore, albeit active in various other C−C bond coupling reactions, involving even alkynes, $[RuCp(CH_3CN)_3]^+$ is an unsuitable catalyst for the cyclotrimerization of alkynes. The formation of arene complexes may be prevented under photochemical conditions since the arene ligands in $[RuCp(\eta^6\text{-arene})]^+$ are known to be photo-labile.[49]

5. What Happens if the Phosphane Ligand is Tethered?

What is the reason for the extraordinary difference in behavior between the two fragments RuCpCl and $[RuCp(PR_3)]^+$? There are at least two reasons for this: the first is the charge on the complex: clearly, a cationic complex will be more electrophilic than a neutral complex; the other is the greater steric requirements of the tertiary phosphane ligand than the chloride ligand. To elucidate this point further, we tethered the phosphane ligand onto the Cp ring via a two-carbon linker under, otherwise, the same

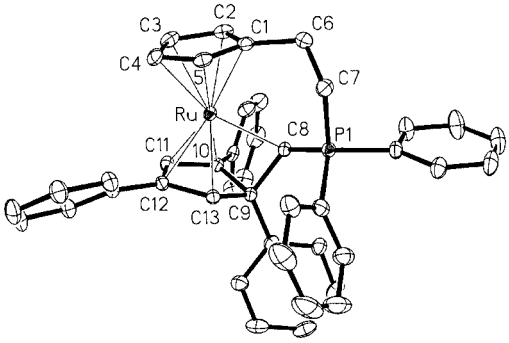

Figure 14. Structural view of $[Ru(\eta^5\text{-}C_5H_4CH_2CH_2PPh_2\text{-}\kappa^1C\text{-}CH\text{-}\eta^4\text{-}C_5Ph_3H_2)]PF_6$ (PF_6^- omitted for clarity)

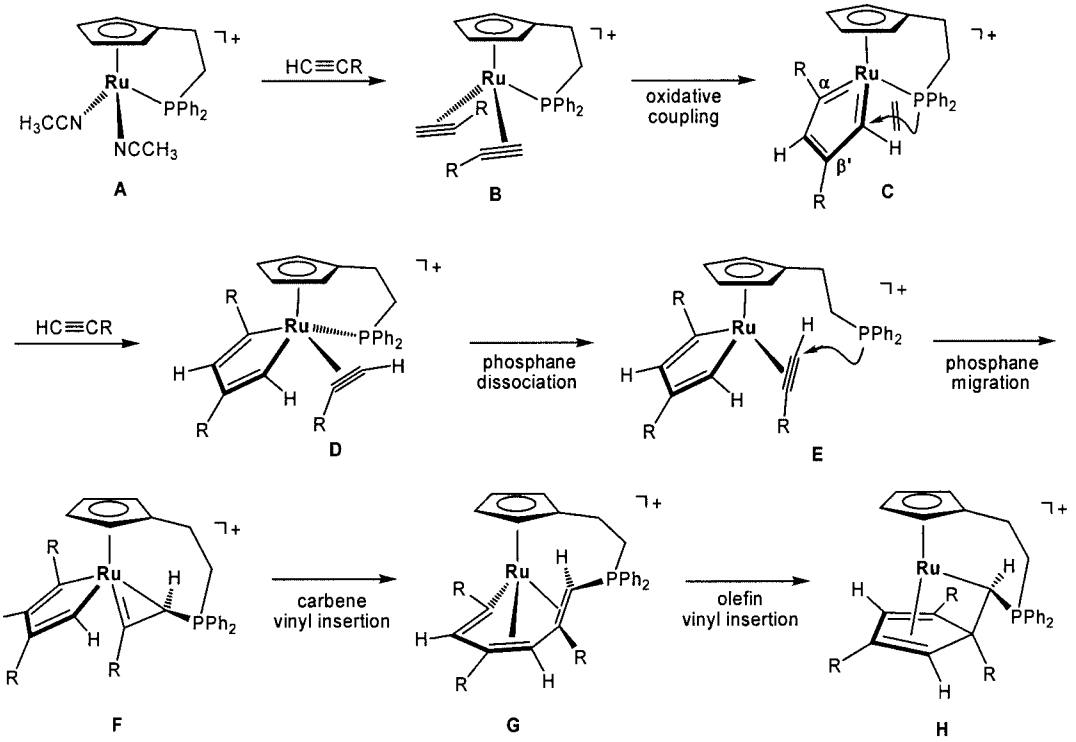

Scheme 24

 © 2004 Wiley-VCH Verlag GmbH & Co. KGaA, Weinheim

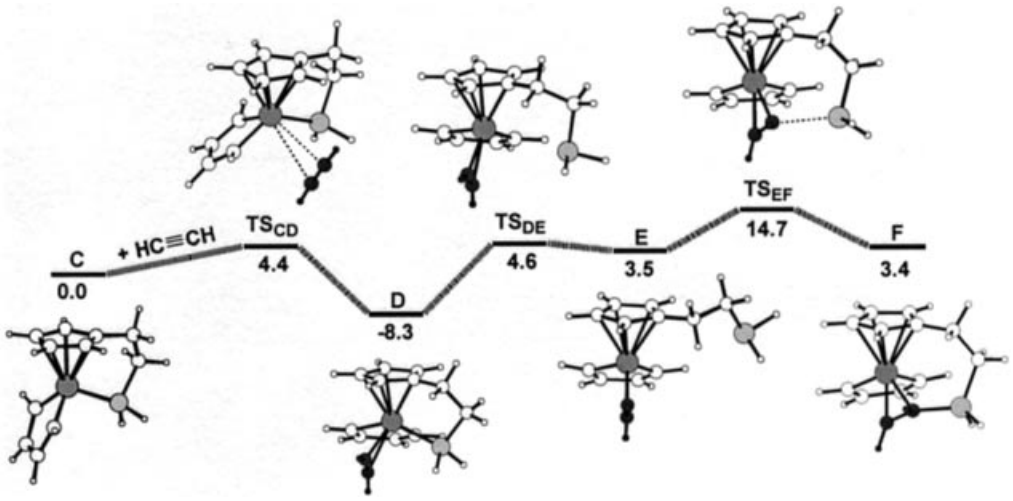

Figure 15. Energy profile of the B3LYP potential energy surfaces for the conversion of the ruthenacyclopentatriene complex **C** into the 1-metallacyclopropene **F**

reaction conditions.[50] In fact, the arrested phosphorus moiety diverts the previously direct nucleophilic attack of the coordinated trialkylphosphane to the α-carbon atom of the metallacyclopentatriene. Instead, a third alkyne molecule is added, which finally leads to an unusual C−C coupling process that involves three alkynes and the tethered phosphane, to give the cycloaddition product **H** as shown in Scheme 24. A structural view of [Ru(η^5-$C_5H_4CH_2CH_2PPh_2$-κ^1C−CH-η^4-$C_5Ph_3H_2$)]PF_6 is given in Figure 14.

According to DFT/B3LYP calculations (Figure 15 and Figure 16), this intriguing [2+2+1] alkyne cyclotrimerization proceeds through Ru−P bond dissociation, phosphane attack at the coordinated acetylene to yield the 1-metallacyclopropene **F**, carbene vinyl insertion, and olefin vinyl insertion processes. Thus, in the present case, tethering can be considered to delay phosphane migration. The tethering of the phosphane ligand opens the interligand space between the metallacycle plane and the Ru−P vector and is depicted in Scheme 25. It is interesting to note that the corresponding angle of 103° in the tethered complex parallels that in RuCpCl, which mediates the cyclotrimerization of alkynes (vide supra).

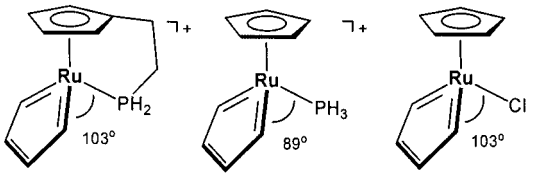

Scheme 25

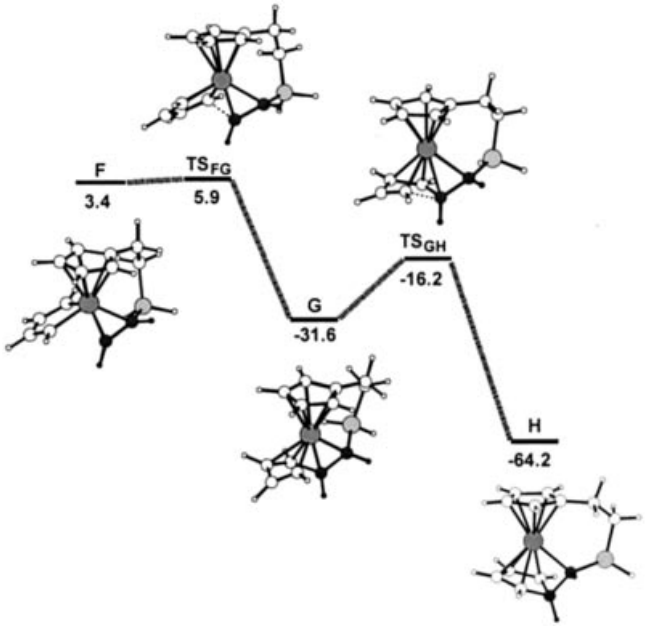

Figure 16. Energy profile of the B3LYP potential energy surfaces for the conversion of the 1-metallacyclopropene **F** into the final cyclotrimerization product **H**

Complex **C** is easily able to accommodate a third alkyne to afford the metallacyclopentadiene acetylene complex **D**. In the crowded complex **D**, the Ru−P bond is labilized, giving a free phosphane arm in **E** through an endothermic reaction,. The effect of ring strain introduced by a two-carbon tether has been demonstrated recently by Casey et al.[51] The subsequent reaction steps are quite straightforward: Nucleophilic attack of the pendant phosphane ligand at the coordinated acetylene results in the formation of the novel metallacyclopentadiene 1-metallacyclopropene complex **F**. The activation energy for this intramolecular process is 11.2 kcal/mol. It should be noted that related coupling reactions between a coordinated alkyne and a coordinated phosphane to yield 1-metallacyclopropenes and vinyl complexes have been reported in the literature.[52,53] Further, intermolecular nucleophilic additions of phosphanes and phosphites to alkyne ligands are feasible.[54] Complex **F** is prone to C−C coupling between the carbene carbon atom of the 1-metallacyclopropene moiety and the α-carbon

 © 2004 Wiley-VCH Verlag GmbH & Co. KGaA, Weinheim

atom of the metallacyclopentadiene unit bearing no substituent, to give **G**. This reaction requires an activation energy of only 2.5 kcal/mol and is energetically very favorable releasing 35.0 kcal/mol. The final and rate-determining step is the insertion of the vinyl moiety into the η^2-olefin unit to give **H**, thus completing the [2+2+1] cyclotrimerization.

6. Outlook

It is highly fascinating to witness the vast and diversified varieties of rearrangements within and between molecules ligated to the ruthenium(II) center. Tertiary phosphanes and carbon monoxide, which ordinarily are spectator ligands, function here as active ligands and give rise to a wide array of scenarios that compete with the process of trimerization. This may be compared with the behavior of other metal centers so as to arrive at a deeper understanding of the individuality of the various transition metals. Unfortunately, experimental results are often difficult to compare directly because of the variable reactions conditions applied. The better choice may involve the use of reliable theoretical studies which, however, are still in their infancy and hence scarce.

The reactions surveyed here may be compared with the theoretical study of acetylene trimerization with $CpCoL_2$ (L = CO, PR_3, olefin). At least two fundamental differences are obvious: (i) for $CpCoL_2$, the coligands L serve as leaving ligands only, that give way to the incoming acetylenes; (ii) there is a larger variety of intermediates for the ruthenium system. This may partly be related to the atomic radii; the smaller radius of Co (1.09 vs. 1.21 Å for Ru)[55] may control interligand interactions (through-space coupling)[56] in a different way. In this respect, it might be relevant to undertake investigations of the rhodium analog CpRh.

We can be convinced that in the future an ever-increasing number of theoretical treatments will follow, which ultimately will help us understand chemical periodicity from first principles.

Acknowledgments

Financial support by the "Fonds zur Förderung der wissenschaftlichen Forschung" (Project No. P16600-N11) is gratefully acknowledged.

[1] R. H. Grubbs, *C&EN* **2003**, *81*, 112.
[2] Y. Yamamoto, H. Takagishi, K. Itoh, *Org. Lett.* **2001**, *3*, 2117.
[3] Y. Yamamoto, H. Takagishi, K. Itoh, *J. Am. Chem. Soc.* **2002**, *124*, 28.
[4] S. Niu, M. B. Hall, *Chem. Rev.* **2000**, *100*, 353.
[5] S. W. Benson, *Thermochemical Kinetics*, Wiley, New York, **1968**.
[6] [6a] K. N. Houk, R. W. Gandour, R. W. Strozier, N. G. Rondan, L. A. Paquette, *J. Am. Chem. Soc.* **1979**, *101*, 6797. [6b] R. D. Bach, G. J. Wolber, H. B. Schlegel, *J. Am. Chem. Soc.* **1985**, *107*, 2837.
[7] H. Jiao, P. v. R. Schleyer, *J. Phys. Org. Chem.* **1998**, *11*, 655.
[8] [8a] W. Reppe, O. Schlichting, K. Klager, T. Toepel, *Justus Liebigs Ann. Chem.* **1948**, *560*, 1. [8b] W. Reppe, W. Schweckendiek, *Justus Liebigs Ann. Chem.* **1948**, *560*, 104.
[9] [9a] S. Saito, Y. Yamamoto, *Chem. Rev.* **2000**, *100*, 2901. [9b] N. E. Schore, *Chem. Rev.* **1988**, *88*, 1081. [9c] D. B. Grotjahn, "Transition metal alkyne complexes: transition meta-catalyzed cyclotrimerization", in *Comprehensive Organometallic Chemistry II* (Eds.: E. W. Abel, F. G. A. Stone, G. Wilkonson, L. S. Hegedus), Pergamon, Oxford, **1995**, vol. 12, pp. 741−770.
[10] [10a] K. P. C. Vollhardt, *Acc. Chem. Res.* **1977**, *10*, 1. [10b] K. P. C. Vollhardt, *Angew. Chem. Int. Ed. Engl.* **1984**, *23*, 539.
[11] [11a] Y. Wakatsuki, H. Yamazaki, *J. Chem. Soc., Chem. Commun.* **1973**, 280. [11b] H. Bönnemann, *Angew. Chem. Int. Ed. Engl.* **1978**, *17*, 505. [11c] H. Bönnemann, *Angew. Chem. Int. Ed. English.* **1985**, *24*, 248.
[12] Y. Yamamoto, R. Ogawa, K. Itoh, *Chem. Commun.* **2000**, 549.
[13] [13a] Y. Yamamoto, H. Kitahara, R. Ogawa, H. Kawaguchi, K. Tatsumi, K. Itoh, *J. Am. Chem. Soc.* **2000**, *122*, 4310. [13b] Y. Yamamoto, H. Kitahara, R. Hattori, K. Itoh, *Organometallics* **1998**, *17*, 1910.
[14] Y. Yamamoto, H. Kitahara, R. Ogawa, K. Itoh, *J. Org. Chem.* **1998**, *63*, 9610.
[15] Y. Yamamoto, R. Ogawa, K. Itoh, *J. Am. Chem. Soc.* **2001**, *123*, 6189.
[16] Y. Yamamoto, S. Okuda, K. Itoh, *Chem. Commun.* **2001**, 1102.
[17] Y. Yamamoto, H. Takagishi, K. Itoh, *J. Am. Chem. Soc.* **2002**, *124*, 6844.
[18] D. Suzuki, H. Urabe, F. Sato, *J. Am. Chem. Soc.* **2001**, *123*, 7925.
[19] B. M. Trost, F. D. Toste, *Angew. Chem. Int. Ed.* **2001**, *40*, 1114.
[20] J. H. Hardesty, J. B. Koerner, A. Albright, G.-Y. Lee, *J. Am. Chem. Soc.* **1999**, *121*, 6055.
[21] K. Kirchner, M. J. Calhorda, R. Schmid, L. F. Veiros, *J. Am. Chem. Soc.* **2003**, *125*, 11721.
[22] Y. Yamamoto, T. Arakawa, R. Ogawa, K. Itoh, *J. Am. Chem. Soc.* **2003**, *125*, 12143.
[23] For metallacyclopentatriene complexes see: [23a] M. O. Albers, P. J. A. deWaal, D. C. Liles, D. J. Robinson, E. Singleton, M. B. Wiege, *J. Chem. Soc., Chem. Commun.* **1986**, 1680. [23b] C. Gemel, A. LaPensée, K. Mauthner, K. Mereiter, R. Schmid, K. Kirchner, *Monatsh. Chem.* **1997**, *128*, 1189. [23c] L. Pu, T. Hasegawa, S. Parkin, H. Taube, *J. Am. Chem. Soc.* **1992**, *114*, 2712. [23d] W. Hirpo, M. D. Curtis, *J. Am. Chem. Soc.* **1988**, *110*, 5218. [23e] J. L. Kerschner, P. E. Fanwick, I. P. Rothwell, *J. Am. Chem. Soc.* **1988**, *110*, 8235. [23f] B. Hessen, A. Meetsma, F. van Bolhuis, J. H. Teuben, G. Helgesson, S. Jagner, *Organometallics* **1990**, *9*, 1925. [23g] C. Ernst, O. Walter, E. Dinjus, S. Arzberger, H. Görls, *J. Prakt. Chem.* **1999**, *341*, 801. [23h] Y. Yamada, J. Mizutani, M. Kurihara, H. Nishihara, *J. Organomet. Chem.* **2001**, *637-639*, 80.
[24] Y. Yamamoto, K. Hata, T. Arakawa, K. Itoh, *Chem. Commun.* **2003**, 1290.
[25] [25a] J. L. Paih, F. Monnier, S. Derien, P. H. Dixneuf, E. Clot, O. Eisenstein, *J. Am. Chem. Soc.* **2003**, *125*, 11964. [25b] J. L. Paih, S. Derien, P. H. Dixneuf, *Chem. Commun.* **1999**, 1437.
[26] B. M. Trost, M. T. Rudd, *J. Am. Chem. Soc.* **2002**, *124*, 4178.
[27] B. M. Trost, M. T. Rudd, *J. Am. Chem. Soc.* **2003**, *125*, 11516.
[28] C. S. Yi, R. Torres-Lubian, N. Liu, A. L. Rheingold, I. A. Guzei, *Organometallics* **1998**, *17*, 1257.
[29] M. Paneque, M. L. Poveda, N. Rendón, K. Mereiter, *J. Am. Chem. Soc.* **2003**, *125*, 1610.
[30] M. E. Stoll, P. Belanzoni, M. J. Calhorda, M. G. B. Drew, V. Félix, W. E. Geiger, C. A. Gamelas, I. S. Gonçales, C. C. Romão, L. F. Veiros, *J. Am. Chem. Soc.* **2001**, *123*, 10959.
[31] E. Rüba, R. Schmid, K. Kirchner, M. J. Calhorda, *J. Organomet. Chem.* **2003**, *682*, 204.
[32] K. Ferré, L. Toupet, V. Guerchais, *Organometallics* **2002**, *21*, 2578.
[33] R. Schmid, K. Kirchner, *J. Org. Chem.* **2003**, *68*, 8339.
[34] C. Slugovc, E. Rüba, R. Schmid, K. Kirchner, *Organometallics* **1999**, *18*, 4230.
[35] E. Becker, C. Slugovc, E. Rüba, C. Standfest-Hauser, K. Mere-

 © 2004 Wiley-VCH Verlag GmbH & Co. KGaA, Weinheim

iter, R. Schmid, K. Kirchner, *J. Organomet. Chem.* **2002**, *649*, 55.
[36] [36a] E. Rüba, K. Mereiter, R. Schmid, V. N. Sapunov, K. Kirchner, H. Schottenberger, M. J. Calhorda, L. F. Veiros, *Chem. Eur. J.* **2002**, *8*, 3948. [36b] E. Rüba, K. Mereiter, R. Schmid, K. Kirchner, *Chem. Commun.* **2001**, 1996. [36c] E. Rüba, K. Mereiter, R. Schmid, K. Kirchner, H. Schottenberger, *J. Organomet. Chem.* **2001**, *637-639*, 70. [36d] K. Mauthner, K. M. Soldouzi, K. Mereiter, R. Schmid, K. Kirchner, *Organometallics* **1999**, *18*, 4681.
[37] [37a] E. Becker, K. Mereiter, M. Puchberger, R. Schmid, K. Kirchner, *Organometallics* **2003**, *22*, 2124. [37b] E. Becker, E. Rüba, K. Mereiter, R. Schmid, K. Kirchner, *Organometallics* **2001**, *20*, 3851.
[38] E. Rüba, K. Mereiter, R. Schmid, K. Kirchner, E. Bustelo, M. C. Puerta, P. Valerga, *Organometallics* **2002**, *21*, 2912.
[39] For related $PAr_2(\eta^2$-arene) complexes see: [39a] N. Feiken, P. S. Pregosin, G. Trabesinger, M. Scalone, *Organometallics* **1997**, *16*, 537. [39b] N. Feiken, P. S. Pregosin, G. Trabesinger, A. Albinati, G. L. Evoli, *Organometallics* **1997**, *16*, 5756. [39c] T.-Y. Cheng, D. J. Szalda, R. M. Bullock, *Chem. Commun.* **1999**, 1629. [39d] H. Aneetha, M. Jimenez-Tenorio, M. C. Puerta, P. Valerga, K. Mereiter, *Organometallics* **2002**, *21*, 628.
[40] [40a] T. Arliguie, B. Chaudret, G. Chung, F. Dahan, *Organometallics* **1991**, *10*, 2973. [40b] M. L. Christ, S. Sabo-Etienne, B. Chaudret, *Organometallics* **1995**, *14*, 1082. [40c] A. F. Borowski, S. Sabo-Etienne, M. L. Christ, *Organometallics* **1996**, *15*, 1427. [40d] S. Hietkamp, D. J. Hufkens, K. Vrieze, *J. Organomet. Chem.* **1978**, *152*, 347. [40e] C. Six, B. Gabor, H. Görls, R. Mynott, P. Philipps, W. Leitner, *Organometallics* **1999**, *18*, 3316.
[41] [41a] P. N. Riley, J. R. Parker, P. E. Fanwick, I. P. Rothwell, *Organometallics* **1999**, *18*, 3579 and references cited therein. [41b] A. H. Klahn, B. Oelckers, F. Godoy, M. T. Garland, A. Vega, R. Perutz, C. L. Higgitt, *J. Chem. Soc., Dalton Trans.* **1998**, 3079 and references cited therein.
[42] For related ruthenium tetramethylfulvene complexes see: [42a] C. Li, L. Luo, S. P. Nolan, W. Marshall, P. J. Fagan, *Organometallics* **1996**, *15*, 3456. [42b] L. Fan, M. L. Turner, M. B. Hursthouse, K. M. A. Malik, O. V. Gusev, P. M. Maitlis, P. M, *J. Am. Chem. Soc.* **1994**, *116*, 385. [42c] L. Fan, C. Wei, F. I. Aigbirhio, M. L. Turner, O. V. Gusev, L. N. Morozova, D. R. T. Knowles, P. M. Maitlis, *Organometallics* **1996**, *15*, 98. [42d] D. M. Hankin, A. A. Danopoulos, G. Wilkinson, T. K. N. Sweet, M. B. Hursthouse, *J. Chem. Soc., Dalton Trans.* **1996**, 4063. [42e] C. Gemel, K. Mereiter, R. Schmid, K. Kirchner, *Organometallics* **1997**, *16*, 5601. [42f] U. Kölle, B.-S. Kang, *J. Organomet. Chem.* **1990**, *386*, 267.
[43] S. Pavlik, K. Mereiter, R. Schmid, K. Kirchner, *Organometallics* **2003**, *22*, 1771.
[44] [44a] J. R. Fritch, K. P. C. Vollhardt, *Angew. Chem. Int. Ed. Engl.* **1979**, *18*, 409. [44b] G. Ville, K. P. C. Vollhardt, *J. Am. Chem. Soc.* **1981**, *103*, 5267. [44c] G. Ville, K. P. C. Vollhardt, M. J. Winter, *Organometallics* **1984**, *3*, 1177. [44d] B. K. Campion, R. H. Heyn, T. D. Tilley, *Organometallics* **1990**, *9*, 1106.
[45] E. Rüba, K. Mereiter, K. M. Soldouzi, C. Gemel, R. Schmid, K. Kirchner, E. Bustelo, M. C. Puerta, P. Valerga, *Organometallics* **2000**, *19*, 5384.
[46] W. Reppe, H. Vetter, *Justus, Liebigs Ann. Chem.* **1953**, *582*, 133.
[47] [47a] M. L. H. Green, L. Pratt, G. Wilkinson, *J. Chem. Soc.* **1960**, 989. [47b] E. Weiss, R. Merenyi, W. Huebel, *Chem. Ber.* **1962**, *95*, 1170. [47c] Y. Blum, Y. Shvo, D. F. Chodosh, *Inorg. Chim. Acta* **1985**, *97*, L25. [47d] A. J. Pearson, R. J. Shively, R. A. Dubbert, *Organometallics* **1992**, *11*, 4096.
[48] [48a] R. Markby, H. W. Sternberg, I. Wender, *Chem. Ind.* **1959**, 1381. [48b] R. S. Dickson, G. R. Tailby, *Aust. J. Chem.* **1970**, *23*, 1531. [48c] J. H. Bieri, A. Dreiding, T. C. C. Gartenmann, E. R. F. Gesing, R. Kunz, R. Prewo, *J. Organomet. Chem.* **1986**, *306*, 241. [48d] H. Borwieck, O. Walter, E. Dinjus, J. Rebizant, *J. Organomet. Chem.* **1998**, *570*, 121. [48e] E. R. R. F. Gesing, J. P. Tane, K. P. C. Vollhardt, *Angew. Chem.* **1980**, *92*, 1057.
[49] T. P. Gill, K. R. Mann, *Organometallics* **1982**, *1*, 485.
[50] E. Becker, K. Mereiter, M. Puchberger, R. Schmid, K. Kirchner, *Organometallics* **2003**, *22*, 2124.
[51] For [2+2+1] cyclotrimerization reactions of alkynes see: [51a] J. M. O'Connor, A. Closson, K. Hiibner, R. Merwin, P. K. Gantzel, D. M. Roddick, *Organometallics* **2001**, *20*, 3710. [51b] H. J. Kim, N. S. Choi, S. W. Lee, *J. Organomet. Chem.* **2000**, *616*, 67. [51c] J. M. O'Connor, K. Hiibner, R. Merwin, P. K. Gantzel, B. S. Fong, M. Adams, A. L. Rheingold, *J. Am. Chem. Soc.* **1997**, *119*, 3631. [51d] G. Moran, M. Green, A. G. Orpen, *J. Organomet. Chem.* **1983**, *250*, C15. [51e] J. Moreto, K. Maruya, P. M. Bailey, P. M. Maitlis, *J. Chem. Soc., Dalton Trans.* **1982**, 1341. [51f] L. S. Liebeskind, R. Chidambaram, *J. Am. Chem. Soc.* **1987**, *109*, 5025.
[52] H. Ishino, S. Kuwata, Y. Ishii, M. Hidai, *Organometallics* **2001**, *20*, 13.
[53] J. M. O'Connor, K. D. Bunker, *J. Organomet. Chem.* **2003**, *671*, 1.
[54] [54a] J. L. Davidson, *J. Chem. Soc., Dalton Trans.* **1986**, 2423. [54b] J. L. Davidson, G. Vasapollo, L. Manojlovic-Muir, K. W. Muir, *J. Chem. Soc., Chem. Commun.* **1982**, 1025. [54c] S. R. Allen, R. G. Beevor, M. Green, N. C. Norman, A. G. Orpen, *J. Chem. Soc., Dalton Trans.* **1985**, 435. [54d] J. R. Morrow, T. L. Tonker, J. L. Templeton, W. R. Kenan, *J. Am. Chem. Soc.* **1985**, *107*, 6956.
[55] C. H. Suresh, N. Koga, *J. Phys. Chem. A* **2001**, *105*, 5940.
[56] V. N. Sapunov, R. Schmid, K. Kirchner, H. Nagashima, *Coord. Chem. Rev.* **2003**, *238-239*, 363.

Received March 19, 2004

 © 2004 Wiley-VCH Verlag GmbH & Co. KGaA, Weinheim

A Structural Study of Bisphosphonate Metal Complexes − Three New Polymeric Structures of the Calcium Complex of Clodronic Acid

Mervi Kontturi,*[a] Sirpa Peräniemi,[b] Jouko J. Vepsäläinen,[b] and Markku Ahlgrén[a]

Keywords: Bisphosphonate / Clodronate / Calcium / Layered compounds / X-ray diffraction

Three novel calcium complexes of clodronic acid were prepared and their structures determined by single-crystal X-ray diffractometry. Previously, a monomeric structure, $[Ca\{Cl_2C(PO_3H)_2\}(H_2O)_5]$ (**1**), has been determined, but the new structures are polymeric: $[\{Ca_2[Cl_2C(PO_3)_2](H_2O)_6\}\cdot 4.5H_2O]_n$ (**2**), $[\{Ca_2Na_{0.5}[Cl_2C(PO_3)_2](H_2O)_8\}Cl_{0.5}\cdot 4H_2O]_n$ (**3**) and $[\{Ca_5[Cl_2C(PO_3)_2]_2(H_2O)_{15}\}(NO_3)_2\cdot 1.5H_2O]_n$ (**4**); and they provide new, important information about the binding abilities of clodronic acid. Compounds **2**–**4** crystallise in the triclinic crystal system, the space group being $P\bar{1}$ with $Z = 2$. Compound **2** consists of Ca atoms and Cl_2MBP ligands connected to one-dimensional chains. The chains are held together by hydrogen bonds formed by aqua ligands and lattice water molecules. The structure of **3** consists of similar calcium clodronate chains forming two-dimensional layers through additional, six-coordinate Na atoms. Compound **4** consists of two-dimensional calcium clodronate layers, the calcium atoms are connected by Cl_2MBP– and aqua ligands. The nitrate groups and lattice water molecules lie between the layers and hold them together. The layered compounds **3** and **4** reveal substantial porosity.
(© Wiley-VCH Verlag GmbH & Co. KGaA, 69451 Weinheim, Germany, 2004)

Introduction

Bisphosphonates, BP, are an interesting class of compounds due to their pharmaceutical applications,[1−4] and also due to their potential chemical applications in ion exchange, sorption, catalysis, and so forth.[5−8] Typically, bisphosphonates are used to inhibit the mineralization of soft tissues and as a therapy for bone-formation and resorption disorders.[1−4] It has been proposed that one stage of the mechanism of action of the non-nitrous methylenebisphosphonates (MBP) is that they are rapidly adsorbed onto the hydroxyapatite surface of bone by forming a layered structure.[4,9−11] Recently, new insights have been reported concerning the molecular mechanism of action of MBPs.[12]

The use of BPs in ion exchange, sorption and catalysis is based on their ability to form porous materials when complexing with metal atoms and their effectiveness is related to the degree of porosity. The structures of these materials consist of chains, layers or pillared layers; dimensionality depends on the number of donor atoms of the ligands, but also on the size of the organic group between the phosphonate groups and on the degree of protonation of the phosphonate group.[5−8]

Clodronate, disodium dichloromethylenebisphosphonate tetrahydrate, is one of the best-documented MBP derivatives that is used effectively in medical applications.[13] However, there are no studies on how clodronate can form a layered structure on the hydroxyapatite surface of bone. Clodronate has six possible O-donor atoms, and therefore we can presume that it also forms polymeric structures to be utilized in chemical applications. The previously reported crystal structure of calcium clodronate, $[Ca\{Cl_2C(PO_3H)_2\}(H_2O)_5]$ (**1**), revealed that Cl_2MBP itself acted only as a bidentate chelating ligand with Ca, forming a monomeric complex.[14] However, we have reported structures of alkaline earth metal complexes of a symmetrical diethyl ester derivative of clodronic acid in which one O atom of each of the two phosphonate groups is masked by an ethyl group, and the results showed that this ligand provides 3−5 donor O atoms, producing dimeric and polymeric structures.[15] In the present study, three new polymeric structures of the calcium complex of clodronic acid, $[\{Ca_2[Cl_2C(PO_3)_2](H_2O)_6\}\cdot 4.5H_2O]_n$ (**2**), $[\{Ca_2Na_{0.5}[Cl_2C(PO_3)_2](H_2O)_8\}Cl_{0.5}\cdot 4H_2O]_n$ (**3**) and $[\{Ca_5[Cl_2C(PO_3)_2]_2(H_2O)_{15}\}(NO_3)_2\cdot 1.5H_2O]_n$ (**4**), are depicted.

Results and Discussion

The previously-published calcium clodronate **1** was prepared from calcium monohydrogenphosphate and the disodium salt of clodronic acid by slow evaporation at 60 °C.[14,16] We prepared this monomeric structure and the new polymeric calcium clodronate compounds from the disodium salt of clodronic acid (clodronate) and calcium nitrate (compounds **1**, **2** and **4**) or from clodronate and calcium

[a] Department of Chemistry, University of Joensuu
P. O. Box 111, 80101 Joensuu, Finland
Fax: (internat.) +35813-2513377
E-mail: mervi.kontturi@joensuu.fi
[b] Department of Chemistry, University of Kuopio
P. O. Box 1627, 70211 Kuopio, Finland

chloride (compound **3**) using a gel method. The gel-crystallisation tests revealed that concentrated solutions of the starting materials always produced calcium complex **1**. On the other hand, the new polymeric compounds were prepared under carefully controlled conditions; the effective factors are the pH of the ligand solution, the metal concentration and the rate of the diffusion and precipitation processes. In the preparation of **1**, clodronate (0.069 mmol) was used in the gel (pH 4.2, 1 mL), and the metal salt was offered as a concentrated $Ca(NO_3)_2 \cdot 4H_2O$ solution (3.34 M, 1 mL), which was placed above the gel and after one week was replaced by an acetone/ethanol (1:1) solution. Compound **4** was prepared under similar conditions, but using only a quarter of the amount of clodronate (0.017 mmol) in pH 5.0 and by placing a pure tetramethoxysilane (TMOS)-gel layer between the original gel and the precipitants. Compound **2** was also prepared from clodronate (0.017 mmol) but in pH 6.2. A pure TMOS-gel layer was placed above the native gel, and the concentration of the Ca solution was 1/75 of the former. No organic precipitant was needed to obtain the crystals of **2**. Compound **3** was prepared using the same amount of clodronate as in **1** and $CaCl_2$ (0.14 mmol), both of which were in the gel (pH 3.2, 1 mL), and acetone was placed above the gel immediately after gelation.

The calcium clodronate compound **1** consists of monomeric units,[14] while calcium compounds **2**−**4** are polymeric. The density increases with the dimensionality: it is lowest for **1** (1.86 g/cm^3) and highest for **4** (2.04 g/cm^3). Compound **2**, $[\{Ca_2[Cl_2C(PO_3)_2](H_2O)_6\} \cdot 4.5H_2O]_n$, consists of infinite chains, the asymmetric unit containing two independent Ca atoms and one Cl_2MBP ligand (see Figure 1, left). Compound **3**, $[\{Ca_2Na_{0.5}[Cl_2C(PO_3)_2](H_2O)_8\}Cl_{0.5} \cdot 4H_2O]_n$ (see Figure 2, left), consists of chains similar to those in **2**, the chains being connected to a two-dimensional layered structure by six-coordinate Na centres. Compound **4**, $[\{Ca_5[Cl_2C(PO_3)_2]_2(H_2O)_{15}\}(NO_3)_2 \cdot 1.5H_2O]_n$, consists of two-dimensional layers of calcium clodronate, the asymmetric unit containing five independent calcium atoms connected to each other by Cl_2MBP− and aqua ligands (see Figure 3, left).

In compounds **1**−**4**, the calcium atoms are hepta-coordinated, the geometry around the metal atom is a distorted, monocapped trigonal prism, and the average Ca−O bond length is 2.41(6) Å. In **2** and **3** there are two crystallographically independent Ca atoms in the asymmetric unit (see Figure 1, right, and Figure 2, right). Four of the O atoms around the two Ca atoms are from the chelating Cl_2MBP ligands, and the coordination sphere is completed by three aqua ligands. The coordinated Cl_2MBP ligands form both four- and six-membered chelate rings with the metal atoms. In **3** one aqua ligand of Ca1 also acts as a bridge between Ca1 and an additional, six-coordinate Na atom [Na−O 2.44(2) Å], which lies in the centre of symmetry. The rest of the coordination sites around Na are occupied by aqua ligands.

In **4** there are five crystallographically independent Ca atoms (see Figure 3, left). The coordination sphere of calcium atoms 1, 2, 4 and 5 consists of four oxygen atoms from two chelating ligands, forming both four- and six-membered chelate rings. The coordination spheres of the Ca atoms are completed with three aqua ligands. The coor-

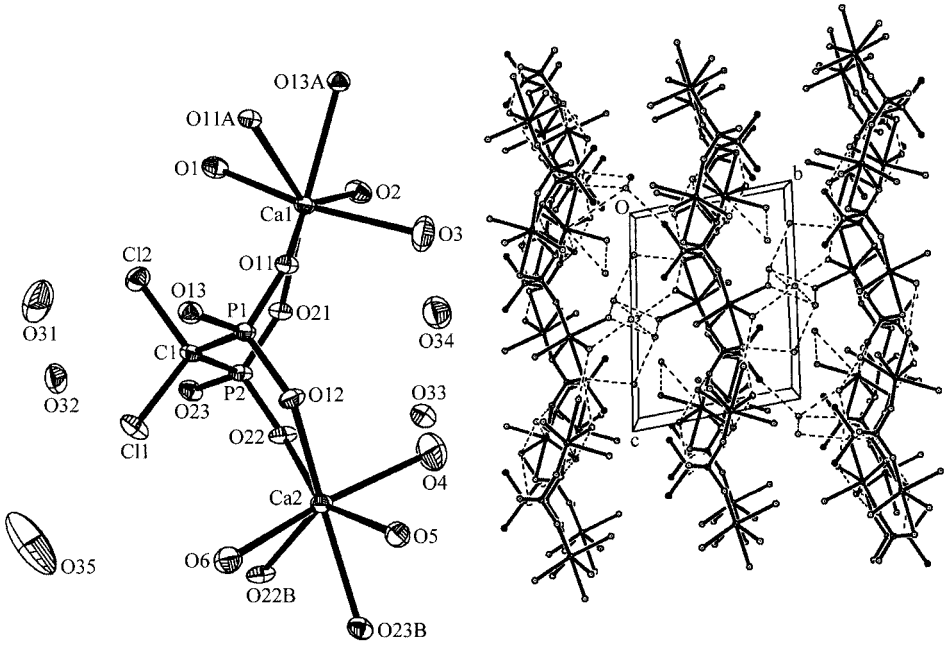

Figure 1. The structure of the asymmetric unit of **2** with numbering scheme and thermal ellipsoids (50 %; left) and packing of **2** (right); hydrogen atoms and water molecules O33′, O34′ and O35′ are omitted for clarity; selected bond lengths (Å): Ca1−O11 2.380(2), Ca1−O21 2.332(2), Ca1−O11A 2.482(2), Ca1−O13A 2.502(2), Ca1−O1 2.426(3), Ca1−O2 2.421(3), Ca1−O3 2.390(3), Ca2−O12 2.334(2), Ca2−O22 2.360(2), Ca2−O22B 2.481(2), Ca2−O23B 2.492(2), Ca2−O4 2.392(3), Ca2−O5 2.435(2), Ca2−O6 2.435(2) [A refers to atom at ($-x$, $1 - y$, $-z$) and B at ($1 - x$, $1 - y$, $1 - z$)]

 © 2004 Wiley-VCH Verlag GmbH & Co. KGaA, Weinheim

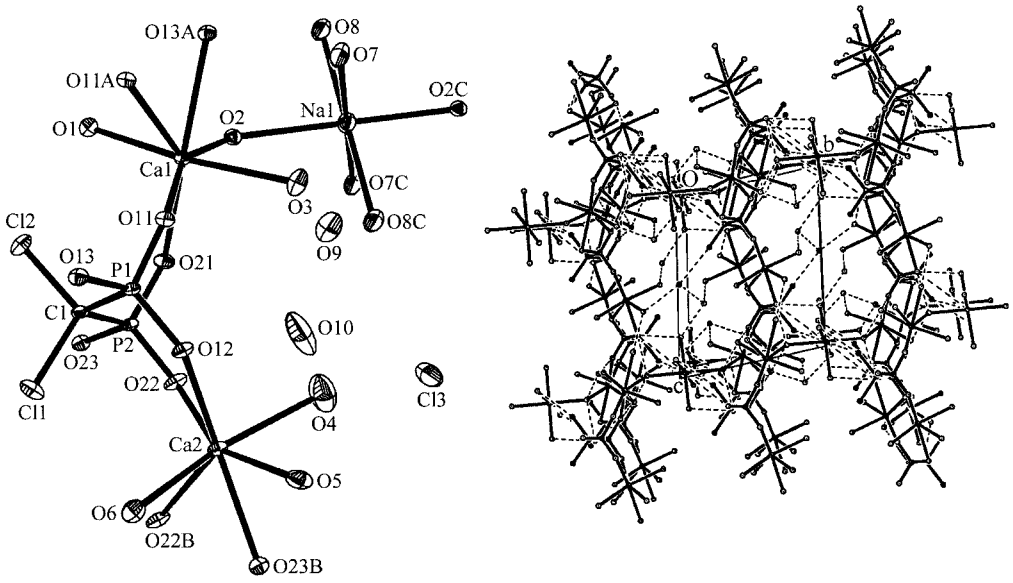

Figure 2. The structure of the asymmetric unit of **3** with numbering scheme and thermal ellipsoids (50 %; left) and packing of **3** in the direction of the *a* axis (right); hydrogen atoms are omitted for clarity; selected bond lengths (Å): Ca1−O11 2.339(1), Ca1−O21 2.340(1), Ca1−O11A 2.435(1), Ca1−O13A 2.545(1), Ca1−O1 2.445(1), Ca1−O2 2.458(1), Ca1−O3 2.407(2), Ca2−O12 2.335(1), Ca2−O22 2.357(1), Ca2−O22B 2.519(1), Ca2−O23B 2.471(1), Ca2−O4 2.395(1), Ca2−O5 2.408(1), Ca2−O6 2.419(2), Na1−O2 2.448(1), Na1−O7 2.454(2), Na1−O8 2.393(2) [A refers to atom at ($-x$, $1 - y$, $-z$), B at ($1 - x$, $1 - y$, $1 - z$) and C at ($1 - x$, $2 - y$, $-z$)]

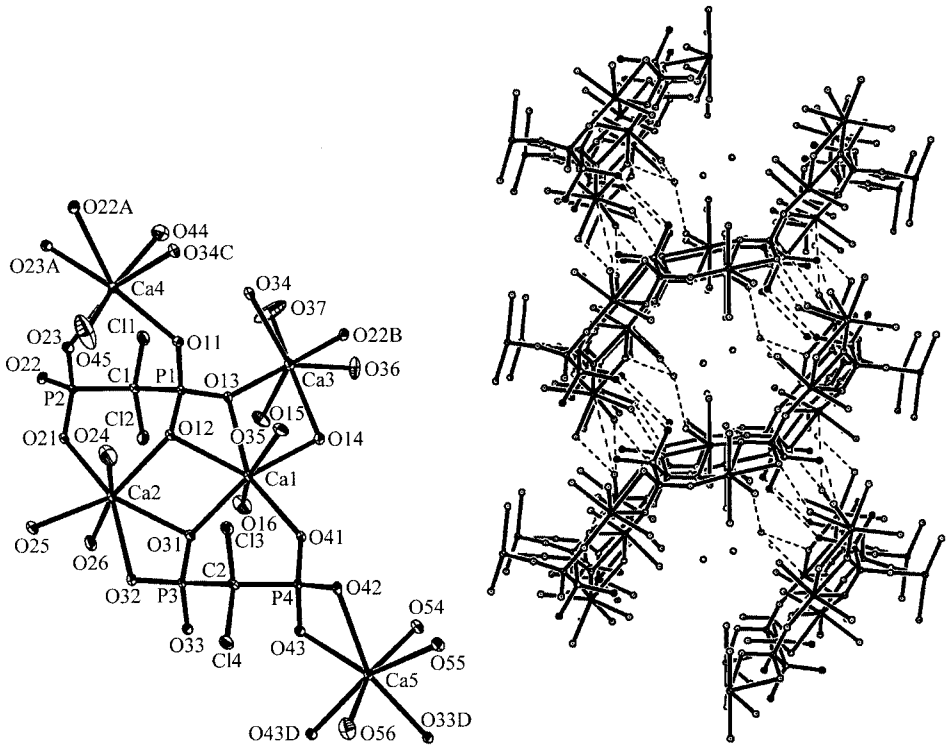

Figure 3. The structure of the asymmetric unit of **4** with numbering scheme and 50 % thermal ellipsoids (hydrogen atoms and nitrate ions are omitted for clarity; left) and packing of **4** in the direction of the *a* axis (hydrogen atoms and oxygen atoms of nitrate ions are omitted for clarity; right); selected bond lengths (Å): Ca1−O12 2.494(3), Ca1−O13 2.491(3), Ca1−O31 2.313(3), Ca1−O41 2.336(3), Ca1−O14 2.483(3), Ca1−O15 2.414(3), Ca1−O16 2.354(3); Ca2−O12 2.321(3), Ca2−O21 2.369(3), Ca2−O31 2.425(3), Ca2−O32 2.532(3), Ca2−O24 2.420(4), Ca2−O25 2.399(3), Ca2−O26 2.408(3); Ca3−O13 2.292(3), Ca3−O22B 2.310(2), Ca3−O14 2.532(3), Ca3−O34 2.576(3), Ca3−O35 2.408(3), Ca3−O36 2.392(3), Ca3−O37 2.370(3); Ca4−O11 2.349(3), Ca4−O22A 2.499(3), Ca4−O23 2.310(3), Ca4−O23A 2.456(3), Ca4−O34C 2.450(3), Ca4−O44 2.381(3), Ca4−O45 2.370(4); Ca5−O33D 2.338(3), Ca5−O42 2.528(3), Ca5−O43 2.440(3), Ca5−O43D 2.356(3), Ca5−O54 2.451(3), Ca5−O55 2.425(3), Ca5−O56 2.435(3) [A refers to atom at ($1 - x$, $1 - y$, $-z$), B at ($x - 1$, y, z), C at ($-x$, $1 - y$, $-z$) and D at ($-x$, $-y$, $1 - z$)]

 © 2004 Wiley-VCH Verlag GmbH & Co. KGaA, Weinheim

dination sphere of calcium atom 3 consists of only two phosphonate oxygen atoms originating from two different Cl_2MBP ligands and the rest of the sites are occupied by five aqua ligands.

In the monomeric compound **1**, one of the oxygen atoms of both phosphonate groups of Cl_2MBP is coordinated to the Ca atom, the second oxygen atom being unbound and the third protonated.[14] In the case of the polymeric compounds **2**−**4**, there are neither unbound nor protonated oxygen atoms: the Cl_2MBP ligands are coordinated to the ambient calcium atoms through all six oxygen atoms, acting as chelating and bridging ligands. In **2** and **3** all Cl_2MBP ligands form two six-membered and two four-membered chelate rings simultaneously and are coordinated to four metal atoms. In **4** one ligand acts similarly to these, while the other one is connected to six Ca atoms. The bond lengths and angles of the Cl_2MBP ligand in compounds **2**−**4** are all typical.

Some porosity was found in all compounds. In **2** the chains are connected to each other by intermolecular hydrogen bonds, forming layers parallel to the (010) plane. The chlorine atoms and aqua ligands point towards the interlayer section, and the space is filled with lattice water molecules (Figure 1, right). Between the infinite chains there are intermolecular hydrogen bonds involving the aqua ligands and phosphonate O atoms [O···O distances 2.603(12)−3.051(8) Å and angles 118−179°]. In **3** the layers are parallel to the (−111) plane. The structure reveals substantial porosity in the packing diagram, as seen in Figure 2, right. Along the *a* axis, the layers are packed one on top of the other, forming pillars where two Na and four Ca atoms in a 24-membered ring define a cavity on the plane. The aqua ligands of each metal atom point into the cavity, and the Cl3 ions sit in the middle of the opening surrounded by lattice water molecules. There are also smaller pores between the layers. Intramolecular hydrogen bonds are formed between the aqua ligands, and the intermolecular hydrogen bonds involve both water molecules and chlorine Cl3 atoms [O···O/Cl distances 2.718(2)−3.339(4) Å and angles 119−170°] holding the layers together. In compound **4**, the layers are parallel to the (011) plane, and tunnels are formed between the layers along the *a* axis. The tunnels are filled with nitrate molecules and lattice water molecules (see Figure 3, right). Both inter- and intramolecular hydrogen bonds are found, the O···O distances being 2.457(12)−3.084(4) Å and the angles 117−177°. The intermolecular hydrogen bonds hold the adjacent calcium clodronate layers together, and involve water molecules and the O atoms of nitrate.

Conclusion

The previously-published structure and the present ones clearly differ: in compound **1**, the Cl_2MBP ligand provides only two donor O atoms, being chelated to one Ca atom;[14] while in the new polymeric compounds **2**−**4**, all Cl_2MBP ligands provide six donor O atoms, forming two six-membered and two four-membered chelate rings and acting as mono- and polyatomic bridges between the Ca atoms. As a result, the Cl_2MBP ligands in **2**−**4** are tightly bound to several Ca atoms through all O atoms, resulting in one-dimensional chains or two-dimensional layers, connected to a three-dimensional open network through hydrogen bonds. In compound **3**, the porosity is marked. These new findings concerning the coordination abilities of clodronic acid may explain its activity in forming a layered structure on the hydroxyapatite surface of bone and also provide new information about the ability of clodronic acid to form porous materials that can be used in chemical applications.

Experimental Section

General Remarks: All reagents used for the synthesis and characterisation of compounds **2**−**4** were of analytical reagent grade. The synthesis and characterisation of clodronic acid and its disodium salt $Na_2[CCl_2(PO_3H_2)]\cdot 4H_2O$ have been reported earlier.[14] The metal complexes were crystallised using gel methods **A** (**3**) and **C** (**1**, **2**, and **4**). In method **A**, a carefully weighed amount of $Na_2[CCl_2(PO_3H)_2]\cdot 4H_2O$ and metal salt were dissolved in water (2 × 0.45 mL) and warmed to 40 °C in a water bath. The solutions were then mixed together, and the TMOS (0.1 mL) was added. The two-phase system was shaken until homogeneous, and the emulsion was left to form a gel. Crystallisation was induced by adding an organic precipitant (1 mL) above the gel. In method **C**, $Na_2[CCl_2(PO_3H)_2]\cdot 4H_2O$ was dissolved in water (0.9 mL); and if necessary, the pH was adjusted with NaOH (0.02−1.0 M). TMOS (0.1 mL) was added; and the two-phase system was shaken until homogeneous. The emulsion was left to form a gel. In the preparation of **2** and **4**, after gelation a pure TMOS-gel layer (0.5 mL, 20 % v/v) was added above the native gel. The metal salt was dissolved in water (1.0 mL), added above the gel, and after 1−2 weeks replaced with organic precipitant (1.0 mL).

$[Ca\{Cl_2C(PO_3H)_2\}(H_2O)_5]$ (1): Preparation of **1** by slow evaporation at 60 °C has been described previously.[14,16] In this investigation, **1** was prepared with method **C** by placing clodronate (0.069 mmol, pH 4.5) in TMOS-gel and adding a water solution of $Ca(NO_3)_2\cdot 4H_2O$ (3.34 M, pH 4.2) above the gel. After one week the metal salt solution was replaced with a 1:1 acetone/ethanol solution. In a few weeks the crystals formed in the shape of cubes. The measured cell dimensions and results of elemental analysis agree with the earlier results.[14]

$[\{Ca_2[Cl_2C(PO_3)_2](H_2O)_6\}\cdot 4.5H_2O]_n$ (2): In the preparation of **2** with method **C**, clodronate (0.017 mmol) was dissolved in water and the pH was adjusted to 6.2. A water solution of $Ca(NO_3)_2\cdot 4H_2O$ (0.043 M, pH 4.5) was added above a pure TMOS-gel layer. Two days later the colourless, plank-like crystals were formed above the gel. $CH_{21}Ca_2Cl_2O_{16.5}P_2$ (510.18): calcd. C 2.35, H 4.15; Ca, 15.7; found C 2.11, H 3.90; Ca, 15.6.

$[\{Ca_2Na_{0.5}[Cl_2C(PO_3)_2](H_2O)_8\}Cl_{0.5}\cdot 2H_2O]_n$ (3): In the preparation of **3** with method **A**, both clodronate (0.069 mmol) and calcium chloride (0.14 mmol) were dissolved in water (pH 3.2) and TMOS was added. After gelation, acetone was placed above the gel, and in six months thin crystals were formed above the gel. $CH_{20}Ca_2Cl_{2.5}Na_{0.5}O_{16}P_2$ (530.39): calcd. C 2.26, H 3.80; found C 2.04, H 4.12.

$[\{Ca_5[Cl_2C(PO_3)_2]_2(H_2O)_{15}\}(NO_3)_2\cdot 1.5H_2O]_n$ (4): In the preparation of **4** with method **C**, clodronate (0.017 mmol) was dissolved

 © 2004 Wiley-VCH Verlag GmbH & Co. KGaA, Weinheim

Table 1. Crystal data of compounds **2**, **3** and **4**

	2	**3**	**4**
Empirical formula	$CH_{21}Ca_2Cl_2O_{16.5}P_2$	$CH_{20}Ca_2Cl_{2.5}Na_{0.5}O_{16}P_2$	$C_2H_{33}Ca_5Cl_4N_2O_{34.5}P_4$
M_r	510.18	530.39	1103.38
Crystal system	Triclinic	Triclinic	Triclinic
Space group	$P\bar{1}$	$P\bar{1}$	$P\bar{1}$
a (Å)	8.8019(3)	8.7689(3)	8.7757(3)
b (Å)	8.8977(3)	9.2561(3)	10.4116(5)
c (Å)	11.9694(4)	11.9222(4)	20.2680(9)
α (°)	98.640(2)	97.976(2)	89.337(2)
β (°)	106.681(2)	106.357(2)	88.556(3)
γ (°)	92.886(2)	97.496(2)	75.815(3)
V (Å^3)	883.43(5)	904.77(5)	1794.8(1)
Z	2	2	2
D_m (g cm^{-3})[a]	1.89(4)	–	2.00(8)
D_c (g cm^{-3})	1.92	1.95	2.04
F (000)	526	544	1126
μ(Mo-K_α) (mm^{-1})	1.204	1.259	1.338
Crystal size (mm^3)	0.20 × 0.20 × 0.10	0.20 × 0.20 × 0.10	0.20 × 0.20 × 0.20
θ Range (°)	3.70–26.00	2.57–26.00	2.25–25.00
Temperature (K)	120(2)	120(2)	120(2)
No. of unique data	3399	3561	5782
No. of obs. reflections	2999	3249	5206
No. of parameters	235	223	466
R_1 (Fo) > 4σ(Fo)	0.0428	0.0253	0.0447
ωR_2 (all data)	0.1169	0.0660	0.1040
Goodness-of-fit	1.087	1.043	1.010
Largest diff. peak and hole (e·Å^{-3})	0.606 and −0.612	0.587 and −0.433	1.723 and −0.909

Measured at room temperature.

in water and the pH adjusted to 5.0. A water solution of $Ca(NO_3)_2{\cdot}4H_2O$ (3.34 M, pH 4.2) was placed above a pure TMOS-gel layer. After two weeks the metal salt solution was replaced with a 1:1 acetone/ethanol solution. About two months later colourless crystals were formed as thin plates in and above the gel. $C_2H_{33}Ca_5Cl_4N_2O_{34.5}P_4$ (1103.38): calcd. C 2.18, H 3.01, N 2.54, Ca, 18.2; found C 2.20, H 3.13, N 2.48, Ca, 18.1.

X-ray Crystallographic Study: Single-crystal x-ray diffraction studies were performed on a Nonius Kappa CCD diffractometer using Mo-K_α radiation (λ = 0.71073 Å). Denzo and Scalepack[17] programs were used for cell refinements and data reduction. The structures were solved by direct methods with SHELXS 97.[18] Structural refinements were carried out with SHELXL 97.[19] The hydrogen atoms were placed in calculated positions and not refined. In **2** two water molecules, O33 and O34 are disordered over two positions with population parameters 50/50 and water molecule O35 is disordered around a centre of symmetry. The hydrogen atoms of the disordered water molecules were omitted in the calculations. In **3** the Cl3 atom is disordered around a centre of symmetry. Crystallographic data of compounds **2**–**4** are summarised in Table 1.

CCDC-233048 (compound **2**), -233049 (compound **3**), -233050 (compound **4**) contain the supplementary crystallographic data for this paper. These data can be obtained free of charge at www.ccdc.cam.ac.uk/conts/retrieving.html [or from the Cambridge Crystallographic Data Centre, 12 Union Road, Cambridge CB2 1EZ, UK; Fax: +44 1223/336-033; E-mail: deposit@ccdc.cam.ac.uk].

[1] H. Fleisch, *Bisphosphonates in Bone Disease: From the Laboratory to the Patient*, The Parthenon Publishing Group Inc., New York, **1995**.
[2] H. Fleisch, R. G. G. Russel, B. Simpson, R. C. Muehlbauer, *Nature* **1969**, *223*, 211–212.
[3] J. A. Kanis, E.V. McCloskey, *Prog. Basic Clin. Pharmacol*, 4th ed., Karger, Basel, **1990**, 89–136.
[4] O. L. M. Bijvoet, H. A. Fleisch, R. E. Canfield, R. G. G. Russell, *Bisphosphonates on Bones*, Elsevier, Amsterdam, **1995**.
[5] B. Zhang, A. Clearfield, *J. Am. Chem. Soc.* **1997**, *119*, 2751–2752.
[6] G. Alberti, M. Casciola, U. Constantino, R. Vivani, *Adv. Mater.* **1996**, *8*, 291–303.
[7] J. L. Snover, H. Byrd, E. P. Suponeva, E. Vicenzi, M. E. Thompson, *Chem. Mater.* **1996**, *8*, 1490–1499.
[8] C. Serre, G. Férey, *J. Mater. Chem.* **2002**, *12*, 2367–2369.
[9] J. C. Frith, J. Mönkkönen, S. Auriola, H. Mönkkönen, M. J. Rogers, *Arthritis Rheum.* **2001**, *44*, 2201–2210.
[10] H. L. Benfor, J. C. Frith, S. Auriola, J. Mönkkönen, M. J. Rogers, *Mol. Pharmacol.* **1999**, *56*, 131–140.
[11] J. C. Frith, J. Mönkkönen, G. M. Blackburn, R. G. Russell, M. J. Rogers, *J. Bone. Miner. Res.* **1997**, *12*, 1358–1367.
[12] M. J. Rogers, *Curr. Pharm. Des.* **2003**, *9*, 2643–2658.
[13] P. P. Major, A. Lipton, J. Berenson, G. H. Hortobagyi, *Cancer* **2000**, *88*, 6–14.
[14] M. Nardelli, G. Pelizzi, G. Staibano, E. Zucchi, *Inorg. Chim. Acta* **1983**, *80*, 259–271.
[15] M. Kontturi, E. Vuokila-Laine, S. Peräniemi, T. T. Pakkanen, J. J. Vepsäläinen, M. Ahlgrén, *J. Chem. Soc., Dalton Trans.* **2002**, 1969–1973.
[16] V. A. Uchtman, *J. Phys. Chem.* **1972**, *76*, 1304–1310.
[17] Z. Otwinowski, W. Minor, *Methods Enzymol.* **1997**, *276*, 307–326.
[18] G. M. Sheldrick, *SHELXS 97, Program for Crystal Structure Determination*, University of Göttingen, **1997**.
[19] G. M. Sheldrick, *SHELXS 97, Program for Crystal Structure Refinement*, University of Göttingen, **1997**.

Received March 24, 2004

 © 2004 Wiley-VCH Verlag GmbH & Co. KGaA, Weinheim

Synthesis and Crystal Structure of $Cs_2(CN_3H_6)_3[(C_2H_5)_2NH_2][W_7O_{22}(O_2)_2]\cdot 3H_2O$

Hiroyuki Suzuki,[a] Masato Hashimoto,*[a] and Seichi Okeya[a]

Keywords: Polyoxometallates / Peroxoisopolytungstates / Clathrates / Crystal structures

A novel diperoxoheptatungstate was crystallised as a Cs^+–$CN_3H_6^+$–$(C_2H_5)_2NH_2^+$ salt and characterised by a single-crystal X-ray diffraction method. The anion has a Lindqvist heptametallate structure. The metal atoms are located in a bent 2-3-2 arrangement with the central W_3 section (W3, W4 and W5) as the hinge. The peroxo groups coordinate the tungsten atoms at both ends of the W_3 section (W3 and W5). In the crystal polyanions, caesium and guanidinium cations, and water of crystallisation form tunnel-like cavities, and the diethylammonium cations are accommodated in the cavities, suggesting a clathrate-like feature for the compound.
(© Wiley-VCH Verlag GmbH & Co. KGaA, 69451 Weinheim, Germany, 2004)

Introduction

Polyoxometallates are aggregates of oxo anions involving transition metals of groups 5 and 6. By substituting oxo groups in a polyoxometallate with peroxo groups, a peroxopolyoxometallate is formed. The peroxopolyoxometallates are known to be effective oxidising agents. Several peroxopolyoxometallates have thus been examined as oxidation catalysts, and epoxidation of alkene and hydroxylation of benzene are mentioned as examples of catalytic reactions.[1−3]

Peroxopolyoxometallates constructed from only oxoanions of addenda atoms such as V, Mo and W are called peroxoisopolyoxometallates, and from both addenda and hetero atoms such as P, S and As are called peroxoheteropolyoxometallates. The catalytic properties of the peroxopolyoxometallates depend on their components; generally, peroxoheteropolyoxometallates are more active than peroxoisopolyoxometallates, and tungstates are more active than molybdates.[4,5] Other than functioning as catalysts, the peroxopolyoxometallates have application in photoresist materials and as precursors of oxides.[6]

While extensive research in the application of peroxopolyoxometallates has been done, the basic chemistry of peroxopolyoxometallates has not been well-investigated. Especially, the chemistry of peroxoisopolytungstates is not well-known and only four anionic structures, $[W(O_2)_4]^{2-}$,[7] $[W_2O_3(O_2)_2(H_2O)_2]^{2-}$,[8] $[W_4O_6(O_2)(OH)_2(H_2O)_2]^{2-}$ [9] and $[W_4O_{12}(O_2)_2]^{4-}$ [10] have been reported so far, probably due to the instability of the system and compounds formed, and the slow formation of the anions. On the other hand, a spectroscopic work has been reported and a number of structurally unknown species have been detected.[11,12]

The authors have therefore been working with isolating peroxoisopolytungstates as single crystals to elucidate synthetic conditions and structures of the complexes. In the course of the investigation on peroxoisopolytungstates formed in aqueous medium, a novel diperoxoheptatungstate anion was isolated as a ceasium/diethylammonium/guanidinium salt. The preparation and structure of this compound is described here.

Results and Discussion

An ORTEP[13] diagram of all non-H atoms in the asymmetric unit is shown in Figure 1 with atom numbering. The anion has a Lindqvist heptametallate structure. The metal atoms are located in a bent 2-3-2 arrangement in which the central W_3 section (W3, W4 and W5) acts as a hinge. The dihedral angle between least-squares planes defined by W1−W2−W5−W4−W3 and W3−W4−W5−W6−W7 is 84.67(1)°. The peroxo groups coordinate the tungsten atoms at both ends of the W_3 section (W3 and W5), protruding from opposite sides of the W_2 units. The two W atoms are thus heptacoordinated with a pentagonal bipyramidal geometry. The other W atoms are hexacoordinate. Selected bond lengths are listed in Table 1. The ranges of the bond lengths of W−O (terminal) and W−O (bridge) are 1.713(4)−1.751(4) Å and 1.758(4)−2.324(4) Å, respectively.

Although O10 and O12 are asymmetrically bridging, the short bond lengths W4−O10 [1.784(4) Å] and W4−O12 [1.758(4) Å] indicate that these O atoms behave like the terminal oxygen atoms of W4. The long W−O bond lengths *trans* to W4−O10 and W4−O12, W4−O13 [2.222(4) Å]

[a] Department of Material Science and Chemistry, Faculty of Systems Engineering, Wakayama University,
930 Sakaedani, Wakayama 640-8510, Japan
Fax: (internat.) +81-73-457-8259
E-mail: mh1043@sys.wakayama-u.ac.jp

 © 2004 Wiley-VCH Verlag GmbH & Co. KGaA, Weinheim **DOI: 10.1002/ejic.200400050**

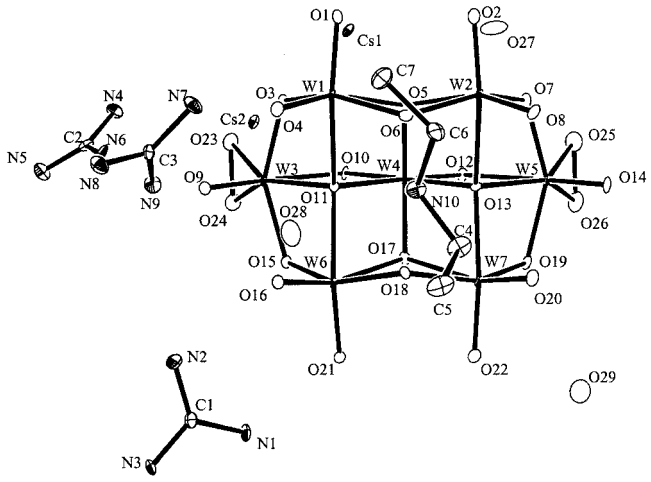

Figure 1. An ORTEP view of $Cs_2(CN_3H_6)_3[(C_2H_5)_2NH_2][W_7O_{22}(O_2)_2]\cdot 3H_2O$, displacement ellipsoids are drawn at the 50% probability level; selected bond lengths (Å) and angles (°): W(1)−O(1) 1.742(4), W(1)−O(4) 1.742(4), W(2)−O(2) 1.747(5), W(2)−O(8) 1.732(4), W(3)−O(9) 1.723(4), W(5)−O(14) 1.713(4), W(6)−O(16) 1.745(4), W(6)−O(21) 1.751(4), W(7)−O(20) 1.744(5), W(7)−O(22) 1.744(5), W(1)−O(3) 1.947(4), W(1)−O(6) 1.938(4), W(1)−O(5) 2.283(4), W(1)−O(11) 2.208(4), W(2)−O(5) 2.285(4), W(2)−O(6) 1.953(4), W(2)−O(7) 1.947(4), W(2)−O(13) 2.207(4), W(3)−O(3) 1.973(4), W(3)−O(10) 2.3237(4), W(3)−O(11) 2.081(4), W(3)−O(15) 1.984(4), W(4)−O(5) 1.883(4), W(4)−O(10) 1.784(4), W(4)−O(11) 2.252(4), W(4)−O(12) 1.758(4), W(4)−O(13) 2.222(4), W(4)−O(17) 1.898(4), W(5)−O(7) 1.964(4), W(5)−O(12) 2.367(4), W(5)−O(13) 2.110(4), W(5)−O(19) 1.993(4), W(6)−O(11) 2.204(4), W(6)−O(15) 1.950(4), W(6)−O(17) 2.227(4), W(6)−O(18) 1.935(4), W(7)−O(13) 2.174(4), W(7)−O(17) 2.280(4), W(7)−O(18) 1.930(4), W(7)−O(19) 1.951(4), W(3)−O(23) 1.955(5), W(3)−O(24) 1.943(5), W(5)−O(25) 1.948(5), W(5)−O(26) 1.942(5), O(23)−O(24) 1.479(7), O(23)−O(24) 1.468(7), O(23)−W(3)−O(24) 44.3(2), O(25)−W(5)−O(26) 44.6(2)

and W4−O11[2.252(4) Å], are the result of the *trans* influence of O10 and O12. The same phenomenon has been observed in peroxoheptamolybdates.[14−16]

In the vicinity of the peroxo groups (O23−O24 and O25−O26), the W−O bond lengths are in the range of 1.942(5)−1.955(5) Å, and the O23−O24 and O25−O26 bond lengths are 1.479(7) Å and 1.467(7) Å, respectively. The angles O23−W3−O24 and O25−W5−O26 of the peroxo group are 44.6(2)° and 44.3(2)°, respectively. These values are normal for compounds of this type.

The existence of such a polyanion has been predicted by an ^{17}O NMR study.[11,12] However, this is the first example of the isolation and structural analysis of this type of anion. On the other hand, the corresponding molybdates have already been isolated and structurally analysed.[14] Structures of heptatungstates without peroxo groups have also been reported.[17,18] The bond lengths in peroxoheptamolybdate, heptatungstate and the present peroxoheptatungstate are compared in Table 1;[17−21] no significant differences are observed, and any discrepancies may be partly due to the accuracy of the measurements. The slightly shorter bond lengths in the present compound are a result of the low temperature at the time of the measurement.

Packing diagrams are shown in Figures 2 and 3. Three H_2O molecules, three $CN_3H_6^+$ and two Cs^+ ions, and one $(C_2H_5)_2NH_2^+$ ion surround the anion. The polyanions, cations and water of crystallisation are linked by hydrogen bonds and electrostatic interactions (Table 2) to stabilise the whole crystal structure. Generally, the peroxoheptatungstate was considered to be difficult to isolate in the solid state and it has not been achieved before, although the existence of the anion in aqueous solution has been determined by spectroscopic methods.[11,12] The reason for the isolation of the peroxoheptatungstate as single crystals this time may have depended on the stabilisation of the whole crystal structure by the coexistence of not a single but several kinds of cations in the composition. As can be seen in Figure 3, the polyanions, the caesium and guanidinium cations, and the water of crystallisation form tunnel-like cavities, and the diethylammonium cations are accommodated in these cavities. The ammonium cation is held in the structure by hydrogen bonds with the polyanion and water of crystallisation in the walls of the tunnels. The bond lengths are listed in Table 2. The compound thus has a

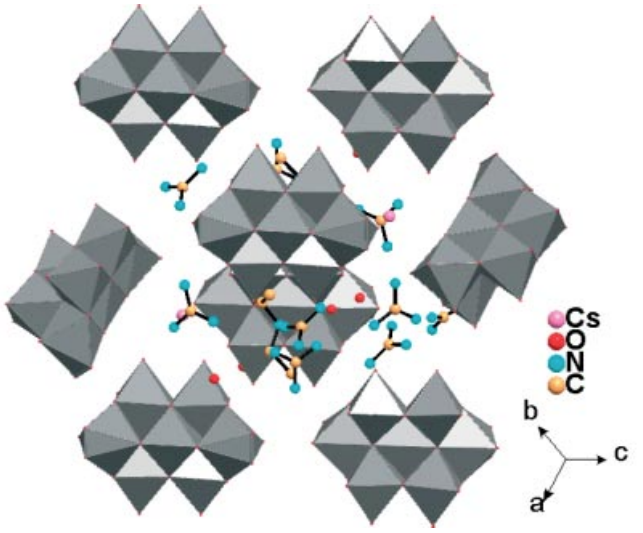

Figure 2. A packing diagram of $Cs_2(CN_3H_6)_3[(C_2H_5)_2NH_2][W_7O_{22}(O_2)_2]\cdot 3H_2O$

Table 1. Comparison of bond lengths (Å) in heptametallates

	M−O (terminal)	M−O−M (bridging)	Peroxo M−O	Peroxo O−O	Ref.
Peroxoheptatungstate	1.713(4)−1.751(4)	1.758(4)−2.324(4)	1.942(5)−1.955(5)	1.467(7)−1.479(7)	this work
Heptatungstate	1.523−1.884	1.661−2.616	−	−	[17,18]
Peroxoheptamolybdate	1.640−1.757	1.743−2.509	1.864−1.975	1.376−1.511	[19−21]

 © 2004 Wiley-VCH Verlag GmbH & Co. KGaA, Weinheim

clathrate nature. This suggests that these compounds may be obtained with other monovalent cations in combination with caesium and guanidinium cations. We are therefore attempting to obtain such compounds with monovalent cations having various features; the results will be published elsewhere.

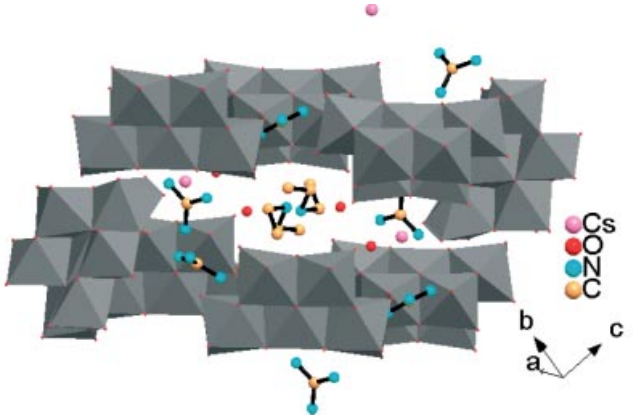

Figure 3. A packing diagram of $Cs_2(CN_3H_6)_3[(C_2H_5)_2NH_2]$-$[W_7O_{22}(O_2)_2]\cdot 3H_2O$; the tunnel-like cavity formed by polyanions, caesium and guanidinium cations and water is shown

Table 2. Distances involved in hydrogen bonding and electrostatic interactions (Å)

	Oaq	Oani	Cs
Gu−N[a]	2.868(8)−3.315(8)	2.827(7)−3.159(8)	3.403(6)−3.868(6)
Am−N[b]	2.731(8)	2.873(7)	−
Oaq[c]	2.730(8)	2.734(7)−2.878(7)	3.503(6)
Oani[d]			2.990(4)−3.712(5)

[a] Gu−N···nitrogen of guanidinium. [b] Am-N···nitrogen of ammonium. [c] Oaq···oxygen of water molecule. [d] Oani···oxygen of anion.

Experimental Section

Preparation of $Cs_2(CN_3H_6)_3[(C_2H_5)_2NH_2][W_7O_{22}(O_2)_2]\cdot 3H_2O$: Tungsten powder (1.83 g) was slowly dissolved in 30% hydrogen peroxide (25 mL), and the mixture was diluted to 100 mL with H_2O. Care must be taken here because of a vigorous reaction. The pH of the solution was adjusted to ca. 4.0 with aqueous LiOH (2.7 M). CsCl, $(CN_3H_5)\cdot HCl$, $(C_2H_5NH)\cdot HCl$ (molar ratio W/cation = 1:0.5 for each) were then added to the resulting solution. Colourless plate-shaped crystals appeared at room temperature in about 40 days.

Crystallographic Data for $Cs_2(CN_3H_6)_3[(C_2H_5)_2NH_2][W_7O_{22}(O_2)_2]\cdot 3H_2O$: M_r = 2276.77, monoclinic, $P2_1/c$, a = 13.4459(3), b = 11.3009(2), c = 25.0294(2) Å, β = 90.4760(10)°, V = 3803.11(11) Å^3, Z = 4, D_x = 3.977 g/cm^3, T = 100(2) K, μ (Mo-K_α) = 23.08 mm^{-1}, R_1 [$F_o > 4.0\sigma(F_o)$] = 0.0270, wR_2 (all data) = 0.0627, goodness of fit = 0.998, R(int.) = 0.0643, reflections measured 63317, unique reflection 11647, parameter 497.

Intensity data of $Cs_2(CN_3H_6)_3[(C_2H_5)_2NH_2][W_7O_{22}(O_2)_2]\cdot 3H_2O$ was collected on SMART CCD SYSTEM. Data reduction and absorption correction based on psi-scans were applied with TEXSAN.[22] All calculations were performed with SHELX97.[23] Cs and W atoms were located by a direct method and all other atoms by successive Fourier syntheses. All non-H atoms were refined anisotropically by full-matrix least-squares based on F^2.

CCDC-227357 contains the supplementary crystallographic data for this paper. These data can be obtained free of charge at www.ccdc.cam.ac.uk/conts/retrieving.html [or from the Cambridge Crystallographic Data Center, Union Road, Cambridge CB2 1EZ, UK; Fax: (internat.) +44-1223-336-033; E-mail: deposit@ccdc.cam.ac.uk].

Acknowledgments

The authors are grateful to Dr. Tomoji Ozeki, The Tokyo Institute of Technology, for the measurement of X-ray intensity data.

[1] G. Gelbard, F. Raison, E. Roditi-Lachter, R. Thouvenot, L. Ouahab, D. Grandjean, *J. Mol. Catal. A: Chemical* **1996**, *114*, 77.
[2] Y. Matsumoto, M. Asami, M. Hashimoto, M. Misono, *J. Mol. Catal. A: Chemical* **1996**, *114*, 161.
[3] K. Nomiya, H. Yanagibayashi, *J. Mol. Catal. A: Chemical* **1996**, *114*, 181.
[4] N. M. Gresley, W. P Griffith, B. C. Parkin, A. J. P. White, D. J. Williams, *J. Chem. Soc., Dalton Trans.* **1996**, 2039.
[5] D. V. Deubel, J. Sundermeyer, G. Frenking, *Inorg. Chem.* **2000**, *39*, 2314.
[6] *Kikan Kagaku Sousetu No.20, Polyoxometallate Chemistry* (Ed.: T. Kudou), Gakkaisyuppan Center, Tokyo, **1993**.
[7] R. Stomberg, *J. Less-Common Metals* **1988**, *143*, 363.
[8] F. W. B. Einstein, B. R. Penfold, *Acta Crystallogr.* **1964**, *17*, 1127.
[9] T. Ozeki, T. Yamase, *Bull. Chem. Soc. Jpn.* **1997**, *70*, 2101.
[10] W. P. Griffith, B. C. Parkin, A. J. P. White, D. J. Williams, *J. Chem. Soc., Dalton Trans.* **1995**, 3131.
[11] O. W. Howarth, L. Pettersson, I. Andersson, *Polyoxometalate Chemistry From Topology via Self-Assembly to Applications* (Eds.: M. T. Pope, A. Müller), Kluwer Academic Publishers, Dordrecht, The Netherlands, **2001**, pp. 145.
[12] O. W. Howarth, *Dalton Trans.* **2004**, 476.
[13] C. K. Johnson, *ORTEPII*, Report ORNL-5138, Oak Ridge National Laboratory, Tennessee, USA, **1976**.
[14] R. Stomberg, L. Trysberg, I. Larking, *Acta Chem. Scand.* **1970**, *24*, 2678.
[15] I. Larking, R. Stomberg, *Acta Chem. Scand.* **1972**, *26*, 3708.
[16] L. Trysberg, R. Stomberg, *Acta Chem. Scand., Ser. A* **1981**, *35*, 823.
[17] J. Fuchs, E. P. Flindt, *Z. Naturforsch., Teil B* **1979**, *34*, 412.
[18] K. G. Burtseva, T. S. Chernaya, M. I. Sirota, *Dokl. Akad. Nauk SSSR.* **1978**, *243*, 104.
[19] I. Larking, R. Stomberg, *Acta Chem. Scand.* **1972**, *26*, 3708.
[20] I. Persdotter, L. Trysberg, R. Stomberg, *Acta Chem. Scand., Ser. A* **1986**, *40*, 335.
[21] S. Olson, R. Stomberg, *Z. Kristallogr.* **1997**, *212*, 311.
[22] Molecular Structure Corporation, *TEXSAN*, Version 1.7−2, MSC, 3200 Research Forest Drive, The Woodlands, TX 77381, USA, **1995**.
[23] G. M. Sheldrick, *SHELX97*, University of Göttingen, Germany, **1997**.

Received January 20, 2004

 © 2004 Wiley-VCH Verlag GmbH & Co. KGaA, Weinheim

Cobalt-Mediated Cyclooligomerization Reactions of Borylacetylenes

Avijit Goswami,[a] Claus-Jürgen Maier,[a] Hans Pritzkow,[a] and Walter Siebert*[a]

Dedicated to Professor Helmut Werner on the occasion of his 70th birthday

Keywords: Boranes / Catalysts / (Cyclobutadiene)cobalt complexes / Mono(boryl)acetylenes / Triborylbenzenes

Reaction of bis(diethylamino)acetylene (**1**) with lithium and chlorobis(dimethylamino)borane yields 1-[bis(dimethylamino)boryl]-2-(diethylamino)acetylene (**2**). Treatment of 1-aryl-2-(trimethylstannyl)acetylenes **3** with chlorobis(diisopropylamino)borane results in the quantitative formation of 1-aryl-2-[bis(diisopropylamino)boryl]acetylene compounds **4**. The 1-aryl-2-borylacetylene derivatives **5**, **6**, and **7** are obtained by the reaction of **3** with the appropriate haloborane, or by reacting **4** with two equivalents of HCl and one equivalent of catechol, dithiocatechol and 2-hydroxythiophenol. The catalytic cyclotrimerizations of **5a–d** with $[CpCo(CO)_2]$ or $[Co_2(CO)_8]$ lead to isomeric mixtures of the triborylbenzene derivatives **8a–d** and **8a′–d′**, whereas **6a–d** and **7a–b** undergo cyclotrimerization only with catalytic amount of $[Co_2(CO)_8]$, to give isomeric mixtures of the triborylbenzene derivatives **12a–d/12a′–d′** and **13a–b/13a′–b′**, respectively. The reaction of **2** with a stoichiometric amount of (η^5-cyclopentadienyl)bis(ethene)cobalt leads to (η^5-cyclopentadienyl)(η^4-cyclobutadiene)cobalt complexes **9**. The analogous complexes **10** and **11** are obtained by the reactions of **6** and **7** with a stoichiometric amount of (η^5-cyclopentadienyl)dicarbonylcobalt. Treatment of $Co_2(CO)_8$ with **5a**, **6a**, and **7a** yields the dicobaltatetrahedranes **14a**, **15a** and **16a**. Compound **15a** reacts with two equivalents of diphenylacetylene and 1-(1,3,2-benzodioxaborolyl)-2-phenylacetylene (**5a**), to furnish (1,3,2-benzodithiaborolyl)pentaphenylbenzene (**17**) and bis(1,3,2-benzodioxaborolyl)(1,3,2-benzodithiaborolyl)-triphenylbenzene (**18**), respectively. The new compounds have been characterized by NMR spectroscopy and mass spectrometry, as well as by X-ray structural analyses for **4a**, **5a**, **6a**, and **10a**.

(© Wiley-VCH Verlag GmbH & Co. KGaA, 69451 Weinheim, Germany, 2004)

Introduction

Over the past decades, the cyclooligomerization reactions of alkynes with transition metal complexes have received considerable attention.[1] $[CpCo(CO)_2]$[2] is a convenient and efficient reagent for the syntheses of CpCo−cyclobutadiene complexes,[3] cyclopentadienones,[4] and benzene derivatives,[5] whereas $[Co_2(CO)_8]$ is used in Pauson−Khand[6] and [2+2+2] cyclotrimerization reactions.

Recently, we reported the Co-catalyzed [2+2+2] cyclotrimerization of mono-[7] and bis(catecholboryl)acetylenes.[8] With both types of acetylenes, only benzene derivatives were obtained — no CpCo-cyclobutadiene complexes were observed — even when using stoichiometric amounts of $[CpCo(CO)_2]$ and the corresponding acetylene.

To study the influence of the substituents with respect to the formation of CpCo−cyclobutadiene and/or benzene derivatives, we have synthesized new mono(boryl)acetylene derivatives with terminal boryl and amino or aryl substituents. Compound **2**, which has both amino and boryl substituents (Scheme 1), can react similarly to the push−pull acetylene $Me_2N-C\equiv C-COOMe$,[9] and undergoes dimerization.

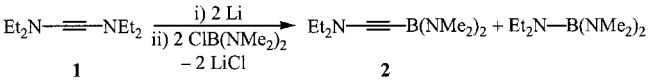

Scheme 1

The influence of the substituents at the boryl group is of particular interest, as amino groups at the boron center may reduce its Lewis acidity. A large part of this work concentrates on the reactivity of arylalkynyl boranes **5**, **6**, and **7**, in which two oxygen atoms (in **5**), two sulfur atoms (in **6**) and one oxygen and one sulfur atom (in **7**) are bound to the boron atom. It is expected that the heteroatoms have different electronic and steric effects on the reactivity of the acetylenes **5**−**7**. In this paper, we report the syntheses, structures and reactivities of the monoborylacetylene derivatives **2** and **4**−**7**.

[a] Anorganisch-Chemisches Institut der Universität,
Im Neuenheimer Feld 270, 69120 Heidelberg, Germany
Fax: (internat.) +49-(0)6221-54-5609
E-mail: walter.siebert@urz.uni-heidelberg.de

Results and Discussion

Synthesis and Properties of Mono(boryl)acetylene Derivatives 2, 4, 5, 6 and 7

Bis(diethylamino)acetylene (**1**) is obtained by treating 2-fluoro-1,1-dichloroethene or trichloroethene with *N*,*N*-disubstituted lithium amides and secondary amines.[10] In **1**, the N−C≡C bond is cleaved by lithium in THF to give two lithium compounds (Et_2NLi and $Et_2N-C{\equiv}CLi$), which react with various electrophiles. The mixture was treated with chlorobis(dimethylamino)borane to give $Et_2N-B(NMe_2)_2$ (70%) and 1-amino-2-borylacetylene (**2**) (43%), which were separated by fractional distillation (Scheme 1). Their compositions were determined by mass spectrometric and NMR spectroscopic data.

The reactions of chlorobis(diisopropylamino)borane with 1-trimethylstannyl-2-arylacetylenes **3** led to light-yellow compounds **4** in quantitative yields (Scheme 2). Compounds **4**[11] were characterized by ^1H, ^{13}C, and ^{11}B NMR spectroscopy, as well as by mass spectrometry.

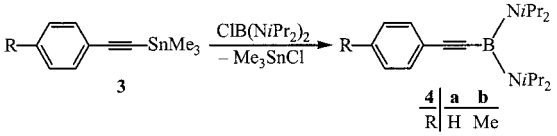

Scheme 2

In the ^{11}B NMR spectrum, the signal at δ = 26 ppm of **4a** indicates a trigonal-planar boryl group, which we confirmed by X-ray structural analysis. In the linear B−C≡C−C moiety (Figure 1) the C≡C bond is slightly widened relative to other R−C≡C−R compounds (1.18 Å).[12]

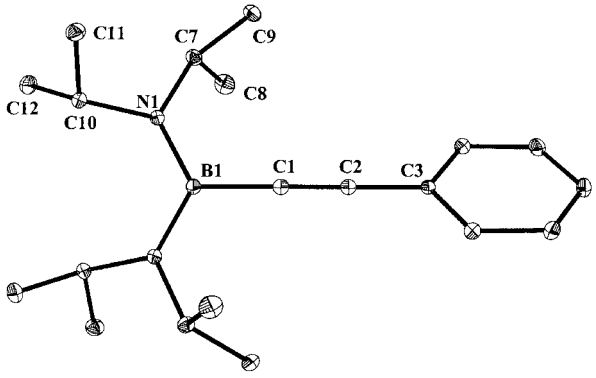

Figure 1. Molecular structure of **4a** in the solid state; hydrogen atoms are omitted for clarity; selected bond lengths [Å] and bond angles [°]: C1−C2 1.210(14), C2−C3 1.434(14), N1−B1 1.434(8), B1−C1 1.559(15), C1−C2−C3 180.0, C2−C1−B1 180.0

The syntheses of compounds **5**, **6**, and **7** were achieved by two reaction procedures. A solution of 1-aryl-2-(trimethylstannyl)acetylene (**3**) in toluene was reacted with the corresponding haloborane to give **5**−**7**. When compound **4** was treated with two equivalents of HCl and one equivalent of catechol or dithiocatechol or 2-hydroxythiophenol in THF, the corresponding alkynes **5**, **6**, and **7** were obtained as crystalline solids (Scheme 3). These compounds are soluble in benzene and toluene, but are less soluble in hexane and pentane. The ^1H NMR spectra of **5**−**7** show the expected multiplicities of the aromatic protons in the region δ = 6.9−7.9 ppm. In the ^{13}C NMR spectra, the signals for the boron-bound carbon atoms were not observed; the signals for the β carbon atoms (δ = 84−109 ppm) are shifted to lower fields relative to the alkylacetylenes (δ = 70−80 ppm),[13] which may indicate an interaction of the empty orbital at the boron atom with the π system of the triple bond.

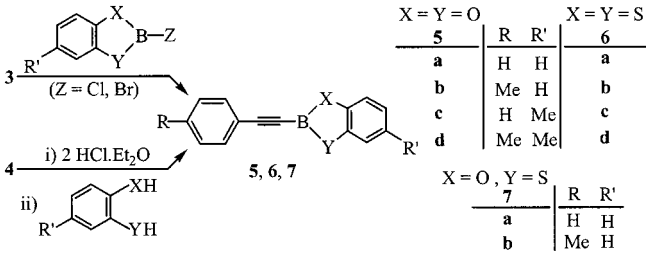

Scheme 3

The structures of **5a** and **6a** were determined by performing single-crystal X-ray analyses (Figures 2 and 3). Each compound has a linear B−C≡C−C moiety (**5a**: exactly; **6a**: approximately) and the C≡C bond lengths are slightly longer than those of normal alkyne compounds. The B−C bonds are rather short. This finding is in agreement with structural data for oxygen-substituted bis(catecholboryl)acetylenes.[14]

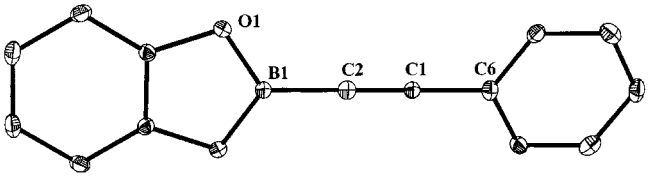

Figure 2. Molecular structure of **5a** in the solid state; hydrogen atoms are omitted for clarity; selected bond lengths [Å] and bond angles [°]: C1−C2 1.196(5), C1−C6 1.447(5), B1−C2 1.513(5), B1−O1 1.383(15), C1−C2−C6 180.0, C1−C2−B1 180.0

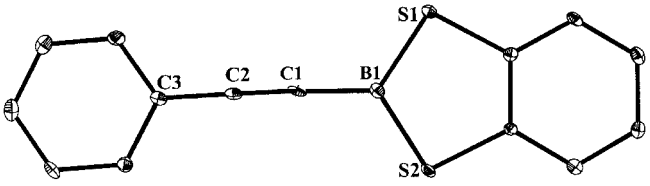

Figure 3. Molecular structure of **6a** in the solid state; hydrogen atoms are omitted for clarity; selected bond lengths [Å] and bond angles [°]: C1−C2 1.207 (8), C2−C3 1.423(7), B1−C1 1.521(8), B1−S1 1.796(6), C1−C2−C3 178.5(5), C2−C1−B1 177.6(5)

 © 2004 Wiley-VCH Verlag GmbH & Co. KGaA, Weinheim

Trimerization of 5 to Triboryl-triarylbenzene Derivatives 8

Only a few triborylbenzene derivatives are known,[15] of which some have been prepared in low yields by Grignard reactions. Recently, we obtained triborylbenzene derivatives[7] by cyclotrimerization of monoborylacetylenes in the presence of catalytic amount of dicarbonyl(η^5-cyclopentadienyl)cobalt. Analogously, in refluxing toluene, the monoborylalkyne derivatives **5a**−**d** formed isomeric mixtures of the 1,3,5- and 1,2,4-triborylbenzene derivatives **8a**−**d** and **8a′**−**d′** in the presence of a catalytic amount of $[CpCo(CO)_2]$ or $[Co_2(CO)_8]$ (Scheme 4). The isomers could not be separated.

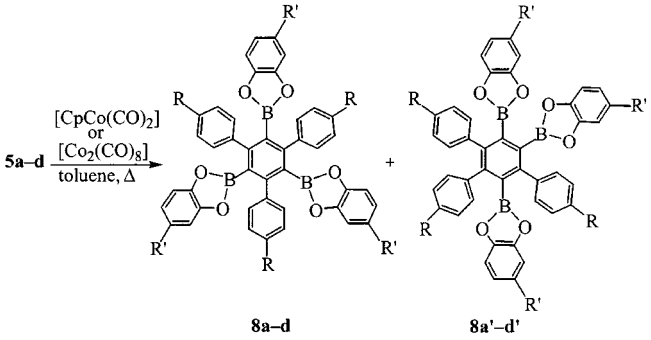

Scheme 4

The air-stable solids **8a**−**d** and **8a′**−**8d′** are light-yellow in color and are not soluble in most organic solvents; **8a**/**8a′** dissolve partially in chloroform, whereas **8b**−**d** and **8b′**−**d′** are slightly soluble in dichloromethane and toluene. Compounds **8a**−**d** and **8a′**−**d′** were characterized by ^{1}H, ^{13}C, and ^{11}B NMR spectroscopy, elemental analysis, and mass spectrometry. The ^{11}B NMR spectra exhibit broad signals at δ = 24 ppm for **8a**/**8a′**, δ = 22 ppm for **8b**/**8b′** and **8d**/**8d′**, and δ = 23 ppm for **8c**/**8c′**. In the ^{1}H NMR spectrum of **8a**/**8a′**, several peaks appear in the region δ = 7.2−7.6 ppm that are due to aromatic protons of the catechol and phenyl substituents. In the ^{13}C NMR spectrum, three signals at δ = 112.7, 123.2, and 147.8 ppm are observed for the carbon atoms of the catechol groups. The signal at δ = 139.9 ppm is assigned to the *ipso*-carbon atoms of the central ring of the isomer **8a** and three signals at δ = 134.6, 137.3, and 142.5 ppm to the *ipso*-carbon atoms of the central ring of the isomer **8a′**. The ^{13}C NMR spectroscopic signals of the carbon atoms of the phenyl substituents appear at δ = 121.2, 128.5, 130.0, and 132.8 ppm. Similarly, the ^{1}H NMR spectra of **8b**−**d** and **8b′**−**d′** show the expected multiplets (in the region δ = 6.9−7.6 ppm for the aromatic protons) and singlets near δ = 2.3−2.4 ppm (methyl groups). The ^{13}C NMR spectra reveal chemical shifts of the *ipso*-carbon atoms of the central ring of the isomers **8b**−**d** near δ = 140−141 ppm and the *ipso* carbon atoms of the isomers **8b′**−**d′** in the region δ = 136−148 ppm.

Thermal reactions of **5a**−**d** with a stoichiometric amount of $[CpCo(CO)_2]$ did not provide any (cyclobutadiene)cobalt complex: only the cyclotrimerization products were found. Likewise, photochemical activation of $[CpCo(CO)_2]$ and **5a**−**d** did not yield (cyclobutadiene)cobalt complexes: only the starting materials were recovered.

Catalytic Cycles with $[CpCo(CO)_2]$ and $[Co_2(CO)_8]$

The postulated mechanism of $[CpCo(CO)_2]$-catalyzed cyclotrimerization[5a,16] of acetylene is suggested for **5a**. Under thermal conditions, two alkyne ligands displace the CO groups to form a bis(alkyne)cobalt complex, followed by reductive coupling of the alkyne units to give a coordinatively unsaturated cobaltacyclopentadiene complex. Coordination of a third molecule of **5a** could then lead to an 18-VE complex, which undergoes alkyne insertion to form the corresponding cobaltacycloheptatriene compound. Subsequent reductive elimination of the CpCo complex fragment leads to the formation of the triborylbenzene derivatives **8a**/**8a′**. Recently, Vollhardt et al.[17] reported the synthesis of a (η^2-alkyne)cobaltacyclopentadiene complex, which indirectly proves the proposed catalytic cycle, although no direct evidence for the intermediacy of the postulated cobaltacycloheptatriene was obtained. According to ab initio and density functional theory (DFT) investigations of the mechanism,[16] a cobaltacycloheptatriene is in fact very unlikely to form.

Analogously, the catalytic oligomerization of **5a** with octacarbonyldicobalt led to the triborylbenzene derivatives **8a**/**8a′** in 71% yield. One of our aims is to isolate intermediates to shed more light on the catalytic cycle proposed in Scheme 5, which is a short version of the Knox−Pauson−Spicer mechanism.[18] In the first step, elimination of two CO ligands leads to the unsaturated species $[Co_2(CO)_6]$, which reacts with **5a** to give the boryl-substituted dicobaltatetrahedrane complex **14a** (**A**). Subsequent elimination of CO and insertion of one molecule of **5a** should yield the intermediate **B**, of which many examples are known.[19] However, under our conditions, **B** was not detected. A Diels−Alder-type reaction of **B** with **5a** may

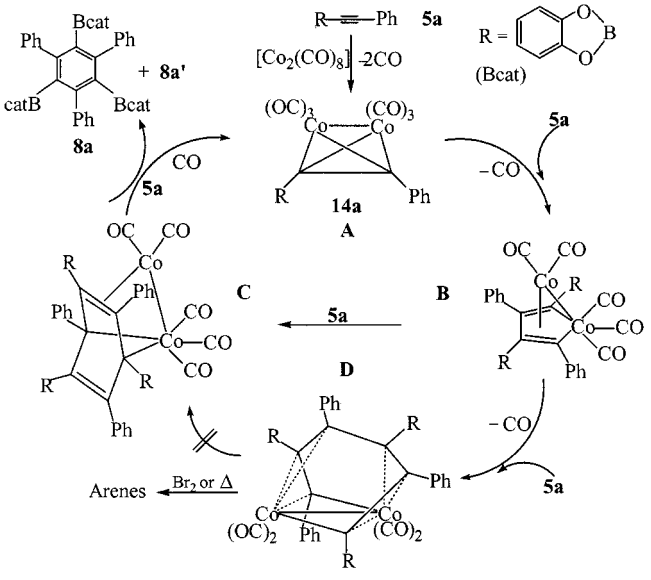

Scheme 5

 © 2004 Wiley-VCH Verlag GmbH & Co. KGaA, Weinheim

lead to **C**, which eliminate **8a/8a′** and the pentacarbonyldicobalt fragment reacts with CO and **5a** to give **14a**. We did not observe the postulated intermediates **C** and the "flyover" dicobaltacyclooctadiene complex **D**; several examples have been reported of the latter species.[18,20] It has been demonstrated that drastic conditions[21] or chemical promoters[18] transform **D** into arenes and, therefore, **D** is not on the main path of the catalytic reaction to arenes.[18]

Synthesis of CpCo−Diborylcyclobutadiene Complexes 9, 10 and 11

In 1965, Pettit et al.[22] reported the first generation of the tricarbonyl(η^4-cyclobutadiene)iron complex. Among the various synthetic methods, the reactions of alkynes with transition metal carbonyl complexes in particular have been studied extensively during the last three decades.[23] In an analogous manner, compound **2** was treated with (η^5-cyclopentadienyl)bis(ethene)cobalt in hexane and compounds **6** and **7** with dicarbonyl(η^5-cyclopentadienyl)cobalt in refluxing toluene to give the corresponding (η^4-cyclobutadiene)(η^5-cyclopentadienyl)cobalt complexes **9**, **10**, and **11** in good yields (Scheme 6). Purification of compounds **9a/9a′** by column chromatography on aluminum oxide led to decomposition. Because of a paramagnetic impurity in the crude product, compounds **9a/9a′** could not be characterized by NMR spectroscopy. EI-MS data confirm the identity of **9a/9a′** through the appearance of the molecular ion peaks with the expected isotopic patterns. Compounds **10** and **11** are partially soluble in toluene and chloroform; in methanol, a fast reaction, leading to the formation of $B(OMe)_3$, takes place.

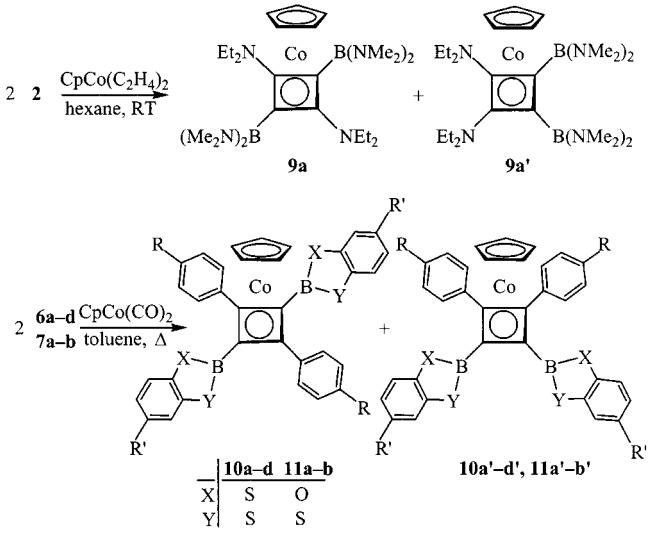

Scheme 6

Purification of **10** and **11** can be accomplished by washing repeatedly with hexane. Complexes **10** and **11** were characterized by ^1H, ^{13}C, and ^{11}B NMR spectroscopy, elemental analysis, and mass spectrometry. The ^{11}B NMR spectra show broad signals at $\delta = 58$ ppm for **10a/10d**, and $\delta = 57$ ppm for **10b/10c**. The ^1H NMR spectra of **10** exhibit multiplets in the region $\delta = 7.0-7.9$ ppm that are due to the aromatic protons, in addition to the Cp resonances ($\delta = 4.6-4.9$ ppm). Four quaternary carbon atoms of diboryl-substituted (η^4-cyclobutadiene)cobalt complexes **10** were detected in the ^{13}C NMR spectrum in the region $\delta = 79-89$ ppm. From the NMR spectra, it is not possible to make a distinction between the *trans* (**10a−d**) and *cis* isomers (**10a′−d′**) of the cyclobutadiene complexes. For steric reason, the *trans* isomers **10a−d** seem to be more favored, which is confirmed by the solid state structure of **10a**. However, several complexes are known that have *cis*-bis(trimethylsilyl)cyclobutadiene ligands.[1c,24] The problem was resolved unequivocally by analyzing the major peaks in terms of the degradation of the cyclobutadiene ring in the mass spectra. In general, three different acetylenes are released from the molecular ion of the *cis* isomer, but only a single acetylene is released from the *trans* isomer.[25] Here, in all cases, three kinds of acetylenes were released from the molecular ion. Therefore, mass spectra gave evidence for both the *cis* isomer and the *trans* isomers, but the *cis* isomer could not be identified by NMR spectroscopic measurements.

The structure of **10a** was characterized by performing a single-crystal X-ray diffraction analysis. Two independent molecules were found; the structure of one is shown in Figure 4. The solid state structure of **10a** reveals that both phenyl groups, as well as one of dithiacatecholboryl groups, do not lie in the plane of the cyclobutadiene ring. From the internal bond angles of the cyclobutadiene ring of **10a**, it is found that there is a little deviation from the exact square-planar shape because the internal bond angles for both the carbon atoms attached to the boron atom are smaller than those attached to the phenyl groups.

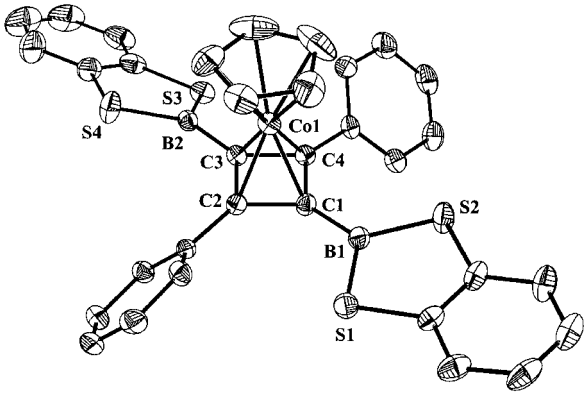

Figure 4. Molecular structure of **10a** in the solid state; hydrogen atoms are omitted for clarity; selected bond lengths [Å] and bond angles [°]: C1−C2 1.460 (5), C2−C3 1.465(5), C3−C4 1.476(5), C4−C1 1.462(5), C1−B1 1.528(6), C3−B2 1.527(6), C2−C1−C4 89.2(3), C1−C2−C3 91.4(3), C2−C3−C4 88.5(3), C1−C4−C3 90.9(3)

Similarly, ^{11}B NMR spectra show broad signals at $\delta = 45$ ppm for **11a/11a′** and $\delta = 46$ ppm for **11b/11b′**. The ^1H NMR spectra exhibit multiplets in the region $\delta =$

7.1−7.9 ppm that are due to aromatic protons. In the ^{13}C NMR spectra of **11a/11a′** and **11b/11b′**, the signals in the region δ = 84−86 ppm are assigned to the *ipso*-carbon atoms of the central C_4 ring and to the signals of the Cp carbon atoms (δ = 83−87 ppm). The EI mass spectra of **11a**−**b** and **11a′**−**b′** show ion fragmentations similar to those mentioned above, with the expected isotopic patterns. It is important to mention that no benzene derivatives were observed in the reactions of $[CpCo(CO)_2]$ with the alkynes **6** and **7** (Scheme 6).

$[Co_2(CO)_8]$-Catalyzed Cyclotrimerization of 6 and 7 to Triborylbenzenes 12 and 13

Arnett et al.[26] prepared the sterically encumbered hexaisopropylbenzene by $[Co_2(CO)_8]$-catalyzed trimerization of bis(isopropyl)acetylene. Analogously, in refluxing toluene, the mono(boryl)acetylene derivatives **6** and **7** formed the triborylbenzene derivatives **12** and **13** in the presence of a catalytic amount of $[Co_2(CO)_8]$ (Scheme 7). The isomeric mixture (1,3,5- and 1,2,4-substituted) could not be separated. Purifications of **12** and **13** were achieved by washing repeatedly with hexane, toluene and CH_2Cl_2.

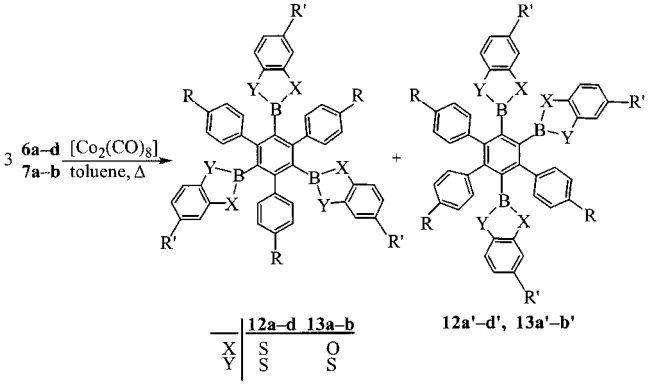

Scheme 7

The compounds **12** and **13** are air-stable solids and are not soluble in most common organic solvents; slight solubility in chloroform enables NMR spectra to be measured. All compounds were characterized by ^1H, ^{13}C, and ^{11}B NMR spectroscopy, elemental analysis, and mass spectrometry. The ^{11}B NMR spectra show broad signals at δ = 62 ppm for **12a/12a′** and δ = 60 ppm for **12b/12b′**, **12c/12c′**, and **12d/12d′**. In the ^1H NMR spectra, multiplets (δ = 6.9−7.9 ppm) are observed for the aromatic protons of **12a**−**d** and **12a′**−**d′**. In the ^{13}C NMR spectra, the signals in the region δ = 126−128 ppm are assigned to the *ipso*-carbon atoms of the central ring of the isomers **12a**−**c** and those in the region δ = 128−141 ppm to the *ipso* carbon atoms of the isomers **12a′**−**c′**. The quaternary carbon atoms of **12d/12d′** were not observed.

The ^{11}B NMR spectra of **13a/13a′** exhibit broad signals at δ = 53 ppm and of **13b/13b′** at δ = 52 ppm. The ^1H NMR spectra show multiplets in the aromatic region for the aryl protons of **13a/b** and **13a′/b′**. The ^{13}C NMR spectra reveal the signals of the *ipso*-carbon atoms of the central ring of **13a** at δ = 132.8 ppm and at δ = 132.7 ppm for **13b**.

Synthesis and Properties of Dicobaltatetrahedranes 14a, 15a, and 16a

(Alkyne)hexacarbonyldicobalt complexes are obtained by treating alkynes with $Co_2(CO)_8$.[27] Analogously, the mono(boryl)acetylene derivatives **5a**, **6a**, and **7a** reacted with $Co_2(CO)_8$ in CH_2Cl_2; elimination of two CO units resulted in the corresponding complexes **14a**, **15a** and **16a** (Scheme 8). These compounds were isolated by column chromatography as brown-red oils,[28] which we characterized by ^1H, ^{13}C, and ^{11}B NMR spectroscopy, IR spectroscopy, and mass spectrometry.

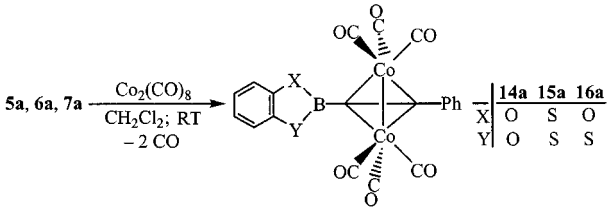

Scheme 8

The ^{11}B NMR spectrum of **14a** shows a broad signal at δ = 33 ppm. The ^1H NMR spectrum exhibits the signals of the aromatic protons in the region δ = 7.2−7.7 ppm. In the ^{13}C NMR spectrum, the arene carbon atoms give rise to signals at δ = 112.6, 123.2, and 147.8 ppm for the catechol unit and at δ = 121.2, 128.5, 130.0, and 130.2 ppm for the phenyl group. The signal of the carbon atom bound to the boron atom are not observed, while the carbon atom attached directly to the phenyl group appears at δ = 104.3 ppm. The carbonyl ligands exhibit a signal in the ^{13}C NMR spectrum at δ = 200.2 ppm.

Similarly, in their ^{11}B NMR spectra, the signals of the complexes **15a** and **16a** appear at δ = 59 and 47 ppm, respectively. The ^1H NMR spectra show multiplets in the regions δ = 7.1−7.8 ppm for **15a** and δ = 7.1−7.5 ppm for **16a**. The characteristic carbonyl ligands in the ^{13}C NMR spectra appear at δ = 199.5 ppm for **15a** and δ = 200.6 ppm for **16a**.

Complex **14a** can also act as a catalyst for the cyclotrimerization of **5a**. When a catalytic amount of **14a** and 1-(catecholboryl)-2-phenylacetylene (**5a**) were heated in toluene, the triborylbenzene derivatives **8a/8a′** were obtained in good yield (Scheme 9).

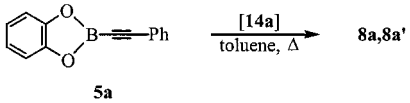

Scheme 9

 © 2004 Wiley-VCH Verlag GmbH & Co. KGaA, Weinheim

(1,3,2-Benzodithiaborolyl)pentaphenylbenzene and Bis(1,3,2-benzodioxaborolyl)(1,3,2-benzodithiaborolyl)triphenylbenzene (17 and 18)

Recently, we have shown the use of C_2Co_2 clusters for the preparation of different substituted arenes.[8] Analogously, we have heated diphenylacetylene and a stoichiometric amount of **15a** in toluene, which resulted in the formation of (1,3,2-benzodithiaborolyl)pentaphenylbenzene (**17**) in good yield (Scheme 10). Compound **17** is not soluble in common organic solvents and, therefore, NMR spectroscopic measurements were not possible. Compound **17** was characterized by mass spectrometry, which confirms the identity of **17** through the appearance of the molecular ion peak at $m/z = 608$.

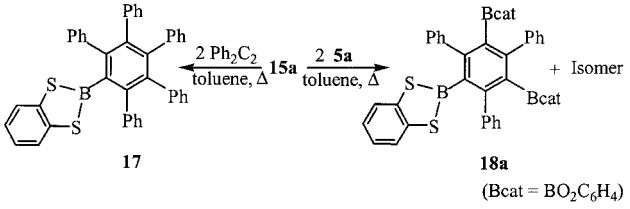

Scheme 10

Similarly, compound **15a** was treated with two equivalents of 1-(catecholboryl)-2-phenylacetylene (**5a**) in toluene under reflux, which led to the formation of an isomeric mixture **18** in moderate yield. Because of the complete insolubility of compound **18**, NMR spectroscopic measurements were not possible. Compound **18** was characterized by EI mass spectrometry, which indicated the molecular ion peak of **18** at $m/z = 692$.

Conclusions

We have studied the reactions of boryl-substituted acetylenes with catalytic and stoichiometric amounts of $[CpCo(C_2H_4)_2]$, $[CpCo(CO)_2]$, and $[Co_2(CO)_8]$. [2+2+2] Cyclotrimerization products **8** are obtained from the reactions of (catecholboryl)acetylenes **5** with a catalytic amount of $[CpCo(CO)_2]$ or $[Co_2(CO)_8]$. (η^4-Cyclobutadiene)cobalt complexes are not formed from (thermal and photochemical) reactions of **5** with stoichiometric amount of $[CpCo(CO)_2]$. Treatment of nitrogen- and sulfur-bound borylacetylenes **2**, **6**, and **7** with a stoichiometric amount of $[CpCo(C_2H_4)_2]$ or $[CpCo(CO)_2]$ opened a long-sought route to the new class of boryl-substituted (η^4-cyclobutadiene)cobalt complexes. Possibly because of steric reasons, the nitrogen-substituted borylacetylene **2** does not undergo catalytic cyclotrimerization with $[CpCo(C_2H_4)_2]$ or $[CpCo(CO)_2]$. On the other hand, triborylbenzene derivatives **12** and **13** are obtained from the reactions of **6** and **7**, respectively, with a catalytic amount of $[Co_2(CO)_8]$. Surprisingly, we found that changing the heteroatom(s) bound to the boron atom causes a remarkable difference in the reactivities of **6** and **7** when compared to that of **5**. Most likely, this behavior of **6** and **7** arises from interactions of the sulfur atom(s) with the cobalt center, which might prevent the formation of coordinatively unsaturated cobaltacyclopentadiene complexes (the postulated precursor en route to cyclotrimerization products). Instead of cyclotrimerization products, (η^4-cyclobutadiene)cobalt complexes **10** and **11** are obtained. Reactions of **5a**, **6a**, and **7a** with a stoichiometric amount of $[Co_2(CO)_8]$ lead to the Co_2C_2 clusters **14a**, **15a**, and **16a**, respectively.

Experimental Section

General: All reactions were performed under nitrogen using standard Schlenk techniques. Solvents were dried with the appropriate drying agents and distilled under nitrogen. Glassware was dried with a heat gun under high vacuum. ^1H, ^{13}C, and ^{11}B NMR spectroscopy: Bruker AC 200 spectrometer; ^1H and ^{13}C spectra were referenced to $(CH_3)_4Si$ and ^{11}B spectra to $F_3B{\cdot}OEt_2$. IR spectra were recorded on a Bruker IFS 28 FT spectrometer. Mass spectra were obtained on Finnigan MAT 8230 plus spectrometers using the EI technique. Elemental analyses were carried out at the Microanalytical Laboratory, University of Heidelberg. Melting points (uncorrected) were obtained on a Büchi apparatus, using capillaries that were filled under nitrogen and sealed. Bis(diethylamino)acetylene[10] (**1**), $(i\mathrm{Pr}_2\mathrm{N})_2\mathrm{BCl}$,[29] 1-aryl-2-(trimethylstannyl)acetylenes[30] **3**, and chlorocatecholborane[31] were prepared according to literature procedures. Bromo(dithiocatechol)borane and bromo(1,3,2-benzothiaoxaborol), which have not been reported previously in the literature, were prepared by the reactions of dithiocatechol and 2-hydroxythiophenol with excess BBr_3. Catechol, 4-methylcatechol, dithiocatechol, 4-methyldithiocatechol, and 2-hydroxymercaptanol were purchased from Aldrich.

1-[Bis(dimethylamino)boryl]-2-(diethylamino)acetylene (2): Bis(diethylamino)acetylene (**1**, 1.18 g, 7.0 mmol) was added slowly at room temperature to a stirred suspension of lithium powder (0.34 g, 49.7 mmol) in diethyl ether (20 mL). The reaction mixture was heated under reflux for 3 h. After cooling, the mixture was stirred at ambient temperature for 40 h. The ether was evaporated by vacuum, THF (20 mL) was added, and the THF solution was heated for 1 h. The solid that formed was separated by filtration and washed with a small amount of THF. After drying under high vacuum, a green solid (a mixture of Et_2NC_2Li and $LiNEt_2$) was obtained. Chlorobis(dimethylamino)borane (1.26 g, 9.4 mmol) was added within 10 min at −60 °C to a solution of lithium compounds (0.85 g, 4.7 mmol) in THF (10 mL). The reaction mixture was stirred for 16 h. After filtration, the solvent was evaporated under high vacuum. Compound **2** and $Et_2B(NMe)_2$ were obtained by fractional distillation. Yield 0.39 g (43%), colorless liquid, b.p. 50 °C/0.2 Torr. ^1H NMR (200.1 MHz, $CDCl_3$): δ = 1.18 (t, $^3J_{H,H}$ = 7.2 Hz, 6 H, CH_2CH_3), 2.68 (s, 12H, NCH_3), 2.90 (q, $^3J_{H,H}$ = 7.2 Hz, 4 H, CH_2CH_3) ppm. ^{13}C NMR (50.3 MHz, $CDCl_3$): δ = 12.90 (CH_2CH_3), 40.60 (NCH_3), 48.20 (CH_2CH_3) ppm. ^{11}B NMR (64.2 MHz, $CDCl_3$): δ = 26 ppm. MS (70 eV, EI): m/z (%) = 195 (100) [M^+], 180 (31) [$M^+ - CH_3$], 123 (93) [$M^+ - NEt_2$].

1-[Bis(diisopropylamino)boryl]-2-phenylacetylene (4a) and 1-[Bis(diisopropylamino)boryl]-2-tolylacetylene (4b): Chlorobis(diisopropylamino)borane (2.59 g, 10.5 mmol) in toluene (10 mL) was added slowly at −78 °C to a stirred solution of 1-trimethylstannyl-2-arylacetylene (**3a**: 2.80 g; **3b**: 2.94 g; 10.5 mmol) in toluene (40 mL). The reaction mixture was stirred overnight to reach room temperature, the solvent was evaporated under high vacuum, and the residue was distilled.

 © 2004 Wiley-VCH Verlag GmbH & Co. KGaA, Weinheim

4a: Yield 3.1 g (94%), pale-yellow liquid, b.p. 102 °C/0.01 Torr. ^{1}H NMR (200.1 MHz, $CDCl_3$): δ = 1.38 [d, $^3J_{H,H}$ = 6.9 Hz, 24 H, $CH(CH_3)_2$], 3.55 [sept., $^3J_{H,H}$ = 6.9 Hz, 4 H, $CH(CH_3)_2$], 7.4−7.5 (m, C_6H_5, 5H) ppm. ^{13}C NMR (50.3 MHz, $CDCl_3$): δ = 24.23 [$CH(CH_3)_2$], 46.71 [$CH(CH_3)_2$], 104.6 (C_{sp}−C_i), 125.1, 127.8, 128.3, 130.9 (C_6H_5) ppm; C_{sp}−B not found. ^{11}B NMR (64.2 MHz, $CDCl_3$): δ = 26 ppm. MS (70 eV, EI): *m*/*z* (%) = 312 (13) [M^+], 297 (100) [$M^+ - CH_3$], 269 (87) [$M^+ - i$Pr], 212 (31) [$M^+ - N(i\text{Pr})_2$]. MS (70 eV, HR-EI): *m*/*z* (%) = 312.2759 (8) [M^+; $^{12}C_{20}{}^1H_{33}{}^{11}B^{14}N_2$: 312.2736]; Δmmu = 2.3.

4b: Yield: 3.0 g (87%), yellow liquid, b.p. 112 °C/0.02 Torr. ^{1}H NMR (200.1 MHz, $CDCl_3$): δ = 1.35 [d, $^3J_{H,H}$ = 7.0 Hz, 24H, $CH(CH_3)_2$], 2.32 (s, CH_3, 3 H), 3.53 [sept., $^3J_{H,H}$ = 6.9 Hz, 4H, $CH(CH_3)_2$], 7.3−7.6 (m, 4H, C_6H_5) ppm. ^{13}C NMR (50.3 MHz, $CDCl_3$): δ = 21.32 (CH_3), 24.25 [$CH(CH_3)_2$], 46.81 [$CH(CH_3)_2$], 104.5 (C_{sp}−C_i), 125.3, 127.5, 128.7, 131.2 (C_6H_4) ppm; C_{sp}−B not found. ^{11}B NMR (64.2 MHz, $CDCl_3$): δ = 26 ppm. MS (70 eV, EI): *m*/*z* (%) = 326 (100) [M^+]. MS (70 eV, HR-EI): *m*/*z* (%) = 326.2899 (100) [M^+; $^{12}C_{21}{}^1H_{35}{}^{11}B^{14}N_2$: 326.2893]; Δmmu = 0.6.

Two General Procedures for 1-Aryl-2-borylacetylenes 5, 6, and 7. Procedure A: The appropriate 1-aryl-2-(trimethylstannyl)acetylene **3** was dissolved in toluene (50 mL) and then the corresponding haloborane in toluene (10 mL) was added slowly at −20 °C. The reaction mixture was stirred overnight at ambient temperature. After evaporation of the solvent under high vacuum, a crystalline solid was obtained.

Procedure B: The appropriate 1-aryl-2-[bis(diisopropylamino)-boryl]acetylene **4** was dissolved in THF (50 mL) and then 2 equiv. of HCl·Et_2O (2 M) was added slowly at −78 °C. Stirring was continued for 45 min and NH_2iPr_2Cl formed as a white solid. The corresponding aromatic diol in THF (15 mL) was then added dropwise and the reaction mixture was stirred overnight at room temperature. After filtration of the solid, the solution was reduced to near dryness, and a crystalline product was obtained.

1-(Catecholboryl)-2-phenylacetylene (5a): Starting materials: **3a** (4.8 g, 18 mmol), $H_4C_6O_2BCl$ (2.78 g, 18 mmol). Yield 2.8 g (71%), orange-red solid, m.p. 76 °C. ^{1}H NMR (200.1 MHz, $CDCl_3$): δ = 7.2−7.7 (m, 9 H, H_{aryl}) ppm. ^{13}C NMR (50.3 MHz, $CDCl_3$): δ = 105.1 (C_{sp}−C_i), 112.7, 123.3, 147.9 (catechol), 121.2, 128.6, 130.1, 132.8 (C_6H_5) ppm; C_{sp}−B not observed. ^{11}B NMR (64.2 MHz, $CDCl_3$): δ = 25 ppm. MS (70 eV, EI): *m*/*z* (%) = 220 (100) [M^+]. MS (70 eV, HR-EI): *m*/*z* (%) = 220.0715 (100) [M^+; $^{12}C_{14}{}^1H_9{}^{11}B^{16}O_2$: 220.0695]; Δmmu = 2.0.

1-(Catecholboryl)-2-tolylacetylene (5b): Starting materials: **3b** (2.4 g, 8.6 mmol), $H_4C_6O_2BCl$ (1.32 g, 8.6 mmol). Yield 1.4 g (69%), yellow solid, m.p. 72 °C (dec.). ^{1}H NMR (200.1 MHz, $CDCl_3$): δ = 2.35 (s, 3 H, CH_3), 7.0−7.5 (m, 8 H, H_{aryl}) ppm. ^{13}C NMR (50.3 MHz, $CDCl_3$): δ = 21.67 (CH_3), 103.4 (C_{sp}−C_i), 112.6, 123.1, and 147.8 (catechol), 115.5, 121.3, 129.2, 132.7 (tolyl) ppm; C_{sp}−B not observed. ^{11}B NMR (64.2 MHz, $CDCl_3$): δ = 25 ppm. MS (70 eV, EI): *m*/*z* (%) = 234 (100) [M^+]. MS (70 eV, HR-EI): *m*/*z* (%) = 234.0833 (100) [M^+; $^{12}C_{15}{}^1H_{11}{}^{11}B^{16}O_2$: 234.0852]; Δmmu = 1.9.

1-(4-Methylcatecholboryl)-2-phenylacetylene (5c): Starting materials: **3a** (4.1 g, 15.4 mmol), $CH_3C_6H_3O_2BCl$ (2.59 g, 15.4 mmol). Yield 2.4 g (66%), yellow solid, m.p. 75 °C. ^{1}H NMR (200.1 MHz, $CDCl_3$): δ = 2.39 (s, CH_3, 3 H), 6.9−7.6 (m, 8 H, H_{aryl}) ppm. ^{13}C NMR (50.3 MHz, $CDCl_3$): δ = 21.38 (CH_3), 93.37 (C_{sp}−C_i), 111.9, 113.2, 123.6, 130.0, 145.7, 147.8 (catechol), 121.2, 128.8, 132.7, 133.2 (C_6H_5) ppm; C_{sp}−B not observed. ^{11}B NMR (64.2 MHz, $CDCl_3$): δ = 24 ppm. MS (70 eV, EI): *m*/*z* (%) = 234 (100) [M^+]. MS (70 eV, HR-EI): *m*/*z* (%) = 234.0834 (100) [M^+; $^{12}C_{15}{}^1H_{11}{}^{11}B^{16}O_2$: 234.0852]; Δmmu = 1.8.

1-(4-Methylcatecholboryl)-2-tolylacetylene (5d): Starting materials: **4b** (4.44 g, 13.6 mmol), HCl·OEt_2 (13.6 mL, 27.2 mmol), 4-methylcatechol (1.68 g, 13.6 mmol). Yield 2.1 g (62%), brown solid, m.p. 73 °C (dec.). ^{1}H NMR (200.1 MHz, $CDCl_3$): δ = 2.35 (s, 3 H, CH_3), 2.37 (s, 3 H, CH_3), 6.9−7.5 (m, 7 H, H_{aryl}) ppm. ^{13}C NMR (50.3 MHz, $CDCl_3$): δ = 21.40 and 21.65 (CH_3), 83.81 (C_{sp}−C_i), 111.9, 113.1, 123.1, 138.9, 145.4, 147.5 (catechol), 119.0, 129.2, 132.0, 132.8 (tolyl) ppm; C_{sp}−B not observed. ^{11}B NMR (64.2 MHz, $CDCl_3$): δ = 23 ppm. MS (70 eV, EI): *m*/*z* (%) = 248 (100) [M^+]. MS (70 eV, HR-EI): *m*/*z* (%) = 248.1008 (100) [M^+; $^{12}C_{16}{}^1H_{13}{}^{11}B^{16}O_2$: 248.1015]; Δmmu = 0.7.

1-(Dithiocatecholboryl)-2-phenylacetylene (6a): Starting materials: **3a** (4.1 g, 15.4 mmol), $H_4C_6S_2BBr$ (3.55 g, 15.4 mmol). Yield 2.8 g (72%), brown-red solid, m.p. 82 °C. ^{1}H NMR (200.1 MHz, $CDCl_3$): δ = 7.4−7.8 (m, 9 H, H_{aryl}) ppm. ^{13}C NMR (50.3 MHz, $CDCl_3$): δ = 84.01 (C_{sp}−C_i), 125.7, 126.5, 140.9 (dithiocatechol), 128.4, 129.7, 131.1, 132.2 (C_6H_5) ppm; C_{sp}−B not observed. ^{11}B NMR (64.2 MHz, $CDCl_3$): δ = 47 ppm. CI-MS: *m*/*z* (%) = 252.1 [M^+] (70)

1-(Dithiocatecholboryl)-2-tolylacetylene (6b): Starting materials: **3b** (1.7 g, 6.09 mmol), $H_4C_6S_2BBr$ (1.4 g, 6.09 mmol). Yield 1.2 g (74%), light-yellow solid, m.p. 86 °C. ^{1}H NMR (200.1 MHz, $CDCl_3$): δ = 2.38 (s, 3 H, CH_3), 7.15−7.50 (m, 8 H, H_{aryl}) ppm. ^{13}C NMR (50.3 MHz, $CDCl_3$): δ = 21.07 (CH_3), 92.43 (C_{sp}−C_i), 122.2, 126.0, 140.9 (dithiocatechol), 126.8, 127.1, 128.4, 132.2 (tolyl) ppm; C_{sp}−B not observed. ^{11}B NMR (64.2 MHz, $CDCl_3$): δ = 48 ppm. MS (70 eV, EI): *m*/*z* (%) = 266 (100) [M^+]. MS (70 eV, HR-EI): *m*/*z* (%) = 266.0401 (100) [M^+; $^{12}C_{15}{}^1H_{11}{}^{11}B^{32}S_2$: 266.0395]; Δmmu = 0.6.

1-(4-Methyldithiocatecholboryl)-2-phenylacetylene (6c): Starting materials: **4a** (3.5 g, 11.2 mmol), HCl·OEt_2 (11.2 mL, 22.4 mmol), 4-methyldithiocatechol (1.75 g, 11.2 mmol). Yield 2.3 g (77%), yellow solid, m.p. 88 °C. ^{1}H NMR (200.1 MHz, $CDCl_3$): δ = 2.42 (s, 3 H, CH_3), 7.13, 7.41, 7.64 (m, 8 H, H_{aryl}) ppm. ^{13}C NMR (50.3 MHz, $CDCl_3$): δ = 21.07 (CH_3), 93.37 (C_{sp}−C_i), 126.1, 126.8, 127.1, 135.9, 137.6, 140.9 (dithiocatechol), 122.2, 128.4, 129.7, 132.2 (C_6H_5) ppm; C_{sp}−B not observed. ^{11}B NMR (64.2 MHz, $CDCl_3$): δ = 47 ppm. MS (70 eV, EI): *m*/*z* (%) = 266 (100) [M^+]. MS (70 eV, HR-EI): *m*/*z* (%) = 266.0399 (100) [M^+; $^{12}C_{15}{}^1H_{11}{}^{11}B^{32}S_2$: 266.0395]; Δmmu = 0.4.

1-(4-Methyldithiocatecholboryl)-2-tolylacetylene (6d): Starting materials: **3b** (3.05 g, 10.9 mmol), $CH_3C_6H_3S_2BBr$ (2.66 g, 10.9 mmol). Yield 2.2 g (72%), brown solid, m.p. 93 °C. ^{1}H NMR (200.1 MHz, $CDCl_3$): δ = 2.28 (s, 3 H, CH_3), 2.38 (s, 3 H, CH_3), 7.1−7.6 (m, 7 H, H_{aryl}) ppm. ^{13}C NMR (50.3 MHz, $CDCl_3$): δ = 21.07, 21.67 (CH_3), 83.81 (C_{sp}−C_i), 126.0, 126.8, 127.0, 135.8, 137.6, 140.9 (thiocatechol), 119.1, 129.2, 132.1, 140.2 (tolyl) ppm; C_{sp}−B not observed. ^{11}B NMR (64.2 MHz, $CDCl_3$): δ = 48 ppm. MS (70 eV, EI): *m*/*z* (%) = 280 (100) [M^+]. MS (70 eV, HR-EI): *m*/*z* (%) = 280.0562 (100) [M^+; $^{12}C_{16}{}^1H_{13}{}^{11}B^{16}S_2$: 280.0551]; Δmmu = 1.1.

1-(1,3,2-Benzothiaoxaborolyl)-2-phenylacetylene (7a): Starting materials: **4a** (3.1 g, 9.93 mmol), HCl·OEt_2 (9.93 mL, 19.86 mmol), 2-hydroxyphenol (1.25 g, 9.93 mmol). Yield 1.8 g (76%), brown-red solid, m.p. 66 °C. ^{1}H NMR (200.1 MHz, $CDCl_3$): δ = 7.2−7.6 (m, 9 H, H_{aryl}) ppm. ^{13}C NMR (50.3 MHz, $CDCl_3$): δ = 108.9 (C_{sp}−C_i), 114.2, 123.5, 125.4, 126.3, 126.9, 156.7 (2-hydroxythio-

 © 2004 Wiley-VCH Verlag GmbH & Co. KGaA, Weinheim

phenol), 119.7, 128.5, 129.9, 132.6 (C_6H_5) ppm; C_{sp}−B not observed. ^{11}B NMR (64.2 MHz, $CDCl_3$): δ = 38 ppm. MS (70 eV, EI): *m/z* (%) = 236 (100) [M^+]. MS (70 eV, HR-EI): *m/z* (%) = 236.0462 (100) [M^+; $^{12}C_{14}{}^1H_9{}^{11}B^{16}O_1{}^{32}S_1$: 236.0467]; Δmmu = 0.5.

1-(1,3,2-Benzothiaoxaborolyl)-2-tolylacetylene (7b): Starting materials: **3b** (2.75 g, 9.85 mmol), H_4C_6OSBr (2.0 g, 9.85 mmol). Yield: 2.1 g (86%), yellow solid, m.p. 71 °C. ^{1}H NMR (200.1 MHz, $CDCl_3$): δ = 2.39 (s, 3 H, CH_3), 7.2−7.6 (m, 8 H, H_{aryl}) ppm. ^{13}C NMR (50.3 MHz, $CDCl_3$): δ = 21.66 (CH_3), 109.3 ($C_{sp}-C_i$), 114.8, 123.8, 125.4, 126.2, 126.9, 156.6 (2-hydroxythiophenol), 118.4, 129.3, 132.5, 140.4 (tolyl) ppm; C_{sp}−B not observed. ^{11}B NMR (64.2 MHz, $CDCl_3$): δ = 38 ppm. MS (70 eV, EI): *m/z* (%) = 250 (100) [M^+]. MS (70 eV, HR-EI): *m/z* (%) = 250.0622 (100) [M^+; $^{12}C_{15}{}^1H_{11}{}^{11}B^{16}O_1{}^{32}S_1$: 250.0627]; Δmmu = 0.5.

Isomers of Tris(catecholboryl)triphenylbenzene (8a/8a′), Tris(catecholboryl)tritolylbenzene (8b/8b′), Tris(4-methylcatecholboryl)triphenylbenzene (8c/8c′), and Tris(4-methylcatecholboryl)tritolylbenzene (8d/8d′). Catalyst = [CpCo(CO)$_2$]: Borylacetylene (**5a:** 1.32 g; **5b**: 1.42 g; **5c**: 1.42 g; **5d**: 1.50 g; 6 mmol) and dicarbonylcobalt(η^5-cyclopentadienyl) (0.055 g, 0.3 mmol, 5 mol%) were heated at 90 °C in toluene (20 mL) for 3 days. The solid that formed was separated and washed several times with small amount of solvents (**8a/8a′**: toluene and CH_2Cl_2; **8b/8b′**: hexane and toluene; **8c/8c′** and **8d/8d′**: hexane) and dried in vacuo.

8a/8a′: Yield 1.02 g (77%), yellow solid, m.p. 230 °C. ^{1}H NMR (200.1 MHz, $CDCl_3$): δ = 7.2−7.6 (m, 27 H, H_{aryl}) ppm. ^{13}C NMR (50.3 MHz, $CDCl_3$): δ = 112.7, 123.2, 147.8 (catechol), 121.2, 128.5, 130.0, 132.8 (C_6H_5), 139.9 (central benzene, symm.), 134.6, 137.3, 142.5 (central benzene, unsymm.) ppm. ^{11}B NMR (64.2 MHz, $CDCl_3$): δ = 24 (br.) ppm. MS (70 eV, EI): *m/z* (%) = 660 (100) [M^+], 542 (42) [M^+ − catB + 1], 424 (15) [M^+ − 2catB + 1]. MS (70 eV, HR-EI): *m/z* (%) = 660.2087 (100) [M^+; $^{12}C_{42}{}^1H_{27}{}^{11}B_3{}^{16}O_6$: 660.2086]; Δmmu = 0.1. $C_{42}H_{27}B_3O_6$ (660.1): calcd. C 76.42, H 4.12; found C 76.15, H 4.75.

8b/8b′: Yield 1.10 g (78%), yellow solid, m.p. 241 °C. ^{1}H NMR (200.1 MHz, $CDCl_3$): δ = 2.35 (s, 9 H, CH_3), 7.0−7.4 (m, 24 H, H_{aryl}) ppm. ^{13}C NMR (50.3 MHz, $CDCl_3$): δ = 21.67 (CH_3), 112.6, 123.1, 147.8 (catechol), 118.1, 129.2, 132.0, 132.7 (tolyl), 140.6 (central benzene, symm.), 135.9, 139.2, 147.5 (central benzene, unsymm.) ppm. ^{11}B NMR (64.2 MHz, $CDCl_3$): δ = 22 (br.) ppm. MS (70 eV, EI): *m/z* (%) = 702 (8) [M^+], 584 (65) [M^+ − catB + 1], 466 (100) [M^+ − 2catB + 1]. MS (70 eV, HR-EI): *m/z* (%) = 702.2551 (5) [M^+; $^{12}C_{45}{}^1H_{33}{}^{11}B_3{}^{16}O_6$: 702.2556]; Δmmu = 0.5. $C_{45}H_{33}B_3O_6$ (702.2): calcd. C 76.97, H 4.74; found C 77.95, H 4.98.

8c/8c′: Yield 0.95 g (67%), yellow solid, m.p. 245 °C. ^{1}H NMR (200.1 MHz, $CDCl_3$): δ = 2.42 (s, 9 H, CH_3), 7.1−7.6 (m, 24 H, H_{aryl}) ppm. ^{13}C NMR (50.3 MHz, $CDCl_3$): δ = 21.60 (CH_3), 112.0, 113.3, 123.3, 129.4, 145.6, 147.7 (catechol), 123.7, 129.2, 132.2, 132.9 (C_6H_5), 140.7 (central benzene, symm.), 139.1, 146.0, 148.0 (central benzene, unsymm.) ppm. ^{11}B NMR (64.2 MHz, $CDCl_3$): δ = 23 (br.) ppm. MS (70 eV, EI): *m/z* (%) = 702 (100) [M^+], 570 (95) [M^+ − $H_3CC_6H_3O_2B$ + 1]. MS (70 eV, HR-EI): *m/z* (%) = 702.2596 (100) [M^+; $^{12}C_{45}{}^1H_{33}{}^{11}B_3{}^{16}O_6$: 702.2556]; Δmmu = 4.0. $C_{45}H_{33}B_3O_6$ (702.2): calcd. C 76.97, H 4.74; found C 76.45, H 5.08.

8d/8d′: Yield 1.12 g (75%), pale yellow solid, m.p. 261 °C. ^{1}H NMR (200.1 MHz, $CDCl_3$): δ = 2.35 (s, 9 H, CH_3), 2.39 (s, 9 H, CH_3), 6.9−7.5 (m, 21 H, H_{aryl}) ppm. ^{13}C NMR (50.3 MHz, $CDCl_3$): δ = 21.37 and 21.48 (CH_3), 111.9, 113.2, 123.1, 133.1, 145.7, 147.8 (catechol), 118.1, 129.0, 132.0, 132.7 (tolyl), 140.5 (central benzene, symm.), 138.9, 145.3, 147.5 (central benzene, unsymm.) ppm. ^{11}B NMR (64.2 MHz, $CDCl_3$): δ = 22 (br.) ppm. MS (70 eV, EI): *m/z* (%) = 744 (100) [M^+], 612 (49) [M^+ − $H_3CC_6H_3O_2B$ + 1]. MS (70 eV, HR-EI): *m/z* (%) = 744.3028 (100) [M^+; $^{12}C_{48}{}^1H_{39}{}^{11}B_3{}^{16}O_6$: 744.3025]; Δmmu = 0.3. $C_{48}H_{39}B_3O_6$ (744.2): calcd. C 77.46, H 5.28; found C 77.05, H 5.59.

Catalyst = [Co$_2$(CO)$_8$]: Mono(boryl)acetylene (**5a:** 1.76 g; **5b:** 1.87 g; **5c:** 1.87 g; **5d:** 1.98 g; 8 mmol) and octacarbonyldicobalt (0.136 g, 0.4 mmol, 5 mol%) were heated at 90 °C in toluene (20 mL) for 2 days. Workup was carried out as above.

Yields: 1.25 g (71%) of **8a/8a′**; 1.45 g (77%) of **8b/8b′**; 1.32 g (70%) of **8c/8c′**; 1.49 g (75%) of **8d/8d′**.

[η^4-Bis(diethylamino)bis(dimethylaminoboryl)cyclobutadiene](η^5-cyclopentadienyl)cobalt(I) (9): A solution of **2** (0.39 g, 2 mmol) in hexane (5 mL) was added within 15 min at room temparature to a solution of $CpCo(C_2H_4)_2$ (0.36 g, 2 mmol) in hexane (20 mL). The reaction mixture was stirred for 3 h. After filtration, the solvent was evaporated under high vacuum and a brown-green cobalt complex **9** was obtained. MS (70 eV, EI): *m/z* (%) = 515 (5) [M^+ + 1], 341 (4) [$C_{15}H_{24}B_2CoN_4{}^+$], 205 (7) [$C_9H_{19}B_2N_4{}^+$], 58 (37) [$C_3H_8N^+$], 28 (100) [$C_2H_4{}^+$].

[η^4-Bis(dithiocatecholboryl)diphenylcyclobutadiene](η^5-cyclopentadienyl)cobalt(1) (10a/10a′), [η^4-Bis(dithiocatecholboryl)ditolylcyclobutadiene](η^5-cyclopentadienyl)cobalt(1) (10b/10b′), [η^4-Bis(4-methyldithiocatecholboryl)diphenylcyclobutadiene](η^5-cyclopentadienyl)cobalt(1) (10c/10c′), [η^4-Bis(4-methyldithiocatecholboryl)ditolylcyclobutadiene](η^5-cyclopentadienyl)cobalt(1) (10d/10d′), [η^4-bis(1,3,2-benzo-thiaoxaborolyl)diphenylcyclobutadiene](η^5-cyclopentadienyl)cobalt(1) (11a/11a′), and [η^4-Bis(1,3,2-benzothiaoxaborolyl)ditolylcyclobutadiene](η^5-cyclopentadienyl)cobalt(1) (11b/11b′): Borylalkyne (**6a:** 2.01 g; **6b:** 2.12 g; **6c:** 2.12 g; **6d:** 2.24 g; **7a:** 1.88 g; **7b:** 2.00 g; 8 mmol) was added at room temperature to a solution of dicarbonylcobalt(η^5-cyclopentadienyl) (0.72 g, 4 mmol) in toluene (30 mL). The reaction mixture was heated under reflux for 3 d. After cooling, the precipitate was collected by filtration, washed several times with hexane, and dried in vacuo.

10a/10a′: Yield 1.42 g (56%), orange solid, m.p. 241 °C. ^{1}H NMR (200.1 MHz, $CDCl_3$): δ = 4.72 (s, 5 H, Cp−H), 7.4−7.9 (m, 18 H, H_{aryl}) ppm. ^{13}C NMR (50.3 MHz, $CDCl_3$): δ = 81.05, 82.10 (C_{4ring}), 86.25 (Cp−C), 125.7, 126.5, 140.9 (dithiocatechol), 128.4, 129.7, 131.1, 132.2 (C_6H_5) ppm. ^{11}B NMR (64.2 MHz, $CDCl_3$): δ = 58 (br.) ppm. MS (70 eV, EI): *m/z* (%) = 628 (100) [M^+], 478 (50) [M^+ − $BS_2C_6H_4$ + 1], 450 (2) [M^+ − PhC≡CPh], 376 (70) [M^+ − $C_6H_4S_2BC{\equiv}CPh$], 302 (4) [M^+ − $C_6H_4S_2BC{\equiv}CBS_2C_6H_4$]. MS (70 eV, HR-EI): *m/z* (%) = 628.0222 (100) [M^+; $^{12}C_{33}{}^1H_{23}{}^{11}B_2{}^{59}Co^{32}S_4$: 628.0200]; Δmmu = 2.2. $C_{33}H_{23}B_2CoS_4$ (628.0): calcd. C 63.06, H 3.39; found C 62.21, H 3.58.

10b/10b′: Yield 1.53 g (58%), orange-red solid, m.p. 245 °C. ^{1}H NMR (200.1 MHz, $CDCl_3$): δ = 2.35 (s, 6 H, CH_3), 4.82 (s, 5 H, Cp−H), 6.9−7.3 (m, 16 H, H_{aryl}) ppm. ^{13}C NMR (50.3 MHz, $CDCl_3$): δ = 21.69 (CH_3), 84.86 (Cp−C), 82.84, 83.41 (CBD), 124.8, 125.6, 139.9 (dithiocatechol), 127.5, 128.8, 130.2, 131.2 (tolyl) ppm. ^{11}B NMR (64.2 MHz, $CDCl_3$): δ = 57 (br.) ppm. MS (70 eV, EI): *m/z* (%) = 656 (100) [M^+], 506 (30) [M^+ − $BS_2C_6H_4$ + 1], 450 (3) [M^+ − $H_3CC_6H_4C{\equiv}CC_6H_4CH_3$], 390 (70) [$M^+$ − $C_6H_4S_2BC{\equiv}CC_6H_4CH_3$], 330 (5) [$M^+$ − $C_6H_4S_2BC{\equiv}CBS_2C_6H_4$]. MS (70 eV, HR-EI): *m/z* (%) = 656.0519 (100) [M^+; $^{12}C_{35}{}^1H_{27}{}^{11}B_2{}^{59}Co^{32}S_4$: 656.0513]; Δmmu = 0.6. $C_{35}H_{27}B_2CoS_4$ (656.0): calcd. C 64.02, H 4.15; found C 64.34, H 4.59.

10c/10c′: Yield 1.45 g (55%), yellow solid, m.p. 247 °C. ^{1}H NMR (200.1 MHz, $CDCl_3$): δ = 2.36 (s, 6 H, CH_3), 4.86 (s, 5 H, Cp−H),

 © 2004 Wiley-VCH Verlag GmbH & Co. KGaA, Weinheim

7.1−7.9 (m, 16 H, H_{aryl}) ppm. ^{13}C NMR (50.3 MHz, $CDCl_3$): δ = 20.96 (CH_3), 79.72 (Cp−C), 82.45, 83.23 (C_{4ring}), 124.5, 126.8, 127.0, 135.9, 137.7 (dithiocatechol), 122.2, 128.8, 129.3, 132.8 (C_6H_5) ppm. ^{11}B NMR (64.2 MHz, $CDCl_3$): δ = 57 (br.) ppm. MS (70 eV, EI): *m/z* (%) = 656 (100) [M^+], 492 (50) [M^+ − $BS_2C_6H_3CH_3$ + 1], 478 (5) [M^+ − PhC≡CPh], 390 (70) [M^+ − $H_3CC_6H_3S_2BC$≡CPh], 302 (10) [M^+ − $H_3CC_6H_3S_2BC$≡$CBS_2C_6H_3CH_3$]. MS (70 eV, HR-EI): *m/z* (%) = 656.0533 (100) [M^+; $^{12}C_{35}{}^1H_{27}{}^{11}B_2{}^{59}Co^{32}S_4$: 656.0513]; Δmmu = 2.0. $C_{35}H_{27}B_2CoS_4$ (656.0): calcd. C 64.02, H 4.15; found C 64.49, H 4.77.

10d/10d′: Yield 1.56 g (57%), orange solid, m.p. > 300 °C. ^1H NMR (200.1 MHz, $CDCl_3$): δ = 2.38 (s, 6 H, CH_3), 2.42 (s, 6 H, CH_3), 4.68 (s, 5 H, Cp−H), 7.0−7.8 (m, 14 H, H_{aryl}) ppm. ^{13}C NMR (50.3 MHz, $CDCl_3$): δ = 21.07 and 21.56 (CH_3), 83.90 (Cp−C), 79.72, 89.76 (C_{4ring}), 125.7, 126.4, 126.5, 135.2, 137.2, 140.8 (dithiocatechol), 128.2, 129.0, 130.0, 132.7 (tolyl) ppm. ^{11}B NMR (64.2 MHz, $CDCl_3$): δ = 58 (br.) ppm. MS (70 eV, EI): *m/z* (%) = 684 (15) [M^+], 520 (18) [M^+ − $BS_2C_6H_3CH_3$ + 1], 478 (10) [M^+ − $H_3CC_6H_4C$≡$CC_6H_4CH_3$], 404 (100) [M^+ − $H_3CC_6H_3S_2$-BC≡$CC_6H_4CH_3$], 330 (22) [M^+ − $H_3CC_6H_3S_2BC$≡$CBS_2C_6H_3CH_3$]. MS (70 eV, HR-EI): *m/z* (%) = 684.0851 (100) [M^+; $^{12}C_{37}{}^1H_{31}{}^{11}B_2{}^{59}Co^{16}S_4$: 684.0826]; Δmmu = 2.5. $C_{37}H_{31}B_2CoS_4$ (684.4): calcd. C 64.90, H 4.57; found C 64.38, H 5.07.

11a/11a′: 1.64 g (68%), red-brown solid, m.p. 210 °C. ^1H NMR (200.1 MHz, $CDCl_3$): δ = 5.35 (s, 5 H, Cp−H), 7.4−7.9 (m, 18 H, H_{aryl}) ppm. ^{13}C NMR (50.3 MHz, $CDCl_3$): δ = 83.98, 85.26 (C_{4ring}), 87.26 (Cp−C), 113.8, 122.8, 125.3, 125.9, 127.4, 155.6 (2-hydroxythiophenol), 120.5, 124.4, 128.9, 131.5 (C_6H_5) ppm. ^{11}B NMR (64.2 MHz, $CDCl_3$): δ = 45 (br.) ppm. MS (70 eV, EI): *m/z* (%) = 596 (50) [M^+], 462 (50) [M^+ − $BSOC_6H_4$ + 1], 418 (3) [M^+ − PhC≡CPh], 360 (65) [M^+ − C_6H_4SOBC≡CPh], 302 (4) [M^+ − C_6H_4SOBC≡$CBOSC_6H_4$]. MS (70 eV, HR-EI): *m/z* (%) = 596.0665 (82) [M^+; $^{12}C_{33}{}^1H_{23}{}^{11}B_2{}^{59}Co^{16}O_2{}^{32}S_2$: 596.0657]; Δmmu = 0.8. $C_{33}H_{23}B_2CoO_2S_2$ (596.2): calcd. C 66.44, H 3.89; found C 65.89, H 4.56.

11b/11b′: 1.56 g (62%), red solid, m.p. 221 °C. ^1H NMR (200.1 MHz, $CDCl_3$): δ = 2.32 (s, 6 H, CH_3), 5.37 (s, 5 H, Cp−H), 7.1−7.5 (m, 16 H, H_{aryl}) ppm. ^{13}C NMR (50.3 MHz, $CDCl_3$): δ = 21.39 (CH_3), 83.86 (Cp−C), 84.49, 86.23 (C_{4ring}), 114.5, 123.5, 125.1, 125.9, 126.7, 156.3 (2-hydroxythiophenol), 118.1, 128.9, 132.2, 140.1 (tolyl) ppm. ^{11}B NMR (64.2 MHz, $CDCl_3$): δ = 46 (br.) ppm. MS (70 eV, EI): *m/z* (%) = 624 (80) [M^+], 490 (50) [M^+ − $BSOC_6H_4$ + 1], 418 (2) [M^+ − $H_3CC_6H_4C$≡$CC_6H_4CH_3$], 374 (45) [M^+ − C_6H_4SOBC≡$CC_6H_4CH_3$], 330 (9) [M^+ − C_6H_4SOBC≡$CBOSC_6H_4$]. MS (70 eV, HR-EI): *m/z* (%) = 624.0985 (100) [M^+; $^{12}C_{35}{}^1H_{27}{}^{32}S_2{}^{16}O_2{}^{11}B_2{}^{59}Co$: 624.0970]; Δmmu = 1.5. $C_{35}H_{27}B_2CoO_2S_2$ (624.2): calcd. C 67.30, H 4.36; found C 66.95, H 4.72.

Isomers of Tris(dithiocatecholboryl)triphenylbenzene (12a/12a′), Tris(dithiocatecholboryl)tritolylbenzene (12b/12b′), Tris(4-methyldithiocatecholboryl)triphenylbenzene (12c/12c′), Tris(4-methyldithiocatecholboryl)tritolylbenzene (12d,12d′), Tris(1,3,2-benzothiaoxaborolyl)triphenylbenzene (13a/13a′), and Tris(1,3,2-benzothiaoxaborolyl)tritolylbenzene (13b/13b′). Catalyst = [$Co_2(CO)_8$]: Borylalkyne (**6a:** 2.26 g; **6b:** 2.39 g; **6c:** 2.39 g; **6d:** 2.52 g; **7a:** 2.12 g; **7b:** 2.25 g; 9 mmol) and octacarbonyldicobalt (0.155 g, 0.45 mmol, 5 mole-%) were heated under reflux in toluene (20 mL) for 48 h. The solid was separated and washed several times with small amounts of solvents (**12a/12a′**: toluene and CH_2Cl_2; **12b/12b′**: hexane and toluene; **12c/12c′** and **12d/12d′**: hexane; **13a/13a′**: toluene and CH_2Cl_2; **13b/13b′**: hexane and toluene) and dried in vacuo.

12a/12a′: 1.74 g (77%), black solid, m.p. > 300 °C. ^1H NMR (200.1 MHz, $CDCl_3$): δ = 7.4−7.9 (m, 36 H, H_{aryl}) ppm. ^{13}C NMR (50.3 MHz, $CDCl_3$): δ = 125.8, 126.6, 141.0 (dithiocatechol), 126.9 (central benzene, symm.), 128.4, 128.9, 138.0 (central benzene, unsymm.), 128.6, 129.9, 131.2, 132.3 (C_6H_5) ppm. ^{11}B NMR (64.2 MHz, $CDCl_3$): δ = 62 (v. br.) ppm. MS (70 eV, EI): *m/z* (%) = 756 (100) [M^+]. MS (70 eV, HR-EI): *m/z* (%) = 756.0742 (100) [M^+; $^{12}C_{42}{}^1H_{27}{}^{11}B_3{}^{32}S_6$: 756.0716]; Δmmu = 2.6. $C_{42}H_{27}B_3S_6$ (756.4): calcd. C 66.66, H 3.60; found C 65.21, H 3.84.

12b/12b′: 1.83 g (76%), black solid, m.p. 295 °C. ^1H NMR (200.1 MHz, $CDCl_3$): δ = 2.39 (s, 9 H, CH_3), 7.2−7.5 (m, 24 H, H_{aryl}) ppm. ^{13}C NMR (50.3 MHz, $CDCl_3$): δ = 21.27 (CH_3), 122.4, 127.3, 141.2 (dithiocatechol), 126.3 (central benzene, symm.), 136.0, 137.8, 140.6 (central benzene, unsymm.), 127.0, 128.6, 129.9, 132.4 (tolyl) ppm. ^{11}B NMR (64.2 MHz, $CDCl_3$): δ = 60 (v. br.) ppm. MS (70 eV, EI): *m/z* (%) = 798 (100) [M^+]. MS (70 eV, HR-EI): *m/z* (%) = 798.1197 (100) [M^+; $^{12}C_{45}{}^1H_{33}{}^{11}B_3{}^{32}S_6$: 798.1185]; Δmmu = 1.2. $C_{45}H_{33}B_3S_6$ (798.5): calcd. C 67.66, H 4.17; found C 67.74, H 4.59.

12c/12c′: 1.90 g (79%), black solid, m.p. 297 °C. ^1H NMR (200.1 MHz, $CDCl_3$): δ = 2.33 (s, 9 H, CH_3), 6.9−7.6 (m, 24 H, H_{aryl}) ppm. ^{13}C NMR (50.3 MHz, $CDCl_3$): δ = 21.77 (CH_3), 122.9, 126.8, 127.8, 136.6, 138.3, 141.7 (dithiocatechol), 128.5 (central benzene, symm.), 136.2, 138.0, 141.1 (central benzene, unsymm.), 127.5, 129.1, 130.4, 132.9 (C_6H_5) ppm. ^{11}B NMR (64.2 MHz, $CDCl_3$): δ = 60 (v. br.) ppm. MS (70 eV, EI): *m/z* (%) = 798 (100) [M^+]. MS (70 eV, HR-EI): *m/z* (%) = 798.1185 (100) [M^+; $^{12}C_{45}{}^1H_{33}{}^{11}B_3{}^{32}S_6$: 798.1185]; Δmmu = 0.0. $C_{45}H_{33}B_3S_6$ (798.5): calcd. C 67.66, H 4.17; found C 67.89, H 4.75.

12d/12d′: 2.05 g (81%), black solid, m.p. > 310 °C. ^1H NMR (200.1 MHz, $CDCl_3$): δ = 2.38 (s, 9 H, CH_3), 2.41 (s, 9 H, CH_3), 7.2−7.7 (m, 21 H, H_{aryl}) ppm. ^{13}C NMR (50.3 MHz, $CDCl_3$): δ = 21.17 and 21.78 (CH_3), 126.2, 126.9, 127.1, 135.9, 137.7, 141.0 (dithiocatechol), 119.2, 129.3, 132.2, 140.3 (tolyl) ppm; because of the low solubility, the *ipso*-carbon atoms were not observed. ^{11}B NMR (64.2 MHz, $CDCl_3$): δ = 60 (v. br.) ppm. MS (70 eV, EI): *m/z* (%) = 840 (100) [M^+]. MS (70 eV, HR-EI): *m/z* (%) = 840.1680 (100) [M^+; $^{12}C_{48}{}^1H_{39}{}^{11}B_3{}^{16}S_6$: 840.1655]; Δmmu = 2.5. $C_{48}H_{39}B_3S_6$ (840.6): calcd. C 68.56, H 4.68; found C 67.38, H 5.15.

13a/13a′: 1.50 g (70%), red solid, m.p. 282 °C. ^1H NMR (200.1 MHz, $CDCl_3$): δ = 7.2−7.6 (m, 27 H, H_{aryl}) ppm. ^{13}C NMR (50.3 MHz, $CDCl_3$): δ = 113.8, 122.8, 124.4, 125.3, 125.9, 155.6 (2-hydroxythiophenol), 132.8 (central benzene, symm.), 135.2, 138.4, 141.2 (central benzene, unsymm.), 120.5, 128.0, 128.9, 131.5 (C_6H_5) ppm. ^{11}B NMR (64.2 MHz, $CDCl_3$): δ = 53 (br.) ppm. MS (70 eV, EI): *m/z* (%) = 708 (100) [M^+], 574 (10) [M^+ − $OSBC_6H_4$ + 1]. MS (70 eV, HR-EI): *m/z* (%) = 708.1415 (100) [M^+; $^{12}C_{42}{}^1H_{27}{}^{11}B_3{}^{16}O_3{}^{32}S_3$: 708.1401]; Δmmu = 1.4. $C_{42}H_{27}B_3O_3S_3$ (708.2): calcd. C 71.17, H 3.84; found C 71.07, H 4.26.

13b/13b′: Yield: 1.85 g (82%), red solid, m.p. 293 °C. ^1H NMR (200.1 MHz, $CDCl_3$): δ = 2.38 (s, 9 H, CH_3), 7.2−7.6 (m, 24 H, H_{aryl}) ppm. ^{13}C NMR (50.3 MHz, $CDCl_3$): δ = 21.39 (CH_3), 114.5, 123.5, 125.1, 125.9, 131.7, 156.3 (2-hydroxythiophenol), 132.7 (central benzene, symm.), 118.1, 126.7, 128.9, 132.2 (tolyl) ppm; *ipso* carbon atoms of unsymm. ring were not observed. ^{11}B NMR (64.2 MHz, $CDCl_3$): δ = 52 (br.) ppm. MS (70 eV, EI): *m/z* (%) = 750 (70) [M^+]. MS (70 eV, HR-EI): *m/z* (%) = 750.1872 (100) [M^+; $^{12}C_{45}{}^1H_{33}{}^{11}B_3{}^{16}O_3{}^{32}S_3$: 750.1871]; Δmmu = 0.1. $C_{45}H_{33}B_3O_3S_3$ (750.3): calcd. C 71.98, H 4.43; found C 71.09, H 4.93.

3-(1,3,2-Benzodioxaborolyl)-4-phenyl-1,2-bis(tricarbonylcobalta)-tetrahedrane (14a), 3-(1,3,2-Benzodithiaborolyl)-4-phenyl-1,2-bis-

 © 2004 Wiley-VCH Verlag GmbH & Co. KGaA, Weinheim

(tricarbonylcobalta)tetrahedrane (15a), and 3-(1,3,2-Benzothiaoxaborolyl)-4-phenyl-1,2-bis(tricarbonylcobalta)tetrahedrane (16a): A solution of an alkyne (**5a:** 1.29 g; **6a:** 1.48 g; **7a:** 1.39 g; 5.9 mmol) in CH_2Cl_2 (10 mL) was added at −20 °C to a solution of $Co_2(CO)_8$ (2.03 g, 5.9 mmol) in CH_2Cl_2 (20 mL). The mixture was stirred for 48 h at room temperature and the solvent was evaporated to near dryness. The residue was separated by column chromatography (Florisil®; hexane) to give two fractions. Using hexane as the eluent, $[Co_2(CO)_8]$ was obtained first. The second fraction (hexane/toluene, 1:4) contained the corresponding dicobalt complex.

14a: Yield 1.51 g (50%), red oil. ^{1}H NMR (200.1 MHz, $CDCl_3$): δ = 7.2−7.7 (m, 9 H, H_{aryl}) ppm. ^{13}C NMR (50.3 MHz, $CDCl_3$): δ = 104.3 (C_{ipso}), 112.7, 123.2, 147.8 (catechol), 121.2, 128.5, 130.0, 132.8 (C_6H_5), 200.1 (CO) ppm; CB was not observed. ^{11}B NMR (64.2 MHz, $CDCl_3$): δ = 33 ppm. IR (hexane): $\tilde{\nu}$ = 2021 (vs), 2039 (s), 2057 (vs), 2081 (w), 2098 (s) cm^{-1}. MS (70 eV, EI): *m/z* (%) = 506 (2) [M$^+$], 478 (16) [M$^+$ − CO], 450 (6.5) [M$^+$ − 2 CO], 422 (13) [M$^+$ − 3 CO], 394 (30) [M$^+$ − 4 CO], 366 (53) [M$^+$ − 5 CO], 338 (27) [M$^+$ − 6 CO], 279 (30) [M$^+$ − 6 CO − Co], 220 (100) [M$^+$ − 6 CO − 2 Co]. MS (70 eV, HR-EI): *m/z* (%) = 505.9105 (2) [M$^+$; $^{12}C_{20}{}^1H_9{}^{11}B^{59}Co_2{}^{16}O_8$: 505.9054]; Δmmu = 5.1.

15a: Yield 1.52 g (48%), brown-red oil. ^{1}H NMR (200.1 MHz, $CDCl_3$): δ = 7.1−7.8 (m, 9 H, H_{aryl}) ppm. ^{13}C NMR (50.3 MHz, $CDCl_3$): δ = 72.56 (br., CB), 122.5 (C_{ipso}), 125.5, 126.9, 137.4 (dithiocatechol), 128.1, 128.3, 130.2, 131.2 (C_6H_5), 199.5 (CO) ppm. ^{11}B NMR (64.2 MHz, $CDCl_3$): δ = 59 ppm. IR (hexane): $\tilde{\nu}$ = 2007 (s), 2025 (s), 2044 (vs), 2060 (vs), 2088 (w) cm^{-1}. MS (70 eV, EI): *m/z* (%) = 538 (2) [M$^+$], 510 (3) [M$^+$ − CO], 482 (5) [M$^+$ − 2 CO], 454 (2) [M$^+$ − 3 CO], 426 (7) [M$^+$ − 4 CO], 398 (12) [M$^+$ − 5 CO], 370 (15) [M$^+$ − 6 CO], 311 (4) [M$^+$ − 6 CO − Co], 252 (100) [M$^+$ − 6 CO − 2 Co]. MS (70 eV, HR-EI): *m/z* (%) = 537.8536 (2) [M$^+$; $^{12}C_{20}{}^1H_9{}^{11}B^{59}Co_2{}^{16}O_6{}^{32}S_2$: 537.8597]; Δmmu = 6.1.

16a: 1.40 g (45%), brown-red oil. ^{1}H NMR (200.1 MHz, $CDCl_3$): δ = 7.1−7.5 (m, 9 H, H_{aryl}) ppm. ^{13}C NMR (50.3 MHz, $CDCl_3$): δ = 108.7 (C_{ipso}), 114.8, 123.8, 125.4, 126.2, 126.9, 156.6 (2-hydroxythiophenol), 121.5, 128.4, 129.9, 132.5 (C_6H_5), 200.6 (CO) ppm; CB was not observed. ^{11}B NMR (64.2 MHz, $CDCl_3$): δ = 47 ppm. IR (hexane): $\tilde{\nu}$ = 2007 (s), 2022 (vs), 2044 (vs), 2060 (vs), 2076 (s) cm^{-1}. MS (70 eV, EI): *m/z* (%) = 522 (3) [M$^+$], 494 (7) [M$^+$ − CO], 466 (10) [M$^+$ − 2 CO], 438 (12) [M$^+$ − 3 CO], 410 (31) [M$^+$ − 4 CO], 382 (15) [M$^+$ − 5 CO], 354 (13), [M$^+$ − 6 CO], 295 (6) [M$^+$ − 6 CO − Co], 236 (100) [M$^+$ − 6 CO − 2 Co]. MS (70 eV, HR-EI): *m/z* (%) = 521.8856 (3) [M$^+$; $^{12}C_{20}{}^1H_9{}^{11}B^{59}Co_2{}^{16}O_7{}^{32}S_1$: 521.8826]; Δmmu = 3.0.

(1,3,2-Benzodithiaborolyl)pentaphenylbenzene and Bis(1,3,2-benzodioxaborolyl)(1,3,2-benzodithiaborolyl)triphenylbenzene (17 and 18): Diphenylacetylene (0.75 g, 4.2 mmol) or 1-(catacholboryl)-2-phenylacetylene (**5a**; 0.92 g, 4.2 mmol) was added at room temperature to a solution of **15a** (1.12 g, 2.1 mmol) in toluene (30 mL). The resulting mixture was stirred for 48 h under reflux. After cooling, the dark-black precipitate was collected by filtration and washed several times with hexane and toluene, and then dried in vacuo.

17: 0.90 g (70%), dark solid, m.p. > 300 °C. MS (70 eV, EI): *m/z* (%) = 608 (100) [M$^+$]. MS (70 eV, HR-EI): *m/z* (%) = 608.1818 (100) [M$^+$; $^{12}C_{42}{}^1H_{29}{}^{11}B^{32}S_2$: 608.1803]; Δmmu = 1.5.

18: 1.10 g (75%), black solid, m.p. > 300 °C. MS (70 eV, EI): *m/z* (%) = 692 (100) [M$^+$]. MS (70 eV, HR-EI): *m/z* (%) = 692.1633 (100) [M$^+$; $^{12}C_{42}{}^1H_{27}{}^{11}B_3{}^{16}O_4{}^{32}S_2$: 692.1629]; Δmmu = 0.4.

Crystal Structure Determinations of 4a, 5a, 6a, and 10a: Crystal data and details of the structure determinations are listed in Table 1. Unique sets of intensity data were collected using a Bruker−AXS SMART 1000 diffractometer (Mo-K_α radiation, λ = 0.71073 Å, graphite monochromator, ω-scan). Empirical absorp-

Table 1. Crystal data and structural refinement for **4a, 5a, 6a**, and **10a**

	4a	**5a**	**6a**	**10a**
Empirical formula	$C_{20}H_{33}N_2B$	$C_{14}H_9O_2B$	$C_{14}H_9S_2B$	$C_{33}H_{23}B_2CoS_4$
Molecular mass	312.29	220.02	252.14	628.30
Crystal system	monoclinic	orthorhombic	monoclinic	triclinic
Space group	*C*2/*c*	F*dd*2	$P2_1$	$P\bar{1}$
Unit cell				
a [Å]	13.9717(7)	19.626(5)	14.419(2)	12.7008(7)
b [Å]	14.9033(8)	7.1519(18)	5.4955(8)	15.9541(9)
c [Å]	11.0036(6)	15.422(4)	15.466(2)	17.364(1)
α [°]	90	90	90	87.270(1)
β [°]	118.881(1)	90	102.885(3)	69.319(1)
γ [°]	90	90	90	88.105(1)
Volume [Å^3]	2006.25(18)	2164.8(9)	1194.6(3)	3287.5(3)
Z	4	8	4	4
Calcd. density [g cm^{-3}]	1.034	1.350	1.402	1.269
μ [mm^{-1}]	0.059	0.088	0.414	0.796
F(000)	688	912	520	1288
Crystal size [mm]	0.50 × 0.34 × 0.26	0.35 × 0.23 × 0.07	0.17 × 0.10 × 0.01	0.18 × 0.07 × 0.05
$\theta_{max.}$ [°]	32.01	32.10	27.11	25.03
Index ranges	−20/18, 0/22, 0/16	0/29, 0/10, −21/22	−18/17, −7/ 6, 0/19	−14/15, −18/18, 0/20
Reflections collected	9223	5076	7208	35994
independent	3421(0.0216)	1717(0.0673)	4370(0.0625)	11615(0.0763)
Parameters	173	98	308	725
Goodness-of-fit on F^2	1.045	1.072	0.993	0.870
R_1 [$I > 2\sigma_I$]	0.0438	0.0713	0.0532	0.0503
wR_2 (all reflections)	0.1230	0.1678	0.1195	0.1162
T [K]	103(2)	103(2)	103(2)	298(2)
Residual electron density [e/A^3]	0.532/−0.125	0.926/−0.367	0.462/−0.581	0.281/−0.542

 © 2004 Wiley-VCH Verlag GmbH & Co. KGaA, Weinheim

tion corrections were applied. The structures were solved by direct methods (SHELXS-86)[32] and refined by least-squares methods based on F^2 with all measured reflections (SHELXL-97).[33] All non-hydrogen atoms were refined anisotropically.

CCDC-227235 (for **4a**), -227236 (for **5a**), -227237 (for **6a**), and -227238 (for **10a**) contain the supplementary crystallographic data for this paper. These data can be obtained free of charge at www.ccdc.cam.ac.uk/conts/retrieving.html [or from the Cambridge Crystallographic Data Centre, 12 Union Road, Cambridge CB2 1EZ, UK; Fax: (internat.) +44-1223-336-033; E-mail: deposit@ccdc.cam.ac.uk].

Acknowledgments

This work was supported by the SFB 623 and the Fonds der Chemischen Industrie. We thank Prof. R. Gleiter for fruitful discussions.

[1] [1a] S. Saito, Y. Yamamoto, *Chem. Rev.* **2000**, *100*, 2901−2915. [1b] Y. Yamamoto, A. Nagata, H. Nagata, Y. Ando, Y. Avikawa, K. Tatsumi, K. Itoh, *Chem. Eur. J.* **2003**, *9*, 2469−2483. [1c] E. R. F. Gesing, K. P. C. Vollhardt, *J. Organomet. Chem.* **1981**, *217*, 105−118. [1d] L. P. M. Bushnell, E. R. Evirt, R. G. Bergman, *J. Organomet. Chem.* **1978**, *157*, 445−456.

[2] [2a] T. S. Piper, F. A. Cotton, G. Wilkinson, *J. Inorg. Nucl. Chem.* **1955**, *1*, 165−174. [2b] E. O. Fischer, R. Jira, *Z. Naturforsch., Teil B* **1955**, *10*, 355.

[3] [3a] A. Efraty, *Chem. Rev.* **1977**, *77*, 691−744. [3b] R. Gleiter, *Angew. Chem.* **1992**, *104*, 29−46; *Angew. Chem. Int. Ed. Engl.* **1992**, *31*, 27−44. [3c] A. Nakamura, N. Hagihara, *Bull. Chem. Soc., Jpn.* **1961**, *34*, 452−453. [3d] M. D. Rausch, R. A. Genetti, *J. Am. Chem. Soc.* **1967**, *89*, 5502−5503. [3e] J. L. Boston, D. W. A. Sharp, G. Wilkinson, *J. Chem. Soc.* **1962**, 3488−3494.

[4] N. Schore, *Chem. Rev.* **1988**, *88*, 1081−1119.

[5] [5a] K. P. C. Vollhardt, *Angew. Chem.* **1984**, *96*, 525−542; *Angew. Chem. Int. Ed. Engl.* **1984**, *23*, 539−644. [5b] H. Bönnemann, W. Brijoux, R. Brinkmann, W. Meurers, R. Mynott, W. Von Phillipsbon, T. Egolf, *J. Organomet. Chem.* **1984**, *272*, 231−249.

[6] [6a] I. U. Khand, G. R. Knox, P. L. Pauson, W. E. Watts, *J. Chem. Soc., Chem. Commun.* **1971**, 36. [6b] I. U. Khand, G. R. Knox, P. L. Pauson, W. E. Watts, *J. Chem. Soc., Perkin Trans. 1* **1973**, 975−977. [6c] P. L. Pauson, *Tetrahedron* **1985**, *41*, 5855−5860.

[7] Y. Gu, H. Pritzkow, W. Siebert, *Eur. J. Inorg. Chem.* **2001**, 373−379.

[8] C. Ester, A. Maderna, H. Pritzkow, W. Siebert, *Eur. J. Inorg. Chem.* **2000**, 1177−1184.

[9] [9a] M. Neuenschwander, P. Bigler, *Helv. Chim. Acta* **1973**, *56*, 959−965. [9b] A. Niederhauser, M. Neuenschwander, *Helv. Chim. Acta* **1973**, *56*, 1331−1343.

[10] S. Y. Delavarenne, H. G. Viehe, *Chem. Ber.* **1970**, *103*, 1209−1215.

[11] C. Blanchard, E. Framery, M. Vaultier, *Synthesis* **1996**, 45−47.

[12] F. H. Allen, O. Kennard, D. G. Watson, L. Brammer, A. G. Orpen, R. Taylor, *J. Chem. Soc., Perkin Trans. 2* **1987**, S1−S19.

[13] M. Hesse, H. Meier, B. Zeeh, *Spektroskopische Methoden in der Organischen Chemie,* 4th ed., Thieme Verlag, Stuttgart, **1991**.

[14] [14a] H. Schulz, G. Gabbert, H. Pritzkow, W. Siebert, *Chem. Ber.* **1993**, *126*, 1593−1595. [14b] M. Bluhm, A. Maderna, H. Pritzkow, S. Bethke, R. Gleiter, W. Siebert, *Eur. J. Inorg. Chem.* **1999**, 1693.

[15] K. Okada, T. Sugawa, M. Oda, *J. Chem. Soc., Chem. Commun.* **1992**, 74.

[16] J. H. Hardesty, J. B. Koerner, T. A. Albright, G. Y. Lee, *J. Am. Chem. Soc.* **1999**, *121*, 6055− 6067.

[17] R. Diercks, B. E. Eaton, S. Gürtzgen, S. Jalisatgi, A. J. Matzger, R. H. Radde, K. P. C. Vollhardt, *J. Am. Chem. Soc.* **1998**, *120*, 8247−8248.

[18] R. J. Baxter, G. R. Knox, J. H. Mori, P. L. Pauson, M. D. Spicer, *Organometallics* **1999**, *18*, 206−214.

[19] [19a] R. J. Baxter, G. R. Knox, P. L. Pauson, M. D. Spicer, *Organometallics* **1999**, *18*, 197−205. [19b] M. A. Bennett, P. B. Donaldson, *Inorg. Chem.* **1978**, *17*, 1995−2000. [19c] R. J. Kaufman, R. S. Sidhu, *J. Org. Chem.* **1982**, *47*, 4941−4947.

[20] [20a] O. S. Mills, G. Robinson, *Proc. Chem. Soc.* **1964**, 187. [20b] G. Gervasio, E. Sappa, L. Marko, *J. Organomet. Chem.* **1993**, *444*, 203−209. [20c] R. S. Dickson, P. J. Fraser, *Aust. J. Chem.* **1972**, *25*, 1179.

[21] [21a] W. Hübel, C. Hoogzand, *Chem. Ber.* **1960**, *93*, 103. [21b] U. Krüerke, W. Hübel, *Chem. Ber.* **1961**, *94*, 2829. [21c] U. Krüerke, W. Hübel, *Chem. Ber.* **1961**, *94*, 2917.

[22] G. F. Emerson, L. Watts, R. Pettit, *J. Am. Chem. Soc.* **1965**, *87*, 131.

[23] F. L. Bowden, A. B. P. Lever, *Organomet. Chem. Rev.* **1968**, *3*, 227.

[24] J. R. Fritch, K. P. C. Vollhardt, *J. Am. Chem. Soc.* **1978**, *100*, 3643.

[25] H. Sakurai, J. Hayashi, *J. Organomet. Chem.* **1972**, *39*, 365−370.

[26] M. E. Arnett, J. M. Bollinger, *J. Am. Chem. Soc.* **1964**, *86*, 4729−4731.

[27] [27a] P. Galow, A. Sebald, B. Wrackmeyer, *J. Organomet. Chem.* **1983**, *259*, 253. [27b] H. Greenfield, H. W. Sternberg, R. A. Friedel, J. H. Wotiz, R. Markby, I. Wender, *J. Am. Chem. Soc.* **1956**, *78*, 120.

[28] [28a] J. Perez, L. Riera, V. Riera, S. G. Granda, E. G. Rodriguez, D. G. Churchill, M. R. Churchill, T. S. Janik, *Inorg. Chim. Acta* **2003**, *347*, 189−193. [28b] M. Akita, M. Terada, M. Tanaka, Y. Moro-Oka, *Organometallics* **1992**, *11*, 3468.

[29] P. Y. Chavant, M. Vaultier, *J. Organomet. Chem.* **1993**, *455*, 37−46.

[30] M. Younus, N. J. Long, P. R. Raithby, J. Lewis, N. A. Page, A. J. P. White, D. J. Williams, M. C. B. Colbert, A. J. Hodge, M. S. Khan, D. G. Parker, *J. Organomet. Chem.* **1999**, *578*, 198−209.

[31] W. Gerrard, M. F. Lappert, B. A. Mountfield, *J. Chem. Soc., II* **1959**, 1529−1535.

[32] G. M. Sheldrick, *SHELXS-86*, University of Göttingen, **1986**.

[33] G. M. Sheldrick, *SHELXL-97*, University of Göttingen, **1997**.

Received January 23, 2004
Early View Article
Published Online May 25, 2004

 © 2004 Wiley-VCH Verlag GmbH & Co. KGaA, Weinheim

Novel Bonding Modes between Tetrathiafulvalenes (TTFs) and Transition Metal Centers: π-Bonding and Covalent $TTFSiMe_2-ML_n$ Coordination to Platinum

Mathuresh N. Jayaswal,[a] Harmel N. Peindy,[a] Fabrice Guyon,*[a] Michael Knorr,*[a] Narcis Avarvari,[b] and Marc Fourmigué[b]

Keywords: Platinum / Tetrathiafulvalene / pi interactions / Si ligands / X-ray diffraction

Two novel strategies for coordinating TTF to transition metal centers have been developed. The reaction of tetrathiafulvalene (TTF) or 3,4-dimethyltetrathiafulvalene (*o*-Me_2TTF) with [Pt(η^2-C_2H_4)(PPh_3)$_2$] leads to the π complexes [Pt(η^2-TTF)(PPh_3)$_2$] (**1**) and [Pt(η^2-*o*-Me_2TTF)(PPh_3)$_2$] (**2**), respectively. An X-ray crystallographic study performed on **2** confirmed, that TTFs act as a π acidic ligand. NMR studies revealed the existence, in solution, of an equilibrium between free and complexed TTF. Dilithiation of *o*-Me_2TTF and subsequent silylation with $ClSiMe_2H$ afforded 3,4-dimethyl-3′,4′-(dimethylsilyl)tetrathiafulvalene (**3**), which has been structurally characterized. **3** reacts by oxidative addition across [Pt(η^2-C_2H_4)(PPh_3)$_2$] to give [Pt{η^2-*o*-($SiMe_2$)$_2$-$TTFMe_2$}(PPh_3)$_2$] (**4**), in which the TTF ligand is covalently ligated to platinum via $SiMe_2$ bridges. The redox properties of **3** and **4** have been investigated by cyclic voltammetry. Strong cathodic shifts of the two redox processes were observed for **4**, implying the TTF core.
(© Wiley-VCH Verlag GmbH & Co. KGaA, 69451 Weinheim, Germany, 2004)

Introduction

From the research devoted to novel functionalized tetrathiafulvalenes (TTFs) has emerged, in the past few years, the synthesis of derivatives incorporating substituents allowing the coordination to transition metal fragments.[1] Such molecules are particularly interesting in molecular materials science for the elaboration of hybrid organic/inorganic multifunctional materials.[2] Two main strategies have been used for the synthesis of transition metal complexes incorporating the TTF unit: (i) the functionalization of TTFs with phosphane (**A**) or pyridine ligands (**B**) taking advantage of the donor coordinating properties of these substituents,[3] and (ii) the coordination of metal fragments to the tetrathiolate or dithiolate tetrathiafulvalene ($TTFS_4^{4-}$ and $TTFS_2^{2-}$ (**C**), respectively) via covalent metal-ligand bonds (Scheme 1).[4]

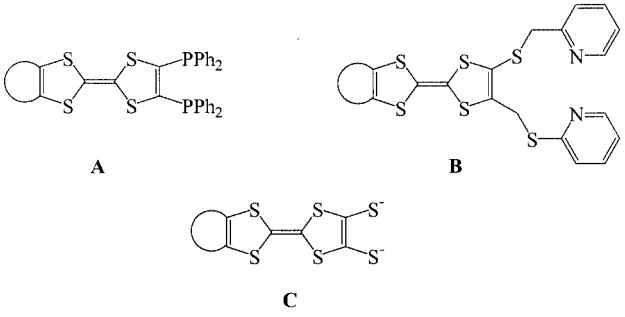

Scheme 1. Schematic drawings of TTF derivatives used as ligands

Organometallic chemistry, however, offers additional alternative routes to link a metal center to an organic substrate, such as oxidative addition and π-coordination. Starting with a $Pt^0(PPh_3)_2$ fragment, we present herein two novel synthetic approaches for the development of organometallic complexes incorporating the TTF unit. Firstly, since there are no reports of studies devoted to the synthesis of transition metal complexes incorporating a π-ligated TTF unit, it was tempting to evaluate the ability of TTF to act as a π-acidic ligand. Our second strategy is based on the functionalization of TTFs with SiR_2-H moieties followed by the oxidative addition of the Si−H bond to the low valent platinum center. In this paper we describe the synthesis and characterization of the complexes [Pt(η^2-TTF)(PPh_3)$_2$], [Pt(η^2-*o*-Me_2TTF)(PPh_3)$_2$], and [Pt{*o*-($SiMe_2$)$_2$$TTFMe_2$}-($PPh_3$)$_2$], which, to the best of our knowledge, represent the first examples of two novel bonding modes between TTF derivatives and transition metal centers i.e. π bonding and covalent bonding via an SiR_2 bridge.

[a] Laboratoire de Chimie des Matériaux et Interfaces, Université de Franche-Comté, Faculté des Sciences et des Techniques, 16, Route de Gray, 25030 Besançon Cedex, France
E-mail: michael.knorr@univ-fcomte.fr
[b] Laboratoire de Chimie Inorganique, Matériaux et Interfaces, Université d'Angers, FRE 2447 CNRS, 2 Boulevard Lavoisier, 49045 Angers, France

 © 2004 Wiley-VCH Verlag GmbH & Co. KGaA, Weinheim **DOI: 10.1002/ejic.200300930**

Results and Discussion

Synthesis and Characterization of $[Pt(\eta^2\text{-TTF})(PPh_3)_2]$ (1) and $[Pt(\eta^2\text{-}o\text{-}Me_2TTF)(PPh_3)_2]$ (2)

The displacement of the ethylene ligand in $[Pt(\eta^2\text{-}C_2H_4)(PPh_3)_2]$ by other olefins such as styrene, propenoates, cycloalkenes, tetracyanoethylene, allenes, and other olefinic compounds represents a convenient method of preparing Pt^0 complexes of the type $[Pt(olefin)PPh_3)_2]$, since volatile ethylene can be easily removed. The olefinic structure of TTF led us to investigate its reactivity towards the reactive starting material $[Pt(\eta^2\text{-}C_2H_4)(PPh_3)_2]$. After stirring a solution of $[Pt(\eta^2\text{-}C_2H_4)(PPh_3)_2]$ in toluene with a slight excess of TTF for 1 hour, concentration and addition of heptane afforded bright yellow $[Pt(\eta^2\text{-TTF})(PPh_3)_2]$ (**1**) (Scheme 2). The coordination of TTF via the H−C=C−H bond can be inferred unambiguously from the NMR spectra. Thus, in the proton NMR spectrum, two olefinic hydrogen atoms give rise to a broadened triplet at δ = 3.96 with a $^3J_{P,H}$ coupling of 2.5 Hz, and an additional $^3J_{Pt,H}$ coupling of 60.2 Hz. For comparison, the ethylene protons of $[Pt(\eta^2\text{-}C_2H_4)(PPh_3)_2]$ resonate at a much higher field (δ = 2.14 ppm), Furthermore, two singlets can be seen at δ = 6.35 and 6.32 ppm in an approximate ratio of 1:1. These resonances can be interpreted by the existence, in solution, of an equilibrium between free and complexed TTF. This is corroborated by the $^{31}P\{^1H\}$ NMR spectrum which displays two singlets at δ 27.8 and 16.1 in an approximate ratio of 3:1, flanked by platinum satellites ($^1J_{P,Pt}$ = 3444 and 4083 Hz, respectively). The more intense system centered at 27.8 ppm can be attributed to the $(PPh_3)_2Pt$ fragment complexed by the TTF. Note that the $^{31}P\{^1H\}$ NMR spectrum of the starting material $[Pt(\eta^2\text{-}C_2H_4)(PPh_3)_2]$ consists of a singlet at δ 35.8 with a $^1J_{P,Pt}$ coupling of 3741 Hz. The second system centered at δ = 16.1 ppm can be tentatively assigned to the platinum fragment $[Pt(PPh_3)_2]$, resulting from the decomplexation of TTF, which may be stabilized by weak interactions with the sulfur atoms. The reversible coordination/decoordination of an olefin has already been reported in the case of the complexes $[Pt(\eta^2\text{-}C_2H_4)(PCy_3)_2]$ and $[Pt(\eta^2\text{-norbornene})(PPh_3)_2]$.[5]

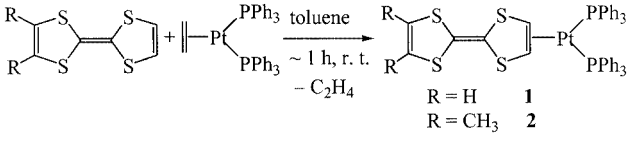

Scheme 2

In order to probe whether, in the case of an asymmetric TTF derivative such as 3,4-dimethyltetrathiafulvalene (*o*-Me_2TTF), coordination to platinum occurs via the double bound substituted with two hydrogens or, alternatively, via the double bond substituted by the two methyl groups, we also treated $[Pt(\eta^2\text{-}C_2H_4)(PPh_3)_2]$ with the 3,4-dimethyltetrathiafulvalene. During the reaction, pure yellow $[Pt(\eta^2\text{-}o\text{-}Me_2TTF)(PPh_3)_2]$ (**2**) precipitated (Scheme 2). The NMR spectra indicate the exclusive coordination of the substituted TTF via the H−C=C−H moiety. Thus, as observed for **1**, the proton NMR spectrum exhibits the signals for the olefinic H atoms centered at δ = 3.95 ($^3J_{P,H}$ = 2.4 Hz and $^3J_{Pt,H}$ = 61 Hz). The resonance of the Me groups appears as a singlet at δ = 2.00. The additional singlets observed at δ 6.30 and 1.96 stemming from 3,4-dimethyltetrathiafulvalene indicate, that as in the case of **1**, an equilibrium occurs in solution between free and complexed 3,4-dimethyltetrathiafulvalene (ratio 1:3.3). Cooling the solution resulted in the progressive increasing of the ratio of complexed to uncomplexed TTF. The $^{31}P\{^1H\}$ NMR spectrum is very similar to that of **1** mentioned above, and requires no special comments.

Molecular Structure of 2

Complex **2** crystallizes, with one solvent molecule (toluene), in the triclinic space group $P\bar{1}$. The molecular structure of the Pt^0 complex is characterized by a trigonal planar ligand arrangement with the alkene in the plane of the triangle (Figure 1). The Pt−P distances [2.293(2) and 2.294(2) Å] lie in the typical range observed in other [Pt(olef-

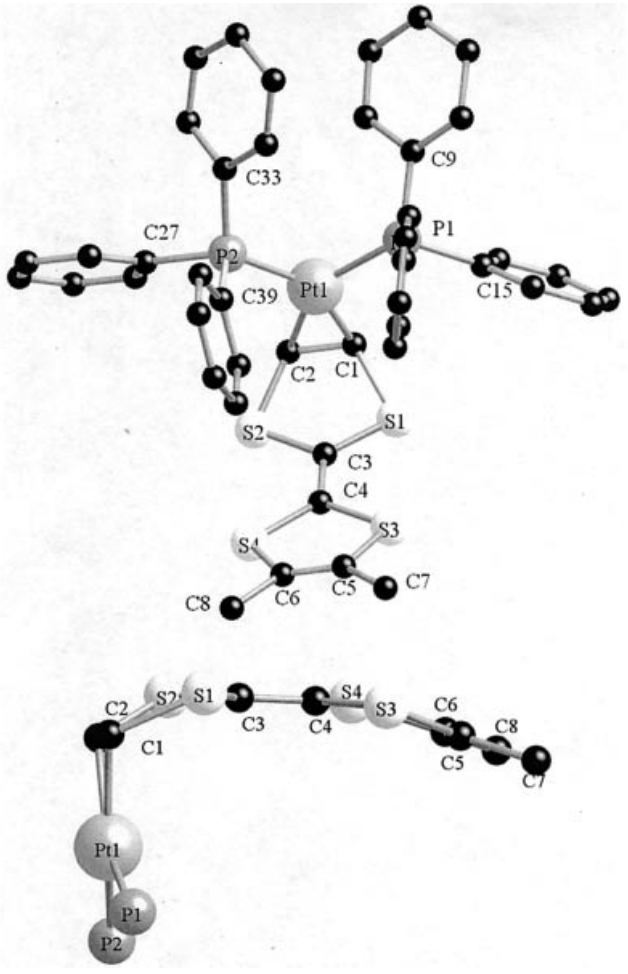

Figure 1. Top: molecular structure of **2** with labelling scheme; bottom: view of the Pt-TTFMe_2 core showing the boat conformation of the TTFs; hydrogen atoms are omitted for clarity

 © 2004 Wiley-VCH Verlag GmbH & Co. KGaA, Weinheim

Table 1. Comparison of selected geometric parameters between **2** and $[Pt(PPh_3)_2(CH_2{=}CH_2)]$[7]

Complex	P−Pt−P	Pt−P	C−Pt−C	C(1)−C(2)	Pt−C
2	103.55(8)	2.293(2) 2.294(2)		1.360(11)	2.059 2.007
$Pt(PPh_3)_2(CH_2{=}CH_2)$	111.6(1)	2.265(2) 2.270(2)	39.7(4)	1.43(1)	2.11(1) 2.12(1)

in)$(PPh_3)_2$] complexes.[6] The P−Pt−P angle [103.55(8)°] is more acute than in the ethylene complex (Table 1). The Pt−C bonds are significantly shorter in **2** in comparison with the starting material $[Pt(CH_2{=}CH_2)(PPh_3)_2]$. The TTF part is strongly folded along the S···S axis of each fulvalene, with values of 31.02(54)° for S(1)···S(2) and 16.52(21)° for S(3)···S(4), while the central core [S(1−4), C(3) and C(4)] is nearly planar (Figure 1, bottom). Thus, the boat conformation is much more pronounced in **2** compared with the geometry of the free *o*-Me_2TTF, for which angles of 0.6° and 1.88° have been reported.[8] These deformations have already been observed with several metal-coordinated TTF derivatives (see for example ref.[3c]) but not with such magnitude. The increasing of the out-of-plane bend leads to significant changes for the other structural parameters. Table 2 provides a comparison of selected bond lengths and angles between **2**, and uncoordinated *o*-Me_2TTF. As can be seen, the external C−S bonds become longer upon coordination. This may be due to a reduction of conjugation within the fulvalene rings, which also leads to a shortening of the C(5)−C(6) bond length [1.305(11) vs. 1.338(4) Å]. Conversely, due to the interaction with the platinum, there is a significant lengthening of the C(1)−C(2) bond as observed in almost all cases of coordinated olefins.[9] In contrast to the symmetrical structure of *o*-Me_2TTF, C(1) and C(2) are not equivalent in **2**: (i) the Pt−C bond lengths are quite different (Table 1), and (ii) the value observed for the S(1)−C(1)−C(2) angle [112.3(6)°] suggests that the C(1) atom approaches a tetrahedral hybridization, whereas the C(1)−C(2)−S(2) angle remains nearly unchanged upon complexation, indicating an sp^2 hybridization for C(2) [119.9(6)°].

Table 2. Selected bond lengths (Å) and angles (°) for 3,4-dimethyltetrathiafulvalene,[8] **2**, and **3**

	3,4-Dimethyltetrathiafulvalene	**2**	**3**
S(1)−C(1)	1.743(4)	1.843(8)	1.762(3)
S(1)−C(3)	1.765(3)	1.729(9)	1.750(3)
S(2)−C(2)	1.739(4)	1.760(9)	1.765(2)
S(2)−C(3)	1.767(3)	1.768(8)	1.749(3)
C(3)−C(4)	1.340(4)	1.366(10)	1.357(4)
C(1)−C(2)	1.308(5)	1.360(11)	1.338(4)
S(3)−C(4)	1.753(3)	1.759(9)	1.751(3)
S(3)−C(5)	1.755(3)	1.781(9)	1.762(3)
S(4)−C(4)	1.762(3)	1.730(10)	1.751(3)
S(4)−C(6)	1.758(3)	1.772(8)	1.750(3)
C(5)−C(6)	1.338(4)	1.305(11)	1.328(4)
C(5)−C(7)	1.500(5)	1.527(10)	1.501(4)
C(6)−C(8)	1.503(5)	1.505(12)	1.506(4)
C(1)−Si(1)			1.886(2)
C(2)−Si(2)			1.873(3)
C(1)−S(1)−C(3)	94.42(17)	93.4(4)	96.21(12)
C(2)−S(2)−C(3)	94.31(17)	91.3(4)	96.37(12)
S(1)−C(1)−C(2)	118.2(3)	112.3(6)	116.92(19)
C(1)−C(2)−S(2)	118.7(3)	119.9(6)	116.5(2)
S(1)−C(3)−S(2)	114.27(17)	114.9(4)	113.34(14)
S(2)−C(3)−S(4)	122.9(3)	120.5(7)	122.6(2)
C(3)−C(4)−S(3)	123.3(3)	120.9(7)	123.5(2)
C(4)−S(4)−C(6)	95.51(15)	95.2(4)	95.46(13)
C(4)−S(3)−C(5)	96.14(15)	94.3(4)	95.63(13)
S(3)−C(4)−S(4)	113.89(17)	113.9(5)	114.14(14)
S(3)−C(5)−C(6)	116.9(2)	117.0(6)	116.7(2)
C(6)−C(5)−C(7)	127.0(3)	129.4(8)	127.0(3)
S(4)−C(6)−C(5)	117.6(2)	117.2(7)	117.9(2)
C(5)−C(6)−C(8)	126.8(3)	128.9(8)	126.7(3)
C(2)−C(1)−Si(1)			127.5(2)
C(1)−C(2)−Si(2)			128.76(19)

 © 2004 Wiley-VCH Verlag GmbH & Co. KGaA, Weinheim

Synthesis and Characterization of a Bis(silylated) Platinum-TTF Complex

One common strategy for the synthesis of substituted TTFs takes advantage of the acidity of the TTF hydrogen atoms.[10] Indeed, treatment with *n* equivalents of strong bases such as LDA at low temperature affords TTF−Li_n, which can be treated with a variety of electrophiles. Using this procedure, 3,4-dimethyltetrathiafulvalene was dilithiated with 2 equivalents of LDA, then silylated with chlorodimethylsilane to give 3,4-dimethyl-3′,4′-(dimethylsilyl)-tetrathiafulvalene (**3**) (Scheme 3).

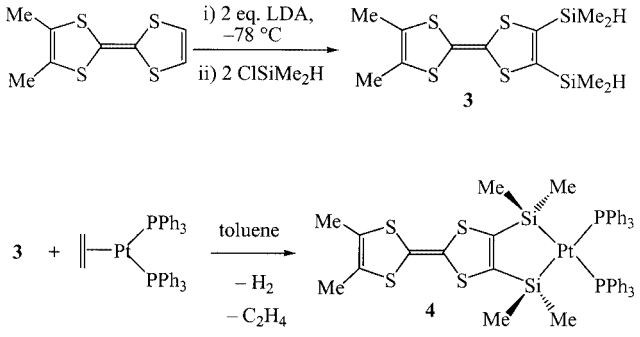

Scheme 3

Compound **3** was isolated in 72% yield as orange air-stable solid, soluble in aliphatic hydrocarbons. Recrystallization from a concentrated hexane solution afforded single-crystals suitable for an X-ray diffraction study. The geometry of **3** is shown in Figure 2, structural parameters are given in Table 2. The framework of 3,4-dimethyltetrathiafulvalene is only slightly influenced by the substitution with the dimethylsilyl functions. The geometry around the Si atoms is essentially tetrahedral, with C−Si−C angle values varying between 108.49(17) and 111.5(2)°. The C(1)−Si(1) and C(2)−Si(2) bond lengths [1.886(2) and 1.873(3) Å] are quite similar to that in $(TTF)_2SiMe_2$ [1.868(5) Å].[11]

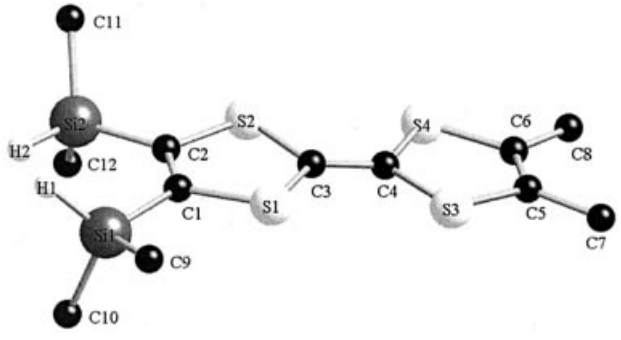

Figure 2. Molecular structure of **3**

By taking advantage of the reactivity of the Si−H bond towards low valent transition metal centers, compound **3** seemed to be a promising precursor to covalently link a platinum fragment to the TTF unit.[12] Thus, **3** reacts by oxidative addition with one equivalent of [Pt(η^2-C_2H_4)$(PPh_3)_2$] in toluene to afford the platinum bis(silyl) complex [Pt{*o*-$(Me_2Si)_2TTFMe_2$}$(PPh_3)_2$] (**4**) (Scheme 3). The chelating coordination of the two $SiMe_2$ groups on each Pt center was confirmed by the ^1H NMR spectrum [singlet, δ = −0.13 ppm, ^3J(Pt−H) = 22.1 Hz], and the $^{31}P\{^1H\}$ NMR spectrum [δ = 30.0 ppm, ^1J(Pt−P) = 1716 Hz].

Cyclic voltammetric data for *o*-Me_2TTF, **3**, and **4** are given in Table 3. In each case, two reversible or quasi reversible single-electron oxidation waves were observed corresponding to the oxidation of the TTF core (Figure 3). Substitution of the olefinic hydrogens in *o*-Me_2TTF by the Si-Me_2H group induces a slight cathodic shift for the first oxidation wave due to the inductive effect of the methyl group, whereas $E_2^{1/2}$ remains unchanged. More interesting is the fact that the bis(silyl) complex **4** shows a strong cathodic shift (nearly 0.2 V) for the two redox processes. This observation is contrary to the tendency reported in the case of TTFs functionalized with phosphane or pyridine. The latter always display shifts towards more anodic potentials upon coordination.[3e,3j] This implies a strong interaction between the TTF core and the metallic fragment. Note also that the second oxidation wave in **4** appears not totally reversible at standard scan rates (50−250 mV·s^{-1}), since an additional reduction peak was observed at $E_{pc} \approx 0$ V. This peak disappeared when the scan rate was faster (= 1 V·s^{-1}) or when the potential was reversed just before the second oxidation wave (Figure 3). Nevertheless the potential, and the reversibility of the first electron transfer offer the possibility of synthesizing open shell species from this organometallic complex.

Table 3. Voltammetric data (*E* in V vs. Ag/0.1 M $AgClO_4$)

Compound	$E_1^{1/2}$	$E_2^{1/2}$
DMTTF	+ 0.05	+ 0.53
3	−0.01	+ 0.53
4	−0.24	+ 0.34

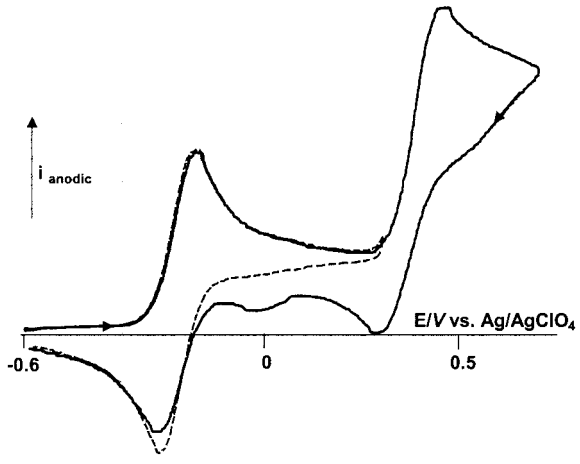

Figure 3. Cyclic voltammograms of **4** in CH_2Cl_2 solution on a platinum electrode; scan rate: 100 mV s^{-1}

 © 2004 Wiley-VCH Verlag GmbH & Co. KGaA, Weinheim

Conclusion

In summary, the bonding modes between tetrathiafulvalenes and transition metal centers described in this paper highlight the possible development of novel classes of TTF derivatives using strategies from organometallic chemistry. For example, insertion of unsaturated organic substrates such as alkynes into the platinum-silicon bond may be an original tool for introducing functionalization to the TTF core.[13] On the other hand, the reactivity of the Si−H bond is not restricted to platinum, and generalization to other metal centers may provide a family of transition metal−silicon complexes in which the redox properties of the TTF may be fine-tuned by the metallic fragment. Both approaches, as well as potential applications in materials science, are currently being pursued in our laboratories.

Experimental Section

General Comments: All reactions were performed under dry nitrogen using standard Schlenk techniques. Solvents were dried by standard methods, freshly distilled, and saturated with nitrogen prior to use. TTF,[14] *o*-Me_2TTF,[15] and [Pt(PPh_3)$_2$(C_2H_4)][16] were prepared according to published procedures. The ^{1}H, ^{31}P{^{1}H}, and ^{195}Pt NMR spectra were recorded at 300.13, 81.01, and 42.95 MHz, respectively, on a Bruker Avance 300 instrument. ^{195}Pt chemical shifts were externally referenced to aqueous K_2PtCl_4 with downfield chemical shifts reported as positive. Elemental analyses were performed at the Université de Bourgogne with an EA 1108 Fisons instrument.

Electrochemical Measurements: Voltammetric analyses were carried out, at ambient temperature, in a standard three-electrode cell with a Radiometer PGP 201 potentiostat. The electrolyte consisted of a 0.2 M *n*Bu_4NPF_6 solution in CH_2Cl_2. The working electrode was a platinum disk electrode, and the auxiliary electrode was a platinum wire. The reference electrode was a silver/silver ion electrode, Ag/Ag^+ (0.1 M $AgClO_4$ in acetonitrile) separated from the solution by a sintered glass disk. After each measurement the reference was checked against the ferrocene-ferrocenium couple (+ 0.16V relative to this reference electrode).

Synthesis of [Pt(η^2-TTF)(PPh_3)$_2$] (1): To a solution of [Pt(η^2-C_2H_4)(PPh_3)$_2$] (375 mg, 0.5 mmol) in toluene (8 mL) was added TTF (110 mg, 0.54 mmol). The solution was stirred at room temperature for 1 h. Hexane was then added and the resultant solution cooled to 4 °C. The solid, which formed, was collected by filtration, washed with hexane and dried to provide **1** as an orange solid. (393 mg, 85% yield).^{1}H NMR ($CDCl_3$): δ = 3.96 (t br., 2 H, H-TTF, $^3J_{H,P}$ = 2.5, $^2J_{H,Pt}$ = 60.2 Hz), 6.32 (s, 2 H, H-TTF) 7.14−7.24 (m, 30 H, Ph). ^{31}P{^{1}H} NMR: δ = 27.85 (s, $^1J_{Pt,P}$ = 3444 Hz) ppm. $C_{42}H_{34}P_2PtS_4$ (924.00): calcd. C 54.60, H 3.71; found C 55.01, H, 3.60.

Synthesis of [Pt(η^2-*o*-Me_2TTF)(PPh_3)$_2$] (2): To a solution of [Pt(η^2-C_2H_4)(PPh_3)$_2$] (337 mg, 0.45 mmol) in toluene (8 mL) was added *o*-Me_2TTF (116 mg, 0.5 mmol). The solution was stirred at room temperature for 0.5 h. The orange complex precipitated gradually from solution. After cooling at 4 °C the supernatant liquid was decanted, and the residue washed with hexane. (381 mg, 89% yield).^{1}H NMR ($CDCl_3$): δ = 2. 00 (s, 6 H, CH_3), 3.95 (t br., 2 H, H-TTF, $^3J_{H,P}$ = 2.4, $^2J_{H,Pt}$ = 61.0 Hz), 7.16−7.24 (m, 30 H, Ph) ppm. ^{31}P{^{1}H} NMR: δ = 27.8 (s, $^1J_{Pt,P}$ = 3450 Hz) ppm. ^{195}Pt{^{1}H} NMR: δ = −3206 (t, $^1J_{Pt,P}$ = 3450 Hz) ppm. $C_{44}H_{38}P_2PtS_4$ (952.05): calcd. C 55.51, H 4.02; found C 55.86, H, 4.17.

Synthesis of 3,4-Dimethyl-3′,4′-(dimethylsilyl)tetrathiafulvalene (3): A solution of *o*-Me_2TTF (0.23 g, 1 mmol) in THF (20 mL) was treated at −78 °C with LDA (2.5 mmol). The yellow precipitate was stirred at −78 °C for 4 h, and then treated with chlorodimethylsilane (2.6 mmol). The reaction temperature was allowed to rise slowly overnight to room temperature. The solvent was then removed under reduced pressure, and the residue was extracted with diethyl ether. After evaporation of the diethyl ether, the resultant solid was recrystallized from hexane to give **3** as orange crystals (250 mg, 72% yield). ^{1}H NMR ($CDCl_3$): δ = 0.34 (d, 12 H, $SiMe_2$, $^3J_{H,H}$ = 3.8 Hz), 1.94 (s, 6 H, Me-TTF), 4.49 (h, 2 H, Si−H) ppm. IR (KBr): $\tilde{\nu}$ = 2163 (Si−H) cm^{-1}. $C_{12}H_{20}S_4Si_2$ (348.70): calcd. C 41.33, H 5.78; found C 41.45, H 5.75.

Synthesis of [Pt{*o*-(Me_2Si)$_2$TTFMe_2}(PPh_3)$_2$] (4): To a solution of 3,4-dimethyl-3′,4′-(dimethylsilyl)tetrathiafulvalene (**3**) (105 mg, 0.3 mmol) in toluene (7 mL) was added [Pt(η^2-C_2H_4)(PPh_3)$_2$] (210 mg, 0.28 mmol) in toluene (7 mL). The resultant orange solution was stirred at room temperature for 2 h. The yellow complex precipitated gradually from solution. The supernatant liquid was decanted and the residue was washed with hexane (224 mg, 75% yield). ^{1}H NMR ($CDCl_3$): δ = −0.13 (s, 12 H, $SiMe_2$, $^2J_{Pt,H}$ = 22.1 Hz), 1.91 (s, 6 H, Me-TTF), 7.16−7.30 (m, 30 H, Ph) ppm. ^{31}P{^{1}H} NMR: δ = 30.0 (s, $^1J_{Pt,P}$ = 1716 Hz) ppm. $C_{48}H_{48}P_2PtS_4Si_2$ (1066.35) calcd. C 54.07, H 4.54; found C 54.40, H 4.65.

Table 4. X-ray structural data for **2** and **3**

Compound	**2**	**3**
Formula	$C_{47.5}H_{42}P_2PtS_4$	$C_{12}H_{20}S_4Si_2$
Fw	998.08	348.70
Crystal size (mm)	0.32 × 0.15 × 0.08	0.77 × 0.37 × 0.19
T (K)	293(2)	293 (2)
Crystal system	triclinic	triclinic
Space group	$P\bar{1}$	$P\bar{1}$
a (Å)	9.4534(19)	5.7661(12)
b (Å)	14.305(3)	9.1180(18)
c (Å)	16.968(3)	18.653(4)
α (deg)	90.33(3)	89.05(3)
β (deg)	101.71(3)	95.87(3)
γ (deg)	108.89(3)	107.54(3)
V (Å^3)	2119.4(7)	930.1(3)
Z	2	2
$\rho_{calcd.}$ (g cm^{-3})	1.564	1.245
μ (mm^{-1})	3.616	0.623
F(000)	998	368
λ (Å)	0.71073	0.71073
θ range, deg	1.87−25.79	2.34−25.84
Index ranges	$-11 \le h \le 11$, $-17 \le k \le 17$, $0 \le l \le 20$	$-7 \le h \le 6$, $-11 \le k \le 11$, $0 \le l \le 22$
No. of reflns. collected	7577	3298
No. of ind. reflns.	4162	2248
Largest diff. peak and hole, e(Å^{-3})	−1.050/1.258	−0.177/0.268
Final *R* indices[a]	0.0446	0.0397
R indices (all data)	0.1030	0.0609
GOF on F^2	0.749	0.990

[a] $R(F) = \Sigma\| F_o| - |F_c\|/ \Sigma|F_o|$.

 © 2004 Wiley-VCH Verlag GmbH & Co. KGaA, Weinheim

Crystallographic Data Collection and Structure Determinations of 2 and 3: Suitable crystals of **2** and **3** for X-ray diffraction were obtained by crystallization from toluene and hexane, respectively. A single-crystal of each compound was mounted in a glass capillary using Araldite glue. Data were collected with a Stoe-IPDS diffractometer, with graphite-monochromated Mo-K_α radiation (λ = 0.71073 Å). Details are given in Table 4. A numerical absorption correction was applied (FACEIT, Stoe). The structures were solved by direct methods, and refined by full-matrix least-squares on F^2 with anisotropic thermal parameters for all non-H atoms. H atoms were included in calculated positions, and constrained to ride on the parent C atoms. All calculations were performed with the SHELTX package.[17] CCDC-226740 for [$Pt(PPh_3)_2$(*o*-Me_2TTF)] and -226741 for [*o*-Me_2TTF($SiMe_2H)_2$] contain the supplementary crystallographic data for this paper. These data can be obtained free of charge at www.ccdc.cam.ac.uk/conts/retrieving.html or from the Cambridge Crystallographic Data Center, 12 Union Road, Cambridge CB2 1EZ, UK [Fax: (internat.) +44-1223-336-033; E-mail: deposit@ccdc.cam.ac.uk].

Acknowledgments

Financial support and a postdoctoral grant for M. N. Jajaswal from the Ministère de la Recherche et de la Technologie are acknowledged.

[1] J. L. Segura, N. Martin, *Angew. Chem. Int. Ed.* **2001**, *40*, 1372−1409.
[2] E. Coronado, J. R. Galan-Mascaros, C. J. Gomez-Garcia, V. Laukhin, *Nature* **2000**, *408*, 447−449.
[3] [3a] M. Fourmigué, P. Batail, *Bull. Soc. Chim. Fr.* **1992**, *129*, 29−36. [3b] M. Fourmigué, C. E. Uzelmeier, K. Boubekeur, S. L. Bartley, K. R. Dunbar, *J. Organomet. Chem.* **1997**, *529*, 343−350. [3c] C. E. Uzelmeier, S. L. Bartley, M. Fourmigué, R. Rogers, G. Grandinetti, K. R. Dunbar, *Inorg. Chem.* **1998**, *37*, 1833−1840. [3d] B. W. Smucker, K. R. Dunbar, *J. Chem. Soc., Dalton Trans.* **2000**, 1309−1315. [3e] N. Avarvari, D. Martin, M. Fourmigué, *J. Organomet. Chem.* **2002**, 643−644, 292−300. [3f] P. Pellon, G. Gachot, J. Le Bris, S. Marchin, R. Carlier, D. Lorcy, *Inorg. Chem.* **2003**, *42*, 2056−2060. [3g] F. Iwahori, S. Golhen, L. Ouahab, R. Carlier, J. P. Sutter, *Inorg. Chem.* **2001**, *40*, 6541−6542. [3h] F. Setifi, L. Ouahab, S. Golhen, Y. Yoshida, G. Saito, *Inorg. Chem.* **2003**, *42*, 1791−1793. [3i] S. Campagna, S. Serroni, F. Puntoriero, F. Loiseau, L. De Cola, C. J. Kleverlaan, J. Becher, A. P. Sorensen, P. Hascoat, N. Thorup, *Chem. Eur. J.* **2002**, *8*, 4461−4469. [3j] S. X. Liu, S. Dolder, P. Franz, A. Neels, H. Stoeckli-Evans, S. Decurtins, *Inorg. Chem.* **2003**, *42*, 4801−4803.
[4] [4a] R. R. Schumaker, E. M. Engler, *J. Am. Chem. Soc.* **1980**, *102*, 6651−6652. [4b] H. Poleschner, W. John, F. Hoppe, E. Fanghänel, S. Roth, *J. Prak. Chem.* **1983**, *6*, 957−975. [4c] R. D. McCullough, J. A. Belot, A. L. Rheingold, G. P. A. Yap, *J. Am. Chem. Soc.* **1995**, *117*, 9913−9914. [4d] R. D. McCullough, J. A. Belot, J. Seth, A. L. Rheingold, G. P. A. Yap, *J. Mater. Chem.* **1995**, *5*, 1581−1587. [4e] S. B. Wilkes, I. R. Butler, A. E. Underhill, M. B. Hursthouse, D. E. Hibbs, K. M. Abdul Malik, *J. Chem. Soc., Dalton Trans.* **1995**, 897−903. [4f] N. Le Narvor, N. Robertson, E. Wallace, J. D. Kilburn, A. E. Underhill, P. N. Bartlett, M. Webster, *J. Chem. Soc., Dalton Trans.* **1996**, 823−828. [4g] A. Kobayashi, H. Tanaka, M. Kumasaki, H. Torii, B. Narymbetov, T. Adachi, *J. Am. Chem. Soc.* **1999**, *121*, 10763−10771. [4h] H. Tanaka, Y. Okano, H. Kobayashi, W. Suzuki, A. Kobayashi, *Science* **2001**, *291*, 285−287. [4i] T. Nakamura, T. Takahashi, T. Yumoto, T. Akutagawa, T. Hasegawa, *Chem. Lett.* **2001**, 134−135. [4j] M. Nakano, A. Kuroda, G. Matsubayashi, *Inorg. Chim. Acta* **1997**, *254*, 189−193. [4k] K. Kubo, N. Nakano, H. Tamura, G. Matsubayashi, M. Nakamoto, *J. Organomet. Chem.* **2003**, *669*, 141−143. [4l] G.-Q. Bian, J. Dai, Q.-Y. Zhu, W. Yang, Z.-M. Yan, M. Munakata, M. Maekawa, *Chem. Commun.* **2002**, 1474−1475.
[5] [5a] H. C. Clark, G. Ferguson, M. J. Hampden-Smith, B. Kaitner, H. Ruegger, *Polyhedron* **1988**, *7*, 1349−1353. [5b] P. G. Gassman, I. G. Cesa, *Organometallics* **1984**, *3*, 119−128.
[6] [6a] F. Caruso, M. Camalli, G. Pellizer, F. Asaro, M. Lenarda, *Inorg. Chim. Acta* **1991**, *181*, 167−176. [6b] G. F de Sousa, C. A. L. Filgueiras, P. B. Hitchcock, J. F. Nixon, *Inorg. Chim. Acta* **1997**, *261*, 217−200.
[7] P. T. Chengu, S. C. Nyburg, *Can. J. Chem.* **1972**, *50*, 912.
[8] C. E. Uzelmeier, M. Fourmigué, K. R. Dunbar, *Acta Crystallogr., Sect. C* **1998**, *54*, 1047−1049.
[9] F. A. Cotton, G. Wilkinson, C. A. Murillo, M. Bochmann, *Advanced Inorganic Chemistry*, 6th edn., John Wiley & Sons, New York, **1999**.
[10] D. C. Green, *J. Org. Chem.* **1979**, *44*, 1476−1479.
[11] M. Fourmigué, Y-S. Huang, *Organometallics* **1993**, *12*, 797−802.
[12] [12a] W. Fink, *Helv. Chim. Acta* **1975**, *58*, 606−613. [12b] C. Eaborn, T. N. Metham, A. Pidcock, *J. Organomet. Chem.* **1973**, *63*, 107−117. [12c] C. Eaborn, B. Rattcliff, A. Pidcock, *J. Organomet. Chem.* **1974**, *65*, 174−180. [12d] M. Tanaka, Y. Uchimaru, H.-J. Lautenschlager, *Organometallics* **1991**, *10*, 16−18. [12e] U. Schubert, C. Müller, *J. Organomet. Chem.* **1991**, *418*, C6−C8. [12f] D. F. Mullica, E. L. Sappenfield, M. J. Hampden-Smith, *Polyhedron* **1991**, *10*, 867−872. [12g] M. Knorr, F. Guyon, I. Jourdain, S. Kneifel, J. Frenzel, C. Strohmann, *Inorg. Chim. Acta* **2003**, *350*, 455−466.
[13] [13a] M. Tanaka, Y. Uchimaru, *Bull. Soc. Chim. Fr.* **1992**, *129*, 667−675. [13b] P. Braunstein, M. Knorr, *J. Organomet. Chem.* **1995**, *500*, 21−38.
[14] A. J. Moore, M. R. Bryce, *Synthesis* **1997**, 407−409.
[15] F. Gerson, A. Lamprecht, M. Fourmigué, *J. Chem. Soc., Perkin Trans. 2* **1996**, 1409−1414.
[16] C. D. Cook, G. S. Jauhal, *J. Am. Chem. Soc.* **1968**, *90*, 1464−1467.
[17] G. M. Sheldrick, *SHELTX*, *Programs for the Refinement of Crystal Structures*, University of Göttingen, Germany, **1997**.

Received December 12, 2003
Early View Article
Published Online May 5, 2004

 © 2004 Wiley-VCH Verlag GmbH & Co. KGaA, Weinheim

Synthesis and Characterization of Potassium Complexes Containing Terminal η^2-Pyrazolato Ligands

Wenjun Zheng,[a] Mary Jane Heeg,[a] and Charles H. Winter*[a]

Keywords: Hydrogen bonds / N ligands / Potassium / Pyrazolato ligands

The potassium complexes [K(η^2-3,5-R_2pz)(η^6-18-crown-6)] (R = Ph, *t*Bu; pz = pyrazolato) were prepared by treatment of 3,5-diphenylpyrazole or 3,5-di-*tert*-butylpyrazole with potassium hydride in the presence of 18-crown-6. These complexes contain η^6-18-crown-6 and terminal η^2-pyrazolato ligands, and constitute the first examples of group 1 metal complexes with this pyrazolato ligand coordination mode. In contrast to [K(η^2-3,5-Ph_2pz)(η^6-18-crown-6)] and [K(η^2-3,5-*t*Bu_2pz)(η^6-18-crown-6)], the aqua complex [K(η^2-3,5-Me_2pz)(H_2O)(η^6-18-crown-6)] was obtained when 3,5-dimethylpyrazole was treated with potassium hydride and 18-crown-6 in the presence of a small amount of water. [K(η^2-3,5-Me_2pz)(H_2O)(η^6-18-crown-6)] contains an η^2-pyrazolato ligand that is bent towards being co-facial with the best plane of the 18-crown-6 ligand, to allow hydrogen bonding between the pyrazolato ligand nitrogen atoms and the coordinated aqua ligand. The hydrogen bonding thus confers a novel terminal π-facial η^2-bonding mode to the pyrazolato ligand. All compounds were characterized by elemental analysis, NMR spectroscopy, and mass spectrometry.
(© Wiley-VCH Verlag GmbH & Co. KGaA, 69451 Weinheim, Germany, 2004)

Introduction

The coordination chemistry of metal complexes with pyrazolato (pz) ligands is currently a topic of considerable interest.[1−6] While many bridging coordination modes have been documented, pyrazolato ligands bonded to single metal centers (terminal coordination) are less common and are restricted to η^1,[1] η^2,[1e,2−4] and η^5.[5] The terminal η^1- and η^2-coordination modes reported to date involve donation of the in-plane nitrogen atom lone pairs to the metal centers, whereas only the rare η^5-bonding mode entails bonding with the out-of-plane π-orbitals of the aromatic pyrazolato ring.[5] Although many main group element pyrazolato complexes have been structurally characterized,[1,2,6] group 1 complexes are limited to a few examples with bridging pyrazolato ligands[7,8] and a small number containing tris(pyrazolyl)borate and related ligands.[9] Structurally characterized potassium pyrazolato complexes are restricted to [(μ-η^2:η^1:η^1-3,5-Ph_2pz)K(THF)]$_6$,[8a] an erbium complex [K{Er(η^2-3,5-*t*Bu_2pz)$_4$}$_n$] with the potassium ion trapped in a bridged η^3-coordination mode,[8b] and a complex in which potassium is bonded to a structurally complex manganese-containing pyrazolato ligand through an η^5-interaction.[5b] No examples of terminal η^2-pyrazolato ligand coordination to a group 1 metal have been reported, most likely due to the propensity of these ligands to bridge between the large group 1 metal ions.

We have recently reported examples of the slipped η^2-coordination mode of triazolato and tetrazolato ligands to the [K(18-crown-6)]$^+$ fragment.[10] In these complexes, there was significant asymmetry in the potassium−nitrogen bond lengths (Δ_{K-N} = 0.35−0.60 Å), and there were no obvious steric interactions that would cause such slipped pyrazolato ligand coordination modes. These results prompted us to investigate the coordination chemistry of analogous potassium pyrazolato complexes. Herein we report the synthesis, structure, and properties of several pyrazolato complexes of the [K(η^6-18-crown-6)]$^+$ fragment. The new complexes contain terminal η^2-pyrazolato ligands, and represent the first structurally characterized group 1 pyrazolato complexes with this coordination mode.

Results and Discussion

The synthetic chemistry is shown in Scheme 1. Treatment of equimolar quantities of potassium hydride, 3,5-diphenylpyrazole or 3,5-di-*tert*-butylpyrazole, and 18-crown-6 in tetrahydrofuran afforded colorless solids after filtration and removal of the solvent. However, the crude products could not be purified by recrystallization in common organic solvents or by other methods. Infrared spectra of the crude products show strong, broad stretches centered at approximately 3400 cm^{-1}, which suggest the presence of water in the products. Since commercial 18-crown-6 could form a hydrate, the solutions were further treated with excess potassium metal in refluxing tetrahydrofuran to eliminate any water that might be associated with the 18-crown-6. Follow-

[a] Department of Chemistry, Wayne State University, Detroit, Michigan 48202, USA
Fax: (internat.) +1-313-577-8289
E-mail: chw@chem.wayne.edu

 © 2004 Wiley-VCH Verlag GmbH & Co. KGaA, Weinheim **DOI: 10.1002/ejic.200400025**

ing this treatment, the products were purified in several different ways. Filtration of the hot reaction solution and then allowing this solution to cool slowly to room temperature led to the direct crystallization of [K(η^2-3,5-Ph_2pz)(η^6-18-crown-6)] (**1**, 96%). The infrared spectrum of **1** does not show any absorption band near 3400 cm^{-1}, suggesting a water-free formulation. The complex [K(η^2-3,5-*t*Bu_2pz)(η^6-18-crown-6)] (**2**) did not crystallize from tetrahydrofuran on cooling after filtration. Removal of the tetrahydrofuran under reduced pressure afforded crude **2** as a colorless solid. Recrystallization from toluene at −20 °C afforded analytically pure **2** in a 81% yield as colorless crystals. There are no absorption bands at around 3400 cm^{-1} in the infrared spectrum of **2**. Due to the presence of the lipophilic *tert*-butyl groups, **2** is soluble in common organic solvents. By contrast, **1** is only soluble in polar solvents such as methanol and hot tetrahydrofuran. Attempts were made to prepare a 3,5-dimethylpyrazolato complex that was analogous to **1** and **2**. Treatment of equimolar quantities of potassium hydride, 3,5-dimethylpyrazole, and 18-crown-6 in tetrahydrofuran, followed by hot filtration of the reaction solution, led to colorless single crystals of [K(η^2-3,5-Me_2pz)(H_2O)(η^6-18-crown-6)] (**3**, 83%) on cooling of the tetrahydrofuran solution, without the need for further treatment with potassium metal. A crystal structure as described below reveals the presence of coordinated water. All attempts to prepare the water-free 3,5-dimethylpyrazolato analogue of **3** have thus far failed, and only **3** has been isolated. Apparently, **3** is highly crystalline and precipitates as soon as it forms. Further treatment of **3** with excess potassium metal as for **1** and **2** afforded a product that was only slightly soluble in tetrahydrofuran. This product gave complex ^1H NMR spectra and was not pursued further. Complexes **1**−**3** are thermally stable at room temperature and are unaffected by exposure to relatively dry ambient air for a few minutes. However, the complexes are hygroscopic and lose crystallinity upon extended exposure to ambient atmosphere. For this reason, **1**−**3** were handled under dry argon in this study.

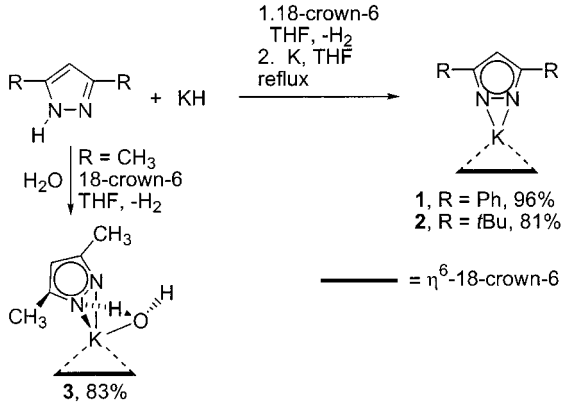

Scheme 1

^1H and $^{13}C\{^1H\}$ NMR spectra, infrared spectra, and element analysis data are consistent with the formulations of **1**−**3**. In addition, the X-ray crystal structures of **1** and **3** were determined and are described below. The ^1H NMR spectra of **1**−**3** show resonance signals for the pyrazolato ligand, as well as resonances at about δ = 3.6 ppm for the protons of the 18-crown-6 ligand. A broad resonance at δ = 5.4 ppm in the ^1H NMR spectrum of **3** in [D_4]methanol is assigned to the protons of the aqua ligand. It is not clear if the water molecule is still coordinated to the potassium ion in **3**, or if it has been displaced by the methanol solvent. The infrared spectrum of **3** displays a broad absorption at 3400 cm^{-1}, which is assigned to the stretches associated with the aqua ligand. This band did not disappear completely even after **3** was heated at 100 °C for 15 h, suggesting strong bonding between the potassium ion and oxygen atom of the aqua ligand. The mass spectra of **1**−**3** show a parent ion at *m*/*z* = 303, which is consistent with the [K(18-crown-6)]$^+$ moiety.

Complexes **1** and **3** were structurally characterized by X-ray crystallography, the crystal data are given in Table 1. Perspective views of **1** and **3** are shown in Figure 1 and Figure 2, respectively, and an extended diagram that emphasizes the hydrogen bonding of **3** is given in Figure 3. We were unable to solve the X-ray crystal structure of **2** due to disorder in the crystals, but its solid-state structure is presumably very similar to that of **1**.

Complex **1** contains the η^2-3,5-diphenylpyrazolato and η^6-18-crown-6 ligands, and there are no significant intermolecular contacts (Figure 1). The potassium−nitrogen bond lengths [2.722(3), 2.766(4) Å] are similar and are consistent with idealized η^2-bonding. These bond lengths are within the range of those found in [(μ-η^2:η^1:η^1-3,5-Ph_2pz)K(THF)]$_6$ (K−N 2.716−2.869 Å).[8a] The potassium−oxygen bond lengths range between 2.78−2.95 Å, and are similar to other structurally characterized complexes containing [K(η^6-18-crown-6)]$^+$ fragments.[11] The angle formed between the plane of the pyrazolato C_3N_2 core and the best plane of the six oxygen atoms of the 18-crown-6 ligand is 85.01(10)°. Such an arrangement is consistent with donation of the in-plane lone pairs of the nitrogen atoms to the potassium ion, and is very similar to the η^2-coordination mode that has been documented in many main group element complexes.[1e,2] The potassium ion is located 0.710(2) Å above the best plane of the 18-crown-6 ligand oxygen atoms, towards the side with the pyrazolato ligand. This arrangement certainly facilitates bonding to the pyrazolato ligand. Selected bond lengths and angles for **1** are presented in Table 2.

Complex **3** contains the η^2-3,5-dimethylpyrazolato, η^6-18-crown-6 and aqua ligands. The aqua ligand hydrogen atoms are engaged in both intramolecular and intermolecular hydrogen bonding with the pyrazolato ligand. A view of the molecular structure is shown in Figure 2 and a view emphasizing the hydrogen bonding is contained in Figure 3. The potassium−nitrogen bond lengths are 2.955(3) and 3.138(3) Å. These bond lengths are longer than those in **1** due to the higher coordination number at the potassium ion (9 versus 8). In fact, the potassium−nitrogen bond lengths in **3** are even longer than would be expected when the coordination number increases by one, and support the idea that

 © 2004 Wiley-VCH Verlag GmbH & Co. KGaA, Weinheim

Table 1. Summary of crystallographic data for **1** and **3**

	1	**3**
Formula	$C_{27}H_{35}KN_2O_6$	$C_{17}H_{33}KN_2O_7$
M	522.67	416.55
T (K)	295(2)	295(2)
Crystal system	monoclinic	monoclinic
Space	$P2_1/n$	$P2_1/n$
a (Å)	9.4714(10)	12.9297(15)
b (Å)	22.622(3)	8.7945(9)
c (Å)	13.9001(18)	19.436(2)
α (°)	90	90
β (°)	108.449(3)	92.730(2)
γ (°)	90	90
V (Å^{-3})	2825.2(6)	2207.6(4)
Z	4	4
$d_{calcd.}$ (g/cm^3)	1.229	1.253
Absorption coefficient (mm^{-1})	0.229	0.278
F(000)	1112	896
Crystal size (mm)	0.40 × 0.20 × 0.10	0.24 × 0.20 × 0.10
θ range (deg)	1.79 to 28.35	1.94 to 28.32
Limiting	$-12 \le h \le 11$; $0 \le k \le 30$; $0 \le l \le 18$	$-17 \le h \le 17$; $0 \le k \le 11$; $0 \le l \le 25$
No. of reflections collected	20327	16023
No. of independent reflections	6564 (*R*int = 0.080)	5264 (*R*int = 0.051)
No. of data/restraints/parameters	6564/0/326	5264/0/355
GOF/F^2	0.866	0.793
R indices [$I > 2\sigma(I)$]	$R_1 = 0.0588$; $wR_2 = 0.1369$	$R_1 = 0.0475$; $wR_2 = 0.1226$
R indices (all data)	$R_1 = 0.2191$; $wR_2 = 0.1957$	$R_1 = 0.1727$; $wR_2 = 0.1859$
Largest diff. peak/hole (e·Å^{-3})	0.213/−0.392	0.205/−0.283

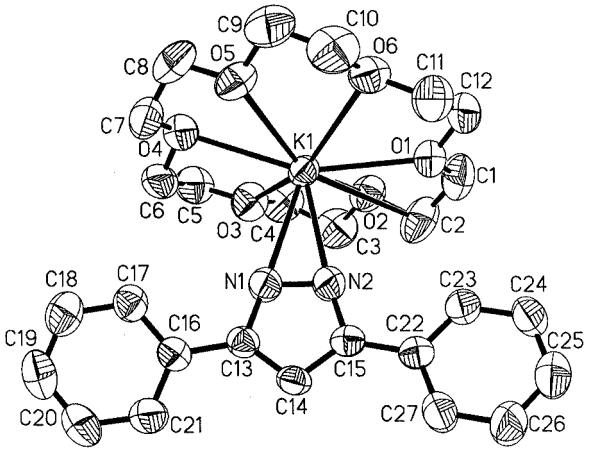

Figure 1. Perspective view of **1** with thermal ellipsoids at the 50% probability level

Table 2. Selected bond lengths (Å) and angles (°) for **1**

K−N(1)	2.766(4)
K−N(2)	2.722(3)
K−O(1)	2.775(3)
K−O(2)	2.860(3)
K−O(3)	2.816(3)
K−O(4)	2.954(3)
K−O(5)	2.864(3)
K−O(6)	2.917(3)
N(1)−N(2)	1.362(4)
N(1)−C(13)	1.351(5)
N(2)−C(15)	1.358(5)
C(13)−N(1)−K(1)	177.3(3)
C(15)−N(2)−K(1)	174.2(3)
N(1)−K−N(2)	28.72(9)

3 contains a new pyrazolato coordination mode. The longer potassium−nitrogen bond lengths in **3** may also arise as a result of the less basic pyrazolato ligand π-orbitals donating to the potassium ion (i.e. less optimum ionic bonding). The potassium−oxygen bond lengths are 2.848(3) Å for the aqua ligand and 2.84−3.07 Å for the 18-crown-6 ligand. These values are similar to or slightly longer than the related values found in **1** and other [K(η^6-18-crown-6)]$^+$ fragments.[11] The angle formed between the plane of the pyrazolato C_3N_2 core and the best plane of the 18-crown-6 ligand oxygen atoms is 24.40(14)°, which indicates that the planes of the 18-crown-6 ligand oxygen atoms and the pyrazolato ligand are almost coplanar. This situation is very different from that of **1**, where the pyrazolato ligand core plane is nearly perpendicular to the best plane of the 18-crown-6 ligand oxygen atoms. The distance of the nitrogen atoms from the best plane of the 18-crown-6 ligand oxygen atoms is 3.409(3) Å for N(1) and 3.711(3) Å for N(2), indicating that the pyrazolato ligand core plane is twisted slightly relative to that of the 18-crown-6 ligand. The potassium ion is located 0.976(1) Å above the best plane of the 18-crown-6

 © 2004 Wiley-VCH Verlag GmbH & Co. KGaA, Weinheim

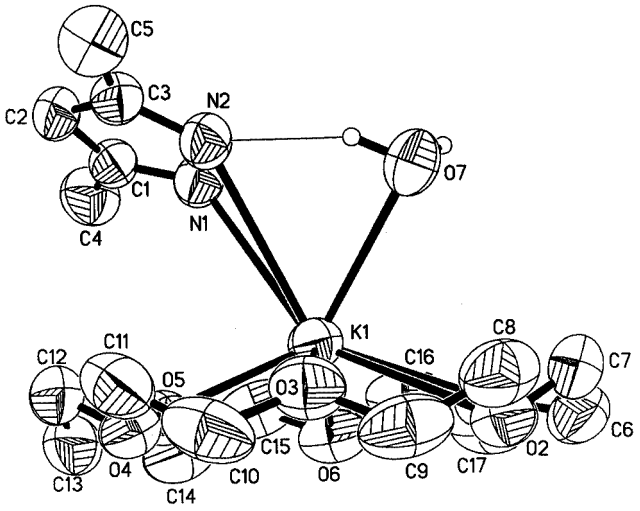

Figure 2. Perspective view of **3** with thermal ellipsoids at the 50% probability level

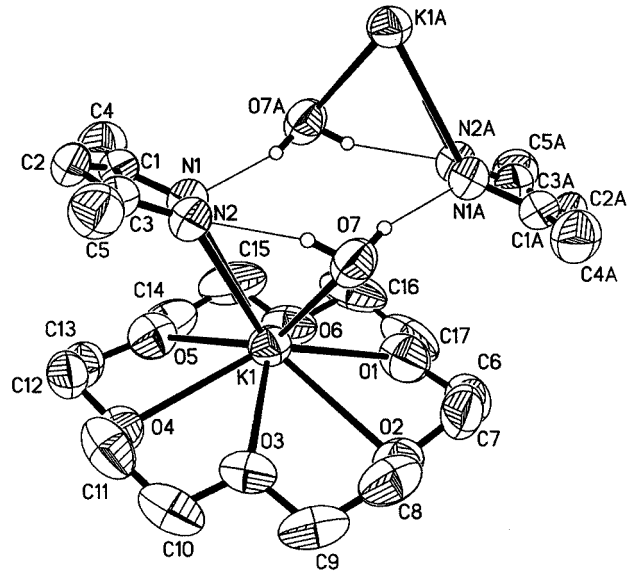

Figure 3. Perspective view of **3** that emphasizes the intramolecular and intermolecular hydrogen-bonding interactions; thermal ellipsoids are at the 50% probability level

Table 3. Selected bond lengths (Å) and angles (°) for **3**

K−N(1)	2.954(3)
K−N(2)	3.138(3)
K−O(1)	2.837(3)
K−O(2)	3.071(3)
K−O(3)	2.912(3)
K−O(4)	2.980(3)
K−O(5)	2.836(3)
K−O(6)	3.045(3)
K−O(7)	2.847(3)
N(1)−N(2)	1.381(4)
C(1)−N(1)−K	140.1(2)
C(3)−N(2)−K	142.8(2)
N(1)−K−N(2)	25.98(7)

ligand oxygen atoms. This value is larger than that of **1**, and reflects the larger coordination number in **3** and the differing coordination modes in the two complexes. Selected bond lengths and angles for **3** are given in Table 3.

Inspection of the hydrogen bonding in **3** reveals that one hydrogen atom of the aqua ligand is intramolecularly hydrogen bonded to N(2) of the pyrazolato ligand, with a nitrogen−hydrogen distance of 2.00(5) Å, a N(2)−O(7) distance of 2.813(7) Å, and a N···H−O angle of 154(3)°. The other hydrogen atom of the aqua ligand is intermolecularly hydrogen bonded to N(1) of an adjacent molecule, with a nitrogen−hydrogen distance of 2.01(5) Å, a N(1′)−O(7) distance of 2.883(7) Å, and N···H−O angle of 164(3)°. The intermolecular hydrogen bonding thus leads to dimeric species within the crystal that are connected by 10-membered $H_4N_4O_2$ rings.

The bending of the pyrazolato ligand in **3** towards the plane of the 18-crown-6 ligand and its slight twisting relative to this plane could have several origins. Accommodation of the aqua ligand in **3** requires that the pyrazolato ligand moves on the face of the coordination sphere to facilitate formation of the new potassium−oxygen bond. Such motion would necessarily lead to a reduction of the angle between the planes of the 18-crown-6 and pyrazolato ligands. However, there is a further bending of the pyrazolato ligand toward the 18-crown-6 ligand, as is seen by the 140.7(3)° angle between the KN_2 and C_3N_2 planes. With the observed distortions, the in-plane (and more basic) nitrogen atom lone pairs point more directly toward the aqua ligand hydrogen atoms, which presumably optimizes intramolecular and intermolecular hydrogen bonding. The stronger intramolecular hydrogen bonding to N(2) could infer some less basic character on this atom, which is a possible origin for the longer K−N(2) bond length and the slight twisting of the C_3N_2 plane relative to that of the 18-crown-6 ligand oxygen atoms. The disposition of the pyrazolato ligand in **3** requires that there is at least some donation of electron density to the potassium ion from the out-of-plane π-orbitals on the nitrogen atoms of the pyrazolato ligand. Idealized π-η^2-pyrazolato ligand coordination to a single metal center would have an angle of about 90° between the MN_2 and C_3N_2 planes. Such a coordination mode has not been reported, although this coordination mode has been documented in an ytterbium complex containing a phosphorus−antimony analog of a pyrazolato ligand.[4c] This ytterbium complex has no hydrogen bonding. However, the pyrazolato ligand in **3** represents a distortion that is significantly towards an idealized π-η^2-pyrazolato ligand, and this bonding arrangement is clearly driven by the hydrogen-bond formation with the aqua ligand. The predominately ionic bonding expected for a group 1 salt probably allows for low energy distortions of the ligands about the coordination sphere. The potassium−nitrogen bonding mode in **3** resembles that observed in lanthanide complexes containing μ-η^2:η^2 pyrazolato ligands,[12] since the latter coordination mode also demands donation of some electron density from the out-of-plane π-orbitals on the nitrogen atoms of the pyrazolato ligand.

 © 2004 Wiley-VCH Verlag GmbH & Co. KGaA, Weinheim

This work documents the first examples of monomeric terminal η^2-pyrazolato ligand coordination to a group 1 metal. The 18-crown-6 ligand saturates the coordination sphere in **1** in such a way that the 3,5-diphenylpyrazolato ligand can just be accommodated by **1**. Optimal ionic bonding then leads to the observed η^2-pyrazolato ligand. In our recent report,[10] the triazolato and tetrazolato complexes [K(*i*Pr$_2$C$_2$N$_3$)(18-crown-6)] and [K(PhCN$_4$)(18-crown-6)] have asymmetric potassium−nitrogen distances (Δ_{K-N} = 0.35−0.60 Å) and there was no evidence for steric interactions that would promote such asymmetric bonding of the heterocyclic ligands. By contrast, **1** contains an essentially idealized η^2-pyrazolato ligand (Δ_{K-N} = 0.044 Å). The nitrogen atom lone pairs in the pyrazolato ligands are definitely more basic than those of the 1,2,4-triazolato and tetrazolato ligands,[13] and the better donor characteristics of the pyrazolato ligands may then facilitate the η^2-coordination mode relative to the more nitrogen-rich heterocyclic ligands. The first examples of terminal η^2-1,2,4-triazolato and tetrazolato ligand coordination have been reported in the past several years.[2d,10,14]

Use of the less sterically demanding 3,5-dimethylpyrazolato ligand leads to the aqua complex **3**, which contains a novel η^2-pyrazolato ligand coordination mode. There is an analogy between **3** and the metal complexes containing slipped cyclopentadienyl ligands.[15−17] In two crystallographically characterized complexes containing terminal η^2-cyclopentadienyl ligands, [Mg(η^5-Cp)(η^2-Cp)(NH$_2$[CH(CH(CH$_3$)$_2$]$_2$)][16a] and [Mg(η^5-Cp)(η^2-Cp)(NH$_2$C(CH$_3$)$_3$](THF)],[16b] the η^2-cyclopentadienyl ligands are stabilized through intramolecular and intermolecular N−H···C hydrogen bonding.[16a] This is similar to the stabilization of the pyrazolato ligand in **3**. The complexes Mg(*t*Bu$_2$pz)$_2$(*t*BupzH)$_2$ [14] and Nd(Me$_2$pz)$_3$(Me$_2$pzH)$_2$(py)[18] contain intramolecular N−H···N hydrogen bonding that appears to enforce η^1-bonding of the pyrazolato ligands.

Experimental Section

General: All reactions were performed under dry argon using standard Schlenk and dry box techniques. Solvents were distilled from various drying agents under argon prior to use. 3,5-Diphenylpyrazole, 3,5-dimethylpyrazole, and 18-crown-6 were purchased from commercial sources. 3,5-Di-*tert*-butylpyrazole was prepared according to literature methods.[19]

^{1}H and ^{13}C{^{1}H} NMR spectra were obtained in dry, degassed [D$_4$]methanol and [D$_8$]tetrahydrofuran, and were referenced to the residual proton or carbon atom resonances of these solvents. Infrared spectra were obtained using Nujol as the medium. Elemental analyses were performed by Midwest Microlab, Indianapolis, IN. Melting points were obtained on a Haake−Buchler HBI digital melting point apparatus and are uncorrected.

[K(η^2-3,5-Ph$_2$pz)(η^6-18-crown-6)] (1): A mixture of 3,5-diphenylpyrazole (2.20 g, 10.0 mmol), potassium hydride (0.42 g, 10.5 mmol), and 18-crown-6 (2.77 g, 10.5 mmol) in tetrahydrofuran (100 mL) was stirred at room temperature for 15 h, after which time hydrogen evolution was complete. This solution was further treated with excess potassium (0.50 g, 13 mmol), and the suspension was refluxed for 0.5 h. The hot solution was filtered through a 2-cm pad of Celite and **1** formed as colorless single crystals as the solution cooled (5.02 g, 96%). M.p.: 173 °C. ^{1}H NMR (CD$_3$OD, 23 °C): δ = 7.35, 7.81 (mult, 10 H, Ph-*H*), 6.94 (s, 1 H, C*H*), 3.53 (s, 24 H, O−CH_2). ^{13}C NMR (CD$_3$OD, 23 °C): δ = 150.73 (s, *C*−Ph), 133.87, 129.77, 128.59, 126.58, (4s, *C*, Phenyl ring), 100.44 (s, *C*H), 71.25 (s, O−*C*H$_2$). MS (EI): *m*/*z*: 303 ([K(18-crown-6)]$^+$, 100%). C$_{27}$H$_{35}$KN$_2$O$_6$ (522.7): calcd. C 62.04, H 6.75, N 5.36; found C 62.18, H 6.82, N, 5.40.

[K(η^2-3,5-*t*Bu$_2$pz)(η^6-18-crown-6)] (2): In a fashion similar to the preparation of **1**, treatment of 3,5-di-*tert*-butylpyrazole (1.80 g, 10.0 mmol) with potassium hydride (0.42 g, 10.5 mmol), 18-crown-6 (2.77 g, 10.5 mmol), and potassium (0.5 g, 13 mmol) in tetrahydrofuran afforded crude **2** as a tetrahydrofuran solution. After removal of the tetrahydrofuran under reduced pressure, the crude material was dissolved in toluene and cooled to −20 °C to afford **2** as colorless crystals (3.92 g, 81%). M.p.: 158 °C. ^{1}H NMR (C$_4$D$_8$O, 23 °C): δ = 5.53 (s, 1 H, C−*H*), 3.62 (s, 24 H, CH_2), 1.25 (s, 18 H, CH_3). ^{13}C NMR (C$_4$D$_8$O, 23 °C): δ = 157.78 (s, *C*−*t*Bu), 92.38 (s, *C*H), 71.02 (s, O−*C*H$_2$), 32.66 (s, *C*−CH$_3$), 25.71 (s, *C*H$_3$). MS (EI): *m*/*z*: 303 ([K(18-crown-6)]$^+$, 100%). C$_{23}$H$_{43}$KN$_2$O$_6$ (482.7): calcd. C 57.23, H 8.98, N 5.80; found C 57.35, H 8.86, N 5.72.

[K(η^2-3,5-Me$_2$pz)(H$_2$O)(η^6-18-crown-6)] (3): Treatment of 3,5-dimethylpyrazole (0.96 g, 10 mmol) with potassium hydride (0.42 g, 10.5 mmol) and 18-crown-6 (2.77 g, 10.5 mmol) in tetrahydrofuran (100 mL) at room temperature for 2 h, followed by reduction in volume to 50 mL under reduced pressure, and after standing for 48 h, afforded **3** as colorless crystals (3.45 g, 83%). M.p.: 145 °C. ^{1}H NMR (CD$_3$OD, 23 °C): δ = 5.80 (s, 1 H, C*H*), 5.4 (br, 2 H, *H*$_2$O), 3.61 (s, 24 H, O−CH_2), 2.19 (s, 6 H, CH_3). ^{13}C NMR (CD$_3$OD, 23 °C): δ = 145.50 (s, *C*−CH$_3$), 104.69 (s, *C*H), 71.35 (s, *C*H$_2$), 11.95 (s, *C*H$_3$). MS (EI): *m*/*z*: 303 ([K(18-crown-6)]$^+$, 100%). IR (Nujol, cm^{-1}): ν_{OH} = 3400 (s). C$_{17}$H$_{33}$KN$_2$O$_7$ (416.6): calcd. C 49.02, H 7.99, N 6.73; found C 48.99, H 7.89, N, 6.64.

X-ray Crystallography: Crystals of **1** (*M* = 522.67) and **3** (*M* = 416.55) were grown as described above and crystallized in the monoclinic crystal system with space group $P2_1/n$. Relevant details and data are summarized in Table 1. The crystals were mounted in thin glass capillaries under an argon atmosphere. Diffraction data were collected on a Bruker P4 four-circle diffractometer coupled to a Bruker CCD area detector at 295(2) K, with graphite-monochromated Mo-K_α radiation (λ = 0.71073 Å). The structures were solved from the Patterson maps using SHELX-97[20] and refined against F^2 on all data by full-matrix least-squares with the same program. All non-hydrogen atoms were refined anisotropically. The hydrogen atoms were included in the model at their geometrically calculated positions and held riding or observed on a difference Fourier and refined. CCDC-201685 (**1**) and CCDC-201686 (**3**) contain the supplementary crystallographic data for this paper. These data can be obtained free of charge on application to CCDC, 12 Union Road, Cambridge CB21EZ, UK [Fax: (internat.) + 44-1223-336-033; E-mail: deposit@ccdc.cam.ac.uk]. Structure searches were performed using the Cambridge Crystallographic Database, Version 5.24, November 2002.

Acknowledgments

We thank the Office of Naval Research (contract No. N00014-21-0-866) for support of this research.

 © 2004 Wiley-VCH Verlag GmbH & Co. KGaA, Weinheim

[1] Reviews of pyrazolato complexes: [1a] S. Trofimenko, *Chem. Rev.* **1972**, *72*, 497−509. [1b] S. Trofimenko, *Progr. Inorg. Chem.* **1986**, *34*, 115−210. [1c] A. P. Sadimenko, S. S. Basson, *Coord. Chem. Rev.* **1996**, *147*, 247−297. [1d] G. La Monica, G. A. Ardizzoia, *Progr. Inorg. Chem.* **1997**, *46*, 151−238. [1e] J. E. Cosgriff, G. B. Deacon, *Angew. Chem. Int. Ed.* **1998**, *37*, 286−287. [1f] A. P. Sadimenko, *Adv. Heterocycl. Chem.* **2001**, *80*, 157−240. [1g] F. Nief, *Eur. J. Inorg. Chem.* **2001**, 891−904.

[2] Main group metal complexes with terminal η^2-pyrazolato ligands: [2a] W. Zheng, N. C. Mösch-Zanetti, T. Blunck, H. W. Roesky, M. Noltemeyer, H.-G. Schmidt, *Organometallics* **2001**, *20*, 3299−3303. [2b] D. Pfeiffer, C. H. Winter, M. J. Heeg, *Inorg. Chem.* **2000**, *39*, 2377−2384. [2c] G. B. Deacon, E. E. Delbridge, C. M. Forsyth, P. C. Junk, B. W. Skelton, A. H. White, *Aust. J. Chem.* **1999**, *52*, 733−739. [2d] D. Pfeiffer, C. H. Winter, M. J. Heeg, *Angew. Chem. Int. Ed.* **1998**, *37*, 2517−2519.

[3] Selected, recent leading references to transition metal complexes with terminal η^2-pyrazolato ligands: [3a] K. Most, N. C. Mösch-Zanetti, D. Vidovic, J. Magull, *Organometallics* **2003**, *22*, 5485−5490. [3b] G. Zhu, J. M. Tanski, G. Parkin, *Polyhedron* **2003**, *22*, 199−203. [3c] K. R. Gust, J. E. Knox, M. J. Heeg, H. B. Schlegel, C. H. Winter, *Eur. J. Inorg. Chem.* **2002**, 2327−2334. [3d] K. R. Gust, J. E. Knox, M. J. Heeg, H. B. Schlegel, C. H. Winter, *Angew. Chem. Int. Ed.* **2002**, *41*, 1591−1594. [3e] C. Yélamos, K. R. Gust, A. G. Baboul, M. J. Heeg, H. B. Schlegel, C. H. Winter, *Inorg. Chem.* **2001**, *40*, 6451−6462.

[4] Selected, leading references to lanthanide and actinide complexes with terminal η^2-pyrazolato ligands: [4a] G. B. Deacon, C. M. Forsyth, D. L. Wilkinson, *Chem. Eur. J.* **2001**, *7*, 1784−1795. [4b] L. Zhang, X. Zhou, R. Cai, L. Weng, *J. Organomet. Chem.* **2000**, *612*, 176−181. [4c] G. B. Deacon, E. E. Delbridge, G. D. Fallon, C. Jones, D. E. Hibbs, M. B. Hursthouse, B. W. Skelton, A. H. White, *Organometallics* **2000**, *19*, 1713−1721. [4d] G. B. Deacon, E. E. Delbridge, B. W. Skelton, A. H. White, *Eur. J. Inorg. Chem.* **1999**, 751−761. [4e] D. Pfeiffer, B. J. Ximba, L. M. Liable-Sands, A. L. Rheingold, M. J. Heeg, D. M. Coleman, H. B. Schlegel, T. F. Kuech, C. H. Winter, *Inorg. Chem.* **1999**, *38*, 4539−4548. [4f] X.-G. Zhou, Z.-E. Huang, R.-F. Cai, L.-B. Zhang, L.-X. Zhang, X.-Y. Huang, *Organometallics* **1999**, *18*, 4128−4133. [4g] G. B. Deacon, E. E. Delbridge, B. W. Skelton, A. H. White, *Eur. J. Inorg. Chem.* **1998**, 543−545. [4h] J. E. Cosgriff, G. B. Deacon, B. M. Gatehouse, H. Hemling, H. Schumann, *Angew. Chem. Int. Ed. Engl.* **1993**, *32*, 874−875. [4i] J. E. Cosgriff, G. B. Deacon, B. M. Gatehouse, H. Hemling, H. Schumann, *Aust. J. Chem.* **1994**, *47*, 1223−1235. [4j] C. W. Eigenbrot Jr., K. N. Raymond, *Inorg. Chem.* **1982**, *21*, 2653−2660.

[5] Ru: [5a] J. R. Perera, M. J. Heeg, H. B. Schlegel, C. H. Winter, *J. Am. Chem. Soc.* **1999**, *121*, 4536−4537. K: [5b] J. C. Röder, F. Meyer, E. Kaifer, *Angew. Chem. Int. Ed.* **2002**, *41*, 2304−2306. Ba: [5c] A. Steiner, G. T. Lawson, B. Walfort, D. Leusser, D. Stalke, *J. Chem. Soc., Dalton Trans.* **2001**, 219−221. Tl: [5d] G. B. Deacon, E. E. Delbridge, C. M. Forsyth, B. W. Skelton, A. H. White, *J. Chem. Soc., Dalton Trans.* **2000**, 745−751.

[6] Selected references about main group element complexes with pyrazolato ligands: [6a] A. Mar, S. J. Rettig, A. Storr, J. Trotter, *Can. J. Chem.* **1988**, *66*, 101−108. [6b] D. A. Atwood, A. H. Cowley, R. A. Jones, *Organometallics* **1993**, *12*, 236−238. [6c] A. Steiner, D. Stalke, *Inorg. Chem.* **1995**, *34*, 4846−4853. [6d] M. V. Capparelli, P. Hodge, B. Piggott, *Chem. Commun.* **1997**, 937−938.

[7] Li: [7a] J.C. Röder, F. Meyer, H. Pritzkow, *Organometallics* **2001**, *20*, 811−817. Na: [7b] A. Fraser, B. Piggott, *J. Chem. Soc., Dalton Trans.* **1999**, 3484−3486. [7c] A. Steiner, D. Stalke, *J. Chem. Soc., Chem. Commun.* **1993**, 1702−1704. [7d] H. Schumann, P. R. Lee, J. Loebel, *Angew. Chem. Int. Ed., Engl.* **1989**, *28*, 1033−1035.

[8] [8a] C. Yélamos, M. J. Heeg, C. H. Winter, *Inorg. Chem.* **1998**, *37*, 3892−3894. [8b] G. B. Deacon, E. E. Delbridge, C. M. Forsyth, *Angew. Chem. Int. Ed.* **1999**, *38*, 1766−1767.

[9] [9a] S. Guo, F. Peters, F. F. D. Biani, J. W. Bats, E. Herdtweck, P. Zanello, M. Wagner, *Inorg. Chem.* **2001**, *40*, 4928−4936. [9b] O. Kuhl, J. Sieler, E. Hey-Hawkins, *Main Group Met. Chem.* **2001**, *24*, 39−42. [9c] Z. Hu, S. M. Gorun, *Inorg. Chem.* **2001**, *40*, 667−671. [9d] C. Janiak, S. Temizdemir, S. Dechert, *Inorg. Chem. Commun.* **2000**, *3*, 271−275. [9e] J. Reglinski, M. D. Spicer, M. Garner, A. R. Kennedy, *J. Am. Chem. Soc.* **1999**, *121*, 2317−2318. [9f] J. L. Kisko, T. Hascall, C. Kimblin, G. Parkin, *J. Chem. Soc., Dalton Trans.* **1999**, 1929−1935. [9g] H. V. R. Dias, H.-Y. Kim, *Organometallics* **1996**, *15*, 5374−5379. [9h] H. V. R. Dias, W. Jin, H.-Y. Kim, H.-L. Lu, *Inorg. Chem.* **1996**, *35*, 2317−2328. [9i] H. V. R. Dias, J. D. Gorden, *Inorg. Chem.* **1996**, *35*, 318−324. [9j] H. V. R. Dias, H.-L. Lu, R. E. Ratcliff, S. G. Bott, *Inorg. Chem.* **1995**, *34*, 1975−1976.

[10] W. Zheng, M. J. Heeg, C. H. Winter, *Angew. Chem. Int. Ed.* **2003**, *42*, 2761−2764.

[11] Recent selected examples: [11a] M. C. Cassani, Y. K. Gun'ko, P. B. Hitchcock, A. G. Hulkes, A. V. Khvostov, M. F. Lappert, A. V. Protechenko, *J. Organomet. Chem.* **2002**, *647*, 71−83. [11b] S. Neander, U. Behrens, F. Olbrich, *J. Organomet. Chem.* **2000**, *604*, 59−67. [11c] C. Downie, Z.-J. Tang, A. M. Guloy, *Angew. Chem. Int. Ed.* **2000**, *39*, 337−340.

[12] For examples of lanthanide complexes with this coordination mode: [12a] G. B. Deacon, A. Gitlits, P. W. Roesky, M. R. Burgstein, K. C. Lim, B. W. Skelton, A. H. White, *Chem. Eur. J.* **2001**, *7*, 127−138. [12b] G. B. Deacon, A. Gitlits, B. W. Skelton, A. H. White, *Chem. Commun.* **1999**, 1213−1214. [12c] G. B. Deacon, E. E. Delbridge, B. W. Skelton, A. H. White, *Angew. Chem. Int. Ed.* **1998**, *37*, 2251−2252.

[13] M. R. Grimmett in *Comprehensive Organic Chemistry* (Eds.: D. Barton, W. D. Ollis), Pergamon Press: Oxford, **1979**, vol. 4, p. 365.

[14] N. C. Mösch-Zanetti, M. Ferbinteanu, J. Magull, *Eur. J. Inorg. Chem.* **2002**, 950−956.

[15] For recent leading references: [15a] L. F. Veiros, *Organometallics* **2000**, *19*, 5549−5558. [15b] L. F. Veiros, *J. Organomet. Chem.* **1999**, *587*, 221−232. [15c] W. Simanko, W. Tesch, V. N. Sapunov, K. Mereiter, R. Schmid, K. Kirchner, J. Coddington, S. Wherland, *Organometallics* **1998**, *17*, 5674−5688.

[16] [16a] A. Xia, M. J. Heeg, C. H. Winter, *J. Am. Chem. Soc.* **2002**, *124*, 11264−11265. [16b] M. M. Olmstead, W. J. Grigsby, D. R. Chacon, T. Hascall, P. P. Power, *Inorg. Chim. Acta* **1996**, *251*, 273−284.

[17] A. D. Bond, R. A. Layfield, J. A. MacAllister, M. McPartlin, J. M. Rawson, D. S. Wright, *Chem. Commun.* **2001**, 1956−1957.

[18] G. B. Deacon, C. M. Forsyth, A. Gitlits, R. Harika, P. C. Junk, B. W. Skelton, A. H. White, *Angew. Chem. Int. Ed.* **2002**, *41*, 3249−3251.

[19] C. Fernàndez-Castaño, C. Foces-Foces, N. Jagerovic, J. Elguero, *J. Mol. Struct. (THEOCHEM)* **1995**, *355*, 265.

[20] G. M. Sheldrick, SHELXL-97; *Program for Crystal Structure Refinement*; University of Göttingen: Göttingen, Germany, **1997**.

Received January 13, 2004
Early View Article
Published Online April 26, 2004

 © 2004 Wiley-VCH Verlag GmbH & Co. KGaA, Weinheim

DFT Calculations on the C−Cl/Si−H Exchange Catalyzed by *P,N*-Chelated Pt^{II} Complexes

Dietmar Sturmayr[a] and Ulrich Schubert*[a]

Keywords: Chlorinated hydrocarbons / Hemilabile ligands / Oxidative addition / Reductive elimination / Silanes

The mechanism of the previously reported C–Cl/Si–H exchange reaction between H_xCCl_{4-x} (x = 0–3) and $HSiMe_2Ph$ catalyzed by [PtMeCl($Ph_2PCH_2CH_2NMe_2$-κ²*P,N*)] [PtMeCl(P∩N)] was investigated by DFT calculations. The energetically less-favored isomer of [PtMeCl(P∩N)], with Cl and P being *cis*, was identified to be the actual catalytic species. The catalytic reaction proceeds by oxidative addition of the silane, de-coordination of the nitrogen atom of the *P,N*-chelating ligand, reductive elimination of the chlorosilane and oxidative addition of the C–Cl bond of H_xCCl_{4-x}. The final step is the reductive elimination of the C–H bond with concomitant re-coordination of the nitrogen atom of the *P,N*-chelating ligand.

(© Wiley-VCH Verlag GmbH & Co. KGaA, 69451 Weinheim, Germany, 2004)

Introduction

We recently reported that the complex [PtMeCl($Ph_2PCH_2CH_2NMe_2$-κ²*P,N*)] [PtMeCl(P∩N)] catalyzes the C−Cl/Si−H exchange reaction between H_xCCl_{4-x} (x = 0−3) and $HSiMe_2Ph$ [Equation (1)].[1] While the chlorinated hydrocarbons are successively dechlorinated, the silane is the chloride sink and $ClSiMe_2Ph$ is formed. The order of reactivity is $CCl_4 > CHCl_3 > CH_2Cl_2 > CH_3Cl$. A related reaction is the [Rh(C_6F_5)(PMe_3)$_3$]-catalyzed hydrodefluorination of C_6F_6 by $HSi(OEt)_3$.[2]

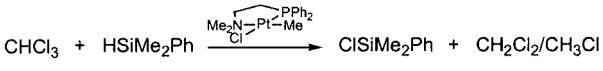

(1)

A remarkable feature of this reaction is that [PtMeCl(P∩N)], where Cl and P are *trans* in the most stable isomer ("*trans*-[PtMeCl(P∩N)]"),[3,4] does not react with either CCl_4 or $HSiMe_2Ph$ alone on a reasonable time scale. The formation of the catalytic species must be the result of an initial reaction of [PtMeCl(P∩N)] with either $HSiMe_2Ph$ or the chlorinated hydrocarbon. We therefore postulated that the energetically less-favored isomer of [PtMeCl(P∩N)] with *cis* Cl and P ("*cis*-[PtMeCl(P∩N)]") might be the actual catalytic species.[1] To shed light on this question and on the further course of the reaction we performed DFT calculations, which are reported in this article.

[a] Institute of Materials Chemistry, Vienna University of Technology,
Getreidemarkt 9/165, 1060 Wien, Austria

Results and Discussion

The theoretical analysis of the catalytic reaction was divided into two parts. In the first part the reaction of both isomers of [PtMeCl(P∩N)] with SiH_4 was analyzed. In the second part the catalytic cycle was studied. SiH_4 and CH_3Cl were used as the reactants to simplify the calculations.

Reaction of [PtMeCl(P∩N)] with SiH_4

When [PtMeCl(P∩N)] is taken as the starting point of the catalytic reaction, the next step must be the reaction with $HSiR_3$. We therefore investigated first the oxidative addition of the silane to the two isomers of [PtMeCl(P∩N)]. Calculations were carried out by method I (see Computational Details) on *P,N*-chelated complexes where the chelate ligand was modeled as $PH_2CH_2CH_2NH_2$.

Reaction of SiH_4 with *trans*-[PtMeCl(P∩N)] (1)

The energy required to form TS_{1-2} from **1** and SiH_4 is 23.6 kcal/mol (Figure 1). A Pt−Si bond of 2.456 Å and a

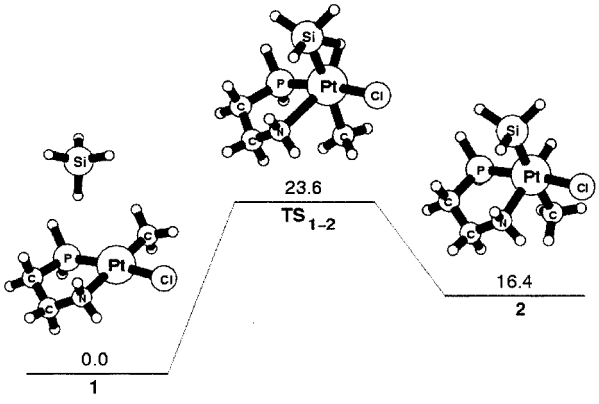

Figure 1. Reaction for the reaction of SiH_4 with **1**; energies in kcal/mol

 © 2004 Wiley-VCH Verlag GmbH & Co. KGaA, Weinheim DOI: 10.1002/ejic.200400029

Pt−H bond of 1.582 Å are formed. The Pt−N bond length is increased to 2.686 Å in $\mathbf{TS}_{1-2}$ compared to 2.267 Å in **1**. The eventually formed Pt^{III} complex **2** is 16.4 kcal/mol higher in energy than the reactants **1** and SiH_4. This, and the high activation energy of 23.6 kcal/mol for the initial reaction step, seems to be the reason why no reaction is observed between **1** and $HSiMe_2Ph$.

Reaction of SiH_4 with cis-[PtMeCl(P∩N)] (3)

The activation energy required to form $\mathbf{TS}_{3-4}$ (22.7 kcal/mol; Figure 2) is similar to that for *trans*-[PtMeCl(P∩N)]. The formed Pt−Si bond in $\mathbf{TS}_{3-4}$ (2.736 Å) and the Pt−H bond (1.827 Å) are much longer than the bonds in the corresponding complex $\mathbf{TS}_{1-2}$ in the previous reaction. This means that the interaction of the SiH_4 molecule with the platinum center is weaker. This is also reflected in a shorter Pt−N bond length of 2.248 Å. The reaction of **3** with SiH_4 eventually results in the six-coordinate Pt^{III} complex **4**, releasing 13.1 kcal/mol. Complex **4**, with the silyl ligand *trans* to Cl, is lower in energy than isomer **1** with the silyl ligand *trans* to a methyl ligand.

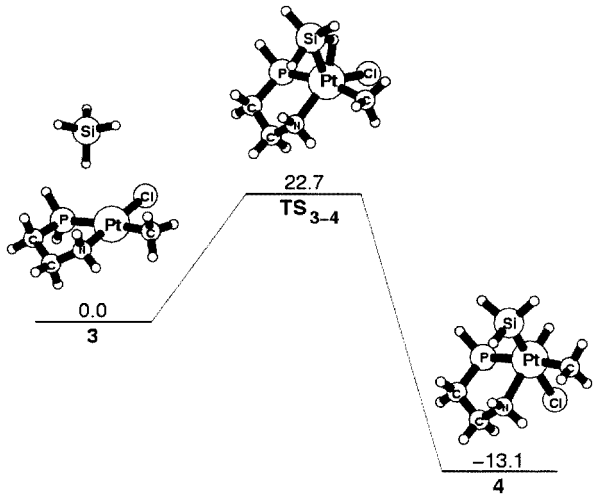

Figure 2. Reaction for the reaction of SiH_4 with **3**; energies in kcal/mol

It appears that the formation of *cis*-[PtMeCl(P∩N)] is necessary for the catalytic reaction to occur. The energy difference between the more stable *trans*-[PtMeCl(P∩N)] (**1**) and *cis*-[PtMeCl(P∩N)] (**3**) is 9.7 kcal/mol, which means that both isomers could be present in the equilibrium. This is in agreement with the fact that hydridosilanes do not react with [PtMeCl(P∩N)], since the activation energy for the reaction of the hydridosilane (22.7 kcal/mol) is quite high. However, when CCl_4 is present, a Cl/H exchange reaction can occur giving the catalytic cycle.

Catalytic Cycle

The mechanism of the Cl/H exchange reaction is examined in this section. The complete cycle was modeled in four steps as described in the following sections. In this part of the work, a much simpler model was used to describe the involved complexes — the *P,N*-chelating ligand was replaced by a PH_3 and an NH_3 ligand, and method II was used.

Oxidative Addition of SiH_4 to [PtMeCl(PH_3)(NH_3)] (5)

The starting point is the catalytic active complex **5** (Figure 3), which is analogous to the previously discussed *cis*-[PtMeCl(P∩N)] (**3**). Complex **5** reacts with SiH_4 to form the transition state $\mathbf{TS}_{5-6}$. The energy required is 24.5 kcal/mol. In $\mathbf{TS}_{5-6}$ a Pt−Si bond of 2.739 Å and a Pt−H bond of 1.822 Å are formed and, as a result, the Si−H bond is stretched to 1.601 Å. The Pt−N bond length is 2.248 Å, therefore the addition of SiH_4 to $\mathbf{TS}_{5-6}$ happens when the *P,N*-ligand is closed. The relaxation of $\mathbf{TS}_{5-6}$ leads to the octahedral Pt^{III} complex [Pt(Me)H(SiH_3)Cl(PH_3)(NH_3)] (**6**). Upon formation of the six-coordinate complex the Pt−Si and Pt−H bonds are shortened to 2.353 and 1.560 Å, respectively, while all other bonds are lengthened. This frees 35.5 kcal/mol, and therefore the energy of **6** is 11.0 kcal/mol lower than that of the starting compounds. Up to this point, the reaction profile is very similar to that discussed before (Figure 3), which shows that the simplification introduced by replacing the chelating $H_2NCH_2CH_2PH_2$ ligand by single NH_3 and PH_3 ligands does not affect the outcome of the calculations very much.

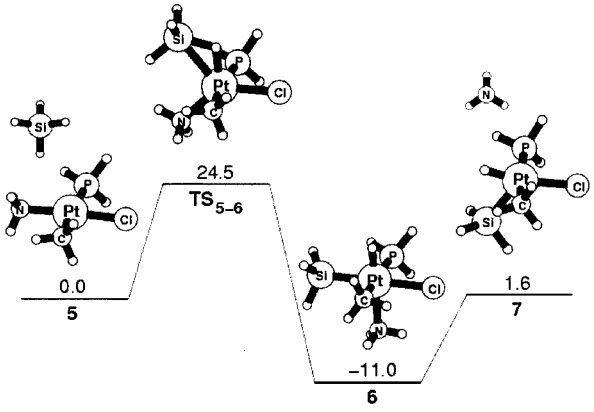

Figure 3. Reaction profile for the oxidative SiH_4 addition to **5**; energies in kcal/mol

The only way for **6** to undergo further reaction is by loss of the NH_3 ligand, which in the real system is the opening of the *P,N*-chelate. The relaxation of **6** after eliminating the NH_3 ligand leads to [Pt(Me)H(SiH_3)Cl(PH_3)] (**7**) which can be described as a distorted trigonal bipyramid. The formation of **7** from **6** is endothermic, and an energy of 12.6 kcal/mol is required for this process.

Reductive H_3SiCl Elimination from 7

The transition state $\mathbf{TS}_{7-8}$ (Figure 4) is formed from **7** by the reorientation of the SiH_3 group towards the chloro ligand, with concomitant increase of the Pt−Si bond length from 2.336 to 2.615 Å and that of the Pt−Cl bond from

 © 2004 Wiley-VCH Verlag GmbH & Co. KGaA, Weinheim

2.423 to 2.554 Å. The other bond lengths are shortened. The formation of a Si−Cl bond is observed, with a bond length of 2.303 Å in the transition state.

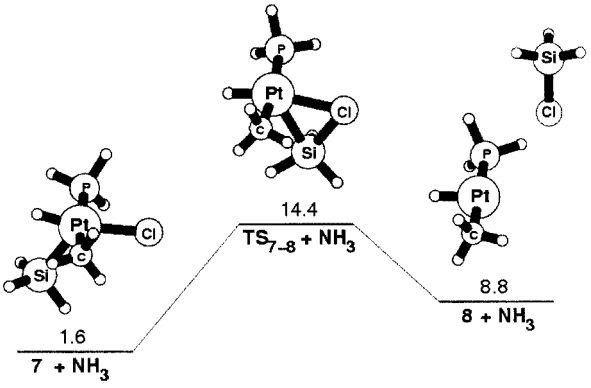

Figure 4. Reaction profile for the reductive H_3SiCl elimination from **7**; energies in kcal/mol

The three-coordinate complex [PtMeH(PH_3)] (**8**) is obtained by elimination of H_3SiCl from $\mathbf{TS}_{7-8}$. An energy of 7.2 kcal/mol is required to eliminate H_3SiCl from **7**. The hydrido ligand in the trigonal-planar complex **8** is *cis* to the phosphorus atom.

Oxidative CH_3Cl Addition to 8

In $\mathbf{TS}_{8-9}$, formed from the oxidative addition of CH_3Cl to **8** (Figure 5), the C−Cl bond is stretched from 1.806 Å in CH_3Cl to 2.284 Å and new Pt−C and Pt−Cl bonds develop (Pt−C: 2.575 Å; Pt−Cl: 2.501 Å). The Pt−P, Pt−C and Pt−H bond lengths are slightly lengthened. The formation of $\mathbf{TS}_{8-9}$ requires 24.9 kcal/mol, which is quite high. On the other hand the relaxation to [Pt(Cl)$Me_2H(PH_3)$] (**9**) frees 36.4 kcal/mol. The five-coordinate complex **9** is a result of the reorientation of the incoming CH_3 group.

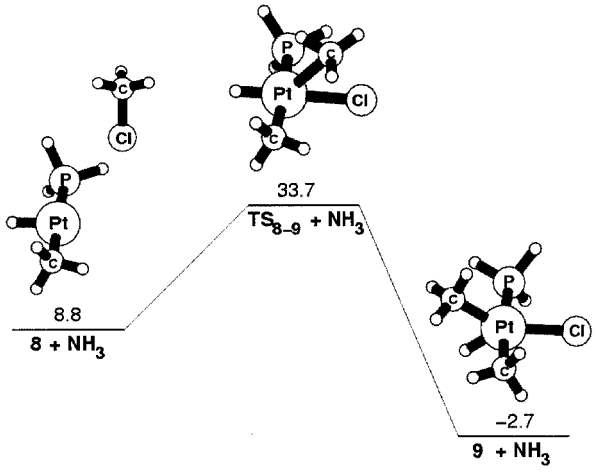

Figure 5. Reaction profile for the oxidative CH_3Cl addition to **8**; energies in kcal/mol

Reductive CH_4 Elimination from 9

The final step, the reductive CH_4 elimination, starts from the five-coordinate complex **9** (Figure 6). Only minor geometric changes are required to form $\mathbf{TS}_{9\text{-}10}$, where the new C−H bond is formed (1.552 Å). The related Pt−H and Pt−C bonds are stretched to 1.585 Å and 2.181 Å respectively. The Cl−Pt−H angle is opened from 139.9° to 153.1° and the Cl−Pt−C angle from 147.6° to 161.2°. An energy of 2.5 kcal/mol is freed by dissociating the CH_4 molecule and, as a result, the three-coordinate complex [PtMeCl(PH_3)] (**10**) is formed.

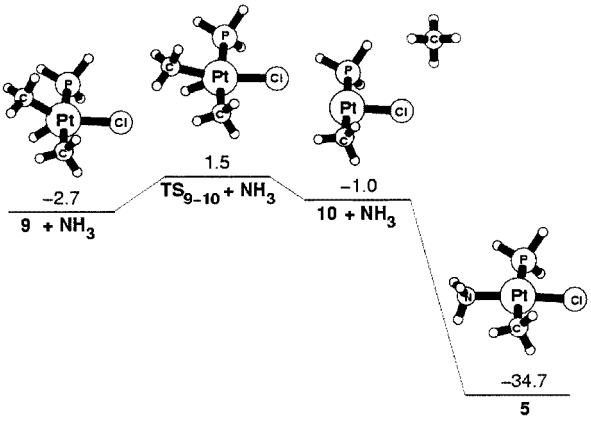

Figure 6. Reaction profile for the reductive CH_4 elimination from **9**; energies in kcal/mol

To close the catalytic cycle, the re-coordination of the NH_3 group is needed (representing the closing of the *P,N*-ligand in the real system). This frees 33.7 kcal/mol and results in the re-formation of the four-coordinate complex **5**, which is the starting point of the catalytic cycle.

Conclusions

Since no intermediates were observed in the [PtMeCl(P∩N)]-catalyzed C−Cl/Si−H exchange between H_xCCl_{4-x} and $HSiMe_2Ph$,[1] theoretical calculations were carried out to elucidate the reaction mechanism and the stereochemistry of the intermediates. Based on these calculations, the mechanism shown in Scheme 1 is proposed, which largely corresponds to our initial suggestion.[1]

The formation of *cis*-[PtMeCl(P∩N)] (**3**) is obviously necessary for the catalytic reaction to occur. This isomer is 9.7 kcal/mol less stable than *trans*-[PtMeCl(P∩N)] (**1**), but its reaction with SiH_4 turns out to be energetically more favorable. The oxidative addition of SiH_4 results in an octahedral Pt^{III} complex, therefore it is not necessary for the NH_3 ligand (corresponding to the amino group of the *P,N*-chelating ligand in the real system) to be eliminated for the reaction to occur. De-coordination of the amino group only occurs after the addition of the silane, and all the subsequent steps in the catalytic cycle — elimination of SiH_3Cl, addition of CH_3Cl and elimination of CH_4 — proceed via three- or five-coordinate complexes. The amino group is re-

 © 2004 Wiley-VCH Verlag GmbH & Co. KGaA, Weinheim

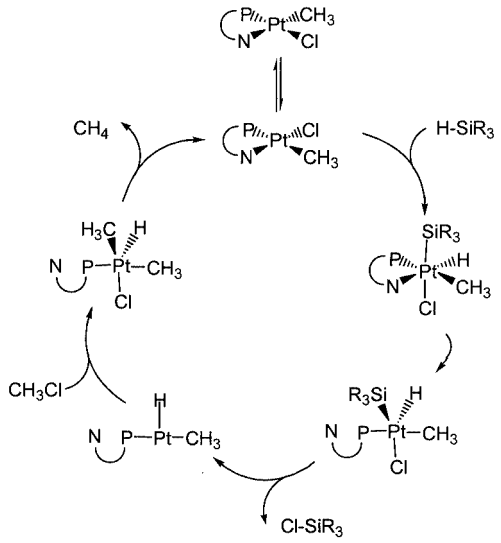

Scheme 1

coordinated in the final step, where the starting complex *cis*-[PtMeCl(P∩N)] (**3**) is regenerated.

The methyl group stays *trans* to phosphorus during the whole reaction. This is obviously a particularly favorable orientation of the ligands, since five-coordinate intermediates with analogous geometries have also been found in the reaction of [$PtMe_2$(P∩N)] and [$Pt(SiH_3)$Me(P∩N)] with chlorinated hydrocarbons and chlorosilanes.[5]

A final point to be made is the importance of the hydrido-methyl intermediate **8**. We have recently postulated such an intermediate, based on spectroscopic evidence, in the reaction of [$PtMe_2$(P∩N)] with $HSiEt_3$ and $HSiMePh_2$. In the first step of this reaction [PtMeH(P∩N)] and Me-SiR_3 are formed; the hydrido-methyl complex may react with a second molecule of silane to give [$Pt(SiR_3)$-Me(P∩N)] and H_2.[6]

Computational Details

The geometry optimizations of the equilibrium geometries and transition structures were performed using the B3LYP version of DFT, which is comprised of Becke's hybrid three-parameter exchange functional and the correlation functional of Lee, Yang and Parr.[7,8] The relativistic effective core potential and basis set of Preuss and co-workers (which is available in the Gaussian 98 software package as the SDD basis set) was used in Methods I and II for platinum.[9] In Method I, the 6-311G++(d) basis set was used for all atoms, except platinum. In Method II, the 6-31G++(d) basis set was used for all atoms, except platinum. Vibrational mode analyses were carried out to confirm that optimized geometries on the potential-energy surfaces correspond to a local minimum without an imaginary frequency mode, or a saddle point with only one imaginary mode. Corrections for zero-point vibrational energies were taken into account in the stationary structures obtained. All the calculations were carried out with the Gaussian 98 package.[10]

Acknowledgments

This work was supported by the Fonds zur Förderung der wissenschaftlichen Forschung (FWF).

[1] F. Stöhr, D. Sturmayr, U. Schubert, *Chem. Commun.* **2002**, 2222.
[2] M. Aizenberg, D. Milstein, *Science* **1994**, *265*, 359.
[3] D. Sturmayr, U. Schubert, *Monatsh. Chem.* **2003**, *134*, 791.
[4] F. Stöhr, D. Sturmayr, G. Kickelbick, U. Schubert, *Eur. J. Inorg. Chem.* **2002**, 2305.
[5] D. Sturmayr, U. Schubert, *Eur. J. Inorg. Chem.* **2004**, in press.
[6] S. M. Thompson, F. Stöhr, D. Sturmayr, G. Kickelbick, U. Schubert, *J. Organomet. Chem.* **2003**, *686*, 183.
[7] A. D. Becke, *J. Chem. Phys.* **1993**, *18*, 5648.
[8] C. Lee, W. Yang, R. G. Parr, *Phys. Rev. B* **1988**, *37*, 785.
[9] D. Andrae, U. Haeussermann, M. Dolg, H. Stoll, H. Preuss, *Theor. Chim. Acta* **1990**, *123*, 123.
[10] M. J. Frisch, G. W. Trucks, H. B. Schlegel, G. E.Scuseria, M. A. Robb, J. R. Cheeseman, V. G. Zakrzewski, J. A. Montgomery, R. E. Stratmann, J. C. Burant, S. Dapprich, J. M. Millam, A. D. Daniels, K. N. Kudin, M. C. Strain, O. Farkas, J. Tomasi, V. Barone, M. Cossi, R. Cammi, B. Mennucci, C. Pomelli, C. Adamo, S. Clifford, J. Ochterski, G. A. Petersson, P. Y. Ayala, Q. Cui, K. Morokuma, D. K. Malick, A. D. Rabuck, K. Raghavachari, J. B. Foresman, J. Cioslowski, J. V. Ortiz, B. B. Stefanov, G. Liu, A. Liashenko, P. Piskorz, I. Komaromi, R. Gomperts, R. L. Martin, D. J. Fox, T. Keith, M. A. Al-Laham, C. Y. Peng, A. Nanayakkara, C. Gonzalez, M. Challacombe, P. M. W. Gill, B. Johnson, W. Chen, M. W. Wong, J. L. Andres, C. Gonzalez, M. Head-Gordon, E. S. Replogle, J. A. Pople, Gaussian, Inc., Pittsburgh, PA, **1998**.

Received January 16, 2004
Early View Article
Published Online May 6, 2004

 © 2004 Wiley-VCH Verlag GmbH & Co. KGaA, Weinheim

Zinc Guanidinate Complexes and Their Application in Ring-Opening Polymerisation Catalysis

Martyn P. Coles*[a] and Peter B. Hitchcock[a]

Keywords: Guanidinate / N ligands / O ligands / Ring-opening polymerisation / Zinc

The insertion reaction between 1 equiv. of carbodiimide, R′N=C=NR′, and the zinc bis(amide) $[Zn\{N(SiMe_3)_2\}_2]$ affords the homoleptic zinc(II) guanidinate compounds $[Zn\{(Me_3Si)_2NC(NR')_2\}_2]$ (**3**, R′ = *i*Pr; **4**, R′ = Cy) in preference to the monosubstituted compounds. Compound **3** also results from the protonation reaction of 1 equiv. of the neutral guanidine $(Me_3Si)_2NC(NiPr)(NHiPr)$ (**2**) with $[Zn\{N(SiMe_3)_2\}_2]$ or $ZnMe_2$. In contrast, the *N*-dimethylguanidine analogue $Me_2NC(NiPr)(NHiPr)$ (**1**) reacts cleanly with 1 equiv. of $ZnMe_2$ to afford the dimeric species $[Zn\{Me_2NC(NiPr)_2\}Me]_2$ (**5**). Attempted protonation of the Zn–C bond in **5** with 2,6-di-*tert*-butylphenol resulted in preferential reaction at the Zn–N bond and formation of the mixed (aryloxo)methyl complex $[Zn(OAr)Me{\cdot}\{Me_2NC(NiPr)(NHiPr)\}]$ (**6**), isolated as the guanidine adduct. Heating of **6**, in an attempt to promote methane elimination, afforded a small amount of the dimetallic complex $[\{Zn(OAr)\}_2(\mu\text{-}\{Me_2NC(NiPr)_2\})(\mu\text{-}NMe_2)]$ (**7**) as a result of the extrusion of NMe_2^- from the guanidine-based ligand. The amine-elimination reaction between $[Zn\{N(SiMe_3)_2\}_2]$ and 1 equiv. of 1,3,4,6,7,8-hexahydro-2*H*-pyrimido[1,2-*a*]pyrimidine (hppH) proceeds smoothly to afford the mixed (guanidinate)(amide) complex $[Zn(hpp)\{N(SiMe_3)_2\}]_2$ (**8**), which forms a dimer in the solid state. Crystal structures of compounds **3**–**8** are reported and a preliminary study of the activity of **8** in the ring-opening polymerisation of lactide is described.
(© Wiley-VCH Verlag GmbH & Co. KGaA, 69451 Weinheim, Germany, 2004

Introduction

There has been a great deal of recent interest in the metal-catalysed ring-opening polymerisation (ROP) of cyclic esters, in particular lactide (LA),[1] as benefits over polymers derived from petrochemical sources include the renewable source of feedstock and the biocompatibility of the resultant polyester material.[2] Well-defined metal catalysts have generally allowed a greater control over the selectivity of the polymerisation process to be achieved, and structure-activity correlation studies associated with the ancillary ligands have been the focus of many of the recent developments in this area. As a consequence, many novel metal alkoxide and amide species have been synthesised and shown to be active catalysts for this process, where monomer insertion into the metal−oxygen or metal−nitrogen bond initiates polymerisation, and propagation ideally occurs in a controlled fashion to furnish stereoregular polylactide (PLA).

Anionic, *N*,*N*′-chelating ligands have thus far proved to be one of the most promising classes of supporting group in metal-catalysed lactide polymerisation. In particular, the β-diketiminate anion,[3] in combination with a zinc centre containing a reactive Zn−X bond, has been pursued in this area, exhibiting varying degrees of activity and selectivity dependant on the nature of the X group (Figure 1).[4,5] In general, it has been found that compounds containing a Zn−OR group, especially when R is a small alkyl group such as isopropyl, are significantly more active than those containing the amide group $[N(SiMe_3)_2]^-$, most likely due to a sluggish insertion of the first monomer into the sterically crowded Zn−N linkage. A recent report has also noted that structurally related bis(phosphanyl)methyl complexes of zinc are also active for the ROP of lactide,[6] although in these cases no evidence of "living" behaviour was observed.

A related class of chelating *N*,*N*′-donor ligands that has received attention in this area is the amidinate anion, $[RC(NR')_2]^-$,[7,8] where the metallacycle formed upon complexation to a metal atom differs principally from β-diketiminate compounds in the number of constituent atoms (i.e. 4 vs. 5). A range of different metals have been investigated including Fe,[9] Sn,[10] and the lanthanides[11] where, as for the β-diketiminate complexes, the coordination sphere is usually completed by either alkoxide or amide substituents at which initial reaction with the monomer is considered to take place (Figure 2). A notable exception is the series of homoleptic lanthanide complexes $[Ln\{RC(NCy)_2\}_3]$ (R = Me, Ln = Nd, Gd, Yb; R = Ph, Ln = Nd, Yb),[12] which are reported to be highly active for the ROP of ε-caprolactone, presumably initiating at one of the M−N

[a] Department of Chemistry,
University of Sussex, Falmer, Brighton BN1 9QJ, UK
Fax: (internat.) + 44-1273-677196
E-mail: m.p.coles@sussex.ac.uk

 © 2004 Wiley-VCH Verlag GmbH & Co. KGaA, Weinheim **DOI: 10.1002/ejic.200400031**

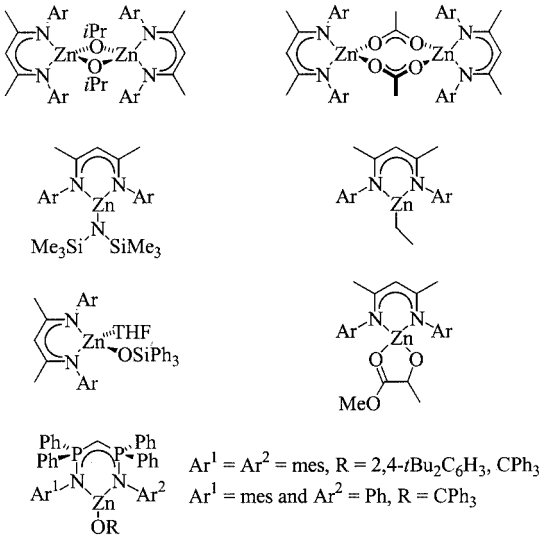

Figure 1. Zinc complexes, supported by β-diketiminate and related ligands, that are active for the ring-opening polymerisation of lactide

metal−amidinate bonds. Extension of this area to include the closely related guanidinate anions, $[R_2NC(NR'_2)]^-$,[13] has focussed mainly on the lanthanides, with catalytic activity observed with examples of both mono-,[14] and bis(ligand)[15] complexes (Figure 3).

Considering the potential for combining an active Zn−X (where X = alkoxide, amide) component with a supporting amidinate or guanidinate ligand set, it came as a surprise to us that no accounts have appeared on the investigation of zinc amidinate and guanidinate complexes as catalysts in this area. Indeed, very few amidine or amidinate complexes of zinc have been reported, with a few notable exceptions being the $[ZnBr_2L_2]$ adduct, where L = neutral *N*,*N*′-di-*p*-tolylformamidine,[16] and the bis(benzamidinate) complex $[Zn\{PhC(NSiMe_3)_2\}_2]$.[17] A report of the reaction between

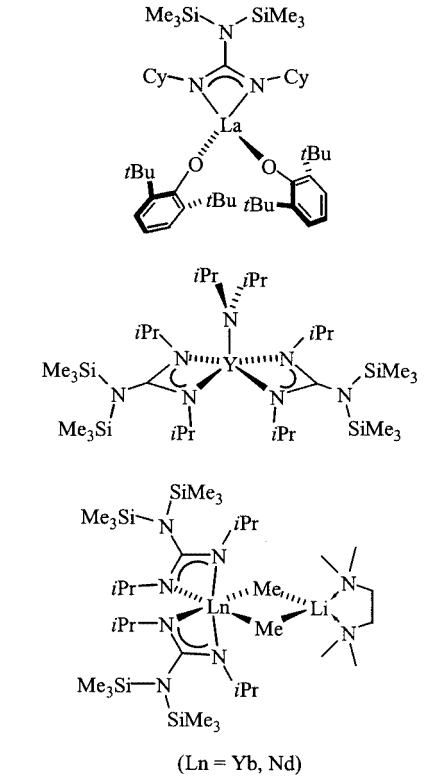

Figure 3. Metal complexes, supported by guanidinate ligands, that are active for ring-opening polymerisation

alkylzinc compounds and amidines to afford Zn(amidinate)$_2$ complexes appeared as unpublished results that, to the best of our knowledge, were never expounded upon.[7]

Recently, the synthesis of tolylformamidinate complexes of zinc was investigated, although the only products forthcoming from the study were cluster species incorporating oxygen.[18] Wheatley and co-workers have investigated mixed Zn/Li species containing *N*,*N*′-diphenylbenzamidin-

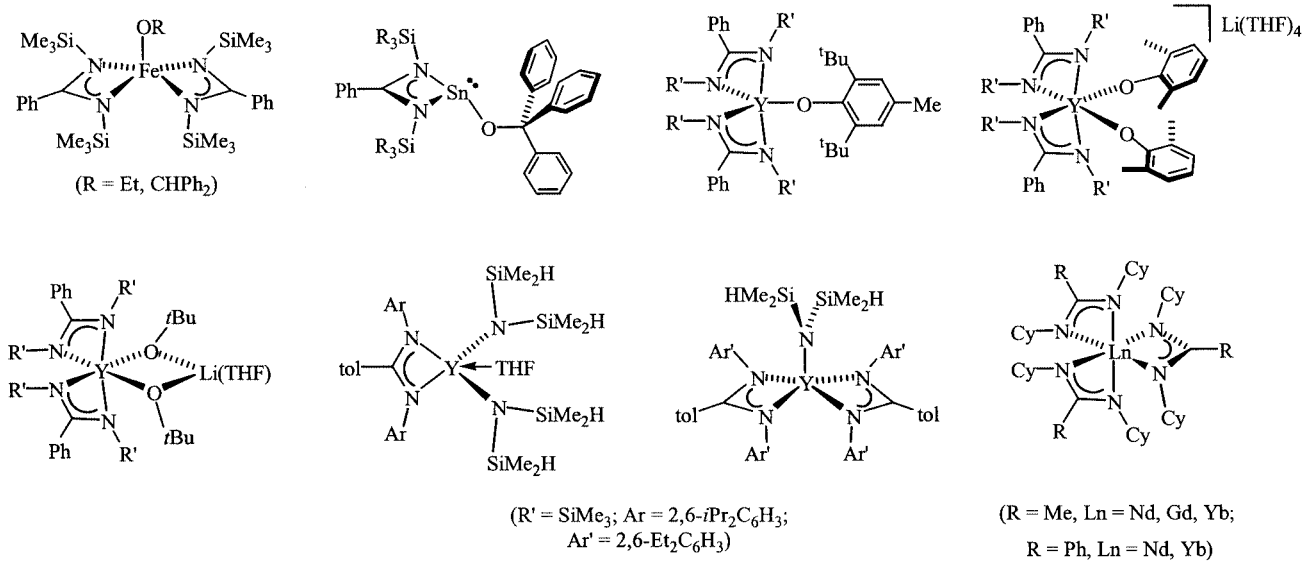

Figure 2. Metal complexes, supported by amidinate ligands, that are active for ring-opening polymerisation

 © 2004 Wiley-VCH Verlag GmbH & Co. KGaA, Weinheim

ate and reported the reactivity with dry oxygen gas to afford similar oligomeric structures.[19] In contrast, a recent review did not report any zinc complexes containing anionic guanidinate ligands in the literature.[13] During the course of our work, we have developed several areas of research based around amidinate[20] and guanidinate chemistry,[21,22] and wish to report the results from a study into the synthesis and catalytic application of guanidinate-containing zinc complexes.

Results and Discussion

An atom-efficient route that has been employed in the synthesis of metal guanidinate complexes is the insertion of a carbodiimide into an existing metal−amide bond,[14,23] first reported by Lappert and co-workers in 1970.[24] The stoichiometric reaction between R′N=C=NR′ (R′ = *i*Pr, Cy) and [Zn{N(SiMe$_3$)$_2$}$_2$] was therefore investigated as a potential route to mono(guanidinato)zinc−amide complexes (Scheme 1). However, after the appropriate workup, the only product isolated from the reaction for each of the carbodiimides investigated was the homoleptic, bis(guanidinate) complex [Zn{(Me$_3$Si)$_2$NC(NR′)$_2$}$_2$] (**3**, R′ = *i*Pr; **4**, R′ = Cy), resulting from insertion of a molecule of carbodiimide into *both* zinc−amide bonds. Compounds **3** and **4** can be purified by crystallisation from hexane at −30 °C affording colourless crystals in moderate yield. The molecular structures are illustrated in Figures 4 and 5, crystal data are summarised in the Exp. Sect. and selected bond lengths and angles in Table 1.

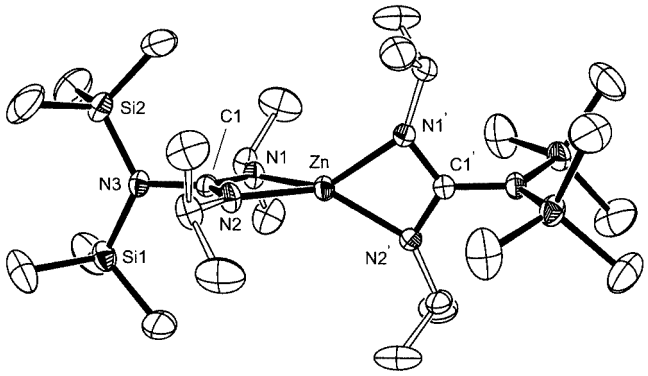

Figure 4. Molecular structure of [Zn{(Me$_3$Si)$_2$NC(N*i*Pr)$_2$}$_2$] (**3**) with thermal ellipsoids drawn at the 30% probability level; hydrogen atoms omitted for clarity

Compounds **3** and **4** are monomeric in the solid state, with the metal coordination sphere consisting of two η^2-guanidinate ligands in a "flattened" tetrahedral geometry. The angles at the metal atom are in the range 66.23(8)−139.32(13)° and 66.03(12)−135.93(12)° for **3** and **4**, respectively, where the lowest value is a consequence of the small bite angle of the ligand. The four-membered metallacycles are essentially planar (largest deviation: **3**, 0.015 Å; **4**, 0 Å) with an angle of 84.06° and 86.95° between the "ZnNCN" least-squares planes for **3** and **4**, respectively. The carbon−nitrogen distances are consistent with delocalisation across the "CN$_2$" fragment of the metallacycle, and the C−N(SiMe$_3$)$_2$ distances [**3**, 1.428(3) Å; **4**, 1.430(5) Å] and large angles between the "CN$_2$" and "NSi$_2$" moieties

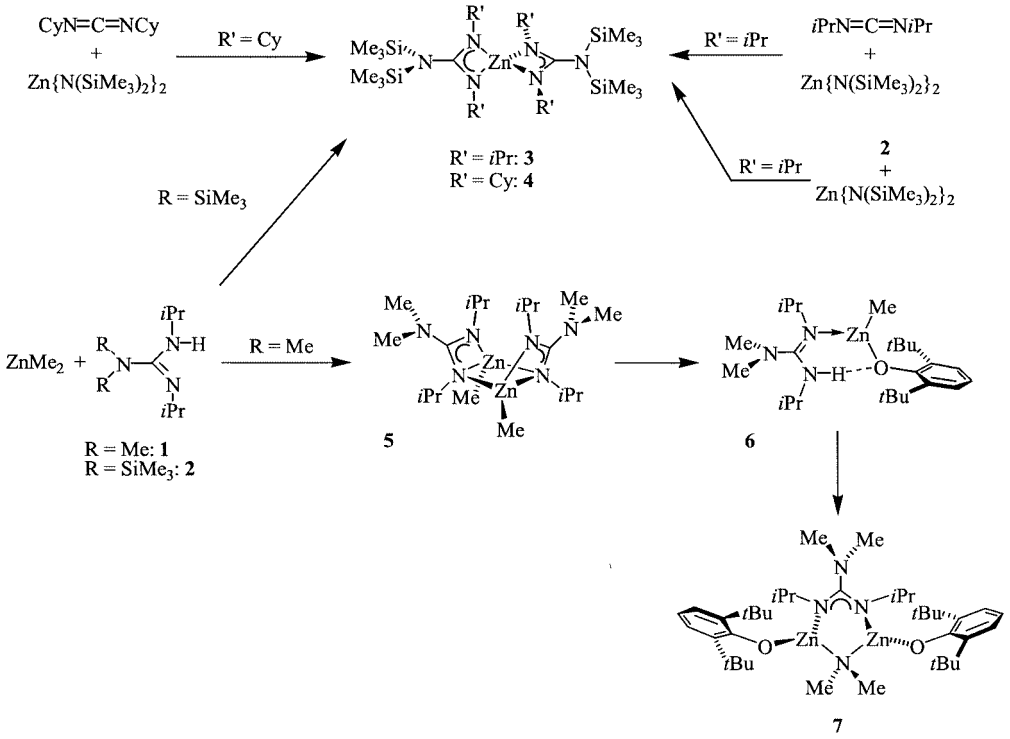

Scheme 1. Summary of the synthesis of zinc guanidinate complexes **3**−**7**

 © 2004 Wiley-VCH Verlag GmbH & Co. KGaA, Weinheim

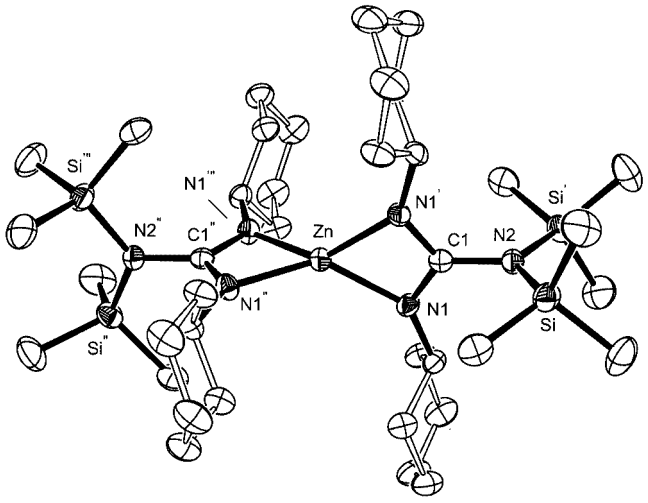

Figure 5. Molecular structure of $[Zn\{(Me_3Si)_2NC(NCy)_2\}_2]$ (**4**) with thermal ellipsoids drawn at the 30% probability level; hydrogen atoms omitted for clarity

Table 1. Selected bond lengths [Å] and angles [°] for **3** and **4**

	3[a]		
Zn−N(1)	2.011(2)	Zn−N(2)	2.021(2)
C(1)−N(1)	1.325(3)	N(3)−Si(1)	1.753(2)
C(1)−N(2)	1.326(3)	N(3)−Si(2)	1.752(2)
C(1)−N(3)	1.428(3)		
N(1)−Zn−N(2)	66.23(8)	N(1)−Zn−N(1′)	134.89(12)
N(1)−Zn−N(2′)	132.05(9)	N(2)−Zn−N(2′)	139.32(13)
N(1)−C(1)−N(2)	112.3(2)		
	4[b]		
Zn−N(1)	2.006(2)	C(1)−N(1)	1.322(3)
N(2)−Si	1.7590(15)	C(1)−N(2)	1.430(5)
N(1)−Zn−N(1′)	66.03(12)	N(1′)−Zn−N(1′′′)	135.93(12)
N(1)−Zn−N(1′′′)	133.45(13)	N(1)−C(1)−N(1′)	111.5(3)

[a] Symmetry elements for **3**: $'\ -x+1, y, -z+1/2$. [b] Symmetry elements for **4**: $'\ -x+5/4, y, -z+1/4$; $''\ -x+5/4, -y+1/4, z$; $'''\ x, -y+1/4, -z+1/4$.

[**3**, 87.61°; **4**, 81.46°] are consistent with a single bond with possible N−Si π-interactions.[25]

An alternative approach to the targeted mono(guanidinate) complexes was subsequently investigated, namely the reaction between dimethylzinc and 1 equiv. of the (neutral) guanidine, predicted to proceed by protonolysis of the zinc−carbon linkage. The ligand precursors, $[R_2NC\{NR'\}\{NHR'\}]$, were prepared from the reaction between the lithium diamide $LiNR_2$ (R = $SiMe_3$, Me) and *i*PrN=C=N*i*Pr, followed by quenching of the intermediate lithium salt with a stoichiometric amount of water, to afford $[Me_2NC(N{i}Pr)(NH{i}Pr)]$ (**1**) and $[(Me_3Si)_2NC(N{i}Pr)(NH{i}Pr)]$ (**2**).[26] The compounds were isolated as colourless and yellow liquids, respectively, and were used without further purification. The reaction between **2** and $[Zn\{N(SiMe_3)_2\}_2]$ or $ZnMe_2$ in a 1:1 ratio did not proceed to the mono(ligand) complex, but afforded only the bis(guanidinate) species **3** after the appropriate workup (Scheme 1). In contrast, the reaction of the dimethylamino analogue **1** with $ZnMe_2$ afforded colourless crystals of **5** suitable for an X-ray diffraction study. The molecular structure is illustrated in Figure 6, crystal data are summarised in the Exp. Sect. and selected bond lengths and angles in Table 2.

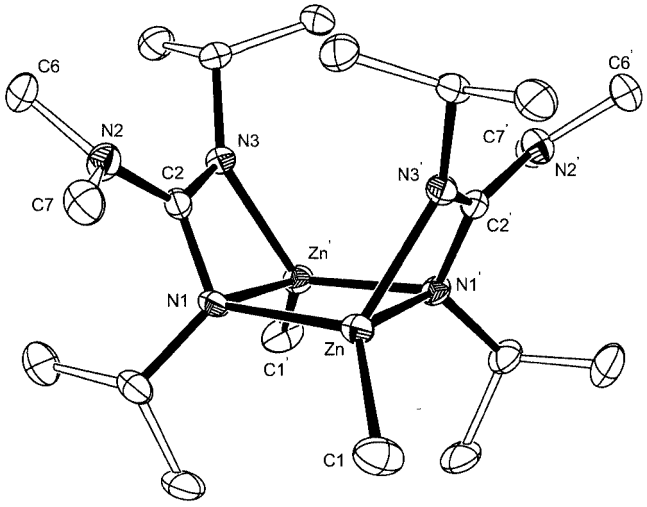

Figure 6. Molecular structure of $[Zn\{Me_2NC(N{i}Pr)_2\}Me]_2$ (**5**) with thermal ellipsoids drawn at the 30% probability level; hydrogen atoms omitted for clarity

Table 2. Selected bond lengths [Å] and angles [°] for **5** and **6**

	5[a]		
Zn−N(1)	2.101(3)	Zn−N(1′)	2.201(3)
Zn−N(3′)	2.063(3)	Zn−C(1)	1.987(5)
C(2)−N(1)	1.393(6)	N(2)−C(6)	1.462(6)
C(2)−N(3)	1.314(5)	N(2)−C(7)	1.461(6)
C(2)−N(2)	1.357(5)		
N(1′)−Zn−N(3′)	63.50(16)	N(1′)−Zn−N(1)	91.80(12)
N(1′)−Zn−C(1)	130.9(2)	N(3′)−Zn−C(1)	126.05(18)
N(3′)−Zn−N(1)	109.42(16)	N(1)−Zn−C(1)	119.74(19)
N(1)−C(2)−N(3)	112.2(4)		
	6		
Zn−O	1.9511(15)	Zn−C(24)	1.955(2)
Zn−N(1)	1.9952(18)	C(1)−N(1)	1.324(3)
C(1)−N(2)	1.353(3)	C(1)−N(3)	1.373(3)
O−C(10)	1.358(3)	H(2A)···O	2.83
O−Zn−C(24)	120.79(9)	O−Zn−N(1)	107.78(7)
N(1)−Zn−C(24)	131.30(9)	Zn−O−C(10)	110.96(12)
C(1)−N(1)−Zn	125.04(15)	C(2)−N(1)−Zn	114.34(13)
C(1)−N(1)−C(2)	119.45(18)	C(1)−N(3)−C(8)	123.0(2)
C(1)−N(3)−C(9)	121.6(2)	C(8)−N(3)−C(9)	115.1(2)

[a] Symmetry elements for **5**: $'\ -x, -y+1, z$.

Compound **5** crystallised as the dimeric compound $[Zn\{Me_2NC(N{i}Pr)_2\}Me]_2$, with a $\mu,\eta^2:\eta^1$-coordination mode of the guanidinate ligand, resulting in an essentially planar Zn_2N_2 ring (largest deviation from least-squares plane: 0.041 Å). Whilst this type of coordination has not previously been observed for monoanionic guanidinate ligands,[27] related tricyclic core structures have been reported

 © 2004 Wiley-VCH Verlag GmbH & Co. KGaA, Weinheim

for amidinate complexes of lithium,[28−30] magnesium[31] and iron,[32] and we have also observed this structural motif in a recently reported lithium phospha(III)guanidinate complex.[33] In contrast to the majority of these structures which contain crystallographic inversion symmetry, a non-centrosymmetric structure is observed for compound **5**, with a *syn* arrangement of the ligands about the central Zn_2N_2 ring.[29,31] The zinc atoms are present in a distorted tetrahedral geometry [angles in the range 63.50(16)−130.9(2)°], with the "ZnNCN" metallacycle at an angle of 66.19° to the central Zn_2N_2 plane. Examination of the Zn−N bond lengths in **5** suggests a strong association of the monomeric units in the solid state. Indeed, if we consider the dimer as consisting of two [Zn(guanidinate)-Me] fragments, based solely upon metal−nitrogen distances there is an apparent stronger interaction between the ligand of one unit and the metal of another [Zn−N(1) = 2.101(3) Å], than within the chelating guanidinate itself [Zn−N(1′) = 2.201(3) Å]. In all cases the Zn−N distances are significantly longer than in the homoleptic compounds **3** (av. 2.016 Å) and **4** (2.006 Å), despite a reduced angle between the NR_2 plane and the metallacycle in **5** (31.60°) that allows contribution from a zwitterionic resonance to the overall bonding.[25] In agreement with this postulate, the C(2)−N(2) bond length of **5** [1.357(5) Å] is intermediate between the value expected for C−N single and C=N double bonds, and is significantly shorter than the corresponding bonds in **3** [1.428(3) Å] and **4** [1.430(5) Å].

Transformation of the zinc−methyl group to a Zn−O linkage, desirable for applications in ROP, was attempted by reaction with 2,6-di-*tert*-butylphenol (Scheme 1). It was anticipated that the steric bulk of the alkyl substituents positioned about the resultant metal−oxygen bond would disfavour a bridging coordination mode for the aryloxide and promote a low aggregation within the final product. The reaction was performed at room temperature and after the appropriate workup colourless crystals of **6** were obtained. The molecular structure is illustrated in Figure 7, crystal data are summarised in the Exp. Sect. and selected bond lengths and angles in Table 2.

The molecular structure of **6** shows retention of the zinc−methyl group and incorporation of the aryloxide ligand in an overall monomeric, distorted trigonal planar zinc complex (Σ_{angles} at Zn: 359.57°). The coordination sphere of the zinc atom is completed by the *neutral* form of the guanidine ligand, $Me_2NC(NiPr)(NHiPr)$ (**1**), bonding through the N_{imino} atom,[34] such that the "CN_2" component is essentially coplanar with the ZnMeON metallacycle [max. deviation at C(1) 0.15 Å]. This arrangement is likely governed by the formation of an intramolecular hydrogen bond between the amino-NH and the aryloxide-O atoms [H(2a)···O 2.83 Å] which results in a widening of the angle between the N(1) and C(24) atoms at the zinc atom from the ideal trigonal planar angle to 131.30(9)°.

Despite coordinating as a neutral ligand in **6**, the Zn−N bond [1.9952(18) Å] is shorter than those observed in **5** (av. 2.12 Å) where it binds as an anionic ligand, reflecting the reduction in coordination number at the metal centre. This

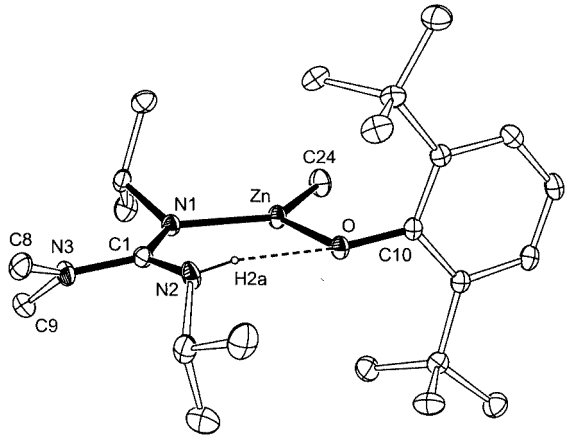

Figure 7. Molecular structure of [Zn(OAr)Me·{Me_2NC-(N*i*Pr)(NH*i*Pr)}] (**6**) with thermal ellipsoids drawn at the 30% probability level; hydrogen atoms, except H(2a), omitted for clarity

shortening may also be enhanced by the intramolecular H-bond noted above. The Zn−O bond [1.9511(15) Å] is relatively long in comparison to related three- and four-coordinate zinc complexes containing this and the similarly substituted 2,4,6-$tBu_3C_6H_2$ aryloxide groups [range: 1.818(1)−1.923(5) Å], and the angle at the oxygen atom [110.96(12)°] is by far the smallest observed [range: 124.04(14)−155.7(10)°].[35] These data suggest that there is a reduced π-donation from the oxygen to the zinc atom in **6** compared with the other examples cited, caused by the localisation of electron density in the hydrogen bond to the amino NH group.

The EI^+ mass spectrum of **6** indicates that, as predicted under these experimental conditions, dissociation of the guanidine occurs resulting in a signal at *m*/*z* (%)= 284 (72) equivalent to the "Zn(OAr)Me" fragment. Slightly more unexpected was the observation of a peak at *m*/*z* (%) = 439 (38) in the same spectrum, corresponding to the monomeric form of the target complex, "Zn{$Me_2NC(NiPr)_2$}(OAr)". This fragment must arise as a result of protonation of the methyl group by the NH functionality, with loss of methane, and prompted us to investigate the thermal stability of **6** in the expectation that, under the correct conditions, reactivity could be promoted at the Zn−C bond. Thus, a mixture of **5** and 1 equiv. of HOAr was heated in toluene, and the resultant solid crystallised from hexane at −30 °C, affording a small number of colourless crystals of **7** that were analysed by NMR spectroscopy and X-ray diffraction. The X-ray diffraction study was performed on representative crystals of **7** to determine the nature of the product; the molecular structure is illustrated in Figures 8 and 9, crystal data are summarised in the Exp. Sect. and selected bond lengths and angles in Table 3.

Compound **7** is a dimetallic zinc complex where the metal atoms are joined by bridging guanidinate and amide groups to generate a six-membered metallacycle. Each zinc atom is also bound by an aryloxide ligand, giving an overall distorted trigonal-planar geometry with the sum of the angles at Zn(1) and Zn(2) equal to 359.54° and 359.37°, respec-

 © 2004 Wiley-VCH Verlag GmbH & Co. KGaA, Weinheim

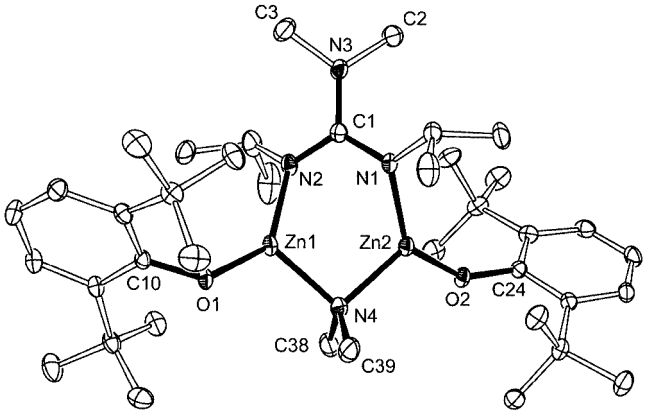

Figure 8. Molecular structure of $[\{Zn(OAr)\}_2(\mu\text{-}\{Me_2NC(NiPr)_2\})(\mu\text{-}NMe_2)]$ (**7**) with thermal ellipsoids drawn at the 20% probability level; hydrogen atoms omitted for clarity

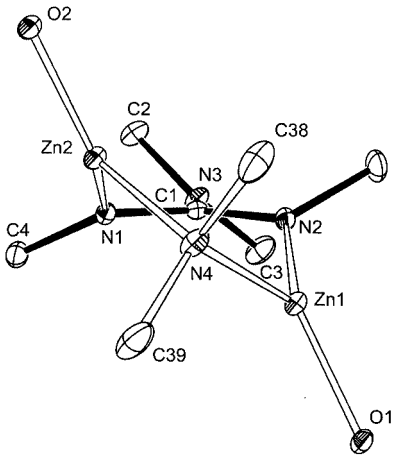

Figure 9. Core of $[\{Zn(OAr)\}_2(\mu\text{-}\{Me_2NC(NiPr)_2\})(\mu\text{-}NMe_2)]$ (**7**) along the approximate N(4)−C(1)−N(3) vector, illustrating the "half-chair" geometry of the metallacycle, and the distribution of the ligand substituents

tively. Overall, the metallacycle adopts a half-chair conformation (Figure 9) with a twist angle of 34.56° between the planes defined by Zn(1)−N(4)−Zn(2) and N(1)−C(1)−N(2). Both the guanidinate and amide bridge symmetrically between the two metal atoms.

Whilst a number of examples of bridging acyclic guanidinates have been reported between Pd, Fe and the s-block metals,[36] by far the most common coordination mode involves chelating to the metal atom,[13] rationalised in terms of the ligand donor orbital pointing towards the "mouth" of the ligand. The C−N distances within the guanidinate ligand (av. 1.35 Å) signify delocalisation of the R_2N lone pair into the core of the ligand, typically observed for this substitution pattern of nitrogen substituents. The average $Zn-N_{amide}$ distance in **7** (1.963 Å) is shorter than that found to the bridging amide group in the homoleptic series $[Zn(NR_2)(\mu\text{-}NR_2)]_2$ (R = Ph,[37] 2.03 Å; R = CH_2Ph,[38] 2.04 Å; R = CH_2iPr,[39] 2.03 Å], a possible consequence of the greater electron-withdrawing ability of the ArO^- ligand. The Zn−O bond lengths (av. 1.843 Å) are within the range

Table 3. Selected bond lengths [Å] and angles [°] for **7** and **8**

7			
Zn(1)−N(2)	1.950(3)	Zn(2)−N(1)	1.946(3)
Zn(1)−O(1)	1.846(2)	Zn(2)−O(2)	1.840(2)
Zn(1)−N(4)	1.990(3)	Zn(2)−N(4)	1.982(3)
C(1)−N(1)	1.352(5)	C(1)−N(2)	1.336(5)
C(1)−N(3)	1.361(5)	N(4)−C(38)	1.470(6)
N(4)−C(39)	1.461(6)		
O(1)−Zn(1)−N(2)	135.79(12)	O(2)−Zn(2)−N(1)	134.73(12)
O(1)−Zn(1)−N(4)	111.24(12)	O(2)−Zn(2)−N(4)	111.50(13)
N(2)−Zn(1)−N(4)	112.51(13)	N(1)−Zn(2)−N(4)	113.14(13)
N(1)−C(1)−N(2)	119.3(3)		
8[a]			
Zn−N(1)	2.1879(18)	Zn−N(2)	2.0486(19)
Zn−N(1′)	2.0831(19)	Zn−N(4)	1.9177(18)
C(1)−N(1)	1.380(3)	N(4)−Si(1)	1.707(2)
C(1)−N(2)	1.318(3)	N(4)−Si(2)	1.702(2)
C(1)−N(3)	1.349(3)		
N(1)−Zn−N(2)	64.20(7)	N(1)−Zn−N(1′)	92.88(7)
N(1)−Zn−N(4)	131.93(8)	N(2)−Zn−N(4)	125.11(8)
N(2)−Zn−N(1′)	104.61(7)	N(1′)−Zn−N(4)	122.41(8)
Zn−N(1)−Zn′	87.12(7)	N(1)−C(1)−N(2)	113.37(19)

[a] Symmetry elements for **8**: ′ $-x + 1, -y, -z + 1$.

associated with this substituent (vide supra), although the angle at the oxygen atom varies significantly between the two ligands [Zn(1)−O(1)−C(10) 130.0(2)°, Zn(2)−O(2)−C(24) 140.9(2)°] indicating the "soft" character of this angle.

Recently, we[21,22] and others[25,40] have utilised the commercially available bicyclic guanidine 1,3,4,6,7,8-hexahydro-2*H*-pyrimido[1,2-*a*]pyrimidine (hppH) as a ligand precursor in the coordination chemistry of transition-metal and main-group complexes. The major difference of this system in comparison with acyclic guanidinates is that the constraint of the amide substituent and the amidine "CN_2" components of the molecule in the cyclic framework is predicted to enhance electron donation to a metal centre by increasing the contribution to the overall bonding from a zwitterionic resonance form. A potential complication in the application of the anionic ligand $[hpp]^-$ in molecular catalysis that arises from the bicyclic nature of the ligand is the propensity to adopt a bridging coordination mode to different metal centres, extensively exploited by Cotton and others in the support of many dimetallic systems.[30,41] Indeed, we have observed that the stoichiometric reaction between neutral hppH and $ZnMe_2$ affords the fully characterised, trimetallic complex $[Zn_3(hpp)_4Me_2]$ containing both two-coordinate $[\mu\text{-hpp}]^-$ and three-coordinate $[\kappa^{1,2}N\text{-}\kappa^3N'\text{-hpp}]^-$ bonding modes; this will be described fully in a forthcoming publication.[42]

In contrast to the reactions between acyclic guanidines and $[Zn\{N(SiMe_3)_2\}_2]$, the reaction with hppH proceeds smoothly at room temperature to afford the mono(guanidinate) species $[Zn(hpp)\{N(SiMe_3)_2\}]_n$ (**8**) in excellent yield. Low-temperature (−30 °C) crystallisation from a concentrated hexane solution affords colourless crystals suitable

 © 2004 Wiley-VCH Verlag GmbH & Co. KGaA, Weinheim

for an X-ray diffraction study. The molecular structure is illustrated in Figure 10, crystal data are summarised in the Exp. Sect. and selected bond lengths and angles in Table 3.

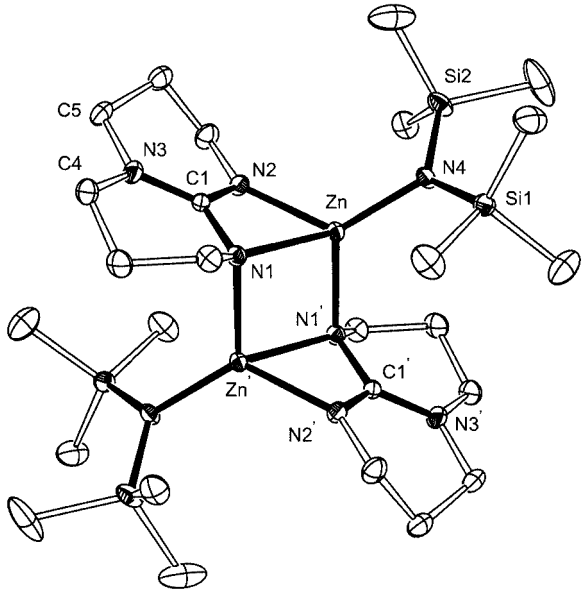

Figure 10. Molecular structure of $[Zn(hpp)\{N(SiMe_3)_2\}]_2$ (**8**) with thermal ellipsoids drawn at the 30% probability level; hydrogen atoms omitted for clarity

Compound **8** crystallised as the dimeric compound $[Zn(hpp)\{N(SiMe_3)_2\}]_2$, with a previously unreported $\mu,\eta^2:\eta^1$-coordination mode for the $[hpp]^-$ anion. Unlike the molecular structure of **5**, complex **8** exists as a centrosymmetric dimer with an *anti* arrangement of ligands about the central Zn_2N_2 metallacycle, a likely consequence of the different steric requirements of the ligands at the zinc centre. The Zn_2N_2 core of the molecule is perfectly planar and forms an angle of 72.9° to the essentially planar ZnN_2C metallacycle (largest deviation from least-squares plane 0.075 Å). The resultant geometry at the zinc centre is therefore best described as distorted tetrahedral with bond angles in the range 64.20(7)° (corresponding to the bite angle of the ligand) to 131.93(8)°.

As in **5**, a strong interaction between the two "monomeric" $[Zn(hpp)\{N(SiMe_3)_2\}]$ units is indicated by the shorter Zn−N(1′) distance [2.0831(19) Å] compared with Zn−N(1) [2.1879(18) Å]. The remaining Zn−N bond of the chelating $[hpp]^-$ anion is shorter [2.0486(19) Å], a probable combination of increased electron donation from $[hpp]^-$ [angle between N(1)−C(1)−N(2) and C(4)−N(3)−C(5) planes 4.57°] and a more electron-deficient zinc atom arising from the presence of the amide vs. the methyl substituent. The $Zn-N_{amide}$ distance [1.9177(18) Å] is slightly longer than the value in related, three-coordinate β-diketiminate[43] and (imine)(oxazoline)[44] zinc amides [1.896(2) and 1.883(3) Å, respectively], which may reflect a weaker bond, more reactive to ROP.

Preliminary NMR investigations of the catalytic activity of **8** towards the ring-opening of D,L-lactide (LA) was performed in CD_2Cl_2 and $[D_8]$toluene. In contrast to many zinc complexes incorporating the relatively bulky $N(SiMe_3)_2$ group, where initiation is reported as being slow,[4] the immediate reaction of **8** to generate a new species (> 98% in ca. 2 min) was observed, as judged by a shift of the $N(Si\mathit{Me}_3)_2$ resonance from δ = −0.02 ppm to δ = 0.05 ppm (CD_2Cl_2). The progress of the reaction was monitored by ^1H NMR spectroscopy, clearly indicating that 45−85 equiv. of LA were polymerised to polylactide (PLA) with more than 95% conversion in less than 2 h. Assuming the rate of initiation is much greater than the rate of propagation, leading to all zinc centres being activated prior to further insertion of monomer, integration of the $N(Si\mathit{Me}_3)_2$ end-group signal versus either the methine or methyl resonances of the growing polymer chain will allow an approximate value of the molecular weight to be calculated. From the ^1H NMR spectra of the polymerisation reactions performed with **8**, this appeared to be a reasonable approximation (vide supra), and a graph of molecular weight vs. conversion was therefore plotted (Figure 11). The straight-line relationships generated for different monomer concentrations and solvents present good evidence that the polymerisation proceeds in a "well-behaved" fashion. In addition, after 18 h at room temperature, a sample of **8** and LA (45 equiv.) that had progressed to more than 98% conversion was able to initiate the polymerisation of a further 50 equiv. of LA in CD_2Cl_2. The fresh monomer was converted into PLA over a period of 2 h, demonstrating the stability of the propagating species over time and providing further indication of the controlled nature of the polymerisation. There was no evidence for a tacticity bias in the ^1H NMR spectrum of the PLA produced by **8**, as indicated by selective decoupling of the methine protons.

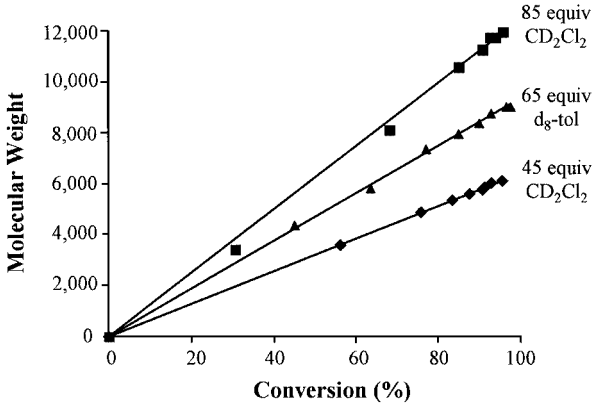

Figure 11. Plot of molecular weight vs. monomer conversion (determined by ^1H NMR spectroscopy) for the polymerisation of LA with **8**

Conclusion

We have demonstrated that the synthesis of mono(guanidinate) complexes of zinc is beleaguered with difficulties,

 © 2004 Wiley-VCH Verlag GmbH & Co. KGaA, Weinheim

and the nature of the product can be highly dependant on the synthetic protocol employed and substitution pattern of the nitrogen groups contained within the ligand precursor. Initial attempts at formation of the mono(ligand) amide only afforded the homoleptic Zn^{II} guanidinate products **3** and **4** under a variety of conditions. Assuming a stepwise reaction pathway is in operation, proceeding by initial formation of one guanidinate anion at the metal atom, this mono(ligand) product evidently activates the metal−amide bond to further insertion relative to the Zn−N bond of the bis(amide) starting material.

An interesting contrast was noted in the protonation reactivity between $ZnMe_2$ and the neutral diisopropylguanidines $R_2NC(NiPr)(NHiPr)$ (R = $SiMe_3$ and Me), where a similar steric environment at the metal atom is anticipated as the metal-bound nitrogen atoms are substituted by isopropyl groups in each instance. Changing the nitrogen substituents of the NR_2 moiety from trimethylsilyl to methyl, however, arrested multiple protonation of the dialkylzinc and provided a clean and efficient route to the first example of a mono(guanidinate) compound **5** of zinc. It has been previously demonstrated in guanidinate chemistry of aluminium that, despite being remote from the metal centre, the nature of the R substituents can strongly influence the distribution of electron density within the $[R_2NC\{NR'\}_2]^-$ anion and the potential therefore exists to "tune" the reactivity of the metal centre.[25] In general, the larger, more electron-withdrawing silyl substituents will reduce the extent of electron donation through the $N_{amino}-C$ bond by disfavouring delocalisation of the N_{amino} lone-pair into the framework of the ligand. The smaller, electron-donating methyl groups, however, allow the NR_2 and CN_2 components of the ligand to approach coplanarity, thus providing the correct orbital alignment for interaction between the nitrogen lone-pair and the empty p-orbital of the sp^2-carbon atom. The result is the potential for greater electron donation for the anion derived from **1** compared with **2**, which is apparently sufficient to prevent activation of the zinc−methyl bond to further protonation in compound **5**. It is curious to note that in **5**, the usually highly reactive $Zn-CH_3$ bond is even resistant to protonation from a bulky phenol derivative and that the acidic proton preferentially reacts at one of the Zn−N bonds of the guanidinate, affording the mixed methyl(aryloxide) compound **6**.

The molecular structure of **6** confirms retention of the neutral ligand at the zinc centre and reveals an intramolecular hydrogen bond to the aryloxide-O atom. Comparison of the Zn−O bond with other examples of compounds containing the same ligand indicates that the bond in **6** is exceptionally long and angular. This is in agreement with the oxygen lone-pairs participating in the hydrogen bond to the NH group, with the result being consistent with a lower Zn−O bond order than noted in previous examples of zinc complexes incorporating this ligand.

Attempts to promote methane elimination by heating a mixture of **5** and ArOH met with partial success. Loss of the zinc−methyl group was achieved with concomitant conversion of the neutral guanidine ligand to the anionic guanidinate and retention of the aryloxide substituent. However, the guanidinate ligand was found to be unstable under the conditions employed, as indicated by the isolation of a small amount of the dimetallic species $[\{Zn(OAr)\}_2(\mu\text{-}\{Me_2NC(NiPr)_2\})(\mu\text{-}NMe_2)]$ (**7**), formed by amide extrusion from the guanidine or guanidinate ligand. As this product was only isolated in low yield, and as such may represent only a minor component of the product mixture, detailed mechanistic studies into its formation were not carried out. However further work in this area is merited due to the possible implications that such a process has in metal-catalysed guanylation of amines and transamination of guanidines,[45] and C=N metathesis of carbodiimides.[46]

Building on the observation that the introduction of a more electron-donating guanidinate ligand caused multiple protonation at the metal centre to be effectively "shut down" during the synthesis of **5**, we turned our attention to the potentially more strongly electron-donating anion $[hpp]^-$. It has been shown that constraining the NR_2 and CN_2 components in the bicyclic framework of this compound promotes an increased contribution from a zwitterionic resonance form, manifested in shorter Ti−N distances in a series of titanium compounds incorporating the $[hpp]^-$ anion in comparison to acyclic amidinates and guanidinates.[21] Thus, synthesis of $[Zn(hpp)\{N(SiMe_3)_2\}]_2$ (**8**), containing the desired combination of a supporting ancillary guanidinate and reactive zinc−amide bond, was achieved. Compound **8** was found to be active in the small-scale polymerisation of lactide and analysis of the NMR spectroscopic data indicated a well-behaved system.

Overall we have therefore exploited the observation that, in order to prevent the formation of homoleptic Zn^{II} guanidinate compounds, more electron-donating guanidinate anions must be employed. Eventually, the correct combination of ligands was found in **8** and we proved the concept that this compound is an active catalyst for the well-behaved ROP of lactide. The application of **8** in the polymerisation of related monomers and an in-depth study of the structure of the polymeric material will be published in due course.

Experimental Section

General Remarks: All manipulations were carried out under dry nitrogen using standard Schlenk and cannula techniques, or in a conventional nitrogen-filled glovebox operating at < 1 ppm oxygen. Solvents were dried with appropriate drying agents, degassed, and stored over a potassium mirror or activated molecular sieves prior to use. R′N=C=NR′ (R′ = *i*Pr, Cy; Aldrich), $LiNMe_2$ (Fluka), $LiN(SiMe_3)_2$ (Aldrich) and $ZnMe_2$ (ca. 2 M solution in toluene; Fluka) were obtained commercially and used as received, unless stated otherwise. The compound $[Zn\{N(SiMe_3)_2\}_2]$ was synthesised from the reaction between $ZnBr_2$ and 2 equiv. of $LiN(SiMe_3)_2$. The crude product was extracted into hexane and used without further purification. Elemental analyses were performed by S. Boyer at The University of North London. NMR spectra were recorded with a Bruker Avance DPX 300 MHz spectrometer. Coupling constants are quoted in Hertz.

 © 2004 Wiley-VCH Verlag GmbH & Co. KGaA, Weinheim

$Me_2NC(NiPr)(NHiPr)$ (1): A slurry of lithium dimethylamide (5.00 g, 98.00 mmol) in Et_2O (100 mL) was cooled to 0 °C and a solution of diisopropylcarbodiimide (12.40 g, 98.00 mmol) in Et_2O (50 mL) was added dropwise with a cannula. The mixture was allowed to warm to room temperature to afford a cloudy yellow solution, that was stirred for a further 14 h under ambient conditions. Degassed water (1.8 mL, 100.00 mmol) was subsequently added dropwise with a syringe causing the formation of a clear yellow solution and a white precipitate. The mixture was filtered through Celite and the volatiles were removed to afford a pale-yellow liquid that was used without further purification. Yield: 11.75 g (70%). ^{1}H NMR ($CDCl_3$, 298 K): δ = 3.37 (sept, $^3J_{H,H}$ = 6.4, 1 H, C*H*Me$_2$), 3.25 (sept, $^3J_{H,H}$ = 6.3, 1 H, C*H*Me$_2$), 2.67 (s, 6 H, N*Me$_2$*), 1.03 (d, $^3J_{H,H}$ = 6.3, 6 H, CH*Me$_2$*), 1.02 (d, $^3J_{H,H}$ = 6.3, 6 H, CH*Me$_2$*) ppm; N*H* signal not observed. ^{13}C NMR ($CDCl_3$, 298 K): δ = 155.8 (*C*N$_3$), 47.3 (*C*HMe$_2$), 45.9 (*C*HMe$_2$), 39.0 (N*Me$_2$*), 25.1 (CH*Me$_2$*), 23.6 (CH*Me$_2$*) ppm.

$(Me_3Si)_2NC(NiPr)(NHiPr)$ (2): Compound **2** was synthesised using a similar procedure to that outlined for the synthesis of **1**, using lithium bis(trimethylsilyl)amide (2.50 g, 14.94 mmol), diisopropylcarbodiimide (1.89 g, 14.94 mmol) and water (0.27 g, 14.94 mmol). The compound was isolated as a colourless liquid and was used without further purification. Yield: 3.21 g (75%). ^{1}H NMR ($CDCl_3$, 298 K): δ = 3.79 (br. sept, $^3J_{H,H}$ = 6.0, 1 H, C*H*Me$_2$), 3.64 (br. sept, $^3J_{H,H}$ = 5.6, 1 H, C*H*Me$_2$), 1.08 (br. d, $^3J_{H,H}$ = 5.9, 6 H, CH*Me$_2$*), 1.04 (br. d, $^3J_{H,H}$ = 5.8, 6 H, CH*Me$_2$*), 1.15 (s, 18 H, Si*Me$_3$*) ppm; N*H* signal not observed. ^{13}C NMR ($CDCl_3$, 298 K): δ = 147.5 (*C*N$_3$), 47.3 (*C*HMe$_2$), 42.0 (*C*HMe$_2$), 24.9 (CH*Me$_2$*), 22.7 (CH*Me$_2$*), 1.6 (Si*Me$_3$*) ppm.

$[Zn\{(Me_3Si)_2NC(NiPr)_2\}_2]$ (3). Method 1: A solution of dimethylzinc (0.9 mL of a 2 M solution in toluene, 1.80 mmol) was further diluted with an additional 20 mL of toluene and cooled to −78 °C. A solution of **2** (0.50 g, 1.74 mmol) in toluene (40 mL) was added dropwise with a cannula and the resultant colourless solution was allowed to warm to room temperature and stirred for 14 h. The mixture was filtered and cooled to −30 °C to afford colourless crystals of $[Zn\{(Me_3Si)_2NC(NiPr)_2\}_2]$. Yield: 0.45 g (48%). $C_{26}H_{64}N_6Si_4Zn$ (638.56): calcd. C 48.91, H 10.10, N 13.16; found C 48.99, H 9.99, N 13.07. ^{1}H NMR (C_6D_6, 298 K): δ = 3.70 (sept, $^3J_{H,H}$ = 6.1, 4 H, C*H*Me$_2$), 1.17 (d, $^3J_{H,H}$ = 6.2, 24 H, CH*Me$_2$*), 0.30 (2, 36 H, Si*Me$_3$*) ppm. ^{13}C NMR (C_6D_6, 298 K): δ = 165.2 (*C*N$_3$), 44.7 (*C*HMe$_2$), 27.0 (CH*Me$_2$*), 2.3 (Si*Me$_3$*) ppm. MS (EI$^+$): *m*/*z* = 636 [M]$^+$, 621 [M − Me]$^+$. **Method 2:** A solution of **2** (0.37 g, 1.29 mmol) in toluene (20 mL) was added dropwise at room temperature to a toluene (25 mL) solution of $[Zn\{N(SiMe_3)_2\}_2]$ (0.50 g, 1.29 mmol) with a cannula. No visible change was observed. The reaction mixture was stirred at room temperature for 18 h, after which time the volatiles were removed to afford a sticky white solid. ^{1}H NMR spectra indicated a 1:1 mixture of **3** (identified from the chemical shift values in comparison with an authentic sample) and unchanged $[Zn\{N(SiMe_3)_2\}_2]$. No further purification was attempted.

$[Zn\{(Me_3Si)_2NC(NCy)_2\}_2]$ (4): A solution of CyN=C=NCy (0.27 g, 1.29 mmol) in toluene (25 mL) was added dropwise to a stirred solution of $[Zn\{N(SiMe_3)_2\}_2]$ (0.50 g, 1.29 mmol) in toluene (25 mL) at room temperature. No visible change was observed, and the resultant colourless solution was stirred at ambient conditions for 16 h. Removal of the volatiles in vacuo afforded crude **2** as a white solid that was crystallised from toluene at −30 °C as analytically pure colourless crystals. Yield: 0.32 g (62%) based on CyN=C=NCy. $C_{38}H_{80}N_6Si_4Zn$ (798.81): calcd. C 57.14, H 10.09, N 10.52; found C 57.05, H 10.09, N 10.56. ^{1}H NMR (C_6D_6, 298 K): δ = 3.37 (m, 4 H, *Cy*), 1.91−1.24 (m, 44 H, *Cy*), 0.33 (s, 36 H, Si*Me$_3$*) ppm.

An analogous reaction procedure using *i*PrN=C=N*i*Pr afforded a colourless crystalline material that analysed for **3**.

$[Zn\{Me_2NC(NiPr)_2\}Me]_2$ (5): A solution of **1** (1.00 g, 5.84 mmol) in toluene (30 mL) was added at room temperature to a solution of dimethylzinc (2.9 mL of a 2 M solution in toluene, 5.80 mmol) that had been further diluted by 50 mL of toluene. Evolution of a gas was observed and the resultant clear yellow solution was stirred under ambient conditions for 12 h. Removal of the volatiles afforded a pale-yellow solid that could be used without further purification. Analytically pure samples were obtained by crystallisation from hexane at −30 °C. Yield 0.98 g (67%). $C_{10}H_{23}N_3Zn$ (501.37): calcd. C 47.91, H 9.25, N 16.76; found C 47.73, H 9.37, N 16.86. ^{1}H NMR (C_6D_6, 298 K): δ = 3.41 (sept, $^3J_{H,H}$ = 6.1, 2 H, C*H*Me$_2$), 2.47 (s, 6 H, N*Me$_2$*), 1.12 (br. d, 12 H, CH*Me$_2$*), −0.12 (s, 3 H, Zn*Me*) ppm. ^{13}C NMR (C_6D_6, 298 K): δ = 166.5 (*C*N$_3$), 47.2 (*C*HMe$_2$), 40.0 (N*Me$_2$*), 25.7 (br., CH*Me$_2$*), −11.2 (Zn*Me*) ppm. MS (EI$^+$): *m*/*z* = 404 $[\{Me_2NC(NiPr)_2\}_2Zn]^+$, 360 $[\{Me_2NC(NiPr)_2\}_2Zn - NMe_2]^+$, 234 $[\{Me_2NC(NiPr)_2\}Zn]^+$.

$[Zn(OAr)Me{\cdot}\{Me_2NC(NiPr)(NHiPr)\}]$ (6): A solution of 2,6-di-*tert*-butylphenol (0.41 g, 2.00 mmol) in toluene (20 mL) was added dropwise at room temperature to a solution of **5** (0.50 g, 2.00 mmol) in toluene (30 mL). The resultant clear, pale-yellow solution was stirred at room temperature for 12 h, after which time the volatile component was removed in vacuo to afford a pale-yellow solid. Crystallisation from hexane afforded **6** as colourless crystals. Despite repeated crystallisations, a persistent, unidentified impurity was observed during the preparation of **6**. As such, accurate analysis was not obtained and the NMR spectroscopic data are reported for the major component, which corresponds to **6**. Yield: 0.43 g (46%) calculated for **6**. $C_{24}H_{45}N_3OZn$ (457.00): calcd. C 63.07, H 9.92, N 9.19; found C 56.74, H 9.39, N 6.73. ^{1}H NMR (C_6D_6, 298 K): δ = 7.46 (d, $^3J_{H,H}$ = 7.8, 2 H, *m*-C_6H_3), 6.92 (t, $^3J_{H,H}$ = 7.7, 1 H, *p*-C_6H_3), 3.29 (sept, $^3J_{H,H}$ = 6.5, 1 H, C*H*Me$_2$), 3.08 (br. sept, 1 H, C*H*Me$_2$), 2.19 (br. s, 6 H, N*Me$_2$*), 1.72 (s, 18 H, C*Me$_3$*), 1.17 (br. d, $^3J_{H,H}$ = 6.4, CH*Me$_2$*), 0.99 (br. d, $^3J_{H,H}$ = 6.0, CH*Me$_2$*), −0.33 (s, 3 H, Zn*Me*) ppm. ^{13}C NMR (C_6D_6, 298 K): δ = 165.7 (*C*N$_3$), 139.0 (*C*), 128.3 (*C*), 125.3 (*C*H), 115.9 (*C*H), 50.1 (br., *C*HMe$_2$), 45.6 (*C*HMe$_2$), 39.8 (N*Me$_2$*), 35.5 (*C*Me$_3$), 32.4 (C*Me$_3$*), 24.9 (CH*Me$_2$*), 22.7 (CH*Me$_2$*), −8.8 (Zn*Me*) ppm. IR (nujol mull, KBr): $\tilde{\nu}$ = 3234 (m), 3140 (m), 1596 (s), 1518 (s), 1404 (s), 1365 (s), 1349 (m), 1318 (m), 1254 (s), 1243 (s), 1198 (w), 1183 (w), 1171 (w), 1136 (w), 1122 (m), 1102 (m), 1064 (w), 1047 (m), 975 (w), 938 (w), 881 (w), 853 (m), 814 (m), 752 (s), 686 (m), 634 (w) cm^{-1}.

$[\{Zn(OAr)\}_2(\mu\text{-}\{Me_2NC(NiPr)_2\})(\mu\text{-}NMe_2)]$ (7): 2,6-Di-*tert*-butylphenol (0.41 g, 2.00 mmol) in toluene (20 mL) was added dropwise at room temperature to a solution of **5** (0.50 g, 2.00 mmol) in toluene (30 mL). The resultant clear, pale-yellow solution was heated at 75 °C for 3 d, after which time a clear colourless solution had formed. The volatiles were removed to afford a waxy solid that was redissolved in hexane. Cooling of this solution to −30 °C afforded a small number of colourless crystals suitable for an X-ray analysis. ^{1}H NMR (C_6D_6, 298 K): δ = 7.36 (d, $^3J_{H,H}$ = 7.7, 4 H, *m*-C_6H_3), 6.86 (t, $^3J_{H,H}$ = 7.7, 2 H, *p*-C_6H_3), 2.98 (sept, $^3J_{H,H}$ = 6.4, 2 H, C*H*Me$_2$), 2.73 (s, 6 H, N*Me$_2$*), 2.16 (s, 6 H, N*Me$_2$*), 1.63 (s, 36 H, C*Me$_3$*), 0.87 (d, $^3J_{H,H}$ = 6.4, 12 H, CH*Me$_2$*) ppm. ^{13}C NMR (C_6D_6, 298 K): δ = 169.8 (*C*N$_3$), 165.6 (*C*), 138.2 (*C*), 125.1 (*C*H), 115.9 (*C*H), 48.6 (*C*HMe$_2$), 44.2 (N*Me$_2$*), 40.2 (N*Me$_2$*), 35.6 (*C*Me$_3$), 31.8 (C*Me$_3$*), 26.1 (CH*Me$_2$*) ppm.

 © 2004 Wiley-VCH Verlag GmbH & Co. KGaA, Weinheim

Table 4. Crystal structure and refinement data for **3**−**8**

	3	**4**	**5**	**6**	**7**	**8**
Empirical formula	$C_{26}H_{64}N_6Si_4Zn$	$C_{38}H_{80}N_6Si_4Zn$	$C_{20}H_{46}N_6Zn_2$	$C_{24}H_{45}N_3OZn$	$C_{39}H_{68}N_4O_2Zn_2$	$C_{26}H_{60}N_8Si_4Zn_2$
Formula mass	638.56	798.81	501.37	457.00	755.71	727.92
Temperature [K]	173(2)	173(2)	173(2)	173(2)	173(2)	173(2)
Wavelength [Å]	0.71073	0.71073	0.71073	0.71073	0.71073	0.71073
Crystal size [mm]	0.40 × 0.35 × 0.20	0.20 × 0.15 × 0.10	0.30 × 0.10 × 0.05	0.30 × 0.30 × 0.25	0.10 × 0.10 × 0.02	0.40 × 0.30 × 0.05
Crystal system	monoclinic	orthorhombic	orthorhombic	triclinic	monoclinic	monoclinic
Space group	*C*2/*c* (No. 15)	*Fddd* (No. 70)	*Fdd*2 (No. 43)	$P\bar{1}$ (No. 2)	$P2_1/c$ (No. 14)	$P2_1/c$ (No. 14)
a [Å]	17.3585(4)	9.8360(3)	21.5372(11)	10.5249(2)	9.7245(2)	10.6494(2)
b [Å]	8.7203(2)	30.3263(9)	27.5586(15)	10.5294(2)	27.4359(6)	11.4158(4)
c [Å]	26.1372(6)	32.0293(9)	8.8220(4)	13.2813(3)	16.0939(2)	15.7858(4)
α [°]	90	90	90	78.008(1)	90	90
β [°]	94.137(1)	90	90	73.935(1)	104.185(1)	100.008(1)
γ [°]	90	90	90	66.487(1)	90	90
V [Å^3]	3946.11(16)	9554.0(5)	5236.2(5)	1288.99(5)	4162.94(14)	1889.90(7)
Z	4	8	8	2	4	2
D_c [Mg·m^{-3}]	1.08	1.11	1.27	1.18	1.21	1.28
Absorption coefficient [mm^{-1}]	0.77	0.65	1.85	0.97	1.19	1.42
θ range for data collection [°]	3.78 to 25.60	3.85 to 25.00	4.28 to 25.02	3.79 to 24.72	3.72 to 25.02	3.80 to 24.73
Reflection collected	11770	10132	14344	16240	61410	11043
Independent reflections	3509 (R_{int} = 0.060)	2079 (R_{int} = 0.0481)	2233 (R_{int} = 0.065)	4347 (R_{int} = 0.050)	7332 (R_{int} = 0.082)	3205 (R_{int} = 0.048)
Reflection with $I > 2\sigma(I)$	2836	1714	2077	3700	5443	2780
Data/restraints/parameters	3509/0/168	2079/0/113	2233/1/128	4347/0/269	7332/0/428	3205/0/181
Goodness-of-fit on F^2	1.017	1.060	1.050	1.018	1.060	1.044
Final *R* indices	R_1 = 0.043,	R_1 = 0.044,	R_1 = 0.038,	R_1 = 0.035,	R_1 = 0.051,	R_1 = 0.030,
[$I > 2\sigma(I)$]	wR_2 = 0.102	wR_2 = 0.099	wR_2 = 0.087	wR_2 = 0.075	wR_2 = 0.105	wR_2 = 0.069
R indices (all data)	R_1 = 0.059,	R_1 = 0.058,	R_1 = 0.044,	R_1 = 0.046,	R_1 = 0.079,	R_1 = 0.039,
	wR_2 = 0.110	wR_2 = 0.107	wR_2 = 0.090	wR_2 = 0.079	wR_2 = 0.117	wR_2 = 0.072
Largest diff. peak/hole [e·Å^{-3}]	0.28/−0.30	0.58/−0.47	0.37/−0.38	0.27/−0.36	0.69/−0.42	0.34/−0.42

[Zn(hpp){N(SiMe$_3$)$_2$}]$_2$ (8): A solution of hppH (0.18 g, 1.29 mmol) in toluene (20 mL) was added dropwise to a toluene solution (25 mL) of [Zn{N(SiMe$_3$)$_2$}$_2$] (0.50 g, 1.29 mmol) at room temperature. No visible change was observed. The solution was stirred at room temperature for 18 h, after which time the volatile components were removed in vacuo to afford [Zn(hpp)N(SiMe$_3$)$_2$]$_2$ as a white powder. Yield: 0.43 g (90%). Analytically pure samples for applications in polymerisation experiments were obtained by recrystallisation of a sample of **7** from hexane at −30 °C, affording colourless parallelepipedal crystals. $C_{26}H_{60}N_8Si_4Zn_2$ (727.92): calcd. C 42.90, H 8.31, N 15.39; found C 43.05, H 8.20, N 15.27. ^{1}H NMR (C_6D_6, 298 K): δ = 3.22 (m, 8 H, hpp-C*H*$_2$), 2.52 (t, $^3J_{H,H}$ = 6.4, 8 H, hpp-C*H*$_2$), 1.61 (quint, $^3J_{H,H}$ = 5.9, 8 H, hpp-C*H*$_2$), 0.36 (s, 36 H, Si*Me*$_3$) ppm. ^{13}C NMR (C_6D_6, 298 K): δ = 161.6 (*C*N$_3$), 47.9 (hpp-*C*H$_2$), 43.7 (hpp-*C*H$_2$), 23.8 (hpp-*C*H$_2$), 5.6 (Si*Me*$_3$) ppm. MS (EI$^+$): *m*/*z* = 347 [(hpp)Zn{N(SiMe$_3$)$_2$ − Me]$^+$.

X-ray Crystallographic Study: Details of the crystal data, intensity collection and refinement for complexes **3**−**8** are listed in Table 4. Crystals were covered with oil and suitable single crystals were selected under a microscope and mounted on a Kappa CCD diffractometer. The structures were refined with SHELXL-97.[47] Additional features are: [Zn{(Me$_3$Si)$_2$NC(N*i*Pr)$_2$}$_2$] (**3**): The molecule lies on a twofold rotation axis. [Zn{(Me$_3$Si)$_2$NC(NCy)$_2$}$_2$] (**4**): The molecule lies on a site of crystallographic 222 symmetry. [Zn{Me$_2$NC(N*i*Pr)$_2$}Me]$_2$ (**5**): The molecule lies on a twofold rotation axis. [Zn(OAr)Me{Me$_2$NC(N*i*Pr)(NH*i*Pr)}] (**6**): H on N(2) freely refined; all other H atoms riding. [Zn(hpp){N(SiMe$_3$)$_2$}]$_2$ (**8**): The molecule lies on a crystallographic inversion centre. CCDC-199300 (**3**), -199299 (**4**), -228536 (**5**), -228537 (**6**), -228538 (**7**) and -199301 (**8**) contain the supplementary crystallographic data for this paper. These data can be obtained free of charge at www.ccdc.cam.ac.uk/conts/retrieving.html [or from the Cambridge Crystallographic Data Centre, 12 Union Road, Cambridge CB2 1EZ, UK; Fax: + 44 -1223-336033; E-mail: deposit@ccdc.cam.ac.uk].

Acknowledgments

We thank the University of Sussex for additional financial support. We also wish to acknowledge the use of the EPSRC's Chemical Database Service at Daresbury.

[1] B. J. O'Keefe, M. A. Hillmyer, W. B. Tolman, *J. Chem. Soc., Dalton Trans.* **2001**, 2215−2224.
[2] R. E. Drumright, P. R. Gruber, D. E. Henton, *Adv. Mater.* **2000**, *12*, 1841−1846.
[3] L. Bourget-Merle, M. F. Lappert, J. R. Severn, *Chem. Rev.* **2002**, *102*, 3031−3066.
[4] M. Cheng, A. B. Attygalle, E. B. Lobkovsky, G. W. Coates, *J. Am. Chem. Soc.* **1999**, *121*, 11583−11584.
[5] B. M. Chamberlain, M. Cheng, D. R. Moore, T. M. Ovitt, E. B. Lobkovsky, G. W. Coates, *J. Am. Chem. Soc.* **2001**, *123*, 3229−3238; M. H. Chisholm, J. C. Huffman, K. Phomphrai, *J. Chem. Soc., Dalton Trans.* **2001**, 222−224.
[6] M. S. Hill, P. B. Hitchcock, *J. Chem. Soc., Dalton Trans.* **2002**, 4694−4702.
[7] J. Barker, M. Kilner, *Coord. Chem. Rev.* **1994**, *133*, 219−300.
[8] F. T. Edelmann, *Coord. Chem. Rev.* **1994**, *137*, 403−481.
[9] B. J. O'Keefe, L. E. Breyfogle, M. A. Hillmyer, W. B. Tolman, *J. Am. Chem. Soc.* **2002**, *124*, 4384−4393.
[10] K. B. Aubrecht, M. A. Hillmyer, W. B. Tolman, *Macromolecules* **2002**, *35*, 644−650.
[11] K. B. Aubrecht, K. Chang, M. A. Hillmyer, W. B. Tolman, *J. Polym. Sci. A: Polym. Chem.* **2001**, *39*, 284−293.
[12] Y. Luo, Y. Yao, Q. Shen, J. Sun, L. Weng, *J. Organomet. Chem.* **2002**, *662*, 144−149.

 © 2004 Wiley-VCH Verlag GmbH & Co. KGaA, Weinheim

[13] P. J. Bailey, S. Pace, *Coord. Chem. Rev.* **2001**, *214*, 91−141.
[14] G. R. Giesbrecht, G. D. Whitener, J. Arnold, *J. Chem. Soc., Dalton Trans.* **2001**, 923−927.
[15] Y. Yao, Y. Luo, J. Chen, Z. Zhang, Y. Zhang, Q. Shen, *J. Organomet. Chem.* **2003**, *679*, 229−237; Y. Luo, Y. Yao, Q. Shen, K. Yu, L. Weng, *Eur. J. Inorg. Chem.* **2003**, 318−323.
[16] G. Minghetti, G. Banditelli, F. Bonati, *Inorg. Chim. Acta* **1975**, *12*, 85−91.
[17] J.-K. Buijink, M. Noltemeyer, F. T. Edelmann, *Z. Naturforsch., Teil B* **1991**, *46*, 1328−1332.
[18] M. L. Cole, D. J. Evans, P. C. Junk, L. M. Louis, *New J. Chem.* **2002**, *26*, 1015−1024.
[19] A. D. Bond, D. J. Linton, P. Schooler, A. E. H. Wheatley, *J. Chem. Soc., Dalton Trans.* **2001**, 3173−3178.
[20] J. Grundy, M. P. Coles, P. B. Hitchcock, *J. Organomet. Chem.* **2002**, *662*, 178−187.
[21] M. P. Coles, P. B. Hitchcock, *J. Chem. Soc., Dalton Trans.* **2001**, 1169−1171; M. P. Coles, P. B. Hitchcock, *Organometallics* **2003**, *22*, 5201−5211.
[22] S. R. Boss, M. P. Coles, R. Haigh, P. B. Hitchcock, R. Snaith, A. E. H. Wheatley, *Angew. Chem. Int. Ed.* **2003**, *42*, 5593−5596; D. B. Soria, J. Grundy, M. P. Coles, P. B. Hitchcock, *Polyhedron* **2003**, *22*, 2731−2737.
[23] M. K. T. Tin, G. P. A. Yap, D. S. Richeson, *Inorg. Chem.* **1999**, *38*, 998−1001; S. M. Mullins, A. P. Duncan, R. G. Bergman, J. Arnold, *Inorg. Chem.* **2001**, *40*, 6952−6963; A. P. Duncan, S. M. Mullins, J. Arnold, R. G. Bergman, *Organometallics* **2001**, *20*, 1808−1819.
[24] G. Chandra, A. D. Jenkins, M. F. Lappert, R. C. Srivastava, *J. Chem. Soc., A* **1970**, 2550−2558.
[25] S. L. Aeilts, M. P. Coles, D. C. Swenson, R. F. Jordan, V. G. Young Jr., *Organometallics* **1998**, *17*, 3265−3270.
[26] G. R. Giesbrecht, G. D. Whitener, J. Arnold, *Organometallics* **2000**, 2809−2812.
[27] For examples of structurally related compounds containing *dianionic* guanidines, see: N. Thirupathi, G. P. A. Yap, D. S. Richeson, *Chem. Commun.* **1999**, 2483−2484; P. J. Bailey, A. J. Blake, M. Kryszczuk, S. Parsons, D. Reed, *J. Chem. Soc., Chem. Commun.* **1995**, 1647−1648.
[28] J. R. Hagadorn, J. Arnold, *Inorg. Chem.* **1997**, *36*, 132−133; J. Barker, D. Barr, N. D. R. Barnett, W. Clegg, I. Cragg-Hine, M. G. Davidson, R. P. Davies, S. M. Hodgson, J. A. K. Howard, M. Kilner, C. W. Lehmann, I. Lopez-Solera, R. E. Mulvey, P. R. Raithby, R. Snaith, *J. Chem. Soc., Dalton Trans.* **1997**, 951−955; D. Stalke, M. Wedler, F. T. Edelmann, *J. Organomet. Chem.* **1992**, *431*, C1−C5.
[29] D. Doyle, Y. K. Gun′ko, P. B. Hitchcock, M. F. Lappert, *J. Chem. Soc., Dalton Trans.* **2000**, 4093−4097.
[30] F. A. Cotton, L. M. Daniels, C. A. Murillo, D. J. Timmons, *Chem. Commun.* **1997**, 1449−1450.
[31] A. R. Sadique, M. J. Heeg, C. H. Winter, *Inorg. Chem.* **2001**, *40*, 6349−6355.
[32] F. A. Cotton, L. M. Daniels, J. H. Matonic, C. A. Murillo, *Inorg. Chim. Acta* **1997**, *256*, 277.
[33] M. P. Coles, P. B. Hitchcock, *Chem. Commun.* **2002**, 2794−2795.
[34] For recent examples of N_{imine}-bound, neutral guanidines, see: S. H. Oakley, D. B. Soria, M. P. Coles, P. B. Hitchcock, *Dalton Trans.* **2004**, 537.
[35] M. H. Chisholm, J. C. Gallucci, H. Zhen, J. C. Huffman, *Inorg. Chem.* **2001**, *40*, 5051−5054; D. J. Darensbourg, M. S. Zimmer, P. Rainey, D. L. Larkins, *Inorg. Chem.* **1998**, *37*, 2852−2853; D. J. Darensbourg, M. W. Holtcamp, G. E. Struck, M. S. Zimmer, S. A. Niezgoda, P. Rainey, J. B. Robertson, J. D. Draper, J. H. Reibenspies, *J. Am. Chem. Soc.* **1999**, *121*, 107−116; D. J. Darensbourg, M. S. Zimmer, P. Rainey, D. L. Larkins, *Inorg. Chem.* **2000**, *39*, 1578−1585; R. L. Geerts, J. C. Huffman, K. G. Caulton, *Inorg. Chem.* **1986**, *25*, 1803−1805; R. L. Geerts, J. C. Huffman, K. G. Caulton, *Inorg. Chem.* **1986**, *25*, 590−591.
[36] K. T. Holman, S. D. Robinson, A. Sahaipal, J. W. Steed, *J. Chem. Soc., Dalton Trans.* **1999**, 15−18; S. R. Foley, G. P. A. Yap, D. S. Richeson, *Chem. Commun.* **2000**, 1515−1516; S. R. Foley, G. P. A. Yap, D. S. Richeson, *Inorg. Chem.* **2002**, *41*, 4149−4157; G. R. Giesbrecht, A. Shafir, J. Arnold, *J. Chem. Soc., Dalton Trans.* **1999**, 3601−3604.
[37] M. A. Putzer, A. Dashti-Mommertz, B. Neumüller, K. Dehnicke, *Z. Anorg. Allg. Chem.* **1998**, *624*, 263−266.
[38] D. R. Armstrong, G. C. Forbes, R. E. Mulvey, W. Clegg, D. M. Tooke, *J. Chem. Soc., Dalton Trans.* **2002**, 1656−1661.
[39] H. Schumann, J. Gottfriedsen, F. Girgsdies, *Z. Anorg. Allg. Chem.* **1997**, *623*, 1881−1884.
[40] S. R. Foley, G. P. A. Yap, D. S. Richeson, *Polyhedron* **2002**, *21*, 619−627.
[41] F. A. Cotton, D. J. Timmons, *Polyhedron* **1998**, *17*, 179−184; F. A. Cotton, J. H. Matonic, C. A. Murillo, *J. Am. Chem. Soc.* **1997**, *119*, 7889−7890; F. A. Cotton, J. H. Matonic, C. A. Murillo, *J. Am. Chem. Soc.* **1998**, *120*, 6047−6052; R. Clérac, F. A. Cotton, L. M. Daniels, J. P. Donahue, C. A. Murillo, D. J. Timmons, *Inorg. Chem.* **2000**, *39*, 2581−2584; J. L. Bear, Y. Li, B. Han, K. M. Kadish, *Inorg. Chem.* **1996**, *35*, 1395−1398; F. A. Cotton, J. Gu, C. A. Murillo, D. J. Timmons, *J. Am. Chem. Soc.* **1998**, *120*, 13280−13281; F. A. Cotton, J. Gu, C. A. Murillo, D. J. Timmons, *J. Chem. Soc., Dalton Trans.* **1999**, 3741−3745; F. A. Cotton, C. A. Murillo, D. J. Timmons, *Chem. Commun.* **1999**, 1427−1428; F. A. Cotton, P. Huang, C. A. Murillo, D. J. Timmons, *Inorg. Chem. Commun.* **2002**, *5*, 501−504; F. A. Cotton, L. M. Daniels, C. A. Murillo, D. J. Timmons, C. C. Wilkinson, *J. Am. Chem. Soc.* **2002**, *124*, 9249−9256; F. A. Cotton, X. Feng, D. J. Timmons, *Inorg. Chem.* **1998**, *37*, 4066−4069; F. A. Cotton, N. E. Gruhn, J. D. Gu, P. Huang, D. L. Lichtenberger, C. A. Murillo, L. O. Van Dorn, C. C. Wilkinson, *Science* **2002**, *298*, 1971−1974.
[42] M. P. Coles, A. E. H. Wheatley, *manuscript in preparation*.
[43] M. Cheng, D. M. Moore, J. J. Reczek, B. M. Chamberlain, E. B. Lobkovsky, G. W. Coates, *J. Am. Chem. Soc.* **2001**, *123*, 8738−8749.
[44] M. Cheng, N. A. Darling, E. B. Lobkovsky, G. W. Coates, *Chem. Commun.* **2000**, 2007−2008.
[45] T.-G. Ong, G. P. A. Yap, D. S. Richeson, *J. Am. Chem. Soc.* **2003**, *125*, 8100−8101.
[46] T.-G. Ong, G. P. A. Yap, D. S. Richeson, *Chem. Commun.* **2003**, 2612−2613; K. R. Birdwhistell, J. Lanza, J. Pasos, *J. Organomet. Chem.* **1999**, *584*, 200−205; J. R. Babcock, L. R. Sita, *J. Am. Chem. Soc.* **1998**, *120*, 5585−5586.
[47] G. M. Sheldrick, *SHELXL-97, Program for the Refinement of Crystal Structures*, Göttingen, **1997**.

Received January 15, 2004
Early View Article
Published Online May 5, 2004

 © 2004 Wiley-VCH Verlag GmbH & Co. KGaA, Weinheim

Synthesis and Structural Characterization of Monomeric Manganese(II) *N*-Heterocyclic Carbene Complexes [MnX_2(C{N(*i*Pr)C(Me)}$_2$)$_2$] (X = Cl, I, and MeCOO)

Jianfang Chai,[a] Hongping Zhu,[a] Ying Peng,[a] Herbert W. Roesky,*[a] Sanjay Singh,[a] Hans-Georg Schmidt,[a] and Mathias Noltemeyer[a]

Keywords: Carbene ligands / Manganese / Halides / Acetate

Reaction of $MnCl_2(THF)_{1.5}$, MnI_2, or $Mn(MeCOO)_2$ with two equivalents of *N*-heterocyclic carbene [C(Me)N(*i*Pr)]$_2$C (**1**) in THF at room temperature readily afforded the corresponding carbene adducts [MnX_2(C{N(*i*Pr)C(Me)}$_2$)$_2$] [X = Cl (**2**); X = I (**3**); X = MeCOO (**4**)] in good yield. Solid-state structural analysis of complexes **2**–**4** reveals that all complexes are monomeric. In complexes **2** and **3** the central manganese atoms are four coordinate and have a distorted tetrahedral geometry. The manganese atom in compound **4** has a coordination number of six and resides in a highly distorted octahedral geometry. The *N*-heterocyclic carbene ligands in these complexes are coordinated differently to the central metal atoms.

(© Wiley-VCH Verlag GmbH & Co. KGaA, 69451 Weinheim, Germany, 2004)

Introduction

The first carbenes were isolated in the late 1980s and early 1990s,[1] and since then there has been a revival of interest in carbene ligands,[2] which are formally neutral, two-electron donors. A major portion of the work has focused on *N*-heterocyclic carbenes due to their easy preparation and good thermal stability, which have been used to prepare a variety of main-group, transition metal, and lanthanide complexes.[2a,2c] A significant number of these complexes, especially the late transition metal complexes, have been shown to be effective catalysts in a number of organic reactions, such as hydrosilylation,[3] hydrogenation and hydroformylation of olefins or copolymerization of ethylene and CO.[2,4] In addition, palladium *N*-heterocyclic carbene complexes have been successfully applied in various C−C bond forming syntheses, in particular the Heck, Suzuki, and Kumada reactions.[2,5] Recently, iron(II) halides possessing *N*-heterocyclic carbenes of composition FeX_2L_2 [X = Cl, Br; L = C{N(*i*Pr)C(Me)}$_2$] were found to be remarkably active and efficient catalysts for atom-transfer radical polymerization.[6]

Manganese(II) complexes bearing tertiary phosphane ligands have been extensively studied.[7] It seems that chelating bidentate phosphane ligands are necessary to prepare monomeric manganese dihalide adducts such as dmpe and diphos. The isolation of [$MnX_2(PPh_3)_2$] has been questioned and it is likely that the complexes are [$MnX_2(OPPh_3)_2$] instead.[8] Until now, only one monomeric manganese(II) dihalide with a nonchelating phosphane ligand of composition [$MnI_2(PEt_3)_2$] has been unambiguously characterized.[8] *N*-Heterocyclic carbenes are considered to be analogues of tertiary phosphanes,[9] although they are stronger σ-donor ligands and therefore, in general, form more stable bonds to metals. Compared with tertiary phosphane ligands, *N*-heterocyclic carbene ligands have better thermal stability and oxidation resistance and a mobile steric effect upon changing the substituents at the nitrogen atoms.[2b] However, manganese *N*-heterocyclic carbene complexes are rare and have not attracted much attention to date.[2a] To the best of our knowledge, only a few manganese *N*-heterocyclic carbene complexes are known including [$Mn(MeC_5H_4)(CO)_2$(C{N(Me)CH_2}$_2$)],[10] [$MnBr(CO)_3$-(C{N(Me)CH_2}$_2$)],[10] and [$Mn(CO)_5$C{N(BH_3)C(Me)-C(Me)N(Me)}][11] with a formal oxidation state of +1 at the manganese. Therefore, we became interested in the synthesis and structures of *N*-heterocyclic carbene complexes containing manganese(II). Recently, we reported the first structurally characterized manganese *N*-heterocyclic carbene complex of composition [Mn(NHAr){HC-(CMeNAr)$_2$}(C{N(*i*Pr)C(Me)}$_2$)] (Ar = 2,6-*i*$Pr_2C_6H_3$), which shows that the Mn−C(carbene) bond length (2.27 Å) is in the range of an Mn−C single bond and that Mn→C(carbene) back-bonding is negligible.[12] For a better understanding of manganese *N*-heterocyclic carbene complexes and for comparison of *N*-heterocyclic carbenes with

[a] Institut für Anorganische Chemie, Universität Göttingen, Tammannstrasse 4, 37077 Göttingen, Germany
Fax: (internat.) + 49-(0)551-393373
E-mail: hroesky@gwdg.de

tertiary phosphane ligands, we describe herein the synthesis and structural characterization of several monomeric adducts of manganese(II) halides and acetate with *N*-heterocyclic carbenes $[MnX_2(C\{N(iPr)C(Me)\}_2)_2]$ [X = Cl (**2**); X = I (**3**); X = MeCOO (**4**)].

Results and Discussion

Synthesis of Compounds 2−4

The isolation of free stable *N*-heterocyclic carbenes enables the easy synthesis of a variety of carbene adducts that were previously inaccessible.[13] The reaction of $[MnCl_2(THF)_{1.5}]$, MnI_2, or $Mn(MeCOO)_2$ with two equivalents of $[C(Me)N(iPr)]_2C$ (**1**) in THF at room temperature readily afforded the corresponding carbene adducts in good yield (91% **2**, 77% **3**, and 81% **4**; Scheme 1). Compounds **2** and **4** are colorless solids and compound **3** is a light-orange solid. Compounds **2** and **3** are moderately air sensitive and can even be exposed to air for a short period of time when in the solid state, while compound **4** is much more sensitive to air. Compounds **2**−**4** are poorly soluble in non-polar solvents, although they are readily soluble in solvents such as CH_2Cl_2 and MeCN. Compound **4** has also a good solubility in THF, but **2** and **3** are sparingly soluble in THF. Complexes **2**−**4** have been characterized by mass spectrometry, IR spectroscopy, X-band EPR spectroscopy, microanalysis and single crystal X-ray structural analysis. The EI mass spectra of these compounds are similar: the molecular ion peak is not observed, but free carbene appears as the most intense signal at m/z = 180 (100%), which indicates the cleavage of the Mn−C(carbene) bond in these compounds under the experimental conditions. This is consistent with the results reported in the literature.[14] The IR spectrum of **4** displays two prominent vibrations for the O−C−O part of the acetate group ν_{as} (1599 cm^{-1}) and ν_s (1406 cm^{-1}). The absorption at about 1600 cm^{-1} is broad.

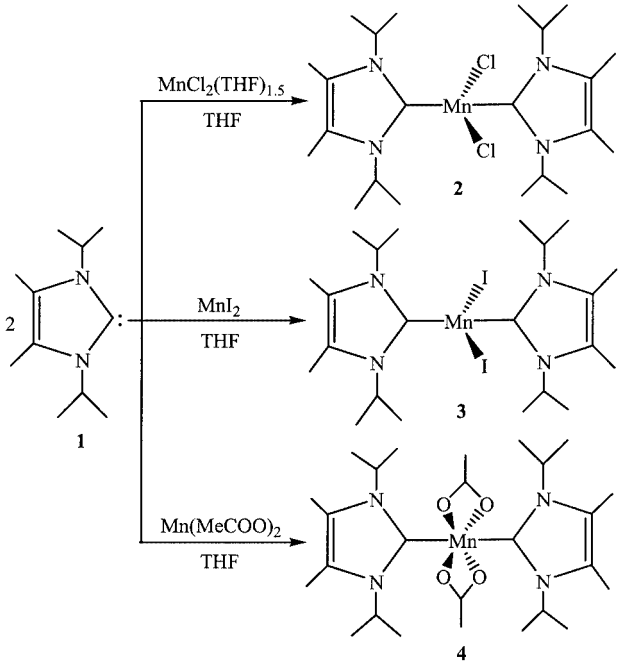

Scheme 1

X-ray Diffraction Analyses for Complexes 2−4

Compounds **2** and **3** are the first structurally characterized manganese halides possessing *N*-heterocyclic carbene ligands. Single crystals of **2** and **3** suitable for X-ray structural analysis were obtained by recrystallization from THF solutions at 4 °C. The molecular structures of **2** and **3** are shown in Figures 1 and 2, respectively; selected bond

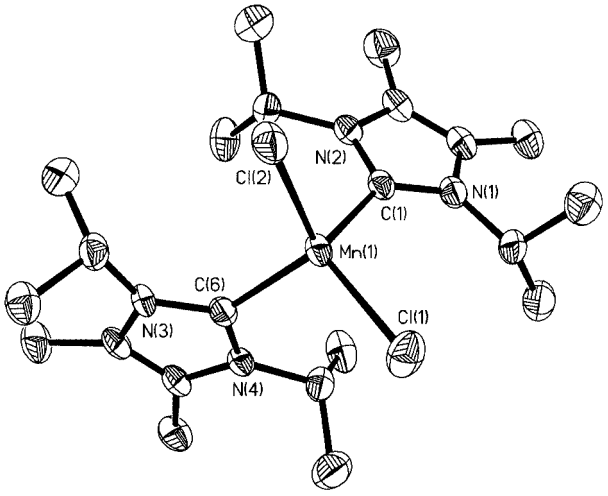

Figure 1. Molecular structure of **2** (50% probability ellipsoids); hydrogen atoms are omitted for clarity

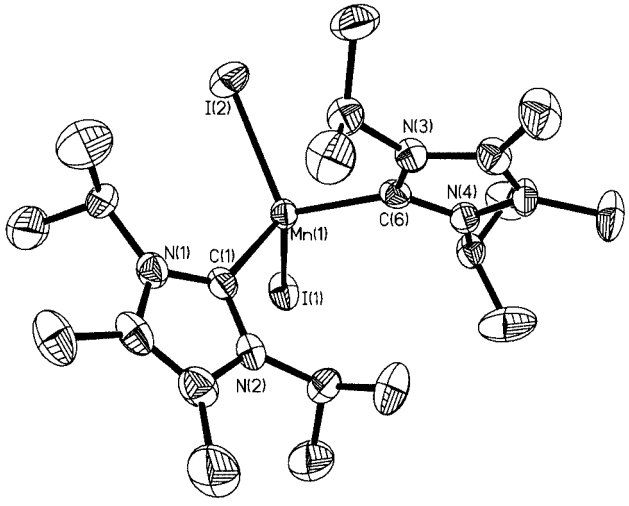

Figure 2. Molecular structure of **3** (50% probability ellipsoids); hydrogen atoms are omitted for clarity

 © 2004 Wiley-VCH Verlag GmbH & Co. KGaA, Weinheim

Table 1. Selected bond lengths (Å) and bond angles (°) for compounds **2** and **3**

Compound **2**			
Mn(1)−Cl(1)	2.3535(11)	N(1)−C(1)	1.355(4)
Mn(1)−Cl(2)	2.3575(10)	N(2)−C(1)	1.355(4)
Mn(1)−C(1)	2.214(3)	N(3)−C(6)	1.355(4)
Mn(1)−C(6)	2.219(3)	N(4)−C(6)	1.359(4)
C(1)−Mn(1)−C(6)	103.02(12)	C(6)−Mn(1)−Cl(2)	114.64(9)
C(1)−Mn(1)−Cl(6)	112.77(9)	Cl(1)−Mn(1)−Cl(2)	111.47(4)
C(6)−Mn(1)−C1(1)	108.92(9)	N(1)−C(1)−N(2)	104.5(3)
C(1)−Mn(1)−Cl(2)	105.78(8)	N(3)−C(6)−N(4)	104.6(3)
N(1)−C(1)−Mn(1)	131.6(2)	N(2)−C(1)−Mn(1)	123.9(2)
N(3)−C(1)−Mn(1)	132.3(2)	N(4)−C(1)−Mn(1)	122.6(2)
Compound **3**			
Mn(1)−I(1)	2.7307(7)	N(1)−C(1)	1.356(5)
Mn(1)−I(2)	2.7114(8)	N(2)−C(1)	1.352(6)
Mn(1)−C(1)	2.210(4)	N(3)−C(6)	1.354(5)
Mn(1)−C(6)	2.204(4)	N(4)−C(6)	1.352(5)
C(1)−Mn(1)−C(6)	102.35(15)	C(6)−Mn(1)−I(2)	105.79(11)
C(1)−Mn(1)−I(1)	106.46(10)	I(1)−Mn(1)−I(2)	109.04(2)
C(6)−Mn(1)−I(1)	116.60(10)	N(1)−C(1)−N(2)	104.7(3)
C(1)−Mn(1)−I(2)	116.89(11)	N(3)−C(6)−N(4)	104.1(3)
N(1)−C(1)−Mn(1)	131.7(3)	N(2)−C(1)−Mn(1)	123.3(3)
N(3)−C(1)−Mn(1)	124.5(3)	N(4)−C(1)−Mn(1)	131.2(3)

lengths and angles are listed in Table 1. The manganese centers are four coordinate and have a distorted tetrahedral geometry in which each manganese is bonded to two halides and two carbene carbons. A crystallographic twofold axis passes through the metal center bisecting the angles X−Mn−X and C−Mn−C. There is a slight difference between the two structures due to the different ionic radius of Cl and I: the X−Mn−X (111.5°) and C−Mn−C (103.0°) angles in **2** are slightly larger than the corresponding ones in **3** (109.0° and 102.4°, respectively). The dihedral angle between the two carbene planes is 84.5° in **2** and 77.0° in **3**. These differences possibly result from the stronger repulsion between iodine and carbene in **3** than that between chlorine and carbene in **2**; this is also reflected in the EPR spectra.

The Mn−C(carbene) bond lengths (av. 2.21 Å) in **2** and **3** are in the expected range of Mn−C single bonds, but significantly shorter than the Mn−P bond lengths found in $[MnI_2(PEt_3)_2]$[8] (av. 2.53 Å) and $[MnI_2(PPhMe_2)]_n$ [15] (av. 2.67 Å). The Mn−I distances (av. 2.72 Å) in **3** are a little longer than those in $[MnI_2(PEt_3)_2]$ (av. 2.67 Å)[8] due to the different *trans* influence. However, the I−Mn−I (109.0°) and C−Mn−C (102.4°) angles in **3** are significantly smaller than the corresponding ones (120.1° and 115.1°, respectively) in $[MnI_2(PEt_3)_2]$.[8]

The N(1)−C(1)−Mn(1) (131.6°) and N(3)−C(6)−Mn(1) (132.3°) angles deviate significantly from their counterparts N(2)−C(1)−Mn(1) (123.9°) and N(4)−C(6)−Mn(1) (122.6°) in **2**, which implies that both the *N*-heterocyclic carbenes undergo *in-plane* bending.[16] However, *out-of-plane* bending is only observed for one *N*-heterocyclic carbene ligand [C(6), N(3), C(7), C(8) and N(4)] and the Mn(1)−C(6) bond lies out of the *N*-heterocyclic carbene plane by 6.4°. The other *N*-heterocyclic carbene and the central manganese atom are coplanar. In **3**, both the *N*-heterocyclic carbene ligands undergo *out-of-plane* bending, as shown by the Mn−C bond angles, which deviate from the corresponding *N*-heterocyclic carbene planes by 4.7° and 4.3°, respectively. These angles are in the normal range.[14]

Compound **4** is the first structurally characterized monomeric manganese complex containing two symmetric chelating acetate groups. Single crystals suitable for X-ray structural analysis were grown from THF solution at −26 °C. The molecular structure is shown in Figure 3; selected bond lengths and bond angles are listed in Table 2. Complex **4** crystallizes in the monoclinic space group *C*2/*c*. The central manganese atom is surrounded by four oxygen atoms from the two chelating carboxy groups and two carbene carbon atoms in a highly distorted octahedral geometry. The complex adopts a symmetric structure. A mirror plane passes through the manganese atom bisecting the two acetate groups and the two carbenes.

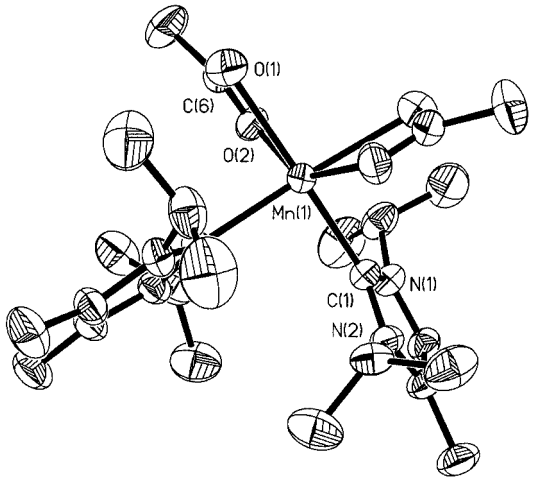

Figure 3. Molecular structure of **4** (50% probability ellipsoids); hydrogen atoms are omitted for clarity

The two acetate groups are symmetrically bonded, in a chelating fashion, to the manganese atom, resulting in the formation of two MnOCO four-membered rings. Both rings are planar and nearly orthogonal, as shown by a dihedral angle of 85.8°. Manganese complexes containing chelating carboxy groups are rare.[17] The Mn−O distances from the O *trans* to the *N*-heterocyclic carbene carbon (2.34 Å) are slightly longer than those (2.23 Å) from the O *cis* to the carbon, probably due to the strong donor property of the *N*-heterocyclic carbene. Accordingly, the shorter Mn−O bond is associated with a longer carboxy C−O bond. The average value (2.29 Å) of the Mn−O distance is significantly longer than that of the bridging carboxyl group in the $[Mn_2(\mu\text{-MeCOO})_x]^{4-x}$ system (1.99−2.13 Å),[18] and is also longer than that (av. 2.07 Å) of the chelating acetate group in $[Mn(MeCOO)(CO)_2(PPh_3)_2]$.[19] The distance from

 © 2004 Wiley-VCH Verlag GmbH & Co. KGaA, Weinheim

Table 2. Selected bond lengths (Å) and bond angles (°) for compound **4**

Mn(1)−O(1)	2.343(2)	Mn(1)−C(1A)	2.254(3)
Mn(1)−O(2)	2.233(2)	Mn(1)−C(6A)	2.612(3)
Mn(1)−O(1A)	2.343(2)	O(1)−C(6)	1.238(4)
Mn(1)−O(2A)	2.233(2)	O(2)−C(6)	1.258(4)
Mn(1)−C(1)	2.254(3)	N(1)−C(1)	1.364(3)
Mn(1)−C(6)	2.612(3)	N(2)−C(1)	1.356(3)
C(1)−Mn(1)−C(1A)	96.68(13)	O(1)−Mn(1)−C(1A)	87.69(9)
C(1)−Mn(1)−O(1)	161.79(9)	O(1)−Mn(1)−O(1A)	93.65(12)
C(1)−Mn(1)−O(1A)	87.69(9)	O(1)−Mn(1)−O(2A)	98.60(8)
C(1)−Mn(1)−O(2)	104.91(9)	O(1A)−Mn(1)−O(2A)	56.92(8)
C(1)−Mn(1)−O(2A)	97.34(8)	O(1A)−Mn(1)−C(1A)	161.79(9)
O(2)−Mn(1)−O(2A)	146.33(12)	O(2A)−Mn(1)−C(1A)	104.91(8)
O(2)−Mn(1)−C(1A)	97.34(8)	O(1)−C(6)−O(2)	122.0(3)
O(2)−Mn(1)−O(1)	56.92(8)	N(1)−C(1)−N(2)	104.0(2)
O(2)−Mn(1)−O(1A)	98.60(8)	N(2)−C(1)−Mn(1)	126.67(18)
N(1)−C(1)−Mn(1)	129.32(18)		

the manganese atom to the central carbon atom of the acetate group (2.61 Å) is in the non-bonding range.[19]

The C−Mn−C angle in **4** is 96.7°, which shows that the two *N*-heterocyclic carbenes are in a *cis* position. The Mn−C distance (2.25 Å) is in the range (2.20−2.27 Å) of the Mn−C(*N*-heterocyclic carbene) distances known and is slightly longer than those in **2** and **3**.

Interestingly, no *in-plane* or *out-of-plane* bending of the *N*-heterocyclic carbenes is found in **4**. The similar N(1)−C(1)−Mn(1) (129.3°) and N(2)−C(1)−Mn(1) (126.7°) angles do not support any *in-plane* bending of the *N*-heterocyclic carbenes.

Solid-State Powder EPR Measurements

Manganese(II) complexes give a great variety of EPR signals related to their structures.[20] The X-band EPR spectra of complexes **2**−**4** were recorded at ambient temperature for powder samples. As expected, a strong resonance in complexes **2** and **3** is observed near $g_{eff} = 4.3$ due to their tetrahedral geometry.[21a] In addition, compound **2** exhibits two shoulders at lower field and several weaker bands at higher field, while the spectrum of **3** is much simpler: another strong resonance ($g_{eff} = 2$) and a very weak one at high field. The spectrum of compound **4** exhibits a very strong band ($g_{eff} = 2$) and a weaker one (near $g_{eff} = 4.3$) and has shoulders at higher and lower field of the main line. The spectrum of **4** is very similar to that of $[Mn(o\text{-phen})_2(NCS)_2]$, which has a very small D value (near zero) and a large λ value (near 1/3) (D and λ are zero-field splitting parameters).[21b] The spectrum is consistent with the symmetric structure of **4** and the *cis* arrangement of the two carbene ligands.

Conclusion

In summary, we have shown that the *N*-heterocyclic carbene ligand $[C(Me)N(i\text{Pr})]_2C$ (**1**) forms stable adducts **2**−**4** with manganese(II) halides and acetate. The X-ray structural analyses show that complexes **2**−**4** are monomeric and the *N*-heterocyclic carbene ligands in these complexes are arranged differently at the central metal atoms. These results indicate that the *N*-heterocyclic carbene ligand is a better ligand to form monomeric adducts than the tertiary phosphane ligand.

Experimental Section

General: All reactions were performed using standard Schlenk and drybox techniques. Solvents were appropriately dried and distilled under dinitrogen prior to use. Elemental analyses were performed by the Analytisches Labor des Instituts für Anorganische Chemie der Universität Göttingen. Mass spectra were obtained on a Finnigan Mat 8230. IR spectra were recorded on a Bio-Rad Digilab FTS-7 spectrometer as Nujol mulls between KBr plates. The EPR spectra were recorded on a Bruker Elexsys E 500 X-band spectrometer. All samples were measured as crystalline powders in an argon atmosphere at room temperature with a modulation frequency of 100 kHz, 3−5 G modulation amplitude, about 9.42 GHz microwave frequency and microwave power in the range between 2 and 10 mW as spectrometer settings. $[C(Me)N(i\text{Pr})]_2C$[22] (**1**) was prepared by the literature protocol.

Preparation of 2: THF (40 mL) was added to a mixture of **1** (0.72 g, 4 mmol) and $[MnCl_2(THF)_{1.5}]$ (0.47 g, 2 mmol) at room temperature. The suspension was stirred for 13 h. The solvent was concentrated to about 3 mL and the colorless precipitate was collected by filtration. Yield: 0.88 g (91%). M.p. 268−270 °C. $C_{22}H_{40}Cl_2MnN_4$ (486.42): calcd. C 54.27, H 8.22, N 11.51; found C 54.32, H 8.23, N 11.52. IR (KBr, Nujol mull): $\tilde{\nu}$ = 1629 cm^{-1} (m), 1552 (w), 1401 (m), 1376 (s), 1360 (s), 1262 (vw), 1218 (m), 1168 (w), 1136 (m), 1107 (w), 1070 (m), 1023 (w), 968 (vw), 931 (vw), 905 (w), 885 (w), 803 (vw), 751 (m), 722 (m), 674 (vw), 544 (m), 412 (w).

Preparation of 3: The procedure is the same as that described for **2**. Yield: 1.03 g (77%). M.p. 273−283 °C. $C_{22}H_{40}I_2MnN_4$ (669.32): calcd. C 39.46, H 5.98, N 8.37; found C 39.54, H 6.00, N 8.34. IR (KBr, Nujol mull): $\tilde{\nu}$ = 1629 cm^{-1} (m), 1552 (w), 1398 (m), 1377 (s), 1364 (s), 1291 (vw), 1262 (vw), 1219 (m), 1191 (vw), 1168 (w), 1136 (m), 1109 (w), 1071 (m), 1023 (w), 968 (vw), 931 (vw), 905 (w), 886 (w), 848 (vw), 803 (vw), 750 (m), 722 (m).

Preparation of 4: THF (40 mL) was added to a mixture of **1** (0.72 g, 4 mmol) and $Mn(MeCOO)_2$ (0.34 g, 2 mmol) at room temperature. A clear solution was obtained immediately and stirred for 6 h. The solution was concentrated to about 5 mL and kept at −26 °C for 3 days to give colorless crystals. Yield: 0.86 g (81%). M.p. 156−158 °C. $C_{26}H_{46}MnN_4O_4$ (532.96): calcd. C 58.54, H 8.63, N 10.51; found C 58.58, H 8.67, N 10.14. IR (KBr, Nujol mull): $\tilde{\nu}$ = 1750 cm^{-1} (vw), 1695 (vw),1628 (s), 1599 (vs), 1573 (s), 1406 (s), 1323 (m), 1260 (m), 1238 (w), 1222 (m), 1195 (w), 1167 (vw), 1138 (m), 1112 (m), 1073 (w), 1048 (vw), 10231 (vw), 917 (w), 908 (w), 888 (vw), 804 (s), 751 (m), 722 (m), 658 (s), 648 (w), 616 (m), 544 (m), 483 (w), 457 (vw), 411 (vw).

X-ray Crystallography: Crystallographic data (see Table 3) for complexes **2**−**4** were collected on a Stoe−Siemens−Huber four-circle diffractometer coupled to a Siemens CCD area detector with graphite-monochromated Mo-K_α radiation (λ = 0.71073 Å). All structures were solved by direct methods (SHELXS-97)[23] and refined against F^2 using SHELXL-97.[24] All non-hydrogen atoms were refined anisotropically. The hydrogen atoms were included at geometrically calculated positions and refined using a riding model.

 © 2004 Wiley-VCH Verlag GmbH & Co. KGaA, Weinheim

Table 3. Crystallographic data for compounds **2**−**4**

	2	**3**	**4**·THF
Empirical formula	$C_{22}H_{40}Cl_2MnN_4$	$C_{22}H_{40}I_2MnN_4$	$C_{30}H_{54}MnN_4O_5$
Molecular mass	486.42	669.32	605.71
Temperature (K)	200(2)	200(2)	203(2)
Wavelength (Å)	0.71073	0.71073	0.71073
Crystal system	monoclinic	monoclinic	monoclinic
Space group	$P2_1/n$	$P2_1/n$	$C2/c$
Unit cell dimensions (Å)	a = 11.2852(17)	a = 11.2771(13)	a = 12.970(2)
	b = 14.867(3)	b = 16.054(3)	b = 14.374(3)
	c = 15.321(3)	c = 15.705(3)	c = 19.322(2)
	β = 90.24(2)°	β = 90.399(14)°	β = 106.070(10)°
Volume (Å^3)	2570.6(9)	2843.1(8)	3461.5(10)
Z	4	4	4
D (calcd. Mg·m^{-3})	1.257	1.564	1.162
Crystal size (mm^3)	1.00 × 0.30 × 0.20	0.80 × 0.60 × 0.30	0.90 × 0.70 × 0.70
Absorption coefficient (mm^{-1})	0.736	2.650	0.421
θ range for data collection (°)	3.54 to 22.53	3.61 to 25.01	3.54 to 24.94
F(000)	1036	1324	1308
Reflections collected	3570	6010	3231
Independent reflections	3348 (R_{int} = 0.0671)	4994 (R_{int} = 0.0660)	3028 (R_{int} = 0.0717)
Data/restraints/parameters	3348/0/274	4994/0/274	3028/0/174
Goodness-of-fit on F^2	1.081	1.065	1.015
Final R indices [$I > 2\sigma(I)$]	0.0460, 0.1150	0.0411, 0.1077	0.0595, 0.1597
R (all data)	0.0544, 0.1233	0.0440, 0.1111	0.0670, 0.1701
Largest diff. peak/hole (e·Å^{-3})	0.673/−0.854	1.161/−1.433	0.762/−0.834

CCDC-222956 (for **2**), -222955 (for **3**), and -222954 (for **4**) contain the supplementary crystallographic data for this paper. These data can be obtained free of charge at www.ccdc.cam.ac.uk/conts/retrieving.html or from the Cambridge Crystallographic Data Centre, 12 Union Road, Cambridge CB2 1EZ, UK [Fax: +44-1223-336033; E-mail: deposit@ccdc.cam.ac.uk].

Acknowledgments

We are grateful to the Deutsche Forschungsgemeinschaft, the Fonds der Chemischen Industrie, the Göttinger Akademie der Wissenschaften, and Ciba company for support of this work.

[1] [1a] A. Igau, H. Grützmacher, A. Baceiredo, G. Bertrand, *J. Am. Chem. Soc.* **1988**, *110*, 6463−6466. [1b] A. J. Arduengo III, R. L. Harlow, M. Kline, *J. Am. Chem. Soc.* **1991**, *113*, 361−363.

[2] See the reviews: [2a] D. Bourissou, O. Guerret, F. P. Gabbaï, G. Bertrand, *Chem. Rev.* **2000**, *100*, 39−91. [2b] L. Jafarpour, S. P. Nolan, *Adv. Organomet. Chem.* **2000**, *46*, 181−222. [2c] W. A. Herrmann, T. Weskamp, V. P. W. Böhm, *Adv. Organomet. Chem.* **2002**, *48*, 1−69. [2d] W. A. Herrmann, *Angew. Chem. Int. Ed.* **2002**, *41*, 1290−1309.

[3] W. A. Herrmann, L. J. Goossen, C. Köcher, G. R. J. Artus, *Angew. Chem. Int. Ed. Engl.* **1996**, *35*, 2805−2807.

[4] J. Huang, E. D. Stevens, S. P. Nolan, J. L. Petersen, *J. Am. Chem. Soc.* **1999**, *121*, 2674−2678.

[5] V. César, S. Bellemin-Laponnaz, L. H. Gade, *Organometallics* **2002**, *21*, 5204−5208.

[6] J. Louie, R. H. Grubbs, *Chem. Commun.* **2000**, 1479−1480.

[7] F. R. Hartley, *The Chemistry of Organophosphorus Compounds Vol. 1*, John Wiley & Sons Ltd. England, **1990**.

[8] N. Hebendanz, F. H. Köhler, G. Müller, *Inorg. Chem.* **1984**, *23*, 3043−3044.

[9] [9a] D. S. McGuinness, B. F. Yates, K. J. Cavell, *Organometallics* **2002**, *21*, 5408−5414. [9b] M. Albrecht, J. R. Miecznikowski, A. Samuel, J. W. Faller, R. H. Crabtree, *Organometallics* **2002**, *21*, 3596−3604.

[10] M. F. Lappert, P. L. Pye, *J. Chem. Soc., Dalton Trans.* **1977**, 2172−2180.

[11] A. Wacker, H. Pritzkow, W. Siebert, *Eur. J. Inorg. Chem.* **1998**, 843−849.

[12] J. Chai, H. Zhu, K. Most, H. W. Roesky, D. Vidovic, H.-G. Schmidt, M. Noltemeyer, *Eur. J. Inorg. Chem.* **2003**, 4332−4337.

[13] A. J. Arduengo III, H. V. R. Dias, F. Davidson, R. L. Harlow, *J. Organomet. Chem.* **1993**, *462*, 13−18.

[14] W. A. Herrmann, K. Öfele, M. Elison, F. E. Kühn, P. W. Roesky, *J. Organomet. Chem.* **1994**, *480*, C7−C9.

[15] B. Beagley, J. C. Briggs, A. Hosseiny, W. E. Hill, T. J. King, C. A. McAuliffe, K. Minten, *J. Chem. Soc., Chem. Commun.* **1984**, 305−306.

[16] W. A. Herrmann, F. C. Munck, G. R. J. Artus, O. Runte, R. Anwander, *Organometallics* **1997**, *16*, 682−688.

[17] B. Albela, M. Corbella, J. Ribas, I. Castro, J. Sletten, H. Stoeckli-Evans, *Inorg. Chem.* **1998**, *37*, 788−798.

[18] L. Dubois, D.-F. Xiang, X.-S. Tan, J. Pécaut, P. Jones, S. Baudron, L. Le Pape, J.-M. Latour, C. Baffert, S. Chardon-Noblat, M.-N. Collomb, A. Deronzier, *Inorg. Chem.* **2003**, *42*, 750−760 and references cited therein.

[19] W. K. Dean, G. L. Simon, P. M. Treichel, L. F. Dahl, *J. Organomet. Chem.* **1973**, *50*, 193−207.

[20] R. M. Wood, D. M. Stucker, L. M. Jones, W. B. Lynch, S. K. Misra, J. H. Freed, *Inorg. Chem.* **1999**, *38*, 5384−5388 and references cited therein.

[21] [21a] R. D. Dowsing, J. F. Gibson, D. M. L. Goodgame, M. Goodgame, P. J. Hayward, *J. Chem. Soc., Dalton Trans.* **1969**, 1242−1248. [21b] R. D. Dowsing, J. F. Gibson, M. Goodgame, P. J. Hayward, *J. Chem. Soc., Dalton Trans.* **1970**, 1133−1138.

[22] N. Kuhn, T. Kratz, *Synthesis* **1993**, 561−562.

[23] G. M. Sheldrick, *Acta Crystallogr., Sect. A* **1990**, *46*, 467−473.

[24] G. M. Sheldrick, SHELXL-97, *Program for Crystal Structure Refinement*, Universität Göttingen, **1997**.

Received November 10, 2003
Early View Article
Published Online May 5, 2004

 © 2004 Wiley-VCH Verlag GmbH & Co. KGaA, Weinheim

Synthesis of a Novel Organoiridium(I) Fluoro Complex

Michael Gorol,[a] Nadia C. Mösch-Zanetti,[a] Herbert W. Roesky,*[a] Mathias Noltemeyer,[a] and Hans-Georg Schmidt[a]

Dedicated to G.-V. Röschenthaler on the occasion of his 60th birthday

Keywords: Syntheses / Crystal structures / Iridium(I) / Fluoro complexes / Pentafluorosilicates

Cyclooctadienefluorotriphenylphosphaneiridium(I) [IrF(C_8H_{12})(PPh_3)] (**3**) was prepared and its structure determined by single crystal X-ray diffraction analysis. Complex **3** crystallises in the monoclinic space group $P2_1/n$. The lattice parameters are a = 931.9(3) pm, b = 1629.4(7) pm, c = 1592.9(7) pm, $\alpha = \gamma = 90°$, β = 92.85(3)°. Number of molecules per unit cell is 4. The square planar iridium complex **3** exhibits an Ir–F bond length of 201.3(5) pm. **3** was obtained in Teflon tubes, whereas the use of glass vessels led to cyclooctadiene-bis(triphenylphosphane)iridium(I)-pentafluorosilicate(IV) ([Ir(C_8H_{12})(PPh_3)$_2$][SiF_5]) (**4**). The composition of **4** was confirmed by single crystal X-ray diffraction analysis. **4** crystallises in the monoclinic space group $P2_1/c$. The lattice parameters are a = 1157.4(9) pm, b = 1864.4(9) pm, c = 1922.5(17) pm, $\alpha = \gamma = 90°$, β = 96.16(7)°. The number of molecules per unit cell is 4. The square-planar coordinated iridium cation [Ir(C_8H_{12})(PPh_3)$_2$]$^+$ is separated from the trigonal bipyramidal [SiF_5]$^-$ anion by 461.1 pm (shortest Ir···F distance) and thus it is assumed that no interactions occur between the fluorine and iridium atoms.
(© Wiley-VCH Verlag GmbH & Co. KGaA, 69451 Weinheim, Germany, 2004)

Introduction

There is ongoing interest in low oxidation state transition metal compounds containing fluorine-metal and carbon-metal bonds as a result of their use in synthesis and catalysis.[1−3] In the presence of π back-bonding ligands fluoro complexes of d^8 metals are stable although they object the predicted hard/soft acid/base (HSAB) rules. This has been shown for the iridium Vaska system $IrF(CO)(PPh_3)_2$, whose derivatives are the only known *organometallic fluorides* in the chemistry of iridium(I).[1,4] Compounds of this type are certainly the most extensively studied and readily prepared systems but structural characterisation has not been accomplished. Thus far, bond length parameters are available only for iridium d^6 centers e.g. Cp*$IrF(Ph)(PMe_3)$,[5] $Ir(Cl)F(NSF_2)(CO)(PPh_3)_2$,[6] [IrF($\eta^2$-NH=$NC_6H_3$-2-$CF_3$)(CO)($PPh_3$)$_2$][$BF_4$],[7] $Ir(FBF_3)Me_2(PMe_2Ph)_3$,[8] and [Ir{C(F)O}F(CO)$_2$(PEt_3)$_2$][BF_4].[9] Iridium(I) complexes with cyclooctadiene or cyclooctene as the stabilising C-based ligands are well-known and widely used as starting materials in organometallic chemistry. However, appropriate fluorides are missing, although some are accessible, as in the case of homologous rhodium(I) olefin complexes.[10−12]

Moreover, complexes of weakly or non-coordinating fluorinated anions such as $[BF_4]^-$, $[PF_6]^-$, $[AsF_6]^-$ and $[SbF_6]^-$ are of special interest in organometallic fluorine chemistry. For instance, the iridium complex [Ir(C_8H_{12})(PCy_3)(py)][PF_6] has been widely used as a catalyst for the reduction of hindered alkenes and [Ir(C_8H_{12})(PPh_3)$_2$][PF_6] has also proven to be useful as a hydrogenation catalyst.[13,14] However, the investigation of pentacoordinate fluorosilicon anions enjoys increasing interest. Large cations are required for the stabilisation of the rather unstable $[SiF_5]^-$ anion ($[SiF_5]^- \rightarrow SiF_4 + F^-$).[15] In recent years a rising number of transition metal complexes containing $[SiF_5]^-$, like in [PtCl(CO)(PEt_3)$_2$][SiF_5],[16] [Ir(H_2)(CO)(PPh_3)$_3$][SiF_5],[17] [Au(PPh_3)$_3$][SiF_5],[18] [Ir(CO)$_2$($PtBu_2Ph$)$_2$][SiF_5],[19] [Ir(H_2)(CO)$_2$($PtBu_2Ph$)$_2$][SiF_5][19] and [Co(NioxH)$_2$(PPh_3)$_2$][SiF_5] ($NioxH_2$ is 1,2-cyclohexanedione dioxime)[20] have been reported.

Herein, we describe the syntheses and characterisations of the novel organoiridium(I) fluoro complex $IrF(C_8H_{12})(PPh_3)$ (**3**) and of the complex salt [Ir(C_8H_{12})(PPh_3)$_2$][SiF_5] (**4**). The crystal structure analysis of **3** lead to the first iridium(I) fluorine bond parameters, whereas that of **4** is probative for the formation of the $[SiF_5]^-$ anion.

Results and Discussion

During our research with the aim of obtaining novel iridium fluorides, the use of most of the usual fluorination ag-

[a] Institut für Anorganische Chemie der Universität Göttingen, Tammannstr. 4, 37077 Göttingen, Germany
Fax: (internat.) +49-(0)551-393373
E-mail: hroesky@gwdg.de

 © 2004 Wiley-VCH Verlag GmbH & Co. KGaA, Weinheim DOI: 10.1002/ejic.200400030

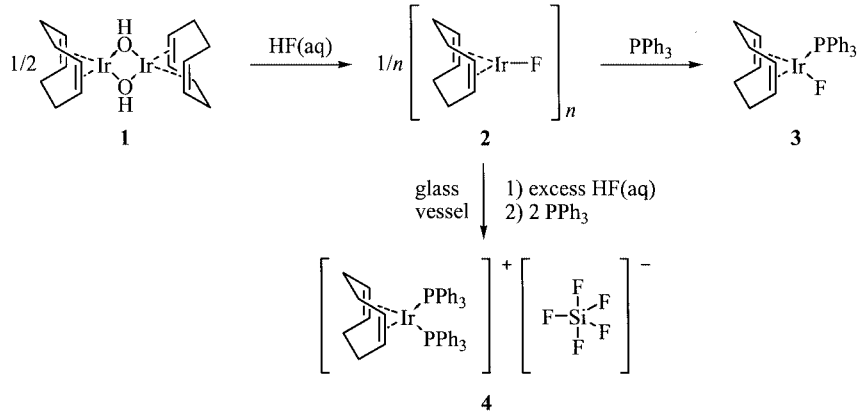

Scheme 1

ents including AgF, Me_3SnF, $(Me_2N)_3S^+(Me_3SiF_2)^-$ (TASF) or XeF_2 failed. The synthesis of $IrF(C_8H_{12})(PPh_3)$ (**3**) was finally successful using aqueous HF as the fluorinating agent, according to the procedure described for the rhodium(I) analogue.[10]

Treatment of a solution of $[Ir(\mu\text{-}OH)(C_8H_{12})]_2$ (**1**)[21] in THF with 73% aqueous HF in a Teflon tube gave compound **2** as a yellow precipitate in virtually quantitative yield (Scheme 1). Due to its insolubility in organic solvents NMR spectroscopic data are not available and, unfortunately, the mass spectrum only shows the fragmentation pattern of the coordinated cyclooctadiene ligand. The formation of an iridium fluoro complex can only be derived from the IR spectrum of compound **2**, which exhibits the $\tilde{\nu}_{IrF}$ stretching mode at 478 cm^{-1} similar to that of $\tilde{\nu}_{IrF}$ = 451 cm^{-1} in $IrF(CO)(PPh_3)_2$.[22] Therefore, a polymeric structure for compound **2** is proposed.

Reaction of triphenylphosphane with a suspension of **2** in THF results in the formation of a reddish solution. After addition of pentane, $IrF(C_8H_{12})(PPh_3)$ (**3**) crystallised as an orange solid. The ^1H NMR spectrum of **3** shows two sets of resonances for the four olefinic protons of the cyclooctadiene ligand. Due to the asymmetric coordination at the iridium(I) centre, one resonance appears at δ = 5.42 ppm (*m*, 2 H), whereas the other one is shifted upfield to δ = 2.59 ppm (*m*, 2 H). These values are similar to those (δ = 5.15 and 2.73 ppm) reported for $IrCl(C_8H_{12})(PPh_3)$.[23] The difference between the two signals is presumably due to the unequal *trans* influence of PPh_3 and F^-. In the ^{19}F NMR spectrum of **3**, a singlet was observed at $\delta = -219.3$ ppm, characteristic of an iridium(I)-bound fluorine atom and the $^{31}P\{^1H\}$ NMR spectrum displays a singlet at δ = 25.1 ppm.

Single crystals suitable for X-ray diffraction analysis of **3** were obtained by slow diffusion of pentane into a concentrated THF solution. Compound **3** crystallises in the monoclinic space group $P2_1/n$. The asymmetric unit contains one molecule of $IrF(C_8H_{12})(PPh_3)$ and half a solvent molecule of THF. Figure 1 shows the molecular structure of $IrF(C_8H_{12})(PPh_3)$ (**3**) along with selected bond lengths and angles. As expected from the larger *trans* influence of PPh_3 with respect to F^-, the Ir(1)−C(5) and Ir(1)−C(6) distances are longer than the Ir(1)−C(1) and Ir(1)−C(2) ones (Figure 1). The Ir(1)−F(1) bond length of 201.3(5) pm in **3** is shorter than those in iridium d^6 compounds, e.g. Cp* $IrF(Ph)(PMe_3)$ 206.9(4) pm,[5] $Ir(Cl)F(NSF_2)(CO)(PPh_3)_2$ 208.9(4),[6] $[IrF(\eta^2\text{-}NH{=}NC_6H_3\text{-}2\text{-}CF_3)(CO)(PPh_3)_2][BF_4]$ 221(4) pm,[7] and $Ir(FBF_3)Me_2(PMe_2Ph)_3$ 238.9(7) pm.[8] This might be due to π back-donation of the olefin ligand in **3**, causing stabilisation of such complexes.[4] The only exception is the iridium(III) fluoro complex $[Ir\{C(F)O\}F(CO)_2(PEt_3)_2][BF_4]$ with an Ir−F separation of 199.8(3) pm.[9] Complex **3** represents the first crystal structure to be determined for an organoiridium(I) fluoro complex.

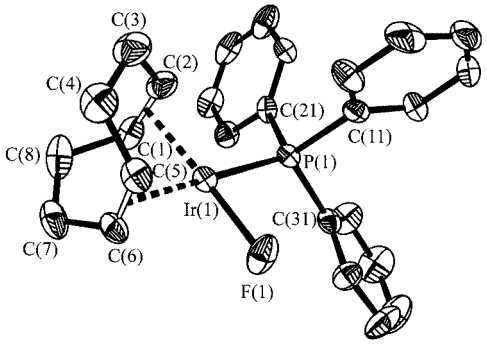

Figure 1. Molecular structure of $IrF(C_8H_{12})(PPh_3)$ (**3**) (without THF) with 50% probability ellipsoids and the labelling scheme; selected bond lengths (pm) and angles (°): Ir(1)−F(1) 201.3(5), Ir(1)−C(1) 209.3(9), Ir(1)−C(2) 208.7(8), Ir(1)−C(5) 218.9(8), Ir(1)−C(6) 217.2(7), C(1)−C(2) 140.0(13), C(5)−C(6) 139.3(12), Ir(1)−P(1) 231.93(19), P(1)−C(11) 181.9(7), P(1)−C(21) 181.7(7), P(1)−C(31) 181.8(8); F(1)−Ir(1)−C(1) 161.2(3), F(1)−Ir(1)−C(2) 157.9(3), F(1)−Ir(1)−C(5) 88.6(3), F(1)−Ir(1)−C(6) 86.6(3), F(1)−Ir(1)−P(1) 90.32(15), C(1)−Ir(1)−P(1) 97.8(2), C(2)−Ir(1)−P(1) 92.3(2), C(5)−Ir(1)−P(1) 159.0(2), C(6)−Ir(1)−P(1) 163.5(2)

However, treatment of **1** with aqueous HF carried out in glass vessels resulted in deep red crystals. This side product is insoluble in THF, but can be recrystallised from a dichloromethane/pentane mixture. This compound was unambiguously identified as the complex salt $[Ir(C_8H_{12})(PPh_3)_2][SiF_5]$ (**4**) by IR and NMR spectroscopy as well as single crystal structure analyses. The formation

 © 2004 Wiley-VCH Verlag GmbH & Co. KGaA, Weinheim

of the cationic iridium complex $[Ir(C_8H_{12})(PPh_3)_2]^+$ in the presence of weakly coordinating anions is well-known.[14] In addition, the appearance of the $[SiF_5]^-$ anion is not unexpected, if reactions involving HF are carried out in glass vessels.[20] Thus, the reaction of **1** in THF with an excess of aqueous HF in a glass vessel affords **4** in quantitative yield, after two equiv. of triphenylphosphane were added (Scheme 1). The ^{1}H NMR spectrum of **4** shows three resonances of equal intensity for the protons of the cyclooctadiene ligand [δ = 4.20 (br. s, 4 H), δ = 2.33 (m, 4 H) and δ = 1.97 ppm (m, 4 H)]. These values are similar to δ = 4.14 (s, 4 H) and δ = 2.12 ppm (m, 8 H) found in $[Ir(C_8H_{12})(PPh_3)_2][BF_4]$.[24] The formation of the cationic bisphosphane complex is best documented by its ^{13}C NMR spectrum. The resonance for the carbon atoms of the =*C*H− groups of the cyclooctadiene ligand appears as a triplet [δ = 87.40 ppm (t, *J* = 5.58 Hz)] indicative of coupling to two phosphorus nuclei, whereas the −*C*H$_2$− groups show a singlet at δ = 31.37 ppm. In the ^{19}F NMR spectrum a broad resonance (δ = −139.1 ppm) is observed. This is in good agreement with that reported (δ = −139 ppm) for the $[SiF_5]^-$ anion in $[Au(PPh_3)_3][SiF_5]$.[18] The ^{31}P NMR resonance is shifted upfield in comparison to that of compound **3** and appears as a singlet at δ = 17.4 ppm. Compound **4** gives rise to bands in the infrared spectrum at ($\tilde{\nu}$ = 879, 790, 479 and 448 cm^{-1} CsI plates), due to Si−F modes similar to those reported in the literature.[16]

Single crystals suitable for X-ray diffraction analyses of **4** were obtained by slow diffusion of pentane into a concentrated CH_2Cl_2 solution. Compound **4** crystallises in the monoclinic space group $P2_1/c$. A structure determination showed one $[Ir(C_8H_{12})(PPh_3)_2]^+$ cation, one non-coordinated $[SiF_5]^-$ anion and a solvent molecule CH_2Cl_2 in the asymmetric unit. The cation is depicted in Figure 2 together with selected bond lengths and angles. The iridium-phosphorus bond lengths [Ir(1)−P(1) 233.1(3) and Ir(1)−P(2) 235.3(3) pm] are similar to those of Ir−P(1) 236.7(2) and Ir−P(2) 232.6(3) pm found in $[Ir(C_8H_{12})(PPh_3)_2][PF_6]$.[14]

The $[SiF_5]^-$ anion is not coordinated to an iridium atom (shortest Ir···F distance is 461.1 pm). The geometry of the silicon atom is regular bipyramidal. The Si−F$_{eq}$ bond lengths are Si(1)−F(1) 158.4(10), Si(1)−F(3) 159.8(10) and Si(1)−F(5) 158.3(10) pm. The Si−F$_{ax}$ distances are longer, with values of Si(1)−F(2) 162.3(10) and Si(1)−F(4) 162.5(11) pm. The bond lengths and angles for the $[SiF_5]^-$ anions in the compounds $[Au(PPh_3)_3][SiF_5]$, $[Ir(CO)_2(PtBu_2Ph)_2][SiF_5]$ and $[Ir(H)_2(CO)_2(PtBu_2Ph)_2][SiF_5]$, are in the same range as those for compound **4**.[18,19]

Once compound **3** has been isolated it does not interact with the glass surface. Evidence for that is derived from NMR and IR spectroscopic data obtained from the oily residue, formed in a glass vessel, as a result of the decomposition of **3** after some weeks. In the ^{19}F NMR spectrum a triplet (δ = −256.3 ppm, t, *J* = 28.8 Hz) and in the ^{31}P{H} NMR spectrum a doublet (δ = 24.5 ppm, d, *J* = 28.7 Hz) suggest the formation of a complex, which has one fluorine atom and two phosphane groups bonded to the iridium atom. The IR spectrum exhibits a band at 1945 cm^{-1} attributable to a $\tilde{\nu}_{CO}$ mode. These data lead to the assumption that one of the products of the decomposition of **3** is the Vaska complex $IrF(CO)(PPh_3)_2$. The formation of a carbonyl complex is in agreement with reports of the ability of rhodium(I) systems to abstract carbon monoxide from oxygen-containing organic solvents.[25]

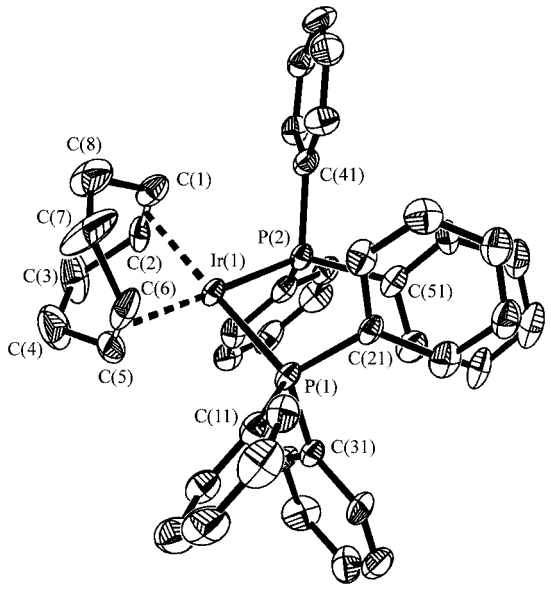

Figure 2. Molecular structure of the $[Ir(C_8H_{12})(PPh_3)_2]^+$ cation in **4** with 50% probability ellipsoids and the labelling scheme; selected bond lengths (pm) and angles (°): Ir(1)−C(1) 221.5(11), Ir(1)−C(2) 223.5(10), Ir(1)−C(5) 216.5(11), Ir(1)−C(6) 219.5(11), Ir(1)−P(1) 233.1(3), Ir(1)−P(2) 235.3(3), C(1)−C(2) 140.8(16), C(5)−C(6) 132.3(19), P(1)−C(11) 184.1(11), P(1)−C(21) 180.6(11), P(1)−C(31) 181.4(10), P(2)−C(41) 183.0(11), P(2)−C(51) 184.3(10), P(2)−C(61) 183.9(11); C(1)−Ir(1)−P(1) 153.7(3), C(2)−Ir(1)−P(1) 168.7(3), C(5)−Ir(1)−P(1) 95.6(3), C(6)−Ir(1)−P(1) 89.5(3), C(1)−Ir(1)−P(2) 93.9(3), C(2)−Ir(1)−P(2) 86.7(2), C(5)−Ir(1)−P(2) 152.0(4), C(6)−Ir(1)−P(2) 170.4(4), P(1)−Ir(1)−P(2) 94.43(9)

Conclusion

The present study describes the synthesis and characterisation of $IrF(C_8H_{12})(PPh_3)$ and provides the first crystallographic data for an organoiridium(I) fluoro complex. The reaction of $[Ir(\mu\text{-}OH)(C_8H_{12})]_2$ with concentrated aqueous HF yields the fluoro complex, only in Teflon tubes, whereas the use of glass vessels led to $[Ir(C_8H_{12})(PPh_3)_2][SiF_5]$. The X-ray diffraction analysis of this iridium(I) complex salt shows that the rather unstable $[SiF_5]^-$ anion can be trapped.

Experimental Section

General Remarks: Solvents were dried and distilled under nitrogen prior to use. All reactions were carried out under dry nitrogen, using standard Schlenk techniques. NMR spectra were recorded using a Bruker Avance 200, Bruker MSL 400 or a Bruker Avance 500 spectrometer and referenced to the resonances of the residual protons in deuterated benzene or CD_2Cl_2. ^{1}H NMR: external

 © 2004 Wiley-VCH Verlag GmbH & Co. KGaA, Weinheim

Table 1. Crystallographic data for **3** and **4**

	3 (incl. THF)	**4** (incl. CH_2Cl_2)
Empirical formula	$C_{28}H_{31}FIrPO_{0.5}$	$C_{45}H_{44}Cl_2F_5IrP_2Si$
Molecular mass [gmol^{-1}]	617.70	1032.93
Temperature [K]	200(2)	200(2)
Wavelength λ [pm]	71.073	71.073
Crystal system	monoclinic	monoclinic
Space group	$P2_1/n$	$P2_1/c$
a [pm]	931.9(3)	1157.4(9)
b [pm]	1629.4(7)	1864.4(9)
c [pm]	1592.9(7)	1922.5(17)
α [°]	90	90
β [°]	92.85(3)	96.16(7)
γ [°]	90	90
V [nm^3]	2.4157(17)	4.125(5)
Z	4	4
Absorption coefficient [mm^{-1}]	5.616	3.529
F(000)	1216	2056
Reflections collected	5803	7556
Independent reflections	4216 [R_{int} = 0.0421]	7149 [R_{int} = 0.1654]
Data/restraints/parameters	4216/0/292	7149/0/505
Goodness-of-fit on F^2	1.111	1.050
Final *R* indices [$I > 2\sigma(I)$]	0.0560, 0.1471	0.0671, 0.1620
Largest diff. Peak/hole [e·Å^{-3}]	5.144/−3.777	3.414/−2.480

standard TMS. ^{13}C NMR: external standard TMS. ^{19}F NMR: external standard CCl_3F. ^{31}P NMR: external standard 85% H_3PO_4. Infrared spectra were recorded on a BIO-RAD Digilab FTS 7 spectrometer. [Ir(μ-OH)(C_8H_{12})]$_2$ (**1**) was prepared by literature methods.[21] All other materials used in the syntheses were reagent grade chemicals and used without further purification.

IrF(C_8H_{12})(PPh_3) (3): Aqueous HF (50.0 μL, 2.00 mmol, 73%) solution was added to a solution of **1** (0.63 g, 1.00 mmol) in THF (10 mL). The reaction mixture was allowed to stand overnight to form a yellow insoluble precipitate **2,** which was filtered off and dried in vacuo. The solid was treated with a solution of PPh_3 (0.52 g, 2.00 mmol) in THF (10 mL) and the mixture was stirred until all solids had dissolved. The resulting reddish solution was layered with pentane (40 mL). After standing overnight orange crystals had formed which were filtered off and dried under reduced pressure. The product was recrystallised from THF/pentane (0.83 g, 71%). M.p. 218 °C (decomp.). $C_{26}H_{27}FIrP$ (581.68): calcd. C 53.69, H 4.68; found C 53.47, H 4.81. ^{1}H NMR (300.13 MHz, C_6D_6): δ = 1.40 (m, 4 H, CH_2), 2.05 (m, 4 H, CH_2), 2.59 (m, 2 H, CH), 5.42 (m, 2 H, *CH*), 7.08 (m, 9 H, C_6H_5), 7.93 (m, 6 H, C_6H_5) ppm. ^{19}F NMR (188.27 MHz, CCl_3F): δ = −219.3 (s, IrF) ppm. ^{31}P NMR (121.50 MHz, C_6D_6): δ = 25.1 (s, IrP). EIMS 70 eV, *m*/*z* (rel. int.): 582 [M] (5), 262 [M − Ir−C_8H_{12}−F] (100), 108 [M − Ir−P(C_6H_5)$_3$−F] (20).

[Ir(C_8H_{12})(PPh_3)$_2$][SiF_5] (4): Aqueous HF (0.50 mL, 20.0 mmol, 73%) solution was added to a solution of **1** (0.63 g, 1.00 mmol) in THF (10 mL) in a glass vessel . The reaction mixture was allowed to stand overnight to form a yellow insoluble precipitate, which was filtered off and dried in vacuo. The solid was treated with a solution of PPh_3 (1.05 g, 4.00 mmol) in THF (10 mL) and the mixture was stirred for 24 h. Deep red crystals formed which were filtered off and dried under reduced pressure. The product was recrystallised from CH_2Cl_2/pentane (1.80 g, 96%). $C_{44}H_{42}F_5IrP_2Si$ (948.05): calcd. C 55.74, H 4.47; found C 55.41, H 4.65. IR (CsI): $\tilde{\nu}$ = 879, 790, 479 and 448 cm^{-1} (SiF_5^-). ^{1}H NMR (300.13 MHz, CD_2Cl_2): δ = 1.97 (m, 4 H, CH_2), 2.32 (m, 4 H, CH_2), 4.20 (s, 4 H, CH), 7.39 (m, 15 H, C_6H_5) ppm. ^{13}C NMR (125.77 MHz, CD_2Cl_2): δ = 31.4 (s, C-3, C-4, C-7, C-8), 87.4 (t, *J* = 5.6 Hz, C-1, C-2, C-5, C-6), 128.9 (t, *J* = 5.2 Hz, C_6H_5), 131.7 (t, *J* = 1.0 Hz, C_6H_5), 134.6 (t, *J* = 5.5 Hz, C_6H_5) ppm. ^{19}F NMR (188.27 MHz, CCl_3F): δ = −139.1 (s, SiF_5) ppm. ^{31}P NMR (121.50 MHz, CD_2Cl_2): δ = 17.8 (s, IrP_2) ppm. FAB$^+$MS 70 eV, *m*/*z* (rel. int.): 825 [Ir(C_8H_{12})(PPh_3)$_2$] (100). FAB$^-$MS 70 eV, *m*/*z* (rel. int.): 123 [SiF_5] (100).

X-ray Crystallographic Study: The single crystals were mounted on a glass fibre in a frozen paraffin drop. Diffraction data were collected on a STOE AED2 four-circle diffractometer with graphite-monochromated Mo-K_α radiation (λ = 71.073 pm). The crystal structures were solved by direct methods using SHELXS-97[26] and refined with SHELXL-97[27] against F^2 for all data by full-matrix least-squares. All non-hydrogen atoms were refined anisotropically. Hydrogen atoms were included in the model at fixed positions. A summary of the crystal data is given in Table 1.

CCDC-228254 (for **3**) and -228255 (for **4**) contain the supplementary crystallographic data for this paper. These data can be obtained free of charge at www.ccdc.cam.ac.uk/conts/retrieving.html [or from the Cambridge Crystallographic Data Centre, 12 Union Road, Cambridge CB2 1EZ, UK; Fax: (internat.) +44-1223-336-033; E-mail: deposit@ccdc.cam.ac.uk].

Acknowledgments

This work was supported by the Deutsche Forschungsgemeinschaft, the Degussa-Hüls AG, the Fonds der Chemischen Industrie, and the Göttinger Akademie der Wissenschaften.

[1] N. M. Doherty, N. W. Hoffman, *Chem. Rev.* **1991**, *91*, 553−573.
[2] E. F. Murphy, R. Murugavel, H. W. Roesky, *Chem. Rev.* **1997**, *97*, 3425−3468.
[3] H. W. Roesky, *J. Fluorine Chem.* **1999**, *100*, 217−226.

 © 2004 Wiley-VCH Verlag GmbH & Co. KGaA, Weinheim

[4] K. Fagnou, M. Lautens, *Angew. Chem.* **2002**, *114*, 26−49; *Angew. Chem. Int. Ed.* **2002**, *41*, 26−47.
[5] J. E. Veltheer, P. Burger, R. G. Bergman, *J. Am. Chem. Soc.* **1995**, *117*, 12478−12488.
[6] P. G. Watson, E. Lork, R. Mews, *J. Chem. Soc., Chem. Commun.* **1994**, 1069−1070.
[7] J. A. Carroll, R. E. Cobbledick, F. W. B. Einstein, N. Farrell, D. Sutton, P. L. Vogel, *Inorg. Chem.* **1977**, *16*, 2462−2469.
[8] E. G. Lundquist, K. Folting, J. C. Huffman, K. G. Caulton, *Organometallics* **1990**, *9*, 2254−2261.
[9] A. J. Blake, R. W. Cockman, E. A. V. Ebsworth, J. H. Holloway, *J. Chem. Soc., Chem. Commun.* **1988**, 529−530.
[10] J. Vicente, J. Gil-Rubio, D. Bautista, *Inorg. Chem.* **2001**, *40*, 2636−2637.
[11] H. L. M. van Gaal, F. L. A. van den Bekerom, J. P. J. Verlaan, *J. Organomet. Chem.* **1976**, *114*, C35−C37.
[12] R. R. Burch, R. L. Harlow, S. D. Ittel, *Organometallics* **1987**, *6*, 982−987.
[13] R. H. Crabtree, *Acc. Chem. Res.* **1979**, *12*, 331−338.
[14] P. A. Chaloner, P. B. Hitchcock, M. Reisinger, *Acta Crystallogr., Sect. C* **1992**, *48*, 735−737.
[15] F. Klanberg, E. L. Muetterties, *Inorg. Chem.* **1968**, *7*, 155−160.
[16] H. C. Clark, P. W. R. Corfield, K. R. Dixon, J. A. Ibers, *J. Am. Chem. Soc.* **1967**, *89*, 3360−3361.
[17] P. Bird, J. F. Harrod, K. A. Than, *J. Am. Chem. Soc.* **1974**, *96*, 1222−1224.
[18] F. Olbrich, R. J. Lagow, *Z. Anorg. Allg. Chem.* **1995**, *621*, 1929−1932.
[19] A. C. Cooper, J. C. Bollinger, J. C. Huffman, K. G. Caulton, *New J. Chem.* **1998**, *22*, 473−480.
[20] Y. A. Simonov, N. V. Gerbeleu, M. Gdaniec, P. N. Bourosh, E. B. Koropchanu, O. A. Bologa, *Russ. J. Coord. Chem.* **2001**, *27*, 341−352.
[21] L. M. Green, D. W. Meek, *Organometallics* **1989**, *8*, 659−666.
[22] L. Vaska, J. Peone Jr., *Inorg. Synth.* **1974**, *15*, 64−68.
[23] K. Vrieze, H. C. Volger, A. P. Praat, *J. Organomet. Chem.* **1968**, *14*, 185−200.
[24] M. Green, T. A. Kuc, S. H. Taylor, *J. Chem. Soc., Sect. A* **1971**, 2334−2337.
[25] J. A. Osborn, F. H. Jardine, J. F. Young, G. Wilkinson, *J. Chem. Soc., Sect. A* **1966**, 1711−1732.
[26] G. M. Sheldrick, *Acta Crystallogr., Sect. A* **1990**, *46*, 467−473.
[27] G. M. Sheldrick, *SHELX*-97, *Program for Crystal Structure Analysis*, University of Göttingen, **1998**.

Received January 15, 2004
Early View Article
Published Online May 5, 2004

 © 2004 Wiley-VCH Verlag GmbH & Co. KGaA, Weinheim

Synthesis and Characterization of Ti Complexes Using 4-*tert*-Butyl-2,6-bis(hydroxymethyl)phenol: X-ray Structures of a Confacial Bioctahedron with Terminal Nucleophilic Phenylmethoxide Ligands, and a Ti_4O_{16} Core Protected by Two Hydrophobic Binding Pockets

Thorsten Glaser,*[a] Ioannis Liratzis,[a] Thomas Lügger,[a] and Roland Fröhlich[b]

Keywords: Tridentate ligands / O ligands / Titanium

Treatment of 4-*tert*-butyl-2,6-bis(hydroxymethyl)phenol (H_3L) with $[TiO(acac)_2]$ in protic solvents at elevated temperatures leads to the formation of the dinuclear complex $(Et_4N)[L_3Ti_2]$ **1**, whereas carrying out the reaction at room temperature or in aprotic solvents leads to the formation of the tetranuclear complex $(Et_4N)_2[L_2(HL)_4Ti_4O_2]$ **2**. Heating **2** in protic solvents leads to the formation of **1**, but **2** is stable in non-protic solvents such as THF even upon heating. Dissolving **1** in an aprotic solvent leads to the formation of **2**. The anion of **1** consists of a confacial bioctahedron with a $[(BzO)_3Ti^{IV}(\mu_2\text{-}OPh)_3Ti^{IV}(OBz)_3]^-$ core. The phenylmethoxide ligands (BzO^-), and the phenolato ligands are bound to the strong Lewis acid Ti^{IV}. The bond lengths are for Ti–OBz ca. 1.83 Å and for Ti–μ_2-OPh ca. 2.11 Å. Despite the highly covalent Ti–OBz bond, the phenylmethoxide ligands exhibit nucleophilic character, and a tendency to bridge two Ti^{IV} ions as demonstrated by the synthesis of the tetranuclear complex **2**. The dianion in **2** consists of a Ti_4O_{16} core with two hydrophobic half-bowl shaped pockets built from three *tert*-butylbenzene units each. The hydrophobic pockets allow access to the Lewis basic $\mu_3\text{-}O^{2-}$ ligands of the Ti_4O_{16} core. In the crystal structure of **2**·$2CH_3CN$, two Et_4N^+ cations occupy these two binding pockets.

(© Wiley-VCH Verlag GmbH & Co. KGaA, 69451 Weinheim, Germany, 2004)

Introduction

In 1970, Robson introduced the concept of dinucleating ligands (compartmental ligands, Robson type ligands).[1] Since then, there has been a steady increase in the number and type of such ligands synthesized in non-cyclic or macrocyclic versions. These ligands are based on the 2,6-bis(iminomethyl)phenol (**A**) and 2,6-bis(aminomethyl)-phenol (**B**) backbones (Scheme 1). The synthesis of homo- and hetero-dinuclear transition metal complexes enabled detailed investigations of their magnetochemical and electrochemical properties. Theses studies provided important insight into the molecular and electronic structure of dinuclear metallo-proteins, and into the cooperativity of such sites in catalysis.[2] The corresponding ligand system based on 2,6-bis(hydroxymethyl)phenol (**C**) (Scheme 1), however, has only recently been used for the synthesis of metal complexes.[3,4] Furthermore, a search of the Cambridge Structural Database indicates that the structural coordination chemistry of phenylmethoxide ligands has, in general, not been well explored.[5] We are interested in dinuclear face-sharing octahedral transition metal complexes (confacial bioctahedra) using ligands based on **C**, because this bridging mode provides short metal-metal distances giving rise to strong electronic communications. The corresponding ligands based on **A** and **B** have already been used for the synthesis of confacial bioctahedra with $N_3M(\mu_2\text{-}OPh)_3MN_3$[6] and $N_3M(\mu_2\text{-}SPh)_3MN_3$cores.[7] Due to their terminal facial $(R_nN)_3$ donor set (n = 1 or 2), these dinuclear complexes cannot be used as ′metal complexes as ligands′ (metallo-ligands). However, confacial bioctahedra with a $O_3M(\mu_2\text{-}OPh)_3MO_3$ core, where the terminal oxygen ligands represent monodentately coordinated alkoxide ligands, represent metallo-ligands, which can be used in a modular approach for the synthesis of larger molecules or even 1D coordination polymers.

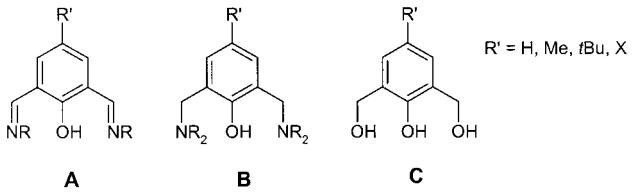

Scheme 1

[a] Institut für Anorganische und Analytische Chemie, Westfälische Wilhelms-Universität Münster,
Wilhelm-Klemm-Straße 8, 48149 Münster, Germany
E-mail: tglaser@uni-muenster.de
[b] Organisch-Chemisches Institut, Westfälische Wilhelms-Universität Münster,
Corrensstr. 40, 48149 Münster, Germany

Herein, we report on the rational synthesis of a confacial bioctahedron with nucleophilic terminal donors. Using the ligand 4-*tert*-butyl-2,6-bis(hydroxymethyl)phenol (H_3L), the complex $(Et_4N)[L_3Ti_2]$ (**1**) with a $[(BzO)_3Ti^{IV}(\mu_2\text{-}OPh)_3\text{-}Ti^{IV}(OBz)_3]^-$ core has been synthesized and characterized. The Ti^{IV} ions are strong Lewis acids. The terminal phenylmethoxide ligands, therefore, have to donate much of their charge to the coordinated Ti^{IV} ions. However, the terminally coordinated phenylmethoxide ligands still possess sufficient nucleophilicity to bridge two Ti^{IV} ions as demonstrated by the synthesis and characterization of $(Et_4N)_2[L_2(HL)_4Ti_4O_2]$ (**2**).

Results and Discussion

Synthesis and Characterization

Treatment of H_3L with $[TiO(acac)_2]$ in a 3:2 molar ratio in the presence of a stoichiometric amount of Et_3N in refluxing MeOH yielded, after addition of excess $(Et_4N)Cl$, filtration, and slow evaporation of the solvent, yellow crystals of **1**. The IR spectrum confirmed the presence of the ligand.[3] The absorptions at 2957, 2876, 1393, and 1363 cm^{-1} are characteristic of the *tert*-butyl groups of the ligand, and the symmetric ring stretch appears at 1479 cm^{-1}. Two strong absorptions for the stretching frequencies of the phenolic C−O bond can be observed at 1252 and 1212 cm^{-1} as well as one broad absorption of the benzylic C−O bond at 1041 cm^{-1}. Three strongly resolved absorptions at 613, 590, and 564 cm^{-1} [ν(Ti−O)][8] indicate the coordination of the ligand to titanium. The electrospray mass spectrum of **1** exhibits a prominent ion at a mass-to-charge ratio (*m*/*z*) of 717.6, with mass and isotope distribution patterns corresponding to $[L_3Ti_2]^-$ (calculated *m*/*z* of 717.2). The ^1H and ^{13}C NMR spectra correspond to a symmetrical coordination of one kind of trianionic ligand L^{3-}. These data are all in agreement with the formulation of **1** containing the symmetric bioctahedral $[L_3Ti_2]^-$ anion.

Treatment of H_3L with $[TiO(acac)_2]$ using similar conditions used for the synthesis of **1**, but stirring the reaction solution at room temperature, yielded yellow needles of **2**. The IR spectrum clearly shows, that this change in the reaction temperature affords a complex different from **1**. Characteristic absorptions show the presence of the ligand but a broad flat absorption at 2600−3200 cm^{-1} indicates, that the ligand is not completely deprotonated. The phenolic C−O stretching region exhibits four absorptions with a different intensity pattern compared with the two absorptions observed in the spectrum of **1**, while the absorption corresponding to the stretching frequency of the benzylic C−O bond at 1040 cm^{-1} becomes smaller and broader in the spectrum of **2**. The three sharp resolved absorptions of the ν(Ti−O) stretches in the spectrum of **1** are replaced by several unresolved transitions in this region in the spectrum of **2**. Thus, the IR spectrum of **2** indicates a more asymmetric coordination mode of the ligand compared with in **1**, and/or the occurrence of more than one set of ligands. This is corroborated by the ^1H NMR spectrum of **2**. The observation of three *tert*-butyl resonances and six different signals for the aromatic protons, demonstrates the presence of three distinguishable sets of ligand molecules in **2**. Additionally, two hydroxy proton resonances suggest, that only seven of the nine possible hydroxy groups of the three ligand molecules are deprotonated in **2**. The benzylic region shows a multitude of sharp signals indicating, that the two protons of each benzylic group are inequivalent, and that no fluxional interconversion occurs between them. Although the IR and NMR spectra of **2** show clear differences from the spectra of **1**, the electrospray mass spectrum of **2** in MeOH exhibits only a prominent ion at a mass-to-charge ratio (*m*/*z*) of 717.1 as in the spectrum of **1**, with mass and isotope distribution patterns corresponding to $[L_3Ti_2]^-$. This indicates the transformation of **2** into **1** under the conditions of the electrospray ionization (high temperature).

Single Crystal X-ray Diffraction Studies

Structure of $(NEt_4)[L_3Ti_2]$ (1)

The crystal structure of **1** consists of dinuclear anions $[L_3Ti_2]^-$ and well separated Et_4N^+ cations. Figure 1 shows two views of the molecular structure of the $[L_3Ti_2]^-$ anion in crystals of **1**, and the labeling scheme used. There is no crystallographic symmetry imposed on the anion. The anion consists of two titanium ions and three ligand molecules L^{3-}, which are the triply-deprotonated form of H_3L. Each ligand acts as a tridentate donor with two terminal phenylmethoxide donors (BzO^-), and one μ_2-bridging phenolato donor (PhO^-). The two titanium ions are bridged in a face-sharing fashion by the three phenolato donors giving rise to an overall bioctahedral core. However, the coordination geometry of the titanium ions deviates severely from octahedral symmetry. Table 1 summarizes selected interatomic distances and angles of the $O_3Ti(\mu_2\text{-}O)_3TiO_3$ core. The Ti−μ_2-OPh bond lengths are in the range of 2.10−2.13 Å while the Ti−OBz bond lengths are 0.3 Å shorter (1.81−1.84 Å). The Ti1···Ti2 distance is 3.04 Å. The short Ti−OBz bond lengths indicate a strong bond between the Lewis acidic Ti^{IV} ions and the Lewis basic BzO^-. The latter

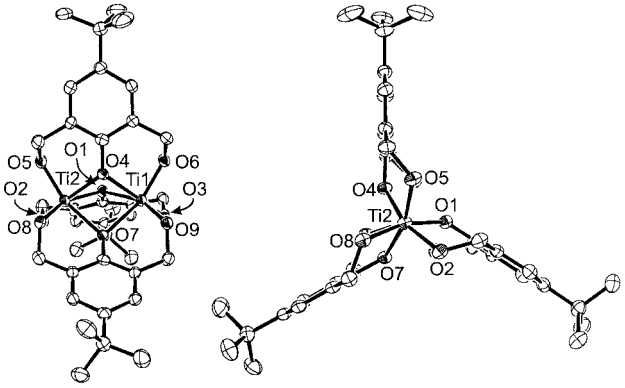

Figure 1. Two views of the molecular structure of the anion $[L_3Ti_2]^-$ in crystals of **1**

 © 2004 Wiley-VCH Verlag GmbH & Co. KGaA, Weinheim

Table 1. Selected interatomic distances (Å) and angles (°) for $(Et_4N)[L_3Ti_2]$ (**1**)

Ti1−O3 (OBz)	1.837(3)	Ti2−O2 (OBz)	1.834(2)
Ti1−O6 (OBz)	1.834(2)	Ti2−O5 (OBz)	1.835(3)
Ti1−O9 (OBz)	1.817(3)	Ti2−O8 (OBz)	1.815(2)
Ti1−O1 (μ2-OPh)	2.133(2)	Ti2−O1 (μ2-OPh)	2.114(2)
Ti1−O4 (μ2-OPh)	2.105(2)	Ti2−O4 (μ2-OPh)	2.104(2)
Ti1−O7 (μ2-OPh)	2.114(2)	Ti2−O7 (μ2-OPh)	2.099(2)
Ti1···Ti2	3.043(1)		
O9−Ti1−O6	97.69(11)	O2−Ti2−O5	97.75(11)
O9−Ti1−O3	95.02(11)	O8−Ti2−O7	86.02(10)
O6−Ti1−O3	94.25(11)	O2−Ti2−O7	102.54(11)
O9−Ti1−O4	107.08(11)	O5−Ti2−O7	159.14(10)
O6−Ti1−O4	85.14(10)	O8−Ti2−O4	104.36(10)
O3−Ti1−O4	157.78(11)	O2−Ti2−O4	158.86(11)
O9−Ti1−O7	85.31(10)	O5−Ti2−O4	85.67(10)
O6−Ti1−O7	158.15(11)	O7−Ti2−O4	73.66(9)
O3−Ti1−O7	107.09(10)	O8−Ti2−O1	160.48(11)
O4−Ti1−O7	73.35(9)	O2−Ti2−O1	85.17(10)
O9−Ti1−O1	158.42(10)	O5−Ti2−O1	102.49(11)
O6−Ti1−O1	103.81(10)	O7−Ti2−O1	74.75(9)
O3−Ti1−O1	85.30(10)	O4−Ti2−O1	73.75(9)
O4−Ti1−O1	73.35(9)	Ti2−O1−Ti1	91.51(9)
O7−Ti1−O1	74.05(9)	Ti2−O4−Ti1	92.60(9)
O8−Ti2−O2	95.98(11)	Ti2−O7−Ti1	92.46(9)
O8−Ti2−O5	96.68(11)		

exhibits no resonance stabilization of the negative charge compared with PhO^-.

An ideal bioctahedron would have all X−M−X angles equal to 90°, and all M−X_{br}−M (br denotes bridging ligand) angles equal to 70.53°. Distortions from this ideal geometry may be attributed to attractive or repulsive M-to-M forces.[9] In order to compare the structure of the anion in **1** with an ideal bioctahedron, four sets of angles have to be considered: Ti1−μ_2-OPh−Ti2 (β, ideal value 70.53°), PhO−Ti−OPh (α′, ideal value 90°), BzO−Ti−OBz (α″, ideal value 90°), and PhO−Ti−OBz (α‴, ideal value 90°). The respective mean values of these angles in **1** are: β = 92.2°, α′ = 73.7°, α″ = 96.2°, and α‴ = 95.0°. The increased value of β and the decreased value of α′ compared with the ideal values of 70.53 ° and 90 °, respectively, are clear evidence of an elongation of the bioctahedron along the C_3-axis, thus indicating repulsive electrostatic interactions between the two Ti^{IV} ions. To interpret the values of α″ and α‴, the steric constraints of the tridentate ligand L^{3-} must be considered. Similar constraints do not occur in confacial bioctahedra with only the monodentate ligands X, $X_3M(\mu_2\text{-}X)_3MX_3$. The steric constraint of the phenyl ring on the methoxide CH_2O^- units pushes the coordinated methoxide oxygen atom towards the phenyl plane of the ligand molecule (Figure 1, right). This is especially apparent with the occurrence of two different types of PhO−Ti−OBz angles (α‴). The mean value of these angles for benzylic and phenolic oxygen atoms belonging to the same ligand molecule is 85.4°, while for benzylic and phenolic oxygen atoms belonging to different ligand molecules it is 104.6°, demonstrating the steric stress on the phenylmethoxide donors.

Structure of $(Et_4N)_2[L_2(HL)_4Ti_4O_2]\cdot 2CH_3CN$ (2·2CH$_3$CN)

The crystal structure of **2**·2CH_3CN consists of tetranuclear dianions $[L_2(HL)_4Ti_4O_2]^{2-}$, Et_4N^+ cations, and CH_3CN molecules. The asymmetric unit consists of one half of the dianion with the other half generated by a center of inversion. The titanium centers are in distorted octahedral coordination environments of six oxygen donors (Figure 2 and Table 2). Ti1 is coordinated by one μ_3-oxo ligand O1′, one non-bridging OPh O10, one μ_2-OPh O50, two non-bridging OBz centers O19 and O51, and one μ_2-OBz O31′, whereas Ti2 is coordinated by two μ_3-oxo ligands O1 and O1′, one non-bridging OPh O30, one μ_2-OPh O50, one non-bridging OBz center O59, and one μ_2-OBz O31. The mean bond lengths for the different kinds of Ti−O bonds are: Ti−OBz 1.86 Å, Ti−OPh 1.90 Å, Ti−μ_3-O 1.97 Å, Ti−μ_2-OBz 2.03 Å, and Ti−μ_2-OPh 2.08 Å. The terminal phenylmethoxide donors form the shortest Ti−O bonds, while the bridging phenolato donors form the longest Ti−O bonds. It is interesting to compare these values with the corresponding values for Ti−OBz (1.83 Å) and Ti−μ_2-OPh (2.11 Å) found in **1**. The Ti−OBz bonds are slightly shorter in **1** compared with those in **2**, and the Ti−μ_2-OPh bonds are slightly longer in **1** compared with those in **2**. There are two other trends observed in the bond lengths in **2**, namely (*i*) the Ti−O bond length of one type of oxygen donor decreases upon going from monodentate to bridging. A ligand bridging two metal ions has to donate charge to both metal ions compared with a monodentate ligand, which only donates charge to one metal ion. Although the bridging ligand donates more overall charge (i.e. the sum of both bonds), the charge donation per bond is less compared with the bond to a monodentate ligand.[10] This results in the observed increase in the bond lengths of the bridging ligand compared with the monodentate ligand. (*ii*) The Ti−O bond length of a phenylmethoxide donor is shorter than of a phenolato donor of the same coordination mode (OBz vs. OPh and μ_2-OBz vs. μ_2-OPh), which is consistent with the stronger donor ability of a phenylmethoxide ligand compared with a phenolato ligand due to the difference in resonance stabilizations of the respective anions.[11]

The three independent ligand molecules in **2** exhibit three different coordination modes. Ligand a (O10, O11, O19) acts as a bidentate chelating ligand via O10 (OPh) and O19 (OBz), while O11 is protonated and forms an intramolecular hydrogen bond with the terminally coordinated phenylmethoxide oxygen atom O59′ (2.83 Å). Ligand b (O30, O31, O39) also coordinates only in a bidentate fashion via O30 (OPh) and O31 (OBz) but the phenylmethoxide donor acts as a bridging ligand between two Ti^{IV} ions. The protonated O39 (BzOH) forms an intramolecular hydrogen bond with the terminally coordinated phenylmethoxide oxygen atom O19 (2.72 Å). The remaining ligand c (O50,

 © 2004 Wiley-VCH Verlag GmbH & Co. KGaA, Weinheim

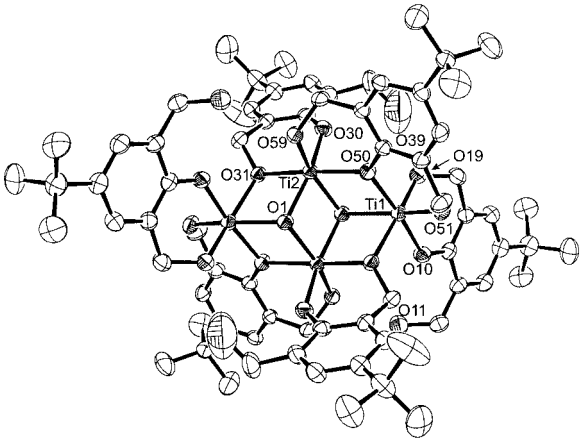

Figure 2. Molecular structure of the dianion $[L_2(HL)_4Ti_4O_2]^{2-}$ in crystals of **2**·2CH_3CN

Table 2. Selected interatomic distances (Å) and angles (°) for $(Et_4N)_2[L_2(HL)_4Ti_4O_2]$·2$CH_3CN$ (**2**·2CH_3CN)
Symmetry transformations used to generate equivalent atoms: $' -x + 1, -y + 1, -z + 1$

Ti1−O1′ (μ_3-O)	1.967(2)	Ti2−O30 (OPh)	1.903(2)
Ti1−O10 (OPh)	1.902(2)	Ti2−O31 (μ_2-OBz)	1.978(2)
Ti1−O19 (OBz)	1.852(3)	Ti2−O50 (μ_2-OPh)	2.049(2)
Ti1−O50 (μ_2-OPh)	2.102(2)	Ti2−O59 (OBz)	1.874(2)
Ti1−O51 (OBz)	1.844(2)	Ti1···Ti2	3.2083(8)
Ti1−O31′ (μ_2-OBz)	2.080(2)	Ti1···Ti2′	3.1226(9)
Ti2−O1 (μ_3-O)	1.949(2)	Ti2···Ti2′	3.0297(11)
Ti2−O1′ (μ_3-O)	1.999(2)		
O51−Ti1−O19	98.27(12)	O59−Ti2−O31	99.72(10)
O51−Ti1−O10	95.82(11)	O30−Ti2−O31	85.61(10)
O19−Ti1−O10	88.97(11)	O1−Ti2−O31	77.58(9)
O51−Ti1−O1′	155.97(11)	O59−Ti2−O1′	158.50(10)
O19−Ti1−O1′	97.72(10)	O30−Ti2−O1′	95.59(11)
O10−Ti1−O1′	102.29(10)	O1−Ti2−O1′	79.76(10)
O51−Ti1−O31′	91.42(11)	O31−Ti2−O1′	100.36(9)
O19−Ti1−O31′	169.01(10)	O59−Ti2−O50	84.47(9)
O10−Ti1−O31′	84.87(10)	O30−Ti2−O50	94.51(10)
O1′−Ti1−O31′	74.81(9)	O1−Ti2−O50	101.67(10)
O51−Ti1−O50	85.36(10)	O31−Ti2−O50	175.80(9)
O19−Ti1−O50	97.34(10)	O1′−Ti2−O50	75.44(9)
O10−Ti1−O50	173.35(10)	Ti2−O1−Ti1′	105.75(11)
O1′−Ti1−O50	74.89(9)	Ti2−O1−Ti2′	100.24(10)
O31′−Ti1−O50	88.56(9)	Ti1′−O1−Ti2′	108.00(10)
O59−Ti2−O30	93.53(11)	Ti2−O31−Ti1′	100.60(10)
O59−Ti2−O1	97.19(10)	Ti2−O50−Ti1	101.23(9)
O30−Ti2−O1	161.34(10)		

O51, O59) exhibits the same tridentate coordination mode as the ligands in **1**.

The structure of **2** may be regarded as consisting of a Ti_4O_{16} core enclosed by an organic shell [Figure 3 (a)]. The oxygen atoms are situated above and below a plane comprised of the four titanium ions. Two half-bowls each formed by three *tert*-butylbenzene moieties are positioned above and below this Ti_4-plane, respectively. Figure 3 (b) demonstrates that the hydrophobic half-bowl allows access to the μ_3-oxo ligand. Thus, two hydrophobic binding pockets for Lewis bases are provided by **2**. In the crystal structure of **2**·2CH_3CN, the two hydrophobic pockets of each dianion are occupied by the two Et_4N^+ cations [Figure 3 (c)]. The Ti_4O_{16} core found in the dianion of **2** represents a relatively common structural motif in Ti−oxygen chemistry since it has been observed in several complexes constructed from varying kinds of alkoxide ligands from monodentate to tridentate.[4,12] These compounds can be used as molecular precursors for metal oxides in sol-gel chemistry or for thin-film preparation.

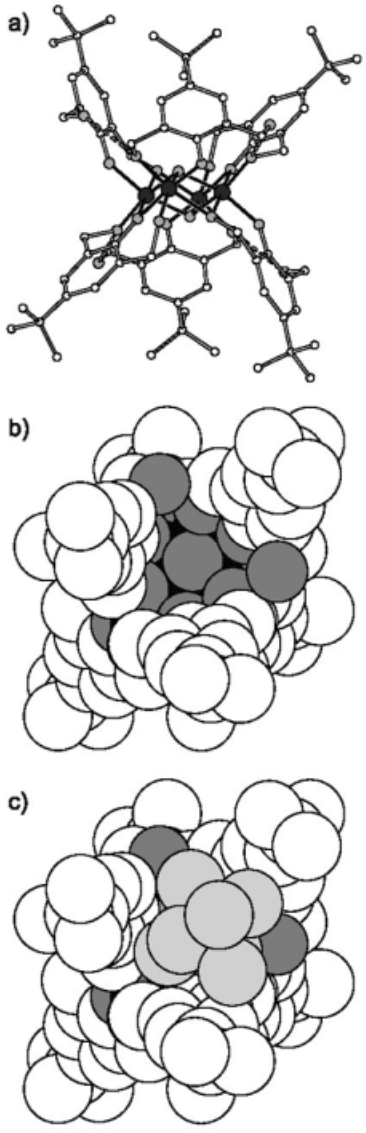

Figure 3. a) Sketch of the molecular structure of the dianion $[L_2(HL)_4Ti_4O_2]^{2-}$ **2**·2CH_3CN illustrating the Ti_4O_{16} core and the two hydrophobic half-bowls each formed by three *tert*-butylbenzene units; b) Space-filling model of this structure [rotated by 90° relative to the view in a)] illustrating the hydrophobic pocket, which allows direct access to the μ_3-oxo oxygen atom of the Ti_4O_{16} core; c) Space-filling model of the dianion, and one Et_4N^+ cation placed in the hydrophobic pockets of the dianion

Solution Properties

The monoanion of **1** has an idealized C_{3h} symmetry in the solid state. If this symmetry were to be retained in solu-

 © 2004 Wiley-VCH Verlag GmbH & Co. KGaA, Weinheim

tion, two sets of signals would be expected for the benzylic protons in the ^{1}H NMR spectrum. However, the ^{1}H NMR spectrum of **1** in [D_6]DMSO exhibits only one broad resonance for the benzylic protons at $\delta = 5.17$ ppm. This indicates that a dynamic equilibrium exists between two forms with different orientations of the methoxide groups relative to the phenolic plane (Scheme 2). On the other hand, the ^{1}H NMR spectrum of **2** in [D_8]THF solution displays all signals predicted for the three different ligand molecules observed in the solid-state structure. This means, that the conformation of the tetranuclear dianion is fixed, which could be a consequence of the four intramolecular hydrogen bonds.

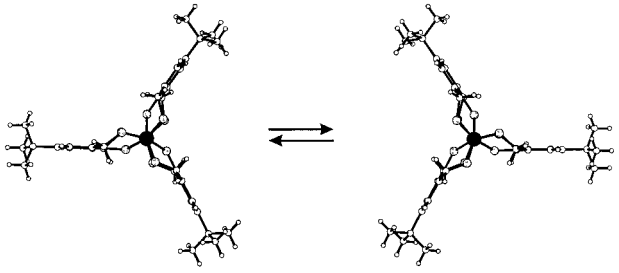

Scheme 2

The UV/Vis absorption spectra of acetonitrile solutions of H_3L, **1**, and **2** are shown in Figure 4. The protonated ligand exhibits absorptions at 309 nm (sh, ≈ 120 M^{-1} cm^{-1}) and 282 nm (2320 M^{-1} cm^{-1}). The spectrum of complex **1** exhibits absorption intensity, which starts to increase starting at ≈ 400 nm with no resolved transitions but shoulders at ≈ 288, 246, and 222 nm. The absorption of the tetranuclear complex **2** starts to increase at ≈ 450 nm with maxima at 333 nm (22200 M^{-1} cm^{-1}), 296 nm (21600 M^{-1} cm^{-1}), and 290 nm (21600 M^{-1} cm^{-1}). The strong low-energy absorptions in the spectra of **1** and **2** are oxygen-to-titanium charge transfer in origin. The main conclusion is that **1** and **2** are clearly distinguishable by their absorption spectra. The spectrum of **2** measured in THF is identical to that measured in CH_3CN.

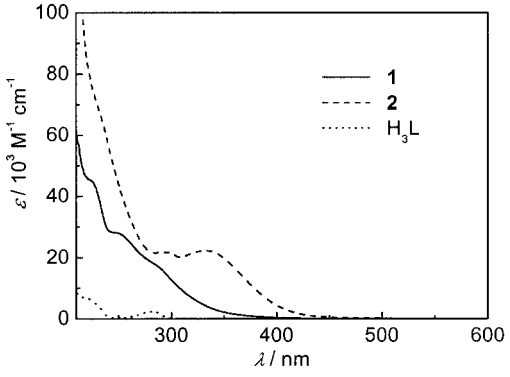

Figure 4. UV-Vis absorption spectra of acetonitrile solutions of H_3L, **1**, and, **2**

Heating **2** in protic solvents leads to the formation of **1**, an essential fact for the controlled synthesis of **1** and **2**, respectively. The reaction between the ligand and [$TiO(acac)_2$] in alcoholic solution at room temperature results in the formation of **2**, whereas **1** is formed by heating the reaction mixture to reflux. This is corroborated with the ESI mass spectrum of a methanolic solution of **2** which, due to heating of the solution in the ESI process, exhibits only the signal corresponding to the anion of **1**. On the other hand, in non-protic solvents **2** is stable even upon heating. Storing the sealed NMR tube of the [D_8]THF solution of **2** at 70 °C overnight does not affect the ^{1}H NMR spectrum. Additionally, **1** can be converted back to **2**. Dissolving **1** in a CH_3CN/MeOH mixture (10:1) leads to the deposition of yellow crystals, which were shown to be pure **2** by FTIR spectroscopy and single-crystal X-ray diffraction. These observations are in agreement with the following equilibrium:

$$[L_2(HL)_4Ti_4O_2]^{2-} \rightleftarrows 2\,[L_3Ti_2]^- + 2\,H_2O$$

The cleavage of the titanium−oxo bond of the former titanyl unit requires some activation energy, and a protic solvent is needed for the formation of water. The dinuclear $[L_3Ti_2]^-$ complex seems to be more stable in protic solvents whereas the tetranuclear $[L_2(HL)_4Ti_4O_2]^{2-}$ complex seems to be more stable in aprotic solvents. The latter might indicate that the two Et_4N^+ cations remain in the hydrophobic binding pockets to give an overall neutrally charged ion triple.

Conclusions

We have shown by the synthesis of complex **1**, that 2,6-bis(hydroxymethyl)-4-*tert*-butylphenol is capable of forming a confacial bioctahedron with a $[(BzO)_3Ti^{IV}(\mu_2\text{-}OPh)_3Ti^{IV}(OBz)_3]^-$ core exhibiting a short Ti···Ti distance of ≈3.0 Å. The coordination of the terminal phenylmethoxide donors to the strong Lewis acid Ti^{IV} still leaves some nucleophilicity at the oxygen atoms. This has been demonstrated with the synthesis of complex **2**, which exhibits μ_2-bridging phenylmethoxide ligands. Work is in progress to prepare coordination polymers using the anion of **1** as a building block.

The tetranuclear dianion in **2** consists of a Ti_4O_{16} core protected by two hydrophobic pockets, which allow access to the μ_3-oxo ligand of the Ti_4O_{16} core. TiO_2 is known as a heterogeneous photocatalyst, e.g. for the oxidation of ethanol.[13] Studies on the binding of ethanol to **2** are in progress to evaluate the potential of **2** as a homogeneous photocatalyst utilizing the strong LMCT absorption band at 333 nm.

Experimental Section

General Methods and Materials: Infrared spectra (400−4000 cm^{-1}) of solid samples were recorded in KBr disks using a Bruker Vector

 © 2004 Wiley-VCH Verlag GmbH & Co. KGaA, Weinheim

22 spectrometer. UV/Vis/NIR-absorption spectra of solutions were measured on a Varian Cary 50 spectrophotometer in the range of 190−1100 nm at ambient temperature. ESI mass spectra were recorded on a Micromass Quattro LC mass spectrometer. ^{1}H and ^{13}C NMR spectra were obtained on a Bruker AC200 or on a Bruker ARX300 spectrometer using the solvent resonances as an internal standard in each case. The ligand H_3L was synthesized according to a published procedure.[3]

$(Et_4N)[L_3Ti_2]$ (1): To a stirred solution of H_3L (500 mg, 2.38 mmol) and $[TiO(acac)_2]$ (415 mg, 1.59 mmol) in MeOH (40 mL) was added Et_3N (1.00 mL, 7.13 mmol). The yellow solution was heated to reflux for 5 h. Addition of $(Et_4N)Cl$ (4.0 g), filtration, and slow evaporation of the solvent yielded yellow crystals of $(Et_4N)[L_3Ti_2]$ (350 mg, 52%). $C_{44}H_{65}NO_9Ti_2$ (847.77): calcd. C 62.34, H 7.73, N 1.65; found C 62.01, H 7.58, N 1.51. MS (ESI in MeOH/CH_3CN solution, negative ion mode): m/z = 749.6 $\{[L_3Ti_2]MeOH\}^-$, 717.6 $[L_3Ti_2]^-$. ^{1}H NMR (300 MHz, [D$_6$]DMSO, 25 °C): δ = 1.13 (t × t, $J_{H,H}$ = 7.4, J_{H-N} = 1.8 Hz, 12 H, NCH_2CH_3), 1.21 (s, 27 H, *tert*-butyl CH_3), 3.17 (q, 8 H, NCH_2CH_3), 5.17 (s, 12 H, br, benz. CH), 6.94 (s, 6 H, arom. CH). ^{13}C NMR (75 MHz, [D$_6$]DMSO, 25 °C): δ = 7.0 (NCH_2CH_3), 31.3 ($C(CH_3)_3$), 33.4 ($C(CH_3)_3$), 51.4 (t, J_{C-N} = 2.6 Hz, NCH_2CH_3), 71.0 (benz. CH_2), 122.2 (C_{Ar}-3), 127.8 (C_{Ar}-4), 139.8 (C_{Ar}-2), 154.5 (C_{Ar}-1). IR: $\tilde{\nu}$ = 2957 s, 2876 m, 2827 m, 1608 w, 1479 vs, 1451 s, 1393 w, 1363 w, 1252 vs, 1212 vs, 1041 vs/br, 871 w, 832 m, 765 m, 755 m, 668 m, 613 vs, 590 vs, 564 s cm^{-1}.

$(Et_4N)_2[L_2(HL)_4Ti_4O_2]\cdot 2EtOH\cdot 2H_2O$ ($2\cdot 2EtOH\cdot 2H_2O$): To a stirred solution of H_3L (500 mg, 2.38 mmol) and $[TiO(acac)_2]$ (415 mg, 1.59 mmol) in EtOH (45 mL) was added Et_3N (1.00 mL, 7.13 mmol). The yellow solution was stirred at room temperature for 5 h. Addition of $(Et_4N)Cl$ (4.0 g), filtration, and slow evaporation of the solvent yielded yellow needles of $(Et_4N)_2[L_2(HL)_4Ti_4O_2]\cdot 2EtOH\cdot 2H_2O$ (300 mg, 42%). $C_{88}H_{142}N_2O_{24}Ti_4$ (1803.61): calcd. C 58.60, H 7.94, N 1.55; found C 58.71, H 7.71, N 1.58. ^{1}H NMR (200 MHz, [D$_8$]THF, 25 °C): δ = 0.35 (m, 24 H, NCH_2CH_3), 1.19 (s, 27 H, *tert*-butyl CH_3), 1.23 (s, 27 H, *tert*-butyl CH_3), 1.25 (s, 27 H, *tert*-butyl CH_3), 3.88 (q, 16 H, NCH_2CH_3), 4.5−6.0 (m, 24 H, benz. CH), 6.8−7.2 (6s, 12 H, arom. CH), 7.87 (s, 2 H, BzOH), 8.42 (s, 2 H, BzOH). IR: $\tilde{\nu}$ = 2953 s, 2904 m, 2866 m, 1606 w, 1479 vs, 1393 w, 1364 w, 1305 w, 1275 s, 1262 s, 1218 vs, 1040 m/br, 1005 w, 877 w, 839 s, 768 m, 540−630 br cm^{-1}. X-ray quality crystals of $2\cdot 2CH_3CN$ were grown from MeOH/CH_3CN, 1:5.

Table 3. Crystal data and structure refinement for **1** and $2\cdot 2CH_3CN$

	1	$2\cdot 2CH_3CN$
Chemical formula	$C_{44}H_{65}NO_9Ti_2$	$C_{92}H_{140}N_4O_{20}Ti_4$
Molecular mass	847.77	1813.68
Crystal system	monoclinic	monoclinic
Space group	*C*2/*c* (No. 15)	*P*21/*c* (No. 14)
a / Å	43.409(7)	14.493(1)
b / Å	9.632(2)	19.454(1)
c / Å	26.008(4)	16.956(1)
β / °	126.122(4)	97.06(1)
V / Å^3	8784(2)	4744.4(5)
Z	8	2
T / K	153	198
μ / cm^{-1}	4.17	3.93
No. data collected	17743	29946
No. unique data	5645	11286
$R_{int.}$	0.054	0.044
Final $R(F)$ obsd.	0.045	0.072
Final $R(F^2)$ all	0.125	0.224

X-ray Crystallographic Data Collection and Refinement of the Structures: A summary of the crystal data, data collection, and refinements of the both structures is given in Table 3. Data sets were collected with Bruker AXS APEX and Nonius KappaCCD diffractometers, equipped with rotating anode generators. Programs used: data collection − SMART[14] and COLLECT,[15] data reduction − SAINT[14] and Denzo-SMN,[16] absorption correction − SADABS[14] and SORTAV,[17] structure solution − SHELXS-97,[18] structure refinement − SHELXL-97.[19] CCDC-220429 (**1**) and -220430 ($\mathbf{2}\cdot 2CH_3CN$) contain the supplementary crystallographic data for this paper. These data can be obtained free of charge at www.ccdc.cam.ac.uk/conts/retrieving.html [or from the Cambridge Crystallographic Data Center, 12 Union Road, Cambridge CB2 1EZ, UK; Fax: (internat.) +44-1223-336-033; E-mail: deposit@ccdc.cam.ac.uk].

Acknowledgments

T. G. gratefully acknowledges generous support from Prof. F. E. Hahn. This work was supported by the Fonds der Chemischen Industrie, the Bundesministerium für Bildung und Forschung, the Dr. Otto Röhm Gedächtnisstiftung, and the Deutsche Forschungsgemeinschaft (Priority Program "Molecular Magnetism'). The skilful technical assistance of Mrs. T. Pape is gratefully acknowledged.

[1] [1a] R. Robson, *Inorg. Nucl. Chem. Lett.* **1970**, *6*, 125−128. [1b] R. Robson, *Aust. J. Chem.* **1970**, *23*, 2217−2224. [1c] N. H. Pilkington, R. Robson, *Aust. J. Chem.* **1970**, *23*, 2225−2236.
[2] [2a] F. L. Urbach in *Metal Ions in Biological Systems* (Ed. H. Sigel), Marcel Dekker, New York, **1981**, vol. 12, p. 73−115. [2b] C. L. Spiro, S. L. Lambert, T. J. Smith, E. N. Duesler, R. R. Gagne, D. N. Hendrickson, *Inorg. Chem.* **1981**, *20*, 1229−1237. [2c] D. E. Fenton, H. Okawa, *Chem. Ber./Recueil* **1997**, *130*, 433−442. [2d] S. Albedyhl, M. T. Averbuch-Pouchot, C. Belle, B. Krebs, J. L. Pierre, E. Saint-Aman, S. Torelli, *Eur. J. Inorg. Chem.* **2001**, 1457−1464. [2e] C. Sudbrake, H. Vahrenkamp, *Eur. J. Inorg. Chem.* **2001**, 751−754. [2f] S. Brooker, P. D. Croucher, T. C. Davidson, G. S. Dunbar, A. James McQuillan, G. B. Jameson, *Chem. Commun.* **1998**, 2131−2132. [2g] I. A. Koval, D. Pursche, A. F. Stassen, P. Gamez, B. Krebs, J. Reedijk, *Eur. J. Inorg. Chem.* **2003**, 1669−1674. [2h] G. Steinfeld, V. Lozan, B. Kersting, *Angew. Chem.* **2003**, *115*, 2363−2365; *Angew. Chem. Int. Ed.* **2003**, *42*, 2261−2263.
[3] T. Glaser, T. Lügger, *Inorg. Chim. Acta* **2002**, *337*, 103−112.
[4] A. Rammel, F. Brisach, J. Henry, *J. Am. Chem. Soc.* **2001**, *123*, 5612−5613.
[5] [5a] B. Müller, A. Schneider, M. Tesmer, H. Vahrenkamp, *Inorg. Chem.* **1999**, *38*, 1900−1907. [5b] R. Walz, K. Weis, M. Ruf, H. Vahrenkamp, *Chem. Ber./Recueil* **1997**, *130*, 975−980.
[6] [6a] C. J. Fahrni, A. Pfaltz, M. Neuburger, M. Zehnder, *Helv. Chim. Acta* **1998**, *81*, 507−524. [6b] P. Chakraborty, S. K. Chandra, *Polyhedron* **1994**, *13*, 683−687. [6c] Q. Zeng, S. Gou, L. He, Y. Gong, X. You, *Inorg. Chim. Acta* **1999**, *287*, 14−20. [6d] M. D. Timken, W. A. Marritt, D. N. Hendrickson, R. A. Gagne, E. Sinn, *Inorg. Chem.* **1985**, *24*, 4202−4208.
[7] [7a] B. Kersting, D. Siebert, *Inorg. Chem.* **1998**, *37*, 3820−3828. [7b] B. Kersting, D. Siebert, D. Volkmer, M. J. Kolm, C. Janiak, *Inorg. Chem.* **1999**, *38*, 3871−3882. [7c] G. Steinfeld, B. Kersting, *Chem. Commun.* **2000**, 205−206. [7d] B. Kersting, G. Siedle, *Z. Naturforsch., Teil B* **2000**, *55*, 1179−1187.

 © 2004 Wiley-VCH Verlag GmbH & Co. KGaA, Weinheim

[8] P. Jeske, G. Haselhorst, T. Weyhermüller, K. Wieghardt, B. Nuber, *Inorg. Chem.* **1994**, *33*, 2462−2471.
[9] [9a] F. A. Cotton, D. A. Ucko, *Inorg. Chim. Acta* **1972**, *6*, 161−172. [9b] R. H. Summerville, R. Hoffman, *J. Am. Chem. Soc.* **1979**, *101*, 3821−3831.
[10] [10a] T. Glaser, K. Rose, S. E. Shadle, B. Hedman, K. O. Hodgson, E. I. Solomon, *J. Am. Chem. Soc.* **2001**, *123*, 442−454. [10b] T. Glaser, B. Hedman, K. O. Hodgson, E. I. Solomon, *Acc. Chem. Res.* **2000**, *33*, 859−868.
[11] K. Rose, S. E. Shadle, T. Glaser, S. de Vries, A. Cherepanov, G. W. Canters, B. Hedman, K. O. Hodgson, E. I. Solomon, *J. Am. Chem. Soc.* **1999**, *121*, 2353−2363.
[12] [12a] S. Weymann-Schildknetch, M. Henry, *J. Chem. Soc., Dalton Trans.* **2001**, 2425−2428. [12b] J. A. Ibers, *Nature* **1963**, *197*, 686−687. [12c] D. A. Wright, D. A. Williams, *Acta Crystallogr., Sect. B* **1968**, *24*, 1107−1114. [12d] T. J. Boyle, R. W. Schwartz, R. J. Doedens, J. W. Ziller, *Inorg. Chem.* **1995**, *34*, 1110−1120. [12e] A. I. Yanovskii, F. M. Dolgushin, M. I. Yanovskaya, N. M. Kotova, Y. T. Struchkov, N. Y. Turova, *Zh. Neorg. Khim.* **1997**, *42*, 450−453.
[13] [13a] M. A. Fox, M. T. Dulay, *Chem. Rev.* **1993**, *93*, 341−357. [13b] D. S. Muggli, J. L. Falconer, *J. Catal.* **1998**, *175*, 213−219. [13c] R. Wittenberg, M. A. Pradera, J. A. Navio, *Langmuir* **1997**, *13*, 2373−2379. [13d] L.-F. Liao, W.-C. Wu, C.-Y. Chen, J.-L. Lin, *J. Phys. Chem. B* **2001**, *105*, 7678−7685.
[14] Bruker AXS, **2000**.
[15] Nonius B. V., **1998**.
[16] Z. Otwinowski, W. Minor, *Methods Enzymol.* **1997**, *276*, 307−326.
[17] [17a] R. H. Blessing, *Acta Crystallogr., Sect. A* **1995**, *51*, 33−37. [17b] R. H. Blessing, *J. Appl. Cryst.* **1997**, *30*, 421−426.
[18] G. M. Sheldrick, *Acta Crystallogr., Sect. A* **1990**, *46*, 467−473.
[19] G. M. Sheldrick, University of Göttingen, Germany, **1997**.

Received December 10, 2003
Early View Article
Published Online May 5, 2004

 © 2004 Wiley-VCH Verlag GmbH & Co. KGaA, Weinheim

Formation of Large Clusters in the Reaction of Lanthanide Cations with Heptamolybdate

Katja Burgemeister,[a] Daniel Drewes,[a] Eva Melanie Limanski,[a] Ina Küper,[a] and Bernt Krebs*[a]

Keywords: Lanthanides / Molybdenum / Polyoxometalates / Structural analysis

A series of new lanthanide polyoxomolybdates was synthesised by reaction of lanthanide cations with the heptamolybdate anion $(Mo_7O_{24})^{6-}$. The heteropolyanions $[Ln_4(MoO_4)(H_2O)_{16}(Mo_7O_{24})_4]^{14-}$ (Ln = La^{III}, Ce^{III}, Pr^{III}, Sm^{III}, Gd^{III}) were isolated as either their ammonium or tetramethylammonium salts and characterised by X-ray structure analysis, energy dispersive X-ray fluorescence analysis, and IR and Raman spectroscopy. The central $[Ln_4(MoO_4)(H_2O)_{16}]^{10+}$ core of the anion is coordinated by four heptamolybdate groups. Each Ln^{III} atom in the core exhibits ninefold coordination by oxygen atoms belonging to H_2O, $(MoO_4)^{2-}$ and $(Mo_7O_{24})^{6-}$ units; the central molybdenum atom is coordinated tetrahedrally by four oxygen atoms.

(© Wiley-VCH Verlag GmbH & Co. KGaA, 69451 Weinheim, Germany, 2004)

Introduction

Because of their multifunctional applications in the fields of catalysis, chemical analysis and medicine, the chemistry of polyoxometalates is a research area of growing interest.[1−3] The selective synthesis of heteropolymetalates is made difficult by the large number of equilibrium reactions during the formation of the resulting anions. The characterisation of novel compounds and functional investigations are required for identification of structural characteristics and for understanding the different mechanisms that are responsible for biological and catalytic activity.

In recent years, a number of very large polyoxomolybdate clusters have been synthesised and structurally characterised. The Müller group has reported several giant mixed-valence nano-structured polyoxomolybdates with well above one hundred molybdenum atoms.[4−7] In polyoxotungstate chemistry quite different structures have been described; the $[As_{12}Ce_{16}(H_2O)_{36}W_{148}O_{524}]^{76-}$ anion is the largest anion yet known.[8]

Lanthanide-containing polyoxometalates constitute a type of compound of great impact.[9] Structural studies of lanthanide polyoxotungstates have been investigated and a number of compounds, for example $Na_6H_2[Ce(W_5O_{18})_2]\cdot 30H_2O$,[10] $K_{16}[Ce(P_2W_{17}O_{61})_2]\cdot 50H_2O$[11] and $K_{15}H_3[Eu_3(H_2O)_3(W_5O_{18})_3(SbW_9O_{33})]\cdot 25.5H_2O$,[12] have been reported. In connection with the discovery of the anti-HIV activity of the polyoxometalate PM-104 by Yamase et al. and of the substances $K_{13}[Ln(SiW_{11}O_{39})_2]\cdot nH_2O$ and $K_{17}[Ln(P_2W_{17}O_{61})_2]\cdot nH_2O$, synthesised by Francesconi et al., investigations relating to structure-activity correlations were reported.[13,14]

There are still only a few crystal structure analyses of lanthanide-containing polyoxomolybdates. In 1991 Yamase et al. reported the synthesis and characterisation of the compound $(NH_4)_{12}H_2[Eu_4(MoO_4)(H_2O)_{16}(Mo_7O_{24})_4]\cdot 18H_2O$, the luminescence properties of which are of great interest.[15] A similar structure of nonluminescent dimeric $[Pr_4(MoO_4)(Mo_7O_{24})_4]_2^{28-}$ was reported in 1987.[16] The synthesis and crystal structure of the neodymium-containing compound $Na_4(NH_4)_{10}[Nd_4(MoO_4)(Mo_7O_{24})_4]\cdot 34H_2O$ was published in 1997.[17]

In this paper we report the syntheses and structural characterisation of five new lanthanide containing polyoxomolybdates of the general structure $[(CH_3)_4N]_x[NH_4]_{14-x}[Ln_4(MoO_4)(H_2O)_{16}(Mo_7O_{24})_4]\cdot nH_2O$. Polyoxoanions of this type, which are isotypic with Yamase's europium compound, were prepared for Ln = La^{III}, Ce^{III}, Pr^{III}, Sm^{III} and Gd^{III} and their complete crystal structures are reported here.

Results and Discussion

$[(CH_3)_4N]_x[NH_4]_{14-x}[Ln_4(MoO_4)(H_2O)_{16}(Mo_7O_{24})_4]\cdot nH_2O$ crystals (Ln = La^{III}, Ce^{III}, Pr^{III}, Sm^{III}, Gd^{III}) were obtained from aqueous solution at a pH of about 5. The syntheses succeeded in a direct and straightforward way from an aqueous solution of heptamolybdate by addition of salts of the trivalent lanthanides in water. The inserted amounts of

[a] Westfälische Wilhelms-Universität, Institut für Anorganische und Analytische Chemie,
Corrensstraße 30, 48149 Münster, Germany
Fax: (internat.) +49-(0)251-83-38366
E-mail: krebs@uni-muenster.de

 © 2004 Wiley-VCH Verlag GmbH & Co. KGaA, Weinheim DOI: 10.1002/ejic.200400037

lanthanide ions in relation to heptamolybdate are not stoichiometric and vary from 1:5 for Ln = Sm^{III}, Ce^{III} and Pr^{III} to 2:5 for Ln = Gd^{III} and La^{III}. $[(CH_3)_4N]_{1.33}[NH_4]_{12.67}[La_4(MoO_4)(H_2O)_{16}(Mo_7O_{24})_4]\cdot 12H_2O$ (**1**), $[(CH_3)_4N]_{3.33}[NH_4]_{10.67}[Sm_4(MoO_4)(H_2O)_{16}(Mo_7O_{24})_4]\cdot 22H_2O$ (**4**) and $[(CH_3)_4N]_{3.33}[NH_4]_{10.67}[Gd_4(MoO_4)(H_2O)_{16}(Mo_7O_{24})_4]\cdot 16H_2O$ (**5**) crystallise in the cubic crystal system, space group $I\bar{4}3d$. The asymmetric unit consists of one quarter of the whole molecule, and the unit cell contains 12 anions. $[NH_4]_{14}[Ce_4(MoO_4)(H_2O)_{16}(Mo_7O_{24})_4]\cdot 36H_2O$ (**2**) crystallises in the triclinic crystal system, space group $P\bar{1}$, containing one formula unit per asymmetric unit and two formula units per unit cell. $[NH_4]_{14}[Pr_4(MoO_4)(H_2O)_{16}(Mo_7O_{24})_4]\cdot 29H_2O$ (**3**) crystallises in the monoclinic crystal system, space group $C2/c$. The asymmetric unit contains half a molecule and the unit cell includes four anions.

The five new heteromolybdate anions $[La_4(MoO_4)(H_2O)_{16}(Mo_7O_{24})_4]^{14-}$ (anion in compound **1**), $[Ce_4(MoO_4)(H_2O)_{16}(Mo_7O_{24})_4]^{14-}$ (anion in compound **2**), $[Pr_4(MoO_4)(H_2O)_{16}(Mo_7O_{24})_4]^{14-}$ (anion in compound **3**), $[Sm_4(MoO_4)(H_2O)_{16}(Mo_7O_{24})_4]^{14-}$ (anion in compound **4**) and $[Gd_4(MoO_4)(H_2O)_{16}(Mo_7O_{24})_4]^{14-}$ (anion in compound **5**) are isostructural to the europium-containing anion that is known from the literature.[15] Figure 1 shows the arrangement of the $[Ln_4(MoO_4)(H_2O)_{16}(Mo_7O_{24})_4]^{14-}$ anion seen from two different directions.

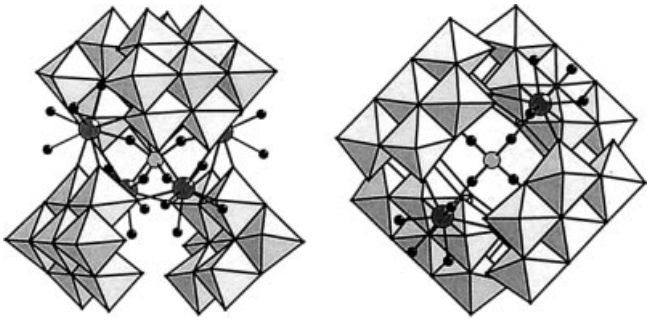

Figure 1. Polyhedron representation of the $[Ln_4(MoO_4)(H_2O)_{16}(Mo_7O_{24})_4]^{14-}$ anion viewed in two different projections

All the examples of this type contain a centered molybdenum atom (Mo1) that is coordinated tetrahedrally by four oxygen atoms. The O−Mo1−O bond angles differ only slightly from the perfect tetrahedral angle. The bond lengths between Mo1 and the four oxygen atoms [1.75(1)−1.77(1) Å] show that these bonds have partial double-bond character. Each oxygen atom of the central $(MoO_4)^{2-}$ unit is bonded to a lanthanide atom; the corresponding Mo1−O bond lengths show that an exchange of lanthanide atoms has no influence on the dπ-pπ bonding between molybdenum and oxygen atoms.

Each of the four lanthanide atoms in the $[Ln_4(MoO_4)(H_2O)_{16}(Mo_7O_{24})_4]^{14-}$ anion shows ninefold coordination by the oxygen atoms, approximating a tricapped trigonal prism, by attachment of one oxygen atom from the central $(MoO_4)^{2-}$ unit, four oxygen atoms from three $(Mo_7O_{24})^{6-}$ units and four oxygen atoms from four aqua ligands. The bond lengths and bond angles of the central $[Ln_4(MoO_4)(H_2O)_{16}]^{10+}$ unit (Ln = La^{III}, Ce^{III}, Pr^{III}, Sm^{III}, Eu^{III}, Gd^{III}) are given in Table 1 and 2. As shown in Table 2, all the lanthanide ions are coordinated by oxygen atoms in a very similar way. The observed decrease of Ln−O and Ln−OH_2 bond lengths in the series La > Ce > Pr > Sm > Eu > Gd is to be expected as an effect of the lanthanide contraction. The lanthanide atoms are well separated, with intramolecular Ln···Ln distances of between 6.28(1) and 7.67(1) Å for **1** and 6.15(1) and 7.50(1) Å for **5**. The decrease of these Ln···Ln distances is also an effect of the lanthanide contraction.

Figure 2 shows a schematic description of the $[Ln_4(MoO_4)(H_2O)_{16}(Mo_7O_{24})_4]^{14-}$ anion. Each $(Mo_7O_{24})^{6-}$ unit can be regarded as a tetradentate ligand bonded to three lanthanide atoms. Two of the seven MoO_6 octahedra of the $(Mo_7O_{24})^{6-}$ unit provide two terminal oxygen atoms for the Ln−O bonds.

It has been shown by Evans et al. that a characteristic feature of the heptamolybdate anion in $(NH_4)_6(Mo_7O_{24})\cdot 4H_2O$ is that all the MoO_6 octahedra contain two terminal or quasi-terminal bonds to oxygen atoms in *cis* positions.[18] This structural signature can also be found in the $(Mo_7O_{24})^{6-}$ units of all $[Ln_4(MoO_4)(H_2O)_{16}(Mo_7O_{24})_4]^{14-}$ anions. The short Mo−O_t bond lengths of the terminal and quasi-terminal oxygen atoms correspond well in the heptamolybdate anion and the $[Ln_4(MoO_4)(H_2O)_{16}(Mo_7O_{24})_4]^{14-}$ anions (Table 3). The coordination of the lanthanide cations by such terminal oxygen atoms does not lead to a significant expansion of these Mo−O bond lengths.

As well as the two short Mo−O bonds, each MoO_6 octahedron contains two intermediate Mo−O bonds and two long Mo−O bonds. The two long Mo−O bonds are located *trans* to the short Mo−O bonds and show Mo−O distances of between 2.09(1) Å and 2.51(1) Å (**1**−**5**) and 2.16(1) Å and 2.42(1) Å $[(NH_4)_6(Mo_7O_{24})\cdot 4H_2O]$. The intermediate Mo−O bonds show Mo−O distances of between 1.87(1) Å and 2.01(1) Å (compounds **1**−**5**) and 1.90(1) Å and 1.97(1) Å $[(NH_4)_6(Mo_7O_{24})\cdot 4H_2O]$.[18]

A comparison of the lanthanide-containing polyoxomolybdates **1**−**5** with the heptamolybdate anion in $(NH_4)_6(Mo_7O_{24})\cdot 4H_2O$ given in Table 3 shows rather similar distances within the limits of error. The variation of the lanthanide atoms belonging to the central $[Ln_4(MoO_4)(H_2O)_{16}]^{10+}$ unit has no significant influence on the coordinating heptamolybdate units.

According to the required charge balance, 14 cations per formula unit are needed. Compounds **2** and **3** contain only ammonium counterions. In this case, the cations cannot be distinguished crystallographically from the water molecules. To achieve better crystallisation, tetramethylammonium ions were added during the preparation of **1**, **4** and **5**. Compounds **4** and **5** contain 3.33 of these counterions each, with the lanthanum-containing compound **1** only having 1.33 tetramethylammonium ions. The fractional numbers result from the special positions of carbon and nitrogen atoms in the unit cell. Elemental analyses validate the content of

 © 2004 Wiley-VCH Verlag GmbH & Co. KGaA, Weinheim

Table 1. Comparison of selected Mo1−O, Ln···Ln, Ln−O and Ln−Ow[b] bond lengths with standard deviations of the anions $[Ln_4(MoO_4)(H_2O)_{16}(Mo_7O_{24})_4]^{14-}$ with Ln = La^{III}, Ce^{III}, Pr^{III}, Sm^{III}, Eu^{III},[15] Gd^{III}

Mo1−O (Å)		Ln···Ln (Å)		Ln−O (Å)		Ln−Ow (Å)	
$Mo1-O_{LaMo}$ [a]	1.76(1)	La···La	6.28(1)−7.67(1)	La−O	2.46(1)−2.57(1)	La−Ow[b]	2.53(1)−2.68(1)
$Mo1-O_{CeMo}$ [a]	1.75(1)−1.76(1)	Ce···Ce	6.25(1)−7.61(1)	Ce−O	2.44(1)−2.46(1)	Ce−Ow[b]	2.52(1)−2.65(1)
$Mo1-O_{PrMo}$ [a]	1.76(1)−1.77(1)	Pr···Pr	6.23(1)−7.60(1)	Pr−O	2.42(1)−2.52(1)	Pr−Ow[b]	2.51(1)−2.62(1)
$Mo1-O_{SmMo}$ [a]	1.77(1)	Sm···Sm	6.19(1)−7.55(1)	Sm−O	2.38(1)−2.50(1)	Sm−Ow[b]	2.44(1)−2.61(1)
$Mo1-O_{EuMo}$ [a]	1.76(2)−1.77(1)	Eu···Eu	6.17(1)−7.51(1)	Eu−O	2.38(1)−2.48(2)	Eu−Ow[b]	2.43(2)−2.59(2)
$Mo1-O_{GdMo}$ [a]	1.76(1)−1.77(1)	Gd···Gd	6.15(1)−7.50(1)	Gd−O	2.36(1)−2.47(1)	Gd−Ow[b]	2.40(1)−2.63(1)

[a] The subscripts indicate the atoms bonded to the oxygen atom. [b] Ow = oxygen atom of a water molecule.

Table 2. Comparison of O−Mo1−O and O−Ln−O bond angles with standard deviations of the anions $[Ln_4(MoO_4)(H_2O)_{16}(Mo_7O_{24})_4]^{14-}$ with Ln = La^{III}, Ce^{III}, Pr^{III}, Sm^{III}, Eu^{III},[15] Gd^{III}

Anion	O−Mo1−O (°)	O−Ln−O (°)	O−Ln−Ow[a] (°)	Ow−Ln−Ow[a] (°)
$[La_4(MoO_4)(H_2O)_{16}(Mo_7O_{24})_4]^{14-}$	109.1(2)−110.3(4)	68.1(2)−136.7(2)	65.0(2)−143.0(2)	66.9(2)−131.4(3)
$[Ce_4(MoO_4)(H_2O)_{16}(Mo_7O_{24})_4]^{14-}$	109.3(4)−110.2(4)	68.7(3)−136.3(3)	65.5(3)−141.1(3)	67.8(3)−138.3(4)
$[Pr_4(MoO_4)(H_2O)_{16}(Mo_7O_{24})_4]^{14-}$	108.6(6)−110.0(4)	68.9(3)−136.7(3)	66.4(3)−140.8(3)	67.7(4)−134.5(4)
$[Sm_4(MoO_4)(H_2O)_{16}(Mo_7O_{24})_4]^{14-}$	108.7(2)−110.0(3)	68.4(2)−137.2(2)	65.3(2)−142.5(2)	67.3(2)−132.6(2)
$[Eu_4(MoO_4)(H_2O)_{16}(Mo_7O_{24})_4]^{14-}$	108.0(7)−110.2(8)	69.4(6)−136.8(6)	67.1(6)−140.4(6)	66.9(6)−135.3(6)
$[Gd_4(MoO_4)(H_2O)_{16}(Mo_7O_{24})_4]^{14-}$	109.0(2)−110.4(4)	70.2(2)−137.2(2)	65.6(2)−143.1(2)	67.4(3)−131.9(3)

[a] Ow = oxygen atom of a water molecule.

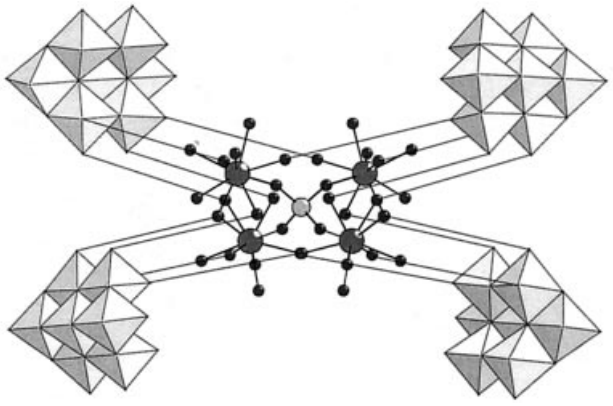

Figure 2. Schematic presentation of the $[Ln_4(MoO_4)(H_2O)_{16}(Mo_7O_{24})_4]^{14-}$ anion

ammonium and tetramethylammonium ions. There is no evidence for protonation of the crystal water molecules or the $[Ln_4(MoO_4)(H_2O)_{16}(Mo_7O_{24})_4]^{14-}$ anions.

The spectroscopic data of all $[Ln_4(MoO_4)(H_2O)_{16}(Mo_7O_{24})_4]^{14-}$ anions show great similarities in the most important bands of the IR and Raman spectra. The characteristic region of the Mo−O vibrations in the Raman spectra are observed in the region between 1000 and 800 cm^{-1} for all analysed compounds. In the IR spectra the characteristic $Mo-O_t$ bands are observed around 893 cm^{-1}.

Conclusion

The selective and aimed syntheses of five novel lanthanide-containing polyoxomolybdates $[(CH_3)_4N]_x[NH_4]_{14-x}[Ln_4(MoO_4)(H_2O)_{16}(Mo_7O_{24})_4]\cdot nH_2O$ **(1−5)** are reported.

Table 3. Mo−O-bond lengths with standard deviations of the heptamolybdate unit of the $[Ln_4(MoO_4)(H_2O)_{16}(Mo_7O_{24})_4]^{14-}$ anion with Ln = La^{III}, Ce^{III}, Pr^{III}, Sm^{III}, Eu^{III},[15] Gd^{III} and the heptamolybdate anion in $(NH_4)_6(Mo_7O_{24})\cdot 4H_2O$[18]

Anion	Region of Mo−O bond lengths (Å) Short bond	Intermediate bond	Long bond
$[La_4(MoO_4)(H_2O)_{16}(Mo_7O_{24})_4]^{14-}$	1.70(1)−1.75(1)	1.88(1)− 2.00(1)	2.11(1)−2.48(1)
$[Ce_4(MoO_4)(H_2O)_{16}(Mo_7O_{24})_4]^{14-}$	1.68(1)−1.74(1)	1.87(1)−1.99(1)	2.09(1)−2.51(1)
$[Pr_4(MoO_4)(H_2O)_{16}(Mo_7O_{24})_4]^{14-}$	1.67(1)−1.74(1)	1.88(1)−2.00(1)	2.12(1)−2.50(1)
$[Sm_4(MoO_4)(H_2O)_{16}(Mo_7O_{24})_4]^{14-}$	1.71(1)−1.74(1)	1.89(1)−1.99(1)	2.12(1)−2.48(1)
$[Eu_4(MoO_4)(H_2O)_{16}(Mo_7O_{24})_4]^{14-}$	1.68(2)−1.75(2)	1.88(3)−1.99(3)	2.13(3)−2.54(2)
$[Gd_4(MoO_4)(H_2O)_{16}(Mo_7O_{24})_4]^{14-}$	1.70(1)−1.74(1)	1.89(1)−2.01(1)	2.12(1)−2.50(1)
$[Mo_7O_{24}]^{6-}$	1.71(1)−1.75(1)	1.90(1)−1.97(1)	2.16(1)−2.42(1)

 © 2004 Wiley-VCH Verlag GmbH & Co. KGaA, Weinheim

All compounds were completely characterised by X-ray structure analysis. The $[Ln_4(MoO_4)(H_2O)_{16}(Mo_7O_{24})_4]^{14-}$ clusters are built up by a central $[Ln_4(MoO_4)(H_2O)_{16}]^{10+}$ unit surrounded by four heptamolybdate groups, each of which can be regarded as a tetradentate ligand. The building blocks are connected by four lanthanide atoms which are coordinated by nine oxygen atoms. Investigations of the oxidation catalysis and anti-tumour and anti-HIV activity of the present compounds are in progress.

Experimental Section

Syntheses of Heteropolymolybdates: All starting materials and chemicals were used without further purification.

$[(CH_3)_4N]_{1.33}[NH_4]_{12.67}[La_4(MoO_4)(H_2O)_{16}(Mo_7O_{24})_4]\cdot 12H_2O$ (1): $(NH_4)_6(Mo_7O_{24})\cdot 4H_2O$ (0.93 g, 0.75 mmol) was dissolved in 20 mL of water, and 1 mL of CH_3OH was added. An aqueous solution (5 mL) containing $La(NO_3)_3\cdot 6H_2O$ (0.13 g, 0.3 mmol) was added dropwise to the above solution with stirring at room temperature. $(NMe_4)Br$ solution (0.5 mL; 1 M in water) was added to the resulting solution (pH ≈ 5). The reaction vessel was kept closed at room temperature for 48 h. Colorless single crystals were obtained from the solution. Yield: 0.37 g (86% based on La). $C_{5.33}H_{122.67}La_4Mo_{29}N_{14}O_{128}$ (5769.6): calcd. C 1.11, H 2.14, N 3.40; found C 1.06, H 2.22, N 3.43. IR data (KBr): $\tilde{\nu}$ = 3423 cm^{-1} (s) [ν(O−H)]; 1614 (s) [δ(N−H)]; 1389 (s) [δ(O−H)]; 941 (m); 893 (s) [ν(Mo-O_t)]; 621 (s) [ν(Mo-O)]; 488 (w). Raman data: $\tilde{\nu}$ = 946 cm^{-1} (s) (Mo-O_t); 891 (m); 863 (w); 363 (w); 222 (m). EDAX: calcd. Mo:La = 7.25:1; found Mo:La = 7.36:1.

$[NH_4]_{14}[Ce_4(MoO_4)(H_2O)_{16}(Mo_7O_{24})_4]\cdot 36H_2O$ (2): $(NH_4)_6(Mo_7O_{24})\cdot 4H_2O$ (0.93 g, 0.75 mmol) was dissolved in 9 mL of water, and 1 mL of CH_3OH was added. An aqueous solution (5 mL) containing $CeCl_3\cdot 7H_2O$ (0.056 g, 0.15 mmol) was added dropwise to the above solution with stirring at room temperature. The resulting solution (pH ≈ 5) was kept in a closed reaction flask at 278 K for 18 h. Red single-crystals were obtained from the solution. Yield: 0.18 g (78% based on Ce). $H_{160}Ce_4Mo_{29}N_{14}O_{152}$ (6132.5): calcd. H 2.63, N 3.20; found H 2.61, N 3.17. IR data (KBr): $\tilde{\nu}$ = 3142 cm^{-1} (s, br) [ν(O−H)]; 1620 (m) [δ(OH_2)]; 1401 (s) [δ(NH_4)]; 893 (s, br) [ν(Mo-O_t)]; 634 (m, br) [ν(Mo-O)]; 486 (w). Raman data: $\tilde{\nu}$ = 944 cm^{-1} (s) (Mo-O_t); 916 (m); 860 (w); 364 (w); 219 (m). EDAX: calcd. Mo:Ce = 7.25:1; found Mo:La = 6.56:1.

$[NH_4]_{14}[Pr_4(MoO_4)(H_2O)_{16}(Mo_7O_{24})_4]\cdot 29H_2O$ (3): This compound was prepared similarly to **2**, with $Pr(NO_3)_3\cdot 5H_2O$ (0.062 g, 0.15 mmol) instead of $CeCl_3\cdot 7H_2O$. Green single-crystals were ob-

Table 4. Crystallographic data for $[(CH_3)_4N]_{1.33}[NH_4]_{12.67}[La_4(MoO_4)(H_2O)_{16}(Mo_7O_{24})_4]\cdot 12H_2O$ (**1**), $[NH_4]_{14}[Ce_4(MoO_4)(H_2O)_{16}(Mo_7O_{24})_4]\cdot 36H_2O$ (**2**), $[NH_4]_{14}[Pr_4(MoO_4)(H_2O)_{16}(Mo_7O_{24})_4]\cdot 29H_2O$ (**3**), $[(CH_3)_4N]_{3.33}[NH_4]_{10.67}[Sm_4(MoO_4)(H_2O)_{16}(Mo_7O_{24})_4]\cdot 22H_2O$ (**4**) and $[(CH_3)_4N]_{3.33}[NH_4]_{10.67}[Gd_4(MoO_4)(H_2O)_{16}(Mo_7O_{24})_4]\cdot 16H_2O$ (**5**)

	1	**2**	**3**	**4**	**5**
Formula	$La_4Mo_{29}O_{128}N_{14}C_{5.33}H_{122.67}$	$Ce_4Mo_{29}O_{152}N_{14}H_{160}$	$Pr_4Mo_{29}O_{145}N_{14}H_{146}$	$Sm_4Mo_{29}O_{138}N_{14}C_{13.33}H_{158.67}$	$Gd_4Mo_{29}O_{132}N_{14}C_{13.33}H_{146.67}$
Mol. mass (g/mol)	5769.56	6132.15	6009.06	6107.79	6027.25
Crystal color/habit	colorless rhombic crystals	red rhombic crystals	light-green rhombic crystals	light-yellow rhombic crystals	colorless rhombic crystals
Crystal size (mm)	0.22 × 0.18 × 0.16	0.15 × 0.10 × 0.10	0.15 × 0.10 × 0.10	0.26 × 0.15 × 0.14	0.48 × 0.44 × 0.40
Crystal system	cubic	triclinic	monoclinic	cubic	cubic
Space group	*I*$\bar{4}$3*d*	*P*$\bar{1}$	*C*2/*c*	*I*$\bar{4}$3*d*	*I*$\bar{4}$3*d*
a (Å)	35.800(4)	17.121(3)	19.781(4)	35.533(4)	35.487(4)
b (Å)	35.800(4)	19.914(4)	43.872(9)	35.533(4)	35.487(4)
c (Å)	35.800(4)	24.328(5)	20.454(4)	35.533(4)	35.487(4)
α (°)	90	84.96(3)	90	90	90
β (°)	90	87.65(3)	117.28(3)	90	90
γ (°)	90	65.25(3)	90	90	90
V (Å^3)	45884(9)	7503.5(25)	15776.2(55)	44864(9)	44689(9)
Z	12	2	4	12	12
$d_{calcd.}$ (g/cm^3)	2.463	2.666	2.538	2.651	2.631
μ (mm^{-1})	3.485	3.639	3.542	4.003	4.217
T (K)	173	213	293	173	213
Measured refl.	237745	41899	36455	234219	163082
Independent refl.	9506	21826	9805	9261	7229
Unique refl. [$I > \sigma(I)$]	9160	16012	8099	9256	7008
R_{int}	0.0574	0.0508	0.1187	0.046	0.2026
Refined parameters	392	1673	854	425	427
2θ range (°)	4.24 < 2θ < 56.69	8 < 2θ < 48	8 < 2θ < 46	5.21 < 2θ < 56.6	8.1 < 2θ < 52.1
R [$I > 2\sigma(I)$]	R_1 = 0.0437[a]	R_1 = 0.0550[a]	R_1 = 0.0576[a]	R_1 = 0.0339[a]	R_1 = 0.0566[a]
	wR_2 = 0.1106[b]	wR_2 = 0.1218[b]	wR_2 = 0.1480[b]	wR_2 = 0.0864[b]	wR_2 = 0.1004[b]
R (all data)	R_1 = 0.0469[a]	R_1 = 0.0853[a]	R_1 = 0.0744[a]	R_1 = 0.0339[a]	R_1 = 0.0579[a]
	wR_2 = 0.1145[b]	wR_2 = 0.1443[b]	wR_2 = 0.1874[b]	wR_2 = 0.0864[b]	wR_2 = 0.1014[b]
Goof[c]	1.092	1.106	1.047	1.236	1.038
$(\Delta\rho)_{max}$ (e$^-$/Å^3)	2.57	1.24	1.39	1.42	1.02
$(\Delta\rho)_{min}$ (e$^-$/Å^3)	−1.81	−2.98	−2.46	−1.76	−1.24

[a] $R_1 = \Sigma||F_{obsd.}| - |F_{calcd.}||/\Sigma|F_{obsd.}|$. [b] $wR_2 = \{\Sigma[w(F_{obsd.}^2 - F_{calcd.}^2)^2]/\Sigma[w(F_{obsd.}^2)^2]\}^{1/2}$. $w = 1/[\sigma^2(F_o^2) + xP + (yP)^2]$; with $P = (F_o^2 + 2F_c^2)/3$ and x = 1053.774, y = 0.0532 (**1**), x = 0.0000, y = 0.0437 (**2**); x = 578.45, y = 0.085 (**3**); x = 792.964, y = 0.0314 (**4**); x = 926.793, y = 0.0597 (**5**). [c] goof = $[\Sigma w(F_{obsd.}^2 - F_{calcd.}^2)^2/(n-p)]^{1/2}$, where n = number of reflections, p = parameter used.

 © 2004 Wiley-VCH Verlag GmbH & Co. KGaA, Weinheim

tained from the solution after 18 h. Yield: 0.18 g (80% based on Pr). $H_{146}Mo_{29}N_{14}O_{145}Pr_4$ (6009.1): calcd. H 2.45, N 3.26; found H 2.49, N 3.17. IR data (KBr): $\tilde{\nu}$ = 3152 cm^{-1} (s, br) [ν(O−H)]; 1621 (m) [δ(OH_2)]; 1401 (s) [δ(NH_4)]; 939 (w); 893 (s, br) [ν(Mo-O_t)]; 634 (m, br) [ν(Mo-O)]; 485 (w). Raman data: $\tilde{\nu}$ = 945 cm^{-1} (s) (Mo-O_t); 922 (m); 860 (w); 365 (w); 219 (m). EDAX: calcd. Mo:Pr = 7.25:1; found Mo:Pr = 7.09:1.

$[(CH_3)_4N]_{3.33}[NH_4]_{10.67}[Sm_4(MoO_4)(H_2O)_{16}(Mo_7O_{24})_4]\cdot 22H_2O$ (4): $(NH_4)_6(Mo_7O_{24})\cdot 4H_2O$ (0.93 g, 0.75 mmol) was dissolved in 20 mL of water, and 1 mL of CH_3OH was added. An aqueous solution (5 mL) containing $Sm(NO_3)_3\cdot 6H_2O$ (0.07 g, 0.15 mmol) was added dropwise to the above solution while stirring at room temperature. $(NMe_4)Br$ solution (0.5 mL; 1 M in water) was added to the resulting solution (pH ≈ 5). The reaction flask was kept closed at 278 K for 24 h. Light-yellow single-crystals were obtained from the solution. Yield: 0.19 (83% based on Sm). $C_{13.33}H_{158.67}Mo_{29}N_{14}O_{138}Sm_4$ (6107.8): calcd. C 2.62, H 2.62, N 3.21; found C 2.55, H 2.44, N 3.17. IR data (KBr): $\tilde{\nu}$ = 3135 cm^{-1} (s) [ν(O−H)]; 1622 (s) [δ(N−H)]; 1385 (s) [δ(O−H)]; 941 (m); 894 (s) [ν(Mo-O_t)]; 629 (s) [ν(Mo-O)]; 485 (w). Raman data: $\tilde{\nu}$ = 951 cm^{-1} (s) (Mo-O_t); 897 (w); 862 (w); 368 (w); 219 (w). EDAX: calcd. Mo:Sm = 7.25:1; found Mo:Sm = 7.53:1.

$[(CH_3)_4N]_{3.33}[NH_4]_{10.67}[Gd_4(MoO_4)(H_2O)_{16}(Mo_7O_{24})_4]\cdot 16H_2O$ (5): This compound was prepared similarly to **1**, with $Gd(NO_3)_3\cdot 5H_2O$ (0.013 g, 0.30 mmol) instead of $La(NO_3)_3\cdot 6H_2O$. Colorless single-crystals were obtained from the solution after 24 h. Yield: 0.31 g (69% based on Gd). $C_{13.33}H_{146.67}Gd_4Mo_{29}N_{14}O_{132}$ (6027.3): calcd. C 2.65, H 2.45, N 3.25; found C 2.45, H 2.37, N 3.23. IR data (KBr): $\tilde{\nu}$ = 3422 cm^{-1} (s) [ν(O−H)]; 1626 (s) [δ(N−H)]; 1408 (s) [δ(O−H)]; 941 (m); 893 (s) [ν(Mo-O_t)]; 634 (s) [ν(Mo-O)]; 485 (w). Raman data: $\tilde{\nu}$ = 951 cm^{-1} (s) (Mo-O_t); 921 (m); 895 (w); 865 (w); 370 (w); 220 (w). EDAX: calcd. Mo:Gd = 7.25:1; found Mo:Gd = 7.79:1.

Instrumentation and Analytical Procedures: IR spectra were measured on a Perkin−Elmer 683 spectrometer as KBr pellets. Elemental analyses were carried out on an Elementar Vario EL III analyzer. The atomic ratios of the heavy elements were determined by energy-dispersive X-ray fluorescence analysis (EDAX).

Diffraction experiments were performed on a STOE IPDS imaging plate system (for **1**, **2** and **3**) and a Bruker Smart Apex diffractometer with CCD detector (for **4** and **5**), both using Mo-K_α radiation (λ = 0.71073 Å). Structures were solved by direct methods with SHELXS-97 and refined with SHELXL-97.[19] No hydrogen atoms were included. The nitrogen atoms of the ammonium cations were modeled as oxygen atoms because nitrogen atoms could not be distinguished from oxygen atoms.

All atoms except the oxygen atoms belonging to water molecules were refined anisotropically by full-matrix least-squares calculations based on F^2. As usual for polyoxometalates, the crystal structures show disorder in the counterions and crystal water part of the structure. The details of data collection and refinement are summarised in Table 4.

Further details on the crystal structure investigations may be obtained from the Fachinformationzentrum Karlsruhe, 76344 Eggenstein-Leopoldhafen, Germany [Fax: +49-(0)7247-808-666; E-mail: crysdata@fiz-karlsruhe.de], on quoting the depository number CSD-413732 (for **1**), -413730 (for **2**), -413733 (for **3**), -413734 (for **4**) or -413731 (for **5**).

Acknowledgments

Support by the Deutsche Forschungsgemeinschaft, the Fonds der Chemischen Industrie, and the Bundesministerium für Bildung und Forschung is gratefully acknowledged.

[1] M. T. Pope, *Heteropoly and Isopoly Oxometalates*, Springer, Berlin **1983**.
[2] *Polyoxometalate Chemistry* (Eds.: M. T. Pope, A. Müller), Kluwer Academic Publishers, Dordrecht **2001**.
[3] *Chem. Rev.* **1998**, *98*, 1−387 (Ed.: C. L. Hill), special edition on polyoxometalates.
[4] A. Müller, P. Kögerler, C. Kuhlmann, *Chem. Commun.* **1999**, 1347−1358.
[5] A. Müller, S. Q. N. Shah, H. Bögge, M. Schmidtmann, *Nature* **1999**, *397*, 48−50.
[6] A. Müller, E. Krickemeyer, H. Bögge, M. Schmidtmann, F. Peters, *Angew. Chem.* **1998**, *110*, 3567−3571; *Angew. Chem. Int. Ed.* **1998**, *37*, 3360−3363.
[7] A. Müller, S. Polarz, S. K. Das, E. Krickemeyer, H. Bögge, M. Schmidtmann, B. Hauptfleisch, *Angew. Chem.* **1999**, *111*, 3439−3443; *Angew. Chem. Int. Ed.* **1999**, *38*, 3241−3245.
[8] K. Wassermann, M. H. Dickman, M. T. Pope, *Angew. Chem.* **1997**, *109*, 1513−1516; *Angew. Chem. Int. Ed. Engl.* **1997**, *36*, 1445−1448.
[9] K. Wassermann, M. T. Pope, *Inorg. Chem.* **2001**, *40*, 2763−2768.
[10] J. Iball, N. J. Low, T. J. R. Weakly, *J. Chem. Soc., Dalton Trans.* **1974**, 2021−2024.
[11] V. N. Molchanov, L. P. Kazanski, E. A. Torchenkova, V. I. Sinonov, *Sov. Phys. Crystallogr.* **1979**, *24*, 96−101; *Chem. Abstr.* **1979**, *90*, 131106v.
[12] T. Yamase, H. Naruke, Y. Sasaki, *J. Chem. Soc., Dalton Trans.* **1990**, 1687−1696.
[13] Y. Inouye, Y. Tokutake, T. Yoshida, A. Yamamoto, T. Yamase, S. Nakamura, *Chem. Pharm. Bull.* **1991**, *39*, 1638−1641.
[14] J. Bartis, S. Sukal, E. Davis, R. Kronzon, M. Blumenstein, L. C. Francesconi, *Preparation, Characterisation and anti-HIV Activity of Lanthanide Polyoxoanions*, 210th ACS National Meeting, Chicago **1995**, 646.
[15] H. Naruke, T. Ozeki, T. Yamase, *Acta Crystallogr., Sect. C* **1991**, *47*, 489−492.
[16] A. M. Fedosseev, M. S. Grigorév, A. I. Yanovskii, T. Struchkovyn, V. I. Spitsin, *Doklady Academii Nauk SSSR* **1987**, 111−114.
[17] X.-Z. Cai, S.-M. Wang, J.-F. Huang, H.-M. Guan, X. Lin, *Chin. J. Struct. Chem.* **1997**, *16*, 328−334; *Chem. Abstr.* **1997**, *127*, 184826u.
[18] H. T. Evans, *J. Am. Chem. Soc.* **1968**, *90*, 3275−3276.
[19] G. M. Sheldrick, *SHELXL 97*, Siemens Analytical X-ray Instruments, **1998**, University of Göttingen.

Received January 15, 2004
Early View Article
Published Online May 13, 2004

 © 2004 Wiley-VCH Verlag GmbH & Co. KGaA, Weinheim

Metal-Directed Self-Assembly: Two New Metal-Binicotinate Grid Polymeric Networks and Their Fluorescence Emission Tuned by Ligand Configuration

Benlai Wu,[a] Daqiang Yuan,[a] Feilong Jiang,[a] Ruihu Wang,[a] Lei Han,[a] Youfu Zhou,[a] and Maochun Hong*[a]

Keywords: Self-assembly / Binicotinic acid / Fluorescence / Coordination polymer / Chirality

Two new 2-D metal-binicotinate coordination polymers, namely, $[Cd^{II}(bpdc)]_n$ (**1**) and $\{[Zn^{II}_8(bpdc)_8(H_2O)_8](H_2O)_8\}_n$ (**2**) (H_2bpdc = binicotinic acid) have been synthesized using hydrothermal and three-layer diffusion methods, respectively. Single-crystal X-ray analyses revealed that both are extended grid networks of the (4,4) topology. Their structures alter with the configuration and function of bpdc. The achiral, free H_2bpdc has axial chirality induced by metal coordination in **1**, and bpdc connects to four metal centers forming a 2-D (4,4) net with three kinds of apertures generated through self-assembly. In **2**, however, bpdc connects to three metal centers, fabricating a microporous framework containing hydrophilic channels. Studies on the solid emission spectra of the free ligand, **1**, and **2** confirmed, that the configuration of bpdc resulting from metal-directed coordination has a profound effect on the fluorescence emissions of **1** and **2**.

(© Wiley-VCH Verlag GmbH & Co. KGaA, 69451 Weinheim, Germany, 2004)

Introduction

The construction of extended metal-organic networks, especially with micropores, is of current interest in the fields of supramolecular chemistry and crystal engineering, because of their exploitable magnetic,[1−3] catalytic,[4] optoelectronic,[5,6] and inclusive properties.[7] The self-assembly of suitable ligands and metal centers has been proved to be an efficient route for the formation of one- to three-dimensional networks with fascinating structural topologies.[8−11]

Recently, interest has increasingly been centered on self-assembly of metal ions with multi-pyridine and multi-carboxylate spacers.[12−15] As exemplified by the successful syntheses of porous networks, the rigid skeletons of multi-pyridine ligands always sustain the frameworks, and the diversely coordinating multi-carboxylate spacers can help enhance the stability of the resultant metal-organic networks.[16,17] The family of binicotinic acid ligands (H_2bpdc) bearing 2,2′-bipyridyl and dicarboxyl functional groups has received considerable attention in photochemistry and crystal engineering.[18−25] On the one hand, owing to the structural features of the strong chelating bipyridyl moiety and the adjacent carboxyl groups, these ligands often acts as bis(monodentate),[18] tridentate[19,20] or bis(bidentate)[20,21] bridging spacers, and facilitate the formation of 1-D catenopolymers, indicating ligand-directed synthesis. On the other hand, the configuration of bpdc can be greatly altered along the 1,1′ bond, while the pyridyl and carboxyl functional groups bind to the selected metal centers. This may also provide a route for metal-directed synthesis, something which has been rarely reported in the literature. In this work we selected Cd^{II} and Zn^{II} as metal nodes for assembly with Me_2bpdc (dimethyl 2,2′-bipyridine-3,3′-dicarboxylate) and H_2bpdc, respectively, and obtained two 2-D novel coordination polymers, namely, $[Cd^{II}(bpdc)]_n$ (**1**) and $\{[Zn^{II}_8(bpdc)_8(H_2O)_8](H_2O)_8\}_n$ (**2**). Complex **1**, which was assembled under hydrothermal conditions, has a (4,4) topological network with three-shaped apertures, while complex **2**, obtained through a three-layer diffusion method, exhibits a microporous framework containing hydrophilic channels.

We also report the interesting results of fluorescence emission experiments, which show that the configuration of bpdc resulting from metal-directed coordination has a profound effect on the emissions of **1** and **2**.

Results and Discussion

Using hydrothermal methods, the crystalline complex **1** was successfully obtained through the reaction of Me_2bpdc with $CdCl_2{\cdot}2.5H_2O$ (ratio 1:1) in the presence of triethylamine at 160 °C, under which conditions Me_2bpdc underwent hydrolytic decomposition to give bpdc. Substituting $CdCl_2{\cdot}2.5H_2O$ with $ZnCl_2$ under the same reaction conditions yielded only a white precipitate. Finally, single crys-

[a] State Key Laboratory of Structural Chemistry, Fujian Institute of the Research on the Structure of Matter, Chinese Academy of Sciences,
Fuzhou, Fujian, 350002, China
Fax: (internat.) + 86-591-371-4946
E-mail: hmc@ms.fjirsm.ac.cn

Supporting information for this article is available on the WWW under http://www.eurjic.org or from the author.

tals of compound **2** were obtained in a three-layer diffusion system with a aqueous solution of H_2bpdc as the bottom layer, a mixture of DMF, water, and methanol as the mesosphere, and a methanol solution of $ZnCl_2$ as the top layer.

Structural Description

A single-crystal X-ray diffraction analysis revealed, that complex **1** crystallizes in the tetragonal space group *P*4(2)/*mnm*, and possesses a 2-D framework with square, rectangular, and rhombohedral apertures (Figure 1). The local coordination geometry around each Cd^{II} center in **1** can be described as distorted trigonal prismatic (Figure 2), in which each Cd^{II} center is coordinated by four O atoms from the chelating carboxyl groups of two bpdc ligands and two N atoms from another two bpdc ligands to complete the coordination sphere. With its two chelating carboxyl groups and bridging 2,2′-pyridyl moiety (the dihedral angle of two pyridine rings being 93.7°), each bpdc is simultaneously bound to four Cd atoms (Scheme 1), resulting in the formation of a 2-D network with three different shaped apertures. To the best of our knowledge, the four-connecting hexadentate coordination pattern of bpdc is the first such example of its kind. The architecture of **1** with the 2,2′-bipyridyl moiety bridging divalent metal centers has rarely been reported.[18−22]

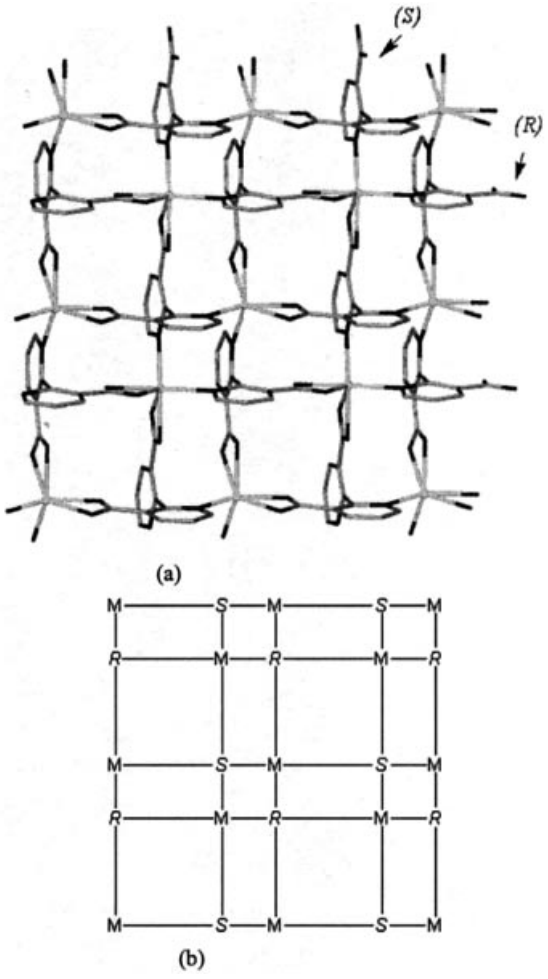

Figure 1. (a) 2-D three-shaped grid network representation of **1** (viewed along the *c* axis); (b) a simplified scheme indicating the construction of **1** interweaved by -*R*-M-*R*- and -*S*-M-*S*- chains [*R* = (*R*)-bpdc, *S* = (*S*)-bpdc and M = Cd^{II}]

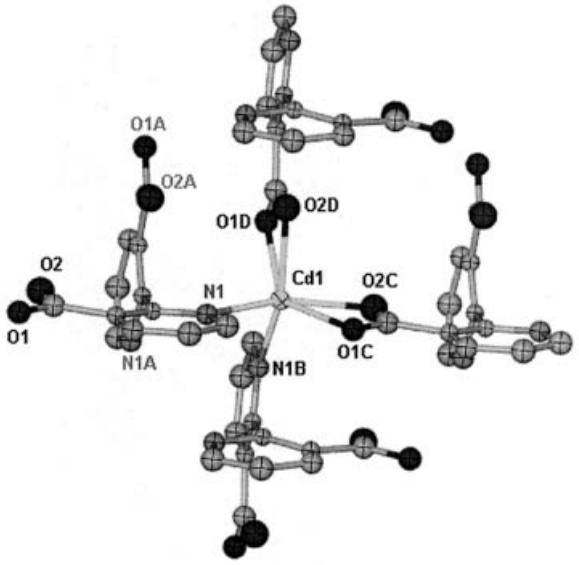

Figure 2. An ORTEP representation of the local geometry around the Cd^{II} center in **1** (50% probability thermal ellipsoids)

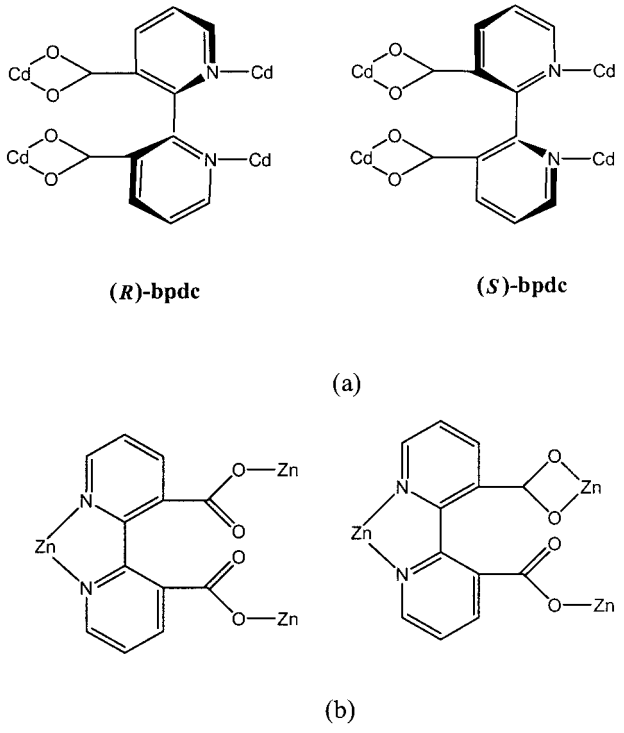

Scheme 1. Coordination modes of bpdc in (a) complex **1** and (b) complex **2**

 © 2004 Wiley-VCH Verlag GmbH & Co. KGaA, Weinheim

Table 1. Selected bond lengths (Å) and angles (°) for **1** and **2**

Complex **1**

Cd1−O1C	2.399(14)	Cd1−O2C	2.305(12)
Cd1−O1D	2.399(14)	Cd1−O2D	2.305(12)
Cd1−N1	2.332(18)	Cd1−N1B	2.332(18)
O2D−Cd1−O2C	93.8(7)	O2D−Cd1−N1B	147.9(4)
O2C−Cd1−N1B	92.2(5)	O2D−Cd1−N1	92.2(5)
O2C−Cd1−N1	147.9(4)	N1B−Cd1−N1	99.1(9)
O2D−Cd1−O1C	95.8(4)	O2C−Cd1−O1C	51.4(4)
N1B−Cd1−O1C	112.4(6)	N1−Cd1−O1C	96.7(6)
O2D−Cd1−O1D	51.4(4)	O2C−Cd1−O1D	95.8(4)
N1B−Cd1−O1D	96.7(6)	N1−Cd1−O1D	112.4(6)
O1C−Cd1−O1D	134.9(8)		

Complex **2**

Zn1−O21A	1.995(6)	Zn1−O15B	2.019(6)
Zn1−O33	2.107(6)	Zn1−N2	2.115(7)
Zn1−N1	2.133(8)	Zn2−O9	1.989(6)
Zn2−O4	2.005(6)	Zn2−N4	2.108(7)
Zn2−O34	2.130(6)	Zn2−N3	2.179(7)
Zn3−O24C	2.008(6)	Zn3−N6	2.087(7)
Zn3−O35	2.094(6)	Zn3−O13	2.132(7)
Zn4−O2	1.956(6)	Zn4−O11	2.009(6)
Zn4−N16	2.088(7)	Zn4−O36	2.165(6)
Zn5−O8D	2.074(8)	Zn5−N14	2.101(8)
Zn5−O37	2.124(6)	Zn5−N13	2.125(7)
Zn6−O28	1.994(6)	Zn6−O17	2.015(6)
Zn6−O38	2.097(6)	Zn6−N8	2.117(7)
Zn6−N7	2.171(7)	Zn7−O31E	1.991(6)
Zn7−O6F	2.004(6)	Zn7−O39	2.063(7)
Zn7−N10	2.077(8)	Zn7−N9	2.178(7)
Zn8−O26	1.963(6)	Zn8−O20	1.995(6)
Zn8−N12	2.104(7)	Zn8−O40	2.139(6)
Zn8−N11	2.189(7)		
O21A−Zn1−O15B	102.3(3)	O21A−Zn1−O33	93.0(3)
O15B−Zn1−O33	97.7(3)	O21A−Zn1−N2	114.4(3)
O15B−Zn1−N2	141.2(3)	O33−Zn1−N2	92.9(3)
O21A−Zn1−N1	92.6(3)	O15B−Zn1−N1	90.3(3)
O33−Zn1−N1	169.0(3)	N2−Zn1−N1	76.2(3)
O9−Zn2−O4	118.5(3)	O9−Zn2−N4	115.4(3)
O4−Zn2−N4	126.0(3)	O9−Zn2−O34	87.4(2)
O4−Zn2−O34	93.1(2)	N4−Zn2−O34	88.3(2)
O9−Zn2−N3	105.9(3)	O4−Zn2−N3	90.6(3)
N4−Zn2−N3	75.7(2)	O34−Zn2−N3	162.4(2)
O24C−Zn3−N6	112.1(3)	O24C−Zn3−O35	95.4(3)
N6−Zn3−O35	94.4(3)	O24C−Zn3−O13	145.1(4)
N6−Zn3−O13	102.4(3)	O35)Zn3−O13	86.6(3)
O24C−Zn3−N5	83.9(3)	N6−Zn3−N5	77.0(3)
O35−Zn3−N5	170.3(3)	O13−Zn3−N5	99.6(3)
O24C−Zn3−O14	88.7(3)	N6−Zn3−O14	150.5(3)
O35−Zn3−O14	104.6(3)	O13−Zn3−O14	57.4(3)
N5−Zn3−O14	85.2(3)	O2−Zn4−O11	116.6(3)
O2−Zn4−N16	105.9(3)	O11−Zn4−N16	137.0(3)
O2−Zn4−O36	93.1(3)	O11−Zn4−O36	90.6(2)
N16−Zn4−O36	93.2(3)	O2−Zn4−N15	103.8(3)
O11−Zn4−N15	86.7(3)	N16−Zn4−N15	77.0(3)
O36−Zn4−N15	162.2(3)	O29−Zn5−O8D	141.8(4)
O29−Zn5−N14	110.5(3)	O8D−Zn5−N14	107.7(4)
O29−Zn5−O37	92.2(2)	O8D−Zn5−O37	84.6(3)
N14−Zn5−O37	94.1(3)	O29−Zn5−N13	93.0(3)
O8D−Zn5−N13	96.3(3)	N14−Zn5−N13	76.2(3)
O37−Zn5−N13	170.1(3)	O28−Zn6−O17	124.3(3)
O28−Zn6−O38	92.8(3)	O17−Zn6−O38	88.5(3)
O28−Zn6−N8	120.4(3)	O17−Zn6−N8	115.2(3)
O38−Zn6−N8	91.1(3)	O28−Zn6−N7	92.3(3)
O17−Zn6−N7	99.1(3)	O38−Zn6−N7	166.3(3)
N8−Zn6−N7	75.3(3)	O31E−Zn7−O6F	101.1(3)
O31E−Zn7−O39	97.5(3)	O6F−Zn7−O39	98.1(3)
O31E−Zn7−N10	116.5(3)	O6F−Zn7−N10	139.0(3)
O39−Zn7−N10	92.5(3)	O31E−Zn7−N9	85.9(3)
O6F−Zn7−N9	91.1(3)	O39−Zn7−N9	169.3(3)
N10−Zn7−N9	77.0(3)	O26−Zn8−O20	110.5(3)
O26−Zn8−N12	107.2(3)	O20−Zn8−N12	142.0(3)
O26−Zn8−O40	91.1(3)	O20−Zn8−O40	92.7(3)
N12−Zn8−O40	91.5(3)	O26−Zn8−N11	107.8(3)
O20−Zn8−N11	87.2(3)	N12−Zn8−N11	76.6(2)
O40−Zn8−N11	159.8(3)		

Symmetry codes: $A = 1 - y, 1 - x, 1 - z$; $B = y, x, 1 - z$; $C = x, y - 1, z$; $D = y - 1, x, 1 - z$ for 1; $A = x - 1, y + 1, z$; $B = x - 1, y, z$; $C = x, y + 1, z$; $D = x, y - 1, z$; $E = x + 1, y, z$; $F = x + 1, y - 1, z$ for 2.

The most interesting feature of **1** is that the achiral free H_2bpdc itself induces axial chirality upon metal coordination. Bpdc links to four metal centers, and exhibits a stereoselective configuration. As shown in Scheme 1, the deprotonated bpdc anions in complex **1** may exhibit (*R*) or (*S*) configurations. Each cadmium(II) center is ligated by two (*R*)-bpdc and two (*S*)-bpdc ligands. Unusually, ligands of the same configuration combine with metal nodes in the same line, so that the 2-D network is interweaved by -(*R*)-bpdc-Cd^{II}-(*R*)-bpdc- and -(*S*)-bpdc-Cd^{II}-(*S*)-bpdc- chains, as shown in Figure 1. Thus, the formation of the framework in **1** is a typical example of a metal-directed stereoselective supramolecular assembly.

In contrast to **1**, complex **2** crystallizes in the monoclinic space group *Pc*, and each asymmetric unit consists of 8 Zn^{II}, 8 bpdc, 8 H_2O, and 8 lattice H_2O units. There are two kinds of coordination geometries around the zinc(II) centers as shown in Figure 3. The Zn3 site exhibits a distorted octahedral geometry, which is surrounded by two nitrogen atoms from a bpdc bipyridyl group, four oxygen atoms from a bpdc monodentate carboxylate group, a bpdc chelating carboxylate group, and a water molecule. In contrast, the other zinc(II) centers, except for the slight difference in bond lengths and angles listed in Table 1, exhibit distorted trigonal bipyramidal environments each of which are surrounded by two nitrogen atoms from a bpdc bipyridyl group, three oxygen atoms from two other bpdc monodentate carboxylate groups, and a water molecule. The Zn−N and Zn−O distances are in the range of 2.077(8)−2.202(7) and 1.963(6)−2.443(10) Å, respectively. Unlike the four-connecting hexadentate pattern in complex **1**, each bpdc anion in complex **2** links three Zn^{II} centers with its chelating 2,2′-pyridyl moiety, asymmetrically chelating monodentate carboxyl groups, or its chelating 2,2′-pyridyl moiety and two monodentate carboxyl groups, displaying pentadentate or tetradentate three-connecting coordination modes

 © 2004 Wiley-VCH Verlag GmbH & Co. KGaA, Weinheim

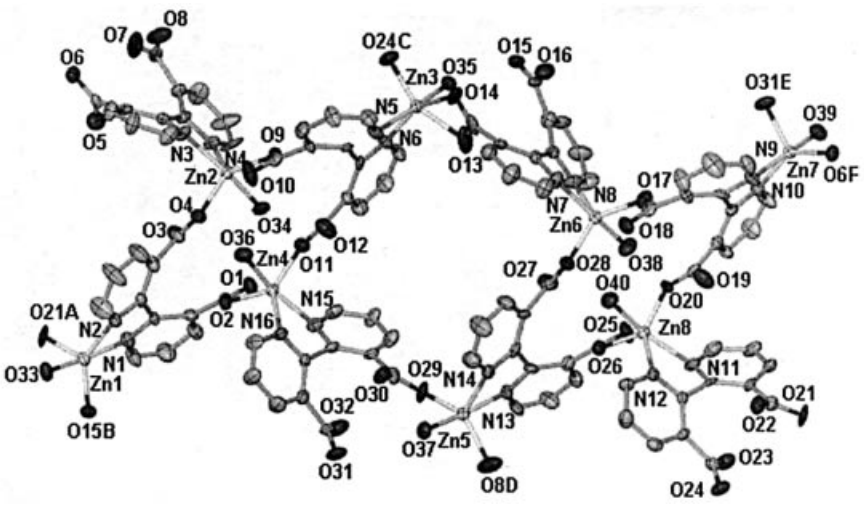

Figure 3. An ORTEP representation of the coordination geometry around the Zn^{II} centers in **2** (50% probability thermal ellipsoids); the solvent water molecules and hydrogen atoms have been omitted for clarity

due to the different coordination patterns of its carboxyl groups (see Scheme 1). The eight bpdc anions in the same asymmetric unit exhibit different distortions of the 2,2′-bipyridyl moiety along the 1,1′ bond, and the dihedral angles between their two pyridine rings are in the range of 30−45°.

The 2-D polymeric structure of **2** can be depicted as a porous grid topology. As shown in Figure 4, two triangular bpdc ligands coordinate to two Zn^{II} nodes with their carboxyl arms to form a rhombus, and further connect to Zn^{II} nodes of adjacent rhombuses with their 2,2′-bipyridyl moieties, resulting in an extended sheet along the *ab*-plane. Furthermore, cage-like pores with a diameter of about 1.2 nm are created through this regular combination of rhombuses. Through the face-to-face packing of 2-D grid sheets along *c*-axis, these cage-like pores run through each other and result in 1-D hydrophilic channels (Figure 5), where the guest water molecules reside. To the best of our knowledge, the framework architectures and unusual coordination modes of bpdc in **1** and **2** are new in the family of bpdc-containing complexes.

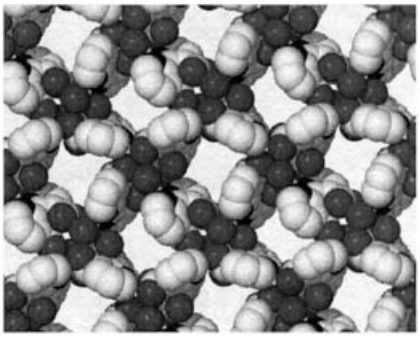

Figure 5. View of the 1-D hydrophilic tunnels along the *c* axis in **2** (guest water molecules have been omitted for clarity)

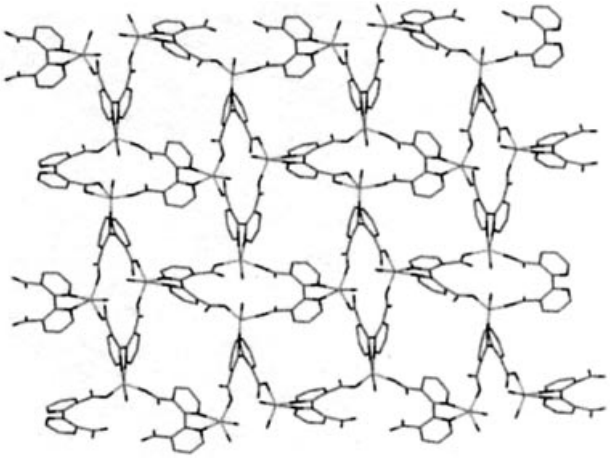

Figure 4. Perspective view of the 2-D network with square cavities and rhombuses in **2**

Fluorescence Properties

Investigations of the solid emissions of Me_2bpdc, **1**, and **2** indicate, that the intraligand fluorescence emission (IL) wavelength and intensity can be tuned by altering the configuration of bpdc, i.e. the dihedral angle between its pyridine moieties. The emissions of **1** [$\lambda_{max.}$ = 404 nm] and **2** [$\lambda_{max.}$ = 448 nm] can be tentatively assigned to the intraligand fluorescence emission, since a similar but weaker emission [$\lambda_{max.}$ = 443 nm for Me_2bpdc] can also be observed for the free ligand (Figure 6). Generally, the intraligand fluorescence emission wavelength of a multi-pyridine ligand is determined by the energy gap between the π and π* molecular orbitals of the free ligand, which is simply related to the extent of π conjugation in the system. For bpdc, however, whose 2,2′-bipyridyl moiety can rotate along the 1,1′ bond, the π and π* energy levels may be perturbed by the dihedral angle between the pyridine rings according to Perkovic's hy-

 © 2004 Wiley-VCH Verlag GmbH & Co. KGaA, Weinheim

pothesis.[23] The unexpected blue-shifted emission of **1** and the slightly red-shifted emission of **2** have been examined. As the dihedral angle of the 2,2′-bipyridyl moiety changes from 53.2° in Me_2bpdc to 93.7° in bpdc in complex **1**,[26] the energy gap between the π* and π molecular orbitals of bpdc increases. Thus, the maximum emission wavelength of **1** undergoes a blue-shift. However, as the dihedral angle of the 2,2′-bipyridyl moiety in **2** decreases to around 30−45°, the energy gap between the π* and π molecular orbitals of bpdc decreases, and the maximum emission wavelength of **2** undergoes a red-shift. The emission intensities of **1** and **2** increase relative to that of Me_2bpdc, and are approximately 1.6 and 1.3 times larger than that of Me_2bpdc, respectively. These enhancements perhaps result from the coordination of bpdc to Cd^{II} or Zn^{II}, which increases the conformational rigidity of the ligands, therefore reducing the non-radiative decay of the intraligand $^1(\pi$-$\pi^*)$ excited state. Similar enhancements of the intraligand fluorescence have also been found in polypyridyl cadmium(II) and polypyridyl zinc(II)polymers.[27−30]

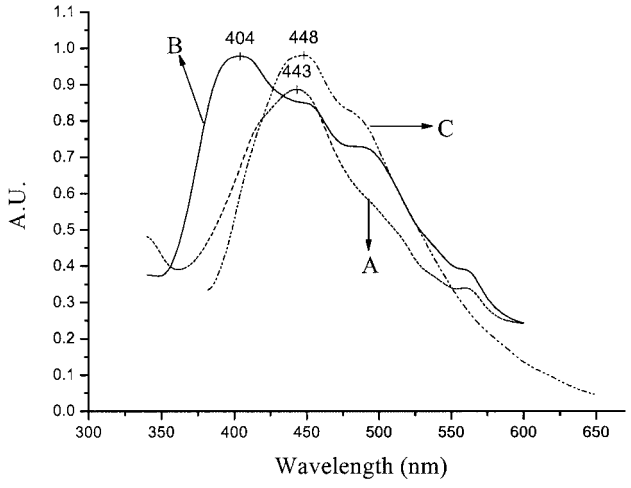

Figure 6. Fluorescence spectra of Me_2bpdc (A), **1** (B), and **2** (C) in the solid state at room temperature (the height of curve A has been reduced for clarity)

Conclusion

Based on the alteration of the configuration of bpdc induced by metal centers, two new 2-D coordination polymers have been obtained by self-assembly of bpdc with Cd^{II} or Zn^{II}. The achiral free H_2bpdc itself causes axial chirality by upon metal coordination in **1**, while in **2** it displays a different distortion of the 2,2′-bipyridyl moiety along the 1,1′ bond to meet the requirements of the final structural motif. Through tuning the configuration of bpdc, complexes **1** and **2** display stronger fluorescence emissions at different wavelengths, which may result in their exploitation in photo-materials.

Experimental Section

General Remarks: Except for binicotinic acid and dimethyl 2,2′-bipyridine-3,3′-dicarboxylate, which were synthesized by literature methods,[31] all other materials were used as received. The IR spectra in KBr disk were recorded with a Magna 750 FT-IR spectrophotometer. C, H and N elemental analyses were determined with an Elementary Vario ELIII elemental analyzer. Fluorescence spectra were measured with an Edinburgh FL-FS90 TCSPC system.

$[Cd^{II}(bpdc)]_n$ (1): Hydrothermal treatment of $CdCl_2{\cdot}2.5H_2O$ (0.2 mmol), Me_2bpdc (0.2 mmol), triethylamine (0.1 mL), and water (15 mL) at 160 °C for 5 days yielded colorless, crystalline blocks of **1** with only one pure phase. The yield of **1** was 55%. $C_{12}H_6CdN_2O_4$ (354.6): calcd. C 40.68, H 1.69, N 7.91; found C 41.10, H 1.44, N 7.91. IR (KBr): $\tilde{\nu}$ = 3093 cm^{-1} (w), 1616 (s), 1577 (s), 1566 (s), 1493 (sh, w), 1431 (m), 1400 (s), 1157 (m), 874 (m), 796 (s), 434 (m).

$\{[Zn^{II}_8(bpdc)_8(H_2O)_8](H_2O)_8\}_n$ (2): With a solution of H_2bpdc (0.2 mmol) in water (20 mL) as the bottom layer in a 50-mL tube, a mixture of water (5 mL), methanol (5 mL), and DMF (10 mL) was added dropwise to the tube along its wall to form a middle layer. A solution of $ZnCl_2$ (0.2 mmol) in methanol (10 mL) was then added as the top layer. After slowly diffusing for two weeks, colorless blocks of **2** appeared in the mesosphere and the yield of **2** was 40%. $C_{96}H_{80}N_{16}O_{48}Zn_8$ (2748.72): calcd. C 41.95, H 2.93, N 8.15; found C 41.70, H 2.84, N 8.18. IR (KBr): $\tilde{\nu}$ = 3461 cm^{-1} (br., s), 3096 (w), 3004 (w), 1653 (s), 1616 (s), 1582 (s), 1432 (m), 1381 (vs), 1161 (m), 1115 (w), 874 (m), 786 (s), 447 (m).

X-ray Crystallographic Determinations: A prismatic crystal of complex **1** with approximate dimensions of 0.46 × 0.28 × 0.04 mm, and a block crystal of complex **2** with approximate dimensions of 0.33 × 0.16 × 0.10 mm, respectively, were selected for X-ray diffraction analysis. The unit-cell parameters and intensities were collected at 298(2) K on a Siemens SMART CCD diffractometer with graphite-monochromated Mo-K_α radiation (λ = 0.71073Å) using the ω-scan mode. The structures were solved by direct methods, and refined on F^2 by full-matrix least-squares procedures using the SHELXTL software suite.[32] All non-hydrogen atoms were refined anisotropically. For complex **1**, no hydrogen atoms were theoretically located, and the maximum and minimum peaks in the final difference maps were 2.211 and −1.573 e·$Å^{-3}$ due to the statistical distribution of the pyridine rings. The largest residual density peak is close to the carboxyl group. For complex **2**, the positions of the hydrogen atoms in the pyridine rings were generated geometrically, and the maximum and minimum peaks in the final difference maps were 1.188 and −0.397 e·$Å^{-3}$ from the disordered solvent water molecule, respectively. The Flack x parameter of complex **2** is 0.3200 with an esd 0.0120 before a twin model refinement, and its absolute structural parameter is 0.00 in the final list of crystal and structural refinement data for complex **2**. A summary of the crystallographic data of complexes **1** and **2** is presented in Table 2, and their selected bond lengths and bond angles are listed in Table 1. CCDC-217300 and CCDC-223662 contain the supplementary crystallographic data for **1** and **2**, respectively. These data can be obtained free of charge at www.ccdc.cam.ac.uk/conts/retrieving.html [or from the Cambridge Crystallographic Data Center, 12 Union Road, Cambridge CB2 1EZ, UK; Fax: (internat.) + 44-1223-336-033; E-mail: deposit@ccdc.cam.ac.uk].

Acknowledgments

This work was supported by grants from the National Natural Science Foundation of China (No.20231020) and the Natural Science Foundation of Fujian Province.

 © 2004 Wiley-VCH Verlag GmbH & Co. KGaA, Weinheim

Table 2. Crystal data and refinement data for **1** and **2**

	1	**2**
Empirical formula	$C_{12}H_6CdN_2O_4$	$C_{96}H_{80}N_{16}O_{48}Zn_8$
Molecular mass	354.6	2748.72
Temperature (K)	298(2)	298(2)
Wavelength (Å)	0.71073	0.71073
Crystal system, space group	tetragonal, *P*4(2)/*mnm*	monoclinic, *Pc*
a (Å)	8.1884(9)	19.6871(10)
b (Å)	8.1884(9)	19.761(0)
c (Å)	16.432(3)	15.543(0)
α (°)	90	90
β (°)	90	101.973(2)
γ (°)	90	90
V (A^3)	1101.8(2)	5915.5(3)
Z, $\rho_{calcd.}$ (Mg m^{-3})	16, 2.101	2, 1.543
μ (Mo-K_α) (mm^{-1})	1.992	1.687
F(000)	664	2784
θ range (°)	2.78 to 25.03	3.05 to 22.50
Reflections collected/unique	2444/ 557 [*R*(int) = 0.0522]	28583/13398 [*R*(int) = 0.0310]
Goodness-of-fit on F^2	1.316	1.076
*R*1, *wR* [$I > 2\sigma(I)$] (all data)	0.0630, 0.1790, 0.0753, 0.1864	0.0497, 0.1320, 0.0535, 0.1356

[1] O. Kahn, C. J. Martinez, *Science* **1998**, *279*, 44−48.
[2] O. Kahn, *Acc. Chem. Res.* **2000**, *33*, 647−657.
[3] O. M. Yaji, G. M. Li, *Angew. Chem. Int. Ed. Engl.* **1995**, *34*, 207−209.
[4] J. S. Seo, D. Whang, H. Lee, S. I. Jun, J. Oh, Y. J. Jeon, K. Kim, *Nature* **2000**, *404*, 982−986.
[5] W.-B. Lin, O. R. Evans, R.-G. Xiong, Z.-Y. Wang, *J. Am. Chem. Soc.* **1998**, *120*, 13272−13273.
[6] J. Zhang, Y.-R. Xie, Q. Ye, R.-G. Xiong, Z. Xue, X.-Z. You, *Eur. J. Inorg. Chem.* **2003**, 2572−2577.
[7] L. C. Tabares, J. A. R. Navarro, J. M. Salas, *J. Am. Chem. Soc.* **2001**, *123*, 383−387.
[8] O. M. Yaghi, H. Li, *J. Am. Chem. Soc.* **1996**, *118*, 295−296.
[9] O. M. Yaghi, H. Li, T. L. Groy, *J. Am. Chem. Soc.* **1996**, *118*, 9096−9101.
[10] O. R. Evans, W. Lin, *Inorg. Chem.* **2000**, *39*, 2189−2198.
[11] P. Ayyappan, O. R. Evans, W. Lin, *Inorg. Chem.* **2002**, *41*, 3328−3330.
[12] K. Biradha, M. Fujita, *Chem. Commun.* **2001**, 15−16.
[13] J. Kim, B. Chen, T. M. Reineke, H. Li, M. Eddaoudi, D. B. Moler, M. O'keeffe, O. M. Yaghi, *J. Am. Chem. Soc.* **2001**, *123*, 8239−8247.
[14] K. Seki, *Chem. Commun.* **2001**, 1496−1497.
[15] C. J. Kepert, M. J. Rosseinsky, *Chem. Commun.* **1998**, 31−32.
[16] M. Eddaoudi, H. Li, O. M. Yaghi, *J. Am. Chem. Soc.* **2000**, *122*, 1391−1397.
[17] Y.-H. Liu, Y.-L. Lu, H.-Ch. Wu, J.-Ch. Wang, K.-L. Lu, *Inorg. Chem.* **2002**, *41*, 2592−2597.
[18] G. Y. S. K. Swamy, K. Chandramohan, N. V. Lakshmi, K. Ravikumar, *Z. Kristallogr.* **1998**, *213*, 191−194.
[19] Zh. J. Zhong, X.-Z. You, Q.-CH. Yang, *Polyhedron* **1994**, *13*, 1951−1955.
[20] X.-M. Zhang, H.-Sh. Wu, X.-M. Chen, *Eur. J. Inorg. Chem.* **2003**, 2959−2964.
[21] B.-L. Wu, H.-Q. Zhang, H.-Y. Zhang, Q.-A. Wu, H.-W. Hou, Y. Zhu, X.-Y. Wang, *Aust. J. Chem.* **2003**, *56*, 335−338.
[22] M.-L. Tong, G. Yang, X.-M. Chen, *Aust. J. Chem.* **2000**, *53*, 607−610.
[23] M. W. Perkovic, *Inorg. Chem.* **2000**, *39*, 4962−4968.
[24] P.-X. Xie, Y.-J. How, B.-W. Zhang, F. Wu, W.-J. Tian, J.-C. Shen, *J. Chem. Soc., Dalton Trans.* **1999**, 4217−4221.
[25] S. Menon, M. V. Rajasekharan, J. P. Tuchagues, *Inorg. Chem.* **1997**, *36*, 4341−4346.
[26] C. R. Rice, K. J. Robinson, J. D. Wallis, *Acta Crystallogr., Sect. C* **1993**, *49*, 1980−1982.
[27] Ch.-G. Zheng, Y.-L. Xie, R.-G. Xiong, X.-Z. You, *Inorg. Chem. Commun.* **2001**, *4*, 405−408.
[28] J. Zhang, Y.-R. Xie, Q. Ye, R.-G. Xiong, Z.-L. Xue, X.-Z. You, *Eur. J. Inorg. Chem.* **2003**, 2572−2577.
[29] J.-H. Luo, M.-Ch. Hong, R.-H. Wang, R. Cao, L. Han, Zh.-Zh. Lin, *Eur. J. Inorg. Chem.* **2003**, 2705−2710.
[30] L. Han, M.-C. Hong, R.-H. Wang, J.-H. Luo, Zh.-Zh. Lin, D.-Q. Yuan, *Chem. Commun.* **2003**, 2580−2581.
[31] S. Dholakia, R. D. Gillard, F. l. Wimmer, *Polyhedron* **1985**, *4*, 791−795.
[32] G. M. Sheldrick, Bruker SHELXTL-PC, University of Göttingen, Germany, **1997**.

Received December 1, 2003
Early View Article
Published Online May 5, 2004

 © 2004 Wiley-VCH Verlag GmbH & Co. KGaA, Weinheim

Film Polymerization − A New Route to the Synthesis of Insoluble Polyimides Containing Functional Nickel(II) Schiff Base Units in the Main Chain

Santo Di Bella,*[a] Giuseppe Consiglio,[b] Nicoletta Leonardi,[a] Salvatore Failla,*[b] Paolo Finocchiaro,[b] and Ignazio Fragalà[a]

Keywords: Coordination polymer / Nickel / Film polymerization / Nonlinear optics

The synthesis and characterization of a new, amino-derivatized functional bis(salicylaldiminato)Ni^{II} complex is reported. It is a useful and reactive precursor in the synthesis of polyimide thermosets. Thus, the first synthesis of a polyimide containing a nonlinear optical Ni^{II} Schiff base complex in the main chain is achieved by thermally controlled film polymerization. Polymerization was monitored on silicon substrates by FT-IR spectroscopy. The polymer film possesses characteristics analogous to those of the insoluble polymer obtained by polymerization in solution, as evidenced by FT-IR spectroscopy and TGA analysis. The present approach might represent a general strategy for achieving thin films of insoluble, functional polymers.

(© Wiley-VCH Verlag GmbH & Co. KGaA, 69451 Weinheim, Germany, 2004)

Introduction

The development of easily processable, functional molecular materials is of central interest in the emerging field of molecular electronics.[1] In this regard, functional polymers are amongst the most promising materials, by virtue of their facile processability into composites,[2] as well as in thin films.[3] The exploration of new polymers with functional transition metal complexes in the main chain is intriguing and the unique electronic properties associated with the metal center certainly deserve to be investigated, especially the distinct or combined, optical (linear and nonlinear), electrical, and magnetic properties.[4]

The very high thermal stability and high glass transition temperature of polyimides makes them well suited for plastic electronics,[2,3,5] although in some cases their low solubility prevents the application as thin-film materials. An alternative synthetic strategy to polyimides is the in situ film polymerization, with the potential to obtaining better thermal and mechanical characteristics of thin films. This strategy involves the choice of suitable and reactive monomers, in order to achieve a thermally controlled polymerization. The appropriate derivatization of starting monomers is thus of relevance for the design and synthesis of new functional thermoset materials.

[a] Dipartimento di Scienze Chimiche, Università di Catania and INSTM UdR di Catania,
95125 Catania, Italy
Fax: (internat.) +39-095-580138
E-mail: sdibella@unict.it
[b] Dipartimento di Metodologie Fisiche e Chimiche per l'Ingegneria (sede Enna), Università di Catania,
95125 Catania, Italy
E-mail: sfailla@dmfci.unict.it

We report here on the synthesis and characterization of novel polyimide thermosets by thermally controlled, film polymerization, which might represent a general method for accomplishing films of insoluble, functional polymers. Moreover this contribution represents the first example of a co-polyimide containing a nonlinear optical Ni^{II} metal complex unit[6] in the main chain.[7,8] To this end, the amino-derivatized Schiff base bis(salicylaldiminato)Ni^{II} complex (**1**) and the bis(maleimide) (**2**) were chosen as starting monomers (Scheme 1).

Results and Discussion

Synthesis of the Derivatized Schiff Base Complex 1

The synthesis of bis(salicylaldiminato), amino-derivatized compounds represents a difficult task. In fact, since these Schiff bases necessarily involve salicylaldehydes as starting compounds, the latter are chemically incompatible with the concurrent existence of free amines. On the other hand, nitrosalicylaldehydes, which could be used as starting materials, give rise to very low soluble Schiff bases. Actually, both the free ligand and the Ni^{II} complex of the related 5-nitro Schiff base, synthesized by standard procedures,[6b,6c] have a very low solubility in most solvents. Consequently, all attempts to obtain the diamine by reduction failed. We have thus developed an alternative route to the synthesis of amino-derivatized, Schiff base Ni^{II} complexes. The adopted synthetic approach is sketched in Scheme 2. It involves protection of the aldehyde function of the starting 5-nitrosalicylaldehyde by acetic anhydride to afford **3**; H_2-catalyzed reduction of the 5-nitro group to the free amine **4**; protection of the amine group with Boc_2O, followed by hydrolysis of the phenol and aldehyde func-

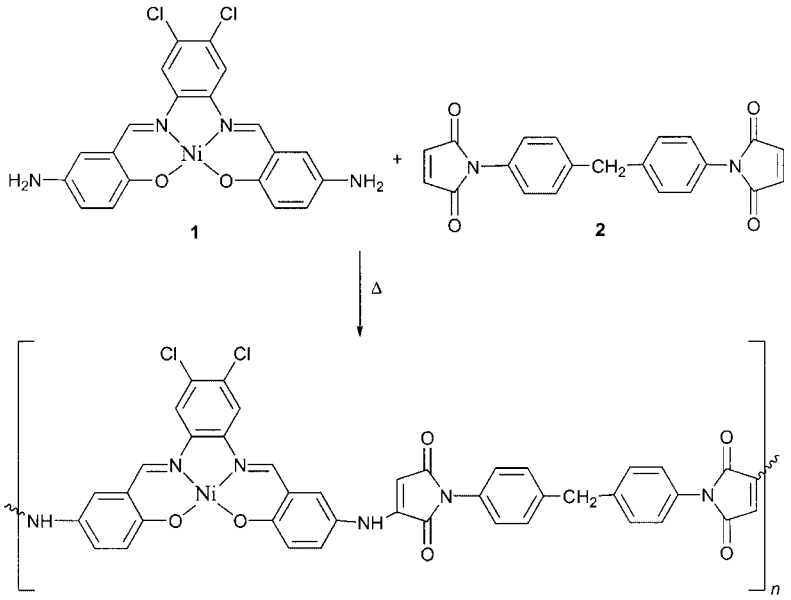

Scheme 1

tionalities with NaOH to get the salicylaldehyde derivative **5**; template reaction with the appropriate 1,2-diamine and Ni^{II} ion affords the 5-amino protected, Schiff base complex **6**; deprotection with trifluoroacetic acid of the amine groups of **6** leads to the 5-amino derivatized Schiff base Ni^{II} complex **1**. All these intermediate precursors **3**−**6**, as well as the amino-derivatized, Schiff base Ni^{II} complex **1**, were obtained in high yields (> 82%), except compound **5** (65%), and fully characterized by mass spectrometry and ^1H NMR spectroscopy, and gave satisfactory microanalyses.

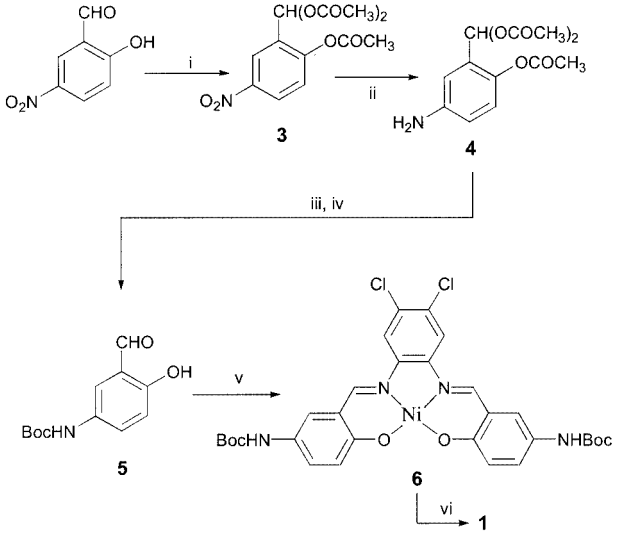

Scheme 2. Reagents and conditions: (i) $(CH_3CO)_2O$, H_2SO_4 cat., room temp.; (ii) H_2 (45 psi), 10% Pd/C, EtOH; (iii) Boc_2O, CH_2Cl_2, room temp.; (iv) MeOH/H_2O, NaOH, reflux; (v) 4,5-dichloro-1,2-phenylenediamine, $NiOAc_2{\cdot}4H_2O$, MeOH; (vi) CF_3COOH, DCM, PhOMe, room temp.; then NaOH, H_2O

INDO/SCI-SOS calculations[9] on **1**, upon geometry optimization, indicate a molecular quadratic hyperpolarizability ($\beta_\mu = -22.8 \times 10^{-30}$ $cm^5{\cdot}esu^{-1}$), which can be compared with the calculated ($\beta_\mu = -17.3 \times 10^{-30}$ $cm^5{\cdot}esu^{-1}$)[6c] and experimental ($\beta_\mu = -20.5 \times 10^{-30}$ $cm^5{\cdot}esu^{-1}$)[6c] values for the unsubstituted Ni(salophen) derivative. The derivatized functional complex **1** is thus a potential candidate for nonlinear optical applications.

Polymerization in Solution

Polymerization was first carried out in solution. This allows for verification of the chemistry involved, by means of the synthesis and analysis of the prepolymer. Partial polymerization was performed by heating a solution of **1** and **2** (0.034 M in each component) in 1-methyl-2-pyrrolidone (NMP) for 1 h, at 90 °C. The prepolymer, that precipitated from chloroform, was analyzed by ^1H NMR and FT-IR spectroscopy. The 500 MHz ^1H NMR of the crude prepolymer in [D_6]DMSO solution shows a partial disappearing of the sharp resonance at $\delta = 7.15$ ppm (olefinic protons of **2**)[10] and the broad resonance (D_2O exchangeable) at $\delta = 4.57$ ppm, assigned to the primary amine protons of **1**. Moreover, the spectrum reveals the presence of new signals, with respect to the starting monomers. In particular, the peaks at $\delta = 2.80$, 3.85, 4.95, and 5.95 ppm, are evidence for the formation of the succinimide ring[11] and the secondary (−NH−) proton of the nitrogen bridge,[10] respectively (see Exp. Sect.). Along with the typical absorption bands,[12] the FT-IR spectrum of **2** also shows a strong absorption at 688 cm^{-1}, from the maleimide ring deformation, and the 1150 cm^{-1} absorption due to asymmetric C−N−C stretching. They represent the reference absorptions used to monitor the reaction between **1** and **2**. The comparison of the FT-IR spectrum of a 1:1 mixture of **1** and **2** with that of the prepolymer indicates an increase of the transmittance of bands at 688 and 1150 cm^{-1}, and the formation of a new band at 1175 cm^{-1} due to the asymmetric C−N−C

 © 2004 Wiley-VCH Verlag GmbH & Co. KGaA, Weinheim

stretching of the succinimide ring.[13] In summary, both the ^{1}H NMR and FT-IR spectroscopic experiments on the prepolymer enable us to establish that the reaction between **1** and **2** involves a Michael addition reaction, as sketched in Scheme 1.

Polymerization was performed by curing a solution of the prepolymer in NMP for 2 h, at 140 °C. The resulting brown material has a low solubility in most solvents, typical of the polyimides, thus preventing, in principle, its application as a functional material. Longer reaction times and higher reaction temperatures did not result in appreciable changes in polymer properties (see infra). Thermogravimetric analysis of the polymer indicates a high thermal stability with a decomposition onset of 380 °C. In comparison with monomers (**2** melts at 157 °C, while **1** starts to decompose, without melting, at 330 °C) the higher thermal stability of the polymer is in agreement with its rigid structure. Accordingly, differential scanning calorimetry analysis indicates the absence of a transition glass temperature in the 30−400 °C range.

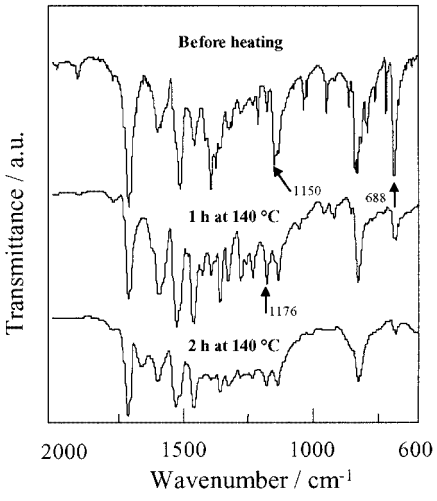

Figure 1. FT-IR spectra of a polyimide thermoset cast film on a silicon substrate at different polymerization stages, using as a reference sample the same substrate before casting. The arrows at 1176, and 1150, 688 cm^{-1} indicate the emerging succinimide function and the disappearing maleimide function, respectively

Film Polymerization

Casting of filtered chloroform solutions of **1** and **2** monomers (0.034 M in each component) on silicon substrates [Czochralsky-grown Si(100), optically transparent in the 600−4000 cm^{-1} IR region of interest, transmittance ≥ 0.90][14] followed by heating, allows the degree of film polymerization to be monitored by FT-IR analysis (Figure 1). When a film of cast monomers is heated at 140 °C for 1 h, the peaks at 688 and 1150 cm^{-1} associated with the maleimide ring decrease, while the peak at 1176 cm^{-1} associated with the succinimide function appears. After the polymer film is further heated at 140 °C for 2 h, the peak at 688 cm^{-1} almost completely disappears, and a band broadening in the range 1100−1600 cm^{-1} is observed, thus indicating an almost complete polymerization. This is also evident from the comparison of this spectrum with the almost identical one of the polymer obtained by polymerization in solution. The further heating of the film does not produce further changes in the FT-IR spectra. The polymer film possesses almost indistinguishable characteristics with respect those of the polymer obtained by polymerization in solution, as confirmed by the TGA analysis.

The polymer films were also characterized by optical spectroscopy. The optical absorption spectrum of the cast film, before heating, shows a band at 380 nm, and two shoulders at about 450 and about 560 nm (Figure 2). After polymerization is complete, the optical spectrum remains almost unchanged, except for a red-shift (≈ 10 nm) of the band at 380 nm along with a better defined structure. This is consistent with a more homogeneous film upon polymerization and good optical quality. These spectral features are similar to those of the optical spectrum of **1** in chloroform solution, thus indicating that the electronic structure of monomer **1** remains essentially unchanged upon polymerization.

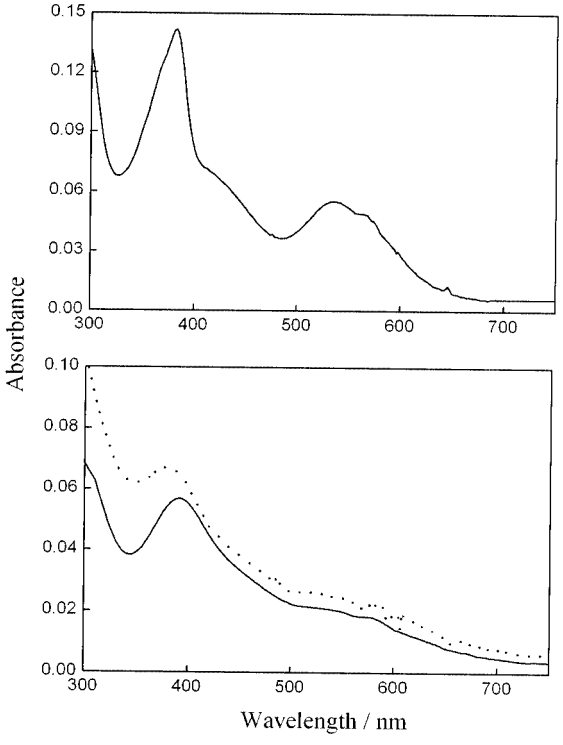

Figure 2. Optical absorption spectra (bottom) of a polyimide thermoset cast film on a glass substrate before heating (- - -) and after 3 h of heating at 140 °C (−). The absorption spectrum of complex **1** (top) in chloroform solution is reported for comparison

Conclusion

In this contribution we have achieved a convenient synthesis for novel functional, amino-derivatized Ni^{II} metal complexes. These complexes can be easily incorporated in the main chain of polyimides and *thermally controlled* film polymerization can be obtained by heating the monomers,

 © 2004 Wiley-VCH Verlag GmbH & Co. KGaA, Weinheim

as monitored by FT-IR spectroscopy. Such an approach might represent a general method for accomplishing films of insoluble, otherwise rather intractable, functional polymers.

Further work is currently in progress with the aim of identifying more flexible monomers, in order to obtain copolymers with definite transition glass temperatures.

Experimental Section

Materials: Nickel(II) acetate tetrahydrate, 2-hydroxy-5-nitrobenzaldehyde, and all the other reagents (Aldrich) were used without purification. 4,5-Dichloro-1,2-phenylenediamine (Aldrich) was purified by sublimation in vacuo. 1,1′-(Methylenedi-4,1-phenylene)bis(maleimide) (**2**) (Aldrich), was purified by recrystallization from toluene. Dichloromethane (DMC) was distilled from CaH_2.

Physical Measurements

Elemental analyses were performed with a Carlo Erba 1106 elemental analyzer. ^{1}H NMR spectra were recorded with a Varian Unity Inova 500 MHz spectrometer, using TMS as internal standard. ESI MS were recorded with an Agilent 1100 Series ESI/MSD spectrometer. Experimental conditions were as follows: Capillary voltage, 3.5 kV; fragmentor, 100 V; source temperature, 350 °C; drying gas, N_2 (10 L/min), carrier solvent, methanol (0.4 mL/min). Samples were dissolved in methanol. For complex **1** the methanol solution was acidified with trifluoroacetic acid. Infrared spectra were recorded with a JASCO FT-IR spectrometer. Thermal measurements were performed with a Mettler Toledo TGA/SDTA85^e system. Thermal analyses were made both in air and under prepurified nitrogen (30 mL/min) using a 10 °C/min heating rate. DSC measurements were obtained from a Mettler DSC 20 calorimeter, under nitrogen atmosphere using a 20 °C/min heating rate. UV-vis spectra were recorded with a Beckman DU 650 spectrophotometer.

Syntheses

Acetyloxy(2-acetyloxy-5-nitrophenyl)methyl Acetate (3): A solution of 2-hydroxy-5-nitrobenzaldehyde (1.67 g, 10.0 mmol), acetic anhydride (50 mL), and H_2SO_4 (3 drops) was stirred under nitrogen for 1 h at room temperature. The solution obtained was poured into ice cold water (500 mL), and stirred for 30 minutes in order to hydrolyze the anhydride. The white solid was collected by filtration, air dried, and crystallized from an EtOAc/cyclohexane mixture to yield 2.55 g (82%) of a white crystalline solid (m.p. 113−115 °C). ESI MS: *m*/*z* (%) = 312 (23) $[MH]^+$. $C_{13}H_{13}NO_8$ (311.24): calcd. C 50.17, H 4.21, N 4.50; found C 50.23, H 4.19, N 4.53.

Acetyloxy(2-acetyloxy-5-aminophenyl)methyl Acetate (4): A solution of compound **3** (2.49 g, 8.00 mmol) in EtOH (40 mL) and THF (10 mL), was hydrogenated (H_2, 45 psi) using 10% Pd/C as catalyst (0.5 g). After 4 h, the filtrate was quickly concentrated to quantitatively give compound **4** (2.25 g) as light brown oil, which was used without any further purification.

***tert*-Butyl (3-Formyl-4-hydroxyphenyl)carbamate (5):** A solution of compound **4** (2.25 g, 8.00 mmol), and di(*tert*-butyl) dicarbonate (1.75 g, 8.00 mmol) in anhydrous DCM (15 mL), was stirred under nitrogen for 8 h. The solvent was evaporated under vacuum, and the oil obtained was dissolved in MeOH (10 mL). Sodium hydroxide (1.6 g, 40 mmol) and water (5 mL) were then added, and the resulting solution refluxed for 5 h. After cooling, the solution was neutralized, and the brown solid was collected by filtration, washed with water, and dried under vacuum. The solid was purified by column chromatography (SiO_2, $CHCl_3$, R_f = 0.22) and crystallized from cyclohexane, to yield 1.23 g (65%) of pale yellow needles (m.p. 122−123 °C). ^{1}H NMR (500 MHz, $CDCl_3$): δ = 10.75 (s, 1 H, O*H*), 9.84 (s, 1 H, C*H*O), 7.82 (d, J_{meta} = 2.8 Hz, 1 H, Ar*H*), 7.24 (dd, J_{ortho} = 9.0, J_{meta} = 2.8 Hz, 1 H, Ar*H*), 6.90 (d, J_{ortho} = 9.0 Hz, 1 H, Ar*H*), 6.39 (br. s, 1 H, N*H*), 1.49 (s, 9 H, CH_3C) ppm. ESI MS: *m*/*z* (%) = 238 (34) $[MH]^+$. $C_{12}H_{15}NO_4$ (237.25): calcd. C 60.75, H 6.37, N 5.90; found C 60.90, H 6.45; N 5.97.

{*N*,*N*′-Bis[5-(*tert*-butoxycarbonylamino)-2-hydroxybenzylidene]-4,5-dichloro-1,2-phenylene-diaminato}Ni^{II} (6): A solution of compound **5** (0.475 g, 2.00 mmol) in 4 mL of methanol was slowly added to a warm solution of 4,5-dichloro-1,2-phenylenediamine (0.177 g, 1.00 mmol) and nickel(II) acetate tetrahydrate (0.250 g, 1.00 mmol) in 10 mL of methanol. The brown suspension obtained was refluxed for 1 h, and then cooled to room temperature. The solid was filtered off, washed with methanol, and dried under vacuum, to yield 0.64 g (95%) of product as red-brown needles. ^{1}H NMR (500 MHz, [D$_6$]DMSO): δ = 9.11 (br. s, 2 H, N*H*), 8.87 (s, 2 H, C*H*=N), 8.57 (s, 2 H, Ar*H*), 7.86 (br. s, 2 H, Ar*H*), 7.22 (dd, J_{ortho} = 9.2, J_{meta} = 2.8 Hz, 2 H, Ar*H*), 6.80 (d, J_{ortho} = 9.2 Hz, 2 H, Ar*H*), 1.48 (s, 18 H, CH_3C) ppm. ESI MS: *m*/*z* (%) = 671 (12), 673 (13) $[MH]^+$. $C_{30}H_{30}Cl_2N_4NiO_6$ (672.18): calcd. C 53.61, H 4.50, N 8.33; found C 53.93, H 4.66, N 8.27.

[*N*,*N*′-Bis(5-amino-2-hydroxybenzylidene)-4,5-dichloro-1,2-phenylenediaminato]Ni^{II} (1): Trifluoroacetic acid (0.81 mL) was added to a suspension of compound **6** (0.540 g, 0.803 mmol) and anisole (0.4 mL) in DCM. The solution obtained was stirred under nitrogen for 24 h, at room temperature. The volatile material was removed under vacuum, and the red solid was collected and washed with diethyl ether. The solid was dissolved in 100 mL of water and filtered. Solid NaOH was added to the aqueous solution (pH ≈ 11), and the dark-brown powder that formed was collected by filtration, washed with water, and dried under high vacuum over P_2O_5, to yield 0.36 g (95%) of **1**. ^{1}H NMR (500 MHz, [D$_6$]DMSO): δ = 8.64 (s, 2 H, C*H*=N), 8.47 (s, 2 H, Ar*H*), 6.87 (d, J_{ortho} = 8.5 Hz, 2 H, Ar*H*), 6.72 (d, J_{ortho} = 8.5 Hz, 2 H, Ar*H*), 6.65 (s, 2 H, Ar*H*), 4.57 (br. s, 4 H, NH_2) ppm. ESI MS: *m*/*z* (%) = 471 (95), 473 (100) $[MH]^+$. UV/vis ($CHCl_3$): $\lambda_{max.}$ = 392, 440 (sh), 544 nm. TGA analysis: $T_{dec.}$ = 330 °C (onset). $C_{20}H_{14}Cl_2N_4NiO_2$ (471.95): calcd. C 50.90, H 2.99, N 11.87; found C 51.03, H 3.02, N 11.79.

Prepolymer: In a two-necked flask (100 mL), equipped with a reflux condenser, magnetic bar and a nitrogen inlet, a solution of **1** (0.25 g, 0.53 mmol) and **2** (0.19 g, 0.53 mmol) in NMP (16 mL) was stirred under nitrogen at 90 °C for 1 h. The mixture was poured into chloroform to give a brown solid, which was collected by filtration, washed with chloroform, several times, and then dried under vacuum (0.40 g). FT-IR (KBr pellet): $\tilde{\nu}$ = 3330 (br. m), 1710 (vs), 1598 (m), 1529 (s), 1460 (s), 1358 (m), 1175 (m), 1136 (m), 825 (s), 688 cm^{-1} (w). ^{1}H NMR (500 MHz, [D$_6$]DMSO), in the spectrum are present new peaks, with respect to the starting monomers: δ = 5.95 (s, D_2O exchangeable, Ar−NH succinimide), 4.95, 3.85 and 2.80 (m, succinimide H) ppm.

Polymer: A solution of **1** (0.25 g, 0.53 mmol) and **2** (0.19 g, 0.53 nmol) in NMP (16 mL) was placed into a two-necked flask (100 mL) equipped with a reflux condenser and a nitrogen inlet. The solution was stirred under nitrogen at 90 °C for 1 h. The temperature was then raised to 140 °C and stirring continued for 2 h. The dark mixture was cooled to room temperature, and then poured into chloroform to give a brown solid. The solid was collected by filtration, washed several times with chloroform, and then

 © 2004 Wiley-VCH Verlag GmbH & Co. KGaA, Weinheim

dried under vacuum (0.42 g). FT-IR (KBr pellet): $\tilde{\nu}$ = 3335 (br. m), 1710 (vs), 1598 (m), 1529 (s), 1460 (s), 1358 (m), 1179 (m), 1137 (m), 825 cm^{-1} (s). TGA analysis: $T_{dec.}$ = 380 °C (onset). Anal. calcd. for a polymer structure as in Scheme 1, $C_{41}H_{28}Cl_2N_6NiO_6$: calcd. C 59.31, H 3.40, N 10.12; found C 59.95, H 3.55; N 10.80.

Film Polymerization: A filtered (0.2-μm syringe filter) chloroform solution of the monomers (0.034 M, 1:1 molar ratio) was cast on 2 × 2 cm silicon substrates. Polymerisation was achieved by heating the film under nitrogen by curing steps of 1 h at 140 °C. Polymerisation was monitored by FT-IR measurements after each step. FT-IR (silicon substrate, after 3 h heating): $\tilde{\nu} \approx$ 3350 (br. w), 1710 (vs), 1593 (m), 1514 (s), 1452 (s), 1340 (m), 1180 (m), 1142 (m), 826 (s), 689 cm^{-1} (vw). TGA analysis: $T_{dec.}$ = 370 °C (onset).

Acknowledgments

We thank the MIUR (PRIN 2001 and FIRB 2002 research programs) for financial support and Prof. E. Scamporrino for helpful discussions.

[1] See, for example: M. A. Ratner, *Mater. Today* **2002**, *5(2)*, 20−27; R. L. Carrol, C. B. Gorman, *Angew. Chem. Int. Ed.* **2002**, *41*, 4378−4400; C. Joachim, J. K. Gimzewski, A. Aviram, *Nature* **2000**, *408*, 541−548.

[2] See, for example: *Materials for Advanced Technologies (ICMAT-2001) Symposium G: Plastic Electronics-Materials and Devices*, in, *Thin Solid Films* **2002**, *417* (1−2) (Eds.: W. Huang, E. T. Kang), Elsevier, Amsterdam, **2002**; *Molecular Materials and Functional Polymers*, in *Monatshefte für Chemie/-Chemical Monthly* **2001**, *132* (1) (Eds.: W. J. Blau, P. Lianos, U. Schubert), Springer-Verlag, Wien, New York, **2001**.

[3] See, for example: *Polymers for Second-Order Nonlinear Optics* (Eds.: G. A. Lindsay, K. D. Singer), *ACS Symposium Series* **1995**, *601*; T. J. Marks, M. A. Ratner, *Angew. Chem. Int. Ed. Engl.* **1995**, *34*, 155−173; D. M. Burland, R. D. Miller, C. A. Walsh, *Chem. Rev.* **1994**, *94*, 31−75.

[4] S. Di Bella, *Chem. Soc. Rev.* **2001**, *30*, 355−366.

[5] For a recent review, see for example: H. Saadeh, D. Yu, L. M. Wang, L. P. Yu, *J. Mater. Chem.* **1999**, *9*, 1865−1873.

[6] [6a] S. Di Bella, I. Fragalà, *New J. Chem.* **2002**, *26*, 285−290. [6b] S. Di Bella, I. Fragalà, I. Ledoux, J. Zyss, *Chem. Eur. J.* **2001**, *7*, 3738−3743. [6c] S. Di Bella, I. Fragalà, I. Ledoux, M. A. Diaz-Garcia, T. J. Marks, *J. Am. Chem. Soc.* **1997**, *119*, 9550−9557.

[7] Cu^{II} Schiff bases were previously inserted in the main chain of polyethers and polycarbonates: D. Vitalini, P. Mineo, S. Di Bella, I. Fragalà, P. Maravigna, E. Scamporrino, *Macromolecules* **1996**, *29*, 4478−4485; E. Scamporrino, S. Bazzano, D. Vitalini, P. Mineo, *Macromol. Rapid Commun.* **2003**, *24*, 236−241.

[8] For comprehensive reviews on polymers involving transition metal complexes, see: P. Nguyen, P. Gómez-Elipe, I. Manners, *Chem. Rev.* **1999**, *99*, 1515−1548; R. P. Kingsborough, T. M. Swager, *Prog. Inorg. Chem.* **1999**, *48*, 123−231.

[9] Calculations on **1** were performed as described in: S. Di Bella, I. Fragalà, *Eur. J. Inorg. Chem.* **2003**, 2606−2611.

[10] J. T. Lin, M. A. Hubbad, T. J. Marks, *Chem. Mater.* **1992**, *4*, 1148−1150.

[11] W. Wu, D. Wang, C. Ye, *J. Appl. Polym. Sci.* **1998**, *70*, 2471−2477.

[12] S. F. Parker, S. M. Mason, K. P. J. Williams, *Spectrochim. Acta* **1990**, *46A*, 315−321.

[13] C. Di Giulio, M. Gautier, B. Jasse, *J. Appl. Polym. Sci.* **1984**, *29*, 1771−1779.

[14] See, for example: F. Schomann, K. Graff, *J. Electrochem. Soc.* **1989**, *136*, 2025−2031.

Received December 22, 2003
Early View Article
Published Online May 5, 2004

 © 2004 Wiley-VCH Verlag GmbH & Co. KGaA, Weinheim

Palladacyclopentadiene Complexes with Mono- and Didentate Imidato Ligands: Synthesis, Hemilabile Behaviour and Catalytic Application in the Stille Reaction

José Luis Serrano,*[a] Ian J. S. Fairlamb,*[b] Gregorio Sánchez,*[c] Luis García,[a] José Pérez,[a] Jorge Vives,[c] Gregorio López,[c] Catherine M. Crawforth,[b] and Richard J. K. Taylor[b]

Keywords: Catalysis / Cross-coupling / N,O ligands / Palladium / Stille reactions

The binuclear hydroxo complex $[NBu_4]_2[Pd_2\{C_4(COOMe)_4\}_2(\mu\text{-}OH)_2]$ (**1**) has been prepared by addition of two equivalents of NBu_4OH to polymeric $[Pd\{C_4(COOMe)_4\}]_n$. Complex **1** has been successfully employed as a precursor to three novel binuclear imidate-bridged complexes $[NBu_4]_2[Pd_2\{C_4(COOMe)_4\}_2(\mu\text{-imidate})_2]$ [imidate = succinimidate (suc) **2**, phthalimidate (pht) **3** or maleimidate (mal) **4**] in which the imidate group displays a bidentate *N*,*O*-coordination mode. The hemilabile behaviour of the imidate ligands has been investigated by reaction with a variety of P, N and S ligands, affording the corresponding mononuclear derivatives $[NBu_4][Pd\{C_4(COOMe)_4\}(imidate)L]$ [L = PPh_3 (**2a**, **3a** or **4a**), $P(p\text{-}C_6H_4F)_3$ (**2b**, **3b** or **4b**), PBu_3 (**2c**, **3c** or **4c**), py (**2d**, **3d** or **4d**), $p\text{-}MeC_6H_4NH_2$ (**2e**, **3e** or **4e**), tetrahydrothiophene (**2f**, **3f** or **4f**)] with terminal *N*-bonded imidate ligands. The characterization of the new complexes involved spectroscopic methods (IR, FAB, ^1H, ^{13}C, ^{19}F and ^{31}P NMR) and X-ray crystallographic analysis for **1**, **4b** and **4e**. The mononuclear derivatives are shown to catalyse the Stille cross-coupling of benzyl bromide **7** with ethyl *Z*-vinylstannyl carboxylate (**8**) in high yields. Yields and reaction times are dependent on the presence and type of imidate ligand, which suggests an important role for it in the catalytic cycle.

(© Wiley-VCH Verlag GmbH and Co. KGaA, 69451 Weinheim, Germany, 2004)

Introduction

Over the last twenty five years great advances in the development of palladium-catalysed carbon−carbon and carbon−heteroatom bond-forming processes have been observed.[1] Palladium-catalysed reactions, such as Stille[2] and Suzuki coupling, have made significant contributions to synthetic chemistry, not least in the synthesis of important natural products and materials.[3] For this reason, highly active, efficient and selective Pd catalysts are continually been sought after. The scope of the Suzuki and Stille reactions — the reaction of organohalides with organoboronic acids or organostannanes, respectively — has been substantially expanded upon in recent years. The design of electron-rich palladium species possessing strong σ-donor ligands that mediate mild cross-coupling reactions of activated and deactivated organohalide substrates with appropriate nucleophiles has contributed to this effort.[4] To date, however, palladacyclopentadiene complexes have not been used in classic carbon−carbon bond-forming processes, although they have been implicated in a number of other catalytic processes.[5]

In this paper, we wish to describe the synthesis of a new class of palladacyclopentadiene complexes that contain imidato ligands (succinimide, maleimide and phthalimide). We have studied in previous work[6] the hemilabile behaviour[7] of such ligands in complexes with a classical cyclometallated backbone. The precursors employed in this case were the well-known complexes with bridging acetate groups. However, regarding the desired palladacyclopentadiene compounds we envisaged that they could be synthesised from binuclear hydroxypalladium complexes, the chemistry of which has been studied recently,[8] by means of a simple acid-base reaction with protic electrophiles.[9] Thus, the preparation of the new organometallic di-μ-hydroxo complex **1** containing a palladacyclopentadiene backbone, its use as a precursor of binuclear di-μ-imidate palladacyclopentadiene complexes **2**−**4**, and their hemilabile behaviour towards monodentate ligands, such as acetonitrile,

[a] Departamento de Ingeniería Minera, Geológica y Cartográfica, Area de Química Inorgánica, Universidad Politécnica de Cartagena,
30203 Cartagena, Spain
E-mail: jose.serrano@upct.es
[b] Department of Chemistry, University of York,
York, Heslington, York, YO10 5DD, UK
E-mail: ijsf1@york.ac.uk
[c] Departamento de Química Inorgánica, Universidad de Murcia, 30071 Murcia, Spain
E-mail: gsg@um.es

 © 2004 Wiley-VCH Verlag GmbH & Co. KGaA, Weinheim DOI: 10.1002/ejic.200300962

phosphanes [Ph_3P, (p-$C_6H_4F)_3P$ and nBu_3P], pyridine, p-toluidine and tetrahydrothiophene, are reported in detail herein. A comparison of the catalytic properties of the new di-μ-imidate palladacyclopentadiene complexes with [1,2,3,4-tetrakis(methoxycarbonyl)-1,3-butadiene-1,4-diyl]-palladium(II) (TCPC), [Pd($NCOC_2H_4CO$)(PPh_3)$_2$Br][10] (**5**) and [Pd($NCOC_2H_4CO$)(dppe)Br] (**6**) in the Stille reaction, is also presented. Fairlamb and Taylor[11] have recently disclosed the first application of imidato-based palladium pre-catalysts **5** and **6** in the Stille reaction,[12] where they found that allylic and benzylic substrates were coupled efficiently.[13] Here the succinimide ligand, a pseudohalide that can be viewed as a strong σ-acceptor and moderate π-donor (stronger π-donor than chlorine), plays an important role.[14] Thus, being able to compare the effect of the palladacyclopentadiene unit and the presence of an imidate ligand, is an important objective of this paper.

Results and Discussion

The novel anionic palladacyclopentadiene complex [Pd_2{C_4(COOMe)$_4$}$_2$(μ-OH)$_2$]$^{2-}$ (**1**) was conveniently prepared by reaction of the polymeric complex [Pd{C_4(COOMe)$_4$}]$_n$ (TCPC) with NBu_4OH in water (Scheme 1).[5d]

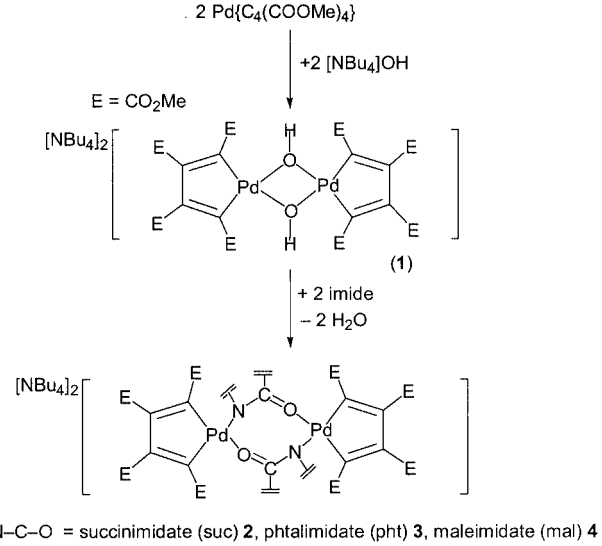

Scheme 1. Hydroxo- and imidate-bridged binuclear complexes

The analytical data for the hydroxo-bridged palladacyclopentadiene dimer **1** are consistent with the proposed formula. Negative-ion FAB mass spectrometry shows a signal at m/z = 725 due to the [Pd_2{C_4{$COOMe)_4$}{C_4{$COOMe}_3${CO}})(μ-$OH)_2$]$^-$ fragment. Evidence for the

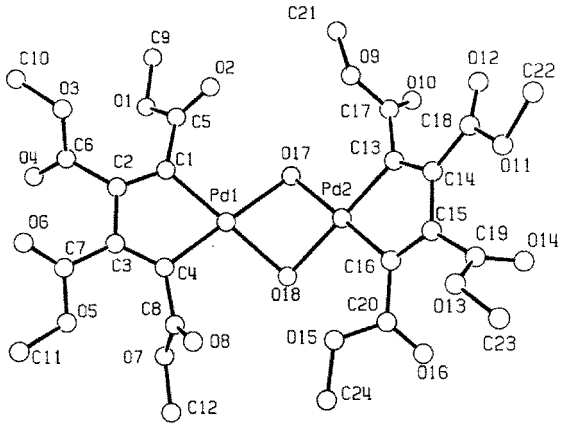

Figure 1. X-ray single-crystal structure of **1**

μ-OH ligand comes from the IR spectrum of **1**, which shows a stretching vibration at $\tilde{\nu}$ = 3600 cm^{-1}. A high-field shielded resonance is also seen at δ = −0.85 ppm in the ^{1}H NMR spectrum, which is attributable to this ligand. Two and four signals for the metallacycle moiety are found in the ^{1}H and ^{13}C NMR spectra, respectively. These attributes are consistent with the symmetrical nature of **1**. X-ray crystallographic analysis on a poor quality crystal of **1** allowed us to unambiguously define the connectivities of the atoms in the anion complex (Figure 1), confirming the proposed molecular structure and its similarity to previously reported halide complexes.[15] It was not possible to refine the structure with acceptable R-values to obtain an adequate data set for an accurate structure determination. Complex **1** crystallized from dichloromethane/diethyl ether as yellow crystals in the monoclinic space group $P2_1/c$ with cell parameters a = 12.8481(6) Å, b = 63.7441(30), c = 16.6102(8) Å, γ = 119.9433(9)°, V = 12618.0(17) Å^3, Z = 8, D_c = 1.369 g·cm^{-3}.

In acetone, **1** reacts with succinimide, phthalimide or maleimide to give the dinuclear complexes **2**, **3** and **4**, respectively, in which the imidato ligands replace the bridging hydroxo groups (as shown in Scheme 1). The imidate complexes are air-stable yellow solids, whose IR spectra exhibit strong bands between $\tilde{\nu}$ = 1700 ± 20 cm^{-1} and 1620 ± 20 cm^{-1}, that are characteristic of the carboxylate and imidate groups, respectively. The dinuclearity of these complexes was confirmed by FAB mass spectrometry. The negative FAB mass spectra of complexes **2**−**4** show peaks corresponding to [(NBu_4)Pd_2{C_4(COOMe)$_4$}$_2$(μ-suc)$_2$]$^-$ (m/z = 1220, **2**), [(NBu_4)Pd_2{C_4(COOMe)$_4$}$_2$(μ-phthal)$_2$-2]$^-$ (m/z = 1314, **3**) and [Pd_2{C_4(COOMe)$_4$}$_2$(mal)]$^-$ (m/z = 876, **4**). The dinuclear complexes **2**−**4** undergo rapid dissociation in acetonitrile to give mononuclear species. In CD_3CN, complex **2** exhibits four singlet resonances (δ = 3.36, 3.46, 3.49 and 3.60 ppm) in the ^{1}H NMR spectrum, which are attributable to the four methoxycarbonyl groups of the asymmetric [Pd{C_4(COOMe)$_4$}(suc)(CD_3CN)]$^-$ complex. Compounds **3** and **4** behave in a similar manner (see Exp. Sect.).

 © 2004 Wiley-VCH Verlag GmbH & Co. KGaA, Weinheim

We have investigated the hemilabile behaviour of the imidato-bridged compounds toward neutral ligands, such as phosphanes, amines and tetrahydrothiophene. These reactions take place in acetone under mild conditions to give the corresponding anionic square-planar complexes $[Pd\{C_4\{COOMe)_4\}(N\text{-imidate})(L)]^-$ (**2a**−**f**, **3a**−**f**, **4a**−**f**, Scheme 2), which are air-stable pale-yellow solids. The IR spectra show bands characteristic of the palladacyclopentadiene backbone and imidate ligands (see Exp. Sect.).

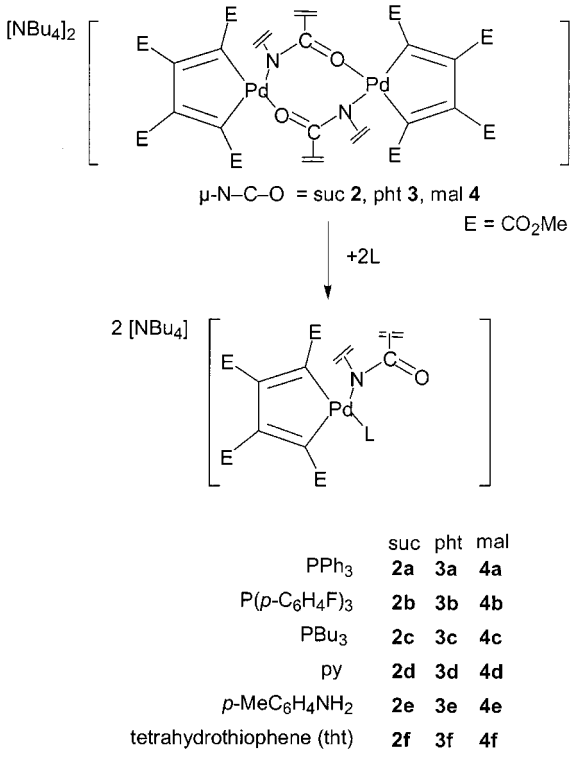

	suc	pht	mal
PPh_3	**2a**	**3a**	**4a**
$P(p\text{-}C_6H_4F)_3$	**2b**	**3b**	**4b**
PBu_3	**2c**	**3c**	**4c**
py	**2d**	**3d**	**4d**
$p\text{-}MeC_6H_4NH_2$	**2e**	**3e**	**4e**
tetrahydrothiophene (tht)	**2f**	**3f**	**4f**

Scheme 2. Mononuclear *N*-imidate complexes

With regard to the ^1H NMR spectra, the expected resonances of the palladacyclopentadiene, imidate and neutral ligands are seen. The resonances of the methoxycarbonyl groups on the carbons *trans* to the imidate units appear between $\delta = 3.25$ and 3.58 ppm, whilst the resonances of the methoxycarbonyl groups on the carbons *trans* to the neutral ligands occur at higher field, particularly in complexes containing PPh_3 and $P(p\text{-}C_6H_4F)_3$ ligands (between $\delta = 2.50$ and 2.62 ppm for complexes **2a**,**b**, **3a**,**b** and **4a**,**b**). The $^{31}P\{^1H\}$ NMR spectra of the phosphane complexes show a single resonance in the usual range for palladium(II) complexes (for PPh_3 (**2a**, **3a**, **4a**), $\delta = 28.1-28.7$ ppm; $P(4\text{-}F\text{-}C_6H_4)_3$ (**2b**, **3b**, **4b**), $\delta = 26.4-26.8$ ppm; $PnBu_3$ (**2c**, **3c**, **4c**), $\delta = 2.5-3.6$ ppm). The molecular structures of **4b** and **4e** were confirmed by X-ray single crystal diffraction (Figure 2 and 3, respectively; data collection and refinement information is given in the Exp. Sect.).

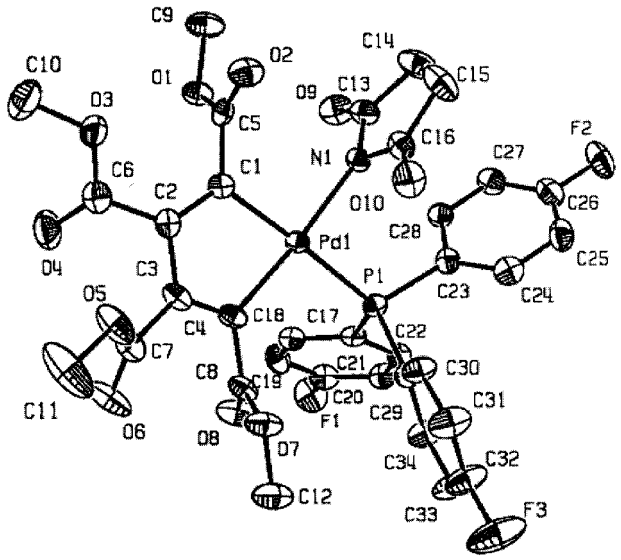

Figure 2. X-ray single crystal structure of **4b**

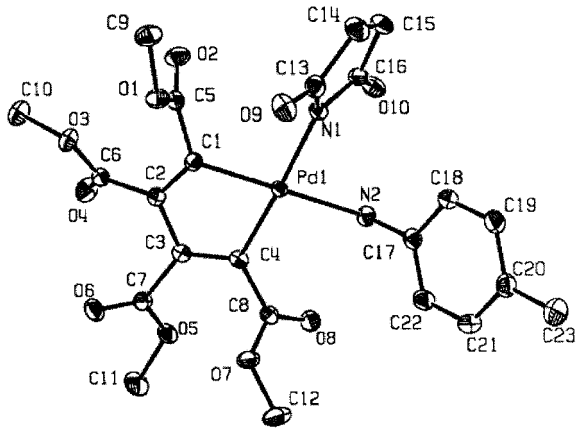

Figure 3. X-ray single crystal structure of **4e**

The X-ray data represent the first description of crystal structures in which the maleimidate ligand appears coordinated to a metal centre in a *N*-monodentate mode (η^2-alkene coordination is common for maleimide ligands).[16] Selected bond lengths and angles are given in Table 1.

The Pd(1)−N(1) distance and the C(1)−Pd(1)−C(4) angle are similar in both compounds and lie close to those determined for related structures.[5n] A slight tetrahedral distortion of the planar palladium environment is observed in **4b**, with torsion angles of −2.13° for P(1)−C(4)−C(1)−Pd(1) and −6.19° for N(1)−C(1)−C(4)−Pd(1).[17] In complex **4e** the coordination around the metal centre is characterised by a plane defined by the C(1)−C(4)−N(1)−Pd(1) atoms, with N(2) out of the plane [torsion angles of −0.30° for N(1)−C(1)−C(4)−Pd(1) and −9.40° for N(2)−C(4)−C(1)−Pd(1)]. Following the recent classification put forward by Dance and Scudder[18] for PPh_3, the conformation of the $Pd-P(p\text{-}C_6H_4F)_3$ group can be de-

 © 2004 Wiley-VCH Verlag GmbH & Co. KGaA, Weinheim

Table 1. Selected bond lengths (Å) and angles (°) for complexes **4b** and **4e**

	4b	**4e**
Pd(1)−C(1)	2.066(4)	2.0154(19)
Pd(1)−C(4)	2.036(4)	2.0095(18)
Pd(1)−N(1)	2.077(3)	2.0900(15)
Pd(1)−P(1)[a]	2.3339(12)	2.1789(16)
N(1)−C(13)	1.378(5)	1.390(2)
N(1)−C(16)	1.357(5)	1.362(2)
C(13)−O(9)	1.213(5)	1.216(2)
C(16)−O(10)	1.224(5)	1.232(2)
C(13)−C(14)	1.521(7)	1.507(3)
C(14)−C(15)	1.308(7)	1.319(3)
C(15)−C(16)	1.511(6)	1.506(3)
C(1)−Pd(1)−C(4)	80.05(17)	79.73(8)
C(1)−Pd(1)−N(1)	167.52(15)	177.16(7)
C(4)−Pd(1)−N(1)	91.05(15)	97.47(7)
C(1)−Pd(1)−P(1)[a]	97.74(13)	94.26(7)
C(4)−Pd(1)−P(1)[a]	176.28(12)	165.48(7)
N(1)−Pd(1)−P(1)[a]	91.58(10)	88.57(6)

[a] N(2) in compound (**4e**)

scribed as a *good rotor* for **4b** (T_1 = 16.96°; T_2 = 36.35°; T_3 = 69.46°), based on the M−P−C_{ipso}−C torsion angle.

Catalytic Properties of the Mononuclear Imidate Complexes

The mononuclear palladacyclopentadiene complexes **2a**, **2d**, **2f**, **3a**−**3f**, **4a**, **4d** and **4f** were evaluated in the Stille coupling of benzyl bromide (**7**) with ethyl *Z*-vinylstannyl carboxylate (**8**) in dry toluene at 60 °C under an atmosphere of nitrogen (Table 2).

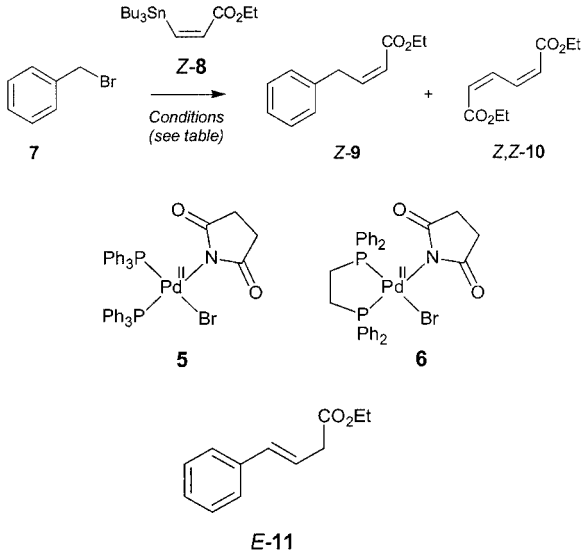

This was achieved under identical reactant concentrations and catalyst loadings to that reported in the successful Stille coupling using **5** and **6** as catalysts.[11] All of the mononuclear complexes were shown to catalyse the cross-coupling reaction. The particular type of imidate (succinimide, maleimide, phthalimide) and the neighbouring ligand attenuated the catalyst activity and overall yields of *Z*-**9**. The tetrahydrothiophene (tht) ligand proved to be the best for all of the imidate complexes, indicating that ligand dissociation is probably important (entries 5, 11 and 14). Credibility for this suggestion is gained by comparing the

Table 2. Palladacyclopentadiene screening against Stille cross-coupling[a]

Entry	Catalyst[b]	Imidate	Time (h)	Yield of (*Z*)-**9** (%)	Yield of (*Z*,*Z*)-**10** (%)
1	[Pd(NCOC$_2$H$_4$CO)(PPh$_3$)$_2$Br] (**5**)	Suc	3	98	–
2	]Pd(NCOC$_2$H$_4$CO)(dppe)Br] (**6**)	Suc	24	90[c]	–
3	**2a** (PPh$_3$)	Suc	22	82[d]	0
4	**2d** (Py)	Suc	1.3	86[e]	4
5	**2f** (tht)	Suc	1.5	95	4
6	**3a** (PPh$_3$)	Pht	3.75	72[f]	0
7	**3b** [P(*p*-C$_6$H$_4$F)$_3$]	Pht	6	99[g]	0
8	**3c** (P*n*Bu$_3$)	Pht	20	80	0
9	**3d** (Py)	Pht	2.75	63	3
10	**3e** (*p*-MeC$_6$H$_4$NH$_2$)	Pht	5.75	84	0
11	**3f** (tht)	Pht	1	81	0
12	**4a** (PPh$_3$)	Mal	21	53	0
13	**4d** (Py)	Mal	20	32	1
14	**4f** (tht)	Mal	3	70[h]	0
15	TCPC	–	15[i]	68	0
16	Pd/P(*t*Bu)$_3$[j]	–	1.5	71	0

[a] Reaction conditions: **7** (0.5 mmol), (*Z*)-**8** (0.6 mmol), $C_6H_5CH_3$ (5 mL) at 60 °C, under an inert atmosphere of N_2. Isolated yields are given after column chromatography in all cases. All reactions were closely monitored by TLC using 5% ethyl acetate/petroleum ether as eluent. The reaction time given is representative of complete reaction, as adjudged by complete disappearance of **7**. [b] 5 mol % [Pd] unless stated otherwise. [c] Isomer ratio [(*E*)-**9**:(*Z*)-**9**, 1:29]. [d] Isomer ratio [(*E*)-**9**:(*Z*)-**9**, 1:3.7]. The *E*-regioisomer **11** was also observed (2%). [e] Isomer ratio [(*E*)-**9**:(*Z*)-**9**, 1:14.3]. [f] Isomer ratio (*E*:*Z*, 1:23). [g] Isomer ratio (*E*:*Z*, 1:2.5). The *E*-regioisomer **11** was also observed (8%). [h] Isomer ratio (*E*:*Z*, 1:12.2). The *E*-regioisomer **11**was also observed (4%). [i] The reaction had to be conducted at 100 °C. Very slow conversion into *Z*-**9** was seen at 60 °C. [j] [Pd$_2$dba$_3$] (2.5 mol %), P(*t*Bu)$_3$ (5.5 mol %), $C_6H_5CH_3$, 60 °C.

 © 2004 Wiley-VCH Verlag GmbH & Co. KGaA, Weinheim

pyridine and triphenylphosphane ligands (entries 3, 4, 6, 9, 12 and 13). The presence of a pyridine ligand in combination with a succinimide or phthalimide provides higher reaction rates than those catalysts containing phosphane ligands (entries 4 and 9). The reaction employing the maleimide-based complex **4d** was surprisingly sluggish and the overall yield was low (entry 13). With the exception of the phthalimide/triphenylphosphane derivative **3a** (entry 6), triphenylphosphane retards the reaction rate (entries 3 and 12). For a number of examples, regio- and/or stereoisomerisation was observed (entries 2−4, 6, 7 and 14) which is a common problem observed with this type of product.[11] We generally found that isomerisation occurs during the latter stages of the reaction (as judged by ^{1}H NMR spectroscopy and TLC analysis). In terms of isolated yields, **3b** is the best catalyst, providing *Z*-**9**/*E*-**11** in 99% combined yield, although extensive isomerisation was observed, which might be related to its high activity. The succinimido catalyst **2f** provided the product *Z*-**9** in 95% yield and no isomerisation was observed (entry 5). This catalyst reduces the reaction time by half in comparison to precatalyst **5** (entries 1 and 5) and is the catalyst of choice. As a control experiment, the TCPC complex was screened for catalytic activity (entry 15). Higher temperatures (100 °C) were required to facilitate the reaction, with the coupling product isolated in 68% yield after 15 h. The requirement for a higher temperature is presumably associated with the polymeric form of TCPC. Against a state-of-the-art catalyst system developed by Fu et al., namely the Pd/P(*t*Bu)$_3$ system,[19] our results compare well (entries 4, 5, 11). Employing an identical catalyst loading to that used in our studies (5 mol % Pd), the product *Z*-**9** was isolated in 71% yield after 1.5 h (entry 16). For catalyst **2f**, containing the tht ligand, lowering the catalyst concentration to 0.5 mol % gives the cross-coupled product in a 93% yield after only 3.25 h. Future studies will be focussed on assessing the effect and impact of catalyst loading on the reaction rates and yields of these reactions.

Generally, the results indicate that a phosphane ligand is *not* a prerequisite (it is usually required to promote the oxidative addition process). The type of imidate seems to affect the yields and reaction times, suggesting that it too plays an important role within the catalytic cycle. The substantially lower activity of TCPC in this reaction also suggests that the imidate and other ligands are important for catalysis. In consideration of the classic catalytic cycle, where a Pd^0/Pd^{II} or related anionic cycle is considered,[20] the palladacyclopentadiene unit would be reduced. However, we have yet to isolate any side-products related to the organic diene fragment of the palladacyclopentadiene unit. In the absence of phosphane ligand, reduction would be expected to release metallic palladium black, particularly towards the latter stages of the reaction when substrate concentration is low. In several reactions (entries 4, 5, 9 and 13, Table 2) small quantities of the homocoupled (self-coupled) product *Z*,*Z*-**10**, derived from the organotin reagent, *Z*-**8**, were isolated. The exact quantity of *Z*,*Z*-**10** varies, but it should be emphasised that we only begin to detect this during the latter stages of the reaction (by TLC).

Conclusion

The new di-μ hydroxo complex $[NBu_4]_2[Pd_2\{C_4(COOMe)_4\}_2(\mu\text{-}OH)_2]$ (**1**) has been synthesised and characterised. Its validity as a precursor in acid-base reactions has been demonstrated by preparation of new imidate-bridged complexes in which an *N*,*O*-bidentate coordination mode is exhibited. Bridge splitting with neutral ligands affords mononuclear *N*-bonded imidate complexes. Two *N*-bonded maleimidate complexes have been described and represent the first such examples where the maleimidate is *N*-bonded to a metal centre. These mononuclear complexes demonstrate very good catalytic properties in the Stille reaction and represent the first uses of anionic palladacyclopentadiene complexes in classical carbon−carbon bond-forming reactions. We intend to extend their use to other important reactions in synthesis, such as the Suzuki and Heck reactions. A number of complexes are more active than the previously described succinimido catalyst **5**. Complexes **2d**, **2f** and **3f** were the most efficient in this respect. Further studies are being carried out to probe whether these catalysts operate by classical or non-classical catalytic pathways, whether the palladacyclopentadiene unit is stable under the catalytic conditions, and which Pd complex is observed after catalysis. These results will be reported in due course.

Experimental Section

General Remarks: C, H, N and S analyses were carried out with a Carlo Erba model 1108 microanalyser. IR spectra were recorded on a Perkin−Elmer spectrophotometer 16F PC FT-IR, using Nujol mulls between polyethylene sheets. NMR spectroscopic data were recorded on a Bruker AC 200E or a Varian Unity 300 spectrometer. Mass spectrometric analyses were performed on a Fisons VG Autospec double-focusing spectrometer, operating in the negative mode. Ions were produced by fast-atom bombardment (FAB) with a beam of 25-KeV Cs atoms. The mass spectrometer was operated with an accelerating voltage of 8 kV and a resolution of at least 1000. The palladacyclopentadiene precursor (TCPC) was prepared by a published method.[4] Dry CH_2Cl_2 and toluene were distilled from calcium hydride. THF was distilled from sodium-benzophenone ketyl. Reagents were purchased from commercial sources and used directly unless stated otherwise in the text.

Catalysis: Nitrogen gas was oxygen-free and was dried immediately prior to use by passing over sodium hydroxide pellets. All TLC analysis was performed using Merck 5554 aluminium-backed silica plates. Compounds were visualised using UV light (254 nm) and either an acidic aqueous solution of vanillin, a basic aqueous solution of potassium permanganate, acidic DNP or iodine silica. Column chromatography was performed with Fisons matrix silica using the eluent specified in the text. The inorganic solutions used were either saturated (NaCl, KF) or of the approximate concentration indicated in the text. PE refers to petroleum ether 40−60 °C.

^{1}H and ^{13}C NMR spectra were recorded on a Jeol EX270 spectrometer operating at 270 and 67.9 MHz, respectively, on a Bruker AMX 500 at 500 and 125 MHz, respectively, or a Jeol EX400 spectrometer operating at 400 and 100 MHz. The solutions were prepared in suitable deuterated solvents. The spectra were referenced

 © 2004 Wiley-VCH Verlag GmbH & Co. KGaA, Weinheim

to either TMS or residual protonated solvent. Proton assignments were based on coupling constants, integration and correlation tables. Carbon spectral assignments were aided using DEPT studies and correlation tables. All melting points were recorded on an Electrothermal IA9000 digital melting point apparatus and are uncorrected. Low- and high-field resolution electron ionisation (EI) and chemical ionisation (CI) mass spectrometry were performed by Dr. T. A. Dransfield and Mr. B. R. Glennie, using a Fisons analytical (VG) Autospec instrument. All values are reported in accordance with convention and high resolution molecular ions given are within ±5 ppm of the required molecular mass. Infrared spectroscopic data were obtained using an ATI Mattson Genesis FT-IR spectrometer. Samples were prepared for analysis as either neat films between NaCl plates, nujol mulls or solutions.

$[NBu_4]_2[Pd_2\{C_4(COOMe)_4\}_2(\mu\text{-}OH)_2]$ (1): $[NBu_4]OH$ (aq) (7.68 mL of 1 M solution, 7.68 mmol) was added to a suspension of $[Pd\{C_4\{COOMe)_4\}]_n$ (1.5 g, 3.84 mmol) in water (15 mL), with constant stirring for 30 min. The solvent was partly evaporated under reduced pressure until a yellow solid began to precipitate. The mixture was then stored overnight at ca. 4 °C and the solid was filtered off, washed with diethyl ether and air-dried. The compound was recrystallised from acetone/diethyl ether. Yield (1.972 g, 79%). M.p. 155 °C (dec.). $C_{56}H_{98}N_2O_{18}Pd_2$ (1300.2): calcd. C 51.7, H 7.6, N 2.1; found C 52.0, H 7.8, N 1.9. IR (nujol): $\tilde{\nu}$ = 3602m (νOH), 1686s (νCO), 1546s (νCO) cm^{-1}. ^1H NMR (200 MHz, $CDCl_3$): δ = −0.85 (s, 2 H, OH), 3.60 (s, 12 H, COOMe), 3.66 (s, 12 H, COOMe) ppm. $^{13}C\{^1H\}$ NMR (200 MHz, $CDCl_3$): δ = 50.5 (COO*Me*), 50.8 (COO*Me*), 50.8 (COO*Me*), 51.0 (COO*Me*) ppm. FAB-MS (negative mode): *m*/*z* = 784 $[Pd_2\{C_4(COOMe)_4\}\{C_4(COOMe)_3(CO)\}(\mu\text{-}OH)_2]^-$, 725 $[Pd_2\{C_4(COOMe)_4\}\{C_4(COOMe)_2(CO)\}(\mu\text{-}OH)_2]^-$, 407 $[Pd\{C_4(COOMe)_4O]^-$.

Complexes $[NBu_4]_2[Pd_2\{C_4(COOMe)_4\}_2(\mu\text{-imidate})_2]$ [imidate = succinimidate (suc) (2), phthalimidate (pht) (3) or maleimidate (mal) (4): These dinuclear complexes were obtained according to the following general method. A stoichiometric amount of imide (0.46 mmol) was added to an acetone solution of hydroxo complex **1** (0.3 g, 0.23 mmol). The solution was stirred at room temperature for 30 min and the solvent was partly evaporated under reduced pressure. Addition of a mixture of diethyl ether and hexane (1:1) caused the formation of yellow-orange solids, which were filtered off, washed with diethyl ether and air-dried. The compounds were recrystallised from acetone/diethyl ether.

$[NBu_4]_2[Pd(C_4\{COOMe\}_4(\mu\text{-suc})]_2$ (2): Yield: 0.239 g (71%), m.p. 95 °C (dec.). $C_{64}H_{104}N_4O_{20}Pd_2$ (1462.4): calcd. C 52.6, H 7.2, N 3.8; found C 52.4, H 7.5, N 3.9. IR (nujol): $\tilde{\nu}$ = 1704 s (νCO), 1598 s (νCO). ^1H NMR (200 MHz, CD_3CN): δ = 2.27 (s, 4 H, suc), 3.36 (s, 3 H, COOMe), 3.46 (s, 3 H, COOMe), 3.49 (s, 3 H, COOMe), 3.60 (s, 3 H, COOMe) ppm. FAB-MS (negative mode): *m*/*z* = 1220 $[(NBu_4)Pd_2\{C_4(COOMe)_4\}_2(\mu\text{-suc})_2]^-$, 880 $[Pd_2\{C_4(COOMe)_4\}_2(suc)]^-$, 488 $[Pd\{C_4(COOMe)_4\}(suc)]^-$.

$[NBu_4]_2[Pd\{C_4(COOMe)_4\}(\mu\text{-pht})]_2$ (3): Yield: 0.229 g (64%), m.p. 147 °C (dec.). $C_{72}H_{104}N_4O_{20}Pd_2$ (1558.5): calcd. C 55.5, H 6.7, N 3.6; found C 55.6, H 6.9, N 3.9. IR (nujol): $\tilde{\nu}$ = 1698 s (νCO), 1634 s (νCO). ^1H NMR (200 MHz, CD_3CN): δ = 3.01 (s, 3 H, COOMe), 3.45 (s, 3 H, COOMe), 3.51 (s, 3 H, COOMe), 3.62 (s, 3 H, COOMe), 7.46 (m, 4 H, pht) ppm. FAB-MS (negative mode): *m*/*z* = 1314 $[(NBu_4)Pd_2\{C_4(COOMe)_4\}_2(\mu\text{-pht})_2 - 2]^-$, 930 $[Pd_2\{C_4(COOMe)_4\}_2(pht) + 1]^-$, 536 $[Pd\{C_4(COOMe)_4\}(pht)]^-$.

$[NBu_4]_2[Pd(C_4\{COOMe\}_4(\mu\text{-mal})]_2$ (4): Yield: 0.208 g (62%), m.p. 79 °C (dec.). $C_{64}H_{100}N_4O_{20}Pd_2$ (1458.6): calcd. C 52.7, H 6.9, N 3.8; found C 52.4, H 7.1, N 3.9. IR (nujol): $\tilde{\nu}$ = 1714 s (νCO), 1626 (νCO). ^1H NMR (200 MHz, CD_3CN): δ = 3.27 (s, 3 H, COOMe), 3.45 (s, 3 H, COOMe), 3.49 (s, 3 H, COOMe), 3.60 (s, 3 H, COOMe), 6.34 (s, 2 H, mal) ppm. FAB-MS (negative mode): *m*/*z* = 876 $[Pd_2\{C_4(COOMe)_4\}_2(mal)]^-$, 486 $[Pd\{C_4(COOMe)_4\}(mal)]^-$.

Complexes $[NBu_4][Pd\{C_4(COOMe)_4\}(suc)L]$ [L = PPh_3 (2a), P(*p*-$C_6H_4F)_3$ (2b), PBu_3 (2c), py (2d), *p*-$MeC_6H_4NH_2$ (2e), tetrahydrothiophene (2f)]: A stoichiometric amount of ligand (0.068 mmol) was added to a solution of the dinuclear complex $[NBu_4]_2[Pd(C_4\{COOMe\}_4(\mu\text{-suc})]_2$ (**2**; 0.05 g, 0.034 mmol) in acetone. The solution was stirred at room temperature for 30 min, and then the solvent was partly evaporated under reduced pressure to approximately one-third of the initial volume. The addition of diethyl ether caused the formation of yellow or pale-yellow solids, which were filtered off, washed with diethyl ether and air-dried. The compounds were recrystallised from dichloromethane/diethyl ether.

$[NBu_4][Pd\{C_4(COOMe)_4\}(suc)(PPh_3)]$ (2a): Yield: 0.046 g (69%). M.p. 103 °C (dec.). $C_{50}H_{67}N_2O_{10}PPd$ (993.48): calcd. C 60.4, H 6.8, N 2.8; found C 60.2, H 7.0, N 3.1. IR (nujol): $\tilde{\nu}$ = 1694 s (νCO), 1614 s (νCO). ^1H NMR (200 MHz, $CDCl_3$): δ = 1.60 (m, 2 H, suc), 2.04 (m, 2 H, suc), 2.50 (s, 3 H, COOMe), 3.49 (s, 3 H, COOMe), 3.51 (s, 3 H, COOMe), 3.56 (s, 3 H, COOMe), 7.30 (m, 9 H, PPh_3), 7.61 (m, 6 H, PPh_3) ppm. $^{31}P\{^1H\}$ NMR (200 MHz, $CDCl_3$): δ = 28.7 (s) ppm. FAB-MS (negative mode): *m*/*z* = 749 $[Pd\{C_4(COOMe)_4\}(suc)(PPh_3) - 1]^-$, 488 $[Pd\{C_4(COOMe)_4\}(suc)]^-$.

$[NBu_4][Pd\{C_4(COOMe)_4\}(suc)\{P(p\text{-}C_6H_4F)_3\}]$ (2b): Yield: 0.057 g (80%). M.p. 164 °C (dec.). $C_{50}H_{64}F_3N_2O_{10}PPd$ (1047.5): calcd. C 57.3, H 6.2, N 2.7 found C 57.0, H 6.5, N 2.5. IR (nujol): $\tilde{\nu}$ = 1698 s (νCO), 1614 s (νCO). ^1H NMR (200 MHz, $CDCl_3$): δ = 1.67 (m, 2 H, suc), 2.04 (m, 2 H, suc), 2.62 (s, 3 H, COOMe), 3.52 (s, 3 H, COOMe), 3.53 (s, 3 H, COOMe), 3.57 (s, 3 H, COOMe), 7.02 [m, 6 H, P(*p*-$C_6H_4F)_3$], 7.62 [m, 6 H, P(*p*-$C_6H_4F)_3$] ppm. $^{19}F\{^1H\}$ NMR (200 MHz, $CDCl_3$): δ = −110.9 (td, ^3J = 5.6, ^5J = 1.9 Hz) ppm. $^{31}P\{^1H\}$ NMR (200 MHz, $CDCl_3$): δ = 26.8 (s) ppm. FAB-MS (negative mode): *m*/*z* = 804 $[Pd\{C_4\{COOMe)_4\}(suc)\{P(p\text{-}C_6H_4F)_3\}]^-$, 488 $[Pd\{C_4(COOMe)_4\}(suc)]^-$.

$[NBu_4][Pd\{C_4(COOMe)_4\}(suc)(PBu_3)]$ (2c): Yield: 0.039 g (62%). M.p. 102 °C (dec.). $C_{44}H_{79}N_2O_{10}PPd$ (933.51): calcd. C 56.6, H 8.5, N 3.0; found C 56.5, H 8.8, N 3.2. IR (nujol): $\tilde{\nu}$ = 1694 s (νCO), 1622 s (νCO). ^1H NMR (200 MHz, $CDCl_3$): δ = 0.88 (t, J = 3.6 Hz, 9 H, PBu_3), 1.32 (m, 6 H, PBu_3), 1.48 (m, 12 H, PBu_3), 2.44 (m, 4 H, suc), 3.53 (s, 3 H, COOMe), 3.57 (s, 3 H, COOMe), 3.60 (s, 3 H, COOMe), 3.63 (s, 3 H, COOMe) ppm. $^{31}P\{^1H\}$ NMR (200 MHz, $CDCl_3$): δ = 2.5 (s) ppm. FAB-MS (negative mode): *m*/*z* = 690 $[Pd\{C_4\{COOMe)_4\}(suc)(PBu_3)]^-$, 488 $[Pd\{C_4\{COOMe)_4\}(suc)]^-$.

$[NBu_4][Pd(C_4\{COOMe\}_4(suc)(py)]$ (2d): Yield: 0.038 g (69%). M.p. 160 °C (dec.). $C_{37}H_{57}N_3O_{10}Pd$ (810.30) calcd. C 54.8, H 7.1, N 5.2; found C 54.5, H 7.4, N 5.2. IR (nujol): $\tilde{\nu}$ = 1692 s (νCO), 1624 s (νCO). ^1H NMR (200 MHz, $CDCl_3$): δ = 2.37 (m, 4 H, suc), 3.14 (s, 3 H, COOMe), 3.56 (s, 3 H, COOMe), 3.57 (s, 3 H, COOMe), 3.58 (s, 3 H, COOMe), 7.21 (m, 2 H, py), 7.63 (m, 1 H, py), 8.73 (d, J = 2.4 Hz, 2 H, py) ppm. $^{13}C\{^1H\}$ NMR (200 MHz, $CDCl_3$): δ = 32.1 (suc), 50.0 (COO*Me*), 50.7 (COO*Me*), 50.8 (COO*Me*), 51.0 (COO*Me*) ppm. FAB-MS (negative mode): *m*/*z* = 567 $[Pd(C_4\{COOMe\}_4(suc)(py)]^-$, 488 $[Pd(C_4\{COOMe\}_4(suc)]^-$.

$[NBu_4][Pd\{C_4(COOMe)_4\}(suc)(p\text{-}MeC_6H_4NH_2)]$ (2e): Yield: 0.038 g (66%). M.p. 155 °C (dec.). $C_{39}H_{61}N_3O_{10}Pd$ (838.35): calcd. C 55.9, H 7.3, N, 5.0; found C 55.6, H 7.6, N 5.2. IR (nujol): $\tilde{\nu}$ =

 © 2004 Wiley-VCH Verlag GmbH & Co. KGaA, Weinheim

1720 s (νCO), 1602 s (νCO). ^{1}H NMR (200 MHz, $CDCl_3$): δ = 2.20 (s, 3 H, *Me*C_6H_4), 2.33 (m, 4 H, suc), 3.54 (s, 3 H, COOMe), 3.55 (s, 3 H, COOMe), 3.66 (s, 3 H, COOMe), 3.68 (s, 3 H, COOMe), 5.18 (br., 2 H, NH_2), 6.75 (d, J = 8.2 Hz, 2 H, C_6H_4), 6.91 (d, J = 8.2 Hz, 2 H, C_6H_4) ppm. ^{13}C{^{1}H} NMR (200 MHz, $CDCl_3$): δ = 20.6 (*Me*C_6H_4), 31.8 (suc), 50.8 (COO*Me*), 51.1 (COO*Me*) ppm. FAB-MS (negative mode): *m*/*z* = 595 [Pd{C_4(COOMe)$_4$}(suc)(*p*-Me$C_6H_4NH_2$)]$^-$, 488 [Pd{C_4(COOMe)$_4$}(suc)]$^-$.

[NBu$_4$][Pd{C_4(COOMe)$_4$}(suc)(tht)] (2f): Yield: 0.044 g (79%). M.p. 185 °C (dec.). $C_{36}H_{60}N_2O_{10}PdS$ (819.36): calcd. C 52.8, H 7.4, N 3.4, S 3.9; found C 53.0, H 7.6, N 3.2, S 4.2. IR (nujol): $\tilde{\nu}$ = 1698 s (νCO), 1620 s (νCO). ^{1}H NMR (300 MHz, $CDCl_3$): δ = 1.86 (m, 4 H, tht), 2.47 (m, 4 H, suc), 2.93 (m, 4 H, tht), 3.54 (s, 3 H, COOMe), 3.56 (s, 3 H, COOMe), 3.60 (s, 3 H, COOMe), 3.67 (s, 3 H, COOMe) ppm. ^{13}C{^{1}H} NMR (300 MHz, $CDCl_3$): δ = 30.2 (tht), 32.4 (suc), 35.1 (tht), 50.6 (COO*Me*), 50.8 (COO*Me*), 50.9 (COO*Me*), 51.0 (COO*Me*) ppm. FAB-MS (negative mode): *m*/*z* = 595 [Pd{C_4(COOMe)$_4$}(suc)(*p*-Me$C_6H_4NH_2$)]$^-$, 488 [Pd{C_4(COOMe)$_4$} (suc)]$^-$.

Complexes [NBu$_4$][Pd(C_4{COOMe}$_4$(pht)L] [L = PPh$_3$ (3a), P(*p*-C_6H_4F)$_3$ (3b), PBu$_3$ (3c), py (3d), *p*-Me$C_6H_4NH_2$ (3e), tetrahydrothiophene (3f)]: A stoichiometric amount of ligand (0.064 mmol) was added to a solution of complex **3** (0.05 g, 0.032 mmol) in acetone. The solution was stirred at room temperature for 30 min and the solvent was then partly evaporated under reduced pressure to approximately one-third of the initial volume. The addition of diethyl ether caused the formation of yellow or pale-yellow solids, which were filtered off, washed with diethyl ether and air-dried. The compounds were recrystallized from dichloromethane/diethyl ether.

[NBu$_4$][Pd{C_4(COOMe)$_4$}(pht)(PPh$_3$)] (3a): Yield: 0.051 g (77%). M.p. 95 °C. $C_{54}H_{67}N_2O_{10}PPd$ (1041.5): calcd. C 62.3, H 6.5, N 2.7; found C 62.0, H 6.8, N 3.1 IR (nujol): $\tilde{\nu}$ = 1694 s (νCO), 1640 s (νCO). ^{1}H NMR (200 MHz, $CDCl_3$): δ = 2.51 (s, 3 H, COOMe), 3.25 (s, 3 H, COOMe), 3.51 (s, 3 H, COOMe), 3.55 (s, 3 H, COOMe), 7.57 (m, 13 H, pht + PPh$_3$), 7.60 (m, 6 H, PPh$_3$) ppm. ^{31}P{^{1}H} NMR (200 MHz, $CDCl_3$): δ = 28.3 (s) ppm. FAB-MS (negative mode): *m*/*z* = 798 [Pd{C_4(COOMe)$_4$}(pht)(PPh$_3$)]$^-$, 536 [Pd{C_4(COOMe)$_4$}(pht)]$^-$.

[NBu$_4$][Pd{C_4(COOMe)$_4$}(pht)(P{*p*-C_6H_4F}$_3$)] (3b): Yield: 0.057 g (81%). M.p. 165 °C (dec.). $C_{54}H_{64}F_3N_2O_{10}PPd$ (1095.5): calcd. C 59.2, H 5.9, N 2.6; found C 59.0, H 6.1, N 2.9. IR (nujol): $\tilde{\nu}$ = 1694 s (νCO), 1640 s (νCO). ^{1}H NMR (200 MHz, $CDCl_3$): δ = 2.61 (s, 3 H, COOMe), 3.26 (s, 3 H, COOMe), 3.52 (s, 3 H, COOMe), 3.55 (s, 3 H, COOMe), 6.86 [m, 6 H, P(*p*-C_6H_4F)$_3$], 7.27 [m, 4 H, pht + P(*p*-C_6H_4F)$_3$], 7.57 [m, 6 H, pht + P(*p*-C_6H_4F)$_3$] ppm. ^{19}F{^{1}H} NMR (200 MHz, $CDCl_3$): δ = −111.2 (td, ^3J = 5.6, ^5J = 3.8 Hz, 3 F) ppm. ^{31}P{^{1}H} NMR (200 MHz, $CDCl_3$): δ = 26.5 (s) ppm. FAB-MS (negative mode): *m*/*z* = 852 [Pd{C_4(COOMe)$_4$}(pht){P(*p*-C_6H_4F)$_3$}]$^-$, 536 [Pd{C_4(COOMe)$_4$}(pht)]$^-$.

[NBu$_4$][Pd{C_4(COOMe)$_4$}(pht)(PBu$_3$)] (3c): Yield: 0.038 g (60%). M.p. 132 °C (dec.). $C_{48}H_{79}N_2O_{10}PPd$ (981.56): calcd. C 58.7, H 8.1, N 2.8; found C 58.5, H 8.4, N 2.7. IR (nujol): $\tilde{\nu}$ = 1692 s (νCO), 1646 s (νCO). ^{1}H NMR (200 MHz, $CDCl_3$): δ = 0.75 (t, J = 7.2 Hz, 9 H, PBu$_3$), 1.19 (m, 6 H, PBu$_3$), 1.46 (m, 12 H, PBu$_3$), 3.07 (s, 3 H, COOMe), 3.45 (s, 3 H, COOMe), 3.57 (s, 3 H, COOMe), 3.60 (s, 3 H, COOMe), 7.40 (m, 2 H, pht), 7.54 (m, 2 H, pht) ppm. ^{31}P{^{1}H} NMR (200 MHz, $CDCl_3$): δ = 3.2 (s) ppm. FAB-MS (negative mode): *m*/*z* = 738 [Pd{C_4(COOMe)$_4$}(pht)(PBu$_3$)]$^-$, 536 [Pd{C_4(COOMe)$_4$}(pht)]$^-$.

[NBu$_4$][Pd{C_4(COOMe)$_4$}(pht)(py)] (3d): Yield: 0.042 g (76%). M.p. 168 °C (dec.). $C_{41}H_{57}N_3O_{10}Pd$ (858.34): calcd. C 57.4, H 6.7, N 4.9; found C 57.1, H 7.0, N 5.0. IR (nujol): $\tilde{\nu}$ = 1698 s (νCO), 1644 s (νCO). ^{1}H NMR (200 MHz, $CDCl_3$): δ = 3.16 (s, 3 H, COOMe), 3.25 (s, 3 H, COOMe), 3.55 (s, 3 H, COOMe), 3.59 (s, 3 H, COOMe), 7.19 (m, 2 H, py), 7.37 (m, 2 H, pht), 7.50 (m, 2 H, pht), 7.59 (m, 1 H, py), 8.74 (m, 2 H, py) ppm. ^{13}C{^{1}H} NMR (300 MHz, $CDCl_3$): δ = 50.1 (COO*Me*), 50.7 (COO*Me*), 50.8 (COO*Me*), 50.9 (COO*Me*) ppm. FAB-MS (negative mode): *m*/*z* = 928 [Pd$_2${C_4(COOMe)$_4$}$_2$(suc)]$^-$, 536 [Pd(C_4{COOMe}$_4$(pht)]$^-$.

[NBu$_4$][Pd{C_4(COOMe)$_4$}(pht)(*p*-Me$C_6H_4NH_2$)] (3e): Yield: 0.037 g (65%). M.p. 93 °C (dec.). $C_{43}H_{61}N_3O_{10}Pd$ (886.40): calcd. C 58.3; H 6.9, N 4.7; found C 58.6, H 7.1, N 5.0. IR (nujol): $\tilde{\nu}$ = 1698 s (νCO), 1646 s (νCO). ^{1}H NMR (200 MHz, $CDCl_3$): δ = 2.11 (s, 3 H, *Me*C_6H_4), 3.24 (s, 3 H, COOMe), 3.52 (s, 3 H, COOMe), 3.66 (s, 3 H, COOMe), 3.71 (s, 3 H, COOMe), 5.34 (br., 2 H, NH_2), 6.75 (m, 4 H, C_6H_4), 7.44 (m, 2 H, pht), 7.56 (m, 2 H, pht) ppm. ^{13}C{^{1}H} NMR (200 MHz, $CDCl_3$): δ = 20.5 (*Me*C_6H_4), 50.7 (COO*Me*), 50.8 (COO*Me*), 51.1 (COO*Me*), 51.2 (COO*Me*) ppm. FAB-MS (negative mode): *m*/*z* = 536 [Pd{C_4(COOMe)$_4$}(pht)]$^-$.

[NBu$_4$][Pd{C_4(COOMe)$_4$}(pht)(tht)] (3f): Yield: 0.036 g (65%). M.p. 180 °C (dec.). $C_{40}H_{60}N_2O_{10}PdS$ (867.41): calcd. C 55.4, H 7.0, N 3.2, S 3.7; found C 55.6, H 7.3, N 3.4, S 4.0. IR (nujol): $\tilde{\nu}$ = 1698 s (νCO), 1644 s (νCO). ^{1}H NMR (200 MHz, $CDCl_3$): δ = 1.82 (m, 4 H, tht), 2.98 (m, 4 H, tht), 3.10 (s, 3 H, COOMe), 3.58 (s, 3 H, COOMe), 3.62 (s, 3 H, COOMe), 3.71 (s, 3 H, COOMe), 7.45 (m, 2 H, pht), 7.58 (m, 2 H, pht) ppm. ^{13}C{^{1}H} NMR (200 MHz, $CDCl_3$): δ = 30.1 (tht), 35.0 (tht), 50.6 (COO*Me*), 50.7 (COO*Me*), 50.9 (COO*Me*) ppm. FAB-MS (negative mode): *m*/*z* = 536 [Pd{C_4(COOMe)$_4$}(pht)]$^-$.

Preparation of the Complexes [NBu$_4$][Pd{C_4(COOMe)$_4$}(mal)L] [L = PPh$_3$ (4a), P(*p*-C_6H_4F)$_3$ (4b), PBu$_3$ (4c), py (4d), *p*-Me$C_6H_4NH_2$ (4e), tetrahydrothiophene (4f)]: A stoichiometric amount of ligand (0.068 mmol) was added to a solution of the dinuclear complex [NBu$_4$]$_2$[Pd(C_4{COOMe}$_4$(μ-mal)]$_2$ (**4**; 0.05 g, 0.034 mmol) in acetone. The solution was stirred at room temperature for 30 min, and then the solvent was partly evaporated under reduced pressure to approximately one-third of the initial volume. The addition of diethyl ether caused the formation of yellow or pale-yellow solids, which were filtered off, washed with diethyl ether and air-dried. The compounds were recrystallised from dichloromethane/diethyl ether.

[NBu$_4$][Pd{C_4(COOMe)$_4$}(mal)(PPh$_3$)] (4a): Yield: 0.043 g (64%). M.p. 140 °C (dec.). $C_{50}H_{65}N_2O_{10}PPd$ (991.47): calcd. C 60.6, H 6.6, N 2.8; found C 60.4, H 6.9, N 3.0. IR (nujol): $\tilde{\nu}$ = 1698 s (νCO), 1636 s (νCO. ^{1}H NMR (300 MHz, $CDCl_3$): δ = 2.50 (s, 3 H, COOMe), 3.43 (s, 3 H, COOMe), 3.49 (s, 3 H, COOMe), 3.55 (s, 3 H, COOMe), 5.91 (s, 2 H, mal), 7.27 (m, 9 H, PPh$_3$), 7.60 (m, 6 H, PPh$_3$) ppm. ^{31}P{^{1}H} NMR (300 MHz, $CDCl_3$): δ = 28.1 (s) ppm. FAB-MS (negative mode): *m*/*z* = 748 [Pd{C_4(COOMe)$_4$}(mal)(PPh$_3$)]$^-$, 486 [Pd{C_4(COOMe)$_4$}(mal)]$^-$.

[NBu$_4$][Pd{C_4(COOMe)$_4$}(mal)(P{*p*-C_6H_4F)$_3$]] (4b): Yield: 0.047 g (66%). M.p. 160 °C (dec.). $C_{50}H_{62}F_3N_2O_{10}PPd$ (1045.4): calcd. C 57.4, H 6.0, N 2.7; found C 57.2, H 6.3, N 2.9. IR (nujol): $\tilde{\nu}$ = 1694 s (νCO), 1632 s (νCO). ^{1}H NMR (200 MHz, $CDCl_3$): δ = 2.60 (s, 3 H, COOMe), 3.43 (s, 3 H, COOMe), 3.51 (s, 3 H, COOMe), 3.55 (s, 3 H, COOMe), 5.99 (s, 2 H, mal), 6.97 [m, 6 H, P(*p*-C_6H_4F)$_3$], 7.56 [m, 6 H, P(*p*-C_6H_4F)$_3$] ppm. ^{19}F{^{1}H} NMR (200 MHz, $CDCl_3$): δ = −111.1 (td, ^3J = 5.6, ^5J = 3.8 Hz, 3 F) ppm. ^{31}P{^{1}H} NMR (200 MHz, $CDCl_3$): δ = 26.4 (s) ppm. FAB-

 © 2004 Wiley-VCH Verlag GmbH & Co. KGaA, Weinheim

MS (negative mode): *m*/*z* = 802 [Pd{C_4(COOMe)$_4$}(mal){P(*p*-$C_6H_4F)_3$}]$^-$, 486 [Pd{C_4(COOMe)$_4$}(mal)]$^-$.

[NBu$_4$][Pd{C_4(COOMe)$_4$}(mal)(PBu$_3$)] (4c): Yield: 0.034 g (54%). M.p. 90 °C (dec.). $C_{44}H_{77}N_2O_{10}PPd$ (931.50): calcd. C 56.7, H 8.3, N 3.0; found C 56.4, H 8.4, N 3.3. IR (nujol): $\tilde{\nu}$ = 1694 s (νCO), 1638 s (νCO). ^{1}H NMR (300 MHz, $CDCl_3$): δ = 0.86 (t, 9 H, J = 4.8 Hz, PBu_3), 1.30 (m, 6 H, PBu_3), 1.48 (m, 12 H, PBu_3), 3.46 (s, 3 H, COOMe), 3.51 (s, 3 H, COOMe), 3.59 (s, 3 H, COOMe), 3.62 (s, 3 H, COOMe), 6.42 (s, 2 H, mal) ppm. ^{31}P{^{1}H} NMR (300 MHz, $CDCl_3$): δ = 3.6 (s) ppm. FAB-MS (negative mode): *m*/*z* = 688 [Pd{C_4(COOMe)$_4$}(mal)(PBu$_3$)]$^-$, 486 [Pd{C_4-(COOMe)$_4$}(mal)]$^-$.

[NBu$_4$][Pd{C_4(COOMe)$_4$}(mal)(py)] (4d): Yield: 0.042 g (76%). M.p. 158 °C (dec.). $C_{37}H_{55}N_3O_{10}Pd$ (808.28): calcd. C 55.0, H 6.9, N 5.2; found C 54.7, H 7.2, N 5.3. IR (nujol): $\tilde{\nu}$ = 1692 s (νCO), 1638 s (νCO). ^{1}H NMR (300 MHz, $CDCl_3$): δ = 3.15 (s, 3 H, COOMe), 3.49 (s, 3 H, COOMe), 3.55 (s, 3 H, COOMe), 3.57 (s, 3 H, COOMe), 6.39 (s, 2 H, mal), 7.20 (m, 2 H, py), 7.61 (m, 1 H, py), 8.66 (m, 2 H, py) ppm. ^{13}C{^{1}H} NMR (300 MHz, $CDCl_3$): δ = 50.1 (COO*Me*), 50.8 (COO*Me*), 50.9 (COO*Me*), 51.1 (COO*Me*) ppm. FAB-MS (negative mode): *m*/*z* = 486 [Pd{C_4(COOMe)$_4$}(mal)]$^-$.

[NBu$_4$][Pd{C_4(COOMe)$_4$}(mal)(*p*-MeC$_6$H$_4$NH$_2$)] (4e): Yield: 0.032 g (56%). M.p. 135 °C (dec.). $C_{39}H_{59}N_3O_{10}Pd$ (836.34): calcd. C 56.0, H 7.1, N 5.0; found C 55.9, H 7.3, N 5.2. IR (nujol): $\tilde{\nu}$ = 1720 s (νCO), 1634 s (νCO). ^{1}H NMR (200 MHz, $CDCl_3$): δ = 2.18 (s, 3 H, *Me*C$_6$H$_4$), 3.47 (s, 3 H, COOMe), 3.54 (s, 3 H, COOMe), 3.66 (s, 3 H, COOMe), 3.69 (s, 3 H, COOMe), 5.23 (br., 2 H, NH$_2$), 6.42 (s, 2 H, mal), 6.70 (d, J = 8.0 Hz, 2 H, C$_6$H$_4$), 6.87 (d, J = 8.0 Hz, 2 H, C$_6$H$_4$) ppm. ^{13}C{^{1}H} NMR (200 MHz, $CDCl_3$): δ = 23.9 (*Me*C$_6$H$_4$), 50.9 (COO*Me*), 51.1 (COO*Me*) ppm. FAB-MS (negative mode): *m*/*z* = 486 [Pd{C_4(COOMe)$_4$}(mal)]$^-$.

[NBu$_4$][Pd{C_4(COOMe)$_4$}(mal)(tht)] (4f): Yield: 0.032 g (57%). M.p. 170 °C (dec.). $C_{36}H_{58}N_2O_{10}PdS$ (817.35): calcd. C 52.9, H 7.1, N 3.4, S 3.9: found C 53.1, H 7.3, N 3.6, S 4.0. IR (nujol): $\tilde{\nu}$ = 1704 s (νCO), 1640 s (νCO). ^{1}H NMR (200 MHz, $CDCl_3$): δ = 1.84 (m, 4 H, tht), 2.91 (m, 4 H, tht), 3.47 (s, 3 H, COOMe), 3.54 (s, 3 H, COOMe), 3.61 (s, 3 H, COOMe), 3.69 (s, 3 H, COOMe), 6.47 (s, 2 H, mal) ppm. ^{13}C{^{1}H} NMR (200 MHz, $CDCl_3$): δ = 30.1 (tht), 34.9 (tht), 50.5 (COO*Me*), 50.7 (COO*Me*), 50.9 (COO*Me*) ppm. FAB-MS (negative mode): *m*/*z* = 486 [Pd{C_4(COOMe)$_4$}(suc)]$^-$.

Preparation of Ethyl (*Z*)-3-(Tributylstannyl)propenoates (8): AIBN (0.073 g (0.4 mmol) was added to a neat mixture of ethyl propiolate (1.74 g, 17.7 mmol) and tributyltin hydride (5 mL, 18.6 mmol) and the mixture heated to 60 °C for 24 h. It was then allowed to cool to ambient temperature and purified by column chromatography using PE/EtOAc (95:5, v/v) as the eluent. This gave the *Z* isomer (2.72 g, 39%) and the *E* isomer (3.89 g, 56%), both as colourless oils. R_f = 0.70, PE/EtOAc (9:1, v/v). ^{1}H NMR (270 MHz, $CDCl_3$): δ = 0.85−0.99 (m, 18 H, 4 × CH_3 and 3 × CH_2), 1.24−1.32 (m, 6 H, 3 × CH_2), 1.43−1.56 (m, 6 H, 3 × CH_2), 4.21 (q, ^3J = 7.0 Hz, 2 H, CH_2), 6.72 (d, ^3J = 13.0 Hz, 1 H, *CH*), 7.15 (d, ^3J = 13.0 Hz, 1 H, *CH*) ppm. These data are consistent with those previously published.[21]

General Procedure for Stille Cross-Coupling: The specified catalyst (5 mol %) was added to a solution of benzyl bromide (0.5 mmol) and the stannane (0.6 mmol) in dry toluene (5 mL) and heated to 60 °C in the dark, under N_2 atmosphere, for the specified time. The reaction was allowed to cool to ambient temperature, then saturated aq. KF (5 mL) was added and the mixture stirred vigorously for 1 h. The mixture was filtered through Celite, washed with saturated aq. NaCl (2 × 5 mL) and dried ($MgSO_4$). Concentration in vacuo and subsequent purification by column chromatography using ethyl acetate/hexane mixtures (1:20 to 1:9, v/v) afforded the desired product along with some minor side-products.

Preparation of Ethyl (2*Z*)-4-Phenyl-2-butenoate (9): Obtained as a colourless oil. R_f = 0.51, PE/EtOAc (9:1, v/v). ^{1}H NMR (270 MHz, $CDCl_3$): δ = 1.32 (t, ^3J = 7.0 Hz, 3 H, CH_3), 4.03 (dd, ^3J = 7.5, 1.5, 2 H, CH_2), 4.22 (q, ^3J = 7.0 Hz, 2 H, CH_2), 5.86 (dt, ^3J = 11.5, ^4J = 1.5 Hz, 1 H, *CH*), 6.36 (dt, ^3J = 11.5, 7.5, 1 H, *CH*), 7.22−7.34 (m, 5 H, *Ph-H*) ppm. ^{13}C{^{1}H} NMR (67.9 MHz, $CDCl_3$): δ = 14.2 (CH_3), 35.1 (CH_2), 59.9 (CH_2), 119.9 (CH), 126.3 (CH), 128.7 (CH), 139.4 (C), 147.9 (CH), 166.3 (C) (*ipso* CH) ppm. These data are consistent with those previously published.[22]

Preparation of Ethyl (2*E*)-4-Phenyl-2-butenoate (9′): Obtained as a colourless oil. R_f = 0.30, PE/EtOAc (9:1, v/v). ^{1}H NMR (270 MHz, $CDCl_3$): δ = 1.27 (t, ^3J = 7.5 Hz, 3 H, CH_3), 3.52 (dd, ^3J = 7.0, 1.0, 2 H, CH_2) 4.18 (q, ^3J = 7.5 Hz, 2 H, CH_2), 5.81 (dt, ^3J = 15.5, ^4J = 1.0 Hz, 1 H, *CH*), 7.10 (dt, ^3J = 15.5, 7.0, 1 H, *CH*), 7.13−7.19 (m, 5 H, *Ph-H*) ppm. ^{13}C{^{1}H} NMR (67.9 MHz, $CDCl_3$): δ = 14.3 (CH_3), 38.6 (CH_2), 60.4 (CH_2), 122.5 (CH), 126.8 (CH), 128.8 (CH), 128.9 (CH), 137.8 (C), 147.4 (CH), 166.6 (C) ppm. These data are consistent with those previously published.[23]

Preparation of Diethyl (2*Z*,4*Z*)-2,4-Hexadienedioate (10): Obtained as a white solid. R_f = 0.10, PE/EtOAc (9:1 v/v). ^{1}H NMR (270 MHz, $CDCl_3$): δ = 1.30 (t, ^3J = 7.0 Hz, 6 H, CH_3), 4.21 (q, ^3J = 7.0 Hz, 4 H, CH_2), 5.52 (m, 2 H, *CH*), 7.89 (m, 2 H, *CH*) ppm. ^{13}C{^{1}H} NMR (100 MHz, $CDCl_3$): δ = 14.3 (CH_3), 61.0 (CH_2), 128.5 (CH), 140.9 (CH), 166.0 (C) ppm. These data are consistent with those previously published.[24]

Preparation of Diethyl (2*E*,4*E*)-2,4-Hexadienedioate (10′): Obtained as a white solid. R_f = 0.09, PE/EtOAc (9:1 v/v). ^{1}H NMR (400 MHz, $CDCl_3$): δ = 1.31 (t, ^3J = 7.0 Hz, 6 H, CH_3), 4.24 (q, ^3J = 7.0 Hz, 4 H, CH_2), 6.19 (m, 2 H, *CH*), 7.31 (m, 2 H, *CH*) ppm. ^{13}C{^{1}H} NMR (100 MHz, $CDCl_3$): δ = 14.3 (CH_3), 61.0 (CH_2), 128.5 (CH), 140.9 (CH), 166.0 (C) ppm. These data are consistent with those previously published.[25]

X-ray Crystallography: Crystals of **4b** and **4e** suitable for a diffraction study were grown from acetone/diethyl ether. Data collection for **4e** was performed at −173 °C on a Bruker Smart CCD diffractometer with a nominal crystal to detector distance of 4.5 cm. Diffraction data were collected based on a ω scan run. A total of 1371 frames were collected at 0.3° intervals and 10 s per frame. The diffraction frames were integrated using the SAINT package[26] and corrected for absorption with SADABS.[27] Data collection for **4b** was performed at −100 °C on a Siemens P4 diffractometer. The structures were solved by the Patterson (**4b**) or direct (**4e**) methods[28] and refined by full-matrix least-squares techniques using anisotropic thermal parameters for non-H atoms[28] (Table 3). Hydrogen atoms were introduced in calculated positions and refined during the last stages of the refinement.

CCDC-218969 (**4b**) and -218971 (**4e**) contain the supplementary crystallographic data for this paper. These data can be obtained free of charge at www.ccdc.cam.ac.uk/conts/retrieving.html [or from the Cambridge Crystallographic Data Centre, 12 Union Road, Cambridge CB2 1EZ, UK; Fax: + 44-1223-336-033; E-mail: deposit@ccdc.cam.ac.uk].

 © 2004 Wiley-VCH Verlag GmbH & Co. KGaA, Weinheim

Table 3. Crystal data and structure refinement for compounds **4b** and **4e**

	4b·$C_4H_{10}O$	**4e**
Formula	$C_{54}H_{72}F_3N_2O_{11}PPd$	$C_{39}H_{59}N_3O_{10}Pd$
Molecular mass	1119.51	836.29
Crystal system	monoclinic	monoclinic
Space group	$P2_1/n$	$C2/c$
a (Å)	11.4262(17)	33.3156(15)
b (Å)	27.753(3)	9.0527(4)
c (Å)	17.5419(17)	27.4288(13)
β (°)	96.140(10)	92.6040(10)
V (Å^3)	5330.9(11)	8263.9(7)
Z	4	8
T (K)	173(2)	100(2)
Reflections collected	10318	25058
μ (mm^{-1})	0.433	0.506
Independent reflections	9724 [R(int) = 0.0410]	9196 [R(int) = 0.0213]
Final $R1$	$R1$ = 0.0451	$R1$ = 0.0315
$wR2$ [$I > 2\sigma(I)$]	$wR2$ = 0.0980	$wR2$ = 0.0785
R indices (all data)	$R1$ = 0.0833	$R1$ = 0.0362
	$wR2$ = 0.1079	$wR2$ = 0.0848

Acknowledgments

Financial support of this work by Dirección General de Investigación (Spain) (project-BQU2001-0979-C02-01/02) is gratefully acknowledged. We are grateful to Dr. Jason M. Lynam (University of York) and Prof. Michael Green (University of Bristol) for useful discussions. We thank the EPSRC for a PhD studentship for C. M. C (GR/N06977). I. J. S. F. acknowledges the University of York for financial support. We further acknowledge the constructive remarks made by the referees regarding the catalysis studies.

[1] [1a] *Metal-Catalyzed Cross-Coupling Reactions* (Eds.: F. Diederich, P. J. Stang), Wiley-VCH, New York, **1998**. [1b] J. Tsuji, *Palladium Reagents and Catalysts, Innovations in Organic Synthesis*, John Wiley & Sons, New York, **1995**.

[2] For a review on the Stille reaction, see: V. Farina, V. Krishnamurthy, W. J. Scott, *Org. React.* **1997**, *50*, 1.

[3] K. C. Nicolaou, E. J. Sorensen, *Classics in Total Synthesis*, VCH Publishers, New York, **1996**, chapter 31.

[4] Recent developments in both the Stille and Suzuki reactions have been reviewed: A. F. Littke, G. C. Fu, *Angew. Chem. Int. Ed.* **2002**, *41*, 4176−4211.

[5] [5a] J. Cámpora, P. Palma, E. Carmona, *Coord. Chem. Rev.* **1999**, *195*, 207−281. [5b] P. W. Jennings, L. L. Johnson, *Chem. Rev.* **1994**, *94*, 2241−2290. [5c] I. Ojima, M. Tzmarioudaki, Z. Li, R. Donovan, *Chem. Rev.* **1996**, *96*, 635−662. [5d] K. Moseley, P. M. Maitlis, *J. Chem. Soc., Dalton Trans.* **1974**, 169−175. [5e] T. S. Ito, S. Hasegawa, Y. Takashi, Y. Ishii, *J. Chem. Soc., Chem. Commun.* **1972**, 629−630. [5f] K. Itoh, in *Fundamental Research in Organometallic Chemistry* (Eds.: M. Tsutsui, Y. Ishii, H. Yaozeng), Science Press and Van Nostrand Reinhold Company, New York, **1982**, p. 149. [5g]B. M. Trost, G. J. Tanoury, *J. Am. Chem. Soc.* **1987**, *109*, 4753−4755. [5h] B. M. Trost, M. K. Trost, *J. Am. Chem. Soc.* **1991**, *113*, 1850−1852. [5i] B. M. Trost, M. Yanai, K. Hoogsteen, *J. Am. Chem. Soc.* **1993**, *115*, 5294−5295. [5j] B. M. Trost, V. K. Chang, *Synthesis* **1993**, 824−832; A. Fürstner, F. Stelzer, H. Szillat, *J. Am. Chem. Soc.* **2001**, *123*, 11863−11869. [5k] M. Rubina, M. Rubin, V. Gevorgyan, *J. Am. Chem. Soc.* **2002**, *124*, 11566−11567. [5l] H. tom Diek, C. Munz, C. Müller, *J. Organomet. Chem.* **1990**, *384*, 243−255. [5m] H. Suzuki, K. Itoh, Y. Ishii, K. Simon, J. A. Ibers, *J. Am. Chem. Soc.* **1976**, *98*, 8494−8500. [5n] R. van Belzen, R. A. Klein, H. Kooijman, N. Veldman, A. L. Speck, C. J. Elsevier, *Organometallics* **1998**, *17*, 1812−1825 and references cited therein. [5o] G. Sánchez, J. Vives, J. L. Serrano, J. Pérez, G. López, *Inorg. Chim. Acta* **2002**, *328*, 74−80.

[6] J. L. Serrano, L. García, J. Pérez, E. Pérez, J. Vives, G. Sánchez, G. López, E. Molins, A. Guy Orpen, *Polyhedron* **2002**, *21*, 1589−1596.

[7] [7a] P. Braunstein, F. Naud, *Angew. Chem. Int. Ed.* **2001**, *40*, 680−699. [7b] C. S. Slone, D. A. Weinberger, C. A. Mirkin, *Prog. Inorg. Chem.* **1999**, *48*, 233−250.

[8] [8a] S. Kannan, A. J. James, P. R. Sharp, *Inorg. Chim. Acta* **2003**, *345*, 8−14. [8b] L. Díez, P. Espinet, J. A. Miguel, *J. Chem. Soc., Dalton Trans.* **2001**, 1189−1195.

[9] [9a] J. Ruiz, V. Rodriguez, N. Cutillas, M. Pardo, J. Pérez, G. López, P. A. Chaloner, P. B. Hitchcock, *Organometallics* **2001**, *20*, 1973−1982. [9b] J. Ruiz, V. Rodríguez, G. López, J. Casabó, E. Molins, C. Miravitlles, *Organometallics* **1999**, *18*, 1177−1184 and references cited therein. [9c] J. Ruiz, N. Cutillas, V. Rodríguez, J. Sampedro, G. López, P. A. Chalonner, P. B. Hitchcock, *J. Chem. Soc., Dalton Trans.* **1999**, 2939−2946. [9d] G. Sánchez, J. L. Serrano, J. García, G. López, J. Pérez, E. Molins, *Inorg. Chim. Acta* **1999**, *287*, 37−46. [9e] G. Sánchez, J. L. Serrano, J. Pérez, M. C. Ramírez de Arellano, G. López, E. Molins, *Inorg. Chim. Acta* **1999**, *295*, 136−145.

[10] The most common route to imidato complexes of palladium(II) and platinum(II) involves oxidative addition of *N*-haloimidates to the low valent precursor (employed in the synthesis of **5** and **6**), see: [10a] J. L. Serrano, Y. Zheng, J. R. Dilworth, G. Sánchez, *Inorg. Chem. Commun.* **1999**, *2*, 407−410, and reference 11. Use of imide salts has also been described, see: [10b] I. Dubuc, M. Dubois, F. Belanger-Gariepy, D. Zargarian, *Organometallics* **1999**, *18*, 30−35; or imide deprotonation reactions, see: [10c] T. Ikariya, S. Takizawa, M. Shirado, S. Yoshikawa, *J. Organomet. Chem.* **1979**, *171*, C47−C49. [10d] G. Carturan, V. Belluco, M. Graziani, *J. Organomet. Chem.* **1976**, *112*, 243−248.

[11] C. M. Crawforth, S. Burling, I. J. S Fairlamb, R. J. K. Taylor, A. C. Whitwood, *Chem. Commun.* **2003**, 2194−2195.

[12] [12a] D. Milstein, J. K. Stille, *J. Am. Chem. Soc.* **1978**, *100*, 3636−3638. [12b] J. K. Stille, *Angew. Chem. Int. Ed. Engl.* **1986**, *25*, 508−523. [12c] J. K. Stille, *Pure Appl. Chem.* **1985**, *57*, 1771−1780.

[13] C. M. Crawforth, I. J. S Fairlamb, R. J. K. Taylor, *Tetrahedron Lett.* **2003**, *45*, 461−465. For references relating to other Stille cross-coupling reactions where benzylic halides have been employed as substrates, see: G. A. Holloway, H. M. Hügel, M. A. Rizzacasa, *J. Org. Chem.* **2003**, *68*, 2200−2204; see also ref. 2

 © 2004 Wiley-VCH Verlag GmbH & Co. KGaA, Weinheim

for a complete list of lead references for the Stille cross-coupling of benzylic and allylic halides.

[14] [14a] D. M. Roundhill, *Inorg. Chem.* **1970**, *9*, 254−258. [14b] H. Adams, N. Bailey, T. N. Briggs, J. A. McCleverty, H. M. Colquhoun, D. J. Williams, *J. Chem. Soc., Dalton Trans.* **1986**, 813−819.

[15] J. Pérez, L. García, J. L. Serrano, E. Pérez, G. Sánchez, J. Vives, *Acta Crystallogr., Sect. C* **2002**, *C58*, 404−406; A. L. Rheinghold, C. J. Baldacchini, J. M. O′Connor, J. Huang, *Acta Crystallogr. C* **2002**, *C45*, 1626.

[16] The Cambridge structural database was checked for related complexes (CSD version 5.24 November 2002; updated Feb. 2003 and Apr. 2003).

[17] J. Pérez, L. García, E. Pérez, J. L. Serrano, J. F. Martínez, G. Sánchez, G. López, A. Espinosa, M. Liu, F. Sanz, *New J. Chem.* **2003**, *27*, 1490−1496.

[18] I. Dance, M. Scudder, *J. Chem. Soc., Dalton Trans.* **2000**, 1579.

[19] A. F. Littke, G. C. Fu, *Angew. Chem.* **1999**, *111*, 2568−2570; *Angew. Chem. Int. Ed.* **1999**, *38*, 2411−2413; A. F. Littke, L. Schwarz, G. C. Fu, *J. Am. Chem. Soc.* **2002**, *124*, 6343−6348.

[20] C. Amatore, A. Jutand, *J. Organomet. Chem.* **1999**, *576*, 254−278.

[21] [21a] J. K. Stille, B. L. Groh, *J. Am. Chem. Soc.* **1987**, *109*, 8132; J. K. Stille, B. L. Groh, *J. Organomet. Chem.* **1967**, *9*, 285.

[22] Z. X. Wang, Y. Shi, *J. Org. Chem.* **1998**, *63*, 3099−3104.

[23] T. Yamane, K. Kikukawa, M. Takagiand, T. Matsuda, *Tetrahedron* **1973**, *29*, 955−962.

[24] S. Zhang, D. Zhang, L. S. Liebeskind, *J. Org. Chem.* **1997**, *62*, 2312−2313.

[25] A. G. M. Barrett, T. D. Hamprech, O. Ohkubo, *J. Org. Chem.* **1997**, *62*, 9376−9378.

[26] *SAINT*, Version 6.22, Bruker AXS Inc.

[27] G. M. Sheldrick, *SADABS*, University of Göttingen, **1996**.

[28] G. M. Sheldrick, *SHELX-97. Programs for Crystal Structure Analysis*, Release 97-2, University of Göttingen, Germany, **1998**.

Received December 12, 2003
Early View Article
Published Online May 5, 2004

 © 2004 Wiley-VCH Verlag GmbH & Co. KGaA, Weinheim

Coordination Chemistry of 1,3-Bis(2-pyridylimino)- and 1,3-Bis-(2-thiazolylimino)isoindole Copper Complexes: Investigation of Their Catalytic Behavior in Oxidation Reactions

Markus B. Meder[a] and Lutz H. Gade*[a,b]

Keywords: Copper / Allylic peroxylation / Coordination polymers / Radical reactions / Oxidation

The copper complexes [Cu(4-MeBPI)(OAc)] (**4**), [Cu(4-Me-10-*t*BuBPI)(OAc)] (**5**) and [Cu(BTI)(OAc)] (**6**) [BPI = 1,3-bis(2-pyridylimino)isoindole, BTI = 1,3-bis(2-thiazolylimino)isoindole] were prepared by reaction of the protio ligands with copper(II) acetate. Compounds **4** and **6** were characterized by X-ray diffraction, establishing distorted square-planar coordination geometries of the copper ions. Two monoclinic modifications of **6** (**6a** and **6b**) were found, both crystallizing in the space group $P2_1/c$, but possessing different cell parameters. In contrast to **6a**, which is monomeric in the crystal, the second monoclinic modification **6b** has a more complicated crystal structure, which is composed of both monomeric complex units such as those found in **6a** and infinite chains of coordination polymers. The copper atoms in the polymeric chains of **6b** display fivefold coordination and a ligand polyhedron that is an intermediate form between a trigonal-bipyramidal and a square-pyramidal geometry. The allylic peroxylation of cyclohexene with *t*BuOOH (70% aqueous solution) catalyzed by **4** and **6** (0.17 mol %) gave *tert*-butylperoxy-3-cyclohexene with selectivities of 86% and 80% (based on cyclohexene) and turnover frequencies of 63 h^{-1} and 18 h^{-1}, respectively. The peroxylation reaction is thought to proceed according to a Haber–Weiss radical chain mechanism.

(© Wiley-VCH Verlag GmbH & Co. KGaA, 69451 Weinheim, Germany, 2004)

Introduction

The direct oxidation of C−H bonds is an important chemical transformation in organic synthesis. A preparatively useful example of such a conversion of hydrocarbons is the copper-catalyzed Kharasch−Sosnovsky reaction, i.e. the allylic acyloxylation of olefins [Equation (1)].[1] In the presence of chiral oxazoline-based ligands it has been possible to render this reaction enantioselective,[2] although a truly efficient asymmetric catalyst has not as yet been found. A much less studied variant of this oxidation is the allylic peroxylation, which is also catalyzed by Cu salts [Equation (2)]. The synthesis of dialkyl peroxides by the oxidation of cycloolefins with *tert*-butyl hydroperoxide, first reported by Kharasch,[3] has recently attracted renewed attention due to the high diastereoselectivity of the subsequent epoxidation or dihydroxylation of the C=C bond.[4] This gives rise to highly functionalized cyclohexane derivatives.

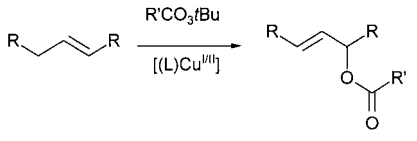

(1)

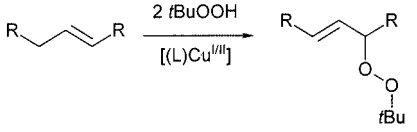

(2)

In the standard reaction protocols for allylic peroxylations, a Cu^I or Cu^{II} salt and, occasionally, an N-donor ligand are added to the reaction mixture which assemble to give the active catalyst, the nature of which is generally not unambiguously established.

In this paper we report the synthesis and structural characterization of several Cu^{II} complexes containing 1,3-bis(2-pyridylimino)isoindole (BPI) and 1,3-bis(2-thiazolylimino)isoindole (BTI) ligands, and their use as selective catalysts in the allylic peroxylation of cyclohexene. First reported in the 1950s,[5] such tridentate ligands have more recently been employed by Siegl and co-workers in the tran-

[a] Laboratoire de Chimie Organométallique et de Catalyse (CNRS UMR 7513), Institut Le Bel, Université Louis Pasteur, 4, rue Blaise Pascal, 67000 Strasbourg, France
[b] Anorganisch-Chemisches Institut, Universität Heidelberg, Im Neuenheimer Feld 270, 69120 Heidelberg, Germany
E-mail: lutz.gade@uni-hd.de

 © 2004 Wiley-VCH Verlag GmbH & Co. KGaA, Weinheim **DOI: 10.1002/ejic.200400012**

sition-metal (mainly cobalt) catalyzed oxidation of saturated hydrocarbons.[6,7] In a systematic study of the cobalt-catalyzed oxidation of cyclohexane and cyclohexene, Mimoun et al. employed *tert*-butyl hydroperoxide as the oxidizing reagent;[8] furthermore, the photoactivation of this kind of BPI-metal peroxo complex for the oxidation of hydrocarbons has also been reported.[9] Given the facile accessibility of well-defined BPI and BTI transition metal complexes and the previous results on copper-catalyzed allylic peroxylations, copper complexes of isoindole-derived tridentate ligands appear to be promising candidates for this type of transformations.

Results and Discussion

Synthesis of the Bis(2-pyridylimino)isoindole (BPI)- and Bis(2-thiazolylimino)isoindole (BTI)-Copper Complexes

For the synthesis of the bis(2-pyridylimino)isoindole and bis(2-thiazolylimino)isoindole ligand precursors, the method previously reported by Siegl was employed.[6,7,10] The phthalodinitrile starting materials were treated with an excess of the corresponding 2-aminopyridines or 2-aminothiazole in the presence of a catalytic amount of $CaCl_2$ (Scheme 1). The use of 1-hexanol as solvent instead of 1-butanol, as is reported in the literature for this type of conversion, gave significantly improved yields of the ligand precursors 4-MeBPI (**1**), 4-Me-10-*t*BuBPI (**2**) and BTI (**3**).

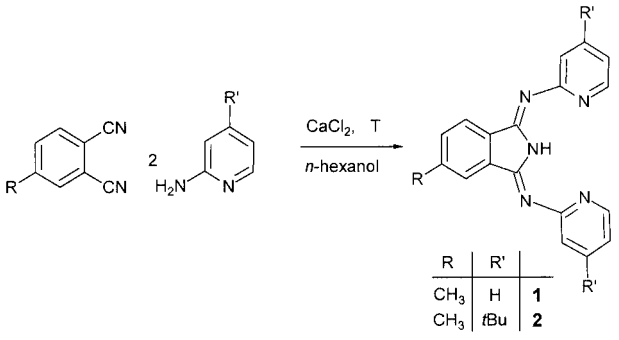

Scheme 1. Synthesis of the BPI ligands **1** and **2**

The BPI- and BTI-copper complexes [(4-MeBPI)-Cu(OAc)] (**4**), [(4-Me-10-*t*BuBPI)Cu(OAc)] (**5**), and [(BTI)-Cu(OAc)] (**6**) were prepared as previously published for similar complexes (Scheme 2 and Scheme 3);[11,12] compound **6** is the first BTI copper complex to be reported. To avoid the formation of the symmetric complexes $[Cu(BPI)_2]$ or $[Cu(BTI)_2]$, the exact metal−ligand stoichiometry was chosen, and the reaction temperature kept below 300 K. The formulation and the identity of **4**−**6** were confirmed by IR spectroscopy and elemental analysis.

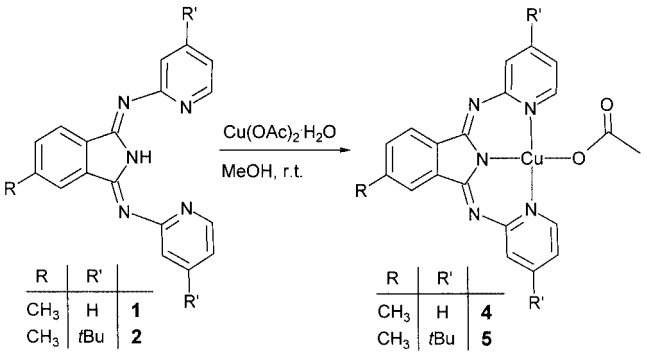

Scheme 2. Synthesis of the (acetato)(BPI)copper complexes **4** and **5**

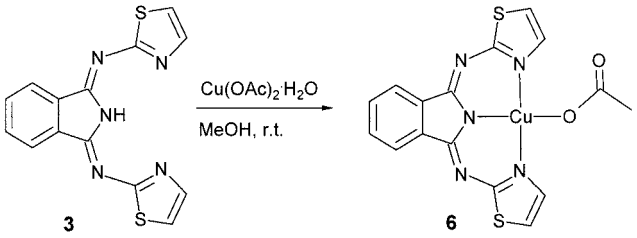

Scheme 3. Synthesis of the (acetato)(BTI)copper complex **6**

Structural Characterization of 4, 6a and 6b

Whereas a considerable number of X-ray diffraction studies have been carried out for transition-metal complexes of BPI, there are only a few previously determined structures for copper complexes. Gagné reported the dimeric structure of a (carbonato)(BPI)copper complex and the molecular structure of a μ-oxo-copper pentamer,[11] while Bereman, in a study aimed at modeling the coordination sphere of the Cu^{II} site in galactose oxidase, reported the crystal structure analysis of a pentacoordinate (acetato)(BPI)-copper complex.[13]

X-ray diffraction studies of both BPI copper compounds **4** and **5** were carried out. However, severe disorder of the *tert*-butyl groups in **5**, as well as disordered solvent in the unit cell, precluded a complete structure analysis of the latter (although the gross structural features displayed in Scheme 2 were confirmed). A single-crystal X-ray structure analysis of complex **4** established the structural details of this class of compounds. Its molecular structure is displayed in Figure 1, along with the principal bond lengths and bond angles.

As is apparent from Figure 1, the molecular structure of **4** is distorted from an ideal square-planar geometry. For instance, the N(1)−Cu−N(5) angle was found to be 158.8(1)°, which is significantly more acute than the corresponding bond angle found by Bereman et al. in the pentacoordinate complex [(10-MeBPI)Cu(OAc)(H_2O)] (169.4°).[13] The acetato ligand is monodentate and the Cu−O(1) distance of 1.956(2) Å is in the expected range.[14] The carboxyl group is arranged orthogonally to the metal complex plane due to steric repulsion with the pyridyl rings. This leads to an axial disposition of the O(2) atom of the carboxyl unit relative to the copper atom. However, the

 © 2004 Wiley-VCH Verlag GmbH & Co. KGaA, Weinheim

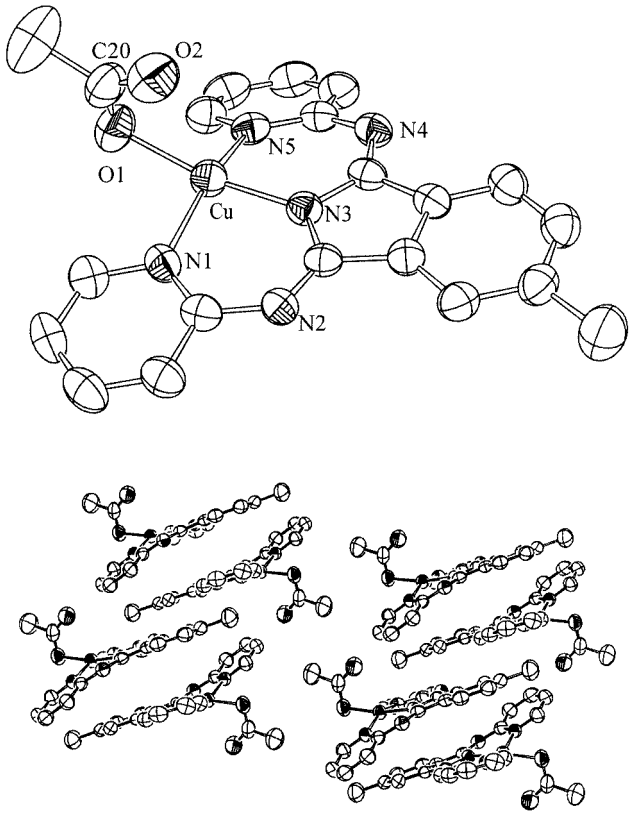

Figure 1. Molecular structure of complex **4** (top); selected bond lengths (Å) and angles (°): Cu−N(1) 2.023(3), Cu−N(3) 1.884(3), Cu−N(5) 2.014(3), Cu−O(2) 2.601(3), Cu−O(1) 1.956(2), C(20)−O(1) 1.249(5), C(20)−O(2) 1.245(5), N(1)−Cu−N(3) 90.6(1), N1−Cu−N5 158.2(1), N(1)−Cu−O(1) 93.3(1), N(3)−Cu−N(5) 89.3 (1), N(3)−Cu−O(1) 166.1(1), N(5)−Cu−O(1) 91.9(1), O(1)−C(20)−O(2) 122.9(4); view of the molecular packing of **4** in the unit cell (bottom)

Cu−O(2) distance of 2.601 Å does not support a significant bonding interaction and should be compared with the Cu−O bond length of 2.466 Å for the weakly axially coordinated water molecule in Bereman's complex.[13] A view of the packing of complex **4** in the unit cell clearly indicates that there are no bridging interactions of the acetato groups between the molecular units that stack in a head-to-tail fashion (Figure 1, bottom).

Since there is no previous report of a fully structurally characterized BTI complex, attempts were made to crystallize compound **6** in order to carry out an X-ray diffraction study. Two monoclinic crystalline modifications, the habits of which differed only marginally and which possessed identical analytical properties, were obtained in varying ratios on slow diffusion of *n*-hexane into a toluene solution of **6**. Mechanical separation of one type of crystal habit and subsequent recrystallization again gave both crystalline forms. Single-crystal X-ray structure analysis of both crystalline modifications **6a** and **6b** were carried out in order to establish the details of the molecular structure of **6** and its arrangement in both solid forms. The molecular structure of **6a** and its molecular packing pattern is displayed in Figure 2, while the principal bond lengths and bond angles are listed in Table 1.

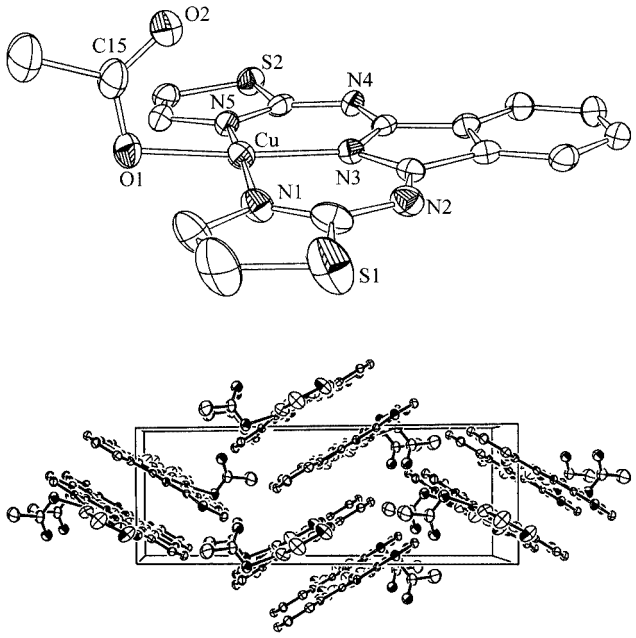

Figure 2. Molecular structure of **6a** (top); selected bond lengths and angles are given in Table 1; view of the molecular packing of **6a** in the unit cell (bottom)

Table 1. Comparison of selected bond lengths (Å) and angles (°) of **6a** and **6b**

	6a	**6b**
Cu−N1	1.991(3)	1.94(1)
Cu−N3	1.931(3)	1.98(1)
Cu−N5	1.989(3)	1.95(1)
Cu−O1	1.948(3)	2.08(1)
Cu−O2	2.595	2.54
Cu−O2′	–	2.23(1)
N1−Cu−N3	89.7(1)	89.1(5)
N1−Cu−N5	172.7(1)	173.0(5)
N3−Cu−O1	175.3(1)	154.2(5)
N3−Cu−O2	–	120.6(5)
O1−Cu−O2′	–	85.2
Cu−O1−C15	104.8(2)	101(1)
O1−C15−O2	122.8(4)	123(1)

The replacement of the pyridyl units by thiazolyl groups leads to a different orientation of the neutral N-donor functions and leaves a more open space for the acetate ligand than in **4**. These two factors lead to a complex geometry, which deviates less from the idealized planar structure than that found for **4**. The angles N(1)−Cu−N(5) and N(3)−Cu−O(1) are 172.7(1) and 175.3(1)°, respectively. Whereas the metal−N distance of the formally anionic donor atom is 0.05 Å greater than in **4** [**6a**: 1.931(3), **4**: 1.884(3) Å], the copper−thiazolyl-N bond lengths are about 0.03 Å shorter than the corresponding bond lengths in the BPI complex. The view of the molecular packing in **6a**, which is displayed in Figure 2, indicates a molecular head−tail stacking with interlayer distances of about 3.7

 © 2004 Wiley-VCH Verlag GmbH & Co. KGaA, Weinheim

Å. There is no indication of bonding interactions through bridging acetato ligands in this structure.

In contrast to **6a**, the second monoclinic modification **6b** has a more complicated crystal structure composed of both monomeric complex units such as those found in **6a** and infinite chains of coordination polymers. A segment of such a chain structure is displayed in Figure 3, while the parameters of the complex within the polymeric structure are listed in Table 1 (those of the monomers are essentially identical to **6a**).

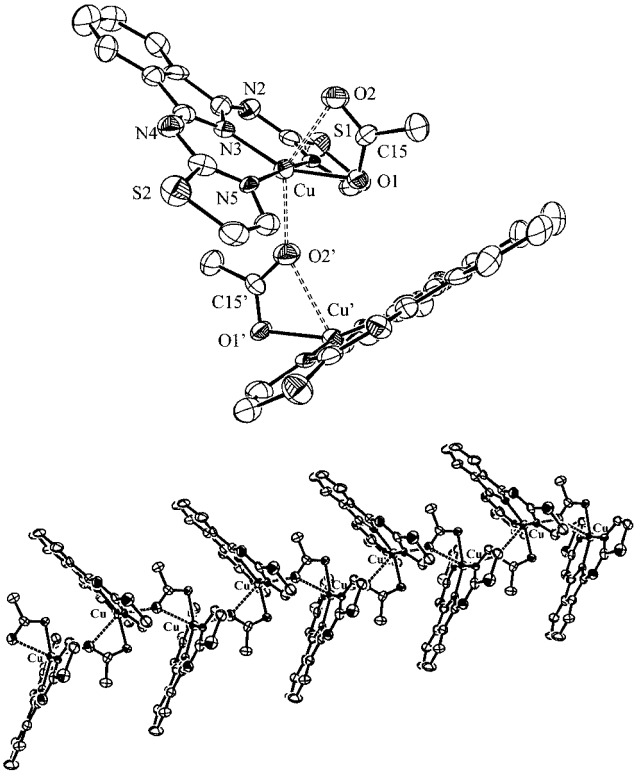

Figure 3. A segment of the chain structure in **6b** (top); selected bond lengths and angles are given in Table 1; polymeric chain structure of the (acetato)(BTI)copper complex in **6b** (bottom)

In contrast to the almost ideally planar four-coordinate structure of **6a**, the copper atoms in the polymeric chains of **6b** display fivefold coordination and a ligand polyhedron which is an intermediate form between a trigonal-bipyramidal and a square-pyramidal geometry. While the arrangement of the three heterocycles of the BTI ligand remains almost planar [N(1)−Cu−N(5), 173.0(5)°], the acetato ligand is tilted out of this plane [N(3)−Cu−O(1), 154.2(5)°], therefore making space for the coordination of the second acetato oxygen atom of a neighboring (acetato)(BTI)copper coordination unit. Significantly, the Cu−O(1) bond length of 2.08(1) Å is longer than in the square-planar monomer, and the Cu−O(2′) distance of 2.23(1) Å is indicative of substantial intermolecular bonding, leading to the polymeric complex. Similar Cu−O bond lengths were reported for two BPI copper complexes: a dimeric carbonato- and an oligomeric hydroxo-bridged complex.[12]

It should be pointed out that upon redissolution of either of the two crystalline modifications of compound **6** and subsequent recrystallization of the material, crystals of both monoclinic forms reprecipitated. The sole species in solution is therefore thought to be the monomer, as observed in **6a**. Exclusive formation of either **6a** or **6b** was not achieved by variation of either the solvent system or the temperature of crystallization.

Allylic Peroxylation of Cyclohexane Catalyzed by Complexes 4−6

In order to assess the catalytic activity of the copper complexes in the allylic peroxylation of alkenes, the Cu^{II}-catalyzed reaction of *t*BuOOH with cyclohexene was studied. In contrast to a previous study on the analogous Co-catalyzed reaction by Mimoun et al., who employed the oxidant in very high concentrations (96%),[8] we chose the commercial aqueous solution of 70% *t*BuOOH. Remarkably, all three complexes gave the dialkyl peroxide, *tert*-butylperoxy-3-cyclohexene, very selectively (Scheme 4). Conversions to this major product (based on cyclohexene) were in the range of 80−90%.

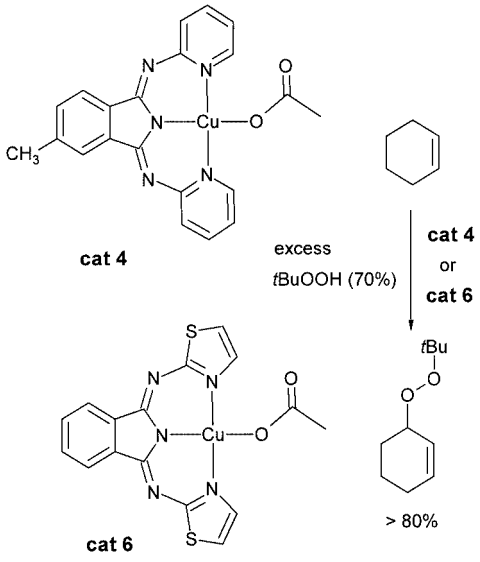

Scheme 4. Allylic peroxylation of cyclohexene catalyzed by complexes **4** and **6** giving the dialkyl peroxide in over 80% yield

The principal difference between the three catalysts was the activity observed: the two BPI derivatives display the same catalytic activity and are significantly more active than the BTI complex as is shown in Figure 4 for catalysts **4** and **6**. Both reactions were carried out with a catalyst loading of 0.17 mol %. Considering the nearly linear part of the conversion curves between 10% and 75%, the turnover frequencies amount to 63 h^{-1} for **4** and 18 h^{-1} for the BTI complex **6**. The maximum conversions of 86% observed for complex **4** and 80% for complex **6** correspond to turnover numbers of 505 and 470, respectively. The reaction product *tert*-butylperoxy-3-cyclohexene was isolated by distillation

 © 2004 Wiley-VCH Verlag GmbH & Co. KGaA, Weinheim

and fully characterized. In order to exclude the possibility that a simple copper salt acts as a catalytic species after initial degradation of the ligands, analogous catalytic runs using the identical reaction parameters were carried out with copper acetate. Very slow oxidation of cyclohexene was observed with low chemoselectivity; the conversion of the starting material was variable, but in all cases well below 10% after 1500 minutes (the time frame of the experiments represented in Figure 4). Thus, for the results presented in this work, the background activity of nonligated copper salts is insignificant.

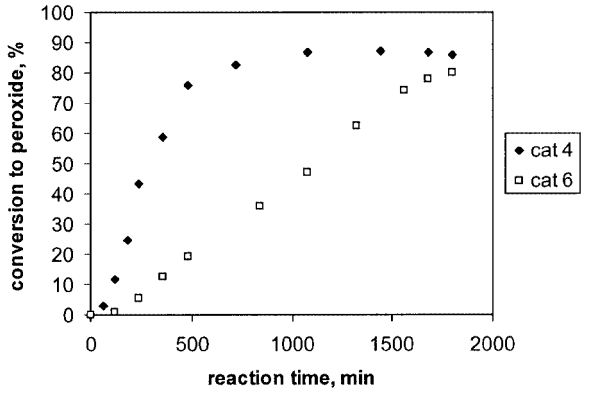

Figure 4. Peroxidation of cyclohexene with the catalysts **4** and **6**

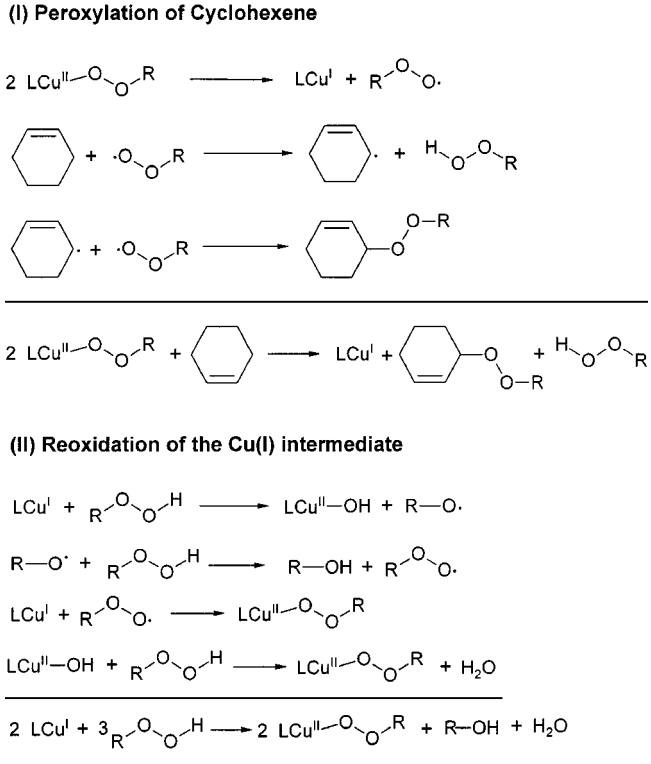

Scheme 5. Postulated Haber−Weiss mechanism for the Cu-catalyzed peroxylation: generation of the alkylperoxycopper(II) complexes as the active species and their degradation to the Cu^{I} species with concomitant transfer of the peroxyl group to the allylic position of cyclohexene

The catalytic reaction most probably proceeds according to a Haber−Weiss chain mechanism, as has been suggested previously, and which depicted in Scheme 5.[15] The active species is the copper(II) *tert*-butyl peroxide complex which thermally decomposes to the Cu^{I} complex and a peroxyl radical. This radical intermediate abstracts a hydrogen atom from the allylic position of cyclohexene, and the cyclohexenyl radical then recombines with a second peroxyl radical generated in the same way. The Cu^{I} product is then re-oxidized by the alkyl hydroperoxide in several steps generating *tert*-butanol and water as reduced products.

When the reaction product *tert*-butylperoxy-3-cyclohexene was exposed to the copper complexes over a longer period of time (> 20 h for **4** and **5** and > 35 h for **6**), slow conversion of the dialkyl peroxide to cyclohexenone and *tert*-butanol was observed (Scheme 6). This slow secondary reaction limits the yields of the dialkyl peroxide which can be isolated from the copper-catalyzed peroxylation described in this work. It was also observed by the addition of the Cu complexes to pure, isolated dialkyl peroxide.

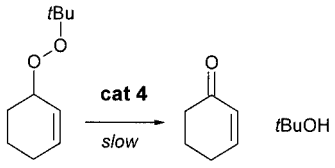

Scheme 6. Copper-catalyzed slow conversion of *tert*-butylperoxy-3-cyclohexene to cyclohexenone and *tert*-butanol

Conclusion

In this work we have presented a detailed study of the coordination chemistry of three BPI and BTI copper complexes and their activity as catalysts for the allylic peroxylation of cyclohexene as substrate of reference. Using the hydroperoxide oxidant as an aqueous solution with a concentration of 70% gave the *tert*-butyl cyclohexenyl peroxide with high selectivity. Other previously described reaction products such as 3-cyclohexenol, 3,3′-dicyclohexenyl were not observed, even in traces, while exposure of the dialkyl peroxide to the copper catalysts for an extended period of time led to a very slow degradation to cyclohexenone as a secondary product. The high selectivity of the peroxylation on use of the BPI copper compounds and the relatively high turnover numbers obtained render these systems competitive catalysts for peroxylation reactions. We are currently studying the regioselectivity of the peroxide formation for nonsymmetrical olefins in order to assess the general applicability of this method.

Experimental Section

All manipulations were performed under a nitrogen atmosphere in standard (Schlenk) glassware. Solvents were dried according to standard procedures and saturated with nitrogen. The deuterated

 © 2004 Wiley-VCH Verlag GmbH & Co. KGaA, Weinheim

solvents used for NMR spectroscopic measurements were degassed by three successive "freeze-pump-thaw" cycles and dried using standard techniques.

The ^1H and ^{13}C NMR spectra were recorded using an AMX 400 FT NMR spectrometer and infrared spectra on a Perkin−Elmer 1600 FT-IR spectrometer. Elemental analyses were carried out in the microanalytical laboratories of the chemistry departments at Würzburg (Germany) and Strasbourg (France). The compounds 2-amino-4-*tert*-butylpyridine[16] and 4-methylphthalonitrile[17] were prepared according to published methods. All other chemicals used as starting materials were obtained commercially and used without further purification.

Preparation of the Ligands: The synthesis of the ligand precursors was carried out by a modified protocol based on the method which was originally published by Siegl.[7,10] This modified reaction protocol will be exemplified for the synthesis of the novel derivative 4-Me-10-*t*BuBPI (**2**).

4-Me-10-*t*BuBPI (2): A suspension of 4-methylphthalonitrile (1.50 g, 10.6 mmol), 2-amino-4-*tert*-butylpyridine (3.96 g, 26.1 mmol) and $CaCl_2$ (0.16 g, 1.36 mmol) in 1-hexanol (50 cm^3) was refluxed for 18 h. After cooling to room temperature, the yellow compound which precipitated was filtered, washed with water (500 cm^3) and dried in vacuo. Yield: 2.53 g (56%). M.p. 204 °C. ^1H NMR (400.16 MHz, C_6D_6, 295 K): δ = 1.1, 1.2 (2 × s, 2 × 9 H, 10-*t*Bu), 2.05 (s, 3 H, 4-CH_3), 6.84 (m, 2 H, 11-H), 6.94 (br. d, $^3J_{H,H}$ = 7.9 Hz, 1 H, 5-H), 7.72 (m, 2 H, 9-H), 8.02 (br. s, 1 H, 3-H), 8.12 (d, $^3J_{H,H}$ = 7.9 Hz, 1 H, 6-H), 8.60 (d, $^3J_{H,H}$ = 5.3 Hz, 2 H, 12-H), 11.91 (br. s, 1 H, N−H). $\{^1H\}^{13}C$ NMR (100.6 MHz, C_6D_6, 295 K): δ = 21.6 (4-*C*H_3), 30.4 (10-C(*C*H_3)$_3$], 34.5 (10-*C*(CH$_3$)$_3$], 117.7 (C-11), 121.1 (C-9), 122.9 (C-5), 123.6 (C-6), 132.8 (C-3), 137.2 (C-1, C-2), 141.9 (C-4), 148.1 (C-12), 154.1 (C-7), 161.8 (C-8, C-10) ppm. IR (KBr): $\tilde{\nu}$ = 3237 (m, br), 2962 (m), 2867 (w), 1633 (m), 1590 (s), 1534 (w), 1477 (w), 1401 (w), 1365 (w), 1354 (w), 1310 (vw), 1285 (w), 1265 (w), 1219 (w), 1201 (vw), 1180 (vw), 1108 (vw), 1037 (vw), 928 (m), 890 (m), 826 (m), 716 (m) cm^{-1}. $C_{27}H_{31}N_5$ (425.57 g mol^{-1}): calcd. C 76.2, H 7.3, N 16.5; found C 76.5, H 7.4, N 16.3.

Preparation of the Copper Complexes

[Cu(4-MeBPI)(OAc)] (4): A suspension of **1** (87.0 mg, 0.28 mmol) was added to a stirred suspension of $Cu(OAc)_2{\cdot}H_2O$ (0.11 g, 0.56 mmol) in 10 mL of methanol at room temperature. After stirring for 16 h at room temperature, the reaction mixture was filtered and the resulting deep brown solution was concentrated in vacuo. The crude product was suspended in toluene and filtered with Celite. Evaporation of the solvent afforded a green-brown solid, which was recrystallized from toluene/*n*-hexane. Yield: 87.0 mg (71%). Green-brown crystals suitable for X-ray diffraction were grown by the slow diffusion of *n*-hexane into a saturated solution of **4** in toluene at room temperature. M.p. 116 °C. IR (KBr): $\tilde{\nu}$ = 2925 (w), 1628 (m), 1597 (m), 1573 (s), 1531 (m), 1467 (m), 1460 (m), 1431 (m), 1398 (vw), 1365 (w), 1280 (w), 1184 (w), 1135 (m), 1077 (w), 1012 (w), 786 (w), 755 (w) cm^{-1}. $C_{21}H_{17}CuN_5O_2$ (434.95 g mol^{-1}): calcd. C 58.0, H 3.5, N 16.1; found C 58.1, H 3.5, N 15.9%.

[Cu(4-Me-10-*t*BuBPI)(OAc)] (5): A suspension of **2** (80.0 mg, 0.19 mmol) was added to a stirred suspension of $Cu(OAc)_2{\cdot}H_2O$ (75.0 mg, 0.38 mmol) in 10 mL of methanol at room temperature. After stirring for 16 h at room temperature, the reaction mixture was filtered and the resulting deep brown solution was concentrated in vacuo. The crude product was suspended in toluene and filtered with Celite. Evaporation of the solvent afforded a green-brown solid, which was recrystallized from toluene/*n*-hexane. Yield: 82.0 mg (79%). M.p. 124 °C. IR (KBr): $\tilde{\nu}$ = 2965 (w), 1671 (m), 1573 (s), 1507 (m), 1478 (m), 1403 (m), 1360 (m), 1326 (w), 1248 (w), 1182 (m), 1143 (m), 1112 (m), 1082 (w), 946 (w), 918 (w), 885 (w), 828 (w), 729 (w) cm^{-1}. $C_{29}H_{33}CuN_5O_2$ (547.15 g mol^{-1}): calcd. C 63.7, H 6.1, N 12.8; found C 63.9, H 6.2, N 12.4%.

[Cu(BTI)(OAc)] (6a) and [Cu(BTI)(OAc)]$_\infty$ (6b): A suspension of BTI (**3**) (0.12 g, 0.38 mmol) in methanol was added to a suspension of $Cu(OAc)_2{\cdot}H_2O$ (0.15 g, 0.76 mmol) in methanol (10 mL). After stirring for 12 h at room temperature, the reaction mixture was dried in vacuo and the residue was redissolved in toluene. After filtration with Celite, the solution was concentrated and the crude product was recrystallized from toluene/*n*-hexane. Orange (**6a**) and yellow (**6b**) crystals suitable for X-ray diffraction were grown by slow diffusion of *n*-hexane into a saturated solution of **6** in toluene at room temperature. Yield: 0.13 g (81%). M.p. 121 °C. IR (KBr): $\tilde{\nu}$ = 3107 (w), 2965 (vw), 1583 (m), 1542 (s), 1494 (m), 1469 (w), 1383 (m), 1308 (w), 1298 (w), 1240 (m), 1190 (m), 1102 (s), 1071 (m), 916 (vw), 877 (m), 813 (vw), 715 (m), 682 (vw) cm^{-1}. $C_{16}H_{11}CuN_5O_2S_2$ (432.97 g mol^{-1}): calcd. C 44.4%; H 2.6%; N 16.2; found C 44.7%; H 2.7%; N 15.9%.

Catalytic Peroxylation of Cyclohexene: The catalytic peroxylations were carried out in neat cyclohexene with catalyst concentrations of 0.17 mol % and a twofold excess of *tert*-butyl hydroperoxide. Samples of ca. 10 μL were taken at the intervals indicated in Figure 4 and dissolved in 2 mL of toluene. The solution was then injected into a Shimadzu GC-17A/GCMS-QP5050A instrument. The measured ratio of the substrate and products was calibrated by comparative measurements with known ratios of pure substances. The conversion (%) generally refers to the generation of *tert*-butyl cyclohex-2-en-1-yl peroxide based on the substrate cyclohexene. The data displayed are average values of two runs.

The reaction product *tert*-butyl cyclohex-2-en-1-yl peroxide was isolated after filtration of the product mixture through a pad of Celite and removal of the solvent in vacuo. The crude product was subjected to a Kugelrohr distillation at 1 mbar (b.p. ca. 60 °C). ^1H NMR (400.16 MHz, $CDCl_3$, 295 K): δ = 1.25 (s, 9 H), 1.56 (m, 1 H), 1.73 (m, 2 H), 1.94 (m, 2 H), 2.06 (m, 12 H), 4.40 (m, 1 H), 5.74 (m, 1 H), 5.95 (m, 1 H). $\{^1H\}^{13}C$ NMR (100.6 MHz, $CDCl_3$, 295 K): δ = 18.8, 25.7, 26.8, 27.3, 76.7, 80.0, 124.5, 133.7 ppm. MS (EI): 170.1 [M^+].

X-ray Diffraction Study of 4, 6a and 6b: The crystal data were collected on a Nonius−Kappa CCD diffractometer at −100 °C and transferred to a DEC Alpha workstation; for all subsequent calculations the Nonius OpenMoleN package was used.[18] The structures were solved by direct methods, and absorption corrections were part of the scaling procedure of the data reductions. After refinement of the heavy atoms, difference Fourier maps revealed the maxima of residual electron density close to the positions expected for the hydrogen atoms; they were introduced as fixed contributors in the structure factor calculations with fixed coordinates (C−H: 0.95 Å) and isotropic temperature factors [B(H) = 1.3 B_{eqv}(C) Å^2], but not refined. Full least-square refinements on F^2. A final difference map revealed no significant maxima of electron density. The scattering factor coefficients and the anomalous dispersion coefficients were taken from the literature.[19] Crystal data and experimental details for the crystals of **4**, **6a** and **6b** are given in Table 2.

CCDC-228180 to -228182 contains the supplementary crystallographic data for this paper. These data can be obtained free of charge at www.ccdc.cam.ac.uk/conts/retrieving.html [or from the

 © 2004 Wiley-VCH Verlag GmbH & Co. KGaA, Weinheim

Table 2. X-ray data collection and processing parameters for **4**, **6a** and **6b**

	4	**6a**	**6b**
Empirical formula	$2(C_{21}H_{17}CuN_5O_2)C_7H_8$	$C_{16}H_{11}CuN_5O_2S_2$	$C_{16}H_{11}CuN_5O_2S_2$
M	962.03	432.97	432.97
Temp. [°C]	21(1)	−100(1)	−100(1)
Wavelength. [Å]	0.71073	0.71073	0.71073
Space group	$P\bar{1}$	$P2_1/c$	$P2_1/c$
a [Å]	8.3873(5)	10.7706(6)	5.4021(6)
b [Å]	9.2129(5)	7.6486(4)	8.4923(2)
c [Å]	14.8935(9)	21.383(1)	25.679(1)
α [°]	92.069(5)	–	–
β [°]	91.730(5)	101.577(5)	91.743(5)
γ [°]	103.686(5)	–	–
V [Å^3]	1116.5(2)	1725.7(2)	3357.2(3)
Z	1	4	8
$D_{calcd.}$ [g cm^{-3}]	1.43	1.67	1.71
Abs. coeff./[mm^{-1}]	1.010	1.529	1.572
R indices	$R_1 = 0.046$ $R_w = 0.065$	$R_1 = 0.035$ $R_w = 0.041$	$R_1 = 0.092$ $R_w = 0.141$

Cambridge Crystallographic Data Centre, 12 Union Road, Cambridge CB2 1EZ, UK; Fax: (internat.) +44-1223-336-033; E-mail: deposit@ccdc.cam.ac.uk].

Acknowledgments

We thank the Deutsche Forschungsgemeinschaft, the CNRS (France) and the Institut Universitaire de France for financial support of this work. We are grateful to Dr. André De Cian and N. Gruber for the X-ray diffraction studies.

[1] [1a] M. S. Kharasch, G. Sosnovsky, *J. Am. Chem. Soc.* **1958**, *80*, 756−757. [1b] M. S. Kharasch, G. Sosnovsky, *J. Am. Chem. Soc.* **1959**, *81*, 5819−5824.

[2] Selected early reports of asymmetric Kharasch−Sosnovsky reactions: [2a] A. S. Gokhale, A. B. E. Minidis, A. Pfaltz, *Tetrahedron Lett.* **1995**, *36*, 1831−1834. [2b] M. B. Andrus, A. B. Argade, X. Chen, M. G. Pamment, *Tetrahedron Lett.* **1995**, *36*, 2945−2948. [2c] K. Kawasaki, S. Tsumura, T. Katsuki, *Synlett* **1995**, 1245−1246. [2d] A. Levina, J. Muzart, *Tetrahedron: Asymmetry* **1995**, *6*, 147−156. Recent reviews: [2e] M. B. Andrus, J. C. Lashley, *Tetrahedron* **2002**, *58*, 845−866. [2f] J. Eames, M. Watkinson, *Angew. Chem. Int. Ed.* **2001**, *40*, 3567−3571.

[3] [3a] M. S. Kharasch, P. Pauson, W. Nudenberg, *J. Org. Chem.* **1953**, *18*, 322−327. [3b] W. Treibs, G. Pellmann, *Chem. Ber.* **1954**, *87*, 1201−1205. [3c] M. S. Kharasch, A. Fono, *J. Org. Chem.* **1958**, *23*, 324−325. [3d] M. S. Kharasch, A. Fono, *J. Org. Chem.* **1959**, *24*, 72−78.

[4] [4a] M. Schulz, R. Kluge, F. G. Gelalcha, *Tetrahedron: Asymmetry* **1998**, *9*, 4341−4360. [4b] M. Schulz, R. Kluge, S. Liebsch, J. Lessig, M. Halik, F. G. Gelalcha, *Tetrahedron* **1996**, *52*, 13151−13166.

[5] J. A. Elvidge, R. P. Linsted, *J. Chem. Soc.* **1952**, 5008−5012.

[6] [6a] W. O. Siegl, *J. Org. Chem.* **1977**, *42*, 1872−1878. [6b] W. O. Siegl, *Inorg. Nucl. Chem. Letters* **1974**, *10*, 825−829.

[7] R. R. Gagné, W. A. Marritt, D. N. Marks, W. O. Siegl, *Inorg. Chem.* **1981**, *20*, 3260−3267.

[8] L. Saussine, E. Brazi, A. Robine, H. Mimoun, J. Fischer, R. Weiss, *J. Am. Chem. Soc.* **1985**, *107*, 3534−3540.

[9] [9a] E. T. Farinas, C. V. Nguyen, P. K. Mascharak, *Inorg. Chim. Acta* **1997**, *263*, 17−21. [9b] F. A. Chavez, P. K. Mascharak, *Acc. Chem. Res.* **2000**, *33*, 539− 545.

[10] W. O. Siegl, *J. Heterocyclic Chem.* **1981**, *18*, 1613−1618.

[11] R. R. Gagné, R. S. Gall, G. C. Lisensky, R. E. Marsh, L. M. Speltz, *Inorg. Chem.* **1979**, *18*, 771−781.

[12] [12a] A. W. Addison, P. J. Burke, K. Henrick, *Inorg. Chem.* **1982**, *21*, 60−63. [12b] E. Balogh-Hergovich, J. Kaiser, G. Speier, G. Huttner, A. Jacobi, *Inorg. Chem.* **2000**, *39*, 4224−4229. [12c] O. P. Anderson, A. la Cour, A. Dodd, A. D. Garrett, M. Wicholas, *Inorg. Chem.* **2003**, *42*, 4513−4515.

[13] [13a] R. D. Bereman, G. D. Shields, J. R. Dorfman, J. Bordner, *J. Inorg. Biochem.* **1983**, *19*, 75−93. [13b] D. M. Baird, W. P. Maehlmann, R. D. Bereman, P. Singh, *J. Coord. Chem.* **1997**, *42*, 107−126.

[14] R. K. Hocking, T. W. Hambley, *Inorg. Chem.* **2003**, *22*, 2833−2835.

[15] [15a] F. Haber, R. Willstädter, *Chem. Ber.* **1931**, *64*, 2844−2856. [15b] F. Haber, J. Weiss, *Naturwiss.* **1932**, *51*, 948−950. [15c] F. Haber, J. Weiss, *Proc. R. Soc.* **1934**, *147*, 332−351.

[16] P. J. Domaille, R. L. Harlow, S. D. Ittel, W. G. Peet, *Inorg. Chem.* **1983**, *22*, 3944−3952.

[17] W. O. Siegl, F. C. Ferris, P. A. Mucci, *J. Org. Chem.* **1977**, *42*, 3442−3443.

[18] Nonius *OpenMoleN, Interactive Structure Solution*, Delft, **1997**.

[19] D. T. Cromer, J. T. Waber, *International Tables for X-ray Crystallography*, The Kynoch Press, Birmingham, **1974**.

Received January 8, 2004
Early View Article
Published Online May 5, 2004

 © 2004 Wiley-VCH Verlag GmbH & Co. KGaA, Weinheim

Can the *cyclo*-P_5 Ligand Introduce Basicity at the Transition Metal Center in Metallocenes? A Hybrid Density Functional Study on the *cyclo*-P_5 Analogues of Metallocenes of Fe, Ru and Os

E. J. Padma Malar[a]

Keywords: Basicity / Density functional calculations / Electronic structure / Metallocenes / Natural charge / Transition metals

Density functional theory (DFT) calculations and natural population analysis (NPA) performed on metallocenes of Fe, Ru and Os triad reveal that the *cyclo*-P_5 ligand introduces basicity at the metal center. All-electron calculations at the B3LYP/6-311+G* level yield NPA charges of 0.28, –0.28 and –0.91 at the iron center in [$FeCp_2$], [$FeCp(\eta^5\text{-}P_5)$] and [$Fe(\eta^5\text{-}P_5)_2$], respectively. The same trend in the charges is observed even when the core electrons of the metal are replaced by effective core potentials (ECPs). The accumulation of negative charge at the metal center is found to be similar in the *cyclo*-P_5 analogues of ruthenocene and osmocene. Thus, for example, the net NPA charges on Ru and Os in the decaphosphametallocenes are predicted to be –0.6 to –0.9, respectively, at different levels of calculations involving ECPs. The natural orbital populations show a small transfer of electron density from each phosphorus atom to the metal center, leading to a significant build-up of negative charge on the metal in [$M(\eta^5\text{-}P_5)_2$]; this is a new feature observed in the transition metals bound to *cyclo*-P_5 ring. This finding is indeed supported by the indirect evidence observed by Scherer and coworkers from the diamagnetic behavior in an iridium derivative of $Fe(P_5)$, that the Fe atom is negatively charged while one of the P atoms is positively charged. Natural bond orbital analysis reveals that the extent of covalent bond formation between the metal and the ligand is more pronounced for the *cyclo*-P_5 than the cyclopentadienyl ligand. While Cp retains 56–68% of aromaticity, the P_5 ring exhibits 26–51% aromaticity as compared to the free anionic rings.
(© Wiley-VCH Verlag GmbH & Co. KGaA, 69451 Weinheim, Germany, 2004)

Introduction

Cyclopentadienyl, C_5H_5 (Cp), is a very common and versatile ligand in the field of organometallic chemistry.[1–4] The inorganic ring *cyclo*-P_5, also known as pentaphospholyl or pentaphosphacyclopentadienyl, is π isoelectronic with Cp and is known to form complexes with several transition metals.[5–7] The first carbon-free entirely inorganic sandwich complex $[Ti(\eta^5\text{-}P_5)_2]^{2-}$ was synthesized and characterized in 2002 by Urnezius et al.[8] The crystal-structure analyses of mixed metallocenes $[M(\eta^5\text{-}C_5Me_4R)(\eta^5\text{-}P_5)]$ (M = Fe, Ru; R = Me, Et) and $[Ti(\eta^5\text{-}P_5)_2]^{2-}$ show a sandwich structure with two parallel η^5- or π-bonded rings.[6a,6b,8] Besides the pentaphospolyl ligand, inorganic rings of the type E_n (E = As, P; $n = 3-6$) are also known to form complexes with transition metals.[7] Numerous transition metal complexes have been studied with heterocyclic ligands of the type $P_n(CH)_{5-n}$ ($n = 1-4$).[9–11] Phosphorus heterocycles are also known to form sandwich complexes with some lanthanides.[10] The similarity between *cyclo*-P_5 and the Cp ligands towards complex formation is a manifestation of the "diagonal relationship" of the elements carbon and phosphorus in the Periodic Table; they have similar electronegativity values.[7,11] In recent years the role of planar aromatic heterocycles possessing novel structural and bonding features in catalysis has been recognised.[12]

Although experimental studies illustrate the potential of the P_5 ring as a ligand and can lead to a wealth of interesting complexes, there is still not much known about the structure and bonding in complexes containing a P_5 ring. Semiempirical and ab initio molecular orbital studies show that *cyclo*-P_5^- is aromatic in nature.[13–15] Early investigations[16] on bonding and stabilities in the pentaphospholyl complexes of iron were based on the extended Hückel theory. A number of studies document the importance of electron-correlation methods in obtaining reliable predictions in transition metal compounds.[17–19] Recent studies show that density functional theory (DFT)[20] calculations are remarkably successful in predicting a variety of properties to an accuracy which rivals that of more expensive correlated ab initio methods. Several recent works reveal that the DFT method provides reliable results in the case of transition metal and lanthanide complexes.[21] DFT analysis

[a] Department of Physical Chemistry, University of Madras, Guindy Campus,
Chennai-600025, India
E-mail: ejpmalar@vsnl.net
Supporting information for this article is available on the WWW under http://www.eurjic.org or from the author.

of the electronic structure and bonding in some azaferrocenes and phosphaferrocenes by Frison et al.[22] has revealed the role of the heteroatom electronegativity as well as the shape of the lone pair in bonding. Frunzke et al.[23] have shown that in the ferrocene analogues $[Fe(\eta^5\text{-}E_5)_2]$ (E = N, P, As, Sb), bis(pentaphospholyl)ferrocene $[Fe(\eta^5\text{-}P_5)_2]$ exhibits the strongest bonding. A DFT study of Lein et al.[24] has shown that the metal−ligand bonding in $[Ti(\eta^5\text{-}E_5)_2]^{2-}$ (E = N, P, As, Sb) is more covalent than electrostatic. In addition to the complexes containing phosphorus rings, those of the analogous aza-rings have also received attention in recent years.[25] The recent DFT study of Malar[26] reveals novel structural and bonding features in the metallocenes of lithium and beryllium containing the *cyclo*-P_5 ligand. In the lowest energy structure, *cyclo*-P_5 exhibits η^1-coordination with the metal center and is perpendicular to the second ligand, which is η^5-coordinated. The absence of a metal−dπ interaction with the ligand results in a tilting of the *cyclo*-P_5 ring such that it becomes perpendicular to the second ligand. The above study shows that the *cyclo*-P_5 ligand behaves as a better donor than Cp and results in a lowering of the net charges on the lithium and beryllium centers.[26] It is of interest to know the influence of *cyclo*-P_5 on the electronic population of the metal centers in the title compounds.

The present study is aimed at getting detailed information on the molecular and electronic structures and the nature of the bonding in metallocenes of Fe, Ru and Os containing the *cyclo*-P_5 ligand. Both the mono- and bis-(*cyclo*-P_5) analogues of ferrocene, ruthenocene and osmocene are examined by hybrid DFT calculations. The electronic structures, properties and stabilities of these compounds are compared with those of the carbocyclic metallocenes Cp_2M, which are well characterized experimentally and theoretically.

Results and Discussion

Energetics

The relative stabilities of the complexes with reference to their ionic components are shown in Table 1. The binding energies ΔE are calculated with reference to the metal dication and the two anionic Cp/P_5 rings using the equation $\Delta E = E(LML') - E(L^-) - E(L'^-) - E(M^{2+})$. The heterolytic dissociation energy in the metallocene is given by $-\Delta E$.

The heterolytic dissociation energy of 615 kcal/mol predicted for the eclipsed geometry of ferrocene, based on the present B3LYP/6-311+G* analysis, agrees very closely with the observed value of 635 ± 15 kcal/mol.[27] Table 1 shows that the binding energies of ferrocene and its *cyclo*-P_5 analogues predicted by Type-II and -III basis sets are close to those of the all-electron 6-311+G* results. Type-I calculations deviate significantly from the B3LYP/6-311+G* values, though the trends in the stabilities are similar. Examination of the present results show that the predictions based on B3LYP/Type-III calculations, which use triple-split valence basis on the metal, agree better with those of the all-electron calculations at the B3LYP/6-311+G* level for ferrocene and its analogues. Although the all-electron calculations are more accurate, in systems with Ru or Os centers that require the use of ECPs, B3LYP/Type-III results are expected to be reliable. The dissociation energies predicted in this work by B3LYP/Type-I, B3LYP/Type-II, B3LYP/Type-III, and B3LYP/6-311+G* for ferrocene (608−638 kcal/mol) show better agreement with the experimental results than the value of 663 kcal/mol reported using the B_PW91 method of density functional theory.[21d] Our study shows that in a series of analogous metallocenes, the heterolytic dissociation energy increases in the order ferrocene < ruthenocene < osmocene; thus osmocenes are pre-

Table 1. Binding energies (kcal/mol) of the metallocenes at the eclipsed and staggered geometries; relative energies are given in parentheses

System	Point group	B3LYP/Type-I	B3LYP/Type-II	B3LYP/Type-III	B3LYP/6-311+G*
$FeCp_2$	D_{5h}	−638.11 (0.0)	−608.23 (0.0)	−606.93 (0.0)	−615.04 (0.0)
	D_{5d}	−637.56 (0.55)	−607.81 (0.42)	−606.47 (0.46)	−614.58 (0.46)
$FeCpP_5$	C_{5v}(e)	−581.55 (0.0)	−574.23 (0.0)	−574.95 (0.0)	−583.60 (0.0)
	C_{5v}(s)	−580.84 (0.71)	−573.48 (0.75)	−574.35 (0.60)	−582.80 (0.80)
$Fe(P_5)_2$	D_{5h}	−507.12 (0.0)	−519.94 (0.0)	−521.99 (0.0)	−530.71 (0.0)
	D_{5d}	−506.14 (0.98)	−519.18 (0.76)	−521.34 (0.73)	−529.79 (0.92)
$RuCp_2$	D_{5h}	−681.25 (0.0)	−650.88 (0.0)	−655.29 (0.0)	
	D_{5d}	−680.91 (0.34)	−650.62 (0.26)	−654.89 (0.40)	
$RuCpP_5$	C_{5v}(e)	−639.29 (0.0)	−629.60 (0.0)	−636.94 (0.0)	
	C_{5v}(s)	−638.65 (0.64)	−629.00 (0.60)	−636.32 (0.62)	
$Ru(P_5)_2$	D_{5h}	−578.34 (0.0)	−591.22 (0.0)	−600.32 (0.0)	
	D_{5d}	−577.28 (1.06)	−590.24 (0.98)	−599.47 (0.85)	
$OsCp_2$	D_{5h}	−728.61 (0.0)	−699.27 (0.0)	−701.30 (0.0)	
	D_{5d}	−727.94 (0.67)	−698.72 (0.55)	−700.75 (0.55)	
$OsCpP_5$	C_{5v}(e)	−692.59 (0.0)	−683.61 (0.0)	−690.64 (0.0)	
	C_{5v}(s)	−691.65 (0.94)	−682.71 (0.90)	−689.80 (0.84)	
$Os(P_5)_2$	D_{5h}	−635.55 (0.0)	−648.07 (0.0)	−659.74 (0.0)	
	D_{5d}	−633.95 (1.60)	−646.56 (0.51)	−658.07 (1.67)	

 © 2004 Wiley-VCH Verlag GmbH & Co. KGaA, Weinheim

dicted to be more stable than the corresponding ferrocenes and ruthenocenes. This is in agreement with the earlier observation of Mayor-López et al[21d] that ruthenocene has a higher heterolytic dissociation energy than ferrocene. The present work shows that the stability of the *cyclo*-P_5 analogues of the metallocenes follows the order: MCp_2 > $MCpP_5$ > $M(P_5)_2$. In the pentaphosphaferrocene [$FeCp(\eta^5$-$P_5)$], the magnitude of the binding energy is 31−35 kcal/mol lower than in ferrocene when Type-II, Type-III, and 6-311+G* basis sets are used. However there is a more pronounced lowering of stability in the carbon-free metallocene [$Fe(\eta^5$-$P_5)_2$], by about 53 kcal/mol relative to the pentaphospha analogue. A similar but less marked lowering in the stabilities of the *cyclo*-P_5 analogues of ruthenocene and osmocene is evident from Table 1. The heterolytic dissociation energies of [$M(\eta^5$-$P_5)_2$] (M = Fe, Ru and Os) are lower than the corresponding values for MCp_2 by 85, 55, and 41 kcal/mol, respectively, according to Type-III calculations. A similar trend in the relative stabilities is also observed in penta- and decaphospha analogues of beryllocene using B3LYP/6-31G*, B3LYP/6-31+G*//B3LYP/6-31G*, B3LYP/6-311+G**//B3LYP/6-31G* and B3LYP/LANL2DZ calculations.[26] The prediction based on the present B3LYP/6-311+G* analysis, that [$Fe(\eta^5$-$P_5)_2$] is about 84 kcal/mol less stable than ferrocene towards heterolytic cleavage, contradicts the conclusion of Frunzke et al.[23] that the former is as stable as ferrocene.

The bonding in metallocenes is generally explained on the basis of interaction between the occupied π-orbitals of the ligands and the vacant d_{xz} and d_{yz} orbitals of the metal, which leads to stabilization of the bonding e_1'' orbitals and destabilization of the antibonding $(e_1'')^*$ orbitals. The earlier study of Mayor-López et al.[21d] on the electronic structures of ferrocene and ruthenocene showed that the HOMO−LUMO gap is about 0.8 eV larger for the latter than for the former. This led the authors to conclude that metal-ligand covalency, and hence the binding energy, is greater in ruthenocene than in ferrocene. Figure 1 depicts the energetics of the highest occupied and lowest vacant MOs generated by the B3LYP/6-311+G* method in the eclipsed structure of ferrocene analogues. The HOMO−LUMO energy gap follows the order $FeCp_2$ (5.09) > $FeCp(P_5)$ (4.35) > $Fe(P_5)_2$ (3.12). The lower HOMO−LUMO gap in the phospha analogues indicates that the interaction between the ligand π-orbitals and the vacant metal orbitals is smaller and it may account for their lower binding energies. The trends in the MO energies in ferrocene and its *cyclo*-P_5 analogues appear to be very similar to those of the beryllocenes with eclipsed structures.[26] The HOMO−LUMO energy gap in the beryllocenes is $BeCp_2$ (6.53) > $BeCp(P_5)$ (3.83) > $Be(P_5)_2$ (2.99) by the B3LYP/6-31G* method.[26] The resemblance in the MO energetics in the two different classes of metallocenes with sandwich structures reveals that the nature of the orbital interactions is quite similar irrespective of the type of the metal center. It is apparent that the ligand donor π-orbitals play a major role in the stabilization of the bonding and the destabilization of the antibonding MOs in these metallocenes.

The relative energies shown in parentheses in Table 1 reveal that the eclipsed sandwich arrangement is more stable than the staggered geometry by 0.3−1.7 kcal/mol. The small energy difference between the eclipsed and staggered arrangements is in agreement with the ^{13}C NMR study of ferrocene at cryogenic temperatures, which shows that ferrocene is freely rotating about its fivefold symmetry axis above 45−50 K.[21b] An eclipsed structure for ferrocene and ruthenocene was confirmed by an electron-diffraction study[28] and a crystal-structure analysis.[29] Negligibly small energy difference between the staggered and eclipsed geometries have been reported in different DFT studies of carbocyclic metallocenes MCp_2 [21b−21g] and in aza- and phosphaferrocenes.[22,23] Analysis of the vibrational frequencies in the present work reveals that all values are real

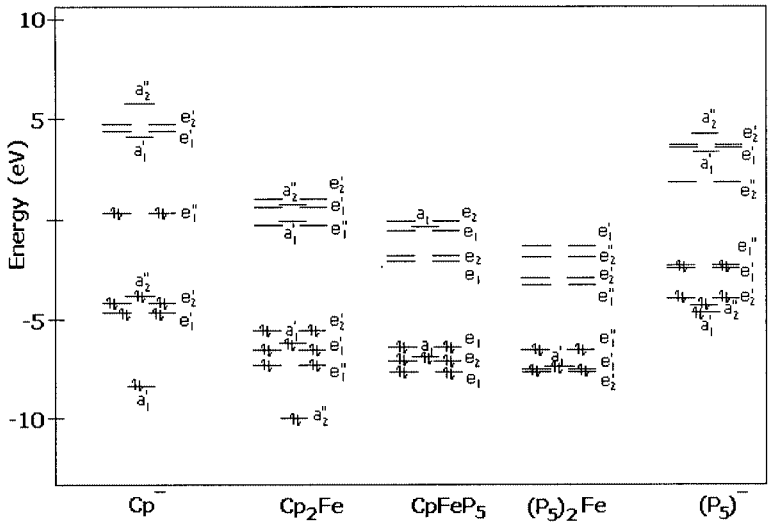

Figure 1. B3LYP/6-311+G* energy level diagram showing the highest occupied and lowest vacant molecular orbitals of the anionic ligands (D_{5h} point group) and their ferrocene analogues in their eclipsed sandwich geometries

 © 2004 Wiley-VCH Verlag GmbH & Co. KGaA, Weinheim

in the eclipsed structure and it is thus a minimum in the potential energy surface. However, the staggered sandwich structure exhibits one imaginary vibrational frequency in the range 20−50 i cm^{-1}, which indicates that the staggered arrangement is not a potential minimum and is likely to be the rotational transition state. In a recent study using different DFT methods, Schaefer and co-workers[21g] found that the eclipsed sandwich structure is the global minimum in the metallocenes of the first transition metal series. These authors have reported that the staggered structure of ferrocene is 0.75−1.13 kcal/mol higher in energy than the eclipsed geometry and is in agreement with the present results.

Geometries of Ferrocene, Ruthenocene and Osmocene and their *cyclo*-P_5 Analogues

Table 2−4 display selected geometrical parameters in the optimized eclipsed sandwich structures. It is found that the structural parameters of the ligands and the metal−ligand separations are nearly identical in both the eclipsed sandwich and the staggered sandwich arrangements. In a given system, the calculations at the different levels yield structures that vary only marginally. The predicted values are found to be closer to experimental results in Type-III calculations when ECPs are used. The computed ring bond lengths for the C−C and P−P bonds in the metallocenes are in the ranges 1.43−1.44 and 2.14−2.16 Å, respectively, and agree satisfactorily with the available experimental and the reported DFT studies.[21b−21d,21g,22−24] Although the C−C and P−P bonds in these complexes are characteristic of aromatic bonds, the present results show that the ligand rings expand along the series Fe, Ru, and Os. Thus the C−C and P−P lengths are the longest in osmium metallocenes. The present P−P bond lengths are very similar to the observed mean value of 2.154(9) Å[8] in the decaphosphatitanium complex $[Ti(\eta^5\text{-}P_5)_2]^{2-}$.

The distance between the metal and the center of the Cp ring (d_C; Table 2) in ferrocene is predicted to be 1.686−1.687 Å and it is 0.026 Å longer than the experimental value of 1.66 Å reported by Haaland.[28] In ruthenocene, there is an elongation of about 0.18 Å in the metal−ring distance as compared to that in ferrocene; this value is similar to the experimental increase of about 0.16 Å. However, the calculations predict that the d_C values are quite similar in $RuCp_2$ and $OsCp_2$. Similar trends in d_C are also maintained in the pentaphosphametallocenes. The longer separation between the metal and Cp ligands in ruthenium and osmium metallocenes leads to an increase of about 0.15 Å in Ru−C and Os−C bond lengths as compared to those of the Fe−C bonds.

The distance between the metal and the center of the P_5 ring, d_P, is shorter than the M−Cp(centre) in pentaphosphametallocenes. The experimental d_P values in the alkyl derivatives of pentaphosphametallocenes are 1.55, 1.65 and 1.66 Å for M = Fe, Ru and Os, respectively.[6a,6b] These values are about 0.20 Å shorter than the corresponding d_C values. The d_P values predicted by B3LYP are 1.597, 1.716 and 1.711 Å in $MCpP_5$ (M = Fe, Ru, Os) by Type-III calculations. The metal−Cp separations are longer than d_P and the values are 1.712, 1.888, and 1.897 Å, respectively. The distances between the metal and P_5 center in decaphosphametallocenes are 1.693, 1.788 and 1.788 Å for Fe, Ru

Table 2. B3LYP optimized geometries and bond orders (in parentheses) in metallocenes MCp_2 with eclipsed sandwich geometries

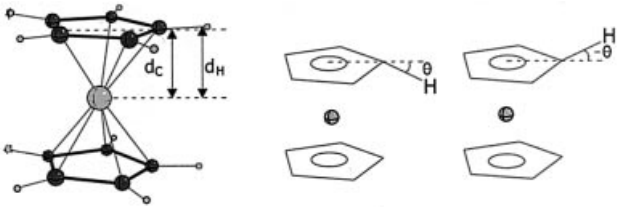

System	Parameter	Type I	Type II	Type III	6-311+G*	Expt.
$FeCp_2$	C−C	1.428 (1.289)	1.427 (1.289)	1.426 (1.285)	1.426 (1.286)	1.440[a]
	Fe−C	2.079(0.285)	2.078 (0.286)	2.078 (0.292)	2.077 (0.295)	2.064[a]
	d_C	1.687	1.687	1.687	1.686	1.660[a]
	d_H	1.660	1.661	1.662	1.664	
	θ	1.8	1.7	1.6	1.4	3.7±0.9[a]
$RuCp_2$	C−C	1.431 (1.278)	1.429 (1.278)	1.430 (1.275)		1.430[b]
	Ru−C	2.233 (0.300)	2.231 (0.302)	2.226 (0.314)		2.186[b]
	d_C	1.872	1.871	1.864		1.816[b]
	d_H	1.882	1.883	1.875		
	θ	−0.7	−0.8	−0.7		
$OsCp_2$	C−C	1.436 (1.255)	1.434 (1.255)	1.434 (1.249)		
	Os−C	2.224 (0.340)	2.220 (0.343)	2.221 (0.352)		
	d_C	1.858	1.855	1.856		
	d_H	1.870	1.872	1.870		
	θ	−0.8	−1.1	−0.8		

[a] Refs.[28a,28b] [b] Ref.[30]

 © 2004 Wiley-VCH Verlag GmbH & Co. KGaA, Weinheim

Table 3. B3LYP optimized geometries and bond orders (in parentheses) in the eclipsed sandwich metallocenes $MCpP_5$

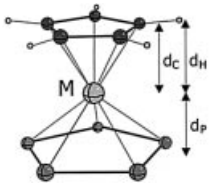

System	Parameter	Type I	Type II	Type III	6-311+G*	Expt.
$FeCpP_5$	C−C	1.427 (1.282)	1.424 (1.284)	1.423 (1.280)	1.423 (1.282)	1.42[a]
	P−P	2.148 (1.227)	2.144 (1.213)	2.143 (1.202)	2.142 (1.207)	2.10,[a] 2.12[b]
	Fe−C	2.093 (0.290)	2.095 (0.288)	2.097 (0.286)	2.097 (0.290)	2.09[a]
	Fe−P	2.444 (0.365)	2.429 (0.381)	2.423 (0.386)	2.419 (0.387)	2.35[a]
	d_C	1.705	1.709	1.712	1.713	1.71,[a] 1.75[b]
	d_P	1.624	1.604	1.597	1.592	1.53,[a] 1.55[b]
	d_H	1.666	1.686	1.679	1.685	
	θ	2.6	1.5	2.2	1.8	
$RuCpP_5$	C−C	1.431 (1.283)	1.428 (1.284)	1.428 (1.280)		1.42[c]
	P−P	2.160 (1.203)	2.160 (1.193)	2.159 (1.180)		2.10[c]
	Ru−C	2.247 (0.263)	2.248 (0.264)	2.245 (0.279)		2.21[c]
	Ru−P	2.528 (0.397)	2.520 (0.408)	2.513 (0.426)		2.43[c]
	d_C	1.888	1.892	1.888		1.85[c]
	d_P	1.737	1.725	1.716		1.65[c]
	d_H	1.881	1.897	1.886		
	θ	0.5	−0.3	−0.1		
$OsCpP_5$	C−C	1.434 (1.272)	1.431 (1.272)	1.431 (1.270)		1.42[d]
	P−P	2.167 (1.161)	2.167 (1.152)	2.162 (1.143)		2.11[d]
	Os−C	2.251 (0.279)	2.248 (0.283)	2.254 (0.291)		2.22[d]
	Os−P	2.522 (0.467)	2.518 (0.474)	2.512 (0.499)		2.44[d]
	d_C	1.890	1.890	1.897		1.86[d]
	d_P	1.722	1.715	1.711		1.66[d]
	d_H	1.892	1.902	1.899		
	θ	−0.1	−0.7	−0.1		

[a] Experimental values for [Fe(η^5-C_5Me_4Et)(η^5-P_5)]. [b] Experimental values for [Fe(η^5-C_5Me_5)(η^5-P_5)].[6a,7b] [c] Experimental values for [Ru(η^5-C_5Me_4Et)(η^5-P_5)].[6a,7b] [d] Experimental values for [Os(η^5-C_5Me_4Et)(η^5-P_5)].[6l]

Table 4. B3LYP optimized geometries and bond orders (in parentheses) in eclipsed metallocenes $M(P_5)_2$

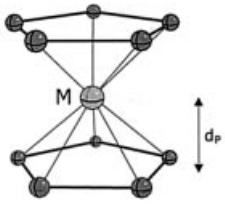

System	Parameter	Type I	Type II	Type III	6-311+G*
$Fe(P_5)_2$	P−P	2.141 (1.229)	2.139 (1.218)	2.137 (1.210)	2.136 (1.211)
	Fe−P	2.488 (0.352)	2.487 (0.369)	2.484 (0.341)	2.481 (0.342)
	d_P	1.694	1.695	1.693	1.689
$Ru(P_5)_2$	P−P	2.157 (1.215)	2.156 (1.207)	2.154 (1.194)	
	Ru−P	2.571 (0.332)	2.566 (0.341)	2.561 (0.346)	
	d_P	1.800	1.795	1.788	
$Os(P_5)_2$	P−P	2.162 (1.181)	2.161 (1.175)	2.158 (1.170)	
	Os−P	2.570 (0.377)	2.569 (0.382)	2.562 (0.408)	
	d_P	1.796	1.795	1.788	

and Os, respectively, according to B3LYP/Type-III calculations. These values are longer than those in the pentaphosphametallocenes by 0.07−0.10 Å. The d_P values in the decaphospa analogues of Ru and Os closely resemble the value of 1.797 Å observed in $[Ti(\eta^5\text{-}P_5)_2]^{2-}$.[8]

The theoretical lengths for d_C, d_P, metal−carbon, and metal−phosphorus deviate from the experimental values by about 0.05 Å. The Ru−P distance in $RuCpP_5$ exhibits a maximum deviation of about 0.08 Å. The experimental data shown in Table 3 are from the crystal structure of the alkyl

 © 2004 Wiley-VCH Verlag GmbH & Co. KGaA, Weinheim

derivatives of $MCpP_5$ that exhibit staggered geometries, and thus a comparison with these values may not be appropriate.

Even though the B3LYP geometries deviate from the experimental results, they nevertheless reveal the right trend regarding the changes in lengths among the homologues. The results obtained are helpful to understand the nature of bonding in these metallocenes.

The complete structural analysis shows that the hydrogen atoms in the Cp ring move away from the plane of the carbon atoms, in agreement with different experimental and theoretical observations in metallocenes of main group elements and transition metals.[31] The bend angle, θ, given in Table 2 and 3 reveals that the hydrogens of the Cp ring are bent away from the metal (θ negative) except in ferrocene and pentaphosphaferrocene. In these two systems, the hydrogens are bent towards Fe by about 1.5°, which results in a lowering of the d_H distance by about 0.02−0.03 Å (Table 2 and 3). Experimental studies show that the hydrogen atoms are bent out of the Cp plane towards the metal center in metallocenes such as $FeCp_2$, $CrCp_2$ and $NiCp_2$ by 3.0−6.5°.[28,31b−31h] The present study predicts the right direction of bending of the hydrogens in ferrocene and the magnitude of the bend angle is also close to the value of 1.6(0.4)° reported in a neutron diffraction study.[32] The hydrogens in ruthenocene and osmocene and their pentaphospha analogues bend away from the metal center and the bend angle is smaller in magnitude (<1°).

Nature of the Bonding in the Complexes

The force constant of the Cp−M stretching vibration is considered to be one of the most important parameters to assign the character of the Cp−M bonding.[18h] NMR and Mossbauer spectroscopic studies of ferrocene and related complexes have shown the covalent nature of the Fe-ligand bonding, originating essentially from the π-contribution of the ligands.[33−35]

The covalent bond orders for the C−C bonds in the different MCp_2 and $MCpP_5$ complexes under study are in the range 1.25 −1.29 (Table 2 and 3). Comparison of these values with the B3LYP/6-31G* and B3LYP/6-311+G* C−C bond orders of 1.406 and 1.405 in the free cyclopentadienyl anion shows that the covalent bonding is reduced in the Cp unit of the complexes studied. The calculations reveal that the build-up of covalent bonding between the metal and the ligand carbons, with M−C bond orders in the range 0.25−0.35, is at the expense of bonding within the ligand. The highest M−C bond order of 0.34−0.35 is observed in osmocene, which has the lowest C−C bond order of 1.25−1.26. The B3LYP/Type-III predicted M−C bond orders of 0.29, 0.31, and 0.35 in ferrocene, ruthenocene and osmocene, respectively, reflect that the metal−ligand covalency increases in the Fe triad, as predicted by Mayor-López et al.[21d]

The M−P bond indices in the metallocenes of *cyclo*-P_5 are in the range 0.37−0.50 (Table 3 and 4). The ligated P_5 rings have P−P bond orders of 1.14−1.23, which are significantly lower than the value in the *cyclo*-P_5 anion (1.409 and 1.406 at B3LYP/6-31G* and B3LYP/6-311+G* levels, respectively). The bond orders for the M−P bonds in $MCpP_5$ are more pronounced than those of the M−C bonds. This is reflected in the shorter separation between the metal and P_5 ring as compared to that of M−Cp(centre), in agreement with the observed distances. The present analysis also reveals that the metal−P_5 covalent bonding increases along the iron triad.

Natural Population and Net Atomic Charges

The natural population of the valence orbitals of the metal and the ligand atoms and their net NPA charges obtained from the NBO analysis are shown in Table 5. It can be seen that the total population on the transition metal on the metallocene $(Cp)_2M$ is less than the free-atom value of eight electrons and that the metal center exhibits a small positive charge of 0.16−0.28 at the different levels of calculations, in agreement with earlier observations.[23] However, the metal d-population increases in the order $MCp_2 < MCpP_5 < M(P_5)_2$. The ns and np valence orbital populations of the metal also increase in the above order, although the contribution of the np orbital is very small. According to B3LYP/Type-III calculations on the decaphosphametallocenes, 0.42, 0.41 and 0.50 electrons populate the ns orbitals in Fe, Ru and Os, respectively. The population of the metal d-orbitals exceeds eight electrons on the Fe and Ru centers and the total valence populations are 8.92, 8.88 and 8.56 for Fe, Ru, and Os, respectively. Thus, the population analysis reveals a significant accumulation of negative charges of −0.92, −0.88 and −0.56 on Fe, Ru and Os, respectively, in the decaphosphametallocenes. In these complexes, the 3s populations of phosphorus are 1.67, 1.68 and 1.69, while the corresponding 3p populations are 3.23, 3.23 and 3.25, respectively. Thus it is seen that the total valence orbital populations of the phosphorus atoms in the above complexes are lower than the free-atom value of five electrons, which indicates a small transfer of electron density from each phosphorus to the metal center. This leads to positive charges of 0.09, 0.09, and 0.06 on the phosphorus atoms of bis(*cyclo*-P_5) metallocenes of Fe, Ru and Os, respectively. Consequently the novel situation arises in which the metal attains significant negative charge (Fe: −0.92; Ru: −0.88; Os: −0.56). The present work establishes the fact that the *cyclo*-P_5 ligand is responsible for accumulation of excess electron density on the transition metal center by a small transfer of electron density from each P atom. This is also observed at B3LYP/Type-I and B3LYP/Type-II levels and even when ECPs are used for phosphorus atoms at the B3LYP/LANL2DZ level. The more reliable B3LYP/6-311+G* study on ferrocenes corroborates this finding. A small negative charge of −0.05 on Fe in both mono- and bis(*cyclo*-P_5) ferrocenes has been reported by Frunzke et al.[23] Our recent work on the phosphorus analogues of lithocene anion and beryllocene also supports the fact that the P_5 ring transfers significant electron density to the metal center.[26] In these cases the metal center becomes less positive when the Cp ligand in the carbocyclic metallocene is replaced by *cyclo*-P_5 ligand. The present calculations

 © 2004 Wiley-VCH Verlag GmbH & Co. KGaA, Weinheim

Table 5. Natural population of valence orbitals of the ligand and metal atoms and their natural charges for the eclipsed sandwich metallocenes by the B3LYP method

System[a]	Element	Natural population Ns	np	$(n-1)d$	Net NPA charge
$FeCp_2$	C	0.96	3.29		−0.25
		0.96	*3.29*		*−0.24*
		0.97	**3.27**		**−0.25**
	Fe	0.17	0.02	7.53	0.28
		0.19	*0.02*	*7.61*	*0.18*
		0.17	**0.01**	**7.61**	0.21
$FeCpP_5$	C	0.97	3.24		−0.22
		0.97	*3.23*		*−0.21*
		0.97	**3.24**		**−0.22**
	P	1.66	3.30		0.03
		1.67	*3.27*		*0.05*
		1.69	**3.31**		**−0.00**
	Fe	0.31	0.06	7.92	−0.28
		0.34	*0.06*	*8.00*	*−0.40*
		0.30	**0.04**	**7.78**	**−0.11**
$Fe(P_5)_2$	P	1.66	3.25		0.09
		1.67	*3.23*		*0.09*
		1.69	**3.26**		**0.04**
	Fe	0.41	0.13	8.39	−0.91
		0.42	*0.12*	*8.39*	*−0.92*
		0.37	**0.11**	**7.87**	**−0.36**
$RuCp_2$	C	*0.97*	*3.28*		*−0.25*
		0.97	**3.27**		**−0.25**
	Ru	*0.21*	*0.01*	*7.54*	*0.25*
		0.18	**0.01**	**7.65**	**0.16**
$RuCpP_5$	C	*0.98*	*3.25*		*−0.24*
		0.98	**3.23**		**−0.22**
	P	*1.69*	*3.29*		*0.01*
		1.68	**3.29**		**0.03**
	Ru	*0.42*	*0.06*	*7.58*	*−0.08*
		0.26	**0.04**	**7.96**	**−0.27**
$Ru(P_5)_2$	P	*1.68*	*3.23*		*0.09*
		1.69	**3.23**		**0.08**
	Ru	*0.41*	*0.10*	*8.37*	*−0.88*
		0.38	**0.08**	**8.32**	**−0.77**
$OsCp_2$	C	*0.97*	*3.29*		*−0.26*
		0.97	**3.29**		**−0.26**
	Os	*0.33*	*0.02*	*7.36*	*0.27*
		0.30	**0.01**	**7.43**	**0.26**
$OsCpP_5$	C	*0.98*	*3.25*		*−0.24*
		0.98	**3.25**		**−0.24**
	P	*1.69*	*3.29*		*0.01*
		1.68	**3.28**		**0.03**
	Os	*0.42*	*0.06*	*7.58*	*−0.08*
		0.38	**0.05**	**7.76**	**−0.19**
$Os(P_5)_2$	P	*1.69*	*3.25*		*0.06*
		1.69	**3.22**		**0.08**
	Os	*0.50*	*0.13*	*7.92*	*−0.56*
		0.51	**0.11**	**8.15**	**−0.76**

[a] Numbers in normal typeface correspond to the 6-311+G* basis set; bold values and those in italics correspond to Type-II and Type-III calculations, respectively.

on the mono(*cyclo*-P_5) metallocenes of Fe, Ru and Os also show that the phosphorus atoms exhibit a small positive charge and the metal center attains a negative charge, although it is less pronounced. Thus the B3LYP/Type-III calculations on $CpMP_5$ yield net charges of −0.40, −0.08 and −0.08 on Fe, Ru and Os, respectively. This finding corroborates the experimental observation of diamagnetic behavior in an iridium derivative of $Fe(P_5)$, which led Scherer and co-workers to conclude that the Fe atom is negatively charged while one of the P atoms is positively charged.[7g] The observation that the metal center is electron rich and the P_5 ring is electron deficient in $M(P_5)_2$ may have an impact in catalysis, since the heterocyclic complexes are increasingly used as catalysts.[12]

Aromaticity in the Ligand Species

There has been a recent surge of interest in the aromaticity of heterocycles containing phosphorus with different coordination numbers.[36] The *cyclo*-P_5 anion contains six π-electrons in the ring and is classified as aromatic, similar to the Cp anion, based on its UV spectrum[5b] and according to geometric, energetic and magnetic criteria of aromaticity.[13−15] However, the change in the degree of aromaticity in the Cp and P_5 ligands in metal complexes has not been explored so far. Knowledge of the degree of aromaticity in the ligand moieties in the complexes will aid in the understanding of the bonding in the metallocenes. The ring expansion and the consequent weakening of ring bonds in the Cp and *cyclo*-P_5 ligands in the different complexes under study shows that the aromaticity of the ligand moieties is lower than in the free anions of Cp and P_5, respectively. We have estimated the relative aromaticity RI_x of the Cp and P_5 rings in the complexes with reference to the free Cp and P_5 anions, respectively, using the relationship

$$RI_x = \frac{I_x\,(\text{complex}) - I_{\text{ethane}}}{I_x\,(\text{anion}) - I_{\text{ethane}}}$$

where x denotes the Cp or P_5 ring and I_x denotes the aromaticity index. Although different geometric, energetic and magnetic criteria are widely used to quantify aromaticity in cyclic systems,[37−41] in the present analysis the aromaticity index is taken as the lowest ring bond-order, in accordance with the ring-current definition of Jug.[37a] I_{ethane} is the C−C bond order in the archetypal nonaromatic compound ethane. The bond orders obtained from the NBO analysis were used in the comparison. Since bond orders are less sensitive to the basis sets than the bond lengths (Table 2−4), meaningful estimates of relative aromaticity can be obtained from this analysis. Table 6 lists the relative aromaticity in the ligands obtained using bond orders at the same level of the theory. These results indicate that the Cp ring retains 56−68% of aromaticity in the complexes MCp_2 and $MCpP_5$ (M = Fe, Ru, Os), and that the aromaticity of the Cp ligand is highest when the central metal is Fe and lowest when it is Os. A similar trend exists in the relative aromaticity of the P_5 ring in the complexes $MCpP_5$ and $M(P_5)_2$ (M = Fe, Ru, Os) but the magnitude is considerably lower (26−51%).

In the metallocenes under study, the decrease of aromaticity is more pronounced in the P_5 ring than in the Cp

 © 2004 Wiley-VCH Verlag GmbH & Co. KGaA, Weinheim

Table 6. Relative aromaticitiy (in %) of Cp and P_5 ligands in the metallocenes of Fe, Ru and Os in an eclipsed sandwich (D_{5h}/C_{5v}) arrangement

[a]	Cp ligand				P_5 ligand			
	Type I	Type II	Type III	6-311+G*	Type I	Type II	Type III	6-311+G*
$FeCp_2$	67.9	67.2	66.1	66.4				
$FeCpP_5$	66.0	65.8	64.7	65.3	50.5	45.6	42.5	43.9
$Fe(P_5)_2$					51.1	47.0	44.8	45.1
$RuCp_2$	64.9	64.1	63.3					
$RuCpP_5$	66.3	65.8	64.7		44.0	40.0	36.3	
$Ru(P_5)_2$					47.3	43.9	40.3	
$OsCp_2$	58.6	57.6	55.9					
$OsCpP_5$	63.3	62.4	61.9		32.6	28.5	25.9	
$Os(P_5)_2$					38.0	34.9	33.5	

[a] C−C bond orders: B3LYP/6-31G*: Cp^- = 1.406; ethane = 1.041; B3LYP/6-311+G*: Cp^- = 1.405; ethane = 1.051. P−P bond orders in P_5 anion: B3LYP/6-31G*: 1.409; B3LYP/6-311+G*: 1.406.

ring. This situation is compensated by stronger metal−P_5 bond formation, as observed earlier. It is evident from the significant bond indexes for M−C and M−P bonds that considerable π-electron density of the ligand moiety is directed towards bonding with the central metal. Even though the ligands are weakened, the complex gains stability due to covalent bonding of the ligand atoms with the central atom.

Conclusions

The present study reveals that the metal attains a negative charge of about one unit in the decaphosphametallocenes [M(η^5-P_5)$_2$] (M = Fe, Ru and Os). The natural population analysis establishes the fact that the *cyclo*-P_5 ligand is responsible for an accumulation of excess electron density on the transition metal center by a small transfer of electron density from each P atom. The observation that the metal center is electron rich and the P_5 ring is electron deficient in $M(P_5)_2$ may have an impact in catalysis, since the heterocyclic complexes are increasingly being used as catalysts.

The B3LYP/6-311+G* bond-dissociation energy of 615 kcal/mol in ferrocene agrees very well with the experimental value of 635 ± 15 kcal/mol. The calculations reveal that the build-up of covalent bonding between the metal and the ligand is at the expense of bonding within the ligand. The present analysis also shows that both the M−Cp and M−P_5 covalent bonding increases along the iron triad.

Computational Aspects

All computations reported in this study were carried out using the Gaussian 03 suite of programs.[42] Hybrid Hartree−Fock−DFT calculations were performed with Becke's three parameter hybrid-exchange functional and the gradient-corrected nonlocal correlation functional of Lee, Yang and Parr (B3LYP).[43] We performed all-electron calculations on ferrocene and its *cyclo*-P_5 analogues [FeCp(η^5-P_5)] and [Fe(η^5-P_5)] with a triple-split valence basis set, which includes polarization and diffuse functions on the heavy atoms, at the B3LYP/6-311+G* level.[44] The calculations make use of the McLean−Chandler[44b,44c] (12s,9p) → (621111, 52111) basis set ("negative-ion" basis set) for phosphorus atoms. The Watchers−Hay all-electron basis set,[44d,44e] including the scaling factor of Raghavachary and Trucks,[44f] was used for the iron center. In the metallocenes of Ru and Os, the calculations invoked an electron core potential (ECP) approximation for the chemically inactive core electrons of the metal. Three different types of calculations were performed using the ECPs: in Type-I, the ligand atoms (H, C, and P) were treated with the split valence basis set including polarization at the 6-31G* level; in Type-II and Type-III, the 6-311+G* basis set was used for the ligand atoms. The core electrons of the metal were treated, in these three types of calculations, by the Los Alamos small-core potentials (LanL2)[45a] which incorporate some relativistic effects for post third-row atoms and are found to be the "best known" ECPs.[44a] In Type-I and Type-II, the metal valence electrons are treated by the double-zeta basis set of Hay and Wadt (LanL2DZ).[45a] The Type-III calculations invoke the Stevens−Basch−Krauss triple-split valence basis[45b−45d] for the valence electrons of the metal. Complete structural optimization was carried out for the eclipsed sandwich (D_{5h}/C_{5v}) and the staggered sandwich (D_{5d}/C_{5v}) geometries of the metallocenes.

Vibrational frequencies were calculated at the optimized geometries and the total energies were corrected for zero-point vibrational energy (ZPE). A scaling factor of 0.98 for ZPE, which is reported to be suitable for B3LYP/6-31G* calculations,[46] was used in the present work. The dications of the metals were calculated at their ^{5}D ground state. The total energies of the complexes E(LML′) and their ionic components E(L^-), E(L'^-) and E(M^{2+}) are included in the Supporting Information (Table S1).

The bonding in the metallocenes was examined by natural atomic orbital (NAO) and natural bond orbital (NBO) analyses using the NBO program incorporated in the Gaussian package.[47] Natural Population Analysis (NPA) performed in the NAO basis is well known to yield reliable estimates of atomic charges, in contrast to the Mulliken Population Analysis (MPA) charges, which are highly sensitive to the basis sets employed.[48] The extent of covalent bond formation between the metal and the ligand atoms was analyzed using bond orders[49] calculated in terms of natural atomic orbitals.

Acknowledgments

This work was initiated when the author was a SERC Visiting Fellow at the Indian Institute of Technology, Chennai, India. I thank

 © 2004 Wiley-VCH Verlag GmbH & Co. KGaA, Weinheim

Professor B. Vishwanathan, Indian Institute of Technology, Chennai, for his keen interest and support of this work. I am grateful to Professors K. Jug, Universität Hannover, Germany, and E. D. Jemmis, University of Hyderabad, India, for interesting discussions. I thank the University Grants Commission, New Delhi, India, and the Department of Science and Technology, New Delhi, India, for financial support.

[1] C. Elschenbroich, A. Salzer, *Organometallics − A Concise Introduction*, VCH Verlagsgesellschaft, Weinheim, Germany, **1989**.
[2] [2a] P. Jutzi, N. Burford, *Chem. Rev.* **1999**, *99*, 969. [2b] J. C. Green, *Chem. Soc. Rev.* **1998**, *27*, 263.
[3] A. Togni, L. Halterman, *Metallocenes: Synthesis, Reactivity, Applications*, Wiley-VCH, Weinheim, **1998**.
[4] N. J. Long, *Metallocenes*, Blackwell Science, Oxford, **1998**.
[5] [5a] M. Baudler, D. Düster, D. Ouzounis, *Z. Anorg. Allg. Chem.* **1987**, *544*, 87. [5b] M. Baudler, S. Akpapoglou, D. Ouzounis, F. Wasgestian, B. Meinigke, H. Budzikiewicz, H. Munster, *Angew. Chem.* **1988**, *100*, 288; *Angew. Chem. Int. Ed. Engl.* **1988**, *27*, 280. [5c] M. Baudler, D. Ouzounis, *Z. Naturforsch., Teil B* **1989**, *44*, 831. [5d] B. M. Gimarc, *Pure Appl. Chem.* **1990**, *62*, 423.
[6] [6a] O. J. Scherer, T. Brück, G. Wolmershäuser, *Chem. Ber.* **1988**, *121*, 935. [6b] B. Rink, O. J. Scherer, G. Wolmershäuser, *Chem. Ber.* **1995**, *128*, 71. [6c] M. Baudler, T. Etzbach, *Angew. Chem.* **1991**, *103*, 590; *Angew. Chem. Int. Ed. Engl.* **1991**, *30*, 580. [6d] B. Rink, O. J. Scherer, G. Heckmann, G. Wolmershäuser, *Chem. Ber.* **1992**, *125*, 1011. [6e] A. K. Hughes, V. J. Murphy, D. O'Hare, *J. Chem. Soc., Chem. Commun.* **1994**, 163. [6f] O. J. Scherer, G. Berg, G. Wolmershäuser, *Chem. Ber.* **1995**, *128*, 635. [6g] O. J. Scherer, T. Hilt, G. Wolmershäuser, *Organometallics* **1998**, *17*, 4110. [6h] O. J. Scherer, S. Wiegel, G. Wolmershäuser, *Chem. Eur. J.* **1998**, *4*, 1910. [6i] A. R. Kudinov, P. V. Petrovskii, M. I. Rybinskaya, *Russ. Chem. Bull.* **1999**, *48*, 1362. [6j] A. R. Kudinov, M. I. Rybinskaya, *Russ. Chem. Bull.* **1999**, *48*, 1615. [6k] A. R. Kudinov, D. A. Loginov, Z. A. Starikova, P. V. Petrovskii, M. Corsini, P. Zanello, *Eur. J. Inorg. Chem.* **2002**, 3018.
[7] [7a] O. J. Scherer, *Comments Inorg. Chem.* **1987**, *6*, 1. [7b] O. J. Scherer, *Angew. Chem.* **1990**, *102*, 1137; *Angew. Chem. Int. Ed. Engl.* **1990**, *29*, 1104. [7c] M. Baudler, K. Glinka, *Chem. Rev.* **1993**, *93*, 1623. [7d] O. J. Scherer, *Acc. Chem. Res.* **1999**, *32*, 751 and references therein. [7e] K. H. Whitemire, *Adv. Organomet. Chem.* **1998**, *42*, 1. [7f] M. Herberhold, G. Frohmader, W. Milius, *J. Organomet. Chem.* **1996**, *522*, 185. [7g] M. Detzel, T. Mohr, O. J. Scherer, G. Wolmershäuser, *Angew. Chem.* **1994**, *106*, 1142; *Angew. Chem. Int. Ed. Engl.* **1994**, *33*, 1110. [7h] L. Weber, *Angew. Chem. Int. Ed. Engl.* **1996**, *35*, 2618.
[8] E. Urnezius, W. W. Brennessel, C. J. Cramer, J. E. Ellis, P. v. R. Schleyer, *Science* **2002**, *295*, 832.
[9] J. F. Nixon, *Chem. Rev.* **1988**, *88*, 1327; A. G. Avent, F. G. N. Cloke, K. R. Flower, P. B. Hitchcock, J. F. Nixon, *Angew. Chem. Int. Ed.* **1994**, *33*, 2330; P. B. Hitchcock, C. Jones, J. F. Nixon, *Angew. Chem. Int. Ed.* **1994**, *33*, 463.
[10] F. T. Edelmann, D. M. M. Freckmann, H. Schumann, *Chem. Rev.* **2002**, *102*, 1851.
[11] K. B. Dillon, F. Mathey, J. F. Nixon, *Phosphorus: The Carbon Copy*, Wiley, Chichester, **1998**.
[12] [12a] L. Weber, *Angew. Chem. Int. Ed.* **2002**, *41*, 563. [12b] Deschamps, L. Ricard, F. Mathey, *J. Organomet. Chem.* **1997**, *548*, 17. [12c] K. Tanaka, G. C. Fu, *J. Org. Chem.* **2001**, *66*, 8177. [12d] K. Tanaka, S. Qiao, M. Tobisu, M. M.-C. Lo, G. C. Fu, *J. Am. Chem. Soc.* **2000**, *122*, 9870. [12e] S. Qiao, G. C. Fu, *J. Org. Chem.* **1998**, *63*, 4168.
[13] E. J. P. Malar, *J. Org. Chem.* **1992**, *57*, 3694.
[14] T. P. Hamilton, H. F. Schaefer III, *Angew. Chem.* **1989**, *101*, 500; *Angew. Chem. Int. Ed. Engl.* **1989**, *28*, 485.
[15] A. Dransfeld, L. Nyulaszi, P. v. R. Schleyer, *Inorg. Chem.* **1998**, *37*, 4413.
[16] [16a] M. C. Kerins, N. J. Fitzpatrick, M. T. Nguyen, *Polyhedron* **1989**, *8*, 1135. [16b] J. A. Chamizo, M. Ruiz-Mazon, R. Salcedo, R. A. Toscano, *Inorg. Chem.* **1990**, *29*, 879.
[17] [17a] C. W. Bauschlicher Jr., S. R. Langhoff, H. Partridge, in *Modern Electronic Structure Theory, Part II* (Ed.: D. R. Yarkony), World Scientific, Singapore **1995**, p. 1280. [17b] M. A. Pietsch, M. Couty, M. B. Hall, *J. Phys. Chem.* **1995**, *99*, 16315. [17c] L. W. Mire, S. D. Wheeler, E. Wagenseller, D. S. Marynick, *Inorg. Chem.* **1998**, *37*, 3099. [17d] M. Couty, C. A. Bayse, R. Jimenez-Catano, M. B. Hall, *J. Phys. Chem.* **1996**, *100*, 13976. [17e] K. Pierloot, B. Persson, B. O. Roos, *J. Phys. Chem.* **1995**, *99*, 3465.
[18] [18a] R. L. Williamson, M. B. Hall, *Int. J. Quantum Chem., Quantum Chem. Symp.* **1987**, *21*, 503. [18b] T. E. Tailor, M. B. Hall, *Chem. Phys. Lett.* **1985**, *114*, 338. [18c] H. P. Lüthi, J. H. Ammeter, J. Almlöf, K. Faegri Jr., *J. Chem. Phys.* **1982**, *77*, 2002. [18d] J. Almlöf, K. Faegri, B. R. Schilling, H. Lüthi, *Chem. Phys. Lett.* **1984**, *106*, 266. [18e] H. Lüthi, P. E. M. Siegbahn, J. Almlöf, K. Faegri Jr., A. Heiberg, *Chem. Phys. Lett.* **1984**, *106*, 1. [18f] M. L. McKee, *J. Phys. Chem.* **1992**, *96*, 1683. [18h] E. Diana, R. Rossetti, P. L. Stanghellini, S. F. A. Kettle, *Inorg. Chem.* **1997**, *36*, 382.
[19] C. Park, J. Almlöf, *J. Chem. Phys.* **1991**, *95*, 1829.
[20] [20a] P. Hohenberg, W. Kohn, *Phys. Rev. B* **1964**, *136*, 864. [20b] R. G. Parr, W. Yang, *Density Functional Theory of Atoms and Molecules*, Oxford University Press, New York, **1989**.
[21] [21a] T. Yasuike, S. Yabushita, *J. Phys. Chem. A* **1999**, *103*, 4533. [21b] A. M. Orendt, J. C. Facelli, Y. J. Jiang, D. M. Grant, *J. Phys. Chem. A* **1998**, *102*, 7692. [21c] N. Matsuzawa, J. Seto, D. A. Dixon, *J. Phys. Chem. A* **1997**, *101*, 9391. [21d] M. J. Mayor-López, J. Weber, *Chem. Phys. Lett.* **1997**, *281*, 226. [21e] L. Maron, O. Eisenstein, *J. Phys. Chem. A* **2000**, *104*, 7140. [21f] M. Kaupp, P. v. R. Schleyer, M. Dolg, H. Stoll, *J. Am. Chem. Soc.* **1992**, *114*, 8202. [21g] Z.-F. Xu, Y. Xie, W.-L. Feng, H. F. Schaefer III, *J. Phys. Chem. A.* **2003**, *107*, 2716.
[22] G. Frison, F. Mathey, A. Sevin, *J. Phys. Chem. A.* **2002**, *106*, 5653.
[23] J. Frunzke, M. Lein, G. Frenking, *Organometallics* **2002**, *21*, 3351.
[24] M. Lein, J. Frunzke, G. Frenking, *Inorg. Chem.* **2003**, *42*, 2504.
[25] [25a] M. Lein, J. Frunzke, A. Timoshkin, G. Frenking, *Chem. Eur. J.* **2001**, *7*, 4155. [25b] L. Gagliardi, P. Pyykkö, *J. Phys. Chem. A* **2002**, *106*, 4690.
[26] E. J. P. Malar, *Inorg. Chem.* **2003**, *42*, 3873.
[27] M. F. Ryan, J. R. Eyler, D. E. Richardson, *J. Am. Chem. Soc.* **1992**, *114*, 8611 and references therein.
[28] [28a] A. Haaland, J. E. Nilsson, *Acta Chem. Scand.* **1968**, *22*, 2653. [28b] A. Haaland, *Acc. Chem. Res.* **1979**, *12*, 415.
[29] A. Hess, J. Sehnert, T. Weyhermüller, N. Metzler-Nolte, *Inorg. Chem.* **2000**, *39*, 5437.
[30] P. Seiler, J. D. Dunitz, *Acta Crystallogr., Sect. B* **1980**, *36*, 2946.
[31] [31a] K. C. Waterman, A. Streitwieser, R. Blom, K. Faegri Jr., T. Midtgaard, *J. Am. Chem. Soc.* **1991**, *113*, 3230. [31b] R. K. Bohn, A. Haaland, *J. Organomet. Chem.* **1966**, *5*, 470. [31c] B. J. Drouin, P. A. Cassak, S. G. Kukolich, *Inorg. Chem.* **1997**, *36*, 2868. [31d] S. Shibata, L. S. Bartell, R. M. Gavin, *J. Chem. Phys.* **1964**, *41*, 717. [31e] A. Haaland, J. Lusztyk, D. P. Norak, J. Brunvoll, *Chem. Commun.* **1974**, 54. [31f] I. A. Ronova, D. A. Bochvar, A. L. Chistjakov, Y. T. Struc, J. Alekseev, *J. Organomet. Chem.* **1966**, *5*, 470. [31g] P. Jutzi, F. Khol, P. Hofmann, C. Kruger, Y. H. Tsay, *Chem. Ber.* **1980**, *113*, 757. [31h] S. Alexandratos, A. Streitwieser Jr., H. F. Schaefer III, *J. Am. Chem. Soc.* **1976**, *98*, 7959. [31i] K. K. Jespersen, J. Chandrashekhar, P. v. R. Schleyer, *J. Org. Chem.* **1980**, *45*, 1608. [31j] K. C. Waterman, A. Streitwieser Jr., *J. Am. Chem. Soc.* **1984**, *106*, 3138.
[32] F. Takusagawa, T. F. Koetzle, *Acta Crystallogr., Sect. B* **1979**, *35*, 1074.
[33] R. H. Herber, I. Gattinger, F. H. Köhler, *Inorg. Chem.* **2000**, *39*, 851.

 © 2004 Wiley-VCH Verlag GmbH & Co. KGaA, Weinheim

[34] A. A. Koridze, P. V. Petrovskii, S. P. Gubin, E. I. Fedin, *J. Organomet. Chem.* **1975**, *93*, C26.
[35] P. S. Nielsen, R. S. Hansen, H. J. Jacobsen, *J. Organomet. Chem.* **1976**, *114*, 145.
[36] [36a] L. Nyulaszi, *Chem. Rev.* **2001**, *101*, 1229 and references therein. [36b] G. Frison, A. Sevin, N. Avarvari, F. Mathey, P. Le Floch, *J. Org. Chem.* **1999**, *64*, 5524. [36c] E. Mattmann, F. Mathey, A. Sevin, G. Frison, *J. Org. Chem.* **2002**, *67*, 1208.
[37] [37a] K. Jug, *J. Org. Chem.* **1983**, *48*, 1344. [37b] K. Jug, A. Köster, *J. Phys. Org. Chem.* **1991**, *4*, 163. [37c] E. J. P. Malar, K. Jug, *J. Phys. Chem.* **1984**, *88*, 3508. [37d] E. J. P. Malar, K. Jug, *J. Phys. Chem.* **1985**, *89*, 5235. [37e] E. J. P. Malar, K. Jug, *Tetrahedron* **1986**, *42*, 417. [37f] K. Jug, E. J. P. Malar, *J. Mol. Struct.* **1987**, *153*, 221. [37g] E. J. P. Malar, F. Neumann, K. Jug, *J. Mol. Struct.* **1995**, *336*, 81. [37h] J. Jeevanandam, E. J. P. Malar, R. Gopalan, *Organometallics* **2003**, *22*, 5454.
[38] [38a] T. M. Krygowski, M. K. Cyranski, *Chem. Rev.* **2001**, *101*, 1385. [38b] J. A. N. F. Gomes, R. B. Mallion, *Chem. Rev.* **2001**, *101*, 1349. [38c] R. H. Mitchel, *Chem. Rev.* **2001**, *101*, 1301. [38d] A. R. Katritzky, K. Jug, D. C. Oniciu, *Chem. Rev.* **2001**, *101*, 1421. [38e] M. Randić, *Chem. Rev.* **2003**, *103*, 3449.
[39] [39a] A. R. Katritzky, P. Barczynski, G. Musamarra, D. Pisano, M. Szafran, *J. Am. Chem. Soc.* **1989**, *111*, 7. [39b] A. R. Katritzky, M. Karelson, S. Sild, T. M. Krygowski, K. Jug, *J. Org. Chem.* **1998**, *63*, 5228.
[40] [40a] P. v. R. Schleyer, P. K. Freeman, H. Jiao, B. Goldfuss, *Angew. Chem. Int. Ed. Engl.* **1995**, *34*, 337. [40b] P. v. R. Schleyer, H. Jiao, *Pure Appl. Chem.* **1996**, *68*, 209. [40c] L. Nyulaszi, P. v. R. Schleyer, *J. Am. Chem. Soc.* **1999**, *121*, 6872.
[41] M. K. Cyranski, T. M. Krygowski, A. R. Katritzky, P. v. R. Schleyer, *J. Org. Chem.* **2002**, *67*, 1333.
[42] M. J. Frisch, G. W. Trucks, H. B. Schlegel, G. E. Scuseria, M. A. Robb, J. R. Cheeseman, J. A. Montgomery, Jr., T. Vreven, K. N. Kudin, J. C. Burant, J. M. Millam, S. S. Iyengar, J. Tomasi, V. Barone, B. Mennucci, M. Cossi, G. Scalmani, N. Rega, G. A. Petersson, H. Nakatsuji, M. Hada, M. Ehara, K. Toyota, R. Fukuda, J. Hasegawa, M. Ishida, T. Nakajima, Y. Honda, O. Kitao, H. Nakai, M. Klene, X. Li, J. E. Knox, H. P. Hratchian, J. B. Cross, C. Adamo, J. Jaramillo, R. Gomperts, R. E. Stratmann, O. Yazyev, A. J. Austin, R. Cammi, C. Pomelli, J. W. Ochterski, P. Y. Ayala, K. Morokuma, G. A. Voth, P. Salvador, J. J. Dannenberg, V. G. Zakrzewski, S. Dapprich, A. D. Daniels, M. C. Strain, O. Farkas, D. K. Malick, A. D. Rabuck, K. Raghavachari, J. B. Foresman, J. V. Ortiz, Q. Cui, A. G. Baboul, S. Clifford, J. Cioslowski, B. B. Stefanov, G. Liu, A. Liashenko, P. Piskorz, I. Komaromi, R. L. Martin, D. J. Fox, T. Keith, M. A. Al-Laham, C. Y. Peng, A. Nanayakkara, M. Challacombe, P. M. W. Gill, B. Johnson, W. Chen, M. W. Wong, C. Gonzalez, J. A. Pople, *Gaussian 03, Revision B.04*, Gaussian, Inc., Pittsburgh PA, **2003**.
[43] [43a] A. D. Becke, *J. Chem. Phys.* **1993**, *98*, 5648. [43b] C. Lee, W. Yang, R. G. Parr, *Phys. Rev. B* **1988**, *37*, 785.
[44] [44a] J. B. Foresman, A. Frisch, *Exploring Chemistry with Electronic Structure Methods*, Gaussian, Inc., Pittsburgh, PA, **1996**. [44b]A. D. McLean, G. S. Chandler, *J. Chem. Phys.* **1980**, *72*, 5639. [44c] R. Krishnan, J. S. Binkley, R. Seeger, J. A. Pople, *J. Chem. Phys.* **1980**, *72*, 650. [44d] A. J. H. Wachters, *J. Chem. Phys.* **1970**, *52*, 1033. [44e] P. J. Hay, *J. Chem. Phys.* **1977**, *66*, 4377. [44f] K. Raghavachari, G. W. Trucks, *J. Chem. Phys.* **1989**, *91*, 1062.
[45] [45a] P. J. Hay, W. R. Wadt, *J. Chem. Phys.* **1985**, *82*, 270, 284, 299. [45b] W. Stevens, H. Basch, J. Krauss, *J. Chem. Phys.* **1984**, *81*, 6026. [45c] W. J. Stevens, M. Krauss, H. Basch, P. G. Jasien, *Can. J. Chem.* **1992**, *70*, 612. [45d] T. R. Cundari, W. J. Stevens, *J. Chem. Phys.* **1993**, *98*, 5555.
[46] C. W. Bauschlicher, H. Patridge, *J. Chem. Phys.* **1995**, *103*, 1788.
[47] [47a] J. P. Foster, F. Weinhold, *J. Am. Chem. Soc.* **1980**, *102*, 7211. [47b] E. D. Glendening, A. E. Reed, J. E. Carpenter, F. Weinhold, *NBO Version 3.1*.
[48] [48a] A. E. Reed, R. B. Weinstock, F. Weinhold, *J. Chem. Phys.* **1985**, *83*, 735. [48b] A. E. Reed, L. A. Curtiss, F. Weinhold, *Chem. Rev.* **1988**, *88*, 899. [48c] C. Lambert, P. v. R. Schleyer, *Angew. Chem. Int. Ed. Engl.* **1994**, *33*, 1129.
[49] [49a] K. B. Wiberg, *Tetrahedron* **1968**, *24*, 1083. [49b] M. S. Gopinathan, K. Jug, *Theor. Chim. Acta* **1983**, *63*, 511.

Received January 22, 2004
Early View Article
Published Online May 5, 2004

 © 2004 Wiley-VCH Verlag GmbH & Co. KGaA, Weinheim

The Hybrid Organic-Inorganic 2-D Material $(CsNa_2[\{Sn(CH_3)_2\}_3(H_2O)_4(\beta\text{-}XW_9O_{33})]\cdot 7H_2O)_\infty$ (X = As^{III}, Sb^{III}) and Its Solution Properties[‡]

Firasat Hussain,[a] Markus Reicke,[a] and Ulrich Kortz*[a]

Keywords: Hybrid materials / Organometallic compounds / Polyoxometalates / Self assembly / Tungsten

We report on the hybrid organic-inorganic 2-D materials $(CsNa_2[\{Sn(CH_3)_2\}_3(H_2O)_4(\beta\text{-}AsW_9O_{33})]\cdot 7H_2O)_\infty$ (**1a**) and the isomorphous $(CsNa_2[\{Sn(CH_3)_2\}_3(H_2O)_4(\beta\text{-}SbW_9O_{33})]\cdot 7H_2O)_\infty$ (**2a**) which crystallize in the orthorhombic system, space group $Pna2_1$, with identical unit cell parameters a = 26.118(2) Å, b = 16.064(1) Å, c = 13.776(1) Å, and Z = 1. Compounds **1a** and **2a** have been synthesized in good yield by crystallization from a reaction mixture of dimethyltin dichloride and $Na_9[\alpha\text{-}XW_9O_{33}]$ (X = As^{III}, Sb^{III}) in aqueous, acidic medium. We have shown by multinuclear NMR spectroscopy (^{183}W, ^{119}Sn, ^{13}C, ^{1}H) that **1a** and **2a** decompose in solution leading to the monomeric species $[\{Sn(CH_3)_2(H_2O)_2\}_3(\beta\text{-}XW_9O_{33})]^{3-}$ [X = As^{III} (**1**), Sb^{III} (**2**)]. Polyanions **1** and **2** consist of a $(\beta\text{-}XW_9O_{33})$ fragment stabilized by three dimethyltin units. The dimethyltin groups are grafted onto the polyanion by two Sn–O(W) bonds on the side of the heteroatom lone pair. Compounds **1** and **2** are rare examples of discrete polyoxoanions which polymerize upon crystallization leading to a 2-D solid-state structure with inorganic and organic surface regions.
(© Wiley-VCH Verlag GmbH & Co. KGaA, 69451 Weinheim, Germany, 2004)

Introduction

Polyoxometalates are of interest because they exhibit a tremendous structural variety and useful properties in different fields, including catalysis and medicine.[1−6] This is most likely the reason why the number of researchers actively involved in polyoxoanion chemistry has increased significantly over the last couple of decades. A study of the literature reveals that the vast majority of reports is devoted to catalytic studies of polyoxoanion salts and acids.

Most likely this is a result of the fact that the synthesis of novel polyoxoanion architectures is not trivial. Although the template effect seems to play an important role during the formation process of polyoxoanions, the detailed mechanism of formation is far from being understood. This is even more surprising as the first polyoxoanions were reported almost two centuries ago.[7] However, it took another 100 years for the first structure (the Keggin ion) to be determined.[8]

It is known that the size, shape and charge density of many polyoxoanions are of interest for pharmaceutical applications (e.g. antiviral, antitumor).[1−6,9] However, the mechanism of action of many polyoxoanions is not selective towards a specific target. In order to improve selectivity it often appears desirable to modify a given polyoxoanion core structure slightly. However, such attempts result frequently in a different polyoxoanion framework. Therefore the most straightforward and promising approach towards systematic derivatization of polyoxoanions involves attachment of organic groups to the surface of the metal-oxo framework. In order to be attractive for pharmaceutical applications the functionalized polyoxoanions should be water soluble and fairly stable at physiological pH.

To date the number of water-soluble polyoxoanions with tightly bound organic functions is rather small. Pope and co-workers were the first to study the interaction of monoorganotin groups with polyoxoanions. They reacted different organotin halide precursors (e.g. $nC_4H_9SnCl_3$, $C_6H_5SnCl_3$) with a large number of lacunary heteropolytungstates in aqueous solution and were able to identify novel, mostly dimeric polyoxoanion structures.[10] Single-crystal X-ray diffraction studies revealed that these products contain tightly anchored organotin fragments. The compounds were also studied in solution by multinuclear NMR spectroscopy. This technique is also very valuable in the evaluation of the stability of polyoxoanions in low concentration at physiological pH for medicinal applications. Liu and co-workers have also synthesized some monoorganotin-substituted polyoxotungstates. They introduced ester functionalities to the organotin fragment and tested the biological (antitumor) activity of their products.[11] Very recently Hasenknopf et al. used the same methodology to introduce peptide functions into organotin units which were incorporated in the monolacunary Wells−Dawson deriva-

[‡] Polyoxoanions Functionalized by Diorganotin Groups, Part 1.

[a] International University Bremen, School of Engineering and Science
P. O. Box 750 561, 28725 Bremen, Germany
Fax: (internat.) + 49-(0)421-200-3229
E-mail: u.kortz@iu-bremen.de

tive $[x\text{-}P_2W_{17}O_{61}]^{10-}$ ($x = \alpha_1, \alpha_2$).[12] Haiduc et al. have also reported some monoorganotin derivatives of polyoxotungstates.[13] However, the proposed structures of Liu and Haiduc need to be confirmed by X-ray diffraction. To date, only a few monoorganotin-substituted polyoxomolybdates and -vanadates are known.[14]

Interestingly there are no reports on diorganotin-substituted polyoxotungstates. Such species could allow for more flexibility regarding the interaction with, and binding to, organic compounds and biomolecules. Therefore we decided to investigate the interaction of dimethyltin groups with lone-pair-containing heteropolytungstates in some detail.

Results and Discussion

Here we report on the novel and isostructural polyoxoanion-based 2-D materials $(CsNa_2[\{Sn(CH_3)_2\}_3(H_2O)_4(\beta\text{-}XW_9O_{33})]\cdot 7H_2O)_\infty$ (X = As, **1a**; Sb, **2a**; see Figure 1). The structure of **1a** and **2a** is best described as a polymeric network composed of $[\{Sn(CH_3)_2\}_3(H_2O)_4(\beta\text{-}XW_9O_{33})]^{3-}$ building blocks ($X = As^{III}, Sb^{III}$) that are linked by Sn−O(W′) bridges. This leads to a 2-D surface which is not planar, but could be described as a ladder with a zig-zag backbone where the individual levels are decorated by methyl groups (see Figure 2). Clearly, the solid-state structure of **1a** and **2a** is governed by the organotin functionalities.

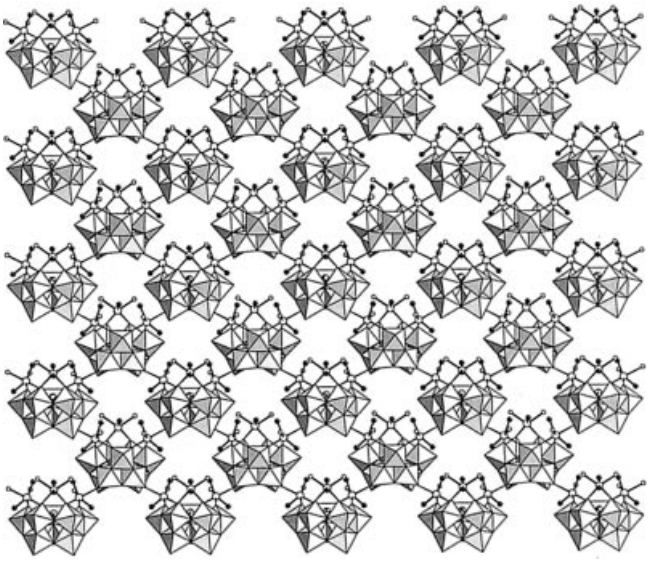

Figure 1. Combined polyhedral/ball-and-stick representation of the 2-D solid-state structure of $(CsNa_2[\{Sn(CH_3)_2\}_3(H_2O)_4(\beta\text{-}XW_9O_{33})]\cdot 7H_2O)_\infty$ (X = As, **1a**; Sb, **2a**); the octahedra represent WO_6 and the balls are tin (diagonally hatched), arsenic/antimony (crosshatched), oxygen (white) and carbon (black); hydrogen atoms are omitted for clarity

Compounds **1a** and **2a** are isostructural, which means that the different sizes of the As and Sb heteroatoms with their associated lone pairs have no significant effect on the solid-state structures.

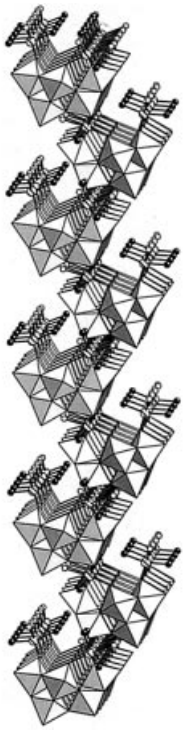

Figure 2. Side view of the 2-D solid-state structure of **1a** and **2a**; the code is the same as in Figure 1

The three organotin groups attached to each monomeric unit of **1a** and **2a** contain tin centers that are octahedrally coordinated by four oxo and two methyl groups which are positioned *trans* to each other. However, only two organotin groups are structurally equivalent and different from the third. The molecular formulae and charges of **1a** and **2a** are supported by bond-valence calculations, which indicate that all terminal oxygen atoms bound to the tin atoms are diprotonated.[15]

Close inspection of **1a** and **2a** indicates that the C−Sn−C bond angles are significantly smaller than 180°, indicating that the interior methyl groups still experience some degree of repulsion (see Figure 1). The C−Sn−C bond angles of the two equivalent organotin groups are very similar for **1a** [149(1)°, 152(1)°] and **2a** [150(1)°, 151(1)°]; however, the C−Sn−C bond angle of the unique organotin unit is distinctly larger in polyanion **1a** [166(1)°] than in **2a** [162(1)°]. This observation reflects (a) the smaller size of the As^{III} atom compared to Sb^{III}, (b) the shorter As^{III}−O bond lengths compared to Sb^{III}, and (c) the smaller size of the As^{III} lone-pair compared to Sb^{III}.

It is known that the α to β isomerization of $[\alpha\text{-}AsW_9O_{33}]^{9-}$ and $[\alpha\text{-}SbW_9O_{33}]^{9-}$ is facilitated in an acidic, aqueous medium.[16,17] This is in complete agreement with the synthetic conditions for **1a** and **2a**, which were isolated at pH 3. The $(\beta\text{-}AsW_9O_{33})$ fragment has so far only been observed in two different polyoxoanion structures.[16,18] The large tungstoarsenate(III) $[As_6W_{65}O_{217}(H_2O)_7]^{26-}$ is the only example of a polyanion that contains both $(\alpha\text{-}AsW_9O_{33})$ and $(\beta\text{-}AsW_9O_{33})$ isomers in the same structure.[18]

 © 2004 Wiley-VCH Verlag GmbH & Co. KGaA, Weinheim

The fact that no cations are involved in the exclusively covalent 2-D network of **1a** and **2a** requires it to possess a negative charge. Indeed the appropriate number of cations (1 Cs, 2 Na) for each polyanionic unit was found by X-ray diffraction and elemental analysis. Therefore **1a** and **2a** are best described as polymeric polyanion salts. This view is further supported by our observation that **1a** and **2a** are soluble in water upon heating.

Clearly, in solution the polymeric structure of **1a** and **2a** decomposes and we identified the likely sites: the very long Sn−O(W′) bonds in **1a** [2.607(3), 2.656(3) Å] and **2a** [2.559(3), 2.633(3) Å]. The question now arises in which form **1a** and **2a** are present in solution: oligomeric or monomeric. The latter requires the existence of the hypothetical, monomeric polyanion $[\{Sn(CH_3)_2(H_2O)_2\}_3(\beta\text{-}XW_9O_{33})]^{3-}$ [X = As^{III} (**1**), Sb^{III} (**2**)]. Polyanion **1** consists of a (β-AsW_9O_{33}) fragment which is stabilized by three dimethyltin fragments, and polyanion **2** represents its antimony derivative (see Figures 3 and 4). The three dimethyltin groups of **1** and **2** are grafted onto the polyanion by two Sn−O(W) bonds each on the side of the heteroatom lone pair.

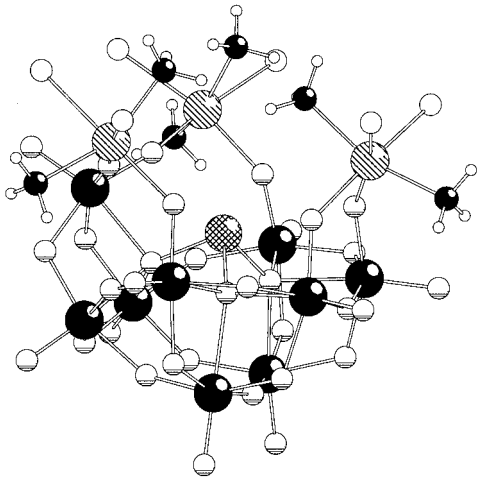

Figure 3. Ball-and-stick representation of $[\{Sn(CH_3)_2(H_2O)_2\}_3(\beta\text{-}XW_9O_{33})]^{3-}$ (X = As^{III}, **1**; Sb^{III}, **2**); the balls represent tungsten (black), tin (diagonally hatched), arsenic/antimony (crosshatched), oxygen (white with shadow), carbon (black) and hydrogen (small white); water molecules are shown as white balls

Solution NMR spectroscopy is the most elegant technique to prove the existence of **1** and **2** in solution. It is well-known that NMR of the addenda atoms (in this case tungsten) is the most sensitive analytical tool to obtain structural information of polyoxoanions in solution. Compounds **1a** and **2a** are ideal for a multinuclear NMR study because they are diamagnetic and contain several NMR-active, spin 1/2 nuclei. Therefore we performed ^{183}W, ^{119}Sn, ^{1}H and ^{13}C NMR studies on (a) freshly synthesized solutions of **1a** and **2a** (see Exp. Sect.) and (b) solid **1a** and **2a** redissolved in water. Interestingly we obtained exactly the same NMR results in both cases.

The ^{183}W NMR spectrum shows five peaks (intensity ratios 2:1:2:2:2) for **1a** at δ = −130.5, −135.2, −138.1, −142.5 and −146.2 ppm and for **2a** at δ = −108.1, −117.4, −120.1, −127.1 and −134.7 ppm (see Figure 5). The latter spectrum shows an additional, very small peak at δ = −124.6 ppm for which we do not yet have a good explanation. We also recorded a ^{119}Sn NMR spectrum and observed two peaks with an intensity ratio of 1:2 at δ = −175.9, −200.0 ppm (**1a**) and δ = −164.6, −205.2 ppm (**2a**), respectively (see Figure 6). Interestingly both signals for **1a** are somewhat broader than those for **2a**. The ^{13}C NMR spectrum shows only one peak for **1a** at δ = 8.5 ppm and for **2a** at δ = 8.7 ppm. As expected, the ^{1}H NMR spectrum also shows only one peak at δ = 4.7 ppm for **1a** and **2a**. All these results indicate that a species with C_s symmetry is present in solution and prove the existence of the discrete, monomeric polyanions **1** and **2**. Furthermore, the above NMR spectra do not change for several months; indicating that the dimethyltin groups are tightly bound to the tungsten-oxo fragment.

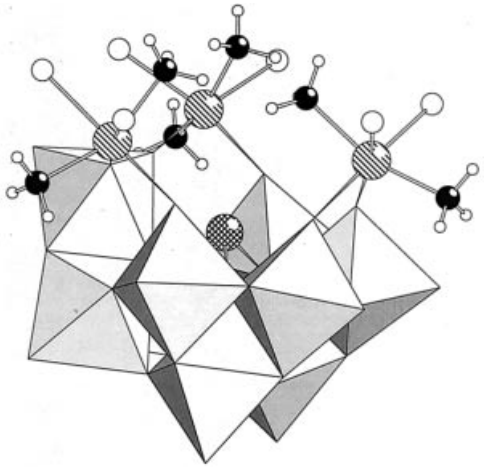

Figure 4. Combined polyhedral/ball-and-stick representation of **1** and **2**; the code is the same as in Figure 3

Polyoxoanions **1** and **2** were synthesized by heating an aqueous solution containing dimethyltin dichloride and $Na_9[\alpha\text{-}XW_9O_{33}]$ (X = As^{III}, Sb^{III}) in the appropriate stoichiometric ratio (3:1) in an aqueous, acidic medium (pH 3). From this solution the polymeric materials **1a** and **2a** were formed upon crystallization and both products could be isolated in good yield (see Exp. Sect.).

Interestingly, formation of **1** and **2** is accompanied by the isomerization (α-XW_9O_{33}) → (β-XW_9O_{33}) (X = As, Sb), and it is likely that steric interactions of the methyl groups do not allow formation of the hypothetical trisubstituted α-derivative $[\{Sn(CH_3)_2(H_2O)_2\}_3(\alpha\text{-}XW_9O_{33})]^{3-}$ (X = As^{III}, Sb^{III}). More precisely, the three "internal" methyl groups would come very close to each other if they were grafted onto a (α-AsW_9O_{33}) or (α-SbW_9O_{33}) fragment (see Figures 3 and 4). Furthermore the lone pair of electrons on the heteroatom may exhibit a repulsive effect on the internal methyl groups. Rotation of one W_3O_{13} triad by 60° results in the β-isomer and then all three dimethyltin units can be bound without steric hindrance, resulting in a stable structure. The terminal oxygens of all tin atoms in **1** and **2** are

 © 2004 Wiley-VCH Verlag GmbH & Co. KGaA, Weinheim

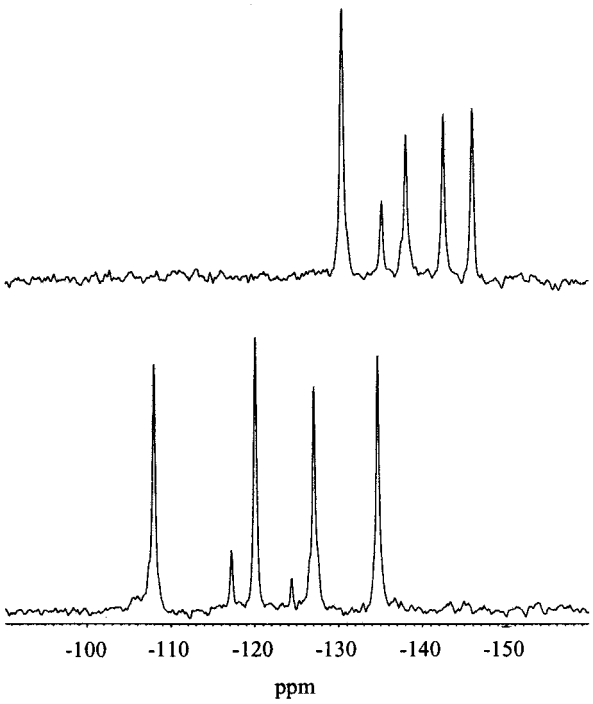

Figure 5. Room-temperature ^{183}W NMR spectra of **1a** (top) and **2a** (bottom) in D_2O

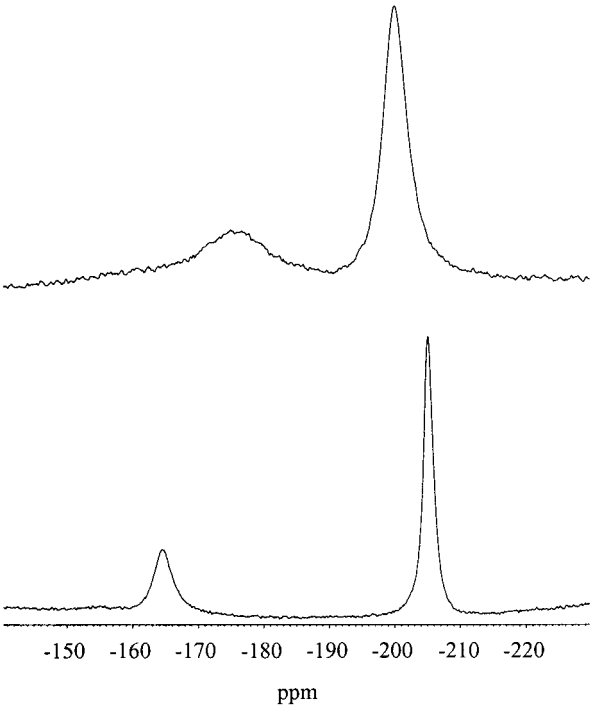

Figure 6. Room-temperature ^{119}Sn NMR spectra of **1a** (top) and **2a** (bottom) in D_2O

almost certainly diprotonated. The presence of labile water ligands explains the tendency of **1** and **2** to polymerize in the solid state.

Conclusions

Our work has shown that diorganotin fragments can be incorporated into polyoxotungstates. Polyanions **1** and **2** represent (a) novel examples of hybrid organic-inorganic polyoxoanions, (b) the first examples of diorganotin-substituted polyoxoanions, (c) the first monomeric organotin derivatives of lone-pair-containing polyoxoanions, and (d) the first organotin derivatives of $[\beta\text{-}AsW_9O_{33}]^{9-}$ and $[\beta\text{-}SbW_9O_{33}]^{9-}$. The compounds presented here are rare examples of discrete polyoxoanions which polymerize upon crystallization, leading to a 2-D structure with inorganic and organic surface regions. We plan to prepare derivatives of polyanions **1** and **2** by attaching organic functional groups (e.g. COOH, NH_2, OH, SH) and chiral subunits (e.g. amino acids) to the organotin fragments. Such species would be of major interest for catalytic and medicinal applications (e.g. stabilization of metal nanoparticles, interaction with biomolecules).

Currently we investigate the possibility of grafting diorganotin units on other lacunary polyoxotungstates.

Experimental Section

The lacunary precursors $Na_9[\alpha\text{-}AsW_9O_{33}]$ and $Na_9[\alpha\text{-}SbW_9O_{33}]$ were synthesized according to published procedures and their purity was confirmed by infrared spectroscopy.[17,20] All other reagents were used as purchased without further purification.

All elemental analyses were performed by Kanti Labs Ltd. in Mississauga, Canada. The IR spectra were recorded on a Nicolet Avatar FTIR spectrophotometer in a KBr pellet. All NMR spectra were recorded, on a 400 MHz JEOL ECX instrument. The ^{183}W NMR measurements were performed at 16.656 MHz in 10 mm tubes and the ^{119}Sn, ^{13}C, and ^{1}H spectra were recorded in 5 mm tubes at 149.081, 100.525 and 399.782 MHz, respectively. The chemical shifts for unbound dimethyltin dichloride at pH 3 are at $\delta = -243.7$ ppm (^{119}Sn), 12.2 ppm (^{13}C) and 0.84 ppm (^{1}H).

$(CsNa_2[\{Sn(CH_3)_2\}_3(H_2O)_4(\beta\text{-}AsW_9O_{33})]\cdot 7H_2O)_\infty$ (1a): $Sn(CH_3)_2Cl_2$ (0.58 g, 2.64 mmol) was dissolved in 40 mL of H_2O and then $Na_9[\alpha\text{-}AsW_9O_{33}]$ (2.00 g, 0.80 mmol) was added. This solution (pH 3) was heated to 80 °C for 1 h and then cooled to room temperature and filtered. A few drops of 0.1 M CsCl were added and then the solution was allowed to evaporate in an open beaker at room temperature. After 1−2 days a white crystalline product started to appear. Evaporation was allowed to continue until the solvent level had approached the solid product, which was filtered off and air-dried. A total of 1.9 g (yield 76%) of crystalline product was obtained. **1a** (3081.0): calcd. Cs 4.3, Na 1.5 Sn 11.6, As 2.4, W 53.7; found Cs 4.0, Na 1.8, Sn 10.9, As 2.1, W 54.0. IR for **1a** (KBr disk): $\tilde{\nu}$ = 954, 909, 870, 829, 760, 727, 688, 518, 476, 430 cm^{-1}. NMR (D_2O, 293 K) for **1a**: ^{183}W (relative intensities in parentheses): $\delta = -130.5$ (2), −135.2 (1), −138.1 (2), −142.5 (2), −146.2 (2) ppm. ^{119}Sn: $\delta = -175.9$ (1), −200.0 (2) ppm. ^{13}C: δ = 8.5 ppm. ^{1}H: δ = 4.7 ppm.

 © 2004 Wiley-VCH Verlag GmbH & Co. KGaA, Weinheim

Table 1. Crystal data and structure refinement for **1a** and **2a**

	1a	**2a**
Formula	$C_6H_{40}AsCsNa_2O_{44}Sn_3W_9$	$C_6H_{40}CsNa_2O_{44}SbSn_3W_9$
Mol. wt. (g/mol)	3081.0	3127.9
Crystal color	colorless	colorless
Crystal system	orthorhombic	orthorhombic
Crystal size (mm^3)	0.10 × 0.06 × 0.02	0.11 × 0.06 × 0.04
Space group (No.)	$Pna2_1$ (33)	$Pna2_1$ (33)
a (Å)	26.118(2)	26.118(2)
b (Å)	16.064(1)	16.064(1)
c (Å)	13.776(1)	13.776(1)
Volume ($Å^3$)	5779.4(7)	5779.4(7)
Z	1	1
D_{calcd} ($Mg·m^{-3}$)	3.561	3.672
Abs. coeff. (mm^{-1})	20.548	20.595
Reflections (unique)	14373	14370
Reflections (obsd.)	11413	12214
$R(F_o)$[a]	0.068	0.052
$R_w(F_o)$[b]	0.1401	0.1078
Diff. peak ($e·Å^3$)	5.248	2.985
Diff. hole ($e·Å^3$)	−5.107	−3.762

[a] $R = \Sigma||F_o| - |F_c||/\Sigma|F_o|$. [b] $Rw = [\Sigma w(F_o^2 - F_c^2)^2/\Sigma w(F_o^2)^2]^{1/2}$.

$(CsNa_2[\{Sn(CH_3)_2\}_3(H_2O)_4(\beta\text{-}SbW_9O_{33})]·7H_2O)_\infty$ (2a): The synthesis was identical to that of **1a**, with the exception that 2.00 g (0.80 mmol) of $Na_9[\alpha\text{-}SbW_9O_{33}]$ was used instead of $Na_9[\alpha\text{-}AsW_9O_{33}]$. A total of 2.0 g (yield 79%) of crystalline product was obtained. **2a** (3127.9): calcd. Cs 4.2, Na 1.5, Sn 11.4, Sb 3.9, W 52.9; found Cs 3.9, Na 1.3, Sn 11.2, Sb 3.8, W 53.4. IR of **2a** (KBr disk): $\tilde{\nu}$ = 951, 865, 820, 747, 677, 520, 473, 457, 422 cm^{-1}. NMR (D_2O, 293 K) for **2a**: ^{183}W: (relative intensities in parenthesis): δ = −108.1 (2), −117.4 (1), −120.1 (2), −127.1 (2), −134.7 (2) ppm. ^{119}Sn: δ = −164.6 (1), −205.2 (2) ppm. ^{13}C: δ = 8.7 ppm. ^1H: δ = 4.7 ppm.

X-ray Crystallography: Crystals of **1a** and **2a** were mounted on a glass fiber for indexing and intensity data collection at 173 K on a Bruker D8 SMART APEX CCD single-crystal diffractometer using Mo-K_α radiation (λ = 0.71073 Å). Direct methods were used to solve the structure and to locate the heavy atoms (SHELXS-97). The remaining atoms were found from successive difference maps (SHELXL-97). Routine Lorentz and polarization corrections were applied and an absorption correction was performed using the SADABS program.[21] Crystal data and structure refinement details for **1a** and **2a** are summarized in Table 1.

CCDC-221555 (for **1a**) and -221556 (for **2a**) contain the supplementary crystallographic data for this paper. These data can be obtained free of charge at www.ccdc.cam.ac.uk/conts/retrieving.html [or from the Cambridge Crystallographic Data Centre, 12 Union Road, Cambridge CB2 1EZ, UK; Fax: (internat.) + 44-1223-336-033; E-mail: deposit@ccdc.cam.ac.uk].

Acknowledgments

U. K. thanks the International University Bremen for research support. U. K. also highly appreciates that the Florida State University Chemistry Department (USA) allowed him unlimited access to the single-crystal X-ray diffractometer. Figure 1−4 were generated by Diamond Version 2.1e (copyright Crystal Impact GbR).

[1] *Polyoxometalate Chemistry for Nano-Composite Design* (Eds.: T. Yamase, M. T. Pope), Kluwer, Dordrecht, **2002**.
[2] *Polyoxometalate Chemistry: From Topology via Self-Assembly to Applications* (Eds.: M. T. Pope, A. Müller), Kluwer, Dordrecht, **2001**.
[3] *Chemical Reviews, Polyoxometalates* (Ed.: C. Hill), **1998**.
[4] *Polyoxometalates: from Platonic Solids to Anti Retroviral Activity* (Eds.: M. T. Pope, A. Müller), Kluwer, Dordrecht, **1994**.
[5] M. T. Pope, A. Müller, *Angew. Chem.* **1991**, *103*, 56−70; *Angew. Chem. Int. Ed. Engl.* **1991**, *30*, 34−48.
[6] M. T. Pope, *Heteropoly- and Isopoly-Oxometalates*, Springer, Berlin, **1983**.
[7] J. Berzelius, *Pogg. Ann.* **1826**, *6*, 369.
[8] [8a] J. F. Keggin, *Nature* **1933**, *131*, 908−909. [8b] J. F. Keggin, *Proc. Roy. Soc., A* **1934**, *144*, 75−77.
[9] D. A. Judd, J. H. Nettles, N. Nevins, J. P. Snyder, D. C. Liotta, J. Tang, J. Ermolieff, R. F. Schinazi, C. L. Hill, *J. Am. Chem. Soc.* **2001**, *123*, 886−897.
[10] [10a] F. B. Xin, M. T. Pope, *Organometallics* **1994**, *13*, 4881−4886. [10b] F. B. Xin, M. T. Pope, G. J. Long, U. Russo, *Inorg. Chem.* **1996**, *35*, 1207−1213. [10c] F. B. Xin, M. T. Pope, *Inorg. Chem.* **1996**, *35*, 5693−5695. [10d] G. Sazani, M. H. Dickman, M. T. Pope, *Inorg. Chem.* **2000**, *39*, 939−943.
[11] [11a] Q. H. Yang, H. C. Dai, J. F. Liu, *Transition Metal Chem.* **1998**, *23*, 93−95. [11b] X. H. Wang, H. C. Dai, J. F. Liu, *Polyhedron* **1999**, *18*, 2293−2300. [11c] X. H. Wang, H. C. Dai, J. F. Liu, *Transition Metal Chem.* **1999**, *24*, 600−604. [11d] X. H. Wang, J. F. Liu, *J. Coord. Chem.* **2000**, *51*, 73−82. [11e] X. H. Wang, J. T. Liu, R. C. Zhang, B. Li, J. F. Liu, *Main Group Met. Chem.* **2002**, *25*, 535−539.
[12] S. Bareyt, S. Piligkos, B. Hasenknopf, P. Gouzerh, E. Lacote, S. Thorimbert, M. Malacria, *Angew. Chem.* **2003**, *115*, 3526−3528; *Angew. Chem. Int. Ed.* **2003**, *42*, 3404−3406.
[13] M. Rusu, A. R. Tomsa, D. Rusu, I. Haiduc, *Synth. React. Inorg. Met.-Org. Chem.* **1999**, *29*, 951−965.
[14] [14a] B. Krebs, B. Lettmann, H. Pohlmann, R. Frohlich, *Z. Kristallogr.* **1991**, *196*, 231−241. [14b] M. Rusu, L. Muresan, A. R. Tomsa, D. Rusu, G. Marcu, *Synth. React. Inorg. Met.-Org.*

 © 2004 Wiley-VCH Verlag GmbH & Co. KGaA, Weinheim

Chem. **2000**, *30*, 499−511. [14c] G. Kastner, H. Reuter, *J. Organomet. Chem.* **2000**, *598*, 381−386. [14d] G. Kastner, H. Reuter, *Main Group Met. Chem.* **2000**, *23*, 383−388.
[15] I. D. Brown, D. Altermatt, *Acta Crystallogr., Sect. B* **1985**, *41*, 244−247.
[16] U. Kortz, M. G. Savelieff, B. S. Bassil, B. Keita, L. Nadjo, *Inorg. Chem.* **2002**, *41*, 783−789.
[17] M. Bösing, I. Loose, H. Pohlmann, B. Krebs, *Chem. Eur. J.* **1997**, *3*, 1232−1237.
[18] U. Kortz, M. G. Savelieff, B. S. Bassil, M. H. Dickman, *Angew. Chem.* **2001**, *113*, 3488−3491; *Angew. Chem. Int. Ed.* **2001**, *40*, 3384−3386.
[19] This conclusion is further supported by a crystal structure which we obtained during the reviewing period of this manuscript. Interaction of $Sn(CH_3)_2Cl_2$ with the well-known $K_{14}[As_2W_{19}O_{67}(H_2O)]$ in aqueous solution at pH 3 resulted in crystals that are composed of discrete polyanions **1** rather than the 2-D material **1a**.
[20] C. Tourné, A. Revel, G. Tourné, M. C. R. Vendrell, *Acad. Sc. Paris, Ser. C* **1973**, *277*, 643−645.
[21] G. M. Sheldrick, SADABS, University of Göttingen, **1996**.

Received January 23, 2004
Early View Article
Published Online April 28, 2004

 © 2004 Wiley-VCH Verlag GmbH & Co. KGaA, Weinheim

An Energy Dispersive X-ray Diffraction Study of Dioxouranium(VI) in 1 M Lithium Citrate

Ermanno Vasca,[a] Giuseppe Palladino,[a] Carla Manfredi,[b] Cecilia Fontanella,[a] Claudia Sadun,[c] and Ruggero Caminiti*[c]

Keywords: X-ray Diffraction / Solution / Uranium / Lithium citrate

An Energy Dispersive X-ray Diffraction (EDXD) study of 0.3 M dioxouranium(VI) in 1 M lithium citrate at pH = 5 is reported. The data are in accordance with the existence of a predominately polynuclear complex containing four U atoms, concluded from potentiometric measurements. The uranium atoms lie at the corners of two triangles sharing one edge. Five O atoms surround each uranyl group, the uranium coordination polyhedron being a pentagonal bipyramid; four U atoms are linked through double or single O bridges. The U–U distances are 3.95 Å and 4.65 Å.
(© Wiley-VCH Verlag GmbH & Co. KGaA, 69451 Weinheim, Germany, 2004)

Introduction

Speciation of dioxouranium(VI) in the presence of organic ligands containing at least one carboxylate group is a topic that is extremely relevant to the safe disposal of nuclear wastes resulting from the use of fission technologies. Actually, modeling the migration of radionuclides in the environment requires an extensive and accurate knowledge of the equilibria involving the contaminating ion, both in solution and at the solid−solution interface. The solution chemistry of highly radioactive actinides, which may be difficult to investigate directly, is frequently simulated by means of the thermodynamic data existing for uranium in the same oxidation state; so, as an example, UO_2^{2+} is often assumed to closely follow the chemical behavior of the NpO_2^{2+} and PuO_2^{2+} ions. Besides the well-established importance of their mononuclear complexes, with a unique or with different ligands, the formation of polynuclear complexes may substantially influence the speciation involved under specific thermodynamic conditions typical of the environment, for instance by enhancing the solubility of a solid phase. In connection with this, the most instructive example is probably represented by the $[(UO_2)_3(CO_3)_6]^{6-}$ complex, which has been since the determination of its formation constant through potentiometry,[1] extensively investigated by a large number of different techniques.[2,3,4] Similar investigations are still performed, first potentiometrically and then by other methods, on the complexes between UO_2^{2+} and acetate, UO_2^{2+} and oxalate, and UO_2^{2+} with ligands containing at least one carboxylic group.

Much interest has also been devoted to the dioxouranium(VI) citrate system,[5] in which the existence of polynuclear species of general stoichiometry $H_x(UO_2)_yL_z^{(x+2y-3z)+}$ (L indicates the citrate ion, $C_6H_5O_7^{3-}$) with different (x,y,z) coefficients [5−11] has been demonstrated. Nevertheless, despite large experimental efforts, the actual composition of polynuclear species with $y > 2$ and $z > 2$ is still a controversial topic: amongst the stoichiometries suggested on the basis of data from potentiometry, spectroscopy and other techniques (e.g. Electrospray Mass Spectrometry) there are $(x,2,1)$,[12] $(x,6,6)$,[7] $(x,3,2)$, and $(x,3,3)$.[11] The problem must certainly be tackled by combining a multiplicity of techniques. Electrochemical methods (mainly potentiometry) can be of fundamental importance in determining the stoichiometry and the formation constants of the complexes existing under different analytical conditions. On the other hand, spectroscopic methods may help to determine the actual structure of the species in solution.

The aim of the present work is to explore the possibility of studying the dioxouranium(VI) citrate system by using an approach like the one just described, by combining potentiometry and the Energy Dispersive X-ray Diffraction (EDXD) technique. The main difficulty lies in needing to work at dioxouranium(VI) concentrations (0.1 mol/dm^3 − 0.3 mol/dm^3) which are about one order of magnitude different from those usually used in each technique. A further goal of this work is to determine if the X-ray diffraction

[a] Dipartimento di Chimica, Università di Salerno, Via S. Allende 43, 84081 Baronissi (SA), Italy
[b] Dipartimento di Chimica, Università di Napoli "Federico II", Via Cinthia, 80126 Napoli, Italy
[c] Dipartimento di Chimica, Istituto Nazionale per la Fisica della Materia, Università degli Studi di Roma "La Sapienza", P.le Aldo Moro 5, 00185 Roma, Italy
E-mail: r.caminiti@caspur.it
Supporting information for this article is available on the WWW under http://www.eurjic.org or from the author.

Table 1. Composition of the solutions analyzed by EDXD; concentrations are given as mol·dm^{-3} (upper values) and as the number of atoms in the stoichiometric unit volume V/Å^3 (lower values)

Solution	Concentrations					Density (g/cm^3)	V (Å^3)
	[Li^+]	[$C_6H_5O_7^{3-}$]	[ClO_4^-]	[UO_2^{2+}]	[H_2O]		
A	3.000	1.000	0.676	–	49.0248	1.161	533.511
	1	0.3333	0.22533	–	16.34163		
B	3.000	1.000	0.6574	0.3004	48.27821	1.228	533.511
	1	0.3333	0.21913	0.10013	16.09276		

pattern of relatively concentrated (about 0.3 molar) uranyl solutions in the presence of a threefold concentration of citrate can be interpreted by assuming the U–U and U–O distances previously reported by a number of authors.[13–16]

1. Results and Discussion

The analysis of the experimental data was performed using the *difference method*. This method has been successfully applied to liquid systems, in neutron diffraction and isotopic substitutions.[17–22] Here the assumption has been made that the perturbations induced by the presence of the solute has a limited influence on the bulk lithium citrate and perchloric acid solution. The structure of the lithium citrate and perchloric acid solution was mainly preserved because it is three times more concentrated than the solute uranyl perchlorate. The experimental curves from the lithium citrate and perchloric acid solutions were then subtracted from the dioxouranium(VI) experimental curves. In so doing all the interactions occurring in both solutions were cancelled, i.e. water–water, water–lithium citrate and perchlorate, lithium citrate–lithium citrate and perchlorate, and perchlorate–perchlorate. It was then possible to exclusively focus attention onto the interactions of the uranyl–uranyl and uranyl–other constituent in solution .The concentrations of the two solutions that were analyzed are reported in Table 1.

In the following the observed structure functions are reported [in the form $qi(q)M(q)$, in Figure 1, along with the radial distribution functions (*rdf*), in the form $D(r)_{\text{difference}} = D(r) - 4\pi r^2(\rho_0)$ for the water citrate solution and the citrate dioxouranium(VI) solution measured under the same experimental conditions.

The main features emerging from a qualitative analysis of both structure functions and radial distribution functions are significant and the presence in the dioxouranium(VI) solution of evident peaks at high values of r, implies an increase of order in solution for the lithium citrate and perchloric acid solution.

This pattern is particularly evident in the $D(r)_{\text{difference}}$ curves. As shown in Figure 1, the lithium citrate and perchloric acid solution (solution **A**) exhibits a large main peak at 2.5–6.0 Å and a second peak at 6.0–8.0 Å. In the dioxouranium(VI) solution *rdf* (solution **B**), we can discern peaks positioned at the same values of those present in the first solution rdf. This is expected because the concentration

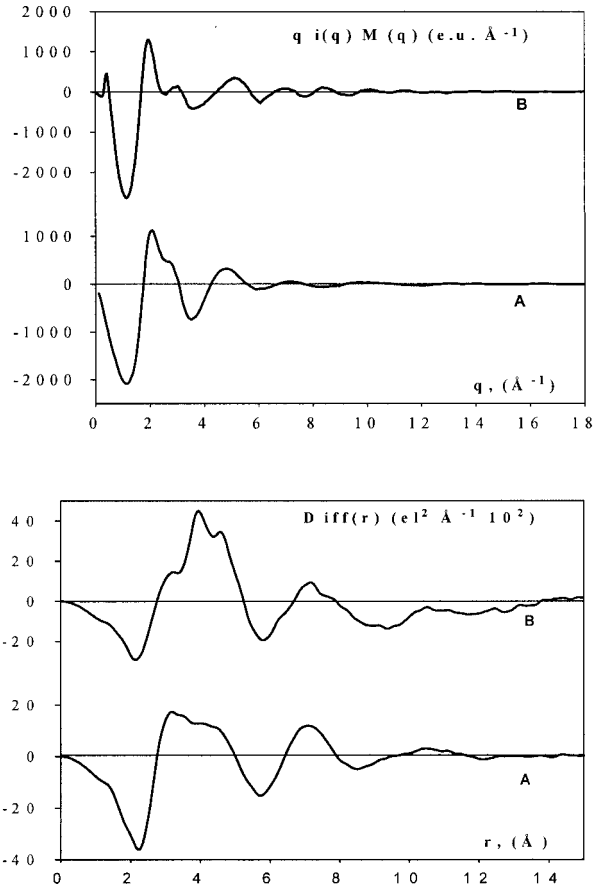

Figure 1. Top: experimental structure function in the form $q\ i(q)\ M(q)$: (**A**) Lithium citrate and perchloric acid solution, (**B**) dioxouranium(VI) solution; bottom: experimental radial distribution function in the form $D(r)_{\text{difference}} = D(r) - 4\pi r^2\rho$: (**A**) lithium citrate and perchloric acid solution, (**B**) dioxouranium(VI) solution

of lithium citrate is equal in the two solutions, and the concentration of ClO_4^- ions of the solution containing perchloric acid (solution **A**) is equivalent to the concentration of ClO_4^- ions due to the presence of dioxouranium(VI) perchlorate in the second solution (solution **B**). In the dioxouranium(VI) solution new peaks appear, namely the peak at 3.95 Å due to the interactions of the U atoms between themselves and between the constituent of the solution: water, lithium, citrate and perchlorate ions.

The features discussed above were used to build a structural model, the theoretical structure function and the theoretical distribution function, which best explained the

 © 2004 Wiley-VCH Verlag GmbH & Co. KGaA, Weinheim

experimental data. Theoretical peaks were calculated by the Fourier transformation of a model structure function obtained by the Debye Equation (1) for pairs of interactions using the same sharpening factor, the same $q_{max.}$ value as for experimental data and assuming σ_{mn} to be the root mean square (r.m.s.) variation in the interatomic distance.

$$i_{mn}(q) = \{f_m \cdot f_n \cdot [\sin(r_{mn} \cdot q)/r_{mn} \cdot q] \cdot \exp(-1/2 \cdot \sigma^2_{mn} q^2)\} \quad (1)$$

Instead of using a σ_{mn} value for each distance r_{mn}, the number of the parameters has been reduced, by assuming the same σ value for distances within predefined ranges; predefined ranges used are reported in Table 2.

Table 2. Final values of the adjusted r.m.s. σ for the model used

σ Values (Å)	Distance range (Å)
0.05	$0.0 < r \leq 1.9$
0.13	$1.9 < r \leq 3.0$
0.20	$3.0 < r \leq 5.6$
0.25	$5.6 < r \leq 9.0$
0.30	$r > 9.0$

As previously noted, the "*difference method*" was used to test the experimental data. The experimental $D(r)$ curves of both solutions, namely (**A**) lithium citrate and perchloric acid solution and (**B**) dioxouranium(VI) solution, and the difference curve between the two experimental $D(r)$ curves are reported in Figure 2.

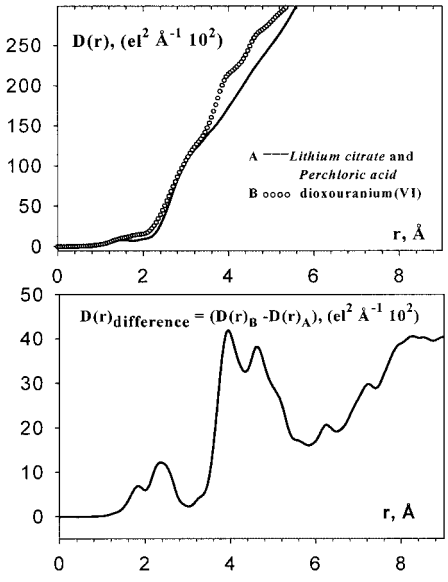

Figure 2. Top: experimental radial distribution function in the form $D(r)$; (**A**) lithium citrate and perchloric acid solution, (**B**) dioxouranium(VI) solution; bottom: experimental difference curve between the experimental radial distribution functions of solution (**B**) [dioxouranium(VI) solution], and solution (**A**) (lithium citrate and perchloric acid solution)

The experimental $D(r)$ difference curve only contains the interactions involving the UO_2^{2+} ions and the other constituent of solution **B**. Thus all the interactions which are also present in solution **A** have been eliminated from solution **B**. In fact the first peak in the difference curve occurs at 1.78 Å and corresponds to the U−O distances in the UO_2^{2+} ion and there are no peaks at lower distances due to the bond lengths in the citrate and perchlorate ions. Hence the first peak is exactly reproduced, in the theoretical peak shape function; on the basis of the two interactions U−O at 1.78 Å, with a σ value 0.05, it can be assumed that the second peak at 2.4 Å represents only the metal O coordination peak. The coordination number has been determined as five; the U−O distances are not equal for all the interactions, but are in the range 2.35−2.50 Å, i.e. two O atoms are coordinated at 2.35 Å, two at 2.40 and one at 2.50, with an average value of 2.40 Å: all these considered distances are in the range 1.9−3.0 Å to which a σ value 0.20 is attributed. The theoretical functions and the experimental one are shown in Figure 3.

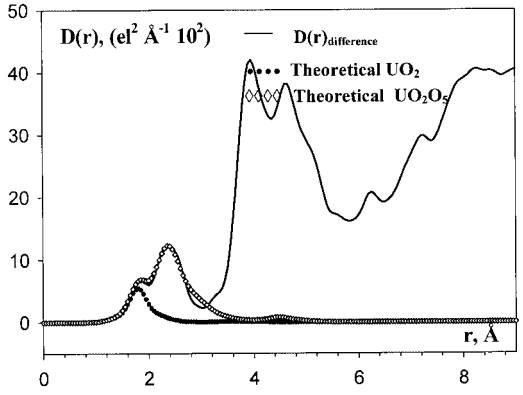

Figure 3. Experimental radial distribution functions difference curve $D(r)_{difference}$ (−−), the theoretical peak shape function of U−O interactions in UO_2^{2+} ion (solid circles), and the theoretical peak shape function of U−O interactions the in UO_2^{2+} ion coordinating five O atoms (open diamonds)

The bond lengths, and their spatial disposition are in good agreement with the literature data: dioxouranium(VI), in solution and in the solid state, is coordinated with five neighbors; the uranium atoms are at the centers of neighboring pentagonal bipyramids.[14]

The large peak at about 3.95Å indicates that the five O atoms, positioned on the equatorial plane of the pentagonal bipyramid, do not belong to the citric anions present in solution. The contributions of the five C atoms, bound to the O atoms, are altogether inadequate to fit the experimental peak.

On the basis of the literature data, tests have been performed for the presence of polynuclear complexes in solution. The first hypothesis tested, was the presence of binuclear complexes; two uranyl groups bonded by two bridging O atoms, with the uranium atoms at the center of neighboring pentagonal bipyramids having one common edge, with an usual U−U distance of 3.95 Å. Calculating the theoretical peak shape function, by a dimeric compound model, with a σ value of 0.20, a peak positioned at

 © 2004 Wiley-VCH Verlag GmbH & Co. KGaA, Weinheim

3.95Å appears, but is still largely inadequate to reproduce the experimental one, as is shown in Figure 4.

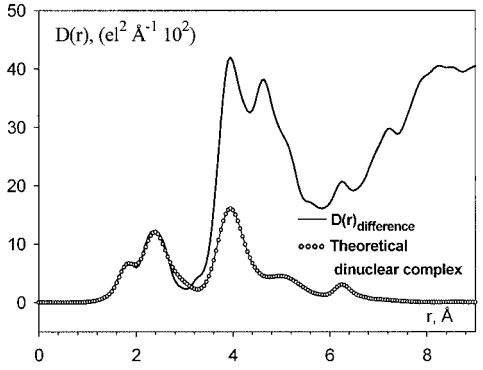

Figure 4. Experimental radial distribution functions difference curve $D(r)_{difference}$ (−−), the theoretical peak shape function of U−O interactions in binuclear complex $[(UO_2^{2+})O_5]_2$ (open circles)

The theoretical peak shape function was calculated for a model containing only the U−O interactions. The model of the binuclear complex is shown in Figure 5. Adding the U−C interactions, arising from the citric anions, bound to the O atoms, the experimental peak height is not reached.

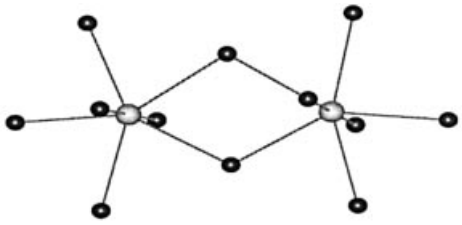

Figure 5. Picture of the model of the binuclear complex

A trinuclear model was successively tested. The position of the three U atoms, in a triangular unit, was supposed to be both symmetric and asymmetric; each U atom was considered to be surrounded by seven O atoms, and the coordination polyhedron was a pentagonal bipyramid, with the two apical O atoms belonging to the uranyl atoms. The model was constructed imposing the distance values previously obtained; 1.78 Å for the uranyl U−O distance and an average value of 2.42 Å, with a variation from 2.35 to 2.50 Å, for the remaining five O atoms. The three U atoms were positioned at the corner of an equilateral triangle with an edge length of 3.95 Å, or at the corner of a scalene triangle with an average edge length of 3.95 Å. The theoretical peak shape function obtained applying the model previously described only reproduces the experimental one with regards to the peak at 3.95. Adding the interactions arising from the citrate anions, belonging to the oxygen atoms that are free in the trinuclear complex, the height of the successive peak in the experimental function is not reached.

On the basis of the former considerations and of the potentiometric results it was supposed that a tetranuclear complex is present in solution of. The complex had to maintain the distorted pentagonal bipyramidal configuration around the U atoms, three U−U interactions at 3.95 Å and it had to create U−U interactions at 4.65 Å.

The structure of the tetramer is shown in Figure 6. The four uranium atoms lie at the corners of two isosceles triangles, with two edge length of 3.95 Å and the other edge length of 4.65 Å. The two triangles share one of the edges measuring 3.95 Å. They are not coplanar showing a dihedral angle of 35.30°. Each uranyl group is surrounded by five O atoms, as in dinuclear and trinuclear tested complexes.

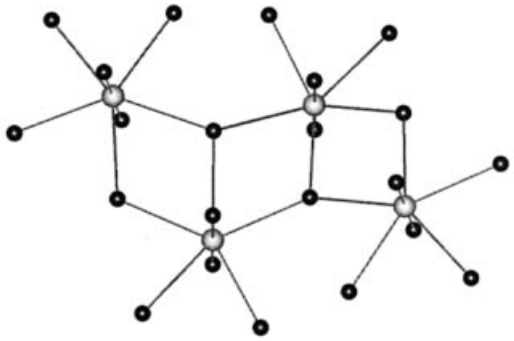

Figure 6. Picture of the model of the tetranuclear complex

In Figure 7 the experimental radial distribution function in the difference form $D(r)_{difference}$ is compared to the theoretical one, obtained from the model shown in Figure 6.

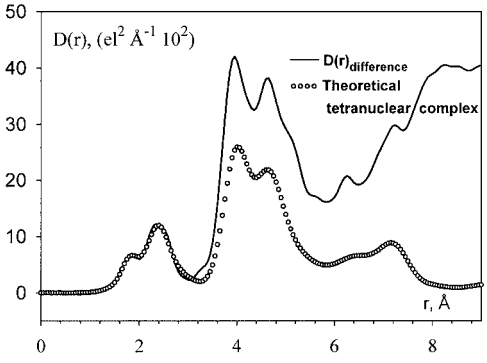

Figure 7. Experimental radial distribution functions difference curve $D(r)_{difference}$ (−−), the theoretical peak shape function of U−O interactions in tetranuclear complex $[(UO_2^{2+})_4O_{14}]$ (open circles)

Even if the trend of the theoretical curve, calculated with the tetranuclear model, is analogous to that of the experimental curve, it is not reproduced. The theoretical peaks are remarkably lower than the experimental ones. For this reason models obtained from a larger number of UO_2 units have been tested. Pentanuclear and esanuclear complexes, arranged according to various geometries, have been tried. The models were constructed imposing the distance values previously obtained (1.78 Å uranyl U···O distance and an average value of 2.42 Å for the remaining five O atoms). The five or six U atoms were positioned at the corners of various geometrical figures with edge lengths of 3.95 Å, or

 © 2004 Wiley-VCH Verlag GmbH & Co. KGaA, Weinheim

4.65 Å opportunely distributed, in order to reproduce the experimental curve. It turns out that these models are not acceptable since the heights of the obtained peaks, in the theoretical peak shape function, were much too high, with respect to the experimental ones, in order to allow for the presence of a second sphere of coordination around the atom of uranium.

Therefore it was decided to return to the study of the tetranuclear complexes, and to reconsider the second coordination sphere. Since the concentration of citrate anions is three times higher than the concentration of the uranyl cations, it was assumed that at least one oxygen atom, between those bound to the uranyl, belong to a citrate carboxylic group. The theoretical peak shape function, calculated by this model, still did not give a good agreement with the experimental data. Models with a greater number of citrate interactions were tested, but these gave way to theoretical functions that exceeded the experimental ones, especially for the peak at 3.95 Å.

Therefore a further hypothesis was considered; that the contributions that were still lacking came from water molecules and due to hydrogen bonds with the oxygen atoms of the uranyl group a first coordination sphere of the complex could still be considered.

The model was constructed with the geometry parameters previously reported when only the U−O interactions were considered. The four O atoms bridging the four uranyl cations belong to OH^- groups that, with the four citrate anions, neutralize the positive charge of the uranyls. The possible model of the citrate coordination in the tetranuclear complex is shown in Figure 8 (see a). Six water molecules supplying the other O atoms that surround the U atoms and sixteen water molecules are bound to the eight O atoms of the uranyl cations by hydrogen bond with a O−O distance of about 2.86 Å and OÔU angle of about 115°.

In order to simplify the model construction, the tetranuclear complex was considered to have a symmetry center and the citrate anions to have the same spatial configuration. This conformational restriction, regarding the citrate anions, leads to the theoretical function not perfectly reproducing the experimental one. Different citrate anion conformations would allow a greater variability of the distances and therefore a better agreement between the experimental data and the theoretical peak shape function.

In Figure 9, the comparison between the experimental function and the theoretical one, calculated for the model previously described, is shown.

On the basis of NMR literature data, the possibility of the hydroxy group and the α-carboxyl group being involved in coordination was tested. The comparison between the experimental function and the theoretical one, calculated for the model proposed by NMR spectroscopic data, maintaining the uranyl first coordination sphere, unaltered with respect to the previously tested model, shows comparable concordance, Figure 9. For this model, the tetranuclear complex was also considered to have a symmetry center, but the conformational restrictions are superior with respect to the other model due to the five atom ring formation, Figure 8 (b). The X-ray diffraction in this case, is unable to discriminate between the two citrate coordination manners: for this purpose the information supplied from NMR spectroscopy may be fundamental. A better agreement between the experimental data and the theoretical function was not attempted since a refined structural analysis exceeded the main interest of this study, whose aim was to determine which form had the prevailing polynuclear uranyl citrate complexes.

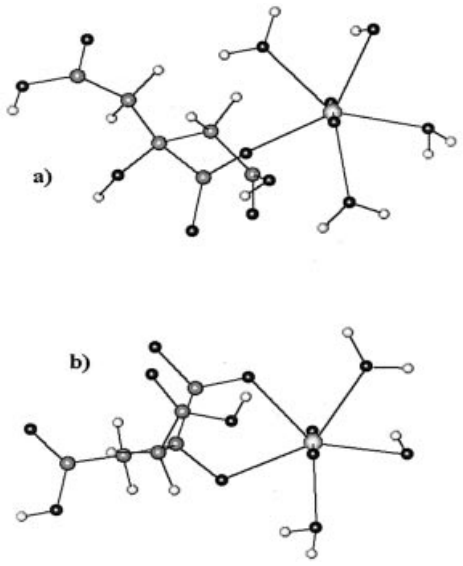

Figure 8. Picture of the models of the citrate coordination in tetranuclear complex: a) $[(UO_2^{2+})_4Cit_4O_6]\cdot 16H_2O$ and b) $[(UO_2^{2+})_4Cit_4O_2]\cdot 16H_2O$

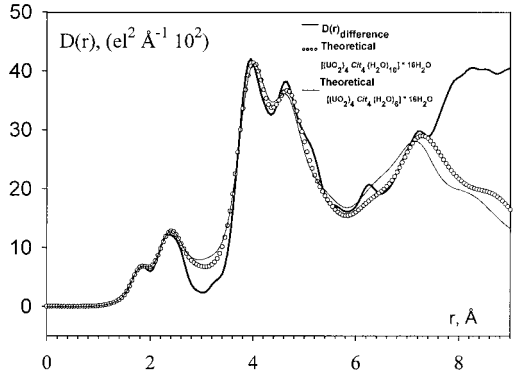

Figure 9. Experimental radial distribution functions difference curve $D(r)_{difference}$ (bold line), the theoretical peak shape functions of the tetranuclear complex $[(UO_2^{2+})_4Cit_4(H_2O)_{10}]\cdot 16H_2O$ (open circles) and $[(UO_2^{2+})_4Cit_4(H_2O)_6]\cdot 16H_2O$ (----)

2. Conclusions

A structural study on a uranyl perchlorate diluted solution in 1 M lithium citrate, with a ratio [total citrate]/[U^{VI}] > 3, has been carried out by means of X ray diffraction, on

 © 2004 Wiley-VCH Verlag GmbH & Co. KGaA, Weinheim

the basis of a preliminary speciation study of the solution performed potentiometrically. The experimental data, treated and interpreted using the *differences method*, shows the occurrence of tetranuclear dioxouranium(VI) citrate complexes in solution. Further data, both potentiometric and spectroscopic, will be needed in order to unequivocally describe the citrate coordination around the dioxouranium(VI) polynuclear complexes.

3. Experimental Section

3.1 Sample Preparation. Reagents and Materials: All the solutions analyzed, Table 1, were prepared by using doubly distilled water. The uranyl perchlorate stock solution was prepared and standardized, with an accuracy of 0.3%, as suggested in ref.[1] starting from $UO_2(NO_3)_2{\cdot}6H_2O$ (Fluka p. a.). Perchloric acid solutions at different concentrations, prepared by diluting the 70% product from Fluka, were standardized using both $KHCO_3$ or HgO as primary standards (Fluka analytical grade) and methyl red or phenolphthalein, respectively, as indicators; analyses agreed within 0.1%. Concentrated lithium citrate and sodium citrate solutions were prepared from $Li_3C_6H_5O_7{\cdot}4H_2O$ (> 99.5%, Fluka) and $Na_3C_6H_5O_7{\cdot}2H_2O$ (> 99.5%, Fluka) respectively, which were not further purified. Sodium perchlorate was prepared and standardized as described elsewhere.[1]

The pH of solution **B** was 5.10±0.02 at 18 °C. It was measured with a Metrohm 691 pH-meter equipped with a 6.0232.100 glass combined electrode (Metrohm); the electrode was calibrated with IUPAC pH standards. The potentiometric data were recorded around the clock using Metrohm 6.0123.100 and 6.0726.100 electrodes, a 34970A Data Acquisition/Switch Unit pursued by Agilent Technologies and automatic burettes 715 Dosimat from Metrohm. Impedance adaptors were used to collect the data with a precision of 0.01 mV. The software TITPOT (by InLab, www.inlab.it) was used to control the experiments through a personal computer.

3.2 Potentiometric Measurements: Potentiometry was used to study the speciation of the uranyl ion in the presence of citrate. While the system is quite well-known at dioxouranium(VI) concentrations lower that 10 mM a preliminary experiments were performed at higher metal concentrations, in order to better define the stoichiometry of the polynuclear complexes other than the dimer. The results of a preliminary experiment are presented here, which is part of a more systematic investigation now in progress.

The experiment has been performed as a potentiometric titration. An accurately known volume of the test solution TS [TS: 0.100 M $UO_2(ClO_4)_2$, 0.100 M $HClO_4$, 2.700 M $NaClO_4$] placed into a vessel thermostatted at (25.00±0.02) °C, has been titrated in the dark, under a nitrogen stream, with known volumes, V_T, of the solution T (T: 0.100 M $UO_2(ClO_4)_2$, 0.700 M Na_3L, 0.150 M NaOH, 2.800 M $NaClO_4$). After each addition the $[H_3O^+]$ was determined from the EMF, E_I (in mV), of the cell (I). Cell I: Glass Electrode/Test Solution/Reference Electrode by using the Nernst Equation (2).

$$E_I = E^0 + 59.16{\cdot}\log[H_3O^+] + Ej \qquad (2)$$

In Equation (2) the cell constant E^0 was determined in two separate experiments performed before and after the titration, while the liquid junction potential Ej was evaluated as described elsewhere.[23] A second type Ag,AgCl electrode was used as the reference electrode; it was external to the cell but in electrical contact with TS through a salt bridge: 3.000 M $NaClO_4$/0.010 M $AgClO_4$, 2.990 M $NaClO_4$/AgCl,Ag.

The primary (V_T, E_I) data collected allowed us to span the $1.14 < -\log[H_3O^+] < 4.34$ range, and was processed using the least-squares program Hyperquad[24] in order to determine the equilibrium constant, β_{xyz}, of the general reaction (3)

$$x{\cdot}[H^+] + y{\cdot}[UO_2^{2+}] + z{\cdot}[L^{3-}] = [H_x(UO_2)_yL_z]^{(x+2y-3z)+} \qquad (3)$$

Several models have been tested. On the basis of the literature data,[5] under the experimental conditions chosen it is expected that the concentration of mononuclear complexes is very small, and hence negligible. In Table 3 the results that gave the least standard deviation are reported, while in Table 4 the proposed model with the formation constant of each species is presented.[25−27]

Table 3. Survey of the standard deviation of different speciation models

Model	σ (mV)
(0,1,1), (0,2,2), (1,3,3), (−2,4,4)	0.2299
(0,2,2), (2,3,2), (1,3,3), (−2,4,4)	0.2254
(1,1,1), (0,2,2), (1,3,3), (−2,4,4)	0.1593
(0,2,2), (0,3,2), (1,3,3), (−2,4,4)	0.1456
(0,2,2), (1,3,2), (1,3,3), (−2,4,4)	0.1158

Table 4. Formation constants of the $H_x(UO_2)_yL_z^{(x+2y-3z)+}$ species at 25 °C in 3 M $NaClO_4$

(*x*,*y*,*z*)	$\log\beta_{xyz} \pm 3\sigma$
(0,2,2)	17.96 ± 0.01
(1,3,2)	20.95 ± 0.06
(1,3,3)	30.19 ± 0.01
(−2,4,4)	28.50 ± 0.02

Owing to the high citrate concentration of the titrant solution, the ionic strength of the titrated solution increased from 3.1 M to about 4.2 M; nevertheless, the actual ionic strength variations are probably smaller, owing to the fact that part of the citrate is not present as the trivalent anion but is in the form of the polynuclear uranyl complexes, variously protonated. Thus the overall accuracy of the reported data is estimated to be of about 2−3%.

Table 5. Auxiliary data used for the calculation of the distribution diagram of Figure 1

Reaction	log *K*	Ref.
$H_2O = H^+ + OH^-$	−14.22	[25]
$H^+ + L^{3-} = HL^{2-}$	5.16 ± 0.03	[26]
$2H^+ + L^{3-} = H_2L^-$	9.46 ± 0.03	[26]
$3H^+ + L^{3-} = H_3L$	12.70 ± 0.04	[26]
$UO_2^{2+} + H_2O = UO_2OH^+ + H^+$	−5.03 ± 0.06	[27]
$2UO_2^{2+} + 2H_2O = (UO_2)_2(OH)^{2+} + 2H^+$	−6.01 ± 0.02	[27]
$3UO_2^{2+} + 5H_2O = (UO_2)_3(OH)_5^+ + 5H^+$	−16.13 ± 0.03	[27]

 © 2004 Wiley-VCH Verlag GmbH & Co. KGaA, Weinheim

By using the set of constants of Table 4 and the auxiliary data of Table 5 the distribution diagram presented in Figure 10 was constructed. The diagram has been calculated by assuming $[U^{VI}] = 0.3$ M and [total citrate] = 1 M.

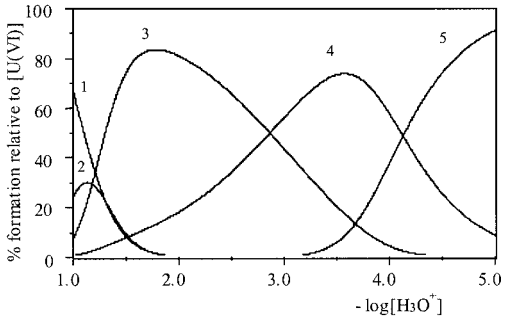

Figure 10. Distribution diagram of the uranyl citrate system; the curves have been calculated by using the data set reported in Tables 3 and 4, and assuming $[U^{VI}] = 0.3$ M and [total citrate] = 1 M; L represents the citrate anion, $C_6H_5O_7^{3-}$; the numbers on the curves indicate the following species: UO_2^{2+} (curve 1); $H(UO_2)_3L_2^{+}$ (curve 2); $H(UO_2)_3L_3^{2-}$ (curve 3); $(UO_2)_2L_2^{2-}$ (curve 4); $(UO_2)_4(OH)_2L_4^{6-}$ (curve 5)

The results of the potentiometric titration suggested the best experimental conditions for the X-ray measurements: a solution containing 0.3 mol dioxouranium(VI) and 1 mol citrate per dm^3, in which sodium should rather be substituted by lithium, because the Li−O distances interfere less with the other ones expected in the system.

3.3 EDXD Measurements: Several examples of the application of Angle Dispersive, or Energy Dispersive X-ray Diffraction to pure liquids and solutions of metal ions in various solvents can be found in the literature.[28−32]

In the present work, the Energy Dispersive X-ray Diffraction (EDXD) technique has been used. Compared with traditional ADXD (angular dispersion), it has several advantages:[33−38] Diffraction patterns are collected in a much shorter period of time, using only a few reflection angles, but still covering q ranges equal to or larger than those obtained by AD; samples are stored in sealed cells, which avoid evaporation and contamination by moisture in the air.

Experiments were performed by using the noncommercial energy-scanning diffractometer built at the Department of Chemistry, Rome University. Detailed descriptions of the instrument and the technique can be found elsewhere.[35−37]

Transmission geometry has been employed. The White Bremsstrahlung component of the radiation emitted by a tungsten tube working at 50 kV and 40 mA was used. Scattered intensities for the samples and the empty cell were measured at seven different angles. This choice allowed us to cover a wide range of the scattering variable q, namely between 0.23−18 $Å^{-1}$. The measuring time at each angle was set so as to obtain a minimum of 1000000 counts per experimental point for $q > 5$ $Å^{-1}$ and 300000 for $q < 5$ $Å^{-1}$, where q is given by Equation (4)

$$q = 4\pi\cdot\sin\theta/\lambda = 1.014\cdot E\cdot\sin\theta \quad (4)$$

When E is expressed in keV and q in $Å^{-1}$, measurement angles, the energy range used and scattering parameters are reported in Table 6.

Table 6. Scattering parameters associated with the energy range used (13.0 −43.7 keV) for each measurement angle

Scattering angles (degree)	q range ($Å^{-1}$)
24.0	5.36−18.00
15.5	3.52−11.84
8.0	1.83−6.17
5.0	1.15−3.86
3.0	0.69−2.32
2.0	0.46−1.55
1.5	0.34−1.16
1.0	0.23−0.77

The primary beam intensity $I(E)$ was measured directly using the same voltage, by reducing the tube current to 10 mA at a zero scattering angle without the sample. Transmission of the sample was measured under the same conditions. Both quantities are needed to carry out necessary conditions to observed scattered intensities.[35−38] After correction of experimental data for escape peak suppression,[35−38] the various angular sets were combined and the re-scaled intensity, in electron units (e. u.), was normalized to a stoichiometric unit volume containing one Li atom. Such correction is performed using our program DIF1, written ad hoc. Detailed description of procedures and formulae used can be found in refs.[25−28]. The atomic and water concentrations, together with stoichiometric volume and density, are reported in Table 1 (in $mol^{-1}\cdot Å^3$ and g/cm^3, respectively). The "static" structure function $I(q)$ was constructed according to Equation (5), where f_i are the atomic scattering factors, x_i are the number of concentrations of i-type atoms in the stoichiometric unit, $I_{e.u.}$ is the observed intensity in electron units.

$$i(q) = I_{e.u.} - \Sigma x_i f_i^2 \quad (5)$$

Fourier transformation of $i(q)$ led to radial distributions (rdf)

$$D(r) = 4\pi r^2\cdot\rho_0 + (2r/\pi)\int_0^{q\,max} qi(q)M(q)\sin(rq)dq \quad (6)$$

In Equation (6) ρ_0 is the bulk number density of stoichiometric units and

$$M(q) = [f_U^2(0)/f_U^2(q)]\exp(-0.01q^2) \quad (7)$$

is the sharpening factor; the value of 18 $Å^{-1}$ was used as the upper limit of integration.

Supporting Information: Primary potentiometric data are available (see footnote on the first page of this article).

Acknowledgments

The authors would like to thank Professor Diego Ferri of the Department of Chemistry of the University of Naples "Federico II" for his helpful comments and discussion.

 © 2004 Wiley-VCH Verlag GmbH & Co. KGaA, Weinheim

[1] L. Ciavatta, D. Ferri, I. Grenthe, F. Salvatore, *Inorg. Chem.* **1981**, *20*, 463−467.
[2] M. Åberg, D. Ferri, J. Glaser, I. Grenthe, *Inorg. Chem.* **1983**, *22*, 3981−3985.
[3] D. Ferri, J. Glaser, I. Grenthe, *Inorg. Chim. Acta* **1988**, *148*, 133−134.
[4] P. G. Allen, J. J. Bucher, D. L. Clark, N. M. Edelstein, S. A. Ekberg, J. W. Gohdes, E. A. Hudson, N. Kaltsoyannis, W. W. Lukens, M. P. Neu, P. D. Palmer, T. Reich, D. K. Shuh, C. D. Tait, B. D. Zwick, *Inorg. Chem.* **1995**, *34*, 4797−4807.
[5] L. Pettit, G. Pettit, K. J. Powell, *IUPAC Stability Constants Database*, IUPAC and Academic Software, Otley (UK), **1994−1999**.
[6] I. Feldman, C. A. North, H. B. Hunter, *J. Phys. Chem.* **1960**, *64*, 1224−1230.
[7] K. S. Rayan, A. E. Martell, *Inorg. Chem.* **1965**, *4*, 462−469.
[8] G. Markovits, P. Klots, L. Newman, *Inorg. Chem.* **1972**, *11*, 2405−2408.
[9] E. Prenesti, P. G. Daniele, S. Berto, *Proceedings of the XIII Spanish-Italian Congress on Thermodynamics of Metal Complexes*, Santiago de Compostela, Spain, 2−6 June, **2002**.
[10] S. Sammartano, University of Messina, *private communication*, Messina, Italy.
[11] S. P. Pasilis, J. E. Pemberton, *Abstract of Papers*, 225th ACS National Meeting, New Orleans, LA, United States, March 23−27, **2003**.
[12] I. Feldman, W. F. Neuman, *J. Am. Chem. Soc.* **1951**, *73*, 2312−2315.
[13] M. Aberg, *Acta Chem. Scand.* **1970**, *24*, 2901−2915.
[14] M. Aberg, *Acta Chem. Scand.* **1971**, *25*, 368−369.
[15] M. Aberg, *Acta Chem. Scand., Ser. A* **1976**, *30(7)*, 507−514.
[16] J. Jiang, M. J. Sarsfield, J. C. Renshaw, F. R. Livens, D. Collison, J. M. Charnock, M. Helliwell, H. Eccles, *Inorg. Chem.* **2002**, *41*, 2799−2806.
[17] L. Gontrani, R. Caminiti, L. Bencivenni, C. Sadun, *Chem. Phys. Lett.* **1999**, *301*, 131−137.
[18] R. Caminiti, M. Carbone, S. Panero, C. Sadun, *J. Phys. Chem.* **1999**, *3*, 10348−10355.
[19] R. H. Tromp, G. W. Neilson, *J. Phy. s Chem.* **1996**, *100*, 7380−7383.
[20] D. Atzei, T. Ferri, C. Sadun, P. Sangiorgio, R. Caminiti, *J. Am. Chem. Soc.* **2001**, *123*, 2552−2558.
[21] R. Saladino, V. Neri, A. R. Pelliccia, R. Caminiti, C. Sadun, *J. Org. Chem.* **2002**, *67*, 1323−1332.
[22] C. Sadun, R. Bucci, A. L. Magrì, *J. Am. Chem. Soc.* **2002**, *124*, 3036−3041.
[23] G. Biedermann, G. Douhéret, *Chem. Scripta* **1980**, *16*, 144−153.
[24] P. Gans, A. Sabatini, A. Vacca, *Talanta* **1996**, *43*, 1739−1753.
[25] N. Ingri, G. Lagerstrom, M. Frydman, L. G. Sillén, *Acta Chem. Scand.* **1957**, *11*, 1034.
[26] F. Pugliese, *Thesis*, **2002**, University of Salerno, Faculty of Sciences, Baronissi (SA) Italy.
[27] G. Palladino, unpublished results.
[28] J. E. Enderby, G. W. Neilson, in *Water-A Comprehensive Treatise* (Ed.: F. Franks), Plenum Press, New York, **1979**, vol. 6, chapter 1.
[29] A. H. Narten, H. A. Levy, *J. Chem. Phys.* **1971**, *55*, 2263.
[30] H. Ohtaki, S. Itoh, T. Yamaguchi, S. Ishiguro, B. M. Rode, *Bull. Chem. Soc. Jpn.* **1983**, *56*, 3406.
[31] R. Caminiti, *Chem. Phys. Lett.* **1982**, *86*, 214.
[32] R. Caminiti, M. Carbone, C. Sadun, *J. Mol. Liquids* **1998**, *75*, 149.
[33] T. Egami, *J. Mater. Sci.* **1978**, *13*, 2587.
[34] T. Ijima, K. Nishikawa, *J. Appl. Cryst.* **1988**, *21*, 943.
[35] G. Fritsch, D. A Keimel, *J. Mater. Sci. Eng.* **1991**, *A 134*, 888.
[36] R. Caminiti, M. Carbone, G. Mancini, C. Sadun, *J. Mat. Chem.* **1997**, *7(8)*, 1331.
[37] R. Caminiti, C. Sadun, V. Rossi, F. Cilloco, R. Felici, XXVth Italian Congress of Physical Chemistry, Cagliari, **1991**, p. 4138; It. Pat 01261484, June 23, **1993**.
[38] K. Nishikawa, T. Iijima, *Bull. Chem. Soc. Jpn.* **1984**, *57*, 1750.

Received October 16, 2003
Early View Article
Published Online May 5, 2004

 © 2004 Wiley-VCH Verlag GmbH & Co. KGaA, Weinheim

Synthesis and Characterization of a Series of Lanthanide Complexes Constructed from Orotic Acid

Xing Li,[a] Qian Shi,[a] Daofeng Sun,[a] Wenhua Bi,[a] and Rong Cao*[a]

Keywords: Lanthanides / O ligands / Polymers / Solvothermal synthesis

The solution reaction of orotic acid (2,6-dioxo-1,2,3,6-tetrahydropyrimidine-4-carboxylic acid, H_3dtpc) and $Ln(NO_3)_3 \cdot 6H_2O$ (Ln = La, Ce) or Ln_2O_3 (Ln = Pr, Nd) yielded five complexes $[\{Ln(^aH_2dtpc)_2(^bH_2dtpc)(H_2O)_4\} \cdot H_2O]_n$ (Ln = La **1**, Ce **3**), $[La(^aH_2dtpc)_2(^cH_2dtpc)(H_2O)_6] \cdot 4H_2O$ (**2**), and $[Ln(^aH_2dtpc)_2(OH)(H_2O)_6] \cdot (H_3dtpc)_2 \cdot 7H_2O$ (Ln = Pr **4**, Nd **5**). Complexes **1** and **3** possess 1D chain structures, **2** is a mononuclear structure, and **4** and **5** are mononuclear complexes that are extended into infinite honeycomb structures through hydrogen bonding interactions. The hydrothermal reaction of orotic acid and Ln_2O_3 (Ln = La, Nd, Eu, Gd, Er) produced five polymeric complexes $[Ln(^dHdtpc)(OH)(H_2O)]_n$ (Ln = La **6**, Nd **7**, Eu **8**, Gd **9**, Er **10**), which contain isostructural 3D frameworks with ladder-like chains formed by Ln^{III}, a μ_3-OH bridge and an orotate spacer.

(© Wiley-VCH Verlag GmbH & Co. KGaA, 69451 Weinheim, Germany, 2004)

Introduction

Lanthanide complexes are of great interest because of their various potential applications in magnetic materials, Ln-doped semiconductor technology, nonlinear optical devices, catalysts, molecular sensors and probes.[1−6] Due to the unique nature of lanthanide ions, such as their large radius, high coordination number and the existence of many single electrons the assembly of lanthanide complexes possessing novel structures and special properties offers great challenges and opportunities in terms of controlling their shapes and dimensions. The selection of an appropriate organic ligand along with different synthetic methods is a key step for the construction of lanthanide complexes with the desired features. It has been proved that ligands containing a combination of nitrogen and oxygen donor atoms are good building blocks for the formation of lanthanide coordination polymers;[7,8] orotic acid (2,6-dioxo-1,2,3,6-tetrahydropyrimidine-4-carboxylic acid, H_3dtpc) may therefore be a good ligand for the construction of lanthanide complexes. Aside from its significance in biological systems,[9] orotic acid possesses a fascinating coordination behavior with potential hydrogen-bonding interactions, such as asymmetric geometry and multiple coordination sites.[10] However, previous studies on the coordination chemistry of orotic acid mainly focused on transition metals[11−19] or alkali metals;[20−22] the lanthanides have been neglected. Recently we began to use orotic acid as an organic ligand for the synthesis of lanthanide complexes with the aim of studying the coordination chemistry of the lanthanide-orotic acid system and to obtain some novel structures. We have successfully synthesized two novel lanthanide polymers containing orotic acid by employing a hydrothermal technique.[23,24] This paper reports systematic studies on the synthesis and characterization of a series of lanthanide-orotic acid complexes. We will show that the structures of lanthanide-orotic acid complexes are influenced by the synthetic methods, the lanthanide contraction and the pH.

Results and Discussion

Preparation of the Complexes

The coordination chemistry of H_3dtpc with transition metals has been studied in detail in recent years,[11−19] although systematic studies on lanthanide systems have received scant attention. Our aim was to investigate the coordination chemistry of Ln-orotate (Ln is a lanthanide metal) and hoped to obtain novel structures with special properties as well as to study the effects of the lanthanide contraction and acidity on the structure formation. Ten complexes with four kinds of structures were successfully isolated by employing different synthetic techniques.

The solution reactions of lanthanide nitrate or oxide and orotic acid generated the lanthanum complexes **1** and **2** (pH 4−5), the cerium complex **3** (pH 4−5), the praseodymium complex **4** (pH 3−4), and the neodymium complex **5** (pH 3−4). The successful isolation of **1**−**5** prompted us to ex-

[a] State Key Laboratory of Structural Chemistry, Fujian Institute of Research on the Structure of Matter, Chinese Academy of Sciences,
Fuzhou, Fujian, 350002, P. R. China

Supporting information for this article is available on the WWW under http://www.eurjic.org or from the author.

tend our work to other metals of the lanthanide series. However, when we carried out similar reactions of $Ln(NO_3)_3{\cdot}nH_2O$ or Ln_2O_3 (Ln = Sm−Lu) and orotic acid in water, only uncharacterized precipitates were obtained, which may be due to the effects of the lanthanide contraction. The lanthanide contraction from La to Lu results in a gradual decrease of the ionic radius and of the pH value of the incipient precipitate with increasing atomic number.[25] We therefore tried to lower the pH value to 2 or 1 by addition of dilute HCl or HNO_3, but only single crystasl of orotic acid itself were isolated,[26] probably because orotic acid is not deprotonated at such low pH values and therefore cannot coordinate to lanthanide ions.

In order to investigate the effects of the lanthanide contraction and acidity on structure formation, similar experiments were carried out under hydrothermal conditions. The hydrothermal reaction of Ln_2O_3 (Ln = La, Nd, Ea, Gd, Er) and orotic acid (1:2) in aqueous solution (pH 7) yielded complexes **6**−**10**, which are all unexpectedly isomorphous. Taking account of the deprotonation process

$$H_3dtpc \rightleftarrows H_2dtpc^- + H^+ \rightleftarrows Hdtpc^{2-} + 2\,H^+ \rightleftarrows dtpc^{3-} + 3\,H^+$$

we tried to lower pH values of the reaction systems, hoping to obtain different structures. However, similar results were obtained although the yields or purity of the products were different. This result illustrates that complexes **6**−**10** are the most stable form under hydrothermal condition and their structures are not affected by the pH values of the reaction systems and lanthanide contraction, in contrast to previous observations.[8a,27]

It is interesting that the pH and the lanthanide contraction do, however, have an effect on the structures observed from the solution reactions: the La and Ce complexes were isolated at pH 4−5 and the Pr and Nd complexes were isolated at pH 3−4; no complexes suitable for X-ray analyses were successfully isolated from the solution reactions for the lanthanide elements heavier than neodymium. The different results between the solution and hydrothermal reactions may be caused by different reaction mechanisms:[28] the hydrothermal reaction mechanism is shifted from the thermodynamic to the kinetic domain when compared to a high-temperature solid-state reaction or from the kinetic to the thermodynamic domain when compared to a conventional solution reaction. Thus, the compounds obtained from hydrothermal reactions are often different to those obtained from conventional solution reactions.

Crystal Structures

X-ray diffraction studies revealed that complexes **1** and **3** are allomers with one-dimensional chain structures. Two types of coordination modes of orotate ligands are present in the structures: one adopts a monodentate fashion to coordinate one Ln^{III} ion through its carboxylate group ($^aH_2dtpc^-$, a in Scheme 1), and the other one acts as a μ_3-bridge to link three Ln^{III} atoms, in which a deprotonated carboxylic group bridges two Ln^{III} ions and the carbonyl oxygen atom connects to another Ln^{III} ion ($^bH_2dtpc^-$, b in Scheme 1). The central La or Ce is coordinated by four carboxylate oxygens and one carbonyl oxygen from different orotate ligands, and four oxygen atoms from coordinated water molecules (see **a** in Figure 1), with the Ln−O distances ranging from 2.497(4) to 2.626(4) Å and from 2.484(2) to 2.598(3) Å for **1** and **3**, respectively. Two Ln^{3+} ions are linked by two bridging carboxylate groups of $^bH_2dtpc^-$ to form a binuclear unit $[Ln_2(^aH_2dtpc)_4(^bH_2dtpc)_2(H_2O)_8]$, which can be viewed as the basic building block for the two complexes. Every two such blocks are connected by $Ln-O_{carbonyl}$ bonding to yield a 1D chain (Figure 2). The chains are further joined by different kinds of hydrogen bonding to generate the final 3D framework (Figure 3).

Complex **2** has a mononuclear structure (see **b** in Figure 1) in which the orotate ligands have two types of modes: one binds in a monodentate fashion to coordinate one Ln^{III} ion through its carboxylate group ($^aH_2dtpc^-$, **a** in Scheme 1), and the other one coordinates to a Ln^{III} ion through its carbonyl oxygen atom ($^cH_2dtpc^-$, **c** in Scheme 1). It should be noted that the carboxylate oxygen atoms in $^cH_2dtpc^-$ remain free and do not coordinate to metal ions; this is the first observation of such an interesting coordination mode for the orotate ligand. The La^{III} atom is nine-coordinate, with bonds to two carboxylate and one carbonyl oxygen atoms of different orotate ligands, and six coordinated water oxygen atoms, with La−O distances ranging from 2.486(4) to 2.610(4) Å. The hydrogen bonding provided by the isolated water molecules in the crystal lattice extends complex **2** into a 3D structure (Figure 4).

Complex **4** is also mononuclear, and each local coordination unit around the metal ion contains four orotate ligands (see **c** in Figure 1), two of which are not engaged in coordination to the metal ion as they are not deprotonated; the other two coordinate to the Pr^{III} ion through the deprotonated carboxylic oxygen atoms ($^aH_2dtpc^-$, **a** in

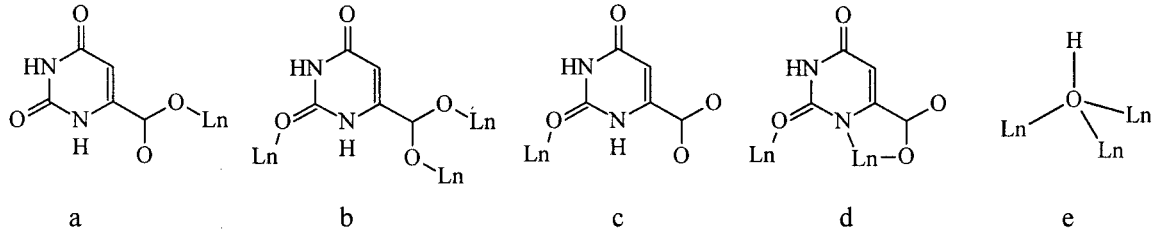

Scheme 1

 © 2004 Wiley-VCH Verlag GmbH & Co. KGaA, Weinheim

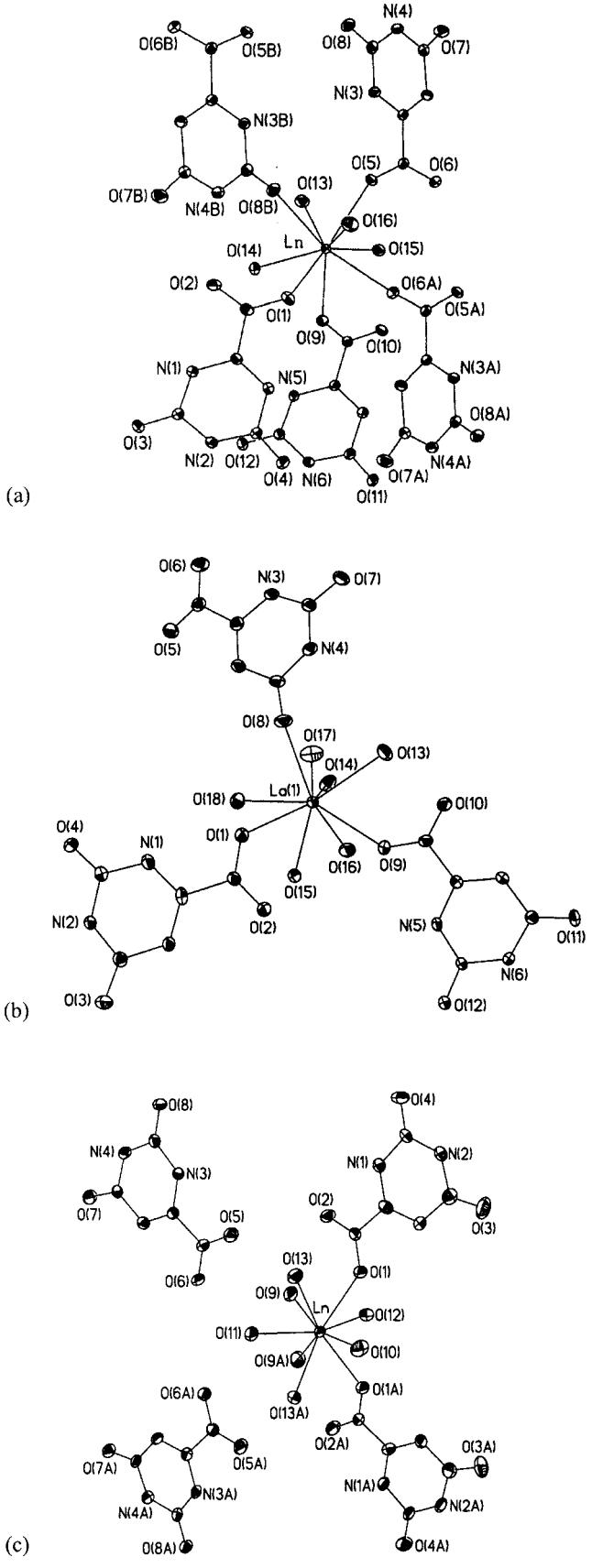

Figure 1. Local coordination environment of metal ions: (a) for **1** and **3**; (b) for **2**; (c) for **4** and **5**

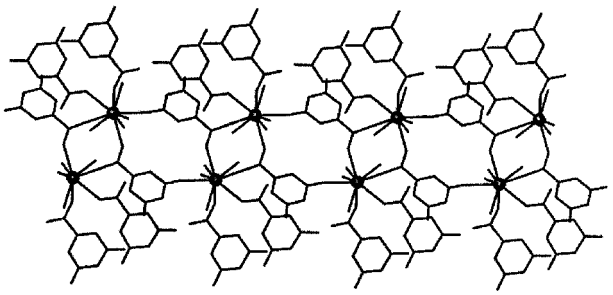

Figure 2. The 1D chain structure for **1** and **3**

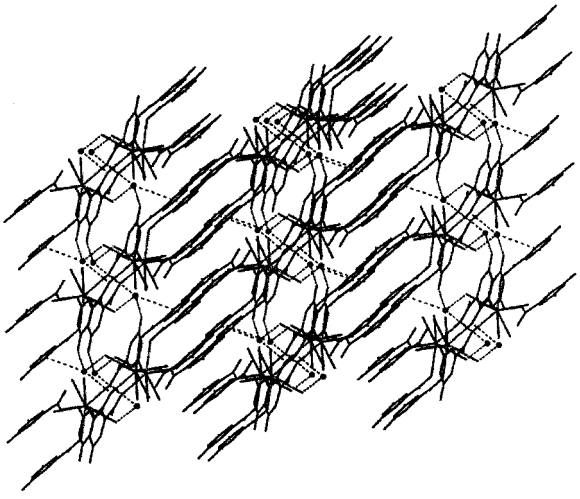

Figure 3. Packing structure along the *b* axis of **1** and **3**

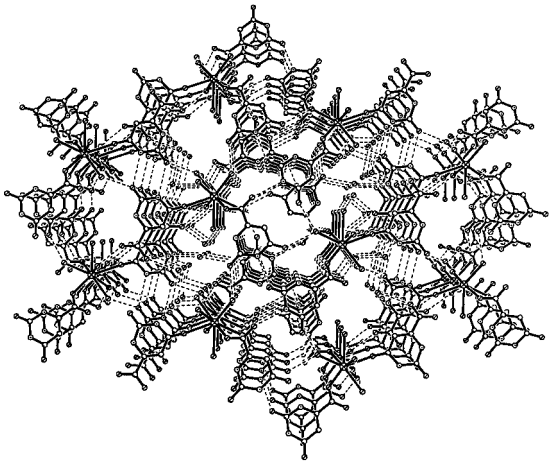

Figure 4. Packing structure along the *a* axis of **2**

Scheme 1). The Pr^{III} ion is nine-coordinate, with bonds to two carboxylate oxygen atoms from different orotate ligands, one oxygen atom from a hydroxyl group and six oxygen atoms from coordinated water molecules, with Pr−O distances ranging from 2.473(6) to 2.620(6) Å. Two coordinated units form a pore-like structure through hydrogen-bonding interactions between orotate ligands and metal ions; such pore-like units are further extended into 2D framework in the *ab* plane. The uncoordinated orotate li-

 © 2004 Wiley-VCH Verlag GmbH & Co. KGaA, Weinheim

gands are located between two neighboring 2D layers, and strong π-π stacking interactions between the heterocyclic rings of uncoordinated and coordinated orotate ligands are observed, with distances from 3.20 to 3.60 Å.

The presence of this intermolecular hydrogen bonding and the π-π stacking interaction finally results in a honeycomb-like 3D structure along the *c* axis with unique quasi-channels (see **a** in Figure 5) accommodating a great number of guest water molecules; the free orotate and coordinated orotate ligands are arranged alternately in the 3D framework (see **b** in Figure 5). Because the hydrogen atoms on the isolated water and coordinated water molecules cannot be assigned completely from the Fourier peaks, the potential hydrogen bonding for complexes **4** and **5** is not discussed.

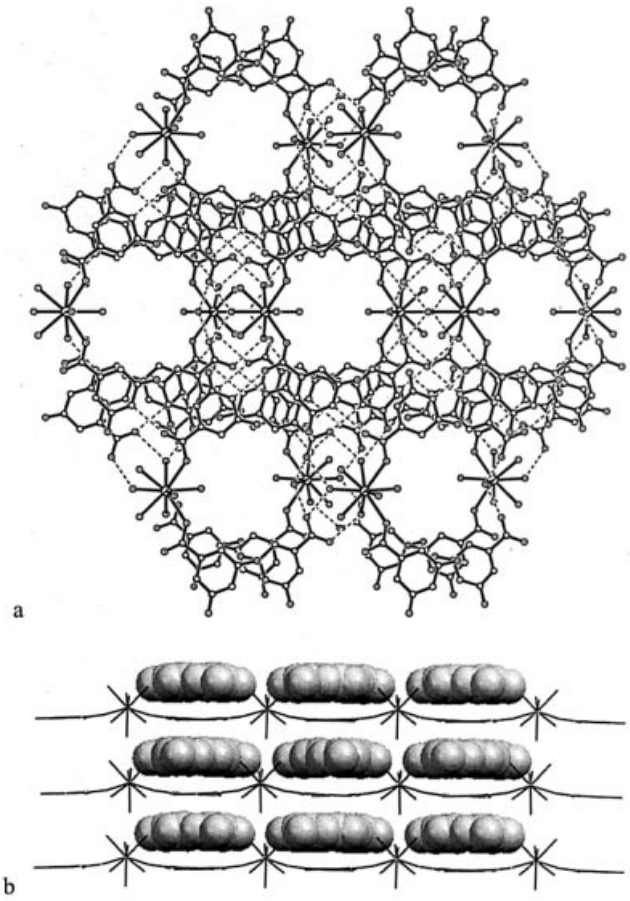

Figure 5. (a) the honeycombed structure with quasi-channels along the *c* axis for **4** and **5**, guest water molecules are omitted for clarity; (b) 3D packing structure along the *b* axis for **4** and **5**, space-filingl sphere (uncoordinated orotate ligands), wire-frame (coordinated orotate ligands)

The crystal structure of **5** is isomorphous to that of **4**; the local coordination environment around the Nd^{III} ion is shown in Figure 1 (see **c**). The Nd^{III} ion is nine-coordinate, with bonds to two carboxylate oxygen atoms from different orotate ligands, one oxygen atom from a hydroxyl group and six oxygen atoms from coordinated water molecules. Hydrogen bonding and π-π stacking interactions between neighboring heterocyclic rings of uncoordinated and coordinated orotate ligands, with distances from 3.22 to 3.61 Å, extend complex **5** into a honeycombed structure with unique quasi-channels accommodating guest water molecules.

It is interesting to observe the effect of the lanthanide contraction on the structures of complexes **1**−**5**. La^{3+} forms one-dimensional, mononuclear structures and Ce^{3+} also forms a one-dimensional structure. However, because of their smaller atomic sizes, Pr^{3+} and Nd^{3+} only form mononuclear structures. This is similar to the observation of Li and co-workers, who have reported the effect of the lanthanide contraction on crystal structure dimensions.[8a]

Complexes **6**−**10** are isostructural, possessing three-dimensional network structures constructed by eight-coordinate Ln^{III} centers. As shown in Figure 6, the Ln^{III} ion is coordinated by one nitrogen and seven oxygen atoms, of which three oxygen atoms come from OH^- groups, three oxygen atoms from different orotate ligands, and one oxygen atom from a coordinated water molecule. The carboxylic group and the adjacent nitrogen of orotic acid are deprotonated during the formation of **6**−**10**, and each orotate ligand acts as a tetradentate ligand linking three metal atoms in a chelating-bridging mode through one carboxylate oxygen, two carbonyl oxygens and the deprotonated nitrogen ($^{d}Hdtpc^{2-}$, d in Scheme 1). Each hydroxyl group acts as a μ_3-bridge linking three Ln^{III} ions (e in Scheme 1). Orotic acid usually acts as a bidentate dianionic ligand chelating to one metal ion through the deprotonated carboxylic group and the adjacent nitrogen atom; the two carbonyl oxygen atoms usually do not engage in coordination owing to their weak coordination ability. Although several examples show the coordination of a carbonyl oxygen,[10a,23,24] at least one of them remains free. In **6**−**10** both carbonyl oxygen atoms engage in coordination to Ln^{III}, and this unusual coordination mode may be ascribed to the high affinity of lanthanide ions for oxygen.

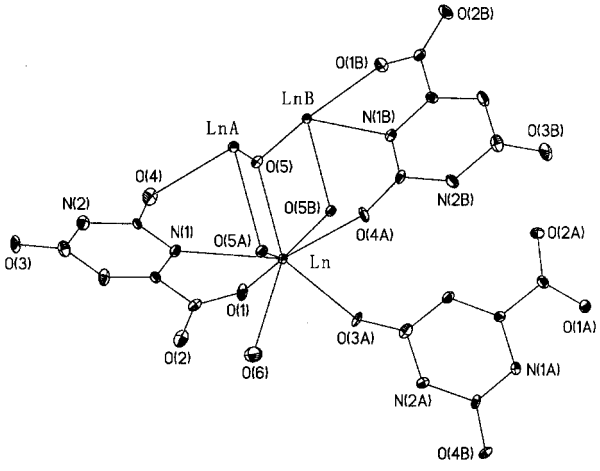

Figure 6. Local coordination environment around metal ions in **6**−**10**

[Ln(Hdtpc)(OH)(H_2O)] can be viewed as the basic building block for complexes **6**−**10**. Every two such blocks are connected by a shared orotate ligand and a μ_3-OH moiety

 © 2004 Wiley-VCH Verlag GmbH & Co. KGaA, Weinheim

to give rise to a zig-zag lathanide chain (Figure 7) with Ln−Ln distances of 4.0065(1) Å for **6**, 3.9117(7) Å for **7**, 3.8466(1) Å for **8**, 3.824(2) Å for **9**, and 3.752(2) Å for **10**. The chains are further joined by the remaining carbonyl oxygen of the orotate ligands in a different direction to complete the eight-coordinate environment of Ln^{III}, forming the final three-dimension frameworks along the *c* axis (Figure 8). In other words, the structures of **6**−**10** can also be regarded as ladder-like chains formed by Ln^{III}−OH and orotate spacers

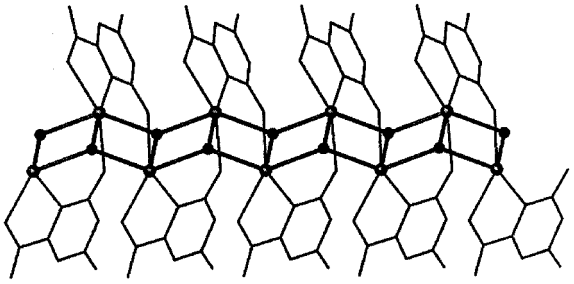

Figure 7. The zig-zag lanthanide chain formed by orotate ligands, μ_3-OH bridges in **6**−**10**

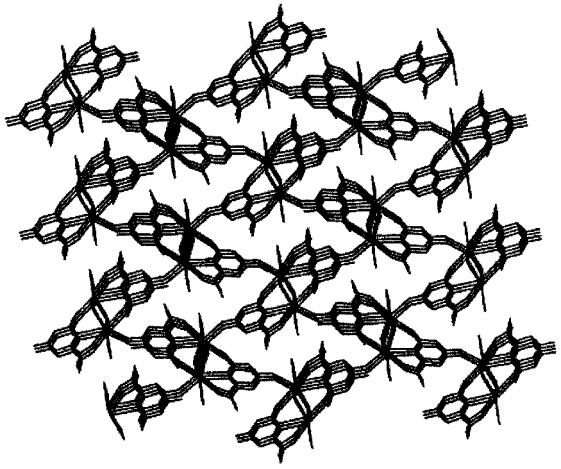

Figure 8. Packing structure along the *c* axis of **6**−**10**

Conclusions

In conclusion, ten lanthanide complexes have been prepared from orotic acid and the appropriate lanthanide salt. Lanthanide complexes with different structures were isolated from aqueous solution due to the effects of the lanthanide contraction. Nevertheless, the same geometries of complexes **6**−**10** were obtained with the hydrothermal method, which implies that the effects of the lanthanide contraction and the solution pH on crystal formation can be ignored in Ln-orotate hydrothermal reactions. The different results between solution and hydrothermal condition may be due to their different reaction mechanisms.

Experimental Section

Preparation of Complexes

General: All chemicals were used as purchased without purification prior to reaction. The infrared spectra were recorded as KBr pellets in the 4000−400 cm^{-1} region on a Magna 750 FT-IR spectrophotometer. The C, H and N microanalyses were carried out with a Perkin−Elmer 240-element analyzer in this institute.

$[\{La(^aH_2dtpc)_2(^bH_2dtpc)(H_2O)_4\}\cdot H_2O]_n$ (1): A mixture of $La(NO_3)_3\cdot 6H_2O$ (0.13 g, 0.3 mmol), H_3dtpc (0.104 g, 0.6 mmol), H_2O (20 mL) and EtOH (10 mL) was heated to boiling with stirring for 30 min. The solution was adjusted to pH 4−5 with 12 M aqueous NH_4OH and allowed to cool to room temperature. After two days colorless sheet-like crystals were obtained. Yield: 65%. $C_{15}H_{19}LaN_6O_{17}$ (694.3): calcd. C 25.95, H 2.76, N 12.11; found C 26.29, H 2.78, N 12.20. IR (KBr): $\tilde{\nu}$ = 1676 cm^{-1} (vs), 1479 (m), 1431 (m), 1379 (s), 1014 (w), 928 (w), 856 (w), 773 (m), 760 (w), 546 (m), 430 (w).

$[La(^aH_2dtpc)_2(^cH_2dtpc)(H_2O)_6]\cdot 4H_2O$ (2): A mixture of $La(NO_3)_3\cdot 6H_2O$ (0.11 g, 0.25 mmol), H_3dtpc (0.044 g, 0.25 mmol), and H_2O (20 mL) was heated in a 25 mL Teflon-lined bomb at 110 °C for 3 days to yield a colorless solution (pH 4−5). After evaporation for several days at room temperature, colorless sheet-like crystals were obtained. Yield: 30%. $C_{15}H_{29}LaN_6O_{22}$ (784.3): calcd. C 22.97, H 3.73, N 10.71; found C 23.17, H 3.61, N 10.93. IR (KBr): $\tilde{\nu}$ = 1705 cm^{-1} (vs), 1635 (vs), 1597 (s), 1491 (m), 1431 (m), 1373 (s), 1012 (w), 935 (w), 868 (w), 777 (w), 648 (w), 550 (m), 517 (w), 426 (w).

$[\{Ce(^aH_2dtpc)_2(^bH_2dtpc)(H_2O)_4\}\cdot H_2O]_n$ (3): A mixture of $Ce(NO_3)_3\cdot 6H_2O$ (0.087 g, 0.2 mmol), H_3dtpc (0.07 g, 0.4 mmol), H_2O (20 mL), and EtOH (10 mL) was heated to boiling with stirring for 30 min. The solution was adjusted to pH 4−5 with 12 M aqueous NH_4OH mixture and allowed to cool slowly to room temperature. After two days colorless sheet-like crystals were obtained. Yield: 60%. $C_{15}H_{19}CeN_6O_{17}$ (695.5): calcd. C 25.91, H 2.75, N 12.08; found C 26.13, H 2.68, N 12.17. IR (KBr): $\tilde{\nu}$ = 1709 cm^{-1} (vs), 1628 (vs), 1439 (s), 1390 (s), 1313 (m), 1018 (w), 856 (w), 931(W), 798 (m), 559 (m), 451 (w).

$[Pr(^aH_2dtpc)_2(OH)(H_2O)_6]\cdot(H_3dtpc)_2\cdot 7H_2O$ (4): A mixture of Pr_2O_3 (0.068 g, 0.2 mmol), H_3dtpc (0.14 g, 0.8 mmol), and water (30 mL) was heated to boiling with stirring for 30 min, the pH was adjusted to 3−4 by addition of 6 M aqueous H_2SO_4 and the mixture was then filtered. The filtrate was allowed to cool to room temperature. After two days light-blue crystals were obtained. Yield: 65%. $C_{20}H_{41}N_8O_{30}Pr$ (1014.5): calcd. C 23.67, H 4.07, N 11.04; found C 23.75, H 3.98, N 11.09. IR (KBr): $\tilde{\nu}$ = 1736 cm^{-1} (vs), 1635 (vs), 1489 (m), 1408 (vs), 1383 (s), 1011 (w), 931 (w), 814 (m), 754 (m), 544 (s), 432 (m).

$[Nd(^aH_2dtpc)_2(OH)(H_2O)_6]\cdot(H_3dtpc)_2\cdot 7H_2O$ (5): This complex was prepared as above by using Nd_2O_3 instead of Pr_2O_3. Yield: 65%. $C_{20}H_{41}N_8NdO_{30}$ (1017.8): calcd. C 23.60, H 4.06, N 11.01; found C 23.77, H 4.01, N 11.16. IR (KBr): $\tilde{\nu}$ = 1739 cm^{-1} (vs), 1670 (vs), 1635 (vs), 1489 (m), 1410 (vs), 1383 (vs), 1011 (w), 930 (w), 818 (m), 754 (m), 544 (s), 432 (m).

$[La(^dHdtpc)(OH)(H_2O)]_n$ (6): A mixture of La_2O_3 (0.0325 g, 0.1 mmol), H_3dtpc (0.035 g, 0.2 mmol) and water (15 mL) was placed in a 25 mL stainless reactor fitted with a Teflon liner and heated to 160 °C for 72 hours. It was then cooled to room temperature, and colorless needle-like crystals were obtained. Yield: 80%.

 © 2004 Wiley-VCH Verlag GmbH & Co. KGaA, Weinheim

$C_5H_5LaN_2O_6$ (328.0): calcd. C 18.31, H 1.54, N 8.54; found C 18.82, H 1.46, N 8.76. IR (KBr): $\tilde{\nu}$ = 1664 cm^{-1} (vs), 1641 (vs), 1581 (s), 1558 (s), 1485 (m), 1407 (s), 1373 (s), 1335 (s), 1011 (m), 955 (w), 845 (m), 575 (m), 540 (w), 426 (w).

[Nd(^{d}Hdtpc)(OH)(H_2O)]$_n$ (7): This complex was prepared in a similar manner to **6** but with Nd_2O_3 instead of La_2O_3. Light-red crystals were obtained in 85% yield . $C_5H_5N_2NdO_6$ (333.3): calcd. C 18.02, H 1.51, N 8.40; found C 18.35, H 1.44, N 8.60. IR (KBr): $\tilde{\nu}$ = 1643 cm^{-1} (vs), 1487 (m), 1412 (s), 1336 (s), 1012 (s), 957 (w), 847 (m), 806 (m), 577 (m), 430 (w).

[Eu(^{d}Hdtpc)(OH)(H_2O)]$_n$ (8): This complex was prepared in a similar manner to **6** but with Eu_2O_3 instead of La_2O_3. Colorless crystals were obtained in 80% yield. $C_5H_5EuN_2O_6$ (341.1): calcd. C 17.61, H 1.48, N 8.21; found C 17.36, H 1.43, N 8.34. IR (KBr): $\tilde{\nu}$ = 1672 cm^{-1} (vs), 1649 (vs), 1487 (m), 1417 (s), 1340 (s), 1157 (w), 1014 (m), 958 (w), 808 (m), 771 (m), 434 (w).

[Gd(^{d}Hdtpc)(OH)(H2O)]$_n$ (9): This complex was prepared in a similar manner to **6** but with Gd_2O_3 instead of La_2O_3. Colorless crystals were obtained in 85% yield. $C_5H_5GdN_2O_6$ (346.4): calcd. C 17.34, H 1.46, N 8.09; found C 16.97, H 1.36, N 7.79. IR (KBr): $\tilde{\nu}$ = 1674 cm^{-1} (vs), 1651 (vs), 1579 (s), 1489 (m), 1417 (s), 1342 (s), 1014 (m), 958 (w), 810 (m), 579 (w), 436 (w).

[Er(^{d}Hdtpc)(OH)(H_2O)]$_n$ (10): This complex was prepared in a similar manner to **6** but with Er_2O_3 instead of La_2O_3. Colorless crystals were obtained in 85% yield. $C_5H_5ErN_2O_6$ (356.4): calcd. C 16.85, H 1.41, N 7.86; found C 16.93, H 1.37, N 7.95. IR (KBr): $\tilde{\nu}$ = 1655 cm^{-1} (vs), 1585 (s), 1487 (m), 1421 (s), 1016 (m), 962 (w), 820 (m), 623 (m), 579 (w), 436 (w).

X-ray Crystallography: Single crystals of complexes **1**−**10** with dimensions 0.8 × 0.16 × 0.1 (**1**), 0.8 × 0.26 × 0.2 (**2**), 0.8 × 0.24 × 0.12 (**3**), 0.6 × 0.24 × 0.16 (**4**), 0.6 × 0.20 × 0.12 (**5**), 0.36 × 0.24 × 0.04 (**6**), 0.24 × 0.08 × 0.06 (**7**), 0.4 × 0.24 × 0.04 (**8**), 0.4 ×

Table 1. Crystal data for **1**−**5**

Complex	**1**	**2**	**3**	**4**	**5**
Empirical formula	$C_{15}H_{19}LaN_6O_{17}$	$C_{15}H_{29}LaN_6O_{22}$	$C_{15}H_{19}CeN_6O_{17}$	$C_{20}H_{43}PrN_8O31$	$C_{20}H_{43}NdN_8O_{31}$
Molecular mass	694.27	784.35	695.48	1014.49	1017.82
Crystal system	triclinic	triclinic	triclinic	orthorhombic	orthorhombic
Space group	$P\bar{1}$	$P\bar{1}$	$P\bar{1}$	*Cmc*2 (1)	*Cmc*2 (1)
a (Å)	8.5991(5)	6.7944(2)	8.5414(17)	22.9991(17)	22.9997(6)
b (Å)	10.2849(6)	10.1432(2)	10.260(2)	12.7674(4)	12.7520(4)
c (Å)	13.4175(8)	20.5961(6)	13.335(3)	12.6962(4)	12.6996(3)
α (°)	90.914(10)	94.731(10)	90.95(3)	90	90
β (°)	99.77(3)	93.44(10)	100.27(3)	90	90
γ (°)	105.69(10)	105.523	105.89(3)	90	90
V (Å^3)	1123.48(11)	1358.00(6)	1103.3(4)	3728.1(2)	3724.69(18)
Z	2	2	2	4	4
D_c (g·cm^{-3})	2.052	1.918	2.094	1.840	1.847
μ (mm^{-1})	2.003	1.682	2.167	1.429	1.516
F(000)	688	788	690	2104	2108
2*θ* range (°)	1.54−25.10	1.00−25.02	1.56−27.51	1.77−25.09	1.77−25.04
*R*1 [$I > 2\sigma(I)$]	0.0379	0.0380	0.0248	0.0318	0.0372
*R*1 (all data)	0.0440	0.0461	0.0303	0.0334	0.0460
S (F^2)	*1.053*	*1.082*	*1.221*	*1.059*	*1.068*

Table 2. Crystal data for **6**−**10**

Complex	**6**	**7**	**8**	**9**	**10**
Empirical formula	$C_5H_5LaN_2O_6$	$C_5H_5NdN_2O_6$	$C_5H_5EuN_2O_6$	$C_5H_5GdN_2O_6$	$C_5H_5ErN_2O_6$
Molecular mass	328.02	333.35	341.07	346.36	356.37
Crystal system	orthorhombic	orthorhombic	orthorhombic	orthorhombic	orthorhombic
Space group	*Pna*2 (1)	*Pna*2 (1)	*Pna*2 (1)	*Pna*2 (1)	*Pna*2 (1)
a (Å)	10.2210(16)	10.1518(13)	10.893(15)	10.654(10)	10.004(7)
b (Å)	16.976(3)	16.763(2)	16.575(5)	16.5208(17)	16.310(8)
c (Å)	4.6996(17)	4.6564(6)	4.6334(7)	4.6223(5)	4.598(3)
β (°)	90	90	90	90	90
V (Å^3)	815.5(3)	792.39(17)	774.9(2)	768.64(14)	750.2(8)
Z	4	4	4	4	4
D_c (g·cm^{-3})	2.672	2.794	2.924	2.993	3.155
μ (mm^{-1})	5.246	6.560	8.102	8.636	11.194
F(000)	616	628	640	644	660
2*θ* range (°)	2.33−25.96	2.35−25.01	2.36−25.02	2.37−25.07	2.39−25.13
*R*1 [$I > 2\sigma(I)$]	0.0375	0.0298	0.0441	0.0506	0.0476
*R*1 (all data)	0.0523	0.0344	0.0626	0.0752	0.0665
S (F^2)	1.066	1.091	1.020	1.036	1.019

 © 2004 Wiley-VCH Verlag GmbH & Co. KGaA, Weinheim

0.36 × 0.04 (**9**), 0.24 × 0.05 × 0.03 mm^3 (**10**) were selected for crystal structure analyses. Data collection for complexes **1**−**5** and **7**−**10** was performed at 293 K on a Siemens Smart CCD diffractometer with graphite-monochromated Mo-K_α radiation (λ = 0.71073 Å). Empirical absorption corrections were applied using the SADABS program. Data collection for **6** was performed at 293 K on a CAD4 four-cycle diffractometer with graphite-monochromated Mo-K_α radiation (λ = 0.71073Å). Corrections for Lorentz polarization factors and empirical absorption were applied to the data. The structures of **1**−**10** were solved by direct methods; the heavy atoms were located from the E-maps; other non-hydrogen atoms were derived from the successive difference Fourier syntheses. All non-hydrogen atoms were refined by full-matrix, least-squares minimizations of $\Sigma(F_o - F_c)^2$ with anisotropic thermal parameters for **1**−**5** and **7**. The metal atoms were refined anisotropically while all other non-hydrogen atoms were refined isotropically for **6**, **8**, **9** and **10** in order to obtain a reasonable data/parameter ratio. One free water molecule (O14) in **4** and **5** was disordered over two sets of positions refined with restraints. The calculations were performed with the SHELXTL-97 program package.[29] The hydrogen atoms were located from the difference Fourier map and refined isotropically. Table 1 summarizes the important crystal data for **1**−**5** and Table 2 the data for **6**−**10**. The selected bond lengths and angles for **1**−**10** are provided in Table S1 in the Supporting Information.

CCDC-202618−202627 (for **1**−**10**) contain the supplementary crystallographic data for this paper. These data can be obtained free of charge at www.ccdc.cam.ac.uk/conts/retrieving.html [or from the Cambridge Crystallographic Data Centre, 12 Union Road, Cambridge CB2 1EZ, UK; Fax: +44 1223 336 033; E-mail: deposit@ccdc.cam.ac.uk].

Acknowledgments

The authors thank the financial support from the National Natural Science Foundation of China (90206040, 20325106, 20333070), the Natural Science Foundation of Fujian Province (B9820003), the Key and the "One-hundred Talent" Projects from CAS.

[1] [1a] J. P. Costes, F. Dahan, A. Dupuis, J. P. Laurent, *Inorg. Chem.* **1997**, *36*, 3429−3433. [1b] A. Bencini, C. Benelli, A. Caneschi, R. L. Carlin, A. Dei, D. Gatteschi, *J. Am. Chem. Soc.* **1985**, *107*, 8128−8136.
[2] M. Taniguchi, K. Takahei, *J. Appl. Phys.* **1993**, *73*, 943−947.
[3] J. Lisowski, P. Starynowicz, *Inorg. Chem.* **1999**, *38*, 1351−1355.
[4] O. R. Evans, R. Xiong, Z. wang, G. K. Wong, W. Lin, *Angew. Chem. Int. Ed.* **1999**, *38*, 536−538.
[5] M. Fujita, Y. J. Kwon, S. Washizu, K. Ogura, *J. Am. Chem. Soc.* **1994**, *116*, 1151−1152.
[6] M. Munakata, L. P. Wu, T. Kuroda-Sowa, M. Maekawa, Y. Suenaga, K. Furuichi, *J. Am. Chem. Soc.* **1996**, *118*, 3305−3306.
[7] [7a] Y. C. Liang, R. Cao, W. P. Su, M. C. Hong, W. J. Zhang, *Angew. Chem. Int. Ed.* **2000**, *39*, 3304−3307. [7b] Y. C. Liang, M. C. Hong, R. Cao, J. B. Weng, W. P. Su, *Inorg. Chem.* **2001**, *40*, 4574−4582.
[8] [8a] L. Pan, X. Y. Huang, J. Li, Y. G. Wu, N. W. Zheng, *Angew. Chem. Int. Ed.* **2000**, *39*, 527. [8b] L. Ma, O. R. Evans, B. M. Foxman, W. B. Lin, *Inorg. Chem.* **1999**, *38*, 5837−5840.
[9] [9a] J. Leberman, A. Kornberg, E. S. Simms, *J. Biol. Chem.* **1955**, *215*, 403. [9b] P. Castan, E. Colacio-Rodriguez, A. L. Beauchamp, J. Wimmer, *J. Inorg. Biochem.* **1990**, *38*, 225−239.
[10] [10a] C. P. Raptopoulou, V. Tangoulis, V. Psycharis, *Inorg. Chem.* **2000**, *39*, 4452−4459. [10b] X. L. Xu, S. L. James, D. M. P. Mingos, A. J. P. White, D. J. Williams, *J. Chem. Soc., Dalton Trans.* **2000**, 3783−3790.
[11] [11a] T. Solin, K. Matsumoto, K. Fuwa, *Bull. Chem. Soc. Jpn.* **1981**, *54*, 3731−3734. [11b] D. J. Darensbourg, D. L. Larkins, J. H. Reibenspies, *Inorg. Chem.* **1998**, *37*, 6125−6128. [11c] D. J. Darensbourg, J. D. Draper, D. L. Larkins, B. J. Frost, J. H. Reibenspies, *Inorg. Chem.* **1998**, *37*, 2538−2546.
[12] [12a] S. L. James, D. M. P. Mingos, X. L. Xu, A. J. P. White, D. J. Williams, *J. Chem. Soc., Dalton Trans.* **1998**, 1335−1340. [12b] A. D. Burrows, D. M. P. Mingos, A. J. P. White, D. J. Williams, *J. Chem. Soc., Dalton Trans.* **1996**, 149−151. [12c] A. D. Burrows, D. M. P. Mingos, A. J. P. White, D. J. Williams, *J. Chem. Soc., Dalton Trans.* **1996**, 3805−3812.
[13] [13a] F. Nepveu, N. Gaultier, N. Korber, J. Jaud, P. Castan, *J. Chem. Soc., Dalton Trans.* **1995**, 4005−4013. [13b] P. Castan, T. Ha, F. Nepveu, G. Semardinelli, *Inorg. Chim. Acta* **1995**, *221*, 173−175. [13c] P. Castan, C. Viala, P. L. Fabre, F. Nepveu, J. P. Souchard, G. Bernardinelli, *Can. J. Chem.* **1998**, *76*, 205−212. [13d] T. T. B. Ha, A. M. Larsonneur-Galibert, P. Castan, J. Jaud, *J. Chem. Cryst.* **1999**, *29*, 565−569. [13e] P. Arrizabalaga, P. Castan, F. Dahan, *Inorg. Chem.* **1983**, *22*, 2245−2252.
[14] [14a] I. Mutikainen, *Inorg. Chim. Acta* **1987**, *136*, 155−158. [14b] I. Mutikainen, P. Lumme, *Acta Crystallogr., Sect. B* **1980**, *36*, 2233−2237.
[15] [15a] A. Karipides, B. Thomas, *Am. Cryst. Assoc., Abstr. Paper (Summer)* **1983**, *11*, 45. [15b] A. Karipides, B. Thomas, *Acta Crystallogr., Sect. C* **1986**, *42*, 1705−1707.
[16] [16a] Y. D. Fridman, E. P. Tsoi, M. G. Levina, *Koord. Khim.* **1984**, *10*, 469. [16b] T. S. Khodashova, M. A. Porai-Koshits, N. K. Davidenko, N. N. Vlasova, *Koord. Khim.* **1984**, *10*, 264.
[17] N. Lalipti, C. P. Raptopoulou, A. Terzis, A. Panagiotopoulos, S. P. Perlepes, E. Manessi-Zoupa, *J. Chem. Soc., Dalton Trans.* **1998**, 1327−1333.
[18] M. Rul, K. Wels, H. Vahrenkamp, *J. Am. Chem. Soc.* **1997**, *36*, 2130−2137.
[19] T. W. Hambley, R. I. Christopherson, E. S. Zvargulis, *Inorg. Chem.* **1995**, *34*, 6550−6552.
[20] S. Bekiroglu, O. Kristiansson, *J. Chem. Soc., Dalton Trans.* **2002**, 1330−1335.
[21] I. Mutikainen, R. Hamalainen, M. Klinga, U. Turpeinen, *Z. Kristallogr.* **1997**, *212*, 65−66.
[22] [22a] I. Bach, O. Kumberger, H. Schmidbaur, *Chem. Ber.* **1990**, *123*, 2267. [22b] O. Kumberger, J. Riede, H. Schmidbaur, *Chem. Ber.* **1991**, *124*, 2739−2742.
[23] X. Li, R. Cao, D. F. Sun, Q. Shi, M. C. Hong, Y. C. Liang, *Inorg. Chem. Commun.* **2002**, *5*, 589−591.
[24] D. F. Sun, R. Cao, Y. C. Liang, H. C. Hong, *Chem. Lett.* **2001**, 878−879.
[25] C. H. Huang, *Rare Earth Coordination Chemistry*, chapter 2, p. 25−26, the Press of Science, **1997**.
[26] J. Solbakk, *Acta Chem. Scand.* **1971**, *25*, 3006.
[27] [27a] L. Pan, T. Frydel, M. B. Sander, X. Y. Huang, J. Li, *Inorg. Chem.* **2001**, *40*, 1271−1283. [27b] R. Cao, D. F. Sun, Y. C. Liang, M. C. Hong, K. Tatsumi, Q. Shi, *Inorg. Chem.* **2002**, *41*, 2087−2094.
[28] [28a] R. M. Barrer, *Hydrothermal Chemistry of Zeolite*, Academic Press, London, **1982**. [28b] G. Bemazeau, *J. Mater. Chem.* **1999**, *9*, 15−18. [28c] S. H. Feng, R. R. Xu, *Acc. Chem. Res.* **2001**, *34*, 239−247.
[29] G. M. Sheldrick, *SHELXS97, Program for Crystal Structure Solution*, University of Göttingen, **1997**.

Received December 3, 2003
Early View Article
Published Online April 26, 2004

 © 2004 Wiley-VCH Verlag GmbH & Co. KGaA, Weinheim

Crystal Structure and Excited Optical Nonlinearity of a 1D Polymeric $[W_2O_2S_6Cu_4(NCMe)_4]_n$ Cluster

Hegen Zheng,*[a] Jianliang Zhou,[a] Michael F. Lappert,[b] Yinglin Song,[c] Yizhi Li,[a] and Xinquan Xin[a]

Keywords: Cluster compounds / Copper / Nonlinear optics / Polymers / Tungsten

The self-assembly reaction of $(NH_4)_2(WOS_3)$ with CuBr in the presence of PCy_3 (PCy_3 = tricyclohexylphosphane) in MeCN gives rise to a novel 1D polymeric compound $[W_2O_2S_6Cu_4(NCMe)_4]_n$ (**1**) with solvent MeCN coordinated to the copper atom. This situation is unprecedented in the W(Mo)/Cu/S system. The excited state absorption and refraction of **1** in CH_3CN solution were studied by using the Z-scan technique with laser pulses of 40 ps pulse-width at a wavelength of 532 nm. The compound possesses an optical self-focusing performance. The positive nonlinear refraction is attributed to population transitions between singlet states. Compound **1** displays a strong excited-state absorption, which induces an asymmetry between the peak and valley.

(© Wiley-VCH Verlag GmbH & Co. KGaA, 69451 Weinheim, Germany, 2004)

Introduction

Polymeric transition-metal chalcogenides have attracted much attention because of their possible applications as catalysts or nonlinear optical devices directly derived from their peculiar solid-state structures.[1,2] Compared with polyoxometalates, polythiometalates are still in their infancy.[3−5] Mo(W)/Cu/S polymeric clusters are scarce and only a few structures have been reported. For example, the linear one-dimensional chains in $[\{WS_4Ag\}\{[H_3NC(CH_2OH)_3\}_n(dmf)_{2n}]$,[6a] $[\{(\eta^5\text{-}C_5Me_5)WS_3\}_2Ag_3(CN)\}_n]$[6b,6c] or $[WOS_3Cu_3(CN)(py)_4]_n$ (M = Mo, W),[7] the two-dimensional framework in $[\{NEt_4\}\{Mo_2O_2S_6Cu_6I_3(4,4'\text{-bipy})_5\}\cdot MeOH\cdot H_2O]_n$,[8a] $[(PPh_4)_2\{(CuNCS)_4WS_4\}]_n$ [8b] or the three-dimensional cross-framework in $[\{NEt_4\}_2\{(\mu_4\text{-}WSe_4)Cu_4(CN)_4\}]_n$.[9] We report here the synthesis and crystal structure of a novel 1D polymeric cluster $[W_2O_2S_6Cu_4(NCMe)_4]_n$ (**1**) with a novel zigzag chain configuration along the *c* axis and solvent as a ligand. Additionally, the excited state nonlinear refraction and absorption of compound **1** were investigated by using the Z-scan technique with picosecond pulses. We also propose a steady-state model of singlet excited state nonlinear refraction, which agrees well with experimental results of the excited-state refraction and absorption.

[a] State Key Laboratory of Coordination Chemistry, Coordination Chemistry Institute, Nanjing University, Nanjing 210093, P. R. China
E-mail: zhenghg@netra.nju.edu.cn
[b] The Chemistry Laboratory, University of Sussex, Brighton, BN1 9QJ, UK
[c] Department of Physics, Harbin Institute of Technology, Harbin 150001, P. R. China

Results and Discussion

Synthesis of Compound 1

The reaction of $(NH_4)_2(WOS_3)$ and CuBr in the presence of PCy_3 (molar ratio of 1:2:2) in MeCN solution led to deep-red crystals of $[W_2O_2S_6Cu_4(NCMe)_4]_n$ (**1**) in 65% yield after allowing the orange-red filtrate to stand under an oxygen-free atmosphere for several days. Surprisingly, the PCy_3 ligand is not present in **1**, and solvent MeCN molecules are the only additional co-ligands present. This differs from our previously reported results when an analogous ligand, PPh_3, was used in place of PCy_3. As shown in Scheme 1, reaction of $[WOS_3]^{2-}$ with CuBr and PPh_3 produced a single cubic-like compound $[WOS_3Cu_3(PPh_3)_3Br]$.[10] When the reaction was performed in the absence of PCy_3 we could not isolate compound **1** or obtain good quality crystals, de-

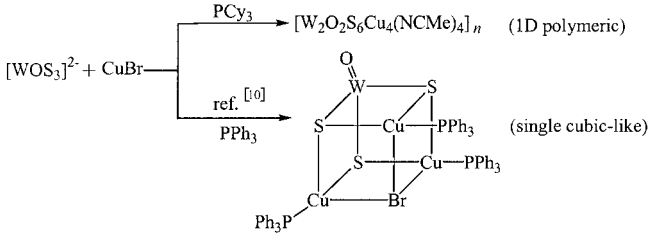

Scheme 1

 © 2004 Wiley-VCH Verlag GmbH & Co. KGaA, Weinheim **DOI: 10.1002/ejic.200300931**

spite several attempts. It is possible that PCy_3 plays a role in the crystal growth.

Single-Crystal X-ray Diffraction Studies

Compound **1** crystallizes in the monoclinic system with space group $P2_1/c$. An ORTEP drawing is shown in Figure 1. The configuration of the polymeric compound can be viewed as a helical chain which is propagated along the crystallographic *c* axis. For clarity, a simplified diagram is shown in Figure 2, with S atoms omitted; the packing diagram of the unit cell is shown in Figure 3. It should be noted that the chain turns at each W atom. The main core in compound **1** may be described as containing a nest-shaped $W_2S_6Cu_4$ fragment, which has been previously been observed in $[(C_7H_7)_3P]_4Cu_4W_2S_6O_2$ [11] and $[Et_4N]_4[Mo_2S_6Cu_6O_2I_6]$.[12] Each approximately tetrahedral W atom is coordinated by one terminal O and three μ_3-S atoms with angles subtended at W of 108.61(10)−110.8(3)°. However, the coordination tetrahedron around the Cu(1) atom, formed by two μ_3-S and two N atoms from MeCN, is much more distorted, the angles of Cu ranging from 105.14(11)° to 116.0(3)°. The average W−Cu−W and Cu−W−Cu angles are 177.05(6)° and 85.80(2)°, respectively. The W=O bond length of 1.718(8) Å is typical of a double bond and is similar to those observed in $[(C_7H_7)_3P]_4Cu_4W_2S_6O_2$,[11] and $[(PPh_3)_4(SCMe_3)_2Cu_6W_2S_6O_2]$.[13] The W−$\mu_3$-S bond lengths are 2.244(2), 2.245(3), and 2.238(3) Å.

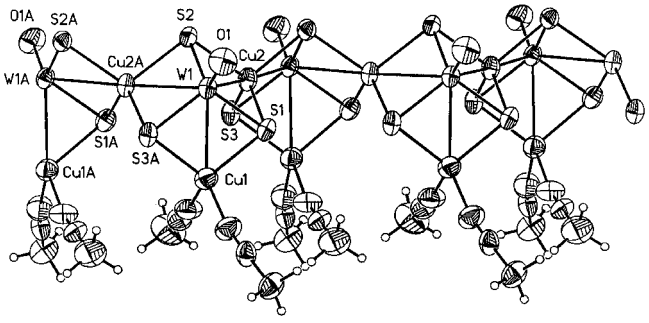

Figure 1. ORTEP drawing of a portion of the anion of $[W_2O_2S_6Cu_4(NCMe)_4]_n$ (**1**) with atomic labeling (30% displacement ellipsoids)

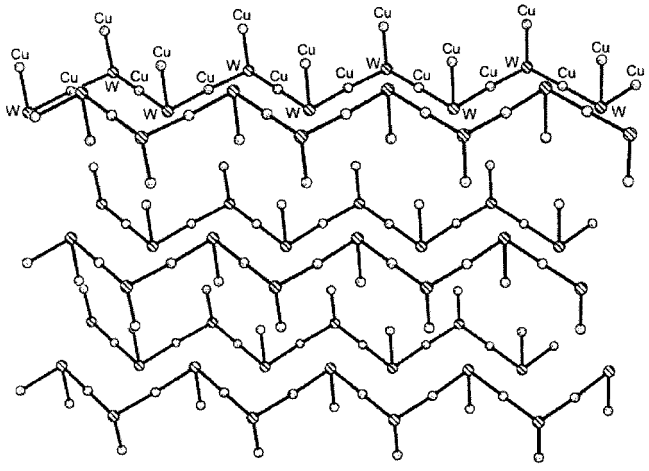

Figure 2. Simplified diagram of the anionic helical chain of **1**; sulfur atoms omitted for clarity

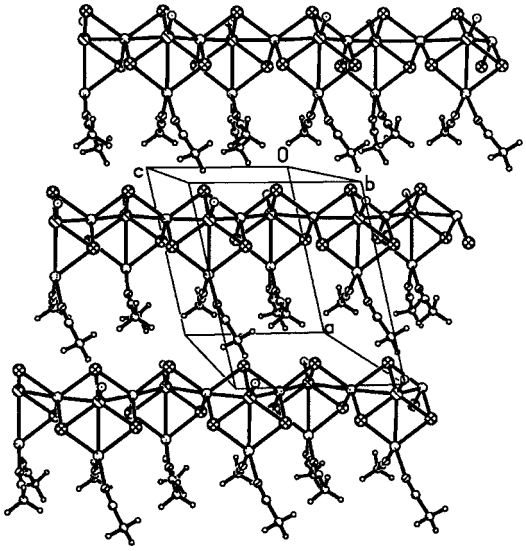

Figure 3. Packing drawing of the unit cell of **1** viewed along the *b* axis

There are two types of copper atoms in the $W_2S_6Cu_4$ core. The Cu(1) atom is tetrahedrally coordinated by two μ_3-S atoms and two nitrogen atoms of the MeCN ligands, resulting in a $(\mu_3\text{-S})_2Cu(NCMe)_2$ arrangement, while the Cu(2) atom is tetrahedrally coordinated by the four μ_3-S atoms resulting in a $(\mu_3\text{-S})_4Cu$ arrangement. Owing to the different coordination modes of the copper atoms, the W−Cu lengths are slightly different; for example, the W1−Cu1 bond length [2.6999(16) Å] is shorter than those for the W1−Cu2 bonds [av. 2.7489(15) Å]. The Cu−S distances also reflect the different coordination modes of the copper atoms, the Cu(2)−S bonds [av. 2.3264(3) Å] are longer than those for Cu(1) [av. 2.292(3) Å]. Selected bond lengths and angles are listed in Table 1.

Nonlinear Optical Properties

The UV/Vis spectrum of the polymeric compound **1** is depicted in Figure 4. It shows two absorption peaks with the first maximum located at 367 nm. The polymer has a relatively low linear absorption in the visible and near-IR regions. Indeed, the solution is nearly transparent in the visible and near infrared range, which qualifies the cluster as a potential optical limiting material.

The open-aperture Z-scan results are shown in Figure 5. The nonlinear transmittances of the sample are dependent only on the incident intensity for nanosecond and picosecond laser pulses, which indicates that the metal cluster possesses excited state absorption and not two-photon absorption. The details will be reported elsewhere. The nonlinear absorption of about 90% at the focus shows that the metal cluster possesses strong excited state absorption and a large optical limiting response. The normalized closed-aperture Z-scan curve (Figure 6) has a pair of sharp peaks and valley and the occurrence of the peak at positive Z indicates that

 © 2004 Wiley-VCH Verlag GmbH & Co. KGaA, Weinheim

Table 1. Selected bond lengths (Å) and angles (°) of $[W_2O_2S_6Cu_4(NCMe)_4]_n$ (**1**)

Cu1−N2	2.006(11)	Cu1−N1	2.027(12)	Cu1−S3A	2.291(3)
Cu1−S1	2.293(3)	Cu1−W1	2.6999(16)	Cu2−S3	2.322(3)
Cu2−S2	2.322(3)	Cu2−S2A	2.329(3)	Cu2−S1	2.330(3)
Cu2−W1	2.7479(15)	Cu2A−W1	2.7494(15)	O1−W1	1.718(8)
S1−W1	2.244(2)	S2−W1	2.245(3)	S2−Cu2	2.329(3)
S3−W1	2.238(3)	S3−Cu1	2.291(3)	W1−S3	2.238(3)
W1−Cu2	2.7494(15)				
N2−Cu1−N1	105.8(4)	N2−Cu1−S3A	116.0(3)	N1−Cu1−S3A	111.7(3)
N2−Cu1−S1	106.3(3)	N1−Cu1−S1	111.9(3)	S3A−Cu1−S1	105.14(11)
S3−Cu2−S2	114.46(11)	S3−Cu2−S2A	103.14(11)	S2−Cu2−S2A	107.88(12)
S3−Cu2−S1	115.21(11)	S2−Cu2−S1	103.36(11)	S2−Cu2−S1A	112.87(11)
O1−W1−S3A	110.3(3)	O1−W1−S1	109.5(3)	S3A−W1−S1	108.61(10)
O1−W1−S2	110.8(3)	S3A−W1−S2	108.72(10)	S1−W1−S2	108.79(10)
Cu1−W1−Cu2	86.45(4)	Cu1−W1−Cu2A	85.84(4)	Cu2−W1−Cu2	85.76(2)

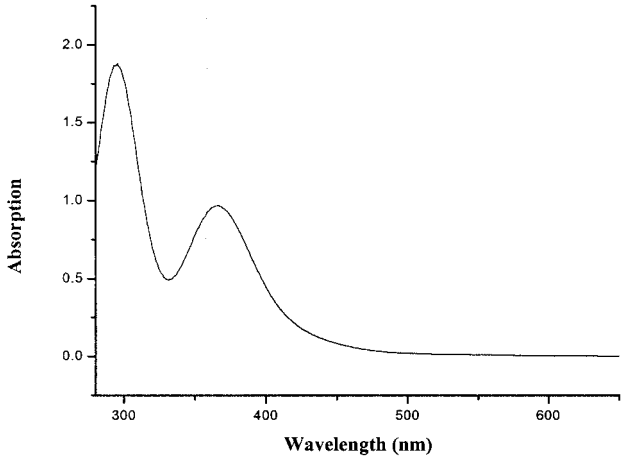

Figure 4. Electronic spectrum of **1** in acetonitrile; concentration 1.2×10^{-4} M

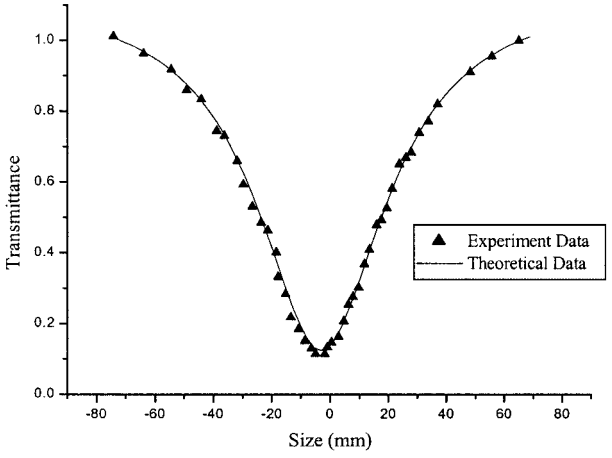

Figure 5. The open-aperture Z-scan results of compound **1**

the cluster possesses positive nonlinear refraction or is self-focusing. Both the peak and the valley are asymmetric, and the width of the valley is widened. The asymmetry of the peak and valley of the normalized Z-scan curve is caused by the strong excited-state absorption. The excited-state optical nonlinearity can be studied by excited-state theory.

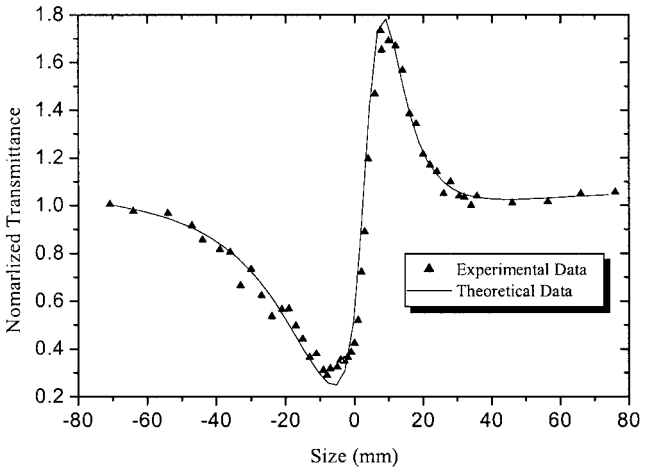

Figure 6. The Z-scan results of compound **1** observed under a closed-aperture configuration divided by those obtained under the open-aperture configuration

Under the excitation of picosecond laser pulses, the contribution of population of the singlet states to optical nonlinearities predominate and that of the triplet is negligible.[14] The nonlinear absorption index and refraction index can be written as shown in Equation (1)[15]

$$\begin{cases} \alpha = \alpha_0 + N_0\sigma_0 + N_1\sigma_S \\ \beta = \beta_0 + N_0\eta_0 + N_1\eta_S \end{cases} \quad (1)$$

where α_0 and α are the absorption coefficients of solvent and solute, respectively, σ_0 and σ_S are the absorption cross-sections of the ground and first singlet excited states, respectively, β_0 and β are the refractive indices of solvent and solution, respectively, and η_0 and η_S are the refrangibilities of the ground and first singlet excited states, respectively.

The light propagation equations are shown in Equation (2)

$$\begin{cases} \frac{\partial I}{\partial z} = -\alpha I \\ \frac{\partial \phi}{\partial z} = k\beta \end{cases} \quad (2)$$

 © 2004 Wiley-VCH Verlag GmbH & Co. KGaA, Weinheim

where k is the wave vector and I is the incident laser density. We performed a Z-scan measurement using TEM_{00}-mode laser pulses with a beam-waist radius of ω_0, a Gaussian temporal profile of duration τ, and a propagation direction along positive z. The irradiance I thus varies with z, r, and t according to Equation (3)

$$I(z,r,t) = \frac{\omega_0^2}{\omega^2(z)} I_{00} \exp\left[-\left(\frac{t}{\tau}\right)^2\right] \exp\left[-\left(\frac{2r^2}{\omega^2(z)}\right)\right] \quad (3)$$

where $\omega(z) = \omega_0[1 + (z/z_0)^2]^{1/2}$ is the beam waist radius at z, $z_0 = \pi\omega_0^2/\lambda$ is the diffraction length of the beam, and I_{00} is the on-axis peak irradiance at the focus.

The lifetime of the second excited singlet-state is of the order of sub-picosecond, and is much shorter than the duration of the picosecond pulses. Hence this problem can be dealt with by a stable-state approximation. For the sake of simplicity, only the case of steady state is considered. In this event, the outcome may be expressed by Equation (4)

$$\begin{cases} \alpha = \alpha_0 + \dfrac{1 + K_a \dfrac{I}{I_s}}{1 + \dfrac{I}{I_s}} \sigma_0 N \\ \beta = \beta_0 + \dfrac{1 + K_r \dfrac{I}{I_s}}{1 + \dfrac{I}{I_s}} \eta_0 N \end{cases} \quad (4)$$

where $I_S = (\eta\nu)/(\sigma_0\tau_{S0})$ is a saturable intensity, and K_a and K_r are defined by $K_a = \sigma_S/\sigma_0$ and $K_r = \eta_S/\eta_0$, which are the ratios of the singlet excited-state absorption cross section and refrangibility to those of the ground state, respectively.

From Equations (1)−(4) we studied the nonlinear optical properties of the excited state of metal clusters, and successfully fitted the experimental results shown in Figure 5 and 6 (solid lines). The ratios K_r and K_a are calculated to be 1.1 and 18 by the fitting curve for picosecond pulses. It can be seen that the ratio of refraction volumes of the singlet excited-state to the ground-state is greater than one for picosecond pulses, so it is self-focusing. The ratio of the singlet excited-state absorption cross-section to the ground-state is very large, so the compound possesses a strong excited-state absorption, which induces the asymmetry of the peak and valley.

Conclusions

In summary, a novel 1D polymeric compound $[W_2O_2S_6Cu_4(NCMe)_4]_n$ (**1**) with solvent MeCN coordinated to the copper atom was obtained through the self-assembly reaction of $(NH_4)_2(WOS_3)$ with CuBr in the presence of PCy_3. Compound **1** exhibits a strong excited-state absorption performance, the ratio of absorption cross-section of the singlet excited-state to that of the ground-state was about 18. Compound **1** is therefore considered to be a promising candidate for picosecond optical-limiting. The ratio of refrangibility of the singlet excited-state to that of the ground state is about 1.1; thus, it possesses a self-focusing property with picosecond pulses. The asymmetry of the peak and valley of the Z-scan curve is caused by the excited-state absorption. The nonlinear refraction and absorption model of the excited-states is presented to simulate the experiment results.

Experimental Section

General: The reagent $(NH_4)_2(WOS_3)$ was prepared according to a literature procedure.[16] Other chemicals were of AR grade and used without further purification. Infrared spectra were recorded with a Fourier transform Nicolet FT-170SX spectrophotometer (KBr pellets). The electronic spectrum was taken on a Shimadzu UV-240 spectrophotometer and elemental analyses (C and H) were performed on a PE-240C elemental analyzer. The ^1H NMR spectra were recorded on a Bruker AC400 spectrometer.

Nonlinear Optical Measurements: The nonlinear optical properties of the metal cluster solution were measured by the Z-scan technique at 532 nm. A continuum ns/ps Nd:YAG laser system with a pulse width of 40 ps was used. The metal complex **1** in CH_3CN solution was filled into a 2-mm cuvette with a linear transmittance of 92%. The input and the output energies of beams were measured with energy meters (Laser Precision Corporation Rjp-735). The focal length of the lens was 90 mm. The laser beam waist was about 36 μm at focus point, and the corresponding Rayleigh length was thus much larger than the thickness of sample. The aperture diameter was 2 mm and this corresponds to a far-field transmittance of 9.8%. The experimental data were collected utilizing a single shot at a rate of 1 pulse per minute to avoid thermal effects. The input pulse energies were 700 μJ for picosecond pulses.

Preparation of Compound 1: A solution of PCy_3 (560 mg, 2 mmol) in MeCN (10 mL) was added to a mixture of $(NH_4)_2(WOS_3)$ (332 mg, 1 mmol) and CuBr (287 mg, 2 mmol) in MeCN (40 mL). The resulting mixture was stirred for 24 h and then filtered. The red filtrate was layered with hexane (20 mL) and allowed to stand at room temperature for several weeks. Deep-red crystals were obtained; yield: 65%. Characteristic infrared absorptions were found at 420 cm^{-1} and 440 cm^{-1} for ν(W−S), 910 cm^{-1} for ν(W−O), and 2100 cm^{-1} for ν(C≡N). ^1H NMR ([D$_6$]DMSO, 25 °C): δ = 1.93 (s, CH_3). $C_4H_6Cu_2N_2OS_3W$ (505.22): calcd. C 9.51, H 1.20, N 5.54; found C 9.21, H 1.23, N 5.32.

Crystal Structure Determination and Refinement: A well-developed single crystal of the polymeric compound with suitable dimensions was mounted on a glass fiber. Cell dimension measurements and data collection were performed on a Siemens Smart CCD diffractomer with graphite monochromatized Mo-K_α radiation (λ = 0.71073 Å) at 20 °C. Intensity data for the crystal were obtained in the range $4.56° < 2\theta < 50°$ using the ω-scan technique. The structure was solved by direct methods using SHELXTL software and refined by full-matrix least-square methods on F^2.[17] All H atoms were geometrically fixed and allowed to ride on their attached atoms. Selected bond lengths and angles are listed in Table 1 and details of the data collection and structure refinement are summarized in Table 2.

CCDC-223470 contains the supplementary crystallographic data for this paper. These data can be obtained free of charge at www.ccdc.cam.ac.uk/conts/retrieving.html [or from the Cambridge Crystallographic Data Centre, 12 Union Road,

 © 2004 Wiley-VCH Verlag GmbH & Co. KGaA, Weinheim

Table 2. Crystal data and standard refinement details for $[W_2O_2S_6Cu_4(NCMe)_4]_n$ (**1**)

Empirical formula	$C_4H_6Cu_2N_2OS_3W$
Molecular mass	505.22
Crystal system	monoclinic
Space group	$P2_1/c$
Unit cell dimensions (Å)	$a = 9.075(2)$
	$b = 17.827(2)$
	$c = 7.481(2)$
β (°)	102.780(10)
Volume (Å^3)	1180.3(4)
Z	4
$D_{calcd.}$ (Mg·m^{-3})	2.843
Absorption coefficient (mm^{-1})	13.786
$F(000)$	928
Crystal size (mm)	$0.30 \times 0.20 \times 0.20$
Crystal colour	red
θ range for data collection (°)	2.28 to 24.99
Reflections collected	5980
Independent reflections	2074
Observed reflections	1643 [$I > 2\sigma(I)$]
Absorption correction	empirical
Transmission factors	$T_{min} = 0.052$; $T_{max} = 0.064$
Data/restraints/parameters	2074/0/120
Goodness-of-fit on F^2	1.057
Final difference map extremes	0.915; −0.633
R_1, wR_2 (all data)	0.0718, 0.0832
R_1, wR_2 [$I > 2\sigma(I)$]	0.0437, 0.0792

Cambridge CB2 1EZ, UK; Fax: +44-1223-336-033; E-mail: deposit@ccdc.cam.ac.uk].

Acknowledgments

Financial support from the National Natural Science Foundation of China, from the State Key Laboratory of Coordination Chemistry, and from Fujian Institute of Research on the Structure of Matter, Chinese Academy of Sciences is gratefully acknowledged.

[1] D. W. Murphy, P. A. Christian, *Science* **1979**, *205*, 651−653.
[2] R. R. Chianelli, T. A. Pecoraro, T. R. Halbert, H. W. Pan, E. I. Stiefel, *J. Catal.* **1984**, *86*, 226−230.
[3] A. Müller, F. Peters, M. I. Pope, D. Gatteschi, *Chem. Rev.* **1998**, *98*, 239−272.
[4] E. Coronado, C. J. Gomes-Carcia, *Chem. Rev.* **1998**, *98*, 273−296.
[5] E. Katsoulis, *Chem. Rev.* **1998**, *98*, 359−388.
[6] [6a] Q. Huang, X.-T. Wu, T.-L. Sheng, Q.-M. Wang, *Inorg. Chem.* **1995**, *27*, 4931−4932. [6b] J. P. Lang, K. Tatsumi, *Inorg. Chem.* **1999**, *38*, 1364. [6c] J.-P. Lang, Q.-F. Xu, W. Ji, H. I. Elim, K. Tatsumi, *Eur. J. Inorg. Chem.* **2004**, 86.
[7] H. W. Hou, H. G. Zheng, H. G. Ang, Y. T. Fan, M. K. M. Low, Y. Zhu, W. L. Wang, X. Q. Xin, W. Ji, W. T. Wong, *J. Chem. Soc., Dalton Trans.* **1999**, 2953−2957.
[8] [8a] Q. F. Zhang, Y. Y. Niu, W. H. Leung, Y. L. Song, I. D. Williams, X. Q. Xin, *Chem. Commun.* **2001**, 1126−1127. [8b] C. Potvin, J. M. Manoli, F. Secheresse, S. Marzak, *Inorg. Chem.* **1987**, *26*, 4370.
[9] Q. F. Zhang, W. H. Leung, X. Q. Xin, H. K. Fun, *Inorg. Chem.* **2000**, *39*, 417−426.
[10] H. W. Hou, X. Q. Xin, S. Shi, *Coord. Chem. Rev.* **1996**, *153*, 25−56.
[11] R. Doherty, C. R. Hubbard, A. D. Mighell, A. R. Siedle, J. Stewart, *Inorg. Chem.* **1979**, *18*, 2991−2995.
[12] H. W. Hou, D. L. Long, X. Q. Xin, X. X. Huang, B. S. Kang, P. Ge, *Inorg. Chem.* **1996**, *35*, 5363−5367.
[13] S. W. Du, N. Y. Zhu, P. C. Chen, X. T. Wu, *Angew. Chem. Int. Ed. Engl.* **1992**, *31*, 1085−1087.
[14] Y. L. Song, M. Yang, R. B. Wang, C. F. Li, *Chin. J. Lasers* **1994**, *A21*, 653−657.
[15] Y. Song, C. Zhang, Y. Wang, G. Fang, G. Jin, X. Zhang, S. Liu, L. Chen, X. Xin, *Opt. Commun.* **2000**, *186*, 105−110.
[16] J. W. McDonald, G. D. Frieson, C. D. Rosenhein, W. E. Newton, *Inorg. Chim. Acta* **1983**, *72*, 205−210.
[17] SHELXTL Version 5.1 Reference Manual, Siemens Analytical X-ray Systems, Inc., Madison, WI, USA, **1996**.

Received December 13, 2003
Early View Article
Published Online May 5, 2004

 © 2004 Wiley-VCH Verlag GmbH & Co. KGaA, Weinheim

Synthesis and Characterisation of the First Three-Dimensional Mixed-Metal-Center Inorganic-Organic Hybrid Framework with *N*-(Phosphonomethyl)iminodiacetate

Filipe A. Almeida Paz,[a] Fa-Nian Shi,[b] Jacek Klinowski,[a] João Rocha,*[b] and Tito Trindade[b]

Keywords: Carboxylate ligands / Crystal engineering / Hydrothermal synthesis / N ligands / Organic-inorganic hybrid composites

Using crystal engineering concepts, the first three-dimensional (3D) mixed-metal-centre inorganic-organic hybrid frameworks incorporating *N*-(phosphonomethyl)iminodiacetate ($pmida^{4-}$) were synthesised under mild hydrothermal conditions (100 °C) and characterised structurally. The crystal structures, obtained by the displacement of the coordinated water molecules in $[Co_2V_2O_2(pmida)_2(H_2O)_{10}]\cdot 2(H_2O)$ (**1**) [$P2_1/c$ monoclinic space group, $Z = 2$, $a = 9.996(2)$ Å, $b = 14.854(3)$ Å, $c = 10.781(2)$ Å, $\beta = 110.90(3)°$ and $V = 1495.5(5)$ Å^3] by the rod-like bridging 4,4′-bipyridine (4,4′-bpy) ligand — $[CdVO(pmida)(4,4'\text{-bpy})(H_2O)_2]\cdot(4,4'\text{-bpy})_{0.5}\cdot H_2O$ (**2**) and $[CoVO(pmida)(4,4'\text{-bpy})(H_2O)_2]\cdot(4,4'\text{-bpy})_{0.5}$ (**3**) — are isostructural and were also determined in the $P2_1/c$ monoclinic space group ($Z = 4$) by single-crystal X-ray diffraction studies at low temperature (180 K): for **2**, $a = 9.1267(18)$ Å, $b = 17.610(4)$ Å, $c = 15.361(3)$ Å, $\beta = 93.06(3)°$ and $V = 2465.3(9)$ Å^3; for **3**, $a = 8.7734(18)$ Å, $b = 17.264(4)$ Å, $c = 15.507(3)$ Å, $\beta = 93.94(3)°$ and $V = 2343.2(8)$ Å^3. All the crystal structures contain centrosymmetric dimeric $[V_2O_2(pmida)_2]^{4-}$ units connected to neighbouring M^{2+} cations (Cd^{2+} for **2**, and Co^{2+} for **1** and **3**) through the phosphonate group. In **2** and **3**, extended two-dimensional $[MVO(pmida)(H_2O)_2]_n$ layers are formed, with the 4,4′-bpy molecules acting as pillars between adjacent layers, leading to porous 3D supramolecular structures, $[MVO(pmida)(4,4'\text{-bpy})(H_2O)_2]_\infty$, with a topology resembling that of the NbO net.

(© Wiley-VCH Verlag GmbH & Co. KGaA, 69451 Weinheim, Germany, 2004)

Introduction

Since Hoskins and Robson reported the first highly ordered organic-inorganic coordination frameworks,[1] there has been a widespread interest in the design, synthesis and characterisation of such compounds.[2,3] The driving force behind this work is the potential application of functional materials for reversible guest-exchange,[4,5] shape selectivity,[5] catalysis,[6] gas storage,[7] molecular recognition,[8] photoluminescence,[9] and/or unusual magnetic,[10−12] nonlinear[11] and semiconducting properties,[13] chirality[12,14] or clathration.[15] While considerable progress has been made in the understanding of the chemical self-assembly of the building blocks of such materials, reliable prediction of their final topology and chemical properties remains one of the greatest challenges to crystal engineers, since several supramolecular isomers of similar energies are usually formed.[3] However, by careful selection of metallic centres with specific coordination geometries and organic ligands with predictable coordination fashions, some supramolecular motifs can be predicted.

We have focused our research on the synthesis of novel highly crystalline organic-inorganic hybrid materials which incorporate, simultaneously, traditional and novel ligands to the field.[16−18] *N*-(Phosphonomethyl)iminodiacetic acid (H_4pmida) is a precursor of a multidentate organic ligand ($pmida^{4-}$) with interesting and flexible coordination properties: apart from the two carboxylic acid groups and the central N-donor atom, it contains a phosphonate group capable of coordinating to several metal centres and to eliminate available coordination sites. Surprisingly, searches in the literature and the Cambridge Structural Database produced only a handful of structures incorporating this organic molecule: $Na_4[V_2O_2(pmida)_2]\cdot 10H_2O$ and $Na_8[V_2O_2(pmida)_2]_2\cdot 16H_2O$;[19] $[Co_2(pmida)(H_2O)_5]\cdot H_2O$ and $[Zn_2(pmida)(CH_3CO_2H)]_2\cdot H_2O$;[20] several zirconium derivatives;[21] $\{K_2[CoO_3(pmida)]\}_6\cdot xH_2O$[22] and $[Pb_2(pmida)]\cdot 1.5H_2O$.[23] The structures reported by Crans and co-workers[19] contain a centrosymmetric dimeric $[V_2O_2(pmida)_2]^{4-}$ unit, in which $pmida^{4-}$ completely traps

[a] Department of Chemistry, University of Cambridge, Lensfield Road, Cambridge CB2 1EW, UK
E-mail: jk18@cam.ac.uk
[b] Department of Chemistry, University of Aveiro, CICECO, 3810-193 Aveiro, Portugal
E-mail: rocha@dq.ua.pt

the vanadium centres inside three five-membered rings formed by the two carboxylate groups and the phosphonate group, closely resembling what we have observed for the *N*′′-carboxymethyldiethylenetriamine-*N*,*N*,*N*′,*N*′′-tetraacetate[17] and nitrilotriacetate[18] ligands. We felt that the $[V_2O_2(pmida)_2]^{4-}$ unit could then be used as a robust building block to construct novel multi-dimensional hybrid materials by replacing the Na^+ counterions with transition metal cations such as Co^{2+} and Cd^{2+}. This was first achieved with Co^{2+} cations which, along with the $[V_2O_2(pmida)_2]^{4-}$ unit, formed centrosymmetric neutral $[Co_2V_2O_2(pmida)_2(H_2O)_{10}]$ species (present in the crystal structure of **1**). Interestingly, each Co^{2+} centre is coordinated to five water molecules, which led us to believe that such weakly bound molecules could be easily displaced by a multitopic rod-like bridging ligand, such as 4,4′-bipyridine (4,4′-bpy). Here, we wish to report the synthesis and structural characterisation of the first two three-dimensional mixed-metallic frameworks incorporating $pmida^{4-}$ and 4,4′-bpy: $[CdVO(pmida)(4,4'\text{-bpy})(H_2O)_2]\cdot(4,4'\text{-bpy})_{0.5}\cdot H_2O$ (**2**) and $[CoVO(pmida)(4,4'\text{-bpy})(H_2O)_2]\cdot(4,4'\text{-bpy})_{0.5}$ (**3**).

Results and Discussion

$[Co_2V_2O_2(pmida)_2(H_2O)_{10}]\cdot 2(H_2O)$ (**1**), $[CdVO(pmida)(4,4'\text{-bpy})(H_2O)_2]\cdot(4,4'\text{-bpy})_{0.5}\cdot H_2O$ (**2**) and $[CoVO(pmida)(4,4'\text{-bpy})(H_2O)_2]\cdot(4,4'\text{-bpy})_{0.5}$ (**3**) were synthesised under mild hydrothermal conditions (see Exp. Sect.) and characterised structurally by single-crystal X-ray diffraction (see Exp. Sect. for further details) [$pmida^{4-}$ = *N*-(phosphonomethyl)iminodiacetate and 4,4′-bpy = 4,4′-bipyridine]. Compounds **2** and **3** have almost identical frameworks, with the most important difference being the extra crystallisation solvent molecule present in **2**. The phase purity and homogeneity of the bulk samples were further confirmed by X-ray powder diffraction analysis and elemental composition studies (EDS and CHN elemental analyses).

All structures contain two crystallographically unique metal centres, M1 and V1 [where M = Co^{2+} (for **1** and **3**) or Cd^{2+} (for **2**)], both in a six-coordination geometry, $\{CoO_6\}$ (in **1**), $\{MO_3N_3\}$ (in **2**/**3**) and $\{VO_5N\}$ [see Figure 1 and (a) in Figure 2; Table 1 and 2]. V1 is always connected to one oxo group and to two $pmida^{4-}$ ligands, with the coordination geometry resembling the typical highly distorted octahedral environment of V^{4+} sites [angles varying from 74.66(8) to 169.94(9)° (for **1**), 75.78(11) to 172.65(13)° (for **2**), and from 75.64(10) to 172.97(12)° (for **3**)], with a short (V=O), four intermediate (V−O) and one long (V−N) bonds (Table 1 and 2), all within the expected ranges reported by Boudin et al.,[24] as found in related compounds. The same authors classify such coordination geometry for V^{4+} as 1+4+1 with, as observed in our struc-

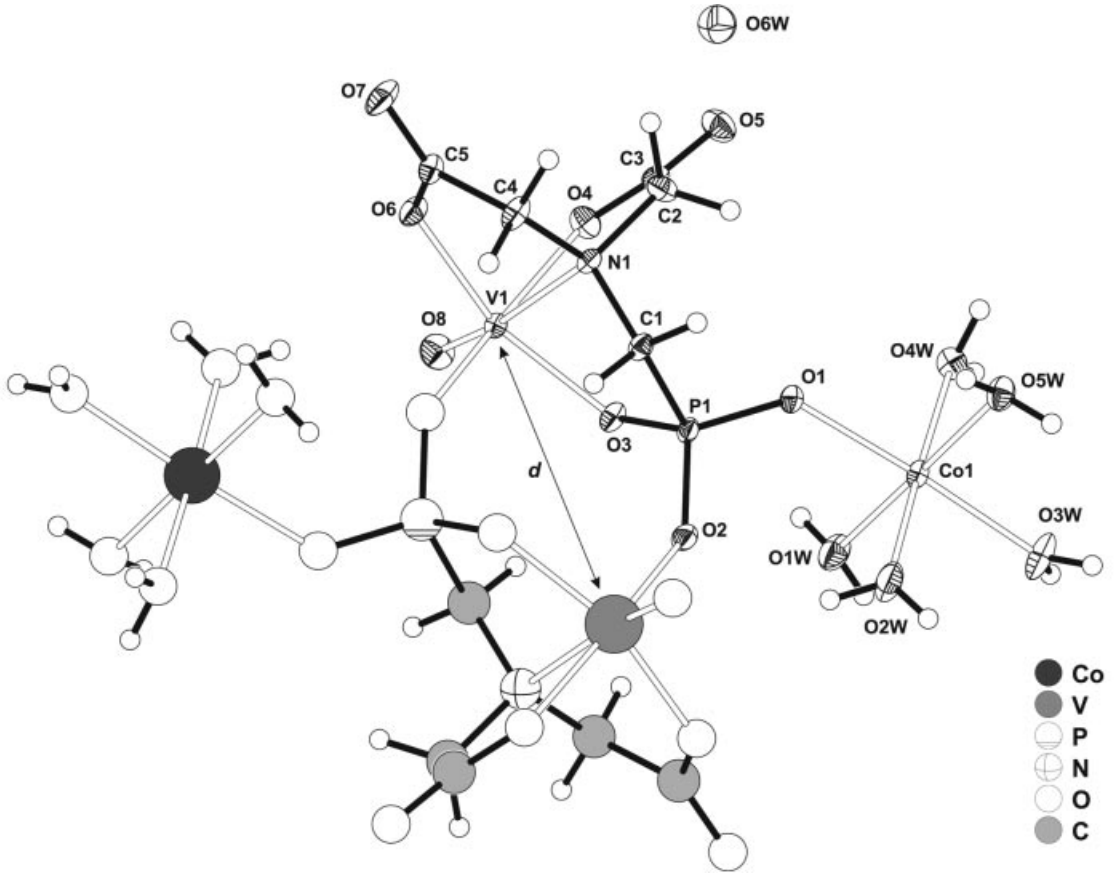

Figure 1. Molecular unit of **1**, showing the labelling scheme for all non-hydrogen atoms belonging to the asymmetric unit [*d* = 5.2285(13) Å]; displacement ellipsoids are drawn at the 50% probability level and H atoms are shown as small spheres; see Table 1 for bond lengths and angles

 © 2004 Wiley-VCH Verlag GmbH & Co. KGaA, Weinheim

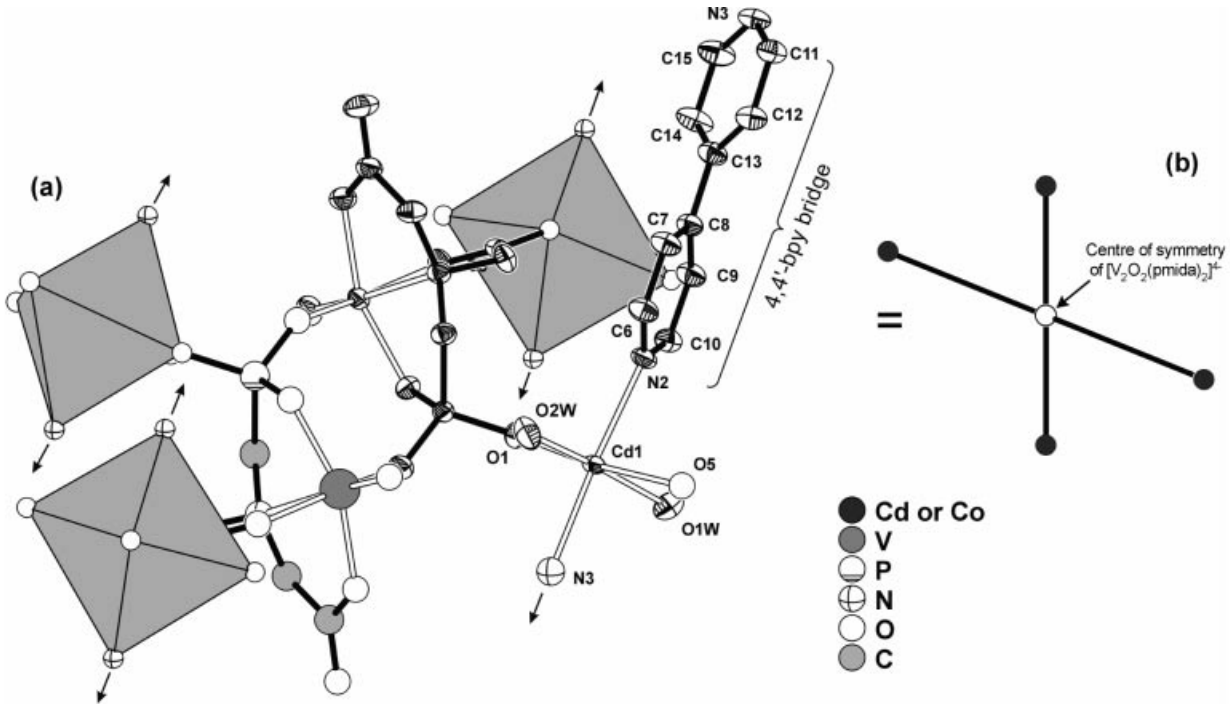

Figure 2. (a) Mixed polyhedral and ball-and-stick, and (b) topological representations of the hexametallic secondary building unit (SBU): section of the [MVO(pmida)(4,4′-bpy)(H_2O)$_2$] framework, showing one $[V_2O_2(pmida)_2]^{4-}$ dimeric unit bridging four $[M(4,4'\text{-bpy})(H_2O)_2]^{2n+}_n$ cationic chains (M = Cd^{2+} and Co^{2+} for **2** and **3**, respectively, represented as grey-filled octahedra); arrows indicate the ditopic bridging 4,4′-bpy ligands; atoms from the asymmetric unit are represented by thermal ellipsoids drawn at the 50% probability level (anisotropic displacement parameters from structure **2**); all hydrogen atoms have been omitted for clarity; see Table 2 for bond lengths and angles

Table 1. Selected bond lengths (Å) and angles (°) for **1**[a]

Co1−O1W	2.095(2)	O3W−Co1−O1W	89.22(9)
Co1−O2W	2.120(2)	O3W−Co1−O2W	87.57(9)
Co1−O3W	2.052(2)	O3W−Co1−O4W	91.57(8)
Co1−O4W	2.139(2)	O3W−Co1−O5W	91.33(8)
Co1−O5W	2.111(2)	O5W−Co1−O2W	88.15(9)
Co1−O1	2.0364(19)	O5W−Co1−O4W	89.81(8)
V1−O2^i	1.9897(19)		
V1−O3	1.9957(19)	O2^i−V1−O3	91.37(8)
V1−O4	2.0273(19)	O2^i−V1−O4	163.89(8)
V1−O6	2.0299(19)	O2^i−V1−O6	86.94(8)
V1−O8	1.604(2)	O2^i−V1−N1	88.14(8)
V1−N1	2.363(2)	O3−V1−O4	86.80(8)
		O3−V1−O6	154.18(8)
O1−Co1−O1W	88.55(8)	O3−V1−N1	79.54(7)
O1−Co1−O2W	90.52(8)	O4−V1−N1	75.79(8)
O1−Co1−O3W	177.01(9)	O6−V1−O4	87.77(8)
O1−Co1−O4W	90.42(8)	O6−V1−N1	74.66(8)
O1−Co1−O5W	90.91(8)	O8−V1−O2^i	101.17(10)
O1W−Co1−O2W	92.31(10)	O8−V1−O3	103.81(10)
O1W−Co1−O4W	89.74(8)	O8−V1−O4	94.81(10)
O1W−Co1−O5W	179.29(8)	O8−V1−O6	101.79(10)
O2W−Co1−O4W	177.77(8)	O8−V1−N1	169.94(9)

[a] Symmetry transformation used to generate equivalent atoms: (i) 2 − *x*, −*y*, 1 − *z*.

tures, the V=O being *trans* to V−N, showing a marked influence of the oxo ligand in the long V−N distance.[24] Such bonds, although longer than those found in compounds with a *trans* amine nitrogen donor atom bound to vanadium as, for example, complexes with nitrilotriacetic acid (2.17−2.30 Å),[25] *N*-(2-hydroxyethyl)iminodiacetic acid (2.17−2.31 Å),[26] *N*-(carbamoylmethyl)iminodiacetic acid (2.19−2.21 Å),[27] *N*-(carbamoylethyl)iminodiacetic acid (2.17−2.19 Å),[28] (*S*)-[1-(2-pyridyl)ethyl]iminodiacetic acid (2.26−2.29 Å)[29] and triethanolamine (2.15−2.28 Å),[30] are similar to the values found by Crans and co-workers for the vanadium compounds containing $pmida^{4-}$ ligands: {$Na_4[V_2O_2(pmida)_2]\cdot 10H_2O$ (**a**) and $Na_8[V_2O_2(pmida)_2]_2\cdot 16H_2O$ (**b**)}.[19] Since for each compound the four V−O bonds are statistically identical, the coordination geometry for V1 can be seen as a highly distorted octahedral environment (Table 1 and 2).

In **1**, the coordination environment of Co1 is composed of five water molecules and one O-donor atom from the phosphonate group (Figure 1), with a coordination geometry of an almost regular octahedron [bond lengths and angles varying from 2.0364(19) to 2.139(2) Å, and 87.57(9) to 179.29(8)°, respectively] (Table 1). As expected, the bridging rod-like 4,4′-bpy ligand has displaced the weakly bound water molecules, introducing significant structural changes in the final compounds. In **2** and **3**, M1 is now coordinated to six independent moieties (two water molecules, two $pmida^{4-}$ and two 4,4′-bpy ligands) with a coordination geometry of a slightly distorted octahedron [bond angles varying from 84.02(12) to 174.82(1)° (for **2**), and from 86.09(11) to 175.02(9)° (for **3**); see (a) in Figure 2 and Table 2]. Interestingly, each pair of ligand types is *trans*-coordinated in the axial positions, with the O-donor atoms

 © 2004 Wiley-VCH Verlag GmbH & Co. KGaA, Weinheim

Table 2. Selected bond lengths (in Å) and angles (in degrees) for **2** and **3**[a]

	2	**3**		**2**	**3**
M1−O1W	2.318(3)	2.117(3)	N2−M1−O2W	94.74(11)	93.40(10)
M1−O2W	2.350(3)	2.128(3)	N2−M1−O5$^{i/iv}$	85.45(11)	86.39(10)
M1−O1	2.252(3)	2.079(2)	N3$^{ii/v}$−M1−O1W	92.14(12)	91.27(10)
M1−O5$^{i/iv}$	2.374(3)	2.218(2)	N3$^{ii/v}$−M1−O2W	84.02(12)	86.09(11)
M1−N2	2.307(3)	2.140(3)	N3$^{ii/v}$−M1−O5$^{i/iv}$	89.42(11)	88.42(10)
M1−N3$^{ii/v}$	2.282(3)	2.129(3)	N3$^{ii/v}$−M1−N2	174.82(12)	174.80(11)
V1−O2$^{iii/vi}$	1.962(3)	1.951(2)			
V1−O3	2.000(3)	2.005(2)	O2$^{iii/vi}$−V1−O3	91.31(11)	91.97(10)
V1−O4	2.032(3)	2.029(2)	O2$^{iii/vi}$−V1−O4	161.34(11)	160.32(10)
V1−O6	2.010(3)	2.026(2)	O2$^{iii/vi}$−V1−O6	88.14(11)	87.41(10)
V1−O8	1.616(3)	1.612(2)	O2$^{iii/vi}$−V1−N1	85.00(11)	84.75(10)
V1−N1	2.341(3)	2.355(3)	O3−V1−O4	88.09(11)	88.20(10)
			O3−V1−O6	153.57(11)	152.36(10)
O1−M1−O1W	91.40(10)	89.59(10)	O3−V1−N1	77.85(11)	76.79(9)
O1−M1−O2W	96.68(10)	95.41(10)	O4−V1−N1	76.64(11)	76.14(9)
O1−M1−O5$^{i/iv}$	174.14(9)	175.02(9)	O6−V1−O4	84.21(12)	83.42(10)
O1−M1−N2	88.81(11)	89.87(10)	O6−V1−N1	75.78(11)	75.64(10)
O1−M1−N3$^{ii/v}$	96.34(11)	95.33(10)	O8−V1−O2$^{iii/vi}$	101.96(13)	101.75(12)
O1W−M1−O2W	171.38(11)	174.54(10)	O8−V1−O3	104.09(13)	105.39(12)
O1W−M1−O5$^{i/iv}$	87.28(10)	87.05(10)	O8−V1−O4	96.26(13)	97.15(12)
O2W−M1−O5$^{i/iv}$	84.98(10)	88.10(10)	O8−V1−O6	101.86(13)	101.77(12)
N2−M1−O1W	88.40(11)	88.80(10)	O8−V1−N1	172.65(13)	172.97(12)

[a] Symmetry transformations used to generate equivalent atoms: (i) x, 1/2 − y, 1/2 + z; (ii) x + 1, 1/2 − y, 1/2 + z; (iii) 2 − x, −y, 1 − z; (iv) x, 1/2 − y, z − *1/2*; (v) x − 1, 1 − y, z − 1/2; (vi) −x, −y, 1 − z. M = Cd^{2+} or Co^{2+} for **2** and **3**, respectively.

from the two pmida^{4-} ligands being from different functional groups inside this molecule [O1 belongs to the phosphonate group, while O5 belongs to the bridging-η^2-*syn*, *anti*-bidentate C3 carboxylate group; see (a) in Figure 2]. The average M−O and M−N distances are 2.09/2.32/2.14 and 2.29/2.13 Å (for **1/2/3**), consistent with values found in similar structures.

The pmida^{4-} anion is a polydentate ligand that completely traps the vanadium centres inside three five-membered rings formed by the two carboxylate and phosphonate groups connected in an *anti*-unidentate coordinative fashion to the vanadium centres [pmida-V moiety; Figure 1 and (a) in Figure 2]. The average bite angles are ca. 76.7/76.8/76.2° (for **1/2/3**, Table 1 and 2), similar to the values for **a** and **b** (ca. 76.7 and 77.0°, respectively).[19] Interestingly, in **2** and **3** each carboxylate group from pmida^{4-} has a different coordination mode: while the C5 group is only coordinated to V1 by the O5 atom in an *anti*-unidentate mode, C3 also forms a bridge with a neighbouring M1 through a bridging-*syn*,*anti*-bidentate coordination mode [V1···Cd1^{i} 5.3463(11) Å, and V1···Co1^{ii} 5.2888(11) Å; symmetry codes: (i) x, 1/2 − y, −1/2 + z; (ii) x, 1/2 − y, 1/2 + z]. All carboxylate groups maintain approximately the equivalence in the C−O bonds, with the distances within the 1.239(3)−1.278(3) Å, 1.239(5)−1.277(5) Å and 1.240(4)−1.277(4) Å ranges for structures **1**−**3**, respectively. This is particularly unexpected for the carboxylate groups adopting the *anti*-unidentate coordinative fashion (C5 for all the structures, plus C1 in **1**), and can be explained by the extensive hydrogen-bonding network in the crystal struc-

Table 3. Hydrogen bonding geometry (distances in Å and angles in degrees)[a]

D−H···A	*d*(D−H)	*d*(H···A)	*d*(D···A)	>(DHA)
1				
O1W−H1C···O5^{i}	0.85(1)	1.932(12)	2.770(3)	171(3)
O1W−H1D···O4W^{i}	0.85(1)	2.004(16)	2.817(3)	160(4)
O2W−H2C···O2	0.83(1)	2.13(3)	2.809(3)	139(3)
O2W−H2D···O6W^{ii}	0.84(1)	2.19(4)	2.633(5)	113(4)
O3W−H3A···O6^{iii}	0.84(1)	1.891(12)	2.723(3)	173(4)
O3W−H3B···O4^{i}	0.84(1)	1.902(13)	2.724(3)	166(4)
O4W−H4C···O3^{i}	0.85(1)	1.923(10)	2.769(3)	179(4)
O4W−H4D···O7^{iv}	0.86(1)	1.868(11)	2.719(3)	172(3)
O5W−H5A···O5^{v}	0.84(1)	1.978(14)	2.791(3)	163(3)
O5W−H5B···O7^{iii}	0.84(1)	2.004(12)	2.840(3)	173(3)
O6W···O5	–	–	2.814(5)	–
O6W···O7^{vi}	–	–	2.985(5)	–
2				
O1W−H1C···N4^{vii}	0.86(3)	1.89(4)	2.732(4)	170(5)
O1W−H1D···O4^{viii}	0.86(3)	1.92(4)	2.744(4)	158(6)
O2W−H2C···O8^{ix}	0.85(3)	2.00(3)	2.838(4)	174(4)
O2W−H2D···O7^{i}	0.85(3)	1.86(3)	2.694(4)	167(5)
O3W···O3^{vi}	–	–	2.916(7)	–
O3W···O8^{vi}	–	–	2.898(7)	–
3				
O1W−H1C···N4^{iv}	0.85(3)	1.91(3)	2.740(3)	167(4)
O1W−H1D···O4^{v}	0.84(3)	1.86(3)	2.669(3)	160(5)
O2W−H2C···O8^{x}	0.83(3)	2.04(3)	2.855(4)	169(4)
O2W−H2D···O7^{xi}	0.84(3)	1.85(3)	2.681(4)	175(5)

[a] Symmetry transformations used to generate equivalent atoms: (i) 1 − x, −y, 1 − z; (ii) x, y, z − *1*; (iii) x − *1*, y, z − 1; (iv) x − 1, 1/2 − y, z − 1/2; (v) x, 1/2 − y, z − 1/2; (vi) x − 1, y, z; (vii) x + 1, y, z; (viii) x, 1/2 − y, 1/2 + z; (ix) 2 − x, −y, 1 − z; (x) −x, −y, 1 − z; (xi) 1 − x, −y, 1 − z.

 © 2004 Wiley-VCH Verlag GmbH & Co. KGaA, Weinheim

tures (Table 3). As in **a** and **b**, the phosphonate group from pmida^{4-} establishes bridges between adjacent vanadium centres (through the O2 and O3 atoms), leading to the formation of a centrosymmetric dimeric unit consisting of two pmida-V moieties, $[V_2O_2(pmida)_2]^{4-}$, and imposing V1···V1$^{iii/iv}$ separations of 5.2285(13)/5.2545(17)/5.2128(16) Å (for **1**/**2**/**3**) [symmetry codes: (iii) $2 - x, -y, 1 - z$; (iv) $-x, -y, 1 - z$; see Figure 1 and (a) in 2].

In the structures reported by Crans and co-workers, the $[V_2O_2(pmida)_2]^{4-}$ dimeric units appear isolated in the crystal structure, interacting only with the neighbouring Na^+ cations and water molecules. Similarly, **1** can be described by the close packing of $[Co_2V_2O_2(pmida)_2(H_2O)_{10}]$ moieties, interacting through the extensive hydrogen-bonding network (not shown; Table 3). However, in **2** and **3** coordinative interactions with Cd^{2+} and Co^{2+} cations from adjacent moieties lead to the formation of extended two-dimensional (2D) $[MVO(pmida)(H_2O)_2]_n$ networks in the *bc* plane of the unit cell (Figure 3). In fact, apart from the bridge created by the C3 *syn*,*anti*-bidentate carboxylate group discussed previously, O1 is also connected to a neighbouring M1 centre, establishing the final tridentate coordination mode for the phosphonate group [V1···M1 6.2903(11)/6.1987(12) Å and M1···V1$^{iii/iv}$ 5.0474(11)/4.9696(11) Å for (**2**/**3**); symmetry codes: (iii) $2 - x, -y, 1 - z$; (iv) $-x, -y, 1 - z$].

As often occurs in other hybrid organic-inorganic materials, **2** and **3** can also be seen as modular structures assembled by the 3D repetition of a discrete hexametallic secondary building unit (SBU) composed of 4 M^{2+} and 2 V^{4+} centres (Figure 2 and 3). Taking the geometrical centres of the $[V_2O_2(pmida)_2]^{4-}$ units (denoted as A) and the M^{2+} metal centres (denoted as X; see Figure 2b and 3b) as network nodes, the $[MVO(pmida)(H_2O)_2]_n$ layers can be seen as undulating plane nets formed by distorted 4-gons assembled by 4- (A) and 2-connected nodes (X) [se (b) in Figure 3]. As expected for a typical AX_2 plane net, A and X are not co-planar, with rows of X-nodes placed above and below the plane of the A-nodes. Such a topological feature has direct consequences in the 3D structure of the compounds. In fact, ditopic bridging 4,4′-bpy molecules [with dihedral angles of ca. 42/44° (**2**/**3**) between the two 4-pyridyl groups; see (a) in Figure 2] establish physical links between consecutive M1 metal centres [see (b) in Figure 2], forming $[M(4,4'\text{-bpy})(H_2O)_2]_n^{2n+}$ cationic chains which run along the crystallographic *a* axis [see (a) in Figure 2 and Figure 4], and act as pillars between consecutive $[MVO(pmida)(H_2O)_2]_n$ layers [M1···M1^{v} 11.613(4)/11.308(4) Å for (**2**/**3**); symmetry code: (v) $1 + x, 1/2 - y, 1/2 + z$] (Figure 4).

The parallel stacking of 4,4′-bpy-pillared $[MVO(pmida)(H_2O)_2]_n$ layers leads to a porous 3D supramolecular structure, $[MVO(pmida)(4,4'\text{-bpy})(H_2O)_2]_\infty$ (Figure 4), with a topology resembling that of the NbO net (Figure 5).[31] This 3D structure contains rectangular channels which run along the *a* direction (average cross-section of ca. 5.0 × 4.0 Å^2), and stack in an [ABAB...] brick-wall-like fashion in the *bc* plane (Figure 6). A search for the solvent accessible voids for $[MVO(pmida)(4,4'\text{-bpy})(H_2O)_2]_\infty$ using the software package PLATON[32] (1.20 Å probe radius) gives 596.2/516.9 Å^3 (24.2/22.1% of the total volume of the unit cell) for **2**/**3**. These channels contain the extra crystallisation solvent molecule (in the case of **2**), and 4,4′-bpy molecules strongly hydrogen bonded to the framework, establishing further interactions between consecutive layers (Figure 6 and Table 3).

Thermal Analysis

The course of thermal decomposition of compounds **1**, **2** and **3** is similar. For **1** and **2**, two mass losses in the 54−336 and 30−280 °C temperature ranges, respectively, correspond to the release of all the water molecules from the crystal structure: for **1**, the combined mass losses (24.2%) are in good agreement with the calculated value (23.8%) for the release of the twelve crystallographic water molecules; for **2**, some lattice water is gradually released between 30 and 180 °C (1.4% observed, 2.6% calculated); between 180 and 280 °C all the remaining water molecules are released in a one-step process (7.5% observed, 7.8% calculated).

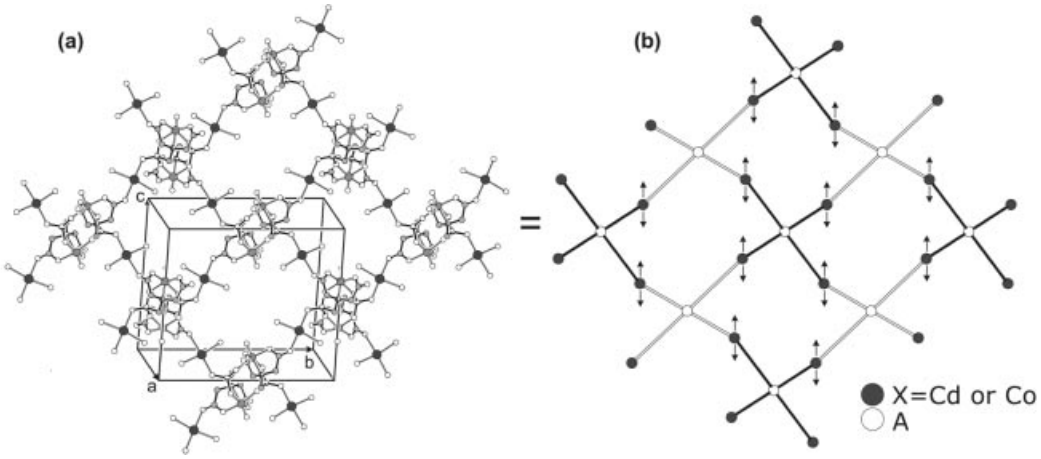

Figure 3. (a) Ball-and-stick and (b) topological representations of 2D $[MVO(pmida)(H_2O)_2]_n$ undulated network; all hydrogen atoms have been omitted for clarity; arrows indicate the ditopic bridging 4,4′-bpy ligands and thus the direction of the $[M(4,4'\text{-bpy})(H_2O)_2]_n^{2n+}$ cationic chains which connect neighbouring $[MVO(pmida)(H_2O)_2]_n$ layers (M = Cd^{2+} and Co^{2+} for **2** and **3**, respectively)

 © 2004 Wiley-VCH Verlag GmbH & Co. KGaA, Weinheim

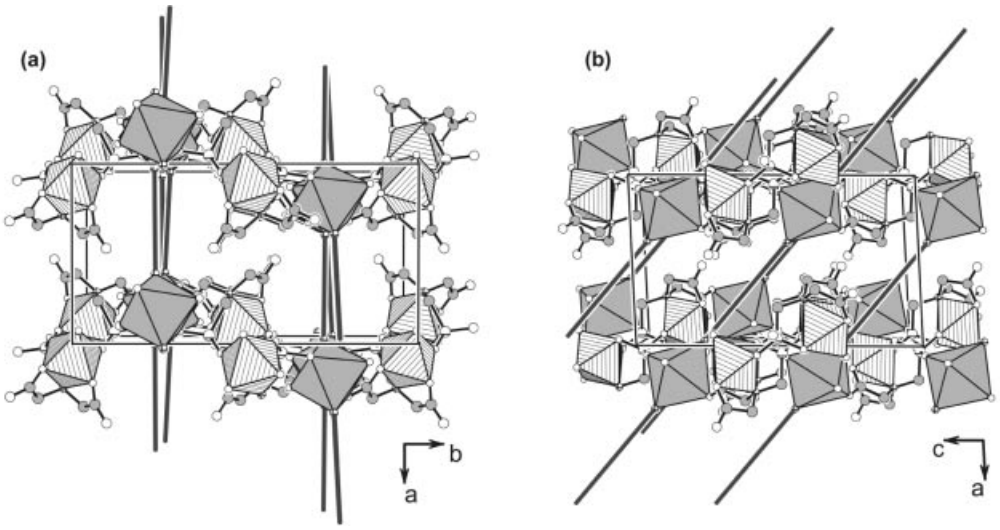

Figure 4. Perspective views along the (a) *c* and (b) *b* crystallographic axes of two consecutive $[MVO(pmida)(H_2O)_2]_n$ layers (M = Cd^{2+} and Co^{2+} for **2** and **3**, respectively), which pack in a parallel fashion along the *a* direction (one layer per *a* axis); the bridging 4,4′-bpy ligands (represented as grey-filled rods) act as pillars between the layers; V^{4+} and M^{2+} centres are represented as white- and grey-filled octahedra, respectively; all hydrogen atoms have been omitted for clarity

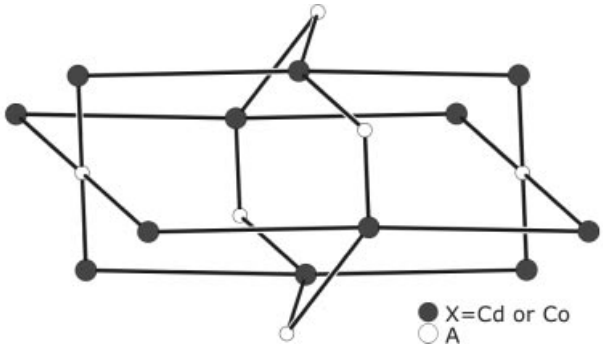

Figure 5. Topological representation of a portion of the $[MVO(pmida)(4,4'\text{-bpy})(H_2O)_2]_\infty$ network (M = Cd^{2+} and Co^{2+} for **2** and **3**, respectively), showing a topology resembling that of the NbO net[31]

Interestingly, in compound **3** the release of the two molecules per formula unit is significantly faster, with the majority of the water molecules being liberated between 30 and 149 °C (4.9% observed, 5.8% calculated). Although the steric hindrance created by the presence of the 4,4′-bpy molecules within the channels is almost the same for **2** and **3**, the hydrogen bonds caused by the presence of extra lattice water in **2** appear to be responsible for the slow kinetics of the dehydration process (Table 3 and Figure 6).

Up to 606 °C, 520 °C and 655 °C total mass losses of 46.6%, 55.7% and 60.9% are registered for **1**, **2** and **3**, respectively, which is attributed to the thermal decomposition of the organic component, leading to the formation of the mixed oxo-metallic phosphates, MVO_2PO_4 (**1**: 52.1% calculated and 53.4% observed residues; **2**: M = Cd^{2+}, 42.2% calculated and 44.3% observed residues; **3**: M = Co^{2+}, 38.3% calculated and 39.1% observed residues).

Vibrational Spectra

FT-IR spectroscopy confirms the presence of the organic ligands used in the synthesis (see Exp. Sect.). The presence of hydrogen-bonding networks is evident from the spectra, not only through the presence of the typical O−H stretching vibrations for water molecules (very broad bands), but also to in-plane (δ) and out-of-plane (γ) O−H···O deformations (see Exp. Sect.). The characteristic antisymmetric and symmetric stretching bands for carboxylate ions are also present, with the corresponding $\Delta[\nu_{assym}(CO_2^-) - \nu_{sym}(CO_2^-)]$ values being 218 cm^{-1}, 246 and 189 cm^{-1}, and 250 and 192 cm^{-1} for **1**, **2** and **3**, respectively. These values are a clear indication of the presence of carboxylate groups in the *anti*-unidentate and bridging-η^2-*syn*,*anti*-chelate coordination modes, respectively, as observed in the crystal structures (Figure 1 and 2).[33] The *anti*-unidentate coordination mode for the carboxylate groups is clearly observed in the IR spectra from the typical stretching vibration for C−O groups (found at 1685, 1670 and 1697 cm^{-1} for structures **1**−**3**, respectively).

Conclusion

Crystal Engineering concepts have been used to examine the assembly of ordered 3D solid organic-inorganic hybrid materials containing $[V_2O_2(pmida)_2]^{4-}$ moieties [where $pmida^{4-}$ is *N*-(phosphonomethyl)iminodiacetate]. Two novel isostructural mixed-metal materials containing Cd^{2+} or Co^{2+} have been prepared by using the rod-like 4,4′-bipyridine ligand to establish physical bridges between adjacent $[M_2V_2O_2(pmida)_2]$ moieties. The 3D structures contain pores along the *a* direction of the unit cell that are filled with uncoordinated 4,4′-bipyridine and solvent molecules.

 © 2004 Wiley-VCH Verlag GmbH & Co. KGaA, Weinheim

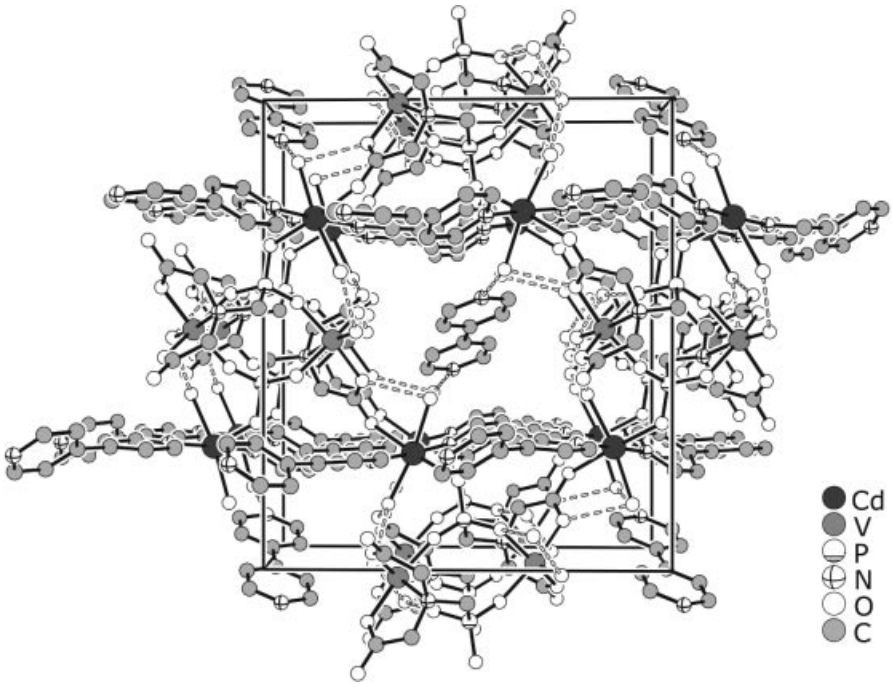

Figure 6. Perspective view along the *a* direction of the unit cell of **2**; hydrogen bonds are represented as white-filled dashed lines (for hydrogen-bonding geometry see Table 3); all hydrogen atoms have been omitted forclarity

Current work is focused on functionalising such materials by selectively controlling the organic pillars and the metal cations bridging adjacent $[V_2O_2(pmida)_2]^{4-}$ moieties.

Experimental Section

General: All reagents were readily available from commercial sources and were used as received without further purification. Syntheses were carried out in PTFE-lined stainless-steel reaction vessels (40 mL) under autogenous pressure and static conditions at 100 °C in a preheated oven. Reactions took place over a period of 4 days after which the vessels were removed from the oven and left to cool to ambient temperature before opening. All compounds proved to be air- and light-stable, and insoluble in water and common organic solvents such as methanol, ethanol, acetone, dichloromethane, toluene, DMSO and chloroform.

Characterisation: Elemental analyses for C, H and N were performed on an Exeter Analytical CE-440 Elemental Analyzer (University of Cambridge). Samples were combusted under oxygen at 975 °C, with He as the purge gas. FT-IR spectra were measured from KBr disks (Aldrich, 99%+, FT-IR grade) on a Matson 700 FTIR spectrometer. Thermogravimetric analyses (TGA) were carried out using a Shimadzu TGA-50, with a heating rate of 10 °C/min, under nitrogen atmosphere with flow rate of 20 mL/min.

Preparation and Structural Characterisation of $[CoVO(pmida)(H_2O)_5]_2\cdot 2(H_2O)$ (1): A mixture of vanadium(IV) oxide sulfate pentahydrate ($VOSO_4\cdot 5H_2O$; 0.40 g, 99% Sigma-Aldrich), cobalt acetate tetrahydrate ($CoC_4H_6O_4\cdot 4H_2O$; 0.620 g, 99.0% Fluka), *N*-(phosphonomethyl)iminodiacetic acid hydrate (H_4pmida; 0.400 g, 97% Fluka), and imidazole ($C_3H_4N_2$; 0.200 g, 99.0% Panreac) in about 8 mL of distilled water, was stirred thoroughly for 30 min at ambient temperature yielding a suspension with a molar composition of 1.00:1.56:1.19:1.86:281, respectively. After the reaction a large amount of big purple crystals of **1** (ca. 0.50 g) were isolated by vacuum filtering, washed with large amounts of distilled water (3 × ca. 50 mL), and air-dried at ambient temperature. Large single-crystals of **1** could also be formed by the slow evaporation of water from the autoclave mother liquor. $C_{10}H_{32}Co_2N_2O_{28}P_2V_2$ (910.06) (based on single-crystal data): calcd. C 13.14, H 3.97, N 3.06; found C 13.63, H 3.72, N 2.89. TGA data (mass losses): 54−169 °C 18.8% (DTG peak at 142 °C); 169−336 °C 5.4% (DTG peak at 171 °C); 336−440 °C 20.4% (DTG peaks at 379 and 403 °C); 440−606 °C 2.0% (DTG peak at 501 °C). Selected FT-IR data (cm^{-1}): ν(O−H, lattice and coordinated water) = 3384 vs (very broad); ν_{sym}(C−H in CH_2) = 2962 m; ν_{asym}(C−H in CH_2) = 2925 m; ν(C−O) = 1695 m; $\nu_{asym}(CO_2^-)$ = 1622 vs; δ(CH_2) = 1427 m; $\nu_{sym}(CO_2^-)$ = 1404 s; δ(O−H···O) = 1389 s and 1343 m; ν(C−O) = 1254 m; δ(C−C−N, amines) = 1145 vs and 1116 s; ν(N−C) = 1103s; ν(P−O) = 1061 vs; ν(V−O) = 955 s; γ(O−H···O) = 909 m; ν(P−C) = 774 m; γ(C−O) = 737 m.

Preparation and Structural Characterisation of $[CdVO(pmida)(4,4'\text{-bpy})(H_2O)_2]\cdot(4,4'\text{-bpy})_{0.5}\cdot H_2O$ (2): A mixture of vanadium(IV) oxide sulfate pentahydrate ($VOSO_4\cdot 5H_2O$; 0.40 g, 99% Sigma−Aldrich), cadmium oxide (CdO; 0.470 g, 99% Fluka), *N*-(phosphonomethyl)-iminodiacetic acid hydrate (H_4pmida; 0.560 g, 97% Fluka) and 4,4′-bipyridine (4,4′-bpy; 0.190 g, 99% Fluka) in about 15 mL of distilled water, was stirred thoroughly for 30 min at ambient temperature yielding a suspension with a molar composition of 1.30:2.77:2.04:1.00:685, respectively. After the reaction the resulting mixture consisted of two distinct phases: a large amount of light-blue crystals of **1** (ca. 0.20 g), and a residual amount of a white powder of unknown composition. The two components were readily separated by vacuum filtering and washing with large amounts of distilled water (3 × ca. 50 mL). Crystals of **2** were manually harvested and then air-dried at 70 °C. $C_{20}H_{22}CdN_4O_{11}PV$ (688.73) (based on single-crystal data): calcd. C 34.78, H 3.50, N 8.11; found C 33.72, H 3.32, N 7.72. TGA data (mass losses): 30−180 °C 1.4% (DTG peak at 50 °C); 180−280 °C 6.1% (DTG peak at 216 °C);

 © 2004 Wiley-VCH Verlag GmbH & Co. KGaA, Weinheim

280−520 °C 48.2% (DTG peaks at 366 °C and 430 °C). Selected FT-IR data (cm^{-1}): ν(O−H, lattice and coordinated water) = 3381 vs (very broad); 3140 vs (very broad); ν(C−H, aromatic compounds) = 3055 s; 3036 s; ν_{sym}(C−H in CH_2) = 2963 m; ν_{asym}(C−H in CH_2) = 2917 m; overtones and combination bands for 4-monosubstituted pyridines = 1966 w and 1940 w; ν(C−O) = 1670 sh; $\nu_{asym}(CO_2^-)$ = 1632 vs and 1601 vs; interactions between ν(C−C) and ν(C−N) for 4-monosubstituted pyridines = 1565 m and 1489 m; ν(C−H, aromatic compounds) = 1535 m; δ(CH_2) = 1428 m; $\nu_{sym}(CO_2^-)$ = 1412 s and 1386 s; δ(O−H···O) = 1343 m and 1325 m; ν(C−O) = 1266 m and 1254 m; δ(C−H, 4-monosubstituted pyridines) = 1219 m and 1099 s; ρ(C−H) = 1160 s and 1050 s; δ(C−C−N, amines) = 1123 s and 1113 s; ν(N−C) = 1098 vs and 1075 vs; ν(P−O) = 1050 vs; interactions between ν(C−C) and ν(C−N) for 4-monosubstituted pyridines = 992 m; ν(V−O) = 946 s; γ(O−H···O) = 911 m; γ(=C−H, 4-monosubstituted pyridines) = 855 m and 805 s; ν(P−C) = 783 vs; γ(C−O) = 732 m; δ(C−N−C, tertiary amines) = 556 m (very broad); ρ[(C−O)−O] 490 m and 514 m.

Preparation and Structural Characterisation of [CoVO(pmida)(4,4′-bpy)(H_2O)$_2$]·(4,4′-bpy)$_{0.5}$ (3): A mixture of vanadium(IV) oxide sulfate pentahydrate ($VOSO_4·5H_2O$; 0.40 g, 99% Sigma−Aldrich), cobalt acetate tetrahydrate ($CoC_4H_6O_4·4H_2O$; 0.310 g, 99.0% Fluka), *N*-(phosphonomethyl)iminodiacetic acid hydrate (H_4pida; 0.280 g, 97% Fluka), 4,4′-bipyridine (4,4′-bpy; 0.100 g, 99% Fluka), and sodium hydroxide (NaOH; 0.20 g, 98.0% Panreac) in ca. 10 g of distilled water, was stirred thoroughly for 30 min at ambient temperature yielding a suspension with a molar composition of 2.47:1.94:1.94:1.00:7.81:867, respectively. After the reaction the resulting mixture consisted of three distinct phases: a large amount of big purple-pink crystals of **2** (ca. 0.21 g), and a residual amount of small mixed particles of unknown microcrystalline compounds. These components were readily separated by vacuum filtering and washing with large amounts of distilled water (3 × ca. 50 mL). Crystals of **3** were manually harvested and air-dried at ambient temperature. $C_{20}H_{22}CoN_4O_{10}PV$ (619.26) (based on single-crystal data): calcd. C 38.79, H 3.58, N 9.05; found C 38.23, H 3.56, N 8.83. TGA data (mass losses): 30−149 °C 4.9% (DTG peak at 119 °C); 215−265 °C 4.7% (DTG peak at 250 °C); 265−335 °C 18.3% (DTG peak at 301 °C); 335−366 °C 10.5% (DTG peak at 343 °C); 366−478 °C 8.0% (DTG peaks at 377 and 400 °C); 478−655 °C 14.5% (broad DTG peak at 575 °C). Selected FT-IR data (cm^{-1}): ν(O−H, lattice and coordinated water) = 3395 vs (very broad); ν(C−H, aromatic compounds) = 3063 s; 3044 s; ν_{sym}(C−H in CH_2) = 2962 m and 2953 m; ν_{asym}(C−H in CH_2) = 2923 m and 2912 m; ν(C−O) = 1697 m; $\nu_{asym}(CO_2^-)$ = 1651 vs and 1610 vs; interactions between ν(C−C) and ν(C−N) for 4-monosubstituted pyridines = 1578 m and 1491 m; ν(C−H, aromatic compounds) = 1536 m; δ(CH_2) = 1428 m; $\nu_{sym}(CO_2^-)$ = 1418 s and 1401 s; δ(O−H···O) = 1358 m and 1336 m; ν(C−O) = 1261 m and 1249 m; δ(C−H, 4-monosubstituted pyridines) = 1221 m and 1205 m; δ(C−C−N, amines) = 1128 s and 1117 s; ν(N−C) = 1103 vs and 1095 vs; ν(P−O) = 1062 vs and 1049 s; ν(V−O) = 949 s; γ(O−H···O) = 910 m; γ(=C−H, 4-monosubstituted pyridines) = 862 m, 821 vs, 800 s; ν(P−C) = 787 m; γ(C−O) = 733 m; δ(ring, 4-monosubstituted pyridines) = 635 s.

X-ray Crystallographic Studies: Suitable single crystals of [$Co_2V_2O_2$(pmida)$_2$(H_2O)$_{10}$]·2(H_2O) (**1**), [CdVO(pmida)(4,4′-bpy)(H_2O)$_2$]·(4,4′-bpy)$_{0.5}$·H_2O (**2**) and [CoVO(pmida)(4,4′-bpy)(H_2O)$_2$]·(4,4′-bpy)$_{0.5}$ (**3**) were mounted on a glass fibre using perfluoropolyether oil.[34] Data were collected at 180(2) K on a Nonius−Kappa charge-coupled device (CCD) area-detector diffractometer (Mo-K_α graphite-monochromated radiation, λ = 0.7107 Å), equipped with an Oxford Cryosystems cryostream and controlled by the Collect software package.[35] Images were processed with Denzo and Scalepack,[36] and the data were corrected for absorption by using the empirical method employed in Sortav.[37] Structures were solved by the direct methods of SHELXS-97,[38] and refined by full-matrix least-squares on F^2 using SHELXL-97.[39] All non-hydrogen atoms were directly located from difference Fourier maps and refined with anisotropic displacement parameters.

In **2** and **3**, the crystallographically unique 4-pyridyl group from the uncoordinated 4,4′-bpy molecule was found to be affected by thermal disorder, with the last difference Fourier map syntheses showing a large residual electron density around the aromatic ring: for **2**, the highest peak (2.661 e·Å^{-3}) was located at 0.67 Å from C17, and the deepest hole (−2.660 e·Å^{-3}) at 0.17 Å from C16; for **3**, the highest peak (1.737 e·Å^{-3}) was located at 0.57 Å from C16, and the deepest hole (−1.079 e·Å^{-3}) at 0.46 Å from C16. In **2**, only N4 was satisfactorily refined using anisotropic treatment, with all the carbon atoms receiving a single common isotropic displacement parameter; in **3**, atoms from the uncoordinated 4-pyridyl group were generally refined using an anisotropic treatment, with the exception of C16 and C17, for which a common isotropic displacement parameter was used instead. AFIX 66 instruction was also applied in the earlier stages of the refinement in order to ensure a reasonable geometry for the uncoordinated 4-pyridyl aromatic rings.

The hydrogen atoms attached to carbon were located at their idealised positions, and included in the refinement in a riding-motion approximation with an isotropic thermal displacement parameter fixed at 1.2-times U_{eq} of the atom to which they are attached. Hydrogen atoms from coordinated water molecules were directly located from difference Fourier maps and refined using independent isotropic displacement parameters. The O−H and H···H distances were restrained to 0.84(2) and 1.37 Å, respectively, to ensure a chemically reasonable geometry for the water molecules. These O−H bonds are intended to provide the best fit for the X-ray data, but they do not reflect the true position of the hydrogen nucleus. For **1** and **2**, the crystallisation water molecules were also directly located from difference Fourier maps. Although in **1** the O-atom could be successfully refined using anisotropic thermal displacement parameters, in **2** such treatment gave large tensors in more than one direction, suggesting that the atom is affected by thermal disorder (the atom was instead refined with isotropic thermal displacement parameters). No attempt was made to place the hydrogens on these oxygen atoms and, consequently, the empirical formulae are four and two H atoms short per formula unit, for **1** and **2**, respectively.

All cavity dimensions were calculated by overlapping rigid spheres with van der Waals radii for each element: O 1.52 Å, N 1.55 Å, C 1.7 Å, Cd 2.2 Å, Co 2.0 Å, V 2.0 Å and P 1.8 Å (hydrogen atoms were omitted in all cases for simplicity). Information concerning crystallographic data collection and structure refinement for structures **1** to **3** is summarised in Table 4. Selected bond lengths and angles are given in Table 1 (for **1**) and 2 (for **2** and **3**), and hydrogen-bonding geometry in Table 3.

CCDC-220439 (for **1**), -214332 (for **2**) and -219881 (for **3**) contain the supplementary crystallographic data for this paper. These data can be obtained free of charge at www.ccdc.cam.ac.uk/conts/retrieving.html [or from the Cambridge Crystallographic Data Centre, 12 Union Road, Cambridge CB2 1EZ, UK; Fax: +44 1223 336 033; E-mail: deposit@ccdc.cam.ac.uk].

 © 2004 Wiley-VCH Verlag GmbH & Co. KGaA, Weinheim

Table 4. Crystal data and structure refinement information for **1**−**3**

	1[a]	**2**[a]	**3**
Formula	$C_{10}H_{32}Co_2N_2O_{28}P_2V_2$	$C_{20}H_{22}CdN_4O_{11}PV$	$C_{20}H_{22}CoN_4O_{10}PV$
Molecular mass	910.06	688.73	619.26
Crystal system	monoclinic	monoclinic	monoclinic
Space group	$P2_1/c$	$P2_1/c$	$P2_1/c$
a (Å)	9.996(2)	9.1267(18)	8.7734(18)
b (Å)	14.854(3)	17.610(4)	17.264(4)
c (Å)	10.781(2)	15.361(3)	15.507(3)
β (°)	110.90(3)	93.06(3)	93.94(3)
Volume (Å^3)	1495.5(5)	2465.3(9)	2343.2(8)
Z	2	4	4
D_c (g cm^{-3})	2.021	1.856	1.755
μ(Mo-K_α) (mm^{-1})	1.916	1.374	1.241
F(000)	920	1376	1260
Crystal size (mm)	0.23 × 0.18 × 0.16	0.32 × 0.28 × 0.23	0.12 × 0.10 × 0.07
Crystal type	purple blocks	green blocks	purple blocks
θ range	3.73 to 27.47	3.52 to 27.47	3.54 to 27.48
Index ranges	$-12 \le h \le 12$	$-11 \le h \le 11$	$-11 \le h \le 11$
	$-19 \le k \le 19$	$-22 \le k \le 22$	$-22 \le k \le 22$
	$-13 \le l \le 13$	$-19 \le l \le 19$	$-20 \le l \le 20$
Reflections collected	8406	14579	19973
Independent reflections	3400 (R_{int} = 0.0243)	5600 (R_{int} = 0.0296)	5336 (R_{int} = 0.0562)
Final R indices [$I > 2\sigma(I)$]	$R1$ = 0.0332	$R1$ = 0.0455	$R1$ = 0.0491
	$wR2$ = 0.0369	$wR2$ = 0.1139	$wR2$ = 0.1100
Final R indices	$R1$ = 0.1011	$R1$ = 0.0494	$R1$ = 0.0701
(all data)	$wR2$ = 0.1040	$wR2$ = 0.1174	$wR2$ = 0.1204
Largest diff. peak and hole	0.562 and −0.924 e·Å^{-3}	2.661 and −2.660 e·Å^{-3}	1.737 and −1.079 e·Å^{-3}

[a] Empirical formula is four (for **1**) and two (for **2**) H atoms short.

Acknowledgments

We are grateful to FEDER, POCTI (Portugal), and to the Portuguese Foundation for Science and Technology (FCT) for their general financial support and also the Ph.D. and Post-Doctoral research grants Nos. SFRH/BD/3024/2000 (to F. A. A. P.) and SFRH/BPD/9309/2002 (to F.-N. S.).

[1] B. F. Hoskins, R. Robson, *J. Am. Chem. Soc.* **1990**, *112*, 1546−1554.
[2] S. R. Batten, R. Robson, *Angew. Chem. Int. Ed.* **1998**, *37*, 1461−1494; S. Kitagawa, M. Kondo, *Bull. Chem. Soc. Jpn.* **1998**, *71*, 1739−1753; M. J. Zaworotko, *Chem. Commun.* **2001**, 1−9; P. J. Hagrman, D. Hagrman, J. Zubieta, *Angew. Chem. Int. Ed.* **1999**, *38*, 2639−2684; O. M. Yaghi, H. L. Li, C. Davis, D. Richardson, T. L. Groy, *Acc. Chem. Res.* **1998**, *31*, 474−484.
[3] B. Moulton, M. J. Zaworotko, *Chem. Rev.* **2001**, *101*, 1629−1658.
[4] Y. B. Dong, M. D. Smith, R. C. Layland, H. C. zur Loye, *Chem. Mat.* **2000**, *12*, 1156−1161; R. Kitaura, K. Fujimoto, S. Noro, M. Kondo, S. Kitagawa, *Angew. Chem. Int. Ed.* **2002**, *41*, 133−135; H. Li, M. Eddaoudi, M. O′Keeffe, O. M. Yaghi, *Nature* **1999**, *402*, 276−279.
[5] O. M. Yaghi, G. M. Li, H. L. Li, *Nature* **1995**, *378*, 703−706.
[6] J. S. Seo, D. Whang, H. Lee, S. I. Jun, J. Oh, Y. J. Jeon, K. Kim, *Nature* **2000**, *404*, 982−986; S. S. Y. Chui, S. M. F. Lo, J. P. H. Charmant, A. G. Orpen, I. D. Williams, *Science* **1999**, *283*, 1148−1150.
[7] R. Kitaura, K. Seki, G. Akiyama, S. Kitagawa, *Angew. Chem. Int. Ed.* **2003**, *42*, 428−431.
[8] O. M. Yaghi, H. L. Li, T. L. Groy, *J. Am. Chem. Soc.* **1996**, *118*, 9096−9101; T. L. Hennigar, D. C. MacQuarrie, P. Losier, R. D. Rogers, M. J. Zaworotko, *Angew. Chem. Int. Ed. Engl.* **1997**, *36*, 972−973.
[9] M. L. Tong, J. X. Shi, X. M. Chen, *New J. Chem.* **2002**, *26*, 814−816; H. F. Zhu, W. Zhao, T. Okamura, B. L. Fei, W. Y. Sun, N. Ueyama, *New J. Chem.* **2002**, *26*, 1277−1279; B. L. Fei, W. Y. Sun, T. Okamura, W. X. Tang, N. Ueyama, *New J. Chem.* **2001**, *25*, 210−212; Z. Y. Fu, X. T. Wu, J. C. Dai, L. M. Wu, C. P. Cui, S. M. Hu, *Chem. Commun.* **2001**, 1856−1857.
[10] G. S. Papaefstathiou, R. Vicente, C. P. Raptopoulou, A. Terzis, A. Escuer, S. P. Perlepes, *Eur. J. Inorg. Chem.* **2002**, 2488−2493; S. Shova, G. Novitchi, M. Gdaniec, A. Caneschi, D. Gatteschi, L. Korobchenko, V. K. Voronkova, Y. A. Simonov, C. Turta, *Eur. J. Inorg. Chem.* **2002**, 3313−3318; T. Ezuhara, K. Endo, K. Matsuda, Y. Aoyama, *New J. Chem.* **2000**, *24*, 609−613.
[11] G. Yang, H. G. Zhu, B. H. Liang, X. M. Chen, *J. Chem. Soc., Dalton Trans.* **2001**, 580−585.
[12] Y. G. Li, H. Zhang, E. Wang, N. Hao, C. W. Hu, Y. Yan, D. Hall, *New J. Chem.* **2002**, *26*, 1619−1623.
[13] C. R. Kagan, D. B. Mitzi, C. D. Dimitrakopoulos, *Science* **1999**, *286*, 945−947.
[14] N. G. Pschirer, D. M. Ciurtin, M. D. Smith, U. H. F. Bunz, H. C. zur Loye, *Angew. Chem. Int. Ed.* **2002**, *41*, 583; C. J. Kepert, T. J. Prior, M. J. Rosseinsky, *J. Am. Chem. Soc.* **2000**, *122*, 5158−5168.
[15] O. Teichert, W. S. Sheldrick, *Z. Anorg. Allg. Chem.* **2000**, *626*, 1509−1513; M. Fujita, Y. J. Kwon, S. Washizu, K. Ogura, *J. Am. Chem. Soc.* **1994**, *116*, 1151−1152.
[16] F. A. A. Paz, J. Klinowski, *Chem. Commun.* **2003**, 1484−1485; F. A. A. Paz, A. D. Bond, Y. Z. Khimyak, J. Klinowski, *Acta Crystallogr. Sect. E.* **2002**, *58*, M730-M732; F. A. A. Paz, Y. Z. Khimyak, A. D. Bond, J. Rocha, J. Klinowski, *Eur. J. Inorg. Chem.* **2002**, 2823−2828.
[17] F. A. A. Paz, A. D. Bond, Y. Z. Khimyak, J. Klinowski, *Acta Crystallogr., Sect. C* **2002**, *58*, M608−M610.
[18] F. A. A. Paz, J. Klinowski, *J. Phys. Org. Chem.* **2003**, *16*, 772−782.
[19] D. C. Crans, F. L. Jiang, O. P. Anderson, S. M. Miller, *Inorg. Chem.* **1998**, *37*, 6645−6655.
[20] J. G. Mao, A. Clearfield, *Inorg. Chem.* **2002**, *41*, 2319−2324.
[21] A. Clearfield, C. V. K. Sharma, B. P. Zhang, *Chem. Mater.*

 © 2004 Wiley-VCH Verlag GmbH & Co. KGaA, Weinheim

2001, *13*, 3099−3112; B. Zhang, D. M. Poojary, A. Clearfield, G. Peng, *Chem. Mater.* **1996**, *8*, 1333−1340; D. M. Poojary, B. Zhang, A. Clearfield, *Angew. Chem. Int. Ed. Engl.* **1994**, *33*, 2324−2326.

[22] S. O. H. Gutschke, D. J. Price, A. K. Powell, P. T. Wood, *Angew. Chem. Int. Ed.* **1999**, *38*, 1088−1090.

[23] J. G. Mao, Z. K. Wang, A. Clearfield, *Inorg. Chem.* **2002**, *41*, 6106−6111.

[24] S. Boudin, A. Guesdon, A. Leclaire, M. M. Borel, *Int. J. Inorg. Mater.* **2000**, *2*, 561−579.

[25] J. M. Shi, J. Q. Xu, W. T. Yu, L. D. Liu, C. J. Wu, *Pol. J. Chem.* **2001**, *75*, 1695−1701; M. H. Lee, N. H. Heo, S. Hayashi, *Polyhedron* **1998**, *17*, 55−62; C. Djordjevic, P. L. Wilkins, E. Sinn, R. J. Butcher, *Inorg. Chim. Acta* **1995**, *230*, 241−244; Y. G. Wei, S. W. Zhang, G. Q. Huang, M. C. Shao, *Polyhedron* **1994**, *13*, 1587−1591; A. E. Lapshin, Y. I. Smolin, Y. F. Shepelev, M. Sivak, D. Gyepesova, *Acta Crystallogr. Sect. C* **1993**, *49*, 867−870; L. Kuchta, M. Sivak, F. Pavelcik, *J. Chem. Res.* (*S*) **1993**, 393−393; K. Okamoto, J. Hidaka, M. Fukagawa, K. Kanamori, *Acta Crystallogr. Sect. C* **1992**, *48*, 1025−1027.

[26] K. Kanamori, K. Ishida, K. Fujimoto, T. Kuwai, K. Okamoto, *Bull. Chem. Soc. Jpn.* **2001**, *74*, 2377−2378; B. J. Hamstra, A. L. P. Houseman, G. J. Colpas, J. W. Kampf, R. LoBrutto, W. D. Frasch, V. L. Pecoraro, *Inorg. Chem.* **1997**, *36*, 4866−4874; M. MahroofTahir, A. D. Keramidas, R. B. Goldfarb, O. P. Anderson, M. M. Miller, D. C. Crans, *Inorg. Chem.* **1997**, *36*, 1657−1668; G. J. Colpas, B. J. Hamstra, J. W. Kampf, V. L. Pecoraro, *J. Am. Chem. Soc.* **1994**, *116*, 3627−3628.

[27] G. J. Colpas, B. J. Hamstra, J. W. Kampf, V. L. Pecoraro, *J. Am. Chem. Soc.* **1996**, *118*, 3469−3478; M. Sivak, J. Tyrselova, F. Pavelcik, J. Marek, *Polyhedron* **1996**, *15*, 1057−1062.

[28] L. Kuchta, M. Sivak, J. Marek, F. Pavelcik, M. Casny, *New J. Chem.* **1999**, *23*, 43−46; M. Sivak, V. Sucha, L. Kuchta, J. Marek, *Polyhedron* **1999**, *18*, 93−99.

[29] A. Kojima, K. Okazaki, S. Ooi, K. Saito, *Inorg. Chem.* **1983**, *22*, 1168−1174.

[30] Y. H. Chen, Q. T. Liu, Y. H. Deng, H. P. Zhu, C. N. Chen, H. J. Fan, D. Z. Liao, E. Q. Gao, *Inorg. Chem.* **2001**, *40*, 3725−3733; W. Plass, *Eur. J. Inorg. Chem.* **1998**, 799−805; D. C. Crans, H. J. Chen, O. P. Anderson, M. M. Miller, *J. Am. Chem. Soc.* **1993**, *115*, 6769−6776; S. Kitagawa, M. Munakata, M. Ueda, *Inorg. Chim. Acta* **1989**, *164*, 49−53; K. Wieghardt, M. Kleineboymann, W. Swiridoff, B. Nuber, J. Weiss, *J. Chem. Soc., Dalton Trans.* **1985**, 2493−2597.

[31] A. F. Wells, *Structural Inorganic Chemistry*, 4th ed., Clarendon Oxford University Press, **1975**.

[32] A. L. Spek, *Acta Crystallogr., Sect. A* **1990**, *46*, C34.

[33] G. B. Deacon, R. J. Phillips, *Coord. Chem. Rev.* **1980**, *33*, 227−250; C. Oldham, *Comprehensive Coordination Chemistry*, vol. 2, 1st ed. (Ed.: S. G. Wilkinson), Pergamon Press, **1987**, pp. 435−459.

[34] T. Kottke, D. Stalke, *J. Appl. Crystallogr.* **1993**, *26*, 615−619.

[35] Collect: Data Collection Software, R. Hooft, Nonius B. V., Delft, The Netherlands, **1998**.

[36] Z. Otwinowski, W. Minor, *Methods in Enzymology*, vol. 276, *Macromolecular Crystallography, Part A* (Eds.: C. W. Carter Jr., R. M. Sweet), Academic Press, New York, **1997**, p. 307.

[37] R. H. Blessing, *Acta Crystallogr., Sect. A* **1995**, *51*, 33−38; R. H. Blessing, *J. Appl. Crystallogr.* **1997**, *30*, 421.

[38] G. M. Sheldrick, *SHELXS 97, Program for Crystal Structure Solution*, University of Göttingen, **1997**.

[39] G. M. Sheldrick, *SHELXL 97, Program for Crystal Structure Refinement*, University of Göttingen, **1997**.

Received January 5, 2004
Early View Article
Published Online May 5, 2004

 © 2004 Wiley-VCH Verlag GmbH & Co. KGaA, Weinheim

Chloride as Supramolecular Glue: Anion-Directed Assembly of a 2D Network of Mn^{III} Complexes

Manuel R. Bermejo,*[a] M. Isabel Fernández,[b] Ana M. González-Noya,[b] Marcelino Maneiro,[b] Rosa Pedrido,[a] M. Jesús Rodríguez,[b] and Miguel Vázquez[a]

Keywords: Supramolecular chemistry / Manganese / Schiff bases / Hydrogen bond / Self-assembly

The Schiff base H_4L [where H_4L = *N*,*N*′-bis(3-hydroxysalicylidene)ethane-1,2-diamine], containing six potential donor atoms, is able to induce the formation of a novel $[Mn^{III}(H_2L)(CH_3OH)_2]Cl$ (**1**) complex, which was characterized by elemental analysis, FAB mass spectrometry, IR, ^1H NMR and electronic spectroscopy, magnetic measurements, X-ray diffraction techniques and conductivity measurements. The study of its redox properties by cyclic and normal pulse voltammetry is also reported. The crystal structure of **1** is formed by monomeric cationic Mn^{III} complexes, where the manganese ion is in an octahedral environment and is coordinated in the equatorial plane to the N_2O_2 donor set of the inner Schiff-base compartment. The neutral condition of the complex is achieved with the presence of the chloride counterion, which behaves as a multiple acceptor of hydrogen bonds. The chloride is involved in four O–H···Cl bonds, connecting three neighbouring cationic complexes. To the best of our knowledge, this constitutes the first example of self-assembly of discrete units of Mn^{III} complexes in a 2D network in the solid state through hydrogen bonding, where the anion is acting as a supramolecular glue.

(© Wiley-VCH Verlag GmbH & Co. KGaA, 69451 Weinheim, Germany, 2004)

Introduction

Of the first-row transition metals, manganese has a particularly appealing coordination chemistry due to its rich redox behaviour, as demonstrated by the variety of structures and oxidation states in polynuclear manganese complexes.[1−3] In particular, manganese(III) derivatives from tetradentate Schiff-base ligands have a clear tendency to form infinite linear or helical chains, due to the predisposition of these ligands to occupy a planar configuration in an octahedral coordination geometry, leaving the axial positions free to develop polymerization through bidentate bridges.[4,5] Occasionally manganese−Schiff-base complexes can produce dimeric structures with μ-phenoxo[4b,4f,5] or μ-oxo bridges with the ligand in the equatorial plane around each metal centre[6] or, alternatively, μ-oxo bridges with the two ligands bridging both metal ions.[4b,4e,8] Moreover, some 2D polymerization processes via coordinative bonding have been reported.[9] In contrast, the aggregation of manganese(III) discrete complexes or infinite chains in multidimensional frameworks by metal-free supramolecular interactions (hydrogen bonding, π-π stacking, and so forth) are particularly rare.[10]

In the last years, part of our research program has been focused on reproducing the reactivity of some manganese redox enzymes, and we have reported an important number of active synthetic models of Mn^{III} systems derived from Schiff-base ligands. With the skill and the motivation acquired due to our recent successes in the construction of very appealing supramolecular architectures,[11] we are now interested in investigating the overlooked supramolecular chemistry of manganese(III). In particular, our new scheme consists in obtaining the aggregation of discrete manganese(III) complexes into multidimensional arrays through metal-free self-assembly.

In this paper we describe the results of this research work. We believed that the insertion of extra donor atoms out of the classical tetradentate compartment of a salen-type ligand would favour the aggregation of neighbouring complexes through hydrogen bonding. This represents a class of weaker, non-covalent interactions that not only induce supramolecular arrays through self-organization of molecules, but also plays a crucial role in fundamental biological processes, such as the expression and transfer of genetic information, and is essential for molecular recognition between receptors and substrates.[12] For this purpose, we designed the ligand H_4L that contains six potential donor atoms: two imine nitrogen and four phenolic oxygen atoms. The reaction of H_4L with manganese(II) chloride, in fact,

[a] Departamento de Química Inorgánica, Facultade de Química, Universidade de Santiago de Compostela, 15782 Santiago de Compostela, Spain
[b] Departamento de Química Inorgánica, Facultade de Ciencias, Universidade de Santiago de Compostela, 27002 Lugo, Spain
Fax: (internat.) +34-981-597525
E-mail: qimb45@usc.es

yields a supramolecular system, which we report herein and where the main intermolecular interactions come from the special role of the halide counterion as a kind of supramolecular glue. This type of networks, which have the ability to bind negatively charged ions, also constitute a hot subject of research in recent years due to their potential ability and selectivity to recognize anion receptors in solution.[13,14]

Results and Discussion

The hexadentate Schiff base, H_4L (see Scheme 1), reacts with the manganese(II) chloride salt to yield a black crystalline complex with the formula $[Mn(H_2L)(CH_3OH)_2]Cl$ (**1**), in accordance with the elemental analysis. The solid appears to be stable in the solid state and in solution; it melts at over 300 °C and is insoluble or sparingly soluble in water and also in common organic solvents, but quite soluble in MeOH, DMF and DMSO.

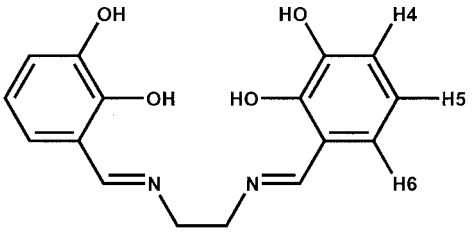

Scheme 1. Structure of the Schiff-base ligand H_4L

Spectroscopy techniques verified the coordination of the ligand to the manganese ion. Thus, the IR spectrum of **1** shows the shift of the $\nu(CN_{imine})$ band to lower frequency (-13 cm^{-1}) and a positive shift of the $\nu(CO_{phenol})$ mode ($+13$ cm^{-1}) with respect to the free ligand. These data suggest the coordination of the Schiff base in its dianionic form through the inner phenol oxygen and the imine nitrogen atoms.[14] The absence of ν(Mn−Cl) bands in the far IR spectrum indicates that the metal is not coordinated to the chloride, as confirmed by the crystal structure of this complex. The FAB mass spectrum shows a peak due to the fragment $[Mn(H_2L)]^+$, which thus further corroborates coordination of the ligand to the manganese ion.

The room temperature magnetic moment of **1** is 4.8 B.M., close to the spin-only value of 4.9 B.M., as expected for a high-spin magnetically diluted d^4 manganese(III) ion. The magnetic behaviour obeys the Curie−Weiss law in the range 40−300 K, showing little or no antiferromagnetic interaction between neighbouring metal centres. The electronic spectrum in methanol solution is also typical of a manganese(III) ion in an octahedral environment. On other hand, the conductivity measurements in DMF give a Λ_M value of 90 μS cm^{-1} for **1**, indicating behaviour that is attributable to 1:1 electrolytes.[16]

X-ray Diffraction Studies

Single crystals of $[Mn(H_2L)(CH_3OH)_2]Cl$ (**1**), suitable for X-ray diffraction studies were obtained as detailed in the Exp. Sect. An ORTEP view of **1**, together with the atomic numbering scheme, is shown in Figure 1. Experimental details are given in Table 1. Main bond lengths and angles are listed in Table 2. This structure reveals the existence of a cationic octahedral $[Mn(H_2L)(CH_3OH)_2]^+$ complex; the neutral condition is achieved by the presence of a chloride anion, which acts as a counterion despite the known tend-

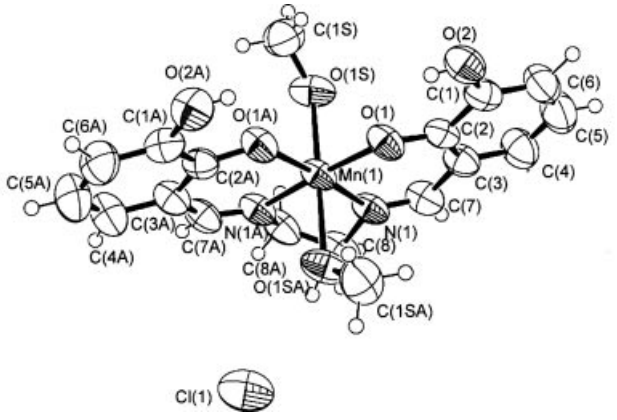

Figure 1. ORTEP plot of **1**; atoms showing the atomic numbering scheme are represented by their 50 % probability ellipsoids; symmetry operation to generate equivalent atoms: A $-$ x + 2, y, $-z$ + 1/2

Table 1. Crystal data and structure refinement for **1**

Empirical formula	$C_{18}H_{22}ClMnN_2O_6$
Molecular weight	452.77
Temperature (K)	298(2)
Wavelength (Å)	0.71073
Crystal system	Orthorhombic
Space group	*Pbcn*
a (Å)	7.6793(7)
b (Å)	14.8888(13)
c (Å)	17.7322(16)
Volume (Å^3)	2027.4(3)
Z	4
$D_{calcd.}$ (g cm^{-3})	1.483
Absorption coefficient (mm^{-1})	0.819
F(000)	936
Crystal size (mm)	0.40 × 0.30 × 0.30
Theta range for data collection	2.30 to 28.30°
Reflections collected	13540
Independent reflections	2527 (R_{int} = 0.0368)
Completeness to θ = 28.30°	99.9 %
Absorption correction	Empirical
Max. and min transmission	0.7911 and 0.7352
Refinement method	Full-matrix least-squares on F^2
Data/restraints/parameters	2527/0/160
Goodness-of-fit on F^2	1.012
Final R_{int} [$I>2\sigma(I)$]	$R1$ = 0.0366, $wR2$ = 0.0888
R_{int} (all data)	$R1$ = 0.0729, $wR2$ = 0.1017
Largest diff. peak and hole	0.213 and −0.190 e·Å^{-3}

 © 2004 Wiley-VCH Verlag GmbH & Co. KGaA, Weinheim

Table 2. Selected bond lengths (Å) and angles (°) for **1**

Mn(1)−O(1)	1.8755(14)	O(1)−Mn(1)−O1(A)	94.06(9)
Mn(1)−O(1A)	1.8755(14)	O(1)−Mn(1)−N(1A)	173.90(7)
Mn(1)−N(1)	1.9809(17)	O(1)−Mn(1)−N(1)	92.00(7)
Mn(1)−N(1A)	1.9809(17)	O(1A)−Mn(1)−N(1)	173.90(7)
Mn(1)−O(1S)	2.2675(19)	O(1A)−Mn(1)−N(1A)	92.00(7)
Mn(1)−O(1SA)	2.2675(19)	N(1)−Mn(1)−N(1A)	81.96(11)
Mn···Mn	7.67(9)	O(1)−Mn(1)−O(1S)	91.18(7)
		O(1A)−Mn(1)−O(1S)	91.21(7)
		N(1)−Mn(1)−O(1S)	89.37(7)
		N(1A)−Mn(1)−O(1S)	87.97(7)
		O(1S)−Mn(1)−O(1SA)	176.48(9)

H bonds D−H···A	*d*(D−H)	*d*(H···A)	*d*(D···A)	<(DHA)
O(1S)−H(1S)···Cl(1)#1[a]	0.73(3)	2.35(3)	3.081(2)	178(3)
O(2)−H(2A)···Cl(1)#2	0.77(3)	2.55(3)	3.218(2)	146(2)
O(2)−H(2A)···O(1)	0.77(3)	2.31(3)	2.668(2)	103.6(10)
C(7)−H(7)···O(2)#3	0.86(2)	2.51(7)	3.143(3)	130.6(2)

[a] Symmetry transformations used to generate equivalent atoms: $^{\#1}x + 1/2, +y + 1/2, -z + 1/2$; $^{\#2}x + 1, +y, +z$; $^{\#3}x + 1/2, -y + 1/2 + 1, -z$.

ency to appear coordinated to the metal ion in similar Mn^{III} compounds.[4b,17]

The structure of discrete mononuclear $[Mn(H_2L)(CH_3OH)_2]^+$ cations comprises the planar Schiff-base ligand tightly bound to manganese(III) through the inner N_2O_2 compartment through the N_{imine} and O_{phenol} atoms ($Mn-N_{imine}$ bond lengths of 1.9809(17) Å and $Mn-O_{phenol}$ 1.8755(14) Å, typical of such complexes).[4,18] The coordination spheres of the slightly distorted octahedral manganese centres are then completed by capping *trans* methanol molecules [$Mn-O_{methanol}$ 2.2675(19) Å]. The elongation in the *trans* $Mn-O_{methanol}$ bonds is usually attributed to a Jahn−Teller distortion for a d^4 high-spin Mn^{III} system but in this case the poor donor strength of the methanol molecules may also contribute to this elongation. The MnN_2O_2 core forms two six-membered chelate rings, which are nearly planar [maximum deviation of any atom from its least-squares calculated plane is −0.1170(11) Å, with the manganese atom 0.1027(09) Å above this plane]. This indicates a slight distortion from the ideal geometry. The slight distortion of the octahedron is also shown by the angles between the manganese and adjacent donor atoms, which range from 81.96(11)° to 94.06(9)°. The angle between the metal atom and the *trans* donor atoms is 176.48(9)°. All distances and angles lie in the range expected for this type of Mn^{III} complexes;[4,17,18] the N(1)−C(7) bond length of 1.277(3) Å suggests a double bond, which is confirmed by the IR spectrum with a strong vibration band at 1620 cm^{-1}.

The $[Mn(H_2L)(CH_3OH)_2]^+$ cations are interconnected through the chloride anions by hydrogen bonds yielding a supramolecular structure. Each chloride anion is involved in four O−H···Cl hydrogen bonds with four different hydroxy groups from three neighbouring cationic complexes (see Figure 2).

Two of these interactions are in the range of strong hydrogen bonds with an almost linear angle O−H···Cl, and involve the hydroxy groups from the axial methanol ligands of two different complexes [H(1S)···Cl(1) 2.35(3), O(1S)···Cl(1) 3.081(2) Å and O(1S)−H(1S)···Cl(1) 178(3)°] (see Table 2).

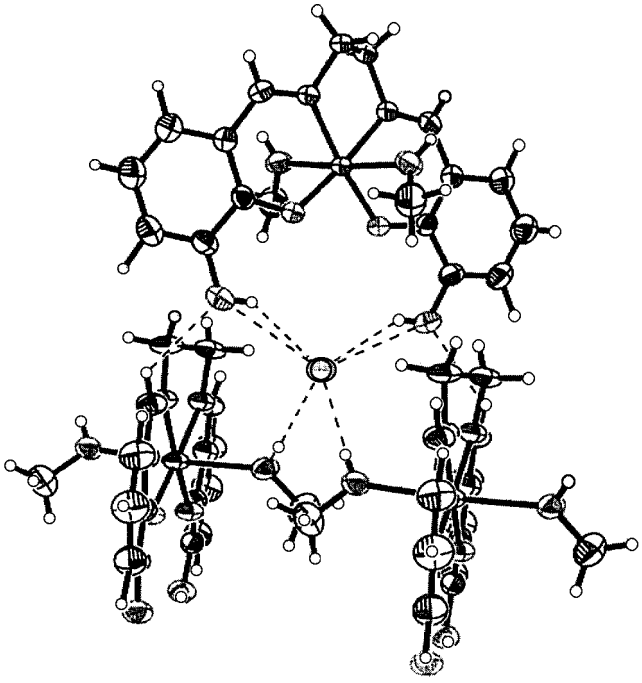

Figure 2. Part of the unit cell of **1**, exhibiting the net of interactions between three neighbouring cationic complexes; the chloride anion is tetra-coordinated to four hydroxy groups through hydrogen bonding

The other two intermolecular contacts imply the outer hydroxy groups of the third complex [H(2A)···Cl(1) 2.55(3), O(2)···Cl(1) 3.218(2) Å and O(2)−H(2A)···Cl(1) 146(2)°], and can be categorized as intermediate in strength,[19] prob-

 © 2004 Wiley-VCH Verlag GmbH & Co. KGaA, Weinheim

ably because of the additional interaction of these outer hydroxy groups with the inner hydroxy groups through intramolecular hydrogen bonding [H(2A)···O(1) 2.31(3), O(2)···O(1) 2.668(2) Å and O(2)−H(2A)···O(1) 103.6(10)°].

This rich supramolecular structure is completed and further stabilized with intermolecular hydrogen bonds between carbon atoms from imine groups and oxygen atoms from the free phenolic sets of adjacent molecules. In this case the H(7)···O(2) distance is of 2.51(7) Å, the C(7)···O(2) distance is of 3.143(3) Å, and the C(7)−H(7)···O(2) angle is 130.6(2)°.

The packing of **1** determines the existence of a supramolecular structure in which the chloride counterions are acting as multiple acceptors, connecting three neighbouring complexes through very different hydrogen bonding. However, the Mn···Mn distances of 7.67(9) Å are too long to establish intermetallic interactions between neighbouring manganese ions, which is in accordance with the non-antiferromagnetic behaviour showed by the magnetic studies.

These multiple intermolecular interactions are extended into the solid to form an infinite array (see Figure 3) constituting, to the best of our knowledge, the first example of an anion-directed assembly of a 2D network of manganese(III) complexes.

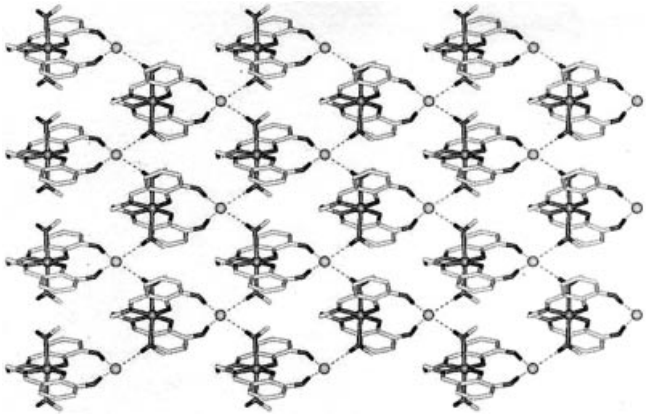

Figure 3. Perspective view of the 2D network formed, which shows the chloride′s role as supramolecular glue in the assembly of the manganese(III) complexes

^{1}H NMR Studies

Paramagnetic ^{1}H NMR studies of **1** were undertaken using [D_6]DMSO as a solvent, and the data serve to substantiate the formation of the manganese(III) complex. The spectrum of **1** is essentially as would be expected, in accordance with the assignments proposed by Pecoraro[20] and also from our own results.[4d,18] The spectrum contains two upfield proton resonances at −16.3 and −28.1 ppm that lie outside the diamagnetic region (δ ca. 0−10) and must arise from the H5 and H4 protons of the aromatic rings, respectively.[4d]

Electrochemical Studies

The electrochemical behaviour of **1** in DMF solution was studied by cyclic and normal pulse voltammetry (see Figure 4). The oxidation state +III for the manganese ion in DMF solutions of **1** is determined by NPV, as it exhibited anodic and cathodic currents when an anodic potential scan was performed (Figure 4b), but when a cathodic potential scan was used, only cathodic current was observed (Figure 4c). This behaviour suggests that only the oxidized form of the implied redox system $Mn^{II}-Mn^{III}$ is present in solution, as we have previously reported.[4b]

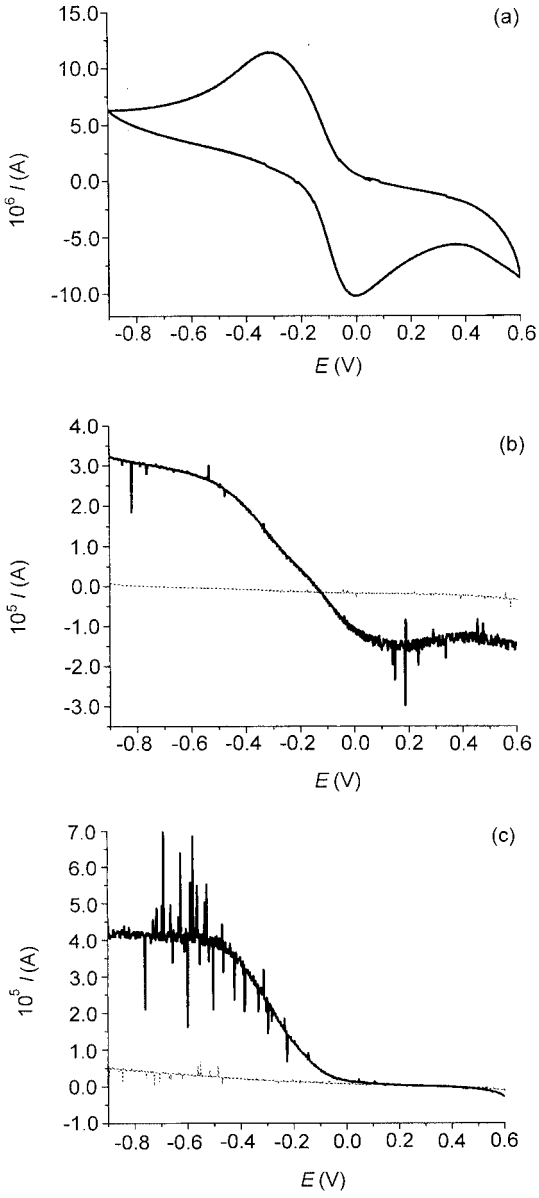

Figure 4. Cyclic voltammogram for **1** at a scan rate of 0.02 V s^{-1} (a); normal pulse voltammogram (NPV) with anodic scan of **1** (b); NPV with cathodic scan of **1** (c)

CV of **1** exhibits a quasi-reversible one-electron reduction−oxidation wave (Figure 4a) centred at $E_{1/2}$ = −0.159 V (versus saturated calomel electrode, SCE). Although this negative potential belongs to the range which would favour the potential catalytic activity, as we have previously reported for other manganese(III)−Schiff base systems,[4g] the peak-to-peak separation of 0.318 V (E_{ox} =

 © 2004 Wiley-VCH Verlag GmbH & Co. KGaA, Weinheim

0.007 V; E_{red} = −0.311 V) becomes a significant handicap for the possible use of this complex in catalysis.

Conclusion

In the present work, we have shown how a ligand such as H_4L is able to induce, simultaneously, the formation of a manganese(III) complex and its aggregation into an infinite 2D array in the solid state through hydrogen bonding. The chloride anions, contrary to their typical behaviour, are not directly coordinated to the manganese atom at the first coordination sphere, but they act as multiple hydrogen-bonding-acceptor counterions as a kind of supramolecular glue, promoting the assembly of the Mn^{III} complexes. Finally, it must be noted that the development of molecular and supramolecular systems, such as this one, with the ability to bind negatively charged ions could play an important role in biology, medicine and the environment.

Experimental Section

General: Elemental analyses were performed on a Carlo Erba EA 1108 analyser. NMR spectra were recorded on a Bruker AC-300 spectrometer using [D_6]DMSO (296 K) as a solvent. Infrared spectra were registered as KBr pellets on a Bio-Rad FTS 135 spectrophotometer in the range 4000−200 cm^{-1}. Fast atom bombardment (FAB) mass spectra were obtained on a Kratos MS-50 mass spectrometer, employing Xe atoms at 70 KeV in *m*-nitrobenzyl alcohol as a matrix. Room-temperature magnetic susceptibilities were measured using a digital measurement system MSB-MKI, calibrated using tetrakis(isothiocyanato)cobaltate(II). Magnetic susceptibility measurements in the 40−300 K temperature range were obtained using a SQUID-QUANTUM model MPMS magnetometer operating at 5000 G. Electronic spectra were recorded on a Cary 230 spectrometer. Conductivities of 10^{-3} M solutions in DMF were measured on a Crison microCM 2200 conductivimeter.

Electrochemical Measurements: Measurements were performed using an EG&G PAR model, 273 potentiostat, controlled by an EG&G PAR model, 270 software. A Metrohm model, 6.1204.000 graphite disc, coupled to a Metrohm model, 628−10 rotating electrolyte device, was used as a working electrode. A saturated calomel electrode was used as a reference and a platinum wire as an auxiliary electrode.
Measurements were made with ca. 10^{-3} M solution of 1 in dimethylformamide using 0.1 M tetraethylammonium perchlorate as a supporting electrolyte. Cyclic voltammetry measurements were performed with a static graphite electrode, whilst direct-current and pulse voltammograms were recorded with the graphite disc rotating at 2000 revolutions per minute.

Syntheses: All solvents, 2,3-dihydroxybenzaldehyde (Maybridge), ethylenediamine (Aldrich), manganese(II) chloride tetrahydrate (Aldrich), and ABTS (Aldrich) were used as received without further purification.

Ligand Synthesis: Ethylenediamine (14.48 mol, 0.97 mL) was added to a methanolic solution (120 mL) of 2,3-dihydroxybenzaldehyde (28.96 mmol, 4 g).[21] This mixture was refluxed in a round bottomed flask fitted with a Dean−Stark trap to remove the water produced during the reaction. After refluxing for 3 h, the solution was concentrated to yield a yellow solid. The product was collected by filtration, washed with diethyl ether and dried in air. The yield was almost quantitative; M.p. 240 °C. $C_{16}H_{16}N_2O_4$ (300.2): calcd. C 63.9, H 5.4, N 9.3; found C 63.3, H 5.6, N 9.4. MS FAB (*m*/*z*): 301.1. IR (KBr): ν(O−H) 3258, 3389 (m), ν(C=N) 1633 (vs), ν(C−O) 1246 (s) cm^{-1}. ^1H NMR ([D_6]DMSO): δ = 3.93 (s, 4 H), 6.65 (t, 2 H), 6.82 (d, 2 H), 6.85 (d, 2 H), 8.54 (s, 2 H), 8.97 (br. s, 2 H), 13.46 (br. s, 2 H) ppm. ^{13}C NMR ([D_6]DMSO): δ = 58.0 (CH_2), 116−122 (C_{ar}), 145.8 (C-OH_{inner}), 151.0 (C-OH_{outer}), 167.2 (C=N) ppm.

Synthesis of the Complex $[Mn(H_2L)(CH_3OH)_2]Cl$ (1): H_4L (1.0 mmol, 0.30 g) was dissolved in methanol (40 mL) and $MnCl_2·4H_2O$ (1.0 mmol, 0.20 g), dissolved in methanol was added to the initial yellow solution, which changed to green. After stirring for 10 min, NaOH (2 mmol, 0.08 g), dissolved in a small quantity of water, was added and the mixture turned dark. The reaction mixture was refluxed for 2 hours, and then concentrated in vacuo to half its volume. The complex was obtained as black crystals, suitable for single X-ray-diffraction studies, after slow concentration of the solution. These crystals were isolated by filtration, washed with diethyl ether and dried in air, yield: 0.23 g, 50 %. $C_{18}H_{22}ClMnN_2O_6$ (452.77): calcd. C 47.7, H 4.9, N 6.2; found C 47.5, H 4.7, N 6.3. MS FAB (*m*/*z*): 353 {$Mn(H_2L)$}, 705 {$Mn_2(H_2L)_2$}. IR (KBr): ν(O−H) 3414 (br), ν(C=N) 1620 (vs), ν(C−O) 1259 (s) cm^{-1}. Magnetic moment μ_{eff} = 4.8 B.M. ^1H NMR (300 MHz, [D_6]DMSO): δ = −28.1, −16.3 ppm. Conductivity (in DMF) Λ_M = 90 μS cm^{-1}. E_{ox} = 0.007 V, E_{red} = −0.311 V, $E_{1/2}$ = −0.159 V.

X-ray Crystallographic Studies: Crystals of **1**, suitable for X-ray diffraction studies, were obtained as described above. Data were collected with a Smart CCD-100 Bruker diffractometer employing graphite-monochromated Mo-K_α (λ = 0.71073 Å) radiation. The structure was solved by direct methods[22] and finally refined by full-matrix least-squares base on F^2. An empirical absorption correction was applied using SADABS.[23] All non-hydrogen atoms were anisotropically refined, and all hydrogen atoms were included in the model at geometrically calculated positions. Detailed data collection and refinement of the compound are summarized in Table 1.
CCDC-212667 contains the supplementary crystallographic data for **1**. These data can be obtained free of charge at www.ccdc.cam.ac.uk/conts/retrieving.html (or from the Cambridge Crystallographic Data Centre, 12 Union Road, Cambridge CB2 1EZ, UK [Fax: (internat.) + 44-1223/336-033; E-mail: deposit@ccdc.cam.ac.uk].

Acknowledgments

We thank Ministerio de Ciencia y Tecnología of Spain (BQU2003-00167) for financial support.

[1] J. D. Crowley, D. A. Traynor, D. C. Weatherburn, *Metal Ions in Biological Systems*, vol. 37 (Eds.: A. Sigel, H. Sigel), Marcel Dekker, New York, **2000**, 209−278.
[2] D. S. Marlin, E. Bill, T. Weyhermuller, E. Rentschler, K. Wieghardt, *Angew. Chem. Int. Ed.* **2002**, *41*, 4775−4779.
[3] M. Maneiro, W. F. Ruettinger, E. Bourles, G. L. McLendon, G. C. Dismukes, *Proc. Acad. Nat. Sci. USA* **2003**, *100*, 3707−3712.
[4] [4a] N. Aurangzeb, C. E. Hulme, C. A. McAuliffe, R. G. Pritchard, M. Watkinson, M. R. Bermejo, A. García-Deibe, M. Rey, J. Sanmartín, A. Sousa, *Chem. Commun.* **1994**, 1153−1155. [4b] M. R. Bermejo, A. Castiñeiras, J. C. García-Monteagudo, M. Rey, A. Sousa, M. Watkinson, C. A. McAuliffe, R. G. Pritch-

 © 2004 Wiley-VCH Verlag GmbH & Co. KGaA, Weinheim

ard, R. L. Beddoes, *J. Chem. Soc., Dalton Trans.* **1996**, 2935−2944. [4c] M. Maneiro, M. R. Bermejo, A. Sousa, M. Fondo, A. M. González, A. Sousa-Pedrares, C. A. McAuliffe, *Polyhedron* **2000**, *19*, 47−54. [4d] M. R. Bermejo, A. M. González, M. Fondo, A. García-Deibe, M. Maneiro, J. Sanmartín, O. L. Hoyos, M. Watkinson, *New J. Chem.* **2000**, *24*, 235−241. [4e] M. Maneiro, M. R. Bermejo, M. Fondo, A. M. González, J. Sanmartín, J. C. García-Monteagudo, R. G. Pritchard, A. M. Tyryshkin, *Polyhedron* **2001**, *20*, 711−719. [4f] M. Maneiro, M. R. Bermejo, M. I. Fernández, A. M. González-Noya, A. M. Tyryshkin, R. G. Pritchard, *Z. Anorg. Allg. Chem.* **2003**, *629*, 285−290. [4g] M. Maneiro, M. R. Bermejo, M. I. Fernández, E. Gómez-Fórneas, A. M. González-Noya, A. M. Tyryshkin, *New J. Chem.* **2003**, *27*, 727−733.

[5] [5a] Q. Shi, R. Cao, X. Li, J. Luo, M. Hong, Z. Chen, *New. J. Chem.* **2002**, *26*, 1397−1401. [5b] S. Sailaja, K. Rajender Reddy, M. V. Rajasekharan, C. Hureau, E. Riviere, J. Cano, J. J. Girerd, *Inorg. Chem.* **2003**, *42*, 180−186.

[6] [6a] A. García-Deibe, A. Sousa, M. R. Bermejo, P. P. MacRory, C. A. McAuliffe, R. G. Pritchard, M. Helliwell, *J. Chem. Soc., Chem. Commun.* **1991**, 728−729. [6b] A. García-Deibe, M. R. Bermejo, A. Sousa, C. A. McAuliffe, P. McGlynn, P. T. Ndifon, P. G. Pritchard, *J. Chem. Soc., Dalton Trans.* **1993**, 1605−1610.

[7] [7a] E. Larson, V. L. Pecoraro, *J. Am. Chem. Soc.* **1991**, *113*, 3810−3818. [7b] N. Aurangzeb, C. A. McAuliffe, R. G. Pritchard, M. Watkinson, M. R. Bermejo, A. García-Deibe, A. Sousa, *Acta Crystallogr., Sect. C* **1993**, *49*, 1945−1947. [7c] T. C. Brunold, D. R. Gamelin, T. L. Stemmler, S. K. Mandal, W. H. Armstrong, J. E. Penner-Hahn, E. I. Solomon, *J. Am. Chem. Soc.* **1998**, *120*, 8724−8738.

[8] M. Watkinson, M. Fondo, M. R. Bermejo, A. Sousa, C. A. McAuliffe, R. G. Pritchard, N. Jaiboon, N. Aurangzeb, M. Naeem, *J. Chem. Soc., Dalton Trans.* **1999**, 31−41.

[9] [9a] H. Miyasaka, N. Matsumoto, H. Okawa, N. Re, E. Gallo, C. Floriani, *J. Am. Chem. Soc.* **1996**, *118*, 981−994. [9b] H. Miyasaka, N. Matsumoto, N. Re, E. Gallo, C. Floriani, *Inorg. Chem.* **1997**, *36*, 670−676.

[10] [10a] H. Miyasaka, H. Ieda, N. Matsumoto, N. Re, R. Crescenzi, C. Floriani, *Inorg. Chem.* **1998**, *37*, 255−263. [10b] C. Zhang, J. Sun, X. Kong, C. Zhao, *J. Coord. Chem.* **2000**, *50*, 353−362.

[11] [11a] J. Sanmartín, M. R. Bermejo, A. M. García-Deibe, O. Piro, E. E. Castellano, *Chem. Commun.* **1999**, 1953−1954. [11b] J. Sanmartín, M. R. Bermejo, A. M. García-Deibe, A. L. Llamas, *Chem. Commun.* **2000**, 795−796. [11c] J. Sanmartín, M. R. Bermejo, A. M. García-Deibe, I. M. Rivas, A. R. Fernández, *J. Chem. Soc., Dalton Trans.* **2000**, 4174−4181. [11d] M. Vázquez, M. R. Bermejo, M. Fondo, A. García-Deibe, A. M. González, R. Pedrido, *Eur. J. Inorg. Chem.* **2002**, 465−472. [11e] M. Vázquez, M. R. Bermejo, J. Sanmartín, A. M. García-Deibe, C. Lodeiro, J. Mahía, *J. Chem. Soc., Dalton Trans.* **2002**, 870−877. [11f] M. Vázquez, A. Taglietti, D. Gatteschi, L. Soraace, C. Sangregorio, A. M. González, M. Maneiro, R. Pedrido, M. R. Bermejo, *Chem. Commun.* **2003**, 1840−1841.

[12] J.-M. Lehn, *Science* **2002**, *295*, 2400−2403.

[13] [13a] *Supramolecular Chemistry of Anions* (Ed.: A. Bianchi, K. Bowman-James, E. García-España) Wiley-VCH, New York, **1997**. [13b]F. D. Schimdtchen, M. Berger, *Chem. Rev.* **1997**, *97*, 1609−1646.

[14] [14a] P. A. Gale, *Coord. Chem. Rev.* **2001**, *213*, 79−128. [14b] P. D. Beer, P. A. Gale, *Angew. Chem. Int. Ed.* **2001**, *40*, 486−516.

[15] J. Sanmartín, M. R. Bermejo, A. M. García-Deibe, O. R. Nascimento, L. Lezama, T. Rojo, *J. Chem. Soc., Dalton Trans.* **2002**, 1030−1035.

[16] W. I. Geary, *Coord. Chem. Rev.* **1971**, *7*, 81−122.

[17] E. N. Jacobsen, *Comprehensive Organometallic Chemistry II* vol. 12 (Eds.: E. W. Abel, F. G. A. Stone, E. Wilkinson), Pergamon Press, New York, **1995**, 1097−1135.

[18] O. L. Hoyos, M. R. Bermejo, M. Fondo, A. García-Deibe, A. M. González, M. Maneiro, R. Pedrido, *J. Chem. Soc., Dalton Trans.* **2000**, 3122−3127.

[19] G. Aullón, D. Bellamy, L. Brammer, E. A. Bruton, A. G. Orpen, *Chem. Commun.* **1998**, 653−654.

[20] J. A. Bonadies, M. J. Maroney, V. L. Pecoraro, *Inorg. Chem.* **1989**, *28*, 2044−2051.

[21] U. Casellato, P. Guerriero, S. Tamburini, S. Sitran, A. Vigato, *J. Chem. Soc., Dalton Trans.* **1991**, 2145−2152.

[22] G. M. Sheldrick, *SHELX-97 (SHELXS 97 and SHELXL 97), Programs for Crystal Structure Analyses*, University of Göttingen, Germany, **1998**.

[23] G. M. Sheldrick, *SADABS, Program for Scaling and Correction of Area Detector Data*, University of Göttingen, Germany, **1996**.

Received January 16, 2004
Early View Article
Published Online April 26, 2004

 © 2004 Wiley-VCH Verlag GmbH & Co. KGaA, Weinheim

Syntheses and Crystal Structures of Diorganotin Derivatives of 2,5-Dimercapto-1,3,4-thiadiazole

Chunlin Ma,*[a,b] Junhong Zhang,[a] Feng Li,[a] and Rufen Zhang[a]

Keywords: Macrocyclic ligands / N ligands / Oxo ligands / S ligands / Tin

Two novel trinuclear tin oxo clusters $[(C_2S_3N_2)R_6Sn_3O(OH)Y]\cdot L$ [R = CH_3, Y = OH, L = $1\cdot5H_2O$ (**1**); R = $PhCH_2$, Y = OEt, L = 0 (**2**)], a pentanuclear tin macrocycle $[(CH_3)_2Sn(C_2N_2S_3)]_5\cdot CH_2Cl_2\cdot3H_2O$ (**3**) and $[(PhCH_2)_4Cl_2Sn(C_2S_3N_2)]$ (**4**) have been synthesized by the reaction of 2,5-dimercapto-1,3,4-thiadiazole with dialkyltin dichloride in ethanol (95%) or dichloromethane. Complexes **1**–**4** have been characterized by elemental analysis and IR, ^1H, ^{13}C and ^{119}Sn NMR spectroscopy. The structures of **1**–**3** have been determined by X-ray crystallography. Complexes **1** and **2** display a unique tricyclic structure consisting of fused five-membered Sn_2ON_2 and four-membered Sn_2O_2 rings that form a planar $N_2Sn_3O_2$ skeleton, with a distorted trigonal bipyramidal coordination at tin. Complex **3** is a pentanuclear 35-membered tin macrocycle containing the crown thioether-type ligand in which all five tin atoms bond to the sulfur and nitrogen atoms with distorted octahedral geometries. The structures of complexes **1** and **3** are stabilized by hydrogen bonds or intermolecular non-bonding S···S interactions.

(© Wiley-VCH Verlag GmbH & Co. KGaA, 69451 Weinheim, Germany, 2004)

Introduction

Recent developments in coordination chemistry have produced numerous supermolecular and macrocyclic complexes through the appropriate combination of organometallic complexes and various organic ligands.[1−6] Organotin macrocycles are attracting more and more attention for their potential industrial applications and biological activities.[7,8] In these metallomacrocyclic systems, ligands with multiply coordinating donor atoms and particular stereochemistry may lead to different specific architectures. Heterocyclic thionate ligands,[5] which contain at least one deprotonated heterocyclic thioamide group $(N-C-S)^-$ and can act as monodentate, chelating or bridging ligands are particularly important.[9] In our previous work, we studied the ligand 2-mercaptonicotinic acid (Hmnc), which possesses one deprotonated heterocyclic thioamide group $(N-C-S)^-$, and found that the primary bond of the ligand to the tin atoms occurs through sulfur rather than through nitrogen. Moreover, different coordination patterns of the ligand in the thiolic form have been found.[10,11]

To continue our study in this field, we chose another ligand: 2,5-dimercapto-1,3,4-thiadiazole (H_2dmt), which possesses a more complex deprotonated heterocyclic thioamide group $(S-C-N-N-C-S)^{2-}$ than Hmnc. The heterocycle of H_2dmt, with four available donors all of which can be utilized in bonding in varying combinations, as shown in Scheme 1),[12] may act as a fulcrum about which lattice construction is orchestrated in two or more dimensions.

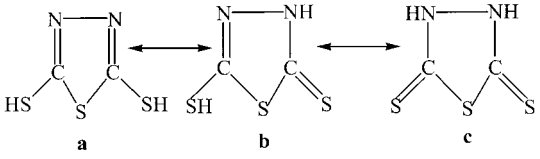

Scheme 1. Tautomeric forms of H_2dmt

In our previous work we reported a pentanuclear tin macrocycle[13] in which the coordination of H_2dmt is through two sulfur atoms of the thiol (**a**) rather than the thione (**c**) tautomer. While continuing our research on other diorganotin complexes of H_2dmt, we surprisingly obtained four novel complexes $[(C_2S_3N_2)(CH_3)_6Sn_3O(OH)_2]\cdot1.5H_2O$ (**1**), $[(C_2S_3N_2)\{(PhCH_2)_6Sn_3O(OH)(OEt)\}]$ (**2**) $[(CH_3)_2Sn(C_2N_2S_3)]_5\cdot CH_2Cl_2\cdot3H_2O$ (**3**) and $[(PhCH_2)_2ClSn(S-C_2SN_2-S)SnCl(PhCH_2)_2]$ (**4**). It is worthwhile to note that complexes **1** and **3** were obtained by the same reactants in different solvents, and the complexes **2** and **4** were obtained by the same reactants in different solvents, too, and that H_2dmt shows different coordination to the tin(IV) atom. All four complexes **1**−**4** were characterized by elemental analysis and IR, ^1H, ^{13}C and ^{119}Sn NMR spec-

[a] Department of Chemistry, Liaocheng University, Liaocheng 252059, P. R. China
Fax: +86-538-671-5521
E-mail: macl@lctu.edu.cn
[b] Department of Chemistry, Taishan University, Taian 271021, P. R. China

troscopy and the structures of **1**, **2** and **3** were determined by X-ray crystallography.

Results and Discussion

Complexes **1**−**4** were prepared by the reaction of dimethyltin dichloride or dibenzyltin dichloride with 2,5-dimercapto-1,3,4-thiadiazole in either EtOH (95%) or CH_2Cl_2. The reaction procedures are shown in Scheme 2.

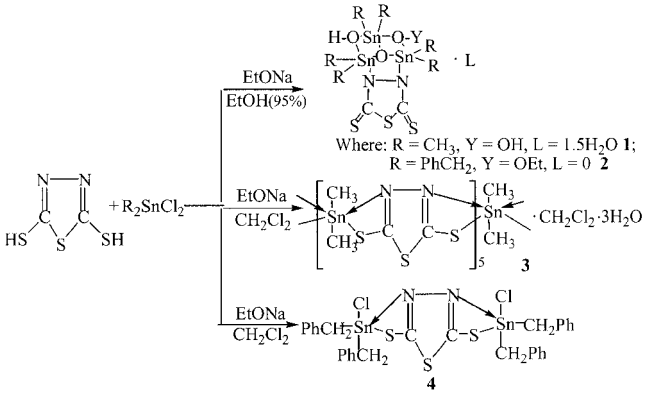

Scheme 2

When the reaction solvent is EtOH (95%), the complexes **1** and **2** were obtained. In view of the results of our present studies[10,14] and those of earlier work,[15] the possible mechanism of formation of complexes **1** and **2** is as follows. Firstly, a hydrolysis reaction of R_2SnCl_2 occurs to form $R_2(Cl)Sn(OH)$, which is then further hydrolyzed to produce $[R_2(OH)SnY]$ (Y = OH or OEt). Two $R_2(Cl)Sn(OH)$ molecules then condense to form $[R_2(Cl)Sn]_2O$, which then reacts with $[R_2(OH)SnY]$ to produce $[R_6Sn_3O(Cl)_2(OH)Y]$.[14] Finally, the two chlorine atoms of $[R_6Sn_3O(Cl)_2(OH)Y]$ are substituted by two nitrogen atoms of the sodium salt of H_2dmt $[Na_2(C_2N_2S_3)]$ to produce the title complexes **1** and **2**. As shown in Scheme 2, the H_2dmt acts as tautomer **c**, bonding to tin(IV) through two nitrogen atoms in both complexes **1** and **2**.

When the reaction solvent was replaced by CH_2Cl_2 we obtained complexes **3** and **4**. In this case the hydrolysis of R_2SnCl_2 does not occur and the ligand coordinates to the tin(IV) center, through two sulfur atoms, as the thiol tautomer (**a**).

Moreover, in complex **4**, the spatial resistances of two benzyl groups are strong enough to prevent another H_2dmt ligand chelating to the central tin atom, which is well consistent with the sequence of steric constraints phenyl ≈ benzyl > *n*-butyl > methyl: the larger the steric constraint of the R groups, the more difficult the substitution of the chlorine atoms.[16]

Description of the Structures

[(C2S3N2)(CH3)6Sn3O(OH)2]·1.5H2O (1) and [(C2S3N2)(PhCH2)6Sn3O(OH)(OEt)] (2)

The molecular structures and unit cells of complexes **1** (Figure 1 and 2) and **2** (Figure 3 and 4) are shown below; selected bond lengths and angles are collected in Table 1 and 2, respectively. Like other trinuclear organotin oxo clusters,[17] complex **1** contains a tricyclic system formed by an N_2Sn_2O ring and two Sn_2O_2 rings, in which the $N_2Sn_3O(OH)_2$ structural motif is almost planar with a mean deviation of ±0.0452 Å. All three tin atoms show severely distorted trigonal bipyramidal configurations.

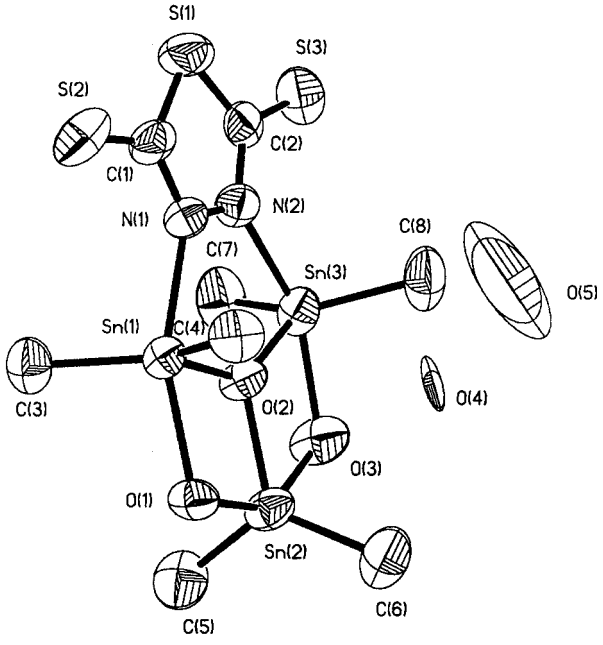

Figure 1. Molecular structure of complex **1**; ellipsoids at 30% probability

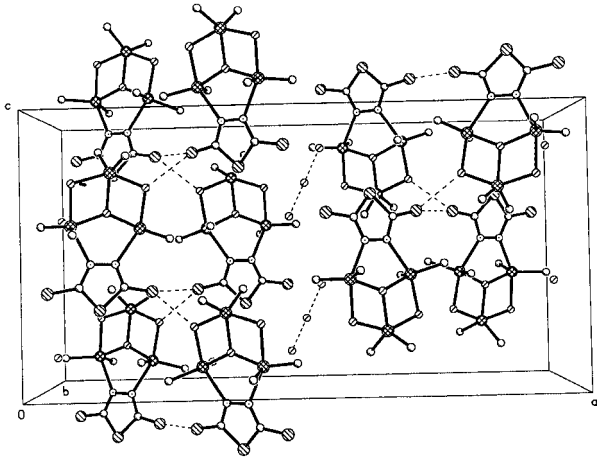

Figure 2. Unit cell of complex **1**

 © 2004 Wiley-VCH Verlag GmbH & Co. KGaA, Weinheim

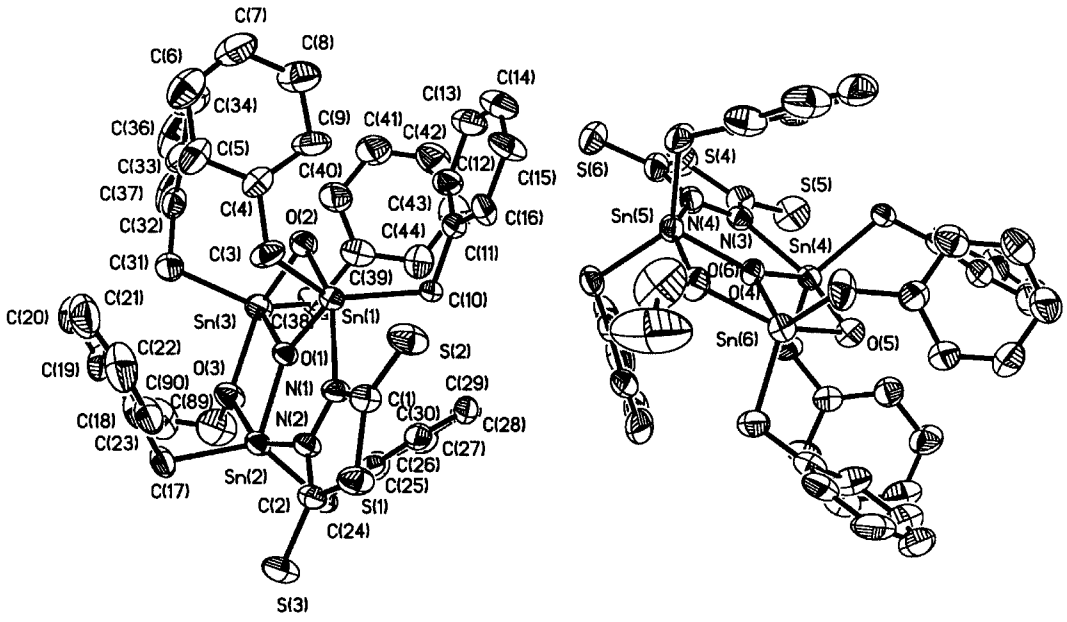

Figure 3. Molecular structure of complex **2**; ellipsoids at 30% probability

Sn(1) and Sn(3) have the same environment, where one μ_3-O atom and two C atoms of the methyl groups occupy the equatorial positions [C(3), C(4) and O(2) for Sn(1); C(7), C(8) and O(2) for Sn(3)], and the axial positions are occupied by one N atom of the H_2dmt and one O atom of the hydroxyl group [N(1) and O(1) for Sn(1); N(2) and O(3) for Sn(3)]. The geometry of Sn(2) is *cis*-R_2SnO_3, in which the axial positions are occupied by the O(3) and O(1) atoms of hydroxyl groups, and two C(5) and C(6) atoms of methyl groups and one μ_3-O(2) atom occupy the equatorial plane. The distortion of the axial angles is very large at the three tin atoms [O(1)−Sn(1)−N(1) 150.4(2)°, O(3)−Sn(3)−N(2) 150.0(2)° and O(3)−Sn(2)−O(1) 144.1(2)° respectively] compared to the ideal angle of 180°.

With regard to the hydrolysis, three [$(CH_3)_2$Sn] units are bridged by one μ_3-O atom and two O atoms of hydroxyl groups, and thus form a trinuclear complex containing two Sn_2O_2 rings. Three Sn atoms and three O atoms [Sn(1), Sn(3), O(2), Sn(2), O(1), O(3)] comprise a fused ring system and are nearly coplanar, with a mean deviation of ±0.0326 Å, which is similar to traditional hydrolytic products with a ladder-type arrangement,[18] but different from the staircase structure of $[Me_4Sn_2(OSiMe_3)_2O]_2$.[19] The Sn−O distances between μ_3-O atom and the tin atoms are similar [Sn(3)−O(2) 2.037(5) Å, Sn(2)−O(2) 2.051(5) Å and Sn(1)−O(2) 2.032 (5) Å], but other Sn−O lengths between the O atoms of the hydroxyl and the tin atoms [Sn(1)−O(1) 2.150(5) Å, Sn(2)−O(1) 2.106(5) Å, Sn(2)−O(3) 2.094(6) Å, Sn(3)−O(3) 2.129(6) Å] are slightly longer, and similar to the Sn−O bonds in the ladder structure $[Me_2ClSnOSnMe_2Cl]_2$ [2.115(9) Å].[20] All of the above indicates that a strong oxo bridge exists in complex **1**.

The two nitrogen atoms of the H_2dmt ligand, which is a five-membered ring, bond to tin atoms to form another five-membered N_2Sn_2O ring. The dihedral angle between the two rings is 1.2°, which indicates that all the atoms of the two rings are almost planar. The Sn−N bond lengths [Sn(1)−N(1) 2.274(6) Å and Sn(3)−N(2) 2.246(7) Å] are similar to the sum of the covalent radii of Sn and N (2.15 Å) and much shorter than the sum of the van der Waals radii of tin and nitrogen atoms (3.74 Å),[21] which proves that the nitrogen atoms coordinate to tin by strong chemical bonds. Furthermore, the C−S bonds [S(2)−C(1) 1.701(10) Å, S(3)−C(2) 1.668(10) Å] are similar to those in thiourea (1.681 Å),[22] suggesting that they are C=S double bonds and therefore retain the thione form. All of above proves

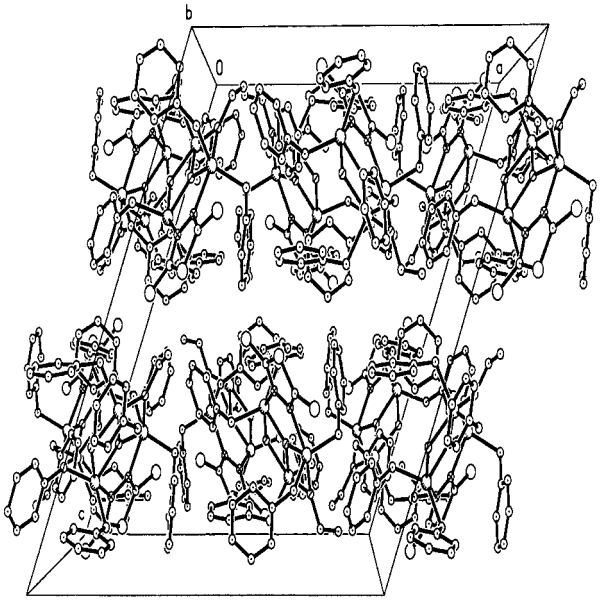

Figure 4. Unit cell of complex **2**

 © 2004 Wiley-VCH Verlag GmbH & Co. KGaA, Weinheim

Table 1. Selected bond lengths (Å) and angles (°) for **1**[a]

Sn(1)−O(2)[a]	2.032(5)	Sn(3)−O(2)	2.037(5)
Sn(1)−C(4)	2.079(8)	Sn(3)−C(8)	2.104(10)
Sn(1)−C(3)	2.096(9)	Sn(3)−C(7)	2.107(10)
Sn(1)−O(1)	2.150(5)	Sn(3)−O(3)	2.129(6)
Sn(1)−N(1)	2.274(6)	Sn(3)−N(2)	2.246(7)
Sn(2)−O(2)	2.051(5)	S(1)−C(1)	1.714(9)
Sn(2)−C(6)	2.075(10)	S(1)−C(2)	1.743(10)
Sn(2)−O(3)	2.094(6)	S(2)−C(1)	1.701(10)
Sn(2)−O(1)	2.106(5)	S(3)−C(2)	1.668(10)
Sn(2)−C(5)	2.121(10)	O(1)···S(2)^{i}	3.178
N(1)−C(1)	1.325(9)	O(3)···S(3)^{ii}	3.206
N(1)−N(2)	1.388(8)	O(4)···O(5)^{iii}	2.085
N(2)−C(2)	1.330(9)	S(3)···S(3)	3.274
O(2)−Sn(1)−C(4)	113.8(3)	O(2)−Sn(3)−C(8)	112.7(3)
O(2)−Sn(1)−C(3)	111.0(3)	O(2)−Sn(3)−C(7)	112.8(3)
C(4)−Sn(1)−C(3)	135.2(4)	C(8)−Sn(3)−C(7)	134.3(4)
O(2)−Sn(1)−O(1)	71.77(18)	O(2)−Sn(3)−O(3)	71.3(2)
C(4)−Sn(1)−O(1)	94.0(3)	C(8)−Sn(3)−O(3)	96.5(4)
C(3)−Sn(1)−O(1)	97.6(3)	C(7)−Sn(3)−O(3)	93.7(4)
O(2)−Sn(1)−N(1)	78.8(2)	O(2)−Sn(3)−N(2)	78.8(2)
C(4)−Sn(1)−N(1)	95.2(3)	C(8)−Sn(3)−N(2)	97.3(4)
C(3)−Sn(1)−N(1)	95.6(3)	C(7)−Sn(3)−N(2)	95.5(4)
O(1)−Sn(1)−N(1)	150.4(2)	O(3)−Sn(3)−N(2)	150.0(2)
O(2)−Sn(2)−C(6)	116.6(4)	C(1)−N(1)−Sn(1)	125.5(6)
O(2)−Sn(2)−O(3)	71.8(2)	N(2)−N(1)−Sn(1)	121.4(5)
C(6)−Sn(2)−O(3)	99.1(4)	C(2)−N(2)−N(1)	115.1(7)
O(2)−Sn(2)−O(1)	72.32(18)	C(2)−N(2)−Sn(3)	121.8(6)
C(6)−Sn(2)−O(1)	98.6(3)	N(1)−N(2)−Sn(3)	123.1(5)
O(3)−Sn(2)−O(1)	144.1(2)	Sn(2)−O(1)−Sn(1)	104.64(19)
O(2)−Sn(2)−C(5)	117.4(3)	Sn(1)−O(2)−Sn(3)	138.0(3)
C(6)−Sn(2)−C(5)	126.0(5)	Sn(1)−O(2)−Sn(2)	111.2(2)
O(3)−Sn(2)−C(5)	97.0(4)	Sn(3)−O(2)−Sn(2)	110.9(2)
O(1)−Sn(2)−C(5)	97.5(3)	Sn(2)−O(3)−Sn(3)	105.7(2)
C(1)−N(1)−N(2)	113.1(7)	O(4)−H(3)···O(5)^{iii}	124.44
O(1)−H(1)···S(2)^{i}	174.32	O(3)−H(2)···S(3)^{ii}	158.81

[a] Symmetry transformations used to generate equivalent atoms: (i) $x, -y, z + 1/2$; (ii) $-x + 1/2, y, z + 1/2$; (iii) $-x + 1, y, -z + 3/2$.

indirectly that H_2dmt bonds to tin as the nitrogen tautomer **c** and not the sulfur tautomer.

As can be seen in Figure 2, molecules of **1** are joined into a network of 2D dimers in a head-to-tail fashion by intermolecular hydrogen bonds. Each monomeric unit forms two weak hydrogen bonds between the O atom of the hydroxyl and the uncoordinated S atom of a neighboring molecule of H_2dmt [O(1)−H(1) 0.897 Å, H···S(2) 2.302 Å, O(1)···S(2) 3.178, O(1)−H(1)···S(2) 174.32°; O(3)−H(2) 0.886 Å, H···S(3) 2.364 Å, O(3)···S(3) 3.206 Å, O(3)−H(2)···S(3) 158.81°]. Moreover, S···S weak intermolecular non-bonding interactions also help to stabilize the structure. The S(3)···S(3) distance of 3.274 Å is significantly shorter than the sum of the van der Waals radii of two sulfur atoms (3.7 Å).[23] Therefore in these two cases hydrogen bonds and intermolecular non-bonding interactions lead to aggregation and formation of a supramolecular assembly.[24]

The tin environment in complex **2** is the same as that of complex **1**. The Sn−N distance [Sn(1)−N(1) 2.224(7) Å, Sn(2)−N(2) 2.230(7) Å], the C−S bonds [S(2)−C(1) 1.673(9) Å, S(3)−C(2) 1.688(9) Å] and the Sn−O distance

Table 2. Selected bond lengths (Å) and angles (°) for **2**

Sn(1)−O(1)	2.047(5)	Sn(2)−O(1)	2.054(5)
Sn(1)−O(2)	2.186(6)	Sn(2)−O(3)	2.223(6)
Sn(1)−C(10)	2.170(8)	Sn(2)−C(24)	2.143(9)
Sn(1)−C(3)	2.136(9)	Sn(2)−C(17)	2.134(9)
Sn(1)−N(1)	2.224(7)	Sn(2)−N(2)	2.230(7)
Sn(3)−O(1)	2.053(5)	S(1)−C(2)	1.747(10)
Sn(3)−O(3)	2.137(6)	S(1)−C(1)	1.755(9)
Sn(3)−O(2)	2.139(6)	S(2)−C(1)	1.672(10)
Sn(3)−C(38)	2.163(12)	S(3)−C(2)	1.687(9)
Sn(3)−C(31)	2.127(11)	N(2)−C(2)	1.317(10)
N(1)−C(1)	1.333(11)	N(1)−N(2)	1.389(9)
C(3)−Sn(1)−C(10)	134.8(4)	C(17)−Sn(2)−C(24)	130.6(4)
O(1)−Sn(1)−C(3)	112.8(3)	O(1)−Sn(2)−C(17)	114.1(3)
O(1)−Sn(1)−C(10)	112.2(3)	O(1)−Sn(2)−C(24)	115.0(3)
O(2)−Sn(1)−C(3)	96.7(3)	O(3)−Sn(2)−C(17)	94.2(3)
O(2)−Sn(1)−C(10)	93.5(3)	O(3)−Sn(2)−C(24)	96.0(3)
O(1)−Sn(1)−O(2)	71.7(2)	O(1)−Sn(2)−O(3)	71.3(2)
O(1)−Sn(1)−N(1)	79.4(2)	O(1)−Sn(2)−N(2)	79.5(2)
O(2)−Sn(1)−N(1)	151.1(2)	O(3)−Sn(2)−N(2)	150.9(2)
C(3)−Sn(1)−N(1)	94.1(3)	C(17)−Sn(2)−N(2)	98.7(3)
C(10)−Sn(1)−N(1)	97.7(3)	C(24)−Sn(2)−N(2)	95.3(3)
C(38)−Sn(3)−C(31)	125.0(5)	Sn(2)−O(1)−Sn(3)	112.4(2)
O(1)−Sn(3)−O(2)	72.7(2)	Sn(2)−O(3)−Sn(3)	103.0(3)
O(1)−Sn(3)−O(3)	73.2(2)	Sn(1)−O(1)−Sn(2)	135.6(3)
O(2)−Sn(3)−O(3)	145.9(2)	Sn(1)−N(1)−N(2)	123.3(5)
C(38)−Sn(3)−O(2)	100.0(3)	Sn(2)−N(2)−N(1)	122.2(5)
C(38)−Sn(3)−O(1)	119.8(4)	N(2)−N(1)−C(1)	114.8(7)
C(38)−Sn(3)−O(3)	97.5(3)	N(1)−N(2)−C(2)	114.3(7)
C(31)−Sn(3)−O(1)	115.2(4)	N(1)−C(1)−S(2)	124.6(7)
C(31)−Sn(3)−O(3)	97.4(4)	N(2)−C(2)−S(3)	124.8(7)
C(31)−Sn(3)−O(2)	96.3(4)	C(1)−S(1)−C(2)	90.6(4)

[from 2.047 Å to 2.224(6) Å] are all similar to those found in complex **1**, which indicates that the $(PhCH_2)_2SnCl_2$ was also hydrolyzed and the ligand coordinates to tin(IV) through two nitrogen atoms as the tautomer **c**. The difference between complexes **1** and **2** lies in the co-ligands formed during the hydrolysis reaction. As shown in Figure 1 and 3 the products of the hydrolysis reaction are $[(CH_3)_2Sn(OH)_2]$ for complex **1** and $[(PhCH_2)_2Sn(OH)(OEt)]$ for complex **2**, respectively. Such a difference may be due to the larger steric constraints of $PhCH_2$ groups than CH_3.

[(CH$_3$)$_2$Sn(C$_2$N$_2$S$_3$)]$_5$·CH$_2$Cl$_2$·3H$_2$O (3)

The molecular structure and unit cell of complex **3** are shown in Figure 5 and 6, respectively; Figure 7 shows the crystal structure of the same component with all co-crystallized solvent molecules omitted. Selected bond lengths and angles are listed in Table 3.

As shown in Figure 5, the coordination of H_2dmt in complex **3** is different from that in complex **1**, but is similar to our previously reported complex $(Bu_2SnC_2N_2S_3)_5$;[13] the ligand is found as the thiol tautomer **a** when bonded to tin. The pentanuclear tin complex is characterized by a 35-membered $C_{10}S_{10}N_{10}Sn_5$ macrocycle ring system with all ten sulfur atoms pointing to the exterior of the cavity, thereby acting as a crown thioether.[25] All five tin atoms have the same arrangement — they are hexacoordinate with

 © 2004 Wiley-VCH Verlag GmbH & Co. KGaA, Weinheim

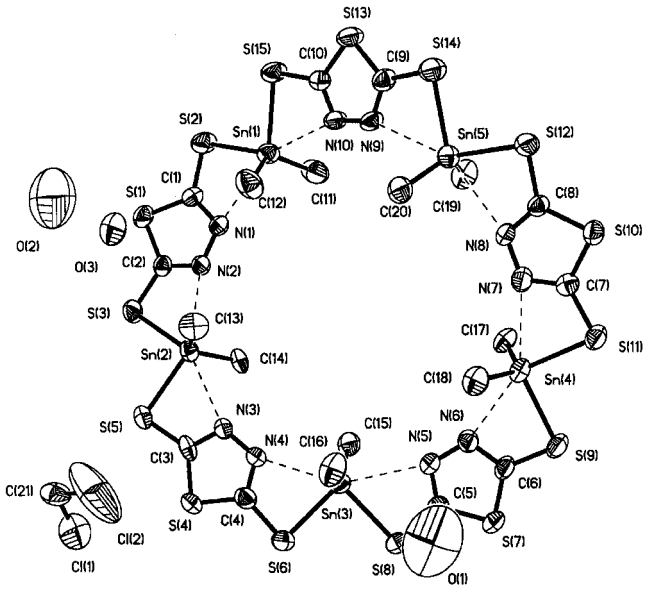

Figure 5. Molecular structure of complex **3**; ellipsoids at 30% probability

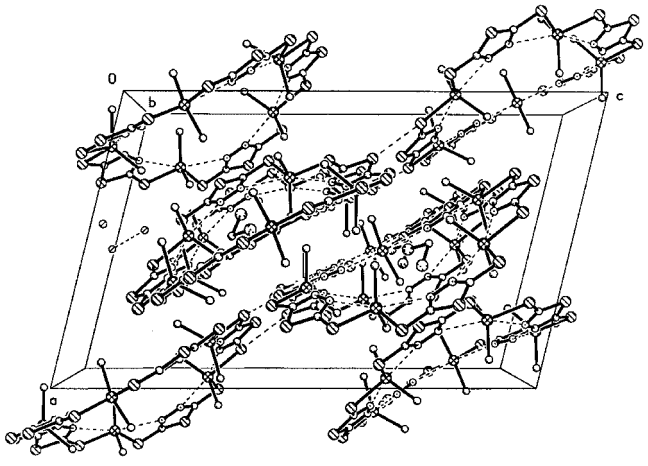

Figure 6. Unit cell of complex **3**

distorted octahedral geometries. Two sulfur atoms and two carbon atoms occupy the equatorial positions and the axial positions are occupied by two azole-N atoms. The deviation from an ideal octahedron is manifested by the bond angles N(1)−Sn(1)−N(10) [149.5(2)°], N(2)−Sn(2)−N(3) [148.7(2)°], N(4)−Sn(3)−N(5) [150.3(2)°], N(6)−Sn(4)−N(7) [147.0(3)°] and N(8)−Sn(5)−N(9) [149.0(2)°], all of which deviate from the ideal value of 180°.

The Sn···S (from 2.483 Å to 2.502 Å) and Sn···N distances (from 2.701 Å to 2.890 Å) are similar to those in the reported complex $(Bu_2SnC_2N_2S_3)_5$ (average value: 2.494 Å and 2.762 Å, respectively).[13] The longest Sn−S distance is slightly longer than the sum of the covalent radii of Sn and S (2.44 Å),[26] but consistent with Sn−S in $tBu_2Sn(S_2CNEt_2)_2$ (2.554 Å),[27] and is much shorter than the sum of the van der waals radii of 4.0 Å.[28] This proves that the sulfur atoms coordinate to the tin atoms by strong

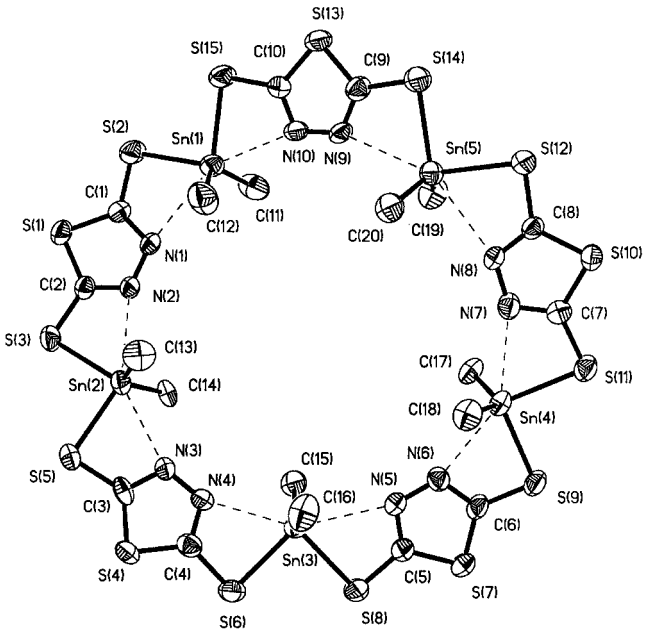

Figure 7. Molecular structure of complex **3** (all solvent molecules omitted)

chemical bonds. The average Sn−N bond length (2.778 Å) is much longer than that in complex **1**, but is similar to the Sn←N (2.787 Å) intermolecular bond found in the trimeric $[Me_3SnSCN_4Ph]_3$ unit.[29] All the Sn−N distances are midway between the covalent radii and the sums of the van der Waals of Sn and N (2.15 and 3.74 Å)[21] and can be regarded as weak coordination bonds. Thus the coordination number of the tin atom is increased to six through Sn←N intermolecular bonds. All above information suggests that the primary bonds of the H_2dmt ligand to tin atoms are through sulfur atoms with the ligand appearing as the thiol tautomer **a**. This situation is similar to that in the reported complex $(Bu_2SnC_2N_2S_3)_5$.[13]

The C−S bond lengths are in the range from 1.695 to 1.750 Å with an average value of 1.723 Å for the chelating ligands, similar to the C−S single bond (1.724 Å) in triphenyltin benzoxazole-2-thiolate,[30] thereby confirming the above proposal.

It is worthwhile to note that the critical cross-ring interatomic distances of the cavity are 10.904 Å [N(1)···Sn(4)] and 10.897 Å [N(4)···Sn(5)], which are larger than those found in dimethyl- and di-*n*-butyltin(IV) complexes with phthalic and isophthalic acid.[8] Furthermore, as shown in Figure 5, there are weak intermolecular non-bonding S···S interactions between the coordinated S atom and the uncoordinated S atom of the neighboring ligand. The S···S distances [S(1)···S(8) 3.489 and S(9)···S(15) 3.449] are all shorter than the sum of the Van der Waals radii of two sulfur atoms (3.7 Å),[23] which indicate that these intermolecular non-bonding interactions lend the crystal stability and compactness and result in a one-dimensional supramolecular polymers arrangement.[5]

 © 2004 Wiley-VCH Verlag GmbH & Co. KGaA, Weinheim

Table 3. Selected bond lengths (Å) and angles (°) for **3**

Sn(1)−C(11)	2.086(11)	Sn(4)−C(18)	2.116(9)
Sn(1)−C(12)	2.090(10)	Sn(4)−C(17)	2.117(9)
Sn(1)−S(15)	2.484(3)	Sn(4)−S(11)	2.492(3)
Sn(1)−S(2)	2.487(3)	Sn(4)−S(9)	2.500(3)
Sn(1)−N(10)	2.722(8)	Sn(4)−N(7)	2.727(8)
Sn(1)−N(1)	2.890(8)	Sn(4)−N(6)	2.770(8)
Sn(2)−C(13)	2.092(9)	Sn(5)−C(19)	2.098(9)
Sn(2)−C(14)	2.124(9)	Sn(5)−C(20)	2.109(9)
Sn(2)−S(3)	2.483(3)	Sn(5)−S(14)	2.489(3)
Sn(2)−S(5)	2.495(3)	Sn(5)−S(12)	2.495(3)
Sn(2)−N(3)	2.777(8)	Sn(5)−N(9)	2.780(8)
Sn(2)−N(2)	2.781(8)	Sn(5)−N(8)	2.797(8)
Sn(3)−C(15)	2.088(9)	S(1)−C(2)	1.735(9)
Sn(3)−C(16)	2.140(9)	S(1)−C(1)	1.743(9)
Sn(3)−S(8)	2.492(3)	S(2)−C(1)	1.742(9)
Sn(3)−S(6)	2.502(3)	S(3)−C(2)	1.733(9)
Sn(3)−N(4)	2.701(8)	S(4)−C(3)	1.695(10)
Sn(3)−N(5)	2.835(8)	S(4)−C(4)	1.719(10)
N(1)−C(1)	1.293(10)	S(5)−C(3)	1.745(10)
N(1)−N(2)	1.373(9)	S(6)−C(4)	1.729(11)
N(2)−C(2)	1.280(10)	S(7)−C(6)	1.707(10)
N(3)−C(3)	1.297(10)	S(7)−C(5)	1.727(10)
N(3)−N(4)	1.330(9)	S(8)−C(5)	1.730(10)
N(4)−C(4)	1.310(10)	S(9)−C(6)	1.715(10)
N(5)−C(5)	1.319(10)	S(10)−C(7)	1.724(9)
N(5)−N(6)	1.371(9)	S(10)−C(8)	1.726(9)
N(6)−C(6)	1.327(10)	S(11)−C(7)	1.715(9)
N(7)−C(7)	1.332(10)	S(12)−C(8)	1.747(9)
N(7)−N(8)	1.377(9)	S(13)−C(9)	1.723(10)
N(8)−C(8)	1.303(10)	S(13)−C(10)	1.727(9)
N(9)−C(9)	1.290(10)	S(14)−C(9)	1.728(10)
N(9)−N(10)	1.357(9)	S(15)−C(10)	1.750(10)
N(10)−C(10)	1.283(10)	O(2)···O(3)	2.361
S(1)···S(8)	3.489	S(9)···S(15)	3.449
C(11)−Sn(1)−C(12)	128.8(5)	N(4)−Sn(3)−N(5)	150.3(2)
C(11)−Sn(1)−S(15)	107.3(3)	S(6)−Sn(3)−N(5)	148.06(18)
C(12)−Sn(1)−S(15)	110.3(3)	S(8)−Sn(3)−N(5)	59.96(18)
C(11)−Sn(1)−S(2)	105.7(3)	C(16)−Sn(3)−N(5)	81.7(3)
C(12)−Sn(1)−S(2)	108.2(3)	C(15)−Sn(3)−N(5)	85.1(3)
S(15)−Sn(1)−S(2)	89.37(10)	S(6)−Sn(3)−N(4)	61.57(18)
C(11)−Sn(1)−N(10)	85.9(4)	S(8)−Sn(3)−N(4)	149.64(18)
C(12)−Sn(1)−N(10)	82.8(3)	C(18)−Sn(4)−C(17)	130.0(4)
S(15)−Sn(1)−N(10)	61.37(19)	C(18)−Sn(4)−S(11)	105.8(3)
S(2)−Sn(1)−N(10)	150.70(19)	C(17)−Sn(4)−S(11)	109.2(3)
C(11)−Sn(1)−N(1)	88.3(3)	C(18)−Sn(4)−S(9)	107.8(3)
C(12)−Sn(1)−N(1)	77.7(3)	C(17)−Sn(4)−S(9)	105.5(3)
S(15)−Sn(1)−N(1)	148.08(17)	S(11)−Sn(4)−S(9)	91.99(9)
S(2)−Sn(1)−N(1)	59.24(16)	C(18)−Sn(4)−N(7)	83.8(3)
N(10)−Sn(1)−N(1)	149.5(2)	C(17)−Sn(4)−N(7)	83.1(3)
C(13)−Sn(2)−C(14)	127.0(4)	S(11)−Sn(4)−N(7)	61.01(19)
C(13)−Sn(2)−S(3)	108.2(3)	S(9)−Sn(4)−N(7)	152.89(19)
C(13)−Sn(2)−S(5)	107.0(3)	C(18)−Sn(4)−N(6)	81.6(3)
C(14)−Sn(2)−S(5)	108.9(3)	C(17)−Sn(4)−N(6)	83.9(3)
S(3)−Sn(2)−S(5)	91.18(9)	S(11)−Sn(4)−N(6)	151.85(19)
C(13)−Sn(2)−N(3)	86.6(3)	S(9)−Sn(4)−N(6)	60.10(19)
C(14)−Sn(2)−N(3)	79.2(3)	N(7)−Sn(4)−N(6)	147.0(3)
S(3)−Sn(2)−N(3)	150.79(17)	C(19)−Sn(5)−C(20)	129.1(4)
S(5)−Sn(2)−N(3)	60.01(17)	C(19)−Sn(5)−S(14)	109.8(3)
C(13)−Sn(2)−N(2)	81.2(3)	C(20)−Sn(5)−S(14)	106.0(3)
C(14)−Sn(2)−N(2)	85.4(3)	C(19)−Sn(5)−S(12)	105.1(3)
S(3)−Sn(2)−N(2)	60.27(17)	C(20)−Sn(5)−S(12)	109.4(3)
S(3)−Sn(2)−N(2)	60.27(17)	S(14)−Sn(5)−S(12)	90.75(9)
S(5)−Sn(2)−N(2)	151.25(18)	C(19)−Sn(5)−N(9)	83.0(3)
N(3)−Sn(2)−N(2)	148.7(2)	C(20)−Sn(5)−N(9)	84.9(3)
C(15)−Sn(3)−C(16)	133.5(4)	S(12)−Sn(5)−N(9)	150.45(18)
C(15)−Sn(3)−S(8)	104.5(3)	S(14)−Sn(5)−N(9)	60.03(18)
C(16)−Sn(3)−S(8)	106.7(3)	C(19)−Sn(5)−N(8)	80.6(3)
C(15)−Sn(3)−S(6)	108.8(3)	C(20)−Sn(5)−N(8)	85.3(3)
C(16)−Sn(3)−S(6)	105.7(3)	S(12)−Sn(5)−N(8)	60.11(18)
S(8)−Sn(3)−S(6)	88.39(10)	S(14)−Sn(5)−N(8)	150.85(18)
C(15)−Sn(3)−N(4)	82.9(3)	N(9)−Sn(5)−N(8)	149.0(2)
C(16)−Sn(3)−N(4)	87.1(3)		

Spectroscopic Data

IR Spectra

The strong broad bands in the IR spectra of complexes **1**−**3** in the region 3440−3000 can be attributed to the O−H stretching vibration. A medium-strength band of δ(H−O−H) is also present at about 1650 cm^{-1} in complexes **1** and **3**; the strong absorption at 1286 cm^{-1} in complex **2** is attributed to the C−O vibration of the EtO group. The main feature in the infrared spectra of complexes **1**−**4** is the absence of a band in the region 2550−2430 cm^{-1}, which appear in the free ligand as the ν(S−H) vibration. In complexes **1** and **2**, the absorption at 1210 cm^{-1} is assigned to the C=S vibration[31] and the new medium-strength band at 445 cm^{-1} for **1** and 480 cm^{-1} for **2** is assigned to the Sn−N stretching,[32] both of which indicate that the $(dmt)^{2-}$ coordinates to tin through its nitrogen atoms as tautomer **c**. The strong absorptions at 597 cm^{-1} for **1** and 627 cm^{-1} for **2** are assigned to Sn−O−Sn stretching. In the far-infrared spectra a strong absorption at 317 cm^{-1} for **3** and 321 cm^{-1} for **4**, which are absent in the spectrum of the ligand, are assigned to the Sn−S stretching vibration. These values are consistent with those reported for a number of organotin(IV) sulfur derivatives.[16,33] The ν(Sn−Cl) absorption at 277 cm^{-1} in complex **4** is close to that found in trichloromethylbis(imidazole)tin·H_2O (275 cm^{-1}).[34] The middle-intensity bands observed at 1635 cm^{-1} in complexes **3** and **4** are assignable to ν(C=N) according to the literature,[35] which suggests that the coordination of dmt to tin is through the sulfur atoms of the thiol tautomer **a**, as reported previously.[36]

NMR Spectra

In the ^1H NMR spectra of complexes **1**−**4** the signal at δ = 1.6 ppm for the -SH protons of the ligand are absent, thus demonstrating that the ligand is deprotonated.

In the ^{13}C NMR spectra of complexes **1**−**4** the chemical shifts of the signals are quite similar to those of the parent ligand. Only a shift in the positions of two carbon atoms in the deprotonated group $(S-C-N-N-C-S)^{2-}$ of H_2dmt are seen; these data reflect the differences between the thiol-C and thione-C atoms. The thiol-to-thione evolution is responsible for the marked deshielding of thione-C,[37] which further proves that the coordination between complexes **1**, **2** and **3**, **4**.

For the methyl derivatives **1** and **3**, substitution of the $^2J_{^{119}Sn,^1}$ (83.2 and 78.1 Hz, respectively) and $^1J_{^{119}Sn,^{13}C}$ values (618.4 and 595.0 Hz, respectively) into the corresponding Lockhart−Manders equations[38] (empirical relationship between the coupling constants and the C−Sn−C angle) gives C−Sn−C angles of 135.0° and 131.5° for complex **1** and 128.5° and 129.0° for complex **3**. These values indicate that the data are reliable.

The ^{119}Sn chemical shifts of tin complexes appear to depend not only on coordination number, but also on the type of donor atoms bonded to the metal ion.[39] As reported in the literature,[40] chemical shifts in the range $\delta = -210$ to

 © 2004 Wiley-VCH Verlag GmbH & Co. KGaA, Weinheim

−400 ppm, −90 to −190 ppm and 200 to −60 ppm have been associated with six-, five- and four-coordinate tin centers, respectively. The value of $\delta = -121.2$ ppm for complex **1**, $\delta = -179.6$ ppm for **2** and $\delta = -187.8$ ppm for **4** are within the range expected for five-coordinate complexes. The chemical shift for complex **3** in $CDCl_3$ indicates a change to a lower coordination than in the solid state, as the value of $\delta = -83.6$ ppm seems to indicate tetracoordination (Me_2S_2)[41] instead of hexacoordination. This change could be explained by the rupture of the weak Sn−N bonds in solution, these bonds being longer than those in other previously published complexes with S,N ligands.[42]

Experimental Section

Materials and Methods: Dimethyltin dichloride (Aldrich) and 2,5-dimercapto-1,3,4-thiadiazole (H_2dmt) were used as received. Dibenzyltin dichloride was prepared by a standard method reported in the literature.[43] The melting points were obtained with a Kofler micro melting point apparatus and are uncorrected. IR spectra were recorded on a Nicolet-460 spectrophotometer using KBr discs and sodium chloride optics. ^{1}H, ^{13}C and ^{119}Sn spectra were recorded on a Bruker AMX-300 spectrometer operating at 300, 75.3 and 111.9 MHz, respectively. The spectra were acquired at room temperature (298 K) unless otherwise specified; ^{13}C spectra are broadband proton decoupled. The chemical shifts are reported in ppm with respect to the references (external tetramethylsilane (TMS) for ^{1}H and ^{13}C NMR and neat tetramethyltin for ^{119}Sn). Elemental analyses were performed with a PE-2400II apparatus.

[{$C_2S_3N_2(CH_3)_2Sn$}$_2$O$(CH_3)_2Sn(OH)_2$]·1.5H_2O (1): Sodium ethoxide (0.136 g, 2 mmol) was added to a solution of 2,5-dimercapto-1,3,4-thiadiazole (0.150 g, 1 mmol) in 95% ethanol (25 mL) and the mixture was stirred for 30 min. $(CH_3)_2SnCl_2$ (0.659 g, 3 mmol) was then added to the mixture, continuing the reaction for 10 h at 40 °C. After cooling to room temperature, the mixture was filtered and the solvent was gradually removed by evaporation under vacuum to give the solid product. The solid was then recrystallized from ethanol to give colorless crystals of **1**. Yield, 80%. m.p. > 220 °C (dec.). IR (KBr): $\tilde{\nu}$ = 3410 (s, O−H), 2923 (m, C−H), 1210 (w, C=S), 561 (m, Sn−C), 597 (s, Sn−O−Sn), 445 (m, Sn−N) cm^{-1}. ^{1}H NMR ($CDCl_3$/D_2O, 300 MHz): δ = 5.15 (s, 2 H, O−H), 0.96 (s, 18 H, CH_3, $^2J^{119}_{Sn,^1}$ = 83.2 Hz) ppm. ^{13}C NMR ($CDCl_3$, 300 MHz): δ = 173.2 (C-1), 173.2 (C-1′), 6.3 [CH_3, $^1J^{119}_{Sn,^{13}C}$ = 618.4 Hz] ppm. ^{119}Sn NMR ($CDCl_3$): $\delta = -121.2$ ppm. $C_8H_{23}N_2O_{4.5}S_3Sn_3$ (671.53): calcd. C 14.31, H 3.45, N 4.20; found C 14.34, H 3.42, N 4.17.

[{$C_2S_3N_2(PhCH_2)_2Sn$}$_2$O$(PhCH_2)_2$Sn(OH)(OEt)] (2): The synthesis procedure was the same as complex **1**. H_2dmt (0.150 g, 1 mmol), sodium ethoxide (0.272 g, 4 mmol), and $(PhCH_2)_2SnCl_2$ (1.116 g, 3 mmol) in 95% ethanol (30 mL); reaction time 10 h; temperature 40 °C. Recrystallized from ethanol as colorless crystals. Yield, 89%. m.p. >200 °C(dec.). IR (KBr): $\tilde{\nu}$ = 3420 (O−H), 3021 (w, Ph−H), 2923 (m, C−H), 1631, 1597, 1491, 1451 (m, Ph), 1286 (s, C−O), 561 (m, Sn−C), 627 (s, Sn−O−Sn), 513 (s, Sn−OR), 480 (m, Sn−N). ^{1}H NMR ($CDCl_3$): δ = 7.15−7.56 (m, 30 H, Ph), 5.15 (s, 1 H, O−H), 3.75 [q, ^3J(^{119}Sn−^{1}H) = 5.8 Hz, 2 H, O−CH_2], 2.28 (m, 12 H, CH_2−Ph, $^2J^{119}_{Sn,^1}$ = 86 Hz,), 1.25 [t, ^4J(^{119}Sn−^{1}H) = 1.2 Hz, 3 H, CH_3] ppm. ^{13}C NMR ($CDCl_3$, 300 MHz): δ = 173.4 (C-1), 173.4 (C-1′), 37.5 [CH_2−Ph, $^1J^{119}_{Sn,^{13}C}$ = 624.1 Hz], 127.4 (*m*-C), 128.2 (*p*-C), 129.3 (*o*-C), 135.2 (*i*-C) ppm. ^{119}Sn NMR ($CDCl_3$): $\delta = -179.6$ ppm. $C_{46}H_{48}N_2O_3S_3Sn_3$ (1129.1): calcd. C 48.93, H 4.29, N 2.48; found C 48.82, H 4.28, N 2.50.

[$(CH_3)_2Sn(C_2N_2S_3)]_5$·CH_2Cl_2·3H_2O (3): The reaction was carried out under nitrogen atmosphere with use of standard Schlenk techniques. H_2dmt (0.30 g, 2 mmol) was added to a solution of dichloromethane (40 mL) and sodium ethoxide (0.272 g, 4 mmol), and the mixture was stirred for 30 minutes. $(CH_3)_2SnCl_2$ (0.439 g, 2 mmol) was then added to the mixture, continuing the reaction for 16 h at 30 °C. After cooling to room temperature the mixture was filtered. The solvent of the filtrate was gradually removed by evaporation under vacuum until a solid product was obtained. The solid was then recrystallized from dichloromethane/ethanol (95%) to give colorless crystals of **3**. Yield, 72%. m.p. > 240 °C (dec.). IR (KBr): $\tilde{\nu}$ = 3430 (s, O−H), 2923 (m, C−H), 1635 (m, C=N), 701 (s, C−S), 563 (m, Sn−C), 317 (m, Sn−S) cm^{-1}. ^{1}H NMR ($CDCl_3$/D_2O): δ = 0.95 [t, 30 H, CH_3, $^2J^{119}_{Sn,^1}$ = 78.1 Hz] ppm. ^{13}C NMR ($CDCl_3$): δ = 168.0 (C-1), 168.0 (C-1′), 5.8 [CH_3, $^1J^{119}_{Sn,^{13}C}$ = 595.0 Hz]. ^{119}Sn ($CDCl_3$): $\delta = -83.6$ ppm. $C_{26}H_{38}Cl_2N_{10}O_3S_{15}Sn_5$ (1683.9): calcd. C 18.55, H 2.27, N 8.32; found C 18.52, H 2.25, N 8.31.

[$(PhCH_2)_2SnCl$(S-C_2SN_2-S)SnCl$(PhCH_2)_2$] (4): The synthesis procedure was the same as that of complex **3**. H_2dmt (0.30 g, 2 mmol) was added to a solution of dichloromethane (40 mL) and sodium ethoxide (0.272 g, 4 mmol), and the mixture was stirred for 30 minutes. $(PhCH_2)_2SnCl_2$ (0.744 g, 2 mmol) was then added; reaction time 16 h; temperature 30 °C. Recrystallized from ether/dichloromethane. M.p. 196−198 °C. Yield, 72%. IR (KBr): $\tilde{\nu}$ = 1635 (C=N), 701 (s, C-S), 561 (m, Sn−C), 321 (m, Sn−S), 277 (m, Sn−Cl) cm^{-1}. ^{1}H NMR ($CDCl_3$): δ = 7.32−7.86 (m, 20 H, aromatic-H), 3.26 [s, 8 H, CH_2−Ph, $^2J^{119}_{Sn,^1}$ = 79.0 Hz] ppm. ^{13}C NMR ($CDCl_3$): δ = 168.5 (C-1), 168.5 (C-1′), 38.5 (CH_2−Ph, $^1J^{119}_{Sn,^{13}C}$ = 546 Hz), 125.4 ($^4J^{119}_{Sn,^{13}C}$ = 30 Hz, *m*-C), 127.0 ($^5J^{119}_{Sn,^{13}C}$ = 26 Hz, *p*-C), 130.5 ($^3J^{119}_{Sn,^{13}C}$ = 44 Hz, *o*-C), 139.0 ($^2J^{119}_{Sn,^{13}C}$ = 36 Hz, *i*-C) ppm. ^{119}Sn NMR ($CDCl_3$): $\delta = -187.8$ ppm. $C_{30}H_{28}Cl_2N_2S_3Sn_2$ (821): calcd. C 43.89, H 3.43, N 3.07; found C 43.86, H 3.40, N 3.05.

Crystal Structures of Complexes 1, 2 and 3: All X-ray crystallographic data were collected on a Bruker SMART-1000-CCD diffractometer. A criterion of observability was used for the solution and refinement. The structure was solved by direct methods and refined by a full-matrix least-squares procedure based on F^2 using the SHELXL-97 program. All data were collected at 298(2) K using graphite-monochromated Mo-K_α radiation (λ = 0.71073 Å) and corrected for Lorentz and polarization effects but not for absorption. All non-H atoms were included in the model at their calculated positions. The positions of the hydrogen atoms were calculated, and their contributions in structural factor calculations were included. Table 4 lists the crystal data and structure refinement parameters.

CCDC-215777 (for **1**), -183604 (for **2**) and -215778 (for **3**) contain the supplementary crystallographic data for this paper. These data can be obtained free of the charge at www.ccdc.cam.ac.uk/conts/retrieving.html [or from the Cambridge Crystallographic Data Center, 12 Union Road, Cambridge, CB2 1EZ, UK; Fax: +44-1223-336-033; E-mail: deposit@ccdc.cam.ac.uk].

Acknowledgments

We thank the National Natural Science Foundation of China (20271025) and the Natural Science Foundation of Shandong Province for financial support.

 © 2004 Wiley-VCH Verlag GmbH & Co. KGaA, Weinheim

Table 4. Crystal data and structure refinement parameters for **1**, **2** and **3**

Empirical formula	$C_8H_{23}N_2O_{4.5}S_3Sn_3$	$C_{46}H_{48}N_2O_3S_3Sn_3$	$C_{26}H_{38}C_{l2}N_{10}O_3S_{15}Sn_5$
Formula mass	671.53	1129.11	1683.91
Temperature (K)	298(2)	293(2)	298(2)
Wavelength (Å)	0.71073	0.71073	0.71073
Crystal system	orthorhombic	monoclinic	monoclinic
Space group	*Pcca*	$P2_1/c$	$P2_1/n$
a (Å)	27.831(15)	20.036(3)	15.856(5)
b (Å)	11.259(6)	23.284(3)	15.207(5)
c (Å)	14.492(8)	22.212(3)	25.173(8)
β (°)	90	114.523(2)	103.611(5)
V (Å^3)	4541(4)	9427(2)	5899(3)
Z	8	8	4
D_c (Mg·m^{-3})	1.964	1.591	1.896
μ (mm^{-1})	3.562	1.750	2.746
F(000)	2552	4480	3248
Crystal size (mm)	0.29 × 0.20 × 0.13	0.40 × 0.30 × 0.20	0.32 × 0.18 × 0.12
θ limits (°)	2.72−25.03	1.33−24.83	2.68−25.03
Index ranges	$-30 \le h \le 33$ $-13 \le k \le 13$ $-17 \le l \le 16$	$-23 \le h \le 23$ $-18 \le k \le 27$ $-26 \le l \le 24$	$-11 \le h \le 18$ $-18 \le k \le 18$ $-29 \le l \le 27$
Max., min. transmission	0.6546,0.4248	0.7210,0.5412	0.7340,0.4736
Refinement method	Full-matrix least-squares on F^2	Full-matrix least-squares on F^2	Full-matrix least-squares on F^2
Reflections collected	22346	48195	30356
Unique reflections	3989 (R_{int} = 0.0686)	16226 (R_{int} = 0.0546)	10294 (R_{int} = 0.0675)
Data, restraints, parameters	3989, 6, 194	16226, 0, 1031	10294, 9, 522
Goodness of fit on F^2	0.914	1.000	0.824
Final *R* indices [$I > 2\sigma(I)$]	R_1 = 0.0420, $wR_2$0.0914	R_1 = 0.0500, wR_2 = 0.1195	R_1 = 0.0472, wR_2 = 0.0920
R indices (all data)	R_1 = 0.0913, wR_2 = 0.1094	R_1 = 0.1204, wR_2 = 0.1537	R_1 = 0.1334, wR_2 = 0.1139
Largest peak, hole difference (e·Å^{-3})	0.616, −0.483	0.875, −0.696	0.960, −0.867

[1] M. Eshel, A. Bino, *Inorg. Chim. Acta* **2001**, *320*, 127−132.
[2] O. I. Shchegolikhina, V. A. Igonin, Yu. A. Molodtsova, Yu. A. Pozdniakova, A. A. Zhdanov, T. V. Strelkova, S. V. Lindeman, *J. Organomet. Chem.* **1998**, *562*, 141−151.
[3] E. Kiss, K. Petrohan, D. Sanna, E. Garribba, G. Micera, T. Kiss, *Polyhedron* **2000**, *19*, 55−61.
[4] D. Dakternieks, A. Duthie, B. Zobel, K. Jurkschat, M. Schürmann, E. R. T. Tiekink, *Organometallics* **2002**, *21*, 647−652.
[5] S. Bhandari, M. F. Mahon, J. G. McGinley, K. C. Molloy, C. E. E. Roper, *J. Chem. Soc., Dalton Trans.* **1998**, 3425−3430.
[6] M. Verdenelli, S. Parola, L. G. Hubert-Pfalzgraf, S. Lecocq, *Polyhedron* **2000**, *19*, 2069−2075.
[7] S. K. Duboy, U. Roy, *Appl. Organomet. Chem.* **2003**, *17*, 3−8.
[8] R. García-Zarracino, J. Ramos-Quiñones, H. Höpfl, *Inorg. Chem.* **2003**, *42*, 3835−3845.
[9] E. S. Raper, *Coord. Chem. Rev.* **1996**, *153*, 199−255.
[10] C. L. Ma, Q. Jiang, R. F. Zhang, D. Q. Wang, *J. Chem. Soc., Dalton Trans.* **2003**, 2975−2978.
[11] C. L. Ma, Q. Jiang, R. F. Zhang, *J. Organomet. Chem.* **2003**, *678*, 148−155.
[12] M. V. Castaño, M. M. Plasencia, A. Macias, J. S. Casas, J. Sordo, E. E. Castellano, *J. Chem. Soc., Dalton Trans.* **1989**, 1409−1411.
[13] C. L. Ma, F. Li, D. Q. Wang, H. D. Yin, *J. Organomet. Chem.* **2003**, *667*, 5−7.
[14] C. L. Ma, F. Li, *Chin. J. Chem.* **2003**, *21*, 146−152.
[15] Y. M Chow, *Inorg. Chem.* **1971**, *10*, 673−677.
[16] A. P. G. de Sousa, R. M. Silva, A. Cesar, J. L. Wardell, J. C. Huffman, A. Abras, *J. Organomet. Chem.* **2000**, *605*, 82−88.
[17] H. Reuter, PhD thesis, University of Bonn, Germany, **1986**.
[18] H. Puff, I. Bung, E. Friedrichs, A. Jansen, *J. Organomet. Chem.* **1983**, *254*, 23−32.
[19] R. Okawara, *Proc. Chem. Soc. London* **1961**, 383−385.
[20] P. G. Harrison, M. J. Begley, K. C. Molloy, *J. Organomet. Chem.* **1980**, *186*, 213−236.
[21] J. E. Hubeey, E. A. Keiter, R. L. Keiter, *Principles and Applications of Inorganic Chemistry*, 4th ed., Harper Collins, New York, **1993**, pp 121−124.
[22] F. H. Allen, O. Kennard, D. G. Watson, L. Brammer, A. G. Orpen, R. J. Taylor, *J. Chem. Soc., Perkin Trans. 2* **1987**, S1.
[23] G. Barone, T. G. Hibbert, M. F. Mabon, K. C. Molloy, I. P. Parkin, L. S. Price, I. Silaghi-Dumitrescu, *J. Chem. Soc., Dalton Trans.* **2001**, 3435−3445.
[24] A. Galani, M. A. Demertzis, M. Kubicki, D. Kovala-Demertzi, *Eur. J. Inorg. Chem.* **2003**, 1761−1767.
[25] G. J. Grant, S. S. Shoup, C. L. Baucom, W. N. Setzer, *Inorg. Chim. Acta* **2001**, *317*, 91−102.
[26] L. Pauling, *The Nature of the Chemical Bond*, 3rd edn., Cornell University Press, Ithaca, **1960**, 64.
[27] S. Z. Hu, D. S. Shi, T. S. Huang, J. Z. Wan, Z. X. Huang, J. L. Yang, C. H. Xu, *Inorg. Chim. Acta* **1990**, *173*, 1−4.
[28] A. Bondi, *J. Phys. Chem.* **1964**, *68*, 441−451.
[29] C. O. Raymando, J. S. Omar, E. P. Georgina, S. Cristiam, *J. Organomet. Chem.* **1994**, *484*, 33−36.
[30] N. G. Fumanova, Yu. T. Strchkov, E. M. Rokhlina, D. N. Kravtsov, *J. Struct. Chem.* **1980**, *21*, 766−772.
[31] H. Hadjiliadis, T. Theophanides, *Can. J. Spectrosc.* **1977**, *22*, 51−57.
[32] J. R. Durig, R. Layton, D. W. Sink, B. R. Mitchell, *Spectrochim. Acta* **1965**, *21*, 1367−1378.
[33] R. Schmiedgen, F. Huber, H. Preut, G. Ruisi, R. Barbieri, *Appl. Organomet. Chem.* **1994**, *8*, 397−401.
[34] R. Visalakshi, V. K. Jain, S. K. Kulshreshtha, G. S. Rao, *Indian J. Chem.* **1989**, *28A*, 51−57.
[35] B. S. Sarawat, G. Srivastava, R. C. Mehrotra, *J. Organoment. Chem.* **1979**, *164*, 153−158.
[36] N. Kottmair, W. Beck, *Inorg. Chim. Acta* **1979**, *34*, 137−144.

 © 2004 Wiley-VCH Verlag GmbH & Co. KGaA, Weinheim

[37] A. Tarassoli, A. Asadi, P. B. Hitchcock, *J. Organomet. Chem.* **2002**, *645*, 105−111.
[38] T. P. Lockhart, W. F. Manders, *Inorg. Chem.* **1986**, *25*, 892−895.
[39] C. H. Yoder, L. A. Margolis, J. M. Horne, *J. Organomet. Chem.* **2001**, *633*, 33−38.
[40] J. Holeček, M. Nádvorník, K. Handlzř, A. Lyčka, *J. Organomet. Chem.* **1986**, *315*, 299−308.
[41] A. Tarassoli, T. Sedaghat, B. Neumüller, M. Ghassemzadeh, *Inorg. Chim. Acta* **2001**, *318*, 15−22.
[42] J. S. Casas, A. Castiñeiras, M. C. Rodríguez-Argüelles, A. Sánchez, J. Sordo, A. Vázquez-López, E. M. Vázquez-López, *J. Chem. Soc., Dalton Trans.* **2000**, 2267−2272.
[43] K. Sisido, *J. Am. Chem. Soc.* **1961**, *83*, 538−541.

Received November 22, 2003
Early View Article
Published Online April 26, 2004

 © 2004 Wiley-VCH Verlag GmbH & Co. KGaA, Weinheim

On the Electronic Structure of Mesitylnickel Complexes of α-Diimines — Combining Structural Data, Spectroscopy and Calculations

Axel Klein,*[a][‡] Martin P. Feth,*[b] Helmut Bertagnolli,[b] and Stanislav Záliš[c]

Keywords: Density functional calculations / Electronic structure / EXAFS / Nickel / Raman spectroscopy

New organometallic nickel complexes of the type [(α-diimine)-Ni(Mes)Br] and [(α-diimine)Ni(Mes)$_2$] (Mes = mesityl = 2,4,6-trimethylphenyl) were prepared and characterised spectroscopically in detail. A combination of spectroscopic techniques (XRD, EXAFS, absorption, resonance Raman) and quantum chemical (DFT) calculations reveals the interplay of the diimine ligands and the mesityl or bromine co-ligands with the nickel centre. The low-lying electronic transitions are assigned as mixed MLCT/L′LCT or MLCT/XLCT due to low-lying accepting π*-orbitals centred on the diimine ligands and mixed metal/co-ligand MOs as donor levels.
(© Wiley-VCH Verlag GmbH & Co. KGaA, 69451 Weinheim, Germany, 2004)

Introduction

Organometallic nickel complexes with α-diimine ligands like 2,2′-bipyridine (bpy), 1,10-phenanthroline (phen) or diazabutadienes (R-DAB) have gained an enormous interest in the last decade. This is mainly due to their success as effective catalysts in olefin polymerisation or olefin/CO copolymerisation.[1−9] It has been established, mainly by Brookhart, that methylnickel complexes with carefully designed diazabutadiene ligands exhibit higher activities than the classical Ziegler catalysts combined with a greatly reduced sensibility towards poisoning by polar functions. Detailed investigations on the activities of various derivatives on polymerisation,[1a] theoretical calculations on the mechanisms and energetics[2] and the use of these compounds for other catalytic purposes[10−13] have been published so far.

In the 1960s these compounds were already known as darkly coloured very reactive materials.[14−17] Detailed investigation of their structures and electronic properties, however, were scarce[15,18−20] until Yamamoto et al. recently reported and discussed the optical spectra of some alkyl and aryl complexes with 2,2′-bipyridine (bpy).[21] In this report the spectra were mainly used to monitor elimination processes. In order to fill that gap we initiated a detailed and combined research project using various spectroscopic techniques (absorption, emission and resonance Raman) and quantum chemical calculations, with a focus on the optical properties.

One reason why such investigations have not been performed so far is probably the high sensitivity of such alkylnickel complexes towards oxygen or moisture.[19] They also easily undergo thermal decomposition by reductive elimination.[21,22] Aryl derivatives are much more inert towards water or oxygen, although the threat of reductive elimination (forming biaryls) remains.[22] We have recently shown that introducing the bulky mesityl co-ligand (Mes = 2,4,6-trimethylphenyl) results in very stable mesityl- and dimesitylnickel complexes[23] of 2,2′-bipyridine, and, with the proper choice of ligands, compounds such as [(N^N)Ni-(Mes)Br] (N^N = α-diimine) have allowed us to carry out a detailed study of the ligand-exchange behaviour of these complexes using EXAFS and spectroscopic techniques like NMR or absorption spectroscopy.[24]

In this paper we wish to report the synthesis and detailed spectroscopic and structural (EXAFS + XRD) characterisation of a series of bromomesityl- and dimesitylnickel complexes of various diimine ligands together with the results of a detailed study of the electronic properties of selected samples using a combination of spectroscopy (absorption, resonance Raman) and quantum chemical calculations. The latter were based on the molecular structures established by single-crystal XRD measurements and EXAFS spec-

[a] Institut für Anorganische Chemie, Universität Stuttgart,
Pfaffenwaldring 55, 70569 Stuttgart, Germany
Fax: +49-(0)711-685-4165
E-mail: aklein@iac.uni-stuttgart.de
[b] Institut für Physikalische Chemie, Universität Stuttgart,
Pfaffenwaldring 55, 70569 Stuttgart, Germany
Fax: +49-(0)711-685-4443
E-mail: m.feth@ipc.uni-stuttgart.de
[c] J. Heyrovský Institute of Physical Chemistry, Academy of Sciences of the Czech Republic,
Dolejškova 3, 18 000 Prague 8, Czech Republic
E-mail: zalis@jh-inst.cas.cz
[‡] Present address: Institut für Chemie, Karl-Franzens-Universität Graz
Schubertstrasse 1, 8010 Graz, Austria
Fax: +43-(0)316-380-9835
E-mail: axel.klein@uni-graz.at
Supporting information for this article is available on the WWW under http://www.eurjic.org or from the author.

 © 2004 Wiley-VCH Verlag GmbH & Co. KGaA, Weinheim **DOI: 10.1002/ejic.200300956**

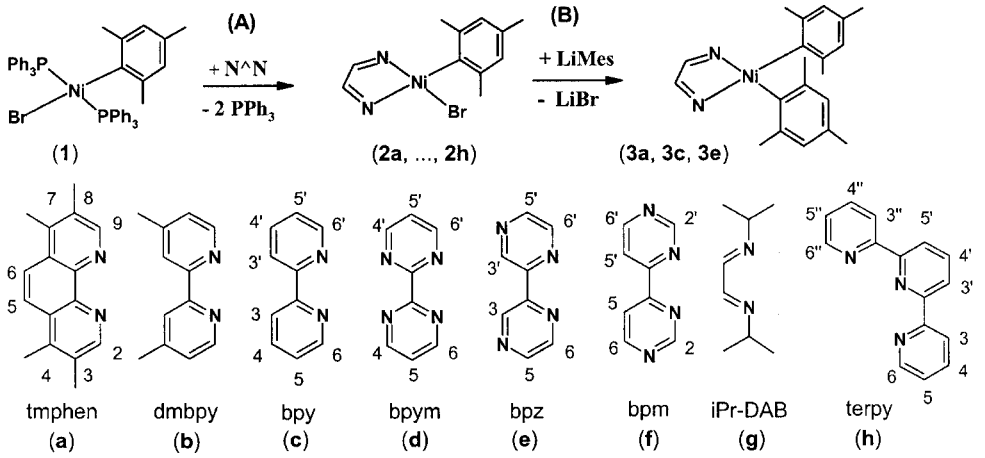

Scheme 1. Preparation of the α-diimine complexes with numbering; tmphen = 3,4,7,8-tetramethyl-1,10-phenanthroline, dmbpy = 4,4′-dimethyl-2,2′-bipyridine, bpy = 2,2′-bipyridine, bpym = 2,2′-bipyrimidine, bpz = 2,2′-bipyrazine, bpm = 4,4′-bipyrimidine, *i*Pr-DAB = *N*,*N*′-diisopropyl-1,2-ethanediimine (*N*,*N*′-diisopropyl-1,4-diazabutadiene), terpy = 2,2′,6′′-terpyridine

troscopy. The compounds under study are bromomesityl complexes of the type [(N^N)Ni(Mes)Br] (N^N = diimine ligands, Mes = mesityl = 2,4,6-trimethylphenyl) with various α-diimine ligands and, additionally, selected dimesityl complexes [(N^N)Ni(Mes)$_2$] (see Scheme 1).

Results and Discussion

Synthesis and General Properties

The neutral complexes [(N^N)Ni(Mes)Br] (N^N = diimine ligands) were synthesised from the precursor complex [(PPh$_3$)$_2$Ni(Mes)Br] (**1**) by ligand-exchange reactions in acetone or toluene solution [see Scheme 1 (A)] and were analysed by ^{1}H and ^{13}C NMR spectroscopy and elemental analysis (see Table 1).

For rather basic diimine ligands like bpy or tmphen reaction A proceeds very smoothly with high yields. The less basic the diimine ligands are (e.g. bpz or bpm) the more the equilibrium tends towards the starting materials. For *i*Pr-DAB the procedure had to be varied to obtain reasonable yields (see Exp. Sect.). With the very weakly basic ligand *N*,*N*′-di(2,6-xylyl)-1,2-ethanediimine (Xyl-DAB) no product was formed upon reaction with [(PPh$_3$)$_2$Ni(Mes)Br] (**1**). Once formed, and in the absence of PPh$_3$ or other strong ligands, the compounds are stable in solvents like CH_2Cl_2, THF, toluene or acetone towards ligand-exchange reactions.[24] The complex [(terpy)Ni(Mes)]Br (**2h**) was prepared following the same method. The ^{1}H NMR spectroscopic data reveal that all three pyridine units bind to nickel and that Br serves only as a counteranion to the cationic complex. The dimesityl complexes [(N^N)Ni(Mes)$_2$] (**3**) were prepared for selected samples by reacting the bromomesityl complexes with mesityllithium as shown in Scheme 1 (B).

The NMR spectroscopic data reflect the geometric properties of the compounds. The bromomesityl complexes

Table 1. ^{1}H NMR spectroscopic data and details of the preparation of complexes [(N^N)Ni(Mes)Br]

	^{1}H NMR δ (ppm)[a]							Yield (%)	Formula (mol. mass)	Elem. anal. found C, H, N (calcd.) (%)
2a	2,9	5,6	Me^{4,7}	Me^{3,8}	*m*-H	*o*-Me	*p*-Me	92	$C_{25}H_{27}BrN_2Ni$	60.79 (60.77), 5.61 (5.51), 5.68 (5.67)
	7.09, 9.28	8.25	2.78	2.65, 2.61	6.50	3.09	2.75		(494.11)	
2b	6,6′	3,3′	Me$^{4,4'}$	5,5′	*m*-H	*o*-Me	*p*-Me	88	$C_{21}H_{23}BrN_2Ni$	57.13 (57.06), 5.25 (5.24), 6.35 (6.34)
	9.20, 6.98	8.18, 8.16	2.51, 2.39	7.49, 7.14	6.43	3.03	2.17		(442.04)	
2c	6,6′	3,3′	4,4′	5,5′	*m*-H	*o*-Me	*p*-Me	95	$C_{19}H_{19}BrN_2Ni$	55.33 (55.12), 4.65 (4.63), 6.72 (6.77)
	9.42, 7.20	8.35, 8.31	8.18, 8.15	7.70, 7.34	6.35	3.05	2.14		(413.98)	
2d	6,6′		4,4′	5,5′	*m*-H	*o*-Me	*p*-Me	75	$C_{17}H_{17}BrN_4Ni$	49.10 (49.09), 4.09 (4.12), 13.13 (13.47)
	9.63, 7.40		9.21, 9.13	7.92, 7.58	6.47	3.02	2.19		(415.97)	
2e	3,3′	6,6′	5,5′		*m*-H	*o*-CH$_3$	*p*-CH$_3$	78	$C_{17}H_{17}BrN_4Ni$	48.92 (49.09), 4.02 (4.12), 13.21 (13.47)
	9.71, 9.52	9.80, 7.33	9.12, 8.75 s		6.50 s	2.91 s	2.20 s		(322.73)	
2f	2,2′	6,6′	5,5′		*m*-H	*o*-CH$_3$	*p*-CH$_3$	75	$C_{17}H_{17}BrN_4Ni$	49.02 (49.09), 4.13 (4.12), 13.41 (13.47)
	10.04 s, 7.85 s	8.08 d, 8.02 d	9.36 d, 9.25 d		6.51 s	2.30 s	2.21 s		(322.73)	
2g	H imine		HC*i*Pr	H$_3$C*i*Pr	*m*-H	*o*-CH$_3$	*p*-CH$_3$	82	$C_{17}H_{27}BrN_2Ni$	56.55 (57.07), 6.29 (6.59), 32.09 (31.60)
	8.55 s, 8.43 s		3.26 m	1.03 d	6.42	2.97 s	2.21 s		(398.03)	
2h	6,6′′;3,3′′	4,4′′	5,5′′	3′,5′;4′	*m*-H	*o*-CH$_3$	*p*-CH$_3$	95	$C_{24}H_{26}BrN_3Ni$	58.73 (59.26), 6.88 (1.18), 30.59 (29.17)
	7.48 qd, 8.69 d	8.35 ddd	7.61	8.72, 8.52	6.72 s	2.96 s	2.29 s		(495.10)	

[a] Measured in [D$_6$]acetone.

 © 2004 Wiley-VCH Verlag GmbH & Co. KGaA, Weinheim

give full sets of ^1H and ^{13}C resonances (see Table 1 and Supporting Information) for the chelate ligands, confirming the planar geometry and C_S symmetry. For the dimesityl complexes C_2 symmetry can be deduced from the NMR spectra.

Structures

The structures of the investigated complexes are essential for the discussion of electronic properties since the molecular entity must be unequivocal. Also, the optical spectroscopy might be affected by intermolecular interactions like stacking and, finally, they serve as a basis for the quantum chemical calculations. Selected samples were therefore submitted to single-crystal XRD or powder EXAFS study.

XRD

The crystal structures of two examples of the series [(N^N)Ni(Mes)Br] with N^N = bpy (**2c**) or *i*Pr-DAB (**2g**)[24] and the structure of [(bpy)Ni(Mes)$_2$] (**3c**)[23] have recently been published. In this paper we report the crystal structure of [(tmphen)Ni(Mes)$_2$] (**3a**; Figure 1). The reason for adding this structure to the series is because of the special character of the tmphen ligand. In the series shown in Scheme 1 tmphen is the most basic ligand and, more importantly, it is a much more rigid ligand than bpy or the bidiazines. This has a strong impact on the molecular structure since previous studies have revealed that the steric demand of two *cis* oriented mesityl substituents in square-planar complexes of nickel, palladium or platinum leads to marked deviations not only in the coordination sphere but also within the diimine ligands.[23–25] This rigidity also has a strong impact on the optical properties, as we will see later.

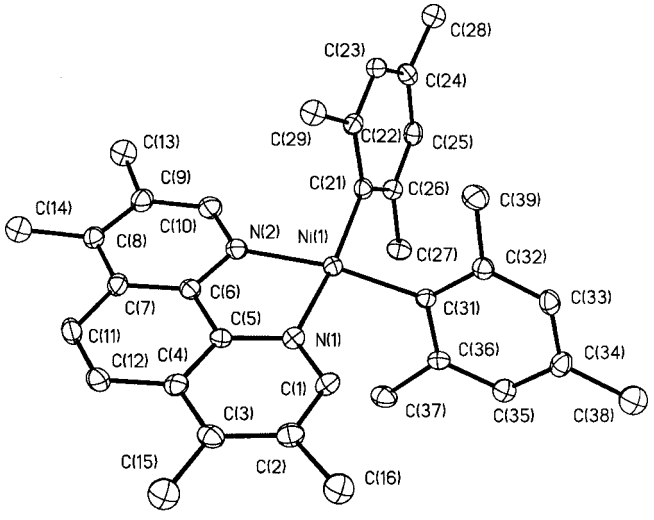

Figure 1. Molecular structure of **3a** (50% probability ellipsoids; H atoms omitted for clarity); selected bond lengths (Å) and angles (deg): Ni−N(1) 1.975(4), Ni−N(2) 1.960(4), Ni−C(11) 1.911(4), Ni−C(21) 1.914(4), N(1)−C(1) 1.337(6), N(2)−C(10) 1.333(6), N1−C(5) 1.345(13), N2−C(6) 1.385(12); N(1)−Ni−N(2) 82.55(16), C(11)−Ni−C(21) 90.47(18), N(1)−Ni−C(11) 94.01(17), N(1)−Ni−C(21) 168.30(17), N(2)−Ni−C(21) 94.79(17), N(2)−Ni−C(11) 169.65(18)

The structure was solved in the orthorhombic *Pbca* space group (for details see Exp. Sect.). A solution in $P2_1/n$, which is the space group obtained for the bpy derivative **3c**, gave slightly worse *R* values. The crystal structure reveals that the complex forms dimers in the unit cell which are π-stacked in a non-graphite-like fashion, with an interplanar distance of 3.49(1) Å. As displayed in Figure 2 the two central rings overlap but are not completely eclipsed (shift of 0.69 Å). The interplanar distance is similar to that in the recently studied isoleptic complex [(tmphen)Pt(Mes)$_2$],[25d] but longer than the distance found in graphite (3.354 Å). For the platinum complex a similar distance of 3.52(1) Å was found but the ligands stack in a staggered fashion and are also not back-to-back, but offset.

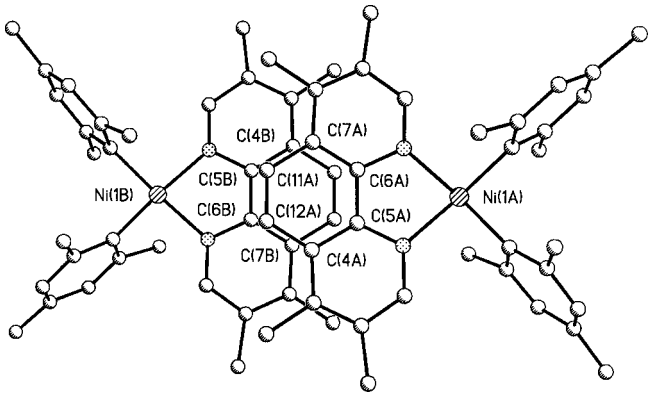

Figure 2. Stacking of two molecules of **3a** in the unit cell

The molecular structure of **3a** resembles in many respects that of the bpy derivative **3c**. The essential distances, for example Ni−N or Ni−C, and the chelate bite angle (around 82°) are very similar. The distortion of the square-planar coordination plane is higher (15.1° vs. 12.4°), as expected. In both cases the distortion of the diimine ligand is quite small (2.8° vs. 3.1°). The mesityl substituents are tilted towards the coordination plane [C(21)−N(2)−Ni(1)−N(1)−C(31)] by 70.0(6)° and 69.0(6)°, respectively, as was observed for other square-planar dimesityl complexes.[23,25] In the related complex [(bpy)Ni(C$_6$F$_5$)$_2$][22a] the C$_6$F$_5$ co-ligands are oriented almost perpendicular to the coordination plane and both the Ni−N distances [1.938(3) and 1.935(3) Å] and the Ni−C distances [1.903(3) and 1.907(3) Å] are markedly shorter. The N−Ni−N bite angle (82.9°) lies in the normal range whereas the C−C bond between the two pyridyl units is noticeably elongated to 1.477(7) Å. The latter is a clear indication of reduced back-bonding to the diimine ligand due to the fact that the fluoroaryl co-ligands donate much less electron density than their mesityl counterpart in the complexes **3a** and **3c**. This is also the reason for the different Ni−C bond lengths in the two types of arylnickel complexes. We thus conclude that the aryl co-ligand strongly governs the geometry around the nickel atom (and also the electron distribution).

 © 2004 Wiley-VCH Verlag GmbH & Co. KGaA, Weinheim

EXAFS Spectroscopy

In the Ni-K edge XANES spectra of all complexes the typical two pre-edge peaks of square-planar Ni^{II} complexes can be observed.[26] The pre-peak at about 8333 eV can be assigned to a 1s→3d electron transition, while the second peak, which occurs at about 8337 eV, is due to a 1s→$4p_z$ transition with shakedown contributions.[26a]

The obtained structural parameters of the investigated complexes determined by curve fitting analysis of the EXAFS spectra at the Ni-K and Br-K edge are summarised in Table 2. [(dmbpy)Ni(Mes)Br] (**2b**), [(bpym)Ni(Mes)Br] (**2d**) and [(bpz)Ni(Mes)Br] (**2e**) show very similar EXAFS functions at the Ni-K and Br-K edge, leading to almost identical structural parameters, which are in very good agreement with values found from single crystal XRD and from the EXAFS analysis of the complex [(bpy)Ni(Mes)Br] (**2c**).[24] As an example, Figure 3 shows the k^3-weighted EXAFS spectra coupled with the magnitudes of the Fourier transforms of **2e** at the Ni-K (a and b) and at the Br-K edge (c and d) The fitting of the Ni-K edge EXAFS spectra was performed using a three-shell model in which the first coordination shell at about 1.9 Å consists of the two coordinating nitrogen atoms of the diimine ligand and the carbon atom of the mesityl group, the second shell contains the bromine backscatterer at about 2.3 Å and the third coordination shell at about 2.8 Å contains the further backbone-carbon atoms of the mesityl and diimine ligand. Because of the quite equal distances and backscatter behaviour of the nitrogen and carbon backscatterers in the first coordination shell, only one shell was fitted with nitrogen amplitude- and phase-functions. The Br-K edge EXAFS spectra were fitted with one coordination shell of nickel at about 2.3 Å. In complex **2a** a slightly higher Ni−C/N distance (1.97 Å) of the first coordination shell was detected, although the Ni−Br distance is of the same order of magnitude.

In Figure 4 (a) a comparison of the experimental k^3-weighted EXAFS functions of [(tmphen)$Ni(Mes)_2$] (**3a**), [(bpy)$Ni(Mes)_2$] (**3c**) and [(bpz)$Ni(Mes)_2$] (**3e**) at the Ni-K edge is shown. The spectra of **3a**, **2h**, **3c** and **3e** were fitted with a two-shell model: the first shell is due to the carbon and nitrogen atoms of the imine and mesityl ligands coordinating directly to the nickel centre atom and the second shell consist of the backbone carbon atoms of the ligands. The structural parameters of **3a**, **2h** and **3c** determined by EXAFS are very similar.

At first sight the complex [(bpz)$Ni(Mes)_2$] (**3e**) seems to deviate from **3a**, **2h** and **3c**. The peak of the first coordination shell in the Fourier-transformed EXAFS spectrum

Table 2. Structural parameters of the solid complexes determined from the Ni-K and Br-K edge EXAFS spectrum

[(N^N)Ni(Mes)Br] N^N	[a]	*r* (Å)	N	σ [Å]	ΔE_0 (eV)	k-range ($Å^{-1}$)	Fit-Index
tmphen (**2a**)	Ni−C/N	1.97 ± 0.02	2.6 ± 0.3	0.108 ± 0.009	22.3	3.90−13.90	37.3
	Ni−Br	2.30 ± 0.02	0.8 ± 0.1	0.071 ± 0.011			
	Ni−C	2.82 ± 0.03	1.9 ± 1.4	0.089 ± 0.027			
	Br−Ni	2.30 ± 0.02	0.9 ± 0.1	0.063 ± 0.006	13.8	4.00−13.10	41.0
dmbpy (**2b**)	Ni−C/N	1.93 ± 0.02	3.1 ± 0.3	0.093 ± 0.006	25.6	3.70−13.00	27.6
	Ni−Br	2.29 ± 0.02	0.9 ± 0.2	0.062 ± 0.008			
	Ni−C	2.79 ± 0.03	3.8 ± 1.1	0.099 ± 0.019			
	Br−Ni	2.29 ± 0.02	1.0 ± 0.1	0.064 ± 0.007	18.5	4.40−13.40	47.8
bpy [24] (**2c**)	Ni−C/N	1.92 ± 0.02	3.1 ± 0.3	0.081 ± 0.008	28.0	3.60−14.90	21.8
	Ni−Br	2.30 ± 0.02	1.0 ± 0.2	0.062 ± 0.011			
	Ni−C	2.81 ± 0.03	5.6 ± 1.7	0.110 ± 0.030			
	Br−Ni	2.30 ± 0.02	0.9 ± 0.1	0.060 ± 0.006	14.5	3.60−11.30	23.5
bpym (**2d**)	Ni−C/N	1.91 ± 0.02	2.8 ± 0.3	0.056 ± 0.006	27.6	3.70−12.50	23.7
	Ni−Br	2.29 ± 0.02	1.2 ± 0.2	0.054 ± 0.008			
	Ni−C	2.82 ± 0.03	2.8 ± 0.8	0.063 ± 0.019			
	Br−Ni	2.29 ± 0.02	0.9 ± 0.1	0.051 ± 0.007	13.5	4.00−12.50	30.6
bpz (**2e**)	Ni−C/N	1.92 ± 0.02	3.3 ± 0.3	0.093 ± 0.009	25.1	3.70−15.00	25.5
	Ni−Br	2.29 ± 0.02	0.8 ± 0.1	0.058 ± 0.008			
	Ni−C	2.80 ± 0.03	4.6 ± 1.4	0.090 ± 0.027			
	Br−Ni	2.29 ± 0.02	1.0 ± 0.1	0.064 ± 0.006	16.5	3.70−14.00	30.6
[(terpy)Ni(Mes)]Br (**2h**)	Ni−C/N	1.89 ± 0.02	3.6 ± 0.4	0.075 ± 0.008	25.6	3.80−14.00	29.9
	Ni−C	2.79 ± 0.03	4.0 ± 1.2	0.060 ± 0.018			
[(N^N)$Ni(Mes)_2$]							
tmphen (**3a**)	Ni−C/N	1.91 ± 0.02	3.5 ± 0.4	0.083 ± 0.008	29.5	3.80−11.90	36.7
	Ni−C	2.81 ± 0.03	3.6 ± 1.1	0.095 ± 0.029			
bpy (**3c**)	Ni−C/N	1.94 ± 0.02	3.7 ± 0.4	0.087 ± 0.009	28.9	3.80−11.50	32.7
	Ni−C	2.85 ± 0.03	5.3 ± 1.6	0.111 ± 0.033			
bpz (**3e**)	Ni−C/N	2.01 ± 0.02	4.4 ± 0.4	0.104 ± 0.009	21.8	3.40−11.00	36.2
	Ni−C	2.90 ± 0.03	4.3 ± 1.6	0.107 ± 0.033			

[a] Absorber−backscatterer distance r, coordination number *N*, Debye−Waller factor σ, with their calculated deviations, shift of the threshold energy ΔE_0 and the fit-index *R*.

 © 2004 Wiley-VCH Verlag GmbH & Co. KGaA, Weinheim

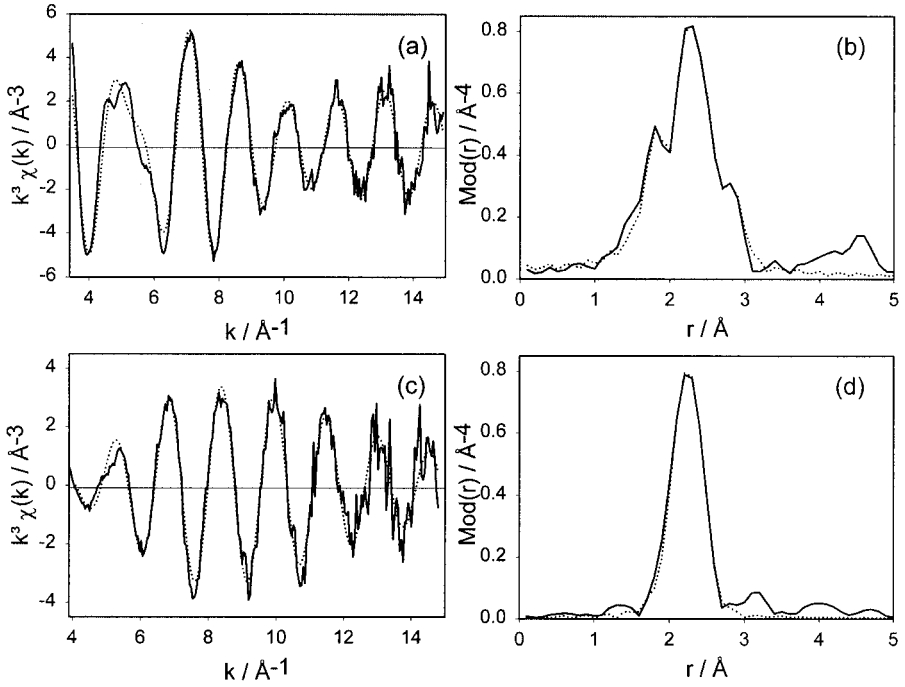

Figure 3. Experimental (solid line) and calculated (dotted line) k^3 χ(k) functions (a,c) and their Fourier transforms (b,d) of solid [(bpz)Ni(Mes)Br] (**2e**) at the Ni-K (a,b) and Br-K edge (c,d)

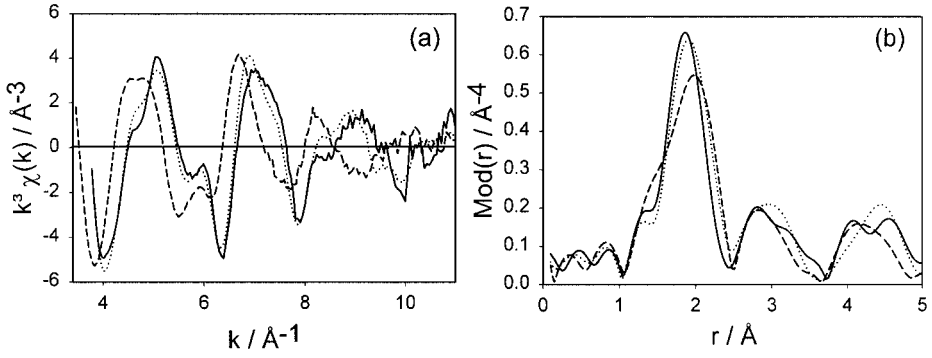

Figure 4. Comparison of the experimental k^3 χ(k) functions (a) and their Fourier transforms (b) of solid [(tmphen)Ni($Mes)_2$] (**3a**) (solid line), solid [(bpy)Ni($Mes)_2$] (**3c**) (dotted line) and solid [(bpz)Ni($Mes)_2$] (**3e**) (dashed line) (Ni-K edge)

of **3e** shows a clear asymmetry, indicating longer and shorter bonded backscatterers in the local environment of the Ni central atoms. However, a fit of two separate coordination shells did not lead to a satisfying result, thus only one coordination shell for the direct environment of nickel was fitted. The determined Ni−C/N distance of 2.01 Å for this shell is significantly longer than in the other dimesityl complexes, such as in [(bpy)Ni($Mes)_2$] (**3c**) (Ni−C/N distance of 1.94 Å). Comparing the bpy complex with the tmphen derivative reveals slightly longer averaged distances for the former. In this series of ligands tmphen represents the high-basicity end and bpy is therefore less basic. Bpz is a much better π-acceptor but therefore a much weaker base, and this gives rise to the lengthening of the Ni−N bonds. The consequences of the basicity of the various ligands for the preparation of the complexes has already been discussed. For the bromomesityl complexes this trend is reversed — the longest average distances are found for the tmphen derivative. This can be explained in the following way. Assuming that the Ni−C and Ni−N bond *trans* to Mes are essentially the same as for the dimesityl complexes, and that the Ni−Br distances are more or less constant, the length of the Ni−N bond *trans* to Br must be the reason for the observed trend. Br is a π-donor which is best accommodated by a good π-acceptor diimine ligand and tmphen in that sense is the worst in our series, whereas bpz is the best.

 © 2004 Wiley-VCH Verlag GmbH & Co. KGaA, Weinheim

Optical Spectroscopy and Calculations

Absorption Spectroscopy and Calculations

Both dimesityl and bromomesityl nickel complexes are brightly coloured, ranging from orange to green in the solid as well as in solution. The absorption spectra (see Figure 5) are dominated by two broad bands of medium intensity in the visible region and an intense band in the UV region. Additional weak, very-long-wavelength bands appear as shoulders in the near IR (NIR) region which, in most cases, are only clearly visible in apolar solvents (Table 3). The two broad bands show a strong negative solvatochromism (see for example Table 4−7) they are red-shifted for the dimesityl complexes relative to their bromomesityl analogues, and in apolar solvents they are partly structured. The UV band is solvent invariant and appears to be characteristic of the ligand.

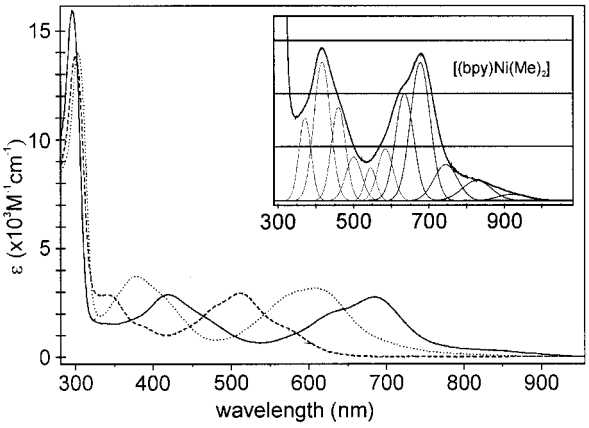

Figure 5. Absorption spectra of [(bpy)Ni(Me$_2$)] (solid line), [(bpy)-Ni(Mes)$_2$] (dotted line) and [(bpy)Ni(Mes)Br] (dashed) in toluene solution; the insert depicts the spectral deconvolution for [(bpy)-Ni(Me)$_2$]

In agreement with recent work by Yamamoto[21] we can assign the two long-wavelength bands to charge-transfer transitions (CT) to the π* orbitals of the diimine ligands and the UV bands to ligand-centred π-π* transitions. In view of the observed solvatochromism of the extremely long-wavelength bands an assignment of these bands to metal-centred (LF) transitions is unlikely.

A closer look at the solvatochromism data (Table 4) reveals that the extent, as derived from the differences of the observed maxima in pentane and DMF solution, increases with the absolute energy, which parallels the series of increasing basicity (or decreasing π-acceptor character; Table 3). Generally the bromomesityl complexes exhibit stronger solvatochromism than the dimesityl derivatives and there is no marked difference between the dimethyl complex [(bpy)Ni(Me)$_2$] and its mesityl analogue. Extreme values are found for **2a**, underlining the special character of the tmphen ligand mentioned above, and for **3e**. All these findings are in full agreement with the simple model of a more or less strong polarisation $M^{(\delta-)}\leftarrow L^{(\delta+)}$ in the ground state, which is transformed to a rather apolar M←L excited state by an MLCT excitation.[28] Strongly basic ligands favour more pronounced polarisation, whereas the donating Mes co-ligands prevent the negative polarisation of the metal by the diimine ligand.

Recently we have discussed the occurrence of mixed MLCT/L′LCT (ligand-to-ligand charge transfer) transitions (instead of pure MLCT transitions) due to contributions of the co-ligands to the frontier orbitals in related diarylplatinum complexes.[29] To probe for such contributions from the mesityl or the bromine co-ligands we have examined the dimesitylnickel complex, the dimethylnickel complex and the bromo(mesityl)nickel complex of 2,2′-bipyridine in a combined spectroscopic and quantum chemical study.

First of all the molecular structures were calculated by both ADF/BP and G03/B3LYP methods. Both methods re-

Table 3. Absorption maxima of the nickel complexes in toluene

[(N^N)Ni(Mes)Br]	λ (ε in 1000 $M^{-1}\cdot cm^{-1}$)[a]				
(N^N)	λ_1	λ_2	λ_3	λ_4	λ_5
tmphen (**2a**)	*300*	*327*, *343*	430 sh, 452	485	527 sh
terpy (**2h**)		341, 365 sh	427, 453	487	531 sh
dmbpy (**2b**)	300	344	456 sh, 486 sh	507	555 sh
bpy (**2c**)	*304* (13.9)	*342* (2.95)	448 sh, 483 sh	*516* (3.01)	571 (1.71)
bpym (**2d**)	*293*	352 sh	490 sh, 507 sh	528	592 sh
bpz (**2e**)	*329*	368 sh	402 sh, 475	*564*, 653 sh	790
*i*Pr-DAB (**2g**)	–	361	427	559 sh, *590*	729 sh
bpm (**2f**)	–	*356*, 401 sh	538 sh, 610 sh	*632*, 650 sh	697 sh, 728 sh
[(N^N)NiMes$_2$]					
(N^N)					
tmphen (**3a**)	297sh	*355*, 378 sh	505 sh, 543,	*564*	
bpy (**3c**)	*307* (14.0)	*377* (3.26)	531 sh, 587 sh	*611* (3.11)	710 sh, 785 sh
bpz (**3e**)	333	408	462 sh, 628 sh	662	
[(bpy)NiMe$_2$]	*294* (15.9)	*416* (2.81)	582 sh, 631 sh	*678* (2.75)	785 sh, 870 sh

[a] Absorption maxima, λ, in nm; main maxima are in italics.

 © 2004 Wiley-VCH Verlag GmbH & Co. KGaA, Weinheim

Table 4. Long-wavelength absorption bands of selected nickel complexes in various solvents — solvatochromism[a]

[(N^N)Ni(Mes)Br] (N^N)	pentane ($E^* = 0$)[b]	λ (in nm) THF (0.59)	$\tilde{\nu}$ (in cm^{-1}) CH_2Cl_2 (0.67)	DMF (0.95)	Δ (cm^{-1})[c]
tmphen (**2a**)	518 (19300)	469 (21310)	423 (23630)	409 (24435)	5135
bpy (**2c**)	558 (17930)	500 (20000)	490 (20410)	464 (21530)	3600
bpz (**2e**)	594 (16850)	545 (18360)	547 (18270)	526 (19030)	2180
*i*Pr-DAB (**2g**)	615 (16250)	572 (17490)	569 (17580)	547 (18270)	2020
[(terpy)Ni(Mes)]$^+$	494 (20240)	450 (22220)	460 (21760)	453 (22090)	1850
[(N^N)Ni($Mes)_2$] (N^N)	pentane	THF	CH_2Cl_2	DMF	Δ (cm^{-1})[c]
tmphen (**3a**)	598 (16720)	546 (18330)	531 (18830)	522 (19160)	2440
bpy (**3c**)	645 (15500)	584 (17120)	576 (17350)	560 (17860)	2360
bpz (**3e**)	681 (14670)	642 (15580)	636 (15720)	629 (15890)	1220
	toluene (0.30)	THF	CH_2Cl_2	DMF	Δ (cm^{-1})[c]
[(bpy)Ni($Me)_2$]	683 (14640)	–	–	615 (16250)	1610
[(bpy)Ni($Mes)_2$]	608 (16450)	584 (17120)	576 (17350)	560 (17860)	1445
[(bpy)Ni(Mes)Br]	516 (19380)	500 (20000)	490 (20410)	464 (21530)	2150

[a] Absorption maxima, λ, in nm; wavenumbers (in cm^{-1}) in parentheses.[b] E^* values are Manuta and Lees' solvent parameters for charge-transfer transitions.[27] [c] $\Delta = E_{(dmf)} - E_{(pentane)}$, or $E_{(toluene)}$ in cm^{-1}. A complete table is provided with the Supporting Information.

Table 5. Selected calculated lowest TD DFT singlet excitation energies for [(bpy)Ni($Mes)_2$]

	Main character (%)	ADF/SAOP Trans. energy in eV (nm)	ADF/SAOP Osc. strength	Experiment λ (nm) in toluene (ε)[a]	Experiment λ (nm) in DMF[a]
^1A	95 (58b → 59b)	1.57 (790)	0.004	789 (200)	745
^1A	38 (57b → 59b); 37 (56b → 59b); 10 (58b → 60b)	2.18 (568)	0.026	611 (2610)	554
^1A	88 (58b → 60b); 3 (57b → 59b)	2.34 (530)	0.005	575 (1990)	535
^1B	87 (58b → 63a); 8 (60a → 60b)	2.54 (488)	0.004	548 (1420)	493
^1A	62 (57b → 60b); 31 (56b → 60b)	2.65 (468)	0.006	445 (1200)	429
^1A	97 (59a → 63a);	2.89 (429)	0.004	410 (2240)	388
^1B	70 (56b → 63a); 26 (57b → 63a)	2.97 (417)	0.012	374 (3000)	362
^1A	53 (60a → 63a); 15 (57b → 60b); 10 (56b → 60b); 7 (57b → 59b);	3.08 (402)	0.130	307 (14000)	306/297

[a] Experimental values from spectral deconvolution. Extinction coefficients, ε, in $M^{-1}\cdot cm^{-1}$.

Table 6. Selected calculated lowest TD DFT singlet excitation energies for [(bpy)Ni($Me)_2$]

	Main character (%)	ADF/SAOP Trans. energy in eV (nm)	ADF/SAOP Osc. strength	G03/B3LYP Trans. energy in eV (nm)	G03/B3LYP Osc. strength	Experiment λ (nm) in toluene (ε)[a]	Experiment λ (nm) in DMF[a]
$^1B_2$	99 ($5a_2 \rightarrow 6b_1$);	1.63 (760)	0.006	1.64 (756)	0.002	785 (380)	760
$^1A_1$	72 ($7b_1 \rightarrow 8b_1$); 17 ($7b_1 \rightarrow 9b_1$); 10 ($5a_2 \rightarrow 6a_2$)	1.87 (663)	0.017	2.24 (553)	0.048	678 (4110)	618
$^1B_2$	97 ($5a_2 \rightarrow 9b_1$); 2 ($7b_1 \rightarrow 6a_2$)	2.02 (614)	0.006	2.75 (451)	0.008	631(3300)	581
$^1B_2$	96 ($7b_1 \rightarrow 6a_2$) 2 ($5a_2 \rightarrow 9b_1$);	2.56 (484)	0.026	3.08 (402)	0.029	461 (2830)	434
$^1A_1$	48 ($5a_2 \rightarrow 6a_2$); 24 ($7b_1 \rightarrow 8b_1$); 24 ($7b_1 \rightarrow 9b_1$)	2.78 (446)	0.125	3.34 (371)	0.119	416 (4280)	392

[a] Experimental values from spectral deconvolution. Extinction coefficients, ε, in $M^{-1}\cdot cm^{-1}$.

produce the experimentally obtained bond lengths and angles well. The biggest difference between the two methods was observed for the Ni–C bond, where ADF/BP gave a value of 1.930 Å and G03/B3LYP yielded 1.906 Å for the dimethyl complex compared to the experimental value of 1.923(4) Å.[30] Approximately the same was found for the dimesityl derivative. For the bromomesityl complex ADF/BP also gave a far more accurate Ni–Br distance (2.324 Å) compared with the experimental value of 2.300(1) Å (G03/BLYP gave 2.399 Å). Comparing the experimental data of the dimethyl derivative [(bpy)Ni($Me)_2$] (monoclinic $P2/c$, $Z = 4$)[30] with all the so far structurally characterised

 © 2004 Wiley-VCH Verlag GmbH & Co. KGaA, Weinheim

Table 7. Selected calculated lowest TD DFT singlet excitation energies for [(bpy)Ni(Mes)Br]

	Main character (%)	ADF/SAOP		G03/B3LYP		Experiment	
		Trans. energy in eV (nm)	Osc. strength	Trans. energy in eV (nm)	Osc. strength	λ (nm) in toluene (ε)[a]	λ (nm) in DMF[a]
^{1}A	48 (104a → 106a); 30 (103a → 106a)	1.64 (756)	0.015	1.82 (682)	0.001	675 (80)	–
^{1}A	89 (102a → 106a); 6 (104a → 106a)	1.69 (734)	0.004	1.85 (669)	0.001	613 (270)	555
^{1}A	83 (100a → 106a); 5 (104a → 107a)	2.13 (582)	0.022	2.04 (607)	0.025	558 (1420)	522
^{1}A	52 (103a → 107a); 36 (104a → 107a)	2.31 (537)	0.005	2.29 (540)	0.001	539 (50)	496
^{1}A	43 (104a → 108a); 31 (103a → 108a); 20 (99a → 106a);	2.56 (484)	0.013	2.46 (502)	0.012	512 (2710)	473
^{1}A	36 (100a → 107a); 36 (99a → 106a)	2.71 (457)	0.010	2.60 (476)	0.040	477 (1830)	447
^{1}A	53 (100a → 107a); 15 (99a → 106a)	2.82 (440)	0.025	2.72 (456)	0.004	449 (960)	427
^{1}A	68 (105a → 109a); 10 (103a → 109a)	2.89 (429)	0.010	–	–	418 (900)	–
^{1}A	70 (100a → 108a); 10 (99a → 107a)	3.14 (395)	0.038	3.01 (412)	0.009	380 (1430)	349
^{1}A	34 (103a → 109a); 30 (102a → 109a); 18 (99a → 107a); 8 (104a → 109a)	3.44 (360)	0.030	–	–	340 (2740)	325

[a] Experimental values from spectral deconvolution. Extinction coefficients, ε, in $M^{-1}\cdot cm^{-1}$.

mesitylnickel complexes reveals markedly shorter Ni−C bonds for the latter. This is in contrast to what would be expected on steric grounds. The C−Ni−C angles in the dimesityl derivatives are slightly enlarged to more than 90° (86.6° for the dimethyl derivative). The N−Ni−N chelate bite and the Ni−N bonds, however, do not differ. As a consequence, it seems that in [(bpy)Ni(Me)$_2$] the inter-ring distance between the pyridine rings is elongated (1.485 Å) which normally means reduced back-bonding. ADF/BP gives a value of 74.4° for the N1−Ni−C11−C12 tilt angle of the mesityl co-ligands (74.9° by G03/B3LYP) and we feel that from these structural data there is already evidence for a notable co-ligand (Mes) contribution to the electronic transitions. The Mes co-ligand therein could act either as a π-donor or π-acceptor. Furthermore, from the EXAFS measurements we have evidence of a strong π-donating interaction of the bromine co-ligand with the nickel atom. Both types of co-ligand contributions will be substantiated by a view of the calculated frontier orbitals. The ground-state one-electron energies and percentage composition of selected highest occupied and lowest unoccupied molecular orbitals have been calculated by DFT methods and the results are shown qualitatively in Figure 6.

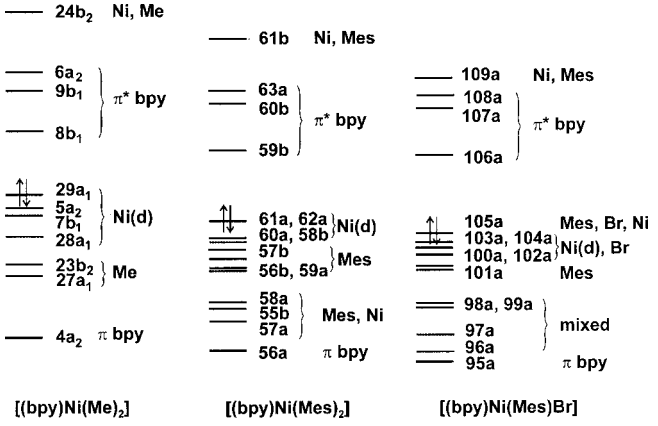

Figure 6. Qualitative MO schemes [(bpy)Ni(Me)$_2$], [(bpy)Ni(Mes)$_2$] (**3c**) and [(bpy)Ni(Mes)Br] (**2c**) based on ADF/SAOP calculated one-electron energies and percentage composition of selected frontier molecular orbitals

The labelling and relative position of ADF/SAOP calculated frontier molecular orbitals is depicted in Figure 6. The calculated composition is available in the Supporting Information. The figure illustrates how the replacement of Mes by other co-ligands influences the composition of the frontier MOs. The character of the LUMO is only moderately influenced by the variation of the co-ligand R.

More substantial changes are observed in the composition of the set of HOMOs which, in the case of [(bpy)Ni(Mes)$_2$] (**3c**), have large contributions of the Mes co-ligand. This is different for [(bpy)Ni(Me)$_2$], where the lower lying occupied orbitals are formed by Me sp^3 orbitals interacting with central metal orbitals. Both ADF/BP and DFT/B3LYP give qualitatively the same composition for the HOMO and LUMO of [(bpy)Ni(Me)$_2$], and the composition of the other frontier orbitals does not differ substantially either. In the case of [(bpy)Ni(Mes)Br] (**2c**) bromine p orbitals contribute to a large extent to the HOMOs whereas the contributions of the mesityl co-ligands are lower than for the dimesityl derivative.

To gain insight to the electronic transitions, lowest TD DFT singlet excitation energies have been calculated and compared to experimentally observed absorption maxima. The results are summarised in Tables 5−7. To this end the absorption spectra of the three compounds have been submitted to a spectral deconvolution, as shown in Figure 5. However, the results of the deconvolutions were not unambiguous since both multiple electronic transitions and vibrational progression could contribute to the various maxima observed as shoulders in the spectra.

All calculated transitions have mixed character. They can be characterised as MLCT excitations for [(bpy)Ni(Me)$_2$], whereas for [(bpy)Ni(Mes)$_2$] (**3c**) and [(bpy)Ni(Mes)Br] (**2c**) the contribution from the Mes or Br co-ligands cannot be neglected and the corresponding transitions should be assigned as mixtures of MLCT/L′LCT [ligand (Mes)-to-li-

 © 2004 Wiley-VCH Verlag GmbH & Co. KGaA, Weinheim

gand charge transfer] or MLCT/XLCT (halogen-to-ligand charge transfer), respectively. Both co-ligands thus act as π-donors. In the bromomesityl complex the donor character of the mesityl group is lower than the dimesityl derivative. The transition energies agree qualitatively quite well with experimental ones for the dimesityl and dimethyl derivatives (Table 5 and 6). Note that the solvatochromic effects are enormous for most absorption bands. Generally, G03/B3LYP predicts larger transition energies than ADF/SAOP, as shown in Table 7. For **2c** the ADF/SAOP calculations predict very low-energy transitions around 1.64 eV (750 nm), which cannot be found in the absorption spectra; the TD-DFT method using "pure" functionals underestimates the transitions energies also in the case of other halide complexes.[31] The transitions calculated at higher energies fit better to experimentally found ones; however the intensity pattern is not reproduced well. G03 calculations using hybrid B3LYP functionals give transitions with high bromine contributions closer to the experimentally measured weak, low-lying absorption bands.

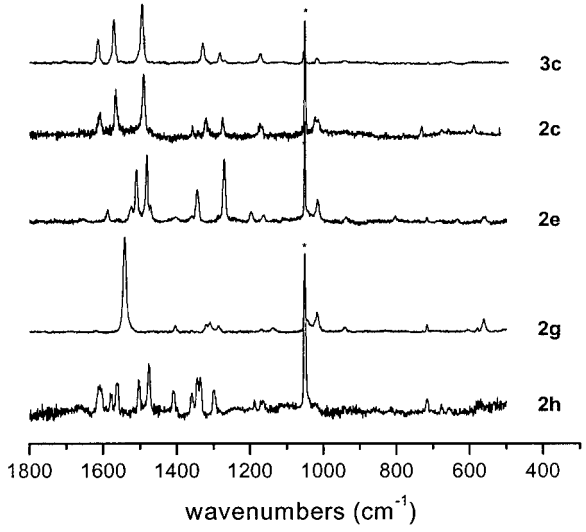

Figure 7. Resonance Raman spectra of the nickel complexes [(bpy)Ni(Mes)$_2$] (**3c**; λ_{ex} = 542 nm), [(bpy)Ni(Mes)Br] (**2c**; λ_{ex} = 488 nm), [(bpz)Ni(Mes)Br] (**2e**; λ_{ex} = 592 nm), [(*i*Pr-DAB)Ni(Mes)Br] (**2g**; λ_{ex} = 598 nm) and [(terpy)Ni(Mes)]Br (**2h**; λ_{ex} = 457.9 nm), obtained from KNO_3 pellets upon irradiation into the long-wavelength absorption bands; * denotes the 1051 cm^{-1} resonance of NO_3^-

Resonance Raman Spectroscopy

In many cases the character of the excited states of transition metal complexes has been studied by emission spectroscopy.[32] However, of the present nickel complexes only **2a**, **2b**, **2h** and **3a** show very weak emission in the solid or solution; the others do not emit either in the solid or in solution, even at 110 K. Additionally, for the weakly emitting compounds the obtained results are ambiguous. We therefore embarked on a combination of resonance Raman (rR) spectroscopy and quantum chemical calculations to probe the character of the excited states. The rR technique allows us to draw direct conclusions about the character of the electronic transitions since it is based on the presumption that only those Raman bands due to vibrations that are influenced by the electronic transition that is excited are enhanced in intensity.[33] The rR spectra of the dimesityl complexes and selected bromomesityl complexes dispersed in KNO_3 were recorded after irradiation of their lowest-energy absorption bands; examples are displayed in Figure 7. Selected data are collected in Table 8 (see also Supporting Information) in comparison to DFT calculated Raman active vibrations for the model system [(bpy)Ni(Me)$_2$] and the resonances of free bpy.[34]

Based on these calculations and data the resonances observed for [(bpy)Ni(Mes)$_2$] (**3c**) at 1608, 1561, 1485, 1322, 1277, 1167, 1015, 655 and 370 cm^{-1} can be assigned to the normal modes of the bpy ligand. They have been observed previously in rR experiments with a number of bpy complexes upon excitation into their metal-to-ligand(bpy) charge-transfer bands.[35] The resonance at highest energy is assigned to the ν(C=N) vibration. Its energy decreases along the series tmphen > bpy > bpz which is caused by the increasing π-accepting abilities from tmphen to bpz. Resonances at 426, 343 and 241 cm^{-1} were assigned to the metal-ligand modes ν(Ni−C), ν(Ni−N) and δ(Ni−N), respectively. For the other diimine ligands the assignment is based on comparison with the bpy analogue.

At first sight (e.g. in Figure 7 for the two bpy complexes) the rR spectra of the bromomesityl complexes of the aromatic diimine ligands are much the same as those recorded for the dimesityl complexes. For the *i*Pr-DAB complex assignment of the observed resonances at 1542 cm^{-1} ν(C=N), or 1170, 1138 and 1020 cm^{-1} ν(C−C) was facilitated by comparison with recently examined organoplatinum(II) and -platinum(IV) complexes.[29b,36] A closer look at the data reveals that in the dimesityl complexes some resonances are observed that do not appear for the bromomesityl derivatives, for example for bpy: 1263, 1114 and 941 and 740 cm^{-1} (marked in italics in Table 8). Such resonances are characteristic of ν(C=C$_{ring}$) or δ$_{ring}$ vibrations and could be assigned to the mesityl co-ligands. They appear only for the dimesityl complexes because the contribution of the mesityl co-ligands to the excited state is markedly higher (mixed MLCT/L′LCT) than for the bromomesityl complexes (mixed XLCT/MLCT) thus supporting the results from quantum chemical calculation (vide supra). The mentioned resonances might also be interpreted as bpy-centred resonances and their occurrence explained by the differences in symmetry between dimesityl (C_2) and bromomesityl (C_s). However, it is unlikely that the higher-symmetry molecules exhibit more resonances than the lower-symmetry ones.

Support for the partial XLCT character of the excited states in the bromomesityl complexes could not be obtained from rR spectra. The only relevant vibration, ν(Ni-Br), which occurs around 160−170 cm^{-1}, is quite weak and therefore hard to detect in the rR experiment due to the closeness to the excitation line. Furthermore, it is also possible that the Ni−Br σ-bond is not much distorted upon π-

 © 2004 Wiley-VCH Verlag GmbH & Co. KGaA, Weinheim

Table 8. Selected resonance Raman data of [(bpy)Ni(Mes)$_2$] (**3c**), [(bpy)Ni(Mes)Br] (**2c**) and [(terpy)Ni(Mes)]Br (**2h**) compared to calculated [(bpy)Ni(Mes)$_2$] and the free ligand[a]

λ_{ex}	**3c** $\tilde{\nu}$ (cm^{-1}) 542 nm	**2c** $\tilde{\nu}$ (cm^{-1}) 488 nm	**2h** $\tilde{\nu}$ (cm^{-1}) 457.9 nm	Calculated[b] $\tilde{\nu}$ (cm^{-1})	bpy[c] $\tilde{\nu}$ (cm^{-1})	Assignment
1	1608	1603	1608	1590	1579	$\nu(C{=}C_{ring}) + \nu(C{=}N_{ring})$
2	1561	1565	1577/1561	1549	1553	$\nu(C{=}C_{ring}) + \nu(C{=}N_{ring})$
3	1485	1490	1503/1475	1463	1448	$\nu(C{=}C_{ring})/\delta(H)$
4	–[c]	–[c]	1408	1414	1401	$\nu(C{=}C_{ring})/\delta(H)$
5	1322	1325	1336	1296	1270	$\nu(C{-}C_{interring})$
6	1277	1280	1299	1273	1248	$\nu(C{=}N_{ring}) + \nu(C{=}C_{ring})$
7	*1263*	–[c]	–[c]	–	–	$\nu(C{=}C_{ring})$
8	1167	1177	1172	1152	1210	$\delta(H)/\nu(C{=}C_{ring})$
9	*1114*	–[c]	–[c]	–	1138	$\delta(H)/\nu(C{=}C_{ring})$
10	1015	1020	1023	1047	1090	δ(H)/ring breathe
11	*941*	–[c]	–[c]	–	–	δ(ring)
12	*740*	–[c]	–[c]	–	–	δ(ring)
13	655	770	676	643	651	δ(ring bend)
14	565	650	654	542	618	ν(Ni–C)
15	426	564	557	421	–	$\delta(N{-}Ni{-}N)_{out\text{-}of\text{-}plane}$
16	370	376	n.m.	383	398	$\nu(Ni{-}N) + \delta(C{-}Ni{-}C)$
17	343	n.m.	n.m.	358	–	ν(Ni–N)
18	241	n.m.	n.m.	224	–	δ(N–Ni–N)

[a] From resonance Raman experiments on KNO_3 pellets at ambient temperature. Excitation wavelengths, λ_{ex}, coincident with the long-wavelength absorption maximum. [b] Calculated for [(bpy)Ni(Mes)$_2$] by G03/B3LYP; scaling factor 0.9613.[37] [c] Not observed. n.m. = not measured; resonances of **3c** marked in *italics* are assigned to mesityl vibrations (see text).

donation by the bromine atom and therefore not resonantly enhanced.

Conclusion

Quantum chemical calculations have revealed the interplay of the metal centre, the chelating diimine ligand and the co-ligands methyl, mesityl or bromine to form the frontier orbitals relevant for the optical transitions and excited states. Strong experimental evidence for the π-accepting mode of the chelate ligand and the π-donating modes of the mesityl and bromine co-ligands comes from a combination of spectroscopic methods. A structural study using EXAFS spectroscopy shows some clear trends for the metal–ligand distances that can be explained by varying σ-donor and/or π-acceptor ability through the series of diimine ligands and π-donating contributions from the bromine co-ligand. Support for a specific electronic contribution from the mesityl co-ligand comes from XRD results. The absorption spectra agree qualitatively well with the calculated transitions. Resonance Raman spectroscopy strongly supports the π-accepting character of the diimine ligands. The evidence for the co-ligand contributions is less strong and should be further substantiated by rR studies on structurally varied derivatives (H/D exchange, other aryl co-ligands, Cl/Br/I exchange). Such studies are already underway.

Experimental Section

Instrumentation: ^{1}H NMR spectra were recorded on Bruker AC250 or AM200 spectrometers. UV/Vis absorption spectra were recorded on Bruins Instruments Omega 10, Hewlett–Packard 8453 Diode Array and Varian Cary 4E spectrophotometers. Resonance Raman spectra of the complexes dispersed in KNO_3 pellets were recorded on a Dilor XY spectrometer equipped with a Wright Instruments CCD detector, using a Spectra Physics 2040E Ar^+ and Coherent CR490 and CR590 dye lasers (with Coumarin 6 and Rhodamine 6G dyes) as excitation sources. Emission spectra were recorded on a Perkin–Elmer LS5B spectrophotometer.

Computational Details: Ground-state electronic structure calculations on complexes [(bpy)Ni(R)$_2$] and [(bpy)Ni(Mes)Br] (**2c**) have been done on the base of density-functional theory (DFT) methods using the ADF2002.03[38] and Gaussian 03[39] program packages. The lowest excited states of the closed-shell complexes were calculated by the time-dependent DFT (TD DFT) method (both ADF and G03 programs).

Within the ADF program, Slater-type orbital (STO) basis sets of triple-ζ quality with polarisation functions were employed; methyl groups on the Mes co-ligands were described by basis sets of double-ζ quality with polarisation functions. The inner shells were represented by a frozen core approximation (1s for C, N, 1s-3p for Br and 1s-3p for Ni were kept frozen). The following density functionals were used within ADF: the local density approximation (LDA) with VWN parametrisation of electron gas data or the functional including Becke's gradient correction[40] to the local-exchange expression in conjunction with Perdew's gradient correction[41] to the LDA expression (ADF/BP). The scalar relativistic (SR) zero-order regular approximation (ZORA) was used within this study. Compositions and energies of molecular orbitals and electronic transition energies and compositions were calculated by the asymptotically correct SAOP functional,[42] which is suitable also for higher-lying MOs and electronic transitions. Core electrons were included in ADF/SAOP calculations.

Within Gaussian 03 6-31G* polarized double-ζ basis sets[43] for C, N, H and Ni atoms; effective core pseudopotentials with corresponding optimised set of basis functions for Br atom[44] were used

 © 2004 Wiley-VCH Verlag GmbH & Co. KGaA, Weinheim

for geometry optimisation and frequency calculations. Correlation consistent polarized double-ζ basis sets[45] (cc-pVDZ) within TD-DFT calculations. Hybrid Becke's three parameter functional with Lee, Yang and Parr correlation functional (B3LYP)[46] was used in Gaussian 03 calculations (G03/B3LYP). Gaussian 03 was also used for the calculations of the vibrations at G03/B3LYP optimised geometries.

The calculations on [(bpy)Ni(Me)$_2$] and [(bpy)Ni(Mes)$_2$] (**3c**) were performed in a C_{2v} or C_2 constrained symmetry, respectively. The z axis is coincident with the C_2 symmetry axis; the central atom and bpy ligand lie in the y,z plane. All results discussed correspond to optimised geometries. The calculations on [(bpy)Ni(Mes)Br] were done without any symmetry constrains.

Crystal Structure Analysis for [(tmphen)Ni(Mes)$_2$] (3a): Data collection was performed at T = 173(2) K on a Siemens P4 diffractometer with Mo-K_α radiation (λ = 0.71073 Å). The structure was solved by direct methods using the SHELXTL-PLUS package[47] and refinement was carried out with SHELXL-97 employing full-matrix least-squares methods on F^2 with $F_o^2 = -3\sigma(F_o^2)$. Formula (M_W) $C_{34}H_{38}N_2Ni_1$ (533.37); cell dimensions (Å): a = 16.297(3), b = 16.578(3), c = 20.732(4); V = 5601.3(19) Å^3; Z = 8; Abs. coefficient = 0.718 mm^{-1}; F(000) = 2272; GooF at F^2 = 1.174; R values [$I > 2\sigma(I)$]: $R1$ = 0.0801, $wR2$ = 0.1679; R values (all data): $R1$ = 0.164, $wR2$ = 0.2076; max./min. 0.609/−0.508 e·Å^{-3}. Empirical absorption correction was performed using Ψ-scans. All non-hydrogen atoms were treated anisotropically, hydrogen atoms were included by using appropriate riding models.

CCDC-226909 (for **3a**) contains the supplementary crystallographic data for this paper. These data can be obtained free of charge at www.ccdc.cam.ac.uk/conts/retrieving.html [or from the Cambridge Crystallographic Data Centre, 12 Union Road, Cambridge CB2 1EZ, UK; Fax: +44-1223-336-033; E-mail: deposit@ccdc.cam.ac.uk].

EXAFS Measurements: The XANES and EXAFS measurements were performed at the beamlines X1.1 (RÖMO II) and E4 at the Hamburger Synchrotronstrahlungslabor des Deutschen Elektronensynchrotrons (HASYLAB at DESY, Hamburg, Germany), at beamline 2−3 at the Stanford Synchrotron Radiation Laboratory (SSRL) at SLAC (Stanford, USA) or at the newly designed EXAFS-beamline KMC-2 at the Berliner Elektronenspeicherring-Gesellschaft für Synchrotronstrahlung m.b.H (BESSY II, Berlin, Germany).

For the measurements at the Ni-K edge (8332.8 eV) a Si(111) double crystal monochromator was used at the SSRL and at DESY. For the measurements at the Br-K edge (13474.0 eV) at beamline X1.1 a Si(311) double crystal monochromator was used. At BESSY a SiGe(220) double graded-crystal (0.5% Ge/cm) monochromator was used for the nickel and the bromine edge. The synchrotron beam current was between 80 and 100 mA at HASYLAB (positron energy 4.45 GeV), between 100 and 250 mA at BESSY (electron energy 1.7 GeV) and between 80 and 100 mA at the SSRL (electron energy 1.7 GeV).

All the experiments were carried out under ambient conditions at 25 °C. The tilt of the second monochromator crystal was set to 30% harmonic rejection. Energy resolution was estimated to be about 0.7−2.0 eV for the Ni-K edge and 4.0 eV for the Br-K edge. The spectra were collected in transmission mode with ion chambers. All ion chambers were filled with nitrogen in the case of the measurements at the Ni-K edge, and the second and third chamber with argon in the case of the measurements at the Br-K edge. Energy calibration was performed with nickel metal foil in the case of measurements at the Ni-K edge and lead metal foil (Pb L_{III}-edge) in the case of the Br-K edge. The solid complexes were embedded in a polyethylene matrix and pressed to pellets. The concentration of all samples was adjusted to yield an absorption jump, $\Delta\mu d$, of about 1.5.

Data evaluation started with background absorption removal from the experimental absorption spectrum by subtraction of a Victoreen-type polynomial. Then, the background-subtracted spectrum was convoluted with a series of increasingly broader Gauss functions and the common intersection point of the convoluted spectra was taken as energy E_0.[48] To determine the smooth part of the spectrum, corrected for pre-edge absorption, a piecewise polynomial was used. It was adjusted in such a way that the low-R components of the resulting Fourier transform were minimal. After division of the background-subtracted spectrum by its smooth part, the photon energy was converted into photoelectron wavenumbers k. The resulting EXAFS function was weighted with k^3. Data analysis in k-space was performed according to the curved wave multiple scattering formalism of the program EXCURV92 with XALPHA phase and amplitude functions.[49] The mean-free path of the scattered electrons was calculated from the imaginary part of the potential (VPI was set to −4.00) and an overall energy shift (ΔE_0) was assumed. The Amplitude Reduction Factor (AFAC) was set to a value of 0.8 in the case of the Ni-K as well as the Br-K edge.

Materials and Procedures: The precursor complex [(PPh$_3$)$_2$Ni(Mes)Br] (**1**) [23] and the ligands bpm,[50] bpz,[51] and *i*Pr-DAB[52] were obtained following literature procedures. Mesityllithium was prepared according to the method of Biali et al.[53] Other reagents were commercially available and used without further purification. All preparations and physical measurements were carried out in dried solvents under an argon atmosphere, using Schlenk techniques.

Preparation of [(N^N)Ni(Mes)Br] (2) [N^N = tmphen (a), dmbpy (b), bpy (c), bpym (d), bpz (e) bpm (f), and terpy (h)]: In a typical reaction 2 g of [(PPh$_3$)$_2$Ni(Mes)Br] (**1**) (2.56 mmol) were suspended in 250 mL of toluene, 1.1 equivalents of the ligand was added and the solution stirred overnight at ambient temperature. The reaction volume was then reduced to 20 mL and the resulting solids were filtered off. They were washed with small amounts of toluene (2 × 5 mL) and *n*-pentane (3 × 20 mL) and dried. For bpz and bpm the products were recrystallised twice from a mixture of CH_2Cl_2 and *n*-heptane (1:8). From the filtrates only small amounts of clean products could be isolated after evaporation to dryness and recrystallisation from CH_2Cl_2/*n*-heptane (1:8). For analytical data see Table 1 and Supporting Information.

Preparation of Bromo-1,4-diisopropyl-1,4-diazabutadienemesitylnickel(II), [(*i*Pr-DAB)Ni(Mes)Br] (2g): *i*Pr-DAB (250 mg, 1.78 mmol) was added to a vigorously stirred suspension of [(PPh$_3$)$_2$Ni(Mes)Br] (**1**; 250 mg, 0.32 mmol) in 500 mL of *n*-pentane. After a few minutes the yellow suspension dissolved leaving a violet voluminous precipitate that was finally filtered off. The obtained violet solid was recrystallised from CH_2Cl_2/*n*-heptane (1:8) and dried, yielding 112 mg of dark-violet microcrystalline material. For nalytical data see Table 1 and Supporting Information.

Preparation of the Dimesitylnickel Complexes 3a, 3c, 3e: The dimesitylnickel complexes [(N^N)Ni(Mes)$_2$] were prepared as described for the bpy complex[23] from the bromomesityl complexes and mesityllithium.

3a: Yield 88%, dark violet powder. $C_{34}H_{38}N_2Ni_1$ (533.40): calcd. C 76.56, H 7.18, N 5.25; found C 76.59, H 7.23, N 5.27. ^{1}H NMR ([D$_6$]DMSO): δ = 8.26 (s, 2 H, H5,6), 7.64 (s, 2 H, H2,9), 6.45 (s, 4 H, *m*-H), 2.67 (s, 6 H, $H_3C^{4,7}$), 2.64 (s, 12 H, *o*-CH_3), 2.29 (s, 6

 © 2004 Wiley-VCH Verlag GmbH & Co. KGaA, Weinheim

H, $H_3C^{3,8}$), 2.13 (s, 6 H, *p*-CH_3) ppm. ^{13}C NMR (CD_2Cl_2): δ = 157.2, 150.5, 142.6, 127.3, 122.7 (all tmphen); 144.9 (Mes-1), 144.1 (Mes-2), 130.9 (Mes-4), 125.3 (Mes-3), 27.3 (*o*-CH_3), 20.8 (*p*-CH_3), 18.1 ($H_3C^{4,7}$), 14.9 ($H_3C^{3,8}$) ppm.

3c: Yield 84%, dark violet powder. $C_{28}H_{30}N_2Ni_1$ (453.27): calcd. C 74.20, H 6.67, N 6.18; found C 74.35, H 6.65, N 6.22. ^1H NMR ([D_6]acetone): δ = 8.38 (d, $^3J_{H3,H4}$ = 8.02 Hz, 2 H, H3,3′), 8.12 (dd,$^3J_{H4,H5}$ = 6.90 Hz, 2 H, H4,4), 7.54 (d, $^3J_{H5,H6}$ = 4.84 Hz, 2 H, H6,6′), 7.44 (dd, 2 H, H5,5′), 6.37 (s, 4 H, *m*-H), 2.53 (s, 12 H, *o*-CH_3), 2.08 (s, 6 H, *p*-CH_3) ppm. ^{13}C NMR ([D_6]acetone): δ = 157.4 (bpy-2,2′), 149.9 (bpy-6,6′), 144.1 (Mes-2), 138.1 (bpy-4,4′), 136.6 (Mes-1), 130.9 (Mes-4), 127.6 (bpy-3,3′), 126.0 (Mes-3), 122.0 (bpy-5,5′), 27.3 (*o*-CH_3), 20.8 (*p*-CH_3) ppm.

3e: Yield 78%, dark green microcrystalline powder. $C_{26}H_{28}N_4Ni_1$ (455.25): calcd. C 68.60, H 6.20, N 12.31; found C 68.72, H 6.22, N 12.41. ^1H NMR ([D_6]acetone): δ = 9.54 (s, 2 H, H3,3′), 8.75 (s, 2 H, H5,5′), 7.53 (s, 2 H, H6,6′), 6.49 (s, 4 H, *m*-H), 2.45 (s, 12 H, *o*-CH_3), 2.28 (s, 6 H, *p*-CH_3) ppm.

Supporting Information: Fourteen tables with comparisons between calculated and experimental structural data for **2c**, **3c**, and [(bpy)-Ni(Me)$_2$]; details of the crystal structure of **3a**; ^{13}C NMR spectroscopic data of selected complexes and absorption spectroscopic data are also given. Furthermore, eight figures are provided showing additional EXAFS spectra and the XANES spectra of **2e** and **2d** and a view of the unit cell of **3a** from the crystal structure determination (see also the footnote on the first page of this article).

Acknowledgments

We wish to thank HASYLAB at DESY (Hamburg, Germany), the SSRL at SLAC (Stanford, USA) and BESSY (Berlin, Germany) for providing synchrotron radiation. The SSRL is operated by the U.S. Department of Energy, Office of Basic Energy Science. Ministry of Education of the Czech Republic and the COST Action D14 is gratefully acknowledged.

[1] [1a] S. D. Ittel, L. K. Johnson, M. Brookhart, *Chem. Rev.* **2000**, *100*, 1169. [1b] C. M. Killian, L. K. Johnson, M. Brookhart, *Organometallics* **1997**, *16*, 2005. [1c] S. Mecking, L. K. Johnson, L. Wang, M. Brookhart, *J. Am. Chem. Soc.* **1998**, *120*, 888. [1d] A. M. LaPointe, M. Brookhart, *Organometallics* **1998**, *17*, 1530.

[2] A. Michalak, T. Ziegler, *Organometallics* **2001**, *20*, 1521.

[3] [3a] S. Mecking, *Angew. Chem.* **2001**, *113*, 550; *Angew. Chem. Int. Ed.* **2001**, *40*, 534. [3b] A. Held, S. Mecking, *Chem. Eur. J.* **2000**, *6*, 4623.

[4] G. J. P. Britovsek, V. C. Gibson, D. F. Wass, *Angew. Chem.* **1999**, *111*, 448; *Angew. Chem. Int. Ed.* **1999**, *38*, 428.

[5] M. Schmid, R. Eberhardt, M. Klinga, M. Leskelä, B. Rieger, *Organometallics* **2001**, *20*, 2321.

[6] J. Heinicke, M. He, A. Dal, H.-F. Klein, O. Hetche, W. Keim, U. Flörke, H.-J. Haupt, *Eur. J. Inorg. Chem.* **2000**, *3*, 431.

[7] C. Wang, S. Friedrich, T. R. Younkin, R. T. Li, R. H. Grubbs, D. A. Bansleben, M. W. Day, *Organometallics* **1998**, *17*, 3149.

[8] M. Schmid, R. Eberhardt, J. Kukral, B. Rieger, *Z. Naturforsch., Teil B* **2002**, *57*, 1141.

[9] L. Johnson, L. Wang, S. McLain, A. Bennett, K. Dobbs, E. Hauptman, A. Ionkin, S. Ittel, K. Kunitsky, W. Marshall, E. McCord, C. Radzewich, A. Rinehart, K.J. Sweetman, Y. Wang, Z. Yin, M. Brookhart, *ACS Symp. Ser.* **2003**, *857*, 131.

[10] [10a] J. L. Davis, B. A. Arndtsen, *Organometallics* **2000**, *19*, 4657. [10b] C. Geyer, S. Schindler, *Organometallics* **1998**, *17*, 4400.

[11] P. T. Matsanuga, J. C. Mavrapoulos, G. L. Hillhouse, *Polyhedron* **1995**, *14*, 175.

[12] P. T. Matsanuga, C. R. Hess, G. L. Hillhouse, *J. Am. Chem. Soc.* **1994**, *116*, 3665.

[13] P. T. Matsanuga, G. L. Hillhouse, *J. Am. Chem. Soc.* **1993**, *115*, 2075.

[14] P. Binger, M. J. Doyle, C. Krüger, Y.-H. Tsay, *Z. Naturforsch., Teil B* **1979**, *34*, 1289.

[15] T. Yamamoto, A. Yamamoto, S. Ikeda, *J. Am. Chem. Soc.* **1971**, *93*, 3350.

[16] W. Seidel, *Z. Chem.* **1985**, *25*, 411.

[17] G. Wilke, G. Herrmann, *Angew. Chem.* **1966**, *78*, 591. G. Wilke, G. Herrmann, *Angew. Chem. Int. Ed. Engl.* **1966**, *5*, 581.

[18] T. R. Miller, I. G. Dance, *J. Am. Chem. Soc.* **1973**, *95*, 6970.

[19] A. Arcas, P. Royo, *Inorg. Chim. Acta* **1978**, *31*, 97.

[20] R. F. de Souza, L.C. Simon, M.C. Alves, *J. Catal.* **2003**, *214*, 165.

[21] T. Yamamoto, M. Abla, Y. Murakami, *Bull. Chem. Soc. Jpn.* **2002**, *75*, 1997.

[22] [22a] T. Yamamoto, M. Abla, *J. Organomet. Chem.* **1997**, *535*, 209. [22b] T. Yamamoto, *Synlett* **2003**, *4*, 425. [22c] T. Yamamoto, S. Wakabayashi, K. Osakada, *J. Organomet. Chem.* **1992**, *428*, 223.

[23] A. Klein, *Z. Anorg. Allg. Chem.* **2001**, *627*, 645.

[24] M. P. Feth, A. Klein, H. Bertagnolli, *Eur. J. Inorg. Chem.* **2003**, 839.

[25] [25a] A. Klein, E. J. L. McInnes, W. Kaim, *J. Chem. Soc., Dalton Trans.* **2002**, 2371. [25b] A. Klein, H.-D. Hausen, W. Kaim, *J. Organomet. Chem.* **1992**, *440*, 207. [25c] A. Klein, M. Niemeyer, *Z. Anorg. Allg. Chem.* **2000**, *626*, 1191. [25d] A. Klein, J. van Slageren, S. Zális, *Eur. J. Inorg. Chem.* **2003**, 1927.

[26] [26a] G. J. Colpas, M.J. Maroney, C. Bagyinka, M. Kumar, W.S. Willis, S.L. Suib, N. Baidya, P. K. Mascharak, *Inorg. Chem.* **1991**, *30*, 920. [26b] M. W. Renner, L. R. Furenlid, K. M. Barkigia, J. Fajer, *J. Phys. IV France* **1997**, *7*, 661. [26c] N. Kosugi, T. Yokoyama, K. Asakura, H. Kuroda, *Chem. Phys.* **1984**, *91*, 249. [26d] H. Nishida, T. Yokoyama, H. Kuroda, *Chem. Phys.* **1986**, *104*, 449.

[27] D. M. Manuta, A. J. Lees, *Inorg. Chem.* **1983**, *22*, 3825.

[28] W. Kaim, S. Ernst, S. Kohlmann, *Chem. unserer Zeit* **1987**, *21*, 50.

[29] [29a] A. Klein, J. van Slageren, S. Záliš, *Eur. J. Inorg. Chem.* **2003**, 1917. [29b] A. Klein, J. van Slageren, S. Záliš, *Inorg. Chem.* **2002**, *41*, 5216.

[30] G. C. Tucci, R. H. Holm, *J. Am. Chem. Soc.* **1995**, *117*, 6489.

[31] M. Turki, C. Daniel, S. Zalis, A. Vlček, Jr, J. Van Slageren, D. J. Stufkens, *J. Am. Chem. Soc.* **2001**, *123*, 11431.

[32] [32a] P. C. Ford, in *Inorganic and Organometallic Photochemistry* (Ed.: M. S. Wrighton), ACS, Washington, D.C., **1978**, vol. 168, 73. [32b] A. B. P. Lever, *Inorganic Electronic Spectroscopy*, Elsevier, Amsterdam, **1984**.

[33] R. J. H. Clark, T. J. Dines, *Angew. Chem.* **1986**, *98*, 131. R. J. H. Clark, T. J. Dines, *Angew. Chem. Int. Ed. Engl.* **1986**, *25*, 131.

[34] [34a] J. S. Strukl, J. L. Walter, *Spectrochim. Acta* **1971**, *27*, 223. [34b] J. S. Strukl, J. L. Walter, *Spectrochim. Acta* **1971**, *27*, 209.

[35] [35a] I. Srnova-Sloufova, B. Vlckova, T. L. Snoeck, D. J. Stufkens, P. Matejka, *Inorg. Chem.* **2000**, *39*, 3551. [35b] R. Hage, J. G. Haasnoot, D. J. Stufkens, T. L. Snoeck, J. G. Vos, J. Reedijk, *Inorg. Chem.* **1989**, *28*, 1413. [35c] P. A. Mabrouk, M. S. Wrighton, *Inorg. Chem.* **1986**, *25*, 526. [35d] R. W. Balk, T. L. Snoeck, D. J. Stufkens, A. Oskam, *Inorg. Chem.* **1980**, *19*, 3015.

[36] [36a] J. van Slageren, D. J. Stufkens, S. Zalis, A. Klein, *J. Chem. Soc., Dalton Trans.* **2002**, 218. [36b] J. van Slageren, A. Klein, S. Zalis, D. J. Stufkens, *Coord. Chem. Rev.* **2001**, *219−221*, 937.

[37] M. W. Wong, *Chem. Phys. Lett.* **1996**, *256*, 391.

[38] [38a] C. Fonseca Guerra, J. G. Snijders, G. Te Velde, E. J. Baerends, *Theor. Chim. Acc.* **1998**, *99*, 391. [38b] S. J. A. van Gisbergen, J. G. Snijders, E. J. Baerends, *Comput. Phys. Commun.* **1999**, *118*, 119.

 © 2004 Wiley-VCH Verlag GmbH & Co. KGaA, Weinheim

[39] Gaussian 03, Revision B.2, M. J. Frisch, G. W. Trucks, H. B. Schlegel, G. E. Scuseria, M. A. Robb, J. R. Cheeseman, J. A. Montgomery, Jr., T. Vreven, K. N. Kudin, J. C. Burant, J. M. Millam, S. S. Iyengar, J. Tomasi, V. Barone, B. Mennucci, M. Cossi, G. Scalmani, N. Rega, G. A. Petersson, H. Nakatsuji, M. Hada, M. Ehara, K. Toyota, R. Fukuda, J. Hasegawa, M. Ishida, T. Nakajima, Y. Honda, O. Kitao, H. Nakai, M. Klene, X. Li, J. E. Knox, H. P. Hratchian, J. B. Cross, C. Adamo, J. Jaramillo, R. Gomperts, R. E. Stratmann, O. Yazyev, A. J. Austin, R. Cammi, C. Pomelli, J. W. Ochterski, P. Y. Ayala, K. Morokuma, G. A. Voth, P. Salvador, J. J. Dannenberg, V. G. Zakrzewski, S. Dapprich, A. D. Daniels, M. C. Strain, O. Farkas, D. K. Malick, A. D. Rabuck, K. Raghavachari, J. B. Foresman, J. V. Ortiz, Q. Cui, A. G. Baboul, S. Clifford, J. Cioslowski, B. B. Stefanov, G. Liu, A. Liashenko, P. Piskorz, I. Komaromi, R. L. Martin, D. J. Fox, T. Keith, M. A. Al-Laham, C. Y. Peng, A. Nanayakkara, M. Challacombe, P. M. W. Gill, B. Johnson, W. Chen, M. W. Wong, C. Gonzalez, J. A. Pople, Gaussian, Inc., Pittsburgh PA, **2003**.
[40] A. D. Becke, *Phys. Rev. A* **1988**, *38*, 3098.
[41] J. P. Perdew, *Phys. Rev. A* **1986**, *33*, 8822.
[42] P. R. T. Schipper, O. V. Gritsenko, S. J. A. van Gisbergen, E. J. Baerends, *J. Chem. Phys.* **2000**, *112*, 1344.
[43] [43a] P. C. Hariharan, J. A. Pople, *Theor. Chim. Acta* **1973**, *28*, 213. [43b] V. A. Rassolov, J. A. Pople, M. A. Ratner, T. L. Windus, *J. Chem. Phys.* **1998**, *109*, 1223.
[44] A. Bergner, M. Dolg, W. Kuechle, H. Stoll, H. Preuss, *Mol. Phys.* **1993**, *80*, 1431.
[45] D. E. Woon, T. H. J. Dunning, *J. Chem. Phys.* **1993**, *98*, 1358.
[46] P. J. Stephens, F. J. Devlin, C. F. Cabalowski, M. J. Frisch, *J. Phys. Chem.* **1994**, *98*, 11623.
[47] [47a] G. M. Sheldrick, SHELXTL, Bruker Analytical X-ray Systems, Madison, Wisconsin, USA, **1998**. [47b] G. M. Sheldrick, SHELXL-97: A program for Crystal Structure Determination, University of Göttingen, Göttingen, Germany, **1997**.
[48] [48a] T. S. Ertel, H. Bertagnolli, S. Hückmann, U. Kolb, D. Peter, *Appl. Spectrosc.* **1992**, *46*, 690. [48b] M. Newville, P. Livins, Y. Yakoby, J. J. Rehr, E. A. Stern, *Phys. Rev. B* **1993**, *47*, 14126.
[49] S. J. Gurman, N. Binsted, I. Ross, *J. Phys. C* **1986**, *19*, 1845.
[50] F. Effenberger, *Chem. Ber.* **1965**, *98*, 2260.
[51] J. J. Lafferty, F. H. Case, *J. Org. Chem.* **1967**, *32*, 1591.
[52] J. M. Kliegman, R. K. Barnes, *Tetrahedron* **1970**, *26*, 2555.
[53] S. E. Biali, Z. Rappoport, *J. Am. Chem. Soc.* **1985**, *107*, 1007.

Received December 19, 2003
Early View Article
Published Online April 26, 2004

 © 2004 Wiley-VCH Verlag GmbH & Co. KGaA, Weinheim

EurJIC
European Journal of Inorganic Chemistry

Issue 14/2004

Pages 2797–2990

Papers available ahead of print in Early View at www.interscience.wiley.com

Earliest available Table of Contents:
Automatically, free of charge by e-mail through
www.interscience.wiley.com/alerts

COVER PICTURE

The cover picture shows the rearrangement of *N*-imidoyl-*N*-heterocyclic carbenes as well as a crystal structures of a palladium complex of a derivative of one of the rearranged carbene ligands. This work was supported by the polymer laboratory of BASF AG, Ludwigshafen, Germany, in search of new imino-*N*-heterocyclic carbene late transition metal complexes as novel polymerization catalysts. Details are discussed in the article by B. Bildstein et al. on p. 2827 ff.

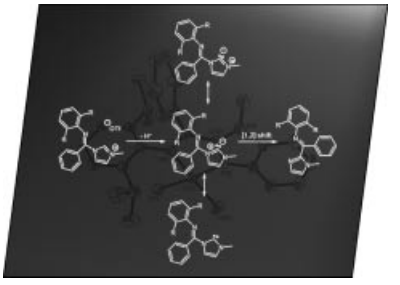

MICROREVIEW

Contents

2811 **R. H. Laye, E. J. L. McInnes***

Solvothermal Synthesis of Paramagnetic Molecular Clusters

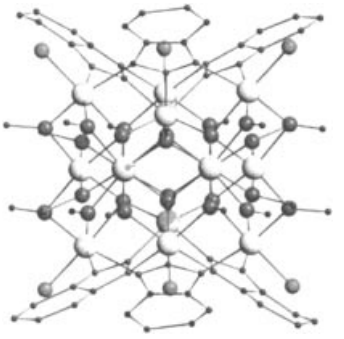

Keywords: Solvothermal synthesis / Hydrothermal synthesis / Clusters / Single-molecule magnets

 © 2004 Wiley-VCH Verlag GmbH & Co. KGaA, Weinheim

SHORT COMMUNICATIONS

2819 **P. Wu, Q. Li, N. Ge, Y. Wei,* Y. Wang, P. Wang, H. Guo***

An Easy Route to Monofunctionalized Organoimido Derivatives of the Lindqvist Hexamolybdate

Keywords: Organoimido Derivatives / Polyoxometalates / Acid Catalysis / Dehydration / Organic−inorganic hybrid

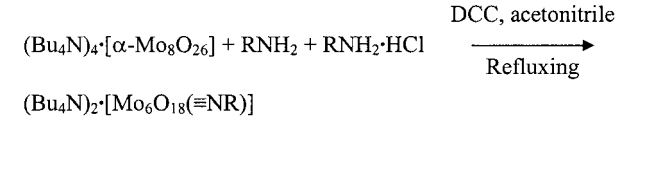

2823 **S. Mazières,* C. Le Roux,* M. Peyronneau, H. Gornitzka, N. Roques**

Structural Characterization of Bismuth(III) and Antimony(III) Chlorotriflates: Key Intermediates in Catalytic Friedel−Crafts Transformations

Keywords: Bismuth / Antimony / Triflate / X-ray diffraction / Friedel−Crafts reactions

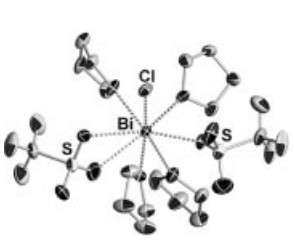

ClBi(OSO2CF3)2·4THF

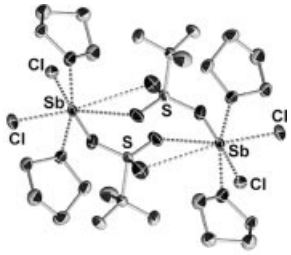

Cl2Sb(OSO2CF3)·2THF

FULL PAPERS

2827 **G. Steiner, A. Krajete, H. Kopacka, K.-H. Ongania, K. Wurst, P. Preishuber-Pflügl, B. Bildstein***

[1,2]-Rearrangement of Imino-*N*-heterocyclic Carbenes − Synthesis and Structures of Chelating Iminoimidazole Pd and Ni Complexes

Keywords: N ligands / Carbenes / Chelates / Transition metals / Rearrangement

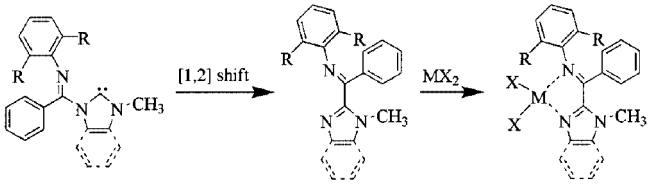

2837 **T. B. Wen, W. Y. Hung, Z. Y. Zhou, M. F. Lo, I. D. Williams, G. Jia***

Synthesis and Characterization of $[OsCl_2(=C=CHR)(PPh_3)_2]$ and Related Complexes

Keywords: Carbyne ligands / Osmium / Vinylidene ligands

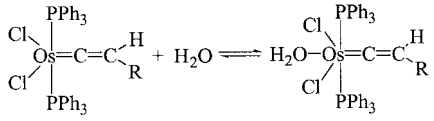

2847 **T. Vermonden, W. M. de Vos, A. T. M. Marcelis,* E. J. R. Sudhölter**

3-D Water-Soluble Reversible Neodymium(III) and Lanthanum(III) Coordination Polymers

Keywords: Lanthanides / NMR spectroscopy / Self-assembly / Tridendate ligands / Viscosity

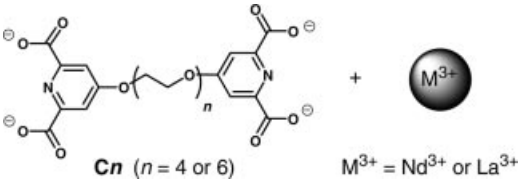

Cn (*n* = 4 or 6) $M^{3+} = Nd^{3+}$ or La^{3+}

2853 **M. Cangiotti, M. Formica, V. Fusi,* L. Giorgi, M. Micheloni,* M. F. Ottaviani,* S. Sampaolesi**

Nitroxide Radicals Interacting with Polyamine-Phenolic Ligands and Their Metal Complexes

Keywords: EPR / Macrocycles / Metal complexes / Nitroxide radicals / Polyamines

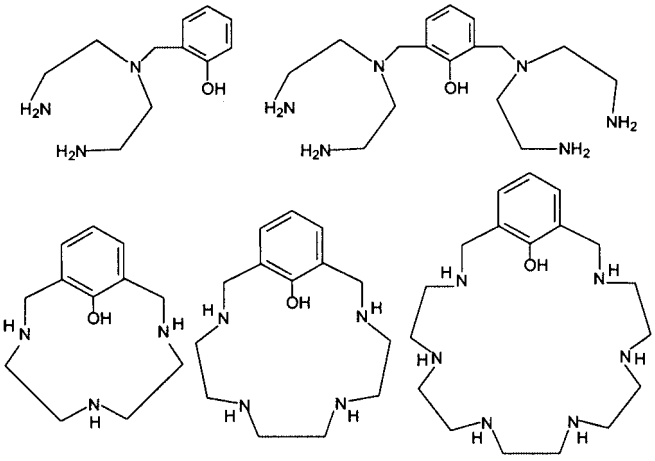

2861 **F. Wolff, C. Lorber,* R. Choukroun,* B. Donnadieu**

Paramagnetic Chloro-, Alkoxo-, or Azidovanadium(IV) Complexes Supported by an [ONNO]-Type Amine Bis(phenolate) Ligand

Keywords: Vanadium / Amines / Paramagnetism

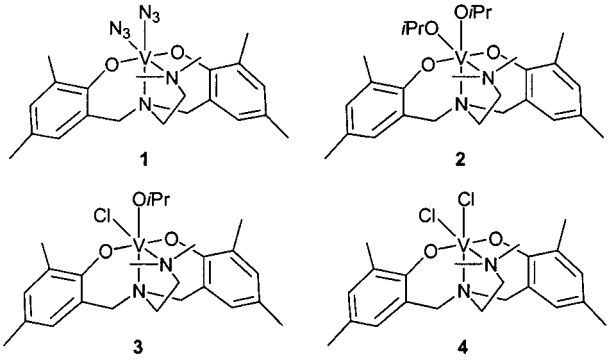

2868 **C. Näther,* I. Jeß**

Synthesis, Crystal Structure and Thermal Reactivity of New Copper(I) Halide Pyrimidine-Containing Coordination Polymers

Keywords: Coordination polymers / Copper / Halides / N ligands / Thermal properties

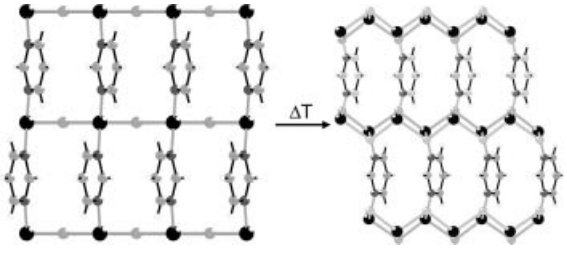

2877 **S. Vagin,* U. Ziener, M. Hanack,* P. A. Stuzhin**

Ruthenium(II) Octaphenylporphyrazine Complexes with Mixed Axial Ligands: Peculiarities of Their Formation and Spectral Properties

Keywords: Isocyanide ligands / N ligands / NMR spectroscopy / Porphyrinoids / Ruthenium / Self-assembly

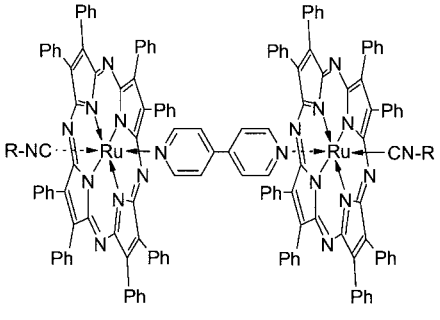

 © 2004 Wiley-VCH Verlag GmbH & Co. KGaA, Weinheim

2885 **C. J. Milios, T. C. Stamatatos, P. Kyritsis, A. Terzis, C. P. Raptopoulou, R. Vicente,* A. Escuer,* S. P. Perlepes***

Phenyl 2-Pyridyl Ketone and Its Oxime in Manganese Carboxylate Chemistry: Synthesis, Characterisation, X-ray Studies and Magnetic Properties of Mononuclear, Trinuclear and Octanuclear Complexes

Keywords: Carboxylate ligands / Magnetic properties / Manganese / N,O ligands / X-ray crystallography

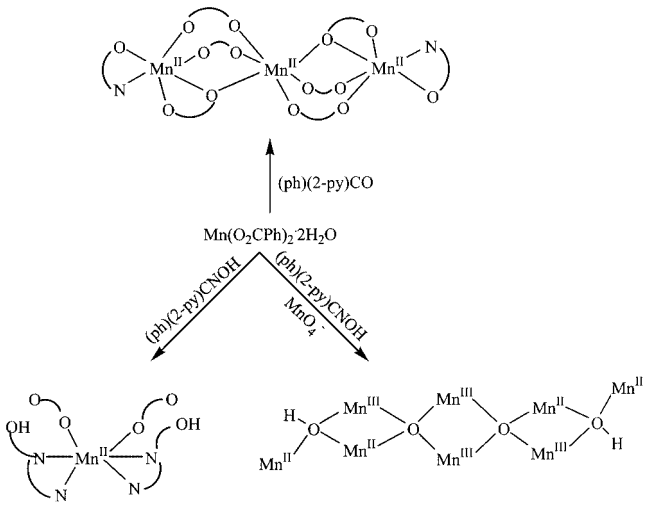

2902 **S. Frantz, B. Sarkar, M. Sieger, W. Kaim,* F. Roncaroli, J. A. Olabe,* S. Záliš**

EPR Insensitivity of the Metal-Nitrosyl Spin-Bearing Moiety in Complexes $[L_nRu^{II}\text{-}NO^{\bullet}]^k$

Keywords: Density functional calculations / EPR spectroscopy / Nitric oxide / Radical complexes / Ruthenium

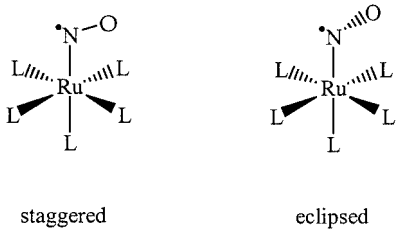

2908 **M. Biesemans,* F. A. G. Mercier, M. Van Poeck, J. C. Martins, G. Dumartin, R. Willem**

Interface Synthesis, Characterization and Catalytic Properties of Dialkyldichlorotin and Tetraalkyl Distannoxane Functionalities Grafted to Insoluble Polystyrene Beads by a Hexamethylene Spacer

Keywords: Catalysis / Heterogeneous catalysis / NMR spectroscopy / Transesterification / Tin

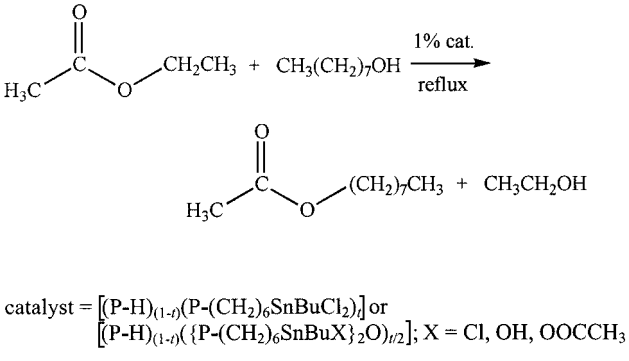

2914 **G. Marinescu, D. Visinescu, A. Cucos, M. Andruh,* Y. Journaux,* V. Kravtsov, Y. A. Simonov, J. Lipkowski**

Oxalato-Bridged $[Cu^{II}Cr^{III}]$ and $[Mn^{II}Cr^{III}]$ Binuclear Complexes: Synthesis, Crystal Structures, Magnetic and EPR Investigations

Keywords: Copper complexes / Magnetic properties / Manganese complexes / Oxalato bridges

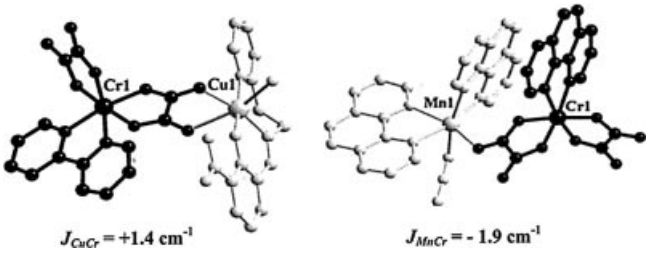

 © 2004 Wiley-VCH Verlag GmbH & Co. KGaA, Weinheim

2923 **E. Sheng, S. Zhou, S. Wang,* G. Yang, Y. Wu, Y. Feng, L. Mao, Z. Huang**

Homolysis of the Ln−N (Ln = Yb, Eu) Bond − Synthesis, Structure, and Catalytic Activity of Ytterbium(II) and Europium(II) Complexes Having (Dimethylamino)propyl- and (Dimethylamino)ethyl-Functionalized Indenyl Ligands

Keywords: Catalyst / Homolysis / Organometallics / Polymer / Polymerization

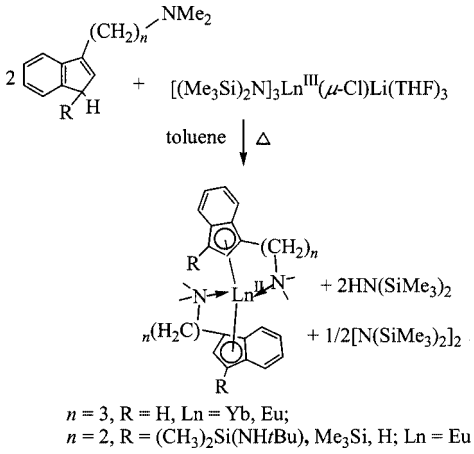

2933 **R. Ahlrichs, C. E. Anson, R. Clerac, D. Fenske,* A. Rothenberger, M. Sierka, S. Wieber**

Molecular Alloys: Syntheses and Structures of the Copper−Antimony Clusters $[Cu_{17}Sb_8(dppm)_6(Ph_2PCHPPh_2)]$ and $[Cu_{20}Sb_{10}(PCy_3)_8]$

Keywords: X-ray diffraction / Cluster compounds / Antimony / Copper

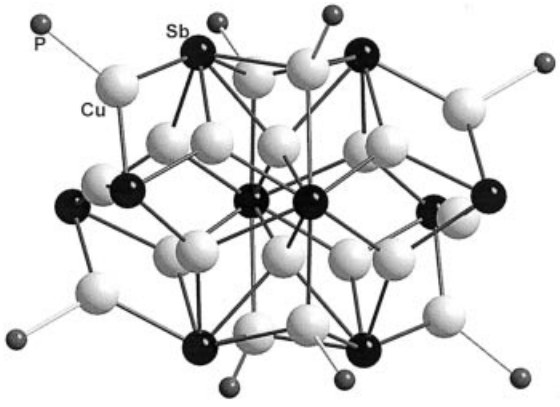

2937 **J. M. Vila,* E. Gayoso, M. T. Pereira, J. M. Ortigueira, G. Alberdi, M. Mariño, R. Alvarez, A. Fernández**

The First Cyclometallated (1-Ferrocenylethanone thiosemicarbazone)palladium(II) Compounds − Crystal and Molecular Structure of $[Pd\{(\eta^5\text{-}C_5H_5)Fe(\eta^5\text{-}C_5H_3)C(Me)=NN=C(S)NHMe\}(PPh_3)]$

Keywords: C−H activation / Ferrocene / Thiosemicarbazone / Palladium / X-ray diffraction

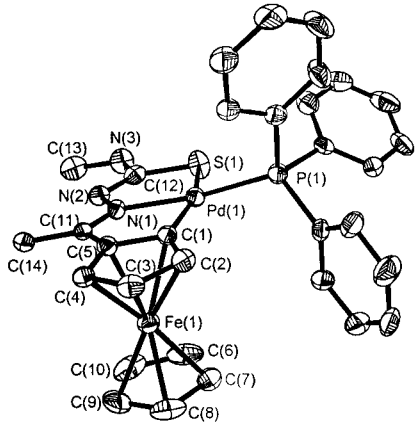

 © 2004 Wiley-VCH Verlag GmbH & Co. KGaA, Weinheim

2943 **D. Vujovic,* H. G. Raubenheimer, L. R. Nassimbeni**

One-Dimensional Cd^{II} Coordination Polymers: Solid Solutions with Ni^{II}, Thermal Stabilities and Structures

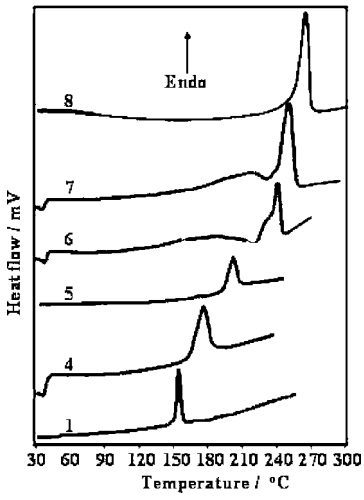

Keywords: Coordination polymers / Solid solutions / Cadmium complexes

2950 **B. B. Dhar, R. Mukherjee, S. Mukhopadhyay,* R. Banerjee**

Kinetics and Mechanism of Oxidation of Fe^{2+} by the Tris(biguanide)manganese(IV) Ion in Aqueous Acid Media

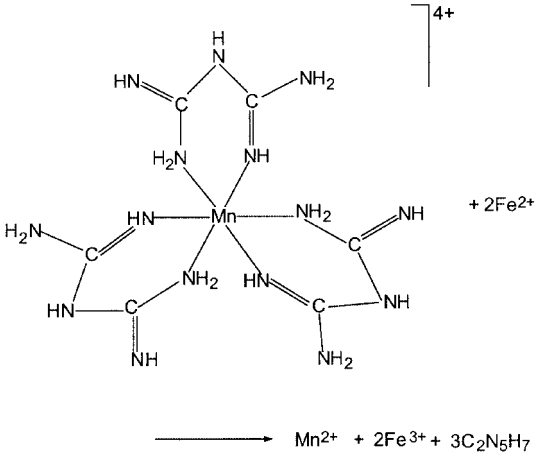

Keywords: Iron / Kinetics / Manganese / Mechanism / Redox chemistry

2956 **K. Huang, J. Yu,* G. Wang, Y. Li, R. Xu***

Covalent Bonding of Phosphonates of L-Proline and L-Cysteine to γ-Zirconium Phosphate

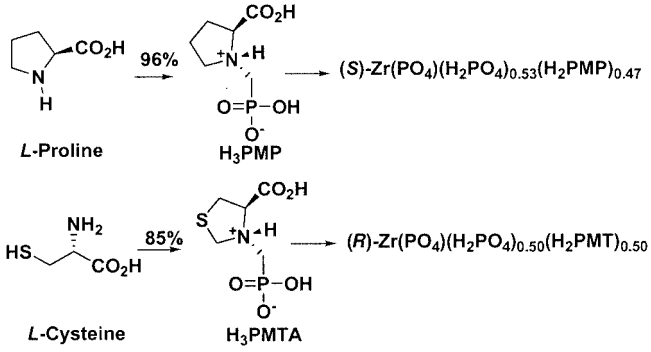

Keywords: Amino acids / Chirality / Phosphates / Phosphonates / Zirconium

 © 2004 Wiley-VCH Verlag GmbH & Co. KGaA, Weinheim

2961 **M. Nanjo,* E. Nanjo, K. Mochida***

Tris(trimethylsilyl)-Substituted Heavy Group 14-Element-Centered Anions: Unsolvated Trimeric Germyllithium and Solvated Dimeric Silyl- and Stannyllithiums

Keywords: Germanium / Lithium / Silicon / Solid-state structures / Tin

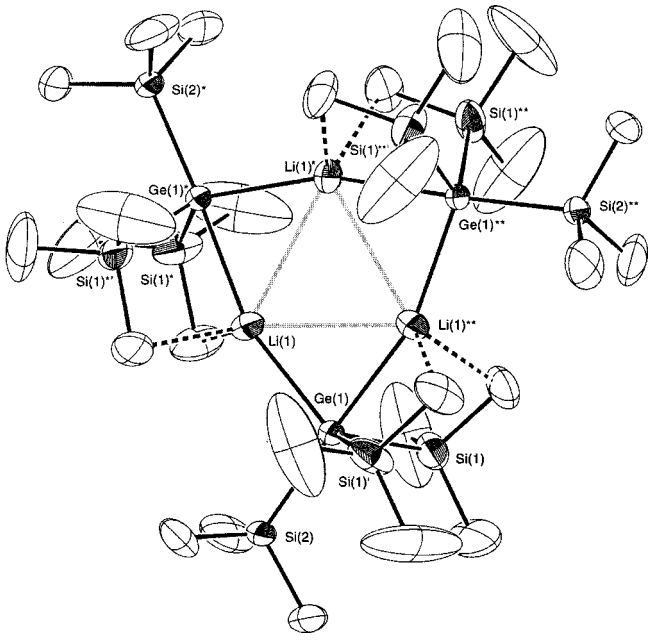

2968 **X.-J. Zheng, Z.-M. Wang, S. Gao, F.-H. Liao, C.-H. Yan, L.-P. Jin***

Hydrothermal Syntheses, Structures, and Properties of Three 3-D Lanthanide Coordination Polymers that Form 1-D Channels

Keywords: Coordination polymer / Hydrothermal synthesis / Lanthanides / 2,6-Naphthalenedicarboxylate / X-ray diffraction

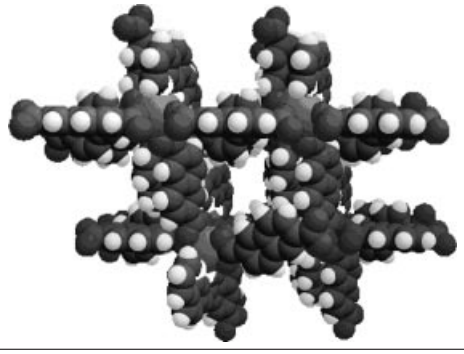

2974 **K. Heinze,* M. Schlenker**

Main Chain Ferrocenyl Amides from 1-Aminoferrocene-1′-carboxylic Acid

Keywords: Metallocenes / Hydrogen bonds / Peptides / Conformation analysis

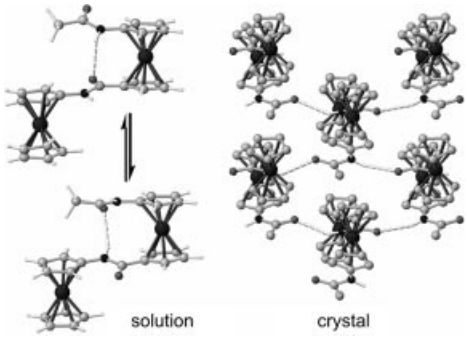

CORRECTION

2989 **P. Kölle, R. Dronskowski***

Synthesis, Crystal Structures and Electrical Conductivities of the Ionic Liquid Compounds Butyldimethylimidazolium Tetrafluoroborate, Hexafluorophosphate and Hexafluoroantimonate

Keywords: Electrochemistry / Ionic liquids / Packing efficiency / X-ray diffraction

 © 2004 Wiley-VCH Verlag GmbH & Co. KGaA, Weinheim

Solvothermal Synthesis of Paramagnetic Molecular Clusters

Rebecca H. Laye[a] and Eric J. L. McInnes*[a]

Keywords: Solvothermal synthesis / Hydrothermal synthesis / Clusters / Single-molecule magnets

A brief overview is given of the literature of the use of solvothermal techniques – chemistry in superheated solvents – towards paramagnetic cluster synthesis. Although these techniques have been used extensively to prepare infinite lattice magnetic materials, there is much less work on preparing discrete molecular clusters other than the polyoxovanadates and -molybdates. This microreview details some of our early success in using these techniques towards high-nuclearity vanadium(III), chromium(III), manganese(II/III), iron(III) and nickel(II) clusters, including some very high spin ground state clusters ($S \leq 25$), and therefore demonstrates the potential in the synthesis of molecular materials such as single-molecule magnets.

(© Wiley-VCH Verlag GmbH & Co. KGaA, 69451 Weinheim, Germany, 2004)

Introduction

Interest in polymetallic cluster complexes of paramagnetic transition metal ions has increased hugely since the discovery of "single-molecule magnets" (SMMs).[1] This remarkable class of molecules displays magnetic bistability that is entirely of a molecular origin, and arises from the combination of a high ground state electron spin (S, resulting from the magnetic exchange interactions between the individual ions within the cluster), and a large negative zero-field splitting (D) within this ground state.[2] The first SMM discovered was the dodecametallic, mixed-valence manganese(III/IV) cluster[1] $[Mn_{12}O_{12}(O_2CMe)_{16}(H_2O)_4]$, trivially known as "Mn12", that has an $S = 10$ ground state. Magnetic hysteresis (due to retention of magnetisation in the absence of an applied magnetic field) in SMMs is only observed below a certain blocking temperature, and in Mn12 this is ca. 4 K − this is still the highest recorded for an SMM. The blocking temperature is controlled in part by the product DS^2. Clearly, if SMMs are to be exploited in, for example, memory devices there is a need to synthesise new SMMs with higher blocking temperatures. Thus, the primary challenge in this field is still the synthesis of new cluster molecules.

The vast majority of paramagnetic cluster compounds have been synthesised by what might be termed "conventional" coordination chemistry techniques − a source of metal ion and bridging and terminal ligands in a common solvent at temperatures limited by the boiling point of that solvent at atmospheric pressure. Although these methods have been superbly successful in producing a bewildering array of clusters (see ref.[3] for a recent review of structures

[a] Department of Chemistry, The University of Manchester, Oxford Road, Manchester M13 9PL, UK
Fax: (internat.) + 44-161-275-4598
E-mail: eric.mcinnes@man.ac.uk

Rebecca Laye has been a post-doctoral researcher with Eric McInnes in the Department of Chemistry at The University of Manchester since 2002. She completed her PhD under the supervision of Prof. Jon A. McCleverty and Prof. Michael D. Ward at the University of Bristol in 2002, and obtained her MChem. in Chemistry at Bristol in 1999. In 2004 she was awarded a Ramsey Fellowship.

Eric McInnes has been a Lecturer in the Department of Chemistry at The University of Manchester since 2000. Prior to this he was a post-doctoral researcher in the School of Chemical Sciences at the University of East Anglia with Prof. Andrew J. Thomson FRS and Prof. Annie K. Powell, and in Manchester with Dr. Frank E. Mabbs and Dr. David Collison. He completed his PhD in 1995 under the supervision of Dr. Lesley J. Yellowlees at the University of Edinburgh, where he also obtained his BSc in 1992.

MICROREVIEWS: This feature introduces the readers to the author's research through a concise overview of the selected topic. Reference to important work from others in the field is included.

with more than 6 metal ions), there is no reason to confine synthetic methods to this limited temperature/pressure regime as this can only limit the range of products available. A few groups have explored higher temperature routes to clusters − for example, high-nuclearity chromium(III) clusters, including very high spin ground state examples,[4] have been made by solid-state thermolysis reactions followed by extraction into a suitable solvent and crystallisation.[5] Although these results demonstrate the possibilities of higher temperature routes, they lack the advantages of solution chemistry, most importantly the direct crystallisation of products. We were inspired by the pioneering work of Zubieta and co-workers in the hydrothermal synthesis of high-nuclearity, high-valent (alkoxo)polyoxovanadates and -molybdates[6] to investigate the use of solvothermal techniques in the synthesis of large paramagnetic clusters of the 1st row transition metal ions. This Microreview summarises the important literature to date, and highlights some of our early successes in this area demonstrating the applicability of these techniques in cluster chemistry of metals across the 1st row, with examples of vanadium(III), chromium(III), manganese(II/III), iron(III) and nickel(II) chemistry, including some of the highest spin ground state molecules known.

Solvothermal Synthesis

Hydrothermal or, more generally, solvothermal techniques involve heating a reaction mixture in a sealed vessel such that reaction temperatures greater than the boiling point of the solvent can be reached (typically between 100 and 250 °C in hydrothermal chemistry), typically under autogenous pressure. [Note that some authors reserve the term hydro(solvo)thermal to refer to supercritical conditions − in this work we merely imply heating beyond the boiling point.] Superheated solvents exhibit (i) reduced viscosity (and therefore enhanced diffusion of chemical species) and (ii) very different solubilising properties (e.g. the dielectric constant of water decreases rapidly with increasing temperature)[7] compared to ambient conditions. These factors can lead to very different chemistry. For example, (ii) can lead to otherwise insoluble reagents being solubilised (which can be exploited to overcome solubility differences between metal salts and ligands), and (i) can lead to enhanced crystal growth from reaction solutions. Furthermore, the temperature regime available in solvothermal techniques, intermediate between low-temperature solution chemistry and high-temperature solid-state chemistry, can favour the formation of metastable kinetic products rather than the thermodynamic products (e.g. metal oxides) favoured at higher temperatures. All these features of hydrothermal chemistry have long been exploited in materials chemistry, e.g. in the preparation of zeolites, and there are several excellent reviews in this area.[7,8] More recently, these techniques have been employed extensively in the synthesis of coordination polymers (or metalorganic frameworks),[9] including magnetic materials.[10]

However, there is much less literature on the solvothermal synthesis of *discrete molecular clusters*, despite the fact that all the above advantages are equally applicable. In particular, the propensity to crystallise products direct from reaction solution is invaluable because product identification in cluster chemistry relies almost entirely on single-crystal X-ray diffraction given the complexity, and unpredictability,[11] of the materials being formed. The literature on solvothermal cluster synthesis is dominated by Zubieta's systematic exploration of the hydrothermal synthesis of polyoxo/alkoxovanadates,[6] although there is also a significant body of work involving metal chalcogenide clusters.[12] Zubieta's work highlights another important advantage of solvothermal conditions for cluster synthesis. From a very simple set of reagents − for example, a source of vanadium(III) (V_2O_3) and vanadium(V) [V_2O_5 or $(NH_4)VO_3$], a bridging ligand (tri- or tetraalcohol, which are readily deprotonated to alkoxides), and a mineraliser salt and source of counterion (alkylammonium halide salt) in superheated water (150−210 °C) − a vast array of vanadium(IV/V) clusters can be formed: for example, $[V_6O_7\{EtC(CH_2O)_3\}_4]^{2-}$ (based on a V_6 octahedron, see Figure 1),[13] $[V_{10}O_{16}\{EtC(CH_2O)_3\}_4]^{2-/4-}$, $[V_{10}O_{13}\{EtC(CH_2O)_3\}_5]^{-}$ (based on V_{10} edge-sharing bioctahedra),[14] and $[V_{16}O_{20}\{CH_2(OH)C(CH_2O)_3\}_8(H_2O)_4]$,[15] amongst many others. Thus, because solvothermal conditions facilitate the isolation of metastable species, the nature of the product (nuclearity, oxidation states, topology) is very sensitive to the specific reaction conditions and there is a vast "parameter space" to explore over and above the obvious variables of reagents and solvent, viz. stoichiometery, temperature, pressure, pH, mineralisers, fill volume of the reaction vessel, etc. O'Hare has also recently highlighted this in hydrothermal syntheses of uranyl-based coordination polymers.[9c]

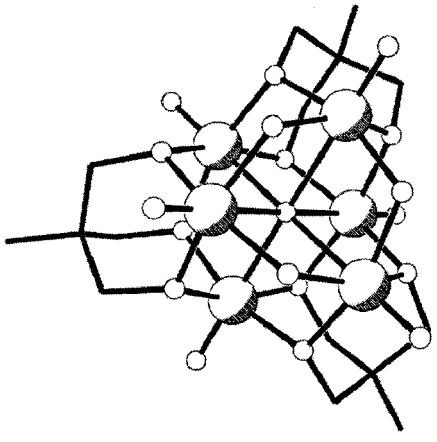

Figure 1. Structure of Zubieta's $[V_6O_7\{MeC(CH_2O)_3\}_4]^{2-}$ anion, after ref.[13]; scheme: V (large shaded circles), O (small open), C (connectivity only), H omitted for clarity

There is now a very large amount of literature on hydrothermally prepared polyoxometallate clusters of the vanadium group − in addition to Zubieta's alkoxide-based work (reviewed in detail elsewhere),[6] there are many polyoxovanadates exploiting inorganic (borate, phosphonate, arsenate, germanate) templates,[16] and several heterometallic vanadate/molybdates[17] and tungstates.[18] (Alkoxo)po-

 © 2004 Wiley-VCH Verlag GmbH & Co. KGaA, Weinheim

lyoxovanadate[19] and -molybdate[20] clusters-of-clusters with nuclearities up to 18 and 42, respectively, have also been prepared by hydrothermally induced condensation of smaller, preformed clusters.

All this work is based on vanadium and molybdenum in the +4 or +5 oxidation state, and even in the fully reduced M^{IV} forms these clusters only have one unpaired electron per metal centre. In our work, where we are targeting very high spin ground state clusters, we require transition-metal ions with several unpaired electrons; thus, we are utilising later transition ions or lower oxidation states of the early transition metals. There are very few solvothermally prepared clusters with later transition ions, but there are a few important examples. Secondary metals − Co^{II}, Mn^{II}, Cu^{II} and Zn^{II} − have been introduced into polyoxovanadates and -molybdates.[21] More significantly in the context of this article, Zubieta has recently extended his poly(alkoxide) work to Fe^{III} in $[\{Fe(OH)(MeCN)_2\}Fe_6OCl_6\{CH_2(OH)C(CH_2O)_3\}_4]$ (based on a face-capped Fe_6 octahedron), $[Fe_{10}O_2Cl_8\{EtC(CH_2O)_3\}_6]$ and the heterometallic $[(VO)_2Fe_8O_2Cl_6\{EtC(CH_2O)_3\}_6]$ (both structurally related to the edge-sharing bioctahedral V_{10} clusters, above) all synthesised from mixtures of $FeCl_2$, V_2O_5 and tri- or tetra-alcohol ligand in MeCN at 120−150 °C.[22] In addition, two hexametallic Co^{II} clusters have been reported by solvothermal routes: Wood et al. prepared the Co_6 ring $[Co_6\{O_3PCH_2N(CH_2CO_2)_2\}_6]^{12-}$ from the potassium salt of the ligand and $Co(NO_3)_2$ in MeOH at 200 °C,[23] while Ōkawa's $[Co_6(OH)_2(phenylcinnamate)_{10}]$ is prepared from the organic acid, $Co(NO_3)_2$ and base in water at 170 °C.[24] It is perhaps significant that several of these latter examples use organic solvents rather than water, as these less polar solvents have been suggested to favour formation of clusters rather than infinite solids under solvothermal conditions,[23] presumably due to the effectively limitless source of O^{2-}/OH^- available in hydrothermal synthesis favouring the formation of polymers.[23]

Our Work

Our rationale was to use the simple triangular clusters $[M_3O(O_2CR)_6L_3]^{n+}$ (Figure 2) as our source of metal ion, in superheated alcohols as solvent and source of bridging ligand. The "basic metal carboxylates"[25] have several advantages as precursors: (i) they are small clusters themselves, (ii) they are known for the 1st row transition metals from vanadium to cobalt, (iii) homovalent M^{III}_3 ($n = 1$) and heterovalent $M^{III}_2M^{II}$ ($n = 0$) triangles are available for V, Mn, and Fe, (iv) heterometallic triangles are known, (v) they can be prepared with a wide range of carboxylates and terminal ligands (L), (vi) the central oxide and bridging carboxylates provide sources of ligands with several potential bridging modes. Hence, these simple metal triangles have been used extensively as precursors to higher nuclearity clusters, particularly with manganese and iron by "conventional" synthetic methods (for example, Mn12 derivatives can be prepared by oxidation of $[Mn_3O(O_2CR)_6L_3]^+$),[1a] and with chromium(III) by high-temperature solid-state routes.[5] There is much less literature[21c,22,23,26] on solvothermal synthesis with alcohols than with water. However, in addition to (perhaps) favouring cluster formation (see above), alcohols obviously provide a source of alkoxide that can bridge in μ_2 and μ_3 modes, thus providing further scope for extensive metal aggregation.

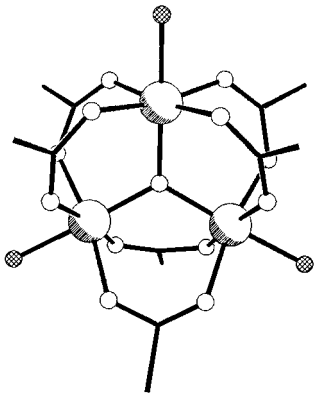

Figure 2. Structure of $[M_3O(O_2CMe)_3L_3]^{+/0}$; scheme: M (large shaded circles), terminal ligands L (cross-hatched circle), others as in Figure 1

Our first efforts employed this simple reaction system of metal triangle in alcohols with no additional source of bridging ligand. For example, reaction of $[Cr_3O(O_2CMe)_6(H_2O)_3]Cl$ in MeOH or EtOH at 200 °C yields the decametallic clusters $[Cr_{10}(OR)_{20}(O_2CMe)_{10}]$, which have a cyclic structure with respect to the metal ions where neighbouring ions are bridged by a μ_2-acetate and two μ_2-alkoxides (Figure 3).[27] Thus, in this example extensive bridging of metal ions has occurred, utilising ligands from both the metal precursor and deprotonated solvent as we had hoped. Furthermore, otherwise identical reactions under reflux only give recrystallised versions of the starting triangle (although Bino has reported that refluxing $[Cr_3O(O_2CMe)_6(H_2O)_3]Cl$ in H_2O yields the octametallic $[Cr_8(OH)_{12}(O_2CMe)_{12}]$)[28]. Therefore, the superheated conditions have allowed us to overcome the kinetic inertness of the Cr^{III} ion to form larger clusters. Alternative routes to Cr^{III} clusters have also been by high temperatures for this reason. For example, heating $[Cr_3O(O_2CCMe_3)_6(H_2O)_3]NO_3$ in the solid state at 300 °C, followed by extraction with and crystallisation from *n*PrOH, gives $[Cr_{12}O_9(OH)_3(O_2CCMe_3)_{15}]$,[5] and refluxing $[Cr_3O(O_2CMe)_6(H_2O)_3]Cl$ in a high-boiling solvent, PhCN at 188 °C, in the presence of 2,2′-bipyridine (bipy) gives the butterfly tetramers $[Cr_4O_2(O_2CMe)_7(bipy)_2]Cl$.[29]

The magnetic properties of the $[Cr_{10}(OR)_{20}(O_2CMe)_{10}]$ clusters are highly unusual.[27] $[Cr_{10}(OEt)_{20}(O_2CMe)_{10}]$ is weakly antiferromagnetically coupled ($J = -0.9$ cm^{-1}), leading to an $S = 0$ ground state. This is the norm for paramagnetic "molecular wheels" in the literature, albeit the magnitude of $|J|$ is small compared to other (octametallic) Cr^{III} examples.[3] However, $[Cr_{10}(OMe)_{20}(O_2CMe)_{10}]$ is weakly ferromagnetically coupled ($J = +4.5$ cm^{-1}). The logical consequence of this is an $S = 15$ ground state, which

 © 2004 Wiley-VCH Verlag GmbH & Co. KGaA, Weinheim

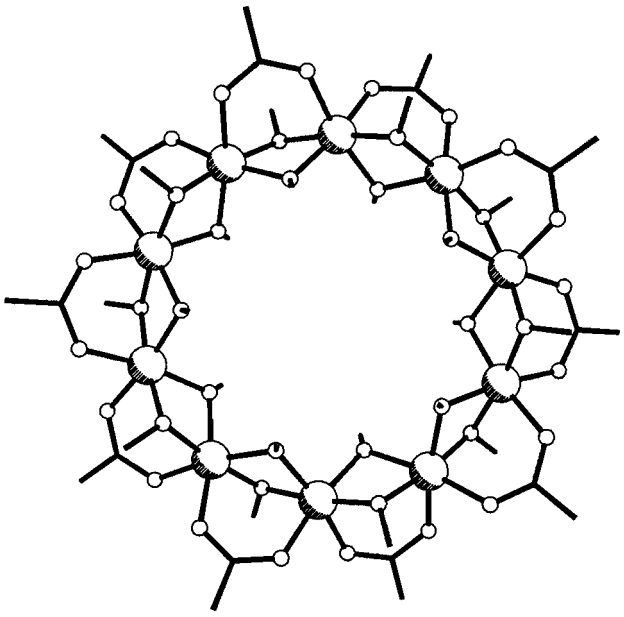

Figure 3. X-ray structure of a molecule of $[Cr_{10}(OMe)_{20}(O_2CMe)_{10}]$; scheme: Cr (large shaded circles), others as in Figure 1

is the highest know for a Cr-based cluster, and among the highest for any metal ion.[30] We have recently confirmed this by inelastic neutron scattering (INS) measurements on $[Cr_{10}(OCD_3)_{20}(O_2CCD_3)_{10}]$,[31] prepared by reaction of $[Cr_3O(O_2CCD_3)_6(H_2O)_3]NO_3$ in CD_3OD at 200 °C. The simplicity of the solvothermal route and the high yield (60−80%) of these clusters is vital in preparing the gram-scale quantities of per-deuterated complex required for INS studies at reasonable cost. This remarkable change from an $S = 0$ to an $S = 15$ ground state by changing the alkoxide bridge is simply a consequence of a small shift in J (ca. 6 cm^{-1}) that happens to cross $J = 0$. The small decrease in the antiferromagnetic contribution to J on changing from OEt to OMe is rationalisable in terms of the decrease in electron density at the bridging atom and consequent poorer overlap of magnetic orbitals, and similar shifts in J have been observed in Cr^{III} dimers.[32] We have now prepared a large family of these compounds $[Cr_{10}(OR)_{20}(O_2CR')_{10}]$ (R′ = Me, Et, $CCMe_3$; R = Me, Et) by the same route, and for each R′ the R = Me species are less antiferromagnetically coupled than the R = Et ones, including a second ferromagnetically coupled example, $[Cr_{10}(OMe)_{20}(O_2CCMe_3)_{10}]$.[31]

The analogous Fe^{III} wheels are known, the first known example being Lippard's $[Fe_{10}(OMe)_{20}(O_2CCH_2Cl)_{10}]$ "ferric wheel",[33] and can be prepared under much more facile conditions reflecting the greater kinetic lability of the ferric ion. Under solvothermal conditions we have only prepared insoluble powders from $[Fe_3O(O_2CMe)_3L_3]X$ in alcohols. Similar results have been reported by others from reactions under reflux − continuous extraction of this mixture is one of the routes to isolating the parent ferric wheel $[Fe_{10}(OMe)_{20}(O_2CMe)_{10}]$.[34] Nevertheless, the isolation of $[M_{10}(OR)_{20}(O_2CR')_{10}]$ with Fe^{III} and Cr^{III} indicates that this should be a stable molecule for a range of M^{III} ions, and indeed we have recently prepared the dark-green V^{III} analogue $[V_{10}(OMe)_{20}(O_2CMe)_{10}]$ by reaction of $[V_3O(O_2CMe)_6(pyridine)_3][ReO_4]$ (we have been exploring perrhenate as a non-explosive analogue of perchlorate) in MeOH at 150 °C (equivalent reactions under reflux only give pale-yellow powders).[35] There is very little V^{III} cluster chemistry in the literature because of the readily oxidisable nature of this ion, and $[V_{10}(OMe)_{20}(O_2CMe)_{10}]$ is the highest nuclearity example reported to date. Here we have exploited the reducing nature of alcohols under solvothermal conditions to stabilise the V^{III} ion − others have used this effect to reduce V^V precursors to make V^{IV} clusters,[36] and V^{III} coordination polymers have also been prepared from VCl_3 under hydrothermal conditions.[37] Similar reactions of $[V_3O(O_2CR')_6L_3]^+$ with carboxylates other than acetate in superheated ROH lead to the formation of the octametallic V^{III} rings $[V_8(OH)_4(OR)_8(O_2CR')_{12}]$ with alternate $(\mu_2\text{-}OH)(\mu_2\text{-}O_2CR')_2$ and $(\mu_2\text{-}OR)_2(\mu_2\text{-}O_2CR')$ bridging (Figure 4) − this is in contrast to the analogous Cr^{III} chemistry where the decametallic wheel is always formed.[35,38] V^{III} clusters are an appealing goal since some V^{III} dimers exhibit very strong ferromagnetic coupling[39] and if this could be introduced into larger clusters it would generate the well-isolated, large spin states necessary for SMM behaviour. Although both the eight and ten-membered V^{III} wheels are antiferromagnetically coupled, the establishment of a reliable synthetic route to high-nuclearity V^{III} clusters is an important step forward.

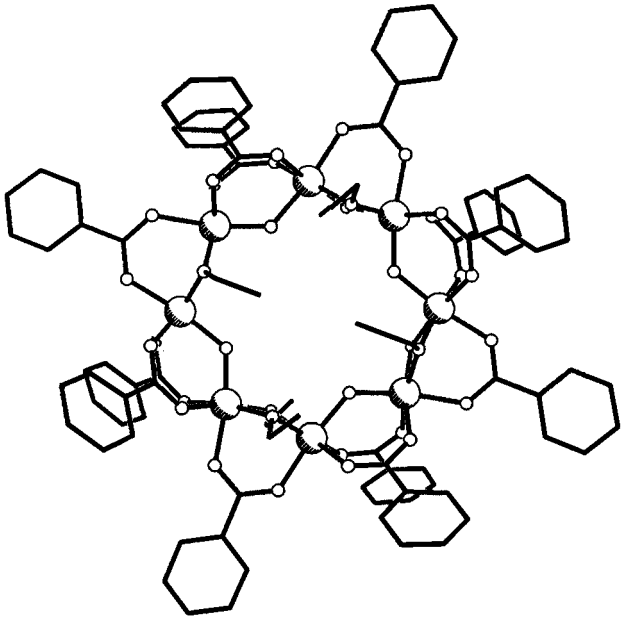

Figure 4. X-ray structure of a molecule of $[V_8(OH)_4(OEt)_8(O_2CPh)_{12}]$; scheme: V (large shaded circles), others as in Figure 1

This simple reaction fails with Mn^{III} for the very reason that it works for V^{III}. The Mn^{III} ions in $[Mn_3O(O_2CR)L_3]X$ (X = anion) are reduced to Mn^{II} in superheated alcohol solutions and only pale-pink solutions are formed. How-

 © 2004 Wiley-VCH Verlag GmbH & Co. KGaA, Weinheim

ever, by changing to a more inert solvent we have shown that solvothermal techniques are also applicable to manganese cluster synthesis. For example, reaction of the mixed-valent $[Mn_3O(O_2CPh)_6(py)_2(H_2O)]$ (py = pyridine) in MeCN at 100 °C gives the hexametallic $[Mn_6O_2(O_2CPh)_{12}(py)_2]$.[40] In contrast to the alcohol-based reactions above, there is very little rearrangement of the precursor, simply a dimerisation of triangle with loss of terminal ligands. The $\{Mn_6O_2\}^{12+}$ core (Figure 5) consists of two planar $\{Mn_3O\}^{6+}$ units linked by four μ_3-carboxylates. Christou has previously shown that the same precursor can undergo thermally induced aggregation by reflux in a relatively high-boiling solvent (PhCN at 188 °C) to give an alternative hexametallic species, $[Mn_6O_2(O_2CPh)_{10}(py)_4]$, based on an edge-sharing bitetrahedral $\{Mn_6O_2\}^{10+}$ core.[41] This higher temperature, but non-solvothermal, reaction has led to more substantial rearrangement, and reduction, of the precursor − the related cluster $[Mn_6O_2(O_2CCMe_3)_{10}(HO_2CCMe_3)_4]$ has also been prepared by reflux in other relatively high-boiling solvents (toluene at 110 °C, dioxane at 100 °C).[42] This illustrates the importance of the temperature regime in cluster formation, and therefore the advantages of the greater range of this parameter in a wider range of solvents afforded by the solvothermal methodology. In this example we have prepared a product of the same nuclearity as higher temperature, non-sovothermal reactions, but with different metal topology and oxidation states. This leads to very different magnetic behaviour − $[Mn_6O_2(O_2CPh)_{10}(py)_4]$ has an S = 0 ground state, while $[Mn_6O_2(O_2CPh)_{12}(py)_2]$ has S = 3 (the parent monomer has an S = 3/2 ground state, so this can be considered as a simple ferromagnetic coupling of the two "halves" in the hexametallic cluster).[40]

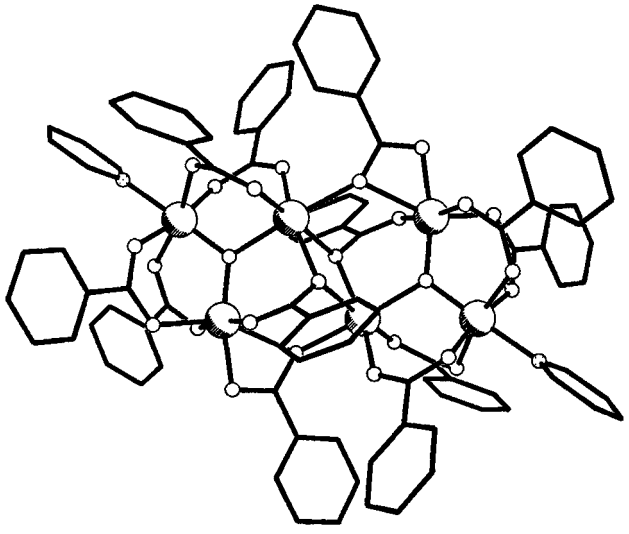

Figure 5. X-ray structure of a molecule of $[Mn_6O_2(O_2CPh)_{12}(py)_2]$; scheme: Mn (large shaded circles), others as in Figure 1

In the examples above we have taken very simple reaction systems involving only a triangular precursor and a solvent. We are now starting to explore analogous reactions but with additional ligands with potential for extensive metal bridging and possible structure-directing properties. For example, we have already shown that reaction of M^{III} acetate triangles in methanol leads to formation of $[M_{10}(OMe)_{20}(O_2CMe)_{10}]$ wheels. If we add an additional ligand which competes with the alkoxides, we should prevent formation of the metal wheels and thus force the formation of clusters of different shape and size. For example, reaction of $[Fe_3O(O_2CMe)_6(H_2O)_3]Cl$ in MeOH at 100 °C, in the presence of benzotriazole (btaH), yields the tetradecametallic Fe^{III} cluster $[Fe_{14}(bta)_6O_6(OMe)_{18}Cl_6]$ (Figure 6).[43] The structure is based on a hexa-capped hexagonal bipyramid of Fe^{III} ions with the caps on alternate faces (Figure 7). The bta^- ligands coordinate in their maximal μ_3-mode to form two $\{Fe_4(bta)_3\}$ moieties (Figure 6b) which sandwich a central Fe_6 ring, bridged by 18 μ_2-methoxides and six μ_4-oxides. The $\{M_4(bta)_3\}$ fragment is well known in M^{II} chemistry in the centred tetrahedral clusters $[M_5(bta)_6(diketonate)_4]$;[44] thus, its formation here is not unexpected and in this case has capped the growth of the iron oxide/alkoxide cluster. However, the absence of carboxylate in the structure is totally unexpected. As with all the reactions above, the product is crystallised directly from the reaction solution. The equivalent reaction under reflux gives only solutions from which we have failed to crystallise any cluster products.

$[Fe_{14}(bta)_6O_6(OMe)_{18}Cl_6]$ has one of the largest ground state spins yet observed, with initial magnetisation data suggesting S = 23 but possibly as high as 25.[43] This higher value can be easily rationalised from competing *anti*ferromagnetic interactions within the cluster: the relative magnitude of the four chemically distinct nearest-neighbour exchange pathways, via μ_2-O(Me) and/or μ_4-O, can be predicted on the basis of the Fe−O−Fe angles (Figure 7). The Fe(apex)−Fe(face cap) (J_1) and Fe(apex)−Fe(ring) (J_3) interactions are expected to be the most antiferromagnetic because of the largest angles, and therefore dominate over the much weaker antiferromagnetic Fe(face cap)−Fe(ring) (J_2) and Fe(ring)−Fe(ring) (J_4) interactions. This would lead to a very simple spin structure in the ground state with the two apical iron ions of the bipyramid "spin up" and all other ions "spin down". Conventional fitting of the experimental magnetic susceptibility data to a spin Hamiltonian to derive the four distinct J values is not possible for this system of 14 S = 5/2 spins. However, density functional theory calculations in tandem with Monte Carlo simulations of the experimental magnetic data to estimate the J values supports this simple model with values of $J_1 = -22$ cm^{-1}, $J_2 = -8.7$ cm^{-1}, $J_3 = -29.7$ cm^{-1} and $J_4 = -3.7$ cm^{-1}.[45] Scheme 1 summarises the clusters prepared above from simple $[M_3O(O_2CR)_6L_3]X$ precursors.

Finally, we give an example of the solvothermal synthesis of a late transition ion cluster, namely nickel(II). The typically large zero-field splitting of Ni^{II} makes this ion a promising building block for SMMs.[46] Since Ni^{II} cannot form M_3 triangles, we have used simple [Ni(diketonate)$_2$] monomers as our precursors − these are known to form heterocubane $[Ni_4(OR)_4(diketonate)_4]$ species in alcohols under

 © 2004 Wiley-VCH Verlag GmbH & Co. KGaA, Weinheim

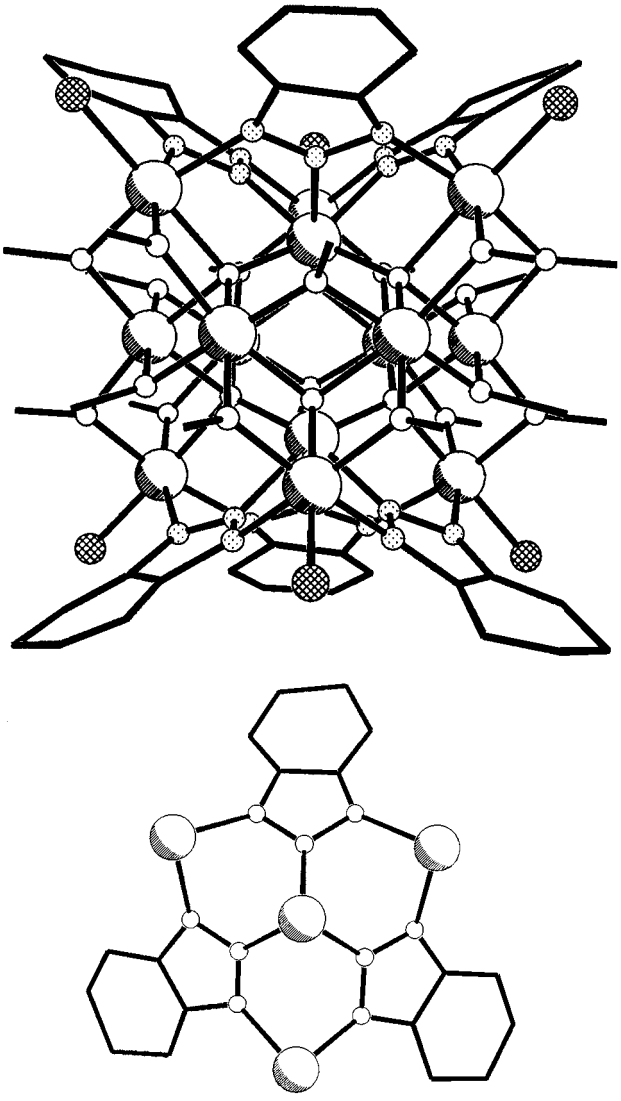

Figure 6. (a) X-ray structure of a molecule of $[Fe_{14}(bta)_6O_6(OMe)_{18}Cl_6]$; (b) the $\{Fe_4(bta)_3\}$ fragment; scheme: Fe (large shaded circles), N (dotted), Cl (cross hatched), others as in Figure 1

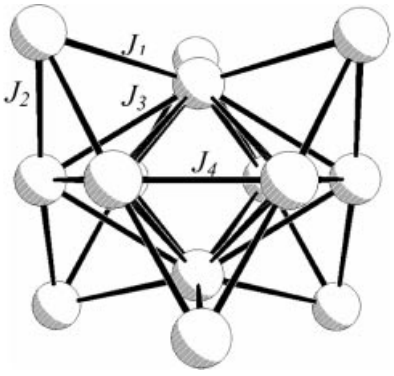

Figure 7. The hexacapped hexagonal-bipyramidal metallic skeleton of $[Fe_{14}(bta)_6O_6(OMe)_{18}Cl_6]$, highlighting the four chemically distinct magnetic exchange interactions

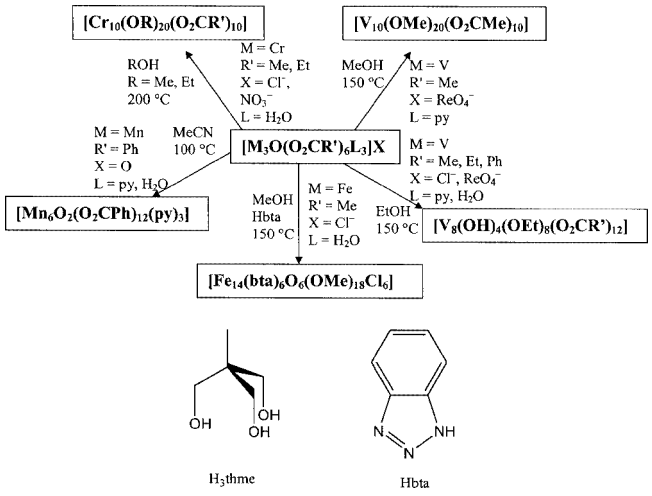

Scheme 1. Summary of clusters prepared solvothermally from $[M_3O(O_2CR)_6L_3]X$ precursors, and structures of the ligands benzotriazole (Hbta) and 1,1,1-tris(hydroxymethyl)ethane (H_3thme)

reflux.[46a] Analogous reactions under solvothermal conditions give identical products. However, in the presence of a competing ligand larger clusters can be obtained. For example, reaction of $[Ni(dbm)_2]$ (Hdbm = dibenzoylmethane) in EtOH at 150 °C with the triol 1,1,1-tris(hydroxymethyl)-ethane (H_3thme) gives the decametallic Ni^{II} cluster $[Ni_{10}(O)(thme)_4(dbm)_4(O_2CPh)_2(EtOH)_6]$ (Figure 8a: note the solvothermal conditions have led to the partial degradation of the diketonate to carboxylate − the cluster can be prepared more rationally with carboxylate as an additional reagent).[47] The analogous reaction under reflux gives only heterocubanes − the solvothermal conditions are essential for preventing the formation of this very stable product. The cluster core is a very regular Ni_{10} supertetrahedron, centred on a μ_6-O, where each (near equilateral) triangular Ni_6 face is bound by a single, fully deprotonated $thme^{3-}$ (Figure 8b). The disposition of the three alkoxide arms of $thme^{3-}$, investigated extensively by Zubieta in polyoxovanadate chemistry (see above), is known to favour the formation of triangular M_3 fragments (with each arm μ_2, the ligand overall being μ_3, for example see Figure 1), which can then condense to form larger clusters (hence the preponderance of clusters based on triangular faces with this ligand − octahedral, edge-sharing bioctahedra, etc.).[6] Hence, this could be anticipated with Ni^{II}. However, the formation of the expanded M_6 triangles, allowing formation of the supertetrahedron, is unprecedented. We have also found that other ligands with a potentially similar trigonal arrangement of alcohol groups can form analogous clusters under solvothermal conditions, e.g. *cis*,*cis*-1,3,5-cyclohexanetriol.[47] The magnetic properties of the Ni_{10} cluster are dominated by the antiferromagnetic exchange interactions across the linear Ni−μ_6-O−Ni groups. Magnetic ordering phenomena below 20 K prevent full characterisation of the molecular behaviour, which is unfortunate because the supertetrahedral topology should lead to extensive spin frustration effects.

 © 2004 Wiley-VCH Verlag GmbH & Co. KGaA, Weinheim

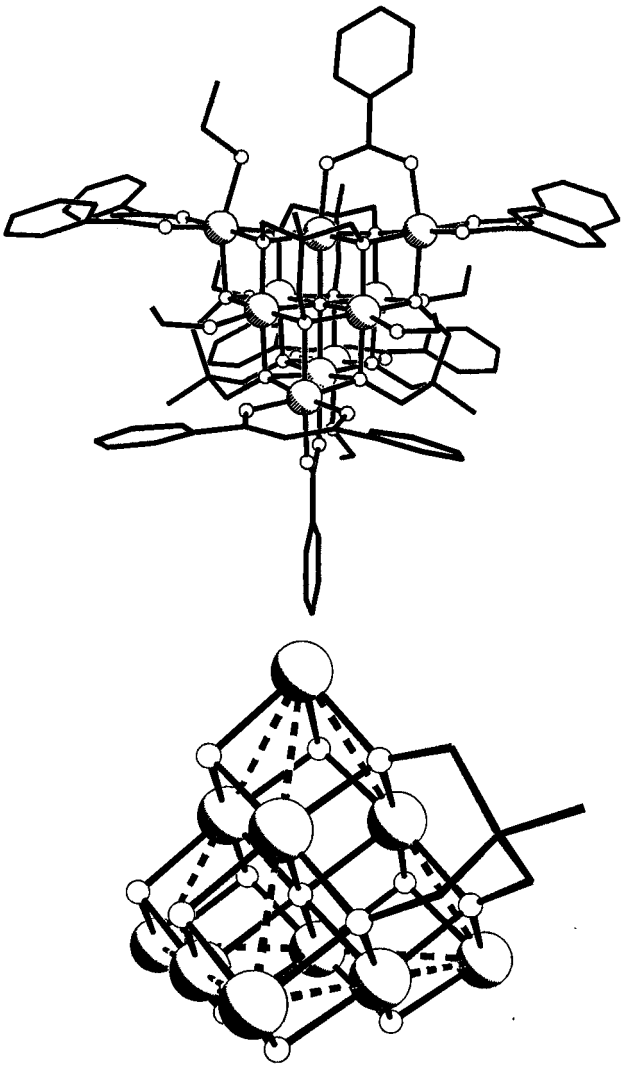

Figure 8. X-ray crystal structure of (a) a molecule of $[Ni_{10}(O)(thme)_4(dbm)_4(O_2CPh)_2(EtOH)_6]$; (b) the Ni_{10} core, highlighting the supertetrahedron and one of the $thme^{3-}$ ligands binding each Ni_6 face; scheme: Ni (large shaded circles), others as in Figure 1

Conclusions

The work above illustrates some of the advantages of solvothermal synthetic techniques in the synthesis of paramagnetic cluster complexes. In every example above, these products are *only* isolated under solvothermal conditions − under less forcing conditions (ambient or under reflux) either no product is isolated or different products are formed. In addition, in each case the products crystallise directly from the reaction solutions as the only solid product, and in the majority of cases in yields of greater than 50% based on total metal content. Over and above these massive advantages, we also have shown examples of exploiting the solvothermal regime (allowing high-temperature reactions in low-boiling solvents) to overcome the kinetic inertness of Cr^{III}, and to isolate clusters in relatively unusual oxidation states such as V^{III} (exploiting the enhanced reducing nature of alcohols under these conditions). Moreover, several of the clusters we are preparing have interesting magnetic properties including some of the highest ground state spins known. Thus, solvothermal techniques will be an important tool in the synthesis of new SMMs and related materials, alongside the more established synthetic routes.

Acknowledgments

We are grateful to The Leverhulme Trust, the EPSRC and the European Community for funding our research, and to several collaborators including Prof. H. U. Güdel (Berne), Prof. R. Sessoli (Firenze), Dr. T. Mallah (Paris-Sud) and Dr. S. Teat (Daresbury). The benzotriazole and triol work is the result of collaboration with our colleagues Dr. E. K. Brechin and Dr. D. Collison at Manchester.

[1] [1a] R. Sessoli, H.-L. Tsai, A. R. Schake, S. Wang, J. B. Vincent, K. Folting, D. Gatteschi, G. Christou, D. N. Hendrickson, *J. Am. Chem. Soc.* **1993**, *115*, 1804. [1b] R. Sessoli, D. Gatteschi, A. Caneschi, M. A. Novak, *Nature* **1993**, *365*, 141.
[2] R. Sessoli, D. Gatteschi, *Angew. Chem. Int. Ed.* **2003**, *42*, 268; *Angew. Chem.* **2003**, *115*, 278.
[3] R. E. P. Winpenny, *Adv. Inorg. Chem.* **2001**, *52*, 1.
[4] D. Collison, M. Murrie, V. S. Oganesyan, S. Piligkos, N. R. J. Poolton, G. Rajaraman, G. M. Smith, A. J. Thomson, G. A. Timko, W. Wernsdorfer, R. E. P. Winpenny, E. J. L. McInnes, *Inorg. Chem.* **2003**, *42*, 5293.
[5] [5a] A. S. Batsanov, G. A. Timko, Y. T. Struchkov, N. V. Gérbéléu, K. M. Indrichan, *Koord. Khim.* **1991**, *17*, 662. [5b] F. E. Mabbs, E. J. L. McInnes, M. Murrie, S. Parsons, G. M. Smith, C. C. Wilson, R. E. P. Winpenny, *Chem. Commun.* **1999**, 643. [5c] I. M. Atkinson, C. Benelli, M. Murrie, S. Parsons, R. E. P. Winpenny, *Chem. Commun.* **1999**, 285.
[6] M. I. Khan, J. Zubieta, *Prog. Inorg. Chem.* **1995**, *43*, 1.
[7] A. Rabenau, *Angew. Chem. Int. Ed. Engl.* **1985**, *24*, 1026; *Angew. Chem.* **1985**, *97*, 1017.
[8] [8a] For example, see: G. Demazeau, *J. Mater. Chem.* **1999**, *9*, 15; J. Gopalakrishnan, *Chem. Mater.* **1995**, *7*, 1265. [8b] J. Livage, *Coord. Chem. Rev.* **1998**, *178−180*, 999. [8c] A. Stein, S. W. Keller, T. E. Mallouk, *Science* **1993**, *259*, 1558. [8d] R. I. Walton, *Chem. Soc. Rev.* **2002**, *31*, 230. [8e] M. Figlarz, *Chem. Scr.* **1988**, *28*, 3.
[9] For example, see: [9a] R. C. Haushlater, K. G. Strohmaier, F. W. Lai, *Science* **1989**, *246*, 1289. [9b] G. M. Yaghi, H. Li, *J. Am. Chem. Soc.* **1995**, *117*, 10401. [9c] M. B. Doran, A. J. Norquist, D. O'Hare, *Inorg. Chem.* **2003**, *42*, 6968.
[10] For example, see: [10a] S. O. H. Gutschke, D. J. Price, A. K. Powell, P. T. Wood, *Angew. Chem. Int. Ed.* **2001**, *40*, 1920; *Angew. Chem.* **2001**, *113*, 1974. [10b] A. Rujiwatra, C. J. Kepert, M. J. Rossiensky, *Chem. Commun.* **1999**, 2307. [10c] R. Kuhlman, G. L. Schimek, J. L. Kolis, *Inorg. Chem.* **1998**, *38*, 194.
[11] R. E. P. Winpenny, *J. Chem. Soc., Dalton Trans.* **2002**, 1.
[12] For examples see: [12a] J.-H. Liao, M. G. Kantzidis, *J. Am. Chem. Soc.* **1990**, *112*, 7400. [12b] P. T. Wood, W. T. Pennington, J. W. Kolis, B. Wu, C. J. O'Connor, *Inorg. Chem.* **1993**, *32*, 129. [12c] B. K. Das, M. G. Kanatzidis, *J. Organomet. Chem.* **1996**, *513*, 1; S. D. Huang, C. P. Lai, C. L. Barnes, *Angew. Chem. Int. Ed. Engl.* **1997**, *36*, 1854; *Angew. Chem.* **1997**, *109*, 1961. [12d] G.-C. Guo, T. C. W. Mak, *J. Chem. Soc., Dalton Trans.* **1997**, 709. [12e] W. Bensch, C. Näther, M. Schur, *Chem. Commun.* **1997**, 1773. [12f] B. K. Das, M. G. Kanatzidis, *Polyhedron* **2000**, *19*, 1995. [12g]M. Emirdag-Eanes, J. A. Ibers, *Inorg. Chem.* **2002**, *41*, 6170; and references cited therein.
[13] [13a] M. I. Khan, Q. Chen, J. Zubieta, D. P. Goshorn, *Inorg. Chem.* **1992**, *31*, 1556. [13b] M. I. Khan, Q. Chen, J. Höpe, S. Parkin, C. J. O'Connor, J. Zubieta, *Inorg. Chem.* **1993**, *32*, 2929.

 © 2004 Wiley-VCH Verlag GmbH & Co. KGaA, Weinheim

[14] [14a] M. I. Khan, Q. Chen, D. P. Goshorn, H. Hope, S. Parkin, J. Zubieta, *J. Am. Chem. Soc.* **1992**, *114*, 3341. [14b] M. I. Khan, Q. Chen, D. P. Goshorn, J. Zubieta, *Inorg. Chem.* **1993**, *32*, 672.
[15] M. I. Khan, Y.-S. Lee, C. J. O'Connor, J. Zubieta, *J. Am. Chem. Soc.* **1994**, *116*, 5001.
[16] For example: [16a] G. Huan, A. J. Jacobson, V. W. Day, *Angew. Chem. Int. Ed. Engl.* **1991**, *30*, 422. [16b] J. Salta, Y.-D. Chang, J. Zubieta, *J. Chem. Soc., Chem. Commun.* **1994**, 1039. [16c] J. T. Rijssenbeek, D. J. Rose, R. C. Haushalter, J. Zubieta, *Angew. Chem. Int. Ed. Engl.* **1997**, *36*, 1008; *Angew. Chem.* **1997**, *109*, 1049. [16d] Y.-M. Chen, E.-B. Wang, B.-Z. Lin, S.-T. Wang, *Chem. Commun.* **2003**, 519.
[17] Y. Zhang, R. C. Haushalter, A. Clearfield, *J. Chem. Soc., Chem. Commun.* **1995**, 1149.
[18] M. I. Khan, S. Cevik, R. J. Doedens, Q. Shen, S. Li, C. J. O'Connor, *Inorg. Chim. Acta* **1998**, *277*, 69.
[19] Q. Chen, J. Zubieta, *Angew. Chem. Int. Ed. Engl.* **1993**, *32*, 261; *Angew. Chem.* **1993**, *105*, 304.
[20] [20a] M. I. Khan, J. Zubieta, *J. Am. Chem. Soc.* **1992**, *114*, 10058. [20b] M. I. Khan, Q. Chen, J. Salta, C. J. O'Connor, J. Zubieta, *Inorg. Chem.* **1996**, *35*, 1880.
[21] [21a] Y. Zhang, P. J. Zapf, L. M. Meyer, R. C. Haushalter, J. Zubieta, *Inorg. Chem.* **1997**, *36*, 2159. [21b] C.-M. Liu, S. Gao, H.-M. Hu, Z.-M. Wang, *Chem. Commun.* **2001**, 1636. [21c] M. I. Kahn, S. Tabussum, R. J. Doedens, *Chem. Commun.* **2003**, 532. [21d] R. S. Rarig, Jr, L. Bewley, V. Golub, C. J. O'Connor, J. Zubieta, *Inorg. Chem. Commun.* **2003**, *6*, 539.
[22] R. C. Finn, J. Zubieta, *J. Cluster Sci.* **2000**, *11*, 4.
[23] S. O. H. Gutshke, D. J. Price, A. K. Powell, P. T. Wood, *Angew. Chem. Int. Ed.* **1999**, *38*, 1088; *Angew. Chem.* **1999**, *111*, 1158.
[24] H. Kumagai, Y. Oka, S. Katawa, M. Ohba, K. Inoue, M. Kurmoo, H. Ōkawa, *Polyhedron* **2003**, *22*, 1917.
[25] R. D. Cannon, R. P. White, *Prog. Inorg. Chem.* **1988**, *36*, 195.
[26] J. Spandl, C. Faniel, I. Brüdgam, H. Hartl, *Angew. Chem. Int. Ed.* **2003**, *42*, 1163; *Angew. Chem.* **2003**, *115*, 1195.
[27] E. J. L. McInnes, C. A. Anson, A. K. Powell, A. J. Thomson, S. Poussereau, R. Sessoli, *Chem. Commun.* **2001**, 89.
[28] M. Eshel, A. Bino, I. Felner, D. C. Johnston, M. Luban, L. L. Miller, *Inorg. Chem.* **2000**, *39*, 1376.
[29] T. Ellis, M. Glass, A. Harton, K. Folting, J. C. Huffman, J. B. Vincent, *Inorg. Chem.* **1994**, *33*, 5522.
[30] [30a] J. C. Goodwin, R. Sessoli, D. Gatteschi, W. Wernsdorfer, A. K. Powell, S. L. Heath, *J. Chem. Soc., Dalton Trans.* **2000**, 1835. [30b] Z. J. Zhong, H. Seino, Y. Mizobe, M. Hidai, A. Fujishima, S. Ohkoshi, K. Hashimoto, *J. Am. Chem. Soc.* **2000**, *122*, 2952. [30c] J. Larianova, M. Gross, M. Pilkington, H. Andres, H. Stoekli-Evans, H. U. Güdel, S. Decurtins, *Angew. Chem. Int. Ed.* **2000**, *39*, 1605; *Angew. Chem.* **2000**, *112*, 1667. [30d] A. J. Tasiopoulos, W. Wernsdorfer, B. Moulton, M. J. Zawortko, G. Christou, *J. Am. Chem. Soc.* **2003**, *125*, 15274.
[31] D. M. Low, G. Rajaraman, R. H. Laye, M. Helliwell, J. van Slageren, R. Sessoli, S. Ochsenbien, H. U. Güdel, E. Ruiz, S. Alvares, G. Timko, E. J. L. McInnes, manuscript in preparation.
[32] [32a] P. J. Hay, J. C. Thilbeault, R. Hoffman, *J. Am. Chem. Soc.* **1975**, *97*, 4884;. [32b] E. D. Estes, R. P. Scaringe, W. E. Hatfield, D. J. Hodgson, *Inorg. Chem.* **1977**, *16*, 1605.
[33] K. L. Taft, C. D. Delfs, G. C. Papaefthymiou, S. Foner, D. Gatteschi, S. J. Lippard, *J. Am. Chem. Soc.* **1994**, *116*, 823.
[34] C. Benelli, S. Parsons, G. A. Solan, R. E. P. Winpenny, *Angew. Chem. Int. Ed. Engl.* **1996**, *35*, 1825; *Angew. Chem.* **1996**, *108*, 1957.
[35] R. H. Laye, M. Murrie, S. Ochsenbein, A. R. Bell, S. J. Teat, J. Raftery, H. U. Güdel, E. J. L. McInnes, *Chem. Eur. J.* **2003**, *9*, 6215.
[36] J. Spandl, I. Brüdgam, H. Hartl, *Angew. Chem. Int. Ed.* **2001**, *40*, 4018; *Angew. Chem.* **2001**, *113*, 4141.
[37] K. Barthelet, J. Marrot, D. Riou, G. Férey, *Angew. Chem. Int. Ed.* **2002**, *41*, 281; *Angew. Chem.* **2002**, *114*, 291.
[38] S. Bartram, R. H. Laye, E. J. L. McInnes, unpublished results.
[39] R. Knopp, K. Wieghardt, B. Nuber, J. Weiss, W. S. Sheldrick, *Inorg. Chem.* **1990**, *29*, 363.
[40] D. M. Low, E. K. Brechin, M. Helliwell, T. Mallah, E. Rivière, E. J. L. McInnes, *Chem. Commun.* **2003**, 2330.
[41] A. R. Schake, J. B. Vincent, Q. Li, P. D. W. Boyd, K. Folting, J. C. Huffman, D. N. Hendrickson, G. Christou, *Inorg. Chem.* **1989**, *28*, 1915.
[42] [42a] A. R. E. Baikie, A. J. Howes, M. B. Hursthouse, A. B. Quick, P. J. Thornton, *J. Chem. Soc., Chem. Commun.* **1986**, 1587. [42b] N. V. Gérbéléu, A. S. Batsanov, G. A. Timko, Y. T. Strutchkov, K. M. Indrichan, G. A. Popovich, *Dokl. Akad. Nauk. SSSR* **1987**, *294*, 256.
[43] D. M. Low, L. F. Jones, A. Bell, E. K. Brechin, T. Mallah, E. Rivière, S. J. Teat, E. J. L. McInnes, *Angew. Chem. Int. Ed.* **2003**, *42*, 3781; *Angew. Chem.* **2003**, *115*, 3911.
[44] [44a] J. Handley, D. Collison, C. D. Garner, M. Helliwell, R. Docherty, J. R. Lawson, P. A. Tasker, *Angew. Chem. Int. Ed. Engl.* **1993**, *32*, 1036; *Angew. Chem.* **1993**, *105*, 1085. [44b] E.G. Bakalbassis, E. Diamantopoulou, S. P. Perlepes, C. P. Raptopoulou, V. Tangoulis, A. Terzis, T. F. Zafiropoulos, *J. Chem. Soc., Chem. Commun.* **1995**, 1347.
[45] G. Rajaraman, J. Cano, E. K. Brechin, E. J. L. McInnes, *Chem. Commun.* **2004**, 1476−1477.
[46] [46a] M. A. Halcrow, J.-S. Sun, J. C. Huffman, G. Christou, *Inorg. Chem.* **1995**, *34*, 4167. [46b] H. Andres, R. Basler, A. J. Blake, C. Cadiou, G. Chaboussant, C. M. Grant, H. U. Güdel, M. Murrie, S. Parsons, C. Paulsen, F. Semadini, V. Villar, W. Wernsdorfer, R. E. P. Winpenny, *Chem. Eur. J.* **2002**, *8*, 4867.
[47] R. Shaw, I. S. Tidmarsh, R. H. Laye, B. Breeze, M. Helliwell, E. K. Brechin, S. L. Heath, M. Murrie, S. Ochsenbein, H. Güdel, E. J. L. McInnes, *Chem. Commun.* **2004**, 1418−1419.

Received March 30, 2004

 © 2004 Wiley-VCH Verlag GmbH & Co. KGaA, Weinheim

An Easy Route to Monofunctionalized Organoimido Derivatives of the Lindqvist Hexamolybdate

Pingfan Wu,[a,c] Qiang Li,[b] Ning Ge,[a] Yongge Wei,*[a] Yuan Wang,[a] Ping Wang,[b] and Hongyou Guo*[b]

Keywords: Organoimido Derivatives / Polyoxometalates / Acid Catalysis / Dehydration / Organic−inorganic hybrid

In the presence of a carbodiimide (DCC) a proton can dramatically speed up the reaction of α-$[Mo_8O_{26}]^{4-}$ with aromatic amines under mild conditions and convenient bench manipulations, which results in the easy synthesis of monofunctionalized organoimido derivatives of $[Mo_6O_{19}]^{2-}$ even bearing an electron-withdrawing group such as bromo or chloro groups.

(© Wiley-VCH Verlag GmbH & Co. KGaA, 69451 Weinheim, Germany, 2004)

Introduction

The surface modification of polyoxometalates, that is, the substitution of a terminal oxo or M=O group with organic species,[1,2] has received increasing interest in recent years because it can afford a way to conveniently and effectively construct novel organic−inorganic hybrid materials[3−9] with the so-called "value-adding properties"[10] and possible synergistic effects.[11] Organoimido derivatives,[8,9,11−24] which were first reported by E. A. Maatta et al.,[15] are amongst the most important organic derivatives of polyoxometalates obtained by surface modification, since the π electrons in the organic component may extend their conjugation to the inorganic framework and thus dramatically modify the electronic structure and redox properties of the corresponding parent polyoxometalates.[10−12] In addition, organoimido derivatives of polyoxometalates with a remote, active functional group may be exploited to prepare covalently-linked nano-dumbbells,[13,14] polymeric chains[9] and even networks of polyoxometalates in more controllable manners.

So far, the synthesis of organoimido derivatives of polyoxometalates has focused mainly on Lindqvist polyoxometalates such as the hexamolybdate ion, $[Mo_6O_{19}]^{2-}$, the hexatungstate ion, $[W_6O_{19}]^{2-}$, and the pentatungstenmolybdate ion, $[MoW_5O_{19}]^{2-}$, obtained by reactions with phosphinimines,[15,16] isocyanates[17−19] or aromatic amines.[20,21] As we know, it is very difficult to prepare organoimido derivatives of polyoxometalates bearing an electron-withdrawing group in reasonable yield and high purity using the three approaches mentioned above. However, one of us, together with his co-workers[22,23] at UMKC, has recently developed an efficient and convenient reaction protocol to give monofunctionalized arylimido derivatives of polyoxometalates with a carbodiimide, that is, DCC (*N*,*N*′-dicyclohexylcarbodiimide), as the dehydrating agent. Furthermore, a first attempt to modify the α-octamolybdate ion, α-$[Mo_8O_{26}]^{4-}$, with this approach resulted in the selective synthesis of bifunctionalized arylimido derivatives of hexamolybdate, in a degradation and re-assembly process, with reasonable yield and high purity.[9] However, under such active reaction conditions, it was still not possible to functionalize polyoxometalates with aromatic amines bearing electron-withdrawing groups, for example, bromo and chloro groups, because of the weak nucleophilicity and easy oxidization of these kinds of amines. In this communication, we report our recent discovery that a proton can dramatically speed up the reaction of α-$[Mo_8O_{26}]^{4-}$ with aromatic amines under much milder conditions and, in the meanwhile, monofunctionalized organoimido derivatives of $[Mo_6O_{19}]^{2-}$, bearing even electron-withdrawing groups such as *para*-chloroaniline, *meta*-chloroaniline, *ortho*-chloroaniline and *para*-bromoaniline, are selectively synthesized in high purity and moderate yield with easy bench manipulations. As examples, the synthesis and structural characterization of five arylimido derivatives, $(Bu_4N)_2[Mo_6O_{18}(=NAR)]$, (where AR = *o*-$CH_3C_6H_4$ **1**, AR = *p*-ClC_6H_4 **2**, AR = *o*-ClC_6H_4 **3**, AR = *m*-ClC_6H_4 **4**, AR = *p*-BrC_6H_4 **5**) will be introduced here.[25]

[a] State Key Laboratory for Structural Chemistry of Unstable and Stable Species, College of Chemistry and Molecular Engineering, Peking University, Beijing 100871, China
Fax: + 86-10-62751708
E-mail: ygwei@pku.edu.cn
[b] Department of Chemistry, Beijing University of Chemical and Technology, Beijing 100029, China
E-mail:guohy@public.fhnet.cn.net
[c] Department of Bioengineering, Hubei Polytechnic University, Wuhan 430068, China

Results and Discussion

When a mixture of $(Bu_4N)_4$·[α-Mo_8O_{26}], an aromatic amine and its hydrochloride salt, and DCC or other carbodiimides is refluxed in anhydrous acetonitrile under nitrogen, the corresponding monofunctionalized organoimido derivative of $[Mo_6O_{19}]^{2-}$ is formed and this reaction is usually complete in about six hours. However, under the same conditions, no anticipatory dehydrating reaction was observed for $(Bu_4N)_2$·$[Mo_6O_{19}]$. Instead, it was reduced, while the aromatic amine was oxidized. The key role of DCC here is to act as a special dehydrating agent with an activating effect on the terminal Mo−O bond, which is similar to its activating effect on the carboxyl group in the synthesis of amide or peptides.[22] In our tests, the amount of DCC is equivalent to, or slightly higher than that of the water needed to be removed from the reaction system because excess DCC usually results in unexpected side reactions and reduces the yield of the products.[22]

It was observed that no hydrochloride salt is present, *o*-toluidine or other active aromatic amines with an electron-donating group, react with α-$[Mo_8O_{26}]^{4-}$ to produce only the bifunctionalized arylimido derivatives of hexamolybdate.[9] On the other hand, under the same conditions, no reaction occurs between α-$[Mo_8O_{26}]^{4-}$ and *para*-chloroaniline or other inert aromatic amines with an electron-withdrawing group, except for the oxidation of the corresponding amines. However, for both types of aromatic amines, the addition of hydrochloride salts to the reaction mixture results in the formation of monofunctionalized organoimido derivatives of hexamolybdate, for instance, **1** and **2**. Moreover, the reaction can be speeded up by increasing the amount of hydrochloride salts. It is also worth pointing out that this novel routine can be carried out even at room temperature. The hydrochloride salt is, in fact, a proton carrier that introduces the proton into the reaction mixture. While more work needs to be done to shed light on the detailed reaction mechanism, the likely role of the proton is to complex with DCC and hence to increase the electrophilic ability of DCC to attack the oxo group of Mo−O. Additionally, it also promotes the conversion of the octamolybdate into the hexamolybdate through a degradation and re-assembly process since in an acidic organic solvent, hexamolybdates and its derivatives are much more stable than octamolybdates.[9]

The optimum reaction conditions, including the amount of each raw material and the reaction time, can be obtained by monitoring the reaction system by TLC, UV or ^{1}H NMR technology and a favorable routine is given in the Exp. Sect. Compared to previous methods presented in the literature,[15−23] this novel reaction route has many advantages: it is faster and is usually complete in less than 6 h, it is more efficient with easy bench manipulations, and the reaction conditions are much milder. Best of all, this approach tolerates electron-withdrawing functional groups such as chloro and bromo. With aromatic amine chlorides or bromides easily accessible, a great number of organoimido derivatives of hexamolybdate bearing halogen groups can now be easily synthesized in reasonable yield. Thus, this reaction opens alternative ways to make organic−inorganic hybrids based on polyoxometalates in a much more controlled fashion.[24] Related work is underway in our laboratory and will be published in subsequent papers.

The composition and structures of compounds **1**, **2**, **3**, **4**, and **5** were initially obtained according to elemental analysis, and IR, ^{1}H NMR, and UV/Vis spectroscopy studies. The IR spectra of the compounds are similar to those of previously reported mono organoimido derivatives, and the strong shoulder peak near 974 cm^{-1} proves them to be the mono-organoimido substitution derivatives.[15,16,21,26] Compared to the ^{1}H NMR spectra of corresponding free amine ligands, the protons of **1**, **2**, **3**, **4**, and **5**, except for those in the tetrabutylammonium cation, all exhibit significantly downfield chemical shifts, indicating that the shielding nature of $[Mo_5O_{18}(Mo{\equiv}N-)]^{2-}$ is much weaker than that of the amino group NH_2-. The fact that the chemical shifts of the aromatic protons in **2**, **3**, **4**, and **5** are higher than in **1** implies that the Mo≡N bond in **2**, **3**, **4**, and **5** is more electron withdrawing than in **1**, which is in good agreement with the electronic character of their imido ligands: **1** has an electron-donating methyl group (CH_3) whereas **2**, **3**, **4**, and **5** have an electron-withdrawing halogen group (Cl or Br). The lowest energy L→M electronic transition at 325 nm in $[Mo_6O_{19}]^{2-}$ is bathochromically shifted by more than 20 nm and becomes considerably more intense in **1** (350 nm), **2** (346 nm), **3** (345 nm), **4** (344 nm), and **5** (345 nm), which indicates that the Mo−N π-bond is formed in these organoimido derivatives. The bathochromic shift on going from **2**, **3**, **4**, and **5** to **1** is consistent with the trend in the π-donor ability of imido ligands.

The molecular structures of **1** and **2** have also been confirmed by single-crystal X-ray diffraction analysis[27] and their cluster anions are shown in Figure 1. In both struc-

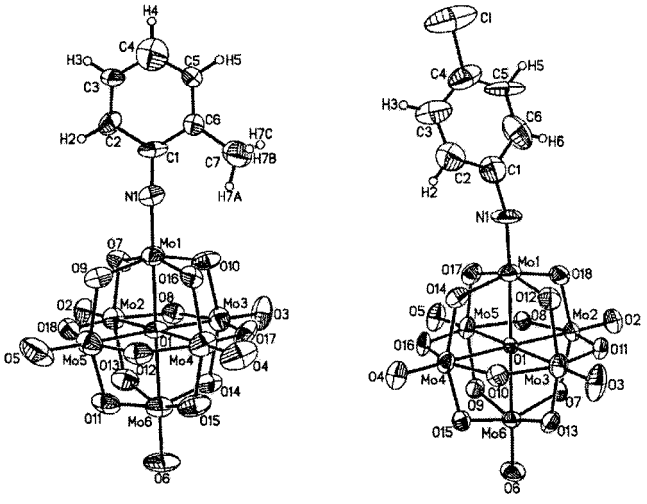

Figure 1. ORTEP drawings of the cluster anions of **1** and **2**

 © 2004 Wiley-VCH Verlag GmbH & Co. KGaA, Weinheim

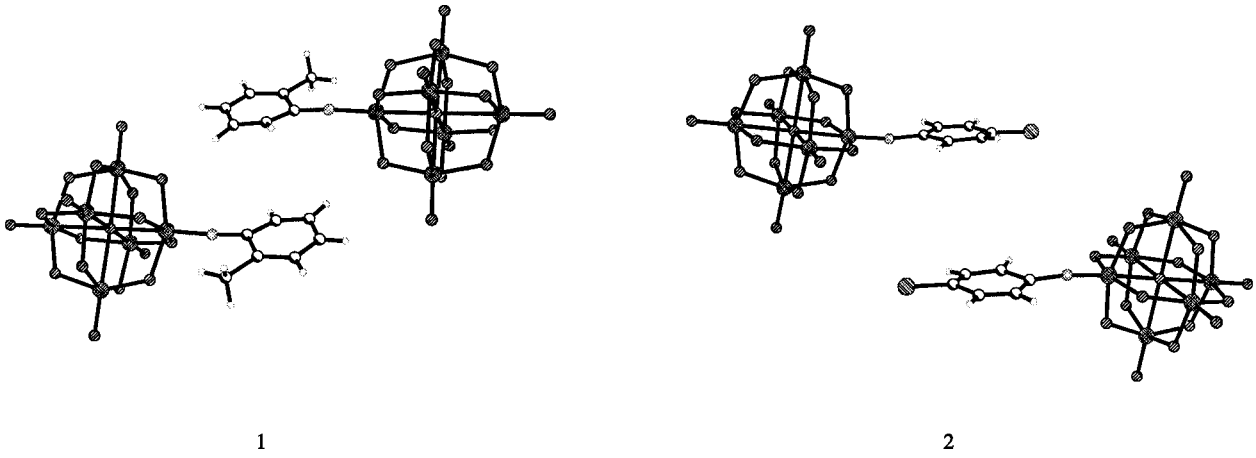

1 **2**

Figure 2. Showing of the dimer structure of cluster anions of **1** and **2**

tures, the arylimido ligands are indeed bound to a terminal position of the hexamolybdate in a monodentate fashion. The short Mo−N bond lengths [1.772(18) Å in **1** and 1.686(5) Å in **2**] and the C−N−Mo bond angles close to 180° (173.9° for **1** and 163.6° for **2**) are typical of organoimido groups bound to an octahedral d^0 metal center and are consistent with a substantial degree of Mo≡N triple bond character.[28] The C(1)−N(1)−Mo(1) bond angle of **2** is in agreement with angles of other derivatives bearing *para*-only-replaced phenylimido ligands and substantially smaller than the angles of **1** and other derivatives bearing *ortho*-replaced phenylimido ligands. Since the shortening of the Mo≡N bond is not observed for *ortho*-replaced phenylimido ligands derivatives, and **2** and other derivatives with *para*-only replaced phenylimido groups all crystallize in the same monoclinic space group of No. 14, this difference is probably due to the force of the crystal packing. Compared to the hexamolybdate and other derivatives, the bond lengths of the five terminal oxo ligands of **1** and **2** do not vary appreciably. The Mo(1)−O(1) distances between the Mo-bearing imido group and the central oxygen atom within the cluster anion cage are both significantly shorter than the other Mo−O(1) distances. An analogous contraction was noticed in the structures of other monofunctionalized imido derivatives of Lindqvist polyoxometalates reported in the literature,[11−24] which implies that there are no appreciable differences in their molecular structures. However, an important feature that should be pointed out here is the dimerization of cluster anions of **1** and **2** in the solid state through the π-π stacking of parallel phenyl rings of two neighboring cluster anions (see Figure 2). The existence of supramolecular π-π interactions between the pairs of cluster anions is clearly indicated by the short vertical phenyl ring separation of 3.136 and 3.796 Å in **1** and **2**, respectively. Such a structural feature has not been mentioned before in the reported mono phenylimido derivatives of hexamolybdate.[11−24]

Conclusion

In summary, we have developed a novel reaction route to give organonimido derivatives of Lindqvist polyoxometalates by introducing a proton. Compared to literature methods, even in the case of aromatic amines with an electron-withdrawing halogen group, this new method allows the reaction to be carried out under much milder conditions, even at room temperature, with much faster reaction rates and reasonable yield. With aromatic amine chlorides or bromides widely accessible and much cheaper than the corresponding iodides, this new approach provides an alternative way to efficiently construct novel, hybrid molecular materials containing covalently-bonded metal−oxygen clusters and organic conjugated segments. Extension of this approach to other polyoxometalates is still under study in our laboratory.

Experimental Section

A typical synthesis is as follows: a mixture of $(Bu_4N)_4$·[α-Mo_8O_{26}] (1.0 mmol), DCC (3.4 mmol), aromatic amine (1.34 mmol) and its salt (1.34 mmol) was refluxed under nitrogen in anhydrous acetonitrile (10 mL) for about 6 h. During the course of the reaction the color of the solution changed into red-brown, and some white precipitates (*N*,*N*′-dicyclohexylurea) were formed. The resulting dark-red solution was cooled down to room temperature and the white precipitates were removed by filtration. While most of the acetonitrile evaporated slowly in the open air, the product precipitated from the filtrate as a red colloid-like solid. The product was collected by filtration, washed successively with EtOH or benzene and Et_2O for several times, and then recrystallized twice from the mixture of acetone and EtOH (1:1), the product deposited as orange crystals usually in moderate yield of ca. 40 to 50 %.

1 (yield, 52 %): $C_{39}H_{79}Mo_6N_3O_{18}$ (1453.7): calcd. C 32.22, H 5.48, N 2.89; found C 32.51, H 5.46, N 2.85. ^{1}H NMR (600 MHz, CD_3CN, 300 K): δ = 0.98 (t, 24 H, CH_3-, $[Bu_4N]^+$), 1.38 (m, 16

 © 2004 Wiley-VCH Verlag GmbH & Co. KGaA, Weinheim

H, -CH_2-, $[Bu_4N]^+$), 1.62 (m, 16 H, -CH_2-, $[Bu_4N]^+$), 2.61 (s, 3 H, CH_3-, CH_3-Ar), 3.12 (t, 16 H, NCH_2-, $[Bu_4N]^+$), 7.26 (m, 1 H, *o*-ArH), 7.21 (m, 2 H, *m*-ArH), 7.04(m, 1 H, *p*-ArH) ppm. IR (KBr pellet, major absorbances): 2961, 2873, 1638, 1619, 1478, 1378, 1323, 1194, 1173, 1118, 1107, 1064, 1027, 997, 952 with shoulder at 973, 883, 794 with shoulder at 710, 661, 599 cm^{-1}. UV/Vis (MeCN): λ_{max}/nm = 235 (3.2×10^4), 245 (3.3×10^4), 350 (2.0×10^4) $\varepsilon/M^{-1}cm^{-1}$. Crystals suitable for single-crystal X-ray diffraction were grown from a mixed solution of acetone and EtOH (1:1).

2 (yield, 45 %): $C_{38}H_{76}ClMo_6N_3O_{18}$ (1474.1): calcd. C 30.96, H 5.20, N 2.85; found C 30.54, H 5.22, N2.49. ^{1}H NMR (600 MHz, CD_3CN, 300 K): δ = 0.98 (t, 24 H, CH_3-, $[Bu_4N]^+$), 1.38 (m, 16 H, -CH_2-, $[Bu_4N]^+$), 1.62 (m, 16 H, -CH_2-, $[Bu_4N]^+$), 3.12 (t, 16 H, NCH_2-, $[Bu_4N]^+$), 7.23, 7.24 (2 H, *o*-H-Ar), 7.40, 7.41 (2 H, *m*-H-Ar) (AA′BB′ "quadruplet', 4 H, Ar) ppm. IR (KBr pellet, major absorbances): 2963, 2874, 1639, 1620, 1473, 1380, 1336, 1171, 1090, 954 with shoulder at 975, 884, 795 with shoulder at 710, 602 with shoulder at 637 cm^{-1}. UV/Vis (MeCN): λ_{max}/nm = 226 (3.5×10^4), 254 (3.5×10^4), 346 (2.2×10^4) $\varepsilon/M^{-1}cm^{-1}$. X-ray quality crystals were obtained from a mixed solution of acetone and EtOH (1:1).

3 (monofunctionalized derivative of *o*-chloroaniline: yield, 50 %): ^{1}H NMR (600 MHz, CD_3CN, 300 K): δ = 0.99 (t, 24 H, CH_3-, $[Bu_4N]^+$), 1.40 (m, 16 H, -CH_2-, $[Bu_4N]^+$), 1.63 (m, 16 H, -CH_2-, $[Bu_4N]^+$), 3.13 (t, 16 H, NCH_2-, $[Bu_4N]^+$), 7.35 (m, 2 H, *p*-H-Ar), 7.47 (m, 2 H, *o*-H-Ar) ppm. UV/Vis (MeCN): λ_{max}/nm = 223, 247, 345.

4 (monofunctionalized derivative of *m*-chloroaniline: yield, 48 %): ^{1}H NMR (600 MHz, CD_3CN, 300 K): δ = 0.99 (t, 24 H, CH_3-, $[Bu_4N]^+$), 1.40 (m, 16 H, -CH_2-, $[Bu_4N]^+$), 1.63 (m, 16 H, -CH_2-, $[Bu_4N]^+$), 3.12 (t, 16 H, NCH_2-, $[Bu_4N]^+$), 7.20(m, 1 H, *m*-*m*-H-Ar), 7.24 (s, 1 H, *o*-*o*-H-Ar), 7.38, 7.39 (d, 2 H, *o*-*p*-H-Ar) ppm. UV/Vis (MeCN): λ_{max}/nm = 225, 248, 344.

5 (monofunctionalized derivative of *p*-bromoaniline: yield, 48 %): ^{1}H NMR (600 MHz, CD_3CN, 300 K): δ = 0.99 (t, 24 H, CH_3-, $[Bu_4N]^+$), 1.40 (m, 16 H, -CH_2-, $[Bu_4N]^+$), 1.63 (m, 16 H, -CH_2-, $[Bu_4N]^+$), 3.12 (t, 16 H, NCH_2-, $[Bu_4N]^+$), 7.14, 7.15 (2 H, *o*-H-Ar), 7.56, 7.57 (2 H, *m*-H-Ar) (AA′BB′ "quadruplet', 4 H, Ar) ppm. UV/Vis (MeCN): λ_{max}/nm = 223, 246, 345.

Acknowledgments

This work is sponsored by NFSC No 20201001, SRF for ROCS of SEM and MOST No TG2000077503. It is also partially supported by the university funding from Hubei Polytechnic University. Y. W. also thanks Prof. Peng for professional support when he was at UMKC.

[1] *Polyoxometalates: From Platonic Solids to Anti-Retroviral Activity* (Eds.: M. T. Pope, A. Müller), Kluwer, Dordrecht, 1994.
[2] P. Gouzerh, A. Proust, *Chem. Rev.* **1998**, *98*, 77.
[3] P. Judeinstein, *Chem. Mater.* **1992**, *4*, 4.
[4] C. R. Mayer, V. Cabuil, T. Lalot, R. Thouvenot, *Angew. Chem.* **1999**, *111*, 3878; *Angew. Chem. Int. Ed.* **1999**, *38*, 3672.
[5] R. C. Schroden, C. F. Blanford, B. J. Melde, B. J. S. Johnson, A. Stein, *Chem. Mater.* **2001**, *13*, 1704.
[6] H. Zeng, G. R. Newkome, C. L. Hill, *Angew. Chem.* **2000**, *112*, 1841; *Angew. Chem. Int. Ed.* **2000**, *39*, 1771.
[7] A. Dolbecq, P. Mialane, L. Lisnard, J. Marrot, F. Sécheresse, *Chem. Eur. J.* **2003**, *9*, 2914.
[8] A. R. Moore, H. Kwen, A. B. Beatty, E. A. Maatta, *Chem. Commun.* **2000**, 1793.
[9] L. Xu, M. Lu, B. Xu, Y. Wei, Z. Peng, D. R. Powell, *Angew. Chem.* **2002**, *114*, 4303; *Angew. Chem. Int. Ed.* **2002**, *41*, 4129.
[10] D. E. Katsouli, *Chem. Rev.* **1998**, *98*, 359.
[11] J. L. Stark, V. G. Young Jr., E. A. Maatta, *Angew. Chem.* **1995**, *107*, 2751; *Angew. Chem. Int. Ed. Engl.* **1995**, *34*, 2547.
[12] J. B. Strong, G. P. A. Yap, R. Ostrander, L. M. Liable-Sands, A. L. Rheingold, R. Thouvenot, P. Gouzerh, E. A. Maatta, *J. Am. Chem. Soc.* **2000**, *122*, 639.
[13] J. L. Stark, A. L. Rheingold, E. A. Maatta, *J. Chem. Soc., Chem. Commun.* **1995**, 1165.
[14] M. Lu, Y. Wei, B. Xu, C. F.-C. Cheung, Z. Peng, D. R. Powell, *Angew. Chem.* **2002**, *114*, 1636; *Angew. Chem. Int. Ed.* **2002**, *41*, 1566.
[15] Y. Du, A. L. Rheingold, E. A. Maatta, *J. Am. Chem. Soc.* **1992**, *114*, 345.
[16] A. Proust, R. Thouvenot, M. Chaussade, F. Robert, P. Gouzerh, *Inorg. Chim. Acta* **1994**, *224*, 81.
[17] W. Clegg, R. J. Errington, K. A. Fraser, C. Lax, D. G. Richards, *Polyoxometalates: From Platonic Solids to Anti-Retroviral Activity* (Eds.: M. T. Pope, A. Müller), Kluwer, Dordrecht, 1994, p 113.
[18] J. B. Strong, R. Ostrander, A. L. Rheingold, E. A. Maatta, *J. Am. Chem. Soc.* **1994**, *116*, 3601.
[19] T. R. Mohs, G. P. A. Yap, A. L. Rheingold, E. A. Maatta, *Inorg. Chem.* **1995**, *34*, 9.
[20] W. Clegg, R. J. Errington, K. A. Fraser, S. A. Holmes, A. Schäfer, *Chem. Commun.*1995, 455.
[21] R. A. Roesner, S. C. McGrath, J. T. Brockman, J. D. Moll, D. X. West, J. K. Swearingen, A. Castineiras, *Inorg. Chim. Acta* **2003**, *342*, 37.
[22] Y. Wei, B. Xu, C. L. Barnes, Z. Peng, *J. Am. Chem. Soc.* **2001**, *123*, 4083.
[23] Y. Wei, L. Meng, C. F.-C. Cheung, C. L. Barnes, Z. Peng, *Inorg. Chem.* **2001**, *40*, 5489.
[24] B. Xu, Y. Wei, C. L. Barnes, Z. Peng, *Angew. Chem.* **2001**, *113*, 2353; *Angew. Chem. Int. Ed.* **2001**, *40*, 2290.
[25] Coupound **2** has been reported briefly without detailed synthesis and characterization by A Proust et al. (see reference[1], p 34).
[26] W. Nugent, J. E. Mayer, *Metal-Ligand Multiple Bonds*, Wiley, New York, 1988, p 123−125.
[27] Crystal structure data for **1**: C_{39} H_{79} Mo_6 N_3 O_{18}, M_r = 1453.69, triclinic, $P\bar{1}$, a = 12.266(3), b = 12.337(3), c = 19.788(4) Å, α = 105.98(3), β = 97.55(3), γ = 98.44(3)°, V = 2800.6(10) Å^3, Z = 2, $\rho_{calcd.}$ = 1.724 Mg/m^3, T = 293(2) K, $R1$= 0.0661, and $wR2$ = 0.1416 with GOF = 0.718. Crystal structure data for **2**: C_{38} H_{76} Cl Mo_6 N_3 O_{18}, M_r = 1474.11, monoclinic, $P2_1/n$, a = 17.615(4), b = 17.623(4), c = 19.284(4) Å, β = 114.35(3)°, V = 5453.5(19) Å^3, Z = 4, $\rho_{calcd.}$ = 1.795 Mg/m^3, T = 293(2)K, $R1$ = 0.0441, and $wR2$ = 0.0783 with GOF = 0.803. CCDC-217580 and -217581 contain the supplementary crystallographic data for compounds **2** and **1**, respectively. These data can be obtained free of charge at www.ccdc.cam.ac.uk/conts/retrieving.html (or from the Cambridge Crystallographic Data Center, 12 Union Road, Cambridge CB 21EZ,UK; Fax: (internat.) + 44-1223-336-033; E-mail: deposit@ccdc.cam. ac.uk).
[28] D. E. Wigley, *Prog. Inorg. Chem.* **1992**, *42*, 239.

Received February 25, 2004

 © 2004 Wiley-VCH Verlag GmbH & Co. KGaA, Weinheim

Structural Characterization of Bismuth(III) and Antimony(III) Chlorotriflates: Key Intermediates in Catalytic Friedel–Crafts Transformations

Stéphane Mazières,*[a] Christophe Le Roux,*[a] Magali Peyronneau,[a] Heinz Gornitzka,[a] and Nicolas Roques[b]

Keywords: Bismuth / Antimony / Triflate / X-ray diffraction / Friedel–Crafts reactions

Chlorotriflates of antimony and bismuth $Cl_nM(OSO_2CF_3)_{3-n}$ (n = 1 or 2) are believed to be metallic intermediates of major importance in Friedel–Crafts reactions that use $Bi(OSO_2CF_3)_3$, $Sb(OSO_2CF_3)_3$, the systems $BiCl_3/CF_3SO_2OH$ or $SbCl_3/CF_3SO_2OH$ as catalysts. Unknown until now, the compounds $ClBi(OSO_2CF_3)_2$ (**1**) and $Cl_2Sb(OSO_2CF_3)$ (**2**) have been synthesized by reaction of MCl_3 (M = Bi, Sb) with triflic acid. After crystallization from THF, **1** and **2** were investigated in the solid state by X-ray crystallography. Their use as catalysts in benzoylation of toluene, acylation of *m*-xylene, and sulfonylation of toluene led to conclusive results, thus giving weight to their key role as intermediates in Friedel–Crafts reactions.
(© Wiley-VCH Verlag GmbH & Co. KGaA, 69451 Weinheim, Germany, 2004)

Introduction

The number of bismuth compounds structurally characterized by X-ray crystallographic methods has greatly increased over the past decades, showing the growing interest in these structures.[1] For our topic, we will focus on Bi^{III} and also Sb^{III} halides, which are found to be useful in a number of applications;[2] of major interest is the use of bismuth or antimony derivatives in catalysis. For Friedel–Crafts acylations, reactions which are mainly developed on an industrial scale using at least a stoichiometric amount of a Lewis acid such as $AlCl_3$ or $TiCl_4$,[3] $BiCl_3$ and recently bismuth(III) trifluoromethanesulfonate (triflate) appeared to be among the best catalysts for the acylation of aromatic compounds.[4–6] In 1988, Olah had already showed the catalytic activity of boron(III), aluminium(III) and gallium(III) triflates in alkylation and acylation reactions with 50mol % metallic triflates.[7] Later various metallic salts of triflic acid such as rare earth[8–11] and antimony(III) triflates[12,13] were reported. The catalytic efficiency of bismuth(III) triflate was confirmed, especially in the sulfonylation of arenes,[14] a reaction that belongs to the most important group of aromatic electrophilic substitutions.[3,4] In the present work we describe the preparation of mixed chlorotriflates of bismuth and antimony, which are involved in the process of acylation and sulfonylation of aromatic compounds that use Bi^{III} and Sb^{III} triflate based catalysts, and their direct use as catalysts in these reactions.

[a] Laboratoire Hétérochimie Fondamentale et Appliquée, UMR 5069,
118 route de Narbonne, 31062 Toulouse Cedex 04, France
Fax: (internat.) +33-5-61-558204
E-mail: mazieres@chimie.ups-tlse.fr
[b] Rhodia Organique Fine, Centre de Recherche de Lyon,
85 rue des frères Perret, 69192 Saint-Fons, France

Results and Discussion

In the mechanism for both acylation and sulfonylation reactions,[6,8–13] it clearly appears that the main electrophilic agent is a mixed anhydride such as trifluoromethanesulfonic carboxylic- or trifluoromethanesulfonic arenesulfonic anhydrides ($RCO-O-SO_2CF_3$ or $ArSO_2-O-SO_2CF_3$), which are known to be strong acylating or sulfonylating reagents.[15] The formation of mixed anhydrides results from ligand exchanges at the metal (Scheme 1, path a).

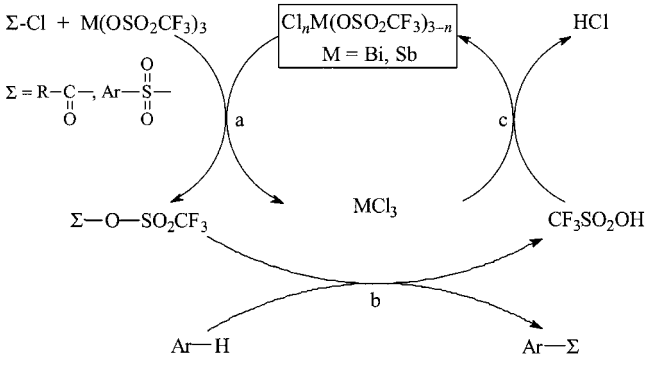

Scheme 1

Following the formation of the anhydride and its reaction with the aromatic compound (Scheme 1, path b), the

mechanism involves the reaction of the metal(III) chloride with triflic acid (CF_3SO_2OH), leading to the mixed metallic intermediate (Scheme 1, path c). The metal acts as a shuttle for the triflic acid. Such types of mixed compounds have been previously related with fluorosulfonic acid and result from the reaction of $BiCl_3$ and fluorosulfonic acid; however, they have been poorly characterized.[16] In fact, it appears that these metallic intermediates play a key role with regard to the entire mechanism. Until now their existence was postulated,[8–13] but no real proof was given for their exact structure. One goal was to isolate such mixed metallic chlorotriflates. The reaction between the metal(III) chloride and an excess of triflic acid did not lead to metal tristriflate[17] but to compounds **1** and **2** in appreciable yields (Scheme 2).

$$MCl_3 + x\,CF_3SO_2OH \xrightarrow[110\ ^\circ C]{C_6H_5CH_3} Cl_nM(OSO_2CF_3)_{3-n}$$

M = Bi, Sb $x > 3$ $n = 1$: M = Bi **1** (89%) $n = 2$: M = Sb **2** (61%)

Scheme 2

With bismuth, the only product is the chlorobistriflate **1**, while antimony leads exclusively to the dichlorotriflate **2**. It appears that the trifluoromethanesulfonate ligand exhibits a strong electronic effect, which modifies the strength of the remaining M–Cl bonds. Only one ligand exchange occurred with antimony, while two with bismuth. **1** is stable up to 250 °C,[18] and this thermostability can indicate the strength of the bonds involved.

In the synthesis of these compounds, the use of toluene as solvent proved to be crucial; while $BiCl_3$ is mainly soluble in π-donor solvents, the solvation of $SbCl_3$ with donor solvents can be greatly compromised by strong complexation, which inhibits further reactivity. Indeed, these complexes known as Mentshutkin complexes[19,20] are responsible for the inefficiency of $SbCl_3$ in the catalysis of Friedel- Crafts reactions of activated aromatics.[21] Compounds **1** and **2** are crystalline, and their THF adducts were obtained from a THF/pentane solution. Single crystals suitable for an X-ray structure determination were grown at −20 °C.

The structure analysis of the THF complexes in the solid state shows a monomeric form in the case of the bismuth compound and a dimeric form for the antimony compound (Figure 1 and Figure 2). In both compounds, primary M–Cl bonds (Bi–Cl1 2.465 Å and Sb–Cl1 2.362 Å, Sb–Cl2 2.363 Å) appear shorter than M–Cl bond lengths in MCl_3 or MCl_3 with oxygen donor interactions;[22] this is in accordance with the observed stability of these M–Cl bonds. For the THF adduct of **1**, the chlorine atom, in good approximation, occupies the axial position of a distorted pentagonal bipyramid (Figure 1).

The two triflate ligands are connected to the bismuth atom through oxygen atoms, Bi–O1 2.386 Å and Bi–O4 2.613 Å, the latter bond length is longer, probably due to another weak interaction (Bi–O5 2.879 Å) which destroys the ideal geometry of the bipyramid.

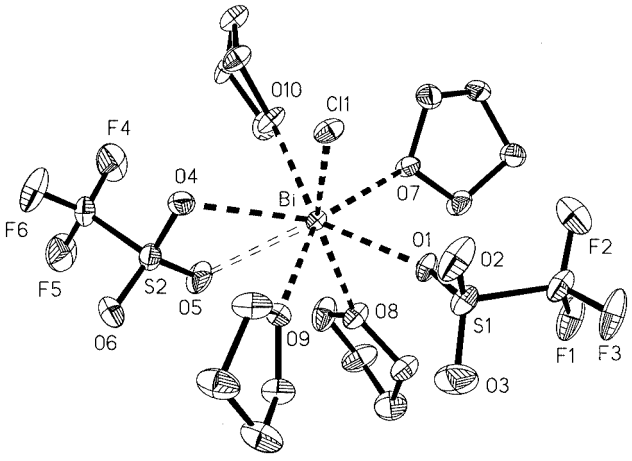

Figure 1. Molecular structure of **1**·4THF in the solid state; selected distances (Å) and angles (°): Bi–Cl1 2.465(4), Bi–O1 2.386(11), Bi–O4 2.613(13), Bi–O5 2.879(15), Cl1–Bi–O8 156.4(3), Cl1–Bi–O4 80.4(3), Cl1–Bi–O5 131.2(3)

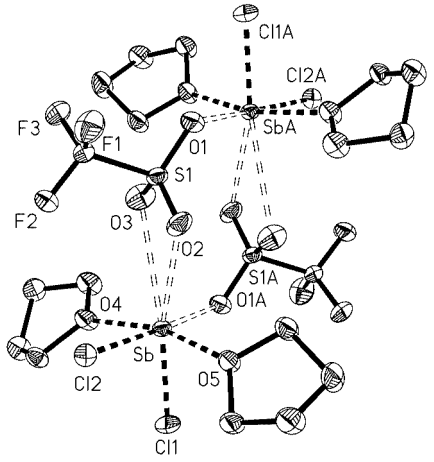

Figure 2. Molecular structure of **2**·2THF in the solid state; selected distances (Å) and angles (°): Sb–Cl1 3.3628(8), Sb–Cl2 2.3629(8), Sb–O1A 2.876(3), Sb–O2 2.911(3), Sb–O3 3.084(3), Cl1–Sb–Cl2 92.75(3), Cl1–Sb–O1A 82.57(5), Cl1–Sb–O2 158.83(5), Cl1–Sb–O3 153.55(5)

The structure of the THF adduct of **2** may be best described as a distorted octahedron in which one SO_2 group occupies an axial position (Figure 2). This structure is associated into dimeric units through two weak coordinations by two triflate ligands of different units thereby bridging the two Sb centers. The antimony atoms are thus seven-coordinate.

These newly synthesized and fully characterized mixed chlorotriflates are believed to be the mixed metallic intermediates involved in the mechanism, but nothing is known about the real mixture in solution during the process. By changing the stoichiometry of the reactants, triflic acid and metal chloride, it was not possible to isolate or even characterize $Cl_2Bi(OSO_2CF_3)$ or $ClSb(OSO_2CF_3)_2$ in solution; this is probably due to their lack of stability. In both cases we only obtained products **1** and **2**.

Finally, experiments were performed in which **1** and **2** were used as catalysts in benzoylation, acylation and sulfon-

 © 2004 Wiley-VCH Verlag GmbH & Co. KGaA, Weinheim

Table 1. Catalytic activity of **1** and **2** in benzoylation, acylation and sulfonylation reactions

Entry	Reaction	Catalyst	Mol (%)	Yield (%)	*o*/*m*/*p*
1	benzoylation of toluene	$Bi(OSO_2CF_3)_3$	10	95[6]	22/2/76
2		**1**	10	60	21/2/77
3	acylation of *m*-xylene	$Sb(OSO_2CF_3)_3$	10	77[13]	
4		**2**	30	74	
5	sulfonylation of toluene	**1**	5	99	39/6/55
6		$BiCl_3/CF_3SO_2OH$	5/10	95[23]	39/6/55
7		**2**	5	99	40/6/54
8		$SbCl_3/CF_3SO_2OH$	5/5	99	38/6/56

ylation of aromatic compounds (Table 1). In these catalytic systems, the ratio of triflate ligand, which leads to the mixed anhydride (Scheme 1, path a) is the main factor that influences the efficiency of the catalytic process.

For the benzoylation of toluene (Table 1, entries 1 and 2), the use of $ClBi(OSO_2CF_3)_2$ **1** at 10 mol % led to 60% yield, and gave a similar result to that obtained with $Bi(OSO_2CF_3)_3$.[6] The yield for **1** is lower, but **1** only has two triflate ligands instead of three as is the case for $Bi(OSO_2CF_3)_3$.

$Cl_2Sb(OSO_2CF_3)$ **2** provided identical results (74% yield) for the acylation of *m*-xylene (Table 1, entries 3 and 4) with *n*-pentCOCl to that obtained by the catalytic system described by Kobayashi.[13] For the sulfonylation of toluene (Table 1, entries 5 to 8), where the mixed species play a key role, a 99% yield of tolylphenylsulfones was obtained with **1** [similar to that obtained by the catalytic system $BiCl_3/CF_3SO_2OH$ (5 mol %/10 mol %)],[23] and a 99% yield was also obtained with **2** [the same as that obtained by the catalytic system $SbCl_3/CF_3SO_2OH$ (5 mol %/5 mol %)]. In addition, all the selectivities proved to be similar.

With regard to the yields and the selectivities, the results for the catalytic activity of **1** and **2** are conclusive, and these mixed metallic chlorotriflates are strongly believed to be the key intermediates in these Friedel−Crafts reactions.

Experimental Section

Syntheses of **1** and **2** were performed under a dry and oxygen-free argon atmosphere. Solvents were dried by appropriate methods. Melting points were determined in capillaries sealed under argon and are uncorrected.

$ClBi(OSO_2CF_3)_2$ (1): Triflic acid (10.5 g, 70.0 mmol) was added dropwise at 0 °C to a solution of bismuth(III) chloride (9.1 g, 28.9 mmol) in toluene (60 mL). The reaction mixture was then stirred for 10 min at room temperature and heated to 110 °C for 90 min. After cooling, the mixture was filtered, and the residue was washed twice with dichloromethane (100 mL). Solvents were removed in vacuo, and **1** was obtained as a white powder (14.0 g, 89% yield) and was recrystallized from a THF/pentane solution at −20 °C. M.p. >250 °C. ^{13}C NMR (100.6 MHz, [D$_6$]DMSO, TMS): δ = 125.9 (q, $^1J_{C,F}$ = 322 Hz) ppm. ^{19}F NMR (376.4 MHz, CD_3CN, CF_3COOH): δ = 0.9 ppm. IR (CH_3CN): $\tilde{\nu}$ = 635, 585, 515 (S−O in OSO_2CF_3), 310 (Bi−Cl) cm^{-1}. RAMAN: $\tilde{\nu}$ = 307 (Bi−Cl) cm^{-1}. MS (DCI/CH_4): *m*/*z* = 543 (4) $[MH]^+$, 507 (5) $[M - Cl]^+$, 393 (8) $[M-Cl-OSO_2CF_3]^+$. $C_2BiClF_6O_6S_2$ (542.57): calcd. C 4.43, Cl 6.53, F 21.01, S 11.82; found C 4.43, Cl 6.05, F 21.09, S 11.87.

$Cl_2Sb(OSO_2CF_3)$ (2): The same procedure was used as for **1**, and the reaction mixture was heated at 110 °C for 5 h. **2** (4.6 g, 61% yield) was recrystallized from a THF/pentane solution at −20 °C. M.p. 61 °C(decomp.). ^{13}C NMR (100.6 MHz, [D$_6$]DMSO, TMS): δ = 120.5 (q, $^1J_{C,F}$ = 322 Hz) ppm. ^{19}F NMR (376.4 MHz, [D$_6$]DMSO, CF_3COOH): δ = 1.5 ppm. IR (CH_3CN): $\tilde{\nu}$ = 588, 515 (S−O in OSO_2CF_3), 353 (Sb−Cl) cm^{-1}. RAMAN: $\tilde{\nu}$ = 356 (Sb−Cl) cm^{-1}. MS (DCI/CH_4): *m*/*z* = 343 (16) $[MH]^+$, 193 (19) $[M - OSO_2CF_3]^+$. It was not possible to obtain satisfactory elemental data.

Benzoylation of Toluene: PhCOCl (1.97 g, 14 mmol), toluene (2.58 g, 28 mmol), and catalyst (14 mmol) were added together in a 20 mL flask. After 5 h at 110 °C, dichloromethane (20 mL) was added, and the organic layer was extracted with a 6% aqueous HCl (2 × 10 mL), dried ($MgSO_4$), and concentrated. After purification by flash chromatography (silica, pentane/ether, 9:1), methylbenzophenones were isolated. The use of 10 mol % of $Bi(OSO_2CF_3)_3$ led to 95% yield (*o*/*m*/*p*, 22/2/76)[6] and 10 mol % of **1** led to 60% yield (*o*/*m*/*p*, 21/2/77).

Acylation of *m*-Xylene: Following the procedure described by Kobayashi,[13] *n*-pentCOCl (0.20 g, 1.49 mmol), *m*-xylene (4.69 g, 44.2 mmol), and $Sb(OSO_2CF_3)_3$ (83 mg, 1.46 mmol) were added together, and the mixture was heated at 100 °C. After 24 hours, 1-(2,4-dimethylphenyl)hexan-1-one was obtained in 77% yield. With the same procedure, the use of 30 mol % of **2** led to 74% yield.

Sulfonylation of Toluene: (a) **1** as the catalyst: following the procedure described in ref. 23, 99% yield (*o*/*m*/*p*, 39/6/55) was obtained using 5 mol % of **1**, the system $BiCl_3/CF_3SO_2OH$ (5 mol %/10 mol %) provided 95% yield (*o*/*m*/*p*, 39/6/55). (b) **2** as the catalyst: following the typical procedure, $PhSO_2Cl$ (3.25 g, 18.4 mmol), toluene (3.39 g, 36.8 mmol) and catalyst (5 mol %, 0.92 mmol) were heated at 110 °C for 12 hours. Dichloromethane (40 mL) was then added, and the organic layer was extracted with aqueous HCl (40 mL of a 2 N solution), neutralized by saturated $NaHCO_3$ solution (40 mL), and analyzed by GC with tetradecane as external standard.

X-ray Structure Determination for the THF Adducts of 1 and 2: Crystal data were collected at low temperatures [*T* = 193(2) K] using an oil-coated shock-cooled crystal on a Bruker-AXS CCD 1000 diffractometer with Mo-K_α radiation (λ = 0.71073 Å). Semi-empirical absorption corrections were employed.[24] The structures were solved by direct methods (SHELXS-97)[25] and refined using the least-squares method on F^2.[26] Experimental details are given in Table 2.

 © 2004 Wiley-VCH Verlag GmbH & Co. KGaA, Weinheim

Table 2. Crystal Data for **1**·4THF and **2**·2THF

	1·4THF	**2**·2THF
Empirical formula	$C_{18}H_{32}BiClF_6O_{10}S_2$	$C_9H_{16}Cl_2F_3O_5SSb$
Molecular mass	830.99	485.93
Crystal system	monoclinic	triclinic
Space group	$P2_1/c$	$P\bar{1}$
a (Å)	17.018(2)	8.299(2)
b (Å)	18.394(2)	9.515(2)
c (Å)	8.960(1)	11.395(2)
α (°)		105.791(2)
β (°)	93.232(2)	96.575(2)
γ (°)		106.136(2)
V (Å^3)	2800.3(5)	814.0(3)
Z	4	2
Abs. coeff. (mm^{-1})	6.626	2.196
Crystal size (mm)	0.1 × 0.2 × 0.6	0.3 × 0.5 × 0.6
Max. and min. transmission	0.377188	0.702541
Reflections collected	24516	7073
Independent reflections	3985	4060
R_{int}	0.0870	0.0269
No. of parameters	343	190
$R1$ [$I > 2\sigma(I)$]	0.0646	0.0330
$wR2$ (all data)	0.1631	0.0906
Largest diff. peak (e Å^{-1})	4.498	2.098
CCDC	199266	199267

CCDC-199266 (for **1**·4THF) and -199267 (for **2**·2THF) contain the supplementary crystallographic data for this paper. These data can be obtained free of charge at www.ccdc.cam.ac.uk/conts/retrieving.html [or from the CCDC, 12 Union Road, Cambridge CB2 1EZ, UK; Fax: (internat.) +44-1223-336-033; E-mail: deposit@ccdc.cam.ac.uk].

Acknowledgments

We gratefully acknowledge the Centre National de la Recherche Scientifique (CNRS) and Rhodia Organique Fine for support of this work.

[1] C. Silverstru, H. J. Breunig, H. Althaus, *Chem. Rev.* **1999**, *99*, 3277−3327.
[2] [2a] M. N. Leonard, L. C. Wieland, R. S. Mohan, *Tetrahedron* **2002**, *58*, 8373−8397. [2b] N. C. Norman in *Chemistry of Arsenic, Antimony and Bismuth*, Blackie Academic and Professional, London, **1998**. [2c] H. Suzuki, Y. Matano, *Organobismuth Chemistry*, Elsevier, Amsterdam, **2001**.
[3] Reviews about the FC acylation and sulfonylation: [3a] G. A. Olah, *Friedel−Crafts and Related Reactions*, John Wiley & Sons, New York, **1963−1965**, vol. 1−4. [3b]S. B. Mahato, *J. Indian Chem. Soc.* **2000**, *77*, 175−191.
[4] C. Le Roux, J. Dubac, *Synlett* **2002**, 181−200.
[5] J. R. Desmurs, M. Labrouillère, H. Gaspard, A. Laporterie, J. Dubac, *Tetrahedron Lett.* **1997**, *38*, 8871−8874.
[6] S. Répichet, C. Le Roux, J. Dubac, J. R. Desmurs, *Eur. J. Org. Chem.* **1998**, 2743−2746.
[7] G. A. Olah, O. Farook, S. Morteza, F. Farnia, J. A. Olah, *J. Am. Chem. Soc.* **1988**, *110*, 2560−2565.
[8] A. Kawada, S. Mitamura, S. Kobayashi, *J. Chem. Soc., Chem. Commun.* **1993**, 1157−1158.
[9] S. Kobayashi, S. Iwamoto, *Tetrahedron Lett.* **1998**, *39*, 4697−4700.
[10] J. Matsuo, K. Odashima, S. Kobayashi, *Synlett* **2000**, *3*, 403−405.
[11] C. J. Chapman, C. G. Frost, J. P. Hartley, A. J. Whittle, *Tetrahedron Lett.* **2001**, *42*, 773−775.
[12] S. Kobayashi, I. Komoto, *Tetrahedron* **2000**, *56*, 6463−6565.
[13] O. Kobayashi, I. Kawamoto, (Sumitomo Chemical) Jpn. Kokai Tokkyo Koho JP 2001 294.548 (Jp. Appl. 2000/31, 800, 09 Feb. 2000) (*Chem. Abstr.* **2001**, *135*, 30367v).
[14] S. Répichet, C. Le Roux, P. Hernandez, J. Dubac, *J. Org. Chem.* **1999**, *64*, 6479−6482.
[15] [15a] F. Effenberger, G. Epple, *Angew. Chem.* **1972**, *84*, 294−295; *Angew. Chem. Int. Ed. Engl.* **1972**, *11*, 299−300. [15b] F. Effenberger, K. Huthmacher, *Angew. Chem. Int. Ed. Engl.* **1974**, *13*, 409−410. [15c] F. Effenberger, K. Huthmacher, *Chem. Ber.* **1976**, *109*, 2315−2326.
[16] R. C. Paul, S. Singh, R. C. Kumar, R. D. Sharma, R. D. Verma, *Ind. J. Chem.* **1979**, 273−275.
[17] Preparation of $M(OSO_2CF_3)_3$ (M = Bi or Sb) is known from $M(C_6H_5)_3$ [12,17a] or from the corresponding oxide. [17a] M. Labrouillère, C. Le Roux, H. Gaspard, A. Laporterie, J. Dubac, J.-R. Desmurs, *Tetrahedron Lett.* **1999**, *40*, 285−286. [17b] S. Répichet, A. Zwick, L. Vendier, C. Le Roux, J. Dubac, *Tetrahedron Lett.* **2002**, *43*, 993−995.
[18] DSC analyses have been performed on compound **1**, and no significant decomposition occurred until 250 °C.
[19] H. Schmidbaur, R. Nowak, B. Huber, G. Müller, *Organometallics* **1987**, *6*, 2266−2267 and references cited therein.
[20] See for historical interest, B. Mentshutkin, *Chem. Zentr.* **1910**, *3*, 378−383.
[21] B. Mentshutkin, *Chem. Zentr.* **1912**, *4*, 1436−1439.
[22] [22a] For examples see: J. R. Eveland, K. H. Whitmire, *Inorg. Chim. Acta* **1996**, *249*, 41−46. [22b] E. Hough, D. G. Nicholson, A. K. Vasudevan, *J. Chem. Soc., Dalton Trans.* **1987**, 427−430. [22c] G. R. Wiley, D. R. Aris, W. Errington, *Inorg. Chim. Acta* **2000**, *300*, 1004−1013.
[23] S. Répichet, C. Le Roux, J. Dubac, *Tetrahedron Lett.* **1999**, *40*, 9233−9234.
[24] *SADABS, Program for Absorption Correction*, Bruker AXS.
[25] G. M. Sheldrick, *Acta Crystallogr., Sect. A* **1990**, *46*, 467−473.
[26] *SHELXL-97, Program for Crystal Structure Refinement*, G. M. Sheldrick, University of Göttingen, Germany, **1997**.

Received April 5, 2004

 © 2004 Wiley-VCH Verlag GmbH & Co. KGaA, Weinheim

[1,2]-Rearrangement of Imino-*N*-heterocyclic Carbenes − Synthesis and Structures of Chelating Iminoimidazole Pd and Ni Complexes

Georg Steiner,[a] Alexander Krajete,[a] Holger Kopacka,[a] Karl-Hans Ongania,[b] Klaus Wurst,[a] Peter Preishuber-Pflügl,[c] and Benno Bildstein*[a]

Keywords: N ligands / Carbenes / Chelates / Transition metals / Rearrangement

Imidazolium and benzimidazolium salts with an *N*-iminoyl and an *N*′-alkyl group are potential precursors for new bidentate [*N*,*C*] ligands which are of interest as novel steering ligands for applications of their metal complexes in homogeneous catalysis. Deprotonation of these azolium salts with potassium hydride does indeed occur, however, the initially formed imino-*N*-heterocyclic carbenes rearrange spontaneously under migration of the *N*-iminoyl group from the nitrogen to the former carbene carbon with the formation of 2-iminoyl(benz)imidazoles. These rearranged compounds are new [*N*,*N*] ligand systems, which can also be synthesized by aluminum-assisted condensation of anilines with the corresponding 2-acylimidazoles. Palladium and nickel [*N*,*N*] complexes have been prepared, characterized by single-crystal X-ray analysis, and briefly evaluated for their catalytic performance in ethylene polymerizations and in Suzuki cross-coupling reactions.

(© Wiley-VCH Verlag GmbH & Co. KGaA, 69451 Weinheim, Germany, 2004)

Introduction

Soon after Arduengo and co-workers[1] isolated the first stable imino-*N*-heterocyclic carbene (NHC) in 1991, the chemistry of these nucleophilic species attracted the interest of many chemists due to their very rich coordination chemistry with almost all elements of the periodic table, and due to the possibility of employing modified and optimized NHC's as steering ligands in metal complexes with catalytic applications, i.e. for carbon-carbon cross-coupling reactions, olefin metathesis, and other reactions.[2] From a historic perspective,[3] metal complexes of simple (in situ generated) NHC's have been studied for over 40 years by the groups of Wanzlick,[4] Lappert,[5] Raubenheimer,[6] Öfele and Herrmann.[2b][2c]

The most common *N*-heterocyclic carbenes are imidazol-2-ylenes containing various *N*-substituents, usually simple alkyl or aryl groups.[2] In recent years tailor-made heterotopic chelating NHCs containing an additional donor functionality gained more and more importance, due to the general focus on applications of NHC metal complexes in catalysis.[2b] Chart 1 gives an overview of selected, recent examples from the current literature[7−9] of [*N*,*C*] and [*C*,*N*,*C*] metal complexes. In addition to the NHC donor, in all reported [*N*,*C*] ligand systems the *N*-donor is part of a planar heterocycle, i.e. pyridine and oxazoline, respectively. To the best of our knowledge, no other *N*-donor functionalities have been investigated as components of heterotopic [*N*,*C*] ligands for potential catalytic applications of their metal complexes, except for one very recent example,[10] published during the preparation of this manuscript.

Conceptually, our motivation for the work reported here is based on the following considerations: We have a general interest in the development of new and improved olefin polymerization catalysts.[11] Up to now, however, there are no NHC metal complexes as olefin polymerization precatalysts, only oligmerization catalysts have been reported.[12] In contrast, ring opening olefin metathesis polymerization (ROMP) is one of the most prominent uses for NHC ruthenium complexes.[13,14] The NHC ligands reported in the literature thus far are not suitable as steering ligands for late transition metal olefin polymerization catalysts based on iron or nickel,[15] because the planar *N*-donor (e.g. pyridine, compare Scheme 1) prevents the axial shielding resulting in suppressed chain termination pathways at the active metal site. The most active non-cyclopentadienyl late transition metal polymerization catalysts are [*N*,*N*,*N*] bis(imino)pyridine iron and [*N*,*N*] bisimine nickel complexes with peripheral sterically demanding *N*-aryl substituents (Scheme 2).[15] We therefore anticipate that [*N*,*C*] and [*N*,*C*,*N*] ligand systems where one *N*-donor is replaced by an NHC moiety will be very promising novel ligands for

[a] Institute of General, Inorganic and Theoretical Chemistry, University of Innsbruck,
Innrain 52a, 6020 Innsbruck, Austria
[b] Institute of Organic Chemistry, University of Innsbruck,
Innrain 52a, 6020 Innsbruck, Austria
[c] BASF Aktiengesellschaft,
67056 Ludwigshafen, Germany

new olefin polymerization precatalysts. In this contribution, we summarize our results on the chemistry of such imino-NHCs and of their metal complexes.

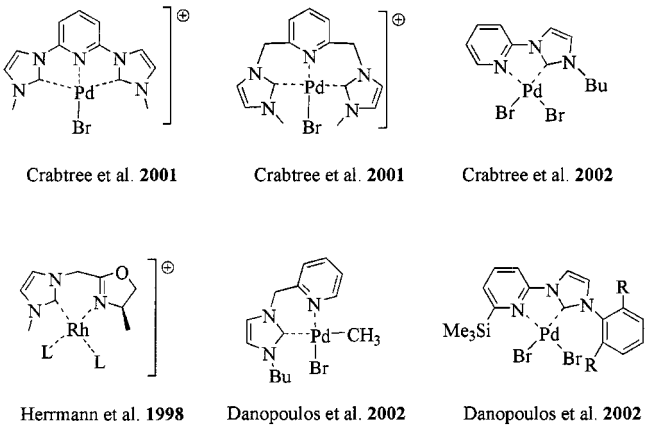

Scheme 1. Recent examples[7−9] of [*N*,*C*] chelating NHC metal complexes

Results and Discussion

The most versatile and common route to imino-*N*-heterocyclic carbenes consists of deprotonation of their corresponding (benz)imidazolium salts by suitable strong bases.[2] Simple azolium salts are easily accessible by alkylation or arylation of the parent heterocycles, whereas introduction of an additional *N*-donor with sterically demanding substituents is more challenging.

In a first approach, one might assume that condensation of known *N*,*N*′-dibenzoylbenzimidazolium salts[16] with anilines might give access to tridentate [*N*,*C*,*N*] ligand precursors (compare Scheme 2). However, it proved impossible to convert mono- or bis-acylated azolium salts into the corresponding iminoyl derivatives under a variety of experimental conditions. Therefore we chose an alternate synthetic strategy which introduces the imino functionality at an early stage in the synthetic sequence (Scheme 3).

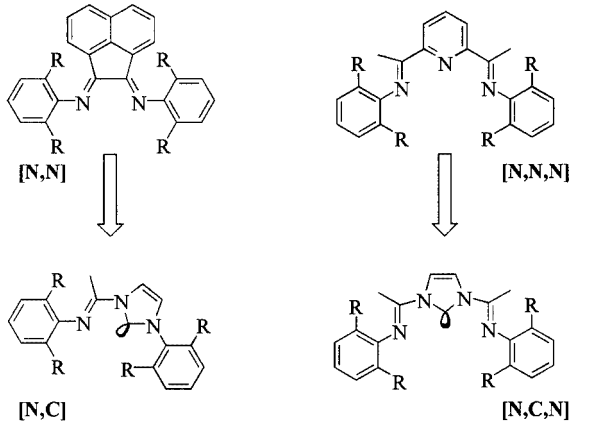

Scheme 2. Design concept for new [*N*,*C*] and [*N*,*C*,*N*] ligands

In other work[11b] we found that iminoyl chlorides **1**[17] are very convenient and useful electrophilic reagents which react quantitatively with *N*-H nucleophiles. They also convert imidazole and benzimidazole to the corresponding *N*-iminoyl heterocycles **2a** and **2b** in very good yield. Both compounds are yellow air-stable organic materials with properties in line with their structure (for details see Exp. Sect.). Spectroscopically, the imine group is clearly evident from a strong stretching vibration in the IR spectrum (**2a**: $\nu_{C=N}$ = 1652 cm^{-1}; **2b**: $\nu_{C=N}$ = 1651 cm^{-1}) and from a low-field ^{13}C chemical shift of the imine carbon (**2a**: δ = 148.6 ppm; **2b**: δ = 149.9 ppm).

Monoiminoylazoles **2a** and **2b** already contain one sterically bulky *N*-arylated donor − in this case 2,6-diisopropylphenyl − in agreement with the design concept outlined in the introduction. To obtain access to azolium precursors for [*N*,*C*] and [*N*,*C*,*N*] ligands according to Scheme 2, either a simple alkylation step or a second acylation with iminoyl chloride is all that is formally needed.

The attempt at forming *N*,*N*′-bisiminoylazolium salts by reaction of **2a** and **2b** with a second equivalent of iminoyl chloride **1** gave inconclusive results: a reaction did occur but the very air-sensitive product could not be characterized and its follow-up chemistry ruled out the formation of an azolium precursor to a [*N*,*C*,*N*] ligand. After half a year of trying to improve reaction conditions and workup procedures we finally concluded that such tridentate ligand systems are unfortunately not accessible due to fragmentation of the precursor imidazolium species.

On the other hand, the use of azolium salts as the required starting materials for [*N*,*C*] ligands produces no major problems: alkylation at the *N*′-position of **2a** and **2b** is indeed possible using methyl triflate as a highly electrophilic reagent, affording *N*-iminoyl-*N*′-methyl-azolium salts **3a** and **3b**, respectively, in high yield (**3a**: 100%; **3b**: 77%). Other, more common alkylating agents like iodomethane yielded no reaction at all under a variety of experimental conditions, including forced conditions like sealed-tube reactions using excess methyl iodide as solvent and reagent. Both azolium salts are yellow, slightly air-sensitive compounds of surprising stability. Key spectroscopic data include the observation of molecular ions of the cations in the positive mode FAB mass spectra (**3a**: *m*/*z* = 346; **3b**: *m*/*z* = 396), detection of the low-field NMR signal of the azolium hydrogen in the 2-position of the heterocycle [**3a**: δ(^{1}H) = 9.09 ppm; **3b**: δ(^{1}H) = 9.50 ppm], and observation of the *N*-methyl NMR signals [**3a**: δ(^{1}H) = 4.08 ppm, δ(^{13}C) = 37.6 ppm; **3b**: δ(^{1}H) = 4.25 ppm, δ(^{13}C) = 34.8 ppm]. Interestingly, the ^{13}C chemical shifts of the imine carbon are almost identical to those of the non-cationic non-methylated starting materials **2a** and **2b** suggesting that the positive charge predominantly located at the *N*-methyl nitrogen. In the case of **3b** suitable crystals for an X-ray structure analysis were obtained (Table 1, Figure 1). In the solid state, the cation of **3b** has a conformation where the imine functionality is oriented away from the 5-ring *N*-heterocycle. Due to steric crowding, the aryl substituents are tilted with respect to the plane of the benzimidazole-imine

 © 2004 Wiley-VCH Verlag GmbH & Co. KGaA, Weinheim

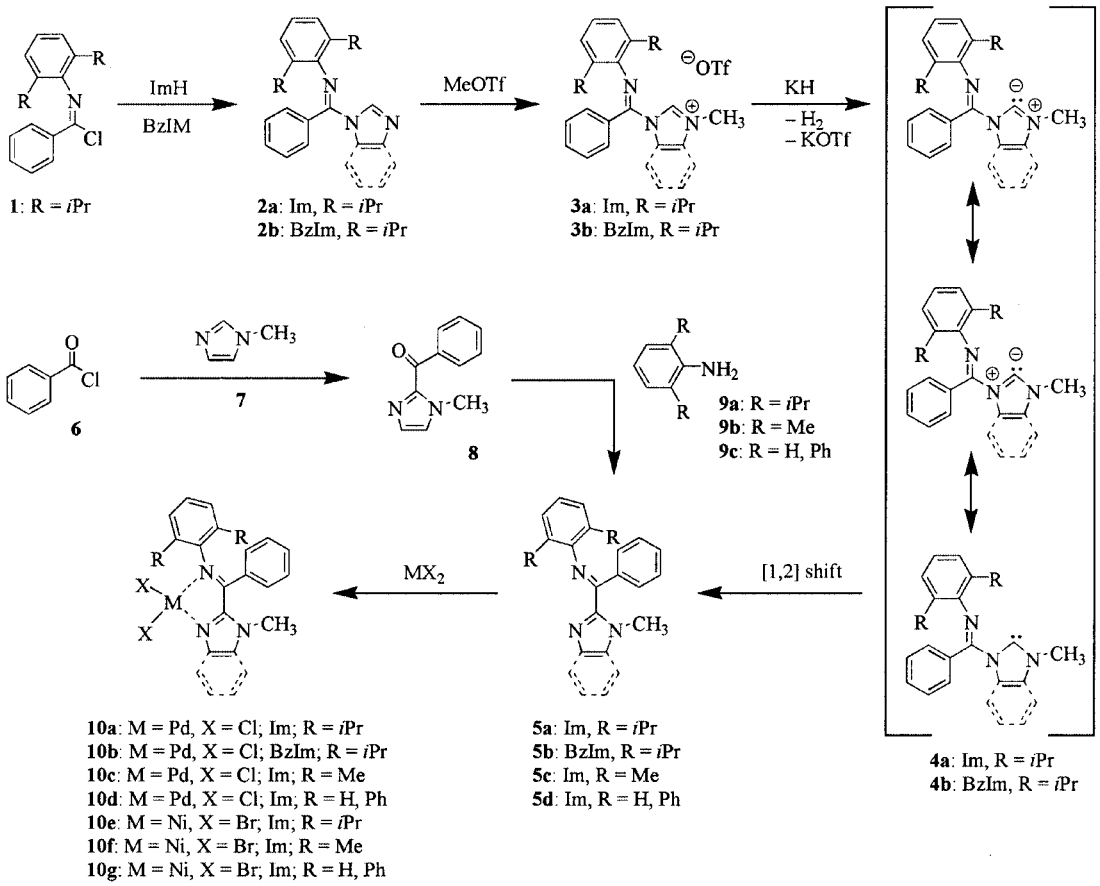

Scheme 3. Synthesis of compounds **2**–**10** (ImH = imidazole, BzImH = benzimidazole, *i*Pr = isopropyl, Me = methyl, Ph = phenyl)

moiety by 39.8° (phenyl group) and 76.6° (2,6-diisopropylphenyl group), respectively. The unsymmetric charge distribution indicated by the NMR spectroscopic data in solution is also evident in the crystalline state: The bond length of C(14)–N(2) equals 133.8(4) pm, slightly longer than the value of C(14)–N(3) with 132.0(4) pm, suggesting more double-bond character to this latter bond and more positive charge on the nitrogen N(3) of the *N*-methyl group.

Both azolium salts **3a** and **3b** serve as the key precursors for the corresponding [*N*,*C*] carbenes **4a** and **4b**, respectively (Scheme 3). Reaction of THF solutions of **3a** or **3b** with potassium hydride as base led to the evolution of H_2 gas, indicating deprotonation at the imidazole C(2) carbon. Subsequent reaction of these deprotonated (benz)imidazolium species with $PdCl_2$ afforded stable palladium complexes, as anticipated, but their properties and structures (vide infra) were not consistent with [*N*,*C*]$PdCl_2$ complexes. It soon became clear that the initial carbenes **4a** and **4b** must have rearranged by a 1,2-iminoyl shift to C(2)-substituted iminoyl(benz)imidazole **5a** and **5b**, and with "regular" [*N*,*N*] ligands easily formed the [*N*,*N*]$PdCl_2$ complexes **10a** and **10b**, respectively. Low temperature reactions aimed at trapping the initial carbenes **4a** or **4b** failed in all cases, suggesting that this 1,2-rearrangement is an unavoidable process under normal experimental conditions, thereby more or less ruling out the existence of iminocarbenes **4a** and **4b** in the condensed phase. The 1,2-shift of the iminoyl moiety of carbenes **4a** or **4b** is reminiscent of the Stevens rearrangement[18] of acceptor-substituted ammonium salts, but to the best of our knowledge no such migration has ever been described for ylides derived from (benz)imidazolium salts.

In addition we report that the attempted preparation of a Pd complex of **4a** by Raubenheimer's methodology[6] was equally unsuccessful: deprotonation of **2a** followed by complexation with $PdCl_2$ and subsequent methylation with methyl triflate did not afford the desired [*N*,*C*]$PdCl_2$ complex, instead a regular non-chelating imidazole–Pd complex was formed.[19]

The rearrangement of [*N*,*C*] carbenes **4a** and **4b** to [*N*,*N*] ligands **5a** and **5b** prompted us to look for a more versatile synthetic route for this potentially useful ligand framework. To this end, benzoyl chloride **6** was reacted with methylimidazole **7** to afford 2-benzoyl-*N*-methylimidazole (**8**) by a published procedure (Scheme 3).[20] Introduction of the imine functionality was achieved with aluminum-metalated

 © 2004 Wiley-VCH Verlag GmbH & Co. KGaA, Weinheim

Table 1. Crystallographic data for **3b**, **10a**, **10b**, **10c**

Compound	**3b**	**10a**	**10b**	**10c**
Molecular formula	$C_{28}H_{30}F_3N_3O_3S$	$C_{23}H_{27}Cl_2N_3Pd$	$C_{27}H_{29}Cl_2N_3Pd$	$C_{19}H_{19}Cl_2N_3Pd$
Molecular mass	545.61	522.78	572.83	466.67
Crystal system	monoclinic	monoclinic	monoclinic	monoclinic
Space group	$P2_1/c$ (No. 14)	$P2_1/c$ (No. 14)	$P2_1/c$ (No. 14)	$P2_1/c$ (No. 14)
a, pm	853.60(2)	1110.34(2)	1122.59(5)	1314.09(4)
b, pm	2896.60(9)	1269.48(3)	1391.70(5)	966.81(2)
c, pm	1185.39(5)	1649.36(3)	1622.83(6)	1518.84(4)
α, deg	90	90	90	90
β, deg	103.800(2)	94.566(1)	91.865(2)	94.852(1)
γ, deg	90	90	90	90
Z	4	4	4	4
V, nm^3	2.84632(16)	2.31748(8)	2.53402(17)	1.92273(9)
ρ_{calcd}, Mg·m^{-3}	1.273	1.498	1.502	1.612
Temp, K	233(2)	233(2)	293(2)	233(2)
Absorption coefficient (mm^{-1})	0.166	1.045	0.963	1.249
F(000)	1144	1064	1168	936
Color, habit	colorless prism	orange prism	yellow prism	orange plate
Crystal size	0.3 × 0.2 × 0.12 mm	0.3 × 0.25 × 0.16 mm	0.08 × 0.06 × 0.05 mm	0.35 × 0.3 × 0.15 mm
θ range for data collection	1.90° to 21.00°	2.03° to 25.00°	1.93° to 22.00°	1.97° to 26.00°
Index ranges	$0 = h = 8$; $-29 = k = 29$; $-11 = l = 11$	$0 = h = 13$; $-15 = k = 15$; $-19 = l = 19$	$0 = h = 11$; $-14 = k = 14$; $-17 = l = 17$	$0 = h = 16$; $-11 = k = 11$; $-18 = l = 18$
Reflections collected	11078	13548	11746	11762
Independent reflections	3042 (R_{int} = 0.0469)	4070 (R_{int} = 0.0243)	3107 (R_{int} = 0.0591)	3768 (R_{int} = 0.0285)
Reflections with $I > 2\sigma(I)$	2291	3631	2434	3235
Absorption correction	none	none	none	none
Refinement method	Full-matrix least-squares on F^2	Full-matrix least-squares on F^2	Full-matrix least-squares on F^2	Full-matrix least-squares on F^2
Data/restraints/parameters	3042/0/345	4070/0/264	3107/0/300	3768/0/231
Goodness-of-fit on F^2	1.083	1.057	1.022	1.062
Final R int [$I > 2\sigma(I)$]	R_1 = 0.0534; wR_2 = 0.1406	R_1 = 0.0239; wR_2 = 0.0590	R_1 = 0.0348; wR_2 = 0.0693	R_1 = 0.0261; wR_2 = 0.0627
R int (all data)	R_1 = 0.0742; wR_2 = 0.1518	R_1 = 0.0291; wR_2 = 0.0608	R_1 = 0.0539; wR_2 = 0.0745	R_1 = 0.0337; wR_2 = 0.0652
Extinction coefficient	0.0043(10)	0.0007(2)	0.00053(19)	0.0038(3)
Largest diff. peak and hole	343 and −282 e nm^{-3}	405 and −356 e nm^{-3}	316 and −260 e nm^{-3}	367 and −339 e nm^{-3}

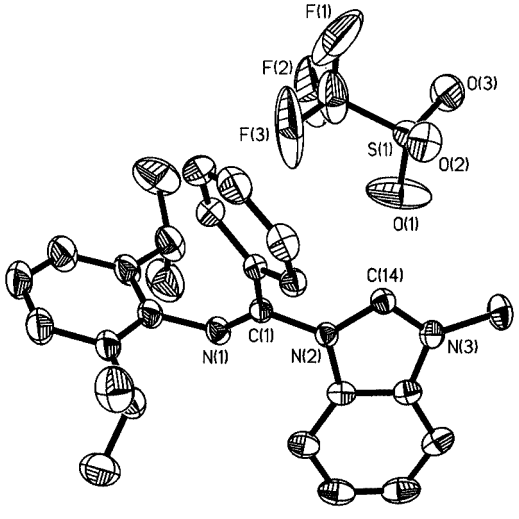

Figure 1. Molecular structure of **3b**; hydrogen atoms are omitted for clarity; selected bond lengths (pm): C(1)−N(1) = 126.1(4), C(1)−N(2) = 145.4(4), N(2)−C(14) = 133.8(4), C(14)−N(3) = 132.0(4); selected angles (°): N(2)−C(14)−N(3) = 110.6(3); tilt angle phenyl group of C(1) versus plane N(1)−C(1)−N(2): 39.8(3); tilt angle 2,6-diisopropylphenyl group of N(1) versus plane N(1)−C(1)−N(2): 76.6(3)

anilines **9a**, **9b**, and **9c** in yields of 68%-85%, thereby allowing steric fine-tuning of these [*N*,*N*] ligand systems. The aluminum-assisted condensation of carbonyl functionalities with primary amines is a very convenient method,[11a,21] which is especially useful for electronically deactivated and sterically crowded systems. Mechanistically it involves a metalation of aniline with trimethylaluminum and sequential formation of the hemiaminal and aminal of the carbonyl moiety, driven by the high oxophilicity of aluminum and by the formation of the thermodynamically very stable Al−O−Al bond of tetramethylaluminoxane.[11a,21] This aluminum-assisted formation of **5a**−**5d** is a necessary synthetic protocol for the chemistry reported in this paper, because standard condensation procedures of **8** with anilines (e.g. acid-catalyzed condensation with aceotropic removal of water) gave only partial conversion into the product in non-useful preparative yields. Compounds **5a**, **5c**, and **5d** are air-stable viscous oils with spectroscopic properties in accordance with their structure (for details see Exp. Sect.). During the course of this work an analogous [*N*,*N*] ligand has been claimed in a patent,[22] although without a phenyl substituent on the imine carbon and without a *N*′-alkyl group. Otherwise the only comparable bidentate *N*-hetero-

 © 2004 Wiley-VCH Verlag GmbH & Co. KGaA, Weinheim

cyclic imine ligands reported in the literature are pyridinylimines published three years ago.[23]

Reaction of **5a**, **5c** and **5d** with either $PdCl_2$ or $NiBr_2$ afforded the [*N*,*N*]MX_2 complexes **10a**, **10c**−**10g**, respectively, in isolated yields of 65−99% (Scheme 3). Complex **10b** with a benzimidazole backbone has been prepared in 85% yield by the one-pot sequence **3b-4b-5b-10b** (vide supra). All four palladium compounds **10a**−**10d** are orange, air-stable and diamagnetic complexes, indicating the expected regular square-planar coordination geometry at the palladium center. In contrast, all three nickel complexes **10e**−**10f** are green-brown, highly air-sensitive and strongly paramagnetic compounds, suggesting a tetracoordinate tetrahedrally distorted geometry in the case of monomeric complexes, or a bromine-bridged pentacoordinate coordination sphere in the case of dimeric complexes. The paramagnetism of these nickel compounds prevented NMR spectroscopic characterization, on the other hand it is clear evidence for the "designed" steric bulk of the [*N*,*N*] ligands **5a**, **5c** and **5d**.

The different substitution patterns of the *N*-aryl groups of palladium complexes **10a**−**10d** is obviously responsible for varying solubility in this series of complexes: compounds **10a** and **10c** are soluble in common organic solvents, allowing their routine characterization by NMR spectroscopic analysis, but complexes **10b** and **10d** showed only insufficient solubilities even in polar solvents like acetonitrile, acetone and dimethyl sulfoxide, preventing detection of their NMR signals. For compounds **10a** and **10c** the ^{13}C signal of the imine carbon (**10a**: $\delta_{C=N}$ = 165.7 ppm; **10c**: $\delta_{C=N}$ = 167.5 ppm) is shifted to lower field by approximately 7 ppm in comparison with the non-complexed free ligands **5a** and **5c**.

Single crystals for X-ray analyses were obtained for complexes **10a**−**10c** (Table 1, Figures 2−4). Overall, all three compounds show the expected square-planar coordination geometry at the palladium centers, deviations from the ideal 90° angle are most pronounced for the structurally enforced [*N*,*N*] chelate (angle N−Pd−N; **10a**: 79.7°, **10b**: 79.8°, **10c**: 79.6°) whereas all other angles are, more or less, close to the ideal value (**10a**: 91.3°-97.4°, **10b**: 89.1°-95.8°, **10c**: 92.2°-95.7°). On the other hand, due to steric crowding, the phenyl groups and the peripheral *N*-aryl groups show large tilt angles of 71.9° to 87.4° in relation to the coordination plane. Clearly visible in Figures 2−4 is the different steric shielding of the palladium metal centers by the differently substituted *N*-aryl groups, indicating "steric control" in these precatalysts by employment of different building blocks. The lengths of the Pd−Cl bonds (226.9−228.4 pm) and of the Pd−N bonds (199.1−207.8 pm) are unexceptional. The bond lengths of the coordinated imine moieties are distinctly shorter (129.7−130.3 pm) in comparison with those of the coordinated N=C double bonds (132.7−133.4 pm) of the (benz)imidazole rings.

Some preliminary catalytic screenings were performed with these new palladium and nickel precatalysts. Ethylene polymerization experiments with methylaluminoxane (MAO) activated nickel complexes **10e**−**10g** in homogeneous solution (70 °C, 20 bar ethylene pressure) showed only very low activities, indicating the predominance of chain termination processes. This result is not too unexpected, because axial shielding of the active metal site in these nickel complexes is insufficient due to the sterically "open"

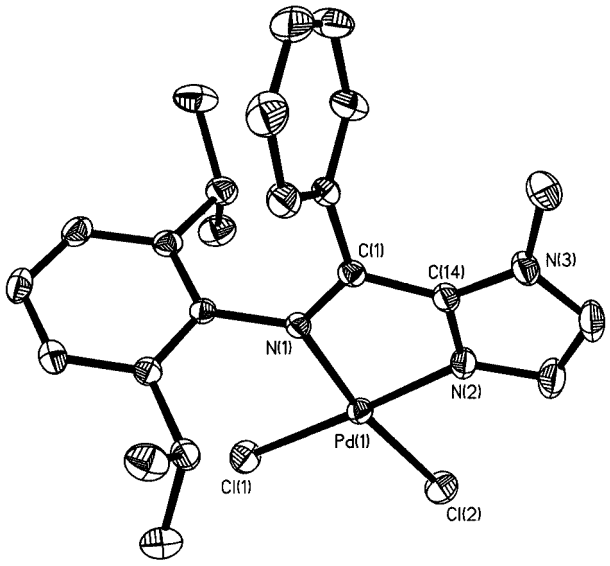

Figure 2. Molecular structure of **10a**; hydrogen atoms are omitted for clarity; selected bond lengths (pm): Pd(1)−Cl(1) = 228.36(6), Pd(1)−Cl(2) = 228.15(6), Pd(1)−N(1) = 207.75(17), Pd(1)−N(2) = 199.20(19), C(1)−N(1) = 130.3(3), C(1)−C(14) = 145.4(3), N(2)−C(14) = 132.7(3), C(14)−N(3) = 136.1(3); selected angles (°): Cl(1)−Pd(1)−Cl(2) = 91.60(2); Cl(1)−Pd(1)−N(1) = 97.40(5); Cl(2)−Pd(1)−N(2) = 91.25(6); N(1)−Pd(1)−N(2) = 79.73(7); N(1)−C(1)−C(14) = 113.86(19); N(2)−C(14)−C(1) = 118.23(19); tilt angle phenyl group of C(1) versus plane N(1)−C(1)−C(14): 71.9(1); tilt angle 2,6-diisopropylphenyl group of N(1) versus plane N(1)−C(1)−C(14): 74.9(2)

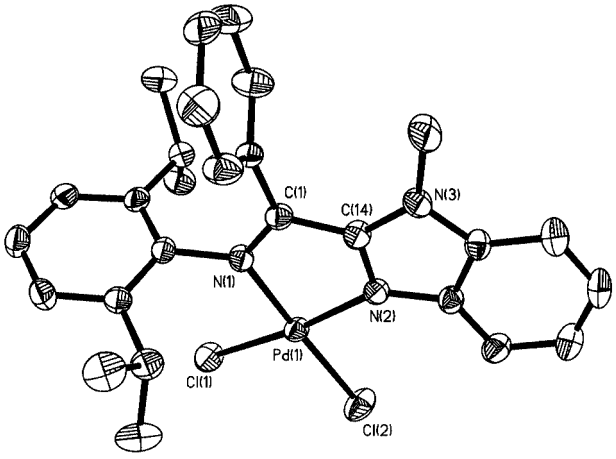

Figure 3. Molecular structure of **10b**; hydrogen atoms are omitted for clarity; selected bond lengths (pm): Pd(1)−Cl(1) = 227.93(12), Pd(1)−Cl(2) = 226.91(13), Pd(1)−N(1) = 204.4(3), Pd(1)−N(2) = 202.6(3), C(1)−N(1) = 129.7(5), C(1)−C(14) = 147.0(6), N(2)−C(14) = 133.1(5), C(14)−N(3) = 136.7(5); selected angles (°): Cl(1)−Pd(1)−Cl(2) = 89.10(5); Cl(1)−Pd(1)−N(1) = 95.52(10); Cl(2)−Pd(1)−N(2) = 95.79(11); N(1)−Pd(1)−N(2) = 79.77(14); N(1)−C(1)−C(14) = 113.8(4); N(2)−C(14)−C(1) = 117.6(4); tilt angle phenyl group of C(1) versus plane N(1)−C(1)−C(14): 86.2(2); tilt angle 2,6-diisopropylphenyl group of N(1) versus plane N(1)−C(1)−C(14): 79.5(3)

 © 2004 Wiley-VCH Verlag GmbH & Co. KGaA, Weinheim

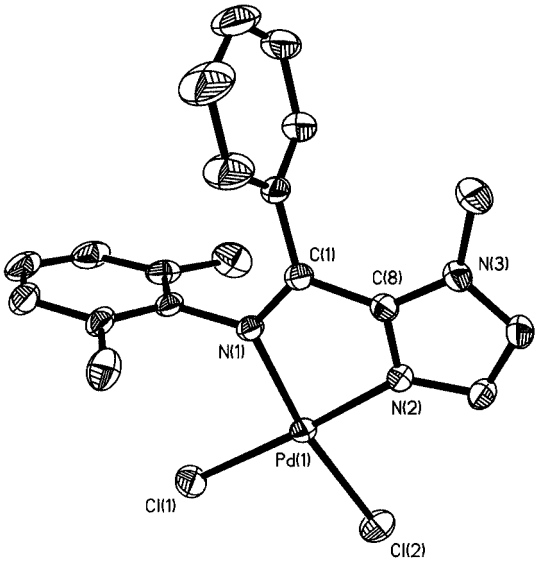

Figure 4. Molecular structure of **10c**; hydrogen atoms are omitted for clarity; selected bond lengths (pm): Pd(1)−Cl(1) = 228.11(7), Pd(1)−Cl(2) = 227.73(7), Pd(1)−N(1) = 205.7(19), Pd(1)−N(2) = 199.1(2), C(1)−N(1) = 130.2(3), C(1)−C(8) = 146.0(3), N(2)−C(8) = 133.4(3), C(8)−N(3) = 135.1(3); selected angles (°): Cl(1)−Pd(1)−Cl(2) = 92.76(3); Cl(1)−Pd(1)−N(1) = 95.65(5); Cl(2)−Pd(1)−N(2) = 92.16(6); N(1)−Pd(1)−N(2) = 79.60(7); N(1)−C(1)−C(8) = 113.1(2); N(2)−C(8)−C(1) = 117.5(2); tilt angle phenyl group of C(1) versus plane N(1)−C(1)−C(8): 76.6(2); tilt angle 2,6-dimethylphenyl group of N(1) versus plane N(1)−C(1)−C(8): 87.4(2)

imidazole side of the bidentate iminoylimidazole ligands. On the other hand, palladium complexes **10a**, **10c**, **10d** are efficient catalysts for Suzuki carbon-carbon cross-coupling reactions: aromatic boronic acids are quantitatively coupled with aryl bromides without formation of undesired homo-coupled products. However, only bromo electrophiles are sufficiently activated for this reaction, attempts to cross-couple boronic acids with the industrially more important chloro aromatics gave no conversion at all.

Conclusion

The work reported in this contribution is motivated by the search for novel bidentate [*N*,*C*] ligand systems as steering ligands for late transition metal complexes with applications in polymerization catalysis and fine chemical synthesis. Conceptually, the new ligands should contain one imine donor with a sterically demanding *N*-aryl substituent and a *N*-heterocyclic carbene (NHC) as the second donor site. Synthetically, imidazole and benzimidazole are *N*-derivatized with iminoyl chloride followed by *N′*-alkylation with methyl triflate, affording novel iminoyl(benz)imidazolium salts of surprising stability. An X-ray structure and NMR spectroscopic data of benzimidazolium triflate indicate that the positive charge resides predominantly at the *N′*-methyl side, suggesting that the *N*-iminoyl moiety is in a "normal" chemical environment, thereby explaining the unusual stability of this azolium salt. Deprotonation of these (benz)imidazolium triflates at the (benz)imidazole C(2) carbon using potassium hydride as base is successful, however, the initially formed imino-NHC rearranges by a Stevens 1,2-shift to 2-iminoyl(benz)imidazoles which are new [*N*,*N*] ligand systems. These are also synthesized by an alternate synthetic route, which introduces the *N*-aryl group by an aluminum-assisted condensation of anilines with 2-benzoyl-1-methylimidazole. The [*N*,*N*] palladium complexes derived from these ligands are regular square-planar, diamagnetic complexes, as shown by single-crystal structure analysis of three representatives. In contrast, the [*N*,*N*] nickel complexes are highly air-sensitive and strongly paramagnetic complexes, due to ligand induced distortions. Preliminary catalytic tests of olefin polymerizations and of C−C cross-coupling reactions are performed, showing that the palladium complexes are useful catalysts for Suzuki reactions, but the nickel complexes are only poor catalysts for MAO-cocatalyzed ethylene polymerizations.

Experimental Section

General: Commercially available starting materials were used as obtained. Solvents were dried, deoxygenated and saturated with argon according to standard procedures in organometallic chemistry. Reactions of air-sensitive materials were performed in Schlenk glassware in an atmosphere of argon by techniques common in inorganic/organometallic chemistry. New compounds were characterized by MS and IR and NMR spectroscopy, etc by current state of the art procedures, details of instrumentation have been published previously.[24]

Imidazole 2a: A Schlenk tube was charged with imidazole (1.76 g, 25.8 mmol) and dry dichloromethane (40 mL). *N*-(2,6-diisopropylphenyl)benziminoyl chloride[11b,16] **1** (12.3 mmol) dissolved in dichloromethane (30 mL) was added to this solution. Imidazolium chloride immediately precipitated, indicating fast formation of the product. Stirring at ambient temperature was continued for 3 hours. Workup: 150 mL of water was added to the mixture to dissolve and remove the imidazolium chloride, the organic product was extracted with three portions of dichloromethane, the combined organic layers were washed with a brine solution, the dichloromethane solution of the product was dried with Na_2SO_4 and concentrated in vacuo to a volume of approximately 5 mL. After an equal volume of *n*-hexane was added, 3.30 g **2a** crystallized in the form of a yellow, microcrystalline solid in 81% yield, m.p: 112−115 °C. IR (KBr): $\tilde{\nu}$ = 2969 (w), 2962 (m), 1652 (s), 1602 (w), 1590 (m), 1515 (m), 1469 (s), 1439 (s), 1376 (s), 1364 (m), 1333 (m), 1314 (s), 1297 (s), 1283 (m), 1239 (s), 1160 (s), 1059 (s), 1023 (s), 940 (m), 918 (s), 835 (s), 706 (s), 700 (s) cm^{-1}. MS (FAB): *m*/*z* = 331 $[M]^+$. ^1H NMR (300 MHz, $CDCl_3$): δ = 0.89 [d, $^3J_{H,H}$ = 6.6 Hz, 6 H, $CH(CH_3)_2$], 1.07 [d, $^3J_{H,H}$ = 6.6 Hz, 6 H, $CH(CH_3)_2$], 2.82 [2 H, sept., 2 × $CH(CH_3)_2$], 6.65−7.71 (m, 10 H, C_6H_5, C_6H_3, $C_3H_3N_2$), 7.91 (s, 1 H, $C_3H_3N_2$) ppm. ^{13}C NMR (75.432 MHz, $CDCl_3$): δ = 21.7, 23.8, 28.4 [$CH(CH_3)_2$], 118.0, 122.8, 124.1, 128.3, 128.9, 129.9, 130.2, 130.7, 136.6, 137.3, 141.9 (C_6H_5, C_6H_3, $C_3H_3N_2$), 148.6 (C=N) ppm. $C_{22}H_{25}N_3$ (331.46): calcd. C 79.72, H 7.60, N 12.68; found C 80.00, H 7.63, N 12.63.

Benzimidazole 2b: A Schlenk tube was charged with benzimidazole (761 mg, 6.44 mmol) and dry dichloromethane (70 mL). *N*-(2,6-diisopropylphenyl)benziminoyl chloride[11b,17] **1** (3.07 mmol) dissolved in dichloromethane (8 mL) was added to this solution.

 © 2004 Wiley-VCH Verlag GmbH & Co. KGaA, Weinheim

Benzimidazolium chloride immediately precipitated, indicating fast formation of the product. Stirring at ambient temperature was continued for 4 hours. Workup: 150 mL of water was added to the mixture to dissolve and remove the benzimidazolium chloride, the organic product was extracted with three portions of dichloromethane, the combined organic layers were washed with a brine solution, the dichloromethane solution of the product was dried with Na_2SO_4 and concentrated in vacuo to a volume of approximately 5 mL. After an equal volume of *n*-hexane was added, 1.12 g **2b** crystallized in the form of a yellow, microcrystalline solid in 96% yield. m.p.: 123−127 °C. IR (KBr): $\tilde{\nu}$ = 2963 (w), 2867 (m), 1651 (s), 1609 (s), 1588 (s), 1493 (s), 1451 (s), 1369 (s), 1290 (m), 1217 (s), 1161 (m), 1057 (m), 931 (s), 800 (s), 764 (s), 708 (s), 698 (s) cm^{-1}. MS (FAB): *m*/*z* = 381 $[M]^+$. ^1H NMR (300 MHz, $CDCl_3$): δ = 0.95−1.27 [m, 12 H, $CH(CH_3)_2$], 2.92−3.19 [m, 2 H, 2 × $CH(CH_3)_2$], 7.02−8.07 (m, 12 H, C_6H_5, C_6H_3, $C_7H_5N_2$) ppm. ^{13}C NMR (75.432 MHz, $CDCl_3$): δ = 21.8, 24.2, 28.4, 28.8 $[CH(CH_3)_2]$, 115.3, 120.4, 122.9, 123.5, 124.0, 124.7, 127.2, 128.6, 128.9, 130.8, 131.7, 136.7, 142.2, 143.0, 146.4 (C_6H_5, C_6H_3, $C_7H_5N_2$), 149.9 (C=N) ppm. $C_{26}H_{27}N_3$ (381.52): calcd. C 81.85, H 7.13, N 11.01; found C 81.98, H 7.15, N 10.97.

Imidazolium Triflate 3a: A Schlenk tube was charged with **2a** (150 mg, 0.453 mmol) and dry dichloromethane (40 mL). The solution was cooled to −80 °C and methyltrifluoromethansulfonate (50 µL, 0.453 mmol) was added via a syringe. After 20 minutes stirring at −80 °C, the cooling bath was removed and the mixture was stirred for a further 2 hours, resulting in a clear bright yellow solution. Thin layer chromatography (TLC) indicated complete reaction, all starting material had been consumed with the formation of a polar non-eluting product. Workup: all volatile materials were removed on a vacuum line, the solid yellow residue was washed with two portions of dry diethyl ether and dried in vacuo, affording 224 mg **3a** as a yellow, moderately air-sensitive powder in 100% yield. MS (FAB): *m*/*z* = 346 [M of cation]$^+$. ^1H NMR (300 MHz, CD_2Cl_2): δ = 0.93 (d, $^3J_{H,H}$ = 6.9 Hz, 6 H, $CH(CH_3)_2$], 1.12 [d, $^3J_{H,H}$ = 6.6 Hz, 6 H, $CH(CH_3)_2$], 2.81 (m, 2 H, 2 × $CH(CH_3)_2$], 4.08 (s, 3 H, CH_3), 7.07−7.87 (m, 10 H, C_6H_5, C_6H_3, $C_3H_3N_2$), 9.09 (s, 1 H, $C_3H_3N_2$) ppm. ^{13}C NMR (75.432 MHz, CD_2Cl_2): δ = 21.9, 24.1, 28.8 $[CH(CH_3)_2]$, 37.6 (N−CH_3), 118.9, 120.5, 123.7, 124.9, 125.8, 129.4, 129.5, 132.7, 136.9, 137.0, 140.8 (C_6H_5, C_6H_3, $C_3H_3N_2$), 147.3 (C=N) ppm. $C_{24}H_{28}F_3N_3O_3S$ (495.56): calcd. C 58.17, H 5.70, N 8.48; found C 58.08, H 5.72, N 8.43.

Benzimidazolium Triflate 3b: A Schlenk tube was charged with **2b** (214 mg, 0.561 mmol) and dry dichloromethane (40 mL). The solution was cooled to −80 °C and methyltrifluoromethansulfonate (62 µL, 0.561 mmol) was added via a syringe. After 20 minutes stirring at −80 °C, the cooling bath was removed and the mixture was stirred for a further 2 hours, resulting in a clear bright yellow solution. Thin layer chromatography (TLC) indicated complete reaction, all starting material had been consumed with the formation of a polar non-eluting product. Workup: all volatile materials were removed on a vacuum line, the solid yellow residue was washed with two portions of dry diethyl ether and dried in vacuo, affording 236 mg **3b** as a yellow, moderately air-sensitive powder in 77% yield. MS (FAB): *m*/*z* = 396 [M of cation]$^+$. ^1H NMR (300 MHz, CD_2Cl_2): δ = 0.95 (d, $^3J_{H,H}$ = 6.9 Hz, 6 H, $CH(CH_3)_2$], 1.14 [d, $^3J_{H,H}$ = 6.6 Hz, 6 H, $CH(CH_3)_2$], 2.92 [m, 2 H, 2 × $CH(CH_3)_2$], 4.25 (s, 3 H, CH_3), 7.11−8.09 (m, 12 H, C_6H_5, C_6H_3, $C_7H_5N_2$), 9.50 (s, 1 H, $C_7H_5N_2$) ppm. ^{13}C NMR (75.432 MHz, CD_2Cl_2): δ = 21.9, 24.4, 28.8 $[CH(CH_3)_2]$, 34.8 (N−CH_3), 113.7, 117.4, 123.7, 125.8, 128.5, 128.9, 129.6, 129.7, 130.7, 132.7, 136.9, 141.1, 143.2 (C_6H_5, C_6H_3, $C_3H_3N_2$), 149.1 (C=N) ppm. $C_{28}H_{30}F_3N_3O_3S$ (545.62): calcd. C 61.64, H 5.54, N 7.70; found C 61.53, H 5.57, N 7.66. Single crystal X-ray structure: Table 1, Figure 1.

Ketone 8:[20] A round-bottom flask was charged (without protection from air) with 1-methylimidazole **7** (10 mL, 0.125 mol) and acetonitrile (125 mL). The stirred solution was cooled to 0 °C and benzoyl chloride **6** (14.6 mL) was added from a dropping funnel within a period of 15 minutes, followed by addition of triethylamine (17.5 mL, 0.125 mol). The mixture was stirred overnight at ambient temperature, resulting in a yellow solution and a white precipitate of triethylammonium chloride. The ammonium salt was filtered off, solvents and other volatile materials were removed on a rotary evaporator, affording crude **8** as a yellow oil. Distillation in an oil pump vacuum gave 17.5 g (75%) pure **8** as a yellow viscous liquid, b.p. 120−125 °C. MS (EI): *m*/*z* = 186 $[M]^+$. ^1H NMR (300 MHz, CD_2Cl_2): δ = 4.03 (s, 3 H, CH_3), 7.13−7.18 (d, 2 H, $C_3H_2N_2$), 7.45−7.58 (m, 3 H, C_6H_5), 8.26−8.29 (d, 2 H, C_6H_5) ppm. ^{13}C NMR (75.432 MHz, CD_2Cl_2): δ = 36.6 (N−CH_3), 127.3, 128.2, 129.3, 131.1, 132.8, 137.8, 143.5 (C_6H_5, $C_3H_2N_2$), 184.1 (C=O) ppm. ^1H NMR spectroscopic data and the boiling point concur with published data.[20]

Imidazole 5a: A Schlenk tube was charged with 2,6-diisopropylaniline **9a** (2 mL, 10.6 mmol), toluene (40 mL), and 5.3 mL of a 2.0 molar toluene solution of trimethylaluminum (10.6 mmol). The stirred solution was heated to 80 °C. After 90 minutes methane evolution was completed and the solution was cooled to ambient temperature. Under protection from air, (1-methyl-2-imidazolyl)-phenylketone (**8**) (986 mg, 5.30 mmol) was added in one portion, and an immediate color change from yellow to burgundy red was observed. The mixture was stirred overnight at ambient temperature and heated to 80 °C for a further three hours, affording a bright yellow solution. Workup: the solution was cooled to 0 °C, the mixture was carefully hydrolyzed with crushed ice, the organic product was extracted with three portions of diethyl ether, the combined organic layers were washed with one portion of a 5% aqueous NaOH solution, the diethyl ether solution was washed with two portions of water, the organic phase was dried with Na_2SO_4, and all volatile materials were removed in vacuo on a rotary evaporator, affording the crude product together with 2,6-diisopropylaniline. Chromatography on alumina with diethyl ether/*n*-hexane (v/v, 1:1) as eluent afforded 1.45 g pure **5a** in 79% yield as a yellow oil. MS (EI): *m*/*z* = 345 $[M]^+$. ^1H NMR (300 MHz, $CDCl_3$): δ = 0.89 [d, $^3J_{H,H}$ = 6.9 Hz, 6 H, $CH(CH_3)_2$], 1.10 [d, $^3J_{H,H}$ = 6.6 Hz, 6 H, $CH(CH_3)_2$], 2.87 [m, 2 H, 2 × $CH(CH_3)_2$], 4.08 (s, 3 H, N−CH_3), 6.98−7.17 (m, 10 H, C_6H_5, C_6H_3, $C_3H_2N_2$) ppm. ^{13}C NMR (75.432 MHz, $CDCl_3$): δ = 21.6, 24.3, 28.2 $[CH(CH_3)_2]$, 36.8 (N−CH_3), 122.6, 123.5, 125.4, 127.3, 128.4, 129.0, 129.2, 134.8, 135.5, 144.6, 144.9 (C_6H_5, C_6H_3, $C_3H_2N_2$), 158.5 (C=N) ppm. $C_{23}H_{27}N_3$ (345.49): calcd. C 79.96, H 7.88, N 12.16; found C 80.05, H 7.86, N 12.12.

Imidazole 5c: A Schlenk tube was charged with 2,6-dimethylaniline (**9b**) (2.5 mL, 20.3 mmol), toluene (40 mL) and 10.2 mL of a 2.0 molar toluene solution of trimethylaluminum (20.3 mmol). The stirred solution was heated to 80 °C. After 90 minutes methane evolution was completed and the solution was cooled to ambient temperature. Under protection from air, (1-methyl-2-imidazolyl)-phenylketone (**8**) (1.89 g, 10.2 mmol) was added in one portion, and an immediate color change from yellow to burgundy red was observed. The mixture was stirred over the weekend at ambient temperature, affording a bright yellow solution. Workup: the solution was cooled to 0 °C, the mixture was carefully hydrolyzed with crushed ice, the organic product was extracted with three portions of diethyl ether, the combined organic layers were washed with one

 © 2004 Wiley-VCH Verlag GmbH & Co. KGaA, Weinheim

portion of a 5% aqueous NaOH solution, the diethyl ether solution was washed with two portions of water, the organic phase was dried with Na_2SO_4, and all volatile materials were removed in vacuo on a rotary evaporator, affording the crude product together with 2,6-dimethylaniline. Chromatography on alumina with diethyl ether/*n*-hexane (v/v, 1:1) as eluent afforded 2.0 g pure **5c** in 68% yield as a yellow oil. MS (EI): m/z = 289 $[M]^+$. ^1H NMR (300 MHz, CD_2Cl_2): δ = 2.09 (s, 6 H, CH_3), 4.15 (s, 3 H, N−CH_3), 6.82−7.24 (m, 10 H, C_6H_5, C_6H_3, $C_3H_2N_2$) ppm. ^{13}C NMR (75.432 MHz, CD_2Cl_2): δ = 18.8 (CH_3), 37.6 (N−CH_3), 123.2, 125.9, 126.1, 127.6, 127.9, 128.5, 128.9, 129.3, 136.7, 144.8, 148.4 (C_6H_5, C_6H_3, $C_3H_2N_2$), 159.8 (C=N) ppm. $C_{19}H_{19}N_3$ (289.38): calcd. C 78.86, H 6.62, N 14.52; found C 78.99, H 6.62, N 14.48.

Imidazole 5d: A Schlenk tube was charged with 2-aminobiphenyl (**9c**) (1.9 g, 11.2 mmol), toluene (40 mL), and 5.6 mL of a 2.0 molar toluene solution of trimethylaluminum (11.2 mmol). The stirred solution was heated to 80 °C. After 90 minutes methane evolution was completed and the solution was cooled to ambient temperature. Under protection from air, (1-methyl-2-imidazolyl)phenylketone (**8**) (1.05 g, 5.61 mmol) was added in one portion, and an immediate color change from yellow to burgundy red was observed. The mixture was stirred for 48 hours at ambient temperature, affording a bright yellow solution. Workup: the solution was cooled to 0 °C, the mixture was carefully hydrolyzed with crushed ice, the organic product was extracted with three portions of diethyl ether, the combined organic layers were washed with one portion of a 5% aqueous NaOH solution, the ether solution was washed with two portions of water, the organic phase was dried with Na_2SO_4, and all volatile materials were removed in vacuo on a rotary evaporator, affording the crude product together with 2-aminobiphenyl. Chromatography on alumina with diethyl ether/*n*-hexane (v/v, 1:1) as eluent afforded 1.61 g pure **5d** in 85% yield as a yellow oil. MS (EI): m/z = 337 $[M]^+$. ^1H NMR (300 MHz, $CDCl_3$): δ = 2.69, 4.15 (s, 3 H, N−CH_3, *E*/*Z* isomers in 1:2 ratio), 6.59−7.72 (m, 16 H, C_6H_5, $C_{12}H_9$, $C_3H_2N_2$) ppm. ^{13}C NMR (75.432 MHz, $CDCl_3$): δ = 33.3, 37.2 (N−CH_3, *E*/*Z* isomers in 1:2 ratio), 120.8, 121.2, 124.2, 125.1, 125.9, 127.0, 127.8, 128.2, 128.8, 128.9, 129.2, 129.4, 129.6, 129.8, 130.4, 131.4, 132.9, 133.5, 135.4, 138.3, 140.1, 140.4, 142.2, 144.8, 147.7, 148.2, 158.3 (C_6H_5, $C_{10}H_9$, $C_3H_2N_2$), 160.2 (C=N) ppm. $C_{23}H_{19}N_3$ (337.42): calcd. C 81.87, H 5.68, N 12.45; found C 81.96, H 5.71, N 12.39.

Palladium(II) Complex 10a. **Method A:** A Schlenk tube was charged with **3a** (145 mg, 0.293 mmol), THF (40 mL), and an excess of potassium hydride (25 mg, 0.62 mmol). H_2 evolution commenced immediately and the mixture was stirred for 3 hours at ambient temperature, after this time no more gas evolution was observed. The slightly yellow suspension was filtered under protection from air through a short plug of glass wool to remove excess KH and most of the potassium trifluoromethanesulfonate. Palladium dichloride (52 mg, 0.293 mmol) was added to the resulting slightly turbid solution and the mixture was stirred at room temperature for 20 hours, resulting in a brown suspension. Workup: the volatiles were removed on a rotary evaporator, the brown residue was chromatographed on alumina with dichloromethane and acetonitrile as eluent, the brown fraction was decolorized with activated charcoal, and the solvents were removed in vacuo, affording 100 mg of **10a** as a tan solid in 65% yield.

Method B: A Schlenk tube was charged with **5a** (630 mg, 1.82 mmol), acetonitrile (30 mL) and $PdCl_2$ (323 mg, 1.82 mmol). The mixture was stirred overnight at ambient temperature to afford an orange solution. Workup: the solution was filtered through celite and chromatographed on silica with dichloromethane and acetonitrile as eluent, the orange fraction was collected, solvents were removed on a rotary evaporator, and the product was dried in vacuo, yielding 800 mg (84%) **10a** as an orange powder.

Data for 10a: MS (FAB): m/z = 522 $[M]^+$ was not observed, due to clustering signals of higher masses were detected. ^1H NMR (300 MHz, CD_2Cl_2): δ = 1.05 [d, $^3J_{H,H}$ = 6.6 Hz, 6 H, $CH(CH_3)_2$], 1.46 (d, $^3J_{H,H}$ = 6.9 Hz, 6 H, $CH(CH_3)_2$], 3.21 [m, 5 H, 2 × $CH(CH_3)_2$, N−CH_3], 6.98−7.93 (m, 10 H, C_6H_5, C_6H_3, $C_3H_2N_2$) ppm. ^{13}C NMR (75.432 MHz, CD_2Cl_2): δ = 23.3, 24.7, 29.1 [$CH(CH_3)_2$], 37.5 (N−CH_3), 123.6, 127.7, 127.9, 128.4, 128.8, 129.5, 129.7, 132.3, 140.3, 140.8, 146.3 (C_6H_5, C_6H_3, $C_3H_2N_2$), 165.7 (C=N) ppm. $C_{23}H_{27}Cl_2N_3Pd$ (522.81): calcd. C 52.84, H 5.21, N 8.04; found C 52.76, H 5.20, N 8.10. Single-crystal X-ray structure: Table 1, Figure 2.

Palladium(II) Complex 10b: A Schlenk tube was charged with **3b** (165 mg, 0.302 mmol), of THF (40 mL) and an excess of potassium hydride (25 mg, 0.62 mmol). H_2 evolution commenced immediately and the mixture was stirred for 3 hours at ambient temperature, after that period no more gas evolution was observed. The slightly yellow suspension was filtered under protection from air through a short plug of glass wool to remove excess KH and most of the potassium trifluoromethanesulfonate. $PdCl_2$ (65 mg, 0.363 mmol) was added to the resulting slightly turbid solution and the mixture was stirred at room temperature for 24 hours, resulting in a brown suspension. Workup: the volatiles were removed on a rotary evaporator, the brown residue was chromatographed on alumina with dichloromethane and acetonitrile as eluent, the brown fraction was decolorized with activated charcoal, and the solvents were removed in vacuo, affording 147 mg of **10b** as a yellow solid in 85% yield. IR (KBr): $\tilde{\nu}$ = 2961 (m), 2869 (m), 1588 (m), 1487 (s), 1410 (m), 1385 (m), 1346 (s), 1011 (s), 789 (m), 746 (s), 713 (s) cm^{-1}. MS (FAB): m/z = 573 $[M]^+$ was not observed, due to clustering signals of higher masses were detected. ^1H and ^{13}C NMR spectroscopy were attempted in deuterated acetonitrile, acetone, and dimethyl sulfoxide, respectively, but the solubility of **10b** was insufficient to obtain meaningful NMR spectroscopic data. $C_{27}H_{29}Cl_2N_3Pd$ (572.87): calcd. C 56.61, H 5.10, N 7.33; found C 56.48, H 5.07, N 7.38. Single crystal X-ray structure: Table 1, Figure 3.

Palladium(II) Complex 10c: A Schlenk tube was charged with **5c** (710 mg, 2.45 mmol), acetonitrile (30 mL), and $PdCl_2$ (435 mg, 2.45 mmol). The mixture was stirred overnight at ambient temperature to afford an orange solution. Workup: the solution was filtered through celite and chromatographed on silica with dichloromethane and acetonitrile as eluent, the orange fraction was collected, solvents were removed on a rotary evaporator, the product was dried in vacuo, and recrystallized from acetonitrile, yielding 1.03 mg (90%) **10c** as orange crystals. MS (FAB): m/z = 467 $[M]^+$ was not observed, due to clustering signals of higher masses were detected. ^1H NMR (300 MHz, CD_3CN): δ = 2.22, 2.34 (6 H, 2 × s, CH_3), 3.11 (s, 3 H, N−CH_3), 6.89−7.47 (m, 10 H, C_6H_5, C_6H_3, $C_3H_2N_2$) ppm. ^{13}C NMR (75.432 MHz, CD_3CN): δ = 19.4 (CH_3), 37.3 (N−CH_3), 127.5, 127.9, 128.2, 128.5, 128.7, 129.8, 130.9, 131.9, 132.5, 144.1, 147.4 (C_6H_5, C_6H_3, $C_3H_2N_2$), 167.5 (C=N) ppm. $C_{19}H_{19}Cl_2N_3Pd$ (466.71): calcd. C 48.90, H 4.10, N 9.00; found C 49.10, H 4.15, N 8.94. Single crystal X-ray structure: Table 1, Figure 4.

Palladium(II) Complex 10d: A Schlenk tube was charged with **5d** (545 mg, 1.62 mmol), acetonitrile (30 mL) and $PdCl_2$ (286 mg, 1.62 mmol). The mixture was stirred overnight at ambient temperature to afford an orange solution. Workup: the solution was filtered through celite and chromatographed on silica with dichlorometh-

 © 2004 Wiley-VCH Verlag GmbH & Co. KGaA, Weinheim

ane and acetonitrile as eluent, the orange fraction was collected, solvents were removed on a rotary evaporator, the product was dried in vacuo, and recrystallized from a mixture of dichloromethane and acetonitrile, yielding 835 mg (98%) **10d** as orange crystals. MS (FAB): m/z = 515 $[M]^+$ was not observed, due to clustering signals of higher masses were detected. ^1H and ^{13}C NMR spectroscopy were attempted, but the solubility of **10d** was insufficient to obtain meaningful NMR spectroscopic data. $C_{23}H_{19}Cl_2N_3Pd$ (514.47): calcd. C 53.67, H 3.72, N 8.16; found C 53.37, H 3.75, N 8.21.

Nickel(II) Complex 10e: A Schlenk tube was charged with **5a** (787 mg, 2.28 mmol), acetonitrile (30 mL) and $NiBr_2$ (550 mg, 2.52 mmol). The mixture was stirred overnight, giving a green suspension. Workup: acetonitrile was removed on a vacuum line, the residue was dissolved in dry dichloromethane, the solution was filtered through a Schlenk frit to remove excess $NiBr_2$, and the solution was evaporated to dryness on a vacuum line, affording 1.22 g (95%) **10e** as a green-brown, paramagnetic, air-sensitive powder. ^1H NMR in deuterated dimethyl sulfoxide showed only very broad signals. $C_{23}H_{27}Br_2N_3Ni$ (563.98): calcd. C 48.98, H 4.83, N 7.45; found C 48.70, H 4.89, N 7.58.

Nickel(II) Complex 10f: A Schlenk tube was charged with **5c** (510 mg, 1.76 mmol), dichloromethane (40 mL) and $NiBr_2$·DME (544 mg, 1.76 mmol). The mixture was stirred for 48 hours at room temperature, giving a brown solution. Workup: dichloromethane was removed on a vacuum line, affording 814 mg (91%) **10f** as a brown, paramagnetic, air-sensitive powder. ^1H NMR spectra, in deuterated dimethyl sulfoxide, showed only very broad signals. $C_{19}H_{19}Br_2N_3Ni$ (507.88): calcd. C 44.93, H 3.77, N 8.27; found C 44.54, H 3.67, N 7.96.

Nickel(II) Complex 10g: A Schlenk tube was charged with **5d** (480 mg, 1.42 mmol), dichloromethane (40 mL) and $NiBr_2$·DME (439 mg, 1.42 mmol). The mixture was stirred for 48 hours at room temperature, giving a green solution. Workup: dichloromethane was removed on a vacuum line, affording 790 mg (99%) **10g** as a green, paramagnetic, air-sensitive powder. ^1H NMR spectra, in deuterated dimethyl sulfoxide, showed only very broad signals. $C_{23}H_{19}Br_2N_3Ni$ (555.92): calcd. C 49.69, H 3.44, N 7.56; found C 49.21, H 3.51, N 7.42.

X-ray Crystallography: Single-crystal X-ray measurements and structure determinations of **3b, 10a, 10b, 10c** (Table 1, Figures 1−4): The data collection was performed on a Nonius Kappa CCD equipped with graphite-monochromatized Mo-K_α-radiation (λ = 0.71073 Å) and a nominal crystal to area detector distance of 36 mm. Intensities were integrated using DENZO and scaled with SCALEPACK.[25] Several scans in the φ and ω directions were made to increase the number of redundant reflections, which were averaged in the refinement cycles. This procedure replaces an empirical absorption correction. The structures were solved with direct methods (SHELXS-86) and refined against F^2 (SHELX-97).[26] Hydrogen atoms at carbon atoms were added geometrically and refined using a riding model. All non-hydrogen atoms were refined with anisotropic displacement parameters.

CCDC-216464 (for **3b**), -216465 (for **10a**), -216466 (for **10b**), -216467 (for **10c**) contain the crystallographic data for this paper. These data can be obtained free of charge at www.ccdc.cam.ac.uk/conts/retrieving.html [or from the Cambridge Crystallographic Data Centre, 12 Union Road, Cambridge CB2 1EZ, UK; Fax: (internat.) +44-1223-336-033; E-mail: deposit@ccdc.cam.ac.uk].

Acknowledgments

We thank BASF Aktiengesellschaft, Ludwigshafen, Germany for financial support and for preliminary ethene polymerizations as well as for investigations of C−C cross-coupling Suzuki reactions.

[1] A. J. Arduengo, R. L. Harlow, M. Kline, *J. Am. Chem. Soc.* **1991**, *113*, 361.
[2] Reviews: [2a] *Carbene Chemistry* (Ed.: G. Bertrand), Marcel Dekker, Inc., New York, **2002**. [2b]W.A. Herrmann, *Angew. Chem.* **2002**, *114*, 1343; *Angew. Chem. Int. Ed.* **2002**, *41*, 1290. [2c] W. A. Herrmann, T. Weskamp, V. P. W. Böhm, *Adv. Organomet. Chem.* **2001**, *48*, 1. [2d] C. J. Carmalt, A. H. Cowley, *Adv. Inorg. Chem.* **2000**, *50*, 1. [2e] D. Bourissou, O. Guerret, F. P. Gabbai, G. Bertrand, *Chem. Rev.* **2000**, *100*, 39. [2f] A. J. Arduengo, *Acc. Chem. Res.* **1999**, *32*, 913. [2g] W. A. Herrmann, C. Köcher, *Angew. Chem.* **1997**, *109*, 2257; *Angew. Chem. Int. Ed. Engl.* **1997**, *36*, 2163.
[3] A. J. Arduengo, R. Krafczyk, *Chemie in unserer Zeit* **1998**, *32*, 6.
[4] H.-W. Wanzlick, E. Schikora, *Angew. Chem.* **1962**, *74*, 129.
[5] M. F. Lappert, *J. Organomet. Chem.* **1988**, *358*, 185.
[6] H. G. Raubenheimer, S. Cronje, *J. Organomet. Chem.* **2001**, *617−618*, 170.
[7] [7a] R. H. Crabtree, *Pure Appl. Chem.* **2003**, *75*, 435. [7b] M. Poyatos, J. A. Mata, E. Falomir, R. H. Crabtree, E. Peris, *Organometallics* **2003**, *22*, 1110. [7c] S. Gründemann, A. Kovacevic, M. Albrecht, J. W. Faller, R. H. Crabtree, *J. Am. Chem. Soc.* **2002**, *124*, 10473. [7d] J. A. Loch, M. Albrecht, E. Peris, J. Mata, J. W. Faller, R. H. Crabtree, *Organometallics* **2002**, *21*, 700. [7e] S. Gründemann, M. Albrecht, J. A. Loch, J. W. Faller, R. H. Crabtree, *Organometallics* **2001**, *20*, 5485.
[8] [8a] A. A. Danopoulos, A. A. D. Tulloch, S. Winston, G. Eastham, M. B. Hursthouse, *Dalton Trans.* **2003**, 1009. [8b] A. A. D. Tulloch, S. Winston, A. A. Danopoulos, G. Eastham, M. B. Hursthouse, *Dalton Trans.* **2003**, 699. [8c] A. A. Danopoulos, S. Winston, W. B. Motherwell, *Chem. Commun.* **2002**, 1376. [8d] A. A. D. Tulloch, A. A. Danopoulos, G. J. Tizzard, S. J. Coles, M. B. Hursthouse, R. S. Hay-Motherwell, W. B. Motherwell, *Chem. Commun.* **2001**, 1270. [8e] A. A. D. Tulloch, A. A. Danopoulos, S. Kleinhenz, M. E. Light, M. B. Hursthouse, G. Eastham, *Organometallics* **2001**, *20*, 2027.
[9] W. A. Herrmann, L. J. Goossen, M. Spiegler, *Organometallics* **1998**, *17*, 2162.
[10] L. G. Bonnet, R. E. Douthwaite, B. M. Kariuki, *Organometallics* **2003**, *22*, 4187.
[11] [11a] G. A. Luinstra, J. Queisser, B. Bildstein, H.-H. Görtz, C. Amort, M. Malaun, A. Krajete, G. Werne, M. O. Kristen, N. Huber, C. Gernert, *Highly Active Ethene Polymerization Catalysts with Unusual Imine Ligands*, in *Late Transition Metal Polymerization Catalysis* (Eds.: B. Rieger, L. S. Baugh, S. Kacker, S. Striegler), Wiley-VCH, Weinheim, **2003**, chapter 3, p. 59. [11b] A. Krajete, G. Steiner, H. Kopacka, K.-H. Ongania, K. Wurst, M. O. Kristen, P. Preishuber-Pflügl, B. Bildstein, *Eur. J. Inorg. Chem. **2004**, 1740.* [11c] U. Siemeling, T.-C. Auch, O. Kuhnert, M. Malaun, H. Kopacka, B. Bildstein, *Z. Anorg. Allg. Chem.* **2003**, *629*, 1334. [11d] C. Amort, M. Malaun, A. Krajete, H. Kopacka, K. Wurst, M. Christ, D. Lilge, M. O. Kristen, B. Bildstein, *Appl. Organomet. Chem.* **2002**, *16*, 506. [11e] U. Siemeling, O. Kuhnert, B. Neumann, A. Stammler, H.-G. Stammler, B. Bildstein, M. Malaun, M. O. Kristen, P. Zanello, *Eur. J. Inorg. Chem.* **2001**, 913.
[12] D. S. McGuinness, V. C. Gibson, D. F. Wass, J. W. Steed, *J. Am. Chem. Soc.* **2003**, *125*, 12716.
[13] [13a] T. Weskamp, F. J. Kohl, W. A. Herrmann, *J. Organomet. Chem.* **1999**, *582*, 362. [13b] T. Weskamp, W. C. Schattenmann, M. Spiegler, W. A. Herrmann, *Angew. Chem.* **1998**, *110*, 2631;

 © 2004 Wiley-VCH Verlag GmbH & Co. KGaA, Weinheim

Angew. Chem. Int. Ed. **1998**, *37*, 2490. [13c] C. W. Bielawski, R. H. Grubbs, *Angew. Chem.* **2000**, *112*, 3025; *Angew. Chem. Int. Ed.* **2000**, *39*, 2903.
[14] Review: M. R. Buchmeiser, *Well-Defined Transition Metal Catalysts for Metathesis Polymerization*, in *Late Transition Metal Polymerization Catalysis* (Eds.: B. Rieger, L. S. Baugh, S. Kacker, S. Striegler), Wiley-VCH, Weinheim, **2003**, chapter 5, p. 155.
[15] Recent reviews: [15a] *Late Transition Metal Polymerization Catalysis* (Eds.: B. Rieger, L. S. Baugh, S. Kacker, S. Striegler), Wiley-VCH, Weinheim, **2003**. [15b]V. C. Gibson, S. K. Spitzmesser, *Chem. Rev.* **2003**, *103*, 283. [15c] S. Mecking, *Angew. Chem.* **2001**, *113*, 550; *Angew. Chem. Int. Ed.* **2001**, *40*, 534. [15d] S. D. Ittel, L. K. Johnson, M. Brookhart, *Chem. Rev.* **2000**, *100*, 1169. [15e] S. Mecking, *Coord. Chem. Rev.* **2000**, *203*, 325. [15f] G. J. P. Britovsek, V. C. Gibson, D. F. Wass, *Angew. Chem.* **1999**, *111*, 448; *Angew. Chem. Int. Ed.* **1999**, *38*, 428.
[16] H. W. Gibson, H. R. Jois, *J. Org. Chem.* **1991**, *56*, 865.
[17] R. T. Boere, V. Klassen, G. Wolmershäuser, *J. Chem. Soc., Dalton Trans.* **1998**, 4147.
[18] *March's Advanved Organic Chemistry: Reactions, Mechanism, and Structure*, 5th ed., (Eds.: M. B. Smith, J. March), John Wiley & Sons, Inc.; New York, **2001**, chapter 16, p. 1419.
[19] G. Steiner, B. Bildstein, K. Wurst, unpublished.
[20] E. Regel, K. H. Büchel, *Justus Liebigs Ann. Chem.* **1977**, 145.
[21] B. Bildstein, P. Denifl, *Synthesis* **1994**, 158.
[22] J. A. Ponasik Jr., J. P. McDevitt, C. M. Killian, P. B. Mackenzie, L. S. Moody (Eastman Chemical Company) US 6372682 B2, example 92, p. 43.
[23] T. V. Laine, U. Piironen, K. Lappalainen, M. Klinga, E. Aitola, M. Leskelä, *J. Organomet. Chem.* **2000**, *606*, 112.
[24] B. Bildstein, M. Malaun, H. Kopacka, K. Wurst, M. Mitterböck, K.-H. Ongania, G. Opromolla, P. Zanello, *Organometallics* **1999**, *18*, 4325.
[25] Processing of X-ray diffraction data collected in oscillation mode: Z. Otwinowski, W. Minor, *Methods Enzymol.* **1997**, *276*, 307.
[26] G. M. Sheldrick, Program package *SHELXTL V.5.1*, Bruker Analytical X-ray Instruments Inc, Madison, USA **1997**.

Received January 28, 2004
Early View Article
Published Online May 13, 2004

 © 2004 Wiley-VCH Verlag GmbH & Co. KGaA, Weinheim

Synthesis and Characterization of $[OsCl_2(=C=CHR)(PPh_3)_2]$ and Related Complexes

Ting Bin Wen,[a] Wai Yiu Hung,[a] Zhong Yuan Zhou,[b] Man Fung Lo,[a] Ian D. Williams,[a] and Guochen Jia*[a]

Keywords: Carbyne ligands / Osmium / Vinylidene ligands

Treatment of $[OsCl_2(PPh_3)_3]$ with HC≡CR (R = Ph, *p*-tolyl, CMe_3) in the presence of HCl gives the corresponding trichloro(carbyne) complexes $[OsCl_3(\equiv CCH_2R)(PPh_3)_2]$ in good yields. The vinylidene complexes $[OsCl_2(=C=CHR)(PPh_3)_2]$ (R = Ph, *p*-tolyl, CMe_3) are, in turn, prepared from the reactions of the carbyne complexes $[OsCl_3(\equiv CCH_2R)(PPh_3)_2]$ with NEt_3. These new vinylidene complexes are hygroscopic and react with H_2O to give (aqua)(vinylidene) complexes $[OsCl_2(H_2O)(=C=CHR)(PPh_3)_2]$. The structures of several of these new complexes have been determined by X-ray diffraction studies.

(© Wiley-VCH Verlag GmbH & Co. KGaA, 69451 Weinheim, Germany, 2004)

Introduction

(Vinylidene)ruthenium complexes[1] of the type $[RuCl_2(=C=CHR)(PR'_3)_2]$ have attracted attention because they are catalytically active for olefin metathesis,[2a−2c] dimerization and carboxylation of terminal alkynes,[2d] and they can be used as precursors to other vinylidene complexes.[2d,2e] A number of such complexes have been prepared from the reactions of HC≡CR with dichlororuthenium complexes such as $[RuCl_2(PPh_3)_3]$,[3,4] $[RuCl_2H_2(PR'_3)_2]$ (R′ = Cy, *i*Pr),[5] $[RuCl_2(PiPr_3)_2]_n$,[6] $[RuCl_2(MeCN)_2(PiPr_3)_2]$,[6] $[RuCl_2(p\text{-cymene})]_2/PR'_3$[6] and $[\{RuCl_2(TPPMS)_2\}Na_2]_2{\cdot}4H_2O$ [TPPMS = $Ph_2P(2\text{-}OSO_2C_6H_4)Na$][7] or from the reaction of $[RuCl_2(=CHPh)(PCy_3)_2]$ with 1,2-propadiene.[2a]

In contrast to ruthenium, the chemistry of related (vinylidene)osmium complexes of the type $[OsCl_2(=C=CHR)(PR'_3)_2]$ is still underdeveloped, despite the fact that a large number of other (vinylidene)osmium complexes have been prepared.[8−21] To the best our knowledge, only $[OsCl_2(=C=CHPh)(PiPr_3)_2]$, which was produced by elimination of the imine ligands from the (imine)(vinylidene) complexes $[OsCl_2(=C=CHPh)(NH=CR_2)(PiPr_3)_2]$ [CR_2 = CMe_2, $C(CH_2)_5$] in refluxing toluene, has been reported by Esteruelas and co-workers.[13]

Prompted by the facile preparation of the (vinylidene)ruthenium complex $[RuCl_2(=C=CHCMe_3)(PPh_3)_2]$ from the reaction of $HC\equiv CCMe_3$ with $[RuCl_2(PPh_3)_3]$, we have attempted to prepare analogous (vinylidene)osmium complexes $[OsCl_2(=C=CHR)(PPh_3)_2]$ from the reactions of $[OsCl_2(PPh_3)_3]$ with HC≡CR. However, it was found that the expected vinylidene complexes $[OsCl_2(=C=CHR)(PPh_3)_2]$ could not be isolated from the reactions of $[OsCl_2(PPh_3)_3]$ with HC≡CR (R = CMe_3,[22] $SiMe_3$ [23]). Instead, the reactions afford a series of complexes including carbyne complexes $[OsCl_3(\equiv CCH_2R)(PPh_3)_2]$, osmabenzyne complexes, and vinyl(vinylidene) complexes $[OsX\{C(C\equiv CR)=CHR\}(=C=CHR)(PPh_3)_2]$ (X = Cl, C≡CR).[22,23] It was suggested that these complexes are formed via vinylidene intermediates $[OsCl_2(=C=CHR)(PPh_3)_2]$, although attempts to isolate them from the reactions failed. In this report, we will show that the vinylidene complexes $[OsCl_2(=C=CHR)(PPh_3)_2]$ can be obtained from the deprotonation reactions of (carbyne)osmium complexes $[OsCl_3(\equiv CCH_2R)(PPh_3)_2]$.

Results and Discussion

Preparation of Carbyne Complexes $[OsCl_3(\equiv CCH_2R)(PPh_3)_2]$

We have previously shown that the carbyne complexes $[OsCl_3(\equiv CCH_2CMe_3)(PPh_3)_2]$ (**4**) and $[OsCl_3(\equiv CCH_3)(PPh_3)_2]$ (**5**) are formed as one of the products from the reaction of $[OsCl_2(PPh_3)_3]$ (**1**) with $HC\equiv CCMe_3$ and $HC\equiv CSiMe_3$, respectively.[22,23] It was suspected that the carbyne complexes were produced by protonation of the vinylidene intermediates $[OsCl_2(=C=CHR)(PPh_3)_2]$ with HCl generated in situ. Thus, it was expected that carbyne

[a] Department of Chemistry and Open Laboratory of Chirotechnology of the Institute of Molecular Technology for Drug Discovery and Synthesis, The Hong Kong University of Science and Technology,
Clear Water Bay, Kowloon, Hong Kong, P. R. China
[b] Department of Applied Biology and Chemical Technology, Hong Kong Polytechnic University,
Kowloon, Hong Kong, P. R. China

complexes $[OsCl_3(\equiv CCH_2R)(PPh_3)_2]$ might be readily prepared from the reaction of $[OsCl_2(PPh_3)_3]$ (**1**) with HC≡CR in the presence of HCl. Indeed, treatment of $[OsCl_2(PPh_3)_3]$ (**1**) with HC≡CR (R = Ph, *p*-tolyl, CMe_3) and HCl gave exclusively the corresponding (carbyne)trichloro complexes $[OsCl_3(\equiv CCH_2R)(PPh_3)_2]$ (**2**−**4**) in good yields [Equation (1)].

$$OsCl_2(PPh_3)_3 + H{\equiv}R \xrightarrow[\text{benzene, } -PPh_3]{\text{HCl (ether solution)}} Cl{-}Os(Cl)(PPh_3)_2{\equiv}C{-}CH_2{-}R \quad (1)$$

1 → **2**, R = Ph; **3**, R = *p*-tolyl; **4**, R = CMe_3

The analogous reaction of **1** with $HC{\equiv}CSiMe_3$ in the presence of HCl led to the known desilylated (carbyne)-trichloro complex $[OsCl_3(\equiv CCH_3)(PPh_3)_2]$ (**5**), which was isolated as a yellow solid in 71% yield [Equation (2)]. It is assumed that reaction of **1** with $HC{\equiv}CSiMe_3$ initially generates the vinylidene intermediate $[OsCl_2(=C=CHSiMe_3)(PPh_3)_2]$, which reacts with HCl to give the (carbyne)-trichloro complex $[OsCl_3(\equiv CCH_2SiMe_3)(PPh_3)_2]$. Desilylation of the later carbyne complex by electrophilic reagents (e.g. HCl or H_2O) produces the carbyne complex **5**. There are many reports on the cleavage of Si−C bonds by H_2O or acids to give C−H bonds.[24−27]

$$OsCl_2(PPh_3)_3 + H{\equiv}SiMe_3 \xrightarrow[\text{benzene, } -PPh_3]{\text{HCl (ether solution)}} Cl{-}Os(Cl)(PPh_3)_2{\equiv}C{-}CH_3 \quad (2)$$

1 → **5**

The new complexes **2** and **3** were characterized by multinuclear NMR spectroscopy. The $^{31}P\{^1H\}$ NMR spectra (in $CDCl_3$) of complexes **2** and **3** display singlet ^{31}P signals at $\delta = -12.9$ and -12.1 ppm, respectively. The ^1H NMR spectra (in $CDCl_3$) display the $\equiv CCH_2$ proton signals at $\delta = 1.77$ (for **2**) and 1.72 ppm (for **3**). The $^{13}C\{^1H\}$ NMR spectra (in CD_2Cl_2) exhibit the resonances of the C-α atoms of the carbyne ligands as a triplet at $\delta = 278.2$ (**2**) and 280.1 ppm (**3**) and the signals of the CH_2 carbon atoms as a singlet at $\delta = 57.3$ (**2**) and 57.1 ppm (**3**). The $^{31}P\{^1H\}$ and $^{13}C\{^1H\}$ NMR spectroscopic data suggest that the two PPh_3 ligands in **2** and **3** are *trans* to each other and that the carbyne ligand is *trans* to a chloro ligand.

The structure of **2** was confirmed by an X-ray diffraction study. A view of the molecular geometry of **2** is shown in Figure 1. Selected bond lengths and angles are given in Table 1. Similarly to **4**,[22] the geometry around the osmium atom in **2** can be viewed as a distorted octahedron with two PPh_3 ligands at the axial positions and the three chlorides and the carbyne ligand in the equatorial plane. The Os−C(1)−C(2) unit in **2** is almost linear with a bond angle of 174.8(3)°. The Os−C(carbyne) bond length in **2** [1.734(3) Å] is nearly identical to that in **4** [1.728(3) Å],[22] and is within the range of those reported previously for other (carbyne)osmium complexes.[10,16,18,22,24,25,27−34] As expected, the Os−Cl(1) bond [2.4621(8) Å] is significantly longer than the mutually *trans* bonds Os−Cl(2) [2.4105(7) Å] and

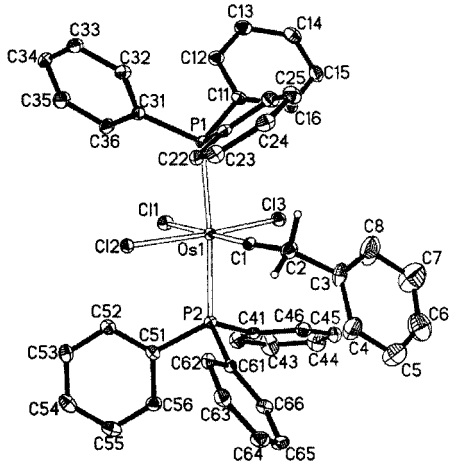

Figure 1. Molecular structure for $[OsCl_3(\equiv CCH_2Ph)(PPh_3)_2]$ (**2**)

Table 1. Selected bond lengths [Å] and bond angles [°] for $[OsCl_3(\equiv CCH_2Ph)(PPh_3)_2]\cdot 1.5C_6H_6$ (**2**·$1.5C_6H_6$) and $[OsCl_3(\equiv CCH_3)(PPh_3)_2]\cdot CH_2Cl_2$ (**5**·CH_2Cl_2)

	2	**5**		**2**	**5**
Os(1)−C(1)	1.734(3)	1.724(5)	C(1)−C(2)	1.457(5)	1.434(7)
Os(1)−P(1)	2.4501(8)	2.4476(14)	Os(1)−P(2)	2.4339(8)	2.4426(14)
Os(1)−Cl(1)	2.4621(8)	2.4827(13)	Os(1)−Cl(2)	2.4105(7)	2.3845(13)
Os(1)−Cl(3)	2.3874(8)	2.4227(14)	C(2)−C(3)	1.515(5)	
P(2)−Os(1)−P(1)	175.83(3)	176.16(4)	Cl(3)−Os(1)−Cl(2)	170.77(3)	178.56(5)
C(1)−Os(1)−Cl(1)	173.84(10)	175.40(17)	C(2)−C(1)−Os(1)	174.8(3)	174.0(5)
P(1)−Os(1)−Cl(1)	92.46(3)	89.57(5)	P(2)−Os(1)−Cl(1)	84.71(3)	87.86(5)
Cl(2)−Os(1)−P(1)	86.72(3)	87.41(5)	Cl(2)−Os(1)−P(2)	90.16(3)	89.74(5)
Cl(3)−Os(1)−P(1)	92.21(3)	91.84(5)	Cl(3)−Os(1)−P(2)	90.43(3)	90.96(5)
Cl(2)−Os(1)−Cl(1)	88.81(3)	88.65(5)	Cl(3)−Os(1)−Cl(1)	82.07(3)	90.12(5)
C(1)−Os(1)−P(1)	89.87(10)	91.32(17)	C(1)−Os(1)−P(2)	93.26(10)	91.47(17)
C(1)−Os(1)−Cl(2)	97.02(10)	94.44(18)	C(1)−Os(1)−Cl(3)	92.14(10)	86.81(18)
C(1)−C(2)−C(3)	111.1(3)				

 © 2004 Wiley-VCH Verlag GmbH & Co. KGaA, Weinheim

Os−Cl(3) [2.3874(8) Å], due to the strong *trans* influence of the carbyne ligand.

The structure of **5** has been previously assigned on the basis of NMR spectroscopic data.[23] Its structure was now also confirmed by an X-ray diffraction study. A view of the molecular geometry of **5** is shown in Figure 2. Selected bond lengths and angles are given in Table 1. Overall, the structural features of **5** are similar to those of **2** and **4**.

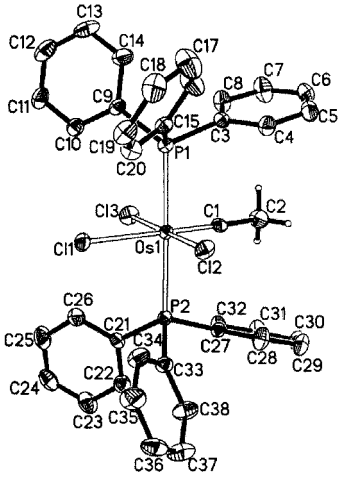

Figure 2. Molecular structure for [$OsCl_3(\equiv CCH_3)(PPh_3)_2$] (**5**)

The chemistry of (carbyne)osmium complexes has received considerable attention, especially in recent years.[8,10,13,15−19,20a,20c,20d,20e,21−25,28−38] Reported compounds closely related to **2**−**5** include [$OsCl_3(\equiv CPh)(PPh_3)_2$],[35] [$OsCl_2(SCN)(\equiv CC_6H_4NMe_2)(PPh_3)_2$],[35] [$OsHCl_2(\equiv CR')(PR_3)_2$] (R = Cy, *i*Pr),[19,24,25,36] [$OsHCl(OPh)(\equiv CMe)(P{i}Pr_3)_2$],[19] and [$OsCl_2(\equiv C-CH=CRPh)[P(iPr)_2CH_2CO_2Me)[P(iPr)_2CH_2CO_2)]$] (R = Ph, Me).[34] The analogous carbyne complex [$OsCl_3(\equiv CPh)(PPh_3)_2$] was previously obtained from the reaction of HCl with [$OsCl(\equiv CPh)(O_2CO)(PPh_3)_2$], which was in turn prepared from the reaction of [$OsCl(\equiv CPh)(CO)(PPh_3)_2$] with O_2.[35b] Thus, the reactions reported here represent a much simpler route to (carbyne)osmium complexes of the type [$OsX_3(\equiv CR')(PR_3)_2$] (X = halide).

Preparation of Vinylidene Complexes [$OsCl_2(=C=CHR)(PPh_3)_2$]

Deprotonation of (carbyne)metal complexes is one of the common routes to prepare vinylidene complexes. For example, deprotonation of [$CpOsH(\equiv CCH_2Ph)[P(iPr_3)]BF_4$, [$OsH(OAc)(\equiv CCH_3)(P{i}Pr_3)_2]BF_4$, [$OsHCl_2(\equiv CCH_2Ph)(P{i}Pr_3)_2$], and [$CpMn(\equiv CCH_3)(CO)_2]BCl_4$ produces the vinylidene complexes [$CpOsH(=C=CHPh)(P{i}Pr_3)$],[17] [$OsH(OAc)(=C=CH_2)(P{i}Pr_3)_2$],[21] [$OsHCl(=C=CHPh)(P{i}Pr_3)_2$][37] and [$CpMn(=C=CH_2)(CO)_2$],[39] respectively. Thus, it was reasoned that the vinylidene complexes [$OsCl_2(=C=CHR)(PPh_3)_2$] might be obtained by treatment of the easily accessible (carbyne)trichloro complexes [$OsCl_3(=CCH_2R)(PPh_3)_2$] with bases. Indeed, the (carbyne)-trichloro complexes **2**−**4** were readily deprotonated by NEt_3 to give the corresponding moisture-sensitive dichloro(vinylidene) complexes **6**−**8**, which can be isolated in good to excellent yields [Equation (3)].

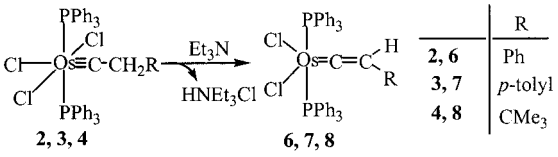

(3)

Our attempt to isolate the vinylidene complex [$OsCl_2(=C=CH_2)(PPh_3)_2$] from the deprotonation reaction of the (carbyne)trichloro complex [$OsCl_3(\equiv CCH_3)(PPh_3)_2$] (**5**) failed, however. The in situ $^{31}P\{^1H\}$ NMR spectrum for the reaction of **5** with NEt_3 in CD_2Cl_2 also showed a new broad peak at $\delta \approx 3.7$ ppm, which is similar to those observed for the in situ reactions of [$OsCl_3(\equiv CCH_2R)(PPh_3)_2$] (R = Ph or *p*-tolyl, CMe_3) with NEt_3, indicative of the formation of the vinylidene complex [$OsCl_2(=C=CH_2)(PPh_3)_2$]. However, after workup with a procedure similar to that used for the isolation of **6**−**8**, the isolated solid showed the $^{31}P\{^1H\}$ NMR signal of **5** and several unidentified broad peaks. Apparently, the initially formed vinylidene complex decomposes during workup.

The solid-state structure of the vinylidene complex **8** was determined by an X-ray diffraction study. A view of the molecular geometry of **8** is shown in Figure 3. Selected bond lengths and angles are given in Table 2. The geometry around the osmium atom in **8** may be described as a distorted trigonal bipyramid with two PPh_3 ligands at the axial positions and the other three ligands in the equatorial plane. The deviation is reflected by the P(1)−Os−P(2) angle [168.13(2)°] (which is bent away from the vinylidene ligand) and the Cl(1)−Os−Cl(2) angle [149.31(2)°]. The Cl−Os−Cl angle is close to that calculated for the model complex [$OsCl_2(=C=CH_2)(PH_3)_2$] (146.9°)[40] and the X−M−X angles observed in the analogous compounds

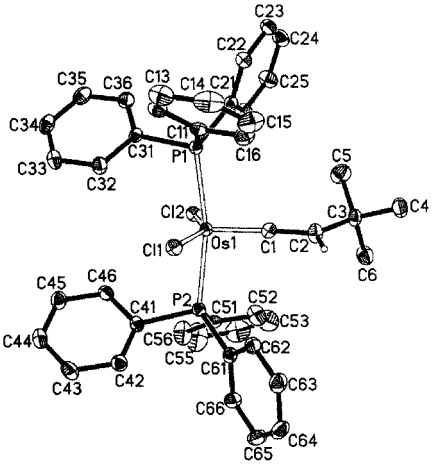

Figure 3. Molecular structure for [$OsCl_2(=C=CHCMe_3)(PPh_3)_2$] (**8**)

 © 2004 Wiley-VCH Verlag GmbH & Co. KGaA, Weinheim

$[RuBr_2(=C=CHCMe_3)(PPh_3)_2]$ [144.81(7)°][3b] and $[RuCl_2(=C=C[Se(iPr)Ph](PPh_3)_2]$ [148.89(6)°].[41] The Cl−Ru−Cl angles in the vinylidene complexes $[RuCl_2(=C=CHPh)(PR_3)_2]$ [PR_3: PCy_3 = 158.31(7)°[5b]/156.93(2)°;[6] $PiPr_3$ = 158.63(4)°[6]] are significantly larger, however. The Os−C(1)−C(2) unit is nearly linear, with an Os−C(1)−C(2) angle of 175.5(2)° and Os−C(1) and C(1)−C(2) bond lengths of 1.796(3) and 1.320(4) Å, respectively, which compare well with those reported for other (vinylidene)osmium complexes.[8−16]

Table 2. Selected bond lengths [Å] and bond angles [°] for $[OsCl_2(=C=CHCMe_3)(PPh_3)_2]$ (**8**)

Os(1)−Cl(1)	2.3399(7)	Os(1)−Cl(2)	2.3457(6)
Os(1)−P(1)	2.3698(7)	Os(1)−P(2)	2.3690(7)
Os(1)−C(1)	1.796(3)	C(1)−C(2)	1.320(4)
C(2)−C(3)	1.521(4)		
P(1)−Os(1)−P(2)	168.13(2)	Cl(1)−Os(1)−Cl(2)	149.31(2)
C(1)−Os(1)−Cl(1)	103.28(8)	C(1)−Os(1)−Cl(2)	107.39(8)
Cl(1)−Os(1)−P(1)	88.22(2)	Cl(2)−Os(1)−P(1)	89.69(2)
Cl(1)−Os(1)−P(2)	87.27(2)	Cl(2)−Os(1)−P(2)	88.61(2)
C(1)−Os(1)−P(1)	96.15(9)	C(1)−Os(1)−P(2)	95.57(9)
C(2)−C(1)−Os(1)	175.5(2)	C(1)−C(2)−C(3)	129.1(3)

As mentioned previously, (vinylidene)osmium complexes with the general composition $[OsCl_2(=C=CHR)(PR_3)_2]$ are still very rare. Esteruelas et al. recently reported the vinylidene complex $[OsCl_2(=C=CHPh)(PiPr_3)_2]$, which was prepared by elimination of the imine ligands from the (imine)(vinylidene) complexes $[OsCl_2(=C=CHPh)(NH=CR_2)(PiPr_3)_2]$ [CR_2 = CMe_2, $C(CH_2)_5$] in a refluxing toluene solution.[13] As far as we know, complex **8** is the first structurally characterized osmium complex of this kind. Other reported five-coordinate (vinylidene)osmium complexes include $[OsHCl(=C=CHR)(PR'_3)_2]$ (PR'_3 = PCy_3, $PiPr_3$],[19,24,37,42] $[OsCl(=N=CR_2)(=C=CHPh)(PiPr_3)_2]$,[13] $[OsCl(=C=CHR)(2,6\text{-}[P(tBu)_2CH_2]_2C_6H_3)]$,[11] [Os[C(≡CR)=CHR)Cl(=C=CHR)$(PPh_3)_2$][22,23] and $[Os(CH=CHSiMe_3)Cl(=C=CHPh)(PiPr_3)_2]$.[43] These compounds adopt a Y-shaped geometry around the osmium atom.

Consistent with the solid-state structure, a freshly prepared and vacuum-dried sample of **8** in freshly distilled dry CD_2Cl_2 at room temperature shows a singlet $^{31}P\{^1H\}$ signal at δ = 3.4 ppm. The ^1H NMR spectrum in CD_2Cl_2 exhibits a triplet at δ = 1.20 ppm with a P-H coupling constant of 3.6 Hz for the vinylidene =CH proton and the $^{13}C\{^1H\}$ NMR spectrum displays two triplets at δ = 274.1 ($J_{P,C}$ = 12.5 Hz) and 120.5 ppm ($J_{P,C}$ = 5.5 Hz), which are due to C-α and -β of the vinylidene ligand, respectively.

Complexes **6** and **7** presumably have similar structures, as indicated by their NMR spectroscopic data. Freshly prepared and vacuum-dried samples of **6** and **7** in freshly distilled CD_2Cl_2 at room temperature show the $^{31}P\{^1H\}$ signals at δ = 9.6 and 9.2 ppm, respectively. The ^1H NMR spectra exhibits triplets at δ = 2.56 and 2.46 ppm for the vinylidene =C*H* protons of **6** and **7**, respectively. The $^{13}C\{^1H\}$ NMR spectra displays C-α signals of the vinylidene ligands at δ = 280.8 and 281.0 ppm for **6** and **7**, respectively.

Preparation of (Aqua)(vinylidene) Complexes $[OsCl_2(H_2O)(=C=CHR)(PPh_3)_2]$

During the process of recording the $^{31}P\{^1H\}$ NMR spectra of the vinylidene complexes **6** and **7** with commercially available CD_2Cl_2, it was found that the chemical shifts of the signals of the vinylidene complexes changed with different batches of solvent and with time when a non-sealed NMR tube was used. It was suspected that this change might be caused by coordination of water present in solution to give the (aqua)(vinylidene) complexes $[OsCl_2(H_2O)(=C=CHR)(PPh_3)_2]$, which equilibrate with $[OsCl_2(=C=CHR)(PPh_3)_2]$. As a result of fast dissociation and association of water, only one ^{31}P signal with an average ^{31}P shift is observed at room temperature. Different amounts of water present in the solution will therefore affect the relative amounts of the five-coordinate vinylidene complexes and the corresponding six-coordinate (aqua)(vinylidene) complexes, therefore resulting in different ^{31}P chemical shifts in the NMR spectra. This speculation was confirmed by experiments. At low temperature, the $^{31}P\{^1H\}$ NMR spectra in commercial CD_2Cl_2 show two singlets. The chemical shift of one of the ^{31}P signals is close to that of $[OsCl_2(=C=CHAr)(PPh_3)_2]$ in freshly dried CD_2Cl_2. The other signal can therefore be attributed to $[OsCl_2(H_2O)(=C=CHR)(PPh_3)_2]$. Treatment of a blue solution of **6** or **7** in CD_2Cl_2 in an NMR tube with a drop of water gave an orange solution immediately, the $^{31}P\{^1H\}$ NMR spectra of which shows sharp singlets at $\delta \approx -3.6$ or -3.8 ppm, respectively. The chemical shifts are very close to those of the ^{31}P signals suspected for the (aqua)(vinylidene) complexes observed at low temperature. The possibility of isomerism arising from the rotation of the vinylidene group at low temperature can be excluded because such a rotation does not generate two different electronically favourable conformers.

The (aqua)(vinylidene) complexes $[OsCl_2(H_2O)(=C=CHPh)(PPh_3)_2]$ (**9**) and $[OsCl_2(H_2O)(=C=CH\text{-}p\text{-}tolyl)(PPh_3)_2]$ (**10**) were isolated as orange solids on a preparative scale by treatment of **6** and **7** with excess water [Equation (4)]. Orange solids of **9** and **10** were also obtained when blue solids of **6** and **7** were exposed to air for 18 h.

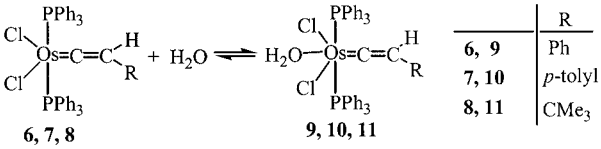

(4)

The solid-state structure of **9** (Figure 4) was confirmed by an X-ray diffraction study. Selected bond lengths and angles are given in Table 3. The geometry around the osmium atom in **9** can be viewed as a distorted octahedron with two PPh_3 ligands *trans* to each other lying in the axial

 © 2004 Wiley-VCH Verlag GmbH & Co. KGaA, Weinheim

positions. The equatorial plane is formed by two chloro, the vinylidene and water ligands with the coordinated water molecule *trans* to the vinylidene ligand [O(1W)−Os−C(1) = 175.8(2)°]. The two mutually *trans*-disposed chloro ligands severely bend away from the vinylidene ligand and toward the water molecule with a Cl(1)−Os−Cl(2) angle of 158.56(5)° and Cl(1)−Os−O and Cl(2)−Os−O angles of 81.13(11)° and 77.53(11)°, respectively. These angles deviate greatly from the ideal value of 180° for a *trans* angle and 90° for a *cis* angle. The vinylidene ligand is bound to the metal atom in a nearly linear fashion with an Os−C(1)−C(2) angle of 174.7(6)°. The Os−C(1) [1.812(7) Å] and C(1)−C(2) [1.298(8) Å] bond lengths are similar to those of **8**, and compare well with those observed in other (vinylidene)osmium complexes.[8−16] The Os−O bond length is 2.289(4) Å, which is close to those in [OsCl(=C=CHPh)(NH=CMe_2)(H_2O)($PiPr_3$)$_2$]OTf [2.281(6) Å],[14] [OsCl(=CHPh)(H_2O)(CO)($PiPr_3$)$_2$]BF_4 [2.182(5) Å],[44a] [OsMe(H_2O)(CO)$_2$(PMe_3)$_2$]OTf [2.155(6) Å],[44b] [Cp*Os(η^3-C_4H_7)Me(H_2O)]BF_4 [44c] [2.158(5) Å] and [$OsCl_2$(H_2O)(≡CCH=CPh_2)(PPh_3)$_2$]BF_4 [2.209(5) Å].[45]

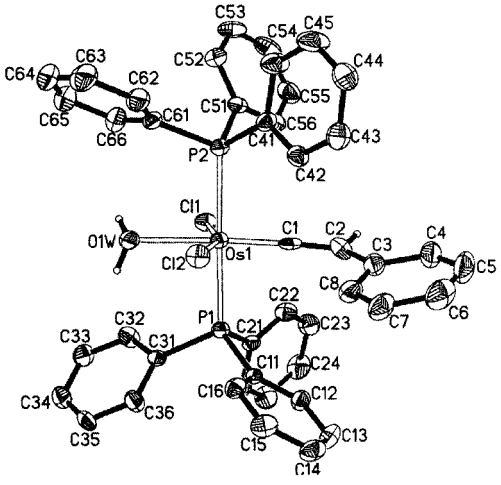

Figure 4. Molecular structure for [$OsCl_2$(H_2O)(=C=CHPh)(PPh_3)$_2$] (**9**)

Table 3. Selected bond lengths [Å] and angles [°] for [$OsCl_2$(H_2O)(=C=CHPh)(PPh_3)$_2$]·C_6H_6 (**9**·C_6H_6)

Os(1)−P(1)	2.3848(15)	Os(1)−P(2)	2.3959(15)
Os(1)−Cl(1)	2.3699(15)	Os(1)−Cl(2)	2.3886(14)
Os(1)−C(1)	1.812(7)	Os(1)−O(1 W)	2.289(4)
C(1)−C(2)	1.298(8)	C(2)−C(3)	1.479(9)
P(1)−Os(1)−P(2)	178.88(5)	Cl(1)−Os(1)−Cl(2)	158.56(5)
C(1)−Os(1)−O(1W)	175.8(2)	C(2)−C(1)−Os(1)	174.7(6)
C(1)−C(2)−C(3)	127.2(7)	O(1W)−Os(1)−P(1)	91.07(9)
O(1W)−Os(1)−Cl(1)	81.13(11)	O(1W)−Os(1)−Cl(2)	77.58(11)
C(1)−Os(1)−Cl(1)	102.54(18)	C(1)−Os(1)−Cl(2)	98.83(19)
C(1)−Os(1)−P(1)	87.08(16)	C(1)−Os(1)−P(2)	91.96(16)
Cl(1)−Os(1)−P(1)	88.84(5)	P(1)−Os(1)−Cl(2)	94.06(6)
Cl(1)−Os(1)−P(2)	90.83(6)	Cl(2)−Os(1)−P(2)	86.64(6)
O(1W)−Os(1)−P(2)	89.93(10)		

The water in **9** and **10** is only weakly bound to the metal center. Thus, when the orange solids of **9** or **10** are placed under vacuum for 3 h, the color changed to blue, indicating the reformation of **6** or **7**. Similarly, if the isolated orange solids of **9** or **10** are redissolved in CD_2Cl_2, the $^{31}P\{^1H\}$ NMR spectra at room temperature show a broad signal with a chemical shift significantly downfield from those observed in the presence of added water, indicating that water is partially dissociated and the equilibrium shown in Equation (4) occurs in solution. Thus, the NMR spectroscopic data of **9** and **10** have to be collected in the presence of added water. The $^{13}C\{^1H\}$ NMR spectrum of **9** in a CD_2Cl_2 solution saturated with H_2O shows the Os=C $^{13}C\{^1H\}$ signal as a triplet at δ = 289.1 ppm ($J_{P,C}$ = 11.4 Hz). The ^1H NMR signal of =C=CH_2 of **9** is observed at δ = 2.48 ppm at room temp. and at δ = 2.61 ppm at 211 K. The ^1H NMR signal of H_2O is observed at δ = 1.95 ppm at 211 K**.** The NMR spectroscopic data of **9** are consistent with the solid-state structure. Complex **10** presumably has a structure similar to that of **9**, as judged by its spectroscopic data.

As indicated by NMR experiments, complex **8** also reacts with water to give the (aqua)(vinylidene) complex [$OsCl_2$(H_2O)(=C=CHCMe_3)(PPh_3)$_2$] (**11**). Thus, the $^{31}P\{^1H\}$ NMR spectrum of a sample of **8** in commercially available CD_2Cl_2 at room temperature shows a singlet at δ = 2.8 ppm which is slightly upfield from that obtained with dry CD_2Cl_2. At 188 K, this singlet splits into two peaks at δ = 3.6 and −10.2 ppm, which can be attributed to [$OsCl_2$(=C=CHCMe_3)(PPh_3)$_2$] (**8**) and [$OsCl_2$(H_2O)-(=C=CHCMe_3)(PPh_3)$_2$] (**11**), respectively. Similarly, the ^1H NMR spectrum in CD_2Cl_2 at room temperature shows one C=CH signal at δ = 1.17 ppm and at 188 K two C=CH signals at δ = 1.50 and 0.91 ppm, which can be assigned to **8** and **11**, respectively. The water proton signal appears as a broad peak at δ = 2.12 ppm at room temperature, which sharpens at low temperature with a similar chemical shift and gives a relative integration of 2:1 with the less-intense vinylidene signal of **11**. As further evidence for the formation of **11**, addition of a drop of water to a solution of **8** in commercial CD_2Cl_2 in an NMR tube causes the ^{31}P signal to shift from δ = 2.8 ppm to −5.8 ppm, and the ^1H signal of =CCH to shift from δ = 1.17 ppm to 0.91 ppm. The upfield shift of the ^{31}P signal is expected because the relative amount of **11** is increased when the concentration of water in the solution is increased. However, the ^{31}P shift cannot, even in the presence of excess water, reach the value of δ = −10.2 ppm observed for **11** at low temperature, suggesting that the equilibrium constant is small (see below).

During the process of the NMR study, it was found that these vinylidene species (**8** and **11**) are unstable in solution, especially in the presence of added water. The major decomposition product is the carbyne complex **4**. Other detectable decomposition species include a small amount of PPh_3 and others showing unidentified doublet and triplet signals. The decomposition is likely initiated by the protonation of the vinylidene ligand of **11** with water present in the solution. Owing to the instability and incomplete

 © 2004 Wiley-VCH Verlag GmbH & Co. KGaA, Weinheim

conversion of **8** to **11**, even in the presence of excess water, complex **11** could not be isolated.

NMR Study of the Equilibria

We carried out variable-temperature $^{31}P\{^1H\}$ and ^1H NMR experiments to study the dynamic process between $[OsCl_2(=C=CHR)(PPh_3)_2]$ and $[OsCl_2(H_2O)(=C=CHR)(PPh_3)_2]$. As an illustration, the $^{31}P\{^1H\}$ NMR spectra of a sample of **6** in wet CD_2Cl_2 (the Os/H_2O molar ratio in solution is 1:0.2) at different temperatures are shown in Figure 5. At room temperature (298 K), the ^{31}P signal is a singlet at δ = 9.1 ppm, which broadens and shifts upfield upon decreasing the temperature to 239 K. The upfield shift of the ^{31}P signal on lowering the temperature indicates that the equilibrium is shifted toward the formation of the (aqua)(vinylidene) complex **9** at lower temperature. The singlet separates into two peaks with unequal intensities when the temperature is lowered below 217 K. At 198 K, two sharp singlets in about a 5:1 ratio at δ = 11.6 and −3.4 ppm are observed, due to the ^{31}P signals of **6** and **9**, respectively. Similarly, in the ^1H NMR spectrum in CD_2Cl_2 at room temperature, the Os=C=CH vinylidene proton displays only one triplet at δ = 2.54 ppm with a P-H coupling constant of 3.3 Hz. This signal is somewhat broader when the temperature is lowered and at 190 K gives rise to two broad singlets (the broadening is probably due to unresolved coupling with the ^{31}P nuclei) at δ = 2.71 and 2.65 ppm in an approximate ratio of 5:1. The water proton signal at 190 K appears as a singlet at δ = 1.88 ppm with a relative integration of 2:1 with the less-intense vinylidene signal at δ = 2.65 ppm. The water content in the solution affects the appearance of the variable-temperature spectra. Thus, when a solution with an Os/H_2O molar ratio of 1:1.6 was used in the variable-temperature experiments, the NMR spectra show a singlet ^{31}P signal with a chemical shift between those of **6** and **9** at room temperature, as one might expect, but only show the signal of the (aqua)(vinylidene) complex **9**, while the signal of **6** cannot be detected, when the temperature is lowered below 255 K, due to the higher affinity of the metal center for H_2O at low temperature. The variable-temperature spectra of **7/10** and **8/11** show spectroscopic features similar to those of **6** and **8**.

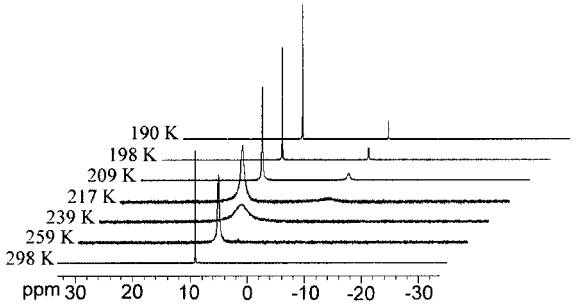

Figure 5. The variable-temperature $^{31}P\{^1H\}$ NMR spectra of $[OsCl_2(=C=CHPh)(PPh_3)_2]$ (**6**) and $[OsCl_2(H_2O)(=C=CHPh)(PPh_3)_2]$ (**9**) in wet CD_2Cl_2 (Os/H_2O molar ratio in solution = 1:0.2) at 121.5 MHz

The equilibrium constants at several temperatures (between 298 and 270 K) were estimated on the basis of variable-temperature $^{31}P\{^1H\}$ and ^1H NMR measurements of samples of **9**, **10** and **11** in CD_2Cl_2. The relative amounts of the five-coordinate vinylidene complexes and their corresponding (aqua)(vinylidene) complexes were calculated from the average ^{31}P chemical shifts assuming that the chemical shifts of five-coordinate vinylidene complexes and their corresponding (aqua)(vinylidene) complexes do not change with temperature.[46] The relative concentrations of coordinated and free water in the solution can be obtained from the integrals of the H_2O signals in the ^1H NMR spectra and the concentrations of the aqua complexes. The equilibrium constants at different temperatures calculated based

Table 4. Parameters for the equilibria between $[OsCl_2(=C=CHR)(PPh_3)_2]$ and $[OsCl_2(H_2O)(=C=CHR)(PPh_3)_2]$

$[OsCl_2(=C=CHPh)(PPh_3)_2] + H_2O \rightleftarrows [OsCl_2(H_2O)(=C=CHPh)(PPh_3)_2]$ (**9**)				
T [K]	298	292	282	270
K[a]	202.7	312.6	788.9	3085
ln$K$	5.312	5.745	6.671	8.034
ΔG^0 [kcal·mol^{-1}]	−3.15	−3.33	−3.73	−4.30
$[OsCl_2\{=C=CH(p\text{-tolyl})\}(PPh_3)_2] + H_2O \rightleftarrows [OsCl_2(H_2O)\{=C=CH(p\text{-tolyl})\}(PPh_3)_2]$ (**10**)				
T [K]	298	287	280	270
K[b]	172.1	506.9	1197	4684
ln$K$	5.148	6.228	7.087	8.452
ΔG^0 [kcal·mol^{-1}]	−3.05	−3.55	−3.94	−4.53
$[OsCl_2(=C=CHCMe_3)(PPh_3)_2] + H_2O \rightleftarrows [OsCl_2(H_2O)(=C=CHMe_3)(PPh_3)_2]$ (**11**)				
T (K)	298	290	285	279	275
K[c]	15.51	35.22	69.37	172.8	416.4
ln$K$	2.741	3.562	4.239	5.152	6.032
ΔG^0 [kcal·mol^{-1}]	−1.62	−2.05	− 2.40	−2.86	−3.30

[a] The values were obtained with a CD_2Cl_2 solution having an Os/H_2O molar ratio of 1:1.6. [b] The values were obtained with a CD_2Cl_2 solution having an Os/H_2O molar ratio of 1:1. [c] The values were obtained with a CD_2Cl_2 solution having an Os/H_2O molar ratio of 1:0.4.

 © 2004 Wiley-VCH Verlag GmbH & Co. KGaA, Weinheim

on these data are summarized in Table 4. A plot of $\ln K$ against reciprocal absolute temperature gave a straight line. According to the equation $\ln K = -(\Delta H^0/R)(1/T) + \Delta S^0/R$, the standard enthalpy and the standard entropy change of the reaction can be calculated from the slope of the straight line and the intercept, respectively. Approximate values of $\Delta H^0 = -22.7$ kcal·mol^{-1} and $\Delta S^0 = -70.96$ cal·mol^{-1}·K^{-1} were calculated for the equilibrium between **8** and **11** in CD_2Cl_2, and the value of ΔG^0 at 298 K was −1.62 kcal·mol^{-1}. For the equilibrium between **6** and **9** in CD_2Cl_2, the relevant values were calculated to be $\Delta H^0 = -15.7$ kcal·mol^{-1}, $\Delta S^0 = -42.3$ cal·mol^{-1}·K^{-1} and $\Delta G^0_{(298)} = -3.15$ kcal·mol^{-1}. These results indicate that formation of the (aqua)(vinylidene) is exothermic and that the equilibria are shifted to the (aqua)(vinylidene) complexes when the temperature is lowered, as mentioned previously.

As can be seen from Table 4, the equilibrium constant at room temperature for **6/9** is similar to that of **7/11** and is about 13 times as large as that of **8/11**, indicating that [$OsCl_2(=C=CHAr)(PPh_3)_2$] (**6** and **7**) have a higher affinity for H_2O than [$OsCl_2(=C=CHCMe_3)(PPh_3)_2$] (**8**). This difference may be related to that fact that CMe_3 is more electron-donating than Ar, thus the Lewis acidities of **6** and **7** are higher than that of **8**.

Conclusions

Reaction of [$OsCl_2(PPh_3)_3$] with terminal acetylenes HC≡CR (R = Ph, *p*-tolyl, CMe_3) in the presence of HCl readily produced the carbyne complexes [$OsCl_3(\equiv CCH_2R)(PPh_3)_2$]. Due to the acidic nature of the protons α to the carbyne carbon atom, the vinylidene complexes [$OsCl_2(=C=CHR)(PPh_3)_2$] (R = CMe_3, Ph, *p*-tolyl) can be easily prepared from these carbyne complexes by treatment with NEt_3. Interestingly, these vinylidene complexes are hygroscopic and react with water to give [$OsCl_2(H_2O)(=C=CHR)(PPh_3)_2$] reversibly. Dynamic NMR studies show that the vinylidene complexes [$OsCl_2(=C=CHR)(PPh_3)_2$] (R = Ph, *p*-tolyl) have a higher tendency to form the aqua complexes than does [$OsCl_2(=C=CHCMe_3)(PPh_3)_2$]. Thus, the (aqua)(vinylidene) complexes [$OsCl_2(=C=CHR)(H_2O)(PPh_3)_2$] (R = Ph, *p*-tolyl) could be isolated by treatment of the anhydrous vinylidene complexes with water.

Experimental Section

General: All manipulations were carried out at room temperature under nitrogen using standard Schlenk techniques, unless otherwise stated. Solvents were distilled under nitrogen from sodium/benzophenone (hexane, diethyl ether, THF, benzene) or calcium hydride (dichloromethane, $CHCl_3$). The starting material [$OsCl_2(PPh_3)_3$][47] was prepared according to literature methods. Microanalyses were performed by M-H-W Laboratories (Phoenix, AZ). ^{1}H, ^{13}C{^{1}H} and ^{31}P{^{1}H} NMR spectra were collected with a Bruker ARX-300 spectrometer (300 MHz) or a JOEL EX-400 spectrometer (400 MHz). ^{1}H and ^{13}C NMR chemical shifts are relative to TMS, and ^{31}P NMR chemical shifts are relative to 85% H_3PO_4.

[$OsCl_3(\equiv C-CH_2Ph)(PPh_3)_2$] (2): HCl·$OEt_2$ (1.00 mL,1.0 M in diethyl ether solution, 1.0 mmol) and HC≡CPh (0.32 mL, 2.9 mmol) were added to a solution of [$OsCl_2(PPh_3)_3$] (0.50 g, 0.48 mmol) in benzene (15 mL). The reaction mixture was stirred at room temperature for 6 h to give a yellow microcrystalline solid, which was collected by filtration, washed with diethyl ether (2 × 20 mL) and dried under vacuum (0.33 g). The filtrate was concentrated to ca. 5 mL, and addition of diethyl ether (20 mL) to the residue produced additional yellow solid, which was collected by filtration, washed with diethyl ether (2 × 20 mL), and dried under vacuum overnight (0.05 g). Total yield: 0.38 g (86%). ^{1}H NMR (399.65 MHz, $CDCl_3$): δ = 1.77 (s, 2 H, Os≡CCH_2), 6.46 (d, $J_{H,H}$ = 7.1 Hz, 2 H, *o*-C_6H_5), 7.08 (t, $J_{H,H}$ = 7.6 Hz, 2 H, *m*-C_6H_5), 7.19 (t, $J_{H,H}$ = 7.6 Hz, 1 H, *p*-C_6H_5), 7.29−7.38 (m, 18 H, P*Ph*$_3$), 7.81−7.86 (m, 12 H, P*Ph*$_3$) ppm. ^{13}C{^{1}H} NMR (100.4 MHz, CD_2Cl_2): δ = 278.2 (t, $J_{P,C}$ = 11.1 Hz, Os≡*C*), 134.9−125.0 (m, C_6H_5, PPh_3), 57.3 (s, Os≡C*C*H_2) ppm. ^{31}P{^{1}H} NMR (121.5 MHz, $CDCl_3$): δ = −12.9 (s) ppm. $C_{44}H_{37}Cl_3OsP_2$ (924.3): calcd. C 57.18, H 4.04; found C 57.35, H 4.19.

[$OsCl_3\{\equiv C-CH_2(p\text{-tolyl})\}(PPh_3)_2$] (3): HCl·$OEt_2$ (1.00 mL, 1.0 M in diethyl ether solution, 1.0 mmol) and 4-ethynyltoluene (0.24 mL, 1.9 mmol) were added to a solution of [$OsCl_2(PPh_3)_3$] (0.50 g, 0.48 mmol) in benzene (15 mL). The reaction mixture was stirred at room temperature for 6 h to give a yellow microcrystalline solid, which was collected by filtration, washed with diethyl ether (2 × 20 mL) and dried under vacuum (0.32 g). The filtrate was concentrated to about 5 mL, and addition of diethyl ether (20 mL) to the residue produced additional yellow solid, which was collected by filtration, washed with diethyl ether (2 × 15 mL), and dried under vacuum overnight (31 mg). Total yield: 0.35 g (78%). ^{1}H NMR (399.65 MHz, $CDCl_3$): δ = 1.72 (s, 2 H, Os≡CCH_2), 2.22 (s, 3 H, $C_6H_4CH_3$), 6.21 (d, $J_{H,H}$ = 8.0 Hz, 2 H, C_6H_4) 6.79 (d, $J_{H,H}$ = 8.0 Hz, 2 H, C_6H_4), 7.30 (m, 18 H, PPh_3), 7.80 (m, 12 H, PPh_3) ppm. ^{13}C{^{1}H} NMR (100.4 MHz, CD_2Cl_2): δ = 280.1 (t, $J_{P,C}$ = 12.0 Hz, Os≡*C*), 138.0−122.1 (m, C_6H_5, PPh_3), 57.1 (s, Os≡C*C*H_2), 21.2 (s, C_6H_4-*C*H_3) ppm. ^{31}P{^{1}H} NMR (121.5 MHz, $CDCl_3$): δ = −12.1 (s) ppm. $C_{45}H_{39}Cl_3OsP_2$ (938.3): calcd. C 57.60, H 4.19; found C 57.40, H 4.34.

[$OsCl_3(\equiv CCH_2CMe_3)(PPh_3)_2$] (4): HC≡$CCMe_3$ (0.28 mL, 2.3 mmol) and HCl·OEt_2 (0.80 mL, 0.80 mmol, 1.0 M in diethyl ether solution) were added to a solution of [$OsCl_2(PPh_3)_3$] (0.40 g, 0.38 mmol) in benzene (15 mL). The reaction mixture was stirred at room temperature for 6 h to give a yellow microcrystalline solid, which was collected by filtration, washed with diethyl ether (2 × 20 mL) and dried under vacuum (0.20 g). The filtrate was concentrated to ca. 3 mL, and addition of diethyl ether (20 mL) to the residue produced additional yellow solid, which was collected by filtration, washed with diethyl ether (2 × 20 mL), and dried under vacuum overnight (0.08 g). Total yield: 0.28 g (82%). The spectroscopic data have been reported previously.[22]

[$OsCl_3(\equiv CCH_3)(PPh_3)_2$] (5): HC≡$CSiMe_3$ (0.27 mL, 1.9 mmol) and HCl·OEt_2 (1.20 mL, 1.0 M in diethyl ether solution, 1.2 mmol) were added to a solution of [$OsCl_2(PPh_3)_3$] (0.50 g, 0.48 mmol) in benzene (15 mL). The reaction mixture was stirred at room temperature for 8 h to give a yellow microcrystalline solid, which was collected by filtration, washed with diethyl ether (2 × 20 mL) and dried under vacuum (0.25 g). The filtrate was concentrated to ca. 3 mL, and addition of diethyl ether (20 mL) to the residue produced additional yellow solid, which was collected by filtration,

 © 2004 Wiley-VCH Verlag GmbH & Co. KGaA, Weinheim

washed with diethyl ether (2 × 15 mL), and dried under vacuum overnight (0.04 g). Total yield: 0.29 g (71%). ^{1}H NMR (300.13 MHz, CD_2Cl_2): δ = 0.04 (t, $J_{P,H}$ = 2.5 Hz, 3 H, CH_3), 7.36−7.43 (m, 18 H, PPh_3), 7.89−7.96 (m, 12 H, PPh_3) ppm. ^{13}C{^{1}H} NMR (100.40 MHz, CD_2Cl_2): δ = 283.7 (t, $J_{P,C}$ = 12.3 Hz, Os≡*C*), 135.1−127.9 (m, PPh_3), 36.9 (s, Os≡C-*C*H_3) ppm. ^{31}P{^{1}H} NMR (121.5 MHz, CD_2Cl_2): δ = −13.5 (s) ppm. $C_{38}H_{33}Cl_3OsP_2$ (848.2): calcd. C 53.81, H 3.92; found C 53.60, H 4.18.

[$OsCl_2$(=C=CHPh)(PPh_3)$_2$] (6): NEt_3 (0.43 mL, 3.1 mmol) was added to a CH_2Cl_2 (40 mL) solution of [$OsCl_3$(≡CCH_2Ph)(PPh_3)$_2$] (0.57 g, 0.62 mmol). The reaction mixture rapidly changed color from yellow to blue. After stirring for 1 h, the solvent was removed completely under vacuum and the resulting blue solid was extracted with benzene (30 mL). The extract was filtered through Celite to remove the insoluble Et_3N·HCl. The filtrate was concentrated to ca. 1 mL and diethyl ether was slowly added to give a blue solid, which was collected by filtration, washed with diethyl ether (2 × 10 mL) and dried under vacuum overnight. Yield: 0.47 g (85%). ^{1}H NMR (300.13 MHz, freshly distilled CD_2Cl_2): δ = 2.56 (t, $J_{P,H}$ = 3.3 Hz, 1 H, Os=C=C*H*), 6.48 (d, $J_{H,H}$ = 7.4 Hz, 2 H, *o*-C_6H_5), 6.71 (t, $J_{H,H}$ = 7.4 Hz, 1 H, *p*-C_6H_5), 7.02 (t, $J_{H,H}$ = 7.4 Hz, 2 H, *m*-C_6H_5), 7.25−7.41 (m, 18 H, PPh_3), 7.57−7.64 (m, 12 H, PPh_3) ppm. ^{13}C{^{1}H} NMR (100.4 MHz, freshly distilled CD_2Cl_2): δ = 280.8 (br., Os=*C*), 135.0−124.3 (m, C_6H_5, PPh_3), 112.1 (t, $J_{P,C}$ = 4.8 Hz, Os=C=*C*H) ppm. ^{31}P{^{1}H} NMR (121.5 MHz, freshly distilled CD_2Cl_2): δ = 9.6 (s) ppm. $C_{44}H_{36}Cl_2OsP_2$ (887.8): calcd. C 59.53, H 4.09; found C 59.54, H 4.01.

[$OsCl_2${=C=CH(*p*-tolyl)}(PPh_3)$_2$] (7): NEt_3 (0.44 mL, 3.2 mmol) was added to a CH_2Cl_2 (40 mL) solution of [$OsCl_3${≡CCH_2(*p*-tolyl)}(PPh_3)$_2$] (0.50 g, 0.53 mmol). The reaction mixture rapidly changed color from yellow to blue. After stirring for 1 h, the solvent was removed completely under vacuum and the resulting blue solid was extracted with benzene (30 mL). The extract was filtered through Celite to remove the insoluble Et_3N·HCl. The filtrate was concentrated to ca. 1 mL and diethyl ether was slowly added to give a blue solid, which was collected by filtration, washed with diethyl ether (2 × 10 mL) and dried under vacuum overnight. Yield: 0.42 g (88%). ^{1}H NMR (300.13 MHz, CD_2Cl_2): δ = 2.39 (s, 3 H, $C_6H_4CH_3$), 2.46 (t, $J_{P,H}$ = 3.4 Hz, 1 H, Os=C=C*H*), 6.40 (d, $J_{H,H}$ = 8.0 Hz, 2 H, C_6H_4), 6.87 (d, $J_{H,H}$ = 8.0 Hz, 2 H, C_6H_4), 7.33−7.41 (m, 18 H, PPh_3), 7.59−7.62 (m, 12 H, PPh_3) ppm. ^{13}C{^{1}H} NMR (100.4 MHz, freshly distilled CD_2Cl_2): δ = 281.0 (br., Os=*C*), 135.0−124.9 (m, C_6H_4, PPh_3), 112.0 (t, $J_{P,C}$ = 4.5 Hz, Os=C=*C*H), 20.9 (s, C_6H_4-*C*H_3) ppm. ^{31}P{^{1}H} NMR (121.5 MHz, freshly distilled CD_2Cl_2): δ = 9.2 (s) ppm. $C_{45}H_{38}Cl_2OsP_2$ (901.8): calcd. C 59.93, H 4.25; found C 59.76, H 4.26.

[$OsCl_2$(=C=CHCMe_3)(PPh_3)$_2$] (8): NEt_3 (0.31 mL, 1.7 mmol) was added with stirring to a solution of [$OsCl_3$(≡CCH_2CMe_3)(PPh_3)$_2$] (0.50 g, 0.55 mmol) in CH_2Cl_2 (50 mL). The reaction solution changed color from orange to brown immediately. The reaction mixture was stirred at room temperature for 1 h and the solvent was removed completely under vacuum. The brown solid was extracted with benzene (15 mL) and the extract filtered through Celite to remove the insoluble Et_3N·HCl. The volume of the brown filtrate was reduced to ca. 1 mL. Addition of diethyl ether (20 mL) to the residue produced a purple solid, which was collected by filtration, washed with diethyl ether (2 × 10 mL) and hexane (20 mL) and dried under vacuum overnight. Yield: 0.29 g (61%). ^{1}H NMR (300.13 MHz, freshly distilled CD_2Cl_2): δ = 0.54 [s, 9 H, C(CH_3)$_3$], 1.20 (t, $J_{P,H}$ = 3.6 Hz, 1 H, Os=C=C*H*), 7.42−7.51 (m, 18 H, PPh_3), 7.66−7.71 (m, 12 H, PPh_3) ppm. The signal of H_2O appears at room temp. at δ = 1.73 ppm and at 211 K at δ = 1.86 ppm with an integral of 2:1 relative to that of the vinylidene signal. ^{13}C{^{1}H} NMR (100.40 MHz, freshly distilled CD_2Cl_2): δ = 274.1 (t, $J_{P,C}$ = 12.5 Hz, Os=*C*), 134.9−128.4 (m, PPh_3), 120.5 (t, $J_{P,C}$ = 5.5 Hz, Os=C=*C*H), 32.60 [s, C(*C*H_3)$_3$], 27.47 [s, *C*(CH_3)$_3$] ppm. ^{31}P{^{1}H} NMR (121.5 MHz, freshly distilled CD_2Cl_2): δ = 3.4 (s) ppm. FAB-MS (NBA): *m*/*z* = 868 [M^+]. $C_{42}H_{40}Cl_2OsP_2$ (867.8): calcd. C 58.13, H 4.65; found C 58.49, H 4.53.

[$OsCl_2$(H_2O)(=C=CHPh)(PPh_3)$_2$] (9): Water (0.2 mL) was added to a blue solution of [$OsCl_2$(=C=CHPh)(PPh_3)$_2$] (0.15 g, 0.17 mmol) in CH_2Cl_2 (10 mL). The solution turned orange immediately. After stirring for 20 min, the solvent was pumped off to give an orange paste. Diethyl ether (10 mL) was added to the residue to give an orange solid, which was collected by filtration, washed with diethyl ether (2 × 5 mL) and dried under vacuum for 30 min. Yield: 0.14 g (91%). ^{1}H NMR (300.13 MHz, CD_2Cl_2): δ = 2.48 (t, $J_{P,H}$ = 3.3 Hz, 1 H, Os=C=C*H*), 6.70 (d, $J_{H,H}$ = 7.2 Hz, 2 H, *o*-C_6H_5), 6.76 (t, $J_{H,H}$ = 7.4 Hz, 1 H, *p*-C_6H_5), 7.08 (t, $J_{H,H}$ = 7.4 Hz, 2 H, *m*-C_6H_5), 7.28−7.40 (m, 18 H, PPh_3), 7.70−7.76 (m, 12 H, PPh_3) ppm. The signal of H_2O appears at room temp. at δ = 1.77 ppm and at 211 K at δ = 1.95 ppm with an integral of 2:1 relative to that of the vinylidene =CH signal. ^{13}C{^{1}H} NMR (100.4 MHz, CD_2Cl_2): δ = 289.1 (t, $J_{P,C}$ = 11.4 Hz, Os=*C*), 134.7−123.8 (m, C_6H_5, PPh_3), 112.3 (t, $J_{P,C}$ = 4.4 Hz, Os=C=*C*H) ppm. ^{31}P{^{1}H} NMR (121.5 MHz, CD_2Cl_2 in the presence of a drop of water): δ = −3.6 (s) ppm. $C_{44}H_{38}Cl_2OOsP_2$ (905.8): calcd. C 58.34, H 4.23; found C 58.54, H 4.42.

[$OsCl_2$(H_2O){=C=CH(*p*-tolyl)}(PPh_3)$_2$] (10): Water (0.2 mL) was added to a blue solution of [$OsCl_2${=C=CH(*p*-tolyl)}(PPh_3)$_2$] (0.15 g, 0.17 mmol) in CH_2Cl_2 (10 mL). The solution turned orange immediately. After stirring for 20 min, the solvent was pumped off to give an orange paste. Diethyl ether (10 mL) was added to the residue to give an orange solid, which was collected by filtration, washed with diethyl ether (2 × 5 mL) and dried under vacuum for 30 min. Yield: 0.14 g (89%). ^{1}H NMR (300.13 MHz, CD_2Cl_2): δ = 2.38 (s, 3 H, $C_6H_4CH_3$), 2.42 (t, $J_{P,H}$ = 3.5 Hz, 1 H, Os=C=C*H*), 6.62 (d, $J_{H,H}$ = 8.0 Hz, 2 H, C_6H_4), 6.92 (d, $J_{H,H}$ = 8.0 Hz, 2 H, C_6H_4), 7.30−7.37 (m, 18 H, PPh_3), 7.70−7.73 (m, 12 H, PPh_3) ppm. The signal of H_2O appears at room temp. at δ = 1.73 ppm and at 190 K at δ = 1.86 ppm with an integral of 2:1 relative to that of the vinylidene =CH signal. ^{13}C{^{1}H} NMR (100.4 MHz, CD_2Cl_2): δ = 293.7 (t, $J_{P,C}$ = 14.1 Hz, Os=*C*), 135.1−125.4 (m, C_6H_4, PPh_3), 112.5 (t, $J_{P,C}$ = 4.5 Hz, Os=C=*C*H), 20.8 (s, C_6H_4-*C*H_3) ppm. ^{31}P{^{1}H} NMR (121.5 MHz, CD_2Cl_2): δ = −3.8 (s) ppm. $C_{45}H_{40}Cl_2P_2OOs$ (919.9): calcd. C 58.76, H 4.38; found C 58.63, H 4.12.

Observation of 11: Owing to the instability and incomplete conversion of **8** to **11**, **11** could not be isolated but could be detected when a solution of **8** in commercially available CD_2Cl_2 was monitored by variable-temperature ^{31}P{^{1}H} and ^{1}H NMR experiments. Characterization data of **11**: ^{1}H NMR (300.13 MHz, CD_2Cl_2, 188 K): δ = 0.91 (br. s, 1 H, Os=C=C*H*), 2.38 (br., 2 H, H_2O) ppm. ^{31}P{^{1}H} NMR (121.5 MHz, CD_2Cl_2, 188 K): δ = −10.2 (br. s) ppm.

Crystal-Structure Analyses: Crystals suitable for X-ray diffraction were grown by layering hexane on CH_2Cl_2 solutions of **2**, **5** and **8**, or cooling a warm solution of **9** in benzene. Data collection was performed with a Bruker Apex CCD Area Detector for **2** and **8** and with a Bruker SMART CCD Area Detector for **5** and **9**, using graphite-monochromated Mo-K_α radiation (λ = 0.71073 Å) in all

 © 2004 Wiley-VCH Verlag GmbH & Co. KGaA, Weinheim

Table 5. Crystallographic details for [$OsCl_3(\equiv CCH_2Ph)(PPh_3)_2$]·1.5$C_6H_6$ (**2**·1.5C_6H_6), [$OsCl_3(\equiv CCH_3)(PPh_3)_2$]·$CH_2Cl_2$ (**5**·CH_2Cl_2), [$OsCl_2(=C=CHCMe_3)(PPh_3)_2$] (**8**) and [$OsCl_2(H_2O)(=C=CHPh)(PPh_3)_2$]·$C_6H_6$ (**9**·C_6H_6)

Compound	**2**·1.5C_6H_6	**5**·CH_2Cl_2	**8**	**9**·C_6H_6
Empirical formula	$C_{44}H_{37}Cl_3OsP_2$·1.5C_6H_6	$C_{38}H_{33}Cl_3OsP_2$·CH_2Cl_2	$C_{42}H_{40}Cl_2OsP_2$	$C_{44}H_{38}Cl_2OOs\ P_2$·C_6H_6
Formula mass	1041.39	933.06	867.78	983.89
Temperature [K]	100(2)	293(2)	180(2)	293(2)
Radiation (Mo-K_α) [Å]	0.71073	0.71073	0.71073	0.71073
Crystal system	triclinic	triclinic	monoclinic	monoclinic
Space group	$P\bar{1}$ (no. 2)	$P\bar{1}$ (no. 2)	$P2_1/c$	$P2_1/n$
a [Å]	9.9952(7)	10.6256(9)	22.2749(10)	16.106(2)
b [Å]	13.9065(10)	12.9185(12)	9.5252(4)	12.3804(14)
c [Å]	17.7242(12)	14.0763(12)	18.7580(8)	21.477(3)
α [°]	110.6600(10)	78.341(2)	90	90
β [°]	97.6520(10)	89.708(2)	113.2070(10)	96.382(3)
γ [°]	98.292(2)	81.302(2)	90°	90
V [Å^3]	2235.6(3)	1869.9(3)	3657.9(3)	4255.9(9)
Z	2	2	4	4
$d_{calcd.}$ [g·cm^{-3}]	1.547	1.657	1.576	1.536
Abs. coeff. [mm^{-1}]	3.139	3.880	3.749	3.234
F(000)	1042	920	1728	1968
Crystal size [mm]	0.36 × 0.10 × 0.08	0.36 × 0.32 × 0.25	0.32 × 0.25 × 0.25	0.32 × 0.32 × 0.10
θ range [°]	1.60 to 27.88	1.94 to 27.53	2.36 to 28.31°	1.90 to 27.57
No. of reflns. collected	19208	12564	21881	27413
No. of indep. reflns.	10057 (R_{int} = 0.0318)	8431 (R_{int} = 0.0353)	8561 (R_{int} = 0.0260)	9785 (R_{int} = 0.0849)
No. of obsd. reflns. [$I > 2\sigma(I)$]	8921	7060	7617	4759
Absorption correction	SADABS	SADABS	SADABS	SADABS
Data/restraints/params	10057/0/532	8431/3/434	8561/0/428	9785/0/506
Goodness-of-fit on F^2	0.992	0.989	1.037	0.764
Final R_{int} [$I > 2\sigma(I)$]	R_1 = 0.0303, wR_2 = 0.0696	R_1 = 0.0428, wR_2 = 0.1021	R_1 = 0.0261, wR_2 = 0.0583	R_1 = 0.0425, wR_2 = 0.0637
Largest peak/hole (e·Å^{-3})	1.798/−0.974	2.236/−0.950	1.639/−0.519	1.312/−0.799

cases. Empirical absorption corrections (SADABS)[48] were applied. All structures were solved by direct methods, expanded by difference Fourier syntheses and refined by full-matrix least-squares on F^2 using the Bruker SHELXTL (Version 5.10)[49] program package. All non-hydrogen atoms were refined anisotropically. Hydrogen atoms were introduced at their geometric positions and refined as riding atoms. Further details on crystal data, data collection and refinements are summarized in Table 5. CCDC-227451 (**2**·1.5C_6H_6), -227452 (**5**·CH_2Cl_2), -227453 (**8**) and -227454 (**9**·C_6H_6) contain the supplementary crystallographic data for this paper. These data can be obtained free of charge at www.ccdc.cam.ac.uk/conts/retrieving.html [or from the Cambridge Crystallographic Data Centre, 12 Union Road, Cambridge CB2 1EZ, UK; Fax: + 44-1223-336033; E-mail: deposit@ccdc.cam.ac.uk].

Acknowledgments

The authors acknowledge financial support from the Hong Kong Research Grants Council.

[1] For reviews on vinylidene complexes, see for example: [1a] M. I. Bruce, *Chem. Rev.* **1991**, *91*, 197−257. [1b] M. I. Bruce, A. G. Swincer, *Adv. Organomet. Chem.* **1983**, *22*, 59−128. [1c] C. Bruneau, P. H. Dixneuf, *Acc. Chem. Res.* **1999**, *32*, 311−323. [1d] M. C. Puerta, P. Valerga, *Coord. Chem. Rev.* **1999**, 193−195, 977−1025.

[2] [2a] P. Schwab, R. H. Grubbs, J. W. Ziller, *J. Am. Chem. Soc.* **1996**, *118*, 100−110. [2b] H. Katayama, F. Ozawa, *Chem. Lett.* **1998**, 67−68. [2c] H. Katayama, H. Urushima, F. Ozawa, *J. Organomet. Chem.* **2000**, *606*, 16−25. [2d] T. Opstal, F. Verpoort, *Synlett* **2003**, 314−320. [2e] J. Louie, R. H. Grubbs, *Angew. Chem. Int. Ed.* **2001**, *40*, 247−249.

[3] [3a] Y. Wakatsuki, H. Yamazaki, N. Kumegawa, T. Satoh, J. Y. Satoh, *J. Am. Chem. Soc.* **1991**, *113*, 9604−9610. [3b] Y. Wakatsuki, N. Koga, H. Yamazaki, K. Morokuma, *J. Am. Chem. Soc.* **1994**, *116*, 8105−8111.

[4] Reactions of [$RuCl_2(PPh_3)_3$] with $HC\equiv CC(OH)Ar_2$ can also lead to related allenylidene complexes: [4a] D. Touchard, S. Guesmi, M. Bouchaib, P. Haquette, A. Daridor, P. H. Dixneuf, *Organometallics* **1996**, *15*, 2579−2581. [4b] K. J. Harlow, A. F. Hill, J. D. E. T. Wilton-Ely, *J. Chem. Soc., Dalton Trans.* **1999**, 285−291. [4c] H. J. Schanz, L. Jafarpour, E. D. Stevens, S. P. Nolan, *Organometallics* **1999**, *18*, 5187−5190. [4d] A. Fürstner, O. Guth, A. Düffels, G. Seidel, M. Liebl, B. Gabor, R. Mynott, *Chem. Eur. J.* **2001**, *7*, 4811−4820.

[5] [5a] C. Grünwald, O. Gevert, J. Wolf, P. González-Herrero, H. Werner, *Organometallics* **1996**, *15*, 1960−1962. [5b] J. Wolf, W. Stüer, C. Grünwald, O. Gevert, M. Laubender, H. Werner, *Eur. J. Inorg. Chem.* **1998**, 1827−1834. [5c] J. Wolf, W. Stüer, C. Grünwald, H. Werner, P. Schwab, M. Schulz, *Angew. Chem. Int. Ed.* **1998**, *37*, 1124−1126.

[6] H. Katayama, F. Ozawa, *Organometallics* **1998**, *17*, 5190−5196.

[7] M. Saoud, A. Romerosa, M. Peruzzini, *Organometallics* **2000**, *19*, 4005−4007.

[8] P. Barrio, M. A. Esteruelas, E. Oñate, *Organometallics* **2003**, *22*, 2472−2485.

[9] J. Gimeno, M. Gonzalez-Cueva, E. Lastra, E. Perez-Carreño, S. García-Granda, *Inorg. Chim. Acta* **2003**, *347*, 99−106.

[10] P. Barrio, M. A. Esteruelas, E. Oñate, *Organometallics* **2002**, *21*, 2491−2503.

[11] D. G. Gusev, T. Maxwell, F. M. Dolgushin, M. Lyssenko, A. J. Lough, *Organometallics* **2002**, *21*, 1095−1100.

 © 2004 Wiley-VCH Verlag GmbH & Co. KGaA, Weinheim

[12] M. Baya, P. Crochet, M. A. Esteruelas, A. M. López, J. Modrego, E. Oñate, *Organometallics* **2001**, *20*, 4291−4294.
[13] R. Castarlenas, M. A. Esteruelas, E. Gutiérrez-Puebla, E. Oñate, *Organometallics* **2001**, *20*, 1545−1554.
[14] R. Castarlenas, M. A. Esteruelas, E. Oñate, *Organometallics* **2000**, *19*, 5454−5463.
[15] T. B. Wen, Y. Y. Cheung, J. Z. Yao, W. T. Wong, Z. Y. Zhou, G. Jia, *Organometallics* **2000**, *19*, 3803−3809.
[16] M. A. Esteruelas, M. Oliván, E. Oñate, N. Ruiz, M. A. Tajada, *Organometallics* **1999**, *18*, 2953−2960.
[17] M. Baya, M. A. Esteruelas, *Organometallics* **2002**, *21*, 2332−2335.
[18] R. Castarlenas, M. A. Esteruelas, E. Oñate, *Organometallics* **2001**, *20*, 3283−3295.
[19] G. Ferrando, H. Gérard, G. J. Spivak, J. N. Coalter III, J. C. Huffman, O. Eisenstein, K. G. Caulton, *Inorg. Chem.* **2001**, *40*, 6610−6621.
[20] For additional examples of recent work on (vinylidene)Os complexes, see for example: [20a] M. Baya, M. A. Esteruelas, E. Oñate, *Organometallics* **2001**, *20*, 4875−4886. [20b] A. V. Marchenko, H. Gérard, O. Eisenstein, K. G. Caulton, *New. J. Chem.* **2001**, *25*, 1244−1255. [20c] M. L. Buil, M. A. Esteruelas, C. García-Yebra, E. Gutiérrez-Puebla, M. Oliván, *Organometallics* **2000**, *19*, 2184−2193. [20d] M. A. Esteruelas, C. García-Yebra, M. Oliván, E. Oñate, M. A. Tajada, *Organometallics* **2000**, *19*, 5098−5106. [20e] M. Baya, P. Crochet, M. A. Esteruelas, E. Gutiérrez-Puebla, A. M. López, J. Modrego, E. Oñate, N. Vela, *Organometallics* **2000**, *19*, 2585−2596. [20f] M. L. Buil, M. A. Esteruelas, *Organometallics* **1999**, *18*, 1798−1800. [20g] C. Bohanna, M. L. Buil, M. A. Esteruelas, E. Oñate, C. Valero, *Organometallics* **1999**, *18*, 5176−5179.
[21] M. L. Buil, O. Eisenstein, M. A. Esteruelas, C. García-Yebra, E. Gutiérrez-Puebla, M. Oliván, E. Oñate, N. Ruiz, M. A. Tajada, *Organometallics* **1999**, *18*, 4949−4959.
[22] T. B. Wen, S. Y. Yang, Z. Y. Zhou, Z. Lin, C. P. Lau, G. Jia, *Organometallics* **2000**, *19*, 3757−3761.
[23] T. B. Wen, Z. Y. Zhou, G. Jia, *Angew. Chem. Int. Ed.* **2001**, *40*, 1951−1954.
[24] H. Werner, S. Jung, B. Weberndörfer, J. Wolf, *Eur. J. Inorg. Chem.* **1999**, 951−957.
[25] J. Espuelas, M. A. Esteruelas, F. J. Lahoz, L. A. Oro, N. Ruiz, *J. Am. Chem. Soc.* **1993**, *115*, 4683−4869.
[26] See for example: [26a] C. Bianchini, A. Marchi, L. Marvelli, M. Peruzzini, A. Romerosa, R. Rossi, *Organometallics* **1996**, *15*, 3804−3816. [26b] Y. Kawata, M. Sato, *Organometallics* **1997**, *16*, 1093−1096.
[27] H. Werner, R. W. Lass, L. O. Gevert, J. Wolf, *Organometallics* **1997**, *16*, 4077−4088.
[28] M. A. Esteruelas, A. I. González, A. M. López, E. Oñate, *Organometallics* **2003**, *22*, 414−425.
[29] P. Crochet, M. A. Esteruelas, A. M. López, M. P. Martínez, M. Oliván, E. Oñate, N. Ruiz, *Organometallics* **1998**, *17*, 4500−4509.
[30] L. J. Baker, G. R. Clark, C. E. F. Rickard, W. R. Roper, S. D. Woodgate, L. J. Wright, *J. Organomet. Chem.* **1998**, *551*, 247−259.
[31] M. A. Esteruelas, A. M. López, N. Ruiz, J. I. Tolosa, *Organometallics* **1997**, *16*, 4657−4667.
[32] A. M. LaPointe, R. R. Schrock, W. M. Davis, *J. Am. Chem. Soc.* **1995**, *117*, 4802−4813.
[33] L. M. Hodges, M. Sabat, W. D. Harmon, *Inorg. Chem.* **1993**, *32*, 371−372.
[34] B. Weber, P. Steinert, B. Windmüller, J. Wolf, H. Werner, *J. Chem. Soc., Chem. Commun.* **1994**, 2595−2596.
[35] [35a] G. R. Clark, N. R. Edmonds, R. A. Pauptit, W. R. Roper, J. M. Waters, A. H. Wright, *J. Organomet. Chem.* **1983**, *244*, C57−C60. [35b] M. A. Gallop, W. R. Roper, *Adv. Organomet. Chem.* **1986**, *25*, 121−198.
[36] G. J. Spivak, J. N. Coalter, M. Oliván, O. Eisenstein, K. G. Caulton, *Organometallics* **1998**, *17*, 999−1001.
[37] M. Bourgault, A. Castillo, M. A. Esteruelas, E. Oñate, N. A. Ruiz, *Organometallics* **1998**, *17*, 636−645.
[38] For additional examples of recent work on (carbyne)Os complexes, see: [38a] M. Baya, M. A. Esteruelas, E. Oñate, *Organometallics* **2002**, *21*, 5681−5684. [38b] H. Chen, R. Liu, W. H. Myers, W. D. Harman, *J. Am. Chem. Soc.* **1998**, *120*, 509−520. [38c] G. J. Spivak, K. G. Caulton, *Organometallics* **1998**, *17*, 5260−5266. [38d] M. L. Spera, H. Chen, M. W. Moody, M. M. Hill, W. D. Harman, *J. Am. Chem. Soc.* **1997**, *119*, 12772−12778.
[39] C. Kelly, L. A. Mercando, M. R. Terry, N. Lugan, G. L. Geoffroy, Z. Xu, A. L. Rheingold, *Angew. Chem. Int. Ed. Engl.* **1992**, *31*, 1053−1054.
[40] S. Y. Yang, T. B. Wen, G. Jia, Z. Lin, *Organometallics* **2000**, *19*, 5477−5483.
[41] A. F. Hill, A. G. Hulkes, A. J. P. White, D. J. Williams, *Organometallics* **2000**, *17*, 371−373.
[42] [42a] M. Oliván, E. Clot, O. Eisenstein, K. G. Caulton, *Organometallics* **1998**, *17*, 3091−3100. [42b] M. Oliván, E. Clot, O. Eisenstein, K. G. Caulton, *Organometallics* **1998**, *17*, 897−901. [42c] M. Oliván, O. Eisenstein, K. G. Caulton, *Organometallics* **1997**, *16*, 2227−2229.
[43] D. Huang, M. Oliván, J. C. Huffman, O. Eisenstein, K. G. Caulton, *Organometallics* **1998**, *17*, 4700−4706.
[44] [44a] H. Werner, W. Stüer, J. Wolf, M. Laubender, B. Weberndörfer, R. Herbst-Irmer, C. Lehmann, *Eur. J. Inorg. Chem.* **1999**, 1889−1897. [44b] G. Bellachioma, G. Cardaci, A. Macchioni, F. Valentini, C. Zuccaccia, E. Foresti, P. Sabatino, *Organometallics* **2000**, *19*, 4320−4326. [44c] H. D. Mui, J. L. Brumaghim, C. J. Cross, G. S. Girolami, *Organometallics* **1999**, *18*, 3264−3272.
[45] T. B. Wen, Z. Y. Zhou, M. F. Lo, I. D. Williams, G. Jia, *Organometallics* **2003**, *22*, 5217−5225.
[46] P. J. Hore, *Nuclear Magnetic Resonance*, Oxford University Press Inc., New York, **1995**, pp. 44−55.
[47] P. R. Hoffmann, K. G. Caulton, *J. Am. Chem. Soc.* **1975**, *97*, 4221−4228.
[48] G. M. Sheldrick, *SADABS, Empirical Absorption Correction Program*, University of Göttingen, Germany, **1996**.
[49] Bruker, *SHELXTL™ Reference Manual* (Version 5.1), Bruker Analytical X-ray Systems Inc., Madison, Wisconsin, USA, **1997**.

Received January 2, 2004
Early View Article
Published Online May 13, 2004

 © 2004 Wiley-VCH Verlag GmbH & Co. KGaA, Weinheim

3-D Water-Soluble Reversible Neodymium(III) and Lanthanum(III) Coordination Polymers

Tina Vermonden,[a] Wiebe M. de Vos,[a] Antonius T. M. Marcelis,*[a] and Ernst J. R. Sudhölter[a]

Keywords: Lanthanides / NMR spectroscopy / Self-assembly / Tridendate ligands / Viscosity

The formation of soluble supramolecular 3-D coordination polymers with Nd^{3+} and La^{3+} in aqueous solution has been studied for two bifunctional ligands consisting of two pyridine-2,6-dicarboxylate groups connected at the 4-position by $O(CH_2CH_2O)_4$ and $O(CH_2CH_2O)_6$ spacers (**C4** and **C6**, respectively). Viscosity measurements were used to monitor the network formation as a function of the ligand concentration, and the ratio between metal ions and ligands. For corresponding conditions **C4** solutions with Nd^{3+} always gave much higher viscosities than **C6** solutions with Nd^{3+}. **C6** is long, and flexible enough to bind with both chelating groups to only one metal ion (ring formation). This causes the polymers to stop growing, resulting in smaller average sizes of the 3-D polymers. The ring-structures could be demonstrated by ^1H NMR spectroscopy using **C6** and La^{3+} at low concentrations.
(© Wiley-VCH Verlag GmbH & Co. KGaA, 69451 Weinheim, Germany, 2004)

Introduction

In the past few decades, the field of supramolecular chemistry has grown into an important part of chemistry. Supramolecular structures can be built using several noncovalent intermolecular interactions such as hydrogen bonding, π−π-stacking interactions, van der Waals interactions, and coordinative bonding (metal−ligand bonding).[1]

Metal−ligand bond strengths span a wide range, with the strength depending on both the metal ion and the ligand. In some cases the bond strengths are comparable to covalent bonds, and the reversibility of the binding can be tuned by the choice of solvent.[1] When a coordinating solvent such as water or acetonitrile is used, the reversibility of the binding increases.

In a previous study, we reported the reversible formation of linear polymers in aqueous solutions of Zn^{2+} ions with bifunctional ligands, consisting of two terdendate pyridine-2,6-dicarboxylate groups connected through an $O(CH_2CH_2O)_4$ or $O(CH_2CH_2O)_6$ spacer, **C4** or **C6**, respectively.[2] The bifunctional ligands can form not only linear polymers through metal ion coordination, but also rings. The rings can be formed by one ligand molecule and one metal ion (monomer rings) if a long and flexible spacer links the ligand groups. If the spacer is shorter or less flexible, at least two ligand molecules and two metal ions are necessary to form rings (dimer and larger rings). We showed, that the amount of ring formation depends on spacer length, concentration, temperature, and the metal ion/ligand molecule (M/L) molar ratio.[2] The total amount of rings is much higher when the ligand is long enough to form monomeric rings than when only dimers and larger rings can be formed. The larger the rings become, the smaller the probability of them being formed. This implies, that the amount of small rings will always be higher than the amount of large rings. When the molecules are able to form monomeric rings, there will still be dimer and larger rings present in solution, but their relative amounts will be much smaller. This also means, that when two ligand molecules differing in spacer length are compared, the solutions with molecules able to form monomeric rings will show a greater overall formation of rings than the solution with molecules able to form only dimer and larger rings.

The rings are dominant at low concentrations, where the probability of meeting a ligand group of another molecule is smaller than at higher concentrations. On going from a low to a high concentration, mainly rings are formed in the first instance and, after reaching a critical concentration, linear polymers are formed in addition. The total amount of rings stays approximately the same, but the amount and average length of the linear polymers increases. By considering the relative amounts we can say, that rings play an important role at low concentrations, but can be ignored at high concentrations. This relation between the formation of rings and linear chains was also found for reversible hydrogen-bonded supramolecular polymers.[3]

Another very important role in the equilibrium between rings and linear polymers is the molar ratio between metal

[a] Laboratory of Organic Chemistry, Contribution from the Dutch Polymer Institute, Wageningen University,
Dreijenplein 8, 6703 HB Wageningen, The Netherlands
Fax: (internat.) + 31-317-484914
E-mail: Ton.Marcelis@wur.nl
Supporting information for this article is available on the WWW under http://www.eurjic.org or from the author.

 DOI: 10.1002/ejic.200400098 © 2004 Wiley-VCH Verlag GmbH & Co. KGaA, Weinheim

ions and ligand molecules (M/L). The ideal ratio for forming linear polymers is 1, but this is also the ideal ratio for ring formation. Overall it can be said, that the influence of rings is largest at a molar ratio of unity and at low concentrations.[2]

In the field of coordination chemistry, interest in the lanthanide metal ions has grown considerably in the last two decades. Because of their large size, lanthanide ions can generally support higher coordination numbers than transition metal ions. Not many self-assembled structures of lanthanide ions in aqueous solution have been reported, although some lanthanide-containing helicates in water have been reported.[4−6] A few lanthanide coordination polymers having 3-D networks have also been reported, but only solid-state properties have been studied.[7−11]

In this paper we describe the reversible formation of 3-D polymers of the bifunctional ligands **C4** and **C6** with Nd^{3+} and La^{3+}. Neodymium(III) and lanthanum(III) are both lanthanide ions, and are large enough to form complexes with three terdendate ligands (9-coordination).[12] Compared with first-row transition metal ions such as Zn^{2+} or Ni^{2+}, which give 6-coordination with terdendate ligands, Nd^{3+} and La^{3+} can bind an additional ligand group by self-assembly, which makes the formation of a 3-D network possible. Additionally, we show that the possibility of ring formation also plays an important role in this system.

Results and Discussion

The ligands we used were **C4** and **C6**, these are represented in Figure 1. The complexing groups are based on 2,6-pyridinedicarboxylic acid. The complexation behavior of this group has been well studied with numerous metal ions. The complexation constants (p*K*) of the subsequent bindings of three 2,6-pyridinedicarboxylic acid molecules to one Nd^{3+} ion are 8.78, 6.72, and 5.06 as reported by Grenthe.[13]

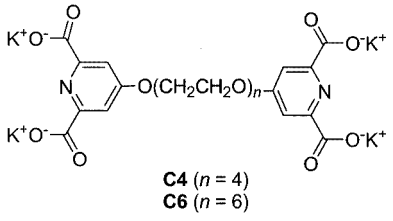

Figure 1. Schematic representation of the bifunctional ligands **C4** and **C6**

In our study we did not verify these stability constants but only the stoichiometry of binding. This was done using a monofunctional ligand with only an ethoxy group at the 4-position of the pyridine moiety in an isothermal titration calorimetric experiment (ITC). As can be seen in Figure 2, an inflection point was found at an Nd^{3+}/monoligand molar ratio of 0.33. This experiment confirms, that the Nd^{3+} center is surrounded by three terdendate monofunctional ligands.

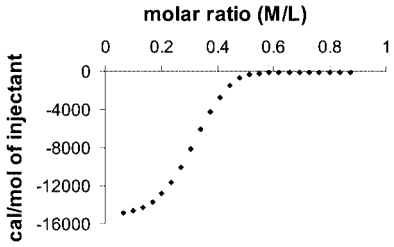

Figure 2. ITC curve of the monofunctional ligand 4-ethoxy-2,6-pyridinedicarboxylic acid (1.07 mM in cell) and $Nd(NO_3)_3$ (9.65 mM in burette) in a 0.1 M PIPES buffer of pH = 5.4 at 298 K

In a previous paper we showed, that **C4** and **C6** display different behavior towards Zn^{2+} although they differ only in spacer length [$O(CH_2CH_2O)_4$ versus $O(CH_2CH_2O)_6$].[2] One **C6** molecule is just long enough to form a ring around one zinc ion (monomer ring). On the other hand **C4** cannot form a monomeric ring, and needs at least two ligand molecules and two zinc ions to form a ring. This implies that the total amount of rings formed is much higher when **C6** is used instead of **C4** at all concentrations, as explained in the Introduction.

The situation is different when Nd^{3+} was used instead of Zn^{2+}. The ligands still form rings with the metal ion, and **C6** more so than **C4**, but the metal ion has still one binding site left. This makes the system more complicated. Although monomer rings alone will not be present anymore, they can act as chain stoppers as shown in Figure 3. **C4** is shorter, and therefore similar chain-stopping rings cannot be formed. The smallest possible rings do not prevent the polymer from growing longer as shown in Figure 3.

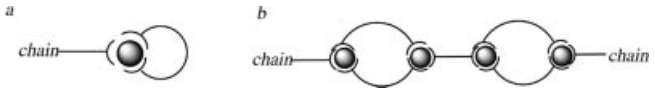

Figure 3. Schematic representation of the smallest possible rings for **C6** (a) and **C4** (b), and their influence on polymer formation

Viscosity measurements were used to study the solution properties as a function of the molar ratio. We titrated a ligand solution in a 0.1 M PIPES buffer of pH = 5.4 with an $Nd(NO_3)_3$ solution in the same buffer. A precipitate was always initially formed upon the addition of neodymium ions, but this completely dissolved after mixing. After each addition the viscosity was measured. Above an M/L molar ratio of 1, the precipitate did not dissolve anymore, and no viscosities could be measured above that ratio. At much larger ratios (M/L > 2) the precipitates dissolved easily again upon shaking. In Figure 4 the reduced viscosity of **C4** and Nd^{3+} has been plotted as a function of the molar ratio at three different concentrations of ligand (20.0 mm, 36.7 mm and 53.6 mm). We found a peak in the viscosity at

 © 2004 Wiley-VCH Verlag GmbH & Co. KGaA, Weinheim

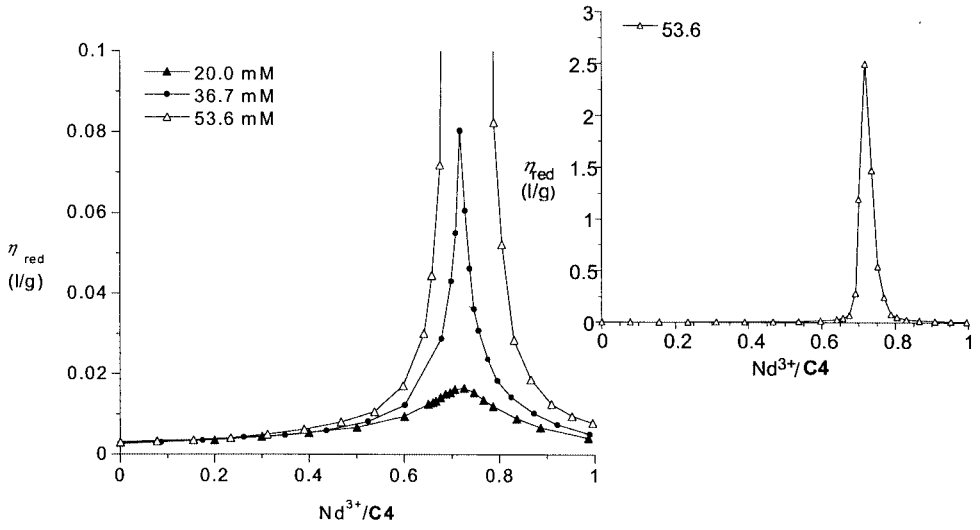

Figure 4. Reduced viscosity of **C4** as a function of molar ratio $Nd(NO_3)_3$/**C4** in a 0.1 M PIPES buffer of pH = 5.4 at 298 K at different concentrations

a molar ratio of about 2:3 (M/L), which can be expected when mixing a bifunctional ligand with a metal ion capable of binding three ligand groups. However, the most noticeable fact is the enormous effect of concentration. At the lowest concentration (20 mM), the highest reduced viscosity was 0.017 L/g. When the concentration was increased further to 37.6 mM, the highest reduced viscosity was already 0.071 L/g, and when the concentration was increased to 53.6 mM, the reduced viscosity went up to at least 2.5 L/g. This shows, that the size of the aggregates increases enormously with concentration through the formation of 3-D networks. The presence of a peak indicates, that the process is reversible. An excess of metal ions (> 0.67) causes the network to break down.

Upon close inspection of the graphs it can be seen, that the peak is shifted a little compared to the 2:3 ratio. With increasing concentration, the peak shifted to a slightly higher molar ratio. We will explain this after discussing the viscosity plots of **C6**.

Figure 5 shows the viscosity of **C6** and Nd^{3+} as a function of molar ratio at four different concentrations. Most noticeable here is, that although the viscosity increases with increasing concentration, this effect is much smaller than observed for **C4**. The curves are also much more asymmetric than those of **C4**. Another effect is the clear shift of the peak to higher molar ratios with increasing concentration. This shift is larger than for **C4**. The shifts of the peaks are plotted in Figure 6 for both ligands as a function of concentration.

The explanation for the low viscosity, asymmetric curves, and the large shift of the peak of **C6** compared with that of **C4** can only be found in the much stronger tendency of **C6** to form small rings. Since **C6** is able to form monomeric rings, which can act as chain stoppers (see Figure 3a), the structures cannot grow as large as for **C4**. This causes the much lower viscosity of **C6** and Nd^{3+} at all concentrations. The ideal molar ratio for formation of those rings is 0.67. At larger molar ratios (M/L), the amount of the rings de-

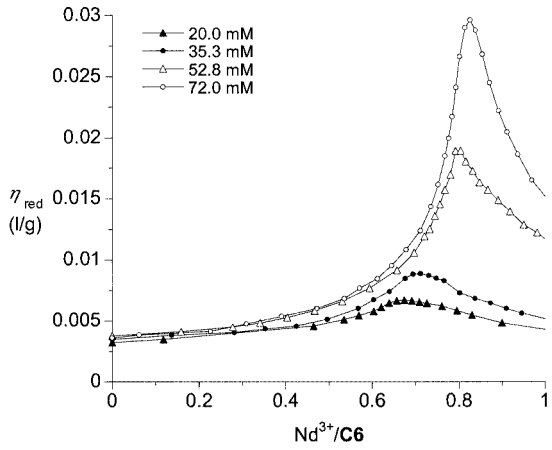

Figure 5. Reduced viscosity of **C6** as a function of molar ratio $Nd(NO_3)_3$/**C6** in a 0.1 M PIPES buffer of pH = 5.4 at 298 K at different concentrations

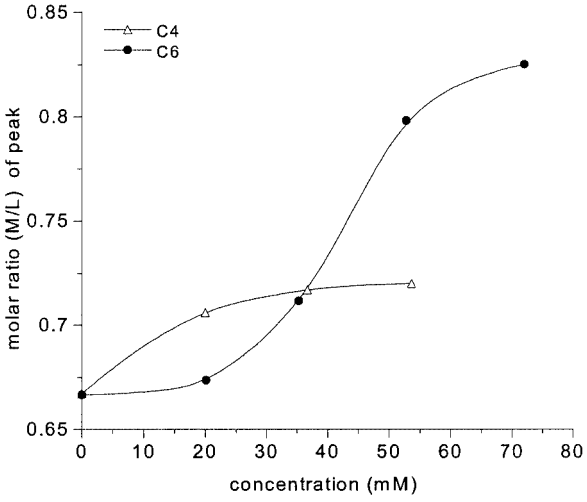

Figure 6. Molar ratio at the highest viscosity of solutions of **C4** and **C6** with Nd^{3+} as a function of concentration

 © 2004 Wiley-VCH Verlag GmbH & Co. KGaA, Weinheim

creases, allowing the formation of longer chains, and therefore the highest reduced viscosity is reached at higher molar ratios. This also explains the asymmetric curves. At higher molar ratios (above 0.67) the rings open and become part of the 3-D polymers. This effect contributes to higher viscosities. At these higher molar ratios, however, the metal ions will not all be coordinated to three chelating groups, which causes the viscosity to drop. Both effects counteract each other, leading to a slower decrease in viscosity than expected based on only the explanation of the excess of metal ions.

C4 also shows a shift in the viscosity peak, but it is much smaller. The origin of the shift here can, however, not be found in end capping by ring formation, since the rings can be part of a polymer chain (see Figure 3b). Therefore, the shift found for **C4** has an explanation different from that for **C6**. The shift for **C4** may be explained by the fact, that more expanded structures can be formed when not every metal ion is complexed with three ligand groups. This expansion causes a higher viscosity even though the molar mass of the structures is not larger. This is also the case for conventional covalently bonded polymer solutions. Expanded polymers take a larger volume, and therefore their solutions give higher viscosities than solutions of polymers with the same length but which are more compact.

For **C4**, a concentration-dependent viscosity plot was also measured at a constant M/L molar ratio of 0.71, corresponding to the average molar ratio of the top of the peak at concentrations above 20 mM. Although the top of the peak for concentrations below 20 mM is lower than at M/L = 0.71, the influence of this is negligible due to the broadness of the peak at lower concentrations. This plot is shown in Figure 7 to illustrate the enormous effect of concentration on the viscosity, and thus on the sizes of the self-assembled structures. With increasing concentration, the influence of the rings becomes smaller, and the 3-D polymers become larger, resulting in the steep increase in viscosity (see Figure 8).

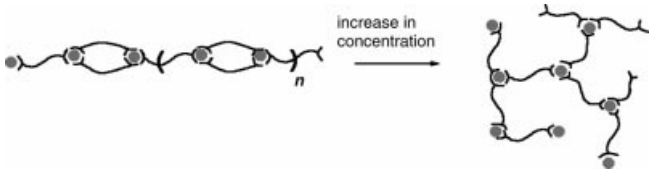

Figure 8. Changes in the structures of **C4**/Nd^{3+} coordination aggregates as a function of concentration

Some NMR experiments were performed in order to examine more closely the shifts of the peaks in the viscosity plots with respect to the molar ratio. The different causes for the shifts for **C6** and **C4** can be illustrated by ^1H NMR experiments. These experiments were performed using lanthanum(III) as the metal ion instead of neodymium(III), because neodymium broadens the signals in the spectrum; La^{3+} has properties similar to those of Nd^{3+}. They both belong to the lanthanides, and are known to exhibit 9-coordination.[12,13] The stoichiometry was checked by isothermal titration calorimetry and indeed showed, that three ligand groups are bound to one lanthanum ion. The curve was less steep than that shown in Figure 2 for neodymium due to lower complexation constants, which is in agreement with reported values in the literature. The reported complexation constants (pK) of La^{3+} with three dipicolinic acid molecules (structure of complexing group similar to the ones we use) are 7.98, 5.81, and 4.27.[13]

The reduced viscosity plots of both metal ions gave comparable results for both ligand molecules. At the measured concentrations, the shift in the molar ratio of the peak was found for both Nd^{3+} and La^{3+} and for both ligands. However, the viscosity of **C4** with lanthanum was found to be lower than for **C4** with neodymium at a concentration of 36.7 mM (Figure 9).

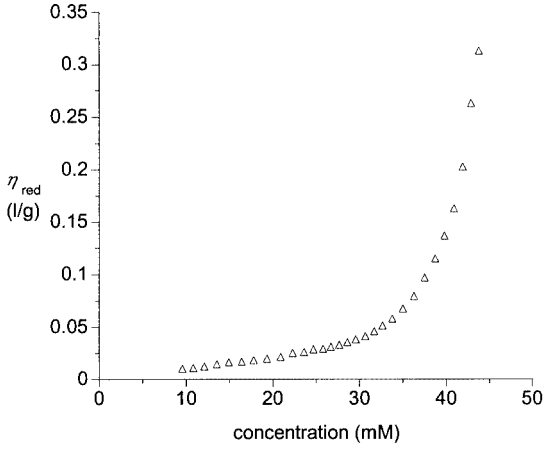

Figure 7. Reduced viscosity of **C4** as a function of concentration at a $Nd(NO_3)_3$/ligand ratio of 0.71 in a 0.1 M PIPES buffer of pH = 5.4 at 298 K

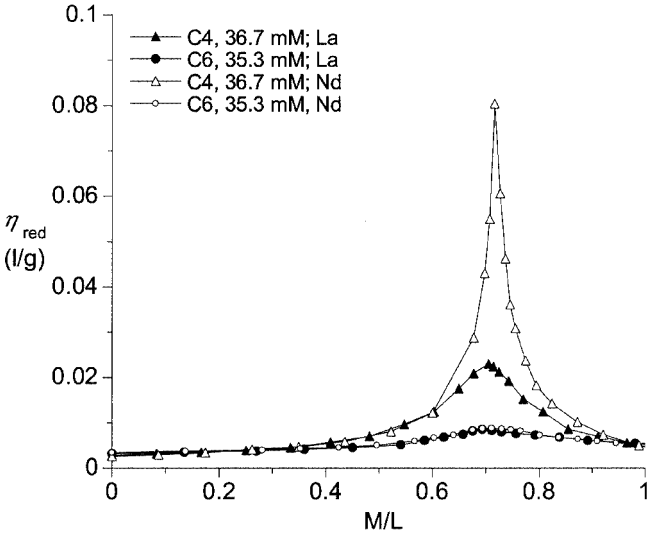

Figure 9. Reduced viscosity of **C4** (triangles) and **C6** (circles) as a function of molar ratio $Nd(NO_3)_3$/ligand (open) and $La(NO_3)_3$/ligand (full) in a 0.1 M PIPES buffer of pH = 5.4 at 298 K

 © 2004 Wiley-VCH Verlag GmbH & Co. KGaA, Weinheim

The NMR spectra in D_2O were recorded for both ligands as a function of concentration at an M/L ratio of 0.71, and as a function of the M/L ratio at a ligand concentration of 40 mM. A precipitate was also formed upon addition of La^{3+} ions to a ligand solution, but this subsequently dissolved after mixing. For ligand **C4** few changes occurred in the spectra when metal ions were added to a 40 mM solution in D_2O at pH = 5.8 (Figure 10). The signals between δ = 3.0 and 4.5 ppm originate from the OCH_2 protons in the spacer, the signal at δ ≈ 7.4 ppm originates from the aromatic protons in the pyridine ring. The signals became a little broader upon addition of La^{3+} ions, but no new signals appeared. The aromatic signal at δ = 7.35 ppm also shifted to 7.45 upon complexation, up to a molar ratio of 0.72. Above that ratio, the signal shifted back to δ = 7.40 ppm. The proton signals of the spacer shifted a little to high field. The broadening of signals instead of the formation of separated signals for free and coordinated ligand upon addition of metal ions, points to an exchange process between the ligand molecules at a moderate rate on the NMR time scale.[14]

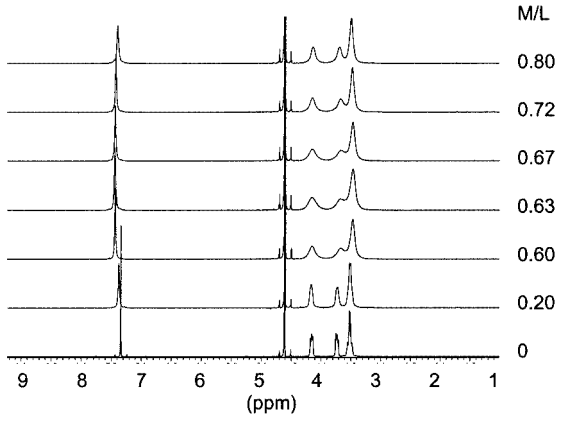

Figure 10. ^1H NMR spectra of compound **C4** with La^{3+} at 40 mM in D_2O at 298 K, pH = 5.8 at various molar ratios

No significant changes occurred in the ^1H NMR spectra upon dilution of a solution with a constant M/L ratio of 0.71 in D_2O (see Supporting Information). This implies that at all concentrations either the exchange between different species is fast, or that only one kind of species (3-D polymer) is present.

For **C6**, a new signal appears both in the molar ratio dependent spectra (Figure 11), and in the dilution spectra (Supporting Information). We observed the new signal as a broad bump in the molar ratio dependent series at δ = 3.1 ppm, with the highest intensity at a molar ratio of 0.67. The highest amount of small ring-like species would be expected at a molar ratio of 0.67, which is the ideal ratio for ring formation around metal ions with 9-coordination. These small structures containing many rings could, for example, look like the representation in Figure 12.

We indeed observed, that upon increasing the molar ratio, the bump became bigger up to a molar ratio of 0.67.

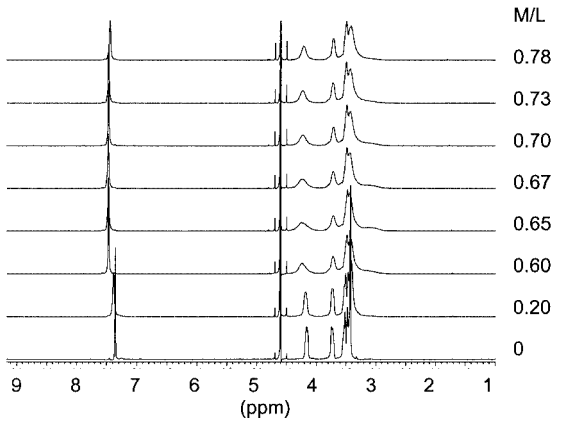

Figure 11. ^1H NMR spectra of compound **C6** with La^{3+} at 40 mM in D_2O at 298 K, pH = 5.8 at various molar ratios

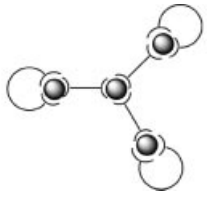

Figure 12. Schematic representation of an example of a small structure containing multiple rings, that can be formed by **C6** and La^{3+} ions at low concentrations and a molar ratio (M/L) close to 0.67

This signal in the NMR spectrum is, therefore, most likely caused by the structure of the rings. At higher ratios the height of the bump decreased rapidly because here, larger open structures are more dominant. The larger structures do not seem to give unique signals; they cause only broadening and slight shifting of the signals, which are also present without metal ions. The broadening of the signals is itself an indication of the formation of large structures. The disappearance of the "ring signal" at δ = 3.1 ppm at M/L > 0.67 is in agreement with the viscosity plots. Here the viscosity increased at a molar ratio of > 0.67 due to the opening of ring structures, which contribute to larger structures with higher viscosities.

Since we did not see this "ring signal" in the NMR spectra of **C4**, the presence of these kinds of structures can be ruled out here. This is logical, because **C4** is not long and flexible enough to act as a chain stopper.

In the dilution series (Supporting Information) no clear signal was found at δ = 3.1 ppm at 40 mM, but a broad bump appeared starting from about 20 mM, which became resolved into two peaks at 5 mM. Upon dilution, the only species that can become dominant in this system are chain-stopping rings. At low concentrations, the probability of a ligand meeting another metal ion is small, and therefore more rings are formed using only one metal ion to bind both chelating groups of a ligand molecule.

 © 2004 Wiley-VCH Verlag GmbH & Co. KGaA, Weinheim

Conclusions

We have reported here the first water-soluble lanthanide-containing reversible 3-D coordination polymers, and the viscosities of their aqueous solutions as a function of both the concentration and the M/L molar ratio. The investigated bifunctional ligands self-assemble in aqueous solution in the presence of neodymium and lanthanum ions to give reversible networks. The use of these ligands in combination with lanthanide ions gives rise to much higher viscosities than when transition metal ions such as zinc are used, that yield linear coordination polymers.[2] A comparison of the viscosities and ^{1}H NMR spectra of **C4** and **C6** shows, that under the same conditions, **C6** always gives smaller structures with lanthanide ions than **C4**. Ligand **C6** has a long enough spacer to bend around one metal ion. In this way it can act as a chain stopper, which causes the structures to stop "growing" and remain small. The ideal M/L ratio for formation of these rings is 0.67. The opening of the rings at higher M/L ratios causes a rather asymmetrical curve, and a shift of the peak in the molar ratio dependent viscosity plots. The ring structures can also be seen in the ^{1}H NMR spectra of **C6** at low concentrations, and at a molar ratio close to 0.67, giving separate signals at $\delta \approx 3.1$ ppm. The ^{1}H NMR spectra of **C4** do not show this signal at any concentration or molar ratio. Also, in the viscosity plots, the shifts of the peaks with respect to the molar ratio are much smaller and the curves are more symmetrical, showing that rings acting as chain stoppers are not present. Coordination structures formed by **C4** and neodymium are therefore able to become much larger. The small shifts of the viscosity peaks here originate from expansion of the structures when metal ions are only slightly in excess.

Experimental Section

The syntheses of compounds **C4** and **C6** have been reported in a previous paper.[2] All commercial chemicals were obtained from Acros or Aldrich, and were used as received. ^{1}H NMR (200 MHz) spectra were recorded with a Bruker AC-E 200 spectrometer. Isothermal titration calorimetry measurements were performed with a Microcal MCS ITC with a cell volume of 1.353 mL. The experiments were performed using injections of 5 μL, 250 s between injections, and a reference offset of 60%. Viscosity measurements were performed in a 100 mM 1,4-piperazinebis(ethanesulfonic acid) buffer (PIPES) of pH = 5.4 with a Schott AVS 360 capillary viscometer. The reduced viscosity is defined as the specific viscosity divided by the ligand concentration C in g/L, i.e. $\eta_{red} = \eta_{sp}/C = (\eta_s - \eta_o)/(\eta_o \cdot C)$, with η_s being the viscosity of the sample, and η_o the viscosity of the solvent.

[1] J.-M. Lehn, *Supramolecular Chemistry*; VCH, Weinheim, **1995**.
[2] T. Vermonden, J. van der Gucht, P. de Waard, A. T. M. Marcelis, N. A. M. Besseling, E. J. R. Sudhölter, G. J. Fleer, M. A. Cohen Stuart, *Macromolecules* **2003**, *36*, 7035−7044.
[3] S. H. M. Söntjens, R. P. Sijbesma, M. H. P. van Genderen, E. W. Meijer, *Macromolecules* **2001**, *34*, 3815−3815.
[4] M. Elhabiri, R. Scopelliti, J.-C. G. Bünzli, C. Piguet, *Chem. Commun.* **1998**, 2347−2348.
[5] J. J. Lessmann, W. De W. Horrocks Jr., *Inorg. Chem.* **2000**, *39*, 3114−3124.
[6] M. Elhabiri, J. Hamacek, J.-C. G. Bünzli, A.-M. Albrecht-Gary, *Eur. J. Inorg. Chem.* **2004**, 51−62.
[7] S. Y. Niu, G. D. Yang, Y. L. Zhang, J. Jin, L. Ye, Z. Z. Yang, *J. Mol. Struct.* **2002**, *608*, 95−99.
[8] L. Pan, X. Huang, J. Li, Y. Wu, N. Zheng, *Angew. Chem. Int. Ed.* **2000**, *39*, 527−530.
[9] P.-R. Wei, D.-D. Wu, Z.-Y. Zhou, T. C. W. Mak, *Polyhedron* **1998**, *17*, 497−505.
[10] C. Seward, N.-X. Hu, S. Wang, *J. Chem. Soc., Dalton Trans.* **2001**, 134−137.
[11] J. Luo, M. Hong, R. Wang, D. Yuan, R. Cao, L. Han, Y. Xu, Z. Lin, *Eur. J. Inorg. Chem.* **2003**, 3623−3632.
[12] J.-C. G. Bünzli, C. Piguet, *Chem. Rev.* **2002**, *102*, 1897−1928.
[13] I. Grenthe, *J. Am. Chem. Soc.* **1961**, *83*, 360−364.
[14] N. Ouali, B. Bocquet, S. Rigault, P.-Y. Morgantini, J. Weber, C. Piguet, *Inorg. Chem.* **2002**, *41*, 1436−1445.

Received February 6, 2004
Early View Article
Published Online May 13, 2004

 © 2004 Wiley-VCH Verlag GmbH & Co. KGaA, Weinheim

Nitroxide Radicals Interacting with Polyamine-Phenolic Ligands and Their Metal Complexes

Michela Cangiotti,[a] Mauro Formica,[a] Vieri Fusi,*[a] Luca Giorgi,[a] Mauro Micheloni,*[a] M. Francesca Ottaviani,*[a] and Sonia Sampaolesi[a]

Keywords: EPR / Macrocycles / Metal complexes / Nitroxide radicals / Polyamines

We have analyzed the interactions of a series of nitroxide radicals with ligands containing a phenol moiety coupled with different polyamine fragments, and their Cu^{II} and Zn^{II} complexes, by EPR experiments. Nitroxide radicals are good mimics of the properties of pollutant molecules, e.g., organic compounds having different polarities and charges, surfactants, and polyaromatics. Charged, polar, and low-polarity sites in the ligands and complexes are all available for interactions; in particular, the ability to entrap the radicals in a vice-like structure, by the formation of phenyl sandwich complexes, determines the type of selective interaction that occurs when a chain or planar aromatic structure is present. For closely packed complexes, Zn^{II} has a cooperative effect in the interaction with the radical; it allows both the entrance of low-polarity radicals at the low-polarity sites of the complex and the interactions of polar or charged radicals at the polar sites of the complexes. Conversely, Cu^{II} coordinates to the amino groups of the ligands and blocks the entry of radicals, which, thus, impedes their insertion into the structure of the complexes. The opposite behavior, with respect to that of Cu^{II} and Zn^{II}, was found for the complexes that have more open structures. The complexes that have cyclic ligands exhibit a poor ability to interact with radicals, but, for the ligands in the absence of the coordinating metals, the interactions are significantly enhanced as a result of the entrance of the radicals into the cyclic structures. In all cases, stronger interactions occur when both hydrophilic and hydrophobic sites are involved. The neutral-surfactant probe forms aggregates mainly with the cooperative effect of the copper complexes. UV/Vis measurements confirmed the results obtained by EPR and indicate that weak interactions occur between the radicals and the complexes or ligands; they also confirmed the formation of 1:1 adducts.

(© Wiley-VCH Verlag GmbH & Co. KGaA, 69451 Weinheim, Germany, 2004)

Introduction

Transition metal complexes can host and bind various organic and inorganic species, which, thus, allows their recognition, transport, and activation.[1−5] In this respect, the most important property of the metal complex is its readiness to interact with the host species through an unsaturated coordination site, which, in turn, is affected by the nature of the metal and the degree of preorganization of the complex that allows it to adapt to the presence of the new species. Because many natural biological sites, such as the active centers of various metalloenzymes, are produced by two transition metal ions, many dinuclear metal complexes have been synthesized and used successfully as devices for the recognition and assembly of external species that have different properties, e.g., inorganic and organic species; therefore, synthetic receptors for metal ions can be used to mimic enzymes' active centers.[6−10] Control over the distance between the two metal ions is crucial to allow the cooperation of both metal ions and, thus, the ability to mimic the reactions of active centers such as those present, for example, in oxygen receptors, activators, and carriers.[11,12] Moreover, the cooperation of the two metal ions permits a stronger complexation of the guest, which is usually coordinated by both metal centers.

Recently, we reported the synthesis and properties of several macrocyclic and noncyclic ligands containing a phenol moiety inserted into a polyamine skeleton.[13−17] Solid-state and solution studies highlighted the ability of these ligands to form complexes with M^{II} cations and, hence, to match the properties above; therefore, these systems may be suitable for interacting with secondary species that are extracted from the environment and then linked at the metal−ligand active sites. In particular, the dinuclear metal complexes we synthesized present the two transition metal ions in close proximity, which allows them to bind cooperatively to at least one substrate that is linked in a bridge disposition between them. In this paper, we report a series of ligands containing phenol moieties coupled with different polyamine fragments, which we term MODEN, DIDEN, ANIDEN, ANITR, and ANIPT (Scheme 1). With the exception of ANITR, which contains a tetraamine chain, these ligands are obtained from a combination of

[a] Institute of Chemical Sciences, University of Urbino, P.zza Rinascimento 6, 61029 Urbino, Italy
E-mail: vieri@chim.uniurb.it
ottaviani@uniurb.it

one or two diethylentriamine (dien) chains linked in different positions to the 2,6-dimethylphenol moiety. For example, ANIDEN can be viewed as the macrocyclic counterpart of MODEN, while ANIPT is the macrocyclic counterpart of DIDEN. ANITR forms only mononuclear species with transition metal ions such as Cu^{II} or Zn^{II} in aqueous or alcoholic solution, whereas the other ligands mainly form dinuclear species that are the only species existing in alcoholic solution. The dinuclear species of ANIPT and DIDEN possess ligand/metal molar ratios of 1:2, while those for ANIDEN and MODEN are 2:2.

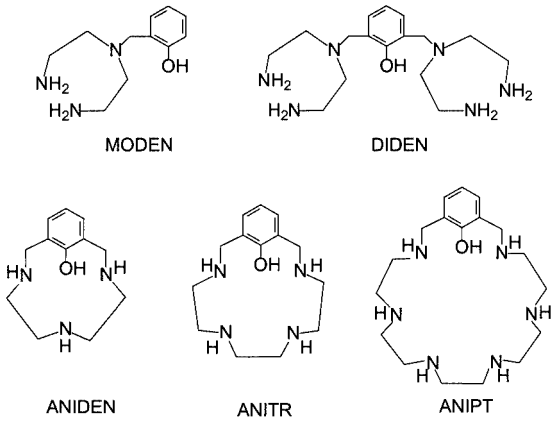

Scheme 1

Electron paramagnetic resonance (EPR) spectroscopy is a powerful tool for the analysis of the binding of nitroxide radicals to coordination sites and ligand groups.[18,19] Several studies have dealt with the magnetic and structural properties of complexes formed from metal complexes and nitroxide radicals.[20−25] To the best of our knowledge, however, no efforts have as yet been devoted to studying the interactions of heterocyclic ligands, and their dinuclear metal complexes, with differently structured nitroxide radicals.

Therefore, in an effort to analyze the ability of these ligands — and, more specifically, their complexes with Cu^{II} or Zn^{II} — to interact with pollutant molecules extracted selectively from the environment, in this study we applied the EPR technique while using selected nitroxide radicals that mimic well the properties of pollutant molecules, e.g., organic species that have different polarities and charges, surfactants, and polyaromatics (their formulas and acronyms are presented in Scheme 2).

Results and Discussion

EPR Spectroscopy

Figure 1 shows examples of the EPR spectra obtained for the complexes in the presence of the CATn radicals (radical concentration, 1 mM; complex concentration, 8 mM) at 263 K: (a) CAT1 with DIDEN-Cu, DIDEN-Zn, MODEN-Cu, and MODEN-Zn and (b) CAT12 with DIDEN-Zn and MODEN-Zn. The full lines in the Figure are the experimental spectra and the dashed lines represent the computed ones. The computation of the spectral line shape was

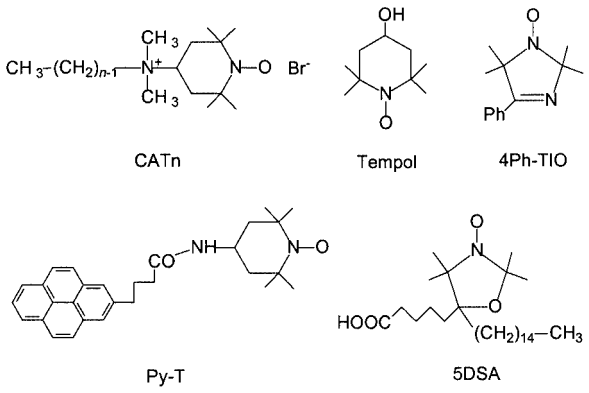

Scheme 2

performed by means of a well-established procedure that was reported by Budil et al.[26] The **g** tensor components (for the coupling between the electron spin and the magnetic field) were assumed to be constants (g_{ii} = 2.009, 2.006, 2.003). The **A** tensor components (for the coupling between the electron spin and the nuclear spin of the nitrogen atom) mainly reflect the variations in polarity of the nitroxide environment: an increase in A_{ii} values (accuracy: 3%) corresponds to an increase in the environmental polarity. For instance, the A_{ii} values found for CAT1 are greater than those evaluated for CAT12; the presence of the hydrophobic chain attached to the positively charged CAT group favors the localization of the nitroxide group in a less polar environment. An increase in line width arises from spin−spin interactions; the presence of paramagnetic copper ions in the vicinity of the nitroxide moiety may be responsible for this effect. A partial self-aggregation of surfactant radicals is also responsible for spin-exchange interactions. The variation in line width among the samples is very small, between 1 and 2 G, which gives, on average, a value of 1.5 G (reported in Figure 1). This value indicates that the spin−spin effects are quite negligible in the CAT*n* samples that we analyzed in this study. The NO group, therefore, does not approach the paramagnetic Cu^{II} center.

A Brownian, or Jump, model for the diffusional rotation of the nitroxide unit was considered and provided the correlation-time components, perpendicular and parallel, of $\tau_i = 1/(6D_i)$ and $\tau_i = 1/D_i$, respectively. These values (accuracy of 3% on the basis of the computation) are the most important parameters for analyses of complex−radical interactions; indeed, an increase in the correlation time for motion reflects a decrease in the radical mobility that is due to the interaction between the radical and the complex, or the ligand. This interaction is mainly physical, that is, dipole−dipole and van der Waals interactions prevail, but ion−dipole interactions are certainly the main driving forces that move the radicals towards the ligand sites.

The spectra recorded at complex/radical molar ratios < 8:1 (not shown) present higher mobilities (lower correlation time for motion) than those recorded at an 8:1 ratio (Figure 1); molar ratios > 8:1 result in almost equivalent spectra (also not shown) as that at an 8:1 molar ratio. We found, however, that already at a 1:1 molar ratio between the com-

 © 2004 Wiley-VCH Verlag GmbH & Co. KGaA, Weinheim

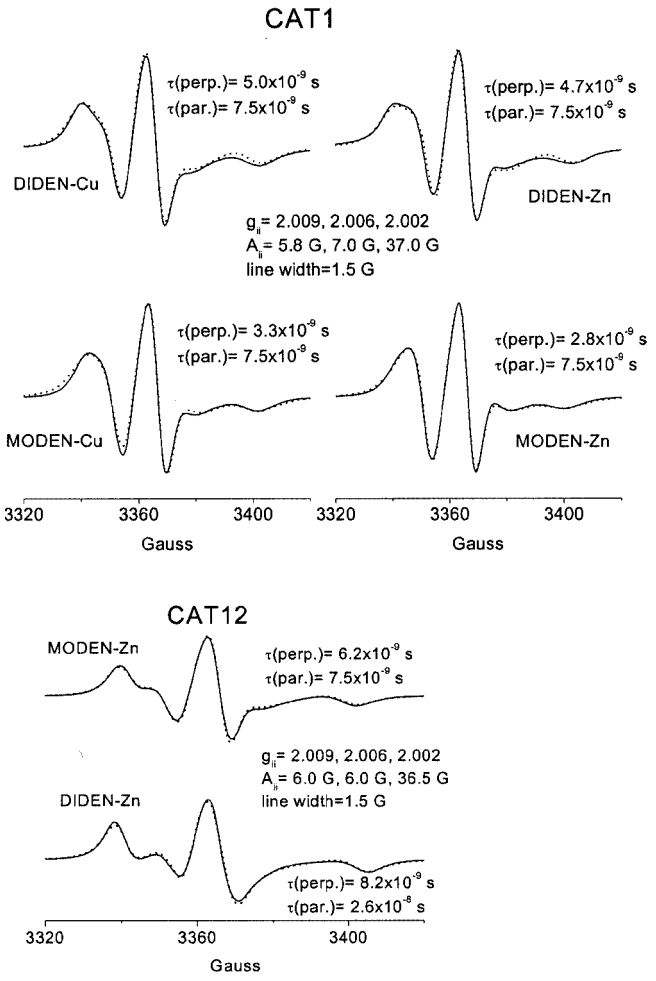

Figure 1. Examples of the EPR spectra obtained for the complexes in the presence of the CAT*n* radicals (radical concentration 1 mM; complex concentration 8 mM) at 263 K; (a) CAT1 with DIDEN-Cu, DIDEN-Zn, MODEN-Cu, and MODEN-Zn; (b) CAT12 with DIDEN-Zn and MODEN-Zn; the full lines in the figure are the experimental spectra, the dashed lines are the computed ones

plex and the radical, a small, but perceptible, quenching of the mobility occurs with respect to that of the radical in the absence of the complexes. On the other hand, we were mainly interested in the differences among the various systems (radicals + complexes or ligands), which showed equivalent trends at the different complex/radical molar ratios. For this reason, we simply compared the spectra obtained for the various radical/complex (or radical/ligand) systems at molar ratios of 1:8.

The first observation we made based on the parameters listed in Figure 1 was a decrease in the mobility on proceeding from CAT1 to CAT12, when comparing the same complex. It must be remembered that a similar difference in rotational mobility is found between the two probes in solution in the absence of the complexes, which occurs as a result of the different structures (size and shape) of the probes. In any case, this difference leads to a lower sensitivity of CAT12 with respect to its ability to differentiate among the various systems; when the interactions are strong, the mobility is very low and all the spectra appear to be similar. Computation of the line shape, however, easily reveals the differences. Problems may arise because the spectral computation of the different samples often requires a different anisotropy of motion, in which case a direct comparison of the perpendicular or parallel correlation times for motion does not work. Similarly, the average correlation time is not a good parameter for comparing the samples because different diffusional models yield different weights to the perpendicular and parallel components. Therefore, for an easier comparison, we simply used $2A_{zz}'$ splitting, i.e., the distance between the low- and high-field absorptions (in several cases, the second derivatives of the signals allowed more-accurate evaluations of this parameter: accuracy within 2−3%), which is related directly to the increased resolution of the anisotropic components of the hyperfine tensor; in turn this increased resolution is due to a progressive quenching of radical mobility: an increase in $2A_{zz}'$ reflects a decrease in mobility of the radical because of its interactions with the complexes or the ligands.

Figure 2 displays the variation of $2A_{zz}'$ for the various CAT*n* complex (or ligand) systems as histograms. Analyses of these histograms allowed us to define some general trends:

1. The DIDEN-Zn complex interacts the most with CAT*n*.
2. MODEN-Zn interacts less than does MODEN-Cu.
3. Cu complexes also interact more than do Zn complexes for the ANITR-M and ANIPT-M systems.
4. Conversely, DIDEN-Zn interacts more than does DIDEN-Cu.
5. ANITR-M and ANIPT-M interact less strongly than do the other complexes.
6. ANIDEN-Cu also interacts quite strongly.

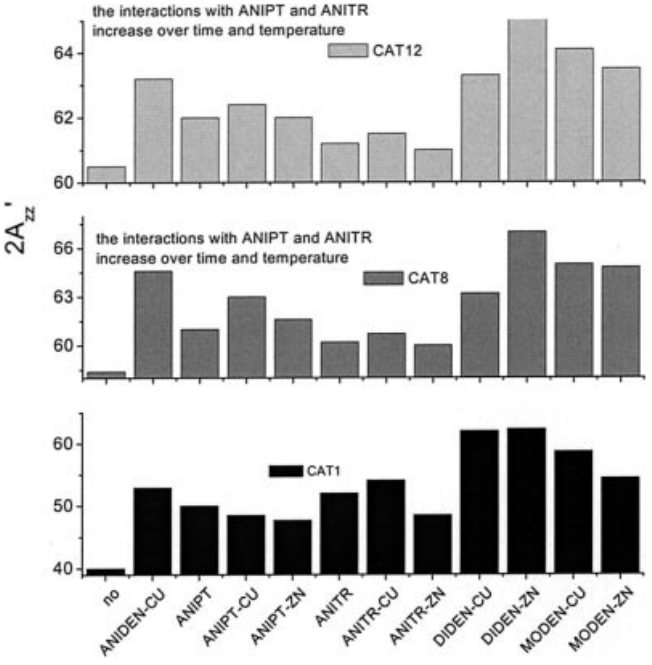

Figure 2. Histograms of the values of $2A_{zz}'$ for the various CAT*n* complex (or ligand) systems

 © 2004 Wiley-VCH Verlag GmbH & Co. KGaA, Weinheim

Before discussing these results, we also stress that different behaviors were found for ANITR and ANIPT (the ligands lacking coordinated metal ions), which interact quite strongly with CAT1, but, initially, the interaction is relatively weak with CAT8 and CAT12. However, increasing the temperature or leaving the samples to equilibrate for longer times leads to a progressive increase in the strength of binding because of the slow kinetics of the interaction.

Since CAT1 behaved similarly to CAT8 and CAT12, we hypothesized that the interaction takes place mainly by means of the charged CAT group; the driving force for the interactions certainly can be ascribed to this moiety. Therefore, we supposed that the hydrophobic chains of CAT8 and CAT12 do not play a substantial role in the binding between the radical and the complexes, but rather they affect only the entrance of ANITR and ANIPT into the macrocycles, as indicated by the slow kinetics of the interactions. Consequently, it is surprising to note that the similar trends observed for CAT*n* also hold for the hydrophobic radicals Py-T and 4Ph-TIO, as is shown in the histograms in Figure 3. Nevertheless, the lower values of $2A_{zz}'$ arose from the much faster mobility of these radicals with respect to the CAT*n* radicals, because 4Ph-TIO is more mobile than Py-T. This faster rotational mobility, in turn, allows a better differentiation of one sample from another. Some further discrepancies were found, however, between the CAT*n* samples and the 4Ph-TIO and Py-T samples:

1. The difference in probe mobility between MODEN-Cu and MODEN-Zn is relatively high.
2. MODEN-Cu exhibits the maximum interaction with 4Ph-TIO.
3. ANITR-Zn interacts more strongly than does ANITR-Cu.
4. The interaction with the ligands ANITR and ANIPT is relatively strong and is constant over time and at different temperatures.

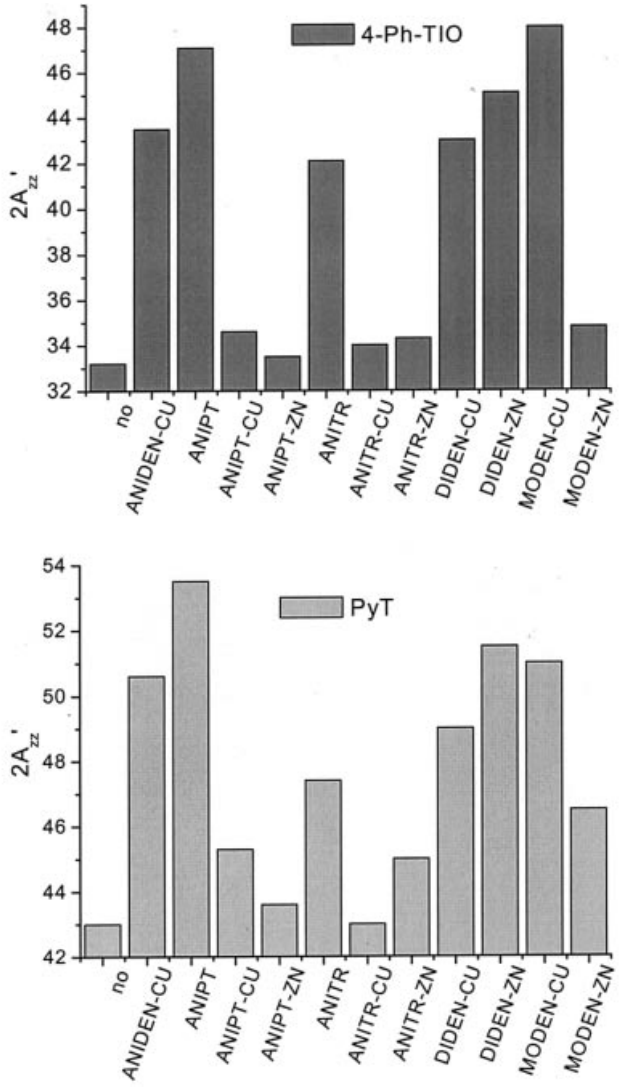

Figure 3. Histograms of the values of $2A_{zz}'$ for the Py-T and 4Ph-TIO complex (or ligand) systems

Before discussing the rationale implicit in these results, and the connections with the structures of the complexes, the results from the last two radicals shown in the histograms in Figure 4, 5DSA and Tempol, deserve separate considerations. First of all, the parameter used for describing the interaction with Tempol is not the $2A_{zz}'$ splitting, but rather the intensity ratio between the two components superimposing to form the overall signal (results not shown). These two components, which arise because the radicals exist in two motion regimes, simply termed fast and slow, originate from the two different radical environments, i.e., in water (bulk, not interacting radicals) and in the complexes (interacting radicals). As has already found in previous studies,[27] the increase in the intensity ratio between the slow and fast components (Is/If) can be interpreted as being due to the an increase in the interactions of the radicals with the complexes or the ligands. These intensities were calculated by a subtraction/addition procedure of the components themselves to separate them and obtain, by double integration, the values of their intensities. The histogram in Figure 4 for Tempol shows the values of Is/If for the different ligands and complexes. It is interesting that, on the basis of the higher Is/If ratio, the interaction of Tempol is stronger for DIDEN-Cu and ANITR-Zn, with respect to the other complexes; this finding is the opposite of the preferential interactions occurring for the other radicals and indicates that the mechanism of interaction is also different.

An introductory description is also needed for the results obtained from 5DSA. In this case, the self-aggregation ability of this radical provides a new contribution appearing as a single line (not shown for brevity). This component, termed the agg. component, arises from spin−spin exchange interactions due to the high local concentration of self-aggregating radicals; since this component is absent in the absence of the complex or the ligand, this observation implies that the complex or the ligand offers an aggregation site for these radicals. This behavior can be described in terms of a cooperative interaction in which the ligand or the complex, by interacting with the radicals, cooperates with them in the formation of the aggregates. This aggre-

 © 2004 Wiley-VCH Verlag GmbH & Co. KGaA, Weinheim

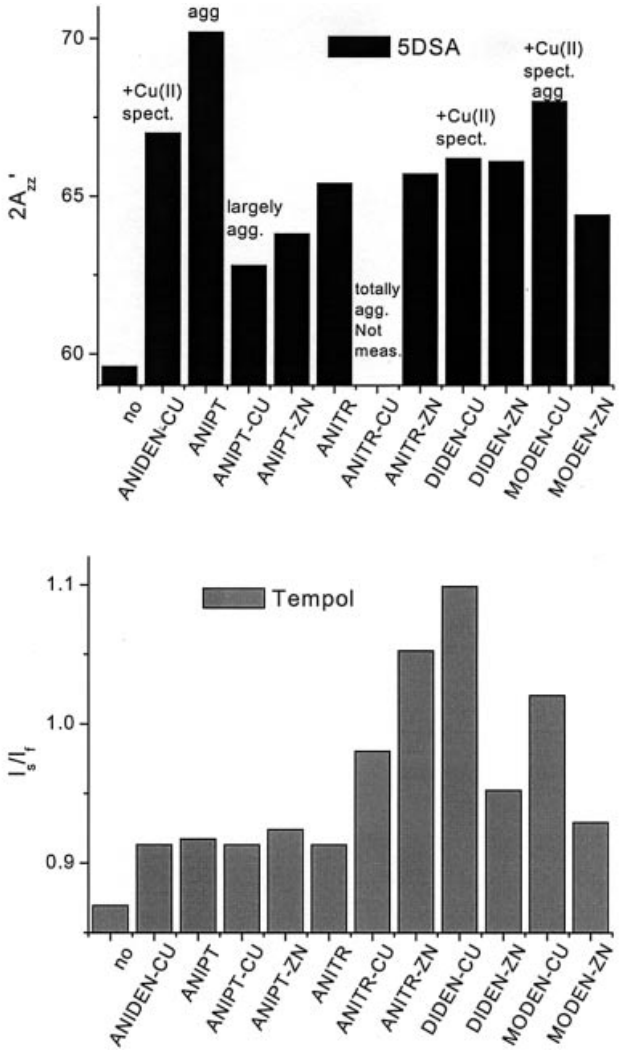

Figure 4. Histograms of the values of $2A_{zz}'$ for the 5DSA and Tempol complex (or ligand) systems

gation, however, is also favored by the repulsive effect of the charged metal sites: the hydrophobic chains escape from contact with the ions by forming aggregates. In cases in which the agg. component contributes to the EPR spectrum, we indicate the presence of aggregated surfactants by the "agg" label at the top of the pertinent bar in the histogram showing the $2A_{zz}'$ values for the different ligands or complexes (Figure 4). Although the strongest interaction for 5DSA is exhibited by ANIPT, which also shows the formation of 5DSA aggregates, the preferential formation of aggregates is presented by ANIPT-Cu and ANITR-Cu, which, conversely, show a weak interaction, as evidenced by the $2A_{zz}'$ values. This finding demonstrates that the mechanism of interaction of 5DSA with these complexes is different from that of the other complexes. Also, it is interesting that the interaction of the copper complexes with 5DSA leads to the appearance of a signal characteristic of monomeric copper complexes. This observation implies that, when interacting with the complex, this surfactant radical functions as a separator of the two Cu^{II} ions. This phenomenon may be related to both a physical separation and an electron transfer between the radical and Cu^{II}. This result holds true also for DIDEN-Cu and ANIDEN-Cu, which show the strongest interactions with the radical. For DIDEN-Cu, the high $2A_{zz}'$ value, the appearance of a signal from monomeric Cu^{II} complexes, and the presence of aggregates characterize the spectrum and are indicative of a very strong interaction.

This interaction can be understood quite easily by considering that it arises from an acid−base interaction between the COOH group of the probe and the amino groups of the ligand. Such an interaction may also involve the Cu^{II} ions, which coordinate well to deprotonated carboxylic groups, and, hence, may be responsible for the appearance of the monomeric copper complexes.

All of the results described above for the different radicals can be analyzed, for each complex or ligand, by proposing a suitable mechanism of interaction.

The structure of DIDEN-M characterizes a quite strong interaction with almost all the nitroxide radicals: charged, polar, and low-polarity interacting sites are all available for the interaction, but, mainly, the ability to entrap the radicals in a vice- or pliers-like structure determines the preferential interactions of the radicals with this complex. MODEN-M and ANIDEN-M may also create a similar interacting effect, but, in these cases, the possibility of forming phenyl sandwiches with the radicals also enhances the interactions.

Perhaps surprisingly, DIDEN-Zn generally interacts more readily than does DIDEN-Cu, whereas the opposite holds true for MODEN-M (i.e., the Cu complex interacts more readily than does the Zn complex). For DIDEN-Zn, the high ability to interact arises from two synergic effects: (1) Zn^{II} has a cooperative effect in the interaction with the radical and allows both the entrance of the low-polarity radicals at the low-polarity binding sites of the complex and (2) the interactions of the polar or charged radicals at the polar sites of the complex; conversely, Cu^{II} readily coordinates to the amino groups of the ligands and blocks the entrance of the radicals, which, thus, impedes their insertion in the complex structure. The Cu and Zn complexes of MODEN behave in an opposite way because the more open MODEN structure allows the entrance of the radicals into the structure of the Cu complex. Essentially, the coordinative requirement of Cu^{II} is not saturated by the donor atoms of the ligands and the radical behaves as an extra ligand. On the basis, however, of the strength of the interaction, as measured by EPR spectroscopy, the binding site of the radicals is not located directly at the NO moiety.

In the cases of ANITR and ANITP, their monomeric nature does not allow either a sandwich- or vice-like interaction. Therefore, the presence of the chain for the CAT or 5DSA does not favor the interaction and the ANITR-M and ANTP-M complexes show a weak interaction with the probes. Nevertheless, it is interesting that ANITP-M, which has the larger cycle, increases its interacting ability with respect to ANITR-M, by increasing the chain length of the

 © 2004 Wiley-VCH Verlag GmbH & Co. KGaA, Weinheim

CAT*n* probes, because both hydrophilic and hydrophobic interactions become active.

Two other interesting features in the interactions of the radicals with the ANITR and ANITP ligands and complexes are noteworthy.

(a) Cu complexes are more interacting than Zn complexes for CAT*n*, but this trend is reversed for ANITR-M with respect to the hydrophobic probes (ANITR-Zn is more interacting than ANITR-Cu for 5DSA, Py-T, and 4Ph-TIO); this observation means that the mechanism of interaction is different because ANITR-Cu is more selective for the interaction with hydrophilic substances and ANITR-Zn is more selective in respect to the hydrophobic molecules. In relation to the different mechanisms of interaction of the copper and zinc complexes, the behavior of 5DSA is very informative: the copper complexes promote the self-aggregation of the probes, i.e., it is favored by repulsion of the charged copper site.

(b) In the absence of the metal ion, the ligands ANITR and ANIPT show a significant interaction with the hydrophobic probes; in these cases, the macrocycles offer a comfortable binding site for the probes that have a prevalently hydrophobic nature. The CAT*n* probes are less interactive, but it is interesting to note that, in the presence of the chain, a slow kinetic process (which takes hours at room temperature) allows the progressive entrance of these probes so that they can be hosted by the macrocycles. As expected, an increase in temperature accelerates this process.

With regard to the mechanism of the interaction process, further information was provided by Tempol, which, in several cases, behaved in a manner opposite to that of the CAT*n* probes. We propose that, for Tempol, the interactions occur through the hydroxyl moiety, whereas the CAT*n* probes promote the interactions via their positively charged group.

UV/Vis Spectroscopy

The interaction of the radicals with the metal complexes was also supported by UV/Vis spectroscopy experiments, in which we observed the d−d electronic transitions of the coordinated Cu^{II} chromophore in the complexes in the absence and presence of the radicals. Table 1 shows λ_{max} (nm) and $\varepsilon_{\lambda max}$ ($mol^{-1}dm^3cm^{-1}$) values of DIDEN-Cu in methanol solution in the absence and in the presence of Tempol, CAT1, and Py-T. This complex in methanol shows a band at λ_{max} = 623 nm for the d−d transitions (ε = 150 $mol^{-1}dm^3$ cm^{-1}), while a shift towards lower energy was observed in the presence of Tempol and, moreover, for CAT1, but the effect was lower for Py-T, which is in agreement with the EPR spectroscopic results. Figure 5 shows the UV/Vis electronic spectra of the system Tempol-DIDEN-Cu upon addition of different quantities of Tempol to a methanol solution of the DIDEN-Cu complex. A constant profile was obtained at high Tempol/DIDEN-Cu molar ratio, which indicates the weak complexation of Tempol by DIDEN-Cu, as we had found also by EPR spectroscopy. The increase in absorbance at 669 nm, as a function of the number of equivalents of Tempol added, provided evidence for the formation of a Tempol/DIDEN-Cu adduct having 1:1 stoichiometry. CAT1 and Py-T provided similar results to those obtained with Tempol, as a function of the relative molar ratio with respect to the complex.

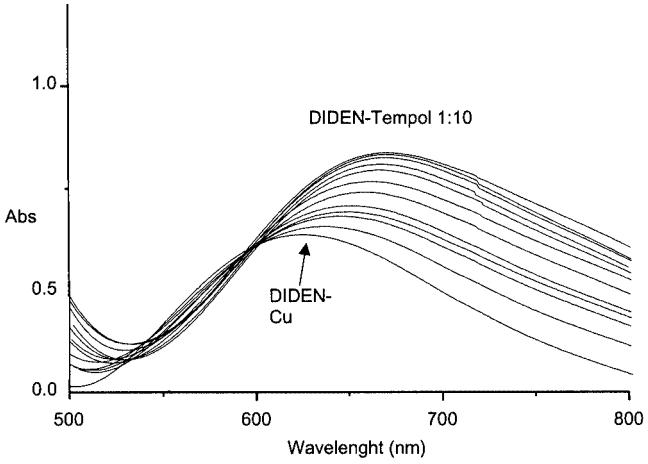

Figure 5. UV/Vis electronic spectra obtained upon addition of different quantities of Tempol to a methanol solution of the DIDEN-Cu complex; [DIDEN-Cu] = 5×10^{-3} M

The shift in the d−d band was slightly smaller for ANIPT-Cu and ANITR-Cu, with respect to those of DIDEN-Cu, ANIDEN-Cu and MODEN-Cu, but this variation was not as significant as expected on the basis of the EPR spectroscopy results, which indicates that the "copper side" (tested by the UV/Vis spectroscopic analysis) was less sensitive to the complexation behavior of the radicals with respect to the "radical side" (tested by the EPR analysis).

Conclusions

We have demonstrated that ligands containing a phenol moiety coupled to different polyamine fragments, namely DIDEN, MODEN, ANIDEN, ANIPT, and ANITR

Table 1. Values of λ_{max} [nm] and $\varepsilon_{\lambda max}$ [mol^{-1} dm^3 cm^{-1}] obtained from the UV/Vis spectra of DIDEN-Cu in methanol solution in the absence and presence of Tempol, CAT1, and Py-T

DIDEN-Cu[a]		DIDEN-Cu/Tempol		DIDEN-Cu/CAT1		DIDEN-Cu/Py-T	
$\lambda_{max.}$	ε	$\lambda_{max.}$	ε	$\lambda_{max.}$	ε	$\lambda_{max.}$	ε
623	150	669	350	683	360	663	200

[a] Charges have been omitted for clarity.

 © 2004 Wiley-VCH Verlag GmbH & Co. KGaA, Weinheim

(Scheme 1), and their Cu^{II} and Zn^{II} dinuclear complexes, bind differently to nitroxide radicals, namely Tempol, 4Ph-TIO, CAT1, CAT8, CAT12, 5DSA, and Py-T (Scheme 2), that mimic well the properties of pollutant molecules, e.g., organic species having different polarities and charges, surfactants, and polyaromatics.

Computer-aided analysis of the EPR spectra provided indications of the different strengths of interactions as a function of the complex or ligand structure, and of the structure, polarity, and charge of the radical. The interactions between the radicals and the complexes or the ligands were dynamic in nature.

The structure of DIDEN-M allows a quite strong interaction with almost all the nitroxide radicals: charged, polar, and low-polarity interacting sites are all available for the interaction, but, mainly, the ability to entrap the radicals in a vice- or pliers-like structure determines the preferential interaction of the radicals with this complex. Also, MODEN-M and ANIDEN-M may also create a similar interaction effect, but, in these cases, the possibility of phenyl sandwiches existing also enhances the interactions.

In DIDEN-Zn, the metal ion has a cooperative effect in the interaction with the radical and allows both the entrance of the low-polarity radicals at the low-polarity interacting sites of the complex and the interactions of polar or charged radicals at the polar sites of the complexes; conversely, in DIDEN-Cu, the metal readily coordinates the amino groups of the ligands and, because of the packing of the resulting structure, it blocks the entry of the radicals, which, thus, impedes their insertion into the structure of the complexes. The more open MODEN structure allows the entrance of the radicals in the structure of the Cu complex; MODEN-Cu is able to interact more strongly than is MODEN-Zn. Essentially, Cu^{II} presents a coordinative requirement that is not saturated by the donor atoms of the ligand and the radical functions as an extra ligand. On the basis of the strength of interaction as measured by EPR spectroscopy, however, the binding site of the radicals is not on the NO side.

ANITR-M and ANIPT-M complexes undergo weak interactions with the nitroxide probes. ANIPT-M, however, which has the larger cycle, has increased interacting ability with respect to ANITR-M when the chain length of the CAT*n* probes is increased, because, in these cases, both the hydrophilic and hydrophobic interactions become active. ANITR-Cu was revealed to be more selective for interactions with hydrophilic substances, whereas ANITR-Zn was more selective in interactions with hydrophobic molecules. For the ANITR and ANIPT ligands, in the absence of the coordinating metal ions, the interactions are significantly enhanced because of the entrance of the radicals in the cyclic structure. The kinetics of the entrance processes are slow (it takes hours at room temperature) for CAT8 and CAT12 radicals.

With the copper complexes of MODEN, DIDEN, and ANIDEN, the interaction of 5DSA induces the appearance of the EPR spectroscopic signal of a monomeric Cu complex, which is due to magnetic separation and/or electron transfer occurring at the two Cu^{II} ions. For the copper complexes of ANITR and ANIPT, the main effect of the ion is to promote the self-aggregation of the 5DSA radicals.

The interactions between Tempol and the complexes or the ligands are weak and occur through the hydroxyl moiety, which has a negative potential for interaction, whereas CAT*n* promotes interactions via the positively charged group.

The positively charged moiety of the radicals undoubtedly promotes the interactions with the complexes and the ligands, but stronger interactions occurred when both hydrophilic and hydrophobic sites were involved.

UV/Vis spectroscopic measurements confirmed the results obtained by EPR spectroscopy, i.e., they indicate that weak interactions occur between the radicals and the complexes or the ligands, and they also confirm the formation of 1:1 adducts.

Experimental Section

General: The ligands MODEN,[13] DIDEN,[14] ANIDEN,[15] ANITR,[16] and ANIPT[17] (Scheme 1) and their metal complexes used in the present study were synthesized as previously reported. 5-Doxylstearic acid (5DSA) and 4-hydroxy-2,2,6,6-tetramethylpiperidine-*N*-oxyl (Tempol) were purchased from Sigma and used without any further purification. 4-Trimethylammonio-Tempo bromide (CAT1), its derivatives bearing C_8 and C_{12} chains (CAT8 and CAT12, respectively), and pyrene-Tempo (Py-T) were kindly provided by Dr. X. Lei, Columbia University, NY. 4-Phenyl-2,2,5,5-tetramethyl-3-imidazolin-1-yloxy (4Ph-TIO) was kindly provided by Prof. L. Greci, University of Ancona, Italy. Methanol solutions of the complexes or the ligands (initial concentration: 0.05 M) and of the radicals (initial concentration: 5 mM; deoxygenated and stored in a refrigerator under nitrogen in the dark) were added together to obtain molar ratios, between the complex or ligand and the radical, from 1:1 to 10:1 at a constant radical concentration of 1 mM. The complex solutions in the absence of the radicals were also analyzed by EPR spectroscopy for the sake of comparison. The solutions were processed by EPR spectroscopy (glass tube: 2 mm diameter; sealed and inserted in the EPR spectrometer's cavity) immediately after preparation and 1 and 2 d after preparation. The EPR spectra were recorded with an EMX-Bruker spectrometer operating at the X band (9.5 GHz) and interfaced to a PC (Bruker software) for data acquisition and handling. The temperature was controlled by means of a Bruker ST3000 variable-temperature assembly. Experiments were carried out as a function of temperature (between 293 and 163 K) and a progressive quenching of the mobility was observed as the temperature decreased. The room-temperature spectra, however, did not indicate a significant variation in mobility among the various samples (results not shown), which suggests that the interactions between the complexes (or ligands) and the radicals were dynamic in nature, i.e., the radical undergoes fast exchange between the ligand site and the bulk solution, and/or the formed complex structure allowed fast rotation of the radical at the ligand site. The spectra recorded at 263 K, however, still do not indicate a frozen environment, but rather slow-exchange conditions that suggest a wide range of mobilities exist between samples; these spectra permitted an analysis of the behavior of the different interactions of the different samples. Both progressive cooling and direct cooling at 263 K in the EPR cavity were per-

 © 2004 Wiley-VCH Verlag GmbH & Co. KGaA, Weinheim

formed. The latter procedure ensured a reproducible response and, therefore, a better comparison could be made among the samples.

Electronic Spectroscopy: UV absorption spectra were recorded at 298 K with a Varian Cary-100 spectrophotometer equipped with a temperature control unit. The samples tested by UV/Vis spectroscopy were obtained using a constant concentration of the complex in methanol (between 1 and 5 mM) and variable concentrations of the radicals, which allowed us to obtain radical/complex molar ratios from 10:1 to 1:1.

Acknowledgments

The authors thank the Italian Ministero dell'Istruzione dell'Università e della Ricerca (MIUR), PRIN2002, for financial support.

[1] [1a] C. J. Pedersen, *J. Am. Chem. Soc.* **1967**, *89*, 7017. [1b] J. M. Lehn, *Pure Appl. Chem.* **1977**, *49*, 857. [1c] D. J. Cram, J. M. Cram, *Science* **1984**, *183*, 4127. [1d] J. M. Lehn, *Angew. Chem. Int. Ed. Engl.* **1988**, *27*, 89.
[2] P. Guerriero, S. Tamburini, P. A. Vigato, *Coord. Chem. Rev.* **1995**, *110*, 17.
[3] C. Bazzicalupi, A. Bencini, V. Fusi, C. Giorgi, P. Paoletti, B. Valtancoli, *Inorg. Chem.* **1998**, *37*, 941 and references cited therein.
[4] S. Aoki, E. Kimura, *J. Am. Chem. Soc.* **2000**, *122*, 4542.
[5] N. M. Murthy, M. Mahroof-Tahir, K. D. Karlin, *Inorg. Chem.* **2001**, *40*, 628.
[6] S. J. Lippard, J. M. Berg, *Principles of Bioinorganic Chemistry*, University Science Books, CF, **1994**.
[7] J. Reedijk E. Bouwman, *Bioinorganic Catalysis*, Marcel Dekker, New York, **1999**.
[8] [8a] K. D. Karlin, *Science* **1993**, *261*, 701. [8b] D. E. Wilcox, *Chem. Rev.* **1996**, *96*, 2435.
[9] M. N. Hughes, *The Inorganic Chemistry of the Biological Processes*, Wiley, New York, **1981**.
[10] [10a] Y. L. Agnus, *Copper Coordination Chemistry: Biochemical and Inorganic Perspective*, Adenine Press, New York, **1983**. [10b] *Zinc Enzymes* (Eds.: I. Bertini, C. Luchinat, W. Marek, M. Zeppezauer), Birkhäuser, Boston, MA, **1986**.
[11] A. E. Martell, D. T. Sawyer, *Oxygen Complexes and Oxygen Activation by Transition Metals*, Plenum Press, New York, **1987**.
[12] [12a] S. Schindler, *Eur. J. Inorg. Chem.* **2000**, 2311. [12b] M. B. Davies, *Coord. Chem. Rev.* **1996**, 1.
[13] [13a] K. Zeng, M. Qian, S. Gou, H.-K. Fun, C. Duan, X. You, *Inorg. Chim. Acta* **1999**, *294*, 1. [13b] E. Berti, A. Caneschi, C. Daiguebonne, P. Dapporto, M. Formica, V. Fusi, L. Giorgi, A. Guerri, M. Micheloni, P. Paoli, R. Pontellini, P. Rossi, *Inorg. Chem.* **2003**, *42*, 348.
[14] [14a] P. Dapporto, M. Formica, V. Fusi, M. Micheloni, P. Paoli, R. Pontellini, P. Rossi, *Inorg. Chem.* **2000**, *39*, 4663. [14b] P. Dapporto, M. Formica, V. Fusi, L. Giorgi, M. Micheloni, P. Paoli, R. Pontellini, P. Rossi, *Inorg. Chem.* **2001**, *40*, 6186. [14c] N. Ceccanti, M. Formica, V. Fusi, L. Giorgi, M. Micheloni, R. Pardini, R. Pontellini, M. R. Tiné, *Inorg. Chim. Acta* **2001**, *321*, 153. [14d] M. Formica, L. Giorgi, V. Fusi, M. Micheloni, R. Pontellini, *Polyhedron* **2002**, *21*, 1351.
[15] V. Fusi, A. Llobet, J. Mahia, M. Micheloni, P. Paoli, X. Ribas, P. Rossi, *Eur. J. Inorg. Chem.* **2002**, 987.
[16] P. Dapporto, M. Formica, V. Fusi, M. Micheloni, P. Paoli, R. Pontellini, P. Romani, P. Rossi, *Inorg. Chem.* **2000**, *39*, 2156.
[17] J. A. Aguilar, A. B. Descalzo, P. Diaz, V. Fusi, E. Garcia-España, S. V. Luis, M. Micheloni, J. A. Ramirez, P. Romani, C. Soriano, *J. Chem. Soc., Perkin Trans. 2* **2000**, 1187.
[18] [18a] L. J. Berliner, *Spin Labeling. Theory and Applications*, Academic Press, New York, **1976**, vol. 1, **1979**, vol. 2. [18b] L. J. Berliner, J. Reuben, *Biological Magnetic Resonance. Spin Labeling. Theory and Applications*, Plenum Press, New York, **1989**, vol. 8, p. 1.
[19] [19a] M. F. Ottaviani, E. Cossu, N. J. Turro, D. A. Tomalia, *J. Am. Chem. Soc.* **1995**, *117*, 4387. [19b] M. F. Ottaviani, M. Garcia-Garibay, N. J. Turro, *Colloids Surf.* **1993**, *72*, 321.
[20] [20a] M. Fettouhi, B. El Ali, M. Morsy, S. Golhen, L. Ouahab, B. Le Guennic, J.-Y. Saillard, N. Daro, J.-P. Sutter, E. Amouyal, *Inorg. Chem.* **2003**, *42*, 1316. [20b] Y. Tsukahara, T. Kamatani, A. Iino, T. Suzuki, S. Kaizaki, *Inorg. Chem.* **2002**, *41*, 4363.
[21] [21a] C. Stroh, P. Turek, P. Rabu, R. Ziessel, *Inorg. Chem.* **2001**, *40*, 5334. [21b] C. Stroh, E. Belorizky, P. Turek, H. Bolvin, R. Ziessel, *Inorg. Chem.* **2003**, ASAP Article.
[22] F. Lanfranc de Panthou, E. Belorizky, R. Calemczuk, D. Luneau, C. Marcenat, E. Ressouche, P. Turek, P. Rey, *J. Am. Chem. Soc.* **1995**, *117*, 11247.
[23] [23a] D. Zhang, W. Liu, W. Xu, X. Jin, D. Zhu, *Inorg. Chim. Acta* **2001**, *318*, 84. [23b] Y. Sueishi, H. Inoue, T. Oka, H. Tsukube, S. Yamamoto, *Bull. Chem. Soc. Jpn.* **1998**, *71*, 817.
[24] [24a] P. F. Richardson, R. W. Kreilick, *J. Phys. Chem.* **1978**, *82*, 1149. [24b] G. Francese, F. M. Romero, A. Neels, H. Stoeckli-Evans, S. Decurtins, *Inorg. Chem.* **2000**, *39*, 2087.
[25] D. A. Shultz, K. E. Vostrikova, S. H. Bodnar, H.-J. Koo, M.-H. Whangbo, M. L. Kirk, E. C. Depperman, J. W. Kampf, *J. Am. Chem. Soc.* **2003**, *125*, 1607.
[26] D. E. Budil, S. Lee, S. Saxena, J. H. Freed, *J. Magn. Res. A.* **1996**, *120*, 155.
[27] M. F. Ottaviani, F. Furini, A. Casini, N. J. Turro, S. Jockusch, D. A. Tomalia, L. Messori, *Macromolecules* **2000**, *33*, 7842.

Received December 2, 2003
Early View Article
Published Online May 13, 2004

 © 2004 Wiley-VCH Verlag GmbH & Co. KGaA, Weinheim

Paramagnetic Chloro-, Alkoxo-, or Azidovanadium(IV) Complexes Supported by an [ONNO]-Type Amine Bis(phenolate) Ligand

Fabien Wolff,[a] Christian Lorber,*[a] Robert Choukroun,*[a] and Bruno Donnadieu[a]

Keywords: Vanadium / Amines / Paramagnetism

The reactions between $V(N_3)_2(NMe_2)_2$ or $V(OiPr)_4$ and the chelating dianionic bis(phenoxy)amine ligand $[ONNO]H_2$ afford complexes formulated as $[V(N_3)_2\{ONNO\}]$ (**1**) and $[V(OiPr)_2\{ONNO\}]$ (**2**). When refluxed in toluene with an excess of Me_3SiCl, compound **2** leads to mono- or dichloro derivatives $[V(Cl)(OiPr)\{ONNO\}]$ (**3**) and $[VCl_2\{ONNO\}]$ (**4**) depending on the experimental conditions. The crystal structures of complexes **1**–**4** were solved and show in all cases an [ONNO] ligand that has phenolate groups in a *trans* configuration, with both amino-nitrogen donor atoms of the ligand coordinated to the octahedral vanadium center. Complexes **1**–**4** were further characterized by EPR spectroscopy and susceptibility measurement studies typical of d^1-paramagnetic V^{IV} species.
(© Wiley-VCH Verlag GmbH & Co. KGaA, 69451 Weinheim, Germany, 2004)

Introduction

In the past decade, ''non-metallocene'' complexes have attracted considerable attention due to their activity as α-olefin polymerization catalysts.[1] Chelating diamide,[1a,2–4] dialkoxide,[1a,5–6] or phenoxyimine[7,8] ligands in particular have been extensively studied as rigid supporting environments for group 4 transition metals. As a result a great deal of novel and useful chemistry has emerged, including the discovery of highly active olefin polymerization precatalysts. Among these new ligands, chelating dianionic [ONNO]-type amine bis(phenolate) ligands, recently introduced by Kol et al.[5] and associated to group 4 metal complexes, have proved to give highly active 1-hexene polymerization catalysts, and in some cases even isospecific living polymerization was possible.[5a] As our interest lies strongly in vanadium chemistry with various supporting ligand environments,[9] in particular those that could help stabilize the formal oxidation state (+III or +IV) of the vanadium center (and thus avoid the reduction to inactive V^{II} species by the alkylaluminum cocatalyst) during the vanadium-catalyzed polymerization of olefins,[10,11] we have recently described the synthesis of a series of oxovanadium(V) complexes with the ancillary amine bis(phenolate) [ONNO]-type ligand (Figure 1),[12] and demonstrated interesting features in the solution and the solid-state structure of these complexes. In the present article, we wish to report on the synthesis, structure, EPR spectroscopy, and magnetism of new d^1-paramagnetic vanadium(IV) complexes supported by the same [ONNO]-type bis(phenoxy)amine ligand.

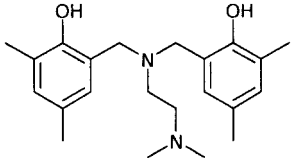

[ONNO]H$_2$

Figure 1. Structure of [ONNO]-type bis(phenoxy)amine ligand

Results and Discussion

1. Syntheses

In the past few years we have successfully used tetrakis(dialkylamido)vanadium(IV) $V(NR_2)_4$ as a precursor to various families of vanadium complexes.[9b,19,20] Logically, therefore, we first attempted the reaction between $V(NR_2)_4$

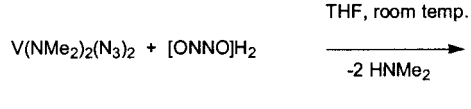

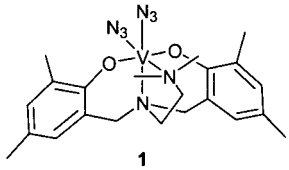

1

Scheme 1. Synthesis of azido-[ONNO] vanadium(IV) complex

[a] Laboratoire de Chimie de Coordination du CNRS, UPR 8241, 205 route de Narbonne, 31077 Toulouse Cedex 04, France
Fax: (internat) +33-5-61553003
E-mail: lorber@lcc-toulouse.fr
choukrou@lcc-toulouse.fr

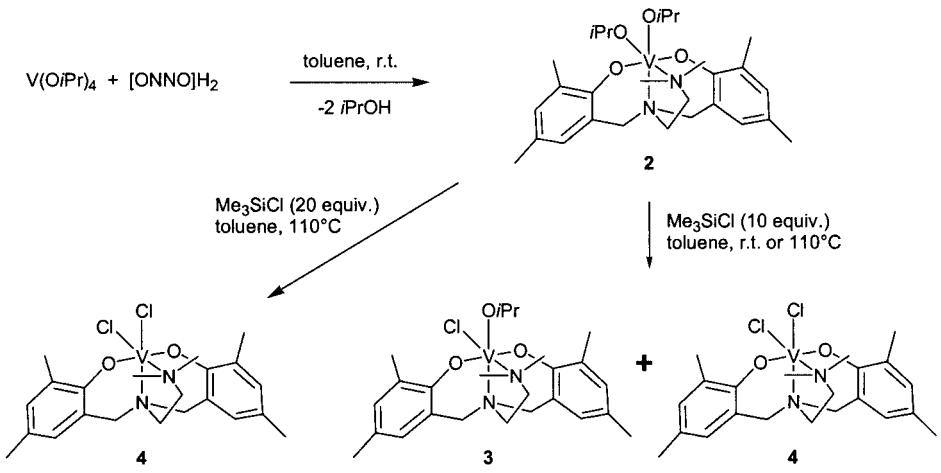

Scheme 2. Synthesis of alkoxo- and chloro- [ONNO] vanadium(IV) complexes

(R = Me; Et)[21] and an equimolar amount of the bisphenol ligand [ONNO]H_2, but although a reaction occurred we failed to isolate the pure [V(NMe_2)$_2${ONNO}] derivatives resulting from the amine elimination reaction. We then conducted the room temperature reaction of the new [V(N_3)$_2$(NMe_2)$_2$] complex (see Exp. Sect.) with [ONNO]H_2 in THF, which yielded the brown microcrystalline vanadium(IV) complex [V(N_3)$_2${ONNO}] (**1**) (yield: 40%) (Scheme 1). Brown crystals were further obtained by slow diffusion of pentane into a THF solution of **1**.

Reacting [ONNO]H_2 with an equimolar amount of V(O*i*Pr)$_4$ in toluene at room temperature for two hours afforded a dark red solution from which the complex [V(O*i*Pr)$_2${ONNO}] (**2**) was isolated with good yield (86%) as a dark red microcrystalline solid (Scheme 2). Compound **2** was recrystallized from a concentrated cold (−40 °C) pentane solution as dark red crystals.

Trimethylchlorosilane is known for its ability to substitute −NMe_2, −OR, or oxo groups by chlorine atoms in lanthanides [22] and in group 4−6 transition metal complexes;[3,4,9b,23] for vanadium complexes forcing conditions are generally required.[9b,20] We showed previously that Me_3SiCl could replace an azido group by a chlorine atom in oxo-vanadium(V) complexes,[12] and thus it was interesting to react the bis-azido complex **1** with Me_3SiCl. Unfortunately, the reaction did not proceed to completion even under forcing conditions in refluxing toluene.[24] However, when 10 equiv. of Me_3SiCl were used to chlorinate complex **2** in toluene at room temp. or 110 °C, a reaction occurred giving a mixture of the monochloro [V(Cl)(O*i*Pr){ONNO}] (**3**) and the dichloro [VCl_2{ONNO}] (**4**) derivatives. From that mixture of complexes, compound **3** was accidentally isolated as purple crystals (Scheme 2). In order to achieve a complete chlorination of **2**, a larger excess of Me_3SiCl (20 equiv.) was necessary, in dilute refluxing toluene solution, followed by slow cooling of the solution to room temperature, to afford dark blue crystals of the dichloro complex [VCl_2{ONNO}] (**4**) (yield: 96%) (Scheme 2).

In solution, [ONNO]-vanadium(IV) compounds **1**−**4** are all d^1-paramagnetic species presenting well-resolved electron paramagnetic resonance (EPR) spectra with the characteristic octet pattern at about g = 1.97 [A_{iso}(^{51}V) = 94.0 G (**1**), 70.9 G (**2**), 77.3 G (**3**), 82.7 G (**4**)] expected for the interaction of an unpaired electron of V^{IV} with the ^{51}V nucleus (I = 7/2). Accordingly, susceptibility measurements show magnetic moments consistent with a d^1 electronic configuration [μ_{eff} = 1.80 μ_B (**1**), 1.79 μ_B (**2**), 1.77 μ_B (**3**), 1.82 μ_B (**4**)].

Addition of pyridine or PMe_3 to complex **2** did not affect its EPR spectrum (in particular, no coupling with the ^{31}P phosphorus nucleus of PMe_3 was observed) or the color of the solution, suggesting that the sidearm NMe_2 group is sufficiently tightly bound to the metal not to be displaced by strong donors (as in our vanadium(V)[ONNO] complexes[12]).

2. Solid State Structures

In contrast to diamagnetic [ONNO]-vanadium(V) complexes for which ^{1}H NMR spectroscopy and NOESY experiments are very helpful tools in determining the structure in solution and in particular the conformation of the [ONNO] fragment, for paramagnetic d^1-vanadium(IV) species it is of tremendous importance to have a crystal structure in order to assess their formulation without ambiguity, as we have already stated in other articles dealing with vanadium(IV) complexes.[9a,9b]

Crystals suitable for X-ray structure determination were obtained for all complexes described in this article, either by diffusion of pentane into a THF solution of the complex (for **1** and **3**), cold pentane solution (for **2**), or slow cooling of a toluene solution from 110 °C to ambient temperature (for **4**). ORTEP drawings are given in Figure 2−5, with selected bond lengths and angles in Table 1 (complex **2** presents two independent molecules in the cell with very similar structural parameters, therefore only one of these molecules will be described here).

 © 2004 Wiley-VCH Verlag GmbH & Co. KGaA, Weinheim

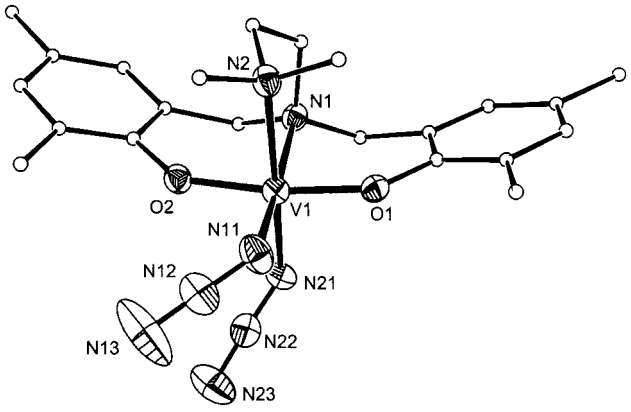

Figure 2. ORTEP drawing of the molecular structure of **1** showing 50% probability ellipsoids (except on C atoms for clarity) and partial atom-labeling schemes. Hydrogen atoms are omitted for clarity

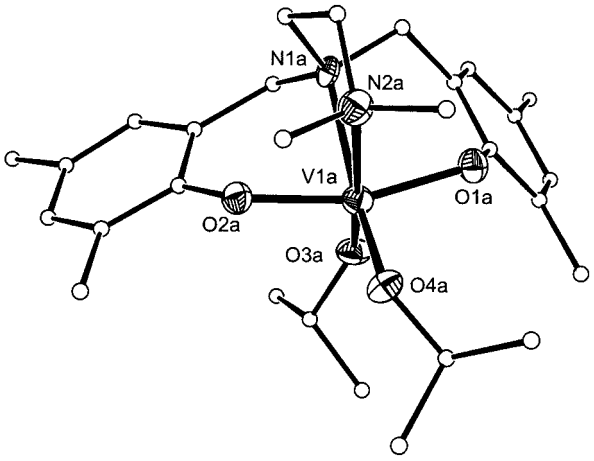

Figure 3. ORTEP drawing of the molecular structure of **2** (independent molecule A) showing 50% probability ellipsoids (except on C atoms for clarity) and partial atom-labeling schemes. Hydrogen atoms are omitted for clarity

The solid-state structures confirm our first formulation for complexes **1**−**4** as mononuclear vanadium complexes with one [ONNO] ligand in association with either two N_3 groups (**1**), two O*iPr* groups (**2**), two Cl groups (**4**), or one chlorine atom and one O*iPr* group (**3**). Furthermore, all complexes have a slightly distorted octahedral geometry with a *trans* configuration for the two phenolate rings of the [ONNO] ligand, as well as coordination of both amino-nitrogen donor atoms to the metal center, features that they share with their group 4 and oxo-[ONNO] vanadium(V) analogs.[5b,5d,5e,5f,12]

In contrast to the latter oxo complexes in which a *trans* effect due to the oxo ligand was observed, resulting in an elongated V−N bond of the amino-nitrogen atom of the [ONNO] ligand *trans* to the oxo group compared to the one in *cis*, here in the vanadium(IV) systems the two V−N bonds (formed between the metal center and the tripodal

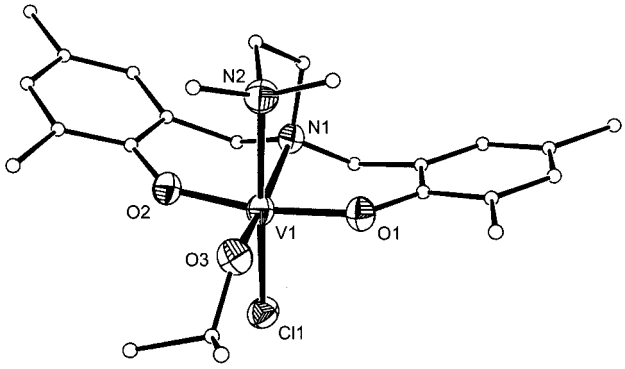

Figure 4. ORTEP drawing of the molecular structure of **3** showing 50% probability ellipsoids (except on C atoms for clarity) and partial atom-labeling schemes. Hydrogen atoms are omitted for clarity

Table 1. Selected structural parameters for complexes [V(X)(Y){ONNO}], X = Y = N_3 (**1**), O*i*Pr (**2**), or Cl (**4**), or X = O*i*Pr and Y = Cl (**3**) (distances are given in Å and angles in deg, X is the group *cis* to the NMe_2 sidearm whereas Y is the group *trans*)

	[V(N_3)$_2${ONNO}] (**1**)	[V(O*iPr*)$_2${ONNO}] (**2**)[a]	[V(Cl)(O*iPr*){ONNO}] (**3**)	[VCl_2{ONNO}] (**4**)
V−O1	1.780(2)	1.919(4)	1.801(1)	1.794(2)
V−O2	1.816(2)	1.882(4)	1.794(1)	
V−N1	2.193(3)	2.273(4)	2.226(1)	2.209(4)
V−N2	2.224(3)	2.313(5)	2.227(2)	2.209(4)
V−X	1.981(3) (*N11*)	1.793(4) (*O4*)	1.782(1) (*O3*)	2.308(2) (*Cl2*)
V−Y	2.029(3) (*N21*)	1.787(4) (*O3*)	2.3468(9) (*Cl1*)	2.354(2) (*Cl1*)
O1−V−O2	170.7(1)	162.6(2)	167.32(5)	168.9(2) [b]
N1−V−N2	82.0(1)	76.8(2)	80.11(5)	82.1(2)
X−V−Y	96.0(1)	104.1(2)	98.38(4)	95.51(6)
V−O1−C7	143.2(2)	116.6(3)	142.7(1)	143.2(2)
V−O2−C8	141.4(2)	129.8(4)	142.0(1)	
V−O3−C23		133.9(4)	131.7(1)	
V−O4−C26		131.0(3)		
α, β[c]	+6.5, −3.1	+2.6, +3.6	−4.0, +9.4	+4.1, −4.1
δ [d]	−148	+106	−149	−140

[a] For independent molecule A. [b] For **4**, angle O1−V−O1′. [c] Dihedral angle: α = C1−C2−C7−O1, β = C14−C13−C8−O2. [d] Angle defined by the two planes containing the two phenolate aromatic rings, the + sign refers to a folding away from the NMe_2 sidearm whereas the − sign refers to a folding in towards the NMe_2 sidearm.

 © 2004 Wiley-VCH Verlag GmbH & Co. KGaA, Weinheim

amino-N atom and the dimethylamino sidearm N atom) have almost identical distances ranging from 2.19 to 2.31 Å. Short phenoxide V−O bond lengths of 1.78 to 1.82 Å are found in **1**, **3** and **4** (which correspond to the complexes that adopt a similar "symmetric" configuration, vide infra),[25] whereas they are about 0.1 Å longer in complex **2**. All other bonds are in the normal range; alkoxide V−O bond lengths are about 1.79 Å, V−Cl bond lengths are about 2.35 Å, and V−N_{azido} bond lengths are about 2.00 Å. V−O−$C_{phenolate}$ angles are around 141−143° in **1**, **3** and **4**, whereas for **2** they are 117−130° (vide infra). In **2**−**3**, V−O−C_{iPr} angles are between 132−134° which reflect only weak π interactions in the V−alkoxide bonds.

More importantly, if we have a closer look at the four crystal structures of **1**−**4** [see also Figure 6 that represents a view along the tripodal nitrogen atom N1−V−X axis for **1**−**4**, X being N11 (**1**), O4 (**2**), O3 (**3**), Cl2 (**4**)], in complexes **1**, **3** and **4** the [ONNO] fragment adopts the same, almost superimposable, configuration which is probably due to the very similar electronegativity of the chloride and azide ligands. Interestingly, the arrangement of the three groups attached to the tripodal N donor atom (the two benzylic groups and the ethylenic arm) is not helicoidal as observed in the crystal structure of **2**. As a result, the phenolate groups of the [ONNO] framework in **1**, **3** and **4** fold in towards the pendant (dimethylamino)ethyl sidearm, the angle between the two planes of the aromatic rings is about −148° (**1**), −149° (**3**) and −140° (**4**) (the minus sign refers to a folding towards the NMe_2 sidearm, in contrast to the folding away from the NMe_2 sidearm that has a positive sign), whereas in complex **2** the phenolate groups of the tetradentate ligand fold back away from the pendant (dimethylamino)ethyl sidearm, the angle δ between the two planes of the aromatic rings is about +106°. As a consequence, the V−$O_{phenolate}$ and V−N_{amino} bond lengths are longer by about 0.05−0.10 Å in **2** (compared to **1**, **3** or **4**), and the O1−V−O2 angle are smaller in **2** by about 5−10° as well as the V−O−$C_{phenolate}$ by 13° (V−O2−C8) to 26° (V−O1−C7).

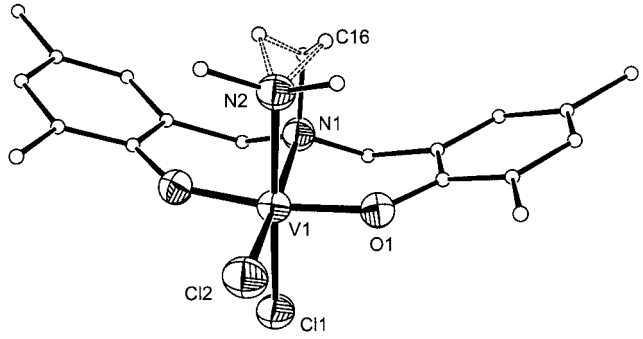

Figure 5. ORTEP drawing of the molecular structure of **4** showing 50% probability ellipsoids (except on C atoms for clarity) and partial atom-labeling schemes. Hydrogen atoms are omitted for clarity

A similar observation was already mentioned in our oxo-[ONNO]-vanadium(v) series of complexes in which, in the solid state and in solution, the amine(bisphenolate) ligand accommodates different arrangements that allows the aromatic rings to flip above and under the plane defined by the vanadium center, the tripodal N atom and the two phenolate O atoms. Now, on the basis of all the crystal structures collected on our [ONNO]-vanadium systems,[26] it ap-

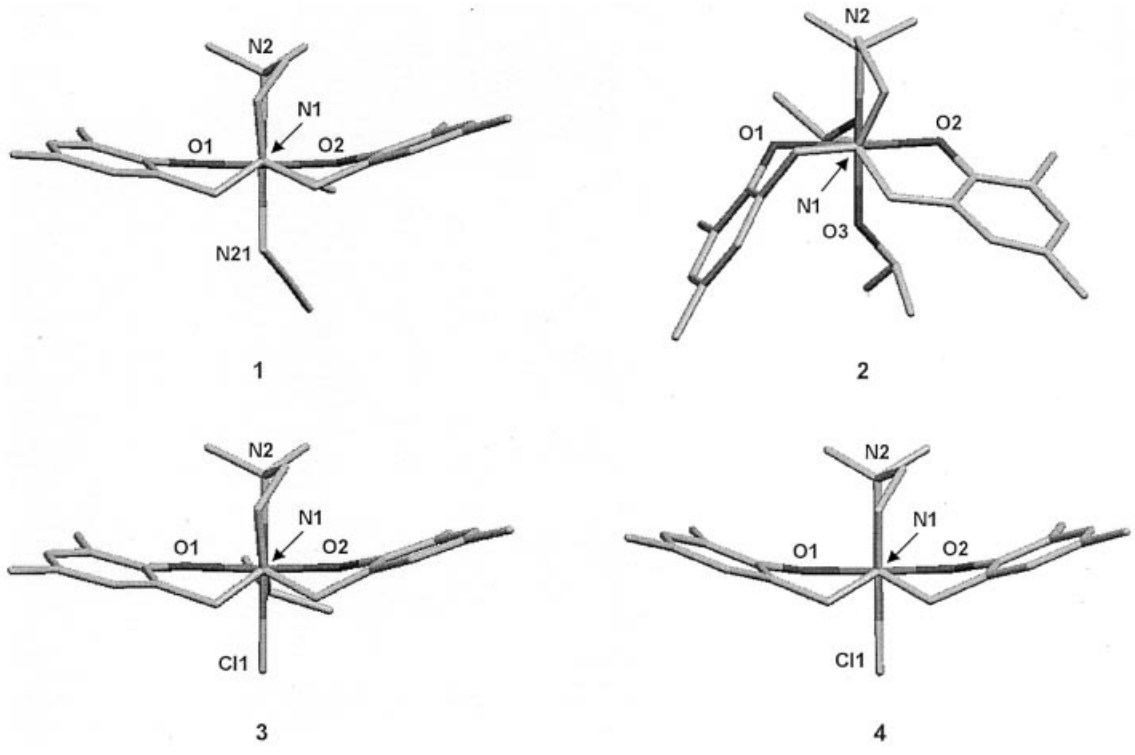

Figure 6. View along the tripodal N1−V−X axis of complexes **1**−**4** [X = N11 (**1**), O4 (**2**), O3 (**3**), Cl2 (**4**)]

 © 2004 Wiley-VCH Verlag GmbH & Co. KGaA, Weinheim

pears that the "dissymmetric" configuration (never observed for group 4 metal complexes) in which the phenolate ligand folds back away from the pendant (dimethylamino)-ethyl sidearm (as in complex **2** and *cis*-[$V^{V}O(OiPr)\{ONNO\}$][12]) is due to the presence of an *O*-ligated anionic ligand (alkoxo, oxo, ···) *trans* to the (dimethylamino)ethyl sidearm nitrogen donor atom in these complexes.

Interestingly, we crystallized only one isomer for [V(Cl)(O*i*Pr){ONNO}] (**3**) although we could expect the formation of two isomers during the chlorination process with Me_3SiCl. Nevertheless, as the two groups (Cl and O*i*Pr) are *trans* to amino nitrogen donor atoms of similar electronic properties, there is probably no reason why in solution the two isomers would not coexist (and have not been distinguished by EPR spectroscopy).

Conclusion

New vanadium(IV) complexes **1**−**4** containing the amine bis(phenolate) [ONNO] ligand and additional azido, isopropoxo or chloro groups are reported. All complexes are d^1-paramagnetic species, whose crystal structures show an [ONNO] moiety that can adopt two different geometries depending on the nature of the ligand located *trans* to the NMe_2 sidearm nitrogen donor atom. Next, we will present the reactivity of these [ONNO]-vanadium complexes towards olefin polymerization.

Experimental Section

General Remarks: All manipulations were carried out using standard Schlenk line or drybox techniques under argon. Starting materials were purchased from Aldrich Inc. or Fluka Inc. and used without further purification. Solvents were refluxed and dried with appropriate drying agents under argon, collected by distillation and stored in a drybox over activated 4-Å molecular sieves. Trimethylchlorosilane and azidotrimethylsilane were distilled and stored over 4-Å molecular sieves under argon. $[ONNO]H_2$ and $V(OiPr)_4$ were prepared according to known procedures.[5e,13] EPR spectra were recorded on a Bruker ESP300E spectrometer. Infrared spectra were prepared as KBr pellets under argon in a glove box and were recorded on a Perkin−Elmer Spectrum GX FT-IR spectrometer. Infrared data are quoted in wavenumber (cm^{-1}). Elemental analyses were performed at the Laboratoire de Chimie de Coordination (Toulouse, France). Magnetic susceptibility data were collected on powdered samples of the different compounds using a homemade Faraday-type automatic magnetometer with mercury tetra(thiocyanato)cobaltate susceptibility (at 20 °C, 16.44×10^{-6} $cm^3 \cdot mol^{-1}$). Diamagnetic corrections were applied using Pascal's constants as described previously.[9b]

CAUTION: Organic and inorganic azides are potentially explosive compounds and should be handled with great care.[14]

$[V(N_3)_2(NMe_2)_2]$: A large excess of azidotrimethylsilane (2.5 g, 22.0 mmol) was added to a pentane solution (15 mL) of $V(NMe_2)_4$ (1.1 g, 5.0 mmol). The solution was kept at room temperature overnight without stirring. A brown-red microcrystalline solid was filtered off, washed with pentane and dried (yield 96%). IR: $\tilde{\nu}$ = 2050 (s, ν_{N3}) cm^{-1}. $C_4H_{12}N_8V$ (223.1): calcd. C 21.53, H 5.42; found C 21.51, H 5.25 (Caution: we encountered an explosion during the combustion analysis).

$[V(N_3)_2\{ONNO\}]$ (1): Solid $[ONNO]H_2$ ligand (195 mg, 0.45 mmol) was added at room temperature to a THF suspension (2 mL) of $[V(N_3)_2(NMe_2)_2]$ (100 mg, 0.45 mmol). The brown solution was stirred at room temperature for 2 h and a brown solid was filtered off (yield 40%). EPR (THF, 20 °C): g = 1.968, $A(^{51}V)$ = 94.0 G. IR: $\tilde{\nu}$ = 2057 (s, ν_{N3}) cm^{-1}. μ_{eff} (20 °C) = 1.80 μ_B. $C_{22}H_{30}N_8O_2V$ (489.5): calcd. C 53.98, H 6.18, N 22.89; found C 53.81, H 6.31, N 23.11.

$[V(OiPr)_2\{ONNO\}]$ (2): Solid $[ONNO]H_2$ ligand (125 mg, 0.35 mmol) was added at room temperature to a toluene solution (2 mL) of $V(OiPr)_4$ (100 mg, 0.35 mmol). The blue-green solution immediately turned dark red and was stirred at room temperature for 2 h. Removal of the volatiles under vacuum and washing with pentane afforded a dark red solid (yield 86%). EPR (pentane, 20 °C): g = 1.967, $A(^{51}V)$ = 70.9 G. μ_{eff} (20 °C) = 1.79 μ_B. $C_{28}H_{44}N_2O_2V$ (491.6): calcd. C 64.23, H 8.47, N 5.35; found C 63.97, H 8.40, N 5.49.

[V(O*i*Pr)(Cl){ONNO}] (3): An excess of Me_3SiCl (1.90 mmol) was slowly added at room temperature to a toluene solution (2 mL) of **2** (100 mg, 0.19 mmol). The reaction mixture was placed in a 25 mL screw-cap vial and heated at 110 °C for 14 h. Removal of the volatiles afforded a dark solid containing a mixture of **3** and **4** from which **3** could be recrystallized from a pentane/THF solution at room temperature giving 11 mg of **3** (yield 11%). EPR (CH_2Cl_2, 20 °C): g = 1.973, $A(^{51}V)$ = 77.3 G. μ_{eff} (20 °C) = 1.77 μ_B. $C_{25}H_{37}ClN_2O_3V$ (500.0): calcd. C 60.06, H 7.46, N 5.60; found C 59.72, H 7.51, N 5.44.

$[VCl_2\{ONNO\}]$ (4) (*CAUTION*: *closed flask heating*): A large excess of Me_3SiCl (3.80 mmol) was slowly added at room temperature to a toluene solution (4 mL) of $[V(OiPr)_2\{ONNO\}]$ (100 mg, 0.19 mmol). The reaction mixture was placed in a 25 mL screw-cap vial and heated at 110 °C for 14 h and then cooled to room temperature. Dark blue needles were filtered off, washed with pentane and dried under vacuum (yield 96%). EPR (CH_2Cl_2, 20 °C): g = 1.975, $A(^{51}V)$ = 82.7 G. μ_{eff} (20 °C) = 1.82 μ_B. $C_{22}H_{30}Cl_2N_2O_2V$ (476.3): calcd. C 55.47, H 6.35, N 5.88; found C 55.60, H 6.33, N 5.96.

Crystal Structure Determination of 1−4: For the four compounds, data were collected at low temperature (T = 180 K) on a Stoe Imaging Plate Diffraction System (IPDS), equipped with an Oxford Cryosystems Cryostream Cooler Device and using graphite-monochromated Mo-K_α radiation (λ = 0.71073Å). Final unit cell parameters were obtained by means of a least-squares refinement of a set of 8000 well-measured reflections. The crystal decay was monitored during data collection by measuring 200 reflections by image; no significant fluctuation of intensities was observed. Structures were solved by means of Direct Methods with the program SIR92.[15] Subsequent difference Fourier maps and models were refined by least-squares procedures on F^2 by using SHELXL-97[16] integrated in the package WINGX version 1.64,[17] and empirical absorption corrections were applied to the data.[18] All hydrogen atoms were located on difference Fourier maps, and introduced in the refinement as fixed contributors using a riding model with an isotropic thermal parameter fixed at 20% higher than those of the C sp^2 atoms and 50% for the C sp^3 atoms to which they were connected. The methyl groups were refined with the torsion angle as free variable. For the four compounds all non-hydrogens atoms were anisotropically refined, and in the last cycles of refinement weighting schemes were used, where weights were calculated from

 © 2004 Wiley-VCH Verlag GmbH & Co. KGaA, Weinheim

Table 2. Crystal data and structure refinement parameters for **1**−**4**

	1	**2**	**3**	**4**
Empirical formula	$C_{22}H_{30}N_8O_2V$	$C_{56}H_{88}N_4O_8V_2$	$C_{50}H_{74}Cl_2N_4O_6V_2$	$C_{22}H_{26}Cl_2N_2O_2V$
Molecular mass	489.48	1047.18	999.91	476.32
Crystal system	monoclinic	triclinic	tetragonal	orthorhombic
Space group	$P2_1/n$	$P\bar{1}$	$I4_1/a$	$Pnma$
a (Å)	19.703(5)	9.411(5)	28.174(5)	16.455(2)
b (Å)	14.479(5)	12.537(5)	28.174(5)	16.2959(15)
c (Å)	8.321(5)	24.800(5)	12.630(5)	8.1845(7)
α (deg)	90.0	80.763(5)	90.0	90.0
β (deg)	92.875(5)	83.429(5)	90.0	90.0
γ (deg)	90.0	77.161(5)	90.0	90.0
V (Å)^3	2370.8(17)	2806.4(19)	10025(5)	2275.2(4)
Z	4	2	8	8
$D_{calcd.}$ (g·cm^{-3})	1.371	1.239	1.325	1.379
μ (Mo-K_α) (mm^{-1})	0.454	0.387	0.531	0.691
F(000)	1028	1124	4240	980
θ Range (deg)	2.07 to 23.26	2.82 to 22.46	1.65 to 26.05	2.48 to 25.97
Measured reflections	13661	15083	40093	16946
Unique reflections/R_{int}	3398/0.0672	7296/0.0951	5097/0.0352	2237/0.1104
Parameters/restraints	304/0	651/0	297/0	158/0
Final R indices [$I > \sigma 2(I)$]	$R_1 = 0.0392$ $wR_2 = 0.0791$	$R_1 = 0.0712$ $wR_2 = 0.1081$	$R_1 = 0.0353$ $wR_2 = 0.0928$	$R_1 = 0.0546$ $wR_2 = 0.1409$
Final R indices all data	$R_1 = 0.0753$ $wR_2 = 0.0909$	$R_1 = 0.1396$ $wR_2 = 0.1277$	$R_1 = 0.0425$ $wR_2 = 0.0980$	$R_1 = 0.0808$ $wR_2 = 0.1556$
Goodness of fit	0.925	0.962	1.018	1.051
$\Delta\rho_{max.} - \Delta\rho_{min.}$, e·Å^3	0.222 and −0.233	0.340 and −0.296	0.507 and −0.363	0.478 and −0.416

the following formula: $w = 1/[\sigma^2(F_o^2) + (aP)^2 + bP]$ where $P = (F_o^2 + 2F_c^2)/3$.

CCDC-226148, -226149, -226150 and -226151 contain the supplementary crystallographic data for this paper. These data can be obtained free of charge at www.ccdc.cam.ac.uk/conts/retrieving.html [or from the Cambridge Crystallographic Data Centre, 12 Union Road, Cambridge CB2 1EZ, UK; Fax: +44-1223-336-033; E-mail: deposit@ccdc.cam.ac.uk].

Acknowledgments

This research was supported by the Centre National de la Recherche Scientifique (CNRS).

[1] For recent reviews see: [1a] V. C. Gibson, S. K. Spitzmesser, *Chem. Rev.* **2003**, *103*, 283−315. [1b] G. J. P. Britovsek, V. C. Gibson, D. F. Wass, *Angew. Chem. Int. Ed.* **1999**, *38*, 429−447.

[2] [2a] J. D. Scollard, D. H. McConville, *J. Am. Chem. Soc.* **1996**, *118*, 10008−10009. [2b] J. D. Scollard, D. H. McConville, N. C. Payne, J. J. Vittal, *Macromolecules* **1996**, *29*, 5241−5243.

[3] [3a] R. Baumann, W. M. Davis, R. R. Schrock, *J. Am. Chem. Soc.* **1997**, *119*, 3830−3831. [3b] R. R. Schrock, F. Schattenmann, M. Aizenberg, W. M. Davis, *Chem. Commun.* **1998**, 1999−2000. [3c] R. Baumann, R. R. Schrock, *J. Organomet. Chem.* **1998**, *557*, 69−75. [3d] R. R. Schrock, R. Baumann, S. M. Reid, J. T. Goodman, R. Stumpf, D. M. Davis, *Organometallics* **1999**, *18*, 3649−3670. [3e] J. T. Goodman, R. R. Schrock, *Organometallics* **2001**, *20*, 5205−5211.

[4] [4a] A. Shafir, M. P. Power, G. D. Whitener, J. Arnold, *Organometallics* **2001**, *20*, 1365−1369. [4b] R. M. Gauvin, C. Lorber, R. Choukroun, B. Donnadieu, J. Kress, *Eur. J. Inorg. Chem.* **2001**, 2337−2346. [4c] Y. M. Jeon, S. J. Park, J. Heo, K. Kim, *Organometallics* **1998**, *17*, 3161−3163. [4d] S. Tinkler, R. J. Deeth, D. J. Duncalf, A. McCamley, *Chem. Commun.* **1996**, 2633−2634. [4e] F. G. N. Clocke, T. J. Geldbach, P. B. Hitchcock, J. B. Love, *J. Organomet. Chem.* **1996**, *506*, 343−345. [4f] N. A. H. Male, M. Thornton-Pett, M. Bochmann, *J. Chem. Soc., Dalton Trans.* **1997**, 2487−2494. [4g] V. C. Gibson, B. S. Kimberley, A. J. P. White, D. J. Williams, P. Howard, *Chem. Commun.* **1998**, 313−314. [4h] C. H. Lee, Y.-H. La, S. J. Park, J. W. Park, *Organometallics* **1998**, *17*, 3648−3655.

[5] [5a] E. Y. Tshuva, I. Goldberg, M. Kol, *J. Am. Chem. Soc.* **2000**, *122*, 10706−10707. [5b] E. Y. Tshuva, I. Goldberg, M. Kol, H. Weitman, Z. Goldschmidt, *Chem. Commun.* **2000**, 379−380. [5c] E. Y. Tshuva, I. Goldberg, M. Kol, Z. Goldschmidt, *Chem. Commun.* **2001**, 2120−2121. [5d] E. Y. Tshuva, S. Groysman, I. Goldberg, M. Kol, Z. Goldschmidt, *Organometallics* **2002**, *21*, 662−670. [5e] E. Y. Tshuva, I. Goldberg, M. Kol, Z. Goldschmidt, *Organometallics* **2001**, *20*, 3017−3028. [5f] E. Y. Tshuva, I. Goldberg, M. Kol, Z. Goldschmidt, *Inorg. Chem.* **2001**, *40*, 4263−4270.

[6] [6a] Y. Nakayama, K. Watanabe, N. Ueyama, A. Nakamura, A. Harada, J. Okuda, *Organometallics* **2000**, *19*, 2498−2503. [6b] R. M. Gauvin, J. A. Osborn, J. Kress, *Organometallics* **2000**, *19*, 2944−2946. [6c] H. Mack, M. S. Eisen, *J. Chem. Soc., Dalton Trans.* **1998**, 917−921. [6d] M. G. Thorn, Z. C. Etheridge, P. E. Fanwick, I. P. Rothwell, *Organometallics* **1998**, *17*, 3636−3638. [6e] X. Bei, D. C. Swenson, R. F. Jordan, *Organometallics* **1997**, *16*, 3282−3302.

[7] See for example: [7a] M. Mitani, R. Furuyama, J-I. Mohri, J. Saito, S. Ishii, H. Terao, H. Tanaka, T. Fujita, *J. Am. Chem. Soc.* **2003**, *125*, 4293−4305. [7b] S. Matsui, Y. Tohi, M. Mitani, J. Saito, H. Makio, H. Tanaka, M. Nitabaru, T. Nakano, T. Fujita, *Chem. Lett.* **1999**, 1065−1066. [7c] S. Matsui, T. Fujita, *Catal. Today* **2001**, *66*, 63−73. [7d] J. Saito, M. Mitani, S. Matsui, J-I. Mohri, S. Kojoh, N. Kashiwa, T. Fujita, *Angew. Chem. Int. Ed.* **2001**, *40*, 2918−2920. [7e] Y. Susuki, N. Kashiwa, T. Fujita, *Chem. Lett.* **2002**, 358−359. [7f] M. Mitami, T. Nakano, T. Fujita, *Chem. Eur. J.* **2003**, *9*, 2396−2402.

[8] [8a] J. Tian, G. W. Coates, *Angew. Chem. Int. Ed.* **2000**, *39*, 3626−3629. [8b] M. Fujita, G. W. Coates, *Macromolecules* **2002**, *35*, 9640−9647. [8c] J. Tian, P. D. Hustad, G. W. Coates, *J. Am. Chem. Soc.* **2002**, *124*, 3614−3621.

[9] [9a] C. Lorber, R. Choukroun, B. Donnadieu, *Inorg. Chem.* **2003**, *42*, 673−675. [9b] C. Lorber, R. Choukroun, B. Donnad-

 © 2004 Wiley-VCH Verlag GmbH & Co. KGaA, Weinheim

ieu, *Inorg. Chem.* **2002**, *41*, 4217−4226. [9c] R. Choukroun, B. Donnadieu, C. Lorber, P.-M. Pellny, W. Baumann, U. Rosenthal, *Chem. Eur. J.* **2000**, *6*, 4505−4509. [9d] R. Choukroun, B. Donnadieu, C. Lorber, *Chem. Eur. J.* **2002**, *8*, 2700−2704. [9e] R. Choukroun, C. Lorber, B. Donnadieu, *Organometallics* **2002**, *21*, 1124−1126. [9f] F. Wolff, R. Choukroun, C. Lorber, B. Donnadieu, *Eur. J. Inorg. Chem.* **2003**, 628−632.

[10] C. Lorber, B. Donnadieu, R. Choukroun, *Organometallics* **2000**, *19*, 1963−1966.

[11] C. Lorber, B. Donnadieu, R. Choukroun, *J. Chem. Soc., Dalton Trans.* **2000**, 4497−4498.

[12] F. Wolff, C. Lorber, R. Choukroun, B. Donnadieu, *Inorg. Chem.* **2003**, *42*, 7839−7845.

[13] I. M. Thomas, *Can J. Chem.* **1961**, *39*, 1386−1388.

[14] For a discussion of the hazards associated with HN_3 and related azides, see: [14a] L. Bretherick, *Handbook of Reactive Chemical Hazards*; Butterworth: London, **1975**; pp. 775−776. [14b] Committee on Prudent Practices for Handling, Storage, and Disposal of Chemicals in Laboratories *Prudent Practices in the Laboratory, Handling and Disposal of Chemicals*; National Academic Press: Washington, D. C. **1995**; pp. 165 and 102.

[15] A. Altomare, G. Cascarano, G. Giacovazzo, A. Guagliardi, M. C. Burla, G. Polidori, M. Camalli, *J. Appl. Crystallogr.* **1994**, *27*, 435.

[16] *SHELX97* [includes *SHELXS-97*, *SHELXL-97*, *CIFTAB*], Programs for Crystal Structure Analysis (Release 97−2); G. M. Sheldrick, University of Göttingen, Institut für Anorganische Chemie, Tammanstraße 4, 3400 Göttingen, Germany, **1998**.

[17] L. J. Farrugia, *J. Appl. Crystallogr.* **1999**, *32*, 837−838.

[18] N. Walker, D. Stuart, *Acta Crystallogr., Sect. A* **1983**, *39*, 158−166.

[19] R. Choukroun, P. Moumboko, S. Chevalier, M. Etienne, B. Donnadieu, *Angew. Chem. Int. Ed.* **1998**, *37*, 3169.

[20] C. Lorber, R. Choukroun, unpublished results.

[21] D. C. Bradley, M. H. Gitlitz, *J. Chem. Soc., A* **1969**, 980−985.

[22] W. J. Evans, L. A. Edinger, J. W. Ziller, *Polyhedron* **1999**, *18*, 1475−1477.

[23] C. Lorber, J. P. Donahue, C. A. Goddard, E. Nordlander, R. H. Holm, *J. Am. Chem. Soc.* **1998**, *120*, 8102−8112.

[24] **caution**: Organic and inorganic azides are potentially explosive compounds and should be handled with great care. Reflux in toluene was realized on a 20 mg scale to prevent any explosion and in a stainless steel reactor for safety.

[25] Generally, phenoxide bond lengths are ca 1.90 Å. Very few vanadium compounds are known with phenoxide V−O bond lengths < 1.79 Å, among which: [25a] V. Vergopoulos, S. Jantzen, N. Julien, E. Rose, D. Rehder, *Z. Naturfosh. B* **1994**, *49*, 1127−1130. [25b] N. F. Choudhary, N. G. Connelly, P. B. Hitchcock, G. J. Leigh, *J. Chem. Soc., Dalton Trans.* **1999**, 4437−4446. [25c] A. Hills, D. L. Hughes, G. J. Leigh, J. R. Sanders, *J. Chem. Soc., Dalton Trans.* **1991**, 61−64. [25d] P. J. Toscano, E. J. Schermerhorn, C. Dettelsbach, D. Macherone, J. Zubieta, *J. Chem. Soc., Chem. Commun.* **1991**, 933−934. [25e] V. J. Murphy, H. Turner, *Organometallics* **1997**, *16*, 2495−2497.

[26] This rule is also true for V^{III} and V^{II} related systems (C. Lorber, R. Choukroun, *Organometallics*, submitted).

Received December 10, 2003
Early View Article
Published Online May 13, 2004

 © 2004 Wiley-VCH Verlag GmbH & Co. KGaA, Weinheim

Synthesis, Crystal Structure and Thermal Reactivity of New Copper(I) Halide Pyrimidine-Containing Coordination Polymers

Christian Näther*[a] and Inke Jeß[a]

Keywords: Coordination polymers / Copper / Halides / N ligands / Thermal properties

Reaction of copper(I) chloride with pyrimidine in acetonitrile leads to the formation of the ligand-rich 1:1 compound poly-[CuCl(μ_2-pyrimidine-*N*,*N*′)] (**1**). "Zig-zag"-like CuCl chains are found in the crystal structure that are connected by the pyrimidine ligands to form layers. This compound loses half of its ligands upon heating and transforms into the new l2:1 coordination polymer poly[$(CuCl)_2$(μ_2-pyrimidine-*N*,*N*′)] (**2**). In this structure, ladder-like CuCl double chains occur which are connected by the pyrimidine ligands to form layers. If copper(I) iodide is used in the synthesis, the new 1:1 coordination polymer poly[CuI(μ_2-pyrimidine-*N*,*N*′)] (**3**) forms. In contrast to compound **1**, CuI single chains and $(CuI)_2$ dimers are found as the CuX substructure, and these are connected by the ligands to form sheets. On heating this compound a similar behaviour as for compound **1** is observed, and a transformation into the new 2:1 compound poly[$(CuI)_2$(μ_2-pyrimidine-*N*,*N*′)] (**4**) occurs. This compound is not isotypic to **2** even though the topology of the coordination network is identical (CuI double chains are connected into layers by the pyrimidine ligands). The thermal behaviour of the known compounds poly[CuBr(μ_2-pyrimidine-*N*,*N*′)] (**5**) and poly-[$(CuBr)_2$(μ_2-pyrimidine-*N*,*N*′)] (**6**) was also investigated. A transformation of the ligand-rich 1:1 compound **5** into the 2:1 compound **6** is also observed in the thermal decomposition reaction.

(© Wiley-VCH Verlag GmbH & Co. KGaA, 69451 Weinheim, Germany, 2004)

Introduction

Inorganic-organic coordination polymers based on copper(I) halides or pseudohalides and aromatic nitrogen-donor ligands are well-known and several of them have been synthesised and structurally characterised in the past.[1−38] These compounds consist of CuX substructures such as four- or six-membered rings, "zig-zag"-like or helical single chains, or "ladder-like" double chains, which are connected by the nitrogen-donor ligands to give one-, two- or three-dimensional coordination polymers. For each combination of copper(I) halide or pseudohalide and nitrogen-donor ligand several different compounds are frequently found, each of which has a different ratio — 1:1, 1:2, 2:1, 3:2 or 4:1 — between the copper(I) halide or pseudohalide and the organic ligand. We have found that most ligand-rich copper(I) halide or pseudohalide compounds can be transformed into ligand-poorer compounds by thermal decomposition, whereas others loses all their ligands in one step forming the pure copper(I) halides or pseudohalides.[26−38] This method is therefore an alternative route for the preparation of new CuX (X = Cl, Br, I, SCN, CN) coordination polymers that cannot be prepared in solution or that are always obtained as mixtures. We have found, for example, no simple relationship between the structure of the starting compound and its thermal reactivity or the structure of the decomposition product.[26−38] However, our investigations do show that the product formation depends on the kinetics of all the reactions involved.[31] In some cases several ligand-poorer intermediates (2:1 or 4:1) or different polymorphic modifications can be isolated.[32−34] In order to investigate the influence of the coordination behaviour of the organic ligands on the structure and the thermal reactivity of these coordination polymers we have prepared and structurally characterised several of them. In most cases we have used small six-membered nitrogen heterocycles (e.g. pyrazine or its derivatives). To investigate the influence of the position of the nitrogen-donor atoms on the structure we were also interested in the pyridazine or pyrimidine coordination compounds. With pyrimidine only the 1:1 compound [CuBr(pyrimidine)][9] the 2:1 compound [$(CuBr)_2$(pyrimidine)][37] and the 2:1 compound [$(CuCN)_2$(pyrimidine)][18,24] have been structurally characterized. The amine-poorer compounds [$(CuX)_2$pyrimidine] (X = Cl, Br, I) were also prepared and characterised by elemental analysis and thermogravimetric measurements.[25] It was shown that these compounds lose all of the pyrimidine ligands in one step forming the pure copper(I)-halides. Here we report on the synthesis, the crystal structure and the thermal reactivity of CuX and $(CuX)_2$ pyrimidine-containing coordination polymers.

[a] Institut für Anorganische Chemie der Christian-Albrechts-Universität zu Kiel,
Olshausenstraße 40, 24098 Kiel, Germany
E-mail: cnaether@ac.uni-kiel.de

Results and Discussion

Crystal Structures

The 1:1 compound poly[CuCl(μ_2-pyrimidine-*N*,*N*′)] (**1**) crystallizes in the orthorhombic space group *Pma*2 with two formula units in the unit cell. The compound is not isotypic with the 1:1 coordination polymer poly[CuBr(μ_2-pyrimidine-*N*,*N*′)] (**5**), and the topology of the coordination network is also different.[9] The asymmetric unit consists of one copper and one chlorine atom as well as one pyrimidine ligand, all of which are located in special positions. Each copper(I) atom is coordinated by two chlorine atoms and two nitrogen atoms of pyrimidine ligands within a distorted tetrahedron (Figure 1, top).

The bond lengths and angles are similar to those of related compounds (Table 1). The copper atoms are connected through the chlorine atoms forming "zig-zag" CuCl chains in the direction of the crystallographic *b*-axis (Figure 1, bottom). These chains are connected by the pyrimidine ligands to form layers that are parallel to (001) (Figure 1, bottom).

The ligand-poorer 2:1 compound poly[$(CuCl)_2$(μ_2-pyrimidine-*N*,*N*′)] (**2**) crystallizes in the orthorhombic space group *Pnma* with four formula units in the unit cell. The asymmetric unit consists of one crystallographically independent Cu and Cl atom in general positions and one pyrimidine ligand which is located in a special position (Figure 2, top). The compound is not isotypic with the previously reported compound poly[$(CuBr)_2$(μ_2-pyrimidine-*N*,*N*′)] (**6**)[37] but contains an identical topology of the coordination network. The copper atoms are coordinated by three chlorine atoms and one nitrogen atom of the pyrimidine ligand within strongly distorted tetrahedra (Table 1). The Cu−N bond length is significantly shorter than that observed in compound **1**, whereas the Cu−Cl bond lengths are longer.

The CuX substructure consists of CuCl double chains which are connected by the pyrimidine ligands to form layers which are parallel to the *bc* plane (Figure 2, bottom). This topology of the coordination network is frequently found in such ligand-poorer 2:1 compounds.

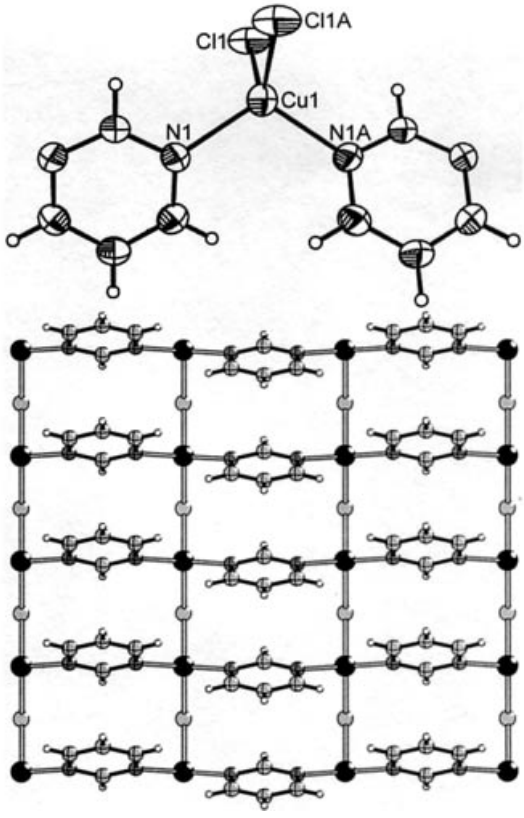

Figure 1. Crystal structure of poly[CuCl(μ_2-pyrimidine-*N*,*N*′] (**1**) showing the coordination sphere of the copper atoms with labelling and displacement ellipsoids drawn at the 50% probability level (top); view of the coordination network along the crystallographic *c*-axis (bottom)

The 1:1 compound poly[CuI(μ_2-pyrimidine-*N*,*N*′)] (**3**) crystallizes in the monoclinic space group $P2_1/c$ with eight formula units in the unit cell. The asymmetric unit consists

Table 1. Selected bond lengths (Å) and angles (°) for poly[CuCl(μ_2-pyrimidine-*N*,*N*′] (**1**) and poly[$(CuCl)_2$(μ_2-pyrimidine-*N*,*N*′] (**2**)

poly[CuCl(μ_2-pyrimidine-*N*,*N*′] (**1**)			
Cu(1)−N(1A)	2.060(2)	Cu(1)−N(1)	2.060(2)
Cu(1)−Cl(1)	2.337(1)	Cu(1)−Cl(1A)	2.337(1)
N(1A)−Cu(1)−N(1)	112.91(9)	N(1A)−Cu(1)−Cl(1)	111.40(4)
N(1)−Cu(1)−Cl(1)	106.18(5)	N(1A)−Cu(1)−Cl(1A)	106.18(5)
N(1)−Cu(1)−Cl(1A)	111.40(4)	Cl(1)−Cu(1)−Cl(1A)	108.79(3)
Cu(1)−Cl(1)−Cu(1A)	108.79(3)		
poly[$(CuCl)_2$(μ_2-pyrimidine-*N*,*N*′] (**2**)			
Cu(1)−N(1)	2.011(2)	Cu(1)−Cl(1A)	2.293(1)
Cu(1)−Cl(1B)	2.447(1)	Cu(1)−Cl(1)	2.476(1)
Cu(1)−Cu(1A)	2.887(1)		
N(1)−Cu(1)−Cl(1A)	126.02(8)	N(1)−Cu(1)−Cl(1A)	104.67(8)
Cl(1A)−Cu(1)−Cl(1B)	105.61(4)	N(1)−Cu(1)−Cl(1)	104.95(8)
Cl(1A)−Cu(1)−Cl(1)	109.26(3)	Cl(1A)−Cu(1)−Cl(1)	104.42(3)
Cu(1A)−Cl(1)−Cu(1B)	105.61(4)	Cu(1A)−Cl(1)−Cu(1)	74.39(3)
Cu(1B)−Cl(1)−Cu(1)	71.81(3)		

 © 2004 Wiley-VCH Verlag GmbH & Co. KGaA, Weinheim

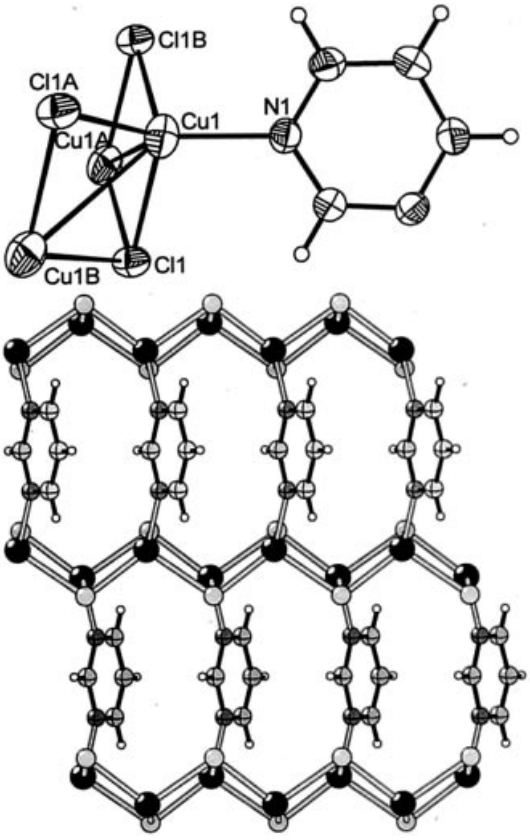

Figure 2. Crystal structure of poly[$(CuCl)_2(\mu_2$-pyrimidine-*N*,*N*′] (**2**) showing the coordination sphere of the copper atoms with labelling and displacement ellipsoids drawn at the 50% probability level (top); view of the coordination network along the crystallographic *a*-axis (bottom)

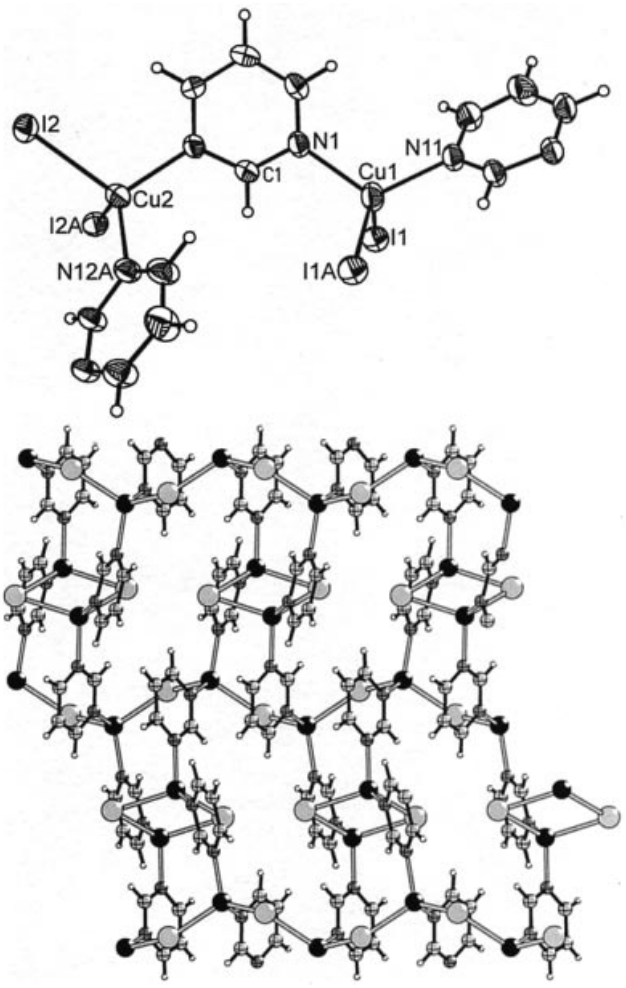

Figure 3. Crystal structure of poly[CuI(μ_2-pyrimidine-*N*,*N*′] (**3**) showing the coordination sphere of the copper atoms with labelling and displacement ellipsoids drawn at the 50% probability level (top); view of the coordination network along the crystallographic *a*-axis (bottom)

of two crystallographically independent Cu atoms and one I atom as well as two pyrimidine ligands located in general positions (Figure 3, top). This compound is isotypic to the 1:1 coordination polymer poly[CuBr(μ_2-pyrimidine-*N*,*N*′)] (**1**).[9] Each of the two crystallographically independent copper atoms is coordinated by two iodine atoms and two organic ligands within a distorted tetrahedra (Table 2 and Figure 3, top). In contrast to compound **1**, two different building units are found as the CuX substructure. Cu1 and I1 form coplanar $(CuI)_2$ dimers which are located on centres of inversion, whereas Cu2 and I2 are connected to "zig-zag"-like CuI single chains which propagate in the direction of the crystallographic *c*-axis (Figure 3, bottom). The dimers and single chains are connected by the pyrimidine ligands into corrugated layers in the *bc* plane.

The ligand poorer 2:1 compound poly[$(CuI)_2(\mu_2$-pyrimidine-*N*,*N*′)] (**4**) crystallizes in the monoclinic space group $P2_1/m$ with two formula units in the unit cell (Table 3). The asymmetric unit contains one copper atom and one iodine in general positions as well as one pyrimidine ligand which is located in the crystallographic mirror plane. The compound is isotypic with the previously reported coordination polymer poly[$(CuBr)_2(\mu_2$-pyrimidine-*N*,*N*′)] (**6**).[37] The copper atoms are surrounded by three iodine atoms and one nitrogen atom of the pyrimidine ligand within a distorted tetrahedron (Figure 4, top). The bond lengths and angles are similar to those observed in other ligand-poorer 2:1 CuX compounds. As in the CuCl compound **1** and the CuI compound **4**, CuX double chains are found as the CuX substructure, and these are connected to form layers by the pyrimidine ligands. Therefore, the topology of the coordination network is identical in all ligand-poorer 2:1 compounds.

If the crystal structures of the present pyrimidine compounds are compared with those of the previously reported pyrazine and pyridazine compounds some interesting features become obvious. The ligand-rich 1:2 coordination polymers with pyrazine have an identical topology of the coordination network to the present pyrimidine compounds. CuX single chains (X = Cl,[39] Br[15]) are observed as the CuX substructure, and these are connected into layers by the pyrazine ligands. If the N-donor atoms are located in the 1- and 2-positions, like in pyridazine, the topology of the coordination network in the 1:1 compounds is completely different.[9,34] Due to steric restrictions no layered structures can be formed and typical one-dimensional

 © 2004 Wiley-VCH Verlag GmbH & Co. KGaA, Weinheim

Table 2. Selected bond lengths (Å) and angles (°) for poly[CuI(μ_2-pyrimidine-*N*,*N*′] (**3**) and poly[$(CuI)_2$(μ_2-pyrimidine-*N*,*N*′] (**4**)

poly[CuI(μ_2-pyrimidine-*N*,*N*′] (**3**)			
Cu(1)−N(11)	2.047(4)	Cu(1)−N(1)	2.078(4)
Cu(1)−I(1)	2.653(1)	Cu(1)−I(1A)	2.668(1)
Cu(2)−N(2)	2.059(4)	Cu(2)−N(12A)	2.063(4)
Cu(2)−I(2A)	2.601(1)	Cu(2)−I(2)	2.614(1)
N(11)−Cu(1)−N(1)	117.9(2)	N(11)−Cu(1)−I(1)	105.1(2)
N(1)−Cu(1)−I(1)	106.3(2)	N(11)−Cu(1)−I(1A)	107.5(2)
N(1)−Cu(1)−I(1A)	100.9(2)	I(1)−Cu(1)−I(1A)	120.0(1)
N(2)−Cu(2)−N(12A)	107.4(2)	N(2)−Cu(2)−I(2A)	114.3(2)
N(12A)−Cu(2)−I(2A)	112.1(2)	N(2)−Cu(2)−I(2)	106.8(2)
N(12A)−Cu(2)−I(2)	110.7(2)	I(2A)−Cu(2)−I(2)	105.5(1)
poly[$(CuI)_2$(μ_2-pyrimidine-*N*,*N*′] (**4**)			
Cu(1)−N(1)	2.058(6)	Cu(1)−I(1)	2.620(2)
Cu(1)−I(1A)	2.634(2)	Cu(1)−I(1B)	2.691(2)
Cu(1)−Cu(1A)	2.722(2)	Cu(1)−Cu(1B)	2.776(2)
N(1)−Cu(1)−I(1)	107.7(2)	N(1)−Cu(1)−I(1A)	110.0(2)
I(1)−Cu(1)−I(1A)	117.6(1)	N(1)−Cu(1)−I(1B)	100.6(2)
I(1)−Cu(1)−I(1B)	117.0(1)	I(1A)−Cu(1)−I(1B)	102.6(1)
Cu(1)−I(1)−Cu(1A)	62.4(1)	Cu(1)−I(1)−Cu(1B)	63.0(1)
Cu(1A)−I(1)−Cu(1B)	102.6(1)		

Table 3. Selected crystal data and results of the structure refinements for compounds **1**−**4**

Compound	**1**	**2**	**3**	**4**
Formula	$C_4H_4N_2CuCl$	$C_4H_4N_2Cu_2Cl_2$	$C_4H_4N_2CuI$	$C_4H_4N_2Cu_2I_2$
Mol. mass (g·mol^{-1})	179.08	278.08	270.53	460.97
Crystal colour	orange	yellow	yellow	yellow
Crystal size (mm^{-1})	0.07 × 0.10 × 0.13	0.05 × 0.09 × 0.12	0.07 × 0.10 × 0.13	0.07 × 0.10 × 0.13
Diffractometer	STOE AED-II	STOE IPDS	STOE AED-II	STOE AED-II
Crystal system	orthorhombic	orthorhombic	monoclinic	monoclinic
Space group	*Pma*2	*Pnma*	$P2_1/c$	$P2_1/m$
a (Å)	11.610 (1)	14.737 (1)	9.564 (2)	4.1554 (7)
b (Å)	3.8000 (6)	13.379 (1)	17.689 (3)	15.159 (2)
c (Å)	6.4900 (8)	3.7772 (2)	8.073 (1)	7.049 (1)
α (°)	−	−	−	−
β (°)	−	−	108.47 (1)	96.81 (2)
γ (°)	−	−	−	−
V (Å^3)	283.33 (6)	744.72 (8)	1295.4 (4)	440.9 (1)
Temperature (K)	room temp.	room temp.	room temp.	room temp.
Z	2	4	8	2
$D_{calcd.}$ (g·cm^{-3})	2.077	2.480	2.774	3.472
F(000)	176	536	992	412
2θ range (°)	3-60	3−56	3-56	3−54
h/k/l ranges	−16/16	−19/19	−12/11	−2/5
	−5/5	−17/17	−15/23	−19/5
	−9/9	−4/4	−0/10	−8/8
μ(Mo-K_α) (mm^{-1})	4.15	6.34	8.03	11.75
Absorption corr.	numerical	−	numerical	numerical
Min./max. transm.	0.4858/0.5930	−	0.2671/0.3970	0.1503/0.2451
Measured refl.	3360	6535	6133	2098
$R_{int.}$	0.0529	0.0342	0.0376	0.0481
Independent refl.	884	914	3143	996
Refl. with $I > 2\sigma(I)$	755	742	2065	733
Parameters	42	50	146	50
R_1 [$I > 2\sigma(I)$]	0.0189	0.0332	0.0274	0.0310
wR_2 [all data]	0.0499	0.0955	0.0674	0.0771
Goof	1.058	1.067	0.971	1.088
Res. elec. den. (e·Å^{-3})	0.24 / −0.17	0.62 / −0.66	0.78 / −0.86	1.23 / −0.97

 © 2004 Wiley-VCH Verlag GmbH & Co. KGaA, Weinheim

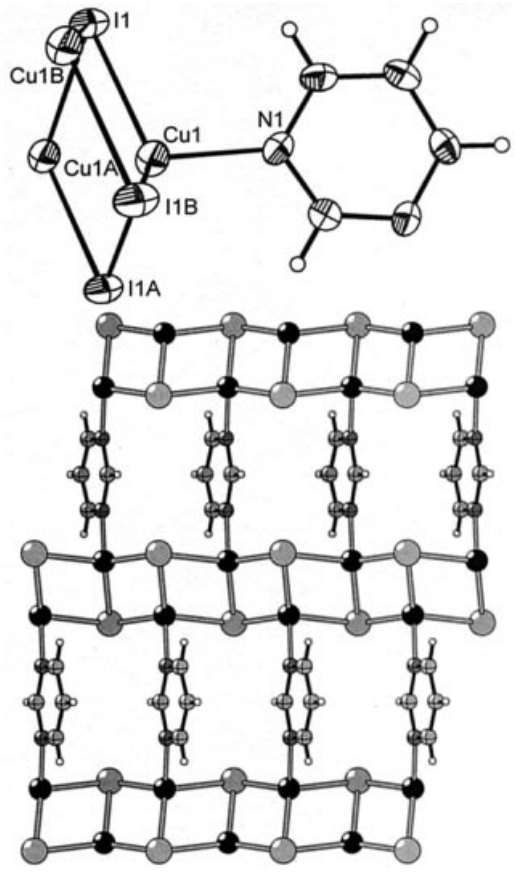

Figure 4. Crystal structure of poly[$(CuI)_2(\mu_2$-pyrimidine-*N*,*N*′] (**4**) showing the coordination sphere of the copper atoms with labelling and displacement ellipsoids drawn at the 50% probability level (top); view of the coordination network along the crystallographic *a*-axis (bottom)

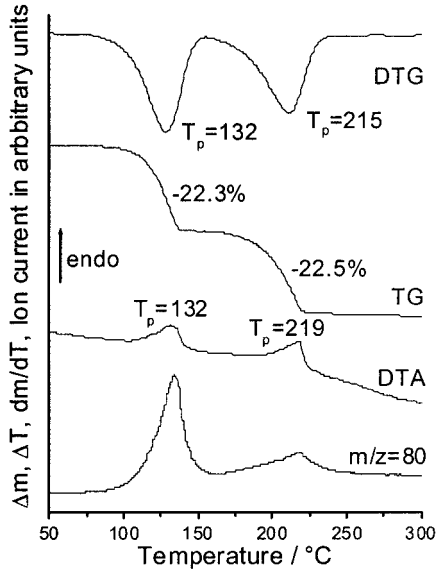

Figure 5. DTA, TG, DTG and MS trend scan curves for poly[CuCl(μ_2-pyrimidine-*N*,*N*′] (**1**) (weight: 19.98 mg; heating rate: 4 °C/min.; MS: m/z = 80 (pyrimidine); T_p = peak temperature)

structures result. A similar observation is made for the ligand-poorer 2:1 compounds. The topology of the structures with pyrazine is identical to that of the structures with pyrimidine. CuX double chains (X = Cl,[40] Br[11]) are observed that are connected to form layers. This arrangement cannot be formed with pyridazine as ligand and therefore completely different CuX substructures (X = Cl, Br,[34] I[9]) and a completely different coordination network result.

Thermal Properties

The thermal properties of compounds **1**−**5** were investigated by simultaneous differential thermoanalysis, thermogravimetry and mass spectrometry, as well as temperature-dependent X-ray powder diffraction.

On heating poly[CuCl(μ_2-pyrimidine-*N*,*N*′] (**1**) in a thermobalance two mass steps are observed, which are accompanied by two endothermic events in the DTA curve at peak temperatures of 132 and 219 °C (Figure 5).

The experimental mass-loss of 22.3 and 22.5% in both steps is in good agreement with that calculated for the removal of half of the pyrimidine ligands in each step [Δm_{theo} = 22.3%]. The DTG curve shows that both steps are well resolved and that only pyrimidine (m/z = 80) is emitted. The final product of this reaction was identified as $Cu^{I}Cl$ by X-ray powder diffraction. These results suggest that in the first step the ligand-poorer 2:1 compound poly[$(CuCl)_2(\mu_2$-pyrimidine-*N*,*N*′] (**2**) is formed, which on further heating loses its remaining pyrimidine ligands. The results found for the decomposition of the amine-poorer 2:1 compound are in agreement with those found by Mayer et al.[25]

To identify the intermediate after the first TG step a second TG experiment was performed which was stopped after the first TG step. The residue isolated was investigated by elemental analysis and X-ray powder diffraction. When this experimental powder pattern was compared with that calculated for the 2:1 compound **2** from single crystal data, it was confirmed that the ligand poorer coordination polymer **2** had formed (Figure 6).

On heating the 1:1 compound poly[CuI(μ_2-pyrimidine-*N*,*N*′] (**3**) a similar behaviour as for compound **1** was found. Two endothermic events were observed at peak temperatures of 110 and 215 °C which are accompanied by two well-resolved mass steps in the TG curve (Figure 7). The MS spectra show that in both steps only pyrimidine ligands are emitted and the experimental mass loss is in good agreement with that calculated for the emission of half of the pyrimidine ligands in each step (Δm_{theo} = 14.8%). Therefore, the first TG step should lead to the formation of the ligand-poorer compound **4**. The residue after the second TG step was identified as CuI by X-ray powder diffraction, which is in agreement with previous investigations.[25]

 © 2004 Wiley-VCH Verlag GmbH & Co. KGaA, Weinheim

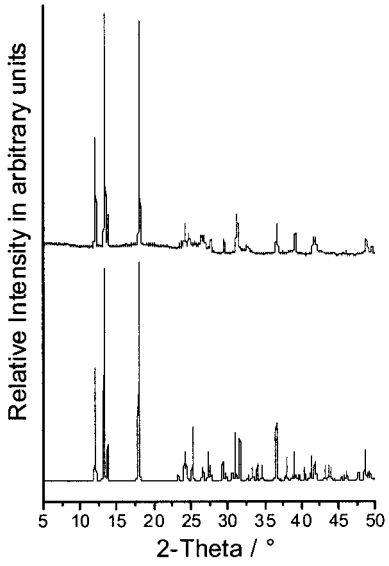

Figure 6. Powder pattern of the residue isolated after the first TG step during the thermal decomposition of poly[CuCl(μ_2-pyrimidine-*N*,*N*′] (**1**) (top), and calculated pattern for the ligand-poorer 2:1 compound poly[(CuCl)$_2$(μ_2-pyrimidine-*N*,*N*′] (**2**) (bottom)

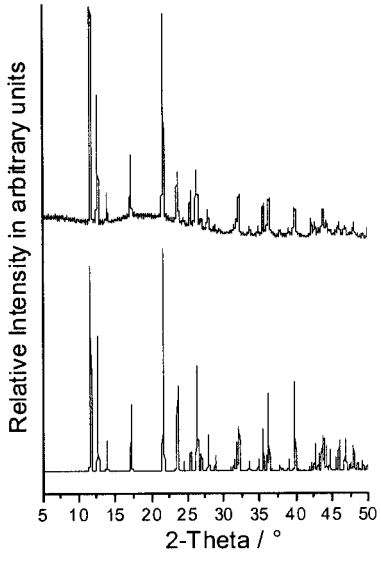

Figure 8. Powder pattern of the residue isolated after the first TG step during the thermal decomposition of poly[CuI(μ_2-pyrimidine-*N*,*N*′] (**3**) (top), and calculated pattern for the ligand-poorer 2:1 compound poly[(CuI)$_2$(μ_2-pyrimidine-*N*,*N*′] (**4**) (bottom).

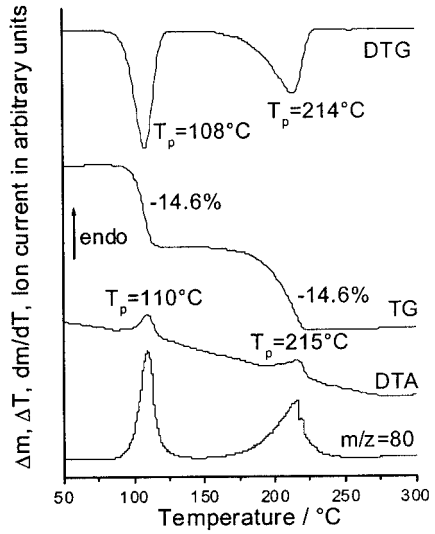

Figure 7. DTA, TG, DTG and MS trend scan curves for poly[CuI(μ_2-pyrimidine-*N*,*N*′] (**3**) (weight: 19.98 mg; heating rate: 4 °C/min.; MS: *m*/*z* = 80 (pyrimidine); T_p = peak temperature)

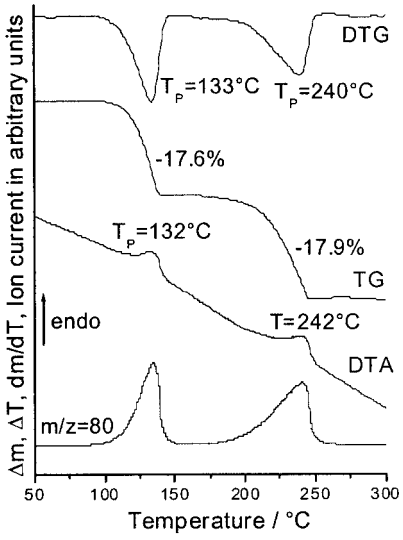

Figure 9. DTA, TG, DTG and MS trend scan curves for poly[CuBr(μ_2-pyrimidine-*N*,*N*′] (**5**) (weight: 19.98 mg; heating rate: 4 °C/min.; MS: *m*/*z* = 80 (pyrimidine); T_p = peak temperature)

In a second TG run the experiment was stopped after the first TG step and the intermediate was investigated by X-ray powder diffraction and elemental analysis. The CHN content is in agreement with that calculated for a ligand-poorer 2:1 compound and the experimental powder pattern is identical with that calculated for compound **4** (Figure 8).

If the known 1:1 compound poly[CuBr(μ_2-pyrimidine-*N*,*N*′)] (**5**) is heated in a thermobalance two well-resolved mass steps occur which are accompanied by two endothermic events in the DTA curve (Figure 9). The MS curve shows that only the N-donor ligands are removed and the experimental mass loss of 17.6 and 17.9% in both steps is in good agreement with that calculated for the removal of half of the pyrimidine ligands in each step (Δm_{theo} = 17.9%). The residue formed after the first TG step was identified as the ligand-poorer 2:1 compound poly[(CuBr)$_2$(μ_2-pyrimidine-*N*,*N*′)] (**6**; Figure 10).

Because in previous investigations we have shown that the product formation sometimes depends on the kinetics of all the reactions involved[31] heating-rate-dependent studies were performed for all compounds at rates of between 0.5 and 16 °C/min. However, these experiments showed no changes in the TG curves and gave no hints for the presence of additional intermediates during the thermal reactions.

To investigate if the reaction is more complex and, for example, different polymorphic modifications occur, temperature-dependent X-ray powder measurements were performed[33–35] (Figure 11).

 © 2004 Wiley-VCH Verlag GmbH & Co. KGaA, Weinheim

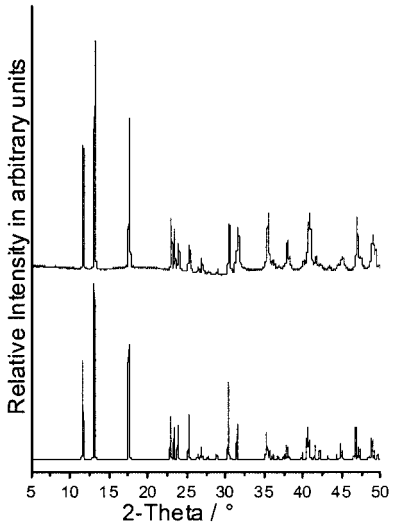

Figure 10. Powder pattern of the residue isolated after the first TG step during the thermal decomposition of poly[CuBr(μ_2-pyrimidine-*N*,*N*′] (**5**) (top), and calculated pattern for the ligand-poorer 2:1 compound poly[(CuBr)$_2$(μ_2-pyrimidine-*N*,*N*′] (**6**) (bottom)

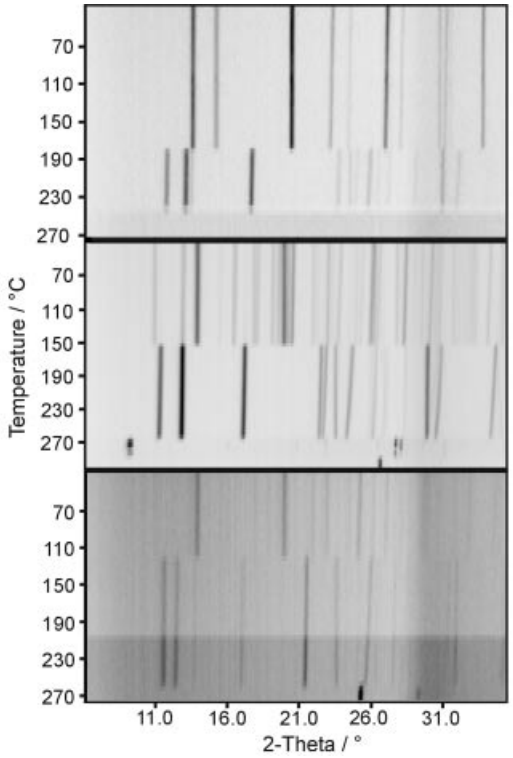

Figure 11. Temperature-resolved X-ray powder pattern for poly[CuCl(μ_2-pyrimidine-*N*,*N*′] (**1**) (top), poly[CuBr(μ_2-pyrimidine-*N*,*N*′] (**5**) (middle) and poly[CuI(μ_2-pyrimidine-*N*,*N*′] (**3**) (bottom); heating rate: 5 °C/min; the diffraction pattern was measured every 5 °C

It must be noted that the decomposition temperatures cannot be compared with those from the DTA-TG-MS measurements because different conditions, for example static or flowing atmosphere, are used. On heating the CuCl compound **1** the formation of the 2:1 compound is observed at about 180 °C, which is obvious from the dramatic change of the diffraction pattern (Figure 11, top). The 2:1 compound **2** is stable up to about 250 °C and then formation of CuCl is observed. The formation of CuCl is not visible in the presented pattern because in this experiment the gaseous product blows out the powder from the X-ray beam. However, this was proven in additional experiments. When poly[CuBr(μ_2-pyrimidine-*N*,*N*′] (**5**) was heated similar observations were made. The 1:1 compound is stable up to about 150 °C before the transformation into the 2:1 compound occurs. On further heating the ligand-poorer compound **6** decomposes at about 260 °C. Decomposition of the iodine compound **3** starts at about 120 °C (Figure 11, bottom). The 2:1 phase **4** is stable up to 260 °C and then the formation of CuI is observed. From these experiments there is no hint of additional intermediates or the occurrence of different polymorphic modifications. However, it should be noted that the stability range of the ligand-poorer 2:1 compounds increases from CuCl to CuI, whereas for the 1:1 compounds an opposite trend is observed. This is in agreement with previous results which shows that the stability of the ligand-poorer coordination polymers increases from CuCl to CuI.

Conclusion

In the present work we have prepared several new coordination polymers based on copper(I) halides and pyrimidine as the N-donor ligand. Comparison of these structures with those of the previously reported compounds with pyrazine and pyridazine as the organic ligands shows that the structure of these coordination polymers can be understand to some extent by taking into account the coordination behaviour of the N-donor ligands. However, the influence of the ligands on the actual CuX substructure is difficult to predict.

For all of these compounds ligand-poorer 2:1 compounds are observed during the thermal decomposition, which, on further heating, decompose to the pure copper(I) halides. The results observed for the amine-poorer 2:1 compounds are in agreement with those of previous investigations.[25] However, our investigations shows that this is a general phenomena and that there is no simple relationship between the structure of the ligand-rich phases and their thermal reactivity. Because the topology of the coordination network in the ligand-poorer coordination polymers is identical, whereas that of the ligand-rich coordination polymers is different, there is also no obvious relationship between the structures of the starting compounds and those formed by the thermal decomposition reaction. However, our investigation shows that new ligand-poorer coordination polymers can be prepared by thermal decomposition of suitable ligand-rich precursor compounds.

Experimental Section

Synthesis of poly[CuCl(μ_2-pyrimidine-*N*,*N*′)] (1): CuCl (49.5 mg, 0.5 mmol), pyrimidine (160 μL, 2 mmol) and 2 mL of acetonitrile

 © 2004 Wiley-VCH Verlag GmbH & Co. KGaA, Weinheim

were placed into a glass ampoule which was sealed and heated for 1 week at 100 °C. The reaction mixture was cooled to room temp. and the orange-red residue was filtered off and washed with ethanol and diethyl ether. Yield: 79.3% based on CuCl. $C_4H_4ClCuN_2$ (179.08): calcd. C 26.8, H 2.2, N 15.6; found C 26.5, H 2.2, N 15.5.

Synthesis of poly[(CuCl)$_2$(μ$_2$-pyrimidine-*N*,*N*′)] (2): Single crystals were prepared by the reaction of CuCl (98.9 mg, 1.0 mmol), pyrimidine (40 μL, 0.5 mmol) and 2 mL acetonitrile in a glass ampoule which was sealed and heated for 4 days at 100 °C. The reaction mixture was cooled to room temp. and the yellow residue was filtered off and washed with ethanol and diethyl ether. Under these conditions the precipitate consists of a mixture of the 1:1 compound **1** and the 2:1 compound **2**. If an excess of CuCl is used the product is contaminated with a small amount of unchanged copper(I) chloride. However, this compound can be prepared in large amounts and very pure by thermal decomposition of **1**.

Synthesis of poly[CuI(μ$_2$-pyrimidine-*N*,*N*′)] (3): CuI (95.2 mg, 0.5 mmol), pyrimidine (160 μL, 2 mmol) and 2 mL of acetonitrile were stirred together at room temp. for 3 days. The yellow residue was filtered off and washed with ethanol and diethyl ether. Yield: 84.3% based on CuI. $C_4H_4CuIN_2$ (270.53): calcd. C 17.8, H 1.5, N 10.4; found C 17.7, H 1.4, N 10.3. Single crystals were prepared by the reaction of CuI (47.6 mg, 0.25 mmol) and pyrimidine (80 μL, 1 mmol) in 2 mL of acetonitrile. After 5 days yellow single crystals were grown.

Synthesis of poly[(CuI)$_2$(μ$_2$-pyrimidine-*N*,*N*′)] (4): CuI (190.5 mg, 1.0 mmol), pyrimidine (40 μL, 0.5 mmol) and 3 mL of acetonitrile were placed into a glass ampoule which was sealed and heated for 3 days at 110 °C. The reaction mixture was cooled to room temp. and the yellow residue was filtered off and washed with ethanol and diethyl ether. The product consists of yellow needles and a yellow microcrystalline powder. Yield: 84.5%. $C_4H_4Cu_2I_2N_2$ (460.97): calcd. C 10.4, H 0.9, N 6.1; found C 10.4, H 0.8, N 6.2.

Synthesis of poly[CuBr(μ$_2$-pyrimidine-*N*,*N*′)] (5): CuBr (71.7 mg, 0.5 mmol), pyrimidine (160 μL, 2 mmol) and 3 mL of acetonitrile were placed into a glass ampoule which was sealed and heated for 4 days at 100 °C. The reaction mixture was cooled to room temp. and the orange residue was filtered off and washed with ethanol and diethyl ether. Yield: 86.8%. $C_4H_4BrCuN_2$ (223.54): calcd. C 21.5, H 1.8, N 12.5; found C 20.4, H 1.8, N 12.4.

Single-Crystal Structure Analysis: All structure solutions were performed with direct methods using SHELXS-97.[41] Further details are given in Table 3. Structure refinement was done against F^2 using SHELXL-97.[42] All non-hydrogen atoms were refined with anisotropic displacement parameters. The C−H hydrogen atoms were positioned with idealised geometry and were refined with isotropic displacement parameters using the riding model. For compounds **1**, **3** and **4** a numerical absorption correction was performed using X-RED and X-SHAPE.[43] The absolute structure for compound **1** was determined and is in agreement with the selected setting [Flack *x* parameter = −0.047(15)]. In addition, refinement of the inverted structure leads to significant poorer reliability factors [*R*1 for 755 $F_o > 4\sigma(F_o)$ = 0.0440, *wR*2 for all 884 reflections = 0.1525, Flack *x* parameter = 1.026 (0.042)].
CCDC-226928 (for **1**), -226929 (for **2**), -226926 (for **3**) and -226927 (for **4**) contain the supplementary crystallographic data for this paper. These data can be obtained free of charge at www.ccdc.cam.ac.uk/conts/retrieving.html [or from the Cambridge Crystallographic Data Centre, 12 Union Road, Cambridge CB2 1EZ, UK; Fax: +44-1223-336-033; E-mail: deposit@ccdc.cam.ac.uk].

X-ray Powder Diffraction: X-ray powder diffraction experiments were performed using a STOE STADI P transmission powder diffractometer equipped with a 4° PSD (position sensitive detector) using Cu-K_α radiation (λ = 1.540598 Å). For the temperature-dependent X-ray powder measurements a 45° PSD and a graphite furnace from STOE & CIE were used. These measurements were carried out in glass capillaries under a static air atmosphere.

Differential Thermal Analysis, Thermogravimetry and Mass Spectrometry: DTA-TG-MS measurements were performed using an STA-409CD with Skimmer coupling from Netzsch, equipped with a quadrupole mass spectrometer QMA 400 (max. 512 amu) from Balzers. The MS measurements were performed in analog and trend scan mode, in Al_2O_3 crucibles under helium atmosphere (purity: 4.6) at heating rates of 4 °C/min. The heating-rate-dependent measurements were performed with the same instrument in a Pt-Rh furnace in flowing nitrogen (purity: 5.0). All measurements were performed with a flow rate of 75 mL/min. and were corrected for buoyancy and current effects. The instrument was calibrated using standard reference materials.

Elemental Analysis: C, H and N analysis was performed using a CHN-O-RAPID combustion analyser from Heraeus and EDAX was performed using a Philips XL30 Environmental Scanning Electron Microscope (ESEM) equipped with an EDAX system from Philips.

Acknowledgments

This work was supported by the State of Schleswig-Holstein. We are very thankful to Professor Dr. Wolfgang Bensch for financial support and for use of his equipment.

[1] J. M. J. Amoore, L. R. Hanton, M. D. Spicer, *Dalton Trans.* **2003**, *6*, 1056.
[2] F. Tuna, J. Hamblin, A. Jackson, G. Clarkson, N. W. Alcock, M. J. Hannon, *Dalton Trans.* **2003**, *11*, 2141.
[3] M. Maekawa, H. Konaka, Y. Suenaga, T. Kuroda-Sowa, M. Munakata, *J. Chem. Soc., Dalton Trans.* **2000**, *22*, 4160.
[4] T. Kuroda-Sowa, T. Horino, M. Yamamoto, Y. Ohno, M. Maekawa, M. Munakata, *Inorg. Chem.* **1997**, *36*, 6382.
[5] Z.-R. Qu, Z.-F. Chen, J. Zhang, R.-G. Xiong, B. F. Abrahams, Z.-L. Xue, *Organometallics* **2003**, *22*, 2814.
[6] A. J. Blake, N. R. Brooks, N. R. Champness, L. R. Hanton, P. Hubberstey, M. Schröder, *Pure Appl. Chem.* **1998**, *70*, 2351.
[7] A. J. Blake, N. R. Brooks, N. R. Champness, P. A. Cook, A. M. Deveson, D. Fenske, P. Hubberstey, W.-S. Li, M. Schröder, *J. Chem. Soc., Dalton Trans.* **1999**, 2103.
[8] B. Roßenbeck, W. S. Sheldrick, *Z. Naturforsch., Teil B* **2000**, *55*, 467.
[9] T. Kromp, W. S. Sheldrick, *Z. Naturforsch., Teil B* **1999**, *54*, 1175.
[10] A. J. Blake, N. R. Brooks, N. R. Champness, P. A. Cooke, M. Crew, A. M. Deveson, L. R. Hanton, P. Hubberstey, D. Fenske, M. Schröder, *Cryst. Eng.* **1999**, *2*, 181.
[11] N. S. Persky, J. M. Chow, K. A. Poschmann, N. N. Lacuesta, S. L. Stoll, *Inorg. Chem.* **2001**, *40*, 29.
[12] O. M. Yaghi, G. Li, *Angew. Chem.* **1995**, *107*, 232 and, *Angew. Chem. Int. Ed. Engl.* **1995**, *34*, 207.
[13] S. R. Batten, J. C. Jeffery, M. D. Ward, *Inorg. Chim. Acta* **1999**, *292*, 231.
[14] Y. L. Jack, B. R. Cabrera, R.-J. Wang, J. Li, *Inorg. Chem.* **1999**, *38*, 4608.
[15] P. M. Graham, R. D. Pike, M. Sabat, R. D. Bailey, W. T. Pennington, *Inorg. Chem.* **2000**, *39*, 5121.
[16] O. Teichert, W. S. Sheldrick, *Z. Anorg. Allg. Chem.* **2000**, *626*, 1509.

 © 2004 Wiley-VCH Verlag GmbH & Co. KGaA, Weinheim

[17] O. Teichert, W. S. Sheldrick, *Z. Anorg. Allg. Chem.* **1999**, *625*, 1860.
[18] O. Teichert, W. S. Sheldrick, *Z. Anorg. Allg. Chem.* **2000**, *626*, 2196.
[19] T. Röttgers, W. S. Sheldrick, *Z. Anorg. Allg. Chem.* **2001**, *627*, 1976.
[20] C. Näther, I. Jeß, *Acta Crystallogr., Sect. C* **2002**, *58*, m190.
[21] K. Wasielewski, R. Mattes, *Z. Naturforsch., Teil B* **1992**, *47*, 1795.
[22] K. Nieminen, *Acta Chem. Scand., Ser. A* **1981**, *35*, 753.
[23] M. D. Vaira, F. Mani, *J. Chem. Soc., Dalton Trans.* **1985**, 2327.
[24] S. A. Barnett, A. J. Blake, N. R. Champness, C. Wilson, *Cryst. Eng. Commun.* **2000**, 5.
[25] J. T. Maeyer, T. J. Johnson, A. K. Smith, B. D. Borne, R. D. Pike, W. T. Pennington, M. Krawiec, *Polyhedron* **2003**, *22*, 419.
[26] C. Näther, J. Greve, I. Jeß, *Polyhedron* **2001**, *20*, 1017.
[27] C. Näther, I. Jeß, *Monatsh. Chem.* **2001**, *132*, 897.
[28] C. Näther, I. Jeß, H. Studzinski, *Z. Naturforsch., Teil B* **2001**, *56*, 997.
[29] C. Näther, M. Wriedt, I. Jeß, *Z. Anorg. Allg. Chem.* **2002**, *628*, 394.
[30] C. Näther, I. Jeß, *Z. Naturforsch., Teil B* **2002**, *57*, 1133.
[31] C. Näther, I. Jeß, *J. Solid State Chem.* **2002**, *169*, 103.
[32] C. Näther, J. Greve, I. Jeß, *Solid State Sc.* **2002**, *4*, 813.
[33] C. Näther, M. Wriedt, I. Jeß, *Inorg. Chem.* **2003**, *42*, 2391.
[34] C. Näther, I. Jeß, *Inorg. Chem.* **2003**, *42*, 2968.
[35] C. Näther, I. Jeß, N. Lehnert, D.-H. Hübner, *Solid State Sci.* **2003**, *5*, 1343.
[36] C. Näther, J. Greve, I. Jeß, C. Wickleder, *Solid State Sci.* **2003**, *5*, 1167.
[37] C. Näther, J. I. Jeß, M. Bolte, *Z. Naturforsch., Teil B* **2003**, *58*, 1105.
[38] T. Kromp, W. S. Sheldrick, C. Näther, *Z. Anorg. Allg. Chem.* **2003**, *629*, 45.
[39] J. M. Moreno, J. Suarez-Varela, E. Colacio, J. C. Avila-Roson, M. A. Hidalgo, D. Martin-Ramos, *Can. J. Chem.* **1995**, *73*, 1591.
[40] S. Kawata, S. Kitagawa, H. Kurnagai, S. Iwabuchi, M. Katada, *Inorg. Chim. Acta* **1998**, *267*, 143.
[41] G. M. Sheldrick, SHELXS 97: *Program for Crystal Structure Solution*, University of Göttingen, Germany, **1997**.
[42] G. M. Sheldrick, SHELXL-97: *Program for the Refinement of Crystal Structures*, University of Göttingen, Germany, **1997**.
[43] XRED and XEMP: Programs for numerical absorption correction, STOE & CIE GmbH, Darmstadt, Germany, **1998**.

Received December 17, 2003
Early View Article
Published Online May 13, 2004

 © 2004 Wiley-VCH Verlag GmbH & Co. KGaA, Weinheim

Ruthenium(II) Octaphenylporphyrazine Complexes with Mixed Axial Ligands: Peculiarities of Their Formation and Spectral Properties

Sergej Vagin,*[a,b] Ulrich Ziener,[a,c] Michael Hanack,*[a] and Pavel A. Stuzhin[b]

Keywords: Isocyanide ligands / N ligands / NMR spectroscopy / Porphyrinoids / Ruthenium / Self-assembly

A series of new axially bis-coordinated (octaphenylporphyrazinato)ruthenium(II) complexes {[(Ph_8Pz)RuL_2], L = cyclohexyl isocyanide, CyNC, (**1b**); 4,4′-bipyridine, bpy, (**2c**); *N*-methylimidazole, CH_3Im, (**3a**)} was prepared and characterized. The reaction of the bis-isocyanide adducts [(Ph_8Pz)Ru(*t*-BuNC)$_2$] (**1a**) or [(Ph_8Pz)Ru(CyNC)$_2$] (**1b**) with monodentate N-heterocycles gave, under certain conditions, the mixed-ligand complexes [(Ph_8Pz)Ru(Py)(*t*BuNC)] (**4a**), [(Ph_8Pz)Ru(Py)-(CyNC)] (**4b**) and [(Ph_8Pz)Ru(CH_3Im)(CyNC)] (**3b**). The reaction of **1a** or **1b** with an excess of bidentate 4,4′-bipyridine under the same conditions resulted in the formation of the corresponding dimeric species [(Ph_8Pz)Ru(*t*BuNC)]$_2$(μ-bpy) (**2a**) and [(Ph_8Pz)Ru(CyNC)]$_2$(μ-bpy) (**2b**) in high yield. The structures of all the complexes were unambiguously proved by ^{1}H NMR spectroscopy, and the possibility of their self-assembly is discussed. All mixed-ligand compounds were also characterized by UV/Vis and IR spectroscopy, as well as elemental analysis. The ^{1}H NMR spectra of these compounds are discussed in detail.

(© Wiley-VCH Verlag GmbH & Co. KGaA, 69451 Weinheim, Germany, 2004)

Introduction

The high interest in complexes of porphyrins (Por), and their analogues, with transition metals such as Co, Fe, Ru, Os, etc. has arisen, especially in recent years, due to their possible application in materials science and industry. Many peculiar properties of these compounds appear to be a consequence of their ability to bind additional axial ligands, as well as to change the oxidation state of the central metal relatively easily. In particular, a high catalytic activity in different processes — decarbonylation of aldehydes,[1a] isomerization of epoxides,[1b] oxidation of different organic substrates,[1c,1d] etc. — has been observed for transition-metal complexes with porphyrin-type macrocycles, including phthalocyanines (Pc).[1e] Polymeric axially linked complexes of iron, cobalt and ruthenium with phthalocyanines and naphthalocyanines (Nc) possess semiconducting properties in the solid state.[2] Porphyrin complexes of ruthenium and osmium have also been used to construct different self-organized multimacrocyclic assemblies through axial coordination,[3] in which energy- or electron-transfer effects can appear due to the special intramolecular interaction between face-to-face or side-to-face oriented macrocycles, leading to the possibility of light harvesting and efficient photocurrent generation by these systems.[4] Additionally, the important role played by porphyrin-like complexes with different transition metals, especially iron and cobalt, in many biological processes has led to a vast amount of research on analogous model compounds, including phthalocyanines. This research was aimed mainly at the investigation of the axial-ligand-exchange rules and mechanisms in macrocyclic systems.[5]

Complexes of alkyl- and aryl-substituted porphyrazines (Pz), which have an intermediate structure between porphyrins and phthalocyanines, have been less-well investigated and only a few studies on the synthesis and properties of these compounds are available. We have previously prepared and characterized a series of monomeric and oligomeric iron and ruthenium complexes with octaphenylporphyrazine (Ph_8Pz), containing different axial ligands,[6] and investigated the axial-ligand-exchange processes in [(Ph_8Pz)Fe(L)(L′)], where L and L′ are isocyanides or N-heterocycles.[7] Here we continue the study of axially coordinated complexes of octaphenylporphyrazine with iron subgroup metals. We have reported previously that "crude" [(Ph_8Pz)Ru], which can be prepared by template condensation of diphenylfumaronitrile and [$Ru(NH_3)_5(N_2)$]Cl_2,[6e] is a very convenient starting material for the synthesis of hexacoordinate (octaphenylporphyrazinato)ruthenium(II) complexes [(Ph_8Pz)RuL_2], where L is one of various N-heterocycles or isocyanides. Thus, refluxing crude [(Ph_8Pz)Ru]

[a] Universität Tübingen, Institut für Organische Chemie,
Auf der Morgenstelle 18,
72076 Tübingen, Germany
E-mail: hanack@uni-tuebingen.de
[b] Ivanovo State University of Chemistry and Technology,
Organic Chemistry Department,
153460 Ivanovo, F. Engels 7, Russia
[c] Universität Ulm, Organische Chemie III / Makromolekulare Chemie der Universität,
Albert-Einstein-Allee 11, 89081 Ulm, Germany

in pyridine for 24 h gave the corresponding bis-pyridine adduct [(Ph_8Pz)Ru($Py)_2$] (**4c**) and heating [(Ph_8Pz)Ru] with *tert*-butyl isocyanide resulted in the formation of [(Ph_8Pz)-Ru(tBuNC)$_2$] (**1a**).[6c] A similar route was chosen in the present work to prepare bis adducts of (octaphenylporphyrazinato)ruthenium(II) with cyclohexyl isocyanide {[(Ph_8Pz)Ru-(CyNC)$_2$] (**1b**)}, 4,4′-bipyridine {[(Ph_8Pz)Ru(bpy)$_2$] (**2c**)} and *N*-methylimidazole {[(Ph_8Pz)Ru($CH_3Im)_2$] (**3a**)}. The bis-isocyanide complexes **1a** and **1b** were utilized to prepare the mixed axial ligand complexes [(Ph_8Pz)Ru(Py)(tBuNC)] (**4a**), [(Ph_8Pz)Ru(Py)(CyNC)] (**4b**), [(Ph_8Pz)Ru(CH_3Im)-(CyNC)] (**3b**), [(Ph_8Pz)Ru(tBuNC)$_2$(bpy) (**2a**) and [(Ph_8Pz)Ru(CyNC)]$_2$(bpy) (**2b**) shown in Scheme 1. The structure of these compounds was verified by means of UV/Vis, IR and NMR spectroscopy (see discussion below), as well as by elemental analysis. Mass spectrometry was found not to give enough information on the structure of axially coordinated ruthenium octaphenylporphyrazines due to a complete loss of axial ligands even under the relatively soft conditions of the FD technique.[6c] Therefore, we did not apply this method of analysis for the compounds reported here.

Results and Discussion

Ruthenium complexes of porphyrins or phthalocyanines are, in general, more stable towards the loss of axial ligands than their iron analogues.[5e,10] This is also true for octaphenylporphyrazine systems. For example, the complete substitution of axially coordinated isocyanides by pyridine, or vice versa, in iron complexes proceeds with rather high rates ($\tau_{1/2} \approx 1-10$ min) even at room temperature.[7] On the other hand bis-isocyanide adducts [(Ph_8Pz)Ru($RNC)_2$] with ruthenium as a central metal remain unchanged in pyridine solution at room temperature at least for several hours. Early investigations on axial-ligand-exchange in iron or ruthenium phthalocyanines allowed the proposal of a dissociative mechanism for these processes.[5] Additionally, in complexes with axial ligands that exhibit a strong *trans* effect, substitution usually proceeds in two well-separated steps, as shown in Scheme 2, where Pz is a porphyrazine-type macrocycle and M is iron or ruthenium. We have also observed this mechanism for the substitution of axially coordinated isocyanides by N-heterocycles in (octaphenylporphyrazinato)iron complexes.[7]

In this work we studied the substitution behavior of axially coordinated isocyanides in (octaphenylporphyrazinato)-ruthenium(II) complexes. Although these compounds remain spectroscopically unchanged at room temperature in pyridine solution for a relatively long time, as pointed out above, heating them to elevated temperatures (but below 100 °C) results in modest changes in their UV/Vis spectra (see **a** in Figure 1, dotted line), although the resulting spectra do not correspond to that of the bis-pyridine adduct **4c**. The spectra were, however, found to be similar to the spec-

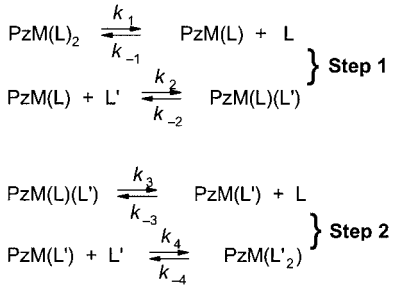

Scheme 2

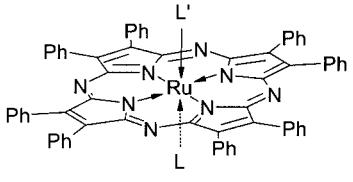

1a, 1b, 2c, 3a, 3b, 4c, 4a, 4b

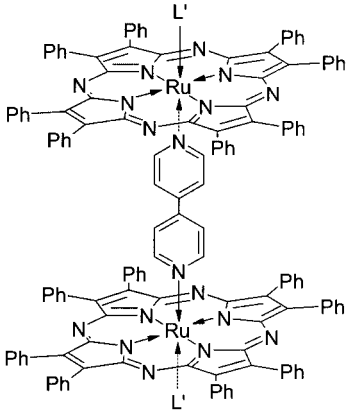

2a, 2b

L =	tBuNC	CyNC	bpy	CH_3Im	CH_3Im	Py	Py	Py	---	---
L' =	*t*BuNC	CyNC	bpy	CH_3Im	CyNC	Py	*t*BuNC	CyNC	*t*BuNC	CyNC
Nr.	**1a**	**1b**	**2c**	**3a**	**3b**	**4c**	**4a**	**4b**	**2a**	**2b**

Scheme 1. Structure and numbering of the prepared complexes

 © 2004 Wiley-VCH Verlag GmbH & Co. KGaA, Weinheim

tra of solutions of (octaphenylporphyrazinato)iron(II) complexes [(Ph_8Pz)Fe(L)(L′)] with two different axial ligands — one isocyanide and one nitrogen heterocycle, such as pyridine. These spectra were observed in our titration experiments on [(Ph_8Pz)Fe($RNC)_2$] with nitrogen heterocycles, in which we were not able to isolate the mixed-ligand compounds in the solid state due to their high lability.[7] Additionally, the formation of [(Ph_8Pz)Fe(L)(L′)] adducts from [(Ph_8Pz)Fe($RNC)_2$] was found to be so fast that we were not able to study the kinetics of this process by common spectroscopic techniques. In contrast, the reaction of [(Ph_8Pz)Ru(tBuNC)$_2$] with pyridine could be followed easily. The reaction was found to be first order in ruthenium complex {a linear dependence of ln(C^o/C) on reaction time was observed, where C^o and C are the starting and current concentrations of [(Ph_8Pz)Ru(tBuNC)$_2$] respectively} and zero order in pyridine (see Figure 2). This, and the observed spectral changes, allowed us to assume that under these reaction conditions only the first step shown in Scheme 2 {formation of the mixed-ligand complex [(Ph_8Pz)Ru(Py)(tBuNC)] (**4a**)} takes place. The activation energy of this process is rather high (see Table 1), which explains the observed high kinetic stability of ruthenium complexes **1a** and **1b** at room temperature. However, a comparison of the kinetic parameters of the described reaction with those of analogous reactions of [PcRu($BzNC)_2$] (Bz = benzyl) reveals a higher lability of the porphyrazine complex.[10] A similar trend was observed in our studies on (octaphenylporphyrazinato)iron complexes.[7]

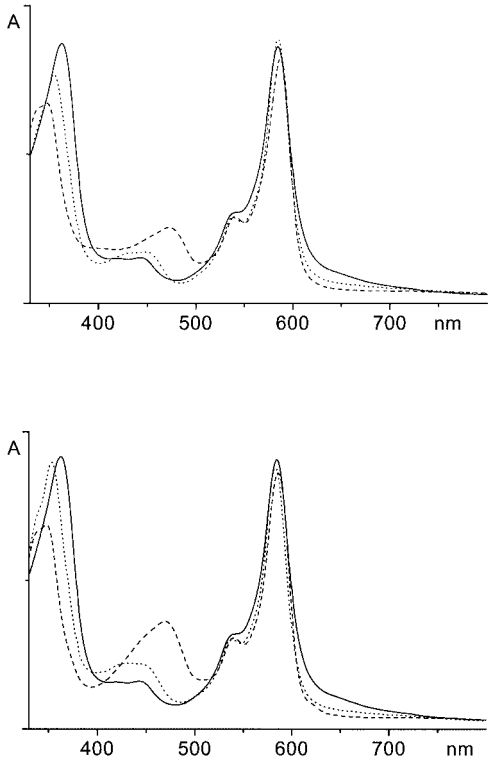

Figure 1. Comparison of the UV/Vis spectra in dichloromethane: a) [(Ph_8Pz)Ru(tBuNC)$_2$] (**1a**, solid line), [(Ph_8Pz)Ru(Py)$_2$] (**4c**, dashed line) and [(Ph_8Pz)Ru(Py)(tBuNC)] (**4a**, dotted line); b) [(Ph_8Pz)Ru(tBuNC)$_2$] (**1a**, solid line), [(Ph_8Pz)Ru(bpy)$_2$] (**2c**, dashed line) and [(Ph_8Pz)Ru(tBuNC)]$_2$(μ-bpy) (**2a**, dotted line)

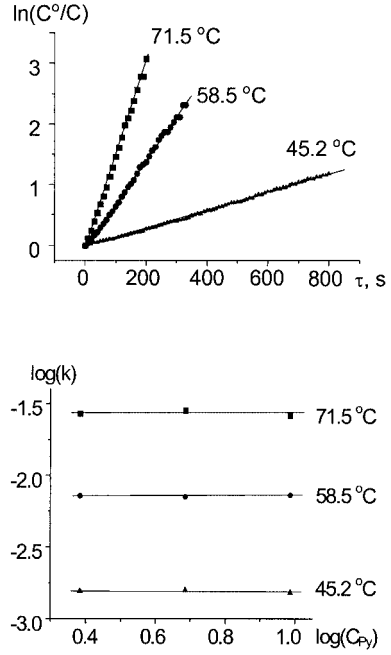

Figure 2. Kinetics results for the reaction of [(Ph_8Pz)Ru(tBuNC)$_2$] (**1a**) with pyridine in toluene; top: the dependence of ln(C^o/C) on reaction time; bottom: the dependence of the rate constant on the concentration of pyridine

Table 1. Kinetic parameters of reaction of [(Ph_8Pz)Ru(tBuNC)$_2$] (**1a**) with pyridine in toluene

Concentration of pyridine (mol/L)	Temperature (K)	$k_1 \times 100$ (s^{-1})	E^o_a (kJ/mol)
9.68	344.7	2.60 ± 0.03	99 ± 3
	331.7	0.729 ± 0.006	
	318.4	0.151 ± 0.001	
4.84	344.7	2.82 ± 0.05	
	331.7	0.713 ± 0.006	
	318.4	0.158 ± 0.001	
2.42	344.7	2.69 ± 0.04	
	331.7	0.722 ± 0.005	
	318.4	0.155 ± 0.001	

[(Ph_8Pz)Ru(Py)(tBuNC)] (**4a**) was isolated and its IR and NMR spectra were recorded. The obtained spectroscopic data proved the mixed-ligand nature of the compound. The analogous complexes of iron or ruthenium phthalocyanine or porphyrins have been described previously.[10] Several other compounds, such as CO, nitroso derivatives and phosphites,[10–12] can also be utilized as strong-field axial ligands to build similar mixed-ligand complexes. Here (octaphenylporphyrazinato)ruthenium mixed-ligand complexes with axially coordinated isocyanides and nitrogen heterocycles have been isolated and characterized for the first time.

 © 2004 Wiley-VCH Verlag GmbH & Co. KGaA, Weinheim

It is remarkable that upon heating the reaction mixture above 100 °C in the presence of an excess of the nitrogen heterocycle the second step in Scheme 2 can also take place to yield the bis adduct of the corresponding heterocycle, which does not happen under milder conditions with the same concentration of heterocycle. Therefore, and in contrast to iron complexes, in the case of porphyrazinatoruthenium isocyanides the kinetic control of the substitution reaction becomes obvious. This allowed us to prepare and isolate mixed-ligand complexes of (octaphenylporphyrazinato)ruthenium(II) with axially coordinated alkyl isocyanides and nitrogen heterocycles, namely [(Ph_8Pz)Ru(Py)(CyNC)] (**4b**) and [(Ph_8Pz)Ru(CH_3Im)(CyNC)] (**3b**). Interestingly, the reaction of [(Ph_8Pz)Ru(RNC)$_2$] even with a large excess of 4,4′-bipyridine (see Exp. Sect.) under mild conditions results in an almost quantitative yield of the dimeric bipyridine-bridged complexes **2a** or **2b** with no monomeric mixed-ligand species. The structure of these self-assembled dimers was determined from their ^{1}H NMR spectra.

The position of the ^{1}H NMR resonances of the axial ligands depends strongly on the distance of the protons from the coordinating metal because of the different shielding effect of the porphyrazine macrocycle ring current. This allows, for example, to use iron and ruthenium phthalocyanines as shift reagents in NMR spectroscopy for some coordination compounds.[13a,13b] The protons closest to the center of the macrocycle undergo the strongest shielding ring-current effect, which can be as much as 9 ppm, as was observed, for example, for the α-protons in dioctylgermanium phthalocyanine.[13c] Dependence of the ring-current shielding effect on the position of the proton about phthalocyanines or naphthalocyanines was also calculated.[13d,13e] Accordingly, the observed ^{1}H NMR signals of coordinated axial ligands in different complexes of (octaphenylporphyrazinato)ruthenium(II) can be assigned as shown in Table 2. The signals of coordinated pyridine appear as three multiplets, which have slightly different positions for the bis-pyridine adduct **4c** and the mixed-ligand species **4a** and **4b**. The position of the α-proton signals was found to be the most sensitive to the nature of the *trans* ligand (see Table 2 and Scheme 3). The resonance of the α-proton in **4a**, for example, is shifted upfield by 0.28 ppm relative to **4c**. Therefore, taking into account also the integration, it can clearly be seen that the mixed-ligand complexes **4a** and **4b** do not contain any admixture of bis-pyridine adduct **4c** or of starting material **1a** or **1b** (see also **a** in Figure 3).

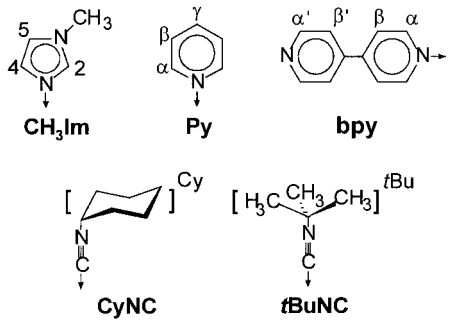

Scheme 3. Designation of protons in axially coordinated molecules used for ^{1}H NMR signals' assignment

Similarly, the proton signals of the coordinated *N*-methylimidazole undergo a noticeable upfield shift when going from the bis(*N*-methylimidazole) adduct **3a** to the mixed-ligand complex **3b** (see Table 2). Their shifts are even stronger than for the pyridine adducts. In contrast, the signals of coordinated alkyl isocyanides do not depend as strongly on the nature of the *trans* ligand. Thus, the difference in position of the singlet of coordinated *t*BuNC in **1a** and **4a** is only 0.04 ppm. The signals of coordinated CyNC appear as several broad multiplets in the region $\delta = -0.6$ to 0.9 ppm and their assignment is complicated because of

Table 2. ^{1}H NMR spectroscopic data of the prepared compounds; intervals are given for broad multiplets or groups of multiplets; middle position is given for narrow multiplets

Compound	Macrocycle resonances (ppm)[a]	N-Heterocycle signals (ppm); assignment and multiplicity	Resonances of alkyl isocyanide (ppm)	Solvent/frequency
[(Ph_8Pz)Ru(*t*BuNC)$_2$] (**1a**)[6c]	8.33 (*o*-Ph); 7.42−7.57 (*m*-, *p*-Ph)	−	−0.16 (*t*Bu), s	$CDCl_3$/250 MHz
[(Ph_8Pz)Ru(CyNC)$_2$] (**1b**)	8.31 (*o*-Ph); 7.44−7.53 (*m*-, *p*-Ph)	−	−0.38 − 0.86 (Cy), m	$CDCl_3$/250 MHz
[(Ph_8Pz)Ru(bpy)$_2$] (**2c**)	8.23 (*o*-Ph); 7.56 (*m*-Ph); 7.45 (*p*-Ph)	3.14 (α), m; 5.82 (β), m; 6.67 (β′), m; 8.28 (α′), m	−	CD_2Cl_2/400 MHz
[(Ph_8Pz)Ru(*t*BuNC)]$_2$(bpy) (**2a**)	8.17 (*o*-Ph); 7.35−7.50 (*m*-, *p*-Ph)	2.40 (α, α′), m; 4.95 (β, β′), m	−0.28 (*t*Bu), s	$CDCl_3$/250 MHz
[(Ph_8Pz)Ru(CyNC)]$_2$(bpy) (**2b**)	8.10 (*o*-Ph); 7.48 (*m*-Ph); 7.40 (*p*-Ph)	2.44 (α, α′), m; 4.94 (β, β′), m	−0.65 − 0.80 (Cy), m	CD_2Cl_2/400 MHz
[(Ph_8Pz)Ru(CH_3Im)$_2$] (**3a**)	8.18 (*o*-Ph); 7.53 (*m*-Ph); 7.41 (*p*-Ph)	2.42 (−C*H*$_3$), s; 2.69 (*4*), m; 3.11 (*2*), m; 5.09 (*5*), m	−	CD_2Cl_2/400 MHz
[(Ph_8Pz)Ru(CH_3Im)(CyNC)] (**3b**)	8.30 (*o*-Ph); 7.43−7.56 (*m*-, *p*-Ph)	2.35(−C*H*$_3$), s; 2.13 (*4*), m; 2.53 (*2*), m; 4.97 (*5*), m	−0.44 − 0.95 (Cy), m	$CDCl_3$/250 MHz
[(Ph_8Pz)Ru(Py)$_2$] (**4c**)[6c]	8.25 (*o*-Ph); 7.37−7.53 (*m*-, *p*-Ph)	3.03 (α), m; 5.56 (β), m; 6.30 (γ), m	−	$CDCl_3$/250 MHz
[(Ph_8Pz)Ru(Py)(*t*BuNC)] (**4a**)	8.33 (*o*-Ph); 7.43−7.58 (*m*-, *p*-Ph)	2.75 (α), m; 5.59 (β), m; 6.33 (γ), m	−0.20 (*t*Bu), s	$CDCl_3$/250 MHz
[(Ph_8Pz)Ru(Py)(CyNC)] (**4b**)	8.30 (*o*-Ph); 7.40−7.56 (*m*-, *p*-Ph)	2.77 (α), m; 5.61 (β), m; 6.34 (γ), m	−0.55 − 0.96 (Cy), m	$CDCl_3$/250 MHz

[a] Signals appear as multiplets.

 © 2004 Wiley-VCH Verlag GmbH & Co. KGaA, Weinheim

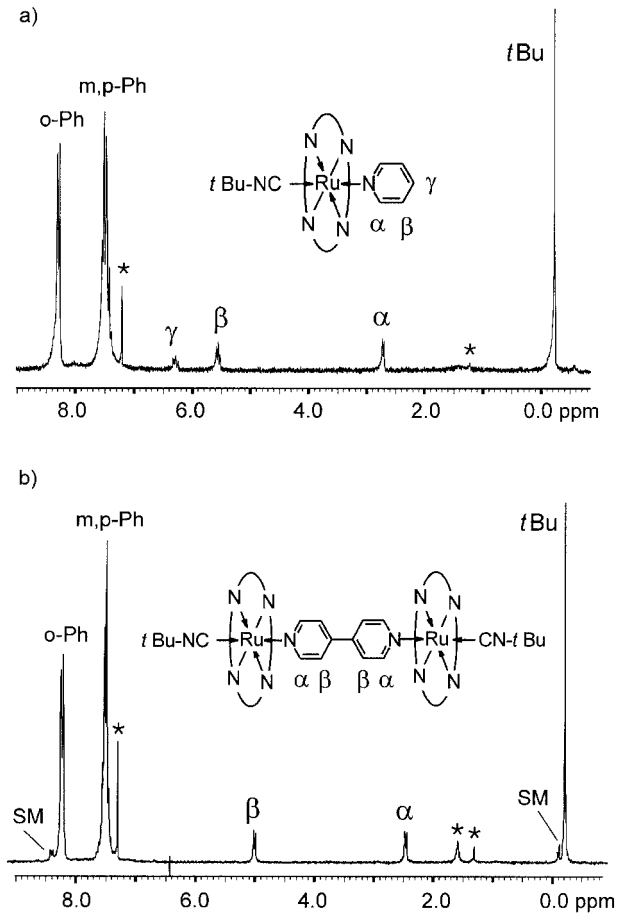

Figure 3. ^{1}H NMR spectra of [(Ph_8Pz)Ru(Py)(*t*BuNC)] (a) and [(Ph_8Pz)Ru(*t*BuNC)]$_2$(μ-bpy) (b) in $CDCl_3$ (250 MHz); signals of impurities ($CHCl_3$, H_2O etc.) are marked with an asterisk; signals of starting materials are denoted as SM

the different possible conformations of CyNC (axial and equatorial position of NC group, for example).

The upfield shift of the proton signals of nitrogen heterocycles upon *trans* substitution with isocyanide can be explained as an effect of the displacement of the central metal from the macrocycle plane towards a stronger coordinating axial ligand, which is an isocyanide in our case. The crystal-structure parameters summarized in ref.[10] clearly show, for example, a tendency of carbonyl coordinated *trans* to pyridine, THF or DMF in Fe, Ru or Os complexes to pull the metal out of the Por or Pc plane. In our case, the nitrogen heterocycle *trans* to the isocyanide ligand is closer to the macrocycle plane than in the bis-heterocycle adduct, and therefore is more strongly affected by the ring-current of the macrocycle. Additional effects of electron redistribution between axial ligands can also play a role. For example, the binding energy of isocyanide in these mixed-ligand complexes is higher than that in bis-isocyanide adducts due to the weaker *trans* effect of the nitrogen heterocycle, resulting in a stronger π-back bonding effect of isocyanide. Therefore, a shorter bond between the coordinating carbon of the isocyanide and the central metal should be expected. Indeed, an increase of the π-back bonding effect of the isocyanide in mixed-ligand complexes of (Ph_8Pz)Ru compared to the corresponding bis-isocyanide adducts can be observed as a lowering of the stretching vibration frequency of the NC group.[6c,14] Thus, ν_{NC} was found to be 2135 cm^{-1} and 2120 cm^{-1} for [(Ph_8Pz)Ru(*t*BuNC)$_2$] (**1a**) and [(Ph_8Pz)Ru(Py)(*t*BuNC)] (**4a**), respectively. Similarly, for cyclohexyl isocyanide-containing complexes **1b** and **4b** it is 2151 and 2128 cm^{-1}, respectively.

Products **2a** and **2b** from the reaction of 4,4′-bipyridine with bis-isocyanide adducts **1a** and **1b** exhibit an analogous decrease of the NC-group vibration frequency, indicating the substitution of one molecule of isocyanide. In their ^{1}H NMR spectra only two multiplets (doublets of doublets) belonging to the coordinated bipyridine were observed at approximately δ = 2.4 and 4.9 ppm, whereas in the ^{1}H NMR spectrum of the bis adduct **2c** with 4,4′-bipyridine four multiplets (doublets of doublets) of bipyridine were observed at δ = 3.14, 5.82, 6.67 and 8.28 ppm (α, β, β′ and α′ respectively, see Scheme 3). Additionally, integration of the signals in the ^{1}H NMR spectra of **2a** and **2b** shows that the ratio between the macrocycle and bipyridine in these compounds is 2:1. This allowed us to ascribe a dimeric structure to these compounds with bipyridine as bridging ligand (see **b** in Figure 3). For **2a** and **2b** the α and α′ protons become magnetically equivalent, as do the β and β′ protons, giving only two signals, α and β, for the coordinated bridging bipyridine. The shielding effect of two macrocycles towards the protons of the bridging ligand is almost additive, which can be seen as follows:

δ_d (β, β′) ≈ δ_m (β) − [δ_m (β′) − δ_m (β)], or 4.9 ≈ 5.82 − (6.67 − 5.82)

where δ_d is the chemical shift of the corresponding proton in the dimers **2a** and **2b** and δ_m is the chemical shift of the corresponding protons in the monomeric compound **2c**. This was also observed in our previous work on iron complexes of octaphenylporphyrazine with diisocyanodurole as axial ligand, where a mixture of corresponding linear oligomers was analyzed by means of ^{1}H NMR spectroscopy.[6d] In the present case, self-assembly of ruthenium porphyrazine complexes to give the dimeric structures **2a** or **2b** occurs, even in the presence of excess 4,4′-bipyridine, with practically no formation of monomeric mixed-ligand complexes, as was mentioned above and can also be seen from the ^{1}H NMR spectra of the products (see **b** in Figure 3 for example). This fact, to the best of our knowledge, has not been observed before for phthalocyanine complexes of ruthenium, although the preferential formation of a dimeric species upon interaction of *trans*-(ethanol)(carbonyl)(octaethylporphyrinato)ruthenium(II) with an excess of different diaza compounds has been reported previously.[15] In our case the self-assembly leading to the symmetric dimers **2a** or **2b** could be realized either during the reaction of bis-isocyanide adducts **1a** or **1b** with 4,4′-bipyridine (thermodynamically controlled possibility of error-correction towards more organized system[16]) or during purification of the reaction product, for example when removing the excess bipyridine and column chromatography (shifting the equilibrium towards dimeric species by removal of the excess of bridging ligand). However, for realization of the latter case it is

 © 2004 Wiley-VCH Verlag GmbH & Co. KGaA, Weinheim

necessary that the corresponding monomeric mixed-ligand complexes [(Ph_8Pz)Ru(bpy)(RNC)] are labile enough towards splitting off the coordinated axial ligand (bipyridine) even at room temperature, which is not the case for the starting bis-isocyanide adducts **1a** and **1b**, as mentioned above. On the other hand, the additional forces leading to a stabilization of the dimeric structures **2a** and **2b** (e.g. van der Waals interaction of the macrocycles in the dimer) are required to shift the equilibrium from the monomeric towards the dimeric species.

The chemical shifts of the protons in the peripheral phenyl groups also depend on the structure of the complexes and the nature of the axial ligands. In general, in the spectra recorded at 250 MHz the phenyl protons appear as two multiplets: a downfield-shifted multiplet for the *ortho* protons, and a multiplet for the *meta* and *para* protons in the region $\delta = 7.4-7.6$ ppm. At 400 MHz these signals become better resolved giving three multiplets, which can be considered as a doublet (*ortho* protons) and two triplets (*meta* and *para* protons) showing an upfield shift of the same order. The chemical shift of the *ortho* protons appears to be the most sensitive to the nature of the axial ligands: axial ligands exhibiting stronger π-acceptor properties, such as isocyanides, lead to a slight downfield shift of the *ortho* proton signals. For example, their resonances in [(Ph_8Pz)Ru(*t*BuNC)$_2$] (**1a**), [(Ph_8Pz)Ru(Py)(*t*BuNC)] (**4a**), [(Ph_8Pz)Ru(Py)$_2$] (**4c**) and [(Ph_8Pz)Ru(CH_3Im)$_2$] (**3**) are observed at $\delta = 8.33$, 8.33, 8.25 and 8.18 ppm, respectively. In the dimeric species **2a** and **2b** they are shifted upfield because of the mutual shielding effect of the neighboring macrocycles and appear at $\delta = 8.17$ and 8.10 ppm, respectively (see Table 2).

No mutual co-facial electronic interaction of the neighboring macrocycles in the dimeric species **2a** and **2b** was observed in the UV/Vis spectra (no noticeable broadening or blue shift of the dimer's Q-band), probably due to the comparatively large distance between the macrocycles. The UV/Vis spectral pattern displayed by these compounds was found to be practically the same as that of the monomeric mixed-ligand complexes, such as [(Ph_8Pz)Ru(Py)(*t*BuNC)] (**4a**). The molar-absorption coefficients for the most intense bands are almost double those of the monomeric species.

The most noticeable changes in the UV/Vis spectra of all prepared compounds, caused by axial-ligand exchange, occur in the region of the B-band (350−360 nm) and charge-transfer (CT) band[6c] (400−500 nm). The Q-band experiences only a slight red shift if a strong π-accepting axial ligand is substituted by a weaker acceptor, whereas the B-band shifts noticeably to the blue if axially coordinated isocyanides are substituted by nitrogen heterocycles. The explanation for these observations is given in our previous work.[6c] The CT bands between 400 and 500 nm are perhaps the most sensitive to the nature of the axial ligands. Their intensity and bathochromic shift increase unambiguously with decreasing π-accepting properties of the axial ligands. However, even one coordinated molecule of isocyanide is enough to noticeably shift these CT-bands hypsochromically due to its pronounced π-accepting effect. Therefore, the position and intensity of the CT bands in mixed-ligand complexes is closer to those in bis-isocyanide adducts than in bis-heterocycle adducts (see Figure 1). The spectral changes shown in Figure 1 are typical for the whole series of adducts (bis-isocyanide → mixed-ligand → bis-heterocycle) and independent of the nature of the isocyanide or the heterocycle. This also allows us to see whether one or two isocyanide molecules are substituted by nitrogen heterocycles by UV/Vis spectroscopy. The obtained UV/Vis data for the prepared complexes are summarized in Table 3.

Experimental Section

The following equipment was used for the characterization of compounds: UV/Vis: Hitachi U-2000 and Specord M-40. IR: Specord M-80, Bruker IFS-48. ^1H and ^{13}C NMR: Bruker AC 250 and AC 400; elemental analysis: Carlo−Erba Elemental Analyzer 1104, 1106.

The kinetics of axial ligand substitution in [(Ph_8Pz)Ru(*t*BuNC)$_2$] was studied spectrophotometrically, registering the changes in optical density at the wavelength of the absorption maximum growth during the course of the reaction, using a computer-linked Hitachi U-2000 spectrophotometer with a thermostatted probe-holder. A series of experiments with constant concentrations of starting [(Ph_8Pz)Ru(*t*BuNC)$_2$] (approx. 2×10^{-5} M) in toluene and three different concentrations of pyridine in toluene were carried out at three different temperatures. Before mixing, the solutions of [(Ph_8Pz)Ru(*t*BuNC)$_2$] and pyridine were thermostatted separately. Toluene and pyridine for kinetic studies and for the syntheses were purified by standard procedures.[8] Other solvents were used without additional purification. Cyclohexyl isocyanide was prepared ac-

Table 3. UV/Vis data of the prepared compounds

Compound	Absorption maxima, nm (log ε)	Solvent
[(Ph_8Pz)Ru(*t*BuNC)$_2$] (**1a**)[6c]	276 (4.80); 364 (4.97); 421 (4.05); 443 (4.07); 540 (4.47); 585 (5.00)	CH_2Cl_2
[(Ph_8Pz)Ru(CyNC)$_2$] (**1b**)	365; 421; 445; 542; 588	$CHCl_3$
[(Ph_8Pz)Ru(bpy)$_2$] (**2c**)	286 (4.76); 349 (4.79); 470 (4.50); 541 (4.41); 587 (4.91)	CH_2Cl_2
[(Ph_8Pz)Ru(*t*BuNC)]$_2$(bpy)] (**2a**)	276 (5.16); 353 (5.27); 431 (4.63); 538 (4.78); 583 (5.26)	CH_2Cl_2
[(Ph_8Pz)Ru(CyNC)]$_2$(bpy)] (**2b**)	357; 449; 541; 587	$CHCl_3$
[(Ph_8Pz)Ru(CH_3Im)$_2$] (**3a**)	301 (4.82); 349 (4.86); 503 (4.55); 546 (4.43); 594 (4.89)	CH_2Cl_2
[(Ph_8Pz)Ru(CH_3Im)(CyNC)] (**3b**)	359; 450; 542; 588	$CHCl_3$
[(Ph_8Pz)Ru(Py)$_2$] (**4c**)[6c]	288 (4.79); 349 (4.86); 407 (4.21); 473 (4.41); 541 (4.49); 588 (4.98)	CH_2Cl_2
[(Ph_8Pz)Ru(Py)(*t*BuNC)] (**4a**)	277 (4.79); 354 (4.93); 448 (4.25); 538 (4.50); 585 (5.02)	CH_2Cl_2
[(Ph_8Pz)Ru(Py)(CyNC)] (**4b**)	358 (4.91); 449 (4.25); 541 (4.48); 588 (5.01)	$CHCl_3$

 © 2004 Wiley-VCH Verlag GmbH & Co. KGaA, Weinheim

cording to the literature procedure.[9] Other chemicals were acquired from commercial sources.

Synthesis of the starting material {"crude" [(Ph_8Pz)Ru]} for the preparation of the axially coordinated complexes [(Ph_8Pz)RuL_2], as well as the synthesis of [(Ph_8Pz)Ru(*t*BuNC)$_2$] (**1a**), have been described before.[6c] Other complexes were prepared as described below.

Bis(cyclohexyl isocyanide)(octaphenylporphyrazinato)ruthenium(II) [(Ph_8Pz)Ru(CyNC)$_2$] (1b): Crude [(Ph_8Pz)Ru] (65 mg) was refluxed in a mixture of cyclohexyl isocyanide (2 mL) and toluene (5 mL) for 24 h. After cooling, 100 mL of CH_2Cl_2 was added to the reaction mixture and stirred for 24 h to dissolve the product as completely as possible. The formed solution was filtered and chromatographed on Al_2O_3 with CH_2Cl_2 as eluent The blue-colored fraction was collected, the solvent was partially evaporated and methanol (ca. 100 mL) was added to precipitate the product, which was filtered off, washed with methanol and dried. Yield 37 mg (49%) of a dark-violet powder. IR (KBr): $\tilde{\nu}$ = 3048 w, 2936 m, 2856 w, 2152 vs, 1600 w, 1560 w, 1472 s, 1448 m, 1368 m, 1320 w, 1168 s, 1088 m, 992 s, 912 w, 888 w, 832 w, 768 w, 744 m, 696 s cm^{-1}. $C_{78}H_{62}N_{10}Ru$ (1240.5): calcd. C 75.52, H 5.04, N 11.29; found C 75.06, H 5.29, N 10.93.

Bis(4,4′-bipyridine)(octaphenylporphyrazinato)ruthenium(II) [(Ph_8Pz)Ru(bpy)$_2$] (2c): Crude [(Ph_8Pz)Ru] (150 mg) was stirred in molten 4,4′-dipyridine hydrate (4 g) at 130 °C for 10 h. After cooling, the reaction mixture was suspended in 200 mL of methanol. The insoluble residue was filtered off, washed thoroughly with methanol and chromatographed as described for [(Ph_8Pz)Ru(CyNC)$_2$]. Yield 120 mg (63%) of a dark-red powder. IR (KBr): $\tilde{\nu}$ = 3049 m, 1594 m, 1468 s, 1448 m, 1405 m, 1367 m, 1171 s, 1066 w, 1004 s, 991 s, 912 w, 887 w, 829 m, 808 m, 779 m, 770 m, 741 m, 693 s, 623 w, 608 m, 542 m cm^{-1}. $C_{84}H_{56}N_{12}Ru{\cdot}2H_2O$ (1334.5 + 36): calcd. C 73.61, H 4.41, N 12.26; found C 73.26, H 4.26, N 11.95.

Bis(*N*-methylimidazole)(octaphenylporphyrazinato)ruthenium(II) [(Ph_8Pz)Ru(CH_3Im)$_2$] (3a): Crude [(Ph_8Pz)Ru] (120 mg) and *N*-methylimidazole (1 mL) were refluxed in 15 mL of toluene for 24 h. After cooling, 25 mL of CH_2Cl_2 was added to the reaction mixture and the formed solution was chromatographed on Al_2O_3 with CH_2Cl_2 as eluent The first colored fraction was collected, diluted slightly with toluene and left to evaporate to dryness in the air at room temperature to give dark-violet rhombic crystals. Yield 45 mg (33%). IR (KBr): $\tilde{\nu}$ = 3129 w, 3047 w, 1601 m, 1575 w, 1534 w, 1495 w, 1468 s, 1448 m, 1420 w, 1368 m, 1287 w, 1241 w, 1174 s, 1107 m, 1094 m, 1066 w, 1028 w, 1004 s, 992 s, 911 w, 888 w, 829 m, 779 m, 768 m, 740 m, 693 s, 661 w, 616 w, 608 m, 542 m, 524 w, 467 w cm^{-1}. $C_{72}H_{52}N_{12}Ru{\cdot}2.5C_7H_8$ (toluene) (1186.4 + 230.4): calcd. C 75.88, H 5.12, N 11.86; found C 75.54, H 5.17, N 11.62.

***trans*-(*tert*-Butyl isocyanide)(octaphenylporphyrazinato)pyridineruthenium(II) [(Ph_8Pz)Ru(Py)(*t*BuNC)] (4a):** [(Ph_8Pz)Ru(*t*BuNC)$_2$] (**1a**; 64 mg, 54 μmol) in 15 mL of pyridine was heated at 80 °C for 8 h. After cooling, the pyridine was removed in vacuo and the residue was chromatographed as described for [(Ph_8Pz)Ru(CyNC)$_2$] (**1b**). Yield 53 mg (83%). IR (KBr): $\tilde{\nu}$ = 3048 w, 2120 s, 1600 m, 1576 w, 1472 s, 1368 s, 1168 s, 1064 w, 992 s, 912 m, 888 w, 832 m, 744 m, 692 s, 608 m, 544 s, 456 w cm^{-1}. $C_{74}H_{54}N_{10}Ru{\cdot}H_2O$ (1184.4 + 18): calcd. C 73.92, H 4.69, N 11.65; found C 74.18, H 4.61, N 11.58.

***trans*-(Cyclohexyl isocyanide)(octaphenylporphyrazinato)pyridineruthenium(II) [(Ph_8Pz)Ru(Py)(CyNC)] (4b):** [(Ph_8Pz)Ru(CyNC)$_2$] (**1b**; 50 mg, 40 μmol) was heated in 50 mL of pyridine at 100 °C for 5 h. After cooling, the reaction mixture was filtered and the product was isolated from solution as described for [(Ph_8Pz)Ru(Py)(*t*BuNC)] (**4a**). Yield 44 mg (88%). IR (KBr): $\tilde{\nu}$ = 3056 w, 2928 m, 2848 w, 2128 s, 1600 w, 1168 s, 992 s, 696 s cm^{-1}. $C_{76}H_{56}N_{10}Ru{\cdot}H_2O$ (1210.4 + 18): calcd. C 74.31, H 4.76, N 11.40; found C 73.93, H 4.70, N 11.71.

***trans*-(Cyclohexyl isocyanide)(*N*-methylimidazole)(octaphenylporphyrazinato)ruthenium(II) [(Ph_8Pz)Ru(CH_3Im)(CyNC)] (3b):** (Ph_8Pz)Ru(CyNC)$_2$ (**1b**; 25 mg, 20 μmol) and 1 mL of *N*-methylimidazole were heated in 50 mL of toluene at 80 °C for 10 h. The product was isolated as described for [(Ph_8Pz)Ru(Py)(CyNC)] (**4b**). Yield 15 mg (62%). $C_{75}H_{57}N_{11}Ru{\cdot}H_2O$ (1213.4 + 18): calcd. C 73.15, H 4.83, N 12.51; found C 73.51, H 5.25, N 12.88.

(μ-4,4′-Bipyridyl)bis[(*tert*-butyl isocyanide)(octaphenylporphyrazinato)ruthenium(II)] [(Ph_8Pz)Ru(*t*BuNC)]$_2$(μ-bpy) (2a): [(Ph_8Pz)Ru(*t*BuNC)$_2$] (**1a**; 100 mg, 84 μmol) and 4,4′-bipyridine (3 g) were heated in 30 mL of toluene at 90 °C for 16 h. The toluene was then removed under vacuum, and the excess of bipyridine was removed by washing with methanol. The residue was chromatographed (Al_2O_3, dichloromethane), precipitated with methanol and dried. Yield 80 mg (80%). $C_{148}H_{106}N_{20}Ru_2$ (2366.7): calcd. C 75.11, H 4.51, N 11.84; found C 74.79, H 4.90, N 12.02.

(μ-4,4′-Bipyridyl)bis[(cyclohexyl isocyanide)(octaphenylporphyrazinato)ruthenium(II)] [(Ph_8Pz)Ru(CyNC)]$_2$(μ-bpy) (2b): [(Ph_8Pz)Ru(CyNC)$_2$] (**1b**; 100 mg, 81 μmol) was used following the same procedure as described for **2a**. Yield 72 mg (73%). IR (KBr): $\tilde{\nu}$ = 3050 cm^{-1} w, 2931 m, 2853 w, 2135 s, 1602 m, 1470 s, 1448 m, 1365 m, 1168 s, 1004 s, 990 s, 829 m, 743 m, 692 s, 607 m, 543 m. $C_{152}H_{110}N_{20}Ru_2{\cdot}H_2O$ (2418.8 + 18): calcd. C 74.92, H 4.63, N 11.50; found C 75.08, H 5.03, N 11.25.

[1] [1a] G. Domazetis, B. Tarpey, D. Dolphin, B. James, *J. Chem. Soc., Chem. Commun.* **1980**, 939−940. [1b] J. T. Groves, K. H. Ahn, R. Quinn, *J. Am. Chem. Soc.* **1988**, *110*, 4217−4220. [1c] T. Higuchi, H. Ohtake, M. Hirobe, *Tetrahedron Lett.* **1991**, *32*, 7435−7438. [1d] B. Meunier, *Chem. Rev.* **1992**, *92*, 1411−1456. [1e] K. Hanabusa, H. Shirai, in *Phthalocyanines: Properties and Applications* (Eds.: C. C. Leznoff, A. B. P. Lever), VCH Publishers, Inc., New York, **1993**, vol. 2, pp. 197−222.

[2] [2a] M. Hanack, S. Deger, A. Lange, *Coord. Chem. Rev.* **1988**, *83*, 115−136. [2b] M. Hanack, M. Lang, *Adv. Mater.* **1994**, *6*, 819−833.

[3] [3a] K. Funatsu, A. Kimura, T. Imamura, A. Ichimura, Y. Sasaki, *Inorg. Chem.* **1997**, *36*, 1625−1635. [3b] N. Kariya, T. Imamura, Y. Sasaki, *Inorg. Chem.* **1997**, *36*, 833−839. [3c] K. Funatsu, T. Imamura, A. Ichimura, Y. Sasaki, *Inorg. Chem.* **1998**, *37*, 1798−1804. [3d] K. Funatsu, T. Imamura, A. Ichimura, Y. Sasaki, *Inorg. Chem.* **1998**, *37*, 4986−4995.

[4] [4a] A. Prodi, M. T. Indelli, C. J. Kleverlaan, E. Alessio, F. Scandola, *Coord. Chem. Rev.* **2002**, *229*, 51−58. [4b] Y. Kobuke, K. Ogawa, *Bull. Chem. Soc. Jpn.* **2003**, *76*, 689−708.

[5] [5a] J. G. Jones, M. V. Twigg, *Inorg. Chim. Acta* **1974**, *10*, 103−108. [5b] D. A. Sweigart, *J. Chem. Soc., Dalton Trans.* **1976**, 1476−1477. [5c] D. V. Stynes, *Inorg. Chem.* **1977**, *16*, 1170−1173. [5d] J. G. Jones, M. V. Twigg, *J. Chem. Soc., Dalton Trans.* **1978**, 1709−1714. [5e] M. M. Doeff, D. A. Sweigart, *Inorg. Chem.* **1981**, *20*, 1683−1687. [5f] J. Martinsen, M. Miller, D. Trojan, D. A. Sweigart, *Inorg. Chem.* **1980**, *19*, 2162−2168. [5g] T. Nyokong, *J. Chem. Soc., Dalton Trans.* **1983**, 3601−3604. [5h] T. Nyokong, J. Guthrie-Strachan, *Inorg. Chim. Acta* **1993**, *208*, 239−242. [5i] G. Pennesi, C. Ercolani, G. Rossi, P. Ascenzi, M. Brunori, F. Monacelli, *J. Chem. Soc., Dalton Trans.* **1985**,

 © 2004 Wiley-VCH Verlag GmbH & Co. KGaA, Weinheim

1113−1118. [5j] P. Ascenzi, M. Brunori, G. Pennesi, C. Ercolani, F. Monacelli, *J. Chem. Soc., Dalton Trans.* **1987**, 369−371.
[6] [6a] P. A. Stuzhin, I. S. Migalova, B. D. Berezin, *Russ. J. Inorg. Chem.* **1993**, *38*, 1877−1883. [6b] P. A. Stuzhin, M. Hamdush, U. Ziener, *Inorg. Chim. Acta* **1995**, *236*, 131−139. [6c] P. A. Stuzhin, S. I. Vagin, M. Hanack, *Inorg. Chem.* **1998**, *37*, 2655−2662. [6d] S. I. Vagin, P. A. Stuzhin, M. Hanack, *Russ. J. Gen. Chem.* **1999**, *69*, 308−313. [6e] P. A. Stuzhin, H. Homborg, *Russ. J. Coord. Chem.* **1997**, *23*, 623−628.
[7] [7a] S. I. Vagin, Diss. Kand. Khim. Nauk (PhD thesis), Ivanovo, Russia, **2000**. [7b] Results to be published.
[8] *Organikum, Organisch-chemisches Grundpraktikum*, 16., bearbeitete Auflage, VEB Deutscher Verlag der Wissenschaften, Berlin, **1986**, pp. 751.
[9] I. Ugi, R. Meyr, *Chem. Ber.* **1960**, *93*, 239−248.
[10] F. Pomposo, D. Carruthers, D. V. Stynes, *Inorg. Chem.* **1982**, *21*, 4245−4248.
[11] S. Omiya, M. Tsutsui, E. F. Meyer, I. Bernal, D. L. Cullen, *Inorg. Chem.* **1980**, *19*, 134−142.
[12] J. J. Watkins, A. L. Balch, *Inorg. Chem.* **1975**, *14*, 2720−2723.
[13] [13a] J. E. Maskasky, J. R. Mooney, M. E. Kenney, *J. Am. Chem. Soc.* **1972**, *94*, 2132−2133. [13b] C. K. Choy, J. R. Mooney, M. E. Kenney, *J. Magn. Reson.* **1979**, *35*, 1−12. [13c] J. E. Maskasky, M. E. Kenney, *J. Am. Chem. Soc.* **1973**, *95*, 1443−1448. [13d] T. R. Janson, A. R. Kane, J. F. Sullivan, K. Knox, M. E. Kenney, *J. Am. Chem. Soc.* **1969**, *91*, 5210−5214. [13e] T. Koyama, T. Suzuki, K. Hanabusa, H. Shirai, N. Kobayashi, *Inorg. Chim. Acta* **1994**, *218*, 41−45.
[14] U. Keppeler, W. Kobel, H. U. Siehl, M. Hanack, *Chem. Ber.* **1985**, *118*, 2095−2104.
[15] A. Endo, Y. Okamoto, K. Suzuki, J.-I. Shimamura, K. Shimizu, G. P. Sato, *Chem. Lett.* **1994**, 1317−1320.
[16] [16a] S. Leininger, B. Olenyuk, P. J. Stang, *Chem. Rev.* **2000**, *100*, 853−908. [16b] S. S. Sun, A. J. Lees, *J. Am. Chem. Soc.* **2000**, *122*, 8956−8967.

Received January 15, 2004
Early View Article
Published Online May 13, 2004

 © 2004 Wiley-VCH Verlag GmbH & Co. KGaA, Weinheim

Phenyl 2-Pyridyl Ketone and Its Oxime in Manganese Carboxylate Chemistry: Synthesis, Characterisation, X-ray Studies and Magnetic Properties of Mononuclear, Trinuclear and Octanuclear Complexes

Constantinos J. Milios,[a] Theocharis C. Stamatatos,[a] Panayotis Kyritsis,[b] Aris Terzis,[c] Catherine P. Raptopoulou,[c] Ramon Vicente,*[d] Albert Escuer,*[d] and Spyros P. Perlepes*[a]

Keywords: Carboxylate ligands / Magnetic properties / Manganese / N,O ligands / X-ray crystallography

The use of phenyl 2-pyridyl ketone [(ph)(2-py)CO] and its oxime [(ph)(2-py)CNOH] in manganese benzoate chemistry has been investigated. The reaction of an excess of (ph)(2-py)CNOH with $Mn(O_2CPh)_2{\cdot}2H_2O$ affords the mononuclear complex $[Mn^{II}(O_2CPh)_2\{(ph)(2\text{-py})CNOH\}_2]{\cdot}1.2H_2O$ (**1**·1.2H_2O) in high yield. The Mn^{II} ion is coordinated by two monodentate benzoates and two *N,N′*-bidentate chelating (ph)(2-py)CNOH molecules in a *cis-cis-trans* fashion. The comproportionation reaction between $Mn(O_2CPh)_2{\cdot}2H_2O$ and N*n*Bu_4MnO_4 (3:1) in the presence of (ph)(2-py)CNOH in MeCN/EtOH/CH_2Cl_2 leads to the isolation of the mixed-valent cluster $[Mn_8O_2(OH)_2(O_2CPh)_{10}\{(ph)(2\text{-py})CNO\}_4]{\cdot}4CH_2Cl_2$ (**2**·4CH_2Cl_2) in about 55% yield. A second synthetic procedure that leads to pure **2** involves the reaction between the known starting material (N*n*Bu_4)$[Mn_4^{III}O_2(O_2CPh)_9(H_2O)]$ and four equivalents of the oxime ligand in CH_2Cl_2. The centrosymmetric octanuclear molecule contains four Mn^{II} and four Mn^{III} ions held together by two μ_4-O^{2-} ligands and two μ_3-OH^- ions to give the unprecedented $[Mn_8(\mu_4\text{-}O)_2(\mu_3\text{-}OH)_2]^{14+}$ core, with peripheral ligation provided by ten $PhCO_2^-$ (two η^1, four *syn,syn* $\eta^1{:}\eta^1{:}\mu_2$ and four $\eta^1{:}\eta^2{:}\mu_3$) and four $\eta^1{:}\eta^1{:}\eta^1{:}\mu_2$ (ph)(2-py)CNO^- ions. The 1:1 reaction between $Mn(O_2CPh)_2{\cdot}2H_2O$ and the ketone (ph)(2-py)CO affords the trinuclear complex $[Mn_3(O_2CPh)_6\{(ph)(2\text{-py})CO\}_2]$ (**3**) in more than 80% yield. As judged from single-crystal X-ray crystallography, the complex adopts a linear structure with one $\eta^1{:}\eta^2{:}\mu_2$ and two $\eta^1{:}\eta^1{:}\mu_2$ benzoates spanning each pair of metal ions. The terminal Mn^{II} ions are capped by bidentate chelating (ph)(2-py)CO ligands. The three complexes have been characterised by IR spectroscopy. The CV study of complex **2** in CH_2Cl_2 reveals irreversible reduction and oxidation processes. The magnetic properties of **2** and **3** have been studied by variable-temperature dc magnetic-susceptibility techniques. As the temperature approaches zero, the value of the $\chi_M T$ product for **2** approaches zero and, thus, the octanuclear complex has an $S = 0$ ground state. This $S = 0$ ground state is explained in terms of the magnetic behaviour of the central, butterfly-like $[Mn_4^{III}(\mu_3\text{-}O)_2]^{8+}$ subcore. The results for **3** reveal weak antiferromagnetic coupling, with $J = -2.7$ cm^{-1} for adjacent Mn^{II} ions.
(© Wiley-VCH Verlag GmbH & Co. KGaA, 69451 Weinheim, Germany, 2004)

Introduction

There are several reasons why manganese carboxylate chemistry is the focus of such great research interest at present. One such reason is that a tetranuclear Mn carboxylate cluster is an integral component of the photosystem II reaction centre of green plants (and cyanobacteria), where it is responsible for the light-driven oxidation of water to dioxygen gas.[1] This Mn_4 water oxidation complex (WOC) is the site of substrate (water) binding, deprotonation and oxidative coupling to O_2, although the exact structure of the cluster[2] and its precise mechanism[1] of action are currently unknown. The synthesis and structural/spectroscopic characterisation of Mn model complexes[1,3] have provided a wealth of data for comparison and contrast with the corresponding characteristics for the native WOC. In the last ten years, the synthesis and study of polynuclear Mn carboxylate complexes have also been stimulated by the discovery that some of them exhibit the new magnetic phenomenon of single-molecule magnetism.[4] This property is the ability of discrete molecules to exhibit the superparamagnet-like property of slow magnetisation relaxation and thus to behave as magnets below their blocking temperature by exhibiting magnetisation vs. field hysteresis. Such properties do not arise from intermolecular exchange interactions and long-range ordering, but instead from a combination of two intramolecular properties, namely a

[a] Department of Chemistry, University of Patras, 265 04 Patras, Greece
E-mail: perlepes@patreas.upatras.gr
[b] Department of Chemistry, University of Athens, 15771 Athens, Greece
E-mail: kyritsis@chem.uoa.gr
[c] Institute of Materials Science, NCSR "Demokritos", 15310 Aghia Paraskevi Attikis, Greece
[d] Departament de Quimica Inorganica, Universitat de Barcelona, Diagonal 647, 08028 Barcelona, Spain
E-mail: ramon.vicente@qi.ub.es and albert.escuer@qi.ub.es

large ground-state spin (S) and a significant magnetoanisotropy of the Ising (easy-axis) type, the latter being reflected in a large and negative value of the zero-field splitting parameter D.[4] The first single-molecule magnet (SMM) was $[Mn_{12}O_{12}(O_2CMe)_{16}(H_2O)_4]$, which possesses an $S = 10$ ground state,[5] and a number of other Mn_x carboxylate SMMs have since been discovered.[4,6] There is thus a continuing need to develop new synthetic methods for the preparation of new polynuclear Mn carboxylate compounds.

Among the many synthetic lines currently being pursued by our groups and others in this field is the reaction of a bridging ligand containing both chelating sites and ionizable hydrogens with a simple Mn carboxylate "salt" or a preformed Mn carboxylate cluster that does not already incorporate any chelating ligand.[6,8] As long as the RCO_2^-/bridging ligand ratio is high enough to leave an amount of non-protonated RCO_2^- ions in the reaction mixture, this approach normally leads to heteroleptic RCO_2^-/deprotonated bridging ligand metal clusters. One of the ligands that has previously proved to be useful in these syntheses, giving many new polynuclear complexes, is di-2-pyridyl ketone [$(2\text{-py})_2CO$; Figure 1]. Our groups have been exploring "ligand blend" reactions involving the monoanion $(2\text{-py})_2C(OH)O^-$ or the dianion $(2\text{-py})_2CO_2^{2-}$ of the *gem*-diol form of $(2\text{-py})_2CO$ (these anions are stabilized *only* in the presence of metal ions[8]) *and* carboxylates. These reaction schemes have led[9] to a variety of Fe, Co, Ni, Cu, Zn clusters with nuclearities ranging from three to twelve and with interesting magnetic properties, including SMM behaviour.[9j] In Mn carboxylate chemistry the most impressive cluster isolated[10] is $[Mn_{10}^{II}Mn_4^{III}O_4(O_2CMe)_{20}\{(2\text{-py})_2C(OH)O\}_4]$; the observed tetradecanuclearity is extremely rare in 3d-metal chemistry. Recently we have extended our efforts to ligands (Figure 1) that present a structural similarity to $(2\text{-py})_2CO$; our goals are to investigate to what extent the use of such ligands might affect the identity of the obtained products compared with $(2\text{-py})_2CO$ and to what extent this might thus prove to be a route to new cluster types. Our initial work was concentrated on di-2-pyridyl ketone oxime, $(2\text{-py})_2CNOH$, a ligand whose employment in Mn carboxylate chemistry gave the new family of valence-trapped, mixed-valence complexes[11] $[Mn_2^{II}Mn_2^{III}(O_2CR)_2X_2\{(2\text{-py})_2CNO\}_2\{(2\text{-py})_2CO_2\}_2]$, where X^- is Cl^-, Br^- or RCO_2^-; it has been of great interest that an appreciable quantity of the oxime ligand undergoes transformation to yield the coordinated dianion of the *gem*-diol form of $(2\text{-py})_2CO$. The mechanism of this transformation probably involves reaction(s) of the electrophilically activated coordinated oxime group. In attempting to extend the above-mentioned chemistry, and to create new topologies, we have begun reactions featuring phenyl 2-pyridyl ketone oxime, (ph)(2-py)CNOH, and its ketone, (ph)(2-py)CO. These ligands have different electronic properties to those of $(2\text{-py})_2CNOH$ and $(2\text{-py})_2CO$, respectively, and have never been employed in polynuclear 3d-metal chemistry.

Herein we describe our efforts toward the use of (ph)(2-py)CNOH and (ph)(2-py)CO in Mn benzoate chemistry. In particular, we report the synthesis, structure and characterisation of one mononuclear Mn^{II} complex, one trinuclear Mn^{II} complex and one octanuclear $Mn^{II/III}$ cluster featuring a novel core. A small portion of this work has been communicated previously.[10] There is currently a renewed interest in the coordination chemistry of oximes.[12] This interest is driven by a number of considerations.[12,13] In contrast to the great number of studies concerning metal complexes of single oximes and salicylaldoxime, little is known[12,13] about complexes of pyridyloximes, although this class of compounds could offer unique features in terms of structural and physical properties.

Results and Discussion

Synthesis

The initial reaction explored was that between $Mn(O_2CPh)_2{\cdot}2H_2O$ and one equivalent of (ph)(2-py)CNOH in MeCN/EtOH. The pale-orange solution obtained gradually turned brown due to slow oxidation of Mn^{II} under the normal laboratory atmosphere. Evaporation of the resulting solution under reduced pressure, redissolv-

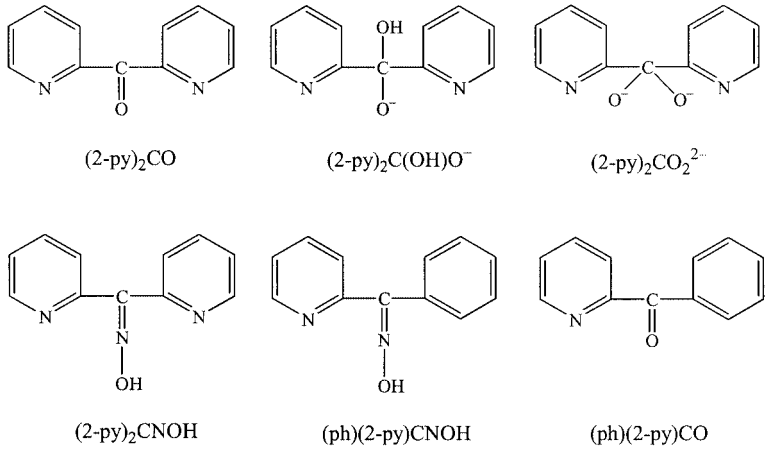

Figure 1. Some of the ligands discussed in the text; note that $(2\text{-py})_2C(OH)O^-$ and $(2\text{-py})_2CO_2^{2-}$ do not exist as free species — they exist only in their metal complexes

 © 2004 Wiley-VCH Verlag GmbH & Co. KGaA, Weinheim

$$Mn(O_2CPh)_2{\cdot}2H_2O + 2\ (ph)(2\text{-}py)CNOH \xrightarrow{EtOH} [Mn(O_2CPh)_2\{(ph)(2\text{-}py)CNOH\}_2] + 2\ H_2O \quad (1)$$

1

ing the residue in CH_2Cl_2 and layering the solution with Et_2O/*n*-hexane gave a mixture of yellow and dark-brown crystals, which were readily separated manually and crystallographically identified as $[Mn(O_2CPh)_2\{(ph)(2\text{-}py)CNOH\}_2]{\cdot}1.2H_2O$ (**1**·$1.2H_2O$) and $[Mn_8O_2(OH)_2(O_2CPh)_{10}\{(ph)(2\text{-}py)CNO\}_4]{\cdot}4CH_2Cl_2$ (**2**·$4CH_2Cl_2$), respectively. The latter is a mixed-valence ($4Mn^{II}$, $4Mn^{III}$) complex (vide infra). With the identities of **1** and **2** established, alternative and convenient syntheses of pure materials were sought. The mononuclear product contains a (ph)(2-py)CNOH/Mn ratio of 2:1, whereas the reaction solution had a ratio of 1:1; thus, attempts to obtain pure **1** were made by increasing the ligand/Mn reaction ratio. The preparation of pure **1** *under aerobic conditions* was achieved by the reaction of $Mn(O_2CPh)_2{\cdot}2H_2O$ with an excess of oxime in EtOH [Equation (1)].

Two procedures were developed that lead to preparation of pure **2**. The first one involves a comproportionation reaction between $Mn(O_2CPh)_2{\cdot}2H_2O$ and NBu_4MnO_4 [14] in a 3:1 ratio in the presence of (ph)(2-py)CNOH. This ratio, on paper, gives an average Mn oxidation state in solution of $Mn^{+3.25}$, higher than that ($Mn^{+2.5}$) observed in solid **2**. The source of the reducing agent is probably EtOH from the solvent mixture, solvent impurities or excess ligand groups, facilitated by the strongly oxidizing nature of Mn^{III}.[15] It is also likely, as with many other reactions in higher oxidation state Mn chemistry, that the reaction solution contains a complicated mixture of several species in equilibrium, with factors such as relative solubility, lattice energies, crystallisation kinetics and others determining the identity of the isolated product.[16] Comproportionation reactions between Mn^{II} and Mn^{VII} sources have found extensive use to produce $Mn/O^{2-}/RCO_2^-$ clusters of various nuclearities.[15,16] Complex **2** was isolated from the above reaction solution in 55% yield. In an attempt to increase further the yield of the product, the Mn^{II}/MnO_4^- ratio was increased to that which would give an average Mn oxidation state of +2.5, as found in **2**, but this instead led to crystallisation of $[Mn_6O_2(O_2CPh)_{10}(MeCN)_4]$[17a] and/or $[Mn_6O_2(O_2CPh)_{10}(EtOH)_4(H_2O)]{\cdot}EtOH$[17b] containing $4Mn^{II}$, $2Mn^{III}$, and no bound (ph)(2-py)CNO^- groups. These and similar hexanuclear species differing in the identity of the bound neutral monodentate ligands have been previously observed and are common products at this oxidation level with benzoate groups.[17c] Attempts to obtain clusters with higher average Mn oxidation states were also made by decreasing the Mn^{II}/MnO_4^- ratio; for example, a ratio of 3:2 (this ratio on paper gives an average Mn oxidation state in solution of Mn^{4+}) again resulted in the isolation of **2** in low (< 30%) yields. The second procedure that leads to pure **2** involves the conversion of $(NBu_4)[Mn_4O_2(O_2CPh)_9(H_2O)]$ into a higher nuclearity product. The anion $[Mn_4O_2(O_2CPh)_9(H_2O)]^-$ contains only Mn^{III} ions, and only $PhCO_2^-$ and H_2O peripheral ligation.[15] The latter fact makes it especially useful for synthesising higher nuclearity products: it has, for example, permitted the isolation of $(NBu_4)[Mn_8O_6Cl_6(O_2CPh)_7(H_2O)_2]$,[18a] $(NBu_4)[Mn_8O_4(O_2CPh)_{12}(Et_2mal)_2(H_2O)_2]$[15] ($Et_2malH_2$ = 2,2-diethylmalonic acid) and $K_4[Mn_{18}O_{16}(O_2CPh)_{22}(phth)_2(H_2O)_4]$[18b] ($H_2phth$ = phthalic acid) when treated with Me_3SiCl, $Na_2(Et_2mal)$ and KH(phth), respectively. Treatment of complex $(NBu_4)[Mn_4O_2(O_2CPh)_9(H_2O)]$ with four equivalents of (ph)(2-py)CNOH in CH_2Cl_2 leads to subsequent isolation of pure crystalline **2** in acceptable yield (ca. 30%). The formation of **2** by this route can be summarised in Equation (2).

It seems that the core of **2** can be thought of as being derived from the "butterfly" $[Mn_4(\mu_3\text{-}O)_2]^{8+}$ core[15] of the starting tetranuclear material by dimerisation/reduction / protonation steps (the order is arbitrary). The $4Mn^{II}$, $4Mn^{III}$ description of **2** requires the reduction of four Mn^{III} ions to have occurred; as stated above, it is not uncommon to find Mn^{III} — a strong oxidizing agent — being reduced by ligand groups, solvent impurities, etc.[15] An alternative means for the generation of the Mn^{II} ions in **2** is disproportionation of Mn^{III}, in which case Mn^{IV}-containing species would be in the filtrate.[15] We have not attempted to identify the exact origin of the Mn^{II} ions in the product, nor would it be a simple matter to do so. The excess of (ph)(2-py)CNOH (oxime/Mn_4 = 4:1) is beneficial to the preparation, because use of a stoichiometric amount (oxime/Mn_4 = 2:1) yields an oxime-free product analysed as $[Mn_6O_2(O_2CPh)_{10}(H_2O)_x]$ (x = 2−3).

The structure of **2** was shown by crystallography (vide infra) to contain an octanuclear core in which two $[Mn_4(\mu_3\text{-}O)(\mu_3\text{-}OH)]$ units have been linked together. Although **2** is a new and interesting complex, the question that arose after its characterisation was whether a discrete tetranuclear product containing this unit might be attainable by suitable alteration of the reaction conditions. A number of such at-

$$2\ [Mn_4^{III}O_2(O_2CPh)_9(H_2O)]^- + 4\ (ph)(2\text{-}py)CNOH \xrightarrow{+4\ e} [Mn_4^{II}Mn_4^{III}O_2(OH)_2(O_2CPh)_{10}\{(ph)(2\text{-}py)CNO\}_4] + 2\ PhCO_2H + 6\ PhCO_2^- + 2\ H_2O \quad (2)$$

2

 © 2004 Wiley-VCH Verlag GmbH & Co. KGaA, Weinheim

$$3\ Mn(O_2CPh)_2{\cdot}2H_2O + 2\ (ph)(2\text{-}py)CO \xrightarrow{MeOH} \underset{\mathbf{3}}{[Mn_3(O_2CPh)_6\{(ph)(2\text{-}py)CO\}_2]} + 4\ H_2O \quad (3)$$

tempts were made, but with no successful isolation of any other species; in particular, increasing the (ph)(2-py)CNOH/Mn_4 reaction ratio further still gives complex **2** as the isolable product. Thus, complex **2** remains the only polynuclear Mn/$PhCO_2^-$/(ph)(2-py)CNO^- species to have been identified to date.

The next goal of this work was to synthesise Mn complexes of the ketone of (ph)(2-py)CNOH, i.e., (ph)(2-py)CO (Figure 1). The reaction used to prepare the trinuclear manganese(II) complex $[Mn_3(O_2CPh)_6\{(ph)(2\text{-}py)CO\}_2]$ (**3**) is shown in Equation (3).

The "wrong" reaction ratio employed experimentally (Mn/ketone= 1:1), compared to the stoichiometric ratio (Mn/ketone= 1.5:1) required by Equation (3), obviously did not prove detrimental to the isolation of the trinuclear product. We have not explored reactions in any solvent (complex **3** can be isolated from a variety of solvents including EtOH, MeCN and CH_2Cl_2) using Mn^{II}:(ph)(2-py)CO ratios other than 1:1.

Attempts to oxidize one or more Mn^{II} ions of **3** failed to give a crystalline compound. Several 3:1 and 3:2 **3**/N*n*Bu_4MnO_4 reaction mixtures were studied under various conditions, but almost all led to a mixture of the starting trinuclear complex and an as-yet unidentified reddish, non-crystalline material; we did not study this material further. Thus, complex **3** does not appear promising for the isolation of other (possibly larger) Mn clusters. We also investigated in situ reactions between $Mn(O_2CPh)_2{\cdot}2H_2O$ and (ph)(2-py)CO in the presence of N*n*Bu_4MnO_4 at various Mn^{II}/Mn^{VII} ratios, but, somewhat to our surprise, the only isolable product remained complex **3**, thus proving the great thermodynamic stability of the $[Mn_3^{II}(\eta^1{:}\eta^1{:}\mu_2\text{-}O_2CR)_4(\eta^1{:}\eta^2{:}\mu_2\text{-}O_2CR)_2]$ core. Along these lines, it is worth noting that reactions of the preformed, mixed-valence compound $[Mn_3^{II,III,III}O(O_2CPh)_6(py)_2(H_2O)]$[19] (py = pyridine) and (ph)(2-py)CO led to fading of the reaction solutions and subsequent isolation of **3**.

X-ray Crystal Structures

$[Mn(O_2CPh)_2\{(ph)(2\text{-}py)CNOH\}_2]{\cdot}1.2H_2O$ (**1**·1.2H_2O)

A labelled plot of the structure of the mononuclear compound **1** is shown in Figure 2. Selected bond lengths and angles are listed in Table 1. The structure consists of well-separated $[Mn(O_2CPh)_2\{(ph)(2\text{-}py)CNOH\}_2]$ moieties and solvate H_2O molecules. The Mn^{II} atom is coordinated by two monodentate benzoates and two *N*,*N*′-bidentate chelating (ph)(2-py)CNOH molecules. The six-coordinate molecule is the *cis*-*cis*-*trans* isomer considering the positions of the oxygen, pyridyl nitrogen and oxime nitrogen atoms, respectively. An analogous *cis*-*cis*-*trans* arrangement has also been observed in the molecular structure of $[Mn(O_2CCF_3)_2\{(py)CHNOH\}_2]$,[13] where (py)CHNOH is 2-pyridinealdoxime. The molecule has no imposed sym-

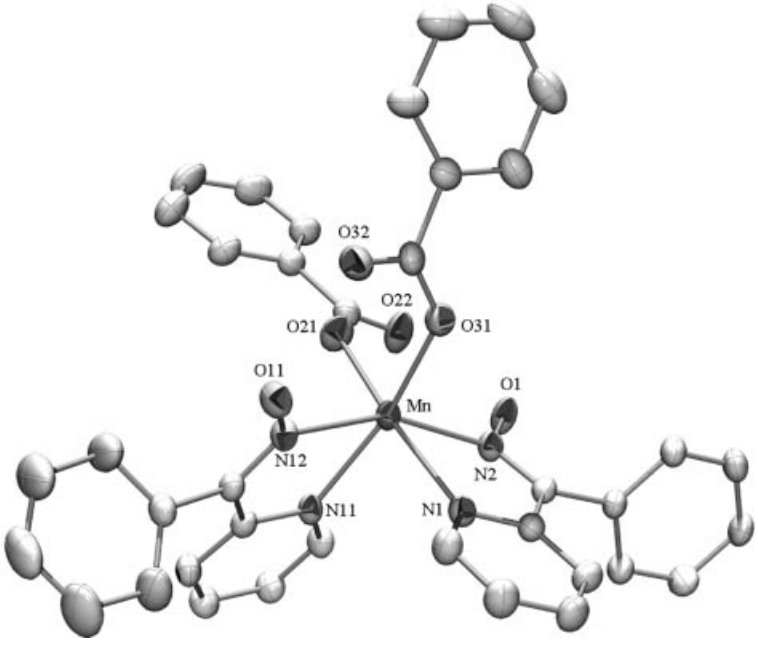

Figure 2. ORTEP plot of the molecule of complex **1**·1.2H_2O at the 30% probability level

 © 2004 Wiley-VCH Verlag GmbH & Co. KGaA, Weinheim

metry, although it approximates closely to C_2 symmetry, with the C_2 axis bisecting the O(21)−Mn−O(31) angle. The four Mn−N bond lengths [2.255(3)−2.319(4) Å] are similar. The distortion from a perfect octahedral geometry is primarily a consequence of the small bite-angle of the chelating ligands, which leads to acute N(1)−Mn−N(2) and N(11)−Mn−N(12) angles of 70.6(1)° and 70.8(1)°, respectively. There are two strong intramolecular hydrogen bonds with the uncoordinated oxime oxygens as donors and the "free" carboxylate oxygens as acceptors. Their dimensions are: O(1)···O(22) 2.524 Å, H(O1)···O(22) 1.735 Å, O(1)−H(O1)···O(22) 169.4° and O(11)···O(32) 2.532 Å, H(O11)···O(32) 1.519 Å, O(11)−H(O11)···O(32) 153.1°. The existence of these strong hydrogen bonds most likely explains the isolation of the *cis-cis-trans* isomer.

Table 1. Selected bond lengths (Å) and angles (°) for $[Mn(O_2CPh)_2\{(ph)(2\text{-py})CNOH\}_2]\cdot 1.2H_2O$ (**1**·1.2H_2O)

Mn−O(21)	2.093(4)	Mn−N(2)	2.255(3)
Mn−O(31)	2.087(3)	Mn−N(12)	2.274(4)
Mn−N(1)	2.319(4)	N(2)−O(1)	1.372(5)
Mn−N(11)	2.281(4)	N(12)−O(11)	1.392(3)
O(21)−Mn−O(31)	90.9(2)	O(31)−Mn−N(12)	96.8(1)
O(21)−Mn−N(1)	171.2(1)	N(1)−Mn−N(11)	94.0(1)
O(21)−Mn−N(11)	87.1(1)	N(1)−Mn−N(2)	70.6(1)
O(21)−Mn−N(2)	100.6(1)	N(1)−Mn−N(12)	91.8(1)
O(21)−Mn−N(12)	96.8(1)	N(11)−Mn−N(2)	97.2(1)
O(31)−Mn−N(1)	89.9(3)	N(11)−Mn−N(12)	70.8(1)
O(31)−Mn−N(11)	167.2(3)	N(2)−Mn−N(12)	158.3(1)
O(31)−Mn−N(2)	95.6(1)		

$[Mn_8O_2(OH)_2(O_2CPh)_{10}\{(ph)(2\text{-py})CNO\}_4]\cdot 4CH_2Cl_2$ (**2**·4CH_2Cl_2)

A partially labelled plot of the octanuclear complex **2** is shown in Figure 3. Selected interatomic distances and angles are listed in Table 2. Complex **2**·4CH_2Cl_2 crystallises in the monoclinic space group *C*2/*c*. Its structure consists of the octanuclear $[Mn_8O_2(OH)_2(O_2CPh)_{10}\{(ph)(2\text{-py})CNO\}_4]$ moiety and solvate CH_2Cl_2 molecules; the latter will not be further discussed. The molecule lies on an inversion centre; it comprises eight Mn ions held together by two μ_4-O^{2-} ions [O(21), O(21′)] and two μ_3-OH^- ions [O(22), O(22′)] to give a $[Mn_8(\mu_4\text{-}O)_2(\mu_3\text{-}OH)_2]^{14+}$ core, with peripheral ligation provided by ten $PhCO_2^-$ groups and four (ph)(2-py)CNO^- ligands. Bond-valence sum (BVS) calculations[20] give values of 1.9 and 1.3 for O(21) and O(22), respectively, supporting their assignments as oxo [O(21), theoretical value: 2.0] and hydroxo [O(22), theoretical value: 1.0] oxygen atoms. The ten $PhCO_2^-$ groups are arranged in three classes: (i) two are monodentate with O(71) and O(71′) being the ligated atoms; (ii) four [those containing O(31)/O(32), O(41)/O(42) and their symmetry-related partners] bridge two Mn ions and are in their familiar *syn*,*syn*-$\eta^1{:}\eta^1{:}\mu_2$ binding modes; and (iii) four (the rest) are in the fairly rare $\eta^1{:}\eta^2{:}\mu_3$ modes, one O bridging two Mn ions and

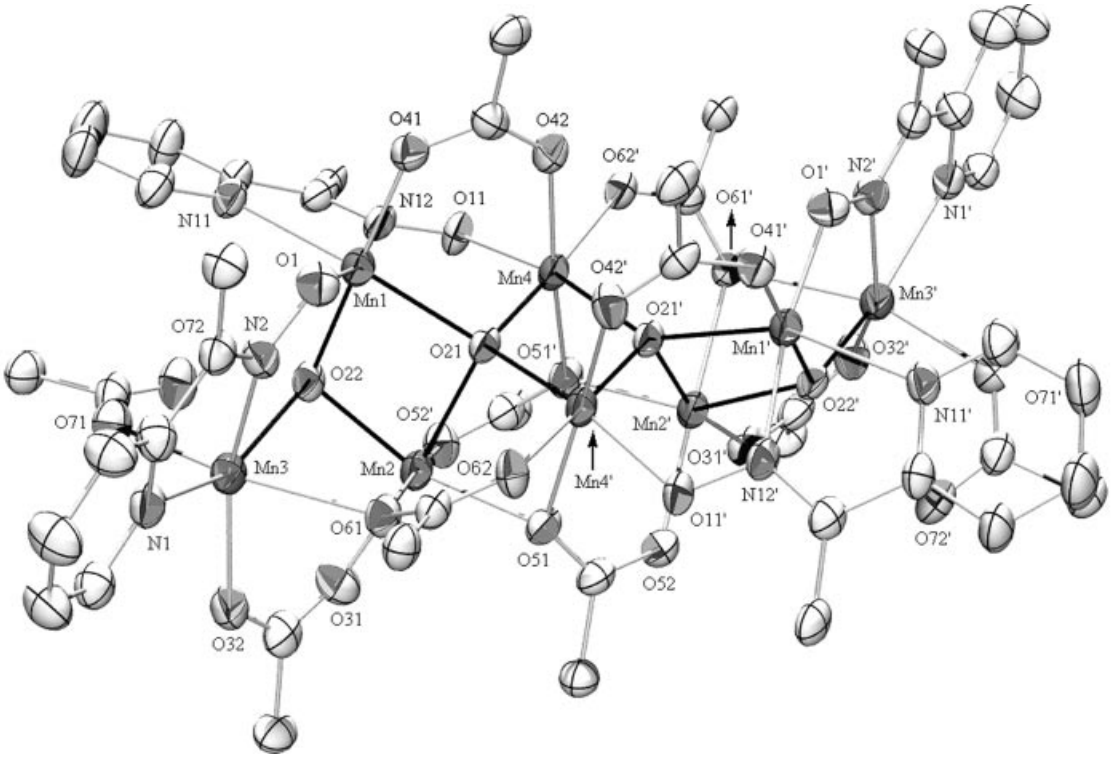

Figure 3. ORTEP representation of complex **2**; thermal ellipsoids are at the 30% probability level; primed and unprimed atoms are related by a crystallographic inversion centre; only the *ipso* carbon atoms of the phenyl groups of the benzoato and oximato ligands are shown

 © 2004 Wiley-VCH Verlag GmbH & Co. KGaA, Weinheim

Table 2. Selected interatomic distances (Å) and angles (°) for $[Mn_8O_2(OH)_2(O_2CPh)_{10}\{(ph)(2\text{-py})CNO\}_4]\cdot 4CH_2Cl_2$ (**2**·$4CH_2Cl_2$)[a]

Mn(1)···Mn(2)	3.270(2)	Mn(2)−O(22)	2.155(5)
Mn(1)···Mn(3)	3.556(2)	Mn(2)−O(31)	2.087(6)
Mn(1)···Mn(4)	3.307(1)	Mn(2)−O(51)	2.133(5)
Mn(2)···Mn(3)	3.368(2)	Mn(2)−O(52′)	2.140(6)
Mn(2)···Mn(4)	3.575(2)	Mn(2)−O(61)	2.308(5)
Mn(3)···Mn(4)	6.062(2)	Mn(3)−O(22)	2.195(5)
Mn(1)···Mn(4′)	3.945(2)	Mn(3)−O(32)	2.067(6)
Mn(2)···Mn(4′)	3.187(2)	Mn(3)−O(61)	2.408(5)
Mn(3)···Mn(4′)	5.367(2)	Mn(3)−O(71)	2.139(6)
Mn(4)···Mn(4′)	2.791(3)	Mn(3)−N(1)	2.269(7)
Mn(1)−O(1)	1.891(6)	Mn(3)−N(2)	2.223(7)
Mn(1)−O(21)	2.235(5)	Mn(4)−O(11)	1.937(5)
Mn(1)−O(22)	1.913(5)	Mn(4)−O(21)	1.872(5)
Mn(1)−O(41)	1.925(5)	Mn(4)−O(21′)	1.898(5)
Mn(1)−N(11)	2.301(6)	Mn(4)−O(42)	2.164(6)
Mn(1)−N(12)	2.050(7)	Mn(4)−O(51′)	2.315(6)
Mn(2)−O(21)	2.274(5)	Mn(4)−O(62′)	1.951(5)
O(1)−Mn(1)−O(21)	107.8(2)	O(32)−Mn(3)−O(61)	80.3(2)
O(1)−Mn(1)−O(22)	95.0(2)	O(32)−Mn(3)−O(71)	97.5(2)
O(1)−Mn(1)−O(41)	83.6(2)	O(32)−Mn(3)−N(1)	98.7(3)
O(1)−Mn(1)−N(11)	94.1(2)	O(32)−Mn(3)−N(2)	156.2(2)
O(1)−Mn(1)−N(12)	166.1(2)	O(61)−Mn(3)−O(71)	161.0(2)
O(21)−Mn(1)−O(22)	83.0(2)	O(61)−Mn(3)−N(1)	107.9(2)
O(21)−Mn(1)−O(41)	96.3(2)	O(61)−Mn(3)−N(2)	82.2(2)
O(21)−Mn(1)−N(11)	156.2(2)	O(71)−Mn(3)−N(1)	91.1(2)
O(21)−Mn(1)−N(12)	85.3(2)	O(71)−Mn(3)−N(2)	104.2(2)
O(22)−Mn(1)−O(41)	178.2(3)	N(1)−Mn(3)−N(2)	71.7(2)
O(22)−Mn(1)−N(11)	85.9(2)	O(11)−Mn(4)−O(21)	93.6(2)
O(22)−Mn(1)−N(12)	91.2(2)	O(11)−Mn(4)−O(21′)	165.2(2)
O(41)−Mn(1)−N(11)	95.3(2)	O(11)−Mn(4)−O(42)	95.2(2)
O(41)−Mn(1)−N(12)	90.4(2)	O(11)−Mn(4)−O(51′)	82.2(2)
N(11)−Mn(1)−N(12)	73.9(2)	O(11)−Mn(4)−O(62′)	86.2(2)
O(21)−Mn(2)−O(22)	77.0(2)	O(21)−Mn(4)−O(21′)	84.4(2)
O(21)−Mn(2)−O(31)	166.8(2)	O(21)−Mn(4)−O(42)	92.4(2)
O(21)−Mn(2)−O(51)	79.5(2)	O(21)−Mn(4)−O(51′)	96.9(2)
O(21)−Mn(2)−O(52′)	100.3(2)	O(21)−Mn(4)−O(62′)	175.5(2)
O(21)−Mn(2)−O(61)	85.8(2)	O(21′)−Mn(4)−O(42)	99.5(2)
O(22)−Mn(2)−O(31)	94.3(2)	O(21′)−Mn(4)−O(51′)	83.5(2)
O(22)−Mn(2)−O(51)	152.2(2)	O(21′)−Mn(4)−O(62′)	97.0(2)
O(22)−Mn(2)−O(52′)	106.4(2)	O(42)−Mn(4)−O(51′)	170.5(2)
O(22)−Mn(2)−O(61)	76.2(2)	O(42)−Mn(4)−O(62′)	82.8(2)
O(31)−Mn(2)−O(51)	105.8(2)	O(51′)−Mn(4′)−O(62′)	87.9(2)
O(31)−Mn(2)−O(52′)	91.7(2)	Mn(1)−O(21)−Mn(2)	93.0(2)
O(31)−Mn(2)−O(61)	82.3(2)	Mn(1)−O(21)−Mn(4)	106.9(2)
O(51)−Mn(2)−O(52′)	92.1(2)	Mn(1)−O(21)−Mn(4′)	145.2(3)
O(51)−Mn(2)−O(61)	87.5(2)	Mn(2)−O(21)−Mn(4)	118.8(2)
O(52′)−Mn(2)−O(61)	173.7(2)	Mn(2)−O(21)−Mn(4′)	99.2(2)
O(22)−Mn(3)−O(32)	109.2(2)	Mn(4)−O(21)−Mn(4′)	95.5(2)
O(22)−Mn(3)−O(61)	73.5(2)	Mn(1)−O(22)−Mn(2)	106.8(2)
O(22)−Mn(3)−O(71)	89.8(2)	Mn(1)−O(22)−Mn(3)	119.7(3)
O(22)−Mn(3)−N(1)	151.7(2)	Mn(2)−O(22)−Mn(3)	101.5(2)
O(22)−Mn(3)−N(2)	80.8(2)		

[a] Primed atoms are related to the unprimed ones by the symmetry transformation $-x, y, -z - 1/2$.

the other O terminal to a third Mn ion, with the bridging carboxylate O atoms being O(51), O(51′), O(61) and O(61′). The four (ph)(2-py)CNO^- ions behave as $\eta^1{:}\eta^1{:}\eta^1{:}\mu_2$ ligands; each ligand chelates one metal ion through its nitrogen atoms forming a five-membered ring and bridges this metal ion with a second one through the terminally ligated, deprotonated O atom [O(1), O(1′), O(11), O(11′)]. For convenience, the six coordination modes exhibited by the four different ligands of **2** are presented in Figure 4.

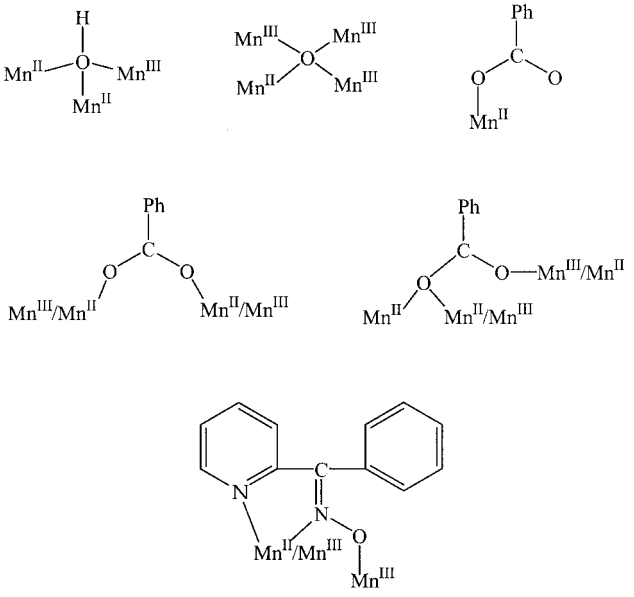

Figure 4. The crystallographically established coordination modes of the hydroxo, oxo, benzoato and phenyl 2-pyridyl ketone oximato ligands present in complex **2**

Mn(1) and Mn(3) are bound to an O_4N_2 set of donor atoms, while Mn(2) and Mn(4) are bound to an O_6 set. Charge considerations require a $4Mn^{II}$, $4Mn^{III}$ oxidation-state description, and Mn(2) and Mn(3) [and their symmetry related Mn(2′) and Mn(3′)] are assigned as the Mn^{II} ions on the basis of: (i) the longer average Mn−O bond lengths at these ions (average 2.190 Å and no individual value shorter than 2.07 Å) compared with those of the other Mn ions (average 2.010 Å), (ii) the clear presence of a Jahn−Teller (JT) axial elongation at Mn(1) and Mn(4) [and their symmetry-related partners], as expected for a high-spin d^4 ion in near-octahedral geometry; the JT elongation axes are O(21)−Mn(1)−N(11) and O(42)−Mn(4)−O(51′), with the axially elongated Mn−O bonds being longer than the equatorial Mn−O bonds by at least 0.21 Å, and (iii) BVS calculations[20] which give values of 3.21, 2.12, 1.75 and 3.20 for Mn(1), Mn(2), Mn(3) and Mn(4), respectively, in good agreement with the above assignments.

The above assignments of the Mn oxidation states reveal that the hydroxo ligand bridges two Mn^{II} and one Mn^{III} ions, while the oxo ligand bridges one Mn^{II} and three Mn^{III} ions (Figure 4). The four $\eta^1{:}\eta^1{:}\mu_2$ $PhCO_2^-$ groups separate further into two subclasses: The groups bearing O(31), O(32) and O(31′), O(32′) each bridge two Mn^{II} ions and those bearing O(41), O(42) and O(41′), O(42′) each bridge two Mn^{III} ions. Similarly, there are two types of $\eta^1{:}\eta^2{:}\mu_3$ $PhCO_2^-$ groups, which all bridge one Mn^{III} and two Mn^{II} ions: the μ_2-O [O(51), O(51′)] of the carboxylate groups bearing O(51), O(52) and O(51′), O(52′) bridges one Mn^{II} and one Mn^{III} ion, whereas the μ_2-O [O(61), O(61′)] of the

 © 2004 Wiley-VCH Verlag GmbH & Co. KGaA, Weinheim

groups bearing O(61), O(62) and O(61′), O(62′) bridges two Mn^{II} ions. The four $\eta^1{:}\eta^1{:}\eta^1{:}\mu_2$ (ph)(2-py)CNO^- ligands also separate further into two subclasses: The anions bearing N(1), N(2), O(1) and their symmetry-related partners each bridge one Mn^{II} and one Mn^{III} ion, while those bearing N(11), N(12), O(11) and N(11′), N(12′), O(11′) each bridge two Mn^{III} ions; in both cases the deprotonated oximate oxygen atom is terminally ligated to a Mn^{III} ion (Figure 4).

The molecular structure of **2** leads to diverse Mn···Mn distances (Table 2), which depend on the number and nature of the bridges between the two metal centres and on the oxidation state of each Mn atom. The central Mn(4)···Mn(4′) separation is the shortest [2.791(3) Å]; this separation is almost identical to the Mn···Mn distances observed for other polynuclear complexes containing the $[Mn_2^{III}(\mu_4\text{-}O)_2]^{2+}$ subunit.[17] The other two $Mn^{III}\cdots Mn^{III}$ distances are 3.307(2) [Mn(1)···Mn(4)] and 3.945(2) Å [Mn(1)···Mn(4′)]; the shorter Mn···Mn separation corresponds to the pair bridged by one oxo, one $\eta^1{:}\eta^1{:}\mu_2$ benzoato and one oximato groups, whereas the larger distance corresponds to that linked by only one oxo group. The shortest $Mn^{II}\cdots Mn^{III}$ distance is Mn(2)···Mn(4′) [3.187(2) Å]; this pair is bridged by one oxo group and the μ_2-O of an $\eta^1{:}\eta^2{:}\mu_3$ benzoato group. The μ_2-benzoate oxygen atom O(61) [and O(61′)] does not bridge the two Mn^{II} ions symmetrically, and Mn(2)−O(61) [2.308(5) Å] is noticeably shorter than Mn(3)−O(61) [2.408(5) Å]. The Mn(2,3)−O(22) distances [2.155(5), 2.195(5) Å] are noticeably longer than the Mn(1)−O(22) distance [1.913(5) Å], consistent with the lower oxidation state in the former. Similarly, Mn(2,3)-carboxylate distances (average 2.190 Å) are longer than Mn(1,4)-carboxylate distances (average 2.090 Å). It is interesting that the μ_4-O^{2-} ions [O(21), O(21′)] bridge the Mn^{III} ions asymmetrically. Thus, Mn(4)−O(21) and Mn(4′)−O(21) are 1.872(5) and 1.898(5) Å, respectively, whereas Mn(1)−O(21) is much longer at 2.235(5) Å. This is the result of O(21) lying on the JT elongation axis of Mn(1); Mn^{III}−O^{2-} distances greater than 2.2 Å are extremely rare.[21] This JT-elongated Mn(1)−O(21) bond contributes to the relatively long Mn(1)···Mn(4′) distance [3.945(2) Å].

The uncoordinated O atoms of the monodentate $PhCO_2^-$ groups [O(72) and O(72′)] are hydrogen-bonded to the μ_3-OH^- ligands, with the O(72)···O(22) distance being 2.610 Å.

The novel Mn_8 topology in **2** can be described in a number of ways, but the following three are particularly useful. As is emphasised in Figure 5, the $[Mn_8O_2(OH)_2]^{14+}$ core can be conveniently described as two $\{Mn_2^{II}Mn_2^{III}(\mu_3\text{-}O)(\mu_3\text{-}OH)\}^{7+}$ units [atoms Mn(1)−Mn(4) and their symmetry-related partners] becoming linked through the μ_3-O^{2-} in each unit converting to a μ_4 mode and thus providing the two "inter-fragment' bonds Mn(4)−O(21′) and Mn(4′)−O(21). The four metal ions in each unit are nearly coplanar with the torsion angle Mn(1)−Mn(2)−Mn(3)−Mn(4) being 9.4°. Although tetranuclear complexes containing the $[Mn_4(\mu_3\text{-}O)_2]$ core, where the metals are arranged in either planar or nonplanar ("butterfly") fashion and the metal oxidation levels are $Mn_2^{II}Mn_2^{III}$,[22] $Mn^{II}Mn_3^{III}$ [23] or Mn^{III},[15,22] have been reported, the $\{Mn_2^{II}Mn_2^{III}(\mu_3\text{-}O)(\mu_3\text{-}OH)\}^{7+}$ unit present in **2** has not been observed either in a discrete tetranuclear complex or encountered as a recognizable sub-fragment of higher nuclearity Mn clusters. A second way of describing the core emphasises its "central" $\{Mn_2^{II}Mn_4^{III}(\mu_4\text{-}O)_2\}^{12+}$ subunit, which is the currently unknown (in either a discrete hexanuclear complex or in a higher nuclearity cluster) oxidized version of the familiar[17] $[Mn_4^{II}Mn_2^{III}(\mu_4\text{-}O)_2]^{10+}$ core; extension of the former at each end with an additional Mn^{II} ion through the μ_3-OH^- gives the core of **2**. In view of the magnetochemical discussion presented below (vide infra), it is of interest and beneficial to consider a third, alternate description of the core of complex **2** which emphasises its structural relationship to a well-known smaller nuclearity Mn/O unit. The molecule can be described as consisting of a central, butterfly-like[15,22] $[Mn_4^{III}(\mu_3\text{-}O)_2]^{8+}$ subunit [atoms Mn(1), Mn(1′), Mn(4), Mn(4′), O(21), O(21′); see Figure 5]. The $[Mn_8(\mu_4\text{-}O)_2(\mu_3\text{-}OH)_2]^{14+}$ core of **2** is then completed by the attachment of two additional $[Mn_2^{II,II}(\mu_2\text{-}OH)]^{3+}$ subunits to the butterfly-like central sub-core via the inter-fragment bonds Mn(1)−O(22), Mn(2)−O(21) and their symmetry equivalents. As a result, each OH^- ligand becomes μ_3, forming a bond with a "wing-tip" Mn^{III} ion [Mn(1), Mn(1′)], and each O^{2-} ligand is converted to μ_4, forming a bond with one of the Mn^{II} ions [Mn(2), Mn(2′)].

Complex **2** joins a very small family of Mn clusters of nuclearity eight, which currently comprise the metal oxi-

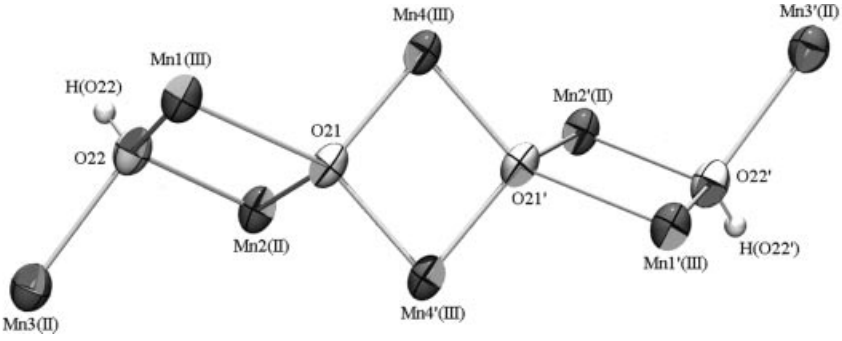

Figure 5. ORTEP representation of the $[Mn_4^{II}Mn_4^{III}(\mu_4\text{-}O)_2(\mu_3\text{-}OH)_2]^{14+}$ core of **2**

 © 2004 Wiley-VCH Verlag GmbH & Co. KGaA, Weinheim

dation states Mn_8^{II},[24] $Mn_6^{II}Mn_2^{III}$,[6a,25] $Mn_2^{II}Mn_6^{III}$,[15,26] Mn_8^{III} [18a,27] and $Mn_2^{III}Mn_6^{IV}$,[28] and thus becomes the first member of the $Mn_4^{II}Mn_4^{III}$ subfamily. Since most of these were reported only recently, we felt it timely to collect the octanuclear $Mn^{II/III}$, Mn^{III} and $Mn^{III/IV}$ clusters in Table 3, together with their cores for convenient comparison; we have not included the Mn_8^{II} complexes. The $[Mn_4^{II}Mn_4^{III}(\mu_4\text{-}O)_2(\mu_3\text{-}OH)_2]^{14+}$ core of **2** bears some similarity to the $[Mn_2^{II}Mn_6^{III}(\mu_3\text{-}O)_2(\mu_4\text{-}O)_2]^{14+}$ core present[15] in the anion $[Mn_8O_4(O_2CPh)_{12}(Et_2mal)_2(H_2O)_2]^{2-}$, where Et_2mal is the dianion of 2,2-diethylmalonic acid; the former can be thought of as being derived from the latter by reduction/protonation steps. Complex **2** is also one of the rare examples of polynuclear Mn complexes that contain oxo and hydroxo bridges simultaneously,[29] other such complexes being $[Mn_8O_4(OH)_2(O_2CMe)_{12}(DMHP)_2(py)_2]$ (DMHP = 2,6-dimethyl-6-hydroxypyrimidine; py = pyridine),[26] $[Mn_4O_5(OH)(tame)_4](CF_3SO_3)_5$ [tame= 1,1,1-tris(aminomethyl)ethane],[30] $[Mn_4O_5(OH)(tacn)_4](ClO_4)_5$ (tacn = 1,4,7-triazacyclononane)[30] and $[Mn_{10}O_4(OH)_2(O_2CMe)_8(hmp)_8](ClO_4)_4$ [hmp = the anion of 2-(hydroxymethyl)pyridine].[16]

The Mn_8 nuclearity of **2** can be put into context by noting that the largest molecular Mn cluster currently known is $[Mn_{30}O_{24}(OH)_8(O_2CCH_2But)_{32}(H_2O)_2(MeNO_2)_4]$,[31a] followed by $[Mn_{26}O_{16}(OH)_{10}(OMe)_6F_{10}(bta)_2(btaH)_2(MeOH)_{13}(H_2O)]$, where btaH is benzotriazole;[31b] these two clusters are also mixed oxo/hydroxo species.

$[Mn_3(O_2CPh)_6\{(ph)(2\text{-}py)CO\}_2]$ (3)

A partially labelled plot of the trinuclear complex **3** is shown in Figure 6. Selected interatomic distances and angles are listed in Table 4. The complex crystallises in the monoclinic space group $P2_1/a$. The central metal ion, Mn(2), which is located on a crystallographic inversion centre, is coordinated octahedrally by six oxygen atoms belonging to six different benzoates. Thus, the trinuclear molecule adopts a linear structure, with one $\eta^1{:}\eta^2{:}\mu_2$ and two *syn*,*syn*-$\eta^1{:}\eta^1{:}\mu_2$ carboxylate groups spanning each pair of Mn^{II}. The termini of the $\{Mn(O_2CPh)_3Mn(O_2CPh)_3Mn\}$ unit are capped by bidentate chelating (ph)(2-py)CO ligands, resulting in six-coordination at these sites.

Table 3. Formulae, cores and core description for structurally characterised octanuclear $Mn^{II/III}$, Mn^{III} and $Mn^{III/IV}$ clusters

Complex[a]	Core	Core description	Ref.
$[Mn_8O_2(O_2CCH_2tBu)_{14}(ButCH_2CO_2H)_4]$	$[Mn_6^{II}Mn_2^{III}(\mu_4\text{-}O)_2(\mu_2\text{-}O)_8]^{10+}$[b]	extension of the $[Mn_4^{II}Mn_2^{III}(\mu_4\text{-}O)_2]^{10+}$ core at one end with two additional Mn^{II} ions	[25]
$[Mn_8O_2(O_2CEt)_8(py)_4(L)_2]^{2+}$	$[Mn_6^{II}Mn_2^{III}(\mu_4\text{-}O)_2(\mu_3\text{-}O)_4(\mu_2\text{-}O)_4]^{6+}$[c]	two distorted cubanes edge-linked together at two Mn−O edges	[6a]
$[Mn_8O_2(OH)_2(O_2CPh)_{10}\{(ph)(2\text{-}py)CNO\}_4]$	$[Mn_4^{II}Mn_4^{III}(\mu_4\text{-}O)_2(\mu_3\text{-}OH)_2]^{14+}$	two $\{Mn_2^{II}Mn_2^{III}(\mu_3\text{-}O)(\mu_3\text{-}OH)\}^{7+}$ units linked *via* the O^{2-} in each unit	this work
$[Mn_8O_4(OH)_2(O_2CMe)_{12}(DMHP)_2(py)_2]$	$[Mn_2^{II}Mn_6^{III}(\mu_3\text{-}O)_4(\mu_2\text{-}OH)_2]^{12+}$	two $[Mn^{II}Mn_3^{III}(\mu_3\text{-}O)_2]^{7+}$ "butterfly" units linked by the two μ_2-OH^- ligands	[26]
$[Mn_8O_4(O_2CPh)_{12}(Et_2mal)_2(H_2O)_2]^{2-}$	$[Mn_2^{II}Mn_6^{III}(\mu_4\text{-}O)_2(\mu_3\text{-}O)_2]^{14+}$	two $[Mn^{II}Mn_3^{III}(\mu_3\text{-}O)_2]^{7+}$ "butterfly" units linked by one O^{2-} in each unit	[15]
$[Mn_8O_4(O_2CMe)_{12}(pic)_4]$	$[Mn_4^{III}(\mu_3\text{-}O)_2]_2^{8+}$	two $[Mn_4^{III}(\mu_3\text{-}O)_2]^{8+}$ units linked through two picolinates bridges	[27a]
$[Mn_8O_6Cl_6(O_2CPh)_7(H_2O)_2]^-$	$[Mn_8^{III}(\mu_4\text{-}O)_2(\mu_3\text{-}O)_4(\mu_2\text{-}Cl)_2(\mu_3\text{-}Cl)(\mu_4\text{-}Cl)]^{8+}$	two $[Mn_4^{III}(\mu_3\text{-}O)_2]^{8+}$ "butterfly" units fused by sharing one "body" Mn; an eighth Mn^{III} ion is connected to the resultant $\{Mn_7O_7\}^{7+}$ unit by two additional bridging O^{2-} ions	[18a]
$[Mn_8O_4(piv)_{10}(thme)_2(py)_2]$	$[Mn_8^{III}(\mu_3\text{-}O)_4]^{16+}$	six edge-sharing triangles or three edge-sharing "butterfly" units (ladder-like unit)	[27b]
$[Mn_8O_4(O_2CPh)_{12}(dbm)_4(bpe)_2]$	$[Mn_4^{III}(\mu_3\text{-}O)_2]_2^{8+}$	two "butterfly" $[Mn_4^{III}(\mu_3\text{-}O)_2]^{8+}$ units with the two bpe ligands attached *syn* about the central $[Mn_2O_2]$ rhomboids	[27c]
$[Mn_8O_4(O_2CEt)_{14}(py)_4(L')_2]^{2+}$	$[Mn_4^{III}(\mu_3\text{-}O)_2]_2^{8+}$	two butterfly-like cores arranged face-to-face and bridged by two bis-bidentate L ligands	[27d]
$[Mn_8O_{10}(O_2CMe)_6(bpy)_2(H_2O)_2]^{4+}$	$[Mn_2^{III}Mn_6^{IV}(\mu_2\text{-}O)_8(\mu_3\text{-}O)_2]^{10+}$	five $[Mn_2O_2]$ rhombs linked and fused to give a core with a serpentine topology	[28]

[a] Counterions and solvate molecules omitted; bpe = *trans*-1,2-bis(4-pyridyl)ethene; bpy = 2,2′-bipyridine; dbm = the anion of dibenzoylmethane; DMHP = 2,6-dimethyl-6-hydroxypyrimidine; Et_2mal = the dianion of 2,2-diethylmalonic acid; L = the dianion of (6-hydroxymethylpyridin-2-yl)-(6-hydroxymethylpyridin-2-yl methoxymethanol); L′ = 1,2-bis(5-methyl-2,2′-bipyridyl-5-yl)ethane; pic = the picolinate anion; piv = the pivalate anion; py = pyridine. [b] The μ_2-O atoms belong to carboxylates. [c] The μ_3-O atoms belong to the L^{2-} ligands, while the μ_2-O atoms are from $EtCO_2^-$ ligands.

 © 2004 Wiley-VCH Verlag GmbH & Co. KGaA, Weinheim

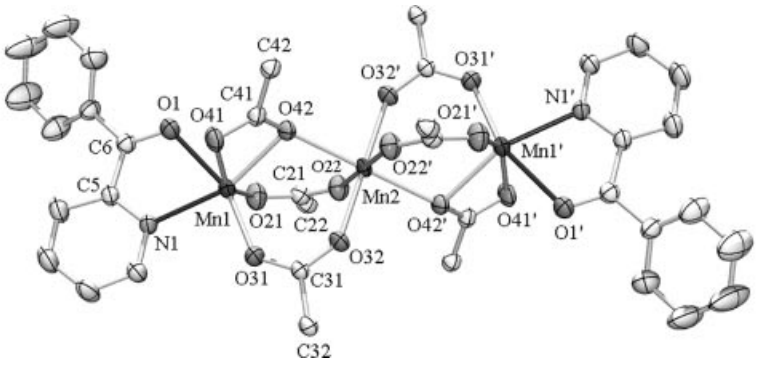

Figure 6. ORTEP drawing showing 30% probability ellipsoids and labelling scheme for complex **3**; primed and unprimed atoms are related by a crystallographic inversion centre; only the *ipso* carbon atoms of the phenyl rings of the benzoato ligands are shown

Table 4. Selected interatomic distances (Å) and angles (°) for $[Mn_3(O_2CPh)_6\{(ph)(2\text{-}py)CO\}_2]$ (**3**)[a]

Mn(1)···Mn(2)	3.603(5)	Mn(2)−O(32)	2.136(3)
Mn(1)···Mn(1′)	7.205(5)	Mn(2)−O(42)	2.240(3)
Mn(1)−O(1)	2.339(4)	C(6)−O(1)	1.224(5)
Mn(1)−N(1)	2.256(4)	C(21)−O(21)	1.258(5)
Mn(1)−O(21)	2.058(4)	C(21)−O(22)	1.239(5)
Mn(1)−O(31)	2.086(3)	C(31)−O(31)	1.249(5)
Mn(1)−O(41)	2.249(4)	C(31)−O(32)	1.247(5)
Mn(1)−O(42)	2.261(3)	C(41)−O(41)	1.247(5)
Mn(2)−O(22)	2.156(3)	C(41)−O(42)	1.275(5)
O(1)−Mn(1)−N(1)	70.4(1)	O(22)−Mn(2)−O(22′)	180.0(1)
O(1)−Mn(1)−O(21)	88.1(1)	O(22)−Mn(2)−O(32)	91.3(1)
O(1)−Mn(1)−O(31)	159.7(1)	O(22)−Mn(2)−O(32′)	88.7(1)
O(1)−Mn(1)−O(41)	81.3(1)	O(22)−Mn(2)−O(42)	89.6(1)
O(1)−Mn(1)−O(42)	96.6(1)	O(22)−Mn(2)−O(42′)	90.5(1)
N(1)−Mn(1)−O(21)	103.1(2)	O(22′)−Mn(2)−O(32)	88.7(1)
N(1)−Mn(1)−O(31)	89.8(1)	O(22′)−Mn(2)−O(32′)	91.3(1)
N(1)−Mn(1)−O(41)	99.5(1)	O(22′)−Mn(2)−O(42)	90.5(1)
N(1)−Mn(1)−O(42)	156.2(1)	O(22′)−Mn(2)−O(42′)	89.6(1)
O(21)−Mn(1)−O(31)	101.2(2)	O(32)−Mn(2)−O(32′)	180.0(1)
O(21)−Mn(1)−O(41)	150.1(1)	O(32)−Mn(2)−O(42)	93.0(1)
O(21)−Mn(1)−O(42)	96.2(1)	O(32)−Mn(2)−O(42′)	87.0(1)
O(31)−Mn(1)−O(41)	98.2(1)	O(32′)−Mn(2)−O(42)	87.0(1)
O(31)−Mn(1)−O(42)	100.3(1)	O(32′)−Mn(2)−O(42′)	93.0(1)
O(41)−Mn(1)−O(42)	57.9(1)	O(42)−Mn(2)−O(42′)	180.0(1)
C(21)−O(21)−Mn(1)	130.6(3)	C(21)−O(22)−Mn(2)	142.0(3)
C(31)−O(31)−Mn(1)	130.9(3)	C(31)−O(32)−Mn(2)	142.3(3)
C(41)−O(41)−Mn(1)	91.6(3)	C(41)−O(42)−Mn(1)	90.3(3)
O(21)−C(21)−O(22)	125.4(5)	C(41)−O(42)−Mn(2)	140.2(3)
C(22)−C(21)−O(21)	116.2(4)	O(41)−C(41)−O(42)	119.9(4)
C(22)−C(21)−O(22)	118.4(4)	C(42)−C(41)−O(41)	119.9(4)
O(31)−C(31)−O(32)	124.7(4)	C(42)−C(41)−O(42)	120.2(4)
C(32)−C(31)−O(31)	117.7(4)	Mn(1)−O(42)−Mn(2)	106.3(4)
C(32)−C(31)−O(32)	117.6(4)		

[a] Primed atoms are related to the unprimed ones by the symmetry transformation $-x, -y + 1, -z$.

The Mn(1) polyhedron is significantly distorted. The main distortions arise from the five-membered chelating ring with a narrow O(1)−Mn(1)−N(1) bond angle [70.4(1)°] and an acute O(41)−Mn(1)−O(42) angle [57.9(1)°]. The Mn−N and Mn−O bond lengths agree well with values expected for high-spin Mn^{II}.[13] The Mn(2)−O bond lengths are in the narrow 2.136(3)−2.240(3) Å range, with the Mn(2)−O(42) distance longer, as expected. The coordination of the bridging benzoate oxygen, O(42) [and O(42′)], is somewhat pyramidal [Σ°O(42) = 336.8°].

Complex **3** joins a small family[32−34] of trinuclear Mn^{II} carboxylate complexes containing the $[Mn_3(\eta^1{:}\eta^1{:}\mu_2\text{-}O_2CR)_4(\eta^1{:}\eta^2{:}\mu_2\text{-}O_2CR)_2]^0$ core. The members of this family are listed in Table 5. This structural motif was also confirmed[35] for complexes $[Mn_3(O_2CPh\text{-}3\text{-}Cl)_6(bpy)_2]$ and $[Mn_3(O_2CPh\text{-}3\text{-}Cl)_6(Me_2\text{-}bpy)_2]$ (Me_2-bpy = 4,4′-dimethyl-2,2′-bipyridine) by analysis of the XANES and EXAFS spectra at the Mn K-edge; since only average distances could be derived, these two complexes are not included in Table 5. Some of the listed complexes have been important in the establishment of the "carboxylate shift" model.[34] Of the various types of metal-carboxylate binding modes, monodentate(monoatomic) bridging between metal centres offers unique flexibility. Analysis[34] of the structural characteristics of discrete compounds containing monodentate (monoatomic) bridging carboxylates shows that they can be arranged into three classes, depending upon the strength of the interaction of the non-bridging, or dangling (O_d), oxygen atom [O(42) in complex **3**] with one of the bridged metal ions [Mn(1) in **3**]. The application of this analysis to trinuclear Mn^{II} carboxylate complexes is demonstrated in Figure 7 and Table 5. The monodentate bridging mode is postulated to be an important intermediate between the other, more common, carboxylate attachment modes, based on observed variations of the geometry for monodentate bridges in structurally characterised complexes. The movement from monodentate to these other binding modes has been termed the "carboxylate shift";[34] such a shift could be kinetically important in carboxylate-containing metalloproteins.

Complex **3** is characterised by a small *D* value, $B > D$, a rather large Mn···Mn distance, a small difference between $C-O_d$ and $C-O_b$ (indicating significant delocalisation of the double bond), a large tilt (α-β) of the $\eta^1{:}\eta^2{:}\mu_2$ carboxylate toward Mn(1) and a significant distortion of the coordination geometry of Mn(1). Thus, complex **3** has a

 © 2004 Wiley-VCH Verlag GmbH & Co. KGaA, Weinheim

Table 5. Pertinent structural[a] and magnetic properties for trinuclear manganese(II) complexes containing the $[Mn_3(\eta^1{:}\eta^1{:}\mu_2\text{-}O_2CR)_4(\eta^1{:}\eta^2{:}\mu_2\text{-}O_2CR)_2]^0$ core; bpy = 2,2′-bipyridine; L = 2,2′-bis(1-methylimidazolyl)phenylmethoxymethane; phen = 1,10-phenanthroline; pybim = 2-(2-pyridyl)benzimidazole

Complex	*B* (Å)	*D* (Å)	*A* (Å)	Mn···Mn (Å)	C−O_b (Å)	C−O_d (Å)	θ (°)	β (°)	α (°)	*J* (cm^{-1})	*S*	Ref.
$[Mn_3(O_2CMe)_6(pybim)_2]$	2.132	2.283	2.235	3.558	[b]	[b]	109.1	[b]	[b]	−1.9	5/2	[32a]
$[Mn_3(O_2CMe)_6(bpy)_2]$	2.155	2.605	2.200	3.614	1.276	1.228	112.2	[b]	[b]	−4.4	5/2	[32b]
anti-$[Mn_3(O_2CMe)_6L_2]$ (A)[c]	2.172	2.488	2.205	3.635	1.28(1)	1.22(1)	112.3	98.9	136.1			[32c]
anti-$[Mn_3(O_2CMe)_6L_2]$ (B)[c]	2.263[d]	2.325[d]	2.236[d]	3.708[d]	1.272[d]	1.250[d]	111.0[d]	92.0[d]	131.1[d]	−2.8[e]		[32c]
syn-$[Mn_3(O_2CMe)_6L_2]$[c]	2.190[f]	2.580[f]	2.191[f]	3.465[f]	1.27(1)[f]	1.25(1)[f]	104.6[f]	102.0[f]	143.4[f]			[32c]
$[Mn_3(O_2CMe)_6(phen)_2]$[g]	2.285	2.425	2.133	3.387	1.263	1.224	100.1	99.9	144.9	[h]	[h]	[32c]
$[Mn_3(O_2CPh)_6(bpy)_2]$	2.285	2.274	2.239	3.588	1.284	1.257	104.9	90.5	135.0	[h]	[h]	[32d]
$[Mn_3(O_2CPh)_6\{(ph)(2\text{-}py)CO\}_2]$	2.261	2.249	2.240	3.603	1.275	1.247	106.3	90.3	140.2	−2.7	5/2	this work
$(Et_4N)_2[Mn_3(O_2CMe)_8]$	2.17	2.14	2.11	3.569	[b]	[b]	[b]	[b]	[b]	−5.6	5/2	[32e]

[a] See Figure 7 for the definition of the structural parameters given in this table. [b] Not reported. [c] Three isomers of $[Mn_3(O_2CMe)_6L_2]$ have been crystallised and structurally characterised; they are designated *anti* and *syn* based on the disposition of the L imidazole groups with respect to the best plane passing through the three metal ions and the two monodentate acetate oxygen bridges. The A designation indicates the *anti* isomer where the central metal is located on a crystallographic inversion centre; no such inversion centre exists in the B form. [d] Average value for one of the two crystallographically independent trinuclear molecules present in the unit cell. [e] Variable-temperature magnetic-susceptibility data are available for a bulk sample of $[Mn_3(O_2CMe)_6L_2]$ possibly containing all three isomers. [f] Average value. [g] The single-crystal structure of this complex was also reported by Miyamae and co-workers;[32f] the quoted bond lengths and angles do no differ much from those reported by Lippard and co-workers. [h] Variable-temperature magnetic susceptibility data are not available.

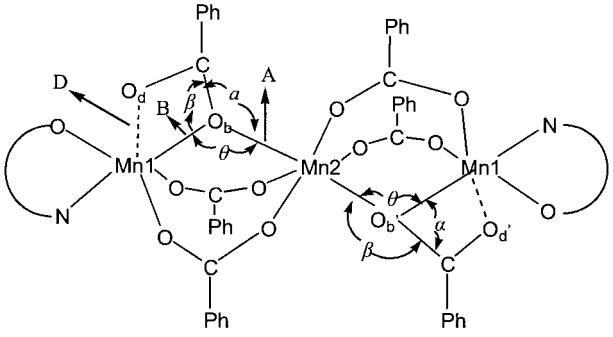

Figure 7. The schematic structure of complex **3** showing the dangling (O_d) and the bridging (O_b) oxygen atoms of the $\eta^1{:}\eta^2{:}\mu_2$ carboxylate groups, and defining the geometry of monoatomic carboxylate-bridged polymetallic centres in relation to the "carboxylate shift" mechanism proposed by Lippard;[32c,34] the values of the relevant structural parameters for **3** and other trinuclear complexes containing the $[Mn_3(\eta^1{:}\eta^1{:}\mu_2\text{-}O_2CR)_4(\eta^1{:}\eta^2{:}\mu_2\text{-}O_2CR)_2]^0$ core are listed in Table 5.

strong interaction between Mn(1) and O_d, i.e. O(42), and can be placed in class III in Lippard's classification scheme.[34]

IR Spectra

The presence of both neutral oxime and solvate H_2O molecules in **1**·1.2H_2O is manifested by a broad IR band of medium intensity at 3434 cm^{-1}, assigned to $\nu(OH)_{oxime}$ [13]/$\nu(OH)_{water}$.[36] The IR spectrum of **2** exhibits a medium band at 3438 cm^{-1} assignable[37] to $\nu(OH)_{OH^-}$; the broadness and relatively low frequency of this band are both indicative of strong hydrogen bonding.

The $\nu(C{=}O)$ mode is found at a lower wavenumber (1648 cm^{-1}) in the spectrum of **3** than for free (ph)(2-py)CO (1668 cm^{-1}); this shift is consistent with ketone-O coordination.[38]

Several bands appear in the 1610−1390 cm^{-1} range in the spectra of **1**−**3**. Contributions from the $PhCO_2^-$ $\nu_{as}(CO_2)$ and $\nu_s(CO_2)$ modes would be expected in this region, but overlap with the stretching vibrations of the aromatic rings and $\nu(C{=}N)_{oxime}$ (in **1** and **2**) renders assignments tentative and application of the spectroscopic criterion of Deacon and Phillips[39a] difficult. In all spectra, the very strong band at 1404−1400 cm^{-1} should have a high $\nu_s(CO_2)$ character.[13,39b]

A medium-intensity band at 606 cm^{-1} is present in the spectrum of **2**. This band is absent from the spectra of **1**·1.2H_2O and can be tentatively assigned to a vibration involving a $Mn^{III}-O^{2-}$ stretch.[40]

Magnetic Properties

Complex 2

Solid-state variable-temperature dc magnetic-susceptibility measurements were performed on a microcrystalline sample of **2** in a 0.1 T field in the range 2.0−300 K. The $\chi_M T$ vs. T and χ_M vs. T plots are shown in Figure 8. The value of $\chi_M T$ gradually decreases from 25.2 $cm^3{\cdot}mol^{-1}{\cdot}K$ at room temperature to 0.82 $cm^3{\cdot}mol^{-1}{\cdot}K$ at 2.0 K. The value of $\chi_M T$ at room temperature is lower than that expected for a cluster of $4Mn^{II}$ and $4Mn^{III}$ non-interacting ions (29.5 $cm^3{\cdot}mol^{-1}{\cdot}K$ for $g = 2$). A well-defined maximum of χ_M appears at 16 K. The $\chi_M T$ vs. T plot extrapolates to $\chi_M T \approx 0$ as the temperature approaches zero, indicating an $S = 0$ ground state. The intense drop of $\chi_M T$ with decreasing temperature reflects the presence of strong antiferromagnetic interactions within the cluster.

Complex **2** contains $4Mn^{II}$ and $4Mn^{III}$ centres, with total spin values ranging from 0 to 18. Owing to the size and low symmetry of the molecule, it is not possible to apply the Kambe method[41] or otherwise evaluate the individual

 © 2004 Wiley-VCH Verlag GmbH & Co. KGaA, Weinheim

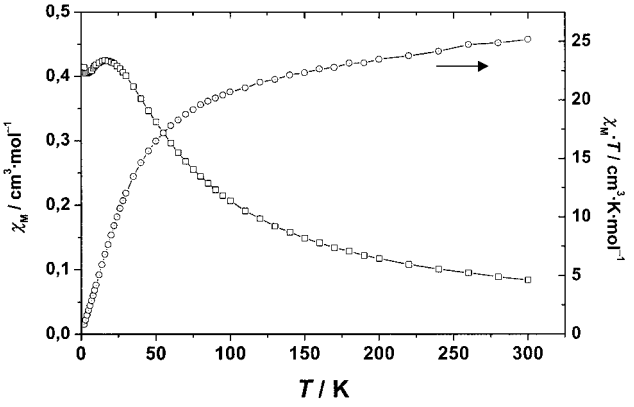

Figure 8. $\chi_M T$ vs. T and χ_M vs. T plots for complex **2**; the solid lines are guides for the eye

pairwise Mn_2 exchange interactions. Magnetisation data were collected in the magnetic field and temperature ranges 1−50 KG and 2.0−4.0 K, respectively. These measurements are poorly indicative, because they reveal a continuous increase of M with a change in the slope at 20 KG, up to an $M/N\beta$ value of 5.2 at 50 KG, far from saturation, indicating that several spin-states different from zero are very close to the ground state.

For the present $Mn_4^{II}Mn_4^{III}$ complex **2** it is important to rationalize the apparent $S = 0$. As indicated above, complex **2** can be described as arising from the linkage of the central $[Mn_4^{III}(\mu_3\text{-}O)_2]^{8+}$ subunit with two $[Mn_2^{II,II}(\mu_2\text{-}OH)]^{3+}$ subunits. Since $Mn^{II}\cdots Mn^{II}$ and $Mn^{II}\cdots Mn^{III}$ exchange interactions are typically weak and antiferromagnetic,[6a] the apparent $S = 0$ ground state of **2** can be rationalised taking as a starting point the well-established magnetic behaviour of the central, butterfly-like $[Mn_4^{III}(\mu_3\text{-}O)_2]^{8+}$ sub-core.

Table 6 conveniently summarises all previous magnetochemically characterised, *discrete* $[Mn_4^{III}(\mu_3\text{-}O)_2]^{8+}$ complexes.[22,42] There are two main exchange parameters: a body-body interaction parameter, J_{bb}, and a wing-tip-body parameter, J_{wb}. It has been found in all studied complexes that both types of interaction are antiferromagnetic and that $|J_{bb}|$ is appreciably larger than $|J_{wb}|$. In the format[42d] (S, S_{bb}, S_{ww}), the ground state of most complexes is (3, 1, 4). Even though both types of pairwise exchange interactions are antiferromagnetic, the ground state of these complexes has six unpaired electrons ($S = 3$). Because the J_{bb} interaction is greater than J_{wb} ($J_{bb}/J_{wb} = 3.0-5.0$), the spins on the two Mn_b ions have a greater tendency to pair up. Each Mn_w ion interacts with both the Mn_b ions and would align its spin antiparallel to both if possible, but it cannot do so. The net result is that the spin alignments of the Mn_w ions are frustrated. Overall, the unpaired electrons on the Mn_b ions are essentially paired up (actually the resultant spin vector S_{bb} is 1, not 0), and this leaves the unpaired electrons on the Mn_w ions. The S_{bb} resultant spin then couples with the $S_{ww} = 4$ to give the resultant $S = 3$ ground state of the complete molecule.[18a] The (3, 1, 4) ground state can be depicted diagrammatically as shown in **I** of Figure 9. In one complex, namely $[Mn_4O_2(O_2CEt)_7(bpya)_2](ClO_4)$ [bpya = bis(2-pyridyl)-amine],[42c] the J_{bb}/J_{wb} ratio is large (7.8) and there is also a very small J_{ww} interaction (-0.8 cm^{-1}); in this case, the spins of the Mn_b ions are fully antiparallel-aligned, i.e. $S_{bb} = 0$, and the ground state is then determined by the interaction of the Mn_w ions via the J_{ww} exchange, giving an $S = 0$ ground state since J_{ww} is antiferromagnetic (**II** in Figure 9). In effect, this (0, 0, 0) ground state can be described as the result of a weak, long-distance J_{ww} interaction between the wing-tip Mn^{III} ions through a strongly coupled, diamagnetic ($S_{bb} = 0$) central unit.[42c] In complex $[Mn_4O_2(O_2CPh)_6(dpm)_2]$ (dpm is the anion of dipivaloylmethane),[42d] the J_{bb}/J_{wb} ratio is much larger (ca. 70) and J_{ww} is negligible, i.e. $J_{ww} = 0$; the (n, 0, n) ground state is best described as fivefold degenerate (**III** in Figure 9). An alternative and completely equivalent description is to suggest that the ground state is composed of two non-interacting independent Mn^{III} ions.[42d]

The core of complex **2** (Figure 5) is more complicated than the $[Mn_4^{III}(\mu_3\text{-}O)_2]^{8+}$ core present in the *discrete* tetranuclear manganese(III) clusters mentioned above. However, the magnetic study of the latter has shown two important features. First, the J_{bb} coupling constant is always negative and relatively strong, and second, ground states with $S \neq 0$ are strongly dependent on the presence of competitive interactions in the coupling scheme. Complex **2** has two possible ligand types which may be involved in competitive interactions; these are the $\mu_4\text{-}O^{2-}$ and the $\mu_3\text{-}OH^-$ ligands. Spin frustration derived from competitive interactions involving the $\mu_4\text{-}O^{2-}$ ligand can be excluded because Mn(1) and Mn(2) are asymmetrically linked to the central Mn(4) and Mn(4′) ions, breaking the possible spin frustration. In fact, due to the fact that the oxo group O(21) lies on the JT

Table 6. Exchange interaction constants and ground state spin for the previous magnetochemically characterised, discrete $[Mn_4^{III}(\mu_3\text{-}O)_2]^{8+}$ complexes; bpy = 2,2′-bipyridine; bpya = bis(2-pyridyl)amine; dbm = the anion of dibenzoylmethane; pic = the picolinate anion; py = pyridine

Complex[a]	J_{wb} (cm^{-1})	J_{bb} (cm^{-1})	J_{bb}/J_{wb}	(S, S_{bb}, S_{ww})	Ref.
$[Mn_4O_2(O_2CMe)_7(bpy)_2]^+$	−7.8	−23.5	3.0	(3, 1, 4)	[22]
$[Mn_4O_2(O_2CMe)_7(pic)_2]^-$	−5.3	−24.6	4.6	(3, 1, 4)	[42a]
$[Mn_4O_2(O_2CMe)_6(py)_2(dbm)_2]$	−5.0	−24.9	5.0	(3, 1, 4)	[42b]
$[Mn_4O_2(O_2CEt)_7(bpya)_2]^+$	−3.3	−25.7	7.8	(0, 0, 0)	[42c]
$[Mn_4O_2(O_2CPh)_6(dpm)_2]$	−0.4	−27.5	68.8	(n, 0, n)	[42d]

[a] Counterions and solvate molecules omitted.

 © 2004 Wiley-VCH Verlag GmbH & Co. KGaA, Weinheim

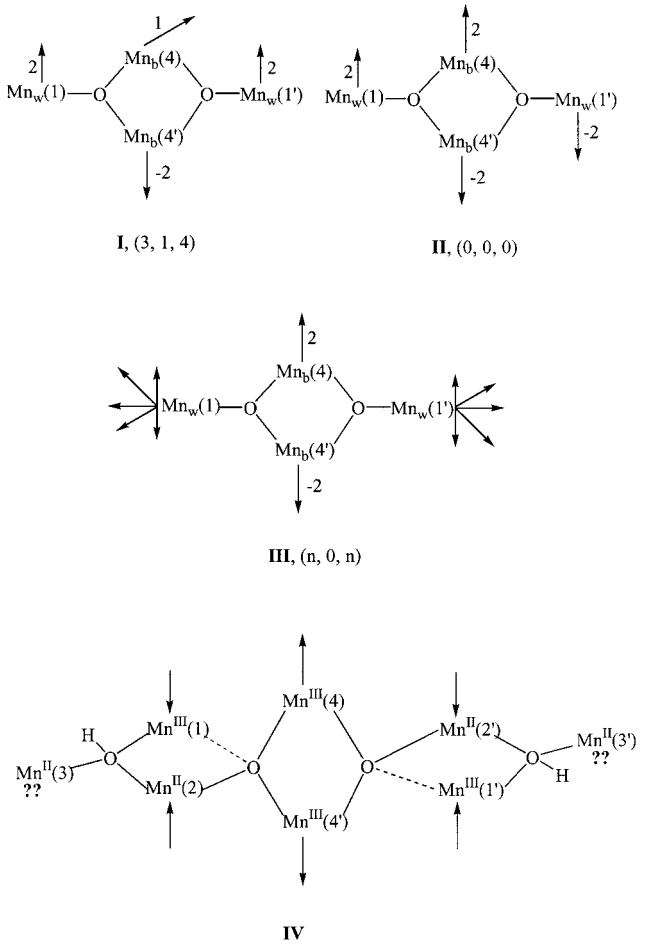

Figure 9. The spin ground states established for *discrete* tetranuclear manganese(III) clusters containing the butterfly-like $[Mn_4^{III}(\mu_3\text{-}O)_2]^{8+}$ core (**I**, **II**, **III**) and a tentative coupling scheme for complex **2** (**IV**); the numbering scheme (in parentheses) for the Mn^{III} ions in the tetranuclear complexes is the same as that used for the central, Mn^{III}-containing subunit of complex **2** (see Figure 5), while the subscripts b and w denote body and wing-tip Mn^{III} ions, respectively; in **IV** the oxidation states of the Mn atoms are also denoted by superscripts

elongation axis of Mn(1), the interaction of Mn(1) with Mn(4′) should be very weak and clearly weaker than the interaction between Mn(1) and Mn(4) through the oximato/carboxylate bridges; an antiparallel alignment of the Mn(1) spin vector with respect to Mn(4) should be expected. Mn(2) is also asymmetrically linked to Mn(4) and Mn(4′) [for example, the Mn(2)−O(21)−Mn(4) bond angle is 118.8°, whereas the Mn(2)−O(21)−Mn(4′) one is 99.2°] and therefore different antiferromagnetic coupling with each of these Mn^{III} centres should be expected. These latter competitive interactions, combined with the antiferromagnetic coupling expected through the double oxo-hydroxo bridge within the Mn(2)···Mn(1) pair, make an antiparallel alignment of the Mn(2) spin vector with respect to Mn(1) reasonable. At this point, a reasonable coupling scheme for **2** can be as shown in **IV** of Figure 9, on the basis of the strong antiferromagnetic coupling within the Mn(4)···Mn(4′) pair (Table 6) and the expected antiferromagnetic interactions. The alignment of the Mn(3) spin vector, mainly determined by its interactions with Mn(1) and Mn(2) through the hydroxo oxygen [O(22), triangular arrangement], is not clear; however, for symmetry reasons, the orientation for Mn(3) and Mn(3′) should be related by the inversion centre of the molecule, resulting in an $S = 0$ ground state.

In summary, it is tempting to assume that the $S = 0$ ground state observed for **2** arises mainly from the reasonable antiferromagnetic interaction between Mn(1) and Mn(2) [and their symmetry-related partners], assuming a strongly coupled, diamagnetic ($S_{bb} = 0$) [Mn(4)Mn(4′)-O(21)O(21′)]$^{2+}$ central subunit and excluding the possibility of spin frustration due to the asymmetry of the interactions. We would like to emphasise that this discussion is only intended to qualitatively show a possible origin of the $S = 0$ ground state observed for complex **2**.

The $S = 0$ ground state is not uncommon in octanuclear Mn clusters and has been established in $[Mn_8O_2(O_2CEt)_8(py)_4(L)_2]^{2+}$,[6a] $[Mn_8O_2(O_2CCH_2But)_{14}(t\text{BuCH}_2CO_2H)_4]$[25] and $[Mn_8O_{10}(O_2CMe)_6(bpy)_2(H_2O)_2]^{4+}$.[28]

Complex 3

The variable-temperature magnetic-susceptibility data for compound **3** also reveal an overall antiferromagnetic behaviour. The $\chi_M T$ vs. T plot is shown in Figure 10. The value of $\chi_M T$ decreases from 12.1 $cm^3 \cdot mol^{-1} \cdot K$ at room temperature to 4.6 $cm^3 \cdot mol^{-1} \cdot K$ at 6.0 K. The room-temperature $\chi_M T$ value is slightly lower than the expected value $\chi_M T = (N\beta^2/3k)3g_i^2S_i(S_i + 1) = 13.125$ $cm^3 \cdot mol^{-1} \cdot K$ for three uncoupled Mn^{II} ions with $S_i = 5/2$ and $g_i = 2$ each. This value is already indicative of substantial antiferromagnetic coupling. The antiferromagnetic behaviour is further confirmed by the dramatic decrease of $\chi_M T$ when T decreases. At low temperature, the value of $\chi_M T$ almost corresponds to the expected value $\chi_M T = (N\beta^2/3k)g_i^2S(S + 1) = 4.375$ $cm^3 \cdot mol^{-1} \cdot K$ for an $S = 5/2$ spin state with $g = 2$.

Taking into account the molecular structure of **3**, the Kambe vector-coupling scheme shown in Figure 11 was considered. The spin Hamiltonian that describes the low-lying electronic states is given by Equation (4), where S_i is

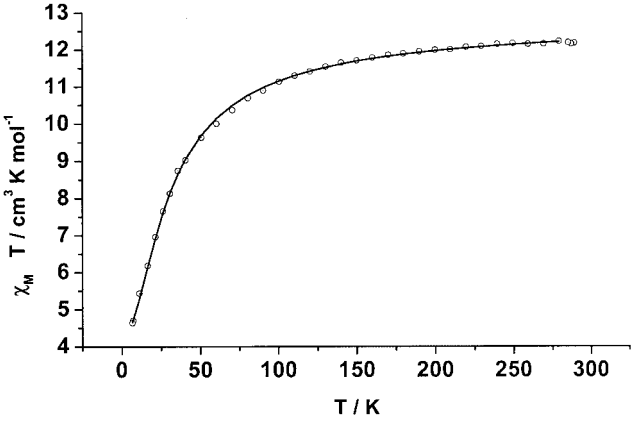

Figure 10. $\chi_M T$ vs. T plot for complex **3**; the solid line is the best theoretical fit to the data (see text for details)

 © 2004 Wiley-VCH Verlag GmbH & Co. KGaA, Weinheim

the spin of the Mn^{II} ion with number i (Figure 11) and $J_{12} = J_{21'} = J$.

$$H_s = -J(S_1S_2 + S_2S_{1'}) - J_{11'}S_1S_{1'} \quad (4)$$

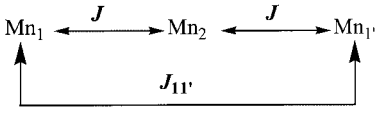

Figure 11. The Kambe vector-coupling scheme used for the interpretation of the magnetic behaviour of complex **3**

The experimental data were fitted with the susceptibility expression derived from the Van Vleck formula for three $S = 5/2$ spins. The best fit was obtained for $J = -2.74$ cm^{-1}, $J_{11'} = 0.7$ cm^{-1} and $g = 1.99$. The agreement between this calculation and experimental data is excellent, as can be judged from Figure 10. The agreement factor, defined as $R = \Sigma(\chi_M^{calcd.} - \chi_M^{exp})^2/\Sigma(\chi_M^{exp})^2$ is 4×10^{-4}. The J value obtained leads to a total-spin ground state of $S = 5/2$. The system can be reasonably fitted with only one J value ($J_{11'} = 0$) but this gives a worse agreement with experimental data. We refrain from analyzing further the magnetic properties of **3**, since detailed studies are available[32a,32b,35] for trinuclear Mn^{II} carboxylate complexes with similar structures.

The J value of **3** is well within the reported range (-5.6 to -1.9) reported for other trinuclear manganese(II) complexes containing the $[Mn_3(\eta^1{:}\eta^1{:}\mu_2\text{-}O_2CR)_4(\eta^1{:}\eta^2{:}\mu_2\text{-}O_2CR)_2]^0$ core[32] (see also Table 5). This indicates that weak antiferromagnetic coupling is mediated by the bridging carboxylate groups, which is as expected, since the Mn−O distances are relatively long in such compounds.[32] J values reported in the manganese(II) literature with *only* carboxylate groups as bridging ligands are always small and negative, between approximately -0.2 and -5 cm^{-1},[13] indicating weak antiferromagnetic coupling.

Electrochemistry of Complex 2

Complex **2** was investigated by cyclic voltammetry (CV), in CH_2Cl_2, and the corresponding voltammogram is shown in Figure 12. It should be stressed at this point that there is no actual proof that complex **2** retains its structure in solution. However, the non-coordinating nature of CH_2Cl_2 and the fact that solutions of **2** in CH_2Cl_2 are non-conducting both provide strong evidence that the structure of the complex is retained in solution. The cyclic voltammogram shows only broad, irreversible features — two oxidations at about 1.24 and 0.57 V, and three reductions at -0.69, 0.06, and 0.98 V, vs. a calomel electrode (4 M KCl). Since complex **2** is valence-trapped, probably owing to the increase in the barrier to intramolecular electron transfer resulting from the JT distortion of Mn^{III},[18a] it is likely that the reduction and oxidation of **2** will be centred at particular Mn ions. It is relatively rare for high-nuclearity $Mn/O/RCO_2^-$ aggregates to exhibit reversible redox processes, and thus the observed behaviour is typical of polynuclear Mn carboxylate complexes.[18a]

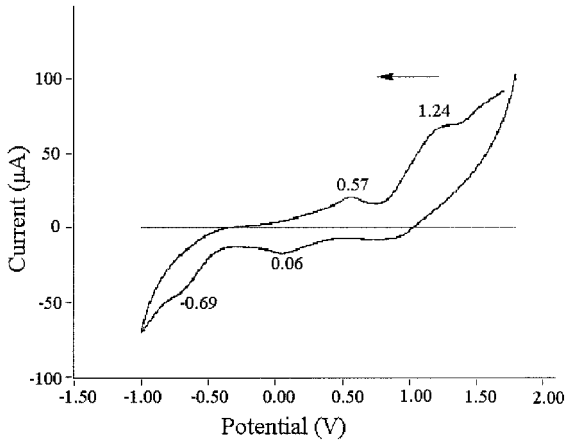

Figure 12. Cyclic voltammogram of complex **2** in CH_2Cl_2; scan rate: 100 mV s^{-1}; the potentials are given vs. a calomel electrode (4 M KCl)

Conclusions and Perspectives

The first use of (ph)(2-py)CNOH in Mn carboxylate chemistry has provided access to new complexes, one mononuclear (**1**) containing Mn^{II}, and the other octanuclear (**2**) with an unprecedented $[Mn_4^{II}Mn_4^{III}(\mu_4\text{-}O)_2(\mu_3\text{-}OH)_2]^{14+}$ core. In the former case, the ligand is neutral and chelates through its nitrogen atoms; in the latter case, the ligand is monoanionic chelating and bridging $Mn^{II}Mn^{III}$ or Mn_2^{III} pairs (Figure 4). Although the octanuclear cluster has been found to possess an $S = 0$ ground state, the bridging mode of (ph)(2-py)CNO^- nevertheless suggests possibilities for other Mn_x species that might exist (e.g. clusters containing the strongly coordinating inorganic anions NO_3^-, N_3^- and SO_4^{2-}) and which may have high-spin ground states. In addition, it provides encouragement for believing that a variety of carboxylate and non-carboxylate M_x^{II} and M_x^{III} clusters (M^{II} = Co^{II}, Ni^{II}; M^{III} = Cr^{III}, Fe^{III}) should also be accessible with this anionic ligand, leading to species with new topologies and exciting magnetic properties. Results with $Co^{II,II/III}$ and Ni^{II} at the time of writing reveal that the nature of (ph)(2-py)CNO^- makes it a versatile ligand for a variety of objectives/advantages, including μ_2 and μ_3 behaviour, high-nuclearity cluster formation, linking of clusters into polymeric arrays, 3d-4f mixed-metal chemistry and ferromagnetic exchange interactions. Clearly, the use of other pyridyl- or polypyridyl oximes offers a potential route to other new polynuclear metal complexes, and such studies are currently under progress.

Analogues of compound **2** with acetates or substituted benzoates are not known, at least to date, and it is currently not evident whether the preparation and the stability of this Mn_8 species are dependent on the particular nature of the $PhCO_2^-$ ligand.

 © 2004 Wiley-VCH Verlag GmbH & Co. KGaA, Weinheim

Complex **3** is a new addition to the growing family of trinuclear complexes with the $[M_3(\eta^1{:}\eta^1{:}\mu_2\text{-}O_2CR)_4(\eta^1{:}\eta^2{:}\mu_2\text{-}O_2CR)_2]^0$ core (M = Mn, Fe, Co), providing a useful new datum point for the ongoing objective of fully understanding the ground-state spin value of transition metal carboxylate clusters as a function of metal, oxidation state and topology of the polynuclear metal core. The structural motif of the linear trinuclear $[M_3(O_2CR)_6]^0$ unit turns out to be as important as that of the triangular basic carboxylate motif, which is characteristic of the trivalent and mixed-valent $M^{II}M_2^{III}$ analogues. Clearly, the inability of phenyl 2-pyridyl ketone, (ph)(2-py)CO, to give the *gem*-diol form [(ph)(2-py)C(OH)$_2$] in solution in the presence of metal ions, restricts its utility to the synthesis of polynuclear metal complexes, in contrast with its bis(2-pyridyl) analogue, (2-py)$_2$CO.

Experimental Section

Materials and Physical Measurements: All manipulations were performed using materials (Merck, Aldrich) as received. Compounds $Mn(O_2CPh)_2{\cdot}2H_2O$,[15] N*n*Bu$_4$MnO$_4$ [14] and (N*n*Bu$_4$)[Mn$_4$O$_2$(O$_2$CPh)$_9$(H$_2$O)][15] were synthesised according to published methods. Elemental analysis (C, H, N) were performed by the University of Ioannina (Greece) Microanalytical Laboratory using an EA 108 Carlo Erba analyzer. IR spectra (4400−450 cm^{-1}) were recorded from KBr pellets on a Perkin−Elmer PC 16 FT-IR spectrometer. Magnetic susceptibility measurements in the range of 2−300 K and magnetisation measurements (2−4 K) in the field range of 0.1−5 T for complex **2** were performed with a Quantum Design SQUID magnetometer at the Magnetochemistry Service of the University of Barcelona. Magnetic susceptibility measurements for complex **3** were performed with a DSM8 pendulum-type susceptometer operating in the range 6−300 K at magnetic fields of approximately 1 T. All measurements were performed on polycrystalline samples. Data were corrected for diamagnetic contributions calculated from Pascal constants. The cyclic voltammogram of complex **2** was recorded on a AFCBP1 Biopotentiostat and a standard three-electrode assembly (glassy carbon working, platinum wire auxiliary, SCE reference) with 0.1 M N*n*Bu$_4$PF$_6$ in distilled CH$_2$Cl$_2$ as supporting electrolyte.

$[Mn(O_2CPh)_2\{(ph)(2\text{-}py)CNOH\}_2]{\cdot}1.2H_2O$ (1·1.2H$_2$O) and $[Mn_8O_2(OH)_2(O_2CPh)_{10}\{(ph)(2\text{-}py)CNO\}_4]{\cdot}4CH_2Cl_2$ (2·4CH$_2$Cl$_2$) as a Mixture: Treatment of a stirred, colourless solution of $Mn(O_2CPh)_2{\cdot}2H_2O$ (0.166 g, 0.50 mmol) in EtOH/MeCN (15 mL, 2:1 v/v) with solid (ph)(2-py)CNOH (0.099 g, 0.50 mmol) resulted in a pale-orange solution, which, upon slow evaporation at room temperature, turned brown due to slow oxidation of Mn^{II} under aerobic conditions. The resulting solution was evaporated to dryness under reduced pressure and the residue redissolved in CH$_2$Cl$_2$ (25 mL) to give a red-brown solution. This was layered with a mixture (50 mL, 1:1 v/v) of Et$_2$O and *n*-hexane. After several days yellow and dark-brown crystals were formed; they were carefully collected by filtration. The two products were readily separable manually, and the yellow and dark brown crystals proved by single-crystal crystallography to be complexes **1**·1.2H$_2$O and **2**·4CH$_2$Cl$_2$, respectively.

$[Mn(O_2CPh)_2\{(ph)(2\text{-}py)CNOH\}_2]{\cdot}1.2H_2O$ (1·1.2H$_2$O): A colourless solution of $Mn(O_2CPh)_2{\cdot}2H_2O$ (0.166 g, 0.50 mmol) in EtOH (10 mL) was treated with solid (ph)(2-py)CNOH (0.297 g, 1.50 mmol). The solid soon dissolved. The resulting yellow solution was stirred for about 10 min and was then allowed to stand undisturbed at 5 °C for several days. Well-formed yellow crystals appeared, which were collected by filtration, washed with Et$_2$O (2 × 5 mL) and dried in air. Yields (based on Mn^{II}) as high as 0.27 g (75%) were obtained. $C_{38}H_{32.4}MnN_4O_{7.2}$ (715.22): calcd. C 63.8, H 4.6, N 7.8; found C 64.1, H 4.6, N 7.7. Main IR data (KBr pellet): $\tilde{\nu}$ = 3434 (m, broad), 2924 (w), 1594 (m), 1538 (s), 1468 (w), 1436 (w), 1402 (s), 1332 (w), 1256 (w), 1190 (w), 1062 (m), 1026 (m), 965 (w), 834 (w), 792 (w), 776 (w), 722 (m), 706 (m), 674 (m), 636 (w), 500 (w) cm^{-1}.

$[Mn_8O_2(OH)_2(O_2CPh)_{10}\{(ph)(2\text{-}py)CNO\}_4]{\cdot}4CH_2Cl_2$ (2·4CH$_2$Cl$_2$). ***Method A*:** Treatment of a stirred, colourless solution of $Mn(O_2CPh)_2{\cdot}2H_2O$ (0.166 g, 0.50 mmol) in EtOH/MeCN (15 mL, 2:1 v/v) with N*n*Bu$_4$MnO$_4$ (0.060 g, 0.16 mmol) resulted in a dark-brown solution. Solid (ph)(2-py)CNOH (0.099 g, 0.50 mmol) was slowly added to this mixture, and it soon dissolved to give a solution of essentially the same colour. The solvents were then evaporated under reduced pressure. The obtained residue was dissolved in CH$_2$Cl$_2$ (25 mL), filtered, and the filtrate layered with a mixture of Et$_2$O and n-hexane (50 mL, 1:1 v/v); slow mixing gave dark-brown crystals of the product, which were collected by filtration, washed with cold CH$_2$Cl$_2$ (2 mL) and Et$_2$O (2 × 5 mL), and dried in vacuo over silica gel. Yield (based on the oxime): 0.17 g (55%). The dried solid analysed as CH$_2$Cl$_2$-free **2**. $C_{118}H_{88}Mn_8N_8O_{28}$ (2505.66): calcd. C 56.6, H 3.6, N 4.5; found C 57.0, H 3.5, N 4.6. The crystals of **2**·4CH$_2$Cl$_2$ were found to lose solvent readily, and they were kept in the mother liquor until a suitable crystal had been found for X-ray crystallography. Main IR data (KBr pellet): $\tilde{\nu}$ = 3438 (m, broad), 3060 (w), 1596 (s), 1552 (s), 1490 (m), 1468 (m), 1444 (m), 1404 (s), 1200 (w), 1174 (w), 1110 (w), 1094 (m), 1070 (s), 1026 (m), 978 (w), 818 (w), 788 (m), 744 (w), 716 (s), 676 (s), 638 (w), 606 (m), 552 (w) cm^{-1}.

***Method B*:** Treatment of a stirred, brown solution of (N*n*Bu$_4$)[Mn$_4$O$_2$(O$_2$CPh)$_9$(H$_2$O)] (0.110 g, 0.07 mmol) in CH$_2$Cl$_2$ (20 mL) with solid (ph)(2-py)CNOH (0.060 g, 0.03 mmol) gave a solution of essentially the same colour. The solution was stirred vigorously for about 45 min, and layered with a mixture of Et$_2$O and *n*-hexane (40 mL, 2:1 v/v) to give X-ray quality, dark-brown crystals of **2**·4CH$_2$Cl$_2$. The crystals were collected by filtration, washed with Et$_2$O (2 × 5 mL) and dried in vacuo over silica gel. The dried solid analysed satisfactorily as **2**. The identity of the product was confirmed by IR spectroscopic comparison with the authentic sample prepared according to Method A.

$[Mn_3(O_2CPh)_6\{(ph)(2\text{-}py)CO\}_2]$ (3): A colourless solution of (ph)(2-py)CO (0.090 g, 0.50 mmol) in MeOH (15 mL) was added to a colourless solution of $Mn(O_2CPh)_2{\cdot}2H_2O$ (0.166 g, 0.50 mmol) in the same solvent (15 mL). The resulting yellow solution was stirred for 1 h. Slow evaporation of this solution at room temperature gave large yellow needles suitable for crystallography. When precipitation was judged complete, the crystals were collected by filtration, washed with Et$_2$O and dried in air. Yields (based on Mn^{II}) as high as 0.18 g (85%) were obtained. $C_{66}H_{48}Mn_3N_2O_{14}$ (1257.88): calcd. C 63.0, H 3.9, N 2.2; found C 62.7, H 3.8, N 2.2. Main IR data (KBr pellet): $\tilde{\nu}$ = 3058 (w), 1648 (m), 1606 (s), 1566 (s), 1536 (s), 1448 (w), 1400 (s), 1316 (m), 1250 (m), 1170 (m, broad), 1068 (w), 1016 (m), 952 (m), 936 (w), 858 (w), 822 (w), 768 (w), 748 (sh), 718 (s), 700 (m), 674 (m), 656 (w), 572 (wb) cm^{-1}.

X-ray Crystallographic Studies: Crystals of **1**·1.2H$_2$O and **3** were mounted in air and covered with epoxy glue, while a crystal of **2**·4CH$_2$Cl$_2$ was mounted in a capillary filled with drops of mother liquor. Diffraction measurements for **1**·1.2H$_2$O and **3** were made

 © 2004 Wiley-VCH Verlag GmbH & Co. KGaA, Weinheim

Table 7. Crystal data and structure refinement for $[Mn^{II}(O_2CPh)_2\{(ph)(2\text{-}py)CNOH\}_2]\cdot 1.2H_2O$ (**1**·1.2H_2O), $[Mn_8O_2(OH)_2(O_2CPh)_{10}\{(ph)(2\text{-}py)CNO\}_4]\cdot 4CH_2Cl_2$ (**2**·4CH_2Cl_2) and $[Mn_3(O_2CPh)_6\{(ph)(2\text{-}py)CO\}_2]$ (**3**)

	1·1.2H_2O	**2**·4CH_2Cl_2	**3**
Empirical formula	$C_{38}H_{32.4}MnN_4O_{7.2}$	$C_{122}H_{96}Cl_8Mn_8N_8O_{28}$	$C_{66}H_{48}Mn_3N_2O_{14}$
Mol. mass	715.22	2845.19	1257.88
Colour and habit	yellow prisms	brown prisms	yellow needles
Crystal size (mm)	0.50 × 0.30 × 0.10	0.06 × 0.12 × 0.50	0.10 × 0.25 × 0.55
Crystal system	monoclinic	monoclinic	monoclinic
Space group	*I*2/*a*	*C*2/*c*	$P2_1/a$
a (Å)	34.73(2)	32.898(8)	15.74(1)
b (Å)	10.645(5)	16.543(4)	17.29(1)
c (Å)	22.834(9)	33.206(8)	11.095(6)
α (°)	90	90	90
β (°)	107.78(2)	136.09(1)	101.75(2)
γ (°)	90	90	90
V (Å^3)	8039(6)	12530(5)	2956(3)
Z	8	4	2
ρ (Mg·m^{-3})	1.182	1.508	1.413
T (°C)	25	25	25
λ (Mo-K_α) (Å)	0.71073		0.71073
λ (Cu-K_α) (Å)		1.54180	
μ (mm^{-1})	0.377	8.544	0.700
F(000)	2968	5776	1290
$2\theta_{max}$ (°)	43	103	47
Index ranges (°)	$-35 \le h \le 34$	$0 \le h \le 33$	$-17 \le h \le 17$
	$0 \le k \le 10$	$0 \le k \le 16$	$0 \le k \le 19$
	$0 \le l \le 23$	$-33 \le l \le 23$	$0 \le l \le 12$
No. of reflections collected	4687	6602	4645
No. of indep. refls./R_{int}	4538/0.0140	6462/0.0220	4391/0.0288
Data with $I > 2\sigma(I)$	3303	4495	3132
Parameters refined	467	797	390
$[\Delta/\sigma]_{max}$	0.002	0.001	0.001
GOF (on F^2)	1.037	1.055	1.080
*R*1[a]	0.0550	0.0650	0.0508
*wR*2[b]	0.1534	0.1643	0.1242
Residuals [e·Å^{-3}]	0.405/-0.270	0.646/-0.603	0.553/-0.269

[a] $R1 = \Sigma(||F_o| - |F_c||)/\Sigma(|F_o|)$. [b] $wR2 = \{\Sigma[w(F_o^2 - F_c^2)^2]/\Sigma[w(F_o^2)^2]\}^{1/2}$.

on a Crystal Logic Dual Goniometer diffractometer using graphite-monochromated Mo-K_a radiation. The X-ray data set for **2**·4CH_2Cl_2 was collected on a $P2_1$ Nicolet diffractometer upgraded by Crystal Logic using graphite monochromated Cu-K_a radiation. Complete crystal data and parameters for data collection and refinement are listed in Table 7. Unit-cell dimensions were determined and refined by using the angular settings of 25 automatically centred reflections in the ranges $11 < 2\theta < 23°$ (for **1**·1.2H_2O and **3**) and $22 < 2\theta < 54°$ (for **2**·4CH_2Cl_2). Intensity data were recorded using the θ-2θ scan method. Three standard reflections monitored every 97 reflections showed less than 3% variation and no decay. Lorentz, polarisation and Ψ-scan absorption corrections were applied using the Crystal Logic software package.

The structures were solved by direct methods using SHELXS-86[43a] and refined by full-matrix least-squares techniques on F^2 with SHELXL-93.[43b] For all three structures, all hydrogen atoms [except those of O(1) and O(11) for **1**·1.2H_2O and the μ_3-OH^- hydrogen for **2**·4CH_2Cl_2 which were located by difference maps and refined isotropically] were introduced at calculated positions as riding on their parent atoms. All non-hydrogen coordinated atoms of **1**·1.2H_2O were refined anisotropically. The solvate oxygen atoms were refined isotropically. Two of them were refined with occupation factors of a total sum one; the third one, sitting on an inversion centre of symmetry, was refined with a freely refined occupation factor of about 0.20. All non-hydrogen atoms of **2**·4CH_2Cl_2 and **3** were refined anisotropically.

CCDC-227429 (**1**·1.2H_2O), -195209 (**2**·4CH_2Cl_2) and -227430 (**3**) contain the supplementary crystallographic data for this paper. These data can be obtained free of charge at www.ccdc.cam.ac.uk/conts/retrieving.hmtl [or from the Cambridge Crystallographic Data Centre, 12 Union Road, Cambridge CB2 1EZ, UK; Fax: +44 1223 336033; E-mail: deposit@ccdc.cam.ac.uk].

Acknowledgments

This work was supported by the Spanish Ministerio de Ciencia y Tecnología, BQU2003/0538 project. P. K. would like to thank the Specific Account of the University of Athens for financial support (Grant 70/4/5728).

[1] [1a] T. G. Carrell, A. M. Tyryshkin, G. C. Dismukes, *J. Biol. Inorg. Chem.* **2002**, *7*, 2−22. [1b] V. K. Yachandra, K. Sauer, M. P. Klein, *Chem. Rev.* **1996**, *96*, 2927−2950.

[2] A. Zouni, H.- T. Witt, J. Kern, P. Fromme, N. Krauss, W. Sanger, P. Orth, *Nature* **2001**, *409*, 739−743.

[3] [3a] S. Wang, M. S. Wemple, J. Yoo, K. Folting, J. C. Huffman, K. S. Hagen, D. N. Hendrickson, G. Christou, *Inorg. Chem.* **2000**, *39*, 1501−1513, and references cited therein. [3b] T. Afrati, C. Dendrinou-Samara, C. P. Raptopoulou, A. Terzis, V. Tangoulis, D. Kessissoglou, *Angew. Chem. Int. Ed.* **2002**, *41*, 2148−2150, and references cited therein.

 © 2004 Wiley-VCH Verlag GmbH & Co. KGaA, Weinheim

[4] [4a] D. Gatteschi, R. Sessoli, *Angew. Chem. Int. Ed.* **2003**, *42*, 268−297. [4b] G. Christou, D. Gatteschi, D. N. Hendrickson, R. Sessoli, *MRS Bull.* **2000**, *25*, 66−71.
[5] [5a] R. Sessoli, D. Gatteschi, A. Caneschi, M. A. Novak, *Nature* **1993**, *365*, 141−143. [5b] R. Sessoli, H.-L. Tsai, A. R. Schake, S. Wang, J. B. Vincent, K. Folting, D. Gatteschi, G. Christou, D. N. Hendrickson, *J. Am. Chem. Soc.* **1993**, *115*, 1804−1816.
[6] [6a] C. Boskovic, W. Wernsdorfer, K. Folting, J. C. Huffman, D. N. Hendrickson, G. Christou, *Inorg. Chem.* **2002**, *41*, 5107−5118, and references cited therein. [6b] E. K. Brechin, M. Soler, J. Davidson, D. N. Hendrickson, S. Parsons, G. Christou, *Chem. Commun.* **2002**, 2252−2253. [6c] E. K. Brechin, C. Boskovic, W. Wernsdorfer, J. Yoo, A. Yamaguchi, E. C. Sanudo, T. R. Concolino, A. L. Rheingold, H. Ishimoto, D. N. Hendrickson, G. Christou, *J. Am. Chem. Soc.* **2002**, *124*, 9710−9711. [6d] C. J. Milios, C. P. Raptopoulou, A. Terzis, F. Lloret, R. Vicente, S. P. Perlepes, A. Escuer, *Angew. Chem. Int. Ed.* **2004**, *43*, 210−212.
[7] C. Boskovic, E. K. Brechin, W. E. Streib, K. Folting, J. C. Bollinger, D. N. Hendrickson, G. Christou, *J. Am. Chem. Soc.* **2002**, *124*, 3725−3736.
[8] G. S. Papaefstathiou, S. P. Perlepes, *Comments Inorg. Chem.* **2002**, *23*, 249−274.
[9] [9a] V. Tangoulis, C. P. Raptopoulou, A. Terzis, S. Paschalidou, S. P. Perlepes, E. G. Bakalbassis, *Inorg. Chem.* **1997**, *36*, 3996−4006. [9b] V. Tangoulis, C. P. Raptopoulou, S. Paschalidou, E. G. Bakalbassis, S. P. Perlepes, A. Terzis, *Angew. Chem. Int. Ed. Engl.* **1997**, *36*, 1083−1085. [9c] A. Tsohos, S. Dionyssopoulou, C. P. Raptopoulou, A. Terzis, E. G. Bakalbassis, S. P. Perlepes, *Angew. Chem. Int. Ed.* **1999**, *38*, 983−985. [9d] G. S. Papaefstathiou, S. P. Perlepes, A. Escuer, R. Vicente, M. Font-Bardia, X. Solans, *Angew. Chem. Int. Ed.* **2001**, *40*, 884−886. [9e] G. S. Papaefstathiou, A. Escuer, R. Vicente, M. Font-Bardia, X. Solans, S. P. Perlepes, *Chem. Commun.* **2001**, 2414−2415. [9f] G. S. Papaefstathiou, A. Escuer, C. P. Raptopoulou, A. Terzis, S. P. Perlepes, R. Vicente, *Eur. J. Inorg. Chem.* **2001**, 1567−1574. [9g] N. Lalioti, C. P. Raptopoulou, A. Terzis, A. E. Aliev, I. P. Gerothanassis, E. Manessi-Zoupa, S. P. Perlepes, *Angew. Chem. Int. Ed.* **2001**, *40*, 3211−3214. [9h] G. S. Papaefstathiou, A. Escuer, M. Font-Bardia, S. P. Perlepes, X. Solans, R. Vicente, *Polyhedron* **2002**, *21*, 2027−2032. [9i] A. K. Boudalis, F. Dahan, A. Bousseksou, J.-P. Tuchagues, S. P. Perlepes, *Dalton Trans.* **2003**, 3411−3418. [9j] A. K. Boudalis, B. Donnadieu, V. Nastopoulos, J. M. Clemente-Juan, A. Mari, Y. Sanakis, J.-P. Tuchagues, S. P. Perlepes, *Angew. Chem. Int. Ed.* **2004**, *43*, 2266−2270.
[10] C. J. Milios, E. Kefalloniti, C. P. Raptopoulou, A. Terzis, R. Vicente, N. Lalioti, A. Escuer, S. P. Perlepes, *Chem. Commun.* **2003**, 819−820.
[11] C. J. Milios, C. P. Raptopoulou, A. Terzis, R. Vicente, A. Escuer, S. P. Perlepes, *Inorg. Chem. Commun.* **2003**, *6*, 1056−1060.
[12] [12a] Y. Yu. Kukushkin, A. J. L. Pombeiro, *Coord. Chem. Rev.* **1999**, *181*, 147−175. [12b] P. Chaudhuri, *Coord. Chem. Rev.* **2003**, *243*, 143−190.
[13] C. J. Milios, E. Kefalloniti, C. P. Raptopoulou, A. Terzis, A. Escuer, R. Vicente, S. P. Perlepes, *Polyhedron* **2004**, *23*, 83−95, and references cited therein.
[14] J. B. Vincent, K. Folting, J. C. Huffman, G. Christou, *Inorg. Chem.* **1986**, *25*, 996−999.
[15] M. W. Wemple, H.-L. Tsai, S. Wang, J. P. Claude, W. E. Streib, J. C. Huffman, D. N. Hendrickson, G. Christou, *Inorg. Chem.* **1996**, *35*, 6437−6449.
[16] N. C. Harden, M. A. Bolcar, W. Wernsdorfer, K. A. Abboud, W. E. Streib, G. Christou, *Inorg. Chem.* **2003**, *42*, 7067−7076.
[17] [17a] M. A. Halcrow, W. E. Streib, K. Folting, G. Christou, *Acta Crystallogr., Sect. C* **1995**, *51*, 1263−1267. [17b] A. G. Blackman, J. C. Huffman, E. B. Lobkovsky, G. Christou, *Polyhedron* **1992**, *11*, 251−255. [17c] A. R. Schake, J. B. Vincent, Q. Li, P. D. W. Boyd, K. Folting, J. C. Huffman, D. N. Hendrickson, G. Christou, *Inorg. Chem.* **1989**, *28*, 1915−1923.
[18] [18a] H.-L. Tsai, S. Wang, K. Folting, W. E. Streib, D. N. Hendrickson, G. Christou, *J. Am. Chem. Soc.* **1995**, *117*, 2503−2514. [18b] R. C. Squire, S. M. J. Aubin, K. Folting, W. E. Streib, G. Christou, D. N. Hendrickson, *Inorg. Chem.* **1995**, *34*, 6463−6471.
[19] J. B. Vincent, H.-R. Chang, K. Folting, J. C. Huffman, G. Christou, D. N. Hendrickson, *J. Am. Chem. Soc.* **1987**, *109*, 5703−5711.
[20] H. H. Thorpe, *Inorg. Chem.* **1992**, *31*, 1585−1588.
[21] H. J. Eppley, S. M. J. Aubin, W. E. Streib, J. C. Bollinger, D. N. Hendrickson, G. Christou, *Inorg. Chem.* **1997**, *36*, 109−115.
[22] J. B. Vincent, C. Christmas, H.-R. Chang, Q. Li, P. D. W. Boyd, J. C. Huffman, D. N. Hendrickson, G. Christou, *J. Am. Chem. Soc.* **1989**, *111*, 2086−2097.
[23] B. Albela, M. S. El Fallah, J. Ribas, K. Folting, G. Christou, D. N. Hendrickson, *Inorg. Chem.* **2001**, *40*, 1037−1044.
[24] For example, see: [24a] R. W. Saalfrank, N. Löw, B. Demleitner, D. Stalke, M. Teichert, *Chem. Eur. J.* **1998**, *4*, 1305−1311. [24b] R. W. Saalfrank, N. Löw, S. Trummer, G. M. Sheldrick, M. Teichert, D. Stalke, *Eur. J. Inorg. Chem.* **1998**, 559−563.
[25] C. Boskovic, J. C. Huffman, G. Christou, *Chem. Commun.* **2002**, 2502−2503.
[26] E. K. Brechin, G. Christou, M. Soler, M. Helliwell, S. J. Teat, *Dalton Trans.* **2003**, 513−514.
[27] [27a] E. Libby, K. Folting, C. J. Huffman, J. C. Huffman, G. Christou, *Inorg. Chem.* **1993**, *32*, 2549−2556. [27b] E. K. Brechin, M. Soler, G. Christou, M. Helliwell, S. J. Teat, W. Wernsdorfer, *Chem. Commun.* **2003**, 1276−1277. [27c] S. Wang, H.-L. Tsai, K. Folting, J. D. Martin, D. N. Hendrickson, G. Christou, *J. Chem. Soc., Chem. Commun.* **1994**, 671−673. [27d] V. A. Grillo, M. J. Knapp, J. C. Bollinger, D. N. Hendrickson, G. Christou, *Angew. Chem. Int. Ed. Engl.* **1996**, *35*, 1818−1820.
[28] A. J. Tasiopoulos, K. A. Abboud, G. Christou, *Chem. Commun.* **2003**, 580−581.
[29] R. E. P. Winpenny, *Adv. Inorg. Chem.* **2001**, *52*, 1−111.
[30] K. S. Hagen, T. D. Westmoreland, M. J. Scott, W. H. Armstrong, *J. Am. Chem. Soc.* **1989**, *111*, 1907−1909.
[31] [31a] M. Soler, E. Rumberger, K. Folting, D. N. Hendrickson, G. Christou, *Polyhedron* **2001**, *20*, 1365−1369. [31b] L. F. Jones, E. K. Brechin, D. Collison, A. Harrison, S. J. Teat, W. Wernsdorfer, *Chem. Commun.* **2002**, 2794−2795.
[32] [32a] V. Tangoulis, D. A. Malamatari, K. Soulti, V. Stergiou, C. P. Raptopoulou, A. Terzis, Th. A. Kabanos, D. P. Kessissoglou, *Inorg. Chem.* **1996**, *35*, 4974−4983. [32b] S. Menage, S. E. Vitols, P. Bergerat, E. Codjovi, O. Kahn, J.-J. Girerd, M. Guillot, X. Solans, T. Calvet, *Inorg. Chem.* **1991**, *30*, 2666−2671. [32c] R. L. Rardin, P. Poganiuch, A. Bino, D. P. Goldberg, W. B. Tolman, S. Li, S. J. Lippard, *J. Am. Chem. Soc.* **1992**, *114*, 5240−5249. [32d] J. B. Vincent, G. Christou, *Adv. Inorg. Chem. Radiochem.* **1989**, *33*, 197−257. [32e] R. A. Reynolds III, W. R. Dunham, D. Coucouvanis, *Inorg. Chem.* **1998**, *37*, 1232−1241. [32f] K. Tsuneyoshi, H. Kobayashi, H. Miyamae, *Acta Crystallogr., Sect. C* **1993**, *49*, 233−236.
[33] For an excellent review on trinuclear Mn complexes, see: D. P. Kessissoglou, *Coord. Chem. Rev.* **1999**, *185−186*, 837−858.
[34] For a review on the "carboxylate shift" mechanism, see: R. L. Rardin, W. B. Tolman, S. J. Lippard, *New J. Chem.* **1991**, *15*, 417−430.
[35] B. Albela, M. Corbella, J. Ribas, I. Castro, J. Sletten, H. Stockli-Evans, *Inorg. Chem.* **1998**, *37*, 788−798.
[36] Z. Sun, P. K. Gantzel, D. N. Hendrickson, *Polyhedron* **1998**, *17*, 1511−1516.
[37] I. Chadjistamatis, A. Terzis, C. P. Raptopoulou, S. P. Perlepes, *Inorg. Chem. Commun.* **2003**, *6*, 1365−1371.
[38] M. Tiliakos, P. Cordopatis, A. Terzis, C. P. Raptopoulou, S. P. Perlepes, E. Manessi-Zoupa, *Polyhedron* **2001**, *20*, 2203−2214.
[39] [39a] G. B. Deacon, R. J. Phillips, *Coord. Chem. Rev.* **1980**, *33*, 227−250. [39b] H. Sakiyama, K. Tokuyama, Y. Matsumura, H. Okawa, *J. Chem. Soc., Dalton Trans.* **1993**, 2329−2334.

 © 2004 Wiley-VCH Verlag GmbH & Co. KGaA, Weinheim

[40] R. D. Cannon, R. P. White, *Prog. Inorg. Chem.* **1988**, *36*, 195−298.
[41] K. Kambe, *J. Phys. Soc. Jpn.* **1950**, *48*, 15.
[42] [42a] E. Libby, J. K. McCusker, E. A. Schmitt, K. Folting, D. N. Hendrickson, G. Christou, *Inorg. Chem.* **1991**, *30*, 3486−3495. [42b] S. Wang, K. Folting, W. E. Streib, E. A. Schmitt, J. K. McCusker, D. N. Hendrickson, G. Christou, *Angew. Chem. Int. Ed. Engl.* **1991**, *30*, 305−306. [42c] G. Aromi, S. Bhaduri, P. Artus, J. C. Huffman, D. N. Hendrickson, G. Christou, *Polyhedron* **2002**, *21*, 1779−1786. [42d] C. Cañada-Vilalta, J. C. Huffman, G. Christou, *Polyhedron* **2001**, *20*, 1785−1793.
[43] [43a] G. M. Sheldrick, *SHELXS-86*, Program for the Solution of Crystal Structures, University of Göttingen, Germany, **1986**. [43b] G. M. Sheldrick, *SHELXL-93*, Program for the Refinement of Crystal Structures, University of Göttingen, Germany, **1993**.

Received January 15, 2004
Early View Article
Published Online May 13, 2004

 © 2004 Wiley-VCH Verlag GmbH & Co. KGaA, Weinheim

EPR Insensitivity of the Metal-Nitrosyl Spin-Bearing Moiety in Complexes $[L_nRu^{II}\text{-}NO^{\cdot}]^k$

Stéphanie Frantz,[a] Biprajit Sarkar,[a] Monika Sieger,[a] Wolfgang Kaim,*[a] Federico Roncaroli,[b] José A. Olabe,*[b] and Stanislav Záliš[c]

Keywords: Density functional calculations / EPR spectroscopy / Nitric oxide / Radical complexes / Ruthenium

A survey of 18 paramagnetic species $[L_nRu(NO)]^k$, including seven new examples studied by in situ electrolysis, reveals a surprisingly narrow range of EPR parameters despite a wide variety of ligands such as pyridine, polypyridines, imines, amines, nitriles, phosphanes, carbonyl, cyclopentadienides, halides, hydride, hydroxide, thiocyanate or cyanide: g_1 = 2.015 ± 0.02, g_2 = 1.990 ± 0.015, g_3 = 1.892 ± 0.03, g_{av} = 1.968 ± 0.02, $\Delta g = g_1 - g_3 = 0.122 \pm 0.037$, $A_2(^{14}N) = 3.3 \pm 0.5$ mT. This rather small variability, smaller still if the organometallic compounds are excluded, differs from the wider range of EPR data reported for nitrosyliron species with $S = 1/2$; apparently, the $\{RuNO\}^7$ configuration involves a rather invariant and relatively covalent metal–NO interaction. DFT calculations were employed for $[(NC)_5Ru(NO)]^{3-}$ to reproduce the EPR data, to evaluate the spin distribution (58% spin density on NO), and to reveal structural changes on reduction such as the Ru–N–O bending and Ru–NO bond lengthening. In addition, the possibility of staggered and eclipsed conformations is discussed.

(© Wiley-VCH Verlag GmbH & Co. KGaA, 69451 Weinheim, Germany, 2004)

Introduction

The formation, reactivity, spectroscopy and structures of nitrosyliron complexes have been investigated for more than a century.[1−3] The question of the appropriate electronic description of such species in terms of oxidation and spin states has been highlighted recently by the examples of simple $[(H_2O)_5Fe(NO)]^{2+}$,[4] of complexes $[(L)Fe(NO)]^{n+}$ with multidentate N-, S- or O-donor ligands L,[5] and of nitrosyliron porphyrins inside or outside of heme proteins.[6,7] Various iron oxidation states, from −II[8] to +IV,[9] can be discussed in conjunction with nitrosonium (NO^+), nitric oxide ($NO^{\cdot}$) or nitroside (NO^-) ligands.[10] Paramagnetic neutral $NO^{\cdot}$ is of particular interest, and its presence has been observed frequently by vibrational or EPR spectroscopy.[11−13]

The current surge in such studies is attributed to the recognition of the essential role of iron−NO interactions in a physiological context,[13] including the formation,[14] binding, and release[15] of this ubiquitous messenger (neurotransmitter) molecule.[16] Copper-[17] or iron-coordinated NO also play an important role in the biological nitrogen cycle.[18] In yet another line of interest, the metal-influenced chemistry of NO is of relevance for catalytic exhaust-gas conversion.[19]

Recently, corresponding compounds of the higher homologue ruthenium have also been studied in the search for NO-scavenging[20] or NO-releasing (delivering) agents.[14,15,21] Scavenging by specifically designed ruthenium(III) aqua complexes containing polycarboxylate coligands was reported recently to involve a fast NO coordination, leading to formally $Ru^{II}(NO^+)$ complexes. However, the potential $Ru^{II}(NO^{\cdot})$ product accessible by electrochemically reversible reduction[20c] was not studied further.[20a]

Photochemical or electron-transfer activation can be envisaged for the labilization of bound NO from its usual, kinetically stable $Ru^{II}(NO^+) = \{RuNO\}^6$ configuration.[21] Following more recent assumptions[22] on the transition from $Ru^{II}-(NO^+)$ to $Ru^{II}-(NO^{\cdot})$ some EPR data on chemically generated $Ru^{II}(NO^{\cdot})$ species and pertinent quantum-chemical calculations have been published in the last few years.[21b,23−30] Herein we describe EPR results from the in situ reduction of several more such complexes $[L_nRu(NO)]^k$, we summarize and critically discuss the data of 18 different such species and compare the unexpectedly

[a] Institut für Anorganische Chemie, Universität Stuttgart, Pfaffenwaldring 55, 70550 Stuttgart, Germany
E-mail: kaim@iac.uni-stuttgart.de
[b] Departamento de Química Inorgánica, Analítica y Química Física, (INQUIMAE), Facultad de Ciencias Exactas y Naturales, UBA,
Pabellón 2, Ciudad Universitaria, C1428EHA Buenos Aires, Republic of Argentina
E-mail: olabe@qi.fcen.uba.ar
[c] J. Heyrovský Institute of Physical Chemistry, Academy of Sciences of the Czech Republic,
Dolejškova 3, 18223 Prague, Czech Republic
E-mail: stanislav.zalis@jh-inst.cas.cz

 © 2004 Wiley-VCH Verlag GmbH & Co. KGaA, Weinheim DOI: 10.1002/ejic.200400042

uniform result with the situation in corresponding iron complexes. Results for the reduction and oxidation of $[Cl_5Ru(NO)]^{2-}$ are also presented, as are improved DFT calculations of the *g* and hyperfine properties of $[(NC)_5Ru(NO)]^{3-}$, including their orientation dependence (eclipsed vs. staggered conformation).

Results and Discussion

Although the new $Ru^{II}-(NO^+)$ precursor complexes referred to in the Exp. Sect. are reduced reversibly at room temperature, no EPR signals were detectable for the one-electron-reduced forms under those conditions. EPR silence at room temperature has been reported before for the related species from Table 1.[22−25] In glassy frozen solution a typical pattern[17,23−30] of rhombic *g* splitting with ^{14}N nitrosyl hyperfine coupling of the central component emerges, a representative spectrum from the in situ electrolysis of a precursor, $[(terpy)(bpz)Ru(NO)]^{3+}$, in CH_3CN/0.1 M Bu_4NPF_6, is shown together with a computer simulation in Figure 1.

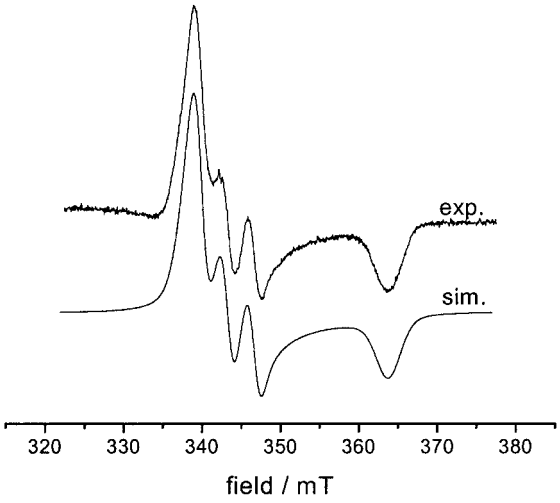

Figure 1. EPR spectrum of $[(terpy)(bpz)Ru(NO)]^{2+}$ at 110 K in CH_3CN/0.1 M Bu_4NPF_6 (top); computer simulation (bottom)

Conversion of commercially available $K_2[Cl_5Ru(NO)]$ into its tetrabutylammonium salt allowed us to additionally study its reduction behavior in acetonitrile. Even at −40 °C the electrochemical reduction proved to be irreversible,

Table 1. EPR spectroscopic data[a] of nitrosylruthenium complexes; n.o. not observed

Complex	g_1	g_2	g_3	g_{av}	Δg	A_1	A_2	A_3	Ref.
$[(py)_4(NH_3)Ru(NO)]^{2+}$	2.0215	1.9875	1.878	1.963	0.1435	n.o.	3.0	n.o.	this work[b]
$[(py)_4(SCN)Ru(NO)]^{+}$	2.0225	1.9895	1.877	1.963	0.1455	n.o.	2.9	n.o.	this work[b]
$[(py)_4ClRu(NO)]^{+}$	2.025	1.990	1.886	1.967	0.139	n.o.	3.1	n.o.	this work[b]
$[(py)_4ClRu(NO)]^{+}$	2.033	1.989	1.874	1.965	0.159	1.51	3.18	1.07	[28][c]
$[(py)_4(OH)Ru(NO)]^{+}$	2.0235	1.991	1.886	1.967	0.1375	n.o.	3.2	n.o.	this work[b]
$[(bpy)_2(CH_3CN)Ru(NO)]^{2+}$	2.028	1.9925	1.882	1.968	0.146	n.o.	3.3	n.o.	this work[b]
$[(bpy)_2ClRu(NO)]^{+}$	2.029	1.992	1.881	1.968	0.148	n.o.	3.2	n.o.	this work[b]
$[(terpy)(bpy)Ru(NO)]^{2+}$	2.0175	1.998	1.883	1.967	0.1345	n.o.	3.4	n.o.	this work[b]
$[(terpy)(bpz)Ru(NO)]^{2+}$	2.0215	1.999	1.886	1.969	0.1355	n.o.	3.4	n.o.	this work[b]
$[(NC)(py)_4Ru(\mu\text{-}CN)(py)_4Ru(NO)]^{2+}$	2.024	1.990	1.865	1.960	0.159	1.55	3.39	0.97	[28][c]
$[(cyclam)ClRu(NO)]^{+}$	2.035	1.995	1.883	1.971	0.152	1.7	3.21	1.5	[24,25b][d]
$[(bpydip)ClRu(NO)]^{+}$	2.027	1.991	1.889	1.969	0.138	1.69	3.23	1.48	[29][e]
$[(dppe)_2ClRu(NO)]^{+}$	2.011	1.976	1.867	1.951	0.144	1.71	1.85[f]	1.43	[25b][g]
$[(depe)_2ClRu(NO)]^{+}$	2.010	1.984	1.888	1.961	0.122	1.8	3.5	1.9	[25b][d]
$[(NC)_5Ru(NO)]^{3-}$	2.004	2.002	1.870	1.959	0.134	n.o.	3.8	n.o.	[27][h]
$[(Ph_3P)_2(C_5Me_5)Ru(NO)]^{+}$	2.0115	1.983	1.900	1.965	0.111	1.63	2.10[f]	2.29	[30a][i]
	1.995	1.995	1.896	1.962	0.099	n.o.	2.85	n.o.	[30a][j]
$[(PhMe_2P)_2(C_5Me_5)Ru(NO)]^{+}$	2.000	1.998	1.915	1.970	0.085	1.06	3.38	1.07	[30a][i]
	1.996	1.996	1.964[f]	1.985[f]	0.032[f]	n.o.	3.25	n.o.	[30a][j]
$[(Me_3P)_2(C_5Me_5)Ru(NO)]^{+}$	2.007	2.002	1.918	1.976	0.089	1.15	3.37	1.20	[30a][i]
	2.001	1.994	1.912	1.969	0.089	0.6	3.3	1.3	[30a][j]
$[HCl(OC)(PiPr_3)_2Ru(NO)]$	2.006	1.993	1.910	1.970	0.096	n.o.	3.45	n.o.	[30b][k]
$[DCl(OC)(PiPr_3)_2Ru(NO)]$	2.001	1.994	1.910	1.968	0.091	n.o.	3.45	n.o.	[30b][k]

[a] ^{14}N hyperfine coupling *A* in mT. [b] In CH_3CN/0.1 M Bu_4NPF_6, measured at 110 K. [c] In CH_3CN/0.1 M Bu_4NPF_6, measured at 10 K. [d] In ethylene glycol + 30% H_2O, measured at 77 K; cyclam = 1,4,8,11-tetraazacyclotetradecane; depe = 1,2-bis(diethylphosphanyl)-ethane. [e] In CH_3CN, measured at 110 K; bpydip = *N*,*N*′-bis(7-methyl-2-pyridylmethylene)-1,3-diiminopropane. [f] Probably erroneous value. [g] In CH_2Cl_2, measured at 77 K; dppe = 1,2-bis(diphenylphosphanyl)ethane. [h] In CH_3CN/0.1 M Bu_4NPF_6, measured at 3.5 K. [i] In CH_2Cl_2, measured at 113 K. [j] In acetone, measured at 100 K. [k] In toluene, measured at 77 K. Additional ^1H hyperfine coupling observed at about 3.5 mT.

 © 2004 Wiley-VCH Verlag GmbH & Co. KGaA, Weinheim

presumably due to the facile dissociation of chloride. In contrast, reversible oxidation produced a species with an EPR signal ($g_{1,2}$ = 2.1075, g_3 = 2.0577) which will have to be analyzed further.

The results for the reversibly reduced systems are summarized, together with literature data, in Table 1; most previously reported species were obtained by chemical reduction with, for example, Zn/Hg[29] or Eu^{2+}.[21b,24,25b]

The spectra reported here were simulated without incorporating unresolved nitrosyl ^{14}N hyperfine splitting of the g_1 and g_3 components. Such incorporation has been reported in the literature;[25,29][30b] however, the corresponding values between 1 and 2 mT, or even below, may rather serve as an approximation or upper limit and they will not be discussed further. Accuracy of the g factors is assumed to be ±0.0005 (g_1), ±0.0002 (g_2) and ±0.001 (g_3); the A_2 values are given with a ±0.1 mT error margin.

Given the wide variety of ligands L for the species $[L_nRu(NO)]^k$ in Table 1 (L = pyridine, polypyridines, imines, amines, nitriles, phosphanes, carbonyl, cyclopentadienide, halides, hydride, hydroxide, thiocyanate, cyanide), the small degree of EPR parameter variation is surprising:
$g_1 = 2.015 \pm 0.02$, $g_2 = 1.990 \pm 0.015$, $g_3 = 1.892 \pm 0.03$, $g_{av} = 1.968 \pm 0.02$, $\Delta g = g_1 - g_3 = 0.122 \pm 0.037$, $A_2(^{14}N) = 3.3 \pm 0.5$ mT.

The variance is still smaller if organometallic derivatives[30] are excluded.

Paramagnetic nitrosyliron complexes, even those involving only low-spin systems,[4,5,7,31] exhibit a distinctly greater variation. In part this may reflect contributions from the more accessible valence-tautomeric $M^I(NO^+)$ state for M = Fe which has a $(d_z^2)^1$ configuration and leads to $g_{1,2} \approx 2.07$, $g_3 \approx 2.0$ and $g_{av} \approx 2.03$ for clearly established $Fe^I(NO^+)$ cases.[25,31b]

On average, the g anisotropy, $\Delta g = g_1 - g_3$, is about twice as large for the ruthenium complexes as for related nitrosyliron(II) species.[27] This is an immediate consequence of the higher spin-orbit coupling constant $\xi(Ru) \approx 2\xi(Fe)$.[32] The deviation of g from the free-electron value of 2.0023 results from admixtures of higher excited states with nonzero angular momentum; according to the approximation in Equation (1) the spin-orbit coupling constant, ξ, is a crucial factor.[33]

$$g = g_e - \frac{2}{3}\sum_i \sum_n \sum_{kj} \frac{\langle \psi_0 | \xi_k \mathbf{L} \delta_k | \psi_n \rangle \langle \psi_n | \mathbf{L}_{ij} \delta_j | \psi_0 \rangle}{E_n - E_0} = g_e + \Delta g \quad (1)$$

ξ: spin orbit coupling constant
L: angular momentum operator
E_0: energy of singly occupied molecular orbital (SOMO)

Unrestricted ADF/BP calculations for the most symmetric species $[(NC)_5Ru(NO)]^{3-}$ have confirmed the expected[11] and recently experimentally confirmed[30b] bending of the RuNO moiety to 146.1° [138.75(11)° for $[HCl(OC)(PiPr_3)_2Ru(NO)]$[30b]) and the lengthening of the Ru−NO bond by 0.128 Å to 1.899 Å [1.8566(11) Å for $[HCl(OC)(PiPr_3)_2Ru(NO)]$[30b]), in agreement with the established NO labilization on reduction for potential medical applications.[20,21] G98/B3LYP calculations give an RuNO angle of 146.7° and a Ru−NO bond length of 1.915 Å. ADF/SAOP calculations indicated about 29% metal and 58% NO contributions to the singly occupied molecular orbital (SOMO), suggesting $Ru^{II}-(NO^{\cdot})$ as the dominant oxidation state formulation, albeit with considerable mixing.[27] The lowest (completely) unoccupied molecular orbital (LUMO) is the second NO-based π* MO (25% metal and 62% NO contribution), originating from the degenerate e level of $[(NC)_5Ru(NO)]^{2-}$. The calculated values (g_n, A_n) are listed in Table 2.

Table 2. Comparison of experimental and calculated g values and hyperfine constants A (mT) for $[(NC)_5Ru(NO)]^{3-}$ at optimized geometry (eclipsed conformation)

	Exp.	Calcd.[a]	Calcd.[b]	Calcd.[c]
g_1	2.004	2.000	2.006	2.007
g_2	2.002	1.993	1.996	1.997
g_3	1.870	1.814	1.845	1.890
$g_1 - g_3$	0.134	0.186	0.161	0.117
g_{iso}[d]	1.959	1.936	1.949	1.965
A_1 (^{101}Ru)	n.o.	0.96	–	1.13
A_2 (^{101}Ru)	n.o.	1.61	–	1.67
A_3 (^{101}Ru)	n.o.	0.24	–	0.46
A_1 (^{14}N)	n.o.	0.51	–	1.28
A_2 (^{14}N)	3.8	3.23	–	4.04
A_3 (^{14}N)	n.o.	0.35	–	1.14

[a] ADF/BP calculations: g values calculated using spin-restricted approach including spin-orbit coupling; A values calculated within the UKS-ZORA approach with core electrons included. [b] ADF/SAOP spin-restricted ZORA calculations including spin-orbit coupling. [c] UKS-Pauli approach. [d] Calculated from $<g> = [(g_1^2 + g_2^2 + g_3^2)/3]^{1/2}$.

The well-known bending of the M−N−O moiety in $\{MNO\}^7$ species with approximately octahedral configuration at M produces a conformational isomerism characterized by variations of the C(CN)−Ru−N−O dihedral angle, θ, with the eclipsed (θ = 0°) and staggered (θ = 45°) conformations as the two extreme cases (Scheme 1). G98/B3LYP geometry optimization shows the eclipsed conformation to be more stable by 0.041 eV (as in $[HCl(OC)(PiPr_3)_2Ru(NO)]$[30b]), the rotational barrier being highly dependent on the functional used. The calculated g_n, $A_n(^{14}N)$ and $A_n(^{101}Ru)$ parameters depend only slightly on the conformation.

The analysis of individual contributions to the Δg values was performed within the UKS-Pauli approach, indicating that the largest contribution arises from the paramagnetic orbital-orbital coupling between the SOMO and LUMO of the same spin polarization. The experimental g values are well reproduced by the calculations. Table 2 shows how the functional and the type of approach influence the calculated values. The best agreement between experimental and calculated g values was achieved using either the ADF/

 © 2004 Wiley-VCH Verlag GmbH & Co. KGaA, Weinheim

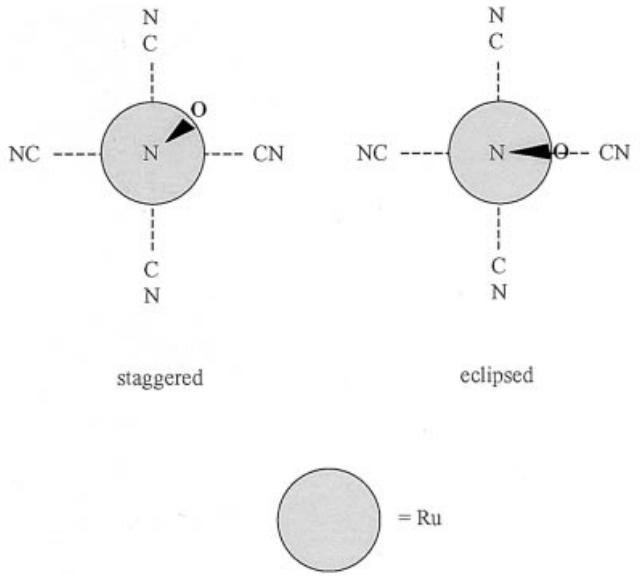

Scheme 1

SAOP spin-restricted ZORA spin-orbit calculation or the UKS-Pauli approach.

The spin distribution in complexes $[L_nRu(NO)]^k$ = $\{RuNO\}^7$ seems to be rather invariant throughout the complexes of Table 1, reflecting the high degree of covalency of the Ru−N bond in the $\{RuNO\}^{[7]}$ configuration with 19 valence electrons. Increasing covalency is also responsible for the general shift to higher g values on going from $Na^+-NO^{\cdot}$ via Cu^I complexes[34] to the Ru^{II} compounds summarized here. In comparison to the results given here, some other calculations[26,29] seem to underestimate the NO contributions. In that context, some conclusions based on very small ν(NO) shifts on reduction such as a $Ru^{III}(NO^{\cdot})$ formulation for $[(cyclam)ClRu(NO)]^{2+}$ or a ligand-delocalized description $(L^{\cdot-})Ru^{II}(NO^+)$ suggested for $[(bpydip)ClRu(NO)]^+$ [29] are not supported by the EPR data [cyclam = 1,4,8,11-tetraazacyclotetradecane; bypdip = *N*,*N*′-bis(7-methyl-2-pyridylmethylene)-1,3-diiminopropane].

Despite the rather uniform EPR results for the species in Table 1 there are some slight variations. The most symmetrical species $[(NC)_5Ru(NO)]^{3-}$ displays a g component splitting approaching the axial limit, with $g_{\perp} > g_{\|}$. The average value of g is smallest for this species whereas it is slightly larger (in 0.012) for $[(cyclam)ClRu(NO)]^+$; however, all $Ru^{II}(NO^{\cdot})$ complexes have g_{av} below 2, indicating the closeness of both π* orbitals of NO[27] and thus of both $^2\Pi_x$ and $^2\Pi_y$ states.[34,35] The presence of states lying close to the radical ground state is also responsible for the rapid relaxation as evident from the EPR silence at room temperature. The relatively large A_2 hyperfine value of 3.8 mT for $^{14}N(NO)$ may in part reflect the reluctance of negatively charged cyanide ligands in $[(NC)_5Ru(NO)]^{3-}$ to accommodate the unpaired electron. On the other hand, the A_2 values are smallest, at about 3.0 mT, for the series of complexes $[(py)_4XRu(NO)]^+$ with rather weak donor ligands (Table 1).

The total g anisotropy $\Delta g = g_1 - g_3$ is highest for the dinuclear complex $[(NC)(py)_4Ru(CN)(py)_4Ru(NO)]^{2+}$, possibly reflecting an effect of the second, non-NO-coordinating metal center with its high spin-orbit coupling constant. $[(NC)_5Ru(NO)]^{3-}$ and the phosphane-containing compound $[(depe)_2ClRu(NO)]^+$ [depe = 1,2-bis(diethylphosphanyl)ethane], both with strong σ donor/π acceptor ligation, display relatively small Δg values, indicating smaller metal contributions; this is also supported by rather high nitrosyl ligand coupling constants $A_2(^{14}N)$.

Changing the solvent from CH_3CN to DMF in the case of $[(py)_4ClRu(NO)]^+$ yielded identical EPR parameters. Although the cyanoiron compounds $[(NC)_5Fe(L)]^{2-}$ [L = NO^+ or *N*-methylpyrazinium (mpz)] can lose one cyanide ligand on reduction[36,37] we found no evidence for conversion into a five-coordinate complex in the paramagnetic ruthenium species studied here. The new calculated metal hyperfine coupling constants $A_n(^{101}Ru)$ (Table 2) confirm the failure to observe such splittings experimentally. Even the calculated A_2 value of 1.61 mT would be difficult to detect because of the line-width, the relatively low natural abundance of only 17% and the distribution of signal intensity over six lines (I = 5/2). The isotope ^{99}Ru (12.7% natural abundance, I = 5/2) has a 10% smaller hyperfine coupling[45] and would be still harder to detect. The maximum calculated isotropic hyperfine splitting of 0.94 mT according to Table 2 is only slightly larger than the $A_{iso}(^{101}Ru)$ parameters measured for radical complexes containing cyanoruthenium[37,38] (≤0.52 mT) or other ruthenium(II) complex fragments (≤0.86 mT).[39] Species with metal-centered spin containing ruthenium(I)[40] are expected to have isotropic metal coupling constants of several milliteslas.

In summary, the small variation in g tensor splitting and hyperfine coupling for all 18 compounds in Table 1 suggest very similar electronic structures, described essentially by the $Ru^{II}(NO^{\cdot})$ formulation. The surprising invariance of EPR parameters points to a higher degree of covalency in the $\{RuNO\}^7$ situation than in the corresponding $\{FeNO\}^7$ arrangements, the latter having more accessible options between the limiting structures $Fe^{II}(NO^{\cdot})$ and $Fe^{I}(NO^+)$ and between low-spin and high-spin states. Perspectives for future work will include nitrosylruthenium complexes with strongly dominant co-ligands such as porphyrins or other macrocycles[41] and the study of osmium analogues with their much higher spin-orbit coupling contributions from the 5d metal.

Experimental Section

Instrumentation: IR spectra were recorded with KBr pellets on a Thermo Nicolet model Avatar 320 FT-IR instrument. ^1H NMR spectra were obtained on a Bruker 500 MHz spectrometer. Electrochemical studies were performed with a Princeton Applied Research potentiostat 273A, by square-wave voltammetry (SWV) at 60 Hz, with vitreous carbon as working electrode and Ag/AgCl (3 M KCl) as reference. The electrolyte was an aqueous solution that was 1 M in NaCl and 0.01 M in HCl. Elemental analyses were done on a Carlo Erba elemental analyser, model 1106. EPR spec-

 © 2004 Wiley-VCH Verlag GmbH & Co. KGaA, Weinheim

troscopy: The nitrosylruthenium complexes were reduced for in situ EPR studies in a two-electrode capillary described earlier.[42] The electrolyte was CH_3CN/0.1 M Bu_4NPF_6. Whereas the brief (ca. 10 min) electrolysis was performed at 295 K, the EPR spectra were recorded at 110 K in glassy frozen solutions due to the EPR silence of the complexes at room temperature. A Bruker ESP 300 spectrometer was used. The *g* factor determination was carried out with a Bruker ER035M gaussmeter and a HP 5350B microwave counter. The spectra were simulated (program Bruker WinSimfonia) without incorporating the unresolved hyperfine splitting of the g_1 and g_3 components.

The complexes *trans*-$[(py)_4ClRu(NO)](PF_6)_2$,[43] *trans*-$[(py)_4(OH)Ru(NO)](PF_6)_2$,[43] *trans*-$[(py)_4(NH_3)Ru(NO)](BF_4)_3$,[44a] *cis*-$[(bpy)_2ClRu(NO)](PF_6)_2$,[23] *cis*-$[(bpy)_2(CH_3CN)Ru(NO)](PF_6)_2$[44b] and $[(terpy)(bpy)Ru(NO)](PF_6)_3$[45] were prepared as described previously.

[(terpy)(bpz)Ru(NO)](PF$_6$)$_3$: $[RuCl_3(terpy)]$[46] (100 mg, 0.227 mmol) and bpz (2,2′-bipyrazine, 60 mg, 0.379 mmol) were heated to reflux for 3 h in 50 mL of EtOH/H_2O (1:1). $NaNO_2$ (150 mg) was added to the red-brown solution and refluxing was continued for 2 h. The red solution was then filtered and a concentrated solution of NH_4PF_6 was added until complete precipitation of the product was ensured. The red solid was suspended in 3 M HCl and NH_4PF_6 was added in the same way as before to afford a brown solid. The product was further purified by recrystallization from acetonitrile/diethyl ether. IR: ν(NO) = 1957 cm^{-1}. $E_{1/2}$ = 0.46 V vs. Ag/AgCl. $C_{28}H_{17}F_{18}N_8OP_3Ru$ (957.40): calcd. C 28.85, N 1.79, N 11.71; found C 27.66, N 1.74, N 11.04. ^{1}H NMR (CD_3CN): δ = 10.12 (s, 1 H), 9.96 (s, 1 H), 9.51 (d, 1 H), 9.38 (d, 1 H), 8.99 (t, 1 H), 8.87 (d, 2 H), 8.82 (d, 1 H), 8.71 (d, 2 H), 8.47 (t, 2 H), 8.06 (d, 2 H), 7.73 (t, 2 H), 7.22 (t, 1 H) ppm.

***trans*-[(py)$_4$(SCN)Ru(NO)](PF$_6$)$_2$:** *trans*-$[(py)_4Ru(NO_2)_2]$[43] (100 mg, 0.0106 mmol) and NaSCN (300 mg, 3.7 mmol) were suspended in 20 mL of acetonitrile, and 0.5 mL of concentrated HPF_6 was added. After mixing, the sample was evaporated to dryness. The solid residue was suspended in water and filtered. 700 mg of NH_4PF_6 was added to the solution and a yellow solid was obtained. This compound was further purified by loading onto a DOWEX 50 WX2 cation exchanger (100−200 mesh) in acid form eluting with 1 M HCl. The main orange fraction was collected and precipitated with NH_4PF_6. $C_{21}H_{20}F_{12}N_6OP_2RuS$ (795.49): calcd. C 31.69, H 2.01, N 10.56, S 4.03; found C 31.90, H 2.27, N 10.12, S 3.63. IR: ν(NO) = 1902 cm^{-1}. $E_{1/2}$ = 0.12 V and −0.35 V vs. Ag/AgCl. ^{1}H NMR (CD_3CN): δ = 8.29 (t, 4 H, H^4), 8.26 (d, 8 H, $H^{2,6}$), 7.70 (t, 8 H, $H^{3,5}$) ppm.

DFT Calculations: Ground state electronic structure calculations on $[(NC)_5Ru(NO)]^{3-}$ have been done on the basis of density-functional theory (DFT) methods using the ADF2002.03[47,48] and Gaussian 98 program packages.[49]

Within the ADF program, Slater-type orbital (STO) basis sets of triple-quality with polarization functions were employed. Basis I was represented by the frozen-core approximation (1s for C, N O and 1s−3d for Ru), basis II also includes core electrons. The following density functionals were used within ADF: the local density approximation (LDA) with VWN parametrization of electron gas data or the functional including Becke's gradient correction[50] to the local exchange expression in conjunction with Perdew's gradient correction[51] to the LDA expression (ADF/BP). The scalar relativistic (SR) zero-order regular approximation (ZORA) was used within the geometry optimization. The *g*-tensor calculations were also performed using the asymptotically correct functional SAOP (statistical average of orbital potentials),[52] which gives better energies of the frontier MOs. Core electrons were included in the ADF/SAOP calculations.

The *g*-tensor was obtained from a spin-nonpolarized wave function after incorporating the spin-orbit (SO) coupling. *A* tensors and *g* tensors were obtained by first-order perturbation theory from the ZORA Hamiltonian in the presence of a time-independent magnetic field.[53,54] The analysis of individual contributions to the *g* tensor was done by the UKS-Pauli approach using gauge-including atomic orbitals.[55]

Within Gaussian-98 Dunning's polarized valence double-ζ basis sets[56] were used for the C, N and O atoms and the quasi-relativistic effective core pseudopotentials with a correspondingly optimized set of basis functions[57] for Ru. The hybrid Becke three-parameter functional with Lee, Yang and Parr correlation functional (B3LYP)[58] was used in the Gaussian-98 calculations (G98/B3LYP).

The geometry of $[(NC)_5Ru(NO)]^{3-}$ was optimized without any symmetry restrictions using the spin-unrestricted open-shell Kohn−Sham (UKS) approach.

Acknowledgments

This work was supported by a grant from Volkswagenstiftung (I/76674), by the FCI, the European Union (COST action D14), the Ministry of Education of the Czech Republic (grant COST OC14.20), and by the Argentine Agencies CONICET and FONCYT (Grant 06−06817).

[1] [1a] L. Playfair, *Proc. Roy. Soc., (London)* **1849**, *5*, 846. [1b] L. Playfair, *Ann. Pharm.* **1850**, *74*, 317.
[2] J. H. Swinehart, *Coord. Chem. Rev.* **1967**, *2*, 385.
[3] [3a] J. A. McCleverty, *Chem. Rev.* **1979**, *79*, 53. [3b] R. D. Feltham, J. H. Enemark, *Top. Stereochem.* **1981**, *12*, 155.
[4] A. Wanat, T. Schneppensieper, G. Stochel, R. van Eldik, E. Bill, K. Wieghardt, *Inorg. Chem.* **2002**, *41*, 4.
[5] [5a] M. Li, D. Bonnet, E. Bill, F. Neese, T. Weyhermüller, N. Blum, D. Sellmann, K. Wieghardt, *Inorg. Chem.* **2002**, *41*, 3444. [5b] T. Schneppensieper, A. Wanat, G. Stochel, S. Goldstein, D. Meyerstein, R. van Eldik, *Eur. J. Inorg. Chem.* **2001**, 2317.
[6] [6a] B. A. Averill, *Chem. Rev.* **1996**, *96*, 2951. [6b] N. S. Trofimova, A. Y. Safronov, O. Ikeda, *Inorg. Chem.* **2003**, *42*, 1945, and references cited therein.
[7] [7a] W. R. Scheidt, M. K. Ellison, *Acc. Chem. Res.* **1999**, *32*, 350. [7b] B. B. Wayland, L. W. Olson, *J. Am. Chem. Soc.* **1974**, *96*, 6037. [7c] Y. Chen, M. A. Sweetland, R. E. Shepherd, *Inorg. Chim. Acta* **1997**, *260*, 163.
[8] [8a] C. Couture, J. R. Morton, K. F. Preston, S. J. Strach, *J. Magn. Reson.* **1980**, *41*, 88. [8b] H. tom Dieck, H. Bruder, E. Kühl, D. Junghans, K. Hellfeldt, *New. J. Chem.* **1989**, *13*, 259.
[9] C. Hauser, T. Glaser, E. Bill, T. Weyhermüller, K. Wieghardt, *J. Am. Chem. Soc.* **2000**, *122*, 4352.
[10] [10a] J. A. Olabe, L. Slep, *Comprehensive Coordination Chemistry II* (Eds.: J. A. McCleverty, T. J. Meyer), Pergamon, **1993**, vol. 1, p. 603−623. [10b] J. A. Olabe, *Adv. Inorg. Chem.*, in press.
[11] J. H. Enemark, R. D. Feltham, *Coord. Chem. Rev.* **1974**, *13*, 339.
[12] G. B. Richter-Addo, P. Legzdins, *Metal Nitrosyls*, Oxford University Press, New York, **1992**.
[13] *Methods in Nitric Oxide Research* (Eds.: M. Feelisch, J. S. Stamler), Wiley, Chichester, **1996**.
[14] P. C. Ford, I. M. Lorkovic, *Chem. Rev.* **2002**, *102*, 993.
[15] [15a] P. G. Wang, M. Xian, X. Tang, X. Wu, Z. Wen, T. Cai, A. Janczuk, *Chem. Rev.* **2002**, *102*, 1091. [15b] J. A. Hrabie, L. K. Keefer, *Chem. Rev.* **2002**, *102*, 1135.
[16] F. Murad, *Angew. Chem. Int. Ed.* **1999**, *28*, 1856.
[17] C. E. Ruggiero, S. M. Carrier, W. E. Antholine, J. W. Whittaker,

 © 2004 Wiley-VCH Verlag GmbH & Co. KGaA, Weinheim

C. J. Cramer, W. B. Tolman, *J. Am. Chem. Soc.* **1993**, *115*, 11285.
[18] S. J. Ferguson, *Curr. Opin. Chem. Biol.* **1998**, *2*, 182.
[19] [19a] M. Iwamoto, H. Hamada, *Catal. Today* **1991**, *10*, 57. [19b] M. H. Groothaert, J. A. van Bokhoven, A. A. Battiston, B. M. Weckhuysen, R. A. Schoonheydt, *J. Am. Chem. Soc.* **2003**, *125*, 7629.
[20] [20a] B. R. Cameron, M. C. Darkes, H. Yee, M. Olsen, S. P. Fricker, R. T. Skerlj, G. J. Bridger, N. A. Davies, M. T. Wilson, D. J. Rose, J. Zubieta, *Inorg. Chem.* **2003**, *42*, 1868. [20b] B. Serli, E. Zangrando, T. Gianferrara, L. J. Yellowlees, E. Alessio, *Coord. Chem. Rev.* **2003**, *245*, 73. [20c] M. R. Rhodes, M. H. Barley, T. J. Meyer, *Inorg. Chem.* **1991**, *39*, 629.
[21] [21a] M. Wolak, R. van Eldik, *Coord. Chem. Rev.* **2002**, *230*, 263. [21b] E. Tfouni, M. Krieger, B. R. McGarvey, D. W. Franco, *Coord. Chem. Rev.* **2003**, *236*, 57.
[22] [22a] S. S. S. Borges, C. U. Davanzo, E. E. Castellano, J. Z. Schpector, S. C. Silva, D. W. Franco, *Inorg. Chem.* **1998**, *37*, 2670. [22b] C. W. B. Bezerra, C. S. Silva, M. T. P. Gambardella, R. H. A. Santos, L. M. A. Plicas, E. Tfouni, D. W. Franco, *Inorg. Chem.* **1999**, *38*, 5660.
[23] R. W. Callahan, T. J. Meyer, *Inorg. Chem.* **1977**, *16*, 574. The EPR spectrum of $[(bpy)_2ClRu(NO)]^+$ shown in this publication was not analyzed.
[24] D. R. Lang, J. A. Davis, L. G. F. Lopes, A. A. Ferro, L. C. G. Vasconcellos, D. W. Franco, E. Tfouni, A. Wieraszko, M. J. Clarke, *Inorg. Chem.* **2000**, *39*, 2294.
[25] [25a] R. C. L. Zampieri, G. Von Poelhsitz, A. A. Batista, O. R. Nascimento, J. Ellena, E. E. Castellano, *J. Inorg. Biochem.* **2002**, *92*, 82. [25b] B. R. McGarvey, A. A. Ferro, E. Tfouni, C. W. Brito Bezerra, I. Bagatin, D. W. Franco, *Inorg. Chem.* **2000**, *39*, 3577.
[26] J. A. Gomez, D. Guenzburger, *Chem. Phys.* **2000**, *253*, 73.
[27] M. Wanner, T. Scheiring, W. Kaim, L. D. Slep, L. M. Baraldo, J. A. Olabe, S. Zalis, E. J. Baerends, *Inorg. Chem.* **2001**, *40*, 5704.
[28] F. Roncaroli, L. M. Baraldo, L. D. Slep, J. A. Olabe, *Inorg. Chem.* **2002**, *41*, 1930.
[29] V. R. de Souza, A. M. de Costa Ferreira, H. E. Toma, *Dalton Trans.* **2003**, 458.
[30] [30a] P. Diversi, M. Fontani, M. Fuligni, F. Laschi, F. Marchetti, S. Matteoni, C. Pinzino, P. Zanello, *J. Organomet. Chem.* **2003**, *675*, 21. [30b] A. V. Marchenko, A. N. Vedernikov, D. F. Dye, M. Pink, J. M. Zaleski, K. G. Caulton, *Inorg. Chem.* **2004**, *43*, 351.
[31] [31a] J. D. W. van Voorst, P. J. Hemmerich, *Chem. Phys.* **1966**, *45*, 3914. [31b] N. Reginato, C. T. C. M. cCrory, D. Pervitsky, L. Li, *J. Am. Chem. Soc.* **1999**, *121*, 10217.
[32] D. W. Pipes, T. J. Meyer, *Inorg. Chem.* **1984**, *23*, 2466.
[33] W. Kaim, *Coord. Chem. Rev.* **1987**, *76*, 187.
[34] K. M. Neyman, D. I. Ganyushin, V. A. Nasluzov, N. Rösch, A. Pöppl, M. Hartmann, *Phys. Chem. Chem. Phys.* **2003**, *5*, 2429.
[35] P. Pietrzyk, W. Piskorz, Z. Sojka, E. Broclawik, *J. Phys. Chem. B* **2003**, *107*, 6105.
[36] EPR of $[(NC)_4Fe(NO)]^{2-}$: C. Glidewell, I. L. Johnson, *Inorg. Chim. Acta* **1987**, *132*, 145.
[37] E. Waldhör, W. Kaim, J. A. Olabe, L. D. Slep, J. Fiedler, *Inorg. Chem.* **1997**, *36*, 2969.
[38] E. Waldhör, J. Poppe, W. Kaim, E. Cutin, M. Garcia Posse, N. E. Katz, *Inorg. Chem.* **1995**, *34*, 3093.
[39] M. Krejcik, S. Zalis, J. Klima, D. Sykora, W. Matheis, A. Klein, W. Kaim, *Inorg. Chem.* **1993**, *32*, 3362.
[40] C. Bianchini, F. Laschi, M. Peruzzini, P. Zanello, *Gazz. Chim. Ital.* **1994**, *124*, 271.
[41] [41a] K. M. Kadish, V. A. Adamian, E. V. Caemelbecke, Z. Tan, P. Tagliatesta, P. Bianco, T. Boschi, G. Yi, M. A. Khan, G. Richter-Addo, *Inorg. Chem.* **1996**, *35*, 1343. [41b] K. M. Miranda, X. Bu, I. Lorkovic, P. C. Ford, *Inorg. Chem.* **1997**, *36*, 4838. [41c] D. S. Bohle, C. H. Hung, B. D. Smith, *Inorg. Chem.* **1998**, *37*, 5798. [41d] G. B. Richter-Addo, R. A. Wheeler, C. A. Hixson, L. Chen, M. A. Kahn, M. K. Ellison, C. E. Schulz, W. R. Scheidt, *J. Am. Chem. Soc.* **2001**, *123*, 6314. [41f] J. C. Patterson, I. M. Lorkovic, P. C. Ford, *Inorg. Chem.* **2003**, *42*, 4902.
[42] W. Kaim, S. Ernst, V. Kasack, *J. Am. Chem. Soc.* **1990**, *112*, 173.
[43] F. Bottomley, M. Mukaida, *J. Chem. Soc., Dalton Trans.* **1982**, 1933.
[44] [44a] H. Nishimura, H. Matsuzawa, T. Togano, M. Mukaida, H. Kakihana, *J. Chem. Soc., Dalton Trans.* **1990**, 137. [44b] H. Nagao, K. Ito, N. Tsuboya, D. Ooyama, N. Nagao, S. F. Howell, M. Mukaida, *Inorg. Chim. Acta* **1999**, *290*, 113.
[45] J. A. Weil, J. R. Bolton, J. E. Wertz, *Electron Paramagnetic Resonance*, Wiley, New York, **1994**.
[46] C. A. Bessel, R. A. Leising, L. F. Szczepura, W. J. Perez, H. Vo, H. My, K. J. Takeuchi, *Inorg. Synth.* **1988**, *32*, 186.
[47] G. te Velde, F. M. Bickelhaupt, S. J. A. van Gisbergen, C. Fonseca Guerra, E. J. Baerends, J. G. Snijders, T. Ziegler, *J. Comput. Chem.* **2001**, *22*, 931.
[48] C. Fonseca Guerra, J. G. Snijders, G. te Velde, E. J. Baerends, *Theor. Chim. Acc.* **1998**, *99*, 391.
[49] M. J. Frisch, G. W. Trucks, H. B. Schlegel, G. E. Scuseria, M. A. Robb, J. R. Cheeseman, V. G. Zakrzewski, J. A. Montgomery, Jr., R. E. Stratmann, J. C. Burant, S. Dapprich, J. M. Millam, A. D. Daniels, K. N. Kudin, M. C. Strain, O. Farkas, J. Tomasi, V. Barone, M. Cossi, R. Cammi, B. Mennucci, C. Pomelli, C. Adamo, S. Clifford, J. Ochterski, G. A. Petersson, P. Y. Ayala, Q. Cui, K. Morokuma, D. K. Malick, A. D. Rabuck, K. Raghavachari, J. B. Foresman, J. Cioslowski, J. V. Ortiz, A. G. Baboul, B. B. Stefanov, G. Liu, A. Liashenko, P. Piskorz, I. Komaromi, R. Gomperts, R. L. Martin, D. J. Fox, T. Keith, M. A. Al-Laham, C. Y. Peng, A. Nanayakkara, C. Gonzalez, M. Challacombe, P. M. W. Gill, B. Johnson, W. Chen, M. W. Wong, J. L. Andres, C. Gonzalez, M. Head-Gordon, E. S. Replogle, J. A. Pople, Gaussian 98, Revision A.11; Gaussian. Inc.: Pittsburgh, PA, **1998**.
[50] A. D. Becke, *Phys. Rev. A* **1988**, *38*, 3098.
[51] J. P. Perdew, *Phys. Rev. A* **1986**, *33*, 8822.
[52] P. R. T. Schipper, O. V. Gritsenko, S. J. A. van Gisbergen, E. J. Baerends, *J. Chem. Phys.* **2000**, *112*, 1344.
[53] E. van Lenthe, A. van der Avoird, P. E. S. Wormer, *J. Chem. Phys.* **1997**, *107*, 2488.
[54] E. van Lenthe, A. van der Avoird, P. E. S. Wormer, *J. Chem. Phys.* **1998**, *108*, 4783.
[55] G. Schrenkenbach, T. Ziegler, *J. Phys. Chem. A* **1997**, *101*, 3388.
[56] D. E. Woon, T. H. Dunning Jr., *J. Chem. Phys.* **1993**, *98*, 1358.
[57] D. Andrae, U. Häussermann, M. Dolg, H. Stoll, H. Preuss, *Theor. Chim. Acta* **1990**, *77*, 123.
[58] P. J. Stephens, F. J. Devlin, C. F. Cabalowski, M. J. Frisch, *J. Phys. Chem.* **1994**, *98*, 11623.

Received January 16, 2004
Early View Article
Published Online May 13, 2004

 © 2004 Wiley-VCH Verlag GmbH & Co. KGaA, Weinheim

Interface Synthesis, Characterization and Catalytic Properties of Dialkyldichlorotin and Tetraalkyl Distannoxane Functionalities Grafted to Insoluble Polystyrene Beads by a Hexamethylene Spacer

Monique Biesemans,*[a] Frédéric A. G. Mercier,[a] Manu Van Poeck,[a] José C. Martins,[b] Gilles Dumartin,[c] and Rudolph Willem[a]

Keywords: Catalysis / Heterogeneous catalysis / NMR spectroscopy / Transesterification / Tin

Insoluble polystyrene-grafted compounds of the type $[(P–H)_{(1-t)}\{P–(CH_2)_6SnBuCl_2\}_t]$ and $[(P–H)_{(1-t)}(\{P–(CH_2)_6SnBuX\}_2O)_{t/2}]$, where (P–H) represents a cross-linked polystyrene, X is Cl, OH or $OOCCH_3$, and t is the degree of functionalization, were synthesized from Amberlite XE-305, a polystyrene cross-linked with divinylbenzene. The compounds were characterized by elemental analysis, IR and Raman spectroscopy, solid-state ^{13}C and ^{117}Sn NMR spectroscopy and, where appropriate, by ^{119}Sn hr-MAS NMR spectroscopy. The influence of the variable t and tin functionality on the catalytic activity of these compounds was assessed in the transesterification reaction of ethyl acetate with octanol.
(© Wiley-VCH Verlag GmbH & Co. KGaA, 69451 Weinheim, Germany, 2004)

Introduction

While organotin compounds enjoy widespread use as versatile reagents or catalysts in a large variety of organic transformations,[1,2] their application is sometimes limited by their toxicity.[3,4] This adverse feature is further aggravated by the generally difficult quantitative removal of organotin reagents and their by-products from the reaction mixture,[5] often making them unsuitable for the synthesis of biological or pharmaceutical derivatives.[3,6] These concerns can be alleviated by grafting the organotin reagent onto a solid support, thereby creating so-called "clean" organotin reagents, which can be removed completely from reaction products by simple filtration. In a previous paper we reported on the synthesis[7] and characterization[7,8] of $[(P–H)_{(1-t)}\{P–(CH_2)_nSnBuX_2\}_t]$ (n = 4, 6; X = Ph, Cl; t (degree of functionalization) = 0.25–0.30]. The catalytic activity of these compounds in the transesterification reaction of ethyl acetate with simple alcohols such as octanol appeared reasonably good.[7] The work presented here describes the synthesis of analogues with a lower degree of functionalization, with the aim of evaluating the effect of t on the catalytic activity of these compounds. Furthermore, based on the work of Otera and co-workers,[9] which proposes the use of distannoxanes $[XR_2SnOSnR_2Y]_2$ (R = Bu, Me; X = Cl, NCS; Y = OH, Cl, NCS) as efficient catalysts in transesterification reactions, distannoxanes grafted to insoluble polystyrene, of the type $[(P–H)_{(1-t)}(\{P–(CH_2)_6SnBuX\}_2O)_{t/2}]$ (X = Cl, OH, $OOCCH_3$) were synthesized from the dialkyldichlorotin precursors. Their characterization and catalytic activity are also discussed.

[a] High Resolution NMR Centre (HNMR), Department of Polymer Science and Structural Chemistry (POSC), Vrije Universiteit Brussel (VUB), Room 10G720, Pleinlaan 2, 1050 Brussels, Belgium
[b] NMR and Structure Analysis Unit, Vakgroep Organische Chemie, University of Ghent, Krijgslaan 281 S4, 9000 Gent, Belgium
[c] Laboratoire de Chimie Organique et Organométallique, CNRS UMR 5802, Université Bordeaux 1, 351 Cours de la Libération, 33405 Talence Cedex, France

Results and Discussion

Synthesis and Characterization

A series of five dialkyldichlorotin compounds $[(P–H)_{(1-t)}\{P–(CH_2)_6SnBuCl_2\}_t]$ (**1a–e**) with t varying between 0.03 and 0.31 was synthesized[7,8] according to Scheme 1.

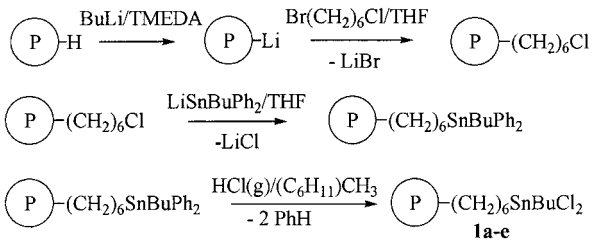

Scheme 1

 © 2004 Wiley-VCH Verlag GmbH & Co. KGaA, Weinheim **DOI: 10.1002/ejic.200400049**

Different degrees of functionalization were obtained by controlled variation of the amount of BuLi in the first lithiation step, resulting in five $(P-H)_{(1-t)}(P-Li)_t$ precursor compounds. The dependence of t on the BuLi/P−H molar ratio in this step is illustrated in Figure 1.

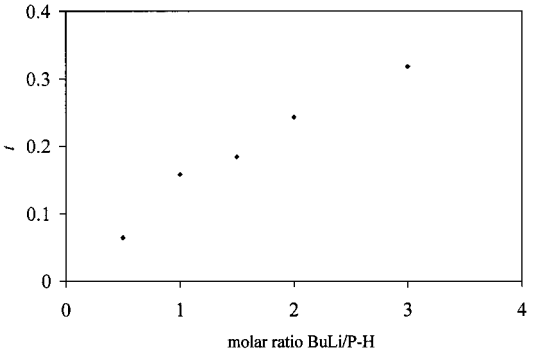

Figure 1. The experimental degree of functionalization (t) as a function of the molar ratio BuLi/P−H in the first reaction step of Scheme 1

The substitution of the phenyl groups by chlorine in the last step of the reaction in Scheme 1, previously performed by reaction with HCl in methanol, suffered from sluggish reactivity leading to polymers with a slight but significant chlorine deficit.[7] In the present synthesis route, pure HCl gas is bubbled for 15 minutes through a suspension of beads of $[(P-H)_{(1-t)}\{P-(CH_2)_6SnBuPh_2\}_t]$ in methylcyclohexane at −80 °C. Using this new route, a better control over the desired substitution reaction was obtained, since less than 2% of grafted R_3SnCl side-functionality was obtained instead of 6−7 % by the HCl/CH_3OH method, as assessed by solid state ^{117}Sn MAS NMR spectroscopy and elemental analysis. Moreover, any possible inconvenience arising from moisture can be better avoided with the latter synthesis route. The determination of t of all precursor compounds and of **1a**−**e** (**1a**, t = 0.03; **1b**, t = 0.10; **1c**, t = 0.12; **1d**, t = 0.21; **1e**, t = 0.31) was performed, as described previously,[7] from experimentally obtained elemental mass fractions of all elements involved, using a mathematical non-linear least-squares procedure, minimizing the impact of the elements leading to larger uncertainty margins.

Since distannoxanes, with general formula $YR_2Sn-O-SnR_2Y$, have also proved to be efficient transesterification catalysts,[9] we were interested in the conversion of compounds **1a**−**e** into compounds of the type $[(P-H)_{(1-t)}(\{P-(CH_2)_6SnBuX\}_2O)_{t/2}]$ with X = Cl, OH, $OOCCH_3$. The synthetic procedures leading to the different Sn−O−Sn-bridged compounds are given in Scheme 2. The reactions were performed twice successively, in order to achieve full conversion as far as possible. IR and Raman spectroscopy were used to monitor the reactions: in the Raman spectra the evolution of the ν(Sn−Cl) band was monitored, while in the IR spectra the appearance of new bands characteristic of the different Sn−O−Sn-bridged compounds can be observed. The purity of the compounds in Scheme 2 was determined by elemental analysis, solid state ^{117}Sn MAS NMR spectroscopy and, where appropriate, by ^{119}Sn hr-MAS NMR spectroscopy. The latter technique is a high resolution liquid NMR technique that is used to obtain NMR spectra of tin-containing grafts dipped in solution, in situ at the solid−liquid interface, provided sufficient local rotational mobility can be achieved on the grafts through matrix pore swelling by the solvent.[8]

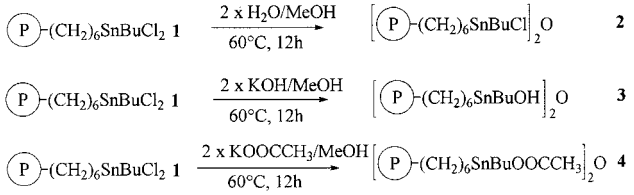

Scheme 2

Whereas the reaction with H_2O and KOH was complete for the compounds with high t value (0.31, compounds **2e** and **3e**), incomplete conversion was observed for the compounds with lower t value (0.03−0.21, compounds **2a**−**d**, **3a**−**d**). This was shown by the presence of residual ν(Sn−Cl) bands in the Raman spectra of **3a**−**d** and the detection of residual amounts of chlorine for **3a**−**d** or too high amounts for **2a**−**d** by elemental analysis; the conversion degree appears to be dependent on t, as illustrated in Figure 2 and 3.

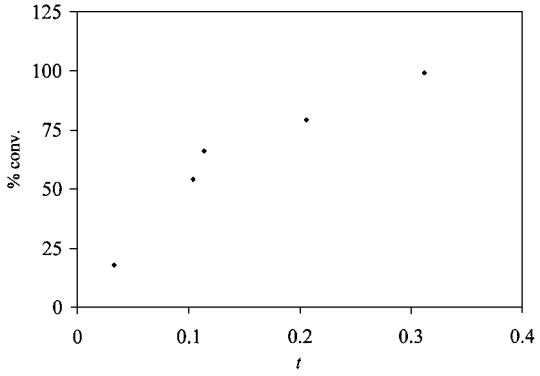

Figure 2. Percentage conversion of **1** into **2** as a function of t

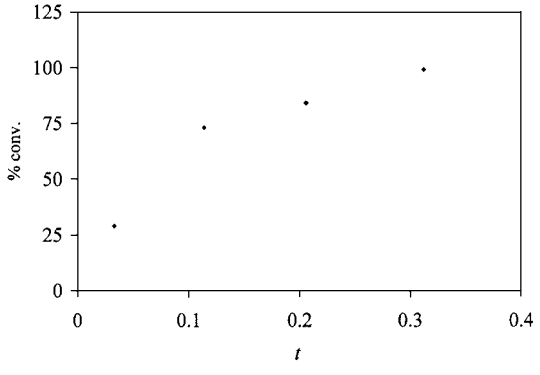

Figure 3. Percentage conversion of **1** into **3** as a function of t

 © 2004 Wiley-VCH Verlag GmbH & Co. KGaA, Weinheim

The explanation for this observation is to be found in the lack of sufficient neighbouring grafted functionalities, which are necessary to generate Sn−O−Sn cross-links, in the compounds with low functionality.

Further evidence for residual $-SnCl_2$ functionalities was found in the ^{119}Sn hr-MAS spectra of **2a**−**d** and **3a**−**d**, which still show resonances for this functionality. This technique, which is used to obtain high resolution liquid-like ^{119}Sn NMR spectra of solvent-swollen beads of $[(P-H)_{(1-t)}\{P-(CH_2)_6SnBuCl_2\}_t]$,[8] in which the tin functionality acquires local rotational mobility, was disappointingly uninformative for **2e** and **3e**, where complete conversion was obtained. In fact, no ^{119}Sn NMR resonance could be generated, probably due to the rigidity of the distannoxane moiety by the additionally introduced Sn−O−Sn cross-linking, preventing sufficient rotational mobility necessary for this technique to be successful.

When reacting **1e** with CH_3COOK in methanol, it was unclear beforehand whether grafted tin compounds of the distannoxane type, $[P-(CH_2)_6SnBuOOCCH_3]_2O$, or of the tin dicarboxylate type, $P-(CH_2)_6SnBu[OOCCH_3]_2$, with both chlorides substituted by acetate, would be obtained, since the synthesis of a compound similar to the latter has already been described in the literature, although in this case the tin moiety is grafted directly to the phenyl rings of an insoluble polystyrene matrix.[10] Therefore, the theoretical mass fractions were calculated for both models using the functionalization degree of the precursor **1e**. When these calculated values were compared to those determined by elemental analysis, the mass fractions, especially the ones for carbon and tin calculated for the Sn−O−Sn model, fitted the experimental values better (see Table 1). Moreover, the positions of the ν(C=O) bands in the IR spectrum of **4e** differ from those of the model dicarboxylate compound $Bu_2Sn(OOCCH_3)_2$, while other characteristic bands of the latter are not found. This favours the proposal that the obtained compound is indeed of the distannoxane type, as is the case for those obtained by reaction of **1** with H_2O or KOH.

Table 1. Comparison of the experimental mass fractions of compound **4e** with the theoretical ones using different models

Model	γ_C (%)	γ_H (%)	γ_{Sn} (%)
Experimental mass fractions	68.80	7.54	18.50
$[P-(CH_2)_6SnBuOOCCH_3]_2O$	68.52	7.43	17.99
$P-(CH_2)_6SnBu[OOCCH_3]_2$	66.98	7.32	16.70

Catalytic Activity

In order to evaluate the catalytic activity of the grafted organotins in **1**−**4**, the reaction between ethyl acetate and octanol (Scheme 3) was investigated. The degree of conversion was calculated from the ratio of initial alcohol to obtained ester by integration of the respective CH_2O ^{1}H NMR resonances. The results are summarized in Table 2.

For the compounds $[(P-H)_{(1-t)}\{P-(CH_2)_6SnBuCl_2\}_t]$ with variable functionalization degree, two types of experiments were performed. Entries 1−4 (type A) were carried out with a constant mass of catalyst (367 mg, corresponding to 1 mol % of **1e**), and consequently a variable molar amount of tin sites. Entries 5−7 (type B) describe reactions with 1 mol % of catalyst (% Sn with respect to octanol). In the first series reasonably good results were obtained for all compounds, with a maximum conversion obtained for t = 0.21, which appears to be the optimal functionalization degree for the catalytic activity (see Table 2). In the second series a slight decrease in conversion was observed with increasing t. Both data sets are in agreement with a better accessibility of the reagents to the catalytic centre at a moderate degree of functionalization, emphasizing the need to find the optimum compromise between having a sufficient number of catalytic sites and avoiding side-chain entanglement due to a too high degree of functionalization.

As far as the distannoxanes are concerned, the catalytic activity is reported for the functionally pure compounds **2e**, **3e** and **4e** only. Although a decreased molecular mobility of the grafted tin functionality is to be expected due to the introduction of Sn−O−Sn bridges, good conversion degrees, comparable (or slightly higher) to those of the precursor compound **1e**, were obtained when using these compounds as catalysts in the transesterification reaction of ethyl acetate with octanol (Table 2; entries 8−11).

The chemical stability of the catalysts under reaction was assessed by solid state ^{117}Sn CP-MAS NMR spectroscopy, at least within the signal-to-noise conditions under which the spectra were obtained. The spectra of compounds **1e** and **2e**, after their use as a catalyst, are reasonably superimposable on the spectra of the same compounds before catalysis. The isotropic chemical shift is found at the same position and no evidence for significant generation of new functionalities can be seen. By way of an example, Figure 4 shows the ^{117}CP-MAS spectrum of **2e** prior to and after a transesterification experiment for 48 hours.

In contrast, the grafted $HOSn-O-SnOH$ (**3e**) and $CH_3COOSn-O-SnOOCCH_3$ (**4e**) compounds are chemically modified during the reaction. Only very ill-defined noisy spectra of these compounds could be obtained, under

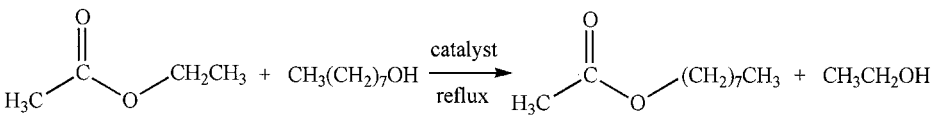

Scheme 3

Table 2. Catalytic activities of dialkyltin- and distannoxane-functionalized polystyrenes in the transesterification of ethyl acetate with octanol

Entry	Catalyst	Type[a]	t	Conv. after 24 h (%)	Conv. after 48 h (%)
1	**1b**	A	0.10	58	87
2	**1c**	A	0.12	65	88
3	**1d**	A	0.21	89	94
4	**1e**	A	0.31	74	89
5	**1c**	B	0.12	84	95
6	**1d**	B	0.21	80	94
7	**1e**	B	0.31	74	89
8	**2e**	B	0.31	78	96
9	**3e**	B	0.31	72	94
10	**4e**	B	0.31	54	90
11	**4e** (re-used)	B	0.31	58	87

[a] A: 367 mg of catalyst, corresponding to 1 mol % Sn with respect to octanol for **1e**, was used; B: 1 mol % Sn (variable mass) with respect to octanol.

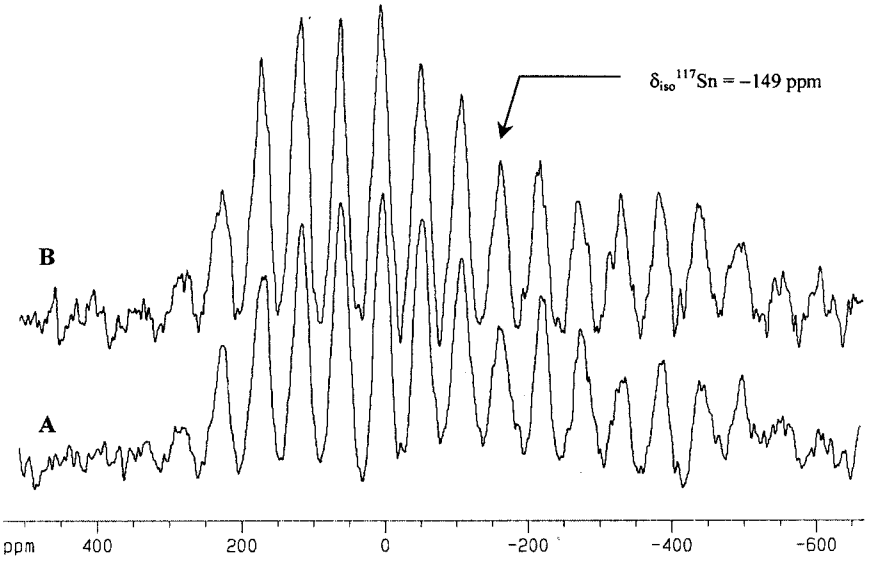

Figure 4. ^{117}Sn CP-MAS spectra of **2e** prior to (A) and after (B) a transesterification experiment

identical acquisition conditions as for the compound before its use as a catalyst, indicating that the organotin grafts are altered during the activation process. The identification of the distannoxane compounds was therefore impossible. Notwithstanding this observation, the catalyst was amenable to a second transesterification run to provide an identical conversion yield as in the first run within experimental error (entry 11 in Table 2). However, as they are chemically unstable, their potential as catalysts is less reliable than for **2e**, which appears to be both efficient and reasonably chemically stable, at least for the model reaction investigated during this work.

Conclusion

Dialkyldichlorotin-grafted polystyrene compounds were obtained with variable degree of functionalization. All compounds showed reasonable catalytic activity in the transesterification reaction of ethyl acetate with octanol. Evidence was found for the existence of an optimal degree of functionalization, interpreted as a compromise between having a sufficient number of catalytic sites and avoiding side-chain entanglement due to a too high degree of functionalization.

The dialkyldichlorotin-grafted polystyrenes were converted into three types of tetraalkyldistannoxanes by reaction with water, hydroxide or acetate. Complete conversion could only be obtained with a sufficiently high degree of functionalization. Their catalytic activity was similar to that of the dialkyldichlorostannanes.

Experimental Section

Synthesis of $[(P-H)_{(1-t)}\{P-(CH_2)_6SnBuCl_2\}_t]$ (1a−e): The polymers were synthesized as summarized in Scheme 1, following a procedure described previously,[7] modified in the last step to allow for a better control of possible side-reactions.[8] In all cases, a divi-

 © 2004 Wiley-VCH Verlag GmbH & Co. KGaA, Weinheim

nylbenzene cross-linked polystyrene, Amberlite XE305 (PolySciences Inc.), was used as the insoluble solid support P−H. In short, a hexamethylene spacer with terminal chloride was grafted onto the insoluble polystyrene P−H, preliminarily lithiated to different extents in the *para* position, by varying the amount of BuLi. In the next step a stannylation reaction with $Ph_2SnBuLi$ in THF substituted the chlorine atom for the $BuPh_2Sn$ group. The $BuCl_2Sn$ functionality in compound **1** was obtained by reaction with HCl gas at −78 °C in methylcyclohexane.[8] IR (cm^{-1}): $\nu_{(Sn-Cl)}$ 340 (m); $\nu_{sym(Sn-Bu)}$ 515 (w); $\nu_{asym(Sn-Bu)}$ 595 (w). $(C_8H_8)_{(1-t)}(C_{18}H_{28}Cl_2Sn)_t$ **1a** (t = 0.033): calcd. C 86.97, H 7.59, Cl 2.03, Sn 3.40; found C 86.96, H 7.78, Cl 3.07, Sn 2.63. **1b** (t = 0.104): calcd. C 78.42, H 7.34, Cl 5.33, Sn 8.92; found C 78.19, H 7.51, Cl 5.44, Sn 7.73. **1c** (t = 0.117): calcd. C 77.16, H 7.30, Cl 5.81, Sn 9.73; found C77.47, H 7.34, Cl 6.32, Sn 9.53. **1d** (t = 0.206): calcd. C 70.21, H 7.10, Cl 8.49, Sn 14.21; found C 70.34, H 7.19, Cl 7.86, Sn 14.46. **1e** (t = 0.312): calcd. C 64.50, H 6.93, Cl 10.68, Sn 17.88; found C 64.51, H 7.24, Cl 10.56, Sn 18.08. ^{119}Sn hr-MAS NMR: δ = 124 ppm.

Synthesis of $[(P-H)_{(1-t)}(\{P-(CH_2)_6SnBuCl\}_2O)_{t/2}]$ (2): Typically, 0.7 g of **1** was covered by MeOH (30 mL) and heated to 60 °C. Water (4 mL) was then added to the reaction mixture. The reaction mixture was stirred magnetically at 60 °C for 6 hours. The solution was removed with a capillary tube and then MeOH (30 mL) and water (4 mL) were again added successively to the polymer beads. The reaction mixture was kept at 60 °C for 18 hours. The obtained target polymer $[(P-H)_{(1-t)}(\{P-(CH_2)_6SnBuCl\}_2O)_{t/2}]$ (**2**) was washed 8 times with methanol (20 mL) and dried under vacuum at 60 °C. $(C_8H_8)_{(1-t)}(C_{18}H_{28}SnClO_{0.5})_t$ (t = 0.31): calcd. C 67.29, H 7.23, Cl 5.57, Sn 18.65; found C 66.98, H 7.32, Cl 6.13, Sn 18.30. IR (cm^{-1}): $\nu_{(Sn-Cl)}$ 337 (m); $\nu_{(Sn-O-Sn)}$ 602 (m); $\nu_{sym(SnBu)}$ 522(w); $\nu_{asym(SnBu)}$ 600 (w). ^{117}Sn MAS NMR: δ_{iso} = −149 ppm.

Synthesis of $[(P-H)_{(1-t)}(\{P-(CH_2)_6SnBuOH\}_2O)_{t/2}]$ (3): The procedure was identical to that described for **2**, but instead of water a solution of KOH (229 mg, 4.08 mmol) in MeOH (20 mL) was added to the reaction mixture. $(C_8H_8)_{(1-t)}(C_{18}H_{29}SnO_{1.5})_t$ (t = 0.31): calcd. C 69.37, H 7.61, Cl 0, Sn 19.15; found C 69.62, H 7.74, Cl 0.33, Sn 19.05. IR (cm^{-1}): $\nu_{(OH)}$ 3650 (w); $\nu_{(Sn-O)}$ 448 (w); $\nu_{asym(Sn-O-Sn)}$ 581 (w); $\nu_{sym(SnBu)}$ 506 (w); $\nu_{asym(SnBu)}$ 601 (w). ^{117}Sn MAS NMR: δ_{iso} = −171 ppm.

Synthesis of $[(P-H)_{(1-t)}(\{P-(CH_2)_6SnBuOOCCH_3\}_2O)_{t/2}]$ (4): The procedure was identical to that described for **2**, but instead of water a solution of CH_3COOK (400 mg, 4.08 mmol) in MeOH (20 mL) was added to the reaction mixture. $(C_8H_8)_{(1-t)}(C_{20}H_{31}SnO_{2.5})_t$ (t = 0.31): calcd. C 68.52, H 7.43, Cl 0, Sn 17.99; found C 68.80, H 7.54, Cl 0.40, Sn 18.50. IR (cm^{-1}): $\nu_{sym(CO)}$ 1319 (w); $\nu_{asym(CO)}$ 1630 (w); $\Delta\nu_{(CO)}$ = 311; $\nu_{(Sn-O)}$ 481 (m); $\nu_{asym(Sn-O-Sn)}$ 608 (w); $\nu_{sym(SnBu)}$ 517 (w); $\nu_{asym(SnBu)}$ 598 (w). ^{117}Sn MAS NMR: δ_{iso} = −167 ppm.

Catalysis Experiments on Transesterification Reactions: Ethyl acetate, used both as reactant ester and solvent, and 1-octanol (Aldrich) were used in a 7:1 molar ratio. A mixture of ethyl acetate (34.1 g, 388 mmol), octanol (7.2 g, 55 mmol) and insoluble Amberlite-supported catalyst (1 mol % Sn with respect to octanol; 367 mg for **1e**) was refluxed for 24 or 48 hours. The catalyst was filtered off and washed with $CHCl_3$, THF and ethanol. The ethyl acetate was distilled off from the reaction mixture. The ratio of initial alcohol to obtained ester was determined by integration (±1 %) of the respective CH_2O ^{1}H NMR resonances.

IR and Raman Spectra: IR spectra were recorded on a Perkin−Elmer System 2000 FT-IR spectrometer (MIR beam) from 200 mg dry KBr pellets containing about 5 mg of substance. The Raman spectra were recorded on a Perkin−Elmer 2000 NIR FT-RAMAN spectrometer using a Raman dpy2 beam with 310 mW power.

NMR Spectroscopic Data: Samples used for the determination of the initial alcohol to obtained ester ratio were prepared by dissolving about 10 mg of mixture in 0.5 mL of $CDCl_3$. Quantitative ^{1}H NMR spectra were recorded on a Bruker AMX500 instrument. The ^{119}Sn hr-MAS spectra were recorded on the same instrument (186.50 MHz) with a specially dedicated Bruker ^{1}H/^{13}C/^{119}Sn hr-MAS probe equipped with gradient coils, by using full rotors containing approximately 20 mg of resin beads, swollen in approximately 100 μL of $CDCl_3$ and spinning at 4000 Hz around the magic angle. External referencing with Ξ = 37.290665 MHz was used. The solid state (CP)-MAS spectra were recorded on a Bruker DRX250 spectrometer, operating at 62.90 and 89.15 MHz for ^{13}C and ^{117}Sn nuclei, respectively, using procedures described previously.[11,12] The solid state ^{117}Sn MAS NMR spectra were deconvoluted by total-lineshape (TLS) fitting[13,14] of the experimental spectra using the PERCH[15] software package.

Acknowledgments

M. B. and R. W. are indebted to the Fund for Scientific Research Flanders (Belgium) (FWO) for financial support (Grant no. 9.0016.02) as well as the Research Council of the VUB for matching funds.

[1] [1a] A. G. Davies, in *Chemistry of Tin*, 2nd ed. (Ed.: P. J. Smith), Blackie, London, **1998**, pp. 265−289. [1b] A. G. Davies, *Organotin Chemistry*, VCH, Blackie, Weinheim, **1997.** [1c]O. A. Mascaretti, R. E. Furlan, *Aldrich Chim. Acta* **1997**, *30*, 55−68.
[2] B. Jousseaume, M. Pereyre, in *Chemistry of Tin*, 2nd ed. (Ed.: P. J. Smith), Blackie, London, **1998**, pp. 290−387.
[3] W. P. Neumann, M. Peterseim, *React. Polym.* **1993**, *20*, 189−205.
[4] [4a] M. Hoch, *Appl. Geochem.* **2001**, 719−743. [4b] Y. Arakawain, in *Chemistry of Tin*, 2nd ed. (Ed.: P. J. Smith), Blackie, London, **1998**, pp. 388−428. [4c] M. A. Champ, P. F. Seligman, *Organotin: Environmental Fate and Effects*, Chapman & Hall, London, **1996**.
[5] C. J. Salomon, G. O. Danelon, O. A. Mascaretti, *J. Org. Chem.* **2000**, *65*, 9220−9222 and references cited therein.
[6] B. Delmond, G. Dumartin, in *Solid-State Organometallic Chemistry: Methods and Applications* (Eds.: M. Gielen, R. Willem, B. Wrackmeyer), Wiley, Chichester, **1999**, pp. 445−471, and references cited therein.
[7] F. A. G. Mercier, M. Biesemans, R. Altmann, R. Willem, R. Pintelon, J. Schoukens, B. Delmond, G. Dumartin, *Organometallics* **2001**, *20*, 958−962.
[8] J. C. Martins, F. A. G. Mercier, A. Vandervelden, M. Biesemans, J.-M. Wieruszeski, E. Humpfer, R. Willem, G. Lippens, *Chem. Eur. J.* **2002**, *8*, 3431−3441.
[9] [9a] J. Otera, T. Yano, A. Kawabata, H. Nozaki, *Tetrahedron Lett.* **1986**, *27*, 2383−2386. [9b] J. Otera, S. Ioka, H. Nozaki, *J. Org. Chem.* **1989**, *54*, 4013−4014. [9c] J. Otera, N. Dan-Oh, H. Nozaki, *J. Org. Chem.* **1991**, *56*, 5307−5311. [9d] J. Otera, N. Dan-Oh, H. Nozaki, *J. Chem. Soc., Chem. Commun.* **1991**, 1742−1743. [9e] J. Otera, N. Dan-Oh, H. Nozaki, *Tetrahedron* **1993**, *49*, 3065−3074.
[10] W. M. Macindoe, A. Williams, R. Khan, *Carbohydr. Res.* **1996**, *283*, 17−25.
[11] G. Dumartin, J. Kharboutli, B. Delmond, M. Pereyre,

 © 2004 Wiley-VCH Verlag GmbH & Co. KGaA, Weinheim

M. Biesemans, M. Gielen, R. Willem, *Organometallics* **1996**, *15*, 19−23.
[12] M. Biesemans, R. Willem, S. Damoun, P. Geerlings, M. Lahcini, P. Jaumier, B. Jousseaume, *Organometallics* **1996**, *15*, 2237−2245.
[13] R. Laatikainen, *J. Magn. Reson.* **1991**, *92*, 1−9.
[14] R. Laatikainen, M. Niemitz, U. Weber, J. Sundelin, T. Hassinen, J. Vepsäläinen, *J. Magn. Reson.* **1996**, *A120*, 1−10.
[15] PERCH Version 1/99; University of Kupio, Finland, **1999**.
Received January 26, 2004
Early View Article
Published Online May 6, 2004

 © 2004 Wiley-VCH Verlag GmbH & Co. KGaA, Weinheim

Oxalato-Bridged [$Cu^{II}Cr^{III}$] and [$Mn^{II}Cr^{III}$] Binuclear Complexes: Synthesis, Crystal Structures, Magnetic and EPR Investigations

Gabriela Marinescu,[a,b] Diana Visinescu,[a,b] Andrei Cucos,[a] Marius Andruh,*[a] Yves Journaux,*[c] Victor Kravtsov,[d] Yurii A. Simonov,[d] and Janusz Lipkowski[e]

Dedicated to Professor Herbert W. Roesky

Keywords: Copper complexes / Magnetic properties / Manganese complexes / Oxalato bridges

Two new heterobinuclear complexes, [(bipy)(C_2O_4)Cr(μ-C_2O_4)Cu(Hfsaaep)(H_2O)]·2H_2O (**1**) and [(phen)(C_2O_4)Cr(μ-C_2O_4)Mn(phen)$_2$(N_3)]·H_2O (**2**) have been obtained by using bis(oxalato)chromium(III) anions, [Cr(AA)(C_2O_4)$_2$]$^-$, as building blocks [AA = 2,2′-bipyridine (bipy); 1,10-phenanthroline (phen)]. The crystal structures of the two complexes have been solved. These complexes comprise neutral oxalato-bridged Cr^{III}–Cu^{II} and Cr^{III}–Mn^{II} units. The [Cr(AA)(C_2O_4)$_2$]$^-$ anion acts as a bidentate ligand toward Cu^{II} in compound **1** and as a monodentate ligand toward Mn^{II} in compound **2**. The copper(II) ion in **1** exhibits a slightly distorted square bipyramidal stereochemistry, with the aqua ligand and one of the bridging oxalato oxygen atoms disposed in the apical positions [Cu(1)–O(1w) = 2.360(3) Å and Cu(1)–O(4) = 2.504(2) Å]. The second bridging oxalato oxygen atom [Cu(1)–O(2) = 2.0747(18) Å] and the *N*,*N*,*O*-type Hfsaaep ligand are located in the basal plane. The distance between the Cr^{III} and Cu^{II} ions across the bridging oxalate unit is 5.506 Å. The Mn^{II} ion in compound **2** is hexacoordinate (two chelating phen ligands, one oxalato bridging oxygen, and one terminal azido group). The intermolecular Cr^{III}···Mn^{II} distance is 5.257 Å. The magnetic properties of the two complexes have been investigated. The magnetic coupling between Cr^{III} and Cu^{II} in **1** was found to be ferromagnetic (J = +1.4 cm^{-1}). The nature of the ground state (S = 2) has been further confirmed by plotting the magnetization-versus-field curve. An antiferromagnetic interaction was found between Cr^{III} and Mn^{II} in compound **2** (J = –1.9 cm^{-1}). The magnetization-versus-field curve indicates the occurrence of a crossover between the Zeeman components: M_S = –1 (ground state S = 1), M_S = –2, from the first excited state (S = 2), and M_S = –3, from the second excited state. The EPR spectra of the two compounds are discussed.

(© Wiley-VCH Verlag GmbH & Co. KGaA, 69451 Weinheim, Germany, 2004)

Introduction

The ability of the oxalato anion to generate homo- and heteropolynuclear complexes with various nuclearities or dimensionalities is well known.[1] This chemistry has been stimulated mainly by the interesting magnetic properties exhibited by such compounds.[2] A plethora of oxalato-bridged homopolynuclear complexes has been characterized so far. These compounds are generally obtained through reactions involving a cationic complex, with potentially free coordination sites, and the oxalate anion. The presence of an ancillary ligand in the coordination sphere of the metallic ion, other than the water molecules, prevents the formation of the insoluble oxalates, and, moreover, influences the nuclearity, as well as the topology, of the metallic centers. As far as the heterometallic complexes are concerned, their synthesis raises an important point: the one-pot procedure, that is, the reaction of two different metal complexes with the oxalate anion, most frequently leads to mixtures of compounds and it is, therefore, inappropriate. To overcome this difficulty, an alternative synthetic approach has been developed: it employs anionic oxalato complexes as ligands toward the second metal ion ("complexes as ligands"; "building-block approach"). Particularly useful for the design of heterometallic systems are homoleptic and heteroleptic anionic complexes of chromium(III) containing potentially bridging oxalato groups. These sys-

[a] Inorganic Chemistry Laboratory, Faculty of Chemistry, University of Bucharest,
Str. Dumbrava Rosie nr. 23, 020464 Bucharest, Romania
E-mail: marius.andruh@dnt.ro
[b] Institute of Physical Chemistry "I. G. Murgulescu", Romanian Academy,
Splaiul Independentei 202, 060021 Bucharest, Romania
[c] Laboratoire de Chimie Inorganique, UMR CNRS 8613, Université de Paris-Sud,
Bât. 420,
91405 Orsay, France
E-mail: jour@icmo.u-psud.fr
[d] Institute of Applied Physics, Academy of Sciences of Moldova, Academy str. 5, 2028 Chisinau, R. Moldova
[e] Institute of Physical Chemistry, Polish Academy of Sciences, Str. Kasprzaka 44/52, 01−224 Warsaw, Poland

 © 2004 Wiley-VCH Verlag GmbH & Co. KGaA, Weinheim **DOI: 10.1002/ejic.200400061**

tems are relatively stable towards substitution reactions and allow a good control over the reaction products. Three types of mononuclear chromium(III) oxalato complexes have been employed as building-blocks in obtaining heteropolynuclear systems: mono-oxalato, $[Cr(salen)(C_2O_4)]^-$ [H_2salen = *N*,*N*′-ethylenebis(salicylideneimine)][3] and $[Cr(acac)_2(C_2O_4)]^-$ (Hacac = acetylacetone),[4] bis(oxalato), $[Cr(AA)(C_2O_4)_2]^-$ [AA = 2,2′-bipyridine (bipy),[5] 1,10-phenanthroline (phen),[6] 2,2′-bipyrimidine (bpym),[7] and 2,2′-dipyridylamine (dpa)[8]], and tris(oxalato), $[Cr(C_2O_4)_3]^{3-}$, species.[9] While the homoleptic complex, $[Cr(C_2O_4)_3]^{3-}$, with three potentially bridging groups, is extensively used to generate two- or three-dimensional networks, the mono-oxalato species are appropriate for the synthesis of heterobinuclear complexes.

In a series of papers, it has been shown that bis-oxalato complexes of chromium(III), $[Cr(AA)(C_2O_4)_2]^-$ (AA = 2,2′-bipy, 1,10-phen, bpym, dpa), are extremely versatile building-blocks for the synthesis of heteropolynuclear complexes having a rich variety of structures.[5–8] The self-assembly processes between these species and mono- or dipositive hydrated cations led to two series of heteropolynuclear complexes: $[M^{I}Cr(bipy)(C_2O_4)_2(H_2O)_x]\cdot yH_2O$ (M = K, Na, Ag) and $[M^{II}Cr_2(bipy)_2(C_2O_4)_4(H_2O)_n]\cdot mH_2O$ (M = Ba, Mn, Co, Ni, Cu). Within each series, completely different structures have been obtained, according to the coordination algorithm of the assembling cation. We have also shown that the structures of the heterometallic complexes can be further influenced by using ancillary ligands attached to the assembling cation. For example, the reaction between Mn^{2+}(aq), 2,2′-bipyridine, and $[Cr(phen)(C_2O_4)_2]^-$ in the presence of sodium oxalate led to a tetranuclear [$Cr^{III}-C_2O_4-Mn^{II}-C_2O_4$-$Mn^{II}-C_2O_4-Cr^{III}$] complex.[6]

In this paper we report two new heterobinuclear complexes, which have been obtained by using bis-oxalato building blocks and ancillary ligands attached to the second metal ion: $[(bipy)(C_2O_4)Cr(\mu\text{-}C_2O_4)Cu(Hfsaaep)(H_2O)]\cdot 2H_2O$ {H_2fsaaep = 3-[*N*-2-(pyridylethyl)formimidoyl]salicylic acid} and $[(phen)(C_2O_4)Cr(\mu\text{-}C_2O_4)Mn(phen)_2(N_3)]\cdot H_2O$.

Results and Discussion

The complexes reported here have been obtained through reactions involving the $[Cr(AA)(C_2O_4)_2]^-$ building blocks and cationic complex species of Cu^{II} and Mn^{II}.

The [CuCr] complex has been synthesized by reacting the bis-oxalato chromium precursor, $[NaCr(bipy)(C_2O_4)_2(H_2O)]\cdot 2H_2O$[5c] with the binuclear chloro-bridged copper(II) complex, $[Cu(Hfsaaep)Cl]_2$ {H_2fsaaep is a Schiff base ligand derived from 3-formylsalicylic acid: 3-[*N*-2-(pyridylethyl)formimidoyl]salicylic acid}.[10] The chloro anion in the {Cu(hfsaaep)Cl} moiety was substituted by the $[Cr(bipy)(C_2O_4)_2]^-$ unit, resulting in a neutral [CuCr] heterobinuclear complex, **1**.

In the attempt to synthesize a $Mn^{II}_2Cr^{III}_2$ tetranuclear complex, with two different bridges connecting the metal ions (oxalato and azido), we have obtained a binuclear complex having an oxalato bridge between the two metal ions and a terminal azido ligand bound to manganese: $[(phen)(C_2O_4)Cr(\mu\text{-}C_2O_4)Mn(phen)_2(N_3)]\cdot H_2O$ (**2**). The phen:Mn^{II} molar ratio has been chosen to be 1:1 to prevent the formation of the tris-chelated manganese complex.

Description of the Structures

$[(Bipy)(C_2O_4)Cr(\mu\text{-}C_2O_4)Cu(Hfsaaep)(H_2O)]\cdot 2H_2O$ (1): The structure of **1** consists of neutral [CuCr] binuclear entities and uncoordinated water molecules (Figure 1). Crystal data, data collection parameters, and structure refinement details are given in Table 3. Selected bond lengths and angles are collected in Table 1. The $[Cr(bipy)(C_2O_4)_2]^-$ ion acts as a bidentate ligand toward the copper(II) ion, that is, one oxalato group acts simultaneously as a bidentate ligand toward chromium and copper. The distance between the Cr^{III} and Cu^{II} ions across the bridging oxalate is 5.506 Å. This distance is longer than those found in the trinuclear complex $[CuCr_2(bipy)_2(C_2O_4)_4(H_2O)_2]\cdot 1.5H_2O$ (Cu···Cr = 5.328 Å), where the two metal ions are bridged by a bis-chelating oxalato group,[5a] and in the binuclear $[(bipy)_2Cu(\mu\text{-}C_2O_4)Cr(C_2O_4)_2]^+$ species (5.056 Å).[11] We recall that in the last compound,[11] the oxalato group behaves as a monodentate ligand toward the copper and its bridging mode differs from that found in complex **1**. The copper atom is coordinated by two oxygen atoms arising from the oxalato bridge, one phenolic oxygen and two nitrogen atoms arising from the organic ligand (one nitrogen atom from the azomethine group, and the other one from the pyridyl ring), and one aqua ligand. The coordination polyhedron of the copper atom may be described as a distorted square-based bipyramid. The apical positions are occupied by the aqua ligand [Cu(1)–O(1w) = 2.360(3) Å] and one oxygen atom from the bridging oxalato group, Cu(1)–O(4) = 2.504(2) Å. The phenolic group of the Schiff base ligand is deprotonated, while the carboxylic group is protonated. The strong intramolecular hydrogen bond,

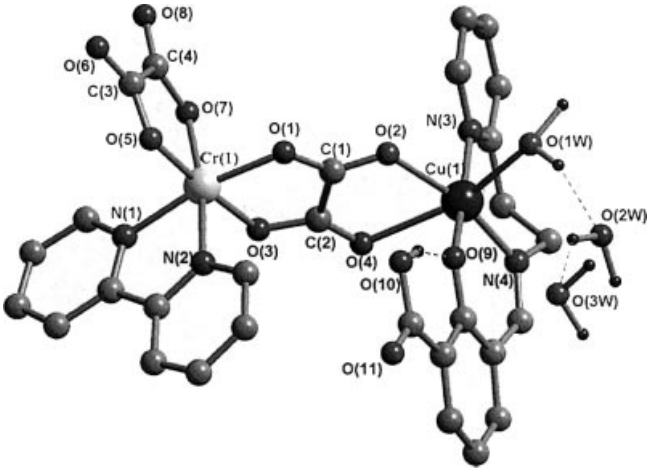

Figure 1. Perspective view of a molecule in crystal **1**, along with the atom numbering scheme

 © 2004 Wiley-VCH Verlag GmbH & Co. KGaA, Weinheim

Table 1. Selected bond lengths (Å) and angles (°)

1		2	
Cu(1)−O(9)	1.9282(18)	Mn(1)−N(7)	2.1592(19)
Cu(1)−N(4)	1.971(2)	Mn(1)−O(4)	2.1883(15)
Cu(1)−N(3)	2.015(2)	Mn(1)−N(5)	2.2385(18)
Cu(1)−O(2)	2.0747(18)	Mn(1)−N(4)	2.2424(18)
Cu(1)−O(1 W)	2.360(3)	Mn(1)−N(3)	2.2937(18)
Cu(1)−O(4)	2.504(2)	Mn(1)−N(6)	2.2944(18)
Cr(1)−O(5)	1.939(2)	Cr(1)−O(5)	1.9300(15)
Cr(1)−O(7)	1.941(2)	Cr(1)−O(7)	1.9081(14)
Cr(1)−O(3)	1.9720(17)	Cr(1)−O(3)	1.9466(14)
Cr(1)−O(1)	1.9786(18)	Cr(1)−O(1)	2.0064(15)
Cr(1)−N(1)	2.057(2)	Cr(1)−N(1)	2.1344(18)
Cr(1)−N(2)	2.064(2)	Cr(1)−N(2)	2.0435(17)
		N(7)−N(8)	1.198(3)
		N(8)−N(9)	1.207(3)
O(9)−Cu(1)−N(4)	91.88(8)	N(7)−Mn(1)−O(4)	89.92(7)
O(9)−Cu(1)−N(3)	171.18(9)	N(7)−Mn(1)−N(5)	167.52(7)
N(4)−Cu(1)−N(3)	95.60(9)	O(4)−Mn(1)−N(5)	88.13(6)
O(9)−Cu(1)−O(2)	83.16(8)	N(7)−Mn(1)−N(4)	91.50(7)
N(4)−Cu(1)−O(2)	166.08(8)	O(4)−Mn(1)−N(4)	156.85(6)
N(3)−Cu(1)−O(2)	90.58(8)	N(5)−Mn(1)−N(4)	95.13(6)
O(9)−Cu(1)−O(1 W)	83.99(9)	N(7)−Mn(1)−N(3)	90.72(7)
N(4)−Cu(1)−O(1 W)	106.63(10)	O(4)−Mn(1)−N(3)	81.83(6)
N(3)−Cu(1)−O(1 W)	89.38(9)	N(5)−Mn(1)−N(3)	101.20(6)
O(2)−Cu(1)−O(1 W)	85.84(9)	N(4)−Mn(1)−N(3)	75.05(7)
O(9)−Cu(1)−O(4)	91.01(8)	N(7)−Mn(1)−N(6)	96.35(7)
N(4)−Cu(1)−O(4)	92.91(8)	O(4)−Mn(1)−N(6)	111.54(6)
N(3)−Cu(1)−O(4)	93.27(8)	N(5)−Mn(1)−N(6)	72.98(6)
O(2)−Cu(1)−O(4)	74.25(6)	N(4)−Mn(1)−N(6)	91.26(7)
O(1 W)−Cu(1)−O(4)	159.93(9)	N(3)−Mn(1)−N(6)	164.78(7)
O(5)−Cr(1)−O(7)	83.66(10)	O(5)−Cr(1)−O(7)	84.65(6)
O(5)−Cr(1)−O(3)	176.23(8)	O(5)−Cr(1)−O(3)	173.92(6)
O(7)−Cr(1)−O(3)	94.75(9)	O(7)−Cr(1)−O(3)	90.57(6)
O(5)−Cr(1)−O(1)	94.21(8)	O(5)−Cr(1)−O(1)	93.96(6)
O(7)−Cr(1)−O(1)	92.56(9)	O(7)−Cr(1)−O(1)	94.03(6)
O(3)−Cr(1)−O(1)	82.43(7)	O(3)−Cr(1)−O(1)	82.60(6)
O(5)−Cr(1)−N(1)	92.96(9)	O(5)−Cr(1)−N(1)	89.43(6)
O(7)−Cr(1)−N(1)	95.34(9)	O(7)−Cr(1)−N(1)	93.63(7)
O(3)−Cr(1)−N(1)	90.59(8)	O(3)−Cr(1)−N(1)	94.63(6)
O(1)−Cr(1)−N(1)	169.87(8)	O(1)−Cr(1)−N(1)	171.88(6)
O(5)−Cr(1)−N(2)	90.37(9)	O(5)−Cr(1)−N(2)	89.11(7)
O(7)−Cr(1)−N(2)	171.55(9)	O(7)−Cr(1)−N(2)	170.92(7)
O(3)−Cr(1)−N(2)	91.56(8)	O(3)−Cr(1)−N(2)	96.05(6)
O(1)−Cr(1)−N(2)	93.84(8)	O(1)−Cr(1)−N(2)	92.97(7)
N(1)−Cr(1)−N(2)	78.95(8)	N(1)−Cr(1)−N(2)	79.69(7)

O(10)−H···O(9) (Table 2), binds this moieties and contributes to their planar arrangement.

The chromium atom is coordinated by two bipy nitrogen and four oxygen atoms, adopting a distorted octahedral geometry. The short bites of the bipy [78.95(8)°] and oxalato ligands [82.43(7) and 83.65(10)°] are the main factors responsible for the distortion of the $[CrN_2O_4]$ chromophore. The Cr−N bond lengths [2.057(2) and 2.064(2) Å] are somewhat longer than the Cr−O(ox) ones (Table 1). The Cr−O bond lengths are slightly shorter for the terminal oxalato ligand [1.939(2) and 1.941(2) Å] than for the bridging one [1.9720(17) and 1.9786(18) Å]. Both Cu^{II} and Cr^{III} ions reside close to the plane of the bridging oxalato ligand and deviate from it by 0.209(3) and 0.018(3) Å, respectively.

The heterobinuclear [CuCr] entities are interconnected through hydrogen bonding interactions involving the two water molecules, the oxygen atoms from the terminal oxalato group, and the aqua ligand coordinated to copper, which results in infinite chains (Figure 2). The distances associated with these interactions are summarized in Table 2. The chains are interconnected in a layer parallel to the (*ab*) crystallographic plane by week π−π stacking interactions (3.57 Å) between pyridine moieties of Hfsaaep and bifurcated O(3 W)···O(7), O(3 W)···O(8) hydrogen bonds (Table 2). The water molecules and hydrophilic fragments of **1** dwell inside such layers, while the hydrophobic bipy entities point outside. The bipy ligands from neighboring layers are arranged in a parallel mode and mutually intercalate with alternating spacings of 3.44 and 3.59 Å (Figure 3). These π−π stacking interactions between the bipy ligands act as a 2-D zipper and join the layers in the direction of the *c* axis (Figure 3).

$[(Phen)(C_2O_4)Cr(\mu\text{-}C_2O_4)Mn(phen)_2(N_3)]\cdot H_2O$ (2): The crystal structure of **2** consists of neutral [MnCr] heterobinuclear entities and crystallization water molecules. The $[Cr(phen)(C_2O_4)_2]^-$ ion acts as a monodentate ligand through an oxalato oxygen atom toward the $[Mn(phen)_2(N_3)]^+$ moiety (Figure 4). The intramolecular Cr···Mn distance is 5.257 Å. Selected bond lengths and angles are gathered in Table 1. The parameters of the hydrogen bonds are listed in Table 2. The manganese(II) ion is hexacoordinated by four nitrogen atoms arising from the phen molecules, one from the azido ion, and by one oxygen atom from the bridging oxalato group. The Mn(1)−N(phen) distances are in the range 2.2385(18)−2.2944(18) Å, while the Mn(1)−N(azido) bond is shorter [2.1592(19) Å]. The Mn−O(oxalato) distance is 2.1883(15) Å. The azido group is almost linear (the N−N−N angle is 178.4(2)°]. The connection between Mn and the azido ligand is bent: the value of the Mn(1)−N(7)−N(8) angle is 117.20(15)°. The bite angles of the phen ligands are 75.05(7) and 72.98(6)°.

As far as the chromium environment is concerned, it exhibits the same characteristic features observed for other compounds containing the $\{Cr(phen)(C_2O_4)_2\}$ moiety.[6] The dihedral angles between the plane of the 1,10-phenanthroline ligand and the planes of the bridging and terminal oxalato groups are 71.72(3)° and 85.13(4)°, respectively. The dihedral angle between oxalato groups is 85.07(4)°.

The 1,10-phenanthroline ligands associated with N(1)/N(2) and N(5)/N(6) atoms are almost parallel in complex **2** and partially overlap. The corresponding dihedral angle [12.51(6)°] and the interplanar spacing of 3.44−4.01 Å in the overlapped area suggest the possibility of intramolecular π−π stacking interactions, which seems to be an interesting characteristic feature of this complex.

Several $Mn^{II}-Cr^{III}$ oxalato-bridged complexes are known.[5a,6,9] To the best of our knowledge, this Mn^{II}−(μ-oxalato)−Cr^{III} binuclear complex is the first to be structurally characterized.

The intermolecular π−π stacking interactions play an important role in controlling the packing of compound **2** in the crystal. The phenanthroline ligands coordinated to the

 © 2004 Wiley-VCH Verlag GmbH & Co. KGaA, Weinheim

Table 2. Hydrogen bonds in the structures of **1** and **2**

D−H···A	*d*(D−H)	*d*(H···A)	*d*(D···A)	Angle (°) (D−H···A)
1				
O(10)−H(10)···O(9)	0.815(19)	1.72(2)	2.494(3)	159(4)
O(1 W)−H(1 W1)···O(2 W)	0.87(5)	1.89(5)	2.723(4)	160(5)
O(1 W)−H(2 W1)···O(8)#1	1.09(5)	2.04(5)	3.016(4)	146(4)
O(2 W)−H(1 W2)···O(3 W)	1.05(2)	1.97(5)	2.886(6)	143(5)
O(2 W)−H(2 W2)···O(6)#2	1.03(2)	2.06(4)	2.965(5)	145(5)
O(3 W)−H(1 W3)···O(6)#2	1.04(2)	1.93(5)	2.799(5)	139(6)
O(3 W)−H(2 W3)···O(8)#3	1.05(2)	2.42(5)	3.257(5)	136(5)
O(3 W)−H(2 W3)···O(7)#3	1.05(2)	2.36(5)	3.093(5)	126(4)
2				
O(1 W)−H(1 W)···N(9)	0.83(4)	2.16(4)	2.975(3)	164(4)
O(1 W)−H(2 W)···O(2)	0.84(4)	2.15(4)	2.939(3)	155(4)

Symmetry transformations used to generate equivalent atoms:
(#1) $-x+1, -y, -z$; (#2) $x, y+1$, z; (#3) $x-1, y+1, z$.

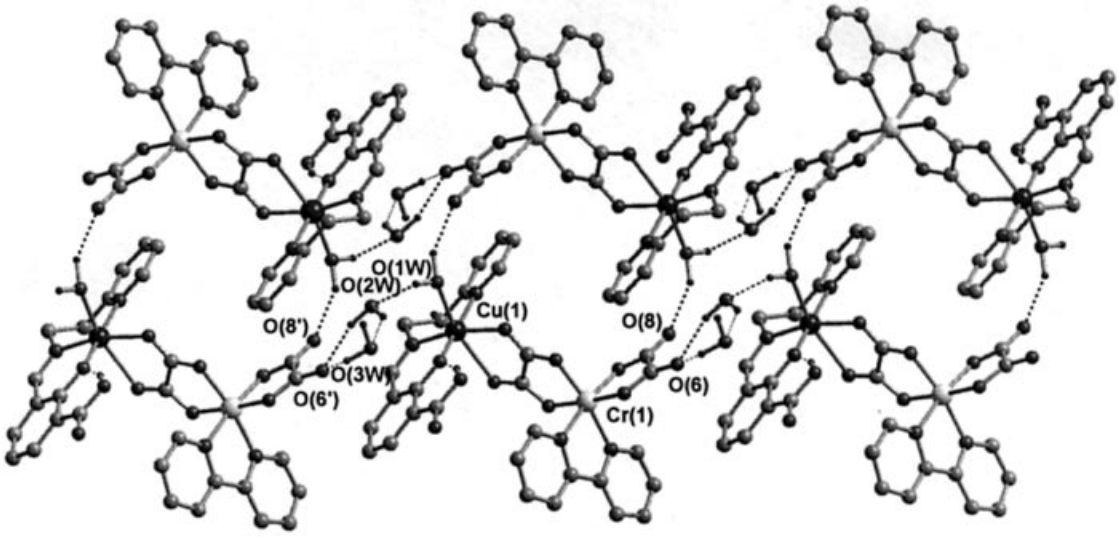

Figure 2. Hydrogen bonding interactions established between the [CuCr] units and the uncoordinated water molecules in crystal **1**

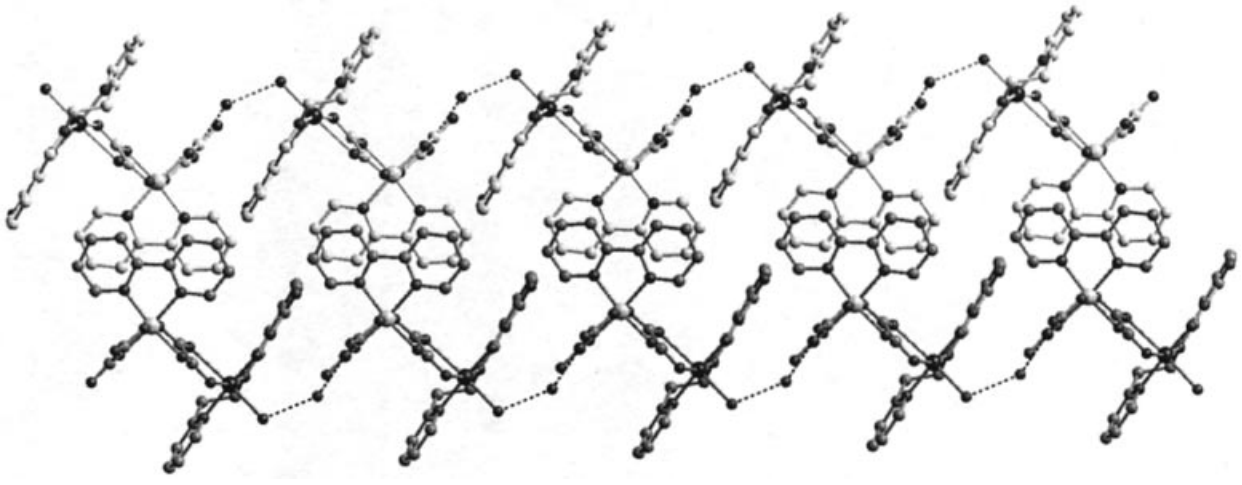

Figure 3. Packing diagram for compound **1**, showing the π−π stacking interactions between the bipy ligands

 © 2004 Wiley-VCH Verlag GmbH & Co. KGaA, Weinheim

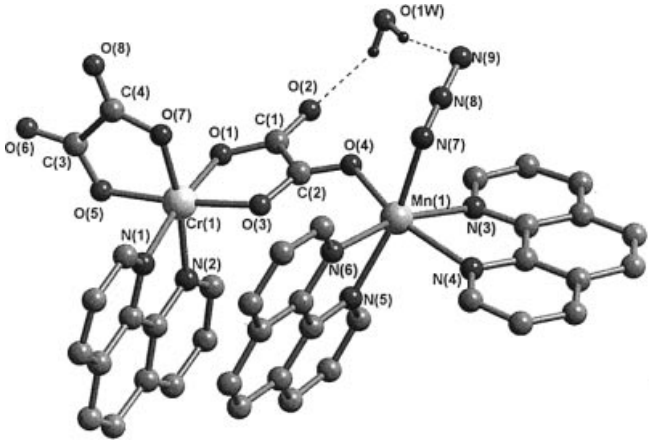

Figure 4. Molecular structure of the binuclear complex in crystal **2**

manganese ions, associated with the N(3) and N(4) atoms, are partially overlapped. The small separation between these phen molecules (3.38 Å), which are related by a center of symmetry, indicate the occurrence of strong π−π interactions (Figure 5). In addition, the phen molecules coordinated to chromium and manganese atoms belonging to two different binuclear units also interact through π−π stacking. The interplanar spacing in this case is in the range of 3.17−4.14 Å. The convolution of the stacking interactions between the phenanthroline molecules coordinated to Mn and Cr atoms results in well-defined layers, which parallel the (*bc*) crystallographic plane (Figure 5). The repeating motif consists of four [MnCr] binuclear units that are interconnected through the aromatic−aromatic interactions established between six phenanthroline moieties. The water molecules occupy the space between the layers.

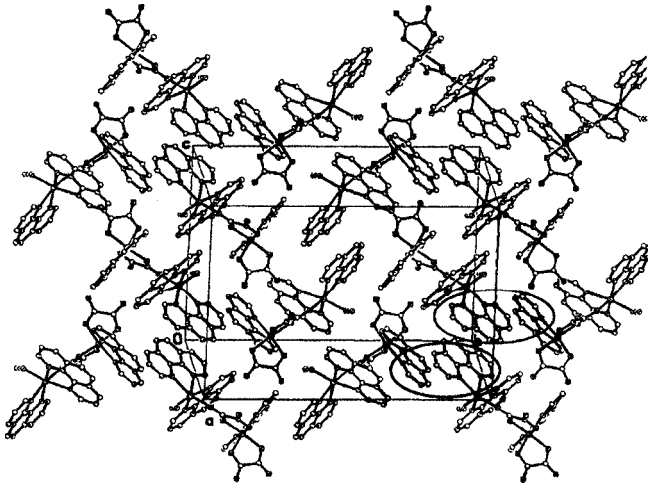

Figure 5. Packing diagram for compound **2**; the two pairs of phen ligands that interact through intermolecular π−π stacking are indicated by circles

Magnetic Properties

The cryomagnetic properties of compounds **1** and **2** deserve to be deeply investigated for two special reasons. (i) Although the bridging mode of the oxalato ligand in compound **1** has been observed with several other [CuCr] complexes,[11−13] the axial coordination of the oxalato oxygen atom to the square-pyramidal copper(II) ion in such compounds leads to the lack of any exchange interaction between Cr^{III} and Cu^{II} ions. In compound **1**, one of the oxygen atoms arising from the oxalato group is coordinated in the basal plane of the coordination polyhedron of copper and can efficiently mediate the exchange interaction between the $d_{x^2-y^2}$ magnetic orbital of Cu^{II} and the magnetic orbitals of Cr^{III}. (ii) The low nuclearity of compound **2** makes it a good candidate for studying the magnetic interactions in Mn^{II}−(μ-oxalato)−Cr^{III} complexes, because the data on such compounds is rather scarce. The plots of $\chi_M T$ versus T for compounds **1** and **2** are given in Figures 6 and 7.

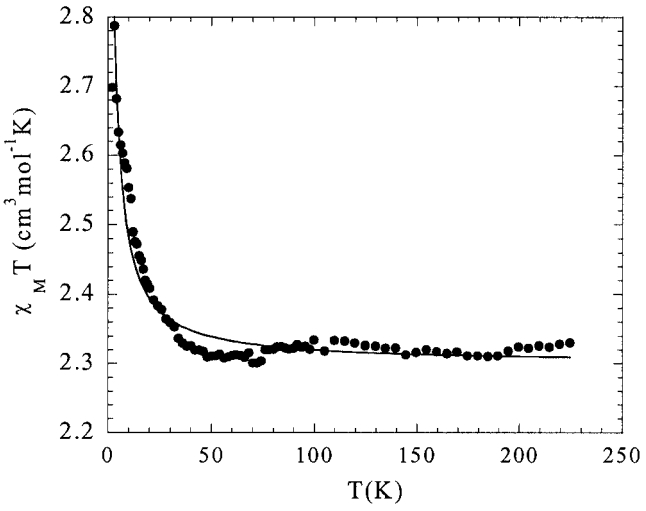

Figure 6. Plots of $\chi_M T$ vs. T for compound **1**; the solid line represents the curve of best fit

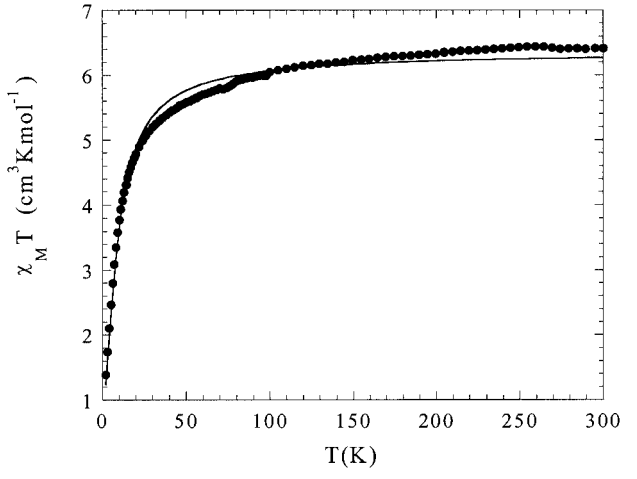

Figure 7. Plots of $\chi_M T$ vs. T for compound **2**; the solid line represents the curve of best fit

At 225 K the value of the $\chi_M T$ product for compound **1** is equal to 2.33 $cm^3 \cdot mol^{-1}K$, which corresponds to the ex-

 © 2004 Wiley-VCH Verlag GmbH & Co. KGaA, Weinheim

pected value for a spin doublet and spin quadruplet isolated magnetically (the calculated value is 2.25 $cm^3 \cdot mol^{-1}K$, assuming, in a first approximation, $g_{Cu} = g_{Cr} = 2$). By decreasing the temperature, $\chi_M T$ remains constant down to 50 K and then it increases, reaching a value of 2.7 $cm^3 \cdot mol^{-1}K$ at 2 K. This behavior indicates a ferromagnetic intramolecular interaction. For the Cu^{II} ($S = 1/2$)−Cr^{III} ($S = 3/2$) system, the energies of the low-lying spin states are obtained by using the isotropic spin Hamiltonian: $\boldsymbol{H} = -J\boldsymbol{S}_{Cu}\mathbf{S}_{Cr}$, which leads to Equation (1) describing the temperature dependence of the $\chi_M T$ product, where $g_1 = (5g_{Cr} - g_{Cu})/4$ and $g_2 = (3g_{Cr} + g_{Cu})/4$.

$$\chi_M T = \frac{2N\beta^2}{k}\frac{5g_2^2 + g_1^2 e^{-2J/kT}}{5 + 3e^{-2J/kT}} \quad (1)$$

Least-squares fitting to the data leads to the following values: $J = +1.4\ cm^{-1}$; $g_{Cr} = 1.99$ (fixed); $g_{Cu} = 2.1$, with $R = 2.2 \times 10^{-4}$ {R is the agreement factor defined as $\Sigma_i[(\chi_M T)_{obsd.}(i) - (\chi_M T)_{calcd.}(i)]^2/\Sigma_i[(\chi_M T)_{obsd.}(i)]^2$}.

To confirm the nature of the ground state, we investigated the variation of the magnetization, M, with respect to the field, at 2 K (Figure 8). The $M = f(H)$ curve closely follows the Brillouin function for a $S = 2$ system, and it is situated above the Brillouin function constructed for two independent $S = 1/2$ and $S = 3/2$ systems.

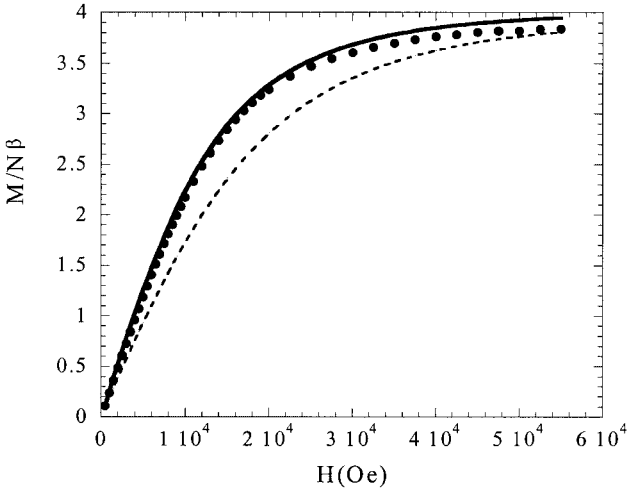

Figure 8. Magnetization-vs.-field curve for compound **1**; solid line: the Brillouin function for $S = 2$; dashed line: Brillouin functions for $S = 1/2$ and $S = 3/2$

Most of the μ-oxalato Cr^{III}−Cu^{II} complexes reported in the literature[5a,11,13] show either no or antiferromagnetic interactions. Only **1** and the Cu^{II}-(μ-oxalato)-Cr^{III} complexes reported by Okawa et al.[3b][3c] show a ferromagnetic interaction. For the latter two compounds, the copper $d_{x^2-y^2}$ orbital interacts with the σ-type orbitals of the oxalato group; on the other hand, the t_{2g} metallic orbitals of the Cr^{III} ions interact with the π-type orbitals of the oxalato bridge, leading to the classical example of ferromagnetic coupling due to the strict orthogonality of the magnetic orbitals. For the other Cr^{III}−Cu^{II} complexes described in the literature, the symmetry conditions are not fulfilled and the interaction is antiferromagnetic.

The value of the $\chi_M T$ product at room temperature for compound **2** is 6.41 $cm^3 \cdot mol^{-1}K$. This value corresponds to the one expected for two uncoupled Mn^{II} and Cr^{III} ions. Upon decreasing the temperature, $\chi_M T$ decreases, reaching a value of 1.38 $cm^3 \cdot mol^{-1}K$ at 2 K. This behavior indicates the occurrence of an antiferromagnetic coupling between Mn^{II} and Cr^{III}. The data were fitted using Equation (2), which gives the temperature dependence of the $\chi_M T$ product:

$$\chi_M T = \frac{2N\beta^2 g^2}{k}\frac{e^{-21J/4kT} + 5e^{-13J/4kT} + 14e^{-J/4kT} + 30e^{15J/4kT}}{3e^{-21J/4kT} + 5e^{-13J/4kT} + 7e^{-J/4kT} + 9e^{15J/4kT}} \quad (2)$$

Least-squares fitting leads to the following values: $J = -1.9\ cm^{-1}$ and $g = 2.01$, with $R = 5.6 \times 10^{-4}$. This value of the J parameter is close to the one found for a tetranuclear μ-oxalato Mn^{II}−Cr^{III} complex ($J = -1.1\ cm^{-1}$).[6]

The magnetization curve, $M = f(H)$, for compound **2**, recorded at 2 K (Figure 9), looks unusual: when increasing the field, instead of reaching the saturation corresponding to $S = 1$, M increases continuously to a value of 5 $N\beta$ at 6 T. This behavior can be explained by the crossover between the Zeeman components $M_S = -1$ (ground state $S = 1$), $M_S = -2$, from the first excited state ($S = 2$), and $M_S = -3$ from the second excited state (Figure 10). The crossover of the first two states occurs at $H = -2J/g\beta$, while that of the $M_S = -1$ and $M_S = -3$ occurs at $H = -3J/g\beta$. Least-squares fitting of the $M = f(H)$ curve, using a model taking into account all of the levels, leads to the following parameters: $J = -1.6\ cm^{-1}$ and $g = 1.99$. These values are in reasonable agreement with those found by the fitting of the magnetic susceptibility data.

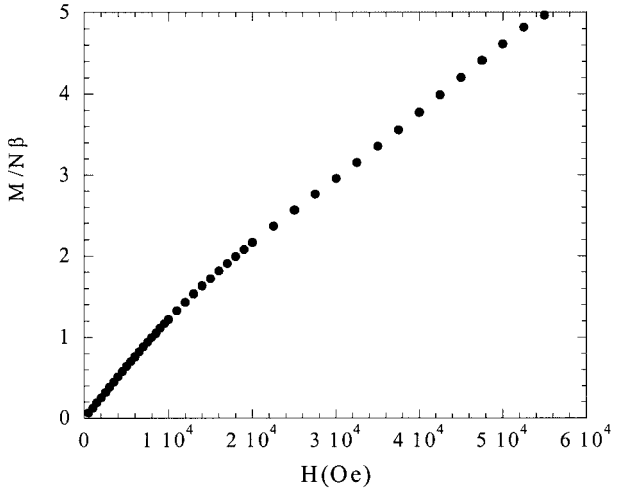

Figure 9. Magnetization-vs.-field curve for compound **2**

 © 2004 Wiley-VCH Verlag GmbH & Co. KGaA, Weinheim

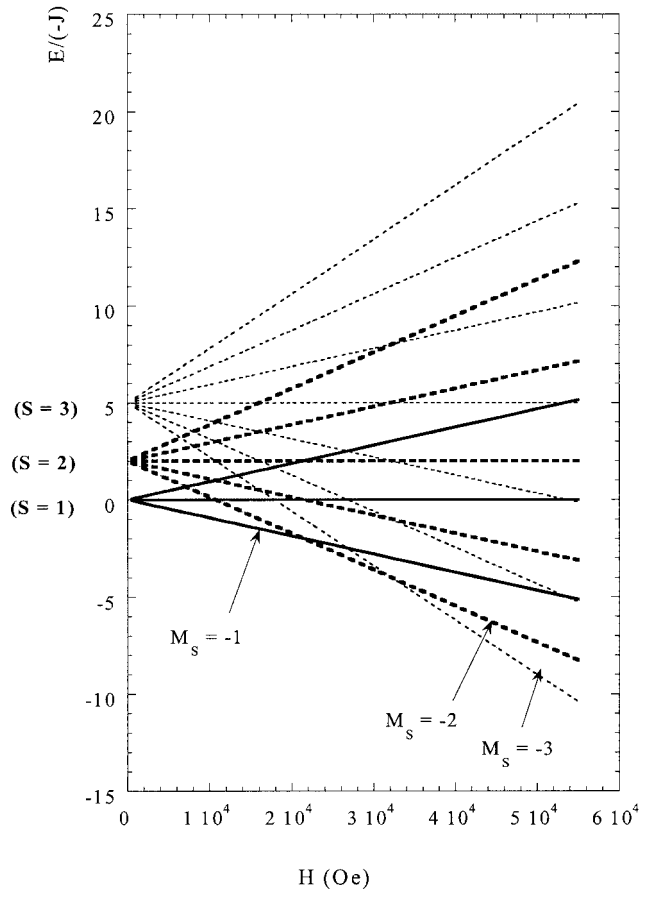

Figure 10. Energies of the lowest spin states ($S = 1$, $S = 2$, $S = 3$) as a function of the applied magnetic field for compound **2**

EPR Spectra

The X-band powder spectra for **1** were recorded between 5 K and room temperature. The spectrum at 5 K, depicted in Figure 11, exhibits features between 0 and 1100 mT. Upon increasing the temperature, the resonances detected at 5 K vary in their relative intensities, especially the signal around 320 mT, which, in contrast to the others signals, increases in intensity between 5 and 10 K. This behavior clearly indicates that this signal belongs to the excited triplet state. The EPR spectra of **1** are difficult to interpret because, even at 5 K, there are two EPR-active states and only one signal can be attributed without doubt to a precise state (triplet state). Moreover, these two states are separated only by 3.8 cm^{-1} and the strong exchange limit condition ($J >> D$) is probably not fulfilled and additional transitions could be observed. Nevertheless we tried to treat the triplet and the quintet states independently and, in a first step, we also assumed that the anisotropy of the two states comes from the zero field splitting of the chromium ion. Starting from the line at 320 mT, we tried to determine the D_1 value of the triplet state. Several possibilities can be considered to label this signal. The presence of high-field transition precludes the solutions that correspond to a small D_1 value. Furthermore, solutions with D_1 values > 1 cm^{-1} do not give satisfactory simulation. Only the solutions with D_1 values in the range from 0.6 to 0.68 cm^{-1} are able to reproduce the lines in the low- and high-field regions. The former value corresponds to axial symmetry and the latter to the rhombic one. The D_1 value of the triplet state is expected to be three-times larger than the D_2 value of the quintet state:[14a]

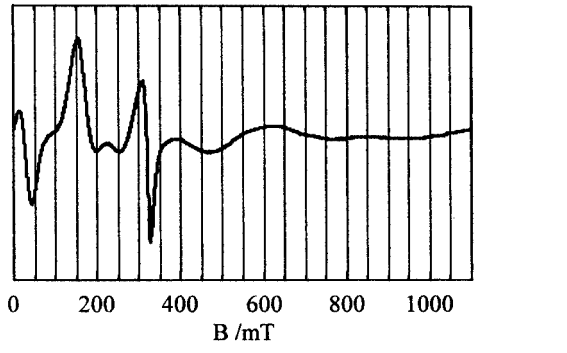

Figure 11. EPR spectrum for compound **1** at 5 K

$$D_1 = 3D_2 = \frac{3D_{cr}}{2} \quad (3)$$

From this formula, we calculate the D_2 value using the previous range for the D_1 values and simulate the spectra of the quintet state. In all cases, the combined spectra of the simulated quintet- and triplet-states spectra do not correspond to the experimental one. In particular, the intense lines at 45 and 150 mT are not well reproduced. Only D_2 values close to 0.15 cm^{-1} are able to reproduce these lines. This finding clearly indicates that there is another contribution to the D values of the two states, namely the anisotropic exchange interaction. Taking this interaction into account, D_2 and D_1 are given by the following relationships:[14a]

$$D_1 = \frac{3D_{cr}}{2} - \frac{D_{CuCr}}{4} \quad (4)$$

$$D_2 = \frac{D_{Cr}}{2} + \frac{D_{CuCr}}{4} \quad (5)$$

These relationships show that the anisotropic exchange provides opposite contributions to the quintet and the triplet states, and this feature could explain why $D_2 < D_1/3$. Because of the large number of parameters to optimize (g_{Cu}, g_{Cr}, D_{Cr}, and D_{CuCr} tensors, and their orientations) we obtained only a rough agreement between our simulation and the experimental spectrum with D_{Cr} and D_{CuCr} values around 0.4 cm^{-1} and -0.15 cm^{-1}, respectively. Nevertheless, it seems impossible to get a good simulation without a noticeable value for the anisotropic exchange. It is well established that the anisotropic exchange in a pair is pro-

 © 2004 Wiley-VCH Verlag GmbH & Co. KGaA, Weinheim

portional to the exchange interaction in an excited state of the pair, where one ion is in its fundamental state and the other in an excited state.[14b,15] In **1**, because of the relative orientation of the magnetic orbitals in the excited state, for which one electron of the chromium ion is in the d_{xy} orbital, there is a strong overlap between this orbital and the $d_{x^2-y^2}$ of the copper ion. This large antiferromagnetic interaction in an excited state of **1** leads to an important value of the anisotropic exchange in **1**.

The X-band powder spectra for **2** were recorded at several temperatures. The spectrum at 5 K exhibits a broad band at $g = 2.0$ and features of lower intensity between 0 and 1180 mT. An increase of the temperature does not induce any noticeable changes in the spectrum. The absence of thermal variation precludes any thorough analysis of the X-band powder spectra of **2**. The compounds discussed here illustrate once more that $[Cr(AA)(C_2O_4)_2]^-$ ions are very useful and versatile building blocks in designing heterometallic complexes.

Experimental Section

General Remarks: All the chemicals used for the present study were purchased from commercial sources and used without further purification. $Na[Cr(bipy)(C_2O_4)_2(H_2O)]\cdot 2H_2O$ and $Ba[Cr_2(phen)_2(C_2O_4)_4(H_2O)]\cdot H_2O$ were prepared as outlined in the literature.[5c,16] $[Cu(Hfsaaep)Cl]_2$ has been obtained as already reported.[17]

$[(Bipy)(C_2O_4)Cr(\mu\text{-}C_2O_4)Cu(Hfsaaep)(H_2O)]\cdot 2H_2O$ (1): A solution of $[Cu(Hfsaaep)Cl]_2$ (1 mmol) in methanol/water (1:1, 10 mL) was added to an aqueous solution of $Na[Cr(bipy)(C_2O_4)_2(H_2O)]\cdot 2H_2O$ (1 mmol, 10 mL). Slow evaporation of the resultant solution led to dark-blue single crystals of $[Cu(Hfsaaep)(H_2O)Cr(bipy)(C_2O_4)_2]\cdot 2H_2O$. IR data (KBr): $\tilde{\nu}$ = 3474 m, 3113 w, 1691 s, 1680 vs, 1639 s, 1565 m, 1447 m, 1395 s, 1383 s, 1324 w, 1238 m, 1027 w, 889 w, 810 m, 771 m, 667 w, 547 m cm^{-1}.

$[(Phen)(C_2O_4)Cr(\mu\text{-}C_2O_4)Mn(phen)_2(N_3)]\cdot H_2O$ (2): A suspension of $[BaCr_2(phen)_2(C_2O_4)_4(H_2O)]\cdot H_2O$ (1 mmol) in water (50 mL) was reacted with a stoichiometric amount of $MnSO_4\cdot 4H_2O$ (1 mmol) dissolved in water (10 mL). The resulting mixture was stirred for 4 h to promote the complete precipitation of barium sulfate, which was removed by filtration. An ethanolic solution of 1,10-phenanthroline (2 mmol, 10 mL), an aqueous solution of $MnCl_2\cdot 4H_2O$ (1 mmol, 10 mL), and aqueous sodium azide (2 mmol, 10 mL) were added successively to the red solution. Slow evaporation of the resultant solution led to orange-red single crystals of $[(phen)(C_2O_4)Cr(\mu\text{-}C_2O_4)Mn(phen)_2(N_3)]\cdot H_2O$. IR data (KBr): $\tilde{\nu}$ = 3479 m, 2038 s, 1705 s, 1679 vs, 1647 s, 1512 m, 1404 s, 1346 s, 1250 s, 1213 w, 1140 w, 1101 w, 851 m, 802 m, 724 s, 640 w, 482 m, 401 w cm^{-1}.

Physical Techniques: The IR spectra (KBr pellets) were recorded with a BIO-RAD FTS 135 spectrophotometer. UV/Vis spectra (diffuse reflectance technique) were recorded using a UV4 (Unicam) spectrophotometer and employing MgO as a standard. Magnetic measurements were carried out with a Quantum Design MPMS-5S SQUID magnetometer. The diamagnetic corrections for the compounds were estimated using Pascal's constants, and magnetic data were corrected for the diamagnetic contributions of the sample holder. EPR spectra were recorded using a Bruker Elexsys 500 spectrometer at the X band.

X-ray Crystallographic Study: X-Ray diffraction measurements were performed at room temperature and at 150 K for **1** and **2**, respectively, with a Nonius Kappa CCD diffractometer equipped with graphite-monochromated Mo-K_α radiation and using φ and ω scans. Crystal data, data collection parameters, and structure refinement details are given in Table 3. Lattice parameters were determined by the least-squares method from 8414 (**1**) and 5830 (**2**) reflections. The structures were solved by direct methods and refined by full-matrix, least-squares techniques based on F^2. The non-hydrogen atoms were refined using anisotropic displacement parameters. In all cases, hydrogen atoms on carbon atoms were calculated and allowed to ride. The other hydrogen atoms were found from difference Fourier maps and refined isotropically. Calculations were performed using SHELX-97 crystallographic software package.[18]

Table 3. Crystallographic data, details of data collection, and structure refinement parameters for compounds **1** and **2**

Compound	**1**	**2**
Chemical formula	$C_{29}H_{27}CrCuN_4O_{14}$	$C_{40}H_{26}CrMnN_9O_9$
M (g mol^{-1})	771.09	883.64
Temperature (K)	293(2)	150(2)
Wavelength (Å)	0.71073	0.71073
Crystal system	triclinic	monoclinic
Space group	$P\bar{1}$	$P2_1/c$
a (Å)	7.9198(2)	9.84960(10)
b (Å)	12.8396(4)	23.4248(3)
c (Å)	16.6094(6)	16.2377(2)
α (°)	87.755(2)	90
β (°)	76.679(2)	106.1134(6)
γ (°)	73.419(19)	90
V ($Å^3$)	1574.54(8)	3599.26(7)
Z	2	4
$D_{calcd.}$ (g·cm^{-3})	1.626	1.631
μ (mm^{-1})	1.098	0.727
F(000)	788	1800
Goodness-of-fit on F^2	1.063	0.974
Final $R1$, wR_2 $[I > 2\sigma(I)]$	0.0461, 0.1104	0.0419, 0.0881
$R1$, wR_2 (all data)	0.0601, 0.1166	0.0626, 0.0943
Largest diff. peak and hole (e $Å^{-3}$)	0.461 and −0.558	0.286 and −0.464

CCDC-206308 (for **1**) and -206309 (for **2**) contain the supplementary crystallographic data for this paper. These data can be obtained free of charge at www.ccdc.cam.ac.uk/conts/retrieving.html [or from the Cambridge Crystallographic Data Centre, 12 Union Road, Cambridge CB2 1EZ, UK; Fax: (internat.) +44-1223-336-033; E-mail: deposit@ccdc.cam.ac.uk].

Acknowledgments

Financial support from the INTAS program (Project 2000−00375) as well as from the CERES Program, Romania (Project 30) is acknowledged graciously.

[1] See, for example: [1a] G. De Munno, R. Ruiz, F. Lloret, J. Faus, R. Sessoli, M. Julve, *Inorg. Chem.* **1995**, *34*, 408 and references cited therein. [1b] J. Y. Lu, M. A. Lawandy, J. Li, T. Yuen, C. L. Lin, *Inorg. Chem.* **1999**, *38*, 2698. [1c] O. Castillo, A. Luque, J. Sertucha, P. Román, F. Lloret, *Inorg. Chem.* **2000**, *39*, 6142. [1d] O. Castillo, A. Luque, F. Lloret, P. Román, *Inorg. Chem. Commun.* **2001**, *4*, 350.

 © 2004 Wiley-VCH Verlag GmbH & Co. KGaA, Weinheim

[2] [2a] O. Kahn, *Adv. Inorg. Chem.* **1995**, *43*, 179. [2b] O. Kahn, *Angew. Chem. Int. Ed. Engl.* **1985**, *24*, 834. [2c] O. Kahn, *Inorg. Chim. Acta* **1982**, *62*, 3. [2d] M. Julve, J. Faus, M. Verdaguer, A. Gleizes, *J. Am. Chem. Soc.* **1984**, *106*, 8306. [2e] J. Glerup, P. A. Goodson, D. J. Hodgson, K. Michelsen, *Inorg. Chem.* **1995**, *34*, 6255. [2f] M. Julve, M. Verdaguer, A. Gleizes, M. Philoche-Levisalles, O. Kahn, *Inorg. Chem.* **1984**, *23*, 3808. [2g] J. Cabrero, N. Ben Amor, C. de Graaf, F. Illas, R. Caballol, *J. Phys. Chem. A* **2000**, *104*, 9983, and references cited therein.

[3] [3a] F. Lloret, M. Julve, M. Mollar, I. Castro, J. Lattore, J. Faus, *J. Chem. Soc., Dalton Trans.* **1989**, 729. [3b] M. Ohba, H. Tamaki, N. Matsumoto, H. Okawa, S. Kida, *Chem. Lett.* **1991**, 1157. [3c] M. Ohba, H. Tamaki, N. Matsumoto, H. Okawa, *Inorg. Chem.* **1993**, *32*, 5385.

[4] T. Sanada, T. Suzuki, T. Yoshida, S. Kaizaki, *Inorg. Chem.* **1998**, *37*, 4712.

[5] [5a] M. Andruh, R. Melanson, C. V. Stager, F. D. Rochon, *Inorg. Chim. Acta* **1996**, *251*, 309. [5b] F. D. Rochon, R. Melanson, M. Andruh, *Inorg. Chem.* **1996**, *35*, 6086. [5c] M. C. Muñoz, M. Julve, F. Lloret, J. Faus, M. Andruh, *J. Chem. Soc., Dalton Trans.* **1998**, 3125.

[6] G. Marinescu, M. Andruh, R. Lescouëzec, M. C. Muñoz, J. Cano, F. Lloret, M. Julve, *New J. Chem.* **2000**, *24*, 527.

[7] G. De Munno, D. Armentano, M. Julve, F. Lloret, R. Lescouëzec, J. Faus, *Inorg. Chem.* **1999**, *38*, 2234.

[8] R. Lescouëzec, G. Marinescu, M. C. Muñoz, D. Luneau, M. Andruh, F. Lloret, J. Faus, M. Julve, J. A. Mata, R. Llusar, J. Cano, *New J. Chem.* **2001**, *25*, 1224.

[9] See, for example: [9a] Z. J. Zhong, N. Matsumoto, H. Okawa, S. Kida, *Chem. Lett.* **1990**, 87. [9b] S. Decurtins, H. W. Schmalle, H. R. Oswald, A. Linden, J. Ensling, P. Gütlich, A. Hauser, *Inorg. Chim. Acta* **1994**, *216*, 65. [9c] S. Decurtins, H. W. Schmalle, P. Schneuwly, J. Ensling, P. Gütlich, *J. Am. Chem. Soc.* **1994**, *116*, 9521. [9d] S. Decurtins, M. Gross, H. W. Schmalle, S. Ferlay, *Inorg. Chem.* **1998**, *37*, 2443. [9e] M. Pilkington, S. Decurtins, in *Magnetism: Molecules to Materials II* (Eds.: J. S. Miller, M. Drillon), Wiley-VCH, Weinheim, **2001**, p. 339.

[10] M. Andruh, I. Ramade, E. Codjovi, O. Guillou, O. Kahn, J. C. Trombe, *J. Am. Chem. Soc.* **1993**, *115*, 1822.

[11] O. Costisor, K. Mereiter, M. Julve, F. Lloret, Y. Journaux, W. Linert, M. Andruh, *Inorg. Chim. Acta* **2001**, *324*, 352.

[12] B. J. Hathaway, in *Comprehensive Coordination Chemistry* (Eds.: G. Wilkinson, R. D. Gillard, J. A. McCleverty), Pergamon, Oxford, **1987**, vol. 5, pp. 607.

[13] [13a] R. Lescouëzec, G. Marinescu, J. Vaissermann, F. Lloret, J. Faus, M. Julve, M. Andruh, *Inorg. Chim. Acta* **2003**, *250*, 131. [13b] E. Coronado, M. C. Giménez, C. T. Gómez-García, F. M. Romero, *Polyhedron* **2003**, *22*, 3115.

[14] [14a] A. Bencini, D. Gatteschi, in *EPR of Exchange Coupled Systems*, Springer-Verlag, Berlin, Heidelberg, **1990**, p. 55. [14b] A. Bencini, D. Gatteschi, in *EPR of Exchange Coupled Systems*, Springer-Verlag, Berlin, Heidelberg, **1990**, p. 28.

[15] J. Kanamori, in *Magnetism* (Eds.: G. T. Rado, H. Suhl), Academic Press, New York, **1963**, vol. I, p. 127.

[16] J. A. Broomhead, *Aust. J. Chem.* **1962**, *15*, 228.

[17] F. Tuna, L. Patron, Y. Journaux, M. Andruh, W. Plass, J. C. Trombe, *J. Chem. Soc., Dalton Trans.* **1999**, 539.

[18] *SHELX97 − Program for the Solution and Refinement of the Crystal Structures*, G. M. Sheldrick, University of Göttingen, Germany, **1997**.

Received January 23, 2004
Early View Article
Published Online May 5, 2004

 © 2004 Wiley-VCH Verlag GmbH & Co. KGaA, Weinheim

Homolysis of the Ln−N (Ln = Yb, Eu) Bond − Synthesis, Structure, and Catalytic Activity of Ytterbium(II) and Europium(II) Complexes Having (Dimethylamino)propyl- and (Dimethylamino)ethyl-Functionalized Indenyl Ligands

Enhong Sheng,[a] Shuangliu Zhou,[a] Shaowu Wang,*[a,b] Gaosheng Yang,[a] Yongyong Wu,[a] Yan Feng,[a] Lili Mao,[a] and Zixiang Huang[c]

Dedicated to Professor Changtao Qian on the occasion of his 70th birthday

Keywords: Catalyst / Homolysis / Organometallics / Polymer / Polymerization

We have synthesized a new series of ytterbium(II) and europium(II) complexes by tandem silylamine elimination/homolysis of Ln–N (Ln = Yb, Eu) bonds. The interaction of 2 equiv. of $C_9H_7CH_2CH_2CH_2NMe_2$ (**1**) with $[(Me_3Si)_2N]_3Ln(\mu\text{-}Cl)Li(THF)_3$ (Ln = Yb, Eu) in toluene under reflux produced lanthanide(II) complexes $[(\eta^5{:}\eta^1\text{-}C_9H_6CH_2CH_2CH_2NMe_2)_2\text{-}Ln]$ [Ln = Yb (**2**), Eu(**3**)] in 67 and 74% yields, respectively. Treatment of 2 equiv. of $Me_2Si(Me_2NCH_2CH_2C_9H_6)(NHtBu)$ with $[(Me_3Si)_2N]_3Eu(\mu\text{-}Cl)Li(THF)_3$ in toluene at 80 °C afforded a europium(II) complex $[\eta^5{:}\eta^1\text{-}Me_2Si(Me_2NCH_2\text{-}CH_2C_9H_5)(NHtBu)]_2Eu{\cdot}(OC_4H_8)_{0.5}$ (**4**) in 46% yield. The interaction of 2 equiv. of $Me_2NCH_2CH_2C_9H_6SiMe_3$ with $[(Me_3\text{-}Si)_2N]_3Eu(\mu\text{-}Cl)Li(THF)_3$ produced a europium(II) compound $[\eta^5{:}\eta^1\text{-}(Me_2NCH_2CH_2C_9H_5SiMe_3)]_2Eu$ (**5**) in 49% yield. Treatment of 2 equiv. of $Me_2NCH_2CH_2C_9H_7$ with $[(Me_3Si)_2N]_3Eu(\mu\text{-}Cl)Li(THF)_3$ in toluene gave a europium(II) complex $(\eta^5{:}\eta^1\text{-}Me_2NCH_2CH_2C_9H_6)_2Eu$ (**6**) in 57% yield. All the compounds were fully characterized by spectroscopic methods and elemental analyses. The structures of the complexes **4**, **5**, and **6** were determined by single-crystal X-ray analyses. The catalytic activities of organometallic complexes were examined; we found that all of the complexes can function as single-component MMA polymerization catalysts with good activity. We studied the effects of solvent and temperature on the catalytic activities and the stereochemistries of the polymers.
(© Wiley-VCH Verlag GmbH & Co. KGaA, 69451 Weinheim, Germany, 2004)

Introduction

Organolanthanide complexes have attracted much attentions for their potential applications as catalysts for olefins transformations.[1] The Ln−N bonds in lanthanide complexes have been demonstrated to exhibit unique reactivity and selectivity for chemo-, regio-, and enantioselective hydroamination of olefins and alkynes,[2] hydrosilylations of olefins,[3] and hydrophosphinations of olefins and alkynes,[4] as well as for olefin polymerization,[5] Tishchenko reactions,[6] ring opening polymerization of ε-caprolactone and δ-valerolactone,[7] and insertion reactions.[8] All of these reactions occur because of the heterolytic reactivity of Ln−N bonds.

We have reported that the interactions of (dimethylamino)ethyl-functionalized indene compounds with ytterbium(III) amide $[(Me_3Si)_2N]_3Yb(\mu\text{-}Cl)Li(THF)_3$ lead to the isolation and characterization of a new class of ytterbium(II) complexes having indenyl ligands; the interactions of methoxyethyl-functionalized indene compounds with $[(Me_3Si)_2N]_3Ln(\mu\text{-}Cl)Li(THF)_3$ (Ln = Yb, Eu) results in the synthesis of a new series of ytterbium(II) and europium(II) complexes.[9] On the basis of a mechanistic study, the pathway for the formation of the ytterbium(II) and europium(II) complexes is believed to proceed through tandem silylamine elimination[10]/homolysis of the Ln−N (Ln = Yb, Eu) bonds; this reaction provides a new methodology for the preparation of lanthanide(II) complexes. Extension of the process of homolysis of the Yb−N bond to europium chemistry, by studying the interactions of the indene compounds C_9H_6-1-R-3-$CH_2SiMe_2NC_4H_8$ (R = H, Me) with europium(III) amide $[(Me_3Si)_2N]_3Eu(\mu\text{-}Cl)Li(THF)_3$, has led to the isolation and characterization of novel europium(II) complexes.[11] The formation of different kinds

[a] Institute of Organic Chemistry, School of Chemistry and Materials Science, Anhui Normal University,
Wuhu, Anhui 241000, China
Fax: (internat.) + 86-553-3883517
E-mail: swwang@mail.ahnu.edu.cn
[b] State Key Laboratory of Organometallic Chemistry, Shanghai Institute of Organic Chemistry,
Shanghai 200032, China
[c] Fujian Institute of Research on the Structure of Matters, Chinese Academy of Sciences,
Fuzhou 350002, China

of lanthanide(II) complexes presumably is due to the ligands' effects on the reactivity. As part of our continued interest in the effects of ligands on the homolytic reactivity of Ln−N bonds, we have turned our attention to the interactions of (dimethylamino)propyl-functionalized indene compounds with $[(Me_3Si)_2N]_3Ln(\mu\text{-}Cl)Li(THF)_3$ (Ln = Yb, Eu) and the interactions of (dimethylamino)ethyl-functionalized indene compounds with europium(III) amide $[(Me_3Si)_2N]_3Eu(\mu\text{-}Cl)Li(THF)_3$.

Herein, we report that interacting (dimethylamino)propyl- and (dimethylamino)ethyl-functionalized indene compounds with $[(Me_3Si)_2N]_3Ln(\mu\text{-}Cl)Li(THF)_3$ (Ln = Yb, Eu) results in the isolation of a new series of ytterbium(II) and europium(II) complexes, which we have characterized. We propose that the pathway for the formation of the lanthanide(II) complexes proceeds through tandem silylamine elimination/homolysis of the Ln−N (Ln = Yb, Eu) bonds. The catalytic activity of the ytterbium(II) and europium(II) complexes as single-component MMA polymerization catalysts is also reported.

Results and Discussion

Synthesis of $Me_2NCH_2CH_2CH_2C_9H_7$ (1)

The interaction of C_9H_7Li with $Me_2NCH_2CH_2CH_2Cl$ in THF produced, after workup, the indene compound $Me_2NCH_2CH_2CH_2C_9H_7$ (**1**) in good yield (Scheme 1). The compound was fully characterized by spectroscopic methods and elemental analysis; the ^1H NMR spectrum showed that the substituent group connects to the sp^2-hybridized carbon atom of the five-membered ring of the indene compound.

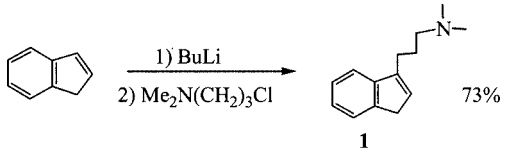

Scheme 1

Reactions of the Indene Compounds with $[(Me_3Si)_2N]_3Ln(\mu\text{-}Cl)Li(THF)_3$ (Ln = Yb, Eu). Synthesis of Ytterbium(II) and Europium(II) Complexes

The interaction of 2 equiv. of $Me_2NCH_2CH_2CH_2C_9H_7$ (**1**) with lanthanide(III) amides $[(Me_3Si)_2N]_3Ln(\mu\text{-}Cl)Li(THF)_3$ (Ln = Yb, Eu) in toluene afforded, after workup, ytterbium(II) and europium(II) compounds $[(\eta^5{:}\eta^1\text{-}C_9H_6CH_2CH_2CH_2NMe_2)_2Yb]$ (**2**) and $[(\eta^5{:}\eta^1\text{-}C_9H_6CH_2CH_2CH_2NMe_2)_2Eu]$ (**3**) in 67 and 74% yields, respectively (Scheme 2). The complexes are sensitive to air and moisture, and they are soluble in THF, DME, and toluene. The complexes were fully characterized by spectroscopic methods and elemental analyses. A ^1H NMR spectroscopic study of complex **2** indicated the diamagnetic property of the complex and the +2 oxidation state of the ytterbium center. The results of elemental analyses are in agreement with the formulas of the ytterbium(II) and europium(II) complexes, which indicates that the reactions occur through a reductive process. All attempts to grow crystals suitable for X-ray analyses to confirm the structures of the complexes failed as a result the severe twinning problems. To overcome this difficulty and to extend the reaction chemistry, we studied the following reactions.

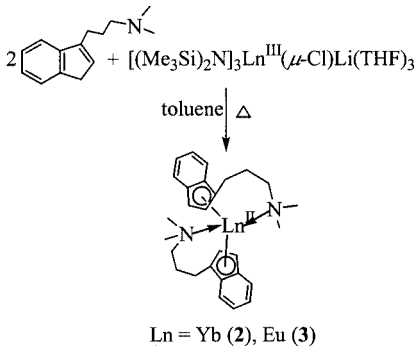

Scheme 2

Treatment of 2 equiv. of $Me_2Si(Me_2NCH_2CH_2C_9H_6)(NHtBu)$ with $[(Me_3Si)_2N]_3Eu(\mu\text{-}Cl)Li(THF)_3$ in toluene at 80 °C afforded, after workup, a europium(II) complex $[\{\eta^5{:}\eta^1\text{-}Me_2Si(Me_2NCH_2CH_2C_9H_5)(NHtBu)\}_2Eu]\cdot(OC_4H_8)_{0.5}$ (**4**) in 46% yield (Scheme 3). The complex is sensitive to air and moisture, and is soluble in THF, DME, pyridine, and toluene, but only slightly soluble in *n*-hexane. The compound was fully characterized by spectroscopic methods and elemental analysis. NMR spectra are not informative because of a lack of locking signals for the paramagnetic solutions of this compound. The elemental analysis of the product is in agreement with the formula of europium(II) complex being $Me_2Si(Me_2NCH_2CH_2C_9H_5)(NHtBu)]_2Eu$, which indicates that the reaction occurs through a reductive process. The structure of the europium(II) complex was confirmed by X-ray analysis. To extend the chemistry, we investigated the interaction of $Me_2NCH_2CH_2C_9H_6SiMe_3$ with $[(Me_3Si)_2N]_3Eu(\mu\text{-}Cl)Li(THF)_3$.

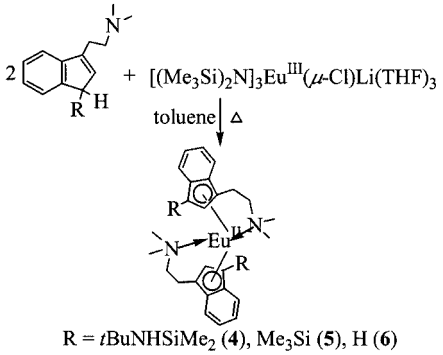

Scheme 3

 © 2004 Wiley-VCH Verlag GmbH & Co. KGaA, Weinheim

Treatment of 2 equiv. of $Me_2NCH_2CH_2C_9H_6SiMe_3$ with $[(Me_3Si)_2N]_3Eu(\mu\text{-}Cl)Li(THF)_3$ produced a europium(II) compound $[\{\eta^5{:}\eta^1\text{-}(Me_2NCH_2CH_2C_9H_5SiMe_3)\}_2Eu]$ (**5**) in 49% yield (Scheme 3). The compound is sensitive to air and moisture, and is soluble in THF, DME, pyridine, and toluene, but is only slightly soluble in *n*-hexane. The complex was fully characterized by spectroscopic method and elemental analysis. Although NMR spectra are not informative because of the paramagnetic property of the complex, the elemental analysis of the complex is in agreement with the formula above; details of the structure were further confirmed by an X-ray diffraction study. These results suggest that the formation of the europium(II) complex occurs through a reductive reaction process. To probe the effects of the silyl substituent and the ligands on the reaction, we studied the interaction of $Me_2NCH_2CH_2C_9H_7$ with $[(Me_3Si)_2N]_3Eu(\mu\text{-}Cl)Li(THF)_3$.

Treatment of 2 equiv. of $Me_2NCH_2CH_2C_9H_7$ with $[(Me_3Si)_2N]_3Eu(\mu\text{-}Cl)Li(THF)_3$ in toluene gave the europium(II) complex $[(\eta^5{:}\eta^1\text{-}Me_2NCH_2CH_2C_9H_6)_2Eu]$ (**6**) in 57% yield (Scheme 3). The complex is sensitive to air and moisture; it is soluble in THF, DME, and pyridine, but it is only slightly soluble in toluene and insoluble in *n*-hexane. The complex was fully characterized by spectroscopic methods and elemental analysis. Although NMR spectra are not informative because of the paramagnetic property of the complex, the results of elemental analysis are in agreement with a monomeric europium(II) complex; the structure of this europium(II) complex was further confirmed by a X-ray diffraction study. The fact that a triple-decker tetranuclear europium(II) complex was not isolated as the product of the reaction between $C_9H_7CH_2SiMe_2NC_4H_8$ and europium(III) amide $[(Me_3Si)_2N]_3Eu(\mu\text{-}Cl)Li(THF)_3$ [11] may be due to the ligands' effects on the reactivity.

The formation of all of the ytterbium(II) and europium(II) complexes above is believed to occur through a reductive process. Several experiments were initiated to probe the reaction mechanism. The indene compounds, the amine $HN(SiMe_3)_2$, and the coupling product $[N(SiMe_3)_2]_2$ were detected by GC-MS analyses of the reaction mixtures after hydrolysis. The formation of the coupling product may be due to homolysis of the $Ln-N(SiMe_3)_2$ bond to produce the radical $N(SiMe_3)_2$, which then couples to give the coupling product; it should be noted, however, that the amount of coupling product $[N(SiMe_3)_2]_2$ is less than that expected, probably as a result of the free radical abstraction of a hydrogen atom from solvent. Homolysis of the Ln−N bond has not been observed, however, when heating the corresponding lanthanide(III) amides $[(Me_3Si)_2N]_3Ln(\mu\text{-}Cl)Li(THF)_3$ (Ln = Yb, Eu) in toluene under reflux for 2 days or when subliming the lanthanide(III) amides $[(Me_3Si)_2N]_3Ln(\mu\text{-}Cl)Li(THF)_3$ (Ln = Yb, Eu) at 100 °C and 10^{-4} Torr; instead, $[(Me_3Si)_2N]_3Ln$ was isolated,[5] indicating that homolysis of the $Ln-N(SiMe_3)_2$ bond occurs after the interaction of the indene compounds with $[(Me_3Si)_2N]_3Ln(\mu\text{-}Cl)Li(THF)_3$ (Ln = Yb, Eu). Our previous work has indicated that the interaction of 1,2-bis(indenyl)ethane with $[(Me_3Si)_2N]_3Yb(\mu\text{-}Cl)Li(THF)_3$ does not produce the ytterbium(II) compound: the ytterbium(III) amides, *meso*-$(EBI)Yb^{III}N(SiMe_3)_2$, were isolated,[9] which suggests an effect of the heteroatom on the reductive reaction.

On the basis of the evidence above, we propose the following pathway for the formation of the lanthanide(II) complexes: The interactions of the (dimethylamino)propyl- or (dimethylamino)ethyl-functionalized indene compounds with $[(Me_3Si)_2N]_3Ln(\mu\text{-}Cl)Li(THF)_3$ (Ln = Yb, Eu) produces the lanthanide(III) amides $(Indenyl')_2LnN(SiMe_3)_2$ [Indenyl' = (dimethylamino)ethyl- or (dimethylamino)propyl-functionalized indenyl ligands] as intermediates and $HN(SiMe_3)_2$ by a silylamine elimination reaction.[10] Coordination of the nitrogen atoms of the (dimethylamino)ethyl or (dimethylamino)propyl groups to the central lanthanide metal ions promotes homolysis of the Ln−N (Ln = Yb, Eu) bonds to give the lanthanide(II) complexes and the radical $N(SiMe_3)_2$, which then couples to form the coupling product (Scheme 4).

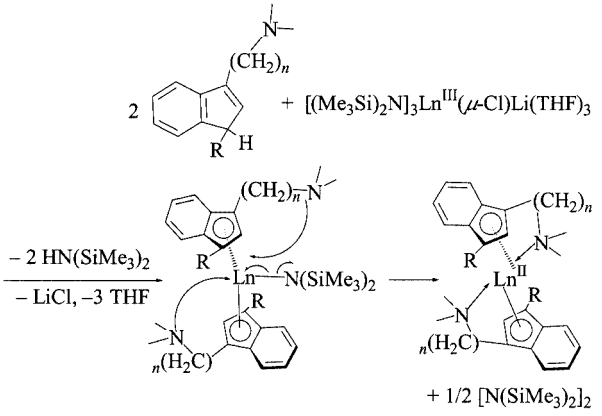

n = 3, R = H, Ln = Yb (**2**), Eu (**3**);
n = 2, Ln = Eu, R = *t*BuNHSiMe$_2$ (**4**), Me$_3$Si (**5**), H (**6**),

Scheme 4. Proposed mechanism for the reductive reaction

Molecular Structures of Complexes 4, 5, and 6

The structures of lanthanide(II) complexes **4** (Figure 1), **5** (Figure 2), and **6** (Figure 3) were determined by X-ray diffraction studies. X-Ray analyses revealed that the central metal ion of each complex exists in a +2 oxidation state. We found that there are two independent molecules in the unit cell of complex **6** that differ by the effects of the substituent groups of the indenyl ligands upon crystallization. The selected bond lengths and angles are listed in the Table 1. Some of the important structural parameters are compiled in Table 2 for a comparison of the structural parameters.

From Table 1 and 2, we see that the Eu−C bond lengths range from 2.827(10) to 2.944(11) Å, with an average of 2.883(11) Å in **4**; this distance is slightly different to those found in **5** [2.873(10) Å] and in **6** [2.841(7) Å]. Similarities are found in the average Eu−N bond lengths of **4** [2.748(9) Å], **5** [2.744(8) Å], and **6** [2.711(6) Å], which indicate the effect of the substituent groups on the bonding between the

 © 2004 Wiley-VCH Verlag GmbH & Co. KGaA, Weinheim

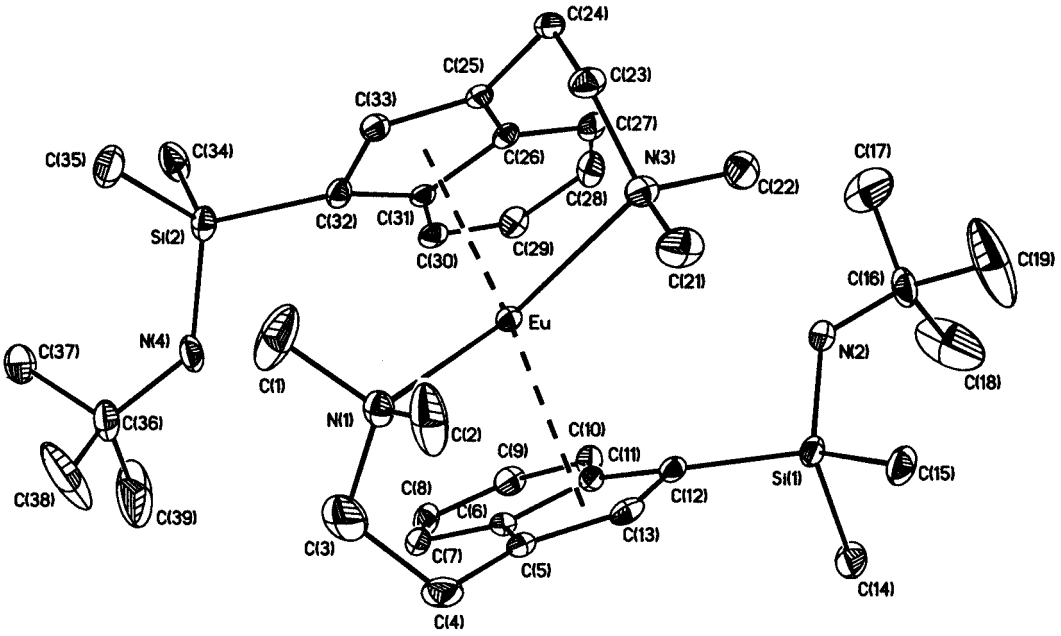

Figure 1. Molecular structure of complex **4**; hydrogen atoms and the solvated THF molecule have been omitted for clarity

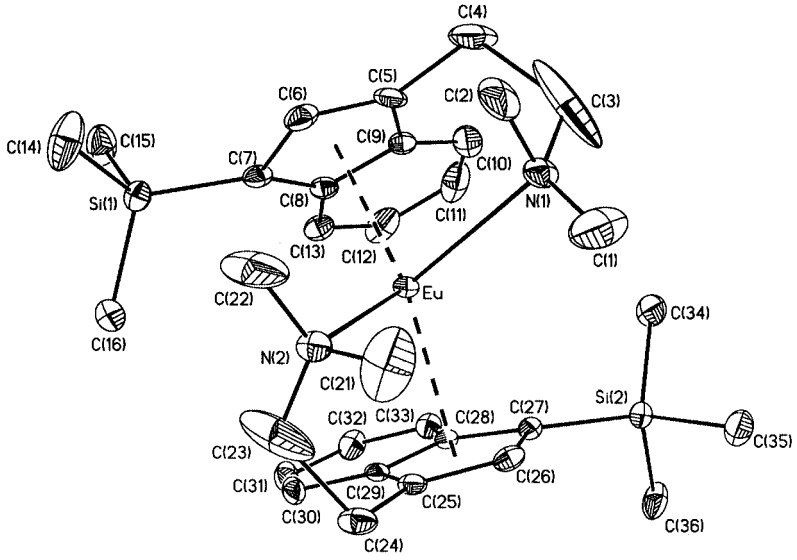

Figure 2. Molecular structure of complex **5**; hydrogen atoms have been omitted for clarity

ligands and the central metal ions. The N−Eu−N angle of 96.1(3)° in **4** is larger than the corresponding angle [92.9(3)°] in **5**, but it is smaller than these angles [102.1(2)° and 107.3(2)°] in **6**. Similar results have been found in the ytterbium(II) analogues (Table 2), suggesting an effect of the substituent groups on the configuration of the ytterbium(II) and europium(II) complexes. From Table 2, we see that, as the substituent groups on the indenyl rings change from *t*BuNHSiMe$_2$ to Me$_3$Si to H, the differences of either the average Ln−C or the average Ln−N bond lengths between **4** and **5**, **4** and **6**, and **5** and **6** are smaller than those values found in their ytterbium(II) analogues, which suggests that the effect of the substituent groups on the bonding between the ligands and the central metal ion becomes weaker as the ionic radii[12] of the central metal ion increases.

The average Eu−C distances found in **4** [2.883(11) Å], **5** [2.873(10) Å], and **6** [2.841(7) Å] are smaller than the corresponding value of 2.911(18) Å found in [(η^5:η^1-C$_9$H$_5$-1-Me-3-CH$_2$SiMe$_2$NC$_4$H$_8$)$_2$Eu], but are longer than the corresponding average values found in [{η^5:η^1-(MeOCH$_2$CH$_2$C$_9$H$_5$SiMe$_3$)}$_2$Yb] [**10**; 2.741(14) Å],[9b] [{η^5:η^1-Me$_2$Si(MeOCH$_2$CH$_2$C$_9$H$_5$)(NH*t*Bu)}$_2$Eu] [**11**; 2.858(8) Å],[9b] and [{η^5:η^1-(MeOCH$_2$CH$_2$C$_9$H$_5$-SiMe$_3$)}$_2$Eu] [**12**; 2.857(11) Å][9b] (Table 2); these difference may be due to steric effects and the different ionic radii. The average Eu−N distances found in **4** [2.748(9) Å], **5** [2.744(8) Å], and **6** [2.711(6) Å] are also smaller than the corresponding value of 2.754(16) Å found in [(η^5:η^1-C$_9$H$_5$-1-Me-3-CH$_2$SiMe$_2$NC$_4$H$_8$)$_2$Eu],[11] but are longer than the corresponding Ln−O bond lengths found in [η^5:η^1-(Me-

 © 2004 Wiley-VCH Verlag GmbH & Co. KGaA, Weinheim

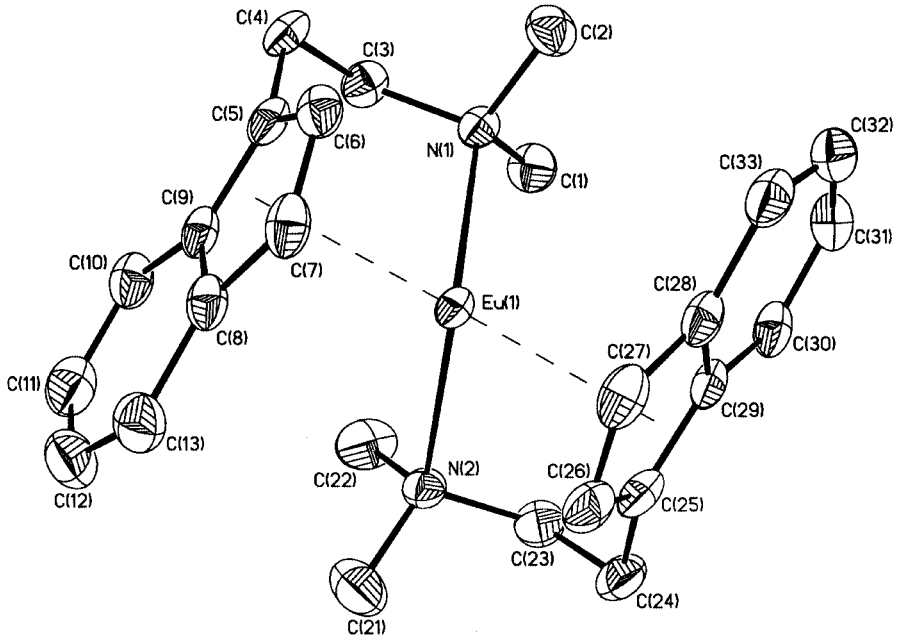

Figure 3. One of the molecular structures of complex **6** in the unit cell; hydrogen atoms have been omitted for clarity

Table 1. Selected bond lengths (Å) and angles (°) for **4**, **5**, and **6**

4		**5**		**6**			
Eu−N(1)	2.789(9)	Eu−N(1)	2.765(8)	Eu(1)−N(1)	2.726(6)	Eu(2)−N(3)	2.677(5)
Eu−N(3)	2.707(9)	Eu−N(2)	2.724(8)	Eu(1)−N(2)	2.742(5)	Eu(2)−N(4)	2.700(5)
Eu−C(5)	2.827(10)	Eu−C(5)	2.817(10)	Eu(1)−C(5)	2.820(6)	Eu(2)−C(45)	2.836(6)
Eu−C(6)	2.870(10)	Eu−C(6)	2.856(10)	Eu(1)−C(6)	2.823(7)	Eu(2)−C(46)	2.786(6)
Eu−C(11)	2.911(10)	Eu−C(7)	2.940(9)	Eu(1)−C(7)	2.822(7)	Eu(2)−C(47)	2.797(6)
Eu−C(12)	2.918(11)	Eu−C(8)	2.913(8)	Eu(1)−C(8)	2.859(7)	Eu(2)−C(48)	2.888(6)
Eu−C(13)	2.829(11)	Eu−C(9)	2.848(10)	Eu(1)−C(9)	2.850(6)	Eu(2)−C(49)	2.887(6)
Eu−C(25)	2.832(10)	Eu−C(25)	2.832(8)	Eu(1)−C(25)	2.821(7)	Eu(2)−C(65)	2.820(6)
Eu−C(26)	2.881(9)	Eu−C(26)	2.852(8)	Eu(1)−C(26)	2.814(7)	Eu(2)−C(66)	2.800(6)
Eu−C(31)	2.911(9)	Eu−C(27)	2.903(8)	Eu(1)−C(27)	2.837(7)	Eu(2)−C(67)	2.846(6)
Eu−C(32)	2.944(11)	Eu−C(28)	2.900(7)	Eu(1)−C(28)	2.864(6)	Eu(2)−C(68)	2.911(6)
Eu−C(33)	2.908(11)	Eu−C(29)	2.867(7)	Eu(1)−C(29)	2.853(6)	Eu(2)−C(69)	2.885(6)
N(1)−Eu−N(3)	96.1(3)	N(1)−Eu−N(2)	92.9(3)	N(1)−Eu(1)−N(2)	102.1(2)	N(3)−Eu(2)−N(4)	107.3(2)

Table 2. A comparison of the structural parameters of the ytterbium(II) and europium(II) complexes incorporating (dimethylamino)ethyl- and methoxyethyl-functionalized indenyl ligands

Complex[a]	Ln−C(av.)	Ln−A(av.)	A−Ln−A	Ref.
4 (Ln = Eu, A = N)	2.883(11)	2.748(9)	96.1(3)	this work
5 (Ln = Eu, A = N)	2.873(10)	2.744(8)	92.9(3)	this work
6 (Ln = Eu, A = N)	2.836(7); 2.846(6)	2.734(6); 2.688(5)	102.1(2); 107.3(2)	this work
7 (Ln = Yb, A = N)	2.806(12)	2.673(11)	95.1(4)	[9a]
8(Ln = Yb, A = N)	2.778(14)	2.650(12)	92.8(5)	[9a]
9(Ln = Yb, A = N)	2.722(10)	2.588(7)	103.7(2)	[9a]
10(Ln = Yb, A = O)	2.741(14)	2.462(9)	84.5(3), 86.3(3)	[9b]
11(Ln = Eu, A = O)	2.858(8)	2.559(6)	88.6(2)	[9b]
12(Ln = Eu, A = O)	2.857(11)	2.588(8)	88.1(3), 83.3(3)	[9b]

[a] **7**: $[\eta^5{:}\eta^1\text{-}Me_2Si(Me_2NCH_2CH_2C_9H_5)(NHtBu)]_2Yb$; **8**: $[\eta^5{:}\eta^1\text{-}(Me_2NCH_2CH_2C_9H_5SiMe_3)]_2Yb$; **9**: $(\eta^5{:}\eta^1\text{-}Me_2NCH_2CH_2C_9H_6)_2Yb$; **10**: $[\eta^5{:}\eta^1\text{-}(MeOCH_2CH_2C_9H_5SiMe_3)]_2Yb$; **11**: $[\eta^5{:}\eta^1\text{-}Me_2Si(MeOCH_2CH_2C_9H_5)(NHtBu)]_2Eu$; **12**: $[\eta^5{:}\eta^1\text{-}(MeOCH_2CH_2C_9H_5SiMe_3)]_2Eu$.

 © 2004 Wiley-VCH Verlag GmbH & Co. KGaA, Weinheim

$OCH_2CH_2C_9H_5SiMe_3)]_2Yb$ [**10**; 2.462(9) Å],[9b] [{η^5:η^1-$Me_2Si(MeOCH_2CH_2C_9H_5)(NHtBu)$}$_2$Eu] [**11**; 2.559(6) Å],[9b] and [{η^5:η^1-$(MeOCH_2CH_2C_9H_5SiMe_3)$}$_2$Eu] [**12**; 2.588(8) Å][9b] (Table 2); these values reflect are steric and ionic radii effects on the bonding. The N−Eu−N angles in **4** [96.1(3)°], **5** [92.9(3)°], and **6** [102.1(2)° and 107.3(2)°] are smaller than the value of 110.19(15)° found in [η^5:η^1-C_9H_5-1-Me-3-$CH_2SiMe_2NC_4H_8)_2$Eu],[11] but are larger than the O−Ln−O (Ln = Yb, Eu) angles found in the methoxyethyl-functionalized (indenyl)ytterbium(II) and -europium(II) complexes[9b] (Table 2); these observations indicate that the substituent groups have an influence on the configuration of complexes having indenyl ligands.

MMA Polymerization

We have studied the activity of the complexes as single-component MMA polymerization catalysts by performing polymerizations in a series of solvents. The polymer products were quenched with acidified methanol after a fixed time and analyzed by obtaining ^{1}H NMR spectra of the microstructures.[13] We found that some polymers cannot be dissolved in THF or passed through GPC columns. We also found that all of the complexes can function as single-component MMA polymerization catalysts and that each has good catalytic activity. It is interesting to note that solvents influence the catalytic activity of the complexes: complexes **2** and **3** display catalytic activity in DME, THF, and toluene; complex **4** exhibits catalytic activity in THF; complexes **5** and **6** possess catalytic activity only in DME. The results are listed in Table 3.

We also examined the effects of temperature on the catalytic activities of the complexes. The catalytic activity of the complexes is temperature dependent: the catalytic activity of the complexes increases as the polymerization temperatures decrease; they possess poor catalytic activities in the temperature range 0−30 °C and exhibit relative higher catalytic activity at lower temperatures. These results are similar to those found when using other ytterbium(II) and eu-

Table 3. Data for the polymerizations of methyl methacrylate (MMA)

Entry[a]	Catalyst	Solvent	t_p (min)	T_p (°C)	$M_w \times 10^{-3}$	$M_n \times 10^{-3}$	M_w/M_n	Conv. (%)	Activity ($\times 10^{-5}$)	Stereochemistry (%) *rr*	*rm*	*mm*
1	**2**	DME	40	30				6	0.04	51	35	14
2		DME	30	0	48.13	20.63	2.33	24	0.24	59	31	10
3		DME	3	−30	69.50	23.85	2.91	6143	3.70	62	28	10
4		DME	5	−60	88.26	37.73	2.34	1743	2.50	67	25	8
5		DME	6	−80	102.30	38.57	2.65	50	2.20	68	24	8
6	**2**	THF	30	0	88.46	38.41	2.30	38	0.38	55	32	13
7		THF	20	−30	85.31	33.34	2.56	23	0.36	60	28	12
8		THF	6	−60	106.30	56.88	1.87	67	3.30	66	27	7
9		THF	2	−80	185.50	75.09	2.47	60	8.90	73	21	6
10	**2**	toluene	40	30				44	0.34	58	28	14
11		toluene	2	0	33.48	9.95	3.36	63	9.50	67	25	8
12		toluene	8	−30				93	3.40	68	26	6
13		toluene	30	−60	69.84	48.41	1.44	5	0.05	65	23	12
14	**3**	DME	30	30	38.21	15.49	2.47	15	1.40	34	36	30
15		DME	30	0	50.96	20.79	2.45	23	3.40	35	43	22
16		DME	2	−30	93.55	42.57	2.20	51	7.70	37	31	32
17		DME	2	−60	109.40	55.28	1.98	84	13.0	42	33	25
18	**3**	THF	30	30	49.86	23.17	2.15	24	0.25	40	30	30
19		THF	2	0	47.46	23.76	2.00	48	7.20	41	31	28
20		THF	2	−30	109.50	55.01	1.96	34	5.10	44	40	16
21		THF	2	−60	154.80	86.12	1.80	63	9.40	47	35	18
22	**3**	toluene	2	30	56.18	25.71	2.18	23	3.40	8	15	77
23		toluene	5	0	93.27	39.52	2.36	13	0.83	10	18	72
24		toluene	30	−30	104.60	46.09	2.27	8	0.09	14	23	63
25	**4**	THF	10	0	40.12	20.42	1.96	12	0.27	29	37	34
26		THF	10	−15	53.58	24.79	2.16	44	1.06	28	33	39
27		THF	10	−30	58.81	27.33	2.15	100	4.82	33	39	28
28		THF	10	−45	96.92	40.46	2.40	100	5.18	40	42	18
29		THF	10	−60	131.19	72.09	1.82	72	1.72	51	37	12
30	**5**	DME	5	0				18	0.88	32	32	36
31		DME	5	−15				16	0.78	32	32	36
32		DME	5	−30	174.21	62.14	2.80	50	2.40	36	35	29
33		DME	5	−45				6	0.32	50	34	16
34	**6**	DME	5	−30				2	0.09	58	27	15
35		DME	5	−45				77	3.59	64	25	11
36		DME	5	−60				18	0.87	75	19	6

[a] Conditions: MMA/solvent = 1:3 (v/v) for catalysts **2** and **3**; MMA/solvent = 1:2 (v/v) for catalysts **4**, **5**, and **6**; cat./MMA (mole ratio) = 1:500 for catalysts **2** and **3**; cat/MMA (mole ratio) = 1:400 for catalysts **4**, **5**, and **6**; activity: g PMMA·mol^{-1}(cat)·h^{-1}; stereoregularity is based on ^{1}H NMR spectroscopic analyses. T_p: Polymerization temperature.

 © 2004 Wiley-VCH Verlag GmbH & Co. KGaA, Weinheim

ropium(II) catalyst systems.[9,11] We also found that the catalytic activity increases as the ionic radii of the catalysts' central metal ion increases; for example, the ytterbium(II) catalyst **2** displayed an activity of 2.5×10^5 g PMMA·mol^{-1}(cat)·h^{-1} in DME at −60 °C, but the europium(II) catalyst **3** bearing the same indenyl ligand exhibited an activity of 13.0×10^5 g PMMA·mol^{-1}(cat)·h^{-1} in the same solvent at the same temperature. These results also support the conclusion that the larger the substituent group of the indenyl ligand, the higher the catalytic activity of the catalyst.

The microstructures of the polymers were studied by ^{1}H NMR spectral analyses.[13] The spectra showed that a mostly syndiotactic polymers were obtained when using the ytterbium catalyst **2** in either polar (THF, DME) or nonpolar (toluene) solvents and when using the europium(II) catalyst **6** in the polar solvent DME. Almost a 1:1:1 ratio of isotactic, syndiotactic, and atactic polymers were obtained, however, when applying the europium(II) catalysts **3**, **4**, and **5** in polar solvents (DME, THF); in contrast, isotactic polymers dominated when using the europium(II) catalyst **3** in toluene. These findings indicate that the donor solvents have an effect on the stereochemistry of the polymers and that this phenomenon may arise from the donor solvents' effects on the epimerization process of the catalysts.[4b,14] The different tacticities of the polymers obtained when using the ytterbium(II) and europium(II) catalysts probably is due to the different ionic radii of the ytterbium(II) and europium(II) ions; these differences affect the epimerization process of the catalysts during the polymerization process.

The molecular weights of the polymers were analyzed by GPC; we found that the molecular weights of the polymers were dependent on the choice of catalyst, solvent, and polymerization temperature. The molecular weights of the polymers generally increase as the polymerization temperature decreases. The results of the polymer molecular mass studies support the supposition that initiation with a divalent lanthanidocence complex occurs through reductive dimerization of MMA to form a bis-initiator, comprising two lanthanide(III) enolates joined through their double-bond termini.[15] The fact that the values of M_w/M_n (1.80 to 3.36) are far from unity may be explained by the effect of partial chain termination caused by deactivation of the catalysts with trace amounts of impurities present in the system: lanthanide(II) complexes and their intermediates formed during the polymerization process are very sensitive to these impurities.

Conclusion

The interactions of the indene compound $Me_2NCH_2CH_2CH_2C_9H_7$ (**1**) with lanthanide(III) amides $[(Me_3Si)_2N]_3Ln(\mu\text{-}Cl)Li(THF)_3$ (Ln = Yb, Eu) and indene compounds $Me_2Si(Me_2NCH_2CH_2C_9H_6)NHtBu$, $Me_2NCH_2CH_2C_9H_6SiMe_3$, and $Me_2NCH_2CH_2C_9H_7$ with europium(III) amide $[(Me_3Si)_2N]_3Eu(\mu\text{-}Cl)Li(THF)_3$ resulted in the isolation of a series of new europium(II) complexes, which we characterized. The formation of the lanthanide(II) complexes is proposed to proceed through tandem silylamine elimination/homolysis of the Ln−N (Ln = Yb, Eu) bonds, as deduced by a mechanistic study. The lanthanide(II) complexes obtained from the reactions function as single-component MMA polymerization catalysts. We examined the effects of temperature, solvent, and substituent groups on the catalysts' activities and the polymers' stereochemistries, molecular weights, and molecular weight distributions.

Experimental Section

General Remarks: All the syntheses and manipulations of air- and moisture-sensitive materials were carried out using flamed Schlenk-type glassware on a Schlenk line. All the solvents were refluxed over and distilled from finely divided $LiAlH_4$ or sodium benzophenone ketyl under argon prior to use, unless otherwise noted. $CDCl_3$ was dried with activated 4-Å molecular sieves. MMA was dried with finely divided CaH_2 and distilled before use. $Me_2Si(Me_2NCH_2CH_2C_9H_6)NHtBu$,[9] $Me_2NCH_2CH_2C_9H_6SiMe_3$,[9] $Me_2NCH_2CH_2C_9H_7$,[16] and $[(Me_3Si)_2N]_3Ln(\mu\text{-}Cl)Li(THF)_3$ (Ln = Yb,[9] Eu[5h]) were prepared according to reported procedures. Elemental analyses were obtained with a Perkin−Elmer 2400 Series II Elemental Analyzer. IR spectra were recorded with a Perkin−Elmer 983(G) spectrometer (CsI crystal plate, Nujol and fluoroble mulls). Melting points were determined using sealed capillaries and uncorrected. GC-MS analyses were carried out with an Agilent 6890/Micromass GCT-MS instrument. ^{1}H NMR and ^{13}C NMR spectra were recorded with a Bruker AV-300 NMR spectrometer in C_5D_5N (pyridine-d_5) for lanthanide complexes and in $CDCl_3$ for polymers and indene compounds; the chemical shifts are listed relative to the internal solvent resonances. Gel permeation chromatography (GPC) analyses of polymer samples were performed at 30 °C using THF as the eluent on a Waters-150C instrument that was calibrated using monodisperse polystyrene (PS) standards at a flow rate of 1.0 mL·min^{-1}. Number-average molecular weights and polydispersities of polymers are given relative to PS standards. The polymers were analyzed according to the literature.[13]

$C_9H_7CH_2CH_2CH_2NMe_2$ (1): A 1.57 M hexane solution of *n*BuLi (54.0 mL, 85.2 mmol) was added slowly at 0 °C to a solution of indene (10.0 mL, 85.2 mmol) in THF (80.0 mL). The reaction mixture was stirred at room temperature overnight and then the solution was cooled to 0 °C and $Me_2NCH_2CH_2CH_2Cl$ (10.4 g, 85.2 mmol) was added in one portion. The reaction mixture was stirred at room temperature for 10 h and then it was hydrolyzed. The organic layer was separated and the aqueous layer was extracted with diethyl ether (2×15.0 mL). The organic fractions were combined and dried with anhydrous $MgSO_4$, filtered, and evaporated to dryness. The colorless oily product (12.5 mg, 73%) was obtained after distillation under reduced pressure. ^{1}H NMR (300.17 MHz, $CDCl_3$, 295 K): δ = 7.50 (d, J = 7.23 Hz, 1 H), 7.44 (d, J = 7.38 Hz, 1 H), 7.34 (m, 1 H), 7.24 (m, 1 H), 6.26 (s, 1 H) 3.36 (s, 2 H), 2.62 (m, 2 H), 2.42 (m, 2 H), 2.30 (s, 6 H), 1.94 (m, 2 H) ppm. ^{13}C NMR (75.48 MHz, $CDCl_3$, 295 K): δ = 145.55, 144.55, 144.38, 127.76, 126.76, 126.07, 124.58, 123.79, 119.04, 59.80, 45.66, 37.77, 26.25, 25.62 ppm. IR (Nujol and Fluroble mulls): $\tilde{\nu}$ = 3065 (m), 3017 (m), 2942 (s), 2857 (s), 2764 (s), 1881 (w), 1790 (w), 1682 (w), 1609 (m), 1460 (s), 1377 (m), 1264 (m), 1169 (m), 1097 (w), 1042 (m), 963 (m), 827 (w), 718 (m), 617 (w),

 © 2004 Wiley-VCH Verlag GmbH & Co. KGaA, Weinheim

504 (w) cm^{-1}. $C_{14}H_{19}N$ (201.31): calcd. C 83.53, H 9.51, N 6.96; found C 83.15, H 9.45, N 7.02.

[(η⁵:η¹-$C_9H_6CH_2CH_2CH_2NMe_2$)$_2$Yb] (2): A solution of $C_9H_7CH_2CH_2CH_2NMe_2$ (**1**; 490 mg, 2.40 mmol) in toluene (10.0 mL) was added slowly to a solution of $[(Me_3Si)_2N]_3Yb(\mu\text{-}Cl)Li(THF)_3$ (1100 mg, 1.20 mmol) in toluene (50.0 mL) . The reaction mixture was stirred at room temperature for 6 h and then under reflux for 24 h. The color of the reaction mixture gradually changed from yellow to blue and finally to dark red. The solvent was evaporated to give a red solid that was washed with *n*-hexane (10.0 mL). The solid was extracted with toluene (2 × 15.0 mL); the extracts were combined and concentrated to ca. 15.0 mL. A red crystalline solid was obtained after cooling the solution to −10 °C. Yield: 460 mg (67%). M.p. 143−144 °C. ^{1}H NMR (300.17 MHz, C_5D_5N, 295 K): δ = 7.55 (m, 4 H), 7.35 (m, 4 H), 7.18 (m, 2 H), 6.16 (m, 2 H, C_9H_6), 3.24 (m, 4 H), 2.57 (m, 4 H), 1.81 (m, 4 H, $CH_2CH_2CH_2$), 2.13 [s, 12 H, $N(CH_3)_2$] ppm. IR (Nujol and Fluroble mulls): $\tilde{\nu}$ = 2947 (m), 2821 (m), 2777 (m), 1612 (m), 1461 (m), 1262 (m), 1152 (m), 1097 (m), 1042 (m), 965 (m), 914 (m), 769 (s), 719 (m), 411 (m) cm^{-1}. $C_{28}H_{36}N_2Yb$ (573.65): calcd. C58.63, H 6.33, N 4.88; found C 58.79, H 5.99, N 4.82.

[(η⁵:η¹-$C_9H_6CH_2CH_2CH_2NMe_2$)$_2$Eu] (3): This compound was prepared as a yellow crystalline solid in 74% yield from the reaction of $[(Me_3Si)_2N]_3Eu(\mu\text{-}Cl)Li(THF)_3$ (1.250 g, 1.40 mmol) and $C_9H_7CH_2CH_2CH_2NMe_2$ (570 mg, 2.80 mmol) in toluene at 50 °C by employing procedures similar to those used for the preparation of **2**. NMR spectra were not informative because of the lack of locking signals that arises from the paramagnetic property of the europium(II) complex. M.p. 335−337 °C (dec.). IR (Nujol and Fluroble mulls): $\tilde{\nu}$ = 3065 (m), 2954 (m), 2859 (m), 1789 (m), 1531 (m), 1460 (s), 1402 (s), 1265 (m), 1151 (m), 1042 (m), 963 (m), 847 (m), 769 (s), 719 (s), 412 (w) cm^{-1}. $C_{28}H_{36}EuN_2$ (552.57): calcd. C 60.86, H 6.57, N 5.07; found C 60.58, H 6.42, N 5.06.

[{η⁵:η¹-$Me_2Si(Me_2NCH_2CH_2C_9H_5)(NHtBu)$}$_2$Eu]·$(OC_4H_8)_{0.5}$ (4): This compound was prepared as yellow crystals in 46% yield from the reaction of $[(Me_3Si)_2N]_3Eu(\mu\text{-}Cl)Li(THF)_3$ (3.010 g, 3.38 mmol) and $Me_2Si(Me_2NCH_2CH_2C_9H_6)(NHtBu)$ (2.140 g, 6.76 mmol) in toluene at 60 °C by employing procedures similar to those used for the preparation of **2**. M.p. 252−254 °C. ^{1}H NMR (300.17 MHz, C_5D_5N, 295 K): δ = 7.54 (br. s, 4 H), 7.19 (br. s, 4 H), 6.57 (m, 2 H, C_9H_5), 4.00 (m, 4 H), 2.88 (m, 4 H, CH_2CH_2), 3.63 (s, 2 H, N*H*), 2.22 [br. s, 12 H, $N(CH_3)_2$], 1.18 [br. s, 18 H, $C(CH_3)_3$], −0.001 [br. s, 12 H, $Si(CH_3)_2$] ppm. IR (Nujol and Fluroble mulls): $\tilde{\nu}$ = 3377 (w), 3063 (w), 2963 (s), 2765 (m), 1600 (m), 1461 (s), 1377 (s), 1249 (s), 1097 (s), 1021 (vs), 864 (s), 764 (s), 721 (m), 615 (m), 435 (w) cm^{-1}. $C_{38}H_{60}EuN_4Si_2$ (**4**·0.5THF) (781.05): calcd. C 58.44, H 7.74, N 7.17; found C 58.05, H 7.76, N 6.90.

[{η⁵:η¹-$(Me_2NCH_2CH_2C_9H_5SiMe_3)$}$_2$Eu] (5): This compound was prepared as yellow crystals in 49% yield from the reaction of $[(Me_3Si)_2N]_3Eu(\mu\text{-}Cl)Li(THF)_3$ (6.870 g, 7.72 mmol) and $Me_2NCH_2CH_2C_9H_6SiMe_3$ (4.000 g, 15.44 mmol) in toluene at 60 °C by using procedures similar to those used for the preparation of **2**. ^{1}H NMR (300.17 MHz, C_5D_5N, 295 K): δ = 7.55 (br. s, 4 H), 7.18 (br. s, 4 H), 6.48 (m, 2 H, C_9H_5), 4.30 (m, 4 H), 2.90 (m, 4 H, CH_2CH_2), 2.24 [br. s, 12 H, $N(CH_3)_2$], 0.57 (br. s, 6 H), −0.03 [br. s, 12 H, $Si(CH_3)_3$] ppm. IR (Nujol and Fluroble mulls): $\tilde{\nu}$ = 3066 (w), 2954 (s), 1628 (m), 1455 (s), 1374 (m), 1260 (m), 1247 (vs), 1070 (m), 1018 (m), 838 (vs), 765 (m), 719 (m), 431 (w) cm^{-1}. $C_{32}H_{48}EuN_2Si_2$ (668.86): calcd. C 57.45, H 7.23, N 4.19; found C 57.02, H 6.93, N 4.02.

[(η⁵:η¹-$Me_2CH_2CH_2C_9H_6$)$_2$Eu] (6): This compound was prepared as yellow crystals in 57% yield from the reaction of $[(Me_3Si)_2N]_3Eu(\mu\text{-}Cl)Li(THF)_3$ (1.29 g, 1.91 mmol) and $Me_2NCH_2CH_2C_9H_7$ (720 mg, 3.82 mmol) in toluene under reflux by employing procedures similar to those used for the preparation of **2**. NMR spectra were not informative because of the lack of locking signals that arises from the paramagnetic property of the compound. IR (Nujol and Fluroble mulls): $\tilde{\nu}$ = 3180 (m), 2919 (vs), 1609 (m), 1459 (vs), 1375 (vs), 1265 (m), 1073 (m), 1018 (m), 863 (m), 769 (s), 718 (m), 386 (w) cm^{-1}. $C_{26}H_{32}EuN_2$ (524.50): calcd. C 59.54, H 6.15, N 5.34; found C 59.30, H 6.10, N 5.38.

Table 4. X-ray experimental data of compounds **4**, **5** and **6**

	4	**5**	**6**
Empirical formula	$C_{40}H_{66}EuN_4O_{0.5}Si_2$	$C_{32}H_{48}EuN_2Si_2$	$C_{26}H_{32}EuN_2$
Molecular mass	819.11	668.86	524.50
Crystal system	orthorhombic	tetragonal	monoclinic
Space group	*Fdd*2	$I\bar{4}$	$P2_1/n$
a (Å)	32.70000(10)	21.2723(5)	16.8056(2)
b (Å)	35.6054(7)	21.2723(5)	15.77160(10)
c (Å)	14.8446(4)	15.9895(5)	18.84910(10)
β (deg)			110.4200(10)
V (Å^3)	17283.5(6)	7235.4(3)	4682.03(7)
Temperature (K)	293(2)	293(2)	293(2)
$D_{calcd.}$ (g cm^{-3})	1.259	1.228	1.488
Z	16	8	8
F(000)	6864	2760	2120
No. of refls. collected	10029	8853	16822
No. of unique refls.	4793 (R_{int} = 0.047)	5426 (R_{int} = 0.024)	8219 (R_{int} = 0.035)
No. of parameters	416	334	523
λ (Å); Mo-K_α	0.71073	0.71073	0.71073
μ (mm^{-1})	1.538	1.820	2.693
Theta limits (deg)	2.39/25.04	2.89/25.06	1.40/25.04
GOF	1.064	1.102	1.140
R [$I > 2\sigma(I)$]	0.048	0.039	0.042
wR_2	0.100	0.085	0.083
Largest diff. peak and hole (e·Å^{-3})	0.687 and −0.411	0.562 and −0.334	0.788 and −0.861

 © 2004 Wiley-VCH Verlag GmbH & Co. KGaA, Weinheim

High-Resolution GC-MS Analyses: Small portions of the reaction mixtures of the preparations of **2** to **6** were hydrolyzed and analyzed by GC-MS techniques. In addition to the corresponding indene compounds and $HN(SiMe_3)_2$, a small amount of coupling product $[(Me_3Si)_2N]_2$ was detected in each component. Retention time for $[(Me_3Si)_2N]_2$: 15.57 min; calcd. $[\{(Me_3Si)_2N\}_2 - Me]^+$ m/z = 306.1799; found 306.1838.

MMA Polymerization: MMA polymerization reactions were performed in a 50.0-mL Schlenk flask, placed in an external temperature-controlled bath, on a Schlenk line or in a glovebox. In a typical procedure, the catalyst (20−50 mg) was loaded into the Schlenk flask and the solvent was added. After the external bath temperature had stabilized, MMA was added through a gastight syringe. The polymerization was terminated by the addition of acidic methanol after a measured interval. The polymer product was precipitated into methanol (50.0 mL), washed with methanol, and then dried to a constant weight in a vacuum oven at 50 °C. The stereochemistry of the polymers and their molecular weights were analyzed by ^1H NMR spectroscopy and GPC techniques, respectively.

X-Ray Crystallography: Suitable crystals of the complexes **4**, **5**, and **6** were each mounted in a sealed capillary. Diffraction was performed on a Siemens SMART CCD-area detector diffractometer using graphite-monochromated Mo-K_α radiation (λ = 0.71073 Å); temperature 293(2) K; φ and ω scan technique; SADABS effects and empirical absorption were applied in the data corrections. All structures were solved by direct methods (SHELXS-97),[17] completed by subsequent difference Fourier syntheses, and refined by full-matrix least-squares calculations based on F^2 (SHELXS-97).[17] See Table 4 for crystallographic data.

CCDC-229706 (for **4**), -195752 (for **5**), and -195751 (for **6**) contain the supplementary crystallographic data for this paper. These data can be obtained free of charge at www.ccdc.cam.ac.uk/conts/retrieving.html [or from the Cambridge Crystallographic Data Centre, 12 Union Road, Cambridge CB2 1EZ, UK; Fax: +44-1223-336-033; E-mail: deposit@ccdc.cam.ac.uk].

Acknowledgments

This work was cosponsored by the National Natural Science Foundation of China (Project Nos. 20271003 and 20072001), the Excellent Young Scholars Foundation of Anhui Province, and a grants from the Anhui Education Department and the Anhui Normal University. We are grateful to Professors Jiping Hu and Baohui Du for their help in obtaining NMR and IR spectra.

[1] [1a] H. Schumann, J. A. Meese-Martscheffel, L. Esser, *Chem. Rev.* **1995**, *95*, 865. [1b] G. Bombieri, G. Paolucci, in *Handbook on the Physics and Chemistry of Rare Earths 25* (Eds.: K. A. Gschneidner, L. Eyring, Jr.), Elsevier, Amsterdam, **1998**, p. 265. [1c]W. J. Evans, *Polyhedron* **1987**, *6*, 803. [1d] W. J. Evans, *Coord. Chem. Rev.* **2000**, *206−207*, 263. [1e] W. J. Evans, *J. Organomet. Chem.* **2002**, *652*, 61. [1f] T. G. Wetzel, S. Dehnen, P. W. Roesky, *Angew. Chem. Int. Ed.* **1999**, *38*, 1086−1088. [1g] M. R. Bürgstein, P. W. Roesky, *Organometallics* **2003**, *22*, 1372−1375. [1h] F. Estler, G. Eickerling, E. Herdtweck, R. Anwander, *Organometallics* **2003**, *22*, 1212−1222.

[2] [2a] Y. K. Kim, T. Livinghouse, Y. Horino, *J. Am. Chem. Soc.* **2003**, *125*, 9560. [2b] P. N. O'Shaughnessy, P. Scott, *Tetrahedron: Asymmetry* **2003**, *14*, 1979−1983. [2c] Y. K. Kim, T. Livinghouse, J. E. Bercaw, *Tetrahedron Lett.* **2001**, *42*, 2933. [2d] S. Tian, V. M. Arredondo, C. L. Stern, T. J. Marks, *Organometallics* **1999**, *18*, 2568. [2e] J. S. Ryu, T. J. Marks, F. E. McDonald, *Org. Lett.* **2001**, *3*, 3091. [2f] V. M. Arredondo, F. E. McDonald, T. J. Marks, *Organometallics* **1999**, *18*, 1949. [2g] V. M. Arredondo, S. Tian, F. E. McDonald, T. J. Marks, *J. Am. Chem. Soc.* **1999**, *121*, 3633. [2h] M. R. Gagne, C. L. Stern, T. J. Marks, *J. Am. Chem. Soc.* **1992**, *114*, 275. [2i] M. R. Gagne, L. Brard, V. P. Conticello, M. A. Giardello, C. L. Stern, T. J. Marks, *Organometallics* **1992**, *11*, 2003. [2j] M. A. Giardello, V. P. Conticello, L. Brard, M. R. Gagne, T. J. Marks, *J. Am. Chem. Soc.* **1994**, *116*, 10241X. [2k] P. N. O'Shaughnessy, P. D. Knight, C. Morton, K. M. Gillespie, P. Scott, *Chem. Commun.* **2003**, 1770−1771. [2l] P. W. Roesky, T. E. Müller, *Angew. Chem. Int. Ed.* **2003**, *42*, 2708−2710. [2m] M. R. Bürgstein, H. Berberich, P. W. Roesky, *Eur. J. Chem.* **2001**, *7*, 3078−3085.

[3] Y. Horino, T. Livinghouse, *Organometallics* **2004**, *23*, 12−14.

[4] [4a] M. R. Douglass, T. J. Marks, *J. Am. Chem. Soc.* **2000**, *122*, 1824−1825. [4b] M. R. Douglass, M. Ogasawara, S. Hong, M. V. Metz, T. J. Marks, *Organometallics* **2002**, *21*, 283−292. [4c] A. M. Kawaoka, M. R. Douglass, T. J. Marks, *Organometallics* **2003**, *22*, 4630−4632.

[5] [5a] H. Yasuda, in *Lanthanides: Chemistry and Use in Organic Synthesis* (Ed.: S. Kobayashi), Springer-Verlag, Heidelberg, **1999**, p. 255. [5b]H. Yasuda, *J. Organomet. Chem.* **2002**, *647*, 128. [5c] Z. Hou, Y. Wakatsuki, *Coord. Chem. Rev.* **2002**, *231*, 1. [5d] M. A. Giardello, Y. Yamamoto, L. Brard, T. J. Marks, *J. Am. Chem. Soc.* **1995**, *117*, 3276. [5e] C. T. Qian, G. Zuo, Y. F. Chen, J. Sun, *Organometallics* **2001**, *20*, 3106. [5f] C. Boisson, F. Barbotin, R. Spitz, *Macromol. Chem. Phys.* **1999**, *200*, 1163. [5g] C. T. Qian, W. L. Nie, J. Sun, *Organometallics* **2000**, *19*, 4134. [5h] S. Zhou, S. Wang, G. Yang, X. Liu, E. Sheng, K. Zhang, L. Cheng, Z. Huang, *Polyhedron* **2003**, *22*, 1019−1024. [5i] Y. Yao, Y. Zhang, Z. Zhang, Q. Shen, K. Yu, *Organometallics* **2003**, *22*, 2876−2882. [5j] Y. Yao, Y. Luo, J. Chen, Z. Zhang, Y. Zhang, Q. Shen, *J. Organomet. Chem.* **2003**, *679*, 229−237.

[6] [6a] H. Berberich, P. W. Roesky, *Angew. Chem. Int. Ed.* **1998**, *37*, 1569. [6b] M. R. Bürgstein, H. Berberich, P. W. Roesky, *Eur. J. Chem.* **2001**, *7*, 3078. [6c] G. B. Deacon, A. Gitlits, P. W. Roesky, M. R. Bürgstein, K. C. Lim, B. W. Skelton, A. H. White, *Chem. Eur. J.* **2001**, *7*, 127−138.

[7] [7a] K. C. Hultsch, T. P. Spaniol, J. Okuda, *Organometallics* **1997**, *16*, 4845. [7b] E. Martin, P. Dubois, R. Jerome, *Macromolecules* **2000**, *33*, 1530. [7c] H. Noss, M. Oberthür, C. Fischer, W. P. Kretschmer, R. Kempe, *Eur. J. Inorg. Chem.* **1999**, 2283−2288. [7d] Y. Luo, Y. Yao, Q. Shen, J. Sun, L. Weng, *J. Organomet. Chem.* **2002**, *662*, 144−149.

[8] [8a] J. Zhang, R. Cai, L. Weng, X. Zhou, *Organometallics* **2003**, *22*, 5385−5391. [8b] H. R. Li, Y. M. Yao, Q. Shen, L. H. Weng, *Organometallics* **2002**, *21*, 2529−2532. [8c] L. S. Mao, Q. Shen, M. Q. Xue, *Organometallics* **1997**, *16*, 3711. [8d] J. Zhang, R. Cai, L. Weng, X. Zhou, *J. Organomet. Chem.* **2003**, *672*, 94−99.

[9] [9a] E. Sheng, S. Wang, G. Yang, S. Zhou, L. Cheng, K. Zhang, Z. Huang, *Organometallics* **2003**, *22*, 684−692. [9b] K. Zhang, W. Zhang, S. Wang, E. Sheng, G. Yang, M. Xie, S. Zhou, Y. Feng, L. Mao, Z Huang, *J. Chem. Soc., Dalton Trans.* **2004**, 1029−1037.

[10] [10a] J. Eppinger, M. Spiegler, W. Hieringer, W. A. Herrmann, R. Anwander, *J. Am. Chem. Soc.* **2000**, *122*, 3080. [10b] W. A. Herrmann, J. Eppinger, M. Spiegler, O. Runte, R. Anwander, *Organometallics* **1997**, *16*, 1813. [10c] R. Anwander, O. Runte, J. Eppinger, G. Gerstberger, M. Spiegler, E. Herctweck, *J. Chem. Soc., Dalton Trans.* **1998**, 847.

[11] S. Wang, S. Zhou, E. Sheng, G. Yang, M. Xie, K. Zhang, L. Cheng, Y. Feng, L. Mao, Z. Huang, *Organometallics* **2003**, *22*, 3546−3552.

[12] R. D. Shannon, *Acta Crystallogr., Sect. A* **1976**, *32*, 751−767.

[13] F. A. Bovey, P. A. Mirau, *NMR of Polymers*, Academic Press, San Diego, **1996**.

[14] [14a] M. A. Giardello, V. P. Conticello, L. Brard, M. Sabat, A. L. Rheingold, C. L. Stern, T. J. Marks, *J. Am. Chem. Soc.* **1994**,

 © 2004 Wiley-VCH Verlag GmbH & Co. KGaA, Weinheim

116, 10212X. [14b] C. M. Haar, C. L. Stern, T. J. Marks, *Organometallics* **1996**, *15*, 1765. [14c] K. C. Hultzsch, T. P. Spaniol, J. Okuda, *Organometallics* **1997**, *16*, 4845. [14d] J. C. Yoder, M. W. Day, J. E. Bercaw, *Organometallics* **1998**, *17*, 4946. [14e] S. Wang, Q. Yang, T. C. W. Mak, Z. Xie, *Organometallics* **2000**, *19*, 334−343.
[15] L. S. Boffa, B. M. Novak, *Macromolecules* **1994**, *27*, 6993.
[16] C. Qian, G. Zuo, J. Sun, *J. Organomet. Chem.* **1999**, *585*, 59−62.
[17] G. M. Sheldrick, *SHELXTL*, Version 5.10; Bruker Analytical X-ray Systems, Inc., Madison, WI, **1997**.

Received January 30, 2004
Early View Article
Published Online June 1, 2004

 © 2004 Wiley-VCH Verlag GmbH & Co. KGaA, Weinheim

Molecular Alloys: Syntheses and Structures of the Copper−Antimony Clusters $[Cu_{17}Sb_8(dppm)_6(Ph_2PCHPPh_2)]$ and $[Cu_{20}Sb_{10}(PCy_3)_8]$

Reinhart Ahlrichs,[a] Christopher E. Anson,[b] Rodolphe Clerac,[c] Dieter Fenske,*[b] Alexander Rothenberger,[b] Marek Sierka,[a] and Stephan Wieber[b]

Keywords: X-ray diffraction / Cluster compounds / Antimony / Copper

The syntheses, structures and theoretical investigations of the copper-antimony clusters $[Cu_{17}Sb_8(dppm)_6(Ph_2PCHPPh_2)]$ [**1**, dppm = bis(diphenylphosphanyl)methane] and $[Sb_{10}Cu_{20}(PCy_3)_8]$ (**2**, Cy = Cyclohexyl) are reported.

(© Wiley-VCH Verlag GmbH & Co. KGaA, 69451 Weinheim, Germany, 2004)

Introduction

Over the last decade our major field of interest has been the synthesis and structural analysis of metal clusters in which metal atoms are bridged by main-group elements. Special focus was placed on Group 15 and Group 16 bridged metal arrangements, and examples for both cluster classes are numerous.[1] Examples of copper clusters bridged by higher homologues of Group 15 are scarce. Yamada et al. have studied cluster cations of the type $Cu_nSb_m^+$ produced by a gas aggregation source and found that the magic numbers [n, m = (4, 1), (5, 6), (6, 7)] reflect the stability of jellium-shell closings.[2] However, only recently were we able to synthesise and structurally characterise the first Cu−Sb cluster $[Cu_{10}(Sb_3)_2(SbSiMe_3)_2(dppm)_6]$ using Schlenk techniques.[3] All these Cu−Sb cluster species contain Sb−Sb bonds as a common structural motif.

Our approach to Group 15/coinage metal clusters generally involves the reaction of a metal salt MX (M = transition metal; X = halide, carboxylate, alkoxide) with a trimethylsilyl derivative of a main-group element in the presence of a tertiary phosphane. A second route is the metathesis reaction of a transition-metal salt with alkali-metallated Group 15 trimethylsilyl compounds.

Results and Discussion

During the course of the investigations into the syntheses of copper−antimony clusters we explored the potential of both routes. The compounds presented in this communication have all been prepared using the first route.

The reactions of dppm and PCy_3 with one equivalent of CuO*t*Bu and subsequent reaction with $Sb(SiMe_3)_3$ produced the copper−antimony clusters $[Cu_{17}Sb_8(dppm)_6(Ph_2PCHPPh_2)]$ **1** and $[Cu_{20}Sb_{10}(PCy_3)_8]$ **2** (Scheme 1).

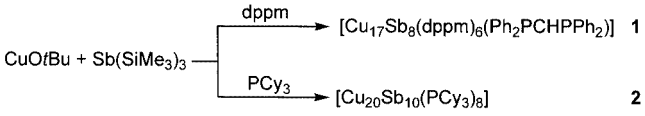

Scheme 1. Syntheses of the Cu−Sb clusters in a THF/hexane solution

Compound **1** crystallizes in the triclinic space group $P\bar{1}$ with two molecules in the unit cell and nine lattice-bound THF molecules (Figure 1). The copper atoms are located on faces and edges of a central trigonal antiprismatic arrangement of Sb(2−7). The trigonal faces Sb(2,3,4) and Sb(5,6,7) are capped by Sb(1) and Sb(8). Cu(13) is located in the centre of a Sb(5,6,7) triangle. Cu(17) is the only copper atom in **1** that is coordinated to a carbon atom [Cu(17)−C(138) 2.08(2) Å] and does not bridge at least two Sb centres.[4] Observed Sb−Cu bond lengths and Cu···Cu distances of **1** are in the ranges 2.561(4)−3.086(4) and 2.515(4)−3.041(5) Å, respectively, and are similar to those observed in the cluster $[Cu_{10}(Sb_3)_2(SbSiMe_3)_2(dppm)_6]$ [Cu−Sb av. 2.60 Å, Cu···Cu 2.583(2)−2.675(2) Å].[3] It is noteworthy in this context that the short Cu···Cu distances of **1** (ca. 2.5 Å) are predominantly between tetrahedral and trigonal Cu centres, and are more likely to be the result of geometric requirements than of Cu−Cu bonding. During the course of the reaction partial deprotonation of dppm by CuO*t*Bu occurred, and the structure of **1** is composed

[a] Institut für Physikalische Chemie, Universität Karlsruhe, Fritz-Haber-Weg 4, 76131 Karlsruhe, Germany
[b] Institut für Anorganische Chemie, Universität Karlsruhe, Engesserstraße 15, 76131 Karlsruhe, Germany
E-mail: dieter.fenske@chemie.uni-karlsruhe.de
[c] Centre de Recherche Paul Pascal-CNRS UPR 8641, 115 Avenue du Dr A. Schweitzer, 33600 Pessac, France

of a $[Cu_{16}Sb_8(dppm)_6]$ unit and metallated dppm [Cu(dppm)]. The structure of the $[Cu_{16}Sb_8(dppm)_6]$ unit in **1** is similar to the structure found for the Group 16 bridged copper cluster $[Cu_{16}Te_8(P^nPr_2Ph)_{10}]$, thus raising questions about the oxidation state of the metal atoms in **1**.[5] In the neutral copper cluster $[Cu_{16}Te_8(P^nPr_2Ph)_{10}]$ the situation is clear with eight formally Te^{2-} centres coordinated to 16 Cu^I centres.[5] The core of **1**, however, consists of eight Sb centres and sixteen Cu centres arranged in the subunit $[Cu_{16}Sb_8(dppm)_6]$. Additional [Cu(dppm)] gives the neutral complex $[Cu_{17}Sb_8(dppm)_6(Ph_2PCHPPh_2)]$ (**1**). The presence of both Cu^I and Cu^{II} centres in the structure cannot be detected. The UV spectra of brown crystals of **1** (200−900 nm) do not show charge-transfer bands similar to those observed in Cu−Te clusters or absorption maxima characteristic for Cu^{II} centres.[5] A similar situation was found for $[Cu_{20}Sb_{10}(PCy_3)_8]$ (**2**), which crystallizes in the monoclinic space group $P2_1/n$ with four molecules of THF as lattice-bound solvent (Figure 2).

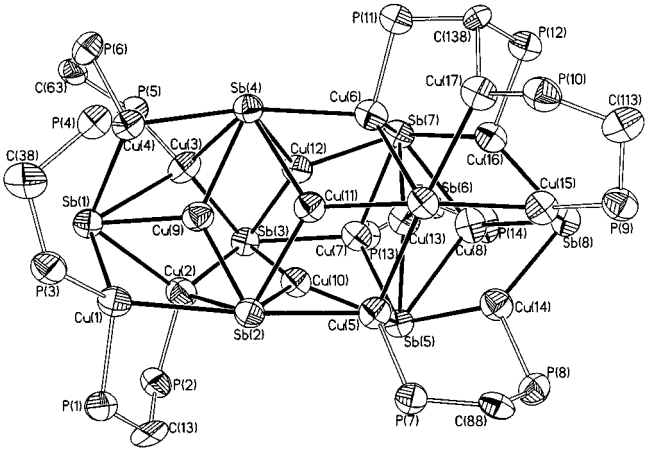

Figure 1. Molecular structure of $[Cu_{17}Sb_8(dppm)_6(Ph_2PCHPPh_2)]$ (**1**); phenyl groups have been omitted; ellipsoids at 50% probability level; selected bond lengths (Å): Cu−Sb 2.561(4) [Sb(2)−Cu(9)] to 3.086(4) [Sb(2)−Cu(2)], shortest Cu−Cu distance 2.515(4) [Cu(2)−Cu(9)], Cu(17)−C(138) 2.08(2), av. Cu−P 2.25

The solid-state structure of **2** consists of two distorted edge-sharing Sb_6 octahedra [Sb(2,3,3a,1,5a,4a) and Sb(4,5,1a,3a,3,2a)] in which the trigonal faces are capped by μ_3-Cu(1,5,6). In the centrosymmetric cluster **2**, the shared edge of the Sb_6 octahedra is bridged by Cu(3) [Cu(3)−Sb(3) 2.7009(19) Å]. The peripheral Cu(2,4,8,10) are coordinated by phosphane ligands. The cyclohexyl substituents of the phoshine ligands form an organic shell preventing the central $Cu_{20}Sb_{10}$ core from further aggregation. Cu(9) exhibits a distorted linear coordination environment [Sb(1A)−Cu(9)−Sb(5): 164.86(7)°] and would perhaps show a similar coordination environment to Cu(3) in a more extended solid-state structure than that of **2**. To elucidate the electronic structure and in particular the oxidation state of the copper atoms involved in the formation of **2**, further experiments (measurement of the temperature dependence of the magnetic susceptibility and of the field dependence of the magnetization between 1.83 K and 100 K) were carried out on polycrystalline samples of **2** (crystals of **1** are contaminated with an amorphous precipitate, so we focused on samples of **2**). As a result, we found that **2** has a diamagnetic ground state with an average susceptibility of −0.003 emu/mol (value in agreement with that expected for a diamagnetic material).

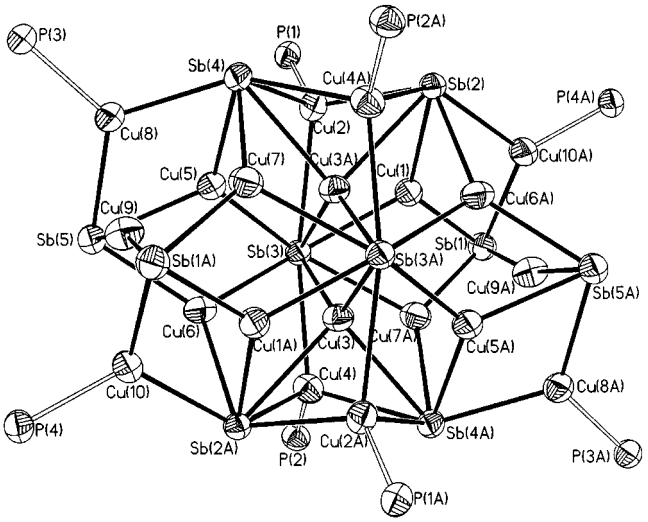

Figure 2. Molecular structure of $[Cu_{20}Sb_{10}(PCy_3)_8]$ (**2**); cyclohexyl groups have been omitted; ellipsoids at 50% probability level; selected bond lengths (Å): Cu−Sb 2.457(2) [Cu(9)−Sb(5)] to 3.106(2) [Cu(2)−Sb(3)], shortest Cu···Cu distance 2.517(2) [Cu(5)−Cu(6)], av. Cu−P 2.24

Independently, a DFT study was carried out to probe these findings.[6] To analyse the properties of the Cu−Sb bond we started with a set of small clusters Cu_nSb_m, n = 1−3; m = 1, 2 summarized in Table 1. Such clusters can provide information about the nature of the Cu−Sb bond with increasing cluster size and different compositions in the absence of ligand effects. Since the electronegativities of Cu and Sb are identical (Pauling scale), no significant charge transfer is expected upon formation of the Cu−Sb bond.[7] This is reflected by the results of Mulliken population analyses (Table 1), which predicts only negligible charge transfer in all small clusters. This confirms the covalent, alloy-like nature of the cores of the Cu−Sb compounds **1** and **2**.

Table 1. Calculated properties of small Cu−Sb clusters: spin state and molecular symmetry, Cu−Sb and Cu−Cu bond lengths (Å) and Mulliken atomic charges

	CuSb	Cu_2Sb	Cu_3Sb	Cu_3Sb_2
State (symmetry)	$^3\Sigma^-$	$^2B_2$ (C_{2v})	$^1A_1$ (C_{3v})	$^2B_2$ (C_{2v})
Cu−Sb	2.43	2.45	2.47	2.51; 2.60
Cu−Cu	−	2.49	2.50	2.55
q_{Cu}	0.07	0.03	0.005	0.02−0.03
q_{Sb}	−0.07	−0.06	−0.01	−0.04

 © 2004 Wiley-VCH Verlag GmbH & Co. KGaA, Weinheim

To investigate the electronic properties of **2** we performed calculations on the model complex **2a** in which the PCy_3 ligands were replaced by PMe_3. The experimental structure of **2** shows a C_i molecular symmetry which was also kept during structure optimisations of **2a**. The calculated ground state of **2a** is ^1A_g with close-lying triplet ^3A_g (0.2 eV higher). Since the BP86 functional is known to stabilise lower spin states, this result just indicates singlet and triplet states that are similar in energy. However, the magnetic measurements indicate a diamagnetic nature of **2** and confirm the singlet ground state. The calculated structural parameters (Table 2) of **2a** are generally in good agreement with the experimental results for **2**.

Table 2. Comparison of selected calculated and experimental structural parameters of **2a** and **2**; bond lengths in Å and bond angles in degrees

Parameter	Calculated (**2a**)	Experimental (**2**)
Cu(3)−Cu(3A)	2.50	2.53
Cu(3A)−Cu(5)	2.61	2.63
Cu(9)−Sb(5)	2.53	2.46
Cu(3)−Sb(3)	2.75	2.70
Sb(1A)−Cu(9)−Sb(5)	171.6	164.9

Conclusion

Based on these results and the UV spectra we suggest that the concept of oxidation numbers and localised Cu^{II} and Cu^{I} centres cannot be applied to the Sb−Cu clusters presented here. Instead, **1** and **2** represent intermediates in the reaction of $Sb(SiMe_3)_3$ and Cu*O*t*Bu* that gives the Cu_2Sb alloy which is still under investigation.[8] The results presented here demonstrate that reactions of $Sb(SiMe_3)_3$ with Cu*O*t*Bu* in the presence of tertiary phosphanes can give rise to a class of Sb−Cu clusters that can be regarded as the first representatives of a possibly larger family of phosphane-stabilised molecular alloys with the metal composition $[Cu_2Sb]_n$.

Experimental Section

General Remarks: All operations were carried out in an atmosphere of purified argon. THF was refluxed over potassium and freshly distilled. Hexane was dried with $LiAlH_4$. $P(Cy)_3$ and dppm were purchased from Aldrich and used without further purification. $Sb(SiMe_3)_3$ was prepared according to a literature procedure.[9] Magnetic susceptibility measurements were performed using a Quantum Design SQUID magnetometer MPMS-XL. The magnetic data were corrected for the sample holder (plastic bag) and the diamagnetic contribution calculated from the Pascal constants.[10]

1: A solution of dppm (0.49 g, 1.27 mmol) in 3 mL THF was added to a solution of Cu*O*t*Bu* (0.27 g, 2.00 mmol) tin 5 mL THF. The brown solution was briefly heated to reflux and then allowed to cool down to room temperature. $Sb(SiMe_3)_3$ (3.85 mL, 0.66 mmol, 0.17 M in hexane) was then added at −78 °C. After storage at −40 °C for two weeks, the mixture was allowed to stand at room temperature for another two weeks to produce dark brown crystals of $[Cu_{17}Sb_8(dppm)_6(Ph_2PCHPPh_2)]$ **1** (nine molecules of THF as lattice-bound solvent) (0.10 g, 16%), decomposition at room temperature. The UV/Vis spectrum of **1** does not show any bands. $C_{211}H_{225}Cu_{17}O_9P_{14}Sb_8$:calcd. C 47.0, H 4.2; found C 44.1, H 3.4.

2: A solution of PCy_3 (0.56 g, 2.00 mmol) in 5 mL THF was added to a solution of Cu*O*t*Bu* (0.27 g, 2.00 mmol) *t*in 10 mL THF_3. The reaction mixture was briefly heated to reflux and then allowed to cool down to room temperature. $Sb(SiMe_3)_3$ (3.85 mL, 0.66 mmol, 0.17 M in hexane) was then added at −78 °C. After storage at −40 °C for two weeks, the mixture was allowed to stand at room temperature for another two weeks to produce dark brown crystals of **2** (0.15 g, 31%). The UV/Vis spectrum of **2** does not show any bands. $C_{304}H_{560}P_{16}Cu_{40}Sb_{20}O_4$: calcd. C 37.4, H 5.8; found C 37.0, H 5.7.

Deviations in the elemental analyses from the calculated values show loss of lattice-bound solvent. Crystals of **1** and **2** were dried under vacuum.

X-ray Crystallographic Study: Data for both compounds were collected on a Stoe IPDS II diffractometer using graphite-monochromated Mo-K_α radiation (λ = 0.71073 Å). The structures were solved by direct methods and refined by full-matrix least-squares on F^2 (all data) using the SHELXTL software package.[11] Hydrogen atoms were placed in calculated positions, non-hydrogen atoms were assigned anisotropic thermal parameters.

Crystal data for 1: $C_{211}H_{225}Cu_{17}O_9P_{14}Sb_8$; M = 5392.67; triclinic, space group $P\bar{1}$, Z = 2; a = 17.503(2) Å, b = 22.469(3) Å, c = 29.642(4) Å, α = 80.80(1)°, β = 76.70(1)°, γ = 69.20(1)°; V = 10567(2) Å^3; T = 150(2) K; $F(000)$ = 5348; $D_{calcd.}$ = 1.695 g cm^{-3}. Of 38611 reflections measured 26935 were unique (R_{int} = 0.1025). 1655 parameters; final wR_2 = 0.2404 (all data); R_1 = 0.0974 [$I > 2\sigma(I)$]; largest difference peak and hole 1.44 and −1.26 e·Å^{-3}; disordered components were refined with isotropic thermal parameters.

Crystal data for 2: $C_{152}H_{280}Cu_{20}O_2P_8Sb_{10}$; M = 4875.82; monoclinic, space group $P2_1/n$; Z = 2; a = 15.984(3) Å, b = 28.640(6) Å, c = 19.444(4) Å, β = 100.60(3)°; V = 8749(3) Å^3; T = 123(2) K; $F(000)$ = 4836; $D_{calcd.}$ = 1.851 g·cm^{-3}. Of 30565 reflections measured 15110 were unique (R_{int} = 0.0681). 865 parameters; final wR_2 = 0.1472 (all data); R_1 = 0.0631 [$I > 2\sigma(I)$]; largest difference peak and hole 1.855 and −1.335 e·Å^{-3}.

CCDC-216800 and -216801 contain the supplementary crystallographic data for this paper. These data can be obtained free of charge at www.ccdc.cam.ac.uk/conts/retrieving.html [or from the Cambridge Crystallographic Data Centre, 12 Union Road, Cambridge CB2 1EZ, UK; Fax: (int.) +44-1223-336-033; E-mail: deposit@ccdc.cam.ac.uk].

Acknowledgments

We would like to thank the DFG (Center for Functional Nanostructures) and the Fonds der Chemischen Industrie for funding.

[1] S. Dehnen, A. Eichhöfer, D. Fenske, *Eur. J. Inorg. Chem.* **2002**, 279−317.
[2] Y. Yamada, H. T. Deng, E. M. Snyder, A. W. Castleman Jr., *Chem. Phys. Lett.* **1993**, *203*, 330−336.

 © 2004 Wiley-VCH Verlag GmbH & Co. KGaA, Weinheim

[3] J. Besinger, J. Treptow, D. Fenske, *Z. Anorg. Allg. Chem.* **2002**, *628*, 512−515.
[4] Cu−C distances in the complex [Cu(dppm)] are 1.96(2) and 2.00(2) Å: A. Camus, N. Marsich, G. Nardin, L. Randaccio, *J. Organomet. Chem.* **1973**, *60*, C39−C42.
[5] A. Eichhöfer, J. F. Corrigan, D. Fenske, E. Tröster, *Z. Anorg. Allg. Chem.* **2000**, *626*, 338−348.
[6] All calculations were performed with the TURBOMOLE program package: [6a] R. Ahlrichs, M. Bär, M. Häser, H. Horn, C. Kölmel, *Chem. Phys. Lett.* **1989**, *162*, 165−169. [6b] O. Treutler, R. Ahlichs, *J. Chem. Phys.* **1995**, *102*, 346−354. We used the Becke−Perdew (BP86) exchange-correlation functional within the resolution of the identity (*R*I) approximation. [6c] A. D. Becke, *Phys. Rev. A* **1988**, *38*, 3098−3100. [6d] S. H. Vosko, L. Wilk, M. Nusair, *Can. J. Phys.* **1980**, *58*, 1200−1211. [6e] J. P. Perdew, *Phys. Rev. B* **1986**, *33*, 8822−8824; erratum: J. P. Perdew, *Phys. Rev. B* **1986**, *34*, 7406. [6f] K. Eichkorn, O. Treutler, H. Öhm, M. Häser, R. Ahlrichs, *Chem. Phys. Lett.* **1995**, *242*, 652. The basis and auxiliary basis set used in the DFT calculations was triple-valence basis and auxiliary basis sets with one polarization function (TZVP). [6g] A. Schäfer, H. Horn, R. Ahlrichs, *J. Chem. Phys.* **1992**, *97*, 2571−2577. [6h] A. Schäfer, C. Huber, R. Ahlrichs, *J. Chem. Phys.* **1994**, *100*, 5829−5835. [6i] K. Eichkorn, F. Weigend, O. Treutler, R. Ahlrichs, *Theor. Chem. Acc.* **1997**, *97*, 119−124.
[7] [7a] L. Pauling, *The Nature of the Chemical Bond*, Cornell University Press, New York, **1960**, pp. 644. [7b] L. Pauling, *General Chemistry*, Freeman, San Francisco, **1970**.
[8] Cu−Sb distances in Cu_2Sb alloy are 2.701(1)−2.834(1) Å, Cu···Cu 2.602(1): [8a] W. B. Pearson, *A Hanbook of Lattice Spacings and Structures of Metals and Alloys*, Pergamon Press, New York, **1967**, vol. 2. [8b] J. Nuss, M. Jansen, *Z. Anorg. Allg. Chem.* **2002**, *628*, 1152−1157 and references cited therein.
[9] G. Becker, A. Münch, C. Witthauer, *Z. Anorg. Allg. Chem.* **1982**, *492*, 15−27.
[10] E. A. Boudreaux, L. N. Mulay (eds.), *Theory and Applications of Molecular Paramagnetism*, John Wiley & Sons, New York, **1976**.
[11] SHELXTL-97, G. M. Sheldrick, University of Göttingen, **1997**.

Received February 2, 2004
Early View Article
Published Online May 13, 2004

 © 2004 Wiley-VCH Verlag GmbH & Co. KGaA, Weinheim

The First Cyclometallated (1-Ferrocenylethanone thiosemicarbazone)-palladium(II) Compounds − Crystal and Molecular Structure of [Pd{(η^5-C_5H_5)Fe(η^5-C_5H_3)C(Me)=NN=C(S)NHMe}(PPh_3)]

José M. Vila,*[a] Eduardo Gayoso,[a] M. Teresa Pereira,[a] Juan M. Ortigueira,[a] Gemma Alberdi,[a] Marta Mariño,[a] Reyes Alvarez,[a] and Alberto Fernández[b]

Keywords: C−H activation / Ferrocene / Thiosemicarbazone / Palladium / X-ray diffraction

Treatment of the 1-ferrocenylethanone thiosemicarbazone ligands (η^5-C_5H_5)Fe(η^5-C_5H_4)C(Me)=NN(H)C(=S)NHR [R = H (**a**), Me (**b**)] with $K_2[PdCl_4]$ gave the novel heterometallic octanuclear palladium(II) compounds [Pd{(η^5-C_5H_5)Fe(η^5-C_5H_3)C(Me)=NN=C(S)NHR}]$_4$ [R = H (**1a**), Me (**1b**)] as tetramers, after deprotonation of the NH group, with the ligands acting as terdentate donors through the [C,N,S] atoms. Treatment with nucleophiles cleaves the tetrameric clusters giving compounds in which splitting only of the Pd–$S_{bridging}$ bonds has occurred. The strength of the Pd–$S_{chelating}$ bond hinders its cleavage. Thus, treatment of **1a** or **1b** with $Ph_2P(CH_2)_nPPh_2$ [*n* = 2 (dppe), 3 (dppp), 4 (dppb)] in a 1:2 molar ratio gave the tetranuclear species **2a**–**4a** and **2b**–**4b**, respectively, and treatment with PPh_2R gave the dinuclear compounds **5a**–**7a** and **5b**–**6b** [R = Ph (**5a**, **5b**), Et (**6a**, **6b**), Me (**7a**)]. The complexes described are the first fully characterized cyclometallated palladium(II) complexes with 1-ferrocenylethanone thiosemicarbazone ligands. The crystal and molecular structure of compound **5b** have been determined by X-ray crystallography.
(© Wiley-VCH Verlag GmbH & Co. KGaA, 69451 Weinheim, Germany, 2004)

Introduction

The synthesis, isolation and characterization of ferrocene[1] marked an important milestone in the evolution of modern organometallic chemistry. One of the developments in this area over the last two decades has been the cyclometallation of ferrocene derivatives. The cyclometallation reaction has been widely investigated in view of the growing chemistry[2] and the novel and outstanding applications which the resultant compounds present. To name but a few examples: the synthesis of new organometallic and organic compounds, many of which can be obtained by insertion reactions of unsaturated species to the metal−carbon bond,[3] the design of complexes with specific antitumor activity towards some forms of cancer[4] or their promising properties as liquid crystals,[5] and their use in the isolation of enantiomerically pure chiral compounds[6] or as efficient catalytic materials.[7]

In the past years, great efforts have been made in order to achieve the isolation and characterization of palladacycles derived from [C,N,X] terdentate ligands (C = phenyl C; X = N,[8] P,[9] O,[10] S[11]), mainly due to the potential hemilability of the Pd−X bond in these systems, which plays an important role in homogeneous catalysis.[12] The reported examples of those complexes containing terdentate [$C_{ferrocene}$,N,X] ligands are scarce, and only compounds with X = N have been described.[13] In some instances potentially terdentate [C,N,N] ferrocenyl ligands do not undergo cyclometallation reactions and only complexes with *N*,*N*-coordination could be isolated.[14] More recently, insertion of alkynes into the $C_{ferrocene}$−Pd bond has given new insights into the chemistry of cyclometallated ferrocene compounds such as the influence of the binding mode of the ferrocenyl ligand.[15]

As a continuation of our studies related to cyclometallated compounds with terdentate [C,N,S] ligands, we have extended our work in this area aimed at incorporating the −C(Me)=NN(H)C(=S)NHR system into the ferrocene ring, to give (η^5-C_5H_5)Fe(η^5-C_5H_4)C(Me)=NN(H)C(=S)-NHR (R = H, Me), with the purpose of producing the hitherto unknown cyclometallated 1-ferrocenylethanone thiosemicarbazone complexes by treatment with an appropriate palladium(II) salt. These compounds turned out to be octanuclear species, and we wished to further explore their reactivity with tertiary mono- and diphosphane ligands which affords the corresponding dinuclear and tetranuclear complexes, respectively. Our report includes a description of the first known crystal structure of this kind of compounds.

[a] Departamento de Química Inorgánica, Universidad de Santiago de Compostela,
15782 Santiago de Compostela, Spain
Fax: (internat.) + 34-981-595012
E-mail: qideport@usc.es
[b] Departamento de Química Fundamental, Universidad de A Coruña,
15071 A Coruña, Spain

Results and Discussion

For convenience, the compounds and reactions are shown in Scheme 1. The compounds described in this paper were characterized by elemental analyses (C, H, N, S), mass spectrometry (in part), IR spectroscopy, and ^1H and $^{31}P\{^1H\}$ NMR spectroscopy (data in the Exp. Sect.).

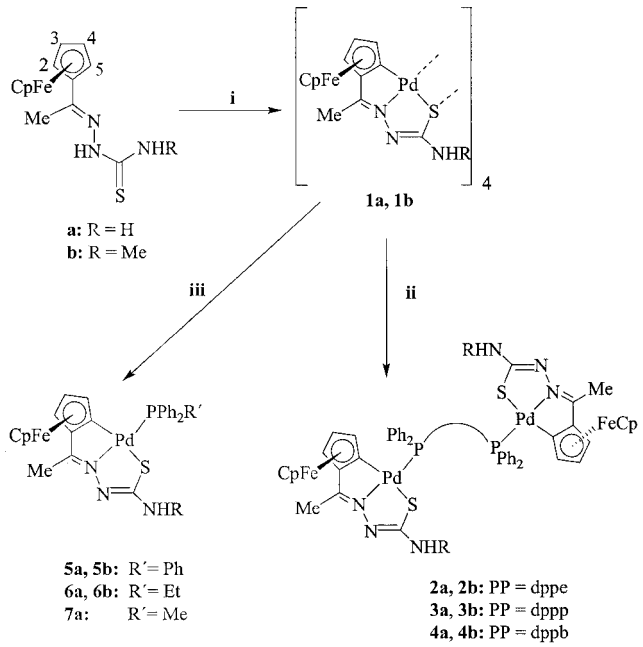

Scheme 1. i) K_2PdCl_4, ethanol/water; ii) $Ph_2P(CH_2)_nPPh_2$ (n = 2, 3, 4), 1:2 ratio, acetone; iii) PPh_2R' (R′ = Me, Et, Ph), 1:4 ratio, acetone

The 1-ferrocenylethanone thiosemicarbazones[16] **a** and **b** were prepared by treatment of thiosemicarbazide or 4-methylthiosemicarbazide, respectively, with acetylferrocene in water in the presence of a few drops of hydrochloric acid, and obtained as air-stable solids, which were fully characterized (see Exp. Sect.). In particular, the IR spectra showed the typical ν(C=N) and ν(C=S) stretches,[17] and the ^1H NMR spectra revealed the NH resonances at δ = 7.38 (**a**) and 6.20 (**b**) ppm.

Cyclopalladated compounds derived from ferrocenyl ligands may be prepared by cyclomercuration and ulterior transmetallation reactions or by direct treatment with a palladium salt. The additional presence of a base such as NaOAc may be necessary.[13f] In the latter case, M_2PdCl_4 (M = Li, Na, K) proved to be a convenient reagent, as well as in the synthesis of cyclopalladated compounds derived from thiosemicarbazone ligands. Thus, treatment of a suspension of potassium tetrachloropalladate in ethanol/water with the corresponding 1-ferrocenylethanone thiosemicarbazone ligand yielded complexes **1a** and **1b** as brown air-stable solids, with the ligand in an (*E*,*Z*) configuration and the sulfur atom of each cyclometallated moiety displaying two different coordination modes: chelating, as part of the Pd*N*NC(NHR)*S* coordination ring, and bridging, linking two cyclometallated moieties through the metal atoms. We tentatively assigned a tetrameric structure for these species in accordance with the results reported by us[18] and others[19] in related complexes derived from terdentate [C,N,S] ligands, as shown by the spectroscopic data. Hence **1a** and **1b** should be considered as novel octanuclear cyclometalled palladium(II) compounds.

The IR spectra showed, as the main difference from the starting material, the disappearance of the ν(N−H) bands due to the −NH group[20] and the ν(C=S) band at 900−800 cm^{-1}, which indicated deprotonation and loss of the C=S double bond character, respectively. The position of the NH_2 and NH bands showed that the former group was not coordinated. The displacement of the ν(C=N) band towards lower wavenumbers upon complex formation[21] is in contrast with other thiosemicarbazone complexes in which the shift is towards higher wavenumbers, probably due to the presence of the five-membered metallacycle in compounds **1a** and **1b**.[22] No ν(Pd−Cl) band was found in the IR spectra of the compounds, indicating the absence of a chloride ligand in the coordination sphere of the metal center. The FAB mass spectra of **1a** and **1b** showed clusters of peaks, centered at 1622 and 1678 amu, which both correspond to $[M]^+$.[23] The ^1H NMR spectra showed only one set of signals, although the activation of the $C_{ferrocene}-H$ bond promotes planar chirality (R_s or R_p) in the ferrocenyl moiety.[24] This issue has been dealt with elsewhere.[25] In the ^1H NMR spectra, the absence of the −NH proton resonance confirms deprotonation as observed in other coordination and organometallic compounds with similar ligands.[26] Broad signals at δ ≈ 6.60 ppm were assigned to the NH_2 (**1a**) and N*H*Me (**1b**) proton resonances, shifted upfield with respect to their positions in the free ligands. A group of three signals at δ ≈ 4.50−4.10 ppm, integrating for one proton each, and a singlet at δ = 4.22 ppm assigned to the C_5H_5 group in each case were consistent with 1,2-disubstituted ferrocenes.[27] These facts provided evidence of metallation of the ligand. Variable-temperature NMR experiments did not produce any significant changes in the spectra.

Treatment of **1a** or **1b** with $Ph_2P(CH_2)_nPPh_2$ [n = 2 (dppe), 3 (dppp), 4 (dppb)] in a 1:2 molar ratio gave the tetranuclear species **2a**−**4a** and **2b**−**4b**, respectively (see Scheme 1). These reactions confirm the different reactivities of the chelating and bridging Pd−S bonds, the former being retained in the final products, even when a large excess of diphosphane was used, whilst the latter was cleaved in all instances, in agreement with the tendency observed in other cyclometallated Pd_4 cluster complexes derived from thiosemicarbazone ligands, indicating once again the greater strength of the $Pd-S_{chelating}$ bond.[18] All compounds were fully characterized by elemental analyses, and by IR and NMR spectroscopy. The ^1H NMR spectra showed only one set of signals in each case. The metallated cyclopentadienyl ring protons appeared as three signals at δ ≈ 4.67−3.48 ppm, with the 4-H proton resonance experiencing an upfield shift and appearing at lower frequency values than the C_5H_5 signal (see Exp. Sect.), due to the shielding effect of the phosphane phenyl rings, consistent with a P

 © 2004 Wiley-VCH Verlag GmbH & Co. KGaA, Weinheim

trans to N arrangement within the terms of the "transphobic effect".[28] Unfortunately, the coupling constants to the phosphorus nuclei could not be assigned, in contrast with related complexes with diphosphane ligands.[29] The $^{31}P\{^{1}H\}$ NMR spectra showed singlets for the two equivalent phosphorus nuclei, shifted to higher frequency compared with those in the spectrum of the free phosphane, in agreement with the phosphorus atom coordinating to the metal center.[30] Based on the ^{1}H and $^{31}P\{^{1}H\}$ NMR spectroscopic data we propose a centrosymmetric arrangement for the compounds (see Scheme 1). Variable-temperature NMR experiments failed to show any noteworthy changes in the spectra. Also, the ^{1}H NMR spectra for compounds **2a**−**4a** and **2b**−**4b** were recorded in the presence of an NMR shift reagent {tris[3-heptafluoropropylhydroxymethylene-*d*-camphorato]europium(III), [Eu(hfc)$_3$]} and the appearance of the resultant spectra in terms of the positions of the signals and the presence of new signals remained unchanged upon varying the quantity of the chiral ligand.

Treatment of **1a** and **1b** with PPh_2R gave the dinuclear air-stable solids **5a**−**7a**, **5b**−**6b** [R = Ph (**5a**, **5b**), Et (**6a**, **6b**), Me (**7a**)] (see Scheme 1). Characteristic microanalytical, IR and NMR spectroscopic data are given in the Exp. Sect. Important spectroscopic features include the absence of the ν(NH) and ν(C=S) bands in the IR spectra (vide supra), the shift of the 4-H signal in the ^{1}H NMR spectra, which appears to high field of the non-substituted C_5H_5 resonance, and the chemical shift value of the ^{31}P singlets in the $^{31}P\{^{1}H\}$ NMR spectra, the latter two being consistent with a P *trans* to N geometry (vide supra). The molecular structure of compound **5b** has been determined by a single-crystal X-ray diffraction analysis.

Molecular Structure of Complex 5b

Suitable crystals of **5b** were grown by slowly concentrating a chloroform solution. The crystal structure has been determined (Figure 1) and confirms the geometry predicted from spectroscopic studies. Selected bond lengths and angles are listed in Table 1. The structure is comprised of a molecule of **5b** per asymmetric unit, with discrete molecules separated by van der Waals distances. Chirality is introduced in the complex due to activation of the C(sp^2)−H bond. The centrosymmetric space group of the crystal structure, however, indicates that both enantiomers are present in the solid state. The palladium atom Pd(1) is in an approximately square-planar coordination environment (r.m.s. = 0.0845 Å, plane 1) bonded to a terdentate 1-ferrocenylethanone thiosemicarbazone ligand through the ferrocene carbon atom C(1), the nitrogen atom N(1) of the C=N moiety, and the thioamide sulfur atom S(1), all of which pertain to the thiosemicarbazone ligand, with the remaining site occupied by the phosphorus atom P(1) of the triphenylphosphane group. Each molecule contains a [5,5,5] tricyclic system which includes the three fused ferrocenyl, cyclometallated and chelate rings, with the *C*,*N*-metallacycle and the *N*,*S*-chelate rings sharing the Pd(1) atom. The cyclometallated [Pd(1),C(1),C(5),C(11),N(1), plane 2], coordination [Pd(1),N(1),N(2),C(12),S(1), plane 3] and metallated ferrocenyl [C(1)−C(5), plane 4] rings are also planar (r.m.s. = 0.0208, 0.0076 and 0.0039 Å, respectively) and coplanar with the palladium coordination plane (angles between planes: 1/2 = 6.2°, 1/3 = 5.5°, 2/3 = 1.2°, 1/4 = 9.5°, 2/4 = 3.8°, 3/4 = 5.0°). The angles between adjacent atoms in the coordination geometry of the metal atom are close to the expected value of 90°, with the most noticeable distortion in the P(1)−Pd(1)−S(1), C(1)−Pd(1)−N(1) and N(1)−Pd(1)−S(1) angles of 103.47(8), 81.0(3) and 81.3(2)°, respectively. The sum of the angles around the palladium atom is approximately 360°. All bond lengths are within the expected ranges, allowing for the strong *trans* influence of the phosphorus donor ligand,[18] which is reflected in the Pd(1)−N(1) distance of 2.067(6)Å (cf. sum of the covalent radii for palladium and nitrogen, 2.01 Å[31]). The Pd(1)−C(1) bond of 2.001(8) Å is shorter than the expected value of 2.081 Å based on the sum of the covalent radii of carbon (sp^2) and palladium, 0.771 and 1.31 Å, respectively,[31] but similar to values reported for other cyclometallated complexes.[25,32] The Pd(1)−P(1) distance, 2.245(2) Å, is also shorter than the expected value of 2.41 Å.[31] The S(1)−C(12) bond length of 1.764(8) Å, and the N(2)−C(12) length of 1.305(9) Å, are consistent with increased single- and double-bond character, respectively, resulting from deprotonation of the ligand. The two C_5H_5 rings are parallel with a tilt angle of 0.8°. They are also nearly eclipsed, being skewed 8.9° form an eclipsed conformation.

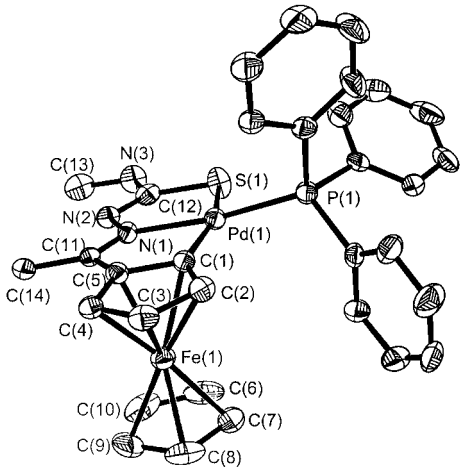

Figure 1. Molecular structure of [Pd{(η^5-C_5H_5)Fe(η^5-C_5H_3)C(Me)=NN=C(S)NHMe}(PPh_3)] (**5b**) with labeling scheme; hydrogen atoms have been omitted for clarity

Table 1. Selected bond lengths [Å] and angles [°] for **5b**

Pd(1)−C(1)	2.001(8)	C(1)−C(5)	1.438(9)
Pd(1)−N(1)	2.067(6)	C(5)−C(11)	1.441(9)
Pd(1)−P(1)	2.245(2)	C(11)−N(1)	1.285(8)
Pd(1)−S(1)	2.343(2)	N(2)−C(12)	1.305(9)
C(12)−S(1)	1.764(8)		
C(1)−Pd(1)−N(1)	81.0(3)	C(1)−Pd(1)−S(1)	162.1(2)
C(1)−Pd(1)−P(1)	94.4(2)	N(1)−Pd(1)−S(1)	81.3(2)
N(1)−Pd(1)−P(1)	170.0(2)	P(1)−Pd(1)−S(1)	103.47(8)

 © 2004 Wiley-VCH Verlag GmbH & Co. KGaA, Weinheim

Experimental Section

General Remarks: All solvents were distilled prior to use from appropriate drying agents.[33] Chemicals were used as supplied from commercial sources. Elemental analyses (C, H, N, S) were carried out at the Servicio de Análisis Elemental at the University of Santiago de Compostela using a Carlo−Erba Elemental Analyzer, model 1108. IR spectra were recorded as KBr discs or Nujol mulls with a Perkin−Elmer 1330 spectrophotometer. NMR spectra were recorded with a Bruker WM250 or AMX-300 spectrometer in $CDCl_3$ and were referenced to $SiMe_4$ (^1H) or 85% H_3PO_4 ($^{31}P\{^1H\}$). The FAB mass spectra were recorded with a Fisons Quatro mass spectrometer with a Cs ion gun; 3-nitrobenzyl alcohol was used as the matrix.

Synthesis of $(\eta^5\text{-}C_5H_5)Fe(\eta^5\text{-}C_5H_4)C(Me)=NN(H)C(=S)NH_2$ (a): A suspension of thiosemicarbazide (0.19 g, 2.19 mmol) and hydrochloric acid (0.1 mL) in water (40 mL) was stirred at room temperature. Acetylferrocene (0.5 g, 2.19 mmol) was added and the mixture stirred for 4 h, filtered and the resultant orange solid dried in vacuo. Yield 603.8 mg, 91.2%. $C_{13}H_{15}FeN_3S$ (301.2): calcd. C 51.8, H 5.0, N 13.9, S 10.7; found C 52.2, H 4.9, N 13.6, S 10.5. IR: $\tilde{\nu}$ = 3406 s, 3221 s [ν(N−H)], 1590 s [ν(C=N)], 819 m [ν(C=S)] cm^{-1}. ^1H NMR ($CDCl_3$): δ = 8.54 (br., 1 H, NH), 7.38 (br., 1 H, NH_2), 6.20 (br., 1 H, NH_2), 4.57 [d, ^3J(HH) = 1.6 Hz, 2 H, 2-H, 5-H], 4.39 (br., 2 H, 3-H, 4-H), 4.16 (s, 5 H, C_5H_5), 2.18 (s, 3 H, Me).

Synthesis of $(\eta^5\text{-}C_5H_5)Fe(\eta^5\text{-}C_5H_4)C(Me)=NN(H)C(=S)NHMe$ (b): Thiosemicarbazone **b** was synthesized as an orange solid in a similar fashion. Yield 673 mg, 97.4%. $C_{14}H_{17}FeN_3S$ (315.2): calcd. C 53.3, H 5.4, N 13.3, S 10.2; found C 53.2, H 5.3, N 12.9, S 9.9. IR: $\tilde{\nu}$ = 3361 s, 3235 m [ν(N−H)], 1663 w [ν(C=N)], 897 m [ν(C=S)] cm^{-1}. ^1H NMR ($CDCl_3$): δ = 8.23 (br., 1 H, NH), 7.64 (br., 1 H, N*H*Me), 4.55 (br., 2 H, 2-H, 5-H), 4.37 (br., 2 H, 3-H, 4-H), 4.14 (s, 5 H, C_5H_5), 3.34 [d, ^3J(HH) = 3.9 Hz, 3 H, NH*Me*], 2.26 (s, 3 H, Me).

Preparation of $[Pd\{(\eta^5\text{-}C_5H_5)Fe(\eta^5\text{-}C_5H_3)C(Me)=NN=C(S)NH_2\}]_4$ (1a): To a stirred solution of potassium tetrachloropalladate (0.2 g, 0.61 mmol) in water (6 mL) were added ethanol (40 mL) and ligand **a** (0.2 g, 0.67 mmol) and the mixture was stirred at room temperature for 24 h. The dark brown precipitate was filtered, washed with cold ethanol and dried in vacuo. Yield 581.3 mg, 58.7%. $C_{52}H_{52}Fe_4N_{12}Pd_4S_4$ (1622.4): calcd. C 38.5, H 3.2, N 10.4, S 7.9; found C 38.3, H 3.1, N 10.2, S 7.7. IR: $\tilde{\nu}$ = 3434 s [ν(N−H)], 1569 w [ν(C=N)] cm^{-1}. ^1H NMR ($CDCl_3$): δ = 6.50 (br., 2 H, NH_2), 4.45 (br., 1 H, 2-H), 4.32 (br., 1 H, 3-H), 4.22 (s, 5 H, C_5H_5), 4.12 (br., 1 H, 4-H), 2.13 (s, 3 H, Me) ppm. FAB-MS: *m*/*z* = 1622 $[M]^+$.

Preparation of $[Pd[\{\eta^5\text{-}C_5H_5)Fe(\eta^5\text{-}C_5H_3)C(Me)=NN=C(S)NHMe\}]_4$ (1b): Complex **1b** was prepared as a brown solid in a similar manner. Yield 678.2 mg, 66.2%. $C_{56}H_{60}Fe_4N_{12}Pd_4S_4$ (1678.5): calcd. C 40.1, H 3.6, N 10.0, S 7.6; found C 40.0, H 3.4, N 9.8, S 7.8. IR: $\tilde{\nu}$ = 3402 m [ν(N−H)], 1588 s [ν(C=N)] cm^{-1}. ^1H NMR ($CDCl_3$): δ = 6.78 (br., 1 H, N*H*Me), 4.45 [d, ^3J(HH) = 1.1 Hz, 1 H, 2-H], 4.33 (br., 1 H, 3-H), 4.22 (s, 5 H, C_5H_5), 4.11 (br., 1 H, 4-H), 2.73 [d, ^3J(H,H) = 4.6 Hz, 3 H, NH*Me*], 2.16 (s, 3 H, Me) ppm. FAB-MS: *m*/*z* = 1678 $[M]^+$.

Preparation of $[\{Pd[(\eta^5\text{-}C_5H_5)Fe(\eta^5\text{-}C_5H_3)C(Me)=NN=C(S)NH_2]\}_2\{\mu\text{-}Ph_2P(CH_2)_2PPh_2\}]$ (2a): 1,2-Bis(diphenylphosphanyl)ethane (14.7 mg, 0.037 mmol) was added to a suspension of **1a** (30.0 mg, 0.0185 mmol) in acetone (8 mL). The mixture was stirred for 24 h and the resultant orange solid filtered and dried. Yield 28.7 mg, 64.2%. $C_{52}H_{50}Fe_2N_6P_2Pd_2S_2$ (1209.6): calcd. C 51.6, H 4.2, N 6.9, S 5.3; found C 51.5, H 4.2, N 6.9, S 5.5. IR: $\tilde{\nu}$ = 3428 s [ν(N−H)], 1572 sh [ν(C=N)] cm^{-1}. ^1H NMR ($CDCl_3$): δ = 5.78 (br., 2 H, NH_2), 4.54 [d, ^3J(HH) = 1.7 Hz, 1 H, 2-H], 4.40 (br., 1 H, 3-H), 4.14 (s, 5 H, C_5H_5), 4.01 (br., 1 H, 4-H), 2.01 (s, 3 H, Me) ppm. ^{31}P NMR ($CDCl_3$): δ = 58.7 (s).

Preparation of $[\{Pd[(\eta^5\text{-}C_5H_5)Fe(\eta^5\text{-}C_5H_3)C(Me)=NN=C(S)NH_2]\}_2\{\mu\text{-}Ph_2P(CH_2)_3PPh_2\}]$ (3a), $[\{Pd[(\eta^5\text{-}C_5H_5)Fe(\eta^5\text{-}C_5H_3)C(Me)=NN=C(S)NH_2]\}_2\{\mu\text{-}Ph_2P(CH_2)_4PPh_2\}]$ (4a), $[\{Pd[(\eta^5\text{-}C_5H_5)Fe(\eta^5\text{-}C_5H_3)C(Me)=NN=C(S)NHMe]\}_2\{\mu\text{-}Ph_2P(CH_2)_2PPh_2\}]$ (2b) $[\{Pd[(\eta^5\text{-}C_5H_5)Fe(\eta^5\text{-}C_5H_3)C(Me)=NN=C(S)NHMe]\}_2\{\mu\text{-}Ph_2P(CH_2)_3PPh_2\}]$ (3b), $[\{Pd[(\eta^5\text{-}C_5H_5)Fe(\eta^5\text{-}C_5H_3)C(Me)=NN=C(S)NHMe]\}_2\{\mu\text{-}Ph_2P(CH_2)_4PPh_2\}]$ (4b): Compounds **3a**, **4a** and **2b**−**4b** were synthesized as air-stable orange solids according to a similar procedure for the preparation of **1a**, but using the appropriate diphosphane ligand. In the case of **3a** and **3b** no solid precipitated and so the solvent was removed at reduced pressure from the resultant solution and the residue recrystallized from dichloromethane/hexane.

3a: Yield 30.8 mg, 68.0%. $C_{53}H_{52}Fe_2N_6P_2Pd_2S_2$ (1223.6): calcd. C 52.0, H 4.3, N 6.9, S 5.2; found C 51.9, H 4.0, N 6.7, S 5.3. IR: $\tilde{\nu}$ = 3443 s [ν(N−H)],] 1570 sh [ν(C=N) cm^{-1}. ^1H NMR ($CDCl_3$): δ = 5.81 (br., 2 H, NH_2), 4.46 [d, ^3J(HH) = 0.9 Hz, 1 H, 2-H], 4.35 (br., 1 H, 3-H), 4.12 (s, 5 H, C_5H_5), 3.83 (m, 1 H, 4-H), 2.29 (s, 3 H, Me) ppm. ^{31}P NMR ($CDCl_3$): δ = 5.8 s.

4a: Yield 36.1 mg, 78.9%. $C_{54}H_{54}Fe_2N_6P_2Pd_2S_2$ (1237.7): calcd. C 52.4, H 4.4, N 6.8, S 5.2; found C 52.3, H 4.3, N 6.5, S 5.1. IR: $\tilde{\nu}$ = 3439 m [ν(N−H)], 1570 m [ν(C=N)] cm^{-1}. ^1H NMR ($CDCl_3$): δ = 4.82 (br., 2 H, NH_2), 4.25 [d, ^3J(HH) = 2.3 Hz, 1 H, 2-H], 4.12 (br., 1 H, 3-H), 3.81 (s, 5 H, C_5H_5), 3.49 [d, ^4J(PH) = 1.9 Hz, 1 H, 4-H], 2.20 (s, 3 H, Me) ppm. ^{31}P NMR ($CDCl_3$): δ = 27.0 (s).

2b: Yield 41.2 mg, 93.2%. $C_{54}H_{54}Fe_2N_6P_2Pd_2S_2$ (1237.7): calcd. C 52.4, H 4.4, N 6.8, S 5.2; found C 52.6, H 4.3, N 6.7, S 5.1. IR: $\tilde{\nu}$ = 3376 m [ν(N−H)], 1628 sh [ν(C=N)] cm^{-1}. ^1H NMR ($CDCl_3$): δ = 5.81 (br., 1 H, N*H*Me), 4.61 [d, ^3J(HH) = 3.2 Hz, 1 H, 2-H], 4.13 (br., 1 H, 3-H), 4.06 (s, 5 H, C_5H_5), 3.99 (br., 1 H, 4-H), 2.87 [d, ^3J(HH) = 4.5 Hz, 3 H, NH*Me*], 2.37 (s, 3 H, Me) ppm. ^{31}P NMR ($CDCl_3$): δ = 62.9 (s).

3b: Yield 32.3 mg, 72.2%. $C_{55}H_{56}Fe_2N_6P_2Pd_2S_2$ (1251.7): calcd. C 52.8, H 4.5, N 6.7, S 5.1; found C 52.6, H 4.4, N 6.5, S 5.0. IR: $\tilde{\nu}$ = 3418 m [ν(N−H)], 1626 w [ν(C=N)] cm^{-1}. ^1H NMR ($CDCl_3$): δ = 6.01 (br., 1 H, N*H*Me), 4.67 [d, 1 H, 2-H, ^3J(HH) = 3.6 Hz], 4.31 (br., 1 H, 3-H), 4.17 (s, 5 H, C_5H_5), 3.81 (br., 1 H, 4-H), 2.99 [d, ^3J(HH) = 4.6 Hz, 3 H, NH*Me*], 2.16 (s, 3 H, Me) ppm. ^{31}P NMR ($CDCl_3$): δ = 3.71 (s).

4b: Yield 36.8 mg, 81.3%. $C_{56}H_{58}Fe_2N_6P_2Pd_2S_2$ (1265.7): calcd. C 53.1, H 4.6, N 6.6, S 5.1; found C 53.0, H 4.5, N 6.4, S 5.1. IR: ν(N−H) 3434 s, ν(C=N) 1629 w cm^{-1}. ^1H NMR ($CDCl_3$): δ = 4.67 (br., 1 H, N*H*Me), 4.25 (br., 1 H, 2-H), 4.10 (br., 1 H, 3-H), 3.82 (s, 5 H, C_5H_5), 3.48 (m, 1 H, 4-H), 2.97 [d, 3 H, NH*Me*, ^3J(HH) = 4.9 Hz], 2.24 (s, 3 H, Me) ppm. ^{31}P NMR ($CDCl_3$): δ = 24.7 (s).

Preparation of $[Pd\{(\eta^5\text{-}C_5H_5)Fe(\eta^5\text{-}C_5H_3)C(Me)=NN=C(S)NH_2\}(PPh_3)]$ (5a): Triphenylphosphane (19.4 mg, 0.0739 mmol) was added to a suspension of **1a** (30.0 mg, 0.0185 mmol) in acetone (8 mL). The mixture was stirred for 24 h and the resultant orange solid filtered and dried. The residue was recrystallized from dichloromethane/hexane. Yield 35.7 mg, 72.3%. $C_{31}H_{28}FeN_3PPdS$ (667.9): calcd. C 55.8, H 4.2, N 6.3, S 4.8; found C 55.5, H 4.1, N

 © 2004 Wiley-VCH Verlag GmbH & Co. KGaA, Weinheim

6.2, S 4.8. IR: $\tilde{\nu}$ = 3346 s [ν(N−H)], 1594 m [ν(C=N)] cm^{-1}. ^1H NMR ($CDCl_3$): δ = 5.05 (br., 2 H, NH_2), 4.29 (br., 1 H, 2-H), 4.11 (m, 1 H, 3-H), 3.90 (s, 5 H, C_5H_5), 3.30 [d, ^3J(HH) = 2.2 Hz, 1 H, 4-H], 2.25 (s, 3 H, Me) ppm. ^{31}P NMR ($CDCl_3$): δ = 30.6 (s).

Preparation of [Pd{(η^5-C_5H_5)Fe(η^5-C_5H_3)C(Me)=NN=C(S)NH_2}(PEtPh_2)] (6a), [Pd{(η^5-C_5H_5)Fe(η^5-C_5H_3)C(Me)=NN=C(S)NH_2}(PMePh_2)] (7a), [Pd{(η^5-C_5H_5)Fe(η^5-C_5H_3)C(Me)=NN=C(S)NHMe}(PPh_3)] (5b), [Pd{(η^5-C_5H_5)Fe(η^5-C_5H_3)C(Me)=NN=C(S)NHMe}(PEtPh_2)] (6b): Compounds **5a**−**7a**, **5b** and **6b** were obtained as air-stable orange solids according to a similar procedure for the synthesis of **1a**, but using the appropriate phosphane ligand. In the case of **6a** no solid precipitated so the solvent was removed at reduced pressure from the resultant solution and the residue recrystallized from dichloromethane/hexane.

6a: Yield 29.5 mg, 64.3%. $C_{27}H_{28}FeN_3PPdS$ (619.8): calcd. C 52.3, H 4.5, N 6.8, S 5.2; found C 52. 3, H 4.2, N 6.7, S 5.1. IR: $\tilde{\nu}$ = 3367 m [ν(N−H)], 1579 m [ν(C=N)] cm^{-1}. ^1H NMR ($CDCl_3$): δ = 4.58 (br., 1 H, 2-H), 4.38 (br., 1 H, 3-H), 4.15 (s, 5 H, C_5H_5), 3.86 (br., 1 H, 4-H), 2.37 (s, 3 H, Me) ppm. ^{31}P NMR ($CDCl_3$): δ = 33.6 (s).

7a: Yield 30.8 mg, 68.7%. $C_{26}H_{26}FeN_3PPdS$ (605.8): calcd. C 51.6, H 4.3, N 6.9, S 5.3; found C 51.4, H 4.1, N 6.8, S 5.2. IR: $\tilde{\nu}$ = 3409 m [ν(N−H)], 1564 m [ν(C=N)] cm^{-1}. ^1H NMR ($CDCl_3$): δ = 4.83 (br., 2 H, NH_2), 4.28 [d, ^3J(HH) = 1.9 Hz, 1 H, 2-H], 4.13 (m, 1 H, 3-H), 3.97 (s, 5 H, C_5H_5), 3.51 [d, ^3J(HH) = 2.1 Hz, 1 H, 4-H], 2.32 (s, 3 H, Me) ppm. ^{31}P NMR ($CDCl_3$): δ = 29.3 (s).

5b: Yield 35.7 mg, 73.3%. $C_{32}H_{30}FeN_3PPdS$ (681.9): calcd. C 56.4, H 4.4, N 6.2, S 4.7; found C 56.0, H 4.4, N 6.1, S 4.6. IR: $\tilde{\nu}$ = 3352 m [ν(N−H)], 1625 w [ν(C=N)] cm^{-1}. ^1H NMR ($CDCl_3$): δ = 4.63 (br., 1 H, N*H*Me), 4.28 [d, ^3J(HH) = 2.1 Hz, 1 H, 2-H], 4.07 [t, ^3J(HH) = 2.1 Hz, 1 H, 3-H], 3.89 (s, 5 H, C_5H_5), 3.27 [d, ^3J(HH) = 2.1 Hz, 1 H, 4-H], 2.93 [d, ^3J(HH) = 4.9 Hz, 3 H, NH*Me*], 2.26 (s, 3 H, Me) ppm. ^{31}P NMR ($CDCl_3$): δ = 30.7 (s).

6b: Yield 30.0 mg, 66.2%. $C_{28}H_{30}FeN_3PPdS$ (633.9): calcd. C 53.1, H 4.8, N 6.6, S 5.1; found C 53.2, H 4.7, N 6.5, S 5.1. IR: $\tilde{\nu}$ = 3345 s [ν(N−H)], 1575 w [ν(C=N)] cm^{-1}. ^1H NMR ($CDCl_3$): δ = 4.70 (br., 1 H, N*H*Me), 4.26 (br., 1 H, 2-H), 4.12 (br., 1 H, 3-H), 3.84 (s, 5 H, C_5H_5), 3.52 (br., 1 H, 4-H), 2.98 [d, ^3J(HH) = 4.9 Hz, 3 H, NH*Me*], 2.25 (s, 3 H, Me) ppm. ^{31}P NMR ($CDCl_3$): δ = 27.8 (s).

X-ray Crystallographic Study:[34] Three-dimensional, room-temperature X-ray data were collected in the range 2.28° < θ < 25.87° with a Bruker CCD diffractometer using the ω-scan method. Reflections were measured from a hemisphere of data collected in frames each covering 0.3° in ω. The 5968 reflections measured were corrected for Lorentz and polarization effects and for absorption using a semiempirical correction based on symmetry-equivalent and repeated reflections (max/min transmissions: 0.95/0.63). The structure was solved by direct methods and refined by full-matrix least-squares unique data (354 parameters) with allowance for the thermal anisotropy of all non-hydrogen atoms. Hydrogen atoms were included in calculated positions and refined using the riding mode. The refinement was carried out taking into account the minor components of the disorder. Minimum/maximum final electron density: −1.204/0.564 e·Å^{-3}. The structure solution and refinement were carried out using the SHELX-97 program package.[35] Crystal data are given in Table 2.

Table 2. Crystal data and structure refinement data for compound **5b**

Empirical formula	$C_{32}H_{30}N_3Cl_2PSFePd$
Formula mass	681.87
Temperature	293(2) K
Wavelength	0.71073 Å
Crystal system	triclinic
Space group	$P\bar{1}$
Unit cell	a = 11.134(2) Å
	b = 11.807(3) Å
	c = 12.418(4) Å
	α = 75.781(19)°
	β = 75.92(2)°
	γ = 70.355(19)°
Volume	1467.1(7) Å^3
Z	2
Density (calculated)	1.544 Mg cm^{-3}
Absorption coefficient	1.259 mm^{-1}
F(000)	692
Crystal size	0.40 × 0.12 × 0.04 mm
θ range for data collection	2.28−25.87°
hkl	−13/0, −14/13, −15/14.
Number of reflections collected	5968
Number of independent reflections	5660 [R(int) = 0.0977]
Max/min transmission	0.422/1.0
Completeness to θ = 25.87°	99.4%
Refinement method	full-matrix least-squares on F^2
Data/restraints/parameters	5660/0/354
Goodness-of-fit	0.927
Final R indices [$I > 2\sigma(I)$]	R_1 = 0.0511, wR_2 = 0.0888
R indices (all data)	R_1 = 0.2655, wR_2 = 0.1229
Largest difference peak/hole	0.564/−1.203 e/Å^3

Acknowledgments

We thank the DGESIC (Ministerio de Ciencia y Tecnología) Proyecto BQU2002-04533-C02-01 and the Xunta de Galicia, incentive PGIDIT03PXIC20912PN, for financial support. M. M. acknowledges a fellowship from the Xunta de Galicia (Spain). We also thank Dr. Susana López-Estévez for helpful NMR discussions.

[1] [1a] T. Kealy, P. L. Pauson, *Nature* **1951**, *168*, 1039−1040. [1b] S. Miller, *J. Chem. Soc.* **1952**, *74*, 632−635. [1c] G. Wilkinson, *J. Am. Chem. Soc.* **1952**, *74*, 2125−2126. [1d] R. Woodward, *J. Am. Chem. Soc.* **1952**, *74*, 3458−3459. [1e] P. Eiland, *J. Am. Chem. Soc.* **1952**, *74*, 4971. [1f] G. Wilkinson, *J. Am. Chem. Soc.* **1952**, *74*, 6148−6149. [1g] E. Fischer, W. Pfab, *Z. Naturforsch., Teil B* **1952**, *7*, 377−379. [1h] J. Dunitz, L. E. Orgel, *Nature* **1953**, *171*, 121−2.

[2] [2a] E. C. Constable, *Polyhedron* **1984**, *3*, 1037−1057. [2b] I. Omae, "Organometallic Intramolecular-Coordination Compounds", in *J Organomet. Chem. Library*, Elsevier, Amsterdam, **1986**. [2c]V. V. Dunina, O. A. Zalewskaya, V. M. Potapov, *Russ. Chem. Rev.* **1988**, *57*, 250−269.

[3] [3a] A. D. Ryabov, *Synthesis* **1985**, *3*, 233−252. [3b] J. Spencer, M. Pfeffer, *Adv. Met.-Org. Chem.* **1994**, *3*, 1−50. [3c] J. Spencer, M. Pfeffer, *Adv. Met.-Org. Chem.* **1998**, *6*, 103−144.

[4] [4a] C. Navarro-Ranninger, I. López-Solera, V. M. González, J. M. Pérez, J. H. Rodríguez, J. L. García-Ruano, P. Raithby, J. R. Masaguer, C. Alonso, *J. Med. Chem.* **1993**, *36*, 3795−3801. [4b] C. Navarro-Ranninger, I. López-Solera, V. M. González, J. M. Perez, A. Alvarez-Valdés, A. Martin, P. Raithby, J. R. Masaguer, C. Alonso, *Inorg. Chem.* **1996**, *35*, 5181−5187.

 © 2004 Wiley-VCH Verlag GmbH & Co. KGaA, Weinheim

[5] M. Marcos, *Metallomesogens − Synthesis, Properties and Applications* (Ed. J. L. Serrano), VCH, Weinheim, **1996**.
[6] [6a] W. A. Herrmann, C. Brossmer, K. Ökefe, C. P. Reisinger, T. Priermeier, M. Beller, M. H. Fischer, *Angew. Chem. Int. Ed. Engl.* **1995**, *107*, 1844−1848. [6b] S. B. Wild, *Coord. Chem. Rev.* **1997**, *166*, 291−311.
[7] [7a] J. Dupont, M. Pfeffer, J. Spencer, *Eur. J. Inorg. Chem.* **2001**, 1917−1927. [7b] L. Botella, C. Nájera, *Angew. Chem. Int. Ed.* **2002**, *41*, 179−181.
[8] A. Fernández, P. Uría, J. J. Fernández, M. López-Torres, A. Suárez, D. Vázquez-García, M. T. Pereira, J. M. Vila, *J. Organomet. Chem.* **2001**, *620*, 8−19.
[9] A. G. J. Ligtenbag, E. K. van Beuken, A. Meetsma, N. Veldman, W. J. J. Smeets, A. Spek, B. L. Feringa, B. L, *J. Organomet. Chem.* **1998**, *556*, 21−30.
[10] [10a] C. Cativiela, L. R. Falvello, J. C. Ginés, R. Navarro, E. P. Urriolabeitia, *New. J. Chem.* **2001**, *25*, 344−352. [10b] A. Fernández, D. Vázquez-García, J. J. Fernández, M. López-Torres, A. Suárez, S. Castro-Juiz, J. M. Vila, *New. J. Chem.* **2002**, *26*, 398−404.
[11] [11a] X. Riera, C. Lopez, A. Caubet, V. Moreno, X. Solans, M. Font-Bardia, *Eur. J. Inorg. Chem.* **2001**, 2135−2141. [11b] A. Fernández, D. Vazquez-Garcia, J. J. Fernández, M. López-Torres, A. Suarez, S. Castro-Juiz, J. M. Ortigueira, J. M. Vila, *New. J. Chem.* **2002**, *26*, 105−112.
[12] C. S. Stone, D. A. Weinberger, C. A. Mirkin, *Progr. Inorg. Chem.* **1999**, *48*, 233.
[13] [13a] I. R. Butler, *Organometallics* **1992**, *11*, 74−83. [13b] C. J. Isaac, C. Price, B. R. Horrocks, A. Houlton, M. R. J. Ebegood, W. Clegg, *J. Organomet. Chem.* **2000**, *598*, 248−253. [13c] A. Caubet, C. López, J. Sales, X. Solans, M. Font-Bardia, *J. Organomet. Chem.* **1999**, *577*, 292−304. [13d] C. López, A. Caubet, X. Soláns, M. Font-Bardia, *J. Organomet. Chem.* **2000**, *598*, 87−102. [13e] C. López, A. Caubet, S. Pérez, X. Soláns, M. Font-Bardia, *J. Organomet. Chem.* **2002**, *651*, 105−113.
[14] Bosque, A. Caubet, C. López, E. Espinosa, E. Molíns, *J. Organomet. Chem.* **1997**, *544*, 233−241.
[15] S. Pérez, C. López, A. Caubet, A. Pawelczyk, R. Bosque, X. Soláns, M. Font-Bardiá, *Organometallics* **2003**, *22*, 2396−2408.
[16] For earlier reports and reactions of ligands **a** and **b** see for example: [16a] J. Boichard, J-P. Monin, J. Tirouflet, *Bull. Soc. Chim. Fr.* **1963**, 851−856. [16b] J. S. Casas, M. V. Castaño, M. C. Cifuentes, A. Sánchez, J. Sordo, *Polyhedron* **2002**, *21*, 1651−1660. [16c] R. Carballo, J. S. Casas, E. García-Martínez, G. Pereiras-Gabién, A. Sánchez, J. Sordo, E. M. Vázquez-López, J. C. García-Monteagudo, U. Abram, *J. Organomet. Chem.* **2002**, *656*, 1−10.
[17] K. Nakamoto, *Infrared and Raman Spectra of Inorganic and Coordination Compounds*, 5th ed., Wiley & Sons, New York, **1997**.
[18] [18a] J. M. Vila, M. T. Pereira, J. M. Ortigueira, M. Graña, D. Lata, A. Suárez, A. Fernández, J. J. Fernández, M. López-Torres, H. Adams, *J. Chem. Soc., Dalton Trans.* **1999**, 4193−4201. [18b] A. Amoedo, M. Graña, J. Martínez, T. Pereira, M. López-Torres, A. Fernández, J. J. Fernández, J. M: Vila, *Eur. J. Inorg. Chem.* **2002**, 613−620.
[19] [19a] K. Kawamoto, Y. Nagasawa, H. Kuma, Y. Kushi, *Inorg. Chem.* **1996**, *35*, 2427−2432. [19b] A. G. Quiroga, J. M. Pérez, I. López-Solera, J. R. Masaguer, A. Luque, P. Román, A. Edwards, C. Alonso, M. C. Navarro-Ranninger, *J. Med. Chem.* **1998**, *41*, 1399−1408.
[20] T. S. Lobana, A. Sánchez, J. S. Casas, A. Castiñeiras, J. Sordo, M. S. García-Tasende, E. Vázquez-López, *J. Chem. Soc., Dalton Trans.* **1997**, 4289−4299.
[21] D. X. West, J. S. Ives, G. A. Bain, A. E. Liberta, J. Valdés-Martínez, K. H. Ebert, S. Hernández-Ortega, *Polyhedron* **1997**, *16*, 1895−1905.
[22] H. Onoue, I. Moritani, *J. Organomet. Chem.* **1972**, *43*, 431−436.
[23] Mass electrospray measurements were also performed with an HP Series 1100 MSD instrument, using dichloromethane/formic acid (1%) as the matrix. Alternatively, molecular weight determinations were also carried out with a Knauer osmometer. In both cases analogous results to the FAB data were obtained.
[24] M. Benito, C. López, X. Morván, *Polyhedron* **1999**, *18*, 2583−2595.
[25] [25a] G. Zhao, Q. G. Wang, T. C. W. Mak, *J. Chem. Soc., Dalton Trans.* **1998**, 3785−3789. [25b] R. Bosque, C. Lopez, X. Solans, M. Font-Bardia, *Organometallics* **1999**, *18*, 1267−1274.
[26] [26a] D. Kovala-Demertzi, A. Domopoulou, M. A. Demertzis, C. P. Raptopoulou, A. Terzis, *Polyhedron* **1994**, *13*, 1917−1925. [26b] F. Hueso-Ureña, N. A. Illán-Cabeza, M. Moreno-Carretero, A. M. Peñas-Chamorro, R. Faure, *Inorg. Chem. Commun.* **1999**, *2*, 323−326.
[27] *Gmelin Handbuch der Anorganische Chemie*, "Eisen Organische-Verbindungen − Ferrocen", Springer-Verlag, Heidelberg, Germany, **1977−1986**, part A1−A8.
[28] J. Vicente, J. A. Abad, A. D. Frankland, M. C. Ramirez de Arellano, *Chem. Eur. J.* **1999**, *5*, 3067−3076.
[29] J. M. Vila, E. Gayoso, T. Pereira, M. Mariño, J. Martínez, J. J. Fernández, A. Fernández, M. López-Torres, *J. Organomet. Chem.* **2001**, *637−639*, 577−585.
[30] P. S. Pregosin, R. W. Kuntz, "^{31}P and ^{13}C NMR of Transition Metal Phosphane Complexes", in *NMR 16* (Eds. P. Diehl, E. Fluck, R. Kosfeld), Springer, Berlin, **1979**.
[31] L. Pauling, *The Nature of the Chemical Bond*, 3rd ed., Cornell University Press, Ithaca, New York, **1960**, pp.224.
[32] [32a] C. Lopez, R. Bosque, X. Solans, M. Font-Bardia, *J. Organomet. Chem.* **1997**, *547*, 309−317. [32b] G. Zhao, F. Xue, Z. Y. Zhang, T. C. W. Mak, *Organometallics* **1997**, *16*, 4023−4026. [32c] C. Lopez, R. Bosque, X. Solans, M. Font-Bardia, *New J. Chem.* **1998**, *22*, 977−982.
[33] W. L. F. Armarego, D. D. Perrin, *Purification of Laboratory Chemicals*, 4th ed., Butterworth-Heinemann, Oxford, **1997**.
[34] Crystallographic data (excluding structure factors) for the structure reported in this paper have been deposited with the Cambridge Crystallographic Data Center as supplementary publication no. CCDC-220842. Copies of the data can be obtained free of charge on application to CCDC, 12 Union Road, Cambridge CB2 1EZ, UK [Fax: (internat.) + 44-1223-336-033; E-mail: deposit@ccdc.cam.ac.uk].
[35] G. M. Sheldrick, *SHELX-97, An integrated system for solving and refining crystal structures from diffraction data*, University of Göttingen, Germany, **1997**.

Received October 7, 2003
Early View Article
Published Online May 5, 2004

 © 2004 Wiley-VCH Verlag GmbH & Co. KGaA, Weinheim

One-Dimensional Cd^{II} Coordination Polymers: Solid Solutions with Ni^{II}, Thermal Stabilities and Structures

Dejana Vujovic,*[a] Helgard G. Raubenheimer,[a] and Luigi R. Nassimbeni[b]

Keywords: Coordination polymers / Solid solutions / Cadmium complexes

Reactions of $Cd(NCS)_2$ with 2-, 3- and 4-aminobenzonitrile ligands (2ABN, 3ABN and 4ABN respectively) have produced one-dimensional chain polymers of the general formula $[M(NCS)_2(ABN)_2]_n$ with the metal centres linked by double NCS^- bridges. The three cadmium polymers $[Cd(NCS)_2(3ABN)_2]_n$ (**1**), $[Cd(NCS)_2(2ABN)_2]_n$ (**2**) and $[Cd(NCS)_2(4ABN)_2]_n$ (**3**) all differ in their hydrogen-bonding patterns. In terms of ABN coordination, both **1** and **2** exhibit terminal amine coordination while in **3** the ABNs are coordinated through the cyano groups. Crystalline solid solutions of **1** of general formula $[Cd_{1-x}Ni_x(NCS)_2(3ABN)_2]_n$, containing nickel and cadmium in varying proportions, have also been prepared in order to establish the influence of the metal ratio on the thermal stability and bonding parameters of the polymers. The coordination polymers are not good candidates for forming clathrates while their thermal stability (ranging between 147 and 244 °C) depends on the position of functional groups on the ABN ligands and on the Cd:Ni ratio in the solid solutions. The new polymers have been characterised by single crystal X-ray diffraction, X-ray powder diffraction, electron microscopy, infrared spectroscopy, thermogravimetry and differential scanning calorimetry.
(© Wiley-VCH Verlag GmbH & Co. KGaA, 69451 Weinheim, Germany, 2004)

Introduction

Self-assembled coordination polymers have attracted considerable recent interest due to both their many interesting architectures[1−6] and numerous applications.[7−9] Such systems are often tunable by making subtle changes to the reaction conditions, such as the choice of counterion and solution pH, that allow the deliberate design of compounds with luminescent,[10] superconducting[11,12] or magnetic properties[13,14] and also compounds that can be used as nanofibres,[15] in catalysis,[16] in separation processes,[17,18] for gas and liquid storage[19] and in nonlinear optics.[20,21]

We have prepared previously one-dimensional coordination polymers of Ni^{II} with aminobenzonitrile isomers and thiocyanate ions as ligands.[22] The structural features and thermal stability of the polymers were determined by the position of the functional groups on the ABN isomers as well as the introduction of guest molecules into the structures. Furthermore, the ABN isomers not only afford hydrogen-bonded networks, but also lead to the possible formation of 1-, 2- and 3-dimensional polymer networks due to different coordination preferences such as coordination to the metal centre in monodentate (albeit ambidentately using either amine or cyanide nitrogens), bidentate (2ABN) or in a bridging fashion (using both nitrogen donors).

Most studied coordination polymers are unimetallic. Addition of a second metal to inorganic compounds is a well-established procedure in industry to modify and improve material properties. Studies on bimetallic coordination polymers usually involve either two different metals in different[23] or similar[24] oxidation states or the same metal in two different oxidation states.[25] The resultant new structure usually differs significantly from the starting one, with the two metals located in different positions along the polymeric chain. Coordination compounds with both metals at the same site of an unchanged structure have also been investigated; this work also concentrates on such bimetallic compounds. Magnetic phase transition studies are an example of this type of work. They involve Hofmann-type clathrates of the general formula $M(NH_3)_2M'(CN)_4{\cdot}2G$ (where M and M′ are transition metals), the magnetic properties of which are affected by diluting one of the metal sites with another metal located at the same position in the overall structure.[26−29]

Extensive studies have been carried out over the past three decades on coordination compounds of SCN^- using various transition metals. Most early work again involved Hofmann-type compounds, which, over the years, has expanded to include the design of materials and architectures with specific properties. SCN^- is a highly versatile ligand with both terminal and bridging coordination possibilities. As a terminal ligand it is either *S*- or *N*-coordinated, while as a bridging ligand it is most often coordinated in a bidentate or tridentate fashion (however, 13 possible bonding

[a] Department of Chemistry, University of Stellenbosch, Private Bag X1, Matieland 7602, South Africa
[b] Department of Chemistry, University of Cape Town, Rondebosch 7701, South Africa

modes have been identified).[30] The result is a wide variety of possible complexes, clusters and polymers (1-D single, double and triple bridged chains and 2-D and 3-D networks).[31,32]

Here, as part of a continuing study, we report on the structural and thermal influence of a metal on coordination polymers. This has been achieved by (i) changing the metal centre from Ni^{II} to Cd^{II} and/or (ii) introducing both metals in different ratios into the starting mixtures. Changing the metal centre from Ni^{II} to Cd^{II} afforded dramatically different polymeric structures **2** and **3** with 2ABN and 4ABN ligands in the presence of thiocyanate. Conversely, when $Cd(NCS)_2$ is treated with 3ABN the resultant polymer **1** is isostructural with its nickel counterpart, giving the option of introducing both metals in different proportions into such structures. Crystal structures, thermodynamic stabilities and metal concentrations in structures of the general formula $[Cd_{1-x}Ni_x(NCS)_2(3ABN)_2]_n$ have been determined by experimental methods (**4**−**7**).

Results and Discussion

Crystal Structure Analysis

Crystalline samples of the cadmium polymers were prepared by slow evaporation of mixtures of ethanolic ABN and $Cd(NCS)_2$ solutions. The crystals grew over a period of 1−3 days. Salient crystal and experimental data (Table 1) and hydrogen-bonding details (Table 2) are summarised here.

Crystal structure analysis revealed that **1** is isostructural with its previously reported nickel analogue **8**.[22] One-dimensional, double-stranded chain polymers were formed with a metal-to-3ABN ratio of 1:2. Thiocyanate double bridges propagate the chain along the crystallographic *b*-axis with the amine-bonded 3ABN ligands at axial positions. Adjacent polymer units are hydrogen-bonded through their amine and nitrile moieties, producing sheets parallel to the (011) plane. The structure of the coordination polymer **1** is shown in Figure 1.

Table 2. Hydrogen-bond lengths and angles

	Donor (D)	Acceptor (A)	D−H (Å)	D···A (Å)	D−H···A (°)
1	N(7A)	N(9A)#[1]	0.87(1)	3.159(3)	174(2)
2	N(7B)	N(9B)#[2]	0.90	3.14(3)	154
	N(7A)	N(9A)#[3]	0.90	3.16(2)	146
	N(7A)	N(9A)#[4]	0.90	3.126(17)	167
3	N(7A)	S1#[5]	0.92(3)	3.569(4)	157(4)
4	N(7A)	N(9A)#[6]	0.90(2)	3.149(3)	174(3)
5	N(7A)	N(9A)#[7]	0.88(2)	3.152(2)	169(2)
6	N(7A)	N(9A)#[8]	0.90(2)	3.150(3)	172(3)
7	N(7A)	N(9A)#[9]	0.88(1)	3.144(1)	169(1)
8[22]	N(7A)	N(9A)#[6]	0.82(1)	3.125(2)	171(2)

#1: $-x+1, y+1, -z+1/2$; #2: $x+1, y, z$; #3: $-x+1, -y-1, -z$; #4: $x-1, y, z$; #5: $x+1/2, -y-1/2, z+1/2$. #6: $-x, y+1, -z+3/2$; #7: $-x+1, y-1, -z+3/2$; #8: $-x, y-1, -z+1/2$; #9: $-x+1, y+1, -z+3/2$.

Polymers **2** and **3** are also one-dimensional chain structures with double thiocyanate bridges. 2ABN ligands in **2** are coordinated to the metal through the amine nitrogens and are disordered over two positions (Figure 2) while 4ABN molecules in **3** are coordinated to the cadmium centres through the cyanide nitrogens (Figure 3). The disordered 2ABN molecules have site occupancies of 50% for each of the two disordered positions, A and B, with the whole structure stabilised by inter- and intramolecular hydrogen bonding. When 2ABN are in position A, each amine group is hydrogen-bonded to two adjacent cyanide ni-

Table 1. Crystallographic data

Compound	**1**	**2**	**3**	**4**	**5**	**6**	**7**	**8**[22]
Empirical formula	$CdC_{16}H_{12}N_6S_2$	$CdC_{16}H_{12}N_6S_2$	$CdC_{16}H_{12}N_6S_2$	$Cd_{0.70}Ni_{0.30}C_{16}H_{12}N_6S_2$	$Cd_{0.59}Ni_{0.41}C_{16}H_{12}N_6S_2$	$Cd_{0.51}Ni_{0.49}C_{16}H_{12}N_6S_2$	$Cd_{0.23}Ni_{0.77}C_{16}H_{12}N_6S_2$	$NiC_{16}H_{12}N_6S_2$
Molecular mass	464.84	464.84	464.84	448.73	442.82	438.53	423.49	411.15
T (K)	173(2)	173(2)	173(2)	173(2)	173(2)	173(2)	173(2)	173(2)
Crystal system	monoclinic	triclinic	monoclinic	monoclinic	monoclinic	monoclinic	monoclinic	monoclinic
Space group	*C*2/*c*	$P\bar{1}$	$P2_1/n$	*C*2/*c*	*C*2/*c*	*C*2/*c*	*C*2/*c*	*C*2/*c*
a (Å)	17.1917(3)	5.9978(3)	7.5212(4)	17.1187(5)	17.0903(3)	17.0787(3)	17.0122(3)	16.9554(3)
b (Å)	5.6604(1)	7.3826(1)	5.7460(3)	5.6369(1)	5.6208(1)	5.6204(1)	5.5829(1)	5.5542(1)
c (Å)	18.5651(3)	9.9158(3)	20.6145(12)	18.4892(5)	18.4630(4)	18.4439(4)	18.3755(4)	18.2897(3)
α (°)	90	88.927(2)	90	90	90	90	90	90
β (°)	92.428(1)	84.145(2)	93.284(3)	92.445(1)	92.426(1)	92.453(1)	92.485(1)	92.491(1)
γ (°)	90	78.552(3)	90	90	90	90	90	90
V (Å^3)	1805.0(1)	428.1(1)	889.4(1)	1782.5(1)	1772.0(1)	1768.8(1)	1743.6(1)	1720.8(1)
Z	4	1	2	4	4	4	4	4
$D_{calcd.}$ (Mg·m^{-3})	1.711	1.803	1.736	1.672	1.660	1.645	1.613	1.587
μ (mm^{-1})	1.452	1.531	1.474	1.429	1.423	1.413	1.396	1.381
F(000)	920	230	460	896	887	881	858	840
Refl. collected	4076	3700	3916	3362	3585	3939	3785	5462
Unique reflections	2145	1958	2176	1801	1926	2101	1992	2120
R_{int}	0.019	0.019	0.021	0.021	0.017	0.012	0.011	0.018
Data/restraints/parameters	2145/2/123	1958/2/197	2176/2/123	1801/2/130	1926/2/129	2101/2/129	1992/2/129	2120/0/123
R [$I > 2\sigma(I)$]	0.0232	0.0248	0.0376	0.0281	0.0224	0.0204	0.0199	0.0226
R (all data)	0.0346	0.0280	0.0508	0.0433	0.0307	0.0256	0.0238	0.0254
wR' [$I > 2\sigma(I)$]	0.0499	0.0476	0.0789	0.0543	0.0550	0.0440	0.0478	0.0587
wR' (all data)	0.0528	0.0484	0.0848	0.0585	0.0580	0.0461	0.0492	0.0602

 © 2004 Wiley-VCH Verlag GmbH & Co. KGaA, Weinheim

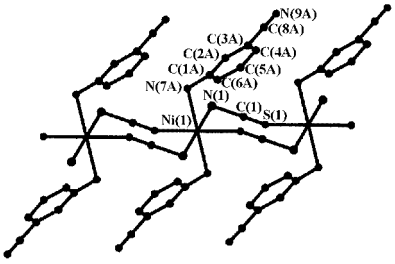

Figure 1. Section of the molecular structure of polymer **1**, showing the numbering scheme (the same numbering scheme was used for all compounds)

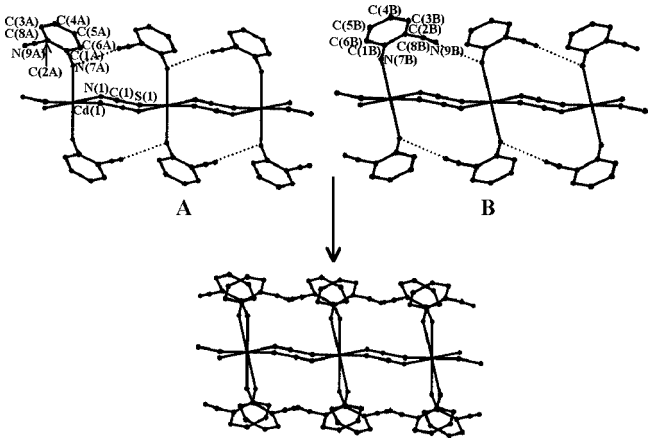

Figure 2. Section of the molecular structure of polymer **2**, showing disorder, hydrogen bonding and the numbering scheme

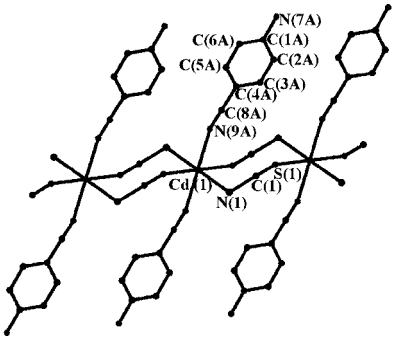

Figure 3. Section of the molecular structure of polymer **3**, showing the numbering scheme

trogens − one on the adjacent monomer unit of the same polymer strand and the other on a symmetry related strand. Intermolecular hydrogen bonding gives rise to the sheets parallel to the (110) plane. Position B only leads to intramolecular hydrogen-bonding. For **3**, only weak hydrogen bonds are present between the amine groups of one polymer strand and the thiocyanate sulfur atoms of another.

The introduction of several compounds (benzene, ABN, chloroform, toluene, naphthalene and linear and aromatic alcohols) into the respective starting mixtures afforded the polymers **1**−**6** (except for **7**) but gave no inclusion compounds. Thus, the cadmium-polymer formation is unaffected by potential guest molecules in the crystallisation medium. The only exception occurs for compound **7** when benzene is used as a guest and the nickel content in the mixed metal exceeds 75%. Here, two products are formed: the original Cd polymer **1** and the previously reported[22] nickel inclusion compound $[Ni(NCS)_2(3ABN)_2]_n$·(benzene). Interestingly, by changing the metal centre, we can suppress or activate the inclusion capability of a polymer. In addition, the introduction of a guest species in nickel polymers resulted in a structural change, due to differences in the modes of ligand coordination around the metal centre,[22] while the same was not observed with cadmium.

These results indicate different behaviours of cadmium and nickel in saturated solutions: nickel polymers can be tuned in terms of both their polymer structure and the formation of cavities, due to inclusion, while such a process is not useful for cadmium-containing compounds.

Solid solutions **4**−**7** were prepared as described in the Exp. Sect. The crystals are green, the colour intensity increasing with increasing concentration of nickel. Relatively large crystals of these bimetallic polymers were selected and then cut in two: one part for single-crystal X-ray analysis and the other for electron microscopy. This is important in avoiding ambiguous results as the ratio of each metal in the crystal could vary from batch to batch and also within the same batch. Crystals chosen for analysis were approximately 2.2 × 1.4 × 0.5 mm before cutting. The Cd:Ni ratio, determined at four sites for each crystal by electron microscopy, was reasonably homogeneous (Figure 4).

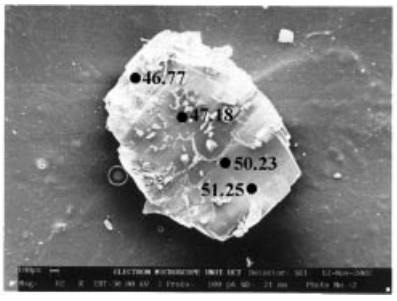

Figure 4. Electron microscopy image of a crystal of polymer **4**, showing the location and the results of measurements (as % Cd)

All four bimetallic compounds **4**−**7** are isostructural with the parent cadmium (**1**) and nickel (**8**) polymers, with the two metals occupying the same site. Structures were solved and refined by first locating all non-hydrogen atoms, then refining them anisotropically, and adding all the hydrogens to the final model. The relative metal composition in the structure was determined as the final part of refinement. The metal site was treated as being disordered as it may be occupied by a different metal atom in different unit cells. We attempted several different methods outlined in the literature:[33] (i) site occupancy values were allowed to refine while the displacement parameters remained fixed, having the same value; (ii) site occupancy values and the displacement parameters were refined simultaneously; (iii) once the site occupancy values were refined according to (i) the displacement parameters were also allowed to refine. All three

 © 2004 Wiley-VCH Verlag GmbH & Co. KGaA, Weinheim

methods were unsuccessful in refining the four structures and, therefore, the following procedure was adopted: Site occupancies of the Ni and Cd atoms were systematically changed from 0 to 1 in 5% increments and the isotropic parameters were not constrained but instead allowed to refine. When these were in the range $0.01 < U_{iso} < 0.03$, the site occupancies were analysed in 1% increments. This technique allowed a final refinement in which the metal atoms had unconstrained anisotropic thermal parameters.

The Cd:Ni ratios determined by crystal structure refinement and electron microscopy are in very good agreement (Figure 5).

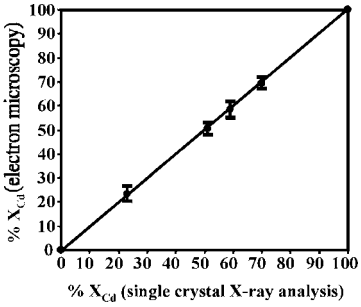

Figure 5. Percentage mol fraction cadmium, X_{Cd}, determined by electron microscopy and by single crystal X-ray diffraction refinement

For two isostructural parent compounds, where one ion is substituted by another at some sites, previous studies of inorganic solid solutions indicate that ions that can substitute one another[34] should not differ in size by more than 10−15%, so as to prevent drastic lattice distortions or changes in packing. These lattice distortions were not observed in our study even though the radii[35] of Cd^{2+} and Ni^{2+} are 0.95 and 0.69 Å, respectively, corresponding to a 38% difference in size. This could be because the volume occupied by the two metal atoms in the unit cell is relatively small compared with that of all the other atoms (in thiocyanate and 3ABN ligands).

Table 3. Selected bond lengths and angles

	Bond lengths (Å)			Bond angles (°)
	M−NCS	M−SCN	M−NH_2	N−M−S
1	2.293(1)	2.709(2)	2.389(2)	93.91(4)
2	2.313(1)	2.719(5)	2.391(5)[a] 2.445(6)[b]	91.03(4)
3	2.290(3)	2.722(1)	[c]	90.92(9)
4	2.215(3)	2.662(1)	2.320(2)	93.69(6)
5	2.158(4)	2.633(1)	2.273(3)	93.35(4)
6	2.159(2)	2.631(1)	2.272(2)	93.37(4)
7	2.065(1)	2.577(1)	2.188(1)	93.08(3)
8[22]	2.016(1)	2.544(1)	2.137(1)	92.98(3)

[a] Ring A. [b] Ring B. [c] Cd−NC = 2.341(3) Å.

Table 3 shows selected bond lengths and angles involving the metal centre; all values are typical for such types of interactions.

Vegard's Law[36] states that in solid solutions of isostructural compounds (i) the unit cell volume is proportional to the cube of the mean ionic radius and (ii) the unit cell dimensions (as well as mean bond lengths involving the metal atom) are linearly dependent on metal ion concentrations that are being substituted. We found that the unit cell dimensions (Table 1), unit cell volumes (Figure 6) and mean metal−ligand bond lengths (Figure 7) are indeed linearly dependent on the relative concentrations of the central cations, decreasing as Cd^{2+} is increasingly replaced by Ni^{2+}.

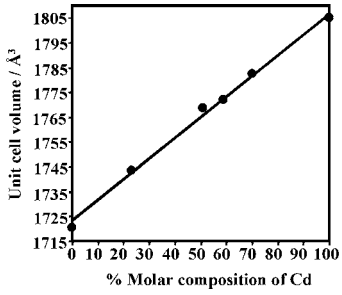

Figure 6. Unit cell volume vs. percentage molar composition of Cd

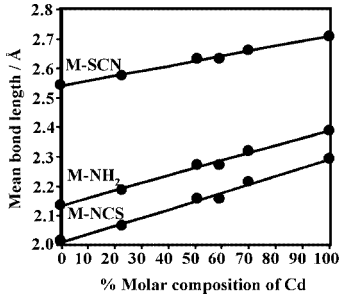

Figure 7. M−NCS bond length vs. percentage molar composition of Cd

We found parabolic behaviour instead of a linear correlation for the volume/ionic radii relationship (Figure 8). This has been observed in other situations before and is probably due the large difference in Cd and Ni ionic radii.[28]

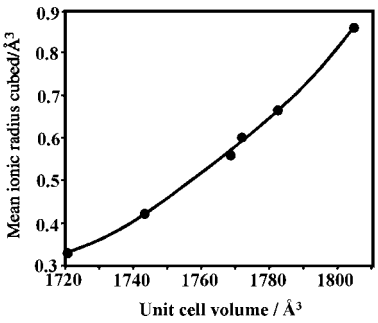

Figure 8. Cube of the mean ionic radii vs. unit cell volume

 © 2004 Wiley-VCH Verlag GmbH & Co. KGaA, Weinheim

Infrared spectroscopy data substantiates a previous finding that NCS^- ligands acting as end-to-end bridging groups have CN stretching vibrations greater than 2100 cm^{-1}.[37] $\tilde{\nu}$(CN) for polymers **1**−**8** is 2124, 2125, 2123, 2124, 2122, 2121, 2118 and 2119 cm^{-1} respectively.

Elemental analysis results agree with the theoretical values. For **4**−**7**, calculated values were based on the relative amounts of cadmium and nickel determined by X-ray analysis, and were found to be in remarkably good agreement with the experimental values, indicating that the average composition of each batch is very close to that of the crystal chosen for X-ray analysis.

X-ray powder diffraction was used to confirm that all samples were uniform in that no structurally different compounds were present in the batch. In all instances, the calculated and experimental XRPD traces of product mixtures agreed; all peaks were present at the correct angular positions and with the correct relative intensities. For solid solutions **4**−**7** the calculated XRPD patterns are virtually identical, with only slight variations in some of the relative peak intensities. Therefore, this method was not sufficiently sensitive to differentiate between different ratios of the two metals present.

Thermal Analysis

Thermal analysis results are summarised in Table 4. For all compounds, the TG and DSC traces have the same profiles. TG traces consist of one-step mass losses due to the loss of two ABN ligands and a corresponding endotherm in the DSC trace. Experimental and calculated mass loss values are in good agreement (based on the composition determined by X-ray analysis).

We were able to determine the thermal stability of the polymers by measuring the onset temperature[38] (T_{on}) of decomposition due to the loss of two ABN ligands. The results show that thermal degradation of **1** and **2** occurs at the same onset temperature while polymer **3** is the most stable. For bimetallic polymers **4**−**7**, the results (Figure 9) indicate that their thermal stability is proportional to the amount of nickel present. This is to be expected as the higher percentage of cadmium causes the bonds (M−NCS, M−SCN and M−NH_2) around the metal centre to lengthen and, therefore, to weaken (Table 3). This result also accords with the rationalisation usually given for the relative positions of the main group cations in the Irving−Williams series.

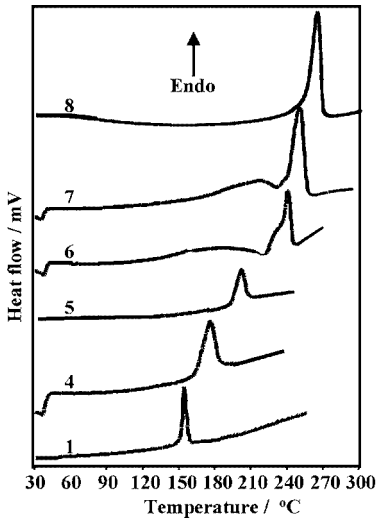

Figure 9. DSC results: migration of decomposition endotherm with changing Cd:Ni ratio

Conclusion

Aminobenzonitrile ligands can be used in the design and manipulation of new polymer architectures and their properties. In addition, the choice of metal ion influences the inclusion properties, thermal stability and structural features of the resultant coordination polymer. For example, at least one of the following is observed for the nickel and cadmium polymers (presented here and previously reported[22]): (i) the functionality through which ABNs are coordinated changes; (ii) both ABN and NCS^- ligands change their bonding environments from bidentate to monodentate coordination and vice versa; (iii) bridging and axial ligands are interchanged, (iv) inclusion properties are drastically affected and (v) thermal stability is influenced.

Comparison of all Ni and Cd polymer structures shows that, by changing the metal centre and/or adding a guest to the starting mixture, we can obtain three different polymer motifs (Scheme 1) that have different hydrogen-bonding capabilities, metal coordination environments and possible magnetic properties. [The nickel(II) coordination polymer, $Ni(NCS)_2(imidazole)_2$, which contains double thiocyanate bridges has been shown to exhibit long-range magnetic ordering.[39]]

Table 4. Thermal analysis data

	Polymer	**1**	**2**	**3**	**4**	**5**	**6**	**7**	**8**[22]
	M:L ratio	1:2	1:2	1:2	1:2	1:2	1:2	1:2	1:2
TG	Exp. mass loss (%)	50.1	50.4	50.9	52.1	53.7	53.1	56.2	57.3
	Calcd. mass loss (%)	50.8	50.8	50.8	52.7	53.3	53.9	55.8	57.5
DSC	T_{on} (°C)	147.9	148.0	182.9	160.0	190.3	239.5	244.2	246.6

 © 2004 Wiley-VCH Verlag GmbH & Co. KGaA, Weinheim

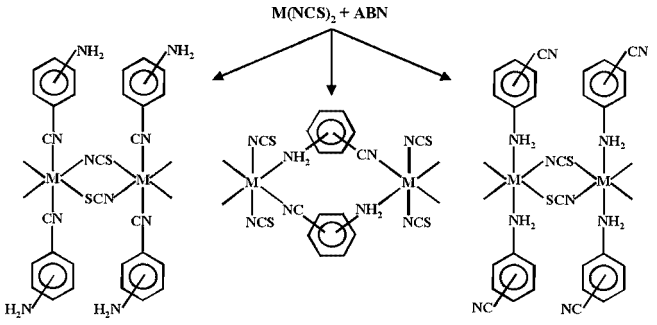

Scheme 1

By means of Vegard's Law,[36] it is possible to predict the composition of these solid solutions and, conversely, to ascertain their thermal stability from their composition.

We are currently attempting to develop a crystallisation methodology that would result in 2- and 3-dimensional ABN coordination polymers.

Experimental Section

Preparation of $[Cd(NCS)_2(3ABN)_2]_n$ (1), $[Cd(NCS)_2(2ABN)_2]_n$ (2) and $[Cd(NCS)_2(4ABN)_2]_n$ (3): The appropriate ABN isomer (0.047 g, 0.4 mmol) was dissolved in ethanol (0.5 mL) and added to ethanolic $Cd(NCS)_2$ solution (0.10 mmol·mL^{-1}, 1 mL). The resultant solution was then left to evaporate slowly, and gave colourless rectangular plate crystals within 24−72 h. Yield: **1**: 69%; **2**: 52%; **3**: 78%. **1:** $C_{16}H_{12}CdN_6S_2$; (464.84): calcd. C 41.34, H 2.60, N 18.08, S 13.80; found: C 41.34, H 2.41, N 18.06, S 13.73. **2**: $CdC_{16}H_{12}N_6S_2$ (464.84); for **2**: calcd. C 41.34, H 2.60, N 18.08 and S 13.80; found C 41.34, H 2.22, N 18.06, S 13.73. **3:** $CdC_{16}H_{12}N_6S_2$ (464.84):calcd. C 41.34, H 2.60, N 18.08, S 13.80 found C 41.35, H 2.52, N 18.10, S 13.77.

Preparation of Solid Solutions $[Cd_{1-x}Ni_x(NCS)_2(3ABN)_2]$ 4−7: 3ABN (0.35 g, 3.0 mmol) was dissolved in ethanol (3 mL) and added to solutions containing Ni^{II} and Cd^{II} in different ratios. To prepare the required metal ratios, ethanolic solutions of $Cd(NCS)_2$ (0.10 mmol·mL^{-1}) and $Ni(NCS)_2$ (0.20 mmol·mL^{-1}) were used. The solution of **4** contained $Ni(NCS)_2$ (1.25 mL) and $Cd(NCS)_2$ (7.50 mL) so that the Ni:Cd ratio was 25:75 while for **5** (Ni:Cd = 37:63) $Ni(NCS)_2$ (1.85 mL) and $Cd(NCS)_2$ (6.30 mL) were used. Compounds of **6** and **7** were prepared by adding $Ni(NCS)_2$ (2.50 and 3.75 mL) to $Cd(NCS)_2$ (5.0 and 2.5 mL) to give Ni:Cd ratios of 50:50 and 75:25 respectively. Crystals were obtained after 2−5 days for **4** and **5**, two weeks for **6** and approximately four weeks for **7**. The crystals varied from light green (**4**) to dark green (**7**) depending on the amount of nickel present. **4:** $C_{16}H_{12}Cd_{0.70}N_6Ni_{0.30}S_2$ (448.73): calcd. C 42.83, H 2.70, N 18.73, S 14.29; found C 42.72, H 2.58, N 18.69 and S 14.45. **5:** $C_{16}H_{12}Cd_{0.59}N_6Ni_{0.41}S_2$: (442.82): calcd. C 43.40, H 2.73, N 18.98, S 14.48; found C 43.21, H 2.52, N 19.05 and S 14.58. **6:** $C_{16}H_{12}Cd_{0.51}N_6Ni_{0.49}S_2$ (438.53): calcd. C 43.82, H 2.76, N 19.16, S 14.62; found C 43.94, H 2.48, N 19.24 and S 14.53. **7:** $C_{16}H_{12}Cd_{0.23}N_6Ni_{0.77}S_2$ (429.49): calcd. C 45.38, H 2.86, N 19.85, S 15.14; found C 45.62, H 2.52, N 19.58, S 15.26.

Thermal Analysis: Samples were crushed, blotted dry and sieved (Nybolt mesh) prior to analysis and then placed in open platinum pans for thermogravimetric (TG) experiments and in crimped but vented aluminium pans for differential scanning calorimetry (DSC). TG and DSC were carried out on a Perkin−Elmer PC7-Series system over the range 30−500 °C, at a heating rate of 20 °C min^{-1}, with a purge of dry nitrogen (30 mL·min^{-1}). Thermal analysis experiments depend on sample preparation, instrument geometry and heating rates. Particle size in particular can have a significant influence on the onset temperature of the thermal events[40]. Therefore, care was taken to prepare all samples in the same, reproducible manner. Each sample was sieved through a Nybolt mesh with a pore size of 17−80 μm.

Structure Determination: Cell dimensions were obtained from the intensity data measurements on a Nonius−Kappa CCD diffractometer using graphite-monochromated Mo-K_α radiation (λ = 0.71069 Å). The strategy for data collection was evaluated using the COLLECT[41] software. For all five structures, data were collected at 173(2) K using standard φ-scan and ω-scan techniques. All sets of data were scaled and reduced using DENZO-SMN.[42] Structures were solved by direct methods using SHELX-86[43] and refined by full-matrix least-squares with the program SHELX-97,[44] refining on F^2. The program X-Seed[45] was used as a graphical interface for structure solution and refinement using SHELX. No absorption corrections were necessary. Important crystal and experimental data for all five structures are given in Table 1.

Elemental Analysis: Elemental analyses to determine the percentages of C, H, N, and S were made on a Carlo−Erba 1106 Elemental Analyser. For each sample, the analysis was carried out in duplicate.

Infrared Spectroscopy: IR spectra were recorded using a Perkin−Elmer 983 IR spectrophotometer and NaCl plates. Samples were run as Nujol mulls over the range 4000−400 cm^{-1} and analysed for the mode of thiocyanate coordination.

Electron Microscopy: Single crystals were mounted using carbon glue and coated with a layer of pure carbon by vacuum evaporation. The analysis was performed on a Leo S440, fully analytical electron microscope with a KEVEX energy dispersive spectrometer. Data were collected at 30 kV with a beam current of 100 pA at a distance of 20 mm, tilt angle of 0° and a take-off angle of 35°. The results were analysed using the KEVEX Sigma Quasar Pro program.

X-ray Powder Diffraction (XRPD): X-ray powder diffraction patterns were measured using a Philips PW1050/25 goniometer with nickel-filtered Cu-K_α radiation. Samples were packed in aluminium sample holders and a step size of 0.1° at a scan rate of 1 s per step in the 2θ range 6−40° was employed for analysis. Calculated XRPD traces were generated for comparison purposes from the crystal structure results using the program LAZYPULVERIX.[46] CCDC-233623 to -233629 contain the supplementary crystallographic data for this paper. These data can be obtained free of charge at www.ccdc.cam.ac.uk/conts/retrieving.html [or from the Cambridge Crystallographic Data Centre, 12 Union Road, Cambridge CB2 1EZ, UK; Fax: (internat.) +44-1223-336-033; E-mail: deposit@ccdc.cam.ac.uk].

Acknowledgments

We thank the Claude Harris Leon Foundation for financial support.

[1] D. K. Chand, K. Biradha, M. Fujita, S. Sakamoto, K. Yamaguchi, *Chem. Commun.* **2002**, 2486.

[2] B. Moulton, M. J. Zaworotko, *Chem. Rev.* **2001**, *101*, 1629.
[3] H. Hou, Y. Fan, L. Zhang, C. Du, Y. Zhu, *Inorg. Chem. Commun.* **2001**, *4*, 168.
[4] G. F. Swiegers, T. J. Malefetse, *Chem. Rev.* **2000**, *100*, 3483.
[5] M. J. Zaworotko, *Angew. Chem. Int. Ed.* **2000**, *39*, 3053.
[6] K. Biradha, Y. Hongo, M. Fujita, *Angew. Chem. Int. Ed.* **2000**, *39*, 3843.
[7] B. Moulton, M. J. Zaworotko, *Curr. Opin. Solid State Mater. Sci.* **2002**, *6*, 117.
[8] J. D. Hartgerink, E. R. Zubarev, S. I. Stupp, *Curr. Opin. Solid State Mater. Sci.* **2001**, *5*, 355.
[9] S. R. Batten, *Curr. Opin. Solid State Mater. Sci.* **2001**, *5*, 107.
[10] L. Ma, O. R. Evans, B. M. Foxman, W. Lin, *Inorg. Chem.* **1999**, *38*, 5837.
[11] N. Singh, R. K. Sinha, *Inorg. Chem. Commun.* **2003**, *6*, 97.
[12] N. Singh, R. K. Sinha, *Inorg. Chem. Commun.* **2002**, *5*, 255.
[13] B. Żurowska, J. Mroziński, M. Julve, F. Lloret, A. Maslojeva, W. Sawska-Dobrowolska, *Inorg. Chem.* **2002**, *41*, 1771.
[14] M. A. Lawandy, X. Huang, R.-J. Wang, J. Li, J. Y. Lu, *Inorg. Chem.* **1999**, *38*, 5410.
[15] J. Y. Lu, C. Norman, K. Abboud, A. Ison, *Inorg. Chem. Commun.* **2001**, *4*, 459.
[16] M. Fujita, J. W. Kwon, S. Washizu, *J. Am. Chem. Soc.* **1994**, *116*, 1151.
[17] B. F. Abrahams, B. F. Hoskins, D. M. Michail, R. Robson, *Nature* **1994**, *369*, 727.
[18] S. Subramanian, M. J. Zaworotko, *Angew. Chem. Int. Ed. Engl.* **1995**, *34*, 2127.
[19] J. L. Atwood, L. J. Barbour, A. Jerga, *Science* **2002**, *296*, 2367.
[20] W. Lin, Z. Wang, L. Ma, *J. Am. Chem. Soc.* **1999**, *121*, 11249.
[21] H. Hou, Y. Wei, Y. Fan, C. Du, Y. Zhu, Y. Song, Y. Niu, X. Xin, *Inorg. Chim. Acta* **2001**, *319*, 212.
[22] D. Vujovic, H. G. Raubenheimer, L. R. Nassimbeni, *Dalton Trans.* **2003**, 631.
[23] Y.-B. Dong, M. D. Smith, H.-C. zur Loye, *Inorg. Chem.* **2000**, *39*, 1943.
[24] N. Singh, S. Gupta, *Inorg. Chem. Commun.* **2000**, *3*, 446.
[25] D. M. Ciurtin, M. D. Smith, H.-C. zur Loye, *Inorg. Chim. Acta* **2001**, *324*, 46.
[26] S. Nagata, *J. Phys. Soc., Jpn.* **1974**, *37*, 645.
[27] Y. Mathey, C. Mazieres, *Bull. Soc. Chim. France* **1973**, *11*, 2918.
[28] T. Miyoshi, T. Iwamoto, Y. Sasaki, *Inorg. Chim. Acta* **1973**, 97.
[29] T. Miyoshi, T. Iwamoto, Y. Sasaki, *Inorg. Chim. Acta* **1968**, 329.
[30] H. Zhang, X. Wang, K. Zhang, B. K. Teo, *Coord. Chem. Rev.* **1999**, 157.
[31] W. Chen, F. Liu, X. You, *Bull. Chem. Soc., Jpn.* **2002**, *75*, 1559.
[32] M. A. S. Goher, F. A. Mautner, M. A. M. Abu-Youssef, A. K. Hafez, A. M.-A. Badr, C. Gspan, *Polyhedron* **2003**, *22*, 3137.
[33] S. G. Bott, B. D. Fahlman, M. L. Pierson, A. R. Barron, *J. Chem. Soc., Dalton Trans.* **2001**, 2148.
[34] B. K. Vainshtein, V. M. Fridkin, V. L. Indenbom, *Modern Crystallography 2, Structure of Crystals*, Springer-Verlag, Berlin, **1995**, ch. 1, pp. 113.
[35] R. Shannon, *Acta Crystallogr., Sect. A* **1976**, *32*, 751.
[36] R. M. Hazen, L. W. Finger, in *Comparative Crystal Chemistry: Temperature, Pressure, Composition and the variation of Crystal Structure*, Wiley-VCH, Weinheim, **1982**, ch. 8, pp. 168.
[37] K. Nakamoto, *Infrared and Raman Spectra of Inorganic and Coordination Compounds*, Wiley, New York, **1978**, ch. 3, pp. 270.
[38] M. R. Caira, L. R. Nassimbeni, in *Comprehensive Supramolecular Chemistry* (Eds. J. L. Atwood, J. E. D. Davies, D. D. MacNicol, F. Vögtle), Elsevier Science, Oxford, **1996**, vol. 6, ch. 25, pp. 825.
[39] B. Żurowska, J. Mroziński, M. Julve, F. Lloret, A. Maslojeva, W. Sawska-Dobrowolska, *Inorg. Chem.* **2002**, *41*, 1771.
[40] M. E. Brown, *Introduction to Thermal Analysis*, Academic Press, Boston, **1990**, ch. 1, pp. 15.
[41] COLLECT, data collection software, Nonius, **1998**.
[42] Z. Otwinowski, W. Minor, in *Methods in Enzymology*, vol. 276: *Macromolecular Crystallography*, part A (Eds.: C. W. Carter Jr., R. M. Sweet), Academic Press, **1997**, pp. 307.
[43] G. M. Sheldrick, SHELX-86, in *Crystallographic Computing 3* (Eds.: G. M. Sheldrick, C. Kruger, R. Goddard), Oxford University Press, Oxford, **1985**, pp. 75.
[44] G. M. Sheldrick, T. R. Schneider, in *SHELXL: High-Resolution Refinement, Methods in Enzymology*, vol. 277 (Macromolecular Crystallography, Part B (Eds.: C. W. Carter, R. M. Sweet), **1997**, pp. 319.
[45] L. J. Barbour, *J. Supramol. Chem.* **2001**, *1*, 189.
[46] K. Yvon, W. Jeitschko, E. Parthe, *J. Appl. Cryst.* **1977**, *10*, 73.

Received October 29, 2003
Early View Article
Published Online May 5, 2004

 © 2004 Wiley-VCH Verlag GmbH & Co. KGaA, Weinheim

Kinetics and Mechanism of Oxidation of Fe^{2+} by the Tris(biguanide)manganese(IV) Ion in Aqueous Acid Media

Basab Bijayi Dhar,[a] Ritam Mukherjee,[a] Subrata Mukhopadhyay,*[a] and Rupendranath Banerjee[a]

Keywords: Iron / Kinetics / Manganese / Mechanism / Redox chemistry

Tris(biguanide)manganese(IV), $[Mn(LH_2)_3]^{4+}$ (LH_2 = biguanide, $C_2N_5H_7$), quantitatively oxidises Fe^{2+} to Fe^{3+} and is itself reduced to Mn^{2+} with almost quantitative (> 95%) release of biguanide. The reaction rate strongly depends on added Fe^{3+}; in the presence of externally added Fe^{3+}, the reaction shows a clear first-order dependence in $[Mn^{IV}]$, whereas in the absence of any added Fe^{3+}, an initial quick loss of Mn^{IV} is associated with a subsequent very sluggish decay. Two consecutive one-electron transfer inner-sphere steps are proposed for the entire redox process where $[Mn(LH_2)_3]^{3+}$, the initial one-electron-reduced product of Mn^{IV}, is believed to be a steady-state intermediate.
(© Wiley-VCH Verlag GmbH & Co. KGaA, 69451 Weinheim, Germany, 2004)

Introduction

The aqueous solution chemistry of mononuclear Mn^{IV} is very scarce due to the extreme paucity of soluble Mn^{IV} species. However, the recently reported[1] tris(biguanide)-manganese(IV) complex $[Mn(LH_2)_3]^{4+}$ (**1**; Figure 1, LH_2 = biguanide, $C_2N_5H_7$) is structurally well characterised and is a rare example of a water-soluble mononuclear Mn^{IV} complex that is stable over a wide range of acidity (10^{-6} to 2 M). Figure 2 displays its UV/Vis spectrum at pH 2.0. Some oxo-bridged di-, tri- and tetranuclear Mn^{IV} complexes[2] are also stable in aqueous solution and have interesting solution chemistry,[3] but their mononuclear counterparts are unknown.

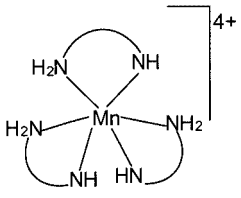

Figure 1. Structure of $[Mn(LH_2)_3]^{4+}$ (**1**)

We report here the kinetics of oxidation of Fe^{2+} by the title Mn^{IV} complex in aqueous acidic media to elucidate the mechanistic aspects of the process as a part of our continued interest[3] in the aqueous solution chemistry of higher-valent manganese species.

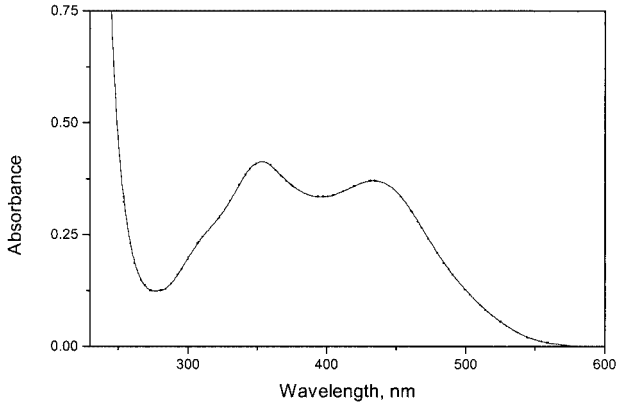

Figure 2. UV/Vis spectrum of 0.050 mM complex at pH 2.0

Results and Discussion

Equilibrium Studies

The built-in program of the Metrohm 736 GP Titrino autotitrator yielded two pK_a values for the title complex from the pH-titration curve: pK_{a1} = 5.30 ± 0.20 and pK_{a2} = 7.60 ± 0.30. The Mn^{IV} in the complex is coordinatively saturated and any deprotonation should thus arise from the ligand biguanide moiety, possibly from protons bound to sp^2 nitrogens as in an analogous Ag^{III} complex or in $[Co^{III}(am)(LH_2)_2]^{2+}$ (am = amino acids like glycine,

[a] Department of Chemistry, Jadavpur University, Calcutta 700032, India
E-mail: subrataju@vsnl.net

 © 2004 Wiley-VCH Verlag GmbH & Co. KGaA, Weinheim DOI: 10.1002/ejic.200300887

alanine, etc.).[4a,4b] In $[Co^{III}(LH_2)_2(H_2O)_2]^{3+}$, however, coordinated water is deprotonated.[4c] Table 1 summarises the known acidity constants of some biguanide complexes.

Table 1. Deprotonation constants of metal biguanide complexes[a]

Metal complex	pK_{a1}	pK_{a2}	Reference
$[Ag^{III}(enbbg)]^{3+}$	3.80	6.30	[4a]
$[Co^{III}(gly)(LH_2)_2]^{2+}$	9.06	10.4	[4b]
$[Co^{III}(L\text{-ala})(LH_2)_2]^{2+}$	9.07	10.4	[4b]
$[Co^{III}(LH_2)_2(H_2O)_2]^{3+}$	5.86	7.92	[4c]
$[Mn^{IV}(LH_2)_3]^{4+}$	5.30	7.60	this work

[a] enbbg = ethylenebis(biguanide), gly = glycine, L-ala = L-alanine.

Stoichiometry and Reaction Products

The results of the stoichiometry experiments (Table 2) yielded $\Delta[Mn^{IV}]/\Delta[Fe^{2+}] = 0.49 \pm 0.03$ and $\Delta[Mn^{IV}]/\Delta[Fe^{3+}] = 0.53 \pm 0.04$. The product solution, after removing iron, displays a typical six-line EPR spectrum of Mn^{II} ($I = 5/2$). Hence, Equation (1) describes the overall redox process.

$$Mn^{IV} + 2Fe^{2+} \rightarrow Mn^{II} + 2Fe^{3+} \quad (1)$$

Iodometric determination of copper in the cupric biguanide precipitated from the product solution indicated release of more than 95% of the biguanide.

Kinetics

The reaction of complex **1** reacting with excess Fe^{2+} does not represent well-behaved kinetics; an initial quick loss in absorbance of **1** is followed by a sluggish phase, and the absorbance vs. time data do not follow first-order kinetics, as shown in Figure 3. In the presence of added Fe^{3+}, the initial loss in absorbance is prevented and the whole reaction course follows first-order kinetics (Figure 3) — the $\ln(A_t - A_\infty)$ vs. time plots were found to be linear to more than 90% completion of the reactions. In all kinetic runs A_∞ values were less than 0.01. Most of the kinetics were therefore determined in the presence of added Fe^{3+}. The first-order rate constants, k_o, defined by Equation (2) were obtained from least-squares slopes of these plots and are presented in Table 3. Moreover, a tenfold variation in the initial Mn^{IV} concentration (0.02 −0.20 mM) gave no change in the k_o values within experimental uncertainty (± 5%). This indicates a first-order decay of Mn^{IV} concentration.

$$-d[Mn^{IV}]/dt = k_o[Mn^{IV}] \quad (2)$$

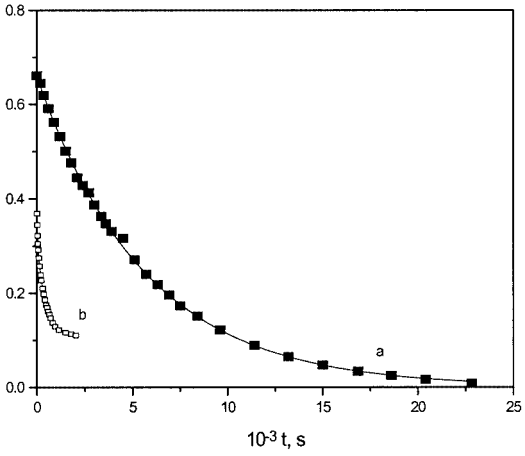

Figure 3. Absorbance vs. time graph for the reduction of $[Mn(LH_2)_3]^{4+}$ (0.10 mM) by Fe^{2+} (5.0 mM): a) in the presence of added Fe^{3+} (0.50 mM); b) in the absence of added Fe^{3+}; $[H^+]$ = 1.3 mM, I = 1.0 M, T = 25.0 °C

At fixed $[Fe^{3+}]_T$ (= $[Fe^{3+}]_{aq}$ + $[Fe(OH)^{2+}]_{aq}$) and $[H^+]$, the plot of $[Fe^{2+}]_T^2/k_o$ vs. $[Fe^{2+}]_T$, (= $[Fe^{2+}]_{aq}$ + $[Fe(OH)^+]_{aq}$) is a straight line with definite intercept and slope (Figure 4). Also, at fixed $[Fe^{2+}]_T$ and $[H^+]$, the plot of $1/k_o$ vs. $[Fe^{3+}]_T$ is a straight line with finite intercept. Plots of k_o versus $[H^+]$ at fixed $[Fe^{2+}]_T$ and $[Fe^{3+}]_T$ have a bell shape (Figure 5) indicating the involvement of at least two protic equilibria[5] in the reaction. We also observed that in the presence of 6% (v/v) acrylonitrile no polymeric products were formed, thus perhaps eliminating any detectable generation of free radicals during the reaction. Equations (3)−(8) provide a reasonable explanation of the kinetic observations.

Table 2. Stoichiometry of the reduction of $[Mn(LH_2)_3]^{4+}$ by Fe^{2+} at pH 2.4−2.7 and T = 25 °C; all concentrations are in mM

$[Mn^{IV}]$	pH	$[Fe^{2+}]_T$	$[Fe^{2+}]_{Left}$	$[Fe^{3+}]_{Produced}$	$\Delta[Mn^{IV}]/\Delta[Fe^{2+}]$	$\Delta[Mn^{IV}]/\Delta[Fe^{3+}]$
0.05	2.4	0.20	0.10	0.09	0.50	0.56
0.06	2.5	0.40	0.27	0.12	0.46	0.50
0.12	2.6	0.80	0.57	0.21 0.52	0.57	
0.20	2.6	1.20	0.73	0.38	0.48	0.57
0.28	2.7	1.30	0.73	0.57	0.49	0.49
					average: 0.49 ± 0.03	average: 0.53 ± 0.04

 © 2004 Wiley-VCH Verlag GmbH & Co. KGaA, Weinheim

$$Fe^{2+}_{aq} \overset{K_a}{\rightleftharpoons} Fe(OH)^{+}_{aq} + H^{+} \quad (3)$$

$$[Mn(LH_2)_3]^{4+} + Fe^{2+}_{aq} \underset{k_{-1}}{\overset{k_1}{\rightleftharpoons}} [Mn(LH_2)_3]^{3+} + Fe^{3+}_{aq} \quad (4)$$

$$[Mn(LH_2)_3]^{4+} + Fe(OH)^{+}_{aq} \underset{k_{-2}}{\overset{k_2}{\rightleftharpoons}} [Mn(LH_2)_3]^{3+} + Fe(OH)^{2+} \quad (5)$$

1

$$Fe^{3+}_{aq} \overset{K_h}{\rightleftharpoons} Fe(OH)^{2+}_{aq} + H^{+} \quad (6)$$

$$[Mn(LH_2)_3]^{3+} + Fe^{2+}_{aq} \xrightarrow{k_3} \text{Products} \quad (7)$$

$$[Mn(LH_2)_3]^{3+} + Fe(OH)^{+}_{aq} \xrightarrow{k_4} \text{Products} \quad (8)$$

Combining these equations leads to Equation (9), assuming a steady state for $[Mn(LH_2)_3]^{3+}$

$$k_o(K_a + [H^+])/(K_h + [H^+]) = (A + B[H^+] + C[H^+]^2)/(D + E[H^+] + F[H^+]^2) \quad (9)$$

where $A = [Fe^{2+}]_T^2 K_a^2 k_2 k_4$, $B = [Fe^{2+}]_T^2 K_a(k_2 k_3 + k_1 k_4)$, $C = [Fe^{2+}]_T^2 k_1 k_3$, $D = [Fe^{3+}]_T k_{-2} K_h K_a + [Fe^{2+}]_T K_h K_a k_4$, $E = [Fe^{3+}]_T(k_{-1} K_a + k_{-2} K_h) + [Fe^{2+}]_T(k_3 K_h + k_4 K_a)$ and $F = [Fe^{3+}]_T k_{-1} + [Fe^{2+}]_T k_3$.

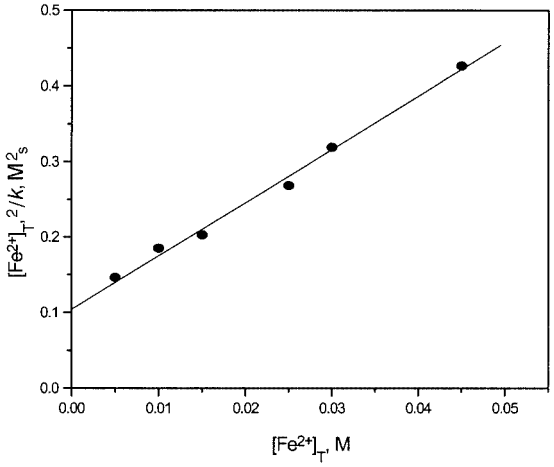

Figure 4. Plot of $[Fe^{2+}]_T^2/k_o$ vs. $[Fe^{2+}]_T$; [complex] = 0.10 mM, $[Fe^{2+}]_T$ = (5.0−45.0) mM, $[Fe^{3+}]_T$ = 0.50 mM, $[H^+]$ = 1.3 mM, I = 1.0 M, T = 25.0 °C

Table 3. First-order rate constants (k_o)[a] at T = 25.0 °C, I = 1.0 M ($NaClO_4$) and λ = 433 nm

$[H^+]$ (mM)	$[Fe^{2+}]_T$ (mM)	$[Fe^{3+}]_T$ (mM)	$10^4 k_o$ [s^{-1}]
1.56	30	1.00	21.6 (21.5)
2.90			18.0 (17.6)
5.27			16.1 (16.8)
8.19			17.3 (17.9)
12.1			20.0 (20.2)
1.30		0.50	28.4 (29.0)
2.23			23.9 (23.5)
5.14			20.8 (21.2)
7.60			22.2 (22.3)
10.1			22.7 (24.1)
12.6			25.7 (26.1)
1.56	45	1.00	38.7 (39.1)
3.37			31.7 (31.3)
5.27			29.7 (30.7)
8.19			32.0 (32.7)
11.2			36.5(35.9)
1.30	60	0.50	63.0 (65.1)
2.23			52.4 (52.2)
3.19			50.0 (48.0)
5.14			45.8 (46.6)
10.1			51.1(52.3)
12.6			56.8 (56.5)
15.1			61.5 (61.0)
1.19		0.30	80.4 (81.2)
4.10			56.5 (56.1)
8.06			58.5 (59.7)
12.0			69.0 (67.7)
15.0			77.6 (74.5)
1.30	5	0.50	1.79 (1.71)
	10		5.68 (5.41)
	15		11.0 (11.1)
	25		23.2 (23.3)
	30		28.2 (29.7)
	45		47.5 (49.9)

[a] Concentration of complex used: 0.10 mM. The k_o values calculated using Equation (9a) are given in parentheses.

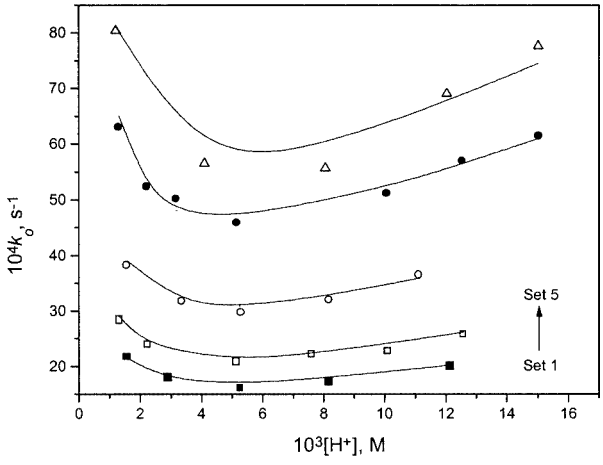

Figure 5. Plot of k_o vs. $[H^+]$; [complex] = 0.10 mM. set 1: $[Fe^{2+}]_T$ = 30.0 mM, $[Fe^{3+}]_T$ = 1.0 mM, $[H^+]$ = (1.5−12.2) mM; set 2: $[Fe^{2+}]_T$ = 30.0 mM, $[Fe^{3+}]_T$ = 0.50 mM, $[H^+]$ = (1.3−12.6) mM; set 3: $[Fe^{2+}]_T$ = 45.0 mM, $[Fe^{3+}]_T$ = 1.0 mM, $[H^+]$ = (1.5−11.2) mM; set 4: $[Fe^{2+}]_T$ = 60.0 mM, $[Fe^{3+}]_T$ = 0.50 mM, $[H^+]$ = (1.3−15.0) mM; set 5: $[Fe^{2+}]_T$ = 60.0 mM, $[Fe^{3+}]_T$ = 0.30 mM, $[H^+]$ = (1.2−15.0) mM. I = 1.0 M, T = 25.0 °C for all experiments

 © 2004 Wiley-VCH Verlag GmbH & Co. KGaA, Weinheim

The plots of the left-hand-side of Equation (9) versus $[H^+]$ at different, fixed $[Fe^{2+}]_T$ and $[Fe^{3+}]_T$ are excellent straight lines (Figure 6; $r > 0.98$), which indicates that $C[H^+]^2 << (A + B[H^+])$ and $(E[H^+] + F[H^+]^2) << D$. Equation (9) therefore simplifies to Equation (10) as K_a $(= 10^{-8.1})$[6] $<<$ $[H^+]$.

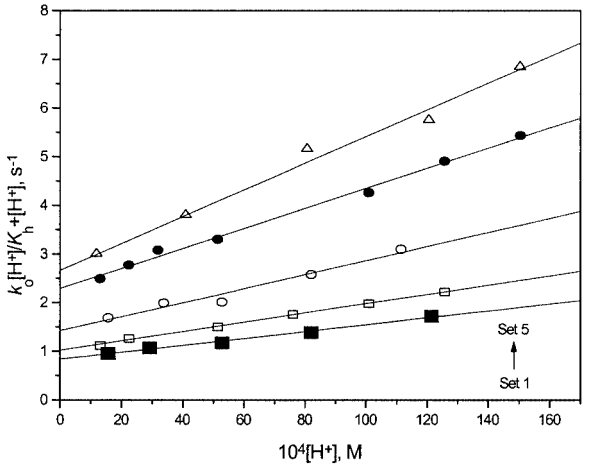

Figure 6. Plot of Y vs. $[H^+]$; [complex] = 0.10 mM; set 1: $[Fe^{2+}]_T$ = 30.0 M, $[Fe^{3+}]_T$ = 1.0 mM, $[H^+]$ = (1.5−12.2) mM; set 2: $[Fe^{2+}]_T$ = 30.0 mM, $[Fe^{3+}]_T$ = 0.50 mM, $[H^+]$ = (1.3−12.6) = mM; set 3: $[Fe^{2+}]_T$ = 45.0 mM, $[Fe^{3+}]_T$ = 1.0 mM, $[H^+]$ = (1.5−11.2) mM, Set 4: $[Fe^{2+}]_T$ = 60.0 mM, $[Fe^{3+}]_T$ = 0.50 mM, $[H^+]$ = (1.3−15.0) mM; set 5: $[Fe^{2+}]_T$ = 60.0 mM, $[Fe^{3+}]_T$ = 0.30 mM, $[H^+]$ = (1.2−15.0) mM. I = 1.0 M, T = 25.0 °C for all experiments

$$k_o[H^+]/(K_h + [H^+]) = (A + B[H^+])/D \quad (10)$$

The elaborated form of Equation (10) is:

LHS = Y (for example) = $[Fe^{2+}]_T^2\{K_a^2k_2k_4 + K_a(k_2k_3 + k_1k_4)[H^+]\}/[Fe^{3+}]_Tk_{-2}K_hK_a + [Fe^{2+}]_TK_hK_aK_4$

or

$$[Fe^{2+}]_T^2/Y = (k_{-2}K_hK_a/a)\,[Fe^{3+}]_T + (k_4K_hK_a/a)\,[Fe^{2+}]_T \quad (11)$$

where $a = K_a^2k_2k_4 + K_a(k_2k_3 + k_1k_4)[H^+]$. Equation (11) explains the observed linear plots of $[Fe^{2+}]_T^2/k_o$ versus $[Fe^{2+}]_T$ at fixed $[Fe^{3+}]_T$ and $[H^+]$ and also the linear plots of $1/k_o$ versus $[Fe^{3+}]_T$ at fixed $[Fe^{2+}]_T$ and $[H^+]$. From the linear plots of Y versus $[H^+]$ (Figure 6), the slopes and intercepts yielded, respectively, $B/D = \{[Fe^{2+}]_T^2(k_2k_3 + k_1k_4)/K_h([Fe^{3+}]_Tk_{-2} + [Fe^{2+}]_Tk_4)\}$ and $A/D = \{[Fe^{2+}]_T^2K_ak_4k_2/K_h([Fe^{3+}]_Tk_{-2} + [Fe^{2+}]_Tk_4)\}$. The slope/intercept of these plots yield B/A $[= (k_2k_3 + k_1k_4)/K_a\,k_2k_4] = 92.6 \pm 2.0\ M^{-1}$ at 25.0 °C and I = 1.0 M. We determined A/D and B/D values at different, fixed $[Fe^{2+}]_T$ and $[Fe^{3+}]_T$. These values were used to plot $[Fe^{2+}]_T/(A/D)$ vs. $[Fe^{3+}]_T/[Fe^{2+}]_T$ and $[Fe^{2+}]_T/(B/D)$ vs. $[Fe^{3+}]_T/[Fe^{2+}]_T$. As expected, these were found to be good straight lines ($r > 0.98$) and yielded k_{-2}/k_4 (= 28.0 ± 2.0) and k_2 $[= (1.28 \pm 0.1) \times 10^4\ M^{-1}s^{-1}]$ from their slopes and intercepts using known K_a and K_h $(= 10^{-2.7})$[7] values. The composite constants $(k_3k_2 + k_4k_1)/k_4$ $[= (1.0 \pm 0.01) \times 10^{-2}]$ and $(k_3k_2 + k_4k_1)/k_{-2}$ (= 3007 ± 150) were also determined from the slopes and intercepts.

Equations (12)−(16) can explain the kinetic observations equally well. Here, Fe^{2+} hydrolysis is neglected and replaced by the deprotonation equilibrium of **1**.

$$[Mn(LH_2)_3]^{4+} \underset{}{\overset{K_a}{\rightleftharpoons}} [Mn(LH_2)_2(LH)]^{3+} + H^+ \quad (12)$$
1 **1a**

$$[Mn(LH_2)_3]^{4+} + Fe^{2+}_{aq} \underset{k_{-1}}{\overset{k_1}{\rightleftharpoons}} [Mn(LH_2)_3]^{3+} + Fe^{3+}_{aq} \quad (13)$$

$$[Mn(LH_2)_2(LH)]^{3+} + Fe^{2+}_{aq} \underset{k_{-2}}{\overset{k_2}{\rightleftharpoons}} [Mn(LH_2)_3]^{3+} + Fe(OH)^{2+}_{aq} \quad (14)$$
1a

$$Fe^{3+}_{aq} \overset{K_h}{\rightleftharpoons} Fe(OH)^{2+}_{aq} + H^+ \quad (15)$$

$$[Mn(LH_2)_3]^{3+} + Fe^{2+}_{aq} \xrightarrow{k_3} \text{Products} \quad (16)$$

Proceeding in the same way as above gives $k_1 = (1.0 \pm 0.01) \times 10^{-2}\ M^{-1}s^{-1}$, $k_2 = 21.5 \pm 0.5\ M^{-1}s^{-1}$ and $k_{-2}/k_3 = 28.0 \pm 2.0$.

Mechanism

We like to allow less importance to Equations (12)−(16) as it is unusual[8] that a deprotonated species of a higher valent transition metal complex is more reactive (k_2) than its conjugate acid (k_1). Further, this flouts the well-known fact that $Fe(OH)^+_{aq}$ is much more reactive than Fe^{2+}_{aq} in redox reactions and $Fe(OH)^+_{aq}$ is a kinetically reactive species even in moderately acidic media.[6]

The value of k_2 evaluated from Equations (3)−(8) indicates a very high reactivity of $Fe(OH)^+_{aq}$ in reducing the title Mn^{IV} complex. A similar situation has been found with the reduction of Ni^{IV}-oxime.[6] There, $Fe(OH)^+_{aq}$ is about 10^5 times more reactive than Fe^{2+}_{aq}. Although it was not possible to extract the absolute value of k_4, we expect it also to be high. Our results also indicate, at best, a poor contribution of Fe^{3+}_{aq} (k_{-1} path) in reoxidising the Mn^{III} species; $Fe(OH)^{2+}_{aq}$ (k_{-2} path) is almost wholly responsible for this. The pattern of reactivity established with Fe^{III}, Mn^{III}, Ag^{II} and Co^{III} as inner-sphere oxidants also revealed a significant contribution of the M−OH path to the overall rate.[9] In contrast, aqua complexes generally predominate for outer-sphere reactions, with little or no contribution from the M−OH path. In the present case, the hydroxo species $Fe(OH)^{2+}_{aq}$ and $Fe(OH)^+_{aq}$ are kinetically superior to their corresponding conjugate acids. Such a situation is likely with inner-sphere reactions, possibly by hydrogen bonding of the OH group to an NH or NH_2 group of the ligand biguanide.

 © 2004 Wiley-VCH Verlag GmbH & Co. KGaA, Weinheim

Experimental Section

Materials: The complex salt $[Mn(C_2N_5H_7)_3]_2SO_4(NO_3)_6{\cdot}3H_2O$ was prepared by a known procedure.[1] The crystals obtained were sufficiently pure, as indicated by satisfactory elemental analysis (calcd. C 11.63, H 3.88, N 40.71; found C 11.3, H 3.9, N 39.9). A stock solution of $Fe(ClO_4)_2$ was prepared by dissolving pure iron powder (G. R., E. Merck) in a slight stoichiometric excess of $HClO_4$ under an N_2 atmosphere. These solutions were prepared just prior to use for kinetic measurements. This solution was estimated by the dichromate oxidation method.[10] $Fe(ClO_4)_3$ solutions were prepared by dissolving freshly precipitated $Fe(OH)_3$ in a stoichiometric excess of $HClO_4$. In solution, Fe^{3+} was estimated by measuring the absorbance of $[Fe(SCN)]_{aq}^{2+}$ (ε = 5000 $M^{-1}cm^{-1}$) at 460 nm after the addition of NH_4SCN solution.[11,12] The free-acid content in both of these iron solutions were measured by passing them separately through a Dowex 50 W X-8 strong cation-exchange resin in the H^+ form to obtain $[H^+]$ equivalent to the metal-ion concentration along with free acid and then subtracting the metal equivalent from these. An aqueous solution of $NaClO_4$ (G. R., E. Merck) was standardised by passing through a Dowex 50 W X-8 strong cation-exchange resin in the H^+ form and titrating the liberated acid with standard NaOH to a phenolphthalein end-point. The total acid content of the reaction mixtures was calculated as added acid plus that produced by the hydrolysis of ferric ion. All other chemicals were of reagent grade and used as received. Doubly distilled, freshly boiled water was used throughout.

Physical Measurements and Kinetics: All absorbances and electronic spectra were recorded with a Shimadzu (1601 PC) spectrophotometer using 1.00 cm quartz cells. The kinetics were monitored in situ in the "kinetic mode" of the instrument at 433 nm, one of the absorption peaks (Figure 2) of the complex **1**, in an electrically controlled thermostatted (25.0 ± 0.1 °C) cell housing (CPS-240A). For faster reactions, Fe^{2+} solution was injected directly into the spectrophotometer cell containing the other components of the reaction mixture. The desired concentration of the complex and the reducing agent was achieved after mixing. All kinetics were monitored in the presence of excess Fe^{2+} over **1** at an ionic strength 1.0 M ($NaClO_4$).

Stoichiometry and Reaction Products: The stoichiometry was measured by estimating unchanged Fe^{2+} spectrophotometrically. Reaction mixtures containing 4−10 times Fe^{2+} over **1** were allowed to react completely under an N_2 atmosphere until the solution turned colourless. Excess 1,10-phenanthroline was then added along with potassium hydrogen phthalate (pH ≈ 4). The red colour of $[Fe(phen)_3]^{2+}$ was then measured at 510 nm (ε = 11100 $M^{-1}cm^{-1}$).[11,13] In another aliquot of product solution, the Fe^{3+} produced was quantified by adding NH_4SCN and measuring the absorbance of $[Fe(SCN)]_{aq}^{2+}$ so formed at 460 nm.[11,12] A reaction mixture, initially containing 2.5 mM [Mn^{IV}], 100 mM [Fe^{2+}] and 10 mM [Fe^{3+}], stored till colourless (absorption < 0.01 at 433 nm), was treated with NaOH solution at about 50 °C with constant stirring. The pH was thus raised to about 5 and the solution was kept for about 24 hours, after which all the iron had precipitated as iron(III) hydroxide. This was removed by filtration. The pH of the resulting solution was lowered to about 1 to avoid the complexation of biguanide with Mn^{2+} and an EPR spectrum was recorded. The biguanide ligand in the product was quantitatively isolated as $[Cu(LH_2)_2]SO_4$ by the addition of $CuSO_4$. The amount of Cu^{II} thus held was determined iodometrically after decomposing the copper complex.[14]

Equilibrium Measurements: A 15 mL mixture of 1.00 mM complex and 3.00 mM $HClO_4$ was titrated with a standard NaOH solution to determine the acid dissociation constants of the title complex. The titration was carried out at 25.0 °C and I = 1.0 M ($NaClO_4$) with a Metrohm 736 GP Titrino autotitrator.

Acknowledgments

Financial assistance from the Department of Science and Technology, New Delhi, India, and the award of a junior research fellowship to B. B. D. by the University Grants Commission, New Delhi are gratefully acknowledged. S. M. acknowledges the Council of Scientific and Industrial Research, New Delhi for funding.

[1] [1a] G. Das, P. K. Bharadwaj, D. Ghosh, B. Chaudhuri, R. Banerjee, *Chem. Commun.* **2001**, 323−324 (Addendum: *Chem. Commun.* **2002**, 2278). [1b] L.-P. Lu, M.-L. Zhu, P. Yang, *Acta Crystallogr., Sect. C* **2004**, *60*, 18−20.

[2] [2a] K. R. Reddy, M. V. Rajasekharan, S. Padhye, F. Dahan, J. P. Tuchagues, *Inorg. Chem.* **1994**, *33*, 428−433. [2b] K. R. Reddy, M. V. Rajasekharan, N. Arulsamy, D. J. Hodgson, *Inorg. Chem.* **1996**, *35*, 2283−2286. [2c] K. Wieghardt, *Angew. Chem. Int. Ed. Engl.* **1994**, *33*, 725−728.

[3] [3a] A. K. Bhattyacharya, A. B. Mondal, R. Banerjee, *J. Chem. Soc., Dalton Trans.* **1997**, 2351−2355. [3b] B. Mondal, S. Kundu, R. Banerjee, *J. Chem. Soc., Dalton Trans.* **1997**, 4341−4344. [3c] S. Banerjee, U. Roy Choudhury, R. Banerjee, S. Mukhopadhyay, *J. Chem. Soc., Dalton Trans.* **2002**, 2047−2052. [3d] B. Mondal, A. K. Bhattyacharya, R. Banerjee, *Polyhedron* **2000**, *19*, 1213−1218. [3e] D. Maji, P. K. Das, R. Banerjee, *Transition Met. Chem.* **2002**, *27*, 80−84. [3f] U. R. Choudhury, S. Banerjee, R. Banerjee, *Transition Met. Chem.* **2002**, *27*, 42−46. [3g] D. Maji, R. Banerjee, *Transition Met. Chem.* **2001**, *26*, 544−550. [3h] U. R. Choudhury, S. Banerjee, R. Banerjee, *J. Chem. Soc., Dalton Trans.* **2000**, 589−592.

[4] [4a] S. Mukhopadhyay, R. Banerjee, *Polyhedron* **1993**, 1−4. [4b] H. Kawaguchi, M. Matsuki, T. Ama, J. Yasui, *Bull. Chem. Soc., Jpn.* **1986**, *59*, 31−38. [4c] B. Chakravarty, I. Ghosh, U. K. Kar, *Indian J. Chem.* **1986**, *25A*, 725−728.

[5] R. G. Wilkins, *The Study of Kinetics and Mechanism of Reactions of Transistion Metal Complexes*, Allyn and Bacon, Boston, **1974**, chapter 1, p. 460.

[6] D. H. Macartney, A. McAuley, *Inorg. Chem.* **1983**, *22*, 2062−2066.

[7] M. R. Grace, T. W. Swaddle, *Inorg. Chem.* **1992**, *31*, 4674−4678.

[8] [8a] K. Lemma, A. M. Sargeson, L. I. Elding, *J. Chem. Soc., Dalton Trans.* **2000**, 1167−1172. [8b] T. Shi, J. Berglund, L. I. Elding, *Inorg. Chem.* **1996**, *35*, 3498−3503. [8c] J. Berglund, L. I. Elding, *Inorg. Chem.* **1995**, *34*, 513−519. [8d] S. Mukhopadhyay, R. Banerjee, *J. Chem. Soc., Dalton Trans.* **1994**, 1349−1353. [8e] P. Bandyopadhyay, B. B. Dhar, J. Bhattacharyya, S. Mukhopadhyay, *Eur. J. Inorg. Chem.* **2003**, 4308−4312.

[9] [9a] G. Bengtsson, S. Fronaeus, L. Bengtsson-Kloo, *J. Chem. Soc., Dalton Trans.* **2002**, 2548−2552. [9b] U. El-Ayaan, R. F. Jameson, W. Linert, *J. Chem. Soc., Dalton Trans.* **1998**, 1315−1319. [9c] B. Bansch, P. Martinez, J. Zuluaga, D. Uribe, R. van Eldik, *Inorg. Chem.* **1991**, *30*, 4555−4559. [9d] R. Banerjee, R. Das, A. K. Chakraborty, *J. Chem. Soc., Dalton Trans.* **1991**, 987−992. [9e] D. H. Macartney, N. Sutin, *Inorg. Chem.* **1985**, *24*, 3403−3409. [9f] C. Dulz, N. Sutin, *J. Am. Chem. Soc.* **1964**, *86*, 829−832. [9g] E. Mentasti, E. Pelizzetti,

 © 2004 Wiley-VCH Verlag GmbH & Co. KGaA, Weinheim

C. Baiocchi, *J. Chem. Soc., Perkin Trans. 2* **1976**, 1841−1845. [9h] R. N. Mehrotra, *J. Chem. Soc., Dalton Trans.* **1981**, 897−901. [9i] G. Davies, B. Warnqvist, *Coord. Chem. Rev.* **1970**, *5*, 349−378. [9j] L. E. Bennett, J. C. Sheppard, *J. Phys. Chem.* **1962**, *66*, 1275−1279.
[10] V. Alexeyev, *Quantitative Analysis*, 2nd ed., MIR Publishers: Moscow, **1985**, p. 365.
[11] A. I. Vogel, *Vogel's Textbook of Quantitative Chemical Analysis*, 5th ed., ELBS and Longman, London, **1989**, p. 690−691.
[12] J. F. Below Jr., R. E. Connick, C. P. Coppel, *J. Am. Chem. Soc.* **1958**, *80*, 2961− 2967.
[13] K. W. Hicks, J. R. Sutter, *J. Phys. Chem.* **1971**, *75*, 1107−1113.
[14] [14a] B. Rathke, *Ber.* **1879**, *12*, 774. [14b] P. Ray, *Chem. Rev.* **1961**, *61*, 314−359. [14c] R. Banerjee, K. Das, A. Das, S. Dasgupta, *Inorg. Chem.* **1989**, *28*, 585−588.

Received December 2, 2003
Early View Article
Published Online May 13, 2004

 © 2004 Wiley-VCH Verlag GmbH & Co. KGaA, Weinheim

Covalent Bonding of Phosphonates of L-Proline and L-Cysteine to γ-Zirconium Phosphate

Kunlin Huang,[a] Jihong Yu,*[a] Guangmei Wang,[a] Yi Li,[a] and Ruren Xu*[a]

Keywords: Amino acids / Chirality / Phosphates / Phosphonates / Zirconium

This paper describes the synthesis and characterization of γ-zirconium phosphate-phosphonates based on chiral *N*-phosphonomethyl-L-proline [(–)-$HO_3PCH_2NHC_4H_7CO_2H$; H_3PMP] from L-proline, and *N*-phosphonomethyl-1,3-thiazolidine-4-carboxylic acid [(–)-$HO_3PCH_2NHCH_2SC_2H_3CO_2H$; H_3PMTA] from L-cysteine. Two compounds formulated as $[Zr(PO_4)(H_2PO_4)_{0.53}(H_2PMP)_{0.47}\cdot 2.0H_2O]$ [γ-ZrPMP (**1**)] and $[Zr(PO_4)(H_2PO_4)_{0.50}(H_2PMT)_{0.50}\cdot 1.6H_2O]$ [γ-ZrPMT (**2**)] were obtained by topotactic reaction of H_3PMP and H_3PMTA, respectively, with γ-ZrP in the presence of water/acetone. They possess intercalation capabilities and optical activities.

(© Wiley-VCH Verlag GmbH & Co. KGaA, 69451 Weinheim, Germany, 2004)

Introduction

Recently, there has been tremendous interest in the design and synthesis of chiral solids for their important applications in enantioseparation and asymmetric catalysis.[1] The chirality of these compounds mostly results from chiral organic groups,[2] therefore one strategy for obtaining solid materials with optical activity is to incorporate optically active organic moieties into the organic-inorganic hybrid frameworks.[1–3]

Zirconium phosphate (ZrP) derivatives incorporating organic functional groups are very promising materials.[4] The layered structure of ZrP provides a template surface where organic structures of virtually any nature can be chemically deposited in an orderly and predictable manner. Among the different zirconium phosphates, the high rigidity of the lamellae of γ-zirconium phosphate $[Zr(PO_4)(H_2PO_4)\cdot 2H_2O]$ allow the preparation of stable hybrid materials by topotactic exchange of dihydrogenphosphates with mono- or diphosphonic acids.[5] Their replacement may be total or partial, depending on the amount and steric volume of the phosphonate used in the topotactic exchange. Many functional groups, such as biphenylphosphonate,[6] poly(ethylene oxide) chains[7] and C_{60},[8] have been integrated into the frameworks. We therefore aimed to prepare functionalized layered γ-zirconium phosphate-phosphonates anchored with chiral groups.

Proline and its analogs or homologs are very important chiral sources that have wide applications, for instance in stereoselective synthesis,[2,9] enantioseparation[10] and biochemistry.[11] Phosphonic acid derivatives of proline are analogs of amino acids with biological activities.[12] Herein we wish to report the synthesis of functionalized γ-zirconium phosphate-phosphonates based on chiral *N*-phosphonomethyl-L-proline (H_3PMP), formed from L-proline, and *N*-phosphonomethyl-1,3-thiazolidine-4-carboxylic acid (H_3PMTA), formed from L-cysteine. The optical activity and intercalation properties are also discussed.

Results and Discussion

Preparation and Characterization of H_3PMP, H_3PMTA, γ-ZrPMP and γ-ZrPMT

The preparation of these compounds is outlined in Scheme 1. This method, which is based on a literature technique,[13] gave H_3PMP and H_3PMTA from the corresponding amino acids in a Mannich-type reaction in yields of 96% and 85%, respectively. γ-ZrP was prepared according to the reported procedure.[14] The specific rotations $[\alpha]_D$ of H_3PMP and H_3PMTA are −63 and −105, respectively, in aqueous solution 25 °C.

Highly crystalline $[Zr(PO_4)(H_2PO_4)_{0.53}(H_2PMP)_{0.47}\cdot 2.0H_2O]$ [γ-ZrPMP (**1**)] and $[Zr(PO_4)(H_2PO_4)_{0.50}(H_2PMT)_{0.50}\cdot 1.6H_2O]$ [γ-ZrPMT(**2**)] were prepared by treatment of H_3PMP or H_3PMTA with γ-ZrP in water/acetone (1:1, v/v) at 80 °C for 14 d, with a phosphonic acid to γ-ZrP ratio of 1. Their $[\alpha]_D$ values in HF/H_2O solution of are −16 and −21, respectively, at 25 °C.

The X-ray powder diffraction patterns of **1** and **2**, as shown in Figure 1b and c, are characteristic of layered structures[4] with a *d*-spacing of 14.2 Å and 14.1 Å, respectively.

[a] State Key Laboratory of Inorganic Synthesis and Preparative Chemistry, College of Chemistry, Jilin University
Changchun 130023, P. R. China
Fax: (internat.) + 86-0431-5168609
E-mail: rrxu@mail.jlu.edu.cn
jihong@mail.jlu.edu.cn

 © 2004 Wiley-VCH Verlag GmbH & Co. KGaA, Weinheim **DOI: 10.1002/ejic.200300906**

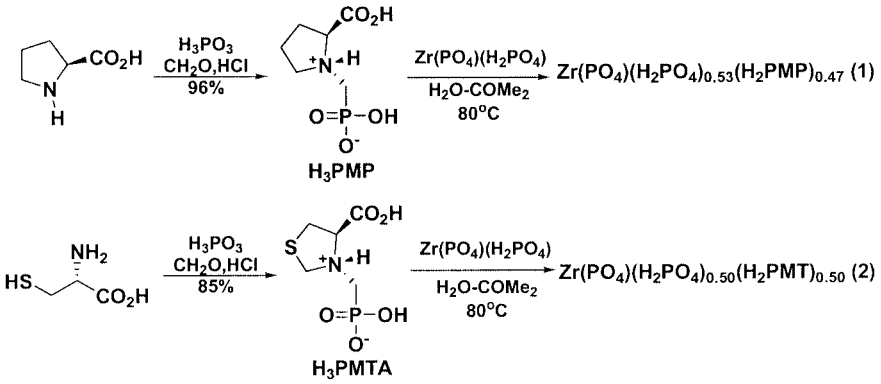

Scheme 1

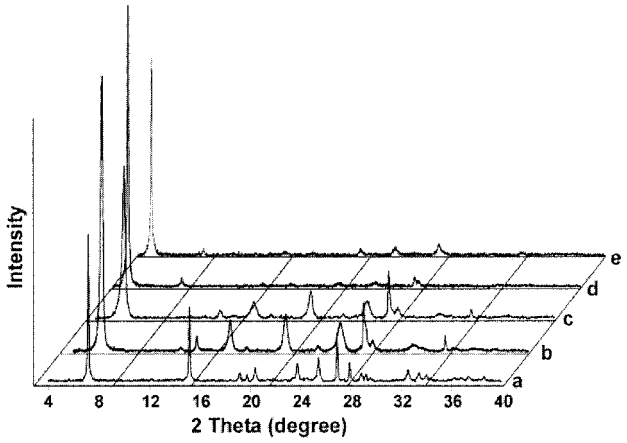

Figure 1. X-ray power diffraction patterns of: (a) γ-ZrP (*d*-spacing 12.2 Å), (b) γ-ZrPMP (**1**) (*d*-spacing 14.2 Å), (c) γ-ZrPMT (**2**) (*d*-spacing 14.1 Å), (d) **3** (*d*-spacing 21.65 Å) and (e) **4** (*d*-spacing 20.94 Å)

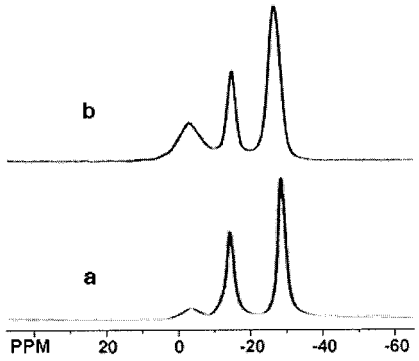

Figure 2. ^{31}P MAS NMR spectra of: (a) γ-ZrPMP (**1**) and (b) γ-ZrPMT (**2**) (δ = −28.8 ppm for PO_4^{3-}, −15.5 ppm for $H_2PO_4^-$, and −5.4 ppm for R-PO_3H^-)

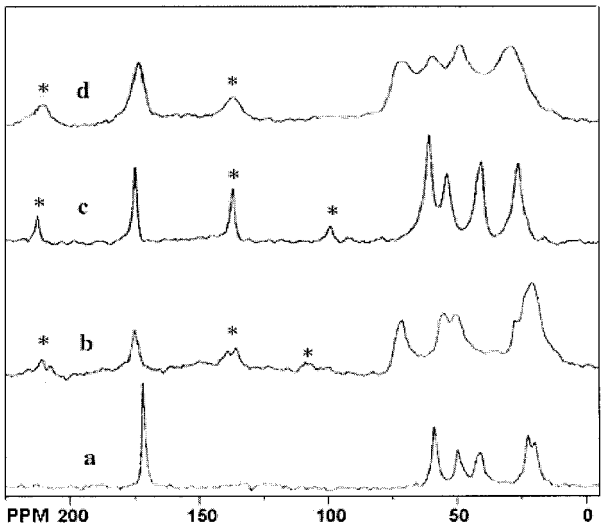

Figure 3. ^{13}C CP/MAS NMR spectra of: (a) H_3PMP, (b) γ-ZrPMP (**1**), (c) H_3PMTA, and (d) γ-ZrPMT (**2**) (asterisks denote spinning sidebands)

As shown in Figure 2, the ^{31}P solid-state MAS NMR spectra of **1** and **2** are similar: each shows three main resonances, one at δ = −28.8 ppm for PO_4^{3-}, one at δ = −15.5 ppm attributed to $H_2PO_4^-$ and one at δ = −5.4 ppm due to the phosphonate phosphorus atom. The ^{31}P MAS NMR spectra of **1** and **2** are similar to that observed for $[Zr(PO_4)(H_2PO_4)_{0.49}(C_6H_5PO_3H)_{0.51}]$.[15] Analyses on the basis of solid-state ^{31}P MAS NMR and high-resolution ^{31}P NMR spectroscopy give $H_2PO_4^-$ to R-PO_3H^- ratios of 1.13 and 1.01 for **1** and **2**, respectively.

The ^{13}C MAS NMR spectra of **1** and **2** indicate that COOH groups (δ = 173 ppm) exist inside the layers (Figure 3b and d). In the FT-IR spectra of **1** and **2**, the absorption at 1730 cm^{-1} is attributed to COOH (Figure 4d and e). The IR and Raman spectra are in good agreement with the ^{13}C MAS NMR spectra.

On the basis of X-ray diffraction data, inductively coupled plasma (ICP), elemental analysis, TGA data and the ^{31}P NMR spectra, **1** and **2** are formulated as (*S*)-$[Zr(PO_4)(H_2PO_4)_{0.53}(HO_3PCH_2NC_4H_7COOH)_{0.47}\cdot 2.0H_2O]$ (**1**; mol. wt. = 371.39) and (*R*)-$[Zr(PO_4)(H_2PO_4)_{0.50}(HO_3PCH_2NCH_2SC_2H_3COOH)_{0.50}\cdot 1.6H_2O]$ (**2**; mol. wt. = 376.52). The BET surface areas of **1** and **2** are 14 and 12 $m^2\cdot g^{-1}$, respectively. Such small surface areas indicate that organic groups are closely packed in the interlayer spaces of **1** and **2**.

 © 2004 Wiley-VCH Verlag GmbH & Co. KGaA, Weinheim

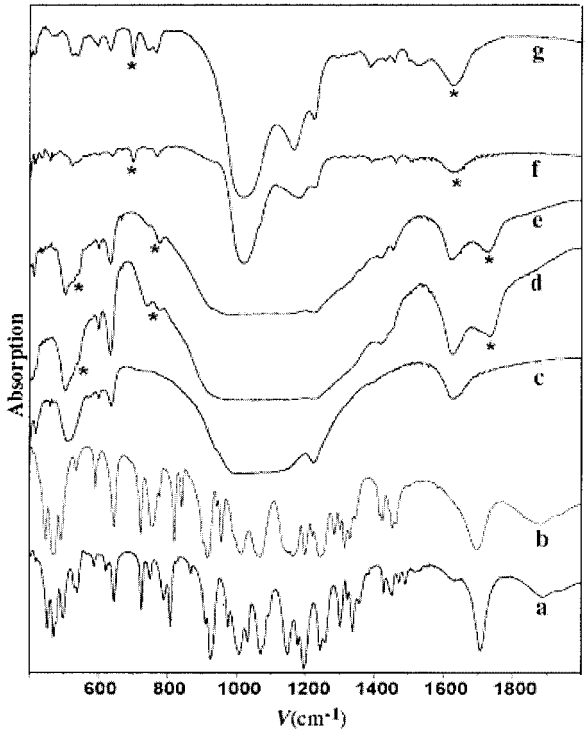

Figure 4. FT-IR spectra of: (a) H_3PMP, (b) H_3PMTA, (c) γ-ZrP, (d) γ-ZrPMP (**1**), (e) γ-ZrPMT (**2**), (f) **3** and (g) **4**; the bands at 1710 and 1730 cm^{-1} are attributed to CO_2H (a−e), and those at 1635 cm^{-1} to $-CO_2^-$ and 701 cm^{-1} to $C_6H_5CH(CH_3)NH_2$ (f and g)

Based on the above experimental data and the structure of γ-ZrP, a schematic representation of the proposed structural character of **2** is shown in Figure 5 (**1** is similar to **2**). In **2**, the nitrogen atoms are protonated by $H_2PO_4^-$ groups. These results are supported by the ^{13}C MAS NMR and IR spectra of **2** (Figures 3 and 4).

Molecule modeling of **2** is carried out based on γ-zirconium phosphate. Figure 6 shows the simulated structure model of **2**. This model shows that the heterocycles are closely packed, in good agreement with small BET surface areas.

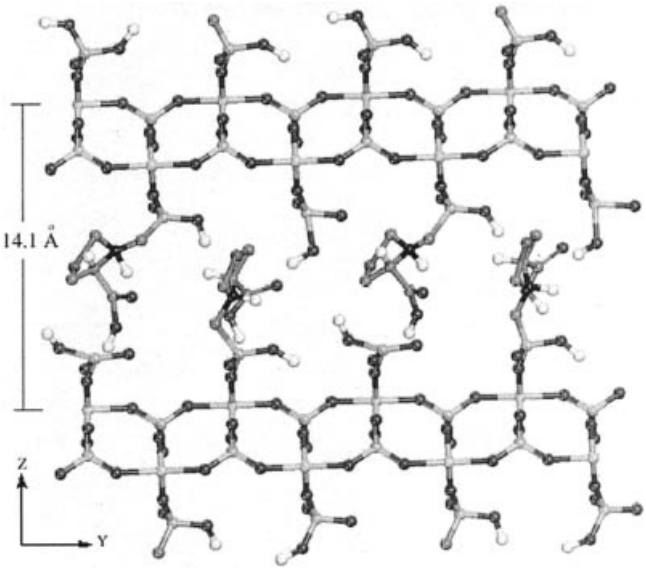

Figure 6. Simulated structural model of γ-ZrPMT (**2**) on the basis of γ-ZrP

Intercalation Capability and Optical Activity of γ-ZrPMP (1) and γ-ZrPMT (2)

A racemic mixture of 1-phenylethylamine [$C_6H_5CH(CH_3)NH_2$] (PEA) was used for the intercalation studies. The compounds $[Zr(PO_4)(H_2PO_4)_{0.53}(HO_3PCH_2NC_4H_7COOH)_{0.47}\cdot 0.56C_6H_5CH(CH_3)NH_2\cdot 0.75H_2O]$ (**3**) and $[Zr(PO_4)(H_2PO_4)_{0.50}(HO_3PCH_2NCH_2SC_2H_3COOH)_{0.50}\cdot 0.51C_6H_5CH(CH_3)NH_2\cdot 0.90H_2O]$ (**4**) were prepared from **1** and **2**, respectively, upon intercalation of PEA in ethanol solution at 55 °C for 24 h and 35 °C for 48 h, respectively. The *d*-spacings of intercalated **3** and **4** are 21.65Å and 20.94 Å, respectively (Figure 1d and e). In the IR spectra of **3** and **4**, the peaks at 1457, 1383 and 701 cm^{-1} are new and the

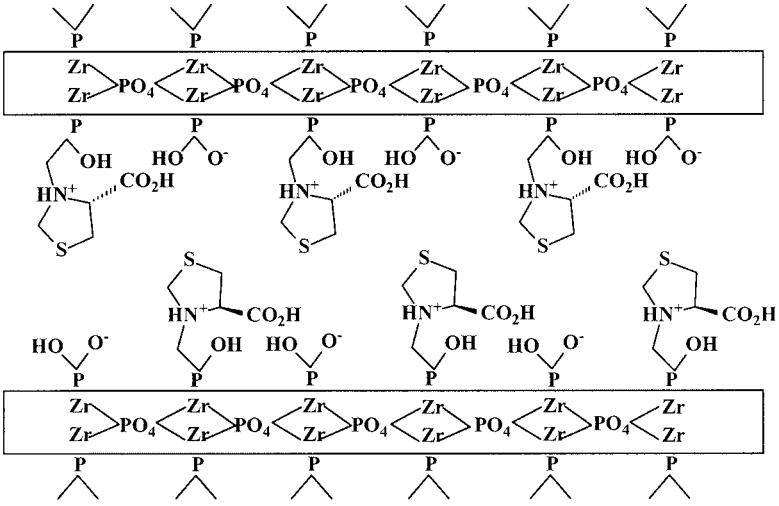

Figure 5. Schematic representation of the interlayer arrangement of γ-ZrPMT (**2**)

 © 2004 Wiley-VCH Verlag GmbH & Co. KGaA, Weinheim

peaks at 1730 cm^{-1} disappear. (Figure 4f and g), which suggests that PEA exists inside the layers.[16]

Deintercalation was achieved by suspending **3** or **4** in 0.5 M HCl at 55 °C. The $[\alpha]_D^{25}$ values of deintercalated **3** and **4** are −15.6 and −21.2 (c = 1.3 in aqueous HF solution; pH ≈ 1.0), respectively. Compared to the $[\alpha]_D^{25}$ values of −16 for **1** and −21 for **2**, these results show that no racemization occurs during the whole experimental process.

Optical measurements show that the mother liquor obtained after the intercalation or deintercalation has no optical activity, which suggests that neither enantiomer is preferred under the above intercalation condition. In-depth studies of enantioseparation need appropriate guests and special techniques, such as high-performance liquid chromatography (HPLC).[3a,17]

Conclusion

In summary, two new compounds, formulated as $[Zr(PO_4)(H_2PO_4)_{0.53}(HO_3PCH_2NC_4H_7COOH)_{0.47}\cdot 2.0H_2O]$ (**1**) and $[Zr(PO_4)(H_2PO_4)_{0.50}(HO_3PCH_2NCH_2SC_2H_3COOH)_{0.50}\cdot 1.6H_2O]$ (**2**) were obtained. The host materials possess intercalation-deintercalation properties and optical activity.

Experimental Section

Materials and Methods: L-Proline, L-cysteine and 1-phenylethylamine $[C_6H_5CH(CH_3)NH_2]$ (PEA) were purchased from Acros, and used as received; PEA was racemic. The content of zirconium and phosphorus was analyzed with a Perkin−Elmer 3300 DV ICP analyzer, and C, H and N by a Perkin−Elmer 2400 analyzer. The IR spectra were recorded as KBr pellets with a Nicolet Impact 410 FT IR spectrometer. X-ray powder diffraction data were collected with a Siemens D5005 diffractometer with Cu-K_α radiation (λ = 1.54178 Å), a 0.03° 2θ-step size, and a 1-s counting time in the 3−40° 2θ range. Thermogravimetric analysis was performed with a NETZSCH STA 449C thermoanalyzer under a 20 mL min^{-1} air flow with a heating rate of 10 °C·min^{-1}. ^{13}C and ^{31}P MAS NMR spectra were recorded with a Bruker-MSL 400 MHz spectrometer. Solution ^{31}P NMR spectra were recorded with an AVANCE 500 spectrometer. BET was carried out under an N_2 flow with a Micro ASAP 2010 M at 77 K. Specific rotation was measured with a WWW-1S digital spectrometer. Solid **1** or **2** was dissolved in about 1.0 mL of HF (40% in water), and deionized water was added up to 50.0 mL. The path length was 20 cm.

Preparation of H_3PMP: This compound was obtained using our modified method based on a literature procedure.[13] CH_2O (40 mmol, 36% in water) was added dropwise to a mixture of L-proline (10 mmol), H_3PO_3 (11 mmol) and HCl (30 mL of a 6.0 M aqueous solution) under reflux. The resultant solution was then heated at reflux for a further 12 h. A white solid with a yield of 96% was recovered after removal of water, and recrystallized from an EtOH/propylene oxide (2:1, v/v) mixture. M.p. 257−259 °C. $C_6H_{12}NO_5P$ (209.14): calcd. C 34.44, N 6.69, H 5.74; found C 34.25, N 6.80, H 5.67. $[\alpha]_D^{25}$ = −63 (c = 1.6, in water). ^{31}P MAS NMR (161.9 MHz, 298 K): δ = 8.7 ppm.

Preparation of H_3PMTA: A mixture of L-cysteine (10 mmol), CH_2O (11 mmol, 36% in water) and HCl (10 mL of a 1.0 M aqueous solution) was allowed to stand at room temperature for 24 h. HCl (10 mL of a 6.0 M aqueous solution) and H_3PO_3 (11 mmol) were then added. CH_2O (40 mmol, 36% in water) was added dropwise to the resultant mixture at reflux over 5 min. The solution was then heated at reflux for a further 5 min. The product (yield: 85%) was recovered by removing the water. M.p. 198−200 °C. $C_5H_{10}NO_5PS$ (227.17): calcd. C 26.44, H 4.44, N 6.17, S 14.11; found C 26.49, H 4.62, N 6.01, S 13.95. $[\alpha]_D^{25}$ = −105 (c = 1.0, in water). ^1H NMR (D_2O + K_2CO_3, 500 MHz, 298 K): δ = 2.23−2.48 (m, 2 H), 3.02−3.20 (m, 2 H), 4.01 (d, $J_{H,H}$ = 6.50 Hz, 1 H), 4.12 (d, $J_{H,H}$ = 9.5 Hz, 1 H), 4.32 (d, J = 9.5 Hz, 1 H) ppm. ^{13}C NMR (D_2O + K_2CO_3, 125.8 MHz, 298 K): δ = 31.9, 53.1 (d, $J_{C,P}$ = 147.7 Hz), 60.3, 76.1, 178.9 ppm. ^{31}P NMR (D_2O, 202.4 MHz, 298 K): δ = 7.7 ppm (t, $J_{H,P}$ = 12.1 Hz). MS: calcd. 228.12 $[M + H]^+$; found 228.14.

Preparation of γ-ZrPMP (1): H_3PMP (0.17 g) and γ-ZrP (0.25 g) were added to a distilled water/acetone solution (1:1, v/v; 35 mL). The resultant solution was kept at 80 °C in a Teflon-lined container in an oil bath for 14 d. A white crystalline solid was recovered after washing with water and drying at room temperature. $Zr(PO_4)(H_2PO_4)_{0.53}(HO_3PCH_2NC_4H_7COOH)_{0.47}\cdot 2H_2O$ (371.39): calcd. C 9.11, H 2.75, N 1.77, P 16.69, Zr 24.56; found C 9.23, H 2.55, N 1.72, P 16.32, Zr 24.17. $[\alpha]_D^{25}$ = −16 (c = 1.2 in HF aqueous solution, pH = 1.5).

Preparation of γ-ZrPMT (2): The experimental procedure for the preparation of **2** was similar to that of **1**, but with H_3PMTA (0.19 g) instead of H_3PMP. $Zr(PO_4)(H_2PO_4)_{0.50}(HO_3PCH_2NCH_2SC_2H_3COOH)_{0.50}\cdot 1.6H_2O$ (376.52): calcd. C 7.97, H 2.31, N 1.86, P 16.47, S 4.25, Zr 24.23; found C 7.89, H 2.40, N 1.78, P 16.19, S 4.40, Zr 24.09. $[\alpha]_D^{25}$ = −21 (c = 1.4 in HF aqueous solution, pH = 1.5)

Intercalation and Deintercalation Studies with γ-ZrPMP (1). Formation of γ-ZrPMP·0.56$C_6H_5CH(CH_3)NH_2$ (3): Compound **1** (100 mg, 0.27 mmol) was intercalated with 1-phenylethylamine (0.14 mL, 1.08 mmol, c = 0.108 mol·L^{-1}) in ethanol solution (10 mL) at 55 °C for 24 h. Compound **3** (91 mg) was recovered by centrifugal separation, and dried at room temperature for 24 h. $Zr(PO_4)(H_2PO_4)_{0.53}(HO_3PCH_2NC_4H_7COOH)_{0.47}\cdot 0.56C_6H_5CH(CH_3)NH_2\cdot 0.75H_2O$ (416.88): calcd. C 21.01, H 3.33, N 3.46, P 14.87, Zr 21.88; found C 21.42, H 2.98, N 3.16, P, 15.03, Zr 22.41. Deintercalation was achieved by suspending **3** in 0.5 M HCl at 55 °C for 2 h. $[\alpha]_D^{25}$ = −15.6 (c = 1.3 in HF aqueous solution, pH ≈ 1.0).

Intercalation and Deintercalation Studies with γ-ZrPMT (2). Formation of γ-ZrPMT·0.51$C_6H_5CH(CH_3)NH_2$ (4): Compound **2** (102 mg, 0.27 mmol) was intercalated with PEA (0.14 mL, 1.08 mmol, c = 0.108 mol·L^{-1}) in ethanol solution (10 mL) at 35 °C for 48 h. Compound **4** (88 mg) was recovered by centrifugal separation, and dried at room temperature for 24 h. $Zr(PO_4)(H_2PO_4)_{0.50}(HO_3PCH_2NCH_2SC_2H_3COOH)_{0.50}\cdot 0.51C_6H_5CH(CH_3)NH_2\cdot 0.90H_2O$ (425.59): calcd. C 19.96, H 3.03, N 3.32, P 14.57, S 3.76, Zr 21.43; found C 20.21, H 2.80, N 3.11, P 14.91, S 3.32, Zr 21.31. Deintercalation was achieved by suspending **4** in 0.5 M HCl at 55 °C for 2 h. $[\alpha]_D^{25}$ = −21.2 (c = 1.3 in HF aqueous solution, pH ≈ 1.0).

Molecular Modeling: Computer modeling procedures were employed for the structure study. Using the Cerius² program,[18] a supercell was created including four cells of γ-ZrP (a = 5.3825, b = 26.5348, c = 12.4102 Å), and then 50% of $H_2PO_4^-$ was replaced

 © 2004 Wiley-VCH Verlag GmbH & Co. KGaA, Weinheim

by H_2PMTA. The H_2O molecules were not taken into account in the modeling procedures. The lattice parameters *a* and *b* of the supercell were fixed, and *c* was changed to 14.1 Å on the basis of X-ray powder diffraction analysis. After fixing the inorganic matrix, the organic moieties were optimized to achieve the minimum geometry using the Universal Forcefield[18] supplied as part of the Cerius^2 program package.

Acknowledgments

This work was supported by the National Natural Science Foundation of China and the State Basic Research Project of China (G2000077507). The help of Ms. Caijin Li, Ms. Lu Tao, Mr. Yongchun Zhou (^{31}P and ^{13}C MAS NMR), Chunyu Wang (solution ^{31}P NMR), Hong Ding and Weijie Jin is greatly acknowledged.

[1] [1a] S. Xiang, Y. Zhang, Q. Xin, C. Li, *Angew. Chem. Int. Ed.* **2002**, *41*, 821−824. [1b] R. Xiong, X. You, B. F. Abrahams, Z. Xue, C. Che, *Angew. Chem. Int. Ed.* **2001**, *40*, 4423−4425.
[2] [2a] K. Soal, S. Niwa, *Chem. Rev.* **1992**, *92*, 833−856. [2b] L. Pu, H.-B. Yu, *Chem. Rev.* **2001**, *101*, 757−824.
[3] [3a] O. R. Evans, H. L. Ngo, W. Lin, *J. Am. Chem. Soc.* **2001**, *123*, 10395−10396. [3b] U. Costantino, M. Nocchetti, F. Marmottini, R. Vivani, *Eur. J. Inorg. Chem.* **1998**, 1447−1452.
[4] [4a] G. Alberti, in *Comprehensive Supramolecular Chemistry*, vol. 7 (Ed.: J. M. Lehn), Pergamon, **1996**, chapt. 5. [4b] A. Clearfield, in *Progress in Inorganic Chemistry*, vol. 47 (Ed.: K. D. Karlin), Wiley, **1998**, pp. 371−510. [4c]A. Clearfield, Z. Wang, *J. Chem. Soc., Dalton Trans.* **2002**, 2937−2947.
[5] [5a] G. Alberti, E. Giontella, S. Murcia-Mascarós, *Inorg. Chem.* **1997**, *36*, 2844−2849. [5b] G. Alberti, R. Vivani, S. Murcia-Mascarós, *J. Mol. Struct.* **1998**, *470*, 81−92.
[6] G. Alberti, F. Marmottini, S. Murcia-Mascarós, R. Vivani, *Angew. Chem. Int. Ed. Engl.* **1994**, *33*, 1594−1597.
[7] G. Alberti, E. Brunet, C. Dionigi, O. Juanes, M. J. Mata, J. C. Rodríguez-Ubis, R. Vivani, *Angew. Chem. Int. Ed.* **1999**, *38*, 3351−3353.
[8] E. Brunet, M. Alonso, M. J. Mata, S. Fernández, O. Juanes, O. Chavanes, J.-C. Rodríguez-Ubis, *Chem. Mater.* **2003**, *15*, 1232−1234.
[9] [9a] B. M. Trost, V. S. C. Yeh, *Angew. Chem. Int. Ed.* **2002**, *41*, 861−863. [9b] B. List, *J. Am. Chem. Soc.* **2002**, *124*, 5656−5657.
[10] [10a] T. Fukuhara, S. Yuasa, *J. Chromatogr. Sci.* **1990**, *28*, 114−117. [10b] R. Herráez-Hernández, P. Campíns-Falcó, L. A. Tortajada-Genaro, *Analyst* **1998**, *123*, 2131−2137.
[11] [11a] R. Zhang, F. Brownewell, J. S. Madalengoitia, *J. Am. Chem. Soc.* **1998**, *120*, 3894−3902. [11b] R. Zhang, J. S. Madalengoitia, *J. Org. Chem.* **1999**, *64*, 330−331.
[12] U. Groth, L. Richter, U. Schollkopf, *Tetrahedron* **1992**, *48*, 117−122.
[13] A. Turner, P. Jafrès, E. J. MacLean, D. Villemin, V. Mckee, G. B. Hix, *Dalton Trans.* **2003**, 1314−1319.
[14] D. M. Poojary, B. Shepeizer, A. Clearfield, *J. Chem. Soc., Dalton Trans.* **1995**, 111−113.
[15] N. J. Clayden, *J. Chem. Soc., Dalton Trans.* **1987**, 1877−1881.
[16] R. A. Condrate, K. Nakamoto, *J. Chem. Phys.* **1965**, *42*, 2590−2598.
[17] M. E. Garcia, J. L. Naffn, N. Deng, T. E. Mallouk, *Chem. Mater.* **1995**, *7*, 1968−1973.
[18] *Cerius^2 Program Package*, Molecular Simulations, Inc., San Diego, CA, **1997**.

Received December 7, 2003
Early View Article
Published Online May 5, 2004

 © 2004 Wiley-VCH Verlag GmbH & Co. KGaA, Weinheim

Tris(trimethylsilyl)-Substituted Heavy Group 14-Element-Centered Anions: Unsolvated Trimeric Germyllithium and Solvated Dimeric Silyl- and Stannyllithiums

Masato Nanjo,*[a] Emi Nanjo,[a] and Kunio Mochida*[a]

Keywords: Germanium / Lithium / Silicon / Solid-state structures / Tin

Tris(trimethylsilyl)-substituted group 14-element-centered anion monomers [LiE($SiMe_3$)$_3$·3THF] (E = Si, Ge, and Sn) can be distilled under reduced pressure to give dimeric silyllithium **4** and stannyllithium **6**, and trimeric germyllithium **5** without pyrolysis products such as dilithiometallanes. The molecular structures of **4**, **5**, and **6** were unequivocally determined by X-ray diffraction. Dimer **4** has a symmetrical bent four-membered-ring structure consisting of two anionic silicon atoms and two cationic lithium atoms with coordinated THF molecules. Dimer **6** has an unsymmetrical distorted four-membered-ring structure consisting of two anionic tin atoms, a bridged unsolvated lithium atom, and a bridged lithium atom solvated by a THF molecule. Interestingly, **6** aggregates to form dimers of dimers by an intermolecular CH_3···Li interaction. Trimeric germyllithium **5** forms an equilateral triangular lithium cluster without solvation. Compound **5** has a crystallographic threefold axis with three anionic germanium atoms and three cationic lithium atoms lying in the same plane. The lithium atoms in **5** are stabilized by an intramolecular CH_3···Li interaction.
(© Wiley-VCH Verlag GmbH & Co. KGaA, 69451 Weinheim, Germany, 2004)

Introduction

Heavy group 14-element-centered anionic species, especially the lithium derivatives, are useful in some applications not only in organic synthesis but also in organometallic chemistry.[1] Despite the large number of reports on syntheses of silyl,[2] germyl,[3] and stannyl[4] anions, much less attention has been paid to their structural studies, which are of special interest for comparing with those of organolithium compounds.[5] Tris(trimethylsilyl)silyllithium (**1**), whose synthesis was first reported by Gilman and Smith in 1967[6] and then modified by Brook in 1982,[7] has been well studied from the viewpoint of its molecular structure,[8] NMR spectroscopic behavior,[9] and its application to the synthesis of the first stable silene species,[10] polysilane dendrimers,[11] and transition metal complexes.[12] Interestingly, thermolysis of **1** leads to the formation of bis(trimethylsilyl)dilithiosilane, which was trapped by [D_1]-ethanol and iodomethane to give the corresponding dideuteriosilane and dimethylsilane, respectively.[13] The structural studies on bis(trimethylsilyl)dilithiosilane were performed by mass spectrometry, suggesting that it forms both monomers and dimers, as determined by the molecular-ion peaks. Recently, the crystal structures of dilithiosilanes were revealed by X-ray diffraction method by using more bulky substituents at the anionic silicon center.[14]

Despite the large number of reports on silyllithium compounds, far less attention has been devoted to their germanium and tin analogues. Tris(trimethylsilyl)germyllithium (**2**) was first prepared by Brook et al. in 1986,[15a] and tris(trimethylsilyl)stannyllithium (**3**) by Preuss et al. in 1992.[16a] However, the solvent-separated ion pair [(Me_3Si)$_3$Ge][Li·[12]crown-4)$_2$][15b] and the monomeric solvated germyllithiums[15c] have only recently been reported by Stalke et al. More recently still, the solvated monomeric structure of the stannyllithium **3**·3THF has been published.[16b] However, the systematic study of lithium derivatives of the heavy group 14-elements is even more scarce. In the course of the thermolyses of [LiE($SiMe_3$)$_3$·3THF] (E = Si, Ge, Sn), we found the formation of aggregated structures of heavy group 14-element-centered anionic species, which include a rare trimeric structure of unsolvated germyllithium **5** and an unsymmetrical dimer of stannyllithium **6**. We report herein the structural study of **5** and **6** together with that of a solvated dimer of silyllithium **4**.

Results and Discussion

Synthesis of [LiE(Me_3Si)$_3$·3THF] (E = Si, Ge, and Sn)

[LiSi($SiMe_3$)$_3$·3THF] (**1**), was synthesized by a published procedure,[7] and was purified by recrystallization from *n*-pentane at −20 °C to give colorless crystals. Similarly,

[a] Department of Chemistry, Faculty of Science, Gakushuin University,
Mejiro, Toshima-ku, Tokyo 171-8588, Japan
Fax: +81-3-5992-1029
E-mail: kunio.mochida@gakushuin.ac.jp
masato.nanjo@gakushuin.ac.jp

$[LiGe(SiMe_3)_3 \cdot 3THF]$ (**2**)[15a] and $[LiSn(SiMe_3)_3 \cdot 3THF]$ (**3**)[16a] were also obtained as colorless crystals. The characterization of **1**−**3** was performed by ^1H, ^{13}C, ^{29}Si, and ^7Li NMR spectroscopy.

Tris(trimethylsilyl)silyllithium

The pyrolysis of **1** in an inert atmosphere at 140−150 °C leads to the formation of dilithiosilane $Li_2Si(SiMe_3)_2$ together with $(Me_3Si)_2$, $Si(SiMe_3)_4$, and $[Si(SiMe_3)_3]_2$, as reported by Lagow et al. in 1990.[13] We also examined the thermolysis of **1** under reduced pressure. Crystals of **1** were placed in a reaction vessel attached to vacuum line and heated slowly under reduced pressure (0.01 Torr). The crystals began to melt at 85 °C, and they completely melted at 100 °C. Bubbles from the interior of the liquid were observed. When the oil bath was heated to 150 °C, the oil of **1** boiled and we were able to obtain colorless crystals by distillation in vacuo. No pyrolysis products such as dilithiosilane, disilane, or tetrakis(trimethylsilyl)silane were detected in the ^1H NMR spectra. One THF molecule is coordinated to each $LiSi(SiMe_3)_3$ unit, as determined by ^1H NMR spectroscopy. The ^{29}Si NMR resonance of the central anionic silicon is observed at $\delta = -183.9$ ppm as a broad signal; this value is intermediate between the value of $\delta = -189.4$ ppm[8b] for monomeric silyllithium **1** and $\delta = -181.7$ ppm[9] for the unsolvated dimer $[(Me_3Si)_3Si(\mu\text{-}Li)]_2$.

The resulting crystals were recrystallized from *n*-hexane to give colorless single crystals. The distilled silyllithium was characterized by X-ray diffraction, and the molecular structure of $[(Me_3Si)_3Si(\mu\text{-}Li\cdot THF)]_2$ (**4**) is shown in Figure 1. The structural parameters are listed in Table 1. The silyllithium **4** is dimeric in the solid state, although the structure is different from that of the unsolvated dimer $[(Me_3Si)_3Si(\mu\text{-}Li)]_2$.[8d] Two lithium atoms bridge two anionic silicon atoms, and each lithium atom is coordinated by one THF molecule with an O(1)−Li(1) distance of 1.914(5) Å. The lithium-lithium distance is 2.695(9) Å. Up to now, six dimeric silyllithiums have been reported: $[(Me_3Si)_3Si(\mu\text{-}Li)]_2$,[8d] $[tBu_3Si(\mu\text{-}Li)]_2$,[17] $[(PhMe_2Si)_2MeSi(\mu\text{-}Li)]_2$,[18] $[(Me_3Si)_2PhSi(\mu\text{-}Li)]_2$,[18] $[(Me_3SiMe_2Si)_3Si(\mu\text{-}Li)]_2$,[19] and $[(tBuMe_2Si)_2HSi(\mu\text{-}Li\cdot THF)]_2$,[20] all of them containing planar four-membered rings consisting of two anionic silicon and two cationic lithium atoms. However, the silyllithium **4** possesses a folded four-membered ring. The sum of the angles of the tetragon is 354.6(4)° and the dihedral angle between the Li(1)−Si(1)−Li(1)* and Li(1)−Si(1)*−Li(1)* planes is 19°. Both the coordinated THF molecules lie on one side of the ring in order to avoid a steric repulsion of the bulky hypersilyl groups. The Li−O distance of 1.914(5) Å is somewhat shorter than that found in $[LiSi(SiMe_3)_3 \cdot 3THF]$ [1.94(1)−1.97(1) Å][8b][8c] and $[LiSi(SiMe_3)_3 \cdot DME]_2 \cdot (\mu\text{-}DME)$ [1.993(6)−2.003(5) Å].[8a] The Si−Si bond lengths of **4** [2.3406(9)−2.3509(9) Å] are normal. The angles around the anionic silicon atom are significantly contracted, the sum of the Si−Si−Si angles being only 307.68(9)°, a value that is closer to that in monomeric $[LiSi(SiMe_3)_3 \cdot 3THF]$ [307.9(3)°] than that in solvent-free dimeric $[LiSi(SiMe_3)_3]_2$ (322.5°).

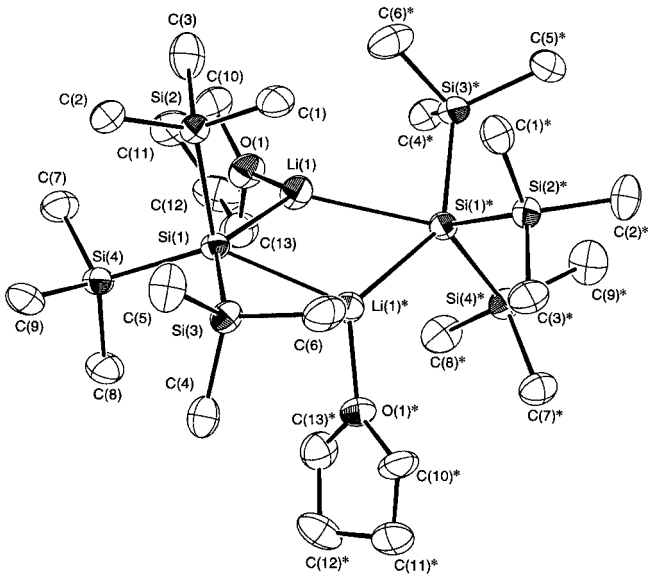

Figure 1. Molecular structure of **4** with 50% probability ellipsoids (H atoms omitted for clarity)

Table 1. Selected atomic distances (Å) and bond angles (°) for **4**; atoms labeled with * are symmetry-equivalent according to the operation $x, -y, -z + 1/2$

Si(1)−Si(4)	2.3406(9)
Si(1)−Si(3)	2.3464(9)
Si(1)−Si(2)	2.3509(9)
Si(1)−Li(1)	2.689(4)
Si(1)−Li(1)*	2.729(4)
O(1)−Li(1)	1.914(5)
Li(1)−Li(1)*	2.695(9)
Si(4)−Si(1)−Si(3)	102.84(3)
Si(4)−Si(1)−Si(2)	103.98(3)
Si(3)−Si(1)−Si(2)	100.86(3)
Si(4)−Si(1)−Li(1)	108.86(10)
Si(3)−Si(1)−Li(1)	141.29(10)
Si(2)−Si(1)−Li(1)	92.59(10)
Si(4)−Si(1)−Li(1)*	127.60(10)
Si(3)−Si(1)−Li(1)*	83.54(9)
Si(2)−Si(1)−Li(1)*	126.13(10)
Li(1)−Si(1)−Li(1)*	59.66(16)
O(1)−Li(1)−Si(1)	117.8(2)
O(1)−Li(1)−Si(1)*	119.14(19)
Si(1)−Li(1)−Si(1)*	117.64(15)

Tris(trimethylsilyl)germyllithium

Colorless crystals of $[LiGe(SiMe_3)_3 \cdot 3THF]$ (**2**) were placed in a reaction vessel attached to a vacuum line and heated slowly under reduced pressure (0.01 Torr). The crystals began to melt at 90 °C, and they completely melted at 100 °C with bubbling from the interior of the liquid. Similar to the case of **4**, we distilled the liquid at 150 °C under reduced pressure (0.01 Torr) to give colorless crystals. The ^1H NMR spectrum of the crystals shows only a singlet at $\delta = 0.41$ ppm assigned to the $SiMe_3$ group; no resonance of coordinated THF molecules was detected. The ^7Li NMR sig-

 © 2004 Wiley-VCH Verlag GmbH & Co. KGaA, Weinheim

nal is observed at $\delta = 2.16$ ppm, which is different from that of **2** ($\delta = 0.58$ ppm), suggesting that the distillate is a solvent-free germyllithium. The resulting crystals were recrystallized from *n*-pentane at −20 °C to give single crystals suitable for X-ray crystallographic analysis.

The molecular structure of $[(Me_3Si)_3Ge(\mu\text{-}Li)]_3$ (**5**) is shown in Figure 2 and the structural parameters are listed in Table 2. Surprisingly, unsolvated germyllithium **5** is a trimeric aggregate in the solid state. The crystal system is hexagonal with the space group $P6_3/m$, and the trimer has a crystallographic threefold axis and a mirror plane. It should be noted that such a trimeric structure is the first such example among all structurally characterized heavy group 14-element-centered anionic species. Trimeric organolithium compounds in the solid state are scarcely known, to the best of our knowledge only three aryllithiums — 2,6-bis(dimethylamino)phenyllithium,[21a] 2,6-di-*tert*-butoxyphenyllithium,[21b] and 2-dimethylamino-6-*tert*-butoxyphenyllithium[21c] — have been characterized by X-ray diffraction. Each lithium atom in **5** is bridging, and three lithium atoms form an equilateral triangle with a Li···Li distance of 3.29(2) Å, which is somewhat longer than those in trimeric aryllithiums (2.96−3.17 Å). Substitution of a carbon in trimeric aryllithiums for a germanium should lead to expansion of the lithium core due to the increased bond length of Li−Ge compared with that of Li−C. Interestingly, each of the lithium atoms is coordinated by carbon atoms on the trimethylsilyl groups, with a C−Li distance of 2.587(10) Å. Although this value is longer than covalent C−Li bond lengths (2.13−2.48 Å) of typical organolithium compounds,[22] it is short enough to be a true CH_3···Li interaction between the lithium and carbon atoms. This is in contrast to the case of trimeric aryllithiums, which are stabilized by coordination of a lone pair of the alkoxy or amino group to the cationic lithium atoms. In **5** the three cationic lithium atoms and three anionic germanium atoms lie in the same plane and one of the trimethylsilyl groups (Si2) is also located in this plane as shown in Figure 2 (bottom). The geometry of the anionic germanium atoms is distorted trigonal bipyramid. The apical Si(2)−Ge(1)−Li(1)** bond angle is 177.6(3)° and equatorial Si(1)−Ge(1)−Li(1), Si(1)′−Ge(1)−Li(1), and Si(1)−Ge(1)−Si(1)′ bond angles are 120.1 (1)°, 120.1 (1)°, and 104.7 (1)°, respectively. The Si(1)−Ge(1)−Si(1)′ angle is very small due to a contribution of the *s*-characteristic anionic charge. The apical bonds Ge(1)−Si(2) and Ge(1)−Li(1)** are slightly longer than the equatorial bonds Ge(1)−Si(1) and Ge(1)−Li(1). The Ge(1)−Li(1) bond of 2.613(10) Å is slightly longer than that found in the monomeric germyllithium **2**.

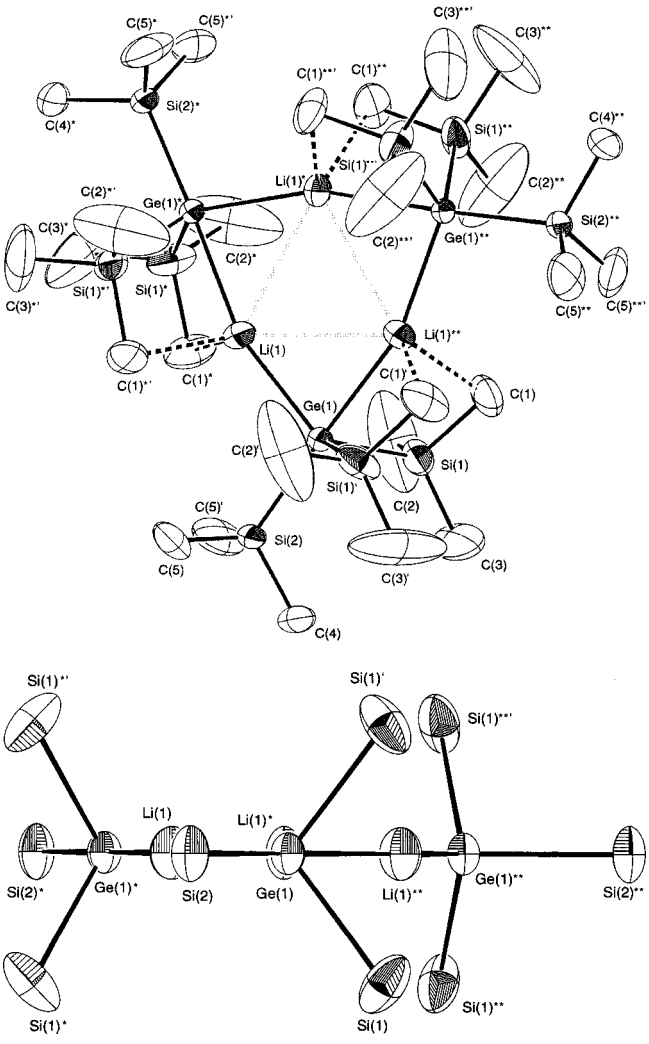

Figure 2. Molecular structure of **5** with 50% probability ellipsoids (H atoms omitted for clarity); dotted lines indicate short intramolecular CH_3···Li interaction

Table 2. Selected atomic distances (Å) and bond angles (°) for **5**; atoms labeled with *, **, and ′ are symmetry-equivalent according to the operations $-y + 1, x - y, z$; $-x + y + 1, -x + 1, z$; and $x, y, -z + 3/2$; respectively

Ge(1)−Si(1)	2.3801(15)
Ge(1)−Si(1)′	2.3801(15)
Ge(1)−Si(2)	2.3909(17)
Ge(1)−Li(1)	2.613(10)
Ge(1)−Li(1)**	2.623(10)
C(1)−Li(1)**	2.587(10)
C(1)′−Li(1)**	2.587(10)
Li(1)−Li(1)*	3.29(2)
Li(1)−Li(1)**	3.29(2)
Si(1)′−Ge(1)−Si(1)	104.73(12)
Si(1)′−Ge(1)−Si(2)	102.23(4)
Si(1)−Ge(1)−Si(2)	102.23(4)
Si(1)′−Ge(1)−Li(1)	120.12(12)
Si(1)−Ge(1)−Li(1)	120.12(12)
Si(2)−Ge(1)−Li(1)	104.4(3)
Si(1)′−Ge(1)−Li(1)**	76.38(16)
Si(1)−Ge(1)−Li(1)**	76.38(16)
Si(2)−Ge(1)−Li(1)**	177.6(3)
Li(1)−Ge(1)−Li(1)**	77.9(5)
Ge(1)−Li(1)−Ge(1)*	162.1(5)
Li(1)*−Li(1)−Li(1)**	60.001(4)

Tris(trimethylsilyl)stannyllithium

Colorless crystals of $[LiSn(SiMe_3)_3 \cdot 3THF]$ (**3**) were placed in a reaction vessel attached to a vacuum line and

 © 2004 Wiley-VCH Verlag GmbH & Co. KGaA, Weinheim

heated slowly under reduced pressure (0.01 Torr). The crystals began to melt with bubbling from the interior of the liquid and the colorless oil gradually changed to pale yellow. Colorless crystals were obtained by distillation under reduced pressure. From the ^{1}H NMR spectrum it was concluded that only one THF molecule is coordinated to the two $LiSn(SiMe_3)_3$ units. The ^{119}Sn NMR resonance is observed at $\delta = -878.2$ ppm as an unresolved multiplet due to coupling with the ^{7}Li nuclei. The resulting crystals were recrystallized from *n*-hexane at room temperature for an X-ray analysis. We also succeeded in the structural characterization of the distilled stannyllithium (**6**). The structural parameters are listed in Table 3.

Table 3. Selected atomic distances (Å) and bond angles (°) for **6**; atoms labeled with * are symmetry-equivalent according to the inversion center at $-x + 2, -y, -z$

Sn(1)−Si(1)	2.558(2)	Sn(2)−Si(5)	2.582(3)
Sn(1)−Si(2)	2.573(3)	Sn(2)−Li(1)	2.764(15)
Sn(1)−Si(3)	2.583(3)	Sn(2)−Li(2)	2.857(17)
Sn(1)−Li(1)	2.796(15)	O(1)−Li(2)	1.907(17)
Sn(1)−Li(2)	2.926(18)	C(3)−Li(1)*	2.392(17)
Sn(2)−Si(4)	2.570(3)	Li(1)−C(3)*	2.392(17)
Sn(2)−Si(6)	2.575(3)	Li(1)−Li(2)	2.74(2)
Si(1)−Sn(1)−Si(2)	102.48(9)	Si(4)−Sn(2)−Li(2)	118.8(4)
Si(1)−Sn(1)−Si(3)	101.70(10)	Si(6)−Sn(2)−Li(2)	136.4(4)
Si(2)−Sn(1)−Si(3)	99.63(12)	Si(5)−Sn(2)−Li(2)	88.3(4)
Si(1)−Sn(1)−Li(1)	127.4(3)	Li(1)−Sn(2)−Li(2)	58.2(4)
Si(2)−Sn(1)−Li(1)	125.5(3)	C(19)−O(1)−C(22)	111.2(10)
Si(3)−Sn(1)−Li(1)	91.2(3)	C(19)−O(1)−Li(2)	119.1(11)
Si(1)−Sn(1)−Li(2)	109.6(3)	C(22)−O(1)−Li(2)	129.7(10)
Si(2)−Sn(1)−Li(2)	89.1(4)	Si(1)−C(3)−Li(1)*	175.7(7)
Si(3)−Sn(1)−Li(2)	144.8(3)	C(3)*−Li(1)−Li(2)	133.2(9)
Li(1)−Sn(1)−Li(2)	57.1(5)	C(3)*−Li(1)−Sn(2)	114.2(6)
Si(4)−Sn(2)−Si(6)	101.24(10)	C(3)*−Li(1)−Sn(1)	116.2(6)
Si(4)−Sn(2)−Si(5)	101.79(9)	Sn(2)−Li(1)−Sn(1)	122.8(5)
Si(6)−Sn(2)−Si(5)	100.38(10)	O(1)−Li(2)−Sn(2)	117.8(9)
Si(4)−Sn(2)−Li(1)	125.7(3)	O(1)−Li(2)−Sn(1)	122.3(8)
Si(6)−Sn(2)−Li(1)	85.3(3)	Sn(2)−Li(2)−Sn(1)	115.2(5)
Si(5)−Sn(2)−Li(1)	130.2(3)		

The stannyllithium $\{[(Me_3Si)_3Sn]_2(\mu\text{-Li})(\mu\text{-Li}\cdot THF)\}$ (**6**) is dimeric in the solid state and the dimer has an unsymmetrical structure, as shown in Figure 3. Although each lithium atom is coordinated by a THF molecule in the case of silyllithium **4**, stannyllithium dimer **6** has only one THF molecule bound to Li(2), with an O(1)−Li(2) bond length of 1.907(17) Å. The two anionic tin and two cationic lithium atoms make a four-membered ring, which has a bent structure with a dihedral angle of 21° between the Sn(1)−Li(1)−Li(2) and Sn(2)−Li(1)−Li(2) planes. The Li(1)−Sn(1)−Li(2) and Li(1)−Sn(2)−Li(2) bond angles are 57.1(5)° and 58.2(4)°, respectively. These values are smaller than that found in silyllithium **4**. The sum of the three Si−Sn−Si angles in **6** is 303.8(3)° at Sn(1) and 303.4(2)° at Sn(2); these values are significantly contracted from the ideal tetrahedral value of 328.5° and are less than that found in silyllithium **4** [the sum of three angles of Si−Si−Si is 307.68(9)°]. However, they are larger than that found in the monomeric structure of **3** (total 296.2°).[16b] Of particular interest is the fact that two $[(Me_3Si)_3Sn(\mu\text{-Li})]_2$ dimers construct aggregates through short Li(1)···C(3)* and C(3)···Li(1)* interactions, as shown in Figure 4. The Li(1)···C(3)* distance of is 2.392(17) Å and the Si(1)−C(3)−Li(1)* angle is 175.7(7)°. These structures are therefore so-called "super-dimers"; super-dimeric structures of group 14-element-centered anionic species have also been observed in the series $[(Me_3Si)_3Si(\mu\text{-M})]_2$ (M = Li, Na, K, Rb, and Cs)[8d] and $[Ph(Me_3Si)_2Si(\mu\text{-Li})]_2$.[23] In his paper[8d] Klinkhammer described CH_3···M interactions, which include a dipole-ion component and C−H donor/M^+ − acceptor component. Although these CH_3···M interactions are weaker than the coordination of solvent molecules, they are strong enough to stabilize a naked lithium atom Li(1) in the case of **6**. The conformation of the trimethylsilyl groups at the anionic Sn(1) and Sn(2) centers is eclipsed. The Sn(1)−Li(2) [2.926(18) Å] and Sn(2)−Li(2) [2.857(17) Å] bond lengths are somewhat longer than those of Sn(1)−Li(1) [2.796(15) Å] and Sn(2)−Li(1) [2.764(17) Å] for steric reasons. The Sn(1)−Li(1)−Sn(2) angle of 122.8(5)° is larger than that of Sn(1)−Li(**2**)−Sn(2) [115.2(5)°].

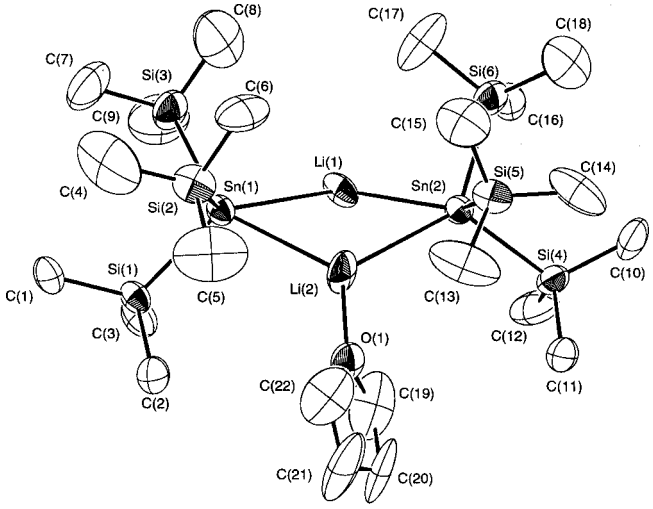

Figure 3. Molecular structure of **6** with 50% probability ellipsoids (H atoms omitted for clarity)

It is interesting that all three group 14-element-centered anionic species $LiE(SiMe_3)_3$ (E = Si, Ge, and Sn) **4**−**6** represent different aggregates in the solid state. It is not clear for the moment why they form different types of clusters. One of the possible reasons might be associated with the difference in Allred−Rochow electronegativities[24] of the central elements (Si = 1.74, Ge = 2.02, Sn = 1.72): the more electronegative germanium atom forms amore stable germyllithium, which does not require additional stabilization by a polar solvent (THF).

Conclusion

Tris(trimethylsilyl)-substituted group 14-element-centered anionic species $[LiE(SiMe_3)_3\cdot 3THF]$ (E = Si, Ge, Sn)

 © 2004 Wiley-VCH Verlag GmbH & Co. KGaA, Weinheim

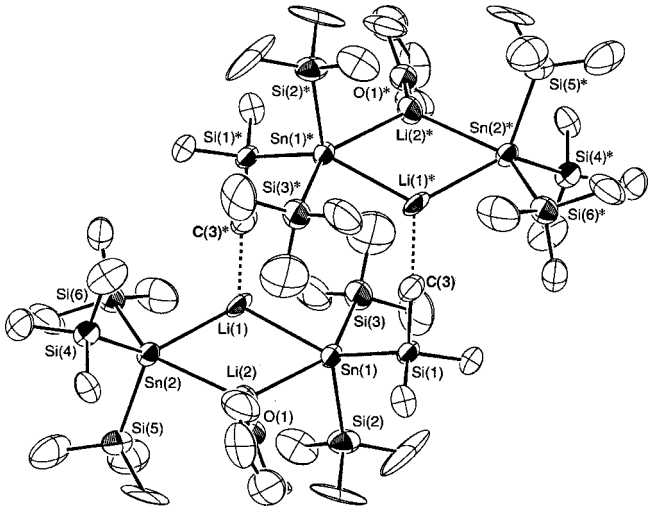

Figure 4. Formation of a dimer of dimers found in **6**; dotted lines indicate short intermolecular $CH_3\cdots Li$ interactions; C−Li distances are listed in Table 3

were heated at 150 °C under reduced pressure to give the corresponding aggregated anionic species with loss of coordinated THF molecules. The dimeric structures of silyllithium $[(Me_3Si)_3Si]_2(\mu\text{-Li}\cdot THF)_2$ (**4**) and stannyllithium $[(Me_3Si)_3Sn]_2(\mu\text{-Li})(\mu\text{-Li}\cdot THF)$ (**6**) and the trimeric strucrture of unsolvated germyllithium $[(Me_3Si)_3Ge]_3(\mu\text{-Li})_3$ (**5**) were unequivocally determined by X-ray crystallographic analyses. Silyllithium **4** and stannyllithium **6** contain distorted four-membered rings consisting of two anionic center atoms and two bridged lithium atoms. Both lithium atoms in **4** are coordinated by a THF molecule; **6** has only one coordinated THF molecule connected to a lithium atom and forms a dimer of dimers by an intermolecular $CH_3\cdots Li$ interaction. Trimeric germyllithium **5** has a crystallographic threefold axis and three anionic germanium atoms and three cationic lithium atoms lying in the same plane. The lithium atoms in **5** are stabilized by an intramolecular $CH_3\cdots Li$ interaction.

Experimental Section

General Procedure: All experiments were performed under an inert atmosphere of argon by standard vacuum-line techniques. *n*-Pentane and *n*-hexane were dried over potassium mirrors and degassed by freeze-pump-thaw cycles and then distilled prior to use. ^1H (400 MHz), ^{13}C (100 MHz), and ^7Li (155 MHz) NMR spectra were recorded on a Varian Inova 400 spectrometer, and ^{29}Si (60 MHz) and ^{119}Sn (112 MHz) NMR spectra were recorded on a JEOL AL-300 spectrometer. ^1H, ^{13}C, and ^{29}Si chemical shifts are referenced to $SiMe_4$ as an external standard. The chemical shifts in the ^7Li NMR spectra are referenced to external LiCl (1.0 M in methanol). The ^{119}Sn NMR chemical shifts are referenced to $SnMe_4$ as an external standard. Elemental analyses could not be performed because of the high instability of the anion species in air.

Preparation of $[(Me_3Si)_3Si(\mu\text{-Li}\cdot THF)]_2$ (4): Tris(tetrahydrofuran)-tris(trimethylsilyl)silyllithium (**1**)[7] (0.110 g, 0.234 mmol) was placed in a dry 6-mm diameter reaction vessel equipped with a side tube. After evacuation of the tube with a rotary pump, it was heated slowly in an oil bath to 150 °C in vacuo. Melting of **1** was observed at 85 °C, and bubbling from the interior of the liquid was observed at 100 °C. When the temperature of the oil bath had reached 150 °C, the vapor went to the top of the vessel and was cooled in the side tube to become a colorless oil, and then colorless crystals of **4** were obtained (0.066 g, 86%) at room temperature. The resulting crystals were recrystallized from *n*-hexane (0.15 mL) to give single crystals suitable for an X-ray crystallographic analysis. ^1H NMR ([D$_6$]benzene): δ = 0.46 (s, 54 H), 1.3−1.4 (m, 9.4 H, THF), 3.4−3.5 (m, 9.4 H, THF) ppm. ^7Li NMR ([D$_6$]benzene): δ = 1.99 ppm. ^{13}C NMR ([D$_6$]benzene): δ = 6.5, 25.2 (THF), 68.7 (THF) ppm. ^{29}Si NMR ([D$_6$]benzene): δ = −5.9 (Me_3Si), −183.9 (br., SiLi) ppm.

Preparation of $[(Me_3Si)_3Ge(\mu\text{-Li})]_3$ (5): Tris(tetrahydrofuran)tris-(trimethylsilyl)germyllithium (**2**)[15] (0.105 g, 0.204 mmol) was placed in a dry 7-mm diameter reaction vessel equipped with a side tube. After evacuation of the tube with a rotary pump, it was heated slowly in an oil bath to 150 °C in vacuo. Melting of **2** was observed at 90 °C, and bubbling from the interior of the liquid was observed at 100 °C. When the temperature of the oil bath had reached 140 °C, the vapor went to the top of the vessel and was cooled in the side tube to become a colorless oil, and then colorless crystals of **5** were obtained (0.060 g, 98%) at room temperature. The resulting crystals were recrystallized from *n*-pentane (0.3 mL) to give single crystals suitable for an X-ray crystallographic analysis. ^1H NMR ([D$_6$]benzene): δ = 0.41 (s, 27 H) ppm. ^7Li NMR ([D$_6$]benzene): δ = 2.16 ppm. ^{13}C NMR ([D$_6$]benzene): δ = 6.4 ppm. ^{29}Si NMR ([D$_6$]benzene): δ = −4.9 ppm.

Preparation of $\{[(Me_3Si)_3Sn]_2(\mu\text{-Li})(\mu\text{-Li}\cdot THF)\}$ (6): Tris(tetrahydrofuran)tris(trimethylsilyl)stannyllithium (**3**)[16] (0.130 g, 0.232 mmol) was placed in a dry 6-mm diameter reaction vessel equipped with a side tube. After evacuation of the tube with a rotary pump, it was heated slowly in an oil bath to 150 °C in vacuo. Melting of **3** was observed at 100 °C, and bubbling from the interior of the liquid was observed. When the temperature of the oil bath had reached 140 °C, the vapor went to the top of the vessel and was cooled in the side tube to become a colorless oil, and then colorless crystals of **6** were obtained (0.056 g, 63%) at room temperature. The resulting crystals were recrystallized from *n*-pentane (0.1 mL) to give single crystals suitable for an X-ray crystallographic analysis. ^1H NMR ([D$_6$]benzene): δ = 0.56 (s, 54 H). 1.2−1.3 (m, 4.6 H, THF), 3.5−3.6 (m, 4.6 H, THF) ppm. ^7Li NMR ([D$_6$]benzene): δ = 1.20 ppm. ^{13}C NMR ([D$_6$]benzene): δ = 7.3, 25.1 (THF), 69.2 (THF) ppm. ^{29}Si NMR ([D$_6$]benzene): δ = −12.4 ppm. ^{119}Sn NMR ([D$_6$]benzene): δ = −878.2 (br) ppm.

X-ray Crystal Structure Analyses for 4, 5, and 6: Crystal data for all structures are presented in Table 4. Data were collected with a MacScience DIP2030 imaging plate diffractometer employing graphite-monochromated Mo-K_α radiation (λ = 0.71073 Å). The structures were solved by direct methods by means of SIR-92[25] (for **4** and **5**) and Multan78[26] (for **6**) refined with all data on F^2 by means of SHELXL-97.[27]

CCDC-225267, -225265, and -225266 (for **4**, **5**, and **6**, respectively) contain the supplementary crystallographic data for this paper. These data can be obtained free of charge at www.ccdc.cam.ac.uk/conts/retrieving.html [or from the Cambridge Crystallographic Data Centre, 12, Union Road, Cambridge CB2 1EZ, UK; Fax: +44-1223-336033; E-mail: deposit@ccdc.cam.ac.uk].

 © 2004 Wiley-VCH Verlag GmbH & Co. KGaA, Weinheim

Table 4. Summary of crystallographic data for **4**, **5**, and **6**

	4	**5**	**6**
Formula	$C_{32}H_{82}Li_2O_2Si_8$	$C_9H_{27}GeLiSi_3$	$C_{22}H_{62}Li_2OSi_6Sn_2$
Mol. mass	737.58	299.11	762.52
Cryst system	orthorhombic	hexagonal	monoclinic
Space group	*Pcan*	$P6_3/m$	$P2_1/n$
a (Å)	15.8010(7)	13.8490(8)	14.136(1)
b (Å)	16.4830(8)	13.849	19.776(2)
c (Å)	18.6960(5)	16.3550(8)	15.246(1)
α (°)	90	90	90
β (°)	90	90	97.608(6)
γ (°)	90	120	90
V (Å^3)	4869.3(3)	2716.5(2)	4224.6(7)
Z	4	6	4
T (K)	295	200	295
$\rho_{calcd.}$ (g cm^{-3})	1.006	1.097	1.199
F(000)	1632	948	1568
θ range (deg)	2.80−26.45	2.11−27.96	2.70−26.45
No. of unique reflns	5000	4358	8550
No. of reflns used for refinement	4101	2261	4564
No. of refined params	201	71	299
*R*1 [$I > 2\sigma(I)$]	0.0581	0.0570	0.0732
*wR*2 (all data)	0.1790	0.1901	0.1636
GOF	1.345	1.412	1.407
Max/min $\Delta\rho$ (e·Å^{-3})	0.763/−0.383	0.627/−0.539	0.596/−0.597

Acknowledgments

We thank the Ministry of Education, Culture, Sports, Science and Technology, Japan, for Grants-in Aid for Scientific Research (Grant No. 13740359). We wish to thank Dr. V. Ya. Lee of the University of Tsukuba for helpful discussions and for comments on this manuscript.

[1] [1a] B. J. Wakefield, in *Comprehensive Organic Chemistry*, vol. 3 (Eds.: D. Barton, W. D. Ollis, D. N. Jones), Pergamon, Oxford, **1979**, p. 987. [1b] D. A. Armitage, in *Comprehensive Organometallic Chemistry*, vol. 2 (Eds.: G. Wilkinson, F. G. A. Stone, E. W. Abel), Pergamon, New York, **1982**, p. 99.

[2] [2a] J. Belzner, U. Dehnert, in *The Chemistry of Organic Silicon Compounds*, vol. 2 (Eds.: Z. Rappoport, Y. Apeloig), Wiley, Chichester, **1998**, p. 779. [2b]K. Tamao, A. Kawachi, *Adv. Organomet. Chem.* **1995**, *38*, 1. [2c] P. Lickiss, C. Smith, *Coord. Chem. Rev.* **1995**, *145*, 75. [2d] A. Sekiguchi, V. Ya. Lee, M. Nanjo, *Coord. Chem. Rev.* **2000**, *210*, 11. [2e] P. Riviere, A. Castel, M. Riviere-Baudet, in *The Chemistry of Organic Germanium, Tin, and Lead Compounds*, vol. 2 (Ed.: Z. Rappoport), Wiley, **2002**, chapter 11, p. 653.

[3] P. Riviere, M. Riviere-Baudet, J. Satge, in *Comprehensive Organometallic Chemistry II* (Ed.: A. G. Davies), Elsevier, Oxford, **1995**, vol. 2, chapter 5.

[4] M. A. Paver, C. A. Russell, D. S. Wright, *Angew. Chem. Int. Ed. Engl.* **1995**, *34*, 1545.

[5] [5a] W. N. Setzer, P. v. R. Schleyer, *Adv. Organomet. Chem.* **1985**, *24*, 353. [5b] E. Weiss, *Angew. Chem. Int. Ed. Engl.* **1993**, *32*, 1501.

[6] [6a] H. Gilman, C. L. Smith, *J. Organomet. Chem.* **1967**, *8*, 245. [6b] H. Gilman, C. L. Smith, *J. Organomet. Chem.* **1968**, *14*, 91.

[7] G. Gutekunst, A. G. Brook, *J. Organomet. Chem.* **1982**, *225*, 1.

[8] (**1**·DME)$_2$·(μ-DME): [8a] G. Becker, H.-M. Hartmann, A. Münch, H. Z. Riffel, *Z. Anorg. Allg. Chem.* **1985**, *530*, 29. **1**·(THF)$_3$: [8b] A. Heine, R. Herbst-Irmer, G. M. Sheldrick, D. Stalke, *Inorg. Chem.* **1993**, *32*, 2694. [8c] H. V. R. Dias, M. M. Olmstead, K. Ruhlandt-Senge, P. P. Power, *J. Organomet. Chem.* **1993**, *462*, 1. Unsolvated dimer of **1**: [8d] K. W. Klinkhammer, *Chem. Eur. J.* **1997**, *3*, 1418.

[9] M. Nanjo, A. Sekiguchi, H. Sakurai, *Bull. Chem. Soc. Jpn.* **1998**, *71*, 741.

[10] A. G. Brook, S. C. Nyburg, F. Abdesaken, B. Gutekunst, G. Gutekunst, R. Krishna, M. R. Kallury, Y. C. Poon, Y.-M. Chang, W.-N. Winnie, *J. Am. Chem. Soc.* **1982**, *104*, 5668.

[11] [11a] J. B. Lambert, J. L. Pflug, C. L. Stern, *Angew. Chem. Int. Ed. Engl.* **1995**, *34*, 98. [11b] H. Suzuki, Y. Kimata, S. Satoh, A. Kuriyama, *Chem. Lett.* **1995**, 293.

[12] T. D. Tilley, in *The Chemistry of Organic Silicon Compounds* (Eds.: S. Patai, Z. Rappoport), Wiley, New York, **1989**, p. 1415.

[13] S. K. Mehrotra, H. Kawa, J. R. Baran Jr., M. M. Ludvig, R. J. Lagow, *J. Am. Chem. Soc.* **1990**, *112*, 9003.

[14] A. Sekiguchi, M. Ichinohe, S. Yamaguchi, *J. Am. Chem. Soc.* **1999**, *121*, 10231.

[15] [15a] A. G. Brook, F. Abdesaken, H. Salradl, *J. Organomet. Chem.* **1986**, *299*, 9. [15b] A. Heine, D. Stalke, *Angew. Chem. Int. Ed. Engl.* **1994**, *33*, 113.; *Angew. Chem.* **1994**, *106*, 121. [15c] S. Freitag, R. Herbst-Irmer, L. Lameyer, D. Stalke, *Organometallics* **1996**, *15*, 2839.

[16] [16a] F. Preuss, T. Wieland, J. Perner, G. Z. Heckmann, *Z. Naturforsch., Teil B* **1992**, *47*, 1355. [16b] C. J. Cardin, D. J. Cardin, W. Clegg, S. J. Coles, S. P. Constantine, J. R. Rowe, S. J. Teat, *J. Organomet. Chem.* **1999**, *573*, 96.

[17] N. Wiberg, K. Amelunxen, H.-W. Lerner, H. Schuster, H. Nöth, I. Krossing, M. Schmidt-Amelunxen, T. Seifert, *J. Organomet. Chem.* **1997**, *542*, 1.

[18] A. Sekiguchi, M. Nanjo, C. Kabuto, H. Sakurai, *Angew. Chem. Int. Ed. Engl.* **1997**, *36*, 113.

[19] Y. Apeloig, M. Yuzefovich, M. Bendikov, D. Bravo-Zhivotovskii, D. Bläser, R. Boese, *Angew. Chem. Int. Ed.* **2001**, *40*, 3016.

[20] T. Iwamoto, J. Okita, C. Kabuto, M. Kira, *J. Am. Chem. Soc.* **2002**, *124*, 11604.

[21] [21a] S. Harder, J. Boersma, L. Brandsma, J. A. Kanters, W.

 © 2004 Wiley-VCH Verlag GmbH & Co. KGaA, Weinheim

Bauer, P. v. R. Schleyer, *Organometallics* **1989**, *8*, 1696. [21b] S. Harder, J. Boersma, L. Brandsma, J. A. Kanters, A. J. M. Duisenberg, J. H. van Lenthe, *Organometallics* **1991**, *10*, 1623. [21c] S. Harder, P. F. Ekhart, L. Brandsma, J. A. Kanters, A. J. M. Duisenberg, P. v. R. Schleyer, *Organometallics* **1992**, *11*, 2623.
[22] W. N. Setzer, P. v. R. Schleyer, *Adv. Organomet. Chem.* **1985**, *24*, 353.
[23] M. Nanjo, A. Sekiguchi, H. Sakurai, *Bull. Chem. Soc. Jpn.* **1999**, *72*, 1387.
[24] A. L. Allred, E. G. Rochow, *J. Inorg. Nucl. Chem.* **1958**, *5*, 264.
[25] A. Altomare, M. C. Burla, M. Camalli, M. Cascarano, C. Giacovazzo, A. Guagliardi, G. Polidoro, *J. Appl. Crystallogr.* **1994**, *27*, 435.
[26] P. Main, S. E. Hull, I. Lessinger, G. Germain, J.-P. Declercq, M. M. Woolfson, *Multan78*, University of York, York, U. K., **1978**.
[27] G. M. Sheldrick, *SHELXL-97, Program for Crystal Structure Refinement*, University of Göttingen, **1997**.

Received December 10, 2003
Early View Article
Published Online May 13, 2004

 © 2004 Wiley-VCH Verlag GmbH & Co. KGaA, Weinheim

Hydrothermal Syntheses, Structures, and Properties of Three 3-D Lanthanide Coordination Polymers that Form 1-D Channels

Xiang-Jun Zheng,[a] Zhe-Ming Wang,[b] Song Gao,[b] Fu-Hui Liao,[b] Chun-Hua Yan,[b] and Lin-Pei Jin*[a]

Keywords: Coordination polymer / Hydrothermal synthesis / Lanthanides / 2,6-Naphthalenedicarboxylate / X-ray diffraction

We report the hydrothermal synthesis and crystal structure of isostructural lanthanide coordination polymers $[Ln_2(NDC)_3(phen)_2]\cdot H_2NDC$ [Ln = Tb (**1**), Ho (**2**) and Yb (**3**)] that feature 2,6-naphthalenedicarboxylate (NDC) and 1,10-phenanthroline (phen) ligands. The NDC ligands bridge the lanthanide ions in two different modes to form a 3-D porous framework that accommodates large, neutral 2,6-naphthalenedicarboxylic acid molecules as guests in the channels, stabilized through O–H···O hydrogen bonds to the NDC ligand. The effective dimension of the channel is ca. 6.0×8.2 Å. Thermogravimetric analysis shows that complex **2** remains stable up to 330 °C, which we confirmed also by powder X-ray diffraction analyses. The framework collapsed upon the loss of the coordinating phen molecules. The Tb complex shows strong evidence of ferromagnetic coupling interactions.
(© Wiley-VCH Verlag GmbH & Co. KGaA, 69451 Weinheim, Germany, 2004)

Introduction

The synthesis of coordination polymers remains a subject of intense interest. Accordingly, a large number of coordination polymers of different dimensions and various topologies have been reported.[1−19] Recent research in this field has focused on producing materials designed to perform highly specific and cooperative functions.[20−25] Advances in the design and synthesis of metal-organic frameworks (MOFs) has led to numerous practical and conceptual developments in that direction.[26−30] Specifically, the chemistry of MOFs provides an extensive array of crystalline materials that have high stability, tunable metrics, organic functionalities, and porosity.[31] The wide variety of possible organic linkers and the multiple physical properties of inorganic metal ions make it feasible to modulate both the dimensions of the pores and the properties of the final porous coordination polymers. In such structures, organic species act as either pillars or linkers to arrange inorganic layers, chains, or clusters of transition or lanthanide ions.[32] Polycarboxylic acids are frequently utilized to construct microporous compounds.[33−36] In the study of lanthanide-organic frameworks, rigid polycarboxylic acids, especially dicarboxylic acids, are frequently used to link lanthanide ions[17,37] or lanthanide cubane-like clusters.[38,39] Considering the high coordination numbers of lanthanide ions, ancillary ligands also can be incorporated into the lanthanide coordination networks. Bulky ancillary ligands can occupy some coordination sites and reduce the interpenetration of frameworks, which results in an increase in the dimensions of the pores in the framework. 2,6-Naphthalenedicarboxylate is a rigid linear ligand whose transition metal coordination polymers, both binary and ternary, have been studied extensively,[40−46] but only three binary coordination polymers of its lanthanide analogues have been reported.[47−49] No ternary lanthanide coordination polymers of 2,6-naphthalenedicarboxylate have been described in the literature. In this study, we selected 2,6-naphthalenedicarboxylate as the linker and a chelating ligand, 1,10-phenanthroline, as the ancillary ligand to construct a ternary lanthanide-organic framework that is thermally stable and exhibits interesting magnetic behavior.

Results and Discussion

Synthetic Considerations

Dipotassium 2,6-naphthalenedicarboxylate readily forms a precipitate upon the addition of lanthanide chlorides. Therefore, for the preparation of our coordination polymers, first we acidified dipotassium 2,6-naphthalenedicarboxylate to prevent it from reacting too quickly with the lanthanide chloride; this process facilitates coordination of phen molecules and leads to the growth of crystals of the ternary complex. In this approach, some phen molecules

[a] Department of Chemistry, Beijing Normal University, Beijing 100875, P. R. China
Fax: (internat.) + 86-1062202075
E-mail: lpjin@bnu.edu.cn
[b] State Key Laboratory of Rare Earth Materials Chemistry and Applications, College of Chemistry and Molecular Engineering, Peking University, Beijing, 100871, P. R. China

 © 2004 Wiley-VCH Verlag GmbH & Co. KGaA, Weinheim DOI: 10.1002/ejic.200300876

act as ligands to coordinate with lanthanide ions, while others act as mild organic bases that deprotonate H_2NDC units to give NDC ions that then coordinate with lanthanide ions.

Crystal Structures

The three complexes are isomorphous and isostructural; we describe in detail only the structure of complex **2**. The asymmetric unit of **2** consists of one Ho^{III} center, 1.5 NDC anions, one phen ligand, and 0.5 H_2NDC guest units. Around the central metal ion, there is a bidentate chelating phen ligand and four bridging NDC anions (Figure 1). The Ho^{III} ion is eight-coordinate with two ligating nitrogen atoms from a phen molecule and six oxygen atoms from four NDC anions; this arrangement results in a triangular dodecahedral coordination polyhedron. For convenience, the NDC anions having the oxygen atoms labeled O1, O3, and O5 (Figure 1) are named NDC1, NDC2, and NDC3, respectively. These structures represent the three orientations of NDC anions in the crystal; the dihedral angles between the naphthalene rings of NDC1 and NDC2, NDC2 and NDC3, and NDC1 and NDC3 are 108.2, 68.0, and 94.7 °C, respectively. In the title coordination polymers, the NDC anions adopt two coordination modes: bis(bridging bidentate) (I) and bis(chelating bidentate) (II), as depicted in Scheme 1. NDC1 ligands adopt the type I binding mode, whereas NDC2 and NDC3 ligands adopt type II binding.

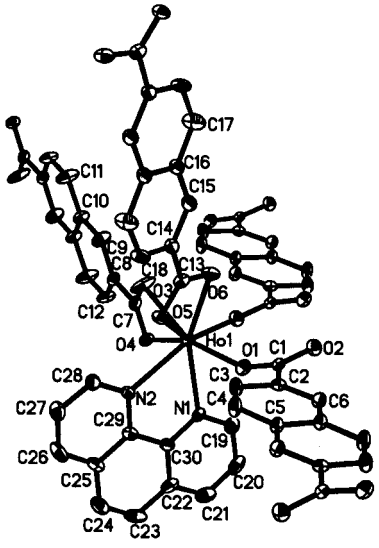

Figure 1. Coordination environment of complex **2**; the asymmetric unit and the related coordination atoms are labeled; guest molecules and all hydrogen atoms have been omitted for clarity; thermal ellipsoids are drawn at 30% probability

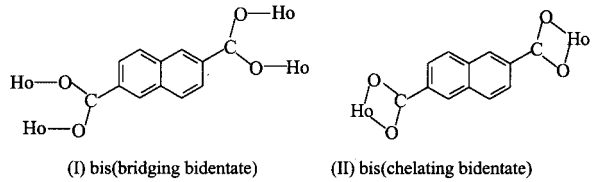

Scheme 1. Coordination modes of the NDC ligand in complex **2**

The framework structure of **2** is built from a dinuclear unit, $Ho_2(NDC)_3(phen)_2$, which results from the linking of two asymmetric units through two carboxylate units of two NDC1 anions. First, the NDC1 ligands link the dinuclear building units to form 1-D chains along the *c*-axis (Figure 2). The distance between the adjacent dinuclear units in the chain is 12.25 Å. Next, the NDC2 ligands link two Ho^{III} ions (Ho···Ho, 13.34 Å), in the [01$\bar{1}$] direction, of two adjacent chains to form 2-D layers that feature 44-membered

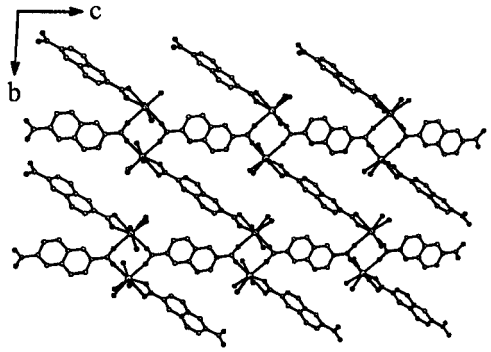

Figure 2. 2-D layers, viewed along the *a*-axis, featuring 44-membered ring channels constructed with Ho^{III}, NDC1, and NDC2 ligands

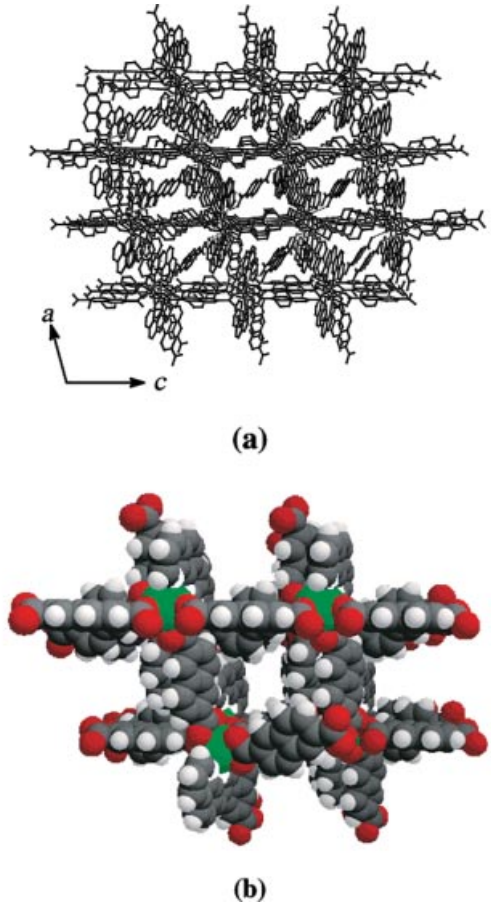

Figure 3. (a) 3-D porous framework of complex **2**, viewed along the *b*-axis, showing the guest molecules accommodated in the 1-D channels; all hydrogen atoms have been omitted for clarity; (b) space-filling model of complex **2** showing the 1-D channel; the guest molecules have been omitted for clarity

 © 2004 Wiley-VCH Verlag GmbH & Co. KGaA, Weinheim

parallelogram channels (Figure 2). Finally, the NDC3 ligands, which act as pillars, link the Ho^{III} ions (Ho···Ho, 13.35 Å), in the [$\bar{1}$10] direction, from two adjacent layers to form the porous 3-D framework (Figure 3).

When viewed along the *b*-axis, complex **2** exhibits many 1-D channels. Despite the large dimensions of the cross-section of the channel (internuclear separation: 13.34 × 13.35 Å) arising from the long span of the NDC ligand (ca. 9.0 Å), the effective dimension of the channel is only 6.0 × 8.2 Å (van der Waals free space) because of the presence of the bulky phen molecules in the channel. The large neutral guest molecules (H_2NDC), which are hydrogen bonded to the coordinating oxygen atoms of the NDC3 ligands in the framework, are accommodated within the channels. The two carboxyl groups of the guest molecule are arrayed in the diagonal direction of the parallelogram channel. The geometries of the hydrogen bonds in complexes **1**, **2**, and **3** are listed in Table 1. Selected bond lengths within **1**, **2**, and **3** are listed in Table 2.

Table 1. The geometries of hydrogen bonds in complexes **1**, **2**, and **3** [Å; °] (symmetry operations: #1 $-x, -y, -z$; #2 $-x, -y+1, -z$)

Complex	D−H···A	*d*(D−H)	*d*(H···A)	*d*(D···A)	<(DHA)
1	O7−H7···O4#1	0.820	1.870	2.637	156.0
2	O7−H7···O6#2	0.820	1.978	2.660	140.11
3	O7−H7···O4#1	0.820	1.810	2.660	179.9

Analysis of the Thermal Stability of 2

The existence of guest molecules in the channels inspired us to investigate the thermal stability of the coordination polymers; we took complex **2** as a representative example to carry out the TG analysis. We observe from the thermogravimetric curve of **2** (Figure 4) that this complex remains stable up to 330 °C, at which temperature the first weight loss occured, i.e., loss of the H_2NDC guest molecule. A second weight loss occurred when the temperature reached 357 °C. The H_2NDC guest molecule was not completely removed before the loss of two coordinating phen molecules occurred. One H_2NDC guest molecule and two coordinating phen molecules were completely removed at 460 °C; this process occurs with a weight loss of 35.2% (calculated: 37.2%). The decomposition of the complex continued at

Table 2. Selected bond lengths [Å] and bond angles [°] for complexes **1**, **2**, and **3** (symmetry operations: #1 $-x, -y, -z$ #2 $-x, -y+2, -z$)

1		**2**		**3**	
Tb(1)−O(1)	2.454(3)	Ho(1)−O(1)	2.227(5)	Yb(1)−O(1)	2.465(3)
Tb(1)−O(2)	2.383(3)	Ho(1)−O(2)#2	2.238(5)	Yb(1)−O(2)	2.374(4)
Tb(1)−O(3)	2.391(3)	Ho(1)−O(3)	2.336(5)	Yb(1)−O(3)	2.388(3)
Tb(1)−O(4)	2.476(3)	Ho(1)−O(4)	2.437(5)	Yb(1)−O(4)	2.475(3)
Tb(1)−O(5)	2.262(3)	Ho(1)−O(5)	2.356(5)	Yb(1)−O(5)	2.261(3)
Tb(1)−O(6)#1	2.272(3)	Ho(1)−O(6)	2.439(5)	Yb(1)−O(6)#1	2.271(3)
Tb(1)−N(1)	2.535(3)	Ho(1)−N(1)	2.496(6)	Yb(1)−N(1)	2.539(4)
Tb(1)−N(2)	2.524(3)	Ho(1)−N(2)	2.496(5)	Yb(1)−N(2)	2.539(4)
O(5)−Tb(1)−O(6)#1	89.54(10)	O(1)−Ho(1)−O(2)#2	89.45(18)	O(5)−Yb(1)−O(6)#1	89.60(12)
O(5)−Tb(1)−O(2)	153.10(11)	O(1)−Ho(1)−O(3)	152.56(19)	O(5)−Yb(1)−O(2)	152.71(14)
O(6)#1−Tb(1)−O(2)	90.35(11)	O(2)#2−Ho(1)−O(3)	88.7(2)	O(6)#1−Yb(1)−O(2)	89.11(15)
O(5)−Tb(1)−O(3)	81.26(10)	O(1)−Ho(1)−O(5)	82.06(18)	O(5)−Yb(1)−O(3)	81.71(12)
O(6)#1−Tb(1)−O(3)	138.04(9)	O(2)#2−Ho(1)−O(5)	138.61(17)	O(6)#1−Yb(1)−O(3)	138.28(12)
O(2)−Tb(1)−O(3)	80.93(10)	O(3)−Ho(1)−O(5)	81.36(18)	O(2)−Yb(1)−O(3)	81.22(13)
O(5)−Tb(1)−O(1)	151.44(10)	O(1)−Ho(1)−O(4)	151.49(17)	O(5)−Yb(1)−O(1)	151.72(12)
O(6)#1−Tb(1)−O(1)	77.96(9)	O(2)#2−Ho(1)−O(4)	78.55(17)	O(6)#1−Yb(1)−O(1)	78.45(12)
O(2)−Tb(1)−O(1)	53.81(9)	O(3)−Ho(1)−O(4)	53.94(17)	O(2)−Yb(1)−O(1)	53.72(12)
O(3)−Tb(1)−O(1)	124.84(9)	O(5)−Ho(1)−O(4)	123.67(16)	O(3)−Yb(1)−O(1)	123.90(12)
O(5)−Tb(1)−O(4)	79.32(10)	O(1)−Ho(1)−O(6)	79.29(17)	O(5)−Yb(1)−O(4)	79.36(13)
O(6)#1−Tb(1)−O(4)	84.48(9)	O(2)#2−Ho(1)−O(6)	84.29(17)	O(6)#1−Yb(1)−O(4)	84.81(12)
O(2)−Tb(1)−O(4)	73.89(10)	O(3)−Ho(1)−O(6)	73.28(18)	O(2)−Yb(1)−O(4)	73.37(14)
O(3)−Tb(1)−O(4)	53.62(9)	O(5)−Ho(1)−O(6)	54.35(16)	O(3)−Yb(1)−O(4)	53.50(11)
O(1)−Tb(1)−O(4)	124.03(9)	O(4)−Ho(1)−O(6)	124.31(16)	O(1)−Yb(1)−O(4)	124.18(12)
O(5)−Tb(1)−N(2)	99.89(10)	O(1)−Ho(1)−N(1)	76.39(18)	O(5)−Yb(1)−N(1)	76.27(12)
O(6)#1−Tb(1)−N(2)	148.72(10)	O(2)#2−Ho(1)−N(1)	87.82(19)	O(6)#1−Yb(1)−N(1)	88.04(13)
O(2)−Tb(1)−N(2)	94.05(12)	O(3)−Ho(1)−N(1)	130.86(19)	O(2)−Yb(1)−N(1)	130.92(13)
O(3)−Tb(1)−N(2)	73.16(10)	O(5)−Ho(1)−N(1)	128.38(19)	O(3)−Yb(1)−N(1)	128.30(12)
O(1)−Tb(1)−N(2)	79.81(10)	O(4)−Ho(1)−N(1)	77.38(17)	O(1)−Yb(1)−N(1)	77.77(12)
O(4)−Tb(1)−N(2)	126.45(9)	O(6)−Ho(1)−N(1)	154.47(17)	O(4)−Yb(1)−N(1)	154.62(13)
O(5)−Tb(1)−N(1)	76.14(10)	O(1)−Ho(1)−N(2)	99.71(18)	O(5)−Yb(1)−N(2)	99.21(13)
O(6)#1−Tb(1)−N(1)	88.65(10)	O(2)#2−Ho(1)−N(2)	148.46(19)	O(6)#1−Yb(1)−N(2)	148.39(12)
O(2)−Tb(1)−N(1)	130.75(11)	O(3)−Ho(1)−N(2)	96.1(2)	O(2)−Yb(1)−N(2)	96.07(16)
O(3)−Tb(1)−N(1)	127.61(10)	O(5)−Ho(1)−N(2)	72.85(18)	O(3)−Yb(1)−N(2)	73.28(12)
O(1)−Tb(1)−N(1)	77.97(9)	O(4)−Ho(1)−N(2)	79.26(18)	O(1)−Yb(1)−N(2)	79.68(12)
O(4)−Tb(1)−N(1)	154.55(11)	O(6)−Ho(1)−N(2)	126.96(18)	O(4)−Yb(1)−N(2)	126.56(11)
N(2)−Tb(1)−N(1)	65.27(10)	N(1)−Ho(1)−N(2)	65.58(19)	N(1)−Yb(1)−N(2)	65.12(13)

 © 2004 Wiley-VCH Verlag GmbH & Co. KGaA, Weinheim

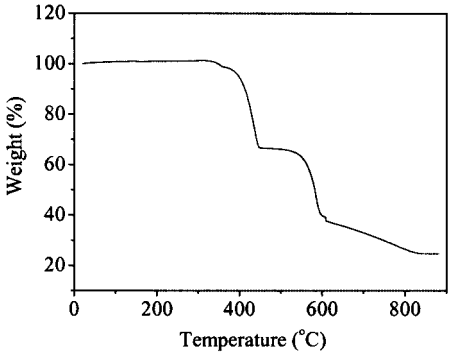

Figure 4. Thermogravimetric curve of complex **2**

491 °C and ended at 840 °C, at which point a residue, Ho_2O_3, was obtained in 24.8% yield (calculated: 24.4%).

To further test the thermal stability of **2**, we examined powder samples by variable-temperature X-ray diffraction analysis. The powder XRD patterns of **2** (Figure 5) at 27, 300, 350, 400, and 500 °C were recorded. We see in Figure 5 that when the temperature rose from 27 to 300 °C, the positions of the major peaks undergo no significant changes, but some peaks shift slightly to lower or higher 2θ values. This observation indicates that a possible distortion of the structure had occurred, but it did not affect the existence of the framework. The similarities between the powder XRD patterns obtained at 300 and 350 °C also suggest that the framework remains stable at 350 °C, i.e., when phen molecules are still present, which is in accordance with the results of the thermogravimetric analysis. Above 400 °C, however, the PXRD patterns are changed completely, which indicates that a collapse of the framework has occurred. The loss of the coordinating phen molecules may account for the framework's collapse, i.e., the presence of the coordinating phen molecules is required for a stabile framework.

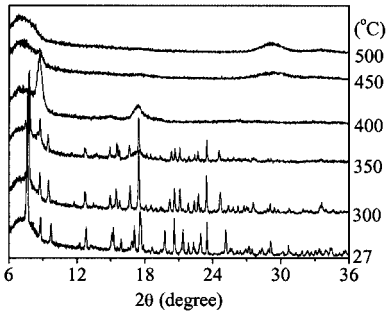

Figure 5. Powder X-ray diffraction patterns of **2** at different temperatures [the large broad peak at < 10° (2θ) arose from the use of the position scan detector]

Because of similarities between the frameworks of the title complexes, we deduced that **1** and **3** have stabilities similar to that of **2**.

Magnetic Properties

We investigated the magnetic properties of complexes **1** and **2** in the solid state at 1 T within the temperature range 2−300 K (Figure 6).

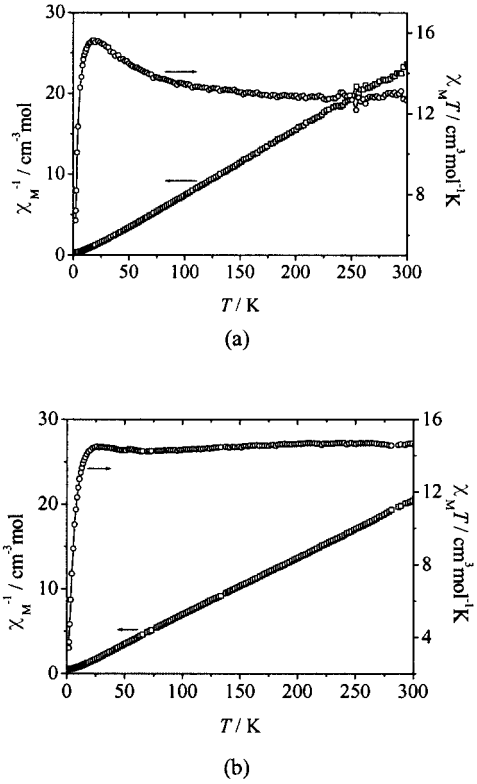

Figure 6. Plots of the temperature dependences of χ_M^{-1} (open squares) and $\chi_M T$ (open circles) for complexes **1** (a) and **2** (b)

For **1**, the observed value of $\chi_M T$ per [Tb] unit is 12.82 cm^3·K·mol^{-1} at room temperature (Figure 6a), which is slightly larger than the value expected for a free Tb^{3+} ion (11.82 cm^3·K·mol^{-1}).[50] Upon cooling, the value of $\chi_M T$ increases up to a maximum of 15.62 cm^3·K·mol^{-1} at ca. 18 K. The plot of χ_M^{-1} vs. T over the temperature range 30−300 K obeys the Curie−Weiss law [$\chi = C/(T - \theta)$] with C = 12.5 cm^3·K·mol^{-1} and θ = 6.5 K. All of these results indicate that there is ferromagnetic coupling between the Tb^{3+} ions. The value of $\chi_M T$ decreases abruptly at temperatures below 18 K to reach 6.70 cm^3·K·mol^{-1} at 2 K. This feature is due primarily to the splitting of the ligand field of the Tb^{3+} ion as a result of strong spin-orbital coupling. For **2**, the observed value of $\chi_M T$ per [Ho] unit is 14.65 cm^3·K·mol^{-1} at room temperature (Figure 6b), which is close to the value expected (14.07 cm^3·K·mol^{-1}) for a free Ho^{3+} ion.[50] The value of $\chi_M T$ decreases slowly as the temperature decreases to ca. 26 K (14.48 cm^3·K·mol^{-1}) and then it drops rapidly below 26 K to reach a value of 3.40 cm^3·K·mol^{-1} at 2 K. The plot of χ_M^{-1} vs. T over the temperature range 30−300 K obeys the Curie−Weiss law with C = 14.76 cm^3·K·mol^{-1} and θ = −2.21 K. The decrease of $\chi_M T$ and the negative value of θ are due primarily to splitting of the ligand field of the Ho^{3+} ion as a result of strong spin-orbital coupling, and is attributed partly to the poss-

 © 2004 Wiley-VCH Verlag GmbH & Co. KGaA, Weinheim

Table 3. Crystal data for complexes **1**, **2**, and **3**

	1	**2**	**3**
Empirical formula	$C_{36}H_{21}N_2O_8Tb$	$C_{36}H_{21}HoN_2O_8$	$C_{36}H_{21}N_2O_8Yb$
Formula mass	768.47	774.48	782.59
Temperature [K]	293(2)	293(2)	293(2)
Wavelength [Å]	0.71073	0.71073	0.71073
Crystal system	triclinic	triclinic	triclinic
Space group	$P\bar{1}$	$P\bar{1}$	$P\bar{1}$
a [Å]	10.7822(2)	10.802(6)	10.8762(2)
b [Å]	12.1806(3)	12.143(6)	12.2294(3)
c [Å]	12.3369(3)	12.245(7)	12.3328(3)
α [°]	94.2028(9)	94.031(11)	93.9317(11)
β [°]	106.3049(9)	106.641(9)	106.6736(11)
γ [°]	100.9193(12)	101.356(9)	101.2612(13)
V [Å^3]	1513.12(6)	1495.0(14)	1527.54(6)
Z	2	2	2
$D_{calcd.}$ [g·cm^{-3}]	1.687	1.720	1.701
μ [mm^{-1}]	2.396	2.706	3.120
Reflections collected, unique, R_{int}	28830, 6894, 0.0759	6266, 5260, 0.0440	28225, 6857, 0.0684
R indices [$I > 2\sigma(I)$]	$R_1 = 0.0377$, $wR_2 = 0.0830$	$R_1 = 0.0492$, $wR_2 = 0.0846$	$R_1 = 0.0415$, $wR_2 = 0.0968$
R indices (all data)	$R_1 = 0.0517$, $wR_2 = 0.0883$	$R_1 = 0.0806$, $wR_2 = 0.0949$	$R_1 = 0.0601$, $wR_2 = 0.1032$

ibly weak antiferromagnetic coupling between the Ho^{3+} ions in **2**.

Conclusion

We have synthesized novel 3-D porous lanthanide coordination polymers, $[Ln_2(NDC)_3(phen)_2]\cdot H_2NDC$ (Ln = Tb, Ho, and Yb), incorporating 2,6-naphthalenedicarboxylate and 1,10-phenanthroline units by hydrothermal reactions; we characterized the complexes by single-crystal X-ray diffraction analysis. The results show that the three complexes are isostructural and that the NDC^{2-} unit is a good spacer for the construction of porous lanthanide coordination polymers. Large, neutral guest molecules (2,6-naphthalenedicarboxylic acid units) are accommodated within the 1-D channels, which are rarely found in lanthanide coordination polymers. These lanthanide coordination polymers remain thermally stable up to ca. 330 °C.

Experimental Section

General Remarks: $TbCl_3\cdot 6H_2O$, $HoCl_3\cdot 6H_2O$, and $YbCl_3\cdot 6H_2O$ were each prepared by dissolving their respective oxides in concentrated hydrochloric acid and then evaporating the solvent to dryness. All the other reagents were commercially available and were used without further purification.

Instrumentation: Elemental analyses were obtained with an Elementar Vario EL analyzer. IR spectra were recorded with a Nicolet Avatar 360 FT-IR spectrometer by using the KBr pellet technique. Thermogravimetric analyses were performed with a TGA 951 thermogravimetric analyzer. The magnetic susceptibilities were obtained on crystal samples by using an Oxford MagLab System 2000 magnetometer. The experimental susceptibilities were corrected for the presence of the sample holder and the diamagnetism contributions were estimated from Pascal's constants. The powder X-ray diffraction patterns were recorded using a Bruker AXS D8 ADVANCE diffractometer.

$[Tb_2(NDC)_3(phen)_2]\cdot H_2NDC$ (1): Hydrochloric acid (1.65 mol·L^{-1}, 4 drops) was added with stirring to a mixture of dipotassium 2,6-naphthalenedicarboxylate (0.044 g, 0.15 mmol) and H_2O (10 mL). $TbCl_3\cdot 6H_2O$ (0.038 g, 0.1 mmol) and phen·H_2O (0.04 g, 0.2 mmol) were then added. The mixture was sealed in a 25-mL stainless steel reactor equipped with a Teflon liner and heated at 170 °C for 72 h. Light-yellow crystals of **1** were obtained (0.015 g, 26.0%). $C_{36}H_{21}N_2O_8Tb$ (768.47): calcd. C 56.27, H 2.75, N 3.65; found C 55.98, H 2.53, N 3.55. IR (KBr pellet): $\tilde{\nu}$ = 3433 m, 1705 m, 1617 m, 1548 m, 1493 m, 1422 s, 1362 m, 805 m, 792 m, 727 m cm^{-1}.

$[Ho_2(NDC)_3(phen)_2]\cdot H_2NDC$ (2): The same procedure was applied as that for **1**, but with the following quantities: dipotassium 2,6-naphthalenedicarboxylate (0.044 g, 0.15 mmol), H_2O (10 mL), hydrochloric acid (1.65 mol·L^{-1}, 4 drops), $HoCl_3\cdot 6H_2O$ (0.038 g, 0.1 mmol), and phen·H_2O (0.04 g, 0.2 mmol). Light-yellow crystals of **2** were obtained (0.018 g, 31.0%). $C_{36}H_{21}HoN_2O_8$ (774.48): calcd. C 55.83, H 2.73, N 3.62; found C 55.56, H 2.37, N 3.54. IR (KBr pellet): $\tilde{\nu}$ = 3439 m, 1705 m, 1619 m, 1552 m, 1494 m, 1423 s, 1362 m, 806 m, 792 m cm^{-1}.

$[Yb_2(NDC)_3(phen)_2]\cdot H_2NDC$ (3): The same procedure was applied as that for **1**, but with the following quantities: dipotassium 2,6-naphthalenedicarboxylate (0.044 g, 0.15 mmol), H_2O (10 mL), hydrochloric acid (1.65mol·L^{-1}, 4 drops), $YbCl_3\cdot 6H_2O$ (0.039 g, 0.1 mmol), and phen·H_2O (0.04 g, 0.2 mmol). Light-yellow crystals of **3** were obtained (0.016 g, 27.3%). $C_{36}H_{21}N_2O_8Yb$ (782.59): calcd. C 55.25, H 2.70, N 3.58; found C 55.63, H 2.91, N 3.72. IR (KBr pellet): $\tilde{\nu}$ = 3427 m, 1548 s, 1492 m, 1415 s, 1354 s, 1195 m, 921 w, 796 m, 775 m, 565 m cm^{-1}.

X-Ray Crystallography: The single-crystal X-ray data collection of complexes **1** and **3** was performed using a Nonius−Kappa CCD diffractometer, and that of **2** using a Bruker Smart 1000 CCD diffractometer, and graphite-monochromated Mo-K_α radiation (λ = 0.71073 Å). Semiempirical absorption corrections were applied. The structures were solved by direct methods and refined by full-matrix least-squares methods on F^2 using the SHELXTL-97 program.[51] All non-hydrogen atoms were refined using anisotropic displacement parameters. The hydrogen atoms were generated geometrically and treated by a mixture of independent and constrained

 © 2004 Wiley-VCH Verlag GmbH & Co. KGaA, Weinheim

refinements. Experimental details of the X-ray data collected for **1**, **2**, and **3** are presented in Table 3. CCDC-224511 to -224513 contain the supplementary crystallographic data for this paper. These data can be obtained free of charge at www.ccdc.cam.ac.uk/conts/retrieving.html [or from the Cambridge Crystallographic Data Centre, 12 Union Road, Cambridge CB2 1EZ, UK; Fax: (internat.) + 44-1223-336-033; E-mail: deposit@ccdc.cam.ac.uk].

Acknowledgments

This work is supported by the National Natural Science Foundation of China (20331010) and the State Key Project of Fundamental Research (G1998061308).

[1] M. D. Ward, *Science* **2003**, *300*, 1104−1105.
[2] N. L. Rosi, J. Eckert, M. Eddaoudi, D. T. Vodak, J. Kim, M. O'Keeffe, O. M. Yaghi, *Science* **2003**, *300*, 1127−1129.
[3] R. Kitaura, S. Kitagawa, Y. Kubota, T. C. Kobayashi, K. Kindo, Y. Mita, A. Matsuo, M. Kobayashi, H. C. Chang, T. C. Ozawa, M. Suzuki, M. Sakata, M. Takata, *Science* **2002**, *298*, 2358−2361.
[4] S. A. Bourne, J. J. Lu, B. Moulton, M. J. Zaworotko, *Chem. Commun.* **2001**, 861−862.
[5] Y. Cui, H. L. Ngo, P. S. White, W. B. Lin, *Chem. Commun.* **2003**, 994−995.
[6] B. Rather, M. J. Zaworotko, *Chem. Commun.* **2003**, 830−831.
[7] J. Perles, M. Iglesias, C. Ruiz-Valero, N. Snejko, *Chem. Commun.* **2003**, 346−347.
[8] E. J. Cussen, J. B. Claridge, M. J. Rosseinsky, C. J. Kepert, *J. Am. Chem. Soc.* **2002**, *124*, 9574−9581.
[9] M. Eddaoudi, H. L. Li, O. M. Yaghi, *J. Am. Chem. Soc.* **2000**, *122*, 1391−1397.
[10] M. Eddaoudi, J. Kim, M. O'Keeffe, O. M. Yaghi, *J. Am. Chem. Soc.* **2002**, *124*, 376−377.
[11] L. R. MacGillivray, R. H. Groeneman, J. L. Atwood, *J. Am. Chem. Soc.* **1998**, *120*, 2676−2677.
[12] Y. C. Liang, R. Cao, W. P. Su, M. C. Hong, W. J. Zhang, *Angew. Chem. Int. Ed.* **2000**, *39*, 3304−3307.
[13] R. G. Xiong, X. Xue, H. Zhao, X. Z. You, B. F. Abrahams, Z. L. Xue, *Angew. Chem. Int. Ed.* **2002**, *41*, 3800−3803.
[14] Y. Cui, O. R. Evans, H. L. Ngo, P. S. White, W. B. Lin, *Angew. Chem. Int. Ed.* **2002**, *41*, 1159−1162.
[15] S. O. H. Gutschke, D. L. Price, A. K. Powell, P. T. Wood, *Angew. Chem. Int. Ed.* **2001**, *40*, 1920−1923.
[16] Y. H. Wan, L. P. Zhang, L. P. Jin, S. Gao, S. Z. Lu, *Inorg. Chem.* **2003**, *42*, 4985−4994.
[17] X. J. Zheng, L. P. Jin, S. Z. Lu, *Eur. J. Inorg. Chem.* **2002**, 3356−3363.
[18] Y. B. Wang, X. J. Zheng, W. J. Zhuang, L. P. Jin, *Eur. J. Inorg. Chem.* **2003**, 1355−1360.
[19] Y. B. Wang, X. J. Zheng, W. J. Zhuang, L. P. Jin, *Eur. J. Inorg. Chem.* **2003**, 3572−3582.
[20] L. G. Westin, M. Kritikos, A. Caneschi, *Chem. Commun.* **2003**, 1012−1013.
[21] R. G. Xiong, X. Z. You, B. F. Abrahams, Z. L. Xue, C. M. Che, *Angew. Chem. Int. Ed.* **2001**, *40*, 4422−4425.
[22] P. C. R. Soares-Santos, H. I. S. Nogueira, V. Felix, M. G. B. Drew, R. A. Sa Ferreira, L. D. Carlos, T. Trindade, *Chem. Mater.* **2003**, *15*, 100−108.
[23] O. M. Yaghi, M. O'Keeffe, M. G. Kanatzidis, *J. Solid State Chem.* **2000**, *152*, 1−2.
[24] S. Nishihara, T. Akutagawa, T. Nakamura, *Inorg. Chem.* **2003**, *42*, 2480−2482.
[25] R. T. Song, K. M. Kim, Y. S. Sohn, *Inorg. Chem.* **2003**, *42*, 821−826.
[26] O. M. Yaghi, H. Li, C. Davis, D. Richardson, T. L. Groy, *Acc. Chem. Res.* **1998**, *31*, 474−484.
[27] S. T. Batten, R. Robson, *Angew. Chem. Int. Ed.* **1998**, *37*, 1460−1494.
[28] G. Férey, *J. Solid State Chem.* **2000**, *152*, 37−48.
[29] S. Kitagawa, M. Kondo, *Bull. Chem. Soc. Jpn.* **1998**, *71*, 1739−1753.
[30] B. L. Chen, M. Eddaoudi, S. T. Hyde, M. O'Keeffe, O. M. Yaghi, *Science* **2001**, *291*, 1021−1023.
[31] O. M. Yaghi, M. O'Keeffe, N. W. Ockwig, H. K. Chae, M. Eddaoudi, J. Kim, *Nature* **2003**, *423*, 705−714.
[32] C. Serre, F. Millange, J. Marrot, G. Férey, *Chem. Mater.* **2002**, *14*, 2409−2415.
[33] A. Dimos, D. Tsaousis, A. Michaelides, S. Skoulika, S. Golhen, L. Ouahab, C. Didierjean, A. Aubry, *Chem. Mater.* **2002**, *14*, 2616−2622.
[34] L. Pan, K. M. Adams, H. E. Hernandez, X. T. Wang, C. Zheng, Y. Hattori, K. Kaneko, *J. Am. Chem. Soc.* **2003**, *125*, 3062−3067.
[35] M. Eddaoudi, J. Kim, N. Rosi, D. Vodak, J. Wachter, M. O'Keeffe, O. M. Yaghi, *Science* **2002**, *295*, 469−472.
[36] R. Cao, D. F. Sun, Y. C. Liang, M. C. Hong, K. Tatsumi, Q. Shi, *Inorg. Chem.* **2002**, *41*, 2087−2094.
[37] L. Pan, E. B. Woodlock, X. Wang, *Inorg. Chem.* **2000**, *39*, 4174−4178.
[38] B. Q. Ma, D. S. Zhang, S. Gao, T. Z. Jin, C. H. Yan, G. X. Xu, *Angew. Chem. Int. Ed.* **2000**, *39*, 3644−3646.
[39] R. Wang, H. Liu, M. D. Carducci, T. Jin, C. Zheng, Z. Zheng, *Inorg. Chem.* **2001**, *40*, 2743−2750.
[40] K. O. Kongshaug, H. Fjellvag, *Solid State Sci.* **2002**, *4*, 443−447.
[41] D. W. Min, S. S. Yoon, C. Lee, C. Y. Lee, M. Suh, Y. J. Hwang, W. S. Han, S. W. Lee, *Bull. Korean Chem. Soc.* **2001**, *22*, 531−533.
[42] J. A. Kaduk, J. A. Hanko, *J. Appl. Crystallogr.* **2001**, *34*, 710−714.
[43] S. L. Zheng, M. L. Tong, S. D. Tan, Y. Wang, J. X. Shi, Y. X. Tong, H. K. Lee, X. M. Chen, *Organometallics* **2001**, *20*, 5319−5325.
[44] Y. K. Lee, S. W. Lee, *Bull. Korean Chem. Soc.* **2003**, *24*, 906−910.
[45] S. W. Lee, H. J. Kim, Y. K. Lee, K. Park, J. H. Son, Y. U. Kwon, *Inorg. Chim. Acta* **2003**, *353*, 151−158.
[46] K. O. Kongshaug, H. Fjellvag, *Solid State Sci.* **2003**, *5*, 303−310.
[47] D. W. Min, S. W. Lee, *Bull. Korean Chem. Soc.* **2002**, *23*, 948−952.
[48] A. Deluzet, W. Maudez, C. Daiguebonne, O. Guillou, *Cryst. Growth Des.* **2003**, *3*, 475−479.
[49] F. A. A. Paz, J. Klinowski, *Chem. Commun.* **2003**, 1484−1485.
[50] O. Kahn, *Molecular Magnetism*, VCH Publishers, New York, **1993**.
[51] G. M. Sheldrick, *SHELXTL-97*, *Program for the Refinement of Crystal Structures*, University of Göttingen, Germany, **1997**.

Received November 26, 2003
Early View Article
Published Online May 13, 2004

 © 2004 Wiley-VCH Verlag GmbH & Co. KGaA, Weinheim

Main Chain Ferrocenyl Amides from 1-Aminoferrocene-1′-carboxylic Acid

Katja Heinze*[a] and Manuela Schlenker[a]

Keywords: Metallocenes / Hydrogen bonds / Peptides / Conformation analysis

The non-natural amino acid 1-aminoferrocene-1′-carboxylic acid is synthesised from ferrocene in eight steps. The folding and association phenomena of amido-substituted ferrocenes in the crystal as well as in solution are studied by X-ray crystallography, IR and NMR spectroscopy and DFT calculations. The amino acid is selectively protected at the amino group with the use of the fluorenyl-9-methoxycarbonyl (Fmoc) group. An amide-linked ferrocene dimer is prepared using the HOBt/DCC protocol for amide formation. In the crystal the dimer forms a hydrogen-bonded sheet structure, while in solution dynamic intramolecular hydrogen bonds are observed by VT ^{1}H NMR and IR spectroscopy. The dynamic flipping process has been rationalised by DFT calculations.

(© Wiley-VCH Verlag GmbH & Co. KGaA, 69451 Weinheim, Germany, 2004)

Introduction

Natural materials are often superior to their artificial synthetic counterparts. The structural and functional variety of peptides is very impressive, especially when considering that only a few α-amino acids are incorporated. Introduction of non-natural amino acids into peptides may lead to novel biomaterials or hybrid materials with some properties that are similar to those of natural proteins such as folding, or with additional properties such as conductive, optical or magnetic properties.[1] The latter properties may be obtained through incorporation of transition metals in the main chain,[2] while folding and supramolecular organisation into stable conformations may be achieved by forming intra- and intermolecular hydrogen bonds to control morphological aspects e.g. formation of nanotubes,[3] fibres,[4] or hydrogels.[5]

Ferrocene derivatives[6] have advantageous characteristics such as excellent stability in water and air, and favourable electrochemical properties which have led to applications of ferrocene in molecular receptors, in sensor devices with electrochemical detection,[7−10] and in labelling of biomolecules.[11,12] Furthermore, the inter-ring separation of ferrocene of about 3.3 Å (close to the N···O distance in β-sheets of peptides) and the rotational freedom of the cyclopentadienyl rings has allowed to use ferrocene 1,1′-dicarboxylic acid as an organometallic β-turn mimetic in ferrocene conjugates of amino acids and peptides,[13−16] and as a molecular pair of scissors.[17]

In our approach peptides with ferrocene moieties in the backbone are sequentially built up by a stepwise synthesis giving a well-defined chain length and a primary structure of the peptide which allows full structural characterisation by NMR spectroscopic methods and X-ray crystallography, as well as high-level calculations. The key ferrocene building block is the non-natural amino acid 1-aminoferrocene-1′-carboxylic acid. Its optimised synthesis and the full characterisation of all intermediates using X-ray structural techniques, VT NMR spectroscopy[18] and DFT calculations is reported here, along with the application of fluorenyl-9-methoxycarbonyl (Fmoc)[19] solution-phase chemistry for *N*-protection and acid activation via benzotriazole ester.

Results and Discussion

Synthesis of 1-Aminoferrocene-1′-carboxylic Acid, Hydrochloride

In 1998 the first synthesis of 1-aminoferrocene-1′-carboxylic acid **9** was reported by Butler and Quayle.[20] However, the method yielded a mixture of compounds which could not be separated and purified. In the same year a different synthetic approach was used by Ueyama et. al, which gave pure 1-aminoferrocene-1′-carboxylic acid, hydrochloride **9** but in quite a low yield (28% from **6**[21]). As the yields of the reactions were unsatisfactory for a broader investigation and only few spectroscopic data were given,[20−22] we report on the optimised synthesis (51% from **6**) and detailed characterisation of **9** and all synthetic intermediates.

Scheme 1 summarises the reaction sequence starting from ferrocene **1** to give 1-aminoferrocene-1′-carboxylic acid, hydrochloride **9·HCl**. The key synthon in this synthesis is 1-aminoferrocene (**5**). Although aminoferrocene is a known compound, the main drawback for further preparative work is the tedious multistage preparation starting from ferro-

[a] Anorganisch-Chemisches Institut der Universität Heidelberg, Im Neuenheimer Feld 270, 69120 Heidelberg, Germany
Fax: (internat.) + 49-6221-545707
E-mail: katja.heinze@urz.uni-heidelberg.de

Supporting information for this article is available on the WWW under http://www.eurjic.org or from the author.

 © 2004 Wiley-VCH Verlag GmbH & Co. KGaA, Weinheim **DOI: 10.1002/ejic.200300897**

cene, with ferrocenylazide[23,24], *N*-ferrocenylacetamide[25] or *N*-ferrocenylphthalimide[26] as key intermediates. The best method for a multigram synthesis of aminoferrocene proves to be the Gabriel synthesis from *N*-ferrocenylphthalimide (**4**), although this route necessitates the synthesis of 1-haloferrocene or ferrocene boronic acid as precursors of **4**. A high-yield synthesis of iodoferrocene **3** has been reported by Bildstein et. al.[26] starting with the selective mono-lithiation of ferrocene **1** with *t*BuLi, then isolating the solid lithio-ferrocene **2** and quenching of **2** with iodine. The reaction in pyridine of **3** with phthalimide and Cu_2O as catalyst has been reported to give the *N*-ferrocenylphthalimide **4**.[26] However, the reaction is accompanied by the formation of biferrocenes by copper-mediated C−C coupling even in the presence of excess phthalimide. The product **4** is thus contaminated with biferrocenes and phthalimide which could not be removed. To circumvent these problems, **4** is prepared in the absence of solvent directly from **3** and pre-formed Cu−phthalimide.[27,28] Hydrazinolysis of **4** in ethanol gives pure **5**, which is then *N*-acetylated with acetic anhydride to form 1-(acetylamino)ferrocene **6**. The *N*-acetylamino group deactivates the substituted Cp ring, allowing the selective Friedel−Crafts acylation of **6** with 2,6-dichlorobenzoyl chloride[21,24,29] at the unsubstituted Cp ring giving 1-(acetylamino)-1′-(2,6-dichlorobenzoyl)ferrocene (**7**). Basic hydrolysis of **7** introduces the desired COOH group seen in **8**. However, the yield of this reaction depends highly on the exact stoichiometric amount of added water. Removal of the acetyl protection group with hydrochloric acid furnishes the ferrocene-containing amino acid **9** as the hydrochloride.[21]

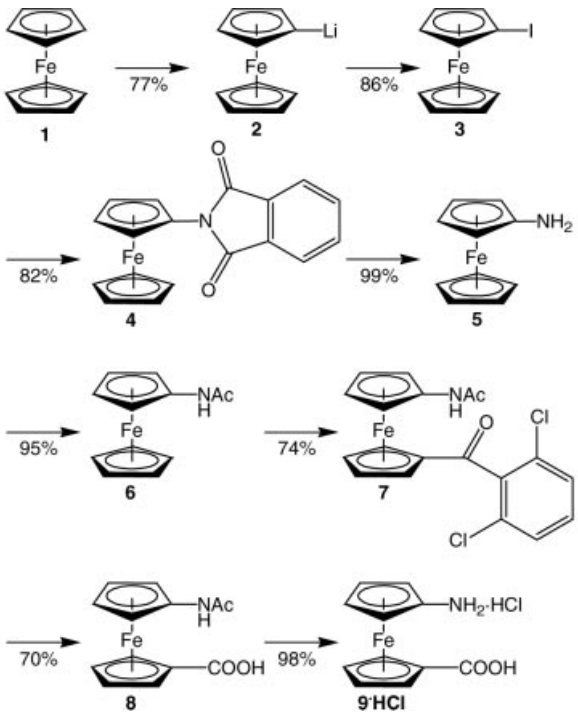

Scheme 1

Crystal Structures of 4-8

2-Ferrocenyl-isoindole-1,3-dione (**4**) crystallises in the monoclinic space group $P2_1/n$ without inclusion of solvent

Table 1. Selected bond lengths (Å) and angles (°) of complexes **4**, **5**, **6**, **7**, **8**, **10**, **11**, **12** and **13**

	4	**5**	**6**	**7**	**8**	**10**(A)	**10**(B)	**11**	**12**	**13**(Fe1)	**13**(Fe2)[d]
Fe1−C1	2.040(4)	2.097(3)	2.04(2)	2.101(3)	2.073(3)	2.064(2)	2.060(2)	2.067(4)	2.078(2)	2.082	2.087
Fe1−C2	2.044(4)	2.061(4)	2.05(2)	2.071(3)	2.056(4)	2.050(2)	2.061(2)	2.071(4)	2.069(3)	2.055	2.041
Fe1−C3	2.043(4)	2.033(4)	2.02(2)	2.044(4)	2.033(4)	2.037(2)	2.038(2)	2.043(4)	2.036(3)	2.019	2.026
Fe1−C4	2.033(4)	2.028(4)	2.02(2)	2.032(4)	2.041(4)	2.038(2)	2.036(2)	2.029(4)	2.033(2)	2.028	2.021
Fe1−C5	2.043(4)	2.056(4)	2.04(2)	2.051(3)	2.064(4)	2.043(2)	2.032(2)	2.037(4)	2.052(2)	2.039	2.032
Fe1−C6	2.039(4)	2.048(4)	2.07(2)	2.040(3)	2.043(4)	2.024(2)	2.023(2)	2.010(4)	2.047(2)	2.014	2.053
Fe1−C7	2.044(4)	2.051(4)	2.00(2)	2.050(4)	2.040(4)	2.033(2)	2.035(2)	2.017(4)	2.035(2)	2.032	2.053
Fe1−C8	2.042(4)	2.043(4)	2.03(2)	2.054(4)	2.047(4)	2.062(2)	2.063(2)	2.054(4)	2.045(3)	2.034	1.999
Fe1−C9	2.043(4)	2.042(4)	2.04(2)	2.053(4)	2.052(4)	2.059(2)	2.055(2)	2.061(4)	2.059(2)	2.017	2.002
Fe1−C10	2.032(4)	2.042(4)	2.04(2)	2.035(4)	2.035(4)	2.038(2)	2.041(2)	2.040(4)	2.058(2)	2.032	2.065
C1−N1	1.421(5)	1.405(5)	1.56(4)	1.405(4)	1.413(5)	1.407(2)	1.409(2)	1.399(5)	1.405(3)	1.395	1.408
N1−C11	1.416(5)	–	1.25(4)	1.351(5)	1.350(5)	1.349(2)	1.348(2)	1.370(6)	1.347(4)	1.347	1.370
N1−C12	1.409(5)	–	–	–	–	–	–	–	–	–	–
C11−O1	1.196(5)	–	1.26(4)	1.236(4)	1.228(5)	1.226(2)	1.225(2)	1.203(5)	1.233(3)	1.229	–
C12−O2	1.211(5)	–	–	–	–	–	–	–	–	–	–
C13−O2	–	–	–	1.221(4)	1.217(4)	1.252(2)	1.248(2)	1.206(4)	1.238(3)	–	–
C13−O3	–	–	–	–	1.335(5)	1.301(2)	1.300(2)	1.424(5)	–	–	–
N1−C11−O1	126.6(4)	–	126(4)	122.8(3)	122.5(4)	123.5(2)	123.3(2)	122.5(4)	123.0(2)	124.0	122.1
N1−C12−O2	125.6(4)	–	–	–	–	–	–	–	–	–	–
O2−C13−O3	–	–	–	–	122.9(4)	123.3(2)	123.6(2)	120.3(4)	–	–	–
C1−C5/subst1[a]	18.1	–	161.2	162.3	17.8	173.7	11.8	16.8	177.3	5.9	168.6
C6−C10/subst2[b]	–	–	–	13.4	174.2	172.5	7.0	171.6	36.3	178.3	–
δ[c]	−6.0	25.2	−34.6	−18.6	−4.8	16.3	11.2	21.0	8.2	−4.2	28.6

[a] Subst1 is the plane defined by the first three atoms of the substituent at C1. [b] Subst2 is the plane defined by the first three atoms of the substituent at C6. [c] δ is defined as the relative rotation of Cp rings (0° = fully eclipsed; 36° = fully staggered). [d] C1−C10, C11, N1, O1 stand for the atoms C21−C30, C13, N2, O2, respectively.

 © 2004 Wiley-VCH Verlag GmbH & Co. KGaA, Weinheim

molecules (Figure 1). Bond lengths and angles in this compound compare well with similar systems (Table 1).[30] The plane of the phthalimido ring system is slightly rotated out of the adjacent Cp ring plane (angle between planes 18°). In a similar ferrocenyl-(2,3-naphthalimide) system with a CH_2 link between ferrocene and the naphthalimide, the substituent ring plane is located almost perpendicular to the Cp ring plane.[30]

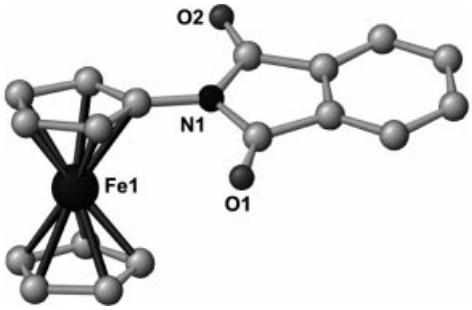

Figure 1. Molecular structure of **4** in the crystal

Aminoferrocene **5** crystallises in the tetragonal space group $I4_1/a$ (Figure 2). The bond lengths and angles are comparable with those found for 1,1′-diaminoferrocene (Table 1).[31] In the crystal the individual molecules of **5** are connected through N−H···N hydrogen bonds forming a helical arrangement along the crystallographic 4_1 screw axis (Figure 2) with a helical pitch of 5.93 Å (corresponding to the crystallographic *c*-axis). The N to N distance is 3.26 Å, and are in agreement with the distances found in the structure of 1,1′-diaminoferrocene (3.26, 3.10, 3.39 Å).[31]

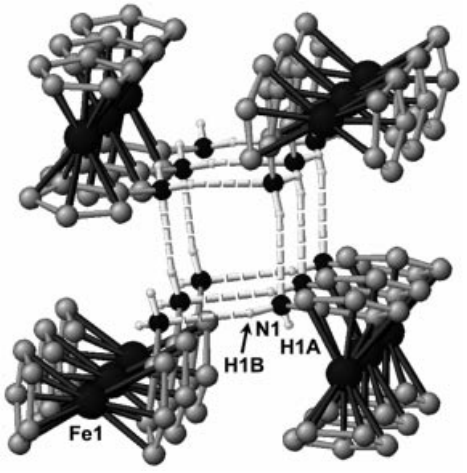

Figure 2. Hydrogen bonding of **5** in the crystal; view approximately along *c*

Compound **6** crystallises in the monoclinic space group $P2_1/n$ (Figure 3, Table 1). The molecules of **6** are connected through intermolecular N−H···O hydrogen bonds that connect the NH_{amide} group and the CO_{amide} group of a neighbouring molecule, forming chains along the *n* glide plane with a repeating distance of 9.54 Å (Figure 3). However, the $NH-CO-CH_3$ group is disordered over two positions, giving two different hydrogen bonds in the crystal: N1H1···O1X (N1 to O1X distance: 2.87 Å) and N1XH1X···O1 (N1X···O1 2.73 Å). A similar hydrogen-bonded chain has been observed in the related iodo-substituted complex $CpFeCpC(=O)NHCH_2I$ with a repeating distance of 9.55 Å and a N to O distance of 2.96 Å.[32]

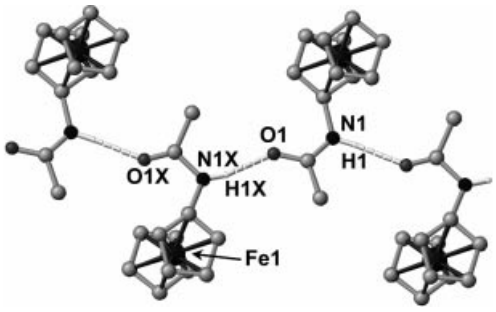

Figure 3. Hydrogen bonding of **6** in the crystal

The disubstituted ferrocene **7** crystallises in the monoclinic space group $P2_1/c$ (Figure 4, Table 1). Due to steric interactions the plane of the dichlorobenzene substituent is located almost perpendicular to the plane of the C6−C10 cyclopentadienyl ring (angle between planes: 82.9°). The molecules of **7** are connected through intermolecular N−H···O hydrogen bonds between the NH_{amide} group and the CO_{amide} group of a neighbouring molecule, forming chains along the 2_1 screw axis with a repeating distance of 9.02 Å; this is similar to that observed in structure **6** (Figure 3). The O1 to N1 distance is 2.88 Å and is similar to those found in **6** and the related complexes $H_3CC(=O)NHCpFeCpC(=O)NHCH_3$ (2.85 and 2.87 Å)[21] and $H_3CC(=O)NHCpFeCpC(=O)OCH_3$ (2.93 Å[33]).

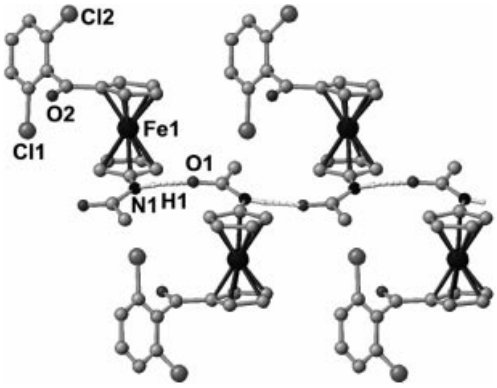

Figure 4. Hydrogen bonding of **7** in the crystal

 © 2004 Wiley-VCH Verlag GmbH & Co. KGaA, Weinheim

The acid **8** crystallises in the orthorhombic space group *Pbca* with inclusion of one methanol molecule (Figure 5, Table 1). The ferrocene complexes are connected through O−H···O hydrogen bonds between the acid OH group (O3H6···O4; O3 to O4 distance: 2.56 Å) over the methanol and the amide CO group (O4H23···O1; O4 to O1 distance: 2.69 Å) to form a helical chain along a twofold axis (parallel to the *b* axis). These chains are further connected through NH···O hydrogen bonds between the amide NH group and the acid CO group (N1H1···O2; N1 to O2 distance: 2.91 Å). The same NH···O hydrogen-bonding motif has also been observed in the crystal structure of the corresponding methyl ester $H_3CC(=O)NHCpFeCp-C(=O)OCH_3$ that forms a dimer with an N to O distance of 2.93 Å.[33]

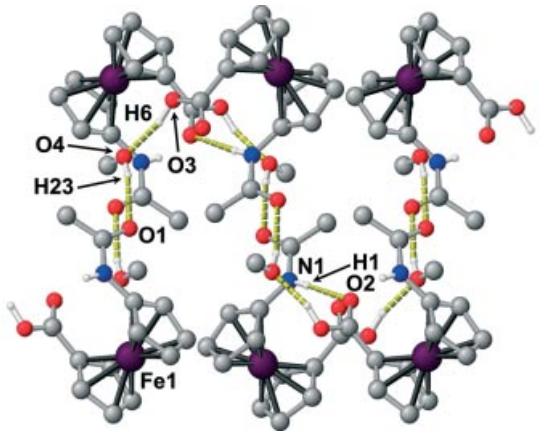

Figure 5. Hydrogen bonding of **8** in the crystal

Properties of 4−9

NMR spectroscopic data of compounds **4**−**13** are collected in Table 2 and Table 3, while UV/Vis spectroscopic and cyclic voltammetric data of **4**−**13** are given in Table 4.

In solution, the phthalimide substituent of **4** undergoes an easy torsional vibration around the C1−N1 bond leading to a time-averaged C_s symmetry of the molecule. Thus, in the ^1H and ^{13}C NMR spectra signal sets for a C_s-symmetric molecule are observed, e.g. only one ^{13}C resonance for the carbonyl carbon nuclei at δ = 167.0 is seen (Table 3; in contrast to the two erroneous reported values of δ = 165.1 and 167.0[26]). The IR absorption spectrum shows the signals assigned to the symmetric and asymmetric CO vibrations at 1778 cm^{-1} and 1717 cm^{-1}, respectively. In the UV/Vis spectrum of **4** bands corresponding to the ferrocene unit and to the phthalimide substituent are observed, and are in agreement with those reported for a similar ferrocenyl-1,8-naphthalimide (Table 4).[30] Further, the cyclic voltammogram of **4** displays waves corresponding to the oxidation of the ferrocene moiety at $E_{1/2}$ = 450 mV and the reduction of the phthalimide group at $E_{1/2}$ = −1470 mV (Table 4).[30]

The hydrogen bonding observed in the crystal of aminoferrocene **5** is also seen in the solid-state IR absorption spectrum: the signals for the NH stretching vibrations appear at 3400 cm^{-1} and 3336 cm^{-1}. The signal for the NH_2 deformation vibration is observed at 1621 cm^{-1}. In concen-

Table 2. ^1H NMR spectroscopic data of complexes **4**−**13**, atom numbering according to the numbering in the crystal structures

	$\Delta\delta_{NH\text{-}1}$[b]	H-1	H-2/5	H-3/4	H-7/10	H-8/9	H-12	Substituent(s)
4[b]	–	–	5.01		4.21 (br. s, 7 H)		–	7.74 (m, 2 H, H-15), 7.86 (m, 2 H, H-14)
5[b]	–	2.63 (br. s, 2 H)	3.98 (pt, 2 H)[a]	3.83 (pt, 2 H)[a]	4.09 (br. s, 5 H)		–	–
6[b]	−2.9	6.59 (br. s, 1 H)	4.53 (br. s, 2 H)	3.97 (br. s, 2 H)	4.15 (br. s, 5 H)		2.00 (s, 3 H)	–
7[b]	−3.4	6.73 (br. s,1 H)	4.69 br. s, 2 H)	4.15 (br. s, 2 H)	4.60 (br. s, 4 H)		2.02 (s, 3 H)	7.33−7.42 (m, 3 H, H-16/17/18)
8[b]	−12	7.15 (br. s, 1 H)	4.65 (br. s, 2 H)	4.07 (br. s, 2 H)	4.46/4.79 (br. s, 2 × 2 H)		2.11 (s, 3 H)	–
9[c]	–	–	4.30/4.51/4.63/4.89 (pt, 4 × 2 H)[a]				–	–
10[d]	−7.0	8.13 (br. s, 1 H)	4.55 (br. s, 2 H)	3.91 (br. s, 2 H)	4.25/4.66 (br. s, 2 × 2 H)		–	4.30 (br. s, 1 H, H-14), 4.47(d[e], 2 H, H-13), 7.32 (m, 4 H, H-17/18), 7.68 (d[f], 2 H, H-16), 7.78(d[f], 2 H, H-19)
11[b]	−3.9	7.42 (br. s, 1 H)	4.91 (br. s, 2 H)	4.15 (br. s, 2 H)	4.72/5.08 (br. s, 2 × 2 H)		1.90 (s, 3 H)	7.44−7.64 (m, 3 H, H-16/17/18), 8.08 (d[g], 1 H, H-15)
12[b]	−5.7	7.78 (br. s, 1 H)	4.44 (br. s, 2 H)	4.03 (br. s, 2 H)	4.34/4.66 (br. s, 2 × 2 H)		2.02 (s, 3 H)	1.05−1.80 (m, 20 H, Cy−CH_2), 3.48−3.59 (m, 1 H, H-15), 4.26 (m, 1 H, H-21), 5.88 (d[h], 1 H, NH)
13[b]	−6.6	7.13 (br. s, 1 H)	4.49 (br. s, 2 H)	4.17 (br. s, 2 H)	4.44/4.68 (br. s, 2 × 2 H)		2.10 (s, 3 H)	–
	−11	8.33 (br. s, 1 H)	4.89 (br. s, 2 H)	4.12 (br. s, 2 H)	4.26 (br. s, 5 H)		–	–

[a] A non-resolved duplet of duplets is denoted pseudo-triplet "pt". [b] In CD_2Cl_2. [c] In D_2O. [d] In $[D]_8THF$. [e] $^3J_{H,H}$ = 6.2 Hz. [f] $^3J_{H,H}$ = 6.8 Hz. [g] $^3J_{H,H}$ = 8.4 Hz. [h] $^3J_{H,H}$ = 7.4 Hz.

 © 2004 Wiley-VCH Verlag GmbH & Co. KGaA, Weinheim

Table 3. ^{13}C NMR spectroscopic data of complexes **4**−**13**; atom numbering according to the numbering in the crystal structures

	C-1	C-2/5	C-3/4	C-6	C-7/10	C-8/9	C-11	C-12	C-13	Substituent(s)
4[a]	89.3	63.4	65.9		69.9		–	–	–	123.5 (C-14), 132.5 (C-13), 134.6 (C-15), 167.0 (C-11)
5[a]	106.5	58.7	63.6		69.2		–	–	–	–
6[b]	95.0	62.1	65.0		69.6		168.9	24.5	–	–
7[a]	96.3	64.1	67.5	80.6	71.8/74.6		168.9	24.1	197.3	129.0 (C-16), 131.1 (C-17), 132.3 (C-15), 138.9 (C-14)
8[c]	98.1	62.3	66.3	74.0	71.5/72.9		168.9	24.3	172.5	–
9[d]		63.7, 68.2, 70.5, 72.7, 81.3, 86.4					–	–	175.0	–
10[e]	99.1	61.2	65.9	73.2	71.3/72.3		–	–	171.6	47.9 (C-14), 120.1 (C-19), 125.4 (C-16), 127.3 and 127.8 (C-17/18), 141.8 (C-20), 144.8 (C-15), 154.0 (C-12)[f]
11[a]	98.6	63.4	67.2	65.6	72.4/74.9		169.4	24.0	167.3	109.2, 120.8, 125.5, 129.5 (C-15/16/17/18), 129.6, 144.1 (C-14/19)
12[a]	94.1	66.0	66.9	79.4	71.3/71.7		169.3	23.8	169.8	25.1, 25.9, 26.6, 31.4, 32.8 ($Cy-CH_2$), 50.7 (C-15), 55.7 (C-21)
13[e]	97.8	63.2	65.9	80.8	70.1/71.0		169.4	23.6	174.9	–
	98.3	61.5	64.4		69.6		–	–	–	–

[a] In CD_2Cl_2. [b] In $CDCl_3$. [c] In $[D]_8$DMSO. [d] In D_2O. [e] In $[D]_8$THF. [f] C^{13} under THF signal.

Table 4. UV/Vis and cyclic voltammetric data of complexes **4**−**13**

	λ_{max} (ε)[a]	λ_{max} (ε)[b]	$E_{1/2}$[c]	$E_{1/2}$[d]
4	443 (370)	325 (1670)	450	−1470
5	443 (195)	–	130	–
6	441 (215)	–	325	–
7	480 (755)	358 (1400)	585	−1480
8	441 (350)	–	525	–
9	431 (160)[e]	–	220[5)]	–
10	441 (230)	347 (590)	525	–
11	457 (430)	370 (555)	670	–
12	441 (450)[f]	–	465	–
13	451 (650)[f]	–	285/590	–

[a] λ_{max}(ferrocene) in nm, ε in $M^{-1}cm^{-1}$ in CH_2Cl_2; extinction conforms to Lambert-Beer's law in the concentration range 2−10 mM. [b] λ_{max}(substituent) in nm, ε in $M^{-1}cm^{-1}$ in CH_2Cl_2. [c] Oxidation $E_{1/2}$(ferrocene) in mV vs. SCE 10^{-3}M in $CH_3CN/n-Bu_4NPF_6$. [d] Reduction $E_{1/2}$(substituent) in mV vs. SCE 10^{-3}M in $CH_3CN/n-Bu_4NPF_6$. [e] In H_2O. [f] In THF.

Table 5. Characteristic IR spectroscopic data of the amide groups of complexes **6**, **7**, **8**, **11**, **12** and **13**

	6	**7**	**8**	**11**	**12**	**13**
amide A (solid)[a]	3262	3275	3322	3359	3319	3327/3316
amide A (CH_2Cl_2)[a]	3435	3431	3303	3428/3363	3291	3430/3292
amide I (solid)[b]	1655	1659	1666	1682	1672	1660/1646
amide I (CH_2Cl_2)[b]	1685	1687	1691	1689	1677	1679/1660
amide II (solid)[c]	1580	1574	1569	1548	1569	1560
amide II (CH_2Cl_2)[c]	1532	1531	1557	1536	1526	1559/1529

[a] Amide A = $\tilde{\nu}_{NH,stretching}$. [b] Amide I = $\tilde{\nu}_{CO,stretching} + \tilde{\nu}_{NH,bending} + \tilde{\nu}_{CN,stretching}$. [c] Amide II = $\tilde{\nu}_{NH,bending} + \tilde{\nu}_{CN,stretching}$.

trated solutions the bands of the NH stretching vibrations are slightly shifted to 3425 and 3354 cm^{-1} showing the presence of hydrogen bonding (in dilute solutions these bands are observed at 3757 and 3692 cm^{-1})[24]. Compound **5** is oxidised at +130 mV (vs. SCE), a much more positive potential than 1,1′-diaminoferrocene (approximately −200 mV vs. SCE[31]). Obviously, the electron-donating effect of the amino groups to the metal centre is additive.[34]

In the solid-state IR absorption spectrum of **6** the characteristic amide vibrations confirm the presence of hydrogen bonds (Table 5). In dilute solutions, however, the bands assigned to amide A and amide I are shifted to higher energies, while that of amide II is shifted to a lower energy, suggesting that hydrogen bonding is absent (Table 5). This finding is also corroborated by the ^1H NMR spectrum of **6** as the signal for the amide proton appears at δ = 6.59 in CD_2Cl_2 at 293 K (Table 2). A weak temperature dependence is indicative of either a non-bonded hydrogen atom or a hydrogen atom involved in a locked hydrogen bond.[13,18] For **6**, the weak temperature dependence of $\Delta\delta_{NH} = -2.9$ ppb K^{-1} is interpreted in terms of the absence of hydrogen bonding (Table 2); thus, **6** is not associated in solution. The cyclic voltammogram of **6** shows that it is oxidised at +325 mV (vs. SCE), a much more positive potential than the amino compound **5** (Table 4).

An IR spectroscopic investigation of **7** shows the presence of hydrogen bonds in the solid state, while in solution no hydrogen bonding is detected (Table 5). This is also verified by the ^1H chemical shift of the amide proton resonating at δ = 6.73 with $\Delta\delta_{NH} = -3.4$ ppb K^{-1} in CD_2Cl_2 (Table 2). Thus, **7** like **6** does not associate in solution. The UV/Vis absorption band for the ferrocene unit of **7** at 480 nm is probably admixed with a charge transfer component (from the electron-rich ferrocene to the electron-deficient aromatic system), and thus appears at a relatively low energy and with a high intensity (Table 4).[35] The absorption band for the aromatic substituent appears at 358 nm. The ferrocene moiety is oxidised at 585 mV and the aromatic substituent is reduced at −1480 mV (Table 4).

The hydrogen bonding observed in the crystal of **8** is also apparent in the solid-state IR absorption spectrum (Table 5). In solution the IR absorption data suggest a hydrogen bond involving the amide hydrogen atom (Table 5). In the proton NMR spectrum a signal at δ = 7.15 in CD_2Cl_2 (δ = 8.40 in THF, Table 2) is observed which is assigned to the amide proton on the basis of the NOESY spectrum (correlation between NH and CH_3). This low-field chemical shift as well as the large temperature depen-

dence $\Delta\delta_{NH} = -12$ ppb K^{-1} confirm that the NH proton is involved in a dynamic hydrogen bond in solution, which can arise from either intermolecular association or intramolecular folding processes.[13,18] The characteristic signal for the vibration of the acid carbonyl group appears at 1715 cm^{-1} in CH_2Cl_2 and in THF, and is similar to that found for ferrocenedicarboxylic acid (1720 cm^{-1} in THF), and suggests the formation of carboxylic acid dimers. As both functional groups are involved in hydrogen bonding, a dynamic intermolecular aggregation in solution is proposed (Scheme 2). The *cis* orientation of the amide groups necessary for intermolecular dimerisation (Scheme 2) is confirmed by NOESY spectroscopy (correlation peak between the CH_3 group and Cp protons H-2/5).

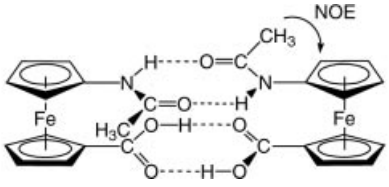

Scheme 2

DFT calculations (see Supporting Information) on monomeric **8** show that the non-hydrogen-bonded structure is the global minimum and the $O_{acid}-H\cdots O_{amide}$ hydrogen-bonded structure is a local minimum 13 kJ mol^{-1} higher in energy, while no minimum is found for the $N_{amide}-H\cdots O_{acid}$ hydrogen-bonded structure. However, the dimeric fourfold hydrogen-bonded structure is calculated to be a minimum 73 kJ mol^{-1} more stable than two isolated molecules of **8** (although this might be an overestimated stabilisation energy due to the basis set superposition error BSSE[36]), confirming the presence of intermolecular hydrogen bonds.

The amino acid **9** can be isolated as the hydrochloride salt **9·HCl** which is soluble and stable in water and dimethyl sulfoxide. Neutralisation of an aqueous solution of **9·HCl** with sodium hydroxide immediately leads to the precipitation of the zwitterionic compound, which rapidly decomposes to a black material at pH > 7. The solid-state IR absorption spectrum of **9·HCl** shows absorption bands that are assigned to the NH and OH groups at 3366, 3177 and 3135 cm^{-1}, indicating extensive hydrogen bonding which is probably intermolecular in nature. The UV/Vis absorption band for the ferrocene moiety of **9·HCl** appears at 431 nm, and is blue-shifted by more than 500 cm^{-1} relative to the bands of e.g. **4**−**6** (441−443 nm) probably due to the cationic nature of the complex.

Peptide Chemistry

A) N-Protection, Crystal and Solution Structure of 10

Since the stability of **9** in alkaline solution is rather poor, *N*-protection of **9** with fluorenyl-9-methyl chloroformate (Fmoc-Cl) has been carried out in buffered solution (phosphate buffer, pH 7) to give the *N*-protected amino acid 1-[(fluoren-9-yl)methyloxycarbonylamino]ferrocene-1′-carboxylic acid (**10**) (Scheme 3).

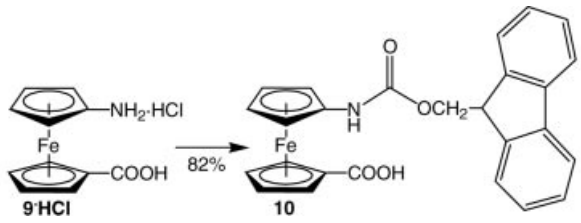

Scheme 3

Compound **10** crystallises in the monoclinic space group $P2_1/c$ with the inclusion of half a molecule dichloromethane per molecule (Figure 6, Table 1). The asymmetric unit contains two independent molecules **10(A)** and **10(B)** which are connected through double O−H···O hydrogen bonds involving the carboxylic acid functions (O3H6···O102, O3···O102 distance: 2.63 Å; O103H106···O2, O103···O2 distance: 2.59 Å) and double N−H···O hydrogen bonds involving the *cis*-orientated urethane HNCO groups (N1H1···O101; N1···O101 distance: 2.83 Å; N101H101···O1; N101-to-O1 distance: 2.86 Å) to form a dimer of approximate C_2 symmetry (Figure 6). The same two eight-membered rings have been detected in the crystal structure of the related Boc-protected complex HOOC−CpFeCpNH(C=O)O*t*Bu (Boc = *tert*-butoxycarbonyl) with O···O distances of 2.66 and 2.66 Å and N···O distances of 2.83 and 2.85 Å.[37] The planes of the fluorenyl substituents are located almost perpendicular to the planes of the cyclopentadienyl rings to which they are attached [**10(A)**: 91.2°, **10(B)**: 83.4°].

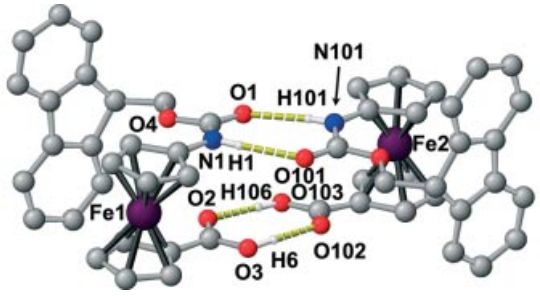

Figure 6. Hydrogen bonding of **10** in the crystal

The hydrogen bonding observed in the crystal of **10** is also confirmed by the IR absorption spectrum which shows the absorption bands assigned to the NH and OH groups between 3500−2800 cm^{-1}, signals for the carbonyl groups at 1707 (vs) and 1664 (s) cm^{-1}, and signals at 1560 (w) and 1544 (w) cm^{-1}. This pattern in the spectral region 1800−1500 cm^{-1} is in accordance with the pattern for a *cis*-orientation of the urethane moiety of **10** calculated by

 © 2004 Wiley-VCH Verlag GmbH & Co. KGaA, Weinheim

DFT [1682 (1.00), 1668 (0.46), 1548 (0.11), 1510 (0.09) cm^{-1}; see Supporting Information].

In CH_2Cl_2 solution two dominant bands are observed at 1707 (vs) and 1673 (s) cm^{-1} and two weak bands at 1570 and 1542 cm^{-1}, suggesting that a *cis*-urethane conformation is the major species. In addition, a shoulder at 1735 cm^{-1} is observed indicating the presence of another species in CH_2Cl_2 solution. In THF solution, however, a different pattern is observed: 1735 (s), 1716 (s) and 1563 (s) cm^{-1}. DFT calculations on **10** with a *trans*-orientated urethane group predict a comparable pattern: 1715 (0.78), 1694 (0.67), 1569 (0.73) cm^{-1} (see Supporting Information). Thus, **10** prefers the *cis*-conformation in CH_2Cl_2 solution and in the crystal and the *trans*-conformation in THF.[38,39] In all cases the acid group appears to be hydrogen bonded via carboxylic acid dimers. In the NH/OH region of the IR absorption spectrum bands are observed at 3266, 3316 and 3425 cm^{-1} in CH_2Cl_2 and at 3269, 3504 and 3573 cm^{-1} in THF. Thus hydrogen bonding involving the NH group exists in CH_2Cl_2 and is absent in THF. NMR spectroscopy supports this interpretation: in CD_2Cl_2 solution two resonances[38,39] assigned to the NH protons are observed at δ = 6.95 (free NH group; *trans* conformation; $\Delta\delta_{NH}$ could not be determined as the signal moves into the multiplet for the fluorenyl protons) and δ = 7.99 (hydrogen-bonded NH group; *cis* conformation; $\Delta\delta_{NH} = -7$ ppb K^{-1}) with equal intensity, together with a doubled signal set for all Cp protons and the CH_2 group, while in THF solution only a single signal set for the NH, Cp and CH_2 protons is observed (Table 2). Based on the experimental data, the proposed dynamic solution structure of **10** is depicted in Scheme 4. The *cis*-orientated species which has the opportunity to form hydrogen bonds is the dominant species in CH_2Cl_2, while the *trans*-orientated conformer without NH hydrogen bonds is the major species in THF. These bonding motifs can be derived from the crystal structure of **10** (Figure 6) by cleaving one and two N−H···O hydrogen bonds, respectively, concomitant with a *cis*/*trans* rearrangement. A similar type of aggregation − albeit more stable − has been proposed for the similar complex **8** (Scheme 2).

B) COOH Activation, Crystal and Solution Structures of 11 and 12

Reaction of the *N*-acetylated amino acid **8** with 1-hydroxybenzotriazole (HOBt) in the presence of 1,3-dicyclohexylcarbodiimide (DCC) leads to the formation of the isolable ferrocenoyl benzotriazole ester **11** (Scheme 5). This reaction is similar to that of ferrocene carboxylic acid with HOBt/DCC.[40] In the absence of HOBt **8** reacts with

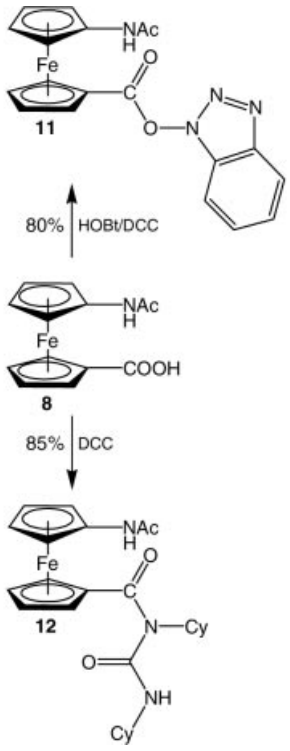

Scheme 5

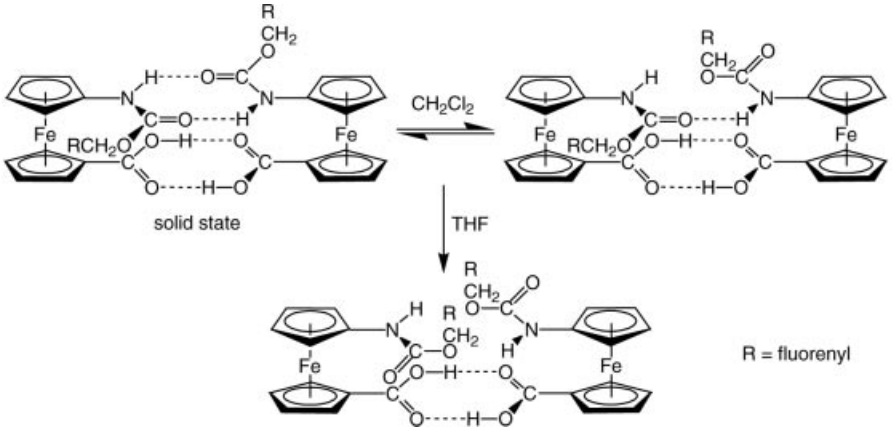

Scheme 4

 © 2004 Wiley-VCH Verlag GmbH & Co. KGaA, Weinheim

DCC to give 1-[1′-(acetylamino)ferrocenylcarbonyl]-1,3-dicyclohexylurea (**12**) in a reaction similar to that of ferrocenecarboxylic acid with DCC.[41−43]

The activated ester **11** crystallises in the monoclinic space group $P2_1/n$ as discrete molecules (Table 1). The benzotriazole substituent is rotated out of the ester plane by 88.6°, similar to Fc-COOBt (96.6°[40]) but pointing in the opposite direction. This orientation allows for an intramolecular hydrogen bond from the amide NH to the central nitrogen atom of the Bt group (N1 to N3 distance: 3.06 Å, Figure 7).

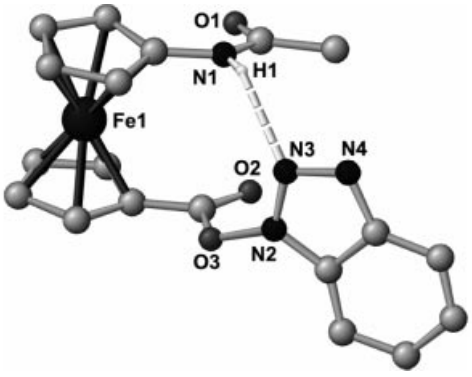

Figure 7. Molecular structure of **11** in the crystal

In the solid state the characteristic IR absorption bands of **11** appear at 3359 (amide A), 1764 (CO_{ester}), 1682 (amide I) and 1548 (amide II) cm^{-1}, while in solution these bands are shifted to 3428, 3363 (amide A), 1787 (CO_{ester}), 1689 (amide I) and 1536 (amide II) cm^{-1} (Table 5). These data show that in the solid state and in solution hydrogen bonding involving the NH part of the amide group occurs. DFT calculations suggest that the solution structure is identical to the crystal structure (Figure 8, see Supporting Information). This intramolecular hydrogen-bonded system is stabilised by 19 kJ mol^{-1} relative to the open form according to DFT calculations. The activation barrier for the hydrogen-bond dissociation is calculated to be 27 kJ mol^{-1}. This interpretation is supported by NMR spectroscopy: the signal for the amide proton appears at $\delta = 7.42$ in CD_2Cl_2 suggesting the presence of hydrogen bonding in dilute solution (Table 2). The signal is temperature dependent, with $\Delta\delta_{NH} = -3.4$ ppb K^{-1} when excluding intermolecular hydrogen bonding (a larger temperature dependence is expected when intermolecular hydrogen bonding is included[13,18]). In the VT-^{1}H NMR spectra the proton signals for the cyclopentadienyl rings H-2/5, H-3/4, H-7/10 and H-8/9 disappear at low temperature with a coalescence temperature (T_C) of 223, 213, 213 and 203 K, respectively, and reappear as separate signals with $\Delta\nu = 168$, 57, 39 and 9 Hz at lower temperature (Figure 8). This finding can be interpreted as a "frozen" interconversion of the enantiomeric hydrogen-bonded structures of **11** rendering the protons pairs H-2/5, H-3/4, H-7/10 and H-8/9 magnetically different (Figure 8). The activation barrier for this process can be estimated to be $\Delta G^{\neq}(T_C) = 43$ kJ mol^{-1}.

In the UV/Vis spectrum the absorption band for the ferrocene unit of **11** appears at 457 nm (probably admixed

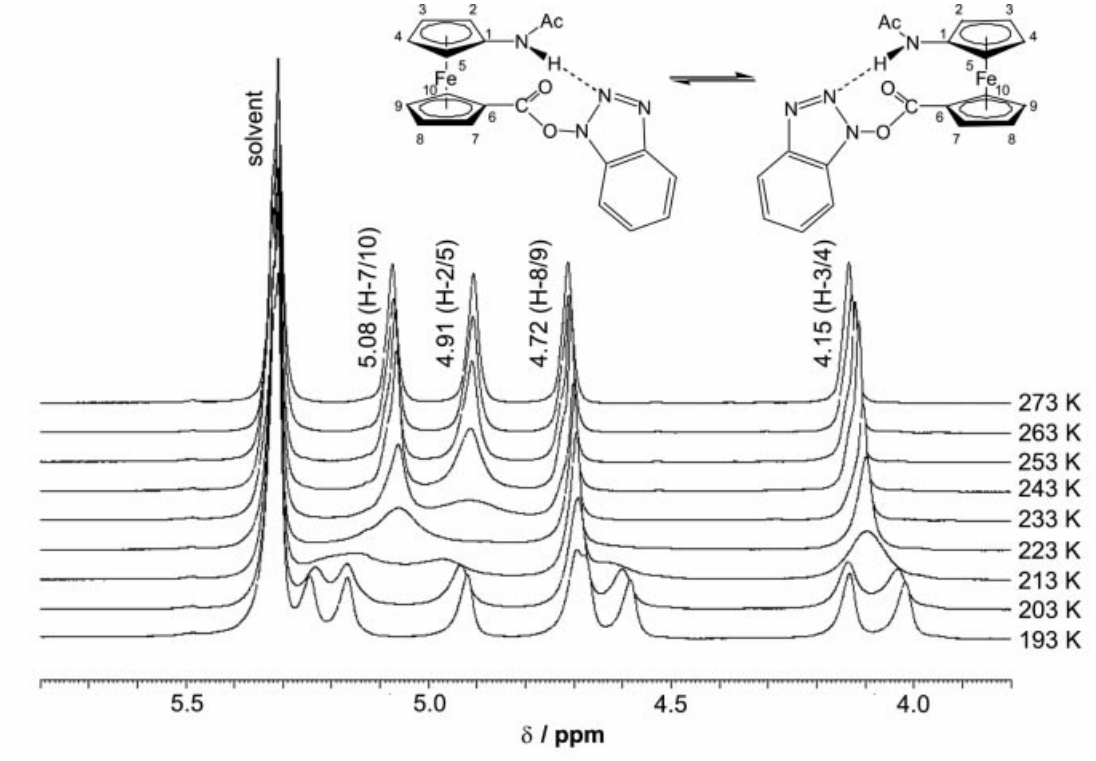

Figure 8. Partial VT-^{1}H NMR spectra of **11** (CD_2Cl_2, 500 MHz) and proposed interconversion of the enantiomeric hydrogen-bonded structures of **11**

 © 2004 Wiley-VCH Verlag GmbH & Co. KGaA, Weinheim

with a charge-transfer component); the absorption band for the benzotriazole group is observed at 370 nm (Table 4). In the cyclic voltammogram the oxidation potential of the ferrocene moiety is 670 mV (Table 4).

The urea derivative **12** crystallises in the monoclinic space group $P2_1/c$ (Table 1). An intramolecular hydrogen bond from the amide proton (N1H1) to the carbonyl oxygen atom O2 is observed (N1···O2 distance: 3.02 Å, Figure 9). This intramolecular hydrogen bond in the crystal structure of **12** proves that such strongly bent connections are indeed possible (cf. proposed solution structures of **11** and **13** and the crystal structure of **11**). The molecules of **12** are connected through two different intermolecular hydrogen-bonding motifs (Figure 10): a centrosymmetric dimeric aggregate through double hydrogen bonds N1H1···O2 (N1···O2 2.96 Å), resulting in bifurcated hydrogen bonds at O2 and H1 and a connection of molecules along the *b*-axis through the NH group of urea (N3H6) and the carbonyl oxygen atom of the *N*-acetyl group (O1) with a donor acceptor distance N3···O1 of 2.95 Å.

The characteristic IR absorption bands in the solid state arise from the hydrogen-bonded NH groups (3319 cm^{-1}), CH_2 and CH groups of the cyclohexyl rings (2934, 2886 cm^{-1}), CO groups (1699, 1672, 1625 cm^{-1}) and CN groups (1569, 1543 cm^{-1}); this is consistent with the observed hydrogen bonding in the crystal structure (Table 5). In solution two absorption bands are observed for the NH stretching vibrations at 3426 and 3291 cm^{-1}. The former is assigned to the non-hydrogen-bonded NH group of the urea moiety and the latter to the hydrogen-bonded NH group of the *N*-acetyl group. Three signals assigned to the carbonyl vibrations appear at 1697, 1677 and 1619 cm^{-1}. The low-energy vibration is assigned the hydrogen-bonded carbonyl group C13−O2. Thus, the IR absorption data suggest a solution structure with an intramolecular hydrogen bond N1−H1···O2 similar to that found in the crystal (Figure 9). The IR spectroscopic data are also in agreement with the DFT-calculated frequencies of the hydrogen-bonded structure (see Supporting Information). NMR experiments confirm this proposed structure as two signals for the amide protons are observed at $\delta = 5.88$ (H^6, NOE correlation to cyclohexyl protons) and $\delta = 7.78$ (H^1), with temperature dependences of $\Delta\delta_{NH} = -13$ and -5.7 ppb K^{-1}, respectively. The large $\Delta\delta_{NH}$ observed for the urea proton H^6 is probably due to the start of intermolecular association at lower temperatures. A static structure as found for **11** was not observed for **12** in the NMR experiments at lower temperatures implying that the activation barrier for the analogous interconversion of hydrogen-bonded structures of **12** is smaller than 40 kJ mol^{-1}.

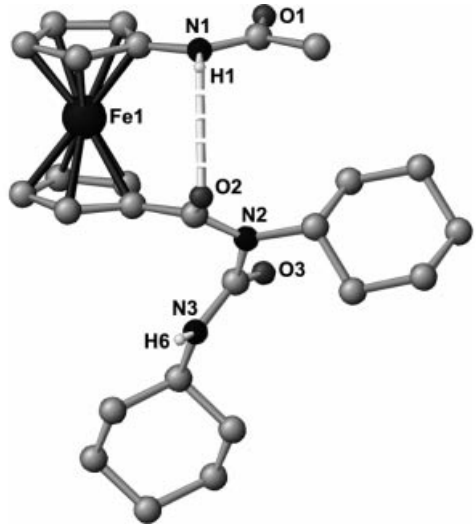

Figure 9. Molecular structure of **12** in the crystal

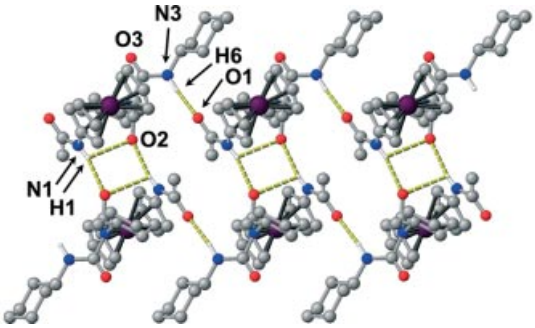

Figure 10. Hydrogen bonding of **12** in the crystal

C) Amide Formation, Crystal and Solution Structure of 13

In the activated ester **11** the C−O ester bond to the benzotriazole is very long (1.423 Å), therefore allowing a facile reaction with amines. Thus, **11** cleanly reacts with aminoferrocene **5** to give the biferrocene **13** (Scheme 6).

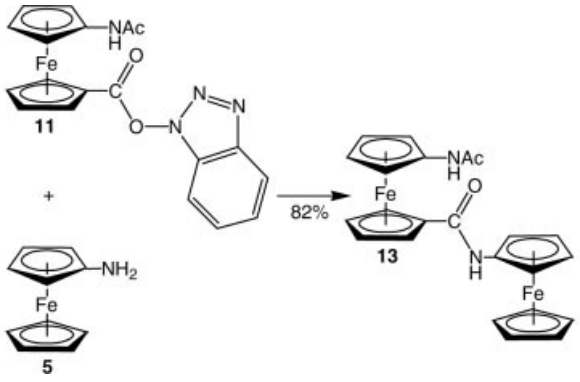

Scheme 6

The diamide **13** crystallises in the polar orthorhombic space group $P2_12_12_1$ as a twinned racemic crystal (Figure 11). The individual molecules are connected through intermolecular hydrogen bonds between the NH-acetyl group and the amide carbonyl oxygen atom (N1···O2 distance: 3.04 Å) and between the NH-amide group and the carbonyl oxygen atom of the acetyl group (N2···O1 distance: 3.03 Å) resulting in a sheet structure (Figure 12).

 © 2004 Wiley-VCH Verlag GmbH & Co. KGaA, Weinheim

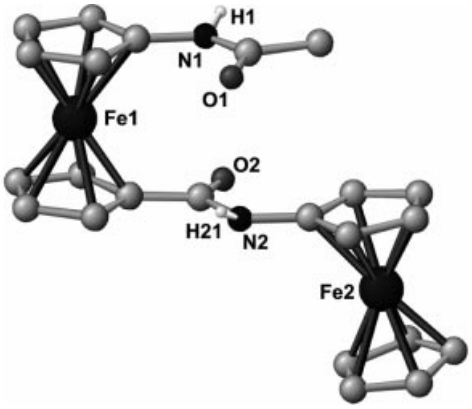

Figure 11. Molecular structure of **13** in the crystal

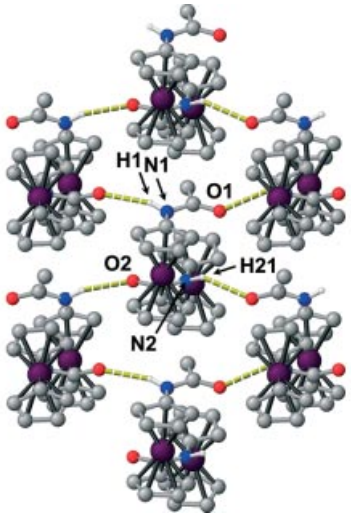

Figure 12. Hydrogen bonding of **13** in the crystal

In the solid-state IR absorption spectrum of **13** the characteristic absorption bands confirm a hydrogen-bonded structure involving all NH protons and all carbonyl groups

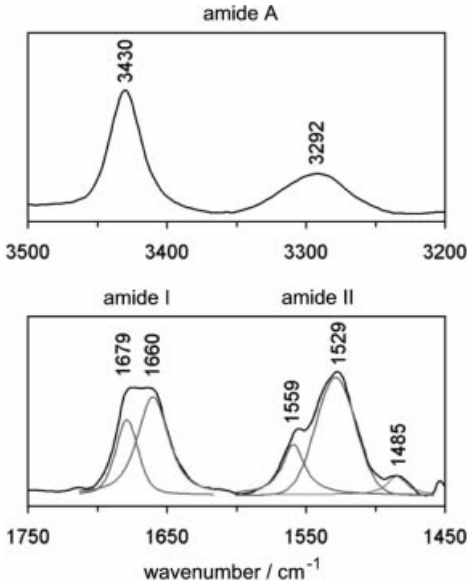

Figure 13. IR spectrum of **13** in CH_2Cl_2

(Table 5). In solution, however, one signal set for a hydrogen-bonded NHCO group (3292, 1660, 1559 cm^{-1}) and one set for a non-hydrogen-bonded NHCO group (3430, 1679, 1529 cm^{-1}) is observed (Table 5, Figure 13). These findings can be accounted for by one of the intramolecularly hydrogen-bonded structures **13a/13b**, as shown in Figure 14, or by a mixture of both structures which are indistinguishable by IR spectroscopy.

In the ^1H NMR spectrum of **13** in CD_2Cl_2 two NH resonances are observed at $\delta = 7.13$ and 8.33 with temperature dependences of $\Delta\delta_{NH} = -6.6$ and -11 ppb K^{-1}, respectively (Table 2). The former signal is assigned to the proton of the NH-acetyl group (NOESY correlation peak between CH_3 and NH) and the latter to the NH proton of the amide bond. The chemical shifts and their temperature dependences suggest that *both* protons are involved in *dynamic* hydrogen bonding. This can be rationalised by a flipping

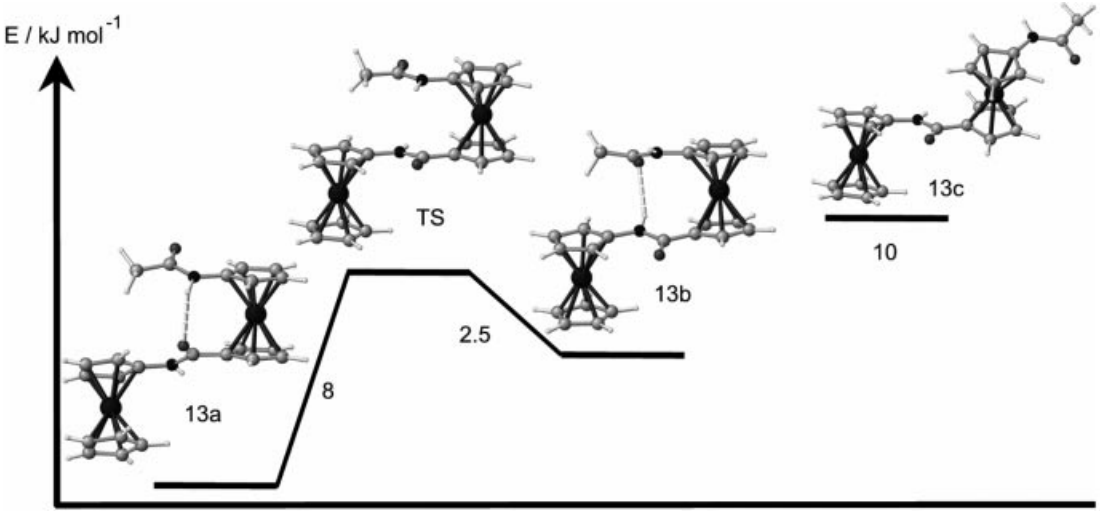

Figure 14. Interconversion of the two hydrogen-bonded structures of **13** (**13a/b**) and the extended form **13c** (DFT: B3LYP, LanL2DZ)

 © 2004 Wiley-VCH Verlag GmbH & Co. KGaA, Weinheim

process that occurs between the two hydrogen-bonded structures **13a** and **13b**, as shown in Figure 14. This equilibrium is fast on the NMR time scale, averaging the NMR signals for free and hydrogen-bonded amide protons. DFT calculations on these two conformers confirm that both are minima on the potential energy surface with **13b** slightly higher in energy than **13a**. The activation barrier for the flipping process **13a** → **13b** is calculated to be only 8 kJ mol^{-1}, supporting the interpretation of a fast equilibrium (Figure 14, see Supporting Information). High-temperature NMR and IR studies show that the folded structures are stable up to 55 °C in chloroform. DFT calculations confirm the stability of **13a/13b** towards unfolding into the extended structure **13c** (Figure 14, $\Delta E_{\mathbf{13a/13c}}$ = 10 kJ mol^{-1}). From these energies, equilibrium compositions of 100:11:2 (**13a**:**13b**:**13c**) at 20 °C and 100:13:3 (**13a**:**13b**:**13c**) at 55 °C can be estimated which explain the experimental findings.

In addition to the folding characteristics imposed by the amide groups, the biferrocene compound **13** shows metal specific properties: (i) **13** absorbs at 451 nm with a small bathochromic shift relative to e.g. **12** (Table 4) and (ii) **13** can be oxidised in two reversible steps at 285 and 590 mV (Table 4). These values are different from the oxidation potentials of comparable mononuclear complexes e.g. **6** and **12** (Table 4). The constant for the comproportionation equilibrium K_C can be estimated to be 1.4×10^5, showing that $\mathbf{13^+}$ is stable towards disproportionation into **13** and $\mathbf{13^{2+}}$.

Conclusion

The optimised synthesis of the non-natural amino acid **9** reported here offers the possibility to incorporate ferrocenes in the main chain of peptides. Standard reactions of peptide synthesis (*N*-protection with Fmoc and acid activation with HOBt/DCC) have been applied to this ferrocene amino acid. The crystal structures of NHC(=O)R-substituted ferrocenes **6**−**13** have been determined by X-ray crystallography in order to elucidate hydrogen-bonding motifs. In most cases hydrogen bonding is found to be intermolecular, except in the case of the active ester **11** (only intramolecular) and the urea derivative **12** (both types). The solution structures have been investigated by a combination of IR and NMR spectroscopy, together with DFT calculations. In solution **6** and **7** are monomeric and non-hydrogen-bonded, **8** and **10** with C(=O)OH groups at the 1′ position form dimers via O−H···O and N−H···O hydrogen bonds, the active ester **11** forms an intramolecular hydrogen bond to the benzotriazole substituent, and **12** and **13** with C(=O)NRR′ groups at the 1′ position form intramolecular N−H···O hydrogen bonds. The structure of the diamide **13** in solution and in the crystal is reminiscent of the typical structures of peptides built from α-amino acids, i.e. α-helix and β-sheet structures, respectively.

This chemistry is currently extended to build ferrocene containing peptides in order to study their folding, electron-transfer and anion-sensing properties.[44]

Experimental Section

Unless noted otherwise, all manipulations were carried out under argon by means of standard Schlenk techniques. All solvents were dried by standard methods and distilled under argon prior to use. Iodoferrocene **3** was prepared by a literature method.[26] All other reagents were used as received from commercial sources. NMR spectra were recorded on Bruker Avance DPX 200 at 200.15 MHz (^{1}H), 50.323 MHz (^{13}C) at 303 K; chemical shifts (δ) in ppm with respect to residual solvent peaks as internal standards: CD_2Cl_2 (^{1}H: δ = 5.32; ^{13}C: δ = 53.5 ppm), $CDCl_3$ (^{1}H: δ = 7.24; ^{13}C: δ = 77.0 ppm), [D]$_6$DMSO (^{1}H: δ = 2.49; ^{13}C: δ = 39.7 ppm), [D]$_8$THF (^{1}H: δ = 1.73, 3.58; ^{13}C: δ = 25.5, 67.7), D_2O (^{1}H: δ = 4.65 ppm). Proton NMR spectra were measured at a concentration of 10 mM. Assignments are based on 2D NMR spectra and by comparison with spectra of similar compounds. IR absorption spectra were recorded on a BioRad Excalibur FTS 3000 spectrometer using CaF_2 cells (concentration < 10 mM) or CsI discs. UV/Vis/NIR spectra were recorded on a Perkin−Elmer Lambda 19, 0.2 cm cells (Hellma, suprasil). Cyclic voltammetry was performed using a glassy carbon electrode, a platinum electrode and a SCE electrode, 10^{-3} M in 0.1 M nBu$_4$NPF$_6$/CH_3CN, potentials are given relative to that of SCE. Mass spectra were recorded on a Finnigan MAT 8400 spectrometer, 4-nitrobenzyl alcohol (FAB). Elemental analyses were performed by the microanalytical laboratory of the Organic Chemistry Department, University of Heidelberg. Melting points were determined with a Gallenkamp capillary melting point apparatus MFB 595 010 and are uncorrected.

Computational Method: Density functional calculations were carried out with the Gaussian98/DFT[45] series of programs. The B3LYP formulation of density functional theory was used employing the LanL2DZ basis set.[45] Harmonic vibrational frequencies and infrared intensities were calculated by numerical second derivatives using analytically calculated first derivatives. Frequencies are not scaled.

Crystallographic Structure Determinations: The measurements were carried out on an Enraf−Nonius Kappa CCD diffractometer using graphite monochromated Mo-K_α radiation. The data were processed using the standard Nonius software.[46] All calculations were performed with the SHELXT PLUS software package. Structures were solved using direct or Patterson methods with the SHELXS-97 program and refined with the SHELXL-97 program.[47] Graphical handling of the structural data during refinement was performed using XMPA[48] and WinRay[49]. Atomic coordinates and anisotropic thermal parameters of the non-hydrogen atoms were refined by full-matrix least-squares calculations. Data relating to the structure determinations are collected in Table 6 and Table 7.

CCDC-225594−225602 contain the supplementary crystallographic data for this paper. These data can be obtained free of charge at www.ccdc.cam.ac.uk/conts/retrieving.html [or from the Cambridge Crystallographic Data Centre, 12 Union Road, Cambridge CB2 1EZ, UK; Fax: (internat.) +44-1223-336-033; E-mail: deposit@ccdc.cam.ac.uk].

Copper Phthalimide: (modified literature procedure)[27,28] A solution of potassium phthalimide (20 g, 107 mmol) in water (50 mL) was added to an aqueous solution of $CuSO_4 \cdot 5H_2O$ (8 g, 32 mmol) in water (50 mL). The mixture was stirred for 30 min and the resulting light blue precipitate was filtered, washed with water and ethanol and dried in vacuo. Yield: 10.8 g (93%).

2-Ferrocenylisoindole-1,3-dione (4): Copper phthalimide (20 g) and iodoferrocene (7 g, 22 mmol) were made into a powder and heated

 © 2004 Wiley-VCH Verlag GmbH & Co. KGaA, Weinheim

Table 6. X-ray crystallographic data of complexes **4**, **5**, **6** and **7**

	4	**5**	**6**	**7**
Formula	$C_{18}H_{13}FeNO_2$	$C_{10}H_{11}FeN$	$C_{12}H_{10}FeNO$	$C_{19}H_{15}Cl_2FeNO_2$
Molecular mass	331.14	201.05	240.06	416.07
Crystal dimension /mm	0.15 × 0.05 × 0.05	0.15 × 0.10 × 0.05	0.10 × 0.03 × 0.03	0.15 × 0.05 × 0.05
Crystal system	monoclinic	tetragonal	monoclinic	monoclinic
Space group (no.)	$P2_1/n$ (14)	$I4_1/a$ (88)	$P2_1/n$ (14)	$P2_1/c$ (14)
a /Å	5.740(1)	23.632(3)	5.913(1)	16.027(3)
b /Å	18.406(4)	23.632(3)	7.488(2)	9.023(2)
c /Å	13.078(3)	5.931(1)	23.405(6)	11.917(2)
β /°	96.91(3)	90.0	92.44(3)	100.55(3)
Cell volume /Å^3	1371.7(5)	3312.3(9)	1035.3(4)	1694.2(6)
Molecular units per cell	4	16	4	4
μ /mm^{-1}	1.105	1.754	1.424	1.218
Density (calcd.) /g cm^{-3}	1.604	1.613	1.540	1.631
T /K	200	200	200	200
Scan range (2Θ)	3.8−54.9	3.4−55.1	5.7−55.0	5.2−55.0
Scan speed /sec frame^{-1}	20	20	40	30
Measured reflections	5748	3488	3740	6587
Unique reflections	3091	1912	2229	3862
Obs. reflections ($I \geq 2\sigma$)	1984	1202	1112	2366
Parameters refined	251	153	154	267
Max. residual electron density/e Å^{-3}	0.55/−0.53	0.31/−0.37	1.92/−0.75	0.46/−0.43
Agreement factors (F^2 refinement)	R_1 = 6.0% R_w = 15.0%	R_1 = 4.9% R_w = 11.3%	R_1 = 15.8% R_w = 40.3%	R_1 = 5.4% R_w = 12.2%

Table 7. X-ray crystallographic data of complexes **8**, **10**, **11**, **12** and **13**

	8	**10**	**11**	**12**	**13**
Formula	$C_{13}H_{13}FeNO_3{\cdot}CH_3OH$	$C_{26}H_{21}FeNO_4{\cdot}0.5CH_2Cl_2$	$C_{19}H_{16}FeN_4O_3$	$C_{26}H_{35}FeN_3O_3$	$C_{23}H_{22}Fe_2N_2O_2$
Molecular mass	319.14	509.75	404.21	493.43	470.13
Crystal dimension /mm	0.05 × 0.02 × 0.02	0.30 × 0.20 × 0.20	0.30 × 0.20 × 0.02	0.35 × 0.15 × 0.06	0.20 × 0.15 × 0.02
Crystal system	orthorhombic	monoclinic	monoclinic	monoclinic	orthorhombic
Space group (no.)	*Pbca* (61)	$P2_1/c$ (14)	$P2_1/n$ (14)	$P2_1/c$ (14)	$P2_12_12_1$ (19)
a /Å	27.396(6)	16.785(2)	9.667(2)	15.867(1)	7.489(2)
b /Å	10.228(2)	16.287(2)	16.146(3)	7.7275(6)	10.286(2)
c /Å	9.5500(19)	17.149(2)	11.253(2)	19.824(2)	24.761(5)
β /°	90.0	106.918(2)	101.85(3)	103.496(2)	90.0
Cell volume /Å^3	2676.0(9)	4485.2(8)	1719.0 (6)	2363.6(3)	1907.4(7)
Molecular units per cell	8	8	44	4	4
μ /mm^{-1}	1.139	0.827	0.906	0.665	1.544
Density (calcd.) /g cm^{-3}	1.584	1.510	1.562	1.327	1.637
T /K	200	173	200	103	200
Scan range (2Θ)	3.0−55.0	3.5−56.6	4.5−54.1	4.2−61.0	4.3−55.4
Scan speed /sec frame^{-1}	30	20	60	20	50
Measured reflections	6102	47935	6127	27762	3031
Unique reflections	3074	11134	3728	7206	3012
Obs. reflections ($I \geq 2\sigma$)	1773	8535	1920	5011	1897
Parameters refined	249	780	251	438	267
Max. residual electron density /e Å^{-3}	0.56/−0.32	0.43/−0.29	0.57/−0.30	1.58/−1.19	0.54/−0.52
Agreement factors (F^2 refinement)	R_1 = 5.3% R_w = 13.9%	R_1 = 3.4% R_w = 7.3%	R_1 = 6.5% R_w = 13.4%	R_1 = 5.2% R_w = 15.2%	6.6 17.7

in vacuo at 135−140 °C for two hours. After cooling to room temperature, the mixture was washed with petroleum ether (boiling range 40−60 °C) to remove unchanged iodoferrocene. The residue was extracted with diethyl ether (5 ×). The combined extracts were evaporated in vacuo to give an orange solid. Yield: 6 g, 18 mmol (82%). $C_{18}H_{13}NO_2Fe$ (331.15): calcd. C 65.29, H 3.96, N 4.23; found C 64.88, H 4.06, N 4.87. IR (CsI): $\tilde{\nu}$ = 3095 (w, CH), 1778 (w, CO_{sym}), 1717 (vs, CO_{asym}), 1479 (s, CN) cm^{-1}. IR (CH_2Cl_2): $\tilde{\nu}$ = 1780 (w, CO_{sym}), 1720 (vs, CO_{asym}), 1484 (s, CN) cm^{-1}. MS (FAB): *m*/*z* (%) = 331 (100) [M$^+$], 266 (64) [M$^+$ − C_5H_5]. M.p. 148−151 °C.

1-Aminoferrocene (5): Compound **4** (3.57 g, 11 mmol) was dissolved in dry ethanol (50 mL). Hydrazine monohydrate (20 mL) was added and the mixture was heated under reflux for two hours. After cooling to ambient temperature, water (80 mL) was added

 © 2004 Wiley-VCH Verlag GmbH & Co. KGaA, Weinheim

and the mixture was extracted with diethyl ether (3 ×). The combined organic phases were dried over Na_2SO_4, filtered and the solvents evaporated to dryness under reduced pressure to give a yellow solid which darkens on storage. Yield: 2.2 g, 10.9 mmol (99%). $C_{10}H_{11}NFe$ (201.05): calcd. C 59.74, H 5.51, N 6.97; found C 59.64, H 5.46, N 7.07. IR (CsI): $\tilde{\nu}$ = 3400, 3336 (w, NH), 3085 (w, CH), 1621 (br., NH_{2def}), 1500 (s, CN) cm^{-1}. IR (CH_2Cl_2): $\tilde{\nu}$ = 3425, 3354 (w, NH), 1616 (br., NH_{2def}), 1497 (s, CN) cm^{-1}. MS (EI): *m/z* (%) = 201 (100) [M^+], 121 (26) [$M^+ - CpNH_2$], 80 (24) [$C_5H_6N^+$].M.p. 153−155 °C.

1-(Acetylamino)ferrocene (6): Compound **5** (2.2 g, 10.9 mmol) was treated with acetic anhydride (20 mL) in the presence of sodium acetate (0.1 g, 1.2 mmol) for 18 hours. After removal of the solvent, the crude pale brown product was purified by recrystallisation from diethyl ether/petroleum ether (40:60) to give a golden powder. Yield: 2.5 g, 10.3 mmol (95%). $C_{12}H_{13}NOFe$ (243.09): calcd. C 59.29, H 5.39, N 5.76; found C 58.80, H 5.41, N 5.81. IR (CsI): $\tilde{\nu}$ = 3262, 3216 (m, NH), 3094, 2854 (w, CH), 1655 (s, CO), 1580 (s, CN) cm^{-1}. IR (CH_2Cl_2): $\tilde{\nu}$ = 3435 (m, NH), 1685 (s, CO), 1532 (s, CN) cm^{-1}. MS (FAB): *m/z* (%) = 243 (100) [M^+]. M.p. 169−171 °C.

1-(Acetylamino)-1′-(2,6-dichlorobenzoyl)ferrocene (7): A solution of **6** (4 g, 16 mmol) in dichloromethane (30 mL) was treated with 2,6-dichlorobenzoyl chloride (2.56 mL, 16 mmol) and $AlCl_3$ (3.06 g, 23 mmol) at 0 °C. The resulting blue solution was stirred for 30 minutes at 0 °C and for two hours at room temperature. The mixture was cooled by carefully adding cold water (50 mL). The colour of the solution turned red immediately. The aqueous solution was extracted with dichloromethane (3 ×) and the combined organic phases were washed with water and 10% NaOH (aq.). After drying over $MgSO_4$ and filtering, the solution was evaporated under reduced pressure to obtain a red oil. Repeated washing with diethyl ether gave a red microcrystalline product. Yield: 4.9 g, 11.8 mmol (74%). $C_{19}H_{15}Cl_2NO_2Fe$ (416.09): calcd. C 54.85, H 3.63, N 3.37; found C 54.78, H 3.81, N 3.35. IR (CsI): $\tilde{\nu}$ = 3275, 3223 (m, NH), 3105, 2853 (w, CH), 1659 (s, CO), 1638 (sh, CO), 1574 (s, CN) cm^{-1}. IR (CH_2Cl_2): $\tilde{\nu}$ = 3431 (w, NH), 1687 (s, CO), 1655 (s, CO), 1531 (s, CN) cm^{-1}. MS (EI): *m/z* (%) = 415 (100) [M^+], 373 (22) [$M^+ - C_2H_2O$], 293 (16) [$M^+ - CpNHCOCH_3$], 178 (100) [$M^+ - CpCOAr$]. M.p. 160 °C.

1-(Acetylamino)-ferrocene-1′-carboxylic Acid (8): A solution of **7** (3.5 g, 8.4 mmol) in 1,2-dimethoxyethane (20 mL) was added to a slurry of potassium *tert*-butoxide (3.8 g, 33 mmol) and water (0.15 mL) while cooling under ice. The red solution was heated under reflux for one hour. A colour change from red to brown was observed. After cooling to ambient temperature, water (20 mL) was added and the solution was washed with diethyl ether. The organic phase was back extracted with 10% NaOH (aq.) and water. The combined aqueous phases were acidified with dilute HCl. The crude product was obtained by extraction with ethyl acetate, drying over $MgSO_4$ and evaporation to dryness. After repeated washing with diethyl ether, an orange-brown product was obtained. Yield: 1.7 g, 5.9 mmol (70%). $C_{13}H_{13}NO_3Fe$ (287.10): calcd. C 54.39, H 4.56, N 4.88; found C 54.38, H 4.55, N 4.83. IR (CsI): $\tilde{\nu}$ = 3322, 3225 (m, NH), 3300−2500 (br., OH), 1698 (sh, CO), 1666 (s, CO), 1569 (s, CN) cm^{-1}. IR (CH_2Cl_2): $\tilde{\nu}$ = 3303 (w, NH), 3235 (w, OH), 1715 (s, CO), 1691 (sh, CO), 1557 (s, CN) cm^{-1}. MS (EI): *m/z* (%) = 287 (100) [M^+], 245 (4) [$M^+ - C_2H_2O$], 178 (28) [$M^+ - CpCOOH$], 165 (4) [$M^+ - CpNHCOCH_3$], 135 (22) [$M^+ - CpCOOH - C_2H_2O$]. M.p. 146−147 °C.

1-Aminoferrocene-1′-carboxylic Acid, Hydrochloride (9·HCl): Compound **8** (0.6 g, 2 mmol) was heated under reflux in 6 N HCl (aq.) (15 mL) for 30 minutes. The mixture turned to a clear brown solution. After filtration, the solvents were evaporated to dryness and the brown residue was washed with tetrahydrofuran and diethyl ether to obtain the product as a light brown solid. Yield: 0.55 g, 1.96 mmol (98%). $C_{11}H_{11}NO_2Fe$ (245.06)·2HCl·0.5H_2O: calcd. C 40.41, H 4.32, N 4.28; found C 39.98, H 4.52, N 4.78. IR (CsI): $\tilde{\nu}$ = 3366 (vs, OH), 3177, 3135, 3030 (m, NH_3^+), 1628 (m, CO) cm^{-1}. MS (FAB): *m/z* (%) = 245 (100) [M^+], 228 (24) [$M^+ - NH_4$]. M.p. 165 °C (dec.).

1-[(Fluoren-9-yl)methyloxycarbonylamino]ferrocene-1′-carboxylic Acid (10): 1-Aminoferrocene-1′-carboxylic acid, hydrochloride **9·HCl** (1.1 g, 3.9 mmol) was dissolved in phosphate buffer (20 mL) and the pH was adjusted to 7. 9-Fluorenylmethyl chloroformate (1.03 g, 3.98 mmol) dissolved in dioxane (10 mL) was added to the solution. A bright orange solid separated from the solution immediately after the addition. After stirring overnight, the precipitate was collected by filtration and washed twice with diethyl ether. Recrystallisation from dichloromethane gave an orange powder. Yield: 1.5 g, 3.2 mmol (82%). $C_{26}H_{21}NO_4Fe$ (467.30)·0.5CH_2Cl_2: calcd. C 62.44, H 4.35, N 2.75; found C 62.25, H 4.34, N 2.87. IR (CsI): $\tilde{\nu}$ = 3263, 3153 (m, NH), 3400−2800 (br., OH), 1707 (s, CO), 1664 (s, CO), 1560 (w, CN) cm^{-1}. IR (CH_2Cl_2): $\tilde{\nu}$ = 3425, 3316 (w, NH), 3266 (w, OH), 1735 (s, CO), 1707 (s, CO), 1673 (s, CO), 1570, 1544 (m, CN) cm^{-1}. IR (THF): $\tilde{\nu}$ = 3573, 3504 (w, NH), 3269 (w, OH), 1735 (s, CO), 1717 (s, CO), 1563 (m, CN) cm^{-1}. MS (FAB): *m/z* (%) = 467 (100) [M^+]. M.p. 118 °C.

Benzotriazol-1-yl 1-(Acetylamino)ferrocene-1′-carboxylate (11): Dicyclohexylcarbodiimide (0.86 g, 4.2 mmol) and *N*-hydroxybenztriazole (0.415 g, 4.2 mmol) was added to a solution of **8** (1.1 g, 3.8 mmol) in dichloromethane (10 mL). The mixture was stirred at room temperature overnight. After filtering, the solution was washed with aqueous $NaHCO_3$, saturated NaCl (aq.) and 2% HCl (aq.). After drying over $MgSO_4$, the solvent was removed in vacuo and the crude product was purified by column chromatography on silica gel with ethyl acetate as eluent. After removal of the solvent under reduced pressure an orange red powder was obtained. Yield: 1.23 g, 3.0 mmol (80%). $C_{19}H_{16}N_4O_3Fe$ (404.21): calcd. C 56.46, H 3.99, N 13.86; found C 57.13, H 4.47, N 13.17. IR (CsI): $\tilde{\nu}$ = 3359 (m, NH), 1764 (s, CO), 1682 (s, CO), 1548 (s, CN), 1491 (m) cm^{-1}. IR (CH_2Cl_2): $\tilde{\nu}$ = 3428, 3363 (w, NH), 1787 (s, CO), 1689 (s, CO), 1536 (s, CN),1485(m) cm^{-1}. MS (FAB): *m/z* (%) = 404 (100) [M^+]. M.p. 133 °C.

1-[1′-(Acetylamino)ferrocenylcarbonyl]-1,3-dicyclohexylurea (12): Compound **8** (1.02 g, 3.5 mmol) was dissolved in tetrahydrofuran (20 mL) and 1,3-dicyclohexylcarbodiimide (0.73 g, 3.5 mmol) was added to the stirred solution. After standing overnight at room temperature, the solvent was removed in vacuo and the crude product was purified by column chromatography on silica gel with ethyl acetate as eluent. The solvent was removed under reduced pressure and an orange-brown product was obtained. Yield: 1.46 g, 3.0 mmol (85%). $C_{26}H_{35}N_3O_3Fe$·0.18CH_2Cl_2 (493.43·0.18CH_2Cl_2): calcd. C 61.80, H 7.00, N 8.26; found C 61.84, H 6.75, N 7.85. IR (CsI): $\tilde{\nu}$ = 3319 (s, NH), 2934 (vs, CH_2), 2856 (s, CH), 1699 (s, CO), 1672 (vs, CO), 1625 (s, CO), 1569 (s, CN), 1541 (m, CN) cm^{-1}. IR (CH_2Cl_2): $\tilde{\nu}$ = 3426 (m, NH), 3291 (m, NH), 2936 (s, CH_2), 2858 (m, CH), 1697 (s, CO), 1677 (s, CO), 1619 (m, CO), 1526 (s, CN), 1510 (s, CN) cm^{-1}. MS (FAB): *m/z* (%) = 493 (20) [M^+], 368 (93) [$M^+ - CyNCO$], 178 (100) [FeCpNHAc]. M.p. 158 °C.

($CH_3CONH-C_5H_4$)Fe(C_5H_4-$CONH-C_5H_4$)Fe(C_5H_5) (13): Compound **11** (1.20 g, 2.9 mmol) and aminoferrocene **5** (0.59 g, 2.9 mmol) were dissolved in tetrahydrofuran (10 mL) and stirred

 © 2004 Wiley-VCH Verlag GmbH & Co. KGaA, Weinheim

for 12 h at ambient temperature. The solvent was removed in vacuo and the residue was dissolved in dichloromethane. The solution was washed with water, aqueous $NaHCO_3$, saturated NaCl and 2% HCl. The organic layer was dried over $MgSO_4$ and the solvent was removed under reduced pressure. Recrystallisation from dichloromethane gave an orange-brown product. Yield: 1.1 g, 2.4 mmol (82%). $C_{23}H_{22}N_2O_2Fe_2$ (470.13): calcd. C 58.76, H 4.72, N 5.96; found C 58.51, H 5.53, N 6.40. IR (CsI): $\tilde{\nu}$ = 3327, 3316 (m, NH), 1660 (s, CO), 1646 (s, CO), 1560 (vs, CN) cm^{-1}. IR (CH_2Cl_2): $\tilde{\nu}$ = 3430, 3292 (w, NH), 1679, (s, CO), 1660 (s, CO), 1559, 1529 (s, CN), 1485 (w) cm^{-1}. MS (FAB): *m*/*z* (%) = 470 (100) [M^+], 405 (38) [M^+ − Cp]. M.p. 196 °C.

Acknowledgments

This work was supported by the Deutsche Forschungsgemeinschaft and the Fonds der Chemischen Industrie. The permanent, generous support from Prof. Dr. G. Huttner is gratefully acknowledged. We thank Simone Leingang for preparative assistance.

[1] H.-A. Klok, *Angew. Chem. Int. Ed.* **2002**, *114*, 1579−1583; *Angew. Chem. Int. Ed.* **2002**, *41*, 1509−1513.
[2] P. Nguyen, P. Gómez-Elipe, I. Manners, *Chem. Rev.* **1999**, *99*, 1515−1548.
[3] D. T. Bong, T. D. Clark, J. R. Granja, M. R. Ghadiri, *Angew. Chem. Int. Ed.* **2001**, *113*, 1016−1041; *Angew. Chem. Int. Ed.* **2001**, *40*, 988−1011.
[4] A. Aggeli, M. Bell, N. Boden, J. N. Keen, P. F. Knowles, T. C. B. McLeish, M. Pitkeathly, S. E. Radford, *Nature* **1997**, *386*, 259−262.
[5] T. C. Holmes, S. de Lacalle, X. Su, G. Liu, A. Rich, S. Zhang, *Proc. Natl. Acad. Sci. USA* **2000**, *97*, 6728−6733.
[6] T. J. Peckham, P. Gómez-Elipe, I. Manners in *Metallocenes* (Eds.: A. Togni, R. L. Haltermann), Wiley-VCH, Weinheim, **1998**, pp. 723−771.
[7] P. D. Beer, *Acc. Chem. Res.* **1998**, *31*, 71−80.
[8] P. D. Beer, J. J. Davis, D. A. Drillsma-Milgrom, F. Szemes, *Chem. Commun.* **2002**, 1716−1717.
[9] T. Ihara, M. Nakayama, M. Murata, K. Nakano, M. Maeda, *Chem. Commun.* **1997**, 1609−1610.
[10] K. Kavallieratos, S. Hwang, R. H. Crabtree, *Inorg. Chem.* **1999**, *38*, 5184−5186.
[11] K. Severin, R. Bergs, W. Beck, *Angew. Chem. Int. Ed.* **1998**, *110*, 1722−1743, *Angew. Chem. Int. Ed.* **1998**, *37*, 1634−1654.
[12] O. Brosch, T. Weyhermüller, N. Metzler-Nolte, *Inorg. Chem.* **1999**, *38*, 5308−5313.
[13] D. R. van Staveren, T. Weyhermüller, N. Metzler-Nolte, *Dalton Trans.* **2003**, 210−220.
[14] A. Nomoto, T. Moriuchi, S. Yamazaki, A. Ogawa, T. Hirao, *Chem. Commun.* **1998**, 1963−1964.
[15] T. Moriuchi, A. Nomoto, K. Yoshida, T. Hirao, *Organometallics* **2001**, *20*, 1008−1013.
[16] T. Moriuchi, A. Nomoto, K. Yoshida, A. Ogawa, T. Hirao, *J. Am. Chem. Soc.* **2001**, *123*, 68−75.
[17] T. Muraoka, K. Kinbara, Y. Kobayashi, T. Aida, *J. Am. Chem. Soc.* **2003**, *125*, 5612−5613.
[18] E. S. Stevens, N. Sugawara, G. M. Bonora, C. Toniolo, *J. Am. Chem. Soc.* **1980**, *102*, 7048−7050.
[19] *Fmoc Solid Phase Peptide Synthesis* (Eds.: W. C. Chan, P. D. White), Oxford University Press, Oxford, **2000**.
[20] J. R. Butler, S. C. Quayle, *J. Organomet. Chem.* **1998**, *552*, 63−68.
[21] T. Okamura, K. Sakauye, N. Ueyama, A. Nakamura, *Inorg. Chem.* **1998**, *37*, 6731−6736.
[22] L. Barisić, V. Rapić, V. Kovač, *Croat. Chem. Acta* **2002**, *75*, 199−210.
[23] D. W. Hall, J. H. Richards, *J. Org. Chem.* **1963**, *28*, 1549−1554.
[24] D. C. D. Butler, C. J. Richards, *Organometallics* **2002**, *21*, 5433−5436.
[25] M. Herberhold, M. Ellinger, W. Kremnitz, *J. Organomet. Chem.* **1983**, *241*, 227−240.
[26] B. Bildstein, M. Malaun, H. Kopacka, K. Wurst, M. Mitterböck, K.-H. Onania, G. Opromolla, P. Zanello, *Organometallics* **1999**, *18*, 4325−4336.
[27] A. N. Nesmeyanov, W. A. Ssazonova, D. N. Drosa, *Chem. Ber.* **1960**, *93*, 2717−2729.
[28] N. Monserrat, A. W. Parkins, A. R. Tomkins, *J. Chem. Res. Synop.* **1995**, 336−337.
[29] M. Derenberg, P. Hodge, *Tetrahedron. Lett.* **1971**, *41*, 3825−3828.
[30] C. J. McAdam, B. H. Robinson, J. Simpson, *Organometallics* **2000**, *19*, 3644−3653.
[31] A. Shafir, M. P. Power, G. D. Whitener, J. Arnold, *Organometallics* **2000**, *19*, 3978−3982.
[32] K. Kam-Wing Lo, J. Shing-Yip Lau, D. Chun-Ming Ng, N. Zhu, *J. Chem. Soc., Dalton Trans.* **2002**, 1753−1756.
[33] G. Pavlović, L. Barisić, V. Rapić, I. Leban, *Acta Crystallogr., Sect. E* **2002**, *58*, m13−m15.
[34] S. Lu, V. V. Strelets, M. F. Ryan, W. J. Pietro, A. B. P. Lever, *Inorg. Chem.* **1996**, *35*, 1013−1023.
[35] Semiempirical ZINDO calculations confirm this assignment: see for example: D. R. Kanis, M. A. Ratner, T. J. Marks, *J. Am. Chem. Soc.* **1990**, *112*, 8203−8204.
[36] W. Koch, M. C. Holthausen, *A Chemist's Guide to Density Functional Theory*, Wiley-VCH, Weinheim, **2001**.
[37] G. Pavlović, L. Barisić, V. Rapić, V. Kovač, *Acta Crystallogr., Sect. C* **2003**, *59*, m55−m57.
[38] *cis*/*trans*-Conformers of urethane derivatives have been observed in the crystal: H. Oku, K. Yamada, R. Katakai, *Acta Crystallogr., Sect. E* **2003**, *59*, o1130−o1132.
[39] *cis*/*trans*-Conformers of Fmoc protected amino acids have been observed in solution: G. Valle, G. M. Bonora, C. Toniolo, *Can. J. Chem.* **1984**, *62*, 2661−2666.
[40] H.-B. Kraatz, J. Lusztyk, G. D. Enright, *Inorg. Chem.* **1997**, *36*, 2400−2405.
[41] A. F. Neto, J. Miller, V. Faria de Andrade, S. Yumi Fujimoto, M. M. de Freitas Alfonso, F. C. Archanjo, V. A. Darin, M. L. Andrade de Silva, Á. D. L. Borges, G. Del Ponte, *Z. Anorg. Allg. Chem.* **2002**, *628*, 209−216.
[42] E. M. Acton, R. M. Silverstein, *J. Org. Chem.* **1959**, *24*, 1487−1490.
[43] H. H. Lau, H. Hart, *J. Org. Chem.* **1959**, *24*, 280−281.
[44] P. D. Beer, P. A. Gale, *Angew. Chem. Int. Ed.* **2001**, *113*, 502−532; *Angew. Chem. Int. Ed.* **2001**, *40*, 486−516.
[45] M. J. Frisch, G. W. Trucks, H. B. Schlegel, G. E. Scuseria, M. A. Robb, J. R. Cheeseman, V. G. Zakrzewski, J. A. Montgomery Jr., R. E. Stratmann, J. C. Burant, S. Dapprich, J. M. Millam, A. D. Daniels, K. N. Kudin, M. C. Strain, O. Farkas, J. Tomasi, V. Barone, M. Cossi, R. Cammi, B. Mennucci, C. Pomelli, C. Adamo, S. Clifford, J. Ochterski, G. A. Petersson, P. Y. Ayala, Q. Cui, K. Morokuma, D. K. Malick, A. D. Rabuck, K. Raghavachari, J. B. Foresman, J. Cioslowski, J. V. Ortiz, B. B. Stefanov, G. Liu, A. Liashenko, P. Piskorz, I. Komaromi, R. Gomperts, R. L. Martin, D. J. Fox, T. Keith, M. A. Al-Laham, C. Y. Peng, A. Nanayakkara, C. Gonzalez, M. Challacombe, P. M. W. Gill, B. Johnson, W. Chen, M. W. Wong, J. L. Andres, C. Gonzalez, M. Head-Gordon, E. S. Replogle, J. A. Pople, Gaussian 98, revision A.6, Gaussian, Inc., Pittsburgh PA, **1998**, http://www.gaussian.com.
[46] R. Hooft, Collect, Data Collection Software, Nonius, The Netherlands, **1998**, http://www. nonius. com.
[47] G. M. Sheldrick, *SHELXS-97, Program for Crystal Structure Solution*, University of Göttingen, Germany, **1997**, http://www.shelx.uni-ac.gwdg.de/shelx/index.html; G. M. Sheldrick, *SHELXL-97, Program for Crystal Structure Refinement*, University of Göttingen, Germany, **1997**, http://www.shelx.uni-

 © 2004 Wiley-VCH Verlag GmbH & Co. KGaA, Weinheim

ac.gwdg.de/shelx/index.html; *International Tables for X-ray Crystallography*, Kynoch Press, Birmingham, U. K., **1974**, vol. 4.
[48] L. Zsolnai, G. Huttner, *XPMA*, University of Heidelberg, Germany, **1998**, http://www.rzuser.uni-heidelberg.de/~il1/laszlo/xpm.html.
[49] R. Soltek, G. Huttner, *WinRay*, University of Heidelberg, Germany, **1999**, http://www.uni-heidelberg.de/institute/fak12/AC/huttner/frame/frame_soft.html

Received December 4, 2003
Early View Article
Published Online May 13, 2004

 © 2004 Wiley-VCH Verlag GmbH & Co. KGaA, Weinheim

Synthesis, Crystal Structures and Electrical Conductivities of the Ionic Liquid Compounds Butyldimethylimidazolium Tetrafluoroborate, Hexafluorophosphate and Hexafluoroantimonate

Philipp Kölle[a] and Richard Dronskowski*[a]

Keywords: Electrochemistry / Ionic liquids / Packing efficiency / X-ray diffraction

The unit of the conductivities in Figure 7 on p. 2317 and in Table 3 on p. 2318 of the original article[1] is incorrect; the correct unit is mS cm^{-1}.

[1] P. Kölle, R. Dronskowski, *Eur. J. Inorg. Chem.* **2004**, 2313−2320 (DOI: 10.1002/ejic.200300940).

Received June 11, 2004
The Authors

[a] Institut für Anorganische Chemie, Rheinisch-Westfälische Technische Hochschule
52056 Aachen, Germany
E-mail: drons@HAL9000.ac.rwth-aachen.de

 DOI: 10.1002/ejic.200400507 © 2004 Wiley-VCH Verlag GmbH & Co. KGaA, Weinheim

EurJIC
European Journal of Inorganic Chemistry

Issue 15/2004

Pages 2991–3186

Papers available ahead of print in Early View at www.interscience.wiley.com

Earliest available Table of Contents:
Automatically, free of charge by e-mail through
www.interscience.wiley.com/alerts

COVER PICTURE

The cover picture shows a view in perspective of a novel phosphovanadate layered structure intercalated by 4,4′-bipyridinium cations which act as hydrogen-bonded pillars between adjacent layers. These inorganic layers are constructed by an unprecendented secondary tetrametallic V^V building unit exhibiting a distorted cubane-type structural motif. Details are discussed in the article by J. Rocha et al. on p. 3031 ff.

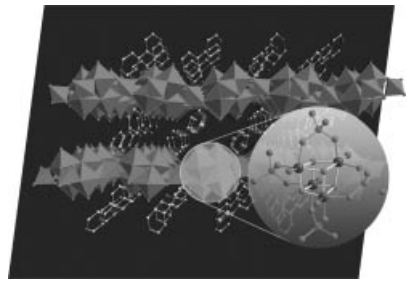

MICROREVIEW

Contents

3003 **C. J. Marmion,* D. Griffith, K. B. Nolan***

Hydroxamic Acids – An Intriguing Family of Enzyme Inhibitors and Biomedical Ligands

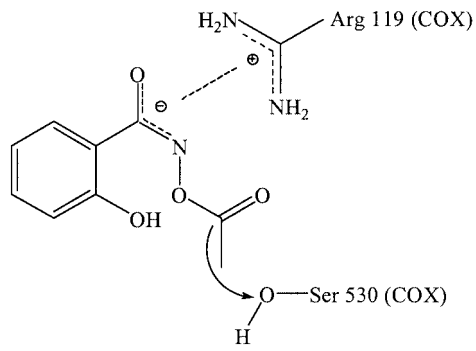

Keywords: Hydroxamic acids / Chelates / Siderophores / Enzyme inhibitors / Nitric oxide donors / Cyclooxygenase

 © 2004 Wiley-VCH Verlag GmbH & Co. KGaA, Weinheim

SHORT COMMUNICATIONS

3017 **P. Rosa, A. Debay, L. Capes, G. Chastanet, A. Bousseksou, P. Le Floch, J.-F. Létard***

Heat- and Light-Induced Spin Transition of an Iron(II) Polymer Containing the 1,2,4,5-Tetrakis-(diphenylphosphanyl)benzene Ligand

Keywords: Spin crossover / Phosphane ligands / Iron / Photomagnetism / Coordination polymers

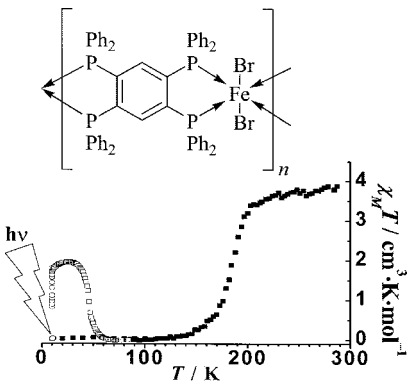

3020 **A. Dahlén, G. Hilmersson***

Microwave-Assisted Generation of Lanthanide(II) Halides in THF and Simple Quantitative Determination

Keywords: Microwave-assisted reactions / Lanthanides / Halides / Titrations / Quantitative determinations

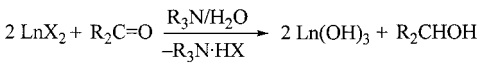

3025 **Y. Song, C. Massera, P. Gamez, A. M. M. Lanfredi, J. Reedijk***

Stabilization of a Copper(II) Complex by Hydrogen Bonds between the Axial Tetrafluoroborate Anion and the Ammonium Group from the Coordinated Cationic Ligand Bis(imidazol-2-yl)-methyl(isopropyl)ammonium

Keywords: Hydrogen bonds / Copper / EPR / N ligands

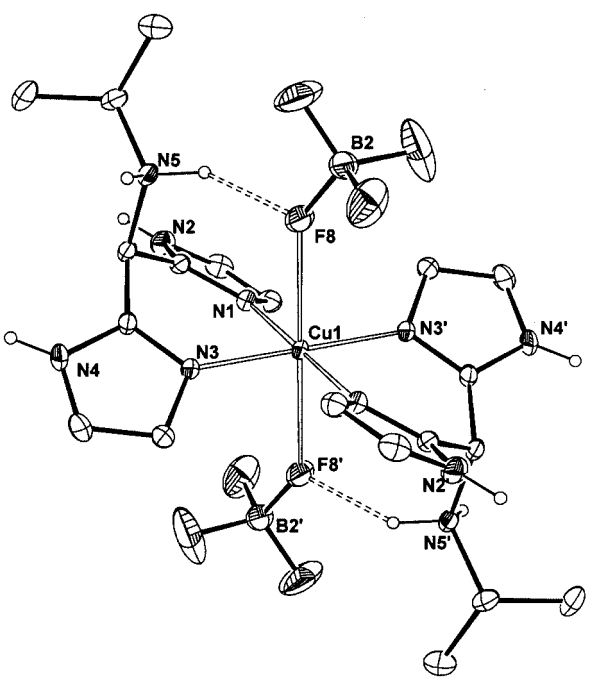

FULL PAPERS

3031 **F.-N. Shi, F. A. A. Paz, J. Rocha,* J. Klinowski, T. Trindade**

Novel Phosphovanadate Layered Structure Assembled from a Tetrametallic Cubane-Like V^{V} Cluster

Keywords: Organic-inorganic hybrid / Hydrothermal synthesis / Oxo ligands / Vanadium

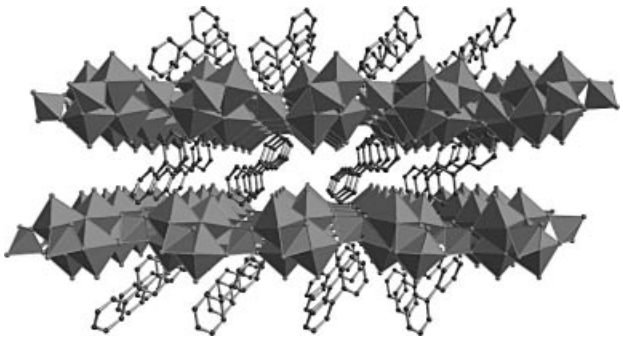

3038 **J. E. Aguado, M. J. Calhorda, P. J. Costa, O. Crespo, V. Félix, M. C. Gimenco, P. G. Jones, A. Laguna***

Synthesis and Theoretical Studies of a Double Helical Complex with the Ligand 4′,4‴-Bis-(ferrocenyl)-2,2′:6′,2″:6″,2‴:6‴,2⁗-quinquepyridine

Keywords: Quinquepyridine / Silver / Helical complexes / Ferrocenyl derivatives / Theoretical studies

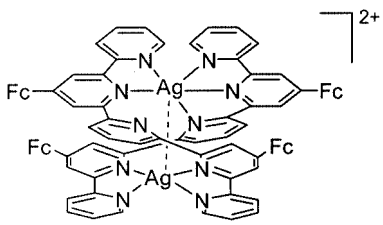

3048 **H. V. Nanishankar, M. Nethaji, B. R. Jagirdar***

Synthesis and Characterization of the First Examples of Dicationic Dihydrogen Complexes of Iron and Ruthenium with the PF_3 Ligand

Keywords: Dihydrogen complexes / H−H activation / Hydride ligands / Iron / Phosphane ligands / Ruthenium

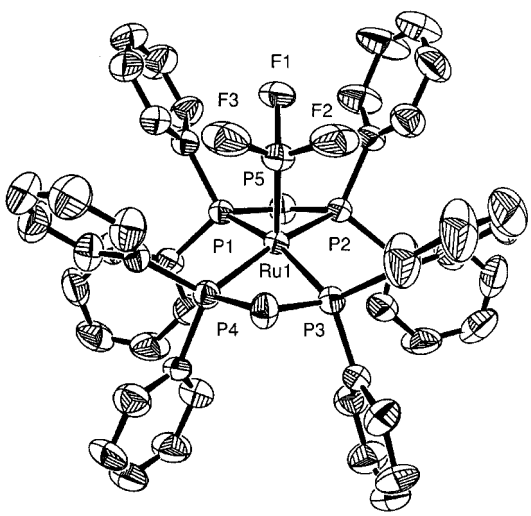

3057 **U. W. Meier, U. Thewalt, T. Debaerdemaeker, B. Rieger***

Synthesis and Polymerization Performance of Pd^{II} Complexes of New 2-Hydroxyethyl-Substituted Diphosphane Ligands

Keywords: Homogeneous catalysis / Palladium / Phosphane ligand / Polyketone / Polymerization

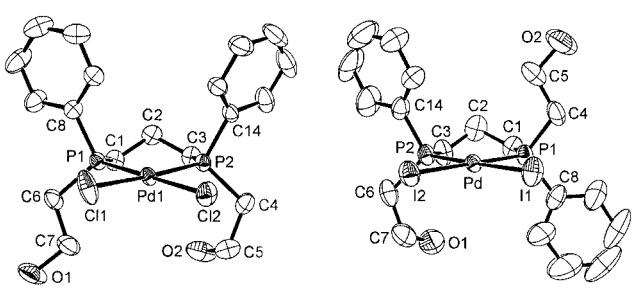

 © 2004 Wiley-VCH Verlag GmbH & Co. KGaA, Weinheim

3063 C. Präsang, Y. Sahin, M. Hofmann, G. Geiseler, W. Massa, A. Berndt*

Syntheses and Reactions of a Stable 1,2-Dichloro-1,2-diborolane and Aromatic Tetraboranes

Keywords: Aromatics / Boranes / Carbanions / Cyclizations / Heterocycles / Rearrangements

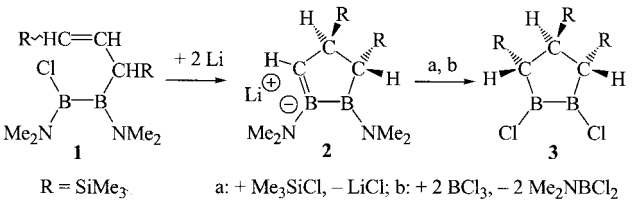

3074 M. Sudupe, J. Cano, P. Royo,* E. Herdtweck

Studies Related to the Chloro Titanium and Zirconium Complexes with [η^5-Cyclopentadienyldi(silylamido)] Ligands

Keywords: Zirconium / Titanium / Silylamido / Cyclopentadienyl-N ligands

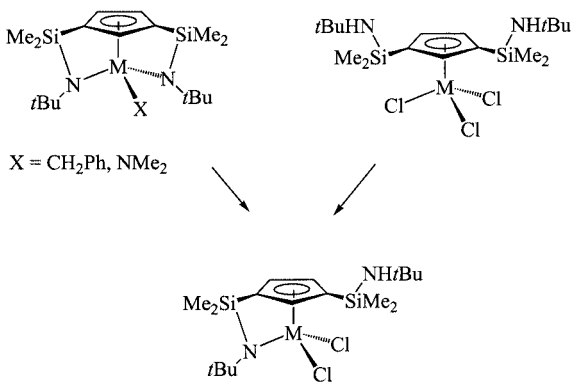

3084 T. Kajiwara,* T. Ito

1,3,5-Triazapentanediene, A Novel Tridentate Ligand that Bridges Two Metal Ions in a $\kappa^1N:\kappa^2N$ Bridging Mode with C_2 Symmetry

Keywords: Chelates / Coordination modes / N ligands / Nickel

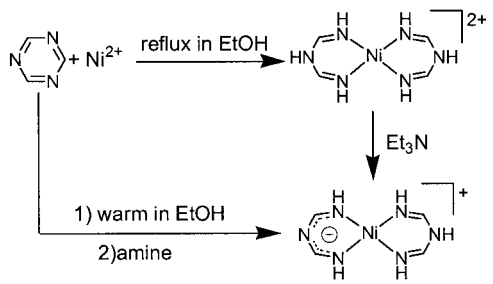

3089 M. L. Gallego, P. Obejero, M. Cano,* J. V. Heras, J. A. Campo, E. Pinilla, M. R. Torres

(Pyrazole)silver(I) and -gold(I) Complexes with Strong and Weak Hydrogen-Bonding Interactions as the Basis of One- or Two-Dimensional Structures

Keywords: Hydrogen bonds / N ligands / Silver / Supramolecular chemistry

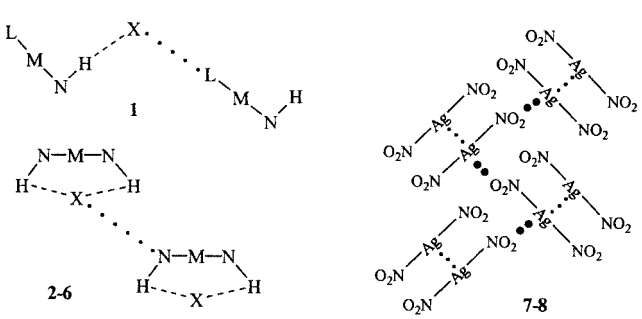

 © 2004 Wiley-VCH Verlag GmbH & Co. KGaA, Weinheim

3099 **M. C. Aragoni, M. Arca,* F. Demartin, F. A. Devillanova, F. Lelj, F. Isaia, V. Lippolis, A. Mancini, L. Pala, G. Verani**

A Theoretical Investigation of the Donor Ability of [M(R,R′timdt)$_2$] Dithiolene Complexes towards Molecular Diiodine (M = Ni, Pd, Pt; R,R′timdt = Formally Monoreduced Disubstituted Imidazolidine-2,4,5-trithione)

Keywords: Charge transfer / Density functional calculations / Dithiolenes / Iodine / Raman spectroscopy / X-ray diffraction

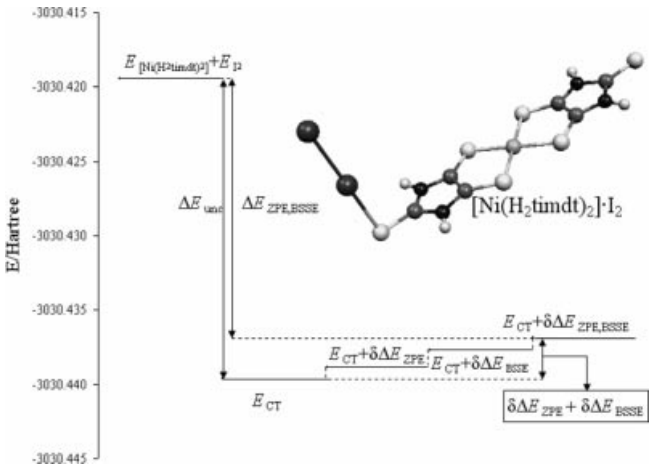

3110 **M. S. Ray, A. Ghosh,* S. Chaudhuri, M. G. B. Drew, J. Ribas***

Supramolecular Hydrogen-Bond Structures and Magnetic Interactions in Basal-Apical, Dinuclear, Azide-Bridged Copper(II) Complexes

Keywords: Azides / Copper / Hydrogen bonds / Magnetic properties / N,O ligands / Schiff bases

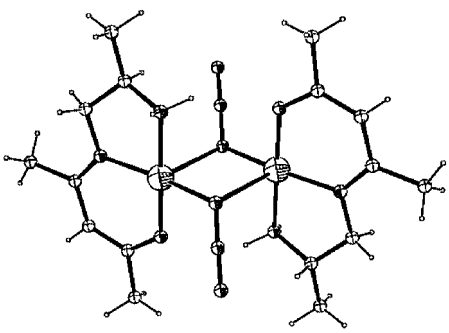

3118 **A. Papakyriakou, I. Bratsos, M. Katsarou, N. Katsaros***

Preparation, Structure Determination and Cytotoxicity of the Pd^{II}·Bleomycin A2 Complex

Keywords: Bleomycin / Palladium / Molecular modelling / Cytotoxicity

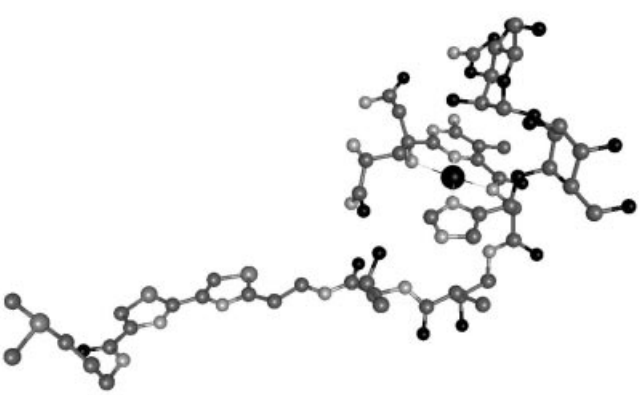

 © 2004 Wiley-VCH Verlag GmbH & Co. KGaA, Weinheim

3127 **A. Maldotti,* A. Molinari, I. Vitali, E. Ganzaroli, P. Battioni, D. Mathieu, D. Mansuy**

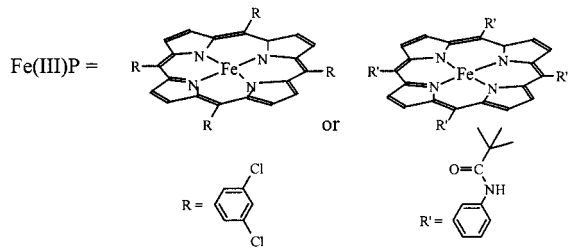

Oxidation of *N*-(4-Chlorophenyl)-*N'*-hydroxyguanidine to *N*-(4-Chlorophenyl)urea and Nitric Oxide by Photoexcited Iron Porphyrins

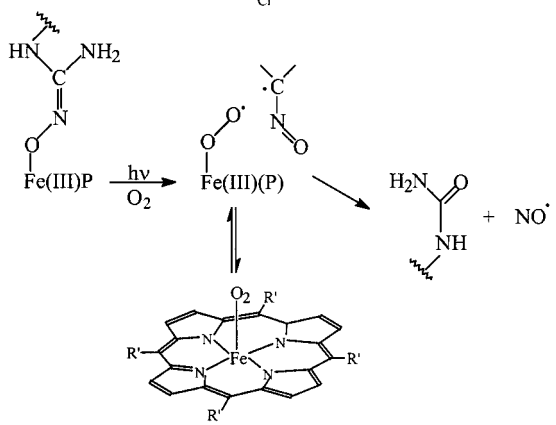

Keywords: O−O activation / Nitric oxide / Photooxidation / Porphyrins / Protein models

3136 **D. Sellmann, K. Hein,* F. W. Heinemann**

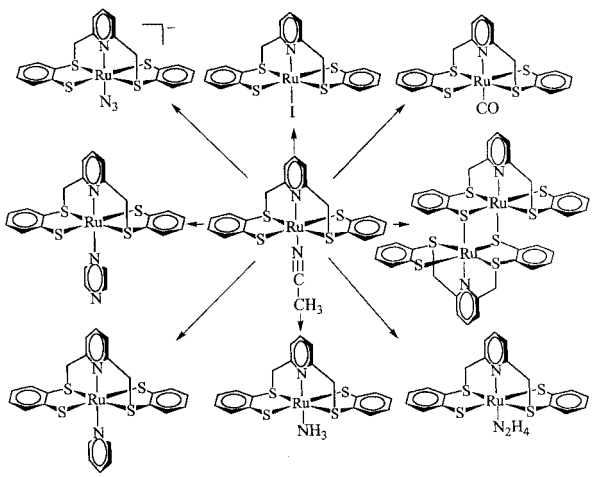

Ruthenium(II) and Ruthenium(III) Complexes Containing the $[pyS_4]^{2-}$ Ligand [pyS_4^{2-} = 2,6-Bis(2-mercaptophenylthio)dimethylpyridine(2−)]

Keywords: Ruthenium / S ligands / Oxidation reactions

3147 **L.-C. Song,* H.-W. Cheng, X. Chen, Q.-M. Hu**

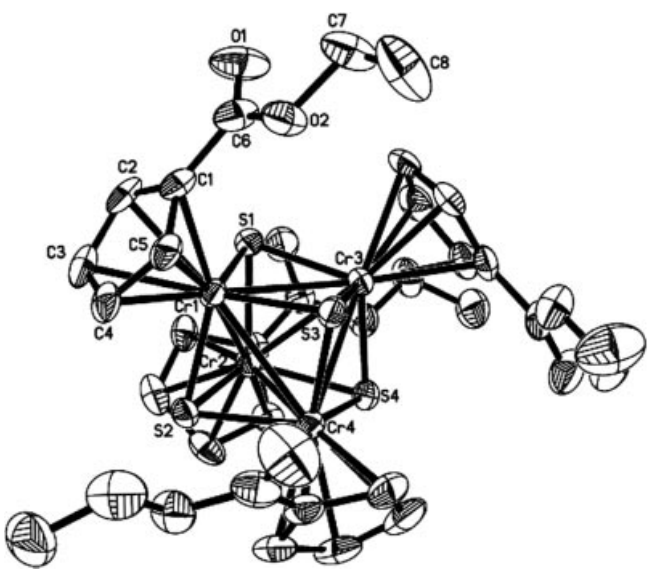

Synthesis and Characterization of Cubane-Like Cr_4E_4 (E = S, Se) Clusters − Molecular Structures of $(\eta^5\text{-}RC_5H_4)_4Cr_4E_4$ (E = S, R = MeCO, MeO_2C, EtO_2C; E = Se, R = H)

Keywords: Clusters compounds / Chromium / Selenium / Cp ligands / Cluster-forming reactions

 © 2004 Wiley-VCH Verlag GmbH & Co. KGaA, Weinheim

3154 **V. Tabernero, T. Cuenca,* E. Herdtweck**

Preparation of Diamidochloro(cyclopentadienyl)-titanium Derivatives as Pre-Catalysts for Olefin Polymerization − X-ray Molecular Structure of $[Ti(\eta^5\text{-}C_5H_5)\{1,2\text{-}C_6H_4(NCH_2CH_2CH_3)_2\}Cl]$ and $[Ti\{\eta^5\text{-}C_5H_4(SiMe_3)\}\{1,2\text{-}C_6H_4(NCH_2CH_2\text{-}CH_3)_2\}Cl]$

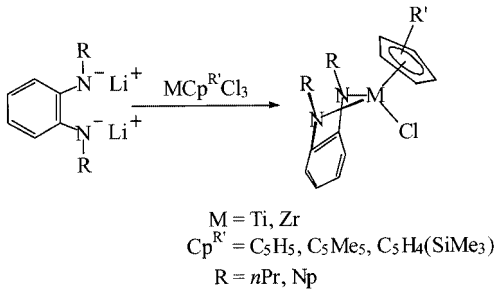

Keywords: Cyclopentadienyl ligands / N ligands / Olefin polymerization / Titanium

3163 **Y. Mekmouche, S. Ménage,* J. Pécaut, C. Lebrun, L. Reilly, V. Schuenemann, A. Trautwein, M. Fontecave**

Mechanistic Tuning of Hydrocarbon Oxidations with H_2O_2, Catalyzed by Hexacoordinate Ferrous Complexes

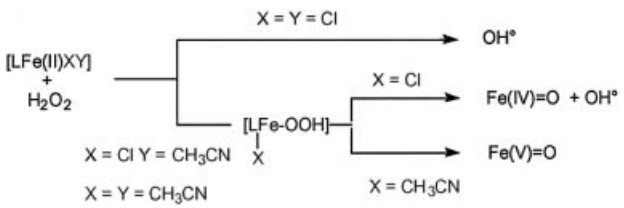

Keywords: Iron catalysts / Hydrogen peroxide / Oxidation / Non-heme iron / Monooxygenase

3172 **J. Mathieu, N. Ghermani, N. Bouhmaida, B. Fenet, A. Marsura***

An Attempt to Programme the Orientation of Bis(heterocyclic) Azine Heterotopic Sequences around Ag^I, Cu^I and Zn^{II} Metal Centres

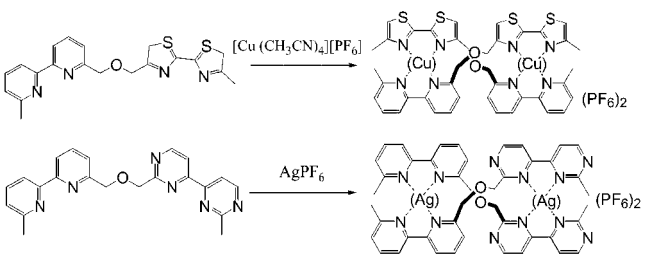

Keywords: Self-assembly / Self-recognition / Heterocyclic bidentate sequences / Cu^I, Ag^I, Zn^{II} metal complexes

 © 2004 Wiley-VCH Verlag GmbH & Co. KGaA, Weinheim

Hydroxamic Acids − An Intriguing Family of Enzyme Inhibitors and Biomedical Ligands

Celine J. Marmion,*[a] Darren Griffith,[a] and Kevin B. Nolan*[a]

Keywords: Hydroxamic acids / Chelates / Siderophores / Enzyme inhibitors / Nitric oxide donors / Cyclooxygenase

This review on hydroxamic acids deals with their efficacy as inhibitors of enzymes including cyclooxygenases, their synthesis, the complexity and structural diversity of their metal complexes, and their ability to act as effective nitric oxide donors.

(© Wiley-VCH Verlag GmbH & Co. KGaA, 69451 Weinheim, Germany, 2004)

1. Introduction

Hydroxamic acids, RCONR′OH, have been known since 1869 with the discovery of oxalohydroxamic acid by Lossen.[1] Despite this, research on these compounds was lacking until the 1980's, after which an enormous amount of information has accumulated with respect to their biomedical applications, their synthesis and the synthesis and structures of their metal complexes. As a result, these weak acids, whether naturally occurring or synthetic, constitute one of the most important families of organic bioligands.

[a] Centre for Synthesis and Chemical Biology, Department of Pharmaceutical & Medicinal Chemistry, Royal College of Surgeons in Ireland,
123 St. Stephen's Green, Dublin 2, Ireland
Fax: (internat.) + 353-1-4022168
E-mail: cmarmion@rcsi.ie
kbnolan@rcsi.ie

One of the first physiological roles of hydroxamic acids was associated with their use as siderophores, a class of low molecular-weight iron-sequestering agents. In the early stages of life, iron, an essential element required by proteins for electron transport, oxygen transport and other life sustaining processes, was in much demand but in poor supply, mainly due to its insolubility under physiological conditions. To circumvent this, organisms, mainly microbial and bacterial, developed a method of effectively assimilating iron in soluble form by synthesising and utilising siderophores.[2,3] These compounds possess either hydroxamate or catecholate groups that are capable of coordinating to iron(III) to give water-soluble, very stable, high-spin octahedral complexes. The desferrioxamine B (a trishydroxamate siderophore, Figure 1) complex of iron(III), for example, has a formation constant log $\beta \approx 30.4$.[4] Complexes

Celine J. Marmion graduated with a BSc. degree in 1990 and a Ph.D. in 1994 from the University of Surrey. She carried out her Ph.D. under the supervision of Prof. L. F. Larkworthy and Prof. G. J. Leigh. She held a lecturing position in chemistry (1994−1995) in St. Mary's College, Strawberry Hill and then graduated with a Postgraduate Certificate in Education from the University of Kingston in 1996. She took up a lecturing position in chemistry at the Royal College of Surgeons in Ireland in 1997 and was promoted to senior lecturer in 2003. Her current research interests include the role of hydroxamic acids as nitric oxide donors, the structural diversity of hydroxamate complexes and the synthesis of metal-based anti-cancer complexes.

Darren Griffith graduated with a BSc degree from University College Dublin in 2000 and obtained his Ph.D. under the supervision of Dr. C. J. Marmion at the Royal College of Surgeons in Ireland in 2004. Research interests include the coordination modes of hydroxamic acids, and the role that hydroxamic acids can play in enhancing the activity of ruthenium and platinum anti-cancer complexes.

Kevin B. Nolan graduated with a BSc degree from University College Galway in 1969 and obtained his Ph.D. under the supervision of Prof. Sean O'Cinneide from the same University in 1972. He carried out post-doctoral research with Prof. R. W. Hay at the University of Stirling and held lecturing positions at University College London (1974−1975) and the University of Surrey (1975−1987) before taking up his present appointment as Professor of Chemistry at the Royal College of Surgeons in Ireland in 1987. His current research interests are in the design and synthesis of hydroxamic acid inhibitors of cyclooxygenase, in the structures of hydroxamate complexes and in the synthesis of metal-based drugs.

MICROREVIEWS: This feature introduces the readers to the authors' research through a concise overview of the selected topic. Reference to important work from others in the field is included.

of iron(II) with hydroxamate ligands are much less stable than those of iron(III), e.g. the desferrioxamine-iron(II) complex has a log $\beta \approx 10$.[5] Even under anaerobic conditions, above pH 4, in the iron(II)-desferrioxamine B system, oxidation of iron(II) to iron(III) by hydroxamate occurs to give the iron(III)-desferrioxamine B complex and desferrioxamine B monoamide.[5] The iron siderophore complex, once inside the cell, undergoes reduction, releasing iron and making it accessible to metabolic demands within the cell.[6] A remarkable feature of siderophores, which is crucial to their function, is their ability to selectively bind iron(III) over other metal ions, which may be "poisonous". Siderophores also have high affinities for other tripositive metal ions such as aluminium(III), but their complexes are less stable than those of iron(III).[7]

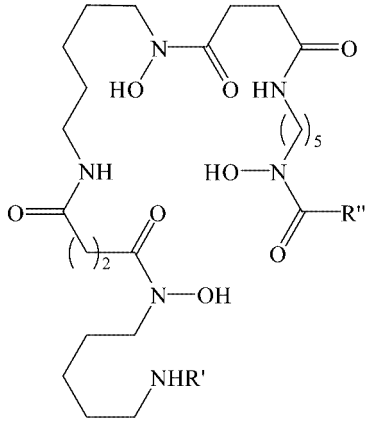

Figure 1. Hydroxamate siderophore, Desferrioxamine B

Siderophores and their analogues have vast therapeutic potential, yet few practical applications of siderophores have been realised. One example is the use of the trishydroxamate siderophore desferrioxamine B (Desferal) to deal with iron-overload in transfusion-dependent patients such as those suffering from thalassaemia.

Thalassaemia, an inherited disease affecting 100,000 babies annually, is characterized by an abnormality in one or more of the globin genes resulting in the inability to synthesise haemoglobin properly, and the patients becoming anaemic.[8] Thalassaemic patients have regular blood transfusions to supplement their haemoglobin levels but this can result in a toxic buildup of iron in the blood, and its accumulation in the heart, liver, endocrine glands and other vital organs eventually resulting in death. Desferrioxamine B, which is administered by prolonged subcutaneous infusion 3 to 7 times per week or by daily intramuscular injections due to its instability in stomach acid, forms a water-soluble iron(III) complex at physiological pH, which is readily excreted in bile and urine. Whilst treatment of thalassaemic patients with regular blood transfusions prolongs their life expectancy by about 20 years, treatment of the resulting iron overload with desferrioxamine B dramatically increases their life expectancy as shown in Figure 2.[9]

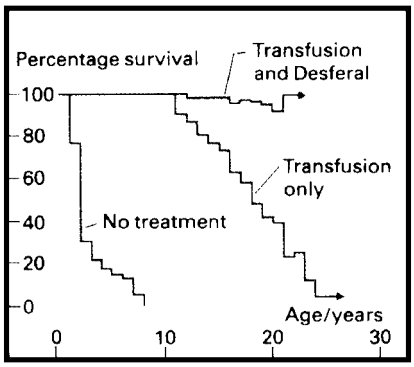

Figure 2. Patient survival rate for treatment of thallasaemia by transfusion only and by both transfusion and administration of desferrioxamine B; taken from ref.[9], reproduced by permission of The Royal Society of Chemistry

The major disadvantage of desferrioxamine B, which has over the past 30 years been the most widely used iron chelator in haematology, is that it is orally inactive.[10] Analogues of desferrioxamine B and a family of compounds known as *N*-hydroxypyrid-2-ones, which are considered to be aromatic hydroxamates are stable in acid and orally active, and are currently being considered as viable alternatives to desferrioxamine B.[11] A related compound deferiprone (not a hydroxamate but a hydroxypyrid-4-one) has been developed as an orally active iron chelator[12,13] but its efficacy has been challenged, and this has resulted in well-publicised acrimony and indeed lawsuits. Analogues of deferiprone are currently under investigation.[11]

Another more recent and potentially powerful application of hydroxamate-containing siderophores is the development of bioconjugates, which are synthesised by covalently linking siderophores with antimicrobial agents. Because microbes have a unique ability to distinguish and employ only certain siderophores, such conjugates could be utilised as carriers to selectively deliver antimicrobial prodrugs to their site of action. The scientific methodology and subsequent syntheses of a number of siderophores, including aerobactin, arthrobactin, schizokinen, a mycobactin, foroxymithine, all of the components of pseudobactin and several analogues, has recently been reported by Miller et al.[14] This group is currently devoting its efforts towards the syntheses and investigation of siderophore antimicrobial agent conjugates in a programme designed to develop iron transport-mediated selective drug delivery systems such as those shown in Figure 3.

This alternative approach to drug delivery may lead to the development of a novel class of selective antimicrobial agents based on active transport of an essential nutrient. The synthesis of such bioconjugates may in addition revitalise old drugs that relied on passive diffusion, and to which resistance has developed. Interestingly, preliminary studies of some of the synthetic siderophore analogues developed by Miller et al. indicate that they have considerable potential as nontoxic, organ selective magnetic resonance imaging (MRI) contrast agents.

 © 2004 Wiley-VCH Verlag GmbH & Co. KGaA, Weinheim

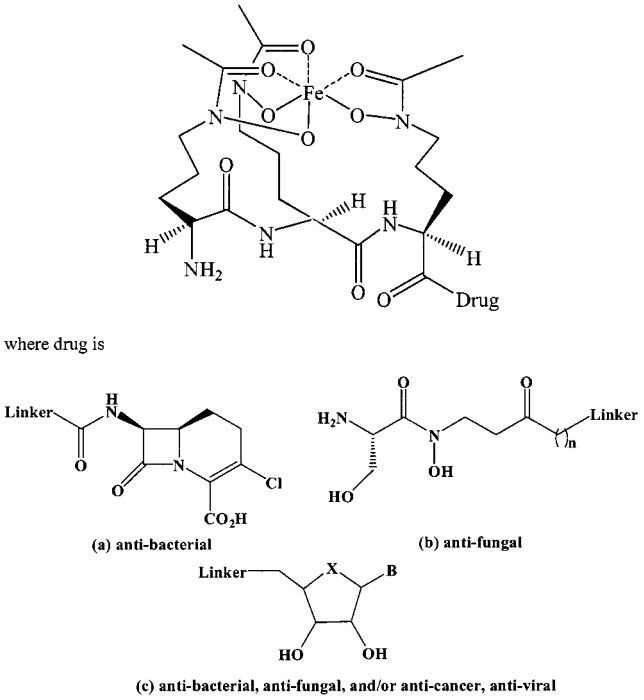

Figure 3. Representative siderophore antimicrobial/anticancer/antiviral agent conjugates as potential iron transport-mediated selective drug delivery systems

The biomedical applications of hydroxamic acids are no longer solely associated with the uptake or removal of iron from the body. In recent years, there has been increasing interest in their roles as potent and selective inhibitors of a range of enzymes including matrix metalloproteases,[15−19] peroxidases,[20−22] hydrolases,[23,24] ureases,[25−28] lipoxygenases,[15] cyclooxygenases[29,30] and peptide deformilases.[31] The basic medicinal chemistry and pharmacology of hydroxamic acid derivatives that act as enzyme inhibitors has recently been the subject of two reviews by Williamson et al.[15] and Lou et al.[32] Hydroxamic acids also represent a wide spectrum of bioactive compounds that have hypotensive,[33] anti-cancer,[16,34−37] anti-malarial,[38−42] anti-tuberculosis and antifungal properties,[43] and have been identified as key functional groups of potential chemotherapeutics targeting cardiovascular diseases, HIV and Alzheimer's disease.[44,45]

Our interest in hydroxamic acids lies in their versatility as ligands, their ability to act as effective nitric oxide donors, and in their potential as specific inhibitors of a class of enzymes known as cyclooxygenases.

2. Syntheses and Structures

Hydroxamic acids are generally considered to be derivatives of hydroxylamine and carboxylic acids, although their metal chelating ability is significantly stronger than the corresponding carboxylic acids. Typically, reaction between hydroxylamine or *O*/*N*-protected hydroxylamines (generated in situ by the addition of base to the hydrochlorides) and an activated acyl group (such as an ester, acid halide, amide) results in the formation of the corresponding hydroxamic acid, Equation (1).

$$RCOX + NH_2OH \rightarrow RCONHOH + HX \quad (1)$$

Recently, a convenient two-step procedure for the parallel synthesis of low molecular-weight hydroxamic acids from carboxylic acids and hydroxylamine with the use of polymer-supported 1-hydroxybenzotriazole has been reported (Figure 4).[46]

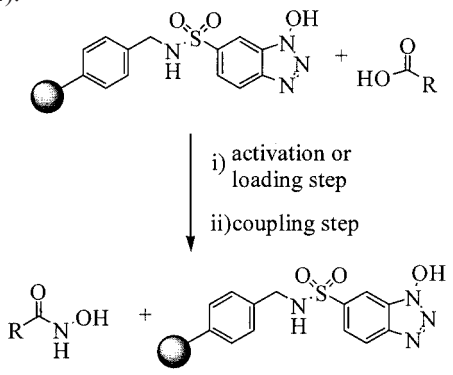

Figure 4. Parallel synthesis of low molecular-weight hydroxamic acids from carboxylic acids and hydroxylamine; reagents and conditions: i. PS-HOBt (1 equiv.), carboxylic acid (1.5 equiv.), DIC (4.5 equiv.), DMAP (0.6 equiv.), DCM/DMF (1:1), 3 h; ii: hydroxylamine (0.6−0.8 equiv.), THF, 5 h

Variations of these methods have been reported and are summarised in a recent paper that describes a simple one-pot method for the syntheses of hydroxamic acids in high yields.[47] The formation of hydroxamic acids and bioactive hydroxamate-containing compounds in both solution and solid phase has also recently been the subject of a comprehensive review by Lou et al.[48]

Two possible hydroxamic acid tautomers exist (Figure 5); the keto tautomer, which is predominant under acidic conditions, and the enol form, which is more stable in alkaline media.[49] Furthermore, NMR spectroscopic studies have shown that each tautomer can exist as (*E*) and (*Z*) isomers (Figure 5), further extending their structural diversity.[50] The conformational preferences of some hydroxamic acids have recently been investigated by density functional and empirical methods.[51]

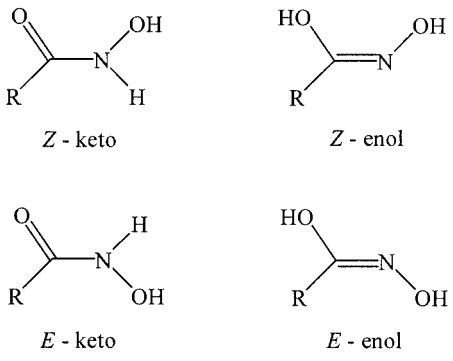

Figure 5. Tautomeric forms of hydroxamic acids

 © 2004 Wiley-VCH Verlag GmbH & Co. KGaA, Weinheim

The acid−base equilibria and associated tautomeric forms have also been extensively described.[52−54] Semi-quantitative comparisons of the acidities of hydroxamic acids, amides and carboxylic acids have recently been reported.[55]

3. Complexation Behaviour

Hydroxamate ligands show a diversity of coordination behaviour that results in a rich array of metal complex structures. The complexing behaviour of hydroxamic acids and, in particular, aminohydroxamic acids has been comprehensively reviewed.[56]

3.1 Bidentate Coordination

It is hardly surprising that many biomedical applications of hydroxamic acids arise as a result of the strong chelating ability of the hydroxamate group. By far the most common mode of metal binding is through the deprotonated hydroxamate and carbonyl oxygen atoms (Figure 6), forming very stable five-membered chelates.

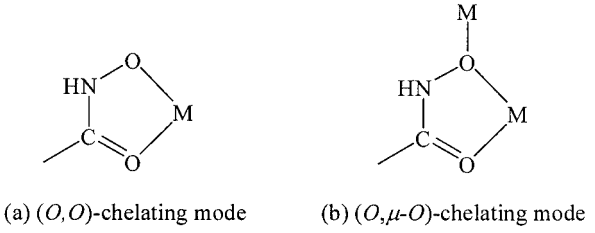

Figure 6. Modes of hydroxamate binding

The hydroxamato(1−) mode of coordination arises from the first deprotonation step involving coordination of the NHO^- moiety. Further metal-induced deprotonation of the NHO^- group leads to hydroximato(2−) complexes.[57]

Furthermore, the hydroxamate moiety possesses several sites for potential hydrogen-bond interactions with, for example, the backbone of enzymes, and these can be critical to their selectivity as enzyme inhibitors (Figure 7).

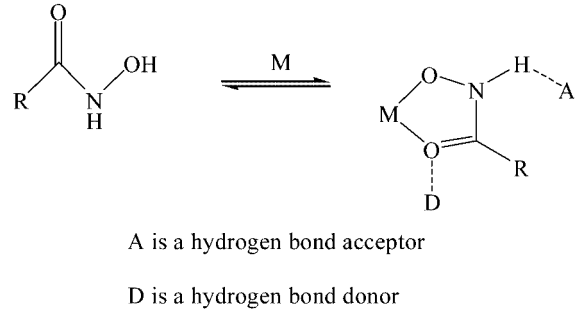

Figure 7. Sites for potential hydrogen-bonding interactions

Bidentate coordination of monohydroxamic acids to a number of transition-metal ions such as iron(III), cobalt(II) and nickel(II) generally results in the ready formation of 3:1 octahedral complexes,[58−60] while in the case of copper(II), 2:1 tetragonal complexes that have two additional monodentate ligands is the preferred geometry.[56,61]

3.2 Monodentate Coordination

Other modes of coordination, including monodentate binding through the deprotonated nitrogen or oxygen atom, have also been reported but these require specially designed coordination environments to provide additional stabilisation. The monodentate *N*-bonded trifluoroacetohydroxamate complex of carbonic anhydrase (a mimic of the hydrogen carbonate−enzyme product complex) is stabilised by hydrogen bonding with Thr-199 and by a weak F to Zn^{II} interaction (2.8 Å) [Figure 8 (a)].[62] A similar complex of acetohydroxamate has also been characterised. The reaction of the octaethylporphyrin (OEP) complex Fe(OEP)Cl, which does not contain two adjacent vacant coordination sites to accommodate normal bidentate coordination, with benzohydroxamic acid gave [Fe(OEP)PhCONHO]·

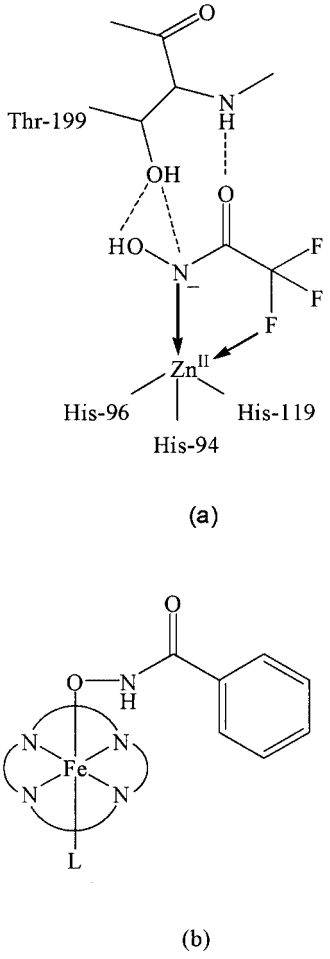

Figure 8. (a) Monodentate *N*-bonded trifluoroacetohydroxamate complex of carbonic anhydrase (a mimic of the hydrogen carbonate−enzyme product complex); (b) monodentate *O*-bonded benzohydroxamate in [Fe(OEP)PhCONHO]·PhCONHOH

 © 2004 Wiley-VCH Verlag GmbH & Co. KGaA, Weinheim

PhCONHOH, which contains monodentate *O*-bonded hydroxamate stabilised by hydrogen bonding with free benzohydroxamic acid in the lattice [Figure 8 (b)].[63]

3.3 Hydroxamate Ligands with Other Coordinating Groups; Metallacrowns

The coordination behaviour of the hydroxamate group can be dramatically enriched by the incorporation of secondary coordinating groups at adjacent sites in the molecule. Dinuclear copper(II) complexes of α-aminohydroxamic acids that exhibit two modes of hydroxamate coordination (Figure 9), both giving five-membered rings, have been characterised. Under alkaline conditions, *N*,*N*- over *O*,*O*-coordination by copper(II) for α-aminohydroxamate ligands is preferred.[64,65]

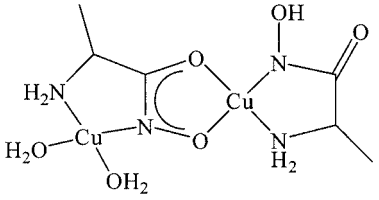

Figure 9. Two distinct bidentate binding modes observed in some complexes of α-aminohydroxamic acids

In the case of nickel(II), α-aminohydroxamate ligands produce bis *N*,*N*-bidentate square-planar complexes[59,66] rather than octahedral complexes containing *O*,*O*-bonded hydroxamates. With these ligands, the cobalt(III) complex forms tris complexes that have *N*,*N*-bidentate coordination.

The coordination properties of β-aminohydroxamic acids are, in general, similar to those of the α derivatives. Whilst β-aminohydroxamic acids can act as *N*,*N*-donors, this involves a six-membered ring, and *O*,*O*-bidentate coordination is generally preferred. A remarkable complex with the general formula $[Cu_5(LH_{-1})_4]$ was reported to be formed from the reaction of copper(II) salts with β-alaninehydroxamic acid (HL).[67] This complex, which is the major species in solution at pH 4.5−9, contains a twelve-membered ring made up of four metal ions linked in pairs by doubly deprotonated NO groups of hydroxamate ligands and another metal ion in a central cavity bonded by the four hydroxamate oxygen atoms. The amino nitrogen atom of one ligand and the carbonyl oxygen atom of another complete basal coordination around each outer copper ion, with the axial coordination of an oxygen atom (from water, perchlorate or a vicinal aminohydroximato ligand) completing the square-pyramidal coordination (Figure 10). This complex is the prototype for a remarkable family of compounds called metallacrowns subsequently developed by Pecoraro and co-workers.[68]

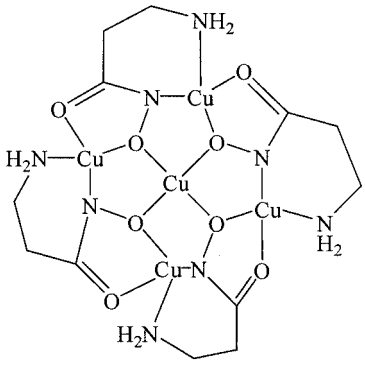

Figure 10. Structure of the copper(II) β-alaninehydroxamic acid complex displaying both *N*,*N*- and *O*,*O*-bidentate coordination through the hydroxamate

Following this, metallacrowns emerged as a new family of molecular recognition agents where hydroxamic acid ligands provided the structural support upon which the supramolecular metallacrown was constructed.[68−71] Salicylhydroxamic acid [Figure 11 (a)], which contains both hydroximato and phenolate donor atoms, is particularly well suited to the synthesis of metallacrowns because (i) three binding sites that are capable of stabilising high valent metal ions are available in the triply deprotonated ligand, and (ii) it is a dinucleating agent with all four heteroatoms as potential metal binding sites [Figure 11 (b)].

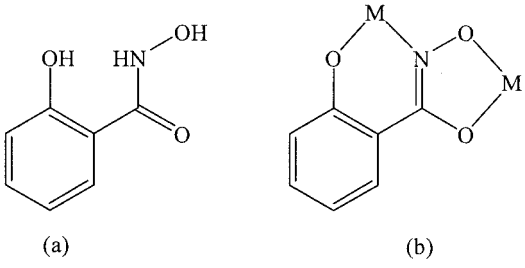

Figure 11. (a) Salicylhydroxamic acid; (b) salicylhydroxamic acid as a dinucleating agent with all four heteroatoms as potential metal binding sites

The ability of salicylhydroxamic acid to form a five-membered chelate ring with one metal through the hydroximate group and a six-membered ring to another metal through the substituted iminophenolate ring facilitates the formation of metal clusters with $M_A-N-O-M_B$ networks that link the ring metals [Figure 11 (b)]. The synthesis of most metallacrowns utilizes base to facilitate deprotonation of the ligand and counterions for charge balance in addition to metal salt and ligand.[68] Replacement of the phenolic group of salicylhydroxamic acid by an amino group affords a family of 2-aminophenylhydroxamic acid (anthranilic hydroxamic acid) metallacrowns. Other scaffolds such as 2-pyridylacetohydroxamic acid and 3-hydroxy-2-naphthohydroxamic acid have also been used in metallacrown synthesis. Although there is a change in charge from −3 to −2 on going from salicylhydroximato to anthranilic hydroximato

 © 2004 Wiley-VCH Verlag GmbH & Co. KGaA, Weinheim

ligands, this does not have a pronounced impact on the resulting metallacrown structures but does result in the complex being uncharged. Recent work involving planar ligands such as picolinehydroxamic acid (picha) or nonplanar α-aminohydroxamic acids, e.g. glycinehydroxamic acid (glyha), afforded a new family of metallacrowns that are capable of accommodating a series of lanthanides in their cavities. The reaction of the appropriate hydroxamic acid with copper acetate and 1/5 equivalent of gadolinium(III) or europium(III) nitrates, for example, afforded $Gd(NO_3)_3$[15-MCCu^{II}N(picha)-5], $Eu(NO_3)_3$[15-MCCu^{II}N(picha)-5], and $Eu(NO_3)_3$[15-MC$_{Cu^{II}N(glyha)}$-5], all of which have been structurally characterized. Several other 15-metallacrown-5 complexes were synthesized with (i) Cu^{II} or Ni^{II} in the peripheral ring metal position, (ii) various lanthanides, La^{III}, Nd^{III}, Sm^{III}, Eu^{III}, Gd^{III}, Dy(III), Ho^{III}, Er^{III}, and Yb^{III}, encapsulated in the center of the ring, and (iii) chiral α-aminohydroxamic acids, e.g. phenylalaninehydroxamic acid, leucinehydroxamic acid and tyrosinehydroxamic acid as scaffolding. The complexes containing Cu^{II} ions have the ring metals either in square-planar environments, bound to two hydroximato ligands, or in square-pyramidal geometries with solvent coordinated. The Ni^{II} complexes appear to be either five- or six-coordinate. The encapsulated lanthanides are generally pentagonal bipyramidal, with five oxygen donors from the metallacrown ring, and solvent or bidentate nitrate ions in the axial positions. These complexes exhibit interesting magnetic behaviour due to the circular arrangement of ions. With Dy(III) encapsulated in the center of the ring, for example, a magnetic moment as high as 10.9 BM is achieved.[72]

Originally it was thought that metallacrowns could only be obtained from β-aminohydroxamic acids but a recent study has shown that in aqueous solution α-aminohydroxamic acids are also capable of forming metallacrowns, but these are less stable.[71]

3.3.1 Aminophenylhydroxamic Acid Complexes

As illustrated by the above structures the diversity of hydroxamate coordination modes can be enriched by the presence of secondary donor groups in the ligand. The influence of the position of these donors relative to the hydroxamate on the resulting structures is illustrated by the copper(II) complexes of isomeric aminophenylhydroxamic acids AphaH, which we recently reported.[73] The structures include a novel helical polymer formed by 3-AphaH, a dimeric copper(II)-metallacrown formed by 2-AphaH, and a simple mononuclear complex formed by 4-AphaH.

Reaction of $CuSO_4{\cdot}5H_2O$ with 3-AphaH in aqueous solution gave a helical polymer with the formula $[Cu_3(3\text{-Aphha})_4(H_2O)SO_4]_n{\cdot}8H_2O$ (Figure 12), the monomeric unit of which has three interlinked unique copper(II) sites. These are the neutral square-planar complex $Cu(3\text{-Apha})_2$, the anionic square-pyramidal complex $[Cu(3\text{-Apha})SO_4(NH_2)(\cdots NH_2)]^-$ and the cationic square-pyramidal complex $[Cu(3\text{-Apha})(H_2O)(NH_2)(\cdots NH_2)]^+$, where NH_2 represents amino groups from neighbouring molecules forming both normal and elongated (···) bonds. The Cu(2)−Cu(3) helical backbones are connected by Cu^I square-planar sites. An extensive network of hydrogen bonds involving hydroxamate nitrogen and oxygen atoms, sulfate oxygen atoms, and both coordinated and lattice waters link the polymer chains. The copper(II) ions in this complex are magnetically independent.

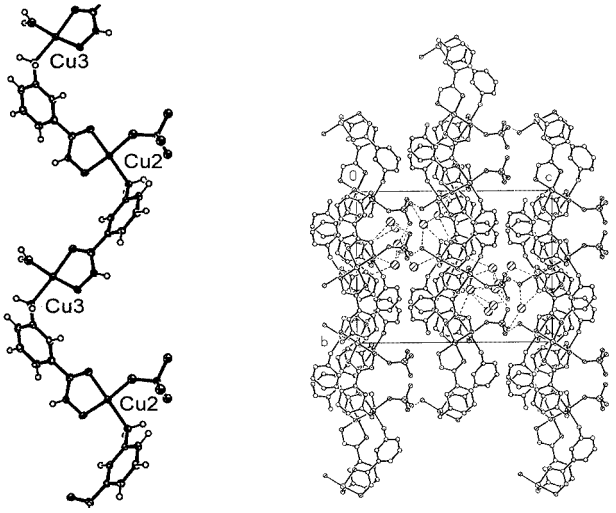

Figure 12. Molecular structure of $[Cu_3(3\text{-Aphha})_4(H_2O)SO_4]_n{\cdot}8H_2O$

The dimeric copper(II)-metallacrown complex $[Cu_5(2\text{-AphaH}_{-1})_4(\mu\text{-}SO_4)(H_2O)_2]_2{\cdot}10H_2O$ (Figure 13) was obtained by reaction of $CuSO_4{\cdot}5H_2O$ and 2-AphaH in aqueous solution. In this case, each monomeric unit contains a square of copper(II) ions, Cu1−4, linked by doubly deprotonated hydroximate ligands 2-AphaH_{-1} and a central copper(II) ion Cu5, which is coordinated by four hydroxamate oxygen atoms and the oxygen atom of a bridging sulfate that is also weakly bonded to Cu4. Pecoraro et al. reported a similar monomeric metallacrown structure, synthesised from $Cu(OAc)_2$.[74] The structure of $[Cu_5(2\text{-AphaH}_{-1})_4(\mu\text{-}SO_4)(H_2O)_2]_2{\cdot}10H_2O$, however, differs from that reported by Pecoraro et al. It is a fused dimeric metallacrown that has a novel "clam-like' structure, the closed end of which arises from the binding of ring copper atoms Cu2 and Cu2A in two metallacrown units to oxygen atoms O2A and O2, respectively, in adjacent units, and the open end of which accommodates bridging sulfate ligands. The external faces of the metallacrown dimer are involved in hydrogen bonding with other metallacrown units through hydroxamate nitrogen and oxygen atoms, resulting in intermolecular Cu−Cu bond lengths of approximately 3.9 Å. The complex is strongly antiferromagnetic. The only other reported dimeric metallacrown is that of a nickel(II) complex in which the metallacrown rings are parallel.[75]

In contrast to the above structures, reaction of 4-AphaH with $CuSO_4{\cdot}5H_2O$ resulted in the formation of a simple mononuclear complex $Cu(4\text{-Apha})_2{\cdot}H_2O$ (Figure 14). An extensive hydrogen-bonding network leads to an overall stacked structure containing internal cavities.

 © 2004 Wiley-VCH Verlag GmbH & Co. KGaA, Weinheim

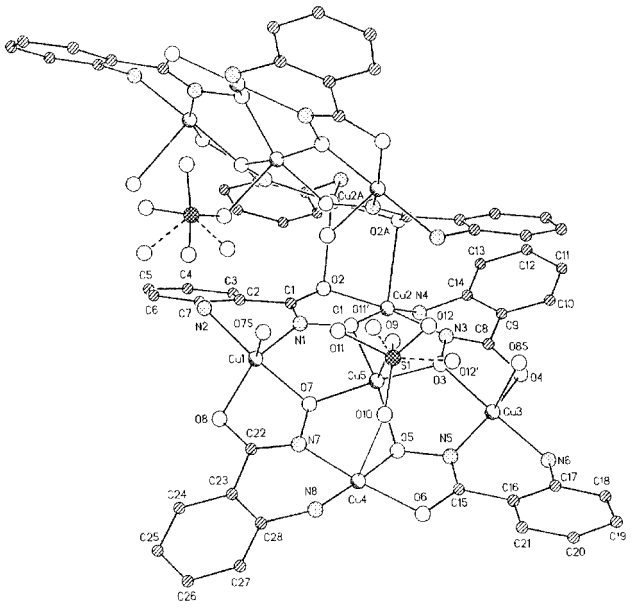

Figure 13. A novel dimeric copper(II)-metallacrown type complex $[Cu_5(2\text{-}AphaH_{-1})_4(\mu\text{-}SO_4)(H_2O)_2]_2\cdot 10H_2O$

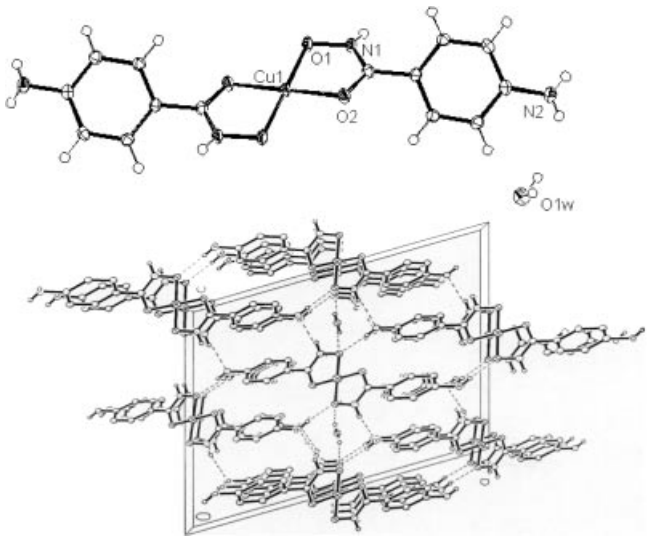

Figure 14. Mononuclear $Cu(4\text{-}Apha)_2\cdot H_2O$ exhibiting an extensive hydrogen-bonding network that leads to an overall stacked structure, which contains internal cavities

An intriguing heptanuclear nickel(II) complex that uniquely exhibits four distinct hydroxamate binding modes, two of which are novel, and which shows both antiferromagnetic and ferromagnetic interactions has also recently been reported by us.[76] Reaction of 2-(dimethylamino)-phenylhydroxamic acid (2-dmAphaH) with $NiSO_4\cdot 6H_2O$ results in the formation of $[Ni_7(2\text{-}dmAphaH_{-1})_2(2\text{-}dmApha)_8(H_2O)_2]SO_4\cdot 15H_2O$ (Figure 15), which contains a trigonal-bipyramidal array of nickel(II) ions with another two nickel(II) ions annexed to the apical sites. This complex in which each nickel ion is octahedrally coordinated contains monodeprotonated 2-dmApha and doubly deprotonated 2-dmAphaH$_{-1}$ hydroxamate ligands.

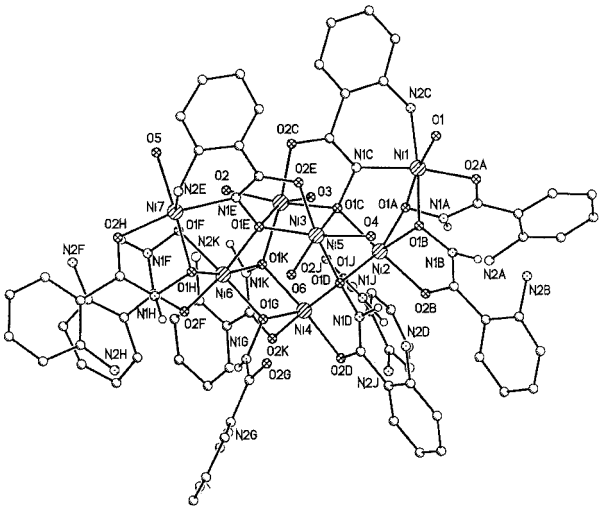

Figure 15. Molecular structure of $[Ni_7(2\text{-}dmAphaH_{-1})_2(2\text{-}dmApha)_8(H_2O)_2]SO_4\cdot 15H_2O$

The hydroxamate binding modes may be categorised as follows. One of the doubly deprotonated hydroxamate ligands C (Figure 15−17) is doubly bidentate with respect to nickel ions, Ni1/Ni3 when all of its donor atoms are involved, and is triply bridging to Ni2/Ni5/Ni3, when the hydroxamate oxygen atom is involved (Figure 17). Ligand E is similarly bonded to Ni5/Ni7 and Ni6/Ni3/Ni5. The remaining eight hydroxamate ligands are singly deprotonated and are coordinated through the hydroxamate group only. Ligand D is bidentate with respect to Ni4 and triply bridging through the hydroxamate oxygen atom with respect to Ni4/Ni2/Ni5. Ligand K is similarly coordinated to Ni4 and Ni4/Ni6/Ni3. Ligand G bridges Ni4 and Ni6 through the hydroxamate oxygen atom, while ligand J is similarly coordinated to Ni2 and Ni4. The four remaining hydroxamate

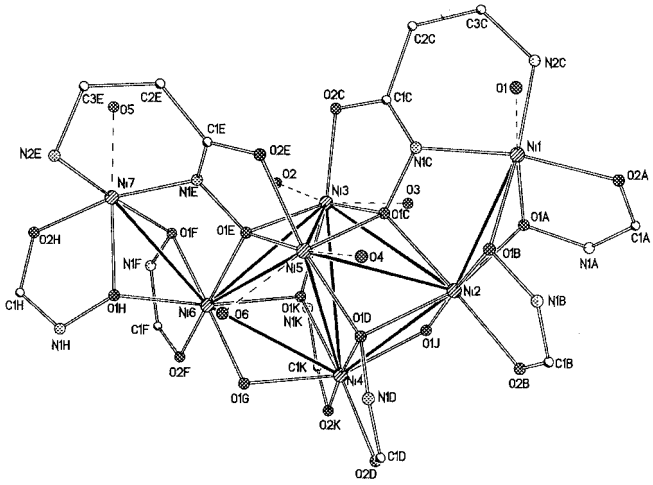

Figure 16. Molecular structure of $[Ni_7(2\text{-}dmAphaH_{-1})_2(2\text{-}dmApha)_8(H_2O)_2]SO_4\cdot 15H_2O$ illustrating the trigonal-bipyramidal arrangement of the five central Ni^{II} ions, and an additional ion annexed to each apex

 © 2004 Wiley-VCH Verlag GmbH & Co. KGaA, Weinheim

ligands coordinate pairs of Ni ions in a bidentate bridging manner. Ligands A and B are bidentate with respect to Ni1 and Ni2, respectively, and both ligands bridge these Ni ions through the hydroxamate oxygen atom. Ligands F and H exhibit the same coordination towards Ni6 and Ni7, respectively. The two binding modes observed for ligands D/K and G/J had not previously been reported for hydroxamate ligands, whilst a similar binding mode for ligands C/E, which involves an additional coordinating group, had only once previously been reported (for a nickel(II) metallacrown with salicylhydroxamic acid).[77] The double hydroxamate bridging of Ni1−Ni2 and Ni6−Ni7 by ligands A and B and F and H, respectively, is similar to that observed in some dinickel model systems for urease inhibition,[28,78] which also contain two hydroxamate bridges and for which inter nickel distances of 3.016 and 3.005 Å have been reported. These values are very similar to the values of 2.958(3) and 2.944(2) Å in the present case.

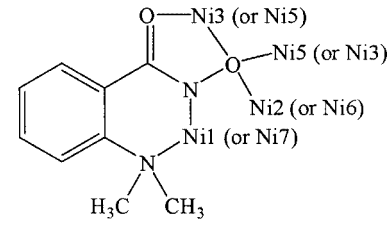

C (or E)

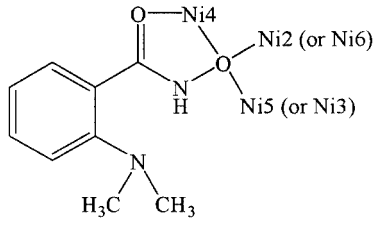

D (or K)

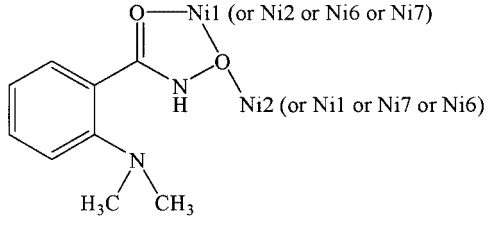

A (or B or F or H)

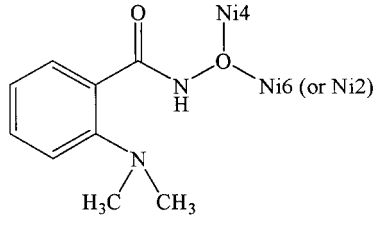

G (or J)

Figure 17. Binding modes of hydroxamate ligands (2-dmApahaH$_{-1}$ and 2-dmApha) in [Ni$_7$(2-dmAphaH$_{-1}$)$_2$(2-dmApha)$_8$(H$_2$O)$_2$]-SO$_4$·15H$_2$O

In contrast to the nickel product, reaction of 2-dmAphaH with CuSO$_4$·5H$_2$O gave the metallacrown [Cu$_5$(2-dmAphaH$_{-1}$)$_4$(HSO$_4$)$_2$(MeOH)$_2$]·2MeOH.[68] The presence of the methyl substituents preclude the formation of a dimeric metallacrown analogous to [Cu$_5$(2-AphaH$_{-1}$)$_4$(μ-SO$_4$)(H$_2$O)$_2$]$_2$·10H$_2$O, which we previously reported for 2-aminophenylhydroxamic acid (Figure 18).[73]

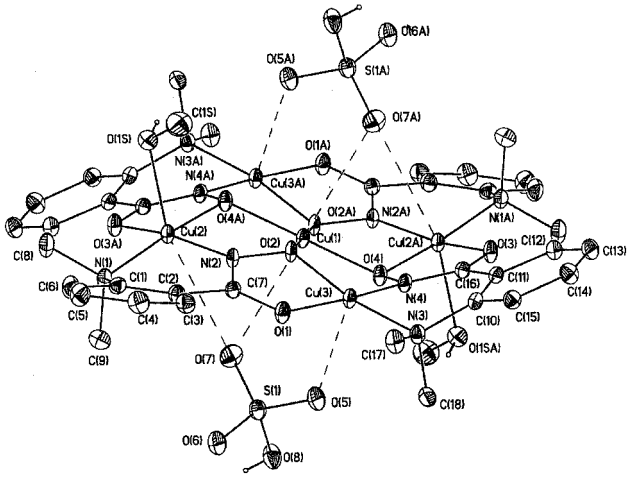

Figure 18. Molecular structure of [Cu$_5$(2-dmAphaH$_{-1}$)$_4$-(HSO$_4$)$_2$(MeOH)$_2$]·2MeOH

3.6 Hydroxamate Complexes of Ruthenium(III), Platinum(II), Palladium(II), Rhodium(I) and Rhodium(III)

Hydroxamate complexes of ruthenium(III), platinum(II) and palladium(II) were recently reported for the first time.[79−81] The fact that no ruthenium(III) hydroxamates had previously been reported is surprising in view of the extensive library of known iron(III) hydroxamates, and this is probably due to nitrosyl abstraction from hydroxamic acids by ruthenium(III) to give ruthenium(II)-nitrosyls as described in section 4. We have recently reported the structure of the first ruthenium(III) hydroxamate complex Ru(H$_2$edta)(2-OMepha) (Figure 19) from the reaction of NH$_4$[Ru(Hedta)Cl] with 2-methoxyphenylhydroxamic acid (2-OmephaH), and the synthesis and characterisation of several other complexes.

Upon addition of base, the hydroxamate ligand in this complex undergoes further deprotonation to give the hydroximato complex [Ru(edta)(2-OMephaH$_{-1}$)]$^{3-}$, Equation (2).

$$[Ru(edta)(2\text{-}OMephaH)]^{2-} \rightleftharpoons [Ru(edta)(2\text{-}OMephaH_{-1})]^{3-} \quad (2)$$

 © 2004 Wiley-VCH Verlag GmbH & Co. KGaA, Weinheim

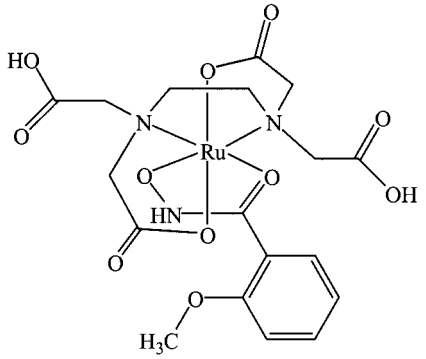

Figure 19. Structure of Ru(H_2edta)(2-OMepha)

The formation of hydroximato complexes, although common in metallacrown chemistry, has been reported in only a few cases for mononuclear complexes.[82−84] The affinity of phenylhydroxamic acid for $[Ru^{III}(edta)(H_2O)]^-$ (hexacoordinate) was found to be much greater than for $[Fe^{III}(edta)(H_2O)]^-$ (heptacoordinate), but this was largely due to differences in charge and coordination numbers of the immediate metal coordination environments rather than intrinsic affinity differences between ruthenium(III) and iron(III) for hydroxamate ligands. The stability of ruthenium(III)-hydroxamate complexes is dependent on the substituent on the aryl ring.

Hydroxamic acid complexes of platinum(II) and palladium(II) have also recently been reported. It was revealed by ^{1}H NMR spectroscopic studies that salicylhydroxamic acid (shaH) does not coordinate to chloro complexes of platinum(II) but can form complexes of the type $[Pt(shaH_{-1})(PPh_3)_2]$, the crystal structure of which was determined. In this complex, $shaH_{-1}$ binds through an (*O*,*O*) coordination mode in its hydroximate form, and the phenolic group remains protonated. Stabilisation of hydroximate binding to platinum is facilitated by the presence of soft ligands. In contrast, the palladium complex $[Pd(sha)_2]$ is readily synthesized and crystallizes as $[Pd(sha)_2](DMF)_4$, with the unexpected (*N*,*O*) binding mode of the salicylhydroxamate ligand.[80] Two novel platinum(II)-diamine benzohydroxamate complexes were reported, namely $[\{Pt(en)\}_2(\mu\text{-bha})]ClO_4\cdot H_2O$ (en = ethane-1,2-diamine, bha = benzohydroxamic acid) (Figure 20), and $[\{Pt(RRchxn)\}_2(\mu\text{-bha})]\cdot 2H_2O$ (chxn = cyclohexane-1,2-diamine) in which Pt−C bonds are present in the dinuclear structures. The two Pt centres are linked through the bha via (*O*,*O*) and (*C*,*N*) coordination modes, the latter involving formation of a Pt−C(*ortho*) bond. Both dinuclear complexes are less cytotoxic than their corresponding dichloro parent complexes. While the mechanism of action of the dinuclear species remains unclear, it has been suggested that the platinum(amine) moieties affect the activity but the presence of the hydroxamate bridge alters the rate of aquation and DNA binding of these species.[81] From these studies, it appears that only aryl hydroxamates readily bind to Pt^{II}. Furthermore, the hydroximate form of the ligand in these complexes appears to be stabilized by the binding of the second platinum centre bridged through the benzohydroximato ligand.

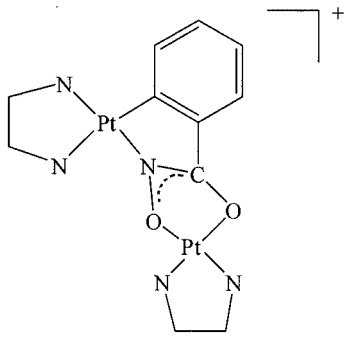

Figure 20. Structure of $[\{Pt(en)\}_2(\mu\text{-bha})]ClO_4\cdot H_2O$ (en = ethane-1,2-diamine, bha = benzohydroxamic acid)

A recent study involving the reaction of *N*-phenylbenzohydroxamic acids with rhodium showed that the oxidation state of the metal ion dictated the type of reaction involved. For rhodium(I), the *N*-phenylbenzohydroxamic acids serve as oxidizing agents and oxidise rhodium(I) to rhodium(III), and are themselves reduced to the corresponding amides. In the presence of rhodium(III), the same hydroxamic acids undergo typical bidentate hydroxamate coordination.[85] Interestingly, an unusual transformation of *N*-arylbenzohydroxamic acids, mediated by osmium(II), affords a family of cyclometalates in which the transformed hydroxamic acids are coordinated as doubly deprotonated benzanilides of osmium(III).[86]

4. Hydroxamic Acids as Nitric Oxide Donors

While some of the physiological roles of hydroxamic acids are undoubtedly due to the chelating ability of the hydroxamate group, others such as their hypotensive effects[33] (a known nitric oxide property) may be due to their ability to release nitric oxide (NO), a view strengthened by the now established importance of NO in many physiological processes. In fact, it is now well recognised that there are probably few pathological conditions where NO does not play an important role.[87−89]

Ruthenium(III) readily forms nitrosyls and there are more known nitrosyl complexes of ruthenium than any other metal.[90] The Ru−NO bond is generally very stable and is easily detected by infrared spectroscopy, ν(NO) at about 1880 cm^{-1}. We have recently shown that hydroxamic acids are effective NO donors by virtue of the fact that they readily transfer NO to ruthenium(III) forming highly stable ruthenium(II)-nitrosyls and by their ability to cause vascular relaxation of rat aorta by NO-mediated activation of the iron(II) haem-containing enzyme guanylate cyclase.[91] In doing so, we effectively used ruthenium(III) as a tool to abstract NO from hydroxamic acids. A similar reaction of hydroxamic acids with $K_3[Fe(CN)_6]$ to give $[Fe(CN)_5NO]^{3-}$ was reported independently at the same time.[92]

 © 2004 Wiley-VCH Verlag GmbH & Co. KGaA, Weinheim

Reaction of the well-characterised $K[Ru(Hedta)Cl]\cdot 2H_2O$ with benzohydroxamic acid in aqueous solution at room temperature resulted in the unambiguous formation of a ruthenium nitrosyl complex. The microanalysis, IR, mass and ^1H NMR spectra are consistent with the formation of $K_2[Ru(edta)(NO)Cl]$, containing a linear, diamagnetic $Ru^{2+}-NO^+$ group (distinctive ν_{NO} at 1880 cm^{-1}) and no absorption at 1730 cm^{-1}, which confirms fully deprotonated edta. This complex is similar to the previously reported six-coordinate $Ru(H_2edta)(NO)Cl\cdot 2H_2O$,[93] but contains fully deprotonated tetradentate edta with two pendant carboxylate groups. A related complex $[Ru(edta)NO]^-$ was formed in solution by reaction of NO with K[Ru(Hedta)Cl].[94] Similar reactions of $K[Ru(Hedta)Cl]\cdot 2H_2O$ with acetohydroxamic acid and salicylhydroxamic acid also gave the same product in high yields. The products of the denitrosylation reactions were shown to be the corresponding carboxylic acids, Equation (3).

$$[Ru(Hedta)Cl]^- + RCONHOH \rightarrow [Ru(edta)(NO)Cl]^{2-} + RCOOH \quad (3)$$

Reaction of $RuCl_3\cdot xH_2O$ with aceto-, benzo-, salicyl- and anthranilic hydroxamic acids in ethanol, followed by purification on Sephadex LH 20 columns also gave ruthenium(II) nitrosyl complexes, all of which have very distinctive ν_{NO} bands at approximately 1885 cm^{-1}.

The ability of hydroxamic acids to release nitric oxide in simple biological systems was shown by vascular relaxation of endothelium-denuded rings (to remove endogenous nitric oxide) of rat aorta. These were set up in organ baths for isometric tension recording. Rings were contracted with the α-1-adrenoreceptor agonist phenylephrine (1μM), and the ability of increasing concentrations of hydroxamic acid derivatives to produce relaxation was examined (the results are shown in Figure 21). Of the hydroxamic acids investigated, benzohydroxamic acid proved most effective, causing approximately 45% relaxation of rat aorta at a concentration of 300 μM. Although this value is higher than that quoted for the well-known NO donor 3-morpholinosydnonimine, SIN-1 (1 μM), it compares favourably with that of another NO donor 4-(3-butoxy-4-methoxybenzo)-2-imidazolidilone, Ro-20−1724 (100 μM). Relaxation occurred by activation of the enzyme guanylate cyclase (a definitive receptor for NO) as shown by the fact that methylene blue (10μM), a known inhibitor of this enzyme, prevented the relaxation (e.g. relaxation to 300μM acetohydroxamic acid: vehicle treated, 31.4 ± 10.9% relaxation; methylene blue treated, 6.4 ± 3.1% relaxation, $n = 4$, $P < 0.05$).

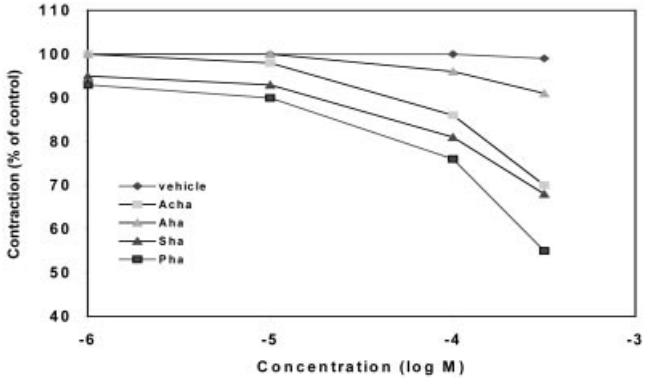

Figure 21. The effects of hydroxamic acids on relaxation of rat aorta

We have therefore shown conclusively that hydroxamic acids can act as effective NO donors by virtue of the fact that they can readily transfer NO to ruthenium(III). Furthermore, hydroxamic acids can cause vascular relaxation in rat aorta by NO-mediated activation of the iron-containing enzyme guanylate cyclase, thus confirming the biological relevance of our novel results.

5. Hydroxamic Acids as Inhibitors of Cyclooxygenase

Cyclooxygenase (COX) is the enzyme responsible for the generation of prostaglandins (Figure 22), bioactive lipids that are involved in many pathophysiological processes including vascular thrombosis, nocioception and temperature control.[95−97]

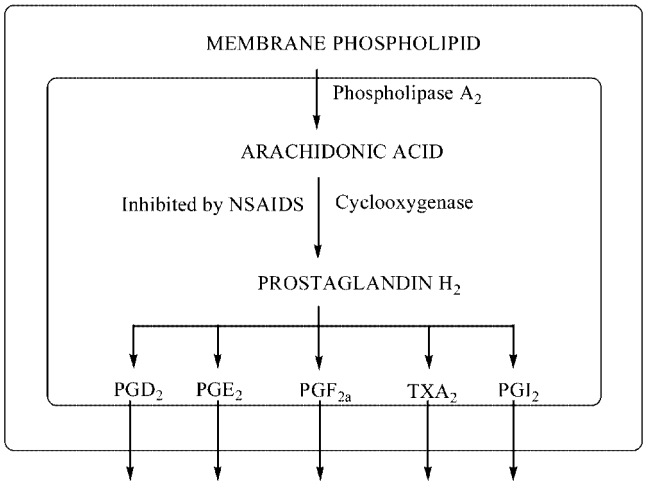

Figure 22. Production of prostaglandins by COX

Two isoforms of the enzyme have been identified: COX-1, which is expressed ubiquitously and is the only form in platelets where it generates thromboxane, a potent platelet activator; and COX-2, which was initially thought to be rare in normal tissue, but expressed at sites of inflammation, in tumours and in response to tissue injury. Both isoforms of COX are inhibited by nonsteroidal anti-inflammatory drugs (NSAIDs)[98] such as aspirin, which were initially thought to have beneficial therapeutic effects due to COX-2 inhibition and side effects due to inhibition of COX-1. There has therefore been intense interest in the development of selective COX-2 inhibitors on the basis that prostaglandins that contribute to inflammation are produced by COX-2, while prostaglandins essential for normal

 © 2004 Wiley-VCH Verlag GmbH & Co. KGaA, Weinheim

physiological processes are produced by COX-1. Several selective COX-2 inhibitors have resulted, including Celecoxib, Nimesulide and a range of modified NSAIDs such as aspirin analogues that have *o*-alkynyl ether or thioether substituents.[99] Aspirin (acetylsalicylic acid) is unique amongst the NSAIDs in that it covalently modifies the enzyme, irreversibly acetylating a serine residue in the substrate channel.[100]

Aspirin and other NSAIDS do not influence the peroxidase site of the enzyme. Therefore, after NSAID treatment, peroxidase (POX) activity can continue to generate damaging free radical species. There is therefore a need for dual COX and POX site inhibition. The hydroxamic acid Tepoxalin is such an inhibitor (Figure 23).[101]

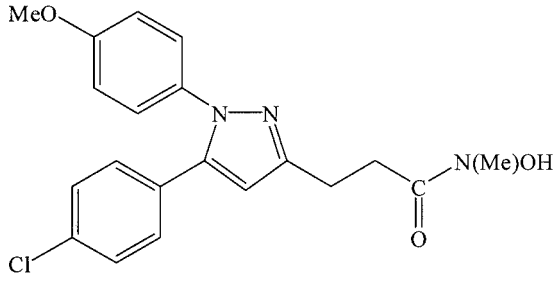

Figure 23. Structure of Tepoxalin

The rationale for the synthesis of selective COX-2 inhibitors has recently been thrown into doubt as it has been shown that COX-2 is expressed constitutively in many tissues and has important physiological roles, and that indeed COX-1 contributes to inflammatory processes. Therefore, it now appears that a combination of selective COX-1 and COX-2 inhibitors may possess greater efficacy than selective COX-2 inhibitors alone.[102]

We decided to investigate hydroxamic acid analogues of aspirin as COX inhibitors for the reasons that: (i) the hydroxamic acid group is less acidic than the carboxylic acid group and should cause less topical irritation; (ii) acetylated hydroxamic acid should, like aspirin, inhibit the COX site by acetylation of Ser-529; (iii) the acetylated hydroxamic acid should also inhibit the POX site since hydroxamic acids are known to inhibit peroxidases; (iv) since we showed that hydroxamic acids are potential NO donors, their aspirin analogues could behave like previously described NO-aspirins with anti-inflammatory effects but devoid of topical irritation, nonulcerogenic, and protective of the stomach.[103,104]

Acetylation of salicylhydroxamic acid with acetyl chloride afforded not the aspirin analogue but instead *O*-acetylsalicylhydroxamic acid, AcSHA, (Figure 24) in which the hydroxamic acid rather than the phenolic group was acetylated. This product was found, however, to be almost as potent as aspirin in the inhibition of cyclooxygenase and was found to require Arg-119 and Ser-529 for activity since the S529A and R119Q mutants were found to be inactive. A crystal structure of the inhibitor-COX-1 complex confirms that acetylation of Ser-529 had occurred, but that instead of the salicylhydroxamate metabolite being trapped in the active site, as was found in the case of bromoaspirin, a fresh molecule of inhibitor is found in this position. This is probably due to the fact that the active site pocket is positively charged and attracts the negatively charged acetylsalicylhydroxamate (i.e. a fresh molecule of inhibitor) with the exclusion of the neutral salicylhydroxamic acid. A mechanism of enzyme inhibition is shown in Figure 25.

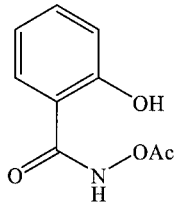

Figure 24. Structure of acetylsalicylhydroxamic acid

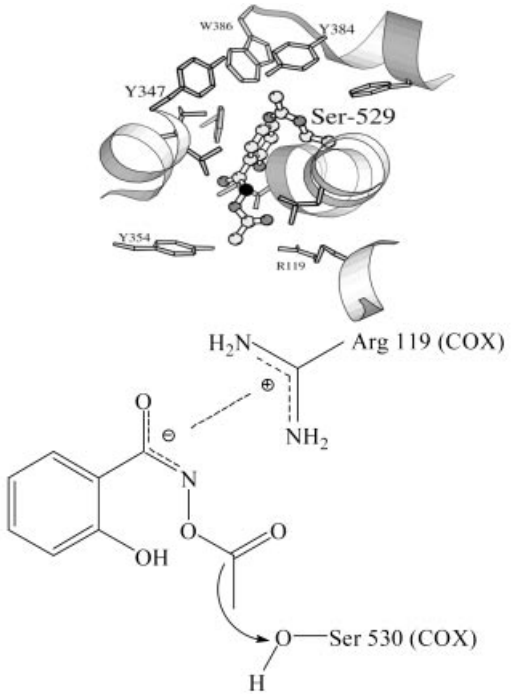

Figure 25. Structure of the COX-1 AcSHA complex, and the mechanism of inhibition of cyclooxygenase

Based on the results obtained with *O*-acetylsalicylhydroxamic acid (AcSHA), we synthesised triacetylsalicylhydroxamic acid (TriAcSHA) (Figure 26), and this was found to be much more effective than both aspirin (ASA) and AcSHA in inactivating both COX-1 and COX-2.[105,106] Hence, preincubation of COX-1 with inhibitor for 5 minutes yielded IC_{50} values of 18 μM for TriAcSHA, and 60 μM for ASA. As with aspirin, mutation of serine-530 of COX-1 to an alanine abolished the activity of TriAcSHA. Mutation of arginine-119 to a glutamine markedly reduced the sensitivity towards TriAcSHA, therefore suggesting that this residue was necessary for interaction with the enzyme. Tri-

 © 2004 Wiley-VCH Verlag GmbH & Co. KGaA, Weinheim

AcSHA was also more effective than aspirin as an inhibitor of platelet aggregation induced by arachidonic acid. The related diacetylated phenylhydroxamates, *N*-methyl-*O*,*O*-diacetylsalicylhydroxamic acid, *N*,*O*-diacetylbenzohydroxamic acid and 2-methyl-*O*,*N*-diacetylbenzohydroxamic acid showed reduced or absent activity against COX-1 (Figure 26). These data together suggest a mechanism of activity which involves Arg-119-assisted *N*-deacetylation of TriAcSha, followed by acetyl group transfer from the phenolate group of the inhibitor to Ser-529, possibly intramolecularly assisted by the anionic deacetylated nitrogen atom (Figure 26).

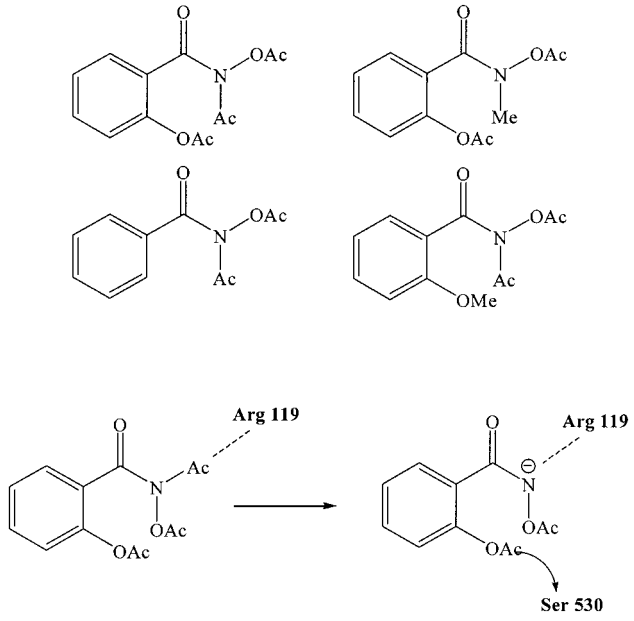

Figure 26. Acetylated salicylhydroxamic acid inhibitors of cyclooxygenase

We synthesized a series of triacylsalicylhydroxamic acids with progressively longer acyl groups (3−6 carbon atoms) (Figure 27). All of the compounds inhibited COX-1 and demonstrated progressively greater COX-1 selectivity with increasing number of carbon atoms (Figure 27). Hence, salicylhydroxamic acid provides a versatile backbone for the generation of a family of acylating inhibitors of COX.

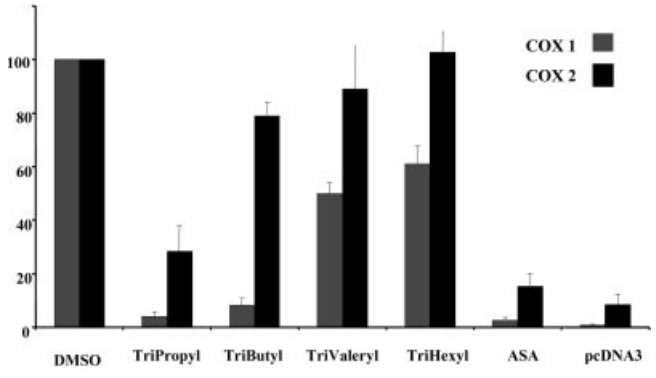

Figure 27. Triacyl derivatives of SHA are selective for COX-1

5. Conclusion

Hydroxamic acids are versatile ligands that give rise to a diverse range of metal complex structures, particularly if there are other metal binding groups present in the molecule. Their biomedical applications, once confined to treatment of metal overload conditions, have been extended to cover inhibition of a wide range of enzymes.

Acknowledgments

We thank Enterprise Ireland (SC/2000/196/Y), EU COST D20, EU COST D21, The Research Committee of the Royal College of Surgeons in Ireland, Centre for Synthesis and Chemical Biology, and Higher Education Authority, Ireland (Programme for Research in Third Level Institutions, Cycle 3) for financial support. We thank Professor Marvin J. Miller for kind permission to use the structures shown in Figure 3.

[1] H. Lossen, *Liebigs Ann. Chem.* **1869**, *150*, 314.
[2] G. Winkelmann, D. van der Helm, J. B. Nielands, *Iron transport in microbes, plants and animals*, New York, **1987**.
[3] A.-M. Albrecht-Gary, A. L. Crumbliss, in *Metal Ions in Biological Systems* (Eds.: A. Sigel, H. Sigel), Marcell Dekker, New York, **1998**, vol. 35, p. 239.
[4] W. R. Harris, C. J. Carrano, S. R. Cooper, S. R. Sofen, A. E. Avdeef, J. E. McArdle, K. N. Raymond, *J. Am. Chem. Soc.* **1979**, *101*, 6097−6104.
[5] E. Farkas, E. A. Enyedy, L. Zekany, G. Deak, *J. Inorg. Biochem.* **2001**, *83*, 107−114.
[6] A. Hartmann, V. Braun, *J. Bacteriol.* **1980**, *143*, 246.
[7] P. Rubini, A. Lakatos, D. Champmartin, T. Kiss, *Coord. Chem. Rev.* **2002**, *228*, 137−152.
[8] L. Lo, S. T. Singer, *Pediatr. Clin. North Am.* **2002**, *49*, 1165−1191, v.
[9] P. S. Dobbin, R. C. Hider, *Chem. Br.* **1990**, *26*, 565−568.
[10] Z. D. Liu, R. C. Hider, *Coord. Chem. Rev.* **2002**, *232*, 151−171.
[11] R. C. Hider, Z. D. Liu, *Curr. Med. Chem.* **2003**, *10*, 1051−1064.
[12] A. Ceci, M. Felisi, V. De Sanctis, D. De Mattia, *Expert Opin. Pharmacother.* **2003**, *4*, 1763−1774.
[13] J. A. Barman Balfour, R. H. Foster, *Drugs* **1999**, *58*, 553−578.
[14] J. M. Roosenberg, 2nd, Y. M. Lin, Y. Lu, M. J. Miller, *Curr. Med. Chem.* **2000**, *7*, 159−197.
[15] E. M. Muri, M. J. Nieto, R. D. Sindelar, J. S. Williamson, *Curr. Med. Chem.* **2002**, *9*, 1631−1653.
[16] W. P. Steward, A. L. Thomas, *Expert. Opin. Investig. Drugs* **2000**, *9*, 2913−2922.
[17] I. Botos, L. Scapozza, D. Zhang, L. A. Liotta, E. F. Meyer, *Proc. Natl. Acad. Sci. USA* **1996**, *93*, 2749−2754.
[18] M. Sani, D. Belotti, R. Giavazzi, W. Panzeri, A. Volonterio, M. Zanda, *Tetrahedron Letters* **2004**, *45*, 1611−1615.
[19] M. Tegoni, F. Dallavalle, A. Santos, *J. Inorg. Biochem.* **2004**, *98*, 209−218.
[20] C. Indiani, E. Santoni, M. Becucci, A. Boffi, K. Fukuyama, G. Smulevich, *Biochemistry* **2003**, *42*, 14066−14074.
[21] E. C. O′Brien, E. Farkas, M. J. Gil, D. Fitzgerald, A. Castineras, K. B. Nolan, *J. Inorg. Biochem.* **2000**, *79*, 47−51.
[22] K. Tsukamoto, H. Itakura, K. Sato, K. Fukuyama, S. Miura, S. Takahashi, H. Ikezawa, T. Hosoya, *Biochemistry* **1999**, *38*, 12558−12568.
[23] D. A. Brown, W. K. Glass, N. J. Fitzpatrick, T. J. Kemp, W. Errington, G. J. Clarkson, W. Haase, F. Karsten, A. H. Mahdy, *Inorg. Chim. Acta* **2004**, in press.
[24] D. A. Brown, L. P. Cuffe, N. J. Fitzpatrick, A. T. Ryan, *Inorg. Chem.* **2004**, *43*, 297−302.
[25] Z. Amtul, A. U. Rahman, R. A. Siddiqui, M. I. Choudhary, *Curr. Med. Chem.* **2002**, *9*, 1323−1348.

 © 2004 Wiley-VCH Verlag GmbH & Co. KGaA, Weinheim

[26] S. Benini, W. R. Rypniewski, K. S. Wilson, S. Miletti, S. Ciurli, S. Mangani, *J. Biol. Inorg. Chem.* **2000**, *5*, 110−118.
[27] D. A. Brown, L. P. Cuffe, N. J. Fitzpatrick, W. K. Glass, K. Herlihy, H. Namir, O. Deeg, W. Errington, T. J. Kemp, *Chem. Commun.* **1998**, 2433.
[28] M. Arnold, D. A. Brown, O. Deeg, W. Errington, W. Haase, K. Herlihy, T. J. Kemp, H. Nimir, R. Werner, *Inorg. Chem.* **1998**, *37*, 2920.
[29] C. M. Dooley, M. Devocelle, B. McLoughlin, K. B. Nolan, D. J. Fitzgerald, C. T. Sharkey, *Mol. Pharmacol.* **2003**, *63*, 450−455.
[30] P. J. Connolly, S. K. Wetter, K. N. Beers, S. C. Hamel, R. H. Chen, M. P. Wachter, J. Ansell, M. M. Singer, M. Steber, D. M. Ritchie, D. C. Argentieri, *Bioorg. Med. Chem. Lett.* **1999**, *9*, 979−984.
[31] D. Chen, C. Hackbarth, Z. J. Ni, C. Wu, W. Wang, R. Jain, Y. He, K. Bracken, B. Weidmann, D. V. Patel, J. Trias, R. J. White, Z. Yuan, *Antimicrob. Agents. Chemother.* **2004**, *48*, 250−261.
[32] B. Lou, K. Yang, *Mini Rev. Med. Chem.* **2003**, *3*, 609−620.
[33] R. Zamora, A. Grzesiok, H. Weber, M. Feelisch, *Biochem. J.* **1995**, *312 (Pt. 2)*, 333−339.
[34] G. Bouchain, D. Delorme, *Curr. Med. Chem.* **2003**, *10*, 2359−2372.
[35] W. P. Steward, *Cancer Chemother. Pharmacol.* **1999**, *43 Suppl*, S56−60.
[36] R. Brammer, J. Buckels, S. Bramhall, *Int. J. Clin. Pract.* **2000**, *54*, 373−381.
[37] J. Holms, K. Mast, P. Marcotte, I. Elmore, J. Li, L. Pease, K. Glaser, D. Morgan, M. Michaelides, S. Davidsen, *Bioorg. Med. Chem. Lett.* **2001**, *11*, 2907−2910.
[38] R. C. Mishra, R. Tripathi, D. Katiyar, N. Tewari, D. Singh, R. P. Tripathi, *Bioorganic & Medicinal Chemistry* **2003**, *11*, 5363−5374.
[39] C. Apfel, D. W. Banner, D. Bur, M. Dietz, T. Hirata, C. Hubschwerlen, H. Locher, M. G. P. Page, W. Pirson, G. Rosse, J.-L. Specklin, *J. Med. Chem.* **2000**, *43*, 2324−2331.
[40] K. P. Holland, H. L. Elford, V. Bracchi, C. G. Annis, S. M. Schuster, D. Chakrabarti, *Antimicrob. Agents Chemother.* **1998**, *42*, 2456−2458.
[41] A. Tsafack, J. Golenser, J. Libman, A. Shanzer, Z. I. Cabantchik, *Mol. Pharmacol.* **1995**, *47*, 403−409.
[42] J. Golenser, A. Tsafack, Y. Amichai, J. Libman, A. Shanzer, Z. I. Cabantchik, *Antimicrob. Agents Chemother.* **1995**, *39*, 61−65.
[43] M. J. Miller, *Chem. Rev.* **1989**, *89*, 1563−1579 and references cited therein.
[44] J. El Yazal, Y.-P. Pang, *J. Phys. Chem. A* **1999**, *103*, 8346−8350.
[45] J. El Yazal, Y.-P. Pang, *J. Phys. Chem. B* **2000**, *104*, 6499−6504.
[46] M. Devocelle, B. M. McLoughlin, C. T. Sharkey, D. J. Fitzgerald, K. B. Nolan, *Org. Biomol. Chem.* **2003**, *1*, 850−853.
[47] G. Giacomelli, A. Porcheddu, M. Salaris, *Org. Lett. (Communication)* **2003**, *5*, 2715−2717.
[48] K. Yang, B. Lou, *Mini Rev. Med. Chem.* **2003**, *3*, 349−360.
[49] A. E. Harvey, D. L. Manning, *J. Am. Chem. Soc.* **1950**, *72*, 4498.
[50] D. Brown, W. Glass, B. G. R. Mageswaren, *Mag. Res. Chem.* **1988**, *26*, 1705.
[51] R. Kakkar, R. Grover, P. Chadha, *Org. Biomol. Chem.* **2003**, *1*, 2200−2206.
[52] D. A. Brown, R. A. Coogan, N. J. Fitzpatrick, W. K. Glass, D. E. Abukshima, L. Shiels, M. Ahlgren, K. Smolander, T. T. Pakkanen, T. A. Pakkanen, M. Perakyla, *J. Chem. Soc., Perkin Trans.* **1996**, *2*, 2673−2679.
[53] O. N. Ventura, J. B. Rama, L. Turi, J. J. Dannenberg, *J. Am. Chem. Soc.* **1993**, *115*, 5754−5761.
[54] D. A. Brown, W. K. Glass, R. Mageswaran, S. i. p. Ali Mohammed, *Mag. Res. Chem.* **1991**, *29*, 40−45.
[55] S. Bohm, O. Exner, *Org. Biomol. Chem.* **2003**, *1*, 1176−1180.
[56] B. Kurzak, H. Kozlowski, E. Farkas, *Coord. Chem. Rev.* **1992**, *114*, 169−200.
[57] E. Farkas, E. A. Enyedy, G. Micera, E. Garribba, *Polyhedron* **2000**, *19*, 1727−1736.
[58] D. A. Brown, D. McKeith (née Byrne), W. K. Glass, *Inorg. Chim. Acta* **1979**, *35*, 5.
[59] D. A. Brown, A. L. Roche, *Inorg. Chem.* **1983**, *22*, 2199−2202.
[60] C. J. Marmion, T. Murphy, Z. Starikova, K. B. Nolan, *Acta Crystallogr., Sect. C* **2000**, *56*, E491−E492.
[61] M. C. M. M. Fernandes, E. B. Paniago, S. Carvalho, *J. Braz. Chem. Soc.* **1997**, *8*, 537−548.
[62] L. R. Scolnick, A. M. Clements, J. C. Liao, L. M. Hellberg, J. May, T. R. Dean, D. W. Christianson, *J. Am. Chem. Soc. (Communication)* **1997**, *119*, 850−851.
[63] L. Cheng, M. A. Khan, D. R. Powell, R. W. Taylor, G. B. Richter-Addo, *Chem. Commun.* **1999**, 1941−1942.
[64] B. Kurzak, K. Kurzak, J. Jezierska, *Inorg. Chim. Acta* **1986**, *125*, 77−82.
[65] B. Kurzak, K. Kurzak, J. Jezierska, *Inorg. Chim. Acta* **1987**, *130*, 189−193.
[66] B. Kurzak, W. Bal, H. Kozlowski, *J. Inorg. Biochem.* **1990**, *38*, 9−16.
[67] B. Kurzak, E. Farkas, T. Glowiak, H. Kozlowski, *J. Chem. Soc., Dalton Trans.* **1991**, 163−167.
[68] V. L. Pecoraro, A. J. Stemmler, B. R. Gibney, J. J. Bodwin, H. Wang, J. W. Kampt, A. Barwinski, in *Prog. Inorg. Chem.*(Ed.: K. Karlin), Pergamon Press, **1996**, vol. 45, pp. 83−177.
[69] G. Psomas, A. J. Stemmler, C. Dendrinou-Samara, J. J. Bodwin, M. Schneider, M. Alexiou, J. W. Kampf, D. P. Kessissoglou, V. L. Pecoraro, *Inorg. Chem.* **2001**, *40*, 1562−1570.
[70] B. R. Gibney, V. L. Pecoraro, in *Inorganic Syntheses*, McGraw-Hill Book Company, Inc., New York, **2002**, vol. 33, pp. 70−74.
[71] M. Careri, F. Dallavalle, M. Tegoni, I. Zagnoni, *J. Inorg. Biochem.* **2003**, *93*, 174−180.
[72] A. J. Stemmler, J. W. Kampf, M. L. Kirk, B. H. Atasi, V. L. Pecoraro, *Inorg. Chem.* **1999**, *38*, 2807−2817.
[73] D. Gaynor, Z. A. Starikova, W. Haase, K. B. Nolan, *J. Chem. Soc., Dalton Trans.* **2001**, 1578−1581.
[74] B. R. Gibney, D. P. Kessissoglou, J. W. Kampt, V. L. Pecoraro, *Inorg. Chem.* **1994**, *33*, 4840−4849.
[75] C. P. Raptopoulou, A. N. Papadopoulos, D. A. Malamatari, E. Ioannidis, G. Moisidis, A. Terzis, D. P. Kessissoglou, *Inorg. Chim. Acta* **1998**, *272*, 283−290.
[76] D. Gaynor, Z. A. Starikova, S. Ostrovsky, W. Haase, K. B. Nolan, *Chem. Commun.* **2002**, 506−507.
[77] G. Psomas, C. Dendrinou-Samara, M. Alexiou, A. Tsohos, C. P. Raptopoulou, A. Terzis, D. P. Kessissoglou, *Inorg. Chem.* **1998**, *37*, 6556−6557.
[78] A. J. Stemmler, J. W. Kampt, M. L. Kirk, V. L. Pecoraro, *J. Am. Chem. Soc.* **1995**, *117*, 6368−6369.
[79] J. Comiskey, E. Farkas, K. A. Krot-Lacina, R. G. Pritchard, C. A. McAuliffe, K. B. Nolan, *Dalton Trans.* **2003**, 4243−4249.
[80] M. D. Hall, T. W. Failes, D. E. Hibbs, T. W. Hambley, *Inorg. Chem.* **2002**, *41*, 1223−1228.
[81] T. W. Failes, M. D. Hall, T. W. Hambley, *Dalton Trans.* **2003**, 1596−1600.
[82] E. Farkas, E. Kozma, M. Petho, K. M. Herlihy, G. Micera, *Polyhedron* **1998**, *48*, 3331−3342.
[83] E. Farkas, H. Csóka, I. Tóth, *Dalton Trans.* **2003**, *8*, 1645−1652.
[84] A. Dessì, G. Micera, D. Sanna, L. S. Erre, *J. Inorg. Biochem.* **1992**, *48*, 279−287.
[85] A. Das, F. Basuli, S.-M. Peng, S. Bhattacharya, *Inorg. Chem.* **2002**, *41*, 440−443.
[86] A. Das, F. Basuli, L. R. Falvello, S. Bhattacharya, *Inorg. Chem.* **2001**, *40*, 4085−4088.
[87] D. R. Adams, M. Brochwicz-Lewinski, A. R. Butler, *Fortschr. Chem. Org. Naturst.* **1999**, *76*, 1−211.
[88] D. J. Stuehr, *Biochim. Biophys. Acta (BBA) − Bioenergetics* **1999**, *1411*, 217−230.
[89] J. Saavedra, L. Keefer, *Chemistry in Britain* **2000**, 30.
[90] M. Schroder, T. A. Stephenson, *Comprehensive Coord. Chem.*, Pergamon Press, **1987**, vol. 4.
[91] C. J. Marmion, T. Murphy, J. R. Docherty, K. B. Nolan, *Chem. Commun.* **2000**, 1153−1154.

 © 2004 Wiley-VCH Verlag GmbH & Co. KGaA, Weinheim

[92] L. N. Koikov, N. V. Alekseeva, E. A. Lisitza, E. S. Krichevsky, N. B. Grigoriev, A. V. Danilov, I. S. Severina, N. V. Pyatakova, V. G. Granik, *Mendeleev Commun.* **1998**, 165−168.
[93] A. A. Diamantis, J. V. Dubrawski, *Inorg. Chem.* **1981**, *20*, 1142−1150.
[94] N. A. Davies, M. T. Wilson, E. Slade, S. P. Fricker, B. A. Murrer, N. A. Powell, G. R. Henderson, *Chem. Commun.* **1997**, 47−48.
[95] D. M. Aronoff, E. G. Neilson, *Am. J. Med.* **2001**, *111*, 304−315.
[96] G. A. FitzGerald, S. Austin, K. Egan, Y. Cheng, D. Pratico, *Ann. Med.* **2000**, 21−26.
[97] F. A. Fitzpatrick, *Curr. Pharm. Des.* **2004**, *10*, 577−588.
[98] L. J. Marnett, A. S. Kalgutkar, *Trends Pharmacol. Sci.* **1999**, *20*, 465−469.
[99] A. S. Kalgutkar, B. C. Crews, S. W. Rowlinson, C. Garner, K. Seibert, L. J. Marnett, *Science* **1998**, *280*, 1268−1270.
[100] P. J. Loll, D. Picot, R. M. Garavito, *Nat. Struct. Biol.* **1995**, *2*, 637−643.
[101] S. C. C. Tam, D. H. S. Lee, E. Y. Wang, D. G. Munroe, C. Y. Lau, *J. Biol. Chem.* **1995**, *270*, 13948−13955.
[102] J. L. Wallace, *Am. J. Med.* **1999**, *107*, 11S−16S; discussion 16S−17S.
[103] K. Takeuchi, H. Ukawa, A. Konaka, M. Kitamura, Y. Sugawa, *J. Pharmacol. Exp. Ther.* **1998**, *286*, 115−121.
[104] C. Lavagna, P. Del Soldato, J. L. Burgaud, P. Rampal, *Curr. Cancer Drug Targets* **2003**, *3*, 407−426.
[105] C. M. Dooley, M. Devocelle, B. McLoughlin, K. B. Nolan, D. J. Fitzgerald, C. T. Sharkey, *Mol. Pharmacol.* **2003**, *63*, 450−455.
[106] P. J. Loll, C. T. Sharkey, S. J. O'Connor, C. M. Dooley, E. O'Brien, M. Devocelle, K. B. Nolan, B. S. Zelinsky, D. J. Fitzgerald,*Mol. Pharmacol.* **2001**, *60*, 1407−1413.

Received March 19, 2004

 © 2004 Wiley-VCH Verlag GmbH & Co. KGaA, Weinheim

Heat- and Light-Induced Spin Transition of an Iron(II) Polymer Containing the 1,2,4,5-Tetrakis(diphenylphosphanyl)benzene Ligand

Patrick Rosa,[a] Amy Debay,[a] Laurence Capes,[b] Guillaume Chastanet,[a] Azzedine Bousseksou,[c] Pascal Le Floch,[d] and Jean-François Létard*[a]

Dedicated to Philipp Gütlich in the occasion of his 70th birthday

Keywords: Spin crossover / Phosphane ligands / Iron / Photomagnetism / Coordination polymers

A new iron(II) spin-crossover compound containing a phosphane ligand has been synthesized and characterized by magnetic susceptibility, Mössbauer spectroscopy, and heat capacity and photomagnetic experiments. The $[Fe(tppb)Br_2]$ complex [tppb = 1,2,4,5-tetrakis(diphenylphosphanyl)benzene] exhibits a gradual spin conversion at $T_{1/2}$ = 184 K, and displays at low temperature a partial photoconversion of the low-spin (LS) state into the metastable high-spin (HS) state by irradiating the sample at 530 nm.

(© Wiley-VCH Verlag GmbH & Co. KGaA, 69451 Weinheim, Germany, 2004)

Introduction

Iron(II) spin-crossover (SC) compounds have numerous potential applications as display devices, optical switches, and magneto-optical storage systems, since heat- and light-induced spin transitions occur in the solid state without any fatigue.[1] The possibility to convert the spin state by irradiating with light is now reported in a large number of spin-crossover complexes. The major drawback of this process up to now is that optical switching requires that it be carried out at very low temperatures. Nevertheless, it has been theoretically predicted and experimentally confirmed that HS → LS relaxation rates k_{HL} can at least be controlled by the energy difference $\Delta E_{HL}°$ between the lowest vibrational levels of HS and of LS states, and by the change of the metal−ligand bond length Δr_{HL}.[2] In this particular context, iron(II) spin-crossover compounds containing phosphorus atoms are very attractive since a large Δr_{HL} is expected. Unfortunately, to date, spin transition has only been reported for solvated $[FeX_2(dppen)_2]\cdot n$S compounds with dppen = *cis*-1,2-bis(diphenylphosphanyl)ethylene, X = Cl or Br, and solvent molecules (S) = $CHCl_3$, CH_2Cl_2, or $(CH_3)_2CO$.[3−7] In the particular case of $[Fe(dppen)_2Cl_2]\cdot 2(CH_3)_2CO$, single-crystal structures determined both in HS and LS states showed a large Δr_{HL}(Fe−P) variation (0.3 Å),[4] and relaxation kinetics of the HS → LS conversion that occurs after the LIESST effect were slower than for classical FeN_6 complexes.[7]

In this work, we report the preparation of a new iron(II) spin-crossover complex containing phosphorus atoms with the 1,2,4,5-tetrakis(diphenylphosphanyl)benzene (tppb) ligand (Figure 1). The thermal spin-crossover properties were studied by magnetic susceptibility measurements,

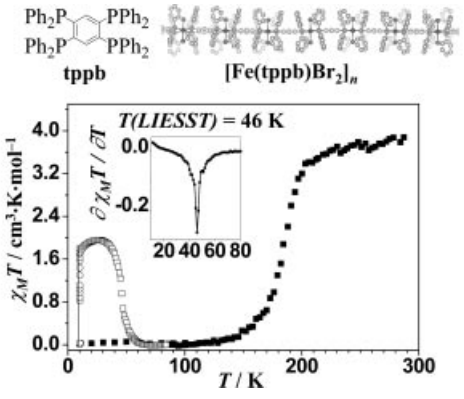

Figure 1. Top left: schematic view of ligand tppb; top right: optimized structure[8] of complex $[Fe(tppb)Br_2]_n$; bottow: molar magnetic susceptibility χ_M vs. temperature T before (filled squares), during (unfilled circles) and after (unfilled squares) light irradiation

[a] Groupe des Sciences Moléculaires, Institut de Chimie de la Matière Condensée de Bordeaux, UPR 9048 CNRS − Université de Bordeaux 1,
87 Av. du Doc. A. Schweitzer, 33608 Pessac, France
Fax: (internat.) + 33-1-40002649
E-mail: letard@icmcb-bordeaux.cnrs.fr
[b] DRECAM/SCM, CEA Saclay,
91191 Gif-sur-Yvette Cedex, France
[c] Laboratoire de Chimie de Coordination, CNRS UPR 8241,
31077 Toulouse Cedex, France
[d] Laboratoire Hétéroéléments et Coordination, UMR 7653 CNRS − Ecole Polytechnique,
91128 Palaiseau Cedex, France

Mössbauer spectroscopy, and heat capacity experiments. Photomagnetic investigations are also reported.

Results and Discussion

Complex $[Fe(tppb)Br_2]_n$ was obtained by mixing equimolar amounts of $FeBr_2$ and tppb in a mixture of chloroform and absolute ethanol (see Exp. Sect.). The elemental analysis (C, H, Cl and Fe) was consistent with the expected composition of a polymeric structure. Crystallization was attempted several times by slow diffusion of solutions of $FeBr_2$ and tppb in ethanol into an H-shaped double-tube glass. An amorphous powder was always obtained, certainly due to the expected low solubility of the polymeric structure. Figure 1 shows a polymeric model built up with the CERIUS 4.0 program.[8] Energy minimization suggests at first a linear organization of the iron(II) atoms along the polymeric chain, with Fe−P bond lengths of 2.5 Å, which are within the 2.3−2.6 Å range reported for $[Fe(dppen)_2Br_2]\cdot 2CHCl_3$ by X-ray diffraction.[4] It also shows that the Fe−Fe distance along the polymer chain is 9 Å, which is longer than that in iron(II)−triazole polymers (3.6 Å[9,10]) since the bridging phosphorus atoms are kept apart by the rigid phenylene structure.

The magnetic properties of $[Fe(tppb)Br_2]_n$ are presented in Figure 1. The value of the molar magnetic susceptibility product with temperature ($\chi_M T$) varies from 3.8 $cm^3\cdot K\cdot mol^{-1}$ at room temperature to nearly 0 $cm^3\cdot K\cdot mol^{-1}$ at 80 K. The room-temperature value is consistent with a high-spin Fe^{II} complex with a $^5T_2$ quintet (assuming octahedral symmetry) ground state. At low temperature, the $\chi_M T$ value corresponds to a low-spin Fe^{II} complex with a $^1A_1$ singlet ground state. The $\chi_M T$ curves recorded in the cooling and warming modes are identical, and no hysteresis is detected. The temperature at which there are equal amounts of HS and LS complexes $T_{1/2}$ is 184 K.

Figure 2 displays the Mössbauer spectra recorded at temperatures of 293 K, 180 K and 80 K. This series of data confirms the occurrence of a temperature-controlled singlet/quintet equilibrium with complete conversion. The single doublet recorded at room temperature is typical of iron(II) in the HS (S = 2) ground state with a quadrupole splitting of $\Delta E_Q = 2.773 \pm 0.007\ mm\cdot s^{-1}$ and an isomer shift of $\delta = 0.663 \pm 0.004\ mm\cdot s^{-1}$ relative to natural iron ($-0.13\ mm\cdot s^{-1}$). In contrast, at 80 K, the unique doublet found with $\Delta E_Q = 0.740 \pm 0.002\ mm\cdot s^{-1}$ and $\delta = 0.396 \pm 0.001\ mm\cdot s^{-1}$ is typical of iron(II) in the LS (S = 0) ground state. At an intermediate temperature (180 K), the inner and outer doublets are observed, as expected. This thermal spin transition was also investigated by DSC techniques. The temperature dependence of the molar heat capacity C_p in the cooling and warming modes was examined in the 120−290 K temperature range. The enthalpy variation associated with the spin transition is $\Delta H = 5.6\ kJ\cdot mol^{-1}$, and the entropy change is $\Delta S = 31\ J\cdot mol^{-1}.K^{-1}$. The value for ΔS is smaller than those obtained in strongly cooperative compounds ($50-80\ J\cdot mol^{-1}\cdot K^{-1}$)[11]. Since it is very close to the electronic-only value (ΔS_{el}) of 13.4 $J\cdot mol^{-1}\ K^{-1}$,[1] the weakness of the vibrational component ΔS_{vib} supports the poorly cooperative behavior of $[Fe(tppb)Br_2]_n$.

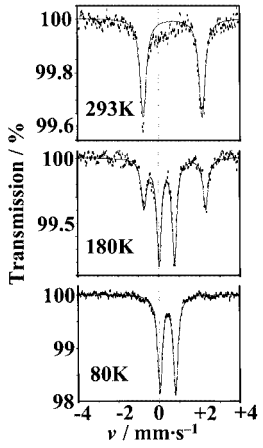

Figure 2. ^{57}Fe Mössbauer spectra for a powder sample of complex **2**; an HS doublet is observed at 293 K, whereas cooling the sample to 80 K gives an LS doublet; at 180 K, both doublets are present with 37% of the HS state

Photomagnetic properties were investigated by irradiating the sample in a SQUID cavity coupled to a Krypton Laser through an optical fiber. The compound was first slowly cooled in the dark from room temperature to 10 K, then irradiated for 1 h. The magnetic response was found to increase rapidly until a value of about 1.8 $cm^3\cdot K\cdot mol^{-1}$ was reached (Figure 1). This indicates a partial conversion (50%) of the LS state into the metastable HS state according to the Light-Induced Excited-Spin-State Trapping (LIESST) process.[12] To increase the level of photoexcitation different experiments were performed: an increase in the irradiation time, an increase in the power (up to $30\ mW\cdot cm^{-2}$), and/or a change in the excitation wavelength (488.0−514.5 nm, 647.1−676.4 nm, 752.5−799.3 nm). Unfortunately, the highest photoinduced LS → HS conversion rate remained at around 50%. The light irradiation was then switched off and the critical LIESST temperature value *T(LIESST)* was recorded.[13] In fact, we recently proposed that the capacity of a compound to retain the light-induced HS information may be estimated through the determination of the *T(LIESST)* value.[14] With this procedure, $\chi_M T$ was found to remain constant at low temperature (tunneling domain) and to drop within a few Kelvin when the thermally activated region was reached. The value of *T(LIESST)*, determined as the minimum of the derivative $\partial\chi_M T/\partial T$, was estimated as 46 K (Figure 1). Such a value, in comparison to the other iron(II) spin-crossover complexes from our database,[14] is unfortunately not exceptional. A study of the kinetics in the vicinity of *T(LIESST)* showed that the relaxation curves strongly deviate from single exponentials, with a fast initial decay and a long tail with a much slower decay, typical of a relaxation following a stretched exponential law. This behavior has, in fact, been reported in many other noncooperative spin-crossover complexes and has been attributed to a distribution of activation energies due to some local inhomogeneity of the

 © 2004 Wiley-VCH Verlag GmbH & Co. KGaA, Weinheim

iron(II) surroundings.[15] In our case, this finding is in good agreement with the gradual character of the thermal spin transition and proves once more the absence of significant cooperativity in the $[Fe(tppb)Br_2]_n$ polymer, certainly because of the long Fe−Fe distances along the chain.

Conclusion

In this work, we have reported the heat- and light-induced spin-crossover properties of a new iron(II) polymeric complex based on a tetraphosphane. This polymer represents an important step towards the design of polynuclear systems combining magnetic interaction and spin conversion under light irradiation. Moreover, it is also a new example of a spin-crossover material involving phosphorus atoms. Synthetic efforts are currently under way to investigate the properties of other complexes based on di- and tetraphosphane ligands.

Experimental Section

General Remarks: All reactions and manipulations were carried out under dry nitrogen. Magnetic susceptibility measurements were carried out by using a MPMS-55 Quantum Design SQUID magnetometer operating at approximately 2 Tesla in the 2−300 K temperature range. Irradiation in the SQUID cavity was done with a 530.9 nm wavelength krypton laser, and the power on the sample was adjusted to 5 $mW{\cdot}cm^{-2}$. Bulk attenuation of light intensity was limited by the preparation of a thin layer of the compound. Its weight was obtained by comparing its thermal spin-crossover curve with the curve recorded with a heavier sample of the same compound. The heat capacities were measured with a Perkin−Elmer DSC-7 calorimeter, and the cell was cooled to the velocity of 2 $K{\cdot}min^{-1}$. Elemental analyses were performed by the Service Central d'Analyse (CNRS) in Vernaison, France.

1,2,3,4-Tetrakis(diphenylphosphanyl)benzene: The synthesis of tppb[16] was modified as follows. Ph_2PNa was obtained starting from Ph_2PCl (6 mL, 32 mmol) in THF (50 mL) and Na (1.5 g, 65.2 mmol) while monitoring by ^{31}P NMR spectroscopy. After 10 h at room temperature, the excess sodium was removed and 1,2,4,5-tetrafluorobenzene (0.71 mL, 6.4 mmol) was added. After 1 h at 70 °C and one night at room temperature, ^{31}P NMR spectroscopic data showed completion of the reaction. A few drops of MeOH were then added, the solvent was removed, and the solid extracted with dichloromethane and water. The organic layer was dried with $MgSO_4$, filtered and concentrated. Recrystallization at −18 °C with the addition of a minimum amount of methanol yielded 2.5 g (47%) of the white product, identified by NMR spectroscopy as tppb.[16]

$\{[Fe(tppb)Br_2]{\cdot}0.16CHCl_3\}_n$: The complex was prepared from a solution of tppb (0.1 g, 0.12 mmol) in $CHCl_3$ (20 mL), which was slowly added to a solution of $FeBr_2$ (0.026 g, 0.12 mmol) in warm (45 °C) absolute ethanol (10 mL) in the presence of a few crystals of ascorbic acid (to prevent oxidation of Fe^{II} to Fe^{III}). Upon addition of the ligand, the reaction mixture changed immediately from an orange color to a cloudy mixture, which yielded a yellow precipitate. The powder was then filtered off, washed with a few milliliters of absolute ethanol, and dried under a stream of nitrogen (yield 106 mg, 84%). $C_{54.16}H_{42.16}Br_2Cl_{0.48}FeP_4$ (1049.56): calcd. C 61.98, H 4.05, Cl 1.62, Fe 5.32; found C 61.86, H 4.11, Cl 1.55, Fe 4.93.

Acknowledgments

The authors would like to acknowledge the Aquitain region for funding.

[1] P. Gütlich, A. Hauser, H. Spiering, *Angew. Chem. Int. Ed. Engl.* **1994**, *33*, 2024−2054; *Angew. Chem.* **1994**, *106*, 2109−2141.
[2] A. Hauser, A. Vef, P. Adler, *J. Chem. Phys.* **1991**, *95*, 8710−8717.
[3] W. Levason, C. McAuliffe, M. Mahfooz Khan, S. M. Nelson, *J. Chem. Soc., Dalton Trans.* **1975**, 1778−1783.
[4] F. Cecconi, M. Di Vaira, S. Midollini, A. Orlandini, L. Sacconi, *Inorg. Chem.* **1981**, *20*, 3423−3430.
[5] E. König, G. Ritter, S. K. Kulshreshtha, J. Waigel, L. Sacconi, *Inorg. Chem.* **1984**, *23*, 1241−1246.
[6] E. König, G. Ritter, S. K. Kulshreshtha, J. Waigel, L. Sacconi, *Inorg. Chem.* **1989**, *28*, 1380−1384.
[7] C.-C. Wu, J. Jürgen, P. K. Gantzel, P. Gütlich, D. N. Hendrickson, *Inorg. Chem.* **1997**, *36*, 5339−5347.
[8] Cerius[2] Molecular Mechanics, Month **1997**. San Diego: Molecular Simulations Inc. **1997**. Energy minimization was done by molecular mechanics technique using the universal force field (UFF), see: A. K. Rappé, C. J. Casewit, K. S. Colwell, W. A. Goddard, W. M. Skiff, *J. Am. Chem. Soc.* **1992**, *114*, 10024−10035.
[9] A. Michalowicz, J. Moscovici, B. Ducourant, D. Cracco, O. Kahn, *Chem. Mater.* **1995**, *7*, 1833−1842.
[10] M. Verelst, L. Sommier, P. Lecante, A. Mosset, O. Kahn, *Chem. Mater.* **1998**, *10*, 980−985.
[11] P. Gütlich, Y. Garcia, H. A. Goodwin, *Chem. Soc. Rev.* **2000**, *29*, 419−427.
[12] A. Hauser, *Chem. Phys. Lett.* **1986**, *124*, 543−548.
[13] At 10 K, after one hour of photoexcitation, the light irradiation was turned off and the temperature was slowly increased at the rate of 0.3 $K{\cdot}min^{-1}$, see: J.-F. Létard, L. Capes, G. Chastanet, N. Moliner, S. Létard, J.-A. Real, O. Kahn, *Chem. Phys. Lett.* **1999**, *313*, 115−120.
[14] S. Marcén, L. Lecren, L. Capes, H. A. Goodwin, J.-F. Létard, *Chem. Phys. Lett.* **2002**, *358*, 87−95.
[15] A. Hauser, J. Adler, P. Gütlich, *Chem. Phys. Lett.* **1988**, *152*, 468−472.
[16] H. Christina, E. McFarlane, W. McForlane, *Polyhedron* **1988**, *7*, 1875−1879.

Received April 6, 2004

 © 2004 Wiley-VCH Verlag GmbH & Co. KGaA, Weinheim

Microwave-Assisted Generation of Lanthanide(II) Halides in THF and Simple Quantitative Determination

Anders Dahlén[a] and Göran Hilmersson*[a]

Keywords: Microwave-assisted reactions / Lanthanides / Halides / Titrations / Quantitative determinations

Lanthanide(II) reagents (SmI_2, $SmBr_2$, YbI_2, EuI_2) have been prepared rapidly in high yields using microwave-assisted heating. Samarium diiodide is obtained as a saturated solution in THF (0.13 M) within 5 min and ytterbium diiodide (0.065 M) after 45 min. A simple method for quantitative determination of LnX_2 in THF is also described by utilizing the instantaneous reaction with ketones in the presence of an amine and water. This method establishes the concentration of the active single-electron-donor species, i.e. Ln^{2+}.

(© Wiley-VCH Verlag GmbH & Co. KGaA, 69451 Weinheim, Germany, 2004)

Introduction

The introduction of the versatile and highly selective single-electron-transfer reagent SmI_2 has had a great impact on the development of organic chemistry during the last 10−15 years.[1−4] The reduction potential of SmI_2 is in the range of −1.3 to −2.2 V,[5] depending on solvents and ligands, which makes SmI_2 particularly useful for selective reduction and various coupling reactions.[6,7] Since SmI_2 has become commercially available, the development of SmI_2-mediated reactions has rapidly entered different areas of organic synthesis. Recently, there have also been reports on the use of other anions (Br^- and amides)[8−10] and lanthanides (Yb, Nd and Dy)[11−13] for various selective reduction reactions. However, reagents such as $SmBr_2$, YbI_2, EuI_2 and ThI_2 are still far from being widely used, much due to the lack of simple methods and long reaction times needed for their preparation. Recent progress in microwave-assisted synthesis is particularly attractive due to dramatically shorter reaction times and higher yields relative to conventional reaction conditions.[14,15]

We have realised that research groups that currently explore the chemistry mediated by e.g. SmI_2 are lacking a reliable method for a simple, rapid and quantitative determination of the concentration of the reducing reagent itself. It is important that the concentration of the reducing reagent is known before the success of a new SmI_2-mediated reaction can be fully evaluated. The concentration of the commercially available SmI_2 reagent (0.1 M) has been found to vary from 0.05 to 0.10 M. (Evaluating the concentrations from several different batches from commercial sources showed that the concentration of SmI_2 varied dramatically.) Today there are only a few volumetric titration methods known for e.g. SmI_2; however, these methods only establish the total concentration of I^- or Sm^{2+} and Sm^{3+} (i.e. they also measure inactive reagents such as SmI_3).[16−18] There is, to the best of our knowledge, no method known for a direct and quantitative method for the titration of the single-electron-transfer reagent Ln^{2+} itself. Recently, we reported on the SmI_2/amine/water instantaneous reduction of ketones.[19] This reaction constitutes a key for quantitative determination of the concentration of various LnX_2 solutions, since the reduction of simple ketones is very clean and proceeds extremely fast. Furthermore, the progress of the reaction may be monitored by the disappearance of the characteristic dark blue colour of SmI_2 in THF (Scheme 1).

$$2\ SmI_2\ (dark\ blue) + R_2C{=}O \xrightarrow[-R_3N{\cdot}HI]{R_3N/H_2O} 2\ Sm(OH)_3\ (white) + R_2CHOH$$

Scheme 1. The colour changes from dark blue to white during the reduction of ketones

Results and Discussion

Generation of LnX_2

Microwave-assisted heating of THF mixtures of samarium metal and iodine, iodoform or diiodoethane for 5 min (at 180 °C) results in rapid formation of dark blue solutions of SmI_2. The resulting SmI_2 solutions are of similar quality whether they are made from iodine, iodoform or diiodoethane. However, the use of iodine is preferred since this source of I^- does not involve the generation of gaseous

[a] Organic Chemistry, Department of Chemistry, Göteborg University,
41296 Göteborg, Sweden
Fax: (internat.) + 46-31-772-3840
E-mail: hilmers@chem.gu.se

Supporting information for this article is available on the WWW under http://www.eurjic.org or from the author.

 © 2004 Wiley-VCH Verlag GmbH & Co. KGaA, Weinheim DOI: 10.1002/ejic.200400309

by-products (i.e. acetylene or ethene)[20,21] that may cause the maximum pressure allowed in the microwave reaction vessel to be exceeded during heating. Crystals of iodine are also more easily handled inside the glove box. There is a significant difference in the rate of SmI_2 formation from samarium metal if it is used as chunks or as a powder. The formation of SmI_2 using powder of mesh −40 is rapid; the reaction is complete within 3−5 min, while chunks require about 20−30 min. When SmI_2 is generated from more than the necessary amount of I_2 and Sm, the excess SmI_2 precipitates leaving a saturated THF solution. After centrifugation of excess undissolved SmI_2, the maximum concentration of SmI_2 in THF is 0.13 M. The UV/Vis spectrum of the microwave-generated SmI_2 was identical to that previously reported (Supporting Information; for Supporting Information see also the footnote on the first page of this article).[22]

Ytterbium diiodide (YbI_2) has not been used much in organic synthesis since the first report by Kagan.[21] This is in part due to its reported low solubility in THF (0.040 M) and lower reactivity than that of SmI_2. In contrast to the large number of reports on SmI_2-mediated reactions, the development of YbI_2 as a single-electron-transfer reagent is still in its infancy. It was, therefore, with great interest that we prepared YbI_2 from ytterbium metal and iodine crystals using microwave-assisted heating. The saturated clear yellow THF solution of YbI_2 (maximum solubility 0.065 M in THF) is formed in less than 45 min under microwave heating at 180 °C, which results in a pressure of 13 bar. YbI_2 can be stored for extended periods of time inside the glove box without any observable change in colour, concentration or reactivity, as long as there is a slight excess of ytterbium metal present. The UV/Vis spectrum of the microwave-generated YbI_2 is identical to that previously reported (Supporting Information).[22]

We were also interested in the preparation of $SmBr_2$ since it is known to have a considerably larger oxidation potential (−2.07 V) than SmI_2 in THF.[23] Recently, Namy and co-workers reported on the preparation of $SmBr_2$ from tetrabromoethane.[10] We found that the predicted concentration of $SmBr_2$ has to be significantly higher than that of SmI_2, otherwise the preparation failed; the use of approximately 0.45 mmol of $SmBr_2$ per mL of THF gives reproducible results. The samarium bromide could be prepared in a microwave oven from samarium powder and either bromine or tetrabromoethane. However, we recommend preparation of $SmBr_2$ from tetrabromoethane since it gives somewhat cleaner reactions relative to $SmBr_2$ prepared from bromine. (The GC chromatograms of reduced 2-heptanone with $SmBr_2$/triethylamine/water shows no impurities for tetrabromoethane-generated $SmBr_2$, while $SmBr_2$ generated from bromine gives several smaller, unidentified peaks.) In agreement with previous studies we conclude that the solubility of $SmBr_2$ is very low in THF, and it exists predominantly as a suspension. The UV/Vis spectrum agrees with the spectrum for $SmBr_2$ prepared from SmI_2 and LiBr previously reported by Flowers and co-workers (Supporting Information).[23]

Table 1. Microwave-assisted generation of LnX_2 and the resulting concentration in THF[a]

Entry	Ln (mmol)	X_2 (mmol)	V [mL]	$[LnX_2]_{theor.}$ [M]	$[LnX_2]_{titrated}$ [M]
1	Sm (1.3)[b]	I_2 (0.10)	10.0	0.010	0.010
2	Sm (1.0)	I_2 (0.32)	5.0	0.063	0.063
3	Sm (1.0)	I_2 (0.39)	5.0	0.078	0.076
4	Sm (1.0)	I_2 (0.47)	5.0	0.094	0.091
5	Sm (1.1)	I_2 (0.50)	5.0	0.100	0.099
6	Sm (13)[b]	I_2 (11.0)	100.0	0.110	0.108
7	Sm (5.0)	I_2 (0.25)	5.0	0.050	0.048
8	Sm (5.0)	I_2 (0.50)	5.0	0.100	0.102
9	Sm (5.0)	I_2 (0.75)	5.0	0.15	0.15[c]
10	Sm (5.0)	I_2 (1.00)	5.0	0.20	0.21[c]
11	Sm (5.0)	I_2 (1.50)	5.0	0.30	0.31[c]
12	Sm (5.0)	I_2 (2.00)	5.0	0.40	0.36[c]
13	Sm (5.0)[b]	I_2 (1.50)	5.0	0.30	0.29[c]
14	Sm (5.0)[b]	I_2 (2.00)	5.0	0.40	0.35[c]
15	Sm (3.0)	$C_2H_2Br_4$ (0.75)	3.5	0.43	0.42[c]
16	Sm (3.0)[b]	$C_2H_2Br_4$ (0.75)	3.5	0.43	0.43[c]
17	Sm (2.3)[d]	$C_2H_2Br_4$ (0.75)	3.5	0.43	0.44[c]
18	Sm (2.3)[d]	Br_2 (1.50)	3.5	0.43	0.40[c]
19	Yb (2.9)	I_2 (0.16)	5.0	0.032	0.031
20	Yb (2.9)	I_2 (0.276)	5.0	0.055	0.057
21	Yb (2.9)	I_2 (0.33)	5.0	0.063	0.064
22	Yb (2.9)	I_2 (0.355)	5.0	0.071	0.069[c]
23	Yb (2.9)	I_2 (0.48)	5.0	0.100	0.108[c]
24	Yb (2.9)	I_2 (0.59)	5.0	0.118	0.119[c]

[a] The starting materials were mixed inside a glove box. YbI_2 was microwave-irradiated for 45 min, and SmI_2 and $SmBr_2$ for 5 min. $[LnX_2]$ was titrated according to the method described below to yield the concentration with an error of approximately ±2%. [b] Prepared in ultrasonic bath for 2−4 h. [c] Suspension, maximum solubility is exceeded, and the given value is an expected concentration provided that all reagents would dissolve. [d] Prepared inside a glove box with magnetic stirring for at least 15 h.

 © 2004 Wiley-VCH Verlag GmbH & Co. KGaA, Weinheim

The use of microwave heating was also explored in the preparation of EuI_2. We found that EuI_2 is prepared within 45 min (this reaction time was not optimised) to yield a clear, light yellow solution. The UV/Vis spectrum is identical to that previously reported (Supporting Information).[22]

Volumetric Titration of SmI_2 Solutions

The reduction of 2-heptanone has been studied using mixtures of SmI_2, amine and water. There is no side-reaction, thus two molecules of SmI_2 are consumed for every reduced molecule of ketone. An excess of I^-, I_2, Sm^0 or Sm^{3+} is not capable of reducing even trace amounts of ketone, hence the reduction of the ketone proceeds only by reaction with the single-electron-transfer reagent SmI_2, and the amount of reduced ketone is directly proportional to the molar concentration of SmI_2 in THF according to Equation (1).

$$R_2C{=}O + 2\,SmI_2 + 6\,H_2O + 4\,R_3N \rightleftharpoons R_2CH_2OH + 2\,Sm(OH)_3 + 4\,R_3N{\cdot}HI \quad (1)$$

Triethylamine (approximately 3 equiv.) and water (approximately 4 equiv.) were added to a solution of unknown concentration of SmI_2 in THF (10−130 mM). The resulting mixture of unknown concentration of the single-electron-transfer reagent SmI_2 was volumetrically titrated with a ketone (2-heptanone) dissolved in THF until the end point, i.e. when the characteristic dark blue colour of SmI_2 had disappeared and a white precipitate and colourless liquid remained. The reduction is instantaneous, even when there is excess precipitated SmI_2 present, which therefore allows rapid titration. The titrant reacts immediately, and there is no delay time during the titration. The added titrant volume was read when the colour changed from light green to white (Table 2).

Table 2. Comparison of volumetric titration with GC-based determinations of $[SmI_2]$[a]

$[SmI_2]_{Volumetric\ titration}$ [M][b]	$[SmI_2]_{Conversion}$ [M][c]	$[SmI_2]_{Internal\ standard}$ [M][d]
0.077	0.075	0.074
0.077	0.076	0.075
0.074	0.074	0.075
0.074	0.075	0.074

[a] SmI_2 (5 mL) was added to a dry Schlenk tube, then Et_3N (3 equiv.) and water (4 equiv.) were added by syringe. [b] 2-heptanone was dissolved in dry THF (0.070 M) and added dropwise to the SmI_2/H_2O/amine mixture. The colour of the solution changed from dark blue to green and finally white. The added titrant volume was noted when the colour changed from light green to white. $[SmI_2]$ was calculated according to the balanced Equation (1). [c] The determined $[SmI_2]$ calculated from the conversion of 2-heptanone to 2-heptanol after integration of the separate peaks of the GC chromatogram. [d] The determined $[SmI_2]$ based on the concentration of unreduced 2-heptanone relative to an internal standard (1-hexanol) after integration of the separate peaks of the GC chromatogram.

It may be argued that SmI_2 decomposes rapidly in the presence of excess water and amine. The stability of the reagent mixture of SmI_2 with excess water and amine in THF was therefore also studied (Figure 1). There is an observed decomposition of a 0.075 M solution of SmI_2 in THF in the presence of 4 equiv. of water and 3 equiv. of amine. However, the decomposition of SmI_2 after 1 h is only about 5%. We therefore conclude that the decomposition of SmI_2 is only of marginal consequence for the analysis. The volumetric addition of the ketone to the THF solution should only require approximately 1−2 min, which corresponds to a maximum error of about 1% in the analysis.

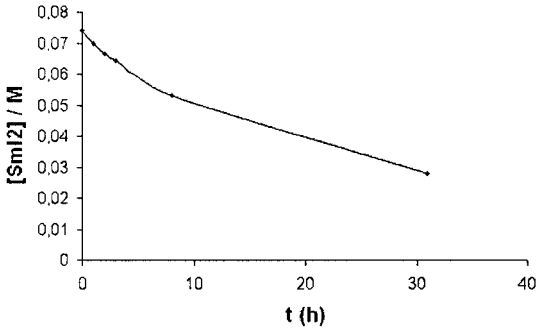

Figure 1. Decomposition of SmI_2 in the presence of triethylamine (3 equiv.) and water (4 equiv.) over an extended period of time (30 h)

GC-Based Titration of SmI_2 and YbI_2

Since the other lanthanide(II) halides do not have such a characteristic colour as SmI_2, another method for the determination of their concentrations was developed. Triethylamine (3 equiv.), water (4 equiv.) and 2-heptanone (1 equiv.) were added to a 5 mL solution or suspension of SmI_2 or YbI_2 in THF (10−400 mM). Provided that the amount of ketone is more than half of the actual amount of LnX_2, the instantaneous reaction of the excess ketone with SmI_2/amine/water results in a mixture of 2-heptanol and 2-heptanone (Scheme 2). Analysis of the amounts of 2-heptanol and 2-heptanone by GC chromatography (verified by an internal standard) yields the initial concentration of LnX_2 (Tables 1 and 2).

$$2\,LnX_2 + R_2C{=}O \xrightarrow[-R_3N{\cdot}HX]{R_3N/H_2O} 2\,Ln(OH)_3 + R_2CHOH$$

Scheme 4. Unbalanced formula for the LnX_2/amine/H_2O reductions

GC-Based Titration of Suspensions of $SmBr_2$, SmI_2 and YbI_2

Initially, we did not expect to be able to determine the amount of precipitated SmI_2 or $SmBr_2$ utilizing the reduction of 2-heptanone in the presence of amine and water. On the contrary, the reduction of the ketone is extremely fast (instantaneous), even with suspensions of YbI_2, SmI_2 and $SmBr_2$; this allows the quantitative titration of suspen-

 © 2004 Wiley-VCH Verlag GmbH & Co. KGaA, Weinheim

sions of up to at least 0.4 M (Table 1). These results also indicate that suspensions of either YbI_2, SmI_2 or $SmBr_2$ can be used as single-electron-transfer reagents in the instantaneous reduction of, for example, ketones by the amine/water method.

Titration of EuI_2

Titrations of EuI_2 in THF were unsuccessful. Apparently, the oxidation potential of Eu^{2+} is too low to mediate the reduction of, for example, 2-heptanone in the presence of triethylamine and water.

Conclusion

There should be numerous reduction reactions for which the oxidation potential of SmI_2 is nonideal, and in which other lanthanide halides and also samarium with different counter anions may play a crucial role. We believe that the exploration of the chemistry mediated by these reagents is dependent on simple methods for their preparation. Due to the very low oxidation potential of EuI_2 its synthetic utility as a single-electron-reagent is somewhat limited, nevertheless its use may increase once this rapid and reliable method of preparation is known. Microwave-assisted generation of LnX_2 from metal (Ln = Sm, Yb and Eu) and halides (I_2 and Br_2) appear to be a viable alternative to the recently reported fast sonication technique.[20] Preliminary results indicate that LnX_2 reagents can be prepared in situ in the presence of reducible substrates. In an ideal situation that would allow the use of less solvent as the actual concentration of LnX_2 could be kept low during the reaction.

The direct method of determining the concentration of LnX_2 solutions by utilizing the instantaneous reaction between, for example, SmI_2 and ketones in the presence of excess amine and water has proven to be a very powerful and reliable method. The major advantage with this method is that the determination is made only on the active single-electron-donor species, i.e. LnX_2. Previously reported methods also include inactive species such as LnX_3 and therefore tend to overestimate the concentration of the reagent. This simple method of determining accurate concentrations of LnX_2 will therefore become useful among those working with single-electron-transfer reagents.

Experimental Section

Generation of SmI_2: Samarium powder (113 mg, 0.75 mmol, 1.5 equiv.) and iodine (127 mg, 0.5 mmol, 1 equiv.) were weighed and diluted with dried THF (5 mL) in a microwave-approved vessel inside a glove box under nitrogen. A magnetic stirrer bar was added, and the vessel was sealed. The mixture was inserted in the microwave oven and irradiated at 180 °C for 5 min to yield a dark blue solution of SmI_2 in THF, which could be used without further purification.

Volumetric Titration of SmI_2: SmI_2 was centrifuged, and the solution (5 mL) was added to a test tube containing a magnetic stirrer bar, located inside a glove box and fitted with a septum. Triethylamine (approximately 3 equiv.) and water (approximately 4 equiv.) were then added to the SmI_2 solution by syringe. While vigorously stirring, 2-heptanone diluted in THF (0.07 M) was added dropwise until the dark blue solution turned colourless with the formation of a white suspension, and the volume of added 2-heptanone was read. The final calculation of [SmI_2] could then be carried out using the balanced formula [Equation (1)].

General GC-Based Determination of the Active Amount of $SmBr_2$, SmI_2 and YbI_2: A solution or suspension of SmI_2 (5 mL) was added to a test tube containing a magnetic stirrer bar, located inside a glove box and fitted with a septum. Triethylamine (approximately 3 equiv.) and water (approximately 4 equiv.) were added into the SmI_2 solution by syringe. While vigorously stirring, excess 2-heptanone diluted in THF (0.070 M) (i.e. more ketone than would be possible to reduce with the estimated amount of the prepared lanthanide reagent) was added in one portion, which caused the solution to decolourise. With the use of gas chromatography, the amount of consumed 2-heptanone was determined with an internal standard added, e.g. 1-hexanol. The final calculation of [SmI_2] could then be performed according to Equation (1).

Supporting Information Available (see also the footnote on the first page of this article): UV/Vis spectra of THF solutions of SmI_2, YbI_2, $SmBr_2$ and EuI_2. Further experimental details are also included.

Acknowledgments

We thank the Swedish Research Council (Vetenskapsrådet) for financial support, and Knut and Alice Wallenberg for funding of the glove box. We also thank Personal Chemistry AB and AstraZeneca R&D in Mölndal for the microwave equipment.

[1] G. A. Molander, *Radicals in Organic Synthesis* (Eds.: P. Renaud, M. P. Sibi), Wiley-VCH, Weinheim, **2001**, vol. 1, pp. 153−182.
[2] P. G. Steel, *J. Chem. Soc., Perkin Trans. 1* **2001**, 2727−2751.
[3] B. K. Banik, *Eur. J. Org. Chem.* **2002**, 2431−2444.
[4] G. A. Molander, *Organic Reactions* (Ed.: L. A. Paquette), John Wiley & Sons, Inc., New York, **1994**, vol. 46, pp. 211−367.
[5] M. Shabangi, J. M. Sealy, J. R. Fuchs, R. A. Flowers II, *Tetrahedron Lett.* **1998**, *39*, 4429−4432.
[6] A. Krief, A.-M. Laval, *Chem. Rev.* **1999**, *99*, 745−777.
[7] G. A. Molander, *Chem. Rev.* **1992**, *92*, 29−68.
[8] W. J. Evans, D. K. Drummond, H. Zhang, J. L. Atwood, *Inorg. Chem.* **1988**, *27*, 575−579.
[9] E. Prasad, B. W. Knettle, R. A. Flowers II, *J. Am. Chem. Soc.* **2002**, *124*, 14663−14667.
[10] F. Hélion, M.-I. Lannou, J.-L. Namy, *Tetrahedron Lett.* **2003**, *44*, 5507−5510.
[11] A. Ogawa, S. Ohya, Y. Sumino, N. Sonoda, T. Hirao, *Tetrahedron Lett.* **1997**, *38*, 9017−9018.
[12] W. J. Evans, P. S. Workman, N. T. Allen, *Organic Lett.* **2003**, *5*, 2041−2042.
[13] W. J. Evans, N. T. Allen, J. W. Ziller, *J. Am. Chem. Soc.* **2000**, *122*, 11749−11750.
[14] P. Lidström, J. Tierney, B. Wathey, J. Westman, *Tetrahedron* **2001**, *57*, 9225−9283.
[15] M. Larhed, C. Moberg, A. Hallberg, *Acc. Chem. Res.* **2002**, *35*, 717−727.

 © 2004 Wiley-VCH Verlag GmbH & Co. KGaA, Weinheim

[16] W. J. Evans, N. T. Allen, *J. Am. Chem. Soc.* **2000**, *122*, 2118−2119.
[17] I. M. Kolthoff, L. H. van Berk, *Z. Anal. Chem.* **1927**, *70*, 369−394.
[18] J. Tillmans, O. Heublein, *Chem.-Ztg.* **1913**, *37*, 901−903.
[19] A. Dahlén, G. Hilmersson, *Tetrahedron Lett.* **2002**, *43*, 7197−7200.
[20] J. M. Concellón, H. Rodríguez-Solla, E. Bardales, M. Huerta, *Eur. J. Org. Chem.* **2003**, 1775−1778.
[21] P. Girard, J. L. Namy, H. B. Kagan, *J. Am. Chem. Soc.* **1980**, *102*, 2693−2793.
[22] Y. Okaue, T. Isobe, *Inorg. Chim. Acta* **1988**, *144*, 143−146.
[23] B. W. Knettle, R. A. Flowers II, *Org. Lett.* **2001**, *3*, 2321−2324.
Received April 15, 2004

 © 2004 Wiley-VCH Verlag GmbH & Co. KGaA, Weinheim

Stabilization of a Copper(II) Complex by Hydrogen Bonds between the Axial Tetrafluoroborate Anion and the Ammonium Group from the Coordinated Cationic Ligand Bis(imidazol-2-yl)methyl(isopropyl)ammonium

Yufei Song,[a] Chiara Massera,[b] Patrick Gamez,[a] Anna Maria Manotti Lanfredi,[b] and Jan Reedijk*[a]

Keywords: Hydrogen bonds / Copper / EPR / N ligands

A new mononuclear copper complex [Cu(HIm-*i*Pr)$_2$(BF$_4$)$_2$](BF$_4$)$_2$·2CH$_3$OH {where Im-*i*Pr is [bis(imidazol-2-yl)methyl](isopropyl)amine} has been obtained by diethyl ether diffusion into a methanol solution of Im-*i*Pr and Cu(BF$_4$)$_2$. The complex has been characterized by X-ray analysis, UV/Vis, IR and EPR spectroscopy. Its crystal structure is built up by centrosymmetric [Cu(HIm-*i*Pr)$_2$(BF$_4$)$_2$]$^{2+}$ complex cations, BF$_4^-$ counterions and methanol lattice molecules. In the cation, the Cu atom exhibits a distorted octahedral CuN$_4$F$_2$ chromophore coordinated by two axial BF$_4^-$ ions and by four equatorial imidazole nitrogen atoms from two cationic HIm-*i*Pr ligands. The complex is stabilized by two intramolecular pseudo-chelate hydrogen bonds between the axial BF$_4^-$ ions and the ammonium nitrogen atoms of the HIm-*i*Pr ligand [N5···F8 = 2.761(5) Å].

(© Wiley-VCH Verlag GmbH & Co. KGaA, 69451 Weinheim, Germany, 2004)

Introduction

Copper ions, as centers of the active site of various metalloproteins, play an essential role in biological processes such as electron transfer, oxidation catalysis and dioxygen transport.[1] All copper proteins studied so far, except for the copper(I) metallothioneins, contain one or more imidazole residues of histidine, coordinated to the copper ions.[2] In the active site of the type-3 copper proteins, each copper ion is coordinated by three imidazole nitrogen atoms.[3]

Considerable progress in modeling the features of copper centers of type-3 copper proteins has been made, especially with the characterization of synthetic copper−dioxygen complexes.[4] In bioinorganic modeling studies frequently used ligand systems are based on pyridine, pyrazole,[5] and benzimidazole moieties.[6] Since side-chain imidazole coordination derived from histidine is very common in the active-site chemistry of copper proteins,[7] and imidazole-based ligand systems are relatively less reported,[8,9] there has recently been a great deal of interest in polyimidazole copper chemistry.

In the course of our research, [bis(imidazol-2-yl)methyl](isopropyl)amine (Im-*i*Pr, Figure 1), a bulky ligand with one amine and four imidazole nitrogen atoms, was synthesized by reaction of isopropylamine with the intermediate bis(imidazol-2-yl)nitromethane unit.[10] This potential tridentate ligand has been designed to investigate the coordination behavior and the binding properties of the bis(imidazol-2-yl) unit, which is present in most of the designed polyimidazole ligands.[11,12] Furthermore, the electronic effects of replacing aromatic rings like pyridine or imidazole with a short aliphatic chain such as isopropyl can be examined. All these studies are likely to provide important information for dioxygen binding chemistry. In this study, the crystal structure of the copper complex [Cu(HIm-*i*Pr)$_2$(BF$_4$)$_2$](BF$_4$)$_2$·2CH$_3$OH is presented. The complex is stabilized by hydrogen bonding between the axial BF$_4^-$ ions and the ammonium group from the cationic HIm-*i*Pr ligands that is thought to be the driving force for the formation of this unusual copper complex.

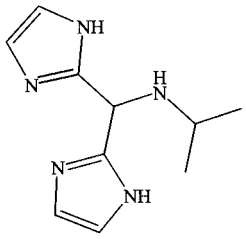

Figure 1. Molecular structure of the ligand Im-*i*Pr

[a] Leiden Institute of Chemistry, Gorlaeus Laboratories, Leiden University,
P. O. Box 9502, 2300 RA Leiden, The Netherlands
Fax: (internat.) + 31-71-5274451
E-mail: reedijk@chem.leidenuniv.nl
[b] Dipartimento di Chimica Generale ed Inorganica, Chimica Analitica, Chimica Fisica, Universita' degli Studi di Parma, Parco Area delle Scienze 17/A, 43100 Parma, Italy

Results and Discussion

X-ray Crystal Structure Studies

The mononuclear copper complex with the formula $[Cu(HIm\text{-}iPr)_2(BF_4)_2](BF_4)_2{\cdot}2CH_3OH$ was obtained by reaction of 1 equiv. of Im-*i*Pr with 1 equiv. of $Cu(BF_4)_2$ in methanol. Diethyl ether diffusion into the methanolic solution led to the formation of blue crystals suitable for X-ray diffraction analysis. The structure formally contains two units of HBF_4. A molecular plot representing the complex, together with the atom-labeling scheme is shown in Figure 2.

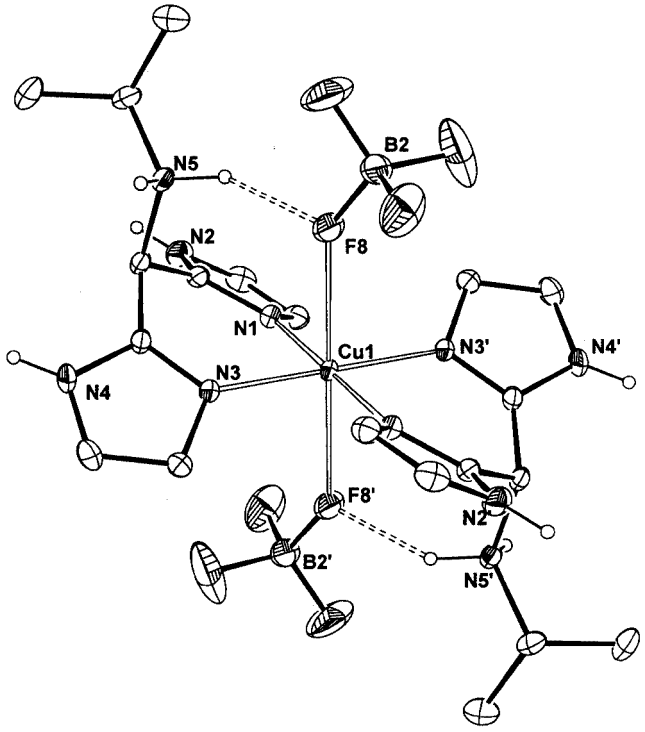

Figure 2. Thermal ellipsoid plot (20% probability level) of the mononuclear copper complex $[Cu(HIm\text{-}iPr)_2(BF_4)_2](BF_4)_2{\cdot}2CH_3OH$ showing the crystallographic numbering scheme; the hydrogen atoms at the C atoms, the non-coordinating BF_4^- ions and the methanol molecules have been omitted for clarity; selected bond lengths [Å] and angles [°]: Cu1−F8 2.493(3), Cu1−N1 2.011(3), Cu1−N3 1.995(3), N5···F8 2.761(5) (hydrogen bond); F8−Cu1−N1 91.4(1), F8−Cu1−N3 86.7(1), N1−Cu1−N3 86.4(1), N1−Cu1−N3a 93.56(11)

Its crystal structure consists of the $[Cu(HIm\text{-}iPr)_2(BF_4)_2]^{2+}$ cation (the −NH group of the Im-*i*Pr ligand is protonated in the course of the reaction to become an ammonium ion), free BF_4^- anions, and crystallization methanol molecules. The Cu^{II} ion, which in the $[Cu(HIm\text{-}iPr)_2(BF_4)_2]^{2+}$ moiety occupies the inversion center, is equatorially coordinated by four imidazole nitrogen atoms (N1, N3, N1′ and N3′) from two organic ligands [Cu1−N1 2.011(3), Cu1−N3 1.995(3) Å]. The coordination sphere is completed by coordination of two BF_4^- anions with a copper−fluoride distance of 2.493(3) Å, which is in good agreement with other values found in the literature,[13] to give a distorted octahedral environment. The complex is stabilized by two intramolecular interactions. The N5−H and N5′−H groups of the ammonium ions are in fact involved in pseudo-chelate hydrogen bonds with fluoride ions from the coordinated BF_4^- anions [N5···F8 2.761(4), H5···F8 1.94(4) Å; N5−H5···F8 144(3)°]. The cationic complexes are packed by weak intermolecular hydrogen bonds involving NH or CH groups from the cations, BF_4^- ions and methanol molecules. Also stacking interactions between the imidazole rings are present. The distance of the centroids between two least-squares imidazole planes is 3.532 Å.

The neutral ligand Im-*i*Pr has been designed to provide new information (for instance the coordinating behavior) in the field of the dioxygen binding chemistry. A general feature that is present in some imidazole-based ligands studied by our group is the [bis(imidazol-2-yl)methyl]amine unit; some examples are 1,1-bis(imidazol-2-yl)-4-(imidazol-4-yl)-2-azabutane (biib), 1,1-bis(imidazol-2-yl)-4-(pyrazol-1-yl)-2-azabutane (bipab), and 1,1-bis(imidazol-2-yl)-4-(pyridine-2-yl)-2-azabutane (bipyb).[9,11] With the potentially tetradentate ligands biib, bipab, and bipyb, dinuclear copper(II) complexes were formed by the sharing of two ligands between two Cu^{II} ions.[11] Due to steric effects, none of these tetradentate ligands can coordinate to a single Cu^{II} ion, but upon dimerization of the complexes, all four nitrogen donors of the ligands are able to coordinate to the copper atoms in a square-planar fashion. This coordination behavior, i.e. ligand sharing, is not observed with the present complex. Im-*i*Pr coordinates to the copper(II) ions in a bidentate fashion. The characteristic of the title complex $[Cu(HIm\text{-}iPr)_2(BF_4)_2](BF_4)_2{\cdot}2CH_3OH$ is that it contains a double intramolecular hydrogen-bond system, which is believed to be the driving force for the formation of the mononuclear copper complex.

Electronic Properties, EPR Spectra, ESI-MS and Conductivity Measurements

The UV/Vis spectrum of the complex in a methanol solution shows absorption bands centered at approximately 365 nm (ε = 2070 M^{-1} cm^{-1}) and 675 nm (ε = 460 M^{-1} cm^{-1}) in the range 300−800 nm. The absorption band at 365 nm is assigned to the charge-transfer transition from the imidazole nitrogen atoms to Cu^{II},[14] while the very weak absorption peak at 675 nm in the visible region of the electronic spectrum of the complex is assigned to d−d transitions of the Cu^{II} octahedral species.[15,16]

The EPR spectrum of a polycrystalline powder of the complex recorded at room temperature shows a typical axial spectrum with $g_{\|}$ = 2.22, $g_{\perp}$ = 2.07, and $A_{\|}$ = 200 G. The signals become sharper upon cooling to 77 K, but the hyperfine signals have not all been resolved.

The EPR analysis of the complex in a frozen solution of MeOH/DMSO (8:2) at 77 K shows a well-resolved axial spectrum with superhyperfine splitting superimposed on the equatorial absorption. The spectrum of the complex is redrawn in Figure 3 with $g_{\|}$ = 2.33, $g_{\perp}$ = 2.06, and $A_{\|}$ = 160 G as the dominant signals; the larger $g_{\|}$ values and the smaller $A_{\|}$ value already indicate a species different from

 © 2004 Wiley-VCH Verlag GmbH & Co. KGaA, Weinheim

that in the solid state. Further, not all nine expected superhyperfine lines with $A_{N\perp}$ = 15 G are resolved, not even at high dilution; this strongly suggests that the copper complex partly dissociates in the MeOH solution. At high dilution, the characteristic EPR lines for the Cu^{2+}−MeOH species ($g_{\|}$ = 2.42, $A_{\|}$ = 115 G)[15] become visible. The fact that the $g_{\|}$ value in the solid state is lower and the $A_{\|}$ value is larger than those in solution may suggest that two axially coordinated BF_4^- anions are dissociated in the methanol solution of the complex, as further confirmed by the ESI-MS and conductivity measurements.

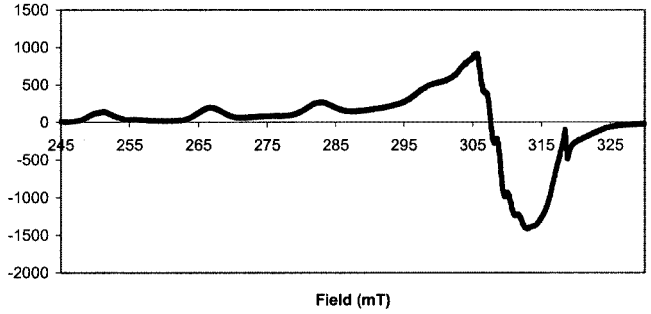

Figure 3. The EPR spectrum of the complex in a frozen solution of MeOH/DMSO (8:2) at 77 K

The conductivity measurement was performed at 25 °C on a 1 mM solution of the complex in MeOH. The value for the equivalent conductivity of the complex was found to be 275 $S{\cdot}cm^2{\cdot}mol^{-1}$, which agrees with a 3:1 type electrolyte in MeOH as the solvent.[17] The result indicates that at least one of the two axially coordinated BF_4^- anions are dissociated from the copper ion in the MeOH solution to form the 3:1 electrolyte (two non-coordinated BF_4^- anions in the crystal lattice of the complex already would have resulted in a 2:1 electrolyte).

The ESI mass spectrum of the complex was measured in MeOH. The most intensive peak at m/z = 206 corresponds to the free ligand Im-*i*Pr. Other major peaks observed at m/z = 450, 419, 391, and 325 correspond to the $[Cu(Im\text{-}iPr)(BF_4)(MeOH)_3]^+$, $[Cu(Im\text{-}iPr)(BF_4)(MeOH)_2]^+$, $[Cu(Im\text{-}iPr)(BF_4)(H_2O)_2]^+$, and $[Cu(HIm\text{-}iPr)_2(BF_4)_2]^{2+}$ cations, respectively; in fact the experimentally observed isotopic pattern is in very good agreement with the theoretical result of the isotope pattern calculation. The ESI mass spectrum of a mixture of the free ligand and $Cu(BF_4)_2$ gave very similar results. It seems that several species are present in the methanolic solution, which may arise from the electrochemical reduction of the copper complex during the electrospray process. Due to the very low solubility of the complex in non-coordinating solvents such as CH_2Cl_2, no information could be obtained with our experimental setup. Extensive studies would be needed to give more detailed information about the solution chemistry of the complex.

Conclusion

In summary, a new mononuclear copper complex has been obtained from the ligand Im-*i*Pr and $Cu(BF_4)_2$. The protonated cationic ligands HIm-*i*Pr coordinate to the copper(II) ion in a bidentate fashion, while two BF_4^- groups complete the distorted octahedral geometry around the metal atom. The complex is stabilized by intramolecular hydrogen bonds formed between the axially coordinated BF_4^- anions and the ammonium group of the ligand HIm-*i*Pr. The frozen-solution EPR spectrum of the complex in MeOH shows dissociation of the tetrafluoroborate anions. The higher $g_{\|}$ value in the solid state than in solution agrees with at least partial dissociation of the BF_4^- anions from the copper ion of the complex in MeOH, which is supported by solution conductivity data. Further studies on the dioxygen binding properties of the corresponding Cu^I complex are currently being carried out in our laboratories.

Experimental Section

General Remarks: All reagents and solvents were purchased from commercial sources and used as received. C, H, N analyses were carried out with a Perkin−Elmer 2400 series II analyzer. IR spectra were recorded with a Perkin−Elmer Paragon 1000 spectrophotometer equipped with a Golden Gate Diamond ATR device, using the diffuse reflectance technique. X-band EPR spectra were recorded at room temperature and at 77 K with a Jeol RE2X ESR spectrometer with DPPH (g = 2.0036) as a standard. The UV/Vis spectrum of the compound was recorded in the 250−800 nm range with a Cary 50 Varian UV/Vis/NIR spectrometer. Electrospray ionization mass spectra (ESI-MS, positive ion) in a methanol solution was recorded with a Thermo Finnigan AQA apparatus. The conductivity measurement was performed with a Philips PW 9526 digital conductivity meter and PW 9551/60 measuring cell with a 1 mM solution of the complex in methanol.

Synthesis of [Bis(imidazol-2-yl)methyl](isopropyl)amine (Im-*i*Pr): Isopropylamine (0.26 g, 4.36 mmol) was added to a solution of the hydrochloride salt of bis(imidazol-2-yl)nitromethane[10] (1.0 g, 4.36 mmol) in sodium hydroxide (10 mL of a 2.0 M of solution). The solution was stirred at 80 °C for more than 2 h and then cooled to room temperature. A white product precipitated from the solution. The precipitate was filtered, and the desired product was washed with small amounts of ethanol and diethyl ether. Yield: 40% (0.36 g). ^1H NMR (200 MHz, CD_3OD, 25 °C, 0−10 ppm): δ = 7.10 (s, 4 H, Im-H), 5.28 (s, 1 H, CH), 2.66 (m, 1 H, CH), 1.10 (d, 6 H, CH_3) ppm. ESI-MS: m/z = 206.1 $[M + H]^+$.

Preparation of the Copper Complex $[Cu(HIm\text{-}iPr)_2(BF_4)_2]\cdot(BF_4)_2\cdot 2CH_3OH$: A solution of the ligand Im-*i*Pr (16.4 mg, 0.08 mmol) in MeOH (5 mL) was added to a solution of $Cu(BF_4)_2\cdot 6H_2O$ (27.6 mg, 0.08 mmol) in MeOH (5 mL). The reaction mixture was stirred for 15 min until the solution was completely clear, then it was filtered. Slow diethyl ether diffusion into the filtrate for several days led to the formation of blue crystals suitable for X-ray analysis. Yield: 30% (10.6 mg). $C_{22}H_{40}B_4CuF_{16}N_{10}O_2$ (887.42): calcd. C 29.8, H 4.5, N 15.8; found

 © 2004 Wiley-VCH Verlag GmbH & Co. KGaA, Weinheim

C 30.2, H 4.9, N 15.3. IR (solid): $\tilde{\nu}$ = 3339.9, 1569.5, 1471.3, 1393.7, 1009.6, 764.3, 697.1, 519.8, 442.2 cm^{-1}.

X-ray Crystallographic Study: The molecular structure of $[Cu(HIm\text{-}iPr)_2(BF_4)_2](BF_4)_2\cdot 2CH_3OH$ was determined by single-crystal X-ray diffraction methods. Crystallographic and experimental details for the structure are summarized in Table 1. Intensity data and cell parameters were recorded at room temperature (25 °C) with a Philips PW 1100 single-crystal diffractometer using graphite-monochromated Mo-K_α radiation and the θ/2θ scan technique. A correction for absorption was made (maximum and minimum value for the transmission coefficient was 1.000 and 0.5472).[18] The structure was solved by Direct Methods using the SIR97 program[19] and refined on F_o^2 by full-matrix least-squares procedures, with the SHELXL-97 program.[20] All non-hydrogen atoms were refined with anisotropic atomic displacements. The hydrogen atoms were included in the refinement at idealized geometry (C−H 0.95 Å) and refined "riding" on the corresponding parent atoms, with the exception of H4, H5NA, H5NB, H8, and H1S, which were located in the difference Fourier map. The weighting scheme used in the last cycle of refinement was $w = 1/[\sigma^2F_o^2 + (0.1758P)^2]$ [where $P = (F_o^2 + 2F_c^2)/3$]. Molecular geometry calculations were carried out with the PARST97 program[21]. Drawings were obtained by ORTEP3 in the WinGX suite.[22] All calculations were carried out with a DIGITAL Alpha Station 255 computer. CCDC-235117 contains the supplementary crystallographic data for this paper. These data can be obtained free of charge at www.ccdc.cam.ac.uk/conts/retrieving.html [or from the Cambridge Crystallographic Data Centre, 12 Union Road, Cambridge CB2 1EZ, UK; Fax: (internat.) + 44-1223-336-033; E-mail: deposit@ccdc.cam.ac.uk].

Table 1. Crystallographic data for $[Cu(HIm\text{-}iPr)_2(BF_4)_2](BF_4)_2\cdot 2CH_3OH$

	$[C_{20}H_{32}Cu_1N_{10}B_2F_8](BF_4)_2\cdot 2CH_3OH$
Formula mass	887.42
Crystal system	monoclinic
Space group	$P21/n$
a [Å]	8.583(5)
b [Å]	13.832(5)
c [Å]	15.573(5)
β [°]	91.133(5)
V [Å^3]	1848.5(14)
Z	2
$D_{calcd.}$ [g·cm^{-3}]	1.594
Linear absorption coeff. [mm^{-1}]	0.711
$F(000)$	902
Crystal size [mm]	0.15 × 0.20 × 0.24
Index ranges	$-12 \le h \le 12$, $0 \le k \le 19$, $0 \le l \le 21$
θ range for data collection[°]	3.06−30.00
Reflections collected	5530
Independent reflections	5364 (R_{int} = 0.0852)
Observed reflections [$I > 2\sigma(I)$]	3551
Data/restraints/parameters	5364/0/276
Goodness-of-fit on F^2 [a]	1.002
Final R indices (obsd. data)[b]	R_1 = 0.0848, wR_2 = 0.2304
R indices (all data)[b]	R_1 = 0.1167, wR_2 = 0.2495
Largest diff. peak/hole [e/Å^{-3}]	1.011/−1.941

[a] Goodness-of-fit $S = [\Sigma w(F_o^2 - F_c^2)^2/(n-p)]^{1/2}$, where n is the number of reflections and p the number of parameters. [b] $R_1 = \Sigma||F_o| - |F_c||/\Sigma|F_o|$, $wR_2 = [\Sigma w(F_o^2 - F_c^2)^2/\Sigma wF_o^4]^{1/2}$.

Acknowledgments

The work described here has been supported by the Leiden University Study group WFMO (Werkgroep Fundamenteel Materialen-Onderzoek). Support from the NRSC Catalysis (a Research School Combination of HRSMC and NIOK) is kindly acknowledged. The project is financially supported by the Dutch Economy, Ecology, Technology (EET) program, a joint program of the Ministry of Economic Affairs, the Ministry of Education, Culture and Science, and the Ministry of Housing, Spatial Planning and the Environment.

[1] J. Reedijk, E. Bouwman (Eds.), *Bioinorganic Catalysis*, Marcel Dekker, New York, Basel, **1999**; E. I. Solomon, M. J. Baldwin, M. D. Lowery, *Chem. Rev.* **1992**, *92*, 521.
[2] K. D. Karlin, Z. Tyeklar, *Bioinorganic Chemistry of Copper*; Chapman & Hall, New York, **1993**.
[3] K. A. Magnus, B. Hazes, H. Tonthat, C. Bonaventura, J. Bonaventura, W. G. J. Hol, *Proteins* **1994**, *19*, 302; K. A. Magnus, H. Tonthat, J. E. Carpenter, *Chem. Rev.* **1994**, *94*, 727.
[4] L. M. Mirica, M. Vance, E. I. Solomon, T. D. P. Stack, *Abstr. Pap. − Am. Chem. Soc.* **2002**, *224*, 040; L. M. Mirica, M. Vance, D. J. Rudd, B. Hedman, K. O. Hodgson, E. I. Solomon, T. D. P. Stack, *J. Am. Chem. Soc.* **2002**, *124*, 9332; L. Que, L. Banci, *Curr. Opin. Chem. Biol.* **2002**, *6*, 169; L. Que, W. B. Tolman, *Angew. Chem. Int. Ed.* **2002**, *41*, 1114; H. C. Liang, C. X. Zhang, M. J. Henson, R. D. Sommer, K. R. Hatwell, S. Kaderli, A. D. Zuberbuhler, A. L. Rheingold, E. I. Solomon, K. D. Karlin, *J. Am. Chem. Soc.* **2002**, *124*, 4170; H. C. Liang, E. Kim, C. D. Incarvito, A. L. Rheingold, K. D. Karlin, *Inorg. Chem.* **2002**, *41*, 2209; T. Osako, K. Ohkubo, M. Taki, Y. Tachi, S. Fukuzumi, S. Itoh, *J. Am. Chem. Soc.* **2003**, *125*, 11027.
[5] N. K. Kitajima, K. Fujisabbla, Y. Moro-oka, *J. Mol. Catal. A.* **1992**, *74*, 143; N. Kitajima, Y. Moro-oka, *Chem. Rev.* **1994**, *94*, 737.
[6] G. A. van Albada, W. J. J. Smeets, A. L. Spek, J. Reedijk, *J. Coord. Chem.* **1999**, *48*, 375; G. Battaini, E. Monzani, A. Perotti, C. Para, L. Casella, L. Santagostini, M. Gullotti, R. Dillinger, C. Nather, F. Tuczek, *J. Am. Chem. Soc.* **2003**, *125*, 4185; L. Santagostini, M. Gullotti, E. Monzani, L. Casella, R. Dillinger, F. Tuczek, *Chem. Eur. J.* **2000**, *6*, 519; E. Monzani, G. Battaini, A. Perotti, L. Casella, M. Gullotti, L. Santagostini, G. Nardin, L. Randaccio, S. Geremia, P. Zanello, G. Opromolla, *Inorg. Chem.* **1999**, *38*, 5359; E. Monzani, L. Casella, G. Zoppellaro, M. Gullotti, R. Pagliarin, R. P. Bonomo, G. Tabbi, C. Nardin, L. Randaccio, *Inorg. Chim. Acta* **1998**, *282*, 180; E. Monzani, L. Quinti, A. Perotti, L. Casella, M. Gullotti, L. Randaccio, S. Geremia, G. Nardin, P. Faleschini, G. Tabbi, *Inorg. Chem.* **1998**, *37*, 553; M. C. Mimmi, M. Gullotti, L. Santagostini, R. Pagliarin, L. De Gioia, E. Monzani, L. Casella, *Eur. J. Inorg. Chem.* **2003**, 3934.
[7] A. Volbeda, W. G. J. Hol, *J. Mol. Biol.* **1989**, *209*, 249; K. D. Karlin, Y. Gultneh, *Prog. Inorg. Chem.* **1987**, *35*, 219.
[8] G. Koolhaas, *Recl. Trav. Chim. Pays-Bas* **1996**, *115*, 381; M. Beretta, E. Bouwman, L. Casella, B. Douziech, W. L. Driessen, L. Gutierrez-Soto, E. Monzani, J. Reedijk, *Inorg. Chim. Acta* **2000**, *310*, 41; E. Bouwman, B. Douziech, L. Gutierrez-Soto, M. Beretta, W. L. Driessen, J. Reedijk, G. Mendoza-Diaz, *Inorg. Chim. Acta* **2000**, *304*, 250.
[9] G. J. A. A. Koolhaas, W. L. Driessen, J. Reedijk, H. Kooijman, A. L. Spek, *J. Chem. Soc., Chem. Commun.* **1995**, 517.
[10] M. Joseph, T. Leigh, M. L. Swain, *Synthesis* **1977**, 459.
[11] G. J. A. A. Koolhaas, P. M. v. Berkel, S. C. v. d. Slot, G. Mendoza-Diaz, W. L. Driessen, J. Reedijk, H. Kooijman, N. Veldman, A. L. Spek, *Inorg. Chem.* **1996**, *35*, 3525.
[12] G. J. A. A. Koolhaas, W. L. Driessen, J. Reedijk, J. van der Plas, R. A. G. de Graaff, D. Gatteschi, H. Kooijman, A. L. Spek, *Inorg. Chem.* **1996**, *35*, 1509; Y. F. Song, P. Gamez, A. F. Stassen, M. Lutz, A. L. Spek, J. Reedijk, *Eur. J. Inorg. Chem.* **2003**, 4073.

 © 2004 Wiley-VCH Verlag GmbH & Co. KGaA, Weinheim

[13] A. M. Mills, K. Flinzner, A. F. Stassen, J. G. Haasnoot, A. L. Spek, *Acta Crystallogr., Sect. C* **2002**, *58*, 243; C. Bucher, E. Duval, E. Espinosa, J. M. Barbe, J. N. Verpeaux, C. Amatore, R. Guilard, *Eur. J. Inorg. Chem.* **2001**, 1077; C. C. Su, T. T. Hwang, O. Y. P. Wang, S. L. Wang, F. L. Liao, *Transit. Met. Chem.* **1992**, *17*, 91; A. J. Jircitano, S. O. Sommerer, K. A. Abboud, *Acta Crystallogr., Sect. C* **1997**, *53*, 434; J. A. Campo, M. Cano, J. V. Heras, M. C. Lagunas, J. Perles, E. Pinilla, M. R. Torres, *Helv. Chim. Acta* **2002**, *85*, 1079.
[14] A. B. P. Lever, *Inorganic Electronic Spectroscopy*, 2nd ed., Elsevier, Amsterdam **1986**; W. Linert, R. F. Jameson, A. Taha, *J. Chem. Soc., Dalton Trans.* **1993**, 3181.
[15] B. J. Hathaway, *Comprehensive Coordination Chemistry*, Pergamon Press, Oxford, **1987**, vol. 5.
[16] L. P. Wu, P. Field, T. Morrissey, C. Murphy, P. Nagle, B. Hathaway, C. Simmons, P. Thornton, *J. Chem. Soc., Dalton Trans.* **1990**, 3835.
[17] W. J. Geary, *Coord. Chem. Rev.* **1971**, *7*, 81.
[18] F. Ugozzoli, *Comput. Chem.* **1987**, *11*, 109; N. Walker, D. Stuart, *Acta Crystallogr., Sect. A.* **1983**, *39*, 158.
[19] A. Altomare, M. C. Burla, M. Camalli, G. L. Cascarano, C. Giacovazzo, A. Guagliardi, A. G. G. Moliterni, G. Polidori, R. Spagna, *J. Appl. Crystallogr.* **1999**, *32*, 115.
[20] G. M. Sheldrick, *SHELXL-97, Program for Crystal Structure Refinement*, University of Göttingen, Germany, **1997**.
[21] M. Nardelli, *J. Appl. Crystallogr.* **1995**, *28*, 659.
[22] L. J. Farrugia, *J. Appl. Crystallogr.* **1997**, *30*, 565.

Received April 7, 2004

 © 2004 Wiley-VCH Verlag GmbH & Co. KGaA, Weinheim

Novel Phosphovanadate Layered Structure Assembled from a Tetrametallic Cubane-Like V^V Cluster

Fa-Nian Shi,[a] Filipe A. Almeida Paz,[b] João Rocha,*[a] Jacek Klinowski,[b] and Tito Trindade[a]

Keywords: Organic-inorganic hybrid / Hydrothermal synthesis / Oxo ligands / Vanadium

A novel phosphovanadate layered structure intercalated by 4,4′-bipyridinium cations, $(C_{10}H_{10}N_2)[(VO_2)_4(PO_4)_2]$, was synthesised under hydrothermal conditions and its crystal structure determined using single-crystal X-ray diffraction. The anionic $[(VO_2)_4(PO_4)_2]_n^{2n-}$ perforated layers are strongly hydrogen bonded to the interlayer 4,4′-bipyridinium cations and are assembled by an unprecedented secondary tetrametallic V^V building unit constructed from a distorted cubane-like $\{V_4O_4\}$ cluster. The compound was further characterised by IR, Raman, ^1H, ^1H-^{13}C, ^{31}P and ^{51}V MAS NMR spectroscopy, and by thermal and elemental analysis.

(© Wiley-VCH Verlag GmbH & Co. KGaA, 69451 Weinheim, Germany, 2004)

Introduction

Much attention has been given to the synthesis of organic-inorganic hybrid compounds given their ability to combine features from both organic and inorganic building units, leading to novel materials with interesting architectures and potential applications. Vanadium, one of the most versatile transition metals through the combination of its three distinct oxidation states with the several possible coordination geometries,[1] has been extensively used as one of the primary building blocks in transition metal phosphates, which can be employed in functional materials due to their unusual catalytic, magnetic, electrical and optical properties.[2] Solvothermal synthetic conditions provide a versatile route for the synthesis of such materials; organic molecules are usually added to the reactive mixtures. These molecules can coordinate to the metal centres,[3] or act as structure-directing agents, templates, counterions or simply as space-filling molecules.[1,4] In this context, special interest has been given to layered structures and their intercalation by a variety of guest molecules.[1]

Following our interest in hybrid materials containing bridging organic ligands[5,6] and, in particular, vanadium centres,[6,7] we wish to report the preparation and structural characterisation of a novel phosphovanadate layered structure intercalated by 4,4′-bipyridinium cations, $(C_{10}H_{10}N_2)[(VO_2)_4(PO_4)_2]$ (**I**). The anionic layers are assembled by an unprecedented secondary tetrametallic V^V building unit that exhibits a distorted cubane-type structural motif. Other tetrametallic vanadium cores of the $\{V_4O_4\}$ type have already been investigated: those that exhibit the boat conformation (involving two pairs of edge-sharing octahedra connected by two corner-sharing oxygen atoms) or the chair conformation (where each VO_6 octahedron is edge-shared by two neighbouring octahedra).[8] Although the formation of cubane-type clusters is a characteristic structural motif in the coordination chemistry of many different metal centres,[9] only vanadium thiocubane clusters $\{V_4S_4\}$ have been described.[10] Thus, to the best of our knowledge, compound **I** is the first material containing such a structural motif assembled by VO_6 octahedra that are further bridged by phosphate groups (Scheme 1).

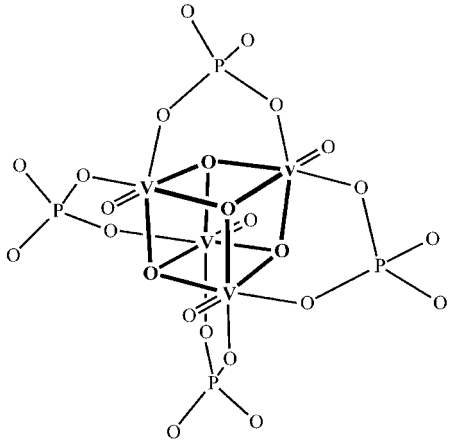

Scheme 1

[a] Department of Chemistry, University of Aveiro, CICECO, 3810-193 Aveiro, Portugal
E-mail: rocha@dq.ua.pt
[b] Department of Chemistry, University of Cambridge, Lensfield Road, Cambridge CB2 1EW, U.K.
E-mail: jk18@cam.ac.uk

Results and Discussion

Crystal Description

The product of the hydrothermal reaction between vanadium(v) oxide, phosphoric acid and 4,4′-bipyridine (4,4′-bpy; see Exp. Sect.) was analysed by single-crystal X-ray diffraction (Table 1) and elemental analysis, and formulated as $(C_{10}H_{10}N_2)[(VO_2)_4(PO_4)_2]$ (**I**) (where $C_{10}H_{10}N_2^{2+}$ = 4,4′-$bpyH_2^{2+}$ = 4,4′-bipyridinium). A direct comparison between the experimental powder X-ray diffraction (PXRD) pattern and a simulation based on single-crystal data confirms phase purity and homogeneity of the bulk sample, despite the presence of a few reflections attributed to strong preferential orientation of the compound.

Table 1. Crystal data and structure refinement information

Formula	$C_{10}H_{10}N_2O_{16}P_2V_4$
Molecular weight	679.90
Crystal system	Monoclinic
Space group	*P*2/c
a (Å)	14.797(3)
b (Å)	7.4178(15)
c (Å)	18.613(4)
β (°)	102.20(3)
Volume (Å^3)	1996.8(7)
Z	4
D_c (g cm^{-3})	2.262
μ(Mo-K_α) (mm^{-1})	2.063
F(000)	1336
Crystal size (mm)	0.12 × 0.12 × 0.10
Crystal type	orange blocks
θ range	3.54 to 27.48
Index ranges	$-19 \le h \le 18$
	$-8 \le k \le 9$
	$-19 \le l \le 24$
Reflections collected	11350
Independent reflections	4559 (R_{int} = 0.0583)
Final R_{int} [$I > 2\sigma(I)$]	$R1$ = 0.0463
	$wR2$ = 0.0888
Final R_{int} (all data)	$R1$ = 0.0805
	$wR2$ = 0.1022
Largest diff. peak and hole	0.641 and −0.666 e·Å^{-3}

The compound contains four crystallographically unique V^V centres distributed along two independent, but topologically identical, tetrametallic secondary building units (SBUs, {V(1),V(4)} and {V(2),V(3)}) that exhibit a distorted cubane-type structural motif (Figure 1) in which each VO_6 octahedron shares edges (belonging to the same face) with the three neighbouring octahedra (Figure 2). In these clusters, formed by twofold rotation axes perpendicu-

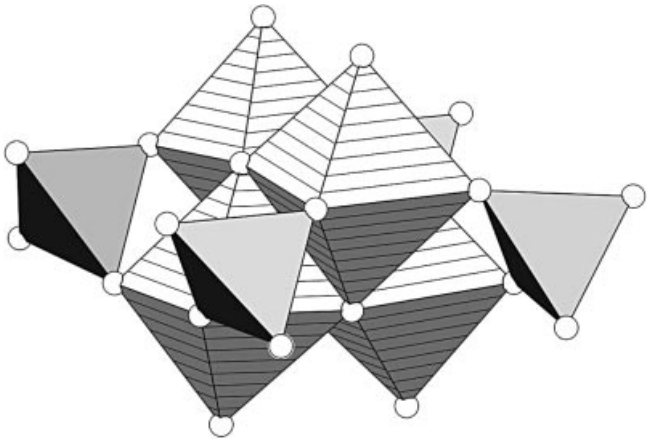

Figure 2. Polyhedral representation of a $\{(V_4O_8)(PO_4)_4\}$ secondary building unit; each VO_6 octahedron is edge-shared (from the same face) with the three neighbouring octahedra, leading to a tetrametallic tetrahedral V^V core

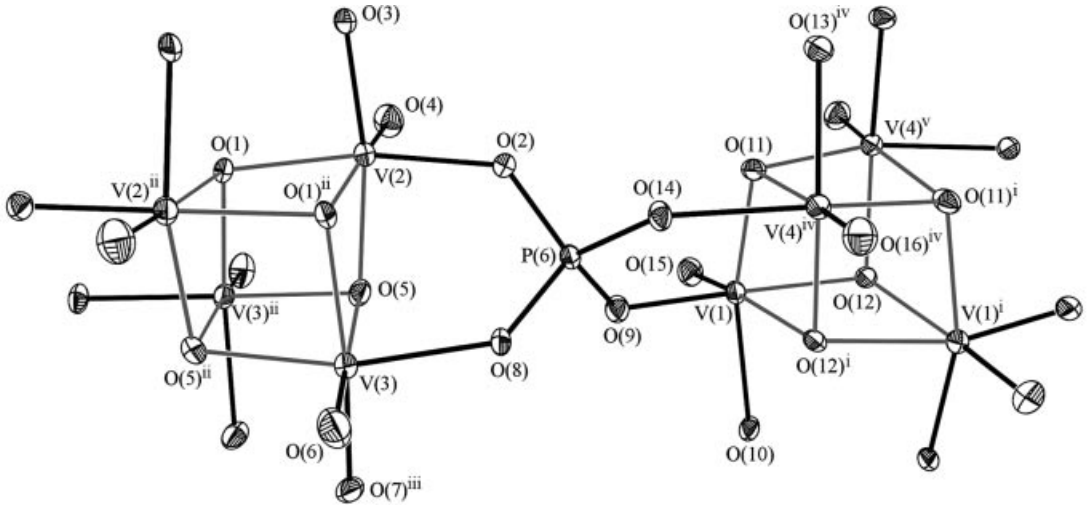

Figure 1. Tetrametallic secondary building units {V(1),V(4)} and {V(2),V(3)}, which form the two-dimensional perforated $[(VO_2)_4(PO_4)_2]_n^{2n-}$ anionic layer; atoms are represented as ellipsoids drawn at the 50% probability level; V···V distances within each SBU: V(1)···V(1)^i 3.3619(18) Å, V(1)···V(4)^{iv} 3.3593(12) Å, V(1)···V(4)^v 2.8031(11) Å, V(4)^{iv}···V(4)^v 3.3758(16) Å, V(2)···V(2)^{ii} 3.3543(16) Å, V(2)···V(3) 3.3322(11) Å, V(2)···V(3)^{ii} 2.8162(11) Å, V(3)···V(3)^{ii} 3.3628(18) Å; for bond lengths and angles see Tables 2 and 3; symmetry codes used to generate equivalent atoms: (i) 1 − *x*, *y*, 1/2 − *z*, (ii) −*x*, *y*, 1/2 − *z*, (iii) *x*, −1 + *y*, *z*, (iv) 1 − *x*, 1 + *y*, 1/2 − *z*, (v) *x*, 1 + *y*, *z*

 © 2004 Wiley-VCH Verlag GmbH & Co. KGaA, Weinheim

lar to the *ac* plane, the coordination environment of each V^V centre resembles the typical 1+4+1 coordination type described by Boudin et al., with the observed short, intermediate and long (V−O) bonds within the expected ranges reported by the same authors (Table 2 and Table 3).[11] The core of each cluster consists of a tetrametallic V_4 tetrahedron: each face is capped by a μ_3−O ligand that is equatorially coordinated to two octahedra, $O_{equatorial}$, and also occupies the *trans* position to the oxo group of a third octahedron, O_{trans} (Figure 1). The registered V···V, V−$O_{equatorial}$ and V−O_{trans} distances are within the ranges, 2.8031(11)−3.3758(16) Å, 1.841(3)−1.933(3) Å and 2.426(3)−2.462(3) Å, respectively (Table 2; see caption of Figure 1 for detailed V···V distances). Phosphate groups appear with two distinct structural functions: on the one hand, within each SBU, they link adjacent V^V centres along the edges of the V_4 tetrahedra (Scheme 1, Figures 1 and 2); on the other hand, they establish physical links between adjacent V_4 tetrahedra. In fact, the parallel linking in the *ab* plane through the phosphate groups of the two previously mentioned SBUs leads to a two-dimensional (2D) anionic $[(VO_2)_4(PO_4)_2]_n^{2n-}$ layer, topologically described as a distorted (4,4) net,[12] which is further perforated by eight-membered rings to form pores with an effective cross-section of ca. 2.5 × 2.5 Å (Figure 3).

Table 2. Bond lengths (in Å) for the two-dimensional $[(VO_2)_4(PO_4)_2]_n^{2n-}$ anionic layer; symmetry codes used to generate equivalent atoms: (i) $1-x, y, 1/2-z$, (ii) $-x, y, 1/2-z$, (iii) $x, -1+y, z$, (iv) $1-x, 1+y, 1/2-z$

V(1)−O(9)	1.932(3)	V(3)−O(1)^{ii}	1.855(3)
V(1)−O(10)	1.932(3)	V(3)−O(5)	2.426(3)
V(1)−O(11)	1.841(3)	V(3)−O(5)^{ii}	1.912(3)
V(1)−O(12)	1.877(3)	V(3)−O(6)	1.589(3)
V(1)−O(12)^{i}	2.451(3)	V(3)−O(7)^{iii}	1.918(3)
V(1)−O(15)	1.585(3)	V(3)−O(8)	1.905(3)
V(2)−O(1)	1.857(3)	V(4)^{iv}−O(11)	1.868(3)
V(2)−O(1)^{ii}	2.462(3)	V(4)^{iv}−O(12)^{i}	1.877(3)
V(2)−O(2)	1.933(3)	V(4)^{iv}−O(13)^{iv}	1.908(3)
V(2)−O(3)	1.911(3)	V(4)^{iv}−O(14)	1.923(3)
V(2)−O(4)	1.590(3)	V(4)^{iv}−O(16)^{iv}	1.583(3)
V(2)−O(5)	1.875(3)		

Table 3. Bond angles (in degrees) for the two-dimensional $[(VO_2)_4(PO_4)_2]_n^{2n-}$ anionic layer; symmetry codes used to generate equivalent atoms: (i) $1-x, y, 1/2-z$, (ii) $-x, y, 1/2-z$

O(9)−V(1)−O(10)	90.38(12)	O(1)^{ii}−V(3)−O(5)	79.63(11)
O(9)−V(1)−O(12)^{i}	79.07(11)	O(1)^{ii}−V(3)−O(5)^{ii}	80.07(12)
O(10)−V(1)−O(12)^{i}	77.18(11)	O(1)^{ii}−V(3)−O(7)^{iii}	157.00(12)
O(11)−V(1)−O(9)	89.62(12)	O(1)^{ii}−V(3)−O(8)	89.83(12)
O(11)−V(1)−O(10)	156.61(13)	O(5)^{ii}−V(3)−O(5)	78.66(12)
O(11)−V(1)−O(12)^{i}	79.87(11)	O(5)^{ii}−V(3)−O(7)^{iii}	88.26(12)
O(11)−V(1)−O(12)	80.88(12)	O(6)−V(3)−O(1)^{ii}	102.61(15)
O(12)−V(1)−O(9)	156.87(12)	O(6)−V(3)−O(5)	177.66(14)
O(12)−V(1)−O(10)	90.20(12)	O(6)−V(3)−O(5)^{ii}	100.99(14)
O(12)−V(1)−O(12)^{i}	78.52(12)	O(6)−V(3)−O(7)^{iii}	99.01(15)
O(15)−V(1)−O(9)	100.07(14)	O(6)−V(3)−O(8)	100.50(14)
O(15)−V(1)−O(10)	99.54(14)	O(7)^{iii}−V(3)−O(5)	78.68(11)
O(15)−V(1)−O(11)	103.49(15)	O(8)−V(3)−O(5)	80.09(11)
O(15)−V(1)−O(12)	102.64(14)	O(8)−V(3)−O(5)^{ii}	157.78(12)
O(15)−V(1)−O(12)^{i}	176.56(13)	O(8)−V(3)−O(7)^{iii}	93.88(13)
O(1)−V(2)−O(1)^{ii}	78.52(12)	O(11)−V(4)^{iv}−O(12)^{i}	80.20(12)
O(1)−V(2)−O(2)	157.49(13)	O(11)−V(4)^{iv}−O(13)^{iv}	88.85(12)
O(1)−V(2)−O(3)	89.39(12)	O(11)−V(4)^{iv}−O(14)	157.37(12)
O(1)−V(2)−O(5)	80.98(12)	O(12)^{i}−V(4)^{iv}−O(13)^{iv}	156.73(12)
O(2)−V(2)−O(1)^{ii}	79.47(11)	O(12)^{i}−V(4)^{iv}−O(14)	89.48(12)
O(3)−V(2)−O(1)^{ii}	79.03(11)	O(13)^{iv}−V(4)^{iv}−O(14)	93.12(12)
O(3)−V(2)−O(2)	90.99(12)	O(16)^{iv}−V(4)^{iv}−O(11)	104.01(14)
O(4)−V(2)−O(1)	103.03(14)	O(16)^{iv}−V(4)^{iv}−O(12)^{i}	101.70(14)
O(4)−V(2)−O(1)^{ii}	178.42(13)	O(16)^{iv}−V(4)^{iv}−O(13)^{iv}	100.84(14)
O(4)−V(2)−O(2)	99.01(15)	O(16)^{iv}−V(4)^{iv}−O(14)	97.75(14)
O(4)−V(2)−O(3)	100.63(15)		
O(4)−V(2)−O(5)	102.17(15)		
O(5)−V(2)−O(1)^{ii}	78.31(11)		
O(5)−V(2)−O(2)	90.05(12)		
O(5)−V(2)−O(3)	156.72(13)		

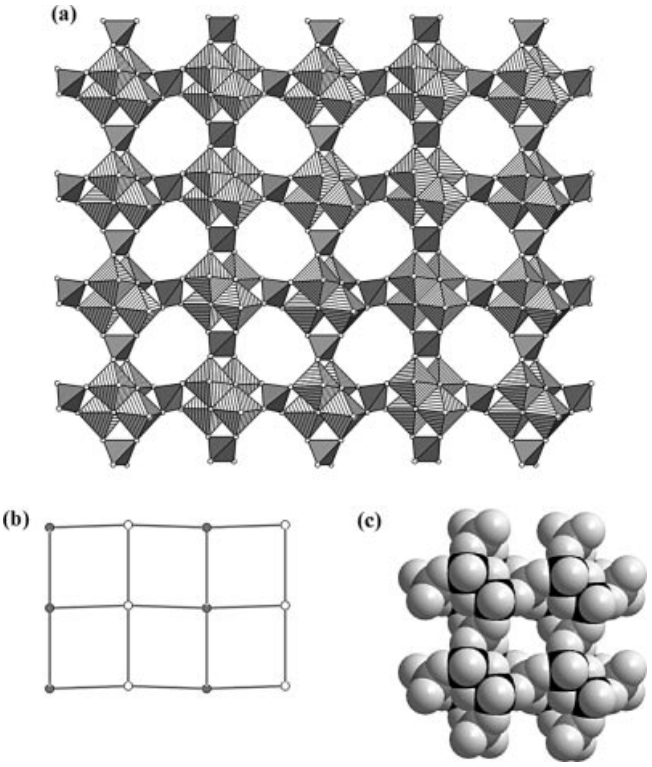

Figure 3. (a) View along the *c* direction of a polyhedral representation of the $[(VO_2)_4(PO_4)_2]_n^{2n-}$ anionic layer, (b) topological representation of the anionic layer which describes a typical (4,4) net (the grey- and white-filled nodes represent the two distinct tetrametallic SBUs), (c) space-fill representation of a portion of the anionic layer showing the pores which have a cross-section of about 2.5 × 2.5 Å

Charge-balancing and space-filling 4,4′-bipyridinium cations are positioned above and below the anionic $[(VO_2)_4(PO_4)_2]_n^{2n-}$ layers, just over the previously mentioned pores (Figure 4). These cations are further connected to the layers through two very strong and highly directional N^+−H···O hydrogen bonds, thus acting as a hydrogen-bonded pillar. The caption of Figure 5 contains further details of the hydrogen-bonding geometry.

 © 2004 Wiley-VCH Verlag GmbH & Co. KGaA, Weinheim

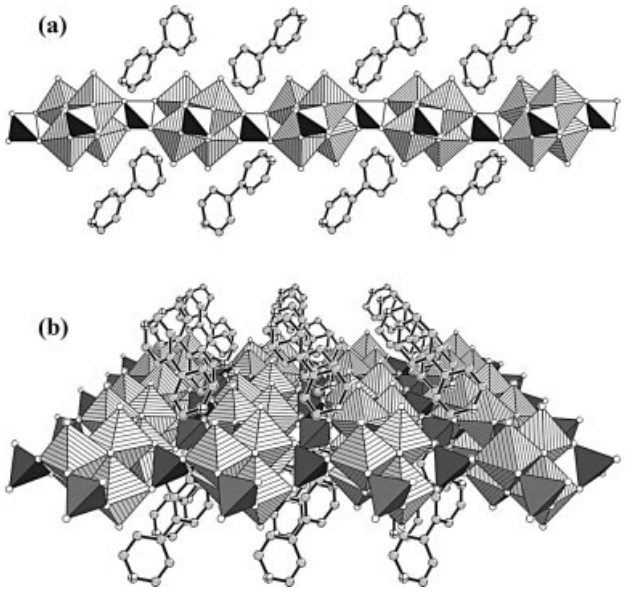

Figure 4. Perspective views along the (a) *b* direction and (b) towards the (100) plane showing the distribution of the 4,4′-bipyridinium cations placed above and below the $[(VO_2)_4(PO_4)_2]_n^{2n-}$ anionic layer

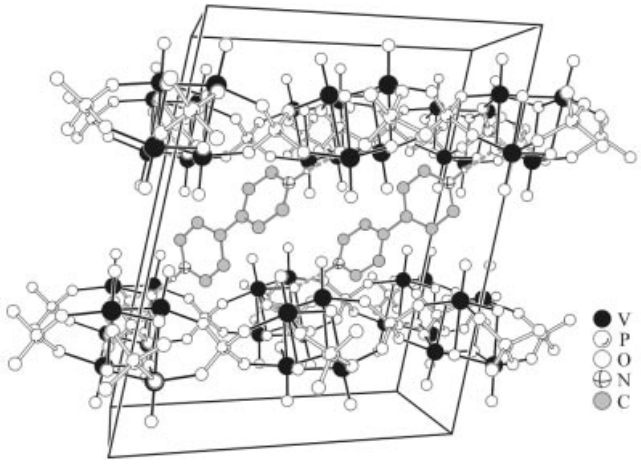

Figure 5. Unit cell contents showing the pillar nature of the interlayer 4,4′-bipyridinium cations through two strong $N^+-H\cdots O$ hydrogen bonds (dashed lines); hydrogen-bonding geometry: N(1)−H(98)···O(12)[i] with *d*(D−H) = 0.976(10) Å, *d*(H···A) = 1.772(12) Å, *d*(D···A) = 2.746(5) Å and <(DHA) = 176(5)°, N(2)−H(99)···O(5)[ii] with *d*(D−H) = 0.974(10) Å, *d*(H···A) = 1.779(12) Å, *d*(D···A) = 2.750(5) Å and <(DHA) = 175(5)°; symmetry codes used to generate equivalent atoms: (i) $1-x$, $1+y$, $1/2-z$. (ii) x, $-y$, $1/2+z$

Solid-State MAS NMR Spectroscopy

The ^1H, ^{13}C, ^{31}P and ^{51}V NMR spectra fully support the crystal structure. Fast (30 kHz) sample spinning averages out the $^1H-^1H$ dipolar interaction, leading to a highly resolved ^1H MAS NMR spectrum (Figure 6a). The 4,4′-bipyridinium cation contains three magnetically nonequivalent ^1H nuclei, labelled H_a, H_b and H_c, which resonate at ca. 15.5, 9.3 (shoulder) and 8.8 ppm, respectively. The $(H_b + H_c)/H_a$ intensity ratio is 4, in accordance to the expected site populations. The ^{13}C CP/MAS NMR spectrum exhibits peaks at ca. 150.6, 145.0 and 124.7 ppm, which are assigned to C_a, C_b and C_c, respectively (Figure 6b). Together, the ^1H and ^{13}C NMR spectra confirm the integrity of the 4,4′-bipyridinium cation.

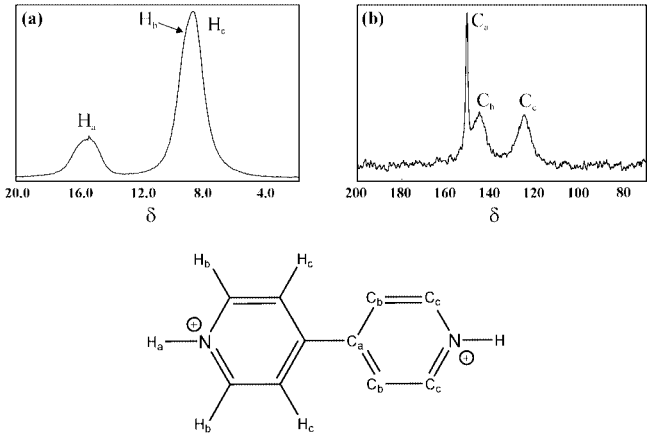

Figure 6. (a) ^1H MAS and (b) ^1H-^{13}C CP MAS NMR spectra, showing the assignment of ^1H and ^{13}C resonances

The ^{31}P MAS NMR spectrum consists of a single peak centred at about −5.2 ppm with a shoulder at about −6.8 ppm which was deconvoluted into three resonances at −6.4, −5.5 and −4.5 in a 1:2:1 intensity ratio, respectively. This is in good agreement with the crystal structure (Figure 7).

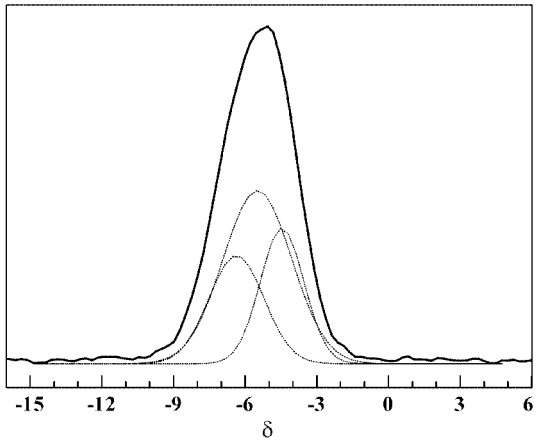

Figure 7. Experimental and simulated ^{31}P MAS NMR spectra

Because of relatively large chemical shift anisotropy, the ^{51}V MAS NMR spectrum exhibits strong spinning sidebands even with MAS at 30 kHz. Three peaks are observed at −580.1, −593.4 and −599.2 ppm in a 2:1:1 intensity ratio, respectively. Since the crystal structure calls for the presence of four nonequivalent V sites, we assume that the peak

 © 2004 Wiley-VCH Verlag GmbH & Co. KGaA, Weinheim

at δ = −579.9 ppm consists of two overlapping resonances (Figure 8).

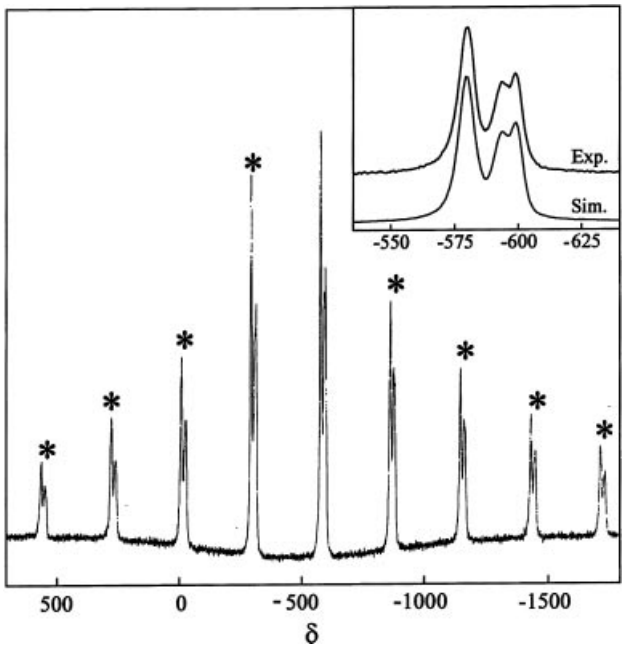

Figure 8. ^{51}V MAS NMR spectrum; the inset shows a magnification of the isotropic peaks (top) and a simulation (bottom) performed with Lorentzian-Gaussian lines (a fair assumption because the second-order quadrupole effects are not significant); asterisks depict spinning sidebands

Thermal Analysis

Thermal treatment reveals that **I** is stable up to ca. 370 °C, as no weight losses were registered. In the 370−800 °C temperature range, the compound undergoes thermal decomposition through five distinct and well-defined steps (as observed in the derivative thermogravimetric analysis), with a total weight loss of 28.3%. This decomposition is attributed to the simultaneous oxidation of the organic component and reduction of half of the V^V centres, leading to the formation of an intermediate inorganic $(V^{IV}_2V^V_2)O_{14}P_2$ phase that contains mixed-valence vanadium centres [72.0% calculated and 71.7% observed residues; Equation (1)]. Between 800 and 900 °C, a continuous weight increase of ca. 1.3% clearly indicates the occurrence of an oxidative process. Indeed, as usually observed in related compounds, traces of oxygen within the apparatus promotes partial oxidation of some V^{IV} centres from the $(V^{IV}_2V^V_2)O_{14}P_2$ intermediate phase, leading to a new mixed-valence phase formulated as $(V^{IV}V^V_3)O_{14.5}P_2$ [73.0% calculated and 73.2% observed residues; Equation (2)].

$$(C_{10}H_{10}N_2)\left[(VO_2)_4(PO_4)_2\right] \xrightarrow[(decomposition\ in\ 5\ steps)]{\Delta} (V^{IV}_2V^V_2)O_{14}P_2 \quad (1)$$

$$(V^{IV}_2V^V_2)O_{14}P_2 \xrightarrow[traces\ of\ O_2]{\Delta} (V^{IV}V^V_3)O_{14.5}P_2 \quad (2)$$

Vibrational Spectroscopy

The IR and Raman spectra contain the most significant diagnostic bands associated with the primary building units of $(C_{10}H_{10}N_2)[(VO_2)_4(PO_4)_2]$. On the one hand, strong bands centred at 990, 970 and 943 cm^{-1} in the IR spectrum (in 976 and 991 in the Raman spectrum) are due to the typical stretching vibrational mode of terminal $V^V{=}O$ double bonds; on the other, bands at 1088 and 1061 cm^{-1} are assigned to the PO_4^{3-} antisymmetric stretching vibrational modes, while those found at 856 and 839 cm^{-1} can be attributed to the related PO_4^{3-} symmetric stretching modes. Several bands observed in the 650−500 cm^{-1} region are also associated with V−O−V stretching vibrational modes, and several intense bands between 1300 and 1640 cm^{-1} arise from the presence of the 4,4′-bipyridinium cations that occupy the interlayer spaces.

Conclusion

A new structure containing 2D anionic $[(VO_2)_4(PO_4)_2]_n^{2n-}$ layers intercalated by 4,4′-bpyH_2^{2+} cations was synthesised by the hydrothermal method and characterised structurally using a variety of techniques. This intercalated phosphovanadate is an important addition to vanadium coordination chemistry as it constitutes the first report of typical $\{V_4O_4\}$ cubane-like clusters. We are currently investigating the intercalation reactions of this compound, particularly the possibility of replacing the 4,4′-bpyH_2^{2+} cations by other organic molecules, and the corresponding structural modifications.

Experimental Section

General: Chemicals were readily available from commercial sources and were used as received without further purification. Syntheses were carried out in PTFE-lined stainless steel reaction vessels (40 cm^3), under autogenous pressure and static conditions in a preheated oven at 140 °C. Reactions took place over a period of 3 days, after which the vessels were removed from the oven and left to cool to ambient temperature before opening. Compounds proved to be air- and light-stable, and insoluble in water and common organic solvents.

Preparation and Structural Characterisation of $(C_{10}H_{10}N_2)[(VO_2)_4(PO_4)_2]$ (I): A yellow suspension containing V_2O_5 (0.140 g, Aldrich), H_3PO_4 (0.450 g, min. 85% Merck) and 4,4′-bipyridine (0.120 g, Fluka) in distilled water (ca. 10 g) was stirred thoroughly for 30 minutes at ambient temperature. The suspension, with a molar composition of ca. 1.0:6.0:1.0:722, respectively, was transferred to the reaction vessel, which was then placed inside the preheated oven. After reacting, the vessel was allowed to cool slowly to ambient temperature to yield a large amount of yellow blocks, which were manually harvested, air-dried for X-ray diffraction analysis and identified as **I**, and a small amount of an unknown pale-green microcrystalline powder. The two phases were readily ultrasonically separated (for 10 minutes), followed by vacuum filtration and washing with copious amounts of distilled water. $C_{10}H_{10}N_2O_{16}P_2V_4$ (based on single-crystal data, 679.90): calcd. C 17.67, N 4.14,

 © 2004 Wiley-VCH Verlag GmbH & Co. KGaA, Weinheim

H 1.48; found C 18.07, N 4.26, H 1.49. TGA data (weight losses and increases) and derivative thermogravimetric peaks (DTG; in parenthesis): 370−450 °C, −8.4% (425 °C); 450−800 °C, −19.9% (540, 621, 661 and 771 °C); 800−900 °C, +1.3% (849 °C).

Selected IR and Raman data in cm^{-1}): 1639 vs (1645), 1620 vs (1623), 1488 s, 1459 m, 1417 m, 1375 s (1367), 1340 m, 1088 vs (1074), 1061 vs, 990 vs, 970 vs, 943 s, 856 m, 839 m, 793 s, 654 m, 622 s, 610 m, 590 m, 503 vs.

Characterisation: Elemental analyses for C, H and N were performed on an Exeter Analytical CE-440 Elemental Analyser (University of Cambridge). Samples were combusted under oxygen at 975 °C, with He as the purge gas.
FT-IR spectra were measured from KBr disks (Aldrich, 99%+, FT-IR grade) on a Matson 700 FTIR spectrometer, and FT-Raman spectra were collected on a Bruker RFS 100 with a Nd:YAG coherent laser (λ = 1064 nm).
Thermogravimetric analyses (TGA) were carried out on Shimadzu TGA-50, with a heating rate of 10 °C/min, under nitrogen with a flow rate of 20 cm^3/min.
Powder X-ray diffraction patterns were recorded at room temperature on a Philips X'Pert diffractometer, operating with a monochromated Cu-K_α radiation source at 40 kV and 50 mA. Simulated powder patterns were based on single-crystal data, and calculated with the STOE Win XPOW software package.[13]
^{1}H, ^{13}C, ^{31}P and ^{51}V solid-state NMR spectra were recorded at 400.12, 100.61, 160.0 and 105.24 MHz, respectively, on a Bruker Avance 400 spectrometer. ^{1}H and ^{31}P MAS NMR spectra were recorded with a 30 kHz spinning rate, 40° rf pulses and recycle delays of 6 and 70 s, respectively. ^{1}H- ^{13}C cross-polarisation (CP) MAS NMR spectra were acquired with 4 μs ^{1}H 90° pulses, a contact time of 2 ms and a recycle delay of 5 s. ^{51}V MAS NMR spectra were recorded with short, 0.6 μs (equivalent to 10°), pulses and a recycle delay of 5 s. Chemical shifts are quoted in ppm from TMS (^{1}H and ^{13}C), 85% H_3PO_4 (^{31}P) and $VOCl_3$ (^{51}V).

X-ray Crystallographic Studies: Suitable single crystals were mounted on a glass fibre using perfluoropolyether oil.[14] Data were collected at 180(2) K on a Nonius Kappa charge-coupled device (CCD) area-detector diffractometer (Mo-K_α graphite-monochromated radiation, λ = 0.7107 Å) equipped with an Oxford Cryosystems cryostream and controlled by the Collect software package.[15] Images were processed with the software packages Denzo and Scalepack,[16] and the data were corrected for absorption by the empirical method employed in Sortav.[17] The structure was solved by the direct methods of SHELXS-97[18] and refined by full-matrix least-squares on F^2 using SHELXL-97.[19]

All non-hydrogen atoms were directly located from difference Fourier maps and refined with anisotropic displacement parameters. The crystallographically unique H-atoms associated with the 4-pyridinium groups were also located from difference Fourier maps, and refined with independent isotropic displacement parameters and a common N−H distance restrained to 0.98(1) Å. Hydrogen atoms attached to carbon were located at their idealised positions using the HFIX 43 instruction in SHELXL, and included in the refinement in riding-motion approximation with an isotropic thermal displacement parameter fixed at 1.2 times U_{eq} of the atom to which they are attached. The last difference Fourier map synthesis shows the highest peak (0.641 e·Å^{-3}) located at 1.42 Å from O(11), and the deepest hole (−0.666 e·Å^{-3}) at 0.79 Å from V(2). Cavity dimensions were calculated by overlapping rigid spheres with van der Waals radii for each element: O 1.52 Å, P 1.8 Å and V 2.0 Å. CCDC-221172 contains the supplementary crystallographic data for this paper. These data can be obtained free of charge at www.ccdc.cam.ac.uk/conts/retrieving.html [or from the Cambridge Crystallographic Data Centre, 12 Union Road, Cambridge CB2 1EZ, UK; Fax: (internat.) + 44-1223-336-033; E-mail: deposit@ccdc.cam.ac.uk].

Acknowledgments

We are grateful to FEDER, POCTI (Portugal) and to the Portuguese Foundation for Science and Technology (FCT) for their general financial support, and also for the Ph.D. and postdoctoral research grants Nos. SFRH/BD/3024/2000 (to F. A. A. P.) and SFRH/BPD/9309/2002 (to F.-N. S.).

[1] P. J. Hagrman, R. C. Finn, J. Zubieta, *Solid State Sci.* **2001**, *3*, 745−774.
[2] A. K. Cheetham, G. Ferey, T. Loiseau, *Angew. Chem. Int. Ed.* **1999**, *38*, 3269−3292; G. Centi, F. Trifiro, J. R. Ebner, V. M. Franchetti, *Chem. Rev.* **1988**, *88*, 55−80; F. Garbassi, J. C. J. Bart, F. Montino, G. Petrini, *Applied Catalysis* **1985**, *16*, 271−287.
[3] C. Qin, L. Xu, Y. G. Wei, X. L. Wang, F. Y. Li, *Inorg. Chem.* **2003**, *42*, 3107−3110; Z. Shi, S. H. Feng, L. R. Zhang, G. Y. Yang, J. Hua, *Chem. Mat.* **2000**, *12*, 2930−2935; R. Finn, J. Zubieta, *Chem. Commun.* **2000**, 1321−1322.
[4] Y. J. Lu, R. C. Haushalter, J. Zubieta, *Inorg. Chim. Acta* **1998**, *268*, 257−261; V. Soghomonian, R. C. Haushalter, J. Zubieta, C. J. Oconnor, *Inorg. Chem.* **1996**, *35*, 2826−2830; V. Soghomonian, Q. Chen, R. C. Haushalter, J. Zubieta, *Angew. Chem. Int. Ed., Engl.* **1993**, *32*, 610−612.
[5] F. A. Almeida Paz, Y. Z. Khimyak, A. D. Bond, J. Rocha, J. Klinowski, *Eur. J. Inorg. Chem.* **2002**, 2823−2828; F. A. Almeida Paz, J. Klinowski, *J. Phys. Org. Chem.* **2003**, *16*, 772−782; F. A. Almeida Paz, J. Klinowski, *Chem. Commun.* **2003**, 1484−1485; F. A. Almeida Paz, J. Klinowski, *Inorg. Chem.* **2004**, in press, DOI: 10.1021/ic049523o; F. A. Almeida Paz, J. Klinowski, *Inorg. Chem.* **2004**, in press, DOI: 10.1021/ic049794z; F. A. Almeida Paz, J. Klinowski, *J. Solid. State Chem.* **2004**, in press.
[6] F. A. Almeida Paz, F.-N. Shi, J. Klinowski, J. Rocha, T. Trindade, *Eur. J. Inorg. Chem.* **2004**, DOI: 10.1002/ejic.200400005.
[7] F.-N. Shi, F. A. Almeida Paz, J. Klinowski, J. Rocha, T. Trindade, *Inorg. Chim. Acta* **2004**, submitted.
[8] M. J. Manos, A. L. Tasiopoulos, E. L. Tolis, N. Lalioti, J. D. Woollins, A. M. Z. Slawin, M. P. Sigalas, T. A. Kabanos, *Chem. Eur. J.* **2003**, *9*, 695−703; M. Worle, F. Krumeich, F. Bieri, H. J. Muhr, R. Nesper, *Z. Anorg. Allg. Chem.* **2002**, *628*, 2778−2784; F. L. Jiang, O. P. Anderson, S. M. Miller, J. Chen, M. Mahroof-Tahir, D. C. Crans, *Inorg. Chem.* **1998**, *37*, 5439−5451; W. Plass, *Eur. J. Inorg. Chem.* **1998**, 799−805; W. Plass, *Inorg. Chem.* **1997**, *36*, 2200−2205; D. C. Crans, F. L. Jiang, J. Chen, O. P. Anderson, M. M. Miller, *Inorg. Chem.* **1997**, *36*, 1038−1047; N. P. Luneva, S. A. Mironova, A. E. Shilov, M. Y. Antipin, Y. T. Struchkov, *Angew. Chem. Int. Ed., Engl.* **1993**, *32*, 1178−1179; M. Mikuriya, T. Kotera, F. Adachi, S. Bandow, *Chem. Lett.* **1993**, 945−948; I. Cavaco, J. C. Pessoa, M. T. Duarte, P. M. Matias, R. T. Henriques, *Polyhedron* **1993**, *12*, 1231−1237; D. C. Crans, R. W. Marshman, M. S. Gottlieb, O. P. Anderson, M. M. Miller, *Inorg. Chem.* **1992**, *31*, 4939−4949; F. Bottomley, D. F. Drummond, D. E. Paez, P. S. White, *J. Chem. Soc., Chem. Commun.* **1986**, 1752−1753; F. Bottomley, D. E. Paez, P. S. White, *J. Am. Chem. Soc.* **1985**, *107*, 7226−7227; F. Bottomley, D. E. Paez, P. S. White, *J. Am. Chem. Soc.* **1982**, *104*, 5651−5657; F. Bottomley, P. S. White, *J. Chem. Soc., Chem. Commun.* **1981**, 28−29; Y. Chang, Q.

 © 2004 Wiley-VCH Verlag GmbH & Co. KGaA, Weinheim

Chen, M. I. Khan, J. Salta, J. Zubieta, *J. Chem. Soc., Chem. Commun.* **1993**, 1872−1874; H. Rieskamp, P. Gietz, R. Mattes, *Chem. Ber.* **1976**, *109*, 2090.
[9] F. H. Allen, *Acta Crystallogr., Sect. B* **2002**, *58*, 380−388.
[10] H. P. Zhu, Q. T. Liu, C. N. Chen, D. X. Wu, *Inorg. Chim. Acta* **2000**, *306*, 131−136; S. A. Duraj, M. T. Andras, B. Rihter, *Polyhedron* **1989**, *8*, 2763−2767; A. A. Pasynskii, I. L. Eremenko, A. S. Katugin, G. S. Gasanov, E. A. Turchanova, O. G. Ellert, Y. T. Struchkov, V. E. Shklover, N. T. Berberova, A. G. Sogomonova, O. Y. Okhlobystin, *J. Organomet. Chem.* **1988**, *344*, 195−213; J. Darkwa, J. R. Lockemeyer, P. D. W. Boyd, T. B. Rauchfuss, A. L. Rheingold, *J. Am. Chem. Soc.* **1988**, *110*, 141−149.
[11] S. Boudin, A. Guesdon, A. Leclaire, M. M. Borel, *Int. J. Inorg. Mater.* **2000**, *2*, 561−579.
[12] A. F. Wells, *Structural Inorganic Chemistry Fourth ed.,* Clarendon Oxford University Press, **1975**.
[13] STOE, *Win XPOW THEO Version 1.15*, STOE & Cie GmbH, **1999**.
[14] T. Kottke, D. Stalke, *J. Appl. Crystallogr.* **1993**, *26*, 615−619.
[15] R. Hooft, *Collect: Data Collection Software, Nonius B. V.,* Delft, The Netherlands, **1998**.
[16] Z. Otwinowski, W. Minor, *Methods in Enzymology*, Vol. 276, *Macromolecular Crystallography, Part A* (Eds.: C. W. Carter Jr., R. M. Sweet), Academic Press, New York, **1997**, pp. 307.
[17] R. H. Blessing, *J. Appl. Crystallogr.* **1997**, *30*, 421; R. H. Blessing, *Acta Crystallogr., Sect. A* **1995**, *51*, 33−38.
[18] G. M. Sheldrick, *SHELXS-97*, *Program for Crystal Structure Solution*, University of Göttingen, University of Göttingen, **1997**.
[19] G. M. Sheldrick, *SHELXL-97*, *Program for Crystal Structure Refinement*, University of Göttingen, University of Göttingen, **1997**.

Received March 29, 2004
Early View Article
Published Online June 17, 2004

 © 2004 Wiley-VCH Verlag GmbH & Co. KGaA, Weinheim

Synthesis and Theoretical Studies of a Double Helical Complex with the Ligand 4′,4′′′-Bis(ferrocenyl)-2,2′:6′,2′′:6′′,2′′′:6′′′,2′′′′-quinquepyridine

Javier E. Aguado,[a] Maria José Calhorda,[b] Paulo J. Costa,[b] Olga Crespo,[a] Vitor Félix,[c] M. Concepción Gimeno,[a] Peter G. Jones,[d] and Antonio Laguna*[a]

Keywords: Quinquepyridine / Silver / Helical complexes / Ferrocenyl derivatives / Theoretical studies

4′,4′′′-Bis(ferrocenyl)-2,2′:6′,2′′:6′′,2′′′:6′′′,2′′′′-quinquepyridine (Fc_2qpy) reacts with AgOTf (OTf = trifluoromethylsulfonate) to give a complex of stoichiometry [Ag(Fc2qpy)]-OTf. The crystal structure reveals a dinuclear arrangement among the cations with an Ag···Ag close contact of 3.089(2) Å. The ligands are wrapped around the silver atoms in a double helical array. Further hydrogen bonding between triflate units and the protons of the ferrocene or pyridine moieties results in a supramolecular structure. Theoretical studies confirm the existence of a weak Ag–Ag bond, and show that the dinuclear form can be more stable than the mononuclear one, when there is a favorable balance between the reorganization energy of the two quinquepyridine chains and the energy released by the formation of stronger Ag–N bonds and the new Ag–Ag interaction in the helix.

(© Wiley-VCH Verlag GmbH & Co. KGaA, 69451 Weinheim, Germany, 2004)

Introduction

The construction of inorganic supramolecular arrays based on covalent interactions, hydrogen bonding, or other intermolecular interactions is a very interesting area of functional materials.[1−6] Oligopyridines have been used as building blocks for the self-assembly of double helical transition-metal complexes.[3−6] The close proximity between the bipyridine or terpyridine units, which is essential for the formation of the double helical complexes, leads to substantial π-π interactions, but also to some constraints upon complex formation. 2,2′:6′,2′′:6′′,2′′′:6′′′,2′′′′-quinquepyridine (qpy) has a rich transition metal coordination chemistry because of its ability to promote tetrahedral, square planar or octahedral geometries.[7−31] There are several coordination modes, the important ones in the formation of metal helicates being those which lead to the partitioning of the ligand into bidentate and tridentate units. This happens, for example, with several first row transition metals. For metals that have no electronic preference for geometry, the assembly is dictated by the size of the metal ion and the available bonding cavity. For the quinquepyridine ligand in a planar configuration, Constable et al. have shown that the five nitrogen atoms form an effective hole-size ca. of 2.45 Å which corresponds to a pentagonal-planar geometry for metals with an ionic radius 1.0 ± 0.1 Å, and such a geometry has been demonstrated for silver(I) in the complex [Ag(qpy)]PF_6.[7] The introduction of sterically demanding substituents to the quinquepyridine can be expected to increase the effective hole-size of the bonding cavity. Consequently, silver(I) is too small to be accommodated by the ligand in a planar pentadentate mode, and supramolecular helical structures can then be achieved. There are few examples of doubly helical silver complexes with quinquepyridine ligands. In the complex $[Ag_2(dmpqpy)_2](ClO_4)_2 \cdot 2H_2O$ (dmpqpy = 6,6′′′′-dimethyl-4′,4′′′-diphenyl-2,2′:6′,2′′:6′′,2′′′:6′′′,2′′′′-quinquepyridine)[31] the ligand acts as tetradentate donor, and the central pyridine nitrogen atoms play the role of rigid spacers, rather than of donor atoms. The silver center is also tetracoordinate in the heterodinuclear derivative $[AgCo(qpy)_2]^{3+}$.[19] Pentacoordinated silver atoms are present in $[Ag_2(dmqpy)_2](ClO_4)_2$ (dmqpy = 6,6′′′′-dimethyl-2,2′:6′,2′′:6′′,2′′′:6′′′,2′′′′-quinquepyridine).[31]

Here we report on the synthesis of the Ag^I complex of the 4′,4′′′-bis(ferrocenyl)-2,2′:6′,2′′:6′′,2′′′:6′′′,2′′′′-quin-

[a] Departamento de Química Inorgánica, Instituto de Ciencia de Materiales de Aragón, Universidad de Zaragoza, C.S.I.C., 50009 Zaragoza, Spain
[b] ITQB, Av. da República, EAN, Apart. 127, 2781−901, Oeiras, and Departamento de Química e Bioquímica, Facultade de Ciências, Universidade de Lisboa, Campo Grande 1749−016 Lisboa, Portugal
[c] Departamento de Química, Universidade de Aveiro, CICECO, 3810−193 Aveiro, Portugal
[d] Institut für Anorganische und Analytische Chemie der Technischen Universität, Postfach 3329, 38023 Braunschweig, Germany
Supporting information for this article is available on the WWW under http://www.eurjic.org or from the author.

 © 2004 Wiley-VCH Verlag GmbH & Co. KGaA, Weinheim **DOI: 10.1002/ejic.200400057**

quepyridine ligand. The crystal structure of the silver(I) derivative shows a double helical arrangement with a short Ag···Ag interaction. Both silver(I) atoms have slightly different geometries. One can be considered as pentacoordinate with an elongated trigonal bipyramidal geometry, and the other as tetracoordinate with a tetrahedral geometry. Theoretical studies have been carried out addressing the formation of the silver(I)-silver(I) interaction as well as the difference in energy between the mononuclear and the dinuclear complexes.

Results and Discussion

Synthesis

The ligand 4′,4′′′-bis(ferrocenyl)-2,2′:6′,2′′:6′′,2′′′:6′′′,2′′′′-quinquepyridine (Fc_2qpy) reacts with AgOTf to give a deep-red solution, from which a complex of stoichiometry [Ag(Fc_2qpy)]OTf was isolated. The X-ray structure confirms that the complex is in fact dimeric with a double helical structure [Equation (1)].

The positive liquid secondary-ion mass spectrum (LSIMS+) exhibits a peak at m/z = 863 (100%), which can be assigned to the cationic molecular peak $[Ag(Fc_2qpy)]^+$. No peaks corresponding to the dinuclear species $[Ag_2(Fc_2qpy)_2]^{2+}$ or $[Ag_2(Fc_2qpy)_2(OTf)]^+$ were detected. The ^{1}H NMR spectrum of [Ag(Fc_2qpy)]OTf shows the signals arising from the protons of the ferrocenyl moieties at δ = 4.12, 4.63, and 4.95 ppm in a ratio 10:4:4. This corresponds to the unsubstituted cyclopentadienyl, and to the α and β protons of the substituted cyclopentadienyl groups, respectively. Five multiplets arise from the quinquepyridine protons, although some of them are overlapping.

Crystal Structure of [Ag(Fc_2qpy)]OTf

The crystal structure of $[Ag\{Fc_2(qpy)\}]_2(OTf)_2 \cdot 3CH_2Cl_2$ has been determined by X-ray diffraction (Figure 1). A selection of bond lengths and angles appears in Table 1. The cation displays a double-helical arrangement, achieved by a series of twists. The dihedral angles between adjacent pyridine planes 8 and 7 (9.5°), 7 and 6 (28.4°), 6 and 9 (38.6°), and 9 and 10 (5°) in one ligand, and between planes 5 and 4 (3.5°), 4 and 1 (32°), 1 and 2 (35.5°), and 2 and 3 (14.2°) in the other (planes are numbered after the nitrogen atoms they contain) confirm that the major twisting in each ligand occurs between the central pyridyl ring and the 2,2′-bipyridyl fragments.

The twisting can be seen more clearly from the space-filling diagram (Figure 2). The helical radius is about a/3,

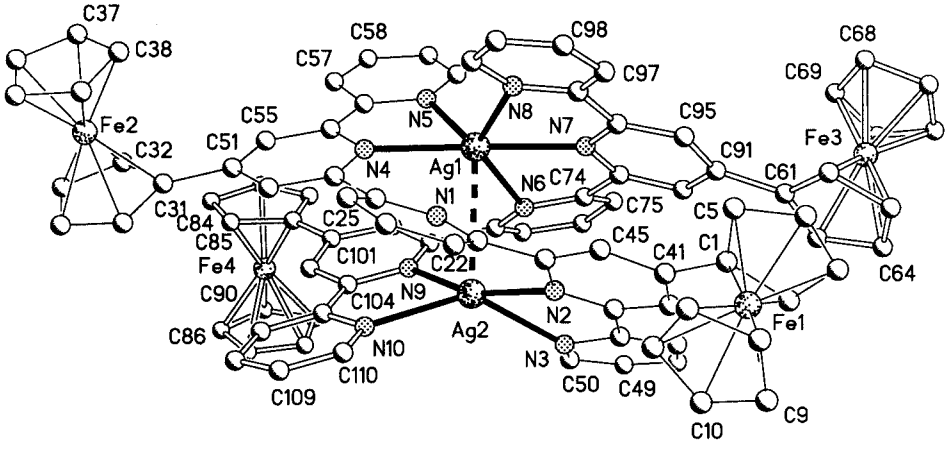

Figure 1. Structure of the cation of $[Ag_2(Fcqpy)_2](OTf)_2$

 © 2004 Wiley-VCH Verlag GmbH & Co. KGaA, Weinheim

Table 1. Selected bond lengths (Å) and angles (°) for compound $[Ag_2(Fc_2qpy)_2](OTf)_2$

Ag(1)−N(7)	2.323(9)	Ag(1)−Ag(2)	3.089(2)
Ag(1)−N(4)	2.341(9)	Ag(2)−N(2)	2.329(9)
Ag(1)−N(5)	2.395(11)	Ag(2)−N(9)	2.341(9)
Ag(1)−N(8)	2.516(11)	Ag(2)−N(10)	2.376(10)
Ag(1)−N(6)	2.550(10)	Ag(2)−N(3)	2.418(11)
N(7)−Ag(1)−N(4)	169.2(3)	N(8)−Ag(1)−Ag(2)	118.1(3)
N(7)−Ag(1)−N(5)	119.7(3)	N(6)−Ag(1)−Ag(2)	61.1(2)
N(4)−Ag(1)−N(5)	70.0(4)	N(2)−Ag(2)−N(9)	161.7(4)
N(7)−Ag(1)−N(8)	68.8(3)	N(2)−Ag(2)−N(10)	123.5(3)
N(4)−Ag(1)−N(8)	102.3(3)	N(9)−Ag(2)−N(10)	71.2(3)
N(5)−Ag(1)−N(8)	124.1(4)	N(2)−Ag(2)−N(3)	69.7(4)
N(7)−Ag(1)−N(6)	68.9(3)	N(9)−Ag(2)−N(3)	108.3(3)
N(4)−Ag(1)−N(6)	119.5(3)	N(10)−Ag(2)−N(3)	135.7(4)
N(5)−Ag(1)−N(6)	80.2(3)	N(2)−Ag(2)−Ag(1)	86.3(3)
N(8)−Ag(1)−N(6)	137.6(3)	N(9)−Ag(2)−Ag(1)	78.3(3)
N(7)−Ag(1)−Ag(2)	91.8(3)	N(10)−Ag(2)−Ag(1)	107.8(3)
N(4)−Ag(1)−Ag(2)	87.1(3)	N(3)−Ag(2)−Ag(1)	115.6(3)
N(5)−Ag(1)−Ag(2)	116.7(3)		

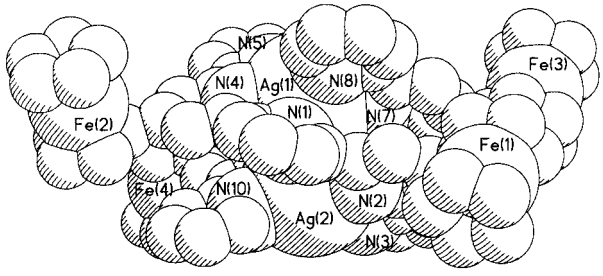

Figure 2. Space filling diagram of the cation in $[Ag_2(Fcqpy)_2](OTf)_2$

4.5 Å and the pitch height about *a*/2, 7 Å. A very distorted trigonal bipyramidal disposition results for one silver atom, upon coordination to three nitrogen atoms of one [Fc_2qpy] ligand, and two from the other [equatorial Ag−N distances 2.323(9), 2.341(9), 2.395(11) Å, axial 2.516(11), 2.550(10) Å]. The atoms N4, N5, N7, and Ag1 lie in the same plane, and the angle between this plane and the plane N8, N6, N7, Ag1 is 60.2°. The other silver atom is bonded to two nitrogen atoms from each ligand. This four-coordinate metal center [Ag−N distances 2.329(9)−2.418(11) Å] shows a very irregular geometry. The dihedral angle between planes N9−Ag2−N10 and N2−Ag2−N3 is 55.3°. This points to a geometry intermediate between tetrahedral and square planar. Thus, in this complex, the two silver(I) atoms exhibit different coordination modes to the quinquepyridine moieties. This is unprecedented since, in metal complexes with this type of ligand, the same coordination has always been observed for both metal ions, for example in $[M_2X(qpy)]^{3+}$ (M = Cu, Co, Ru),[9,10,13,20] or $[M_2X\{(SMe)_2qpy\}_2]^{3+}$ (M = Cu, Ni),[28,29] where the metallic centers are hexacoordinate. Only in complexes which contain two metals in different oxidation states, such as in $[Cu_2(R_2qpy)_2]^{3+}$ (R = SMe, Ph),[28,30] is it possible to find different geometries. Here Cu^{I} is tetrahedral, whereas Cu^{II} is octahedral.

Despite the covalence of the bonding to each silver atom in the compound, the Ag−N distances are within the expected range. The Ag(1)···Ag(2) contact of 3.089(2) Å in $[Ag_2(Fc_2qpy)_2](OTf)_2$ is shorter than in the related examples with qpy derivatives, i.e. 3.48 Å in $[Ag(dmqpy)_2](ClO_4)_2$,[31] and 3.22 Å in $[Ag(dmpqpy)_2](ClO_4)_2\cdot 2H_2O$,[31] but close to those found in complexes with ligands based on terpyridine (terpy) or quaterpyridine (qtpy) units, e.g. $[Ag_2(qtpy)_2](BF_4)_2$ [3.107(2) Å],[34] and $[Ag_2(terpy)_2](PF_6)_2$ (2.914−2.940 Å in each double helical di-silver unit, Ag···Ag contacts of 3.107, 3.156 Å with a second dinuclear unit to form tetranuclear blocks).[33] The distances of the silver atoms Ag1 or Ag2 to the same silver atoms of different units are 7.47 and 6.57 Å, respectively. In $[Ag_2(Fc_2qpy)_2](OTf)_2$ the twisting angles are smaller than in the silver derivatives $[Ag_2(dmqpy)_2](ClO_4)_2$,[31] (major twist angle 47.2°, between terpyridyl and bipyridyl fragments) or $[Ag(dmpqpy)_2](ClO_4)_2\cdot 2H_2O$ (major twist angles 36.8°, 36.1°, in this case between the two bipyridyl fragments and the central ring).[31] These values are in accordance with a shorter silver···silver contact. It has been suggested that it is the steric effect of the terminal groups in flexible ligands with various donor atoms that forces the ligand to adopt a double helical disposition, since the planar configuration is not possible. Four factors seem to govern the formation of a double helical complex, namely the ligand donor set, the coordination geometry of the metal ion, the metal-ion radius, and the substituent effects. These three helical complexes allow an analysis of the effect of the substituents, since the ligand (qpy) and the metal ion (Ag^+) are common to all. The bulkier ferrocene moiety affords the smallest twist angles and, thus, the shortest silver···silver interaction. The presence of four substituents (methyl and phenyl) in qpy, in the 6,6′′′′ and 4′,4′′′ positions, produces a milder effect in the twisting of the ligand than the case with only two ferrocene substituents in the 4′,4′′′ positions.

Stacking interactions between the planar parts of the ligands, reminiscent of the base-pair stacking of nucleic acids, are usual in these helical geometries, sometimes as marked interactions. In $[Ag_2(Fc_2qpy)_2](OTf)_2$ the rings that contain the nitrogen atoms N7 and N2 are almost coplanar (angle between planes 7°), and one lies approximately above the other. The same situation can be observed for the planes that contain N9 and N4 (angle between the planes = 5.6°). The distances between the ring centroids are 3.43 Å and 3.98 Å, respectively. The shorter distance is similar to the stacking distances in $[Ag_2(dmqpy)_2](ClO_4)_2$ (3.38−3.42 Å), and the larger distance is similar to those between di-silver units in the same compound (3.70 Å).[31] No such interactions were observed between di-silver units, since the rings of those which are adjacent are not coplanar. These interactions between di-units are not present in $[Ag(dmpqpy)_2](ClO_4)_2\cdot 2H_2O$, probably due to the presence of the bulky substituents.

Helices are chiral although, normally, a mixture of both enantiomers is obtained, and only the presence of a chiral substituent makes it possible to obtain only one enantiomer. In $[Ag_2(Fc_2qpy)_2](OTf)_2$, the two enantiomers are alternately (Figure 3) disposed. The presence of C−H···O and C−H···F hydrogen bonds (Table 2) results in a supramolecular structure.

 © 2004 Wiley-VCH Verlag GmbH & Co. KGaA, Weinheim

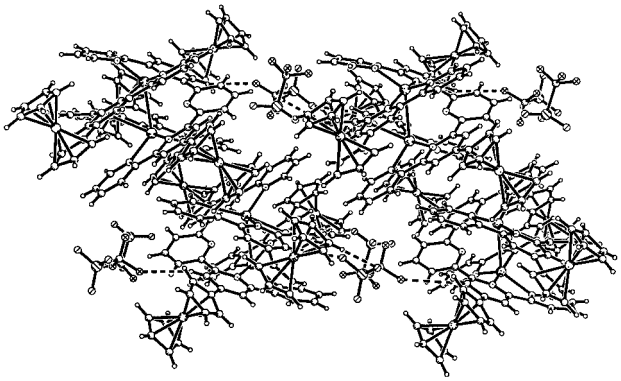

Figure 3. Packing diagram of $[Ag_2(Fcqpy)_2](OTf)_2$

Table 2. Hydrogen bonds [Å and °]

D−H···A	*d*(D−H)	*d*(H···A)	*d*(D···A)	<(DHA)
C(35)−H(35)···O(2)	0.95	2.58	3.415(15)	147.3
C(52)−H(52)···O(2)	0.95	2.54	3.459(16)	162.7
C(25)−H(25)···O(3)	0.95	2.51	3.152(15)	124.7
C(75)−H(75)···O(4)#1	0.95	2.58	3.415(15)	146.7
C(92)−H(92)···O(4)#1	0.95	2.48	3.372(16)	157.3
C(70)−H(70)···O(5)#1	0.95	2.54	3.490(19)	174.3
C(22)−H(22)···F(6)#2	0.95	2.46	3.198(16)	134.1

Symmetry transformations used to generate equivalent atoms: #1: $-x, -y + 1, -z$, #2: $-x + 1, -y + 1, -z$

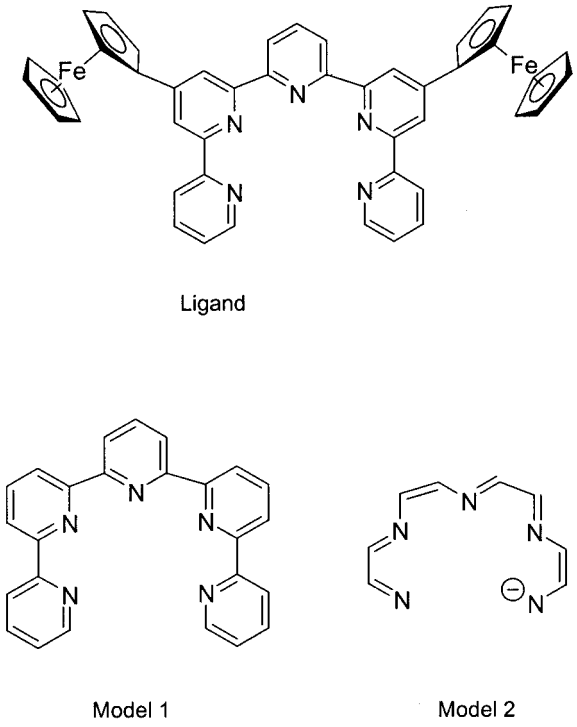

Scheme 1. Theoretical models

Electrochemistry

The electrochemical behavior of the silver complex has been studied by cyclic voltammetry at a platinum electrode in CH_2Cl_2. It shows two oxidation waves. The first is a quasi-reversible two-electron oxidation wave at +0.6 V based on the ferrocene units, a potential slightly higher than that of the free ferrocene (0.47 V). The second is an irreversible oxidation wave at +1.1 V attributable to the oxidation of the silver(I) to silver(II). These reduction waves overlap at around +0.4 V.

Theoretical Studies

Theoretical calculations were performed in order to understand the factors leading to the helical structure observed, and to establish the nature of the Ag···Ag interaction. Several approaches were used, taking into account the size of the system and the adequacy of the method. Geometry optimizations were mainly performed using DFT[34] methods (ADF program[35]), although HF (Gaussian 98[36]) was also tested. Single point MP2[37] calculations were carried out in order to account for correlation effects in the Ag···Ag interactions. The complete structure consists of a large number of atoms, so that models had to be built in such a way as to preserve the features of the experimental structure. For instance, the ferrocenyl units are directed toward the outside of the helices, and were therefore removed. The pyridines were also simplified, keeping the same bonding modes, which implied changing the charge. These models are shown in Scheme 1.

Model 1 was used in a molecular dynamics study of the isolated ligands, aimed at measuring the tendency of the two ligands to preserve the helical arrangement even in the absence of the metal. Model 2 was used in all the quantum calculations.

The quality of the model was addressed first. The structure with two chains and two silver atoms was fully optimized (ADF program; for details see Exp. Sect.). In Figure 4,

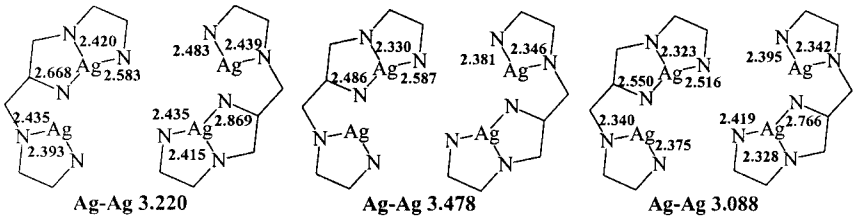

Figure 4. Ag−N distances (Å): calculated using DFT methods (left); in the X-ray structure of $[Ag_2(Fc_2qpy)_2]^{2+}$ (center); in the X-ray structure of $[Ag_2(dmqpy)_2]^{2+}$ (right)

 © 2004 Wiley-VCH Verlag GmbH & Co. KGaA, Weinheim

we show a comparison of the calculated Ag−Ag and Ag−N distances (Å) with those found in the corresponding section of the experimental structure of the $[Ag_2(Fc_2qpy)_2]^{2+}$ helix (notice that for clarity, silver atoms are represented twice, as each chain binds two silvers), and also of the $[Ag_2(dmqpy)_2]^{2+}$ complex (owing to symmetry, only one set of distances is given).[31]

Although the Ag−Ag distance is either slightly too long or too short, depending on the structure considered, some Ag−N distances compare relatively well. Each helix binds two different Ag atoms, using three N atoms for the first Ag, and two N atoms for the second. One of the Ag−N distances in each chain is too long for a bond (2.869, 2.668 Å, and 2.766, 2.550 Å, respectively, for the calculated and experimental distances of $[Ag_2(Fc_2qpy)_2]^{2+}$). A similar binding mode was found in the $[Ag_2(dmqpy)_2]^{2+}$ complex (TEPDUN; there is another complex with the same stoichiometry but a less similar environment). The agreement with respect to distances appears acceptable. The helical arrangement is also retained in this simple model, as can be seen in Figure S1 (See Supporting Information, for Supp. Inf. see also the footnote on the first page of this article).

In the following step, we separated the two chains from the original structure, as shown in Scheme 2, and allowed each fragment to relax in order to optimize the structure.

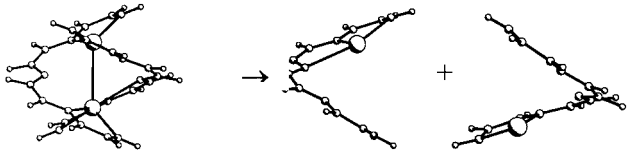

Scheme 2. Separation of the two fragments

The optimized structure consists of an almost flat pentacoordinate Ag complex of the qpy ligand, very similar to the X-ray structure of $[Agqpy]^+$, and is shown in Figure 5.

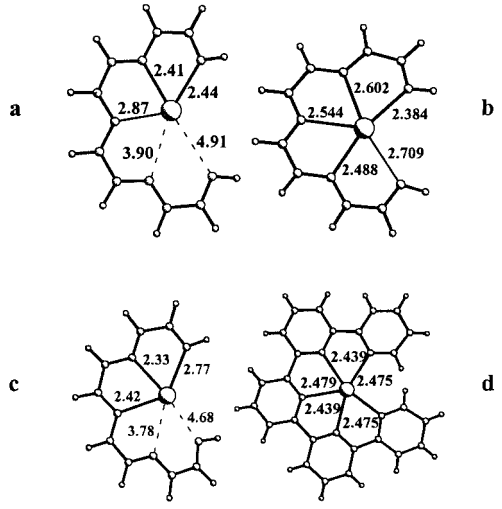

Figure 5. Structures containing one ligand chain and one silver atom: optimized in the helical structure of $[Ag_2(Fc_2qpy)_2]^{2+}$ (a), optimized alone (b), cut from the X-ray structure of the $[Ag_2(Fc_2qpy)_2]^{2+}$ helix (c), X-ray structure of the $[Agqpy]^+$ complex (d).

The Ag−N bond lengths are quite different from those in the helix, also shown in Figure 5, but very close to the distances in the $[Agqpy]^+$ complex, with the exception of one very long bond. Both in the calculated and the experimental helices, there are two Ag−N distances outside the bonding range (3.62, 4.65, or 3.90, 4.91, in the X-ray and calculated structures, respectively). Silver forms extra bonds with nitrogen atoms from the second chain. When the second chain is absent, the five possible Ag−N bonds are formed, and the energy decreases significantly (166 kcal mol^{-1}). How does the formation of the helical structure compete with the formation of two pentacoordinate monomers? Using the ADF optimized structures, we also performed single point HF and MP2 calculations on the monomer, the dimer, and the observed structure. The binding energy of the helical species relative to the sum of the energies of the single chains with the structure they have in the helix (see a in Figure 5) is represented by ΔE_1, and follows directly from Scheme 2. ΔE_2 represents the binding energy relative to two optimized single chains (see b in Figure 5). The difference between these two terms reflects the reorganization energy of each chain from flat to helical, and will be discussed again later. These binding energies are shown in Table 3.

Table 3. Binding energies (kcal·mol^{-1}) of the optimized helical structures relative to the monomer with the geometry in the optimized helical structure (ΔE_1) and the optimized AgL monomer (ΔE_2)

	DFT(ADF)	HF	MP2
ΔE_1	−51.1	−40.4	−90.4
ΔE_2	−5.9	8.5	−26.8

The ΔE_1 values are less relevant, since they give us the interaction energy for adding together the two chains shown in Scheme 2. They are always negative indicating that the formation of the four extra Ag−N bonds (each chain makes two bonds to the second silver atom), and eventually the new Ag−Ag bond, is an exothermic process. ΔE_2 values are much more interesting, because they include the reorganization energy of going from the flat pentacoordinate complex to a helix. This energy may be compensated for by stronger Ag−N bonds (same number, but organized differently) and a new Ag−Ag interaction. HF values give a positive energy, meaning that the helical structure is not favorable. On the other hand, both DFT and MP2 results agree on the higher stability of the double helix relative to the flat monomer, the interaction energy being larger in the MP2 calculation. This indicates that there is some weak Ag−Ag interaction, which relies on correlation and other effects, which are not all described by HF methods, but are fully taken into account by MP2, and only partly by the DFT functionals used. In the absence of this Ag−Ag interaction, the double helix is not favored, which follows from the HF data. Introduction of correlation (DFT) leads to the detection of the Ag−Ag interaction. A better description of cor-

 © 2004 Wiley-VCH Verlag GmbH & Co. KGaA, Weinheim

relation by MP2 increases the exothermiticity of the process.

The existence of the Ag−Ag interaction can be further probed by indicators of bond strength, such as overlap populations or related indices. The experimental distance is relatively long (3.09 Å). Therefore, we performed a natural population analysis,[38] and calculated Wiberg[39] and Mayer[40,41] indices. The Wiberg index, calculated with the MP2 method, was 0.022 for both the optimized structure (model 2) and the $[Ag_2(Fc_2qpy)_2]^{2+}$ helix, indicating a weak bond. The Mayer index, a generalization of the Wiberg index calculated by the ADF program, led to values of 0.066 and 0.086 for the optimized structure and the helix, respectively. These results are all consistent with the existence of a weak Ag···Ag interaction. We may therefore conclude that the helical structure can become energetically more favorable than the existence of monomers, owing to the strong Ag−N bonds that can also be formed in this arrangement, and the extra development of a metal−metal interaction. There is a balance between these terms and the reorganization energy of each chain, which opposes helix formation.

After analyzing the preferences of silver, we address the preferences of the chain in the absence of silver, by means of molecular mechanics and dynamics simulations using the Universal Force Field,[42] within the Cerius2 software package.[43]

A conformational analysis of a single qpy chain (model 1) was undertaken following quench dynamics techniques at 3000 K. The five pyridine rings can adopt *cis* or *trans* arrangements, depending of values of the N−C−C−N torsion angles between adjacent pyridine rings. When the two nitrogen atoms of two contiguous pyridines are opposite to each other, with an almost co-planar arrangement of the aromatic rings, the N−C−C−N torsion angle is near 180°, and the configuration is *trans* (*t*). If they are on the same side, the N−C−C−N torsion angle is near 0°, and the configuration is *cis* (*c*). Apart from changes in the signs of the torsion angles, there are ten unique possible conformations, which are listed in Table 4 together with their energies.

Table 4. The unique MM energy conformations for one qpy chain (torsion angles are listed successively, starting at a terminal pyridine ring)

Conformer	Energy (kcal·mol^{-1})	N−C−C−N torsion angles (°)			
tttt	114.76	180.0	179.9	180.0	180.0
ttct	114.95	−179.7	178.5	22.8	178.6
tttc	117.09	179.9	−179.3	179.2	21.7
tccc	120.32	179.9	18.9	−7.7	21.7
cctc	121.70	19.7	22.2	179.4	−21.3
tcct	116.37	−178.0	10.8	10.8	−178.0
tctc	117.99	−178.9	−23.3	−179.2	22.1
ttcc	118.76	−179.4	178.7	22.7	−20.6
cttc	119.75	−19.9	179.4	−179.4	19.9
cccc	124.89	−21.1	−19.8	14.0	−21.0

The results show that the steric energy increases with the number of *cis* torsion angles present in each conformation. Thus, the lowest energy conformation has an energy of 114.76 kcal·mol^{-1}, and exhibits a *tttt* conformation. In the crystal structure of $[H_2(qpy)][PF_6]_2$,[14] the qpy chain (model 1) exhibits a *cttc* conformation with N−C−C−N torsion angles of 3.5, 177.8, 174.5, and 6.9°. This conformation has an energy of 119.77 kcal·mol^{-1} in the gas phase but, in the crystal, two symmetry related $[H_2(qpy)]^{2+}$ cations are assembled face to face through a π-stacking arrangement with an interplanar distance ca. 3.89 Å, and by hydrogen bonding interactions involving the PF_6^- counterions and N−H groups. Therefore, the observed conformation is probably stabilized by these intermolecular interactions and avoids the low energy *tttt* conformation.

In the structure of $[Ag(qpy)][PF_6]$,[7] the qpy ligand adopts a helical shape, with four N−C−C−N torsion angles of −19.7, 1.1, 1.1, and −19.7° defining a *cccc* conformation. An energy of 125.20 kcal mol^{-1} and N−C−C−N torsion angles of −21.1, −19.8, 14.0, and −21.0° were calculated for this conformation, which is the highest energy conformation, and is forced by the binding of silver to the five nitrogen donors.

Having established the structural preferences of the monomeric chain, we then evaluated the stability of a dimeric model involving the self-assembling of two chains of qpy. The energy minimization of the supramolecular aggregate composed of two $[Fc_2(qpy)]$ units, from the X-ray structure of $[Ag_2(Fc_2qpy)_2]^{2+}$ after removing the two silver atoms, was first attempted in the Universal Force Field, parameterized for the full periodic table, using the default parameters available for $FeCp_2$ fragments. Since convergence was not achieved, a model was created by replacing the two ferrocenyl units with hydrogen atoms. This model structure was subsequently minimized by molecular mechanics calculations, and submitted to a dynamics simulation at room temperature (300 K) during 500 ps. Conformational changes were observed with torsion angles varying from −60 to 60°. Surprisingly, the two chains retained the double helical arrangement, and no *cis* to *trans* isomerization was observed. The overall conformation remained *cisoid*. The simulation was repeated for longer simulation periods of 800 and 1000 ps, respectively, and the chains kept their helical topology in both runs. This was only lost when the temperature was raised above 400 K. The changes of N−C−C−N torsion angles with time are given in Figure 6, for a simulation carried out at 500 K, together with snapshots of the most relevant structures. After the first 144.5 ps, two terminal pyridine rings from different chains experienced a conformational change from *cis* to *trans*, but the double-helix structure was retained. Subsequently, during a period of ca. 42 ps, further conformational changes occurred, until the two chains unfolded completely, adopting an almost parallel arrangement, which remained until the end of the simulation. During this period, the arrangement of the two chains changed from *ctttcttt* → *tttttttt* → *tttttttct*, but the *transoid* conformation of the eight torsion angles was retained for a considerable time. In order to evaluate the steric stability of the different arrangements observed in the molecular dynamics simulation, all the

 © 2004 Wiley-VCH Verlag GmbH & Co. KGaA, Weinheim

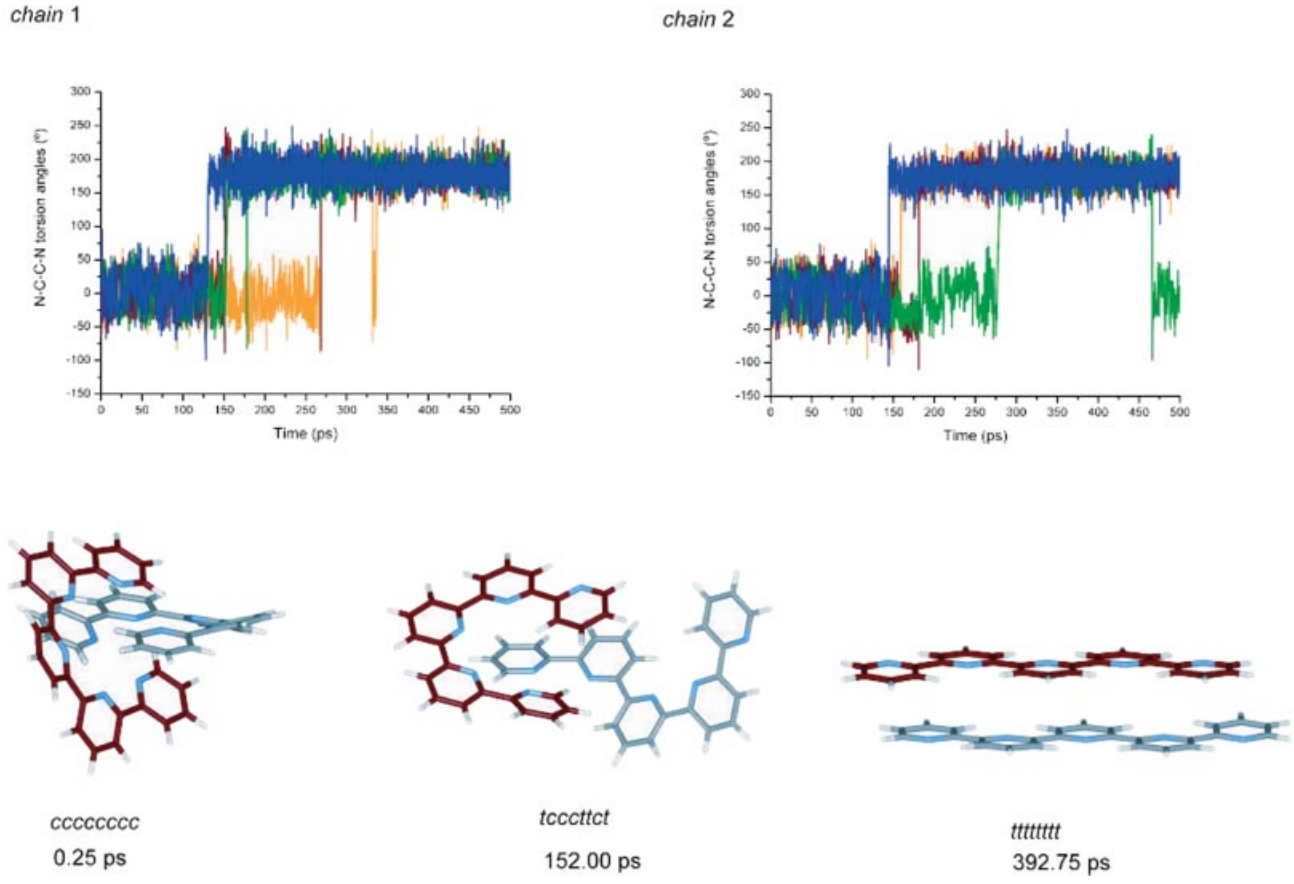

Figure 6. Changes in the N−C−C−N torsion angles during the 500 ps simulation at 500 K, with relevant snapshots showing the unfolding process of the dimeric qpy chain; the yellow, red, green, and blue curves represent the torsion angles from 2,2′, 6,2′, 6′′,2′′′, and 6′′′′, 2′′′′ C−C interannular bonds, respectively; carbon atoms of chains 1 and 2 are red and gray, respectively

frames collected were subsequently minimized by molecular mechanics (MM).

The lowest energy structure (215.94 kcal·mol^{-1}) corresponds to a *tttttttt* conformation, in which the pyridine rings of both chains are π-stacked, with the nitrogen atoms in a *trans* arrangement. In fact, the two terminal pyridine rings subtend a dihedral angle of 4.3°, and the chains are separated by a distance of ca. 3.732 Å. In other words, this supramolecular dimer is stabilized by π-π interactions.

In contrast, the double helix structure *cccccccc*, with torsion angles of −22.8, 22.1, −24.9, −18.9, −22.8, 22.1, −24.9, and −18.9°, is among those with the highest energies (223.97 kcal·mol^{-1}), as reported for the monomer. This conformation was observed in the solid state for $[Ag_2(Fc_2qpy)_2](OTf)_2$ with torsion angles of −1.8 −23.9 −35.9 −3.9 −4.8 −40.2, −28.5, and −1.8°. Therefore, in spite of the apparent stability shown by the double-helix *cccccccc* conformer in the gas phase, dynamics and mechanics results suggest that the silver atoms are, apparently, crucial for this conformational preference.

Selected geometric arrangements of the dimeric qpy chain were also optimized by DFT calculations, the results

Table 5. Low-energy MM structures resulting from self-assembling of two qpy chains

Conformer	Energy (kcal·mol^{-1})	N−C−C−N torsion angles (°)							
tttttttt	215.94	−176.1	−179.5	−178.6	176.5	−176.5	178.7	179.6	176.1
tcttttttt	219.58	174.8	13.9	179.6	178.3	−177.7	−175.4	−170.0	−178.5
tcctttttt	220.36	−175.3	−25.5	12.4	175.2	165.5	−160.1	166.9	−174.2
tcctttct	220.55	168.8	20.7	−20.8	175.5	176.8	179.6	17.3	171.7
ccctccc	220.90	15.6	−21.8	−23.7	−175.3	−175.4	−23.7	−21.8	15.6
ccccctccc	223.15	12.9	−22.4	−26.7	15.1	−168.3	−23.5	−21.4	12.2
cccccccc	223.97	−22.8	22.1	−24.9	−18.9	−22.8	22.1	−24.9	−18.9
tcttcttt	225.02	179.7	−176.6	−179.5	16.9	178.3	−165.3	24.4	175.8
ccctttttt	225.17	−18.1	14.3	11.8	−177.8	179.1	−166.7	170.2	−173.2
tccctttct	227.38	−169.4	−16.7	−11.2	15.7	−177.4	178.1	21.2	173.5
tccccctct	232.03	−176.4	−15.7	−2.4	−19.0	−22.8	−149.9	31.2	176.3

 © 2004 Wiley-VCH Verlag GmbH & Co. KGaA, Weinheim

Table 6. DFT minimized conformations of the supramolecular aggregate of two qpy chains

Conformer	Relative energy (kcal·mol^{-1})	N−C−C−N torsion angles (°)							
ttttttt	0.0	−178.3	−178.9	178.4	179.6	−179.7	−178.6	179.3	177.7
tcttttt	6.6	172.3	17.7	179.1	178.6	178.9	−166.8	−179.6	−179.3
tcttcttt	15.9	173.9	30.8	−165.8	−179.5	16.6	−178.4	−177.0	−178.8
tcccctct	22.6	−174.1	−12.7	−12.6	−21.3	178.6	33.2	−158.2	26.0
cccccccc	41.1	14.6	−26.1	−26.1	14.4	13.7	−25.9	−26.2	14.1

being similar to those discussed above. The *ttttttt* conformation is again the most stable, with an energy lower than that of the *cccccccc* conformer by 44.13 kcal·mol^{-1}. The resultant structures together with their relative energies are given in Table 6.

Conclusions

Although silver helical complexes of the type described here have been known for some years, no previous theoretical evaluation has, to the best of our knowledge, been carried out. DFT calculations were performed with a relatively small model, required by the large size of the real system, but were still able to reveal the main patterns. Optimized DFT geometries were very close to those observed experimentally, both in the case of the monomeric species, and of the double helical chain complex with two silver atoms. In our model, the optimized monomer (Figure 5, b) was found to be more stable than a related complex with a helical structure (Figure 5, a). Molecular dynamics and molecular mechanics also showed that the two chains in the helix (experimental structure or DFT optimized) exhibit a high energy conformation, while the planar arrangement of two chains is stabilized by π-π stacking interactions between the aromatic rings, and it is the lowest energy one. Thus, the preference for a dimeric structure depends on the balance between the reorganization energy of the two chains, i.e. between the preferred *tttt* conformation and the high energy *cccc*, and the energy released by the formation of globally stronger Ag−N bonds and the new Ag−Ag bond. The balance of these terms, accompanied by subtle factors not considered in our models, such as packing effects or π-π stacking, will strongly depend on the substituents.

Experimental Section

Instrumentation: Infrared spectra were recorded in the range 4000−200 cm^{-1} with a Perkin−Elmer 883 spectrophotometer using nujol mulls between polyethylene sheets. Conductivities were measured in ca. 5×10^{-4} mol·dm^{-3} solutions with a Philips 9509 conductimeter. C, N, and S analyses were carried out with a Perkin−Elmer 2400 microanalyzer. Mass spectra were recorded with a VG Autospec instrument with the liquid secondary-ion mass spectra (LSIMS) technique, using nitrobenzyl alcohol as matrix. NMR spectra were recorded with a Varian Unity 300 spectrometer or a Bruker ARX 300 spectrometer in CD_2Cl_2. Chemical shifts are cited relative to $SiMe_4$ (^{1}H, external). Cyclic voltammetric experiments were performed by employing an EG&PARC model 273 potentiostat. A three-electrode system was used, which consists of a platinum disk working electrode. The measurements were carried out in CH_2Cl_2 solutions with 0.1 mol·dm^{-3} Bu_4NPF_6 as a supporting electrolyte. Under the present experimental conditions, the ferrocenium/ferrocene couple was located at 0.47 V relative to the SCE.

Synthesis of $[Ag_2(Fc_2qpy)_2](OTf)_2$: To a solution of 4′,4‴-bis-(ferrocenyl)-2,2′:6′,2″:6″,2‴:6‴,2⁗-quinquepyridine (0.075 g, 0.1 mmol) in dichloromethane (20 mL) was added AgOTf (0.026 g, 0.1 mmol), and the mixture was stirred for 1 h. Evaporation of the solvent to ca. 5 mL, and addition of hexane gave $[Ag_2(Fc_2qpy)_2](OTf)_2$ as an orange-red solid. Yield 89 %. Δ_M 110 Ω^{-1} cm^2·mol^{-1}. $C_{92}H_{66}Ag_2F_6Fe_4N_{10}O_6S_2$ (2024.836): calcd. C 54.57, H 3.28, N 6.91, S 3.16; found C 54.19, H 3.14, N 6.85, S 3.09. ^{1}H NMR: δ = 4.12 (br. m, 10 H, C_5H_5), 4.63 (br. m, 4 H, C_5H_4), 4.95 (br. m, 4 H, C_5H_4), 6.89 (m, 2 H, 5 and 5⁗ of qpy), 7.15 (m, 2 H, 4 and 4⁗ pd qpy), 7.33 (m, 1 H, 4″), 7.6−8.8 (br. m, 10 H, qpy) ppm.

Crystal Data for $[Ag_2(Fc_2qpy)_2](OTf)_2·3CH_2Cl_2$: Empirical formula $C_{95}H_{72}Ag_2Cl_6F_6Fe_4N_{10}O_6S_2$, M = 2279.59, triclinic, space group $P(-1)$, a = 14.917(3), b = 16.205(3), c = 20.572(4) Å, α = 99.71(2), β = 105.46(2), γ = 103.86(2)°, U = 4507.4(15) Å^3, Z = 2, $D_{calcd.}$ = 1.680 Mg·m^{-3}, λ(Mo-K_α) = 0.07173 Å, μ = 1.351 mm^{-1}, F(000) = 2292, T = −130 °C, orange prism, 0.35 × 0.20 × 0.20 mm. 12234 intensities were recorded to $2\theta_{max.}$ 45° (Siemens P4 diffractometer), of which 11739 were unique (R_{int} = 0.0589) after absorption corrections using SHELXA. The structure was solved by heavy-atom methods, and subjected to full-matrix least-squares refinement on F^2 (program SHELXL-97).[44] All non-hydrogen atoms were refined anisotropically. H atoms were included using a riding model. Refinement proceeded to $wR(F^2)$ 0.2101, conventional $R(F)$ 0.0743 for 1180 parameters and 2254 restraints (to light atom U values and local ring geometry), $S(F^2)$ = 0.827; maximum Δρ = 1.384 e·Å^{-3}. CCDC-218940 contains the supplementary crystallographic data for this paper. These data can be obtained free of charge at www.ccdc.cam.ac.uk/conts/retrieving.html [or from the Cambridge Crystallographic Data Center, 12 Union Road, Cambridge CB2 1EZ, UK; Fax: +44-1223/336-033; E-mail: deposit@ccdc.cam.ac.uk].

Computational Details: Density functional calculations[34] were carried out with the Amsterdam Density Functional program (ADF-2000).[35] The Local Spin Density (LSD) exchange correlation potential was used with the Local Density Approximation of the correlation energy (Vosko, Wilk and Nusair's).[45] Gradient corrected geometry optimizations,[46] without symmetry constrains, were performed using the Generalized Gradient Approximation (Becke's non-local exchange[47] and Perdew's correlation corrections).[48] A triple-ζ Slater-type orbital (STO) basis set was used for all atoms, augmented by one polarization function. A frozen core approximation was used to treat the core electrons: (1s) for N and C; ([1−3]s [2−3]p 3d) for Ag.

 © 2004 Wiley-VCH Verlag GmbH & Co. KGaA, Weinheim

Single point calculations at the Hartree−Fock (HF)[49] and second order Møller−Plesset (MP2)[37] levels were performed on the ADF optimized geometries using Gaussian 98.[36] The standard LanL2DZ basis set was used for all atoms.[50] A Natural Population (NPA) analysis,[38] and the evaluation of the Wiberg indices[39] (using the MP2 density) were used as bond strength indicators. Mayer indices were calculated with the ADF densities.[40,41]

HF structure optimizations were also performed, but the agreement between calculated and experimental data was worse than that obtained with the DFT methods (longer distances, especially Ag···Ag). They were, therefore, not considered in further single point energy calculations.

The molecular dynamics simulations and mechanics calculations were carried out using the Cerius2 software[43] with parameters from the Universal Force Field.[42] The atomic charges were calculated with the Qeq method implemented in Cerius2. The conformational analysis of model 1 was performed via quench dynamics techniques. A molecular dynamics run was carried out using a time step of 1 fs and 2000 conformations were generated at 0.25 ps intervals at 3000 K. Concomitantly, the generated conformations were minimized by molecular mechanics calculations. The dynamics simulations with model 2 were carried out at temperatures of 300, 400, and 500 K, respectively, using a time step of 1fs, and a set of atomic positions were saved every 0.25 ps over the entire period of the simulation of 500 ps. The simulation runs at 300 and 400 K were repeated for 800 and 1000 ps. An NVT thermostat was used for all simulations. The structures collected in dynamics run at 500 K were subsequently minimized by molecular mechanics.

Acknowledgments

We thank the Dirección General de Investigación Científica y Técnica (No. BQU2001−2409-C02-C01) and the Fonds der Chemischen Industrie for financial support. We thank Acções-Integradas Luso-Espanholas for a bilateral project.

[1] J. M. Lehn, *Supramolecular Chemistry*, Wiley-VCH, Weinheim, **1995**.
[2] I. Haiduc, F. T. Edelmann, *Supramolecular Organometallic Chemistry*, Wiley-VCH, Weinheim, **1999**.
[3] E. C. Constable, *Prog. Inorg. Chem.* **1994**, *42*, 67.
[4] E. C. Constable, in *Comprehensive Supramolecular Chemistry*, vol. 9 (Ed.: J. M. Lehn), Pergamon, Oxford, **1996**, p. 213.
[5] M. Munakata, L. P. Wu, T. Kuroda-Sowa, *Adv. Inorg. Chem.* **1999**, *46*, 173.
[6] C. Piguet, G. Bernardinelli, G. Hopfgartner, *Chem. Rev.* **1997**, *97*, 2005.
[7] E. C. Constable, M. G. B. Drew, G. Forsyth, M. D. Ward, *J. Chem. Soc., Chem. Commun.* **1988**, 1450.
[8] E. C. Constable, J. Lewis, M. Schröder, *Polyhedron* **1982**, *1*, 311.
[9] E. C. Constable, M. G. B. Drew, M. D. Ward, *J. Chem. Soc., Chem. Commun.* **1987**, 1600.
[10] M. Barley, E. C. Constable, S. A. Corr, R. C. S. McQueen, J. C. Nutkins, M. D. Ward, M. G. B. Drew, *J. Chem. Soc., Dalton Trans.* **1988**, 2655.
[11] E. C. Constable, M. D. Ward, M. G. B. Drew, G. A. Forsyth, *Polyhedron* **1989**, *8*, 2551.
[12] E. C. Constable, S. M. Elder, J. Healy, M. D. Ward, D. A. Tocher, *J. Am. Chem. Soc.* **1990**, *112*, 4590.
[13] E. C. Constable, S. M. Elder, P. R. Raithby, M. D. Ward, *Polyhedron* **1991**, *10*, 1395.
[14] E. C. Constable, S. M. Elder, J. V. Walker, P. D. Wood, D. A. Tocher, *J. Chem. Soc., Chem. Commun.* **1992**, 229.
[15] E. C. Constable, J. V. Walker, D. A. Tocher, M. A. M. Daniels, *J. Chem. Soc., Chem. Commun.* **1992**, 768.
[16] E. C. Constable, J. V. Walker, *J. Chem. Soc., Chem. Commun.* **1992**, 884.
[17] E. C. Constable, M. A. M. Daniels, M. G. B. Drew, D. A. Tocher, J. V. Walker, P. D. Wood, *J. Chem. Soc., Dalton Trans.* **1993**, 1947.
[18] E. C. Constable, R. Martínez-Máñez, A. M. W. Cargill Thompson, J. V. Walker, *J. Chem. Soc., Dalton Trans.* **1994**, 1585.
[19] E. C. Constable, A. J. Edwards, P. R. Raithby, J. V. Walker, *Angew. Chem. Int. Ed. Engl.* **1993**, *32*, 1465.
[20] P. K. K. Ho, K. K. Cheung, C. M. Che, *Chem. Commun.* **1996**, 1197.
[21] P. K. K. Ho, K. K. Cheung, S. M. Peng, C. M. Che, *J. Chem. Soc., Dalton Trans.* **1996**, 1411.
[22] Y. Fu, Q. Li, Z. Zhou, W. Dai, D. Wang, T. C. W. Mak, H. Hu, W. Tang, *Chem. Commun.* **1996**, 1549.
[23] E. C. Constable, A. J. Edwards, P. R. Raithby, D. R. Smith, J. V. Walker, L. Whall, *Chem. Commun.* **1996**, 2551.
[24] E. C. Constable, M. Neuburger, L. A. Whall, M. Zehnder, *New J. Chem.* **1998**, *22*, 219.
[25] C. J. Cathey, E. C. Constable, M. J. Hannon, D. A. Tocher, M. D. Ward, *J. Chem. Soc., Chem. Commun.* **1990**, 621.
[26] E. C. Constable, C. J. Cathey, M. J. Hannon, D. A. Tocher, J. V. Walker, M. D. Ward, *Polyhedron* **1999**, *18*, 159.
[27] E. C. Constable, J. V. Walker, *Polyhedron* **1998**, *17*, 3089.
[28] K. T. Potts, M. Keshavarz, K. F. S. Than, H. D. Abruna, C. R. Arana, *Inorg. Chem.* **1993**, *32*, 4422.
[29] K. T. Potts, M. Keshavarz, K. F. S. Than, H. D. Abruna, C. R. Arana, *Inorg. Chem.* **1993**, *32*, 4436.
[30] W. Dai, H. Hu, X. Wei, X. Zhu, D. Wang, K. Yu, N. R. Dalley, X. Kou, *Polyhedron* **1997**, *16*, 2059.
[31] Y. Fu, J. Sun, Q. Li, Y. Chen, W. Dai, D. Wang, T. C. W. Mak, W. Tang, H. Hu, *J. Chem. Soc., Dalton Trans.* **1996**, 2309.
[32] E. C. Constable, S. M. Elder, M. J. Hannon, A. Martin, P. R. Raithby, D. A. Tocher, *J. Chem. Soc., Dalton Trans.* **1996**, 2423.
[33] G. Baum, E. C. Constable, D. Fenske, C. E. Housecroft, T. Kulke, *Chem. Commun.* **1998**, 2659.
[34] R. G. Parr, W. Yang, *Density Functional Theory of Atoms and Molecules*, Oxford, University Press, New York, **1989**.
[35] [35a] *ADF-2000*: E. J. Baerends, A. Bérces, C. Bo, P. M. Boerrigter, L. Cavallo, L. Deng, R. M. Dickson, D. E. Ellis, L. Fan, T. H. Fischer, C. Fonseca Guerra, S. J. A. van Gisbergen, J. A. Groeneveld, O. V. Gritsenko, F. E. Harris, P. van den Hoek, H. Jacobsen, G. van Kessel, F. Kootstra, E. van Lenthe, V. P. Osinga, P. H. T. Philipsen, D. Post, C. C. Pye, W. Ravenek, P. Ros, P. R. T. Schipper, G. Schreckenbach, J. G. Snijders, M. Sola, D. Swerhone, G. te Velde, P. Vernooijs, L. Versluis, O. Visser, E. van Wezenbeek, G. Wiesenekker, S. K. Wolff, T. K. Woo, T. Ziegler. [35b] C. Fonseca Guerra, O. Visser, J. G. Snijders, G. te Velde, E. J. Baerends, *Parallelisation of the Amsterdam Density Functional Program in: Methods and Techniques for Computational Chemistry* (Eds.: E. Clementi, C. Corongiu), p. 303−395, STEF, Cagliari, **1995**. [35c] C. Fonseca Guerra, J. G. Snijders, G. te Velde, E. J. Baerends, *Theor. Chem. Acc.* **1998**, *99*, 391. [35d] E. J. Baerends, D. Ellis, P. Ros, *Chem. Phys.* **1973**, *2*, 41. [35e] E. J. Baerends, P. Ros, *Int. J. Quantum Chem.* **1978**, *S12*, 169. [35f] P. M. Boerrigter, G. te Velde, E. J. Baerends, *Int. J. Quantum Chem.* **1988**, *33*, 87. [35g] G. te Velde, E. J. Baerends, *J. Comp. Phys.* **1992**, *99*, 84.
[36] *Gaussian 98* (Revision A.7): M. J. Frisch, G. W. Trucks, H. B. Schlegel, G. E. Scuseria, M. A. Robb, J. R. Cheeseman, V. G. Zakrzewski, J. A. Montgomery, R. E. Stratmann, J. C. Burant, S. Dapprich, J. M. Millam, A. D. Daniels, K. N. Kudin, M. C. Strain, O. Farkas, J. Tomasi, V. Barone, M. Cossi, R. Cammi, B. Mennucci, C. Pomelli, C. Adamo, S. Clifford, J. Ochterski, G. A. Petersson, P. Y. Ayala, Q. Cui, K. Morokuma, D. K. Malick, A. D. Rabuck, K. Raghavachari, J. B. Foresman, J. Cioslowski, J. V. Ortiz, B. B. Stefanov, G. Liu, A. Liashenko, P. Piskorz, I. Komaromi, R. Gomperts, R. L. Martin, D. J. Fox, T. Keith, M. A. Al-Laham, C. Y. Peng, A. Nanayakkara, C.

 © 2004 Wiley-VCH Verlag GmbH & Co. KGaA, Weinheim

Gonzalez, M. Challacombe, P. M. W. Gill, B. G. Johnson, W. Chen, M. W. Wong, J. L. Andres, M. Head-Gordon, E. S. Replogle, J. A. Pople, Gaussian, Inc., Pittsburgh, PA, **1998**.
[37] [37a] C. Møller, M. S. Plesset, *Phys. Rev.* **1934**, *46*, 618. [37b] J. S. Binkley, J. A. Pople, *Int. J. Quantum Chem.* **1975**, *9*, 229. [37c] J. S. Binkley, J. A. Pople, R. Seeger, *Int. J. Quantum Chem.* **1976**, *S10*, 1. [37d] R. Krishnan, J. A. Pople, *Int. J. Quantum Chem.* **1978**, *14*, 91. [37e] R. Krishnan, M. Frisch, J. A. Pople, *J. Chem. Phys.* **1980**, *72*, 4244.
[38] [38a] J. E. Carpenter, F. Weinhold, *Mol. Struct. (Theochem)* **1988**, *169*, 41. [38b] J. E. Carpenter, *PhD Thesis, University of Wisconsin (Madison WI)*, **1987**. [38c] J. P. Foster, F. Weinhold, *J. Am. Chem. Soc.* **1980**, *102*, 7211. [38d] A. E. Reed, F. Weinhold, *J. Chem. Phys.* **1983**, *78*, 4066. [38e] A. E. Reed, F. Weinhold, *J. Chem. Phys.* **1983**, *78*, 1736. [38f] A. E. Reed, R. B. Weinstock, F. Weinhold, *J. Chem. Phys.* **1985**, *83*, 735. [38g] A. E. Reed, L. A. Curtiss, F. Weinhold, *Chem. Rev.* **1988**, *88*, 899. [38h] F. Weinhold, J. E. Carpenter, *The Structure of Small Molecules and Ions*, Plenum, **1988**, 227.
[39] K. B. Wiberg, *Tetrahedron* **1968**, *24*, 1083.
[40] I. Mayer, *Chem. Phys. Lett.* **1983**, *97*, 270; I. Mayer, *Int. J. Quantum Chem.* **1984**, *26*, 151.
[41] *MAYER*: A. J. Bridgeman, C. J. Empson, University of Hull (**2002**). Freely available on the worldwide web from http://www.hull.ac.uk/php/chsajb/mayer/.
[42] A. K. Rappe, C. J. Casewit, K. S. Colwell, W. A. Goddard III, W. M. Skiff, *J. Am. Chem. Soc.* **1992**, *114*, 10024.
[43] *CERIUS2*, version 4.2, Molecular Simulations Inc, San Diego, **2000**.
[44] G. M. Sheldrick, *SHELXL-97, A Program for Crystal Structure Refinement*, University of Göttingen, **1997**.
[45] S. H. Vosko, L. Wilk, M. Nusair, *Can. J. Phys.* **1980**, *58*, 1200.
[46] [46a] L. Versluis, T. Ziegler, *J. Chem. Phys.* **1988**, *88*, 322. [46b] L. Fan, T. Ziegler, *J. Chem. Phys.* **1991**, *95*, 7401.
[47] A. D. Becke, *Phys. Rev. A.* **1988**, *38*, 3098.
[48] J. P. Perdew, *Phys. Rev. B.* **1986**, *33*, 8822.
[49] W. J. Hehre, L. Radom, P. v. R. Schleyer, J. A. Pople, *Ab Initio Molecular Orbital Theory*, John Wiley & Sons, New York, **1986**.
[50] [50a] T. H. Dunning, Jr., P. J. Hay, *Modern Theoretical Chemistry* (Ed.: H. F. Schaefer III), Plenum, New York, **1976**, vol. 3, p. 1. [50b] P. J. Hay, W. R. Wadt, *J. Chem. Phys.* **1985**, *82*, 270. [50c] W. R. Wadt, P. J. Hay, *J. Chem. Phys.* **1985**, *82*, 284. [50d] P. J. Hay, W. R. Wadt, *J. Chem. Phys.* **1985**, *82*, 2299.

Received January 22, 2004
Early View Article
Published Online June 1, 2004

 © 2004 Wiley-VCH Verlag GmbH & Co. KGaA, Weinheim

Synthesis and Characterization of the First Examples of Dicationic Dihydrogen Complexes of Iron and Ruthenium with the PF_3 Ligand

H. V. Nanishankar,[a] Munirathinam Nethaji,[a] and Balaji R. Jagirdar*[a]

Keywords: Dihydrogen complexes / H−H activation / Hydride ligands / Iron / Phosphane ligands / Ruthenium

New dicationic dihydrogen complexes of the type *trans*-$[M(\eta^2\text{-}H_2)(PF_3)(diphosphane)_2]^{2+}$ [M = Ru, diphosphane = dppm ($Ph_2PCH_2PPh_2$); M = Fe, Ru, diphosphane = dppe ($Ph_2PCH_2CH_2PPh_2$)] have been prepared from the precursor hydrides *trans*-$[M(H)(PF_3)(diphosphane)_2]^+$ upon reaction with HOTf. In the case of dppm, in addition to the *trans*-dihydrogen complex *cis*-$[Ru(\eta^2\text{-}H_2)(PF_3)(dppm)_2]^{2+}$ was also obtained in the protonation reaction. The intact nature of the H–H bond in these derivatives has been established using the spin–lattice relaxation time measurements (short T_1 values) and the large $J_{H,D}$ coupling constant of the H–D isotopomers. The H–H bond lengths and the stabilities of the dihydrogen complexes are discussed in terms of the π-acidity of the PF_3 ligand and compared with other systems possessing *trans* CO and CNH ligands. The *trans*-$[Ru(\eta^2\text{-}H_2)(PF_3)(dppe)_2]^{2+}$ complex was found to be remarkably stable with respect to the loss of bound H_2 for a period of about 16 h. The H–D isotopomer of this complex exhibits small temperature variations in the $J_{H,D}$ coupling constant. The X-ray crystal structure of *trans*-$[Ru(H)(PF_3)(dppm)_2][BF_4]$ has been determined.

(© Wiley-VCH Verlag GmbH & Co. KGaA, 69451 Weinheim, Germany, 2004)

Introduction

The heterolytic activation of molecular hydrogen by transition metal centers to give a proton and a metal hydride is one of the most intriguing reactions of dihydrogen complexes. Highly electrophilic metal centers have been found to greatly promote heterolysis of dihydrogen.[1,2] This activation pathway leads to interesting reactivity, including catalysis and selective proton transfer to an ancillary ligand.[3,4] The ligand *trans* to the $\eta^2\text{-}H_2$ moiety has a significant role in dictating the properties of the dihydrogen complex, including the heterolytic cleavage of the bound dihydrogen.

We have been interested in preparing systems that are capable of activating H_2 in a heterolytic fashion. Toward this goal, we have reported certain dicationic dihydrogen complexes of iron and ruthenium bearing *trans*-phosphite, phosphane,[5−7] and nitrile[8] ligands that were found to be quite acidic. Numerous examples of highly acidic $\eta^2\text{-}H_2$ complexes have been reported in the literature.[9−14] Rocchini et al.[12] have reported two highly acidic dihydrogen complexes *trans*-$[M(\eta^2\text{-}H_2)(CO)(dppp)_2]^{2+}$ [M = Ru, Os; dppp = 1,3-bis(diphenylphosphanyl)propane]. The ruthenium derivative was found to be stable only at low temperatures whereas the osmium complex is stable even at room temperature. The strong π-accepting tendency of the CO ligand *trans* to the H_2 imparts the high acidity to the dihydrogen ligand. Morris and co-workers have reported an iron dihydrogen complex *trans*-$[Fe(\eta^2\text{-}H_2)(CO)(dppe)_2]^{2+}$ that was found to be quite acidic.[14] In addition to this species, they also prepared a highly acidic dicationic dihydrogen complex, *trans*-$[Ru(\eta^2\text{-}H_2)(CNH)(dppe)_2]^{2+}$ that was found to be stable with respect to the loss of protons or H_2 under strongly acidic conditions (excess triflic acid).[13] A ligand that has similar π acidity to both CO and CNH is PF_3. Dihydrogen complexes with the PF_3 ligand are limited to only one example, the rhenium complex *fac*-$[Re(H_2)(PPh_3)(PF_3)(dien)]^+$.[15,16] As yet there are no reports in the literature of dicationic dihydrogen complexes of transition metals with the PF_3 ligand. Therefore, in continuation of our investigations on the heterolytic activation of molecular hydrogen we report here the first examples of dicationic dihydrogen complexes of iron and ruthenium with a *trans*-PF_3 ligand *trans*-$[M(\eta^2\text{-}H_2)(PF_3)(diphosphane)_2]^{2+}$ (M = Fe, diphosphane = dppe; M = Ru, diphosphane = dppm, dppe).

Results and Discussion

Preparation and Properties of the Hydride Complexes

The new hydride complexes *trans*-$[M(H)(PF_3)(diphosphane)_2][BF_4]$ (M = Fe, diphosphane = dppe **1**; M = Ru, diphosphane = dppm **2**, dppe **3**) were prepared by substitution of the bound H_2 ligand in *trans*-$[M(H)(\eta^2\text{-}H_2)(diphosphane)_2][BF_4]$ with excess PF_3 gas [Equation (1)]. The

[a] Department of Inorganic & Physical Chemistry,
Indian Institute of Science, Bangalore 560 012, India
Fax: (internat.) + 80-2360-0683
E-mail: jagirdar@ipc.iisc.ernet.in

 © 2004 Wiley-VCH Verlag GmbH & Co. KGaA, Weinheim DOI: 10.1002/ejic.200400130

products were obtained as colorless solids that were purified by crystallization from a CH_2Cl_2/Et_2O mixture to give colorless crystals.

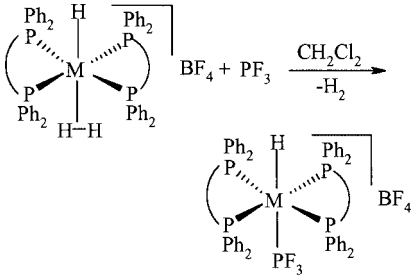

(1)

M	diphosphane	compd.
Fe	dppe	**1**
Ru	dppm	**2**
	dppe	**3**

The ^1H NMR spectra of the hydride complexes show a doublet of multiplets pattern for the hydride moiety due to coupling with the phosphorus (*trans* and *cis*) and fluorine nuclei. The $J_{H,P_{trans}}$ coupling constants were found to be 155.6 and 171.9 Hz whereas the $J_{H,P_{cis}}$ coupling constants were found to be 21.0 and 19.1 Hz for **2** and **3**, respectively. The $^1H\{^{31}P\}$ NMR spectra gave a quadruplet in the hydride region due to H, F coupling, with $J_{H,F}$ equal to 33.1 and 34.4 Hz for **2** and **3**, respectively. In the case of **1**, a multiplet at $\delta = -7.06$ ppm in the ^1H NMR spectrum with an average $J_{H,P}$ coupling constant (H,P_{trans} and H,P_{cis}) of 50.0 Hz was observed. The $^{31}P\{^1H\}$ NMR spectrum consists of one doublet for the dppe P nuclei coupled to the PF_3 ligand and a quadruplet of quintets for the PF_3 moiety coupled to three fluorine and the four dppe P nuclei. The $J_{P,F}$ coupling constant was found to be in the range 1267.0−1307.9 Hz, which is typical for compounds having direct P−F bonds.[17−20] The ^{19}F NMR spectra of the hydride complexes consist of a doublet of doublets for the PF_3 ligand and a broad singlet for the BF_4^- counterion. The NMR spectroscopic data for these complexes are summarized in Table 1. In order to get an insight into the structural aspects, we carried out an X-ray crystallographic study of **2**.

Structure of *trans*-[Ru(H)(PF_3)(dppm)$_2$][BF_4] (2)

The ORTEP diagram of the *trans*-$[Ru(H)(PF_3)(dppm)_2]^+$ cation is shown in Figure 1. In addition to a discrete BF_4^- counterion, two molecules of H_2O were also found (the source of these water molecules could be the solvent used for crystallization because strict measures were not taken to exclude the moisture). The structure is a highly distorted square pyramid defined by the four nearly coplanar dppm phosphorus atoms, with the PF_3 group almost perpendicular to this plane. The hydride ligand that occupies the sixth coordination site on the metal was not located, although its presence was confirmed by ^1H NMR spectroscopy. The Ru−P(dppm) bond lengths vary from 2.3302(18) to

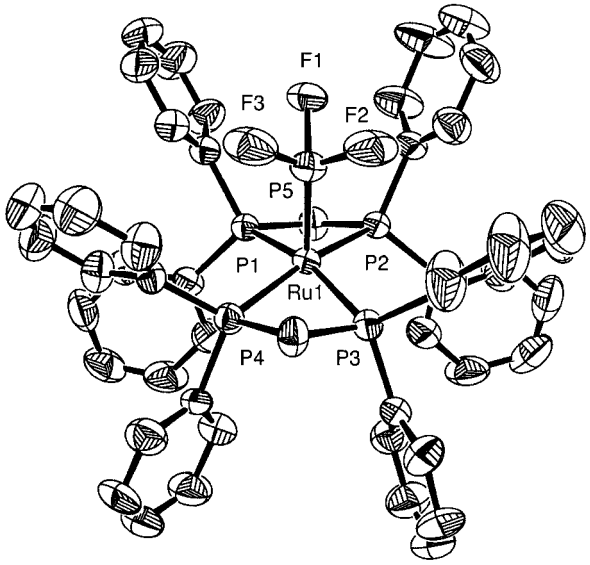

Figure 1. ORTEP view of the *trans*-$[(dppm)_2Ru(H)(PF_3)]^+$ (**2**) cation at the 50% probability level

Table 1. ^1H, $^{31}P\{^1H\}$, and ^{19}F NMR spectral data (δ) for *trans*-[M(H)(PF_3)(diphosphane)$_2$][BF_4] complexes in CD_2Cl_2

	Fragment	**1**	**2**	**3**
^1H	δ(M−H)	−7.06 (m, 1 H)	−2.95 (dm, 1 H)	−6.73 (dm, 1 H)
	$J_{H,P_{trans}}$ (Hz)	50.0[a]	155.6	171.9
	$J_{H,P_{cis}}$ (Hz)		21.0	19.1
	$J_{H,F}$ (Hz)	20.2	33.1	34.4
	δ(CH_2)	2.30 (m, 4 H)	4.64 (m, 2 H)	2.29 (m, 4 H)
		2.60 (m, 4 H)	4.97 (m, 2 H)	2.61 (m, 4 H)
	δ(Ph)	6.60−8.20 (m, 40 H)	7.11−7.57 (m, 40 H)	6.66−7.30 (m, 40 H)
^{31}P	δ(diphosphane)	77.9 (d, 4 P)	−3.8 (d, 4 P)	57.7 (d, 4 P)
	$J_{P,P}$ (Hz)	44.2	32.1	29.2
	δ(PF_3)	149.0 (q quint, 1 P)	132.9 (q quint, 1 P)	126.8 (q quint, 1 P)
	$J_{P,F}$ (Hz)	1267.0	1307.9	1304.6
^{19}F	δ(PF_3)	−12.13 (dd)	−19.00 (dd)	−18.20 (dd)
	δ(BF_4)	−159.28 (br)	−161.18 (br)	−166.07 (br)

[a] Average; no separate H,P_{trans} and H,P_{cis} couplings seen.

 © 2004 Wiley-VCH Verlag GmbH & Co. KGaA, Weinheim

2.352(2) Å whereas the Ru−P(PF_3) distance was found to be 2.206(2) Å. The bond lengths of certain analogous ruthenium derivatives fall in the following order: 2.3153(17) Å {Ru−P($OMe)_3$ in *trans*-[Ru(H){P($OMe)_3$}($dppm)_2$][BF_4]}[7] > 2.264(2) Å {Ru−P($OMe)_2$ in *trans*-[Ru(H){P($OMe)_2$}($dppe)_2$][BF_4]}[5] > 2.206(2) Å {Ru−PF_3 in *trans*-[Ru(H)(PF_3)($dppm)_2$][BF_4]}. This order is a combined effect of the progressive increase in the π-accepting ability as well as the decrease in the steric crowding due to the reduction in the cone angles[21,22] of the *trans*-phosphorus ligands. The dppm bite angles P(1)−Ru(1)−P(2) and P(3)−Ru(1)−P(4) are 71.87(6)° and 70.48(5)°, respectively. The P(1)−C(25)−P(2) and P(3)−C(50)−P(4) bond angles are 96.6(3)° and 94.4(3)°, respectively, falling at the lower end of the range of P−C−P angles (92−133°) that the dppm ligand exhibits in its complexes. The crystallographic data are given in the Exp. Sect. and selected bond lengths and angles are summarized in Table 2.

Table 2. Selected bond lengths (Å) and angles (°) for *trans*-[Ru(H)(PF_3)($dppm)_2$][BF_4] (**2**)

Ru(1)−P(1)	2.3302(18)
Ru(1)−P(2)	2.3481(17)
Ru(1)−P(3)	2.352(2)
Ru(1)−P(4)	2.3437(18)
Ru(1)−P(5)	2.206(2)
P(5)−F(1)	1.554(4)
P(5)−F(2)	1.552(5)
P(5)−F(3)	1.549(5)
P(1)−Ru(1)−P(2)	71.87(6)
P(3)−Ru(1)−P(4)	70.48(5)
P(1)−Ru(1)−P(3)	165.15(6)
P(2)−Ru(1)−P(4)	168.11(6)
P(1)−Ru(1)−P(5)	100.70(7)
P(2)−Ru(1)−P(5)	96.78(7)
P(3)−Ru(1)−P(5)	93.78(7)
P(4)−Ru(1)−P(5)	95.05(7)

Protonation Reactions of *trans*-[Fe(H)(PF_3)($dppe)_2$][BF_4] and *trans*-[Ru(H)(PF_3)($dppm)_2$][BF_4].

The protonation of the hydrides with HOTf in CD_3CN or with HBF_4·Et_2O in CD_2Cl_2 did not afford the dihydrogen complexes; even with large excesses of the acid, no reaction took place. These experiments indicate that the pK_a of the protonating agent must be less than −2.4 in order to obtain the dihydrogen complexes since the pK_a of HOTf in CH_3CN is 2.6[23] and that of HBF_4·Et_2O is −2.4.[24] When the hydrides were protonated with excess triflic acid under H_2 atmosphere in CD_2Cl_2 at room temperature, the corresponding dihydrogen complexes *trans*-[Fe(η^2-H_2)(PF_3)($dppe)_2$]$^{2+}$ (**4**) and *trans*-[Ru(η^2-H_2)(PF_3)($dppm)_2$]$^{2+}$ (**5**) were presumably formed, although we found that they lose the H_2 ligand quite rapidly thus precluding the NMR spectroscopic characterization of these complexes. The singlet at δ = 4.6 ppm in the ^{1}H NMR spectrum due to free H_2 grew in intensity in these experiments. In the case of protonation of **1**, the resulting mixture gave NMR signals that were extensively broadened upon loss of H_2 due to the generation of some Fe^{III} species, amongst others. In an attempt to observe the dihydrogen complexes spectroscopically, the addition of the protonating agent was done at liquid N_2 temperature and then the mixture was slowly warmed up to 0 °C; the NMR spectral studies were also carried out at this temperature. Under these conditions, we observed signals corresponding to the dihydrogen complexes only in the case of **2**.

The protonation of **2** with HOTf under an atmosphere of H_2 resulted in a mixture of *trans*-[Ru(η^2-H_2)(PF_3)($dppm)_2$]$^{2+}$ (**5**) and *cis*-[Ru(η^2-H_2)(PF_3)($dppm)_2$]$^{2+}$ (**6**) in a ratio of 1:3. We have previously observed a similar behavior in certain analogous ruthenium complexes with *trans* phosphite ligands.[7] The complexes of the type *trans*-[Ru(H)[P($OR)_3$]($dppm)_2$][BF_4] isomerize under thermal conditions (in the presence of small amounts of acid impurities in the solvent) to give a mixture of the *trans* and the *cis* hydride phosphite derivatives. We traced the origin of this isomerization to the lability of the *trans* phosphite ligand. The addition of acid accelerated the isomerization reaction in those derivatives resulting in the corresponding *trans* and *cis* dihydrogen complexes *trans*/*cis*-[Ru(η^2-H_2)[P($OR)_3$]($dppm)_2$][BF_4]$_2$.[7] The mechanism of the isomerization in the current work, however, seems to be different. The PF_3 ligand was not found to be labile; refluxing solutions containing the starting *trans* hydride complexes did not give any isomerized species, thus suggesting that the isomerization occurs only upon addition of the acid. We monitored the loss of the bound H_2 ligand and found that it was faster in the case of **5** than **6**. A plausible mechanism could involve the loss of H_2 ligand from the *trans* dihydrogen complex, rearrangement of the five-coordinate species, followed by the re-binding of the H_2 *cis* to the PF_3 moiety. When the protonation was carried out under an Ar atmosphere, we found no evidence of isomerization except for the loss of H_2 ligand from **5**; a singlet at δ = 4.6 ppm due to free H_2 was observed in the ^{1}H NMR spectrum in this case. This suggests that the isomerization is effected upon loss of H_2 from the *trans* dihydrogen complex followed by the rebinding of H_2 *cis* to PF_3 only when there is excess H_2. The mechanism is illustrated in Scheme 1.

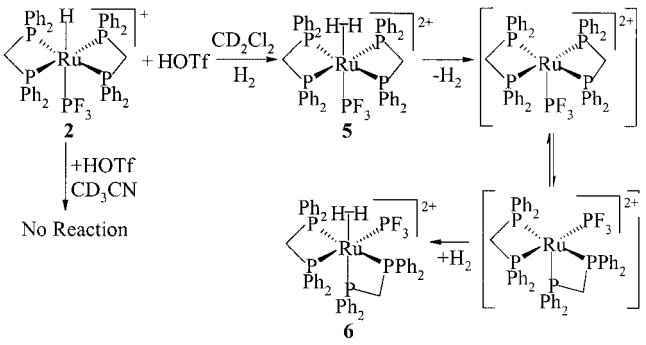

Scheme 1

 © 2004 Wiley-VCH Verlag GmbH & Co. KGaA, Weinheim

Another possible mechanism for the isomerization could involve the protonation of one of the dppm P atoms, opening up of the chelate arms to give Ru−(η^1-dppmH$^+$), followed by the isomerization. The dppmH$^+$ could then protonate the hydride ligand and close its arm. The pK_{a1} of dppmH$^+$ has been reported to be 3.81.[25] The protonated dppm P ([$Ph_2PCH_2PHPh_2$]$^+$) undergoes a dramatic downfield shift with respect to the bound dppm P chemical shifts in the ^{31}P NMR spectroscopy, as has been observed by Rottink and Angelici earlier.[26] We did not find any evidence for a dangling dppmH$^+$ in our ^{31}P NMR spectral studies. In addition, since the pK_a of the protonating agent needs to be lower than −2.4 in order to obtain the dihydrogen complexes, we can rule out this mechanism.

The protonation of **2** in CD_2Cl_2 followed by the addition of CD_3CN gave *trans*-[Ru(CD_3CN)(PF_3)(dppm)$_2$]$^{2+}$ (major product)[27] and the precursor hydride **2** (minor product). The observation of a small amount of the precursor hydride could be due to a part of **2** remaining unchanged under these conditions. These results are summarized in Scheme 2.

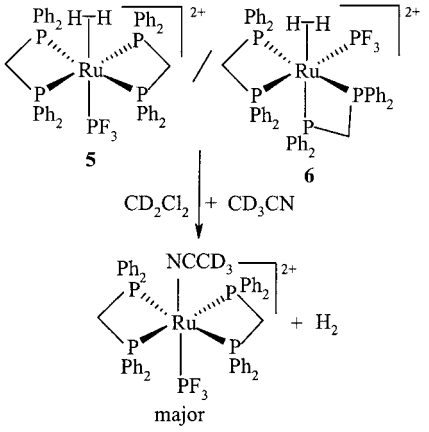

Scheme 2

trans-[Ru(η^2-H_2)(PF_3)(dppm)$_2$]$^{2+}$ (**5**) gives a broad doublet at δ = −1.75 ppm in the ^{1}H NMR spectrum for the bound H_2 ligand coupled to the *trans*-PF_3 ligand ($J_{H_2,P_{trans}}$ = 56.4 Hz). We have observed such strong couplings in the past.[5−7] The ^{31}P{^{1}H} NMR spectrum displays a single signal for all the four dppm phosphorus atoms indicating that they are coplanar. On the other hand, *cis*-[Ru(η^2-H_2)(PF_3)(dppm)$_2$]$^{2+}$ (**6**) shows a broad singlet at δ −4.86 ppm for the bound H_2 ligand in the ^{1}H NMR spectrum and two multiplets for the dppm P atoms in the ^{31}P{^{1}H} NMR spectrum. The NMR spectroscopic data for these derivatives are summarized in Table 3.

Protonation Reaction of *trans*-[Ru(H)(PF_3)(dppe)$_2$][BF_4]

The protonation of **3** was attempted with various protonating agents such as HCl, HBr, HI, CF_3COOH, and HBF_4·Et_2O; once again, the behavior of this hydride was similar to that of **1** and **2**. The dihydrogen complex *trans*-[Ru(η^2-H_2)(PF_3)(dppe)$_2$]$^{2+}$ (**7**) was obtained upon protonation with excess triflic acid. Titration of the hydride complex with triflic acid revealed that it requires 50 equivalents of the acid for the complete conversion of the hydride to the dihydrogen complex. This suggests that the pK_a of **7** must be much less than −5 since the aqueous pK_a of HOTf has been estimated to be about −5.[12]

Basallote and co-workers[28] obtained similar results in the protonation of CpRuHL complexes (L = dppm, dppe, $2PPh_3$) with various acids. They suggested that the lack of formation of the dihydrogen complexes in the presence of a large excess of HCl, HBr, or CF_3COOH was unlikely to be due to kinetic reasons because they observed protonation of certain other metal hydrides with these acids to be usually faster than with HBF_4·Et_2O. The failure of the protonation was related to the thermodynamics of the process. There have been other reports in the literature of the formation of dihydrogen complexes upon protonation of the hydrides with both strong and weak acids.[29,30] The fact that protonation of our hydride complexes failed with all acids except HOTf, and that the complete conversion of the hydrides to the corresponding η^2-H_2 derivatives requires large excesses of the acid (HOTf), indicates that our dihydrogen complexes are extremely strong acids, being roughly similar to HOTf.[31] It is intriguing to note that **7** was found to be stable at room temperature under H_2 atmosphere for about

Table 3. ^{1}H, ^{31}P{^{1}H}, and ^{19}F NMR spectral data (δ) for [M(η^2-H_2)(PF_3)(diphosphane)$_2$]$^{2+}$ complexes in CD_2Cl_2

	Fragment	**5**	**6**	**7**
^{1}H	δ(Ru−H_2)	−1.75 (br. d, 2 H)	−4.86 (br. s, 2 H)	−4.33 (br. d, 2 H)
	$J_{H,P_{trans}}$ (Hz)	56.4		63.0
	δ(CH_2)	4.86 (m, 2 H) 5.08 (m, 2 H)	5.93 (m, 4 H)	2.83 (m, 4 H) 3.00 (m, 4 H)
	δ(Ph)	6.35−7.76 (m, 40 H)	6.35−7.76 (m, 40 H)	6.24−7.82 (m, 40 H)
^{31}P	δ(diphosphane)	−15.6 (d, 4 P)	−13.9 (m, 2 P) −16.2 (m, 2 P)	49.3 (d, 4 P)
	$J_{P,P}$ (Hz)	40.0	45.0	29.2
	δ(PF_3)	134.4 (q quint, 1 P)	130.8 (m, 1 P)	127.4 (q quint, 1 P)
	J(P,F) (Hz)	1261.5	1286.0	1262.5
^{19}F	δ(PF_3)	−16.20 (d)	−20.80 (d)	−5.50 (d)
	δ(OTf)	−90.54 (br)	−91.10 (br)	−91.71 (br)
	δ(BF_4)	−160.14 (br)	−144.25 (br)	−144.77 (br)

 © 2004 Wiley-VCH Verlag GmbH & Co. KGaA, Weinheim

16 h after which time it begins to decompose. We found evidence for some dppeH$^+$ in the ^{31}P NMR spectrum (singlet at δ = 10.0 ppm).[14] We attempted to isolate **7** by precipitation with Et_2O; our attempts, however, failed, and only the starting hydride complex **3** was recovered. In this case, the dihydrogen complex **7** protonates the Et_2O to give Et_2OH^+.

The NMR spectral features of **7** (Table 3) are quite similar to those of **5**; the $J_{H_2,P_{trans}}$ coupling constant of 63.0 Hz is even larger than the values (49−51 Hz) we found earlier in the cases of *trans*-[Ru(η^2-H$_2$)(P)(diphosphane)$_2$]$^{2+}$ complexes [diphosphane = dppe, P = PF(OR)$_2$; diphosphane = dppm, P = P(OR)$_3$, PF(OR)$_2$].[5−7] This stronger coupling could be due to the presence of the more electronegative F substituents in the PF_3 complex, which results in an enormous enhancement of the "s" character of the bonding orbitals in comparison to the PF(OR)$_2$ complexes if it is assumed that the coupling is dominated by the Fermi contact term.[32] No observable H$_2$−F couplings were observed. In an attempt to look for H$_2$−F couplings in the ^{1}H NMR spectrum, we decoupled all the P nuclei and obtained a broad singlet, indicating that the $J_{H_2,F}$ coupling constant is smaller than the line-width of the signal.

Rate Constant for the Decomposition of *trans*-[Ru(η^2-H$_2$)(PF$_3$)(dppe)$_2$]$^{2+}$ (7)

We studied the kinetics of the decomposition of **7** by monitoring the decrease in the integrals of the dihydrogen complex for the η^2-H$_2$ ligand in the ^{1}H NMR spectrum and the dppe phosphorus in the ^{31}P{gated ^{1}H} NMR spectrum. From the kinetics data, the pseudo-first-order rate constant was found to be 4×10^{-5} s^{-1} with a half-life of about 4.45 h. The residual material in the NMR tube after 16 h consisted of dppeH$^+$ (ca. 46%), *trans*-[RuCl(PF$_3$)(dppe)$_2$]$^+$ (**8**; ca. 36%), and *trans*-[Ru(OTf)(PF$_3$)(dppe)$_2$]$^+$ (**9**; <5%) along with certain other unidentifiable Ru^{III} species. The source of the chloride in **8** is the solvent, CD_2Cl_2.

Variable Temperature Spin−Lattice Relaxation Time Measurements.

The variable temperature spin−lattice relaxation times (T_1) for the η^2-H$_2$ moiety were determined; the data are summarized in Table 4. T_1 minima of 10.1, 7.2, and 13.0 ms (at 400 MHz and 273 K) were obtained for **5**, **6**, and **7**, respectively. The H−H distances for the slow- and fast-rotation regimes thus calculated[33] from the T_1 minima are tabulated in Table 5.

HD Isotopomers

In an attempt to prepare the HD isotopomers of **5**, **6**, and **7**, we purged the respective CD_2Cl_2 solutions containing the H_2 complexes with HD gas (generated from NaH and D_2O). Despite purging with HD for a considerable period of time, no observable HD isotopomer was obtained. Therefore, we reacted the starting hydride complexes **2** and **3** with excess F_3CSO_3D in CD_2Cl_2 to obtain the *trans*-[Ru(η^2-HD)(PF$_3$)(dppm)$_2$]$^{2+}$ **5-D$_1$**, *cis*-[Ru(η^2-HD)(PF$_3$)-(dppm)$_2$]$^{2+}$ **6-D$_1$**, and *trans*-[Ru(η^2-HD)(PF$_3$)(dppe)$_2$]$^{2+}$ **7-D$_1$** derivatives, respectively. The ^{1}H NMR spectrum of the hydride region of **5-D$_1$** and **7-D$_1$** is expected to show a doublet of 1:1:1 triplets pattern: the doublet due to the coupling of H with the *trans* phosphorus, and 1:1:1 triplet from the coupling of the proton with deuterium. Figure 2a displays this pattern in the case of **7-D$_1$**. An overlap of the signals is the cause of the poor resolution of the six lines. Upon decoupling the phosphorus atoms, the ^{1}H NMR spectrum shows an approximate 1:1:1 triplet pattern due to

Table 4. Variable-temperature spin−lattice relaxation times (T_1, ms; 400 MHz) of the dihydrogen ligand in [M(η^2-H$_2$)(PF$_3$)-(diphosphane)$_2$]$^{2+}$ complexes in CD_2Cl_2[a]

T (K)	T_1(**5**)	T_1(**6**)	T_1(**7**)
298			18.0
284			17.3
283	12.3	8.7	
273	*10.1*	*7.2*	*13.0*
263	10.8	7.5	
258			15.9
243	11.5	8.7	20.2
233	13.0	8.7	
228			28.9
223	14.4	10.8	
200	18.7	14.4	

[a] Italicized data indicate T_1 minima.

Table 5. d_{HH} values from T_1 (min) (400 MHz) for [M(η^2-H$_2$)(PF$_3$)(diphosphane)$_2$]$^{2+}$ complexes in CD_2Cl_2

	T_1 min	d_{HH} (slow) Å	d_{HH} (fast) Å
5	10.1	0.99	0.79
6	7.2	0.94	0.79
7	13.0	1.03	0.81

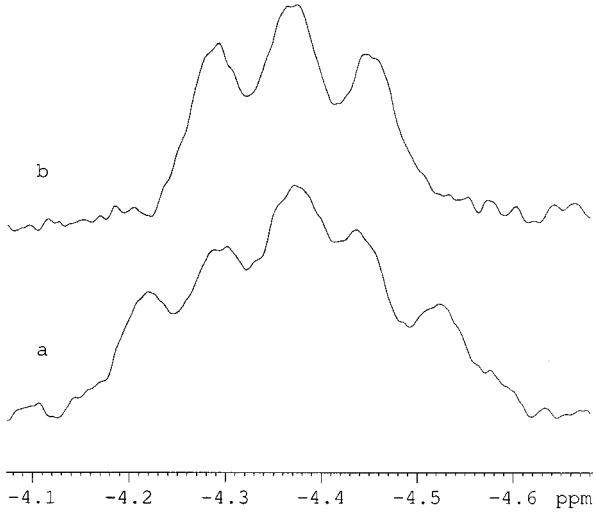

Figure 2. (a) ^{1}H NMR spectrum of *trans*-[Ru(η^2-HD)(PF$_3$)(dppe)$_2$]$^{2+}$ (**7-D$_1$**); (b) ^{1}H{^{31}P} NMR spectrum of *trans*-[Ru(η^2-HD)(PF$_3$)(dppe)$_2$]$^{2+}$ (**7-D$_1$**)

 © 2004 Wiley-VCH Verlag GmbH & Co. KGaA, Weinheim

H−D coupling (Figure 2b). The complex **6-D$_1$** exhibits only a 1:1:1 triplet pattern due to the presence of a *trans* phosphane that is not as strong an acceptor as PF_3. The $J_{H,D}$ coupling constants were found to be 27.0, 28.0, and 30.0 Hz at 273 K for **5-D$_1$**, **6-D$_1$**, and **7-D$_1$**, respectively. The H−H distances calculated from the H−D coupling constant[34,35] are 0.97, 0.96, and 0.92 Å for **5-D$_1$**, **6-D$_1$**, and **7-D$_1$**, respectively. In addition, we carried out variable temperature $J_{H,D}$ measurements for **7-D$_1$**; the data are summarized in Table 6 and show an interesting temperature dependence.

Table 6. Temperature dependence of $J_{H,D}$ for *trans*-[Ru(η^2-H_2)(PF_3)(dppe)$_2$]$^{2+}$ in CD_2Cl_2

T (K)	$J_{H,D}$	d_{HH} (Å)
298	29.8	0.922
273	30.0	0.919
258	30.4	0.912
243	31.0	0.902
228	31.4	0.895
213	32.0	0.885

There have been a few reports on the unusual temperature dependence of $J_{H,D}$ coupling in the case of elongated dihydrogen complexes, for example [RuCp*(H···D)(dppm)]$^+$,[36] *trans*-[Os(H)(H···D)(dppe)$_2$]$^+$,[37] *trans*-[Os(Cl)(H···D)(dppe)$_2$]$^+$,[36] and [RuCp/Cp*(H···D/T)(PP)]$^+$.[38] Based on the theoretical studies by Gelabert et al.,[39] it was interpreted that the varying thermal population of the vibrational excited states of the M-H_2 unit results in the unusual temperature dependence of $J_{H,D}$ of the elongated dihydrogen complexes. The data presented in Table 6 show that the variations in $J_{H,D}$ with temperature are small and close to the error in the determination of the H−D coupling constant.

H−H Distances and the Stabilities of the Dihydrogen Complexes

The H−H distances obtained from the T_1(min) data fall in the range 1.03−0.75 Å (see Table 5) for the slow- and the fast-rotation regimes. A correlation between the H−H distances calculated from $J_{H,D}$ and T_1(min) and $\Delta G^{\ddagger}$ for the loss of the H_2 ligand from the metal center has been reported by Gusev et al.[40] The d_{HH} values calculated from $J_{H,D}$ in the current work are of the order of 0.92−0.97 Å (273 K) which are intermediate between the values of 1.03 and 0.75 Å obtained using the slow- and the fast-spinning approximations of H_2. Morris and Wittebort[33] have suggested that H−H distances obtained from $J_{H,D}$ that are intermediate between those derived from the T_1(min) data indicate that librational motion significantly influences the H_2 relaxation process. In addition to these complexes, several examples have been reported earlier where such a situation has been observed.[33]

The effect of the ligand *trans* to H_2 on the properties of the dihydrogen complex, for example d_{HH} and stability, can be interpreted in terms of the σ donation (η^2-H_2 → empty metal d orbital) and the back-donation (filled metal d orbital → σ* orbital of η^2-H_2) components. Woska et al.[41] have determined the stereoelectronic parameters of a series of phosphorus ligands and concluded that PF_3 is the weakest σ donor and the strongest π acid. Thus, the *trans*-PF_3 ligand exerts a high *trans* influence due to its strong π-acidity; in addition, it is also expected to stabilize the metal d orbitals resulting in reduced overlap with the antibonding orbitals of the H_2. Consequently, a strengthening of the H−H bond and a weakening of the M−H_2 interaction occurs giving rise to dihydrogen complexes with short d_{HH} values. The dihydrogen complexes **5**, **6**, and **7** show H−H distances of 0.97, 0.96, and 0.92 Å, respectively, at 273 K. These distances, rather surprisingly, are not appreciably short. We have also measured the $J_{H,D}$ coupling constant of **7-d$_1$** at various temperatures and obtained a d_{HH} of 0.88 Å at 213 K. This distance is similar to the H−H distance found in the case of *trans*-[Ru(η^2-H_2)(CO)(dppp)$_2$]$^{2+}$ (0.85 Å) reported by Rocchini et al.[12] and *trans*-[Ru(η^2-H_2)(CNH)(dppm)$_2$]$^{2+}$ (0.88 Å) reported by Morris and coworkers.[13] Both of these compounds are unstable with respect to the loss of H_2. Since **7** loses H_2 as noted earlier, we attempted to determine the equilibrium constant for the substitution of the bound H_2 with CH_3CN as this could provide insight into the relative M−H_2 bond strength for the complexes prepared in this study. However, we found that CH_3CN substitutes H_2 completely even under stoichiometric conditions (1:1 molar ratio, complex:CH_3CN) thus precluding the measurement of the equilibrium constant. We earlier found that the H_2 ligand in complexes of the type *trans*-[Ru(η^2-H_2)[P(OR)$_3$](dppm)$_2$]$^{2+}$ and *cis*-[Ru(η^2-H_2)[PF(OR)$_2$](dppm)$_2$]$^{2+}$ is labile; however, upon loss of the H_2 ligand (typically loss of H_2 starts to occur after 24−36 h), the dihydrogen complex could be recovered by purging the solutions containing the five-coordinate species with H_2 gas.[7] Considering the greater π-acidity of the PF_3 ligand in comparison to P(OR)$_3$ or PF(OR)$_2$, it is not surprising to find that **7** is stable only for about 16 h before it starts to decompose. Thus, the π-acidities of the CO, CNH, and PF_3 ligands account for the trend in the stability of the M−H_2 bond for the above three complexes, which increases in the order CO ≤ CNH < PF_3. We found that the protonation of **1** with HOTf resulted in extensive broadening of the ^{1}H NMR signals due to the presence of Fe^{III} species that are generated quite rapidly from a highly unstable iron dihydrogen complex. We believe that the origin of the Fe^{III} species is a dihydrogen complex since, upon its (Fe^{III} species) generation, a singlet at δ = 4.6 ppm was observed, indicating the evolution of H_2. This observation further supports the earlier suggestion that the M−H_2 interaction becomes stronger on going down the group, as has been found earlier.[12,42] We speculate that a compound of formula *trans*-[Os(η^2-H_2)(PF_3)(diphosphane)$_2$]$^{2+}$, if realized, could be isolable. Efforts toward this goal are in progress in our laboratories.

 © 2004 Wiley-VCH Verlag GmbH & Co. KGaA, Weinheim

Conclusion

The complexes *trans*-[Ru(η^2-H_2)(PF_3)(dppm)$_2$]$^{2+}$ (**5**), *cis*-[Ru(η^2-H_2)(PF_3)(dppm)$_2$]$^{2+}$ (**6**), and *trans*-[Ru(η^2-H_2)(PF_3)(dppe)$_2$]$^{2+}$ (**7**) are formulated as dihydrogen complexes based on their short T_1 values and the observation of substantial H−D coupling in the corresponding HD isotopomers. *trans*-[Ru(η^2-HD)(PF_3)(dppe)$_2$]$^{2+}$ shows a temperature-dependent $J_{H,D}$ coupling, although this effect is only small. All of these derivatives, including *trans*-[Fe(η^2-H_2)(PF_3)(dppe)$_2$]$^{2+}$ (**4**), are unstable at room temperature. The dihydrogen complexes are formed only upon addition of excess HOTf to the precursor hydrides and they protonate Et_2O in solution, indicating the high acidities of these derivatives.

Experimental Section

General Remarks: All reactions were carried out under N_2 at room temperature using standard Schlenk[43,44] and inert atmosphere techniques unless otherwise noted. Solvents used for the preparation of dihydrogen complexes were thoroughly saturated with either H_2 or Ar just before use. The ^{1}H, ^{31}P, and ^{19}F NMR spectroscopic data were obtained using AMX Bruker 400 MHz or Avance Bruker 400 MHz instruments. The shift of the residual protons of the deuterated solvent was used as an internal reference. Variable-temperature proton T_1 measurements were carried out at 400 MHz using the inversion recovery method (180°-τ-90° pulse sequence at each temperature)[45] and the data are summarized in Table 4; the d_{HH} values obtained from the T_1 minima are given in Table 5. All ^{31}P NMR spectra were proton decoupled, unless otherwise specified. ^{31}P NMR chemical shifts were measured relative to 85% H_3PO_4 (as an aqueous solution, external reference) in CD_2Cl_2. ^{19}F NMR spectra were recorded with respect to $CFCl_3$ (external reference) in CD_2Cl_2. Satisfactory elemental analysis data for the samples could not be obtained because of the formation of non-combustible metal fluorides during combustion. The mass spectral studies of the compounds were carried out using a Micromass Q-TOF instrument. 1,2-Bis(diphenylphosphanyl)ethane[46] (dppe), bis(diphenylphosphanyl)methane[47] (dppm), *trans*-[Fe(H)(η^2-H_2)(dppe)$_2$][BF_4], *trans*-[Ru(H)(η^2-H_2)(dppe)$_2$][BF_4],[48] *trans*-[Ru(H)(η^2-H_2)(dppm)$_2$][BF_4],[7] and PF_3 [49] were prepared according to literature procedures.

Preparation of *trans*-[Fe(H)(PF_3)(dppe)$_2$][BF_4] (1): *trans*-[Fe(H)(η^2-H_2)(dppe)$_2$][BF_4] (0.100 g, 0.1 mmol) was dissolved in CH_2Cl_2 (8 mL) under an atmosphere of H_2. PF_3 gas was then purged through this solution at a steady rate for about 10 min after which time it was stirred for 2 h. Concentration of the reaction mixture to about 2 mL and addition of Et_2O (20 mL) caused the complete precipitation of a cream-colored product of **1**. The product was dried in vacuo and recrystallized from a CH_2Cl_2 solution by slow diffusion of Et_2O over a period of several days. Yield 0.082 g (75%). ES-MS: m/z = 941 [$M^+ - BF_4$], 853 [$M^+ - PF_3 + BF_4$]. The NMR spectroscopic data of **1** are summarized in Table 1.

Preparation of *trans*-[Ru(H)(PF_3)(diphosphane)$_2$][BF_4] (diphosphane = dppm 2, dppe 3): These compounds were prepared in a similar manner to that of **1** starting from *trans*-[Ru(H)(η^2-H_2)(diphosphane)$_2$][BF_4]. Yields of **2** and **3** were 0.075 g (69%) and 0.080 g (73%), respectively. ES-MS of **2**: m/z = 871 [$M^+ - PF_3 + BF_4$]. ES-MS of **3**: m/z = 897 [$M^+ - PF_3 + HBF_4$]. The NMR spectroscopic data of **2** and **3** are given in Table 1.

Attempt to Prepare *trans*-[Fe(η^2-H_2)(PF_3)(dppe)$_2$]$^{2+}$ (4): A sample of *trans*-[Fe(H)(PF_3)(dppe)$_2$][BF_4] (15 mg) was placed in a 5 mm NMR tube capped with a septum. The tube was then evacuated and filled with H_2 in three cycles. The hydride complex was then dissolved in 0.6 mL of CD_2Cl_2 and the solution was frozen in a liquid-nitrogen bath. About 20 μL (16 equiv.) of triflic acid (HOTf) was added and the tube was warmed up to 273 K slowly. It was then transferred to the NMR probe precooled to 273 K. ^{1}H NMR spectroscopy revealed a decrease in the intensity of the hydride resonances, whereas the ^{31}P{^{1}H} NMR spectrum showed the appearance of an intense signal at δ = 10.0 ppm due to dppeH$^+$. At the same time, the lock signal deteriorated, signaling the formation of some Fe^{III} species. No evidence of the formation of a dihydrogen complex was apparent, although the singlet at δ = 4.6 ppm due to free H_2 increased in intensity. Upon addition of a further 10 μL (8 equiv.) of HOTf, the lock signal deteriorated further and all the ^{1}H NMR signals broadened. The intensity of the dppeH$^+$ in the ^{31}P NMR spectrum increased significantly.

Preparation of *trans*- and *cis*-[Ru(η^2-H_2)(PF_3)(dppm)$_2$]$^{2+}$ (5 and 6): The preparation of these two complexes was carried out as described above. Upon addition of 30 μL (60 equiv.) of HOTf the tube was warmed up to 273 K and then transferred to the NMR probe precooled to 273 K. The dihydrogen complexes formed were observed by NMR spectroscopy. The NMR spectroscopic data of **5** and **6** are summarized in Table 3.

Preparation of *trans*-[Ru(η^2-H_2)(PF_3)(dppe)$_2$]$^{2+}$ (7): The dihydrogen complex **7** was prepared as described above starting from *trans*-[Ru(H)(PF_3)(dppe)$_2$][BF_4], except that the protonation was carried out at room temperature and a large excess of HOTf (100 μL, 80 equiv.) was used. The resulting solution was analyzed by NMR spectroscopy. The NMR spectroscopic data of **7** are summarized in Table 3.

Attempted Protonation of *trans*-[Ru(H)(PF_3)(dppe)$_2$][BF_4] with HCl/HBr/HI/CF_3CO_2H: The protonation of *trans*-[Ru(H)(PF_3)(dppe)$_2$][BF_4] was attempted with various other acids such as HCl, HBr, HI, and CF_3CO_2H in addition to HOTf as described above. The corresponding dihydrogen complex *trans*-[Ru(η^2-H_2)(PF_3)(dppe)$_2$]$^{2+}$ (**7**) was obtained only in the case of HOTf, whereas only the starting hydride was recovered with the other acids. The addition of a large excess of acid (HCl, HBr, HI, and CF_3CO_2H) also did not afford the corresponding dihydrogen complex.

Attempt to Isolate *trans*-[Ru(η^2-H_2)(PF_3)(dppe)$_2$]$^{2+}$ (7): The dihydrogen complex **7** was prepared as described above. NMR spectroscopy revealed the complete conversion of the starting hydride into the dihydrogen complex. In an attempt to isolate it, excess Et_2O was added to the reaction mixture to precipitate the colorless dihydrogen complex. The supernatant solution was carefully removed with a syringe and the precipitate was washed a few times with Et_2O and then dried under a stream of H_2 gas. The NMR spectrum revealed the presence of only the starting hydride complex *trans*-[Ru(H)(PF_3)(dppe)$_2$][BF_4] and no other species, suggesting that complete deprotonation had taken place upon addition of Et_2O. The dihydrogen complex was found to be stable with respect to deprotonation only in the presence of a large excess of acid.

Measurement of the Rate Constant for the Decomposition of *trans*-[Ru(η^2-H_2)(PF_3)(dppe)$_2$]$^{2+}$ (7): A sample of *trans*-[Ru(H)(PF_3)(dppe)$_2$][BF_4] (6 mg) was placed in a 5 mm NMR tube

 © 2004 Wiley-VCH Verlag GmbH & Co. KGaA, Weinheim

capped with a septum. The tube was evacuated and filled with dihydrogen gas in three cycles. The hydride complex was then dissolved in CD_2Cl_2 (0.6 mL). Excess HOTf (15 μL, 30 equiv.) was added and the tube was transferred immediately to the NMR probe. The ^1H and the $^{31}P\{gated\ ^1H\}$ NMR spectra were recorded at intervals of 30 min. The rate constant for the decomposition of *trans*-$[Ru(\eta^2\text{-}H_2)(PF_3)(dppe)_2]^{2+}$ was determined from the integrals of the η^2-H_2 signal with respect to the residual $CDHCl_2$ resonance (δ = 5.32 ppm) in the ^1H NMR spectra and those of the dppe P signal with respect to externally added $[Ph_3PH][OTf]$ (δ = 7.11 ppm) in the $^{31}P\{gated\ ^1H\}$ NMR spectra. After about 16 h, the NMR spectra showed the formation of $dppeH^+$ (ca. 40%), *trans*-$[Ru(Cl)(PF_3)(dppe)_2]^+$ (**8**; ca. 36%), and *trans*-$[Ru(OTf)(PF_3)(dppe)_2]^+$ (**9**; <5%).

8: ^1H NMR (CD_2Cl_2): δ = 3.01 (m, 4 H, $Ph_2PCH_2CH_2PPh_2$), 6.81−7.91 (m, 40 H, $PhPCH_2CH_2PPh_2$) ppm. ^{19}F NMR (CD_2Cl_2): δ = −18.57 (d, PF_3) ppm. $^{31}P\{^1H\}$ NMR (CD_2Cl_2): δ = 64.3 (d, $J_{P,P}$ = 41.0 Hz, $Ph_2PCH_2CH_2PPh_2$), 127.9 (q quint, $J_{P,F}$ = 1308.0 Hz, PF_3) ppm.

9: ^1H NMR (CD_2Cl_2): δ = 2.94 (m, 2 H, $Ph_2PCH_2CH_2PPh_2$), 3.13 (m, 2 H, $Ph_2PCH_2CH_2PPh_2$), 6.81−7.91 (m, 40 H, $PhPCH_2CH_2PPh_2$) ppm. ^{19}F NMR (CD_2Cl_2): δ = −21.81 (d, PF_3), −75.70 (br. s, OTf − coordinated) ppm. $^{31}P\{^1H\}$ NMR (CD_2Cl_2): δ = 46.6 (d, $J_{P,P}$ = 41.3 Hz, $Ph_2PCH_2CH_2PPh_2$), 132.1 (q quint, $J_{P,F}$ = 1312.0 Hz, PF_3) ppm.

Attempt to Determine the Equilibrium Constant for the Substitution of η^2-H_2 with CH_3CN in *trans*-$[Ru(\eta^2\text{-}H_2)(PF_3)(dppe)_2]^{2+}$: The dihydrogen complex *trans*-$[Ru(\eta^2\text{-}H_2)(PF_3)(dppe)_2]^{2+}$ was prepared starting from *trans*-$[Ru(H)(PF_3)(dppe)_2][BF_4]$ (20 mg) and HOTf (50 μL, 30 equiv.) as described above. After ensuring that the starting hydride complex had been completely converted into the dihydrogen complex, the solution was frozen in a liquid-nitrogen bath. Then, CH_3CN (1 μL, 1 equiv.) was added and the NMR tube was slowly warmed up to 253 K. It was then transferred to the NMR probe precooled to 253 K. NMR spectroscopy revealed the complete disappearance of the resonances due to the dihydrogen complex and the appearance of signals due to the nitrile complex *trans*-$[Ru(CH_3CN)(PF_3)(dppe)_2]^{2+}$ (**10**) thus precluding the measurement of the equilibrium constant for the substitution of the coordinated H_2 ligand with CH_3CN.

10: ^1H NMR (CD_2Cl_2): δ = 1.45 (s, 3 H, CH_3CN), 3.05 (m, 4 H, $Ph_2PCH_2CH_2PPh_2$), 6.91−7.91 (m, 40 H, $PhPCH_2CH_2PPh_2$) ppm. ^{19}F NMR (CD_2Cl_2): δ = −13.51 (d, PF_3), −91.03 (br. s, OTf), −144.62 (br. s, BF_4) ppm. $^{31}P\{^1H\}$ NMR (CD_2Cl_2): δ = 38.2 (d, $J_{P,P}$ = 42.5 Hz, $Ph_2PCH_2CH_2PPh_2$), 132.8 (q quint, $J_{P,F}$ = 1258.0 Hz, PF_3) ppm.

Observation of the HD Isotopomers, *trans*-$[Ru(\eta^2\text{-}HD)(PF_3)(dppm)_2]^{2+}$ (5-D_1), *cis*-$[Ru(\eta^2\text{-}HD)(PF_3)(dppm)_2]^{2+}$ (6-D_1), and *trans*-$[Ru(\eta^2\text{-}HD)(PF_3)(dppe)_2]^{2+}$ (7-D_1): The HD isotopomers were prepared using similar procedures as the corresponding H_2 complexes except that appropriate quantities of DOTf were used. The HD isotopomers formed were observed by NMR spectroscopy. The temperature dependent $J_{H,D}$ data for *trans*-$[Ru(\eta^2\text{-}H_2)(PF_3)(dppe)_2]^{2+}$ are summarized in Table 6.

X-ray Crystallographic Study: Colorless crystals were obtained by slow diffusion of Et_2O into a CH_2Cl_2 solution of *trans*-$[Ru(H)(PF_3)(dppm)_2][BF_4]$ (**2**) in an H-tube at room temperature. The unit-cell parameters and intensity data were collected on a Bruker SMART APEX CCD diffractometer equipped with a fine-focus Mo-K_α X-ray source. The SMART software was used for data acquisition and the SAINT software for data abstraction.[50] Absorption corrections were made using the psi-scans method.[51] The structure was solved and refined using the SHELX program suite.[52] The Ru atom position was located from the Patterson map and the non-hydrogen atoms were located from successive difference-Fourier maps and were refined anisotropically. All other hydrogen atoms were fixed in idealized positions and refined in a riding model. Additional details of data collection and structure refinements are listed in Table 7.

Table 7. Crystallographic data for *trans*-$[Ru(H)(PF_3)(dppm)_2][BF_4]$ (**2**)

Formula	$C_{50}H_{48}BF_7O_2P_5Ru$
Mol. wt.	1080.61
Crystal system	orthorhombic
Space group	$P2_12_12_1$
a (Å)	11.845(5)
b (Å)	16.252(6)
c (Å)	27.617(10)
α (°)	90.00
β (°)	90.00
γ (°)	90.00
V (Å^3)	5316(3)
Z	4
D_{calcd} (g/cm^3)	1.350
T (K)	293(2)
λ (Å)	0.71073
μ (mm^{-1})	0.506
R[a]	0.0607
R_w[b]	0.1726

[a] $R = (F_o - F_c)/F_o$. [b] $Rw = [w(F_o - F_c)^2/wF_o^2]^{1/2}$ [based on reflections with $I > 2\sigma(I)$].

CCDC-231476 contains the supplementary crystallographic data for this paper. These data can be obtained free of charge at www.ccdc.cam.ac.uk/conts/retrieving.html [or from the Cambridge Crystallographic Data Centre, 12 Union Road, Cambridge CB2 1EZ, UK; Fax: +44-1223-336033; E-mail: deposit@ccdc.cam.ac.uk].

Acknowledgments

Financial support from the Council of Scientific and Industrial Research, India, is gratefully acknowledged. Acquisition of a 400 MHz NMR spectrometer was supported by the Department of Science and Technology, India, under the "FIST" program.

[1] P. G. Jessop, R. H. Morris, *Coord. Chem. Rev.* **1992**, *121*, 155−284.
[2] D. M. Heinekey, W. J. Oldham Jr., *Chem. Rev.* **1993**, *93*, 913−926.
[3] P. G. Jessop, R. H. Morris, *Inorg. Chem.* **1993**, *32*, 2236−2237.
[4] M. Schlaf, R. H. Morris, *J. Chem. Soc., Chem. Commun.* **1995**, 625−626.
[5] N. Mathew, B. R. Jagirdar, R. S. Gopalan, G. U. Kulkarni, *Organometallics* **2000**, *19*, 4506−4517.
[6] N. Mathew, B. R. Jagirdar, *Inorg. Chem.* **2000**, *39*, 5404−5406.
[7] N. Mathew, B. R. Jagirdar, A. Ranganathan, *Inorg. Chem.* **2003**, *42*, 187−197.
[8] K. K. Majumdar, H. V. Nanishankar, B. R. Jagirdar, *Eur. J. Inorg. Chem.* **2001**, 1847−1853.
[9] M. S. Chinn, D. M. Heinekey, N. G. Payne, C. D. Sofield, *Organometallics* **1989**, *8*, 1824−1826.
[10] M. S. Keady, J. D. Koola, A. C. Ontko, R. K. Merwin, D. M. Roddick, *Organometallics* **1992**, *11*, 3417−3421.

 © 2004 Wiley-VCH Verlag GmbH & Co. KGaA, Weinheim

[11] M. Schlaf, A. J. Lough, P. A. Maltby, R. H. Morris, *Organometallics* **1996**, *15*, 2270−2278.
[12] E. Rocchini, A. Mezzetti, H. Rüegger, U. Burckhardt, V. Gramlich, A. Del Zotto, P. Martinuzzi, P. Rigo, *Inorg. Chem.* **1997**, *36*, 711−720.
[13] T. P. Fong, C. E. Forde, A. J. Lough, R. H. Morris, P. Rigo, E. Rocchini, T. Stephan, *J. Chem. Soc., Dalton Trans.* **1999**, 4475−4486.
[14] S. E. Landau, R. H. Morris, A. J. Lough, *Inorg. Chem.* **1999**, *38*, 6060−6068.
[15] R. M. Chin, J. Barrera, R. H. Dubois, L. E. Helberg, M. Sabat, T. Y. Bartucz, A. J. Lough, R. H. Morris, W. D. Harman, *Inorg. Chem.* **1997**, *36*, 3553−3558.
[16] The *mer* isomer of this complex was obtained in very small concentrations thus precluding its thorough characterization: R. H. Morris, *personal communication*.
[17] R. Mathieu, R. Poilblanc, *Inorg. Chem.* **1972**, *11*, 1858−1861.
[18] P. Meakin, E. L. Muetterties, J. P. Jesson, *J. Am. Chem. Soc.* **1972**, *94*, 5271−5285.
[19] J. F. Nixon, *Adv. Inorg. Chem. Radiochem.* **1970**, *13*, 363−469.
[20] V. F. Bystrov, A. A. Neimysheva, A. U. Stepanyants, I. L. Knunyants, *Dokl. Akad. Nauk. SSSR* **1964**, *156*, 637−640; *Chem. Abstr.* **1964**, *61*, 6548c.
[21] Cone angles: 107° $[P(OMe)_3]$ > 106° $[PF(OMe)_2]$ > 104° (PF_3).[22]
[22] C. A. Tolman, *Chem. Rev.* **1977**, *77*, 313−348.
[23] T. Fujinaga, I. Sakamoto, *J. Electroanal. Chem.* **1977**, *85*, 185−201.
[24] G. Perdoncin, G. Scorrano, *J. Am. Chem. Soc.* **1977**, *99*, 6983−6986.
[25] S. J. Berners-Price, R. E. Norman, P. J. Sadler, *J. Inorg. Biochem.* **1987**, *31*, 197−209.
[26] M. K. Rottink, R. J. Angelici, *Inorg. Chem.* **1993**, *32*, 2421−2425.
[27] Characterization of *trans*-$[Ru(NCCD_3)(PF_3)(dppm)_2]^{2+}$. ^1H NMR (CD_2Cl_2): δ = 4.91 (m, 2 H, $Ph_2PCH_2PPh_2$), 5.08 (m, 2 H, $Ph_2PCH_2PPh_2$), 6.48−7.81 (m, 40 H, $Ph_2PCH_2PPh_2$) ppm. ^{31}P NMR (CD_2Cl_2): δ = −13.9 (d, $J_{P,P}$ = 34.4 Hz, 4 P, $Ph_2PCH_2PPh_2$), 135.1 (q quint, $J_{P,F}$ = 1303.0 Hz, 1 P, PF_3).
[28] M. G. Basallote, J. Durán, J. Fernández-Trujillo, M. A. Máñez, *Organometallics* **2000**, *19*, 695−698.
[29] G. Jia, R. H. Morris, *J. Am. Chem. Soc.* **1991**, *113*, 875−883.
[30] G. Jia, R. H. Morris, *Inorg. Chem.* **1990**, *29*, 581−582.
[31] R. M. Bullock, J.-S. Song, D. J. Szalda, *Organometallics* **1996**, *15*, 2504−2516.
[32] S. Berger, S. Braun, H. -O. Kalinowski, *NMR Spectroscopy of the Non-Metallic Elements*, Wiley, Chichester, **1996**, pp. 895−981.
[33] R. H. Morris, R. Wittebort, *J. Magn. Reson.* **1997**, *35*, 243−250 and references cited therein.
[34] P. A. Maltby, M. Schlaf, M. Steinbeck, A. J. Lough, R. H. Morris, W. T. Klooster, T. F. Koetzle, R. C. Srivastava, *J. Am. Chem. Soc.* **1996**, *118*, 5396−5407.
[35] $d_{HH} = -0.0167J_{H,D} + 1.42$.
[36] W. T. Klooster, T. F. Koetzle, G. Jia, T. P. Fong, R. H. Morris, A. Albinati, *J. Am. Chem. Soc.* **1994**, *116*, 7677−7681.
[37] K. A. Earl, G. Jia, P. A. Maltby, R. H. Morris, *J. Am. Chem. Soc.* **1991**, *113*, 3027−3039.
[38] J. K. Law, H. Mellows, D. M. Heinekey, *J. Am. Chem. Soc.* **2002**, *124*, 1024−1030.
[39] R. Gelabert, M. Moreno, J. M. Lluch, A. Lledós, *J. Am. Chem. Soc.* **1997**, *119*, 9840−9847.
[40] D. G. Gusev, R. L. Kuhlman, K. B. Renkema, O. Eisenstein, K. G. Caulton, *Inorg. Chem.* **1996**, *35*, 6775−6783.
[41] D. Woska, A. Prock, W. P. Giering, *Organometallics* **2000**, *19*, 4629−4638.
[42] E. P. Cappellani, S. D. Drouin, G. Jia, P. A. Maltby, R. H. Morris, C. T. Schweitzer, *J. Am. Chem. Soc.* **1994**, *116*, 3375−3388.
[43] D. F. Shriver, M. A. Drezdon, *The Manipulation of Air-Sensitive Compounds*, 2nd ed., Wiley, New York, **1986**.
[44] S. Herzog, J. Dehnert, K. Luhder, in *Techniques of Inorganic Chemistry* (Ed.: H. B. Johnassen), Interscience, New York, **1969**, vol. VII.
[45] D. G. Hamilton, R. H. Crabtree, *J. Am. Chem. Soc.* **1988**, *110*, 4126−4133.
[46] J. Chatt, F. A. Hart, *J. Chem. Soc.* **1960**, 1378−1389.
[47] W. Hewertson, H. R. Watson, *J. Chem. Soc.* **1962**, 1490−1494.
[48] M. T. Bautista, E. P. Cappellani, S. D. Drouin, R. H. Morris, C. T. Schweitzer, A. Sella, J. Zubkowski, *J. Am. Chem. Soc.* **1991**, *113*, 4876−4887.
[49] R. J. Clark, H. Belefant, S. M. Williamson, *Inorg. Synth.* **1990**, *28*, 310.
[50] Bruker SMART and SAINT Versions 6.22a, BRUKER AXS Madison, Wisconsin, USA, **1999**.
[51] A. C. T. North, D. C. Phillips, F. S. Mathews, *Acta Crystallogr., Sect. A* **1968**, *24*, 351−359.
[52] G. M. Sheldrick, SHELXL-97 Program for the solution of crystal structures, University of Göttingen, Germany.

Received February 17, 2004
Early View Article
Published Online May 25, 2004

 © 2004 Wiley-VCH Verlag GmbH & Co. KGaA, Weinheim

Synthesis and Polymerization Performance of Pd^{II} Complexes of New 2-Hydroxyethyl-Substituted Diphosphane Ligands

Uwe W. Meier,[a] Ulf Thewalt,[b] Tony Debaerdemaeker,[b] and Bernhard Rieger*[a]

Keywords: Homogeneous catalysis / Palladium / Phosphane ligand / Polyketone / Polymerization

We have synthesized a new diphosphane ligand, 1,3-bis[(2-hydroxyethyl)(phenyl)phosphanyl]propane (**2***) (*****: mixture of *meso*- and racemic diastereoisomers), and its corresponding neutral dichloro palladium(II) (**3***), diiodo palladium(II) (**4***), and dicationic diacetonitrile palladium(II) ditetrafluoroborate (**5***) complexes. Separation of the **4** ***rac*** and **4** ***meso*** diastereoisomers was achieved by column chromatography and subsequent crystallization. Assignments of the particular complex geometries of **3** ***meso*** and **4** ***rac*** were facilitated by single-crystal X-ray diffraction analysis. After activation with MAO, complex **3*** exhibits superior activity in the homopolymerization of 2-norbornene relative to that of the dichloro Pd^{II} derivative of 1,3-bis(diphenylphosphanyl)propane (dppp). Compound **5*** and the dppp-analogue possess similar catalytic potentials in ethylene/CO copolymerization experiments. Applying complex **5*** to propylene/CO copolymerization leads to highly regio- and predominantly stereoregular polyketone materials.
(© Wiley-VCH Verlag GmbH & Co. KGaA, 69451 Weinheim, Germany, 2004)

Introduction

Bridged bisphosphane ligands play an important role in homogeneous catalysis. The variety of tools available for tailoring their structures makes these ligands ideal platforms upon which to design selective, molecularly defined catalysts for small-molecule transformations and for polymerization reactions.[1] Until now, the functionalities that have been attached, such as oxygen-containing or fluorinated substituents, have been used primarily to impart particular steric and electronic properties to the ligands, as well as solubility properties of the complexes.[2] A novel approach for further developments is the introduction of suitable functional groups that help to open up selective reaction channels by reversible interactions with either the metal center, the incoming substrate, or the growing polymer chain. In this paper we report the synthesis and structural characterization of Pd^{II} complexes of a new bisphosphane ligand, which bears (2-hydroxyethyl)(phenyl)phosphane units (Scheme 1). We have performed 2-norbornene homopolymerizations, as well as ethylene/CO and propylene/CO copolymerization experiments, to investigate the catalytic potential of these novel complex structures.

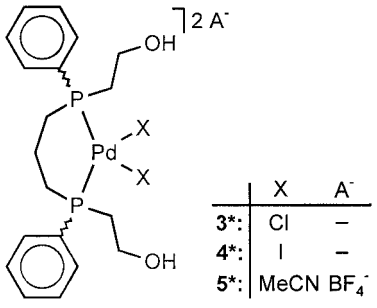

	X	A⁻
3*:	Cl	–
4*:	I	–
5*:	MeCN	BF_4^-

Scheme 1. Novel hydroxy-functionalized bisphosphane Pd^{II} complexes

Results and Discussion

Ligand and Complex Synthesis

Nucleophilic attack of the dilithium diphosphide, which is accessible from 1,3-bis(phenylphosphanyl)propane (**1**) by deprotonation with 2 equiv. of *n*BuLi, on ethylene oxide[3] gave, after aqueous workup, the desired bisphosphane **2*** (Scheme 2). We obtained the ligand as a mixture of the racemic (*R*,*R*;*S*,*S*) and *meso* (*R*,*S*) components in a 1:1.3 ratio (^{31}P NMR: $\delta_{rac} = -32.50$, $\delta_{meso} = -32.64$ ppm).

Complexation of **2*** with $(COD)PdCl_2$ in CH_2Cl_2 gave the corresponding neutral dichloro palladium(II) complex (**3***) in the expected ratio of diastereoisomers (1:1.3, Scheme 3). Extraction of the mixture **3*** with DMSO and subsequent crystallization from DMSO/CH_2Cl_2 gave pure **3** ***meso***. Replacement of the chloro ligands in **3*** by treat-

[a] Department of Inorganic Chemistry II, Materials and Catalysis, University of Ulm,
Albert-Einstein-Allee 11, 89069 Ulm, Germany
Fax: (internat.) + 49-(0)731-502-3039
E-mail: bernhard.rieger@chemie.uni-ulm.de
[b] Sektion Röntgen- und Elektronenbeugung, University of Ulm, Albert-Einstein-Allee 11, 89069 Ulm, Germany

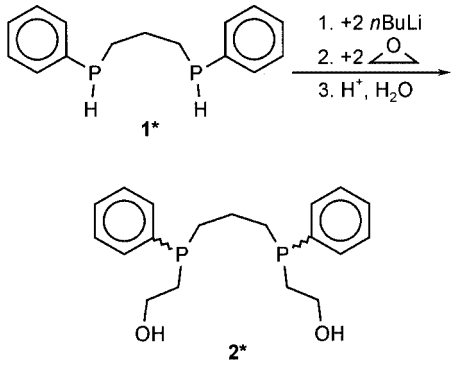

Scheme 2. Synthesis of 2-hydroxyethyl-substituted bisphosphane **2***

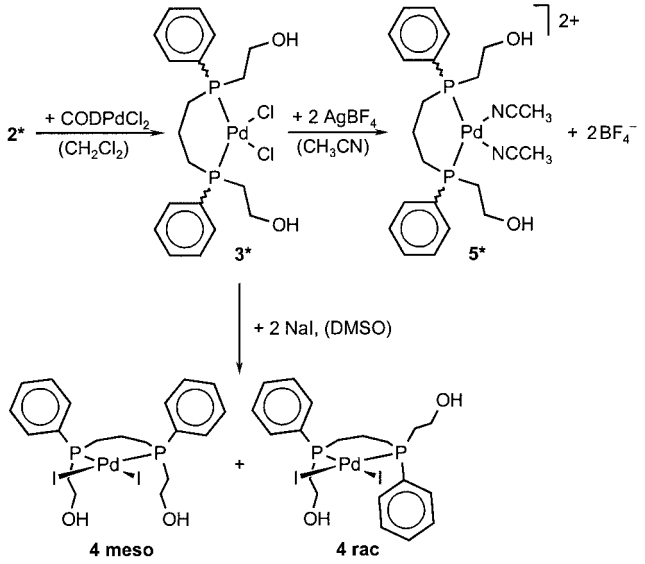

Scheme 3. Preparation of the neutral and dicationic Pd^{II} complexes of ligand **2***

ment with sodium iodide in DMSO affords the corresponding diiodo palladium(II) compounds **4***. Separation into pure racemic (**4** ***rac***) and *meso* fractions (**4** ***meso***) was performed by crystallization and subsequent chromatography over silica (CH_2Cl_2/acetone).[4] The dicationic complex **5*** was obtained from **3*** by halide abstraction using $AgBF_4$ in acetonitrile.

Single crystals of **3** ***meso*** (Figure 1, left) were grown from a DMSO extract of **3*** after treatment with CH_2Cl_2. Suitable crystals of **4** ***rac*** (Figure 1, right) were obtained by slow evaporation of the solvent from a CH_2Cl_2/acetone (1:1) solution. The coordination geometry around the Pd^{II} center is nearly square planar, as expected for palladium complexes of non-rigid diphosphanes. Both complexes show Pd−P and Pd−Hal bond lengths (Table 1) that resemble those of the symmetric [1,3-bis(diphenylphosphanyl)propane]$PdCl_2$ (Pd−P: 2.244(1)/2.249(2) Å; Pd−Cl: 2.351(1)/2.358(2) Å] and [1,2-bis(diphenylphosphanyl)ethane]PdI_2 (Pd−P: 2.2608(14)/2.2756(12) Å; Pd−I: 2.6649(8)/2.6446(10) Å] analogues.[5,6] The corresponding bond angles at the Pd centers of the complexes **3** ***meso*** and **4** ***rac*** are similar, i.e., they are independent of the nature of the chloro or iodo ligands, but the bond angle X−Pd−X is slightly enlarged in case of X = Cl [91.24(5)°] relative to X = I [90.46(2)°]. The orientation of the hydroxyethyl substituents is fixed in the solid state by intermolecular hydrogen bonding between neighboring complexes. Pairs of two

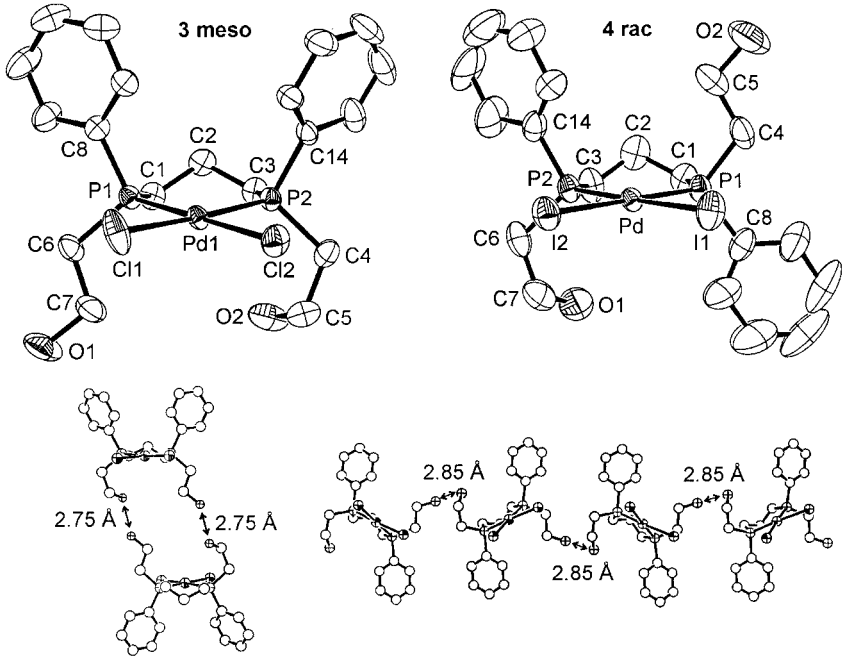

Figure 1. ORTEP plots of ***3 meso*** (left) and ***4 rac*** (right) complexes and arrangements of the complexes in the solid state; thermal ellipsoids are depicted at the 50% probability level; hydrogen atoms are omitted

 © 2004 Wiley-VCH Verlag GmbH & Co. KGaA, Weinheim

Table 1. Selected bond lengths (Å) and angles (deg) for **3** ***meso*** and **4** ***rac***

3 ***meso***		**4** ***rac***	
Bond lengths			
Pd(1)−P(1)	2.243(1)	Pd−P(1)	2.268(2)
Pd(1)−P(2)	2.254(1)	Pd−P(2)	2.264(2)
Pd(1)−Cl(1)	2.354(1)	Pd−I(1)	2.661(1)
Pd(1)−Cl(2)	2.381(1)	Pd−I(2)	2.657(1)
P(1)−C(1)	1.815(5)	P(1)−C(1)	1.827(6)
P(1)−C(6)	1.827(5)	P(1)−C(4)	1.801(6)
P(1)−C(8)	1.805(5)	P(1)−C(8)	1.792(6)
P(2)−C(3)	1.825(5)	P(2)−C(3)	1.816(6)
P(2)−C(4)	1.832(5)	P(2)−C(6)	1.822(6)
P(2)−C(14)	1.817(5)	P(2)−C(14)	1.813(6)
Bond angles			
P(1)−Pd(1)−P(2)	94.54(4)	P(1)−Pd−P(2)	94.89(6)
Cl(1)−Pd(1)−Cl(2)	91.24(5)	I(1)−Pd−I(2)	90.46(2)
P(1)−Pd(1)−Cl(1)	87.25(5)	P(1)−Pd−I(1)	87.07(4)
P(1)−Pd(1)−Cl(2)	178.41(5)	P(1)−Pd−I(2)	177.47(4)
P(2)−Pd(1)−Cl(2)	86.94(4)	P(2)−Pd−I(2)	87.55(4)
P(2)−Pd(1)−Cl(1)	175.61(5)	P(2)−Pd−I(1)	177.08(4)

complex molecules are bridged by two hydrogen bonds in the unit cell of **3** ***meso***. The intermolecular oxygen−oxygen distance is 2.754 Å. In **4** ***rac***, one molecule is bridged by hydrogen bonding with two other complex units, which, thus, forms a linear polymeric chain. The intermolecular oxygen−oxygen distance in **4** ***rac*** (2.853 Å) is slightly enlarged relative to that in **3** ***meso***.

Homo- and Copolymerization Experiments

The use of bulky, substituted chelating ligands is a prerequisite for achieving polymeric products in late transition metal catalyzed ethylene polymerization reactions.[7] Therefore, we chose 2-norbornene to be the first monomer we applied to verify the homopolymerization capabilities of these new complexes. In addition, chain termination induced by β-hydride elimination is thermodynamically unfavorable when using this monomer.[8] The active complex species was obtained by treating the dichloropalladium(II) compound **3*** with MAO in toluene. As expected, polymerization of 2-norbornene resulted in a completely insoluble poly(norbornene) material[9] (Table 2). The monomer conversion is more than twice as high as that obtained when using the structurally related dichloro(dppp)palladium(II) complex, under analogous experimental conditions.

Table 2. Results of 2-norbornene and ethylene homopolymerization experiments using **3*** and the reference dpppPd^{II}Cl$_2$ after activation with MAO in toluene

Run[a]	Monomer	Catalyst	Al:Pd[b]	Yield[c]	Activity[d]
1	norbornene	**3***	500	0.5	180
2	norbornene	(dppp)PdCl$_2$	500	0.2	80
3	norbornene	**3***	1000	0.8	320
4	norbornene	(dppp)PdCl$_2$	1000	0.3	130

[a] Toluene (100 mL), catalyst (15 μmol), 2-norbornene (5 g), 25 °C, 10 min. [b] Ratio Al(MAO):Pd. [c] [g]. [d] [kg[mol(Pd)h]$^{-1}$].

The dicationic complex **5*** shows a satisfying activity in the alternating copolymerization of ethylene and carbon monoxide after activation with methanol; it is similar to the results obtained when using the standard polyketone catalyst [(dppp)Pd(NCCH$_3$)$_2$](BF$_4$)$_2$ (Table 3). In the propylene/CO copolymerization reaction, complex **5*** shows a completely different behavior than that of the dppp-ligated catalyst, which is known to produce regio-irregular polyketones.[10] In contrast, the propylene/CO material resulting from **5*** is brittle and insoluble in common solvents, which we attribute to a polyspiroketal chain structure. ^{13}C NMR spectroscopy investigations in [D$_2$]hexafluoro-2-propanol (HFIP) proved that the product has high regioregularity (head−tail sequences >97%; Figure 2). Interestingly, the methyl area is dominated by a single resonance,[11] which indicates a stereoregular, isotactic microstructure. This finding is supported by the relatively high melting transition temperature (T_m = 169 °C).[12]

One reason for the observed regioregular microstructure could be the alkyl substitution on the phosphorus moieties, which is known to produce regioregular polyketones.[13] We have no genuine explanation for the high stereoregularity of the propylene/CO copolymer material (PCO). The chiral cage, formed by the phenyl- and 2-hydroxyethyl P-substituents around the Pd^{II} center is not significantly pronounced to explain the isotacticity of the PCO product. One possible explanation is that the C_2-symmetric *rac*-catalyst species

Table 3. Ethylene/CO and propylene/CO copolymerization performance of **5*** in comparison to the related dpppPd^{II} complex

Run	Monomer	Catalyst	Amount[a]	Yield[b]	Activity[c]	M_w[d]	M_w/M_n	Regio[e]
5[f]	E/CO	**5***	20	1.3	21	–[g]	–[g]	–
6[f]	E/CO	dppp[h]	20	1.2	20	–[g]	–[g]	–
7[i]	P/CO	**5***	40	0.15	0.2	–[i]	–[i]	97
8[i]	P/CO	dppp[h]	20	1.3	3.4	65	1.8	56

[a] [μmol]. [b] [g]. [c] [kg[mol(Pd)h]$^{-1}$]. [d] [kg mol^{-1}]. Determined by GPC in CHCl$_3$. [e] Regioregularity (head−tail units) [%]. Determined by ^{13}C NMR spectroscopy in [D$_2$]HFIP and CDCl$_3$. [f] 100-mL Steel autoclave, CH$_2$Cl$_2$ (40 mL), MeOH (1 mL), ethylene (40 bar), CO (80 bar), 25 °C, 3 h. [g] Not determined. [h] (NCCH$_3$)$_2$(dppp)Pd(BF$_4$)$_2$. [i] 100-mL Steel autoclave, CH$_2$Cl$_2$ (40 mL), MeOH (run 7: 1 mL; run 8: 0.12 mL), propylene (saturated for 30 min), CO (60 bar), 25 °C, 19 h.

 © 2004 Wiley-VCH Verlag GmbH & Co. KGaA, Weinheim

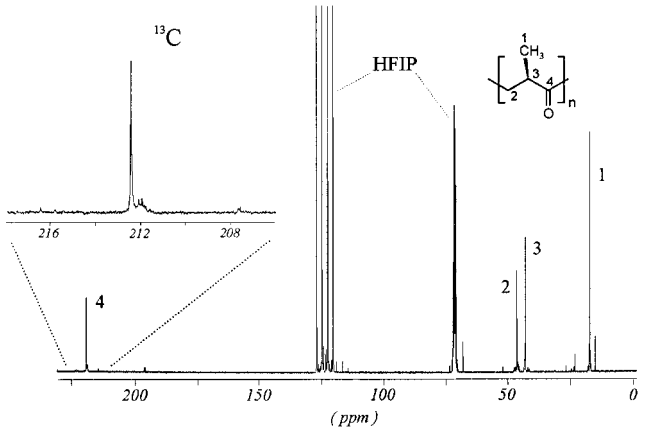

Figure 2. ^{13}C NMR spectrum ([D_2]HFIP) of a propylene/CO-copolymer resulting from the use of **5*** in methanol

has a higher activity than the *meso* complex and leads to the observed isotacticity through interaction of the 2-hydroxy ethyl substituents with the Pd^{II} dicationic metal center (O-coordination). This situation would afford the reversible formation of a chiral and stereorigid metallacycle that might lead to an effective enantiofacial differentiation of the incoming propylene monomer. A second explanation involves reversible interactions of the same OH groups with the coordinated acyl species after CO insertion. Further work toward gaining a deeper insight into these mechanisms is underway.

Conclusion

Our research on multifunctional chelating ligands resulted in the preparation of a 2-hydroxyethyl-substituted bisphosphane **2*** that is accessible by nucleophilic attack of the corresponding dilithium bisphosphide on ethylene oxide. The new ligand exists as a mixture of racemic and *meso* diastereoisomers in a 1:1.3 ratio. Separation of the diastereoisomeric compounds was performed by crystallization and column chromatography of the diiodo Pd^{II} complexes **4***. The neutral dichloro **3*** and the dicationic diacetonitrile Pd^{II} ditetrafluoroborate complexes **5*** are active for the homopolymerization of norbornene and CO/olefins, respectively. Interestingly, the application of complex **5*** affords isotactic propylene/CO copolymers. Elucidating the different polymerization behavior of the *rac* and *meso* isomers and studying the influence of the 2-hydroxyethyl P-substituents will be the subjects of further investigations.

Experimental Section

General: Reactions were performed under argon using standard Schlenk techniques. Solvents were dried by distillation from CaH_2 (dichloromethane) and $LiAlH_4$ (diethyl ether, *n*-pentane). Dry acetonitrile was received from Roth, deoxygenated in vacuo, and stored over molecular sieves (3 Å). H_2O was deoxygenated in vacuo and saturated with argon. 1,3-Bis(phenylphosphanyl)propane (**1**; Strem Chemicals), ethylene oxide (Fluka), $AgBF_4$ and (dppp)$PdCl_2$ (Aldrich), and 2-norbornene (Merck) were used as received. (COD)$PdCl_2$ [14] and $(CH_3CN)_2$(dppp)$Pd(BF_4)_2$ [15] were prepared according to literature procedures. ^1H, ^{13}C, ^{19}F, and ^{31}P NMR spectra were recorded on either a Bruker DRX 400 or an AMX 500 spectrometer. TMS was used as internal standard for the ^1H and ^{13}C spectra. ^{31}P NMR spectroscopic shifts were referenced to the external standard H_3PO_4 (85%). ^{19}F NMR spectra were calibrated to CCl_3F as the internal standard. Mass spectra were acquired using Varian MAT 711 and Finnigan TSQ 7000 instruments. X-Ray structural analyses were performed as described. MAO (in toluene) was supplied by WITCO. Ethylene (2.7), propylene (2.6), and carbon monoxide (2.0) were used without further purification as received from BASF.

1,3-Bis[(2-hydroxyethyl)(phenyl)phosphanyl]propane (2*): 1,3-Bis(phenylphosphanyl)propane (**1**) (11.3 g, 43.4 mmol) was dissolved in THF (400 mL) and cooled to −78 °C. Subsequently, 1.6 M *n*-butyllithium in hexane (53.4 mL, 86.8 mmol) was added to the mixture, which was warmed to room temperature overnight. The orange solution was then cooled to −18 °C and ethylene oxide (7.63 g, 174 mmol, 2 equiv.) was condensed into the reaction mixture. After stirring the resulting white suspension for 1 h at room temperature, all the solvents are removed in vacuo. The residue was hydrolyzed with water and deoxygenated 1 M hydrochloric acid was added, to pH 1, to protonate the bisphosphane. The aqueous solution was extracted with CH_2Cl_2 to remove impurities. Subsequently, after adding CH_2Cl_2 (100 mL) to the resulting acidic water phase, the mixture was adjusted to pH 7, to deprotonate the bisphosphane, by adding deoxygenated aqueous NaOH. The mixture was extracted with CH_2Cl_2 and the combined organic layers were dried over Na_2SO_4. Evaporation of the solvent in vacuo gave ligand **2*** as a colorless, highly viscous oil. Yield 12.2 g (82%). ^1H NMR ($CDCl_3$): δ = 7.47−7.39 (m, 4 H, Ph), 7.33−7.25 (m, 6 H, Ph), 3.68−3.59 (m, 4 H, CH_2O), 2.30−2.15 (br. s, 2 H, OH), 2.01−1.88 (m, 4 H, PCH_2), 1.87−1.72 (m, 4 H, PCH_2, bridge), 1.52−1.39 (m, 2 H, CH_2, bridge) ppm. ^{13}C NMR ($CDCl_3$): δ = 137.7−137.4 (2 × d, *rac*/*meso*, *ipso* Ph), 132.4−132.1 (2 × d, *rac*/*meso*, *ortho* Ph), 128.9 (s, *para* Ph), 128.5−128.3 (2 × d, *rac*/*meso*, *meta* Ph), 60.0 (d, CH_2-OH), 32.0 (vt, *rac*/*meso*, PCH_2), 29.5 (vt, PCH_2, bridge), 22.4−22.1 (m, CH_2, bridge) ppm. $^{31}P\{^1H\}$ NMR ($CDCl_3$): δ = −32.50 (s, *rac*), −32.64 (s, *meso*) ppm; ratio *rac*:*meso* = 1:1.3. IR (film): $\tilde{\nu}$ = 3344 cm^{-1} (br., OH). MS (FD): *m*/*z* (%) = 348 (100) $[M]^+$, 303 (5) $[M - CH_2CH_2OH]^+$. $C_{19}H_{26}O_2P_2$ (348.4): calcd. C 65.51, H 7.52; found C 65.23, H 7.35.

Dichloro{1,3-Bis[(2-hydroxyethyl)(phenyl)phosphanyl]propane}-palladium(II) (3*): Ligand **2*** (9.42 g, 27.1 mmol) was dissolved in CH_2Cl_2 (50 mL) and then added to a solution of (COD)$PdCl_2$ (7.72 g, 27.1 mmol) in CH_2Cl_2 (450 mL). After stirring the mixture for 1 h, the precipitated product was separated. Washing with CH_2Cl_2 and pentane and then drying in vacuo gave complex **3*** as a yellow solid. Yield:13.5 g (95%). Extraction of compound **3*** with a small amount of DMSO, followed by crystallization from the DMSO extract by the addition of CH_2Cl_2, gave the pure *meso* complex (**3** ***meso***) containing single-crystals suitable for X-ray diffraction analysis. ^1H NMR ([D_6]DMSO): δ = 8.00−7.91 [m, 4H (*rac*) +4H (*meso*), Ph], 7.55−7.39 [m, 6H (*rac*) + 6H (*meso*), Ph], 5.10 (t, 2 H, *rac*, OH), 5.05 (t, 2 H, *meso*, OH), 4.08−3.85 [m, 4H (*rac*) + 4H (*meso*), CH_2O], 2.91−2.78 (m, 2 H, *rac*), 2.77−2.64 (m, 2 H, *meso*), 2.64−2.40 [m, 2H (*rac*) + 2H (*meso*)], 2.40−2.26 (m, 2 H, *meso*), 2.22−2.07 [m, 2H (*rac*) + 3H (*meso*)], 2.07−1.90 (m, 2 H, *rac*), 1.88−1.70 (m, 2 H, *rac*), 1.20−0.96 (m, 1 H, *meso*) ppm. $^{31}P\{^1H\}$ NMR ([D_6]DMSO): δ = 17.0 (s, *rac*), 13.6 (s, *meso*) ppm;

 © 2004 Wiley-VCH Verlag GmbH & Co. KGaA, Weinheim

ratio *rac*:*meso* = 1:1.3. IR (KI): $\tilde{\nu}$ = 3422 cm^{-1} (br., OH). MS (FAB): *m*/*z* (%) = 491 (76) $[M - Cl]^+$, 453 (100) $[M - 2Cl]^+$. $C_{19}H_{26}Cl_2O_2P_2Pd$ (525.7): calcd. C 43.41, H 4.99; found C 43.30, H 4.93.

{1,3-Bis[(2-hydroxyethyl)(phenyl)phosphanyl]propane}diiodopalladium(II) (4*) and Its Separation into 4 *meso* and 4 *rac*: The following procedure was performed using solvents as supplied without further purification. Complex **3*** (7.0 g, 13.3 mmol) was dissolved in DMSO (200 mL). After adding NaI (7.97 g, 53.2 mmol), the reaction mixture was stirred for 15 h at room temperature. The DMSO was separated from the crude product by successive extraction with ether and removal of the resulting DMSO-containing ether layers. Extracting of the resulting solid with CH_2Cl_2 and acetone, followed by crystallization, led to an enrichment of the two diastereoisomers in different product fractions. Complete separation and purification of the diastereoisomers was performed by chromatography over silica (CH_2Cl_2/acetone, 1:2) and subsequent crystallization.

{(P*S*,P′*S*)-1,3-Bis[(2-hydroxyethyl)(phenyl)phosphanyl]propane}diiodopalladium(II) and {(P*R*,P′*R*)-1,3-Bis[(2-hydroxyethyl)(phenyl)phosphanyl]propane}diiodopalladium(II) (4 *rac*): Yield: 2.8 g (30%). ^1H NMR ([D$_6$]DMSO): δ = 7.93−7.90 (m, 4 H, Ph), 7.51−7.42 (m, 6 H, Ph), 5.14 (t, br, 2 H, OH), 4.11−3.96 (m, 4 H, CH_2O), 3.14−2.84 (m, 4 H, PCH_2), 2.24−2.11 (m, 2 H, bridge), 2.00−1.72 (m, 4 H, bridge) ppm. $^{31}P\{^1H\}$ NMR ([D$_6$]DMSO): δ = 7.27 (s) ppm. IR (KI): $\tilde{\nu}$ = 3425 cm^{-1} (br., OH). MS (FAB): *m*/*z* (%) = 581 (100) $[M - I]^+$, 454 (10) $[M - 2I]^+$. $C_{19}H_{26}I_2O_2P_2Pd$ (708.6): calcd. C 32.21, H 3.70; found C 32.07, H 3.62.

{(P*S*,P′*R*)-1,3-Bis[(2-hydroxyethyl)(phenyl)phosphanyl]propane}diiodopalladium(II) (4 *meso*): Yield 2.1 g (23%). ^1H NMR ([D$_6$]DMSO): δ = 7.98−7.91 (m, 4 H, Ph), 7.50−7.42 (m, 6 H, Ph), 5.11 (t, br, 2 H, OH), 4.07−3.87 (m, 4 H, CH_2O), 3.08−2.82 (m, 4 H, PCH_2), 2.24−2.02 (m, 5 H, bridge), 1.22−1.00 (m, 1 H, bridge) ppm. $^{31}P\{^1H\}$ NMR ([D$_6$]DMSO): δ = 5.48 (s) ppm. IR (KI): $\tilde{\nu}$ = 3347 cm^{-1} (br., OH). MS (FAB): *m*/*z* (%) = 581 (100) $[M - I]^+$, 454 (7) $[M - 2I]^+$. $C_{19}H_{26}I_2O_2P_2Pd$ (708.6): calcd. C 32.21; H 3.70; found C 32.26; H 3.74.

Diacetonitrile{1,3-bis[(2-hydroxyethyl)(phenyl)phosphanyl]propane}palladium(II) Ditetrafluoroborate (5*): $AgBF_4$ (1.48 g, 7.62 mmol) was added to a suspension of **3*** (2.00 g, 3.81 mmol) in acetonitrile (80 mL). After stirring for 1 h, the reaction mixture was filtered and concentrated in vacuo. The concentrated solution was filtered again and then the complex was precipitated with ether. The solid was washed with diethyl ether and *n*-pentane and then dried in vacuo to give **5***. Yield 2.4 g (89%). ^1H NMR (CD_3OD): δ = 8.17−7.39 (m, 10 H, *meso*/*rac*, Ph), 4.26−3.92 (m, 2 H, *meso*/*rac*, CH_2), 3.78−3.61 (m, 2 H, *meso*/*rac*, CH_2), 3.19−2.15 and 1.64−1.45 (2 × m, 10 H, *meso*/*rac*, CH_2), 2.06 (CH_3CN) ppm. $^{19}F\{^1H\}$ NMR (CD_3OD): δ = −155.55 (s) ppm. $^{31}P\{^1H\}$ NMR (CD_3OD): δ = 44.30 (s, *rac*), 33.37 (s, *meso*) ppm; ratio *rac*:*meso* = 1:1.3. IR (KI): $\tilde{\nu}$ = 3481 (br., OH), 2325, 2297 (w, C≡N), 1076 (br., BF_4) cm^{-1}. MS (FAB): *m*/*z* (%) = 453 (100) $[M - 2CH_3CN,2BF_4]^+$.

2-Norbornene Polymerization Experiments: The corresponding dichloro Pd^{II} complex (15 μmol) was dissolved in toluene (final total volume including MAO: 100 mL), treated with MAO solution

Table 4. Summary of crystal data and structural refinement parameters for **3** ***meso*** and **4** ***rac***

	3 ***meso***	**4** ***rac***
Empirical formula	$C_{19}H_{26}Cl_2O_2P_2Pd$	$C_{19}H_{26}I_2O_2P_2Pd$
Molecular mass	525.64	708.54
Crystal color and shape	colorless prism	orange needle fragment
Crystal size (mm)	0.15 × 0.31 × 0.46	0.26 × 0.19 × 0.12
Crystal system	monoclinic	orthorhombic
Space group	*I*2/*a*	*Pbcn*
a (Å)	13.946(1)	18.322(4)
b (Å)	11.120(1)	18.947(3)
c (Å)	30.962(2)	15.425(2)
α (°)	90	90
β (°)	101.23(1)	90
γ (°)	90	90
V (Å^3)	4709.5(5)	5354.7(17)
Z	8	8
Calculated density [g/cm^3]	1.483	1.758
Absorption coefficient [mm^{-1}]	1.161	3.128
F(000)	2128	2704
θ range (°)	2.57−25.96	2.76−26.00
Index range	−16 = *h* = 16	−22 = *h* = 22
	−13 = *k* = 13	−23 = *k* = 23
	−38 = *l* = 32	−18 = *l* = 18
Reflections collected	13855	39740
Reflections unique	4538 [*R*(int) = 0.0267]	5109 [*R*(int) = 0.0825]
Goodness-of-fit on F^2	1.093	0.935
Final R_{int} [$I > 2\sigma(I)$]	*R*1 = 0.0446	*R*1 = 0.0311
	*wR*2 = 0.1583	*wR*2 = 0.0660
R_{int} (all data)	*R*1 = 0.0497	*R*1 = 0.0644
	*wR*2 = 0.1650	*wR*2 = 0.0704
Largest diff peak and hole (e/Å^3)	3.340 and −1.232	1.036 and −0.478

 © 2004 Wiley-VCH Verlag GmbH & Co. KGaA, Weinheim

(Al:Pd = 1000), and stirred 2 min to form the active species. 2-Norbornene (5 g) was then added to the solution. The polymerization reaction was quenched after 10 min by pouring the mixture into a glass beaker containing MeOH (500 mL)/conc. hydrochloric acid (5 mL). Separation and drying in vacuo at 80 °C gave the polymer as a white powder.

Ethylene/CO Copolymerization Experiments: The corresponding dicationic diacetonitrile palladium(II) ditetrafluoroborate complex was dissolved in a mixture of CH_2Cl_2 (40 mL) and MeOH (1 mL). The activated catalyst solution was transferred into a 100-mL steel autoclave equipped with a magnetic stirring bar. After pressurizing with ethylene (40 bar) for 5 min, the reactor was charged with carbon monoxide at 80 bar. Following a polymerization time of 3 h, the remaining gases were vented off and the reaction mixture was poured into MeOH. The copolymer was isolated by filtration and then it was dried in vacuo at 60 °C.

Propylene/CO Copolymerization Experiments: The catalyst solution was prepared and transferred into the autoclave as described above for the ethylene/CO copolymerization experiments. The reactor was saturated with propene (30 min) and charged with carbon monoxide at 60 bar. The remaining gases were vented off after a reaction time of 19 h at 25 °C. The resulting reaction mixture was diluted with CH_2Cl_2 and stirred with water for 2 h. The organic phase was separated, the solvent evaporated in vacuo, and the copolymer dried in vacuo at 60 °C.

X-ray Crystallography of 3 *meso* and 4 *rac*: The crystals used in this study were mounted onto the ends of a glass fiber. X-Ray diffraction data were collected on a STOE IPDS unit (Imaging Plate Diffraction System) at 20 °C. Graphite-monochromatized Mo-K_α radiation (λ = 0.71073 Å) was used. Crystal data are listed in Table 4 together with refinement details. An absorption correction (analytical method) was applied. The structure of **3** ***meso*** was solved by direct methods using XMY93[16] and that of **4** ***rac*** by the Patterson method. The atomic coordinates and anisotropic thermal parameters of the non-hydrogen atoms were refined using the SHELXL-97 program[17] (full-matrix method on F^2 data). Hydrogen atoms, except those attached to oxygen atoms, were included at their calculated positions in the final refinement cycles. The riding model was used to locate the other hydrogen atoms.

CCDC-224744 (for **3** ***meso***) and -224402 (for **4** ***rac***) contain the supplementary crystallographic data for this paper. These data can be obtained free of charge at www.ccdc.cam.ac.uk/conts/retrieving.html [or from the Cambridge Crystallographic Data Centre, 12 Union Road, Cambridge CB2 1EZ, UK; Fax: (internat.) +44-1223-336-033; E-mail: deposit@ccdc.cam.ac.uk].

[1] [1a] C. Bianchini, A. Meli, *Coord. Chem. Rev.* **2002**, *225*, 35. [1b] E. Drent, P. H. M. Budzelaar, *Chem. Rev.* **1996**, *96*, 663. [1c] K. Cavell, *J. Coord. Chem. Rev.* **1996**, *155*, 209.

[2] [2a] A. Bader, E. Lindner, *Coord. Chem. Rev.* **1991**, *108*, 27. [2b] P. C. Casey, E. L. Paulsen, E. W. Beuttenmueller, B. R. Proft, B. A. Matter, D. R. Powell, *J. Am. Chem. Soc.* **1999**, *121*, 63. [2c] C. Gambs, S. Chaloupka, G. Consiglio, A. Togni, *Angew. Chem.* **2000**, *112*, 2602; *Angew. Chem. Int. Ed.* **2000**, *39*, 2486. [2d] E. Lindner, M. Schmid, J. Wald, J. A. Queisser, M. Geprägs, P. Wegner, C. Nachtigal, *J. Organomet. Chem.* **2000**, *602*, 173. [2e] I. T. Horváth, J. Rábai, *Science* **1994**, *266*, 72. [2f] J. J. J. Juliette, D. Rutherford, I. T. Horváth, J. A. Gladysz, *J. Am. Chem. Soc.* **1999**, *121*, 2696.

[3] [3a] T. Kauffmann, E. Antfang, J. Olbrich, *Chem. Ber.* **1985**, *118*, 1022. [3b] T. Kauffmann, E. Antfang, J. Olbrich, *Tetrahedron Lett.* **1984**, *25*, 1963.

[4] [4a] U. Nagel, B. Rieger, *Chem. Ber.* **1988**, *121*, 1123. [4b] U. Nagel, B. Rieger, A. Bublewitz, *J. Organomet. Chem.* **1989**, *370*, 223. [4c] U. Nagel, T. Krink, *Chem. Ber.* **1993**, *126*, 1091.

[5] W. L. Steffen, G. J. Palenik, *Inorg. Chem.* **1976**, *15*, 2432.

[6] W. Oberhauser, C. Bachmann, T. Stampfl, R. Haid, P. Brügeller, *Polyhedron* **1997**, *16*, 2827.

[7] *Late Transition Metal Polymerization Catalysis* (Eds.: B. Rieger, L. S. Baugh, S. Kacker, S. Striegler), Wiley-VCH, Weinheim, New York, **2003**.

[8] J. Melia, E. Conner, S. Rush, S. Breunig, C. Mehler, W. Risse, *Macromol. Symp.* **1995**, *89*, 433.

[9] R. Wursche, T. Debaerdemaeker, M. Klinga, B. Rieger, *Eur. J. Inorg. Chem.* **2000**, 2063.

[10] A. S. Abu-Surrah, B. Rieger, *Top. Catal.* **1999**, *7*, 165.

[11] [11a] C. Gambs, S. Chaloupka, G. Consiglio, A. Togni, *Angew. Chem.* **2000**, *112*, 2602; *Angew. Chem. Int. Ed.* **2000**, *39*, 2486. [11b] Z. Jiang, A. Sen, *J. Am. Chem. Soc.* **1995**, *117*, 4455.

[12] [12a] Z. Jiang, M. T. Boyer, A. Sen, *J. Am. Chem. Soc.* **1995**, *117*, 7037. [12b] A. Batistini, G. Consiglio, U. W. Suter, *Angew. Chem.* **1992**, *104*, 306.

[13] [13a] S. Bronco, G. Consiglio, R. Hutter, A. Batistini, U. W. Suter, *Macromolecules* **1994**, *27*, 4436. [13b] M. Barsacchi, A. Batistini, G. Consiglio, U. W. Suter, *Macromolecules* **1992**, *25*, 3604.

[14] D. Drew, J. R. Doyle, *Inorg. Synth.* **1972**, *13*, 52.

[15] F. Y. Xu, A. X. Zhao, J. C. W. Chien, *Macromol. Chem.* **1993**, *194*, 2579.

[16] T. Debaerdemaeker, *XMY93, XMY93-Program*, University of Ulm, Germany.

[17] M. Sheldrick, *SHELXL-97*, *Program for the Refinement of Crystal Structures*, Göttingen, **1997**.

Received December 5, 2003
Early View Article
Published Online May 25, 2004

 © 2004 Wiley-VCH Verlag GmbH & Co. KGaA, Weinheim

Syntheses and Reactions of a Stable 1,2-Dichloro-1,2-diborolane and Aromatic Tetraboranes

Carsten Präsang,[a] Yüksel Sahin,[a] Matthias Hofmann,[b] Gertraud Geiseler,[a] Werner Massa,[a] and Armin Berndt*[a]

Keywords: Aromatics / Boranes / Carbanions / Cyclizations / Heterocycles / Rearrangements

The 1,2-dichloro-1,2-diborolane **1b** was isolated in good yield after the reaction of the 1,2-bis(dimethylamino)-1,2-diborolane **2c** with BCl_3. We prepared **2c** from 1,2-bis(dimethylamino)-1,2-dichlorodiborane(4) (**3**) and TMEDA-free [1,3-bis(trimethylsilyl)allyl]lithium (**5a·Li**), which is accessible by deprotonation of 1,3-bis(trimethylsilyl)propene (**4a**) with *n*-butyllithium in diethyl ether. Upon its reaction with lithium in THF, the 1-allyl-2-chlorodiborane(4) **6a** obtained in the first step undergoes an unprecedented ring closure with 1,2-migration of a trimethylsilyl substituent to yield the boron-stabilized carbanion **7a**. Reaction of **7a** with either chlorotrimethylsilane or HCl gives **2c** or **2d**, respectively. The latter compound cannot be transformed into an isolable 1,2-dichloro-1,2-diborolane; this observation demonstrates that a trimethylsilyl substituent next to each boron atom is essential for the stability of 1,2-dichloro-1,2-diborolanes. Compound **1b** is a versatile starting material, inter alia for the syntheses of the aromatic tetraboranes(6) *cis*-**11** and *trans*-**13** and the aromatic tetraborane(4) *cis*-**12**. The isomerization *cis*-**11** → *trans*-**13** can be explained on the basis of reactions occurring under the conservation of two-electron aromaticity.

(© Wiley-VCH Verlag GmbH & Co. KGaA, 69451 Weinheim, Germany, 2004)

Introduction

1,2-Dichloro-1,2-diborolanes appear to be versatile starting materials for the syntheses of 1,2-diborolanes that lack strong donor substituents at the boron centers, but only 1,2-diborolanes possessing such donors, i.e., 1,2-diamino-1,2-diborolanes, are known experimentally.[1−3] Computations have revealed a strong tendency for the unsubstituted 1,2-diborolane to isomerize to nonclassical forms that have two-electron homoaromatic structures.[4] Attempts to prepare 1,2-dichloro-1,2-diborolane (**1a**) by reaction of the 1,2-diamino-1,2-diborolane **2a** with BCl_3 were unsuccessful,[2] as were efforts to obtain **2b** by reaction of 1,2-dichloro-1,2-bis(dimethylamino)diborane(4) (**3**) with 1,3-dilithio-2-methylenepropane (Scheme 1).[3]

In this paper we describe the synthesis of the stable 1,2-dichloro-1,2-diborolane **1b** (Scheme 3) via the new 1,2-diamino-1,2-diborolane **2c** (Scheme 2). Compound **1b** turned out to be a versatile starting material, inter alia for the syntheses of the aromatic tetraboranes *cis*-**11**,[5] *cis*-**12**,[6] and *trans*-**13**[5] as well as for triboracyclopropanates[7] and a pentaborane(7).[6]

Syntheses

The TMEDA-free allyllithium compounds **5a·Li** and **5b·Li** were prepared by deprotonation of 1,3-bis(silyl)propenes **4a**[8,9] and **4b**[10] with *n*-butyllithium in diethyl ether at room temperature. Compound **4b** was synthesized from 3-[dimethyl(phenyl)silyl]propene,[11] which was deprotonated in the same way and then treated with chlorodimethyl(phenyl)silane.

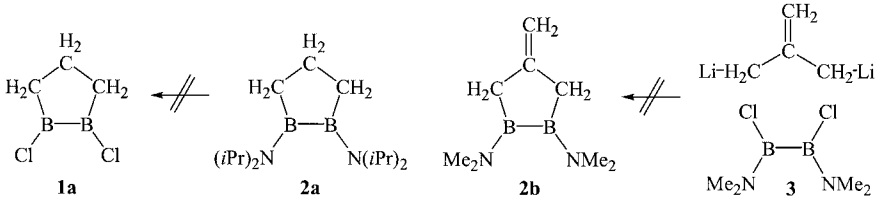

Scheme 1

The bis(trimethylsilyl)propene **4a** is deprotonated usually in the presence of *N*,*N*,*N*,*N*-tetramethylethylenediamine (TMEDA), THF, or HMPA.[8,12−14] The deprotonation

[a] Fachbereich Chemie der Philipps-Universität Marburg, Hans-Meerwein-Strasse, 35032 Marburg
Fax: (internat.) + 49-(0)6421-2828917
E-mail: berndt@chemie.uni-marburg.de
[b] Anorganisch-Chemisches Institut, Universität Heidelberg, Im Neuenheimer Feld 270, 69120 Heidelberg, Germany

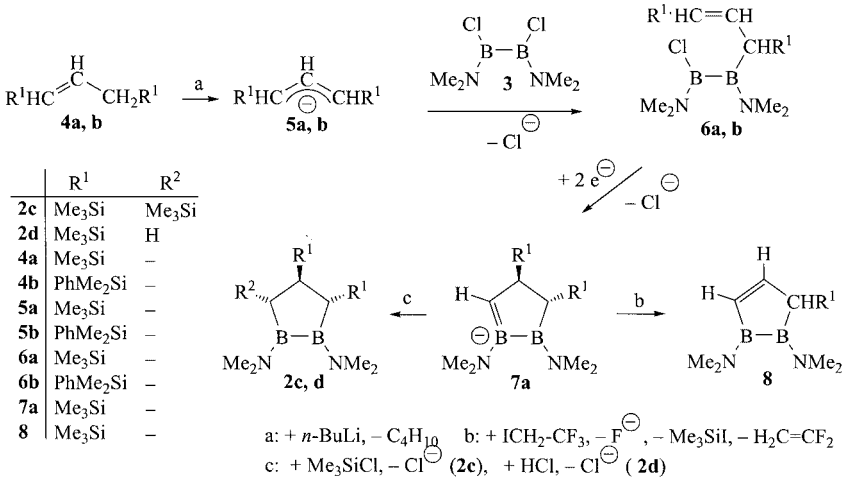

	R^1	R^2
2c	Me_3Si	Me_3Si
2d	Me_3Si	H
4a	Me_3Si	–
4b	$PhMe_2Si$	–
5a	Me_3Si	–
5b	$PhMe_2Si$	–
6a	Me_3Si	–
6b	$PhMe_2Si$	–
7a	Me_3Si	–
8	Me_3Si	–

Scheme 2

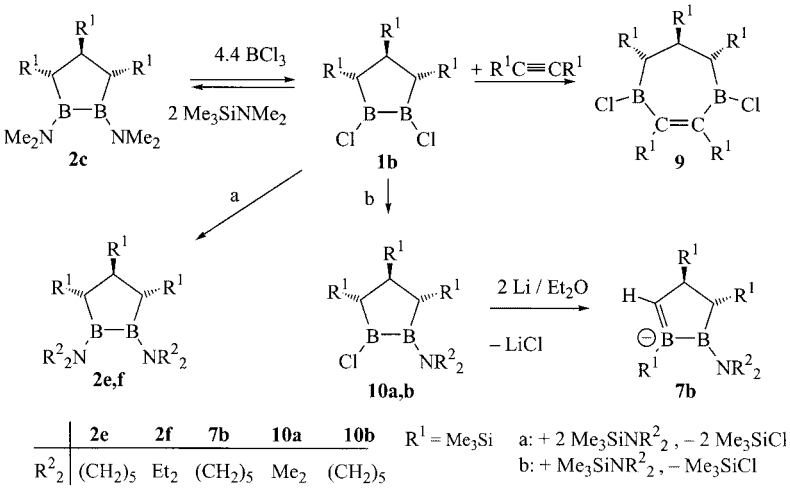

	2e	**2f**	**7b**	**10a**	**10b**
R^2_2	$(CH_2)_5$	Et_2	$(CH_2)_5$	Me_2	$(CH_2)_5$

Scheme 3

with *n*-butyllithium in diethyl ether requires a reaction time of 8 d, but the workup of the products obtained after the reaction of lithiopropene **5a·Li** with 1,2-dichloro-1,2-bis(dimethylamino)diborane(4) (**3**) is considerably easier and yields of allylchlorodiboranes(4) **6a,b** are much higher than they are when using the lithium salts of **5a**,**b** containing TMEDA. The 1-allyl-2-chlorodiboranes(4) **6a**,**b** thus obtained are mixtures of (*E*) and (*Z*) stereoisomers, which could not be separated by distillation. The constitutions of (*E*/*Z*)-**6a**,**b** were deduced from their ^1H and ^{13}C NMR spectra and confirmed by the X-ray crystal structure analysis of the product obtained by reaction of the former with lithium in THF (see below). Nearly identical coupling constants $J(^1H,^1H)$ of the alkene moieties of the isomers prevented assignments of configurations by means of ^1H NMR spectroscopy. Probably, the main products (**6a**: 85%; **6b**: 90%) are the (*E*) isomers because of their lower degree of steric hindrance when compared to the (*Z*) isomers.

Reaction of (*E*/*Z*)-**6a** with lithium powder in THF at room temperature yielded 1,2-diborolan-3-ide **7a** as the sole product. This ring-closing reaction was not observed with **6b** even when stoichiometric amounts of lithium naphthalenide were used. The constitution of **7a** is in agreement with all the NMR spectroscopic data and was confirmed definitely by an X-ray crystal structure analysis (see below). While the methyl groups of the dimethylamino substituent of the uncharged boron atom of **7a** show two signals in the ^1H and ^{13}C NMR spectra (300 K, 300/75 MHz), those of the charged boron atom are averaged, which indicates a less hindered rotation.

During the formation of **7a** from (*E*/*Z*)-**6a**, a C−B bond, as well as a boron-stabilized carbanion, is formed, and a trimethylsilyl group must migrate from a carbon atom to the neighboring carbon atom, which, for **6a**, does not possess a silyl substituent. A mechanism for this unprecedented ring closure is proposed below.

The reaction of the anion **7a** with either chlorotrimethylsilane or HCl gave 1,2-diborolanes **2c** and **2d**, respectively. Their constitutions and stereochemistries are in agreement with all of their NMR spectroscopic data. The ^1H NMR spectrum of **2c** exhibits two signals for the silyl groups (2:1), the aminomethyl groups (1:1), and the ring protons (2:1; d

 © 2004 Wiley-VCH Verlag GmbH & Co. KGaA, Weinheim

and t, respectively). The crude product of **2c** was used for subsequent reactions without further purification because it contained very few impurities after removal of the volatile components and filtration.

Reaction of **7a** with 1,1,1-trifluoro-2-iodoethane did not yield the expected 3-iodo-1,2-diborolane after warming to room temperature, but, instead, the elimination product diboracyclopentene **8**. The constitution of compound **8** was derived from its one- and two-dimensional ^{1}H, ^{11}B, and ^{13}C NMR spectra.

After the addition of ca. 4 equiv. of neat boron trichloride to a solution of **2c** in *n*-pentane at −78 °C, the solution was warmed to ambient temperature during which time both amino groups were replaced cleanly by chlorine atoms. While small-scale experiments yielded nearly pure **1b**, the crude products of experiments starting with > 10 g of **2c** had to be crystallized from *n*-pentane at −30 °C to obtain satisfactory yields (ca. 68%) of pure **1b**. Diborolane **2d**, which lacks one trimethylsilyl group when compared to **2c**, could not be chlorinated in a similar manner. Reaction with BCl_3 resulted in the recovery of **2d** or led to an inseparable mixture of products containing varying amounts of starting material.

The diborolane **1b** reacts with bis(trimethylsilyl)ethyne at room temperature to form the 3,7-diboracycloheptene **9**. Its constitution was confirmed by NMR spectroscopy experiments. Compound **9** displays three signals for the trimethylsilyl groups (ratio: 2:1:2) and two for the methylene groups (2:1; d and t). Formation of the isomeric 1-methylene-2,6-diboracyclohexane, i.e., the product of the often observed 1,1-diborylation of bis(trimethylsilyl)ethyne,[15,16] was ruled out by $^{13}C\{^{11}B\}$ NMR spectroscopy experiments. The signals of the boron-bound carbon atoms at δ = 181.2 and 34.8 ppm sharpened considerably, but no sharp signal appears for a tricoordinated carbon atom that is not bound to boron atoms (i.e., for an $Si_2C{=}CB_2$ moiety). Similar 1,2-diborylations of ethynes are known to occur from 1,2-diamino-1,2-diborolanes, which, however, require $BF_3{\cdot}OEt_2$ as catalyst and elevated temperatures.[1]

One or both chlorine atoms in **1b** can be exchanged with amino groups by adding stoichiometric amounts of silylamines. In this way, we synthesized the monoaminodiborolanes **10a**,**b** and the diaminodiborolanes **2c**,**e**,**f**. Reaction of **10a** with lithium powder in diethyl ether did not yield a tetraborane(6) by dimerization,[5] but gave the 1,2-diborolan-3-ide **7b**, as proven by its X-ray structural analysis. This transformation, like that of **6a** to **7a**, requires the 1,2-migration of a trimethylsilyl substituent (here to a neighboring boron atom) and the generation of a boron-stabilized carbanion. The NMR spectroscopic data of **7b** are similar to those of **7a**, but some of the chemical shifts differ distinctly. The stronger acceptor in **7b** [$B(SiMe_3)$], when compared to $B(NMe_2)$ in **7a**, causes a downfield shift of the signals of the sp^2-hybridized carbon atom and its proton relative to those signals for **7a** (^{13}C: δ = 149.2 vs. 109.0 ppm; ^{1}H: δ = 6.57 vs. 4.58 ppm). The boron atom bearing the trimethylsilyl group, however, is more shielded (δ = 33 vs. 38 ppm), even though it lacks a second π-donating group. Attempts to let **7b** react with electrophiles (MeI, Me_3SiCl, Me_3SnCl) to yield a *B*-trimethylsilyldiborolane were unsuccessful. The mixtures of products obtained obviously contained no compounds featuring a $B{-}B(SiMe_3)C$ moiety, which would result in a ^{11}B NMR signal for a strongly deshielded boron center.[17]

Reactions of **1b** with $K_{2.8}Na$ in *n*-pentane at room temperature yielded the nonclassical dichlorotetraborane(6) *cis*-**11** (Scheme 4).[5,18,19] As seen from its classical isomer **11***, there are only six electrons to connect the four centers of the B_4 ring of *cis*-**11**. Four of them are used for two three-center two-electron (3c2e) σ-bonds and the remaining two for a 4c2e π-bond.[5] Thus, *cis*-**11** is a 2e-aromatic system having a nonclassical σ-skeleton. Computations for model molecules show the energetic advantage of 2e-aromatic compounds of type **11** over orthogonal classical isomers, which benefit only from twofold B−B hyperconjugation (see below). The aromatic tetraborane(4) *cis*-**12** was obtained by reaction of *cis*-**11** with 2 equiv. of lithium naphthalenide at low temperatures.[6] Reduction of *cis*-**12** to its

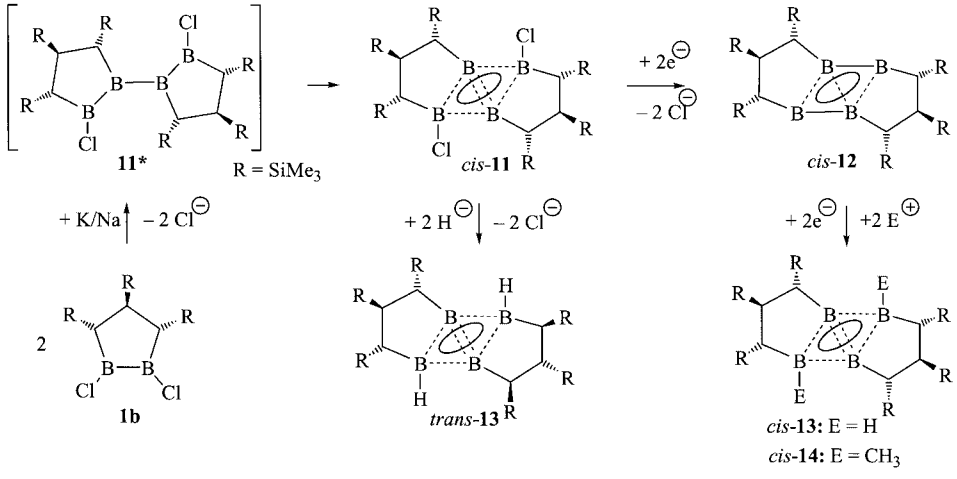

Scheme 4

 © 2004 Wiley-VCH Verlag GmbH & Co. KGaA, Weinheim

dianion and a subsequent reaction with either HCl or methyl iodide leads to the tetraborane(6) *cis*-**13** or *cis*-**14**, respectively.[20] Surprisingly, the stereoisomer *trans*-**13** was obtained by exchange of the Cl atoms of *cis*-**11** for hydrogen by use of sodium triethylhydroborate.[5] A reasonable mechanism for this stereoisomerization is presented below.

Crystal Structures

The lithium cations of all the derivatives of allyllithium analyzed by crystal structure determination so far are coordinated by ligands like TMEDA or diethyl ether.[14,21–24] The structure of **5b·Li** is the first one of a solvent-free allyllithium derivative. Attempts to obtain single crystals of **5a·Li** were unsuccessful: it is insoluble, even in boiling *para*-xylene, and it decomposed in boiling mesitylene.

The **5b·Li** complex exhibits a polymeric structure in the solid state with two independent spiral Li−allyl−Li chains parallel to the *c* axis (Figure 1). According to the space group $I4_1$, one spiral chain with Li1 turns around clockwise (4_1 screw axis at 1/4, 1/4, *z*, 90° rotation of subsequent allyl groups); the second one with Li2 turns anticlockwise (4_3 screw axis at 3/4, 1/4, *z*). By the twofold axis in 0.5,0.5,*z*, a second pair of equivalent chains is generated in 3/4,1/4,*z* (Li2) and 3/4,3/4,*z* (Li1) leading to a tetragonal chain packing of alternating 4_1 and 4_3 spirals (Figure 2). Figure 1 displays a section of the Li1 chain that indicates the η^3-connection of the allyl moieties; the C_3 planes are located at an angle of 60.4(3)° [61.7(3)° for the Li2 chain] with respect to the chain axis. In contrast, the structure of (1,3-diphenylallyl)lithium·OEt_2 [22] possesses chains having 2_1-symmetry (180° rotation of subsequent allyl groups); the inclination of the allyl planes to the chain axis is similar (60°).

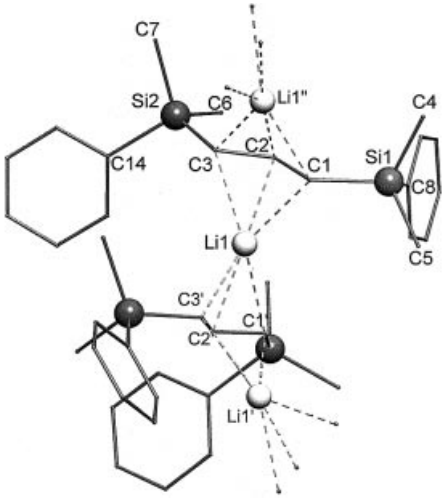

Figure 1. Section of the spiral chain with Li1 in the crystal structure of **5b·Li**; selected bond lengths [pm] and angles [°], the corresponding values for the second spiral chain with Li2 are provided in brackets (same e.s.d.s): C1−C2 140.6(4) [140.2], C2−C3 140.0(4) [139.9], C1−Li1 231.4(6) [233.9], C2−Li1 215.8(6) [215.6], C3−Li1 231.8(6) [228.7], C1′−Li1 228.8(6) [229.7], C2′−Li1 219.3(6) [216.2], C3′−Li1 235.3(6) [229.7]; C1−C2−C3 129.9(3) [128.9], C2−C1−Si1 123.2(2) [124.4], C2−C3−Si2 123.8(2) [123.5], Si1−C1−C2−C3 −176.1(2) [177.9]

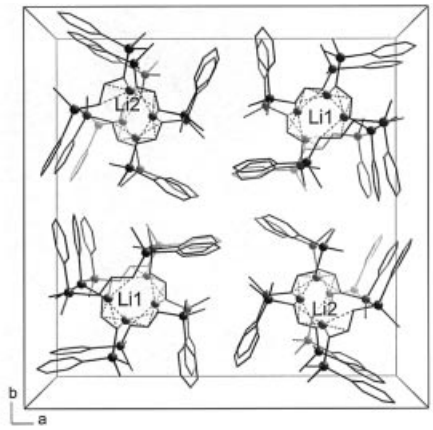

Figure 2. Perspective view along the *c* axis of the unit cell of **5b·Li** having alternating clockwise (Li1) and anticlockwise (Li2) spiral chains

While the differences in the C_3 moieties are not worth mentioning, the absence of an additional ligand coordinating the cation in **5b·Li** has a distinct effect, unsurprisingly, on the C−Li distances. In (1,3-diphenylallyl)lithium·OEt_2, the cation is ca. 10 to 20 pm more remote from the carbon atoms [C−Li: 230(3), 232(3), 248(3), 240(3), 250(3), 252(3) pm].

Compound **7a**·Li[THF]$_2$ forms a contact ion pair; the cation is coordinated by N1, B1−C1, C1−H1, and two molecules of THF, one of which shows disorder. The bond B1−C1 [146.6(3) pm] is significantly shorter than the B2−C3 bond [160.8(3) pm] because of its double bond character. This situation results in a long N1−B1 bond [153.1(2) pm] while the N2−B2 distance [140.8(2) pm] is in the typical range of N−B bonds having a strong π-interaction.

Like **7a**·Li[THF]$_2$, compound **7b**·Li[Et_2O]$_2$ forms a contact ion pair: the cation is coordinated by C1−B1 and two molecules of diethyl ether in this case. The unit cell contains two independent molecules of **7b**·Li[Et_2O]$_2$ with only slightly different bond lengths and bond angles (the second set of data is given in brackets in the following discussion). Complexes **7a**·Li[THF]$_2$ and **7b**·Li[Et_2O]$_2$ are similar with regard to their B_2C_3 rings (see Figures 3 and 4); while the Li cation of the latter is placed approximately above the C−B double bond {B1−Li1: 238.9(5) pm [238.3(4)]; C1−Li1: 239.7(5) pm [243.1(4)]; B2−B1−C1−Li1: 101.9(2)° [101.0(2)°]}, the cation in **7a**·Li[THF]$_2$ is located nearer to the ring plain because of the coordination to the amino group [Li1−C1−B1−B2 146.5 (2)].

In the structure of **1b** (Figure 5), the B−B [169.2(4) pm] and B−Cl [175.9(3), 176.0(3) pm] bond lengths are quite similar to those found in 1,2-dichloro-1,2-dimesityldiborane(4)[25] [168.0(6), 177.0(5) and 177.4(4) pm, respectively]. Compound **1b** deviates from C_s symmetry in the solid state mainly because the orientations of the $SiMe_3$ groups at C1 and C3 break the symmetry of a mirror plane, but also because of slight nonplanarity around the B−B moiety [Cl1−B1−B2−Cl2: 5.8(3)°] and the inequivalent B−C and

 © 2004 Wiley-VCH Verlag GmbH & Co. KGaA, Weinheim

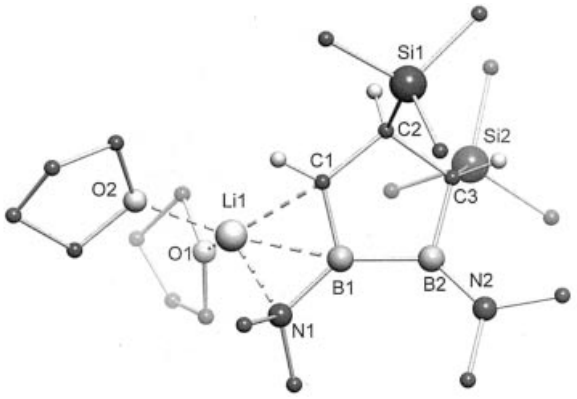

Figure 3. Structure of **7a**·Li[THF]$_2$ in the crystal (most H atoms have been omitted for clarity); selected bond lengths [pm] and angles [°]: B1−B2 169.1(3), B1−C1 146.6(3), B2−C3 160.8(3), C1−C2 152.4(2), C2−C3 156.8(3), N1−Li1 203.3(4), B1−Li1 230.2(4), C1−Li1 223.6(4); C1−B1−B2 103.1(2), C3−B2−B1 105.1(2), C2−C1−B1 115.4(2), C2−C3−B2 104.9(2), sum of angles (without Li1) C1 359.6, N1 344.7, N2 359.8

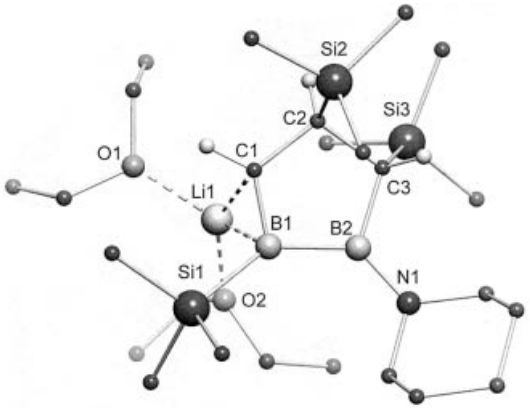

Figure 4. Structure of **7b**·Li[Et$_2$O]$_2$ in the crystal; selected bond lengths [pm] and angles [°], the corresponding values for the second independent ion pair are provided in brackets: B1−B2 171.3(3) [170.0(4)], B1−C1 146.1(3), B2−C3 160.1(3), C1−C2 151.9(3) [152.3(3)], C2−C3 157.4(3) [156.2(3)], B1−Si1 200.9(2) [201.2(2)], B1−Li1 238.9(5) [238.3(4)], C1−Li1 239.7(5) [243.1(4)]; C1−B1−B2 101.4(2) [101.8(2)], C3−B2−B1 107.2(2) [106.9(2)], C2−C1−B1 117.2(2) [116.9(2)], C2−C3−B2 105.1(2) [104.9(2)]; sum of angles (without Li1) C1 359.6 [359.2], N1 359.1 [359.3]

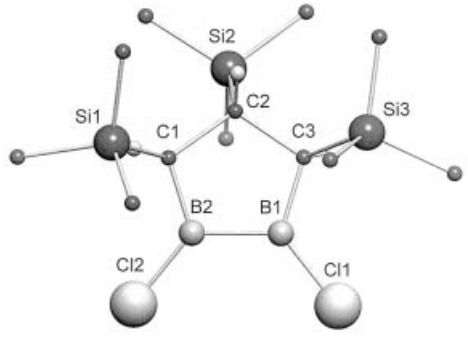

Figure 5. Structure of **1b** in the crystal; selected bond lengths [pm] and angles [°]: B1−B2 169.2(4), B2−C1 150.1(4), C1−C2 156.0(3), C2−C3 157.7(3), C3−B1 151.6(3), B1−Cl1 176.0(3), B2−Cl2 175.9(3), C1−Si1 193.0(2), C2−Si2 189.9(2), C3−Si3 192.5(2); B1−B2−C1 107.2(2), B1−B2−Cl2 128.3(2), B2−B1−C3 106.4(2), B2−B1−Cl1 128.3(2), B1−C3−C2 107.4(2), C3−C2−C1 109.8(2), C2−C1−B2 107.5(2), C1−B2−B1−C3 4.5(2)

C−C bond lengths (see caption to Figure 5). The short B−C [B2−C1: 150.1(4) pm; B1−C3: 151.6(3) pm; usually 158−160 pm] and long C−Si bonds [C1−Si1 193.0(2) pm; C3−Si3 192.5(2) pm; usually 186−187 pm] are mainly the result of C−Si hyperconjugation of the boron atoms with the C−Si bonds.

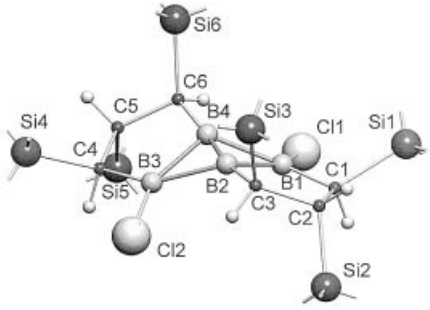

Figure 6. Structure of *cis*-**11** in the crystal; selected bond lengths [pm] and angles [°]: B1−B2 182.6(2), B2−B3 186.3(2), B3−B4 182.2(2), B4−B1 186.0(2), B2−B4 150.2(2), B1−Cl1 179.8(2), B3−Cl2 179.8(2), B1−C1 157.1(2), C1−C2 155.6(2), C2−C3 157.1(2), C3−B2 156.4(2); Cl1−B1−C1 112.1(1), Cl2−B3−C4 112.0(1), C3−B2−B4 169.4(1), C6−B4−B2 170.1(1), B1−B2−B4−B3 135.2(1)

Compound *cis*-**11** (Figure 6) possesses a folded [135.2(1)°] diamond-like structure that has a remarkably short diagonal of only 150.2(2) pm. The edges of this diamond are considerably longer [182.2(2) to 186.3(2) pm] than the B−B bond in **1b** [169.2(4) pm], which indicates multicenter bonding. The boron centers that carry chloro substituents show an approximately planar surrounding by their four neighbors [Cl1−B1−B4−B2: 174.1(1)°; Cl2−B3−B2−B4: 176.7(1)°]. All trimethylsilyl substituents at carbon atoms bound to boron atoms lie on the same side of the B_4 ring. We refer to this stereochemistry as "*cis*" in this text.

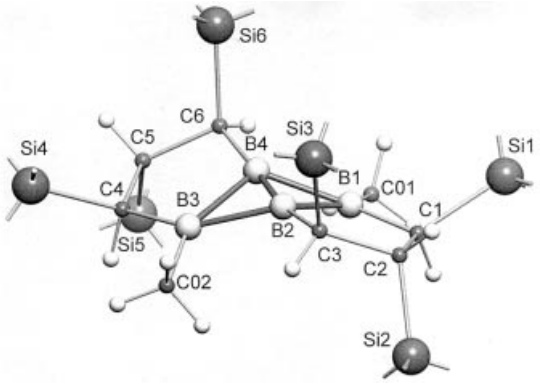

Figure 7. Structure of *cis*-**14** in the crystal; selected bond lengths [pm] and angles [°]: B1−B2 179.9(3) B2−B3 183.0(3), B3−B4 180.2(3), B4−B1 183.5(3), B2−B4 150.1(3), B1−C01 164.8(3), B3−C02 160.9(3), B1−C1 159.6(2), C1−C2 156.1(2), C2−C3 157.0(2), C3−B2 158.0(2); C01−B1−C1 112.0(2), C02−B3−C4 113.0(2), C3−B2−B4 169.4(2), C6−B4−B2 170.1(2), B1−B2−B4−B3 140.2(1)

Compound *cis*-**14** (Figure 7) is isostructural to *cis*-**11** and has a similar folding angle of 140.2(1)° for the B_4 diamond. Its diagonal is short [150.1(3) pm], and the edges of the

 © 2004 Wiley-VCH Verlag GmbH & Co. KGaA, Weinheim

diamond are a bit shorter [179.9(3) to 183.5(3) pm] than those in *cis*-**11**. The boron centers that carry methyl substituents are almost planar-tetracoordinate (max. deviations from best planes: B1,B2,B4,C01,C1, 9.9(2) pm; B2,B3,B4,C02,C4, 5.3(2) pm].

Discussion

The ring closure, accompanied by an 1,2-migration of a trimethylsilyl group, which takes place upon reaction of **6a** with lithium metal and leads to the boron-stabilized carbanion **7a**, is unprecedented to the best of our knowledge. It may be explained, however, by analogy to reactions of carbon electrophiles with allylsilanes,[26] by invoking the borylborenate **15a** as an intermediate (Scheme 5). Since borylborenates are isoelectronic with methyleneboranes[27] and vinyl cations, their dicoordinate boron center can be expected to react intramolecularly as a strong electrophile with the allylsilane moiety to generate a carbocation in the β-position relative to a silyl substituent. 1,2-Migration of silyl substituents in cations of this type are well-known processes in the chemistry of allylsilanes.[26]

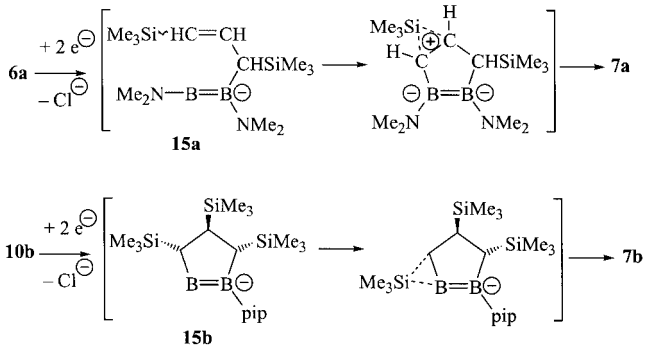

Scheme 5

By analogy, the formation of the boron-stabilized carbanion **7b** upon reaction of **10b** with lithium metal can be rationalized by assuming that the borylborenate **15b** is the intermediate. In this case, the silyl substituent migrates to the neighboring electrophilic dicoordinate boron center.

Obviously, the first 1,2-dichloro-1,2-diborolane, **1b**, owes its persistence to the trimethylsilyl substituents at all of the carbon atoms. All attempts to generate a derivative lacking this substituent next to one of the boron centers were unsuccessful. This result explains the failure of earlier efforts to prepare **1a** lacking any substituents.[2]

So far, reaction of metals with 1,2-dichloro-1,2-diboranes(4) having appropriate substituents, like sterically demanding amino or *tert*-butyl substituents, have led to the elimination of both chlorine atoms and generation of folded or tetrahedral tetraboranes(4).[28,29] The reductive dimerization of **1b** to *cis*-**11** is the first example where only one chlorine atom of each 1,2-dichloro-1,2-diborane(4) is eliminated. The dichlorotetraborane(6) *cis*-**11** is a 2e-aromatic tetraborane(6) that has a nonclassical σ-skeleton. Computations (B3LYP/6-311+G**//B3LYP/6-31G*+ZPE)[30] of model molecules lacking silyl substituents show that the aromatic folded diamond **11u** is preferred over the classical planar **11u*p** by 24.7 kcal·mol^{-1}. The orthogonal **11u*o** (Scheme 6), which benefits from twofold B–B hyperconjugation, is only 13.2 kcal·mol^{-1} lower in energy than **11u*p**.

While the *cis* configuration is retained during the transformations of *cis*-**11** to *cis*-**13** and *cis*-**14** via *cis*-**12** and its dianion,[20] the stereoisomer *trans*-**13** is obtained upon reaction of *cis*-**11** with 2 equiv. of sodium triethylhydroborate. All transformations leading to *cis*-**13** occur with conservation of 2e-aromaticity and retention of the stereochemistry in the four-membered rings. The inversion of the stereochemistry of three adjacent centers during the formation of *trans*-**13** requires opening of one ring and then reclosure after inversion at these three centers. This process is possible without loss of 2e-aromaticity by formation of three-membered aromatic systems as intermediates. The initially formed *cis*-**17** can open to *syn*-**18** with conservation of 2e-aromaticity. Rotation about the B–C bond marked with a curved arrow in Scheme 7 in *syn*-**18** leads to *anti*-**18** in which three trimethylsilyl substituents pointing in opposite directions relative to those in *syn*-**18**. This stereochemistry is locked by the reaction to form *trans*-**13**; thus, the transformation of *cis*-**11** into *trans*-**13** occurs with conservation of 2e-aromaticity in all steps. Our mechanism is supported by computations that show that the prototype molecules **17u** and **18u** are low-energy minima.[31] In addition, attack of electrophiles at the 2c2e B–B bond of triboracyclopropanates **18**, like that which occurs during the transformation of *anti*-**18** into *trans*-**13**, are well known experimentally.[7]

Our assumption that the stereoisomerization does not take place during the substitution of the *first* chloride by

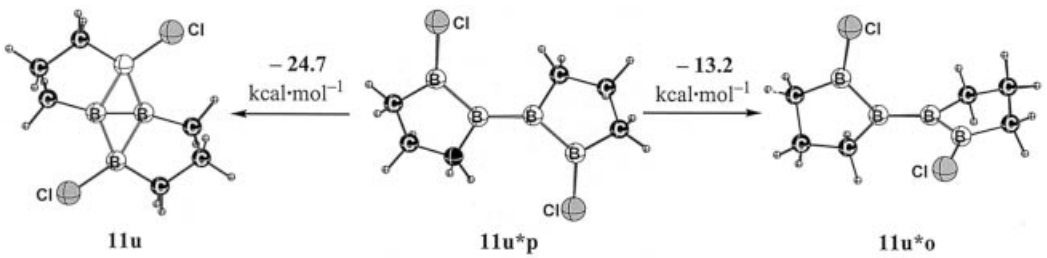

Scheme 6

 © 2004 Wiley-VCH Verlag GmbH & Co. KGaA, Weinheim

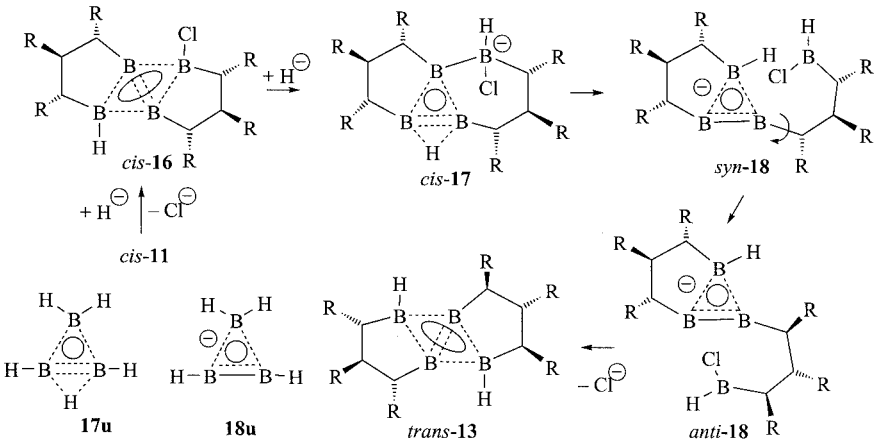

Scheme 7

hydride, but requires a hydrogen atom for the transformation *cis*-**17** → *syn*-**18** to be easy, is supported by the following observation. Substitution of one chloride in *cis*-**11** for CH_2SiMe_3, by reaction with $LiCH_2SiMe_3$, occurs with conservation of the *cis* configuration, as is evidenced by the X-ray structure determination of the obtained monochlorotetraborane(6).[32]

Transformation of the versatile **1b** into 1,2-diorganyl-1,2-diborolanes and their spontaneous and thermally induced reactions will be described in a forthcoming paper.

Experimental Section

General: All reactions were carried out under argon, using standard Schlenk techniques. Solvents were dried, distilled, and saturated with argon. Glassware was dried using a heat gun under high vacuum. ^1H, ^{11}B, and ^{13}C NMR: Bruker ARX 300 and AMX 500 spectrometers. NMR references: Me_4Si, $BF_3{\cdot}OEt_2$.

(*E*)-1,3-Bis[dimethyl(phenyl)silyl]propene (4b): *n*-Butyllithium solution (1.6 N in hexanes, 73.1 mL 117 mmol) was added to a solution of 3-(dimethylphenylsilyl)propene (20.6 g, 116.9 mmol) in *n*-pentane/diethyl ether (1:1, 100 mL) at 0 °C within 2 h. After the solution had been stirred at room temperature for 3 d, chlorodimethyl(phenyl)silane (20.5 g, 120 mmol) was added at −78 °C and the mixture was warmed to room temperature. The organic layer was washed with water (2 × 200 mL), dried with $MgSO_4$, and distilled at 1 × 10^{-3} mbar. Yield: 29.8 g (82%); colorless oil (b.p. 98 °C). For spectroscopic data, see ref.[10]

[1,3-Bis(trimethylsilyl)allyl]lithium (5a·Li): *n*-Butyllithium solution (1.6 N in hexanes, 45 mL 72 mmol) was added at 0 °C to a solution of **4a** (11.9 g, 64.0 mmol) in *n*-pentane/diethyl ether (1:1, 100 mL). After the solution had been stirred at room temperature for 8 d, all volatile components were evaporated in vacuo and the residue was suspended in *n*-pentane (100 mL) and stirred for 2 h. Insoluble **5a·Li** was separated using a reverse glass frit and washed with *n*-pentane (2 × 30 mL). Yield: 9.6 g (78%); colorless, pyrophoric powder. ^1H NMR (200 MHz, [D_8]THF, 300 K): δ = −0.11 (s, 18 H, $SiMe_3$), 2.64 (d, $^3J_{H,H}$ = 16 Hz, 2 H, CHSi), 6.57 (t, $^3J_{H,H}$ = 16 Hz, 1 H, C_2CH) ppm. ^{13}C NMR (75 MHz, [D_8]THF, 300 K): δ = 2.1 (q, $SiMe_3$), 67.3 (d, $^1J_{C,H}$ = 128 Hz, CHSi), 154.3 (d, $^1J_{C,H}$ = 137 Hz, C_2CH) ppm.

1,3-Bis[dimethyl(phenyl)silyl]allyllithium (5b·Li): In a similar reaction to the preparation of **5a·Li**, **4b** (12.0 g, 38.6 mmol) was treated with *n*-butyllithium solution (1.6 N in hexanes, 26.3 mL 42.1 mmol) for 4 d. After workup, **5b·Li** (8.56 g, 70%) was obtained as a slightly yellow, pyrophoric powder. ^1H NMR (300 MHz, [D_8]THF, 300 K): δ = 0.20 (s, 12 H, SiMe), 2.95 (d, $^3J_{H,H}$ = 16 Hz, 2 H, CHSi), 6.77 (t, $^3J_{H,H}$ = 16 Hz, 1 H, C_2CH), 7.15−7.65 (m, 10 H, Ph) ppm.

(*E*/*Z*)-1-[1,3-Bis(trimethylsilyl)allyl]-2-chloro-1,2-bis(dimethylamino)diborane(4) (6a): 1,2-Dichloro-1,2-bis(dimethylamino)diborane(4) (**3**)[33] (17.2 g, 95.0 mmol) was added dropwise to a solution of [1,3-bis(trimethylsilyl)allyl]lithium (**5a·Li**) (18.0 g, 93.6 mmol) in diethyl ether (150 mL) at −78 °C. The mixture was warmed to room temperature and all volatile compounds were evaporated in vacuo. After filtration and washing the residue with *n*-pentane (2 × 50 mL), the filtrate was distilled at 1 × 10^{-1} mbar to yield allyldiborane(4) (*E*/*Z*)-**6a** (29.4 g, 95% relative to **3**; 85:15) as a colorless oil (b.p. 68−72 °C). **(*E*)-6a:** ^1H NMR (300 MHz, $CDCl_3$, 300 K): δ = −0.01, 0.02 (each s, each 9 H, $SiMe_3$), 2.00 (d, $^3J_{H,H}$ = 11 Hz, 1 H, BCHSi), 2.68, 2.69, 2.77, 2.88 (each s, each 3 H, NMe), 5.20 (d, $^3J_{H,H}$ = 18 Hz, 1 H, C=CHSi), 6.09 (dd, $^3J_{H,H}$ = 18, 11 Hz, 1 H, C*H*=CHSi) ppm. ^{11}B NMR (96 MHz, $CDCl_3$, 300 K): δ = 42, 46 ppm. ^{13}C NMR (75 MHz, $CDCl_3$, 300 K): δ = −1.1, −0.8 (each q, $SiMe_3$), 41.2 (br. d, $^1J_{C,H}$ = 94 Hz, BCHSi), 37.6, 39.3, 42.2, 44.6 (each q, NMe), 123.3 (d, $^1J_{C,H}$ = 132 Hz, CH=*C*HSi), 149.3 (d, $^1J_{C,H}$ = 148 Hz, *C*H=CHSi) ppm.

(*E*/*Z*)-1-{1,3-Bis[dimethyl(phenyl)silyl]allyl}-2-chloro-1,2-bis(dimethylamino)diborane(4) (6b): (*E*/*Z*)-**6b** was synthesized by a similar procedure to that of (*E*/*Z*)-**6a** from **3** (4.42 g, 24.44 mmol) and {1,3-bis[dimethyl(phenyl)silyl]allyl}lithium (**5b·Li**, 6.9 g, 22.2 mmol). Distillation at 1 × 10^{-3} mbar yielded (*E*/*Z*)-**6b** (8.29 g, 82% relative to **3**; 9:1) as a colorless oil (b.p. 105−110 °C). **(*E*)-6b:** ^1H NMR (300 MHz, $CDCl_3$, 300 K): δ = 0.27, 0.29, 0.37 (each s, total 12 H, SiMe), 2.28 (d, $^3J_{H,H}$ = 11 Hz, 1 H, BCHSi), 2.35, 2.62, 2.71, 2.85 (each s, each 3 H, NMe), 5.29 (d, $^3J_{H,H}$ = 18 Hz, 1 H, CH=C*H*Si), 6.24 (dd, $^3J_{H,H}$ = 18, 11 Hz, 1 H, C*H*=CHSi), 7.25−7.60 (m, 10 H, Ph) ppm. ^{11}B NMR (96 MHz, $CDCl_3$, 300 K): δ = 42 ppm. ^{13}C NMR (75 MHz, $CDCl_3$, 300 K): δ = −3.4, −2.5, −2.2, −2.1 (each q, SiMe), 40.9 (br. d, $^1J_{C,H}$ = 126 Hz, BCHSi), 37.6, 39.0, 42.1, 44.5 (each q, NMe), 122.2 (d, $^1J_{C,H}$ = 136 Hz, CH=*C*HSi), 127.3, 127.6, 128.6, 128.6, 133.8, 134.0 (each d, *o*-, *m*-, *p*-C), 139.6, 139.9 (each s, *i*-C), 150.9 (d, $^1J_{C,H}$ = 150 Hz, *C*H=CHSi) ppm.

 © 2004 Wiley-VCH Verlag GmbH & Co. KGaA, Weinheim

Lithium 1,2-Bis(dimethylamino)-4,5-bis(trimethylsilyl)diborolan-3-ide (7a·Li): Naphthalene (ca. 10 mg) was added to a mixture of lithium powder (600 mg, 86.4 mmol) in THF (150 mL) and then the suspension was stirred until it turned dark-green (5−30 min). The flask was then placed in a big water bath and allyldiborane(4) **6a** (12.0 g, 36.3 mmol) was added within 2 min. After the mixture had been stirred overnight, all volatile compounds were evaporated in vacuo and the residue was suspended in *n*-pentane (150 mL). After filtration, a stable solution of **7a** was obtained, which was used for further syntheses. Crystallization from *n*-pentane at −30 °C yielded **7a**·Li[THF]$_2$ (8.76 g, 50%) as colorless crystals (m.p. 43 °C). ^{1}H NMR (300 MHz, C_6D_6, 300 K): δ = 0.31, 0.33 (each s, each 9 H, $SiMe_3$), 1.20 (s, 1 H, BCHSi), 1.41 (m, 8 H, THF), 2.08 (d, $^3J_{H,H}$ = 3 Hz, 1 H, C_2CHSi), 2.78, 3.03, 3.25 (each s, total 12 H, NMe), 3.48 (m, 8 H, THF), 4.58 (d, $^3J_{H,H}$ = 3 Hz, 1 H, B=CH) ppm. ^{11}B NMR (96 MHz, C_6D_6, 300 K): δ = 38, 52 ppm. ^{13}C NMR (75 MHz, C_6D_6, 300 K): δ = −2.5, 0.8 (each q, $SiMe_3$), 25.4 (t, THF), 30.4 (br. d, $^1J_{C,H}$ = 109 Hz, BCHSi), 33.6 (d, $^1J_{C,H}$ = 115 Hz, C_2*C*HSi), 42.5, 46.5, 46.8 (each q, NMe), 68.5 (t, THF), 109.0 (br. d, $^1J_{C,H}$ = 118 Hz, B=CH) ppm.

3,4-Bis(dimethylamino)-5-(trimethylsilyl)-3,4-diboracyclopentene (8): 1,1,1-Trifluoro-2-iodoethane (8.19 g, 39.0 mmol) was added to a solution of **7a** (prepared from 12.9 g **6a**) in diethyl ether (100 mL) at −78 °C. The mixture was warmed to room temperature within 10 min by using a water bath and then distilled at 20 mbar to yield **8** (4.33 g) as colorless liquid (b.p. 60−62 °C). ^{1}H NMR (300 MHz, $CDCl_3$, 300 K): δ = −0.08 (s, 9 H, $SiMe_3$), 1.45 (d, $^3J_{H,H}$ = 3 Hz, 1 H, BCHSi), 2.78, 2.87, 2.95, 2.99 (each s, each 3 H, NMe), 6.13 (d, $^3J_{H,H}$ = 9 Hz, 1 H, BCH), 7.01 (dd, $^3J_{H,H}$ = 9, 3 Hz, 1 H, C_2CH) ppm. ^{11}B NMR (96 MHz, $CDCl_3$, 300 K): δ = 46, 51 ppm. ^{13}C NMR (75 MHz, $CDCl_3$, 300 K): δ = −1.3 (q, $SiMe_3$), 34.4 (br. d, $^1J_{C,H}$ = 112 Hz, BCHSi), 41.2, 41.4, 44.9, 45.5 (each q, NMe), 137.1 (br. d, $^1J_{C,H}$ = 149 Hz, BCH), 159.5 (d, $^1J_{C,H}$ = 152 Hz, C_2*C*H) ppm.

1,2-Bis(dimethylamino)-3,4,5-tris(trimethylsilyl)-1,2-diborolane (2c): A solution of **7a·Li** [prepared from **6a** (12.0 g, 36.3 mmol)] in *n*-pentane/diethyl ether (2:1, 150 mL) was cooled to −78 °C and mixed with 1.1 equiv. of chlorotrimethylsilane (4.34 g, 39.9 mmol). After warming to room temperature, all volatile components were evaporated in vacuo and the residue was suspended in *n*-pentane (100 mL). Filtration and evaporation of the solvent yielded **2c** (12.43 g, 93% relative to **6a**) as a highly viscous oil that crystallized overnight (m.p. 42 °C). Usually, the *n*-pentane solutions were used for the synthesis of **1b** without further workup. ^{1}H NMR (300 MHz, $CDCl_3$, 300 K): δ = −0.15, 0.04 (each s, total 27 H, $SiMe_3$), 0.64 (d, $^3J_{H,H}$ = 3 Hz, 2 H, BCHSi), 1.46 (t, $^3J_{H,H}$ = 3 Hz, 1 H, C_2CHSi), 2.82, 2.90 (each s, each 6 H, NMe) ppm. ^{11}B NMR (96 MHz, $CDCl_3$, 300 K): δ = 54 ppm. ^{13}C NMR (75 MHz, $CDCl_3$, 300 K): δ = −3.3, 1.5 (each s, $SiMe_3$), 23.6 (br. d, $^1J_{C,H}$ = 123 Hz, BCHSi; d, $^1J_{C,H}$ = 123 Hz, C_2*C*HSi), 42.7, 45.5 (each q, NMe) ppm.

1,2-Bis(dimethylamino)-3,4-bis(trimethylsilyl)-1,2-diborolane (2d): Starting from **6a** (12.2 g), **2d** was synthesized by a similar procedure to that of **2c** from **7a** and 6 N HCl (1 equiv., diethyl ether). Distillation (10 mbar, 65−70 °C) yielded **2d** (8.53 g, 78%) as a colorless liquid. ^{1}H NMR (300 MHz, $CDCl_3$, 300 K): δ = −0.15, 0.13 (each s, each 9 H, $SiMe_3$), 0.76 (s, 1 H, BCHSi), 0.77 (dd, $^2J_{H,H}$ = 17, $^3J_{H,H}$ = 4 Hz, 1 H, BCH*H′*), 1.05 (dd, $^2J_{H,H}$ = 17, $^3J_{H,H}$ = 10 Hz, 1 H, BC*H*H′), 1.17 (dd, $^3J_{H,H}$ = 10, 4 Hz, 1 H, C_2CHSi), 2.75, 2.79, 2.89, 2.91 (each s, each 3 H, NMe) ppm. ^{11}B NMR (96 MHz, $CDCl_3$, 300 K): δ = 53 ppm. ^{13}C NMR (75 MHz, $CDCl_3$, 300 K): δ = −3.3, −0.9 (each q, $SiMe_3$), 20.5 (br. pseudo t, $^1J_{C,H}$ = 117 Hz, BCH_2), 20.9 (d, $^1J_{C,H}$ = 120 Hz, C_2*C*HSi), 27.0 (br. d, $^1J_{C,H}$ = 109 Hz, BCHSi), 40.7, 40.9, 45.1, 45.6 (each q, NMe) ppm.

1,2-Dichloro-3,4,5-tris(trimethylsilyl)-1,2-diborolane (1b): A solution of **2c** (6.8 g, 18.5 mmol) in *n*-pentane (150 mL) was mixed with neat BCl_3 (8.67 g, 74 mmol, 4.4 equiv.) at −78 °C and then warmed to 0 °C within 3 h. All volatile components were evaporated at this temperature and then the residue was warmed to room temperature in vacuo and evacuation was continued for 2 h. The residue was treated with *n*-pentane (50 mL) and the insoluble byproducts were filtered off. Evaporation of the solvent yielded **1b** (6.2 g, 96%) as a highly viscous oil, which was essentially pure based on its ^{1}H NMR spectra. Crystallization from *n*-pentane (necessary for reactions starting with more than 10 g of **2c**) at −30 °C gave light-yellow crystals [68%; m.p. 44 °C (decomposition)]. ^{1}H NMR (300 MHz, $CDCl_3$, 300 K): δ = −0.15, 0.16 (each s, total 27 H, $SiMe_3$), 1.92 (t, $^3J_{H,H}$ = 1 Hz, 1 H, C_2CHSi), 2.13 (d, $^3J_{H,H}$ = 2 Hz, 2 H, BCHSi) ppm. ^{11}B NMR (96 MHz, $CDCl_3$, 300 K): δ = 84 ppm. ^{13}C NMR (75 MHz, $CDCl_3$, 300 K): δ = −3.4, 1.0 (each q, $SiMe_3$), 28.4 (d, $^1J_{C,H}$ = 124 Hz, C_2*C*HSi), 53.2 (br. d, $^1J_{C,H}$ = 117 Hz, BCHSi) ppm.

3,7-Dichloro-1,2,4,5,6-pentakis(trimethylsilyl)-3,7-diboracycloheptene (9): **1b** (ca. 4.5 g, 12.8 mmol) dissolved in *n*-pentane (50 mL) was treated with bis(trimethylsilyl)ethyne (3.27 g, 19.2 mmol, 1.5 equiv.) at 0 °C. After warming to room temperature, all volatile components were evaporated in vacuo, to yield **9** (6.35 g, 95%) as a highly viscous oil that contained some minor impurities. ^{1}H NMR (300 MHz, $CDCl_3$, 300 K): δ = 0.10, 0.18, 0.33 (each s, total 45 H, $SiMe_3$), 1.26 (t, $^3J_{H,H}$ = 7 Hz, 1 H, C_2CHSi), 1.43 (d, $^3J_{H,H}$ = 7 Hz, 2 H, BCHSi) ppm. ^{11}B NMR (96 MHz, $CDCl_3$, 300 K): δ = 67 ppm. ^{13}C NMR (75 MHz, $CDCl_3$, 300 K): δ = 0.7, 1.6, 3.0 (each q, $SiMe_3$), 18.4 (d, $^1J_{C,H}$ = 127 Hz, C_2*C*HSi), 34.8 (br. d, $^1J_{C,H}$ = 112 Hz, BCHSi), 181.2 (br. s, BCSi) ppm.

1,2-Dipiperidino-3,4,5-tris(trimethylsilyl)-1,2-diborolane (2e): *N*-(Trimethylsilyl)piperidine (ca. 4 equiv.) was added to a stirred solution of **2c** (2.2 g, 6.27 mmol) in *n*-pentane (50 mL) at room temperature. After 24 h, all volatile components were evaporated in vacuo to yield **2e** (2.64 g, 94%) as a slightly yellow solid. ^{1}H NMR (300 MHz, C_6D_6, 300 K): δ = 0.26, 0.43 (each s, total 27 H, $SiMe_3$), 1.00 (d, $^3J_{H,H}$ = 5 Hz, 2 H, BCHSi), 1.5−1.7 (m, 12 H, pip), 1.91 (t, $^3J_{H,H}$ = 5 Hz, 1 H, C_2*C*HSi), 3.3−3.5 (m, 8 H, pip) ppm. ^{11}B NMR (96 MHz, C_6D_6, 300 K): δ = 53 ppm. ^{13}C NMR (75 MHz, C_6D_6, 300 K): δ = −2.6, 2.0 ($SiMe_3$), 22.7 (br., BCHSi), 24.3 (C_2*C*HSi), 25.3, 27.8, 28.2, 51.9, 53.9 (pip) ppm.

1,2-Bis(diethylamino)-3,4,5-tris(trimethylsilyl)-1,2-diborolane (2f): By a procedure analogous to that for the preparation of **2e**, **2f** was synthesized from **2c** (4.0 g, 11.39 mmol) and diethyl(trimethylsilyl)amine (4 equiv.) to yield **2f** (4.59 g, 95%) as a slightly yellow solid. ^{1}H NMR (300 MHz, $CDCl_3$, 300 K): δ = −0.14, 0.03 (each s, total 27 H, $SiMe_3$), 0.65 (d, $^3J_{H,H}$ = 3 Hz, 2 H, BCHSi), 1.05 (t, 12 H, NCH_2CH_3), 1.47 (t, $^3J_{H,H}$ = 3 Hz, 1 H, C_2CHSi), 3.22 (q, 8 H, NCH_2CH_3) ppm. ^{11}B NMR (96 MHz, $CDCl_3$, 300 K): δ = 54 ppm. ^{13}C NMR (75 MHz, $CDCl_3$, 300 K): δ = −2.8, 1.5 (each q, $SiMe_3$), 14.6, 15.0 (each q, NCH_2CH_3), 22.8 (br. d, $^1J_{C,H}$ = 110 Hz, BCHSi), 23.8 (d, $^1J_{C,H}$ = 122 Hz, C_2*C*HSi), 43.2, 45.8 (each t, NCH_2CH_3) ppm.

1-Chloro-2-(dimethylamino)-3,4,5-tris(trimethylsilyl)-1,2-diborolane (10a): Dimethyl(trimethylsilyl)amine (530 mg, 4.52 mmol) was added to a solution of **1b** (1.6 g, 4.56 mmol) in *n*-pentane (50 mL) at room temperature. After the mixture had been stirred overnight, all the volatile components were evaporated in vacuo and the residue was treated with *n*-pentane (25 mL) and filtered. Crystalliza-

 © 2004 Wiley-VCH Verlag GmbH & Co. KGaA, Weinheim

tion from *n*-pentane (5 mL) at −30 °C yielded **10a** (990 mg, 60%) as slightly yellow crystals [m.p. 52 °C (some decomposition)]. ^{1}H NMR (300 MHz, C_6D_6, 300 K): δ = −0.05, 0.25, 0.31 (each s, each 9 H, $SiMe_3$), 1.29 (s, 1 H, NBCHSi), 1.67 (d, $^3J_{H,H}$ = 2 Hz, 1 H, ClBCHSi), 1.79 (d, $^3J_{H,H}$ = 2 Hz, 1 H, C_2CHSi), 2.62, 3.04 (each s, each 3 H, NMe) ppm. ^{11}B NMR (96 MHz, C_6D_6, 300 K): δ = 48, 91 ppm. ^{13}C NMR (75 MHz, C_6D_6, 300 K): δ = −4.6, 0.1, 0.2 ($SiMe_3$), 24.4 (C_2*C*HSi), 27.9 (br., NBCHSi), 40.7, 41.4 (NMe), 46.8 (br., ClBCHSi) ppm.

1-Chloro-2-piperidino-3,4,5-tris(trimethylsilyl)-1,2-diborolane (10b): *N*-(Trimethylsilyl)piperidine (2.62 g, 16.7 mmol) was added to a solution of **1b** (5.85 g, 16.7 mmol) in *n*-pentane (50 mL) at −78 °C. After warming to room temperature, the mixture was stirred for an additional 18 h and then all the volatile components were evaporated in vacuo. Crystallization of the residue from *n*-pentane (15 mL) at −30 °C yielded **10b** (4.86 g, 73%) as colorless crystals [m.p. 72 °C (some decomposition)]. ^{1}H NMR (300 MHz, $CDCl_3$, 300 K): δ = −0.15, 0.01, 0.13 (each s, each 9 H, $SiMe_3$), 1.21 (d, $^3J_{H,H}$ = 2 Hz, 1 H, BCHSi), 1.43 (d, $^3J_{H,H}$ = 2 Hz, 1 H, BCHSi), 1.62 (dd, $^3J_{H,H}$ = 3, 2 Hz, 1 H, C_2CHSi), 1.32−1.75 [m, 6 H, $N(CH_2)_5$], 3.06, 3.29, 3.95 [each m, total 4 H, $N(CH_2)_5$] ppm. ^{11}B NMR (96 MHz, $CDCl_3$, 300 K): δ = 47, 92 ppm. ^{13}C NMR (75 MHz, $CDCl_3$, 300 K): δ = −3.4, 1.1, 1.3 (each q, $SiMe_3$), 25.1 (d, $^1J_{C,H}$ = 123 Hz, C_2*C*HSi), 27.9 (br. d, $^1J_{C,H}$ = 123 Hz, NBCHSi), 47.3 (br. d, $^1J_{C,H}$ = 104 Hz, ClBCHSi), 25.1, 28.1, 28.6, 51.1, 51.7 [each d, $N(CH_2)_5$] ppm.

Lithium 1-Piperidino-2,4,5-tris(trimethylsilyl)-1,2-diborolan-3-ide (7b·Li): A solution of **10b** (2.42 g, 6.1 mmol) in diethyl ether (25 mL) was added to a suspension of lithium powder (ca. 500 mg) in diethyl ether (25 mL) at room temperature. After the mixture had been stirred for 2 h, all the volatile components were evaporated in vacuo. The residue was treated with *n*-pentane (50 mL) and the excess lithium powder and LiCl were filtered off. Crystallization from *n*-pentane (20 mL) at −30 °C yielded **7b**·Li[Et_2O]$_2$ (1.67 g, 62%) as colorless crystals (m.p. 93 °C). ^{1}H NMR (400 MHz, C_6D_6, 300 K): δ = 0.15, 0.23, 0.45 (each s, each 9 H, $SiMe_3$), 0.86 (t, 6 H, Et_2O), 1.26 (s, 1 H, BCHSi), 1.55−1.87 [m, 6 H, $N(CH_2)_5$], 2.33 (d, $^3J_{H,H}$ = 3 Hz, 1 H, C_2CHSi), 3.01 (q, 4 H, Et_2O), 3.13, 3.42, 3.66, 4.21 [each m, each 1 H, $N(CH_2)_5$], 6.57 (d, $^3J_{H,H}$ = 3 Hz, 1 H, BCH) ppm. ^{11}B NMR (96 MHz, C_6D_6, 300 K): δ = 33, 58 ppm. ^{13}C NMR (75 MHz, C_6D_6, 300 K): δ = −2.5, 0.3, 3.2 (each q, $SiMe_3$), 14.4 (q, Et_2O), 27.5 (br., BCHSi), 26.3, 28.8, 29.3, [each t, $N(CH_2)_5$], 42.3 (d, $^1J_{C,H}$ = 119 Hz, C_2*C*HSi), 51.8, 56.2 [each t, $N(CH_2)_5$], 66.1 (t, Et_2O), 149.2 (br. d, $^1J_{C,H}$ = 122 Hz, BCH) ppm.

Dichlorotetraborane(6) (*cis*-11): $K_{2.8}Na$ (3 mL) was added to a solution of **1b** (5.92 g, 16.9 mmol) in *n*-pentane (150 mL; water bath, reflux condensor) at room temperature. After the reaction started (reflux, precipitation of a deep-blue salt), the mixture was stirred for an additional 30 min. The insoluble components were filtered off and washed with *n*-pentane (3 × 50 mL). Removal of the solvent yielded *cis*-**11** (5.11 g, 96%) as a yellow solid, essentially pure based on its ^{1}H NMR spectra. The use of larger quantities (> 10 g) of **1b** in this reaction caused the formation of some impurities. In this case, crystallization from *n*-pentane at −30 °C yielded **1b** (ca. 75%) as yellow crystals. Spectroscopic data: see ref.[5]

Tetraborane(6) (*trans*-13): $NaBEt_3H$ solution (1.0 N in toluene, 6 mL, 6 mmol) was added to a solution of *cis*-**11** (1.9 g, 3 mmol) in diethyl ether (50 mL) at −78 °C. The mixture was warmed slowly (12 h) to room temperature and then all the volatile components were evaporated in vacuo. The residue was treated with *n*-pentane (50 mL) and then the solution was separated from the solids using a pipette. After washing the solids with additional *n*-pentane (25 mL), the combined solutions were reduced to a volume of 20 mL. Crystallization at −30 °C yielded *trans*-**13** (1.02 g, 60%) in three fractions. Spectroscopic data: see ref.[5]

Tetraborane(4) (*cis*-12): Lithium naphthalenide solution (1.0 N, 26.7 mL, 26.7 mmol) was added to a suspension of *cis*-**11** (8.4 g, 13.3 mmol) in diethyl ether (150 mL) at −100 °C. After warming to room temperature, all of the volatile components were evaporated in vacuo and the naphthalene was sublimed (60 °C/1 × 10^{-3} mbar). The residue was treated with *n*-pentane (120 mL) and the insoluble solids were filtered off. Crystallization at −30 °C yielded *cis*-**12** (7.08 g, 95%) as a yellow solid. Spectroscopic data: see ref.[6]

Dimethyltetraborane(6) (*cis*-14): A solution of *cis*-**12** (1.9 g, 3.39 mmol) in THF (25 mL) was treated with lithium naphthalenide (2 equiv.), followed by iodomethane (0.95 g, 6.79 mmol), at −100 °C. After warming to room temperature, all of the volatile compounds were evaporated in vacuo, the residue was treated with *n*-pentane, and the insoluble material was filtered off. Crystallization from *n*-pentane (10 mL) at −30 °C yielded *cis*-**14** (1.60 g, 80%) as yellow crystals [m.p. 125 °C (decomposition)]. Spectroscopic data: see ref.[20]

Tetraborane(6) (*cis*-13): A solution of *cis*-**12** (1.1 g, 1.96 mmol) in THF (25 mL) was treated with lithium naphthalenide (2 equiv.) followed by HCl solution (2 N in diethyl ether, 0.99 mL, 1.98 mmol). After warming to room temperature and evaporation of the volatile compounds in vacuo, the naphthalene was separated by sublimation (60 °C/1 × 10^{-3} mbar). The residue was treated with *n*-pentane and the insoluble compounds were filtered off. *cis*-**13** of only 95% parity was obtained by crystallization from *n*-pentane at −30 °C. Yield (^{1}H NMR spectroscopy): 90%. ^{1}H NMR (300 MHz, C_6D_6, 300 K): δ = 0.07, 0.24, 0.28 (each s, each 18 H, $SiMe_3$), 1.74 (pseudo t, $^3J_{H,H}$ = 4 Hz, 2 H, C_2CHSi), 1.93 (d, $^3J_{H,H}$ = 4 Hz, 2 H, B_3BCHSi), 2.23 (m, 2 H, HBC*H*Si), 7.01 (very br. s, 2 H, BH) ppm. ^{11}B NMR (96 MHz, C_6D_6, 300 K): δ = 27, 51 ppm. ^{13}C NMR (75 MHz, C_6D_6, 300 K): δ = −3.6, 0.4, 0.5 ($SiMe_3$), 28.9 (d, $^1J_{C,H}$ = 123 Hz, C_2*C*HSi), 30 (br., BCHSi), 41.6 (br. d, $^1J_{C,H}$ = 110 Hz, BCHSi) ppm.

Crystal Structure Determinations: All single-crystal diffraction experiments were performed with an image plate area detector system (IPDS, Stoe) using an Mo-K_α radiation source equipped with a graphite monochromator. Crystals were selected from dry inert paraffin oil, mounted on top of a quartz capillary, and measured with φ scans. All crystal and experimental data of the six structure determinations are listed in Table 1. The structures were all solved by direct methods using the SHELXS program[34] and refined by the full-matrix least-squares method against all F^2 data.[35] "Interesting" hydrogen atoms at the nuclei of the structures were localized from difference Fourier maps and refined using individual isotropic displacement parameters; those of peripheral moieties, like the $SiMe_3$ groups, were treated as riding on idealized calculated positions. Their displacement parameters were fixed to 1.2- or (for methyl groups) 1.5-times the U_{eq} values of their bonding partners. All heavier atoms were refined using anisotropic displacement parameters. Images of the structure were drawn using DIAMOND.[36] Crystals of **1b** suitable for X-ray analysis were grown from an *n*-pentane solution at −30 °C. Single crystals of **5b·Li** were obtained by dissolving **5b·Li** (ca. 2 g) in boiling toluene (80 mL) and then keeping the solution at 95 °C for 18 h. The diffraction pattern of the very sensitive crystal showed weak powder rings, which probably caused the somewhat reduced quality of the results, especially

 © 2004 Wiley-VCH Verlag GmbH & Co. KGaA, Weinheim

Table 1. Crystal data and experimental details of the crystal structure determinations; all crystals were measured at $T = 193(1)$ K

	1b	**5b·Li**	**7a·Li[THF]$_2$**	**7b·Li[Et$_2$O]$_2$**	*cis*-**11**	*cis*-**14**
Empirical formula	$C_{12}H_{30}B_2Cl_2Si_3$	$C_{19}H_{25}Li_1Si_2$	$C_{21}H_{49}B_2LiN_2O_2Si_3$	$C_{25}H_{60}B_2LiN_2O_2Si_3$	$C_{24}H_{60}B_4Cl_2Si_6$	$C_{26}H_{66}B_4Si_6$
Formula mass	351.15	316.51	446.36	519.57	631.40	590.57
Crystal system	monoclinic	tetragonal	triclinic	triclinic	triclinic	triclinic
Space group	$P2_1/n$	$I4_1$ ($I4_3$)	$P\bar{1}$	$P\bar{1}$	$P\bar{1}$	$P\bar{1}$
Unit cell [pm, °]	$a = 909.6(1)$	2447.8(1)	973.2(1)	1011.5(1)	1015.6(1)	1014.5(1)
	$b = 1762.4(1)$	2447.8(1)	1126.0(1)	1768.5(2)	1273.5(1)	1280.6(1)
	$c = 1325.3(1)$	1289.8(1)	1426.2(1)	1986.4(2)	1652.0(1)	1643.9(1)
	$\alpha = 90$	90	94.46(1)	83.09(1)	103.10(1)	103.40(1)
	$\beta = 90.650(10)$	90	98.76(1)	90.00(1)	90.28(1)	90.05(1)
	$\gamma = 90$	90	104.04(1)	81.67(1)	109.30(1)	108.69(1)
V [Å^3]	2124.4(3)	7728.1(7)	1487.7(2)	3489.8(6)	1956.7(3)	1961.4(3)
Z	4	16	2	4	2	2
Calculated density [g·cm^{-3}]	1.098	1.088	0.996	0.989	1.072	1.000
Absorption coefficent [mm^{-1}]	0.462	0.177	0.136	0.155	0.363	0.227
$F(000)$	752	2720	492	1152	684	652
Crystal size [mm]	0.12 × 0.10 × 0.03	0.65 × 0.30 × 0.25	0.45 × 0.30 × 0.30	0.55 × 0.45 × 0.30	0.45 × 0.40 × 0.40	0.35 × 0.30 × 0.30
$\Theta_{max.}$ [°]	26.13	25.90	25.92	25.93	25.91	25.92
Index range	$-11 < h < 11$,	$-29 < h < 29$	$-11 < h < 11$	$-12 < h < 12$	$-12 < h < 12$	$-12 < h < 11$
	$-21 < k < 21$	$-29 < k < 30$	$-13 < k < 13$	$-21 < k < 21$,	$-15 < k < 15$,	$-15 < k < 15$
	$-16 < l < 15$	$-15 < l < 15$	$-17 < l < 17$	$-24 < l < 24$	$-20 < l < 20$	$-20 < l < 20$
Scan type	φ scans	φ scans	φ scans	φ scans	φ scans	φ scans
No. of reflections	16576	22589	16018	34646	17996	11838
Unique reflections (R_{int})	4133 (0.061)	7427 (0.0511)	5411 (0.0490)	12717 (0.0718)	7099 (0.0289)	7067 (0.0306)
Observed reflections [$I > 2\sigma(I)$]	2472	6331	3349	7402	5674	5125
Parameters, data/param. ratio	193, 21	430, 17	303, 18	655, 19	367, 19	371, 19
Goodness-of-fit (F^2)	0.818	1.023	0.885	0.827	0.966	0.947
R [$I > 2\sigma(I)$]	0.0327	0.0463	0.0427	0.0427	0.0298	0.0348
wR_2 (all refl.)	0.0648	0.1236	0.1156	0.0974	0.0770	0.0878
Largest diff. peak/hole [e·Å^{-3}]	+0.221/−0.261	+0.690/−0.220	+0.329/−0.238	+0.419/−0.285	+0.286/−0.225	+0.340/−0.252

the relatively high residual electron density of 0.69 e/Å^3. The absolute structure could not be determined clearly because of the absence of suitably strong anomalous scatters [Flack parameter $x = 0.21(11)$]. Possible twinning by merohedry could be excluded. Crystals of **7a**·Li[THF]$_2$ suitable for X-ray analysis were grown from an *n*-pentane solution at −30 °C. In its structure, one of the THF molecules coordinated to lithium shows disorder: C15 has two alternative positions (1:1) above and below the plane of the remaining atoms. A single crystal of **7b**·Li[Et$_2$O]$_2$ was obtained from an *n*-pentane/diethyl ether (1:1) solution at −30 °C. Crystals of the isostructural compounds *cis*-**11** and *cis*-**14** were grown from an *n*-pentane solution at −30 °C. CCDC-225331 (**1b**), -225332 (**5b·Li**), -225333 (**7a·Li[THF]$_2$**), -225334 (**7a·Li[Et$_2$O]$_2$**), -225335 (*cis*-**11**), and -225336 (*cis*-**14**) contain the supplementary crystallographic data for this paper. These data can be obtained free of charge at www.ccdc.cam.ac.uk/conts/retrieving.html [or from the Cambridge Crystallographic Data Centre, 12 Union Road, Cambridge CB2 1EZ, UK; Fax: (internat.) + 44-1223-336-033; E-mail: deposit@ccdc.cam.ac.uk].

Acknowledgments

This work was supported by the Deutsche Forschungsgemeinschaft (Schwerpunktprogramm Polyeder) and the Fonds der Chemischen Industrie.

[1] G. E. Herberich, C. Ganter, L. Wesemann, *Chem. Ber.* **1990**, *123*, 49−51.
[2] G. Knörzer, H. Seyffer, W. Siebert, *Z. Naturforsch., Teil B* **1990**, *45*, 1136−1138.
[3] G. E. Herberich, C. Ganter, L. Wesemann, R. Boese, *Angew. Chem.* **1990**, *102*, 914−915; *Angew. Chem. Int. Ed. Engl.* **1990**, *29*, 912−913.
[4] D. Steiner, C. Balzereit, H.-J. Winkler, N. Stamatis, M. Hofmann, P. v. R. Schleyer, A. Berndt, *Angew. Chem.* **1994**, *106*, 2391−2394; *Angew. Chem. Int. Ed. Engl.* **1994**, *33*, 2303−2306.
[5] C. Präsang, M. Hofmann, G. Geiseler, M. Massa, A. Berndt, *Angew. Chem.* **2002**, *114*, 1597−1599; *Angew. Chem. Int. Ed.* **2002**, *41*, 1526−1529.
[6] C. Präsang, M. Hofmann, G. Geiseler, W. Massa, A. Berndt, *Angew. Chem.* **2003**, *115*, 1079−1082; *Angew. Chem. Int. Ed.* **2003**, *42*, 1049−1052.
[7] C. Präsang, A. Mlodzianowska, Y. Sahin, M. Hofmann, G. Geiseler, W. Massa, A. Berndt, *Angew. Chem.* **2002**, *114*, 3529−3531; *Angew. Chem. Int. Ed.* **2002**, *41*, 3380−3382.
[8] G. Fraenkel, A. Chow, W. R. Winchester, *J. Am. Chem. Soc.* **1990**, *112*, 1382−1386.
[9] N. Shimizu, S. Imazu, F. Fumihiro, Y. Tsuno, *Bull. Chem. Soc. Jpn.* **1991**, *64*, 1122−1128.
[10] M. A. C. de Dios, I. Fleming, W. Friedhoff, P. D. W. Woode, *J. Organomet. Chem.* **2001**, *624*, 60−72.

 © 2004 Wiley-VCH Verlag GmbH & Co. KGaA, Weinheim

[11] M. Sugawara, J. Yoshida, *J. Org. Chem.* **2000**, *65*, 3135−3142.
[12] H. J. Carter, I. Flemming, A. Percival, *J. Chem. Soc., Perkin Trans. 1* **1981**, 2415−2434.
[13] T.-H. Chan, J.-S. Li, *J. Chem. Soc., Chem. Commun.* **1982**, 969−970.
[14] P. B. Hitchcock, M. F. Lappert, W.-P. Leung, D.-S. Liu, T. C. W. Mak, Z.-X. Wang, *J. Chem. Soc., Dalton Trans.* **1999**, 1257−1262.
[15] H. Klusik, C. Pues, A. Berndt, *Z. Naturforsch., Teil B* **1984**, *39*, 1042−1045.
[16] W. Siebert, M. Hildenbrand, P. Hornbach, G. Karger, H. Pritzkow, *Z. Naturforsch., Teil B* **1989**, *44*, 1179−1186.
[17] W. Biffar, H. Nöth, H. Pommerening, *Angew. Chem.* **1980**, *92*, 63−64; *Angew. Chem. Int. Ed. Engl.* **1980**, *19*, 56−57.
[18] Classical dichlorotetraboranes(6) have been known for a long time; see ref.[19]
[19] [19a] K. H. Hermannsdörfer, E. Matejcikova, H. Nöth, *Chem. Ber.* **1970**, *103*, 516−527. [19b] G. Linti, D. Loderer, H. Nöth, K. Polborn, W. Rattay, *Chem. Ber.* **1994**, *127*, 1909−1922.
[20] W. Mesbah, C. Präsang, M. Hofmann, G. Geiseler, W. Massa, A. Berndt, *Angew. Chem.* **2003**, *115*, 1758−1760; *Angew. Chem. Int. Ed.* **2003**, *42*, 1717−1719.
[21] H. Köster, E. Weiss, *Chem. Ber.* **1982**, *115*, 3422−3426.
[22] G. Boche, H. Etzrodt, M. Marsch, W. Massa, G. Baum, H. Dietrich, W. Mahdi, *Angew. Chem.* **1986**, *98*, 84−85; *Angew. Chem. Int. Ed. Engl.* **1986**, *25*, 104−105.
[23] U. Schümann, E. Weiss, *J. Organomet. Chem.* **1987**, *322*, 299−307.
[24] G. Boche, G. Fraenkel, J. Cabral, K. Harms, N. J. R. v. Eikema Hommes, J. Lohrenz, M. Marsch, P. v. R. Schleyer, *J. Am. Chem. Soc.* **1992**, *114*, 1562−1565.
[25] H. Hommer, H. Nöth, J. Knizek, W. Ponikwar, H. Schwenk-Kircher, *Eur. J. Inorg. Chem.* **1998**, 1519−1527.
[26] H.-J. Knölker, N. Foitzik, R. Graf, J.-B. Pannek, P. G. Jones, *Tetrahedron* **1993**, *49*, 9955−9972 and references cited therein.
[27] A. Berndt, *Angew. Chem.* **1993**, *105*, 1034−1058; *Angew. Chem. Int. Ed. Engl.* **1993**, *32*, 985−1009.
[28] T. Mennekes, P. Paetzold, R. Boese, D. Bläser, *Angew. Chem.* **1991**, *103*, 199−200; *Angew. Chem. Int. Ed. Engl.* **1991**, *30*, 173−175.
[29] C.-J. Maier, H. Pritzkow, W. Siebert, *Angew. Chem.* **1999**, *111*, 1772−1774; *Angew. Chem. Int. Ed.* **1999**, *38*, 1666−1668.
[30] All geometries were optimized by employing the B3LYP hybrid functional together with the 6-31G(d) basis set. Relative energies are based on energy computations at the 6-311+G(d,p) level and are corrected for zero-point vibrational energies. [30a] M. J. Frisch, G. W. Trucks, H. B. Schlegel, G. E. Scuseria, M. A. Robb, J. R. Cheeseman, V. G. Zakrzewski, J. A. Montgomery, Jr., R. E. Stratmann, J. C. Burant, S. Dapprich, J. M. Millam, A. D. Daniels, K. N. Kudin, M. C. Strain, O. Farkas, J. Tomasi, V. Barone, M. Cossi, R. Cammi, B. Mennucci, C. Pomelli, C. Adamo, S. Clifford, J. Ochterski, G. A. Petersson, P. Y. Ayala, Q. Cui, K. Morokuma, D. K. Malick, A. D. Rabuck, K. Raghavachari, J. B. Foresman, J. Cioslowski, J. V. Ortiz, A. G. Baboul, B. B. Stefanov, G. Liu, A. Liashenko, P. Piskorz, I. Komaromi, R. Gomperts, R. L. Martin, D. J. Fox, T. Keith, M. A. Al-Laham, C. Y. Peng, A. Nanayakkara, C. Gonzalez, M. Challacombe, P. M. W. Gill, B. Johnson, W. Chen, M. W. Wong, J. L. Andres, C. Gonzalez, M. Head-Gordon, E. S. Replogle, J. A. Pople, *Gaussian 98*, Revision A.7, Gaussian, Inc., Pittsburgh PA, **1998**. [30b]A. D. Becke, *J. Chem. Phys.* **1993**, *98*, 1372, 5648. [30c] C. Lee, W. Yang, R. G. Parr, *Phys. Rev. B* **1988**, *37*, 785.
[31] A. A. Korkin, P. v. R. Schleyer, M. L. McKee, *Inorg. Chem.* **1995**, *34*, 961−977.
[32] C. Präsang, A. Mlodzianowska, G. Geiseler, W. Massa, M. Hofmann, A. Berndt, *Pure Appl. Chem.* **2003**, *75*, 1175−1182.
[33] H. Nöth, W. Meister, *Z. Naturforsch., Teil B* **1992**, *17*, 714−718.
[34] G. M. Sheldrick, *SHELXS-97, Program for the solution of crystal structures*, University of Göttingen, **1997**.
[35] G. M. Sheldrick, *SHELXL-97, Program for refinement of crystal structures*, University of Göttingen, **1997**.
[36] K. Brandenburg, *DIAMOND 2.1c*, Crystal Impact GbR, Bonn, **1999**.

Received January 30, 2004
Early View Article
Published Online May 25, 2004

 © 2004 Wiley-VCH Verlag GmbH & Co. KGaA, Weinheim

Studies Related to the Chloro Titanium and Zirconium Complexes with [η^5-Cyclopentadienyldi(silylamido)] Ligands

María Sudupe,[a] Jesús Cano,[a] Pascual Royo,*[a] and Eberhardt Herdtweck[b]

Dedicated to Professor José Vicente on the occasion of his 60th birthday

Keywords: Zirconium / Titanium / Silylamido / Cyclopentadienyl-N ligands

Trichloro complexes [M{η^5-C_5H_3[$SiMe_2$(NH*t*Bu)]$_2$}Cl_3] [M = Zr (**2**), Ti (**3**)] have been synthesized by reaction of the corresponding chlorides MCl_4 with the lithium salt LiC_5H_3[$SiMe_2$(NH*t*Bu)]$_2$ (**1**). Complexes **2** and **3** react with 2 equiv. of $TiCl_4$ in toluene at 110°C to afford the di(chlorosilyl) derivatives [M{η^5-C_5H_3($SiMe_2Cl$)$_2$}Cl_3] [M = Ti (**5**), Zr (**8**)]. Intermediate formation of [Ti{η^5-C_5H_3[$SiMe_2$(NH*t*Bu)]($SiMe_2Cl$)}Cl_3] (**4**) has been proven by NMR spectroscopy. Reaction of **1** with $TiCl_4$ (2 equiv.) in toluene at 110 °C in the presence of excess NEt_3 has yielded the chloro-silyl complex [Ti{η^5-C_5H_3($SiMe_2Cl$)($SiMe_2$-η^1-N*t*Bu)}Cl_2] (**7**) through the intermediate formation of the amino-silyl derivative [Ti{η^5-C_5H_3[$SiMe_2$(NH*t*Bu)] ($SiMe_2$-η^1-N*t*Bu)}Cl_2] (**6**). Reactions of di-*ansa*-[M{η^5-C_5H_3($SiMe_2$-η^1-N*t*Bu)$_2$}R] and *ansa*-[M{η^5-C_5H_3[$SiMe_2$(NH*t*Bu)] ($SiMe_2$-η^1-N*t*Bu)}R_2] (M = Ti, Zr; R = NMe_2, CH_2Ph) complexes with NEt_3·HCl have afforded the dichloro derivatives [M{η^5-C_5H_3[$SiMe_2$(NH*t*Bu)] ($SiMe_2$-η^1-N*t*Bu)}-Cl_2] [M = Ti (**6**), Zr (**12**)], the amine-coordinated zirconium compound [Zr{η^5-C_5H_3 [$SiMe_2$(NH*t*Bu)]($SiMe_2$-η^1-N*t*Bu)} Cl_2(NMe_2H)] (**9**) and the chloro-benzyl titanium complex [Ti{η^5-C_5H_3[$SiMe_2$(NH*t*Bu)]($SiMe_2$-η^1-N*t*Bu)}Cl-(CH_2Ph)] (**11**). Formation of the mono-substituted chloro-amido zirconium complex [Zr{η^5-C_5H_3[$SiMe_2$ (NH*t*Bu)]-($SiMe_2$-η^1-N*t*Bu)}Cl(NMe_2)] (**10**) by the reaction of [Zr{η^5-C_5H_3[$SiMe_2$(NH*t*Bu)] ($SiMe_2$-η^1-N*t*Bu)}(NMe_2)$_2$] with $SiClMe_3$ has been monitored in C_6D_6 by NMR spectroscopy. All of the new chloro complexes have been characterized by elemental analyses and NMR spectroscopy and the X-ray crystal structure of [Ti(η^5-C_5H_3{$SiMe_2$(NH*t*Bu)}$_2$)Cl_3] (**3**) has been studied by diffraction methods.
(© Wiley-VCH Verlag GmbH & Co. KGaA, 69451 Weinheim, Germany, 2004)

Introduction

Alkylamido-dimethylsilyl-cyclopentadienyl and indenyl group 4 metal complexes and their catalytic applications in olefin polymerization processes have been widely studied.[1−3] The most efficient method of synthesizing these compounds uses the dimetallated anion [$CpSiMe_2$(NR)]$^{2-}$ to transfer the (η^5-Cp-η^1-N) bidentate ligand by reaction with metal chlorides MCl_4 or $MCl_2(NR_2)_2$ to give the dichloro[1a] and diamido[4] derivatives, respectively. However, this method is not recommended in several particular cases and such anion transfers cannot be used when tridentate η^5-Cp(η^1-N)$_2$ ligands are involved in the isolation of cyclopentadienyl-bis(silyl-η^1-amido) metal compounds of the type reported[5] by our group.

An alternative route, avoiding the metathesis step, uses the direct double deprotonation of the amino-dimethylsilyl-cyclopentadiene [$C_5H_5SiMe_2NHR$] with group 4 metal compounds containing strongly basic substituents. Accordingly, metal tetraamides $M(NR_2)_4$ have been extensively used[6] to deprotonate cyclopentadienes,[7] amino-alkyl and -silylcyclopentadienes and different protonated ligands[8] with amine elimination to give amido-silyl ring-closed diamido complexes. The double deprotonation of the cyclopentadiene and the aminosilyl groups may take place in either one or two steps, depending on the acidity of the proton bound to the functional group.[9,10] Similar reactions using metal tetraalkyls[11,12] afford the corresponding dialkyl compounds and are even more useful due to their higher basicity and irreversible elimination of the resulting alkane. However, the use of these deprotonating reagents requires further metathesis of the diamido and dialkyl compounds to access the more versatile dichloro compounds.

We have reported[13] the synthesis of two types of amido and benzyl titanium and zirconium derivatives (Scheme 1), containing the bidentate η^5-C_5H_3[$SiMe_2$(NH*t*Bu)]($SiMe_2$-η^1-N*t*Bu) (**II**) and tridentate η^5-C_5H_3($SiMe_2$-η^1-N*t*Bu)$_2$ (**I**) ligands, by deprotonation of the bis(aminosilyl)cyclopentadiene C_5H_4[$SiMe_2$(NH*t*Bu)]$_2$ with metal amides $M(NMe_2)_4$

[a] Departamento de Química Inorgánica, Facultad de Química, Universidad de Alcalá,
Campus Universitario, 28871 Alcalá de Henares, Spain
Fax: (internat:) +34-91-8854683
E-mail: pascual.royo@uah.es
[b] Anorganisch-Chemisches Institut der Technischen Universität München,
Lichtenbergstrasse 4, 85747 Garching bei München, Germany
Fax: (internat.) +49-(0)89-289-13473
E-mail: eberhardt.herdtweck@ch.tum.de

 © 2004 Wiley-VCH Verlag GmbH & Co. KGaA, Weinheim **DOI: 10.1002/ejic.200400083**

and benzyls $M(CH_2Ph)_4$ (M = Ti, Zr). To access the related chloro compounds, it is convenient to prepare a new type of monocyclopentadienyl compound **III** that may interconvert **I** − **II** − **III** by ring-closing and ring-opening reactions of the M-amidosilyl-Cp system and to compare its reactivity with complexes containing M−Cl, M−NMe_2 and M−CH_2Ph bonds.

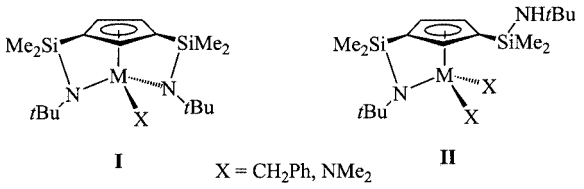

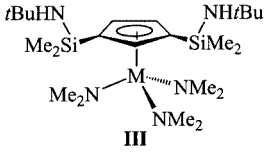

Scheme 1

Halogenation of M−NMe_2 bonds in [M(η5-$C_5H_4SiMe_2$-η1-N*t*Bu)$(NMe_2)_2$] complexes with NMe_2H·HCl is reported[9c] to afford the dichloro zirconium derivative, leaving the silyl-η1-amido bridge unaltered, whereas partial simultaneous halogenation of the Si−N bond yields the corresponding chlorosilyl-η5-cyclopentadienyl dichloro-amido titanium complex with amine elimination. In both cases, the liberated amine NMe_2H remained coordinated to the metal centre. Similar behaviour has also been observed for related cyclopentadienyl-alkyl-η1-NR zirconium and hafnium diamides[9a] and for cyclopentadienyl-Si-O-alkyl-η1-NR zirconium diamides.[10a] Alternatively, $SiClMe_3$[14,15] and $SiCl_2Me_2$[16] are efficient chlorinating agents that do not modify the Cp-silyl-η1-amido chelate.

Conversion of M-alkyl into M-halide bonds in group 4 [M{η5-$C_5H_4SiMe_2$(N*t*Bu)}R_2] complexes without alteration of the Cp-silyl-η1-amido chelate is easily achieved in high yields by reactions with protic acids[17] and I_2.[18]

We describe here the results of our aim to isolate new chloro derivatives of the mono- and di-(η1-amidosilyl)cyclopentadienyl titanium and zirconium complexes. We report the synthesis and structural characterization of a new type of monocyclopentadienyl trichloro complex, [M{η5-C_5H_3[$SiMe_2$(NH*t*Bu)]$_2$}Cl_3] (M = Ti, Zr), and studies related to its ring-closing reactions in order to coordinate the silyl-amido arms to the metal centre. We also report the transformation of the reported[5,13] *ansa*-[M{η5-C_5H_3[$SiMe_2$(NH*t*Bu)](SiMe2-η1-N*t*Bu)}R_2] and di-*ansa*-[M{η5-C_5H_3($SiMe_2$-η1-N*t*Bu)$_2$}R] (R = NMe_2, CH_2Ph) complexes into the chloro compounds by reaction with chlorinating agents.

Results and Discussion

Reactions of the bis(aminosilyl)cyclopentadiene C_5H_4[$SiMe_2$(NH*t*Bu)]$_2$ with metal halides MCl_4 follow different reaction pathways to those reported[13] with metal amides $M(NMe_2)_4$ and benzyls $M(CH_2Ph)_4$ (M = Ti, Zr). Group 4 metal halides MCl_4 behave as dehalosilylating agents[19] that can cleave the sp^3-C(Cp)−SiR_3 bonds with the elimination of the halosilane $ClSiR_3$, and $TiCl_4$ is also a useful deamidating reagent for amidosilane derivatives.[20]

The addition of 2 equiv. of $TiCl_4$ to a dichloromethane solution of the bis(aminosilyl)cyclopentadiene produced simultaneous deamidation of the Si−NH*t*Bu bonds and dehalosilylation with elimination of $SiMe_2Cl_2$ to afford a mixture containing C_5H_4[($SiMe_2Cl$)$_2$][21] and [Ti(η5-$C_5H_4SiMe_2Cl$)Cl_3][22] as major products, together with other unidentified minor components, according to ^1H NMR data (Scheme 2).

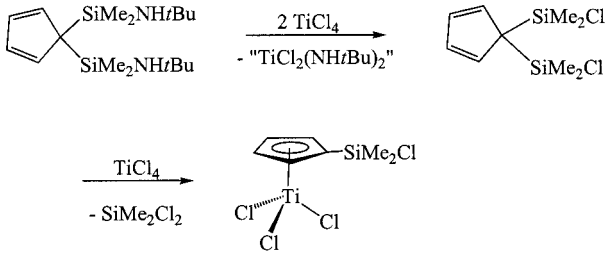

Scheme 2

Reactions with the [M{η5-C_5H_3[$SiMe_2$(NHtBu)]$_2$}Cl_3] (M = Ti, Zr) Complexes

We were first interested in isolating the trichloro [M{η5-C_5H_3[$SiMe_2$(NH*t*Bu)]$_2$}Cl_3] (M = Ti, Zr) complexes to study the possible ring-closing reactions of one or both silyl-amido-metal systems that could give the dichloro(η5-cyclopentadienylsilyl-η1-amido) [M{η5-C_5H_3[$SiMe_2$(NH*t*Bu)](SiMe2-η1-N*t*Bu)}Cl_2] and chloro[η5-cyclopentadienyl bis(silyl-η1-amido)] [M{η5-C_5H_3($SiMe_2$-η1-N*t*Bu)$_2$}Cl] metal complexes, respectively.

With this aim, the higher acidic character of the cyclopentadiene ring proton was used to isolate the required lithium salt LiC_5H_3[$SiMe_2$(NH*t*Bu)]$_2$ (**1**) by selective metallation of the bis(aminosilyl)cyclopentadiene with 1 equiv. of *n*BuLi in hexane−THF for 12 h. Compound **1** was isolated as a white solid and characterized by elemental analysis and NMR spectroscopy (see Exp. Sect.).

Reaction of a toluene suspension of the lithium salt **1** with $ZrCl_4$.2THF afforded the trichloro complex [Zr{η5-C_5H_3[$SiMe_2$(NH*t*Bu)]$_2$}Cl_3] (**2**), which was isolated as a yellow solid in almost quantitative yield and characterized by elemental analysis and NMR spectroscopy. However, a similar reaction of **1** with $TiCl_4$ afforded mixtures of different products depending on the solvent, the molar ratio of both reagents and the reaction conditions (time and temperature). A hexane suspension of the lithium salt **1** reacted

 © 2004 Wiley-VCH Verlag GmbH & Co. KGaA, Weinheim

with $TiCl_4$ (1 equiv.) at room temperature to afford the trichloro derivative [Ti{η^5-C_5H_3[$SiMe_2$(NH*t*Bu)]$_2$}Cl_3] (**3**) as the unique reaction product. Complex **3** was isolated as an orange solid in 70% yield after purification and characterized by elemental analysis and NMR spectroscopy (Scheme 3). ^1H and ^{13}C NMR spectra of complexes **2** and **3** show the behaviour expected for C_s symmetric molecules with two equivalent aminosilyl groups and ring protons. Consequently, two singlets (^1H) and two resonances (^{13}C) for the diastereotopic $SiMe_2$ methyl groups and one singlet (^1H) and two resonances (^{13}C) for the *tert*-butylamino substituents were observed in the NMR spectra of **2** and **3**. In addition, one doublet and one triplet ($J_{H,H}$ = 2.0 Hz) (^1H) are observed for the A_2B spin system of the cyclopentadienyl ring protons and, consistently, three ring carbon resonances appear in the ^{13}C NMR spectra. Recrystallization of **3** using pentane gave crystals appropriate for an X-ray structure determination. The molecular structure of **3** is shown in Figure 1, and selected bond lengths and angles are listed in Table 1.

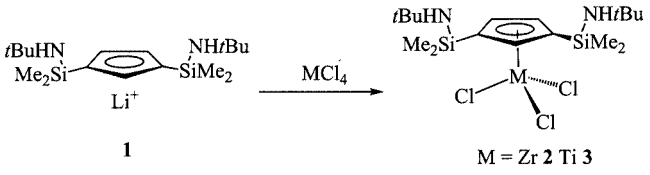

Scheme 3

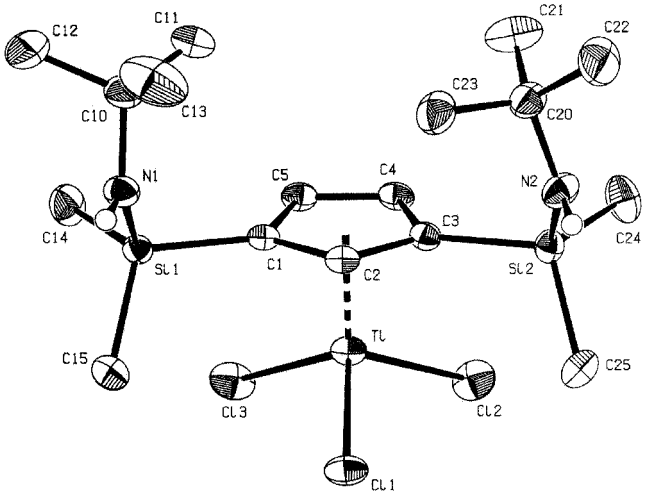

Figure 1. ORTEP drawing of the solid-state molecular structure of **3**; thermal ellipsoids drawn at the 50% probability level and hydrogen atoms are omitted for clarity except for those located at the nitrogen atoms

Complex **3** shows the titanium atom in the well-known pseudo-tetrahedral geometry defined by the centroid of the cyclopentadienyl ring and three coordinated chloro ligands, as reported for many group 4 metal monocyclopentadienyl complexes [Ti(η^5-C_5H_4R)Cl_3] (R = H,[23] Me,[24] $CHPh_2$, CMe_2Ph, $SiMe_2Ph$,[25]), [Ti(η^5-C_5Me_4R)Cl_3] (R = *t*Bu,[26] CH_2CH_2Ph,[27] SiMeClH, $SiMe_3$,[20] [Ti(η^5-1,3-$R_2C_5H_3$)Cl_3] (R = $SiMe_3$,[28] *t*Bu[29]). The Cp ring in an η^5-coordination mode is not distorted, although the C4−C5 distance [1.403(2)] Å is slightly shorter than the other C−C distances of 1.420(2)−1.430(2) Å. Ti−Cl bond lengths (2.23−2.24 Å) and the Cl−Ti−Cl angles (102−104°) are in the typical range for compounds of this type. Si−N bond lengths (1.70−1.71Å) are also in the range known for terminal amino−silyl bonds. Most significantly, the metal fragment and $SiMe_2NH$*t*Bu substituents are at opposite faces of the cyclopentadienyl ring, adopting a conformation that minimizes interaction with the chloro ligands and prevents the nitrogen atoms acting as σ-donor ligands, which would elongate the Ti−Cl bonds and close the Cl−Ti−Cl bond angles, as with [Ti(η^5-C_5H_4R)Cl_3] compounds containing *O*- and *N*-functionalized R groups.[30] In addition, this structural disposition also prevents possible bridging hydrogen-bond interactions between Cl and the NH groups.

Table 1. Characteristic bond lengths (Å) and angles (°) for [Ti(η^5-C_5H_3{$SiMe_2$(NH*t*Bu)}$_2$)Cl_3] (**3**)

Bond lengths		Bond angles	
Ti−Cl1	2.2366(5)	Cl1−Ti−Cl2	102.69(2)
Ti−Cl2	2.2416(6)	Cl1−Ti−Cl3	103.64(2)
Ti−Cl3	2.2396(6)	Cl2−Ti−Cl3	102.45(2)
Si1−N1	1.702(2)	N1−Si1−C1	108.72(7)
Si2−N2	1.707(2)	N2−Si2−C3	110.15(8)
C1−C2	1.420(2)	Si1−N1−C10	131.96(15)
C1−C5	1.430(2)	Si2−N2−C20	133.15(14)
C2−C3	1.420(2)		
C3−C4	1.427(2)		
C4−C5	1.403(2)		

The same reaction of the lithium salt **1** with 1 equiv. of $TiCl_4$ in hexane at 45 °C gave, after 1 h, the bis(chlorosilyl) derivative [Ti{η^5-C_5H_3($SiMe_2Cl$)$_2$}Cl_3] (**5**) as the main reaction product together with a mixture containing various unidentifiable species. The presence in this mixture of the (aminosilyl)(chlorosilyl)cyclopentadienyl titanium complex [Ti{η^5-C_5H_3[$SiMe_2$(NH*t*Bu)]($SiMe_2Cl$)}Cl_3] (**4**) (Scheme 4) could not be verified.4

Pure complex **5** could be isolated from this mixture as a light brown solid in very low yield (10%) after repeated recrystallizations; it was characterized by elemental analysis and NMR spectroscopy. These results demonstrate that complex **3** reacted with unchanged $TiCl_4$ immediately after its formation, when the hexane solution was heated to 45 °C, producing deamidation of both amido-silane groups. Under these conditions, the preferential deamidation of complex **3** prevented the ring-closing formation of *ansa*-cyclopentadienylsilyl-η^1-amido compounds.

Similar behaviour occurs for the same reaction with 1 equiv. of $TiCl_4$ when using a toluene suspension of **1** at room temperature (Scheme 4). The resulting reaction product was a mixture containing almost equal molar proportions of the trichloro complexes **3**−**5**, although in this case formation of small but significant amounts of the also deamidated *ansa*-silyl-η^1-amido complex [Ti{η^5-C_5H_3(SiMe_2Cl)($SiMe_2$-η^1-N*t*Bu)}Cl_2] (**7**) was also observed and

 © 2004 Wiley-VCH Verlag GmbH & Co. KGaA, Weinheim

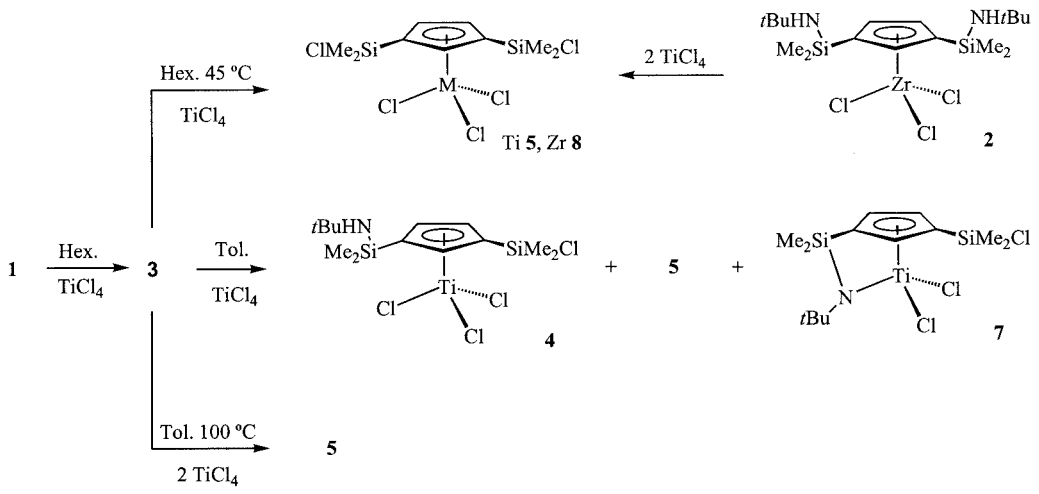

Scheme 4

identified by NMR spectroscopy (see below). The formation of complex **4**, which could not be isolated, was confirmed by a low intensity set of signals in the ^{1}H NMR spectrum, which includes four singlets for the methyl protons of two different $SiMe_2Cl$ and $SiMe_2(NHtBu)$ groups, one singlet for the $NHtBu$ substituent and three multiplets for the non-equivalent ring protons of an asymmetric molecule (see Exp. Sect.). When this mixture containing complexes **3**−**5** and **7** was heated in a Teflon-sealed Schlenk tube at 100 °C for 5 h, compound **3** disappeared completely to give a mixture containing **7** as the major component together with **5** and traces of **4**.

To check the deamidating role of the starting $TiCl_4$ a toluene solution of the isolated complex **3** was reacted with 2 equiv. of $TiCl_4$, heating the solution at 100 °C for 8 h to give an insoluble green product and a solution containing **5**, which was isolated in 65% yield after purification (Scheme 4). Under similar conditions, the zirconium complex **2** did not react with excess $ZrCl_4$ but an almost quantitative deamidation reaction occurred when its toluene solution was heated to 110 °C for 8 h with 2 equiv. of $TiCl_4$. The resulting complex $[Zr\{\eta^5\text{-}C_5H_3(SiMe_2Cl)_2\}Cl_3]$ (**8**) was isolated as a yellow solid in 69% yield and was characterized by elemental analysis and NMR spectroscopy. The ^{1}H NMR spectra of complexes **5** and **8** correspond to molecules with C_s symmetry and show two $SiMe_2$ singlets corresponding to diastereotopic methyl groups of two equivalent chlorosilyl substituents and one doublet and one triplet with relative intensity 2:1, corresponding to the A_2B spin system of the ring protons. Consistently, two $SiMe_2$ and three ring carbon resonances appear in the ^{13}C NMR spectrum (see Exp. Sect.).

$TiCl_4$ is, therefore, the deamidating agent responsible for the transformation of **3** into, successively, **4** and **5**. Moreover, in the presence of excess $TiCl_4$, formation of the *ansa* complexes is totally inhibited.

The thermal behaviour of **2** and **3** in the absence of $TiCl_4$ is also important. Complex **2** is thermally stable, remaining unaltered after heating for 6 h at 125 °C in a Teflon-sealed Schlenk tube. This is consistent with the known high stability of Zr−Cl bonds. However, monitoring the ^{1}H NMR spectrum of a sample of **3**, in a Teflon-sealed NMR tube in C_6D_6 at room temperature, revealed a very slow transformation that gave increasing amounts of a mixture containing one new major compound and a small amount of a second new derivative, along with traces of other components. According to ^{1}H NMR data in the highfield $SiMe_2$ region, the new compounds could be formulated as complexes $[Ti\{\eta^5\text{-}C_5H_3[SiMe_2(NHtBu)](SiMe_2\text{-}\eta^1\text{-}NtBu)\}Cl_2]$ (**6**), and $[Ti\{\eta^5\text{-}C_5H_3(SiMe_2Cl)(SiMe_2\text{-}\eta^1\text{-}NtBu)\}Cl_2]$ (**7**) as the major and minor components, respectively (Scheme 5). This suggests that, in the absence of $TiCl_4$, partial formation of *ansa* complexes takes place with elimination of HCl, which, under these conditions, protonates the free amino Si-$NHtBu$ group of **6** to give the Si−Cl group of **7**. Some of the HCl generated in the previous reaction has to be used to neutralize the eliminated NH_2tBu, otherwise only compound **7** should be observed. After 2 days, this transformation afforded, according to ^{1}H NMR data, an approximately 2:1:1 molar ratio of **6**:**3**:**7**. These data confirmed that formation of the first silyl-η^1-amido bridge occurs at room temperature albeit it is very slowly.

To favour the formation of the *ansa* compounds we studied the same reaction, heating a toluene suspension of the lithium salt **1** with 1 equiv. of $TiCl_4$ at 110 °C in the presence of NEt_3 (3 equiv.) (Scheme 5). Under these conditions no deamidation of complex **3** was observed − instead a mixture was obtained that contained the *ansa* complexes **7** and **6** in a molar ratio 3:1, from which complex **7** was isolated after extraction into pentane, as a yellow solid in 60% yield. Better results were obtained for the same reaction using 2 equiv. of $TiCl_4$ because further deamidation of **6** afforded pure complex **7** as the unique reaction product. Complex **7** is a disymmetric molecule due to the enantioface of the cyclopentadienyl ring. Its ^{1}H NMR spectrum shows the expected four singlets for the $SiMe_2$ groups, one

 © 2004 Wiley-VCH Verlag GmbH & Co. KGaA, Weinheim

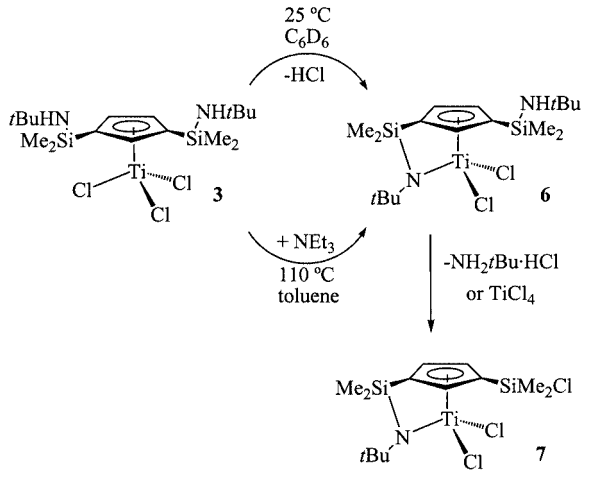

Scheme 5

singlet for the *tert*-butyl substituent and three low-field multiplets for the ring protons. Consistently, four $SiMe_2$ resonances, two N*t*Bu signals and five ring carbon resonances appear in the ^{13}C NMR spectrum of **7** (see Exp. Sect.). Pure samples of complex **6** could not be isolated from the sticky residue, in which it was the minor component. However, complex **6** was identified by its ^1H NMR spectrum, which shows the expected four $SiMe_2$, two *t*Bu singlets and three Cp ring proton multiplets, consistent with its proposed formulation and coincident with those of the pure complex isolated by an alternative method (see below).

Therefore, reactions in the presence of excess NEt_3 yielded the *ansa* complexes, preventing deamidation of complex **3**, even when excess $TiCl_4$ was used to favour the total deamidation of *ansa* complex **6**. However, NEt_3 did not prevent protonation and deamination of the Si−NH*t*Bu group. Indeed, a mixture of **7** and **6** in a molar ratio 1:1 was formed when a toluene suspension of **3** was heated to 110 °C in the presence of 5 equiv. excess NEt_3.

All these results suggest the following sequence of reactions: initially the reaction of $TiCl_4$ with the lithium salt **1** gives the trichloro complex **3**, which is deamidated by excess $TiCl_4$ to give, successively, complexes **4** and **5**. However, ring-closing reactions to give *ansa* complexes require elimination of HCl, this being favoured in the presence of NEt_3, which prevents the deamidation of complex **3** to give **6**. Complex **6** is also deamidated by excess $TiCl_4$, to afford pure complex **7**.

In summary, the ring-closing reaction of the first silyl-η^1-amido arm of the trichloro complex **3** is a selective reaction in the presence of excess NEt_3, although under these conditions simultaneous deamidation of the remaining amido-silane system gives the mono-silyl-η^1-amido complex **7**, preventing the formation of the second silyl-η^1-amido bridge. In contrast, deamidation of both amido-silane groups of complex **3** is a selective reaction in the presence of excess $TiCl_4$, giving the bis(chlorosilyl) derivative **5** while suppressing the formation of silyl-η^1-amido bridges.

Reactions with the [M{η^5-C_5H_3($SiMe_2$-η^1-NtBu)$_2$}R] and [M{η^5-C_5H_3[$SiMe_2$(NHtBu)]($SiMe_2$-η^1-NtBu)}R_2] (M = Ti, Zr; R = NMe_2, CH_2Ph) Complexes

The amido zirconium compound [Zr{η^5-C_5H_3($SiMe_2$-η^1-N*t*Bu)$_2$}(NMe_2)][13] reacted with 1 equiv. of NEt_3·HCl in toluene at 70 °C to produce the simultaneous protonation of both the terminal Zr−NMe_2 and one of the bridging Zr−N*t*Bu−Si bonds, affording a mixture that contained half of the unchanged starting compound and a new zirconium complex.

The starting bis(silyl-η^1-amido) compound was completely transformed into the new zirconium derivative, with elimination of NEt_3, when a second equiv. of NEt_3·HCl was added (Scheme 6), giving an 82% yield of a light brown solid that was characterized by elemental analysis and NMR spectroscopy as the dichloro compound [Zr{η^5-C_5H_3[$SiMe_2$(NH*t*Bu)]($SiMe_2$-η^1-N*t*Bu)}Cl_2(NMe_2H)] (**9**). Compound **9**, which contains the amine coordinated to the metal, was also obtained when the same reaction was carried out with one equiv. of NEt_3·HCl and the diamido compound [Zr{η^5-C_5H_3[$SiMe_2$(NH*t*Bu)]($SiMe_2$-η^1-N*t*Bu)}-(NMe_2)$_2$].[13] The simultaneous reaction of both Zr−NMe_2 bonds also occurred, leaving half of the starting complex unaltered, although one of the two amido groups could be sterically protected by the uncoordinated aminosilyl group. Probably, the increased acidity of the metal centre in the resulting chloro-amido intermediate favours the coordination of chloride with protonation and displacement of the second amido group. The reaction was complete after addition of a second equivalent of NEt_3·HCl, affording pure **9**.

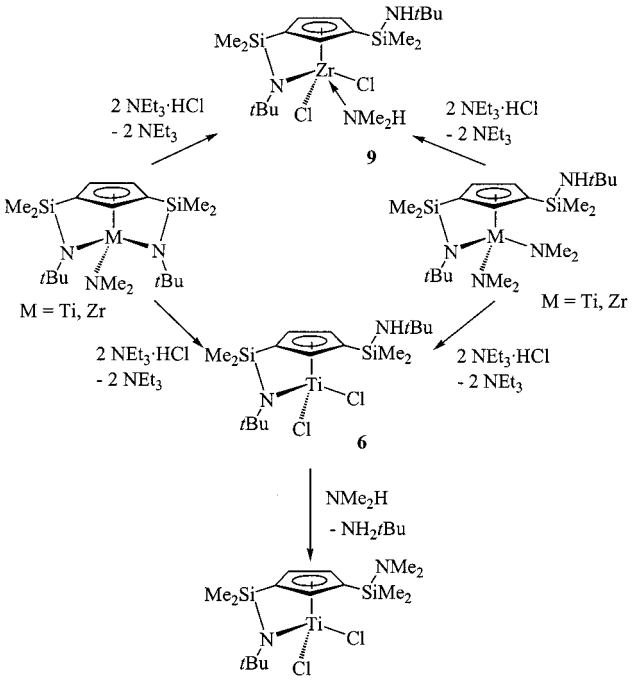

Scheme 6

Similar behaviour was observed for the titanium derivatives [Ti{η^5-C_5H_3($SiMe_2$-η^1-N*t*Bu)$_2$}(NMe_2)] and [Ti{η^5-

 © 2004 Wiley-VCH Verlag GmbH & Co. KGaA, Weinheim

$C_5H_3[SiMe_2(NHtBu)](SiMe_2\text{-}\eta^1\text{-}NtBu)\}(NMe_2)_2]$.[13] However, the resulting product, $[Ti(\eta^5\text{-}C_5H_3\{SiMe_2(NHtBu)\}\text{-}\{SiMe_2(\eta^1\text{-}NtBu)\})Cl_2]$ (**6**), did not contain coordinated amine, and it was always accompanied by variable, small amounts of a second component that could not be isolated but was identified by NMR spectroscopy as $[Ti\{\eta^5\text{-}C_5H_3[SiMe_2(NMe_2)](SiMe_2\text{-}\eta^1\text{-}NtBu)\}Cl_2]$. This last compound resulted from a simultaneous exchange reaction between the amino-silyl Si-NH*t*Bu group of **6** and the liberated amine $NHMe_2$. Complex **6** was isolated as a red solid and characterized by elemental analysis and NMR spectroscopy (see Exp. Sect.).

Reactions with $SiClMe_3$ are reported[14,15] to be a convenient method of converting metal−amido into metal−chloro bonds. The reaction of the diamido zirconium complex $[Zr\{\eta^5\text{-}C_5H_3[SiMe_2(NHtBu)](SiMe_2\text{-}\eta^1\text{-}NtBu)\}(NMe_2)_2]$ with one equivalent of $SiClMe_3$ was monitored by ^1H NMR spectroscopy in C_6D_6 at room temperature (Scheme 7). After 1 h, formation of the chloro-amido derivative $[Zr\{\eta^5\text{-}C_5H_3[SiMe_2(NHtBu)](SiMe_2\text{-}\eta^1\text{-}NtBu)\}\text{-}Cl(NMe_2)]$ (**10**) with elimination of $SiMe_3(NMe_2)$ was confirmed by ^1H and ^{13}C NMR. Addition of a second equiv. of $SiClMe_3$ produced a very slow reaction, which after 4 d afforded a mixture of unidentified reaction products in which $SiMe_3$-NH*t*Bu (δ_{SiMe} = 0.11 ppm; δ_{NHtBu} = 1.09 ppm) and $SiMe_3-NMe_2$ (δ_{SiMe} = 0.04 ppm; δ_{NMe} = 2.37 ppm) were observed in the ^1H NMR spectrum. This suggests that, probably, the first substitution is a fast diastereoselective reaction at the amido ligand unprotected by the noncoordinated silyl-amino group, which gives one single diastereomer (see below). However, the second substitution at the sterically protected amido ligand is very slow and exchange takes place between the amino groups bound to the silylcyclopentadienyl ligand CpSi−NH*t*Bu of **10** and the trimethylsilyl fragment of the liberated silane $Me_3Si-NMe_2$. Similar studies could not be extended to the related diamido titanium derivative as it was always accompanied by variable amounts of the monoamido complex.

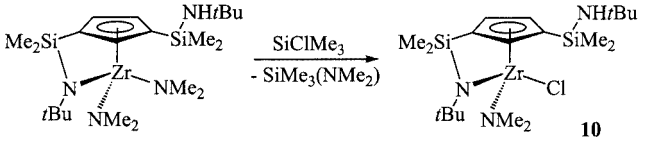

Scheme 7

The reactivity of the benzyl derivatives was also studied (Scheme 8). When 1 equiv. of NEt_3·HCl was added to a toluene solution of the benzyl titanium complex $[Ti\{\eta^5\text{-}C_5H_3(SiMe_2\text{-}\eta^1\text{-}NtBu)_2\}(CH_2Ph)]$,[13] one of the silyl-amido arms was protonated to afford the chloro-benzyl derivative $[Ti\{\eta^5\text{-}C_5H_3[SiMe_2(NHtBu)](SiMe_2\text{-}\eta^1\text{-}NtBu)\}Cl(CH_2Ph)]$ (**11**), which was isolated as a red solid (77% yield) and characterized by elemental analysis and NMR spectroscopy. In this reaction the benzyl−titanium bond was unaltered although it could also be protonated with elimination of toluene when the same reaction was carried out using 2 equiv. of NEt_3·HCl, at 80 °C for 12 h, to afford the dichloro derivative $[Ti(\eta^5\text{-}C_5H_3\{SiMe_2(NHtBu)\}\text{-}\{SiMe_2(\eta^1\text{-}NtBu)\})Cl_2]$ (**6**) described above. Reaction of the related zirconium complex $[Zr\{\eta^5\text{-}C_5H_3(SiMe_2\text{-}\eta^1\text{-}NtBu)_2\}(CH_2Ph)]$[13] was not selective; simultaneous protonation of the η^1-amido and benzyl ligands required the addition of 2 equiv. of NEt_3·HCl, in toluene at 70 °C, to give the dichloro complex $[Zr\{\eta^5\text{-}C_5H_3[SiMe_2(NHtBu)]\text{-}(SiMe_2\text{-}\eta^1\text{-}NtBu)\}Cl_2]$ (**12**), which is similar to **9** but without coordinated amine. Compound **12** was isolated as a brown solid and characterized by NMR spectroscopy. In the light of these results, the reactivity of related dibenzyl complexes $[M\{\eta^5\text{-}C_5H_3[SiMe_2(NHtBu)](SiMe_2\text{-}\eta^1\text{-}NtBu)\}\text{-}(CH_2Ph)_2]$ (M = Ti, Zr) was not studied.

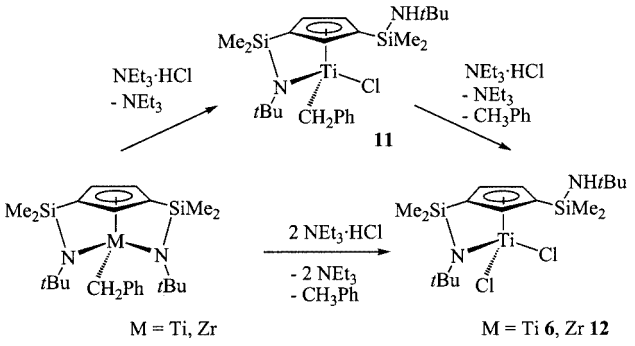

Scheme 8

The new complexes **6** and **9**−**12** belong to the well-known type of *ansa*-cylopentadienylsilyl-η^1-amido compounds with one additional noncoordinated silyl-amino substituent, which makes the face of the cyclopentadienyl ring enantiotopic. Therefore, the dichloro complexes $[M\{\eta^5\text{-}C_5H_3[SiMe_2(NHtBu)](SiMe_2\text{-}\eta^1\text{-}NtBu)\}Cl_2]$ [M = Ti (**6**), Zr (**12**)], and the amine-coordinated zirconium derivative $[Zr\{\eta^5\text{-}C_5H_3\ [SiMe_2(NHtBu)](SiMe_2\text{-}\eta^1\text{-}NtBu)\}\text{-}Cl_2(NMe_2H)]$ (**9**) are disymmetric molecules, in agreement with the observed ^1H and ^{13}C NMR spectra (see Exp. Sect.). The chloro-amido $[Zr\{\eta^5\text{-}C_5H_3[SiMe_2(NHtBu)]\text{-}(SiMe_2\text{-}\eta^1\text{-}NtBu)\}Cl(NMe_2)]$ (**10**) and -benzyl $[Ti\{\eta^5\text{-}C_5H_3[SiMe_2(NHtBu)](SiMe_2\text{-}\eta^1\text{-}NtBu)\}Cl(CH_2Ph)]$ (**11**) complexes exhibit one additional stereogenic centre at the metal, although only one isomer was formed in the diastereoselective reactions discussed above. Accordingly, the NMR spectra of **10** and **11** show the expected four Si-Me signals (^1H, ^{13}C), two singlets (^1H) and four signals (^{13}C) for the N*t*Bu groups, and three (^1H) or five signals (^{13}C) for the cyclopentadienyl ring proton and carbon atoms respectively, along with the typical diastereotopic CH_2Ph doublets for **11**.

All these *ansa* complexes exhibit a ^{13}C signal due to the ring C_{ipso} that is shifted upfield with respect to the other ring-carbon signals,[31] and the metal−amido π-bonding contribution is evidenced by $\Delta(\delta C_{tert} - \delta C_{Me})$[32] of 22.8 (**10**)−30.0 (**6**) compared with those of the Si-NH*t*Bu group [15.9 (**10**)−18.5 (**9**)].

 © 2004 Wiley-VCH Verlag GmbH & Co. KGaA, Weinheim

Conclusion

Monolithium salt $LiC_5H_3[SiMe_2(NHtBu)]_2$ (**1**) reacts with the corresponding tetrachlorides MCl_4 in a straightforward method of synthesizing bis(dimethylsilylamino) monocyclopentadienyl titanium and zirconium complexes $[M\{\eta^5\text{-}C_5H_3[SiMe_2(NHtBu)]_2\}Cl_3]$ (M = Ti, Zr). However, simultaneous reaction of the titanium derivative with the starting $TiCl_4$ produces partial conversion of one or both Si-NH*t*Bu into Si−Cl groups. This is a quantitative transformation when the isolated titanium and zirconium complexes are treated with 2 equiv. of $TiCl_4$.

Ring-closing coordination of one of the silyl-amido arms to the metal by elimination of HCl is very slow at room temperature for the titanium complex and does not occur for the zirconium one. However, this reaction is complete when the titanium compound is heated in toluene to 110 °C in the presence of excess NEt_3, although simultaneous partial conversion of the free Si−NH*t*Bu into Si−Cl is unavoidable. Under these conditions, addition of $TiCl_4$ gives the chloro-silyl complex $[Ti\{\eta^5\text{-}C_5H_3(SiMe_2Cl)(SiMe_2\text{-}\eta^1\text{-}NtBu)\}Cl_2]$ in quantitative yield.

Ring-closing coordination of the second silyl-amido arm was never observed, which is consistent with the very easy ring-opening de-coordination that takes place by protonation with $NEt_3{\cdot}HCl$ of one of the silyl-η^1-amido−titanium and zirconium bonds of the cyclopentadienyl bis(silyl-η^1-amido) di-*ansa*-$[M\{\eta^5\text{-}C_5H_3(SiMe_2\text{-}\eta^1\text{-}NtBu)_2\}R]$ (R = NMe_2, CH_2Ph) complexes. In contrast, the single silyl-η^1-amido-titanium system of the *ansa*-$[M\{\eta^5\text{-}C_5H_3[SiMe_2(NHtBu)](SiMe_2\text{-}\eta^1\text{-}NtBu)\}(NMe_2)_2]$ (M = Ti, Zr) derivatives remains unaltered in these protonation reactions.

Alternative methods to synthesize the elusive di-*ansa*-$[M\{\eta^5\text{-}C_5H_3(SiMe_2\text{-}\eta^1\text{-}NtBu)_2\}Cl]$ complex and its alkyl derivatives are being studied and will be reported in a future paper.

Experimental Section

General Remarks: All manipulations were performed under an inert atmosphere of argon using standard Schlenk techniques or a dry box. Solvents were dried and freshly distilled under argon before use: tetrahydrofuran from sodium benzophenone ketyl; toluene from sodium; hexane from sodium-potassium amalgam. Unless otherwise stated, reagents were obtained from commercial sources and used as received. $C_5H_4[SiMe_2(NHtBu)]_2$, $[M\{\eta^5\text{-}C_5H_3(SiMe_2\text{-}\eta^1\text{-}NtBu)_2\}R]$ and $[M\{\eta^5\text{-}C_5H_3[SiMe_2(NHtBu)](SiMe_2\text{-}\eta^1\text{-}NtBu)\}R_2]$ (M = Ti, Zr; R = CH_2Ph, NMe_2) were prepared by previously reported methods.[13] ^1H and ^{13}C NMR spectra were recorded on a Varian Unity VXR-300 or Varian Unity 500 Plus. Chemical shifts, in ppm, are relative to residual ^1H and ^{13}C resonances for C_6D_6 used as solvent: 7.15 (^1H) and 128.0 (^{13}C), and coupling constants are in Hz. C, H and N analyses were carried out with a Perkin-Elmer 240 C analyzer.

$LiC_5H_3[SiMe_2(NHtBu)]_2$ (1): A hexane solution (1.6 M) of *n*BuLi (11.0 mL, 17.6 mmol) was added dropwise to a yellow solution of $C_5H_4[SiMe_2(NHtBu)]_2$ (5.80 g, 17.6 mmol) in a mixture of hexane (150 mL) and THF (25 mL) at −78 °C. This reaction mixture was then warmed to room temperature and stirred for 12 h. The volatiles were then removed under vacuum to give **1** as a white solid, which was washed with hexane and dried under vacuum (5.72 g, 17.30 mmol, 98%). $C_{17}H_{35}LiN_2Si_2$ (330.6): calcd. C 61.76, H 10.67, N 8.47; found C 61.02, H 10.46, N 8.27. ^1H NMR (C_6D_6/NC_6D_5, 20 °C): δ = 0.49 (s, 12 H, SiMe_2), 0.88 (br. s, 2 H, NH*t*Bu), 1.21 (s, 18 H, NHCMe_3), 6.75 (d, $J_{H,H}$ = 2.0 Hz, 2 H, C_5H_3), 6.90 (t, $J_{H,H}$ = 2.0 Hz, 1 H, C_5H_3) ppm. ^{13}C NMR (C_6D_6/NC_6H_5, 20°): δ = 4.2 (SiMe_2), 34.1 (NHCMe_3), 49.4 (NH*C*Me$_3$), 115.2 (C_5H_3), 115.8 (C_5H_{3ipso}), 120.4 (C_5H_3) ppm.

$[Zr\{\eta^5\text{-}C_5H_3[SiMe_2(NHtBu)]_2\}Cl_3]$ (2): Toluene (100 mL) was added to a mixture of $ZrCl_4{\cdot}2THF$ (2.08 g, 5.52 mmol) and the lithium salt **1** (1.82 g, 5.52 mmol) at room temperature. The reaction mixture was subsequently stirred for a further 12 h. The solvent of the resulting white suspension was then removed under vacuum and the residue extracted into hexane (2 × 50 mL). After filtration and removal of the solvent, complex **2** was isolated as a light yellow solid (2.46 g, 4.33 mmol, 86%). $C_{17}H_{35}Cl_3N_2Si_2Zr$ (521.2): calcd. C 39.17, H 6.77, N 5.37; found C 39.03, H 6.72, N 5.34. ^1H NMR ($CDCl_3$, 20 °C): δ = 0.35 (s, 6 H, SiMe_2), 0.39 (s, 6 H, SiMe_2), 1.02 (br. s, 2 H, NH*t*Bu), 1.08 (s, 18 H, NHCMe_3), 6.52 (d, $J_{H,H}$ = 1.6 Hz, 2 H, C_5H_3), 7.16 (t, $J_{H,H}$ = 1.6 Hz, 1 H, C_5H_3) ppm. ^{13}C NMR ($CDCl_3$, 20 °C): δ = 1.99 (SiMe_2), 3.43 (SiMe_2), 33.6 (NHCMe_3), 49.6 (NH*C*Me$_3$), 120.5 (C_5H_3), 129.3 (C_5H_{3ipso}), 145.1 (C_5H_3) ppm.

$[Ti\{\eta^5\text{-}C_5H_3[SiMe_2(NHtBu)]_2\}Cl_3]$ (3): A colourless solution of $TiCl_4$ (0.76 mL, 6.99 mmol) in hexane (15 mL) was cooled to −78 °C and added to a cooled (−78 °C) stirred suspension of the lithium salt **1** (2.31 g, 6.99 mmol) in the same solvent (75 mL). The reaction mixture was then warmed slowly to room temperature and stirred for 12 h. The resulting light brown suspension was then filtered and, after removal of the solvent, complex **3** was isolated as an orange solid (2.33 g, 4.87 mmol, 70%). $C_{17}H_{35}Cl_3N_2Si_2Ti$ (477.8): calcd. C 42.73, H 7.38, N 5.86; found C 41.92, H 7.30, N 5.73. ^1H NMR ($CDCl_3$, 20 °C): δ = 0.39 (s, 6 H, SiMe_2), 0.48 (s, 6 H, SiMe_2), 0.84 (br. s, 2 H, NH*t*Bu), 0.94 (s, 18 H, NHCMe_3), 6.89 (d, $J_{H,H}$ = 2.0 Hz, 2 H, C_5H_3), 7.57 (t, $J_{H,H}$ = 2.0 Hz, 1 H, C_5H_3) ppm. ^{13}C NMR ($CDCl_3$, 20 °C): δ = 1.25 (SiMe_2), 1.41 (SiMe_2), 33.7 (NHCMe_3), 49.8 (NH*C*Me$_3$), 132.2 (C_5H_3), 136.6 (C_5H_3), 149.2 (C_5H_{3ipso}) ppm.

$[Ti\{\eta^5\text{-}C_5H_3[SiMe_2(NHtBu)](SiMe_2Cl)\}Cl_3]$ (4): An orange solution of $TiCl_4$ (0.17 mL, 1.55 mmol) in toluene (15 mL) was cooled to −78 °C and added to a cooled (−78 °C) stirred suspension of the lithium salt **1** (0.51 g, 1.55 mmol) in the same solvent (75 mL). The reaction mixture was warmed slowly to room temperature and stirred for a further 12 h. The solvent was then removed under vacuum and the residue extracted into hexane (50 mL). After filtration and removal of the solvent, an unresolvable mixture of **3**−**5** and **7** was obtained. The presence of **4** was detected by NMR spectroscopy. **4**: ^1H NMR (C_6D_6, 20 °C): δ = 0.31 (s, 3 H, SiMe_2), 0.39 (s, 3 H, SiMe_2), 0.54 (s, 3 H, SiMe_2), 0.58 (s, 3 H, SiMe_2), 0.92 (s, 9 H, NHCMe_3), 6.70 (m, 1 H, C_5H_3), 6.84 (m, 1 H, C_5H_3), 7.47 (m, 1 H, C_5H_3) ppm.

$[Ti\{\eta^5\text{-}C_5H_3(SiMe_2Cl)_2\}Cl_3]$ (5) − Method A: In a Teflon-sealed Schlenk tube, $TiCl_4$ (0.055 mL, 0.50 mmol) was added by syringe to an orange solution of **3** (0.12 g, 0.25 mmol) in toluene (30 mL) cooled to −78 °C. The reaction mixture was then warmed slowly to room temperature, and subsequently heated for 12 h to 110 °C. The volatiles were then removed under vacuum and the residue was extracted into hexane to give **5** as a light brown solid (0.089 g,

 © 2004 Wiley-VCH Verlag GmbH & Co. KGaA, Weinheim

0.22 mmol, 65%). $C_9H_{15}Cl_5Si_2Ti$ (404.5): calcd. C 26.72, H 3.74; found C 27.00, H 3.73. ^{1}H NMR ($CDCl_3$, 20 °C): δ = 0.76 (s, 6 H, Si*Me*$_2$), 0.82 (s, 6 H, Si*Me*$_2$), 7.33 (d, $J_{H,H}$ = 1.8 Hz, 2 H, C_5H_3), 7.56 (t, $J_{H,H}$ = 1.8 Hz, 1 H, C_5H_3) ppm. ^{13}C NMR ($CDCl_3$, 20 °C): δ = 2.36 (Si*Me*$_2$), 2.81 (Si*Me*$_2$), 131.2 (C_5H_3), 135.0 (C_5H_3), 139.3 (C_5H_{3ipso}) ppm.

Method B: In a sealed Schlenk tube, an orange solution of $TiCl_4$ (0.55 mL, 4.99 mmol) in toluene (15 mL) was cooled to −78 °C and added to a cooled (−78 °C) stirred suspension of the lithium salt **1** (0.55 g, 1.66 mmol) in the same solvent (50 mL). The reaction mixture was then warmed slowly to room temperature and then heated for 12 h to 110 °C. Volatiles were then removed under vacuum and the residue extracted into hexane to give **5** (0.66 g, 1.63 mmol, 60%).

Method C: Following the same procedure as method B, the similar reaction of **1** with $TiCl_4$ in hexane (15 mL), heating to 45 °C for 1 h, gave **5** in low yield (10%) after repeated extractions into hexane.

[Ti{η5-C5H3[SiMe2(NHtBu)](SiMe2-η1-NtBu)}Cl2] (6). − Method A: A solution of [Ti{η5-C_5H_3[SiMe_2(NH*t*Bu)](SiMe_2-η1-N*t*Bu)}-(NMe_2)2] (0.60 g, 1.30 mmol) in toluene (40 mL) was added to a suspension of NEt_3·HCl (0.35 g, 2.60 mmol) in the same solvent. The mixture was then stirred for 12 h to 80 °C. After subsequent removal of the solvent under vacuum, the residue was extracted into pentane (70 mL). Following filtration and removal of the solvent, complex **6** was then isolated as a red solid (0.54 g, 1.22 mmol, 94%). $C_{17}H_{34}Cl_2N_2Si_2Ti$ (441.4): calcd. C 46.26, H 7.76, N 6.35; found C 46.52, H 7.68, N 6.13. ^{1}H NMR (C_6D_6, 20 °C): δ = 0.24 (s, 3 H, Si*Me*$_2$), 0.26 (s, 3 H, Si*Me*$_2$), 0.45 (s, 3 H, Si*Me*$_2$), 0.56 (s, 3 H, Si*Me*$_2$), 1.05 (s, 9 H, NHC*Me*$_3$), 1.38 (s, 9 H, NC*Me*$_3$), 6.35 (m, 1 H, C_5H_3), 6.57 (m, 1 H, C_5H_3), 7.17 (m, 1 H, C_5H_3) ppm. ^{13}C NMR (C_6D_6, 20 °C): δ = −0.1 (Si*Me*$_2$), 0.6 (Si*Me*$_2$), 1.5 (Si*Me*$_2$), 1.8 (Si*Me*$_2$), 32.3 (NHC*Me*$_3$), 33.9 (NC*Me*$_3$), 49.8 (NH*C*Me$_3$), 63.9 (N*C*Me$_3$), 112.6 (C_5H_{3ipso}), 126.1 (C_5H_3), 129.4 (C_5H_3), 129.5 (C_5H_{3ipso}), 130.9 (C_5H_3) ppm.

Method B: A solution of [Ti{η5-C_5H_3(SiMe_2-η1-N*t*Bu)2}(CH_2Ph)] (0.58 g, 1.25 mmol) in toluene (40 mL) was added to a suspension of NEt_3·HCl (0.34 g, 2.50 mmol) in the same solvent. The mixture was then stirred for 12 h at 80 °C. The solvent was then removed under vacuum and the residue extracted into hexane (40 mL). After filtration and removal of the solvent, complex **6** was then isolated as a red solid (0.31 g, 0.70 mmol, 70%).

Method C: 6 was formed when the method described below to prepare **7** was followed, using 1 equiv. of $TiCl_4$. The resulting mixture contained **6** and **7** in a 1:3 molar ratio. Pure **6** could not be isolated from this mixture.

[Ti{η5-C5H3(SiMe2Cl)(SiMe2-η1-NtBu)}Cl2] (7): In a sealed Schlenk tube, an orange solution of $TiCl_4$ (0.32 mL, 2.97 mmol) in toluene (50 mL) was cooled to −78 °C and added to a cooled (−78 °C) stirred suspension of the lithium salt **1** (0.49 g, 1.48 mmol) in the same solvent (50 mL). NEt_3 (0.62 mL, 4.45 mmol) was added to this mixture, and finally, it was warmed to room temperature and heated for 12 h to 110 °C. The volatiles were removed under vacuum and the residue was extracted into hexane. After filtration and removal of the solvent complex **7** was isolated as a yellow solid (0.44 g, 1.10 mmol, 75%). $C_{13}H_{24}Cl_3NSi_2Ti$ (404.7): calcd. C 38.58, H 5.98, N 3.46; found C 39.07, H 6.16, N 3.46. ^{1}H NMR ($CDCl_3$, 20 °C): δ = 0.60 (s, 3 H, Si*Me*$_2$), 0.62 (s, 3 H, Si*Me*$_2$), 0.70 (s, 3 H, Si*Me*$_2$), 0.79 (s, 3 H, Si*Me*$_2$), 1.43 (s, 9 H, NC*Me*$_3$), 6.53 (m, 1 H, C_5H_3), 6.63 (m, 1 H, C_5H_3), 7.25 (m, 1 H, C_5H_3) ppm. ^{13}C NMR ($CDCl_3$, 20 °C): δ = 0.13 (Si*Me*$_2$), 0.64 (Si*Me*$_2$), 1.65 (Si*Me*$_2$), 2.65 (Si*Me*$_2$), 32.1 (NC*Me*$_3$), 64.6 (N*C*Me$_3$), 113.1 (C_5H_{3ipso}), 129.4 (C_5H_3), 130.6 (C_5H_3), 132.1 (C_5H_3), 135.5 (C_5H_{3ipso}) ppm.

[Zr{η5-C5H3(SiMe2Cl)2}Cl3] (8): In a sealed Schlenk tube, $TiCl_4$ (0.18 mL, 1.65 mmol) was added by syringe to a cooled (−78 °C) light yellow solution of complex **2** (0.43 g, 0.82 mmol) in toluene (70 mL). The reaction mixture was then warmed to room temperature, followed by heating for 12 h to 110 °C. Volatiles were then removed under vacuum and the residue extracted into hexane. After filtration and removal of the solvent, complex **8** was isolated as a light yellow solid (0.25 g, 0.56 mmol, 69%). $C_9H_{15}Cl_5Si_2Zr$ (447.9): calcd. C 24.14, H 3.38; found C 24.01, H 3.30. ^{1}H NMR ($CDCl_3$, 20 °C): δ = 0.70 (s, 6 H, Si*Me*$_2$), 0.75 (s, 6 H, Si*Me*$_2$), 6.76 (d, $J_{H,H}$ = 1.8 Hz, 2 H, C_5H_3), 7.19 (t, $J_{H,H}$ = 1.8 Hz, 1 H, C_5H_3) ppm. ^{13}C NMR($CDCl_3$, 20 °C): δ = 2.65 (Si*Me*$_2$), 3.83 (Si*Me*$_2$), 121.4 (C_5H_3), 126.6 (C_5H_{3ipso}), 141.8 (C_5H_3) ppm.

[Zr{η5-C5H3 [SiMe2(NHtBu)](SiMe2-η1-NtBu)}Cl2(NMe2H)] (9): A solution of [Zr{η5-C_5H_3 (SiMe_2-η1-N*t*Bu)2}(NMe_2)] (0.74 g, 1.46 mmol) in toluene (40 mL) was added to a suspension of NEt_3·HCl (0.40 g, 2.92 mmol) in the same solvent. The resultant mixture was then stirred for 2 h at 70 °C. The solvent was then removed under vacuum and the residue extracted into pentane (40 mL). After filtration and removal of the solvent, complex **9** was isolated as an ochre microcrystalline solid (0.64 g, 1.21 mmol, 82%). $C_{19}H_{41}Cl_2N_3Si_2Zr$ (529.8): calcd. C 43.07, H 7.80, N 7.93; found C 42.46, H 7.58, N 7.60. ^{1}H NMR (C_6D_6, 20 °C): δ = 0.27 (s, 3 H, Si*Me*$_2$), 0.28 (s, 3 H, Si*Me*$_2$), 0.5 (s, 3 H, Si*Me*$_2$), 0.52 (s, 3 H, Si*Me*$_2$), 1.06 (s, 9 H, NHC*Me*$_3$), 1.50 (s, 9 H, NC*Me*$_3$), 2.25 (s, 3 H, N*Me*$_2$H), 2.27 (s, 3 H, N*Me*$_2$H), 3.58 (s br, 1 H, NMe$_2$*H*), 6.43 (m, 1 H, C_5H_3), 6.81 (m, 1 H, C_5H_3), 6.91 (m, 1 H, C_5H_3) ppm. ^{13}C NMR (C_6D_6, 20 °C): δ = 1.1 (Si*Me*$_2$), 1.4 (Si*Me*$_2$), 1.9 (Si*Me*$_2$), 4.2 (Si*Me*$_2$), 31.6 (NHC*Me*$_3$), 33.6 (NC*Me*$_3$), 39.3 (br., N*Me*$_2$H), 50.1 (NH*C*Me$_3$), 58.3 (N*C*Me$_3$), 114.6 (C_5H_{3ipso}), 123.9 (C_5H_3), 126.3 (C_5H_3), 127.9 (C_5H_{3ipso}), 129.4 (C_5H_3) ppm.

[Zr{η5-C5H3[SiMe2(NHtBu)](SiMe2-η1-NtBu)}Cl(NMe2)] (10): $SiClMe_3$ (15.2 μL, 0.12 mmol) was added by syringe to a solution of [Zr{η5-C_5H_3[SiMe_2(NH*t*Bu)](SiMe_2-η1-N*t*Bu)}(NMe_2)2] (0.059 g, 0.12 mmol) in C_6D_6. The ^{1}H NMR spectrum of this solution was recorded after 1 h of reaction to confirm that **10** was the unique product. ^{1}H NMR (C_6D_6, 20 °C): δ = 0.30 (s, 3 H, Si*Me*$_2$), 0.32 (s, 3 H, Si*Me*$_2$), 0.44 (s, 3 H, Si*Me*$_2$), 0.46 (s, 3 H, Si*Me*$_2$), 1.04 (s, 9 H, NHC*Me*$_3$), 1.27 (s, 9 H, NC*Me*$_3$), 2.75 (d, 6 H, ZrN*Me*$_2$), 6.28 (m, 1 H, C_5H_3), 6.52 (m, 1 H, C_5H_3), 7.02 (m, 1 H, C_5H_3) ppm. ^{13}C NMR (C_6D_6, 20 °C): δ = 2.0 (Si*Me*$_2$), 2.0 (Si*Me*$_2$), 2.1 (Si*Me*$_2$), 2.1 (Si*Me*$_2$), 33.8 (NHC*Me*$_3$), 34.1 (NC*Me*$_3$), 43.3 (N*Me*$_2$), 49.7 (NH*C*Me$_3$), 56.9 (N*C*Me$_3$), 111.6 (C_5H_{3ipso}), 122.6 (C_5H_{3ipso}), 122.9 (C_5H_3), 125.9(C_5H_3), 127.4 (C_5H_3) ppm.

[Ti{η5-C5H3[SiMe2(NHtBu)](SiMe2-η1-NtBu)}Cl(CH2Ph)] (11): A solution of [Ti{η5-C_5H_3(SiMe_2-η1-N*t*Bu)2}(CH_2Ph)] (0.58 g, 1.25 mmol) in toluene (40 mL) was added to a suspension of NEt_3·HCl (0.17 g, 1.25 mmol) in the same solvent. The resultant mixture was stirred for 2 h at 70 °C. The solvent was then removed under vacuum and the residue was extracted into pentane (40 mL). After filtration and removal of the solvent, complex **11** was isolated as a red solid (0.48 g, 0.96 mmol, 77%). $C_{24}H_{41}ClN_2Si_2Ti$ (497.1): calcd. C 57.99, H 8.31, N 5.64; found C 58.10, H 8.03, N 5.77. ^{1}H NMR (C_6D_6, 20 °C): δ = 0.25 (s, 3 H, Si*Me*$_2$), 0.30 (s, 3 H, Si*Me*$_2$), 0.40 (s, 3 H, Si*Me*$_2$), 0.48 (s, 3 H, Si*Me*$_2$), 1.04 (s, 9 H, NHC*Me*$_3$), 1.48 (s, 9 H, NC*Me*$_3$), 2.92 (d, $J_{H,H}$ = 9.6 Hz, 1 H, C*H*$_2$Ph), 3.1 (d, 1 H, C*H*$_2$Ph), 5.91 (m, 1 H, C_5H_3), 6.39 (m, 1 H, C_5H_3), 6.49 (m, 1 H, C_5H_3), 6.88 (m, 1 H, C_6H_5), 6.97 (m, 2 H, C_6H_5), 7.18

 © 2004 Wiley-VCH Verlag GmbH & Co. KGaA, Weinheim

(m, 2 H, C_6H_5) ppm. ^{13}C NMR (C_6D_6, 20 °C): δ = 0.4 (SiMe_2), 0.6 (SiMe_2), 1.4 (SiMe_2), 1.5 (SiMe_2), 33.7 (NHCMe_3), 33.8 (NCMe_3), 49.6 (NHCMe$_3$), 62.3 (NCMe_3), 79.7 (CH$_2$Ph), 111.4 (C_5H_{3ipso}), 122.5 (C_5H_3), 126.1 (C_5H_{3ipso}), 127.0 (C_5H_3), 128.7 (C_5H_4) 128.8 (C_6H_5), 133.1 (C_6H_5), 139.2 (C_6H_5), 149.5 (C_6H_{5ipso}) ppm.

[Zr{η^5-C$_5$H$_3$[SiMe$_2$(NH*t*Bu)](SiMe$_2$-η^1-N*t*Bu)}Cl$_2$] (12): A solution of [Zr{η^5-C$_5$H$_3$(SiMe$_2$-η^1-N*t*Bu)$_2$}(CH$_2$Ph)] (0.32 g, 0.63 mmol) in toluene (40 mL) was added to a suspension of NEt$_3$·HCl (0.17 g, 1.26 mmol) in the same solvent. The resultant mixture was stirred for 12 h at 70 °C. The solvent was then removed under vacuum and the residue extracted into pentane (70 mL). After filtration and removal of the solvent, complex **12** was isolated as a light brown solid (0.27 g, 0.58 mmol, 88%). ^{1}H NMR (C_6D_6, 20 °C): δ = 0.27 (2s, 6 H, SiMe_2), 0.43 (s, 3 H, SiMe_2), 0.53 (s, 3 H, SiMe_2), 1.05 (s, 9 H, NHCMe_3), 1.30 (s, 9 H, NCMe_3), 6.41 (m, 1 H, C_5H_3), 6.60 (m, 1 H, C_5H_3), 6.97 (m, 1 H, C_5H_3) ppm. ^{13}C NMR (C_6D_6, 20 °C): δ = 0.8 (SiMe_2), 1.4 (SiMe_2), 1.9 (SiMe_2), 33.0 (NHCMe_3), 33.9 (NCMe_3), 49.8 (NHCMe$_3$), 57.6 (NCMe$_3$), 112.6 (C_5H_{3ipso}), 120.9 (C_5H_3), 126.7 (C_5H_{3ipso}), 128.3 (C_5H_3) ppm.

X-ray Crystallographic Study: Crystal data and details of the structure determination (Table 2) and bond lengths and bond angles (Table 1) are given here. Suitable single crystals for X-ray diffraction were grown from a saturated solution of **3** in pentane by standard cooling techniques. A clear orange fragment (0.41 × 0.43 × 0.48 mm) was stored under perfluorinated ether, transferred to a Lindemann capillary, fixed and sealed. Preliminary examination and data collection were carried out on an area detecting system (NONIUS, MACH3 κ-CCD) at the window of a rotating anode (NONIUS, FR591) and graphite-monochromated Mo-K_α radiation (λ = 0.71073 Å). Unit cell parameters were obtained by full-matrix least-squares refinement of 2450 reflections. Data collection was performed at 153 K within a Θ-range of 2.77−25.35°. Nine data sets were measured in rotation scan modus with Δφ/ΔΩ = 1.0° controlled by the COLLECT software package.[33] A total of 30285 intensities were integrated. Raw data were corrected for Lorentz, polarization, and during the scaling procedure for latent decay and absorption effects. After merging (R_{int} = 0.043), a sum of 4654 (all data) and 4560 [$I > 2\sigma(I)$] remained and all data were used.[34] The structure was solved by a combination of direct methods[35] and difference Fourier syntheses.[36] All non-hydrogen atoms were refined with anisotropic displacement parameters. All hydrogen atoms were found in the final difference Fourier maps and allowed to refine freely with isotropic displacement parameters. Full-matrix least-squares refinements with 366 parameters were carried out by minimizing $\Sigma w(F_o^2-F_c^2)^2$ with the SHELXL-97 weighting scheme and stopped at shift/err < 0.001. The correct enantiomer was proved by Flack's parameter ε = 0.02(2). Final residual electron density maps showed no remarkable features. Neutral atom scattering factors for all atoms and anomalous dispersion corrections for the non-hydrogen atoms were taken from *International Tables for Crystallography*.[37] CCDC-229361 contains the supplementary crystallographic data for this paper. These data can be obtained free of charge at www.ccdc.cam.ac.uk/conts/retrieving.html [or from the Cambridge Crystallographic Data Centre, 12 Union Road, Cambridge CB2 1EZ, UK; Fax: (internat.) +44-1223-336-033; E-mail: deposit@ccdc.cam.ac.uk].

Table 2. Crystallographic data for [Ti(η^5-C$_5$H$_3${SiMe$_2$(NH*t*Bu)}$_2$)-Cl$_3$] (**3**)

	3
Empirical formula	$C_{17}H_{35}Cl_3N_2Si_2Ti$
Formula mass	477.87
Colour/shape	orange/fragment
Crystal size (mm)	0.41 × 0.43 × 0.48
Crystal system	monoclinic
Space group	$P2_1$ (No. 4)
a (Å)	9.3637(1)
b (Å)	12.4297(2)
c (Å)	11.2252(1)
β (deg)	103.5551(7)
V (Å^3)	1270.09(3)
Z	2
T (K)	153
$\rho_{calcd.}$ (g cm^{-3})	1.250
μ (mm^{-1})	0.751
F_{000}	504
θ Range (°)	2.77−25.35
Data collected (h,k,l)	±11, ±14, ±13
No. of reflns. collected	30285
No. of indep. reflns./R_{int}	4654 (all)/0.043
No. of obsd. reflns. ($I > 2\sigma$ (I)]	4560 (obsd.)
no. of parameters refined	366
R1 (obsd./all)	0.0198/0.0207
wR2 (obsd./all)	0.0450/0.0453
GOF (obsd./all)	1.093/1.093
max/min $\Delta\rho$ (e·Å^{-3})	+0.19/−0.15

Acknowledgments

The authors acknowledge the MCyT (project MAT2001−1309) for financial support. M. S. and J. C. acknowledge MECD and CAM, respectively, for fellowships.

[1] Reviews: [1a] J. Okuda, T. Eberle, *Metallocenes: Synthesis, Reactivity, Applications* (A. Togni, R. L. Haltermann, Eds.), Wiley-VCH, Weinheim, **1998**, *vol.1, chap. 7*, 415−453. [1b]A. L. McKnight, R. M. Waymouth, *Chem. Rev.* **1998**, *98*, 2587−2598.

[2] [2a] W. E. Piers, P. J. Shaphiro, E. E. Bunel, J. E. Bercaw, *Synlett* **1990**, *2*, 74−84. [2b] P. J. Shaphiro, E. E. Bunel, W. P. Schaefer, J. E. Bercaw, *Organometallics* **1990**, *9*, 867−869. [2c] J. Okuda, *Chem. Ber.* **1990**, *123*, 1649−1651. [2d] P. J. Shaphiro, W. D. Cotter, W. P. Schaefer, J. A. Labinger, J. E. Bercaw, *J. Am. Chem. Soc.* **1994**, *116*, 4623−4640.

[3] [3a] J. C. Stevens, F. J. Timmers, D. R. Wilson, G. F. Schmidt, P. N. Nickias, R. K. Rosen, G. W. Knight, S. Lai, *Eur. Patent Appl.* **1991**, EP416815-A2 (Dow Chemical Co.). [3b] J. M. Canich, *Eur. Patent Appl.* **1991**, EP420436-A1(Exxon Chemical Co.). [3c] J. M. Canich, *PCT Int. Appl.* **1996**, WO 96/00244 (Exxon Chemical Co.). [3d] P. N. Nickias, M. H. McAdon, J. T. Patton, B. P. Friedrichsen, J. C. Stevens, D. D. Vanderlende, *PCT Int. APPl.* **1997**, WO 97/15583 (Dow Chemical Co.).

[4] [4a] K. Kunz, G. Erker, S. Döring, R. Fröhlich, G. Kehr, *J. Am. Chem. Soc.* **2001**, *123*, 6181−6182. [4b] K. Kunz, G. Erker, S. Döring, S. Bredeau, G. Erker, R. Fröhlich, *Organometallics* **2002**, *21*, 1031−1041.

[5] J. Cano, P. Royo, M. Lanfranchi, M. A. Pellinghelli, A. Tiripicchio, *Angew. Chem. Int. Ed.* **2001**, *40*, 2495−2497.

[6] M. F. Lappert, P. B. Power, A. R. Sanger, R. C. Srivastava, *Metal and Metalloid Amines* **1980**, Ellis Horwood: Chinchester, West Sussex, UK.

[7] [7a] J. N. Christopher, G. M. Diamond, R. F. Jordan, J. L. Petersen, *Organometallics* **1996**, *15*, 4038−4044. [7b] G. M. Diamond, R. F. Jordan, J. L. Petersen, *J. Am. Chem. Soc.* **1996**,

 © 2004 Wiley-VCH Verlag GmbH & Co. KGaA, Weinheim

118, 8024−8033. [7c] J. N. Christopher, R. F. Jordan, J. L. Petersen, V. G. Young Jr., *Organometallics* **1997**, *16*, 3044−3050.
[8] [8a] C. Li, R. K. Thomson, B. Gillon, B. O. Patrick, L. L. Schafer, *Chem. Commun.* **2003**, 2462−2463. [8b] M. R. Mason, B. N. Fneich, K. Kirschbaum, *Inorg. Chem.* **2003**, *42*, 6592−6594. [8c] T. Patton, M. M. Bokota, K. A. Abboud, *Organometallics* **2002**, *21*, 2145−2148.
[9] [9a] A.K. Hughes, A. Meetsma, J. H. Teuben, *Organometallics* **1993**, *12*, 1936−1945. [9b] W. A. Herrmann, M. J. A. Morawietz, *J. Organomet. Chem.* **1994**, *482*, 169−181. [9c] D. W. Carpenetti, L. Kloppenburg, J. T. Kupec, J. L. Petersen, *Organometallics* **1996**, *15*, 1572−1581.
[10] [10a] Y. Mu, W. E. Piers, L. R. MacGillivray, M. J. Zaworotko, *Polyhedron* **1995**, *14*, 1−10. [10b] A. L. McKnight, M. A. Masood, R. M. Waymouth, D. A. Strauss, *Organometallics* **1997**, *16*, 2879−2885. [10c] A. K. Hughes, S. M. B. Marsh, J. A. K. Howard, P. S. Ford, *J. Organomet. Chem.* **1997**, *528*, 195−198.
[11] [11a] Y.-X. Chen, P.-F. Fu, C. L. Stern, T. J. Marks, *Organometallics* **1997**, *16*, 5958−5963. [11b] Y.-X. Chen, T. J. Marks, *Organometallics* **1997**, *16*, 3649−3657.
[12] Y. Mu, W. E. Piers, D. C. MacQuarrie, M. J. Zaworotko, V. G. Young Jr., *Organometallics* **1996**, *15*, 2720−2726.
[13] J. Cano, P. Royo, H. Jacobsen, O. Blacque, H. Berke, E. Herdtweck, *Eur. J. Inorg. Chem.* **2003**, 2463−2474.
[14] F. Guérin, D. H. McConville, J. J. Vittal, *Organometallics* **1996**, *15*, 5586−5590.
[15] T. H. Warren, G. Erker, R. Fröhlich, B. Wibbeling, *Organometallics* **2000**, *19*, 127−134.
[16] B. Y. Lee, J. W. Han, H. Seo, I. S. Lee, Y. K. Chung, *J. Organomet. Chem.* **2001**, *627*, 233−238.
[17] E. E. C. G. Gielens, J. Y. Tiesnitsch, B. Hessen, J. H. Teuben, *Organometallics* **1998**, *17*, 1652−1654.
[18] B. Tsuie, D. C. Swenson, R. F. Jordan, J. L. Petersen, *Organometallics* **1997**, *16*, 1392−1400.
[19] T. Cuenca, P. Royo, *Coord. Chem. Rev.* **1999**, *193−195*, 447−498.
[20] A. B. Vázquez, P. Royo, E. Herdtweck, *J. Organomet. Chem.* **2003**, *683*, 155−164.
[21] J. M. Rozell, R. R. Jones, *Organometallics* **1985**, *4*, 2206−2210.
[22] S. Ciruelos, T. Cuenca, R. Gómez, P. Gómez-Sal, A. Manzanero, P. Royo, *Organometallics* **1996**, *15*, 5577−5585.
[23] L. M. Englhardt, R. I. Papasergio, C. L. Raston, A. H. White, *Organometallics* **1984**, *3*, 18−20.
[24] K. Kirschbaum, D. M. Giolando, *Acta Crystallogr., Sect. C* **1991**, *47*, 2216−2218.
[25] J. Saßmannshausen, A. K. Powell, C. E. Anson, S. Wocadlo, M. Bochmann, *J. Organomet. Chem.* **1999**, *592*, 84−94.
[26] S. L. Hart, D. J. Duncalf, J. J. Hastings, A. McCamley, P. C. Taylor, *J. Chem. Soc., Dalton Trans.* **1996**, 2843−2849.
[27] J. C. Flores, J. S. Wood, J. C. W. Chien, M. D. Rausch, *Organometallics* **1996**, *15*, 4944−4950.
[28] C. H. Winter, X.-X. Zhou, D. A. Dobbs, M. J. Heeg, *Organometallics* **1991**, *10*, 210−214.
[29] I. Jibril, S. Abu-Orabi, S.A. Klaib, W. Imhof, G. Huttner, *J. Organomet. Chem.* **1992**, *433*, 253−259.
[30] [30a] Y. Qian, G. Li, W. Chen, B. Li, X. Jin, *J. Organomet. Chem.* **1989**, *373*, 185−191. [30b] H. Qichen, Q. Yanglong, L. Guisheng, T. Youqui, *Transition Met. Chem.* **1999**, *15*, 483−485. [30c] M. Enders, R. Rudolf, H. Pritzkow, *J. Organomet. Chem.* **1997**, *549*, 251−256. [30d] W. A. Herrmann, M. J. A. Morawietz, T. Priermeier, K. Mashima, *J. Organomet. Chem.* **1995**, *486*, 291−295.
[31] C. S. Bajgur, W. R. Tikannen, J. L. Petersen, *Inorg. Chem.* **1985**, *24*, 2539−2546.
[32] D. E. Wigley, *Prog. Inorg. Chem.* **1994**, *42*, 239−482.
[33] R. Hooft, *COLLECT: Data Collection Software for Nonius* κ-CCD *Devices*, Nonius B. V., Delft, The Netherlands, **1998**.
[34] Z.·Otwinowski, W. Minor, *Processing of X-ray Diffraction Data Collected in Oscillation Mode, Methods in Enzymology: Macromolecular CrystallograPhy*, part A (Eds.: C. W. Carter Jr., R. M. Sweet), Academic Press, New York, **1997**, *vol. 276*, 307−326.
[35] G. M. Sheldrick, *SHELXS-97*; University of Göttigen, Germany, **1998**.
[36] G. M. Sheldrick, *SHELXL-97*; University of Göttigen, Germany, **1998**.
[37] A. J. C. Wilson (Ed.), *Interntional Tables for Crystallography*, Kluwer Academic Publisher, Dordrecht, The Netherlands, **1992**, vol. C, Tables 6.1.1.4 (pp. 500−502), 4.2.6.8 (pp. 219−222), 4.2.4.2 (pp. 193−199).

Received February 2, 2004
Early View Article
Published Online May 25, 2004

 © 2004 Wiley-VCH Verlag GmbH & Co. KGaA, Weinheim

1,3,5-Triazapentanediene, A Novel Tridentate Ligand that Bridges Two Metal Ions in a $\kappa^1N:\kappa^2N$ Bridging Mode with C_2 Symmetry

Takashi Kajiwara*[a] and Tasuku Ito[a]

Keywords: Chelates / Coordination modes / N ligands / Nickel

The new mononuclear complexes $[Ni(Htap)_2](ClO_4)_2$ (**1**) and $[Ni(tap)(Htap)]ClO_4$ (**2**) were synthesized by the reaction of nickel(II) perchlorate and 1,3,5-triazine (Htap = 1,3,5-triazapentanediene). In **1** and **2**, neutral Htap and a monoanionic tap^- coordinate in a square-planar mode to the nickel(II) ions (low-spin state) in a bidentate, chelating fashion. Using the central N of tap^- of **2** as a donor atom, multinuclear complexes $[\{Cu(tren)\}_2\{Ni(tap)_2\}](ClO_4)_4$ (**3**) and $[Ni(Htap)_2]_2$-$[Ni\{Ni(tap)(Htap)\}_2(NCS)_4][Ni\{Ni(tap)(Htap)\}(NCS)_5]_2$ (**4**) were synthesized. In both complexes, tap^- binds two metal ions in a $\kappa^1N:\kappa^2N$ bridging mode, with C_2 symmetry along the Ni–Cu axis for **3** and Ni–Ni axis for **4**.
(© Wiley-VCH Verlag GmbH & Co. KGaA, 69451 Weinheim, Germany, 2004)

Introduction

Metal-containing ligands[1] are useful building blocks for making metal-assembled complexes with direct or indirect metal−metal interactions. In our recent studies, we have focused on a metal-containing ligand derived from 1,3,5-tris(2-pyridyl)-2,4,6-triazine (tptz). Upon refluxing, tptz can be converted into bis(2-pyridylcarbonyl)amine (Hpbca, Figure 1) or 2,4-bis(2-pyridyl)-1,3,5-triazapentanediene (Hbptap) in the presence of copper(II) ions; they were isolated as their copper(II) complexes (Scheme 1).[2−4,9] Hbpca was easily obtained as the free ligand,[2] and a variety of metal complexes were synthesized for use as metal-containing ligands.[2,5−8] We have shown that complexes such as $[M(bpca)_2]$,[2,5−7] $[Fe_3(\mu_3\text{-}O)(bpca)_4(OEt)_2Cl_4]^-$,[8] and $[Cu(bptap)_2]$[9,10] potentially act as ligands to build metal-assembled complexes. In the resulting complexes, the two adjacent metal ions are bridged in a $\kappa^1N:\kappa^2O$ mode for $bpca^-$ or $\kappa^1N:\kappa^2N$ mode for $bptap^-$, with local C_2 symmetry along the metal−metal axis (Figure 2). When the two metal ions have dσ spins, this bridging mode causes the dσ orbitals to have different symmetry and thus makes them orthogonal to each other.[2,9,10] As a result, a ferromagnetic interaction occurs between the metal ions. While this coordination mode promotes ferromagnetic interactions, only a few reports have been published concerning either $\kappa^1N:\kappa^2O$ or $\kappa^1N:\kappa^2N$ modes.[11]

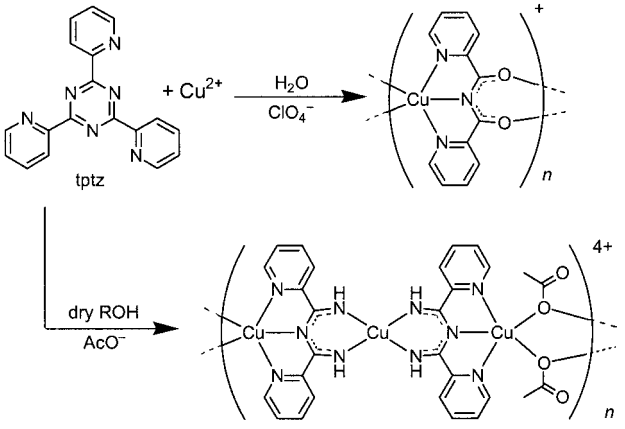

Scheme 1

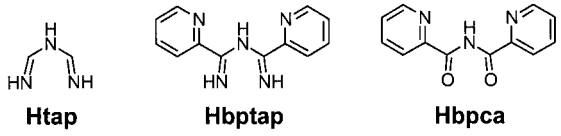

Figure 1. The structures of 1,3,5-triazapentanediene (Htap), 2,4-bis(2-pyridyl)-1,3,5-triazapentandiene (Hbptap), and bis(2-pyridylacarbonyl)amine (Hbpca)

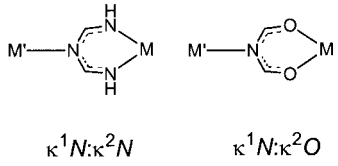

Figure 2. The κ^1N: κ^2N and κ^1N: κ^2O coordination mode with local C_2 symmetry found in complexes of $bpca^-$ and $bptap^-$

This study describes the simplest ligand in the series, 1,3,5-triazapentanediene (Htap, Figure 1), and its metal complexes. This ligand, like Hbptap, can link metals in a $\kappa^1N:\kappa^2N$ mode. Unlike tptz, which requires severe con-

[a] Department of Chemistry, Graduate School of Science, Tohoku University,
Sendai 980-8578, Japan
E-mail: kajiwara@agnus.chem.tohoku.ac.jp

 © 2004 Wiley-VCH Verlag GmbH & Co. KGaA, Weinheim DOI: 10.1002/ejic.200400122

ditions to decompose, 1,3,5-triazine decomposes easily and Htap was first obtained as $[Cu(Htap)_2](ClO_4)_2$.[12] However, this copper(II) complex is not suitable as a metal-containing ligand since it decomposes under basic conditions. We found that 1,3,5-triazine is also converted into Htap in the presence of nickel(II) ions. Herein we report the syntheses of the new nickel(II) complexes $[Ni(Htap)_2](ClO_4)_2$ (**1**) and $[Ni(tap)(Htap)]ClO_4$ (**2**). The syntheses and structures of multinuclear complexes constructed with the complexed ligands, $[\{Cu(tren)\}_2\{Ni(tap)_2\}](ClO_4)_4$ (**3**) and $[Ni(Htap)_2]_2[Ni\{Ni(tap)(Htap)\}_2(NCS)_4][Ni\{Ni(tap)(Htap)\}(NCS)_5]_2$ (**4**), are also described.

Results and Discussion

Synthesis of Complexed Ligands 1 and 2

Unlike tptz, which forms stable metal complexes at room temperature, 1,3,5-triazine readily decomposes in the presence of metal ions to form Htap. At room temperature, the decomposition takes longer with nickel(II) than with copper(II), but upon heating to near reflux it was possible to prepare a new nickel(II) Htap complex, $[Ni(Htap)_2](ClO_4)_2$ (**1**) (Scheme 2).

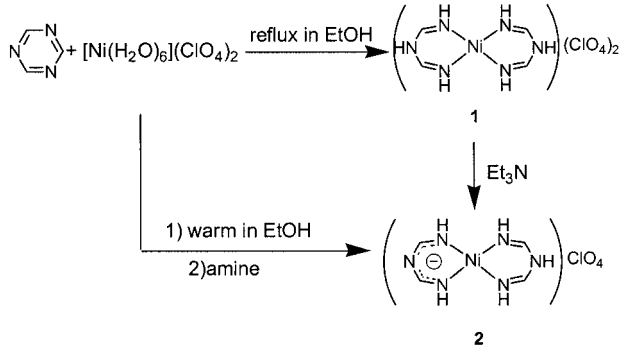

Scheme 2

The mixed-ligand complex $[Ni(tap)(Htap)]ClO_4$ (**2**) was synthesized by controlling the basicity of the solution with ethylenediamine during the decomposition of 1,3,5-triazine. Slow diffusion of triethylamine into an alcoholic solution of **1** also gave the same product.

In order to obtain a pK_a value for **1**, ^1H NMR spectra of **1** and **2** in D_2O were measured. Both complexes have very broad signals at around $\delta = 9.38$ ppm for **1** and $\delta = 8.40$ ppm for **2**, which were not assigned. These broad peaks are indicative of a fast equilibrium between low-spin four-coordinate and high-spin six-coordinate geometries in aqueous solution, and therefore we could not determine a pK_a value for **1**.

Synthesis of Multinuclear Complexes 3 and 4

Complex **2** has a strong ability to act as a complexed ligand through the amide nitrogen atom of tap^-, and the trinuclear complex $[\{Cu(tren)\}_2\{Ni(tap)_2\}](ClO_4)_4$ (**3**) was easily synthesized by the reaction of **2** and $[Cu(tren)](ClO_4)_2$ in $EtOH/H_2O$. In this compound, a neutral $\{Ni(tap)_2\}$ moiety bridges two copper(II) ions to form a linear trinuclear complex acting as a bis-monodentate ligand (see below).

Addition of strong donor ions such as SCN^- to a solution of **2** resulted in the decomposition of **2** to give $\{Ni(NCS)_4\}^{2-}$ and $\{Ni(NCS)_5\}^{3-}$, and by controlling the reaction stoichiometry, a multinuclear complex $[Ni(Htap)_2]_2[Ni\{Ni(tap)(Htap)\}_2(NCS)_4][Ni\{Ni(tap)(Htap)\}(NCS)_5]_2$ (**4**) was obtained as crystals.

Structures of 1 and 2

The structures of complexes **1** and **2** are shown in Figures 3 and 4, respectively. In **1**, the nickel(II) ion is located on a crystallographic inversion center and the two Htap ligands in each molecule are equivalent. Both Htap ligands occupy four coordination sites of the square-planar nickel(II) ion in a bidentate chelating fashion with short Ni−N distances of 1.859(2) Å and 1.8554(18) Å, which results in the nickel(II) ion being in a low-spin state. The central nitrogen atom of the ligand (N2) is protonated, dividing the conjugated π-system, and, as a result, the terminal C−N bonds (C1−N1 and C2−N3) have a double bond character [C−N = 1.278(3) and 1.280(3) Å, respectively]. Each nitrogen atom in Htap is bound to oxygen atom(s) from ClO_4^- by hydrogen bonding(s) [O···N = 2.983(3)−3.136(2) Å].

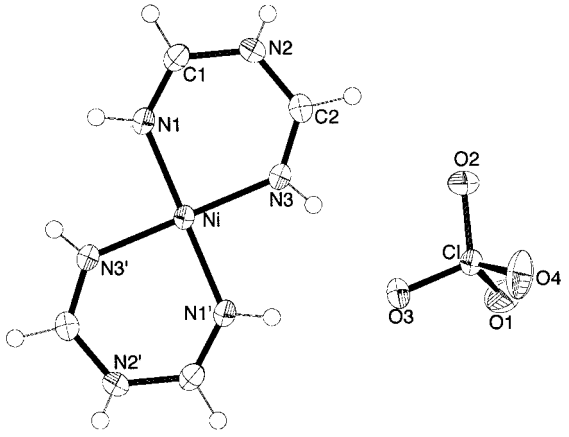

Figure 3. An ORTEP diagram of complex **1** with 50% displacement ellipsoids; relevant bond lengths (Å) and angles (°): Ni−N(1) 1.8554(18), Ni−N(3) 1.859(2), N(1)−C(1) 1.278 (3), C(1)−N(2) 1.348(3), N(2)−C(2) 1.356(3), C(2)−N(3) 1.280(3); N(3)−Ni−N(1) 90.08(9), N(1)−Ni−N(3′) 89.92(9); symmetry transformations used to generate equivalent atoms: ′ $-x, -y + 1, -z$

In **2**, two crystallographically independent cations are present in the unit cell. They have similar structures and are abbreviated as complex **2a** [including Ni(1)] and complex **2b** [including Ni(2)]. $[Ni(tap)(Htap)]^+$ contains both a protonated Htap and a deprotonated tap^-. The structures of the Htap ligands in **2a** and **2b** are similar to that in **1**; however, tap^- shows slight differences from Htap, reflecting the differences in the electronic structures. The minus charge of tap^- is delocalized over the $N_{terminal}-C-N_{central}-C-N_{terminal}$ π-system, and, as a result, the double-bond character of the terminal C−N bonds is reduced and the

 © 2004 Wiley-VCH Verlag GmbH & Co. KGaA, Weinheim

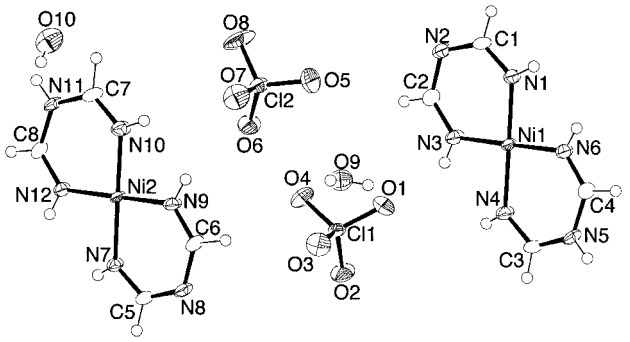

Figure 4. An ORTEP diagram of the complex **2**·H_2O with 50% displacement ellipsoids

bond lengths are slightly elongated [for Htap the $C-N_{terminal}$ bond lengths are in the range between 1.276(4) and 1.285(4) Å; for tap$^-$ the distances are 1.306(4) and 1.297(4) Å for complex **2a** and 1.302(4) and 1.293(4) Å for complex **2b**); see also Table 1]. Both Htap and tap$^-$ coordinate to the nickel(II) ion, with slightly shorter $Ni-N_{terminal}$ bonds for tap$^-$ [1.837(3)−1.843(3) Å] than for Htap [1.860(3)−1.871(3) Å] due to the presence of the negative charge. Because of the strong ligand field, the nickel(II) ions are in a low-spin state. Each of **2a** and **2b** is aligned in a liner manner along the *a* axis and adjoining $N_{central}$(tap) and $N_{central}$(Htap) are connected by a hydrogen bonding [N(2)···N(5)* = 2.775(4) and N8···N(11)* = 2.791(4) Å].

Table 1. Selected bond lengths (Å) and angles (°) for complex **2**

Ni(1)−N(1)	1.837(3)	Ni(1)−N(3)	1.843(3)
Ni(1)−N(4)	1.863(3)	Ni(1)−N(6)	1.871(3)
N(1)−C(1)	1.306(4)	C(1)−N(2)	1.336(4)
N(2)−C(2)	1.338(4)	C(2)−N(3)	1.297(4)
N(4)−C(3)	1.280(4)	C(3)−N(5)	1.351(4)
N(5)−C(4)	1.362(4)	C(4)−N(6)	1.285(4)
Ni(2)−N(7)	1.845(3)	Ni(2)−N(9)	1.845(3)
Ni(2)−N(10)	1.860(3)	Ni(2)−N(12)	1.863(2)
N(7)−C(5)	1.302(4)	C(5)−N(8)	1.350(4)
N(8)−C(6)	1.339(4)	C(6)−N(9)	1.293(4)
N(10)−C(7)	1.282(4)	C(7)−N(11)	1.346(4)
N(11)−C(8)	1.360(4)	C(8)−N(12)	1.276(4)
N(1)−Ni(1)−N(3)	88.87(12)	N(1)−Ni(1)−N(4)	179.09(12)
N(3)−Ni(1)−N(4)	90.24(12)	N(1)−Ni(1)−N(6)	90.72(12)
N(3)−Ni(1)−N(6)	179.41(12)	N(4)−Ni(1)−N(6)	90.17(12)
C(1)−N(2)−C(2)	117.8(3)	C(3)−N(5)−C(4)	124.0(3)
N(9)−Ni(2)−N(7)	89.29(12)	N(9)−Ni(2)−N(10)	89.67(12)
N(7)−Ni(2)−N(10)	178.93(11)	N(9)−Ni(2)−N(12)	179.50(11)
N(7)−Ni(2)−N(12)	91.13(12)	N(10)−Ni(2)−N(12)	89.91(12)
C(6)−N(8)−C(5)	118.8(3)	C(7)−N(11)−C(8)	124.1(3)

Structure of Trinuclear complex 3

Figure 5 shows the crystal structure of trinuclear [{Cu(tren)}$_2${Ni(tap)$_2$}](ClO$_4$)$_4$ (**3**). Complex **3** consists of two terminal copper(II) units and a neutral {Ni(tap)$_2$} moiety acting as a bis-monodentate bridging ligand to form a linear structure. The central nickel(II) ion is on an inversion center. In **3**, the tap$^-$ ligands bind to two metal ions in a $\kappa^1N:\kappa^2N$ bridging mode with local C_2 symmetry along the Ni−Cu axis. The nickel(II) ion is surrounded by four nitrogens from two tap$^-$ ligands, with Ni−N distances of 1.842(2) and 1.852(2) Å (Table 2), which are slightly longer than the values for tap$^-$ in **2** [1.837(3)−1.845(3) Å] and close to those of Htap in **1**. The Cu^{II} ions are in a trigonal-bipyramidal environment and the apical position of each Cu atom is occupied by the tertiary nitrogen from tren and $N_{central}$ from the tap$^-$ ligand, with a distance of 2.009(2) Å for the latter. The minus charge of each tap$^-$ ligand is localized on this nitrogen to bind the Cu atom, and, again, the terminal C−N bonds in the tap$^-$ ligands have double-bond character, with shorter distances [1.283(3) and 1.287(3) Å]. This charge localization causes a slight elongation of the Ni−N distances compared to those of the tap$^-$ ligands of **2a** and **2b**. Each $N_{terminal}$ is bound to an oxygen atom from a perchlorate ion by a hydrogen bonding [N(1)···O(8)′ = 2.987(3) and N(3)···O(7)′′ = 3.017(3) Å].

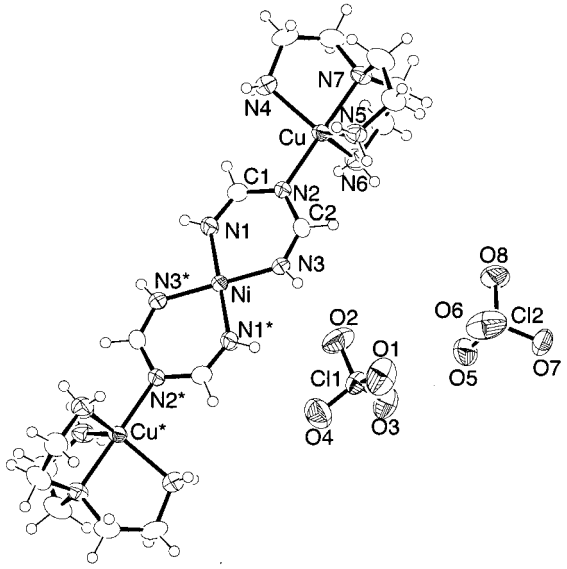

Figure 5. An ORTEP diagram of trinuclear complex **3** with 50% displacement ellipsoids; symmetry transformations used to generate equivalent atoms: * $-x + 1, -y, -z + 1$

Table 2. Selected bond lengths (Å) and angles (°) for complex **3**

Ni−N(1)	1.852(2)	Ni−N(3)	1.842(2)
Cu−N(2)	2.009(2)	Cu−N(5)	2.110(3)
Cu−N(4)	2.098(2)	Cu−N(6)	2.053(3)
Cu−N(7)	2.038(2)		
N(1)−C(1)	1.287(3)	C(1)−N(2)	1.344(3)
N(2)−C(2)	1.346(3)	C(2)−N(3)	1.283(3)
N(1)−Ni−N(3)	88.00(11)	N(1)*−Ni−N(3)[a]	92.00(11)
N(2)−Cu−N(7)	179.11(9)	N(2)−Cu−N(4)	96.28(9)
N(2)−Cu−N(5)	97.30(9)	N(2)−Cu−N(6)	94.87(9)
N(4)−Cu−N(5)	115.86(12)	N(4)−Cu−N(6)	117.65(13)
N(5)−Cu−N(6)	123.09(14)		

[a] Symmetry code: * $-x + 1, -y, -z + 1$.

Structure of Complex 4

Figure 6 shows the structure of multinuclear complex **4**. This complex consists of three independent complexes, di-

 © 2004 Wiley-VCH Verlag GmbH & Co. KGaA, Weinheim

cationic $[Ni(Htap)_2]^{2+}$, including Ni1 (complex $\mathbf{4a^{2+}}$), dianionic dinuclear $[Ni(NCS)_5\{Ni(tap)(Htap)\}]^{2-}$, including Ni2 and Ni3 (complex $\mathbf{4b^{2-}}$), and neutral trinuclear $[Ni(NCS)_4\{Ni(tap)(Htap)\}_2]$, with Ni4 and Ni5 (complex **4c**). Ni5 in **4c** is located on a crystallographic inversion center, therefore complex **4** is formulated as **$(4a)_2(4b)_2(4c)$**. The structure of dicationic $\mathbf{4a^{2+}}$ is similar to **1**, with longer Ni−N distances of 1.842(4)−1.858(4) Å and shorter $C-N_{terminal}$ distances of 1.250(6)−1.277(6) Å showing the double-bonding character of $C-N_{terminal}$ (Table 3). In $\mathbf{4b^{2-}}$, the complexed ligand $\{Ni(tap)(Htap)\}^+$ coordinates to an $\{Ni(NCS)_5\}^{3-}$ moiety through the $N_{central}$ of tap^- (N8) with a bond length of 2.086(3) Å. The $C-N_{terminal}$ distances are short [1.257(6)−1.286(5) Å] due to the localization of the negative charge on $N_{central}$. Trinuclear **4c** consists of an anionic $\{Ni(NCS)_4\}^{2-}$ and two complexed ligands coordinating through N19, with a distance of 2.1048(19) Å. The complexed ligands in **4c** show similar structural features to those in $\mathbf{4b^{2-}}$. Non-coordinating $\mathbf{4a^{2+}}$ and two $\{Ni(tap)(Htap)\}^+$ units from $\mathbf{4b^{2-}}$ and **4c** are arranged almost parallel to each other with close Ni···Ni contacts of 3.7764(10) Å from $\mathbf{4a^{2+}}$ to $\mathbf{4b^{2-}}$ and 3.3328(10) Å from $\mathbf{4b^{2-}}$ to **4c**. The positive charge repulsion between $Ni^{II}\cdots Ni^{II}$ centers is slightly diminished for the **4c**/$\mathbf{4b^{2-}}$ couple compared with $\mathbf{4a^{2+}}$/$\mathbf{4b^{2-}}$.

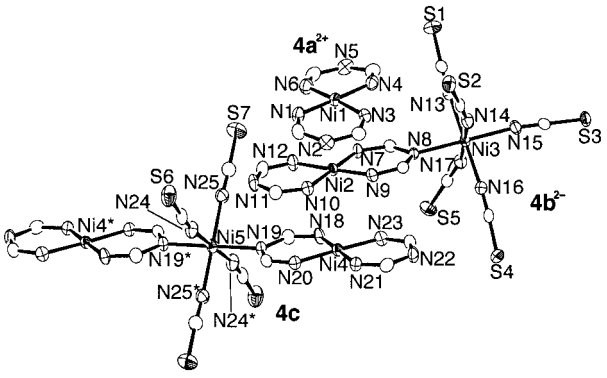

Figure 6. An ORTEP diagram of trinuclear complex **4** with 30% displacement ellipsoids; hydrogen atoms are omitted for clarity; symmetry transformations used to generate equivalent atoms: * $-x + 2, -y + 2, -z$

Conclusion

We have reported the decomposition reaction of triazine in the presence of nickel(II) to give Htap and tap^- complexes. $[Ni(Htap)_2]^{2+}$ and its deprotonated derivatives $[Ni(tap)(Htap)]^+$ and $[Ni(tap)_2]$ were obtained as mononuclear complexes for the former two and as complexed ligands for the latter two species. Two multinuclear complexes **3** and **4** contain the complexed ligands $[Ni(tap)_2]$ and $[Ni(tap)(Htap)]^+$ acting as a bridging ligand and as a terminal ligand, respectively. As expected, the tap^- ligand bridges two metal ions in a $\kappa^1N{:}\kappa^2N$ mode with local C_2 symmetry. The formation of a new complexed ligand should be possible with Htap, which can act as a ferromagnetic coupler like $[Cu(bptap)_2]$. Such investigations are now in progress in our laboratory.

Table 3. Selected interatomic distances(Å) for complex **4**

$\mathbf{4a^{2+}}$	Ni(1)−N(1)	1.844(4)	Ni(1)−N(3)	1.858(4)
	Ni(1)−N(4)	1.848(4)	Ni(1)−N(6)	1.842(4)
	N(1)−C(1)	1.262(6)	C(1)−N(2)	1.351(6)
	N(2)−C(2)	1.348(5)	C(2)−N(3)	1.273(6)
	N(4)−C(3)	1.277(6)	C(3)−N(5)	1.335(6)
	N(5)−C(4)	1.359(6)	C(4)−N(6)	1.250(6)
$\mathbf{4b^{2-}}$	Ni(2)−N(7)	1.828(3)	Ni(2)−N(9)	1.831(3)
	Ni(2)−N(10)	1.850(4)	Ni(2)−N(12)	1.853(4)
	N(7)−C(5)	1.286(5)	C(5)−N(8)	1.334(5)
	N(8)−C(6)	1.328(5)	C(6)−N(9)	1.285(5)
	N(10)−C(7)	1.267(5)	C(7)−N(11)	1.336(6)
	N(11)−C(8)	1.332(6)	C(8)−N(12)	1.257(5)
	Ni(3)−N(8)	2.086(3)	Ni(3)−N(13)	2.054(4)
	Ni(3)−N(14)	2.072(4)	Ni(3)−N(15)	2.080(3)
	Ni(3)−N(16)	2.065(3)	Ni(3)−N(17)	2.108(3)
4c	Ni(4)−N(18)	1.825(4)	Ni(4)−N(20)	1.839(3)
	Ni(4)−N(21)	1.856(4)	Ni(4)−N(23)	1.854(4)
	N(18)−C(14)	1.284(5)	C(14)−N(19)	1.330(5)
	N(19)−C(15)	1.336(5)	C(15)−N(20)	1.281(5)
	N(21)−C(16)	1.268(5)	C(16)−N(22)	1.361(5)
	N(22)−C(17)	1.339(5)	C(17)−N(23)	1.261(5)
	Ni(5)−N(19)	2.104(3)	Ni(5)−N(24)	2.071(4)
	Ni(5)−N(25)	2.075(4)		
	Ni(1)···Ni(2)	3.7763(11)	Ni(2)···Ni(4)	3.3329(11)

Experimental Section

Synthesis of $[Ni(Htap)_2](ClO_4)_2$ (1): A solution of nickel(II) perchlorate hexahydrate in ethanol (0.1 M, 5 mL) and triazine in methanol (0.2 M, 5 mL) were mixed and the resulting pale-green solution was heated to 50 °C for 2 hours, during which time the solution turned yellow. Upon standing overnight, yellow crystals formed. Yield 130 mg (65%). $C_4H_{10}Cl_2N_6NiO_8$ (399.8): calcd. C 12.02, H 2.52, N 21.02; found C 12.17, H 2.71, N 20.87.

Synthesis of $[Ni(tap)(Htap)]ClO_4\cdot H_2O$ ($\mathbf{2}\cdot H_2O$): Three 0.2 M solutions of nickel(II) perchlorate/EtOH (1 mL), ethylenediamine/EtOH (2 mL), and triazine/MeOH (1 mL) were mixed and the resulting blue solution was heated to 70 °C for 1 hour to afford a blue solution. The yellow fraction isolated by column chromatography (Sephadex LH-20/EtOH) was dried. The resulting compound was recrystallized from EtOH/H_2O (1:1, v/v) to give yellow crystals of $\mathbf{2}\cdot H_2O$. Yield 11 mg (35%). $C_4H_{11}ClN_6NiO_5$ (317.3): calcd. C 15.14, H 3.49, N 26.48; found C 15.18, H 3.46, N 26.37.

Synthesis of $[\{Cu(tren)\}_2\{Ni(tap)_2\}](ClO_4)_4$ (3): A yellow suspension of $\mathbf{2}\cdot H_2O$ (3.4 mg, 0.011 mmol) in EtOH/H_2O (1:1, v/v; 1 mL) was added to $[Cu(tren)]ClO_4$ (8.2 mg, 0.027 mmol) in EtOH/H_2O (1:1, v/v; 1 mL). The mixture was stirred to afford a blue-green solution. Blue-green crystals of **3** were obtained from this solution after several days. Yield 6.7 mg (60%). $C_{16}H_{44}Cl_4Cu_2N_{14}NiO_{16}$ (1016.2): calcd. C 18.91, H 4.36, N 19.30; found C 19.10, H 4.45, N 19.21.

Synthesis of $[Ni(Htap)_2]_2[Ni(2)_2(NCS)_4][Ni(2)(NCS)_5]_2\cdot 8H_2O$ ($\mathbf{4}\cdot 8H_2O$): A solution of $\mathbf{2}\cdot H_2O$ (12 mg, 0.038 mmol) in EtOH/ H_2O (1:1, v/v; 1 mL) was added to 0.2 mL of 0.1 M nickel(II) perchlorate/EtOH solution and 0.8 mL of a 0.1 M NH_4SCN/MeOH solution,

 © 2004 Wiley-VCH Verlag GmbH & Co. KGaA, Weinheim

Table 4. Crystallographic data and structural refinement for **1**−**4**

Complex	**1**	**2**·H_2O	**3**	**4**·8H_2O
Enpirical formula	$C_4H_{10}Cl_2N_6NiO_8$	$C_4H_{11}ClN_6NiO_5$	$C_{16}H_{44}Cl_4N_{14}NiCu_2O_{16}$	$C_{38}H_{72}N_{50}Ni_9O_8S_{14}$
Molecular mass	399.77	317.32	1016.22	2334.47
Crystal system	monoclinic	triclinic	monoclinic	triclinic
Space group	$P2_1/n$	$P\bar{1}$	$P2_1/n$	$P\bar{1}$
a (Å)	5.1543(7)	9.3000(16)	9.6351(12)	10.759(3)
b (Å)	9.0810(12)	10.3129(18)	14.7930(18)	11.110(3)
c (Å)	13.5606(18)	12.949(2)	13.0565(16)	20.223(6)
α (°)		74.855(3)		77.971(7)
β (°)	91.997(3)	81.322(3)	95.619(4)	83.374(8)
γ (°)		63.411(3)		70.152(7)
V (Å^3)	634.33(15)	1071.2(3)	1852.0(4)	2221.3(10)
Z	2	4	2	1
T (K)	200(2)	210(2)	223(2)	223(2)
ρ_{calc} (g cm^{-3})	2.093	1.968	1.822	1.745
Reflections collected	5074	10340	13075	22593
Independent reflections	1760 [R_{int} = 0.023]	4699 [R_{int} = 0.030]	4257 [R_{int} = 0.031]	10187 [R_{int} = 0.046]
μ (mm^{-1})	2.004	2.084	2.014	2.264
R_1, wR_2 [$I > 2\sigma(I)$]	0.032, 0.075	0.042, 0.098	0.033, 0.0631	0.040, 0.066
R_1, wR_2 (all data)	0.043, 0.078	0.050, 0.102	0.053, 0.066	0.097, 0.073

and the resulting yellow solution was allowed to evaporate slowly in air. After a week, green crystals of **4**·4H_2O were obtained which were collected by filtration and dried in vacuo. Yield 4.2 mg (30%). $C_{38}H_{56}N_{50}Ni_9S_{14}$ (2190.3): calcd. C 20.90, H 2.59, N 32.09; found C 20.76, H 2.67, N 32.33.

X-ray Crystallography: Data for all the compounds were collected on a Bruker SMART APEX diffractometer employing graphite-monochromated Mo-K_α radiation (λ = 0.71073 Å) at low temperature (200−233 K). The data integration and reduction were undertaken with SAINT and XPREP.[13] An empirical absorption correction determined with SADABS[14] was applied to each data set. The structures were solved by direct methods using SHELXS-97[15] and refined using least-squares methods on F^2 with SHELXL-97.[15] Non-hydrogen atoms were modelled with anisotropic displacement parameters, and hydrogen atoms were placed by difference Fourier syntheses and refined isotropically. Further details can be found in Table 4.

CCDC-230135−230138 (**1**−**4**)contain the supplementary crystallographic data for this paper. These data can be obtained free of charge at www.ccdc.cam.ac.uk/ conts/retrieving.html [or from the Cambridge Crystallographic Data Centre, 12 Union Road, Cambridge CB2 1EZ, UK; Fax: (internat.) + 44-1223-336-033; E-mail: deposit@ccdc.cam.ac.uk].

Acknowledgments

This work was supported by Grants-in-Aid for Scientific Research from the Ministry of Education, Culture, Science, Sports and Technology, Japan.

[1] G. Denti, S. Serroni, S. Campagna, A. Juris, M. Ciano, V. Balzani, in *Perspectives in Coordination Chemistry* (Eds.: A. F. Williams, C. Floriani, A. E. Merbach), VCH, Weinheim, **1992**, p. 153.
[2] A. Kamiyama, T. Noguchi, T. Kajiwara, T. Ito, *Inorg. Chem.* **2002**, *41*, 507−512.
[3] A. Cantarero, J. M. Amigó, J. Faus, M. Julve, T. Debaerdemaeker, *J. Chem. Soc., Dalton Trans.* **1988**, 2033−2039.
[4] I. Castro, J. Faus, M. Julve, J. M. Amigó, J. Sletten, T. Debaerdemaeker, *J. Chem. Soc., Dalton Trans.* **1990**, 891−897.
[5] T. Kajiwara, R. Sensui, T. Noguchi, A. Kamiyama, T. Ito, *Inorg. Chim. Acta* **2002**, *337*, 299−307.
[6] A. Kamiyama, T. Noguchi, T. Kajiwara, T. Ito, *Angew. Chem. Int. Ed.* **2000**, *39*, 3130−3132.
[7] T. Kajiwara, T. Ito, *J. Chem. Soc., Dalton Trans.* **1998**, 3351−3352.
[8] T. Kajiwara, T. Ito, *Angew. Chem. Int. Ed.* **2000**, *39*, 230−233.
[9] T. Kajiwara, A. Kamiyama, T. Ito, *Chem. Commun.* **2002**, 1256−1257.
[10] T. Kajiwara, A. Kamiyama, T. Ito, *Polyhedron* **2003**, *22*, 1789−1793.
[11] ONO^- is known to act as a bridging ligand in a κ^1N-κ^2O fashion. See: [11a] A. Escuer, M. Font-Bardia, E. Penalba, N. Sanz, X. Solans, R. Vicente, *J. Chem. Soc., Dalton Trans.* **1999**, 3115−3119. [11b] O. Kahn, E. Bakalbassis, C. Mathoniere, M. Hagiwara, K. Katsumata, L. Ouahab, *Inorg. Chem.* **1997**, *36*, 1530−1531. [11c] J. A. Halfen, S. Mahapatra, E. C. Wilkinson, A. J. Gengenbach, V. G. Young Jr., L. Que Jr., W. B. Tolman, *J. Am. Chem. Soc.* **1996**, *118*, 763−776. [11d] J. A. Halfen, S. Mahapatra, M. M. Olmstead, W. B. Tolman, *J. Am. Chem. Soc.* **1994**, *116*, 2173−2174.
[12] M. M. Turnbull, M. Y. Wei, R. D. Willett, *J. Coord. Chem.* **1995**, *35*, 11−17.
[13] SMART, SAINT and XPREP, Area detector control and data integration and reduction software, Bruker Analytical X-ray Instruments Inc., Madison, WI, **1995**.
[14] G. M. Sheldrick, SADABS, Empirical absorption correction program for area detector data, University of Göttingen, Germany, **1996**.
[15] G. M. Sheldrick, SHELX97, Programs for Crystal Structure Analysis, University of Göttingen, Germany, **1998**.

Received February 14, 2004
Early View Article
Published Online May 25, 2004

 © 2004 Wiley-VCH Verlag GmbH & Co. KGaA, Weinheim

(Pyrazole)silver(I) and -gold(I) Complexes with Strong and Weak Hydrogen-Bonding Interactions as the Basis of One- or Two-Dimensional Structures

M. Luz Gallego,[a] Paloma Ovejero,[a] Mercedes Cano,*[a] José V. Heras,[a] José A. Campo,[a] Elena Pinilla,[a,b] and M. Rosario Torres[b]

Dedicated to Professor José Vicente on the occasion of his 60th birthday

Keywords: : Gold / Hydrogen bonds / N ligands / Silver / Supramolecular chemistry

New Au^I/Ag^I complexes containing one or two substituted pyrazole ligands $[Au(Hpz^{bp2})(PPh_3)](p\text{-}CH_3C_6H_4SO_3)$ [Hpz^{bp2} = 3,5-bis(4-*n*-butoxyphenyl)pyrazole] (**1**) and $[M(Hpz^{R2})_2]_nX$ [Hpz^{R2} = Hpz^{bp2}, M = Au, *n* = 1, X = *p*-$CH_3C_6H_4SO_3$ (**2**), NO_3^- (**3**); *n* = 2, X = 1,5-naphthalenedisulfonate (1,5nds) (**4**); Hpz^{R2} = Hpz^{bp2}, M = Ag, *n* = 1, X = BF_4^- (**5**), $CF_3SO_3^-$ (**6**); Hpz^{R2} = Hpz^{NO2} (3,5-dimethyl-4-nitropyrazole), M = Ag, *n* = 1, X = BF_4^- (**7**), $CF_3SO_3^-$ (**8**)], have been prepared and characterized. Compounds **1**, **2**, **5** and **8** have been proved to be useful for supramolecular assembly from their single X-ray diffraction analysis. In all cases strong hydrogen bonds maintain the cationic units bonded to their corresponding counterions. The crystal packing arrangement of **1**, **2** and **5** is, however, determined by weak C–H···O/F hydrogen-bonding interactions involving the remaining O/F atoms of the counterion. By contrast, for **8** a two-dimensional layer-type polymeric network is formed by π···π (NO_2···NO_2) and coordinative Ag···O interactions in which the NO_2 substituent on the pyrazole is implicated.

(© Wiley-VCH Verlag GmbH & Co. KGaA, 69451 Weinheim, Germany, 2004)

Introduction

Supramolecular architectures derived from metallic complexes as building blocks are an attractive focus of current research. In this context coordinative interactions and/or hydrogen bonds have been extensively used to produce supramolecular one-, two- or three-dimensional polymeric structures.[1] However, although self-assembly has been well documented,[2] much work remains to extend the knowledge of relevant structures. The nature of the metal, counterions or ligands are factors that can be modulated to determine the molecular assembly.

The silver(I) ion is a favourable building block because of its various potential coordination modes such as linear,[3] trigonal[4] or tetrahedral,[5] and its affinity for hard donor atoms such as nitrogen or oxygen. In addition, some silver(I) derivatives have also been determined to present experimental evidence for an argentophilic attraction[6] and therefore with potential applications for self-assembled nets. In the same context, gold(I) complexes are promising for the construction of supramolecular structures based on the aurophilic nature of gold.[6b,7] Furthermore, experimental evidence from structures of Au/Ag-containing cationic complexes indicates the relevant role of the counterion in the molecular architecture.[2b,6c,8]

It has been postulated that the control and manipulation of weak interactions could be used as the key to tune the properties of the bulk materials. In addition to the classical O/N−H···X (X = O, N or F atoms) hydrogen-bonding interactions, other weaker C−H···X (X = O, N or F atoms) interactions have been shown to control the molecular packing in the solid.[1g,9]

In previous work from our lab we have made use of hydrogen-bonding interactions produced between cationic metal complexes containing pyrazole ligands and the corresponding counterions. Although the strong NH···X (X = O or F atoms from NO_3^- or BF_4^- counterions) hydrogen bonds are the predominant force driving the structure, other different intermolecular interactions, such as C−H···O/F, are also considered to be important for the molecular assembly.[10]

We have now extended these results to the use of new silver(I) and gold(I) pyrazole derivatives of the type $[M(Hpz^{R2})_2]^+$ [Hpz^{R2} = 3,5-bis(4-*n*-butoxyphenyl)pyrazole, Hpz^{bp2}; 3,5-dimethyl-4-nitropyrazole, Hpz^{NO2}) containing different counterions, as well as different substituents on the pyrazole rings. The related complex containing only one

[a] Departamento de Química Inorgánica I, Facultad de Ciencias Químicas, Universidad Complutense,
28040 Madrid, Spain
Fax: (internat.) + 34-91-3944352
E-mail: mmcano@quim.ucm.es
[b] Laboratorio de Difracción de Rayos-X, Facultad de Ciencias Químicas, Universidad Complutense,
28040 Madrid, Spain

pyrazole ligand, [Au(Hpz^{bp2})(PPh$_3$)](*p*-CH$_3$C$_6$H$_4$SO$_3$), has also been prepared and studied (Scheme 1). We report herein how the presence of strong or weak N−H···O/F and C−H···O/F inter- and intramolecular hydrogen-bonding interactions, supported by the different counterions, are responsible for the molecular arrangement in the solid for complexes containing the Hpz^{bp2} ligand. In contrast, the molecular packing of those complexes with Hpz^{NO2} is dominated by interactions through the NO_2 substituents on the ligands.

Compound	Formula
1	[Au(Hpz^{bp2})(PPh$_3$)](*p*-CH$_3$C$_6$H$_4$SO$_3$)
2	[Au(Hpz^{bp2})$_2$](*p*-CH$_3$C$_6$H$_4$SO$_3$)
3	[Au(Hpz^{bp2})$_2$](NO$_3$)
4	[Au(Hpz^{bp2})$_2$]$_2$(1,5nds)[a]
5	[Ag(Hpz^{bp2})$_2$](BF$_4$)
6	[Ag(Hpz^{bp2})$_2$](CF$_3$SO$_3$)
7	[Ag(Hpz^{NO2})$_2$](BF$_4$)
8	[Ag(Hpz^{NO2})$_2$](CF$_3$SO$_3$)

Hpz^{bp2} = 3,5-bis(4-*n*-butoxyphenyl)pyrazole

Hpz^{NO2} = 3,5-dimethyl-4-nitropyrazole

[a] 1,5nds = 1,5-naphthalenedisulfonate ($O_3SC_{10}H_6SO_3$)

Scheme 1

Results and Discussion

Synthetic and Characterization Studies

Complex **1**, containing triphenylphosphane, was obtained from the reaction of [Au(*p*-CH$_3$C$_6$H$_4$SO$_3$)(PPh$_3$)] (prepared by a literature procedure)[8d] and one equivalent of Hpz^{bp2} in dry THF (Scheme 2). Compounds **2**−**4** were prepared by reaction of [AuCl(THT)] (THT = tetrahydrothiophene)[11] with two equivalents of Hpz^{bp2} and one equivalent of the corresponding silver salt in dry THF (Scheme 3). The related silver(I) derivatives **5**−**8** were synthesized by treatment of two equivalents of the corresponding pyrazole ligand with one equivalent of the silver salt in dry THF or acetonitrile (Scheme 4).

$$[Au(p\text{-}CH_3C_6H_4SO_3)(PPh_3)] + Hpz^{bp2} \longrightarrow$$

$$[Au(Hpz^{bp2})(PPh_3)](p\text{-}CH_3C_6H_4SO_3) \quad (\mathbf{1})$$

Scheme 2

$$[AuCl(THT)] + 2\ Hpz^{bp2} + AgX \longrightarrow [Au(Hpz^{bp2})_2]_nX \quad (\mathbf{2}\text{–}\mathbf{4})$$

Scheme 3

$$AgX + 2\ Hpz^{R2} \longrightarrow [Ag(Hpz^{R2})_2]X$$

$$Hpz^{R2} = Hpz^{bp2} \quad (\mathbf{5}\text{–}\mathbf{6})$$
$$Hpz^{R2} = Hpz^{NO2} \quad (\mathbf{7}\text{–}\mathbf{8})$$

Scheme 4

All compounds are air-stable white solids and they were characterized by elemental analysis and IR and ^{1}H NMR spectroscopy. In addition, ^{31}P NMR spectroscopy was also used for **1**. All data are listed in the Exp. Sect. The IR spectra show, amongst others, the characteristic bands of the pyrazole ligands, ν(C=N) + ν(C=C) at ca. 1600 cm^{-1} and ν(N−H) in the range 3112−3308 cm^{-1}, as well as those from the corresponding counterions.[8d,12]

The ^{1}H NMR spectra in $CDCl_3$ solution at room temperature show the expected signals of the ligands. It is interesting to note that the ^{1}H NMR spectra of **5**−**8** at room temperature are consistent with the presence of two equivalent coordinated pyrazole ligands, each of them having two equivalent substituents at the 3- and 5-positions. A related equivalence of the substituents has also been observed for **1**. Thus, it is possible to suggest a metallotropic equilibrium to explain the above behaviour similar to that previously found for related complexes.[13] Lowering the temperature slows down the dynamic process, resulting in the non-equivalence of the substituents, as observed for **5** and **6** at −40 °C by the well-defined signals for the aromatic and alkyl-

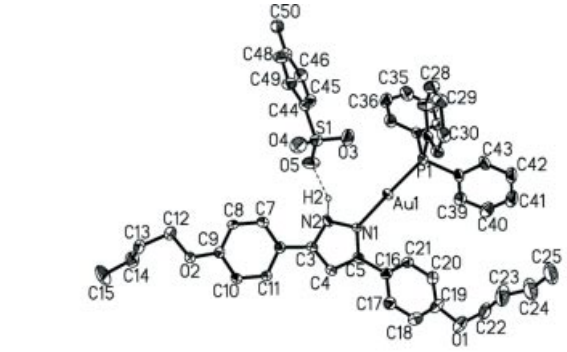

a

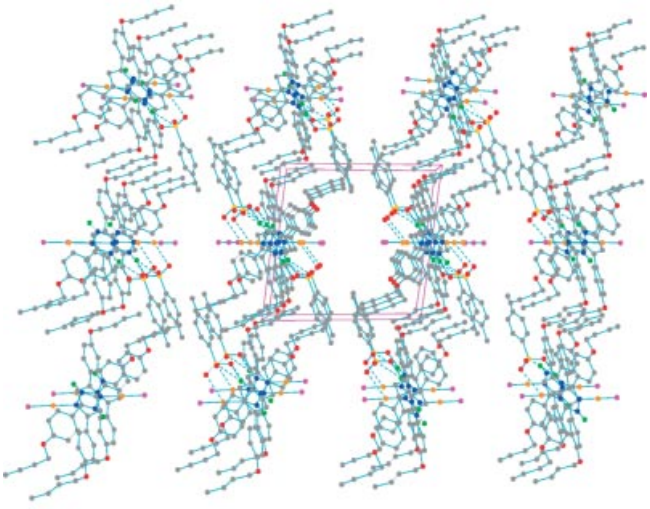

b

Figure 1. a) ORTEP plot of **1** at the 30% probability level; hydrogen atoms, except H2, and the labelling of some atoms have been omitted for clarity; b) view of the packing along the *a* axis (the phenyl groups of the phosphane ligands have been omitted)

 © 2004 Wiley-VCH Verlag GmbH & Co. KGaA, Weinheim

Table 1. Bond lengths (Å) and angles (°) for **1**, **2**, **5** and **8**

[Au(Hpz^{bp2})(PPh$_3$)](*p*-CH$_3$C$_6$H$_4$SO$_3$) (**1**)				[Au(Hpz^{bp2})$_2$](*p*-CH$_3$C$_6$H$_4$SO$_3$) (**2**)			
Au1−N1	2.069(5)	N1−Au1−P1	177.1(2)	Au1−N1	2.019(7)	N1−Au1−N3	176.3(4)
Au1−P1	2.243(2)	O3−S1−O4	111.2(4)	Au1−N3	2.022(7)	O5−S1−O6	111.7(5)
N1−N2	1.396(7)	O3−S1−O5	113.5(4)	N1−N2	1.36(1)	O5−S1−O7	114.5(5)
S1−O3	1.449(5)	O4−S1−O5	113.6(4)	N3−N4	1.36(1)	O6−S1−O7	112.4(5)
S1−O4	1.451(6)	O3−S1−C44	107.1(3)	S1−O5	1.426(6)	O5−S1−C49	105.0(4)
S1−O5	1.433(6)	O4−S1−C44	104.7(3)	S1−O6	1.447(6)	O6−S1−C49	105.7(4)
S1−C44	1.775(7)	O5−S1−C44	106.0(3)	S1−O7	1.416(8)	O7−S1−C49	106.8(5)
				S1−C49	1.77(1)		
[Ag(Hpz^{bp2})$_2$]BF$_4$ (**5**)				[Ag(Hpz^{NO2})$_2$](CF$_3$SO$_3$) (**8**)			
Ag1−N1	2.129(3)	N1−Ag1−N3	170.1(1)	Ag1−N1	2.171(2)	N1−Ag1−N4	163.67(9)
Ag1−N3	2.118(3)	F1−B1−F2	108.5(3)	Ag1−N4	2.161(2)	O1−N3−O2	123.3(3)
N1−N2	1.355(4)	F1−B1−F3	108.9(3)	N1−N2	1.363(3)	O3−N6−O4	124.5(4)
N3−N4	1.359(4)	F1−B1−F4	109.7(3)	N4−N5	1.357(3)	O5−S1−O6	114.0(2)
B1−F1	1.378(4)	F2−B1−F3	111.5(3)	N3−O1	1.223(3)	O5−S1−O7	114.6(2)
B1−F2	1.360(4)	F2−B1−F4	108.8(3)	N3−O2	1.223(3)	O6−S1−O7	115.1(2)
B1−F3	1.354(3)	F3−B1−F4	109.5(3)	N6−O3	1.224(5)	O5−S1−C11	105.3(2)
B1−F4	1.375(4)			N6−O4	1.215(5)	O6−S1−C11	103.0(2)
				S1−O5	1.427(2)	O7−S1−C11	102.9(2)
				S1−O6	1.435(3)		
				S1−O7	1.443(3)		

chain protons of the butoxyphenyl substituents. A similar feature is also present in the gold derivatives **2**−**4**, which exhibit the non-equivalence of the butoxyphenyl substituents at room temperature. The protons at the 4-positions of the pyrazole rings of **2** and **3** show an unusual coupling with the NH proton, which was confirmed by homonuclear decoupling techniques. This situation has also been observed in some metal complexes containing related pyrazole ligands.[14] The ^{31}P NMR spectrum of **1** at room temperature in $CDCl_3$ shows a single resonance at $\delta = 31.06$ ppm in the characteristic region of gold-phosphane complexes.[15]

The photoluminescence study of **1**−**3** in the solid state shows that, under 325−330 nm UV irradiation, all of them emit luminescence in the 440−510 nm range. For **1** this emission occurs both at room temperature and 77 K, while for **2** and **3** this behaviour is only observed at low temperature. The maximum-emission wavelengths are red-shifted by ca. 100 nm relative to the free pyrazole ligands.

Crystal Structure of 1

The molecular structure of [Au(Hpz^{bp2})(PPh$_3$)](*p*-CH$_3$C$_6$H$_4$SO$_3$) (**1**) is depicted in Figure 1a, which also shows the numbering scheme. Selected bond lengths and angles and the hydrogen-bond parameters for all compounds crystallographically characterized in this work are collected in Table 1 and 2, respectively.

The structure of **1** consists of *p*-toluenesulfonate anions and cationic units where the gold(I) atom is two-coordinate. The coordinative environment (shape, Au−P and Au−N distances, and P−Au−N angles) are, as expected, similar to those of the complex [Au(Hpz^{bp2})(PPh$_3$)](NO$_3$) (**A**), previously reported by us,[10b] which contains the same cationic fragment and NO_3^- as counterion [Au1−P1, Au1−N1 and P1−Au1−N1 bond parameters are 2.243(2), 2.069(5) Å and 177.1(2)° in **1**, and 2.239(2), 2.077(5) Å and 178.1(2)° in **A**]. In addition, the cationic unit in both **1** and **A** is bonded to the corresponding counterion by a strong hydrogen bond, with N···O distances of 2.701(7) Å (Table 2) and 2.764(9) Å, respectively.

Table 2. Hydrogen bond geometries for **1**, **2**, **5** and **8** (lengths in Å and angles in degrees)

D−H···A	*d*(D−H)	*d*(H···A)	*d*(D···A)	∠(D−H···A)
[Au(Hpz^{bp2})(PPh$_3$)](*p*-CH$_3$C$_6$H$_4$SO$_3$) (**1**)				
N2−H2···O4	1.02	1.79	2.701(7)	147.2
C29−H29···O3[a]	0.93	2.55	3.39(1)	149.8
C31−H31···O2[b]	0.93	2.48	3.35(1)	156.2
C34−H34···O5[c]	0.93	2.84	3.43(1)	122.0
[Au(Hpz^{bp2})$_2$](*p*-CH$_3$C$_6$H$_4$SO$_3$) (**2**)				
N2−H2···O5	0.99(9)	1.72(9)	2.70(1)	174(8)
N4−H4···O6	0.9(1)	1.7(1)	2.71(1)	175(8)
C4−H4A···O7[d]	0.93	2.51	3.39(2)	158.4
C34−H34···O7[e]	0.93	2.61	3.42(2)	146.9
[Ag(Hpz^{bp2})$_2$]BF$_4$ (**5**)				
N2−H2···F1	0.97	1.88	2.776(4)	152.6
N4−H4···F4	0.95	1.85	2.779(4)	165.3
C7−H7···F3[f]	0.93	2.69	3.40(1)	134.2
[Ag(Hpz^{NO2})$_2$](CF$_3$SO$_3$) (**8**)				
N2−H2···O6	0.93	1.85	2.771(3)	176.0
N5−H5···O7	0.92	1.95	2.852(4)	165.9

[a] $-x, -y + 1, -z + 1$. [b] $-x, -y + 1, -z + 2$. [c] $x + 1, y, z$. [d] $-x + 2, -y + 1, -z + 1$. [e] $x - 1/2, -y + 1/2, z - 1/2$. [f] $-x, -y + 1, -z$.

However, when considering the packing arrangement in the solid several differences are observed. A two-dimensional structure was envisaged for **A** from weak intermolecular C−H···O interactions of 3.31−3.38 Å involving two of the oxygen atoms of the counterion, which were not implicated in the previous hydrogen bond.[10b] In contrast, in **1**

 © 2004 Wiley-VCH Verlag GmbH & Co. KGaA, Weinheim

the *p*-toluenesulfonate counterion forms a weak C−H···O interaction at 3.39(1) Å (Table 2) to produce a columnar one-dimensional arrangement along the *a* axis (see b in Figure 1). These columns are also reinforced by the presence of a new C−H···O interaction between the O2 atom of the substituent on the pyrazole ligand and the C31 atom of the PPh_3 ligand of a neighbouring molecule (Table 2). Throughout this one-dimensional distribution the gold atoms are in a zig-zag disposition at a distance of 5.58(1) Å, which excludes the presence of intermetallic interactions.

The above differences in the supramolecular architectures are clearly dependent on the counterions. It can therefore be suggested that the driving force of the reorientation of cationic entities when the planar NO_3^- is substituted by the bulkier *p*-toluenesulfonate could be related to the pseudo-tetrahedral geometry of the SO_3 group; interactions through this group appear to preclude a layer-like distribution.

However, this result does not exclude the possibility of new contacts involving the remaining free oxygen atom of the SO_3 group (which was not used in the previous interactions). In fact, the columns in **1** are connected to each other by very weak C−H···O interactions at 3.43(1) Å (Table 2).

At this point, it is important to mention that similar weak C−H···O contacts observed in a large variety of compounds have been considered as support of the supramolecular network.[9,16] On these basis, we propose for **1** that the strong N−H···O hydrogen bonds as well as the weak C−H···O inter- and intramolecular contacts through the SO_3 group of the counterion stabilize the crystal structure in the solid state forming a two-dimensional network.

Crystal Structures of 2 and 5

The molecular structures of complexes **2** and **5** are represented in parts a of Figure 2 and 3, respectively. The structures of the mononuclear cations $[M(Hpz^{bp2})_2]^+$ [M = Au (**2**), Ag (**5**)] show similar features. In both cases an angular molecular shape is formed by the two 3,5-disubstituted pyrazole groups bonded through the pyridinic nitrogen to the metal centre. In addition, each cationic unit has both heterocycles in a *cis*-orientation and is bonded to its corresponding counterion by two strong hydrogen bonds using both NH groups and two of the oxygen or fluorine atoms of the counterion, forming an eight-membered metallacycle (O−N−N−Au−N−N−O−S and F−N−N−Ag−N−N−F−B in **2** and **5**, respectively). The molecules have a quasi-linear N−M−N atomic sequence [176.3(4) in **2** and 170.1(1)° in **5**] and the average Au−N (2.02 Å) and Ag−N (2.12 Å) lengths (Table 1) in **2** and **5**, respectively, are similar to those found for related complexes containing pyrazole-type ligands.[10b,15b,15d,17−19] The main difference in the molecular structure of **2** and **5** is related to the orientation of the two pyrazole rings; they are almost parallel in **2** [dihedral angle of 4.5(5)°] but slightly tilted in **5** [dihedral angle of 24.6(1)°]. Other dihedral angles are collected in Table 3.

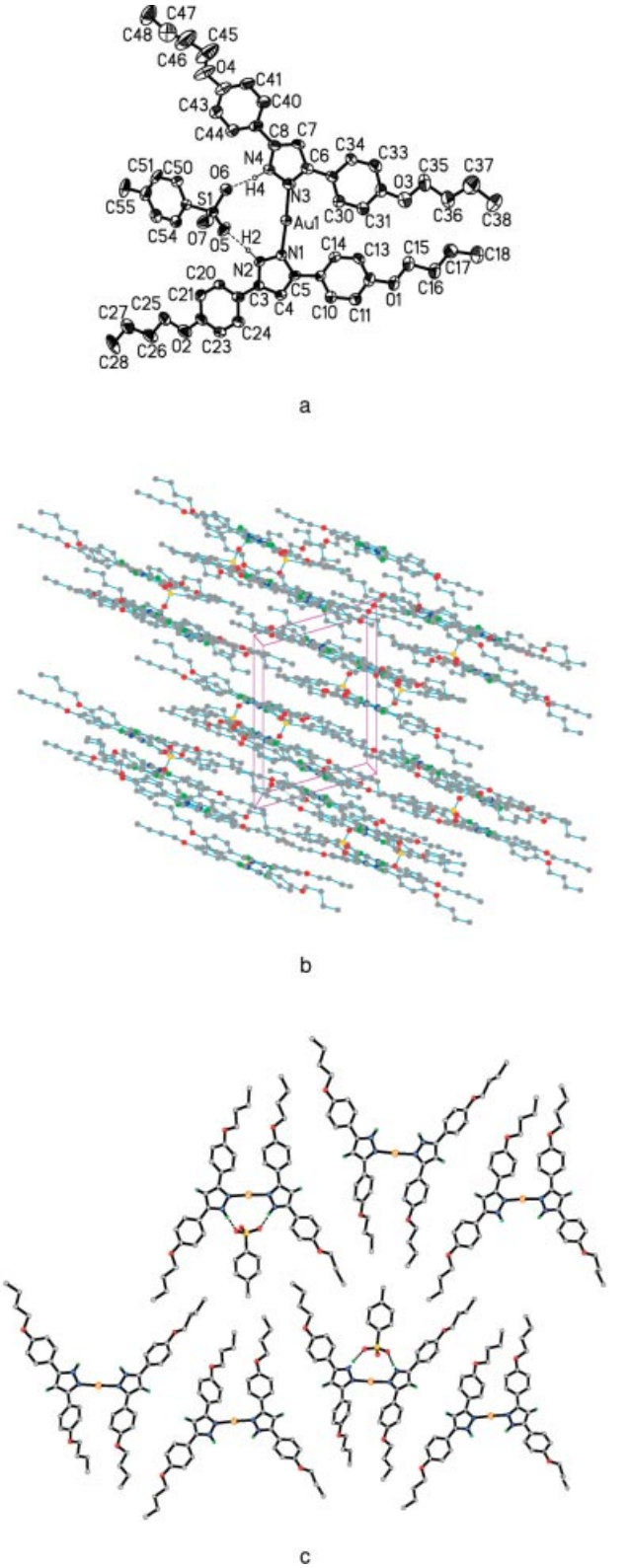

Figure 2. a) ORTEP plot of **2** at the 30% probability level; hydrogen atoms, except H2 and H4, and the labelling of some atoms have been omitted for clarity; b) view of the packing along the *b* axis showing the layer-like arrangement in the (1 0 $\bar{2}$) direction; c) view of the distribution in a layer

The crystal packing of **2** can be defined as layer-like (see b in Figure 2), with the sheet containing the cationic bis(pyrazole)gold units bonded to its corresponding counterion. The layers are situated in the (1 0 $\bar{2}$) direction. The cationic

 © 2004 Wiley-VCH Verlag GmbH & Co. KGaA, Weinheim

Table 3. Dihedral angles (°) between selected planes[a] for **2** and **5**

	$[Au(Hpz^{bp2})_2](p\text{-}CH_3C_6H_4SO_3)$ (**2**)	$[Ag(Hpz^{bp2})_2]BF_4$ (**5**)
1−2	4.5(5)	24.6(2)
1−3	35.8(4)	39.9(2)
1−4	6.1(4)	21.8(2)
3−4	35.8(4)	61.5(2)
2−5	12.7(5)	27.1(2)
2−6	20.1(5)	3.6(2)
5−6	12.9(4)	29.1(2)

[a] Plane 1: N1−N2−C3−C4−C5; plane 2: N3−N4−C6−C7−C8; plane 3: C9−C10−C11−C12−C13−C14; plane 4: C19−C20−C21−C22−C23−C24; plane 5: C29−C30−C31−C32−C33−C34; plane 6: C39−C40−C41−C42−C43−C44.

entities in the layer adopt a head-to-tail alignment with no short contacts between them (see c in Figure 2). However, weak C−H···O interactions between the layers are observed which involve the free O7 atom of the counterion in a bifurcated form [C4···O7 ($-x + 2, -y + 1, -z + 1$) of 3.39(2) Å; C34···O7 ($x - 1/2, -y + 1/2, z - 1/2$) of 3.42(2) Å] (Table 2). These weak intermolecular contacts form a one-dimensional framework.

The crystal packing of **5** also presents similar characteristics, the layers being oriented in the (1 1 $\bar{4}$) direction (see b and c in Figure 3). Weak inter-layer interactions involving the BF_4^- counterion are also observed for this complex. These C−H···F interactions [C7···F3 ($-x, -y + 1, -z$) of 3.40(1) Å] (Table 2) also form a one-dimensional framework.

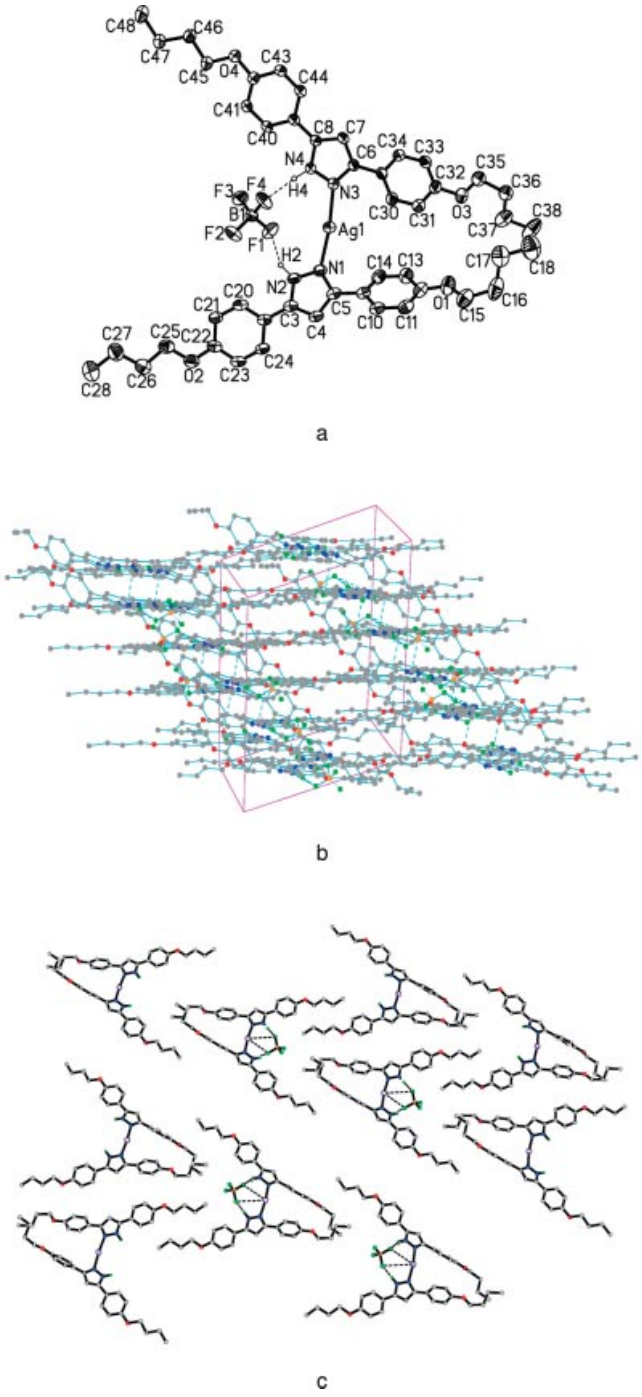

Figure 3. a) ORTEP plot of **5** at the 30% probability level; hydrogen atoms, except H2 and H4, and the labelling of some atoms have been omitted for clarity; b) view of the layer-like packing in the (1 1 $\bar{4}$) direction; c) view of the distribution in a layer

Crystal Structure of 8

The most relevant structure of complexes of the type $[M(Hpz^R)_2]X$ is that of complex **8**, where the pyrazole ligand is 3,5-dimethyl-4-nitropyrazole (Hpz^{NO2}) and X is $CF_3SO_3^-$. The structure of the cation $[Ag(Hpz^{NO2})_2]^+$ is shown in Figure 4 (see part a). The silver atom is coordinated to the two pyridinic nitrogen atoms of the heterocyclic ligands at ca. 2.17 Å (Table 1). The geometry around the metal is distorted lineal with an N1−Ag1−N4 angle of 163.67(9)°. Both pyrazole rings are almost parallel [angle of 4.8(1)°]. They show a *cis* orientation and are bonded through strong hydrogen bonds to the counterion [N2···O6: 2.771(3) Å; N5···O7: 2.852(4) Å] (Table 2). The nitro groups at the 4-position of the heterocyclic rings are almost coplanar with their own pyrazole planes [dihedral angles of 5.1(2) °and 6.3(4)°]; as a consequence the molecule shows a high planarity.

The structure built by the strongest interactions can be considered as that formed by dimers involving coordinative interactions Ag1···O5($-x + 1, -y + 1, -z + 1$) of 2.821(3) Å between the oxygen atom of the counterion (not implicated in the above hydrogen bond) and the silver centre of each molecule, giving rise to a closest distance of the metallic centres in the dimer of 3.7841(4) Å (b in Figure 4).

The next step in the packing is due to π···π contacts between dimers to form columns. The distances between atoms of the nitro groups from two neighbouring molecules, which are not implicated in the same dimer, are 3.268(4) Å [N6···N6($-x + 2, -y + 1, -z + 2$)] and 3.168(6) Å [O3···O3($-x + 2, -y + 1, -z + 2$)]. These are remarkably short distances and show the existence of a π···π interaction between those NO_2 groups,[16e−16g] which are situated in an alternating fashion. This mode of interaction

 © 2004 Wiley-VCH Verlag GmbH & Co. KGaA, Weinheim

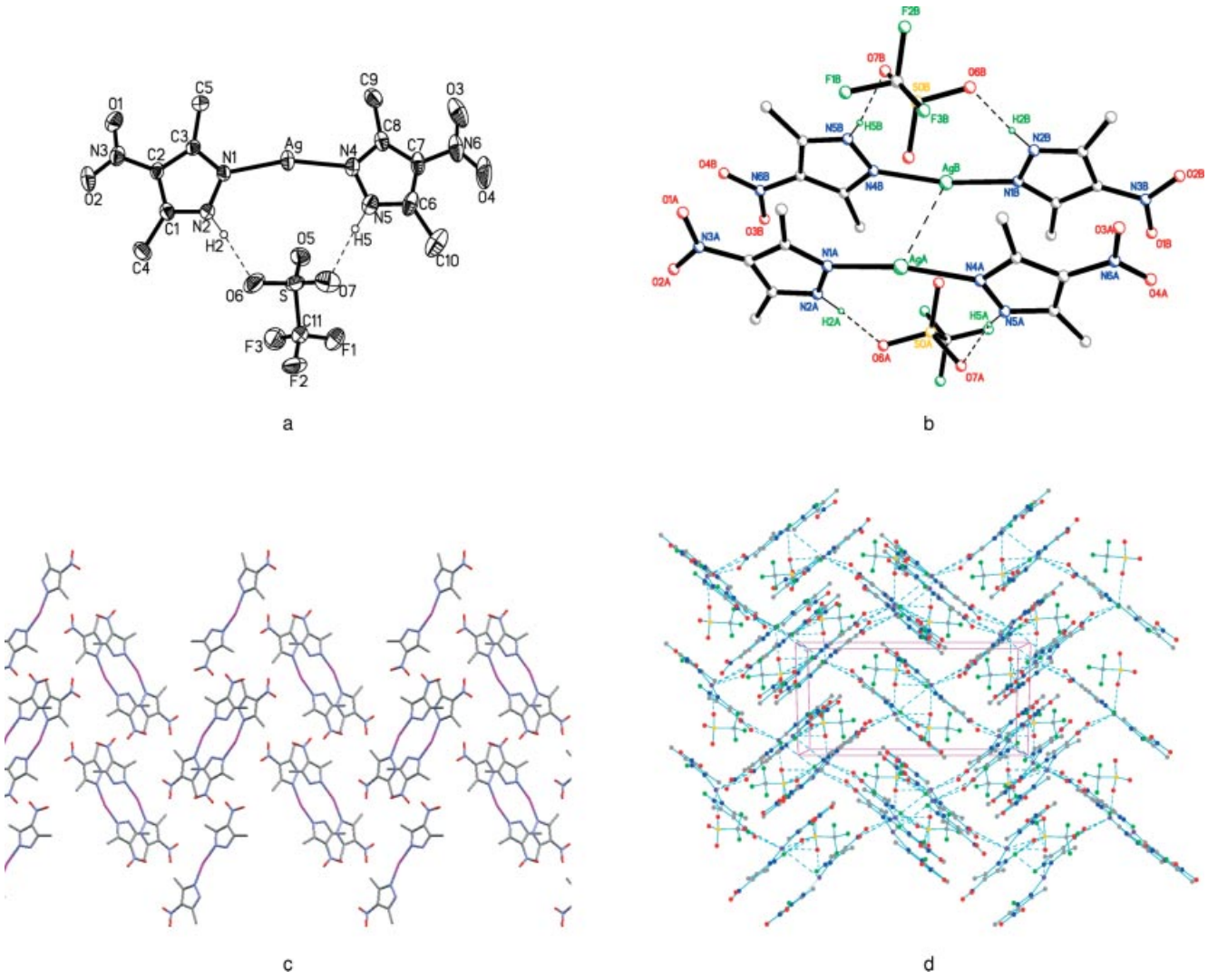

Figure 4. a) ORTEP plot of **8** at the 30% probability level; hydrogen atoms, except H2 and H4, and the labelling of some atoms have been omitted for clarity. b) View of the "dimeric unit" showing the close intermetallic approach. c) View of the two-dimensional network. d) View of the packing along the *c* axis showing the herringbone-type distribution

gives rise to the formation of columns along the (1 0 1) direction.

Finally, the columns are bonded each other to give a two-dimensional network which is extended parallel to the plane (1 0 $\bar{1}$) by long-range coordinative Ag1···O1(x + 1/2, $-y$ + 1/2, z + 1/2) interactions at 2.978(3) Å, produced between an oxygen atom of a NO_2 group, which is not implicated in the previously described π···π interactions, and the metal centre of neighbouring columns (c in Figure 4). This layer-like supramolecular structure can also be described as a herringbone-type arrangement of dimers connected through coordinative Ag···O interactions (d in Figure 4), the dimers being almost orthogonal to the layer as deduced by the angle defined between the C2−C7 line and the *a* axis of 77.01(3)°. No short interlayer distances are observed.

Concluding Remarks

The present work shows that Au/Ag complexes containing pyrazole-type ligands are efficient in constructing one- or two-dimensional networks. Complex **1** is formed by self-assembly of cationic $[Au(Hpz^{bp2})(PPh_3)]^+$ units and *p*-toluenesulfonate counterions, providing linear polymeric chains through N−H···O−S−O···H−C bridges containing both strong and weak hydrogen-bonding interactions. The geometry of the *p*-toluenesulfonate counterion appears to be responsible for the one-dimensional chain, which is different to the two-dimensional network produced by related interactions with the planar NO_3^- counterion. Therefore for cationic complexes containing one pyrazole ligand the one-dimensional supramolecular arrangement appears to be determined not only by the hydrogen-bonding interactions but also by the geometry of the counterion.

For complexes **2**, **5** and **8**, on the basis of the interactions between the counterion and the two NH-pyrazolic groups of each cationic unit, a polymeric chain was expected. However, the molecular conformation is responsible for a different assembly. In fact, in contrast to the observed *trans* disposition of the pyrazole groups found in the $[Ag(Hpz^{R2})_2]^+$

 © 2004 Wiley-VCH Verlag GmbH & Co. KGaA, Weinheim

compounds (Hpz^{R2} = pyrazole, 3,5-dimethylpyrazole),[17] complexes **2**, **5** and **8** present a *cis* orientation, which gives rise to $[M(Hpz^{R2})_2]X$ unities containing the A−N−N−M−N−N−A−B metallacycle (A = donor atom of the counterion; B = central atom of the counterion). The molecular assembly in **2** and **5** is therefore determined by new, weak, intermolecular C−H···O/F contacts through the remaining O/F atoms of the counterion, its geometry being responsible for the polymeric one-dimensional network. Alternatively, an embracing effect of the cations around the anions could also be considered as driving force for encapsulation.

A special behaviour has been found for **8**. The presence of the nitro group on the pyrazoles plays the most relevant role in the formation of its polymeric architecture, which adopts a two-dimensional, herringbone-type structure involving both coordinative Ag···O and π···π interactions. The extensive hydrogen-bonds between the counterions and the cationic unities only determine the formation of dimers.

From the above results we can deduce that, in the absence of coordinative NO_2 groups as substituents on the pyrazole rings, which appear to be determinant for supramolecular interactions, the conformations of the complexes as well as intermolecular orientations between them and the counterions are responsible for the hydrogen-bonding contacts involved in the molecular assembly.

Experimental Section

Materials and Instrumentation: All commercial reagents were used as supplied. The ligands 3,5-bis(4-*n*-butoxyphenyl)pyrazole (Hpz^{bp2})[20] and 3,5-dimethyl-4-nitropyrazole (Hpz^{NO2})[21] as well as the starting gold(I) derivatives [AuCl(THT))][11] and [Au(*p*-$CH_3C_6H_4SO_3$)(PPh_3)][8d] were prepared by literature procedures. Commercial solvents were dried prior to use. Elemental analyses for carbon, hydrogen and nitrogen were carried out by the Microanalytical Service of the Complutense University. IR spectra were performed on a FTIR Nicolet Magna-550 spectrophotometer with samples as KBr pellets in the 4000−400 cm^{-1} region. ^1H and $^{31}P\{^1H\}$ NMR spectra were recorded on Varian VXR-300 or Bruker DPX-300 spectrophotometers of the NMR Service of the Complutense University, from solutions in $CDCl_3$. Chemicals shifts δ(H) are given in ppm relative to $SiMe_4$, with the signal of the deuterated solvent as reference, and δ(P) in ppm relative to 85% H_3PO_4. Coupling constants (*J*) are in Hz. The ^1H and ^{31}P chemical shifts and coupling constants are accurate to ±0.01 ppm and ±0.3 Hz, respectively. Excitation and emission spectra of solid samples placed in capillary tubes were recorded on a Perkin−Elmer LS-55 luminescence spectrometer equipped with a R928 photomultiplier tube.

Synthesis of [Au(Hpz^{bp2})(PPh_3)](*p*-$CH_3C_6H_4SO_3$) (1): Hpz^{bp2} (18 mg, 0.05 mmol) was added to a solution of [Au(*p*-$CH_3C_6H_4SO_3$)(PPh_3)] (30 mg, 0.05 mmol) in freshly distilled THF (20 mL) and stirred for 24 h. The solvent was then removed in vacuo and the product was precipitated by addition of hexane/diethyl ether. Slow diffusion of diethyl ether into a dichloromethane/diethyl ether solution of this product gave colourless crystals suitable for crystallographic studies. $C_{48}H_{50}AuN_2O_5PS$ (994.90): calcd. C 57.95, H 5.02, N 2.82; found C 57.90, H 5.05, N 2.79. IR (KBr): $\tilde{\nu}$ = 3113 cm^{-1} ν(N−H), 1614 ν(C=N) + ν(C=C), 1174, 1162 and 1119 $\nu_d(SO_3)$, 1007 $\nu_s(SO_3)$. ^1H NMR (300 MHz, $CDCl_3$, 25 °C): δ = 1.00 (t, 6 H, CH_3 Hpz^{bp2}), 1.48−1.56 (m, 4 H, CH_2 Hpz^{bp2}), 1.75−1.82 (m, 4 H, CH_2 Hpz^{bp2}), 2.27 (s, 3 H, *p*-$CH_3C_6H_4SO_3$), 3.97 (t, $^3J_{H,H}$ = 6.6 Hz, 4 H, OCH_2 Hpz^{bp2}) 6.71 (s, 1 H, H4 Hpz^{bp2}), 6.86 (d, $^3J_{H,H}$ = 8.5 Hz, 4 H, H_m Hpz^{bp2}), 6.95 (d, $^3J_{H,H}$ = 7.9 Hz, 2 H, *p*-$CH_3C_6H_4SO_3$), 7.60−7.48 (m, 15 H, PPh_3), 7.74 (d, $^3J_{H,H}$ = 7.9 Hz, 2 H, *p*-$CH_3C_6H_4SO_3$), 7.79 (d, $^3J_{H,H}$ = 8.5 Hz, 4 H, H_o Hpz^{bp2}) ppm. ^{31}P NMR (121.49 MHz, $CDCl_3$, 25 °C): δ = 31.06 (s) ppm.

Synthesis of [Au(Hpz^{bp2})$_2$](*p*-$CH_3C_6H_4SO_3$) (2): A THF solution (20 mL) of Hpz^{bp2} (116 mg, 0.32 mmol) was added to a solution of [AuCl(THT)] (50 mg, 0.16 mmol) in dry THF (15 mL), and finally a solution of silver(I) *p*-toluenesulfonate (44 mg, 0.16 mmol) in dry THF (15 mL) was also added. After 24 h of stirring, the resulting mixture was filtered through a plug of Celite and the obtained colourless clear filtrate was evaporated to dryness. The residue was dissolved in dichloromethane and precipitated with hexane. X-ray quality crystals were obtained by slow diffusion of hexane into a dichloromethane solution of the product. $C_{53}H_{63}AuN_4O_7S$ (1097.1): calcd. C 58.02, H 5.79, N 5.11; found C 58.00, H 5.68, N 5.03. IR (KBr): $\tilde{\nu}$ = 3112 cm^{-1} ν(N−H), 1613 ν(C=N) + ν(C=C), 1221, 1174 and 1124 $\nu_d(SO_3)$, 1037 $\nu_s(SO_3)$. ^1H NMR (300 MHz, $CDCl_3$, 25 °C): δ = 1.01 (m, 12 H, CH_3 Hpz^{bp2}). 1.46−1.60 (m, 8 H, CH_2 Hpz^{bp2}), 1.75−1.86 (m, 8 H, CH_2 Hpz^{bp2}), 2.38 (s, 3 H, *p*-$CH_3C_6H_4SO_3$), 3.98 (t, $^3J_{H,H}$ = 6.5 Hz, 8 H, OCH_2 Hpz^{bp2}), 4.01 (t, $^3J_{H,H}$ = 6.5 Hz, 8 H, OCH_2 Hpz^{bp2}), 6.71 (d, $^4J_{H,H}$ = 2.0 Hz, 2 H, H4 Hpz^{bp2}), 6.79 (d, $^3J_{H,H}$ = 8.7 Hz, 4 H, H_m Hpz^{bp2}), 6.96 (d, $^3J_{H,H}$ = 8.7 Hz, 4 H, H_m Hpz^{bp2}), 7.21 (d, $^3J_{H,H}$ = 7.8 Hz, 2 H, *p*-$CH_3C_6H_4SO_3$), 7.76 (d, $^3J_{H,H}$ = 8.7 Hz, 4 H, H_o Hpz^{bp2}), 7.79 (d, $^3J_{H,H}$ = 8.7 Hz, 4 H, H_o Hpz^{bp2}), 7.96 (d, $^3J_{H,H}$ = 7.8 Hz, 2 H, *p*-$CH_3C_6H_4SO_3$), 14.54 (br. s, 2 H, NH Hpz^{bp2}) ppm.

Synthesis of [Au(Hpz^{bp2})$_2$](NO_3) (3): This compound was prepared by the same method previously described for **2**, from [AuCl(THT)] (50 mg, 0.16 mmol), $AgNO_3$ (27 mg, 0.16 mmol) and Hpz^{bp2} (116 mg, 0.32 mmol). $C_{46}H_{56}AuN_5O_7$ (987.96): calcd. C 55.92, H 5.71, N 7.09; found C 55.97, H 5.56, N 7.10. IR (KBr): $\tilde{\nu}$ = 3213 and 3141 cm^{-1} ν(N−H), 1614 ν(C=N) + ν(C=C), 1302 $\nu_{as}(NO_3)$. ^1H NMR (300 MHz, $CDCl_3$, 25 °C): δ = 1.02 (m, 12 H, CH_3 Hpz^{bp2}), 1.46−1.60 (m, 8 H, CH_2 Hpz^{bp2}), 1.78−1.83 (m, 8 H, CH_2 Hpz^{bp2}), 3.99 (t, $^3J_{H,H}$ = 6.5 Hz, 4 H, OCH_2 Hpz^{bp2}), 4.03 (t, $^3J_{H,H}$ = 6.5 Hz, 4 H, OCH_2 Hpz^{bp2}), 6.75 (d, $^4J_{H,H}$ = 1.9 Hz, 2 H, H4 Hpz^{bp2}), 6.84 (d, $^3J_{H,H}$ = 8.9 Hz, 4 H, H_m Hpz^{bp2}), 7.02 (d, $^3J_{H,H}$ = 8.9 Hz, 4 H, H_m Hpz^{bp2}), 7.77 (d, $^3J_{H,H}$ = 8.9 Hz, 4 H, H_o Hpz^{bp2}), 7.80 (d, $^3J_{H,H}$ = 8.9 Hz, 4 H, H_o Hpz^{bp2}), 13.70 (br. s, 2 H, NH Hpz^{bp2}) ppm.

Synthesis of [Au(Hpz^{bp2})$_2$]$_2$(1,5nds) (1,5nds = 1,5-naphthalenedisulfonate) (4): Ag_2O (32 mg, 0.14 mmol) was added to an aqueous solution (25 mL) of 1,5-naphthalenedisulfonic acid (50 mg, 0.14 mmol) with constant stirring until all the solids had dissolved. Acetone was then added to this solution and the resulting white precipitate was filtered off, dried and identified as silver 1,5-naphthalenedisulfonate.

Compound **4** was obtained by the same procedure described for **2**, from [AuCl(THT)] (38 mg, 0.12 mmol), silver 1,5-naphthalenedisulfonate (60 mg, 0.12 mmol) and Hpz^{bp2} (87 mg, 0.24 mmol). $C_{102}H_{118}Au_2N_8O_{14}S_2$ (2138.2): calcd. C 57.30, H 5.56, N 5.24; found C 57.29, H 5.39, N 5.19. IR (KBr): $\tilde{\nu}$ = 3115 cm^{-1} ν(N−H), 1612 ν(C=N) + ν(C=C), 1178 $\nu_d(SO_3)$, 1031 $\nu_s(SO_3)$, 607 $\delta_s(SO_3)$. ^1H NMR (300 MHz, $CDCl_3$, 25 °C): δ = 0.93 (t, $^3J_{H,H}$ = 7.3 Hz, 12 H, CH_3 Hpz^{bp2}), 1.02 (t, $^3J_{H,H}$ = 7.3 Hz, 12 H, CH_3 Hpz^{bp2}),

 © 2004 Wiley-VCH Verlag GmbH & Co. KGaA, Weinheim

1.41−1.58 (m, 16 H, CH_2 Hpz^{bp2}), 1.69−1.84 (m, 16 H, CH_2 Hpz^{bp2}), 3.91 (t, $^3J_{H,H}$ = 6.5 Hz, 8 H, OCH_2 Hpz^{bp2}), 3.97 (t, $^3J_{H,H}$ = 6.5 Hz, 8 H, OCH_2 Hpz^{bp2}), 6.70 (s, 4 H, H4 Hpz^{bp2}), 6.79 (d, $^3J_{H,H}$ = 8.7 Hz, 8 H, H_m Hpz^{bp2}), 6.82 (d, $^3J_{H,H}$ = 8.7 Hz, 8 H, H_m Hpz^{bp2}), 7.47 (t, 2 H, 1,5nds), 7.72 (d, $^3J_{H,H}$ = 8.7 Hz, 8 H, H_o Hpz^{bp2}), 7.77 (d, $^3J_{H,H}$ = 8.7 Hz, 8 H, H_o Hpz^{bp2}), 8.44 (d, $^3J_{H,H}$ = 6.5 Hz, 2 H, 1,5nds), 9.30 (d, $^3J_{H,H}$ = 8.7 Hz, 2 H, 1,5nds), 14.53 (s, 4 H, NH Hpz^{bp2}) ppm.

Synthesis of $[Ag(Hpz^{bp2})_2](BF_4)$ (5): $AgBF_4$ (19 mg, 0.10 mmol) was added under nitrogen to a solution of Hpz^{bp2} (71 mg, 0.20 mmol) in dry THF (10 mL). After 24 h of stirring, the solvent was removed in vacuo, giving rise to an oil from which a white solid was isolated after addition of dichloromethane and pentane. This product was crystallized by diffusion of hexane into a dichloromethane solution. $C_{46}H_{56}AgBF_4N_4O_4$ (923.63): calcd. C 59.83, H 6.11, N 6.07; found C 59.64, H 6.10, N 5.94. IR (KBr): $\tilde{\nu}$ = 3308 cm^{-1} ν(N−H), 1614 ν(C=N) + ν(C=C), 1067 and 1037 ν(BF). ^1H NMR (300 MHz, $CDCl_3$, 25 °C): δ = 1.00 (t, $^3J_{H,H}$ = 7.3 Hz, 12 H, CH_3 Hpz^{bp2}), 1.40−1.60 (m, 8 H, CH_2 Hpz^{bp2}), 1.70−1.90 (m, 8 H, CH_2 Hpz^{bp2}), 3.99 (t, $^3J_{H,H}$ = 6.6 Hz, 8 H, OCH_2 Hpz^{bp2}), 6.69 (s, 2 H, H4 Hpz^{bp2}), 6.70−7.00 (br. s, 8 H, H_m Hpz^{bp2}), 7.62 (d, $^3J_{H,H}$ = 8.8 Hz, 8 H, H_o Hpz^{bp2}), 11.95 (s, 2 H, NH Hpz^{bp2}) ppm. ^1H NMR (300 MHz, $CDCl_3$, −40 °C): δ = 0.95 ppm (t, $^3J_{H,H}$ = 7.2 Hz, 6 H, CH_3 Hpz^{bp2}), 0.96 (t, $^3J_{H,H}$ = 7.2 Hz, 6 H, CH_3 Hpz^{bp2}), 1.40−1.51 (m, 8 H, CH_2 Hpz^{bp2}), 1.68−1.80 (m, 8 H, CH_2 Hpz^{bp2}), 3.86 (t, $^3J_{H,H}$ = 6.6 Hz, 4 H, OCH_2 Hpz^{bp2}), 3.94 (t, $^3J_{H,H}$ = 6.6 Hz, 4 H, OCH_2 Hpz^{bp2}), 6.67 (s, 2 H, H4 Hpz^{bp2}), 6.72 (d, $^3J_{H,H}$ = 8.4 Hz, 4 H, H_m Hpz^{bp2}), 6.95 (d, $^3J_{H,H}$ = 8.7 Hz, 4 H, H_m Hpz^{bp2}), 7.53 (d, $^3J_{H,H}$ = 8.7 Hz, 4 H, H_o Hpz^{bp2}), 7.60 (d, $^3J_{H,H}$ = 8.4 Hz, 4 H, H_o Hpz^{bp2}), 11.86 (s, 2 H, NH Hpz^{bp2}) ppm.

Synthesis of $[Ag(Hpz^{bp2})_2](CF_3SO_3)$ (6): This compound was prepared in a similar way to **5**, from $AgCF_3SO_3$ (21 mg, 0.08 mmol) and Hpz^{bp2} (60 mg, 0.16 mmol). The resulting white solid was purified by washing with dichloromethane. $C_{47}H_{56}AgF_3N_4O_7S$ (985.92): calcd. C 57.26, H 5.73, N 5.68; found C 57.58, H 5.73, N 5.62. IR (KBr): $\tilde{\nu}$ = 3227 cm^{-1} ν(N−H), 1615 ν(C=N) + ν(C=C), 1226 $\nu_s(CF_3)$, 1028 $\nu_s(SO_3)$. ^1H NMR (300 MHz, $CDCl_3$, 25 °C): δ = 1.00 (t, $^3J_{H,H}$ = 7.3 Hz, 12 H, CH_3 Hpz^{bp2}), 1.43−1.61 (m, 8 H, CH_2 Hpz^{bp2}), 1.73−1.87 (m, 8 H, CH_2 Hpz^{bp2}), 3.98 (br. s, 8 H, OCH_2 Hpz^{bp2}), 6.69 (s, 2 H, H4 Hpz^{bp2}), 6.70−7.00 (br. s, 8 H, H_m Hpz^{bp2}), 7.63 (d, $^3J_{H,H}$ = 8.0 Hz, 8 H, H_o Hpz^{bp2}), 12.66 (s, 2 H, NH Hpz^{bp2}) ppm. ^1H NMR (300 MHz, $CDCl_3$, −40 °C): δ = 0.95 (t, $^3J_{H,H}$ = 6.9 Hz, 12 H, CH_3 Hpz^{bp2}), 1.39−1.51 (m, 8 H, CH_2 Hpz^{bp2}), 1.69−1.80 (m, 8 H, CH_2 Hpz^{bp2}), 3.83 (t, $^3J_{H,H}$ = 5.1 Hz, 4 H, OCH_2 Hpz^{bp2}), 3.95 (t, $^3J_{H,H}$ = 5.4 Hz, 4 H, OCH_2 Hpz^{bp2}), 6.67 (s, 2 H, H4 Hpz^{bp2}), 6.69 (d, $^3J_{H,H}$ = 8.7 Hz, 4 H, H_m Hpz^{bp2}), 6.95 (d, $^3J_{H,H}$ = 8.7 Hz, 4 H, H_m Hpz^{bp2}), 7.53 (d, $^3J_{H,H}$ = 8.4 Hz, 4 H, H_o Hpz^{bp2}), 7.61 (d, $^3J_{H,H}$ = 8.4 Hz, 4 H, H_o Hpz^{bp2}), 12.54 (s, 2 H, NH Hpz^{bp2}) ppm.

Synthesis of $[Ag(Hpz^{NO2})_2](BF_4)$ (7): $AgBF_4$ (35 mg, 0.18 mmol) was added under nitrogen to a solution of Hpz^{NO2} (131 mg, 0.36 mmol) in dry acetonitrile (25 mL). After stirring for 24 h, the solvent was removed under vacuum to give an oil from which a white solid was isolated after addition of dichloromethane and pentane. $C_{10}H_{14}AgBF_4N_6O_4$ (476.93): calcd. C 25.18, H 2.96, N 17.62; found C 25.34, H 2.97, N 17.72. IR (KBr): $\tilde{\nu}$ = 3175 cm^{-1} ν(N−H), 1595 ν(C=N) + ν(C=C), 1506 $\nu_{as}(NO)$, 1363 $\nu_s(NO)$, 1034 ν(BF). ^1H NMR (300 MHz, $CDCl_3$, 25 °C): δ = 2.71 (s, 12 H, CH_3 Hpz^{NO2}), 11.67 (s, 2 H, NH Hpz^{NO2}) ppm.

Table 4. Crystal and refinement data for **1**, **2**, **5** and **8**

	1	**2**	**5**	**8**
Formula	$C_{48}AuH_{50}N_2O_5PS$	$C_{53}H_{63}AuN_4O_7S$	$C_{46}H_{56}AgBF_4N_4O_4$	$C_{11}H_{14}AgF_3N_6O_7S$
Mol. mass	994.90	1097.10	923.63	539.21
Crystal system	triclinic	monoclinic	triclinic	monoclinic
Space group	$P\bar{1}$	$P2_1/n$	$P\bar{1}$	$P2_1/n$
a (Å)	11.264(1)	11.518(1)	9.1023(6)	8.8207(6)
b (Å)	13.808(1)	28.170(2)	14.576(1)	18.165(1)
c (Å)	14.633(1)	16.315(1)	19.180(1)	12.3303(8)
α (°)	95.161(1)		111.201(1)	
β (°)	101.889(1)	106.830(2)	92.791(1)	106.143(1)
γ (°)	100.809(1)		105.387(1)	
V (Å^3)	2167.8(3)	5066.9(7)	2257.7(3)	1897.7(2)
Z	2	4	2	4
F(000)	1004	2240	960	1072
D_c (g cm^{-3})	1.524	1.438	1.359	1.887
T (K)	296(2)	296(2)	296(2)	296(2)
μ(Mo-K_α) (mm^{-1})	3.527	2.999	0.509	1.249
Crystal size (mm)	0.35 × 0.12 × 0.04	0.32 × 0.26 × 0.12	0.37 × 0.20 × 0.15	0.38 × 0.18 × 0.12
Scan technique	φ and ω	φ and ω	φ and ω	φ and ω
Data collected	(−14,−14,−19) to (14,18,19)	(−12,−33,−14) to (13,33,19)	(−10,−15,−22) to (10,17,17)	(−8,−22,−15) to (11,20,13)
θ (°)	1.44−28.72	1.45−25.00	1.15−25.00	2.05−26.37
Refls. collected	13974	26518	11769	10664
Refls. indep.	9846 (R_{int} = 0.072)	8933 (R_{int} = 0.084)	7845 (R_{int} = 0.030)	3870 (R_{int} = 0.037)
Data, restraints, parameters	9846/0/527	8933/13/601	7845/16/545	3870/0/216
Refls. observed [$(I) > 2\sigma(I)$]	5854	3716	4737	3068
GOF (F^2)	0.862	0.856	0.903	1.031
$R(F)$[a]	0.054	0.048	0.043	0.033
$wR(F^2)$ (all data)[b]	0.118	0.133	0.111	0.087
Largest residual peak (e·Å^{-3})	1.321	1.359	0.472	0.775

[a] $\Sigma(|F_o| - |F_c|)/\Sigma|F_o|$. [b] $\{\Sigma[w(F_o^2 - F_c^2)^2]/\Sigma[w(F_o^2)^2]\}^{1/2}$.

 © 2004 Wiley-VCH Verlag GmbH & Co. KGaA, Weinheim

Synthesis of $[Ag(Hpz^{NO2})_2](CF_3SO_3)$ (8): The synthetic procedure for **8** was analogous to that used for **5** from $AgCF_3SO_3$ (46 mg, 0.18 mmol) and Hpz^{NO2} (51 mg, 0.36 mmol). Crystals were obtained by the slow diffusion of hexane into a dichloromethane solution of the compound. $C_{11}H_{14}AgF_3N_6O_7S$ (539.21): calcd. C 24.50, H 2.62, N 15.59; found C 24.57, H 2.59, N 15.57. IR (KBr): $\tilde{\nu}$ = 3205 and 3128 cm^{-1} ν(N−H), 1600 ν(C=N) + ν(C=C), 1509 ν_{as}(NO), 1366 ν_s(NO), 1252 $\nu_d(SO_3)$, 1230 $\nu_s(CF_3)$, 1040 $\nu_s(SO_3)$. ^{1}H NMR (300 MHz, $CDCl_3$, 25 °C): δ = 2.70 (s, 12 H, CH_3 Hpz^{NO2}), 12.50 (s, 2 H, NH Hpz^{NO2}) ppm.

X-Ray Structure Determinations: Crystals suitable for X-ray experiments were obtained from dichloromethane/diethyl ether for **1** or dichloromethane/hexane for **2**, **5** and **8**. Data collection was carried out at room temperature on a Bruker Smart CCD diffractometer using graphite-monochromated Mo-K_α radiation (λ = 0.71073 Å) operating at 50 kV and 20 mA. In all cases data were collected over a hemisphere of the reciprocal space by combination of three exposure sets. Each exposure covered 0.3 in ω. The cell parameters were determined and refined by least-squares fit of all reflections collected. The first 50 frames were recollected at the end of the data collection to monitor crystal decay; no appreciable decay was observed. A summary of the fundamental crystal and refinement data is given in Table 4.

The structures were solved by direct methods and refined by full-matrix least-squares methods on F^2.[22] All non-hydrogen atoms were refined anisotropically, with some exceptions due to the thermal and non-resolvable positional disorder found for some atoms. For the C47 atom in **2**, only its coordinates were refined. The fluorine and oxygen atoms in **8** were refined anisotropically over two cycles and in the subsequent cycles their thermal parameters were kept constant. Additionally, for **2** and **5** some carbon atoms of the butoxy chain were refined with geometrical restraints and a variable common carbon−carbon distance. For **5** the BF_4^- group was also refined with geometrical restraints and a variable common boron−fluorine distance. Hydrogen atoms bonded to the nitrogen atoms were located in a Fourier synthesis, included and their coordinates fixed or refined. The remaining hydrogen atoms were included in calculated positions and refined as riding on their respective carbon atoms and the thermal parameters related to the bonded atoms. The largest residual peaks in the final difference map are located close to the metal atoms.

CCDC-226053−226056 (for compounds **1**, **2**, **5** and **8**, respectively) contain the supplementary crystallographic data for this paper. These data can be obtained free of charge at www.ccdc.cam.ac.uk/conts/retrieving.html [or from the Cambridge Crystallographic Data Centre, 12 Union Road, Cambridge CB2 1EZ, UK; Fax: +44 (0)1223 336033; E-mail: deposit@ccdc.cam.ac.uk].

Acknowledgments

Financial support from the Dirección General de Investigación of the Ministerio de Ciencia y Tecnología is gratefully acknowledged (Project BQU2003-07343).

[1] [1a] J. M. Lehn, *Supramolecular Chemistry*, VCH, Weinheim, **1995**. [1b] C. B. Aakeröy, K. R. Seddon, *Chem. Soc. Rev.* **1993**, *22*, 397−407. [1c] M. Fujita, Y. J. Kwon, S. Washizu, K. Ogura, *J. Am. Chem. Soc.* **1994**, *16*, 1151−1152. [1d] G. R. Desiraju, *Angew. Chem.* **1995**, *107*, 2541−2558; *Angew. Chem. Int. Ed. Engl.* **1995**, *34*, 2311−2327. [1e] S. Subramanian, M. J. Zaworotko, *Angew. Chem.* **1995**, *107*, 2295−2297; *Angew. Chem. Int. Ed. Engl.* **1995**, *34*, 2127−2129. [1f] M. A. Withersby, A. J. Blake, N. R. Champness, P. Hubberstey, W. S. Li, M. Schröder, *Angew. Chem.* **1997**, *109*, 2421−2423; *Angew. Chem. Int. Ed. Engl.* **1997**, *36*, 2327−2329. [1g] D. Braga, F. Grepioni, G. R. Desiraju, *Chem. Rev.* **1998**, *98*, 1375−1406. [1h] D. Braga, F. Grepioni, *Acc. Chem. Res.* **2000**, *33*, 601−608. [1i] J. C. MacDonald, P. C. Dorrestein, M. M. Oilley, M. M. Foote, J. L. Lundburg, R. W. Henning, A. J. Schultz, J. L. Manson, *J. Am. Chem. Soc.* **2000**, *122*, 11692−11702. [1j] H. W. Roesky, M. Andruh, *Coord. Chem. Rev.* **2003**, *236*, 91−119.

[2] [2a] J. M. Lehn, *Angew. Chem.* **1990**, *102*, 1347; *Angew. Chem. Int. Ed. Engl.* **1990**, *29*, 1304−1319. [2b] A. J. Blake, N. R. Champness, P. Hubberstey, W. S. Li, M. A. Withersby, M. Schröder, *Coord. Chem. Rev.* **1999**, *183*, 117−138. [2c] B. Moulton, M. J. Zaworotko, *Chem. Rev.* **2001**, *101*, 1629−1658. [2d] P. A. N. Reddy, M. Nethaji, A. R. Chakravarty, *Inorg. Chem. Commun.* **2003**, *6*, 698−701. [2e] W. Bi, R. Cao, D. Sun, D. Yuan, X. Li, M. Hong, *Inorg. Chem. Commun.* **2003**, *6*, 1426−1428.

[3] [3a] T. C. W. Mak, *Inorg. Chim. Acta* **1984**, *84*, 19−23. [3b] W. Bi, D. Sun, R. Cao, M. Hong, *Acta Crystallogr., Sect. E* **2002**, *58*, m324−m325.

[4] [4a] B. L. Fei, W. Y. Sun, T. Okamura, W. X. Tang, N. Uegama, *New J. Chem.* **2001**, *25*, 210−212. [4b] L. Carlucci, G. Ciani, D. M. Prosperio, A. Sironi, *J. Am. Chem. Soc.* **1995**, *117*, 4562−4569.

[5] D. Sun, R. Cao, J. Weng, M. Hong, Y. Liang, *J. Chem. Soc., Dalton Trans.* **2002**, 291−292.

[6] [6a] K. Singh, J. R. Long, P. Stauropoulous, *J. Am. Chem. Soc.* **1997**, *119*, 2942−2943. [6b] P. Pyykkö, *Chem. Rev.* **1997**, *97*, 597−636. [6c] M. L. Tong, X. M. Chen, S. W. Ng, *Inorg. Chem. Commun.* **2000**, *3*, 436−441. [6d] M. Jansen, *Angew. Chem.* **1987**, *99*, 1136−1149; *Angew. Chem. Int. Ed. Engl.* **1987**, *26*, 1098−1110.

[7] [7a] M. A. Bennett, S. K. Bhargava, D. C. R. Hockless, L. L. Welling, A. C. Willis, *J. Am. Chem. Soc.* **1996**, *118*, 10469−10478. [7b] C. F. Shaw, in *Gold: Progress in Chemistry, Biochemistry and Technology* (Ed.: H. Schmidbaur), Wiley, New York, **1999**, p. 259. [7c] S. K. Bhargava, F. Mohr, M. A. Bennett, L. L. Welling, A. C. Willis, *Organometallics* **2000**, *19*, 5628−5635. [7d] W. J. Hunks, M. A. MacDonald, M. C. Jennings, R. J. Puddephatt, *Organometallics* **2000**, *19*, 5063−5070. [7e] S. K. Bhargava, F. Mohr, M. A. Bennett, L. L. Welling, A. C. Willis, *Inorg. Chem.* **2001**, *40*, 4271−4275. [7f] V. W. W. Yam, K. L. Cheung, L. H. Yuan, K. M. C. Wong, K. K. Cheung, *Chem. Commun.* **2000**, 1513−1514. [7g] C. P. McArdle, S. Van, M. C. Jennings, R. J. Puddephatt, *J. Am. Chem. Soc.* **2002**, *124*, 3959−3965. [7h] D. M. P. Mingos, R. Vilar, D. Rais, *J. Organomet. Chem.* **2002**, *641*, 126−133. [7i] F. Mohr, D. J. Eisler, C. P. McArdle, K. Atieh, M. C. Jennings, R. J. Puddephatt, *J. Organomet. Chem.* **2003**, *670*, 27−36.

[8] [8a] O. M. Yaghi, H. Li, *J. Am. Chem. Soc.* **1995**, *117*, 10401−10402. [8b] A. J. Blake, N. R. Champness, M. Crew, S. Parsons, *New J. Chem.* **1999**, *23*, 13−15. [8c] F. Robinson, M. J. Zaworotko, *J. Chem. Soc., Chem. Commun.* **1995**, 2413−2414. [8d] P. Römbke, A. Schier, H. Schmidbaur, *J. Chem. Soc., Dalton Trans.* **2001**, 2482−2486. [8e] W. Schneider, K. Angermaier, A. Sladek, H. Schmidbaur, *Z. Naturforsch., Teil B* **1996**, *51*, 790−800. [8f] M. Preisenberger, A. Schier, H. Schmidbaur, *J. Chem. Soc., Dalton Trans.* **1999**, 1645−1650.

[9] [9a] C. Janiak, T. G. Scharmann, *Polyhedron* **2003**, *22*, 1123−1133. [9b] X. J. Yang, C. Janiak, J. Heinze, F. Drepper, P. Mayer, H. Pietrowski, P. Klüfers, *Inorg. Chim. Acta* **2001**, *318*, 103−116. [9c] N. M. Chowdhry, D. M. P. Mingos, A. J. P. White, D. J. Williams, *Chem. Commun.* **1996**, 899−900. [9d] M. J. Zaworotko, *Chem. Soc. Rev.* **1994**, *23*, 283−288. [9e] D. Braga, L. Scaccianoce, F. Grepioni, S. M. Draper, *Organometallics* **1996**, *15*, 4675−4677.

[10] [10a] M. Cano, J. V. Heras, M. L. Gallego, J. Perles, C. Ruiz-Valero, E. Pinilla, M. R. Torres, *Helv. Chim. Acta* **2003**, *86*, 3194−3203. [10b] R. M. Claramunt, P. Cornago, M. Cano, J. V.

 © 2004 Wiley-VCH Verlag GmbH & Co. KGaA, Weinheim

Heras, M. L. Gallego, E. Pinilla, M. R. Torres, *Eur. J. Inorg. Chem.* **2003**, 2693−2704.

[11] R. Usón, A. Laguna, M. Laguna, *Inorg. Synth.* **1989**, *26*, 85−91.

[12] [12a] L. Malatesta, L. Naldini, G. Simonetta, F. Cariati, *Coord. Chem. Rev.* **1966**, *1*, 255−262. [12b] R. J. Batchelor, J. N. R. Ruddick, J. R. Sams, F. Aubke, *Inorg. Chem.* **1977**, *16*, 1414−1417. [12c] K. Nakamoto, *Infrared and Raman Spectra of Inorganic and Coordination Compounds*, 4th ed., Wiley, New York, **1986**.

[13] [13a] M. Cano, J. V. Heras, M. Maeso, M. Alvaro, R. Fernández, E. Pinilla, J. A. Campo, A. Monge, *J. Organomet. Chem.* **1997**, *534*, 159−172. [13b] M. Cano, J. A. Campo, J. V. Heras, J. Lafuente, C. Rivas, E. Pinilla, *Polyhedron* **1995**, *14*, 1139−1147.

[14] [14a] M. C. Torralba, M. Cano, J. A. Campo, J. V. Heras, E. Pinilla, M. R. Torres, *J. Organomet. Chem.* **2001**, *633*, 91−104. [14b] M. C. Torralba, M. Cano, J. A. Campo, J. V. Heras, E. Pinilla, M. R. Torres, *Inorg. Chem. Commun.* **2002**, *5*, 887−890.

[15] [15a] K. Nomiya, R. Noguchi, K. Ohsawa, K. Tsuda, *J. Chem. Soc., Dalton Trans.* **1998**, 4101−4108. [15b] K. Nomiya, R. Noguchi, K. Ohsawa, K. Tsuda, M. Oda, *J. Inorg. Biochem.* **2000**, *78*, 363−370. [15c] F. Bonati, M. Felici, B. R. Pietroni, A. Burini, *Gazz. Chim. Ital.* **1982**, *112*, 5−8. [15d] P. Ovejero, M. Cano, E. Pinilla, M. R. Torres, *Helv. Chim. Acta* **2002**, *85* 1686−1690.

[16] [16a] T. Steiner, G. R. Desiraju, *Chem. Commun.* **1998**, 891−892. [16b] T. Steiner, B. Lutz, J. van der Maas, A. M. M. Schreurs, J. Kroon, M. Tamm, *Chem. Commun.* **1998**, 171−172. [16c] T. K. Yazicilar, O. Andac, Y. Bekdemir, H. Kutuk, V. T. Yilmaz, W. T. A. Harrison, *Acta Crystallogr., Sect. C* **2002**, *58*, m21−m22. [16d] N. Vembu, M. Nallu, E. C. Spencer, J. A. K. Howard, *Acta Crystallogr., Sect. E* **2003**, *59*, o1192−o1195. [16e] D. C. Zhang, Z. H. Fei, T. Z. Zhang, Y. Q. Zhang, K. B. Yu, *Acta Crystallogr., Sect. C* **1999**, *55*, 102−104. [16f] M. Hörner, I. C. Casagrande, H. Fenner, J. Daniels, J. Beck, *Acta Crystallogr., Sect. C* **2003**, *59*, m424−m426. [16g] M. Hörner, L. Bresolin, J. Bordinhao, E. Hartmann, J. Strähle, *Acta Crystallogr., Sect. C* **2003**, *59*, o426−o427. [16h] S. Y. Wan, Y. Z. Li, T. Okamura, J. Fan, W. Y. Sun, N. Ueyama, *Eur. J. Inorg. Chem.* **2003**, 3783−3789.

[17] [17a] H. Schmidbaur, A. Mair, G. Müller, J. Kachmann, S. Gamper, *Z. Naturforsch., Teil B* **1991**, *46*, 912−918. [17b] A. A. Mohamed, J. P. Fackler Jr., *Acta Crystallogr., Sect. C* **2002**, *58*, m228−m229.

[18] [18a] I. Boldog, E. B. Rusanov, A. N. Chernega, J. Sieler, K. V. Domasevitch, *Polyhedron* **2001**, *20*, 887−897. [18b] D. L. Reger, R. F. Semeniuc, M. D. Smith, *Inorg. Chem.* **2001**, *40*, 6545−6546.

[19] [19a] J. R. Lechar, R. H. de Almeida Santos, *Cryst. Struct. Commun.* **1982**, *11*, 471−477. [19b] G. Yang, R. G. Raptis, *Inorg. Chem.* **2003**, *42*, 261−263. [19c] M. C. Torralba, P. Ovejero, M. J. Mayoral, M. Cano, J. A. Campo, J. V. Heras, E. Pinilla, M. R. Torres, *Helv. Chim. Acta* **2004**, *87*, 250−263.

[20] M. C. Torralba, M. Cano, J. A. Campo, J. V. Heras, E. Pinilla, M. R. Torres, *J. Organomet. Chem.* **2002**, *654*, 150−161.

[21] G. T. Morgan, I. Ackerman, *J. Chem. Soc.* **1923**, 1308−1318.

[22] G. M. Sheldrick, *SHELXTL, Program for Refinement of Crystal Structure*, University of Göttingen, Göttingen, Germany, **1997**.

Received December 17, 2003
Early View Article
Published Online June 1, 2004

 © 2004 Wiley-VCH Verlag GmbH & Co. KGaA, Weinheim

A Theoretical Investigation of the Donor Ability of [M(R,R′timdt)$_2$] Dithiolene Complexes towards Molecular Diiodine (M = Ni, Pd, Pt; R,R′timdt = Formally Monoreduced Disubstituted Imidazolidine-2,4,5-trithione)

M. Carla Aragoni,[a] Massimiliano Arca,*[a] Francesco Demartin,[b] Francesco A. Devillanova,[a] Francesco Lelj,[c] Francesco Isaia,[a] Vito Lippolis,[a] Annalisa Mancini,[a] Luca Pala,[a] and Gaetano Verani[a]

Keywords: Charge transfer / Density functional calculations / Dithiolenes / Iodine / Raman spectroscopy / X-ray diffraction

The σ-type charge-transfer (CT) interaction between [M(R,R′timdt)$_2$] donors (M = Ni, Pd, Pt; R,R′timdt = formally monoreduced disubstituted imidazolidine-2,4,5-trithione) and diiodine has been thoroughly investigated by a large set of theoretical calculations at different levels of theory (HF, pure and hybrid-DFT with different functionals and basis sets) on I_2 (and for the sake of comparison on IBr and Br_2), on the model donor dithiolene complexes [M(H_2timdt)$_2$], and on the adducts [M(H_2timdt)$_2$]·I_2 (M = Ni, Pd, Pt). The computations have accounted for the ability of adducts to assume different stoichiometries and to make up polymeric networks based on sulfur–iodine contacts, as in the case of [Ni(Me,*i*Pr-timdt)$_2$]·I_2, which was also characterised by single-crystal X-ray diffraction. In addition, the strength of the donor–acceptor interaction has been evaluated through the calculated vibrational features of the model adducts, compared with the experimental FT-Raman spectra recorded on the adducts between [M(Et_2timdt)$_2$] and [M(Me,*i*Pr-timdt)$_2$] (M = Ni, Pd, Pt) and diiodine. The frontier-orbital composition, the NBO-charge distribution and bond orders indicate a medium-weak donor ability for the dithiolene donors, which depends only slightly on the nature of the central metal ion, and decreases on passing from M = Ni to M = Pd and Pt, in agreement with the values of the experimental frequencies of the FT-Raman-active I–I stretching vibrations in the adducts [M(Et_2timdt)$_2$]·2I_2 (M = Ni, Pd, Pt). The ZPE- and CP BSSE-corrected binding energy for [Ni(H_2timdt)$_2$]·I_2 has been evaluated as −11 kcal/mol.
(© Wiley-VCH Verlag GmbH & Co. KGaA, 69451 Weinheim, Germany, 2004)

Introduction

Since the pioneering work by Schrauzer and co-workers,[1] the scientific community has become increasingly interested in metal dithiolene complexes.[2] This is justified not only by the essential role of dithiolene ligands in the chemistry of enzymes[3−5] and by the great potential for exploiting these complexes in fields as diverse as nonlinear optics[6,7] and superconductivity,[8] but also by their fascinating electronic structures.[9] In particular, dithiolene complexes containing d^8 metal ions (namely Ni, Pd, and Pt) feature an extended π-electron delocalization involving the organic framework as well as the metal centre.[10] The electronic features are reflected in peculiar molecular properties, such as high thermal and photochemical stabilities, electrochromism,[10] and the ability to undergo multi-step reversible redox processes.[11,12] Square-planar neutral bisdithiolenes feature a peculiar very intense Vis/NIR absorption, which falls at 720, 785, and 680 nm for the simplest [M(edt)$_2$] neutral complexes [edt = ethylenedithiolato; M = Ni (**1**), Pd (**2**), and Pt (**3**), respectively].[1,13] This absorption has been ascribed to a HOMO−LUMO π-π* transition, based on theoretical calculations carried out at several levels of theory, ranging from EHT to TD-DFT.[14,15] The donor ability of the ligand towards the metal centre is tunable through structural modifications of the substituents at the carbon atoms of the dithiolene system, and affects both the Vis/NIR optical properties and the order of the relative stabilities of the available oxidation states (typically dianionic, monoanionic, and neutral).

Since 1995 we have been investigating neutral Ni, Pd, and Pt dithiolene complexes derived from the R,R′timdt ligand (R,R′timdt = formally monoreduced disubstituted imid-

[a] Dipartimento di Chimica Inorganica ed Analitica, Università degli Studi di Cagliari,
S.S. 554 Bivio per Sestu, 09042 Monserrato − Cagliari, Italy
Fax: +39-070-6754456
E-mail: marca@unica.it
[b] Dipartimento di Chimica Strutturale e Stereochimica Inorganica, Università degli Studi di Milano,
Via G. Venezian 21, 20133 Milano, Italy
[c] LAMI Dipartimento di Chimica e LASCAMM-INSTM Sezione Basilicata, Università degli Studi della Basilicata,
Via N. Sauro 85, 85100 Potenza, Italy
Supporting information for this article is available on the WWW under http://www.eurjic.org or from the author.

azolidine-2,4,5-trithione), which differs from the very well-known dmit dithiolenes [dmit = $C_3S_5^{2-}$, 1,3-dithiole-2-thione-4,5-dithiolate;[8] M = Ni (**4**), Pd (**5**), Pt (**6**)] in having NR groups instead of sulfurs in the pentaatomic ligand (Scheme 1).[16−24] Hybrid-DFT[18,19,23] and very recent TD-DFT calculations[21,24] confirmed that the tight HOMO−LUMO energy gap is responsible for the low-energy NIR transition falling at about 1000 nm (extinction coefficients as high as 120000 $M^{-1}\cdot cm^{-1}$ in toluene).[23] In addition, contrary to most dithiolene complexes, and in particular to their dmit analogues, neutral [M(R,R′timdt)$_2$] complexes behave as donors towards molecular acceptors, and some of the authors of this paper have reported the reaction between [Ni(*i*Pr$_2$timdt)$_2$] (**7**) and molecular diiodine, leading to the CT adducts **7**·2I$_2$ and **7**·2I$_2$·1/2I$_2$, and to the mixed-valence complex [Ni(*i*Pr$_2$timdt)$_2$]·2I$_2$·[Ni(I)$_2$(*i*Pr$_2$timdt)$_2$]·3I$_2$.[17] Among Pd complexes, only the CT adduct **8**·I$_2$·CHCl$_3$ (**8** = [Pd(Et$_2$timdt)$_2$]) has been reported,[18] while the reactivity of Pt dithiolene complexes towards diiodine has not been explored to date. In order to rationalize the donor ability of neutral [M(R,R′timdt)$_2$] complexes, we have now carried out a study on the products of the reactions between [M(Et$_2$timdt)$_2$] and [M(Me,*i*Pr-timdt)$_2$] (M = Ni, Pd, Pt) and molecular I$_2$ in several molar ratios (Scheme 1).

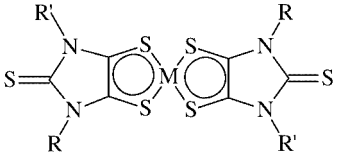

R	R'	M	Dithiolene:I$_2$ reaction ratio			
			1:1	1:2	1:5	1:10
Et	Et	Ni	1:1	1:2	1:2	1:3
		Pd	2:1	2:1	1:2	1:2
		Pt	1:1	1:1	2:3	1:2
Me	i-Pr	Ni	1:1	1:1	1:1	1:4
		Pd	2:5	1:2	1:2	1:2
		Pt	1:3	1:4	1:5	1:5

Scheme 1

Theoretical calculations have recently been proved to be a very valuable tool in interpreting the interactions between chalcogenone donors and molecular halogens,[25] although it seems that the number of papers on complexes containing iodine is limited. Thus, with the aim of understanding the nature of the CT interaction and investigating the effect of the central metal ion and of the substituents on the reactivity of the metal dithiolene complexes [M(R,R′timdt)$_2$] towards molecular diiodine, we performed a large set of theoretical calculations on [M(H$_2$timdt)$_2$]·I$_2$ model adducts.

Results and Discussion

Synthesis

Since the low solubility of neutral [M(R,R′timdt)$_2$] complexes prevents them from reaching the concentrations needed to study their equilibria with iodine in solution,[26] neutral [M(R,R′timdt)$_2$] complexes (M = Ni, Pd, Pt), both symmetrically (R = R′ = Et) and unsymmetrically (R = Me; R′ = *i*Pr) substituted, were reacted with molecular iodine in closed pressure-tubes (to avoid halogen losses) in dithiolene/iodine molar ratios ranging between 1:1 and 1:10, in order to achieve CT adducts with different stoichiometries. Unfortunately, conventional solid-state spectroscopic techniques (such as FT-Raman, FT-IR, and CP MAS ^{13}C NMR) are not useful in clarifying the nature of the final products, which can be only ascertained by elemental analysis and, when possible, by X-ray diffraction. Although the composition of the final products cannot be ascertained clearly in all cases (especially when R = Me, R′ = *i*Pr), an examination of the dithiolene/I$_2$ molar ratios in the adducts (Scheme 1) shows that the halogen content in the final products increases on increasing the starting molar ratio, and that the nature both of the central metal and of the substituents is crucial in determining the final product. It is worthy of note that all the Pt complexes were found to react with I$_2$ yielding reaction products with dithiolene/halogen ratios ranging between 1:0.5 and 1:5 depending on the substituents. The isolation of several adducts with dithiolene/I$_2$ ratios higher than 1:2 suggests that the terminal iodine units of [M(R,R′timdt)$_2$]·2I$_2$ adducts should be able to behave as donors towards further diiodine molecules.

X-ray Diffraction Studies

Crystals having a 1:1 dithiolene/I$_2$ ratio, suitable for X-ray diffraction studies, were obtained by reacting [Ni(Me,-*i*Pr-timdt)$_2$] (**9**) and I$_2$ in molar ratios ranging between 1:1 and 1:5. A perspective view of the 1:1 CT adduct **9**·I$_2$ is depicted in Figure 1. The nickel atom of the [Ni(Me,*i*Pr-timdt)$_2$] molecule is located on a crystallographic inversion centre at 0,0,0 whereas the diiodine molecule lies across a different crystallographic centre at 0, 1/2, 1/2. As expected based on the few previously reported structures of CT adducts between [M(R,R′timdt)$_2$] complexes and diiodine,[17,18] the dithiolene coordinates the iodine molecule through its terminal thiocarbonyl groups with an S(3)···I(1) interaction of 3.098(2) Å. A view of the crystal packing of **9**·I$_2$ (Figure 2) shows the polymeric nature of the adduct. The packing consists of zig-zag polymeric chains made up of complex molecules symmetrically linked by iodine units bridging the terminal sulfur atoms [S(3)] of different molecules. The diiodine moieties are essentially perpendicular to the dithiolene molecular plane and the S(3)···I(1)−I(1)′′···S(3)′′ system is linear. Similar S···I−I···S systems have been isolated in several CT adducts between thioether macrocycles and diiodine.[27] In these systems, which structurally recall the I_4^{2-} anion ($^-$I···I−I···I$^-$),[28]

 © 2004 Wiley-VCH Verlag GmbH & Co. KGaA, Weinheim

the bridging iodine molecule is less elongated than in the corresponding 1:1 CT adducts. Chains of alternating dithiolene and diiodine units are packed by dithiolene stacking interactions analogous to those described for **9**,[19] with the nickel atom sandwiched between two imidazolidine rings of parallel adjacent dithiolene molecules, the distances between each nickel ion and the imidazolidine centroid being 3.72 and 3.77 Å in **9** and **9**·I_2, respectively. A comparison with the crystal structure of **9**[19] shows that the terminal thiocarbonyl group involved in the CT interaction is slightly elongated with respect to the free donor [C(3)−S(3) = 1.644(5) in **9**, 1.674(6) Å in **9**·I_2], in agreement with the situation generally found for CT adducts between thiocarboxyl donors and iodine.[29] However, this lengthening is small and is compatible with a weak sulfur−iodine interaction. The rest of the complex molecule displays bond lengths and angles close to those found in complex **9** [C(1)−C(2), C(1)−S(1), and C(2)−S(2) 1.396(6), 1.682(5), and 1.681(5) Å in **9**; 1.380(7), 1.719(6), and 1.688(5) Å in **9**·I_2]. Due to the bridging role of the halogen in **9**·I_2, the interaction between the metal complex and the diiodine units [S(3)···I 3.098(2) Å] is weaker than that observed in the case of either **7**·2I_2·1/2I_2 [2.825(6) Å] or **8**·I_2·$CHCl_3$ [2.815(3) Å].[17,18] Accordingly, the elongation of the I−I distance due to the CT interaction [2.790(1) Å in **9**·I_2; I−I = 2.715 Å for iodine in the solid state][30] is less than that found for the adducts **7**·2I_2·1/2I_2 and **8**·I_2·$CHCl_3$ [I−I distances 2.815(3) and 2.811(2) Å, respectively].

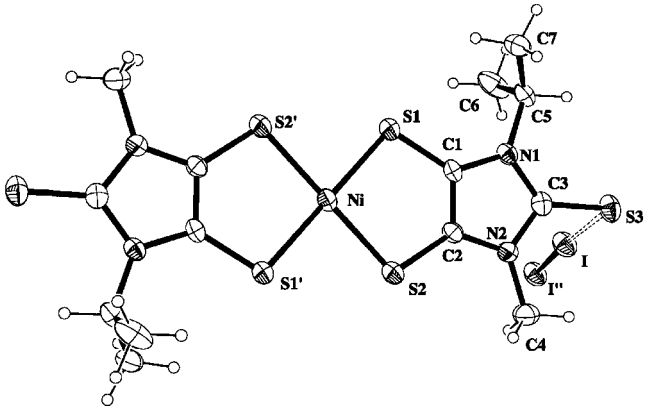

Figure 1. ORTEP structure and atom labelling scheme of **9**·I_2; selected bond lengths (Å): Ni−S(1), 2.176(2); Ni−S(2), 2.170(2); C(1)−S(1), 1.719(6); C(2)−S(2), 1.688(5); C(1)−C(2), 1.380(7); C(1)−N(1), 1.379(7); C(2)−N(2), 1.370(7); N(1)−C(3), 1.376(7); N(2)−C(3), 1.391(6); C(3)−S(3), 1.674(6); S(3)···I, 3.098(2); I−I′′, 2.790(1); selected angles (°): S(1)−Ni−S(2), 94.26(5); S(1)−Ni−S(2)′, 85.74(6); Ni−S(1)−C(1), 101.2(2); Ni−S(2)−C(2), 100.5(2); C(3)−S(3)···I(1), 93.26(8); S(3)···I−I′′, 176.27 (5); symmetry codes: ′ = −*x*, −*y*, −*z*; ′′ −*x*, 1 − *y*, 1 − *z*

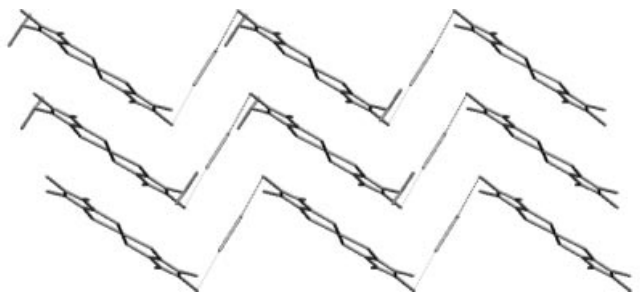

Figure 2. View of the crystal packing of **9**·I_2

FT-Raman Spectroscopy

Because of the resonance Raman effect with the broad NIR absorption at about 1000 nm, the FT-Raman spectra of neutral [M(R,R′timdt)$_2$] complexes recorded with spectrometers based on a Nd:YAG laser (λ_{exc} = 1064 nm) allow us to identify the vibrations due to the MS_4 system.[19] The spectra show only two very intense peaks in the 500−50 cm^{-1} region. The former falls at average values of 435, 427, and 425 cm^{-1} for the Ni, Pd, and Pt complexes, respectively; the latter, which falls at 380 and 340 cm^{-1} for the Ni and Pd complexes, respectively, was not observed for the Pt complex.[19] These peaks have been attributed to the a_g or b_{1g} bending and to the a_g stretching modes of the MS_4C_4 dithiolene system, respectively.[19,24] Analogous peaks also appear in the solid-state FT-Raman spectra of the synthesized CT adducts at frequencies very close to those recorded for the starting dithiolenes. In weak and medium-weak CT adducts, the lengthening of the inter-iodine bond length due to the CT interaction has been correlated to the lowering of the corresponding stretching vibration, which occurs at 180 cm^{-1} for solid iodine, and is shifted towards lower frequencies in CT adducts (140−180 cm^{-1}).[29,31] Unfortunately, when using Nd:YAG FT-Raman spectrometers, the Raman enhancement of the metal-sulfur vibrations makes the peaks due to the I−I stretching mode barely visible. Nonetheless, in the cases of the adducts of the complexes [M(Et_2timdt)$_2$] (M = Ni, Pd, Pt), the peak due to the I−I stretching mode is clearly visible at 139,[32] 153, and 155 cm^{-1}, for M = Ni, Pd, and Pt, respectively (see Figure 3 for [M(Et_2timdt)$_2$]·2I_2 adducts). The position of the peaks indicates a medium-weak interaction between [M(R,R′timdt)$_2$] and I_2, whose strength decreases on passing from Ni to Pt. Unfortunately, the peak due to the I−I vibration is completely absent in the adducts of [M(Me,*i*Pr-timdt)$_2$] dithiolenes.

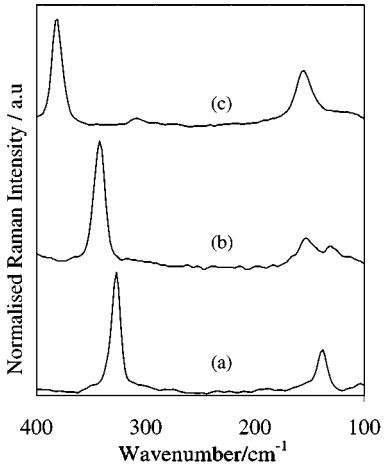

Figure 3. Normalised FT-Raman spectra of the adducts [M(Et_2timdt)$_2$]·2I_2 [M = Ni (a), Pd (b), Pt (c)]

 © 2004 Wiley-VCH Verlag GmbH & Co. KGaA, Weinheim

Theoretical Calculations

A few years ago, we reported[18,19,23] DFT[33,34] calculations performed with the Gaussian 98 package[35] on [M(H_2timdt)$_2$] model complexes [M = Ni (**10**), Pd (**11**), Pt (**12**); R = R′ = H in Scheme 1] using the three-parameter[36] hybrid B3LYP functional (based on the gradient-corrected Becke exchange functional[37] along with the Lee, Yang and Parr correlation functional[38]), and the LanL2DZ basis set (BS) with Effective Core Potentials (ECP)[39] for the central metal ion. With the results of these calculations it was possible to explain the trend in the NIR absorption maxima experimentally found on changing the central metal ion [λ_{max} (Ni) ≈ λ_{max} (Pt) < λ_{max} (Pd)], and the electrochemical behaviour of [M(R,R′timdt)$_2$] complexes compared to other neutral dithiolenes, such as **1**−**3** and **4**−**6**. In fact, TD-DFT calculations showed that the NIR excitation energy is well-represented by an almost pure HOMO−LUMO transition.[21,24] It has been proved that Kohn−Sham (KS) one-electron energies $-\varepsilon$ of occupied orbitals can be interpreted as approximate relaxed vertical ionisation potentials.[40] Thus, the energy of the NIR transition can be estimated as the one-electron energy difference $\Delta\varepsilon$ between the HOMO and the LUMO.[18,19,21,23,24] At any rate, although the previous calculations accounted nicely for the spectroscopic and electrochemical properties of the title dithiolene complexes, the M−S bond lengths were systematically overestimated. Subsequently, we reported relativistic TD-DFT calculations which highlighted how the trend in the metal−sulfur distances is affected by relativistic effects.[21,24] Now, in order to find the best level of theory to deal with adduct formation, new HF and DFT calculations with different basis sets and, in the case of DFT, different functionals of the electron density, were performed on **10**−**12**, on I_2, and, for the sake of comparison, on Br_2 and IBr. The results of the calculations performed separately on **10**−**12** and on I_2 were used to find a suitable theoretical level to approach the donor−acceptor interaction leading to the model CT adducts **10**·I_2, **11**·I_2, and **12**·I_2. As regards DFT calculations, pure (BLYP[37,38] and BPW91[37,41]) and hybrid (mPW1PW[42] and B3LYP)[36−38] functionals were used. The PBE0 GGA functional[43] was not considered, since we have found recently that it gives results close to those obtained at the B3LYP level on the model dithiolene complexes **4** and **10**.[24] For all calculations, the Schafer, Horn and Ahlrichs pVDZ basis sets[44] were used for the organic framework, while for the central metal we tested the LanL2DZ,[39] SBKJC,[45] Stuttgart,[46] CRENBS[47] and CRENBL[47,48] basis sets with the corresponding effective core potential (ECP) sets. For halogens, the all-electron 6-311G**[49] and MIDI![50] and the sets LanL2DZ,[39] SBKJC,[45] and Stuttgart[46] with ECPs were used. Based on the results separately obtained on the interacting molecular units **10**−**12** and I_2,[51,52] the calculations on 1:1 adducts were performed on the model complexes **10**·I_2, **11**·I_2, and **12**·I_2 at the DFT level, using the mPW1PW functional and the LanL2DZ BSs with ECPs both for the central metal ion M and for iodine (see Supporting Information). A comparison between the optimised geometries of the adducts between **10**−**12** and I_2 shows a good agreement between the experimental bond lengths and angles reported previously[17,18] and those of the corresponding calculated values (Table 1). As an example, Figure 4 compares the bond lengths optimised for **11**·I_2 with those determined by X-ray diffraction[18] for **8**·I_2·$CHCl_3$.

Table 1. Optimised[a] bond lengths r (Å) and angles α (°) for the CT adducts **10**·I_2, **11**·I_2, and **12**·I_2, variations Δr (Å) and $\Delta\alpha$ (°) with respect to the free optimised[a] components and corresponding structural data r_{exp} (Å) and α_{exp} (°)[b] [c]

	10·I_2			**11**·I_2			**12**·I_2 [d]	
	$r_{\mathbf{10}\cdot I_2}$[a]	$\Delta r_{\mathbf{10}}$[a]	r_{exp}[b]	$r_{\mathbf{11}\cdot I_2}$[a]	$\Delta r_{\mathbf{11}}$[a]	r_{exp}[c]	$r_{\mathbf{12}\cdot I_2}$[a]	$\Delta r_{\mathbf{12}}$[a]
M−S(1,2)	2.186	−0.075	2.16	2.324	0.006	2.287	2.324	−0.004
M−S(1,2)[e]	2.193	−0.018	−	2.335	0.005	2.286	2.330	0.002
C(1,2)−S(1,2)	1.687	−0.003	1.70	1.700	0.006	1.697	1.701	0.006
C(1,2)−S(1,2)[e]	1.673	−0.017	−	1.685	−0.009	1.689	1.687	−0.008
C(1)−C(2)	1.399	−0.006	1.33	1.399	−0.007	1.343	1.396	−0.006
C(1)−C(2)[e]	1.418	0.013	−	1.418	0.012	1.403	1.413	0.011
C(3)−S(3)	1.669	0.024	1.68	1.675	0.030	1.740	1.676	0.031
C(3)−S(3)[e]	1.631	−0.014	−	1.639	−0.006	1.626	1.640	−0.005
S(3)−I(1)	2.855	−	2.83	2.918	−	2.875	2.918	−
I(1)−I(1)′	2.970	0.074	2.815	2.957	0.061	2.811	2.955	0.059
	$\alpha_{\mathbf{10}\cdot I_2}$[a]	$\Delta\alpha_{\mathbf{10}}$[a]	α_{exp}[b]	$\alpha_{\mathbf{11}\cdot I_2}$[a]	$\Delta\alpha_{\mathbf{11}}$[a]	α_{exp}[c]	$\alpha_{\mathbf{12}\cdot I_2}$[a]	$\Delta\alpha_{\mathbf{12}}$[a]
S(1)−M−S(2)	95.8	0.8	94.5	92.2	0.4	93.0	91.5	0.5
S(1)−M−S(2)[a]	94.8	−0.2	−	91.5	−0.3	92.1	90.7	−0.3
C(3)−S(3)−I(1)	95.9	−	97.4	96.4	−	98.3	96.2	−
S(3)−I(1)−I(1)′	179.6	−	177.5	180.0	−	179.6	179.9	−

[a] mPW1PW functional: Schafer et al. pVDZ BSs for C, H, N and S;[44] LanL2DZ with ECPs for Ni, Pd, and Pt.[39] [b] Average value from the X-ray crystal structure of **7**·2I_2·1/2I_2.[17] [c] Average value from the X-ray crystal structure of **8**·I_2·$CHCl_3$.[18] [d] No CT adduct containing any [Pt(R,R′timdt)$_2$] dithiolene complex has been structurally characterised to date. [e] Bond/angle in the non-interacting ligand.

 © 2004 Wiley-VCH Verlag GmbH & Co. KGaA, Weinheim

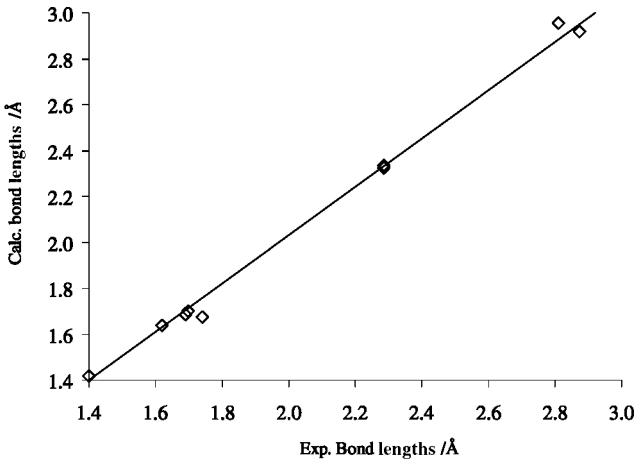

Figure 4. Bond lengths calculated for **11**·I_2 compared with the average structural bond lengths of **8**·I_2·$CHCl_3$ [18]

An interaction diagram (Figure 5 for **10**·I_2) between the molecular orbitals of the dithiolenes **10**−**12** (D_{2h} point group) and those of molecular diiodine ($D_{\infty h}$ point group) shows that the Kohn−Sham HOMO and LUMO in the adducts, depicted in Figure 6 for **10**·I_2, derive from the σ-interaction of the b_{1u} HOMO and b_{2g} LUMO of the dithiolene with the $p\sigma_u$* LUMO of the I_2 molecule, whose energy is just intermediate between those of the two molecular orbitals of the complex. As expected from a qualitative fragment molecular orbital (FMO) interpretation of the donor−acceptor interaction,[53] the electron donation from the filled HOMO of the dithiolene to the antibonding LUMO of diiodine weakens the I−I bond. Due to the compositions of the HOMOs calculated for **10**−**12**, which are very similar in energy and do not contain significant contributions from the central metals, the donor−acceptor interaction between [M(H_2timdt)$_2$] and iodine is not expected to be strongly dependent on M. In fact, the calculated lengthening in the I−I bond length of coordinated diiodine depends only slightly on the nature of the donor dithiolene complex (I−I: 2.830 Å for free I_2; 2.970, 2.957 and 2.955 Å in **10**·I_2, **11**·I_2, and **12**·I_2, respectively). The I−I elongation with respect to free I_2 is small (4.7%, 4.3%, and 4.2% for **10**·I_2, **11**·I_2, and **12**·I_2, respectively) in agreement with the structural results (3.6% and 3.5% for **7**·2I_2·1/2I_2, and **8**·I_2, respectively). As regards the metal dithiolene units, in agreement with the experimental results only very slight modifications are found in the metal−sulfur bond lengths compared to the optimised geometries of the dithiolenes **10**−**12**, which mainly regard the ligand unit interacting with the halogen (M−S = 2.189, 2.313, and 2.328 Å for **10**, **11**, and **12**, respectively, and 2.186, 2.324, and 2.324 Å for **10**·I_2, **11**·I_2, and **12**·I_2, respectively). An examination of all the other bond lengths within the dithiolene ligands shows that an intramolecular charge transfer is induced from the non-interacting H_2timdt moiety to the interacting one, and then to the halogen molecule (intramolecular charge transfer). Thus, the non-interacting unit has a slightly higher trithione character than the interacting one (testified by a slight shortening of all C−S bond lengths, mainly in the terminal one, and a lengthening of the C−C bond length with respect to the other H_2timdt ligand unit interacting with diiodine and to the free dithiolene). On the contrary, in agreement with the structures of **9**·I_2 and **8**·I_2·$CHCl_3$, the C−C bond lengths in the ligand unit interacting with iodine are calculated to be slightly shorter than in the free dithiolene. As expected, the terminal C(3)−S(3) bond interacting with diiodine is the most affected (1.637, 1.637, and 1.645 Å in

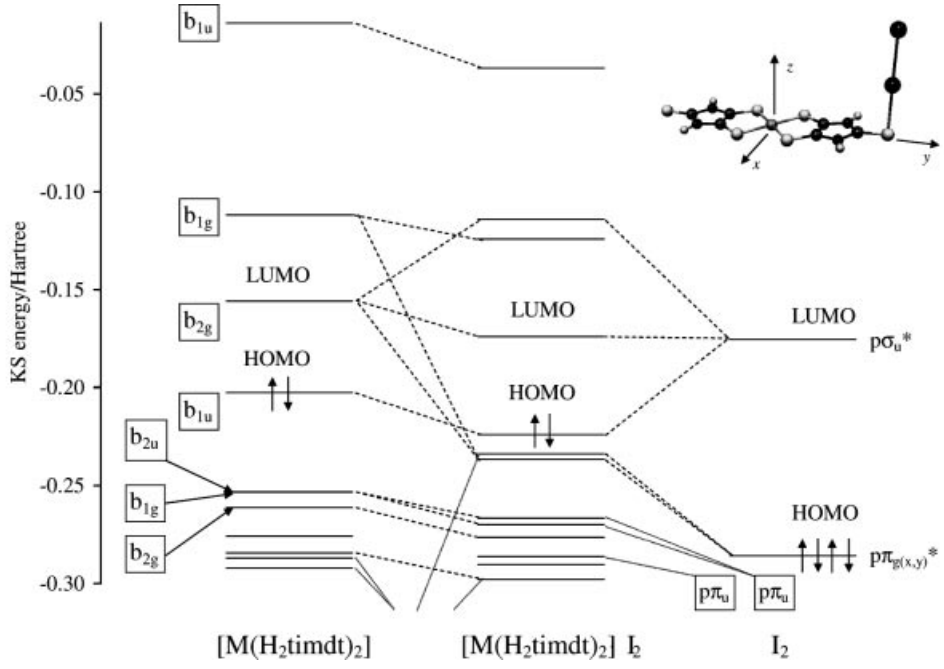

Figure 5. MO diagram showing the interaction between **10** and I_2; symmetry labels are referred to the D_{2h} space group (with the dithiolene on the *xy* plane) for **10** and $D_{\infty h}$ for I_2

 © 2004 Wiley-VCH Verlag GmbH & Co. KGaA, Weinheim

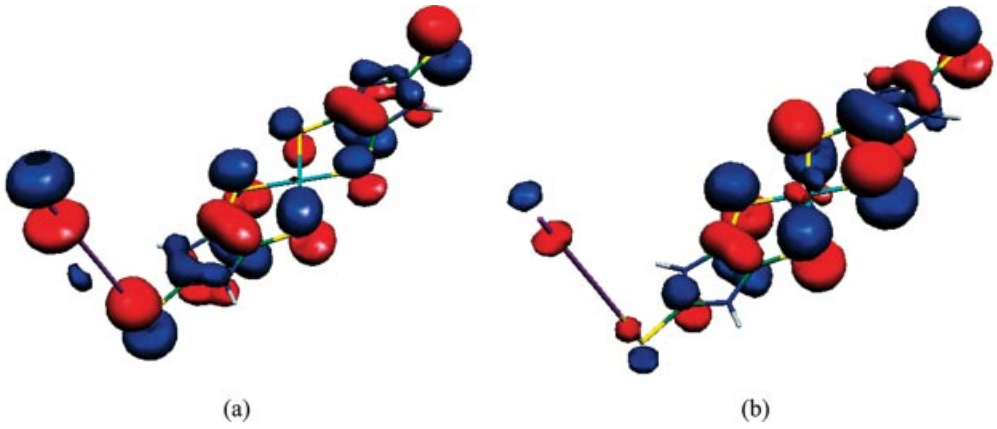

Figure 6. Drawings of Kohn−Sham HOMO (a) and LUMO (b) calculated for **10**·I_2

10, **11**, and **12**; 1.669, 1.675, and 1.676 Å in the interacting unit of **10**·I_2, **11**·I_2, and **12**·I_2, respectively). The strength of the interaction between the dithiolene donors and I_2 is reflected in the Wiberg bond indexes calculated for the involved groups. Thus, bond indexes of 0.287, 0.260, and 0.260 were calculated between the interacting terminal sulfurs and iodine in **10**·I_2, **11**·I_2, and **12**·I_2, respectively. Accordingly, the bond indexes of the interacting terminal thione groups (1.146, 1.391, and 1.388 for **10**·I_2, **11**·I_2, and **12**·I_2, respectively) are smaller than those of the free thione groups (1.639, 1.627, and 1.623 for **10**·I_2, **11**·I_2, and **12**·I_2, respectively), while the I−I bond order assumes fractional values in the three adducts (0.679, 0.702, and 0.704 for **10**·I_2, **11**·I_2, and **12**·I_2, respectively). The overall NBO-charge distribution in the three adducts (Table 2) confirms that the interaction between **10**−**12** and I_2 determines a charge transfer from the dithiolenes to the dihalogen, which depends only very slightly on the central metal ion, and is greater in the case of **10**·I_2 (charge on diiodine −0.295, −0.281, and −0.282 electrons for **10**·I_2, **11**·I_2, and **12**·I_2, respectively). In addition, the most negative charge in the adduct resides on the terminal iodine atom (−0.233, −0.212, and −0.213 for **10**·I_2, **11**·I_2, and **12**·I_2, respectively), which is available for interacting with other iodine molecules. Accordingly, I−I···I−I contacts have been found in the crystal structures of **7**·2I_2·1/2I_2 and **8**·I_2·$CHCl_3$. This type of interaction could also account for the isolation of adducts having dithiolene/I_2 molar ratios higher than 1:2. The partial positive charge remaining on the dithiolene molecule is unevenly distributed over the two ligand units — the most positive being the non-interacting one — in agreement with the differences in the bond lengths described for the two ligands (the charge on the ligand interacting with diiodine is 0.130, 0.120, and 0.123 electrons and that on the non-interacting ligand is 0.166, 0.156, and 0.153 electrons for **10**·I_2, **11**·I_2, and **12**·I_2, respectively). Interestingly, the free terminal sulfur atom of the dithiolene carries a small residual negative charge, which allows for further interaction with a second diiodine molecule to give 1:2 adducts.

The coherent trends in the I−I bond lengths, in the charge transfer from the donor dithiolenes to iodine, and in the S−I and I−I bond indexes, calculated for **10**·I_2, **11**·I_2, and **12**·I_2, clearly indicate that the entity of the donor−acceptor interaction is almost constant on passing from **10**·I_2 to **12**·I_2, and is only slightly higher in the case

Table 2. NBO charge distribution[a] for compounds **4**−**6**, **10**−**12**, and the CT adducts **10**·I_2, **11**·I_2, and **12**·I_2

Atom	**4**	**5**	**6**	**10**	**11**	**12**	**10**·I_2	**11**·I_2	**12**·I_2
M	0.311	0.349	0.311	0.486	0.359	0.303	0.491	0.369	0.312
S(1)	0.037	0.067	0.086	−0.032	−0.003	0.015	0.130	0.120	0.123
S(1)′′[b]	–	–	–	–	–	–	0.010	0.002	0.005
C(1)	−0.391	−0.395	−0.400	−0.004	−0.007	−0.005	−0.008	−0.004	−0.009
C(1)′′[b]	–	–	–	–	–	–	0.006	0.009	0.003
N(1)/S[c]	0.493	0.492	0.490	−0.590	−0.589	−0.587	−0.569	−0.567	−0.567
N(1)′′[b]	–	–	–	–	–	–	−0.588	−0.583	−0.584
C(3)	−0.573	−0.573	−0.572	0.228	0.229	0.235	0.274	0.279	0.279
C(3)′′[b]	–	–	–	–	–	–	0.221	0.226	0.228
S(3)	0.069	0.069	0.063	−0.126	−0.127	−0.139	−0.087	−0.099	−0.105
S(3)′′[b]	–	–	–	–	–	–	−0.072	−0.078	−0.089
I(1)	–	–	–	–	–	–	−0.062	−0.069	−0.069
I[d]	–	–	–	–	–	–	−0.233	−0.212	−0.213

[a] Calculated at DFT/mPW1PW level. pVDZ basis set for C, H, N and S;[44] LanL2DZ with ECP for metal and halogen atoms.[39] Labelling scheme as in Figure 1. [b] For CT adducts, atom in the non-interacting ligand. [c] Endocyclic sulfur of the dmit ligand. [d] Terminal iodine atom.

 © 2004 Wiley-VCH Verlag GmbH & Co. KGaA, Weinheim

of the nickel-dithiolene adduct. This is in agreement with the trend in the wavenumbers of FT-Raman-active stretching I−I frequencies measured for the adducts [M(Et$_2$timdt)$_2$]·2I$_2$. We therefore performed a calculation of the binding energy ΔE between **10** and I$_2$. In order to evaluate this energy, the renowned basis set superposition error (BSSE) has to be taken into account. This occurs when calculating the energy of an assembly of interacting monomers: each unit "borrows" Gaussian basis functions from the other components in order to describe its own electronic structure more accurately.[54] This results in an artificial overestimation of the interaction energies. Due to the computational effort required for these calculations, this correction has only been computed so far for small interacting systems, especially when geometrical deformations are to be taken into account.[54,55]

The BSSE in **10**·I$_2$ has been estimated by adapting the Boys−Bernardi full counterpoise (CP) correction scheme:[56]

$$\Delta E_{BSSE}(\mathbf{10}\cdot I_2) = [E(\mathbf{10}\cdot I_2) - E_{fin}(\mathbf{10})^G - E_{fin}(I_2)^G] + [E_{str}(\mathbf{10}) + E_{str}(I_2) - E(\mathbf{10}) - E(I_2)] = [E(\mathbf{10}\cdot I_2) - E(\mathbf{10}) - E(I_2)] + [E_{str}(\mathbf{10}) + E_{str}(I_2)] - [E_{fin}(\mathbf{10})^G + E_{fin}(I_2)^G] = \Delta E_{unc} + E_{str}(\mathbf{10} + I_2) - E_{fin}(\mathbf{10} + I_2)^G = \Delta E_{unc} + \delta\Delta E_{BSSE}$$

so that the CP-corrected binding energy ΔE_{BSSE} is calculated from the uncorrected value ΔE_{unc} obtained from the total electronic energies calculated for **10**, I$_2$, and **10**·I$_2$ in their optimised geometries, [E(**10**), E(I$_2$) and E(**10**·I$_2$), respectively], adding a BSSE correction term, $\delta\Delta E_{BSSE}$, calculated from the electronic energies computed for **10** and I$_2$ with [E_{fin}(**10** + I$_2$)^G = E_{fin}(**10**)^G + E_{fin}(I$_2$)^G] and without [E_{str}(**10** + I$_2$) = E_{str}(**10**) + E_{str}(I$_2$)], which are the "ghost" electronic functions of iodine and of the dithiolene atoms, respectively, calculated at the "strained" equilibrium geometry assumed in the adduct. Finally, upon adding the Zero Point Energy (ZPE) correction, in order to account for the effects of molecular vibrations at 0 K, a CT-interaction energy $\Delta E_{ZPE,BSSE}$ of −10.94 kcal·mol^{-1} can be evaluated for **10**·I$_2$ (Table 3). It is worth noting that, since large basis sets are used for the organic framework and effective core potentials are used for the central metal and for the halogen atoms, the BSSE correction is small (1.235 kcal·mol^{-1}) compared to the CT-interaction energy. The calculated $\Delta E_{ZPE,BSSE}$ value confirms that the interaction between the dithiolene-complex donor and diiodine is weaker than those of similar systems, such as the CT adduct between imidazoline-2-thione and iodine (ΔE_{unc} = −18.554; $\delta\Delta E_{ZPE}$ = 0.860; $\delta\Delta E_{BSSE}$ = 1.477; $\Delta E_{ZPE,BSSE}$ = −16.216 kcal·mol^{-1}).

Table 3. Electronic energy (E) and electronic energy with ZPE correction (E_{ZPE}) for **10**, I$_2$, and **10**·I$_2$ (Hartree); electronic energy at the adduct geometry with (E_{fin}^G) and without (E_{str}) ghost electronic functions, calculated for **10** and I$_2$ (Hartree); uncorrected interaction energy ΔE_{unc}, ZPE correction $\delta\Delta E_{ZPE}$, BSSE correction $\delta\Delta E_{BSSE}$, and corrected CT-interaction energy $\Delta E_{ZPE,BSSE}$ for **10**·I$_2$ (mHartree and kcal mol^{-1})[a]

	E	E_{ZPE}	E_{str}	E_{fin}^G
10	−3007.6243	−3007.5068	−3007.6231	−3007.6244
I$_2$	−22.7951	−22.7947	−22.7925	−22.7932
10·I$_2$	−3030.4396	−3030.3209	−	−
	ΔE_{unc}	$\delta\Delta E_{ZPE}$	$\delta\Delta E_{BSSE}$	$\Delta E_{ZPE,BSSE}$
E (mHartree)	−20.197	0.800	1.968	−17.429
E (kcal·mol^{-1})	−12.674	0.502	1.235	−10.937

[a] mPW1PW functional: Schafer et al. pVDZ BSs for C, H, N and S;[44] LanL2DZ with ECPs for Ni, Pd, and Pt.[39]

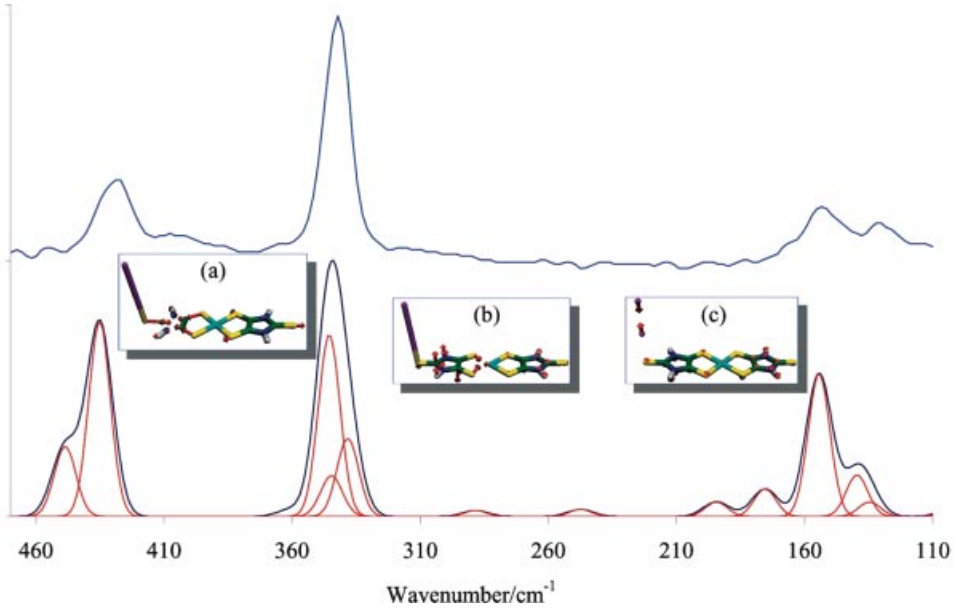

Figure 7. Normalised experimental FT-Raman spectrum recorded for **8**·2I$_2$ and simulated Raman spectrum of **11**·I$_2$ along with the constituent peaks in the range 110−450 cm^{-1}; insets the sketches of the normal harmonic vibrations responsible for the three main groups of bands

 © 2004 Wiley-VCH Verlag GmbH & Co. KGaA, Weinheim

Finally, although the complete assignment of the Raman spectra recorded for the adducts between [M(R,R′timdt)$_2$] and diiodine is beyond the scope of this work, the DFT calculations help us to understand the nature and type of the vibrational FT-Raman peaks. As described above, three groups of Raman peaks are found for all adducts in the far-IR region (500−50 cm^{-1}), although when using an FT-Raman spectrometer exploiting Nd:YAG lasers the lowest-energy peak can only rarely be observed experimentally because of the resonance Raman effect. As regards the two groups of peaks at higher wavenumbers (whose maxima for **10**·I$_2$, **11**·I$_2$, and **12**·I$_2$ are calculated at 450, 508, and 438 cm^{-1} for the first group and 328, 345, and 372 cm^{-1} for the second, respectively), the calculated assignments do not differ from those previously reported for **10**−**12**.[17] Most importantly, the third group of peaks arises from the coupling between the I−I stretching and a waving vibration of the dithiolene complexes, resulting in two overlapping intense peaks, calculated at 146 and 156, 139 and 154, and 151 and 155 cm^{-1} for **10**·I$_2$, **11**·I$_2$, and **12**·I$_2$, respectively. As an example, Figure 7 shows a comparison between the experimental FT-Raman spectrum recorded for **8**·2I$_2$ and the spectrum simulated for **11**·I$_2$. In this case, the two overlapping peaks involving the I−I stretching vibration result in a single peak with a maximum at 155 cm^{-1}, in perfect agreement with the experimental values recorded for the adducts of [Pd(Et$_2$timdt)$_2$].

Conclusions

The interaction between the neutral Ni, Pd, and Pt dithiolene complexes belonging to the general class [M(R,R′timdt)$_2$] and diiodine has been investigated in depth from both an experimental and theoretical point of view. The donor ability of these dithiolenes, previously ascertained for Ni and Pd complexes, has now been confirmed also for Pt complexes. The characterisation of the reaction products has shown that different dithiolene/halogen molar ratios can be reached, depending on the nature of both the central metal ion and of the substituents R and R′. Among the synthesized adducts, [Ni(Me,*i*Pr-timdt)$_2$]·I$_2$ was characterised by X-ray diffraction on a single crystal, showing an unprecedented supramolecular network based on soft S···I interactions and due to the ability of diiodine to bridge different dithiolene stacks. A large set of preliminary calculations proved DFT to be more reliable than HFT in describing the structural and spectroscopic features of the model complexes [M(H$_2$timdt)$_2$] (M = Ni, Pd, Pt) and of dihalogen and interhalogen molecules, such as I$_2$, Br$_2$, and IBr. The mPW1PW functional along with the LanL2DZ basis set adopted for the heaviest atoms have been used to investigate the model CT adducts [M(H$_2$timdt)$_2$]·I$_2$. The computations are in very good agreement with structural and spectroscopic features. DFT calculations have shown that the soft-soft CT interaction involves σ-donation from the HOMO of the dithiolene donor to the LUMO of diiodine. In all cases, the DFT calculations indicate that the title dithiolene complexes are medium-weak donors towards molecular iodine. In accordance with the composition of the Kohn−Sham HOMOs calculated for [M(H$_2$timdt)$_2$], the I−I lengthening with respect to free I$_2$, the change in the Wiberg bond indexes, and the charge transfer calculated on the basis of the NBO-charge distribution, clarify that the donor ability of [M(H$_2$timdt)$_2$] dithiolene complexes depends only marginally on the metal; it is only slightly higher in the case of M = Ni, in agreement with FT-Raman evidence. Thus, a binding energy of −10.83 kcal·mol^{-1} for the adduct [Ni(H$_2$timdt)$_2$]·I$_2$ has been calculated from the electronic energies of the adduct and of the separated synthons, corrected both for ZPE and for BSSE according to the CP scheme.

Experimental Section

Materials and Methods: All solvents, reagents, and pressure tubes were purchased from Aldrich. All operations were carried out under a dry nitrogen atmosphere. The degree of purity of each compound was checked by CHNS and TLC analyses. Elemental analyses were performed on a FISONS EA-1108 CHNS-O instrument. Characterisation of all synthesized compounds was carried out as described previously.[17]

Synthesis of [M(R,R′timdt)$_2$]·*n*I$_2$ Adducts: The dithiolene complexes [M(R,R′timdt)$_2$] (M = Ni, Pd, Pt; R = R′ = Et; R = Me, R′ = *i*Pr) were synthesised as reported previously.[18,19,23] They (15−30 mg) were then reacted with weighed amounts of diiodine in 1:1, 1:2, 1:5, and 1:10 molar ratios, in 30 mL of CHCl$_3$/hexane mixtures (1:3 v/v) according to the procedure described previously for the reaction between **8** and Br$_2$.[22] The stoichiometric ratios of the final products summarised in Scheme 1 were calculated on the basis of the elemental analyses.

[Ni(Et$_2$timdt)$_2$]·I$_2$ (749.20): calcd. C 22.44, H 2.69, N 7.48, S 25.68; found C 21.53, H 2.39, N 6.54, S 24.92.

[Ni(Et$_2$timdt)$_2$]·2I$_2$ (1003.01): calcd. C 16.76, H 2.01, N 5.59, S 19.18; found C 17.12, H 1.95, N 5.06, S 19.09.

[Ni(Et$_2$timdt)$_2$]·3I$_2$ (1256.82): calcd. C 13.38, H 1.60, N 4.46, S 15.31; found C 13.46, H 1.24, N 4.41, S 14.69.

[Pd(Et$_2$timdt)$_2$]·1/2I$_2$ (670.02): calcd. C 25.10, H 3.01, N 8.36, S 28.71; found C 25.75, H 3.04, N 8.52, S 28.55.

[Pd(Et$_2$timdt)$_2$]·2I$_2$ (1050.74): calcd. C 14.76, H 1.77, N 4.92, S 16.88; found C 14.48, H 1.33, N 4.67, S 15.36.

[Pt(Et$_2$timdt)$_2$]·2I$_2$ (1139.40): calcd. C 14.76, H 1.77, N 4.92, S 16.88; found C 14.48, H 1.33, N 4.67, S 15.36.

[Pt(Et$_2$timdt)$_2$]·I$_2$ (885.59): calcd. C 18.99, H 2.28, N 6.33, S 21.72; found C 18.19, H 1.79, N 6.40, S 21.18.

[Pt(Et$_2$timdt)$_2$]·3/2I$_2$ (1012.49): calcd. C 16.61, H 1.99, N 5.53, S 19.00; found C 16.70, H 1.82, N 5.50, S 19.20.

[Ni(Me,*i*Pr-timdt)$_2$]·I$_2$ (749.20): calcd. C 22.44, H 2.69, N 7.48, S 25.68; found C 22.54, H 2.56, N 7.47, S 24.68.

[Ni(Me,*i*Pr-timdt)$_2$]·4I$_2$ (1519.63): calcd. C 11.13, H 1.33, N 3.71, S 12.73; found C 10.76, H 0.95, N 3.30, S 11.60.

[Pd(Me,*i*Pr-timdt)$_2$]·5/2I$_2$ (1177.64): calcd. C 14.28, H 1.71, N 4.76, S 16.33; found C 14.79, H 1.47, N 4.80, S 16.99.

[Pd(Me,*i*Pr-timdt)$_2$]·2I$_2$ (1050.74): calcd. C 16.00, H 1.92, N 5.33, S 18.31; found C 15.47, H 1.60, N 5.03, S 17.35.

[Pt(Me,*i*Pr-timdt)$_2$]·3I$_2$ (1393.21): calcd. C 12.07, H 1.45, N 4.02, S 13.81; found C 12.48, H 1.15, N 3.68, S 13.67.

[Pt(Me,*i*Pr-timdt)$_2$]·4I$_2$ (1647.02): calcd. C 10.21, H 1.22, N 3.40, S 11.68; found C 10.34, H 0.84, N 2.97, S 10.40.

 © 2004 Wiley-VCH Verlag GmbH & Co. KGaA, Weinheim

[Pt(Me,*i*Pr-timdt)$_2$]·5I$_2$ (1900.82): calcd. C 8.85, H 1.06, N 2.95, S 10.12; found C 8.59, H 0.57, N 2.69, S 9.72.

Crystal Data for 9·I$_2$: $C_{14}H_{20}I_2N_4NiS_6$, triclinic, space group $P\bar{1}$ (no. 2), a = 5.519(1), b = 8.667(2), c = 13.685(3) Å, α = 85.30(3)°, β = 80.34(3)°, γ = 72.70(3)°, U = 615.8(7) Å^3, Z = 1, T = 293(2) K, μ = 38.12 cm^{-1}. A needle crystal was mounted on a glass fiber in a random orientation on a Siemens SMART CCD area-detector diffractometer. Graphite monochromated Mo-K_α radiation (λ = 0.71073 Å) was used with the generator working at 45 kV and 40 mA. Cell parameters and orientation matrix were obtained from least-squares refinement on reflections measured in three different sets of 20 frames each in the range $0 < \theta < 28°$. 7082 Intensity data were collected in the full sphere (ω scan method), 2838 of which were unique. 2100 Frames (30 seconds per frame, $\Delta\omega$ = 0.3°) were collected and the first 100 frames recollected to provide crystal decay monitoring, which was not observed. An absorption correction was applied using the SADABS routine.[57] The structure was solved by direct methods (SIR-97)[58] and refined on F^2 using the SHELX-97[59] program implemented in the WINGX suite.[60] Anisotropic displacement parameters were assigned to all non-hydrogen atoms. The hydrogen atoms were included in the structure model riding on their C atoms. The final values for $R1$ and $wR2$ were 0.041 and 0.084, respectively, for 1641 observed reflections [$I > 2\sigma(I)$] and 127 parameters. The maximum and minimum electron-density residual in the final ΔF map were 0.94 and −0.99 e·Å^{-3}, respectively. CCDC-224813 contains the supplementary crystallographic data for this paper. These data can be obtained free of charge at www.ccdc.cam.ac.uk/conts/retrieving.html [or from the Cambridge Crystallographic Data Centre, 12, Union Road, Cambridge CB2 1EZ, UK; Fax: +44 (0)1223 336033; E-mail: deposit@ccdc.cam.ac.uk].

Theoretical Calculations: Our aim was to compare the structures and energetics of model metal-dithiolene complexes **10**−**12**, iodine, and their CT adducts. Therefore, computations were carried out in such a way that the results could be compared reliably. Quantum chemical calculations were carried out on all compounds using the commercially available suite of programs Gaussian 98.[35] Although the use of all-electron basis sets provides better accuracy and efficiency, pseudopotential techniques are useful when relativistic effects have to be taken into account. Thus, the Schafer, Horn, and Ahlrichs all-electron pVDZ basis[44] was used for all calculations for C, N, and S. For Br and I the full-electron 6-311G**[49] and the MIDI![50] BS's, designed as a modification of the MIDI Huzinaga Split Valence basis,[61] and the LanL2DZ,[39] SBKJC,[45] and Stuttgart[46] BSs with effective core potentials (ECPs) were used.[62] For Ni, Pd, and Pt the LanL2DZ,[39] SBKJC,[45] Stuttgart,[46] CRENBS[47] and CRENBL[47,48] BSs were tested.[62] For DFT calculations on **10**−**12** and on the dihalogens Cl_2, Br_2 and I_2, the pure functionals BLYP,[34,36] BPW91,[34,41] and the hybrid ones mPW1PW[42] and B3LYP[36−38] were tested. All geometry optimisations for complexes **10**−**12** were performed starting from the previously reported geometries (D_{2h} point group), computed with the B3LYP functional.[17] Due to a wrong default electronic initial guess, alteration of the initial ground state configurations of dithiolenes **10**−**12** (involving swapping of LUMO, HOMO, and HOMO−1) was needed in some cases. In particular, for HF calculations the "alter" option was used for **11** (SBKJC and Stuttgart BSs for Pd) and **12** (all BSs for Pt). For DFT calculations, the same problems were encountered when the functionals B3LYP (M = Ni, Pd, Pt with all BSs), BLYP (M = Pd with CRENBS, SBKJC and Stuttgart BS; Pt with all BSs), BPW91 (M = Pd with SBKJC BS; Pt with all BSs), and mPW1PW (M = Pd with SBKJC and Stuttgart BSs; M = Pt with all BSs) were used. Interestingly, in the case of **10** and **11**, the removal of the inversion centre in the starting geometries allows the optimisation to converge to slightly lower energies. For the dithiolenes **4**−**6**, for the CT adducts **10·**I$_2$, **11·**I$_2$, and **12·**I$_2$, for imidazoline-2-thione, and for its 1:1 iodine adduct, DFT calculations were performed using the B3LYP and mPW1PW functionals and the LanL2DZ BS's with ECPs for the central metal ion and, if necessary, for halogen atoms. For all molecules, normal mode frequency calculations and NBO[63] charge distributions were calculated at the optimised geometries. The binding energies $\Delta E_{ZPE,BSSE}$, corrected for BSSE and ZPE, were calculated for the CT adducts between either **10** or imidazoline-2-thione and iodine as described above. All calculations were performed on an SGI Origin 3800 equipped with 128 Gb of RAM. The program Molekel 4.3 was used to investigate the shape of the calculated Kohn−Sham orbitals.[64] In order to simulate vibrational IR and Raman spectra starting from Gaussian output files, the program GaussFreq 2003[65] was developed using the RapidQ language. All spectra were simulated as superimposed Gaussian curves with a fixed halfbandwidth of 15 cm^{-1} starting from the calculated unscaled frequencies.

Supporting Information: Details on the criteria followed for choosing the computational level, calculated bond lengths and angles, and KS-orbital energies for dithiolenes **10**−**12**, bond lengths and normal mode frequencies of Br_2, I_2, and IBr have been deposited as Electronic Supporting Information (see also footnote on the first page of this article).

Acknowledgments

CINECA and Dr. Sigismondo Boschi are gratefully acknowledged for the computational resources and continuous help, Prof. Giuseppe Saba for the very useful discussions, and MIUR (Ministero dell'Istruzione, dell'Università e della Ricerca; Fondo Integrativo Speciale per la Ricerca) for funding.

[1] G. N. Schrauzer, V. P. Mayweg, *J. Am. Chem. Soc.* **1965**, *87*, 3585−3592.
[2] U. T. Mueller-Westerhoff, B. Vance, D. Yoon, *Tetrahedron* **1991**, *47*, 909−932.
[3] L. J. Stewart, S. Bailey, B. Bennett, J. M. Charnock, C. D. Garner, A. S. McAlpine, *J. Mol. Biol.* **2000**, *299*, 595−602.
[4] B. S. Lim, J. P. Donahue, R. H. Holm, *Inorg. Chem.* **2000**, *39*, 263−273.
[5] K.-M. Sung, R. H. Holm, *Inorg. Chem.* **2000**, *39*, 1275−1281.
[6] C.-T. Chen, S.-Y. Liao, K.-J. Lin, L.-L. Lai, *Adv. Mater.* **1998**, *3*, 334−338.
[7] Z. Sun, M. Tong, H. Zeng, L. Ding, Z. Wang, Z. Xu, J. Dai, G. Bian, *Chem. Phys. Lett.* **2001**, *343*, 323−327.
[8] P. Cassoux, *Coord. Chem. Rev.* **1999**, *185-186*, 213−232. E. Canadell, *Coord. Chem. Rev.* **1999**, *185-186*, 629−651.
[9] B. S. Lim, D. V. Fomitchev, R. H. Holm, *Inorg. Chem.* **2001**, *40*, 4257−4262.
[10] M. D. Ward, J. A. McCleverty, *J. Chem. Soc., Dalton Trans.* **2002**, 275−288.
[11] R. Kimse, E. Möller, C. Seitz, J. Reinhold, *Z. Anorg. Allg. Chem.* **1997**, *623*, 159−168.
[12] W. E. Geiger, F. Barrière, R. J. LeSuer, S. Trupia, *Inorg. Chem.* **2001**, *40*, 2472−2473.
[13] K. W. Browall, T. Bursh, L. V. Interrante, *Inorg. Chem.* **1972**, *11*, 1800−1806. K. W. Browall, L. V. Interrante, *J. Coord. Chem.* **1973**, *3*, 27−38.
[14] Z. S. Herman, R. F. Kirchner, G. H. Loew, U. T. Mueller-Westerhoff, A. Nazzal, M. C. Zerner, *Inorg. Chem.* **1982**, *21*, 46−56.

 © 2004 Wiley-VCH Verlag GmbH & Co. KGaA, Weinheim

[15] C. Lauterbach, J. Fabian, *Eur. J. Inorg. Chem.* **1999**, 1995−2004.
[16] F. Bigoli, P. Deplano, F. A. Devillanova, V. Lippolis, P. J. Lukes, M. L. Mercuri, M. A. Pellinghelli, E. F. Trogu, *J. Chem. Soc., Chem. Commun.* **1995**, 371−372.
[17] F. Bigoli, P. Deplano, F. A. Devillanova, J. R. Ferraro, V. Lippolis, P. J. Lukes, M. L. Mercuri, M. A. Pellinghelli, E. F. Trogu, J. M. Williams, *Inorg. Chem.* **1997**, *36*, 1218−1226.
[18] M. Arca, F. Demartin, F. A. Devillanova, A. Garau, F. Isaia, F. Lelj, V. Lippolis, S. Pedraglio, G. Verani, *J. Chem. Soc., Dalton Trans.* **1998**, 3731−3736.
[19] M. C. Aragoni, M. Arca, F. Demartin, F. A. Devillanova, A. Garau, F. Isaia, F. Lelj, V. Lippolis, G. Verani, *J. Am. Chem. Soc.* **1999**, *121*, 7098−7107.
[20] M. C. Aragoni, M. Arca, T. Cassano, C. Denotti, F. A. Devillanova, F. Isaia, V. Lippolis, D. Natali, L. Nitti, M. Sampietro, R. Tommasi, G. Verani, *Inorg. Chem. Commun.* **2002**, *5*, 869−872.
[21] T. Cassano, R. Tommasi, L. Nitti, M. C. Aragoni, M. Arca, C. Denotti, F. A. Devillanova, F. Isaia, V. Lippolis, F. Lelj, P. Romaniello, *J. Chem. Phys.* **2003**, *118*, 5995−6002. P. Romaniello, M. C. Aragoni, M. Arca, T. Cassano, C. Denotti, F. A. Devillanova, F. Isaia, F. Lelj, V. Lippolis, R. Tommasi, *J. Phys. Chem.* **2003**, *107*, 9679−9687.
[22] M. C. Aragoni, M. Arca, C. Denotti, F. A. Devillanova, E. Grigiotti, F. Isaia, F. Laschi, V. Lippolis, L. Pala, A. M. Z. Slawin, P. Zanello, J. D. Woollins, *Eur. J. Inorg. Chem.* **2003**, 1291−1295. M. C. Aragoni, M. Arca, F. A. Devillanova, F. Isaia, V. Lippolis, A. Mancini, L. Pala, A. M. Z. Slawin, J. D. Woollins, *Chem. Commun.* **2003**, 2226−2227.
[23] M. C. Aragoni, M. Arca, T. Cassano, C. Denotti, F. A. Devillanova, R. Frau, F. Isaia, F. Lelj, V. Lippolis, L. Nitti, P. Romaniello, R. Tommasi, G. Verani, *Eur. J. Inorg. Chem.* **2003**, 1939−1947.
[24] F. Lelj, P. Romaniello, M. Arca, F. A. Devillanova, *J. Phys. Chem.* **2003**, submitted.
[25] M. C. Aragoni, M. Arca, A. J. Blake, F. A. Devillanova, W.-W. du Mont, A. Garau, F. Isaia, V. Lippolis, G. Verani, C. Wilson, *Angew. Chem. Int. Ed.* **2001**, *40*, 4229−4232. M. C Aragoni, M. Arca, F. Demartin, F. A. Devillanova., A. Garau, F. Isaia, F. Lelj, V. Lippolis, G. Verani, *Chem. Eur. J.* **2001**, *7*, 3122−3133.
[26] M. C. Aragoni, M. Arca, F. A. Devillanova, A. Garau, F. Isaia, V. Lippolis, G. Verani, *Coord. Chem. Rev.* **1999**, *184*, 271−290.
[27] A. J. Blake, F. A. Devillanova, R. O. Gould, W.-S. Li, V. Lippolis, S. Parsons, C. Radek, M. Schröder, *Chem. Soc. Rev.* **1998**, *27*, 195−216.
[28] P. H. Svensson, L. Kloo, *Chem. Rev.* **2003**, *103*, 1649−1684.
[29] M. C. Aragoni, M. Arca, F. Demartin, F. A. Devillanova, A. Garau, F. Isaia, V. Lippolis, G. Verani, *Trends in, Inorg. Chem.* **1999**, *6*, 1−18.
[30] G. van Bolhius, P. B. Koster, T. Michelsen, *Acta Crystallogr.* **1967**, *23*, 90−91.
[31] P. Deplano, J. R. Ferraro, M. L. Mercuri, E. F. Trogu, *Coord. Chem. Rev.* **1999**, *188*, 71−95.
[32] The position of the peak due to the I−I stretching mode in the FT-Raman spectra of the CT adducts of $[Ni(Et_2timdt)_2]$ is in agreement with the value (142 cm^{-1}) for $\mathbf{7}\cdot 2I_2\cdot 1/2I_2$, reported in ref. 31.
[33] E. S. Kryachko, E. V. Ludeña, *Energy Density Function Theory of Many Electron Systems*, Kluwer Academic Publisher, **1990**, NL.
[34] B. Miehlich, A. Savin, H. Stoll, H. Preuss, *Chem. Phys. Lett.* **1989**, *157*, 200−206.
[35] *Gaussian 98* (Revision A.7), M. J. Frisch, G. W. Trucks, H. B. Schlegel, G. E. Scuseria, M. A. Robb, J. R. Cheeseman, V. G. Zakrzewski, J. A. Montgomery, R. E. Stratmann, J. C. Burant, S. Dapprich, J. M. Millam, A. D. Daniels, K. N. Kudin, M. C. Strain, O. Farkas, J. Tomasi, V. Barone, M. Cossi, R. Cammi, B. Mennucci, C. Pomelli, C. Adamo, S. Clifford, J. Ochterski, G. A. Petersson, P. Y. Ayala, Q. Cui, K. Morokuma, D. K. Malick, A. D. Rabuck, K. Raghavachari, J. B. Foresman, J. Cioslowski, J. V. Ortiz, B. B. Stefanov, G. Liu, A. Liashenko, P. Piskorz, I. Komaromi, R. Gomperts, R. L. Martin, D. J. Fox, T. Keith, M. A. Al-Laham, C. Y. Peng, A. Nanayakkara, C. Gonzalez, M. Challacombe, P. M. W. Gill, B. G. Johnson, W. Chen, M. W. Wong, J. L. Andres, M. Head-Gordon, E. S. Replogle, J. A. Pople, Gaussian, Inc., Pittsburgh, PA, **1998**.
[36] A. D. Becke, *J. Chem. Phys.* **1993**, *98*, 5648−5652.
[37] A. D. Becke, *Phys. Rev. A* **1988**, *38*, 3098−3100.
[38] C. Lee, W. Yang, R. G. Parr, *Phys. Rev. B* **1988**, *37*, 785−789.
[39] P. J. Hay, W. R. Wadt, *J. Chem. Phys.* **1985**, *82*, 270−283; *J. Chem. Phys.* **1985**, *82*, 284−298; *J. Chem. Phys.* **1985**, *82*, 299−310.
[40] D. P. Chong, O. V. Gritsenko, E. J. Baerends, *J. Chem. Phys.* **2002**, *116*, 1760−1772.
[41] K. Burke, J. P. Perdew, Y. Wang, in *Electronic Density Functional Theory: Recent Progress and New Directions* (Eds.: J. F. Dobson, G. Vignale, M. P. Das), Plenum Press, New York, **1998**.
[42] C. Adamo, V. Barone, *J. Chem. Phys.* **1998**, *108*, 664−675.
[43] J. P. Perdew, K. Burke, M. Ernzerhof, *J. Phys. Rev. Lett.* **1997**, *77*, 3865−3868.
[44] A. Schafer, H. Horn, R. Ahlrichs, *J. Chem. Phys.* **1992**, *97*, 2571−2577.
[45] W. J. Stevens, H. Basch, M. Krauss, *J. Chem. Phys.* **1984**, *81*, 6026−6033. W. J. Stevens, M. Krauss, H. Basch, P. G. Jasien, *Can. J. Chem.* **1992**, *70*, 612−630. T. R. Cundari, W. J. Stevens, *J. Chem. Phys.* **1993**, *98*, 5555−5565.
[46] P. Fuentealba, H. Preuss, H. Stoll, L. V. Szentpaly, *Chem. Phys. Lett.* **1982**, *89*, 418−422. A. Bergner, M. Dolg, W. Kuechle, H. Stoll, H. Preuss, *Mol. Phys.* **1993**, *80*, 1431−1441. P. Fuentealba, L. V. Szentpaly, H. Preuss, H. Stoll, *J. Phys. B* **1985**, *18*, 1287−1296. G. Igel-Mann, H. Stoll, H. Preuss, *Mol. Phys.* **1988**, *65*, 1321−1328. M. Dolg, U. Wedig, H. Stoll, H. Preuss, *J. Chem. Phys.* **1987**, *86*, 866−872. M. Dolg, H. Stoll, H. Preuss, R. M. Pitzer, *J. Phys. Chem.* **1993**, *97*, 5852−5859.
[47] L. A. LaJohn, P. A. Christiansen, R. B. Ross, T. Atashroo, W. C. Ermlen, *J. Chem. Phys.* **1987**, *87*, 2812−2824. R. B. Ross, J. M. Powers, T. Atashroo, W. C. Ermler, L. A. LaJohn, P. A. Christiansen, *J. Chem. Phys.* **1990**, *93*, 6654−6670.
[48] M. M. Hurley, L. F. Pacios, P. A. Christiansen, R. B. Ross, W. C. Ermler, *J. Chem. Phys.* **1986**, *84*, 6840−6853. W. C. Ermler, R. B. Ross, P. A. Christiansen, *Int. J. Quant. Chem.* **1991**, *40*, 829−846.
[49] L. A. Curtiss, M. P. McGrath, J-P. Blaudeau, N. E. Davis, R. C. Binning Jr., L. Radom, *J. Chem. Phys.* **1995**, *103*, 6104−6113. M. N. Glukhovtsev, A. Pross, M. P. McGrath, L. Radom, *J. Chem. Phys.* **1995**, *103*, 1878−1885.
[50] R. E. Easton, D. J. Giesen, A. Welch, C. J. Cramer, D. G. Truhlar, *Theor. Chim. Acta* **1996**, *93*, 281−301. J. Li, C. J. Cramer, D. G. Truhlar, *Theor. Chem. Acc.* **1998**, *99*, 192−196.
[51] It is worthy of note that the very narrow HOMO−LUMO gap classifies these dithiolene complexes as soft donors (Hardness = 0.674, 0.604, and 0.636 eV, for **10, 11**, and **12**, respectively). In addition, the NBO charge distribution on **10−12** at the optimised geometries shows a negative charge on the terminal sulfur atoms. On the contrary, the charges on the terminal sulfur atoms of neutral dithiolenes **4−6**, calculated at the same level of theory, assume very small positive values. This difference in the charge distributions calculated in the two classes of complexes is in agreement with the donor ability towards halogens found for $[M(R,R'timdt)_2]$ and never reported for dmit metal complexes.
[52] As expected on the basis of the HSAB theory, the hardness estimated from the HOMO and LUMO eigenvalues increases on passing from I_2 to Br_2 (hardness = 1.504, 1.625, and 1.760 eV for I_2, IBr, and Br_2, respectively, at mPW1PW/LanL2DZ level).

 © 2004 Wiley-VCH Verlag GmbH & Co. KGaA, Weinheim

[53] I. Fleming, *Frontier Orbitals and Organic Chemical Reactions*, J. Wiley & Sons, New York, **1976**.
[54] F. F. Muguet, G. W. Robinson, *J. Chem. Phys.* **1995**, *102*, 3648−3654.
[55] A. Karpfner, *J. Phys. Chem. A* **2000**, *104*, 6871−6879.
[56] S. F. Boys, F. Bernardi, *Mol. Phys.* **1970**, *19*, 553−566.
[57] G. M. Sheldrick, SADABS, University of Göttingen, Germany, **1996**, to be published.
[58] A. Altomare, M. C. Burla, M. Camalli, G. L. Cascarano, C. Giacovazzo, A. Guagliardi, A. G. G. Moliterni, G. Polidori, R. Spagna, *J. Appl. Crystallogr.* **1999**, *32*, 115.
[59] G. M. Sheldrick, SHELX-97, *Program for Crystal Structure Refinement*, University of Göttingen, Germany, **1997**.
[60] L. J. Farrugia, *J. Appl. Crystallogr.* **1999**, *32*, 837.
[61] S. Huzinaga, J. Andzelm, M. Klobukowski, E. Radzio-Andzelm, Y. Sakai, H. Takewaki, *Gaussian Basis Sets for Molecular Calculations*, Elsevier, Amsterdam, **1984**.
[62] All BSs were obtained from the Extensible Computational Chemistry Environment Basis Set Database, Version 4/17/03, as developed and distributed by the Molecular Science Computing Facility, Environmental and Molecular Sciences Laboratory which is part of the Pacific Northwest Laboratory, P. O. Box 999, Richland, Washington 99352, USA, and funded by the U. S. Department of Energy. The Pacific Northwest Laboratory is a multi-program laboratory operated by Battelle Memorial Institute for the U. S. Department of Energy under contract DE-AC06-76RLO 1830. Contact David Feller or Karen Schuchardt for further information.
[63] NBO Version 3.1, E. D. Glendening, A. E. Reed, J. E. Carpenter, F. Weinhold.
[64] S. Portmann, H. P. Lüthi, *Chimia* **2000**, *54*, 766−769.
[65] Massimiliano Arca, GaussFreq 2003 for Windows, http://dipcia.unica.it/GaussFreq, **2003**.

Received December 19, 2003
Early View Article
Published Online May 25, 2004

 © 2004 Wiley-VCH Verlag GmbH & Co. KGaA, Weinheim

Supramolecular Hydrogen-Bond Structures and Magnetic Interactions in Basal-Apical, Dinuclear, Azide-Bridged Copper(II) Complexes

Mau Sinha Ray,[a] Ashutosh Ghosh,*[a] Siddhartha Chaudhuri,[b] Michael G. B. Drew,[c] and Joan Ribas*[d]

Keywords: Azides / Copper / Hydrogen bonds / Magnetic properties / N,O ligands / Schiff bases

The synthesis, characterisation, X-ray single crystal structures and magnetic properties of three new basal-apical μ_2-1,1-azide-bridged complexes $[CuL^1N_3]_2$ (**1**), $[CuL^2N_3]_2$ (**2**) and $[CuL^3N_3]_2$ (**3**) with very similar tridentate Schiff-base blocking ligands {HL^1 = *N*-[2-(ethylamino)ethyl]salicylaldimine; HL^2 = 7-(ethylamino)-4-methyl-5-azahept-3-en-2-one; HL^3 = 7-amino-4-methyl-5-azaoct-3-en-2-one} have been reported [complex **1**: monoclinic, $P2_1/c$, a = 8.390(2), b = 7.512(2), c = 19.822(6) Å, β = 91.45(5)°; complex **2**: monoclinic, $P2_1/c$, a = 8.070(9), b = 9.787(12), c = 15.743(17) Å, β = 98.467(10)°; complex **3**: monoclinic, $P2_1/n$, a = 5.884(7), b = 16.147(18), c = 11.901(12) Å, β = 90.050(10)°]. The structures consist of neutral dinuclear entities resulting from the pairing of two mononuclear units through end-on azide bridges connecting an equatorial position of one copper centre to an axial position of the other. The copper ions adopt a (4+1) square-based geometry in all the complexes. In complex **2**, there is no inter-dimer hydrogen-bonding. However, complexes **1** and **3** form two different supramolecular structures in which the dinuclear entities are linked by H-bonds giving one-dimensional systems. Variable temperature (300–2 K) magnetic-susceptibility measurements and magnetisation measurements at 2 K reveal that all three complexes have antiferromagnetic coupling. Magneto-structural correlations have been made taking into consideration both the azido bridging ligands and the existence of intermolecular hydrogen bonds.

(© Wiley-VCH Verlag GmbH & Co. KGaA, 69451 Weinheim, Germany, 2004)

Introduction

The development of supramolecular structures created by hydrogen bonds is a new challenge for the synthesis of non-serendipitous species in order to study their magnetic behaviour;[1,2] control of these hydrogen bonds seems to be very important for synthesising new supramolecular systems. The role played by hydrogen bonds in the transmission of magnetic interactions is still not fully understood. For many years, hydrogen bonds were thought to propagate essentially antiferromagnetic interactions between metal centres,[3] but the number of ferromagnetically coupled hydrogen-bonded systems is growing.[1a,4] A variety of ligands have been employed for preparation of these systems. The azido group is one of the most widely used versatile bridges, which is able to create strong hydrogen bonds between itself and OH or NH_2 of the blocking ligands. As a result, azide-bridged complexes, especially those with copper(II), are one of the most fascinating subjects for studying the magnetic interactions.[5–16] However, there are some misapplications of the magneto-structural correlation for the basal-apical, end-on azide-bridged copper(II) complexes. For example, it is well established that when the azido ligand bridges two Cu^{II} ions in an end-on manner, the nature of the exchange coupling changes from ferromagnetic to antiferromagnetic when the Cu–N–Cu angle is around 108°.[17] This correlation, in principle, is valid only for basal-basal coordination, although it has also sometimes been applied to the basal-apical coordination mode. To understand the controlling factors in such systems it is essential to study dinuclear copper(II) compounds. However, among numerous examples of azide-bridged copper(II) complexes, end-on bridged, basal-apical dimers are rare.[6,10,13] Recently, we found that a group of tridentate Schiff-base blocking ligands, formed by the half condensation of diamines with salicylaldehyde or 2,4-pentandione, provide the desired dimeric species.[18] We have also shown that for basal-apical coordination, the Cu–N–Cu angle is not indicative of the magnetic interaction, nor does it have any controlling structural parameters; instead the supramolecular

[a] Department of Chemistry, University College of Science, University of Calcutta
92 A.P.C. Road, Kolkata 700 009, India
E-mail: ghosh_59@yahoo.com
[b] R.S.I.C, Bose Institute,
Kolkata 700 009, India
[c] School of Chemistry, The University of Reading,
P. O. Box 224, Whiteknights, Reading, RG6 6AD, UK
[d] Departament de Química Inorgànica, Universitat de Barcelona, 08028 Barcelona, Spain
E-mail: joan.ribas@qi.ub.es
Supporting information for this article is available on the WWW under http://www.eurjIc.org or from the author.

 © 2004 Wiley-VCH Verlag GmbH & Co. KGaA, Weinheim **DOI: 10.1002/ejic.200300969**

H-bonding networks between the dinuclear entities play a very important role in magneto-structural correlations.

In order to obtain more insight into the possible control of the H-bonding network and its effect on the magnetism of such systems we have synthesised three new complexes. In this paper we report the synthesis, X-ray crystal-structure analysis, and variable-temperature magnetic behaviour of these basal-apical, dinuclear μ_2-1,1-N_3 copper(II) complexes with three different tridentate Schiff-base blocking ligands (Scheme 1). We found that very subtle differences in the H-bonding network and structural parameters could be responsible for the drastic changes in magnetic behaviour.

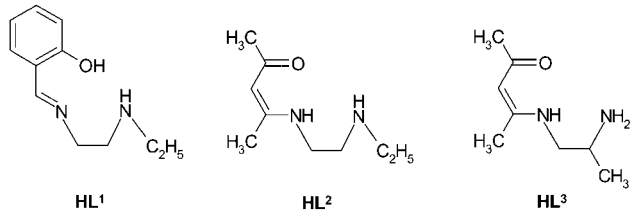

HL¹ **HL²** **HL³**

Scheme 1

Results and Discussion

Infrared Spectra

The coordination mode of azide to transition metal is usually detected by the intense IR band due to $\nu_{as}(N_3)$ which occurs above 2000 cm^{-1}. In general, it appears above 2055 cm^{-1} for μ_2-1,1-azide bridges. However, this generalisation is valid only for symmetric end-on azide bridges where the difference between the two N−N distances ($\Delta d'$) of the azide group is relatively large. In basal-apical-type bridges $\Delta d'$ is smaller and, consequently, ν_{as} appears at lower frequencies.[13,18] All three complexes (**1**, **2** and **3**) that are reported in this paper show only a single absorption band, consistent with the presence of only one type of azide bridge in the structures, and all of them appear at lower frequencies, viz. 2041, 2053 and 2043 cm^{-1} respectively, in agreement with the basal-apical bridging.

Complexes **1** and **2** display a single sharp band at 3239 and 3241 cm^{-1}, respectively, due to the N−H stretching vibration whereas complex **3** shows two bands at 3292 and 3247 cm^{-1} characteristic of the NH_2 group. The band corresponding to the azomethine (C=N) group is distinct in all the three complexes; it occurs at 1630, 1594 and 1593 cm^{-1} for complexes **1**, **2** and **3**, respectively

Description of Structures of Complexes 1, 2 and 3

The structure determination reveals that all the three azido complexes consist of neutral dinuclear entities. Each of them results from the pairing of two mononuclear units related by a crystallographic centre of symmetry. A view of the dinuclear species is given in Figure 1 for complex **1** (complexes **2** and **3** have very similar molecular structures; see Figures S1 and S2 in the Supporting Information). For all three complexes, two centrosymmetrically related Cu^{II} centres are bridged by azide ions in an asymmetric end-on fashion leading to relatively small Cu···Cu distances (Table 1). Within these dimeric units, each of the two trigonally distorted square pyramidal copper(II) centres is coordinated equatorially by three ligating atoms [O(1), N(1) and N(2)] of the corresponding tridentate Schiff-base ligand and a nitrogen atom, N(11), of one of the bridging azides; this comprises the basal plane. A second nitrogen atom, N(11)′, from the centrosymmetrically related bridging azide coordinates axially at a rather long distance [Cu−N(11)′: 2.550(8), 2.447(6), 2.443(9) Å for **1**, **2** and **3** respectively] furnishing

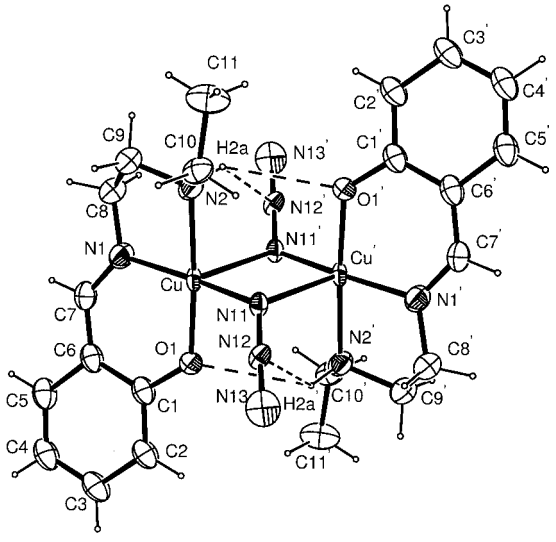

Figure 1. Ortep-3 view of complex **1** (30% thermal ellipsoids) with intramolecular hydrogen bonding (dashed line); atoms marked with a prime are transformed by the symmetry element $-x$, $1-y$, $-z$

Table 1. Main structural and magnetic parameters for complexes **1**, **2** and **3**; parameters for complex **3b** are also included for comparison

Compound	Cu−Cu (Å)	Cu-azido (basal) (Å)	Cu-azido (apical) (Å)	Cu−N−Cu (°)	τ[a]	Angle N_3−basal plane (°)	J_1 cm^{-1}
1	3.106	1.999	2.443	88.3	0.13	47.0	−2.63
2	3.232	1.985	2.447	93.0	0.23	39.0	−1.79
3	3.273	2.016	2.550	90.8	0.21	59.7	−5.37 −3.97
3b[b]	3.318	2.060	2.475	93.6	0.26	57.2	+2.9

[a] τ is the addition parameter.[19] [b] Complex **3** in ref.[18]

 © 2004 Wiley-VCH Verlag GmbH & Co. KGaA, Weinheim

an elongated square-pyramidal (4+1) geometry for each copper(II) centre in all three complexes.

The four basal donor atoms [O(1), N(1), N(2) and N(11)] deviate from the mean coordination plane through them by 0.06(1), −0.10(1), 0.09(1) and −0.05(1) Å, respectively, in complex **1**, 0.08(1), −0.12(1), 0.12(1) and −0.13(1) Å, respectively, in complex **2**, and 0.11(1), −0.14(1), 0.16(1) and −0.12(1) Å, respectively, in complex **3**. The copper atom is slightly pulled out of this plane towards the apical donor atom N(11)′ at a distance 0.125(1), 0.097(1) and 0.108(1) Å in complexes **1**, **2** and **3**, respectively. The distortions of the coordination polyhedron from the square pyramid to the trigonal bipyramid have been calculated by the Addison parameter (τ)[19] as an indication of the degree of trigonality. τ is defined as $(\beta - \alpha)/60$, where β and α are the two trans-basal angles. For a perfectly square pyramidal geometry τ is equal to zero, while it becomes unity for a perfectly trigonal-bipyramidal geometry. The τ values for complexes **1**, **2** and **3** are 0.13, 0.23 and 0.21, respectively.

The five-membered chelate ring Cu−N1−C8−C9−N2 in complex **1** has a half-chair conformation, twisted around C(8)−C(9), with puckering parameters[20] q_2 = 0.383(16) Å and φ_2 = 54.4(2)°. The closest pucker[21] conformation of the five-membered chelate rings Cu−N1−C4−C5−N2 in complexes **2** and **3** is an envelope on C(5); the puckering parameters[20] are q_2 = 0.426(6) Å and φ_2 = 115.3(7)° in the former and q_2 = 0.292(13) Å and φ_2= 71.7(2)° in the latter.

The bridging Cu_2N_2 network is exactly planar as dictated by symmetry. Due to the formation of basal-apical μ_2-1,1-N_3 bridging, the bridging Cu−N bond lengths are significantly different (Δd = 0.46, 0.46 and 0.53 Å for **1**, **2** and **3**, respectively). The bridging N_3^- anions are quasi-linear; the N(11)−N(12)−N(13) angles are 177.5(15)°, 176.8 (7)° and 178.4 (10)° in **1**, **2** and **3**, respectively. The angles subtended at the metal in the coordination sphere are very similar in the three structures. There is, however, a significant difference between the Cu−N(11)−N(12) angles for the axial azide [122.3(9)° in **1**, 115.4(6)° in **2** and 131.9(6)° in **3**].

The three crystal structures exhibit different hydrogen-bonding patterns (Table 2). There is one hydrogen atom, H2a, in each of the complexes **1** and **2** available for hydrogen-bond formation, and two hydrogen atoms, H2a and H2b, in complex **3**. H2a in each of the three complexes is involved in strong intra-dimer N−H···O hydrogen bonding with the ligating oxygen O1 of the corresponding tridentate Schiff-base ligand (Figure 1 and Figures S1 and S2 in the Supporting Information). In addition, in complex **1** a second direct connection is established between the two

Table 2. Hydrogen-bonding distances (Å) and angles (°) for complexes **1**, **2** and **3**

Compound	D−H··· A[a]	D−H	D···A	H···A	∠D−H···A
1	N2−H2a···O1^{i}	0.910	3.233(16)	2.612	126.1
	N2−H2a···N12^{i}	0.910	3.249(16)	2.622	126.7
	N2−H2a···N13^{ii}	0.910	3.533(19)	2.900	127.9
2	N2−H2a···O1^{iii}	0.910	3.221(8)	2.371	155.5
3	N2−H2a···O1^{iv}	0.901	3.260(12)	2.452	149.4
	N2−H2b···N11^{v}	0.899	3.285(13)	2.673	126.2

[a] Symmetry operations for generating equivalent atoms: i) $-x$, $1-y$, $-z$; ii) $1+x$, y, z; iii) $-x$, $-y$, $1-z$; iv) $1-x$, $1-y$, $1-z$; v) $2-x$, $1-y$, $1-z$.

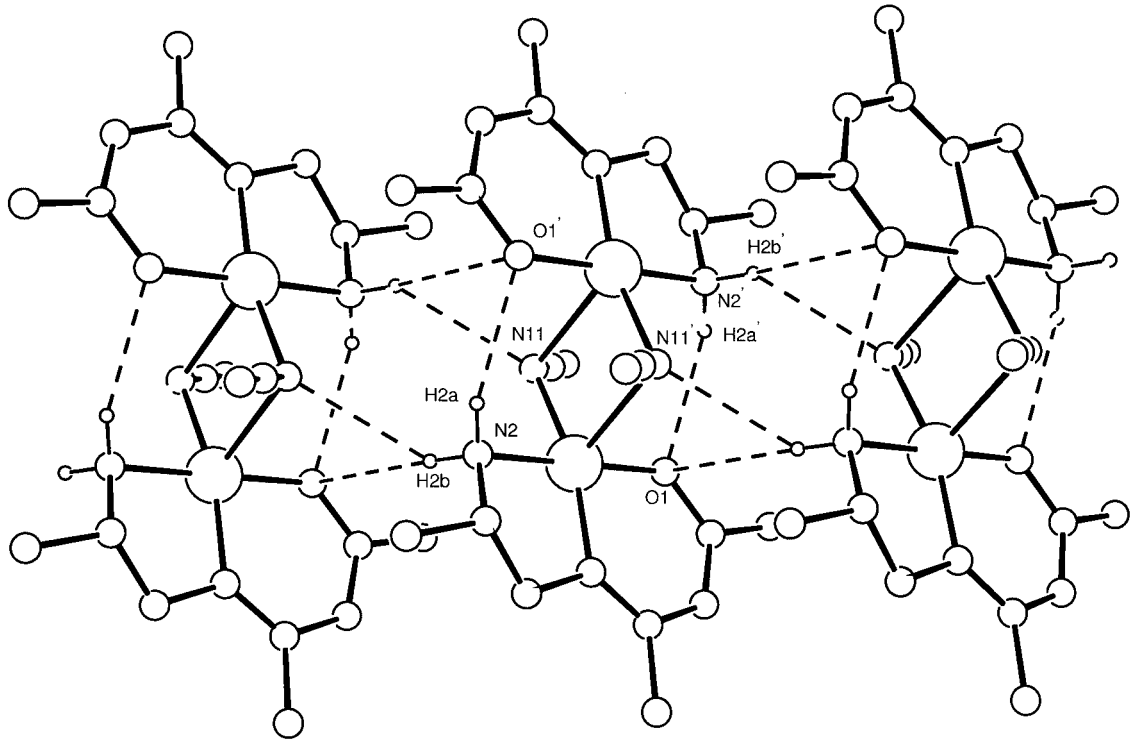

Figure 2. Scheme of the packing (one-dimensional) in complex **3**; the intermolecular hydrogen bonds (magnetic pathways) are shown as dashed lines; atoms marked with a prime are transformed by the symmetry element $1-x$, $1-y$, $1-z$

 © 2004 Wiley-VCH Verlag GmbH & Co. KGaA, Weinheim

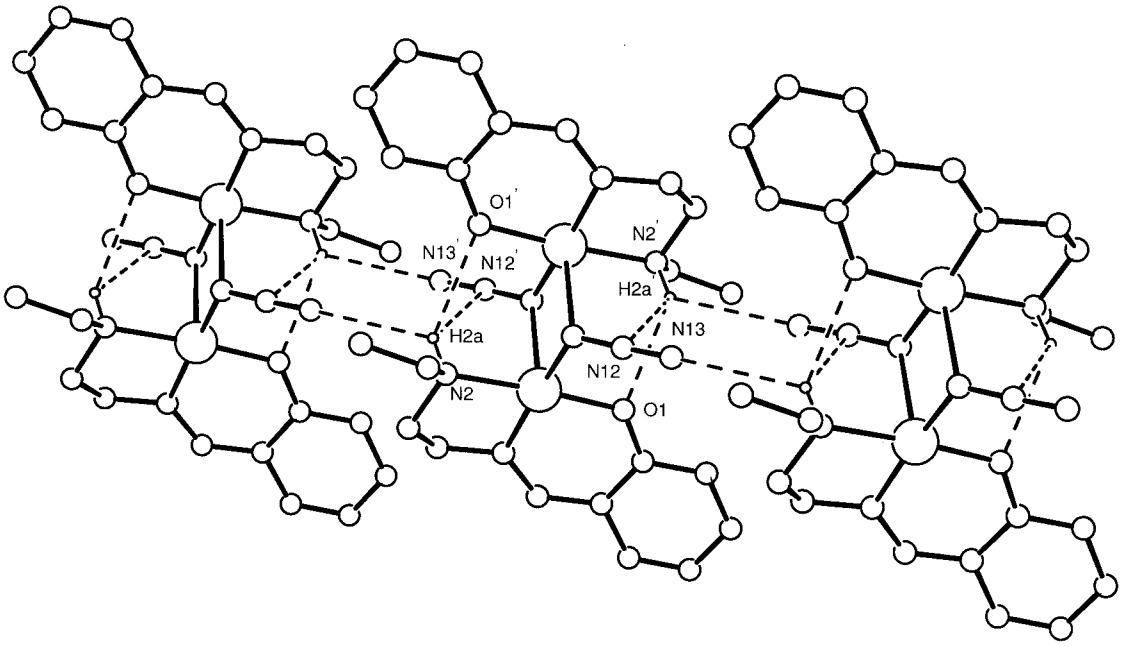

Figure 3. Scheme of the packing (one-dimensional) in complex **1**; the intermolecular hydrogen bonds (magnetic pathways) are shown as dashed lines; atoms marked with a prime are transformed by the symmetry element $-x$, $1 - y$, $-z$

halves of the dinuclear entity through strong intra-dimer N−H···N hydrogen bonding with the middle centrosymmetrically related bridging azido nitrogen N12 (Figure 1).

The inter-dimer interaction is significantly different in complexes **1**, **2** and **3** (Table 2). H2b in complex **3** bridges the symmetry-related dimers through an N2−H2b···N11 [N2···N11:3.285(13) Å] hydrogen bond in a one-dimensional supramolecular entity (Figure 2). H2a in complex **1** is similarly involved in a somewhat weaker N2−H2a···N13 [N2···N13:3.533(19) Å] hydrogen bond-like contact with a neighbouring dimer (Figure 3). Complex **2** does not show any important intermolecular hydrogen bond in the "one-dimensional" net.

Magnetic Properties

Before reporting the experimental data, it is important to underline which are the magnetic pathways in the three complexes, according to the structural data discussed above. Complex **1** can be considered as a dinuclear complex in which the Cu ions are linked by two azido bridging ligands in an end-on equatorial-apical fashion (μ-1,1) through the N11 atom. There are also two short intramolecular hydrogen bonds [O1−H2a(N2): 2.613 Å; N12−H2a(N2): 2.621 Å]. The same H2a(N2) is linked by a weak, hydrogen bond-like contact to N13 (terminal nitrogen of the azido bridging ligand) of another dinuclear complex at 2.934 Å, thus giving a pseudo-one-dimensional supramolecular entity (Figure 3). Complex **2** shows the same intramolecular pathway [Cu−(μ-1,1-N_3)$_2$−Cu]. There is also a short intramolecular hydrogen bond [O1−H2a(N2): 2.37 Å], but in this case there is no appreciable hydrogen bond between adjacent dimers. The shortest H2a(N2) distances are 5.5 Å to N11 and 6.13 Å to O1 of a neighbouring dinuclear entity. Thus, complex **2** can be considered as an isolated dinuclear complex. Complex **3** shows the same intramolecular pathway [Cu−(μ-1,1-N_3)$_2$−Cu] through the N11 atom. There is also a short intramolecular hydrogen bond [O1−H2a(N2): 2.452 Å]. The H2b(N2) atom is linked by a weak hydrogen bond to N11 (first nitrogen of the azido bridging ligand) of another dinuclear complex at 2.673 Å, thus giving a pseudo-one-dimensional supramolecular entity (Figure 2). In this one-dimensional structure H2b(N2) links the O1 of an adjacent unit at 3.063 Å, with H2a···H2a at 3.091 Å and H2a···H2b at 3.323 Å.

Complexes 1 and 2

The magnetic properties of complexes **1** and **2** are very simple and correspond to almost isolated dinuclear entities from the magnetic point of view, at least down to 2 K. A $\chi_m T$ versus T plot (χ_m is the molar magnetic susceptibility for two Cu^{II} ions) for complex **1** is shown in Figure 4 [for the analogous complex **2** the corresponding figure is given in the Supporting Information (Figure S3)]. The value of $\chi_m T$ for **1** at 300 K is 0.83 $cm^3 \cdot mol^{-1} \cdot K$, which is as expected for two magnetically quasi-isolated spin doublets ($g > 2.00$). The $\chi_m T$ values decrease smoothly from 0.83 to 0.35 $cm^3 \cdot mol^{-1} \cdot K$ at 2 K. This global feature is characteristic of very weak antiferromagnetic coupling. Considering the possible interactions through the dinuclear entities as nil, the Bleaney−Bowers formula for a dinuclear $S = 1/2$ system was used.[22] The Hamiltonian employed is $H = -JS_1S_2$. The best-fit parameters were: $J = -2.63 \pm 0.01$ cm^{-1}, $g = 2.11$ and $R = 2.1 \times 10^{-5}$ for **1** and $J = -1.79 \pm 0.01$ cm^{-1}, $g = 2.13$ and $R = 12.1 \times 10^{-5}$ for **2** {R is the agreement factor defined as $\Sigma_i[(\chi_m T)_{obsd.} - (\chi_m T)_{calcd.}]^2 / \Sigma_i[(\chi_m T)_{obsd.}]$, the temperature-independent paramagnetism

 © 2004 Wiley-VCH Verlag GmbH & Co. KGaA, Weinheim

(TIP) was taken as 120×10^{-6} cm^3·mol^{-1}}.[22b] All attempts to improve the fits by introducing a small percentage of mononuclear impurities or a possible intermolecular J' (molecular-field approximation) did not improve the R values, and the intramolecular J values were left unmodified. The reduced molar magnetisation tends to 1.7 $N\beta$ for both **1** and **2** when the fields approach 5 T (see inset in Figure 4 and Figure S3), and they do not follow the de Brillouin formula for two isolated Cu^{II} ions. This feature is also indicative of the small antiferromagnetic coupling in both compounds.

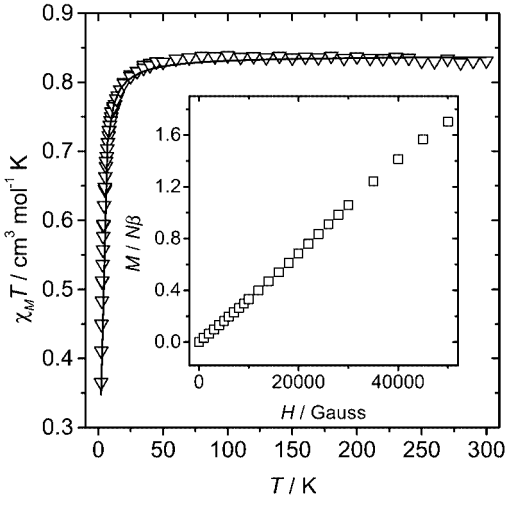

Figure 4. Plot of $\chi_M T$ vs. T for complex **1**; the solid lines represent the best fit and the points the experimental data; inset: plot of $M/N\beta$ vs. H at 2 K for complex **1**

Complex 3

The magnetic properties of complex **3** are different from those of complexes **1** and **2**. The $\chi_m T$ versus T plot (χ_m is the molar magnetic susceptibility for two Cu^{II} ions) is shown in Figure 5. The value of $\chi_m T$ at 300 K is 0.85 cm^3·mol^{-1}·K, which is as expected for two magnetically quasi-isolated spin doublets ($g > 2.00$). The $\chi_m T$ values smoothly decrease from 0.85 to 0.1 cm^3·mol^{-1}·K at 2 K. The global feature is characteristic of weak antiferromagnetic coupling. Considering the possible interactions through the dinuclear entities as nil, all attempts to fit the experimental data with only one $J_{intramolecular}$ value were unsuccessful.[22] The J value was of the order of $4-5$ cm^{-1} but with an unsatisfactory R value. As indicated above, complex **3** is a one-dimensional system formed by dinuclear entities linked by hydrogen bonds. This gives an alternating $S = 1/2$ system (J_1 for azido bridging ligand and J_2 for hydrogen bond). The fit of the magnetic data has been carried out with the Clumag program using a ring of twelve copper(II) ions which is the best way to represent the infinite character of the chain.[23] The best-fit parameters obtained with this computing model are: $J_1 = -5.37 \pm 0.06$ cm^{-1}, $J_2 = -3.97 \pm 0.08$ cm^{-1}, $g = 2.14$ and $R = 0.5 \times 10^{-5}$ (TIP was taken as 60×10^{-6} cm^3 mol^{-1} for the copper ion).[22b] The reduced molar magnetisation (see inset in Figure 5) clearly indicates that the global coupling is more antiferromagnetic than that for complexes **1** and **2**. For **3** the $M/N\beta$ value at 5 T tends to 0.7 $N\beta$, which is very far from the expected value for two isolated copper(II) ions. The shape of the curve formed by the experimental point does not follow the de Brillouin formula, and its convexity is more pronounced than in **1** and **2**. Thus, the global antiferromagnetic coupling is greater than for **1** and **2**.

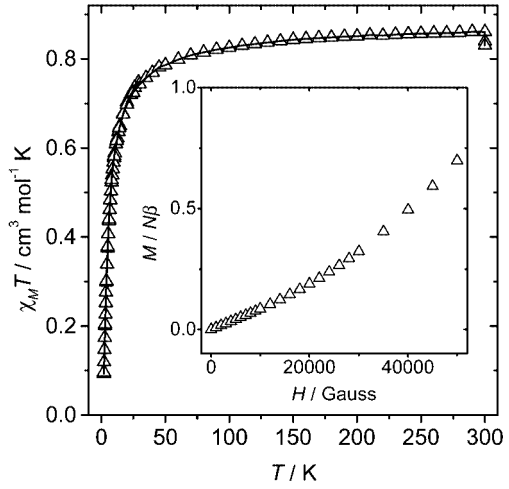

Figure 5. Plot of $\chi_M T$ vs. T for complex **3**; the solid lines represent the best fit and the points the experimental data; inset: plot of the $M/N\beta$ vs. H at 2 K for complex **3**

Magneto-Structural Correlations

Intramolecular Interactions (J_1) through End-On Azido Bridging Ligands

Complexes **1**, **2** and **3** show antiferromagnetic coupling. For complex **3** it is impossible to state if the J value for the azido bridging ligand is -5.38 cm^{-1} or -3.97 cm^{-1} but it seems logical to assume that the intramolecular azido coupling would be greater than the intermolecular hydrogen-bond coupling. In any case both are negative and of the same order of magnitude. When the azido bridge is in a basal-basal position, either the experimental values or the theoretical calculations demonstrate that J can be antiferromagnetic or ferromagnetic depending mainly on the Cu−N_3−Cu angle.[17] This reasoning is not valid when the azido bridges are in basal-apical coordination (such as in **1**, **2** and **3**), although too many papers devoted to this kind of coupling try to relate this angle with the J parameter. The literature data indicate a total dispersion of the J values with regard to the Cu−N−Cu angles.[6−16,18] In equatorial-axial complexes (such as in **1**, **2** and **3**), the distortion parameter τ (square-pyramidal to trigonal bipyramidal)[19] could be important from a magnetic point of view. However, experimentally, the maximum value of τ gives, surprisingly, the minimum value of J. The variations in J are small and, consequently, it would be difficult to establish clear trends connecting theoretical parameters to variations in J.

 © 2004 Wiley-VCH Verlag GmbH & Co. KGaA, Weinheim

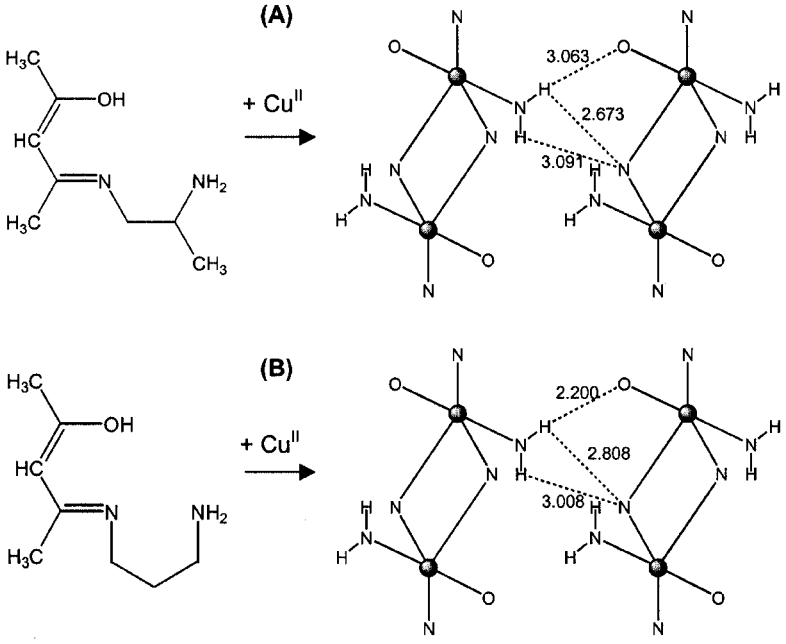

Figure 6. Scheme of the ligands and complex **3** (A) (antiferromagnetically coupled) and complex reported by the authors in ref.[18] (B) (ferromagnetically coupled)

The main structural parameters for the three complexes are gathered in Table 1.

Intermolecular Hydrogen Bonds in Complex 3 − Small Subtleties That Modify the Magnetism

It is well know that the role played by hydrogen bonds in the transmission of magnetic interactions is still not fully understood. For many years, hydrogen bonds were thought to propagate essentially antiferromagnetic interactions between metal centres,[3] but the number of ferromagnetically coupled hydrogen-bonded systems is growing.[1a,4] We decided to compare two very similar complexes, complex **3** and the other one previously reported by us;[18] the ligands and their main structural parameters are schematized in Figure 6. Although the ligands are very similar and the packing of the two complexes is analogous, subtle differences can be found: in **3** the shorter intermolecular hydrogen bond length is N−H···N(azido) (rather long) while in the previous complex,[18] the stronger hydrogen-bond length is N−H···O (very short). The experimental result is that complex **3** clearly shows intermolecular antiferromagnetic coupling while its analogue shows intermolecular ferromagnetic coupling.[18] Although J_{inter} is large, close to -4 cm^{-1} (see above), other much greater J values are reported in literature, such as $J = -90$ cm^{-1} (Cu dimer with O−H···O distance of 2.32 Å).[24] Even for other metals, like chromium(III), considerable large J values are also reported.[3a,25]

Concluding Remarks

Three very similar blocking ligands have been used to synthesise three new, basal-apical, end-on azide-bridged, dinuclear Cu^{II} complexes. The dinuclear entities of all three complexes are very similar but the H-bonding network among the dinuclear entities and consequently their relative orientation in the one dimensional net are very different. From a magnetic point of view, it is important to emphasise that for basal-apical coordination neither the Cu−N−Cu angle nor the τ distortions are clearly indicative of the magnetic interaction.

The difference between the antiferromagnetic character (intra and inter) in **3** with regard to the ferromagnetic character in its homologue[18] is a challenge for experimental and theoretical chemists to synthesise new similar complexes and to try to interpret the subtle differences that cause the drastic change in the magnetic behaviour.

Experimental Section

Caution! *Azido complexes of metal perchlorates in the presence of organic ligands are potentially explosive. Only a small amount of material should be prepared, and it should be handled with care.*

Physical Measurements: Elemental analyses (carbon, hydrogen and nitrogen) were performed using a Perkin−Elmer 240C elemental analyzer and the copper contents in all the complexes were estimated spectrophotometrically.[26] IR spectra of the complexes in KBr (4500−500 cm^{-1}) were recorded using a Perkin−Elmer RXI FT-IR spectrophotometer. Electronic spectra of the complexes in methanol (1200−350 nm) were recorded on a Hitachi U-3501spectrophotometer. The crystallographic data of complex **1** were collected on a Bruker Nonius MACH3 diffractometer and for complexes **2** and **3** were collected on a MAResearch Image Plate system. Magnetic measurements were carried out in the "Servei de Magnetoquímica (Universitat de Barcelona)" on polycrystalline samples (30 mg) with a Quantum Design MPMS XL-5 SQUID susceptometer operating

 © 2004 Wiley-VCH Verlag GmbH & Co. KGaA, Weinheim

at a magnetic field of 0.1 T between 2 and 300 K. The diamagnetic corrections were evaluated from Pascal's constants.

Materials: All the chemicals were of reagent grade and used without further purification. The three monocondensed ligands were synthesised as described below.

Preparation of HL^1 {*N*-[2-Ethylamino)ethyl]salicylaldimine} and HL^2 (7-Ethylamino-4-methyl-5-azahept-3-en-2-one): Both HL^1 and HL^2 were prepared by condensation of the NH_2 group of *N*-ethyl-1,2-ethanediamine (0.45 mL, 5 mmol) with salicylaldehyde (0.53 mL, 5 mmol) and 2,4-pentanedione (0.55 mL, 5 mmol), respectively, in methanol (30 mL) under reflux for 3 h.

Preparation of 7-Amino-4-methyl-5-azaoct-3-en-2-one (HL^3): This ligand was prepared by following a similar method to that adopted for the half condensation of 1,2-ethanediamine or 1,3-propanediamine with 2,4-pentanedione as reported earlier.[27] A solution of 2,4-pentanedione (1.1 mL, 10 mmol) in chloroform (50 mL) was added dropwise to a solution of 1,2-propanediamine (0.80 mL, 10 mmol) in chloroform (50 mL) at ambient temperature. After completion of the addition, the solution was stirred for an additional 3 h and the chloroform was then evaporated under reduced pressure. The resultant viscous oil was collected and dissolved in methanol (30 mL).

Synthesis of $[CuL^1N_3]_2$ (1), $[CuL^2N_3]_2$ (2) and $[CuL^3N_3]_2$ (3): Direct synthesis of the complexes from methanolic solutions of $Cu(ClO_4)_2{\cdot}6H_2O$, NaN_3 and the respective ligands did not allow the formation of sufficiently pure desired products. A mixture of hydrolysed products as well as a small amount of the respective complexes was formed. It was very difficult to separate the mixture. Therefore, to prepare good quality crystalline compounds, we adopted the following procedure.

Addition of copper(II) perchlorate hexahydrate to a methanolic solution of HL^1, HL^2 or HL^3, followed by addition of a stoichiometric amount of triethylamine, gave the dinuclear complex $[(CuL^1)_2](ClO_4)_2$ and the trinuclear complexes $[(CuL^2)_3(OH)](ClO_4)_2{\cdot}H_2O$ and $[(CuL^3)_3(OH)](ClO_4)_2$, respectively, as reported previously for similar compounds.[28]

A methanol/water solution (9:1, v/v) of sodium azide, (0.13 g, 2 mmol) was added to a methanolic solution (30 mL) of $[(CuL^1)_2](ClO_4)_2$ (0.35 g, 0.5 mmol), $[(CuL^2)_3(OH)](ClO_4)_2{\cdot}H_2O$ (0.47 g, 0.5 mmol) or $[(CuL^3)_3(OH)](ClO_4)_2$ (0.44 g, 0.5 mmol) and the mixture was stirred for 30 min. There was no immediate separation of any compounds. The clear solutions were therefore left to stand in a refrigerator overnight. Dark-green plate-shaped single crystals of **1** and blue parallelepiped-shaped single crystals of **2** and **3** suitable for X-ray diffraction were obtained.

Complex 1: Yield: 0.20 g (65%). $C_{22}H_{30}Cu_2N_{10}O_2$ (593.66): calcd. C 44.5, H 5.1, N 23.6, Cu 21.4; found C 44.5, H 5.2, N 23.7, Cu 21.1. UV/Vis (methanol): λ_{max} (ε_{max}) = 613 nm (287 $dm^3{\cdot}mol^{-1}{\cdot}cm^{-1}$). IR: 3239 cm^{-1} ν(N−H); 1630 ν(C=N).

Complex 2: Yield: 0.35 g (80%). $C_{18}H_{34}Cu_2N_{10}O_2$ (549.65): calcd. C 39.3, H 6.2, N 25.5, Cu 23.1; found C 39.2, H 6.0, N 25.6, Cu 22.8. UV/Vis (methanol): λ_{max} (ε_{max}) = 595 nm (334 $dm^3{\cdot}mol^{-1}{\cdot}cm^{-1}$). IR: 3241 cm^{-1} ν(N−H); 1594 ν(C=N).

Complex 3: Yield: 0.27 g (70%). $C_{16}H_{30}Cu_2N_{10}O_2$ (521.60): calcd. C 36.8, H 5.8, N 26.8, Cu 24.3; found C 36.7, H 5.9, N 26.7, Cu 24.0. UV/Vis (methanol): λ_{max} (ε_{max}) = 591 nm (226 $dm^3{\cdot}mol^{-1}{\cdot}cm^{-1}$). IR: 3245 and 3292 cm^{-1} ν(N−H); 1592 ν(C=N).

Crystallographic Studies: The crystallographic data of complex **1** were collected on a Bruker-Nonius MACH3 diffractometer using the ω-2θ scan mode in the θ range 2−25°; a maximum of 60 s were allowed per reflection. The data for complexes **2** and **3** were collected on a MAResearch Image Plate System with the crystals positioned at 70 mm from the plate; 100 frames were measured at 2° intervals with a counting time of 2 min per frame. Mo-K_α radiation was used in all three cases.

The raw intensity data for complex **1** were processed for Lorentz and polarisation effects using the XCAD4 program in the WinGX suite and empirical absorption correction was carried out using ψ-scan data.[29] The data for complexes **2** and **3** were processed using the XDS[30] program and empirical absorption corrections were applied using DIFABS.[31] The number of independent reflections for complexes **1**, **2** and **3** were 2119, 2174 and 1940, respectively.

The structures were solved by direct methods with the SHELXS-97 program.[32] Non-hydrogen atoms were refined with anisotropic thermal parameters. The hydrogen atoms bonded to carbon and nitrogen atoms were included in geometric positions and given thermal parameters equivalent to 1.2-times those of the atom to which they are attached. The crystals of **3** were twinned (*hkl*, *hk*−*l*)

Table 3. Selected crystal parameters, data collection and structure refinement of complexes **1**, **2** and **3**

	1	**2**	**3**
Formula	$C_{22}H_{30}N_{10}O_2Cu_2$	$C_{18}H_{34}N_{10}O_2Cu_2$	$C_{16}H_{30}N_{10}O_2Cu_2$
F_w	593.66	549.65	521.60
T (K)	293	293	293
Space group	$P2_1/c$	$P2_1/c$	$P2_1/n$
Wavelength (Å)	0.70930	0.71073	0.71073
a (Å)	8.390(2)	8.070(9)	5.884(7)
b (Å)	7.512(2)	9.787 (12)	16.147(18)
c (Å)	19.822(6)	15.743(17)	11.901(12)
Crystal system	monoclinic	monoclinic	monoclinic
α (°)	90	90	90
β (°)	91.45(5)	98.467(10)	90.050(10)
γ (°)	90	90	90
V (Å^3)	1248.9(6)	1230(2)	1131(2)
Z	2	2	2
$D_{calcd.}$ (g/cm^3)	1.579	1.484	1.532
μ (mm^{-1})	1.7	1.8	1.9
F(000)	612	572	540
R int[$I > 2\sigma(I)$]	$R1$ = 0.1193	$R1$ = 0.0767	$R1$ = 0.0852
	$wR2$ = 0.2855	$wR2$ = 0.1469	$wR2$ = 0.2145

 © 2004 Wiley-VCH Verlag GmbH & Co. KGaA, Weinheim

Table 4. Selected bond lengths (Å) and angles (°) for complexes **1**, **2** and **3**

	1	**2**	**3**
Cu−O1	1.891(10)	1.929(5)	1.913(8)
Cu−N1	1.950(12)	1.933(5)	1.944(8)
Cu−N2	2.040(12)	2.032(5)	1.994(8)
Cu−N11	1.988(10)	1.985(6)	2.016(8)
Cu−N11\$1′[a]	2.443(9)	2.447(6)	2.550(8)
O1−Cu−N1	93.6(5)	94.7(2)	94.6(3)
O1−Cu−N2	176.2(5)	179.8(2)	178.1(3)
O1−Cu−N11	88.8(4)	90.6(2)	89.9(3)
O1−Cu−N11\$1′	95.1(4)	92.4(2)	90.1(3)
N1−Cu−N2	83.9(5)	85.5(2)	84.6(4)
N1−Cu−N11	168.1(5)	166.0(2)	165.5(3)
N1−Cu−N11\$1′	99.7(5)	105.7(2)	104.5(3)
N2−Cu−N11	93.1(4)	89.2(2)	91.3(3)
N2−Cu−N11\$1′	88.2(4)	87.4(2)	88.4(3)
N11−Cu−N11\$1′	91.7(4)	87.0(2)	89.2(3)
Cu−N11−Cu\$1′	88.3(4)	93.0(2)	90.8(3)

[a] Symmetry elements \$1′: $-x$, $1-y$, $-z$ for complex **1**; $-x$, $-y$, $1-z$ for complex **2**; $1-x$, $1-y$, $1-z$ for Complex **3**.

with a refined ratio of 3:1. The structures were refined on I (= $|F|^2$) using SHELXL-97[33] to $R1$ 0.1193, $wR2$ 0.2855 using 1281 reflections for complex **1**, $R1$ 0.0767, $wR2$ 0.1405 using 1880 reflections for complex **2**, and $R1$ 0.0852, $wR2$ 0.2042, using 1521 reflections for complex **3**. Reflections with $I > 2\sigma(I)$ were considered to be "observed". The relatively high residuals for complex **1** can be attributed to the rather flaky nature of the crystals, which prevented accurate data collection. The crystal structure illustrations were generated using ORTEP-3.[34] The crystallographic data are summarised in Table 3; selected interatomic distances and angles are presented in Table 4.

CCDC-227085 (for **1**), -227086 (for **2**) and -227087 (for **3**) contain the supplementary crystallographic data for this paper. These data can be obtained free of charge at www.ccdc.cam.ac.uk/conts/retrieving.html [or from the Cambridge Crystallographic Data Centre, 12 Union Road, Cambridge CB2 1EZ, UK; Fax: +44-(0)1223-336033; E-mail: deposit@ccdc.cam.ac.uk].

Acknowledgments

One of the authors (M.S.R.) is thankful to UGC, India, for awarding a Senior Research Fellowship (Sanction no. UGC/750/Jr. Fellow Sc.2000/2001).). We also thank EPSRC and the University of Reading for funds for the Image plate system. J.R. also acknowledges financial support from the Spanish Government (Grant BQU2003/00539).

[1] [1a] J. Tercero, C. Diaz, J. Ribas, J. Mahía, M. A. Maestro, *Inorg. Chem.* **2002**, *41*, 5373. [1b] J. Tercero, C. Diaz, J. Ribas, E. Ruiz, J. Mahía, M. Maestro, *Inorg. Chem.* **2002**, *41*, 6780.
[2] H. Kumagai, C. J. Kepert, M. Kurmoo, *Inorg. Chem.* **2002**, *41*, 3410.
[3] Y. Xiu, Q. Liu, H. Jiang, C. Du, X. Xu, M. Yu, Y. Zhu, *New J. Chem.* **2002**, *26*, 176.
[4] [4a] C. Desplanches, E. Ruiz, S. Alvarez, *Chem. Commun.* **2002**, 2614. [4b] D. Maspoch, L. Catalá, P. Gerbier, D. Ruiz-Molina, J. Vidal-Gancedo, K. Wurst, C. Rovira, J. Veciana, *Chem. Eur. J.* **2002**, *8*, 3635. [4c] T. K. Payme, T. Weyhermuller, K. Wieghardt, P. Chaudhuri, *Inorg. Chem.* **2002**, *41*, 6538 and references cited therein.
[5] T. K. Maji, P. S. Mukherjee, G. Mostafa, T. Mallah, J. C. Boquera, N. R. Chaudhuri, *Chem. Commun.* **2001**, 1012.
[6] P. Manikandar, R. Muthukumaran, K. R. J. Thomas, B. Varghese, C. V. R. Chandramouli, P. T. Manoharan, *Inorg. Chem.* **2001**, *40*, 2378.
[7] L. Li, Z. Jiang, D. Liao, S. Yan, G. Wang, Q. Zhao, *Trans. Met. Chem.* **2000**, *25*, 630.
[8] H.-Y. Shen, W. M. Bu, E.-Q. Gao, D. Z. Liao, Z. H. Jiang, S. P. Yan, G. L. Wang, *Inorg. Chem.* **2000**, *39*, 396.
[9] G. de Munno, M. G. Lombardi, M. Julve, F. Lloret, J. Faus, *Inorg. Chim. Acta* **1998**, *282*, 82.
[10] K. Matsumoto, S. Ooi, K. Nakatsuka, W. Mori, S. Suzuki, A. Nakahara, Y. Nakao, *J. Chem. Soc., Dalton Trans.* **1985**, 2095.
[11] R. Cortés, K. K. Urtiaga, L. Lezama, J. I. R. Larramendi, M. I. Arriortua, T. Rojo, *J. Chem. Soc., Dalton Trans.* **1993**, 3685.
[12] L. Li, D. Liao, Z. Jiang, S. Yan, *Polyhedron* **2001**, *20*, 681.
[13] J. P. Costes, F. Dahan, J. Ruiz, J. P. Laurent, *Inorg. Chim. Acta* **1995**, *239*, 53.
[14] A. Escuer, M. Font-Bardía, E. Peñalba, X. Solans, R. Vicente, *Polyhedron* **1998**, *18*, 211.
[15] T. K. Maji, P. S. Mukherjee, S. Koner, G. Mostafa, J. P. Tuchagues, N. R. Chaudhuri, *Inorg. Chim. Acta* **2001**, *314*, 111.
[16] P. S. Mukherjee, T. K. Maji, G. Mostafa, T. Mallah, N. R. Chaudhuri, *Inorg. Chem.* **2000**, *39*, 5147.
[17] [17a] S. S. Tandon, L. K. Thompson, M. E. Manuel, J. N. Bridson, *Inorg. Chem.* **1994**, *33*, 5555. [17b] E. Ruiz, J. Cano, S. Alvarez, P. Alemany, *J. Am. Chem. Soc.* **1998**, *120*, 11122.
[18] M. S. Ray, A. Ghosh, R. Bhattacharya, G. Muthopadhyay, M. G. B. Drew, J. Ribas, *Dalton Trans.* **2004**, 252.
[19] A. W. Addison, T. N. Rao, J. Reedjik, J. van Rijn, C. G. Verschoor, *J. Chem. Soc., Dalton Trans.* **1984**, 1349.
[20] D. Cremer, J. A. Pople, *J. Am. Chem. Soc.* **1975**, *97*, 1354.
[21] G. C. Evans, J. A. Boeyens, *Acta Crystallogr., Sect. B* **1989**, *45*, 581.
[22] [22a] B. Bleaney, K. D. Bowers, *Proc. R. Soc., London, Ser. A* **1952**, *214*, 45. [22b] O. Kahn, *Molecular Magnetism*, VCH Publishers, New York, **1993**.
[23] CLUMAG Program: D. Gatteschi, L. Pardi, *Gazz. Chim. Ital.* **1993**, *123*, 231. This program uses a full-diagonalisation procedure, employing the Irreducible Tensor Operator formalism (ITO).
[24] J. A. Bertrand, T. D. Black, P. G. Eller, T. N. Helm, R. Mahmood, *Inorg. Chem.* **1976**, *15*, 2965.
[25] M. Ardon, A. Bino, K. Michelsen, E. Pedersen, *J. Am. Chem. Soc.* **1987**, *109*, 5855.
[26] *Vogel's Text Book of Quantitative Analysis*, 5th edition, Longman Scientific and Technical, New York, **1989**, p. 689.
[27] N. Matsumoto, T. Akui, H. Murakami, J. Kanesaka, A. Ohyoshi, H. Okawa, *J. Chem. Soc., Dalton Trans.* **1988**, 1021.
[28] [28a] J. P. Costes, F. Dahan, J. P. Laurent, *Inorg. Chem.* **1986**, *25*, 413. [28b] M. Kwiatkowski, E. Kwiatkowski, A. Olechnowicz, *Inorg. Chim. Acta* **1988**, *150*, 65.
[29] L. J. Farrugia, *J. Appl. Cryst.* **1999**, *32*, 837.
[30] W. Kabsch, *J. Appl. Cryst.* **1988**, *21*, 916.
[31] DIFABS program, N. Walker, D. Stuart, *Acta Crystallogr., Sect. A* **1983**, *39*, 158.
[32] A program for automatic solution of crystal structures. G. M. Sheldrick, University of Göttingen, Germany, **1997**, Release 97-2.
[33] A *program for crystal structure refinement.* G. M. Sheldrick, University of Göttingen, Germany, **1997**, Release 97−2.
[34] M. N. Burnett, C. K. Johnson, *ORTEP-3: Oak Ridge Thermal Ellipsoid Plot Program for Crystal Structure Illustrations*, Report ORNL-6895, Oak Ridge National Laboratory, Oak Ridge, TN, USA, **1996**.

Received December 26, 2003
Early View Article
Published Online May 27, 2004

 © 2004 Wiley-VCH Verlag GmbH & Co. KGaA, Weinheim

Preparation, Structure Determination and Cytotoxicity of the Pd^{II}·Bleomycin A2 Complex

Athanasios Papakyriakou,[a] Ioannis Bratsos,[a] Maria Katsarou,[a] and Nikos Katsaros*[a]

Keywords: Bleomycin / Palladium / Molecular modelling / Cytotoxicity

The solution structure of the Pd^{II}·bleomycin A2 complex was resolved by NMR spectroscopy in combination with molecular modelling. The preparation of the complex in 1.0 M NaCl aqueous solutions leads to the formation of a major compound, which is very stable at ambient temperature. Our NMR spectroscopic data demonstrate that bleomycin is coordinated through the β-aminoalanine secondary amine, the pyrimidine ring N1, the deprotonated histidyl amide and the imidazole N1, in contrast to an earlier study that proposed coordination of the valerate amide. 2D NMR spectroscopic data were used as distance constraints in simulated annealing molecular-dynamics calculations and the first solution structure of a square-planar metallo-bleomycin is reported. In order to assess the toxicity of Pd^{II}·bleomycin, cytotoxicity measurements were performed in U937 and K562 leukemia cell lines using two methods. In both cell lines the free drug and the complex exhibit similar toxicity as a function of time.
(© Wiley-VCH Verlag GmbH & Co. KGaA, 69451 Weinheim, Germany, 2004)

Introduction

Bleomycins are a group of antibiotics with clinical use as anticancer drugs.[1−3] The commercial preparation, Bleocin or Blenoxane, consists predominantly of bleomycins A2 and B2 (Scheme 1). Their efficacy is mainly attributed to their ability to mediate cleavage of the DNA backbone by attacking at the deoxyribose 4′-H position and causing single- and double-strand cleavage and base release.[4−8] A number of putative pathways have been proposed to initiate DNA oxidation.[10,11] The drug is activated in the presence of iron and oxygen species as cofactors. Other metals can also facilitate DNA cleavage by bleomycin in vitro, even though their reactions are less well characterized.[12]

Umezawa and co-workers were the first to isolate bleomycins from the culture medium of *Streptomyces verticillus* and to propose the most likely metal-binding sites.[13] The X-ray crystal structure of Cu^{II}·P3A,[14,15] a biosynthetic intermediate of bleomycins lacking the linker, C-terminus and carbohydrate domains, revealed a five-coordinate square-pyramidal complex with five nitrogen donors. Only recently, Suguiyama et al.[16] obtained the X-ray crystal structures of both apo and Cu^{II}·bleomycin A2 bound with a protein and established the proposed metal-binding mode. The equatorial plane comprises the secondary amine of aminoalanine, the pyrimidine N1, the histidine amide and the imidazole N1, while the aminoalanine primary amine occupies the apical position (see Scheme 1). These structures were found to be consistent with the NMR models proposed by Stubbe et al. for the two Co^{III}·bleomycin adducts.[17−19] Among them, HO_2·Co^{III}·bleomycin is considered to be a robust structural analogue of the biologically relevant Fe·bleomycin.[20,21] Although Ga^{III} and In^{III}·bleomycins are not able to mediate DNA degradation, their solution structures were recently shown to bear strong resemblance to these models.[22,23] On the other hand, structural NMR studies on iron species have been carried out for the low-spin CO·Fe^{II}·bleomycin [24] and the paramagnetic Fe^{II}·bleomycin,[25] which exhibited contradictory results. Other direct structural studies on metallo-bleomycins have been performed with manganese,[26−28] ruthenium,[29,30] vanadyl,[31,32] zinc,[33−36] cadmium,[37] nickel,[38,39] calcium and trivalent lanthanides,[40] as well as the paramagnetic Co^{II}·bleomycin complex.[41,42]

In view of the fact that bleomycins are often administered in combination with cisplatin [*cis*-$PtCl_2(NH_3)_2$] for the treatment of malignant tumors,[43] Garnier-Suillerot and Albertini have carried out an investigation on the interaction between the two compounds.[44] Apart from cisplatin, *cis*-$PdCl_2(NH_3)_2$, $PdCl_2$(ethylenediamine) and $PdCl_4^{2-}$ were also used in this study. The final species, resulting from the interaction of these compounds with bleomycin, were suggested to be similar, albeit different reaction rates and formation constants were observed. Spectroscopic and potentiometric data have led the authors to propose a binding mode, which differs from the equatorial plane of most metallo-bleomycins. Instead of the imidazole ring N1, the valerate peptide nitrogen was proposed to be a donor atom of bleomycin, independent of the starting complex.

[a] Institute of Physical Chemistry, NCSR "Demokritos", 153 10 Ag. Paraskevi Attikis, Greece
Fax: (internat.) + 30-210-6511766
E-mail: katsaros@chem.demokritos.gr
Supporting information for this article is available on the WWW under http://www.eurjic.org or from the author.

 © 2004 Wiley-VCH Verlag GmbH & Co. KGaA, Weinheim **DOI: 10.1002/ejic.200400034**

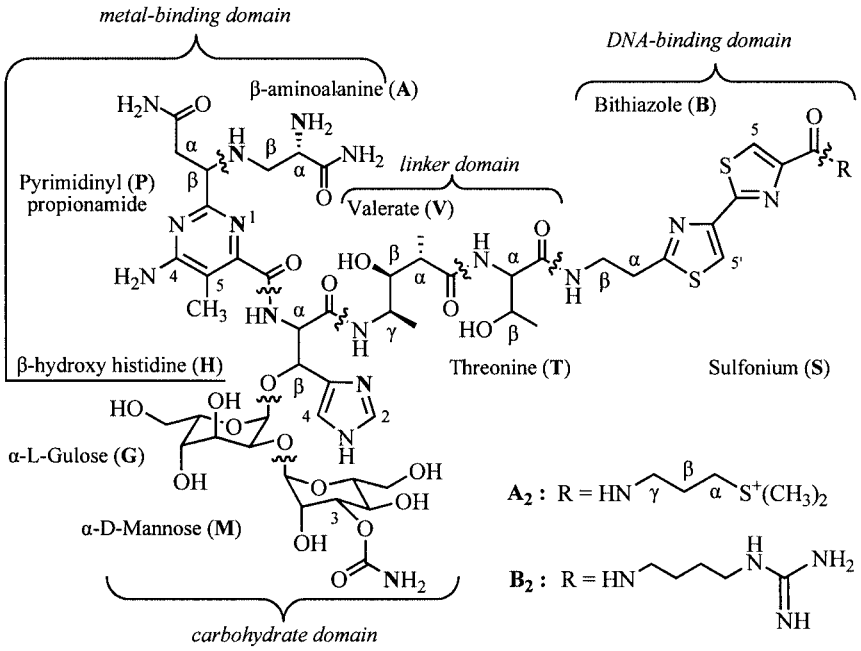

Scheme 1. Structure of bleomycins A2 and B2; the functional groups are separated by wavy lines and the potential N ligands are marked in bold

We have undertaken the preparation and structural characterization of Pd^{II}·bleomycin A2 with the aim to obtain its detailed solution structure through a combined use of NMR spectroscopy and molecular modelling. Our NMR spectroscopic data indicate that bleomycin binds strongly to Pd^{II} and forms a 1:1 adduct through four nitrogen donors, which comprise the equatorial plane of nearly all metallobleomycins. The combination of proton−proton distance constraints obtained by 2D NOESY experiments at low temperature, along with a suitable molecular mechanics force field for the modelling of Pd^{II}·bleomycin A2, have been used in determining its solution structure. Since no cytotoxicity results were reported for Pd^{II}·bleomycin and in pursuing a comparison with a cisplatin−bleomycin complex, we have performed cytotoxicity measurements in two leukemia cell lines using two methods. While complexation of bleomycin and cisplatin results in the decrease of their activity,[44] our data evidences that Pd^{II}·bleomycin exhibits comparable cytotoxicity with that of apo-bleomycin.

Results and Discussion

Interaction of Pd^{II} with Bleomycin

The first step in the structural characterization procedure of Pd^{II}·bleomycin was to prepare a pure and stable complex in aqueous media. Since Pd^{II} tends to undergo hydrolysis reactions,[45,46] addition of a twofold excess of K_2PdCl_4 in bleomycin solutions (1−10 mM concentrations) immediately produced a yellow, fine aggregate. Most likely, the insoluble product consists of hydroxo-bridged polynuclear Pd^{II} species. Even though mixing equimolar amounts of K_2PdCl_4 and bleomycin did not readily result in precipitation, a variety of compounds were formed, even at low pH (< 2). This was evident from the ^1H NMR spectra recorded immediately after mixing, which reveal the presence of at least three different species. Higher pH values and longer periods of time give rise to precipitation or formation of more complex mixtures.

Based on speciation studies of several Pd^{II} compounds analogous to cisplatin as a function of their concentration, pH and $[Cl^-]$,[47−50] we carried out the complex preparation in 1.0 M NaCl, so as to restrict the presence of aqua and/or hydroxo Pd^{II} species. As shown in Figure 1, under these

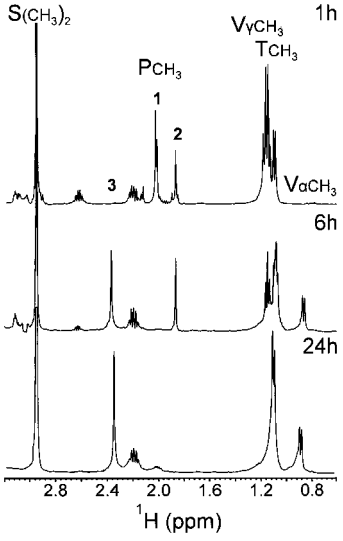

Figure 1. ^1H NMR spectral region of the Pd^{II}·bleomycin A2 system in 1.0 M NaCl at 298 K as a function of time; the resonances of the pyrimidine ring methyl protons ($P-CH_3$) reveal a three-step reaction and are indicated by the numbers 1, 2 and 3

 © 2004 Wiley-VCH Verlag GmbH & Co. KGaA, Weinheim

conditions the ^{1}H NMR spectra indicate a multi-step reaction that occurrs during the first hours after mixing equimolar amounts of K_2PdCl_4 and bleomycin, which eventually leads to a major compound after 24 h at 40 °C. The complex formed is stable over a long period of several months, in neutral aqueous solutions (pH 6.7) of 10 mM concentration and at room temperature. This has allowed us to perform 2D NMR experiments and proceed to the structural determination of Pd^{II}·bleomycin A2.

Assignment and Analysis of the NMR Spectra

A strategy for the assignment of the non-exchangeable protons of bleomycin A2 has been previously presented in detail.[17,24] Combined use of heteronuclear and homonuclear experiments plays a key role in this procedure. A dispersion in the carbon dimension of the HMQC spectra (Figure S1 in the Supporting Information) in combination with the long-range couplings detected in the HMBC and TOCSY experiments have enabled us to assign the signals, especially the crowded disaccharide signals. ^{1}H and ^{13}C chemical shift values of Pd^{II}·bleomycin A2 are given in Tables S1 and S2 of the Supporting Information, in comparison with those reported for the metal-free bleomycin A2.[24,51]

Coordination of bleomycin to Pd^{II} through the pyrimidine and imidazole aromatic rings is readily detected by the changes in the **P**−CH_3 and **H**−C2H chemical shifts. In particular, the former signal appears at considerably lower field regions ($\Delta\delta$ = 0.4 ppm), which indicates a strong electron-withdrawing effect by the metal ion (see Figure 1). Despite the fact that both the ^{1}H and ^{13}C chemical shifts of the histidine **H**−Cα are not significantly affected upon complexation, the deprotonation of the histidine amide nitrogen is evident from the disappearance of its NH resonance. This is a strong indication for the coordination of the amide nitrogen to Pd^{II}, which was also the case for other metallo-bleomycins.[17,19,22−24,33−36] On the other hand, coordination of the β-aminoalanine secondary amine is reflected by the perturbation of the chemical shifts at **P**−CβH ($\Delta\delta$ = 0.4 ppm) and at the two **A**−$CβH_2$ ($\Delta\delta$ = 0.2−0.3 ppm).

Apart from the histidine amide proton, all the others were detected and assigned by observation of scalar couplings with their vicinal protons. Therefore, participation of any other amide nitrogen into the coordination sphere of Pd^{II}, rather than the deprotonated histidine amide, can be excluded. This is also true for the **V**−NH group (δ = 8.01), which has been proposed as a ligand for Pt^{II} and Pd^{II}·bleomycin.[44] The primary amine protons of β-aminoalanine exhibit a single resonance (δ = 6.39) strongly coupled to **A**−CαH. Their degeneration owning to the fast rotation around the C−N bond indicates that the primary amine is not coordinated, in contrast to Ga^{III} and In^{III}·bleomycins for which two strongly coupled signals had been detected.[22,23] Additionally, four pair of signals strongly coupled to each other were assigned to the pyrimidine ring **P**−NH_2 (δ = 7.51, 7.60), **P**−$CONH_2$ (δ = 7.08, 7.69), **A**−$CONH_2$ (δ = 6.93, 7.21) and **M**−$CONH_2$ (δ = 6.16, 6.61). The pyrimidine amine exhibits only medium-size NOEs with the neighbouring methyl group, in accordance with previous NMR studies.[17−19,22,23] **P**−$CONH_2$ and **A**−$CONH_2$ were assigned by virtue of their NOEs with the Cα and Cβ protons of the pyrimidinyl and aminoalanine moieties (see Figure 2). The remaining couple of fast exchanging protons was assigned to **M**−$CONH_2$, which did not show any cross-peak with other protons.

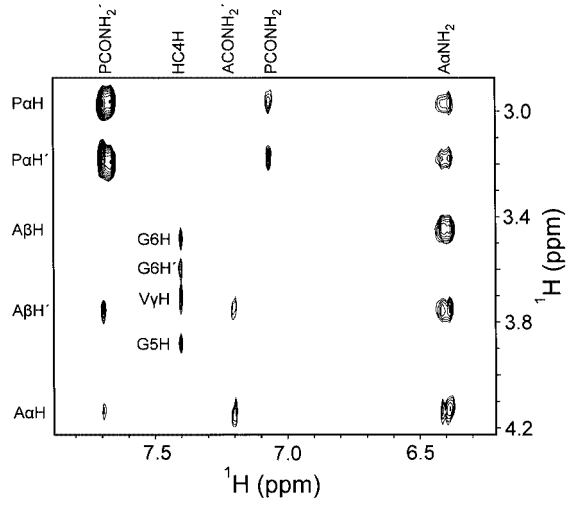

Figure 2. Expanded region from the NOESY spectrum of Pd^{II}·bleomycin A2 in H_2O (10% D_2O), 1.0 M NaCl, pH 6.7 at 278 K; the cross peaks shown are supporting the assignment of the exchangeable primary amine and amide protons

NOESY experiments were performed at 278 K and not only assisted in the assignment procedure, but also provided a wealth of structural information through distance constraints (Table S3 of the Supporting Information). Some common characteristics of metallo-bleomycins, such as the folding of the linker domain under the imidazole ring, were also exhibited by the Pd^{II}·bleomycin adduct. This is indicated by a number of NOEs between the aromatic protons of imidazole and the linker domain, especially by two medium intensity cross-peaks for **H**−C2H···**V**−CαH and **H**−C2H···**T**−CH_3. As a result of shielding by the imidazole ring current, **V**−CαH and **V**−αCH_3 proton signals appear at higher field compared with the metal-free bleomycin. Similarly, **M**−C3H is found to be shielded by the pyrimidine ring current, as the sugars move toward the metal-binding domain. In earlier NMR studies, the even higher upfield shift of the **M**−C3H signal ($\Delta\delta$ > 0.5 ppm) has been used as evidence for the coordination of the 3-*O*-carbamoyl nitrogen,[24] but it was disputed later.[17,19] Such stacking of the carbamoyl moiety over the pyrimidine ring has also been observed in the crystal structure of Cu^{II}·bleomycin A2.[16] Finally, the bithiazole and sulfonium

 © 2004 Wiley-VCH Verlag GmbH & Co. KGaA, Weinheim

moieties of Pd^{II}·bleomycin lack any long-range NOEs with other domains, thus demonstrating a conformational flexibility.

Molecular Modelling and Structure Determination

Having established that the four common nitrogen ligands are involved in Pd^{II}·bleomycin and given that the square-planar geometry is the most favourable, three isomer models were constructed (see Scheme 2). To facilitate more extensive sampling of the conformational space, the disaccharide and β-aminoalanine moieties were placed at different orientations. In models I and II they were placed at opposite sides of the coordination plane, whereas in model III they both share the same side. Models I and II were based on the coordinates of the NMR structure of Co^{II}·bleomycin A2 (PDB code 1DEY),[41] while model III was based on the X-ray crystal structure of Cu^{II}·bleomycin A2 (PDB code 1JIF).[16]

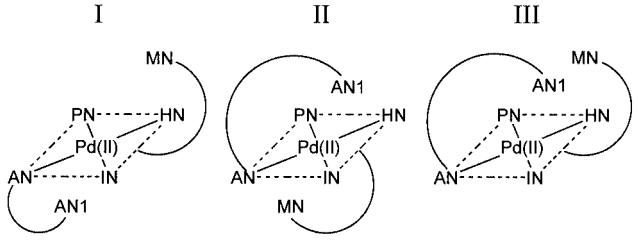

Scheme 2. Starting models employed in the molecular dynamics calculations; the ligands are designated as β-aminoalanine secondary amine (AN), pyrimidine N1 (PN), β-hydroxyhistidine amide (HN) and imidazole N1 (IN); the β-aminoalanine primary amine (AN1) and the mannose carbamoyl nitrogen (MN) occupy different sides of the equatorial plane in models I, II and the same side in model III

Each model was subjected to 20 runs of a simulated annealing calculation following the same protocol as that described for the structural determination of Ga^{III} and In^{III}·bleomycins.[22,23] After minimizing the energy of the initial models without any constraints, a molecular dynamics run was performed while increasing the temperature from 300 to 1000 K. The distance constraints were then gradually introduced and after allowing the system to overcome any potential energy minima, the temperature was decreased to 300 K. From the final 20 ps of the molecular dynamics run (at 300 K with distance constraints) 100 structures were collected and were superimposed by mass-weighted rms fittings of all heavy atoms excluding the bithiazole and C-terminal groups. Their coordinates were averaged and the final model was subjected to energy minimization until the rms gradient became less than 0.01.

The structural and energy statistics of the ten best structures for each model, by virtue of the lowest potential energy and lowest deviation from the restraints, are given in Table 1. Models I and III were found to be more consistent with the NMR constraints and they exhibited the lowest energy structures. Model II resulted in higher strain-energy structures in order to satisfy the restraints and can be readily excluded. Despite the different starting position of β-aminoalanine in models I and III, their final structures were quite similar. As a result, all structures of the isomers I and III exhibit minimal energy differences in comparison with those obtained by model II. Nevertheless, model III exhibits the most favourable results with minor restraint violations and the lowest total potential energy.

The solution structure of Pd^{II}·bleomycin A2 (see Figure 3) resulted by averaging the ten best structures of model III and by minimizing its strain energy. Selected structural data of the coordination plane are presented in Figure S2 (see Supporting Information). Some of the above-mentioned structural features of metallo-bleomycins were also identified in the Pd^{II} adduct. The linker domain of the two Co^{III}·bleomycin complexes is folded under the equatorial plane from the side of the imidazole. The basis of this folding has been related to the interaction of the hydroperoxide or hydroxide axial ligand with the linker backbone.[17,19] In our case, a similar folding of the linker domain can be attri-

Table 1. Structural and energy statistics for the three Pd^{II}·bleomycin A2 models, which were obtained from the simulated annealing molecular dynamics calculations; for each model, ten structures were obtained by mass-weighted rms fitting and averaging the coordinates from the last 20 ps of the trajectory (100 snapshots); statistics were obtained after energy minimization was performed with all the distance restraints applied

	Model I	Model II	Model III
Rmsd. of heavy atoms[a] (Å)	0.77 ± 0.35	1.55 ± 0.44	0.11 ± 0.03
Distance restraint violations > 0.01 Å	7−13	12−16	4−9
Rmsd. from distance restraints (Å)	0.035 ± 0.012	0.040 ± 0.008	0.024 ± 0.004
Potential energy terms: (kcal mol^{-1})	−4.7 ± 4.8	24.6 ± 7.7	−10.4 ± 6.3
Total	13.9 ± 0.4	15.0 ± 1.1	14.6 ± 0.3
Bond	66.1 ± 3.1	71.1 ± 3.2	62.4 ± 1.1
Angle	48.2 ± 2.9	53.6 ± 4.6	44.7 ± 2.6
Dihedral angle[b]	−138.2 ± 6.2	−121.2 ± 7.6	−134.7 ± 7.0
Non-bonded constraint[c]	5.3 ± 3.3	6.1 ± 2.6	2.6 ± 0.7

[a] The atoms of bithiazole and sulfonium moieties were not included due to the disorder of this domain. [b] Including also an improper angle-energy term. [c] The sum of the electrostatic and van der Waals energy terms.

 © 2004 Wiley-VCH Verlag GmbH & Co. KGaA, Weinheim

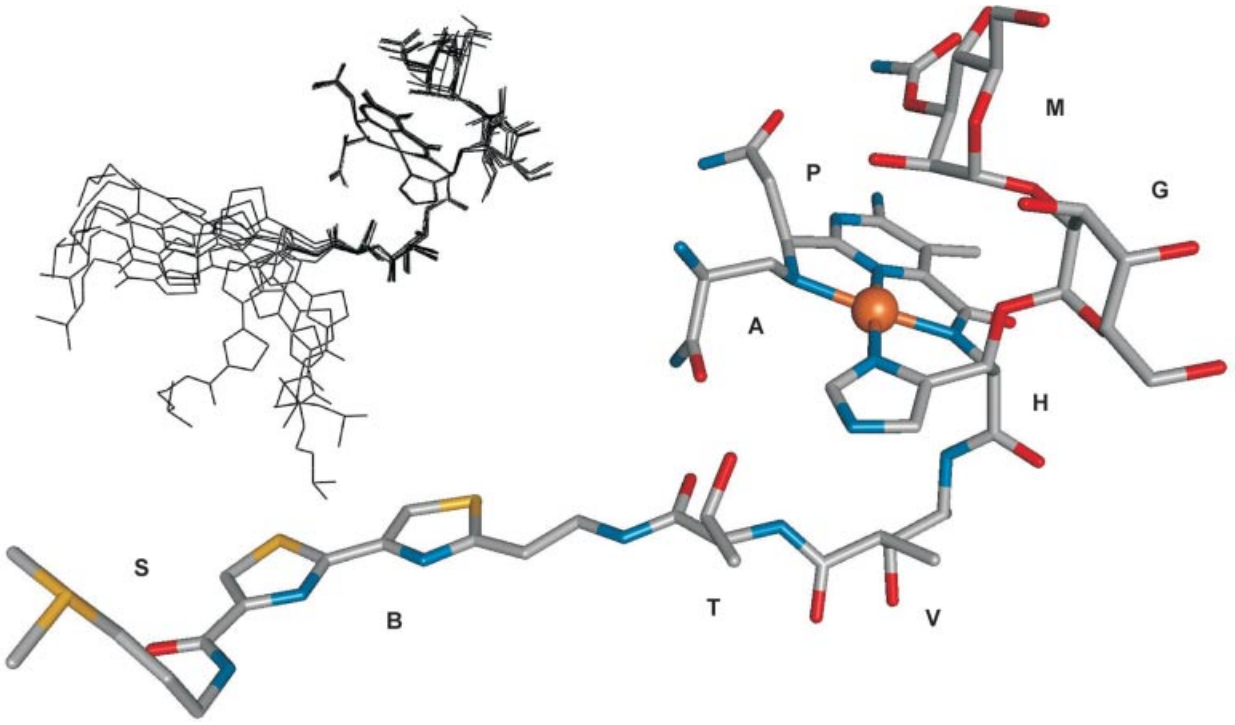

Figure 3. Structure of Pd^{II}·bleomycin A2 calculated from the averaged coordinates of the ten best models of III (shown in the inset) after energy minimization with all the constraints applied; atom colours are grey for C, blue for N, red for O, yellow for S and orange for Pd

buted to the H bonds, which were exhibited between the threonine and aminoalanine moieties (**T**−O−H···O=C−**A** and **T**−C=O···H−N−**A**). Their geometric characteristics indicate a strong interaction, which can account for the folding observed (Figures S3 and S4 in the Supporting Information). This interaction is supported by the strong chemical shift perturbation of **A**−$CONH_2$ protons (Table S1) and by a medium and a weak NOE between the two **A**−$CONH_2$ protons and **T**−NH (Table S3).

The disaccharide moiety of bleomycin is found to be positioned over the plane, which can be due to an additional H bond between the propionamide and carbamoyl moieties (**P**−C=O···H−N−**M**). But since the **P**−$CONH_2$ and **M**−$CONH_2$ signals are marginally perturbed upon complexation (Table S1 in Supporting Information) this interaction cannot be explicitly defined. In addition, it is also possible that water molecules mediate H-bonding interactions between mannose and propionamide domains, an interaction that cannot be simulated without explicit treatment of the solvent. As shown in Figure 3, the aminoalanine moiety is located away from the metal ion. If **A**−αNH_2 occupied the initial position over the metal, then it would be expected to participate in an axial Pd···H−N interaction. This would contradict our NMR spectroscopic data, since one of the degenerate resonances from the interacting amine proton should be shifted to lower field. Indeed, examination of the final model revealed that axial Pd···H−X (X = calcd. C, O, N) interactions are absent. Finally, the thiazolium rings are shown in the *cis* conformation, by virtue of a quite weak NOE detected between their two aromatic protons (not used as distance constraint).

Antitumor Activity

The cytotoxicity of the Pd^{II}·bleomycin A2 complex was screened in two leukemia cell lines, human chronic myeloid leukemia (K562) and human histiocytic lymphoma (U937). K562 cells were incubated with higher concentrations of the drugs (100 and 300 μg/ml) than U937 cells (10 and 100 μg/ml), since the former are less sensitive to several anticancer agents. Incubation times were 6 to 48 hours. Two different methods were used, in order to assess the percentage of total alive cells (MTT) and the number of necrotic cells (Trypan Blue). The MTT assay is based on an enzymatic reaction and is therefore more sensitive and accurate. Since MTT is absorbed by the mitochondria, it is transformed into formazan by the enzyme succinic dehydrogenase. By assessing the activity of the mitochondrial dehydrogenases, the activity of viable cells is screened. The results obtained by both methods are presented in Table S4 (see Supporting Information).

The results obtained using the MTT assay, which are illustrated in Figure 4, show that the cytotoxicity exhibited by Pd^{II}·bleomycin is similar to that of the free drug. For both cell lines, the toxicity of the complex was measured as being 10 % lower than that of bleomycin, following the same trend as a function of time. A plausible explanation for the toxicity demonstrated by Pd^{II}·bleomycin is that the complex dissociates under cellular conditions. By virtue of its lack of redox activity and inability to mediate DNA-strand scission, the cytotoxicity is most probably due to the free drug released into the cells. Based on this hypothesis, the percentage of lower toxicity of Pd^{II}·bleomycin can be

 © 2004 Wiley-VCH Verlag GmbH & Co. KGaA, Weinheim

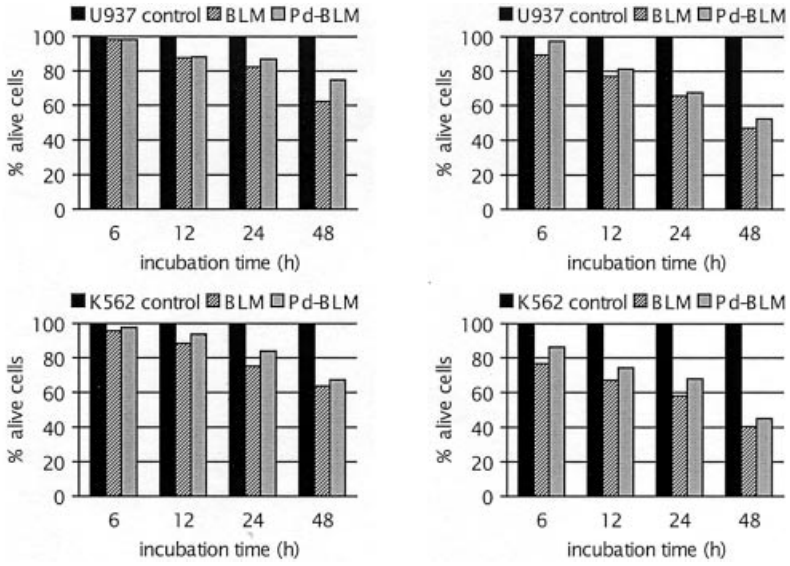

Figure 4. Antitumor activity of the Pd^{II}·bleomycin A2 complex (Pd-BLM) in comparison with that exhibited by the metal-free drug (BLM) as a function of time; the upper diagrams illustrate the results obtained by the MTT assay for U937 cells, after incubation with 10 μg/ml (left) and 100 μg/ml (right) of drugs; the lower diagrams were obtained by the same method as for K562 cells, after incubation with 100 μg/ml (left) and 300 μg/ml (right) of drugs

attributed to the presence of an equilibrium between the metal-bound and the apo-form of bleomycin. It is possible that the stability of the complex observed does not correspond to the same stability under cellular conditions, which are quite different to those of the NMR experiments.

In order to obtain more information on the stability of the complex, we performed NMR and circular dichroism (CD) studies on Pd^{II}·bleomycin in lower salt concentrations. For this reason we diluted a stock 10 mM solution of the complex (1.0 M NaCl, pH = 6.7) in H_2O, so that the final salt concentration was 4−150 mM, while the drug concentration was 0.04−1.5 mM. The pH was adjusted to 7.2 using aliquots from dilute NaOH and the solutions were incubated at 37 °C. All spectra were recorded at room temperature starting one hour after each dilution and lasting up to three days. Seeing that no changes occur either in the CD spectra (solutions with [drug] < 0.5 mM), or the NMR spectra (solutions with [drug] > 0.5 mM), we cannot support the hypothesis that Pd^{II}·bleomycin dissociates under cellular conditions.

On the other hand, we cannot rule out the possibility that Pd^{II}·bleomycin mediates the cytotoxicity observed, without requiring the redox activation of oxygen. Based on observations in vitro that the complex is not only able to bind strongly to DNA, but it can also displace Fe^{III} from its coordination site,[44] the cytotoxicity of Pd^{II}·bleomycin could be attributed to its DNA-binding ability or any other mechanism that may lead to the cell death (such as apoptosis). But taking into consideration that Pt^{II}·bleomycin exhibits a strong affinity for DNA and that the complexation of bleomycin and cisplatin gives rise to a decrease in the cytotoxicity of both drugs,[44] albeit screened in different cell lines, the hypothesis that Pd^{II}·bleomycin dissociates under cellular conditions seems more plausible. Still, further investigations should be carried out, in order to elucidate the mechanism of cytotoxicity. A related paradigm is the case of Cu·bleomycin, which was initially considered as an inhibitor of DNA cleavage.[52] However, later findings have suggested that it may assist in generating an active Fe·bleomycin species in vivo, a mechanism that still remains a puzzle.[12]

Conclusion

Following the procedure described herein, we prepared the Pd^{II}·bleomycin A2 complex in aqueous media and determined its solution structure using NMR spectroscopy in combination with molecular dynamics calculations. Our data reveal that bleomycin binds to Pd^{II} adopting a conformation similar to most of the models proposed either by NMR or X-ray crystallography. The same N ligands involved in the equatorial planes of Cu^{II}, Fe^{II}, Co^{II} and Co^{III}, Ga^{III} and In^{III} metallo-bleomycins are shown to be arranged in a square-planar geometry around Pd^{II}. Cytotoxicity measurements in two leukemia cell lines demonstrate that Pd^{II}·bleomycin is almost as toxic as the free drug, in contrast to Pt^{II}·bleomycin, which was found to have lower toxicity than apo-bleomycin.

Experimental Section

Sample Preparation: Bleocin and pure bleomycin A2 sulfate were a kind offer from Nippon Kayaku Co. Ltd. and were used without further purification. The complex was prepared by mixing equimolar amounts of K_2PdCl_4 (100 mM) and bleomycin (10 mM) in aqueous solutions containing NaCl (1.0 M). The pH of the solution, which immediately dropped below 2.0, was slowly increased to 3.5 using aliquots of dilute NaOH (1.0 M). After heating the mixture at 40 °C for 2 h, its pH, which continuously dropped, was then

 © 2004 Wiley-VCH Verlag GmbH & Co. KGaA, Weinheim

increased to 5.0. This procedure was repeated twice before the pH was finally increased to 7.0. The mixture was then heated at 40 °C for 24 h, so as to assure complete formation of the complex and the pH was finally readjusted to 6.7. Its stability over a period of several months at room temperature is demonstrated by the fact that no changes were detected in the ^{1}H NMR spectra. Using the same procedure, Pd^{II}·bleomycin was also prepared in Millipore water for the cytotoxicity measurements.

NMR Experiments: Samples for the NMR experiments were prepared either in H_2O (10% D_2O) or D_2O 99.99%. All spectra were recorded on a Bruker Avance NMR spectrometer operating at proton frequency of 500.13 MHz. X-WIN NMR 2.6 (Bruker Analytik GmbH) was used to process the spectra and SPARKY 3.1,[53] running on a Linux PC, was used for the assignment and analysis of the 2D spectra. ^{1}H and ^{13}C chemical shift values were referenced to an internal standard, sodium 3-(trimethylsilyl)-1-propanesulfonate (TSP).

Two-dimensional NOESY (100, 200 and 400 ms mixing times), DQF COSY,[54] and TOCSY (MLEV-17 sequence with 35 and 70 ms mixing times)[55] experiments were performed at 278 and 298 K in H_2O and D_2O. Data sets with 2048 × 512 complex points were acquired with 7 KHz-sweep widths in both dimensions and 32 scans per t_1 increment. ^{1}H{^{13}C} HMQC[56] and HMBC[57] spectra were recorded at 278 and 298 K in H_2O and D_2O. Data sets with 1024 × 256 points were collected with 32 or 64 scans per t_1 increment and spectral widths of 6 KHz in the proton and 25 kHz in the carbon dimension. Solvent suppression for the H_2O samples was performed using excitation sculpting with gradients,[58] while for the D_2O samples a pre-saturation pulse was applied during the relaxation delay of 2.0 s. The indirect dimension was zero-filled up to 1024 data points and the FIDs were processed with either a combination of exponential and Gaussian weighting functions or a 90°-shifted sine-bell function.

Force Field Parameters: All molecular modelling calculations were performed with AMBER 6.[59] In order to accurately represent the bleomycin complex, the AMBER-94 force field was modified according to the guidelines of its authors.[60] Standard atom types were assigned to the atoms of bleomycin by analogy with their chemical environment. For the sugar atoms, we used parameters from the GLYCAM force field for modelling carbohydrates.[61] A new atom type was created for Pd^{II} using the van der Waals parameters R^* = 1.65 Å and ε = 0.20 kcal mol^{-1}, based on the crystallographic data of Bondi.[62] According to the calculations of Hambley,[63] these parameters reproduce quite well the metal−ligand separations in molecular mechanics force fields. The bond, angle and dihedral angle parameters of bleomycin were also chosen upon their analogy with existing parameters of AMBER, while those involving Pd^{II} were adapted from parameters developed for platinum compounds.[64] Equilibrium Pd−N bond lengths were set to R_o of 2.01 Å using a relatively low force constant of 100 kcal mol^{-1} Å^{-2}. For the N−Pd−N angles, θ_o of 90° or 180° with 40 kcal mol^{-1} rad^{-2} force constants were used, while dihedral angles involving the metal were set with zero force constants.

The atom-centred point charges of the complex were generated from the electrostatic potential of its molecular fragments. The equatorial plane of Pd^{II}·bleomycin comprising β-aminoalanine, pyrimidinyl propionamide and histidyl moieties was fitted as a whole. For the other domains we used the charges, which had been previously calculated for Ga^{III}·bleomycin.[22] Spin-restricted DFT calculations using Becke's three-parameter-hybrid functional with the correlation functional of Lee, Yang, and Parr (B3LYP)[65−67] were performed using the program package GAMESS.[68] The Los Alamos effective core potentials were applied on palladium,[69−71] and the 6−31G(d) basis set on all other atoms. The point charges were fitted to reproduce the electrostatic potential using the RESP method,[72] a two-stage approach where the equivalent methyl and methylene hydrogen atoms are restrained to have the same charge. In order to reassemble the charges of the entire molecule, the H-neutralization method was used.[73]

Restrained Molecular Dynamics: NOE signals from the NOESY spectrum (200 ms mixing time at 278 K, pH 6.7) were classified as strong, medium and weak by visual inspection of the cross-peak intensities and the constraints were set to an upper distance limit of 3.0, 4.0 and 5.0 Å, respectively. An additional 1.0 Å was allowed for NOEs involving methyl groups and ambiguous methylene protons. A total of 76 distance constraints were applied with a 50 kcal mol^{-1} Å^{-2} force constant, using a square-bottom-well function with parabolic sides out to 0.5 Å and then linear sides beyond that. Molecular dynamics calculations in vacuo were carried out at a time step of 1 fs with the distance-dependent dielectric constant algorithm of AMBER. The cut-off distance was set to 16.0 Å and the non-bonded pair list was updated every ten steps. Temperature regulation was performed using the Berendsen algorithm. For the heating and cooling stages, a bath coupling constant of 0.1−0.5 ps was applied, in order to assure a tighter coupling to the heat bath, while for the equilibration stages it was increased up to 2.0 ps, so as to allow sampling of more natural trajectories. Starting models were energy minimized prior to the simulated annealing calculations without restraints for 500 steps of the steepest descent method, followed by the conjugate gradient method until the rms gradient became less than 0.1.

Each model was subjected to 20 individual runs, while changing the initial velocities assigned. The annealing protocol consisted of five stages: (1) heating the system from 5 K up to 1000 K during the first 20 ps, (2) gradual application of the constraints for a period of 10 ps, (3) high-temperature equilibration for 20 ps, (4) slow cooling down to 300 K during the next 20 ps and (5) final dynamics run for 50 ps at 300 K. A final model from each iteration was generated by mass-weighted rms fitting and averaging the coordinates from the last 20 ps of the trajectory (100 structures). Energy minimization with restraints was performed as above but until the rms gradient became less than 0.01. The results presented in Table 1 were derived from the ten best structures, which were favoured by their low potential energy and minimal deviations from the NMR constraints.

Cell Lines and Cytotoxicity Assays: RPMI 1640, Fetal Bovine Serum (FBS), penicillin, streptomycin, Phosphate Buffered Saline (PBS) and HEPES buffer were purchased from BIOCHROM. L-Glutamine was purchased from AppliChem. Trypan Blue, 3-(4,5-dimethylthiazol-2-yl)-2,5-diphenyl-tetrazolium bromide (MTT), sodium dodecyl sulfate (SDS), formamide and $NaHCO_3$ were purchased from Sigma−Aldrich. Two human cell lines routinely maintained in the Biology department of NCSR "Demokritos" were used in this study. Chronic myelogenic leukemia (K562) and human promyelocytic cell line (U937) were maintained in RPMI 1640 medium containing 10% (v/v) FBS, 2 mM L-glutamine, 0.85 g/l $NaHCO_3$, 25 mM HEPES, 200 U/ml penicillin and 100 μg/ml streptomycin at 37 C in a 5% CO_2 atmosphere. The pH of the medium was adjusted to 7.3. In all experiments, cells were cultured to the logarithmic phase growth over a period of 48 h, starting from a culture density of 3−5 × 10^5 cells/ml.

The viability of the cells was determined by the Trypan Blue dye-exclusion method and cytotoxicity was assessed by the MTT assay.[74−77] Briefly, logarithmically grown cells were plated in 25-

 © 2004 Wiley-VCH Verlag GmbH & Co. KGaA, Weinheim

mL flasks and treated with two concentrations of each drug. Untreated cells were used as a negative control. Incubation was carried out at 37 °C for different time periods, starting from a 6 h incubation up to 50 h. After drug incubation for various time periods at 37 °C, MTT (50 µl, 10 mg/ml) was added to each well, followed by a 4 h incubation at 37 C. The reaction results in the reduction of MTT by the mitochondrial dehydrogenases of viable cells to a purple formazan product. Cells were lysed using DMF solution (55 mL H_2O + 12.5 g SDS + 45 mL formamide, pH 4.7) and left overnight at 37 °C. After centrifugation, 200 µL of each sample were placed in 96-well microtiter plates in duplicate and $OD_{550\ nm}$ was determined in an ELISA plate reader. The results are expressed as the percentage of alive cells, calculated from MTT reduction and it is assumed that the absorbance of control cells is 100%. In addition, cell viability in U937 and K562 cell lines was assessed by the method of Trypan Blue exclusion. Trypan blue (0.2%, 2 µl) was added to aliquots of cell-containing media (18 µl) and the percentage of viable cells was determined by counting the number of cells able to exclude the dye on an hemocytometer. All of the above experiments were performed in duplicate.

Supporting Information (see also the footnote on the first page of this article): Two tables giving the ^1H and ^{13}C chemical shift values of Pd^{II}·bleomycin A2 in comparison with those obtained for the metal-free bleomycin A2, a table with the categorized NOE intensities, a table with all the results from the cytotoxicity measurements, a figure showing an expanded region of the $^1H\{^{13}C\}$ HMQC spectrum and three figures illustrating the solution structure of Pd^{II}·bleomycin A2 along with selected structural data of the coordination sphere, potential intramolecular H-bonds and a comparison with the crystal structure of Cu^{II}·bleomycin.

Acknowledgments

We are grateful to Prof. Ivano Bertini for his hospitality at the University of Florence (CERM) in the framework of the European Large Scale Research Infrastructure. We thank Prof. Enzo Alessio for his critical comments on the manuscript. This work has been supported with a grant by the General Secretariat for Research and Technology of Greece.

[1] H. Umezawa in *Anticancer Agents Based on Natural Product Models* (Eds: J. M. Cassady, J. Douros), Academic Press, New York, **1980**, pp. 147−166.
[2] B. I. Sikic, M. Rosencweig, S. K. Carter, *Bleomycin Chemotherapy*, Academic Press, Orlando, **1985**.
[3] J. S. Lazo, B. A. Chabner in *Cancer Chemotherapy and Biotherapy: Principals and Practice* (Eds.: B. A. Chabner, D. L. Longo), 2nd ed., Lippincott−Raven, Philadelphia, PA, **1996**, p. 379.
[4] S. M. Hecht, *Acc. Chem. Res.* **1986**, *19*, 383−391.
[5] J. Stubbe, J. W. Kozarich, *Chem. Rev.* **1987**, *87*, 1107−1136.
[6] M. J. Absalon, W. Wu, J. W. Kozarich, J. Stubbe, *Biochemistry* **1995**, *34*, 2076−2086.
[7] J. Stubbe, J. W. Kozarich, W. Wu, D. E. Vanderwall, *Acc. Chem. Res.* **1996**, *29*, 322−330.
[8] D. L. Boger, H. Cai, *Angew. Chem.* **1999**, *111*, 470−500; D. L. Boger, H. Cai, *Angew. Chem. Int. Ed.* **1999**, *38*, 448−476.
[9] R. M. Burger, *Chem. Rev.* **1998**, *98*, 1153−1169.
[10] K. E. Loeb, J. M. Zaleski, C. D. Hess, S. M. Hecht, E. I. Solomon, *J. Am. Chem. Soc.* **1998**, *120*, 1249−1259.
[11] N. Lehnert, F. Neese, R. Y. N. Ho, L. Que Jr., E. I. Solomon, *J. Am. Chem. Soc.* **2002**, *124*, 10810−10822.
[12] C. A. Claussen, E. C. Long, *Chem. Rev.* **1999**, *99*, 2797−2816.
[13] H. Umezawa, K. Maeda, T. Takeuchi, Y. Okami, *J. Antibiot.* **1966**, *19*, 200−209.
[14] Y. Iitaka, H. Nakamura, T. Nakatani, Y. Muraoka, A. Fujii, T. Takita, H. Umezawa, *J. Antibiot.* **1978**, *31*, 1070−1072.
[15] T. Takita, Y. Muraoka, T. Nakatani, A. Fujii, Y. Iitaka, H. Umezawa, *J. Antibiot.* **1978**, *31*, 1073−1077.
[16] M. Sugiyama, T. Kumagai, M. Hayashida, M. Maruyama, *Biol. Chem.* **2002**, *277*, 2311−2320.
[17] W. Wu, D. E. Vanderwall, J. W. Kozarich, J. Stubbe, C. J. Turner, *J. Am. Chem. Soc.* **1994**, *116*, 10843−10844.
[18] W. Wu, D. E. Vanderwall, S. M. Lui, X.-J. Tang, C. J. Turner, J. W. Kozarich, J. Stubbe, *J. Am. Chem. Soc.* **1996**, *118*, 1268−1280.
[19] S. M. Lui, D. E. Vanderwall, W. Wu, X.-J. Tang, C. J. Turner, J. W. Kozarich, J. Stubbe, *J. Am. Chem. Soc.* **1997**, *119*, 9603−9613.
[20] D. E. Vanderwall, S. M. Lui, W. Wu, C. J. Turner, J. W. Kozarich, J. Stubbe, *Chem. Biol.* **1997**, *4*, 373−387.
[21] S. T. Hoehn, H.-D. Junker, R. C. Bunt, C. J. Turner, J. Stubbe, *Biochemistry* **2001**, *40*, 5894−5905.
[22] A. Papakyriakou, B. Mouzopoulou, N. Katsaros, *J. Biol. Inorg. Chem.* **2003**, *5*, 549−559.
[23] A. Papakyriakou, N. Katsaros, *Eur. J. Inorg. Chem.* **2003**, *16*, 3001−3006.
[24] M. A. J. Akkerman, E. W. J. F. Neijman, S. S. Wijmenga, C. W. Hilbers, W. Bermel, *J. Am. Chem. Soc.* **1990**, *112*, 7462−7474.
[25] T. E. Lehmann, L.-J. Ming, M. E. Rosen, L. Que Jr., *Biochemistry* **1997**, *36*, 2807−2816.
[26] R. P. Sheridan, R. K. Gupta, *J. Biol. Chem.* **1981**, *256*, 1242−1247.
[27] G. M. Ehrenfeld, N. Murugesan, S. M. Hecht, *Inorg. Chem.* **1984**, *23*, 1496−1498.
[28] R. M. Burger, J. Peisach, *J. Inorg. Chem.* **1984**, *23*, 2215−2217.
[29] H. B. Grey, R. Margalit, J. M. Clarke, L. Podbielski, *Chem. Biol. Interact.* **1986**, *59*, 231−245.
[30] B. Mouzopoulou, H. Kozlowski, N. Katsaros, A. Garnier-Suillerot, *Inorg. Chem.* **2002**, *40*, 6923−6929.
[31] L. Banci, A. Dei, D. Gatteschi, *Inorg. Chim. Acta* **1982**, *67*, L53−L55.
[32] J. Kuwahara, T. Suzuki, Y. Sugiura, *Biochem. Biophys. Res. Commun.* **1985**, *129*, 368−374.
[33] M. A. J. Akkerman, C. A. G. Haasnoot, C. W. Hilbers, *Eur. J. Biochem.* **1988**, *173*, 211−225.
[34] R. A. Manderville, J. F. Ellena, S. M. Hecht, *J. Am. Chem. Soc.* **1994**, *116*, 10851−10852.
[35] R. A. Manderville, J. F. Ellena, S. M. Hecht, *J. Am. Chem. Soc.* **1995**, *117*, 7891−7903.0.
[36] A. M. Calafat, H. Won, L. G. Marzilli, *J. Am. Chem. Soc.* **1997**, *119*, 3656−3664.
[37] J. D. Otvos, W. E. Antholine, S. Wehrli, D. H. Petering, *Biochemistry* **1996**, *35*, 1458−1465.
[38] A. Dei, D. Gatteschi, *J. Inorg. Biochem.* **1982**, *17*, 131−137.
[39] L. L. Guan, J. Kuwahara, Y. Sugiura, *Biochemistry* **1993**, *32*, 6141−6145.
[40] R. E. Lenkinski, B. E. Peerce, R. P. Pillai, J. D. Glickson, *J. Am. Chem. Soc.* **1980**, *102*, 7088−7093.
[41] T. E. Lehmann, M. L. Serrano, L. Que Jr., *Biochemistry* **2000**, *39*, 3886−3898.
[42] T. E. Lehmann, *J. Biol. Inorg. Chem.* **2002**, *7*, 305−312.
[43] G. J. Bosl, D. F. Bajorin, J. Sheinfeld in *Cancer: Principles and Practice of Oncology* (Eds.: V. T. DeVita, S. Hellman, S. A. Rosenberg), 6th ed., Lippincott Williams & Wilkins, Philadelphia, PA, **2001**, pp. 1491−1518.
[44] J. P. Albertini, A. Garnier-Suillerot, *Inorg. Chem.* **1986**, *25*, 1216−1221.
[45] R. B. Martin in *Platinum, Gold and Other Metal Chemotherapeutic Agents* (Ed.: S. J. Lippard), ACS Symposium Series 209, American Chemical Society, Washington, DC, **1983**, pp. 231−244.

 © 2004 Wiley-VCH Verlag GmbH & Co. KGaA, Weinheim

[46] M. Kotowski, R. van Eldik, *Inorg. Chem.* **1984**, *23*, 3310−3312.
[47] H. Hohmann, R. van Eldik, *Inorg. Chim. Acta* **1990**, *174*, 87−92.
[48] T. G. Appleton, A. J. Bailey, D. R. Bedgood, J. R. Hall, *Inorg. Chem.* **1994**, *33*, 217−226.
[49] J. M. Tercero-Moreno, A. Matilla-Hernández, S. González-García, J. Niclós-Gutiérrez, *Inorg. Chim. Acta* **1996**, *253*, 23−29.
[50] M. L. González, J. M. Tercero, A. Matilla, J. Niclós-Gutiérrez, M. T. Fernández, M. C. López, S. González, *Inorg. Chem.* **1997**, *36*, 1806−1812.
[51] C. Xia, F. H. Försterling, D. H. Petering, *Biochemistry* **2003**, *42*, 6559−6564.
[52] E. A. Sausville, J. Peisach, S. B. Horwitz, *Biochemistry* **1978**, *17*, 2740−2746.
[53] T. D. Goddard, D. G. Kneller, *SPARKY 3*, University of California, San Francisco, **2002**.
[54] A. Derome, M. Williamson, *J. Magn. Reson.* **1990**, *88*, 177−185.
[55] A. Bax, D. G. Davis, *J. Magn. Reson.* **1985**, *65*, 355−360.
[56] A. Bax, S. Subramanian, *J. Magn. Reson.* **1986**, *67*, 565−569.
[57] A. Bax, M. F. Summers, *J. Am. Chem. Soc.* **1986**, *108*, 2093−2094.
[58] T. L. Hwang, A. J. Shaka, *J. Magn. Reson.* **1995**, *112*, 275−279.
[59] D. A. Case, D. A. Pearlman, J. W. Caldwell, T. E. Cheatham, W. S. Ross, C. L. Simmerling, T. A. Darden, K. M. Merz, R. V. Stanton, A. L. Cheng, J. J. Vincent, M. Crowley, V. Tsui, R. J. Radmer, Y. Duan, J. Pitera, I. Massova, G. L. Seibel, U. C. Singh, P. K. Weiner, P. A. Kollman, *AMBER 6*, University of California, San Francisco, **1999**.
[60] W. D. Cornell, P. Cieplak, C. I. Bayly, I. R. Gould, K. M. Merz Jr., D. M. Ferguson, D. C. Spellmeyer, T. Fox, J. W. Caldwell, P. A. Kollman, *J. Am. Chem. Soc.* **1995**, *117*, 5179−5197.
[61] R. J. Woods, R. A. Dwek, C. J. Edge, B. Fraser-Reid, *J. Phys. Chem.* **1995**, *99*, 3832−3846.
[62] A. Bondi, *J. Phys. Chem.* **1964**, *68*, 441−451.
[63] T. W. Hambley, *Inorg. Chem.* **1998**, *37*, 3767−3774.
[64] T. W. Hambley, A. R. Jones, *Coord. Chem. Rev.* **2001**, *212*, 35−59.
[65] A. D. Becke, *Phys. Rev. A.* **1988**, *38*, 3098−3100.
[66] A. D. Becke, *J. Chem. Phys.* **1993**, *98*, 1372.
[67] A. D. Becke, *J. Chem. Phys.* **1993**, *98*, 5648−5652.
[68] M. W. Schmidt, K. K. Baldridge, J. A. Boatz, S. T. Elbert, M. S. Gordon, J. J. Jensen, S. Koseki, N. Matsunaga, K. A. Nguyen, S. Su, T. L. Windus, M. Dupuis, J. A. Montgomery, *J. Comput. Chem.* **1993**, *14*, 1347−1363.
[69] P. J. Hay, W. R. Wadt, *J. Chem. Phys.* **1985**, *82*, 270−283.
[70] P. J. Hay, W. R. Wadt, *J. Chem. Phys.* **1985**, *82*, 299−310.
[71] W. R. Wadt, P. J. Hay, *J. Chem. Phys.* **1985**, *82*, 284−298.
[72] C. I. Bayly, P. Cieplak, W. D. Cornell, P. A. Kollman, *J. Phys. Chem.* **1993**, *97*, 10269−10280.
[73] L. Young, I. A. Topol, A. A. Rashin, S. K. Burt, *J. Comput. Chem.* **1997**, *18*, 522−532.
[74] T. Mosmann, *J. Immunol. Methods* **1983**, *65*, 55−63.
[75] H. Tada, O. Shino, K. Kurosima, M. Koyama, K. Tsukamoto, *J. Immunol. Methods* **1986**, *93* 157−165.
[76] M. B. Hansen, S. E. Nielsen, K. Berg, *J. Immunol. Methods* **1989**, *119*, 203−210.
[77] M. B. Hansen, C. Ross, K. Berg, *J. Immunol. Methods* **1990**, *127*, 241−248.

Received January 15, 2004
Early View Article
Published Online May 25, 2004

 © 2004 Wiley-VCH Verlag GmbH & Co. KGaA, Weinheim

Oxidation of *N*-(4-Chlorophenyl)-*N*′-hydroxyguanidine to *N*-(4-Chlorophenyl)urea and Nitric Oxide by Photoexcited Iron Porphyrins

Andrea Maldotti,*[a] Alessandra Molinari,[a] Irene Vitali,[a] Elena Ganzaroli,[a] Pierrette Battioni,[b] Delphine Mathieu,[b] and Daniel Mansuy[b]

Keywords: O−O activation / Nitric oxide / Photooxidation / Porphyrins / Protein models

Photochemical excitation ($\lambda > 350$ nm) of chloro[*meso*-tetrakis(2,6-dichlorophenyl)porphyrin]iron(III) [Fe^{III}(TDCPP)Cl] and chloro[*meso*-tetra(α,α,α,α-pivalamidophenyl)porphyrin]-iron(III) [Fe^{III}(TpivPP)Cl] induces the oxidation of coordinated *N*-(4-chlorophenyl)-*N*′-hydroxyguanidine (**1**) by molecular oxygen, to give iminoxyl radicals and the $Fe^{II}(O_2)$ [or $Fe^{III}(O_2^{\cdot})$] adduct. This complex can be accumulated in significant amounts using [Fe^{III}(TpivPP)Cl]. The primary photoproducts give rise to secondary reactions that lead to the formation of *N*-(4-chlorophenyl)urea (**2**) as the main end-product of **1**. The conversion of **1** into **2** is accompanied by the formation of NO, as revealed both by an ESR spin-trapping technique and in the form of its stable end-products NO_2^- and NO_3^-. The presence of 1-methyl imidazole (1-MeIm) coordinated in axial position has a significant positive effect on the photoinduced production of **2** and NO from the hydroxyguanidine **1**. The observation that radical scavengers inhibit the photooxidation process strongly supports the possibility that the reaction pathway resembles a radical-type autoxidation mechanism, where the very fast reaction of O_2 with the ferrous porphyrin in the presence of the photogenerated iminoxyl radical should yield an iron-peroxo intermediate as precursor of the urea **2** and NO.

(© Wiley-VCH Verlag GmbH & Co. KGaA, 69451 Weinheim, Germany, 2004)

Introduction

The photochemical excitation of iron porphyrin complexes [Fe^{III}(P)] is an important tool for obtaining biomimetic model systems of interest in oxygenase-like catalytic oxidation.[1] All these systems are characterized by common primary photoprocesses. Irradiation in axial ligand (L) to metal charge-transfer bands (λ = 300−400 nm) induces a homolytic cleavage of the Fe^{III}(L) bond, which causes oxidation and detachment of L$^{\cdot}$ as a radical species and reduction of Fe^{III} to Fe^{II} [Equation (1)]. It has been demonstrated that O_2 is able to effectively react with the ferrous intermediate, thus inhibiting solvent-cage effects [back reaction in Equation (1)]. A peculiar aspect of this process is that a monoelectronic reductive activation of O_2 occurs through the formation of a dioxyiron complex $Fe^{II}(P)(O_2)$ or $Fe^{III}(P)(O_2^{\cdot})$ according to Equation (2). A two-electron reduction of O_2 may also be achieved when the described photochemical process is carried out in the presence of suitable hydrocarbons (RH). Under these conditions, alkyl radicals (R$^{\cdot}$) may be formed as a consequence of the reaction between the photogenerated L$^{\cdot}$ radicals and RH. The extremely fast subsequent reaction of O_2 with Fe^{II}(P) in the presence of R$^{\cdot}$ may lead to the formation of alkyl-peroxo complexes according to Equation (3).[2] In all cases, the photoassisted activation of O_2 occurs in a catalytic manner, since the starting iron porphyrin is restored after its reoxidation and after coordination of a new equivalent of axial ligand.

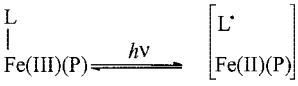

(1)

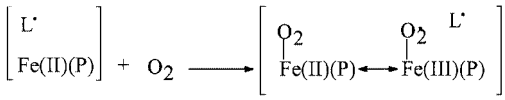

(2)

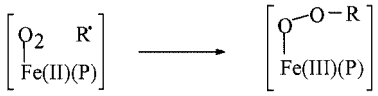

(3)

Chloro[*meso*-tetrakis(2,6-dichlorophenyl)porphyrin]-iron(III) [Fe^{III}(TDCPP)Cl] has been often employed in the photocatalytic activation of O_2 as the bulky chlorine atoms in its *meso*-aryl groups prevent the well-known bimolecular

[a] Dipartimento di Chimica Università di Ferrara, Sezione ISOF−CNR,
Via Luigi Borsari 46, 44100 Ferrara, Italy
[b] Laboratoire de Chimie et Biochimie Pharmacologiques Toxicologiques, UMR 8601 CNRS, Université Paris V,
45 rue des Saints Pères, 75270 Paris Cedex 06, France

reaction of the Fe^{II}dioxy complex to give μ-oxo dimers as the final product.[3] Moreover, they provide a steric protection of the porphyrin ring against its radical-induced oxidative degradation.[4]

One intriguing and up-to-date aspect of the photocatalytic processes described above is their possibility to generate reactive intermediates such as $Fe^{III}(P)(O_2^{\cdot})$, $Fe^{III}(P)$-(OOR) and radical species that might be relevant also to the mechanism of nitric oxide synthases (NOSs), as explained below.

All the three NOS isoforms in mammals catalyse the stepwise oxidation of L-arginine to nitric oxide (NO) by O_2 and NADPH.[5] This process occurs in the NOS oxygenase domain, which contains heme and tetrahydrobiopterin (usually indicated as BH_4) as cofactors.[6] The NO synthesis mechanism is complex and not completely understood. A first step is likely a classical monooxygenation of L-arginine to give *N*-hydroxy-L-arginine, which occurs with the consumption of one mol of O_2 and one mol of NADPH [first step in Equation (4)]. The generally accepted P450 reaction mechanism can account for the stoichiometry and the product formation.[7] Reduction of ferric heme is followed by the formation of a Fe^{II}dioxy complex that accepts a second electron from NADPH to form an iron-peroxo intermediate. The subsequent O−O bond scission yields a presumed iron-oxo species that is able to hydroxylate a guanidinic nitrogen of L-arginine.

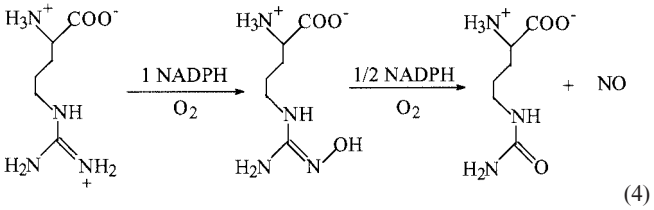

(4)

The second step involves an oxidative cleavage of the C=NOH bond of *N*-hydroxy-L-arginine to give the final products NO and L-citrulline through the consumption of one mol of O_2 and only one electron coming from 0.5 mol of NADPH [second step in Equation (4)].[8] A monoelectronic reduction of ferric heme enables O_2 binding and forms an iron-dioxy complex [$Fe^{II}(P)(O_2)$ or $Fe^{III}(P)(O_2^{\cdot})$]. A number of experimental results are consistent with BH_4 having a redox function in the second step of NO synthesis. Stuehr et al.[9] have proposed that the cofactor BH_4 may be able to provide a second electron to $Fe^{III}(P)(O_2^{\cdot})$ to yield an iron-peroxo intermediate as ultimate oxidant able to react with bound *N*-hydroxy-L-arginine according to Scheme 1 (steps a and b). The subsequent back electron transfer to the $BH_4^{+\cdot}$ radical should yield the final products NO and L-citrulline together with BH_4 and $Fe^{III}(P)$ in their starting conditions (step c).

The formation of radical intermediates has been proposed by Groves et al.[5d,10] for model systems that mimic many important properties of the NOS-catalysed oxidation of *N*-hydroxy-L-arginine. This mechanism, summarized in Scheme 2, involves the oxidation of *N*-hydroxy-L-arginine to the corresponding iminoxyl radical with the simultaneous reduction of $Fe^{III}(P)$ to $Fe^{II}(P)$ (step a). The insertion of O_2 between the ferrous porphyrin and the radical in its α-nitroso form would generate an iron-peroxo intermediate (steps b and c). The subsequent homolytic cleavage of its O−O bond may lead to the formation of NO, L-citrulline and $Fe^{IV}(P)(O)$ (step d), which can immediately undergo a single-electron reduction with, possibly, the involvement of BH_4 (step e).

The very limited number of substrates for NOSs known so far suggests that highly specific structural features are required for NO generation by these enzymes. However, it has been recently shown that NOSs are also able to catalyse the oxidation of some analogues of *N*-hydroxy-L-arginine.[11] In particular, it has been found that mixtures of *N*-arylurea, *N*-arylcyanamide and NO are formed when several *N*-aryl-*N*′-hydroxyguanidines are incubated in the presence of NOS. These substrates are of particular interest in mechanistic studies with model systems since, contrary to *N*-hydroxy-L-arginine, their oxidation products are relatively stable and easy to analyse.

In this work, we have used as oxidizable substrate a simple *N*-aryl-*N*′-hydroxyguanidine: *N*-(4-chlorophenyl)-*N*′-hydroxyguanidine (**1**, see Scheme 3). We have investigated its redox reactivity in the presence of photoexcited iron porphyrins with the aim of inducing the reductive activation of O_2 in order to obtain intermediates analogous to those involved in the NOS-dependent oxidation of *N*-hydroxyarginine. The possibility that the photoinduced redox processes may be affected by the presence of *N*-methyl imidazole (1-MeIm) has also been evaluated.

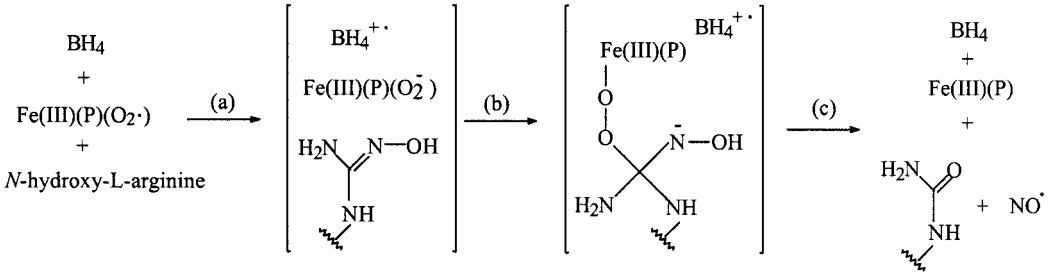

Scheme 1. Proposed mechanism for NOS-assisted oxidation of *N*-hydroxy-L-arginine

 © 2004 Wiley-VCH Verlag GmbH & Co. KGaA, Weinheim

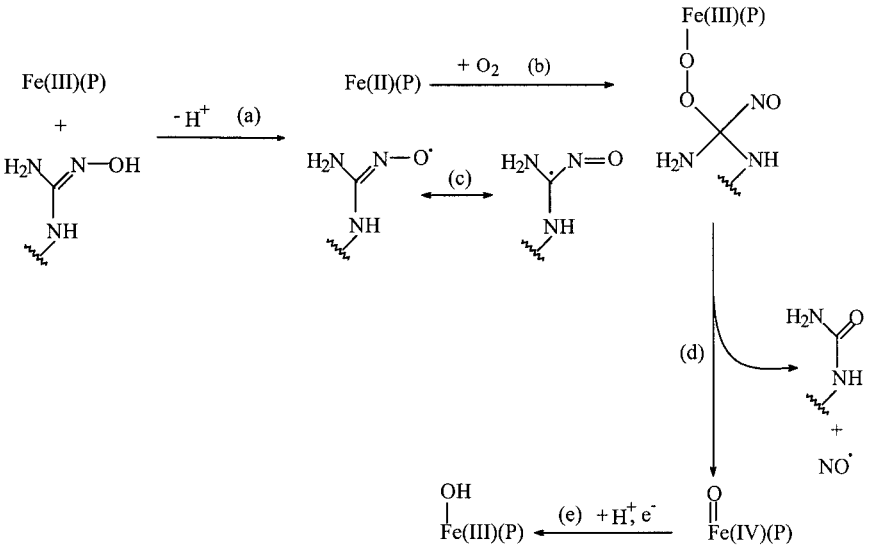

Scheme 2. Proposed radical-type mechanism

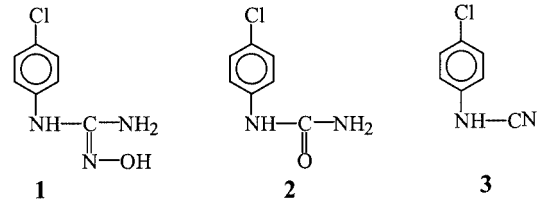

Scheme 3. *N*-(4-Chlorophenyl)-*N*′-hydroxyguanidine (**1**), *N*-(4-chlorophenyl)urea (**2**) and *N*-(4-chlorophenyl)cyanamide (**3**)

The iron porphyrins employed are shown in Figure 1. [Fe^{III}(TDCPP)Cl] has been chosen because of its stability under photocatalytic conditions. The chloro[*meso*-tetra(α,α,α,α-pivalamidophenyl)porphyrin]iron(III) [Fe^{III}(TpivPP)Cl] is expected to give important information about the possible formation and reactivity of $Fe^{II}(P)(O_2)$ adducts as it has a protective enclosure for binding oxygen on one side of the porphyrin ring and it is able to form a stable adduct with O_2.[12]

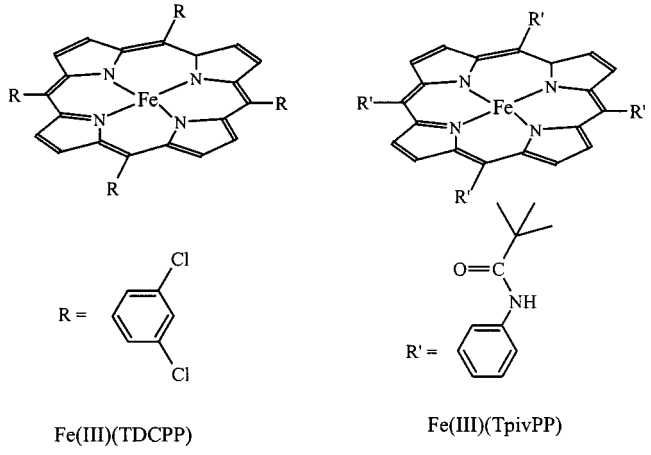

Figure 1. Structure of the investigated iron porphyrins

Results and Discussion

Biomimetic Photooxidation of *N*-(4-Chlorophenyl)-*N*′-hydroxyguanidine (1)

The photochemical experiments described below were carried out by irradiating CH_3CN solutions of [Fe^{III}(TDCPP)Cl] (1×10^{-5} M) and **1** (1×10^{-3} M) in the presence of 1-MeIm, (5×10^{-5} M) [Fe^{III}(TDCPP)Cl/**1**/1-MeIm system] or without 1-MeIm [Fe^{III}(TDCPP)Cl/**1** system] with light of wavelength higher than 350 nm. First of all, we report some UV/Vis results shedding light on the nature of the main light-absorbing species present in these systems. More specifically, we were interested in defining the nature of the iron porphyrin axial ligand that may be involved in the primary photochemical process in Equation (1).

It has been reported previously that numerous *N*-hydroxyguanidines such as **1** are able to bind through their oxygen atom to the ferric heme group of both microperoxidase-8 and NOS itself.[13] The consequent formation of stable, low-spin complexes is accompanied by significant changes in the UV/Vis spectra. In particular, the coordination of *N*-hydroxyguanidines causes red shifts of the Soret peak. Table 1 (runs a and b) provides evidence that the addition of **1** to a [Fe^{III}(TDCPP)Cl] solution induces an analogous shift of the Soret band from 412 nm to 422 nm, thus indicating that **1** is coordinated in the axial position to the metal centre to give the complex [Fe^{III}(TDCPP)(**1**)Cl]. Table 1 (run c) and Figure 2 show that different spectral variations were obtained when both **1** and 1-MeIm were added to [Fe^{III}(TDCPP)Cl]. This result, together with the observation that addition of 1-MeIm alone causes other spectral changes (run d) allows us to infer that solution equilibria in the [Fe^{III}(TDCPP)Cl]/**1**/1-MeIm system lead mainly to the formation of a porphyrin complex that contains hydroxyguanidine and 1-MeIm bound in the two axial positions (step a in Scheme 4).

 © 2004 Wiley-VCH Verlag GmbH & Co. KGaA, Weinheim

Table 1. UV/Vis spectroscopic data of [Fe^{III}(TDCPP)Cl]

Run	System[a]	Absorption maxima (nm)
a	Fe^{III}(TDCPP)Cl	325, 412, 570
b	Fe^{III}(TDCPP)Cl/**1**	422, 541
c	Fe^{III}(TDCPP)Cl/**1**/1-MeIm	426, 535
d	Fe^{III}(TDCPP)Cl/1-MeIm	327, 413, 569
e	Fe^{III}(TDCPP)Cl/**1**/1-MeIm/hν	416, 505, 546

[a] [Fe^{III}(TDCPP)Cl] (CH_3CN): 1×10^{-5} M; [**1**]: 1×10^{-3} M; [1-MeIm]: 5×10^{-5} M. Irradiation in run e was carried out at 22 ± 1 °C in the presence of 760 Torr of oxygen; excitation wavelength: $\lambda > 350$ nm; irradiation time: 30 min.

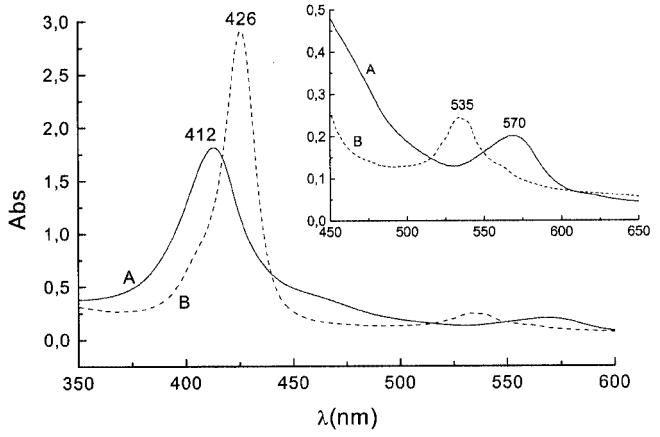

Figure 2. A) UV/Vis spectrum of a CH_3CN solution of [Fe^{III}(TDCPP)Cl] (1×10^{-5} M); B) UV/Vis spectrum of a CH_3CN solution of [Fe^{III}(TDCPP)Cl] (1×10^{-5} M) in the presence of **1** (1×10^{-3} M), and 1-MeIm (5×10^{-5} M)

The [Fe^{III}(TDCPP)Cl]/**1**/1-MeIm system was irradiated for 30 minutes in the presence of 760 torr of O_2. HPLC analyses revealed the formation of both *N*-(4-chlorophenyl)urea (**2**) and *N*-(4-chlorophenyl)cyanamide (**3**; Scheme 3), by comparison of their retention times with those of authentic samples, and by co-injection with the authentic compounds.

Table 2 reports the yields of the described photoprocess in terms of amount of detected products. The first row of this table provides evidence that the urea **2** is the main end-product of the hydroxyguanidine **1**. In agreement with an NOS-like oxidation mechanism, the conversion of **1** to **2** approximately matches the formation of NO, which was revealed in the form of its stable end-products NO_2^- and NO_3^-. Table 2 shows that the cyanamide **3** is a second minor photoproduct. Literature data show that the oxidation of the hydroxyguanidine **1** to the corresponding cyanamide is accompanied by the formation of NO^- instead of NO.[14] This intermediate, after dimerization, protonation and dehydration would release gaseous N_2O without the formation of NO_2^- and NO_3^-.

Control experiments indicated that the formation of **2**, **3**, NO_2^- and NO_3^- from **1** did not occur in appreciable amounts in the dark or in the absence of either [Fe^{III}(TDCPP)Cl] or O_2. We also verified that the photoexciting wavelengths employed here did not cause any appreciable degradation of **2** and **3**. Finally, we found UV/Vis evidence that neither **2** nor **3** competes with **1** in binding the metal centre at the concentrations that they typically reach during the photochemical experiment.

[Fe^{III}(TDCPP)Cl] underwent significant spectral changes when irradiated in the presence of **1** and 1-MeIm. As shown in Table 1 (compare runs c and e), we observed a blue shift

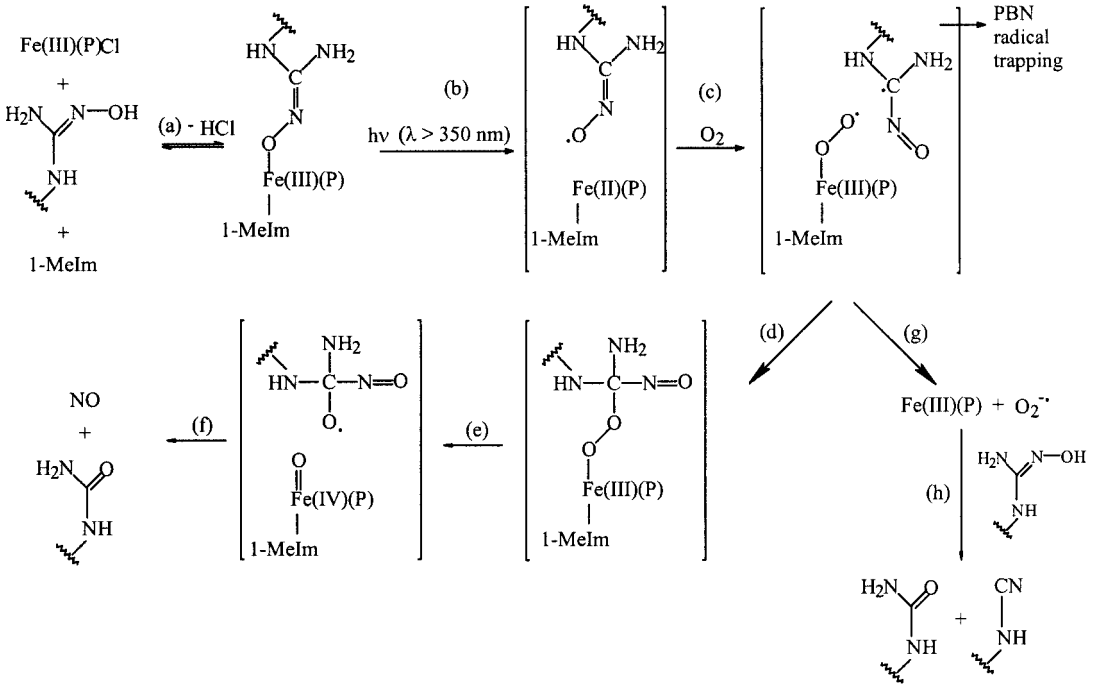

Scheme 4. Proposed photooxidation mechanism

 © 2004 Wiley-VCH Verlag GmbH & Co. KGaA, Weinheim

Table 2. Oxidation of **1** by photoexcited [Fe^{III}(TDCPP)Cl] and by the [Fe^{III}(TpivPP)($O_2^{\cdot}$)(1-MeIm)] adduct

System	Products[a] (μM) Urea **2**	Cyanamide **3**	NO_2^-	NO_3^-
Fe^{III}(TDCPP)Cl/**1**/1-MeIm[b]	6.6 ± 0.6	1.5 ± 0.1	2.2 ± 0.2	2.7 ± 0.2
Fe^{III}(TDCPP)Cl/**1**[b]	1.6 ± 0.1	1.5 ± 0.1	<0.6	<0.6
Fe^{III}(TDCPP)Cl/**1**/1-MeIm/PBN[b]	3.5 ± 0.3	1.5 ± 0.1	1.2 ± 0.2	1.3 ± 0.2
Fe^{III}(TpivPP)($O_2^{\cdot}$)/**1**/1-MeIm[c]	1 ± 0.1	<0.2	<0.6	<0.6

[a] Results are expressed in μmol dm^{-3} of products formed and are averages (± standard deviation) of between three and five experiments. [b] Irradiations were carried out at 22 ± 1 °C in the presence of 760 Torr of oxygen. Excitation wavelength: $\lambda > 350$ nm. Irradiation time: 30 minutes. [Fe^{III}(P)]: 1×10^{-5} M; [**1**]: 1×10^{-3} M; [1-MeIm]: 5×10^{-5} M; [PBN]: 1×10^{-4} M. [c] The [Fe^{III}(TpivPP)($O_2^{\cdot}$)]/1-MeIm adduct was obtained by dissolving [Fe^{III}(TpivPP)Cl] (1×10^{-5} M) in a mixture of acetone and ethanol (95:5, v/v) in the presence of 1-MeIm (5×10^{-5} M). The solution was degassed (less than 1×10^{-5} Torr), irradiated (90 s) and put in contact with O_2 at low temperature (−5 to −8 °C). Then, **1** (1×10^{-3} M) was added to the obtained sample.

of the porphyrin Soret band from 426 nm to 416 nm, as well as the formation of two new bands at 505 and 546 nm. These spectral variations may be ascribed to axial coordination of the end-product NO_2^- anion on the basis of literature data concerning the effect of binding of this anion on the spectroscopic properties of iron porphyrin complexes[15] and by the observation that progressive addition of $NaNO_2$ to the [Fe^{III}(TDCPP)]/**1**/1-MeIm system induced analogous spectral variations.

The data reported in the second line of Table 2 show that the photoinduced oxidation of **1** occurred to some extent also in the absence of 1-MeIm. On the other hand, a significant reduction in the production of **2** and NO was observed in this case, indicating the main role of coordinated 1-MeIm in the photoinduced formation of these products.

Spin-Trapping Investigation and Proposed Reaction Pathways

Evidence for the oxidation of bound *N*-hydroxyguanidine (**1**) to radical species was provided by an ESR spin-trapping investigation. This technique is a powerful tool for detecting the formation of short-lived radicals[16] and has been fruitfully employed in photochemical studies on iron porphyrins.[2a,4] It is based on the ability of some molecules, such as α-phenyl-*N*-*tert*-butylnitrone (PBN), to trap radicals ($R^{\cdot}$) and give paramagnetic nitroxides stable enough to be studied by ESR spectroscopy [Equation (5)].

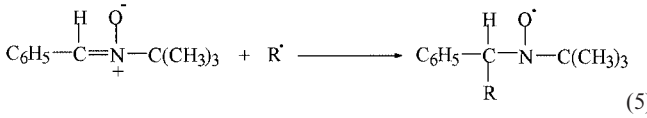

(5)

The [Fe^{III}(TDCPP)Cl]/**1**/1-MeIm system was irradiated in the presence of PBN (5×10^{-3} M) directly in the cavity of an ESR spectrometer. Figure 3 shows that the spectrum obtained consists of a triplet of doublets, with hyperfine splitting constants $a_N = 14.75$ G and $a_H = 2.77$ G. This signal may be ascribed to the trapping of a radical species originating from the photooxidation of the bound hydroxyguanidine **1** according to step b in Scheme 4. In line with this statement, blank experiments carried out without **1** did not give any ESR signal.

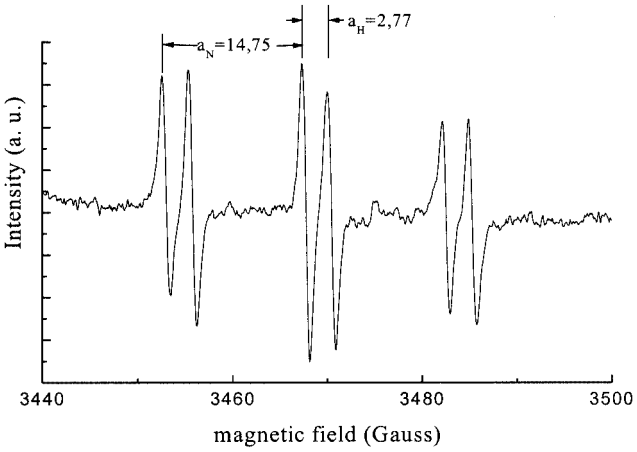

Figure 3. ESR spin-trapping spectrum obtained during irradiation of a CH_3CN solution of [Fe^{III}(TDCPP)Cl] (1×10^{-5} M) in the presence of **1** (1×10^{-3} M), 1-MeIm (5×10^{-5} M) and PBN (5×10^{-3} M)

Row 3 in Table 2 reports the concentration of **2**, **3**, NO_2^- and NO_3^- after 30 minutes irradiation of the [Fe^{III}(TDCPP)Cl]/**1**/1-MeIm system carried out in the presence of PBN (1×10^{-4} M). The radical scavenger did not affect at all the formation of the cyanamide **3**, while it partially inhibited the production of the urea **2**, NO_2^- and NO_3^-.

The above results are consistent with a reaction pathway for the light-induced oxidation of the hydroxyguanidine **1** by [Fe^{III}(TDCPP)Cl] that resembles the radical-type autoxidation mechanism mentioned in the introduction.[5d,10] In line with the general mechanism shown in Equations (1)−(3), peroxidic intermediates should be formed as a consequence of the very fast reaction of O_2 with the photogenerated ferrous porphyrin in the presence of iminoxyl radicals (steps c and d in Scheme 4). The formation of the urea **2** and NO likely occurs as a consequence of a homolytic cleavage of the O−O bond according to steps e and f. The possibility that photogenerated alkyl hydroperoxides may decompose by the above reactions has been reported previously.[1c,2] It seems likely that the well-known ability of

 © 2004 Wiley-VCH Verlag GmbH & Co. KGaA, Weinheim

bound 1-MeIm to stabilize this photogenerated ferrous-dioxy intermediate $Fe^{III}(O_2^{\cdot})$[12b] may be the reason for the observed positive effect of this nitrogen base on the final product yields.

An additional possibility to take into account is that oxidation of **1** may occur as a consequence of its reaction with $O_2^{\cdot -}$, which could originate from $Fe^{III}(O_2^{\cdot})$ dissociation (steps g and h). Indeed, it has been already demonstrated that $O_2^{\cdot -}$ can react with **1** to give the cyanamide **3** as the major product.[17] The low yield of this product indicates that this possibility is only a minor process in the photoinduced oxidation of **1** described here.

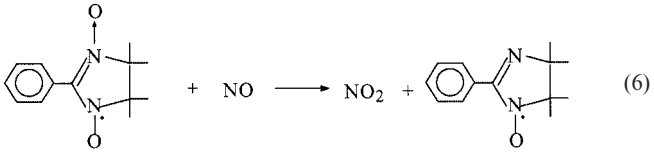

(6)

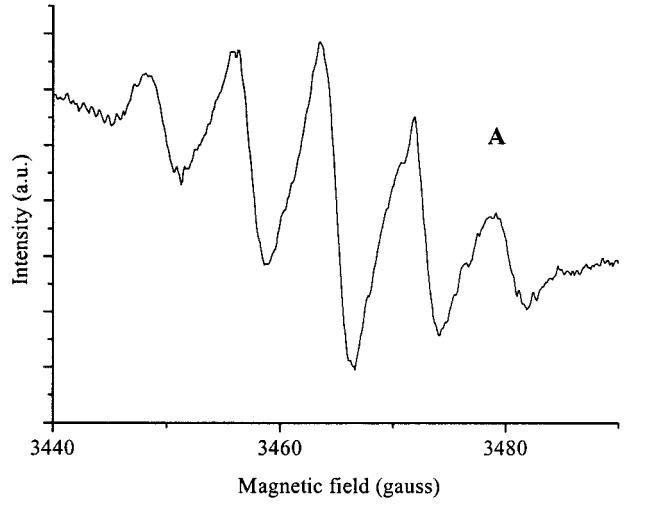

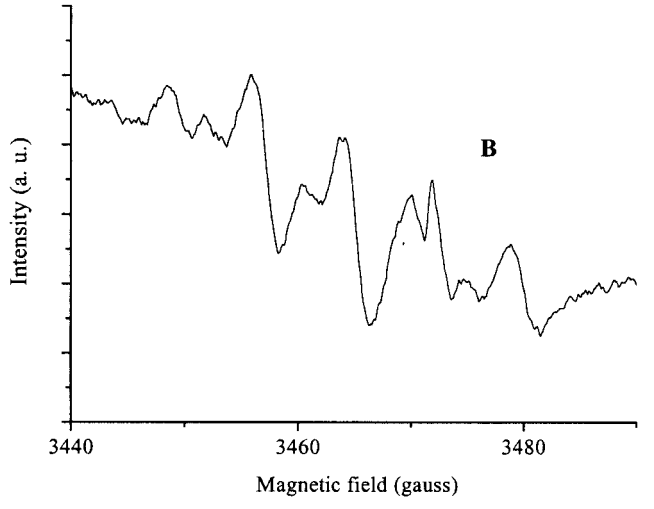

Figure 4. A) ESR spectrum of PTIO (2×10^{-6} M) in a CH_3CN solution containing **1** (1×10^{-3} M), [Fe^{III}(TDCPP)Cl] (1×10^{-5} M) and 1-MeIm (5×10^{-5} M); B) curve A after ten minutes irradiation

The ESR spin-trapping technique was also used to obtain direct evidence for the formation of NO. We employed 2-phenyl-4,4,5,5-tetramethylimidazoline-1-oxyl 3-oxide (PTIO) as an NO-specific reactant.[18] The ESR spectrum of PTIO consists of a 1:2:3:2:1 quintet due to the interaction of one unpaired electron with two equivalent nitrogen atoms (a_N = 8.2 G). Nitric oxide reacts with this compound according to Equation (6) to give an imino-nitroxide (PTI), in which two different nitrogen atoms generate a different and more complex spectrum with nine lines (a_N^1 = 9.8 G and a_N^2 = 4.4 G).

Curve A in Figure 4 shows the five-line ESR spectrum of PTIO (2×10^{-6} M) in the presence of **1** (1×10^{-3} M), [Fe^{III}(TDCPP)Cl] (1×10^{-5} M) and 1-MeIm (5×10^{-5} M). The same signals were obtained when **1** or [Fe^{III}-(TDCPP)Cl] or 1-MeIm were omitted from the reaction mixture. Ten-minute photoexcitation led to a decrease of the intensity of this spectrum together with the growth of new signals, as shown by Curve B in Figure 4. The position of these signals corresponds very well to that expected for the nitroxide PTI.[17] Negligible spectral changes were observed in the dark when the photochemical experiment was carried out in the absence of [Fe^{III}(TDCPP)Cl] or **1**.

Reactivity of Photogenerated [Fe^{II}(TpivPP)(O_2)(1-MeIm)]

Irradiation of [Fe^{III}(TpivPP)Cl] in the presence of **1**, 1-MeIm and O_2 gave results very similar to those obtained with the [Fe^{III}(TDCPP)Cl]/**1**/1-MeIm system from a qualitative point of view. However, experiments carried out with this porphyrin allowed us to accumulate only traces of the end-products, because it undergoes a very fast degradation under aerobic photochemical conditions to give small colourless fragments. This instability may be ascribed to the lack of hindered groups able to protect the *meso* positions from oxidative attacks.

In spite of this limitation, which forced us to limit the photocatalytic characterization previously described to [Fe^{III}(TDCPP)Cl], with [Fe^{III}(TpivPP)Cl] we could obtain direct experimental evidence of the photoinduced formation of a [Fe^{II}(TpivPP)(O_2)(1-MeIm)] adduct, which, in the previous discussion, has only been supposed for [Fe^{III}-(TDCPP)Cl].

The first step for obtaining the [Fe^{II}(TpivPP)(O_2)(1-MeIm)] adduct was the photoinduced reduction of the ferric porphyrin under anaerobic conditions. This result was obtained by irradiating (for 90 s, $\lambda > 350$ nm) deoxygenated solutions of [Fe^{III}(TpivPP)Cl] (1×10^{-5} M) containing 1-MeIm (5×10^{-5} M). We decided to use an acetone/ethanol (95:5) mixture as solvent knowing that, in these conditions, ethanol works as coordinating solvent and that the primary photochemical process is expected to be the reduction of Fe^{III} to Fe^{II} by the bound ethanolate, in line with the general mechanism shown in Equation (1).[2,4] Accordingly, the UV/Vis spectrum observed after irradiation (Curve A in Figure 5) presents the typical absorption at 567 nm of the ferrous porphyrin. The spectral changes (Curve B) that accompany the subsequent oxygenation of the sample at low temperature (−5 to −8 °C) are consistent with the forma-

 © 2004 Wiley-VCH Verlag GmbH & Co. KGaA, Weinheim

tion of [Fe^{II}(TpivPP)(O_2)(1-MeIm)] or [Fe^{III}(TpivPP)-(O_2·)(1-MeIm)] adduct.[12]

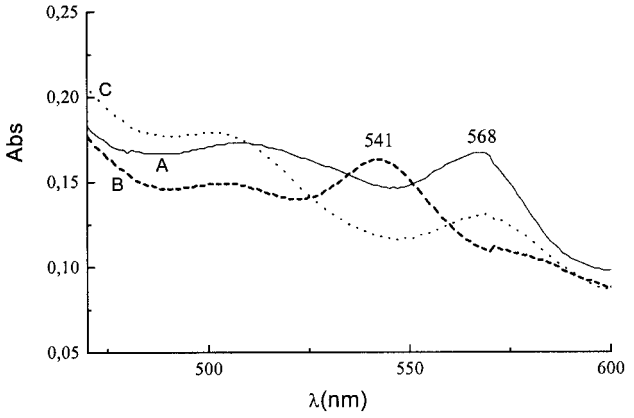

Figure 5. A) UV/Vis spectrum of an acetone/ethanol (95:5) solution of [Fe^{III}(TpivPP)Cl] (1×10^{-5} M) and 1-MeIm (5×10^{-5} M) after 90 s irradiation under anaerobic conditions; B) curve A after subsequent oxygenation of the sample at −8 °C; C) curve B after a second deoxygenation

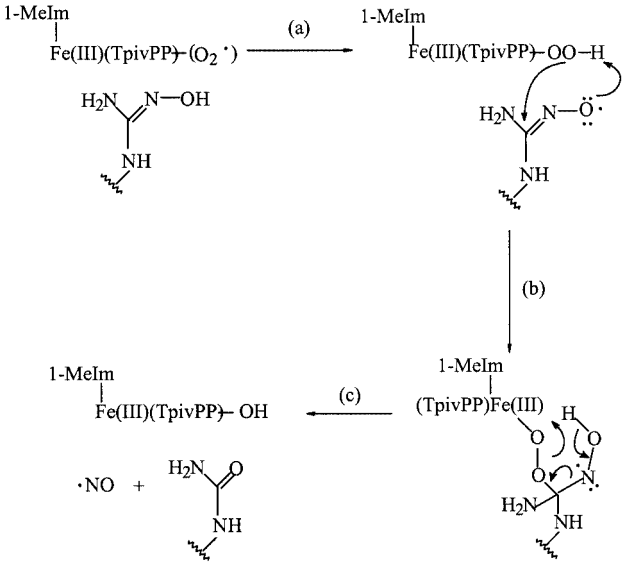

Scheme 5. Oxidation of **1** by the [Fe^{III}(TpivPP)(O_2·)(1-MeIm)] adduct

A second deoxygenation of this solution regenerated the spectrum of the ferrous porphyrin deprived of O_2. Figure 5 shows that this oxygenation/deoxygenation cycle is not completely reversible, probably due to irreversible oxidation of the porphyrin ring. The O_2 binding reversibility to Fe^{II}-(TpivPP) has been demonstrated and discussed in depth by Collman in previous fundamental papers.[12] The novelty of this work is that we observe the same binding reversibility using light rather than chemical reducing agents.

The possibility of accumulating significant amounts of the [Fe^{II}(TpivPP)(O_2)(1-MeIm)] adduct enabled us to investigate its possible reactivity towards the hydroxyguanidine **1**. In fact, it should be taken into account that the [Fe^{II}(TpivPP)(O_2)(1-MeIm)] species might undergo reduction by **1** to give an iron-peroxo intermediate,[19] although a number of results seem to argue against a reaction between the Fe^{III}(P)(O_2·) of NOS and *N*-hydroxy-L-arginine.[9a,9b,20]

Table 2 shows that the addition of **1** to the photogenerated [Fe^{III}(TpivPP)(O_2·)(1-MeIm)] led to a detectable amount of urea **2** with a yield of 80% with respect to the sum of **2** and **3**. A possible reaction pathway explaining this result is given in Scheme 5. The [Fe^{III}(TpivPP)(O_2·)-(1-MeIm)] intermediate might abstract the hydrogen atom of the hydroxyguanidine hydroxy group to furnish a hydroperoxo complex (step a), whose well-known nucleophilicity should allow it to react with the iminoxy radical (step b).[19,21] Finally, a subsequent pericyclic reaction of the peroxy intermediate is expected to form NO and **2** according to step c. The possibility that the conversion of **1** to **2** and NO upon irradiation of the [Fe^{III}(TDCPP)Cl]/**1**/1-MeIm system may also occur, at least in part, through the described mechanism cannot be ruled out.

The formation of urea as a major product of the reaction between [Fe^{II}(TpivPP)(O_2)(1-MeIm)] and **1** was confirmed by an additional experiment where the [Fe^{II}(TpivPP)(O_2)(1-MeIm)] adduct was prepared with a chemical reducing agent according to previous work (see Exp. Sect.).[12b] Addition of the hydroxyguanidine **1** to the chemically obtained [Fe^{II}(TpivPP)(O_2)(1-MeIm)] led to the formation of a detectable amount of the urea **2** with a yield of about the 65% with respect to the sum of **2** and **3**. This chemoselectivity in the production of urea is in line with that obtained using light to form [Fe^{II}(TpivPP)(O_2)(1-MeIm)]. The observed small differences of the **2**:**3** concentration ratios may be ascribed to the experimental error inherent in the HPLC analysis and to the different experimental conditions that we were forced to employ in the two approaches.

Conclusion

The aforementioned results show that photochemical excitation of iron porphyrins is a suitable means of inducing the oxidation of the hydroxyguanidine **1**. This reaction presents important similarities with the oxidation of the endogenous *N*-hydroxy-L-arginine by heme-containing metalloenzyme nitric oxide synthases (NOSs) and their model systems.

Coordinated hydroxyguanidine **1** presents a photoreactivity that typically characterizes many axial ligands, undergoing oxidation to radical species. The simultaneous formation of Fe^{III}(O_2·) is a key point for the oxidation of **1**.

The two iron porphyrin complexes employed here have provided complementary results. Photochemical excitation of [Fe^{III}(TDCPP)Cl] in the presence of O_2 and 1-MeIm revealed that the urea **2** is the main end-product of **1**. In agreement with an NOS-like oxidation mechanism, the conversion of **1** to **2** approximately matches the formation of

 © 2004 Wiley-VCH Verlag GmbH & Co. KGaA, Weinheim

NO, as revealed by both ESR spin-trapping experiments, and in the form of its stable end-products NO_2^- and NO_3^-. A significant reduction in the production of **2** and NO was observed in the absence of 1-MeIm, due to the main role of coordinated 1-MeIm in stabilizing the $Fe^{III}(O_2^{\cdot})$ intermediate.

The ability of radical scavengers to inhibit the production of both the urea **2** and NO strongly supports the possibility that the reaction pathway resembles a radical-type autoxidation mechanism, where the very fast reaction of O_2 with the ferrous porphyrin in the presence of the photogenerated iminoxyl radical should yield an iron-peroxo intermediate as precursor of **2** and NO.

The use of [Fe^{III}(TpivPP)Cl] provides the first experimental evidence for the photoinduced formation of an iron-dioxy adduct. Moreover, the observed reactivity of the [Fe^{II}(TpivPP)(O_2)(1-MeIm)] complex indicates that iron-peroxo species able to generate the urea **2** may be also formed as a consequence of the reduction of the $Fe^{III}(O_2^{-\cdot})$ intermediate by the hydroxyguanidine **1** itself.

The described results give important indications about the reactivity of iron-dioxy complexes that are in good agreement with current opinion on the second step of NOS catalysis. In particular, our results are in line with the hypothesis that the formation of iron-peroxo intermediates is essential for the oxidation of *N*-hydroxy-L-arginine to L-citrulline and NO.

Experimental Section

Materials: The complexes [Fe^{III}(TDCPP)Cl] and [Fe^{III}(TpivPP)Cl] were prepared and purified as described elsewhere.[22,12b] The hydroxyguanidine **1**, the urea **2** and the cianamide **3** were synthesized following previous procedures.[11a] *N*-Methyl imidazole (1-MeIm), α-phenyl-*N*-*tert*-butylnitrone (PBN) and $NaNO_2$ were commercial products (Aldrich), 2-phenyl-4,4,5,5-tetramethylimidazoline-1-oxyl 3-oxide (PTIO) was purchased from Alexis Biochemicals. They were all used as received. Acetonitrile, acetone and ethanol were spectroscopic-grade solvents.

Apparatus: UV/Vis spectra were recorded with a Kontron Model Uvikon 943 spectrophotometer and X-Band electron spin resonance (ESR) spectra with a Bruker 220 SE spectrometer that was calibrated with α,α′-diphenylpicrylhydrazyl. HPLC analysis was carried out with a Thermo Quest instrument, equipped with a UV detector, using a Discovery HS PEG column (Supelco, 25 cm × 4.6 mm, 5 μm).

Irradiation was carried out with a medium-pressure Hanau Q 400 mercury lamp (15 mW/cm^2). The required wavelength interval was selected by using cut-off filters. When necessary, solutions were degassed to less than 1×10^{-5} Torr by means of five vacuum-line freeze-pump-thaw cycles. Low temperature experiments were performed in a Julabo F12 (MP) cryostat.

Photooxidation of *N*-(4-Chlorophenyl)-*N*′-hydroxyguanidine (1): [Fe^{III}(TDCPP)Cl] or [Fe^{III}(TpivPP)Cl] (1×10^{-5} M) was dissolved in a CH_3CN solution (3 mL) containing **1** (1×10^{-3} M), with or without 1-MeIm (5×10^{-5} M). When necessary PBN (1×10^{-4} M) was also added. The solutions thus obtained were irradiated for 30 minutes with wavelengths higher than 350 nm in the presence of 760 Torr of O_2. UV/Vis spectra were recorded during the preparation of the solutions after the addition of each component and at the end of the irradiation. HPLC analysis was performed on the irradiated sample. Separation and detection of **1**, **2** and **3** was achieved by eluting with a mixture of H_2O and CH_3CN (85:15) in the presence of $CH_3COO\,NH_4$ buffer (10 mM), while HPLC analysis of NO_2^- and NO_3^- was realised using a water solution of acetic acid (pH 3) for elution. In both cases the flow rate was 1 mL/min. Compounds **1**, **2** and **3** were identified by injection of authentic samples. Quantitative analysis was performed using calibration curves obtained from the authentic compounds. Control HPLC experiments were carried out in order to verify that no reaction occurred when irradiation was carried out in the absence of [Fe^{III}(TDCPP)Cl] or O_2. Moreover, we verified that no thermal reaction occurred when the reaction mixture was kept in the dark for several hours.

ESR Spin-Trapping: CH_3CN solutions of [Fe^{III}(TDCPP)Cl] (1×10^{-5} M) containing **1** (1×10^{-3} M), 1-MeIm (5×10^{-5} M) and PBN (5×10^{-3} M) were irradiated ($\lambda > 350$ nm, room temperature) inside the ESR cavity using a flat quartz cell. No ESR signal was obtained when performing the described experiment in the absence of **1**.

For NO detection experiments, CH_3CN solutions of [Fe^{III}(TDCPP)Cl] (1×10^{-5} M), 1-MeIm (5×10^{-5} M) and PTIO (2×10^{-6} M) with and without **1** (1×10^{-3} M) were irradiated ($\lambda > 360$ nm) inside the ESR cavity for some minutes.

Preparation of the [Fe^{II}(TpivPP)(O_2)(1-MeIm)] Adduct: [Fe^{III}(TpivPP)Cl] (1×10^{-5} M) dissolved in a mixture of acetone and ethanol (95:5, v/v) in the presence of 1-MeIm (5×10^{-5} M) was degassed to less than 1×10^{-5} Torr by means of five vacuum-line freeze-pump-thaw cycles. Subsequently, it was irradiated (for 90 s) at low temperature (−5 to −8 °C) at wavelengths higher than 350 nm. After irradiation, the solution was put in contact with O_2 at the same low temperature. Finally, a new deoxygenation cycle was carried out. UV/Vis spectra were recorded after each step of the procedure. HPLC analysis was carried out in order to investigate the reactivity of the hydroxyguanidine **1** (1×10^{-3} M) with the Fe^{II}(TpivPP)(O_2) adduct.

The Fe^{II}(TpivPP)(O_2) adduct was also chemically prepared starting from [Fe^{III}(TpivPP)(Br)] and following the procedure already reported by Collman et al.[12b] Here, we employed zinc amalgam as a reducing agent instead of $[Cr(acac)_2]_2$. [Fe^{III}(TpivPP)(Br)] (1×10^{-3} M) and 1-MeIm (3×10^{-3} M) dissolved in acetone were degassed by means of three vacuum-line freeze-pump-thaw cycles. A drop of zinc amalgam was then introduced into the solution kept under argon atmosphere. After a while, the solution became red in colour and the appearance of an intense band at 535 nm was indicative of the formation of the [Fe^{II}(TpivPP)(1-MeIm)$_2$] complex. The solution containing the ferrous complex, separated from the zinc amalgam, in a bath of ethanol/liquid nitrogen at −60 °C was put in contact with O_2. Evidence for the formation of the [Fe^{II}(TpivPP)(O_2)(1-MeIm)] complex was obtained at room temperature by UV/Vis spectroscopy (observation of a new band at 548 nm). Addition of the hydroxyguanidine **1** (2×10^{-2} M) to an acetone solution of [Fe^{II}(TpivPP)(O_2)(1-MeIm)] (1×10^{-3} M) was carried in an ice bath at 0 °C. The reaction mixture was stirred and kept at the same temperature for 30 min before the HPLC analysis.

Acknowledgments

Financial support from MIUR and CNR is gratefully acknowledged.

 © 2004 Wiley-VCH Verlag GmbH & Co. KGaA, Weinheim

[1] [1a] A. Maldotti, A. Molinari, R. Amadelli, *Chem. Rev.* **2002**, *102*, 3811−3836. [1b] B. Meunier, A. Robert, G. Pratviel, J. Bernadou, in *The Porphyrin Handbook* (Eds.: K. M. Kadish, K. M. Smith, R. Guilard), Academic Press, San Diego, **2000**, vol. 4, 119−174. [1c] A. Maldotti, L. Andreotti, A. Molinari, V. Carassiti, *J. Biol. Inorg. Chem.* **1999**, *4*, 154−161. [1d] L. Weber, R. Hommel, J. Behling, G. Haufe, H. Hennig, *J. Am. Chem. Soc.* **1994**, *116*, 2400−2408. [1e] K. S. Suslick, R. A. Watson, *New J. Chem.* **1992**, *16*, 633−642.

[2] [2a] A. Maldotti, C. Bartocci, G. Varani, A. Molinari, P. Battioni, D. Mansuy, *Inorg. Chem.* **1996**, *35*, 1126−1131. [2b] A. Maldotti, A. Molinari, L. Andreotti, M. Fogagnolo, R. Amadelli, *Chem. Commun.* **1998**, 507−508. [2c] A. Maldotti, L. Andreotti, A. Molinari, G. Varani, G. Cerichelli, M. Chiarini, *Green Chem.* **2001**, *3*, 42−46. [2d] R. D. Arasasingham, A. L. Balch, C. R. Cornman, L. Latos-Grazynski, *J. Am. Chem. Soc.* **1989**, *111*, 4357−4363. [2e] A. L. Balch, R. L. Hart, L. Latos-Grazynski, T. G. Traylor, *J. Am. Chem. Soc.* **1990**, *112*, 7382−7388.

[3] R. L. Cheng, L. Latos-Grazynsky, A. L. Balch, *Inorg. Chem.* **1982**, *21*, 2412−2418.

[4] C. Bartocci, A. Maldotti, G. Varani, V. Carassiti, P. Battioni, D. Mansuy, *Inorg. Chem.* **1991**, *30*, 1255−1259.

[5] W. K. Alderton, C. E. Cooper, R. G. Knowles, *Biochem. J.* **2001**, *357*, 593−615. [5b] B. S. S. Masters, K. McMillian, E. A. Sheta, J. S. Nishimura, L. J. Roman, P. Martasek, *FASEB J.* **1996**, *10*, 552−558. [5c] D. Mansuy, J. P. Renaud, in *Cytochrome P450: Structure, Mechanism, and Biochemistry* (Ed.: P. R. Ortiz de Montellano), Plenum Press, New York and London, **1995**, p. 537−574. [5d] J. T. Groves, C. C. Y. Wang, *Curr. Opin. Chem.* **2000**, *4*, 687−695. [5e] G. M. Rosen, P. Tsai, S. Pou, *Chem. Rev.* **2002**, *102*, 1191−1199.

[6] [6a] B. R. Crane, A. S. Arvai, D. K. Ghosh, C. Wu, E. D. Getzoff, D. J. Stuehr, J. A. Tainer, *Science* **1998**, *279*, 2121−2126. [6b] C. S. Raman, H. Li, P. Martasek, V. Kral, B. S. S. Masters, T. L. Poulos, *Cell* **1998**, *95*, 939−950.

[7] [7a] J. T. Groves, Y.-Z. Han in *Cytochrome P450: Structure, Mechanism, and Biochemistry* (Ed.: P. R. Ortiz de Montellano), Plenum Press, New York and London, **1995**, p. 3−48. [7b] M. Sono, M. P. Roach, E. D. Coulter, J. H. Dawson, *Chem. Rev.* **1996**, *96*, 2841−2888. [7c] M. Couture, D. J. Stuehr, D. L. Rousseau, N. Bec, A. C. Gorren, C. Voelker, *J. Biol. Chem.* **2000**, *275*, 3201−3205. [7d] B. Mayer, R. Lange, *J. Biol. Chem.* **1998**, *273*, 13502−13508. [7e] K. M. Ruske, M. M. Spiering, M. A. Marletta, *Biochemistry* **1998**, *37*, 15503−15512.

[8] [8a] D. J. Stuehr, N. S. Kwon, C. F. Nathan, O. W. Griffith, P. L. Feldman, J. Wiseman, *J. Biol. Chem.* **1991**, *266*, 6259−6263. [8b] P. Klatt, K. Schmidt, G. Uray, B. Mayer, *J. Biol. Chem.* **1993**, *268*, 14781−14787.

[9] [9a] C. Wei, Z. Wang, A. Meade, J. McDonald, D. Stuehr, *J. Inorg. Biochem.* **2002**, *91*, 618−624. [9b] C.-C. Wei, B. R. Crane, D. J. Stuehr, *Chem. Rev.* **2003**, *103*, 2365−2375. [9c] D. Mathieu, Y. M. Frapart, J. F. Bartoli, J. L. Boucher, P. Battioni, D. Mansuy, *Chem. Commun.* **2004**, 54−55.

[10] C. C. Y. Wang, D. M. Ho, J. T. Groves, *J. Am. Chem. Soc.* **1999**, *121*, 12094−12103.

[11] [11a] A. Renodon-Corniere, J.-L. Boucher, S. Dijol, D. J. Stuehr, D. Mansuy, *Biochemistry* **1999**, *38*, 4663−4668. [11b] A. Renodon-Corniere, S. Dijol, C. Perollier, D. Lefèvre-Groboillot, J.-L. Boucher, R. Attias, M.-A. Sari, D. J. Stuehr, D. Mansuy, *J. Med. Chem.* **2002**, *45*, 944−954.

[12] [12a] J. P. Collman, R. R. Gagne, T. R. Halbert, J. C. Marchon, C. A. Reed, *J. Am. Chem. Soc.* **1973**, *95*, 7668−7870. [12b] J. P. Collman, R. R. Gagne, C. A. Reed, T. R. Halbert, G. Lang, W. T. Robinson, *J. Am. Chem. Soc.* **1975**, *97*, 1427−1439.

[13] [13a] D. Lefevre-Groboillot, S. Dijols, J. L. Boucher, J. P. Mahy, R. Ricoux, A. Desbois, J. L. Zimmermann, D. Mansuy, *Biochemistry* **2001**, *40*, 9909−9917. [13b] D. Lefevre-Groboillot, Y. Frapart, A. Desbois, J. L. Zimmermann, J. L. Boucher, A. C. F. Gorren, B. Mayer, D. J. Stuehr, D. Mansuy, *Biochemistry* **2003**, *42*, 3858−3867.

[14] [14a] M. J. Clague, J. S. Wishnok, M. A. Marletta, *Biochemistry* **1997**, *36*, 14465−14473. [14b] J. Fukuto, G. C. Wallace, R. Hszieh, G. Chaudhrui, *Biochem. Pharmacol.* **1992**, *43*, 607−613.

[15] Z. Wei, M. D. Ryan, *Inorg. Chim. Acta* **2001**, *314*, 49−53.

[16] E. G. Janzen, *Acc. Chem. Res.* **1971**, *4*, 31−39.

[17] [17a] T. Akaike, M. Yoshida, Y. Miyamoto, K. Sato, M. Kohno, K. Sasamoto, K. Miyazaki, S. Ueda, H. Maeda, *Biochemistry* **1993**, *32*, 827−832. [17b] R. Ricoux, J.-L. Boucher, D. Mandon, Y.-M. Frapart, Y. Henry, D. Mansuy, J.-P. Mahy, *Eur. J. Biochem.* **2003**, *270*, 47−55.

[18] N. Sennequier, J. L. Boucher, P. Battioni, D. Mansuy, *Tetrahedron Lett.* **1995**, *36*, 6059−6062.

[19] [19a] M. A. Marletta, *J. Biol. Chem.* **1993**, *268*, 12231−12234. [19b] H. G. Korth, R. Sustmann, C. Thater, A. R. Butler, K. U. Ingold, *J. Biol. Chem.* **1994**, *269*, 17776−17779. [19c] H. Huang, J. M. Hah, R. B. Silverman, *J. Am. Chem. Soc.* **2001**, *123*, 2674−2676. [19d] A. R. Hurshman, C. Krebs, D. E. Edmondson, B. M. Huynh, M. A. Marletta, *Biochemistry* **1999**, *38*, 15689−15696.

[20] Z.-Q. Wang, C. Wei, S. Ghosh, A. L. Meade, C. Hemann, R. Hille, D. J. Stuehr, *Biochemistry* **2001**, *40*, 12819−12825.

[21] D. L. Wertz, J. S. Valentine, in *Structure and Bonding: Metal-oxo and Metal-peroxo Species in Catalytic Oxidations* (Ed.: B. Meunier), Springer-Verlag, Berlin, Heidelberg, New York, **2000**, *97*, 37−60.

[22] P. Battioni, J. P. Renaud, J. F. Bartoli, J. F. Reina-Artiles, M. Fort, D. Mansuy, *J. Am. Chem. Soc.* **1988**, *110*, 8462−8470.

Received January 21, 2004
Early View Article
Published Online May 27, 2004

 © 2004 Wiley-VCH Verlag GmbH & Co. KGaA, Weinheim

Ruthenium(II) and Ruthenium(III) Complexes Containing the $[pyS_4]^{2-}$ Ligand [pyS_4^{2-} = 2,6-Bis(2-mercaptophenylthio)dimethylpyridine(2−)][‡]

Dieter Sellmann,[†][a] Kinga Hein,*[a] and Frank W. Heinemann[a]

Keywords: Ruthenium / S ligands / Oxidation reactions

In the search for complexes, having sulfur-dominated coordination spheres, that potentially bind, activate, or stabilize nitrogenase-relevant small molecules, we have synthesized several ruthenium–sulfur complexes of the type $[Ru(L)(pyS_4)]$ starting from the labile acetonitrile complex $[Ru(NCMe)(pyS_4)]$ (**2**). Complex **2** was obtained from the reduction of $[Ru(NO)(pyS_4)]Br$ (**1**) by $N_2H_4{\cdot}H_2O$ in the presence of MeCN. The acetonitrile ligand in **2** could be exchanged for the soft σ–π ligand CO to give $[Ru(CO)(pyS_4)]$ (**3**). Attempts to coordinate N_2 to the pyS_4^{2-} fragment of **2** gave $[\{Ru(pyS_4)\}_2]$ (**4**). Complex **2** reacts also with hard σ-ligands, such as N_2H_4, NH_3, pyridine, and pyrazine, to afford mononuclear $[Ru(N_2H_4)(pyS_4)]$ (**5**), $[Ru(NH_3)(pyS_4)]$ (**6**), $[Ru(py)(pyS_4)]$ (**7**), and $[Ru(pyr)(pyS_4)]$ (**8**), respectively. Reaction of **2** with NEt_4N_3 resulted in the formation of $NEt_4[Ru(N_3)(pyS_4)]$ (**9**). The oxidation of **2** with I_2 afforded $[Ru(I)(pyS_4)]$ (**10**). The protonated and alkylated species $[Ru(NCMe)(pyS_4\text{-}H)]BF_4$ (**11**), $[Ru(NCMe)(pyS_4\text{-}Et)]BF_4$ (**12**), and $[\{Ru(pyS_4\text{-}Et)\}_2](BF_4)_2$ (**13**) were obtained from **2** by its treatment with HBF_4 or Et_3OBF_4. The N_2H_4 ligand in **5** could not be oxidized to N_2H_2: the oxidation of the Ru^{II} center to Ru^{III} takes place instead. Attempts to oxidize **5** using either $[FeCp_2]PF_6$ or I_2 gave $[\{Ru^{II/III}(pyS_4)\}_2](PF_6)$ (**14**) and $[Ru^{III}(NH_3)(pyS_4)]X$ (X = PF_6, I) (**15**, **16**). The oxidation of **3** and **6** by $NOBF_4$ gave Ru^{III} species of $[Ru^{III}(CO)(pyS_4)]BF_4$ (**17**) and $[Ru^{III}(NH_3)(pyS_4)]BF_4$ (**18**). The oxidation of **5** and **6** with H_2O_2 afforded $[\{Ru^{II}(pyS_4{-}O_3)\}_2]$ (**19**), $[\{Ru^{II}(pyS_4{-}O_4)\}_2]$ (**20**) and $[Ru^{II}(NH_3)(pyS_4{-}O_4)]$ (**21**). All complexes were characterized by spectroscopic methods and by elemental analysis. The molecular structures of **4**, **6**, **10**, **14**, **15**, **19**, and **20** were determined by X-ray crystallographic analyses.

(© Wiley-VCH Verlag GmbH & Co. KGaA, 69451 Weinheim, Germany, 2004)

Introduction

Transition metals in sulfur-dominated coordination spheres exhibit rich coordination chemistry.[1] Sulfur coordination of transition metals is characteristic of the active sites of metal sulfur oxidoreductases, such as nitrogenases[2] and the nitrile hydratase.[3] To create model compounds, different multidentate organosulfur ligands and their transition metal complexes have been synthesized and investigated.[4] The previously reported $[M(N_HS_4)]$ fragment [$N_HS_4^{2-}$ = 2,2′-bis(2-mercaptophenylthio)diethylamine-(2−)] binds a number of nitrogenase-relevant molecules, such as CO, NO, N_2H_2, N_2H_4, and NH_3, but with the exception of N_2.[5] Moreover, in the case of ruthenium, the diastereoisomerism of the $[M(N_HS_4)]$ fragments leads to the formation of inseparable mixtures of $[Ru(L)(N_HS_4)]$ species. To overcome this problem, the flexible $N(C_2H_4)_2$ bridge was replaced by the rigid $py(CH_2Br)_2$ bridge, which yielded exclusively *trans*-alkylated species. The synthesis of many iron,[6,7c,7e] but only a few ruthenium complexes containing the $[M(pyS_4)]$ fragment have been described.[7a,7b] The extreme lability of important nitrogenase-relevant intermediates, such as $[Fe(N_2H_4)(pyS_4)]$ and $[\mu\text{-}N_2H_2\{Fe(pyS_4)\}_2]$,[8] prompted us to examine the coordination behavior of the pyS_4 ligand towards ruthenium − a homologue of the nitrogenase-dominating iron systems. In the case of ruthenium, the syntheses of $[Ru(L)(pyS_4)]$ complexes, e.g., $[Ru(CO)(pyS_4)]$, require very drastic conditions.[7a] The previous reports have also illustrated the difficulties in finding complexes with labile ligands L. Therefore, our primary aim was to find $[Ru(L)(pyS_4)]$ complexes with labile ligands which are capable of coordinating nitrogenase-relevant small molecules under mild conditions. In this context, we investigated the chemistry of $[Ru(L)(pyS_4)]$ complexes. Herein, we describe the synthesis of labile $[Ru(NCMe)(pyS_4)]$ (**2**) and its reactivity towards various nitrogenase-relevant molecules, such as CO and N_2H_4. We prove also the possibility of coordinating the σ ligands NH_3 and N_3^- to the $[Ru(pyS_4)]$ fragment; these ligands do not coordinate to the Fe analogue.[8] Attempts to oxidize coordinated hydrazine to diazene units led either to the oxidation of Ru^{II} to Ru^{III} or to the oxidation of thiolate donors in the pyS_4 ligand to sulfinates/sulfenates. This is a new observation when compared to the behavior

[‡] Transition Metal Complexes with Sulfur Ligands, 164. Part 163: D. Sellmann, R. Prakash, F. W. Heinemann, M. Moll, M. Klimowicz, *Angew. Chem. Int. Ed.* **2004**, *43*, 1877−1880.

[†] Deceased.

[a] Institut für Anorganische Chemie der Universität Erlangen-Nürnberg,
Egerlandstraße 1, 91058 Erlangen, Germany
Fax: (internat.) + 49-(0)9131-8527367
E-mail: kinga@anorganik.chemie.uni-erlangen.de

 © 2004 Wiley-VCH Verlag GmbH & Co. KGaA, Weinheim **DOI: 10.1002/ejic.200400066**

of other ruthenium sulfur hydrazine complexes, such as $[Ru(N_2H_4)(PPh_3)(tpS_4)]$,[9] $[Ru(N_2H_4)(P\mathit{i}Pr_3)(S_4)]$, $[Ru(N_2H_4)(PCy_3)(S_4)]$,[10] and $[Ru(N_2H_4)(PPh_3)(^{bu}S_4)]$.[11]

Results

Earlier attempts to synthesize the acetonitrile complex **2** directly from $[RuCl_2(CH_3CN)_4]$ and Li_2pyS_4 were unsuccessful.[7a] Now, we have found that **2** can be synthesized from $[Ru(NO)(pyS_4)]Br$ (**1**) by reductive elimination of the NO^+ ligand. Treatment of **1** with two equiv. of $N_2H_4{\cdot}H_2O$ in acetonitrile afforded the target complex **2** (Scheme 1).

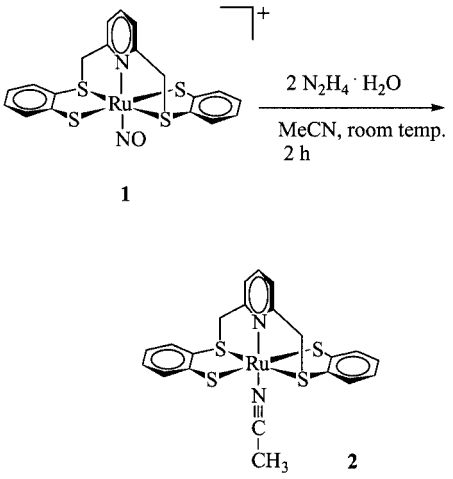

Scheme 1. Synthesis of $[Ru(NCMe)(pyS_4)]$ (**2**)

The NO^+ ligand in **1** is reduced by $N_2H_4{\cdot}H_2O$, giving probably the highly reactive and unstable 19-VE $[Ru(NO)(pyS_4)]^0$ intermediate, which releases NO and coordinates MeCN to afford **2**. The acetonitrile complex **2** is soluble in CH_2Cl_2 and THF, but it is insoluble in MeOH and Et_2O. ^1H and ^{13}C NMR spectra indicate that **2** exhibits C_2 symmetry in solution. In the solid state, **2** can be stored at room temp. for a couple of weeks, but it decomposes in solution over the course of 48 h. Complex **2** is an excellent starting material for the synthesis of numerous complexes that had been inaccessible previously. The reactivity of **2** towards various nucleophiles is depicted in Scheme 2.

Complex **2** reacts with CO instantaneously to give the CO complex **3**; this process indicates the lability of **2**. Attempts to exchange the acetonitrile ligand in **2** by N_2 led to the formation of the stable, dinuclear $[\{Ru(pyS_4)\}_2]$ (**4**). Complex **4** could be obtained in better yield when **2** was heated under reflux in THF for a few days. When **2** was treated with $N_2H_4{\cdot}H_2O$, a mononuclear hydrazine complex formed: $[Ru(N_2H_4)(pyS_4)]$ (**5**). Complex **5** is stable in solution for only a few hours and all attempts to obtain single crystals suitable for X-ray analysis resulted in the formation of crystals of **4**. Although one of the decomposition products of **5** was identified as $[Ru(NH_3)(pyS_4)]$ (**6**), formation of an N_2H_2 complex, resulting from disproportionation, has never been observed. Attempts to synthesize a diazene complex directly from **2** and N_2H_2, generated in situ by hydrolysis of $K_2N_2(CO_2)_2$ with acetic acid, were unsuccessful. Complex **6** could be prepared very simply from **2** in a reaction with gaseous NH_3 under ambient conditions. In contrast to the $[Fe(pyS_4)]$ fragment, which does not coordinate

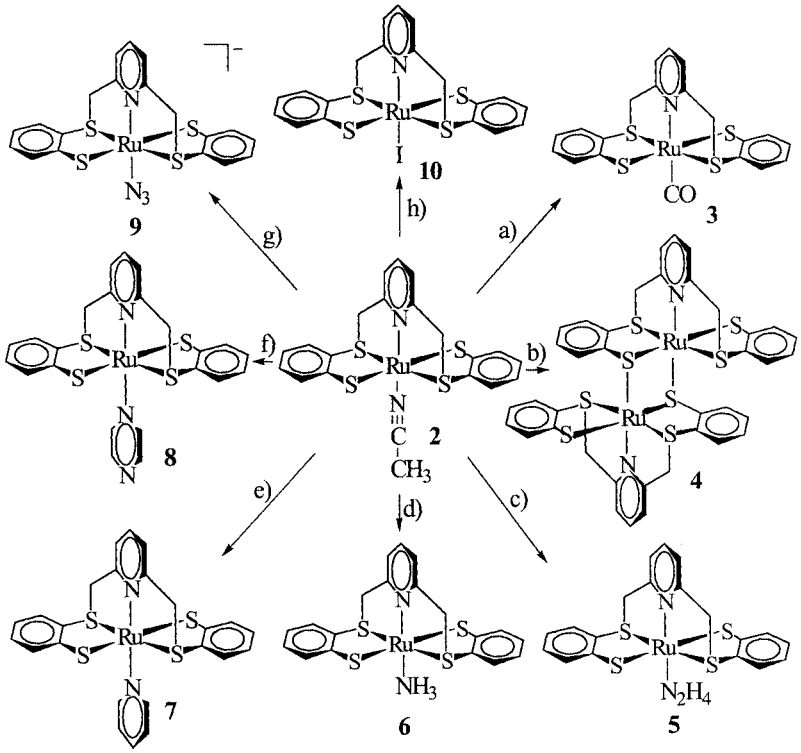

Scheme 2. Reactivity of **2** towards nitrogenase-relevant molecules: a) CO, THF, room temp.; b) N_2, THF, 100 bar; c) $N_2H_4{\cdot}H_2O$, THF, 15 h, room temp.; d) NH_3(g), THF, 2 h, room temp.; e) pyridine, 5 min, reflux; f) pyrazine, 15 min, reflux; g) NEt_4N_3, acetone, 50 °C; h) 0.5 I_2, THF, 30 min, room temp.

 © 2004 Wiley-VCH Verlag GmbH & Co. KGaA, Weinheim

σ ligands at all, the NH_3 ligand in **6** proved to be very inert. The CO exchange reaction takes place very slowly and requires ca. 72 h to reach completion. For that reason, **6** did not afford a dinitrogen complex either. Attempts to exchange NH_3 for N_2 were unsuccessful, even under very drastic conditions, e.g., 100 bar/50 °C. Treatment of **2** with other hard σ ligands, such as pyridine and pyrazine, led to the formation of [Ru(py)(pyS_4)] (**7**) and [Ru(pyr)(pyS_4)] (**8**), respectively. To drive the reactions to completion, the solutions were usually heated under reflux for a short period of time. Azide complexes are used for the preparation of dinitrogen complexes that are not accessible by direct coordination of gaseous nitrogen.[12] Treatment of **2** in acetone with NEt_4N_3 afforded the extremely unstable azide complex NEt_4[Ru(N_3)(pyS_4)] (**9**) whose formation can be ascertained only by IR spectroscopy, which shows a characteristic ν(N_3) absorption at 2026 cm^{-1}. This absorption is in good agreement with those of other [Ru(N_3)(L)]$^-$ complexes, e.g., NEt_4[Ru(N_3)(PPh_3)(tpS_4)] (2029 cm^{-1}),[9] NEt_4[Ru(N_3)(PPh_3)($^{bu}S_4$)] (2034 cm^{-1}),[11] and NEt_4[Ru(N_3)(PCy_3)(S_4)] (2028 cm^{-1}).[13] This reaction took place only when the mixture was heated briefly at 50 °C. The azide complex proved to be too labile to obtain reasonable ^{1}H NMR spectra, and elemental analysis proved also to be very erratic. This situation most certainly is due to the inherent instability of the azide ligand, which proved to be very labile: the compound decomposed when it was dried in vacuo.

Oxidation of **2** with 0.5 equiv. of I_2 in THF led to a color change from orange-red to violet. Addition of *n*-hexane to the filtrate precipitated a violet solid, which we characterized by elemental analysis, mass spectrometry, and X-ray crystallography to be [Ru(I)(pyS_4)] (**10**). Addition of an excess of I_2 to a filtrate after preparation of **10** led to the formation of single crystals, which we identified with the help of an X-ray analysis to be [Ru^{III}(pyS_4)]$_2$(I_3)$_2$ (**22**). In the presence of an excess of iodine, the iodide ligand in **10** dissociates in solution and then two [Ru(pyS_4)] fragments dimerize to form **22**.

We performed protonation and alkylation experiments to further explore the reactivity of [Ru(NCMe)(pyS_4)] (**2**). When **2** was treated with 1 equiv. of HBF_4 at −78 °C, the protonated [Ru(NCMe)(pyS_4-H)]BF_4 (**11**) complex formed; it has a characteristic ν(CN) absorption at 2273 cm^{-1}. Addition of 1 equiv. of Et_3OBF_4 to **2** led to the formation of the monoalkylated species [Ru(NCMe)(pyS_4-Et)]BF_4 (**12**), which has a ν(CN) frequency at 2282 cm^{-1}. To prove the possibility that **2** can be dialkylated, we added an excess (5 equiv.) of Et_3OBF_4 to **2**. In the course of 2 days, the dinuclear complex [{Ru(pyS_4-Et)}$_2$](BF_4)$_2$ (**13**) formed. These observations regarding the reactivity of the [Ru(pyS_4)] acetonitrile complex confirm its wide applicability to the synthesis of other [Ru(L)(pyS_4)] complexes, but only when the entering ligand L is competitive enough to form the desired [Ru(L)(pyS_4)] species.

Our unsuccessful attempts to obtain a [Ru(pyS_4)] dinitrogen complex from its acetonitrile, ammonia, or azide precursors prompted us to return to the hydrazine complex **5** as a starting point. The oxidation of **5** by other oxidants gave unexpected, but interesting, results, which are summarized in Scheme 3.

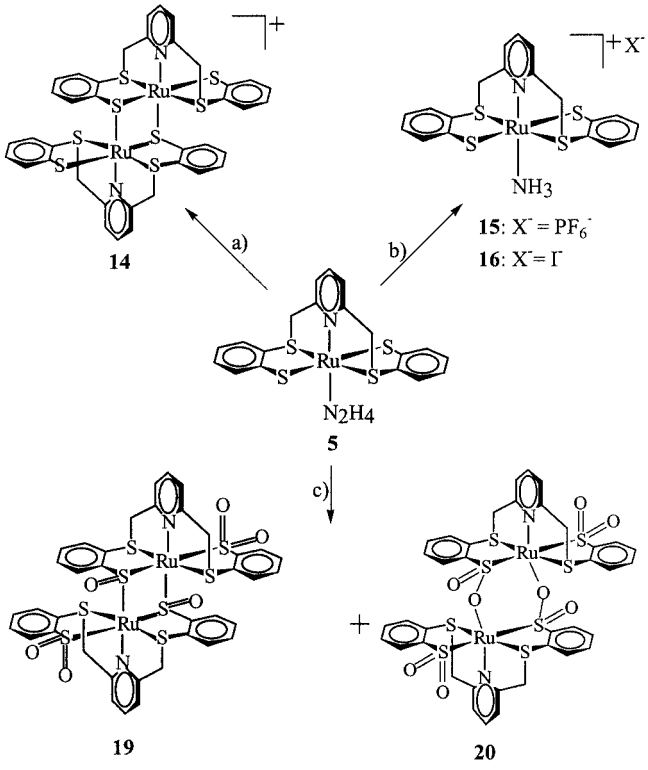

Scheme 3. Oxidation of [Ru(N_2H_4)(pyS_4)] (**5**) with different oxidants: a) [$FeCp_2$]PF_6, LiOMe; b) [$FeCp_2$]PF_6 or I_2; c) H_2O_2

When **5** was treated with 2 equiv. of [$FeCp_2$]PF_6 and 1 equiv. of LiOMe, red microcrystals formed which were identified as **4**. The red solid that precipitated from the filtrate, upon the addition of Et_2O, was separated and characterized as [{$Ru^{II/III}$(pyS_4)}$_2$](PF_6) (**14**). The hydrazine ligand in **5** dissociates in solution and then the resulting two [Ru(pyS_4)] fragments dimerize to form **4**. Overnight, a slow oxidation of the metal centers took place in the mother liquor to produce the mixed-valence species **14**. Treatment of **5** with an excess of either [$FeCp_2$]PF_6 or I_2 gave [Ru^{III}(NH_3)(pyS_4)]X (X = PF_6, I) (**15**, **16**). To gain some understanding of the formation of these stable ammonia complexes (**15**, **16**), we performed some additional oxidation experiments of **3** and **6** using $NOBF_4$. As expected, in both cases [Ru^{III}(CO)(pyS_4)]BF_4 (**17**) and [Ru^{III}(NH_3)(pyS_4)]BF_4 (**18**) formed; these complexes could be isolated and characterized. These results indicate the facility of the oxidation of the Ru center in the [Ru(pyS_4)] fragment when using oxidants such as [$FeCp_2$]PF_6, I_2, and $NOBF_4$. In the case of $NOBF_4$, the oxidation takes place without decoordination of the NH_3 and CO ligands. The formation of stable ammonia complexes, **15** and **16**, from the hydrazine complex **5** is in agreement with the observed decomposition of the hydrazine ligand in **5** to ammonia, and other compounds, mentioned above. A possible explanation for the oxidation

 © 2004 Wiley-VCH Verlag GmbH & Co. KGaA, Weinheim

of **5** to **15** and **16** might be the decomposition of hydrazine to ammonia in the first step and then oxidation of Ru^{II} to Ru^{III} in the resulting ammonia complex — an intermediate species — in the second. The oxidation of **5** and **6** with H_2O_2 leads to oxidation of the thiolate donors. When H_2O_2 is added to a solution of **5** in THF, the initial red color turns to yellow and the formation of a mixture of $[\{Ru(pyS_4-O_3)\}_2]$ (**19**) and $[\{Ru(pyS_4-O_4)\}_2]$ (**20**) is observed. This yellow solid exhibits two new IR bands at 1141 and 1042 cm^{-1} that indicate the oxidation of thiolato sulfur to sulfenato/sulfinato (**19**) and sulfinato groups (**20**).[14] Several examples of the oxidation of thiolate donors in transition metal complexes appear in the literature. Although thiolates are normally oxidized to disulfides, it is known that metal-bound thiolates can be oxidized to sulfinates and sulfenates.[15,16] The X-ray crystallographic structural determination of **19** confirms the formation of dinuclear Ru^{II} species, wherein two $[Ru(pyS_4-O_3)]$ fragments are bridged by the S atom of a sulfenato group. In the case of **20**, two $[Ru(pyS_4-O_3)]$ fragments are bridged by two O atoms. Treatment of **6** with H_2O_2 led also, as in the case of **5**, to the oxidation of the thiolate donors. The elemental analysis of the isolated product was in agreement with the formation of mononuclear $[Ru(NH_3)(pyS_4-O_4)]$ (**21**). The ammonia ligand did not decoordinate during this reaction; this result is in line with our observations, discussed above, on the different stabilities of the ammonia and hydrazine ligands in the $[Ru(pyS_4)]$ fragment.

The various results of the chemical oxidation experiments of the $[Ru(pyS_4)]$ fragment prompted us to undertake electrochemical investigations using the Ru^{II} complexes **2**, **3**, **5**, **6**, **7**, and **8** and the Ru^{III} complexes **15** and **17**. The results support the hypothesis that the metal center is easy oxidized in the $[Ru(pyS_4)]$ fragment. The Ru^{II} CO complex **3** displays one quasireversible redox wave at 0.58 V, which we assign to the redox couple $[Ru(CO)(pyS_4)]^{+/2+}$. The possible chemical oxidation of thiolate donors, which we commented on above, is now corroborated by the results of the electrochemical investigations. $[Ru(NH_3)(pyS_4)]$ (**6**) exhibits an irreversible wave at 0.88 V, which we ascribe to the oxidation of thiolate donors in the pyS_4 ligand. A similar wave at 0.8 V appears in the cyclic voltammogram of the Ru^{III} ammonia complex **15**. The second reversible wave observed for **15** at 0.32 V is assigned to the $[Ru(NH_3)(pyS_4)]^{+/2+}$ redox couple. The cyclic voltammogram of **15** also exhibits one reversible wave in the cathodic region (−0.24 V); it is compatible with the reversible reduction of **15** to the Ru^{II} ammonia complex and can be assigned to the redox couple $[Ru(NH_3)(pyS_4)]^{+/0}$. The cyclic voltammograms of **2**, **7**, and **8** exhibit reversible redox waves in the anodic region that are typical of $[Ru(L)(pyS_4)]$ (L = MeCN, py, pyr): at 0.07, 0.06, and 0.12 V, respectively. In the case of **2**, we also observed a reversible redox wave in the cathodic region at −0.2 V, which we assign to the redox couple $[Ru(NCMe)(pyS_4)]^{0/-1}$. The difficulties in oxidizing the hydrazine complex **5** to a diazene complex are in good agreement with the electrochemical properties of **5**. No redox waves were observable in the anodic region of the voltammogram of **5**. One quasireversible redox wave at −0.13 V is assigned to the redox couple Ru^{II}/Ru^{I}.

Characterization of $[Ru(L)(pyS_4)]$ Complexes

As far as possible, we characterized all of the complexes by elemental analyses and IR, NMR, and mass spectra. The molecular structures of **4**, **6**, **10**, **14**, **15**, **19**, **20**, **22**, **23**, and **24** were determined by X-ray crystallographic analyses. The Ru^{II} complexes (including **6** and **7**) are soluble in CH_2Cl_2, THF, DMF, and DMSO, but they are insoluble in MeOH, Et_2O, and hexane. Complexes **6** and **7** are soluble in all common solvents. The Ru^{III} complexes display better solubility in MeOH and are rather sparingly soluble in CH_2Cl_2 and THF. All Ru^{II} complexes proved to be diamagnetic, while the Ru^{III} complexes are paramagnetic, as indicated by their ^1H NMR spectra. The ^1H NMR spectra of $[Ru^{II}(L)(pyS_4)]$ complexes exhibit a typical set of four or five multiplets for the 11 aromatic protons ($\delta \approx 9-6$ ppm) and two typical patterns for an AB spin system representing the diastereotopic methylene protons ($\delta \approx 5.5-4.5$ ppm). In the case of **20**, all of the pairs of methylene protons of the oxidized pyS_4 ligand are diastereotopic because of the stereogenic center at the S atom of the bridging sulfinic group. Typically, we observed a characteristic triplet that is due to the pyridine H_γ protons. The ^1H NMR spectra of **2**, **6**, and **21** exhibit characteristic singlets at $\delta = 2.16$, 1.54, and 1.52 ppm, respectively, that indicate the coordination of acetonitrile and ammonia ligands. The hydrazine complex **5** gave rise to two singlets at $\delta = 4.86$ and 4.01 ppm, which we assign to the Ru-bound NH_2 group and terminal NH_2 group. In the $^{13}C\{^1H\}$ NMR spectra, the 17 aromatic and 2 aliphatic carbon atoms of the $[Ru(pyS_4)]$ fragments resulted in 10 signals (9 and 1, respectively). The electronic absorption spectra of **5** and **6** in DMF each consist of two strong bands with maxima at 347 and 504 nm; **7** and **8** exhibit absorptions at ca. 400 and 509 nm (for **7**) and 557 nm (for **8**). Absorption at > 500 nm arises from thiolate-to-ruthenium(II) charge-transfer transitions. The blue shift of the pyrazine complex **8** is compatible with its deep violet color compared to the red pyridine complex **7**. The presence of the pyridine unit in the pyS_4 ligand is associated with an absorption at ca. 400 nm. Complex **15** displays absorptions at 596 and 822 nm.

X-ray Structural Analyses

X-ray structural analyses corroborated the spectroscopic results for several of the complexes. Figure 1−3 depict the molecular structures of $[\{Ru(pyS_4)\}_2]\cdot 2$toluene (**4**·2-toluene), $[Ru(NH_3)(pyS_4)]$(**6**), $[Ru(I)(pyS_4)]\cdot 1.5CH_2Cl_2$ (**10**·$1.5CH_2Cl_2$), $[\{Ru(pyS_4)\}_2](PF_6)\cdot CD_2Cl_2$ (**14**·CD_2Cl_2), $[Ru(NH_3)(pyS_4)]PF_6\cdot CH_2Cl_2$ (**15**·CH_2Cl_2), and $0.68[\{Ru(pyS_4-O_3)\}_2]\cdot 0.32[\{Ru(pyS_4-O_4)\}_2]\cdot 2MeOH$ (0.68 **19**·0.32 **20**·2MeOH). We also report the structures of $[\{Ru(pyS_4)\}_2](I_3)_2\cdot 1.8THF$ (**22**·1.8THF), $[\{Ru(pyS_4\text{-}Et)\}_2](BF_4)_2(B_2F_7)\cdot 3CD_2Cl_2$ (**23**·$3CD_2Cl_2$), and $[\{Ru(pyS_4)\}_2](BF_4)(B_2F_7)\cdot 3CH_2Cl_2$ (**24**·$3CH_2Cl_2$), which we only characterized by X-ray crystallography.

 © 2004 Wiley-VCH Verlag GmbH & Co. KGaA, Weinheim

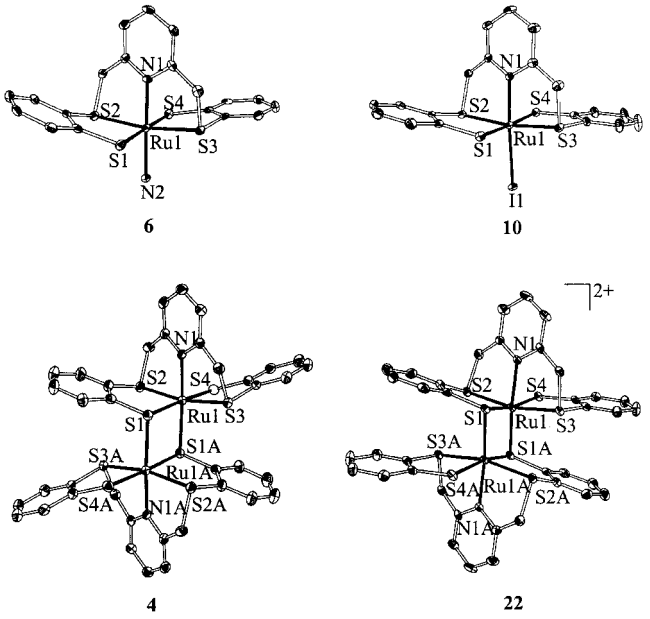

Figure 1. Molecular structures of [{Ru(pyS$_4$)}$_2$]·2 toluene (**4**·2toluene), [Ru(NH$_3$)(pyS$_4$)] (**6**), [Ru(I)(pyS$_4$)]·1.5 CH_2Cl_2 (**10**·1.5CH_2Cl_2), and [{Ru(pyS$_4$)}$_2$](I$_3$)$_2$·1.8THF (**22**·1.8THF); 50% probability ellipsoids, H atoms, solvent molecules, and I_3^- anions omitted

Table 1−3 list selected distances and angles of these complexes.

In all of the complexes, the ruthenium centers exhibit pseudo-octahedral coordination. Thiolate and thioether donors always adopt *trans* positions in the [RuS$_4$] cores. This observation proves the steric rigidity of the py(CH$_2$)$_2$ backbone. In the mononuclear complexes **6**, **10**, and **15**, the Ru centers are coordinated by one N and four S donors of the pentadentate pyS_4^{2-} ligand and a sixth ligand (NH$_3$ or I), while in the dinuclear complexes **4**, **14**, **19**, **20**, **22**, **23**, and **24** the sixth ligand is a thiolate donor of the second [Ru(pyS$_4$)] unit. In mono- and dinuclear Ru^{II} complexes, the Ru−S (thiolate) distances are slightly longer than the Ru−S (thioether) distances, but all the Ru−S distances in the Ru^{III} complexes are of similar length. The Ru−N (pyridine) distances in all the Ru^{II} complexes are slightly shorter (by ca. 4 pm) than in the Ru^{III} complexes.

In the case of **19** and **20**, two different orientations were refined for the oxygen atoms, with an occupancy of 68% for O1, O3, and O4 and 32% for O1′, O2′, O3, and O4. The ethyl groups in **23** are situated at the S atoms S4 and S4A that are *trans* to the bridging S donors S1 and S1A, respectively. The dimer **4** that has two Ru^{II} centers possesses crystallographically imposed C_i symmetry. The mixed-valence complex **14** exhibits approximate C_2 symmetry. The two

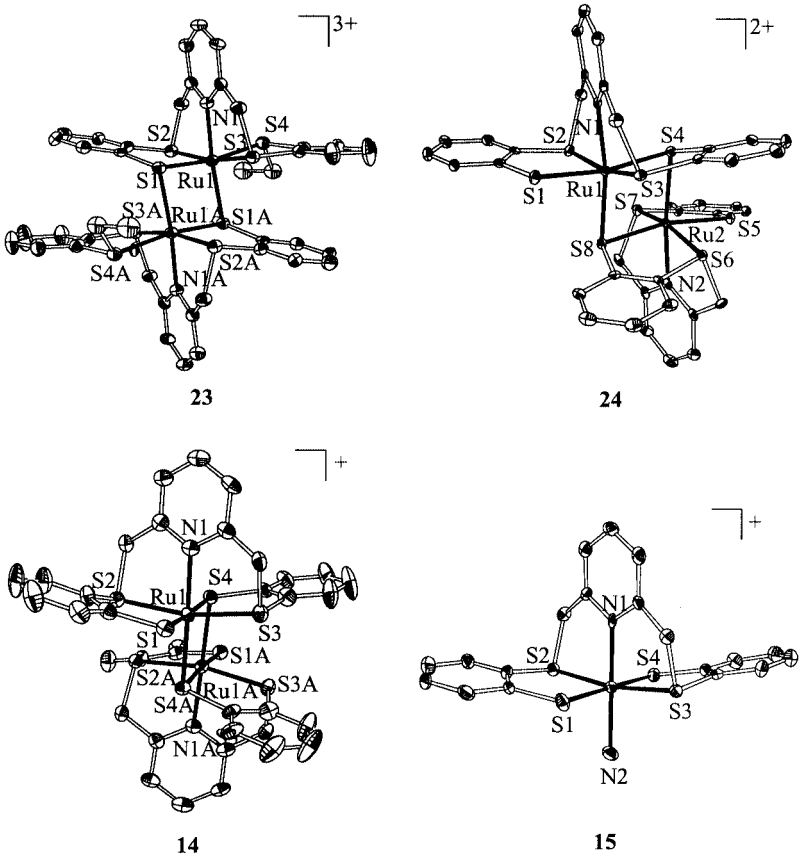

Figure 2. Molecular structures of [{Ru(pyS$_4$)}$_2$](PF$_6$)·CD_2Cl_2 (**14**·CD_2Cl_2), [Ru(NH$_3$)(pyS$_4$)]PF_6·CH_2Cl_2 (**15**·CH_2Cl_2), [{Ru(pyS$_4$-Et)}$_2$](BF$_4$)$_2$(B$_2$F$_7$)·3CD_2Cl_2 (**23**·3CD_2Cl_2), and [{Ru(pyS$_4$)}$_2$](BF$_4$)(B$_2$F$_7$)·3CH_2Cl_2 (**24**·3CH_2Cl_2); 50% probability ellipsoids, H atoms, solvent molecules, and BF_4^-, $B_2F_7^-$, and PF_6^- anions omitted

 © 2004 Wiley-VCH Verlag GmbH & Co. KGaA, Weinheim

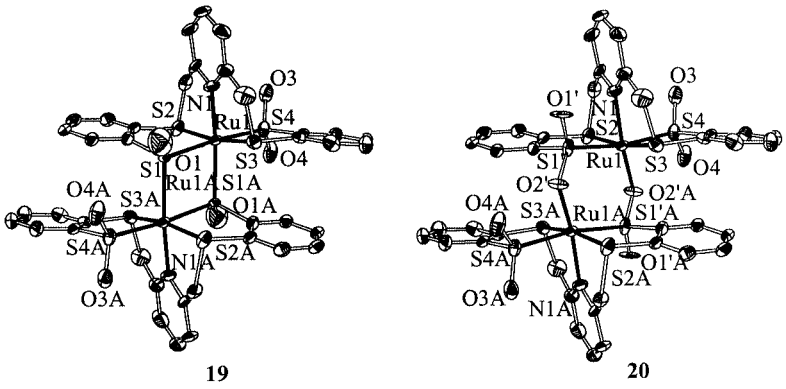

Figure 3. Molecular structures of $[\{Ru(pyS_4-O_3)\}_2]$/$[\{Ru(pyS_4-O_4)\}_2]$·2MeOH (**19**/**20**·2MeOH); 50% probability ellipsoids, H atoms, and solvent molecules omitted

Table 1. Selected distances (pm) and angles (°) in $[Ru(NH_3)(pyS_4)]$ (**6**), $[Ru(I)(pyS_4)]$·$1.5CH_2Cl_2$ (**10**·$1.5CH_2Cl_2$), and $[Ru(NH_3)(pyS_4)]$-PF_6·CH_2Cl_2 (**15**·CH_2Cl_2)

Compound	**6**	**10**·$1.5CH_2Cl_2$	**15**·CH_2Cl_2
Ru1−N1	202.3(3)	207.7(3)	206.7(5)
Ru1−S1	237.7(1)	230.3(1)	232.6(2)
Ru1−S2	231.3(1)	232.9(1)	233.0(2)
Ru1−S3	229.8(1)	231.0(1)	232.2(2)
Ru1−S4	238.7(1)	234.1(1)	229.7(2)
Ru1−L	214.2(3)	271.24(4)	213.2(5)
S1−Ru1−S2	87.08(3)	88.27(4)	88.22(7)
S2−Ru1−S4	93.90(3)	92.71(3)	92.27(7)
S4−Ru1−S3	87.56(3)	88.55(3)	88.76(7)
S1−Ru1−S3	91.65(3)	89.74(4)	90.98(7)
N1−Ru1−S2	84.11(9)	84.38(9)	84.1(2)
N1−Ru1−S1	91.79(9)	89.78(8)	90.7(2)
N1−Ru1−L	178.5(2)	176.51(8)	179.9(3)

Table 2. Selected distances (pm) and angles (°) in $[\{Ru(pyS_4)\}_2]$·2toluene (**4**·2toluene), $[\{Ru(pyS_4-O_3)\}_2]$/$[\{Ru(pyS_4-O_4)\}_2]$·2MeOH (**19**/**20**·2MeOH), and $[\{Ru(pyS_4)\}_2]$-$(I_3)_2$·1.8THF (**22**·1.8THF)

Compound	**4**·2toluene	**19**/**20**·2MeOH	**22**·1.8THF
Ru1−N1	205.3(4)	205.9(5)	210.4(4)
Ru1−S1	237.1(2)	236.2(4)	230.6(2)
Ru1−S2	231.2(2)	231.7(2)	235.9(2)
Ru1−S3	230.6(2)	230.6(2)	234.3(2)
Ru1−S4	238.4(2)	230.4(2)	239.2(2)
Ru1−S1A	240.9(2)	238.4(6)	231.0(2)
S1−O1	–	140.0(2)	–
S4−O3	–	149.3(5)	–
S1−Ru1−S2	87.46(5)	87.5(1)	88.57(5)
S2−Ru1−S4	92.63(5)	94.18(6)	91.65(4)
S4−Ru1−S3	87.18(5)	88.28(6)	87.86(4)
S1−Ru1−S3	93.50(5)	91.1(2)	89.24(4)
N1−Ru1−S2	83.4(2)	84.5(2)	82.6(2)
N1−Ru1−S1	91.7(2)	95.8(2)	86.8(2)
S1−Ru1−S1A	83.80(5)	76.3(2)	105.46(4)
Ru1−S1−Ru1A	96.20(5)	103.7(2)	74.54(4)
O4−S4−O3	–	111.0(3)	–
O1−S1−Ru1A	–	119.6(6)	–

Table 3. Selected distances (pm) and angles (°) in $[\{Ru(pyS_4)\}_2](PF_6)$·CD_2Cl_2 (**14**·CD_2Cl_2), $[\{Ru(pyS_4\text{-}Et)\}_2]$-$(BF_4)_2(B_2F_7)$·$3CD_2Cl_2$ (**23**·$3CD_2Cl_2$), and $[\{Ru(pyS_4)\}_2](BF_4)$-(B_2F_7)·$3CH_2Cl_2$ (**24**·$3CH_2Cl_2$)

Compound	**14**·CD_2Cl_2	**23**·$3CD_2Cl_2$	**24**·$3CH_2Cl_2$
Ru−N1	210.4(6)	208.2(5)	215.5(3)
Ru1−S1	236.4(2)	233.3(2)	239.0(2)
Ru1−S2	232.5(2)	234.4(2)	234.2(2)
Ru1−S3	231.7(2)	231.3(2)	235.4(2)
Ru1−S4	236.6(2)	237.6(2)	233.4(2)
Ru1−S1A	236.4(2)[a]	236.3(2)	234.4(2)[b]
S1−Ru1−S2	88.17(8)	88.10(6)	87.14(4)
S2−Ru1−S4	92.92(8)	93.34(6)	93.83(4)
S4−Ru1−S3	88.36(8)	87.31(6)	87.93(4)
S1−Ru1−S3	89.43(8)	89.14(6)	88.39(4)
N1−Ru1−S2	82.90(2)	83.6(2)	83.0(1)
N1−Ru1−S1	89.8(2)	87.8(2)	82.20(9)
S1−Ru1−S1A	89.16(7)	98.52(5)	88.44(4)[b]
Ru1−S1−Ru1A	84.40(6)	81.48(5)	77.46(3)[c]

[a] S1A = S4A. [b] S1A = S8. [c] S1 = S8, Ru1A = Ru2.

Ru^{III} fragments in dimeric **22** are connected by a crystallographic inversion center. The dinuclear complex **23** contains one *R* and one *S* [Ru(pyS$_4$-Et)] enantiomer, while in the mixed-valence complex **24** always two identical enantiomers [(*R*,*R*) or (*S*,*S*)] occurred.

Conclusion

The aim of this work was the synthesis of new labile $[Ru(L)(pyS_4)]$ complexes. We have found that $[Ru(MeCN)(pyS_4)]$ (**2**) is a good precursor for other complexes. This complex allows the synthesis of $[Ru(CO)(pyS_4)]$ (**3**), $[Ru(N_2H_4)(pyS_4)]$ (**5**), and $[Ru(NH_3)(pyS_4)]$ (**6**), which contain nitrogenase-relevant ligands. The $[Ru(pyS_4)]$ fragment can bind a further σ ligand, such as N_3^-, in contrasting to the $[Fe(pyS_4)]$ fragment, which does not coordinate NH_3 and N_3^- ligands. Moreover, the coordination of the nitrogenase-relevant molecules takes place under rather mild conditions. The replacement of the flexible NH(dialkyl)

 © 2004 Wiley-VCH Verlag GmbH & Co. KGaA, Weinheim

bridge of the former NHS_4^{2-} ligand with the sterically more rigid dialkyl methyl pyridine bridge in the pyS_4^{2-} ligand successfully enforces a *trans*-thiolate configuration in [Ru(L)(pyS_4)] complexes. The synthesis of complexes such as [Ru^{III}(NH_3)(pyS_4)]X (X = PF_6, I, BF_4) (**15**, **16**, **18**) and [Ru^{III}(CO)(pyS_4)]BF_4 (**17**) proves that the oxidation of Ru^{II} to Ru^{III} centers occurs readily in the [Ru(pyS_4)] fragment. Interestingly, both [Ru(N_2H_4)(pyS_4)] (**5**) and [Ru(NH_3)(pyS_4)] (**6**) can be converted readily into the corresponding sulfinato species upon reaction with H_2O_2. We have proven the different lability of hydrazine and ammonia ligands in [Ru(pyS_4)] fragments by studying their reactivity towards a range of oxidants.

Experimental Section

General Methods: Unless noted otherwise, all reactions and operations were carried out under nitrogen and at room temp. using standard Schlenk techniques and absolute solvents. As far as possible, reactions were monitored by IR and NMR spectroscopy. Spectra were recorded using the following instruments: IR (KBr disks or CaF_2 cuvettes, solvent bands were compensated): Perkin−Elmer 16 PC FT IR. NMR: JEOL FT-JNM-GX 270, EX 270, and Lambda LA 400; spectra are referenced to residual protiosolvent signals; chemical shifts are quoted on the δ scale (downfield shifts are positive) relative to tetramethylsilane (^{1}H, ^{13}C{^{1}H} NMR); spectra were recorded at 25 °C. Mass spectra: JEOL JMS 700 spectrometer. UV-Vis-NIR: Varian Cary 50, quartz cuvettes (hellma, d = 1 cm). Elemental Analysis: Carlo−Erba EA 1106 and 1108 analyzer. Cyclic voltammetry was performed with a PAR 264A potentiostat using a three-electrode cell with glassy carbon ROTEL A working, Pt reference, and Pt counter electrodes. The concentration of each complex was 10^{-3} M. NBu_4PF_6 (10^{-1} M) was used as the conducting electrolyte. Potentials are referenced to the NHE via Fc/Fc^+ as internal standard (E = +0.41 V vs. NHE).[17] Reagents (N_2H_4·H_2O, pyridine, pyrazine, LiOMe, Et_3OBF_4, HBF_4/Et_2O, $NOBF_4$, and H_2O_2) were purchased from Merck, Fluka, Aldrich, and Acros. [Ru(NO)(pyS_4)]Br (**1**) was prepared as described in the literature.[7b]

[Ru(NCMe)(pyS_4)] (2): N_2H_4·H_2O (0.034 mL, 0.704 mmol) was added to a brown-violet suspension of **1** (210 mg, 0.352 mmol) in MeCN (20 mL). The color of the suspension turned to carrot-orange. The suspension was stirred for 2 h, during the course of which time an orange solid formed; this solid was filtered, washed with MeOH (2 × 20 mL) and Et_2O (20 mL), and dried in vacuo. Yield: 155 mg of **2** (80%). $C_{21}H_{18}N_2RuS_4$ (527.67): calcd. C 47.80, H 3.43, N 5.31, S 24.31; found C 47.35, H 3.59, N 5.87, S 23.30. IR (KBr): $\tilde{\nu}$ = 2262 cm^{-1} (ν_{CN}). ^{1}H NMR (269.6 MHz, CD_2Cl_2/CD_3CN): δ = 7.63−7.56 (m, 2 H, C_6H_4), 7.41−7.35 (m, 2 H, C_6H_4), 7.11 (t, 1 H, C_5H_3N), 6.93 (d, 2 H, C_5H_3N), 6.88−6.77 (m, 4 H, C_6H_4), 4.64 (d, $^3J_{H,H}$ = 17.8 Hz, 2 H, CH_2), 4.44 (d, $^3J_{H,H}$ = 17.8 Hz, 2 H, CH_2), 2.16 (s, 3 H, CH_3) ppm. ^{13}C{^{1}H} NMR (67.7 MHz, CD_2Cl_2): δ = 158.7, 157.1, 132.2, 131.8, 131.2, 130.2, 127.4, 120.6, 120.1 (C_6H_4), 116.5 (MeCN), 55.6(CH_2) ppm.

[Ru(CO)(pyS_4)] (3): CO gas was bubbled through a red-orange suspension of **2** (200 mg, 0.38 mmol) in THF (20 mL). Instantly, the color of the suspension changed to yellow. After stirring for 24 h under an atmosphere of CO, the resulting yellow suspension was filtered. The filtrate was evaporated to dryness and the resulting yellow powder was washed with MeOH (20 mL) and dried in vacuo. Yield: 178.2 mg of **3**·MeOH (86%). $C_{21}H_{19}NO_2RuS_4$ (546.70): calcd. C 46.14, H 3.50, N 2.56, S 23.46, found C 45.84, H 3.84, N 2.45, S 23.10. IR (KBr): $\tilde{\nu}$ = 1959.4 cm^{-1} (ν_{CO}). ^{1}H NMR (269.6 MHz, CD_2Cl_2): δ = 7.67−7.62 (m, 2 H, C_6H_4), 7.49−7.42, (m, 4 H, C_6H_4), 7.23 (d, $J_{H,H}$ = 13.5 Hz, 2 H, C_5H_3N), 7.03−6.95 (m, 4 H, C_6H_4/C_5H_3N), 5.12 (d, 2 H, CH_2), 5.07 (d, 2 H, CH_2) ppm. ^{13}C{^{1}H} NMR (67.7 MHz, CD_2Cl_2): δ = 201.7 (CO), 156.3, 155.9, 136.8, 132.5, 131.1, 131.0, 129.16, 122.6, 122.0 (C_6H_4) 58.2 (CH_2) ppm. MS (FD, CH_2Cl_2, ^{102}Ru): m/z = 515 [Ru(CO)(pyS_4)]$^+$.

[{Ru(pyS_4)}$_2$] (4): An orange suspension of **2** (250 mg, 0.47 mmol) in THF (30 mL) was heated under reflux for 4 days to give a red-brown suspension. The solid was filtered, washed with Et_2O (2 × 10 mL), and dried in vacuo. Yield: 156 mg of **4** (68%). $C_{38}H_{30}N_2Ru_2S_8$ (973.34): calcd. C 46.89, H 3.11, N 2.88, S 26.36; found C 45.38, H 2.76, N 2.91, S 25.44. MS (FD, DMSO, ^{102}Ru): m/z = 973 [{Ru(pyS_4)}$_2$]$^+$.

[Ru(N_2H_4)(pyS_4)] (5): An excess of N_2H_4·H_2O (0.55 mL, 11.4 mmol) was added to a suspension of **2** (300 mg, 0.57 mmol) in THF (30 mL). After 15 h, the red precipitate was separated, washed with MeOH (3 × 30 mL), and dried in vacuo. Yield: 295 mg of **5** (83%). $C_{19}H_{19}N_3RuS_4$ (518.69): calcd. C 44.00, H 3.69, N 8.10, S 24.72; found C 44.19, H 3.29, N 7.34, S 24.64. IR (KBr): $\tilde{\nu}$ = 3335, 3207, 3102 cm^{-1} (ν_{NH}). ^{1}H NMR (269.6 MHz, [D$_7$]DMF): δ = 7.75−7.72 (m, 2 H, C_6H_4), 7.45−7.42 (m, 2 H, C_6H_4), 7.12−7.06 (t, 3 H, C_5H_3N), 6.91−6.81 (m, 4 H, C_6H_4), 4.86 (s, 2 H, −N*H*$_2$−NH$_2$), 4.72 (d, $^3J_{H,H}$ = 16.2 Hz, 2 H, CH_2), 4.52 (d, $^3J_{H,H}$ = 16.2 Hz, 2 H, CH_2), 4.01 (s, 2 H, −NH$_2$−N*H*$_2$) ppm. ^{13}C{^{1}H} NMR (67.7 MHz, CD_2Cl_2): δ = 159.1, 156.7, 132.5, 132.2, 131.5, 131.2, 128.1, 121.6, 120.5 (C_6H_4), 54.6 (CH_2) ppm. MS (FD, DMF, ^{102}Ru): m/z = 973 [{Ru(pyS_4)}$_2$]$^+$.

[Ru(NH_3)(pyS_4)] (6): NH_3 was bubbled through a suspension of **2** (600 mg, 1.14 mmol) in THF (100 mL) for 15 min. The resulting red suspension was stirred under an NH_3 gas for additional 2 h and then filtered. Addition of *n*-hexane (100 mL) to the red filtrate precipitated a red powder, which was separated, washed with *n*-hexane (3 × 20 mL), and dried in vacuo. Yield: 493 mg of **6** (86%). $C_{19}H_{18}N_2RuS_4$ (503.68): calcd. C 45.31, H 3.60, N 5.56, S 25.46; found C 45.43, H 3.55, N 5.14, S 24.49. IR (KBr): $\tilde{\nu}$ = 3362, 3242, 3161 cm^{-1} (ν_{NH}). ^{1}H NMR (269.6 MHz, CD_2Cl_2): δ = 7.67−7.64 (m, 2 H, C_6H_4), 7.52−7.46 (m, 2 H, C_6H_4), 7.10−7.06 (t, 3 H, C_5H_3N), 6.93−6.88 (m, 4 H, C_6H_4), 4.65 (d, $^3J_{H,H}$ = 16.2 Hz, 2 H, CH_2), 4.46 (d, $^3J_{H,H}$ = 16.2 Hz, 2 H, CH_2), 1.54 (s, 3 H, −NH_3) ppm. MS (FD, CH_2Cl_2, ^{102}Ru): m/z = 973 [{Ru(pyS_4)}$_2$]$^+$, 504 [Ru(NH_3)(pyS_4)]$^+$.

[Ru(py)(pyS_4)] (7): A suspension of **2** (340 mg, 0.64 mmol) in pyridine (25 mL) was heated under reflux for 5 min. The resulting red solution was evaporated to yield a red solid. Yield: 340 mg of **7**·py (82.38%). $C_{29}H_{25}N_3RuS_4$ (644.85): calcd. C 54.02, H 3.91, N 6.52, S 19.89; found C 54.04, H 4.51, N 6.50, S 20.19. ^{1}H NMR (269.6 MHz, CD_2Cl_2): δ = 8.58 (d, $J_{H,H}$ = 5.4 Hz, 2 H, C_5H_5N) 8.41−8.38 (m, 2 H, C_6H_4), 7.69−7.65 (m, 2 H, C_6H_4), 7.52 (d, $J_{H,H}$ = 8.1 Hz, 2 H, C_5H_3N), 7.46−7.40 (t, 1 H, C_5H_5N), 7.31−7.26 (m, 2 H, C_5H_5N), 7.10−7.04 (t, 1 H, C_5H_3N), 6.95−6.89 (m, 4 H, C_6H_4), 4.77 (d, $^3J_{H,H}$ = 16.2 Hz, 2 H, CH_2), 4.47 (d, $^3J_{H,H}$ = 16.2 Hz, 2 H, CH_2) ppm. ^{13}C{^{1}H} NMR (67.7 MHz, CD_2Cl_2): δ = 159.38, 156.74, 150.05, 136.01, 134.82, 132.54, 132.24, 131.55, 128.10, 123.91, 123.77, 120.62 (C_6H_4), 56.5 (CH_2) ppm. MS (FD, CH_2Cl_2, ^{102}Ru): m/z = 973 [{Ru(pyS_4)}$_2$]$^+$.

[Ru(pyrazine)(pyS_4)] (8): An excess of pyrazine (4.0 g, 49 mmol) was added to a suspension of **2** (340 mg, 0.64 mmol) in THF (40 mL).

 © 2004 Wiley-VCH Verlag GmbH & Co. KGaA, Weinheim

The reaction mixture was heated under reflux for 15 min. The resulting deep-violet solution was evaporated to yield a violet powder, which was washed with *n*-hexane (5 × 30 mL) and dried in vacuo. Yield: 210 mg of **8**·0.25 pyrazine (54.22%). $C_{29}H_{25}N_3RuS_4$ (586.78): calcd. C 49.13, H 3.44, N 7.75, S 21.86; found C 48.09, H 3.60, N 7.86, S 20.76. ^{1}H NMR (269.6 MHz, CD_2Cl_2): δ = 8.56 (s, free pyrazine), 8.38 (d, $J_{H,H}$ = 5.4 Hz, 2 H, C_4H_4), 8.07 (d, $J_{H,H}$ = 5.4 Hz, 2 H, C_4H_4), 7.69 (d, $J_{H,H}$ = 16.2 Hz, 2 H, C_6H_4) 7.52 (d, $J_{H,H}$ = 10.8 Hz, 2 H, C_5H_3N), 7.21−7.15 (t, 1 H, C_5H_3N), 6.99−6.88 (m, 6 H, C_6H_4), 4.80 (d, $^3J_{H,H}$ = 16.2 Hz, 2 H, CH_2), 4.50 (d, $^3J_{H,H}$ = 13.5 Hz, 2 H, CH_2) ppm. $^{13}C\{^1H\}$ NMR (67.7 MHz, CD_2Cl_2): δ = 159.14, 156.94, 152.20, 145.40 (free pyrazine), 144.05, 133.14, 132.63, 131.12, 131.00, 121.81, 120.93 (C_6H_4), 56.46 (CH_2) ppm. MS (FD, CH_2Cl_2, ^{102}Ru): *m*/*z* = 973 $[\{Ru(pyS_4)\}_2]^+$, 567 $[Ru(pyr)(pyS_4)]^+$.

[Ru(I)(pyS$_4$)] (10): I_2 (0.27 g, 1.08 mmol) was added to a suspension of **2** (1.15 g, 2.16 mmol) in THF (50 mL). The resulting violet suspension was stirred for 30 min and then filtered. *n*-Hexane (100 mL) was added to the filtrate. After 30 min, the violet precipitate was filtered, washed with *n*-hexane (2 × 20 mL) and Et_2O (2 × 20 mL), and dried in vacuo for 1 h. Yield: 0.65 g of **10** (48.9%). $C_{19}H_{15}NRuS_4I$ (613.55). MS (FD, THF, ^{102}Ru): *m*/*z* = 614 $[Ru(I)(pyS_4)]^+$, 973 $[\{Ru(pyS_4)\}_2]^+$.

[Ru(NCMe)(pyS$_4$-H)]BF$_4$ (11): HBF_4 (0.11 mL, 54% solution in Et_2O, 0.77 mmol) was added to a suspension of **2** (406 mg, 0.77 mmol) in CH_2Cl_2 (20 mL) at −78 °C. The color of the suspension changed to yellow-green. The reaction mixture was stirred for 2 h at −78 °C and then filtered. *n*-Hexane (50 mL) was added to the green filtrate. The green precipitate was separated by filtration and dried in vacuo for 15 min. IR (KBr): $\tilde{\nu}$ = 2472 (ν_{SH}), 2273 (ν_{CN}), 1055 (ν_{BF}) cm^{-1}. MS (FD, DMF, ^{102}Ru): *m*/*z* = 976 $[\{Ru(pyS_4\text{-}H)\}_2]^+$.

[Ru(NCMe)(pyS$_4$-Et)]BF$_4$ (12): Et_3OBF_4 (1.19 mL, 1 M solution in CH_2Cl_2, 1.19 mmol) was added to a suspension of **2** (627 mg, 1.19 mmol) in CH_2Cl_2 (30 mL). The color changed to yellow-brown and, after 2 h, the brown solid was separated by filtration. *n*-Hexane (70 mL) was added to the deep yellow-brown filtrate. The yellow precipitate was filtered, washed with *n*-hexane (20 mL), and dried in vacuo. $C_{23}H_{23}N_2RuS_4BF_4$ (643.56). IR (KBr): $\tilde{\nu}$ = 2282 (ν_{CN}), 1048 (ν_{BF}) cm^{-1}. ^{1}H NMR (269.6 MHz, CD_2Cl_2): δ = 8.25 (d, $J_{H,H}$ = 5.4 Hz, 2 H, C_5H_3N), 7.77−6.93 (m, 9 H, aryl), 5.00, 4.85, 4.73, 4.55 (4 × d, 8 H, CH_2), 3.18 (m, 2 H, CH_2), 2.39 (s, 3 H, coord. CH_3CN), 2.23 (s, 3 H, free CH_3CN), 1.50 (t, 3 H, CH_3) ppm. $^{13}C\{^1H\}$ NMR (67.7 MHz, CD_2Cl_2): δ = 159.2, 155.0, 138.15, 135.6, 134.8, 133.7, 133.5, 133.3, 133.0, 132.9, 132.4, 131.9, 131.6, 130.4, 122.9, 122.3 (C_6H_5), 123.9 (CH_3CN), 55.7 (CH_2), 55.5 (CH_2), 38.1 (CH_2), 13.0 (CH_3), 4.6 (CH_3CN) ppm. MS (FD, CH_2Cl_2, ^{102}Ru): *m*/*z* = 516 $[Ru(pyS_4\text{-}Et)]^+$.

[{Ru(pyS$_4$-Et)}$_2$](BF$_4$)$_2$ (13): Et_3OBF_4 (5.16 mL, 1 M solution in CH_2Cl_2, 6.35 mmol) was added to a suspension of **2** (670 mg, 1.27 mmol) in CH_2Cl_2 (30 mL) and then the mixture was stirred for 2 days. During this period of time, the mixture became a yellow-green solution. Upon addition of Et_2O (20 mL) and THF (30 mL), a yellow solid precipitated; it was filtered and dried in vacuo. $C_{42}H_{40}N_2Ru_2S_8B_2F_8$ (1205.02). IR (KBr): $\tilde{\nu}$ = 1060 cm^{-1} (ν_{BF}). ^{1}H NMR (399.65 MHz, CD_2Cl_2): δ = 8.23 (d, $J_{H,H}$ = 8.1 Hz, 2 H), 7.78−7.25 (m, 9 H, C_6H_5), 5.01 (d, $^3J_{H,H}$ = 24.0 Hz, 2 H, CH_2), 4.84 (d, $^3J_{H,H}$ = 28.0 Hz, 2 H, CH_2), 3.24 (m, 4 H, CH), 2.39 (s, 3 H, free CH_3CN), 1.53 (t, 6 H, CH_3) ppm. $^{13}C\{^1H\}$ NMR (67.7 MHz, CD_2Cl_2): δ = 159.4, 138.3, 134.9, 134.5, 133.4, 133.2, 133.1, 132.5, 130.5 [C_6H_5], 124.0 (free CH_3CN), 55.2 (CH_2), 38.1 (CH_2), 13.0 (CH_3), 4.5 (free CH_3CN) ppm. MS (FD, CH_2Cl_2, ^{102}Ru): *m*/*z* = 585 $[Ru(pyS_4-Et_2)(MeCN)]^{2+}$, 1033 $[\{Ru(pyS_4-Et_2)\}_2]^+$.

[{Ru$^{II/III}$(pyS$_4$)}$_2$](PF$_6$) (14): LiOMe (0.77 mL, 1 M MeOH solution) and $[FeCp_2]PF_6$ (255 mg, 0.77 mmol) were added sequentially to a red solution of **5** (200 mg, 0.386 mmol) in DMF (20 mL) and then the mixture was stirred overnight. During this period of time, red microcrystals formed; they were isolated by filtration and identified as dimeric **4** (ca. 25 mg). Crystals grew from the deep-red filtrate; they were identified by an X-ray structural analysis to be **14**·CD_2Cl_2.

[Ru(NH$_3$)(pyS$_4$)](PF$_6$) (15). From 6: $[FeCp_2]PF_6$ (a small spatula's worth) was added to a red suspension of **6** (80 mg, 0.16 mmol) in THF (10 mL). The resulting green suspension was filtered and Et_2O (30 mL) was added to the green filtrate. The green precipitate was filtered, washed with Et_2O (2 × 10 mL), and dried in vacuo. Yield: 40 mg of **15** (32%). $C_{23}H_{26}F_6N_2OPRuS_4$ (**15**·THF) (720.75): calcd. C 38.33, H 3.89, N 3.64, S 17.79; found C 37.45, H 3.36, N 3.64, S 17.13. IR (KBr): $\tilde{\nu}$ = 3356, 3283, 3187 (ν_{NH}) cm^{-1}. MS (FD, CH_2Cl_2, ^{102}Ru): *m*/*z* = 973 $[\{Ru(pyS_4)\}_2]^+$, 504 $[Ru(NH_3)(pyS_4)]^+$.

From 5: $[FeCp_2]PF_6$ (a small spatula's worth) was added to a red suspension of **5** (230 mg, 0.44 mmol) in THF (30 mL). The resulting green suspension was filtered and then Et_2O (60 mL) was added to the green filtrate. The green precipitate was filtered, washed with Et_2O (2 × 20 mL), and dried in vacuo. Yield: 49 mg of **15** (59%).

[Ru(NH$_3$)(pyS$_4$)](I) (16): I_2 (225 mg, 0.9 mmol) was added to a red suspension of **5** (465 mg, 0.9 mmol) in THF (20 mL) and then the mixture was stirred for 30 min. The resulting yellow-brown solid was separated by filtration, washed with THF (3 × 20 mL), and dried in vacuo. Yield: 140 mg of **15** (47%). $C_{21}H_{22}IN_2O_{0.5}RuS_4$ (**16**·0.5THF) (666.64): calcd. C 37.84, H 3.33, N 4.20, S 19.24; found C 37.84, H 2.89, N 3.99, S 18.44.

[Ru(CO)(pyS$_4$)](BF$_4$) (17): $NOBF_4$ (20.54 mg, 0.17 mmol) was added at 0 °C to a yellow solution of **3** (90 mg, 0.17 mmol) in CH_2Cl_2 (30 mL). The reaction mixture was stirred at room temp. until a green solution formed (ca. 1 h); it was evaporated to yield a green solid. $C_{20.5}H_{16}BCl_2F_4NORuS_4$ (**17**·0.5CH_2Cl_2) (643.93): calcd. C 38.24, H 2.50, N 2.17, S 19.92; found C 35.93, H 2.33, N 2.40, S 18.73. IR (KBr): $\tilde{\nu}$ = 2004.5 cm^{-1}(ν_{CO}).

[Ru(NH$_3$)(pyS$_4$)](BF$_4$) (18): A red solution of **6** (325 mg, 0.65 mmol) in CH_2Cl_2 (30 mL) was combined with $NOBF_4$ (78.54 mg, 0.65 mmol) at 0 °C. The solution was stirred for 1 h at 0 °C and then for an additional 1 h at room temp. until its color had changed to green. Evaporation of the solvent gave a violet oil, which was redissolved in MeOH (30 mL). Et_2O (40 mL) was added to the resulting violet-brown solution. The green precipitate was separated and dried in vacuo. Yield: 130 mg of **18**·CH_2Cl_2 (30%). $C_{23}H_{26}F_6N_2OPRuS_4$ (675.87): calcd. C 35.54, H 2.98, N 4.15, S 18.98; found C 34.55, H 2.70, N 4.17, S 19.05.

[{Ru(pyS$_4$−O$_3$)}$_2$]/[{Ru(pyS$_4$−O$_4$)}$_2$] (19/20): H_2O_2 (1 mL) was added at room temp. to a red suspension of **5** (220 mg, 0.42 mmol) in THF (30 mL) and then the mixture was stirred for 30 min. During this period of time the color of the suspension changed to yellow. The yellow solid was separated by filtration and dried in vacuo. $C_{38}H_{30}N_2O_{8.64}Ru_2S_8$ (0.68[{Ru(pyS$_4$−O$_3$)}$_2$] × 0.32[{Ru(pyS$_4$−O$_4$)}$_2$]) (1143.65). IR (KBr): $\tilde{\nu}$ = 1141, 1042 (ν_{SO}) cm^{-1}. ^{1}H NMR (269.6 MHz, MeOD): δ = 8.09−8.00 (m, 4 H, C_6H_4 × 2),

 © 2004 Wiley-VCH Verlag GmbH & Co. KGaA, Weinheim

7.84−7.77 (m, 8 H, C_6H_4), 7.59−7.47 (m, 16 H, C_6H_4), 7.35−7.23 (m, 4 H, C_5H_3N), 7.14−7.06 (m, 8 H, C_5H_3N), 5.41 (d, $J_{H,H}$ = 16.2 Hz, 2 H, CH_2), 5.40 (d, $J_{H,H}$ = 16.2 Hz, 2 H, CH_2), 4.68 (d, $J_{H,H}$ = 16.2 Hz, 2 H, CH_2), 4.67 (d, $J_{H,H}$ = 18.9 Hz, 2 H, CH_2) ppm. MS (FD, MeOH, ^{102}Ru): *m*/*z* = 1101 $[\{Ru(pyS_4{-}O_4)\}_2]^+$, 1068 $[\{Ru(pyS_4{-}O_3)\}_2]^+$, 974 $[\{Ru(pyS_4)\}_2]^+$, 486 $[Ru(pyS_4)]^+$.

[Ru(NH$_3$)(pyS$_4$−O$_4$)] (21): A red solution of **6** (205 mg, 0.41 mmol) in THF (50 mL) was combined with H_2O_2 (1 mL) at room temp. The resulting yellow precipitate was stirred for 1 h, then filtered, washed with THF (30 mL), and dried in vacuo. Yield: 201.54 mg of **21**·0.5THF (82%). $C_{21}H_{22}N_2RuS_4O_{4.5}$ (603.73): calcd. C 41.78, H 3.67, N 4.64, S 21.24; found C 38.99, H 3.55, N 4.37, S 20.81. IR (KBr): $\tilde{\nu}$ = 3353, 3301, 3188 (ν_{NH}), 1134, 1013 (ν_{SO}) cm^{-1}. ^{1}H NMR (269.6 MHz, CD_2Cl_2): δ = 7.92−7.84 (m, 4 H, C_6H_4), 7.53−7.49 (m, 4 H, C_6H_4), 7.33−7.27 (t, 3 H, C_5H_3N), 7.08 (d, $J_{H,H}$ = 8.1 Hz, 2 H, C_6H_4), 5.82 (d, $J_{H,H}$ = 16.2 Hz, 2 H, CH_2), 4.47 (d, $J_{H,H}$ = 16.2 Hz, 2 H, CH_2), 1.52 (s, 3 H, $-NH_3$) ppm. ^{13}C{^{1}H} NMR (67.7 MHz, CD_3OD): δ = 161.4, 159.7, 136.7, 133.3, 132.5, 132.2, 128.8, 123.8, 122.5 (C_6H_5), 54.9 (CH_2) ppm.

[{Ru(pyS$_4$)}$_2$](I$_3$)$_2$ (22): Black single crystals of **22**·1.8THF that were suitable for X-ray structural analysis were grown from the filtrate after preparation of **10** in the presence of an excess of I_2.

[{Ru(pyS$_4$-Et)}$_2$](BF$_4$)$_2$(B$_2$F$_7$) (23): The single crystals of **23**·3CD_2Cl_2 were obtained during attempts to recrystallize **13** from CD_2Cl_2; spontaneously dealkylation and oxidation of the two Ru centers were observed to occur in the CD_2Cl_2 medium.

[{Ru(pyS$_4$)}$_2$](BF$_4$)(B$_2$F$_7$) (24): The single crystals of **24**·3CH_2Cl_2 were obtained during attempts to recrystallize **13** from CH_2Cl_2; spontaneously dealkylation and oxidation of one of the Ru centers were observed to occur in the CH_2Cl_2 medium.

X-ray Structural Determination of [{Ru(pyS$_4$)}$_2$]·2toluene (4·2toluene), [Ru(NH$_3$)(pyS$_4$)] (6), [Ru(I)(pyS$_4$)]·1.5CH_2Cl_2 (10·1.5CH_2Cl_2), [{Ru(pyS$_4$)}$_2$](PF$_6$)·CD_2Cl_2 (14·CD_2Cl_2), [Ru(NH$_3$)(pyS$_4$)]PF$_6$·CH_2Cl_2 (15·CH_2Cl_2), 0.68[{Ru(pyS$_4$−O$_3$)}$_2$]·0.32[{Ru(pyS$_4$−O$_4$)}$_2$]·2MeOH (0.68 19·0.32 20·2MeOH), [{Ru(pyS$_4$)}$_2$](I$_3$)$_2$·1.8THF (22·1.8THF), [{Ru(pyS$_4$−Et)}$_2$](BF$_4$)$_2$(B$_2$F$_7$)·3CD_2Cl_2 (23·3CD_2Cl_2), and [{Ru(pyS$_4$)}$_2$](BF$_4$)(B$_2$F$_7$)·3CH_2Cl_2 (24·3CH_2Cl_2): Orange rhombs of **4**·2toluene were obtained by recrystallization of a saturated solution of **4** in toluene. Red irregular-shaped crystals of **6** were grown from a saturated H_2O solution of **6**. Black rhombs of **10**·1.5CH_2Cl_2 crystallized from a saturated solution of **10** in CH_2Cl_2. Black blocks of **14**·CD_2Cl_2 were obtained within 10 days from a CD_2Cl_2 solution at room temp. Green fragments of **15**·CH_2Cl_2 formed from a saturated solution of **15** in CH_2Cl_2. Orange prisms of **19/20**·2MeOH formed upon layering a MeOH solution of **19/20** with *n*-hexane. Black crystals of **22**·1.8THF were grown from the filtrate after preparation of **10**. Brown fragments of **23**·3CD_2Cl_2 formed from **13** in a 1:1 mixture of CD_2Cl_2/THF, which was layered with Et_2O. Dark-green platelets of **24**·3CH_2Cl_2 crystallized from a saturated CH_2Cl_2 solution of **13**. Data were collected on a Bruker−Nonius KappaCCD diffractometer using Mo-K_α radiation (λ = 71.073 pm) and a graphite monochromator. Lorentz and polarization corrections were applied for all data sets. A numeric absorption correction was used for **10**·1.5CH_2Cl_2 (Gauss integration).[18] A semiempirical absorption correction has been applied for **14**·CD_2Cl_2 (SORTAV).[19] A semiempirical absorption correction (SADABS)[20] was used for **4**·2toluene, **6**, **15**·CH_2Cl_2, **19/20**·2MeOH, **22**·1.8THF, and **24**·3CH_2Cl_2. All structures were solved by direct methods and refined using full-matrix least-squares procedures on F^2 (SHELXTL NT 6.12).[21] All non-hydrogen atoms were refined anisotropically. The positions of the hydrogen atoms were either taken from the

Table 4. Selected crystallographic data for [{Ru(pyS$_4$)}$_2$] (**4**·2 toluene), [Ru(NH$_3$)(pyS$_4$)] (**6**), and [Ru(I)(pyS$_4$)] (**10**·1.5CH_2Cl_2)

Compound	**4**·2toluene	**6**	**10**·1.5CH_2Cl_2
Formula	$C_{52}H_{46}N_2Ru_2S_8$	$C_{19}H_{18}N_2RuS_4$	$C_{20.5}H_{18}Cl_3INRuS_4$
M_r [g·mol^{-1}]	1157.53	503.66	740.92
Crystal size [mm]	0.14 × 0.10 × 0.05	0.30 × 0.25 × 0.10	0.18 × 0.16 × 0.12
F(000)	588	2032	2880
Crystal system	triclinic	orthorhombic	monoclinic
Space group	$P\bar{1}$	*Pbca*	*C*2/*c*
a [pm]	848.3(1)	1249.9(1)	2163.9(2)
b [pm]	1021.8(1)	1267.8(2)	1366.4(2)
c [pm]	1448.0(2)	2463.9(2)	1763.6(3)
α (°)	103.250(6)	90	90
β (°)	95.209(7)	90	104.626(6)
γ (°)	97.689(6)	90	90
V [nm^3]	1.2011(2)	3.9044(8)	5.0455(9)
Z	1	8	8
$d_{calcd.}$ [g·cm^{-3}]	1.600	1.714	1.951
μ [mm^{-1}]	1.016	1.237	2.505
$T_{min.}/T_{max.}$	0.746/1.000	0.778/1.000	0.602/0.760
Scan technique	ω rotations	φ and ω rotations	φ and ω rotations
2θ Range (°)	6.9−52.8	6.7−56.6	6.8−56.6
Measd. reflections	17246	27662	36368
Indep. reflections	4897	4680	6247
Obsd. reflections[a]	3443	3098	4645
Ref. parameters	290	289	342
*R*1[a]; *wR*2[b] [%]	5.03, 12.73	4.46, 8.94	3.57, 7.28
r_{fin} (max./min.) [e·nm^{-3}]	1.262/−1.199	0.541/−0.542	0.895/−1.046

[a] $[I > 2\sigma(I)]$. [b] All data.

 © 2004 Wiley-VCH Verlag GmbH & Co. KGaA, Weinheim

Table 5. Selected crystallographic data for $[\{Ru(pyS_4)\}_2](PF_6)$ (**14**·CD_2Cl_2), $[Ru(NH_3)(pyS_4)]PF_6$ (**15**·CH_2Cl_2), and $0.68[\{Ru(pyS_4{-}O_3)\}_2]\cdot 0.32[\{Ru(pyS_4{-}O_4)\}_2]$ (**19/20**·2MeOH)

Compound	**14**·CD_2Cl_2	**15**·CH_2Cl_2	**19/20**·2MeOH
Formula	$C_{39}H_{30}Cl_2D_2F_6N_2PRu_2S_8$	$C_{20}H_{20}Cl_2F_6N_2PRuS_4$	$C_{40}H_{38}N_2O_{8.64}Ru_2S_8$
M_r [g·mol^{-1}]	1205.16	733.56	1143.58
Crystal size [mm]	0.38 × 0.12 × 0.08	0.23 × 0.15 × 0.07	0.26 × 0.16 × 0.10
F(000)	4792	1460	1154
Crystal system	orthorhombic	monoclinic	monoclinic
Space group	*Ccca*	$P2_1/n$	$P2_1/c$
a [pm]	1663.4(1)	1287.1(1)	1298.2(2)
b [pm]	2381.3(2)	1382.7(2)	1164.9(1)
c [pm]	2287.6(2)	1617.9(2)	1383.8(1)
α (°)	90	90	90
β (°)	90	111.347(5)	102.263(8)
γ (°)	90	90	90
V [nm^3]	9.061(1)	2.6818(6)	2.0449(4)
Z	8	4	2
$d_{calcd.}$ [g·cm^{-3}]	1.764	1.817	1.857
μ [mm^{-1}]	1.247	1.212	1.207
$T_{min.}/T_{max.}$	0.563/0.902	0.631/1.000	0.852/1.000
Scan technique	ω rotations	ω rotations	ω rotations
2θ range (°)	6.7−51.0	6.9−52.0	6.9−51.4
Measd. reflections	38060	21850	30949
Indep. reflectopms	4219	5246	3873
Obsd. reflections[a]	2852	3204	3006
Ref. parameters	286	354	309
$R1$[a]; $wR2$[b] [%]	6.88, 15.10	5.72, 11.44	5.91, 11.97
$r_{fin.}$ (max./min.) [e·nm^{-3}]	0.863/−0.683	0.728/−0.752	0.552/−0.722

[a] [$I > 2\sigma(I)$]. [b] All data.

Table 6. Selected crystallographic data for $[\{Ru(pyS_4)\}_2](I_3)_2$ (**22**·1.8THF), $[\{Ru(pyS_4\text{-}Et)\}_2](BF_4)_2(B_2F_7)$ (**23**·$3CD_2Cl_2$), and $[\{Ru(pyS_4)\}_2](BF_4)(B_2F_7)$ (**24**·$3CH_2Cl_2$)

Compound	**22**·1.8THF	**23**·$3CD_2Cl_2$	**24**·$3CH_2Cl_2$
Formula	$C_{45.2}H_{44.4}I_6N_2O_{1.8}Ru_2S_8$	$C_{45}H_{40}B_4Cl_6D_6F_{15}N_2Ru_2S_8$	$C_{41}H_{36}B_3Cl_6F_{11}N_2Ru_2S_8$
M_r [g·mol^{-1}]	1864.45	1620.4	1469.47
Crystal size [mm]	0.28 × 0.24 × 0.18	0.15 × 0.07 × 0.05	0.24 × 0.19 × 0.06
F(000)	1756	1606	1456
Crystal system	triclinic	monoclinic	triclinic
Space group	$P\bar{1}$	$P2_1/c$	$P\bar{1}$
a [pm]	1405.1(2)	1233.8(1)	1257.8(2)
b [pm]	1429.7(1)	966.1(1)	1320.4(2)
c [pm]	1508.0(2)	2495.5(3)	1666.1(2)
α (°)	73.33(1)	90	92.19(1)
β (°)	70.66(1)	101.66(1)	94.00(1)
γ (°)	79.61(1)	90	103.55(1)
V [nm^3]	2.7261(6)	2.9132(5)	2.6792(7)
Z	2	2	2
$d_{calcd.}$ [g·cm^{-3}]	2.271	1.840	1.821
μ [mm^{-1}]	4.296	1.166	1.248
$T_{min.}/T_{max}$	0.765/1.000	0.790/1.000	0.783/1.000
Scan technique	φ and ω rotations	φ and ω rotations	φ and ω rotations
2θ range (°)	6.9−56.6	6.6−51.4	6.6−56.6
Measd. refl.	50218	29119	52782
Indep. reflections	13340	5409	12322
Obsd. reflections[a]	9437	3370	7677
Ref. parameters	745	426	785
$R1$[a]; $wR2$[b] [%]	3.48, 7.34	5.84, 11.75	4.78, 9.30
r_{fin}(max./min.) [e·nm^{-3}]	2.144/−1.065	0.764/−0.839	0.853/−0.877

[a] [$I > 2\sigma(I)$]. [b] All data.

 © 2004 Wiley-VCH Verlag GmbH & Co. KGaA, Weinheim

difference Fourier synthesis and refined with a common isotropic displacement parameter (**6**, **10**·1.5CH_2Cl_2, and **24**·3CH_2Cl_2) or were positioned geometrically with isotropic displacement parameters fixed at 1.2 or 1.5 times the value of *U*(eq) of the preceding carbon atom (**4**·2toluene, **14**·CD_2Cl_2, **15**·CH_2Cl_2, **19/20**·2MeOH, **22**·1.8THF, and **23**·3CD_2Cl_2). Complex **4** crystallized with two toluene molecules per formula unit. Four significant residual electron density maxima are found in close vicinity to the central Ru atom. Complex **10** crystallizes with 1.5 molecules of CH_2Cl_2, which are disordered about the crystallographic inversion center. In the case of **22**·1.8THF, the I_3^- anion is disordered on two alternative sites and the solvate THF molecule is disordered on four different sites. Four significant residual electron density maxima are found in close vicinity of the disordered I_3^-/THF units. The $B_2F_7^-$ anion in the structure of **23**·3CD_2Cl_2 is situated on a crystallographic inversion centre and shares its site with one solvate CD_2Cl_2 molecule, with an occupancy of 50% each. The $B_2F_7^-$ anion in the structure of **24**·3CH_2Cl_2 is disordered on two different sites having occupancies of 78(2)% (for C22, C23) and 22(2)% (for C22′, C23′). The CD_2Cl_2 solvent molecule in **14**·CD_2Cl_2 is disordered on a crystallographic C_2 axis. In the case of **15**·CH_2Cl_2, the CH_2Cl_2 solvate molecule is disordered on two different sites having occupancies of 92.1(4)% and 7.9(4)%, respectively. Two different molecules in **19/20**·2MeOH share a single site on a crystallographic inversion center with occupancies of 68(2)% for [{Ru(pS_4−O_3)}$_2$] (**19**) and 32(2)% for [{Ru(pS_4−O_4)}$_2$] (**20**). The solvate MeOH molecules are also disordered. Selected crystallographic data are summarized in Table 4−6.[22]

Acknowledgments

We thank Prof. Dr. Horst Kisch for valuable discussions of many aspects of this work and the Deutsche Forschungsgemeinschaft (SFB 583 "Redoxaktive Metallkomplexe") for financial support.

[1] D. Sellmann, J. Sutter, *Acc. Chem. Res.* **1997**, *30*, 460−469.
[2] [2a] J. B. Howard, D. C. Rees, *Chem. Rev.* **1996**, *96*, 2965−2982. [2b] B. K. Burgess, D. J. Lowe, *Chem. Rev.* **1996**, *96*, 2983−3012. [2c] R. R. Eady, *Chem. Rev.* **1996**, *96*, 3013−3030.
[3] T. Noguchi, J. Honda, T. Nagamune, H. Sasebe, Y. Inoue, I. Endo, *FEBS Lett.* **1995**, *358*, 50−54.
[4] D. Sellmann, J. Sutter, in *Progr. Inorg. Chem. Dithiolenes in More Complex Ligands* (Eds.: E. I. Stiefel, K. D. Karlin), John Wiley & Sons, Inc., Hoboken, New Jersey **2004**, *52*, chapter 11, 585−681.
[5] [5a] D. Sellmann, W. Soglowek, F. Knoch, G. Ritter, J. Dengler, *Inorg. Chem.* **1992**, *31*, 3711. [5b] D. Sellmann, W. Soglowek, F. Knoch, M. Moll, *Angew. Chem.* **1989**, *101*, 1244; *Angew. Chem. Int. Ed. Engl.* **1989**, *28*, 1271. [5c] D. Sellmann, H. Kunstmann, F. Knoch, M. Moll, *Inorg. Chem.* **1988**, *27*, 4183. [5d] D. Sellmann, T. Hofmann, F. Knoch, *Inorg. Chim. Acta* **1994**, *224*, 61.
[6] D. Sellmann, J. Utz, N. Blum, F. W. Heinemann, *Coord. Chem. Rev.* **1999**, *190−192*, 607−627.
[7] [7a] D. Sellmann, K. Engl, F. W. Heinemann, *Eur. J. Inorg. Chem.* **2000**, 423−429. [7b] D. Sellmann, D. Häußinger, T. Gottschalk-Gaudig, F. W. Heinemann, *Z. Naturforsch.* **2000**, *55*, 723−729. [7c] D. Sellmann, N. Blum, F. W. Heinemann, B. A. Hess, *Chem. Eur. J.* **2001**, *7*, 1874−1880. [7d] D. Sellmann, N. Blum, F. W. Heinemann, *Z. Naturforsch., Teil B* **2001**, *56*, 581−588. [7e] D. Sellmann, J. Utz, F. W. Heinemann, *Inorg. Chem.* **1999**, *38*, 5314−5322.
[8] D. Sellmann, N. Blum, F. W. Heinemann, *Z. Naturforsch., Teil B* **2001**, *56*, 581−588.
[9] D. Sellmann, K. Engl, F. W. Heinemann, J. Sieler, *Eur. J. Inorg. Chem.* **2000**, 1079−1089.
[10] T. Gottschalk-Gaudig, PhD Thesis, University of Erlangen-Nürnberg, **1997**.
[11] D. Sellmann, J. Käppler, M. Moll, F. Knoch, *Inorg. Chem.* **1993**, *32*, 960−964.
[12] [12a] P. G. Douglas, R. D. Feltham, H. G. Metzger, *J. Am. Chem. Soc.* **1971**, *93*, 84. [12b] P. G. Douglas, R. D. Feltham, *J. Am. Chem. Soc.* **1972**, *94*, 5254.
[13] D. Sellmann, T. Gottschalk-Gaudig, F. W. Heinemann, *Inorg. Chimica Acta* **1998**, *269*, 63−72.
[14] [14a] R. M. Buonomo, I. Font, M. J. Maguire, J. H. Reibenspies, T. Tuntulani, M. Y. Darensbourg, *J. Am. Chem. Soc.* **1995**, *117*, 963. [14b] S. A. Mirza, M. A. Pressler, M. Kumar, R. O. Day, M. J. Maroney, *Inorg. Chem.* **1993**, *32*, 977.
[15] [15a] L. A. Tyler, J. C. Noveron, M. M. Olmstead, P. K. Mascharak, *Inorg. Chem.* **1999**, *38*, 616−617, [15b] L. A. Tyler, J. C. Noveron, M. M. Olmstead, P. K. Mascharak, *Inorg. Chem.* **2000**, *39*, 357−362. [15c] J. C. Noveron, M. M. Olmstead, P. K. Mascharak, *Inorg. Chem.* **2001**, *123*, 3247−3259.
[16] [16a] G. N. Schrauzer, C. Zhang, R. Chadha, *Inorg. Chem.* **1990**, *29*, 4104−4107. [16b] C. A. Grapperhaus, M. Y. Darensbourg, *Acc. Chem. Res.* **1998**, *31*, 451−459.
[17] M. Koepp, H. Wendt, H. Strehlow, *Z. Elektrochem.* **1960**, *64*, 483.
[18] P. Coppens, in *Crystallographic Computing* (Eds.: F. R. Ahmed, S. R.Hall, C. P. Huber), Munksgaard, Copenhagen, **1970**, pp. 255−270.
[19] R. H. Blessing, *Acta Crystallogr., Sect. A* **1995**, *51*, 33−38.
[20] SADABS, Bruker-Nonius, Inc., **2002**, Madison, WI, USA.
[21] SHELXTL NT 6.12, Bruker AXS, Inc., **2002**, Madison, WI, USA.
[22] CCDC-229802 (for **4**·2toluene), -229803 (for **6**), -229804 (for **10**·1.5 CH_2Cl_2), -229805 (for **14**·CD_2Cl_2), -229806 (for **15**·CH_2Cl_2), -229807 (for **19/20**·2 MeOH), -229808 (for **22**·1.8 THF), -229809 (for **23**·3 CD_2Cl_2), and -229810 (for **24**·3 CH_2Cl_2)contain the supplementary crystallographic data for this paper. These data can be obtained free of charge at www.ccdc.cam.ac.uk/const/retrieving.html [or from the Cambridge Crystallographic Data Centre, 12 Union Road, Cambridge CB2 1EZ, UK; Fax: (internat.) + 44-1223/336-033; E-mail: deposit@ccdc.cam.ac.uk.

Received January 27, 2004
Early View Article
Published Online May 27, 2004

 © 2004 Wiley-VCH Verlag GmbH & Co. KGaA, Weinheim

Synthesis and Characterization of Cubane-Like Cr_4E_4 (E = S, Se) Clusters − Molecular Structures of $(\eta^5\text{-}RC_5H_4)_4Cr_4E_4$ (E = S, R = MeCO, MeO_2C, EtO_2C; E = Se, R = H)

Li-Cheng Song,*[a] Hua-Wei Cheng,[a] Xin Chen,[a] and Qing-Mei Hu[a]

Keywords: Clusters compounds / Chromium / Selenium / Cp ligands / Cluster-forming reactions

Treatment of the Cr–Cr singly-bonded dimers $[\eta^5\text{-}RC_5H_4Cr(CO)_3]_2$ (**1**, R = MeCO; **2**, R = MeO_2C; **3**, R = EtO_2C) with excess sulfur in refluxing THF gave the cubane Cr_4S_4 clusters $(\eta^5\text{-}RC_5H_4)_4Cr_4S_4$ (**4**, R = MeCO; **5**, R = MeO_2C; **6**, R = EtO_2C). The cubane Cr_4S_4 cluster **4** reacted with excess 2,4-dinitrophenylhydrazine to produce the hydrazone derivative $[\eta^5\text{–}2,4\text{-}(NO_2)_2C_6H_3NHN{=}C(Me)C_5H_4]_4Cr_4S_4$ (**7**). The singly-bonded dimers of $[\eta^5\text{-}RC_5H_4Cr(CO)_3]_2$ (**8**, R = Me; **9**, R = EtO_2C), in the presence of excess selenium, reacted similarly to the linear Cr_2Se complexes $[\eta^5\text{-}RC_5H_4Cr(CO)_2]_2Se$ (**10**, R = Me; **11**, R = EtO_2C), which reacted with an equimolar quantity of selenium to afford the cubane Cr_4Se_4 clusters $(\eta^5\text{-}RC_5H_4)_4Cr_4Se_4$ (**12**, R = Me; **13**, R = EtO_2C). A particularly interesting phenomenon is the cross-assembled reaction of the linear Cr_2Se complexes $[\eta^5\text{-}MeC(O)C_5H_4Cr(CO)_2]_2Se$ (**14**) and $[CpCr(CO)_2]_2Se$ (**15**) in the presence of excess selenium in THF that gave rise to a series of cubane Cr_4Se_4 clusters $[\eta^5\text{-}MeC(O)C_5H_4]_nCp_{4-n}Cr_4Se_4$ (**16**, n = 0; **17**, n = 1; **18**, n = 2; **19**, n = 3; **20**, n = 4). The possible pathway for the cross-assembled reaction is suggested. Furthermore the new clusters were characterized by elemental analysis and spectroscopy, and in the case of **4**–**6** and **16** also by X-ray diffraction techniques.

(© Wiley-VCH Verlag GmbH & Co. KGaA, 69451 Weinheim, Germany, 2004)

Introduction

Transition-metal cubane-like cluster complexes containing μ_3-E chalcogen elements (where E = S, Se) have attracted much attention, largely due to their unique structures and novel properties,[1−4] and particularly because of the biological functions played by cubane subclusters, such as Fe_4S_4 and $MoFe_3S_4$, in metalloenzymes of nitrogenase and [Fe]-only hydrogenase.[5−8] Among these transition metal clusters, the Cr_4E_4 cluster complexes (where E = μ_3-S, μ_3-Se) have been studied to a smaller extent, although the parent clusters and the Me-substituted Cp derivatives $Cp_4Cr_4E_4$ (where E = S,[3] E = Se[9]) and $(\eta^5\text{-}MeC_5H_4)_4Cr_4E_4$ (where E = S,[10] E = Se[11]) have been known for many years. In this paper we report the synthesis and spectroscopic characterization of a series of cubane Cr_4E_4 clusters (E = S, Se), $(\eta^5\text{-}RC_5H_4)_4Cr_4S_4$ [where R = MeCO, MeO_2C, EtO_2C, 2,4-$(NO_2)_2C_6H_3NHN{=}CMe$], $(\eta^5\text{-}RC_5H_4)_4Cr_4Se_4$ (where R = Me, EtO_2C) and $[\eta^5\text{-}MeC(O)C_5H_4]_nCp_{4-n}Cr_4Se_4$ (n = 0−4), along with the crystal structures of cubane clusters $(\eta^5\text{-}RC_5H_4)_4Cr_4S_4$ (where R = MeCO, MeO_2C, EtO_2C) and $Cp_4Cr_4Se_4$.

[a] Department of Chemistry, State Key Laboratory of Element-Organic Chemistry, Nankai University,
Tianjin 300071, China
Fax: (internat.) + 86-22-23504853
E-mail: lcsong@nankai.edu.cn

Results and Discussion

Synthesis and Characterization of $(\eta^5\text{-}RC_5H_4)_4Cr_4S_4$ [4, R = MeCO; 5, R = MeO_2C; 6, R = EtO_2C; 7, R = 2,4-$(NO_2)_2C_6H_3NHN{=}CMe$]

The Cr−Cr singly-bonded dimers $[\eta^5\text{-}RC_5H_4Cr(CO)_3]_2$ (**1**, R = MeCO;[12] **2**, R = MeO_2C;[12] **3**, R = EtO_2C[13]) were found to react with an excess amount of elemental sulfur in THF at reflux for 12 h to give cubane clusters **4**−**6** in 81−95 % yields (see Scheme 1), while the functional transformation reaction of cubane cluster **4** with excess 2,4-dinitrophenylhydrazine in CH_2Cl_2 at room temperature for 24 h afforded the phenylhydrazone derivative **7** in 63 % yield (see Scheme 2).

For the above preparations, it is worth pointing out that (i) although clusters **4** and **5** have been previously prepared

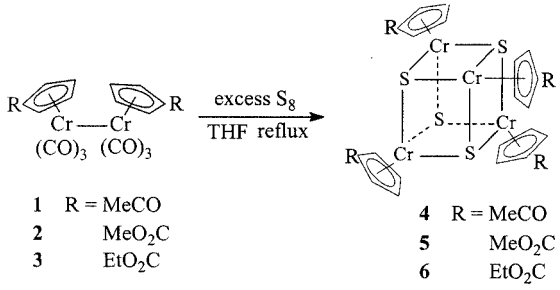

1 R = MeCO
2 MeO_2C
3 EtO_2C

4 R = MeCO
5 MeO_2C
6 EtO_2C

Scheme 1

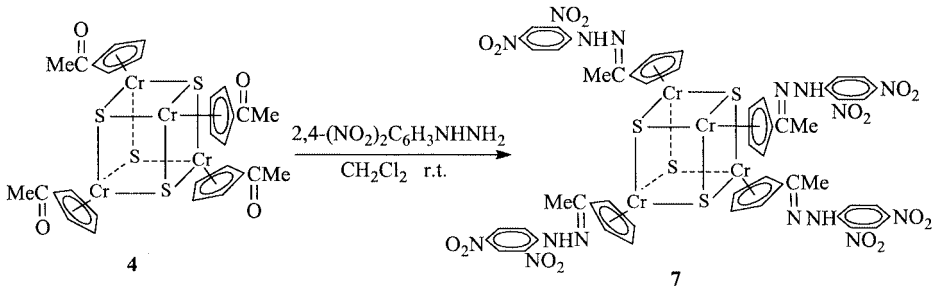

Scheme 2

by another method, the yields were rather low (29 % and 42 %, respectively) and their structures were characterized by combustion analysis and spectroscopy, but not confirmed by X-ray diffraction analysis;[14] and (ii) cluster **7** was the solely isolated product during the course of our study on the functional transformation reactions of the acetyl groups in cluster **4**. The other attempted functional transformation reactions, such as with $NaBH_4$ and with Grignard reagents followed by hydrolysis, led to serious decomposition of the starting cluster **4** and no corresponding hydroxy-containing cluster derivatives were isolated.

The new clusters **6** and **7** were characterized by combustion analysis, IR and ^1H NMR spectroscopy and the structures of clusters **4**−**6** were further confirmed by X-ray crystallographic studies. Similarly to clusters **4** and **5**,[14] the IR spectra of **6** and **7** showed one absorption band at 1708 and 1616 cm^{-1} for the ester C=O and hydrazone C=N groups, while the ^1H NMR spectra of **6** and **7** displayed two singlets at lower and higher fields, attributed respectively to H^2/H^5 and H^3/H^4 protons in the functionally substituted Cp rings.[15]

The ORTEP drawings of **4**−**6** are shown in Figures 1−3, while the selected bond lengths and angles are presented in Table 1.

Figures 1−3 show the molecular structures of clusters **4**−**6**, which are similar to those of the methyl analogs $(\eta^5\text{-}MeC_5H_4)_4Cr_4S_4$,[10] in which the cubane-like Cr_4S_4 cluster core carries four substituted Cp ligands coordinated in an η^5-manner to four chromium atoms. The bond lengths of Cr−Cr are 2.8042−2.8298 Å for **4**, 2.8214−2.8589 Å for **5** and 2.7946−2.8337 Å for **6**, whereas those of Cr−S are 2.2390−2.2540 Å for **4**, 2.2584−2.2747 Å for **5** and 2.2347−2.2478 Å for **6**. The bond angles of Cr−S−Cr are 77.27−78.08° for **4**, 77.03−78.21° for **5** and 77.02−78.49° for **6**, while those of S−Cr−S are 100.69−101.39° for **4**, 100.21−101.95° for **5** and 100.5−101.89° for **6**. The C(1)−C(6) bond of **4** [1.483(11) Å], the C(5)−C(6) bond of **5** [1.494(6) Å] and the C(1)−C(6) bond of **6** [1.477(9) Å] are all shorter than a normal C−C single bond, presumably due to conjugation between the π-electron systems of the functional substituents and the cyclopentadienyl rings.

Table 1. Selected bond lengths (Å) and angles (°) for **4**−**6**

	4	**5**	**6**
Bond lengths			
Cr(1)−Cr(2)	2.8166(18)	2.8379(11)	2.8337(13)
Cr(1)−Cr(3)	2.8042(19)	2.8296(10)	2.7978(12)
Cr(1)−Cr(4)	2.8298(17)	2.8421(12)	2.7946(14)
Cr(2)−Cr(3)	2.8212(17)	2.8589(11)	2.8098(14)
Cr(2)−Cr(4)	2.8212(17)	2.8394(11)	2.8005(14)
Cr(3)−Cr(4)	2.8183(18)	2.8214(12)	2.8175(13)
Cr(1)−S(1)	2.247(2)	2.2637(12)	2.2477(17)
Cr(1)−S(3)	2.248(2)	2.2584(12)	2.2466(17)
Cr(2)−S(1)	2.241(2)	2.2747(12)	2.2462(17)
Cr(2)−S(2)	2.252(2)	2.2669(12)	2.2423(16)
Bond angles			
S(3)−Cr(1)−Cr(2)	98.37(7)	99.01(4)	98.14(5)
S(1)−Cr(1)−S(3)	101.39(9)	100.74(5)	101.89(6)
S(3)−Cr(1)−Cr(3)	51.30(6)	51.41(3)	51.52(4)
S(1)−Cr(1)−Cr(3)	51.19(6)	98.67(4)	51.45(4)
Cr(2)−Cr(1)−Cr(4)	59.95(4)	59.99(2)	59.68(3)
Cr(1)−S(1)−Cr(2)	77.75(8)	77.41(4)	78.18(5)
Cr(2)−S(2)−Cr(4)	77.52(8)	77.65(4)	77.30(5)
Cr(4)−S(3)−Cr(1)	78.08(8)	77.88(4)	77.08(6)
Cr(3)−S(3)−Cr(1)	77.27(8)	77.42(4)	77.00(6)

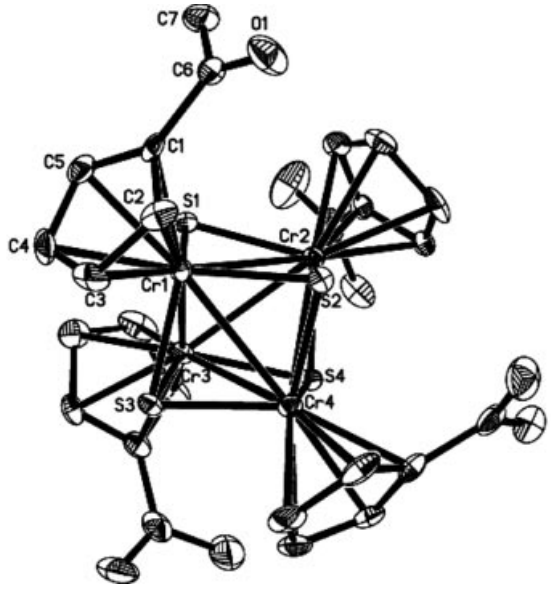

Figure 1. Molecular structure of **4** showing the atom-labeling scheme

 © 2004 Wiley-VCH Verlag GmbH & Co. KGaA, Weinheim

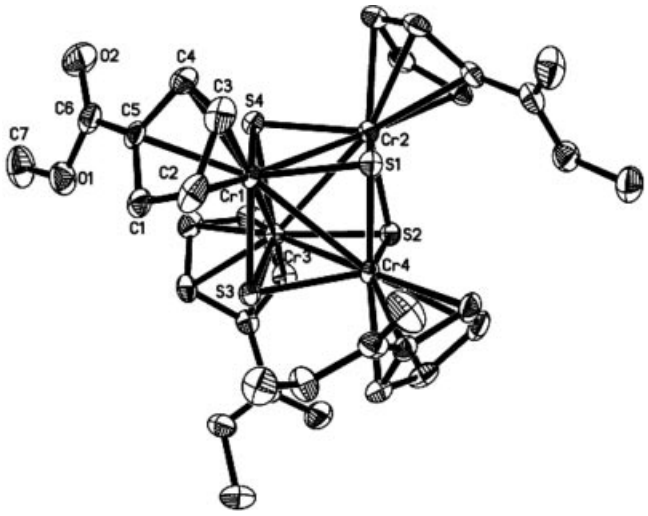

Figure 2. Molecular structure of **5** showing the atom-labeling scheme

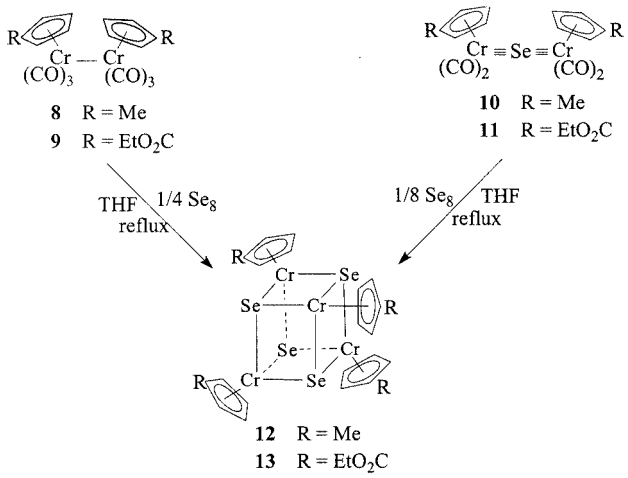

Scheme 3

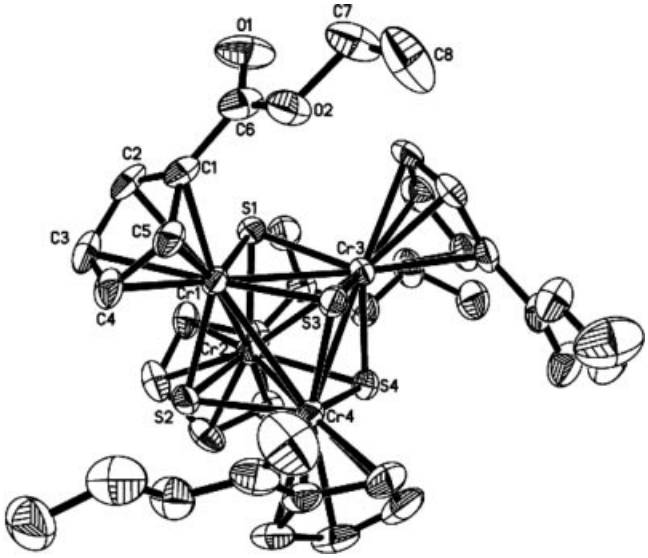

Figure 3. Molecular structure of **6** showing the atom-labeling scheme

Synthesis and Characterization of $(\eta^5\text{-}RC_5H_4)_4Cr_4Se_4$ (12, R = Me; 13, R = EtO_2C) and $[\eta^5\text{-}MeC(O)C_5H_4]_nCp_{4-n}Cr_4Se$ (16, *n* = 0; 17, *n* = 1;18, *n* = 2; 19, *n* = 3; 20, *n* = 4)

When the Cr−Cr singly-bonded dimers $[\eta^5\text{-}RC_5H_4Cr(CO)_3]_2$ (**8**, R = Me;[16] **9**, R = EtO_2C[13]) were refluxed with an equimolar amount of elemental selenium in THF for 8 h or when the linear complexes $[\eta^5\text{-}RC_5H_4Cr(CO)_2]_2Se$ (**10**, R = Me;[17] **11**, R = EtO_2C[17]) were treated with an equimolar quantity of selenium in refluxing THF for 8 h, the corresponding cubane Cr_4Se_4 clusters **12** and **13** were obtained in excellent yield (see Scheme 3).

More interestingly, when an equimolar mixture of the linear acetyl-substituted complex $[\eta^5\text{-}MeC(O)C_5H_4Cr(CO)_2]_2Se$ (**14**)[4] and its parent complex $[CpCr(CO)_2]_2Se$ (**15**)[18] were treated with elemental selenium in refluxing THF for 8 h, a series of Cr_4Se_4 cubane clusters with the general formula $[\eta^5\text{-}MeC(O)C_5H_4]_nCp_{4-n}Cr_4Se_4$ (**16**−**20**, *n* = 0−4) were produced in total 97 % yield (see Scheme 4).

At present, we do not know how clusters **16**−**20** are formed from the reaction described in Scheme 4. We initially thought that the complicated reaction might be similar to that of the linear complexes **10** or **11** with selenium and that cubane clusters **16** and **20** were formed from the corresponding reaction of complexes **14** or **15** with selenium, and clusters **17**−**19** were then produced by ligand exchange between **16** and **20**. However, our experiment showed that the attempted reaction between **16** and **20** in THF at reflux did not afford any cubane clusters bearing mixed-Cp ligands. Therefore, we further suggested that clusters **16**−**20** could possibly be formed by self-tetramerization and cross-tetramerization of the highly unsaturated species η^5-$MeC(O)C_5H_4CrSe$ and CpCrSe, generated in situ from the thermolysis of the mixture of **14**, **15** and elemental selenium. This is because the molar ratio of the five products **16**−**20** is approximately 1:4:6:4:1, which is consistent with the combinatory rule of tetramerization of the two highly unsaturated fragments η^5-$MeC(O)C_5H_4CrSe$ and CpCrSe. However, this pathway is mainly speculative and the detailed mechanism for the cross-assembled reaction needs to be further studied. This cross-assembled reaction is particularly interesting, since it provides evidence for the mechanism for the production of the cubane Cr_4Se_4 clusters[19] and it can also furnish the novel cubane clusters with mixed-Cp ligands.

While the cubane clusters **12**,[11] **16**[9] and **20**[4] have been previously prepared by other methods, clusters **13**, **17**−**19** are new and were characterized by combustion analysis, IR, ^1H NMR spectroscopy and ^{77}Se NMR spectroscopy. The IR spectra of **13** and **17**−**19** display one absorption band

 © 2004 Wiley-VCH Verlag GmbH & Co. KGaA, Weinheim

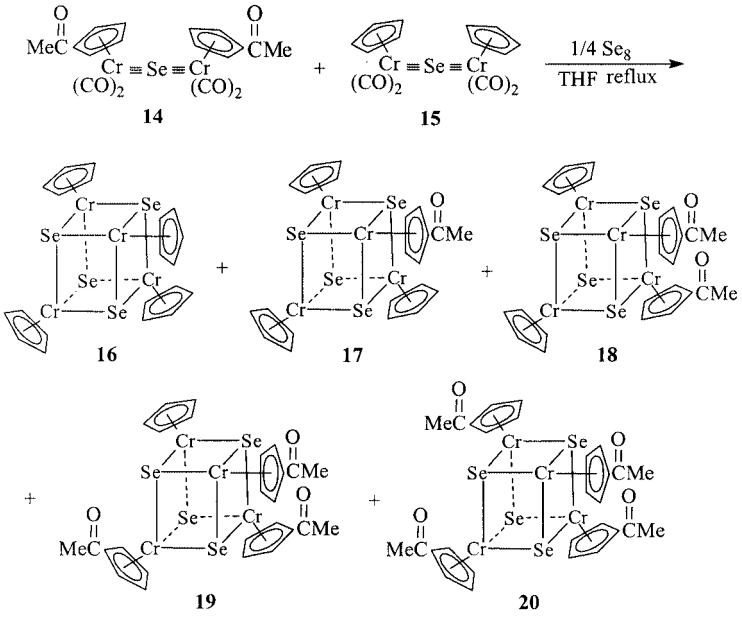

Scheme 4

in the region 1666−1668 cm^{-1} for the ketone carbonyls. The ^1H NMR spectra of **13** and **17−19** show one singlet for the five protons of each Cp ring and two singlets for the H^2/H^5 and H^3/H^4 protons of each substituted Cp ring.[15] It is worthy of note that the ^1H NMR signals of the mixed-Cp cluster **18** appear in the normal range, whereas the signals displayed by **17** and **19** are in the low-field region (12−28 ppm), probably due to traces of paramagnetic species, such as $(CpCr)_mSe_n$ and $(RCpCr)_mSe_n$, generated from the decomposition of the corresponding cubane clusters.

^{77}Se NMR spectroscopy is an important tool for characterizing Se-containing complexes.[20] To examine the influence of different Cp ligands upon ^{77}Se NMR behavior, the ^{77}Se NMR spectra of **12**, **13** and **17−19** were determined. Only one singlet in the range 1009−1241 ppm, which corresponds to the μ_3-Se atoms, was observed. This means that the magnetic environments around the four μ_3-Se atoms in each of the cubane clusters are basically the same, even for the mixed-Cp clusters **17−19**. The ^{77}Se chemical shifts of these clusters are in the order **12** < **17** < **18** < **19** < **13**, which is consistent with the electron-releasing effect of the methyl group and the electron-withdrawing effects of the acetyl and ethoxycarbonyl groups.

Although cluster **16** has been previously prepared,[9] we were the first to confirm its structure by using X-ray crystal-diffraction techniques. This is probably due to its low solubility in common solvents for crystal growing. Figure 4

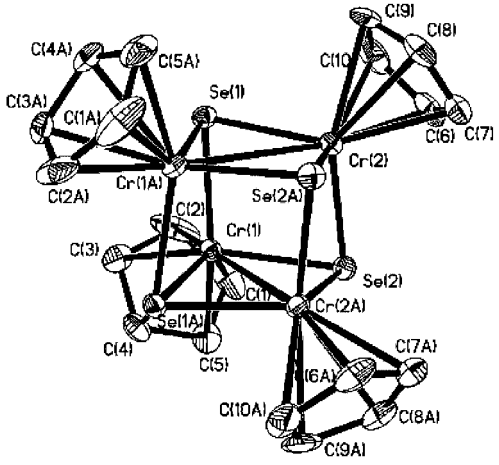

Figure 4. ORTEP drawing of cluster **16**

Table 2. Selected bond lengths (Å) and angles (°) for **16**

Bond lengths			
Se(1)−Cr(2)	2.3983(13)	Se(2)−Cr(2)	2.3972 (14)
Se(1)−Cr(1)	2.3984(13)	C(1)−Cr(1)	2.233(6)
Se(2)−Cr(1)	2.3957(13)	Cr(2)−C(6)	2.245(5)
Bond angles			
Cr(2)−Se(1)−Cr(1)	79.42(3)	C(1)−Cr(1)−Se(1)	115.0(3)
Cr(2)−Se(1)−Cr(1A)	76.32(3)	Se(2)−Cr(1)−Se(1)	98.52(3)
Cr(1)−Se(2)−Cr(2A)	76.56(3)	Se(2)−Cr(1)−Cr(2A)	51.72(3)
Cr(1)−Se(2)−Cr(2)	79.50(3)	Se(1)−Cr(1)−Cr(2A)	99.41(4)
C(1)−Cr(1)−Se(2)	87.5(2)	Se(2)−Cr(2)−Se(1)	98.48(3)

 © 2004 Wiley-VCH Verlag GmbH & Co. KGaA, Weinheim

shows the ORTEP drawing of cluster **16** and Table 2 lists selected bond lengths and angles. Similarly to the methyl derivative,[11] cluster **16** comprises a cubane Cr_4Se_4 cluster core that carries four Cp ligands coordinated in an η^5-fashion to four Cr atoms. The Cr−Cr and Cr−Se bond lengths and the Cr−Se−Cr and Se−Cr−Se bond angles are 2.9683 Å, 2.3957−2.4055 Å, 76.32−79.50° and 98.48−103.12°, respectively. Thus, the cubane Cr_4Se_4 cluster core is just slightly distorted. This molecule has an alternating fourfold axis of symmetry.

Experimental Section

General: All reactions were carried out under an atmosphere of highly purified nitrogen gas using standard Schlenk or vacuum-line techniques. Solvents for preparative use were dried and distilled under nitrogen from Na/benzophenone ketyl or CaH_2 prior to use. Commercial sulfur powder, selenium powder, and 2,4-dinitrophenylhydrazine were used as received. [η^5-$RC_5H_4Cr(CO)_3]_2$ (where R = Me,[16] MeCO,[12] MeO_2C,[12] EtO_2C[13]), [$CpCr(CO)_2]_2Se$[18] and [η^5-$MeC(O)C_5H_4Cr(CO)_2]_2Se$[4] were prepared according to literature procedures. All reactions were monitored by thin layer chromatography (TLC) at intervals. The preparative TLC was carried out on a glass column (2 × 10 cm) packed with silica gel G and glass plates (25 × 20 × 0.25 cm) coated with silica gel H (10−40 μm). Samples for characterization were recrystallized from mixed dichloromethane and hexane. IR spectra were recorded on a Bruker Vector 22 infrared spectrophotometer. While ^{1}H NMR spectra were recorded on a Bruker AC-P 200 NMR spectrometer, ^{77}Se NMR spectra were taken from a Varian Unity-Plus 400 NMR spectrometer with Ph_2Se_2 as external standard and chemical shifts were referenced to Me_2Se (δ = 0 ppm). Elemental analysis was performed on an Elementar Vario EL analyzer. Melting points were determined on a Yanaco MP-500 apparatus.

Preparation of (η^5-$MeCOC_5H_4)_4Cr_4S_4$ (4): A 100-mL Schlenk flask equipped with a magnetic stir bar was charged with [η^5-$MeCOC_5H_4Cr(CO)_3]_2$ (0.423 g, 0.87 mmol), sulfur powder (0.070 g, 2.19 mmol) and THF (20 mL). The mixture was stirred at reflux for 12 h. The solvent was removed under vacuum and the residue was extracted in a minimum volume of dichloromethane, which was then subjected to TLC separation using acetone/petroleum ether (v/v, 1:2) as eluent. Compound **4** (0.287 g, 86 %) was obtained as a black solid from the green band and it was identified by comparing its melting point, ^{1}H NMR and IR spectra with those of the spectroscopically characterized sample.[14]

Preparation of (η^5-$MeO_2CC_5H_4)_4Cr_4S_4$ (5): The same procedure as for the preparation of **4** was followed, but [η^5-$MeO_2CC_5H_4Cr(CO)_3]_2$ (0.450 g, 0.87 mmol) was employed to give **5** (0.342 g, 95 %) as a black solid, which was also identified by comparing its melting point, ^{1}H NMR and IR spectra with those of the spectroscopically characterized sample.[14]

Preparation of (η^5-$EtO_2CC_5H_4)_4Cr_4S_4$ (6): The same procedure as for the preparation of **4** was followed, but [η^5-$EtO_2CC_5H_4Cr(CO)_3]_2$ (0.490 g, 0.90 mmol) was employed to give **6** (0.321 g, 81 %) as a black solid. M.p. 186−188 °C. ^{1}H NMR ($CDCl_3$): δ = 1.32 (t, *J* = 8.0 Hz, 12 H, 4 CH_3), 4.24 (q, *J* = 8.0 Hz, 8 H, 4 CH_2), 4.76 (s, 8 H, 4 H^3, 4 H^4), 5.28 (s, 8 H, 4 H^2, 4 H^5). IR (KBr disk): $\tilde{\nu}$ = 1708 (s) (C=O) cm^{-1}. $C_{32}H_{36}Cr_4O_8S_4$ (884.85): calcd. C 43.44, H 4.10; found C 42.85, H 4.13.

Preparation of [η^5−2,4-$(NO_2)_2C_6H_3NHN{=}CMeC_5H_4]_4Cr_4S_4$ (7): A 2,4-dinitrophenylhydrazine solution (2 mL, ca. 4 mmol), which was prepared by dissolving 1.0 g of 2,4-dinitrophenylhydrazine in 5 mL of 98 % H_2SO_4, 10 mL of H_2O and 35 mL of 95% EtOH, was added to a solution of **4** (0.382 g, 0.50 mmol) in CH_2Cl_2 (10 mL). The mixture was stirred at room temperature for 24 h. The solvent was removed under reduced pressure and the residue was washed carefully by anhydrous ethyl alcohol and was then extracted with a minimum volume of CH_2Cl_2. This extract was subjected to TLC separation using CH_2Cl_2 as eluent. Compound **7** (0.467 g, 63 %) was obtained as a black solid from the main band. M.p. 242−244 °C. ^{1}H NMR ($CDCl_3$): δ = 1.53 (s, 12 H, 4 CH_3), 4.93 (s, 8 H, 4 H^3, 4 H^4), 5.64 (s, 8 H, 4 H^2, 4 H^5), 7.80 (m, 4 H, 4 H^6 of benzene ring), 8.20−8.50 (m, 4 H, 4 H^5 of benzene ring), 9.14 (s, 4 H, 4 H^3 of benzene ring), 11.20 (s, 4 H, 4 NH) ppm. IR (KBr disk): $\tilde{\nu}$ = 3312 (vs) (N−H), 1616 (s) (C=N) cm^{-1}. $C_{52}H_{44}Cr_4N_{16}O_{16}S_4$ (1485.24): calcd. C 42.05, H 2.99, N 15.32; found C 41.74, H 3.51, N 15.09.

Preparation of (η^5-$MeC_5H_4)_4Cr_4Se_4$ (12). Method (i): A mixture of [η^5-$MeC_5H_4Cr(CO)_3]_2$ (0.215 g, 0.50 mmol), selenium powder (0.079 g, 1.00 mmol) and THF (20 mL) was refluxed for 8 h, causing a color change from brown red to dark green. The solvent was removed under vacuum and the residue was extracted with CH_2Cl_2. CH_2Cl_2 was removed under vacuum and the residue was recrystallized from a mixed CH_2Cl_2/hexane solvent to give 0.202 g (96%) of **12** as a black solid. M.p. 179−180 °C. ^{1}H NMR ($CDCl_3$): δ = 2.57 (s, 12 H, 4 CH_3), 30.07 (s, 8 H, 4 H^2, 4 H^5), 30.45 (s, 8 H, 4 H^3, 4 H^4) ppm. ^{77}Se NMR ($CDCl_3$): δ = 1009 (s) ppm. IR (KBr disk): $\tilde{\nu}$ = 1630 (m), 1490 (m), 1449 (s), 1371 (m), 1038 (m), 1024 (s), 802 (vs) cm^{-1}. $C_{24}H_{28}Cr_4Se_4$ (840.30): calcd. C 34.30, H 3.36; found C 34.18, H 3.31. **Method (ii):** A mixture of [η^5-$MeC_5H_4Cr(CO)_2]_2Se$ (0.227 g, 0.50 mmol), selenium powder (0.040 g, 0.50 mmol) and THF (20 mL) was refluxed for 8 h. The same workup as that described in method (i) gave 0.200 g (95%) of **12**.

Preparation of (η^5-$EtO_2CC_5H_4)_4Cr_4Se_4$ (13). Method (i): The same procedure as Method (i) for **12** was followed, but [η^5-$EtO_2CC_5H_4Cr(CO)_3]_2$ (0.273 g, 0.50 mmol) was utilized to give 0.260 g (97%) of **13** as a black solid. M.p. 169−170 °C. ^{1}H NMR ($CDCl_3$): δ = 1.32 (t, *J* = 7.0 Hz, 12 H, 4 CH_3), 4.14 (q, *J* = 7.0 Hz, 8 H, 4 CH_2), 4.95 (s, 8 H, 4 H^3, 4 H^4), 5.83 (s, 8 H, 4 H^2, 4 H^5) ppm. ^{77}Se NMR ($CDCl_3$): δ = 1241 (s) ppm. IR (KBr disk): $\tilde{\nu}$ = 1705 (s) (C=O) cm^{-1}. $C_{32}H_{36}Cr_4O_8Se_4$ (1072.45): calcd. C 35.84, H 3.38; found C 35.41, H 3.16. **Method (ii):** The same procedure as Method (ii) for **12** was followed, but [η^5-$EtO_2CC_5H_4Cr(CO)_2]_2Se$ (0.285 g, 0.50 mmol) was used to afford 0.257 g (96%) of **13**.

Preparation of [η^5-$MeC(O)CC_5H_4]_nCp_{4-n}Cr_4Se_4$ (*n* = 0, 16; *n* = 1, 17; *n* = 2, 18; *n* = 3, 19; *n* = 4, 20): A 100-mL Schlenk flask was charged with [$CpCr(CO)_2]_2Se$ (0.212 g, 0.50 mmol), [η^5-$MeC(O)C_5H_4Cr(CO)_2]_2Se$ (0.255 g, 0.50 mmol), selenium powder (0.158 g, 2 mmol) and THF (30 mL). The mixture was stirred at reflux for 8 h, resulting in a color change from brown red to dark green. The mixture was centrifuged to give a clear centrifugate, which was concentrated to ca. 10 mL and was then subjected to TLC separation using acetone/CH_2Cl_2/petroleum ether (v/v/v, 1:3:3) as eluent to develop four brown-green bands.

[η^5-$MeC(O)C_5H_4]Cp_3Cr_4Se_4$ (17): Compound **17** (0.096 g, 23 %) was obtained from the first band (R_f = 0.81) as a black solid. M.p. 202−203 °C. ^{1}H NMR ($CDCl_3$): δ = 2.17 (s, 3 H, CH_3), 12.27 (s, 2 H, H^3, H^4), 13.17 (s, 15 H, 3 C_5H_5), 15.20 (s, 2 H, H^2, H^5) ppm.

 © 2004 Wiley-VCH Verlag GmbH & Co. KGaA, Weinheim

Table 3. Crystal data and structural refinements details for **4**, **5**, **6** and **16**

	4	**5**	**6**	**16**
Empirical formula	$C_{28}H_{28}Cr_4O_4S_4$	$C_{28}H_{28}Cr_4O_8S_4$	$C_{32}H_{36}Cr_4O_8S_4$	$C_{10}H_{10}Cr_2Se_2$
Formula mass	764.74	828.74	884.85	392.10
Crystal system	monoclinic	triclinic	triclinic	monoclinic
Space group	$P2_1/c$	$P\bar{1}$	$P\bar{1}$	$C2/c$
a(Å)	9.728(3)	10.009(4)	10.384(3)	17.875(7)
b (Å)	9.642(3)	10.798(4)	12.048(4)	8.240(3)
c(Å)	31.097(9)	16.592(6)	15.051(5)	16.184(7)
α (°)	90	73.296(5)	85.127(6)	90
β (°)	97.823(5)	77.332(6)	76.690(5)	116.087(6)
γ (°)	90	66.133(5)	77.264(6)	90
V (Å^3)	2889.7(13)	1559.7(9)	1786.1(10)	2140.9(15)
Z	4	2	2	8
$D_{calcd.}$ (g cm^{-3})	1.758	1.765	1.645	2.433
μ (Mo-K_α) (mm^{-1})	1.788	1.673	1.467	8.782
F(000)	1552	840	904	1488
Reflections collected	14600	6456	9101	4296
Independent reflections	5109	5462	6863	1895
R_{int}	0.0906	0.0225	0.0306	0.0349
$2\theta_{max}$ (°)	50.00	50.06	52.88	50.04
Data/restraints/parameters	5109/0/366	5462/0/397	6863/0/434	1895/0/127
R	0.0619	0.0345	0.0529	0.0308
Rw	0.1250	0.0777	0.1065	0.0700
Goooodness of fit	1.074	0.999	0.986	1.042
Largest difference peak and hole/e·Å^{-3}	0.722 and −0.740	0.373 and −0.396	0.456 and −0.428	0.516 and −0.713

^{77}Se NMR ($CDCl_3$): δ = 1148(s) ppm. IR (KBr disk): ṽ = 1667 (s) (C=O) cm^{-1}. $C_{22}H_{22}Cr_4OSe_4$ (826.24): calcd. C 31.98, H 2.68; found C 31.93, H 2.54.

[η^5-MeC(O)C$_5$H$_4$]$_2$Cp$_2$Cr$_4$Se$_4$ (18): Compound **18** (0.158 g, 36 %) was obtained from the second band (R_f = 0.72) as a black solid. M.p. 214−215 °C. ^{1}H NMR ($CDCl_3$): δ = 2.19 (s, 6 H, 2 CH_3), 5.27 (s, 4 H, 2 H^3, 2 H^4), 5.33 (s, 10 H, 2 C_5H_5), 6.13 (s, 4 H, 2 H^2, 2 H^5) ppm. ^{77}Se NMR ($CDCl_3$): δ = 1178 (s) ppm. IR (KBr disk): ṽ = 1668 (s) (C=O) cm^{-1}. $C_{24}H_{24}Cr_4O_2Se_4$ (868.28): calcd. C 33.20, H 2.79; found C 33.21, H 2.76.

[η^5-MeC(O)C$_5$H$_4$]$_3$CpCr$_4$Se$_4$ (19): Compound **19** (0.112 g, 25 %) was obtained from the third band (R_f = 0.60) as a black solid. M.p. 188−189 °C. ^{1}H NMR ($CDCl_3$): δ = 2.18 (s, 9 H, 3CH_3), 22.17 (s, 6 H, 3 H^3, 3 H^4), 23.75 (s, 5 H, C_5H_5), 27.22 (s, 6 H, 3 H^2, 3 H^5) ppm. ^{77}Se NMR ($CDCl_3$): δ = 1224 (s) ppm. IR (KBr disk): ṽ = 1666 (s) (C=O) cm^{-1}. $C_{26}H_{26}Cr_4O_3Se_4$ (910.31): calcd. C 34.31, H 2.88; found C 34.33, H 2.77.

[η^5-MeC(O)C$_5$H$_4$]$_4$Cr$_4$Se$_4$ (20): Compound **20** (0.031 g, 7 %) was obtained from the fourth band (R_f = 0.45) identified by comparing its IR and ^{1}H NMR spectra with those of the fully characterized sample.[4] The immovable base band was collected and refluxed with 10 mL of bromobenzene for 10 min. Once it had cooled to room temperature, the mixture was filtered and the filtrate was centrifuged to give a clear centrifugate, from which $Cp_4Cr_4Se_4$ (**16**)[9] (0.025 g, 6 %) was obtained.

Attempted Cp/η^5-MeC(O)C$_5$H$_4$ Ligand Exchange Between Cp$_4$Cr$_4$Se$_4$ and [η^5-MeC(O)C$_5$H$_4$]$_4$Cr$_4$Se$_4$: A mixture consisting of $Cp_4Cr_4Se_4$ (0.078 g, 0.10 mmol) and **20** (0.095 g, 0.10 mmol) in THF (20 mL) was stirred at reflux for 10 h. The resulting mixture was concentrated to ca. 5 mL and was subjected to TLC separation using acetone/CH_2Cl_2/petroleum ether (v/v/v, 1:3:3) as eluent to develop only one brown-green band. Compound **20** (0.079 g, 82 %) was recovered from this band, while $Cp_4Cr_4Se_4$ (0.052 g, 67 %) was recovered from the immovable band. No ligand exchange products of [η^5-MeC(O)CC_5H_4]$_n$Cp$_{4-n}$Cr$_4$Se$_4$ (n = 1−3, **17**−**19**) were produced.

Crystal Structure Determination of 4−6 and 16: Single crystals of **4**−**6** and **16**, suitable for X-ray diffraction analysis, were grown by slow evaporation of an acetone/hexane solution at room temperature. Each single crystal was glued to a glass fiber and mounted on a Bruker SMART 1000 automated diffractometer. Data were collected at room temperature, using graphite monochromator Mo-K_α radiation (λ = 0.71073 Å) in the ω-2θ scanning mode. Absorption correction was performed using the SADABS method. The structure was solved by direct methods using the SHELXS-97[21a] program and refined by full-matrix least-squares techniques (SHELXL-97[21b]) on F^2. Hydrogen atoms were located by using the geometric method. The crystal data and structural refinement details are listed in Table 3. The calculations were performed using the TEXSAN crystallographic software package of Molecular Structure Corporation.[22] CCDC-228444, -228445, -228446 and -228990 contain the supplementary crystallographic data for this paper. These data can be obtained free of charge at www.ccdc.cam.ac.uk/conts/retrieving.html [or from the Cambridge Crystallographic Data Centre, 12 Union Road, Cambridge CB2 1EZ, UK; Fax: (internat.) + 44-1223-336-033; E-mail: deposit@ccdc.cam.ac.uk].

Acknowledgments

We are grateful to the National Natural Science Foundation of China and the State Key Laboratory of Organometallic Chemistry for the financial support of this work.

 © 2004 Wiley-VCH Verlag GmbH & Co. KGaA, Weinheim

[1] L. Markó, B. Markó-Monostory, in *The Organic Chemistry of Iron* (Eds.: E. A. K. von Gustorf, F.-W. Grevels, I. Fischer), Academic Press, New York, **1981**, p. 283.
[2] H. Ogino, S. Inomata, H. Tobita, *Chem. Rev.* **1998**, *98*, 2093−2121.
[3] W. Chen, L. Y. Goh, T. C. W. Mak, *Organometallics* **1986**, *5*, 1997−2002.
[4] L.-C. Song, H.-W. Cheng, Q.-M. Hu, *Organometallics* **2004**, *23*, 1072−1080.
[5] J. A. Kovacs, J. K. Bashkin, R. H. Holm, *J. Am. Chem. Soc.* **1985**, *107*, 1784−1786.
[6] J. W. Peters, W. N. Lanzilotta, B. J. Lemon, L. C. Seefeldt, *Science* **1998**, *282*, 1853−1858.
[7] Y. Nicolet, C. Piras, P. Legrand, C. E. Hatchikian, J. C. Fontecilla-Camps, *Structure* **1999**, *7*, 13−23.
[8] Y. Nicolet, A. L. de Lacey, X. Vernède, V. M. Fernandez, E. C. Hatchikian, J. C. Fontecilla-Capms, *J. Am. Chem. Soc.* **2001**, *123*, 1596−1601.
[9] L. Y. Goh, W. Chen, E. Sinn, *J. Chem. Soc., Chem. Commun.* **1985**, 462−464.
[10] A. A. Pasynskii, I. L. Eremenko, Yu. V. Pakitin, V. M. Novotortsev, O. G. Ellert, V. T. Kalinnikov, V. E. Shklover, Yu. T. Struchkov, S. V. Lindeman, T. K. Kurbanov, G. S. Gasanov, *J. Organomet. Chem.* **1983**, *248*, 309−320.
[11] I. L. Eremenko, S. E. Nefedov, A. A. Pasynskii, B. Orazsakhatov, O. G. Ellert, Yu. T. Struchkov, A. I. Yanovsky, D. V. Zagorevsky, *J. Organomet. Chem.* **1989**, *368*, 185−192.
[12] R. M. Medina, J. R. Masaguer, M. Morán, J. Losada, *Inorg. Chim. Acta* **1988**, *146*, 115−118.
[13] L.-C. Song, J.-Q. Wang, Q.-M. Hu, R.-J. Wang, H.-G. Wang, *Chin. J. Struct. Chem.* **1995**, *14*, 15−19.
[14] W.-F. Zhu, G.-H. Zhen, H.-W. Cheng, L.-C. Song, *Chin, J. Org. Chem.* **2001**, *21*, 49−52.
[15] L.-C. Song, J.-Y. Shen, Q.-M. Hu, X.-Y. Huang, *Organometallics* **1995**, *14*, 98−106.
[16] R. Birdwhistell, P. Hackett, A. R. Manning, *J. Organomet. Chem.* **1978**, *157*, 239−241.
[17] L.-C. Song, H.-W. Cheng, Q.-M. Hu, *J. Organomet. Chem.,* manuscript submitted.
[18] W. A. Hermann, J. Rohrmann, H. Nöth, C. K. Nanila, I. Bernal, M. Draux, *J. Organomet. Chem.* **1985**, *284*, 189−211.
[19] W. Chen, L. Y. Goh, E. Sinn, *Organometallics* **1988**, *7*, 2020−2026.
[20] P. A. W. Dean, L. Y. Goh, I. D. Gay, R. D. Sharma, *J. Organomet. Chem.* **1997**, *533*, 1−5.
[21] [21a] G. M. Sheldrick, *Acta Crystallogr., Sect. A* **1990**, *46*, 467−473. [21b] G. M. Sheldrick, *SHELXL-97*, University of Göttingen, **1997**.
[22] *TEXSAN, Crystal Structure Analysis Package,* MSC/AFC Diffractometer Control Software, Molecular Structure Corporation Houston; MSC, 3200 Research Forest Drive, The Woodlands, Texas 77381, USA, **1992**.

Received February 3, 2004
Early View Article
Published Online June 1, 2004

 © 2004 Wiley-VCH Verlag GmbH & Co. KGaA, Weinheim

Preparation of Diamidochloro(cyclopentadienyl)titanium Derivatives as Pre-Catalysts for Olefin Polymerization − X-ray Molecular Structure of [Ti(η^5-C_5H_5){1,2-C_6H_4($NCH_2CH_2CH_3$)$_2$}Cl] and [Ti{η^5-C_5H_4($SiMe_3$)}-{1,2-C_6H_4($NCH_2CH_2CH_3$)$_2$}Cl]

Vanessa Tabernero,[a] Tomás Cuenca,*[a] and Eberhardt Herdtweck[b]

Dedicated to Professor José Vicente Soler on the occasion of his 60th birthday

Keywords: Cyclopentadienyl ligands / N ligands / Olefin polymerization / Titanium

The synthesis of *N*,*N*′-alkyl 1,2-phenylenediamines 1,2-$C_6H_4(NHR)_2$ [R = $CH_2CH_2CH_3$ (*n*Pr), CH_2tBu (Np)] was carried out in three steps by lithiation of the primary 1,2-phenylenediamine, reaction with the appropriate acyl chloride and reduction with $LiAlH_4$. The addition of *n*BuLi to a stirred solution of *N*,*N*′-alkyl diamines in cold hexane resulted in the immediate deposition of the corresponding lithium salts, which react with [$MCp^{R'}Cl_3$] to give the diamidochloro(η^5-cyclopentadienyl)titanium and -zirconium complexes [$MCp^{R'}$\{1,2-$C_6H_4(NR)_2$\}Cl] (**4**–**10**) [M = Ti, Zr; $Cp^{R'}$ = η^5-C_5H_5, η^5-$C_5(CH_3)_5$, η^5-$C_5H_4(SiMe_3)$; R = *n*Pr, Np]. The compound [Ti(η^5-C_5H_5){1,2-C_6H_4(N*n*Pr)$_2$}Cl] (**3**) was obtained by treatment of [Ti(η^5-C_5H_5)Cl_3] with 1,2-C_6H_4(NH*n*Pr)$_2$ in the presence of NEt_3 in toluene. All the reported compounds were characterized by the usual analytical and NMR spectroscopic methods. The molecular structures of **3** and **7** were determined by single-crystal X-ray crystallography. The compounds described here were further investigated as potential olefin polymerization catalysts.

(© Wiley-VCH Verlag GmbH & Co. KGaA, 69451 Weinheim, Germany, 2004)

Introduction

The organometallic chemistry of group 4 transition metals is based largely on η^5-cyclopentadienyl (Cp) complexes, for example [MCp_2R_2] and [$MCpR_3$] derivatives, which doubtless figure among the best known organometallic systems.[1] Chelating diamido ligands are gaining increasing interest in early transition metal chemistry.[2] Bidentate (N^-,N^-) and tridentate (N^-,N^-,X; X = O,N) diamido ligands have been used as alternatives to η^5-cyclopentadienyl-based fragments, and non-η^5-cyclopentadienyl Group 4 metal complexes containing these ligands have been investigated as precursors for living α-olefin polymerization processes.[3] Descriptions of titanium and zirconium derivatives combining η^5-cyclopentadienyl and diamido groups are limited, but they show an interesting chemical reactivity.[4] The well-known amido(η^5-cyclopentadienyl)[5] and the more recently reported diamido(η^5-cyclopentadienyl)[6] derivatives are attracting increasing interest in the context of α-olefin polymerization processes. The vast majority of group 4 metallocene and related complexes used as olefin polymerization precatalysts typically have two or more abstractable or insertable alkyl (or halide) groups attached to the metal. Examples of precatalysts containing only one such group that can be actived for olefin polymerization are scarce.[5h,6,7] This paper expands this class of compounds by reporting monochlorotitanium and -zirconium complexes supported by Cp and chelating diamido ligands which are of potential interest in the context of single-site olefin polymerization catalysis.

We are interested in the synthesis and chemical behaviour of [MCp′(LL)X] derivatives (Cp′ = substituted or unsubstituted η^5-cyclopentadienyl ring; LL = chelating diamido and dialkoxo[7] ligands) and describe herein the synthesis and characterization of new chlorodiamido complexes of titanium and zirconium [$MCp^{R'}$\{1,2-$C_6H_4(NR)_2$\}Cl] [M = Ti, Zr; $Cp^{R'}$ = η^5-C_5H_5, η^5-$C_5(CH_3)_5$, η^5-$C_5H_4(SiMe_3)$; R = *n*Pr, Np]. The X-ray molecular structures of [Ti(η^5-C_5H_5){1,2-C_6H_4(N*n*Pr)$_2$}Cl] and [Ti{η^5-$C_5H_4(SiMe_3)$}{1,2-C_6H_4(N*n*Pr)$_2$}Cl] are also described. All synthesized complexes were tested as potential catalysts for ethylene and styrene polymerization after activation with MAO.

[a] Departamento de Química Inorgánica, Universidad de Alcalá, Campus Universitario, 28871 Alcalá de Henares, Spain
Fax: + 34-91-8854683
E-mail: tomas.cuenca@uah.es
[b] Anorganisch-chemisches Institut, Technische Universität München,
Lichtenbergstrasse 4, 85747 Garching bei München, Germany

 © 2004 Wiley-VCH Verlag GmbH & Co. KGaA, Weinheim **DOI: 10.1002/ejic.200400138**

Results and Discussion

The *N*,*N*′-alkyl-1,2-phenylenediamines 1,2-$C_6H_4(NHR)_2$ [R = *n*Pr (**1**), Np (**2**)] were synthesized in good yield from 1,2-diaminobenzene by successive *N*,*N*′-dilithiation, reaction with propionyl or trimethylacetyl chloride to give the corresponding diamide derivative, and reduction with $LiAlH_4$.[8] The propylamine was obtained as a brown oil and the neopentylamine as an orange solid. The synthesis of *N*,*N*′-bis(neopentyl)-1,2-phenylenediamine has been described previously and it has been used in the synthesis of 1,2-phenylenediaminotin(II) complexes through a transamination process.[9] The amines were spectroscopically and analytically characterized. As it was obtained as an oil, compound **1** could not be recrystallized or subjected to elemental analysis. The phenyl protons and the substituents on the nitrogen atoms exhibit a characteristic set of ^1H and $^{13}C\{^1H\}$ NMR resonances[10] (see Exp. Sect.).

The titanium and zirconium chelating diamido derivatives were synthesized by the usual approach based on the metathetical reaction of the dilithium salts of 1,2-phenylenediamines with the appropriate metal halide. Treatment of **1** and **2**, at −78 °C, successively with *n*BuLi in hexane and the appropriate titanium or zirconium compound $[MCp^{R'}Cl_3]$ in toluene gave the corresponding mono-cyclopentadienyl chlorodiamido titanium and zirconium complexes $[MCp^{R'}\{1,2\text{-}C_6H_4(NR)_2\}Cl]$ (**4**−**10**) [M = Ti, Zr; $Cp^{R'}$ = η^5-C_5H_5, η^5-$C_5(CH_3)_5$, η^5-$C_5H_4(SiMe_3)$; R = *n*Pr, Np] (Scheme 1). Similar attempts to obtain *N*,*N*′-dipropyl-1,2-phenylenediamidozirconium derivatives were unsuccessful, which may be attributed to the larger size of zirconium compared with titanium, favouring β-elimination decomposition pathways. The compound $[Ti(\eta^5\text{-}C_5H_5)\{1,2\text{-}C_6H_4(NnPr)_2\}Cl]$ (**3**) was synthesized by reaction of $[Ti(\eta^5\text{-}C_5H_5)Cl_3]$ with 1,2-$C_6H_4(NHnPr)_2$ in the presence of NEt_3 in toluene. Group 4 metal phenylenediamido complexes of the non-cyclopentadienyl type[2d,9] $M(NN)X_2$ and monocyclopentadienyl[4c] type MCp′′(NN)X have recently been reported.

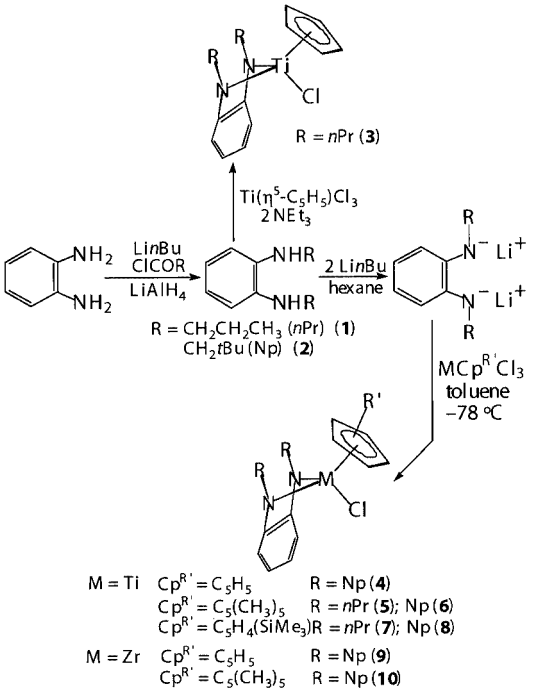

Scheme 1

Complexes **3**−**10** were obtained as black or red-brown solids, soluble in aromatic hydrocarbons, dichloromethane, chloroform, diethyl ether and alkanes (hexane and pentane). Their purification was difficult, as they are highly soluble in alkanes and polar solvents. They are both air and moisture sensitive in solution and in the solid state, although they can be stored unaltered for weeks under an inert atmosphere. The complexes were characterized by the usual analytical and spectroscopic methods. The elemental analysis values found for **8** were inaccurate due to the presence of a small amount of LiCl in the mixture, which could not be removed.

Most importantly in this type of complexes, the diamido ligand can adopt different coordination modes[4e,11] and has two possible conformations (*supine* or*prone*)[12] relative to the cyclopentadienyl ring. The ^1H NMR spectra (C_6D_6 and $CDCl_3$, room temperature) show the presence of only one species, ruling out a mixture of the two rotamers (*supine*-*prone* automerization) observed in solutions of similar monocyclopentadienyl diene complexes.[4d,4e] The spectra show the expected resonances for the cyclopentadienyl rings: one singlet for the C_5H_5 and the C_5Me_5 protons and two sets of pseudo triplets for the $C_5H_4(SiMe_3)$ ring protons, corresponding to an AA′BB′ spin system. The ^1H NMR resonances of the cyclopentadienyl protons appear as signals at δ = 6.20−6.30 ppm for Cp, δ = 6.40−6.73 ppm for $CpSiMe_3$ and δ = 1.65−1.75 ppm for C_5Me_5. Such shifts suggest that the cyclopentadienyl protons are not influenced by phenylene magnetic anisotropy[13] and lead us to propose that the phenylenediamido ligand adopts a *supine* conformation.[4c] The methyl protons of the $SiMe_3$ group exhibit one singlet (δ = 0.25−0.26 ppm). The spectra for compounds **3** and **7** show sets of multiplet, multiplet and triplet for the N-CH_2-CH_2-CH_3 fragment protons, respectively, while two multiplets for the N−CH_2 protons are observed in the spectrum of the pentamethylcyclopentadienyl derivative **5**. These data indicate the diastereotopic nature of the methylene protons bonded to the nitrogen atom. In the spectra of compounds **4**, **6**, and **8**−**10** in C_6D_6, the neopentyl groups show a singlet for the methyl protons and a doublet of doublets corresponding to the diastereotopic methylene protons. Similar spectroscopic features indicate that the neopentyl-group signals in the spectra of compounds **4**, **6**, **8** and **9** in $CDCl_3$ exhibit a diastereotopic behaviour for the N−CH_2 protons, while the spectrum of **10** in $CDCl_3$ shows only one singlet assignable to these protons. Characteristic low-field chemical shift trends are observed for the N−CH_2 protons on going from free diamine (δ = 2.6 ppm for **1** and δ = 2.8 ppm for **2**) to an amido coordination mode to the Lewis acid titanium atom in complexes **3**−**10** (δ = 4−3.5 ppm). The phenyl protons appear as two multiplets in the usual range.

 © 2004 Wiley-VCH Verlag GmbH & Co. KGaA, Weinheim

In the ^{13}C NMR spectra of the free diamines **1** and **2** the signals of the imine C-atoms are observed at δ = 138 and 138.9 ppm, respectively. The corresponding resonances for the titanium and zirconium complexes are found at higher field, at around δ = 125 ppm and δ = 137 ppm for the neopentyl and propyl derivatives, respectively. These spectroscopic data are in agreement with C_s symmetry, consistent with the presence of a mirror plane containing the Ti and Cl atoms and bisecting the N−Ti−N angle of the chelate diamido ligand.

A nuclear Overhauser enhancement (NOE) study of the complexes[12c,12d] containing the Cp ligand confirms this proposal. Irradiation of the Cp signal of the propyl derivative **3** results in a significant NOE enhancement of the CH_2 signals, while irradiation of the Cp signal of the neopentyl derivative **4** results in significant NOE enhancements in the *t*Bu and the CH_2 signals. Irradiation of the Cp signals of **3** and **4** does not cause NOE enhancements in the phenyl signals. These observations suggest that the propyl and neopentyl groups are in close proximity to the Cp ring, with the diamido ligand adopting a *supine* conformation, consistent with the disposition found in the solid state from the X-ray structural analysis of **3** and **7**.

Crystal Structure of [Ti(η^5-C_5H_5){1,2-C_6H_4(N*n*Pr)$_2$}Cl] (3) and [Ti{η^5-C_5H_4(SiMe$_3$)}{1,2-C_6H_4(N*n*Pr)$_2$}Cl] (7)

In order to establish the solid-state molecular geometry for compounds of this type, X-ray crystal-structure analyses of **3** and **7** were carried out. Single crystals of **3** and **7** obtained by slow recrystallization from hexane solution were of good enough quality to be analyzed by X-ray diffraction. The crystal structure of **3** is shown in Figure 1 and Table 1 summarizes selected bond lengths and angles.

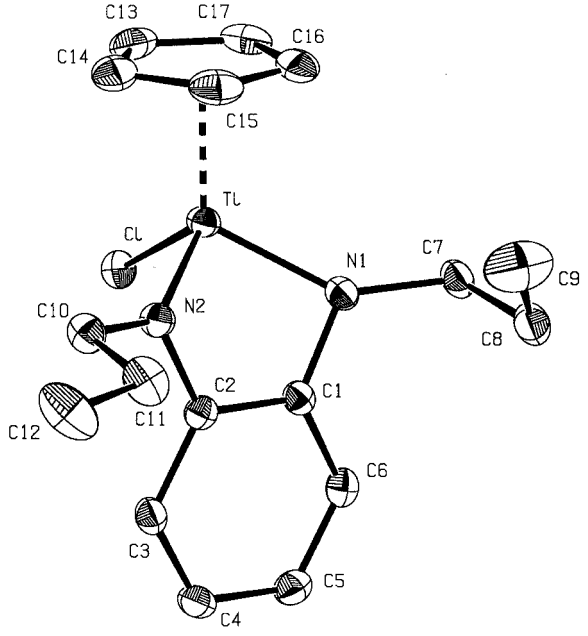

Figure 1. ORTEP representation of [Ti(η^5-C_5H_5){1,2-C_6H_4(NCH$_2$CH$_2$CH$_3$)2}Cl] (**3**) in the solid state; thermal ellipsoids are drawn at the 50% probability level; hydrogen atoms are omitted for clarity

Table 1. Selected interatomic distances (Å) and angles (deg) for complexes **3** and **7**

	3	**7**
Ti−Cl	2.3270(5)	2.3101(5)
Ti−N1	1.9018(14)	1.9034(13)
Ti−N2	1.9014(13)	1.9048(12)
Ti−C13	2.358(2)	2.379(2)
Ti−C14	2.354(2)	2.353(2)
Ti−C15	2.350(2)	2.364(2)
Ti−C16	2.351(2)	2.371(2)
Ti−C17	2.355(2)	2.366(2)
Ti−Cg[a]	2.029	2.038
N1−C1	1.396(2)	1.396(2)
N1−C7	1.461(2)	1.461(2)
N2−C2	1.399(2)	1.398(2)
N2−C10	1.456(2)	1.464(2)
Cl−Ti−N1	104.46(4)	105.64(4)
Cl−Ti−N2	108.22(4)	104.51(4)
Cl−Ti−Cg	117.64	119.77
N1−Ti−N2	89.69(5)	89.48(5)
N1−Ti−Cg	117.46	116.34
N2−Ti−Cg	115.52	116.44
Ti−N1−C1	95.24(9)	97.05(9)
Ti−N1−C7	144.13(10)	142.14(10)
C1−N1−C7	119.01(13)	119.42(12)
Ti−N2−C2	95.37(10)	96.63(9)
Ti−N2−C10	144.51(11)	141.55(11)
C2−N2−C10	118.96(13)	119.59(12)

[a] Cg denotes the centroid of the Cp ligand.

The compound is monomeric with a tetrahedral coordination geometry around the titanium atom which coordinated by an η^5-cyclopentadienyl ring, a chloride ligand and the two nitrogen atoms of the symmetrically chelated diamido ligand. The structure contains a non-crystallographic plane of symmetry containing the cyclopentadienyl and phenylene ring centroids, the metal centre and the chlorine atom. As expected from the NMR spectroscopic data (solution studies), the phenylenediamido ligand adopts a *supine* conformation in the solid state, which minimizes the steric interaction with the Cp ring, although a *prone* conformation of the amido ligand in analogous monocyclopentadienyl diazadiene group 4 and 5 metal complexes has also been observed.[4d,4e] The nature of the alkyl substituents in the nitrogen atom seems to have a dramatic effect on the conformation geometry that the diene ligands adopt in half-sandwich complexes. In the literature, the *supine* conformation preferred for the *n*Pr substituents and the *prone* conformation preferred for the *t*Bu substituents have been found.[12d,14] Unfortunately, we were not successful in preparing crystals of the Np derivatives suitable for X-ray diffraction studies, although we propose that, as in compound **3**, a *supine* conformation can also be expected for Np derivatives in the solid state.

The titanium atom is located out of the plane defined by Cl and the nitrogen atoms [distance from Ti to N(1)−N(2)−Cl plane of 0.923(1) Å] which is almost parallel to the cyclopentadienyl ring with an interplanar angle of 4.6(1)°. The trigonal-planar geometry of the nitrogen atom, corresponding to sp^2 hybridization, is evidenced by the

 © 2004 Wiley-VCH Verlag GmbH & Co. KGaA, Weinheim

sums of the angles at N(1) (358.4°) and N(2) (358.8°) and the comparatively short Ti−N bond lengths of 1.9018(14) and 1.9014(13) Å, which point to a significant pπ-dπ interaction and are in agreement with reported values for related titanium amido[2d,2e,15] complexes. The N−Ti−N angle is 89.69(5)°. The Ti−C(1) and Ti−C(2) distances [2.4600(15) and 2.4635(15) Å] are long enough to allow donation of electron density from the C(1)−C(2) bond to the titanium atom. The phenylene ring shows a marked deformation. Thus, the C(1)−C(2) [1.427(2) Å] distance is significantly elongated with respect to the rest of the C−C distances in the ring (average 1.390 Å). These Ti−C and C(1)−C(2) bond lengths are longer and shorter, respectively, than similar distances reported for related diazadiene complexes[4d,4e] in which a π interaction between the double diene C−C bond and the metal centre is observed. The N−C bond lengths are 1.396(2) and 1.399(2) Å for N(1)−C(1) and N(2)−C(2), respectively, showing slight double-bond character,[16] while the N−C(Pr) bond lengths of 1.461(2) for N(1)−C(7) and 1.456(2) for N(2)−C(10) are consistent with single bonds.

The five-membered chelate ring is not planar and the phenylenediamido ligand is folded along the N(1)···N(2) vector with a fold angle, Θ, of 49.77(7)°. Similar folding has previously been interpreted in terms of κ^4-σ^2(N,N),π(C=C) bonding.[2e,4c,17] However, our results indicate this situation to be unlikely here.[9b]

The titanium-chlorine bond length is 2.3270(5) Å, slightly longer that those found for related monocyclopentadienyl- and dicyclopentadienyl-type chloride complexes.

The crystal structure of **7** is shown in Figure 2 and Table 1 summarizes selected bond lengths and angles. The structural parameters in the Ti-core of **7** are similar to those observed in compound **3**. The Cp ligand is oriented such that the $SiMe_3$ group is located in the plane bisecting the N−Ti−N angle and in a *trans* position with respect to the phenylene ligand.

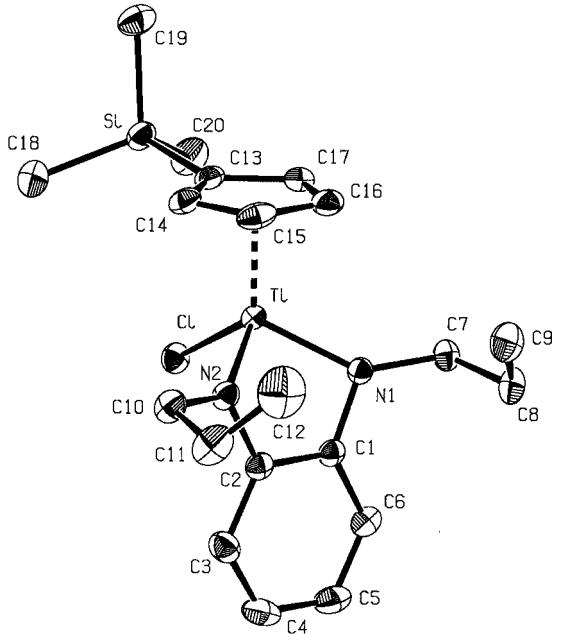

Figure 2. ORTEP representation of [Ti{η^5-$C_5H_4(SiMe_3)$}{1,2-$C_6H_4(NCH_2CH_2CH_3)_2$}Cl] (**7**) in the solid state; thermal ellipsoids are drawn at the 50% probability level; hydrogen atoms are omitted for clarity

Various coordination modes[11] [from η^1-N to η^4-N_2C_2 (σ^2,π)] can be proposed for the diamido ligands, where the N substituents regulate the steric demands at the metal centre. The bonding of the phenylenediamido ligand in compounds **3**−**10** can be best described by a σ^2,*N*,*N* bond with a partial pπ-dπ nitrogen interaction (form **A** in Scheme 2) and electronic density delocalization through the N−C−C−N bond system (form **B** in Scheme 2) consistent with the resonance hybrid form **C**, and such a ligand can therefore produce more electronically saturated complexes, consistent with a dianionic moiety that can donate between four and six electrons to the metal centre. The phenylenediamido ligand can therefore be considered as a σ^2,π-enediamide group structure in which the π-component is mainly contributed by the two nitrogen lone pairs.[18]

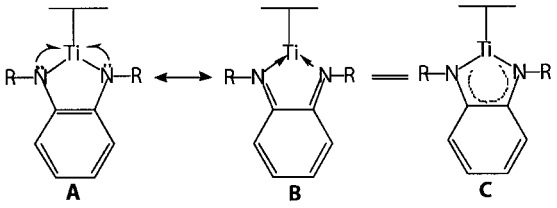

Scheme 2

Olefin Polymerization

Complexes **3**−**8** were studied as α-olefin polymerization pre-catalysts with methylalumoxane (MAO) as cocatalyst.

Ethylene polymerization was investigated using 50 mL total volume of toluene with 10−20 μmol of catalyst, with a Al/Ti molar ratio of 1000 at 25 °C and 1 atm pressure. The results are summarized in Table 2. Only traces of polymer or no polymerization were found when the reaction was carried out with propylene. Polymerization runs with the *n*Pr complexes resulted in moderate[19] activity (approx. 100 g of PE/mmol of Ti·atm·h) of PE with activity increasing in the order **7** < **5** < **3**. This result indicates that the activity is

Table 2. Polymerization of ethylene by [TiCp$^{R'}$\{1,2-$C_6H_4(NR)_2$\}Cl]

Entry	Catalyst[a]	Activity[b]	ΔH_m (J·g^{-1})[c]	α ($\Delta H_m/\Delta H°_m$)	T_m (°C)[c]
1	**3**	150	72.85	25	134
2	**4**	traces	–	–	–
3	**5**	130	100.40	35	131
4	**6**	110	57.56	20	135
5	**7**	70	27.56	95	131
6	**8**	80	116.7	40	130

[a] Reaction conditions: temperature = 25 °C; pressure = 1 atm; 10−20 μmol of catalyst; molar ratio Al:Ti = 1000. [b] gPE/mmol Ti·atm·h. [c] Determined by DSC.

 © 2004 Wiley-VCH Verlag GmbH & Co. KGaA, Weinheim

influenced greatly by the nature of the cyclopentadienyl substituents. A lower activity was observed for the Np derivatives. The activities of these chloro pre-catalyst systems are lower[20] than those found for the well-known non-cyclopentadienyl group 4 complexes containing chelating diamido ligands;[2c,2i,3a,3b,3d,20] rapid deactivation pathways[15d,21] of these chloro compounds after the reaction with MAO or TMA (present in MAO) could be a possible explanation for this behaviour.

The PE polymer samples obtained had melting points of 130−135 °C, characteristic of high density polyethylene, and remarkable differences in the ΔH enthalpy values. The degree of crystallinity (α) found for these PEs was lower than that expected for commercial HDPE, suggesting that chain branching occurs during the polymerization process.[22]

Styrene polymerization was studied using 35 mL total volume of toluene and 5 mL of monomer; the results are summarized in Table 3. For the *n*Pr derivatives, the activity for **3**/MAO was higher than for the system **7**/MAO; a lower activity was found for **5**/MAO (runs 1, 5 and 3, Table 3), indicating that the cyclopentadienyl ligands exert a strong influence on the activity of the catalyst and the order of activity is lower than that obtained for [$CpTiCl_3$] (used as a reference point) under similar conditions.[23] The polymers were precipitated in acidified MeOH, and syndiotactic polystyrene was obtained, as evidenced by NMR spectroscopic analysis and the melting point values.[24]

Table 3. Polymerization of styrene with [$TiCp^{R'}\{1,2\text{-}C_6H_4(NR)_2\}Cl$]

Entry	Catalyst[a]	Activity[b]	T_m (°C)[c]
1	**3**	536	256
2	**4**	146	253
3	**5**	245	274
4	**6**	68	277
5	**7**	480	266
6	**8**	120	266

[a] Reaction conditions: temperature = 50 °C; molar ratio Al:Ti = 1000; solvent = toluene (35 mL); monomer = styrene (5 mL). [b] gPS/mmol Ti·h. [c] Determined by DSC.

It is a general observation that the complexes containing the *n*Pr amido ligand show higher polymerization activities than the Np derivatives, suggesting that the activity is highly influenced by the steric effect[25] at the titanium centre caused by *n*-propyl or neopentyl substituents at the nitrogen atom of the diamido ligand. Similar examples of the influence of bulky substituents on catalytic polymerization activity have been observed for related amidinate complexes.[26]

Attempts to copolymerize styrene/ethylene were unsuccessful and afforded a mixture of the two homopolymers.

The precatalyst complexes **3**−**8** have only one chloro ligand. We assume that initially the MAO cocatalyst reacts with these complexes by methyl−halide exchange to afford Ti−Me derivatives, followed by cleavage of one of the Ti−N bonds by the $AlMe_3$ component in the MAO cocatalyst to generate active cationic alkyl species in a Ziegler−Natta olefin polymerization model.[27]

Conclusions

In this contribution we have described the synthesis and the characterization of new chloro mono(η^5-cyclopentadienyl)phenylenediamidotitanium and -zirconium complexes. X-ray diffraction studies confirm that compounds with *n*Pr substituted at the nitrogen atom adopt a *supine* conformation in the solid state which is maintained in solution, as deduced from the NMR spectroscopic data. The phenylenediamido ligand is bonded to the metal centre as a dianionic ligand showing a σ^2,π structure in which the π-component is mainly contributed by the two nitrogen lone pairs. NMR spectroscopic studies indicate that in solution at room temperature only one species is present, with a *supine* conformation, and no *supine-prone* automerization (flipping of the titanium-diamido framework) is observed. The catalytic activity of these compounds for olefin polymerization, when activated with MAO, was tested and studied. The steric effect of the *n*-propyl or neopentyl substituents at the nitrogen atom of the diamido ligand, and the nature of the cyclopentadienyl ring, strongly influenced catalytic polymerization activity.

Experimental Section

General Considerations: All manipulations were performed under argon using Schlenk and high-vacuum-line techniques or in a glove box model MO40-2. The solvents were purified by distillation under argon before use by employing the appropriate drying/deoxygenated agent. Deuterated solvents were stored over activated 4-Å molecular sieves and degassed by several freeze-thaw cycles. 1,2-Diphenylamine, *n*BuLi, $ClCOCH_2CH_3$, $ClCOC(CH_3)_3$, $LiAlH_4$ and $MgSO_4$ (Aldrich) were purchased from commercial sources and used without further purification. NEt_3 (Aldrich) was distilled before use and stored over 4 Å molecular sieves. [$Ti(\eta^5\text{-}C_5H_5)Cl_3$],[28] [$Ti(\eta^5\text{-}C_5Me_5)Cl_3$],[29] [$Ti(\eta^5\text{-}C_5H_4SiMe_3)Cl_3$],[30] [$Zr(\eta^5\text{-}C_5H_5)Cl_3$]·DME[31] and [$Zr(\eta^5\text{-}C_5Me_5)Cl_3$][32] were prepared by known procedures.

Polymerization-grade ethylene was used as received. Reagent grade styrene (Aldrich) was distilled under reduced pressure from calcium hydride and stored in a refrigerator under argon. The polymerization solvent (toluene) was dried by refluxing over sodium-benzophenone and distilled before used in an inert atmosphere. MAO (Witco 10%) was used as a solution in toluene.

C, H and N microanalyses were performed on a Perkin−Elmer 2400 microanalyzer. The analytical data found for **8** deviated from expected values since LiCl could not be completely removed from the mixture. NMR spectra, measured at 25 °C were recorded on a Varian Unity FT-300 (^{1}H NMR at 300 MHz, ^{13}C NMR at 75 MHz) spectrometer and chemical shifts were referenced to residual solvent protons.

1,2-$C_6H_4(NHCH_2CH_2CH_3)_2$ (1): *n*BuLi (100 mL of a 1.6 M solution, 160 mmol) was added dropwise to a solution of 1,2-pheny-

 © 2004 Wiley-VCH Verlag GmbH & Co. KGaA, Weinheim

lenediamine (8.6 g, 79.27 mmol) in 100 mL of THF at −78 °C. After stirring the reaction mixture for 12 hours, $ClCOCH_2CH_3$ (13.85 mL, 160 mmol) was added and the mixture stirred for an additional 4 h. The reaction mixture was slowly warmed to room temperature to give an orange solution and a white precipitate. After filtration, the solvent was reduced to half of its original volume under vacuum and a suspension of $LiAlH_4$ (10.0 g, 260 mmol) in 50 mL of diethyl ether was added dropwise. After stirring the solution for 12 h at 40 °C, excess $LiAlH_4$ was destroyed by addition of a saturated solution of Na_2SO_4. The solid precipitate was removed by filtration and the solution dried with $MgSO_4$. Removal of the solvent under vacuum gave a brown oil characterized as **1** (1.24 g, 8%). The compound was obtained as an oil that could not be recrystallized, preventing us from obtaining accurate elemental analysis data. ^1H NMR (300 MHz, C_6D_6, 25 °C): δ = 6.96 (m, 2 H, Ph), 6.72 (m, 2 H, Ph), 2.98 (broad, 2 H, NH), 2.78 (t, 4 H, N−CH_2), 1.34 (m, 4 H, CH_2), 0.78 (t, 6 H, CH_3) ppm. ^1H NMR (300 MHz, $CDCl_3$, 25 °C): δ = 6.78 (m, 2 H, Ph), 6.70 (m, 2 H, Ph), 3.24 (broad, 2 H, NH), 3.07 (t, 4 H, N−CH_2), 1.70 (m, 4 H, CH_2), 1.03 (t, 6 H, CH_3) ppm. $^{13}C\{^1H\}$ NMR (75 MHz, C_6D_6, 25 °C): δ = 138.0 (*ipso*-Ph), 119.7−112.2 (Ph), 46.5 (CH_2), 23.2 (CH_2), 11.9 (CH_3) ppm.

1,2-C_6H_4($NHCH_2tBu$)$_2$ (2): The amine *o*-C_6H_4($NHCH_2CtBu$)$_2$ (**2**) was obtained as an orange solid (7.98 g, 32.15 mmol, 41%) following the procedure described for **1**, from *n*BuLi (100 mL, 160 mmol), 1,2-phenylenediamine (8.6 g, 79.0 mmol), $ClCOC(CH_3)_3$ (19.53 mL, 160 mmol) and $LiAlH_4$ (10.0 g, 260 mmol). $C_{16}H_{28}N_2$ (248.16): calcd. C 77.43, H 11.28, N 11.28; found C 76.72, H 11.53, N 11.34. ^1H NMR (300 MHz, C_6D_6, 25 °C): δ = 7.00 (m, 2 H, Ph), 6.74 (m, 2 H, Ph), 3.27 (broad, 2 H, NH), 2.67 (s, 4 H, N−CH_2), 0.88 (s, 18 H, *t*Bu) ppm. ^1H NMR (300 MHz, $CDCl_3$, 25 °C): δ = 6.74 (m, 2 H, Ph), 6.69 (m, 2 H, Ph), 3.30 (broad, 2 H, NH), 2.82 (s, 4 H, N−CH_2), 1.02 (s, 18 H, *t*Bu) ppm. $^{13}C\{^1H\}$ NMR (75 MHz, C_6D_6, 25 °C): δ = 138.9 (*ipso*-Ph), 119.9−113.0 (Ph), 56.6 (CH_2), 31.5 (*ipso*-*t*Bu), 27.9 (*t*Bu) ppm.

[Ti(η^5-C_5H_5){1,2-C_6H_4($NHCH_2CH_2CH_3$)$_2$}Cl] (3): A toluene solution (30 mL) of *o*-C_6H_4($NHPr$)$_2$ (0.84 g, 4.37 mmol) and NEt_3 (1.22 mL, 8.74 mmol) was added to a yellow solution of [Ti(η^5-C_5H_5)Cl_3] (0.96 g, 4.37 mmol) in toluene (60 mL) at −78 °C. The cooling bath was removed and the reaction mixture was allowed to warm to room temperature with stirring for 12 h. The solid formed was collected by filtration and the toluene removed under vacuum. The residue was extracted with pentane (2 × 30 mL). The filtrate was dried and the solid obtained recrystallized from cold pentane to give **3** as a black solid (1.16 g, 3.43 mmol, 78%). $C_{17}H_{23}ClN_2Ti$ (338.49): calcd. C 60.32, H 6.80, N 8.27; found C 60.02, H 6.72, N 8.03. ^1H NMR (300 MHz, C_6D_6, 25 °C): δ = 7.36 (m, 2 H, Ph), 6.97 (m, 2 H, Ph), 6.23 (s, 5 H, C_5H_5), 3.70 (t, 4 H, CH_2), 1.32 (m, 4 H, CH_2), 0.58 (t, 6 H, CH_3) ppm. ^1H NMR (300 MHz, $CDCl_3$, 25 °C): δ = 7.48 (m, 2 H, Ph), 7.11 (m, 2 H, Ph), 6.55 (s, 5 H, C_5H_5), 4.05 (t, 4 H, CH_2), 1.50 (m, 4 H, CH_2), 0.81 (t, 6 H, CH_3) ppm. $^{13}C\{^1H\}$ NMR (75 MHz, C_6D_6, 25 °C): δ = 137.8 (*ipso*-Ph), 127.0, 116.1 (Ph), 114.8 (C_5H_5), 58.9 (N−CH_2), 24.6 (CH_2), 11.6 (CH_3) ppm.

[Ti(η^5-C_5H_5){1,2-C_6H_4(NCH_2tBu)$_2$}Cl] (4): *n*BuLi (4.50 mL of an 1.6 M solution, 7.26 mmol) was added dropwise to a stirred solution of *o*-C_6H_4($NHCH_2tBu$)$_2$ (0.90 g, 3.63 mmol) in 50 mL of hexane at −78 °C. After the addition was complete, the reaction mixture was stirred for 6 hours and then slowly warmed to room temperature; a white precipitate formed. This suspension was cooled to −78 °C and a solution of [Ti(η^5-C_5H_5)Cl_3] (0.80 g, 3.63 mmol) in 50 mL of toluene was added. The reaction mixture was slowly warmed to room temperature and stirred for 12 h. After filtration, the solvent was removed under vacuum to give a red-brown oil which was recrystallized from cold hexane. A red-brown solid was collected which was characterized as **4** (0.64 g, 1.66 mmol, 45%). $C_{21}H_{31}ClN_2Ti$ (394.58): calcd. C 63.92, H 7.86, N 7.10; found C 63.55, H 7.97, N 7.10. ^1H NMR (300 MHz, C_6D_6, 25 °C): δ = 7.33 (m, 2 H, Ph), 7.25 (m, 2 H, Ph), 6.31 (s, 5 H, C_5H_5), 3.88 (dd, 4 H, CH_2), 0.63 (s, 18 H, *t*Bu) ppm. ^1H NMR (300 MHz, $CDCl_3$, 25 °C): δ = 7.48 (m, 2 H, Ph), 7.41 (m, 2 H, Ph), 6.51 (s, 5 H, C_5H_5), 4.17 (dd, 4 H, CH_2), 0.75 (s, 18 H, *t*Bu) ppm. $^{13}C\{^1H\}$ NMR (75 MHz, C_6D_6, 25 °C): δ = 127.8, 119.2 (Ph), 122.3 (*ipso*-Ph), 115.1 (C_5H_5), 67.2 (CH_2), 35.7 (*ipso*-*t*Bu), 28.8 (*t*Bu) ppm.

[Ti(η^5-C_5Me_5){1,2-C_6H_4($NCH_2CH_2CH_3$)$_2$}Cl] (5): Compound **5** was prepared from the reaction of the *o*-C_6H_4($NHPr$)$_2$ amine (0.81 g, 4.22 mmol), 8.44 mmol of *n*BuLi and [Ti(η^5-C_5Me_5)Cl_3] (1.22 g, 4.22 mmol) by the procedure described for **4**, and obtained as a black oil (1.59 g, 3.90 mmol, 92%). $C_{22}H_{33}ClN_2Ti$ (408.54): calcd. C 64.67, H 8.08, N 6.85; found C 64.80, H 8.76, N 6.30. ^1H NMR (300 MHz, C_6D_6, 25 °C): δ = 7.30 (m, 2 H, Ph), 6.89 (m, 2 H, Ph), 3.88 (m, 1 H, N−CH_2), 3.57 (m, 1 H, N−CH_2), 1.75 (s, 15 H, C_5Me_5), 1.64 (m, 4 H, CH_2), 0.80 (t, 6 H, CH_3) ppm. ^1H NMR (300 MHz, $CDCl_3$, 25 °C): δ = 7.26 (m, 2 H, Ph), 7.01 (m, 2 H, Ph), 4.00 (m, 1 H, N−CH_2), 3.81 (m, 1 H, N−CH_2), 1.93 (s, 15 H, C_5Me_5), 1.59 (m, 4 H, CH_2), 0.88 (t, 6 H, CH_3) ppm. $^{13}C\{^1H\}$ NMR (75 MHz, C_6D_6, 25 °C): δ = 124.5, 114.1 (Ph), 122.9 (*ipso*- C_5Me_5), 54.5 (N−CH_2), 23.5 (CH_2), 12.5 (CH_3), 11.4 (C_5Me_5) ppm; the signal for *ipso* Ph was not observed

[Ti(η^5-C_5Me_5){1,2-C_6H_4(NCH_2tBu)$_2$}Cl] (6): Compound **6** was prepared by reacting of the *o*-C_6H_4($NHCH_2tBu$)$_2$ amine (0.85 g, 3.42 mmol), 6.85 mmol of *n*BuLi and [Ti(η^5-C_5Me_5)Cl_3] (1.00 g, 3.45 mmol) by the procedure described for **4**, and obtained as a red-brown oil (0.90 g, 1.94 mmol, 56%). $C_{26}H_{41}ClN_2Ti$ (464.58): calcd. C 67.21, H 8.89, N 6.02; found C 67.26, H 8.84, N 6.17. ^1H NMR (300 MHz, C_6D_6, 25 °C): δ = 7.23 (m, 2 H, Ph), 7.19 (m, 2 H, Ph), 3.97 (dd, 4 H, CH_2), 1.63 (s, 15 H, C_5Me_5), 0.90 (s, 18 H, *t*Bu) ppm. ^1H NMR (300 MHz, $CDCl_3$, 25 °C): δ = 7.38 (m, 2 H, Ph), 7.36 (m, 2 H, Ph), 3.96 (dd, 4 H, CH_2), 1.65 (s, 15 H, C_5Me_5), 0.75 (s, 18 H, *t*Bu) ppm. $^{13}C\{^1H\}$ NMR (75 MHz, C_6D_6, 25 °C): δ = 125.0, 117.4 (Ph), 122.7 (*ipso*-Ph), 121.0 (*ipso*-C_5Me_5), 62.1 (N−CH_2), 37.6 (*ipso*-*t*Bu), 29.6 (*t*Bu), 11.1 (C_5Me_5) ppm.

[Ti{η^5-C_5H_4($SiMe_3$)}{1,2-C_6H_4($NCH_2CH_2CH_3$)$_2$}Cl] (7): Compound **7** was prepared by reacting the *o*-C_6H_4($NHPr$)$_2$ amine (1.7 g, 8.85 mmol), 17.70 mmol of *n*BuLi and [Ti{η^5-C_5H_4($SiMe_3$)}Cl_3] (2.50 g, 8.85 mmol) by the procedure described for **4**, and obtained as a black oil (2.5 g, 6.09 mmol, 69%). $C_{20}H_{31}ClN_2SiTi$ (410.52): calcd. C 58.51, H 7.98, N 6.82; found C 58.61, H 7.98, N 6.26. ^1H NMR (300 MHz, C_6D_6, 25 °C): δ = 7.34 (m, 2 H, Ph), 6.96 (m, 2 H, Ph), 6.57, 6.40 (2 H, 2 H, AA′BB′ spin system, C_5H_4), 3.82 (m, 4 H, CH_2), 1.33 (m, 4 H, CH_2), 0.60 (t, 6 H, CH_3), 0.32 (s, 6 H, $SiMe_3$) ppm. ^1H NMR (300 MHz, $CDCl_3$, 25 °C): δ = 7.43 (m, 2 H, Ph), 7.08 (m, 2 H, Ph), 6.66, 6.65 (2 H, 2 H, AA′BB′ spin system, C_5H_4), 4.08 (m, 4 H, CH_2), 1.46 (m, 4 H, CH_2), 0.78 (t, 6 H, CH_3), 0.25 (s, 6 H, $SiMe_3$) ppm. $^{13}C\{^1H\}$ NMR (75 MHz, C_6D_6, 25 °C): δ = 137.8 (*ipso*-Ph), 125.6 (*ipso*-C_5H_4), 127.0, 116.7 (Ph), 121.8, 116.4 (C_5H_4), 59.3 (CH_2), 24.4 (CH_2), 11.7 (CH_3), −0.04 ($SiMe_3$) ppm.

[Ti{η^5-C_5H_4($SiMe_3$)}{1,2-C_6H_4(NCH_2tBu)$_2$}Cl] (8): Compound **8** was prepared by reacting the *o*-C_6H_4($NHCH_2tBu$)$_2$ amine (0.50 g, 2.00 mmol), 4.03 mmol of *n*BuLi and [Ti{η^5-C_5H_4($SiMe_3$)}Cl_3] (0.59 g, 2.00 mmol) by the procedure described for **4**, and obtained as a red-brown oil (0.60 g, 1.28 mmol, 64%). The isolated oil con-

 © 2004 Wiley-VCH Verlag GmbH & Co. KGaA, Weinheim

sisted mainly of **8**, but it contained some unremovable LiCl as an impurity and therefore correct elemental analysis data could not be obtained, although satisfactory spectroscopic data were obtained. ^{1}H NMR (300 MHz, C_6D_6, 25 °C): δ = 7.31 (m, 2 H, Ph), 7.24 (m, 2 H, Ph), 6.73, 6.38 (2 H, 2 H, AA′BB′ spin system, C_5H_4), 4.02 (dd, 4 H,, CH_2), 0.68 (s, 18 H, *t*Bu), 0.37 (s, 9 H, $SiMe_3$) ppm. ^{1}H NMR (300 MHz, $CDCl_3$, 25 °C): δ = 7.47 (m, 2 H, Ph), 7.40 (m, 2 H, Ph), 6.69, 6.55 (2 H, 2 H, AA′BB′ spin system, C_5H_4), 4.25, 4.11 (2 H, CH_2), 0.77 (s, 18 H, *t*Bu), 0.26 (s, 9 H, $SiMe_3$) ppm. ^{13}C{^{1}H} NMR (75 MHz, C_6D_6, 25 °C): δ = 122.5 (*ipso*-Ph), not observed (*ipso*-C_5H_4), 127.8, 119.1 (Ph), 123.0, 116.3 (C_5H_4), 67.6 (CH_2), 35.9 (*ipso*-*t*Bu), 28.9 (*t*Bu), 0.14 ($SiMe_3$) ppm.

[Zr(η^5-C_5H_5){1,2-C_6H_4(NCH_2tBu)$_2$}Cl] (9): *n*BuLi (5.04 mL of an 1.6 M solution, 8.06 mmol) was added dropwise to a stirred solution of *o*-C_6H_4($NHCH_2t$Bu)$_2$ (1.0 g, 4.03 mmol) in 50 mL of hexane at −78 °C. After the addition was complete, the reaction mixture was stirred for 6 hours and then slowly warmed to room temperature. The white solid formed was filtered and washed with cold hexane. This solid was added to a solution of [Zr(η^5-C_5H_5)Cl_3]·DME (1.4 g, 4.03 mmol) in 50 mL of toluene at −78 °C. The cooling bath was removed and the reaction mixture was allowed to warm to room temperature with stirring for 12 h. The solid formed was insoluble in hexane which made its characterization difficult. Complex **9** was obtained as a yellow solid (0.27 g, 0.62 mmol, 15.4%). $C_{21}H_{31}ClN_2Zr$ (437.67): calcd. C 57.58, H 7.08, N 6.40; found C 57.32, H 8.22, N 6.40. ^{1}H NMR (300 MHz, C_6D_6, 25 °C): δ = 7.39 (m, 2 H, Ph), 7.18 (m, 2 H, Ph), 5.98 (s, 5 H, C_5H_5), 3.80 (dd, 4 H, CH_2), 0.78 (s, 18 H, *t*Bu) ppm. ^{1}H NMR (300 MHz, $CDCl_3$, 25 °C): δ = 7.32 (m, 2 H, Ph), 7.17 (m, 2 H, Ph), 5.82 (s, 5 H, Cp), 3.70 (dd, 4 H, CH_2), 0.72 (s, 18 H, *t*Bu) ppm. ^{13}C{^{1}H} NMR (75 MHz, C_6D_6, 25 °C): δ = 123.5−120.1 (Ph), 124.5 (*ipso*-Ph), 114.0 (C_5H_5), 63.2 (CH_2), 35.4 (*ipso*-*t*Bu), 28.8 (*t*Bu) ppm.

Synthesis of [Zr(η^5-C_5Me_5){1,2-C_6H_4(NCH_2tBu)$_2$}Cl] (10): Compound **10** was prepared by reacting the *o*-C_6H_4($NHCH_2t$Bu)$_2$ amine (1.0 g, 4.03 mmol), 8.06 mmol of *n*BuLi and [Zr(η^5-C_5Me_5)Cl_3] (1.34 g, 4.03 mmol) by the procedure described for **5** and obtained as a black solid (1.66 g, 3.27 mmol, 81%). $C_{26}H_{41}N_2ZrCl$ (507.93): calcd. C 61.48, H 8.07, N 5.51; found C 61.56, H 8.69, N 5.64. ^{1}H NMR (300 MHz, C_6D_6, 25 °C): δ = 7.09 (m, 2 H, Ph), 7.02 (m, 2 H, Ph), 3.65 (dd, 4 H, CH_2), 1.66 (s, 15 H, C_5Me_5), 0.97 (s, 18 H, *t*Bu) ppm. ^{1}H NMR (300 MHz, $CDCl_3$, 25 °C): δ = 7.28 (m, 4 H, Ph), 3.63 (s, 4 H, CH_2), 1.72 (s, 15 H, C_5Me_5), 0.87 (s, 18 H, *t*Bu) ppm. ^{13}C{^{1}H} NMR (75 MHz, C_6D_6, 25 °C): δ = 122.5, 117.2 (Ph), 117.8 (*ipso*- C_5Me_5), 62.1 (CH_2), 34.9 (*ipso*-*t*Bu), 28.9 (*t*Bu), 10.0 (C_5Me_5) ppm; *ipso*-Ph signal not observed.

Polymerization Procedure: Ethylene polymerization was carried out in 100 mL Schlenk flasks with magnetic stirring. Polymerization was carried out as follows: toluene and MAO were injected into the Schlenk flask with magnetic stirring at the desired temperature (25 °C). The solution was then saturated with 1 atmosphere of ethylene, and the monomer pressure was kept constant over the polymerization runs. Polymerization begins with the addition of a toluene solution of the titanium compound into the flask. After the desired reaction time was reached, polymerization was terminated by venting the ethylene gas and quenching with a small volume of a solution of MeOH/HCl. The polymers were isolated by filtration, washed with MeOH, and then dried in vacuo at 50 °C.
Polymerization of styrene was performed in toluene at 50 °C. Polymerization was carried out as follows: toluene (30 mL), styrene (5 mL), and MAO were injected into the Schlenk flasks with magnetic stirring at the desired temperature. The titanium compound dissolved in toluene (5 mL) was added last. All manipulations were performed under an argon atmosphere. The reaction was stopped after 15 minutes by addition of MeOH/HCl, and the polymer prod-

Table 4. Summary of the crystallographic data for compounds **3** and **7**

	3	**7**
Empirical formula	$C_{17}H_{23}ClN_2Ti$	$C_{20}H_{31}ClN_2SiTi$
Formula mass	338.69	410.88
Crystal system	monoclinic	triclinic
Space group	$P2_1/c$ (no. 14)	$P\bar{1}$ (no. 2)
a (Å)	13.0339(2)	10.0673(2)
b (Å)	12.9656(2)	10.3242(2)
c (Å)	10.7520(1)	11.1287(2)
α (°)	90	87.5786(14)
β (°)	110.4105(8)	72.5554(14)
γ (°)	90	88.8736(8)
V (Å^3)	1702.93(4)	1102.47(4)
Z	4	2
$\rho_{calcd.}$ [g cm^{-3}]	1.321	1.238
μ [mm^{-1}]	0.655	0.569
T [K]	123	153
F(000)	712	436
Crystal size (mm)	0.61 × 0.25 × 0.23	0.38 × 0.25 × 0.20
Θ range (°)	2.29/25.41	1.92/25.28
Index ranges	*h*: ±15/*k*: ±15/*l*: ±12	*h*: ±12/*k*: ±12/*l*: ±13
Reflections collected	36764	15832
Independent reflections [$I_o > 2\sigma(I_o)$/all data/R_{int}]	2764/3131/0.038	3616/3989/0.027
Data/restraints/parameters	3131/0/282	3989/0/350
*R*1 [$I_o > 2\sigma(I_o)$/all data]	0.0251/0.0313	0.0251/0.0293
*wR*2 [$I_o > 2\sigma(I_o)$/all data]	0.0605/0.0632	0.0623/0.0648
GOF	1.027	1.077
Weights *a*/*b*	0.0275/0.9782	0.0245/0.4603
$\Delta\rho_{max/min}$ [e·Å^{-3}]	0.26/−0.25	0.26/−0.25

 © 2004 Wiley-VCH Verlag GmbH & Co. KGaA, Weinheim

uct was coagulated with a large excess of acidified methanol and recovered by filtration.

Characterization of Polymers: The thermal properties of the samples were studied in a Du Pont 2920 MDSC instrument calibrated by measuring the melting point of indium. 5−10 mg each of the dried polymer were fused into standard aluminium pans and measured using the following temperature program for polyethylene samples: first a heating phase (10 °C/min) from 50 to 200 °C, followed by a cooling phase (−10 °C/min) to 50 °C. The peak maximum of the second heating curve was taken as the melting point (T_m). To determinate the degree of crystallinity (α) the relationship $\Delta H_m/\Delta H°_m$ was used. ΔH_m was derived from the data of the second heating course of the DSC, and $\Delta H°_m$ was assumed to be the fusion enthalpy[33] (290 J/g) for 100% crystalline polyethylene.
Polystyrene samples were subjected to the following steps: heating at 10 °C/min from 30 to 270 °C and then cooling at 10 °C/min from this temperature to 30 °C, followed by heating at 10 °C/min from 30 to 270 °C to obtain the melting peak temperature (T_m).
The NMR samples were prepared by dissolving the polystyrene sample in tetrachloro-1,2-dideuterioethane. The spectra were recorded at 25 °C.

X-ray Structure Determination of 3 and 7: Details of the X-ray experiment, data reduction, and final structure refinement calculations are summarized in Table 4. Crystals of complex **3** (**7**) suitable for an X-ray single crystal structure determination were obtained from hexane. Preliminary examination and data collection were carried out on a kappa-CCD device (Nonius) at the window of a rotating anode (NONIUS FR591; 50 kV; 60 mA; 3.0 kW) and graphite-monochromated Mo-K_α radiation ($\lambda = 0.71073$ Å).[34] The unit-cell parameters were obtained by full-matrix least-squares refinement of 3274 (3935) reflections. Data collection was performed at 123 (153) K with an exposure time of 60 (80) s per frame, 7 (7) sets; 501 (335) frames; phi and omega scans; 2.0° (2.0°) scan-width. A total number of 36764 (15832) reflections were integrated. Raw data were corrected for Lorentz and polarization effects. If necessary, corrections for absorption and decay effects were applied during the scaling procedure.[35] After merging, a sum of 3131 (3989) independent reflections remained and used for all calculations. The structure was solved by a combination of direct methods[36] and difference-Fourier syntheses.[37] All non-hydrogen atoms of the asymmetric unit were refined with anisotropic thermal displacement parameters. All hydrogen atoms were found in the final Fourier maps and refined with isotropic displacement. Full-matrix least-squares refinements were carried out by minimizing $\Sigma w(F_o^2 - F_c^2)^2$ with the SHELXL-97 weighting scheme and stopped at maximum shift/err < 0.001. Neutral-atom scattering factors for all atoms and anomalous dispersion corrections for the non-hydrogen atoms were taken from the International Tables for Crystallography.[38] All other calculations (including ORTEP graphics) were carried out with the program PLATON.[39]
CCDC-206875 (for **3**) and -206874 (for **7**) contain the supplementary crystallographic data for this paper. These data can be obtained free of charge at www.ccdc.cam.ac.uk/conts/retrieving.html [or from the Cambridge Crystallographic Data Centre, 12 Union Road, Cambridge CB2 1EZ, UK; Fax: +44-1223-336033; E-mail: deposit@ccdc.cam.ac.uk].

Acknowledgments

Financial support for this research by DGICYT (Project MAT2001-1309) is gratefully acknowledged. We are also grateful to Professor Alfonso Grassi (Universtity of Salerno) for facilities to carry out the polymerization experiments.

[1] [1a] P. C. Wailes, R. S. P. Coates, H. Weigold, *Organometallic Chemistry of Titanium, Zirconium and Hafnium*, Academic Press, New York, **1974**. [1b] D. J. Cardin, M. F. Lappert, C. L. Raston, P. I. Riley, in *Comprehensive Organometallic Chemistry* (Eds.: G. Wilkinson, F. G. A. Stone, E. W. Abel), vol. 3, Pergamon, Oxford, **1982**. [1c] D. J. Cardin, M. F. Lappert, C. L. Raston, *Chemistry of Organo-Zirconium and -Hafnium Compounds*, John Wiley & Sons, New York, **1986**. [1d] *Comprehensive Organometallic Chemistry II. A Review of the Literature* (1982−1994) (Eds.: E. W. Abel, F. G. A. Stone, G. Wilkinson), vol. 4, Pergamon, Oxford, **1994**. [1e] *Metallocene: Synthesis, Reactivity and Applications* (Eds.: A. Togni, R. L. Halterman), vol. 1 and 2, Wiley-VCH, New York, **1998**.

[2] [2a] H. C. S. Clark, F. G. N. Cloke, P. B. Hitchcock, J. B. Love, A. P. Wainwright, *J. Organomet. Chem.* **1995**, *501*, 333−340. [2b] F. G. N. Cloke, P. B. Hitchcock, J. B. Love, *J. Chem. Soc., Dalton Trans.* **1995**, 25−30. [2c] J. D. Scollard, D. H. McConville, J. J. Vittal, *Organometallics* **1995**, *14*, 5478−5480. [2d] T. H. Warren, R. R. Schrock, W. M. Davis, *Organometallics* **1996**, *15*, 562−569. [2e] K. Aoyagi, P. Gantzel, K. Kalai, T. D. Tilley, *Organometallics* **1996**, *15*, 923−927. [2f] A. D. Horton, J. de With, A. J. van der Linden, H. van de Weg, *Organometallics* **1996**, *15*, 2672−2674. [2g] F. Guérin, D. H. McConville, N. C. Payne, *Organometallics* **1996**, *15*, 5085−5089. [2h] F. Guérin, D. H. McConville, J. J. Vittal, *Organometallics* **1996**, *15*, 5586−5590. [2i] R. Duchateau, C. T. van Wee, A. Meetsma, P. T. van Duijnnen, J. H. Teuben, *Organometallics* **1996**, *15*, 2279−2290. [2j] J. D. Scollard, D. H. McConville, J. J. Vittal, *Organometallics* **1997**, *16*, 4415−4420. [2k] A. D. Horton, J. de With, *Organometallics* **1997**, *16*, 5424−5436. [2l] R. Baumann, R. Stumpf, W. M. Davis, L.-C. Liang, R. R. Schrock, *J. Am. Chem. Soc.* **1999**, *121*, 7822−7836. [2m] C. Cao, J. T. Ciszewski, A. Odom, *Organometallics* **2001**, *20*, 5011−5013. [2n] J. Scholz, H. Görls, *J. Organomet. Chem.* **2002**, *648*, 87−92. [2o] R. M. Gauvin, J. Kress, *J. Mol. Catal. A* **2002**, *182−183*, 411−417.

[3] [3a] J. D. Scollard, D. H. McConville, *J. Am. Chem. Soc.* **1996**, *118*, 10008−10009. [3b] J. D. Scollard, D. H. McConville, S. J. Rettig, *Organometallics* **1997**, *16*, 1810−1812. [3c] R. Baumann, W. M. Davis, R. R. Schrock, *J. Am. Chem. Soc.* **1997**, *119*, 3830−3831. [3d] V. C. Gibson, B. S. Kimberley, A. J. P. White, D. J. Williams, P. Howard, *Chem. Commun.* **1998**, 313−314. [3e] G. J. P. Britovsek, V. C. Gibson, D. F. Wass, *Angew. Chem. Int. Ed.* **1999**, *38*, 428−447. [3f] P. Mehrkhodavandi, P. Bonitatebus Jr., R. R. Schrock, *J. Am. Chem. Soc.* **2000**, *122*, 7841−7842. [3g] P. Mehrkhodavandi, R. R. Schrock, *J. Am. Chem. Soc.* **2001**, *123*, 10746−10747.

[4] [4a] R. Gómez, R. Duchateau, A. N. Chernega, J. H. Teuben, F. T. Edelman, M. L. H. Green, *J. Organomet. Chem.* **1995**, *491*, 153−158. [4b] F. G. Cloke, T. J. Geldbach, P. B. Hitchcock, J. B. Love, *J. Organomet. Chem.* **1996**, *506*, 343−345. [4c] G. Jiménez-Pindado, M. Thornton-Pett, M. Bochmann, *J. Chem. Soc., Dalton Trans.* **1998**, 393−400. [4d] F. Amor, P. Gómez-Sal, P. Royo, J. Okuda, *Organometallics* **2000**, *19*, 5168−5173. [4e] J. Scholz, G. A. Hadi, K.-H. Thiele, H. Görls, R. Weimann, H. Schumann, J. Sieler, *J. Organomet. Chem.* **2001**, *626*, 243−259.

[5] [5a] P. J. Shapiro, E. E. Bunel, W. E. Piers, J. E. Bercaw, *Synlett* **1990**, *2*, 74−84. [5b] J. Okuda, *Chem. Ber.* **1990**, *123*, 1649. [5c] J. C. Stevens, F. J. Timmers, D. R. Wilson, G. F. Schmidt, P. N. Nickias, R. K. Rosen, G. W. Knight, S. Lai, *Eur. Patent. Appl.* EP **1991**, *416*, 815 (Dow) (*Chem. Abstr.* **1991**, *115*, 93163). [5d] J. M. Canich, *Eur. Patent. Appl.* EP **1991**, *420*, 436 (Exxon) (*Chem. Abstr.* **1991**, *115*, 184145). [5e] R. B. Panell, J. A. M. Canich, G. G. Hlatky (Exxon) *PCT Int. Appl.* **1994**, WO 94/00500. [5f] P. N. Nickias, M. H. McAdon, J. T. Patton (Dow) *PCT Int. Appl.* **1997**, WO 97/15583. [5g]A. L. Mcknight, R. W. Waymouth, *Chem. Rev.* **1998**, *98*, 2587−2598. [5h] J. Jin, D. R. Wilson, E. Y.-X. Chen, *Chem. Commun.* **2002**, 708−709.

[6] J. Cano, P. Royo, M. Lanfranchi, M. A. Pellinghelli, A. Tiripicchio, *Angew. Chem. Int. Ed.* **2001**, *40*, 2495−2497.

 © 2004 Wiley-VCH Verlag GmbH & Co. KGaA, Weinheim

[7] M. González-Maupoey, T. Cuenca, L. M. Frutos, O. Castaño, E. Herdtweeck, *Organometallics* **2003**, *22*, 2694−2704.
[8] [8a] M. Maeda, S. Sasaki, T. Fukumura, E. Fukuzawa, K. Watanabe, M. Kojima, T. Tahara, K. Masuda, Y. Ichiya, *Chem. Pharm. Bull.* **1992**, *40*, 1793−1798. [8b] H. Braunschweig, B. Gehrhus, P. Hitchcock, M. F. Lappert, *Z. Anorg. Allg. Chem.* **1995**, *621*, 1922−1928.
[9] [9a] B. Gehrhus, P. B. Hitchock, M. F. Lappert, J. Heinicke, R. Bolse, D. Bläser, *J. Organomet. Chem.* **1996**, *521*, 211−220. [9b] S. Danièle, P. B. Hitchcock, M. Lappert, P. G. Merle, *J. Chem. Soc., Dalton Trans.* **2001**, 13−19.
[10] A. Bulbarela, H. Tlahuext, H. R. Morales, L. Cuéllar, G. Uribe, R. Contreras, *Magn. Reson. Chem.* **1986**, *24*, 1093.109.
[11] B. Richter, J. Scholz, J. Sieler, K.-H. Thiele, *Angew. Chem.* **1995**, *107*, 2865; *Angew. Chem. Int. Ed. Engl.* **1995**, *34*, 2649.
[12] [12a] H. Yasuda, K. Tatsumi, T. Okamoto, K. Mashima, K. Lee, A. Nakamura, Y. Kai, N. Kanehisa, N. Kasai, *J. Am. Chem. Soc.* **1985**, *107*, 2410−2413. [12b] H. Yasuda, A. Nakamura, *Angew. Chem. Int. Ed. Engl.* **1987**, *26*, 723−742. [12c] T. Okamoto, H. Yasuda, A. Nakamura, Y. Kai, N. Kanehisa, N. Kasai, *J. Am. Chem. Soc.* **1988**, *110*, 5008−5011. [12d] H. Kagawuchi, Y. Yamamoto, K. Asaoka, K. Tatsumi, *Organometallics* **1998**, *17*, 4380−4386. [12e] J. Scholz, H. Görls, *Polyhedron* **2002**, *21*, 305−312.
[13] M. L. H Green, J. Sassmannhausen, *Chem. Commun.* **1999**, 115−116.
[14] A. Nakamura, K. Mashima, *J. Organomet. Chem.* **2001**, *621*, 224−230.
[15] [15a] M. F. Lappert, P. P. Power, A. R. Sanger, R. C. Srivastava, *Metal and Metalloid Amides*, Ellis Horwood, Wiley, New York, **1980**. [15b] R. A. Jones, M. H. Seeberger, J. L. Atwood, W. E. Hunter, *J. Organomet. Chem.* **1983**, *247*, 1−6. [15c] R. M. Pupi, J. N. Coalter, J. L. Petersen, *J. Organomet. Chem.* **1995**, *497*, 17−25. [15d] N. A. H. Male, M. Thornton-Pett, M. Bochmann, *J. Chem. Soc., Dalton Trans.* **1997**, 2487−2494.
[16] G. van Koten, K. Vrieze, *Adv. Organomet. Chem.* **1982**, *21*, 151−239.
[17] [17a] J. M. Boncella, S. Wang, D. D. VanderLende, R. L. Huff, K. A. Abboud, W. M. Vaughn, *J. Organomet. Chem.* **1997**, *530*, 59−70. [17b] C. G. Ortiz, K. A. Abboud, J. M. Boncella, *Organometallics* **1999**, *18*, 4253−4260. [17c] K. Mashima, Y. Matsuo, K. Tani, *Organometallics* **1999**, *18*, 1471−1481.
[18] A. Galindo, A. Ienco, C. Mealli, *New J. Chem.* **2000**, *14*, 73−75.
[19] V. C. Gibson, S. K. Spitzmesser, *Chem. Rev.* **2003**, *103*, 283−315.
[20] [20a] Y. Jeo, J. Heo, W. M. Lee, T. Chang, K. Kim, *Organometallics* **1999**, *18*, 4107−4113. [20b] T. I. Gountchev, T. D. Tilley, *Inorg. Chim. Acta* **2003**, *345*, 81−88. [20c] R. M. Gauvin, R. Choukroun, B. Donadieu, J. Kress, *Eur. J. Inorg. Chem.* **2001**, 2337−2346.
[21] [21a] C. H. Lee, Y. H. La, S. J. Park, J. W. Park, *Organometallics* **1998**, *17*, 3648−3655. [21b] C. Lorber, B. Donnadieu, R. Choukroun, *Organometallics* **2000**, *19*, 1963−1966. [21c] C. H. Lee, Y. H. La, S. J. Park, J. W. Park, *Organometallics* **1999**, *18*, 344−351.
[22] A. Karam, M. Jimeno, J. Lezama, E. Catarí, A. Figueroa, B. R. Gascue, *J. Mol. Catal. A* **2001**, *176*, 65−72.
[23] [23a] P. Longo, A. Proto, A. Zambelli, *Macromol. Chem. Phys.* **1995**, *196*, 3015−3029. [23b] S. Saccheo, G. Goia, A. Grassi, D. E. Bowen, R. F. Jordan, *J. Mol. Catal. A* **1998**, *128*, 111−118. [23c] W. Kamisky, *J. Chem. Soc., Dalton Trans.* **1998**, 1413−1418.
[24] [24a] N. Ishihara, T. Seimiya, M. Kuramoto, M. Uoi, *Macromolecules* **1986**, *19*, 2464−2465. [24b] N. Ishihara, M. Kuramoto, M. Uoi, *Macromolecules* **1988**, *21*, 3356−3360. [24c] N. Tomotsu, N. Ishihara, T. H. Newman, M. T. Malanga, *J. Mol. Catal. A* **1998**, *128*, 167−190.
[25] R. Kleinschmidt, Y. Griebenow, G. Fink, *J. Mol. Catal. A* **2000**, *157*, 83−90.
[26] [26a] J. Richter, F. T. Edelman, M. Noltemeyer, H. G. Schmidt, M. Shmulinson, M. S. Eisen, *J. Mol. Catal. A* **1998**, *130*, 149−162. [26b] S. J. Kim, I. N. Jung, B. R. Yoo, S. H. Kim, J. Ko, D. Byun, S. O. Kang, *Organometallics* **2001**, *20*, 2141.
[27] A. V. Firth, J. C. Stewart, A. J. Hoskin, D. W. Stephan, *J. Organomet. Chem.* **1999**, *591*, 185.
[28] [28a] R. D. Gorsich, *J. Am. Chem. Soc.* **1958**, *80*, 4744−4744. [28b] R. D. Gorsich, *J. Am. Chem. Soc.* **1960**, *82*, 4211−4214.
[29] M. Mena, M. A. Pellinghelli, P. Royo, R. Serrano, A. Tiripicchio, *J. Chem. Soc., Chem. Commun.* **1986**, 1118−1119.
[30] P. Jutzi, M. Kuhn, *J. Organomet. Chem.* **1979**, *173*, 221−229.
[31] E. C. Lund, T. Livinghouse, *Organometallics* **1990**, *9*, 2426−2427.
[32] A. Martín, M. Mena, F. Palacios, *J. Organomet. Chem.* **1994**, *480*, C10−C11.
[33] [33a] G. Luft, M. Dorn, *Angew. Macromol. Chem.* **1991**, *188*, 177. [33b] J. G. Fatou, *Morphology and Crystallization in Polyolefins*, in *Handbook of Polyolefins* (Eds.: C. Vasile, R. B. Seymour), chapter 8, Marcel Dekker, **1993**.
[34] Data Collection Software for Nonius KappaCCD devices, Delft, The Netherlands, **2000**.
[35] Z. Otwinowski, W. Minor, *Methods Enzymol.* **1997**, *276*, 307−326.
[36] A. Altomare, G. Cascarano, C. Giacovazzo, A. Guagliardi, M. C Burla, G. Polidori, M. Camalli, *SIR92, J. Appl. Cryst.* **1994**, *27*, 435−436.
[37] G. M. Sheldrick, *SHELXL-97*, University of Göttingen, Göttingen, Germany, **1998**.
[38] A. J. C. Wilson (Ed.), *International Tables for Crystallography*, Kluwer Academic Publisher, Dordrecht, The Netherlands, **1992**, vol. C, Tables 6.1.1.4 (pp. 500−502), 4.2.6.8 (pp. 219−222), 4.2.4.2 (pp. 193−199).
[39] A. L. Spek, *PLATON A Multipurpose Crystallographic Tool*, Utrecht University, Utrecht, The Netherlands, **2001**.

Received February 18, 2004
Early View Article
Published Online May 25, 2004

 © 2004 Wiley-VCH Verlag GmbH & Co. KGaA, Weinheim

Mechanistic Tuning of Hydrocarbon Oxidations with H_2O_2, Catalyzed by Hexacoordinate Ferrous Complexes

Yasmina Mekmouche,[a] Stéphane Ménage,*[a] Jacques Pécaut,[b] Colette Lebrun,[b] Lee Reilly,[c] Volker Schuenemann,[c] Alfred Trautwein,[c] and Marc Fontecave[a]

Keywords: Iron catalysts / Hydrogen peroxide / Oxidation / Non-heme iron / Monooxygenase

A comparison of the catalytic properties of a series of $Fe^{II}LXY$ complexes on oxidation reactions with H_2O_2, [L = *N*,*N*′-bis(pyridin-2-yl-methyl)-*N*,*N*′-bis(3,4,5-trimethoxybenzyl)-ethane-1,2-diamine] indicates that the lability of the X and Y ligands (Cl^- or CH_3CN) determines the nature of the oxidation pathway. The absence of a labile site in the complex, i.e. when X = Y = Cl^-, causes the reaction to proceed via a Fenton pathway (generation of hydroxyl radicals, exclusively). The presence of two labile CH_3CN ligands (X = Y = CH_3CN) allows the catalysis to proceed through a metal-based mechanism, whereas in the case of a complex with only one labile ligand (X = Cl^- and Y = CH_3CN), the reaction is less controlled by the metal. We wish to emphasize that the cleavage of the O–O bond in the Fe–OOH moeity, a key intermediate in the reaction, is different in the last two cases.

(© Wiley-VCH Verlag GmbH & Co. KGaA, 69451 Weinheim, Germany, 2004)

Introduction

Synthetic non-heme ferrous complexes have been extensively studied due to their ability to mimic some structural and functional properties of non-heme iron monooxygenases or oxygen activating enzymes.[1] Some of the ligands used, mainly polydentate nitrogen-based, are shown in Scheme 1. These complexes have been found to be efficient catalysts for alkane oxidation using hydroperoxides or oxygen-donating reagents.[2] Few catalytic systems, however, allow selective oxidation of alkanes to the corresponding alcohol without formation of secondary products.[3] In the case of Fe and Mn porphyrins, such a selective reaction has been attributed to the involvement of a metal-oxo intermediate as the active species for the hydroxylation.[4] The question of the formation and the stabilization of such a species in non-heme systems has been the subject of extensive studies, and recently an Fe^{IV}=O system has been fully characterized.[5] Nevertheless, as soon as hydrogen peroxide is involved in the catalytic reaction as the oxidant, the nature of the reaction pathway is controversial. It usually alternates between a free radical (Fenton chemistry) or a metal based mechanism.[6] The identification of the essential stereoelectronic parameters, which control the reactivity of the active species, is still an important challenge. In particular, we demonstrated the importance of a labile site on the iron complex in order to allow the oxidant to bind, and to be activated.[7] Here, we will show from the reactivity pattern of a series of six-coordinate iron complexes $[Fe^{II}LXY](ClO_4)_n$ (L designating a tetradentate nitrogen based ligand and X, Y a monodentate ligand) that two labile sites are absolutely required for selective catalysis of alkane oxidation. The ligand L has been designed to serve as a substrate for probing the reaction mechanism. Indeed, L contains sites such as the methylene groups and the phenyl rings from benzylic moieties, which are vulnerable to oxidation. The latter are known to be very reactive towards hydroxyl radicals, leading to the formation of phenol.[8] Three hexacoordinate ferrous complexes, containing the tetradentate ligand L, [L = *N*,*N*′-bis(pyridin-2-yl-methyl)-*N*,*N*′-bis(3,4,5-trimethoxybenzyl)ethane-1,2-diamine],[8] the two remaining coordination sites being occupied either by a solvent molecule (known to be a labile ligand) or a chloride anion (known to be less exchangeable), have also been synthesized and fully characterized (Scheme 1).

The structure and catalytic properties of $FeLCl_2$ (**1**) and $FeL(CH_3CN)_2(ClO_4)_2$ (**2**) have been partly described previously.[9] In this paper they are compared, in more detail, with the structural, spectroscopic, and catalytic properties of a third new complex $FeLCl(CH_3CN)(ClO_4)$ (**3**), containing only one labile site. This complex completes the series.

[a] Laboratoire de Chimie et Biochimie des Centres Rédox Biologiques, Université Joseph Fourier/DRDC/CEA, UMR CNRS 5047,
17 rue des Martyrs, 38054 Grenoble Cédex 9, France
[b] Service de Chimie Inorganique et Biologique, DRFMC CEA-Grenoble, France
[c] Institut für Physik Medizinische Universität, Ratzeburger Allee 160, 23538 Lübeck, Germany
Supporting information for this article is available on the WWW under http://www.eurjic.org or from the author.

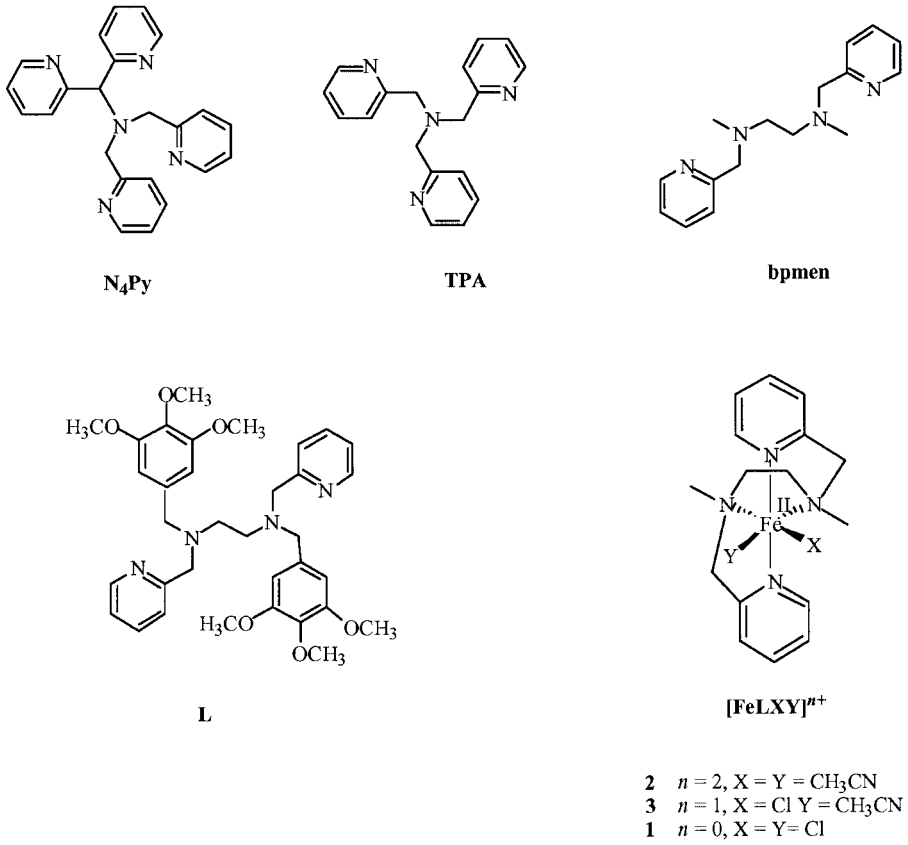

Scheme 1. Ligand used in this study, numbering scheme for the corresponding complexes, and related ligands discussed

Results

Syntheses of Complexes

The syntheses of complexes **1** and **2** are straightforward. Solid products were obtained by simply mixing equimolar amounts of ligand L and $FeCl_2{\cdot}4H_2O$ or $Fe(ClO_4)_2{\cdot}4H_2O$, respectively, in methanol under an inert atmosphere and at room temperature.[9] Complex **3** was synthesized via a two step procedure. When stoichiometric amounts of complexes **1** and **2** were mixed together in CH_2Cl_2 or $CHCl_3$ under argon, a light yellow microcrystalline powder was obtained. The reaction was quantitative, and the complex formed was identified, based on ESI/MS (see Exp. Sect.), as a dinuclear ferrous complex $[Fe_2L_2Cl_2](ClO_4)_2$. When the dinuclear complex was dissolved in acetonitrile it dissociated quantitatively into two identical $FeL(Cl)(CH_3CN)(ClO_4)$ units, i.e. complex **3**, which crystallizes in quantitative yield upon diffusion of ether into the mother liquor.

X-ray Structures of Complexes 1, 2, and 3

The structure of the cation present in the three complexes is represented in Figure 1. The Fe^{II} ion is in a pseudo-octahedral environment with the tetradentate ligand L wrapped around the metal ion. The two remaining coordination sites are filled by two chloride ions for **1**, two acetonitrile molecules for **2**, and one chloride and one acetonitrile for **3**. The topology consists of a *cis* α configuration for the monodentate ligands in each complex. Each one is *trans* with respect to one amine nitrogen atom and the pyridine ligands are *trans* to each other.

The Fe−ligand distances decrease as the number of CH_3CN ligands increases, reflecting the increase in ligand field strength in the following order: **1** < **3** < **2**. Accordingly, the shorter Fe−N distances (1.942−2.060 Å) are found in **2**, consistent with a low-spin configuration for its ferrous ion in the crystalline state, whereas the Fe−N distances (2.212−2.3272 Å) in **1** are longer than in **3** (2.1708−2.2787 Å), a range of distances is in agreement with a high-spin configuration for the ferrous ion in both complexes (see Table 1). Moreover, the $Fe-NCCH_3$ distance is longer in complex **3** [2.1730(8) Å] than in complex **2** [1.942(4) Å], and the Fe−Cl distance is shorter in complex **3** than in complex **1** [2.3383(3) compared with 2.4080(2)−2.4260(2) Å].

The presence of chloride anions is responsible for a distortion from the ideal octahedral geometry as shown by the more acute $N_{pyridine}-Fe-N_{pyridine}$ and $N_{amine}-Fe-N_{amine}$ angles in **1** and **3** compared with those in complex **2**. Accordingly, the presence of two Cl^- ions in a *cis* geometry leads to a larger X−Fe−Y angle [102.274(8) in **1** compared with 96.6(2) in the case of complex **3**].

The structural parameters of the $[Fe^{II}LXY]$ series are similar to those of the previously described $Fe(N_2Py_2)$ family represented, for example, by $[Fe(bpmen)(CH_3CN)_2]^{2+}$ or $(LBzl_2)FeCl_2$ [bpmen = *N*,*N*′-dimethyl-*N*,*N*′-bis(2-pyridyl-

 © 2004 Wiley-VCH Verlag GmbH & Co. KGaA, Weinheim

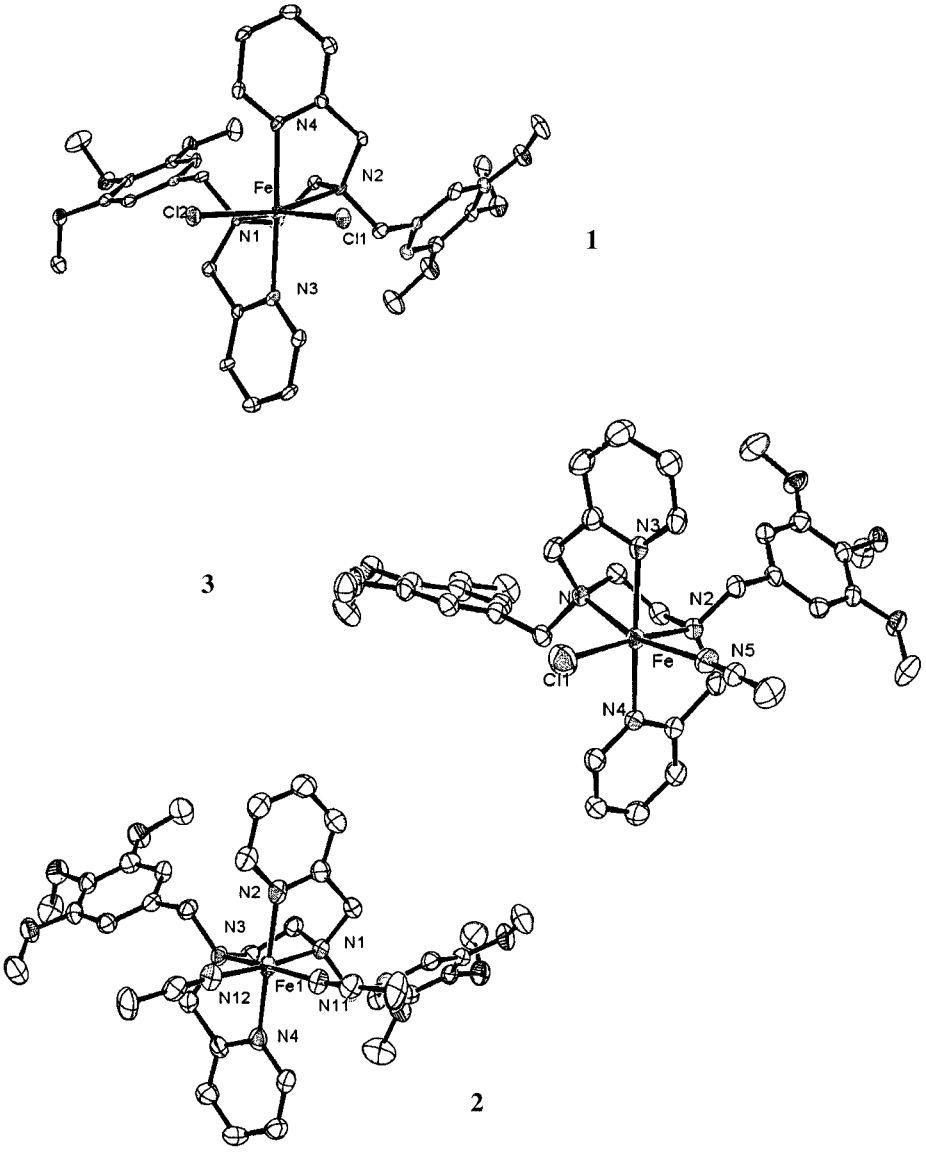

Figure 1. ORTEP representation of the cations of complexes **1**−**3**; all hydrogen atoms have been omitted for clarity

methyl)ethylene-1,2-diamine (Scheme 1), and $LBzl_2$ = *N*,*N*′-dibenzyl-*N*,*N*′-bis(2-pyridylmethyl)ethylene-1,2-diamine].[3b,10]

Spectroscopic Characterization of Complexes 1−3

Solid-state (powder) Mössbauer spectroscopy (77 K) showed a doublet with comparable isomer shifts at about $\delta = 1.1$ mm·s^{-1} for each of the complexes, in accordance with a high spin state for the ferrous ions. Significantly different quadrupole splitting values ΔE_q were observed, however (Table 2).[11] The highest ΔE_q value was found for **3**, in agreement with the lower degree of symmetry resulting from two different monodentate ligands in the iron coordination sphere (see Table 2). It has to be noted that in the solid-state, the spin state of complex **2** differs from that in the crystal, revealing the importance of the packing in the crystal, and suggesting the involvement of a network of hydrogen bonds between the anions. This behavior is characteristic of related spin crossover systems.[12]

The complexes retained their structure in solution as they remained all monomeric in acetonitrile solution as indicated by their ESI/MS spectrum (Table 2). The UV/Visible spectra of acetonitrile solutions exhibit only one intense band in each case at around 400 nm, attributable to a MLCT band from Fe^{II} "t_{2g}" orbitals to π* orbitals of the pyridine ligands. Interestingly, it has been previously shown that the value of the extinction coefficient can be correlated with the ligand field strength.[13] The trend observed here, confirmed the order of the series found in the solid state.

 © 2004 Wiley-VCH Verlag GmbH & Co. KGaA, Weinheim

Table 1. X-ray structural parameters (bond lengths and angles) for FeL(XY) complexes with X and Y = Cl and/or CH_3CN

Bond lengths (Å)	**1**	**3**	**2**
Fe−Cl	2.4260(2) 2.4080(2)	2.3383(3)	
Fe−$NCCH_3$		2.1730(8)	1.942(4) 1.945(4)
Fe−N_{amine}	2.3272(7) 2.3012(6)	2.2475(7) [N1] 2.2787(7)[N2]	2.056(3) 2.060(3)
Fe−$N_{pyridine}$	2.2120(2) 2.2228(6)	2.1708(8) 2.1717(8)	1.982(4) 1.990(4)
Angles (°)			
Cl−Fe−Cl	102.274(8)		
Cl−Fe−$N_{nitrile}$		96.6(2)	
$N_{nitrile}$−Fe−$N_{nitrile}$			91.50(15)
N_{amine}−Fe−N_{amine}	78.07(2)	80.50(2)	86.11(13)
$N_{pyridine}$−Fe−$N_{pyridine}$	169.67(2)	168.69(3)	178.39(15)
$N_{nitrile}$−Fe−$N_{pyridine}$		93.57(3)	94.85(16) 85.41(15)
N_{amine}−Fe−$N_{pyridine}$	75.17(8) 96.70(2)	75.77(3) 96.32(3)	81.04(15) 98.23(14)
$N_{nitrile}$−Fe−N_{amine}		174.94(19)	91.36(14) 175.17(14)
Cl−Fe−N_{amine}	90.40(2) 161.82(2)	95.43(18)	

The three complexes were also characterized by ^{1}H NMR spectroscopy at room temperature in CD_3CN solutions (Figure 2). The spectra show proton resonances between −20 and 140 ppm, a range typical for high spin ferrous (S = 2) complexes. A comparison of ^{1}H NMR spectra showed that the three complexes have different structures in solution. Proton assignments have been carried out from a comparison with related complexes, integrations, and T_1 values (see Table 3).[14] The pyridyl resonances are subject to large isotropic shifts in the following order α > β> γ based on the fact that the paramagnetic contact shifts are governed by σ-delocalization effects, so that the shifts increase with closer proximity to the ferrous ion.[15]

Thus, the α-pyridyl protons were assigned to the resonance at lower field, i.e. above δ = 130 ppm. Moreover, the β-pyridyl proton resonances, easily recognizable as they are usually assigned to two close sharp resonances at around δ = 50 ppm, shifted from 59/53 (β/β′) ppm for complex **1** to 52/44 and 48/40 ppm for complexes **3** and **2**, respectively.[14] Finally, the γ-H resonances were observed at δ = 21 ppm for **1**, and were found upfield for **2** and **3** at δ = 10 ppm and −8 ppm, respectively. The methylene CH_2 resonances can be assigned to the broader resonances spread throughout the spectra (see for example spectrum 2 in Figure 2). The number of these resonances signify the distinction between the two protons of the methylene moieties, a fact which is related to their position with regard to the metal ion. The methylene protons of CH_2−Pyr were tentatively attributed to the broad resonances in the 120−40 ppm region by comparison with the TPA complexes.[14] The methylene protons of the diamino and benzyl moieties of the ligand were less shifted, and were sensitive to the nature of the monodentate ligand set trans to the aliphatic amine.

We have tentatively attributed the upfield shift of the α,β,γ− pyridyl protons and the methylene protons in complex **2** to a lower paramagnetism compared with in **1** and **3**. It should be noted that the resonances of the protons of the trimethoxyphenyl moieties could not be assigned due to the presence of several overlapping peaks in the diamagnetic region of the spectra.

Remarkably, the spectra of **2** and **3** display broader resonances, suggesting ligand exchange in solution. This was confirmed when the NMR spectra were recorded in a non-coordinating solvent, i.e. CD_2Cl_2. Only the spectra of complexes **2** and **3** were different in terms of isomeric shifts and the broadness of the peaks. This is in agreement with the solvent ligand (CH_3CN) being more labile than the coordinated chloride. Conversely, this confirms that the chloride anions in complexes **1** and **3** remain iron-bound in acetonitrile solution, and that solutions of **3** do not contain a mixture of **1** and **2**.

Finally, Table 2 also shows that, as expected, the three complexes have different Fe^{III}/Fe^{II} potentials in acetonitrile. The cyclic voltammograms in CH_3CN/TBAP 0.1 M display one quasi-reversible process (ΔE = 100 mV) for **1** and **2**, whereas two systems of waves were observed on the reverse scan in the case of **3**. The presence of these two reduction peaks was attributed to an EC process, which has been assigned to the minor formation of $[FeLCl_2]^+$ (less than 10%) during the one-electron oxidation process of **3**. Accordingly, the location of the reducing wave of this minor electroactive

Table 2. Physical properties of FeL(XY) complexes with X and Y = Cl and/or CH_3CN

Complex	**1**	**3**	**2**
$\lambda_{max.}$ (ε [$M \cdot cm^{-1}$])	415 nm (1050)	373 nm (1350)	370 nm (1700)
E_{pa} [V/NHE]	0.560	1.12	1.43
E_{pc} [V/NHE]	0.430	0.930; 0.520[a]	1.33
δ [$mm \cdot s^{-1}$] [b]	1.14	1.12	1.15
δ [$mm \cdot s^{-1}$]	3.05	3.24	2.81
ESI/MS fragment	m/z = 693 ($[FeLCl]^+$)	m/z = 693 ($[FeLCl]^+$)	m/z = 757 ($[FeL(ClO_4)]^+$)

[a] Minor wave (less than 10% in intensity compared to the one at 0.930 V). [b] Referenced to α-Fe at 300 K.

 © 2004 Wiley-VCH Verlag GmbH & Co. KGaA, Weinheim

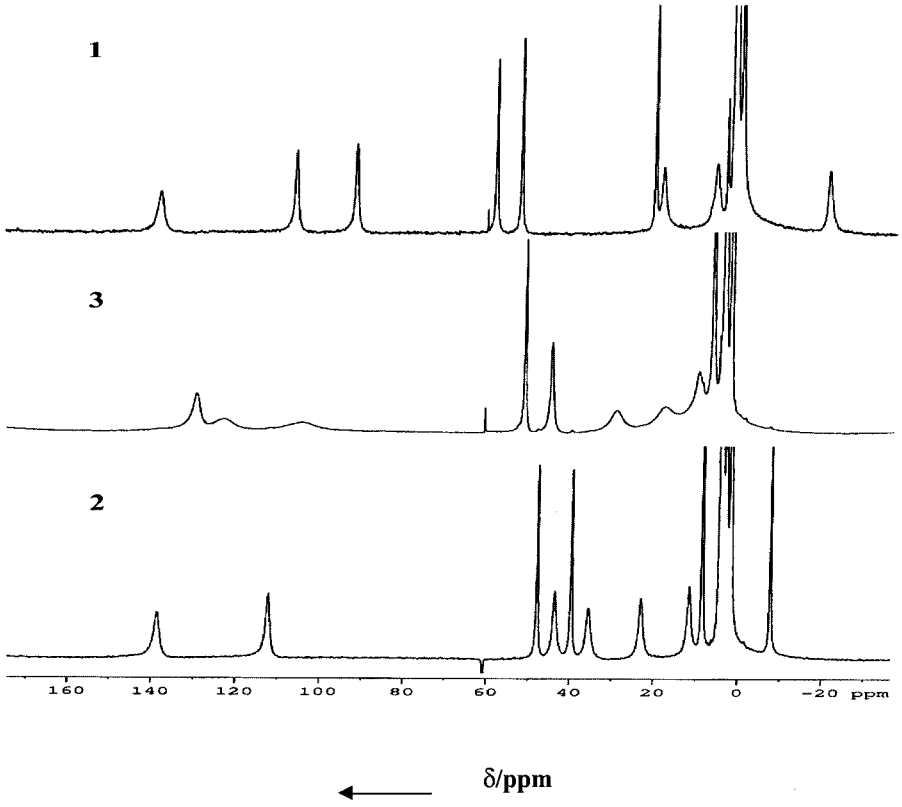

Figure 2. ^{1}H NMR spectra of complexes **1**−**3** in CD_3CN at room temperature

Table 3. ^{1}H NMR spectroscopic data for complexes **1**−**3**

Complex assignment	**1**	**3**	**2**
α-*H*pyr	140	131	138
β,β′-*H*pyr	59; 52	52; 44	48; 39.7
γ-*H*pyr	20.7	10(br)	−8
C*H*$_2$−Pyr	107; 92.7	123; 114	112;43.5
C*H*$_2$−Bz or	19; 6.5	18; 9	35.5; 23
C*H*$_2$-diamine	0.3; −21	4; 3	11.5; 3.2

species was observed close to that observed for **1**. As expected, the easier system to oxidize is **1**, followed by **3** then **2**. The presence of chloride anions in the coordination sphere implicates a decrease in oxidation potential of about 500 mV per anion.

To conclude, the three complexes have different structures in solution. We have thus obtained and fully characterized a series of complexes containing the same tetradentate ligand, and various combinations of chloride and acetonitrile ligands. These complexes can be used to study the effect of the nature of monodentate ligands and the number of labile sites on their ability to catalyze alkane oxidations. It should be noted that they retain their structures during redox processes. These results are presented in the next section.

Ligand Oxidation − A Probe for Hydroxyl Radical Generation

The reaction of complex **1** with hydrogen peroxide in the absence of an external substrate led to the formation of a new chromophore.[9] This chromophore has been characterized as a phenolato complex $[Fe^{III}LOCl]^+$, and resulted from hydroxylation, at the *ortho* position, of one phenyl moiety of the ligand L (Scheme 2). No such species could be observed during reaction of complex **2** with H_2O_2 under the same conditions. On the other hand, in the presence of 10 equivalents of H_2O_2 in acetonitrile, complex **3** was partly converted into this chromophore as shown by ESI-MS with a molecular ion peak at m/z = 708. When $H_2{}^{18}O_2$ was used, only one peak at m/z = 710, corresponding to the $[Fe^{III}(L^{18}O)Cl]^+$ fragment, was present. This signifies that the inserted oxygen came exclusively from the oxidant.

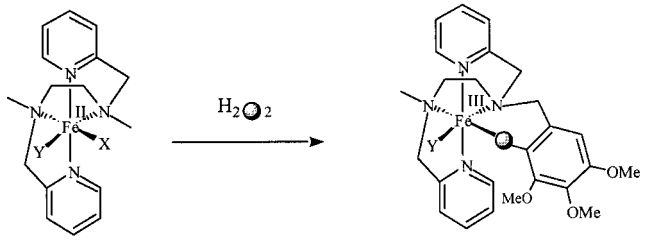

Scheme 2. Chemical transformation of ferrous complexes **1** and **3** using hydrogen peroxide

 © 2004 Wiley-VCH Verlag GmbH & Co. KGaA, Weinheim

However, the yield of ligand hydroxylation was found to be much lower than in the case of **1**. Ligand extraction from the mother liquor confirmed the ligand oxidation, and quantitative analysis showed that the oxidized ligand LOH was preferentially formed with complex **1** (yield = 60%), in contrast to the result with complex **3** (15%) (see Table 4). With all complexes, minor formation of ligand L1, *N*,*N*′-bis(pyridin-2-ylmethyl)-*N*-(3,4,5-trimethoxybenzyl)ethane-1,2-diamine, was detected (<15%).[9] L1 results from an *N*-dealkylation of the ligand L following hydroxylation at one of the benzylic positions.

Table 4. Comparison of the oxidizing properties of complex **1**, **2**, and **3** (experimental conditions: CH_3CN, room temp., Ar; [complex] = 1 mM; [complex]/substrate/H_2O_2, 1:100:10

Complex	**1**	**3**	**2**
Ligand L oxidation[a]			
L (%)	6	60	60
L−OH (%)	70	15	0
L1 (%)	7	14	14
Cyclohexane			
cyclohexanol (% yield[b])	3	7	23
cyclohexanone	1	3	2.5
ol/one [c]	3	2	9.2
cis-DMC			
cis-OH (%[b])	4	7	20
trans-OH	2.5	3	3
% RC[d]	20	40	74
Cyclooctene			
epoxide (%[b])	0	6	31
Cyclohexene			
epoxide (%[b])	0	7	5
2-cyclohexene-1-ol	2	24	9
2-cyclohexene-1-one	0	6	1

[a] Only the three major products analyzed by HPLC have been reported. [b] Yield based on the oxidant. [c] ol/one corresponds to the ratio of cyclohexanol over cyclohexanone. [d] % RC = 100 × (*cis*-OH-*trans*-OH)/(*cis*-OH + *trans*-OH) with an error estimated to be ± 5%; *cis*-OH = (1*R*,2*R*- or 1*S*,2*S*)-1,2-dimethylcyclohexanol. *trans*-OH = (1*R*,2*S*- or 1*S*,2*R*)-1,2-dimethylcyclohexanol.

OH radicals are excellent agents for aromatic hydroxylation.[6] Thus the formation of LOH from the oxidation of L by H_2O_2 was used here as a probe for the presence of $OH^{\cdot}$ radicals derived from H_2O_2. Our results thus show a dramatic difference between **2**, on the one hand, and **1** and **3**, on the other hand, in terms of generation of $OH^{\cdot}$ radicals. Only complex **2** was unable to convert H_2O_2 into $OH^{\cdot}$. It is also important to note that in the case of **3**, LOH is a minor product whereas in the case of **1**, L is extensively converted into LOH, indicating a more significant involvement of $OH^{\cdot}$ radicals in reactions catalyzed by **1**. This is supported by the observations reported below.

Hydrocarbon Oxidation

In a typical reaction, 2 μmol of complex $[FeLXY](ClO_4)_n$ [n = 0 for complex **1**, 1 for **3** and 2 for **2**] in acetonitrile (final volume = 2 mL) was treated with 20 μmol of H_2O_2 (10 equiv.) in the presence of 1100 equiv. of the alkane in acetonitrile at room temperature under argon. All the reactions were complete after 10 minutes by which time the oxidant was completely consumed. No oxidation occurred in the absence of the iron complex. Complex **2** was found to be the most active catalyst during oxidation of cyclohexane with a 30% total yield based on the oxidant, followed by complex **3** (13%), and **1** (4%). The same pattern was observed when the selectivity of the hydroxylation was considered with an alcohol/ketone ratio above 9 for complex **2** (Table 4), whereas much less selectivity was observed with complexes **3** and **1**.

Furthermore, only complex **2** could catalyze stereoselective hydroxylations (Table 4). For example, oxidation of *cis*-1,2-dimethylcyclohexane gave *cis*-1,2-dimethylcyclohexanol (1*R*,2*R* or 1*S*,2*S*) as the major product (%RC over 70%) showing that hydroxylation proceeds preferentially with retention of configuration at C-1, thus excluding a pure radical mechanism. Much less stereoselectivity was observed with complexes **3** and **1** (%RC = 40% and 20%, respectively).

Ligand hydroxylation and alkane oxidation reactions clearly make it possible, therefore, to distinguish **2** from **1** and **3**, but not **1** from **3**. In contrast, alkene epoxidation, as discussed below, provides a convenient reaction probe to make this distinction. Indeed, whereas epoxides are formed during oxidation of cyclohexene and cyclooctene by H_2O_2 in the presence of **2** and **3**, no epoxide could be detected with complex **1** as the catalyst. In the latter case, only very little allylic alcohol could be detected with cyclohexene as the substrate. Here, epoxidation is used as a probe for the involvement of metal-oxo intermediate active species.[16] Thus, these results suggest the presence of such species in reactions catalyzed by **2** or **3**, but not in reactions catalyzed by **1**. The involvement of a $[Fe{=}O]^{n+}$ species is further supported by the observation of ^{18}O labeled cyclohexanol during cyclohexane oxidation by H_2O_2 in the presence of 1000 equivalents of $H_2{}^{18}O$ (complex **2**: 47%, complex **3**: 5%). This is due to the ability of (per)ferryl complexes to exchange O atoms with H_2O.[17] The presence of products labeled with O atoms from both water and the oxidant has already been observed in oxidations dependent on non-heme iron complexes.[18]

Evidence for Iron-Hydroperoxo Complexes During the Reaction

Iron hydroperoxo complexes have been extensively studied during the last decade.[1,19,20] They are usually characterized by a LMCT band in the visible region, from which a resonance Raman spectrum dominated by O−O and Fe−O vibrations may be observed.[21] Using a previously described methodology,[22] which consists of low temperature mixing of the oxidant and the catalyst, we were able to detect such an Fe−OOH species by ESI-MS in some cases. Firstly, fast mixing of complex **3** with 10 equivalents of H_2O_2 resulted in the detection of a new peak at m/z = 726, which we assigned to the $[FeLOOHCl]^+$ fragment, with excellent agreement between its observed and theoretical isotopic patterns (see Supporting Information S1). The assign-

 © 2004 Wiley-VCH Verlag GmbH & Co. KGaA, Weinheim

ment was confirmed, during an MS/MS experiment, by the loss of a fragment of $m/z = 33$ corresponding to the OOH fragment. A corresponding shift of +4 in the parent peak was observed when $H_2{}^{18}O_2$ was used. In contrast, with complex **1**, no Fe−OO(H) could be detected, whereas with complex **2** different fragments were observed at $m/z = 790$ and 345.5. These were assigned to $[FeLOOHClO_4]^+$ and $[FeLOOH]^{2+}$, respectively (Supporting Information S2). The fact that this fragment was absent in the mass spectrum of **3**/H_2O_2 indicates that complex **2** was not a contaminant in solutions of complex **3**.

The presence of a hydroperoxo ferric complex $[X-Fe^{III}-OOH]^{n+}$ in the case of **2** and **3** but not **1**, strongly suggests a distinct reaction pathways in systems dependent on **1** and **3**.

Discussion

Using a variety of reaction probes we have clearly demonstrated that the three complexes under study have very different catalytic properties during oxidation by hydrogen peroxide, even though they contain the same tetradentate nitrogen-based ligand L.

In the case of complex **1**, the extensive conversion of L to LOH by aromatic hydroxylation, the low alcohol/ketone ratio, the low stereoselectivity during alkane oxidation, and the lack of epoxide formation during alkene oxidation suggest that freely diffusing hydroxyl radicals are the active species.[23]

In contrast, in the case of complex **2**, the lack of LOH formation, the high alcohol/ketone ratio, the large stereoselectivity, the fact that oxygens from exogenous water molecules are incorporated into the products, and its ability to epoxidize alkenes are in agreement with a selective metal-based mechanism.

Complex **3** displays some of the properties of complex **1** (formation of LOH, low stereoselectivity), and some of those of complex **2** (epoxidation, formation of an Fe-hydroperoxo complex, and cyclohexanol labeling with $H_2{}^{18}O$). This, then, suggests a third type of mechanism involving both [Fe=O] and OH radical species.

What differentiates complexes **1**−**3** from each other is the number of labile coordination sites. We have shown that in solution, Cl^- ligands are not exchangeable with the solvent even when the iron center is in the ferrous state. In contrast CH_3CN ligands are exchangeable. As a consequence, complex **1** has no exchangeable ligand, complex **3** has one, and complex **2** has two. We thus propose that the number of labile coordination sites defines the type of reaction mechanism, namely the type of active species responsible for substrate activation and oxygen atom insertion (Scheme 3).

In the case of complex **1**, H_2O_2 cannot bind to iron, in agreement with the fact that no Fe−OOH species could be detected. This iron reacts with H_2O_2 via an outer sphere one-electron redox process generating OH radicals with good aromatic hydroxylation and poor epoxidation power. In the case of complex **2**, H_2O_2 can bind to iron to form an intermediate Fe−OOH complex, as shown by ESI-MS. It is proposed that the latter proceeds by heterolytic O−O cleavage to generate an active $[Fe^V=O]$ species, allowing a more selective metal-based oxo transfer process.

In the case of complex **3**, with a single exchangeable coordination site, H_2O_2 can also bind to iron. Indeed an Fe−OOH complex has also been detected in this case by ESI-MS. It can be proposed, however, that the latter proceeds by homolytic (and not heterolytic) cleavage of the O−O bond thus generating both $[Fe^{IV}=O]$ and $OH^{\cdot}$ species, in agreement with the properties of the oxidation reaction catalyzed by **3**.

The question thus arises, whether the rather drastic difference between **2** and **3** results only from the difference in terms of labile sites or for an additional reason. Studies by L. Que Jr. and co-workers have shown the importance of the presence of two labile sites for promoting heterolytic cleavage.[18] In particular, the possibility for the terminal oxygen of the Fe−OOH species to interact with iron via binding to the second site provides a major driving force for the heterolytic cleavage of the O−O bond. A second possibility comes from the binding of a molecule of H_2O to the second site, which can thus promote O−O heterolytic cleavage by donating a proton.

In the case of complex **3**, a Cl−Fe−OOH species is formed, and there is no such driving force for heterolytic cleavage because of the presence of a non-exchangeable Cl ligand. As a consequence, only a homolytic cleavage takes place. We have thus shown here, from a detailed comparison of **2** and **3**, that the number of labile sites has a great impact on the outcome of the oxidation reactions involving Fe−OOH intermediates. Previous studies by Que Jr. and Feringa and co-workers have raised a similar issue. They did it on the basis of the comparison of $[Fe(TPA)(CH_3CN)_2]^{2+}$ complexes with diverse ligand sub-

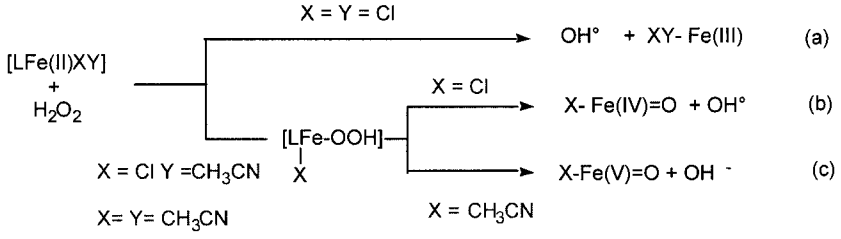

Scheme 3. The three reaction pathways for iron/H_2O_2 systems as a function of the ligands X and Y

 © 2004 Wiley-VCH Verlag GmbH & Co. KGaA, Weinheim

stitutions − which are catalysts of oxidation reactions proceeding by metal-based mechanisms −, with the $[Fe(N4py)(CH_3CN)]^{2+}$ complex, in which N4py is a pentadentate ligand related to TPA (Scheme 1).[18,24] The latter has only one exchangeable site, and is not able to catalyze the epoxidation of alkenes by H_2O_2.

On the other hand, it should be recalled that in the case of reactions of Fe-porphyrins with *m*-chloroperbenzoic acid (*m*CPBA), cleavage of the O−O bond within the intermediate Fe−OOC(O)R complex is dependent on the nature of the axial ligand trans to the acylperoxo ligand.[25] The cleavage is homolytic when this ligand is Cl^-, and heterolytic with less electron donating anions such as ClO_4^-. In the case of **2** and **3**, we might also consider that, rather than the exchangeability of the sites, it is the electronic properties of the ligands (Cl^- vs. CH_3CN) which influence the cleavage of the O−O bond of the X−Fe−OOH species. Further experiments are needed to better establish the importance of such electronic effects in these catalysts.

Conclusion

The structural parameters required for efficient iron catalysts for selective oxidations using hydrogen peroxide as the oxidant have been elucidated. The presence of neutral nitrogen ligands (allowing a high Lewis acidity for the metal for H_2O_2 activation), and the presence of two labile sites (to favor the heterolytic cleavage of the O−O bond) are required for selective and efficient catalysis of alkane hydroxylation. The control of the O−O bond cleavage by anions needs to be better understood, and the charge on the X ligand is probably an important parameter to consider. So far, complex **2** represents one of the more efficient catalyst in its category.

Experimental Section

General: Most of the reagents were of the best commercial grade, and were used without further purification. The synthesis of ligand L has been described previously.[8]

Synthesis of Complex 1: In a glove box, $FeCl_2{\cdot}4H_2O$ (150 μmol) was added to a methanolic solution (8 mL) of ligand L (150 μmol). The solution rapidly turned yellow, and was stirred for two hours under an inert atmosphere at room temperature. The resultant powder was filtered, and washed with diethyl ether. Crystals suitable for X-ray crystallography were obtained by diffusion of diethyl ether into an acetonitrile solution of complex **1**. The powder was found to be stable under aerobic conditions.

Synthesis of Complex 2: In a glove box, $Fe(ClO4)_2{\cdot}4H_2O$ (150 μmol) was added to a methanolic solution (8 mL) of ligand L (150 μmol). The solution was stirred until complete precipitation of a pale yellow powder. After filtration, the powder was washed twice with diethyl ether. Purple crystals of complex **2** were obtained from diffusion of diethyl ether into an acetonitrile solution but the crystals were unsuitable for X-ray crystallography. X-ray quality crystals for **2** were obtained after a metathesis of ClO_4 for PF_6 anions. The powder was found to be less stable in air than complex **1**.

Synthesis of Complex 3: Complex **2** (32 mg, 36 μmol) was added to a $CHCl_3$ or CH_2Cl_2 solution of complex **1** (27 mg, 36 μmol) under an Ar atmosphere, and stirred for 1 h. A light yellow powder progressively appeared (yield >90%). The solid was washed with diethyl ether, and analyzed by ESI-MS and ^{1}H NMR spectroscopy. The spectroscopic data are consistent with the description of the complex as a dinuclear compound $[Fe_2L_2Cl_2(ClO_4)_2]$. The presence of two chloro bridges led, in this case, to a small ferromagnetic coupling as indicated by a CH_2Cl_2 X-band EPR (parallel mode) signal (g = 16, T = 4 K). This is a characteristic signature for an integral spin ground state (data not shown).[26] This was also corroborated by the larger range for the proton resonances observed by ^{1}H NMR spectroscopy in the dinuclear complex, compared with those in complexes **1** and **2** (for example, the α-H resonance of the bound pyridine moieties was observed at δ = 180 ppm, whereas it was found at around δ = 140 ppm in **1** and **2**). Solid-state Mössbauer parameters are in agreement with the high-spin configuration of the two identical ferrous atoms of the dinuclear unit (δ = 1.10 mm·s^{-1} and δ = 1.28 mm·s^{-1}). ESI-MS: m/z = 1485 (50%), $[Fe_2L_2Cl_2ClO_4]^+$: m/z = 1421 (100%) $[Fe_2L_2Cl_3]^+$. ^{1}H NMR (CD_2Cl_2): δ = 180.2 (α-H py); 49.0, 46.5 (β-H py). 155.1, 50.3 (CH_2-py). 31.0, 24.7(CH_2−Et). 70.0, 51.0 [(CH_2−Bz), 10.2 (Ar−O−*Me*), 11.4 (*p*-*H*-Benzyl), −7.2 (γ-*H*-py) ppm.
To obtain complex **3**, the yellow powder was dissolved in acetonitrile, and crystals were grown by diffusion of ether into this acetonitrile solution.

Crystallographic Studies: Data collection and analyses of complexes **1**-**3** were conducted on a Bruker SMART CCD system at the crystallography service of the SCIB laboratory (CEA-Grenoble). Experimental conditions for complex **3**: **3**·0.5$(C_2H_5)_2O$·0.5H_2O ($C_{38}H_{51}Cl_2FeN_5O_{11}$): M = 880.59 g mol^{-1}, yellow plate, triclinic, collection temperature 223 K, space group $P\bar{1}$, a = 10.9451(7) Å, b = 13.3551(8) Å, c = 15.746 (1) Å, α = 94.719 (1)°, β = 105.831(1)°, γ = 97.859(1)°, V = 2176.5(2) Å^3, Z = 2, $R1$ = 0.0515 [I = 2σ(I)]. Pertinent crystallographic data are reported in Table 1, full data can be obtained from the Cambridge Crystallographic Data Centre. The structures were solved by direct methods using the SHELXTL 5.03 software package. All non-hydrogen atoms were refined anisotropically. Hydrogen atoms were placed in ideal positions, and refined as riding atoms with individual (or group) isotropic displacements. CCDC-146454, -146455, and -226070 contain the supplementary crystallographic data for **1**, **2**, and **3**, respectively. These data can be obtained free of charge at www.ccdc.cam.ac.uk/conts/retrieving.html [or from the Cambridge Crystallographic Data Centre, 12 Union Road, Cambridge CB2 1EZ, UK; Fax: (internat.) +44-1223-336-033; E-mail: deposit@ccdc.cam.ac.uk].

Physical Studies: 300-MHz ^{1}H-NMR spectra were recorded on a DPX300 Bruker spectrometer, and the shifts referred to the residual solvent peak. Visible absorption spectra were recorded on Varian Cary1Bio and HP 8453 diode array spectrophotometers. Gas chromatography (GC) was performed on a Perkin−Elmer Autosystem instrument with a FID detector, using an SE 30 column coupled to a Perkin−Elmer Turbomass EI spectrometer. Mössbauer spectra were recorded in 400 μL cups containing the complex as a solid with a conventional constant acceleration spectrometer using a ^{57}Co source in a Rh matrix (1.85 Gbq). ESI-MS spectra were obtained on an LCQ ion trap spectrometer. Cyclic voltammetry experiments were performed using a PAR model 273 potentiostat/galvanostat. The working electrode was a platinum disc.

Ligand Extraction and Titration of the Products After Oxidation Reactions: After the completion of the reaction between the com-

 © 2004 Wiley-VCH Verlag GmbH & Co. KGaA, Weinheim

plex and hydrogen peroxide followed by UV/visible spectroscopy the solvent was removed, and water was added until a concentration of 5 mM, based on starting iron concentration, was reached. Excess dithionite was then added, and 5 equivalents of bathophenanthroline were added. The total complexation of iron by the dinitrogen ligand was followed by UV/Visible spectroscopy (ε_{535nm} = 22140 $M^{-1}\cdot cm^{-1}$) and, when complete, the organic products were extracted with dichloromethane. The products were analyzed by ^1H and ^{13}C NMR spectroscopy and ESI-MS. Quantitative analysis of the components of the mixture was performed using HPLC based on the titration curves of pure samples. The total content never reached 100% due to the presence of minor products observed on the HPLC chromatogram.

Oxidation Reactions: In a typical reaction, 10 equivalents of H_2O_2 were added to a 1 mM solution of complex containing 1100 equivalents of cyclohexane (or 600 equiv. of 1,2-dimethylcyclohexane) or alcene in a glove box. The reaction was complete after 15 minutes, and the oxidation products were analyzed by GC/MS chromatography using benzophenone or acetophenone as an internal standard. The products were identified by ESI-MS, and titration curves were performed using pure samples to enable a quantitative analysis of the products.

Supporting Information: ESI/MS spectrum of **2**/H_2O_2 (S1) and ESI/MS spectrum of **3**/H_2O_2 (S2).

Acknowledgments

We thank the Iron-oxygen protein network (ERBFMRXCT980207) of the T. M. R. program of the E.U.

[1] [1a] E. I. Solomon, T. C. Brunold, M. I. Davis, J. N. Kemsley, S.-K. Lee, N. Lehnert, F. Neese, A. J. Skulan, Y.-S. Yang, J. Zhou, *Chem. Rev.* **2000**, *100*, 235. [1b] L. Que Jr., R. Y. N. Ho, *Chem. Rev.* **1996**, *96*, 2607.

[2] [2a] M. Fontecave, S. Ménage, C. Duboc-Toia, *Coord. Chem. Rev.* **1998**, *178*, 1555. [2b] M. Costas, L. Que Jr., *Coord. Chem. Rev.* **2000**, *200*, 517.

[3] [3a] C. Kim, K. Chen, L. Que Jr., *J. Am. Chem. Soc.* **1997**, *119*, 5964. [3b] K. Chen, L. Que Jr., *Chem. Commun.* **1999**, 1375.

[4] I. Schlichting, J. Brerenzen, K. Chu, A. M. Stock, S. A. Maves, D. E. Benson, R. M. Sweet, D. Ringe, G. A. Petsko, S. G. Sligar, *Science* **2000**, *287*, 1615.

[5] J.-U. Rohde, J.-H. In, M. H. Lim, W. W. Brennessel, M. K. Bukowski, A. Stubna, E. Münck, W. Nam, L. Que Jr., *Science* **2003**, *299*, 1037.

[6] [6a] C. Walling, *Acc. Chem. Res.* **1975**, *8*, 125. [6b] P. A. Mc Faul, D. D. M. Wayner, K. U. Ingold, *Acc. Chem. Res.* **1998**, *31*, 159. [6c] D. T. Sawyer, A. Sobkowiak, T. Matsushita, *Acc. Chem. Res.* **1996**, *29*, 409.

[7] S. Ménage, J.-M. Vincent, C. Lambeaux, G. Chottard, A. Grand, M. Fontecave, *Inorg. Chem.* **1993**, *32*, 4766.

[8] S. Ménage, J. B. Galey, J. Dumats, G. Hussler, M. Seité, I. Gautier-Luneau, G. Chottard, M. Fontecave, *J. Am. Chem. Soc.* **1998**, *120*, 1337.

[9] Y. Mekmouche, S. Ménage, C. Toia-Duboc, M. Fontecave, J.-B Galey, C. Lebrun, J. Pécaut, *Angew. Chem. Int. Ed.* **2001**, *40*, 949.

[10] J. Simaan, S. Poussereau, G. Blondin, J.-J. Girerd, D. Defaye, C. Philouze, J. Guilhem, L. Tchertanov, *Inorg. Chim. Acta* **2000**, *299*, 221.

[11] A. X. Trautwein, E. Bill, E. L. Bominaar, H. Winkler, *Struct. Bonding* **1991**, *78*, 1.

[12] H. R. Chang, J. K. McCuster, H. Toftlund, S. R. Wilson, A. X. Trautwein, H. Winkler, D. N. Hendrickson, *J. Am. Chem. Soc.* **1990**, *112*, 6814.

[13] [13a] P. Mialane, A. Nivorojkine, G. Pratviel, L. Azéma, M. Slany, F. Godde, A. Simaan, F. Banse, T. Kargar-Grisel, G. Bouchoux, J. Sainton, O. Horner, J. Guilhem, L. Tchertanova, B. Meunier, J.-J. Girerd, *Inorg. Chem.* **1999**, *38*, 1085. [13b] H. R. Al-Obaidi, K. B. Jensen, J. J. McGarvey, H. Toftlund, B. Jensen, S. E. J. Bell, J. G. Carroll, *Inorg. Chem.* **1996**, *35*, 5055.

[14] Y. Zang, J. Kim, Y. Dong, E. C. Wilkinson, E. H. Appelman, L. Que Jr., *J. Am. Chem. Soc.* **1997**, *119*, 4197.

[15] L.-J. Ming in *Physical Methods in Bioinorganic Chemistry* (Ed. L. Que Jr.), University Science Book, Sausalito, CA, **2000**, chapter 8.

[16] [16a] M. Sono, M. P. Roach, E. D. Coulter, J. H. Dawson, *Chem. Rev.* **1996**, *96*, 2841. [16b] W. Nam, S.-E. Park, I. K. Lim, M. H. Lim, J. Hong, J. Kim, *J. Am. Chem. Soc.* **2003**, *125*, 14674 and references cited therein.

[17] J. Bernadou, B. Meunier, *Chem. Commun.* **1998**, 2167.

[18] K. Chen, L. Que Jr, *J. Am. Chem. Soc.* **2001**, *121*, 6327.

[19] J.-J. Girerd, F. Banse, A. J. Simaan, *Struct. Bonding* **2000**, *97*, 143.

[20] G. Roelfes, V. Vrajmasu, K. Chen, R. Y. N. Ho, J.-U. Rohde, C. Zondervan, R. M. la Crois, E. P. Schudde, M. Lutz, A. L. Spek, R. Hage, B. L. Feringa, E. Münck, L. Que Jr., *Inorg. Chem.* **2003**, *42*, 2639.

[21] [21a] Y. Mekmouche, H. Hummel, R. Y. N. Ho, L. Que Jr., V. Schüenemann, F. Thomas, A. X. Trautwein, C. Lebrun, K. Gorgy, J. C. Leprêtre, M.-N. Collomb, A. Deronzier, M. Fontecave, S. Ménage, *Chem. Eur. J.* **2002**, *8*, 1196. [21b] R. Y. N. Ho, G. Roelfes, B. L. Feringa, L. Que Jr., *J. Am. Chem. Soc.* **1999**, *121*, 264.

[22] J. Kim, Y. Dong, E. Larka, L. Que Jr., *Inorg. Chem.* **1996**, *35*, 2369.

[23] [23a] A. F. Trotman-Dickenson, *Adv. Free Radical Chem.* **1965**, *1*, 1. [23b] G. V. Buxton, C; L. Greenstock, W. P. Helman, A. B. Ross, *J. Phys. Chem. ref. Data* **1988**, *17*, 513. [23c] S. Miyajima, O. Simamura, *Bull. Chem. Soc. Jpn.* **1975**, *48*, 526.

[24] G. Roelfes, M. Lubben, R. Hage, L. Que Jr., B. L. Feringa, *Chem. Eur. J.* **2000**, *6*, 2152.

[25] [25a] W. Nam, M. H. Lim, S.-Y. Oh, J. H. Lee, H. J. Lee, S. K. Woo, C. Kim, W. Shin, *Angew. Chem. Int. Ed.* **2000**, *39*, 2179. [25b] W. Nam, M. H. Lim, S. K. Moon, C. Kim, *J. Am. Chem. Soc.* **2000**, *122*, 10805.

[26] M. P. Hendrich, P. G. Debrunner, *Biophys. J.* **1989**, *56*, 489.

Received December 11, 2003
Early View Article
Published Online June 1, 2004

 © 2004 Wiley-VCH Verlag GmbH & Co. KGaA, Weinheim

An Attempt to Programme the Orientation of Bis(heterocyclic) Azine Heterotopic Sequences around Ag^{I}, Cu^{I} and Zn^{II} Metal Centres

Julien Mathieu,[b] Noureddine Ghermani,[a] Nouzha Bouhmaida,[c] Bernard Fenet,[d] and Alain Marsura*[b]

Keywords: Self-assembly / Self-recognition / Heterocyclic bidentate sequences / Cu^{I}, Ag^{I}, Zn^{II} metal complexes

Four novel bis(heterocyclic) sequences, which incorporate a 2,2′-bipyridine system with the 2,2′-bithiazole, 4,4′-bithiazole, 2,2′-bipyrazine or 4,4′-bipyrimidine units, have been synthesized. In the presence of stoichiometric amounts of Cu^{I}, Ag^{I} or Zn^{II} cations, fully oriented discrete head-to-head (H-H) or head-to-tail (H-T) species have been observed by NMR and X-ray crystallography. The orientation of the ligands in the Ag^{I}, Cu^{I} or Zn^{II} dinuclear complexes during the self-assembly process appears to be under the control of electronic factors relating to the electronic configuration of the different bis(heterocyclic) sequences.

(© Wiley-VCH Verlag GmbH & Co. KGaA, 69451 Weinheim, Germany, 2004)

Introduction

The design and study of double- and triple-stranded helical complexes obtained by self-assembly of two or three ligand strands with metal ions has been the subject of several recent detailed investigations and literature reviews.[1,2] Architectural information is expressed in the matching between the ligand binding sites and the stereochemical preferences of the metal ion.

Of the numerous helical structures already published, the spontaneous formation of double-stranded homodimetallic[2a−2e] or heterodimetallic[2f−2i] helicates has been studied extensively. The formation of helicates depends on the nature of the metal ions and ligands and sometimes on additional factors introduced by appropriate templating.[3] Some years ago, a first event was observed in the case of Ga^{III} and Ti^{V} aminophenolate/catecholate complexes where the phenolic protons were abstracted allowing the formation of the corresponding dinuclear oriented triple-stranded helicates.[4] The selectivity of these assemblies in discriminating between a nitrogen (amine) and an oxygen (hydroxy) atom of a biphenylene structure was obviously influenced by the difference of reactivity between the two coordinating centres.

Recently, we described another kind of strongly induced selectivity in the case of a Cu^{I} double-stranded head-to-tail (H-T) spontaneous assembly obtained from a bipyridine-bipyrazine sequence.[5] In that case, the final complex was formed solely by the coordination of Cu^{I} to the imino nitrogen lone pairs of the heterocycles without the need for external hindered factors or other stereochemical requirements. Additionally, we have reported ab initio theoretical calculations dealing with the probable origin of the observed selectivity.[6] According to the stereochemistry found in the helicate, an electron back-donating effect was found to be responsible for the better stability of the heterotopic complexes (bipyridine−Cu−bipyrazine) compared to the homotopic ones[6] This feature clearly suggests that the aromatic nature of the heterocycles themselves could play a decisive role on orientation within the final helicate.

In order to verify the generality of this assumption for other ligands, we have prepared four novel bis(heterocyclic) heterotopic saturated sequences, which incorporate a 2,2′-bipyridine nucleus together with a 2,2′-bithiazole, 4,4′-bithiazole, 2,2′-bipyrazine or 4,4′-bipyrimidine bis(heterocyclic) unit. The formation of the corresponding Ag^{I}, Zn^{II}

[a] Laboratoire de Physique Pharmaceutique UMR 8612, Université Paris XI, Faculté de Pharmacie,
5 rue J. B. Clément, 92296 Châtenay-Malabry, France
Fax: (internat.) + 33-1-46835882
E-mail: noureddine.ghermani@cep.u-psud.fr
[b] GEVSM Unité Mixte de Recherche du CNRS, Structure et Réactivité des Systèmes Moléculaires Complexes,
5 rue A. Lebrun, B. P. 403, 54001 Nancy Cedex, France
Fax: (internat.) + 33-3-83682345
E-mail: Alain.Marsura@pharma.uhp-nancy.fr
[c] Laboratoire des Sciences des Matériaux, LSM, Université Cadi Ayyad, Faculté des Sciences Semlalia,
Boulevard Prince Moulay Abdallah, B. P. 2390, 40000 Marrakech, Morocco
E-mail: nouzha@ucam.ac.ma
[d] Centre de RMN Université Claude Bernard, Lyon-1/ESCPE, Domaine Scientifique de la Doua,
Boulevard du 11 Novembre 1918, 69100 Villeurbanne Cedex, France
E-mail: bernard.fenet@univ-lyon1.fr

Supporting information for this article is available on the WWW under http://www.eurjic.org or from the author.

and Cu^I complexes with these ligands and the X-ray structure analysis of the Cu^I and Ag^I dinuclear helicates revealed a fully selective H-T and H-H orientation of the strands within the helicates.

Results and Discussion

Synthesis of Ligands 9 to 12

In order to explore the scope and limitations of a possible programming of oriented double-stranded helicates from discrete bis(heterocyclic) azines, we prepared the new ligands **9**−**12** containing a 2,2′-bithiazole, a 4,4′-bithiazole, a 2,2′-bipyrazine or a 4,4′-bipyrimidine unit, respectively, together with a common 2,2′-bipyridine nucleus. These ligands were designed in order that the non-identical bis(heterocyclic) components present two identical bis(diimine) coordinating centres connected by an oxopropylene bridge. Therefore, in the presence of geometrically tetrahedral coordinating cations, there are two possible orientations for the ligands around the metal atom in a dinuclear complex: H-H (head-to-head) or H-T (head-to-tail) (Figure 1).

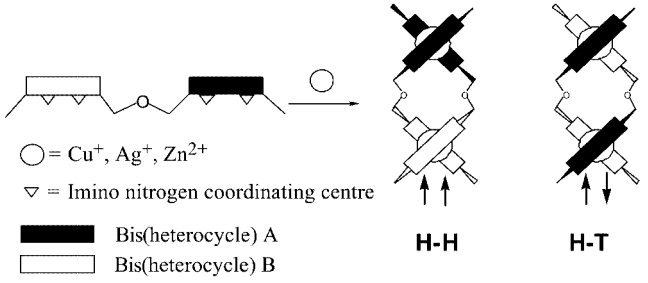

Figure 1. Graphical illustration of the self-assembly strategy

Ligand **9** (Scheme 1) was prepared from the dimethyl-2,2′-bithiazole **1**,[7] ligand **10** from the dimethyl-4,4′-bithiazole **3**,[8] ligand **11** from 2,2′-dimethyl-4,4′-bipyrimidine (**5**)[9] and ligand **12** from 6,6′-dimethyl-2,2′-bipyrazine by a previously reported method[5] The bis(heterocycles) were transformed into 6-(monobromomethyl) **2**, **4** and **6** derivatives or 6-(monohydroxymethyl) derivatives **7** and **8**, respectively. The final ligands were obtained in good yields (70−83%) after Williamson condensation of the (monobromomethyl)bithiazoles, -bipyrimidine or -bipyridine with 6-(hydroxymethyl)-6′-methyl-2,2′-bipyridine[10] or 6-(hydroxymethyl)-6′-methyl-2,2′-bipyrazine,[5] respectively. Addition of previously prepared $[Cu(CH_3CN)_4]PF_6$ or commercially available $Ag(PF_6)$ to solutions of **9**−**12** in anhydrous acetonitrile or addition of $Zn(OTf)_2$ to solutions of the ligands in MeOH affords the corresponding copper, silver or zinc dinuclear complexes (Scheme 2). Addition of the

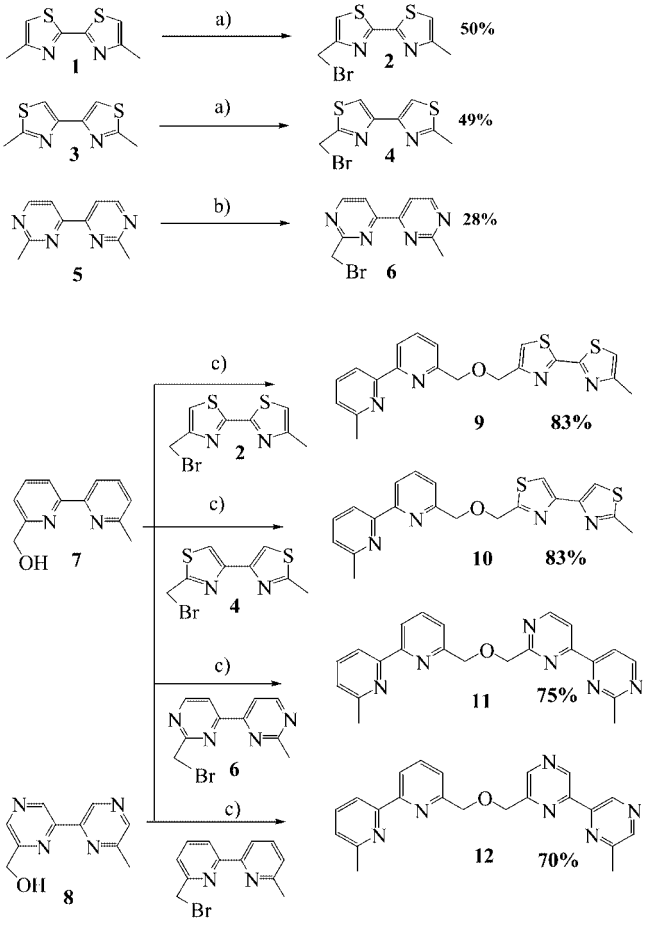

Scheme 1. Synthesis of **7** and **8**: a) NBS, benzoyl peroxide, CCl_4, reflux, hν; b) NBS, AIBN, reflux, hν; c) NaH, THF under Ar, 0 °C

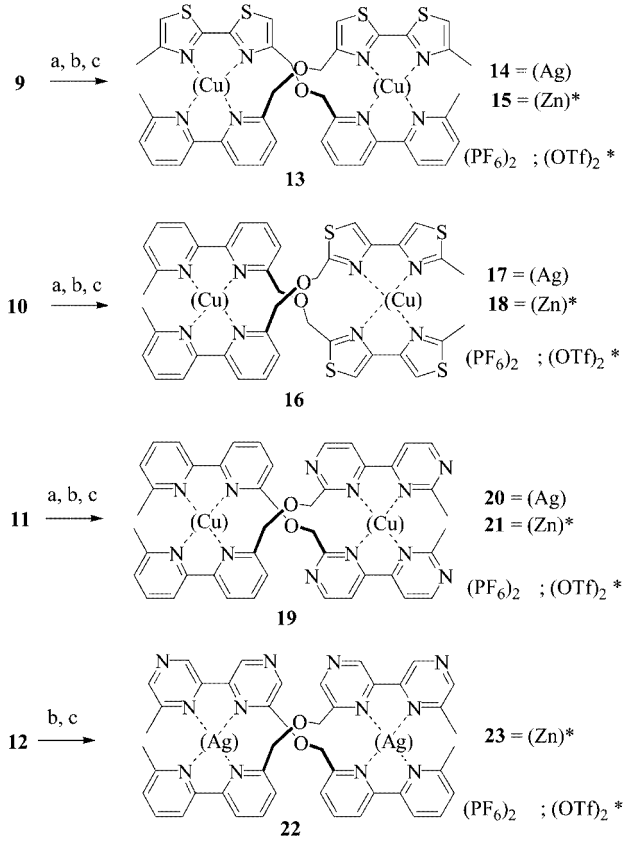

Scheme 2. Synthesis of complexes **13**−**23**: a) $[Cu(CH_3CN)_4]PF_6$; b) $AgPF_6$; c) $Zn(OTf)_2$; (OTf = triflate anion)

 © 2004 Wiley-VCH Verlag GmbH & Co. KGaA, Weinheim

metal ion solutions resulted in instant colour changes from colourless to deep-red or deep-orange in the case of Cu^{I} or colourless to pale yellow in the case of the Ag^{I} and Zn^{II} indicating the effective formation of the complexes. A thin layer chromatographic control showed that the free ligand was totally consumed in the reaction. The crude materials were recrystallized by slow diffusion of diethyl ether into acetonitrile or acetone solutions (copper and silver complexes) or by slow concentration of a methanolic solution in the case of zinc complexes (see Exp. Sect.). The deep red crystals with Cu^{I} and the pale yellow crystals with Ag^{I} and Zn^{II} are stable in air. In each case, the ligands form the expected dinuclear double-stranded helical structures as observed by X-ray diffraction analyses.

Thermodynamic Self-Assembly Processes of Ligands 9−12 with Cu^{I}, Ag^{I} and Zn^{II}

The formation of the double-helical metal complexes **13**−**23** was followed by UV/Vis spectrophotometric titration of ligands **9**−**12** with $Cu[CH_3CN]_4[PF_6]$, $AgPF_6$ in CH_3CN or $Zn(OTf)_2$ in MeOH. Titrations of ligand **9** with $Cu[CH_3CN]_4[PF_6]$ (Figure 2) and ligand **11** with $Zn(OTf)_2$ (Figure 3) are presented as typical examples (see Supporting Information for other titration data; see the footnote on the first page of this article). Spectra obtained during titration of ligand **9** display two sharp isosbestic points between 250 and 600 nm over the duration of the titration. The colourless solution of **9** becomes red instantly upon addition of $Cu[CH_3CN]_4[PF_6]$ owing to the appearance of an MLCT band at $\lambda_{max.}$ = 450 nm (ε = 1700) and indicating coordination of the Cu^{I} atoms. The titration plot (see B in Figure 2) indicates that the species formed has a composition of ca. 1 Cu atom for 1 equiv. of **9** in agreement with the stoichiometry expected for the double-stranded helicate $[Cu_2(\mathbf{9})_2][PF_6]_2$ (**13**). Conversely, the titration spectra of ligand **11** display, on addition of $Zn(OTf)_2$, the successive appearance of two strong and distinct absorptions at $\lambda_{max.}$ = 304 nm (ε = 17650) and $\lambda_{max.}$ = 316 nm (ε = 18970) indicating the effective coordination of the Zn^{II} atoms. The titration plot (B in Figure 3) reveals that the species formed has a composition of ca. 1 Zn atom for 1 equiv. of **11** in agreement with the expected stoichiometry of **21**. A similar difference is observed in the formation of complex **18** containing Zn^{II} but not with the formation of the other zinc complexes or the other metal complexes investigated. This suggests that the two zinc ions were complexed in a different environment in the other species.

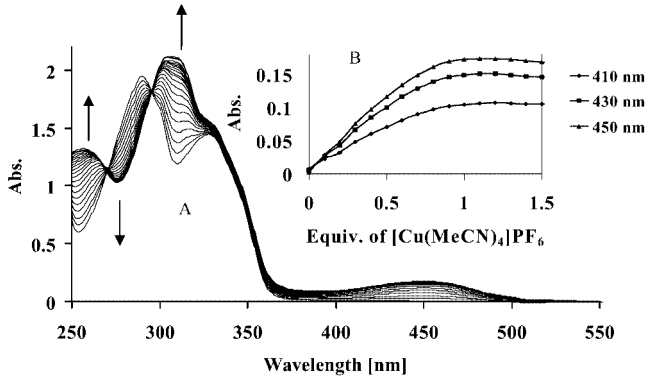

Figure 2. Spectrophotometric titration of ligand **9** with $[Cu(MeCN)_4]PF_6$ (0.1−1.5 equiv.) in acetonitrile: A) UV/Vis absorption spectra and B) Plots of absorbance versus added salt equiv. at three wavelengths

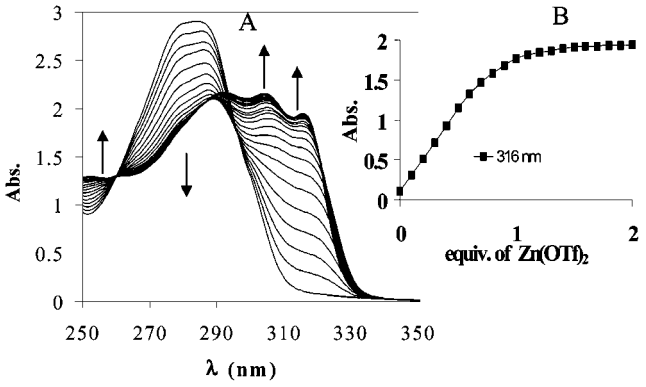

Figure 3. Spectrophotometric titration of ligand **11** with $Zn(OTf)_2$ (0.1−2.0 equiv.) in MeOH: A) UV/Vis absorption spectra and B) plot of absorbance versus added salt equiv. at 316 nm

Analysis of titration data provides the thermodynamic parameters of dihelicate formation. Factor analysis points to the existence of five absorbing species (L, ML, M_2L, ML_2, M_2L_2) and the spectrophotometric data can be fitted to the equilibria given below [Equations (1) and (2)], which characterize the assembly process and are described by stability constants (β_{ml}). Using the SPECFIT program,[11] the binding constants $\log(\beta_{ml})$ for each species M_mL_l have been calculated (Table 1).

$$M + L \rightleftarrows ML \quad \log \beta_{11} \tag{1}$$

$$ML_2 + M \rightleftarrows M_2L_2 \quad \log \beta_{22} \tag{2}$$

The species M_2L and ML_2 were neglected because they

Table 1. Formation constants $\log(\beta_{ml})$ for the complexes $[M_2L_2]^{n+}$ (**13**−**23**) in acetonitrile and methanol (*) at 298 K[11]

$[M_2(L)_2]^{n+}$	$\log \beta_{11}$	$\log \beta_{22}$
$[Cu_2(\mathbf{9})_2]^{2+}$ (**13**)	5.9 ± 0.1	23.7 ± 2.0
$[Ag_2(\mathbf{9})_2]^{2+}$ (**14**)	5.1 ± 0.1	22.5 ± 1.7
$[Zn_2(\mathbf{9})_2]^{4+}$ (**15**)*	6.2 ± 0.3	23.3 ± 1.9
$[Cu_2(\mathbf{10})_2]^{2+}$ (**16**)	3.9 ± 0.2	16.4 ± 1.5
$[Ag_2(\mathbf{10})_2]^{2+}$ (**17**)	5.3 ± 0.1	23.4 ± 1.8
$[Zn_2(\mathbf{10})_2]^{4+}$ (**18**)*	4.9 ± 0.1	21.4 ± 1.4
$[Cu_2(\mathbf{11})_2]^{2+}$ (**19**)	4.3 ± 0.1	19.1 ± 1.9
$[Ag_2(\mathbf{11})_2]^{2+}$ (**20**)	4.8 ± 0.1	21.3 ± 1.4
$[Zn_2(\mathbf{11})_2]^{4+}$ (**21**)*	5.9 ± 0.2	19.3 ± 0.2
$[Cu_2(\mathbf{12})_2]^{2+}$ [5]	5.6 ± 0.1	19.6 ± 1.8
$[Ag_2(\mathbf{12})_2]^{2+}$ (**22**)	5.3 ± 0.4	23.3 ± 1.9
$[Zn_2(\mathbf{12})_2]^{4+}$ (**23**)*	5.2 ± 0.1	23.6 ± 1.9

 © 2004 Wiley-VCH Verlag GmbH & Co. KGaA, Weinheim

were present only in negligible quantities under the experimental conditions used here.

Positive-mode ESI-MS spectra of all the complexes contained doubly charged ions except for the Zn^{II} complexes in which quadruply charged ions were detected. For illustration, mass spectra of the copper and zinc complexes **13** and **15** (Figure 4) reveal the $[Cu_2(\mathbf{9})_2]^{2+}$ doubly charged ion (m/z = 457 a.m.u.) (peak separated by 0.5 a.m.u.) and the $[Cu_2(\mathbf{9})_2\ (PF)_6]^+$ singly charged ion (m/z = 1059 a.m.u.), while for the zinc complex the $[Zn_2(\mathbf{9})_2]^{4+}$ quadruply charged ion (m/z = 229 a.m.u.) (peak separated by 0.25 a.m.u.) and the $[Zn_2(\mathbf{9})_2(OTf)_3]^+$ singly charged ion (m/z = 1364 a.m.u.) are observed. These results are only compatible with the formation of double-stranded helicates.[12] Similar results were obtained with the other complexes.[13]

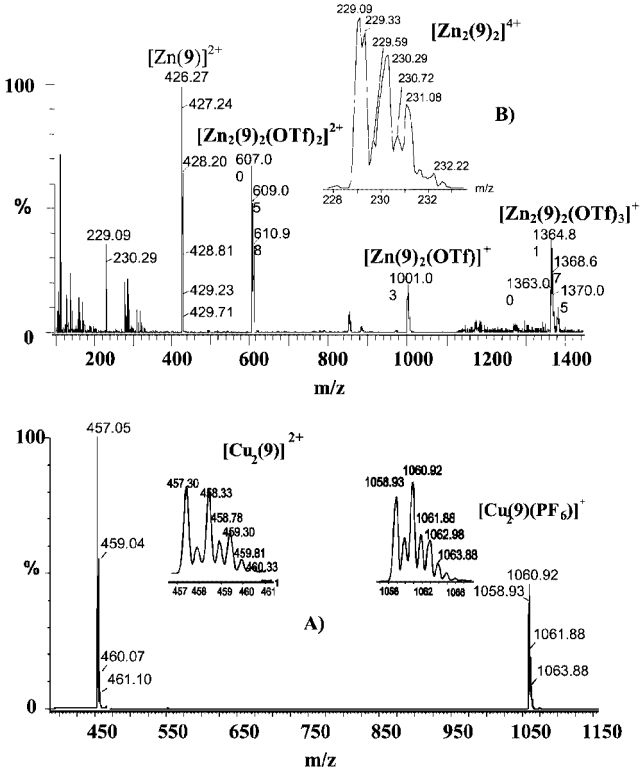

Figure 4. Positive-ion ESI mass spectra of complexes: A) **13** and B) **15**

NMR Analysis

The ^1H NMR spectra of the free ligands **9**−**12** give resolved first-order spectra and each proton of each bis(heterocycle) in the ligand was assigned on the basis of COSY-LR NMR experiments. Complexation of metal ions by the ligand causes upfield or downfield shifts of all the ligand proton ^1H NMR signals indicating the effective formation of the complexes (see for example Figure 5).

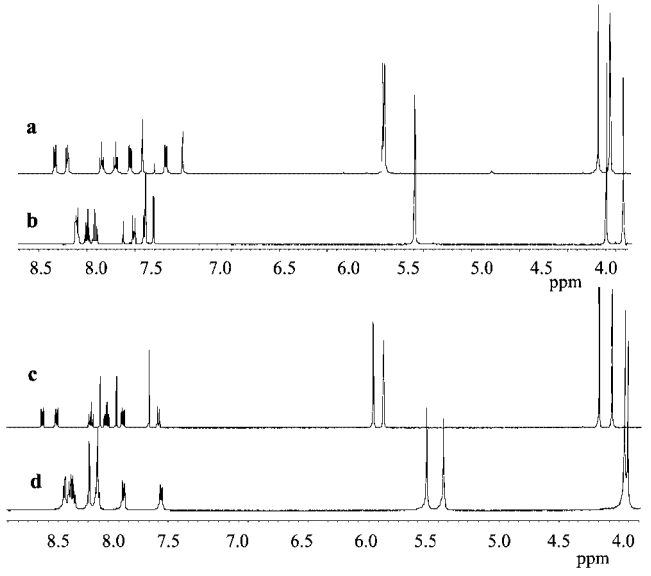

Figure 5. ^1H NMR spectra (400 MHz, 298 K, $CDCl_3/CD_3CN$) of a) ligand **9**; b) $[Ag_2(\mathbf{9})_2][PF_6]_2$ (**14**); c) ligand **10**; d) $[Ag_2(\mathbf{10})_2][PF_6]_2$ (**17**)

Significant shifts of the signals in the ^1H and ^{13}C NMR spectra were observed. Identical spectra were observed from in situ prepared solutions of the complexes by addition of stoichiometric amounts of the metal compound to the free ligand or from redissolution of crystals of the corresponding crystallized metal complex. At room temperature, sharp signals were observed in spectra of the silver and zinc complexes indicating the effective formation of discrete species rather than oligomeric structures. The spectra of the silver complexes **14** and **17** (Figure 5) and **20** and **22** (not shown) obtained from the 2,2′-bithiazolyl and 4,4′-bithiazolyl ligands **9**, **10** and from bipyrimidine and bipyrazine ligands **11**, **12**, respectively, show that only one species is present in solution at room temperature. The methylene protons of the oxopropylene bridges display two A_2 patterns (Figure 5) in place of two AB patterns, which should normally be observed for diastereotopic methylene protons in a chiral heterotopic double-helical structure.[14] This is almost certainly because of a rapid exchange under these experimental conditions as has been reported already for silver helicates.[15] ^1H NMR spectra of the complexes in CD_3CN remain unchanged during a decrease in temperature from 333 to 233 K, and only a negligible broadening of all the signals of the whole spectrum was observed at the lowest temperature with no splitting of the methylene proton resonance into an AB pattern. In the absence of the corresponding X-ray structures for the two (bithiazolyl)silver complexes, no conclusions can be drawn from the above NMR results regarding the conformational preference of these complexes (H-H or H-T). However, variable-temperature results obtained from solutions were compatible with a side-by-side nonhelical achiral structure for these two complexes in solution although a fast exchange between chiral structures cannot be excluded because we did not observe any true line broadening in these experiments. The X-ray structures of

 © 2004 Wiley-VCH Verlag GmbH & Co. KGaA, Weinheim

the silver complexes with bipyrimidyl (**20**) and bipyrazyl (**22**) ligands (see Figures 15 and 16) better corroborated the hypothesis of the existence of a chiral structure undergoing a fast exchange since they reveal that the structures of $[Ag_2(\mathbf{11})_2]^{2+}$ (**20**) and $[Ag_2(\mathbf{12})_2]^{2+}$ (**22**) contain double-stranded helical cations. In each case, only one species is present in the crystals having exclusively an H-H or an H-T conformation, respectively.

As previously observed for the $[Cu_2(\mathbf{12})_2][PF_6]_2$ complex,[5] the NMR signals for compounds $[Cu_2(\mathbf{9})_2][PF_6]_2$ (**13**), $[Cu_2(\mathbf{10})_2][PF_6]_2$ (**16**) and $[Cu_2(\mathbf{11})_2][PF_6]_2$ (**19**) in acetonitrile are broad and poorly resolved at room temperature[16] and display line shapes typical of exchange at moderate rate on the NMR time scale (Figure 6a). Gradually lowering the temperature of the solutions to 233 K gives resolved spectra (Figures b and 7a,b) but which are not identical with the two typical perfect AB patterns previously observed for the $[Cu_2(\mathbf{12})_2][PF_6]_2$ double-stranded helical complex.[5] The spectra observed here display doubling of all signals indicating the presence of two species in solution at 233 K as revealed by the four different signals of methyl protons, AB and A_2 patterns of oxopropylene bridge methylene protons and supplementary signals in the aromatic part of the spectrum (Figures 6b and 7a,b). Increasing the temperature results in the coalescence of the AB spin systems of the methylene protons into two A_2 spin systems. This strongly indicates a loss of chirality during the exchange mechanism[16] so that only one achiral species composes the cations **16** and **19** at 353 K (see Figure 7a,b). Alternatively, there is a fast exchange between chiral structures, as proposed above in the case of the silver complexes.

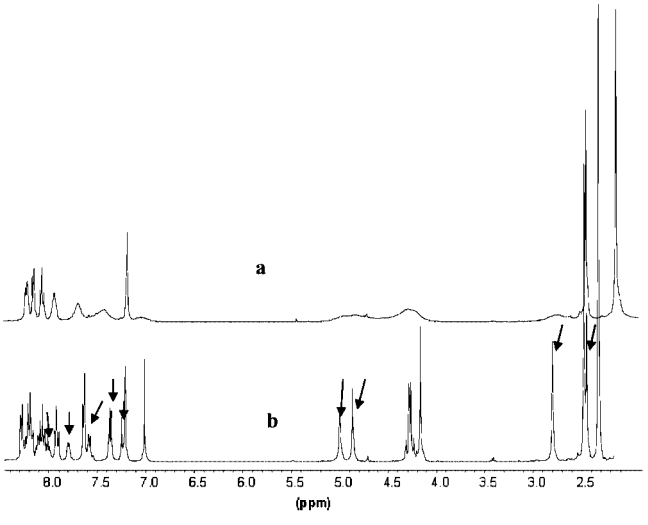

Figure 6. ^1H NMR spectra (400 MHz, CD_3CN) of $[Cu_2(\mathbf{9})_2][PF_6]_2$ (**13**); a) 298 K, b) 233 K (arrows indicate the second species)

A deeper analysis of ^1H NMR data of the Cu^I complexes suggested a dynamic interconversion exchange of enantiomeric helicates should occur at room temperature [dinuclear right-handed (*P*) to dinuclear left-handed (*M*)] on the NMR timescale (unresolved, large methylene proton signals) as observed for the $[Cu_2(\mathbf{12})_2][PF_6]_2$ complex.[5] This

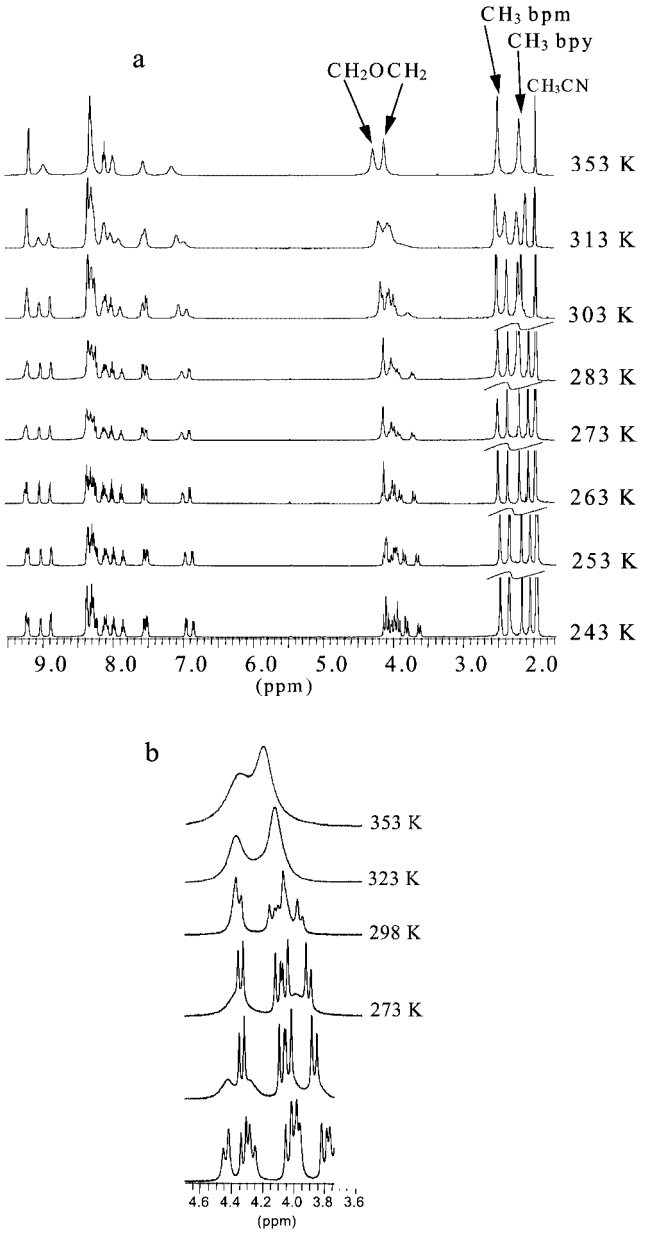

Figure 7. Variable-temperature ^1H NMR spectra of a) $[Cu_2(\mathbf{11})_2][PF_6]_2$ (**19**) (full spectra); b) $[Cu_2(\mathbf{10})_2][PF_6]_2$ (**16**) (selected region of oxapropylene bridges) between 353 and 233 K

was confirmed by recording spectra at different temperatures (down to 233 K) revealing a sharpening of signals and a shifting and characteristic splitting of the signal of the diastereotopic methylene protons of the oxopropylene bridges. Unfortunately, this phenomenon is concomitant with the appearance of supplementary signals (methyl, oxomethylene and aromatic) which correspond to the appearance of a second species in solution. At this stage, two explanations may be advanced.

The first case entails the presence of a mixture of helical and side-by-side double-stranded dinuclear copper complexes, while the second case has a mixture of H-H and H-T conformers undergoing a rapid exchange. It should be kept in mind that the second situation can exist only by a

 © 2004 Wiley-VCH Verlag GmbH & Co. KGaA, Weinheim

total and rapid decomplexation of the components, which allows inversion of the strand orientation. Additionally, it should be mentioned that, for the first hypothesis, a side-by-side complex would be observed in solution during the (*P*) ⇄ (*M*) interconversion process upon depression of the temperature. This might be considered as an intermediate conformer in the exchange mechanism between the two enantiomeric (*P*) and (*M*) helicates. In such a situation, a rapid decomplexation-recomplexation of only one helicate extremity would be sufficient. The first proposal is supported by Harding[17] and later by Greenwald[18] who made similar observations. Despite this, ^{63}Cu NMR spectra of the $[Cu_2(\mathbf{9})_2][PF_6]_2$ (**13**), $[Cu_2(\mathbf{10})_2][PF_6]_2$ (**16**) and the homotopic Cu^I complex were investigated in order to confirm one of the two proposals (see ref.[13] for details). The ^{63}Cu NMR spectra of **13** and **16** exhibit a single resonance at $\delta \approx 0$ ppm, indicating a similar environment for the copper atoms within these helicates. For **13**, this situation is consistent with only an (H-T) orientation of the ligands as was also found in its crystal structure. However, for **16**, we should theoretically observe two resonances with reference to an expected (H−H) orientation as observed in its crystal structure. In any case, these results are obviously not in agreement with the presence of a mixture of (H−H) and (H-T) conformers in which three resonances are normally expected. Considering this, we decided to perform low-temperature ^{1}H NMR ROESY experiments (233 K) on the copper dications **13**, **16**, silver dications **14**, **20** and zinc dication **23**.

In the case of zinc complex **23**, two inter-strand correlations were detected in the (298 K) ^{1}H NMR ROESY spectrum (Figure 8): one between the methyl protons of the bipyrazine unit and 7-H of the bipyridine unit and a second between methyl protons of the bipyridine unit and 1-H of the bipyrazine unit indicating a selective (H-T) orientation of the ligands in this complex. Unfortunately, in the case of the complexes **13**, **16** (copper), **14**, **20** (silver) and **18**, **21** (zinc), we were unable to freeze out the systems, because of a rapid exchange, which operated even at low temperature. Under these conditions, no correlation between terminal methyl protons of one heterocyclic unit and the aromatic protons of the opposite heterocyclic unit were observed by NMR spectroscopy.

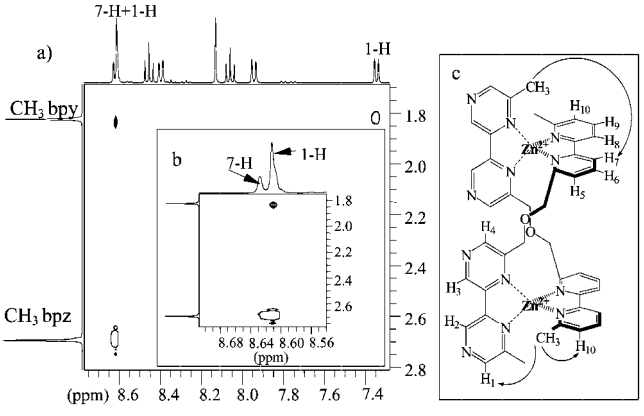

Figure 8. a) ^{1}H NMR ROESY of $[Zn_2(\mathbf{12})_2][OTf]_4$ (**23**) in CD_3OD at 298 K (selected region); b) zoom on correlations between methyl and aromatic protons; c) scheme of the resulting double-stranded helicate structure (arrows indicate specific interactions)

X-ray Structure Analysis

Finally, crystallized helicates $[Ag_2(\mathbf{11})_2][PF_6]_2$ (**20**) and $[Ag_2(\mathbf{12})_2]][PF_6]_2$ (**22**) were obtained by slow diffusion of diethyl ether into acetonitrile solutions of the complexes (see Exp. Sect.) giving light yellow crystals suitable for X-ray crystallography. The two compounds both occupy the centrosymmetric $P\bar{1}$ space group with two PF_6^- counterions in the asymmetric unit. An acetonitrile (C_2H_3N) solvent molecule was found in the asymmetric unit of **20**. However, the presence of PF_6 counterions induces, some disorder in the crystal packing and during the refinements.

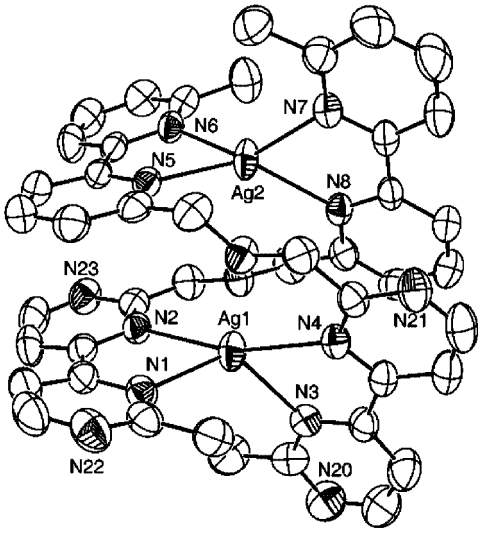

Figure 9. ORTEP drawing of the asymmetric unit of the silver complex $[Ag_2(\mathbf{11})_2][PF_6]_2$ (**20**) (counterions and solvent molecules omitted); thermal ellipsoids are at 50% probability level

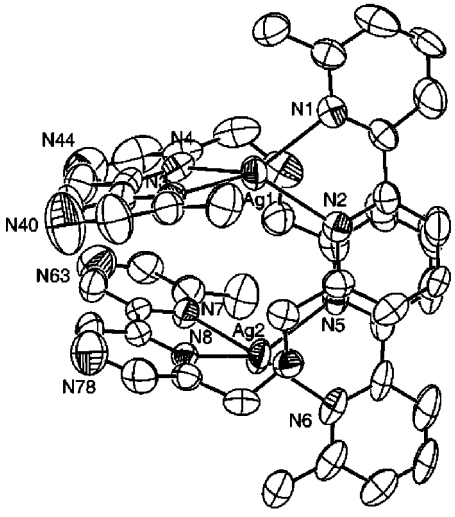

Figure 10. ORTEP drawing of the asymmetric unit of the silver complex $[Ag_2(\mathbf{12})_2][PF_6]_2$ **22** (counterions omitted); thermal ellipsoids are at 50% probability level

 © 2004 Wiley-VCH Verlag GmbH & Co. KGaA, Weinheim

The ORTEP[19] views of the two dinuclear Ag^I complexes **20** and **22** are shown in Figures 9 and 10, respectively. As usual in the case of a chemical system with a large number of heavy atoms, it was impossible to observe all the hydrogen atoms in the Fourier difference maps. This made it particularly difficult to differentiate between N atoms and CH groups of the ligand nuclei without a careful inspection of C−C and C−N bond lengths and thermal displacements, which was done in this case. The complexes **20** and **22** are double-stranded helicates where each Ag^I cation is in tetrahedral coordination involving the nitrogen atoms of the bipyrimidine (bpm), bipyrazine (bpz) and bipyridine (bpy) ligands. However, the complex **20** occupies an (H-H) conformation whereas the complex **22** is in an (H-T) conformation as shown in Figures 9 and 10. The intramolecular Ag−Ag distances are 4.14 and 6.13 Å for the complexes **20** and **22**, respectively. This large difference of 2 Å in the metal−metal spacing of the two helicates can be explained by the π-electronic interactions between the facing heteroatomic rings (bpm−bpy in complex **20** and bpz−bpz in complex **22**), which differ between the two complexes.

In the bpm−bpy interactions in **20**, the nitrogen atoms can avoid a close approach to the opposing π-electronic system.

More precisely, the nucleophilicity of the nitrogen atoms makes the N−N and the N−π-electron repulsions highly involved and favour or disfavour the close approach of the heteroatomic nuclei and the attraction occurred. Conversely, electrostatic repulsion is dominant in the bpz−bpz facing heterocycles in **22**, especially because of the similar positions of the nitrogen atoms in the two facing rings. As a consequence of these interactions, the AgN_4 tetrahedra present distorted geometries as previously reported in our copper helicate studies.[5] The interatomic bond lengths and angles are given.[13] The average values of the Ag−N bond lengths for compound **20** are 2.406(5) Å [$Ag(bpm)_2$], 2.339(5) Å [$Ag(bpy)_2$] and are significantly longer than those in compound **22**, 2.321(7) Å [Ag(bpz−bpy)], 2.317(8) Å [Ag(bpz−bpy)], respectively. All N−Ag−N bond angles are within the range 70−140° except N2−Ag1−N4 = 163° found for the bpm interligand connection. Figures 11 and 12 depict the space-filling representations (MOLEKEL[20]

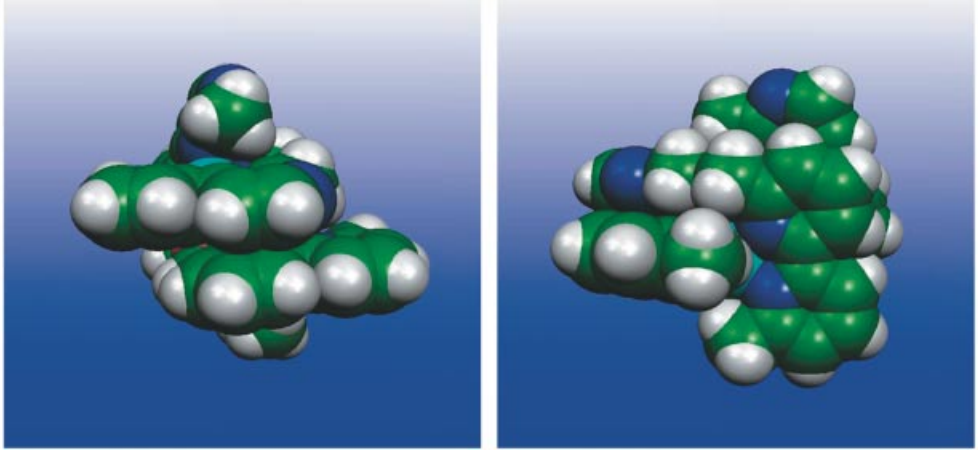

Figure 11. Two views of the space-filling representation of the silver helicate $[Ag_2(\mathbf{11})_2][PF_6]_2$ (**20**) (N atoms blue)

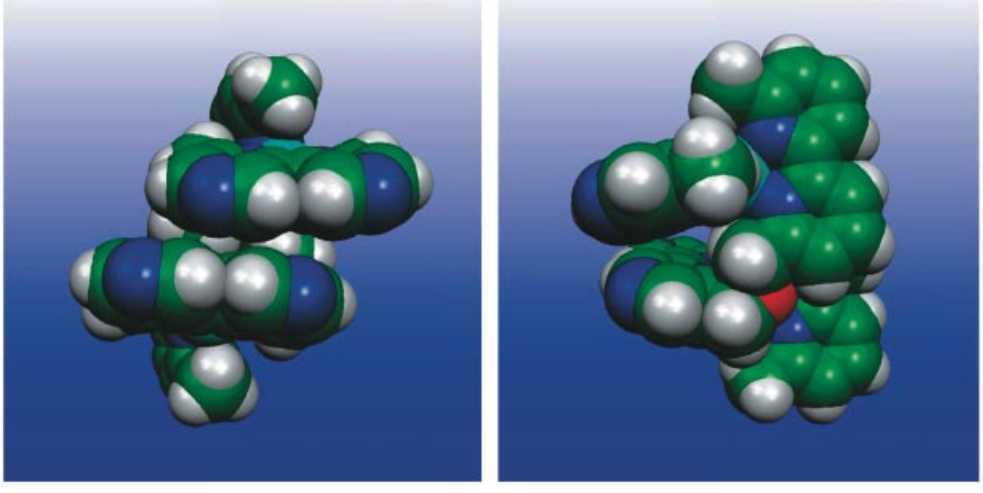

Figure 12. Two views of the space-filling representation of the silver helicate $[Ag_2(\mathbf{12})_2][PF_6]_2$ (**22**) (N atoms blue, O atoms red)

 © 2004 Wiley-VCH Verlag GmbH & Co. KGaA, Weinheim

visualization program) of the structures of **20** and **22** showing the interactions of heteroatomic ring packing and the N−N and N−π-electron repulsions. In Figure 12, the bpm−bpy facing rings are close to each other. The stabilization of the facing rings imposes mutually transverse displacements.

The two helicates $[Cu_2(\mathbf{9})_2][PF_6]_2$ (**13**) and $[Cu_2(\mathbf{10})_2][PF_6]_2$ (**16**), were crystallized by slow diffusion of diethyl ether into acetonitrile or acetone solutions of the complexes (see Exp. Sect.). The resulting crystals were deep-red and fragile. The structures of the copper complexes **13** and **16** were determined from difficult X-ray single-crystal experiments (see Exp. Sect.) because of the poor quality of the crystals. Both compounds crystallized in the triclinic setting and the centrosymmetric $P\bar{1}$ space group. Attempts to resolve and refine the structures in the $P1$ space group did not improve their figures of merit and yielded high R values (see Exp. Sect.), which are expected for such disordered materials especially in the presence of PF_6^- counterions. Twinning was also considered but it was not observed in our samples. However, the helicate structures and conformations could be observed despite the complete disordering of the PF_6^- counterions in the crystal lattices. The asymmetric unit of **13** contains one dinuclear Cu^I complex, two PF_6^- counterions and one residual acetone (C_3H_6O) solvent molecule. The complex **16** contains two dicopper(I) complexes and four PF_6^- counterions in the crystal asymmetric unit. The respective ORTEP[19] views of the two compounds are depicted in Figures 13 and , respectively.

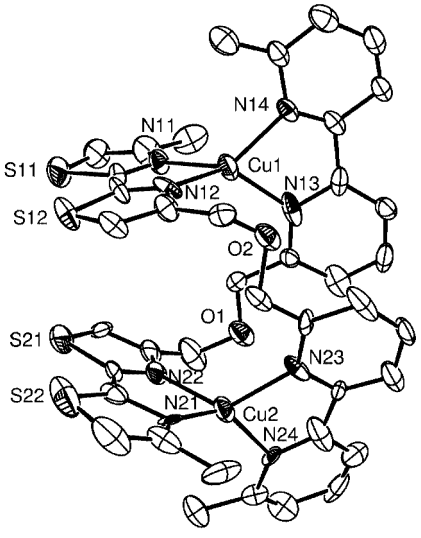

Figure 13. ORTEP drawing of the asymmetric unit of the copper complex $[Cu_2(\mathbf{9})_2][PF_6]_2$ (**13**) (counterions and solvent molecules omitted); thermal ellipsoids are at 50% probability level

The intramolecular Cu−Cu distances are 5.95 Å (complex **13**) and 6.28 (helix **16a**) and 6.24 Å (helix **16b**). The dimetallic cations are double-stranded helicates yielding left- and right-handed units in the crystal because of the presence of the centre of inversion ($P\bar{1}$ space group). It is worth noting that for complex **16**, both dinuclear **16a** and

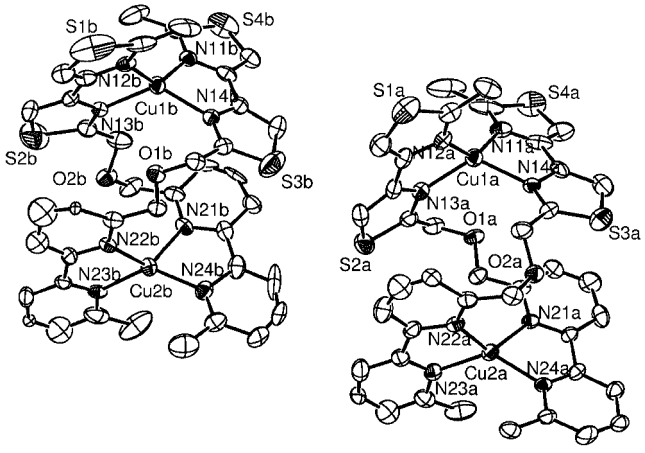

Figure 14. ORTEP drawing of the asymmetric unit contents of the copper complex $[Cu_2(\mathbf{10})][PF_6]_2$ (**16**) (counterions and solvent molecules omitted); thermal ellipsoids are at 50% probability level

16b helices in the asymmetric unit have the same handedness (Figure 14). In the complexes **13** and **16**, the copper ions occupy a distorted tetrahedral coordination involving the nitrogen atoms of the bipyridine and bithiazole heterocyclic ligands. However, the position of the connecting carbon atoms (C-2 or -4) in the bithiazole rings is found to yield to either hetero-ligand (**13**) or homo-ligand (**16**) coordinations of the copper atom as shown in Figures 13 and 14. Consequently, a different ring stacking is obtained as shown in Figures 15 (**13**) and 16 (**16**) generated by the MOLEKEL[20] program. This stacking is due to the π−π and electrostatic interactions between the heterocyclic ligands. Figures 15 and 16 indicate that these interactions are stronger when sulfur atoms are involved: the interactions become attractive. Both transverse and longitudinal displacements of facing heterocyclic ligand planes are observed. This obviously implies CuN_4 distorted tetrahedral geometry especially when the copper atom is connected to one or two bithiazole ligands. These features were also reported in our previous study of the (bipyrazine−bipyridine)copper complex.[5] It is worth noting that the disorder of the PF_6^- counterions results in poor quality structure refinements and has an influence on the precision of the atomic bond lengths and angles in the organic part of the helicates. It can also distort the planarity of the ligand nuclei.

On the other hand, the geometry of the copper environment is much more stable because of the heavy metal contribution to the X-ray diffracting power of the samples. Atomic bond lengths and angles for copper coordination in compounds **13** and **16** are given in the Supporting Information.[13] All Cu−N bond lengths are approximately equal to 2 Å within the estimated error intervals. Similar bond angles in the range from 80 (intra-ligand angles) to 137° (interligand angles) are also found for the two compounds. We note that these structural values do not correlate with the nature of the heterocyclic ligand.

The X-ray structural analyses showed unambiguously that the discrete dinuclear copper helicates **13** and **16** were

 © 2004 Wiley-VCH Verlag GmbH & Co. KGaA, Weinheim

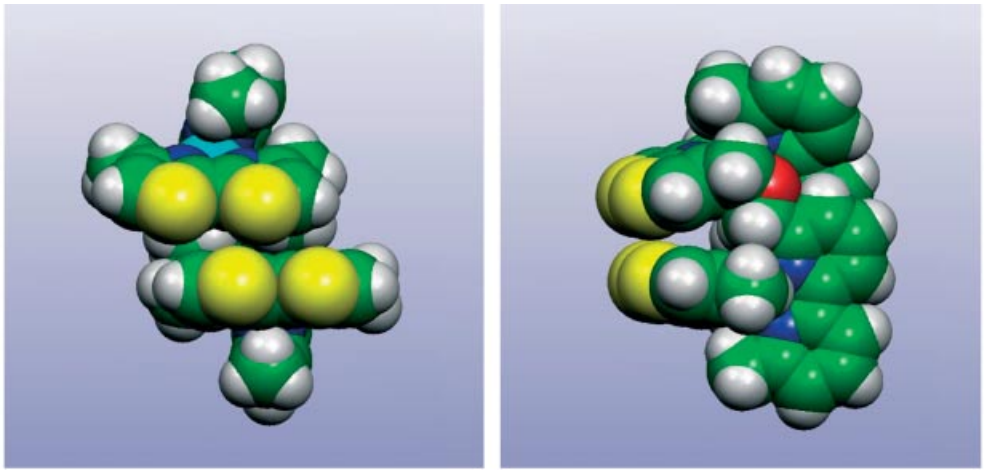

Figure 15. Two views of the space-filling representation of the copper helicate $[Cu_2(\mathbf{9})_2][PF_6]_2$ (**13**) (S atoms yellow, O atoms red)

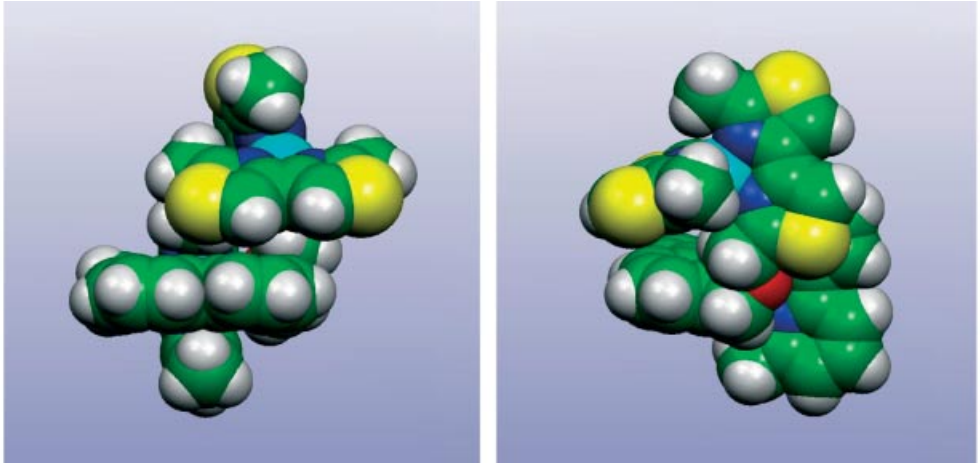

Figure 16. Two views of the space-filling representation of the copper helicate $[Cu_2(\mathbf{10})_2][PF_6]_2$ (**16**) (S atoms yellow, O atoms red)

formed and adopt an (H-T) conformation with the bipyridine-2,2′-bithiazole heterotopic ligand and an (H-H) conformation with the bipyridine-4,4′-bithiazole heterotopic ligand. Both metal centres in the helicates are coordinated to the heterocyclic nitrogen atoms by a distorted tetrahedral geometry.

In unison with experimental[5] and theoretical[6] results obtained previously for the heterotopic bipyrazine−bipyridine ligand self-assembly process with Cu^I, an H-T conformation has also been obtained for this sequence with Ag^I and Zn^{II}. This "programming" was assigned to the electronic properties of the heterocycles on the basis of Cu^I orbital contributions to the HOMO and on the basis of a metal→ligand back-bonding phenomenon,[6] which enhances the stability of the hetero complex (bpz−bpy). Similar reasoning can be applied to the Ag^I and Zn^{II} metal complexes. Conversely, the bipyrimidine−bipyridine sequence **11** exhibits an H-H conformation. The only difference between the bipyrimidine and bipyrazine units lies in the heterocycle electronic configurations. As reported earlier by us,[24,25] both the reactivity and experimental electron density distribution of bipyrazine indicate its less aromatic character compared to other diazines such as bipyrimidine[26] and probably also to other diazines such as bipyridine or phenanthroline. Notably, the topological analysis of the electron density[24] allowed a comparison of the coordination scheme of the inner and outer nitrogen atoms of the bipyrazine and the 4,4′-bipyrimidine rings, respectively,[26] revealing a participation of the outer nitrogen atoms in the coordination of Cu^I only in the bipyrimidine ring. Unfortunately, ab initio DFT calculations on the 4,4′-bipyrimidine homo- and hetero-Cu^I complexes failed and no data could be presented regarding this.

Conclusion

In conclusion, we have demonstrated in this study that four different tetradentate heterotopic ligands containing 2,2-bipyrazine, 2,2′- or 4,4′-bithiazole or 4,4′-bipyrimidine fragments connected to a bipyridine nucleus are very effective for the spontaneous formation of new double-stranded head-to-head (H-H) or head-to-tail (H-T) fully oriented dinuclear helicates in the solid state. Analysis of the spectrophotometric UV/Vis titrations indicate that all the complexes are formed quantitatively at M/L = 1.0 stoichi-

 © 2004 Wiley-VCH Verlag GmbH & Co. KGaA, Weinheim

ometry and that the self-assembly process of the dinuclear double-stranded helicates is driven to completion by positive cooperativity.

However, it was not possible to ascertain the precise nature of the second species which appears in solution at lower temperature (especially in the cases of the silver and copper complexes) because of a very rapid dynamic interconversion equilibrium between conformers. Nevertheless, the structure of one zinc complex **23** with an H-T orientation was fully characterized, which indicates that the helical structures of the dinuclear metal complexes studied may persist in solution. This observation was made possible by the lack of exchange in that particular case.

Considering the X-ray structures of the four complexes, extensive heteroaromatic ring π-stacking and the overlap of near parallel fragments of adjacent ligands govern the metal−metal distance, modulate the pitch and bending of the helix shape and strongly stabilize the molecule. As a direct consequence of this, there is a remarkable and uncommon Ag^{I} cation distorted tetrahedral geometry in the corresponding helicate.

Finally, it is considered that "programming" oriented helicate self-assemblies could be achieved with a high efficiency by the design of heterotopic strands composed only of bis(heterocycles) with different electronic configurations in their structure. Projected investigations include: a) study of the role of the counter-anion in the formation and stability of helicates, b) study of the presented ligands' complexation with hexacoordinating metal atoms. Further work is also in progress to use this property for the construction of other ligands and heterotopic sequences in order to programme novel supramolecularly oriented systems.

Experimental Section

General Remarks: ^{1}H and ^{13}C NMR spectra were recorded with a Bruker DRX 400 spectrometer and ^{63}Cu NMR spectra with a Bruker DRX 500 at −10 °C, UV/Vis spectra were recorded with a Uvmc2 Safas spectrophotometer. Mass spectra (ES) were taken with a Micromass Platform spectrometer. Elemental analyses were obtained with a Perkin−Elmer 240C CHN-O-S analyzer. Solvents were purified by standard methods.

2-(Bromomethyl)-2′-methyl-4,4′-bithiazole (4): NBS (998 mg, 5.61 mmol) was added to a solution of 6,6′-dimethyl-4,4′-bithiazole [9] (1 g, 5.10 mmol) in CCl_4 (100 mL) under Ar. The mixture was refluxed for 30 min, then benzoyl peroxide (85 mg) was added. The mixture was refluxed and irradiated with a tungsten lamp (100 W) for 45 min. The resulting mixture was cooled to 0 °C and the precipitate was filtered, washed with CH_2Cl_2, and the solvent was removed in vacuo. The crude product was purified by chromatography on silica gel (elution: CH_2Cl_2/acetone, 95:5). Yield: 708 mg (50%). M.p. 128 °C. ^{1}H NMR (400 MHz, $CDCl_3$, 25 °C): δ = 7.78 (s, 1 H_{Ar}), 7.62 (s, 1 H_{Ar}), 4.77 (s, 2 H), 2.76 (s, 3 H) ppm. ^{13}C NMR (100 MHz, $CDCl_3$, 25 °C): δ = 166.4 (q), 165.8 (q), 150.8 (q), 149.6 (q), 116.9 (CH_{Ar}), 115.2 (CH_{Ar}), 26.6 (CH_2Br), 19.2 (CH_3) ppm. $C_8H_7BrN_2S_2$ (275.19): calcd. C 34.92, H 2.56, N 10.18; found C 34.9, H 2.54, N 10.12.

2-(Bromomethyl)-2′-methyl-4,4′-bipyrimidine (6): NBS (688 mg, 3.86 mmol) and AIBN were added to a solution of 2,2′-dimethyl-4,4′-bipyrimidine (1.2 g, 6.44 mmol) in CCl_4 (50 mL) under Ar. The mixture was refluxed and irradiated with a tungsten lamp (100 W) for 4 h. The resulting precipitate was filtered, washed with CH_2Cl_2, and the solvent was removed in vacuo. The crude product was purified by chromatography on silica gel (elution: CH_2Cl_2/Et_2O, 75:25), which gave **6** as a white powder. Yield: 480 mg (28%). ^{1}H NMR (400 MHz, $CDCl_3$, 25 °C): δ = 8.94 (d, ^{3}J = 5.1 Hz, 1 H_{Ar}), 8.85 (d, ^{3}J = 4.9 Hz, 1 H_{Ar}), 8.32 (d, ^{3}J = 5.1 Hz, 1 H_{Ar}), 8.24 (d, ^{3}J = 5.2 Hz, 1 H_{Ar}), 4.69 (s, 2 H, CH_2Br), 2.83 (s, 3 H, CH_3) ppm. ^{13}C NMR (100 MHz, $CDCl_3$, 25 °C): δ = 168.5 (q), 166.4 (q), 161.9 (q), 160.4(q), 159.3 (CH_{Ar}), 158.7 (CH_{Ar}), 116.1 (CH_{Ar}), 114.8 (CH_{Ar}), 33.6 (CH_2Br), 26.1 (CH_3) ppm.

6′-Methyl-6-{[(4′-methyl-2,2′-bithiazol-4-yl)methoxy]methyl}-2,2′-bipyridine (9): 6-(Hydroxymethyl)-6′-methyl-2, 2′-bipyridine (300 mg, 1.50 mmol) in THF (10 mL) was added to a suspension of NaH (72 mg, 3.00 mmol) in anhydrous THF (5 mL) under Ar at 0 °C. The mixture was stirred at 0 °C for 1 h, then 6-(bromomethyl)-6′-methyl-2, 2′-bithiazole (413 mg, 1.50 mmol) in THF (10 mL) was added, and the mixture was warmed to room temperature. The mixture was stirred at 40 °C for 4 h. After cooling to room temperature, H_2O (10 mL) was added to the mixture and the phases were separated. The aqueous layer was extracted with CH_2Cl_2 (3 × 30 mL). The combined organic phases were dried with $MgSO_4$ and the solvent was removed in vacuo. The solid was purified by chromatography on silica gel (elution: CH_2Cl_2). Yield: 490 mg (83%). M.p. 118 °C. ^{1}H NMR (400 MHz, $CDCl_3$, 25 °C): δ = 8.32 (d, ^{3}J = 7.8 Hz, 1 H_{Ar}, bpy), 8.19 (d, ^{3}J = 7.6 Hz, 1 H_{Ar}, bpy), 7.83 (t, ^{3}J = 7.8 Hz, 1 H_{Ar}, bpy), 7.69 (t, ^{3}J = 7.6 Hz, 1 H_{Ar}, bpy), 7.53 (d, ^{3}J = 7.6 Hz, 1 H_{Ar}, bpy), 7.41 (s, 1 H_{Ar}, btz), 7.16 (d, ^{3}J = 7.6 Hz, 1 H_{Ar}, bpy), 6.98 (s, 1 H_{Ar}, btz), 4.89 (s, 2 H, CH_2, btz), 4.87 (s, 2 H, CH_2, bpy), 2.63 (s, 3 H, CH_3, bpy), 2.51 (s, 3 H, CH_3, btz) ppm. ^{13}C NMR (100 MHz, $CDCl_3$, 25 °C): δ = 161.6 (q, bpy), 160.4 (q, bpy), 157.8 (q, bpy), 157.5 (q, bpy), 155.8 (q, btz), 155.5 (q, btz), 155.0 (q, btz), 154.1 (q, btz), 137.4 (CH_{Ar}, bpy), 137.0 (CH_{Ar}, bpy), 123.2 (CH_{Ar}, bpy), 121.1 (CH_{Ar}, bpy), 119.8 (CH_{Ar}, bpy), 118.1 (CH_{Ar}, bpy), 117.6 (CH_{Ar}, btz), 115.7 (CH_{Ar}, btz), 73.8 (CH_2, btz), 68.6 (CH_2, bpy), 24.6 (CH_3, bpy), 17.1 (CH_3, btz) ppm. UV/Vis (CH_3CN): $\lambda_{max.}$ ($\varepsilon_{max.}$) = 290 (19500), 328 (14450) nm. $C_{20}H_{18}N_4OS_2 \cdot 0.25CH_2Cl_2$ (415.74): calcd. C 58.50, H 4.49, N 13.48; found C 58.31, H 4.47, N 13.26.

6′-Methyl-6-{[(2′-methyl-4,4′-bithiazol-2-yl)methoxy]methyl}-2,2′-bipyridine (10): 6-(Hydroxymethyl)-6′-methyl-2,2′-bipyridine (268 mg, 1.34 mmol) in THF (10 mL) was added to a suspension of NaH (65 mg, 2.68 mmol) in anhydrous THF (5 mL) under Ar at 0 °C. The mixture was stirred at 0 °C for 1 h, then 6-(bromomethyl)-6′-methyl-4,4′-bithiazole (369 mg, 1.34 mmol) in THF (10 mL) was added, and the mixture was allowed to warm to room temperature. The mixture was stirred at 40 °C for 4 h. After cooling to room temperature, H_2O (10 mL) was added to the mixture and the phases were separated. The aqueous layer was extracted with CH_2Cl_2 (3 × 30 mL). The combined organic phases were dried with $MgSO_4$ and the solvent was removed in vacuo. The solid was purified by chromatography on silica gel (elution: CH_2Cl_2). Yield: 437 mg (83%). M.p. 156 °C. ^{1}H NMR (400 MHz, $CDCl_3$, 25 °C): δ = 8.34 (d, ^{3}J = 7.4 Hz, 1 H_{Ar}, bpy), 8.19 (d, ^{3}J = 7.4 Hz, 1 H_{Ar}, bpy), 7.84 (t, ^{3}J = 7.6 Hz, 1 H_{Ar}, bpy), 7.76 (s, 1 H_{Ar}, btz), 7.68 (d, ^{3}J = 7.2 Hz, 1 H_{Ar}, bpy), 7.60 (s, 1 H_{Ar}, btz), 7.53 (d, ^{3}J = 7.2 Hz, 1 H_{Ar}, bpy), 7.16 (d, ^{3}J = 7.2 Hz, 1 H_{Ar}, bpy), 5.03 (s, 2 H, CH_2, btz), 4.92 (s, 2 H, CH_2, btz), 2.76 (s, 3 H, CH_3, btz), 2.64 (s, 3 H, CH_3, bpy) ppm. ^{13}C NMR (100 MHz, $CDCl_3$, 25 °C): δ = 168.8

 © 2004 Wiley-VCH Verlag GmbH & Co. KGaA, Weinheim

(q, bpy), 166.3 (q, btz), 157.8 (q, bpy), 157.0 (q, bpy), 155.8 (q, bpy), 155.4 (q, bpy), 150.5 (q, btz), 150.1 (q, btz), 137.5 (CH_{Ar}, bpy), 136.9 (CH_{Ar}, bpy), 123.2 (CH_{Ar}, bpy), 121.1 (CH_{Ar}, bpy), 119.9 (CH_{Ar}, bpy), 118.1 (CH_{Ar}, bpy), 115.2 (CH_{Ar}, btz), 114.7 (CH_{Ar}, btz), 74.1 (CH_2, btz), 69.7 (CH_2, bpy), 24.6 (CH_3, bpy), 19.2 (CH_3, btz) ppm. UV/Vis (CH_3CN): $\lambda_{max.}$ ($\varepsilon_{max.}$) = 265 (21100), 287 (18100) nm. $C_{20}H_{18}N_4OS_2 \cdot 1/7CH_2Cl_2$ (406.65): calcd. C 59.49, H 4.53, N 13.78; found C 59.46, H 4.53, N 13.59.

6′-Methyl-6-{[(2′-methyl-4,4′-bipyrimidin-2-yl)methoxy]methyl}-2,2′-bipyridine (11): 6-(Hydroxymethyl)-6′-methyl-2,2′-bipyrazine (348 mg, 1.74 mmol) was added to a suspension of NaH (84 mg, 3.50 mmol) in anhydrous THF (30 mL) under Ar at 0 °C. The mixture was stirred at 0 °C for 1 h, then 2-(bromomethyl)-2′-methyl-4,4′-bipyrimidine (461 mg, 1.74 mmol) was added, and the mixture was allowed to warm to room temperature. The mixture was stirred at 40 °C for 2 h. After cooling to room temperature, H_2O (10 mL) was added to the mixture and the phases were separated. The aqueous layer was extracted with CH_2Cl_2 (3 × 30 mL). The combined organic phases were dried with $MgSO_4$, and the solvent was removed in vacuo. The crude product was purified by chromatography on aluminium oxide gel (elution: CH_2Cl_2), and gave a white powder. Yield 500 mg (75%). M.p. 152 °C. ^{1}H NMR (400 MHz, $CDCl_3$, 25 °C): δ = 8.99 (d, ^3J = 5.1 Hz, 1 H_{Ar}, bpm), 8.82 (d, ^3J = 5.1 Hz, 1 H_{Ar}, bpm), 8.35 (d, ^3J = 4.9 Hz, 1 H_{Ar}, bpm), 8.33 (d, ^3J = 8.0 Hz, 1 H_{Ar}, bpy), 8.24 (d, ^3J = 4.9 Hz, 1 H_{Ar}, bpm), 8.20 (d, ^3J = 7.8 Hz, 1 H_{Ar}, bpy), 7.86 (t, ^3J = 7.8 Hz, 1 H_{Ar}, bpy), 7.69 (t, ^3J = 7.6 Hz, 1 H_{Ar}, bpy), 7.64 (d, ^3J = 7.6 Hz, 1 H_{Ar}, bpy), 7.18 (d, ^3J = 7.6 Hz, 1 H_{Ar}, bpy), 5.04 (s, 2 H, OCH_2, bpm), 5.03 (s, 2 H, OCH_2, bpy), 2.85 (s, 3 H, CH_3, bpm), 2.65 (s, 3 H, CH_3, bpy) ppm. ^{13}C NMR (100 MHz, $CDCl_3$, 25 °C): δ = 168.4 (q, bpm), 167.2 (q, bpm), 161.4 (q, bpm), 160.7 (q, bpm), 159.0 (CH_{Ar}, bpm), 158.6 (CH_{Ar}, bpm), 157.8 (q, bpy), 157.6 (q, bpy), 155.8 (q, bpy), 155.5 (q, bpy), 137.4 (CH_{Ar}, bpy), 136.9 (CH_{Ar}, bpy), 123.1 (CH_{Ar}, bpy), 121.3 (CH_{Ar}, bpy), 119.8 (CH_{Ar}, bpy), 118.1 (CH_{Ar}, bpy), 116.0 (CH_{Ar}, bpm), 114.7 (CH_{Ar}, bpm), 74.4 (OCH_2, bpy), 73.5 (OCH_2, bpm), 26.0 (CH_3, bpm), 24.6 (CH_3, bpy) ppm. UV/Vis (CH_3CN): $\lambda_{max.}$ (ε) = 285 (25117) nm. $C_{22}H_{20}N_6O \cdot 1/9CH_2Cl_2$ (393.87): calcd. C 67.43, H 5.17, N 21.34; found C 67.4, H 5.19, N 21.33.

Compound 12: Data see ref.[5]

$[Cu_2(9)_2][PF_6]_2$ (13): $[Cu(CH_3CN)_4][PF_6]$ (190 mg, 0.51 mmol) was added to the ligand **9** (200 mg, 0.51 mmol) dissolved in anhydrous CH_3CN (50 mL) under Ar. The mixture was stirred at room temperature and instantly yielding a deep-red solution. After evaporation of the solvent, the solid residue was crystallised by slow diffusion of diethyl ether into an acetone solution which gave deep-red crystals. Yield 98%. ^{1}H NMR (A/B = 64:36; 400 MHz, CD_3CN, −30 °C): δ = 8.28 (d, ^3J = 8.0 Hz, 1 H_{Ar}, bpy_A), 8.23−8.16 (m, 1 H_{Ar}, bpy_A, 2 H_{Ar}, bpy_B), 8.11 (t, ^3J = 7.8 Hz, 1 H_{Ar}, bpy_B), 8.07 (t, ^3J = 7.8 Hz, 1 H_{Ar}, bpy_A), 8.01 (t, ^3J = 7.8 Hz, 1 H_{Ar}, bpy_B), 7.92 (t, ^3J = 7.8 Hz, 1 H_{Ar}, bpy_A), 7.81 (d, ^3J = 7.4 Hz, 1 H_{Ar}, bpy_B), 7.64 (d, ^3J = 7.2 Hz, 1 H_{Ar}, bpy_A), 7.63 (s, 1 H_{Ar}, btz_B), 7.58 (d, ^3J = 7.2 Hz, 1 H_{Ar}, bpy_B), 7.37 (d, ^3J = 7.6 Hz, 1 H_{Ar}, bpy_A), 7.24 (s, 1 H_{Ar}, btz_B), 7.21 (s, 1 H_{Ar}, btz_A), 7.01 (s, 1 H_{Ar}, btz_A), 4.99 (s, 2 H, OCH_2, bpy_B), 4.86 (s, 2 H, OCH_2, btz_B), 4.31−4.22 ("q", J_{AB} = 12.8 Hz, 2 H, OCH_2, bpy_A), 4.20−4.13 ("q", J_{AB} = 13.7 Hz, 2 H, OCH_2, btz_A), 2.80 (s, 3 H, CH_3, bpy_B), 2.48 (s, 3 H, CH_3, bpy_A), 2.45 (s, 3 H, CH_3, btz_B), 2.05 (s, 3 H, CH_3, btz_A) ppm. ^{13}C NMR (100 MHz, CD_3CN, −30 °C): δ = 160.7 (q, bpy_B), 160.5 (q, bpy_A, q, bpy_B), 159.1 (q, bpy_A), 157.2 (q, bpy_B), 156.7 (q, bpy_A), 156.5 (q, bpy_B), 155.7 (q, bpy_A), 153.4 (q, btz_A, q, btz_B), 153.2 (q, btz_B), 152.8 (q, btz_A), 150.8 (q, btz_A), 150.5 (q, btz_B), 150.0 (q, btz_A), 149.9 (q, btz_B), 138.6 (CH_{Ar}, bpy_B), 138.2 (CH_{Ar}, bpy_B), 138.1 (CH_{Ar}, bpy_A), 137.7 (CH_{Ar}, bpy_A), 125.4 (CH_{Ar}, bpy_B), 125.3 (CH_{Ar}, bpy_A), 123.2 (CH_{Ar}, bpy_A), 122.4 (CH_{Ar}, bpy_B), 120.4 (CH_{Ar}, bpy_A), 120.0 (CH_{Ar}, bpy_B), 119.2 (CH_{Ar}, bpy_B), 118.9 (CH_{Ar}, bpy_A), 118.7 (CH_{Ar}, btz_B), 118.3 (CH_{Ar}, btz_A), 116.3 (CH_{Ar}, btz_B), 116.1 (CH_{Ar}, btz_A), 71.5 (OCH_2, bpy_B), 71.1 (OCH_2, bpy_A), 67.2 (OCH_2, btz_B), 66.7 (OCH_2, btz_A), 29.5 (CH_3, bpy_B), 24.2 (CH_3, btz_B), 23.7 (CH_3, bpy_A), 15.5 (CH_3, btz_A) ppm. UV/Vis (CH_3CN): $\lambda_{max.}$ ($\varepsilon_{max.}$) = 302, (20200), 450 (MLCT) (1720) nm. ESMS: *m/z* (%) = 1060.7 (60) $[Cu_2(\mathbf{9})_2(PF_6^-)]^+$, 851.0 (80) $[Cu_2(\mathbf{9})]^+$, 457.0 (100) $[Cu_2(\mathbf{9})_2]^{2+}$/2. $C_{40}H_{36}Cu_2F_{12}N_8O_2P_2S_4 \cdot CH_2Cl_2 \cdot H_2O$ (1309.00): calcd. C 37.62, H 3.08, N 8.56; found C 37.78, H 2.95, N 8.57.

$[Ag_2(9)_2][PF_6]_2$ (14): $AgPF_6$ (64.2 mg, 0.25 mmol) was added to the ligand **9** (100 mg, 0.25 mmol) dissolved in anhydrous CH_3CN (20 mL) under Ar. The mixture was stirred at room temperature and after evaporation of the solvent, the solid residue was crystallised by slow diffusion of diethyl ether into an acetone solution which gave white crystals. Yield 99%. ^{1}H NMR (400 MHz, CD_3CN, 25 °C): δ = 8.90 (2 d, 2 H_{Ar}, bpy), 8.08 (t, ^3J = 7.8 Hz, 1 H_{Ar}, bpy), 7.91 (t, ^3J = 7.8 Hz, 1 H_{Ar}, bpy), 7.49 (d, ^3J = 7.6 Hz, 1 H_{Ar}, bpy), 7.39 (d, 1 H_{Ar}, bpy), 7.38 (s, 1 H_{Ar}, btz), 7.30 (s, 1 H_{Ar}, btz), 4.56 (s, 4 H, OCH_2, bpy, OCH_2, btz), 2.55 (s, 3 H, CH_3, bpy), 2.38 (s, 3 H, CH_3, btz) ppm. ^{13}C NMR (100 MHz, CD_3CN, 25 °C): δ = 161.2 (q, bpy), 158.4 (q, bpy), 158.3 (q, bpy), 156.2 (q, bpy), 153.9 (q, btz), 152.6 (q, btz), 151.1 (q, btz), 150.4 (q, bpy), 139.4 (CH_{Ar}, bpy), 139.6 (CH_{Ar}, bpy), 125.4 (CH_{Ar}, bpy), 123.7 (CH_{Ar}, bpy), 121.6 (CH_{Ar}, bpy), 119.9 (CH_{Ar}, bpy), 119.5 (CH_{Ar}, btz), 117.5 (CH_{Ar}, btz), 72.4 (OCH_2, bpy), 66.9 (OCH_2, btz), 25.8 (CH_3, bpy), 15.9 (CH_3, btz) ppm. UV/Vis (CH_3CN): $\lambda_{max.}$ ($\varepsilon_{max.}$) = 300 (18800), 328 (12800) nm. ESMS: *m/z* (%) = 501.2 (60) $[Ag_2(\mathbf{9})_2]^{2+}$/2. $C_{40}H_{36}Ag_2F_{12}N_8O_2P_2S_4 \cdot 5/2\ CHCl_3 \cdot 0.5H_2O$ (1602.30): calcd. C 31.86, H 2.49, N 6.99; found C 31.58, H 2.44, N 7.28.

$[Zn_2(9)_2][OTf]_4$ (15): $Zn(OTf)_2$ (28.2 mg, 0.076 mmol) was added to the ligand **9** (30 mg, 0.076 mmol) dissolved in CH_3OH (10 mL) under Ar. The mixture was stirred at room temperature for 1 h and the solvent was evaporated. Yield 99%. ^{1}H NMR (400 MHz, CD_3OD, 25 °C): δ = 8.76 (d, ^3J = 8.0 Hz, 1 H_{Ar}, bpy), 8.61 (d, ^3J = 8.0 Hz, 1 H_{Ar}, bpy), 8.49 (t, ^3J = 8.0 Hz, 1 H_{Ar}, bpy), 8.20 (t, ^3J = 8.0 Hz, 1 H_{Ar}, bpy), 7.98 (d, ^3J = 7.8 Hz, 1 H_{Ar}, bpy), 7.56 (d, ^3J = 7.8 Hz, 1 H_{Ar}, bpy), 7.27 (s, 1 H_{Ar} btz), 7.25 (s, 1 H_{Ar}, btz), 5.41−5.27 ("q", AB, J_{AB} = 15.2 Hz, 2 H, OCH_2, bpy), 4.30−4.09 ("q", AB, J_{AB} = 13.4 Hz, 2 H, OCH_2, btz), 2.48 (s, 3 H, CH_3, btz), 1.95 (s, 3 H, CH_3, bpy) ppm. ^{13}C NMR (100 MHz, CD_3OD, 25 °C): δ = 162.4 (q, bpy). 159.8 (q, bpy), 157.0 (q, bpy), 154.7 (q, bpy), 148.5 (2 q, btz), 148.2 (2 q, btz), 143.6 (CH_{Ar}, bpy), 142.8 (CH_{Ar}, bpy), 129.0 (CH_{Ar}, bpy), 125.4 (CH_{Ar}, bpy), 122.9 (CH_{Ar}, bpy), 121.6 (CH_{Ar}, bpy), 121.3 (CH_{Ar}, btz), 116.8 (CH_{Ar}, btz), 68.5 (OCH_2, bpy), 67.5 (OCH_2, btz), 22.3 (CH_3, bpy), 15.9 (CH_3, btz) ppm. UV/Vis (CH_3OH): $\lambda_{max.}$ (ε) = 250 (9180), 312 (26062) nm. ESIMS: *m/z* (%) = 1364.0 (36) $[Zn_2(\mathbf{9})_2(OTf)_3]^+$, 1001.0 (19) $[Zn(\mathbf{9})_2(OTf)]^+$, 607.0 (72) $[Zn_2(\mathbf{9})_2(OTf)_2]^{2+}$/2, 426.2 (100) $[Zn\ (\mathbf{9})_2]^{2+}$/2, 229.0 (35) $[Zn_2(\mathbf{9})_2]^{4+}$/4.

$[Cu_2(10)_2][PF_6]_2$ (16): $[Cu(CH_3CN)_4][PF_6]$ (190 mg, 0.51 mmol) was added to the ligand **10** (200 mg, 0.51 mmol) dissolved in anhydrous CH_3CN (50 mL) under Ar. The mixture was stirred at room temperature instantly yielding a deep-orange solution. After evaporation of the solvent, the solid residue was crystallised by slow diffusion of diethyl ether into an acetonitrile solution which gave deep-orange crystals. Yield 92%. ^{1}H NMR (A/B = 51:49; 400 MHz, CD_3CN, −40 °C): δ = 8.34−8.26 (m, 3 H_{Ar}), 8.27 (d, ^3J = 7.8 Hz, 1 H_{Ar}, bpy), 8.20−8.11 (m, 4 H_{Ar}), 8.09−8.06 (m, 2

 © 2004 Wiley-VCH Verlag GmbH & Co. KGaA, Weinheim

H_{Ar}), 7.98 (s, 1 H_{Ar}, btz),7.78 (t, 1 H_{Ar}, bpy), 7.55 (d, 2 H_{Ar}), 7.10 (d, ^3J = 7.3 Hz, 1 H_{Ar}, bpy), 6.76 (d, ^3J = 7.4 Hz, 1 H_{Ar}, bpy), 4.39−3.98 ("q", J_{AB} = 14.3 Hz, 2 H, OCH_2 btz_A), 4.29−4.20 ("q", J_{AB} = 13.3 Hz, 2 H, OCH_2 btz_B), 3.99−3.90 ("q", J_{AB} = 8.2 Hz, 2 H, OCH_2, bpy_B), 3.77−3.68 ("q", J_{AB} = 13.4 Hz, 2 H, OCH_2, bpy_A), 2.48 (s, 3 H, CH_3, btz_B), 2.36 (s, 6 H, CH_3 bpy_B, CH_3, btz_A), 2.15 (s, 3 H, CH_3, bpy_A) ppm. ^{13}C NMR (100 MHz, CD_3CN, −30 °C; A and B could not be differentiated): δ = 166.6 (q, btz), 166.5 (q, btz), 164.4 (q, btz), 164.3 (q, btz), 156.9 (2 q, bpy), 154.4 (q, bpy), 153.9 (q, bpy), 150.8 (q, bpy), 150.5 (q, bpy), 150.4 (q, bpy), 149.9 (q, bpy), 147.4 (q, btz), 146.7 (q, btz), 146.0 (q, btz), 145.6 (q, btz), 138.2 (CH_{Ar}, bpy), 138.0 (CH_{Ar}, bpy), 137.8 (2 CH_{Ar}, bpy), 125.6 (CH_{Ar}, bpy), 125.2 (CH_{Ar}, bpy), 122.9 (CH_{Ar}, bpy), 121.3 (CH_{Ar}, bpy), 120.5 (CH_{Ar}, bpy), 119.9 (CH_{Ar}, bpy), 119.0 (CH_{Ar}, bpy), 118.6 (CH_{Ar}, bpy), 116.0 (CH_{Ar}, btz), 115.8 (CH_{Ar}, btz), 115.5 (CH_{Ar}, btz), 114.8 (CH_{Ar}, btz), 70.6 (OCH_2, bpy), 70.0 (OCH_2, bpy), 65.5 (2 OCH_2, btz), 24.3 (CH_3, bpy), 23.9 (CH_3, bpy), 17.8 (CH_3, btz), 17.6 (CH_3, btz) ppm. UV/Vis (CH_3CN): $\lambda_{max.}$ ($\varepsilon_{max.}$) = 260 (25380), 298 (14650), 448 (MLCT) (1698) nm. ESMS: *m/z* (%) = 1060.9 (45) $[Cu_2(\mathbf{10})_2(PF_6^-)]^+$, 457.0 (100) $[Cu_2(\mathbf{7})_2]^{2+}$/2. $C_{40}H_{36}Cu_2F_{12}N_8O_2P_2S_4$ (1206.05): calcd. C 39.83, H 3.01, N 9.29; found C 39.89, H 3.10, N 9.35.

$[Ag_2(\mathbf{10})_2][PF_6]_2$ (17): $AgPF_6$ (64.2 mg, 0.25 mmol) was added to the ligand **10** (100 mg, 0.25 mmol) dissolved in anhydrous CH_3CN (20 mL) under Ar. The mixture was stirred at room temperature and, after evaporation of the solvent, the solid residue was crystallised by slow diffusion of diethyl ether into an acetonitrile solution which gave white crystals. Yield 95%. ^{1}H NMR (400 MHz, CD_3CN, 25 °C): δ = 8.14−8.04 (m, 3 H_{Ar}, bpy), 7.88 (s, 1 H_{Ar}, btz), 7.82 (t, 1 H_{Ar}, bpy, s, 1 H_{Ar}, btz), 7.54 (d, ^3J = 7.6 Hz, 1 H_{Ar}, bpy), 7.16 (d, ^3J = 6.8 Hz, 1 H_{Ar}, bpy), 4.50 (s, 2 H, OCH_2, btz), 4.34 (s, 2 H, OCH_2, bpy), 2.53 (s, 3 H, CH_3, btz), 2.49 (s, 3 H, CH_3, bpy) ppm. ^{13}C NMR (100 MHz, CD_3CN, 25 °C): δ = 169.1 (q, btz), 167.7 (q, btz), 158.9 (q, bpy), 156.2 (q, bpy), 151.5 (q, bpy), 150.9 (q, bpy), 147.6 (q, btz), 146.8 (q, btz), 140.0 (CH_{Ar}, bpy), 139.9 (CH_{Ar}, bpy), 125.9 (CH_{Ar}, bpy), 123.8 (CH_{Ar}, bpy), 122.1 (CH_{Ar}, bpy), 120.5 (CH_{Ar}, bpy), 117.0 (CH_{Ar}, btz), 116.9 (CH_{Ar}, btz), 73.4 (OCH_2, bpy), 68.1 (OCH_2, btz), 26.5 (CH_3, bpy), 19.2 (CH_3, btz) ppm. UV/Vis (CH_3CN): $\lambda_{max.}$ ($\varepsilon_{max.}$) = 295 (14000) nm. ESMS: *m/z* (%) = 503.2 (20) $[Ag_2(\mathbf{10})_2]^{2+}$/2. $C_{40}H_{36}Ag_2F_{12}N_8O_2P_2S_4{\cdot}2H_2O$ (1330.73): calcd. C 36.10, H 3.03, N 8.42; found C 35.75, H 2.74, N 8.53.

$[Zn_2(\mathbf{10})_2][OTf]_4$ (18): $Zn(OTf)_2$ (28.2 mg, 0.076 mmol) was added to the ligand **10** (30 mg, 0.076 mmol) dissolved in CH_3OH (10 mL) under Ar. The solution was stirred at room temperature for 1 h and the solvent was evaporated giving a yellow powder. Yield 98%. Mixture of diastereoisomers A/B (18:82) in solution. ^{1}H NMR (400 MHz, CD_3OD, 25 °C): δ = 8.71 (d, ^3J = 8.2 Hz, 1 H_{Ar}, bpy_B), 8.52 (d, ^3J = 8.0 Hz, 1 H_{Ar}, bpy_B), 8.45 (t, ^3J = 8.0 Hz, 1 H_{Ar}, bpy_B), 8.15 (t, ^3J = 8.0 Hz, 1 H_{Ar}, bpy_B), 7.89 (d, ^3J = 8.2 Hz, 1 H_{Ar}, bpy_B), 7.67 (s, 1 H_{Ar}, btz_B), 7.57 (s, 1 H_{Ar}, btz_B), 7.51 (d, ^3J = 7.8 Hz, 1 H_{Ar}, bpy_B), 5.51−5.40 ("q", AB, J_{AB} = 15.8 Hz, 2 H, OCH_2, btz_B), 5.13 (s, 4 H, CH_2OCH_2, A), 4.53−4.46 ("q", AB, J_{AB} = 14.7 Hz, 2 H, OCH_2, bpy_B), 2.78 (s, 3 H, CH_3, btz_B), 2.66 (s, 3 H, CH_3, btz_A), 2.14 (s, 3 H, CH_3, bpy_A), 1.91 (s, 3 H, CH_3, bpy_B) ppm. ^{13}C NMR (100 MHz, CD_3OD, 25 °C): δ = 159.8, 159.6, 149.6, 148.7, 148.0 (4 q, btz, 4 q, bpy), 143.8, 143.7, 143.4, 142.9, 142.7 (4 CH_{Ar}, bpy), 129.1, 125.5, 123.3, 122.3, 122.6, 122.3, 121.4, 119.2, 118.1, 117.0, 116.8, 116.2, 116.0 (8 CH_{Ar}, bpy, 4 CH_{Ar}, btz), 69.9, 69.7, 68.9, 68.1 (2 OCH_2, btz, 2 OCH_2, bpy), 23.1, 22.2 (2 CH_3, bpy), 17.9, 16.5 (2 CH_3, btz) ppm. UV/Vis (CH_3OH): λ = 248 nm (24175), 303 (13403) nm. ESIMS: *m/z* (%) = 1363.0 (9) $[Zn_2(\mathbf{10})_2(OTf)_3]^+$, 1001.0 (22) $[Zn(\mathbf{10})_2(OTf)]^+$, 607.0 (100) $[Zn_2(\mathbf{10})_2(OTf)_2]^{2+}$/2, 229.0 (45) $[Zn_2(\mathbf{10})_2]^{4+}$/4.

$[Cu_2(\mathbf{11})_2][PF_6]_2$ (19): $[Cu(CH_3CN)_4][PF_6]$ (145.6 mg, 0.39 mmol) was added to the ligand **11** (150 mg, 0.39 mmol) dissolved in anhydrous CH_3CN (30 mL) under Ar. The mixture was stirred at room temperature, which instantly gave a deep-red solution. After evaporation of the solvent, the solid residue was recrystallised by slow diffusion of diethyl ether into an acetonitrile solution which gave deep-red crystals. Yield 94%. Mixture of diastereoisomers A/B (55:45) in solution. ^{1}H NMR (400 MHz, CD_3CN, −30 °C): δ = 9.25 (d, ^3J = 5.0 Hz, 1 H, bpm_A), 9.22 (d, ^3J = 5.2 Hz, 1 H, bpm_B), 9.05 (d, ^3J = 5.0 Hz, 1 H, bpm_B), 8.90 (d, ^3J = 5.1 Hz, 1 H, bpm_A), 8.40−8.30 (m, 7 H, A and B), 8.25 (d, ^3J = 8.0 Hz, 1 H, bpy_B), 8.16−8.08 (m, 2 H, A and B), 8.00 (t, ^3J = 7.6 Hz, 1 H, bpy_A), 7.87 (t, ^3J = 7.8 Hz, 1 H, bpy_B), 7.57 (d, ^3J = 7.4 Hz, 1 H, bpy_B), 7.53 (d, ^3J = 7.6 Hz, 1 H, bpy_A), 6.97 (d, ^3J = 7.4 Hz, 1 H, bpy_A), 6.87 (d, ^3J = 7.6 Hz, 1 H, bpy_B), 4.15−3.90 (m, 4 H, OCH_2, bpm_A, OCH_2, bpm_B), 4.15 −3.80 ("q", AB, J_{AB} = 13.5 Hz, 2 H, OCH_2, bpy_A), 4.15−3.62 ("q", AB, J_{AB} = 13.2 Hz, 2 H, OCH_2, bpy_B), 2.49 (s, 3 H, CH_3, bpm_A), 2.36 (s, 3 H, CH_3, bpm_B), 2.18 (s, 3 H, CH_3, bpy_B), 2.06 (s, 3 H, CH_3, bpy_A) ppm. ^{13}C NMR (100 MHz, CD_3CN, −30 °C): δ = 167.0, 166.7 (q, bpm_A, q, bpm_B), 163.9, 163.8 (q, bpm_A, q, bpm_B), 159.6, 159.2, 159.0, 158.7 (2 CH, bpm_A, 2 CH, bpm_B), 157.3, 157.0, 156.7, 156.5 (2 q, bpm_A, 2 q, bpm_B), 155.5, 155.2, 154.4, 154.3 (2 q, bpy_A, 2 q, bpy_B), 150.9, 150.8, 150.1, 149.8 (2 q, bpy_A, 2 q, bpy_B), 138.8, 138.4, 138.3, 138.0 (2 CH, bpy_A, 2 CH, bpy_B), 125.8, 125.7 (CH, bpy_A, CH, bpy_B), 123.0, 122.9 (CH, bpy_A, CH, bpy_B), 120.8, 120.7 (CH, bpy_A, CH, bpy_B), 119.2, 119.0 (CH, bpy_A, CH, bpy_B), 117.6, 117.5 (CH, bpm_A, CH, bpm_B), 116.0, 115.8 (CH, bpm_A, CH, bpm_B), 71.6, 71.2 (OCH_2, bpm_A, OCH_2, bpm_B, OCH_2, bpy_A, OCH_2, bpy_B), 26.0, 25.6, 24.4, 23.9 (CH_3, bpm_A, CH_3, bpm_B, CH_3, bpy_A, CH_3, bpy_B) ppm. UV/Vis (CH_3CN): $\lambda_{max.}$ (ε) = 279 (20602), 287 (20838), 450 (MLCT) (1759) nm. ESIMS: *m/z* (%) =447.3 (8) $[Cu_2(\mathbf{11})_2]^{2+}$/2. $C_{44}H_{40}Cu_2F_{12}N_{12}O_2P_2{\cdot}0.25CH_2Cl_2$ (1207.12): calcd. C 44.03, H 3.38, N 13.92; found C 43.84, H 3.42, N 13.99.

$[Ag_2(\mathbf{11})_2][PF_6]_2$ (20): $AgPF_6$ (65.84 mg, 0.26 mmol) was added to the ligand **11** (100 mg, 0.26 mol) dissolved in anhydrous CH_3CN (20 mL) under Ar. The mixture was stirred at room temperature and after evaporation of the solvent, the solid residue was recrystallised by slow diffusion of diethyl ether into an acetonitrile solution which gave white crystals. Yield 92%. ^{1}H NMR (400 MHz, CD_3CN, 25 °C): δ = 9.06 (d, ^3J = 5.4 Hz, 1 H, bpm), 8.95 (d, ^3J = 5.3 Hz, 1 H, bpm), 8.21 (d, ^3J = 5.2 Hz, 1 H, bpm), 8.18 (d, ^3J = 5.3 Hz, 1 H, bpm), 8.06 (d, ^3J = 6.5 Hz, 1 H, bpy), 8.03 (t, ^3J = 8.0 Hz, 1 H, bpy), 7.95 (d, ^3J = 8.0 Hz, 1 H, bpy), 7.62 (t, ^3J = 7.6 Hz, 1 H, bpy), 7.57 (d, ^3J = 7.4 Hz, 1 H, bpy), 6.93 (d, ^3J = 7.4 Hz, 1 H, bpy), 4.45 (s, 4 H, CH_2OCH_2), 2.56 (s, 3 H, CH_3, bpm), 2.35 (s, 3 H, CH_3, bpy) ppm.^{13}C NMR (100 MHz, CD_3CN, 25 °C): δ = 169.2 (q, bpm), 165.8 (q, bpm), 160.8 (CH, bpm), 160.9 (CH, bpm), 158.9 (q, bpm), 158.0 (q, bpm), 156.9 (q, bpy), 155.3 (q, bpy), 151.6 (q, bpy), 150.4 (q, bpy), 139.9 (CH, bpy), 139.8 (CH, bpy), 126.2 (CH, bpy), 124.6 (CH, bpy), 122.3 (CH, bpy), 120.6 (CH, bpy), 118.9 (CH, bpm), 117.1 (CH, bpm), 73.7(OCH_2, bpy), 71.9 (OCH_2, bpm), 26.4 (CH_3, bpm), 26.3 (CH_3, bpy) ppm. UV/Vis (CH_3CN): $\lambda_{max.}$ (ε) = 288 (21700) nm. ESIMS: *m/z* (%) = 491.3 (24) $[Ag_2(\mathbf{11})_2]^{2+}$/2. $C_{44}H_{40}Ag_2F_{12}N_{12}O_2P_2{\cdot}CH_2Cl_2{\cdot}H_2O$ (11377.49): calcd. C 39.24, H 3.22, N 12.20; found C 39.15, H 3.06, N 12.38.

$[Zn_2(\mathbf{11})_2][OTf]_4$ (21): $Zn(OTf)_2$ (89 mg, 0.24 mmol) was added to the ligand **11** (92 mg, 0.24 mmol) dissolved in CH_3OH (30 mL) un-

 © 2004 Wiley-VCH Verlag GmbH & Co. KGaA, Weinheim

der Ar. The mixture was stirred at room temperature for 1 h. After evaporation of the solvent, the solid residue was recrystallised by slow evaporation of a methanolic solution which gave white crystals. Yield 95%. Mixture of diastereoisomers A/B (83:17) in solution. ^{1}H NMR (400 MHz, CD_3OD, 25 °C): δ = 9.32 (d, ^3J = 5.7 Hz, 1 H, bpm_A), 9.02 (d, ^3J = 5.2 Hz, 1 H, bpm_A), 8.89 (d, ^3J = 5.2 Hz, 1 H, bpm_B), 8.84 (d, ^3J = 5.7 Hz, 1 H, bpm_A), 8.72−8.61 (2 H, B), 8.71 (d, ^3J = 7.1 Hz, 1 H, bpy_A), 8.63 (d, ^3J = 8.0 Hz, 1 H, bpy_A), 8.47−8.33 (3 H, B), 8.45 (t, ^3J = 7.8 Hz, 1 H, bpy_A), 8.41 (d, ^3J = 5.2 Hz, 1 H, bpm_A), 8.36 (t, ^3J = 8.0 Hz, 1 H, bpy_A), 8.22 (d, ^3J = 5.0 Hz, 1 H, bpm_B), 8.05−8.00 (m, 2 H, B), 7.93−7.89 (m, 2 H, bpy_A, 1 H, B), 7.37 (d, ^3J = 7.8 Hz, 1 H, bpy_B), 5.69−5.40 ("q", AB, J_{AB} = 15.4 Hz, 2 H, OCH_2, bpm_B), 5.56 (s, 2 H, OCH_2, bpm_A), 5.50 (s, 2 H, OCH_2, bpy_A), 4.61−4.23 ("q", AB, J_{AB} = 15.8 Hz, 2 H, OCH_2, bpy_B), 3.12 (s, 3 H, CH_3, bpy_A), 2.87 (s, CH_3, bpm_A), 2.81 (s, CH_3, bpy_B), 1.89 (s, CH_3, bpm_B) ppm. ^{13}C NMR (100 MHz, CD_3OD, 25 °C): δ = 169.0 (q, bpm_A), 168.7 (q, bpm_B), 165.7 (q, bpm_B), 164.8 (q, bpm_A), 164.7 (q, bpm_A), 161.4 (q, bpm_B), 160.8 (q, bpm_B), 159.8 (q, bpy_B), 159.6 (CH, bpm_A), 159.5 (CH, bpm_B, q, bpm_A), 159.1 (CH, bpm_B), 158.7 (q, bpy_A), 157.7 (CH, bpm_A), 157.0 (q, bpy_B), 154.4 (q, bpy_A), 148.8 (q, bpy_A), 148.5 (q, bpy_B), 148.4 (q, bpy_A), 148.0 (q, bpy_B), 143.6 (CH, bpy_B), 143.0 (CH, bpy_A), 142.7 (CH, bpy_B), 142.6 (CH, bpy_A), 128.8 (CH, bpy_B), 128.2 (CH, bpy_A), 125.5 (CH, bpy_B), 124.2 (CH, bpy_A), 122.8 (CH, bpy_B), 122.0 (CH, bpy_A), 121.0 (CH, bpy_B), 120.9 (CH, bpy_A), 119.28 (CH, bpm_A), 116.8 (CH, bpm_B), 115.8 (CH, bpm_A), 115.1 (CH, bpm_B), 72.4 (OCH_2, bpm_B), 70.5 (OCH_2, bpm_A), 70.3 (OCH_2, bpy_B), 68.8 (OCH_2, bpy_A), 25.0, 24.7, 22.3 (CH_3, bpm_A, CH_3, bpm_B, CH_3, bpy_A, CH_3, bpy_B) ppm. UV/Vis (CH_3CN): $\lambda_{max.}$ (ε) = 298 (21000), 305 (18971), 316 (17651) nm. ESIMS: *m*/*z* (%) = 1342.1 (4) $[Zn_2(\mathbf{11})_2(OTf)_3]^+$, 981.3 (42) $[Zn(\mathbf{11})_2(OTf)]^+$, 597.2 (10) $[Zn_2(\mathbf{11})_2(OTf)_2]^{2+}/2$, 416.3 (22) $[Zn(\mathbf{11})_2]^{2+}/2$, 224.3 (100) $[Zn_2(\mathbf{11})_2]^{4+}/4$.

$[Ag_2(\mathbf{12})_2(PF_6)_2]$ (22): Data see ref.[5]

$[Zn_2(\mathbf{12})_2][OTf]_4$ (23): $Zn(OTf)_2$ (89 mg, 0.24 mmol) was added to the ligand **12** (92 mg, 0.24 mmol) dissolved in CH_3OH (30 mL) under Ar. The mixture was stirred at room temperature for 1 h and the solvent was evaporated. Yield 98%. ^{1}H NMR (400 MHz, CD_3OD, 25 °C): δ = 9.31 (s, 1 H, bpz), 8.92 (s, 1 H, bpz), 8.62 (d, ^3J = 7.8 Hz, 1 H, bpy), 8.62 (s, 1 H, bpz), 8.46 (t, ^3J = 8.0 Hz, 1 H, bpy), 8.40 (d, ^3J = 8.0 Hz, 1 H, bpy), 8.13 (s, 1 H, bpz), 8.06 (t, ^3J = 7.8 Hz, 1 H, bpy), 7.95 (d, ^3J = 7.8 Hz, 1 H, bpy), 7.35 (d, ^3J = 7.8 Hz, 1 H, bpy), 5.60−5.45 ("q", AB, J_{AB} = 15.4 Hz, 2 H, OCH_2, bpy), 4.63 −4.44 ("q", AB, J_{AB} = 14.7 Hz, 2 H, OCH_2, bpz), 2.70 (s, 3 H, CH_3, bpz), 1.82 (s, 3 H, CH_3, bpy) ppm. ^{13}C NMR (100 MHz, CD_3OD, 25 °C): δ = 159.7 (q, bpy), 156.7 (q, bpy), 154.6 (q, bpy), 150.5 (q, bpy), 149.0 (q, bpz), 148.6 (q, bpz), 147.9 (q, bpz), 147.8 (q, bpz), 145.5 (CH, bpz), 143.9 (CH, bpy), 143.4 (CH, bpz), 142.9 (CH, bpy), 142.6 (CH, bpz), 139.5 (CH, bpz), 129.0 (CH, bpy), 125.6 (CH, bpy), 123.1 (CH, bpy), 121.2 (CH, bpy), 71.2 (OCH_2, bpz), 70.5 (OCH_2, bpy), 22.2 (CH_3, bpy), 20.7 (CH_3, bpz) ppm. UV/Vis (CH_3OH): $\lambda_{max.}$ (ε) = 233 (16728), 296 (28491) nm. ESIMS: *m*/*z* (%) = 1343.3 (5) $[Zn_2(\mathbf{12})_2(OTf)_3]^+$, 981.4 (64) $[Zn(\mathbf{12})_2(OTf)]^+$, 597.2 (13) $[Zn_2(\mathbf{12})_2(OTf)_2]^{2+}/2$, 416.3 (95) $[Zn(\mathbf{12})_2]^{2+}$, 224.2 (98) $[Zn_2(\mathbf{12})_2]^{4+}/2$.

X-ray Crystallographic Study: The crystal structures of $[Ag(C_{22}H_{20}N_6O)]_2[PF_6]_2[CH_3N]$ (**20**) [$\rho_{calcd.}$ = 1.70 Mg·m^{-3}, μ (Mo-K_α) = 0.924 mm^{-1}] and $[Ag(C_{22}H_{20}N_6O)]_2[PF_6]_2$ (**22**) [$\rho_{calcd.}$ = 1.74 Mg·m^{-3}, μ (Mo-K_α) = 0.926 mm^{-1}] were determined from single-crystal X-ray diffraction experiments using Mo-K_α X-ray radiation (λ = 0.71073 Å) with a Siemens Smart CCD diffractometer. Both compounds crystallized in the triclinic $P\bar{1}$ space group, Z = 2. The cell parameters for complex **20** are a = 13.705(2), b = 14.010(2), c = 14.277(3) Å, α = 90.47(1), β = 96.31(1), γ = 109.83(1)°, V = 2560.1(2) Å^3. The cell parameters for complex **22** are a = 12.019 (1), b = 15.153(2), c = 15.186(2) Å, α = 75.08(1), β = 70.89(1), γ = 71.13(1)°, V = 2437.0(1) Å^3. 11193 and 10720 reflections were collected up to $\theta_{max.}$ = 23.4° for complexes **20** and **22**, respectively. The structures were solved by semi-invariant methods using the SIR92 module in the WINGX package.[21].The structures were refined by the full-matrix least-squares method based on F^2 using the SHELX97[23] program. Thermal displacements of non-hydrogen atoms were refined anisotropically. Hydrogen atoms were included at their idealized positions but not refined. For complex **20**, the final statistical factors were found equal to $R1$(all observed data) = 0.058, $wR2$ = 0.130 for 7349 data and 695 parameters, $R1[F^2 > 2\sigma(I)]$ = 0.050 for 6374 data with $F^2 > 2\sigma(I)$. The final residual densities in the unit cell were +0.81 and −0.58 e·Å^{-3}. For complex **22**, the final statistical factors were found equal to $R1$(all observed data) = 0.095, $wR2$ = 0.170 for 7009 data and 667 parameters, $R1[F^2 > 2\sigma(I)]$ = 0.073 for 5541 data with $F^2 > 2\sigma(I)$. The final residual densities in the unit cell were +0.92 and −0.64 e·Å^{-3}. The crystal structures of $[Cu_2(C_{20}H_{18}N_4OS_2)_2(C_3H_6O)][PF_6]_2$ (**13**) [$\rho_{calcd.}$ = 1.62 g·cm^{-3}, μ (Mo-K_α) = 1.13 mm^{-1}] and $[Cu(C_{20}H_{18}N_4OS_2)]_2[PF_6]_2$ (**16**) [$\rho_{calcd.}$ = 1.55 g·cm^{-3}, μ (Mo-K_α) = 1.13 mm^{-1}], were determined from single-crystal X-ray diffraction experiments performed with an Enraf−Nonius CAD-4F diffractometer at room temperature. Large crystal samples (**13**: red, 0.6 × 0.5 × 0.3 mm; **16**: orange, 0.9 × 0.6 × 0.5 mm) were chosen for the experiments using Mo-K_α X-ray radiation (λ = 0.71073 Å). Both compounds crystallized in the triclinic $P\bar{1}$ space group, Z = 2 (**13**) and 4 (**16**). The unit cell parameters were obtained by least-squares fit to setting angles of 25 reflections in the range 8° < 2θ < 36° (**13**) and 12° < 2θ < 40° (**16**). The cell parameters are a = 13.336(5), b = 13.437(4), c = 15.874(5) Å, α = 90.63(2), β = 98.82(3), γ = 111.96(2)°, V = 2599(2) Å^3 (**13**) and a = 12.682(5), b = 19.688(5), c = 21.624(5) Å, α = 100.810(5), β = 97.364(5), γ = 99.628(5)°, V = 5157(3) Å^3 (**16**). The ω-2θ scan mode was used to record the diffracted intensities. Three standard reflections were monitored every 2 h in order to control the intensity decay, which did not occur significantly. 8485 and 25719 reflections were collected up to $2\theta_{max.}$ = 55.3 (**13**) and 59.9° (**16**). Lorentz-polarisation corrections and data reduction were performed using the WINGX package[26] for CAD4-collected intensities. The structures were solved by direct methods using the SIR92 program[22] and refined by the full-matrix least-squares method based on F^2 using the SHELX97[23] program. Thermal displacements of non-hydrogen atoms were refined anisotropically. Hydrogen atoms were included at their idealized positions. In the last cycles of refinement, the best results were obtained with empirical absorption corrections using the XABS2 (**13**) and DIFABS (**16**) programs in the WINGX package.[21] For the complex **13**, the final statistical factors were found equal to $R1$(all data) = 0.261, $wR2$ = 0.498 for 8485 data and 668 parameters, $R1[F^2 > 2\sigma(I)]$ = 0.183 for 3790 data with $F^2 > 2\sigma(I)$ and the final residual densities in the unit cell were +1.14 and −1.51 e·Å^{-3}. For the complex **16**, the results were $R1$(all data) = 0.258, $wR2$ = 0.419 for 23950 data and 1231 parameters, $R1[F^2 > 2\sigma(I)]$ = 0.122 for 9291 data with $F^2 > 2\sigma(I)$ and the final residual densities in the unit cell were +1.95 and −0.86 e·Å^{-3}. CCDC-205779 (**20**), -205780 (**22**), -201694 (**13**) and -201695 (**16**) contain the supplementary crystallographic data for this paper. These data can be obtained free of charge at www.ccdc.cam.ac.uk/conts/retrieving.html [or from the Cambridge Crystallographic Data Centre, 12 Union Road, Cambridge CB2 1EZ, UK; Fax: (internat.) + 44-1223/336-033; E-mail: deposit@ccdc.cam.ac.uk].

 © 2004 Wiley-VCH Verlag GmbH & Co. KGaA, Weinheim

Acknowledgments

We are grateful to the CNRS and the MESR for financial support. We also thank Mr. J. M. Ziegler for recording ES mass spectra, Mrs. E. Eppiger and P. Mutzenhardt for recording NMR spectra, and Mrs N. Marshall for correcting the manuscript.

[1] J.-M. Lehn, *Supramolecular Chemistry*, Wiley-VCH, Weinheim, **1995**.

[2] Reviews dealing with helicates: [2a] E. C. Constable, *Tetrahedron* **1992**, *48*, 113−159. [2b] C. Piguet, G. Bernardinelli, G. Hopfgartner, *Chem. Rev.* **1997**, *97*, 2005−2062. [2c] M. Albrecht, *Chem. Eur. J.* **2000**, *6*, 3485−3489. [2d] M. Albrecht, M. Schneider, *Eur. J. Inorg. Chem.* **2002**, 1301−1306. [2e] A. Lützen, M. Hapke, J. Griep-Raming, D. Haase, W. Saak, *Angew. Chem. Int. Ed.* **2002**, *41*, 2086−2089, *Angew. Chem.***2002**, *114*, 2190−2194. Reviews dealing with heterodimetallic helicates: [2f] M. Albrecht, *Chem. Rev.* **2001**, *101*, 3457−3497. [2g] E. C. Constable, J. V. Walker, *J. Chem. Soc., Chem. Commun.* **1992**, 884−885. [2h] E. C. Constable, A. J. Edwards, R. Raithby, J. V. Walker, *Angew. Chem. Int. Ed. Engl.* **1993**, *32*, 1465−1466. [2i] C. Piguet, J.-C. G. Bünzli, *Chem. Soc. Rev.* **1999**, *28*, 347−358.

[3] C. R. Rice, S. Wörl, J. C. Jeffery, R. L. Paul, M. D. Ward, *J. Chem. Soc., Chem. Commun.* **2000**, 1529−1530.

[4] M. Albrecht, R. Fröhlich, *J. Am. Chem. Soc.* **1997**, *119*, 1656−1661.

[5] J. Mathieu, A. Marsura, N. Bouhmaida, N. Ghermani, *Eur. J. Inorg. Chem.* **2002**, 2433−2437.

[6] K. Roussel, A. Cartier, A. Marsura, *Chem. Phys. Lett.* **2003**, *367*, 463−467.

[7] M. Wagner, P. Engrand, J.-B. Regnouf de Vains, A. Marsura, *Tetrahedron Lett.* **2001**, *42*, 5207−5209.

[8] L. C. Hensley, N. Y. Binghampton (General Aniline & Film Corp.), US Patent 2,553,502, **1951**, [*Chem. Abstr.* **1958**, *54*, 18378a].

[9] [9a] F. Effenberger, *Chem. Ber.* **1965**, *98*, 2260−2265. [9b] C. Janiak, L. Uhelin, H. Wu, P. Klüfers, H. G. Piotrowski, T. Scharmann, *J. Chem. Soc., Dalton Trans.* **1999**, 3121−3131.

[10] G. R. Newkome, W. E. Puckett, G. E. Kiefer, V. K. Gupta, Y. Xia, M. Coreil, M. A. Hackney, *J. Org. Chem.* **1982**, *47*, 4116−4120.

[11] logβ values were calculated using the SPECFIT® program version 3.0 (Ed.: R. A. Binstead), Spectrum Software Associates, **1993−2001**.

[12] G. Hopfgartner, C. Piguet, J. D. Henion, A. F. Williams, *Helv. Chim. Acta* **1993**, *32*, 1759−1766.

[13] See Supporting Information; see also the footnote on the first page of this aricle.

[14] J.-M. Lehn, A. Rigault, *Angew. Chem. Int. Ed. Engl.* **1988**, *27*, 1095−1097; *Angew. Chem.* **1988**, *100*, 1121−1122.

[15] C. Provent, E. Rivara-Minten, S. Hewage, G. Brunner, A. F. Williams, *Chem. Eur. J.* **1999**, *5*, 3487−3494.

[16] S. Rüttimann, C. Piguet, G. Bernardinelli, B. Bocquet, A. F. Williams, *J. Am. Chem. Soc.* **1992**, *114*, 4230−4237.

[17] [17a] A. Bilyk, M. M. Harding, *J. Chem. Soc., Dalton Trans.* **1994**, 77−82. [17b] A. Bilyk, M. M. Harding, P. Turner, T. W. Hambley, *J. Chem. Soc., Dalton Trans.* **1994**, 2783−2790.

[18] M. Greenwald, D. Wessely, E. Katz, L. Willner, Y. Cohen, *J. Org. Chem.* **2000**, *65*, 1050−1058.

[19] M. N. Burnett, C. K. Johnson, ORTEP-III report ORNL-6895, **1996**, Oak Ridge International Laboratory, Tennessee, USA.

[20] MOLEKEL: An Interactive Molecular Graphic Tool: S. Portmann, H. P. Lüthi, *CHIMIA* **2000**, *54*, 766−770.

[21] L. J. Farrugia, *J. Appl. Crystallogr.* **1999**, *32*, 837−838.

[22] A. Altomare, G. Cascarano, C. Giacovazzo, A. Guagliardi, *J. Appl. Crystallogr.* **1993**, *26*, 343−350.

[23] G. M. Sheldrick, *SHELXL-97* and *SHELXS-97: Program for the Refinement of Crystal Structures*, University of Göttingen, Germany, **1997**.

[24] F. Bodar-Houillon, Y. Elissami, A. Marsura, N. E. Ghermani, E. Espinosa, N. Bouhmaida, A. Thalal, *Eur. J. Org. Chem.* **1999**, 1427−1440.

[25] F. Bodar-Houillon, T. Humbert, A. Marsura, *Inorg. Chem.* **1995**, *34*, 5205−5209.

[26] N. E. Ghermani, N. Bouhmaida, C. Lecomte, A. L. Papet, A. Marsura, *J. Phys. Chem.* **1994**, *98*, 6287−6292.

Received December 22, 2003
Early View Article
Published Online June 1, 2004

 © 2004 Wiley-VCH Verlag GmbH & Co. KGaA, Weinheim

EurJIC
European Journal of Inorganic Chemistry

Issue 16/2004

Pages 3187–3378

Papers available ahead of print in Early View at www.interscience.wiley.com

Earliest available Table of Contents: Automatically, free of charge by e-mail through www.interscience.wiley.com/alerts

COVER PICTURE

The cover picture shows symbolically the activation of an N_2 molecule by igniting a plasma discharge in nitrogen gas. The crystal structure of a new tantalum nitride obtained by the plasma-enhanced CVD method is seen in the background. Details are discussed in the article by G. V. Vajenine et al. on p. 3233 ff. We thank the Alexander von Humboldt Foundation for support through a Sofia Kovalevskaja Research Award.

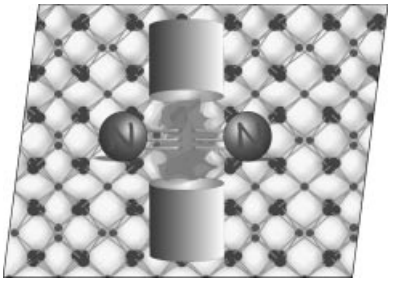

MICROREVIEW

Contents

3201 **R. Leino,* P. Lehmus, A. Lehtonen**

Heteroatom-Substituted Group 4 Bis(indenyl)-metallocenes

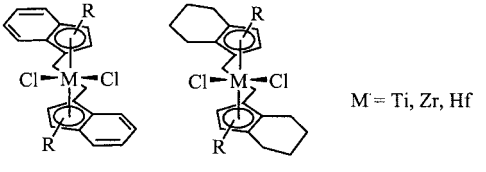

Keywords: Indene / Metallocenes / Zirconium / Olefin polymerization

 © 2004 Wiley-VCH Verlag GmbH & Co. KGaA, Weinheim

SHORT COMMUNICATIONS

3223 **R. Mas-Ballesté, W. Clegg, A. Lledós,* P. González-Duarte***

A Novel Route to Multinuclear d^8 Metal–Chalcogen Compounds with Nuclearity Control

Keywords: Cluster compounds / Platinum / Metalloligands / Self-assembly / Sulfur

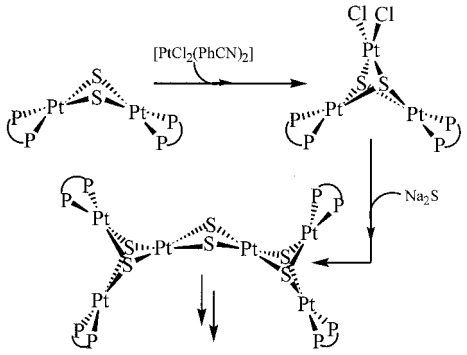

3228 **M. Du, Y.-M. Guo, X.-H. Bu,* J. Ribas**

First Tetranuclear Co^{II} Cluster with Planar Triangular Pattern: Crystal Structure and Ferromagnetic Behavior

Keywords: Carboxylic-functionalized diazamesocyclic ligands / Cobalt / Crystal structure / Magnetic properties / Tetranuclear clusters

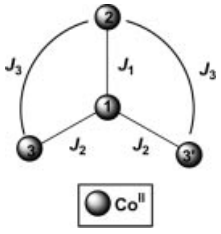

FULL PAPERS

3233 **A. Yu. Ganin, L. Kienle, G. V. Vajenine***

Plasma-Enhanced CVD Synthesis and Structural Characterization of Ta_2N_3

Keywords: Tantalum / Nitrides / Plasma-enhanced chemical vapor deposition / X-ray diffraction / Electron microscopy

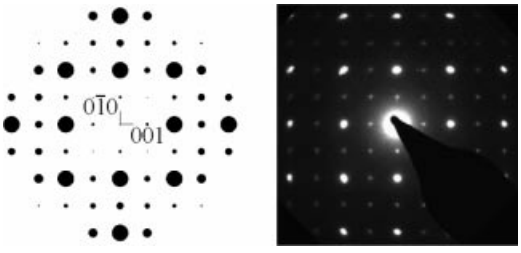

3240 **M. Mehring**

Two- and Three-Dimensional Hydrogen-Bonded Networks Built from 1,3,5-$[(HO)_2(O)P]_3C_6H_3$ and 4-(Dimethylamino)pyridine

Keywords: Phosphonic acid / Hydrogen bonds / Crystal engineering / Supramolecular chemistry

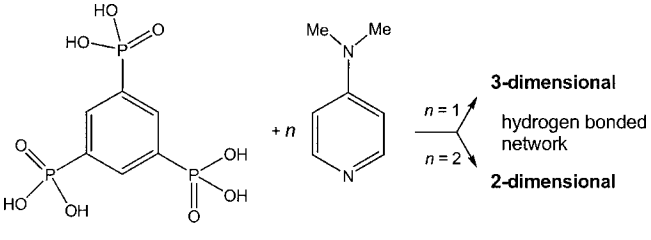

3247 **J. Gromada, A. Mortreux, G. Nowogrocki, F. Leising, T. Mathivet, J.-F. Carpentier***

Binary Neodymium Alkoxide/Dialkylmagnesium Polymerization Systems: Studies on the Nature of the Reaction Intermediates and Active Species

Keywords: Alkoxides / Alkyl complexes / Homogeneous catalysis / Magnesium / Neodymium / Polymerization

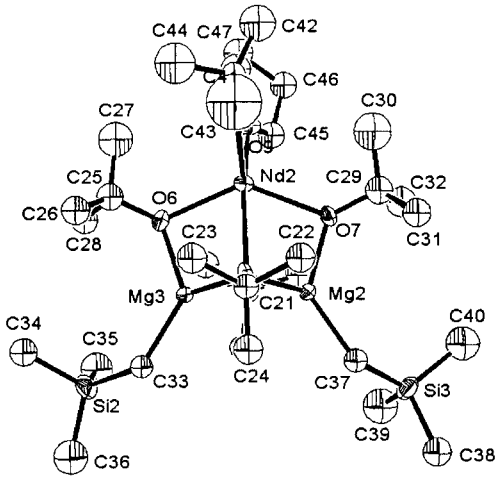

3254 **C. Mechtler, M. Zirngast, J. Baumgartner, C. Marschner***

Synthesis and Reactions of Alkynyl Oligosilanes

Keywords: Alkynes / Anions / Silanes / Polyanions

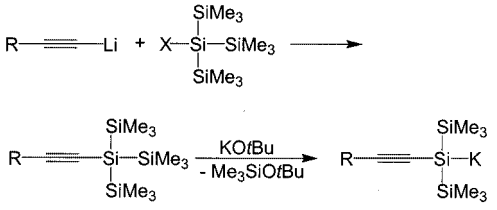

3262 **X. Zheng, C. Sun, S. Lu, F. Liao, S. Gao, L. Jin***

New Porous Lanthanide-Organic Frameworks: Synthesis, Characterization, and Properties of Lanthanide 2,6-Naphthalenedicarboxylates

Keywords: Carboxylate ligands / Coordination polymers / Hydrothermal synthesis / Lanthanides / X-ray diffraction

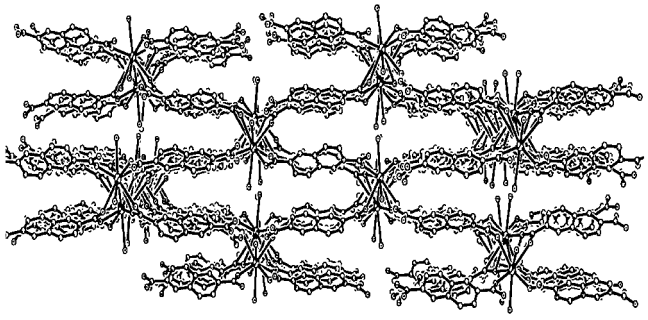

3269 **D. Brown, R. Zong, R. P. Thummel***

Ru^{II} Complexes of Bis(1,10-phenanthrolin-2-yl)-diazines

Keywords: Bridging ligands / Ruthenium / Phenanthrolines / Diazines

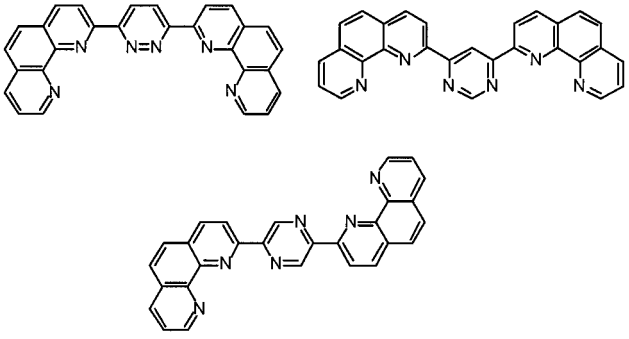

3273 **M. Ponikvar,* J. F. Liebman,* H. D. B. Jenkins***

The Redox Chemistry of SbF_6^- Ion

Keywords: SbF_6^- / Reduction / Redox chemistry / XeF_2 / Stabilisation

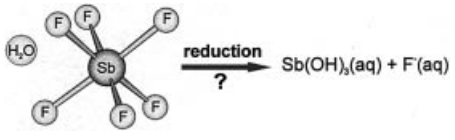

 © 2004 Wiley-VCH Verlag GmbH & Co. KGaA, Weinheim

3277 **R. Wolf, A. Schisler, P. Lönnecke, C. Jones, E. Hey-Hawkins***

Syntheses and Molecular Structures of Novel Alkali Metal Tetraorganylcyclopentaphosphanides and Tetraorganyltetraphosphane-1,4-diides

Keywords: Alkali metals / Phosphorus / P ligands / ^{31}P NMR spectroscopy / Tetraphosphane-1,4-diides

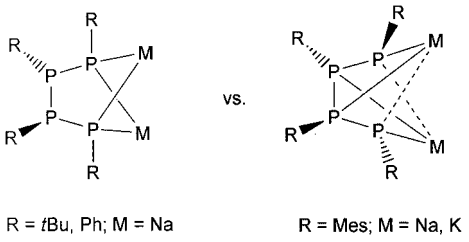

3287 **A. Sánchez-Méndez, G. F. Silvestri, E. de Jesús, F. J. de la Mata, J. C. Flores,* R. Gómez, P. Gómez-Sal**

Tris(pyrazolyl)methane Ligands: Syntheses and Structures of Monometallic and Metallodendritic Complexes

Keywords: N ligands / Titanium / Palladium / Molybdenum / Dendrimers

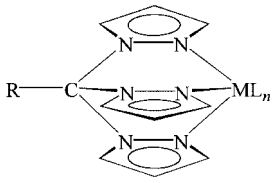

3297 **N. M. Scott, T. Schareina, O. Tok, R. Kempe***

Lithium and Potassium Amides of Sterically Demanding Aminopyridines

Keywords: Amido ligands / Coordination polymers / Lithium / N ligands / Potassium

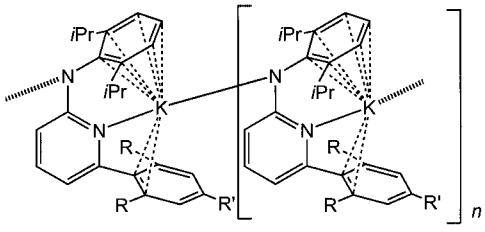

3305 **B. Royo,* E. Herdtweck, C. C. Romão**

Synthesis and Structural Characterization of Novel Oxorhenium(V) Complexes Containing N-Heterocyclic Carbenes

Keywords: Carbene ligands / Oxo ligands / Rhenium

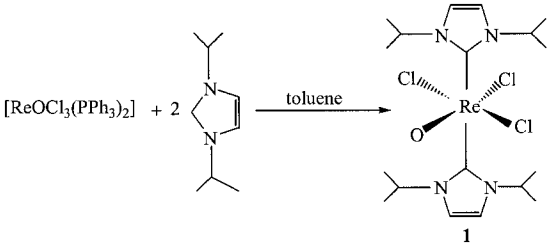

3310 **W. Niu, E. H. Wong,* G. R. Weisman,* Y. Peng, C. J. Anderson, L. N. Zakharov, J. A. Golen, A. L. Rheingold**

Structural and Dynamic Studies of Zinc, Gallium, and Cadmium Complexes of a Dicarboxylate Pendant-Armed Cross-Bridged Cyclen

Keywords: Zinc / Gallium / Cadmium / Cyclen / Cross-bridged ligand / Pendant arms

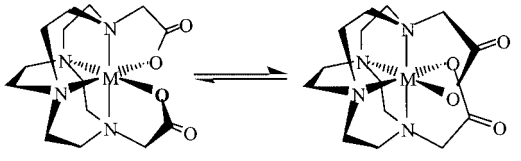

 © 2004 Wiley-VCH Verlag GmbH & Co. KGaA, Weinheim

3316 **C. Ma, C. Chen, Q. Liu,* F. Chen, D. Liao, L. Li, L. Sun**

Synthesis, Structure and Magnetic Properties of a Series of Novel Isophthalate-Bridged Manganese(II) Polymers with Double-Layer or Double-Chain Structures

Keywords: Manganese / Crystal structure / Isophthalic acid / Magnetic properties / Structural topology

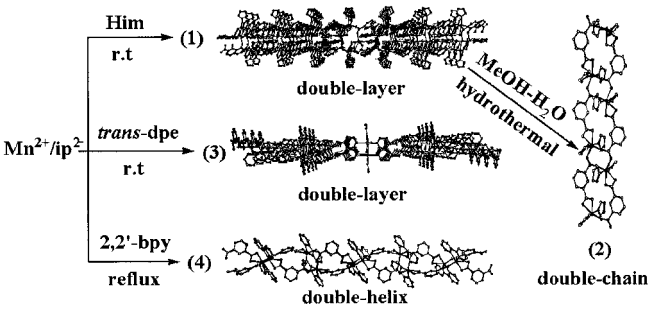

3326 **A. Garoufis,* G. Malandrinos, N. Hadjiliadis**

NMR Evidence for Major Groove Binding of Both Λ- and Δ-$[Ru(bpy)_2(pqx)](PF_6)_2$ to the Oligonucleotide $d(CGCGAATTCGCG)_2$

Keywords: Major groove / N ligands / NMR spectroscopy / Oligonucleotides / Ruthenium

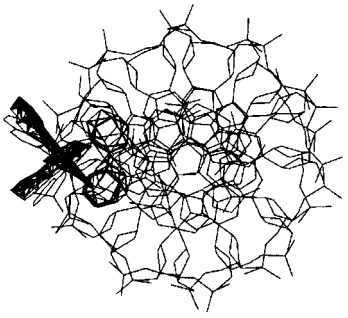

3335 **B. Korybut-Daszkiewicz,* J. Taraszewska,* K. Zięba, A. Makal, K. Woźniak***

Synthesis, Structure and Binding Properties of Nickel and Copper [14]Cyclidene Complexes with Appended Aza Crown Ethers

Keywords: Cyclidene complexes / Crown ether compounds / Copper / Nickel / Electrochemistry

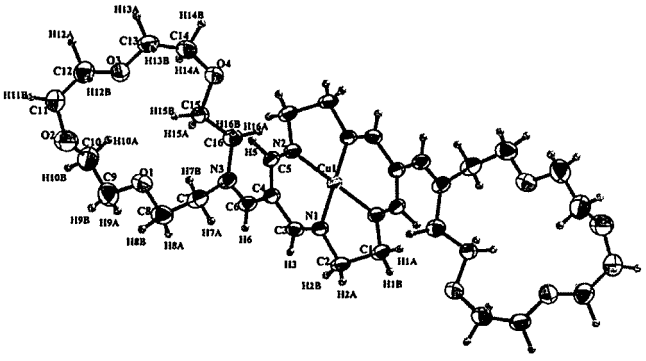

3345 **D. L. Reger,* J. D. Elgin, M. D. Smith, F. Grandjean, L. Rebbouh, G. J. Long***

A Study of the Electronic Spin-State Crossover in $\{Fe[HC(3,4,5\text{-}Me_3pz)_3]_2\}(BF_4)_2$

Keywords: Iron / N ligands / Spin crossover / Magnetic properties / Mössbauer spectroscopy

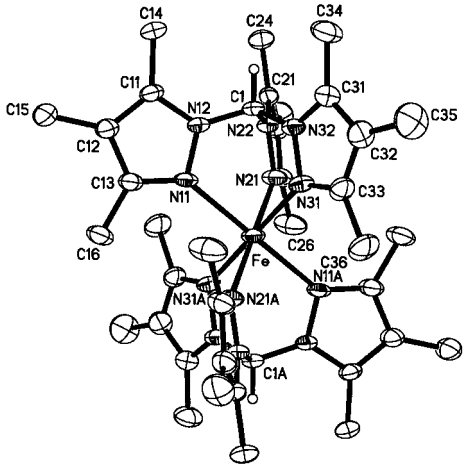

 © 2004 Wiley-VCH Verlag GmbH & Co. KGaA, Weinheim

3353

M. Ortiz, A. Díaz, R. Cao,* R. Suardíaz, A. Otero, A. Antiñolo, J. Fernández-Baeza

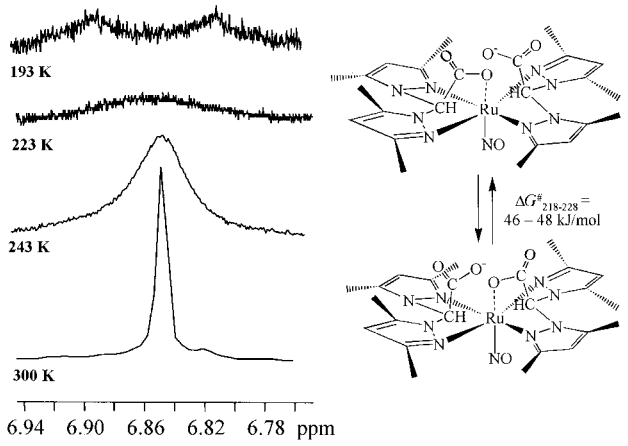

Ruthenium Nitrosyl Complexes of Bis(3,5-dimethylpyrazol-1-yl)methane Oxyanions

Keywords: Ruthenium nitrosyl complexes / Nitric oxide / NNO Scorpionates / Bis(pyrazolic) ligands

3358

L. Baradello, S. Lo Schiavo, F. Nicoló, S. Lanza, G. Alibrandi, G. Tresoldi*

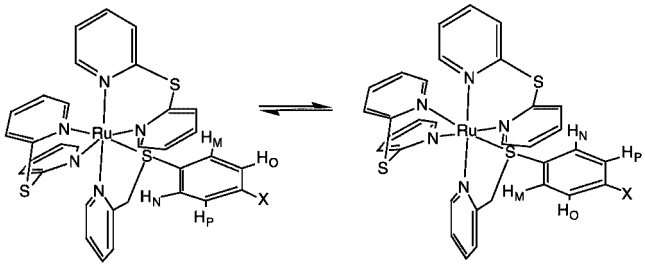

Restricted Phenyl Rotation in Pyridyl Thioether Ligands N,S-Chelated to Congested Diimino-ruthenium Cores

Keywords: Activation barriers / N,S ligands / Restricted rotation / Ruthenium

3370

P. J. Shapiro,* F. Jiang, X. Jin, B. Twamley, J. T. Patton, A. L. Rheingold

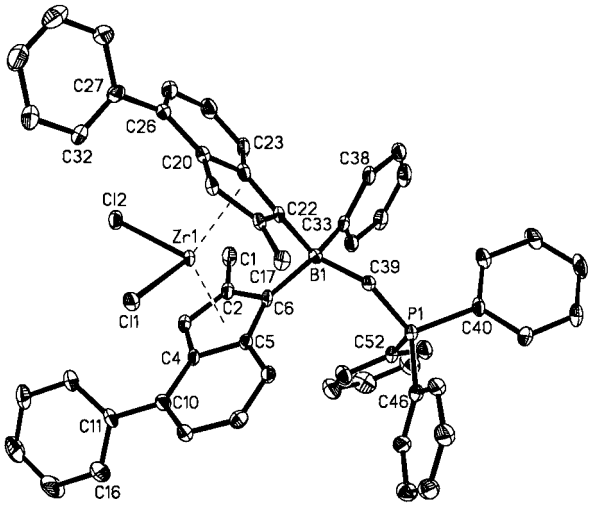

Zwitterionic Phosphorus Ylide Adducts of Boron-Bridged *ansa*-Zirconocene Complexes as Precatalysts for Olefin Polymerization

Keywords: Zirconium / Metallocenes / Boron / Ylides / Catalysis

 © 2004 Wiley-VCH Verlag GmbH & Co. KGaA, Weinheim

Heteroatom-Substituted Group 4 Bis(indenyl)metallocenes

Reko Leino,*[a] Petri Lehmus,[b] and Ari Lehtonen[c]

Keywords: Indene / Metallocenes / Zirconium / Olefin polymerization

The synthesis, characterization and applications of heteroatom-substituted group 4 bis(indenyl)metallocene complexes is reviewed. In recent years, an increasing number of group 4 metallocenes with electronically modified cyclopentadienyl ligands have been reported with, in some cases, considerably altered catalytic properties. This microreview focuses on bis(indenyl) complexes of titanium, zirconium and hafnium that contain nitrogen, oxygen and sulfur atoms directly bonded to the five- or six-membered rings of the indenyl ligand framework. The catalytic performance is briefly reviewed, with emphasis on catalytic olefin polymerization.

(© Wiley-VCH Verlag GmbH & Co. KGaA, 69451 Weinheim, Germany, 2004)

Introduction

The past decades have witnessed an impressive growth in the application of group 4 metallocene complexes in homogeneous catalysis. Of particular significance is the ability of appropriately substituted bridged and unbridged bis(indenyl)-ligated complexes to stereoselectively control the microstructure of poly-α-olefins produced when activated with methylaluminoxane (MAO) or other cocatalysts.[1−6] In enantioselective synthesis, chiral group 4 bis(indenyl)metallocenes are being employed as reagents or catalysts for various applications ranging from enantioselective cyclopolymerization[7] to carbon−carbon, carbon−hydrogen, and carbon−oxygen bond formation in small molecule syntheses.[8,9] Prototypical chiral bis(indenyl) complexes are the now classic ethylene-bridged *ansa*-metallocenes **1**−**3** and their hydrogenated tetrahydroindenyl congeners **4**−**6** (Figure 1) originally described by Brintzinger and co-

[a] Department of Organic Chemistry, Åbo Akademi University, 20500 Åbo, Finland
Fax: (internat.) + 358-2-2154866
E-mail: reko.leino@abo.fi
[b] Borealis Polymers,
P. O. Box 330, 06101 Porvoo, Finland
[c] Department of Chemistry, University of Turku, 20500 Turku, Finland

Reko Leino was born in Turku, Finland in 1969. He received his PhD (Doctor of Science in Technology) at Åbo Akademi University in 1998 with Professor Jan H. Näsman, in the field of organometallic synthesis and catalytic olefin polymerization. After a post-doctoral year at Stanford University with Professor Robert M. Waymouth in 1998-1999 working on stereocontrol in syndiospecific propylene polymerization, he briefly returned to the Laboratory of Polymer Technology, Åbo Akademi University to work on polymer-supported chiral catalysts, then for 18 months during 2001-2002 joined the Biopharmaceutical company Carbion Ltd. (later merged with Biotie Therapies Corp.) focusing on the development of carbohydrate-based pharmaceuticals. Since January 2003 he is Professor of Organic Chemistry at Åbo Akademi University with research interests ranging from synthetic organic and organometallic chemistry to polymer synthesis with current focus on stereoselective catalysis, bioorganometallic and carbohydrate chemistry.

Petri Lehmus was born in Helsinki, Finland in 1970. His interest in the polymerization behavior of single-site catalysts was inspired by his studies at Helsinki University of Technology, where he graduated as Doctor of Science in Technology from the research group of Professor Jukka V. Seppälä. Parts of his Ph.D. work were conducted in the group of Professor Bernhard Rieger at the University of Ulm, Germany. In 2000 he joined Borealis Polymers where he currently acts as research manager for Single Site Technology.

Ari Lehtonen was born in 1966. He obtained his MSc in Chemistry in 1990 from the University of Turku and his Doctorate in 1995, also at the University of Turku. During 1999 he worked as a post-doctoral fellow with Prof. Bohumil Štíbr at the Institute of Inorganic Chemistry, Academy of Sciences of the Czech Republic. Presently, he is a lecturer at the University of Turku. His current research interests include coordination chemistry of catalytically interesting high-valent metal compounds, especially molybdenum and tungsten phenoxides.

MICROREVIEWS: This feature introduces the readers to the author's research through a concise overview of the selected topic. Reference to important work from others in the field is included.

workers 20 years ago.[10−13] In the synthesis, the ethylene-bridged C_2-symmetric complexes, together with an unwanted *meso* diastereomer, are formed as racemates, which in an optimal case may be resolved through diastereomeric derivatives to afford the individual (*R*,*R*) and (*S*,*S*) enantiomers.[10,12,14−16] Since the initial reports, a huge number of substituted chiral and achiral group 4 bis(indenyl) complexes have been prepared and studied, and the structure-property relationships, especially in catalytic olefin polymerization, are now relatively well understood.[3,17−20] An excellent review is available covering the synthesis of chiral titanocene and zirconocene dichlorides and their ligand precursors,[21] including those of the bis(indenyl) type, although, with the exclusion of heteroatom-substituted ligands and complexes. An obvious attractive feature of these catalysts is the relative ease with which variations in the ligand-substitution pattern can be carried out using standard synthetic methodology, although the catalytic performance is very often a complicated and, in many cases, inseparable combination of steric as well as electronic effects.

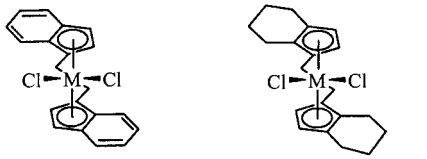

M = Ti (**1**); Zr (**2**); Hf (**3**) M = Ti (**4**); Zr (**5**); Hf (**6**)

Figure 1. Racemic ethylene-bridged bis(indenyl) and bis(tetrahydroindenyl) group 4 *ansa*-metallocenes **1**−**6**; only one enantiomer of the racemic pair is shown

Despite the imminent possibilities, the influence of electronic modification of these systems by direct heteroatom ligand substitution has, until recently, remained less explored. This reluctance may, in part, be due to the anticipated problems associated with the combination of highly electrophilic early transition metals with heteroatom-containing substituents. In recent years, however, a large number of group 4 bis(indenyl) complexes containing oxygen, sulfur as well as nitrogen donor atoms directly bonded to the five- or six-membered rings of the indenyl ligand framework have been reported in the literature; in some cases, the catalytic properties are significantly altered. The purpose of this microreview is to cover the recent synthetic efforts towards these complexes, as well as some of their catalytic applications, with the main focus on olefin polymerization. The emphasis lies on bis(indenyl) and bis(tetrahydroindenyl) complexes of the group 4 metals (Ti, Zr, Hf) that contain N, O and S atoms directly linked to the indenyl ligand. Excluded thus from detailed discussion are complexes containing substituted or unsubstituted cyclopentadienyl, fluorenyl and related ligands, complexes with pendant heteroatom substitution where the functional group is separated from the ligand by an inert linker,[22−25] as well as complexes with directly bonded phosphorus,[26] boron,[27−29] and other heteroatom substituents. The so-called constrained-geometry linked amido-cyclopentadienyl and amido-indenyl complexes,[30,31] as well as cyclopentadienyl complexes containing fused heterocyclic ring systems[32−36] that mimic those of indenyl compounds, are excluded as well. The references have been, with a few exceptions, drawn from the authors' own work in the area and the open scientific literature.

Complex Synthesis and Characterization

Amino-Substituted Group 4 Bis(indenyl)metallocenes

An early example of an amino-substituted group 4 metallocene is the 1,1′-bis(dimethylamino)titanocene dichloride **7** reported by Boche and co-workers in 1984 (Figure 2).[37] Since the first reports by Brintzinger,[38] Näsman,[39] and Plenio groups[40] in 1996, a number of 2-amino-substituted bis(indenyl) complexes of titanium and zirconium have been described and characterized (complexes **8**−**16**).[41−45] Selected compounds have been collected in Figure 3. The numbering system of indene is displayed in Figure 4. Related recently reported complexes include the mixed-ligand titanocene dichloride **17** that incorporates one 2-(dimethylamino)indenyl ligand as described by Bochmann and co-workers,[46] as well as the (aminofluorenyl)zirconium complexes of Miller and Bercaw.[47] Aminocyclopentadienyl compounds have also been incorporated into the donor/acceptor group 4 metallocenes of Ostoja Starzewski, catalyst technology designed for production of thermoplastic elastomers.[48] In addition, a number of mono- and bis(2-aminoindenyl) complexes of manganese, cobalt and iron,[49−52] lithium,[53] and ruthenium[54] have been reported in recent years. Heteroatom-substituted, constrained-geometry titanium complexes including those derived from 2- and 3-aminoindenes have also been described.[55] De Rosa, Resconi and co-workers have recently reported the preparation of a series of silyl-bridged constrained-geometry *tert*-butylamido-indenyl complexes of titanium in which the indenyl ligand has a nitrogen- or sulfur-containing heterocycle condensed onto the five-membered indenyl ring.[56,57]

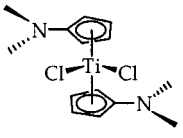

7

Figure 2. 1,1′-Bis(dimethylamino)titanocene dichloride (**7**)

Syntheses of the 2-amino-substituted indenes generally follow the original procedures of Edlund,[58−61] which involve the enamine reaction of 2-indanone with a secondary amine in methanol or toluene to produce the corresponding 2-aminoindenes, typically in excellent yields (Scheme 1).[38−40,42−45,49−53] The reaction is applicable to substituted cyclopentenones and also provides access to a

 © 2004 Wiley-VCH Verlag GmbH & Co. KGaA, Weinheim

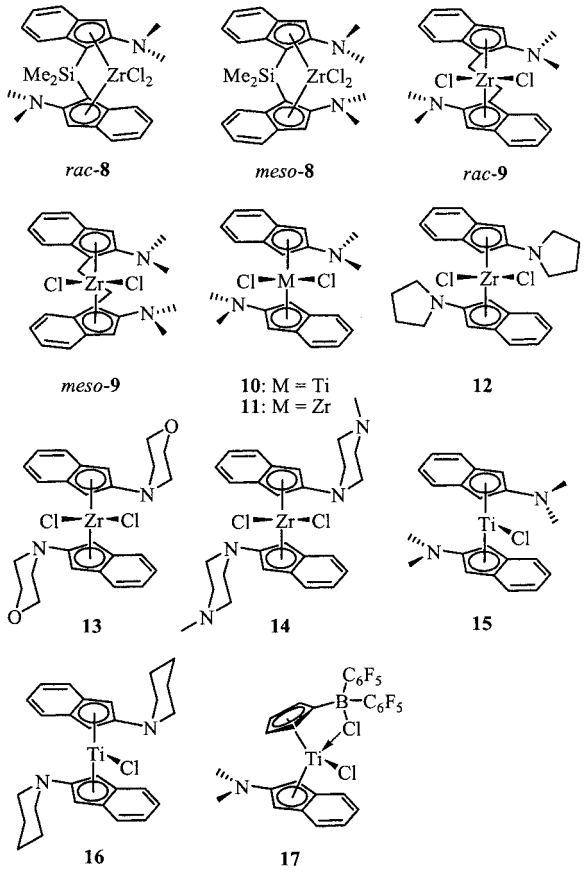

Figure 3. 2-Amino-substituted indenyl complexes of titanium and zirconium described in the literature; for racemic complexes, only one enantiomer of the racemic pair is shown

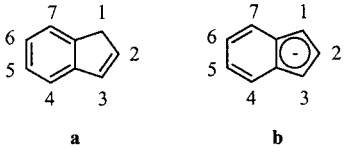

Figure 4. Numbering system for indene (**a**) and the corresponding indenyl anion (**b**)

series of amino-substituted cyclopentadienes.[40,44,49,52] For 2-(dimethylamino)indene, the synthesis of both dimethylsilylene-[38] and ethylene-bridged[39] bis(indenyl) analogues **18** and **19** in good yields (59 and 77%, respectively) has been described that employs standard deprotonation/alkylation and deprotonation/silylation procedures in THF or diethyl ether solution (Scheme 1). The synthesis of 3-aminoindenes by enamine reaction of 1-indanone with secondary amines has also been reported.[55,62,63]

The syntheses of the unbridged bis(2-aminoindenyl)zirconocene dichlorides **11**−**14** proceed in 21−75% yields by reaction of the corresponding 2-aminoindenyllithium salts with $ZrCl_4$ in Et_2O, THF or toluene (Scheme 2) followed by standard workup and crystallization procedures.[38−40,44,45] In terms of metallation yield, toluene appears to be the preferred solvent. The bis(2-dimethylamino)indenyl)titanocene dichloride analogue **10** was obtained in a nearly quantitative yield by oxidation of the corresponding titanium(III) monochloride **15**, which in turn was prepared in over 90% yield by reaction of the 2-(dimethylamino)indenyllithium salt with $TiCl_3$·3THF.[43] The piperidinoindenyl analogue **16** was obtained in 70% yield according to a similar procedure.[64] All zirconium complexes **11**−**14** have been characterized crystallographically (vide infra). The titanium(III) chlorides **15** and **16** reported by Stryker and co-workers have been further converted into a series of (η^3-allyl)titanium and titanacyclobutane complexes, several of which were characterized crystallographically[42,43] and applied in the synthesis of cyclobutanones[64] and substituted cyclobutanimines.[65]

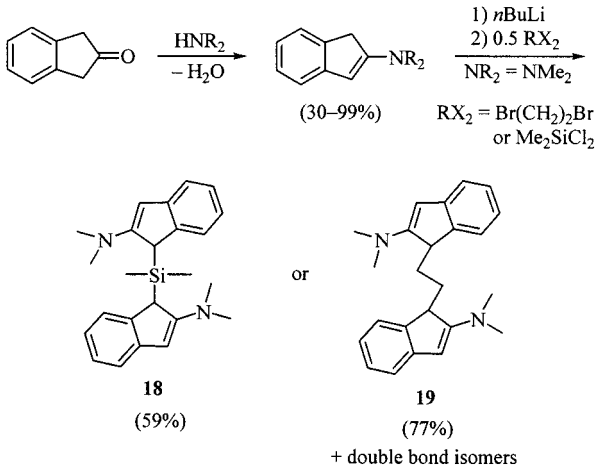

Scheme 1. Synthesis of 2-aminoindenes and the corresponding bridged bis(indenes)

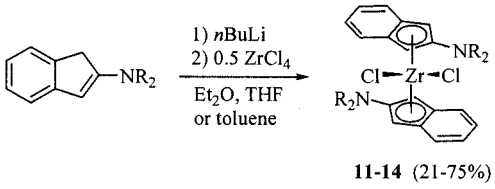

Scheme 2. Synthesis of the unbridged bis(2-aminoindenyl)zirconium dichlorides **11**−**14**

The dimethylsilylene- and ethylene-bridged bis(indenes) **18** and **19** yield, after deprotonation with *n*BuLi and subsequent reactions of the dilithium salts with $ZrCl_4$ in toluene or THF, the corresponding *ansa*-metallocene complexes **8** and **9** (see Figure 3) as mixtures of the racemic and *meso* diastereomers (Scheme 3). In the case of the dimethylsilylene-bridged complex **8**, the reaction in toluene gives a 7:2 *rac*/*meso* mixture in an overall yield of 57%, from which the pure racemic diastereomer *rac*-**8** was obtained in 30% yield by recrystallization, and was characterized crystallographically.[38] The ethylene-bridged analogue **9** in turn shows an unusual case of solvent-dependent *meso* diastereoselectivity in the metallation step, to yield a 1:1 *rac*/*meso* ratio in tolu-

 © 2004 Wiley-VCH Verlag GmbH & Co. KGaA, Weinheim

ene, from which *rac*-**9** was isolated after fractional crystallization in 33% yield.[39] However, when the metallation was carried out in THF, a 3:7 *rac*/*meso* ratio was obtained from which the pure *meso* diastereomer was isolated in 38% yield.[41] Both diastereomers of **9** have been characterized crystallographically.

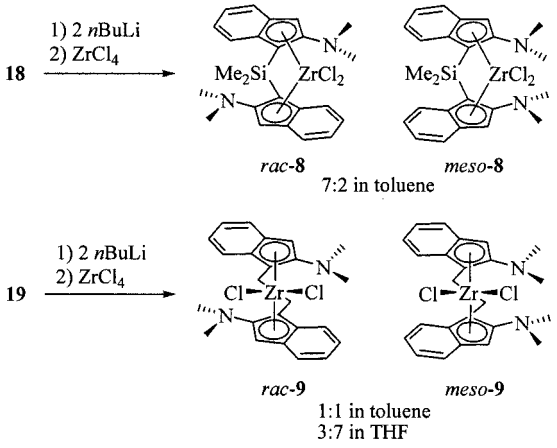

Scheme 3. Synthesis of the *ansa*-bis[2-(dimethylamino)indenyl]zirconocenes **8** and **9**; only one enantiomer of the racemic pair is shown

The ^{1}H and ^{13}C NMR spectra of all unbridged zirconium complexes **11**−**14** show time-averaged molecular C_{2v} symmetry at room temperature, consistent with rapid rotation of the aminoindenyl ligands around the Cp(centroid)−Zr axis. The ^{1}H NMR resonances of the 1-H/3-H protons in the five-membered indenyl ring range from δ = 4.42 (complex **12**) to 4.86 ppm (complex **14**); these protons are considerably shielded relative to those of the 2-hydrocarbon-substituted analogues (commonly δ ≈ 6.0−6.5 ppm), indicating increased electron density in the Cp ring induced by the electron-donating amino substituent. For the complexes **12** and **13**, a detailed 600 MHz ^{1}H NMR spectroscopic study in [D$_8$]toluene by Erker and co-workers reveals two different dynamic processes, which freeze on the NMR timescale when the monitoring temperature is lowered (Scheme 4).[44] For complex **12**, a C−N rotational barrier of $\Delta G^{\ddagger}_{(\text{CN-rot})}$ (338 K) = 16.4 ± 0.2 kcal·mol^{-1} and an activation energy for the rotation about the zirconium−Cp(indenyl) vector of $\Delta G^{\ddagger}_{(\text{Ind-rot})}$ (198 K) = 9.1 ± 0.5 kcal·mol^{-1} was determined. For the 2-morpholinoindenyl complex **13**, the corresponding values were measured as $\Delta G^{\ddagger}_{(\text{CN-rot})}$ (268 K) = 12.9 ± 0.2 kcal·mol^{-1} and $\Delta G^{\ddagger}_{(\text{Ind-rot})}$ (178 K) = 7.6 ± 0.5 kcal·mol^{-1}, indicating that, for both of these complexes, a single metallocene rotamer is present in solution at low temperature within the limits of the ^{1}H NMR detection.

In solution, racemic C_2-symmetric ethylene-bridged bis(indenyl)zirconocenes commonly rapidly interconvert between two limiting conformations, indenyl-forward (Π) and indenyl-backward (Y), which arise from the conformational freedom of the five-membered metallacycle formed by the central metal atom, bridgehead carbon atoms, and the carbon atoms of the ethylene bridge (Scheme 5).[66−68] Simi-

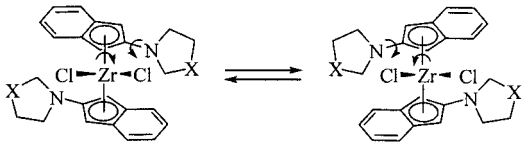

Scheme 4. Dynamic processes in unbridged bis(2-aminoindenyl)zirconium dichlorides

larly, for the *meso* diastereomers, two chiral C_1-symmetric, equienergetic, staggered, mirror-image-limiting conformations exist that interconvert in solution through a completely eclipsed conformation (Scheme 6). Bis(indenyl) complexes having one-membered silicon or carbon bridges are considerably more rigid due to the restricted conformational freedom of the four-membered metallacycle formed by the metal atom, bridgehead carbon atoms, and the bridge.

The ^{1}H NMR spectra of both *rac*- and *meso*-ethylene-bridged 2-dimethylamino-substituted bis(indenyl)zirconocenes *rac*-**9** and *meso*-**9** show at room temperature only one set of highly symmetric ligand resonances, which indicate rapid interconversion between the limiting conformations on the NMR time scale.[39,41] For both diastereomers, only one single resonance is observed for the aminomethyl groups indicating rapid rotation around the η^5-C−N bond as well. The β-protons in the five-membered indenyl rings of both *rac*-**9** (δ = 5.99 ppm) and *meso*-**9** (δ = 5.85 ppm) are considerably shielded relative to those of the racemic and *meso* diastereomers of the unsubstituted bis(indenyl) analogue **2** (δ = 6.58 and 6.70 ppm, respectively);[66] this is consistent with donation of electron density from the amino substituent to the Cp ring. Similarly, the β-H of the dimethylsilylene-bridged analogue *rac*-**8** (δ = 6.4 ppm) is strongly shielded relative to that of the unsubstituted racemic parent complex dimethylsilylenebis(indenyl)zirconium dichloride (δ = 6.90 ppm).[69]

Brintzinger and co-workers have reported cyclic voltammograms of the dimethylamino-substituted complexes *rac*-**8** and **11**.[38] In comparison with the unsubstituted analogues *rac*-dimethylsilylenebis(indenyl)zirconium dichloride and bis(indenyl)zirconium dichloride, an additional irreversible oxidation peak was observed at $E_{1/2} \approx 0$ V, indicating instability against oxidation. The Zr^{IV}/Zr^{III} reduction peaks of these complexes, recorded at $E_{1/2} = -2.48$ V (*rac*-**8**) and −2.42 V (**11**), respectively, are shifted to more negative potentials by 0.28 and 0.43 V relative to the unsubstituted analogues, indicating noticeable increase in the electron density at the Zr centers of the amino-substituted complexes. The electrochemical potentials were measured at a platinum electrode against an Ag/AgNO$_3$ (satd.) reference electrode at 25 °C, with full compensation of the internal resistance (*IR*) of the electrolyte solution, and referenced against the standard potential of the ferrocene/ferrocenium couple ($E_{1/2} = -0.12$ vs. Ag/AgNO$_3$).

 © 2004 Wiley-VCH Verlag GmbH & Co. KGaA, Weinheim

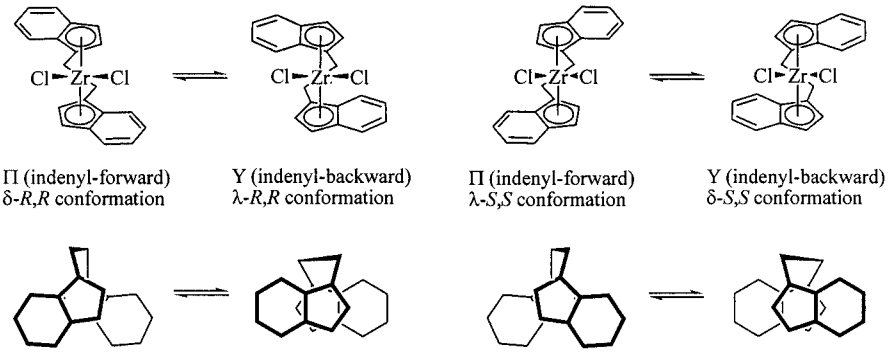

Scheme 5. Schematic presentation of the indenyl-forward/indenyl-backward interconversion for both enantiomers of the racemic ethylene-bis(indenyl)zirconium dichloride **2**

Scheme 6. Conformational freedom in the *meso* diastereomer of ethylene-bridged bis(indenyl)metallocenes

The synthesis of the indenoindole and indenopyrrole ligand precursors **20**–**22** for constrained-geometry type titanium complexes described by Resconi and co-workers are displayed in Schemes 7 and 8, respectively. The indenoindoles **20** and **21** were prepared in high yields by the acid-catalyzed Fischer condensation of 2-indanone with arylhydrazines (Scheme 7). The amines obtained were then alkylated in good yields using methyl iodide or bromoethane.[57]

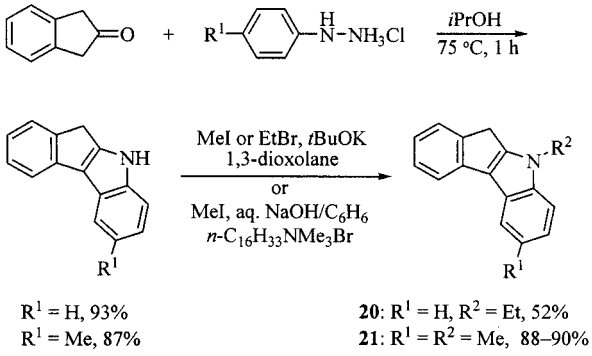

Scheme 7. Synthesis of the indenoindole ligand precursors **20** and **21**

The *N*,2-dimethyldihydroindeno[2,1-*b*]pyrrole ligand precursor **22** was obtained in 25% overall yield (4 steps) by Knorr condensation between 2-aminoindanone hydrochloride and acetoacetic ester followed by *N*-alkylation, hydrolysis, and decarboxylation of carboxylic acid (Scheme 8).[57]

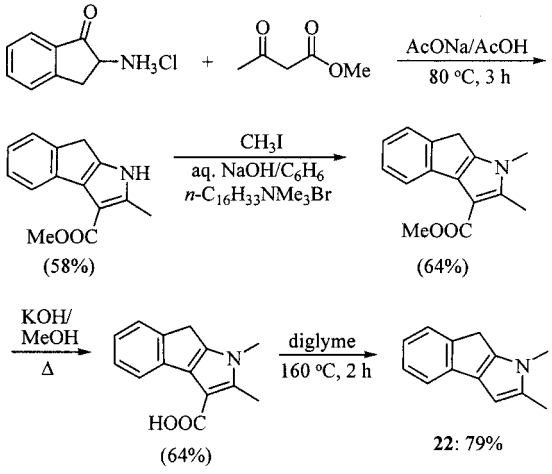

Scheme 8. Synthesis of the indenopyrrole ligand precursor **22**

Alkoxy-Substituted Group 4 Bis(indenyl)metallocenes

Alkoxy-substituted group 4 indenyl complexes **23**–**32** are collected in Figure 5. Detailed information on bis(indenyl) group 4 metallocenes containing direct alkoxy substitution in the five-membered Cp rings has only appeared in the patent literature. The racemic ethylene-bridged 2- and 3-methoxy-substituted zirconium complexes *rac*-**23** and *rac*-**24**[70] displayed in Figure 5 were obtained by recrystallization of the corresponding 1:1 *rac*/*meso* mixtures from toluene.[71] The 1:1 *rac*/*meso* mixtures had been obtained in 35 and 31% yields, respectively, by treating the lithiated ethylene-bridged ligand precursors with $ZrCl_4$ in THF. The syntheses of 2- and 3-methoxyindenes **33** and **34** are displayed in Scheme 9. Reaction of 1-indanone with trimethyl orthoformate in a mixture of methanol, benzene and a small amount of methanol saturated with dry hydrogen chloride yielded, after workup and distillation, a 59% yield of 3-methoxyindene.[72] A similar reaction of 2-indanone with trimethyl orthoformate in methanolic *p*-toluenesulfonic acid solution reportedly yielded 2-methoxyindene

 © 2004 Wiley-VCH Verlag GmbH & Co. KGaA, Weinheim

after purification by preparative GLPC, although the yield of the reaction was not described.[73][74] Subsequent deprotonation with *n*BuLi and reaction with 0.5 equiv. of dibromoethane in THF then gave the corresponding bis(methoxyindenyl)ethanes in 45 and 64% yields, respectively.[71] For the 2- and 3-methoxy-substituted zirconocene dichlorides, the five-membered ring β-protons of **23** (*rac*/*meso* mixture: 6.0/6.1 ppm) and the α-protons of **24** (*rac*/*meso* mixture: δ = 5.7/5.9 ppm) are shielded considerably relative to the corresponding β- and α-protons of the unsubstituted ethylene-bridged *rac*/*meso*-**2** (δ = 6.58/6.70 and 6.20/6.55 ppm, respectively);[66] this is consistent with increased electron density in the η^5-Cp rings. In addition to these, dimethylsilylene-bridged constrained-geometry *tert*-butylamidoindenyl complexes of titanium incorporating both 3-methoxy- and 2-ethoxyindenyl ligands have been reported in the open literature.[55] Synthesis of 2-ethoxyindene in 86% yield by reaction of 2-indanone with ethyl orthoformate in a manner similar to those reported for the 2- and 3-methoxyindenes has been described.[75]

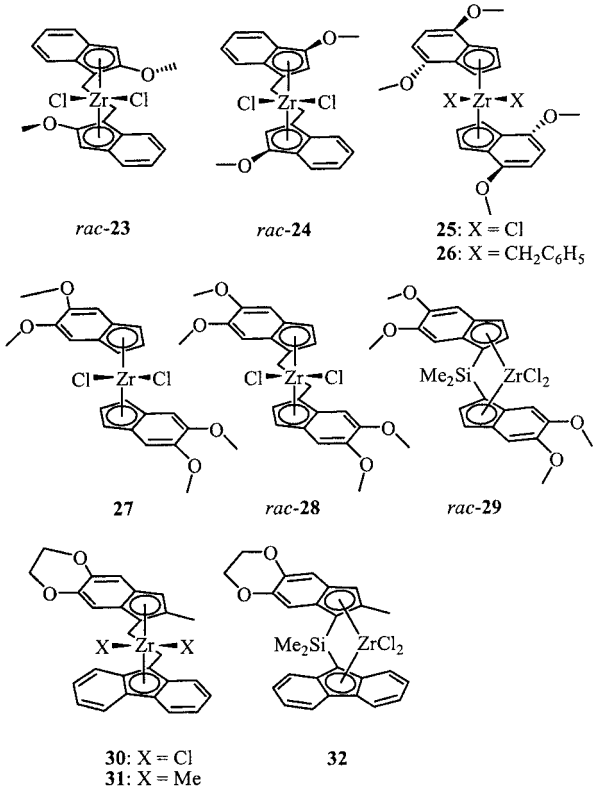

Figure 5. Alkoxy-substituted indenyl complexes of zirconium described in the literature; for racemic complexes only one enantiomer of the racemic pair is shown

Bis(indenyl)zirconium complexes containing alkoxy substitution in the six-membered rings of the indenyl ligand system have been reported in both the open and patent literature (complexes **25**−**29** in Figure 5).[71,76,77] Consiglio and co-workers have described the synthesis of 4,7-dimethoxyindene (**35**) in four steps and in 18% overall yield from *trans*-3-(2,5-dimethoxyphenyl)propanoic acid

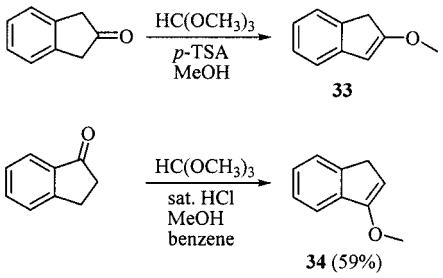

Scheme 9. Synthesis of 2- and 3-methoxyindenes (**33** and **34**)

(Scheme 10),[76] according to a modified literature procedure.[78,79] Deprotonation of **35** with *n*BuLi and subsequent reaction with $ZrCl_4$ in THF then gave, after workup and crystallization from toluene/hexane, a 40% yield of the 4,7-dimethoxy-substituted unbridged bis(indenyl)zirconium dichloride **25**.[76] The benzyl analogue **26** was prepared in 68% yield by reaction of **25** with benzylmagnesium chloride in Et_2O followed by crystallization from toluene/hexane.

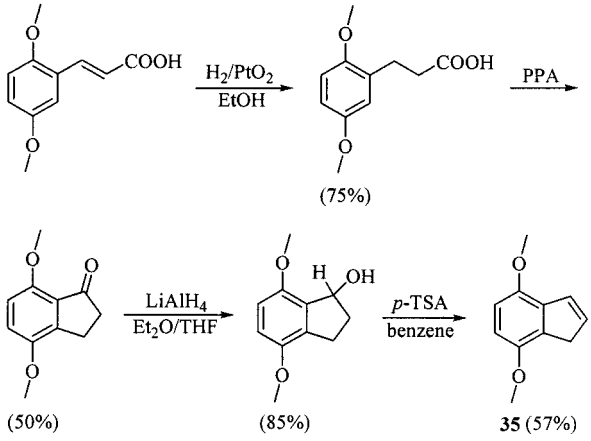

Scheme 10. Synthesis of 4,7-dimethoxyindene (**35**)

Collins and co-workers have reported the synthesis of the unbridged bis(5,6-dimethoxyindenyl)zirconium dichloride (**27**) in 35% yield by deprotonation of 5,6-dimethoxyindene (**36**) with *n*BuLi in THF followed by reaction with $ZrCl_4$ and subsequent workup and crystallization from toluene.[77] The synthesis of **36** is analogous to that of the 4,7-dimethoxy derivative **35**, which involves cyclization of 3-(3,4-dimethoxyphenyl)propanoic acid with polyphosphoric acid to the corresponding 1-indanone followed by reduction and dehydration steps to yield **36** in 49% overall yield (Scheme 11).[80] The ethylene-bridged ligand derivative was then prepared in 56% yield by reaction of the lithium derivative of **36** with dibromoethane in THF/HMPA solution.[77] Subsequent deprotonation with *n*BuLi and reaction with $ZrCl_4$ in THF gave, after workup and washing with

 © 2004 Wiley-VCH Verlag GmbH & Co. KGaA, Weinheim

toluene, the racemic ethylenebis(5,6-dimethoxyindenyl)zirconium dichloride (*rac*-**28**) in 24% yield.

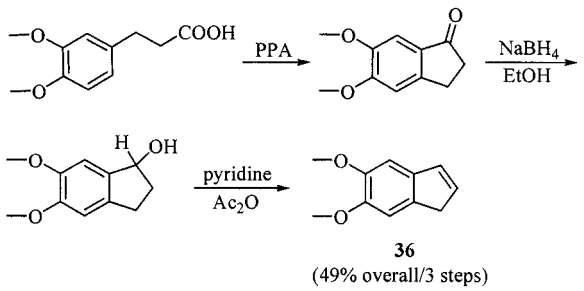

Scheme 11. Synthesis of 5,6-dimethoxyindene (**36**)

The dimethylsilylene-bridged analogue *rac*-**29** has been reported in the patent literature only. It was obtained by deprotonation of the dimethylsilylene-bridged ligand precursor with *n*BuLi and subsequent reaction of the isolated dilithium salt with $ZrCl_4$ in CH_2Cl_2 to give, after workup and crystallization from the same solvent, a 3:1 *rac*/*meso* mixture in 35% yield.[71] The pure racemate was then obtained by recrystallization. The dimethylsilylene-bridged ligand was prepared in 55% yield according to standard procedures by lithiation of **36** with *n*BuLi followed by reaction with dichlorodimethylsilane in THF.

In a recent study, Rieger and co-workers have described a series of C_1-symmetric mixed-ligand *ansa*-zirconium complexes **30**−**32**, which incorporate one 2-methylindenyl ligand with a fused 5,6-ethylenedioxy substituent.[81] The 5,6-(ethylenedioxy)-2-methylindene (**37**) employed was prepared in three steps and 32% overall yield by reaction of 1,2-(ethylenedioxy)benzene with methacryloyl chloride and $AlCl_3$ followed by subsequent reduction and dehydration steps (Scheme 12). The mixed ligand complexes form, upon activation with suitable cocatalysts, active catalyst systems for production of medium-tacticity polypropylenes. A detailed discussion is outside the scope of this review.

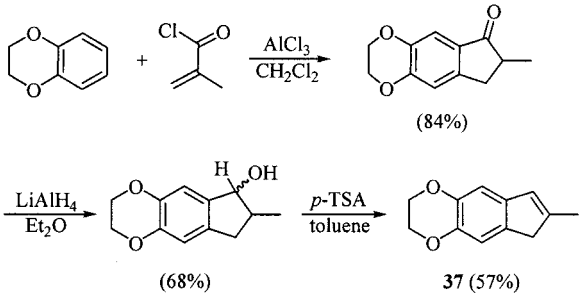

Scheme 12. Synthesis of 5,6-(ethylenedioxy)-2-methylindene (**37**)

All unbridged methoxy-substituted zirconium complexes **25**−**27** give, at room temperature, ^{1}H NMR spectra consistent with time-averaged molecular C_{2v} symmetry and unhindered ligand rotation around the Cp(centroid)−Zr axis. The η^5-Cp ring protons of the dichloride complexes **25** (1-H/3-H: δ = 6.11 ppm; 2-H: δ = 6.30 ppm) and **24** (1-H/3-H: δ = 5.91 ppm; 2-H: δ = 6.15 ppm) are considerably less shielded relative to unsubstituted bis(indenyl)zirconium dichloride (1-H/3-H: δ = 6.20 ppm; 2-H: δ = 6.45 ppm)[76,82] than those of the unbridged 2-amino-substituted complexes **11**−**14** (vide supra). Likewise, the racemic ethylene- and dimethylsilylene-bridged complexes **28** and **29** containing methoxy substituents in the six-membered indenyl rings give resonances in their ^{1}H NMR spectra that indicate that the α-H (δ = 5.98 and 5.82 ppm, respectively) and β-H (δ = 6.45 and 6.75 ppm, respectively) atoms are less shielded than the corresponding H atoms in the 2-aminoindenyl analogues, relative to those of the unsubstituted analogues *rac*-ethylenebis(indenyl)zirconium dichloride (**2**)[66] and *rac*-dimethylsilylenebis(indenyl)zirconium dichloride[69] (α-H: δ = 6.20 and 6.08 ppm; β-H: δ = 6.58 and 6.90 ppm, respectively). In the five-membered ring, however, the electron-releasing effect of the methoxy substituent is similar to that of the amino group, as can be seen by the η^5-Cp ring proton resonances of *rac*/*meso*-**23** (β-H: δ = 6.0/6.1 ppm) and *rac*/*meso*-**24** (α-H: δ = 5.7/5.9 ppm).

In addition to alkoxy groups, sterically hindered ester groups have been incorporated at both the 2- and 3-positions of indene by some of us and others (Figure 6).[83,84] All compounds **38**−**41** can be deprotonated with *n*BuLi to generate the corresponding indenyl anions. In all cases the anions were successfully trapped by addition of chlorotrimethylsilane or iodomethane. Complexation of the ester-functionalized ligands with transition metals has, however, not been described.

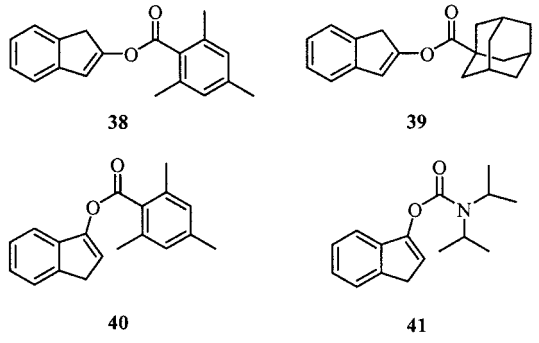

Figure 6. Ester-substituted indenes that can be deprotonated with butyllithium

Siloxy-Substituted Group 4 Bis(indenyl)metallocenes

A series of 1-(3-) and 2-trialkylsiloxy-substituted bis(indenyl) and bis(tetrahydroindenyl) complexes of zirconium and hafnium were reported by Leino, Luttikhedde, Näsman and co-workers between 1996 and 2000, with focus on the electronic effects in catalytic olefin polymerization (Figures 7 and 8).[85−97] Parts of this work have been briefly reviewed previously.[98] Prior to our work, both 2- and 3-trimethylsilylindenes had been reported in the literature;[73,99−103] however, the complexation of silyl ether substituted indenyl ligands with transition metals was undisclosed. Instead of the acid-labile and sterically less shielded trimethylsiloxy group, our initial attempts were focused on the use of the more stable *tert*-butyldimethylsilyl

 © 2004 Wiley-VCH Verlag GmbH & Co. KGaA, Weinheim

ether and its analogues as electron-donating indenyl ligand substituents.[104][105] The synthesis of 2-trialkyl/arylsiloxy-substituted indenes utilizing the keto-enol tautomerism of 2-indanone[73] is shown in Scheme 13. Thus, reaction of 2-indanone with *tert*-butylchlorodimethylsilane,[85] chlorodimethyl(thexyl)silane,[93] chlorotriisopropylsilane,[90] chloro(cyclohexyl)dimethylsilane,[106] and *tert*-butylchlorodiphenylsilane using the base/solvent combinations of DMF/imidazole or DBU/benzene gave the corresponding 2-siloxyindenes **64**−**68** as distillable oils in 69−90% yields. The six-membered ring substituted ligand analogues 2-(*tert*-butyldimethylsiloxy)-4,7-dimethylindene (**69**)[91] (distillable oil) and 2-(*tert*-butyldimethylsiloxy)cyclopenta[*l*]phenanthrene (**70**)[89] (powderous solid) were prepared in 85 and 72% yields, respectively, by reaction of 4,7-dimethyl-2-indanone[91] and 1,3-dihydro-2-oxocyclopenta[*l*]phenanthrene[107,108] (Scheme 14) with *tert*-butylchlorodimethylsilane/DBU in benzene. Analogously, the reaction of 1-indanone with *tert*-butylchlorodimethylsilane[92] and chlorotriisopropylsilane[90] using DBU/dichloromethane gave the corresponding 3-siloxyindenes **72** and **73** in 92 and 70% yields, respectively (Scheme 15). The 2-methyl-substituted analogue 3-(*tert*-butyldimethylsiloxy)-2-methylindene (**73**)[105] was prepared from 2-methyl-1-indanone[109] in 81% yield according to a similar procedure.[110]

The synthesis of the unbridged 2-siloxy-substituted bis(indenyl)zirconium dichlorides **48**,[90] **51**[91] and **52**[89] was carried out using standard procedures involving deprotonation of the indenyl ligand precursor with *n*BuLi in Et_2O or THF followed by metallation with $ZrCl_4$ in the same solvent or toluene (Scheme 16). The unbridged metallocenes were isolated after workup and crystallization in 32−42% yields. Of these, complex **51** was characterized crystallographically (vide infra). Attempts to prepare the analogous unbridged zirconium complexes from 2-(*tert*-butyldimethylsiloxy)indene (**64**) and 2-[dimethyl(thexyl)-siloxy]indene (**65**) likewise resulted in the formation of the desired metallocenes, as evidenced by EIMS, and ^1H and ^{13}C NMR analyses. Due to their extremely high solubilities in all common organic solvents, these complexes were, however, always obtained as inseparable powderous 5:3−5:2 mixtures containing also the unchanged indenyl ligand precursor as the minor component.[110] Obviously, a bulkier substitution pattern, as in complexes **48**, **51** and **52**, is required for obtaining unbridged 2-siloxy-substituted complexes in pure crystalline form.

The unbridged 2-siloxy-substituted zirconocene dichlorides **48**, **51** and **52** show at room temperature highly symmetric ^1H and ^{13}C NMR spectra consistent with time-averaged molecular C_{2v} symmetry and rapid rotation of the siloxyindenyl ligands around the Cp(centroid)−Zr axis. For example, in the ^1H NMR spectrum of complex **51** at ambient temperature five singlets are observed at δ = 6.84, 5.83, 2.32, 1.08 and 0.34 ppm in a 2:2:6:9:6 ratio assigned to the

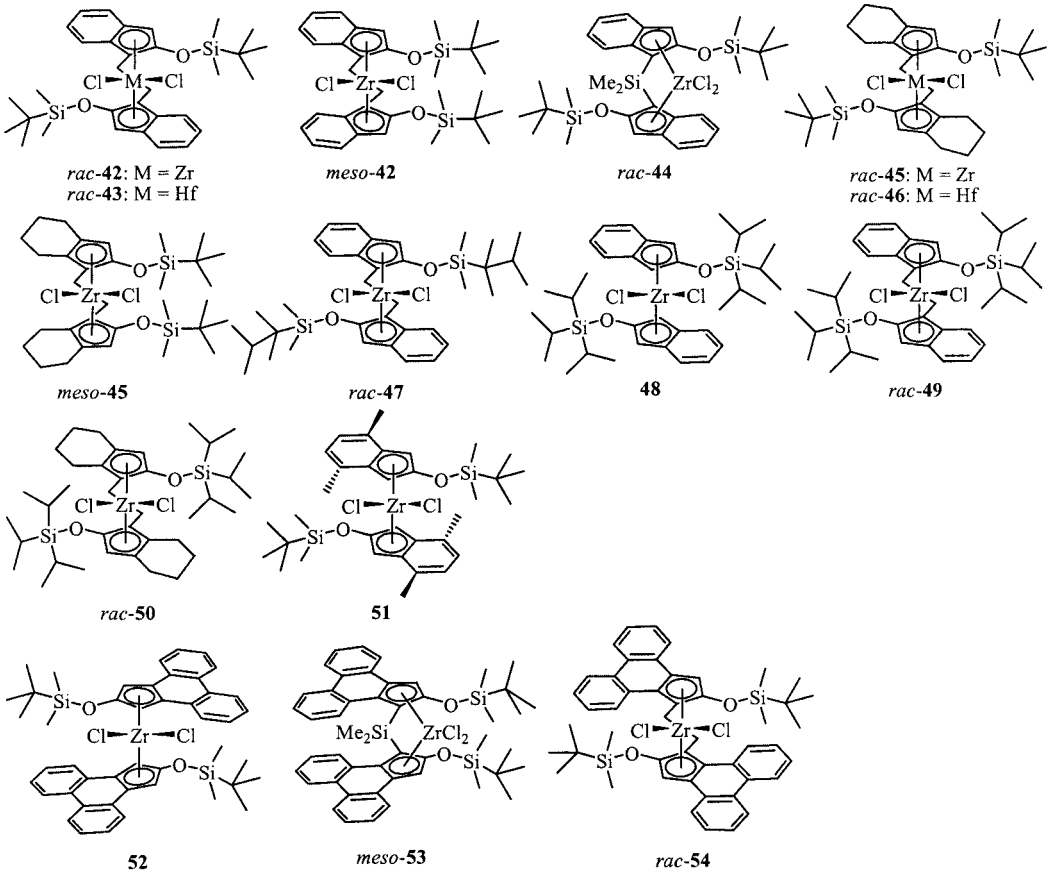

Figure 7. 2-Trialkylsiloxy-substituted bis(indenyl) and bis(tetrahydroindenyl) group 4 metallocenes; for racemic complexes, only one enantiomer of the racemic pair is shown

 © 2004 Wiley-VCH Verlag GmbH & Co. KGaA, Weinheim

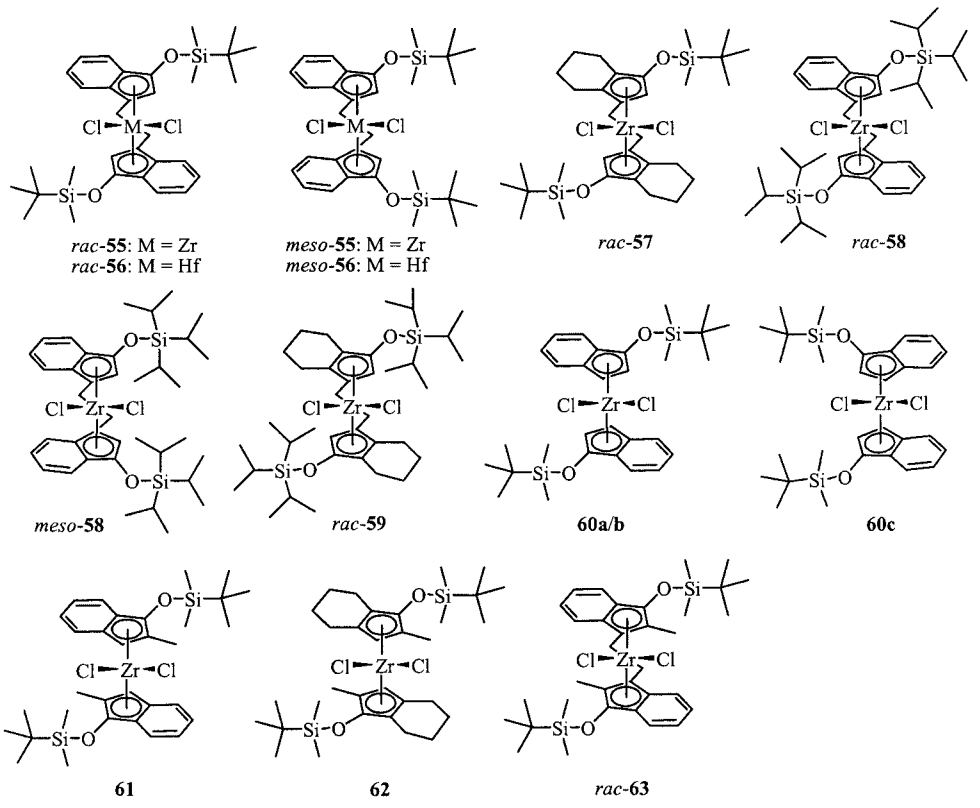

Figure 8. 1-Trialkylsiloxy-substituted bis(indenyl) and bis(tetrahydroindenyl) group 4 metallocenes; for racemic complexes, only one enantiomer of the racemic pair is shown

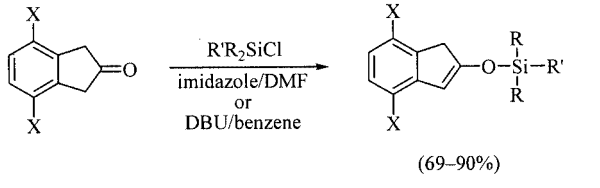

	64	65	66	67	68	69
X	H	H	H	H	H	Me
R'	*t*Bu	thex	*i*Pr	cyhex	*t*Bu	*t*Bu
R	Me	Me	*i*Pr	Me	Ph	Me

Scheme 13. Synthesis of 2-siloxyindenes **64**–**69**

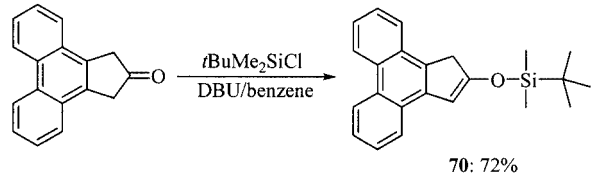

Scheme 14. Synthesis of 2-(*tert*-butyldimethylsiloxy)cyclopenta[*l*]-phenanthrene (**70**)

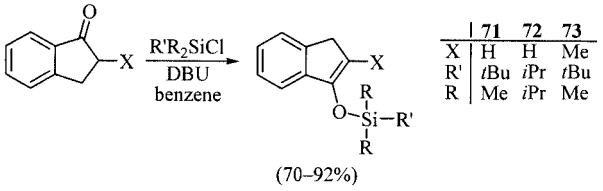

	71	72	73
X	H	H	Me
R'	*t*Bu	*i*Pr	*t*Bu
R	Me	*i*Pr	Me

Scheme 15. Synthesis of 3-siloxyindenes **71**–**73**

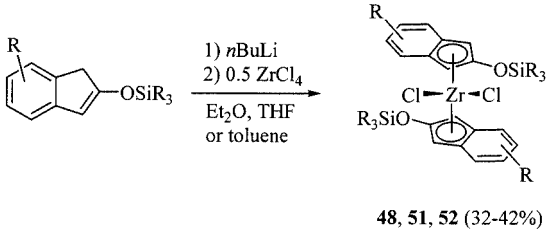

Scheme 16. Synthesis of the unbridged bis(2-siloxyindenyl)zirconium dichlorides

aromatic methine CH, five ring CH, the methyl groups of the aromatic ring, silicon-bound *tert*-butyl and methyl groups, respectively. The 1-H/3-H protons in the five-membered indenyl rings of complexes **48** (δ = 5.51 ppm)[90] and **51** (δ = 5.83 ppm)[91] are considerably more shielded than those observed for the 2-hydrocarbon-substituted analogues (commonly $\delta \approx 6.0-6.5$ ppm), indicating increased electron density in the Cp ring induced by the electron-donating siloxy substituent. In complex **52**, the observed deshielding of this proton resonance (δ = 6.24 ppm)[89] is apparently caused by the increased π-electron delocalization induced by the fused benzo substituents.

Variable-temperature NMR spectroscopic measurements were carried out on both complexes **51**[91] and **52**, and indicate dynamic behavior upon lowering the monitoring temperature. For **51**, the ^{1}H NMR resonance of the methyl sig-

 © 2004 Wiley-VCH Verlag GmbH & Co. KGaA, Weinheim

nal at δ = 2.32 ppm becomes appreciably broadened at 218−198 K, and below coalescence (T_c = 193−190 K) two resonances of equal intensities are observed. In a similar fashion, the methyl signal at δ = 0.34 ppm and the methine signals at δ = 6.84 and 5.83 ppm show considerable broadening at 218−188 K, and split into two resonances below 178 K. Finally, at 173 K a 6.3 Hz ^3J coupling was observed for the methine protons of the six-membered ring. Similar splitting was observed for most of the ^{13}C NMR signals of **51** recorded at 173 K. Analogous to the amino-substituted zirconocenes **12** and **13** described by Erker and co-workers, and discussed earlier in this microreview (vide supra),[44] the signal splitting indicates a single C_2-symmetric bent-metallocene conformation that is detected when the equilibration of **51** with its nonsuperimposable mirror image becomes frozen on the NMR time scale (Scheme 17).[111] The calculated activation barrier for **51**, $\Delta G^{\ddagger}_{(\text{Ind-rot})}$ (190−193 K) = 9.1−9.3 kcal·mol^{-1}, is of similar magnitude to those observed by Erker and co-workers for the amino-substituted complexes,[44] and by Waymouth et al. for dibenzylbis(2-phenylindenyl)zirconium for which $\Delta G^{\ddagger}_{(\text{Ind-rot})}$ (203 K) = 10.7 kcal·mol^{-1} has been reported.[112] For complex **52**, a coalescence temperature of T_c = 173−174 K was estimated from the extensive broadening of the ^{1}H NMR signals at 173 K.[113] An activation barrier $\Delta G^{\ddagger}_{(\text{Ind-rot})}$ (173 K) = 8.91 kcal·mol^{-1} was calculated using the splitting of the ^{13}C NMR Si−CH_3 resonance at this temperature.

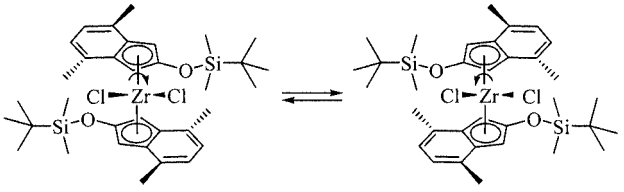

Scheme 17. Dynamic behavior in bis[2-(*tert*-butyldimethylsiloxy)-4,7-dimethylindenyl]zirconium dichloride (**51**)

The 3-(*tert*-butyldimethylsiloxy)indenes **71** and **73** were likewise converted into the corresponding bis(indenyl)zirconium dichlorides **60** and **61** by deprotonation with *n*BuLi in Et_2O followed by reaction of the isolated lithium salts with 0.5 equiv. of $ZrCl_4$ in toluene (Scheme 18). In contrast to 2-substituted indenyl complexes, the presence of a 3-(or 1-)indenyl substituent renders the ligand system prochiral. The attachment of the metal atom can occur from either enantiotopic face of the five-membered ring system, thus resulting in diastereomeric metallocene complexes consisting of a pair of racemic-like enantiomers **A** and **B**, and their *meso*-like diastereomer **C** (Figure 9).[114−116] In the case of complex **60**, workup and crystallization from Et_2O provided a first crop of a diastereomerically pure bright yellow powder in 15% yield, possibly corresponding to the enantiomeric **60a/b** mixture. Further concentration and cooling of the mother liquor then provided the other diastereomer (tentatively **60c**) in 12% yield, contaminated with traces of the other diastereomer.[117] As both diastereomers give highly symmetrical NMR spectra and similar EIMS fragmentation patterns, assignment of the diastereomers is not possible based on the spectroscopic data of the dichlorides only. Similar types of complexes have previously been assigned by Erker and co-workers based on conversion of the dichloride complexes to dimethylzirconium compounds where the *rac*-type isomer exhibits only one ^{1}H NMR resonance, whereas two resonances in a 1:1 ratio are observed for the *meso*-like diastereomer.[116] In the case of the sterically more hindered ligand precursor **73** that contains an additional 2-methyl substituent in the indenyl fragment, the ^{1}H NMR spectrum of the crude product indicates an approximately 1:1 mixture of two metallocene diastereomers. From a crude yield of 40%, diastereomerically pure complex **61** (tentatively the racemic-like isomer) was isolated in 13% yield after recrystallization from toluene. Complex **61** was further hydrogenated to yield the corresponding tetrahydroindenyl complex **62** in 65% isolated yield.[110] Despite several attempts, crystals suitable for X-ray structure determination were not obtained from any of the complexes **60**−**62**.

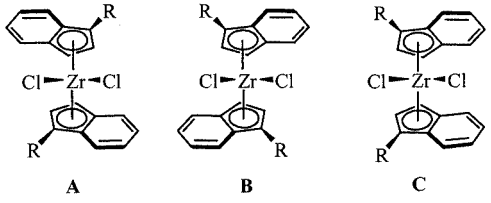

Figure 9. Diastereomers of 3-(1-)substituted bis(indenyl)metallocenes: racemic-like (**A**/**B**) and *meso*-like (**C**)

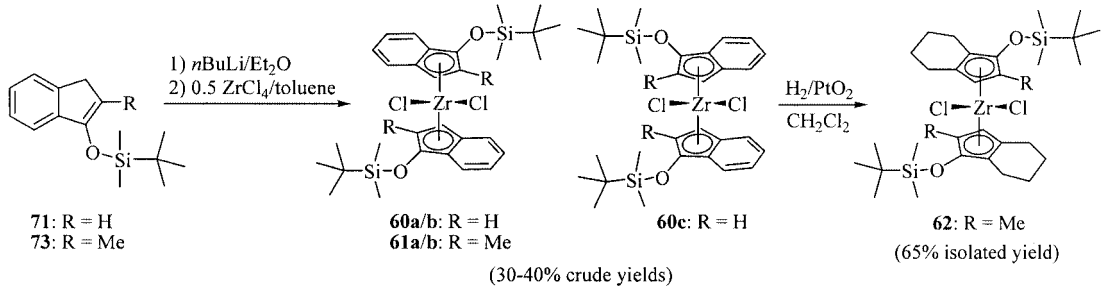

Scheme 18. Synthesis of unbridged 1-siloxy-substituted bis(indenyl) and bis(tetrahydroindenyl)zirconium dichlorides **60**−**62**; for racemic complexes only one enantiomer of the racemic pair is shown

 © 2004 Wiley-VCH Verlag GmbH & Co. KGaA, Weinheim

The synthesis of bridged 2,2′- and 3,3′-siloxy-substituted bis(indenyl) ligands was carried out according to standard procedures. Thus, all 2-siloxy-substituted indenes **64**−**68** were successfully converted into the corresponding ethylene-bridged bis(indenyl) derivatives **74**−**78** in 28−58% yields (crystalline solids) by lithiation with *n*BuLi followed by reaction with 0.5 equiv. of dibromoethane in THF, subsequent workup and purification by crystallization (Scheme 19). In contrast to bis(indenyl)ethane for which the 3,3′-indenyl-bridged isomer predominates,[10,66,118] all siloxy-substituted indenes yield exclusively the 1,1′-bridged product.[85,90,93,106] Only in the case of the six-membered ring substituted 2-siloxyindenes **69**[91] and **70**[106] were the yields for the ethylene-bridged bis(indenyl) ligands **79** and **80** (Figure 10) low (4.8 and 3.9%, respectively), which resulted from the nearly exclusive predomination of the spirocyclopropane adducts formed by intramolecular bis(alkylation) reactions of the substituted indene.[8,67,77,119] Both 2-(*tert*-butyldimethylsiloxy)indene (**64**) and 2-[dimethyl(thexyl)siloxy]indene (**65**) were further converted into the dimethylsilylene-bridged bis(indenyl) ligand analogues **81** and **82** in high yields by deprotonation with *n*BuLi followed by reaction with 0.5 equiv. of dichlorodimethylsilane.[106] The racemic diastereomers of the dimethylsilylene-bridged ligands were obtained as crystalline solids in 42 and 30% yields, respectively, and the *meso* diastereomers were isolated as oils in similar yields after exhaustive washing of the mother liquor with cold pentane. The benzo-fused dimethylsilylene-bridged bis[2-(*tert*-butyldimethylsiloxy)cyclopenta[*l*]phenanthryl] ligand (**83**, Figure 10) was prepared from **70** according to a similar procedure and isolated as a high-melting solid (m.p. 273−274 °C) in 25% yield.[89]

All 3-siloxy-substituted indenes **71**−**73** were converted into the corresponding ethylene-bridged bis(indenyl) analogues **84**,[92] **85**[90] and **86**[110] in variable yields ranging from 14% (compound **86**) to nearly quantitative (compound **85**) by deprotonation with *n*BuLi followed by reaction with dibromoethane in THF (Scheme 20).

The ethylene-bridged bis(2-siloxyindenes) **74**−**76** yield, after deprotonation with *n*BuLi and subsequent reactions of the dilithium salts with $ZrCl_4$ in THF, the corresponding *ansa*-zirconocene complexes **42**, **47** and **49** (Scheme 21).[85,90,93,97] The bulkiness of the siloxy group in the α-position to the ethylene bridge influences the *rac*/*meso* ratio of the metallocenes formed. In the case of the 2-*tert*-butyldimethylsiloxy-substituted complex **42**, metallation with $ZrCl_4$ in THF initially produces a *rac*/*meso* ratio of 14:1 as determined by ^1H NMR spectroscopic analysis of the crude product, whereas an entirely *rac*-selective metall-

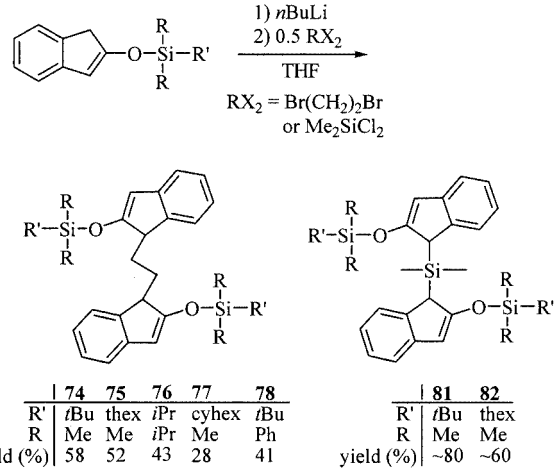

	74	75	76	77	78
R′	*t*Bu	thex	*i*Pr	cyhex	*t*Bu
R	Me	Me	*i*Pr	Me	Ph
yield (%)	58	52	43	28	41

	81	82
R′	*t*Bu	thex
R	Me	Me
yield (%)	~80	~60

Scheme 19. Synthesis of the bis(2-siloxyindenyl)ethanes **74**−**78** and the dimethylbis(2-siloxyindenyl)silanes **81** and **82**

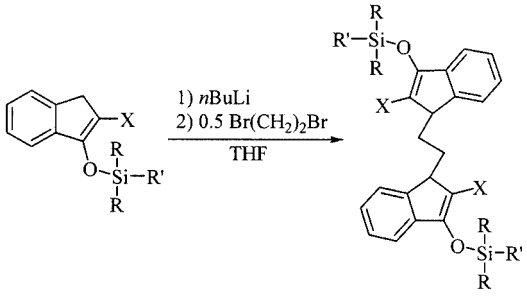

	84	85	86
X	H	H	Me
R′	*t*Bu	*i*Pr	*t*Bu
R	Me	*i*Pr	Me
yield (%)	63	99	14

Scheme 20. Synthesis of the bis(3-siloxyindenyl)ethanes **84**−**86**

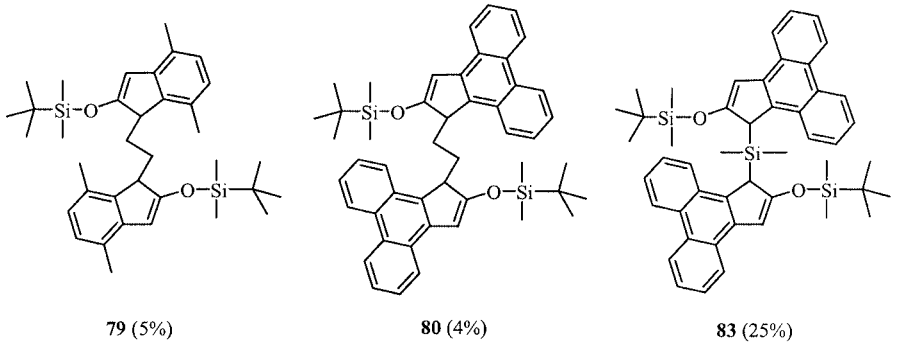

79 (5%) **80** (4%) **83** (25%)

Figure 10. Ethylene- and dimethylsilylene-bridged bis[2-(*tert*-butyldimethylsiloxy)indenes] **79**, **80** and **83**, having substituents in the six-membered rings

 © 2004 Wiley-VCH Verlag GmbH & Co. KGaA, Weinheim

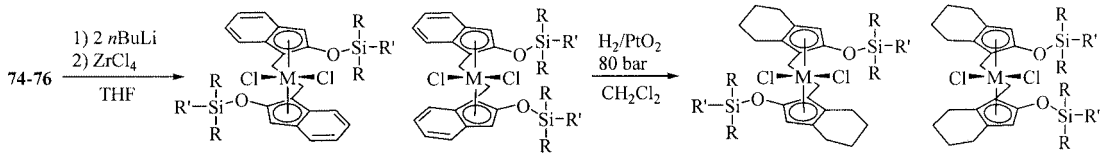

	rac-42	meso-42	rac-43	rac-47	rac-49
R'	tBu	tBu	tBu	thex	iPr
R	Me	Me	Me	Me	iPr
M	Zr	Zr	Hf	Zr	Zr
yield (%)	21-26	-	13	22	28

	rac-45	meso-45	rac-46	rac-49
R'	tBu	tBu	tBu	iPr
R	Me	Me	Me	iPr
M	Zr	Zr	Hf	Zr
yield (%)	80	-	75	67

Scheme 21. Synthesis of the ethylene-bridged 2-siloxy-substituted bis(indenyl)- and bis(tetrahydroindenyl)metallocene complexes **42**, **43**, **45**−**47**, **49** and **50**; for racemic complexes only one enantiomer of the racemic pair is shown

ation was observed for the 2-triisopropylsiloxy-substituted analogue **49**. Pure *rac*-**42** was obtained in 21−26% yield after crystallization/recrystallization from dichloromethane,[85,97] and pure *meso*-**42** after repeated recrystallization from a large-scale synthesis of **42**.[97] The analogous hafnium complex *rac*-**43** was isolated in 13% yield according to a similar procedure.[86] The racemic 2-[dimethyl(thexyl)-siloxy]-[93] and 2-triisopropylsiloxy-substituted[90] zirconium complexes *rac*-**47** and *rac*-**49** were isolated in 22 and 28% yields, respectively, after crystallization from dichloromethane or toluene. All attempts to metallate the dilithium salts of the ligand precursors **77**−**79** failed. The ethylene-bridged benzo-fused ligand precursor **80** was, however, successfully deprotonated with *n*BuLi, and treated with $ZrCl_4$ in THF. Workup and washing of the residue with toluene and hexane provided in total 22 mg of the corresponding metallocene *rac*-**54** (Figure 7) in 7% yield, tentatively assigned as the racemic diastereomer based on the highly isotactic polypropylene obtained upon activation of this complex with MAO and subsequent exposure to gaseous propylene.[113]

The racemic zirconium complexes *rac*-**42** and *rac*-**49** were further hydrogenated to yield the corresponding tetrahydroindenyl analogues *rac*-**45** and *rac*-**50**, isolated in 80% and 67% yields, respectively.[86][90] A small amount of pure *meso*-**45** was isolated after repeated recrystallization of the product obtained from hydrogenation of a *rac*/*meso*-**42** mixture.[120] Hydrogenation of the hafnium complex *rac*-**43** provided the corresponding tetrahydroindenyl complex *rac*-**46** in 75% isolated yield.[121] All of the ethylene-bridged 2-siloxy-substituted bis(indenyl)- and bis(tetrahydroindenyl)-metallocene complexes, with the exception of the bis(indenyl)hafnocene *rac*-**43**, are remarkably stable in air and towards moisture. The 2-siloxy-substituted bis(indenyl) complexes are generally soluble in cyclohexane, diethyl ether, toluene and dichloromethane. The hydrogenated congeners also dissolve readily in aliphatic solvents such as pentane and hexane. The increased stability in polar solvents is exemplified by complex *rac*-**42**, which is readily recrystallized from acetone.

The X-ray crystal structures of complexes *rac*-**42**,[85] *rac*-**45**,[87] *rac*-**46**,[121] *rac*-**47**,[93] *rac*-**49**,[90] *rac*-**50**[90] and *meso*-**45**[120] were determined and are discussed separately (vide infra).

The ^{1}H NMR spectra of all ethylene-bridged racemic and *meso*-2-siloxy-substituted bis(indenyl)- and bis(tetrahydroindenyl)metallocene dichlorides show, at ambient temperature, one set of highly symmetrical ligand resonances indicating rapid interconversion between the limiting ligand conformers on the NMR time scale. The interconversion is analogous to that discussed earlier in this microreview for the 2-dimethylamino-substituted complexes *rac*/*meso*-**9** (Schemes 5 and 6), and by Resconi and co-workers for *rac*/*meso*-ethylenebis(indenyl)zirconium dichloride **2** and its 4,7-dimethyl-substituted analogue.[66,67] Likewise, analogous to the 2-amino-substituted complexes *rac*- and *meso*-**9**, the β-protons in the five-membered rings of all ethylene-bridged *rac*- and *meso*-2-siloxy-substituted bis(indenyl) complexes **42**, **43**, **47** and **49** are shielded and the signals shifted by 0.6−0.7 ppm to a higher field relative to the corresponding resonances of the 2-alkyl or unsubstituted analogues. Similar effects are observed in the ^{13}C NMR spectra for the chemical shifts of the β-carbon atoms of the five-membered rings. The only exception in this series is the benzo-fused complex *rac*-**54**, for which a ^{1}H NMR β-H resonance of δ = 6.51 ppm, similar to that observed for the unsubstituted parent complex *rac*-ethylenebis(indenyl)zirconium dichloride *rac*-**2** (δ = 6.58 ppm),[66][118] was detected.[113] The observed shielding effects are consistent with increased electron densities in the five-membered rings induced by the electron-donating siloxy substituents. For the benzo-fused complex *rac*-**54** the observed deshielding is apparently a consequence of the increased π-electron delocalization, as observed also for its unbridged congener **52** (vide supra). In the ^{29}Si NMR spectrum of the 2-*tert*-butyldimethylsiloxy-substituted ethylene-bridged ligand precursor **74**, the Me_2Si resonance is observed at δ = 22.45 ppm; however, in the corresponding racemic bis(indenyl)- and bis(tetrahydroindenyl)zirconium complexes *rac*-**42** and *rac*-**45**, lower field ^{29}Si NMR resonances of δ = 26.64 and 25.21 ppm, respectively, are observed, which are possibly influenced by electron donation to the aromatic five-membered rings and the Lewis-acidic zirconium atoms.[98] The subsequent decrease in the local electron densities of the oxygen atoms of the metallocene complexes then result in inductive electron withdrawal from the silicon to the oxygen atom, thus contributing to the lower field ^{29}Si NMR resonances.

The dimethysilylene-bridged ligand precursor **81** gave, upon deprotonation and reaction of the dilithium salt with $ZrCl_4$ in CH_2Cl_2 and subsequent workup and crystallization from the same solvent, a 2:1 mixture of fairly pure *rac*-

 © 2004 Wiley-VCH Verlag GmbH & Co. KGaA, Weinheim

and *meso*-dimethylsilylenebis[2-(*tert*-butyldimethylsiloxy)indenyl]zirconium dichlorides (**44**) in approximately 50−55% yield (Scheme 22).[98,106] Surprisingly, in contrast to the ethylene-bridged complexes, the silylene-bridged analogue is highly sensitive towards air and moisture, and only a small sample of fairly pure racemic diastereomer *rac*-**44** was obtained after tedious recrystallization from Et_2O. Likewise, the diastereocontrol in favor of the racemic isomer in the metallation step is inferior to that observed for the ethylene-bridged analogues. The ^1H NMR chemical shift of β-H in *rac*-**44** (δ = 6.22 ppm) is of the same magnitude as that observed for the 2-dimethylamino-substituted analogue *rac*-**8** (δ = 6.4 ppm)[38] (vide supra) and strongly shielded relative to that observed for the parent *rac*-dimethylsilylenebis(-indenyl)zirconium dichloride (δ = 6.90 ppm).[69] The benzo-fused dimethylsilylene-bridged ligand **83** gave after deprotonation with *n*BuLi and subsequent reaction with $ZrCl_4$ in toluene a 1:9 *rac*/*meso* mixture of the corresponding zirconium complex **53**, as indicated by ^1H NMR spectroscopic analysis of the crude product.[89] Both diastereomers of **53** decompose rapidly in common organic solvents; the racemic isomer is the more unstable one. After rapid workup and crystallization from dichloromethane, pure *meso*-**53** was, however, obtained in 40% isolated yield.

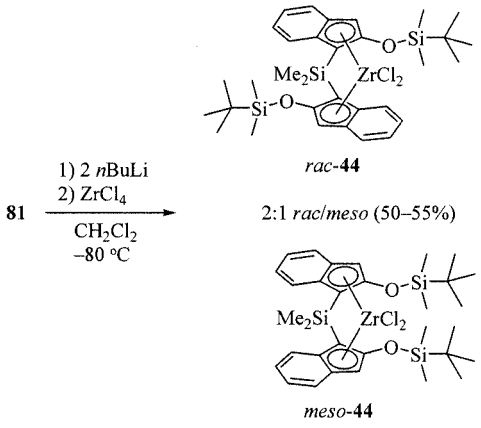

Scheme 22. Synthesis of the dimethylsilylene-bridged 2-*tert*-butyldimethylsiloxy-substituted bis(indenyl) complex **44**; only one enantiomer of the racemic pair is shown

The ethylene-bridged 3-siloxy-substituted ligand precursors **84**−**86** were likewise deprotonated with *n*BuLi in Et_2O or THF, and the obtained dilithium salts reacted with $ZrCl_4$ (ligands **84**−**86**)[90][92][110] and $HfCl_4$ (ligand **84**) in THF or dichloromethane to yield the corresponding 1-(3-)siloxy-substituted *ansa*-metallocene complexes **55**, **56**, **58** and **63** as mixtures of the *rac* and *meso* diastereomers (Scheme 23). In the case of the 1-*tert*-butyldimethylsiloxy-substituted zirconium and hafnium complexes **55** and **56**, metallation of the dilithiated ligand precursor with MCl_4 (M = Zr, Hf) initially produces a 5:1 mixture of the corresponding *rac* and *meso* diastereomers, isolated after workup and crystallization from Et_2O in 20 and 15% yields, respectively. A small amount of analytically pure racemic zirconium complex *rac*-**55** was obtained after tedious recrystallization from toluene.[92] Recrystallization of the *rac*/*meso*-hafnocene mixture from Et_2O finally provided a 28:1 mixture of *rac*-**56**/*meso*-**56** used for characterization of the racemic hafnium complex.[110] Pure *meso* diastereomers *meso*-**55** and *meso*-**56** were obtained in 4 and 8% isolated yields, respectively, after tedious recrystallization from dichloromethane or toluene. Crystals suitable for X-ray structure determination were obtained from the *meso*-zirconocene **55**.[92] Separation of the diastereomers of the *tert*-butyldimethylsiloxy-substituted complexes **55** and **56** is hampered by the *slightly lower solubilities* of the minor *meso* diastereomers in common crystallization solvents such as Et_2O and toluene. An inverse order for the solubilities was observed for the 1-(3-)triisopropylsiloxy-substituted congeners *rac*- and *meso*-**58**, of which the fairly pure racemic diastereomer was obtained in 44% yield by simply washing the crude product with Et_2O.[90] Analytically pure *rac*-**58** was then obtained by recrystallization from toluene. Recrystallization of the Et_2O extracts from hexane provided pure *meso*-**58** in 6% isolated yield. The more highly substituted 1-*tert*-butyldimethylsiloxy-2-methyl-substituted zirconium complex **63** was obtained, after workup and crystallization from hexane, as an inseparable 18:1 mixture of the *rac* and *meso* diastereomers in 7% yield.[110] A 9:1 *rac*/*meso*-**55** mixture and the pure racemic diastereomer of **58** were further hydrogenated to yield the corresponding tetrahydroindenyl complexes **57** and *rac*-**59** in 84 and 67% isolated yields, respectively. The *tert*-butyldimethylsiloxy-substituted tetrahydroindenyl complex was obtained, after crystallization from hexane, as the initial 9:1 *rac*/*meso* mixture. Samples of pure *rac*-**57** were then obtained after careful recrystallization from the same solvent and characterized crystallographically.[92]

The ^1H NMR chemical shifts of the α-protons in the five-membered rings of the racemic 1-siloxy-substituted bis(indenyl)zirconium complexes *rac*-**55** (δ = 5.60 ppm)[92] and *rac*-**58** (δ = 5.63 ppm)[90] are shielded in comparison with those observed for *rac*-ethylenebis(indenyl)zirconium dichloride (**2**) (δ = 6.20 ppm)[66] and *rac*-ethylenebis(1-trimethylsilylindenyl)zirconium dichloride (δ = 6.10 ppm),[70] consistent with electron donation from the siloxy substituent to the aromatic five-membered ring. Similarly, for the tetrahydroindenyl complexes *rac*-**57** (δ = 4.96 ppm)[92] and *rac*-**59** (δ = 5.01 ppm),[90] the α-Hs are shielded relative to that of *rac*-**5** (δ = 5.61 ppm).[118]

In addition to the siloxy-substituted group 4 bis(indenyl) complexes reported by us, a series of siloxy-substituted mono- and bis(cyclopentadienyl) complexes of iron, manganese, tungsten, titanium and zirconium have been described by Plenio and co-workers.[122−125]

Thio-Substituted Group 4 Bis(indenyl)metallocenes

To the best of our knowledge, the only examples of thio-substituted group 4 bis(indenyl)metallocene complexes are those claimed in the patent literature (Figure 11).[126] Explicit yields for the metallation step were not given, characterization data for the ligands and metallocenes were also not given. Complexes **87**−**90** were claimed to be catalysts

 © 2004 Wiley-VCH Verlag GmbH & Co. KGaA, Weinheim

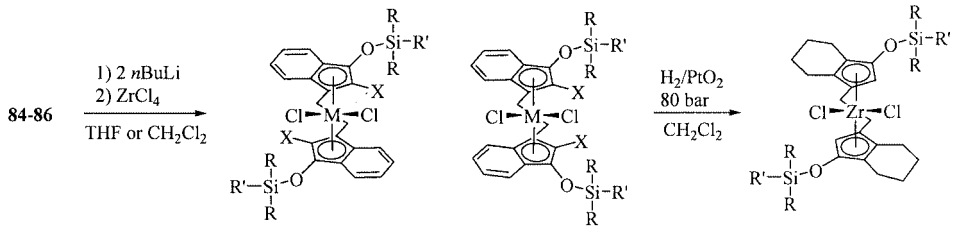

	55	56	*rac*-58	*meso*-58	63
X	H	H	H	H	Me
R'	*t*Bu	*t*Bu	*i*Pr	*i*Pr	*t*Bu
R	Me	Me	*i*Pr	*i*Pr	Me
M	Zr	Hf	Zr	Zr	Zr
rac/*meso*	5:1	5:1			18:1
yield (%)	20	15	44	6	7

	rac-57	*rac*-59
R'	*t*Bu	*i*Pr
R	Me	*i*Pr
rac/*meso*	9:1	
yield (%)	84	67

Scheme 23. Synthesis of the ethylene-bridged 1-siloxy-substituted bis(indenyl)- and bis(tetrahydroindenyl)metallocene complexes **55**−**59** and **63**; for racemic complexes only one enantiomer of the racemic pair is shown

both in solution homopolymerization of ethylene, as well as copolymerization of ethylene and propylene, with few details of polymer characterization given in the patent application.

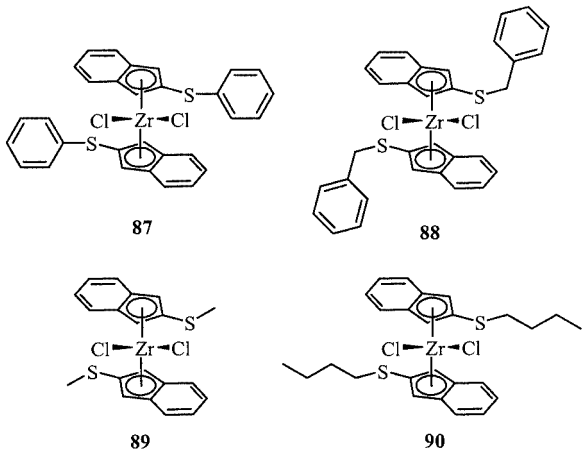

Figure 11. Thio-substituted bis(indenyl)zirconium complexes **87**−**90** reported in the patent literature

Related to these, Rausch and co-workers have reported the synthesis of the monoindenylmetallocene trichloro[1-(thiomethyl)indenyl]titanium (**93**) and its application in the syndiospecific polymerization of styrene (Scheme 24).[127] The 3-(methylthio)indene (**91**) employed as ligand precursor was prepared from indenyllithium and dimethyl disulfide in 76% yield according to the procedure of Hartke.[128] Subsequent deprotonation with *n*BuLi and reaction with chlorotrimethylsilane gave the TMS adduct **92** in 70% yield, which upon reaction with $TiCl_4$ in dichloromethane eliminates TMSCl to form the half-sandwich titanocene **93** in 46% yield after crystallization from toluene. Introduction of the methylthio group appears to have a detrimental effect on the styrene polymerization activity, presumably due to interaction of the sulfur lone pairs with the MAO cocatalyst.

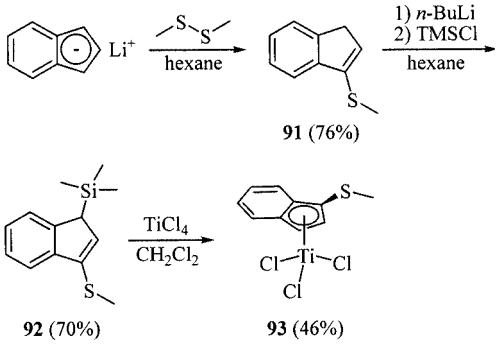

Scheme 24. Synthesis of 3-(methylthio)indene (**91**) and the corresponding half-sandwich titanium dichloride complex **93**

Preparation of C_1-symmetric, mixed-ligand ethylene-bridged group 4 *ansa*-metallocenes (Zr, Hf) **94**−**97** containing one benzothiophene-fused indenyl ligand and one fluorenyl ligand was recently described by Rieger (Figure 12).[129] The 2-methyl-1-*H*-benzo[*b*]indeno[4,5-*d*]thiophene (**98**) precursor was prepared in good yield by Friedel−Crafts acylation of dibenzothiophene with methacrylic chloride in a manner similar to that described for the 5,6-ethylenedioxy-fused ligand (Scheme 10), followed by subsequent Nazarov cyclization, ketone reduction and water elimination (Scheme 25). The mixed-ligand complexes, upon activation with MAO, form high-performance catalysts for production of controlled tacticity polypropylenes. A detailed discussion is outside the scope of this review.

The related indenyl ligand precursor 2-methyl-8*H*-indeno[2,1-*b*]thiophene (**99**), having a sulfur-containing heterocycle condensed to the indenyl *five-membered ring* and reported by Resconi and co-workers for use in constrained-geometry titanium complexes, was prepared from 4-bromo-2-methylthiophene in 30% overall yield (three steps), as displayed in Scheme 26.[57] The 2-methyl-4-phenylthiophene was obtained in 70% yield after reaction of the bromo compound with phenylmagnesium bromide. Sub-

 © 2004 Wiley-VCH Verlag GmbH & Co. KGaA, Weinheim

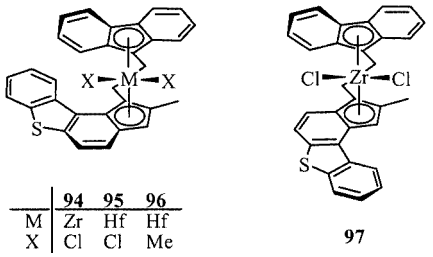

Figure 12. Benzothiophene-fused mixed-ligand *ansa*-(fluorenyl)(indenyl)metallocenes **94**−**97**

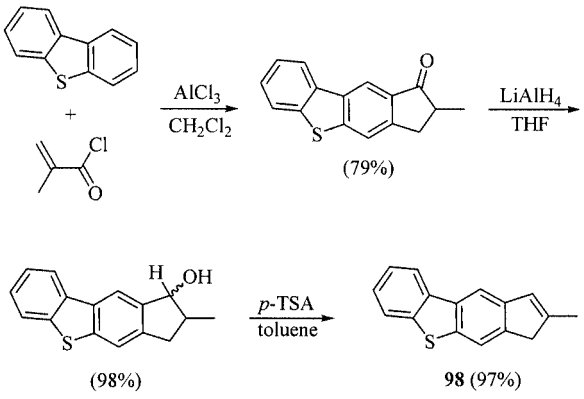

Scheme 25. Synthesis of 2-methyl-1*H*-benzo[*b*]indeno[4,5-*d*]thiophene (**98**)

sequent dimetallation with *n*BuLi was followed by reaction with ethyl *N*,*N*-dimethylcarbamate and Wolff−Kishner reduction of the obtained ketone to furnish **99**.

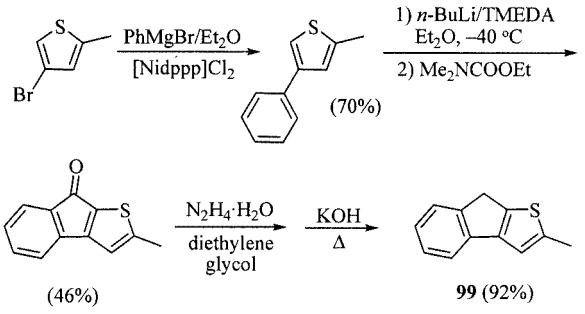

Scheme 26. Synthesis of 2-methyl-8*H*-indeno[2,1-*b*]thiophene (**99**)

Additionally, a few examples of bis(cyclopentadienyl) group 4 metallocenes containing phenylthio-[130] and propylthio-substituted[131,132] Cp ligands have been reported in the literature.

Theoretical Studies

Pakkanen and co-workers have studied the geometry prediction of a large set of bridged zirconocene dichloride complexes by ab initio Hartree−Fock, MP2, BLYP and B3LYP methods; with basis sets range from 3-21G* to 6-311G**.[133] Selected calculated geometrical parameters of close to 60 zirconocene dichloride complexes, including several amino- and siloxy-substituted bis(indenyl) and bis(tetrahydroindenyl)zirconocenes, were compared with the experimentally determined crystal structures. The least expensive HF/3-21G* method was verified to be notably accurate for such predictions by a comprehensive data set of 62 bridged zirconocene dichlorides. In a separate study by the same authors,[134] factors controlling the accessibility of cationic metal sites in zirconocene polymerization catalysts was investigated by the ab initio Hartree−Fock method at the 3-21G* level. Special emphasis was laid on the influence of the electronic effects and the ligand structure on the accessibility, stabilization and destabilization of the active center. Several heteroatom-substituted indenyl complexes, including both amino and siloxy substitution, were modeled successfully. A detailed description is outside the scope of this microreview.

In yet another study by Pakkanen et al., conformational preferences of racemic ethylene-bridged bis(indenyl)zirconocenes were investigated using the ab initio Hartree−Fock method with emphasis on the influence of the ligand-substitution pattern on the relative stabilities of the limiting indenyl-backward (Y) and indenyl-forward (Π) conformations (Scheme 5) and their interconversion.[135] Conformational interconversion of several ethylene-bridged methyl- and 1- or 2-trialkylsiloxy-substituted bis(indenyl)- and bis(tetrahydroindenyl)zirconium dichlorides was evaluated as part of this investigation.

Solid-State Structures

Table 1 presents selected bonding parameters for several unbridged, ethylene-bridged and silicon-bridged bis(indenyl) group 4 metallocene dichlorides and their hydrogenated congeners.[38−41,44,45,6,85,86,88,90,92,93,120,121,136−139] Each studied molecule represents the closely related overall structure of the metal-centered unit, i.e. bent-sandwich geometry around the pseudotetrahedrally coordinated metal ion.

Of the unbridged zirconium complexes, the parent bis(indenyl)zirconium dichloride $(Ind)_2ZrCl_2$ displays a staggered conformation in the solid state,[136] whereas the 2-amino-substituted analogues **11**−**14** all crystallize in an *anti* conformation having a crystallographically imposed C_2-axial symmetry. Crystallization of the unbridged 2-siloxy-substituted zirconium complex bis[2-(*tert*-butyldimethylsiloxy)-4,7-dimethylindenyl]zirconium dichloride (**51**) arranges two rotamers in the asymmetric unit corresponding to a C_1-symmetric, "central/lateral:*gauche*" conformation and a C_2-symmetric, "bis(central):*syn*" conformation, respectively.[114] In both rotamers the metallocene C_5 rings are nearly eclipsed.

The combination of ethylene bridge with bis(indenyl)-based ancillary ligands results in the potential formation of *meso* and *rac* diastereomers. All of the crystallographically characterized *meso* isomers display a chiral C_1-symmetric conformation due to the staggered placement of the two indenyl ligand moieties (Scheme 6). The racemic ethylene-bridged bis(indenyl) and bis(tetrahydroindenyl)metallocenes show the ordinary C_2-symmetric bent-metallocene structure adopting one of the two limiting conformations,

 © 2004 Wiley-VCH Verlag GmbH & Co. KGaA, Weinheim

Table 1. Selected bonding parameters for group 4 bis(indenyl)- and bis(tetrahydroindenyl)metallocene dichlorides

Metallocene	Indenyl conformation	M−Cl [Å]	M−Cn [Å]	Cl−M−Cl [°]	Cn−M−Cn [°]	Cp−Cp [°]	Ref.
$(R^n\text{Ind})_2ZrCl_2$:							
[R = H]	[staggered]	2.440	2.223	94.7	129.1	63.5	[136]
R = 2-Me_2N (**11**)	anti	2.455	2.228	95.1	133.1	49.8	[38]
R = 2-Me_2N (**11**)	anti	2.455	2.229	94.9	132.8	49.1	[39]
R = 2-Pyr (**12**)	anti	2.446	2.233	95.2	133.0	49.6	[40]
R = 2-Morph (**13**)	anti	2.446	2.225	95.8	132.5	50.1	[44]
R = 2-(*N*-Me-Piper) (**14**)	anti	2.440	2.216	94.8	132.4	49.2	[45]
R = 2-TBSO-4,7-Me_2 (**51**)	gauche	2.414	2.253	96.9	130.3	51.5	[91]
R = 2-TBSO-4,7-Me_2 (**51**)	*syn*	2.426	2.242	97.1	127.3	54.9	[91]
rac-Et$(R^n\text{Ind})_2ZrCl_2$:							
R = H (*rac*-**2**)	forward	2.388	2.219	99.1	125.3	63.5	[66]
R = 2-Me_2N (*rac*-**9**)	forward	2.427	2.238	94.8	127.2	62.3	[39]
R = 2-TBSO (*rac*-**42**)	backward	2.412	2.254	99.3	125.9	61.0	[85]
R = 2-TDSO (*rac*-**47**)	backward	2.433	2.243	97.9	120.3	58.6	[93]
R = 2-TIPSO (*rac*-**49**)	forward	2.414	2.237	94.3	125.5	57.7	[90]
rac-Et$(R^n\text{IndH}_4)_2ZrCl_2$:							
R = H (*rac*-**5**)	forward	2.439	2.214	98.6	125.2		[118]
R = 2-TBSO (*rac*-**45**)	backward	2.439	2.231	98.2	125.2	58.6	[86]
R = 2-TIPSO (*rac*-**50**)	backward	2.431	2.228	94.3	125.1	57.8	[90]
R = 1-TBSO (*rac*-**57**)	forward	2.415	2.238	98.7	126.4	63.6	[92]
rac-Et$(R^n\text{IndH}_4)_2HfCl_2$:							
R = 2-TBSO (*rac*-**46**)	backward	2.412	2.210	97.1	126.1	57.6	[121]
meso-Et$(R^n\text{Ind})_2ZrCl_2$:							
R = H (*meso*-**2**)	staggered	2.426	2.227	97.6	126.2	62.3	[66]
R = 2-Me_2N (*meso*-**9**)	staggered	2.440	2.231	96.9	127.5	58.0	[41]
R = 1-TBSO (*meso*-**55**)	staggered	2.431	2.252	96.2	126.4	64.6	[92]
meso-Et$(R^n\text{IndH}_4)_2ZrCl_2$:							
R = H (*meso*-**5**)	staggered	2.439	2.217	98.7	125.2	62.0	[137]
R = 2-TBSO (*meso*-**45**)	staggered	2.439	2.231	98.2	125.2	58.6	[120]
rac-$R_2Si(R'\text{Ind})_2ZrCl_2$:							
R = Me, R′ = H	–	2.431	2.293	98.8	119.0	62.0	[69]
$R^2 = C_4H_8$, R′ = H	–	2.447	2.225	98.2	127.6	64.1	[138]
R = Me, R′ = 2-Me_2N (*rac*-**8**)	–	2.424	2.237	94.9	129.1	59.2	[38]
rac-$R_2Si(R'\text{IndH}_4)_2ZrCl_2$:							
R = Me, R′ = H	–	2.441	2.231	97.3	126.4	62.1	[139]
$R^2 = C_4H_8$, R′ = H	–	2.430	2.231	99.4	126.5	57.2	[138]
meso-$R_2Si(R'\text{Ind})_2ZrCl_2$:							
$R^2 = C_4H_8$, R′ = H	–	2.430	2.250	97.3	127.7	63.1	[138]

indenyl-forward (Π) and indenyl-backward (Y), as discussed previously in this microreview (vide supra). Representative examples of ethylene-bridged parent and heteroatom-substituted bis(indenyl) and bis(tetrahydroindenyl) complexes are displayed in Figures 8 and 9, respectively.

In most cases, racemic ethylene-bridged bis(indenyl)-type metallocenes crystallize in the Π conformation. However, nearly all of the racemic 2-siloxy-substituted complexes crystallize in the less common Y conformation, apparently resulting from the diminished repulsion between the bridge and the 2-substituent of the indenyl ring.[135] As an exception, *rac*-ethylenebis(2-triisopropylsiloxyindenyl)zirconium dichloride *rac*-**49** crystallizes in the indenyl-forward conformation; however, its hydrogenated congener *rac*-**50** again adopts the indenyl-backward conformation in the solid state (Figure 15).[90] Complexes with large equatorial substituents favor the Y conformation, albeit the energy differences between the Π and Y conformations appear to be

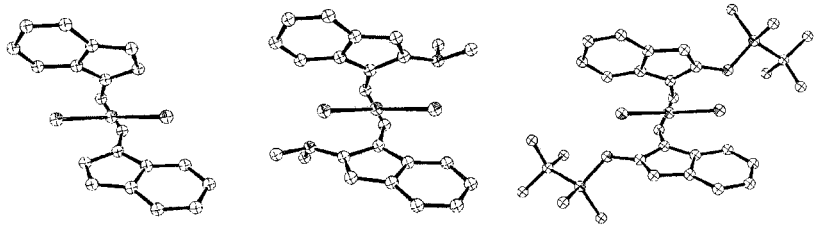

Figure 13. Molecular structures of *rac*-ethylenebis(indenyl)zirconium dichloride (*rac*-**2**) (indenyl-forward conformation),[66] *rac*-ethylenebis(2-dimethylaminoindenyl)zirconium dichloride (*rac*-**9**) (indenyl-forward),[39] and *rac*-ethylenebis(2-*tert*-butyldimethylsiloxyindenyl)-zirconium dichloride (*rac*-**42**) (indenyl-backward)[85]

 © 2004 Wiley-VCH Verlag GmbH & Co. KGaA, Weinheim

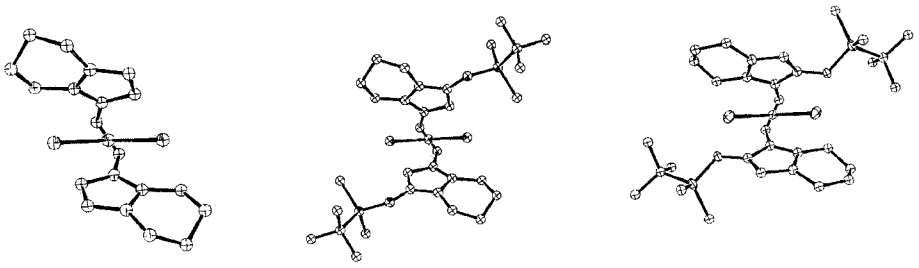

Figure 14. Molecular structures of *rac*-ethylenebis(4,5,6,7-tetrahydroindenyl)zirconium dichloride (*rac*-**5**) (indenyl-forward conformation),[118] *rac*-ethylenebis(1-*tert*-butyldimethylsiloxy-4,5,6,7-tetrahydroindenyl)zirconium dichloride (*rac*-**57**) (indenyl-forward),[92] and *rac*-ethylenebis(2-*tert*-butyldimethylsiloxy-4,5,6,7-tetrahydroindenyl)hafnium dichloride (*rac*-**46**) (indenyl-backward)[121]

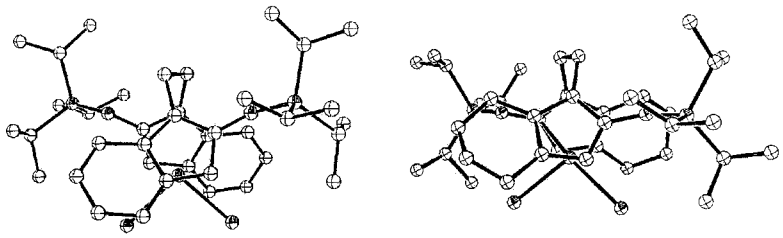

Figure 15. Top views of the molecular structures of *rac*-ethylenebis(2-triisopropylsiloxyindenyl)zirconium dichloride (*rac*-**49**) (indenyl-forward) and of *rac*-ethylenebis(2-triisopropylsiloxy-4,5,6,7-tetrahydroindenyl)zirconium dichloride (*rac*-**50**) (indenyl-backward)[90]

small.[66,67,135] In addition to the siloxy-substituted complexes, the indenyl-backward conformation has also been observed in the solid state by Brintzinger and co-workers for the racemic ethylenebis(4,5,6,7-tetrahydroindenyl)titanium[*O*-acetyl-(*R*)-mandelate],[12,140] by Jordan et al. for the racemic ethylenebis(4,5,6,7-tetrahydroindenyl)zirconium(η^2-CH_2Ph)(CH_3CN)$^+$ cation[141] and racemic ethylenebis(indenyl)hafnium(NMe_2)$_2$,[142] and by Kaminsky and co-workers for racemic ethylenebis(2,4,7-trimethylindenyl)-zirconium dichloride.[68]

X-ray crystal structures of the silicon-bridged bis(indenyl)metallocene derivatives display mainly racemic, C_2-symmetric molecules. The coordination sites are surrounded in an equal fashion, in accordance with the conditions for equivalent enantiofacial coordination of prochiral ligands. Structure determinations of the unbridged, amino-substituted complexes reveal that the amino groups are approximately planar.[38−40,44,45] The short C−N bond lengths of about 1.35 Å indicate that the nitrogen lone pair is considerably delocalized into the indenyl five-membered ring. Even so, related planar amino groups and short N−C distances are not found in the silicon- or ethylene-bridged bis(aminoindenyl)zirconium complexes due to the steric interaction of the amino groups with the interannular bridges.[39,41] The nitrogen−chlorine distances are typically slightly shorter than the sum of their van der Waals radii (3.3 Å), and there is no significant bonding. Aforementioned electron donation from the nitrogen atom may result in adequate electron deficiency that allows these short intermolecular distances. For the C_2-symmetric ethylene-bridged 2-siloxy-substituted complexes, the indenyl-backward conformation brings the chlorine and oxygen atoms in closer contact (3.53−3.85 Å) than in the indenyl-forward conformation (4.06 Å).[85,86,90,93,121] In the unbridged 2-siloxy-substituted complex **51**, the Cl−O distance is even shorter (3.141 Å), being shorter than the sum of their relevant van der Waals radii (3.20 Å).[91] Similar short contacts (3.15−3.30 Å) are also found for 1-siloxy-substituted complexes.[92] Then again, the electron donation from the heteroatom to the zirconocene center can result in a sufficient electron shortage that permits the short intramolecular distances.

UV/Vis Spectroscopic Studies

Recently, Mäkelä-Vaarne and co-workers have utilized UV/Vis spectroscopy to study the activation of siloxy-substituted bis(indenyl) complexes with MAO.[143−145] Interestingly, the position of the siloxy substituent was found to have a drastic influence on the activation behavior of the complex. The activation of 2-siloxy-substituted and unsubstituted bis(indenyl) complexes was observed to proceed relatively quickly, contrary to the slow activation of a 1-siloxy-substituted complex, which showed in the UV/Vis spectrum a sequence of three time-consuming reaction steps. With the aid of molecular modeling studies, the reason for the slow activation of the 1-siloxy-substituted complex was interpreted as resulting from an interaction between the oxygen donor atom of the siloxy group and the electron-deficient zirconium atom. According to UV/Vis studies at ambient temperature, to overcome this interaction took several hours, while formation of the final active species occurred for the 2-siloxy-substituted complex in less than a minute.[145]

On increasing the [Al]/[Zr] ratio for the 1-siloxy-substituted bis(indenyl) complex, the UV/Vis spectrum showed an LMCT band shift to higher energies. This shift is indicative of an interaction between the cocatalyst and the siloxy substituent, the net result of which is a decrease in the cata-

 © 2004 Wiley-VCH Verlag GmbH & Co. KGaA, Weinheim

lytic activity. At low [Al]/[Zr] ratios this band shift was not observed, which can be correlated with the optimum polymerization performance under such conditions in terms of activity and shortened induction times.[86,95,146]

Polymerization Catalysis

Polymerization catalysis will be discussed here with focus on polymerization activity, molecular weight control and copolymerization ability. Optimally, heteroatom substitution can be utilized to tune the electronic properties of catalyst precursors to stabilize the active cationic species by electron donation, which improves the polymerization activity. Noteworthy, it is to a large extent the interaction of the cocatalyst and the functional groups of the catalyst precursor that determine the net result of the electronic effect on the active cationic center.

Olefin Homopolymerization

To study the electronic effects of ligand substituents, Piccolrovazzi et al.[76] and Collins et al.[77] introduced methoxy groups in the 4,7- and 5,6-positions, respectively, of indenyl ligands. Activation with MAO led to a drastic decrease in the polymerization activity relative to the unsubstituted complexes. This was explained by interaction of MAO with the methoxy groups, which resulted in net electron withdrawal and destabilization of the active center. A similar reasoning can also be used to explain the low activities reported for 2-methoxy-substituted bis(indenyl)zirconocenes.[71] Introduction of 2-amino groups into an indenyl ligand framework was found by Brintzinger et al.[38] and Näsman and co-workers[39] to result in modest activity after an induction period of several hours. The induction time was explained to result from inhibition of the reaction generating the active species, probably again as a consequence of an unfavorable interaction of the donor substituents with the cocatalyst MAO. A similar induction period was reported for a 1-siloxy-substituted bis(indenyl) complex,[95,146] and recently explained to be, in addition to an unfavorable interaction with the cocatalyst, a consequence of an interaction between the donor oxygen atom and the electron-deficient zitconium atom.[145]

Increasing the temperature from 40 to 80 °C or adding triisobutylaluminum to the reaction medium was found to shorten the induction period.[95,146] In contrast to 1-siloxy-substituted bis(indenyl) complexes, 2-siloxy-substituted complexes have been reported not to suffer from such induction periods, which according to molecular modeling studies was explained to result from a weaker O(siloxy)−Zr and a weaker (MAO)Al−O(siloxy) interaction of the latter complexes.[145]

Overall, both 1- and 2-siloxy-substituted bis(indenyl) complexes show a considerable increase in ethylene polymerization activity at low [Al]/[Zr] ratios relative to their unsubstituted analogues. Thus, the polymerization behavior of siloxy-substituted bis(indenyl) systems has been extensively studied.[85−89,91,93−98] It was shown that the optimal catalyst activity for siloxy-substituted bis(indenyl) complexes in homogeneous olefin polymerization is achieved at a remarkably low [Al]/[Zr] ratio of 250. A similar low [Al]/[Zr] ratio for the optimal activity was recently reported by Rieger and co-workers for the heteroatom-substituted C_1-symmetric complexes **30** and **32**.[81] Several reasons for the increased polymerization activity at low [Al]/[Zr] ratios have been suggested.[81,85,86,95] Sufficiently shielded heteroatoms, such as oxygen in trialkylated siloxy substituents or oxygen atoms embedded in a dioxane ring, can be understood to be protected against the attack by the Lewis-acidic aluminum cocatalyst. As a result, the heteroatoms preserve their electron-donating nature in the presence of low amounts of MAO, which facilitates the formation of the active site and stabilizes the cationic metal center. In addition, the weaker bonding of the counterion to the cationic alkylmetallocene might increase the rate of monomer insertion into the metal−alkyl bond and thus the chain propagation rate. One further reason could simply be that the polar oxygen substituents promote the approach of the Lewis-acidic aluminum cocatalyst towards the complex and thus promote the activation reaction in the apolar polymerization medium.

Facilitated activation has also been reported by Kallio and co-workers, who showed that siloxy-substituted bis(indenyl) complexes are more readily activated by higher aluminoxanes, such as hexaisobutylaluminoxane than their unsubstituted analogues.[147]

Besides the polymerization activity, the ability to produce sufficiently high-molecular weight polymers is a key factor when evaluating the performance of an olefin polymerization catalyst. Siloxy substitution[85,86,95] and dioxane substitution[81] were found to enhance the probability of chain transfer to aluminum, which was the dominant mechanism for chain termination in propylene polymerization and resulted in rather low polypropylene molecular weights. Chain termination to aluminum has also been reported for 2-amino-substituted complexes in propylene polymeri zation.[38] Rieger et al. reported that borate activation of the dimethylated complex **31** doubled the molecular weight compared with MAO activation of the dichloride.[81] Contrary to propylene polymerization, in ethylene polymerization chain transfer to aluminum has been found to be insignificant for the siloxy-substituted complexes. At 80 °C and with a moderate ethylene concentration of 0.2 mol/dm^3 chain transfer to monomer was found to be the dominant termination mechanism for siloxy-substituted bis(indenyl) complexes, resulting in a number-average molecular weight of 40 kg/mol. For the hydrogenated analogues, chain transfer to monomer was present but less pronounced, and also transfer of β-H to the Zr atom became significant. The number-average molecular weight, 110 kg/mol, was higher than that found for the bis(indenyl) system.[95]

Olefin Copolymerization

Finally, the ability to incorporate comonomers is important when considering the usefulness of a complex to produce linear low-density polyethylene. Table 2 compares the effect of siloxy substituents on the 1-hexene copolymeri-

 © 2004 Wiley-VCH Verlag GmbH & Co. KGaA, Weinheim

zation ability in ethylene polymerization for bis(indenyl)- and bis(tetrahydroindenyl)zirconium complexes.[95,97] Siloxy substitution in the 1-position of the indenyl ligand was found to markedly improve the α-olefin copolymerization ability, reducing the reactivity ratio of ethylene from 48 to 19 for bis(indenyl) complexes, and from 71 to 30 for the corresponding hydrogenated complexes. The reason for the improved copolymerization ability of 1-siloxy-substituted complexes was explained by their increased coordination gap aperture, which is a parameter generally known to affect comonomer accessibility. Replacing the methyl groups at the silicon atom by isopropyl groups has been reported to further improve the copolymerization ability.[94] In contrast to 1-siloxy substitution, 1-*tert*-butyldimethylsilyl substitution, as reported by Ekholm and co-workers for *rac*-ethylenebis(1-*tert*-butyldimethylsilylindenyl)zirconium dichloride (**100**) (Figure 16), clearly reduced the copolymerization ability and resulted in low molecular weight polymers due to excessive chain transfer after primary comonomer insertion, probably as a consequence of the extensive steric hindrance in the vicinity of the active site.[146] Siloxy substitution in the 2-indenyl position resulted in a slightly reduced copolymerization ability relative to that of the unsubstituted complex.[95]

Table 2. Reactivity ratios r_E for MAO-activated racemic ethylene-bridged C_2-symmetric complexes[95,97,148]

	rac-**2**	*rac*-**55**	*rac*-**42**	*rac*-**5**	*rac*-**57**	*rac*-**100**
1-Hexene:						
T_p = 40 °C	–	15	36	–	14	64
T_p = 80 °C	48	19	55	71	30	100
1-Hexadecene:						
T_p = 80 °C	51	25	63	–	–	–

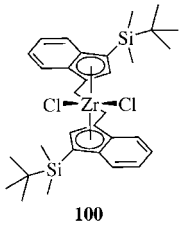

100

Figure 16. *rac*-Ethylenebis(1-*tert*-butyldimethylsilylindenyl)zirconium dichloride (**100**); only one enantiomer of the racemic pair is shown

Conclusions and Outlook

As shown above, modification of group 4 metallocene complexes with electron-donating heteroatom substituents provides an efficient means for modulating the steric as well as electronic features of this class of organometallic compounds. In most cases, the synthesis of such complexes is straightforward employing conventional organic and organometallic synthesis methods for both ligand and metallocene construction. For example, broad varieties of both 2- and 3-amino-, as well as 2- and 3-siloxyindenes, are obtained in high yields in a single reaction step from 2- and 1-indanones and the corresponding secondary amines or chlorosilanes. Accordingly, a large number of bis(indenyl) group 4 complexes, in particular zirconocenes, containing nitrogen and oxygen atoms directly linked to the indenyl ligand have appeared in the literature in recent years. Most recently, while this microreview was being finalized for publication, Erker and co-workers disclosed the synthesis of 4,7-bis(dimethylamino)indene and zirconocene complexes derived thereof.[149]

In terms of the catalytic applications, remarkable effects have been observed in catalytic olefin polymerization where properly shielded electron-donating substituents on the indenyl ligand can be used to control the electron density of the active metal center and thus its ability to control the formation of the cationic active species, monomer-coordination and chain-termination events in the homo- or copolymerization reaction. For example, the siloxy-substituted bis(indenyl)zirconium complexes reach their maximum activities in the polymerizations of ethylene and propylene at significantly reduced concentrations of the expensive MAO cocatalyst, most likely due to the efficient shielding of the donor atoms from unfavorable coordination of alkylaluminum compounds, allowing them to retain the electron-donating character, which in turn facilitates the formation of the active species. Considering the various promising applications of chiral group 4 metallocenes in stereo- and enantioselective organic synthesis, interesting applications for the electronically modified analogues may be anticipated in these areas as well, while such applications hitherto have remained virtually unexplored.

Acknowledgments

Co-authors of our original publications are gratefully acknowledged for their contributions. R. L. wishes to express his sincerest gratitude to his mentor, Professor Jan H. Näsman (1955−2000), whose contribution in the development of the authors' own work reported in this microreview was most influential and whose untimely death a deep loss.

[1] H. H. Brintzinger, D. Fischer, R. Mülhaupt, B. Rieger, R. M. Waymouth, *Angew. Chem. Int. Ed. Engl.* **1995**, *34*, 1143−1170; *Angew. Chem.* **1995**, *107*, 1255−1283.
[2] C. Janiak, in *Metallocenes − Synthesis, Reactivity, Applications* (Eds.: A. Togni, R. L. Halterman), Wiley-VCH, Weinheim, **1998**, vol. 2, chapter 9.
[3] L. Resconi, L. Cavallo, A. Fait, F. Piemontesi, *Chem. Rev.* **2000**, *100*, 1253−1346.
[4] G. W. Coates, *Chem. Rev.* **2000**, *100*, 1223−1252.
[5] S. Lin, R. M. Waymouth, *Acc. Chem. Res.* **2002**, *35*, 765−773.
[6] R. Leino, in *Encyclopedia of Polymer Science and Technology*, 3rd ed. (Ed.: J. I. Kroschwitz), Wiley & Sons, New York, **2003**, vol. 4, pp. 136−179.
[7] G. W. Coates, R. M. Waymouth, *J. Am. Chem. Soc.* **1993**, *115*, 91−98.
[8] R. L. Halterman, *Chem. Rev.* **1992**, *92*, 965−994.
[9] A. H. Hoveyda, J. P. Morken, in *Metallocenes − Synthesis, Reactivity, Applications* (Eds.: A. Togni, R. L. Halterman), Wiley-VCH, Weinheim, **1998**, vol. 2, chapter 10.

 © 2004 Wiley-VCH Verlag GmbH & Co. KGaA, Weinheim

[10] F. R. W. P. Wild, L. Zsolnai, G. Huttner, H. H. Brintzinger, *J. Organomet. Chem.* **1982**, *232*, 233−247.
[11] F. R. W. P. Wild, M. Wasiucionek, G. Huttner, H. H. Brintzinger, *J. Organomet. Chem.* **1985**, *288*, 63−67.
[12] A. Schäfer, E. Karl, L. Zsolnai, G. Huttner, H.-H. Brintzinger, *J. Organomet. Chem.* **1987**, *328*, 87−99.
[13] J. A. Ewen, L. Haspeslach, J. A. Atwood, H. Zhang, *J. Am. Chem. Soc.* **1987**, *109*, 6544−6545.
[14] S. Collins, B. A. Kuntz, Y. Hong, *J. Org. Chem.* **1989**, *54*, 4154−4158.
[15] B. Chin, S. L. Buchwald, *J. Org. Chem.* **1996**, *61*, 5650−5651.
[16] B. Chin, S. L. Buchwald, *J. Org. Chem.* **1997**, *62*, 2267−2268.
[17] W. Spaleck, F. Küber, A. Winter, J. Rohrmann, B. Bachmann, M. Antberg, V. Dolle, E. F. Paulus, *Organometallics* **1994**, *13*, 954−963.
[18] U. Stehling, J. Diebold, R. Kirsten, W. Röll, H.-H. Brintzinger, S. Jüngling, R. Mülhaupt, F. Langhauser, *Organometallics* **1994**, *13*, 964−970.
[19] L. Resconi, F. Piemontesi, I. Camurati, O. Sudmeijer, I. E. Nifant'ev, P. V. Ivchenko, L. G. Kuz'mina, *J. Am. Chem. Soc.* **1998**, *120*, 2308−2321.
[20] C. E. Zachmanoglou, A. Docrat, B. M. Bridgewater, G. Parkin, C. G. Brandow, J. E. Bercaw, C. N. Jardine, M. Lyall, J. C. Green, J. B. Keister, *J. Am. Chem. Soc.* **2002**, *124*, 9525−9546.
[21] R. L. Halterman, in *Metallocenes − Synthesis, Reactivity, Applications* (Eds.: A. Togni, R. L. Halterman), Wiley-VCH, Weinheim, **1998**, vol. 1, chapter 8.
[22] U. Siemeling, *Chem. Rev.* **2000**, *100*, 1495−1526.
[23] H. Butenschön, *Chem. Rev.* **2000**, *100*, 1527−1564.
[24] P. Jutzi, T. Redeker, *Eur. J. Inorg. Chem.* **1998**, 663−674.
[25] C. Müller, D. Vos, P. Jutzi, *J. Organomet. Chem.* **2000**, *600*, 127−143.
[26] C. J. Schaverien, R. Ernst, W. Terlouw, P. Schut, O. Sudmeijer, P. H. M. Budzelaar, *J. Mol. Catal. A: Chem.* **1998**, *128*, 245−256.
[27] R. Duchateu, S. J. Lancaster, M. Thornton-Pett, M. Bochmann, *Organometallics* **1997**, *16*, 4995−5005.
[28] M. T. Reetz, M. Willuhn, C. Psiorz, R. Goddard, *Chem. Commun.* **1999**, 1105−1106.
[29] P. J. Shapiro, *Eur. J. Inorg. Chem.* **2001**, 321−326.
[30] J. Okuda, T. Eberle, in *Metallocenes − Synthesis, Reactivity, Applications* (Eds.: A. Togni, R. L. Halterman), Wiley-VCH, Weinheim, **1998**, vol. 1, chapter 7.
[31] A. L. McKnight, R. M. Waymouth, *Chem. Rev.* **1998**, *98*, 2587−2598.
[32] J. A. Ewen, R. L. Jones, M. J. Elder, A. L. Rheingold, L. M. Liable-Sands, *J. Am. Chem. Soc.* **1998**, *120*, 10786−10787.
[33] J. A. Ewen, M. J. Elder, R. L. Jones, A. L. Rheingold, L. M. Liable-Sands, R. D. Sommer, *J. Am. Chem. Soc.* **2001**, *123*, 4763−4773.
[34] A. N. Ryabov, D. V. Gribkov, V. V. Izmer, A. Z. Voskoboynikov, *Organometallics* **2002**, *21*, 2842−2855.
[35] A. N. Ryabov, V. V. Izmer, A. A. Borisenko, J. A. M. Canich, L. G. Kuz'mina, J. A. K. Howard, A. Z. Voskoboynikov, *J. Chem. Soc., Dalton Trans.* **2002**, 2995−3000.
[36] J. F. van Baar, A. D. Horton, K. P. de Kloe, E. Kragtwijk, S. G. Mkoyan, I. E. Nifant'ev, P. A. Schut, I. V. Taidakov, *Organometallics* **2003**, *22*, 2711−2722.
[37] K.-P. Stahl, G. Boche, W. Massa, *J. Organomet. Chem.* **1984**, *277*, 113−125.
[38] E. Barsties, S. Schaible, M.-H. Prosenc, U. Rief, W. Röll, O. Weyand, B. Dorer, H.-H. Brintzinger, *J. Organomet. Chem.* **1996**, *520*, 63−68.
[39] H. J. G. Luttikhedde, R. P. Leino, C.-E. Wilén, J. H. Näsman, M. J. Ahlgrén, T. A. Pakkanen, *Organometallics* **1996**, *15*, 3092−3094.
[40] H. Plenio, D. Burth, *J. Organomet. Chem.* **1996**, *519*, 269−272.
[41] H. J. G. Luttikhedde, R. Leino, M. J. Ahlgrén, T. A. Pakkanen, J. H. Näsman, *J. Organomet. Chem.* **1998**, *557*, 227−230.
[42] C. A. G. Carter, R. McDonald, J. M. Stryker, *Organometallics* **1999**, *18*, 820−822.
[43] G. Greidanus, R. McDonald, J. M. Stryker, *Organometallics* **2001**, *20*, 2492−2504.
[44] S. Knüppel, J.-L. Fauré, G. Erker, G. Kehr, M. Nissinen, R. Fröhlich, *Organometallics* **2000**, *19*, 1262−1268.
[45] M. Hämäläinen, H. Korpi, M. Polamo, M. Leskelä, *J. Organomet. Chem.* **2002**, *659*, 64−66.
[46] S. J. Lancaster, S. Al-Benna, M. Thornton-Pett, M. Bochmann, *Organometallics* **2000**, *19*, 1599−1608.
[47] S. A. Miller, J. E. Bercaw, *Organometallics* **2000**, *19*, 5608−5613.
[48] K. A. Ostoja Starzewski, W. M. Kelly, A. Stumpf, D. Freitag, *Angew. Chem. Int. Ed.* **1999**, *38*, 2439−2443; *Angew. Chem.* **1999**, *111*, 2588−2592.
[49] H. Plenio, D. Burth, *Angew. Chem. Int. Ed. Engl.* **1995**, *34*, 800−803; *Angew. Chem.* **1995**, *107*, 881−883.
[50] H. Plenio, D. Burth, *Z. Anorg. Allg. Chem.* **1996**, *622*, 225−230.
[51] H. Plenio, D. Burth, *Organometallics* **1996**, *15*, 1151−1156.
[52] H. Plenio, D. Burth, *Organometallics* **1996**, *15*, 4054−4062.
[53] J.-L. Fauré, G. Erker, R. Fröhlich, K. Bergander, *Eur. J. Inorg. Chem.* **2000**, 2603−2606.
[54] M. Kamigaito, Y. Watanabe, T. Ando, M. Sawamoto, *J. Am. Chem. Soc.* **2002**, *124*, 9994−9995.
[55] J. Klosin, W. J. Kruper, Jr., P. N. Nickias, G. R. Roof, P. DeWaele, K. A. Abboud, *Organometallics* **2001**, *20*, 2663−2665.
[56] C. De Rosa, F. Auriemma, O. R. de Ballesteros, L. Resconi, A. Fait, E. Ciaccia, I. Camurati, *J. Am. Chem. Soc.* **2003**, *125*, 10913−10920.
[57] C. Grandini, I. Camurati, S. Guidotti, N. Mascellani, L. Resconi, I. E. Nifant'ev, I. A. Kashulin, P. V. Ivchenko, P. Mercandelli, A. Sironi, *Organometallics* **2004**, *23*, 344−360.
[58] U. Edlund, G. Bergson, *Acta Chem. Scand.* **1971**, *25*, 3625−3633.
[59] U. Edlund, *Acta Chem. Scand.* **1972**, *26*, 2972.
[60] U. Edlund, *Acta Chem. Scand.* **1973**, *27*, 4027−4029.
[61] U. Edlund, *Acta Chem. Scand., Ser. B* **1974**, *28*, 39−44.
[62] W. E. Noland, V. Kaneswaran, *J. Org. Chem.* **1981**, *46*, 1940−1944.
[63] F. G. Bordwell, A. V. Satish, *J. Am. Chem. Soc.* **1992**, *114*, 10173−10176.
[64] C. A. G. Carter, G. Greidanus, J.-X. Chen, J. M. Stryker, *J. Am. Chem. Soc.* **2001**, *123*, 8872−8873.
[65] G. Greidanus-Strom, C. A. G. Carter, J. M. Stryker, *Organometallics* **2002**, *21*, 1011−1013.
[66] F. Piemontesi, I. Camurati, L. Resconi, D. Balboni, A. Sironi, M. Moret, R. Zeigler, N. Piccolrovazzi, *Organometallics* **1995**, *14*, 1256−1266.
[67] L. Resconi, F. Piemontesi, I. Camurati, D. Balboni, A. Sironi, M. Moret, H. Rychlicki, R. Zeigler, *Organometallics* **1996**, *15*, 5046−5059.
[68] W. Kaminsky, O. Rabe, A.-M. Schauwienold, G. U. Schupfner, J. Hanss, J. Kopf, *J. Organomet. Chem.* **1995**, *497*, 181−193.
[69] W. A. Herrmann, J. Rohrmann, E. Herdtweck, W. Spaleck, A. Winter, *Angew. Chem. Int. Ed. Engl.* **1989**, *28*, 1511−1512; *Angew. Chem.* **1989**, *101*, 1536−1538.
[70] W. Spaleck, M. Antberg, M. Aulbach, B. Bachmann, V. Dolle, S. Haftka, F. Küber, J. Rohrmann, A. Winter, in *Ziegler Catalysts* (Eds.: G. Fink, R. Mülhaupt, H. H. Brintzinger), Springer-Verlag, Berlin Heidelberg, **1995**, pp. 83−97.
[71] A. Winter, M. Antberg, W. Spaleck, W. A. Herrmann, H. Riepl, Eur. Pat. Appl. EP582195, **1994**.
[72] L. A. Paquette, A. Varadarajan, E. Bay, *J. Am. Chem. Soc.* **1984**, *106*, 6702−6708.
[73] J. R. Keeffe, A. J. Kresge, Y. Yin, *J. Am. Chem. Soc.* **1988**, *110*, 8201−8206.
[74] B. Eliasson, U. Edlund, *J. Chem. Soc., Perkin Trans. 2* **1981**, 403−408.
[75] W. E. Parham, C. D. Wright, *J. Org. Chem.* **1957**, *22*, 1473−1475.
[76] N. Piccolrovazzi, P. Pino, G. Consiglio, A. Sironi, M. Moret, *Organometallics* **1990**, *9*, 3098−3105.

 © 2004 Wiley-VCH Verlag GmbH & Co. KGaA, Weinheim

[77] I.-M. Lee, W. J. Gauthier, J. M. Ball, B. Iyengar, S. Collins, *Organometallics* **1992**, *11*, 2115−2122.
[78] R. T. Arnold, H. E. Zaugg, *J. Am. Chem. Soc.* **1941**, *63*, 1317−1320.
[79] J. Koo, *J. Am. Chem. Soc.* **1953**, *75*, 1891−1895.
[80] L. Cedheim, L. Eberson, *Acta Chem. Scand., Ser. B* **1976**, *30*, 527−532.
[81] J. Kukral, P. Lehmus, M. Klinga, M. Leskelä, B. Rieger, *Eur. J. Inorg. Chem.* **2002**, 1349−1356.
[82] M. D. Rausch, K. J. Moriarty, J. L. Atwood, W. E. Hunter, E. Samuel, *J. Organomet. Chem.* **1987**, *327*, 39−54.
[83] T. Heinl, S. Retzow, D. Hoppe, G. Fraenkel, A. Chow, *Chem. Eur. J.* **1999**, *5*, 3464−3470.
[84] R. Leino, H. J. G. Luttikhedde, L. Långstedt, A. Penninkangas, *Tetrahedron Lett.* **2002**, *43*, 4149−4151.
[85] R. Leino, H. Luttikhedde, C.-E. Wilén, R. Sillanpää, J. H. Näsman, *Organometallics* **1996**, *15*, 2450−2453.
[86] R. Leino, H. J. G. Luttikhedde, P. Lehmus, C.-E. Wilén, R. Sjöholm, A. Lehtonen, J. V. Seppälä, J. H. Näsman, *Macromolecules* **1997**, *30*, 3477−3483.
[87] R. Leino, H. J. G. Luttikhedde, C.-E. Wilén, J. H. Näsman, *Polym. Mater. Sci. Eng. (Proc. Am. Chem. Soc., Div. Polym. Mater. Sci. Eng.)* **1997**, *76*, 327−328.
[88] R. Leino, H. J. G. Luttikhedde, A. Lehtonen, J. Strandén, J. Mattinen, J. H. Näsman, *Polymer Prepr. (Am. Chem. Soc., Div. Polym. Chem.)* **1998**, *39*, 228.
[89] H. J. G. Luttikhedde, R. Leino, C.-E. Wilén, J. H. Näsman, *Polymer Prepr. (Am. Chem. Soc., Div. Polym. Chem.)* **1998**, *39*, 229−230.
[90] H. J. G. Luttikhedde, R. Leino, A. Lehtonen, J. H. Näsman, *J. Organomet. Chem.* **1998**, *555*, 127−134.
[91] R. Leino, H. J. G. Luttikhedde, A. Lehtonen, R. Sillanpää, A. Penninkangas, J. Strandén, J. Mattinen, J. H. Näsman, *J. Organomet. Chem.* **1998**, *558*, 171−179.
[92] R. Leino, H. J. G. Luttikhedde, A. Lehtonen, P. Ekholm, J. H. Näsman, *J. Organomet. Chem.* **1998**, *558*, 181−188.
[93] R. Leino, H. J. G. Luttikhedde, P. Lehmus, C.-E. Wilén, R. Sjöholm, A. Lehtonen, J. V. Seppälä, J. H. Näsman, *J. Organomet. Chem.* **1998**, *559*, 65−72.
[94] O. Härkki, P. Lehmus, R. Leino, H. J. G. Luttikhedde, J. H. Näsman, J. V. Seppälä, *Macromol. Chem. Phys.* **1999**, *200*, 1561−1565.
[95] P. Lehmus, E. Kokko, O. Härkki, R. Leino, H. J. G. Luttikhedde, J. H. Näsman, J. V. Seppälä, *Macromolecules* **1999**, *32*, 3547−3552.
[96] P. Lehmus, E. Kokko, R. Leino, H. J. G. Luttikhedde, B. Rieger, J. V. Seppälä, *Macromolecules* **2000**, *33*, 8534−8540.
[97] E. Kokko, P. Lehmus, R. Leino, H. J. G. Luttikhedde, P. Ekholm, J. H. Näsman, J. V. Seppälä, *Macromolecules* **2000**, *33*, 9200−9204.
[98] R. Leino, H. J. G. Luttikhedde, in *Olefin Polymerization: Emerging Frontiers*; ACS Symp. Ser., vol. 749 (Eds.: P. Arjunan, J. E. McGrath, J. E. Hanlon), American Chemical Society, Washington, DC, **2000**, pp. 31−47.
[99] W. E. Parham, C. S. Roosevelt, *Tetrahedron Lett.* **1971**, *14*, 923−926.
[100] B. G. Lenz, H. Regeling, B. Zwanenburg, *Tetrahedron Lett.* **1984**, *25*, 5947−5948.
[101] B. Capon, F.-C. Kwok, *J. Am. Chem. Soc.* **1989**, *111*, 5346−5356.
[102] K. Conde-Frieboes, D. Hoppe, *Tetrahedron* **1992**, *48*, 6011−6020.
[103] H. Suginome, T. Takeda, M. Itoh, Y. Nakayama, K. Kobayashi, *J. Chem. Soc., Perkin Trans. 1* **1995**, 49−61.
[104] D. W. Jones, T. C. L. M. Ryder, *Chem. Commun.* **1997**, 1169−1170.
[105] H. Einaga, M. Nojima, M. Abe, *J. Chem. Soc., Perkin Trans. 1* **1999**, 2507−2512.
[106] R. Leino, H. Luttikhedde, C.-E. Wilén, J. Näsman, PCT Int. Appl. FI97/00049; U. S. Pat. 6,277,778 B1.
[107] F. R. Japp, F. W. Streatfeild, *J. Chem. Soc.* **1883**, *43*, 27−34.
[108] A. C. Cope, L. Field, D. W. H. MacDowell, M. E. Wright, *J. Am. Chem. Soc.* **1949**, *71*, 1589−1593.
[109] H. W. Pinnick, S. P. Brown, E. A. McLean, L. W. Zoller III, *J. Org. Chem.* **1981**, *46*, 3758−3760.
[110] R. Leino, H. J. G. Luttikhedde, J. H. Näsman, unpublished results.
[111] C. Fritze, M. Knickmeier, G. Erker, F. Zaegel, B. Gautheron, P. Meunier, L. A. Paquette, *Organometallics* **1995**, *14*, 5446−5449.
[112] M. D. Bruce, G. W. Coates, E. Hauptman, R. M. Waymouth, J. W. Ziller, *J. Am. Chem. Soc.* **1997**, *119*, 11174.
[113] H. J. G. Luttikhedde, R. Leino, J. H. Näsman, unpublished results.
[114] G. Erker, M. Aulbach, M. Knickmeier, D. Wingbermühle, C. Krüger, M. Nolte, S. Werner, *J. Am. Chem. Soc.* **1993**, *115*, 4590−4601.
[115] G. Erker, M. Aulbach, C. Krüger, S. Werner, *J. Organomet. Chem.* **1993**, *450*, 1−7.
[116] C. Krüger, F. Lutz, M. Nolte, G. Erker, M. Aulbach, *J. Organomet. Chem.* **1993**, *452*, 79−86.
[117] R. Leino, H. J. G. Luttikhedde, C.-E. Wilén, J. H. Näsman, K. Kallio, H. Knuuttila, J. Kauhanen, PCT Int. Appl. FI98/00075; U. S. Pat. 6,355,819 B1.
[118] S. Collins, B. A. Kuntz, N. J. Taylor, D. G. Ward, *J. Organomet. Chem.* **1988**, *342*, 21−29.
[119] R. L. Halterman, Z. Chen, M. A. Khan, *Organometallics* **1996**, *15*, 3957−3967.
[120] P. Ekholm, R. Leino, H. J. G. Luttikhedde, A. Lehtonen, J. H. Näsman, unpublished results.
[121] R. Leino, H. J. G. Luttikhedde, A. Lehtonen, unpublished results.
[122] H. Plenio, C. Aberle, *Chem. Commun.* **1996**, 2123−2124.
[123] H. Plenio, A. Warnecke, *Organometallics* **1996**, *15*, 5066−5068.
[124] H. Plenio, C. Aberle, *Organometallics* **1997**, *16*, 5950−5957.
[125] H. Plenio, A. Warnecke, *J. Organomet. Chem.* **1997**, *544*, 133−137.
[126] J. van Beek, J. G. de Vries, J. H. Arts, R. Persad, G. H. J. van Doremaele, PCT Int. Appl. WO94/11406, **1994**.
[127] T. E. Ready, J. C. W. Chien, M. D. Rausch, *J. Organomet. Chem.* **1996**, *519*, 21−28.
[128] K. Hartke, A. Schilling-Pindur, *Liebigs Ann. Chem.* **1984**, 552−563.
[129] S. Deisenhofer, T. Feifel, J. Kukral, M. Klinga, M. Leskelä, B. Rieger, *Organometallics* **2003**, *22*, 3495−3501.
[130] Y. Wielstra, A. Meetsma, S. Gambarotta, S. Khan, *Organometallics* **1990**, *9*, 876−879.
[131] R. Broussier, C. Bourdon, O. Blacque, A. Vallat, M. M. Kubicki, B. Gautheron, *Bull. Soc. Chim. Fr.* **1996**, *133*, 843−851.
[132] R. Broussier, C. Bourdon, O. Blacque, A. Vallat, M. M. Kubicki, B. Gautheron, *J. Organomet. Chem.* **1997**, *538*, 83−90.
[133] M. Linnolahti, P. Hirva, T. A. Pakkanen, *J. Comput. Chem.* **2001**, *22*, 51−64.
[134] M. Linnolahti, T. A. Pakkanen, *Macromolecules* **2000**, *33*, 9205−9214.
[135] M. Linnolahti, T. A. Pakkanen, R. Leino, H. J. G. Luttikhedde, C.-E. Wilén, J. H. Näsman, *Eur. J. Inorg. Chem.* **2001**, 2033−2040.
[136] T. Repo, M. Klinga, I. Mutikainen, Y. Su, M. Leskelä, M. Polamo, *Acta Chem. Scand.* **1996**, *50*, 1116.
[137] S. Collins, W. J. Gauthier, D. A. Holden, B. A. Kuntz, N. J. Taylor, D. G. Ward, *Organometallics* **1991**, *10*, 2061−2068.
[138] H. J. G. Luttikhedde, R. P. Leino, J. H. Näsman, M. Ahlgrén, T. Pakkanen, *J. Organomet. Chem.* **1995**, *486*, 193−198.
[139] H. J. G. Luttikhedde, R. P. Leino, J. H. Näsman, M. Ahlgrén, T. Pakkanen, *Acta Crystallogr., Sect. C* **1995**, *51*, 1488−1490.
[140] H. H. Brintzinger, in *Transition Metals and, Organometallics as Catalysts for Olefin Polymerization* (Eds.: W. Kaminsky, H.-J. Sinn), Springer-Verlag, Berlin, **1988**, pp. 249−256.
[141] R. F. Jordan, R. E. LaPointe, N. Baenziger, G. D. Hinch, *Organometallics* **1990**, *9*, 1539−1545.

 © 2004 Wiley-VCH Verlag GmbH & Co. KGaA, Weinheim

[142] G. M. Diamond, R. F. Jordan, J. L. Petersen, *Organometallics* **1996**, *15*, 4030−4037.
[143] N. I. Mäkelä, H. R. Knuuttila, M. Linnolahti, T. A. Pakkanen, M. A. Leskelä, *Macromolecules* **2002**, *35*, 3395−3401.
[144] N. I. Mäkelä, H. R. Knuuttila, M. Linnolahti, T. A. Pakkanen, *J. Chem. Soc., Dalton Trans.* **2001**, 91−95.
[145] N. I. Mäkelä-Vaarne, M. Linnolahti, T. A. Pakkanen, M. A. Leskelä, *Macromolecules* **2003**, *36*, 3854−3860.
[146] P. Ekholm, P. Lehmus, E. Kokko, M. Haukka, J. V. Seppälä, C.-E. Wilén, *J. Polym. Sci. A: Polym. Chem.* **2001**, *39*, 127−133.
[147] K. Kallio, J. Kauhanen, in *Organometallic Catalysts and Olefin Polymerization* (Eds.: R. Blom, A. Follestad, E. Rytter, M. Tilset, M. Ystenes), Springer, Berlin, **2001**, pp. 14−22.
[148] E. Kokko, P. Lehmus, A. Malmberg, B. Löfgren, J. Seppälä, in *Organometallic Catalysts and Olefin Polymerization* (Eds.: R. Blom, A. Follestad, E. Rytter, M. Tilset, M. Ystenes), Springer, Berlin, **2001**, pp. 335−345.
[149] J. Cano Sierra, S. Gerald Kehr, R. Fröhlich, G. Erker, *Eur. J. Inorg. Chem.* **2004**, 2260−2265.

Received March 16, 2004

 © 2004 Wiley-VCH Verlag GmbH & Co. KGaA, Weinheim

A Novel Route to Multinuclear d^8 Metal−Chalcogen Compounds with Nuclearity Control

Rubén Mas-Ballesté,[a] William Clegg,[b] Agustí Lledós,*[a] and Pilar González-Duarte*[a]

Keywords: Cluster compounds / Platinum / Metalloligands / Self-assembly / Sulfur

We have designed a new synthetic procedure to obtain multinuclear aggregates containing a $\{Pt_2S_2\}_n$ core. The synthetic strategy involves the reaction of [(dppp)Pt(μ-S)$_2$Pt(dppp)] with [PtCl$_2$(PhCN)$_2$] and thus the expansion of the $\{Pt_2S_2\}$ ring to a $[\{Pt_2S_2\}PtCl_2]$ fragment. The lability of the chloride anions allows their replacement by bridging sulfide ligands, thus affording a new $[\{Pt_2(\mu_3\text{-}S)_2\}\{Pt_2(\mu\text{-}S)_2\}\{Pt_2(\mu_3\text{-}S)_2\}]$ core. Its subsequent evolution to $[\{Pt_2S_2\}_3PtCl_2]$ lays the foundation for a new cycle.

(© Wiley-VCH Verlag GmbH & Co. KGaA, 69451 Weinheim, Germany, 2004)

Introduction

Preparation of novel structures in good yields by systematic approaches is relevant in transition-metal sulfide chemistry in view of the current interest and economic importance of these compounds in industrial uses.[1] Although novel approaches to the synthesis of high nuclearity platinum complexes have been reported recently,[2] the chemistry of noble-metal−sulfido clusters has been neglected compared with that of aggregates containing the first transition series metals and molybdenum.[3] Here we report a novel synthetic route based on the behavior of $[L_2Pt(\mu\text{-}S)_2PtL_2]$ compounds as metalloligands, which leads to multinuclear aggregates containing a $\{Pt_2S_2\}_n$ core. The synthetic strategy allows control of the nuclearity of the cluster and can be extended to other metals with square-planar coordination.

The outstanding nucleophilicity of the sulfur atoms in the $\{Pt_2S_2\}$ core accounts for the significant number of known homo- and heterometallic derivatives of $[L_2Pt(\mu\text{-}S)_2PtL_2]$ (L = phosphane) identified to date,[4] as well as for its reaction with organic electrophiles[5] and protons.[6] On the basis of the ability of $[L_2Pt(\mu\text{-}S)_2PtL_2]$ to act as a ligand to metal centers, we now address the use of these compounds for building up multinuclear aggregates containing a $\{Pt_2S_2\}_n$ core. The synthetic strategy involves first expansion of the $\{Pt_2S_2\}$ rings to $[\{Pt_2S_2\}PtL'_2]$ fragments containing labile terminal L′ ligands, which are then replaced by bridging sulfide ligands. As a result, the PtL'_2 fragment evolves to a $\{Pt_2S_2\}$ linking unit between two $\{Pt_2S_2\}$ rings, thus affording a new $[\{Pt_2S_2\}_2\{Pt_2S_2\}]$ core. Its subsequent evolution to $[\{Pt_2S_2\}_3PtL'_2]$ lays the foundation for a new cycle. In this work we present the synthesis and characterization of three complexes derived from $[Pt_2(\mu\text{-}S)_2(dppp)_2]$ (**1**; Scheme 1) and provide evidence for the lability of chloride ligands in the $[\{Pt_2S_2\}PtCl_2]$ fragment.

[a] Departament de Química, Universitat Autònoma de Barcelona, 08193 Bellaterra, Barcelona, Spain
Fax: (internat.) + 34-935-813-101
E-mail: Pilar.Gonzalez.Duarte@uab.es
[b] School of Natural Sciences (Chemistry), University of Newcastle, Newcastle upon Tyne NE1 7RU, UK

Results and Discussion

The reaction of equimolar quantities of $[Pt_2(\mu\text{-}S)_2(dppp)_2]$ (**1**) and $[PtCl_2(PhCN)_2]$ gave the compound $[\{Pt_2(\mu_3\text{-}S)_2(dppp)_2\}PtCl_2]$ (**2**) in good yield. The X-ray crystal structure of this complex consists of discrete trinuclear species and solvent molecules. Although the latter show disorder, the structure of the complex (Figure 1) has been unequivocally determined. Thus, the central Pt_3S_2 unit consists of a nonequilateral triangle of platinum atoms capped above and below by two sulfur atoms, thus forming a trigonal bipyramid. Each platinum atom has approximate square-planar coordination. Significantly, among the wide family of derivatives obtained from $[L_2Pt(\mu\text{-}S)_2PtL_2]$ metalloligands (L = phosphane) no previous example of the $P_4Cl_2Pt_3S_2$ core observed in **2** has been observed by X-ray diffraction. Thus, in the absence of X-ray data, three different alternatives have been proposed as a result of synthetic strategies similar to that followed for the synthesis of **2** (reaction R1). These are: formation of a mixture of hexanuclear $[\{Pt_2(\mu_3\text{-}S)_2[P(tolyl)_3]_4\}M_2(\mu\text{-}Cl)_2\{Pt_2(\mu_3\text{-}S)_2\text{-}[P(tolyl)_3]_4\}]^{2+}$ and trinuclear $[\{Pt_2(\mu_3\text{-}S)_2[P(tolyl)_3]_4\}MCl_2]$ (M = Pd, Pt) species,[7] or formation of only a hexanuclear $[\{Pt_2(\mu_3\text{-}S)_2(PPh_3)_4\}Pd_2(\mu\text{-}Cl)_2\{Pt_2(\mu_3\text{-}S)_2(PPh_3)_4\}]^{2+}$,[8] or a trinuclear $[\{Pt_2(\mu_3\text{-}S)_2(PPh_3)_4\}PtCl_2]$[9] complex. The $^{31}P\{^1H\}$ NMR spectrum of **2** in $CDCl_3$ shows only one signal centered at $\delta = -8.08$ ppm with $^1J_{Pt,P} = 2978$ Hz, thus indicating that the ^{31}P nuclei are equivalent in solution, in agreement with the solid-state structure.

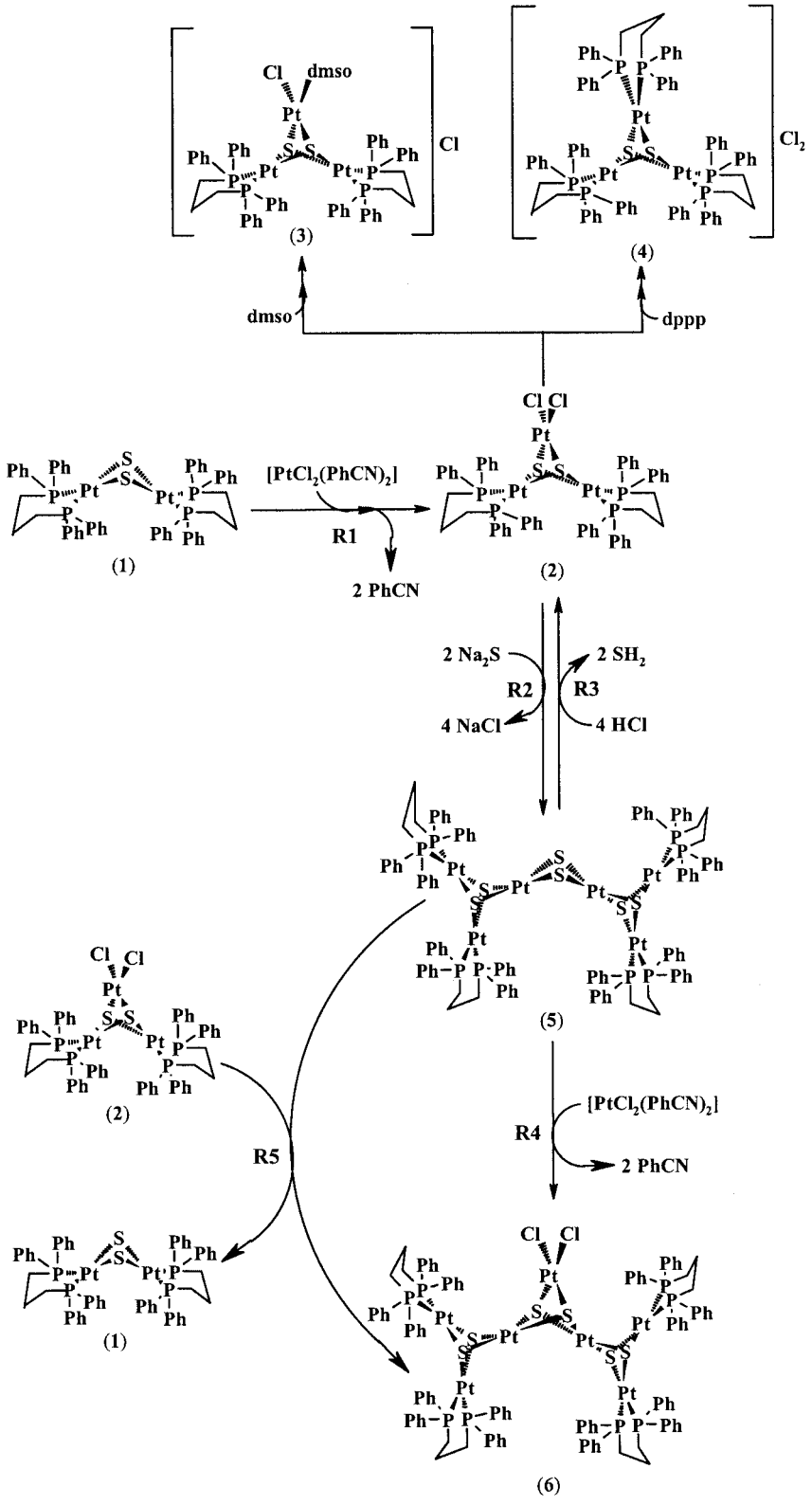

Scheme 1

The lability of the chloro ligands in **2** becomes apparent in the characterization of this compound by ESI-MS. Thus, depending on the recording conditions and on the solvent used to obtain mass data, the following cationic species have been identified: $[\{Pt_2(\mu_3\text{-}S)_2(dppp)_2\}PtCl]^+$ (m/z = 1509.5), $[\{Pt_2(\mu_3\text{-}S)_2(dppp)_2\}PtCl(CH_3CN)]^+$ (m/z = 1550.8), $[\{Pt_2(\mu_3\text{-}S)_2(dppp)_2\}Pt(CH_3CN)_2]^{2+}$ (m/z = 778.2), or $[\{Pt_2(\mu_3\text{-}S)_2(dppp)_2\}PtCl(CH_3OH)]^+$ (m/z = 1541.6).

 © 2004 Wiley-VCH Verlag GmbH & Co. KGaA, Weinheim

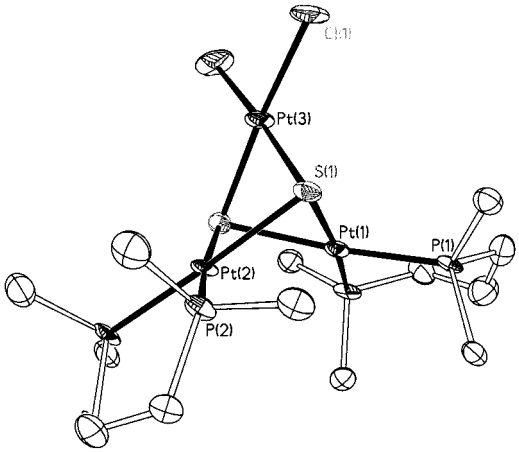

Figure 1. Molecular structure of **2** with the key atoms labeled and 50% probability ellipsoids; H atoms, phenyl rings and CH_2Cl_2 solvent molecules have been omitted; selected structural parameters [Å, °]: Pt−Cl 2.330(7), Pt(1)−S 2.381(7), Pt(2)−S 2.357(6), Pt(3)−S 2.287(6), Pt(1)−P(1) 2.237(7), Pt(2)−P(2) 2.256(7), Pt(1)···Pt(2) 3.124(2), Pt(1)···Pt(3) 2.942(2), Pt(2)···Pt(3) 3.277(2), S···S 2.981; Cl−Pt(3)−Cl 91.1(4), P−Pt(1)−P 93.6(4), P−Pt(2)−P 93.1(3), S−Pt(1)−S 77.5(3), S−Pt(2)−S 78.5(3), S−Pt(3)−S 81.4(3); dihedral (hinge) angles between PtS_2 planes: Pt(1)/Pt(2) 116.0, Pt(1)/Pt(3) 110.1, Pt(2)/Pt(3) 134.0

For the three species a good match between experimental and theoretical isotope distribution has been observed, the above *m*/*z* values corresponding to the major intensity peak. Additional evidence for this lability is provided by the fact that a solution of **2** in DMSO yields the unprecedented complex [{$Pt_2(\mu_3\text{-}S)_2(dppp)_2$}PtCl(dmso)]Cl (**3**), whose synthesis and characterization is reported here. Moreover, the addition of a stoichiometric amount of dppp to **2** affords complex [$Pt_3(\mu_3\text{-}S)_2(dppp)_3$]$Cl_2$ (**4**), already obtained from a different synthetic procedure.[6a]

On the basis of its ability to exchange the chloride ions, the synthesis of [{$Pt_2(\mu_3\text{-}S)_2(dppp)_2$}$_2${$Pt_2(\mu\text{-}S)_2$}] (**5**) was carried out by treating complex **2** with a stoichiometric amount of $Na_2S{\cdot}9H_2O$. The $^{31}P\{^1H\}$ NMR spectrum of **5** in [D_6]DMSO shows a broad signal centered at $\delta = -7.9$ ppm with a $^1J_{Pt,P}$ value of ca. 3000 Hz, and the ^{195}Pt NMR spectrum in the same solvent consists of two signals, one singlet at $\delta = -3524$ ppm (PtS_4) and one triplet centered at $\delta = -4425$ ppm (S_2PtP_2) with $^1J_{Pt,P} = 3002$ Hz. Further evidence for the hexanuclear nature of **5** was provided by the MALDI-TOF mass spectrum, which shows a complex isotope-pattern distribution with a major peak at *m*/*z* = 3013.5. As shown in Figure 2, both features are consistent with the molecular mass of the cation [{$Pt_2(\mu_3\text{-}S)_2(dppp)_2$}Pt(μ-S)(μ-SH)Pt{$Pt_2(\mu_3\text{-}S)_2(dppp)_2$}]$^+$, and thus with the nature of complex **5**.

Comparison of the nucleophilicity of the {Pt_2S_2} core in complexes **5** and **1** was established by determination of their basic character. Thus, titration of **1** and **5** with HCl was monitored by $^{31}P\{^1H\}$ NMR spectroscopy. The addition of a stoichiometric amount of HCl to **5** leads to **2** quantitatively, while formation of [$PtCl_2$(dppp)] from **1** requires a significant excess of HCl.[6a] Additional evidence for the greater basicity of the {Pt_2S_2} core in **5** than in **1** comes

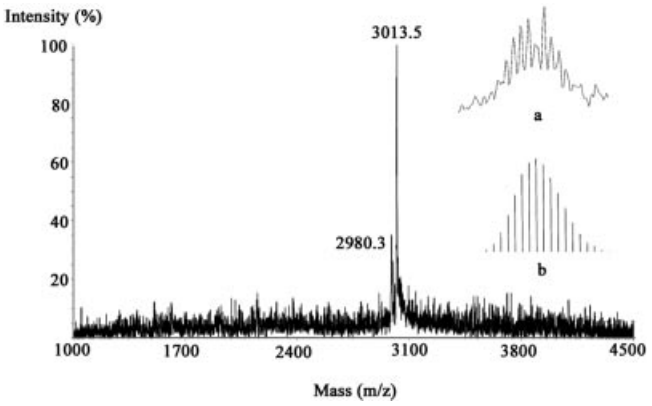

Figure 2. MALDI-TOF spectrum of **5** showing the major intensity peak at *m*/*z* = 3013.5 corresponding to [**5** + H]$^+$; experimental (a) and simulated (b) isotope-distribution patterns are included; the peak at *m*/*z* = 2980 corresponds to [**5** − S]$^+$

from the ability of the former to displace the {$PtCl_2$} fragment from **2** to afford **1** and [{$Pt_2(\mu_3\text{-}S)_2(dppp)_2$}$Pt_2(\mu_3\text{-}S)_2PtCl_2${$Pt_2(\mu_3\text{-}S)_2(dppp)_2$}] (**6**), as indicated in Scheme 1. An alternative way to obtain **6** is by treating **5** with a stoichiometric amount of [$PtCl_2(PhCN)_2$].

Complex **6** was characterized by mass spectrometry and NMR spectroscopy. The MALDI-TOF spectrum has a major signal at *m*/*z* = 1640.2, which can be assigned to the [**6** + 2 H]$^{2+}$ cation (for the major peak, theoretical *m*/*z* = 1640). Comparison of the experimental and theoretical isotope-distribution patterns is given in Figure 3. $^{31}P\{^1H\}$ NMR measurements of **6** in [D_6]DMSO show a broad signal centered at $\delta = -9.3$ ppm with $^1J_{Pt,P}$ of about 3000 Hz. The broadness of this signal, which does not allow us to distinguish the nonequivalence of the phosphorus nuclei, can be attributed to the high number of possible couplings between magnetically active platinum and phosphorus nuclei in **6**. The ^{195}Pt NMR spectrum consists of two singlets ($\delta = -3519$, -3418 ppm) corresponding to the platinum nuclei in the PtS_4 and $PtCl_2S_2$ fragments, respectively, and

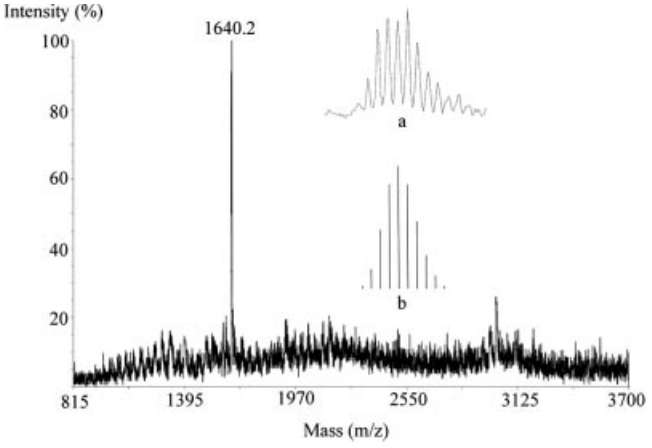

Figure 3. MALDI-TOF spectrum of **6** showing the major intensity peak at *m*/*z* = 1640.3 corresponding to [**6** + 2 H]$^{2+}$; experimental (a) and simulated (b) isotope-distribution patterns are included

 © 2004 Wiley-VCH Verlag GmbH & Co. KGaA, Weinheim

two triplets — $\delta = -4403$ ppm ($^1J_{Pt,P} = 2997$ Hz) and $\delta = -4420$ ppm ($^1J_{Pt,P} = 2970$ Hz) — which can be assigned to the two different platinum nuclei present as S_2PtP_2 in **6**.

The thermodynamic feasibility of the reactions given in Scheme 1 has been corroborated by means of density functional calculations performed for complexes **1**, **2**, **5** and **6**, where dppp is modeled by two PH_3 ligands. The calculated reaction energies are given in Table 1. Geometry optimization of **1t**, **2t**, **5t** and **6t** affords their structural data, that of **2t** being in good agreement with the crystallographically determined data for **2**. As regards the HOMO orbitals of **1t** and **5t**, they essentially consist of an antibonding combination of p_π orbitals of the sulfur atoms pointing outwards from the hinged $\{Pt_2S_2\}$ ring, thus accounting for the observed coordinating ability of the sulfur atoms. Interestingly, the energy level of the HOMO for **5t** (−2.46 eV) is 1.95 eV higher than for **1t** (−4.41 eV), which is in agreement with the greater basicity found experimentally for the $\{Pt_2S_2\}$ core in **5** than in **1**.

Table 1. B3LYP reaction energies in the gas phase

Reaction	R1	R3	R4	R5
Energy [kcal/mol]	−8.3	−41.2	−49.7	−40.4

Conclusion

In this work, we have provided a new insight into the chemistry of $[L_2Pt(\mu\text{-}S)_2PtL_2]$ compounds that goes beyond their usual behavior as metalloligands towards a wide range of transition metals. The synthetic route used demonstrates that the nucleophilicity of the $\{Pt_2S_2\}$ core can be driven to build nuclearity-controlled multinuclear aggregates containing a $\{Pt_2S_2\}_n$ core. This strategy requires replacement of the terminal X ligands in $[\{Pt_2S_2\}_nPtX_2]$ fragments. For X = Cl, this has been achieved by reaction with sodium sulfide.

Characterization of the high nuclearity complexes here obtained has required several spectroscopic techniques, among which MALDI-TOF mass spectrometry has proved very valuable despite its scarce use in coordination chemistry studies.

Finally, on the basis of these results it can be concluded that a similar reaction scheme should be suitable for obtaining macromolecular complexes containing a $\{M_2(\mu\text{-}S)_2\}_n$ core provided M has a preference for square-planar coordination environments.

Experimental Section

General Remarks: All reactions were carried out under pure dinitrogen, and conventionally dried and degassed solvents were used throughout. Complex $[PtCl_2(dppp)]$ was prepared according to published methods.[10] The synthesis of $[(dppp)Pt(\mu\text{-}S)_2Pt(dppp)]$ has already been reported.[5] ^1H, $^{13}C\{^1H\}$ $^{31}P\{^1H\}$ and $^{195}Pt\{^1H\}$ NMR spectra were recorded from samples in $(CD_3)_2SO$ solution at room temperature, using a Bruker 250 spectrometer. ^1H and ^{13}C chemical shifts are relative to $SiMe_4$, ^{31}P chemical shifts to external 85% H_3PO_4 and ^{195}Pt chemical shifts to external H_2PtCl_6. The ESI-MS measurements were performed with a VG Quattro Micromass Instrument. Experimental conditions are given elsewhere.[5] MALDI mass spectra were obtained with a Voyager DE-RP (PerSeptive Biosystems, Framighan) time-of-flight (TOF) mass spectrometer equipped with a nitrogen laser (337 nm, 3 ns pulse). The accelerating voltage in the ion source was 20 kV. Data were acquired in the reflector mode operation with a delay time of 60 ns. Experiments were performed using the matrix 2,5-dihydroxybenzoic acid (DHB; Aldrich). Matrix solutions were prepared by dissolving 10 mg of DHB in 10 mL of CH_3CN/H_2O 50% (v/v). Equal volumes (1 μL + 1 μL) of matrix solution and diluted samples (10^{-2} M in CH_3CN) were mixed and spotted onto the stainless-steel sample plate. The mixture was dried in air before being introduced into the mass spectrometer. Microanalytical data have been omitted because those referring to the carbon content were unsatisfactory, as already reported in some related (phosphane)platinum complexes.[5][6a][6b]

Synthesis of $[\{Pt_2(\mu_3\text{-}S)_2(dppp)_2\}PtCl_2]$ (2): The reaction of equimolar quantities of $[Pt_2(\mu\text{-}S)_2(dppp)_2]$ (**1**; 500 mg, 0.39 mmol) and $[PtCl_2(PhCN)_2]$ (184 mg, 0.39 mmol) in benzene (80 mL) at room temperature for 6 h gave $[\{Pt_2(\mu_3\text{-}S)_2(dppp)_2\}PtCl_2]$ (**2**) as an orange solid, which was filtered off and washed with diethyl ether (532 mg, yield 82%). Slow evaporation of the solvent from a solution of **2** in CH_2Cl_2 afforded yellow X-ray-quality crystals. $^{31}P\{^1H\}$ NMR ($CDCl_3$): $\delta = -8.1$ ppm ($^1J_{Pt,P} = 2978$ Hz). ESI-MS: $m/z = 1509.5$ $[M - Cl]^+$.

Synthesis of $[\{Pt_2(\mu_3\text{-}S)_2(dppp)_2\}PtCl(dmso)]Cl$ (3): Complex **2** (300 mg, 0.19 mmol) was dissolved in the minimum amount of DMSO (1 mL). Addition of diethyl ether caused precipitation of complex **3** as a yellowish solid, which was filtered off and washed with diethyl ether (206 mg, yield 67%). $^{31}P\{^1H\}$ NMR ($CDCl_3$): $\delta_A = -7.1$ ppm ($^1J_{Pt,P_A} = 3022$ Hz); $\delta_B = -7.8$ ppm ($^1J_{Pt,P_B} = 3051$ Hz). ^1H NMR ($CDCl_3$): $\delta = 2.85$ ppm (coordinated dmso). ^{13}C NMR ($CDCl_3$): $\delta = 44.4$ ppm (coordinated dmso). ESI-MS: $m/z = 1587.7$ $[M]^+$.

Synthesis of $[\{Pt_2(\mu_3\text{-}S)_2(dppp)_2\}Pt_2(\mu\text{-}S)_2\{Pt_2(\mu_3\text{-}S)_2(dppp)_2\}]$ (5): A suspension of complex **2** (400 mg, 0.25 mmol) in methanol (50 mL) was allowed to react with a stoichiometric amount of $Na_2S{\cdot}9H_2O$ (61 mg, 0.25 mmol) at room temperature for 1 h. Concentration of the filtered orange solution thus obtained, followed by addition of diethyl ether, allowed isolation and characterization of the title compound (229 mg, yield 61%). $^{31}P\{^1H\}$ NMR ([D$_6$]DMSO): $\delta = -7.9$ ppm. ^{195}Pt NMR ([D$_6$]DMSO): $\delta = -3524$, -4425 ppm ($^1J_{Pt,P} = 3000$ Hz). MALDI: $m/z = 3013.5$ $[M + H]^+$.

Synthesis of $[\{Pt_2(\mu_3\text{-}S)_2(dppp)_2\}Pt_2(\mu_3\text{-}S)_2PtCl_2\{Pt_2(\mu_3\text{-}S)_2(dppp)_2\}]$ (6): A solution of **5** (200 mg, 0.07 mmol) in acetonitrile (50 mL) containing a stoichiometric amount of $[PtCl_2(PhCN)_2]$ (32 mg, 0.07 mmol) was left to react at room temperature for 3 h. The red solution was filtered and the resulting filtrate concentrated. The title compound was isolated after addition of diethyl ether (123 mg, yield 54%). $^{31}P\{^1H\}$ NMR ([D$_6$]DMSO): $\delta = -9.3$ ppm. ^{195}Pt NMR ([D$_6$]DMSO): $\delta = -3519$, -3418, -4403 ppm ($^1J_{Pt,P} = 2997$ Hz), -4420 ($^1J_{Pt,P} = 2970$ Hz) ppm; MALDI: $m/z = 1640.2$ $[M + 2H]^{2+}$.

 © 2004 Wiley-VCH Verlag GmbH & Co. KGaA, Weinheim

X-ray Crystallographic Study of Complex 2: $C_{54}H_{52}Cl_2P_4Pt_3S_2{\cdot}6CH_2Cl_2$, M = 2054.7, orthorhombic, *Pnma*, a = 19.982(3), b = 18.607(2), c = 19.372(2) Å, V = 7202.5(16) Å^3, Z = 4, T = 160 K, R = 0.091. The molecule lies in a crystallographic mirror plane, as do some of the chloroform solvent molecules, while others are in general positions. High displacement parameters suggest possible disorder of the solvent molecules, but this could be resolved only for one, in which one chlorine atom occupies alternative sites on either side of a mirror plane while the carbon atom and the other chlorine atom are in the plane. Restraints on geometry and displacement parameters were used to aid the refinement. The crystallographic analysis was further complicated by the probable occurrence of multiple twinning by exchange among the unit cell axes, all three of which are similar in length; this was indicated by an analysis of the agreement of observed and calculated intensities, but it was not possible to find a simple model for the twinning. This leads to the relatively high R factor. CCDC-221226 contains the supplementary crystallographic data for this paper. These data can be obtained free of charge at www.ccdc.cam.ac.uk/conts/retrieving.html [or from the Cambridge Crystallographic Data Centre, 12 Union Road, Cambridge CB2 1EZ, UK; Fax: (internat.) + 44-1223-336-033; E-mail: deposit@ccdc.cam.ac.uk].

Computational Details: Gas-phase DFT calculations with the B3LYP functional were carried out using the Gaussian 98 suite of programs.[11] Effective core potentials and their related double-ζ basis set known as LANL2DZ were used for Pt, P, Cl and S atoms, supplemented with polarization functions for P, Cl and S atoms. The 6-31G basis set was used for H, C and N atoms with the addition of polarization functions for the N atom. A thermodynamic consideration for the R2 reaction requires taking into account the solvent effects. However, PCM calculation for compound **5** was hindered by the size of the system and thus the reaction energy for R2 could not be obtained.

Acknowledgments

Thanks are due to Prof. O. Rossell and I. Angurell for their assistance in the recording of the ^{195}Pt NMR spectra. Financial support from the Ministerio de Ciencia y Tecnología of Spain (projects BQU2001-1976 and BQU2002-04110-CO2-02) and the EPSRC (UK) is gratefully acknowledged. R. M. B. is indebted to the Universitat Autònoma de Barcelona for a pre-doctoral scholarship.

[1] E. I. Stiefel, *ACS Symp. Ser.* **1996**, *653*, 2.
[2] [2a] C. H. Tao, K. M.-C. Wong, N. Y. Zhu, V. W.-W. Yam, *New J. Chem.* **2003**, *27*, 150. [2b] C.-K. Hui, B. W.-K. Chu, N. Zhu, V. W.-W. Yam, *Inorg. Chem.* **2002**, *41*, 6178. [2c] B. T. Sterenberg, R. Ramachandran, R. J. Puddephatt, *J. Cluster Sci.* **2001**, *12*, 49. [2d] W. Schuh, G. Wachtler, G. Laschober, H. Kopacka, K. Wurst, P. Peringer, *Chem. Commun.* **2000**, 1181.
[3] M. Hidai, S. Kuwata, Y. Mizobe, *Acc. Chem. Res.* **2000**, *33*, 46.
[4] [4a] Z. Li, W. Zheng, H. Liu, K. F. Mok, T. S. A. Hor, *Inorg. Chem.* **2003**, *42*, 8481. [4b] X. Xu, S.-W. A. Fong, Z. Li, Z.-H. Loh, F. Zhao, J. J. Vittal, W. Henderson, S.-B. Khoo, T. S. A. Hor, *Inorg. Chem.* **2002**, *41*, 6838. [4c] M. Capdevila, Y. Carrasco, W. Clegg, R. A. Coxall, P. González-Duarte, A. Lledós, J. A. Ramírez, *J. Chem. Soc., Dalton Trans.* **1999**, 3103. [4d] S.-W. A. Fong, T. S. A. Hor, *J. Chem. Soc., Dalton Trans.* **1999**, 639 and references cited therein. [4e] V. W.-W. Yam, P. K.-Y. Yeung, K.-K. Cheung, *Angew. Chem. Int. Ed. Engl.* **1996**, *35*, 739.
[5] R. Mas-Ballesté, M. Capdevila, P. A. Champkin, W. Clegg, R. A. Coxall, A. Lledós, C. Mégret, P. González-Duarte, *Inorg. Chem.* **2002**, *41*, 3218.
[6] [6a] R. Mas-Ballesté, G. Aullón, P. A. Champkin, W. Clegg, C. Mégret, P. González-Duarte, A. Lledós, *Chem. Eur. J.* **2003**, *9*, 5023. [6b] G. Aullón, M. Capdevila, W. Clegg, P. González-Duarte, A. Lledós, R. Mas-Ballesté, *Angew. Chem. Int. Ed.* **2002**, *41*, 2776. [6c] S.-W. A. Fong, W. T. Yap, J. J. Vittal, T. S. A. Hor, W. Henderson, A. G. Oliver, C. E. F. Rickard, *J. Chem. Soc., Dalton Trans.* **2001**, 1986. [6d] S.-W. A. Fong, J. J. Vittal, W. Henderson, T. S. A. Hor, A. G. Oliver, C. E. F. Rickard, *Chem. Commun.* **2001**, 421.
[7] S. Narayan, V. K. Jain, *Trans. Met. Chem.* **2000**, *25*, 400.
[8] C. E. Briant, T. S. A. Hor, N. D. Howells, D. M. P. Mingos, *J. Chem. Soc., Chem. Commun.* **1983**, 1118.
[9] B. H. Aw, K. K. Looh, H. S. O. Chan, K. L. Tan, T. S. A. Hor, *J. Chem. Soc., Dalton Trans.* **1994**, 3177.
[10] M. P. Brown, R. J. Puddephatt, M. Rashidi, K. R. Seddon, *J. Chem. Soc., Dalton Trans.* **1977**, 951.
[11] M. J. Frisch, G. W. Trucks, H. B. Schlegel, G. E. Scuseria, M. A. Robb., J. R. Cheeseman, V. G. Zakrzewski, J. A. Montgomery, R. E. Stratmann, J. C. Burant, S. Dapprich, J. M. Millam, A. D. Daniels, K. N. Kudin, M. C. Strain, O. Farkas, J. Tomasi, V. Barone, M. Cossi, R. Cammi, B. Mennucci, C. Pomelli, C. Adamo, S. Clifford, J. Ochterski, G. A. Petersson, P. Y. Ayala, Q. Cui, K. Morokuma, D. K. Malick, A. D. Rabuck, K. Raghavachari, J. B. Foresman, J. Cioslowski, J. V. Ortiz, B. B. Stefanov, G. Liu, A. Liashenko, P. Piskorz, I. Komaromi, R. Gomperts, R. L. Martin, D. J. Fox, T. Keith, M. A. Al-Laham, C. Y. Peng, A. Nanayakkara, C. Gonzalez, M. Challacombe, P. M. W. Gill, B. Johnson, W. Chen, M. W. Wong, J. L. Andres, C. Gonzalez, M. Head-Gordon, E. S. Replogle, J. A. Pople, *Gaussian 98*, Revission A.7, Gaussian Inc., Pittsburgh, PA, **1998**.

Received March 30, 2004

 © 2004 Wiley-VCH Verlag GmbH & Co. KGaA, Weinheim

First Tetranuclear Co^{II} Cluster with Planar Triangular Pattern: Crystal Structure and Ferromagnetic Behavior

Miao Du,[a,b] Ya-Mei Guo,[a] Xian-He Bu,*[a] and Joan Ribas[c]

Keywords: Carboxylic-functionalized diazamesocyclic ligands / Cobalt / Crystal structure / Magnetic properties / Tetranuclear clusters

The preparation, crystal structure and magnetic properties of the first tetrameric Co^{II} cluster with a unique planar triangular motif, $[Co_4L_3(H_2O)_2](ClO_4)_2{\cdot}2H_2O$ (**1**), based on a carboxylic-functionalized 1,5-diazacyclooctane (DACO) bridging ligand [1,5-bis(2-carboxyethyl)-DACO], are reported.

(© Wiley-VCH Verlag GmbH & Co. KGaA, 69451 Weinheim, Germany, 2004)

Introduction

The development of routes and strategies for the design and preparation of polynuclear clusters of 3d metals in moderate oxidation states is of great importance in bioinorganic chemistry, magnetochemistry, material chemistry and solid-state chemistry.[1] Tetranuclear systems have attracted particular interest since it was discovered that they are also the smallest aggregates that show single molecular magnet (SMM) behavior.[2] Of the relatively small number of reported tetracobalt(II) compounds, the majority have a dicubane/cubane rather than a square/rhombus-like core.[3] As described by us and others, diazamesocycles, especially 1,5-diazacyclooctane (DACO), modified by suitable functional pendants can be used as building blocks for constructing polymeric systems with unique structures and properties.[4,5] Very recently we have made an attempt to incorporate the carboxylic group, a versatile ligand with various coordination modes, on the backbone of DACO, and some fascinating chemistry of such ligands under self-assembly with metal ions were successfully achieved.[6] In the present contribution, we describe the preparation, crystal structure and magnetic properties of the first tetranuclear Co^{II} cluster $[Co_4L_3(H_2O)_2](ClO_4)_2{\cdot}2H_2O$ (**1**) [H_2L = 1,5-bis(2-carboxyethyl)-DACO; Scheme 1] exhibiting a unique planar-triangular Co_4 topology.

[a] Department of Chemistry, Nankai University,
Tianjin 300071, P. R. China
Fax: (internat.) + 86-22-23502458
E-mail: buxh@nankai.edu.cn
[b] College of Chemistry and Life Science, Tianjin Normal University,
Tianjin 300074, P. R. China
[c] Department de Química Inorgànica, Universitat de Barcelona, 08028 Barcelona, Spain

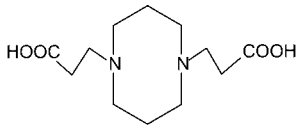

H_2L

Scheme 1

Results and Discussion

The crystal-structure determination of **1** reveals that it is a spontaneously resolved chiral crystal (each individual crystal is a single enantiomer).[7] Four Co^{II} centres are located on an exactly trigonal plane (see Figure 1) with a crystallographic twofold axis passing through Co1 and Co2. Three crystallographically independent Co^{II} ions have different octahedral coordination environments: the central Co1 bonds to six carboxylic oxygen donors, and the vertex Co^{II} ions are coordinated by DACO with unusual *chair*/*chair* configuration,[4] and four $O_{carboxylic}$ (for Co2), and three $O_{carboxylic}$ and one aqua ligand (for Co3). The carboxylato groups bridge the Co^{II} ions in two modes: μ-O,O-μ-O,O′$_{syn}$ (O5−C13−O6 and O3−C12−O4) and μ-O,O (O1−C1−O2) with Co···Co distances of 3.004(5) Å (Co1···Co2), 3.192(6) Å (Co1···Co3) and 4.939(3) Å (Co2···Co3), and Co−O−Co bridging angles of 99.9(2)° (Co1−O1−Co3), 89.3(1)° (Co1−O6−Co2) and 95.3(1)° (Co3−O3−Co1). The Co3···Co3A distance is 6.147(4) Å. The tetramers are well isolated, with the intermolecular contacts between the Co^{II} atoms above 7 Å.

 © 2004 Wiley-VCH Verlag GmbH & Co. KGaA, Weinheim **DOI: 10.1002/ejic.200400274**

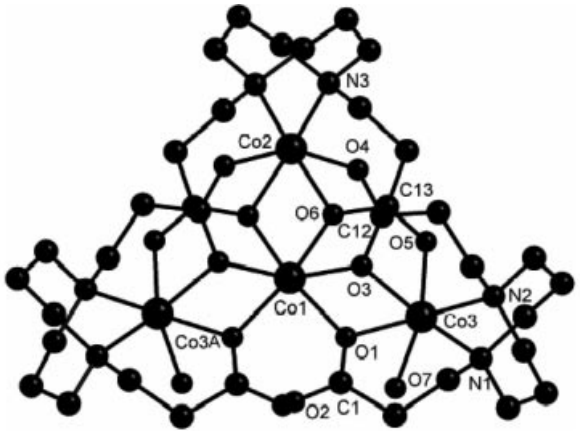

Figure 1. View of the $[Co_4L_3(H_2O)_2]^{2+}$ cation (H atoms omitted for clarity); symmetry code: $-x+1, y, -z+2$; selected bond lengths and angles: Co1−O1 2.070(4), Co1−O3 2.176(4), Co1−O6 2.109(4), Co2−N3 2.097(5), Co2−O4 2.099(4), Co2−O6 2.166(4), Co3−O5 2.119(4), Co3−N1 2.104(5), Co3−O7 2.102(5), Co3−O1 2.101(4), Co3−N2 2.127(5), Co3−O3 2.143(4), Co1−O(1)−Co3 99.9(2), Co1−O(3)−Co3 95.3(1), Co1−O(6)−Co2 89.3(1)

The magnetic properties of **1** in the form of $\chi_M T$ versus T plots (χ_M is the molar magnetic susceptibility for four Co^{II} ions) are shown in Figure 2 (A). The $\chi_M T$ value at 300 K is 11.87 $cm^3 \cdot mol^{-1} \cdot K$, which is larger than the spin-only value for four isolated Co^{II} ions (7.5 $cm^3 \cdot mol^{-1} \cdot K$, assuming artificially $g = 2.00$), indicating an important contribution from the orbital angular momentum typical for the $^4T_{1g}$ ground term. From 300 to 50 K the $\chi_M T$ value is almost constant (close to 12 $cm^3 \cdot mol^{-1} \cdot K$), and from 50 to 2 K it continuously increases (16.2 $cm^3 \cdot mol^{-1} \cdot K$ at 2.0 K). The shape of this curve indicates significant ferromagnetic interactions, because in the presence of spin-orbit interactions the $\chi_M T$ values for any Co^{II} ion tend to decrease with decreasing temperature.[8]

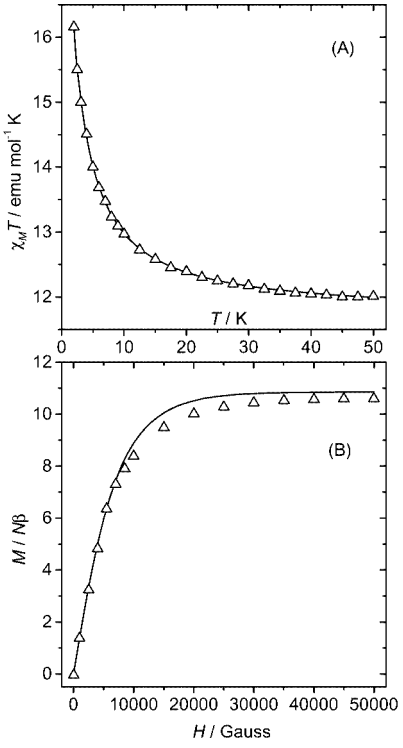

Figure 2. (A) Plot of the $\chi_M T$ vs. T from 50 to 2 K for **1** (the solid line is the best simulation with the following parameters: $J_1 = 2.15 \pm 0.08$ cm^{-1}, $J_2 = 0.40 \pm 0.03$ cm^{-1}, $J_3 = 0.12 \pm 0.02$ cm^{-1}, $g_{\parallel} = 7.3 \pm 0.2$ and $g_{\perp} = 3.5 \pm 0.1$; (B) plot of the reduced magnetisation at 2 K (the solid line is the simulation with J and g values obtained from the $\chi_M T$ vs. T curve)

For the interpretation of the magnetic measurements, the importance of the spin-orbit coupling of Co^{II} must be emphasized. The degeneracy of the $^4T_{1g}$ ground state of the octahedral Co^{II} ion prevents any possible fit in the whole temperature range, except for dinuclear complexes.[9] In the low-temperature region, the overall effect of low-symmetry crystal-field components and spin-orbit coupling produces up to six Kramers doublets and leads to a doublet ground state,[8] which should result in an anisotropic exchange coupling. This anisotropy has been clearly shown by inelastic neutron scattering (INS) studies in many polynuclear Co^{II} systems.[3b,10] For this reason, at low temperature ($< 40-50$ K), Co^{II} systems may be described as having an effective spin of 1/2 with large anisotropy. Thus, for not too complicated systems, it is possible to fit the low-temperature zone with special computational methods, such as the MAGPACK program,[11] as previously done for several di- to pentanuclear Co^{II} systems.[3b,10]

The exchange pathway connecting the Co^{II} ions is depicted in Scheme 2. In the case of tetramer **1**, the exchange Hamiltonian that describes the exchange interactions between the effective $S = 1/2$ spins is:

$$H = -2 \sum_{i=x,y,z} [J_{1i} S_{1i} S_{2i} + J_{2i}(S_{1i} S_{3i} + S_{1i} S_{3'i}) + J_{3i}(S_{2i} S_{3i} + S_{2i} S_{3'i})$$

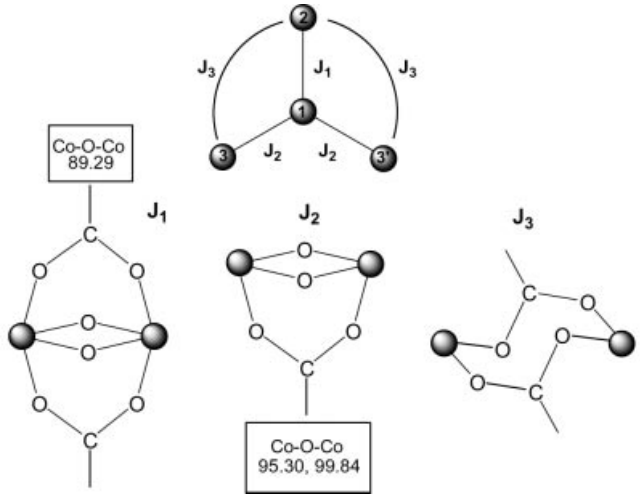

Scheme 2. Spin topology for **1** assuming different J values

When the number of J values is only 1 or 2, it is possible to take into account axial anisotropy of J, since the number of final parameters is still sufficiently small. However, we had to assume here (even artificially) that $J_{x,y} = J_z$, simulat-

 © 2004 Wiley-VCH Verlag GmbH & Co. KGaA, Weinheim

ing with an average J value, such as in an isotropic case. On the other hand, we assumed that $g_{\parallel}$ and $g_{\perp}$ for all four Co^{II} ions were equal. With this hypothesis, the best simulation was obtained with the following parameters: $J_1 = 2.15 \pm 0.08\ cm^{-1}$, $J_2 = 0.40 \pm 0.03\ cm^{-1}$, $J_3 = 0.12 \pm 0.02\ cm^{-1}$, $g_{\parallel} = 7.3 \pm 0.2$ and $g_{\perp} = 3.5 \pm 0.1$. The found g values are very reasonable for Co^{II} sites with distorted octahedral coordination.[12] Moreover, we have obtained the magnetisation vs. H curve at 2 K. At 5 T the $M/N\beta$ (reduced magnetisation) is 10.7. The simulation of the reduced magnetisation vs. H, with J and g values calculated from the susceptibility data, using the same MAGPACK program[11], is given in Figure 2 (B). There is reasonable agreement with the experimental curve.

Taking into account the difficulties for determining the exact J values, it will be interesting to compare this Co_4 cluster with the isostructural Ni_4 analogue.[6a] In the Ni^{II} case the J parameters were: $J_1 = 5.12\ cm^{-1}$, $J_2 = 0.35\ cm^{-1}$, $J_3 = 0.23\ cm^{-1}$ and $g = 2.17$. It was necessary to introduce the D parameter ($7.7\ cm^{-1}$) to explain the magnetic behavior at low temperatures. Thus, it is important to point out that in both cases the three J parameters are ferromagnetic and of the same order of magnitude: $J_1 >> J_2 > J_3$. As in the Ni_4 cluster, in **1** the Co−Co interactions between the corresponding spins are transmitted through the oxo and carboxylato bridges. From the magnetic point of view it is important to distinguish between these pathways. *Co−O−Co angles:* These angles lie close to 90° for J_1 and 95−100° for J_2; they are in the range in which ferromagnetic exchange pathways are dominant (90−100°); large superexchange angles lead to antiferromagnetic interactions while smaller ones induce ferromagnetic coupling.[13] *Acetato bridges*: The effect of the *syn*/*syn* acetato bridge is antiferromagnetic for Co^{II} and, actually, for any metal.[14] Thus, these bridges can mediate an additional exchange pathway and *significantly reduce* the ferromagnetic contribution from μ-oxo ligands. This effect has also been observed in the Ni_4 complex. *Comparison between J_1 and J_2*: J_1 is given by a planar Co−O−Co−O fragment (Scheme 2) with a Co−O−Co angle of 90°. This angle enhances the ferromagnetic coupling, but the presence of *two* carboxylato ligands (*syn*/*syn*) reduces this coupling. On the other hand, J_2 is given by a nonplanar Co−O−Co−O entity, with greater Co−O−Co angles, thus creating low ferromagnetic coupling, which is reduced by the presence of only *one* carboxylato group. Experimentally, both contributions are quasi-balanced, giving a J value that is positive but $< 1\ cm^{-1}$. *Study of J_3*: The carboxylato ligand bridges two Co^{II} ions in a *syn*/*anti* configuration; low antiferro- or ferromagnetic coupling is expected for this kind of coordination mode.[15] To the best of our knowledge, no magnetic studies for *syn*/*anti* carboxylato-bridged Co^{II} complexes have been reported so far.

Experimental Section

Materials and General Methods: H_2L was prepared by a literature method.[6] Other commercially available chemical reagents and solvents were of analytical grade and purified by standard procedures prior to use. FT-IR spectra were recorded with a 170SX (Nicolet) spectrometer at room temperature, and electronic absorption spectra were taken with a Hitachi UV-3010 spectrophotometer. Elemental analyses were carried out with a Perkin−Elmer 240C analyser. TG-DTA experiments were carried out with a Dupont thermal analyser from room temperature to 800 °C under N_2 at a heating rate of 10 °C/min. The variable-temperature magnetic susceptibilities were measured in the "Servei de Magnetoquímica (Universitat de Barcelona)" with a Quantum Design MPMS SQUID susceptometer operating at a magnetic field of 0.1 T between 2 and 300 K. The diamagnetic corrections were evaluated from Pascal's constants for all the constituent atoms.

Preparation of 1: Purple block crystals were obtained in 78% yield (199 mg) by slow concentration of the water solution containing $Co(ClO_4)_2 \cdot 6H_2O$ (300 mg, 0.8 mmol) and $H_2L \cdot 2HCl$ (200 mg, 0.6 mmol) in a 4:3 molar ratio by adjusting the pH to 5−6 with KOH. IR (cm^{-1}): $\tilde{\nu}$ = 1606 vs $\nu_{as}(COO^-)$, 1390 vs $\nu_s(COO^-)$, 1120 vs, 1108 vs and 625 s $\nu(ClO_4^-)$. $C_{36}H_{68}Cl_2Co_4N_6O_{24}$ (1275.6): calcd. C 33.90, H 5.37, N 6.59; found C 33.77, H 5.43, N 6.58. DTA (peak positions): 115, 293, 386 and 545 °C. UV (H_2O): $\lambda_{max.} = 491$ nm.

Crystallographic Study: $C_{36}H_{68}Cl_2Co_4N_6O_{24}$ (**1**), $M_r = 1275.58$, monoclinic, space group C_2, $a = 24.411(5)$, $b = 12.260(2)$, $c = 8.351(2)$ Å, $\beta = 98.738(4)°$, $V = 2470.4(8)$ Å^3, $F(000) = 1320$, $Z = 2$, $\mu = 1.518\ mm^{-1}$, $D_{calcd.} = 1.715\ g \cdot cm^{-3}$, Flack parameter = 0, 2989 reflections measured, 2669 unique ($R_{int} = 0.0186$). Final R, wR and S values are 0.0342, 0.0949 and 1.052, respectively. CCDC-176943 contains the supplementary crystallographic data for this paper. These data can be obtained free of charge at www.ccdc.cam.ac.uk/cons/retrieving.html [or from the Cambridge Crystallographic Data Centre, 12 Union Road, Cambridge CB2 1EZ, UK; Fax: (internat.) + 44-1223-336-033; E-mail: deposit@ccdc.cam.ac.uk].

Acknowledgments

This work was financially supported by the National Science Funds for Distinguished Young Scientist of China (No. 20225101), the Natural Science Foundation of Tianjin (No. 033609711) and the Spanish Government (Grant 2003/00539).

[1] [1a] D. Gatteschi, *Adv. Mater.* **1994**, *6*, 635. [1b] R. E. P. Winpenny, *Comments Inorg. Chem.* **1999**, *20*, 233. [1c] S. Leininger, B. Olenyuk, P. J. Stang, *Chem. Rev.* **2000**, *100*, 853.
[2] [2a] W. Wernsdorfer, N. Aliaga-Alcalde, D. N. Hendrickson, G. Christou, *Nature* **2002**, *416*, 406. [2b] A. L. Barra, A. Caneschi, A. Cornia, F. F. Biani, D. Gatteschi, C. Sangregorio, R. Sessoli, L. Sorace, *J. Am. Chem. Soc.* **1999**, *121*, 5302.
[3] [3a] Z. E. Serna, M. K. Urtiaga, M. G. Barandika, R. Cortes, S. Martin, L. Lezama, M. I. Arriortua, T. Rojo, *Inorg. Chem.* **2001**, *40*, 4550. [3b] H. Andres, J. M. Clemente-Juan, M. Aebersold, H. U. Guedel, E. Coronado, H. Buettner, G. Kearly, J. Melero, R. Burriel, *J. Am. Chem. Soc.* **1999**, *121*, 10028. [3c] R. L. Paul, S. M. Couchman, J. C. Jeffery, J. A. McCleverty, Z. R. Reeves, M. D. Ward, *J. Chem. Soc., Dalton Trans.* **2000**, 845. [3d] G. S. Hanan, D. Volkmer, U. S. Schubert, J.-M. Lehn, G. Baum, D. Fenske, *Angew. Chem. Int. Ed. Engl.* **1997**, *36*, 1842.
[4] [4a] X. H. Bu, M. Du, Z. L. Shang, R. H. Zhang, D. Z. Liao, M. Shionoya, T. Clifford, *Inorg. Chem.* **2000**, *39*, 4190. [4b] X.

 © 2004 Wiley-VCH Verlag GmbH & Co. KGaA, Weinheim

H. Bu, M. Du, L. Zhang, D. Z. Liao, J. K. Tang, R. H. Zhang, M. Shionoya, *J. Chem. Soc., Dalton Trans.* **2001**, 593. [4c] X. H. Bu, M. Du, L. Zhang, Z. L. Shang, R. H. Zhang, M. Shionoya, *J. Chem. Soc., Dalton Trans.* **2001**, 729. [4d] X. H. Bu, M. Du, Z. L. Shang, L. Zhang, Q. H. Zhao, R. H. Zhang, M. Shionoya, *Eur. J. Inorg. Chem.* **2001**, 1551. [4e] M. Du, Y. M. Guo, X. H. Bu, J. Ribas, M. Monfort, *New J. Chem.* **2002**, *26*, 645.

[5] C. A. Grapperhaus, M. Y. Darensbourg, *Acc. Chem. Res.* **1998**, *31*, 451 and references cited therein.

[6] [6a] M. Du, X. H. Bu, Y. M. Guo, L. Zhang, D. Z. Liao, J. Ribas, *Chem. Commun.* **2002**, 1478. [6b] M. Du, X. H. Bu, Y. M. Guo, J. Ribas, C. Diaz, *Chem. Commun.* **2002**, 2550. [6c] M. Du, X. H. Bu, Y. M. Guo, J. Ribas, *Chem. Eur. J.* **2004**, *10*, 1345.

[7] H. D. Flack, *Acta Crystallogr., Sect. A* **1983**, *39*, 876.

[8] [8a] F. E. Mabbs, D. J. Mahin, *Magnetism and Transition Metal Complexes*, Chapman and Hall, Londomn, **1973**. [8b] O. Kahn, *Molecular Magnetism*, VCH, Weinheim, **1993**.

[9] [9a] G. de Munno, M. Julve, F. Lloret, J. Faus, A. Caneschi, *J. Chem. Soc., Dalton Trans.* **1994**, 1175. [9b] M. E. Lines, *J. Chem. Phys.* **1971**, *55*, 2977. [9c] M. J. Hossain, M. Yamasaki, M. Mikuriya, A. Kuribayashi, H. Sakiyama, *Inorg. Chem.* **2002**, *41*, 4058.

[10] [10a] M. J. Plater, M. R. J. Foremn, E. Coronado, C. J. Gómez-García, A. M. Z. Slawin, *J. Chem. Soc., Dalton Trans.* **1999**, 3549. [10b] H. Andres, J. M. Clemente-Juan, R. Basler, M. Aebersold, H. U. Gudel, J. J. Borrás-Almenar, A. Gaita, E. Coronado, H. Buttner, S. Jannse, *Inorg. Chem.* **2001**, *40*, 1943.

[11] [11a] J. J. Borrás-Almenar, J. M. Clemente-Juan, E. Coronado, B. S. Tsukerblat, *Inorg. Chem.* **1999**, *38*, 6081. [11b] J. J. Borrás-Almenar, J. M. Clemente-Juan, E. Coronado, B. S. Tsukerblat, *J. Comput. Chem.* **2001**, *22*, 985.

[12] R. L. Carlin, *Magnetochemistry*, Springer, Berlin, **1986**.

[13] Y.-H. Liu, H.-L. Tsai, Y.-L. Lu, Y.-S. Wen, J.-C. Wang, K.-L. Lu, *Inorg. Chem.* **2001**, *40*, 6426.

[14] [14a] D. Armentano, G. De Munno, F. Lloret, M. Julve, *Inorg. Chem.* **1999**, *38*, 3744. [14b] U. Turpeinen, R. Hamalainen, J. Reedijk, *Polyhedron* **1987**, *6*, 1603.

[15] Y. Pei, K. Nakatani, O. Kahn, J. Sletten, J. P. Renard, *Inorg. Chem.* **1989**, *28*, 3170.

Received April 5, 2004

 © 2004 Wiley-VCH Verlag GmbH & Co. KGaA, Weinheim

Plasma-Enhanced CVD Synthesis and Structural Characterization of Ta_2N_3

Alexei Yu. Ganin,[a] Lorenz Kienle,[a] and Grigori V. Vajenine*[a,b]

Dedicated to Professor Francis J. DiSalvo on the occasion of his 60th birthday

Keywords: Tantalum / Nitrides / Plasma-enhanced chemical vapor deposition / X-ray diffraction / Electron microscopy

Microcrystalline tantalum nitride films were prepared on various substrates from $TaCl_5$ precursor and nitrogen gas using the plasma-enhanced chemical vapor deposition (PECVD) method. Syntheses carried out at 600–650 °C led to single-phase samples of the tantalum nitride Ta_2N_3 with a defect fluorite-type structure. The anion vacancies were found to order resulting in a $2 \times 2 \times 2$ cubic superstructure of the C-Ln_2O_3 type (space group $Ia\bar{3}$, $Z = 16$) with a = 9.8205(4) Å according to a Rietveld refinement of the X-ray powder diffraction data. At higher deposition temperatures (650–700 °C) formation of highly textured orthorhombic Ta_3N_5 was observed. The samples were additionally studied by high-resolution transmission electron microscopy (HRTEM) and selected-area electron diffraction (SAED). The details of the new crystal structure for Ta_2N_3 as well as a possible nitrogen nonstoichiometry are discussed.
(© Wiley-VCH Verlag GmbH & Co. KGaA, 69451 Weinheim, Germany, 2004)

Introduction

The binary Ta−N system is quite rich in compounds with well-defined and variable stoichiometries. The formal oxidation state of tantalum covers the whole range from nearly zero to the maximum of +5. These compounds can be divided into four groups: solid solutions of nitrogen in tantalum, the phase with the approximate stoichiometry Ta_2N, three phases with a nearly 1:1 composition, and nitrogen-rich nitrides. A few comprehensive reviews of tantalum nitride structural chemistry are available.[1−3] Results of the previous structural studies in this binary system are summarized in Table 1.

Up to 5 at.% of nitrogen can be dissolved in the body-centered cubic lattice of elemental tantalum, for example by heating of Ta powder in ammonia at 600−700 °C.[3] The lattice constant of such solid solutions increases slightly to 3.315−3.369 Å compared to that of the pure metal (a = 3.311 Å). Observation of additional weak reflections suggests a cubic superstructure with the unit cell tripled in all directions and with $a_\beta = 3a_\alpha = 10.11$ Å.[1,13]

The γ-phase with the composition range $TaN_{0.41-0.5}$, also denoted as β-Ta_2N,[4] crystallizes with a hexagonal unit cell.[1−4] Its crystal structure can be described as a hexagonal close packing of the tantalum atoms with the nitrogen atoms filling half of the octahedral interstices. While the earlier studies suggested a statistical distribution,[1,2] electron-[3] and neutron-diffraction[4] investigations revealed a trigonal $P\bar{3}1m$ supercell with $a' = \sqrt{3}a$, isostructural to β-Nb_2N[14] and of the anti-Li_2ZrF_6-type.[15] The γ-phase can be obtained by nitriding of tantalum powder in gaseous ammonia at 800−900 °C or from the elements at 2000 °C.[1,3]

The hexagonal ε-phase was proposed by Schoenberg[1] to have a B35 CoSn-type structure with the composition $TaN_{1.00}$; the same description was given by Brauer and Zapp.[2] In this structure type the nitrogen atoms are at the center of slightly distorted tantalum octahedra. Later, Christensen and Lebech[5] showed that the nitrogen atoms are displaced from these ideal positions reducing their coordination sphere to a square pyramid. The unit cell determined by Christensen and Lebech[5] (a = 5.196 Å, c = 2.911 Å) is quite similar to that given by the other authors.[1−3] The ε-phase can be obtained as a product of nitriding of Ta powder at temperatures at > 1100 °C.[1]

Another modification of tantalum mononitride, the δ-phase with a face-centered cubic B1 NaCl-type structure, was observed by Gerstenberg and Calbick[16] in thin films; it was also recently synthesized from the ε-phase by shock compression.[7] The lattice parameter (a = 4.337 Å) for this

[a] Max-Planck-Institut für Festkörperforschung
Heisenbergstraße 1, 70569 Stuttgart, Germany
Fax: (internat.) + 49-711-689-1091
E-mail: G.Vajenine@fkf.mpg.de
A.Ganine@fkf.mpg.de
L.Kienle@fkf.mpg.de
[b] Institut für Anorganische Chemie, Universität Stuttgart,
Pfaffenwaldring 55, 70569 Stuttgart, Germany
Supporting information for this article is available on the WWW under http://www.eurjoc.org or from the author.

Table 1. Structural overview of known tantalum nitrides

Phase	Crystal structure	Composition	Lattice parameters [Å] a	c	Ref.
α-phase	body-centered cubic, A2 W-type	Ta	3.311		[1]
		$TaN_{0.04}$	3.315		[2]
β-phase	α-phase with a cubic 3 × 3 × 3 superstructure	$TaN_{0.05}$	10.11 (3× 3.369)		[1]
γ-phase (β-Ta_2N)	hexagonal close-packing of the tantalum atoms	$TaN_{0.41}$	3.041	4.907	[1]
		$TaN_{0.5}$	3.042	4.905	[2]
	an anti-Li_2ZrF_6-type superstructure with $a' = \sqrt{3}a$	$TaN_{0.5}$	5.283 ($\sqrt{3}$ × 3.050)	4.928	[3]
		$TaN_{0.43}$	5.285 ($\sqrt{3}$ × 3.051)	4.919	[4]
ε-phase	hexagonal, B35 CoSn-type	$TaN_{1.00}$	5.185	2.908	[1]
		$TaN_{1.00}$	5.181	2.905	[2]
		$TaN_{1.00}$	5.188	2.903	[3]
	hexagonal, distorted B35 CoSn-type	$TaN_{1.00}$	5.196	2.911	[5]
δ-phase	face-centered cubic, B1 NaCl-type	$TaN_{0.92}$	4.337		[6]
		$TaN_{0.97}$	4.336		[7]
θ-phase	hexagonal, Bh WC-type	$TaN_{1.00}$	2.936	2.885	[8]
		$TaN_{1.08}$	2.938	2.868	[9]
Ta_3N_5	orthorhombic, Fe_2TiO_5-type	Ta_3N_5	3.8862	b = 10.2118 c = 10.2624	[10]
Ta_4N_5	tetragonal, Nb_4N_5-type	Ta_4N_5	6.835	4.272	[3]
Ta_5N_6	hexagonal, Nb_5N_6-type	Ta_5N_6	5.175	10.307	[3]
TaN_x	cubic, CaF_2-type	TaN_x	5.02		[11]
	CaF_2-type with a body-centered tetragonal superstructure	TaN_x	5.77	5.01	[12]

nitride obtained by Gatterer et al.[6] from the elements at 2000 °C and a pressure of 40 bar, and that obtained by Mashimo et al.[7] (a = 4.336 Å), are almost identical.

Finally, the θ-phase crystallizes hexagonal in the Bh WC-type structure type with a simple hexagonal stacking of the metal layers. The nitrogen atoms center the trigonal prisms formed by the tantalum atoms. The unit cell observed for this hexagonal phase (a = 2.936 Å, c = 2.885 Å) by Brauer et al.[8] is rather similar to that obtained by Mashimo and Tashiro[9] (a = 2.938 Å, c = 2.868 Å). The hexagonal ε-TaN phase transforms into θ-TaN at pressures of 20−100 kbar and at 800−960 °C, or under mechanical alloying conditions.[8,9]

Ta_3N_5, the nitrogen-richest phase, has a pseudobrookite (Fe_2TiO_5)-type[17] structure. This structure contains octahedrally coordinated tantalum atoms, while the nitrogen atoms are both three- and four-coordinate. The TaN_6 octahedra are linked together by sharing edges and corners. Though Brauer and Weidlein[18] reported a tetragonal unit cell, it was later refined as orthorhombic[19] (a = 3.893 Å, b = 10.264 Å, c = 10.264 Å) and monoclinic[20] (a = 10.229 Å, b = 3.875 Å, c = 10.229 Å, β = 90.0°). Brese et al.[10] have shown that both structural models are valid within the accuracy of the data. Ta_3N_5 can be obtained by nitriding of Ta_2O_5 in an ammonia flow at 860−920 °C,[18] for example.

Upon heating in argon or ammonia, Ta_3N_5 decomposes yielding the nitrides Ta_4N_5 and Ta_5N_6.[21] The tetragonal Ta_4N_5[3] phase is isostructural to Nb_4N_5,[22] a defect variant of the NaCl-type structure. The hexagonal Ta_5N_6[3] is isostructural to Nb_5N_6;[22] it is built up from the tantalum atom layers in the stacking ABACABAC.

Yet another binary tantalum nitride, TaN_x, has been reported, although its stoichiometry and crystal structure have not been established reliably. It was first observed in reactive sputtering experiments by Buvinger[11] and appeared to have an fcc-type crystal structure with a = 5.02 Å, which is notably larger than that of the NaCl-type δ-phase (a = 4.34 Å). Coyne and Tauber[12] confirmed the lattice parameter range of 4.98−5.05 Å and proposed a fluorite-type structure for this nitride. Additional reflections led the authors to postulate a body-centered tetragonal supercell with a = 5.77 Å and c = 5.01 Å.

Except for the latter phase, all the above-mentioned tantalum nitrides can be prepared by conventional synthetic routes. In the last few years interest in tantalum nitride films has been sparked by a combination of their mechanical stability, chemical inertness and resistive behavior of these phases. Possible applications in microelectronics as Cu diffusion barriers, for example, has stimulated application of novel techniques such as reactive sputtering,[23,24] rapid thermal processing,[25] and ion-beam-assisted deposition (IBAD)[26] to the synthesis of tantalum nitrides. Another approach, the plasma-enhanced chemical vapor deposition (PECVD) method proved to be useful for the preparation of the cubic δ-phase, for example.[27,28] This contribution describes the application of PECVD to the synthesis of Ta_2N_3, previously known as the "bct-TaN_x" phase, and its structural characterization.

Results and Discussion

Tantalum nitride powder coatings were grown in a PECVD reactor by passing a mixture of nitrogen gas and $TaCl_5$ precursor in the plasma region over the substrate in the temperature range of 600−700 °C. Deposition experiments were carried out on silicon, copper, and quartz glass

 © 2004 Wiley-VCH Verlag GmbH & Co. KGaA, Weinheim

Table 2. PECVD conditions, product composition, and unit cell parameters for selected samples

Sample	Phase composition	N/Ta ratio from EDXS	$a(Ta_2N_3)$ [Å]	Deposition temp. [°C]	Substrate
A	Ta_2N_3	1.35(4)	9.841(4)	630	Si (100)
B	Ta_3N_5	1.48(3)	–	715	Si (100)
C	Ta_2N_3	1.41(3)	9.8205(4)	640	Si (100)
D	Ta_2N_3	1.35(4)	9.822(6)	640	Si (100)
E	Ta_2N_3	1.36(4)	9.850(5)	635	Si (100)
F	Ta_2N_3	1.42(4)	9.862(4)	640	Cu
G	Ta_2N_3	1.28(4)	9.844(4)	620	Cu
H	Ta_2N_3	1.26(4)	9.803(3)	625	quartz glass
I	Ta_2N_3 + Ta_3N_5	1.45(3)	9.863(5)	670	Si (100)
J	Ta_3N_5 + TaN	1.33(4)	–	–	–

substrates. Representative deposition conditions are listed in Table 2.

The phase composition of the coatings varies with the deposition temperature, according to the powder X-ray diffraction investigations. While at higher temperatures of 650−700 °C the orthorhombic Ta_3N_5 phase was predominantly formed, the experiments at lower temperature (600−650 °C) yielded another phase with the strongest reflections corresponding to an fcc lattice with $a \approx 5.0$ Å. This value, which is similar to that observed for the "bct-TaN_x" phase, suggested a nitrogen-rich phase of the fluorite (CaF_2) type. However, the ideal composition "TaN_2" is implausible due to the requirement of the formal oxidation state Ta^{6+}. Indeed, a closer inspection of the additional weak reflections indicated a cubic $2 \times 2 \times 2$ superstructure. The analogy to the well-known bixbyite- or C-Ln_2O_3-type phases[29,30] (space group $Ia\bar{3}$) led us to postulate the same structure and the Ta_2N_3 composition for this tantalum nitride. It was mentioned above that a similar fluorite-based TaN_x phase has been identified by electron diffraction in samples obtained in sputtering experiments.[12] Weak superstructure reflections were observed there as well, but a different body-centered tetragonal supercell with $a = 5.77$ Å and $c = 5.01$ Å was proposed without further structural study.[12] However, these superstructure reflections appear to be identical to those observed in our study; moreover, the c/a ratio of the proposed bct cell is $0.867 \approx \sqrt{3}/2$, indicating the equivalence of the $(200)_{bct}$ and $(111)_{fluorite}$ reflections according to the cell choices of the phases. This would imply non-orthogonality of the proposed a_{bct} and c_{bct} axes, thus making the bct superstructure inadequate.

The product composition was determined by energy-dispersive X-ray spectroscopy (EDXS). Although the formation of nitrogen-rich products could be established, more accurate determination of the composition was not possible. Chlorine contamination was found to be below the detection limit of EDXS (2−3 at.%), whereas the oxygen content did not exceed 5 at.%.

In order to test the proposed structural model for Ta_2N_3, sample A was investigated by HRTEM and was additionally studied with the internal EDX. As before, only a small amount of oxygen (less then 4 at.%) was found in the sample; no other impurities could be detected. Such oxygen content typically results from the surface contamination of thin crystallites. Sample A contains irregular, roundish particles with sizes in the range of 50−500 nm (Figure 1a). Electron-diffraction patterns recorded on aggregates of particles show Bragg intensities located on concentric rings around 000. The d values derived from these patterns are consistent with the metrics of the cubic Ta_2N_3 phase. Applying selected-area electron diffraction (SAED), the larger roundish particles of the sample could be identified as microcrystals of Ta_2N_3. SAED patterns were recorded along different zone axes on these crystallites in order to compare them with simulated patterns. Some crystallites of sample A were sufficiently large and could be tilted in several zone axis orientations. The tilt angles, α, are consistent with the expected cubic metrics, for example with those for the zone axes $[100]_{cubic}$ and $[311]_{cubic}$ ($\alpha = 25.2°$), $[311]_{cubic}$ and $[211]_{cubic}$ ($\alpha = 10°$), and $[111]_{cubic}$ and $[313]_{cubic}$ ($\alpha = 22°$). For all analyzed orientations, we observed a convincing agreement between the simulated and experimental patterns (see Figure 1b for $[100]_{cubic}$).

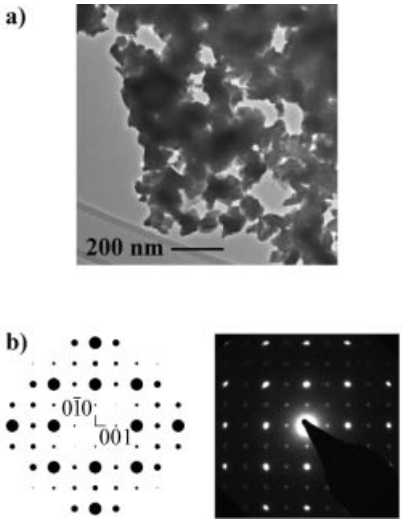

Figure 1. High resolution transmission electron microscopy (HRTEM) micrographs of deposited tantalum nitride: (a) roundish shape of Ta_2N_3 crystallites; (b) simulated and observed selected-area electron diffraction patterns along the [100] axis

 © 2004 Wiley-VCH Verlag GmbH & Co. KGaA, Weinheim

Through-focus HRTEM images, for instance in [110] orientations, are in good agreement with simulated micrographs based on the assumed structure of Ta_2N_3. However, details of the real structure concerning the precise arrangement of the nitrogen atoms cannot be derived from HRTEM micrographs.

The C-Ln_2O_3 structure type is an ordered-defect variant of the fluorite structure. Aside from doubling of the unit cell in all directions, a quarter of the anion positions remain empty. When local coordination of the Ta atoms is considered, this corresponds to removing two of eight nitrogen atoms in the first coordination sphere on going from the ideal TaN_2 composition to the stoichiometry Ta_2N_3. Two types of Ta positions result, as shown in Figure 2a: while two opposing nitrogen atoms of a TaN_8 cube are removed around Ta(1), two nitrogen positions connected by a face diagonal of the cube remain empty for Ta(2). After a relaxation of the crystal structure, Ta(1) occupies the 8*b* position (1/4,1/4,1/4), Ta(2) is shifted to the 24*d* site (*x*,0,1/4), and the nitrogen atoms take the general 48*e* position with $x \approx z \approx 3/8$ and $y \approx 1/8$ (see Table 3). The missing nitrogen atoms would occupy the 16*c* (*x*,*x*,*x*) site with $x \approx 1/8$ in this space group. Partial filling of the latter position is indeed observed in the $U_2N_{3+\delta}$ series, in which both end members, U_2N_3 and UN_2, are known as well.[31]

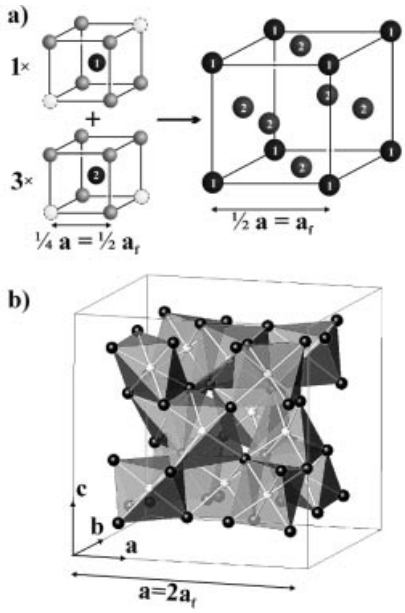

Figure 2. Crystal structure of Ta_2N_3: (a) analogy between the fluorite and Ta_2N_3 structures ["1" and "2" stand for the Ta(1) and Ta(2) positions, respectively]; (b) TaN_6 coordination polyhedra inside the unit cell of Ta_2N_3

While the TEM and SAED investigations confirmed qualitatively the C-Ln_2O_3-type structure for this tantalum nitride, a Rietveld refinement of the powder diffraction data from sample C was carried out in order to elucidate the structural details. It was possible to refine the atomic positions for all atoms; these are shown in Table 3, in comparison with those in related phases.

Table 3. Atomic positions in Ta_2N_3 compared to those in related compounds

	x(24*d*)	*x*(48*e*)	*y*(48*e*)	*z*(48*e*)
Ta_2N_3	−0.0280(3)	0.377(4)	0.153(3)	0.377(6)
Ta_2N_3 model	−0.02686	0.38366	0.14472	0.38061
U_2N_3 [31]	−0.018	0.38	0.167	0.398
Y_2O_3 [32]	−0.0320(1)	0.3911(5)	0.1516(5)	0.3827(6)
Zn_3N_2 [33]	−0.0216(1)	0.3975(1)	0.1498(2)	0.3759(1)
Mg_3N_2 [34]	−0.031(2)	0.38925(6)	0.15217(7)	0.38220(6)
Ca_3N_2 [34]	−0.03826(18)	0.39006(3)	0.15389(3)	0.38242(3)
Ideal fluorite	0	3/8	1/8	3/8

The refinement of the occupation of the 16*c* position was not successful due to the low quality of the powder diffraction data; this position was left empty in the further refinements. The resulting crystal structure of Ta_2N_3 is shown in Figure 2. The structure is built from octants, which have tantalum atoms in their centers. These form a face-centered cubic lattice and are coordinated by distorted octahedra of nitrogen atoms. The TaN_6 units are linked together by sharing edges and corners. The Ta−N distances in two different Ta coordination polyhedron types vary between 2.01(5) and 2.17(4) Å. Similar Ta−N distances were found in the nitrides Ta_3N_5 (1.955−2.240 Å), ε-TaN (2.041−2.163 Å), δ-TaN (2.165 Å), and θ-TaN (2.23 Å). In the Ta(1)N_6 trigonal antiprisms all Ta(1)−N distances are equal to 2.01(5) Å and the bond angles [78(2)−108(2) and 180°] approach those in an ideal octahedron. The Ta(2)N_6 polyhedron is less symmetrical: there are three pairs of Ta(2)−N distances [2 × 2.13(4), 2 × 2.13(5), and 2 × 2.17(4) Å] and the bond angles fall into the ranges 72(2)−116(2) and 129(2)−170(2)°. The coordination of nitrogen atoms remains nearly tetrahedral, as in the parent fluorite structure, with the Ta−N−Ta bond angles ranging from 100(2) to 125(2)°.

Due to a relatively large uncertainty in the nitrogen position, a simple model structure was introduced. First, for each value of $x_{Ta(2)}$, a nitrogen position equidistant from the four tantalum neighbors was calculated. The resulting Ta−N distance was then plotted as a function of $x_{Ta(2)}$ (Figure 3). Remarkably, this function was found to reach a minimum at $x_{Ta(2)} = -0.02686$ with a corresponding Ta−N distance of 2.109 Å. The resulting model structure may be taken as the first approximation to a crystal structure involving chemically similar Ta(1) and Ta(2) atoms. As Table 3 shows, this model reproduces well the observed Ta_2N_3 structure: the corresponding structural parameters compare well with the refined ones, when the respective standard deviations are taken into account.

The question of the exact stoichiometry of Ta_2N_3 remains open: a partial occupation of the 16*c* position, as in $U_2N_{3+\delta}$, leading to $Ta_2N_{3+\delta}$ cannot be excluded. Since the highest formal oxidation state of tantalum is +5, the values of δ from 0 to 1/3 are possible. The EDXS method is not sensitive enough to detect such a small variation of the composition and sufficiently large amounts of Ta_2N_3 for an accurate chemical analysis cannot yet be prepared. Larger

 © 2004 Wiley-VCH Verlag GmbH & Co. KGaA, Weinheim

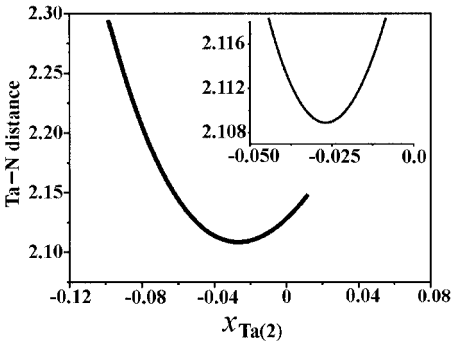

Figure 3. The Ta−N bond length in a Ta_2N_3 model structure in Å as a function of the Ta(2) *x*-coordinate assuming the equality of all Ta−N distances

samples would also be required for accurate measurements of resistivity and magnetic susceptibility. Interestingly, the "bct-TaN_x" phase[12] was found to be conducting, with a ρ(T) behavior corresponding to $\Delta E \approx 0.1-0.3$ eV and with an optical bandgap of 2.0−2.6 eV. Two indirect indications suggest that the formal oxidation state of tantalum in $Ta_2N_{3+\delta}$ is lower than +5. Firstly, the color of the compound (black metallic) compared to that of Ta_3N_5 (red-brown) supports this idea. Secondly, annealing $Ta_2N_{3+\delta}$ samples in vacuo at 700 °C led to an apparent disproportionation to fcc δ-TaN and Ta_3N_5 (see also Table 2), thus also suggesting a lower tantalum oxidation state. Therefore, we designate this phase as Ta_2N_3, keeping the possible nitrogen nonstoichiometry in mind.

In sample B, which contains Ta_3N_5 with a small fraction of Ta_2N_3, nanorods (see Figure 4a) with typical dimensions

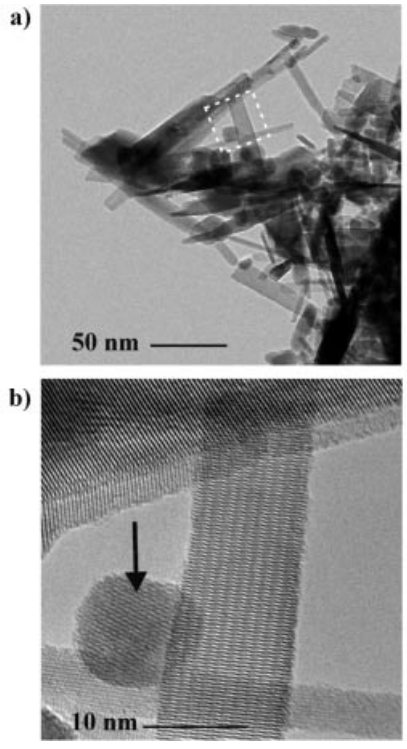

Figure 4. (a) Nanorods of Ta_3N_5; (b) enlarged section: a crystallite of Ta_2N_3 (see arrow) bordered by the Ta_3N_5 nanorods

of 10 nm × 100 nm were observed by HRTEM. In the diffraction patterns of these nanorods strong intensities occur in the positions expected for the orthorhombic Ta_3N_5 phase. All nanorods are highly crystalline (Figure 4b). These microcrystals of Ta_3N_5 exhibit additional features of the micro- and nanostructure which both originate from a lamellar assembly of $(010)_{ortho}$ layers.

Conclusion

Microcrystalline films of a binary tantalum nitride with the composition Ta_2N_3 have been obtained in an RF plasma from $TaCl_5$ and nitrogen gas at 600−650 °C using the PECVD technique. According to X-ray and electron diffraction data, the compound crystallizes in the cubic C-Ln_2O_3 structure type, an ordered defect 2 × 2 × 2 superstructure of the fluorite type. This nitride is thought to be identical with the previously reported "bct-TaN_x" phase obtained in sputtering experiments. Notably, this binary tantalum nitride could not be prepared by conventional synthetic routes so far; plasma activation of the nitrogen gas appears to be essential for the successful synthesis.

Experimental Section

Synthesis: Syntheses were performed in a custom-designed PECVD (Plasma Enhanced Chemical Vapor Deposition) experimental setup, which is schematically illustrated in Figure 5. It consists of a nitrogen gas delivery line, a precursor handling system, and a reactor.

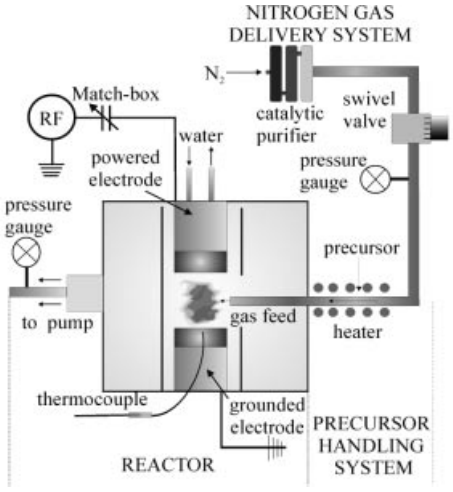

Figure 5. Scheme of the experimental PECVD setup

Nitrogen Gas Delivery Line: Nitrogen gas (Westfalen AG, 99.999%) was further purified by passing it through three separate catalytic columns (silica gel, molecular sieves, and an oxysorb catalyst[35]), in order to remove traces of oxygen and moisture from the nitrogen stream.

 © 2004 Wiley-VCH Verlag GmbH & Co. KGaA, Weinheim

Precursor Handling System: The $TaCl_5$ precursor was loaded in a argon dry box into a glass tube, which was then connected to the setup under nitrogen flow. The precursor was then dropped down into the heated delivery line. Throughout the deposition process the temperature of the precursor handling system was maintained at 70−80 °C by means of a hot air gun in order to prevent the condensation of the precursor.

Reactor: Deposition occurred in a plasma region inside of a quartz tube between two parallel electrodes. This setup was placed in an evacuated glass vessel. The upper of the electrodes was connected to the 13.56 MHz 1000 W RF (radio frequency) source (Hüttinger, PFG-RF1000) through a match box (Hüttinger, PFM 1500A), while the lower electrode was grounded. Substrates were loaded on the lower electrode, the upper electrode was water-cooled. An NiCr/NiAl thermocouple was inserted into the lower electrode for temperature monitoring as shown in Figure 5.

Deposition: Before every deposition, the reactor with a loaded substrate was baked in plasma at 400 °C in the nitrogen gas flow for 1 h. Afterwards, the reactor was cooled and heated up to the deposition temperature by igniting the plasma. Nitrogen carrier gas was mixed with the $TaCl_5$ precursor evaporated at 70−80 °C and delivered into the gap between the two electrodes. The pressure in the system was measured by means of two pressure gauges at the inlet and the outlet of the setup. The deposition time varied depending on the evaporation rate of the $TaCl_5$ precursor. A typical experiment took 2−6 h at an RF power of 500−700 W. The reaction progress could also be monitored by the color change of the plasma from light green to yellow-orange as the precursor was consumed. The conditions of the deposition experiments are summarized in Table 2.

Substrates: Silicon wafer (100), copper (Alfa Aesar, 99.9%), and quartz glass substrates (Heraeus) were used. Their sizes varied from 5 × 10 to 10 × 20 mm. The substrates were prepared for deposition by washing with ethanol in a sonic bath and then rinsing with deionized water and acetone.

Precursor Preparation: Tantalum(v) chloride (Alfa Aesar, 99.99% metals basis) was purified by sublimation. The observed X-ray diffraction pattern of the product matched that of the monoclinic phase reported in the literature.[36]

Scanning Electron Microscopy Analysis: Investigations were performed with a TESCAN 5120MM scanning electron microscope. Quantitative analysis of the samples was done by EDXS with an Oxford Si-detector with an electron-beam energy of 10 keV, and signal accumulation time of 60−120 s.

Transmission Electron Microscopy: Samples A (Ta_2N_3) and B (Ta_3N_5) were crushed in an agate mortar and suspended in *n*-butanol. A perforated carbon/copper net was covered with the suspension, leaving wedge-shaped crystallites in random orientations after drying. HRTEM and SAED investigations were performed with a Philips CM30ST instrument (300 kV, LaB_6 cathode, C_S = 1.15 mm). Computer simulations of the HRTEM images (multislice formalism) and SAED patterns (kinematical approximation) were carried out with the EMS program package[37] (spread of defocus: 70 Å, illumination semiangle: 1.2 mrad). All images were collected with a Multiscan CCD Camera [software Digital Micrograph 3.6.1 (Gatan)].

Sample Appearance: The deposits of Ta_2N_3 were black with a metallic shine; growth of red-brown Ta_3N_5 was also observed in some experiments. Adhesion of all samples to the substrate material was rather low, as evidenced by the "scotch test": the microcrystalline products could be removed from the substrates by a scotch tape.

Annealing: Sample I (Ta_2N_3) was annealed at 700 °C in vacuo (5.0×10^{-8} Torr) for 50 h. X-ray analysis of the sample was carried out before and after the annealing.

X-ray Crystallographic Study: The powder diffraction data were collected with a STADI-P STOE diffractometer using Cu-$K_{\alpha 1}$ radiation at room temperature. The results of the phase analysis are presented in Table 2. The powder diffraction pattern of the single phase sample C is shown in Figure 6, where the reflections corresponding to the 2 × 2 × 2 superstructure of the fluorite unit cell are clearly visible. These data were used for a Rietveld refinement using the CSD package.[38] The C-Ln_2O_3 structure type (space group $Ia\bar{3}$) was chosen as the starting model for Ta_2N_3. The unit cell constant and the atomic positional parameters were refined, while the isotropic temperature displacement factor had to be fixed for the nitrogen atom position; pseudo-Voigt functions were employed to model the reflection profiles. The background was fitted by a parabolic form, and an absorption correction was introduced. Additionally, texture effects along the [100] axis had to be taken into account. Crystal data for the investigated sample are summarized in Table 4. Further details of the crystal structure investigation may be obtained from the Fachinformationzentrum Karlsruhe, 76344 Eggenstein-Leopoldshafen, Germany, on quoting the depository number CSD-413802.

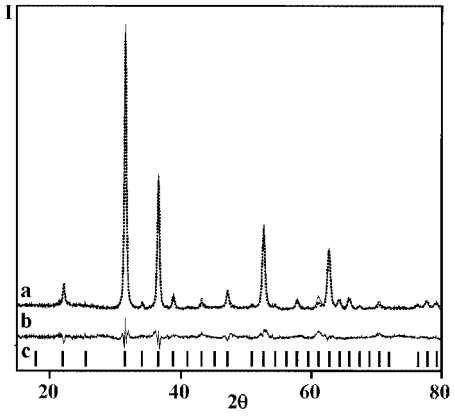

Figure 6. (a) Measured powder X-ray diffraction pattern of Ta_2N_3 (solid line) and the calculated curve (dotted line); (b) the difference curve; (c) positions of the Ta_2N_3 reflections

Table 4. Details of the crystal structure refinement for Ta_2N_3

Radiation, wavelength	Cu-$K_{\alpha 1}$, 1.54051 Å
Crystal system, space group	cubic, $Ia\bar{3}$ (no. 206), Z = 16
Unit cell dimensions [Å]	a = 9.8205(4)
Unit cell volume [Å^3]	947.1(1)
Refinement method	full profile
2θ range [°]	15−80
Free parameters	10
Final R values	R(intensity) = 8.75%; R(profile) = 18.06%

 © 2004 Wiley-VCH Verlag GmbH & Co. KGaA, Weinheim

Acknowledgments

This work was supported by the Sofja Kovalevskaja Research Award of the Alexander von Humboldt Foundation, the Federal Ministry of Education and Research, and Programme for Investment in the Future (ZIP) of the German Government. We also thank Professor Arndt Simon for his support, Mitsuharu Konuma for valuable advice on the PECVD setup, and Viola Duppel and Claudia Kamella for EDX and HRTEM measurements.

[1] N. Schönberg, *Acta Chem. Scand.* **1954**, *8*, 199−203.
[2] G. Brauer, K. H. Zapp, *Z. Anorg. Allg. Chem.* **1954**, *277*, 129−139.
[3] N. Terao, *Jpn. J. Appl. Phys.* **1971**, *10*, 249−259.
[4] L. E. Conroy, A. N. Christensen, *J. Solid State Chem.* **1977**, *20*, 205−207.
[5] A. N. Christensen, B. Lebech, *Acta Crystallogr., Sect. B* **1978**, *34*, 261−263.
[6] J. Gatterer, G. Dufek, P. Ettmayer, R. Kieffer, *Monatsh. Chem.* **1975**, *106*, 1137−1147.
[7] T. Mashimo, S. Tashiro, T. Toya, H. Yamazaki, S. Yamaya, K. Oh-ishi, Y. Syono, *J. Mater. Sci.* **1993**, *28*, 3439−3443.
[8] G. Brauer, E. Mohr, A. Neuhaus, A. Skogan, *Monatsh. Chem.* **1972**, *103*, 794−798.
[9] T. Mashimo, S. Tashiro, *J. Mater. Sci. Lett.* **1994**, *13*, 174−176.
[10] N. E. Brese, M. O'Keeffe, P. Rauch, F. J. DiSalvo, *Acta Crystallogr., Sect. C* **1991**, *47*, 2229−2294.
[11] E. A. Buvinger, *Appl. Phys. Lett.* **1965**, *7*, 14−15.
[12] H. J. Coyne, R. N. Tauber, *J. Appl. Phys.* **1968**, *39*, 5585−5593.
[13] D. P. Seraphim, N. R. Stemple, D. T. Novick, *J. Appl. Phys.* **1962**, *33*, 136−141.
[14] A. N. Christensen, *Acta Chem. Scand., Ser. A* **1976**, *30*, 219−224.
[15] R. Hoppe, W. Daehne, *Naturwissenschaften* **1960**, *47*, 397.
[16] D. Gerstenberg, C. J. Calbick, *J. Appl. Phys.* **1964**, *35*, 402−407.
[17] L. Pauling, *Z. Kristallogr., Kristallgeom., Kristallphys., Kristallchem.* **1930**, *73*, 97−113.
[18] G. Brauer, J. R. Weidlein, *Angew. Chem.* **1965**, *77*, 218−219; *Angew. Chem. Int. Ed. Engl.* **1965**, *4*, 241.
[19] J. Straehle, *Z. Anorg. Allg. Chem.* **1973**, *402*, 47−57.
[20] N. Terao, *C. R. Acad. Sci. Ser. C* **1977**, *285*, 12−20.
[21] J-C. Gilles, *C. R. Acad. Sci. Ser. C* **1968**, *266*, 546−547.
[22] N. Terao, *J. Less-Common Met.* **1971**, *23*, 159−169.
[23] T. Riekkinen, J. Molarius, T. Laurilab, A. Nurmela, I. Suni, J. K. Kivilahti, *Microelectron. Eng.* **2002**, *64*, 289−297.
[24] C. S. Shin, Y. W. Kim, D. Gall, J. E. Greene, I. Petrov, *Thin Solid Films* **2002**, *402*, 172−182.
[25] C. Angelkorta, A. Berendes, H. Lewaltera, W. Bock, B. O. Kolbesen, *Thin Solid Films* **2003**, *437*, 108−115.
[26] K. Volz, M. Kiuchi, W. Ensinger, *Surf. Coat. Technol.* **2000**, *128*, 298−302.
[27] X. Chen, H. L. Frisch, A. E. Kaloyeros, *J. Vac. Sci. Technol. B* **1999**, *17*, 182−185.
[28] X. Chen, G. G. Peterson, C. Goldberg, G. Nuesca, H. L. Frisch, A. E. Kaloyeros, B. Arkles, J. Sullivan, *J. Mater. Res.* **1999**, *14*, 2043−2052.
[29] F. S. Galasso, *Structure and Properties of Inorganic Solids*, 1st ed., Pergamon Press, Oxford, **1970**, p. 99.
[30] A. F. Wells, *Structural Inorganic Chemistry*, 4th ed., Clarendon Press, Oxford, **1975**, p. 451.
[31] R. E. Rundle, N. C. Baenzinger, A. S. Wilson, R. A. McDonald, *J. Am. Chem. Soc.* **1948**, *70*, 99−105.
[32] L. Smrcok, *Cryst. Res. Technol.* **1989**, *24*, 607−611.
[33] D. E. Partin, D. J. Williams, M. O'Keefe, *J. Solid State Chem.* **1997**, *132*, 56−59.
[34] O. Reckeweg, F. J. DiSalvo, *Z. Anorg. Allg. Chem.* **2001**, *687*, 371−377.
[35] B. Horvath, J. Strutz, J. Geyer-Lippmann, E. G. Horvath, *Z. Anorg. Allg. Chem.* **1981**, *209*, 483.
[36] S. Rabe, U. Müller, *Z. Kristallogr. − New Cryst. Struct.* **2000**, *215*, 1−2.
[37] P. A. Stadelmann, *Ultramicroscopy* **1987**, *21*, 131.
[38] L. G. Akselrud, Yu. N. Grin, P. Yu. Zavalij, V. K. Percharsky, V. S. Fundamenskii, "CSD − Universal program package for single crystal and/or powder structure data treatment", *12th European crystallographic meeting: Abstract of papers*, Moscow, **1989**, vol. 3, p. 155.

Received March 22, 2004
Early View Article
Published Online July 12, 2004

 © 2004 Wiley-VCH Verlag GmbH & Co. KGaA, Weinheim

Two- and Three-Dimensional Hydrogen-Bonded Networks Built from 1,3,5-$[(HO)_2(O)P]_3C_6H_3$ and 4-(Dimethylamino)pyridine

Michael Mehring[a]

Keywords: Phosphonic acid / Hydrogen bonds / Crystal engineering / Supramolecular chemistry

Crystallisation of 3,5-bis(phosphonophenyl)phosphonic acid, 1,3,5-$[(HO)_2(O)P]_3C_6H_3$, from $MeOH/H_2O$ in the presence of 4-(dimethylamino)pyridine, 4-$(Me_2N)C_5H_4N$, gave $[1\text{-}\{(HO)_2(O)P\}\text{-}3,5\text{-}\{(HO)(O)_2P\}_2C_6H_3]^{2-}[\{4\text{-}(Me_2N)C_5H_4NH\}^+]_2$ (**2**) and $[1,3\text{-}\{(HO)_2(O)P\}_2\text{-}5\text{-}\{(HO)(O)_2P\}C_6H_3]^-[4\text{-}(Me_2N)\text{-}C_5H_4NH]^+$ (**3**). Single-crystal X-ray diffraction analyses revealed a two- and a three-dimensional hydrogen-bonded network for compounds **2** and **3**, respectively. Compound **2** is composed of layers which are formed by hydrogen-bonded motifs of the type R2,2(8) and R4,4(16). These motifs are connected within the layer by additional hydrogen bonds and the benzene spacer. The cation $[4\text{-}(Me_2N)C_5H_4NH]^+$ is located between the layers and determines the interlayer separation of approximately 6.5 Å. In compound **3** a layered network of the hydrogen-bonded building units R2,3(10) was observed. These units are interconnected by four additional hydrogen bonds within the network. The benzene spacer links the adjacent layers to give a three-dimensional structure. Within this network, channels with internal dimensions of ca. 8.5 × 11.3 $Å^2$ which are occupied by the $[4\text{-}(Me_2N)C_5H_4NH]^+$ cations were observed.

(© Wiley-VCH Verlag GmbH & Co. KGaA, 69451 Weinheim, Germany, 2004)

Introduction

In the last three decades there has been a tremendous interest in the development of new metal phosphonates due to their great potential for applications based on ion exchangers, catalysts, selective adsorbents, sensors, photochemically active materials, proton conductors and materials for non-linear optics.[1,2] Most of the metal phosphonates based on non-functionalised mono(phosphonic acids), RPO_3H_2, and bis(phosphonic acids), $H_2O_3P-R-PO_3H_2$, adopt layered and pillared-layered structures. Recently, a growing interest in metal phosphonate clusters has emerged as well.[3−13] In contrast to the intensive studies of metal phosphonates, little attention was drawn to the structure and properties of simple phosphonic acids. Their crystal structures are characterised by the formation of hydrogen bonds of the type P−O−H···O=P which results in a diverse structural chemistry ranging from hydrogen-bonded clusters[14] to two- and three-dimensional polymers.[15−24] However, the prediction of structures even in the case of non-functionalised mono(phosphonic acids) is far from simple because each phosphonic acid moiety might serve as a hydrogen bond acceptor for one or even two hydrogen bond donors through its P=O group and as a double hydrogen bond donor through its two P−O−H groups. In contrast to crystal engineering approaches to organic solids using phosphonic acids, much effort has been made in the development of organic hydrogen-bonded materials using the carboxylic acid dimer motif. One of the most popular organic acids in this context is trimesic acid, 1,3,5-$(HO_2C)_3C_6H_3$, and a large number of studies based on this carboxylic acid have been reported.[25] Surprisingly, its phosphorus-containing counterpart, the triphosphonic acid 1,3,5-$[(HO)_2(O)P]_3C_6H_3$, has not been the subject of crystal engineering studies. This triphosphonic acid might function as a robust synthon for the construction of two- and three-dimensional networks through the formation of strong hydrogen bonds. The only report on 1,3,5-$[(HO)_2(O)P]_3C_6H_3$ stems from 2002 and deals solely with its synthesis.[26]

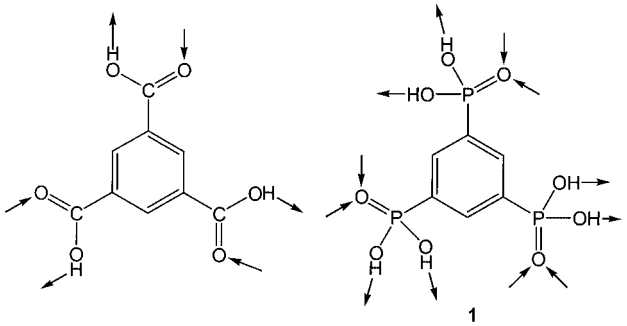

1

A drawback of functional organic solids is often their low thermal stability but it was shown recently that the co-crystallisation of nitrilotri(methylphosphonic acid) with various amines produces aggregates showing thermal stability similar to that obtained for metal phosphonates.[27,28]

[a] Anorganische Chemie II, Universität Dortmund
44221 Dortmund, Germany
Fax: (internat.) + 49-231-755-5048
E-mail: michael.mehring@uni-dortmund.de

Studies of the crystallisation of phosphonic acids in the presence of amines have shown that a proton is transferred from the phosphonic acid to the amine to give anions of the type $[RP(O)_2OH]^-$.[29−35] As result of their self-assembly through strong hydrogen bonds of the type P−O−H···$^-$O−P and the cooperative effect operating within the hydrogen-bonded network, very robust crystalline solids are produced. In a combined theoretical and experimental work on *tert*-butylphosphonic acid we have shown previously that by removal of a proton the hydrogen bond strength in the dimer is increased from ca. 43 kJ·mol^{-1} calculated for $[t\text{BuP(O)(OH)}_2]_2$ to ca. 83 kJ·mol^{-1} calculated for $[\{t\text{BuP(O)}_2\text{(OH)}\}\{t\text{BuP(O)(OH)}_2\}]^-$.[14]

Here we report on the synthesis and characterisation of hydrogen-bonded aggregates of the triphosphonic acid 1,3,5-$[(HO)_2(O)P]_3C_6H_3$ (**1**) with 4-(dimethylamino)pyridine. The phosphonic acid was crystallised in the presence of the amine to give $[1\text{-}\{(HO)_2(O)P\}\text{-}3,5\text{-}\{(HO)(O)_2P\}_2\text{-}C_6H_3]^{2-}[\{4\text{-}(Me_2N)C_5H_4NH\}^+]_2$ (**2**) and $[1,3\text{-}\{(HO)_2\text{-}(O)P\}_2\text{-}5\text{-}\{(HO)(O)_2P\}C_6H_3]^-[4\text{-}(Me_2N)C_5H_4NH]^+$ (**3**). The single-crystal X-ray structure analyses of both compounds as well as their thermal stability are discussed.

Results and Discussion

The triphosphonic acid 1,3,5-$[(HO)_2(O)P]_3C_6H_3$ (**1**) was prepared from the corresponding arylphosphonic ester 1,3,5-$[(i\text{PrO})_2(O)P]_3C_6H_3$[36] by reaction with Me_3SiBr and subsequent reaction with methanol. The ester was prepared by an Ni-mediated variant of the Arbuzov reaction starting from 1,3,5-tribromobenzene in 80% yield. The recently described synthesis of 1,3,5-$[(MeO)_2(O)P]_3C_6H_3$ starting from 1,3,5-trichlorobenzene and trimethyl phosphite under UV irradiation for three weeks was reported to give a mixture of products from which 1,3,5-$[(MeO)_2(O)P]_3C_6H_3$ was isolated in moderate yield and subsequently hydrolysed to give the corresponding triphosphonic acid.[26]

So far, all of our attempts to crystallise the phosphonic acid **1** without the aid of a template have been unsuccessful. However, co-crystallisation of **1** with 4-(dimethylamino)-pyridine from water/methanol gave the 1:2 adduct $[1\text{-}\{(HO)_2(O)P\}\text{-}3,5\text{-}\{(HO)(O)_2P\}_2C_6H_3]^{2-}[\{4\text{-}(Me_2N)C_5H_4NH\}^+]_2$ (**2**) and the 1:1 adduct $[1,3\text{-}\{(HO)_2(O)P\}_2\text{-}5\text{-}\{(HO)(O)_2P\}C_6H_3]^-[4\text{-}(Me_2N)C_5H_4NH]^+$ (**3**). Both salts are soluble in water, but poorly soluble in solvents such as $CHCl_3$, acetone and DMSO. A proton transfer from the phosphonic acid moieties to 4-(dimethylamino)pyridine is observed and thus, in addition to neutral O−H···O hydrogen bonds, ionic hydrogen bonds of the type O−H···O$^-$ and O···H−N$^+$ are formed. Selected bond lengths and angles are given in Table 1. The asymmetric unit of **2** is shown in Figure 1.

Table 1. Hydrogen bond parameters [Å, °] of compounds **2** and **3**

	D−H	H···A	D···A	D−H···A
2				
O(1)−H···O(8A)	0.85(3)	1.70(3)	2.541(2)	172(3)
N(2)−H···O(8A)	0.84(3)	1.99(3)	2.782(3)	158(3)
O(4)−H···O(6A)	0.83(3)	1.72(3)	2.546(3)	174(3)
N(4)−H···O(3A)	0.96(3)	1.71(3)	2.653(3)	167(3)
O(5)−H···O(9A)	1.05(3)	1.39(3)	2.431(2)	170(3)
O(7)−H···O(2A)	0.90(3)	1.55(3)	2.448(2)	179(4)
3				
N(1)−H···O(5)	0.89(2)	1.90(2)	2.778(2)	172(2)
O(2)−H···O(4A)	0.80(2)	1.76(2)	2.568(2)	175(3)
O(3)−H···O(7A)	0.94(3)	1.56(3)	2.495(2)	172(2)
O(5)−H···O(8A)	0.89(3)	1.64(3)	2.523(2)	176(3)
O(6)−H···O(1A)	0.93(2)	1.57(2)	2.496(2)	171(2)
O(9)−H···O(4A)	0.99(3)	1.55(3)	2.536(2)	175(2)

Both amines act as proton acceptors through their pyridine nitrogen atoms to give the cation $[4\text{-}(Me_2N)C_5H_4NH]^+$. It is noteworthy that the oxygen atom O(8) is involved in hydrogen bonds to N(2) and O(1A) with X···O (X = N, O) bond lengths of 2.782(3) and 2.541(2) Å, respectively, thus acting as a double hydrogen bond acceptor. In contrast, the oxygen atom O(3) exclusively forms an O···H−N$^+$ hydrogen bond of 2.653(3) Å with its neighbouring cation $[4\text{-}(Me_2N)C_5H_4NH]^+$. The remaining oxygen atoms form single hydrogen bonds resulting in a total number of eight O−H···O/O−H···O$^-$ hydrogen bonds for each triphosphonic acid molecule. Four of the latter are related by symmetry and the O···O distances range from 2.431(2) to 2.546(3) Å. The dianion $[1\text{-}\{(HO)_2(O)P\}\text{-}3,5\text{-}\{(HO)(O)_2P\}_2C_6H_3]^{2-}$ self-assembles through these hydrogen bonds to give a layered structure with the cations [4-

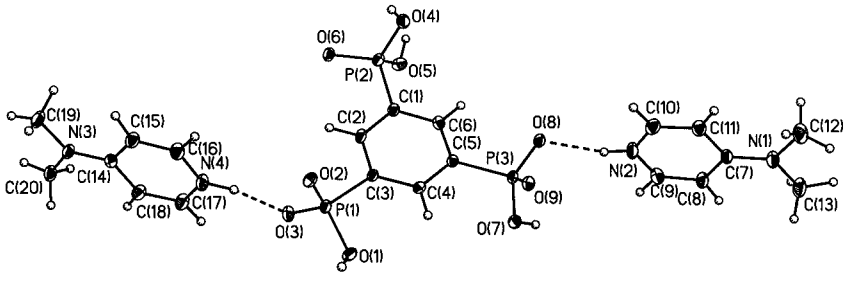

Figure 1. Molecular structure of $[1\text{-}\{(HO)_2(O)P\}\text{-}3,5\text{-}\{(HO)(O)_2P\}_2C_6H_3]^{2-}[\{4\text{-}(Me_2N)C_5H_4NH\}^+]_2$ (**2**): view of the building unit of **2** showing the labeling scheme and the thermal ellipsoids drawn at 30% of probability level; selected bond lengths: P(1)−O(1) 1.570(2) Å, P(1)−O(2) 1.519(2) Å, P(1)−O(3) 1.495(2) Å, P(2)−O(4) 1.552(2) Å, P(2)−O(5) 1.522(2) Å, P(2)−O(6) 1.500(2) Å, P(3)−O(7) 1.538(2) Å, P(3)−O(8) 1.508(2) Å, P(3)−O(9) 1.524(2) Å

 © 2004 Wiley-VCH Verlag GmbH & Co. KGaA, Weinheim

$(Me_2N)C_5H_4NH]^+$ sandwiched between the layers, giving rise to an interlayer distance of ca. 6.5 Å (see Figure 2).

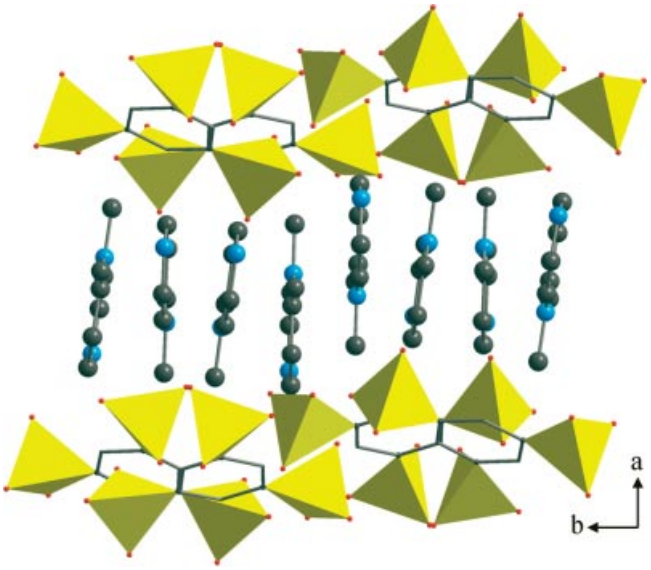

Figure 2. View of the crystal packing diagram of **2** down the *c* axis showing the layered structure; the cations $[4\text{-}(Me_2N)C_5H_4NH]^+$ are intercalated between hydrogen-bonded layers (tetrahedron: PO_3C; phosphorus: yellow; carbon: dark grey; nitrogen: blue; oxygen: red)

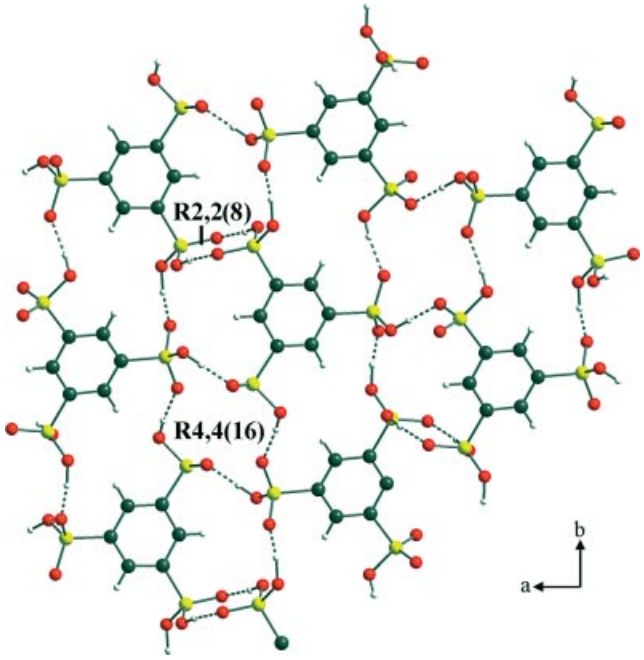

Figure 3. View of the hydrogen-bonded 2-D network in the *b*,*c* plane of **2**; the main structural motifs are dimers having the R2,2(8) notation and tetramers having the R4,4(16) notation; these motifs are linked through an additional hydrogen bond and the benzene spacers within the layer (carbon: dark grey; phosphorus: yellow; oxygen: red; hydrogen: light grey)

The layer shown in Figure 3 is best described as being composed of two hydrogen-bonded ring motifs which are assigned to R2,2(8) and R4,4(16) using the graphset theory (see general remarks).[37] Connecting both ring types with the benzene spacer and an additional hydrogen bond results in the two-dimensional network with the amines stacked above and below the *b*,*c* plane.

The asymmetric unit of compound **3** is shown in Figure 4. Similar to **2**, the cation $[4\text{-}(Me_2N)C_5H_4NH]^+$ is observed as a result of a proton transfer from **1** to the pyridine nitrogen atom of 4-(dimethylamino)pyridine; the N(1)···O(5) distance amounts to 2.778(2) Å. In addition, O(5) is linked to O(8A) showing an intermolecular distance of 2.523(2) Å. The oxygen atom O(4) is involved in two hydrogen bonds to O(2A) and O(9A) with distances of 2.568(2) and 2.536(2) Å, respectively. The remaining oxygen atoms show single O−H···O hydrogen bonds of 2.495(2) Å [O(3)−O(7A)] and 2.496(2) Å [O(6)−O(1A)]. A total of ten O−H···O/O−H···O^- hydrogen bonds for each triphosphonic acid molecule are observed, of which five are related by symmetry. In contrast to the layered structure of **2**, the monoanionic moieties $[1,3\text{-}\{(HO)_2(O)P\}_2\text{-}5\text{-}\{(HO)(O)_2P\}\text{-}C_6H_3]^-$ self-assemble to give a three-dimensional hydrogen-bonded network. This network is composed of layers which are formed by extensive hydrogen bonding (see Figure 5) and which are connected through benzene spacers along the *a* axis.

The main structural feature of the layers is the R2,3(10) ring motif shown in Figure 5. Of note is that this motif was also observed as a structure-directing motif in neutral and anionic clusters of *tert*-butylphosphonic acid.[14] The outer sphere of the R2,3(10) unit is composed of two hydrogen

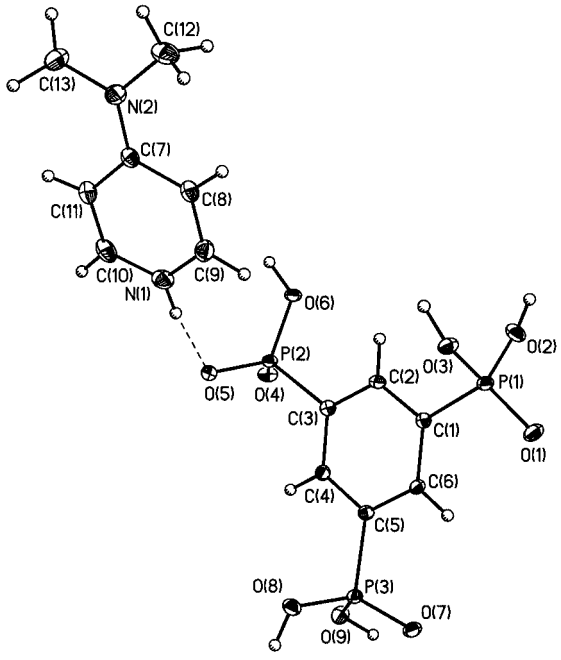

Figure 4. Molecular structure of $[1,3\text{-}\{(HO)_2(O)P\}_2\text{-}5\text{-}\{(HO)(O)_2P\}C_6H_3]^-[4\text{-}(Me_2N)C_5H_4NH]^+$ (**3**): view of the building unit of **3** showing the labeling scheme and the thermal ellipsoids drawn at 30% of probability level; selected bond lengths: P(1)−O(1) 1.481(1) Å, P(1)−O(2) 1.552(2) Å, P(1)−O(3) 1.551(1) Å, P(2)−O(4) 1.514(1) Å, P(2)−O(5) 1.512(1) Å, P(2)−O(6) 1.553(1) Å, P(3)−O(7) 1.495(1) Å, P(3)−O(8) 1.542(1) Å, P(3)−O(9) 1.549(1) Å

 © 2004 Wiley-VCH Verlag GmbH & Co. KGaA, Weinheim

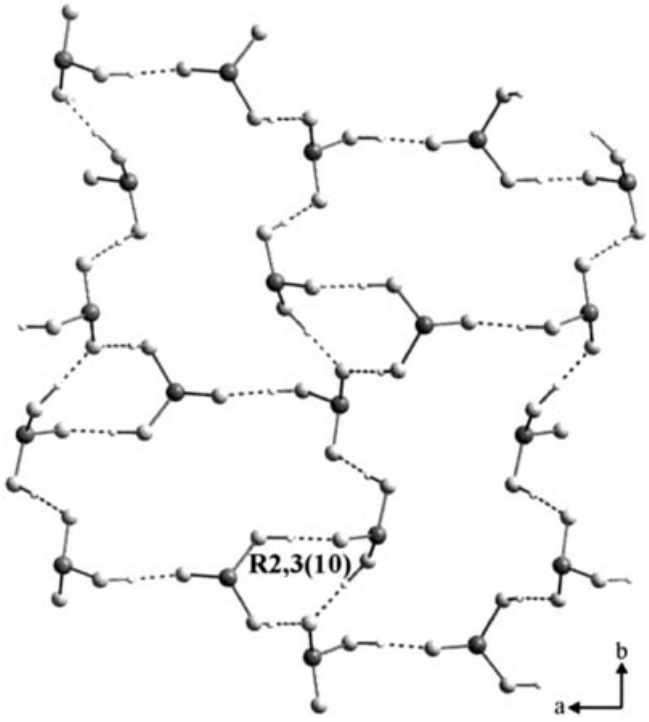

Figure 5. The hydrogen bonded 2-D network of **3**; view of the *a*,*b* plane; the benzene spacer and 4-(dimethylamino)pyridine molecules are omitted for clarity; the main structural motif is a 10-membered ring having the R2,3(10) notation; additional hydrogen bonds link these motifs within the layer; the layers are connected through the benzene spacer along the *c* axis; (phosphorus: grey; oxygen and hydrogen: light grey)

bond acceptors and two hydrogen bond donors. Thus, the R2,3(10) motifs are linked by symmetry-related hydrogen bonds to give the network shown in Figure 5.

The three-dimensional network of compound **3** is illustrated in Figure 6. Large channels with internal dimensions of ca. 8.5 × 11.3 $Å^2$ run along the *a* axis. These channels are occupied by the $[4\text{-}(Me_2N)C_5H_4NH]^+$ cations which are bonded to the triphosphonic acid framework through hydrogen bonds. Interestingly, supramolecular aggregates prepared from nitrilotri(methylphosphonic acid) with various amines were recently reported to give three-dimensional hexagonal structures with channel dimensions close to the values found for compound **3**.[27] A closer look at the structures of compounds **2** and **3** reveals an interesting relationship. Both are composed of similar staircase-type layers as a result of the planar stacking of the benzene rings (Figure 6). In compound **3** hydrogen bonds connect these layers to give the 3-D structure whereas in compound **2** the additional cations prevent the interconnection, resulting in the 2-D structure.

As a result of the proton transfer from the phosphonic acid to 4-(dimethylamino)pyridine, negative charge is introduced into the hydrogen-bonded network resulting in a very robust framework. The hydrogen bond energy of anionic O−H···O^- bonds in phosphonic acids is significantly increased compared with that of the corresponding O−H···O bond and consequently the O−H···O^- bonds are markedly shorter.[14] In agreement with this observation, the average O(H)···O distances in compounds **2** and **3** are 2.492 and 2.523 Å, respectively. Both distances are significantly shorter than the average O(H)···O distance of 2.607 Å calculated for the most stable gas-phase monoanion of *tert*-butylphosphonic acid, $[\{t\text{BuP(O)}_2\text{(OH)}\}\{t\text{BuP(O)(OH)}_2\}_2]^-$.[14] In the solid state typical P−O(H)···O−P distances in the range 2.45−2.60 Å were reported for organic ammonium salts of phosphonic acids. To the best of our knowledge the lower limit is determined by a distance of 2.413 Å reported for an aggregate of nitrilotri(methylphosphonic acid) with phenanthroline.[27,28] The shortest O(H)···O distance in compound **2** amounts to 2.431(2) Å.

The IR spectrum of the triphosphonic acid **1** shows a broad absorption band centred at 3360 cm^{-1}. In contrast, distinct absorption bands at 3240, 3110, 3107 and 2977 cm^{-1} are observed in compound **3** which are red-shifted to

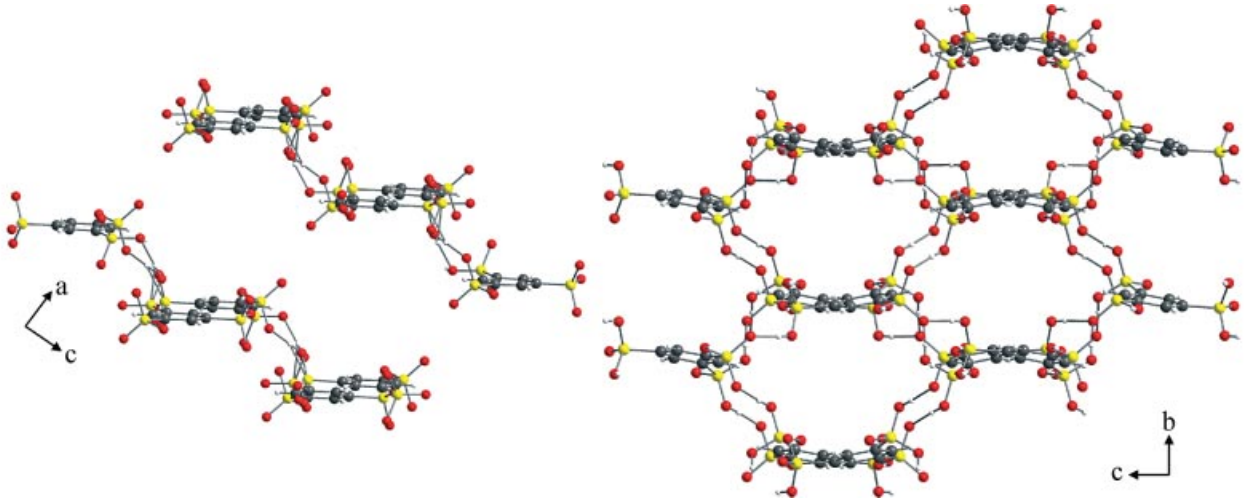

Figure 6. View of the 2-D structure of **2** (left) and the 3-D structure of **3** (right); the cations $[4\text{-}(Me_2N)C_5H_4NH]^+$ are omitted for clarity (carbon: dark grey; phosphorus: yellow; oxygen: red; hydrogen: light grey)

 © 2004 Wiley-VCH Verlag GmbH & Co. KGaA, Weinheim

3213, 3100, 3065 and 2938 cm^{-1} in compound **2**. The bands at 3240 cm^{-1} (**3**) and 3213 cm^{-1} (**2**) are assigned to the O−H stretching of a phosphonic acid moiety. No assignment is made for the bands in the region 2938−3110 cm^{-1} which are associated with the O−H vibration as well as with the C−H vibration of 4-(dimethylamino)pyridine.

The thermal stability of compounds **2** and **3** is increased compared to that of the triphosphonic acid **1**. The latter decomposes at 248 °C. The DTA-TG measurements show that **3** starts to melt at 265 °C; an exothermic peak at 365 °C is indicative of its decomposition. The 1:2 adduct **2** starts to decompose at 319 °C without prior melting at lower temperatures.

Conclusion

The co-crystallisation of 1,3,5-$[(HO)_2(O)P]_3C_6H_3$ and 4-(dimethylamino)pyridine gives a two-dimensional structure for the 1:2 adduct **2** and a three-dimensional network for the 1:1 adduct **3**. Although both compounds **2** and **3** are composed of a large number of different hydrogen bond patterns, their structures are best described by the assembly of simple hydrogen-bonded motifs using the graphset theory. In adduct **2** the motifs R2,2(8) and R4,4(16) are interconnected to give a one-dimensional ribbon and the benzene spacer connects these ribbons to give a layered structure. In adduct **3** the R2,3(10) motif is observed solely. Hydrogen bonding connects the motif into a layer and the benzene spacer connects the layers to give a three-dimensional network. This network contains hexagonal channels which are occupied by 4-(dimethylamino)pyridinium cations, $[4\text{-}(Me_2N)C_5H_4NH]^+$. Our results demonstrate that the phosphorus counterpart of 1,3,5-$(HO_2C)_3C_6H_3$ (H_3TMA), the triphosphonic acid 1,3,5-$[(HO)_2(O)P]_3C_6H_3$ (**1**), is a promising building unit in the growing field of supramolecular chemistry and crystal engineering. In contrast to H_3TMA, it allows the design of 3-D networks. The extension of the reported work to other amines will add to the fundamental understanding of the self-assembly process of phosphonic acids and represents a step towards the rational design of 3-D hydrogen-bonded frameworks. Furthermore, the triphosphonic acid **1** holds potential for the preparation of novel three-dimensional metal phosphonates.

Experimental Section

General Remarks: Solvents were distilled from appropriate drying agents prior to use. Elemental analyses were performed with an instrument from Carlo Erba Strumentzione (model 1106). Thermal analyses were recorded using a vacuum thermoanalyser TA1 from Mettler Instrumente AG. The DTA-TG measurements were performed at a heating rate of 6 °C min^{-1} to a maximum temperature of 700 °C in flowing nitrogen using Al_2O_3 as the reference material. ^1H and ^{31}P NMR spectra were recorded at 200.13 MHz (^1H) and 80.02 MHz (^{31}P) at room temperature. Chemical shifts δ are given in ppm and were referenced against Me_4Si (^1H) and 85% H_3PO_4 (^{31}P). IR spectra were obtained with a Bruker FTIR IFS 113v spectrometer and run as KBr discs. Electrospray ionisation mass spectrometric analyses (ESI-MS) were recorded in the positive and the negative mode with a Thermoquest-Finnigan instrument using MeOH/H_2O (1:1) as the mobile phase. The compounds were dissolved in MeOH/H_2O and then diluted with the mobile phase to give solutions of approximate concentration 0.1 mM. The samples were introduced with a syringe pump operating at 10 μL/min. The capillary voltage was kept at 4.5 kV, while the cone-skimmer voltage was varied in the positive mode between 50 and 110 V, and in the negative mode between −70 and −80 V. The ion source temperature was kept at 280 °C. The *m*/*z* values reported correspond to those of the most intense peaks in the corresponding isotope pattern. Similar ESI-MS spectra of compounds **1**−**3** were obtained in the negative mode. In the positive mode the ESI-MS spectra of compounds **2** and **3** are dominated by the 4-(dimethylamino)pyridinium cation $[4\text{-}(Me_2N)C_5H_4NH]^+$ (*m*/*z* = 122.6), but show a similar peak pattern in the range *m*/*z* = 200−1000 as observed for compound **1**.

Graphset Theory:[37] Graphset descriptors indicate the hydrogen bond motif by the general form *Ga*,*d*(*n*). *G* describes the structural unit: C for a chain, D for a finite dimeric system, R for a cyclic system, S for intramolecular hydrogen bonds. The symbols *d* and *a* define the numbers of hydrogen bond donors and acceptors, respectively. The symbol *n* defines the total number of atoms in a motif.

1,3,5-$[(HO)_2(O)P]_3C_6H_3$ (1): Bromotrimethylsilane (27.9 g, 182.03 mmol) was added with a syringe to a solution of 1,3,5-$[(i\text{Pr}\text{-}O)_2(O)P]_3C_6H_3$ [36] (10.0 g, 18.20 mmol) in 150 mL of CH_2Cl_2 at 0 °C. The solution was stirred at room temperature for 12 h and after the addition of 250 mL of MeOH, the solution was heated at reflux for 4 h. The solvent was removed in vacuo to give a brownish solid. Addition of 100 mL of acetonitrile gave a suspension. The solid material was filtered off and crystallised from water to give **1** (3.5 g, 61%) as a colourless solid which decomposes at 248 °C. $C_6H_9O_9P_3$ (318.1): calcd. C 22.7, H 2.9; found C 22.3, H 2.8. ^1H NMR (200.13 MHz, [D$_4$]MeOH): δ = 8.25−8.47 (m) ppm. ^{31}P NMR (81.02 MHz, [D$_4$]MeOH): δ = 14.1 ppm. ESI-MS (positive mode, 101 V): *m*/*z* (%) = 318.9 (13) $[1,3,5\text{-}\{(HO)_2(O)P\}_3C_6H_3 + H]^+$, 336.6 (8) $[1,3,5\text{-}\{(HO)_2(O)P\}_3C_6H_3 + H_2O + H]^+$, 350.8 (24) $[1,3,5\text{-}\{(HO)_2(O)P\}_3C_6H_3 + CH_3OH + H]^+$, 636.8 (100) $[2 \times 1,3,5\text{-}\{(HO)_2(O)P\}_3C_6H_3 + H]^+$, 954.8 (14) $[3 \times 1,3,5\text{-}\{(HO)_2(O)P\}_3C_6H_3 + H]^+$, 1272.9 (6) $[4 \times 1,3,5\text{-}\{(HO)_2(O)P\}_3C_6H_3 + H]^+$. ESI-MS (negative mode, −71 V): *m*/*z* (%) = 280.7 (3) $[1,3,5\text{-}\{(HO)_2(O)P\}_3C_6H_3 - 2\,H_2O - H]^-$, 289.9 (12) $[2 \times 1,3,5\text{-}\{(HO)_2(O)P\}_3C_6H_3 - 3\,H_2O - 2\,H]^{2-}$, 298.7 (22) $[1,3,5\text{-}\{(HO)_2(O)P\}_3C_6H_3 - H_2O - H]^-$, 316.8 (100) $[1,3,5\text{-}\{(HO)_2(O)P\}_3C_6H_3 - H]^-$, 330.8 (17) $[1,3,5\text{-}\{(HO)_2(O)P\}_3C_6H_3 - H_2O + CH_3CN - H]^-$, 348.8 (8) $[1,3,5\text{-}\{(HO)_2(O)P\}_3C_6H_3 + CH_3CN - H]^-$, 616.8 (4) $[2 \times 1,3,5\text{-}\{(HO)_2(O)P\}_3C_6H_3 - H_2O - H]^-$, 634.9 (46) $[2 \times 1,3,5\text{-}\{(HO)_2(O)P\}_3C_6H_3 - H]^-$. IR (KBr): $\tilde{\nu}$ = 278 (w), 303 (w), 360 (w), 470 (m), 537 (m), 580 (w), 606 (w), 693 (m), 740 (w), 805 (w), 890 (m), 916 (m), 947 (m), 995 (s), 1166 (s, br.), 1400 (w), 1655 (s, br.), 2325 (s, br.), 3360 (vs, br.) cm^{-1}.

$[1\text{-}\{(HO)_2(O)P\}\text{-}3,5\text{-}\{(HO)(O)_2P\}_2C_6H_3]^{2-}[\{4\text{-}(Me_2N)C_5H_4NH\}^+]_2$ (2): A solution of 4-(dimethylamino)pyridine (385 mg, 3.15 mmol) in 1 mL of MeOH was added to a solution of 1,3,5-$[(HO)_2(O)P]_3C_6H_3$ (500 mg, 1.57 mmol) in 25 mL of MeOH. A colourless suspension formed and a mixture of 60 mL of MeOH and 50 mL of H_2O was added. The suspension was heated at reflux for 10 min and filtered. Colourless crystals of **2** (410 mg, 46%), which start to decompose at 319 °C, were formed upon slow evap-

 © 2004 Wiley-VCH Verlag GmbH & Co. KGaA, Weinheim

Table 2. Crystallographic data for compounds **2** and **3**

	2	**3**
Empirical formula	$C_{20}H_{29}N_4O_9P_3$	$C_{13}H_{19}N_2O_9P_3$
Formula mass	526.38	440.22
Crystal system	monoclinic	orthorhombic
Space group	$P2_1/c$	*Pbca*
Cell constants		
a [Å]	10.271(2)	14.681(3)
b [Å]	14.582(3)	14.891(3)
c [Å]	17.041(3)	16.546(3)
β [°]	105.65(3)	
Volume [Å^3]	2457.7(9)	3617.3(12)
Z	4	8
Density(calculated) [Mg·m^{-3}]	1.520	1.617
Absorption coefficient [mm^{-1}]	0.301	0.381
Crystal size [mm]	0.10 × 0.12 × 0.12	0.12 × 0.10 × 0.12
Theta range for data collection	3.02 to 25.35	3.14 to 27.47
Reflections collected	11338	28062
Independent reflections	4583 [R_{int} = 0.035]	4408 [R_{int} = 0.055]
Goodness-of-fit on F^2	0.871	0.917
R indices [$I > 2\sigma(I)$]	*R*1 = 0.0369, *wR*2 = 0.0783	*R*1 = 0.0311, *wR*2 = 0.0634
R indices (all data)	*R*1 = 0.0688, *wR*2 = 0.0634	*R*1 = 0.0783, *wR*2 = 0.0688
Largest diff. peak/hole [e·Å^{-3}]	0.223/−0.384	0.298/−0.376

oration of the solvent. $C_{20}H_{29}N_4O_9P_3$ (562.4): calcd. C 42.7, H 5.2, N 10.0; found C 43.0, H 5.3, N 10.1. ^{1}H NMR (200.13 MHz, D_2O): δ = 3.03 (s, 12 H, NMe_2), 6.70 (d, 4 H, H_{py}), 7.82 (d, 4 H, H_{py}), 7.94−8.07 (m, 3 H, H_{ar}) ppm. ^{31}P NMR (81.02 MHz, D_2O): δ = 13.2 ppm. IR (KBr): $\tilde{\nu}$ = 530 (m, br.), 704 (m), 740 (w), 808 (m), 936 (m), 1065 (m), 1130 (m), 1218 (m), 1401 (w), 1442 (w), 1563 (s), 1648 (s), 1873 (w), 1951 (m), 2051 (m), 2938 (s), 3065 (s), 3100 (s), 3213 (s) cm^{-1}.

$[1,3\text{-}\{(HO)_2(O)P\}_2\text{-}5\text{-}\{(HO)(O)_2P\}C_6H_3]^-[4\text{-}(Me_2N)C_5H_4NH]^+$ (3): A solution of 4-(dimethylamino)pyridine (150 mg, 1.23 mmol) in 1 mL of MeOH was added to a solution of 1,3,5-$[(HO)_2(O)P]_3C_6H_3$ (318 mg, 1.23 mmol) in 10 mL of MeOH. A colourless suspension formed which was dissolved in a mixture of 40 mL of MeOH and 10 mL of H_2O by warming to 50 °C. Colourless crystals of **3** (240 mg, 44%) with a melting point of 265 °C formed upon slow evaporation of the solvent. $C_{13}H_{19}N_2O_9P_3$ (440.2): calcd. C 35.5, H 4.4, N 6.4; found C 35.5, H 4.5, N 6.5. ^{1}H NMR (200.13 MHz, D_2O): δ = 3.00 (s, 6 H, NMe_2), 6.67 (d, 2 H, H_{py}), 7.79 (d, 2 H, H_{py}), 7.96−8.10 (m, 3 H, H_{ar}) ppm. ^{31}P NMR (81.02 MHz, D_2O): δ = 13.6 ppm. IR (KBr): $\tilde{\nu}$ = 405 (w), 446 (w), 487 (w), 540 (m), 696 (m) 811 (w), 948 (m), 998 (s), 1220 (m), 1384 (w), 1401 (w), 1443 (w), 1564 (m), 1599 (w), 1649 (m), 2281 (s, br.), 2977 (s), 3107 (s), 3110 (s), 3240 (s) cm^{-1}.

X-ray Crystallographic Study: Intensity data for the colourless crystals were collected with a Nonius KappaCCD diffractometer with graphite-monochromated Mo-K_α radiation at 173 K. The data collection covered almost the whole sphere of reciprocal space with two (**2**) and four sets (**3**) at different κ angles and 79 (**2**) and 248 (**3**) frames by ω-rotation (Δ/ω = 1°) at two times 110 (**2**) and 30 s (**3**) per frame. The crystal−detector distance was 3.4 cm. Crystal decay was monitored by repeating the initial frames at the end of data collection. Analysis of the duplicate reflections gave no indication of any decay. The structure was solved by direct methods SHELXS-97[38] and successive difference Fourier syntheses. Refinement applied full-matrix least-squares methods (SHELXL-97).[39] The H atoms were located in the difference Fourier map and refined isotropically. Atomic scattering factors for neutral atoms and real and imaginary dispersion terms were taken from *International Tables for X-ray Crystallography*. The figures were created by SHELXTL.[40] Crystallographic data are given in Table 2. CCDC-223048 and -223049 contain the supplementary crystallographic data for this paper. These data can be obtained free of charge at www.ccdc.cam.ac.uk/conts/retrieving.html [or from the Cambridge Crystallographic Data Centre, 12 Union Road, Cambridge CB2 1EZ, UK; Fax: (internat.) + 44-1223-336-033; E-mail: deposit@ccdc.cam.ac.uk].

Acknowledgments

The Deutsche Forschungsgemeinschaft, the Fonds der Chemischen Industrie, the Fachbereich Chemie of the University of Dortmund (Grant for young scientists) and Professor Dr. K. Jurkschat are gratefully acknowledged for support of this work.

[1] A. Clearfield, in *Prog. Inorg. Chem.*, vol. 47 (Ed.: K. D. Karlin), John Wiley and Sons, New York, **1998**, p. 371−510.
[2] G. Alberti, M. Casciola, U. Costantino, R. Vivani, *Adv. Mater.* **1996**, *8*, 291−303.
[3] G. Anantharaman, M. G. Walawalkar, R. Murugavel, B. Gabor, R. Herbst-Irmer, M. Baldus, B. Angerstein, H. W. Roesky, *Angew. Chem. Int. Ed.* **2003**, *42*, 4482−4485.
[4] C. Lei, J. G. Mao, Y. Q. Sun, H. Y. Zeng, A. Clearfield, *Inorg. Chem.* **2003**, *42*, 6157−6159.
[5] E. I. Tolis, M. Helliwell, S. Langley, J. Raftery, R. E. P. Winpenny, *Angew. Chem. Int. Ed.* **2003**, *42*, 3804−3808.
[6] T. Azais, C. Bonhomme, L. Bonhomme-Coury, G. Kickelbick, *Dalton Trans.* **2003**, 3158−3159.
[7] V. Chandrasekhar, S. Kingsley, B. Rhatigan, M. K. Lam, A. L. Rheingold, *Inorg. Chem.* **2002**, *41*, 1030−1032.
[8] V. Chandrasekhar, S. Kingsley, *Angew. Chem. Int. Ed.* **2000**, *112*, 2410−2412.
[9] M. Mehring, M. Schürmann, *Chem. Commun.* **2001**, 2354−2355.
[10] M. Mehring, G. Guerrero, F. Dahan, P. H. Mutin, A. Vioux, *Inorg. Chem.* **2000**, *39*, 3325−3332.

 © 2004 Wiley-VCH Verlag GmbH & Co. KGaA, Weinheim

[11] G. Guerrero, M. Mehring, P. H. Mutin, F. Dahan, A. Vioux, *J. Chem. Soc., Dalton Trans.* **1999**, 1537−1538.
[12] M. G. Walawalkar, H. W. Roesky, R. Murugavel, *Acc. Chem. Res.* **1999**, *32*, 117−126.
[13] M. R. Mason, *J. Cluster Sci.* **1998**, *9*, 1−23.
[14] M. Mehring, M. Schürmann, R. Ludwig, *Chem. Eur. J.* **2003**, *9*, 837−849.
[15] R. Frantz, J. O. Durand, F. Carre, G. F. Lanneau, J. Le Bideau, B. Alonso, D. Massiot, *Chem. Eur. J.* **2003**, *9*, 770−775.
[16] V. A. Uchtman, R. A. Gloss, *J. Phys. Chem.* **1972**, *76*, 1298−1304.
[17] G. Ohms, K. Krüger, A. Rabis, V. Kaiser, *Phosphorus, Sulfur Silicon Relat. Elem.* **1996**, *114*, 75−81.
[18] T. J. R. Weakley, *Acta Crystallogr., Sect. B* **1976**, *32*, 2889−2890.
[19] K. L. Langley, P. J. Squattrito, F. Adani, E. Montoneri, *Inorg. Chim. Acta* **1996**, *253*, 77−85.
[20] R. K. Chadha, G. Ösapay, *Acta Crystallogr., Sect. C* **1995**, *51*, 2340−2342.
[21] D. DeLaMatter, J. J. McCullough, C. Calvo, *J. Phys. Chem.* **1973**, *77*, 1146−1148.
[22] S. W. Peterson, E. Gebert, A. H. Reis Jr., M. E. Druyan, G. W. Mason, D. F. Peppard, *J. Phys. Chem.* **1977**, *81*, 466−471.
[23] E. Gebert, A. H. Reis Jr., M. E. Druyan, S. W. Peterson, G. W. Mason, D. F. Peppard, *J. Phys. Chem.* **1977**, *81*, 471−475.
[24] K. Merz, A. Knüfer, *Acta Crystallogr., Sect. C* **2002**, *58*, o187−o188.
[25] B. Moulton, M. J. Zaworotko, *Chem. Rev.* **2001**, *101*, 1629−1658.
[26] S. A. Reiter, B. Assmann, S. D. Nogai, N. W. Mitzel, H. Schmidbaur, *Helv. Chim. Acta* **2002**, *85*, 1140−1150.
[27] C. V. K. Sharma, A. Clearfield, *J. Am. Chem. Soc.* **2000**, *122*, 4394−4402.
[28] C. V. K. Sharma, A. J. Hessheimer, A. Clearfield, *Polyhedron* **2001**, *20*, 2095−2104.
[29] A. H. Mahmoudkhani, V. Langer, *Crystal Growth Design* **2002**, *2*, 21−25.
[30] A. H. Mahmoudkhani, V. Langer, *J. Mol. Struct.* **2002**, *609*, 97−108.
[31] A. H. Mahmoudkhani, V. Langer, *J. Mol. Struct.* **2002**, *609*, 55−60.
[32] P. S. Wheatley, A. J. Lough, G. Ferguson, C. J. Burchell, C. Glidewell, *Acta Crystallogr., Sect. B* **2001**, *57*, 95−102.
[33] C. Glidewell, G. Ferguson, A. J. Lough, *Acta Crystallogr., Sect. C* **2000**, *56*, 855−858.
[34] G. Ferguson, C. Glidewell, R. M. Gregson, P. R. Meehan, *Acta Crystallogr., Sect. B* **1998**, *54*, 129−138.
[35] J. Beckmann, D. Dakternieks, A. Duthie, *Appl. Organomet. Chem.* **2003**, *17*, 817−818.
[36] M. Henn, K. Jurkschat, D. Mansfeld, M. Mehring, M. Schürmann, *J. Mol. Struct.*, in press.
[37] M. C. Etter, *Acc. Chem. Res.* **1990**, *23*, 120−126.
[38] G. M. Sheldrick, *Acta Crystallogr., Sect. A* **1990**, *46*, 467−473.
[39] G. M. Sheldrick, University of Göttingen, Germany, **1997**.
[40] G. M. Sheldrick, *Release 5.1 Reference Manual*, Bruker AXS, Inc., Madison, Wisconsin, USA **1997**.

Received November 13, 2003
Early View Article
Published Online June 7, 2004

 © 2004 Wiley-VCH Verlag GmbH & Co. KGaA, Weinheim

Binary Neodymium Alkoxide/Dialkylmagnesium Polymerization Systems: Studies on the Nature of the Reaction Intermediates and Active Species

Jérôme Gromada,[a] André Mortreux,[a] Guy Nowogrocki,[b] Frédéric Leising,[c] Thomas Mathivet,[c] and Jean-François Carpentier*[d]

Keywords: Alkoxides / Alkyl complexes / Homogeneous catalysis / Magnesium / Neodymium / Polymerization

Attempts to identify the intermediates and/or active species generated from binary combinations of a lanthanide alk(aryl)-oxide with a dialkylmagnesium reagent, which behave as efficient olefin polymerization systems, are reported. The well-defined trinuclear complex $[Nd_3(\mu_3\text{-}O\textit{t}Bu)_2(\mu_2\text{-}O\textit{t}Bu)_3(\mu\text{-}O\textit{t}Bu)_4(THF)_2]$ (**1**) and the monomeric precursor $[Nd(OC_6H_2\textit{t}Bu_2\text{-}2,6\text{-}Me\text{-}4)_3(THF)]$ (**2**) were used in association with $[Mg(CH_2SiMe_3)_2(Et_2O)]$ (**3**). The new heterodimetallic complex $[(THF)Nd(\mu_3\text{-}O\textit{t}Bu)_2(\mu_2\text{-}O\textit{t}Bu)_2(O\textit{t}Bu)Mg_2(CH_2TMS)_2]$ (**4**) and the alkyllanthanide complex $[Nd(OC_6H_2\textit{t}Bu_2\text{-}2,6\text{-}Me\text{-}4)_2(CH_2SiMe_3)(THF)_2]$ (**5**) have been isolated and characterized in the solid state and in solution. Complex **4** is proposed to be a reaction intermediate in the active species formation, while complex **5** is the first alkyllanthanide species isolated from an "$Ln(OR)_3$"/MgR_2 mixture, consistent with the observed behavior of these combinations in olefin polymerization.

(© Wiley-VCH Verlag GmbH & Co. KGaA, 69451 Weinheim, Germany, 2004)

Introduction

We have recently described new versatile polymerization systems based on combinations of a neodymium alk(aryl)-oxide and a dialkylmagnesium reagent that enable the synthesis of original materials such as high molecular weight poly(ethylene-*b*-methyl methacrylate)[1] and poly(butadiene-*b*-glycidyl methacrylate)[2] diblock copolymers. For this purpose, the well-defined trinuclear complex $[Nd_3(\mu_3\text{-}O\textit{t}Bu)_2(\mu_2\text{-}O\textit{t}Bu)_3(\mu\text{-}O\textit{t}Bu)_4(THF)_2]$ (**1**) and the monomeric precursor $[Nd(OC_6H_2\textit{t}Bu_2\text{-}2,6\text{-}Me\text{-}4)_3(THF)]$ (**2**) were employed.

The active species formed in situ from these combinations act either as initiators with lanthanidocene-like properties, for example for ethylene[1] and methyl methacrylate (MMA)[3] controlled homopolymerizations, or as catalysts for 1,3-diene polymerization[2] along with a fast, reversible transfer reaction to the magnesium centers. From this polymerization behavior, we anticipated that the active species is likely to be a homonuclear alkyllanthanide, or a related mixed alkyl-bridged lanthanide-magnesium species.[1b,1c] Variable-temperature ^1H NMR monitoring experiments of mixtures of a dialkylmagnesium, for example $Mg(n\text{-}Hex)_2$ or *n*BuMgEt, with **1** or **2** showed that fast reactions take place in the absence of monomer.[1b] Complete conversion of the initial alk(aryl)oxides to unidentified species was observed at −70 °C, followed upon raising of the temperature by the appearance of the corresponding 1-alkene (1-hexene, 1-butene; ethylene was immediately polymerized in situ), presumably arising from β-hydride elimination of a putative alkylneodymium species. The release of 1-alkene was observed at temperatures as low as −60 °C with the *tert*-butoxide precursor **1** while a higher temperature, typically 0−20 °C, was required for the aryloxide precursor **2**. As a consequence of this ready decomposition, a reaction product could only be isolated and fully characterized in the case of the **2**/$Mg(n\text{-}Hex)_2$ combination — the alkylmagnesium aryloxide compound $[(n\text{-}Hex)Mg(OC_6H_2\textit{t}Bu_2\text{-}2,6\text{-}Me\text{-}4)]_2$, consistent with the envisioned transmetallation process.[1b] Herein we report further studies of these binary polymerization systems, using $[Mg(CH_2SiMe_3)_2(Et_2O)]$ (**3**) as a co-reagent, and the isolation and structural characterization of two intermediate alkyllanthanide alk(aryl)oxide complexes.

[a] Laboratoire de Catalyse de Lille, UPRESA 8010 CNRS − Université de Lille 1, ENSCL,
B. P. 108, 59652 Villeneuve d'Ascq Cedex, France
[b] Laboratoire de Cristallochimie et Physicochimie du Solide, UPRESA 8012 CNRS − Université de Lille 1, ENSCL,
B. P. 108, 59652 Villeneuve d'Ascq Cedex, France
[c] Rhodia Recherches,
93308 Aubervilliers Cedex, France
[d] Laboratoire Organométalliques et Catalyse, UMR 6509 CNRS − Université de Rennes 1,
35042 Rennes Cedex, France
Fax: (internat.) + 33-2-23236939
E-mail: jean-francois.carpentier@univ-rennes1.fr

Results and Discussion

To obtain a better understanding of these binary catalyst systems, we decided to concentrate our efforts on the iso-

lation of the reaction intermediates and active species. For this purpose, the typical co-reagent Mg(*n*-Hex)$_2$ used for polymerization and initial mechanistic studies was replaced by [Mg(CH$_2$SiMe$_3$)$_2$(Et$_2$O)] (**3**). The latter reagent, in combination with **1** or **2**, has been shown to also generate active polymerization systems towards ethylene, MMA and 1,3-dienes, with properties similar to those of combinations based on Mg(*n*-Hex)$_2$, although somewhat less active.[1b,2] The dialkylmagnesium **3** was selected to stabilize the corresponding alkyllanthanide species, in particular by avoiding β-H elimination reactions.[4] Another potential advantage of **3** over Mg(*n*-Hex)$_2$ and higher long-chain dialkylmagnesium reagents is the better propensity of the CH$_2$SiMe$_3$ moiety for crystallization.

Combinations of [Nd$_3$(OtBu)$_9$(THF)$_2$] and [Mg(CH$_2$SiMe$_3$)$_2$(Et$_2$O)]

Toluene solutions of **1** and **3** in various ratios were prepared and stored at low temperature (−30 °C). When the reaction was performed in a 1:3 molar ratio (i.e. Nd/Mg = 1), as optimized for polymerization purposes, in the absence of additive, it was not possible to isolate any species from the resulting dark-brown solution. On the other hand, in the presence of THF (10 equiv. vs. Nd), the solution remained clear and blue. The ^{1}H NMR spectrum of the blue crystals grown from this solution is identical to the starting trinuclear alkoxide **1**, indicating that an excess of THF prevents the alkylation reaction from taking place. This fact is in direct line with the observed inactivity of the **1**/Mg(*n*-Hex)$_2$ system in the presence of minute amounts of THF for ethylene polymerization.[1b] Evans et al. have observed a similar phenomenon with their [Y(O*t*Bu)$_7$Cl$_2$]/AlMe$_3$ systems and assigned this lack of reactivity to the formation of the unreactive [AlMe$_3$(THF)].[5]

Given the successful isolation by Yasuda et al. of an intermediate in lanthanidocene-based MMA polymerization[6] and the efficient controlled syndiotactic polymerization of this monomer achieved with **1**/Mg(*n*-Hex)$_2$,[3] MMA (0.03 equiv. vs. Nd) was added to some crystallization experiments. Under those conditions, colorless crystals of [(Me$_3$SiCH$_2$)Mg(O*t*Bu)(THF)] (**5**) formed rapidly (15−20% isolated yield vs. Mg) in a reproducible manner, followed after a few weeks by pale-blue crystals of a neodymium complex (**4**; 30−40% yield vs. **1**) [Equation (1)]. As established by NMR spectroscopy and an X-ray diffraction analysis (Figure 1, Table 1), the product **4** corresponds to the new heterodimetallic complex [(THF)Nd(μ$_3$-O*t*Bu)$_2$(μ$_2$-O*t*Bu)$_2$(O*t*Bu)Mg$_2$(CH$_2$SiMe$_3$)$_2$], which obviously, however, does not contain any MMA. The neodymium center in **4** is hexacoordinate, as are most *tert*-butoxyneodymium derivatives,[7] with six oxygen atoms in its environment, one terminal *tert*-butoxy ligand and a THF molecule. Doubly and triply bridging *t*BuO groups link the neodymium atom to the two tetracoordinate magnesium atoms, each of which bears an alkyl chain. Such segregation of the alkoxide and alkyl ligands in complex **4** can be correlated with the higher oxophilicity of Nd vs. Mg (bond disruption energies: Nd−O, 703 ± 13 kJ·mol^{-1}; Mg−O, 363 ± 13 kJ·mol^{-1}).[8]

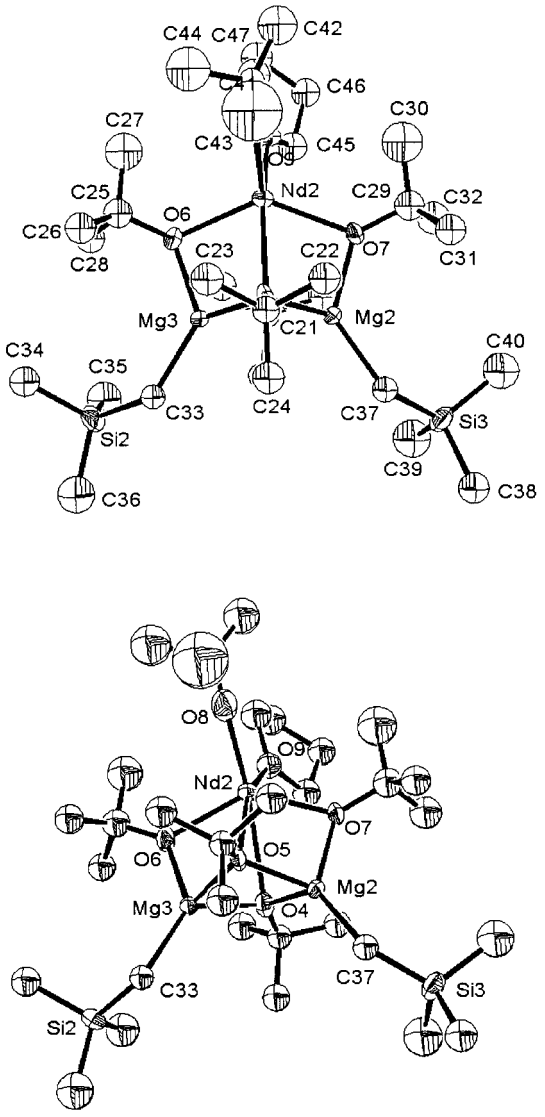

Figure 1. Two views of the molecular structure of [Nd(THF)(μ$_3$-O*t*Bu)$_2$(μ$_2$-O*t*Bu)$_2$(O*t*Bu)Mg$_2$(CH$_2$SiMe$_3$)$_2$] (**4**); ellipsoids are drawn at the 40% probability level and hydrogen atoms omitted for clarity

Several well-characterized aluminium-lanthanide alkyl-alk(aryl)oxide complexes have been described previously, most of which were prepared from the interaction of lanthanide alk(aryl)oxides with AlR$_3$.[9] Examples of heterodimetallic organometallic Ln-Mg complexes are much rarer and none of them contain alk(aryl)oxide ligands as in **4**.[10]

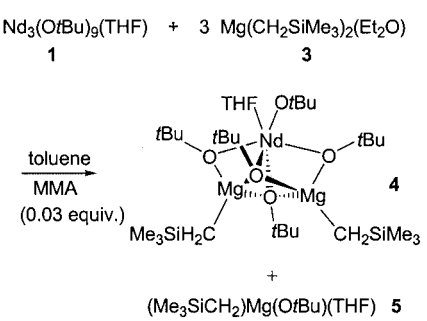

(1)

 © 2004 Wiley-VCH Verlag GmbH & Co. KGaA, Weinheim

Table 1. Selected bond lengths [Å] and angles [°] for **4**

Nd(2)−O(8)	2.241(6)	O(8)−Nd(2)−O(7)	109.5(2)
Nd(2)−O(7)	2.304(3)	O(8)−Nd(2)−O(6)	105.2(2)
Nd(2)−O(6)	2.307(4)	O(7)−Nd(2)−O(6)	135.0(1)
Nd(2)−O(9)	2.350(5)	O(8)−Nd(2)−O(9)	93.3(2)
Nd(2)−O(5)	2.600(4)	O(7)−Nd(2)−O(9)	99.6(1)
Nd(2)−O(4)	2.762(4)	O(8)−Nd(2)−O(5)	107.3(2)
Nd(2)−Mg(2)	3.178(2)	O(7)−Nd(2)−O(5)	71.4(1)
Nd(2)−Mg(3)	3.178(2)	O(8)−Nd(2)−O(4)	162.4(1)
Mg(2)−O(7)	1.984(4)	O(5)−Nd(2)−O(4)	55.3(1)
Mg(2)−O(4)	2.017(4)	O(7)−Mg(2)−O(4)	93.2(2)
Mg(2)−O(5)	2.046(4)	O(4)−Mg(2)−O(5)	75.6(2)
Mg(2)−Mg(3)	3.118(2)	O(6)−Mg(3)−C(33)	130.9(2)
Mg(3)−O(6)	1.974(4)	O(4)−Mg(3)−C(33)	127.9(2)
Mg(3)−O(4)	2.033(4)	O(5)−Mg(3)−C(33)	121.9(2)
Mg(3)−O(5)	2.040(4)	Mg(2)−O(4)−Mg(3)	100.7(2)
Mg(2)−C(37)	2.118(5)	Mg(2)−O(4)−Nd(2)	81.8(1)
Mg(3)−C(33)	2.117(5)	Mg(2)−O(5)−Mg(3)	99.5(2)
O(7)−Mg(2)−C(37)	129.5(2)	Mg(2)−O(5)−Nd(2)	85.4(1)
O(4)−Mg(2)−C(37)	129.8(2)	Mg(3)−O(5)−Nd(2)	85.6(2)
O(5)−Mg(2)−C(37)	121.1(2)	Mg(2)−O(7)−Nd(2)	95.4(1)

In the solid state, complex **4** has basically the same structural framework as the starting trinuclear alkoxide **1**, except that the [Nd(O*t*Bu)(THF)] and [Nd(O*t*Bu)$_2$] moieties have been replaced by two [Mg(O*t*Bu)(CH$_2$SiMe$_3$)] units. It is therefore interesting to compare the geometric features of both structures. The Nd−O distance of the terminal *tert*-butoxide ligand in **4** [Nd(2)−O(8): 2.241(6) Å] is somewhat longer than those found in **1** [2.147(4)−2.163(3) Å],[1b] while the Nd−O(THF) distance is significantly shorter [2.350(5) Å vs. 2.661(4) Å]. It is worthwhile mentioning that these THF and terminal O*t*Bu ligands are statistically disordered (see Exp. Sect.), which may lead to averaged values. The doubly bridging Nd−O distances are, as expected, longer than those for the terminal alkoxide ligand [Nd(2)−O(7): 2.304(3); Nd(2)−O(6): 2.307(4) Å], and slightly shorter than those measured in **1** [2.333(3)−2.458(3) Å]. Also, the nonequivalent triply bridging Nd−O bonds [Nd(2)−O(4): 2.762(4); Nd(2)−O(5): 2.600(4) Å] are the longest ones observed in the structure and longer than the corresponding values in **1** [2.624(3) and 2.409(3) Å],[1b] showing that the Nd atom is highly distorted from an ideal octahedral geometry. The angles around the neodymium center are similar to those observed in **1** except for the O(μ_3)−Nd−O(μ_3) angle, which is smaller in the heterodimetallic complex [55.3(1)° in **4** vs. 66.0(1)° in **1**]. This difference may be ascribed to the asymmetry in the complex caused by the shorter Mg−O bonds compared to the Nd−O ones. The equivalent magnesium atoms are four-coordinate, showing a distorted tetrahedral geometry. This geometry has been observed previously in some mixed alkoxy-amido complexes such as [(CMeNC$_6$H$_3$*i*Pr$_2$-2,6)Mg(μ_2-O*t*Bu)(THF)] and [(CMeNC$_6$H$_3$*i*Pr$_2$-2,6)Mg(μ_2-OC$_6$H$_9$)].[11] The doubly bridging Mg−O distances [Mg(2)−O(7): 1.984(4); Mg(3)−O(6): 1.974(4) Å] and Mg−O−Nd angles [Mg(2)−O(7)−Nd(2): 95.4(1); Mg(3)−O(6)−Nd(2): 95.6(1)°] compare well with the corresponding values observed in [(CMeNC$_6$H$_3$*i*Pr$_2$-2,6)Mg(μ_2-O*t*Bu)(THF)] [Mg−O: 1.997(2) and 1.994(2) Å; Mg−O−Mg: 98.56(6)°].[11]

The solution structure of complex **4** was briefly studied by ^{1}H NMR spectroscopy in [D$_8$]toluene. As shown in Figure 2, interpretation of the variable-temperature NMR spectra is complicated by the high fluxionality of the molecule and, above all, the paramagnetic Nd center, which broadens signals and affects intensity measurements. Thus, the correlation between chemical shift and coordination mode of the alkoxide groups previously noted in diamagnetic yttrium and lanthanum complexes of this type — increased bridging is associated with lower-field shifts[12] — cannot be applied to determine the geometry of **4** in solution unambiguously. Minimal overlapping of the resonances is observed in the NMR spectrum at −80 °C (Figure 2), which features eight major singlet-like resonances **A**−**H** with relative integrations 9:9:18:2:18:4:9:4 (from high field to low field). This pattern is consistent with the structure observed in the solid state, considering that both 18 H singlets **C** and **D** correspond to the μ_3-O*t*Bu and μ_2-O*t*Bu groups, which are magnetically equivalent on the NMR timescale at this low temperature,[12] and that the CH$_2$SiMe$_3$ groups are nonequivalent, one of the methylene resonance being obscured by residual solvent resonances (e.g. **I**) or a stronger intensity signal.

Complex **4** was exposed to ethylene (1 bar) in toluene solution. At room temperature, even after a long time period (48 h), the formation of polyethylene was not observed. This was not unexpected considering that **4** does not contain any Nd−C bond susceptible to insert ethylene. Addition of a slight excess of **3** to **4** under ethylene led to an effective polymerization. We can therefore hypothesize that **4** is an intermediate in the formation of the real active species in **1**/MgR$_2$ systems for ethylene polymerization. On the other hand, the 1:1 Nd/Mg stoichiometry imposed for the reaction between **1** and **3** was not recovered in the final complex **4**, and we cannot discard the potential catalytic activity of other products remaining in the mother solution and so far unidentified, such as species of the type [(*t*BuO)$_2$Nd−R]$_n$.

Combinations of [Nd(OC$_6$H$_2$*t*Bu$_2$-2,6-Me-4)$_3$(THF)] and [Mg(CH$_2$SiMe$_3$)$_2$(Et$_2$O)]

We focused next on [Nd(OC$_6$H$_2$*t*Bu$_2$-2,6-Me-4)$_3$(THF)] (**2**). This precursor, thanks to its bulky and readily displaceable ligand commonly used in the chemistry of group 1−4 metals, might lead to more stable and/or more easily crystallizable complexes, as evidenced by the isolation of [Mg(OC$_6$H$_2$*t*Bu$_2$-2,6-Me-4)(*n*-Hex)]$_2$ from a **2**/Mg(*n*-Hex)$_2$ (1:1) mixture in toluene.[1b] The quantitative formation of the latter compound is in agreement with the assumed in situ formation of a bis(aryloxy)alkylneodymium complex. However, the latter could not be isolated either from Mg(*n*-Hex)$_2$ or upon using the dialkylmagnesium compound **3** in pure toluene, despite repeated efforts. On the other hand,

 © 2004 Wiley-VCH Verlag GmbH & Co. KGaA, Weinheim

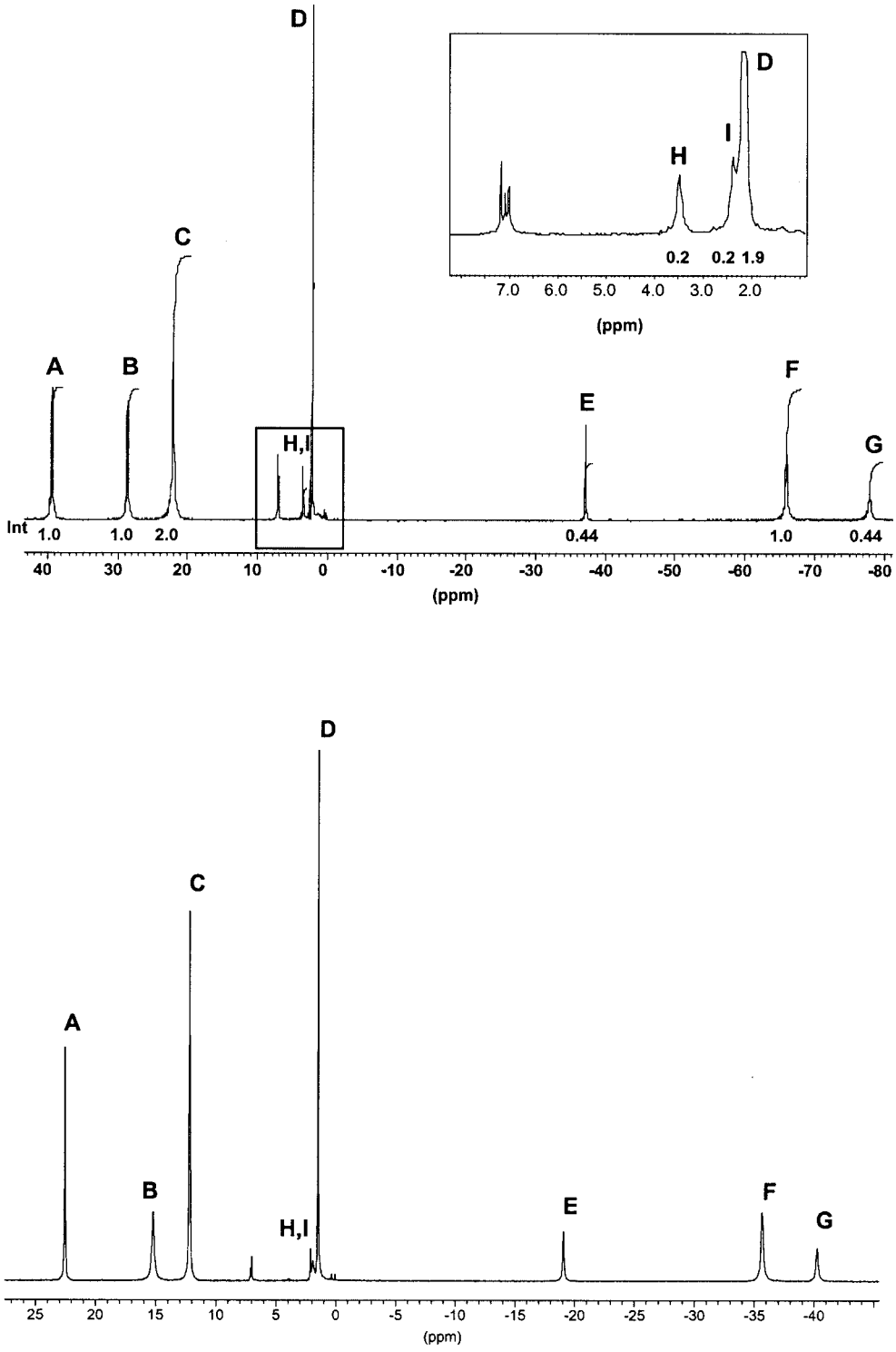

Figure 2. Representative variable-temperature ^{1}H NMR spectra of [Nd(μ_3-O*t*Bu)$_2$(μ_2-O*t*Bu)$_2$(O*t*Bu)Mg$_2$(CH$_2$SiMe$_3$)$_2$(THF)] (**4**) in [D$_8$]-toluene; top: −80 °C; bottom: 0 °C (**I** denotes residual toluene resonance and/or a signal from **4**)

the addition of THF (10 equiv. vs. Nd) to a mixture of **2** and **3** (1:1) enabled the ready crystallization of the pentacoordinate complex [(4-Me-2,6-*t*Bu$_2$C$_6$H$_2$O)$_2$Nd(CH$_2$SiMe$_3$)(THF)$_2$] (**6**) along with [(4-Me-2,6-*t*Bu$_2$C$_6$H$_2$O)Mg(CH$_2$SiMe$_3$)]$_2$ (**7**), isolated in 34% and 39% yields, respectively [Equation (2)].

 © 2004 Wiley-VCH Verlag GmbH & Co. KGaA, Weinheim

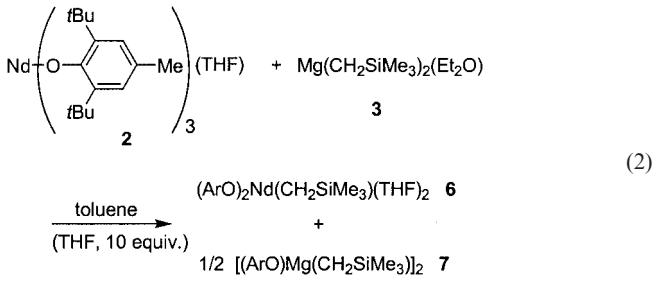

(2)

The solid-state structure of **6** features the metal center coordinated in a slightly distorted trigonal-bipyramidal mode by one equatorial methyltrimethylsilyl and two aryloxy groups (sum of the angles around Nd = 359.49°), and two axial THF ligands (Figure 3, Table 2). A plane of symmetry (noncrystallographic) embraces the Nd, both O(THF) and the C(CH_2SiMe_3) atoms. Similar trigonal-bipyramidal coordination has been observed previously in $Ln(OR)_3L_2$ complexes such as $[Nd(OCtBu_3)_3(CH_3CN)_2]$,[13] as well as in mixed halogen-aryloxide complexes, such as $[SmI(OAr)_2(THF)_2]$ and $[(4\text{-Me-}2,6\text{-}tBu_2C_6H_2\text{-}O)_2LnCl(THF)_2]$ (Ln = Er, Yb),[14] and in the mixed aryl-halogen complex $[(2,6\text{-dimesitylphenyl})YbCl_2(THF)_2]$,[15] in which the chlorine atoms occupy the axial positions. The O(1A)−Nd(1)−O(1B) angle [146.2(1)°] in **6** is much larger than 120°, reflecting the larger steric requirement of the aryloxide ligands compared to the CH_2TMS group. The bulkiness of the equatorial ligands affects the geometry of the axial ligands, with a lower (THF)O−Nd−O(THF) angle [165.46(9)°] than the theoretical value (180°). The increase in coordination number from the four-coordinate, distorted tetrahedral tris(aryloxide) precursor **2** to pentacoordinate complex **6** also likely stems from the decreasing steric requirement of CH_2SiMe_3 compared to the very bulky aryloxide. We assume that this may be the reason why it was not possible to isolate a putative alkyl complex, such as $[(ArO)_2Nd(CH_2SiMe_3)]$, in the absence of THF. The necessary addition of a Lewis base for crystallization has also been claimed in the case of $[Nd(\mu_2\text{-}OAr)(OAr)_2(py)_2]_2$.[9h]

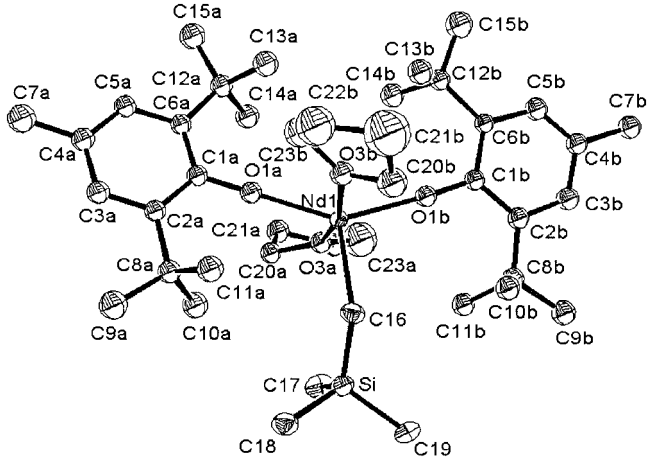

Figure 3. Molecular structure of $[(4\text{-Me-}2,6\text{-}tBu_2C_6H_2O)_3Nd(CH_2SiMe_3)(THF)_2]$ (**6**); ellipsoids are drawn at the 50% probability level and hydrogen atoms omitted for clarity

Table 2. Selected bond lengths [Å] and angles [°] for **6**

Nd(1)−O(1A)	2.235(3)	O(1A)−Nd(1)−O(1B)	146.21(10)
Nd(1)−O(1B)	2.227(3)	O(1A)−Nd(1)−O(3B)	83.70(10)
Nd(1)−O(3A)	2.500(3)	O(1B)−Nd(1)−O(3B)	91.69(10)
Nd(1)−O(3B)	2.487(3)	O(1A)−Nd(1)−C(16)	113.02(12)
Nd(1)−C(16)	2.482(4)	O(1B)−Nd(1)−C(16)	100.26(12)
O(1A)−C(1A)	1.352(5)	O(3B)−Nd(1)−C(16)	88.54(12)
O(1B)−C(1B)	1.355(5)	O(1A)−Nd(1)−O(3A)	84.40(9)
C(16)−Si	1.843(4)	O(1B)−Nd(1)−O(3A)	93.56(10)
C(16)−Nd(1)−O(3A)	103.82(12)	O(3B)−Nd(1)−O(3A)	165.46(9)

The Nd−O(Ar) distances are nearly identical for both ligand units [2.227(3), 2.235(3) Å] and are somewhat longer than those in **2**, but similar to those observed in related complexes.[16] Also, the Nd−O(THF) distances [2.487(3), 2.500(3) Å] are within the range of values reported for Nd−THF complexes.[17] The Nd−C distance of 2.482(4) Å can be compared to the terminal Sm−C distance of 2.45(1) Å in $[Sm(OAr)_3(CH_2SiMe_3)_2][Li(THF)]_2$ (Ar = 2,6-$iPr_2C_6H_3$), reflecting the minimal 2.6% difference in the ionic radii.[18] It is, however, much lower than that of 2.68(1) Å in $[\{1,1'\text{-}(3,5\text{-}tBu_2\text{-}2\text{-}C_6H_2O)_2\}La\{CH(SiMe_3)_2\}(THF)_3]$ due to the larger ionic radius of lanthanum,[18] its hexacoordination and the bulkiness of both aryloxide and alkyl groups.[19]

The characterization of **6** in solution by ^1H NMR spectroscopy was unambiguous and indicated a symmetric structure on the NMR time scale, as observed in the solid state. Complex **6** exhibits the same pattern as **2** for the equivalent aryloxide ligands — narrow signals for the aromatic and Me protons and a broad singlet for the *tert*-butyl groups at higher field. The signals assigned to the alkyl group appear at $\delta = -1.25$ and -7.15 ppm for the methylene and trimethylsilyl groups, respectively, while the two equivalent coordinated THF molecules give broad resonances at $\delta = -6.90$ and -9.66 ppm.

As expected, despite the presence of an Nd−C bond, complex **6** does not initiate ethylene polymerization under the conditions used for catalytic combinations of **2** and **3** (1 atm, 0−80 °C). This is, of course, due to the presence of the two coordinated THF molecules that "block" the active site for the weaker Lewis base ethylene.

In conclusion, some reaction products of the combinations of neodymium alk(aryl)oxides **1** and **2** with $[Mg(CH_2SiMe_3)_2(Et_2O)]$ (**3**) have been isolated and fully characterized. The new heterodimetallic complex **4**, obtained from the association of **1** with **3**, appears to be a plausible intermediate towards the species active in ethylene and methyl methacrylate (co)polymerizations. Indeed, although inert towards ethylene, complex **4** can be further activated upon MgR_2 addition, eventually yielding species that are active in polymerization. The alkylneodymium complex **5** is also inert towards olefins despite its reactive Nd−C bond. The isolation of this complex is, however,

 © 2004 Wiley-VCH Verlag GmbH & Co. KGaA, Weinheim

noteworthy in this area since it is the first example of an alkyl complex prepared from a neodymium alk(aryl)oxide/dialkylmagnesium mixture. Formation of **5** is the strongest evidence to date corroborating that an alkyllanthanide could be the active species in olefin polymerizations initiated by these new binary catalytic systems.

Experimental Section

General: All operations were performed in a glove box under nitrogen. Solvents and deuterated solvents were freshly distilled from sodium-potassium amalgam under argon and degassed prior to use. NMR spectra were recorded in Teflon-valved NMR tubes with a Bruker AC-200 spectrometer. ^{1}H (200 MHz) and ^{13}C{^{1}H} (50 MHz) chemical shifts are expressed in ppm vs. $SiMe_4$ and are referenced to the residual solvent peaks. The complexes [$Nd_3(O\mathit{t}Bu)_9(THF)_2$],[1b] [$Nd(OC_6H_2\mathit{t}Bu_2$-2,6-Me-4)$_3$(THF)],[20] and [$Mg(CH_2SiMe_3)_2(OEt_2)$][21] were prepared according to the reported procedures. Methyl methacrylate (99%, Aldrich) was vacuum-distilled from CaH_2 and stored at −20 °C under argon.

Reaction of [$Nd_3(\mu_3$-O*t*Bu)$_2(\mu_2$-O*t*Bu)$_3(\mu$-O*t*Bu)$_4$(THF)$_2$] (1) with [$Mg(CH_2SiMe_3)_2(Et_2O)$] (3)]. Synthesis of [$Nd(\mu_3$-O*t*Bu)$_2(\mu_2$-O*t*Bu)$_2(\mu$-O*t*Bu)$Mg_2(CH_2SiMe_3)_2$(THF)] (4) and [(Me_3SiCH_2)-Mg(O*t*Bu)(THF)] (5): [$Nd_3(O\mathit{t}Bu)_9(THF)_2$] (**1**; 0.124 g, 0.10 mmol) was dissolved in a minimal amount of toluene (ca. 0.25 ml). Methyl methacrylate (10 μL, 0.010 mmol) and [$Mg(CH_2SiMe_3)_2(OEt_2)$] (**3**; 0.084 g, 0.33 mmol) were then added at room temperature to the resulting deep-blue solution. The solution turned green after addition of the magnesium reagent and was immediately cooled to −30 °C. After 2 d, colorless crystals of [(Me_3SiCH_2)Mg(O*t*-Bu)(THF)] (**5**) were removed from the solution (0.015 g, 17%) and after typically about 10 d, pale-blue crystals of **4** had grown from the dark-green solution (0.027 g, 37%), which proved suitable for X-ray diffraction.

4: ^{1}H NMR (200 MHz, [D$_8$]toluene, 23 °C): δ = 19.56 (s, 1 H), 12.82 (br. s, 0.6 H), 10.40 (s, 2 H), 1.37 (s, 2 H), −15.87 (s, 0.4 H), −30.11 (br. s, 0.7 H), −33.43 (br. s, 0.4 H) ppm. ^{1}H NMR (200 MHz, [D$_8$]toluene, −35 °C): δ = 27.54 (s, 1 H), 19.09 (s, 1 H), 15.16 (s, 2 H), 2.25 (s, 0.2 H), 2.10 (s, 0.1 H), 1.69 (s, 1.5 H), −24.53 (s, 0.4 H), −44.86 (s, 1 H), −51.62 (s, 0.4 H) ppm. ^{1}H NMR (200 MHz, [D$_8$]toluene, −80 °C): δ = 39.38 (s, 9 H), 28.60 (s, 9 H), 22.06 (s, 18 H), 3.48 (s, 2 H), 2.37 (s, 2 H), 2.15 (s, 18 H), −37.21 (s, 4 H), −66.03 (s, 9 H), −78.01 (s, 4 H) ppm. $C_{32}H_{75}Mg_2NdO_6Si_2$ (804.96): calcd. C 47.75, H 9.39; found C 47.1, H 9.11.

5: ^{1}H NMR (200 MHz, [D$_6$]benzene, 23 °C): δ = 3.68 (m, 4 H, THF), 1.29 (s, 9 H, *t*Bu), 1.24 (m, 4 H, THF), 0.41 (s, 9 H, $SiMe_3$), −1.33 (s, 2 H, CH_2) ppm. ^{13}C{^{1}H} NMR (50 MHz, [D$_6$]benzene, 23 °C): δ = 69.7 (*C*H$_2$O, THF), 67.8 (C_q, *t*Bu), 35.3 (*C*H$_3$, *t*Bu), 25.5 (*C*H$_2$, THF), 5.6 [Si(*C*H$_3$)], −6.0 (*C*H$_2$Mg) ppm. $C_{12}H_{28}MgO_2Si$ (256.74): calcd. C 56.14, H 10.99; found C 55.86, H 10.53.

Reaction of [$Nd(OC_6H_2\mathit{t}Bu_2$-2,6-Me-4)$_3$(THF)] (2) with [$Mg(CH_2SiMe_3)_2(Et_2O)$] (3). Synthesis of [$Nd(OC_6H_2\mathit{t}Bu_2$-2,6-Me-4)$_2(CH_2SiMe_3)$(THF)$_2$] (6) and [(4-Me-2,6-*t*Bu$_2$C$_6$H$_2$O)Mg(CH$_2$S-iMe$_3$)]$_2$ (7): [$Nd(OC_6H_2\mathit{t}Bu_2$-2,6-Me-4)$_3$(THF)] (**2**) (0.087 g, 0.10 mmol) was dissolved in a mixture of toluene (0.140 g, 0.16 mL) and THF (0.050 g, 0.70 mmol) THF was weighted to introduce an exact amount. [$Mg(CH_2SiMe_3)_2(Et_2O)$] (**3**) (0.027 g; 0.10 mmol) was added at room temperature to the resulting purple solution, and the mixture was immediately cooled to −30 °C. After a few days, colorless crystals of [(4-Me-2,6-*t*Bu$_2$C$_6$H$_2$O)Mg(CH$_2$S-iMe$_3$)]$_2$ (**7**) were removed from the solution (0.013 g, 39%) and blue crystals of **6** suitable for X-ray analysis were obtained from the blue solution after a month (0.025 g, 34%).

6: ^{1}H NMR (200 MHz, [D$_6$]benzene, 23 °C): δ = 21.36 (s, 2 H, Ar), 10.47 (s, 3 H, Me), 7.99 (br. s, 18 H, *t*Bu), −1.25 (s, 2 H, CH_2), −6.90 (br. s, THF), −7.15 (s, $SiMe_3$), −9.66 (br. s, THF) ppm. $C_{42}H_{73}NdO_4Si$ (814.35): calcd. C 61.94, H 9.04; found C 60.45, H 8.96.

7: ^{1}H NMR (200 MHz, [D$_6$]benzene, 23 °C): δ = 7.19 (s, 2 H, Ar), 2.29 (s, 3 H, Me), 1.59 (s, 18 H, *t*Bu), 0.06 (s, 9 H, $SiMe_3$), −1.16 (s, 2 H, CH_2) ppm. ^{13}C{^{1}H} NMR (50 MHz, C_6D_6, 23 °C): δ = 159.4 (C_{Ar}), 139.8 (C_{Ar}), 128.9 (C_{Ar}), 127.6 (C_{Ar}), 35.7 (C_q, *t*Bu), 33.9 (*C*H$_3$, *t*Bu), 21.9 (*C*H$_3$), 4.1 [Si(*C*H$_3$)], −6.2 (*C*H$_2$-Mg) ppm. $C_{19}H_{34}MgOSi$ (330.86): calcd. C 68.97, H 10.36; found C 68.4, H 9.82.

X-ray Crystal-Structure Determination of 4: A pale-blue crystal of approximate dimensions 0.30 × 0.25 × 0.10 mm was mounted on a glass fiber. X-ray data were collected with a Bruker SMART CCD area-detector diffractometer with Mo-K_α radiation (λ = 0.71073 Å) at T = 100 K. Crystal data: monoclinic, *Cc*; a = 26.312(5), b = 11.595(2), c = 22.888(5) Å; β = 109.127(3)°; V = 6597(2) Å^3; formula unit: $C_{32}H_{75}O_6Mg_2NdSi_2$ with Z = 6; molecular weight: 804.96; calculated density = 1.216 g·cm^{-3}; F(000) = 2562; μ(Mo-K_α) = 1.297 mm^{-1}. 22487 reflections collected (2.27° < Θ < 25.00°). The structure was solved by direct methods.[22] Of the six neodymium atoms in the cell, two are on the twofold axis and the four others are in general positions. The resolution was complicated by the disorder between the monodentate O*t*Bu ions and THF molecules, which had to be refined as independent parts. Hydrogen-atom positions were calculated on a geometrical basis. Full-matrix least-squares refinement on F^2 based on 11197 independent reflections converged with 620 variable parameters and three restraints. $R1$ = 0.0360 [for 10265 data with $I > 2\sigma(I)$]; $wR2$ = 0.0864; GoF (F^2) = 1.057. $\Delta\rho_{max}$ = 1.776 and −0.851 e·Å^{-3}.

X-ray Crystal Structure Determination of 6: A pale-blue crystal of approximate dimensions 0.45 × 0.25 × 0.12 mm was mounted on a glass fiber. X-ray data were collected with a Bruker SMART CCD area-detector diffractometer with Mo-K_α radiation (λ = 0.71073 Å) at T = 100 K. Crystal data: orthorhombic, *Pca2*$_1$; a = 23.732(5), b = 9.799(2), c = 18.902(4) Å; V = 4395.7(16) Å^3; formula unit: $C_{42}H_{73}O_4SiNd$ with Z = 4; molecular weight: 814.33; calculated density = 1.119 g·cm^{-3}; F(000) = 1724; μ(Mo-K_α) = 1.244 mm^{-1}. 30722 reflections collected (2.15° > Θ > 28.04°). The structure was solved by direct methods.[22] Hydrogen-atom coordinates were generated by geometrical calculations. Full-matrix least-squares refinement on F^2 based on 9437 independent reflections converged with 450 variable parameters and one restraint. $R1$ = 0.0339 [for 7321 data with $I > 2\sigma(I)$]; $wR2$ = 0.0637; GoF (F^2) = 1.010. $\Delta\rho_{max}$ = 2.015 and −0.808 e·Å^{-3}. The largest residuals are close to one of the THF molecule and are probably due to some orientational disorder.

CCDC-228005 (**4**) and -228006 (**6**) contain the supplementary crystallographic data for this paper. These data can be obtained free of charge at www.ccdc.cam.ac.uk/conts/retrieving.html [or from the Cambridge Crystallographic Data Centre, 12 Union Road, Cambridge, CB2 1EZ, UK; Fax: (internat.) + 44-1223-336033; E-mail: deposit@ccdc.cam.ac.uk].

 © 2004 Wiley-VCH Verlag GmbH & Co. KGaA, Weinheim

Acknowledgments

We are grateful to Rhodia Electronics and Catalysis for financial support of this research (PhD grant for J. G.).

[1] [1a] J. Gromada, T. Chenal, A. Mortreux, J. W. Ziller, F. Leising, J.-F. Carpentier, *Chem. Commun.* **2000**, 2183−2184. [1b] J. Gromada, A. Mortreux, T. Chenal, J. W. Ziller, F. Leising, J.-F. Carpentier, *Chem. Eur. J.* **2002**, *8*, 3773−3788. [1c] J. Gromada, T. Chenal, A. Mortreux, F. Leising, J.-F. Carpentier, *J. Mol. Catal.* **2002**, *182/183*, 537−543.

[2] J. Gromada, L. Le Pichon, F. Leising, A. Mortreux, J.-F. Carpentier, *J. Organomet. Chem.* **2003**, *683*, 44−55.

[3] J. Gromada, C. Fouga, T. Chenal, A. Mortreux, J.-F. Carpentier, *Macromol. Chem. Phys.* **2002**, *203*, 550−555.

[4] It should be pointed out, as commented by a referee, that numerous *n*-alkyllanthanide complexes, including active polymerization catalysts, are known, which indicates that β-H elimination is not necessarily a problem. Also, β-H elimination is not the only possible decomposition process in the lanthanide *tert*-butoxide/MgR_2 systems described in this paper. When the R alkyl group, transferred from the magnesium to the neodymium atom, does not undergo β-H elimination, a second pathway can take place that involves decomposition of the *tert*-butoxy ligand into isobutene to give the corresponding alkane (RH) and lanthanide oxide. See ref.[1b]

[5] W. J. Evans, T. J. Boyle, J. W. Ziller, *J. Am. Chem. Soc.* **1993**, *115*, 5084−5092.

[6] H. Yasuda, H. Yamamoto, K. Yokota, S. Miyake, A. Nakamura, *J. Am. Chem. Soc.* **1992**, *114*, 4908−4910.

[7] R. Anwander, *Top. Curr. Chem.* **1996**, *179*, 151−245, and references cited therein.

[8] J. A. Kerr, in *CRC Handbook of Chemistry and Physics* (Ed.: D. R. Lide), 81st ed., CRP Press, Boca Raton, Florida, USA, **2000**.

[9] [9a] [(*t*BuO)(THF)Y{(μ_2-O*t*Bu)(μ_2-Me)$AlMe_2$}$_2$], [(*t*BuO)(Cl)-$(THF)_2Y(\mu_2$-O*t*Bu)$_2AlMe_2$]: see ref.[5] [9b][Ln(μ_2-O*t*Bu)$_3$(μ_2-Me)$_3$-$(AlMe_2)_3$] (Ln = Y, Pr, Nd): P. Biagini, G. Lugli, L. Abis, R. Millini, *J. Organomet. Chem.* **1994**, *474*, C16−C18. [9c] [(ArO)Sm{(μ_2-OAr)(μ_2-R)AlR_2}$_2$] (Ar = 2,6-*i*Pr$_2$C$_6$H$_3$, R = Me, Et): J. C. Gordon, G. R. Giesbrecht, J. T. Brady, D. L. Clark, D. W. Keogh, B. L. Scott, J. G. Watkin, *Organometallics* **2002**, *21*, 127−131. [9d] [(ArO)La{(μ-OAr)$AlMe_2$}$_2$]: G. R. Giesbrecht, J. C. Gordon, J. T. Brady, D. L. Clark, D. W. Keogh, R. Michalczyk, B. L. Scott, J. G. Watkin, *Eur. J. Inorg. Chem.* **2002**, 723−731. [9e] [(ArO)Y{(μ_2-OAr)(μ_2-Me)$AlMe_2$}$_2$] (Ar = 2,6-*i*Pr$_2$C$_6$H$_3$), [(ArO)$_2$Ln{(μ_2-Me)$_2AlMe_2$}] (Ln = Y, Lu; Ar = 2,6-*t*Bu$_2$C$_6$H$_3$): A. Fischbach, E. Herdtweck, R. Anwander, G. Eickerling, W. Scherer, *Organometallics* **2003**, *22*, 499−509. [9f] [$(ArO)_2(THF)_2$Ln{(μ_2-OAr)$_2AlMe_2$}] (Ln = Nd, Yb, Ar = 2,6-Me$_2$C$_6$H$_3$, R = Me, Et): W. J. Evans, M. A. Ansari, J. W. Ziller, *Inorg. Chem.* **1995**, *34*, 3079−3082. [9g] [Nd{(μ_2-OAr)$_2AlMe_2$}$_3$] (Ar = 4-MeC$_6$H$_4$): W. J. Evans, M. A. Ansari, J. W. Ziller, *Polyhedron* **1997**, *16*, 3429−3434. [9h] [{(*i*PrO)(*i*Bu)Al(μ_2-O*i*Pr)$_2$Sm(O*i*Pr)(HO*i*Pr)}(μ_2-O*i*Pr)]$_2$, [$(THF)_2$Sm(O*t*Bu)$_2$(μ_2-O*t*Bu)Al(*i*Bu)$_2$]: G. R. Giesbrecht, J. C. Gordon, D. L. Clark, B. L. Scott, J. G. Watkin, K. J. Young, *Inorg. Chem.* **2002**, *41*, 6372−6379.

[10] [10a] W. L. Wu, M. W. Chen, P. Zhou, *Organometallics* **1991**, *10*, 98−104. [10b] J. Lin, Z. Wang, *J. Organomet. Chem.* **1999**, *589*, 127−132.

[11] M. H. Chisholm, J. Gallucci, K. Phomphrai, *Inorg. Chem.* **2002**, *41*, 2785−2794.

[12] [12a] W. J. Evans, M. S. Sollberger, T. P. Hanusa, *J. Am. Chem. Soc.* **1988**, *110*, 1841−1850. [12b] W. J. Evans, M. S. Sollberger, *Inorg. Chem.* **1988**, *27*, 4417−4423. [12c] W. J. Evans, J. M. Olofson, J. W. Ziller, *Inorg. Chem.* **1989**, *28*, 4309−4311. [12d] W. J. Evans, J. M. Olofson, J. W. Ziller, *J. Am. Chem. Soc.* **1990**, *112*, 2308−2314. [12e] W. J. Evans, R. E. Golden, J. W. Ziller, *Inorg. Chem.* **1991**, *30*, 4963−4968.

[13] W. A. Herrmann, R. Anwander, M. Kleine, W. Scherer, *Chem. Ber.* **1992**, *125*, 1971−1979.

[14] Z. M. Hou, A. Fujita, T. Yoshimura, A. Jesorka, Y. G. Zhang, H. Yamazaki, Y. Wakatsuki, *Inorg. Chem.* **1996**, *35*, 7190−7195.

[15] G. W. Rabe, C. D. Berube, G. P. A. Yap, K.-C. Lam, T. E. Concolino, A. L. Rheingold, *Inorg. Chem.* **2002**, *41*, 1446−1453.

[16] [16a] [Nd(Odpp)$_3$(DME)] (Odpp = *O*-2,6-$Ph_2C_6H_3$): 2.191 Å: G. B. Deacon, T. Feng, P. C. Junk, B. W. Skelton, A. H. White, *Chem. Ber./Recueil* **1997**, *130*, 851−857. [16b] [Nd(Odpp)$_3$$(THF)_2$]: 2.190 Å; [Nd(Odpp)$_3$(THF)]: 2.193 Å: G. B. Deacon, T. Feng, B. W. Skelton, A. H. White, *Aust. J. Chem.* **1995**, *48*, 741−756.

[17] [17a] [$NdCl_3(THF)_4$]: C. Wenqi, J. Zhonsheng, X. Yan, F. Yuguo, Y. Guangdi, *Inorg. Chim. Acta* **1987**, *130*, 125−129. [17b] [Nd_2(OCH*i*Pr$_2$)$_6$$(THF)_2$]: D. M. Barnhart, D. L. Clark, J. C. Gordon, J. C. Huffman, J. G. Watkin, B. D. Zwick, *J. Am. Chem. Soc.* **1993**, *115*, 8461−8462.

[18] Effective ionic radii for six-coordinate metal centers: La^{3+}: 1.172 Å; Nd^{3+}: 0.983 Å; Sm^{3+}: 0.958: Å. R. D. Shannon, *Acta Crystallogr., Sect. A* **1976**, *A32*, 751.

[19] C. J. Schaverien, N. Meijboom, A. G. Orpen, *J. Chem. Soc., Chem. Commun.* **1992**, 124−126.

[20] [20a] P. B. Hitchcock, M. F. Lappert, A. Singh, *J. Chem. Soc., Chem. Commun.* **1983**, 1499−1501. [20b] M. F. Lappert, A. Singh, R. G. Smith, *Inorg. Synth.* **1990**, *27*, 164−168.

[21] R. A. Andersen, G. Wilkinson, *J. Chem. Soc., Dalton Trans.* **1977**, 809−811.

[22] [22a] *SMART Software Users Guide*, version 5.0, Bruker Analytical X-ray Systems, Inc., Madison, WI, USA, **1999**. [22b] *SAINT Software Users Guide*, version 6.0, Bruker Analytical X-ray Systems, Inc., Madison, WI, USA, **1999**. [22c] G. M. Sheldrick, *SADABS*, Bruker Analytical X-ray Systems, Inc., Madison, WI, USA, **1999**. [22d] G. M. Sheldrick, *SHELXTL*, version 5.10, Bruker Analytical X-ray Systems, Inc., Madison, WI, USA, **1999**.

Received January 15, 2004
Early View Article
Published Online June 17, 2004

 © 2004 Wiley-VCH Verlag GmbH & Co. KGaA, Weinheim

Synthesis and Reactions of Alkynyl Oligosilanes

Christian Mechtler,[a] Michaela Zirngast,[a] Judith Baumgartner,[a] and Christoph Marschner*[a]

Keywords: Alkynes / Anions / Silanes / Polyanions

Synthesis, properties, and reactions of various alkynyl oligosilanes, and their potassium derivatives are described. A series of tris(trimethylsilyl)silylalkynes have been prepared. Their reaction with potassium *tert*-butoxide leads to the corresponding potassium derivatives, which can be subjected to further derivatization. X-ray structures of three oligosilylalkynes are reported.

(© Wiley-VCH Verlag GmbH & Co. KGaA, 69451 Weinheim, Germany, 2004)

Introduction

Over the last five years we have developed an interest in the chemistry of silyl anions which permits the synthesis of both larger oligosilanes and metal silyl compounds.[1] Besides the advancements in this field it is still desirable to enhance the number of compatible functional groups which can be used. Hence, we decided to study alkynylsilanes. Alkynes can be further functionalized by employing addition and substitution reactions and in the case of metal silyl compounds the triple bond exhibits a charge-stabilizing effect.

Alkynylsilanes are commonly prepared by the reaction of silyl halides or triflates with metal alkynyl compounds in organic solvents.[2−4] However, surprisingly few alkynyl-substituted oligosilanes are known[5] to date and the corresponding anions are almost completely unknown.[1b]

In connection with this we report on the selective synthesis of oligosilyl alkynes and their reactions with potassium *tert*-butoxide to form mono- or di-anions along with the further reactions that they are involved in.

Results and Discussion

Synthesis of Alkynylsilanes

The most convenient method for the synthesis of alkynylsilanes makes use of the reaction of silyl halides with metallated alkynes such as Grignard compounds.[6] Our preferred route was that of the lithiated alkynes. Although a two step synthesis was employed avoiding the use of dilithiated acetylene an excellent yield of over 80% was obtained for **6,** compared with the 5% reported.[7] The nature of the lithium alkyl used for the metallation of the alkyne was not important with the exception of the case of lithiation of phenylated alkynes where the use of methyllithium was found to be crucial. The reacting silanes were usually chlorosilanes, only for the 1-propinyl compound **2,** and also **10**, were the more reactive bromosilanes used (Scheme 1).

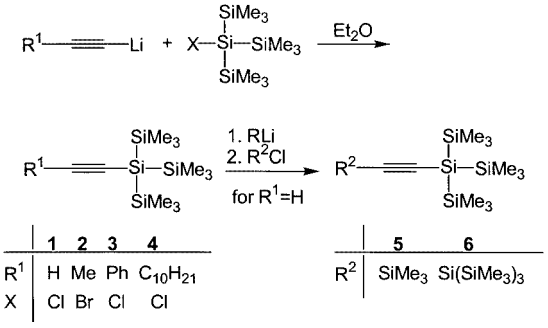

Scheme 1. General scheme for the synthesis of alkynylsilanes

Reaction of propargyl tosylate with potassium tris(trimethylsilyl)silane[1] affords propargylsilane **7** in a yield of 80%. Astonishingly deprotonation of the alkyne by the highly basic silyl anion was not a significant side reaction. Reaction towards the bissilylated compound **8** was easily achieved by lithiation of **7** and reaction with chlorotris(trimethylsilyl)silane (Scheme 2).

In order to obtain a compound bearing two alkynyl groups we treated 2,2-dibromohexamethyltrisilane with two equivalents of lithiated phenylacetylene (Scheme 3).

In an attempt to prepare a higher alkynyl oligosilane, bromopentakis(trimethylsilyl)disilane was treated with phenyl acetylide (Scheme 4).

[a] Institut für Anorganische Chemie, Technische Universität Graz, Stremayrgasse 16, 8010 Graz, Austria
Fax: (internat.) +43-316-8738701
E-mail: marschner@anorg.tu-graz.ac.at

 © 2004 Wiley-VCH Verlag GmbH & Co. KGaA, Weinheim **DOI: 10.1002/ejic.200400107**

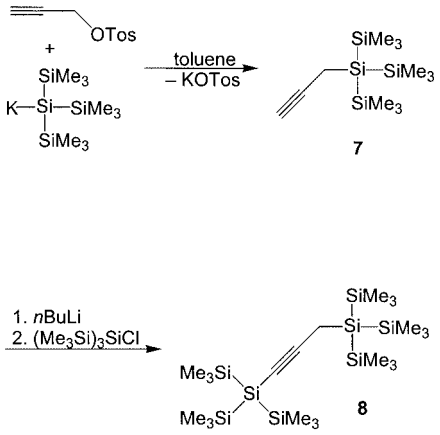

Scheme 2. Preparation of silylated propyne derivatives **7** and **8**

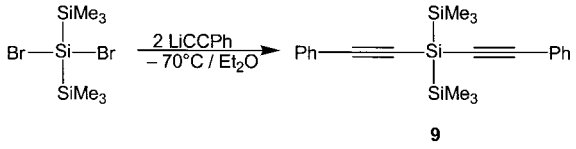

Scheme 3. Preparation of the dialkyne derivative **9**

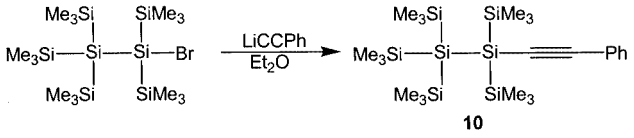

Scheme 4. Preparation of **10**

Preparation of Alkynyl Silyl Anions

Recently, we described the reaction of oligosilanes with one or two molar equivalents of potassium *tert*-butoxide to give the respective mono-[1,16] or dianions[1b] and a silyl ether. Monoanions were formed in THF at ambient temperature, the formation of dianions, however, required a temperature of about 60 °C and reaction times of a few days. The use of benzene or toluene as a solvent and the addition of 18-crown-6 facilitated the formation of dianions so that complete conversion within a few hours at room temperature could be achieved. The alkynylsilanes discussed here proved to be considerably more reactive than the silanes studied so far. The conversion into the respective mono- or dianions proceeded smoothly at room temperature within minutes and even at −20 °C it proceeded within an hour. The alkynyl group seems to enhance reactivity towards the potassium alkoxide significantly. The effect is so pronounced that it is not possible to achieve clean mono metallation for the case of the alkynylidene-bridged compound **6**. Only a mixture of starting material, mono- and dianion could be detected upon reaction with one equivalent of potassium *tert*-butoxide. As already observed for the reactions with other oligosilanes, conversion only occurs in THF, DME or even more polar ethereal solvents. No conversion, even with the more reactive alkynylsilanes occurred in diethyl ether, benzene or toluene.

The metallations of compounds **2**, **3**, **4** and **5** proceeded as expected from our experience gained thus far. A trimethylsilyl group was formally replaced by a negative charge. All reactions were faster than the conversion with tetrakis(trimethylsilyl)silane,[1] with compound **3** being the most reactive. In THF the conversion of **3** at ambient temperature was completed within less than five minutes. Interestingly the reaction of tris(trimethylsilyl)silylacetylene (**1**) with potassium *tert*-butoxide did not yield the expected anion, instead the only product detected was the rearrangement product **5a** which can also be obtained from **5** (Scheme 5). The nature of the rearrangement is still unclear. It is, however, likely that a reaction of the initially formed compound **1a** with *tert*-butyltrimethylsilyl ether occurs.

Tris(trimethylsilyl)propargylsilane (**7**) underwent another unexpected rearrangement. The result of its reaction with potassium *tert*-butoxide was compound **2a**. A closer look at the reaction revealed an initial base catalyzed rearrangement of **7** to **2,** which then was followed by conversion into **2a**. In contrast to the rapid and exclusive reaction of **6** towards the dianion compound **6a**, **8** was showing very different behavior. Addition of one equivalent of potassium *tert*-butoxide did not effect the formation of the expected monoanion **8a**. A second equivalent of the alkoxide eventually resulted in the fast formation of **8a** but even after 72 h no dianion could be observed and complete decomposition had occurred (Scheme 6).

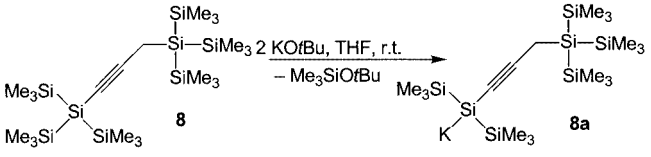

Scheme 6. Monometallation of **8**

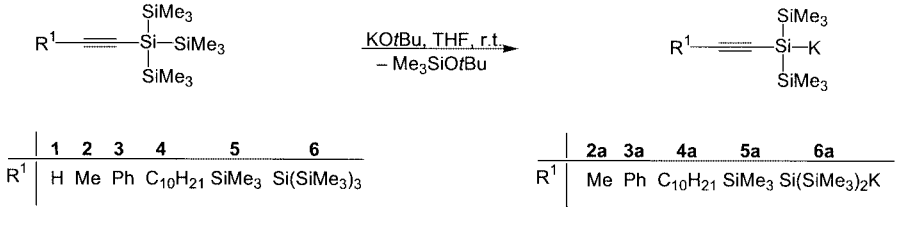

Scheme 5. Synthesis of potassium alkynylsilanes

 © 2004 Wiley-VCH Verlag GmbH & Co. KGaA, Weinheim

The reaction of the dialkyne **9** with potassium *tert*-butoxide did not give a dialkynyl(trimethylsilyl)silyl anion. Although a vigorous and clearly exothermic reaction occurred no soluble silicon containing product was obtained. The brown insoluble material, which could be isolated, seemed to indicate a polymerization reaction. An early and isolated example by Gilman et al.[8] reported addition of two equivalents of triphenylsilyllithium across diphenylacetylene. Besides the addition product almost 90% of polymeric material was obtained. An anionic addition polymerization process may account for the course of reaction in both cases.

The behavior of starting material **10** in its reaction with potassium *tert*-butoxide was of special interest. In the analogous reaction with pentakis(trimethylsilyl)phenyldisilane we have observed a perfect regioselectivity for the cleavage of a trimethylsilyl group in the β-position to the phenyl group. However, for the case of **10** a mixture of the two possible anions **10a** to **10b** was found in a ratio of about 2 to 1 (Scheme 7).

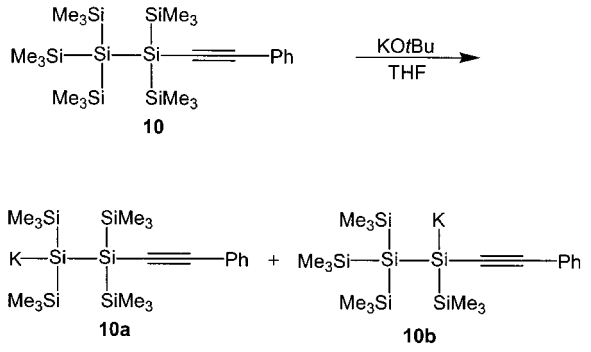

Scheme 7. Reaction of **10** with potassium *tert*-butoxide

NMR Spectroscopy

^{29}Si NMR spectroscopy is most useful for the chemistry of oligosilanes. While the resonances for the tertiary silicon atom of alkylated tris(trimethylsilyl)silanes can be found at around −80 ppm, the alkynyl substituent causes a high-field shift to δ = −101 ppm. Replacement of one trimethylsilyl group by potassium causes another shift to approximately δ = −155 ppm. This behavior is in accordance with our previous observations on other silyl potassium compounds.[1]

Table 1. Increments for the calculation of ^{13}C NMR shifts of substituted alkynes[9,10,16]

Group	α	β
Me	+8.5	−3.6
*n*Bu	+11.1	−5.9
Ph	+12.7	−6.4
$SiMe_3$	+17.4	+21.8
$Si(SiMe_3)_3$	+11.5	+24.9
$CH_2Si(SiMe_3)_3$	+13.0	−4.3

In the case of alkynylsilanes ^{13}C NMR spectroscopy is also of some interest. As acetylenes have only two substituents it is easy to study their influence on the ^{13}C NMR shift. Using acetylene as a parent compound α- and β-shift effects can be observed upon replacement of a proton by another substituent.[9] While alkyl groups cause the α-carbon to resonate at a lower and the β-carbon at a higher field, phenyl groups effect both signals at a lower field with the β-shift being smaller. The trimethylsilyl group again gives rise to a shift to a lower field but the magnitude of the influence is reversed compared to the phenyl group.[10] The tris(trimethylsilyl)silyl group has a similar but even more pronounced influence (Table 1). This plain increment system can also be used advantageously for a rough estimate of disubstituted alkynes, as seen from Table 2, where the observed ^{13}C shift values for the tris(trimethylsilyl)silylated alkynes can be compared to those obtained by simple increment addition to the base value of δ = 71.9 ppm for acetylene.

Table 2. ^{13}C NMR shifts of $(Me_3Si)_3Si-C(A)=C(B)-R$ in ppm; incremental values in brackets

Group R	δ C(A)	δ C(B)
Me	73.1 (79.8)	105.2 (105.3)
$C_{10}H_{19}$	76.5 (77.5)	113.9 (107.9)
Ph	76.5 (89.8)	111.3 (109.5)
$SiMe_3$	107.9 (105.2)	117.7 (114.2)
$Si(SiMe_3)_3$	109.6 (108.3)	109.6 (108.3)
$CH_2Si(SiMe_3)_3$	73.4 (79.1)	110.8 (109.8)

X-ray Crystallography

As has already been mentioned only a few oligosilylacetylenes have been synthesized to date. It is therefore not completely surprising that no crystal structures of tertiary silylacetylenes have been reported so far. Even for secondary silylacetylenes only two examples can be found.[2,11] One reason for this obvious lack of structural investigations may be difficulties in obtaining good quality crystals. Most compounds investigated by us were either oils or solids with melting points close to room temperature. Nevertheless, we were able to determine the first examples of crystal structures of isotetrasilanylacetylenes. Compounds **3**, **6**, and **9** could be subjected to structure analysis (Table 3, Figures 1−3). The structural features of all three compounds are within the ranges of what is expected. Examples of the acetylenic triple bond length of alkynylsilanes range from 1.16 Å to 1.22 Å.[12] **3** [1.185(5) Å], **6** [1.217(6) Å] and **9** [1.205(5), 1.204(5) Å] fit into this range with **6** exhibiting the longest bond, probably reflecting the two bulky silyl groups. The tetrahedral bond angles around the central silicon atoms are clearly a function of the spatial demand of the substituents. This can be observed best for the diacetylene compound **9**, where the two trimethylsilyl groups open up at an angle of 117.4°. Deviations from the expected 180° for the CCSi angle are comparatively small for **3** [176.5(4)°] and **6** [178.9(4)°] and only for **9** [178.7(4), 173.3(3)°] was a

 © 2004 Wiley-VCH Verlag GmbH & Co. KGaA, Weinheim

very slight bending observed. The two tris(trimethylsilyl)silyl groups of **6** exhibit an almost perfectly staggered conformation with respect to each other (Figure 2).

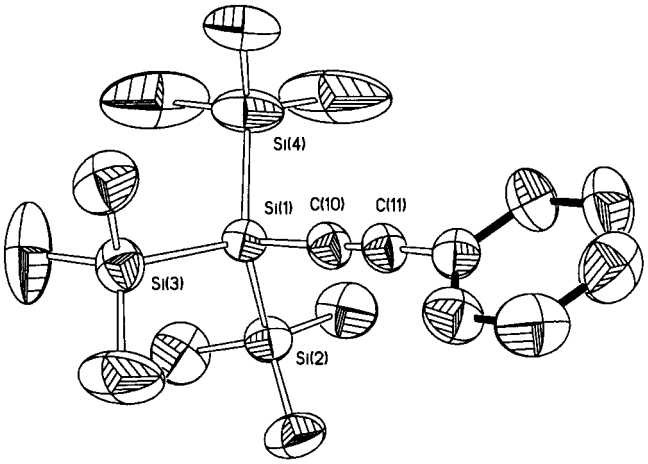

Figure 1. The molecular structure and numbering of **3** with 30% probability thermal ellipsoids; all hydrogen atoms have been omitted for clarity; selected bond lengths (Å) and bond angles (°) with estimated standard deviations: Si(1)−Si(4) 2.317(2), Si(1)−Si(3) 2.3347(19), Si(1)−Si(2) 2.3454(18), Si(1)−C(10) 1.837(5), C(10)−C(11) 1.185(5), C(10)−Si(1)−Si(4) 106.00(15), C(10)−Si(1)−Si(3) 103.18(14), Si(4)−Si(1)−Si(3) 111.59(8), C(10)−Si(1)−Si(2) 107.97(15), Si(4)−Si(1)−Si(2) 114.81(7), Si(3)−Si(1)−Si(2) 112.33(7), Si(1)−C(10)−C(11) 176.5(4), C(10)−C(11)−C(12) 178.3(5)

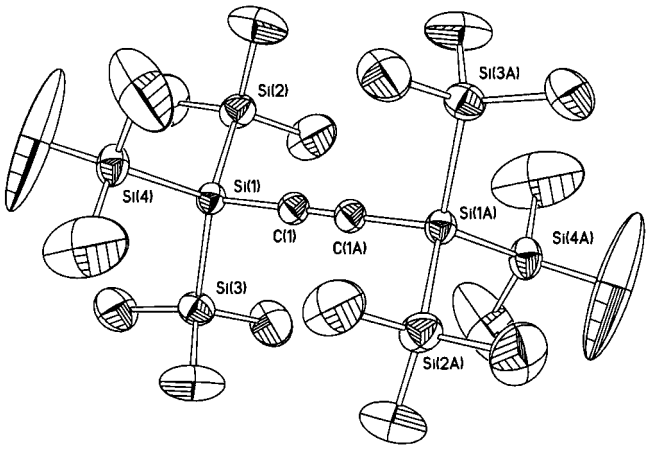

Figure 2. The molecular structure and numbering of **6** with 30% probability thermal ellipsoids; all hydrogen atoms have been omitted for clarity; selected bond lengths (Å) and bond angles (°) with estimated standard deviations: Si(1)−C(1) 1.835(3), Si(1)−Si(2) 2.3430(15), Si(1)−Si(3) 2.3469(16), Si(1)−Si(4) 2.3466(13), C(1)−C(1A) 1.217(6), C(1)−Si(1)−Si(2) 105.73(11), C(1)−Si(1)−Si(3) 104.79(11), Si(2)−Si(1)−Si(3) 113.33(6), C(1)−Si(1)−Si(4) 104.76(10), Si(2)−Si(1)−Si(4) 112.98(6), Si(3)−Si(1)−Si(4) 114.11(6), C(1)−Si(1)−Si(2)−C(4) 178.7(4), Si(1)−C(1)−C(1A) 178.9(4)

Conclusion

A number of alkyne substituted oligosilanes have been prepared mainly by the reaction of lithiated alkynes with chloro- or bromooligosilanes. Reaction of these compounds with potassium *tert*-butoxide showed considerably enhanced reactivity compared to silyl or alkyl-substituted oligosilanes. Usually within minutes formation of a silyl potassium compound and *tert*-butyltrimethylsilyl ether was complete. Phenylacetylene derived compounds (**3, 10**) are the most reactive among all investigated materials. Reaction with a compound possessing two alkynyl substituents (**9**) led to a vigorous and strongly colored reaction which did not yield soluble silicon containing material. The reaction of a propargylsilane (**7**) with the potassium alkoxide gave an initial rearrangement to the propynylsilane (**2**) followed by the formation of a propynylsilyl potassium compound (**2a**). An alkynylidene-bridged bisoligosilyl compound (**6**) could be used to obtain an oligosilyl dianion (**6a**) by means of a smooth reaction. With a similar propargylidene bridged compound (**8**) only mono-metallation could be achieved.

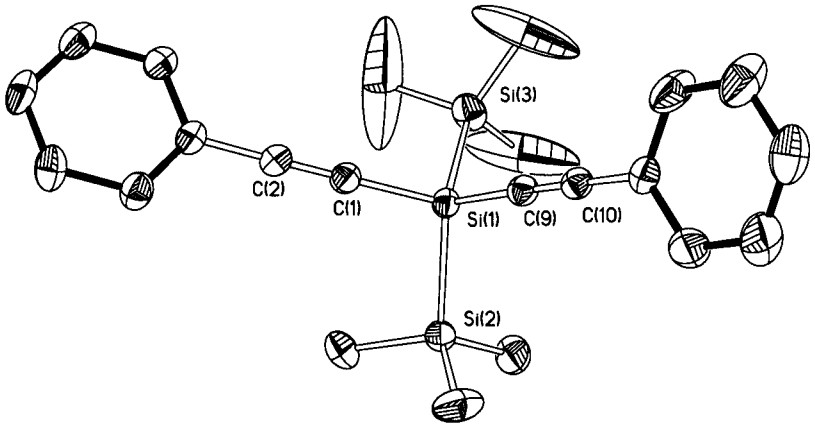

Figure 3. The molecular structure and numbering of **9** with 30% probability thermal ellipsoids; all hydrogen atoms have been omitted for clarity; selected bond lengths (Å) and bond angles (°) with estimated standard deviations: Si(1)−C(9) 1.843(4), Si(1)−C(1) 1.846(4), Si(1)−Si(3) 2.3501(16), Si(1)−Si(2) 2.3539(15), C(1)−C(2) 1.205(5), C(9)−C(10) 1.204(5), C(9)−Si(1)−C(1) 107.70(16), C(9)−Si(1)−Si(3) 109.34(13), C(1)−Si(1)−Si(3) 106.21(13), C(9)−Si(1)−Si(2) 109.38(12), C(1)−Si(1)−Si(2) 106.30(13), Si(3)−Si(1)−Si(2) 117.45(6), Si(1)−C(1)−C(2) 173.3(3), Si(1)−C(9)−C(10) 178.7(3)

 © 2004 Wiley-VCH Verlag GmbH & Co. KGaA, Weinheim

In summary it can be concluded that alkynyl substituents substantially enhance the reactivity of oligosilanes towards potassium alkoxide attack. Given all the possible derivatization reactions of the alkynyl group, its introduction into oligosilyl anions considerably extends the scope of this chemistry.

Experimental Section

General Remarks: All reactions involving air-sensitive compounds were carried out under an atmosphere of nitrogen or argon using either Schlenk techniques or a glovebox. All solvents besides $CDCl_3$ were dried over sodium/potassium alloy under nitrogen and were freshly distilled prior to use. Potassium *tert*-butoxide was purchased from Merck. Other chemicals were obtained from different chemical suppliers and used as received.

Aqueous workup was performed by adding the reaction mixture to 2 M H_2SO_4 followed by separation of the layers. Subsequently, the aqueous layer was extracted twice with the indicated solvent. The combined organic layers were washed with a saturated aqueous sodium hydrogen carbonate solution and then dried over sodium sulfate.

^1H (300 MHz), ^{13}C (75.4 MHz), and ^{29}Si (59.3 MHz) NMR spectra were recorded on a Varian INOVA 300 spectrometer. Samples for ^{29}Si NMR spectra were either dissolved in deuterated benzene or chloroform, or the reaction samples were measured in the presence of a D_2O capillary in order to provide an external lock frequency signal. To compensate for the low isotopic abundance of ^{29}Si the INEPT pulse sequence was used to amplify the signal.[13]

GC analyses were carried out on an HP 5890 series II equipped with capillary column HP-1ms (25 m × 0.251 mm; 0.33 μm) and an HP 5971 mass spectrometer.

GC/MS samples of derivatized silyl anions were obtained by adding a solution of the nucleophile to a mixture of 10% ethyl bromide in diethyl ether or to the organic layer of a mixture of diethyl ether/2 M H_2SO_4 to give the corresponding ethylated or protonated silane species in a very rapid, clean and quantitative reaction.

Elementary analyses were carried out using a Heraeus Vario Elementar. Tetrakis(trimethylsilyl)silane,[14] tris(trimethylsilyl)silane,[1a] chlorotris(trimethylsilyl)silane,[15] tris(trimethylsilyl)silylpotassium,[1,16] propargyltosylate,[17] tris(trimethylsilyl)silylethyne (**1**),[1b] bis[tris(trimethylsilyl)silyl]ethyne (**6**),[1b] and bis[potassiobis(trimethylsilyl)silyl]ethyne (**6a**)[1b] were prepared according to literature procedures.

Propynyltris(trimethylsilyl)silane (2)

Bromotris(trimethylsilyl)silane: Tris(trimethylsilyl)silane (24.0 g, 97.0 mmol) was dissolved at room temperature in bromoform (100 mL). After 16 h the solution was heated to 70 °C for 1 h. After complete conversion (reaction control by GC) bromoform and methylenebromide were distilled off leaving bromotris(trimethylsilyl)silane (28.9 g, 91%) as colorless, deliquescent crystals. ^1H NMR (C_6D_6): δ = 0.29 (s, 27 H) ppm. ^{13}C NMR (C_6D_6): δ = 1.7 ppm. ^{29}Si NMR (THF, D_2O): δ = −12.7, −24.0 ppm. MS: *m*/*z* (%) = 326 (4), 328 (5) [M^+], 313 (6), 311 (5) [M^+ − Me], 174 (93) [Si_3Me_6], 159 (48) [Si_3Me_5], 73 (100) [$SiMe_3$].

Synthesis of 2: A 1-L round-bottomed flask was evacuated and then filled with propyne (approx. 41 mmol). The gas was condensed on diethyl ether (20 mL) at −70 °C in a flask equipped with a dropping funnel. At the same temperature *n*-butyllithium (21 mL, 42 mmol, 2 M in pentane) was added dropwise. The temperature was raised to −50 °C and bromotris(trimethylsilyl)silane (13.1 g, 40.0 mmol) in diethyl ether (20 mL) was added. The mixture was allowed to reach room temperature and was stirred for a further 16 h. Aqueous workup, evaporation of the solvent and distillation (100 °C, 0.05 mbar) yielded **2** (8.51 g, 75%) as a yellowish oil. ^1H NMR (C_6D_6): δ = 1.67 (s, 3 H), 0.44 (s, 27 H) ppm. ^{13}C NMR (C_6D_6): δ = 105.2, 73.1, 5.2, 0.5 ppm. ^{29}Si NMR (THF, D_2O): δ = −11.7, −100.5 ppm. MS: *m*/*z* = 286 (9) [M^+], 271 (20) [M^+ − Me], 213 (18) [M^+ − $SiMe_3$], 174 (75) [$Si(SiMe_3)_2$], 73 (100) [$SiMe_3$].

Tris(trimethylsilyl)silylphenylacetylene (3): Synthesis according to literature.[18] ^1H NMR ($CDCl_3$): δ = 7.46 (m, 2 H), 7.32 (m, 3 H), 0.23 (s, 27 H) ppm. ^{13}C NMR ($CDCl_3$): δ = 132.0, 128.4, 127.9, 124.9, 108.6, 88.4, 0.7 ppm. ^{29}Si NMR ($CDCl_3$): δ = −11.5, −100.5 ppm. MS: *m*/*z* = 348 (13) [M^+], 275 (19) [M^+ − $SiMe_3$], 174 (70) [$Si(SiMe_3)_2$], 135 (25) [$PhSiMe_2$], 129 (26) [Si_3Me_3], 73 (100) [$SiMe_3$].

Dodecynyltris(trimethylsilyl)silane (4): In a 100-mL Schlenk flask equipped with a rubber septum and stirring bar, dodecyne (0.850 g, 5.11 mmol) was dissolved in diethyl ether (30 mL) and methyllithium (3.70 mL, 5.88 mmol, solution, 1.6 M in diethyl ether) was added dropwise via a syringe at −70 °C. After 20 min the temperature was raised to −20 °C followed by addition of chlorotris(trimethylsilyl)silane (1.70 g, 6.00 mmol) in diethyl ether (20 mL). The mixture was then stirred for 16 h at room temperature. Aqueous workup and evaporation of the solvent gave a brown oily solid, which was extracted with pentane (50 mL). Evaporation of the solvent and removal of the volatiles in vacuo (20 °C, 0.05 mbar) yielded **4** (1.84 g, 87%) as a yellow oil. ^1H NMR (C_6D_6): δ = 1.26 (broad signal, 16 H), 0.98 (m, 5 H), 0.32 (s, 27 H) ppm. ^{13}C NMR (C_6D_6): δ = 111.3, 76.5, 32.7, 30.5, 30.4, 30.2, 29.9 (2 ×), 29.4, 23.5, 21.1, 14.8, 1.0 ppm. ^{29}Si NMR (C_6D_6): δ = −11.7, −100.7 ppm. MS: *m*/*z* = 412 (14) [M^+], 339 (10) [M^+ − $SiMe_3$], 174 (100) [$Si(SiMe_3)_2$], 159 (16) [$Si(SiMe_3)_2$ − Me], 73 (100) [$SiMe_3$].

1-Trimethysilyl-2-[tris(trimethylsily)silyl]ethyne (5): Similar procedure as for compound **4** using **1** (1.00 g, 3.67 mmol), methyllithium (2.6 mL, 4.2 mmol, 1.6 M in diethyl ether), and chlorotrimethylsilane (0.33 g, 4.07 mmol) to yield **5** (1.10 g, 87%) as a colorless oil.[19] ^{29}Si NMR (C_6D_6): δ = −12.2, −20.3, −101.2 ppm. MS: *m*/*z* (%) = 344 (26) [M^+], 329 (16) [M^+ − Me], 271 (12) [M^+ − $SiMe_3$], 174 (54) [$Si(SiMe_3)_2$], 73 (100) [$SiMe_3$].

3-Propinyltris(trimethylsilyl)silane (7): Tris(trimethylsilyl)silylpotassium (4.24 mmol) in toluene (20 mL) was added to a solution of propargyltosylate (0.89 g, 4.24 mmol) in toluene (20 mL) at −50 °C. The solution was allowed to reach room temperature and was stirred for a further 16 h before the reaction was subjected to an extractive workup procedure. The residue was filtered through Celite yielding **7** (0.98 g, 81%) as a light yellow oil. ^1H NMR (C_6D_6): δ = 1.68 (t, *J* = 3.0 Hz, 1 H), 1.55 (d, *J* = 3.0 Hz, 2 H), 0.22 (s, 27 H), ppm. ^{13}C NMR (C_6D_6): δ = 84.9, 67.6, 0.8, −3.9 ppm. ^{29}Si NMR (C_6D_6): δ = −12.4, −78.0 ppm. MS: *m*/*z* (%) = 286 (2) [M^+], 271 (19) [M^+ − Me], 213 (100) [M^+ − $SiMe_3$], 197 (26) [$(C_3H_2)Si_3Me_5$], 129 (27) [Si_3Me_3], 73 (100) [$SiMe_3$].

1,3-Bis[tris(trimethylsilyl)silyl]propyne (8): Similar procedure as for the synthesis of **4** employing **7** (3.49 g, 12.3 mmol), butyllithium (7.7 mL, 12.3 mmol, 1.6 M in hexane), and chlorotris(trimethylsilyl)-silane (3.49 g, 12.3 mmol) to give a mixture of **8** and starting materials. Removal of the volatile products by Kugelrohr distillation leaves **8** (3.02 g, 46%) as a yellow oil. ^1H NMR (C_6D_6): δ = 1.80

 © 2004 Wiley-VCH Verlag GmbH & Co. KGaA, Weinheim

(s, 2 H), 0.35 (s, 27 H), 0.24 (s, 27 H) ppm. ^{13}C NMR (C_6D_6): δ = 110.8, 73.4, 0.9, 0.7, −1.3 ppm. ^{29}Si NMR (C_6D_6): δ = −12.3, −12.5, −80.2, −100.4 ppm. MS: *m*/*z* (%) = 532 (2) [M^+], 285 (100) [$(C_3H_2)Si(SiMe_3)_3$], 197 (11) [$(C_3H_2)Si_3Me_5$], 73 (44) [$SiMe_3$].

Hexamethyl-2,2-bis(phenylethynyl)trisilane (9)

2,2-Dibromohexamethyltrisilane: On hexamethyl-2,2-diphenyltrisilane[20] (7.2 g, 21.9 mmol) hydrogen bromide (approx. 20 mL) was condensed at −80 °C. A reflux condenser cooled to −80 °C was put on the flask, the bath removed and the hydrogen bromide was refluxed for 2 h. Subsequently the remaining hydrogen bromide and all volatiles were condensed into a liquid nitrogen cooled trap. The whole procedure was repeated once to ensure complete conversion. The dibromide was obtained as deliquescent crystals at room temperature (7.15 g, 98%). ^{1}H NMR ($CDCl_3$): δ = 0.34 (s, 18 H) ppm. ^{13}C NMR (C_6D_6): δ = −3.0 ppm. ^{29}Si NMR ($CDCl_3$): δ = 23.7, −10.0 ppm. MS: *m*/*z* (%) = 332/334 (8) [M^+], 180/182 (25) [Me_3Si-SiBr], 73 (100) [$SiMe_3$].

Synthesis of 9: Similar procedure as for the synthesis of **4** using phenylacetylene (3.57 g, 35.0 mmol), *n*-butyllithium (22.0 mL, 35.2 mmol, 1.6 M in hexane), and 2,2-dibromohexamethyltrisilane (5.00 g, 15.0 mmol) to give **9** (2.76 g, 49%) as a colorless oil. B.p. 135−142 °C (0.1 bar). ^{1}H NMR (C_6D_6): δ = 7.41 (m, 4 H), 6.91 (m, 6 H), 0.39 (s, 18 H) ppm. ^{13}C NMR (C_6D_6): δ = 132.1, 128.5, 128.4, 123.8, 110.2, 86.9, −1.4 ppm. ^{29}Si NMR ($CDCl_3$): δ = −13.7, −80.8 ppm.

Pentakis(trimethylsilyl)(phenylethynyl)disilane (10)

Bromopentakis(trimethylsilyl)disilane: Pentakis(trimethylsilyl)phenylsilane[16,21] (3.40 g, 6.83 mmol) was treated as described above for the synthesis of 2,2-dibromohexamethyltrisilane. At room temperature colorless, deliquescent crystals (3.30 g, 97%) of the bromo compound were obtained. ^{1}H NMR (C_6D_6): δ = 0.34 (s, 27 H), 0.28 (s, 18 H) ppm. ^{13}C NMR (C_6D_6): δ = 3.9, 2.9 ppm. ^{29}Si NMR ($CDCl_3$): δ = −9.4, −12.5, −69.1, −128.2 ppm.

Synthesis of 10: Similar procedure as for the synthesis of compound **4** using phenylacetylene (1.5 g, 3.48 mmol), methyllithium (9.25 mL, 14.8 mmol, 1.6 M in diethyl ether), and bromopentakis(-trimethylsilyl)disilane (2.20 g, 4.21 mmol) to give **10** (1.11 g, 51%) as colorless crystals. M.p. 75−84 °C. ^{1}H NMR (C_6D_6): δ = 7.68 (m, 1 H), 7.43 (m, 2 H), 6.96 (m, 2 H), 0.41 (s, 18 H), 0.38 (s, 27 H) ppm. ^{13}C NMR (C_6D_6): δ = 137.7, 131.6, 128.4, 124.8, 110.1, 90.9, 3.6, 1.9 ppm. ^{29}Si NMR (C_6D_6): δ = −9.4, −10.4, −98.0, −129.3 ppm.

General Procedure for the Synthesis of Potassium Silyls: In a nitrogen filled glove box the respective silane and potassium *tert*-butoxide (1.05 equiv. for mono-, and 2.10 equiv. for the dipotassium compounds) were dissolved in THF. The solution immediately turned yellow and after some time dark brown. Complete conversion was controlled by ^{29}Si NMR spectroscopy of a small aliquot. Yields were not easily determined by removal of the solvent because different ratios of THF coordinate to the anions. Derivatization reactions with sulfuric acid or ethyl bromide, which were analyzed by GC/MS, showed that formation of the anions was almost quantitative within the limits of detection.

[Propynylbis(trimethylsilyl)silyl]potassium (2a): ^{1}H NMR (C_6D_6): δ = 1.75 (s, 3 H), 0.15 (s, 18 H) ppm. ^{13}C NMR (C_6D_6): δ = 99.6, 95.2, 36.9, 3.4 ppm. ^{29}Si NMR (C_6D_6): δ = −6.8, −155.3 ppm. MS (ethyl bromide quench): *m*/*z* (%) = 242 (31) [M^+], 213 (24) [M^+ − Et], 169 (11) [M^+ − $SiMe_3$], 130 (100) [$Me_3SiSiEt$], 102 (51) [$HSiSiMe_3$], 73 (56) [$SiMe_3$].

[Bis(trimethylsilyl)silylphenylacetylene]potassium (3a): ^{1}H NMR (C_6D_6): δ = 7.00 (m, 2 H), 6.92 (m, 2 H), 6.77 (m, 1 H), 0.04 (s, 18 H) ppm. ^{13}C NMR (C_6D_6): δ = 129.8, 128.7, 127.5, 123.4, 115.2, 106.2, 3.3 ppm. ^{29}Si NMR (C_6D_6): δ = −7.0, −155.1 ppm.

[Dodecynylbis(trimethylsilyl)silyl]potassium (4a): ^{1}H NMR (C_6D_6): δ = 2.1 (m, 2 H), 1.35 (br. s, 4 H), 1.17 (br. s, 12 H), 0.77 (t, 3 H), 0.07 (s, 18 H) ppm. ^{13}C NMR (C_6D_6): δ = 103.7, 96.8, 32.0, 30.8, 29.9, 29.8, 29.6, 29.5, 29.0, 22.7, 21.5, 13.7, 3.4 ppm. ^{29}Si NMR (C_6D_6): δ = −7.3, −156.2 ppm. MS (ethyl bromide quench): *m*/*z* (%) = 368 (22) [M^+], 130 (90) [Si_2Me_3Et], 73 (100) [$SiMe_3$].

{1-Trimethysilyl-2-[bis(trimethylsily)silyl]acetylene}potassium (5a): ^{1}H NMR (C_6D_6): δ = −0.01 (s, 18 H), −0.04 (s, 9 H) ppm. ^{13}C NMR (C_6D_6): δ = 138.0, 109.9, 3.4, 1.1 ppm. ^{29}Si NMR (C_6D_6): δ = −7.6, −27.4, −159.6 ppm. MS (ethyl bromide quench): *m*/*z* (%) = 300 (20) [M^+], 227 (21) [M^+ − $SiMe_3$], 199 (40) [$(Me_3Si)_2$-Si(CC)H], 130 (37) [$Me_3SiSiEt$], 73 (100) [$SiMe_3$].

{1-Bis[bis(trimethylsilyl)silyl]-3-[tris(trimethylsily)silyl]propyne}-potassium (8a): ^{29}Si NMR (C_6D_6): δ = −8.1, −12.7, −82.0, −149.6 ppm.

[1,1,2,2-Tetrakis(trimethylsilyl)-1-(phenylethynyl)disilyl]potassium (10a): ^{29}Si NMR (C_6D_6): δ = −8.0, −13.2, −93.1, −188.9 ppm.

[1,1,1,2-Tetrakis(trimethylsilyl)-1-(phenylethynyl)disilyl]potassium (10b): ^{29}Si NMR (C_6D_6): δ = −6.0, −10.1, −128.4, −151.4 ppm.

Bis[bis(trimethylsilyl)methylsilyl]ethyne (6b): To the dipotassium compound **6a** (0.37 mmol) in diethyl ether (2 mL) dimethylsulfate (0.10 mL, 1.05 mmol) was added at 0 °C. The solution was stirred for 16 h at room temperature before it was subjected to an extractive workup. A colorless oil of **6b** (140 mg, 95%) was obtained. ^{1}H NMR (C_6D_6): δ = 0.26 (s, 6 H), 0.24 (s, 36 H) ppm. ^{13}C NMR (C_6D_6): δ = 114.2, −1.5, −7.8 ppm. ^{29}Si NMR (C_6D_6): δ = −15.6, −65.3 ppm. MS: *m*/*z* (%) = 402 (5) [M^+], 329 (29) [M^+ − $SiMe_3$], 232 (40) [Si − $(SiMe_3)_3$] − Me], 73 (100) [$SiMe_3$].

Bis[bis(trimethylsilyl)silyl]ethyne (6c): 6a (0.39 mmol) was added to a vigorously stirred mixture of H_2SO_4 (2 M, 5 mL) and diethyl ether (5 mL). After 10 min the aqueous layer was removed, the organic residue diluted twice with toluene and the solvent removed under reduced pressure. A colorless oil of **6c** (123 mg, 85%) was obtained. ^{1}H NMR (C_6D_6): δ = 3.83 (s, 2 H), 0.26 (s, 36 H) ppm. ^{13}C NMR (C_6D_6): δ = 110.3, −0.6 ppm. ^{29}Si NMR (C_6D_6): δ = −14.3, −91.0 ppm. MS: *m*/*z* (%) = 374 (5) [M^+], 301 (18) [M^+ − $SiMe_3$], 285 (99) [M^+ − $SiMe_3$ − CH_4], 241 (31) [$Me_3Si(Me)SiC{=}CSiSiMe_3$], 227 (36) [$Me_3Si(H)SiC{=}CSiSiMe_3$], 73 (100) [$SiMe_3$].

X-ray Crystallographic Studies: Measurements were carried out on a Bruker SMART Apex diffractometer with Mo-K_α radiation. The data were reduced to F_o^2 and corrected for absorption effects with SAINT[22] and SADABS,[23] respectively (Table 3). The structures were solved by direct methods and refined by full-matrix least-squares method (SHELXL-97).[24] All non-hydrogen atoms were refined with anisotropic displacement parameters. All hydrogen atoms were located in calculated positions to correspond to standard bond lengths and angles.

Acknowledgments

This study was carried out within the START project *Chiral polysilanes* (Y120) funded by the Austrian ministry of education, science and culture.

 © 2004 Wiley-VCH Verlag GmbH & Co. KGaA, Weinheim

Table 3. Crystallographic data for compounds **3**, **6** and **9**

	3	**6**	**9**
Empirical formula	$C_{17}H_{32}Si_4$	$C_{20}H_{54}Si_8$	$C_{22}H_{28}Si_3$
M_w	348.79	519.35	376.71
Temperature [K]	293(2)	213(2)	150(2)
Size (mm)	0.44 × 0.30 × 0.28	0.66 × 0.49 × 0.10	0.72 × 0.55 × 0.10
Crystal system	monoclinic	triclinic	monoclinic
Space group	$P2_1/c$	$P\bar{1}$	$P2_1/n$
a (Å)	13.829(5)	9.4732(19)	15.949(3)
b (Å)	9.335(3)	9.7130(19)	9.1430(18)
c (Å)	18.912(7)	12.774(3)	17.020(3)
α (°)	90	109.41(3)	90
β (°)	95.550(7)	92.80(3)	103.72(3)
γ (°)	90	119.03(3)	90
V [Å ^{3}]	2430.0(15)	937.3(3)	2411.0(8)
Z	4	1	4
$\rho_{calcd.}$ [gcm^{-3}]	0.953	0.920	1.038
Absorption coefficient [mm^{-1}]	0.240	0.293	0.199
F(000)	760	286	808
θ range	1.48<θ<20.81	1.75<θ<23.26	2.00<θ<26.35
Reflections collected/unique	8327/2540	5750/2674	18232/4893
Completeness to θ [%]	99.7	99.2	99.5
Absorption correction	SADABS	SADABS	SADABS
Data/restraints/parameters	2540/0/199	2674/0/154	4893/0/232
Goodness of fit on F^2	0.980	1.044	1.080
Final R int [$I > 2\sigma(I)$]	$R1$ = 0.0554 $wR2$ = 0.1459	$R1$ = 0.0548 $wR2$ = 0.1594	$R1$ = 0.0845 $wR2$ = 0.2173
R int (all data)	$R1$ = 0.0783 $wR2$ = 0.1585	$R1$ = 0.0600 $wR2$ = 0.1646	$R1$ = 0.1071 $wR2$ = 0.2335
Largest diff. Peak/hole [e$^-$/ Å^3]	0.273/−0.205	0.482/−0.245	0.856/−0.606

[1] [1a] C. Marschner, *Eur. J. Inorg. Chem.* **1998**, 221−226. [1b] R. Fischer, D. Frank, W. Gaderbauer, C. Kayser, C. Mechtler, J. Baumgartner, C. Marschner, *Organometallics* **2003**, *22*, 3723−3731.

[2] E. Hengge, A. Baumegger, M. Eibl, E. Hohenester, C. Kratky, *Angew. Chem.* **1990**, *102*, 722−724; *Angew. Chem. Int. Ed. Engl.* **1990**, *29*, 641−643.

[3] E. Hengge, M. Eibl, F. Schrank, *Spectrochim. Acta Part A* **1991**, *47*, 721−725.

[4] W. Uhlig, C. Tretner, *J. Organomet. Chem.* **1992**, *436*, C1−C4.

[5] For some examples see: [5a] M. Ishikawa, H. Sugisawa, K. Yamamoto, M. Kumada, *J. Organomet. Chem.* **1979**, *179*, 377−390. [5b] M. Ishikawa, K.-I. Nakagawa, M. Kumada, *J. Organomet. Chem.* **1980**, *190*, 117−128. [5c] M. Ishikawa, Y. Nomura, E. Tozaki, A. Kunai, J. Ohshita, *J. Organomet. Chem.* **1990**, *399*, 205−213. [5d] M. Ishikawa, Y. Yuzuriha, T. Horio, A. Kunai, *J. Organomet. Chem.* **1991**, *402*, C20−C22. [5e] M. Ishikawa, J. Ohshita, Y. Ito, J. Iyoda, *J. Am. Chem. Soc.* **1986**, *108*, 7417−7419. [5f] A. Kunai, Y. Yuzuriha, A. Naka, M. Ishikawa, *J. Organomet. Chem.* **1993**, *455*, 77−81. [5g] H. Shizuka, K. Okazaki, H. Tanaka, M. Tanaka, M. Ishikawa, M. Sumitani, K. Yoshihara, *J. Phys. Chem.* **1987**, *91*, 2057−2062. [5h] Y. Apeloig, M. Karni, R. West, K. Welsh, *J. Am. Chem. Soc.* **1994**, *116*, 9719−9729. [5i] J. Ohshita, T. Yoshitomi, M. Ishikawa, *Organometallics* **1994**, *13*, 3227−3232. [5j] G. Hussmann, W. D. Wulff, T. J. Barton, *J. Am. Chem. Soc.* **1983**, *116*, 1263−1269. [5k] Y. Kabe, K. Ohkubo, H. Ishikawa, W. Ando, *J. Am. Chem. Soc.* **2000**, *122*, 3775−3776.

[6] [6a] E. R. H. Jones, L. Skatteböl, M. C. Whiting, *J. Chem. Soc.* **1956**, 4765−4768. [6b] E. A. V. Ebsworth, S. G. Frankiss, *J. Chem. Soc.* **1963**, 661−665.

[7] H. Bock, J. Meuret, H. Schödel, *Chem. Ber.* **1993**, *126*, 2227−2235.

[8] A. G. Brook, K. M. Tai, H. Gilman, *J. Am. Chem. Soc.* **1955**, *77*, 6219−6221.

[9] [9a] E. Pretsch, T. Clerc, J. Seibl, W. Simon, *Spectral Data for Structure Determination of Organic Compounds*, Springer-Verlag, Berlin, Heidelberg, New York, **1989**. [9b] W. Höbold, R. Radeglia, D. Klose, *J. Prakt. Chem.* **1976**, *318*, 519−522.

[10] E. Lukevics, O. Pudova, R. Sturkovich, A. Gaukhman, *J. Organomet. Chem.* **1988**, *346*, 297−304.

[11] P. B. Hitchcock, M. F. Lappert, M. Layh, *Angew. Chem.* **1999**, *111*, 562−565; *Angew. Chem. Int. Ed.* **1999**, *38*, 501−504.

[12] Ranges for the values of known crystal structures have been extracted from the Cambridge Crystallographic Data Base using the *Conquest V1.5* program.

[13] [13a] G. A. Morris, R. Freeman, *J. Am. Chem. Soc.* **1979**, *101*, 760−762. [13b] B. J. Helmer, R. West, *Organometallics* **1982**, *1*, 877−879.

[14] G. Becker, M. Gekeler, H.-M. Hartmann, O. Mund, M. Westerhausen, in *Synthetic Methods of Organometallic and Inorganic Chemistry* (Ed.: W. Herrmann), vol. 2 (chapter 3), Thieme Verlag, Stuttgart, **1996**, p. 187.

[15] H. Gilman, R. L. Harrell, *J. Organomet. Chem.* **1965**, *5*, 199−200.

[16] C. Kayser, R. Fischer, J. Baumgartner, C. Marschner, *Organometallics* **2002**, *21*, 1023−1030.

[17] Propargyltosylate was prepared according to the instructions for diethylene glycolditosylate: J. W. Cornforth, E. D. Morgan, K. T. Potts, R. J. W. Rees, *Tetrahedron* **1973**, *29*, 1659−1667.

[18] M. Ishikawa, S. Matsuzawa, T. Higuchi, S. Kamitori, K. Hirotsu, *Organometallics* **1985**, *4*, 2040−2046.

[19] For ^{1}H NMR and ^{13}C NMR of **5** see ref.[5i]

[20] R. A. Jackson, C. J. Rhodes, *J. Organomet. Chem.* **1987**, *336*, 45−48.

[21] T. Kusukawa, W. Ando, *J. Organomet. Chem.* **1998**, *559*, 11−22.

[22] *SAINTPLUS: Software Reference Manual*, Version 5.054, Bruker-AXS, Madison, WI, **1997−1998**.

[23] R. H. Blessing, *Acta Crystallogr., Sect. A* **1995**, *51*, 33−38; *SADABS*: Bruker AXS **1998**.

[24] G. M. Sheldrick, *SHELX97 Programs for Crystal Structure Analysis (Release 97−2)*, University of Göttingen, Göttingen

 © 2004 Wiley-VCH Verlag GmbH & Co. KGaA, Weinheim

(Germany), **1998**. CCDC-226889 (for **3**), -226890 (for **6**) and -226891 (for **9**) contain the supplementary crystallographic data for this paper. These data can be obtained free of charge at www.ccdc.cam.ac.uk/conts/retrieving.html [or from the Cambridge Crystallographic Data Centre, 12 Union Road, Cambridge CB2 1EZ, UK; Fax: (internat.) +44-1223-336-033; E-mail: deposit@ccdc.cam.ac.uk].

Received February 10, 2004
Early View Article
Published Online June 7, 2004

 © 2004 Wiley-VCH Verlag GmbH & Co. KGaA, Weinheim

New Porous Lanthanide-Organic Frameworks: Synthesis, Characterization, and Properties of Lanthanide 2,6-Naphthalenedicarboxylates

Xiangjun Zheng,[a] Changyan Sun,[a] Shaozhe Lu,[b] Fuhui Liao,[c] Song Gao,[c] and Linpei Jin*[a]

Keywords: Carboxylate ligands / Coordination polymers / Hydrothermal synthesis / Lanthanides / X-ray diffraction

Three porous, 3-D coordination polymers $[Pr_4(NDC)_6(H_2O)_6]\cdot 2H_2O$ (**1**), $[Eu_4(NDC)_6(H_2O)_5]\cdot 3H_2O$ (**2**) and $[Yb_2(NDC)_3(H_2O)]\cdot H_2O$ (**3**) based on lanthanide 2,6-naphthalenedicarboxylates (NDC) were synthesized by hydrothermal reactions of lanthanide chlorides with NDC and their properties were investigated. Polymers **1**, **2** and **3** differ in the coordination environment of the Ln^{III} ions. Their 3-D networks are reminiscent of the shape of a compressed honeycomb, showing 1-D open channels. The guest water molecules and coordinating water molecules are enclathrated in the channels. The photophysical properties of the Eu^{3+} complex were investigated by high-resolution luminescence spectroscopy. The results indicate that there are four Eu^{III} ion sites in complex **2**, which is in accordance with the results of the single-crystal X-ray diffraction studies. Thermogravimetric and variable-temperature powder X-ray diffraction analyses show that the porous frameworks of this series of complexes are relatively stable. The framework remained even when the guest molecules were lost and did not collapse until the temperature reached 430 °C. The magnetic properties of **2** were also investigated.

(© Wiley-VCH Verlag GmbH & Co. KGaA, 69451 Weinheim, Germany, 2004)

Introduction

The assembly of porous networks has been an intriguing field for their potential applications in catalysis,[1,2] adsorption and separation processes,[3−9] ion exchange,[10,11] and sensor technology.[12,13] Many molecular-based porous materials constructed by coordination polymers have been reported.[6−9,14−17] These open-framework coordination polymers possess unprecedented pore size, shape and function. However, the main problem encountered in designing such coordination polymers is the interpenetration of networks or collapse of the framework upon removal of the guest molecules enclathrated in the cavities.[9] The modification of the ligand and the selection of the metal ions are the key points to avoid the interpenetration of networks. Thus far, porous coordination polymers have centered on the assembly of carboxylates and d-block metal ions such as Zn^{II},[9] Cu^{II},[14] and Co^{II} [17,18] as d-block metal ions have low coordination numbers and the coordination sites of d-block metal ions are easily occupied by the carboxylates, therefore interpenetration of the framework is less likely to occur. Lanthanide ions have higher coordination numbers, and it is more difficult to predict or control the coordination frameworks of lanthanide ions than their d-block analogues. The interpenetration of frameworks can frequently be seen in lanthanide coordination polymers because many coordination sites are accessible for the bridging ligand. However, incorporation of ancillary ligands (such as water molecules) into lanthanide coordination networks is also more feasible, and these ancillary ligands can occupy some coordination sites and prevent the frameworks from interpenetrating. At the same time, they may be removed without collapse of the lanthanide-organic framework, thereby generating porous solids with coordinatively unsaturated and Lewis-acidic lanthanide ions that have potential catalytic activity.[19,20] Additionally, the inherent flexibility of their coordination geometry is particularly attractive for the preparation of new network types as this greater structural ambivalence will lead to the synthesis of unprecedented structures. Based on the fact that lanthanide ions have a high affinity for oxygen-containing ligands, we selected a rigid linear ligand, 2,6-naphthalenedicarboxylate, to construct lanthanide coordination polymers. In the present case, we report the synthesis and structure of lanthanide naphthalenedicarboxylates; their properties were inves-

[a] Department of Chemistry, Beijing Normal University, Beijing 100875, People's Republic of China
Fax: +86-10-6220-2075
E-mail: lpjin@bnu.edu.cn
[b] Laboratory of Excited States Processes, Chinese Academy of Sciences; Changchun Institute of Optics, Fine Mechanics and Physics, Chinese Academy of Sciences, Changchun 130021, People's Republic of China
[c] State Key Laboratory of Rare Earth Materials Chemistry and Applications, PKU-HKU Joint Laboratory on Rare Earth Materials and Bioinorganic Chemistry, College of Chemistry, Peking University, Beijing 100871, People's Republic of China

 © 2004 Wiley-VCH Verlag GmbH & Co. KGaA, Weinheim DOI: 10.1002/ejic.200400176

tigated systematically. They are porous and quite thermally stable because they have channels with incorporated solvents, which may be removed without the collapse of the framework.

Results and Discussion

Syntheses and Structures

Dipotassium 2,6-naphthalenedicarboxylate easily forms a precipitate upon the addition of lanthanide chloride, therefore in the preparation of the coordination polymers, the 2,6-naphthalenedicarboxylate was acidified first to facilitate the growth of crystals. 1,10-Phenanthroline (phen), which is a mild organic base, was also added to promote the hydrothermal reaction. Klinowski et al. have reported the crystal structure of $[Yb_2(NDC)_3(H_2O)]\cdot 2H_2O$ from the reaction of $YbCl_3\cdot 6H_2O$, 2,6-naphthalenedicarboxylic acid and triethylamine.[21] The difference between $[Yb_2(NDC)_3(H_2O)]\cdot 2H_2O$ and complex **3** is a lattice water molecule, which cannot have a significant effect on the crystal structure. Therefore, only the structures of complexes **1** and **2** will be discussed here.

There are four crystallographically independent Ln^{III} cations and six NDC anions in the unit cells of **1** and **2**, while for **3** there are only two Yb^{III} ions and three NDC anions in the asymmetric unit. In **1**, **2** and **3**, the Ln^{III} ions are all coordinated to oxygen atoms, with Ln−O distances in the range 2.357(9)−2.745(12) Å for **1**, 2.302(16)−2.625(15) Å for **2** and 2.169(9)−2.323(19) Å for **3**, characteristic of the lanthanide contraction. The NDC ligand adopts a bis(bidentate bridging) coordination mode where every NDC ligand bridges four Ln^{III} cations.

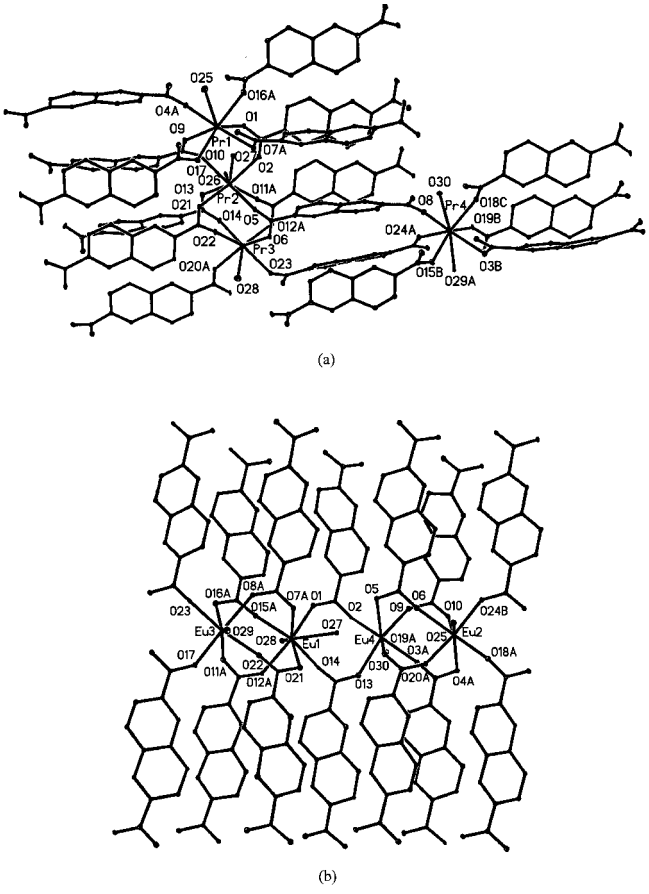

Figure 1. Coordination environment of **1** (a) and **2** (b); lattice water molecules and all hydrogen atoms have been omitted for clarity; thermal ellipsoids are shown at 10% probability

There are four Pr^{III} ions, six NDC anions, six coordinated water molecules and two lattice water molecules in the asymmetric unit of **1**. Pr1 and Pr3 are both sevenfold coordinated, with six oxygen atoms from six NDC ligands and one oxygen atom from a water molecule, while Pr2 and Pr4 are both eightfold coordinated, with six oxygen atoms from six NDC ligands and two oxygen atoms from two water molecules [see (a) in Figure 1]. Pr1 and Pr2 are connected by two μ_2-carboxylates from two NDC ligands. Pr2 and Pr3 are connected by four μ_2-carboxylates from four NDC ligands; Pr4 is connected to Pr2 and Pr3 through the bridging of two NDC ligands. The Pr^{3+} ions along the *a*-axis are bridged together, resulting in an infinite zigzag chain with the order Pr3···Pr2···Pr1···Pr4A···Pr3A···, with Pr···Pr distances of 4.133(2), 4.196(2), 4.131(2) and 5.001(2) Å, respectively. The chains may be viewed as secondary building blocks that are further cross-linked by the $C_{10}H_4$ spacers of the NDC anions. when viewed along the *a*-axis, the resulting 3-D network of **1** is reminiscent of the shape of a compressed honeycomb, showing 1-D open channels (Figure 2). The guest water molecules and coordinated water molecules are enclathrated in the channels.

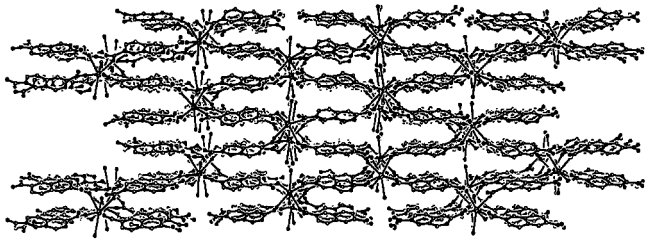

Figure 2. 3-D open-framework of **1** containing 1-D channels viewed along the *a*-axis; all hydrogen atoms and lattice water molecules have been omitted for clarity

There are four Eu^{III} ions, six NDC anions, five coordinated water molecules and three lattice water molecules in the asymmetric unit of **2**. Eu2, Eu3 and Eu4 have a sevencoordinate environment [see (b) in Figure 1] like Pr1 and Pr3 in **1**, while Eu1 is located in an eight-coordinate environment like Pr2 and Pr4 in **1**. Eu1 and Eu3 are connected by four μ_2-carboxylates from four NDC ligands. This is also the case for Eu2 and Eu4; Eu1 and Eu4 are linked by two μ_2-carboxylates from two NDC ligands. The Eu^{3+} ions along the *a*-axis are arranged in the order Eu3···Eu1···Eu4···Eu2···Eu3A···, with Eu···Eu distances of 4.997(2), 4.073(2), 4.805(2) and 4.064(2) Å, respectively. When viewed along the *a*-axis, this complex exhibits the same porous honeycomb-like architecture as **1**. Removing all hydrogen atoms, the coordinated and guest water mol-

 © 2004 Wiley-VCH Verlag GmbH & Co. KGaA, Weinheim

ecules from the crystal structure of **2** gives the ball-and-stick model and the space-filling model shown in Figure 3. The ball-and-stick model shows a quite large opening in the cross section of the open channel, but the space-filling model shows that only the middle part of this is an effective cavity, with dimensions of about 5.0 × 2.1 Å^2.

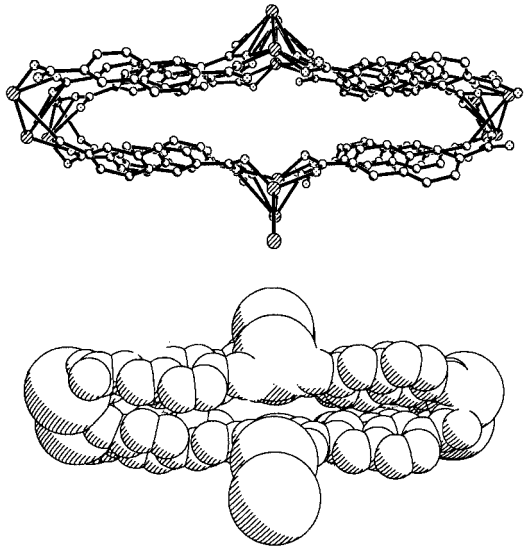

Figure 3. Cross-section of the open channel in **2** (all hydrogen atoms and water molecules have been omitted): ball-and-stick model (top), space-filling model (bottom)

These results show that **1**, **2** and **3** are different in the coordination environment of Ln^{III} ions, but they nevertheless form similar 3-D porous coordination polymers with the same topology. The sizes of the pores are also similar. When viewed along the *b*-axis, the coordination polymers of **1**, **2** and **3** can exhibit 3-D inorganic-organic hybrid architectures (Figure 4). The inorganic sheets are composed of Ln^{3+} ions, and the organic sheets are composed of NDC ligands; the two sheets alternate. The adjacent sheets are linked together through $Ln-O_{COO^-}$ coordination bonds.

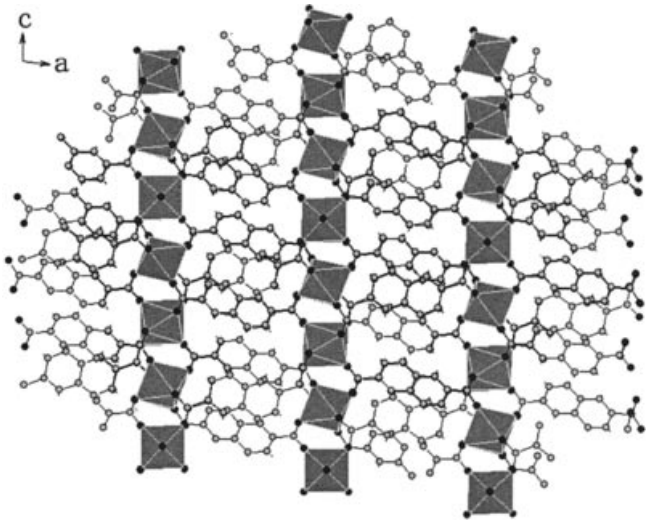

Figure 4. The inorganic-organic hybrid structure of **2**

Photophysical Properties of 2

The Eu^{III} ion is frequently used as a structural probe to investigate local symmetry.[22] The lowest emission level, $^5D_0$, and the ground state, $^7F_0$, are both nondegenerate, therefore the number of excitation peaks corresponding to the $^7F_0 \rightarrow {}^5D_0$ transition will reveal the number of Eu^{3+} ions with different coordination environments in the compound. The high-resolution emission spectrum of **2** corresponding to $^5D_0 \rightarrow {}^7F_J$ (J = 0−4) transitions excited at a wavelength of 355 nm at 77 K is shown in Figure 5. The most intense transition is $^5D_0 \rightarrow {}^7F_2$, which implies red emission light of **2**. No obvious and direct information about the Eu^{3+} ion sites can be obtained from Figure 5, but from the time-resolved spectra (Figure 6) corresponding to $^5D_0 \rightarrow {}^7F_J$ (J = 1, 2) transitions, it can be seen that both the shape and number of the emission peaks change. It can be concluded that there is more than one Eu^{3+} ion site in **2**. Selective excitation techniques were applied to further probe the number of Eu^{3+} ion sites in **2**. With 16107 and 16232 cm^{-1} as the monitoring wavenumbers, and scanning in the range 17280−17229.5 cm^{-1} ($^7F_0 \rightarrow {}^5D_0$), the excitation spectra shown in Figure 7 (a and b) were obtained. There are obviously three groups of peaks located at 17260.7, 17255.4 and 17249.1 cm^{-1}, respectively. Although a broadened $^7F_0 \rightarrow {}^5D_0$ excitation band is often seen in europium coordination polymers, it is worthy of note that there is a shoulder at the peak located at 17253.3 cm^{-1}. The average Eu−O bond lengths for Eu1, Eu2, Eu3 and Eu4 are 2.412, 2.372, 2.372 and 2.391 Å, respectively. However, around Eu2 there is a lattice water molecule, O26, and the distance between Eu2 and O26 [2.80(2) Å] suggests a weak coordination interaction, making the coordination bonds around Eu2 more ionic than those around Eu3. The longer a bond is, the more ionic character the bond possesses and the higher the energy needed to excite the europium ion. Therefore the four peaks at 17260.7, 17255.4, 17253.3 and 17249.1 cm^{-1} in Figure 7a can be ascribed to the $^5D_0$ levels of Eu1, Eu4, Eu2 and Eu3, respectively, confirming that

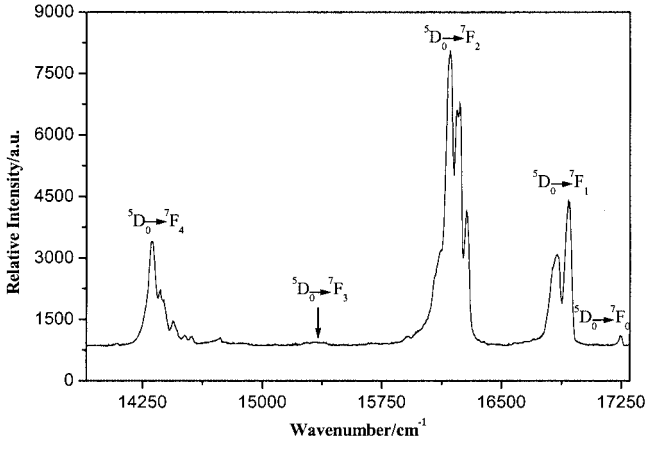

Figure 5. Emission spectrum of **2** corresponding to $^5D_0 \rightarrow {}^7F_J$ (J = 0 ~ 4) transitions at 77 K (λ_{exc} = 355 nm)

 © 2004 Wiley-VCH Verlag GmbH & Co. KGaA, Weinheim

four Eu^{3+} ion sites exist in **2**, which is in agreement with the X-ray diffraction results.

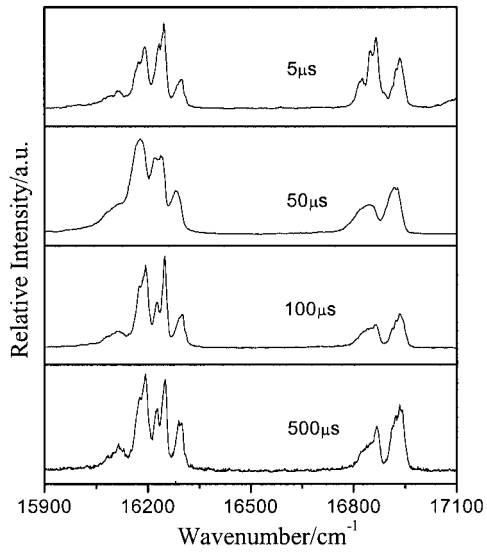

Figure 6. Time-resolved spectra of **2** at 77 K in the range 17100−15900 cm^{-1}; delay time: 5 μs, 50 μs, 100 μs and 500 μs; λ_{exc} = 355 nm

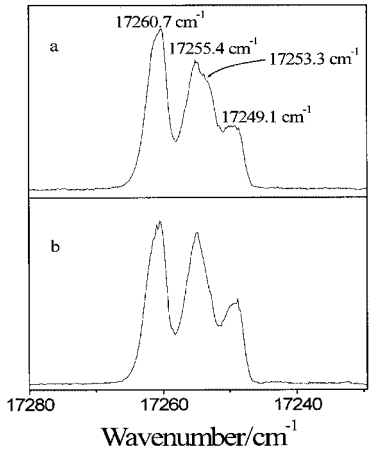

Figure 7. Excitation spectra of **2**; analyzing wavenumbers: a 16107 cm^{-1}; b 16232 cm^{-1}

Thermal Stability Analysis of 2

TG analysis of **2** is consistent with the crystallographic observations. The first weight loss of 5.06% from 103 °C to 186 °C (Figure 8) corresponds to the loss of three lattice water molecules and three coordinated water molecules (calculated: 5.31%), leaving a framework of $[Eu_4(NDC)_6 \cdot 2H_2O]$. Between 271 °C and 308 °C, the sample undergoes a second weight loss of 1.31%. During this process the two coordinated water molecules that have a stronger interaction with the Eu^{3+} ions [Eu1−O28: 2.474(15) Å; Eu2−O25: 2.451(15) Å] and are also involved in hydrogen bonding with carboxylate oxygen atoms [O25···O14 ($-x + 1/2$, $y + 1/2$, $-z + 1/2$) 2.758 Å; O28···O18 ($-x + 3/2$, $y - 1/2$, $-z + 1/2$) 2.844 Å] are removed (calculated: 1.77%), leaving a framework of $[Eu_4(NDC)_6]$. $[Eu_4(NDC)_6]$ remains stable up to 430 °C at which temperature it begins to decompose.

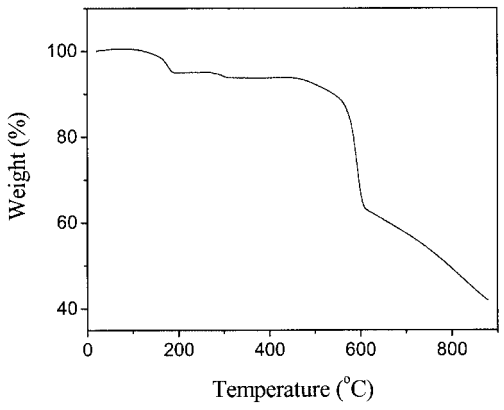

Figure 8. TG curve of **2**

To further test the thermal stability of **2**, powder samples were examined by powder X-ray diffraction analysis. Corresponding to the TG analysis, powder XRD patterns (Figure 9) were recorded at 27, 200, 250, 300, 350, 400, 450, 500 and 700 °C. It can be seen from Figure 9 that the XRD pattern at 200 °C is different from that at room temperature. The major peaks shift a little to higher 2θ value, indicating that a distortion of the structure has occurred, although this does not affect the existence of the framework. From 200 °C to 400 °C the major peaks in the XRD patterns at five different temperatures show no change in their position, indicating that the framework is able to survive the heat treatment and is thermally stable despite the removal of the water molecules. Above 450 °C the XRD pattern changes significantly, revealing the collapse of the framework, which is in accordance with the result of thermogravimetric analysis.

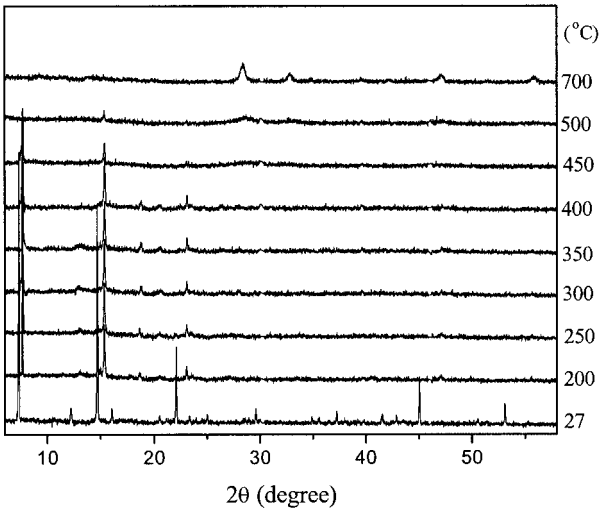

Figure 9. Powder X-ray diffraction patterns of **2** at different temperatures

 © 2004 Wiley-VCH Verlag GmbH & Co. KGaA, Weinheim

The results of thermogravimetric analyses for **1** and **3** show a similar stability to **2**.

Magnetic Properties of 2

The variable temperature magnetic susceptibility of **2** was measured in the range 2−304 K. The plot of $\chi_M T$ vs. T is shown in Figure 10, where χ_M is the corrected molar magnetic susceptibility per $[Eu]_4$ unit. The observed $\chi_M T$ at room temperature is 5.0 $cm^3 \cdot mol^{-1} \cdot K$, less than the value 6.0 for four Eu^{III} ions calculated from the van Vleck equation allowing for population of the lower excited state of ^7F_J (Eu^{3+}) in **2** at 293 K. As the temperature is lowered, $\chi_M T$ decreases continuously due to the depopulation of the Stark levels for a single Eu^{III} ion. At the lowest temperature, $\chi_M T$ is close to zero, indicating a $J = 0$ ground state of the Eu^{III} ion ($^7F_0$). The magnetic susceptibility above 150 K follows the Curie−Weiss law due to the presence of thermally populated excited states.

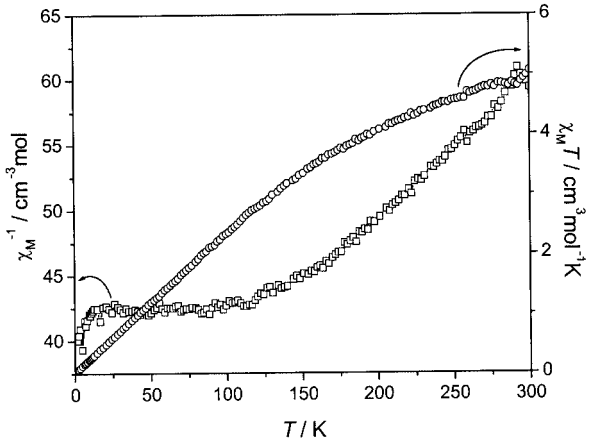

Figure 10. Plot of the temperature dependence of $\chi_M T$ (O) and χ_M^{-1} (□) for the title complex (per $[Eu]_4$unit)

Experimental Section

General: $PrCl_3 \cdot 6H_2O$, $EuCl_3 \cdot 6H_2O$ and $YbCl_3 \cdot 6H_2O$ were prepared by dissolving their oxides in concentrated hydrochloric acid and then evaporating the solvents dryness. All the other reagents are commercially available and were used without further purification. Elemental analyses were obtained on an Elementar Vario EL analyzer. The IR spectra were recorded with a Nicolet Avatar 360 FT-IR spectrometer using the KBr pellet technique. Thermogravimetric analyses were performed with a TGA: 951 Thermogravimetric Analyzer. The magnetic susceptibilities were obtained on a crystalline sample using an Oxford MagLab System 2000 magnetometer. The experimental susceptibilities were corrected for the sample holder and the diamagnetism contributions estimated from Pascal's constants. The powder X-ray diffraction patterns were recorded on a Bruker AXS D8 ADVANCE diffractometer.

$[Pr_4(NDC)_6(H_2O)_6] \cdot 2H_2O$ (1): Two drops of hydrochloric acid (1.65 $mol \cdot L^{-1}$) were added to a mixture of dipotassium 2,6-naphthalenedicarboxylate (0.044 g, 0.15 mmol) and H_2O (3 mL) and the mixture was stirred. $PrCl_3 \cdot 6H_2O$ (0.036 g, 0.1 mmol) and phen·H_2O (0.02 g, 0.1 mmol) were then added. The mixture was sealed in a 25 mL stainless steel reactor with Teflon liner and heated at 200 °C for 72 h. Green crystals of **1** were obtained in 76.3% yield (0.038 g). $C_{72}H_{52}O_{32}Pr_4$ (1992.8): calcd. C 43.40, H 2.63; found C 43.86, H 2.61. IR data (KBr pellet): $\tilde{\nu}$ = 3446 s, 2970 m, 1602 m, 1542 s, 1408 s, 1352 s, 1196 m, 924 m, 797 m, 560 m, 493 m cm^{-1}.

$[Eu_4(NDC)_6(H_2O)_5] \cdot 3H_2O$ (2): Two drops of hydrochloric acid (1.65 $mol \cdot L^{-1}$) were added to a mixture of dipotassium 2,6-naphthalenedicarboxylate (0.044 g, 0.15 mmol) and H_2O (3 mL) and the mixture was stirred. $EuCl_3 \cdot 6H_2O$ (0.037 g, 0.1 mmol) and phen·H_2O (0.04 g, 0.2 mmol) were then added. The mixture was sealed in a 25 mL stainless steel reactor with Teflon liner and heated at 200 °C for 72 h. Light-yellow crystals of **2** were obtained in 78.4% yield (0.04 g). $C_{72}H_{52}Eu_4O_{32}$ (2037.0): calcd. C 42.45, H 2.57; found C 42.99, H 2.24. IR data (KBr pellet): $\tilde{\nu}$ = 3508 m, 1602 m, 1547 s, 1491 s, 1412 s, 1353 s, 1199 m, 927 m, 795 s, 564 m, 492 m cm^{-1}.

$[Yb_2(NDC)_3(H_2O)] \cdot H_2O$ (3): Two drops of hydrochloric acid (1.65 $mol \cdot L^{-1}$) were added to a mixture of dipotassium 2,6-naphthalene-

Table 1. Crystal data for complexes **1**, **2** and **3**

Compound	**1**	**2**	**3**
Empirical formula	$C_{72}H_{52}O_{32}Pr_4$	$C_{72}H_{52}Eu_4O_{32}$	$C_{36}H_{22}O_{14}Yb_2$
Molecular mass	1992.78	2036.98	1024.62
Temperature (K)	293(2)	293(2)	293(2)
Wavelength (Å)	0.71073	0.71073	0.71073
Crystal system	monoclinic	monoclinic	monoclinic
Space group	$P2_1/c$	$P2_1/n$	$C2/c$
a (Å)	17.295(7)	17.006(6)	23.183(9)
b (Å)	15.194(7)	15.130(5)	8.344(4)
c (Å)	26.334(9)	24.973(8)	17.558(8)
α (°)	90	90	90
β (°)	112.35(2)	106.361(6)	98.568(9)
γ (°)	90	90	90
V (Å^3)	6400(4)	6165(3)	3359(3)
Z	4	4	4
D_c [g·cm^{-3}]	2.068	2.194	2.026
μ (mm^{-1})	3.094	4.120	5.607
Reflections collected, unique, R_{int}	26941, 11624, 0.1245	20778, 8866, 0.1549	7617, 2958, 0.0877
R_{int} [$I > 2\sigma(I)$]	R_1 = 0.0493, wR_2 = 0.0588	R_1 = 0.0607, wR_2 = 0.1056	R_1 = 0.0527, wR_2 = 0.1001

 © 2004 Wiley-VCH Verlag GmbH & Co. KGaA, Weinheim

Table 2. Selected bond lengths (Å) and bond angles (°) for complexes **1**, **2** and **3**[a]

1		**2**		**3**	
Pr(1)−O(1)	2.414(7)	Eu(1)−O(14)	2.309(15)	Yb(1)−O(1)	2.169(9)
Pr(1)−O(4)$^{\#1}$	2.419(7)	Eu(1)−O(15)$^{\#10}$	2.313(15)	Yb(1)−O(1)$^{\#16}$	2.169(9)
Pr(1)−O(17)	2.443(8)	Eu(1)−O(7)$^{\#11}$	2.369(16)	Yb(1)−O(3)$^{\#17}$	2.247(11)
Pr(1)−O(7)$^{\#2}$	2.445(8)	Eu(1)−O(1)	2.371(17)	Yb(1)−O(3)$^{\#18}$	2.247(11)
Pr(1)−O(9)	2.452(9)	Eu(1)−O(21)	2.374(17)	Yb(1)−O(5)	2.316(10)
Pr(1)−O(16)$^{\#3}$	2.528(10)	Eu(1)−O(12)$^{\#12}$	2.462(14)	Yb(1)−O(5)$^{\#16}$	2.316(10)
Pr(1)−O(25)	2.636(11)	Eu(1)−O(28)	2.474(15)	Yb(1)−O(7)	2.323(19)
Pr(2)−O(10)	2.400(8)	Eu(1)−O(27)	2.625(15)	Yb(2)−O(6)$^{\#19}$	2.187(10)
Pr(2)−O(11)$^{\#4}$	2.433(7)	Eu(2)−O(24)$^{\#13}$	2.302(16)	Yb(2)−O(6)	2.187(10)
Pr(2)−O(2)	2.435(9)	Eu(2)−O(18)$^{\#13}$	2.335(16)	Yb(2)−O(4)$^{\#20}$	2.206(10)
Pr(2)−O(21)	2.452(8)	Eu(2)−O(4)$^{\#14}$	2.347(15)	Yb(2)−O(4)$^{\#18}$	2.206(10)
Pr(2)−O(5)	2.467(9)	Eu(2)−O(10)	2.383(15)	Yb(2)−O(2)	2.229(10)
Pr(2)−O(13)	2.540(8)	Eu(2)−O(6)	2.388(16)	Yb(2)−O(2)$^{\#19}$	2.229(10)
Pr(2)−O(27)	2.545(8)	Eu(2)−O(20)$^{\#15}$	2.400(14)		
Pr(2)−O(26)	2.714(8)	Eu(2)−O(25)	2.451(14)		
Pr(3)−O(23)	2.403(7)	Eu(3)−O(22)	2.307(16)		
Pr(3)−O(20)$^{\#5}$	2.410(10)	Eu(3)−O(23)	2.328(15)		
Pr(3)−O(22)	2.416(7)	Eu(3)−O(16)$^{\#10}$	2.337(17)		
Pr(3)−O(14)	2.452(8)	Eu(3)−O(17)	2.339(16)		
Pr(3)−O(12)$^{\#4}$	2.460(8)	Eu(3)−O(11)$^{\#12}$	2.345(17)		
Pr(3)−O(6)	2.517(9)	Eu(3)−O(8)$^{\#11}$	2.439(16)		
Pr(3)−O(28)	2.604(11)	Eu(3)−O(29)	2.51(2)		
Pr(4)−O(24)$^{\#6}$	2.357(9)	Eu(4)−O(3)$^{\#14}$	2.317(15)		
Pr(4)−O(15)$^{\#7}$	2.431(9)	Eu(4)−O(2)	2.323(15)		
Pr(4)−O(3)$^{\#8}$	2.432(8)	Eu(4)−O(19)$^{\#15}$	2.365(16)		
Pr(4)−O(19)$^{\#9}$	2.441(8)	Eu(4)−O(13)	2.373(18)		
Pr(4)−O(8)	2.481(7)	Eu(4)−O(5)	2.383(15)		
Pr(4)−O(18)$^{\#2}$	2.483(8)	Eu(4)−O(9)	2.439(16)		
Pr(4)−O(30)	2.513(8)	Eu(4)−O(30)	2.537(19)		
Pr(4)−O(29)$^{\#6}$	2.745(12)				

[a] Symmetry operations: $^{\#1}$ $x, -y + 3/2, z + 1/2$; $^{\#2}$ $-x + 1, -y + 2, -z + 1$; $^{\#3}$ $x - 1, -y + 3/2, z - 1/2$; $^{\#4}$ $x, -y + 3/2, z - 1/2$; $^{\#5}$ $-x + 2, -y + 2, -z + 2$; $^{\#6}$ $-x + 2, -y + 2, -z + 1$; $^{\#7}$ $-x + 2, y + 1/2, -z + 3/2$; $^{\#8}$ $-x + 1, y + 1/2, -z + 1/2$; $^{\#9}$ $x, y, z - 1$; $^{\#10}$ $x + 1/2, -y + 1/2, z + 1/2$; $^{\#11}$ $-x + 1, -y + 1, -z + 1$; $^{\#12}$ $x + 1/2, -y + 1/2, z - 1/2$; $^{\#13}$ $x - 1, y, z$; $^{\#14}$ $x - 1/2, -y + 1/2, z - 1/2$; $^{\#15}$ $-x + 1, -y + 1, -z$; $^{\#16}$ $-x + 1, y, -z + 1/2$; $^{\#17}$ $-x + 3/2, y + 1/2, -z + 1/2$; $^{\#18}$ $x - 1/2, y + 1/2, z$; $^{\#19}$ $-x + 1, -y + 1, -z$; $^{\#20}$ $-x + 3/2, -y + 1/2, -z$.

dicarboxylate (0.044 g, 0.15 mmol) and H_2O (15 mL) and the mixture was stirred. $YbCl_3 \cdot 6H_2O$ (0.039 g, 0.1 mmol) was then added. The mixture was sealed in a 50 mL stainless steel reactor with Teflon liner and heated at 180 °C for 72 h. Light-yellow crystals of **3** were obtained in 29.3% yield (0.015 g). $C_{36}H_{22}O_{14}Yb_2$ (1024.6): calcd. C 42.20, H 2.16; found C 42.08, H 2.31. IR data (KBr pellet): $\tilde{\nu}$ = 3447 m, 2977 m, 1693 s, 1602 s, 1574 s, 1423 s, 1293 s, 1193 m, 775 m, 452 m cm^{-1}.

Measurement of the High-Resolution Luminescence Spectra: The excitation light source was a YAG:Nd laser which emits at 1.064 μm, and the excitation wavelength was 355 nm. The sample was placed in a dewar and cooled with liquid nitrogen. The fluorescence data were collected at right angles through a Spex 1403 monochromator with a photomultiplier tube, then averaged with a Boxcar integrator and finally transferred to a computer.

X-ray Crystallographic Study: The X-ray single-crystal data collection for complexes **1**, **2** and **3** was performed on a Bruker Smart 1000 CCD diffractometer, using graphite-monochromated Mo-K_α radiation (λ = 0.71073Å). Semiempirical absorption corrections were applied using the SADABS program. The structures were solved by direct methods and refined by full-matrix least-squares on F^2 using the SHELXTL-97 program.[23] All non-hydrogen atoms were refined with anisotropic displacement parameters. The hydrogen atoms were generated geometrically and treated by a mixture of independent and constrained refinement. Experimental details for X-ray data collection of **1**, **2** and **3** are presented in Table 1, while selected bond lengths for **1**, **2** and **3** are listed in Table 2.

CCDC-228787−228789 (for **1**−**3**) contains the supplementary crystallographic data for this paper. These data can be obtained free of charge at www.ccdc.cam.ac.uk/conts/retrieving.html [or from the Cambridge Crystallographic Data Centre, 12 Union Road, Cambridge CB2 1EZ, UK; Fax: +44-1223-336033; E-mail: deposit@ccdc.cam.ac.uk].

Acknowledgments

This work is supported by National Natural Science Foundation of China (20331010) and State Key Project of Fundamental Research (G1998061308).

[1] J. S. Seo, D.-M. Whang, H.-Y. Lee, S. I. Jun, J.-H. Oh, Y.-J. Jeon, K.-M. Kim, *Nature* **2000**, *404*, 982.
[2] T. Sawaki, Y. Aoyama, *J. Am. Chem. Soc.* **1999**, *121*, 4793.
[3] H. Li, M. Eddaoudi, M. O'keeffe, O. M. Yaghi, *Nature* **1999**, *402*, 276.
[4] S.-I. Noro, S. Kitagawa, M. Kondo, K. Seki, *Angew. Chem. Int. Ed.* **2000**, *39*, 2082.

 © 2004 Wiley-VCH Verlag GmbH & Co. KGaA, Weinheim

[5] H. J. Choi, T. S. Lee, M. P. Suh, *Angew. Chem. Int. Ed.* **1999**, *38*, 1405.
[6] M. P. Suh, J. W. Ko, H. J. Choi, *J. Am. Chem. Soc.* **2002**, *124*, 10976.
[7] A. Dimos, D. Tsaousis, A. Michaelides, S. Skoulika, S. Golhen, L. Ouahab, C. Didierjean, A. Aubry, *Chem. Mater.* **2002**, *14*, 2616.
[8] E. J. Cussen, J. B. Claridge, M. J. Rosseinsky, C. J. Kepert, *J. Am. Chem. Soc.* **2002**, *124*, 9574.
[9] M. Eddaoudi, J. Kim, N. Rosi, D. Vodak, J. Wachter, M. O'keeffe, O. M. Yaghi, *Science* **2002**, *295*, 469.
[10] K. S. Min, M. P. Suh, *J. Am. Chem. Soc.* **2000**, *122*, 6834.
[11] O. M. Yaghi, H. Li, *J. Am. Chem. Soc.* **1996**, *118*, 295.
[12] M. Albrecht, M. Lutz, A. L. Spek, G. van Koten, *Nature* **2000**, *406*, 970.
[13] J. A. Real, E. Andrés, M. C. Muñoz, M. Julve, T. Granier, A. Bousseksou, F. Varret, *Science* **1995**, *268*, 265.
[14] J. W. Ko, K. S. Min, M. P. Suh, *Inorg. Chem.* **2002**, *41*, 2151.
[15] L. Pan, K. M. Adams, H. E. Hernandez, X. T. Wang, C. Zheng, Y. Hattori, K. Kaneko, *J. Am. Chem. Soc.* **2003**, *125*, 3062.
[16] Y.-H. Liu, Y.-L. Lu, H.-C. Wu, J.-C. Wang, K.-L. Lu, *Inorg. Chem.* **2002**, *41*, 2592.
[17] P. Ayyappan, O. R. Evans, W. B. Lin, *Inorg. Chem.* **2001**, *40*, 4627.
[18] J. Tao, M.-L. Tong, X.-M. Chen, *J. Chem. Soc., Dalton Trans.* **2000**, 3669.
[19] M. Shibasaki, K.-I. Yamada, N. Yoshikawa, *Lanthanide Lewis Acids Catalysis*, in *Lewis Acids in Organic Synthesis* (Ed.: H. Yamamoto), Wiley-VCH: New York, **1999**; vol. 2.
[20] T. Imamoto, *Lanthanides in Organic Synthesis*; Academic: New York, **1994**.
[21] F. A. A. Paz, J. Klinowski, *Chem. Commun.* **2003**, 1484.
[22] G. R. Choppin, D. R. Peterman, *Coord. Chem. Rev.* **1998**, *174*, 283−299.
[23] G. M. Sheldrick, SHELXTL-97, *Program for the refinement of Crystal Structures*, University of Göttingen, Germany, **1997**.

Received March 3, 2004
Early View Article
Published Online June 11, 2004

 © 2004 Wiley-VCH Verlag GmbH & Co. KGaA, Weinheim

Ru^{II} Complexes of Bis(1,10-phenanthrolin-2-yl)diazines

Darren Brown,[a] Ruifa Zong,[a] and Randolph P. Thummel*[a]

Keywords: Bridging ligands / Ruthenium / Phenanthrolines / Diazines

A series of three bis-tridentate bridging ligands has been prepared in which two 1,10-phenanthroline units have been symmetrically appended to a central pyridazine, pyrimidine, or pyrazine ring. These ligands have been treated with [Ru(tpy-d_{11})Cl_3] to afford both mono- and dinuclear complexes whose photo- and electrochemical properties have been evaluated (tpy = 2,2′:6′,2′′-terpyridine). A structural comparison is made between [(tpy)Ru(**3**)Ru(tpy)]$(PF_6)_4$ and a previously reported complex involving 2,2′-bipyridines in place of phenanthrolines on the bridging ligand and surprisingly little difference is found.

(© Wiley-VCH Verlag GmbH & Co. KGaA, 69451 Weinheim, Germany, 2004)

Lehn and co-workers have constructed an elegant series of bis-terdentate ligands (**1**) based on a central pyrimidine ring with the intent of using these systems as bridging ligands for the formation of rack-type polynuclear complexes.[1] An important aspect of constructing such rack systems is the ability to arrange the bridging units in a parallel array to preserve a rectangular rack.[2] They found that the spatial relationship between two bound Ru(tpy) units was governed by the nature of the central substituent R, which was varied between hydrogen, methyl, phenyl, and 9-anthracenyl. When R = H, the planes of the two Ru-bound terpyridines defined a convergence angle of 36.3°, where a parallel arrangement (angle = 0°) was desired for optimum rack formation. This deformation results from a pinching of the ligand which causes the two outer pyridine groups to move closer to one another. We reasoned that further constraining the ligating portion of the system by substituting 1,10-phenanthroline (phen) for the 2,2′-bipyridine (bpy) subunits might offset this pinching effect and result in a more parallel arrayed system.

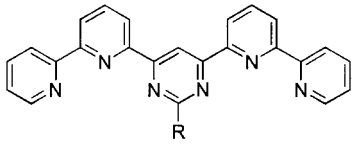

1

In an earlier work we have reported the preparation and Ru^{II} complexation of a series of diphen-substituted diazines **2**−**4**.[3] All three ligands formed mononuclear heteroleptic complexes [Ru(tpy-d_{11})(L)]$^{2+}$ (tpy-d_{11} = perdeuterio-2,2′:6′,2′′-terpyridine), while **3** and **4** also formed dinuclear complexes [(tpy-d_{11})Ru(L)Ru(tpy-d_{11})]$^{4+}$. The use of tpy-d_{11} in place of the protio-analogue greatly facilitated analysis of the NMR spectra. The chemical shifts of the protons on the central pyrimidine or pyrazine ring indicated that these resonances were consistent with the additivity of deshielding effects due to the attached phens with shielding effects from the coordinated tpys. In this paper we report on the structural properties of [(tpy)Ru(**3**)Ru(tpy)]$^{4+}$, as well as on the electronic and photophysical properties of the Ru^{II} complexes of **2**−**4**.

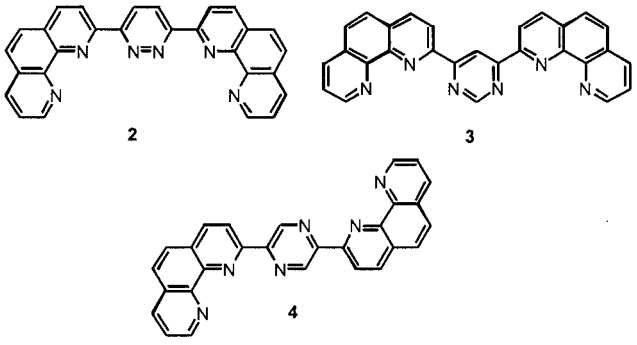

2 **3** **4**

A crystal of [(tpy)Ru(**3**)Ru(tpy)]$(PF_6)_4$ suitable for X-ray analysis was grown from acetonitrile/acetone. In this instance the use of protio-tpy as the auxiliary ligand was preferred. An ORTEP plot showing the structure of the cation is illustrated in Figure 1, and selected structural data is summarized in Table 1 along with the corresponding data from the reported structure for [(tpy)Ru(**1**)Ru(tpy)]$(PF_6)_4$, where R=H.[1] We were quite surprised by the close similarity of the two structures. The central benzo-ring of the phen subunits in **3** pulls C5 and C8 closer by 0.20 Å, and this may straighten out the ligand somewhat. However, this

[a] Department of Chemistry, 136 Fleming Building, University of Houston,
Houston, Texas 77204-5003, USA

change is more than compensated by a lengthening of the C10−C17 bond. The bond angles beyond the chelate rings are found to decrease on the phen side of **3** by about 4.2°, while they increase on the side that pyrazine is coordinated by 1.9°. The overall pinching angle of the molecule actually increases from 25.6° to 30.8° in the complex of **3**. These changes in ligand geometry in going from **1** to **3** are moderated by small adjustments in the Ru−N bond lengths - the Ru−N12 distance is shortened by 0.013 Å and Ru−N15 by 0.015 Å so that the convergence angle remains essentially the same.

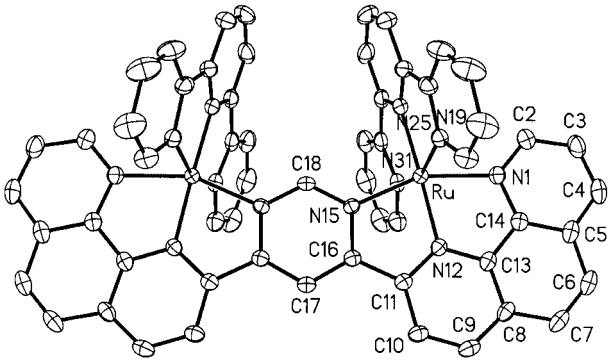

Figure 1. ORTEP diagram of the cation of [(tpy)Ru(**3**)Ru(tpy)]$(PF_6)_4$ with atomic numbering scheme

Table 1. Selected geometric features [bond lengths (Å) and angles (°)] of [(tpy)Ru(**3**)Ru(tpy)]$(PF_6)_4$ compared with analogous features of [(tpy)Ru(**1**)Ru(tpy)]$(PF_6)_4$

	Bridging ligand[a]	
	3	**1**
Ru−N1	2.092(3)	2.090(5)
Ru−N12	1.975(3)	1.988(5)
Ru−N15	2.069(3)	2.084(4)
Ru−N19	2.075(3)	2.090(5)
Ru−N25	1.992(3)	1.993(5)
Ru−N31	2.083(3)	2.092(5)
Ru−Ru	6.0583(5)	6.160
C5−C8	2.863(5)	3.063(10)
C10−C17	3.147(4)	3.075(8)
C28−C28′	3.350(7)	3.405(11)
<C5−C14−C13	119.2(3)	123.5(6)
<C8−C13−C14	122.9(3)	127.1(5)
<C10−C11−C16	129.2(3)	127.3(5)
<C11−C16−C17	125.4(3)	123.5(5)
Convergence angle	36.2	36.3
Pinching angle	30.8	25.6
Bending angle	164.7	170.3

[a] Numbering pattern from Figure 1 with the same relative atom positions for both complexes.

It is interesting to note that the bridging ligand is slightly bent in both complexes, with a larger bend for the complex of **3**. Figure 2 shows how this relatively small deformation is amplified by the tpy ligands which are splayed much farther apart on one side of the complex. On the closer side, the carbon atoms C34 and C34′ are separated by 3.55 Å, while C28 and C28′ are 3.35 Å apart so that some π-stacking effects may be important. On the further side, C22 and C22′ are separated by 7.73 Å. In the complex of **1**, the "open" side of tpy is occupied by a molecule of acetone solvent; this feature is not observed for the complex of **3**. However, the crystal packings are remarkably similar in both cases. It appears that the distortions from ideal octahedral geometry around Ru^{II} caused by tridentate complexation with tpy dictate the shape of the complex, and these effects cannot be greatly influenced by structural modification of the bridging bis-tridentate moiety. The ability of these ligands to participate in rack-type polynuclear structures involving octahedral centers is therefore somewhat compromised.

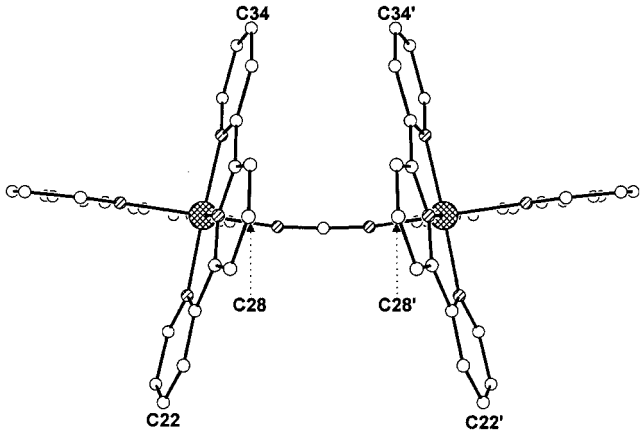

Figure 2. Side view of the cation of [(tpy)Ru(**3**)Ru(tpy)]$(PF_6)_4$

The electronic absorption and emission properties of the mono- and dinuclear complexes of **2**−**4** are summarized in Table 2, and the spectra involving **3** and **4** are illustrated in Figure 3. The mono- and dinuclear complexes all show long wavelength absorption bands that may be attributed to a metal-to-ligand charge-transfer (MLCT) state typically associated with such Ru^{II} polypyridine complexes.[4] This state involves the photoexcitation of an electron from the HOMO, which is a metal-centered d orbital, to the LUMO, which is a π*-orbital localized on one of the ligands. In the cases of the heteroleptic mononuclear complexes of **2**−**4**, the MLCT state consists of two components, one involving the more electronegative and more delocalized bridging diazine and the other involving the tpy-d_{11} ligand. This latter component shows a fairly consistent absorption at higher energy (445−451 nm), reflecting the higher energy of the π*-state for tpy. The lower energy component involving the diazine decreases in energy in the order **2** (522 nm), **4** (530 nm), **3** (538 nm). The energy difference may partly be associated with the disposition of the uncoordinated phen ring. For the complex of **3**, this ring is relatively unhindered in either planar conformation, while the complexes of **4** and **2** show increasing steric hindrance to ligand planarity. The allowed transitions also follows the same trend as can be seen by looking at the ratios of the molar absorptivities for

 © 2004 Wiley-VCH Verlag GmbH & Co. KGaA, Weinheim

Table 2. Photophysical and electrochemical data for Ru^{II} complexes

Complex	Absorption[a] λmax, nm (ε, $M^{-1}\cdot cm^{-1}$)	Emission[a] λ_{em}, nm	Φ≅[c]	$E_{1/2}$[b], V OX	RED
$[Ru(\mathbf{2})(tpy\text{-}d_{11})]^{2+}$	522 (6780), 445 (10580)	737	2.9×10^{-3}	+1.38	−0.84, −1.26, −1.62
$[Ru(\mathbf{3})(tpy\text{-}d_{11})]^{2+}$	538 (11500), 451 (9660)	751	3.1×10^{-3}	+1.40	−0.72, −1.20, −1.60
$[Ru(\mathbf{4})(tpy\text{-}d_{11}]^{2+}$	530 (5950), 451 (6470)	744	3.0×10^{-3}	+1.40	−0.74, −1.18, −1.55
$[(tpy\text{-}d_{11})Ru(\mathbf{3})Ru(tpy\text{-}d_{11})]^{4+}$	647 (10500), 569 (10360) 444 (24040)	842	2.4×10^{-5}	+1.38, +1.56	−0.33, −0.83, −1.56
$[(tpy\text{-}d_{11})Ru(\mathbf{4})Ru(tpy\text{-}d_{11})]^{4+}$	636 (15300), 586sh (6010), 447 (14520)	839	1.1×10^{-4}	+1.36, +1.56	−0.35, −0.76, −1.37

[a] 5×10^{-5} M in CH3CN at 25 °C. [b] Solutions were 0.1 M TBAP in CH_3CN; the sweep rate was 200 mV/s. [c] Referenced to $[Ru(bpy)_3]Cl_2$ in air-equilibrated water (Φ = 0.028).

the two bands for each mononuclear complex. The ratio of the molar absorptivities for the MLCT bands for the tpy vs. the diazine moiety is 1.56 for the complex of **2**, 1.09 for **4**, and 0.84 for **3** which is the most planar.

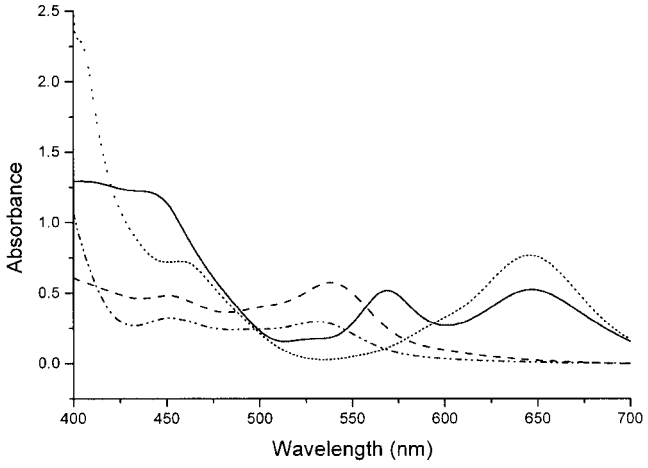

Figure 3. Electronic absorption spectra for Ru^{II} complexes of **3** and **4** in CH_3CN (5×10^{-5} M): $[Ru(\mathbf{3})(tpy\text{-}d_{11})]^{2+}$ (— —), $[Ru(\mathbf{4})(tpy\text{-}d_{11})]^{2+}$ (·· —·· —), $[(tpy\text{-}d_{11})Ru(\mathbf{3})Ru(tpy\text{-}d_{11})]^{4+}$ (—), $[(tpy\text{-}d_{11})Ru(\mathbf{4})Ru(tpy\text{-}d_{11})]^{4+}$ (····)

The dinuclear complexes of **3** and **4** both show enhanced MLCT bands associated with the two auxiliary tpy-d_{11} ligands that are very roughly double their mononuclear counterparts. The longer wavelength components are shifted to much lower energies, hence, the color is green. As has been observed earlier for other diazine-bridged dinuclear Ru^{II} complexes,[4] two bands are seen at longer wavelength. The spectrum for the pyrimidine system shows bands at 647 and 569 nm, whereas that of the pyrazine system shows a strong band at 636 with a shoulder at 586 nm.

All five complexes show weak to medium emission bands when excited at their long wavelength absorption maximum. These emissions follow the expected trend based on the absorptions of the mononuclear complex so that the Stokes shifts remain almost constant at 213−215 nm. The dinuclear complexes show weaker emissions at lower energies, which may be due to quenching by the second metal center.

The redox properties are also consistent and well behaved (reported in Table 2). All five complexes show metal-based Ru^{II}/Ru^{III} oxidations in the range of 1.36−1.40 V. For the dinuclear complexes a second wave at 1.56 V is observed for oxidation of the second metal. This second wave is separated by 0.18−0.20 V from the first wave, indicating a strong interaction between the two metal centers. As observed previously, the interaction is stronger when the metal centers communicate through a pyrazine as opposed to a pyrimidine bridge. Reductions are typically ligand based. For the mononuclear complexes, the first two reductions lie in the range of −0.72 to −0.84 V and −1.18 to −1.26 V, and are associated with the complexed diphen−diazine ligand. The third reduction for these systems is assigned to the tpy-d_{11} ligand (−1.55 to −1.62 V). For the dinuclear complexes, complexation by a second metal increases the reduction potentials associated with the bridging diazine ligand by about +0.4 V.

Experimental Section

The preparation of the ligands **2−4** and their Ru^{II} complexes has been reported.[3] Electronic spectra were obtained on a Perkin−Elmer Lambda 3B spectrophotometer. Emission spectra were obtained on a Perkin−Elmer LS-50 luminescence spectrometer. Cyclic voltammetry was carried out in a conventional three-electrode cell with a BAS-27 voltammeter and a Houston Instruments model 100 X-Y recorder according to a previously described procedure.[5]

X-ray Determination: All measurements were made with a Siemens SMART platform diffractometer equipped with a 1 K CCD area detector. A hemisphere of data (1271 frames at 5 cm detector distance) was collected using a narrow-frame method with scan widths of 0.30° in omega and an exposure time of 30 s/frame. The first 50 frames were remeasured at the end of data collection to monitor instrument and crystal stability, and the maximum correction on I was <1%. The data were integrated using the Siemens SAINT program, and the intensities corrected for Lorentz factor, polarization, air absorption, and absorption due to variation in the path length through the detector faceplate. A psi scan absorption correction was applied based on the entire data set. Redundant reflections were averaged. Final cell constants were refined using 3854 reflections having $I > 10\sigma(I)$, and these, along with other information pertinent to data collection and refinement, are listed in Table 3. The Laue symmetry was determined to be mmm, and from the

 © 2004 Wiley-VCH Verlag GmbH & Co. KGaA, Weinheim

systematic absences noted, the space group was shown to be either *Pna*2(1) or *Pnma*. The asymmetric unit consists of one-half of the Ru_2 tetracation situated about a mirror plane, one PF_6 anion in a general position, two half PF_6 anions situated on mirror planes, a solvent molecule of acetone in a general position, and one-half molecule of acetonitrile on a mirror plane. One of the anions and the acetone are disordered over two slightly different orientations. The acetone had to be treated as an ideal rigid body in order to facilitate refinement. Additionally, the hydrogens on acetonitrile are disordered.

Table 3. Crystallographic data for $[(tpy)Ru(\mathbf{3})Ru(tpy)](PF_6)_4 \cdot 2C_3H_6O \cdot CH_3CN$

Empirical formula	$C_{66}H_{53}F_{24}N_{13}O_2P_4Ru_2$
a, Å	16.0569(10)
b, Å	24.8957(15)
c, Å	17.7269(11)
α, °	90.00
β, °	90.00
γ, °	90.00
V, Å^3	7086.3(8)
Z	4
Molecular weight	1842.23
Space group	*Pnma*
T, °C	−50
λ, Å	0.71073
$\rho_{calcd.}$, g cm^{-3}	1.727
μ, mm^{-1}	0.636
$R_1 = \Sigma\|\|F_o\| - \|F_c\|\|/\Sigma\|F_o\|$	0.0346
$wR_2 = \{[\Sigma[w(F_o^2 - F_c^2)^2]/\Sigma[w(F_o^2)^2]\}^{1/2}$	0.0928
$w = [\sigma^2(F_o^2) + (0.0525P)^2 + (18.5276P)]^{-1}$, where $P = (F_o^2 + 2F_c^2)/3$	

Acknowledgments

We would like to thank the Division of Chemical Sciences, Office of Basic Energy Sciences, U. S. Department of Energy (Contract No. DE-FG03−02ER15334) and the Robert A. Welch Foundation (E-621) for financial support of this work. We also thank Dr. James Korp for assistance with the X-ray determination which required the use of MRSEC/TCSUH Shared Experimental Facilities supported by the National Science Foundation under Award Number DMR-9632667 and the Texas Center for Superconductivity at the University of Houston.

[1] [1a] G. S. Hanan, C. R. Arana, J.-M. Lehn, D. Fenske, *Angew. Chem. Int. Ed. Engl.* **1995**, *34*, 1122−1124. [1b] G. S. Hanan, C. R. Arana, J.-M. Lehn, G. Baum, D. Fenske, *Chem. Eur. J.* **1996**, *2*, 1292−1302.

[2] [2a] S. Leininger, B. Olenyuk, P. J. Stang, *Chem. Rev.* **2000**, *100*, 853−908. [2b] G. F. Swiegers, T. Malefetse, *Chem. Rev.* **2000**, *100*, 3483−3537. [2c] V. Amendola, L. Fabbrizzi, P. Pallavicini, *Coord. Chem. Rev.* **2001**, *216−217*, 435−448. [2d] P. N. W. Baxter, R. G. Khoury, J.-M. Lehn, G. Baum, D. Fenske, *Chem. Eur. J.* **2000**, *6*, 4140−4148. [2e] L. M. Greig, D. Philp, *Chem. Soc. Rev.* **2001**, *30*, 287−302. [2f] T. Bark, M. Düggeli, H. Stoeckli-Evans, A. von Zelewsky, *Angew. Chem. Int. Ed.* **2001**, *40*, 2848−2851.

[3] D. Brown, S. Muranjan, Y. Jang, R. Thummel, *Org. Lett.* **2002**, *4*, 1253−1256.

[4] D. Brown, S. Muranjan, R. P. Thummel, *Eur. J. Inorg. Chem.* **2003**, 3547−3553.

[5] V. Goulle, R. P. Thummel, *Inorg. Chem.* **1990**, *29*, 1767−1772.

Received February 19, 2004
Early View Article
Published Online June 7, 2004

 © 2004 Wiley-VCH Verlag GmbH & Co. KGaA, Weinheim

The Redox Chemistry of SbF_6^- Ion

Maja Ponikvar,*[a][‡] Joel F. Liebman,*[b][‡‡] and H. Donald B. Jenkins*[c][‡‡‡]

Keywords: SbF_6^- / Reduction / Redox chemistry / XeF_2 / Stabilisation

Chemical analysis of Sb in coordination compounds requires quantitative reduction of Sb^V in the form of SbF_6^- (and its related fluoro-hydroxy species) to Sb^{III}. This process, although thermodynamically favoured, appears to be kinetically hindered. The experimentally observed stabilisation of SbF_6^- towards reduction, as happens when the associated metal counterion is complexed by XeF_2 (generally regarded as being an oxidizing agent), is also discussed.
(© Wiley-VCH Verlag GmbH & Co. KGaA, 69451 Weinheim, Germany, 2004)

Introduction

Various coordination compounds have been isolated from MF_q / PnF_5 / anhydrous HF systems (where M = metal in the oxidation state $q+$; PnF_5 = Lewis acid, Pn = P, As, Sb, Bi) because they are interesting as independent products in their own right and because new approaches to the syntheses of these compounds have been established. Such compounds can be further used as starting materials for the syntheses of coordination compounds with fluoro ligands, such as XeF_2 or AsF_3, coordinated to the metal centre. [1−5]

Estimation of the elemental composition of such compounds remains, despite the availability of numerous state-of-the-art, instrumental analytical techniques, still within the domain of classical analysis.[6] Diverse, classical analytical methods are available for the determination of the amounts of total Pn in different oxidation states, usually III or V. Usually, a prior reduction or oxidation of the element being determined has to be initially performed.[7] Problems associated with the determination of the total elemental composition of these compounds, including analytical methods for the determination of the amount of total respectively free fluoride (F_t^- and F_f^-) and the amounts of Pn, were resolved only recently.[8−10] Additional knowledge concerning the chemistry and properties of these compounds in aqueous media[11,12] was gained from the introduction and development of these analytical methods.

The aim of this paper is to explain the tendency shown towards reduction of coordination compounds of the type $M(SbF_6)_2$ (where M = Mg, Ca, Sr, Ba) in relation to their analogues having XeF_2 molecules coordinated in the form $M(SbF_6)_2{\cdot}nXeF_2$ (n = 2−5), as is observed during the process of total chemical analysis employing these compounds. We also examine the thermodynamics of the redox chemistry of SbF_6^- and show that such chemistry may be subject to kinetic rather than thermodynamic barriers.

Results and Discussion

Prior to determination of antimony within coordination compounds containing SbF_6^-, the procedure followed is to quantitatively reduce the Sb^V in the SbF_6^- ion [and the hydrolytically derived Sb(v)-fluoro-hydroxo species] to Sb^{III}. Initially, reduction experiments were conducted according to the standard procedure for the conversion of Sb^V to Sb^{III}, as reported by Hillebrand and Lundell[13] using hydrazine and Na_2SO_3 in acidic (HCl) media. However, the results revealed that hydrazine was completely ineffective as a reductant for the transformation of Sb^V to Sb^{III} in all of the compounds studied, because no Sb^{III} was detected in the sample using redox titration methods once the process of reduction was completed. When the process of reduction of the compounds under study *was* repeated using Na_2SO_3 as a reductant, it was found that Na_2SO_3 was effective for reduction of Sb^V to Sb^{III} in $KSbF_6$ and also in $M(SbF_6)_2$ compounds (where M is Sr or Ba). We can conjecture that the ease of reduction could be related to the nature of the

[a] Jožef Stefan Institute,
Jamova 39, 1000 Ljubljana, Slovenia
Fax: (internat.) + 386-1-423-21-25
E-mail: maja.ponikvar@ijs.si
[b] Department of Chemistry and Biochemistry, University of Maryland,
Baltimore County, Baltimore, MD 21250, USA
Fax: (internat.) + 1-410-455-2608
E-mail: jliebman@umbc.edu
[c] Department of Chemistry, University of Warwick,
Coventry CV4 7AL, West Midlands, UK
Fax: (internat.) + 44-2476-466747
E-mail: Don.Jenkins@warwick.ac.uk
[‡] For all correspondence about experimental measurements.
[‡‡] For all correspondence about the descriptive chemistry and qualitative relations.
[‡‡‡] For all correspondence about the thermochemistry.

M−F bonding. The compounds having a more ionic M−F interaction, that is, $KSbF_6$ and $M(SbF_6)_2$ (where M = Sr, Ba) are reduced more readily than $NaSbF_6$ or than those having M = Mg, Ca with a more significant contribution of covalent fluorine-bridged structures. The M−F bond in $KSbF_6$ is more ionic than in $NaSbF_6$ because the charge−volume ratio of sodium is smaller [$V(Na^+)$ = 0.00394 nm^3 [14]] than the charge−volume ratio of potassium [$V(K^+)$ = 0.00986 nm^3 [14]]. So the Na−F bond is stronger than the K−F bond. As we descend the metal-cation group, the compounds should have an increased contribution to the ionic bond.

In addition, the analogous $M(SbF_6)_2$ compounds with an XeF_2 coordinated to the metal centre M were also examined with respect to their ease of reduction compared to those not having XeF_2 coordinated.

We further report that the reduction of Sb^V in the $M(SbF_6)_2$ compounds (M = Mg or Ca) using 50 mg of metallic Al powder in acid (HCl) media had to be initiated by a gentle heating of the suspension (at approximately 40−50 °C).[9] In contrast, for the compounds where XeF_2 was coordinated as a ligand to the metal centre M, more rigorous conditions were required in order to complete the reduction process: (1) heating to boiling whilst under reflux was required to initiate the reaction and (2) the procedure had to be repeated by one or two subsequent additions of 50 mg of metallic Al.

The tendency of the SbF_6^- ion towards reduction would be more easily rationalized were redox potentials of SbF_6^-/Sb^{III} or $Sb_2F_{11}^-/Sb^{III}$ couples or the other hexafluoropnictates(v) couples listed in the literature. Such is not the case. An alternative understanding of the thermochemistry of the redox chemistry of SbF_6^- and of the apparent resistance of SbF_6^- to reduction by XeF_2 complexation is therefore sought. The aim of the present work is to provide such a rationalisation.

The results of total chemical analysis of the compounds used in this work are presented in Table 1.

These results verify that the analyzed compounds were greater than 99% pure (although their stoichiometry was not always exact).

Conclusion

The Thermochemistry of the Redox Chemistry of SbF_6^-

The likely thermodynamics of three alternative reduction scenarios are considered below. Aqueous N_2H_4, an aqueous SO_3^{2-} salt and metallic Al powder were individually investigated as reducing agents for the purpose of the reduction of Sb^V in the SbF_6^- ion to Sb^{III}, with the assumption that their reaction products are N_2, aqueous SO_4^{2-} and aqueous Al^{III}, respectively. We consider the example of the K^+ salts in reactions (1) − (3), chosen because the relevant thermodynamic data can be estimated. To the extent that hexafluoroantimonate salts are strong electrolytes, the actual choice of counterion is irrelevant since the enthalpy and Gibbs energy of formation of the aqueous salt is the sum of the corresponding quantities for the component ions, in other words, the enthalpy of formation of aqueous K_2SO_3 is the sum of twice the aqueous enthalpies of formation of K^+, and that of SO_3^{2-}. Only enthalpies are discussed in the current study. The three redox reactions are:

$$2\,KSbF_6(aq) + N_2H_4(aq) + 6\,H_2O(l) \rightarrow 2\,Sb(OH)_3(aq) + N_2(g) + 2\,KF(aq) + 10\,HF(aq) \quad (1)$$

$$2\,KSbF_6(aq) + K_2SO_3(aq) + 6\,H_2O(l) \rightarrow 2\,Sb(OH)_3(aq) + K_2SO_4(aq) + 2\,KF(aq) + 10\,HF(aq) \quad (2)$$

$$3\,KSbF_6(aq) + 2\,Al(s) + 3\,H_2O(l) \rightarrow 3\,Sb(OH)_3(aq) + 2\,AlF_3(aq) + 3\,KF(aq) + 6\,HF(aq) \quad (3)$$

All of the desired enthalpy of formation data is available from the archival literature[15] except for that of the standard enthalpy of formation of the aqueous salt containing our anion of interest, that is, $\Delta_fH^0(KSbF_6, aq)$.

Recently, one of us reported a thermochemical study in which the gas-phase enthalpy of formation for SbF_6^-, $\Delta_fH^0(SbF_6^-, g)$, was derived.[16] Taking the standard enthalpy of formation for the solid $KSbF_6$ salt, $\Delta_fH^0(KSbF_6, s) = -2089 \pm 3$ kJ·mol^{-1} (the average value from the refer-

Table 1. The results of elemental chemical analyses of the coordination compounds with SbF_5

	Sb^V [%]				M^{II} [%]				F_t^- [%]				F_f^- [%]			
	Calcd.	Found	Diff.	RSD [%]	Calcd.	Found	Diff.	RSD [%]	Calcd.	Found	Diff.	RSD [%]	Calcd.	Found	Diff.	RSD [%]
$M(SbF_6)_2$ [9]																
$Mg(SbF_6)_2$	49.11	48.8	−0.3	0.20	4.90	4.9	0.0	0.00	45.99	44.4	−1.6	0.26	15.33	16.4	1.1	0.35
$Ca(SbF_6)_2$	47.60	48.3	0.7	0.12	7.83	5.8	−2.0	0.00	44.57	42.0	−2.6	0.14	14.86	11.9	−3.0	0.84
$Sr(SbF_6)_2$	43.55	44.3	0.8	0.00	15.67	13.1	−2.6	0.44	40.78	39.6	−1.2	0.00	13.59	14.8	1.2	0.39
$Ba(SbF_6)_2$	39.99	42.8	2.8	0.14	22.56	19.4	−3.2	0.52	37.45	37.5	0.1	0.27	12.45	19.0	6.6	0.00
$M(SbF_6)_2{\cdot}nXeF_2$																
$Mg(SbF_6)_2{\cdot}2XeF_2$	29.18	29.4	0.2	0.20	2.91	2.8	−0.1	0.00	36.43	35.5	−0.9	0.23	18.22	18.5	0.3	0.00
$Ca(SbF_6)_2{\cdot}3.5XeF_2$	22.05	22.1	0.1	0.00	3.63	3.4	−0.2	0.00	32.70	32.5	−0.2	0.25	18.93	18.8	−0.1	0.00
$Sr(SbF_6)_2{\cdot}3XeF_2$	22.82	20.8	−2.0	0.28	8.21	5.4	−2.8	2.13	32.05	30.8	−1.3	0.16	17.81	18.0	0.2	0.00
$Ba(SbF_6)_2{\cdot}5XeF_2$	16.73	16.7	0.0	0.35	9.44	9.3	−0.1	−	28.78	28.7	−0.1	0.28	18.28	18.2	−0.1	0.32

 © 2004 Wiley-VCH Verlag GmbH & Co. KGaA, Weinheim

ences[17,18] cited therein), in order to estimate $\Delta_f H^0(KSbF_6, aq)$, we then require the corresponding enthalpy of solution for the salt, $\Delta_{soln.}H^0(KSbF_6, s)$. From the data in ref.[15], although we can derive a value of $\Delta_{soln.}H^0(KPF_6, s) = 44\ kJ{\cdot}mol^{-1}$ for the valence isoelectronic KPF_6, in this source we find no additional data for any hexafluoropnictate salt or any other hexafluorometallate salt. The justification for the comparison made is that KPF_6 and $KSbF_6$ are both KEF_6 salts. Further support comes from the fact that a roughly "universal" value for $\Delta_{soln.}H^0(KEO_4, s)$ of about $54 \pm 10\ kJ{\cdot}mol^{-1}$ is found for a set of KEO_4 salts (where E = Cl, Br, I, Mn, Tc, Re) and yet another "universal" value of $\Delta_{soln.}H^0(K_2EO_4, s)$ of about 11 ± 12 kJ/mol for K_2EO_4 salts (where E = S, Se, Cr, Mo, W), where it appears that changing the central metal, E, has a minimal effect on the thermochemical behaviour of these compounds when going into solution. Accordingly, we derive an enthalpy of formation of aqueous $KSbF_6$, $\Delta_f H^0(KSbF_6, aq)$, of about $-2045 \pm 3\ kJ{\cdot}mol^{-1}$ whereupon we find that ΔH for reaction (1) (as written) is exothermic by about 273 kJ, ΔH for reaction (2) by about 513 kJ and ΔH for reaction (3) by 2141 kJ. The uncertainties, although large, indicate that nonetheless these reactions remain unequivocally exothermic and since ΔS for all of them is likely to be positive, they are thermodynamically favoured. We can only conclude that the reduction reactions must be subject to a kinetic barrier. This confirms the long-held view that SbF_6^- is generally an "unreactive" ion.

Stabilization of SbF_6^- to Reduction by XeF_2 Complexation

From the experiments described above, we deduce that aqueous SbF_6^- is stabilized (i.e. more resistant to reduction) when the associated metal counterion is complexed by XeF_2. This is surprising. XeF_2 is generally regarded as being an oxidizing agent, although with the hitherto documented existence of highly stable, higher valence xenon-containing species in aqueous media [both Xe(VII) and Xe(VIII), $HXeO_4^-$ and various protonated forms of XeO_6^{4-}][19] XeF_2 can conceivably also serve as a reducing agent. However, for the counterions we employed for this SbF_6^- study no redox chemistry of any type was seen in the synthesis of the salts (no redox active metal was studied), and so none is expected here. So, why is there any effect at all on the ease of reduction of SbF_6^-? We showed earlier that AsF_6^-, a lighter valence isoelectronic analogue of SbF_6^-, is destabilized with regard to hydrolysis by multiply-charged cations.[12] The same destabilization mechanism may also apply to reduction processes. From elementary chemistry courses, we recall that these multiply-charged, aqueous cations should not be considered as M^{q+} but rather as $[M(H_2O)_n]^{q+}$. Although this is in the absence of XeF_2 as a ligand, we could postulate a similar $[M(H_2O)_w(XeF_2)_x]^{q+}$ ion where w and x are left intentionally unstated because of our admitted ignorance of the constitution of such complex ions in solution. It is clear that the complexing hydrogens are partially positive and so can assist in the decomposition of the anion much as the positive, bare metal cation might be expected to do. There is no reason to doubt that XeF_2 complexes the metal using one of its fluorine atoms whilst the other F atom faces the water molecules: these fluorines are partially negative and the 180° F−Xe−F angle precludes chelation using them both. As such, the metal cation is likely to have a neutral, if not partially negative, exterior and this will not assist in the hydrolytic decomposition of the anion. Indeed, that the exterior of the cationic metal is at least partially fluorinated, as is the anion, suggests they will avoid each other. Such avoidance is documented: Greenberg, Liebman and Van Vechten used similar logic as part of the theoretical interpretation of "the Perfluoroalkyl (R_f) effect" on the thermodynamic and kinetic stability of substituted highly strained organic molecules,[20] a phenomenon first enunciated in an experimental study made by Lemal and Dunlap.[21] Relatedly, where the negative charge on the anion is lessened, as with ion pairing that would arise with the smaller and less electropositive cations Na, Mg and Ca, reduction is also less likely.

Experimental Section

All reagents were of analytical grade and all solutions were prepared using double-distilled water.

Sample Preparation: Except $NaSbF_6$ (tech., Aldrich) and $KSbF_6$ (99%, Aldrich) that are not moisture sensitive, the analyzed coordination compounds are sensitive to traces of moisture. Therefore, the test samples for determination of each constituent were prepared by weighing in a dry box, with a precision of ± 0.05 mg into air and moisture tight Teflon containers. The containers were cooled in liquid nitrogen in order to moderate the subsequent reaction with water (20 mL) during suspension in a closed Erlenmeyer flask.[9]

Analyses: Both accurate and precise results of chemical analyses having an absolute error of less than 0.2−0.3% were obtained using classical analytical methods. A modified analytical technique, involving the use of a fluoride-ion-selective electrode enabled that us to achieve an absolute error of analysis of less than 0.3%, was applied to the determination of fluoride.

The amounts of antimony were determined after reductive decomposition of the acidic (HCl) sample by addition of metallic Al powder (50 mg).[9] If necessary, the sample was either gently heated to approximately 40−50 °C to initiate the reaction or further Al powder (50 mg) was added to the suspension whilst heating to boiling point under reflux to prevent losses of volatile SbF_3. The amount of Sb^{III} obtained was determined by potentiometric titration with $KBrO_3$ after dissolution of the antimony precipitate. The amount of F_t^- was determined after total reductive decomposition of the sample using Devarda alloy in alkaline (KOH) media.[8] The amounts of F_f^- were estimated in aqueous suspensions of the samples. The latter analyses were performed by direct potentiometry using a fluoride-ion-selective electrode.[8] The amounts of other metals (except alkaline metals) were determined using a corresponding complexometric titration with EDTA.[22]

Acknowledgments

We gratefully acknowledge the financial support of the Ministry of Education, Science and Sport of the Republic of Slovenia. We are

 © 2004 Wiley-VCH Verlag GmbH & Co. KGaA, Weinheim

grateful to Dr. Alenka Turičnik for the syntheses of the compounds.

[1] B. Frlec, D. Gantar, J. H. Holloway, *J. Fluorine Chem.* **1982**, *20*, 385−396.
[2] D. Gantar, I. Leban, B. Frlec, *J. Chem. Soc., Dalton Trans.* **1987**, 2379−2383.
[3] M. Tramšek, P. Benkič, A. Turičnik, G. Tavčar, B. Žemva, *J. Fluorine Chem.* **2002**, *114*, 143−148.
[4] A. Turičnik, P. Benkič, B. Žemva, *Inorg. Chem.* **2002**, *41*, 5521−5524.
[5] A. Turičnik, PhD Thesis, University of Ljubljana, Ljubljana, Slovenia, **2003**.
[6] C. M. Beck II, *Anal. Chem.* **1991**, *63*, 993A−1003A.
[7] J. J. Lingane, *Analytical chemistry of selected metallic elements*, Reinhold Publishing Corporation, New York, **1966**, pp. 18−38.
[8] M. Ponikvar, B. Sedej, B. Pihlar, B. Žemva, *Anal. Chim. Acta* **2000**, *418*, 113−118.
[9] M. Ponikvar, B. Pihlar, B. Žemva, *Talanta* **2002**, *58*, 803−810.
[10] M. Ponikvar, B. Pihlar, B. Žemva, *J. Fluorine Chem.* **2003**, *122*, 215−217.
[11] M. Ponikvar, B. Žemva, J. F. Liebman, *J. Fluorine Chem.* **2003**, *123*, 217−220.
[12] M. Ponikvar, B. Sedej, J. F. Liebman, *Eur. J. Inorg. Chem.* **2004**, 1349−1352.
[13] W. F. Hillebrand, G. E. F. Lundell, *Applied Inorganic Analysis with Special Reference to the Analysis of Metals, Minerals and Rocks*, John Wiley & Sons, New York, Chapman & Hall, London, 2nd ed., **1953**, pp. 70−71, 280−281.
[14] H. D. B. Jenkins, H. K. Roobottom, J. Passmore, L. Glasser, *Inorg. Chem.* **1999**, *38*, 3609−3620.
[15] D. D. Wagman, W. H. Evans, V. B. Parker, R. H. Schumm, I. Halow, S. M. Bailey, K. L. Churney, R. L. Nuttall, *J. Phys. Chem. ref. Data* **1982**, *11*, Suppl. 1, 1−200.
[16] H. D. B. Jenkins, H. K. Roobottom, J. Passmore, *Inorg. Chem.* **2003**, *42*, 2886−2893.
[17] W. W. Richards, A. A. Woolf, *J. Fluorine Chem.* **1971**, *1*, 129−139.
[18] J. Burgess, R. D. Peacock, R. J. Sherry, *J. Fluorine Chem.* **1982**, *20*, 541−554.
[19] F. A. Cotton, F. Wilkinson, C. A. Murillo, M. Bochmann, *Advanced Inorganic Chemistry*, 6th ed., John Wiley & Sons, New York, **1999**, pp. 592−593.
[20] A. Greenberg, J. F. Liebman, D. Van Vechten, *Tetrahedron* **1980**, *36*, 1161−1166.
[21] D. M. Lemal, L. H. Dunlap Jr., *J. Am. Chem. Soc.* **1972**, *94*, 6562−6564.
[22] R. Pribil, *Applied Complexometry*, Pergamon Press, Oxford, **1982**, pp. 200−201, 214−216.

Received February 10, 2004
Early View Article
Published Online June 7, 2004

 © 2004 Wiley-VCH Verlag GmbH & Co. KGaA, Weinheim

Syntheses and Molecular Structures of Novel Alkali Metal Tetraorganylcyclopentaphosphanides and Tetraorganyltetraphosphane-1,4-diides[‡]

Robert Wolf,[a] Andrea Schisler,[a] Peter Lönnecke,[a] Cameron Jones,[b] and Evamarie Hey-Hawkins*[a]

In memoriam Professor Marianne Baudler

Keywords: Alkali metals / Phosphorus / P ligands / ^{31}P NMR spectroscopy / Tetraphosphane-1,4-diides

The reaction of sodium with $RPCl_2$ and PCl_3 (12:4:1) in THF gives Na[*cyclo*-(P_5R_4)] [R = *i*Pr (**1**), Ph (**2**)], while four equivalents of $RPCl_2$ [R = Ph, 2,4,6-$Me_3C_6H_2$ (Mes), *t*Bu] react with ten equivalents of sodium sand or elemental potassium in refluxing THF to yield the compounds [$Na_2(THF)_5(P_4Ph_4)$] (**3**), [$Na_2(THF)_4(P_4Mes_4)$] (**4**), and [$Na_2(THF)_4(P_4tBu_4)$] (**5**), or the potassium salt [$K_2(THF)_6(P_4Mes_4)$] (**6**). Recrystallizing **6** from 1,4-dioxane/pentane (1:3) also led to [{$K(L)_2$}$_2${$K(L)$}$_6$(P_4Mes_4)$_4$·0.5THF]$_\infty$ (L = 1,4-dioxane) (**7**). In the solid state, compounds **3**–**6** exist as isolated ion-contact complexes, in which the P_4 chain of the $(P_4R_4)^{2-}$ ligand has a *syn* arrangement, while a polymeric helical arrangement was observed for **7**. A minor product, [{K(pmdeta)(HP_3Mes_3)}$_2${K_2(P_4Mes_4)}]·0.25hexane (**8**), was isolated from the reaction of $MesPCl_2$ and K (1:2.5). Compound **8** contains the first structurally characterized example of a triphosphanide anion, $(HP_3Mes_3)^-$, besides $K_2(P_4Mes_4)$.

(© Wiley-VCH Verlag GmbH & Co. KGaA, 69451 Weinheim, Germany, 2004)

Introduction

Cyclooligophosphanes *cyclo*-$(PR)_n$,[1] which are isolobal with cycloalkanes have attracted the interest of chemists for a long time. Whereas the first example of this class of compounds, *cyclo*-$(PPh)_5$, was synthesized as early as 1877,[2] the first cyclooligophosphanide anions *cyclo*-$(P_nR_{n-1})^-$ were only reported approximately 100 years later.[3,4] Even today, the number of compounds readily accessible in pure form is still small.[5] Thus, the alkali metal compounds K[*cyclo*-(P_3tBu_2)],[3] K[*cyclo*-(P_5Ph_4)],[5] and Li[*cyclo*-(P_ntBu_{n-1})] ($n = 3-5$)[6,7] were only obtained as inseparable mixtures, and characterized by ^{31}P NMR spectroscopy. Only recently, we reported the targeted high-yield synthesis of Na[*cyclo*-(P_5tBu_4)] as well as preliminary results of its use in coordination chemistry.[8]

We have now employed the same synthetic approach for the preparation of other cyclopentaphosphanide anions Na[*cyclo*-(P_5R_4)], starting from *i*PrPCl$_2$, PhPCl$_2$ or MesPCl$_2$ (Mes = 2,4,6-$Me_3C_6H_2$), PCl$_3$, and Na (4:1:12). While Na[*cyclo*-(P_5R_4)] [R = *i*Pr (**1**), Ph (**2**)] are obtained, the tetraphosphane-1,4-diides $Na_2(P_4R_4)$ are the major products for R = Ph (**3**) and R = Mes (**4**).

While a large number of alkali metal phosphanides M(PRR′) (R, R′ = alkyl, aryl, H) have been synthesized and structurally characterized, their structures in solution are largely unknown.[9] In this respect, oligophosphanediides of the general formula $M_2(P_4R_4)$ (M = Li, Na, K; R = Me, Et, Cy, *t*Bu, Ph), which were first obtained by Issleib et al. by reduction of cyclooligophosphanes, *cyclo*-$(PR)_n$, with Li, Na, and K, are of special interest.[10] In contrast to alkali metal phosphanides, M(PRR′),[9] these compounds have been extensively studied by ^{31}P NMR spectroscopy, and their molecular structures in solution were proposed on the basis of the complex spin systems observed.[11] Independently from our own work, the solid-state structures of complexes of the general composition $Na_2(P_nPh_n)$ ($n = 2-4$), which were obtained from the reaction of PhPCl$_2$ and Na, were recently reported.[12]

Although linear and cyclic oligophosphanides are of interest as ligands in main group and transition metal

[‡] This work was presented at the Third International Conference on the Chemistry of the Alkali and Alkaline Earth Metals, 28th September to 2nd October 2003, Würzburg, Germany

[a] Institut für Anorganische Chemie der Universität Leipzig, Johannisallee 29, 04103 Leipzig, Germany
Fax: (internat.) +49-(0)341-9739319
E-mail: hey@rz.uni-leipzig.de
[b] Cardiff University, Chemistry Department, P. O. Box 912, Cardiff CF10 3TB, UK
Fax: (internat.) +44-(0)29-20874030
E-mail: jonesca6@cf.ac.uk

chemistry, there are only a few reports where linear oligophosphanide ligands $(P_nR_n)^{2-}$ have been employed in coordination chemistry. These include the synthesis of metallocene triphosphane-1,3-diyl complexes $[Cp_2M(P_3R_3)]$ (M = Ti, Zr, Hf; R = Me, Et, Ph, *t*Bu),[13] a nickel tetraphosphane-1,4-diyl complex $[Ni(\eta^2\text{-}P_2tBu_2)(P_4tBu_4)]$,[14] the germatetraphospholanes[15] *cyclo*-$(P_4tBu_4GeR_2)$ (R = Et, Ph) and *cyclo*-$\{P_4tBu_4Ge(\eta^2\text{-}P_2tBu_2)\}$, and the stannatetraphospholanes[16] *cyclo*-$(P_4tBu_4SnR_2)$ (R = *t*Bu, *n*Bu, Ph) and *cyclo*-$\{P_4tBu_4Sn(Cl)nBu\}$. In addition, we have shown, that the cyclic oligophosphanide anion *cyclo*-$(P_5tBu_4)^-$ exhibits a rich and unprecedented chemistry.[8,17]

We now report the syntheses of the sodium cyclopentaphosphanides Na[*cyclo*-(P_5R_4)] [R = *i*Pr (**1**), Ph (**2**)], and improved syntheses of the alkali metal tetraphosphane-1,4-diides $[Na_2(THF)_5(P_4Ph_4)]$ (**3**), $[Na_2(THF)_4(P_4Mes_4)]$ (**4**), and $[Na_2(THF)_4(P_4tBu_4)]$ (**5**), and the potassium salts $[K_2(THF)_6(P_4Mes_4)]$ (**6**) and $[\{K(L)_2\}_2\{K(L)\}_6(P_4Mes_4)_4\cdot 0.5THF]_\infty$ (L = 1,4-dioxane) (**7**). The structures of **3**−**6** in solution were established from ^{31}P NMR spectroscopic studies, and were compared with the solid-state structures.

A minor product from the reaction of $MesPCl_2$ and K (1:2.5) with an excess of pmdeta (pmdeta = pentamethyldiethylentriamine) and hexane, namely $[\{K(pmdeta)(HP_3Mes_3)\}_2\{K_2(P_4Mes_4)\}]\cdot 0.25$hexane (**8**), was isolated and structurally characterized. Compound **8** contains the first structurally characterized example of a triphosphanide anion, $(HP_3Mes_3)^-$, besides $K_2(P_4Mes_4)$.

Results and Discussion

Synthesis and Spectroscopic Properties of Na[*cyclo*-(P_5R_4)] [R = *i*Pr (1), Ph (2)]

The reaction of sodium with $RPCl_2$ and PCl_3 (12:4:1) in THF gives Na[*cyclo*-(P_5R_4)] (R = *i*Pr (**1**), Ph (**2**)] in an amount of conversion of 61 and 32%, respectively (as determined by ^{31}P NMR spectroscopy). Besides **1** and **2**, signals of *cyclo*-$(PiPr)_4$,[18] $iPrPH_2$,[19] and $Na_2(P_2iPr_2)$[20] (for **1**) or $Na_2(P_4Ph_4)$ (**3**),[11] Na{PPhP(H)Ph},[20] $Na_2(P_3Ph_3)$,[11] and $Na_2(P_2Ph_2)$[20] (for **2**) were observed in the ^{31}P NMR spectra of the reaction mixtures. Compounds **1** and **2** are very air-sensitive, and even pyrophoric as finely divided powders. They dissolve readily in ethers, aliphatic, and aromatic organic solvents.

In the $^{31}P\{^1H\}$ NMR spectra, **1** and **2** exhibit signals for an ABB′CC′ spin system.[21] Only one conformational isomer was observed, which we propose to be the *all-trans* isomer by comparison with Na[*cyclo*-(P_5tBu_4)].[8] This is also in agreement with the observed coupling constants (Table 1).[5,11c,22]

Table 1. $^{31}P\{^1H\}$ NMR parameters (C_6D_6, 25 °C, δ in ppm, *J* in Hz) of Na[*cyclo*-(P_5R_4)] (R = *i*Pr (**1**), Ph (**2**) or *t*Bu[8])

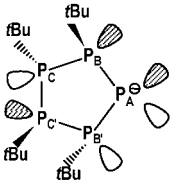

	*i*Pr	Ph	*t*Bu[8]
δ_A	−126.5(1)	−105.6(1)	−105.6(1)
$\delta_B = \delta_{B'}$	+66.3(1)	+72.8(1)	+82.7(1)
$\delta_C = \delta_{C'}$	+42.6(1)	+47.1(1)	+75.0(1)
$^1J_{AB} = {}^1J_{AB'}$	−352.1(1)	−403.2(1)	−379.2(1)
$^1J_{BC} = {}^1J_{B'C'}$	−293.9(2)	−312.3(1)	−317.3(1)
$^1J_{CC'}$	−324.8(2)	−334.2(1)	−309.4(1)
$^2J_{AC} = {}^2J_{AC'}$	−	+9.5(1)	−0.1(1)
$^2J_{BC'} = {}^2J_{B'C}$	−	+11.4(1)	−5.4(1)
$^2J_{BB'}$	−	+1.9(1)	−17.2(1)

Synthesis, Molecular Structures, and Spectroscopic Properties of $[Na_2(THF)_5(P_4Ph_4)]$ (3), $[Na_2(THF)_4(P_4Mes_4)]$ (4), $[Na_2(THF)_4(P_4tBu_4)]$ (5), $[K_2(THF)_6(P_4Mes_4)]$ (6), and $[\{K(L)_2\}_2\{K(L)\}_6(P_4Mes_4)_4\cdot 0.5THF]_\infty$ (L = 1,4-Dioxane) (7)

The reaction of four equivalents of $PhPCl_2$ (**3**), $MesPCl_2$ (**4** and **6**), or $tBuPCl_2$ (**5**) with ten equivalents of sodium sand (**3**−**5**) or elemental potassium (**6**) in refluxing THF yields the compounds **3**−**6** in high purity and moderate yields (27 to 43%, Scheme 1). Compound **7** can be obtained upon recrystallization of **6** from dioxane/pentane (1:3).

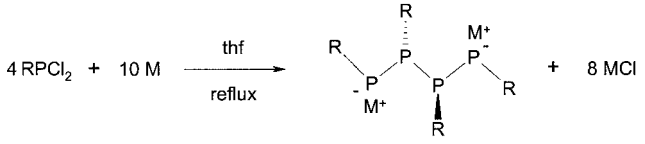

Scheme 1. Synthesis of **3**−**6** [M = Na, R = Ph (**3**), Mes (**4**), *t*Bu (**5**); M = K, R = Mes (**6**)]

In the solid state **3**, **4**, **5**, and **6** exist as isolated ion-contact complexes, in which the P_4 chain of the $(P_4R_4)^{2-}$ ligand has a *syn* arrangement [torsion angles between the planes P1−P2−P3 and P2−P3−P4 or P1−P2−P2′ and P2−P2′−P1′: 32.1° (**3**), 72.7° (**4**), 8.8° (**5**), and 75.1° (**6**)], and is coordinated to two alkali metal cations (Figures 1−5). The coordination spheres of the alkali metal cations are completed by two (**4** and **5**) or three (**3** and **6**) THF molecules. In **3**, a bridging THF molecule can be observed [*d*(Na1−O3) = 301.3(8) pm]. This is a rare situation,[23] and has only been observed twice in the structures of alkali metal phosphanides.[24] Bridging THF molecules were also observed in the molecular structure of the tetrameric sodium and potassium fluorenone ketyls $[Na_4(OC_{13}H_8)_2(THF)_2(\mu_2\text{-}THF)_2(OC_{13}H_8)_4]$ [*d*(Na−O) = 239.1(7)−260.6(7) pm] and $[K_4(hmpa)_4(\mu_2\text{-}THF)(OC_{13}H_8)_4]$ (hmpa = $OP(NMe_2)_3$].[23] The P−P bond lengths, which range from 216.6(1)−226.2(2) pm, are in the typical range for single bond lengths.[25] In spite of these general similarities, there are significant differences between the coordination modes of

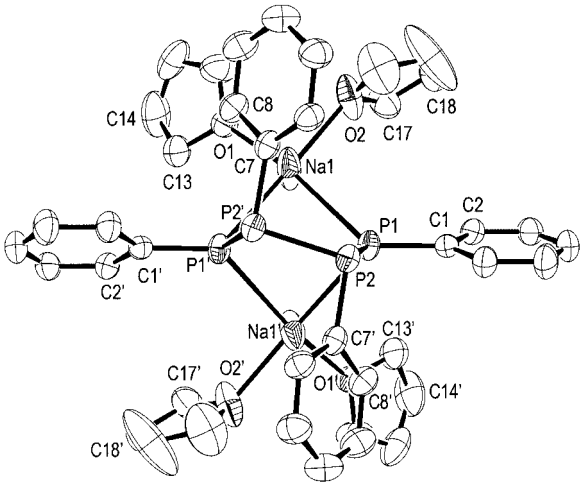

Figure 1. Molecular structure of $[Na_2(THF)_5(P_4Ph_4)]$ (**3**); the bridging THF molecule has been omitted for clarity

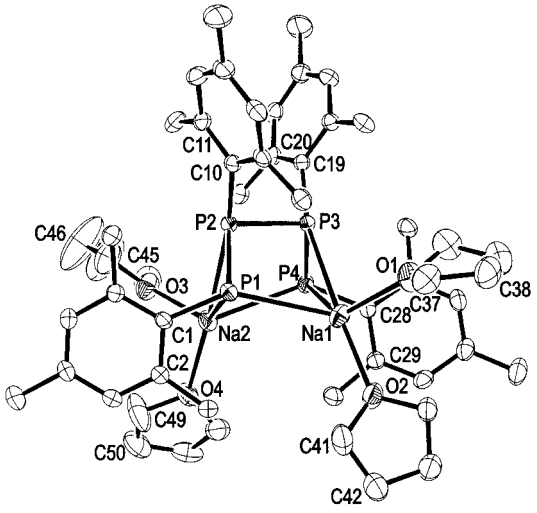

Figure 2. Molecular structure of $[Na_2(THF)_4(P_4Mes_4)]$ (**4**)

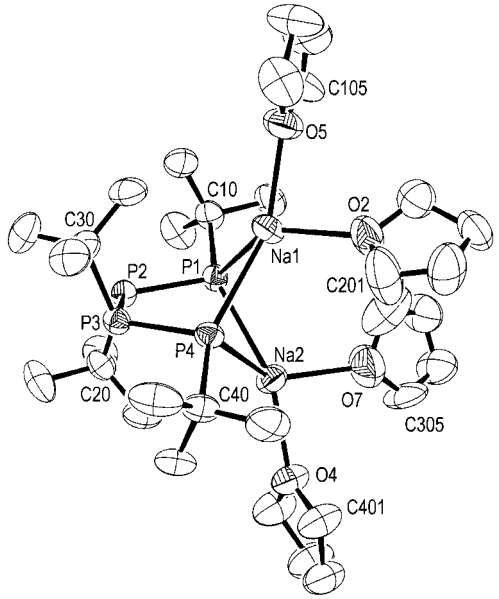

Figure 3. Molecular structure of $[Na_2(THF)_4(P_4tBu_4)]$ (**5**)

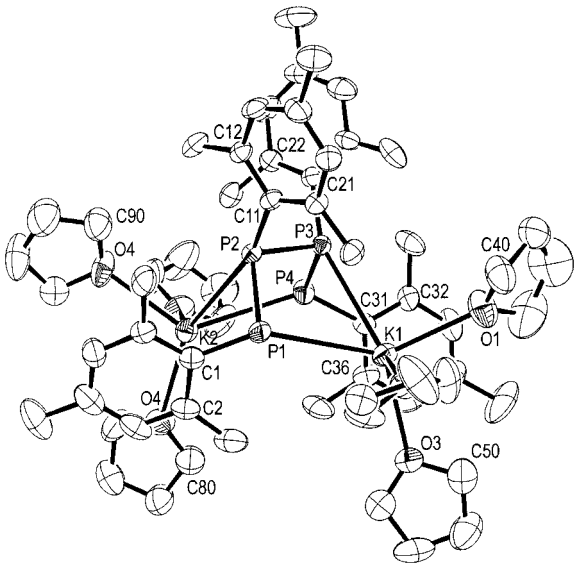

Figure 4. Molecular structure of $[K_2(THF)_6(P_4Mes_4)]$ (**6**)

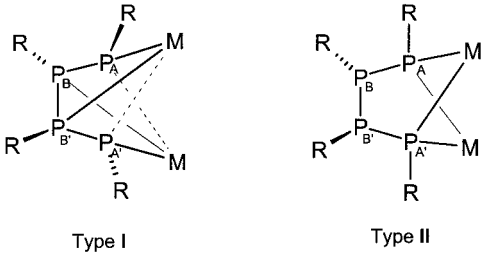

Figure 5. The two structural arrangements observed in the solid-state structures of **3** and **5** (type **II**), and **4** and **6** (type **I**)

Na and K. Whereas for **4** and **6** the phosphorus alkali metal distances are in the typical range for related sodium and potassium phosphanides[9] *both* for the internal and terminal phosphorus atoms of the chain [**4**: *d*(Na1−P1,P3), *d*(Na2−P2,P4) = 289.6(2)−316.6(1) pm, **6**: *d*(K1−P1,P3), *d*(K2−P2,P4) = 331.4(3)−359.8(2) pm], in **3** and **5** the Na cations are exclusively coordinated by the terminal phosphorus atoms [**3**: *d*(Na1−P1) = 290.1(2) pm, *d*(Na1−P1′) = 289.2(2) pm, **5**: *d*(Na1−P1,P4) = 281.9(1)−291.1(1) pm, *d*(Na2−P1,P4) = 284.0(1)−290.1(1) pm] (Figure 5). Thus, for **4** and **6**, the phosphorus atoms in the 1,3 positions coordinate and four-membered MP_3 chelate rings are formed. Additionally, longer contacts can be observed between the alkali metal and the second terminal phosphorus atom [**4**: *d*(Na1−P4) = 331.6(2), *d*(Na2−P1) = 317.3(2) pm, **6**: *d*(K1−P4) = 382.3(3) pm, *d*(K2−P1) = 385.1(2) pm]. The strong interaction with the inner phosphorus atoms is also reflected in the larger torsion angle of the $(P_4R_4)^{2-}$ chain (see above). Solvation of Na and K is completed by short contacts to carbon atoms of the mesityl substituents [**4**: d[Na(1)−C28,C29), *d*(Na2−C1,C2) = 289.6(3)−306.6(3) pm, **6**: *d*(K1−C31,C36), *d*(K2−C1,C2) = 314.2(5)−321.5(6) pm], indicating η^2 interactions of the aryl rings. Interestingly, short K−C contacts were not observed for the phenyl rings of **3**, whereas π coordi-

 © 2004 Wiley-VCH Verlag GmbH & Co. KGaA, Weinheim

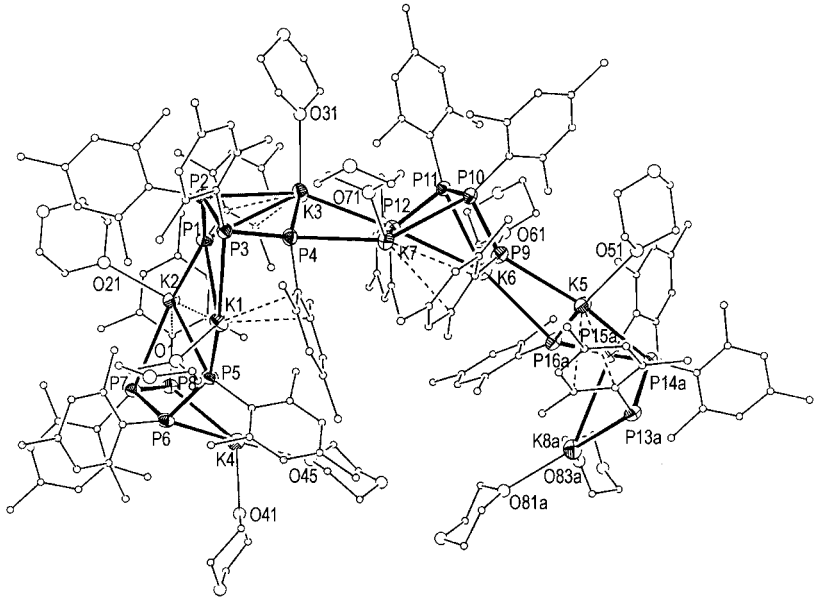

Figure 6. Molecular structure of $[\{K(L)_2\}_2\{K(L)\}_6(P_4Mes_4)_4 \cdot 0.5THF]_\infty$ (L = 1,4-dioxane) (**7**); only one tetrameric unit is shown; the THF solvate molecule has been omitted for clarity; only K−P distances up to 363 pm are shown

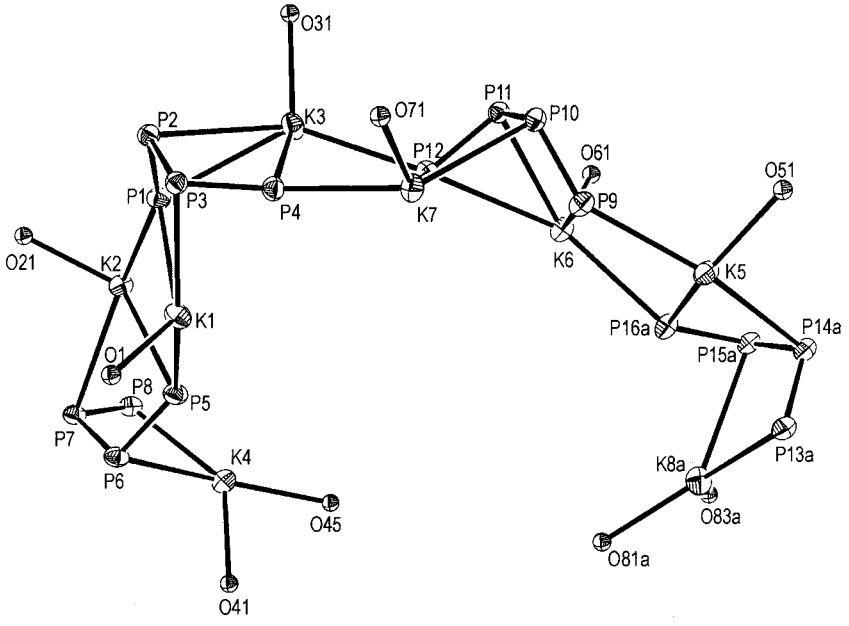

Figure 7. Molecular structure of the tetrameric unit in $[\{K(L)_2\}_2\{K(L)\}_6(P_4Mes_4)_4 \cdot 0.5THF]_\infty$ (L = 1,4-dioxane) (**7**); only the central K, P, O framework and K−P distances up to 363 pm are shown

nation of arene ligands to potassium[26−30] and the heavier alkali metals[31] has often been observed.[32]

When $[K_2(THF)_6(P_4Mes_4)]$ (**6**) was recrystallized from a mixture of 1,4-dioxane and *n*-pentane (1:3), the orange crystalline compound $[\{K(L)_2\}_2\{K(L)\}_6(P_4Mes_4)_4 \cdot 0.5THF]_\infty$ (L = 1,4-dioxane) (**7**) was formed. An X-ray crystal structure analysis revealed, that the asymmetric unit of **7** consists of two crystallographically independent units, $\{K_2(L)_3(P_4Mes_4)\}$ and $\{K_2(L)_2(P_4Mes_4)\}$, both of which are associated *via* K−P interactions. Thus, a tetrameric arrangement is formed in the solid state (Figure 6 and Figure 7), which aggregates *via* further K−P interactions to form a helical, 1-D coordination polymer (Figure 8).

Interestingly, the coordinative arrangement within the monomeric building blocks $\{K_2(L)_3(P_4Mes_4)\}$ and $\{K_2(L)_2(P_4Mes_4)\}$ of the polymeric chain resembles the pattern found in the monomeric THF adduct $[K_2(THF)_6(P_4Mes_4)]$ (**6**). Thus, the K−P distances between one terminal and one internal phosphorus atom are generally significantly shorter [*d*(K5−P16a,P14a;K8a−P15a,P13a) = 324.4(2)−358.9(2) pm, *d*(K6−P9,P11;K7−P10,P12) = 330.8(2)−345.6(2) pm, *d*(K1−P1,P3;K3−P2,P4) = 327.1(2)−355.1(2) pm, *d*(K2−

 © 2004 Wiley-VCH Verlag GmbH & Co. KGaA, Weinheim

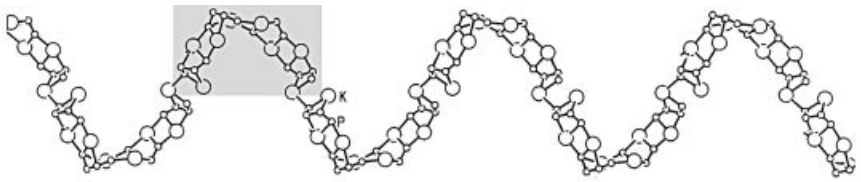

Figure 8. Polymeric helical arrangement in $[\{K(L)_2\}_2\{K(L)\}_6(P_4Mes_4)_4 \cdot 0.5THF]_\infty$ (L = 1,4-dioxane) (**7**); the tetrameric unit is underlain in grey; only K−P distances up to 363 pm are shown

P5,P7;K4−P6,P8) = 323.6(2)−355.8(2) pm] than the K−P distance to the second terminal phosphorus atom [*d*(K8a−P16a;K5−P13a;K4−P5;K2−P8) = 346.5(2)−406.8 pm, *d*(K6−P12;K7−P9;K3−P1;K1−P4) = 360.8(2)−401.3(2) pm]. The torsion angles in the $(P_4Mes_4)^{2-}$ chains are in a range similar to those observed in **4** and **6** [torsion angles between the planes P5−P6−P7 and P6−P7−P8: 70.8°, P1−P2−P3 and P2−P3−P4: 74.4°, P9−P10−P11 and P10−P11−P12: 74.3°, P13a−P14a−P15a and P14a−P15a−P16a: 68.7°]. This seems to indicate the formation of four-membered chelate rings of the dianionic $(P_4Mes_4)^{2-}$ ligands with potassium, a situation that is analogous to the structures of **4** and **6**, and may be described as predominant coordination of the alkali metal by the phosphorus atoms in the 1,3 positions of the chain with additional (weaker) interactions bearing a further phosphorus atom in the terminal position of the chain. The monomeric $\{K_2(L)_3(P_4Mes_4)\}$ and $\{K_2(L)_2(P_4Mes_4)\}$ units are associated *via* a four-membered K_2P_2 ring motif displaying K−P interactions, which are close to the short contacts observed in the monomers themselves [*d*(K5,K6−P16a,P9) = 325.8(2)−340.7(2) pm, *d*(K7,K3−P4,P12) = 324.3(2)−345.6(2) pm, *d*(K1,K2−P1,P5) = 328.6(2)−338.2(2) pm]. In contrast, aggregation of the tetrameric units proceeds through only two K−P interactions [*d*(K8a−P8) = 360.4(2) pm, *d*(K4−P13) = 376.1(2) pm], which are in the upper range of the distances generally observed in related potassium phosphanides.[9] Six potassium atoms within the tetrameric framework are each solvated by one dioxane ligand, whereas the two potassium atoms at the termini of the tetramer are each coordinated by two dioxane ligands. It is noteworthy, that in all the dioxane molecules only *one* oxygen atom coordinates to potassium. Solvation is completed by additional close contacts of some of the potassium cations with the aromatic rings of the mesityl substituents, which may be described as η^2-interactions [(K1−C41,C46) = 308.4(5)−321.7(5) pm, *d*(K3−C11, C12) = 305.8(5)−309.6(5) pm, *d*(K7−C91,C92) = 312.6(5)−316.2(5) pm, *d*(K5−C131a,C132a) = 302.7(5)−309.5(5) pm, *d*(K2−C81,C86) = 302.7(5)−312.1(5) pm].[26−30]

Orange crystals of $[\{K(pmdeta)(HP_3Mes_3)\}_2\{K_2(P_4Mes_4)\}] \cdot 0.25$ hexane (**8**) were obtained from the concentrated reaction mixture of $MesPCl_2$ and K (1:2.5), which also contained an excess of pmdeta and hexane. The crystal structure of this compound displays a co-complex, containing a $[K_2(P_4Mes_4)]$ unit, which is in contact with two $(HP_3Mes_3)^-$ ligands and two K cations, the latter being additionally solvated in each case by one pmdeta ligand (Figure 9 and Fig-

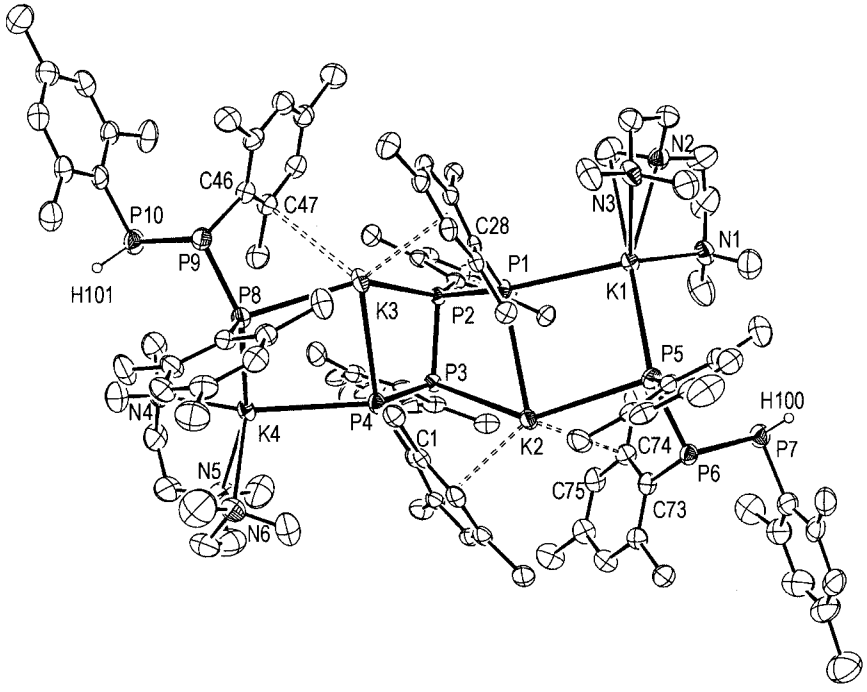

Figure 9. Molecular structure of $[\{K(pmdeta)(HP_3Mes_3)\}_2\{K_2(P_4Mes_4)\}] \cdot 0.25$hexane (**8**) (hexane not shown)

 © 2004 Wiley-VCH Verlag GmbH & Co. KGaA, Weinheim

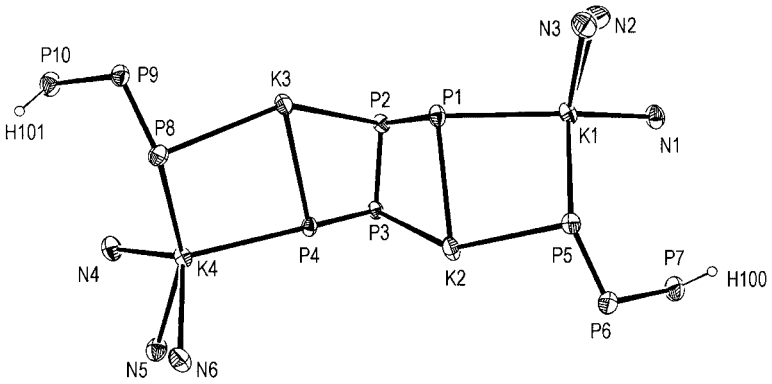

Figure 10. Molecular structure of $[\{K(pmdeta)(HP_3Mes_3)\}_2\{K_2(P_4Mes_4)\}]\cdot 0.25$hexane (**8**); only the central K,P,N framework and the P−H hydrogen atoms are shown.

ure 10). In spite of minor differences, the overall structural arrangement of the $[K_2(P_4Mes_4)]$ core in **8** is similar to those observed in the related compounds **4**, **6**, and **7**: the central $(P_4Mes_4)^{2-}$ dianion is in a *syn* arrangement with a slightly larger torsion angle than in the former structures [torsion angle between the planes P1−P2−P3 and P2−P3−P4: 91.1°]. The K−P distances are short between one terminal and one internal phosphorus atom of the chain and each potassium cation [*d*(K2−P1,P3) = 341.0(2)−342.5(2) pm, *d*(K3−P2,P4) = 339.4(2)−348.3(2) pm], but longer to the second terminal phosphorus atom [*d*(K2−P4) = 385.9(2), *d*(K3−P1) = 393.1(2) pm], indicating the formation of three-membered chelate rings (Figure 10). Additional solvation of the two central potassium cations by the aromatic substituents is indicated by short K−C contacts [*d*(K2−C28,C29,C30,C31,C32,C33) = 297.2(4)−342.3(5) pm, *d*(K2−C47) = 323.3 pm, *d*(K3−C1,C2,C3,C4,C5,C6) = 304.2(5)−334.9(5) pm, *d*(K3−C79) = 312.6 pm].[26−30]

The $[K_2(P_4Mes_4)]$ unit and the two $[K(pmdeta)(HP_3Mes_3]$ units are associated via four-membered K_2P_2 rings with short K−P interactions [*d*(K1,K2−P1,P5) = 321.7(2)−342.5(2) pm, *d*(K3,K4−P4,P8) = 328.5(2)−344.8(2) pm] (Figure 10). The catenated $(HP_3Mes_3)^-$ ligands coordinate to two potassium atoms (K1, K2 and K3, K8, respectively) through the anionic terminal phosphorus atom (P5 or P8), whereas the second terminal phosphorus atom (P7 or P10), which bears the proton of the chain, is uncoordinated. The bond angles about the internal phosphorus atom indicate sp^3 hybridization [angle P5−P6−P7: 107.41(9)°, angle P8−P9−P10: 108.20(8)°], and the P−P bond lengths within the anion are unremarkable [*d*(P5−P6), *d*(P6−P7), *d*(P8−P9), *d*(P9−P10) = 214.5(2)−224.6(2) pm].

The surprising observation of a three-membered monoprotonated $(HP_3Mes_3)^-$ anion in the structure of **8** may be explained by the fact that small amounts of the hitherto unknown compound $K_2(P_3Mes_3)$ were observed as a by-product in the synthesis of **6** when the stoichiometry of the reaction was slightly inaccurate. The anion $(HP_3Mes_3)^-$ may, therefore, have formed by reaction of the $(P_3Mes_3)^{2-}$ dianion with traces of water fortuitously present in the reaction mixture. Unfortunately, complete characterization of **8** was hampered by the impure nature of the isolated solid. Only further investigations will show if **8** can also be produced in a rational fashion.

A comparison of the structures **3**−**8** enables two different structural types to be distinguished: A "quasicyclic" arrangement, in which the ligands form five-membered chelate rings with the alkali metals, was observed for the structures of **3** and **5** (structural type **II**, Table 2 and Figure 5) − an arrangement, which has already been proposed by Baudler et al.[11a,11c] for **3** and related species, on the basis of their $^{31}P\{^1H\}$ NMR spectra (see below). In contrast, a different structural arrangement is present in **4**, **6**, **7**, and **8**, in which coordination occurs through both the internal and the terminal phosphorus atoms of the chain, and four-membered MP_3 chelate rings (M = Na, K) are the predominant structural features (structural type **I**, Table 2 and Figure 5).

Table 2. $^{31}P\{^1H\}$ NMR spectroscopic data (161.9 MHz, 25 °C, δ in ppm, *J* in Hz) of **3**−**6**

	3[11b]	**4**	**5**	**6**
$\delta_{AA'}$	−91.4	−113.1(1)	−78.1(1)	−110.5
$\delta_{BB'}$	−26.6	−13.7(1)	−5.2(1)	−12.6
$^1J_{BB'}$	−310.2(6)	−118.3(1)	−305.5(2)	−127.6(2)
$^1J_{AB} = {}^1J_{A'B'}$	−323.1(6)	−309.8(1)	−341.1(2)	−328.5(2)
$^2J_{AB'} = {}^2J_{A'B}$	−12.3(6)	+120.3(1)	−12.6(1)	+107.2(1)
$^3J_{AA'}$	+310.6(7)	+3.3(1)	+200.9(2)	+1.5(2)
Structural type	**II**	**I**	**II**	**I**

While the $^{31}P\{^1H\}$ NMR spectra of **4**−**6** display well resolved AA′BB′ spin systems at room temperature, the $^{31}P\{^1H\}$ NMR spectrum of **3** exhibits broad signals. Only at −83 °C do signals showing the characteristic AA′BB′ spin system (ca. 80% intensity) appear. These signals compare well with the literature values.[11b] In addition, there are also resonances, which indicate the presence of a second species (δ = −25 to −30, −70; ca. 20% intensity). Since these multiplets were not well resolved, the nature of these

 © 2004 Wiley-VCH Verlag GmbH & Co. KGaA, Weinheim

species could not be confidently ascertained. It seems likely, however, that these signals can be attributed to an ion-separated species $[Na(THF)_n][Na(THF)_m(P_4Ph_4)]$, which is in equilibrium with the ion-contact complex **3**.[12]

Nevertheless, the presence of only one AA′BB′ spin system for **3**−**6** clearly indicates the existence of only one diastereomer in solution. A summary of the chemical shifts and coupling constants of **3**−**6** is displayed in Table 2. While the chemical shifts of these species are in a similar range, a remarkable trend is observed for the coupling constants. Thus, whereas the $^3J(A,A')$ coupling constants (the coupling constants between the two terminal phosphorus atoms of the chain P_A and $P_{A'}$) of **4** and **6** are in the usual range expected for such long-range couplings, the corresponding coupling constants are dramatically larger for **3** and **5**. This unexpected strong coupling between the terminal phosphorus atoms, which has already been noted by Baudler et al. for **3** and related compounds, may indeed be explained by the presence of bridging alkali metal cations in a structure such as **II**, which may mediate an alternative pathway for coupling between the two terminal phosphorus atoms.[11a,11c] This, however, may not only be the case for an ion-contact structure such as **II**, but may also be consistent with alternative structures, such as an ion-separated cyclic arrangement with one bridging alkali metal cation, as suggested by Hoffmann and Caulton.[11b] To distinguish between these different possibilities, the $^2J(A,B')$ coupling constants are particularly informative. Interestingly, Baudler et al. noted that for related five-membered heterocycles *cyclo*-(P_4R_4X) (X = CH_2, R = Me, Cy, *t*Bu, Ph; X = S, Se, R = Ph; X = $P(CF_3)$, R = CF_3) a strict dependence of the $^2J_{P,P}$ coupling constant on structural features may be observed. If the substituents on the respective phosphorus atoms are in a *cisoid* arrangement, the coupling constants appear to attain significantly more positive values than if the substituents on the respective phosphorus atoms are in a *transoid* arrangement[11c] (a relationship, which is also valid for related sila-, stanna- and germatetraphospholanes).[15,16,33] A comparison of the $^2J(A,B')$ coupling constants in **3**−**6** revealed that **3** and **5** display similar negative $^2J(A,B')$ values. In contrast, the $^2J(A,B')$ coupling constants for **4** and **6** are significantly more positive. Hence, assuming that this rule is also valid for the related alkali metal complexes **3**−**6**, the different values for the $^2J(A,B')$ coupling constants may be due to different orientations of the organic substituents on the respective phosphorus atoms. A comparison of the solid-state structures of these compounds shows that a defined *cisoid* orientation of the Mes substituents of the internal and the terminal phosphorus atoms (i.e. between P_A,$P_{B'}$ and $P_{A'}$,P_B respectively) is indeed present in **4**, **6**, **7**, and **8**. However, the substituents on the terminal phosphorus atoms (P_A and $P_{A'}$) of **3** and **5** are approximately coplanar, with an almost coplanar arrangement of the four phosphorus atoms of the $(P_4R_4)^{2-}$ ligand. Thus, a proper *cis*/*trans* relationship between the substituents of P_A,$P_{B'}$ and $P_{A'}$,P_B was not observed for these structures. This characteristic feature of the solid-state structures of **3** and **5** may well be the underlying reason for the smaller values of the $^2J(A,B')$ coupling constants of these compounds in solution.

In general, the main features of the solid-state structures of **3**−**6** appear to reflect the trends observed for the P−P coupling constants of these species in solution quite clearly. This indicates, that the basic structural arrangements in the solid state are indeed retained in solution.

Interestingly, the ^{1}H NMR spectra of **4** and **6** [in C_6D_6 (**4**) and C_7D_8/[D_8]THF, 2:1, (**6**)] exhibit dynamic behavior. At room temperature, the resonances for the *ortho*-methyl groups of the Mes substituents of the terminal phosphorus atoms are inequivalent [**4**: δ = 2.47 (br) and 3.31 (br); **6**: δ = 2.36 and 3.22]. Upon warming the samples to 67 °C (**4**) and 60 °C (**6**), the broad, inequivalent peaks coalesce into a single broad resonance at ca. δ = 2.9 for **4**, while for **6** the previously sharp signals broaden severely, indicating that coalescence apparently requires a higher temperature. The inequivalence and the temperature dependence of the *o*-Me resonances may be the result of hindered rotation of the respective Mes groups in solution. Although a purely steric effect cannot be excluded on the basis of the NMR spectroscopic data alone, this might be caused by the presence of alkali metal-aryl interactions, which were also observed in the solid-state structures of these species.

Conclusions

Investigations of the reactions of *i*PrPCl$_2$, PhPCl$_2$ or MesPCl$_2$ with PCl$_3$ and Na (4:1:12) revealed that the cyclopentaphosphanide salts Na[*cyclo*-(P_5R_4)] [R = *i*Pr (**1**), Ph (**2**)] are formed in yields of 61% and 32%, respectively. In the reactions with PhPCl$_2$ and MesPCl$_2$, however, the catenated tetraphosphanediide salts $[Na_2(THF)_5(P_4Ph_4)]$ (**3**) and $[Na_2(THF)_4(P_4Mes_4)]$ (**4**) were obtained as the major products. Compounds **3**, **4**, $[Na_2(THF)_4(P_4tBu_4)]$ (**5**), and $[K_2(THF)_6(P_4Mes_4)]$ (**6**) were obtained more conveniently in a one-pot reaction of RPCl$_2$ (R = *t*Bu, Ph, Mes) with Na and K (1:2.5), and this represents a general, simplified route to tetraphosphanediide salts $[M_2(P_4R_4)]$.

In the solid state, two different types of coordination of the alkali metals were observed for **3**−**6**. All four phosphorus atoms are employed in the coordination of the alkali metal in **4** and **6**, whereas in **3** and **5**, coordination of Na occurs exclusively through the terminal phosphorus atoms of the chain. Recrystallization of **6** from 1,4-dioxane/pentane and pmdeta/THF/hexane solutions resulted in the isolation of $[\{K(L)_2\}_2\{K(L)\}_6(P_4Mes_4)_4\cdot 0.5THF]_\infty$ (L = 1,4-dioxane) (**7**) and $[\{K(pmdeta)(HP_3Mes_3)\}_2\{K_2(P_4Mes_4)\}]\cdot 0.25$hexane (**8**). The polymeric arrangement of **7** indicates that such compounds may also associate in the solid state, but the basic structural arrangement of the $[K_2(P_4Mes_4)]$ units, displaying four-membered KP_3 chelate rings, is preserved. This is also the case for the structure of **8**, in which one $[K_2(P_4Mes_4)]$ unit is associated with two [K(pmdeta)-(HP_3Mes_3)] moieties. A comparison of the structures of **3**−**8** and of the related compounds $[Na_2(tmeda)_2(P_4Ph_4)]$ and $[Na_2(dme)_3(P_4Ph_4)]$[12] indicates that the M_2P_4 frame-

 © 2004 Wiley-VCH Verlag GmbH & Co. KGaA, Weinheim

works are structurally rather robust, even in the presence of chelating donors and for different modes of association.

The ABB′CC′ (for **1** and **2**) and the AA′BB′ coupling patterns in the ^{31}P NMR spectra of **3**−**6** were analyzed. A comparison of the resultant coupling constants of the latter indicates that the basic structural features of these species are preserved not only in the solid state, but also in solution.

Future investigations will focus on the further elaboration of the structural chemistry of alkali metal oligophosphanediides and on the use of these compounds in the synthesis of phosphorus-rich metal complexes.

Experimental Section

General Methods: All procedures were performed under an inert atmosphere of pure argon with vigorous exclusion of air and moisture. The NMR spectra were recorded with a Bruker AVANCE DRX 400 spectrometer. ^1H NMR (400.13 MHz), internal standard: solvent, external standard: TMS. ^{31}P NMR (161.9 MHz), external standard: 85% H_3PO_4. ^{13}C NMR (100.16 MHz), internal standard: solvent, external standard: TMS. The solvents were saturated with argon and stored over potassium mirrors. *i*PrPCl$_2$,[34] *t*BuPCl$_2$,[34] MesPCl$_2$[35] were prepared by literature methods. PhPCl$_2$ and PCl$_3$ are commercially available and were freshly distilled before use. Elemental analyses were performed on a Heraeus VARIO EL instrument. The melting points were determined in sealed capillaries under argon and are uncorrected.

Data Collection and Structural Refinements of 3−8: Data [λ(Mo-K_α) = 0.71073 Å] were collected with a Siemens CCD (SMART) diffractometer (for **3**−**6**), on a STOE IPDS (**7**) or on a Nonius Kappa CCD (for **8**). All observed reflections were used in the refinements (SAINT) of the unit-cell parameters. Empirical absorption corrections were carried out with SADABS (**3**−**6**) and SORTAV (**8**).[36] The structures were solved by direct methods (**3**−**7**: SHELXTL PLUS. **8**: SHELX-97).[37] Na, K, P, N O, and C atoms were refined anisotropically. Some C atoms of disordered solvent molecules were refined isotropically. H atoms were located using difference maps and refined isotropically. Table 3 lists crystallographic details. The thermal ellipsoids of the molecular structures in Figures 1−4 and 6−10 are shown at the 30% probability level. CCDC-222008 (for **3**), -222009 (for **4**), -222005 (for **5**), -222007 (for **6**), -222006 (for **7**), and -222004 (for **8**) contain the supplementary crystallographic data for this paper. These data can be obtained free of charge via www.ccdc.cam.ac.uk/conts/retrieving.html [or from the Cambridge Crystallographic Data Center, 12 Union Road, Cambridge CB2 1EZ, UK; Fax (internat.): +44-1223-336-033 or E-mail: deposit@ccdc.cam.uk].

Na[*cyclo*-(P$_5$*i*Pr$_4$)] (1) and Na[*cyclo*-(P$_5$Ph$_4$)] (2): PCl$_3$ (2.51 g, 18.2 mmol, 1.6 mL) and Na (5.04 g, 219.0 mmol) were carefully added to *i*PrPCl$_2$ (10.6 g, 73.1 mmol) or PhPCl$_2$ (13.04 g, 72.6 mmol), respectively, in THF (150 mL). The mixture was heated to reflux for 5 days. After 1 day the initially colorless solution had become yellow-green, and after 2 days, dark brown. The solvent was removed under reduced pressure, and the dark brown residue extracted with *n*-pentane (250 mL). The solvent was re-

Table 3. Crystal data and structural refinements for **3**−**8**

	3	**4**	**5**	**6**	**7**	**8**
Formula	$C_{44}H_{60}Na_2O_5P_4$	$C_{52}H_{76}Na_2O_4P_4$	$C_{32}H_{68}Na_2O_4P_4$	$C_{60}H_{92}K_2O_6P_4$	$C_{186}H_{260}K_8O_{20.50}P_{16}$	$C_{109.50}H_{161.50}K_4N_6P_{10}$
M	838.78	934.99	686.72	1111.42	3631.26	2028.05
T [K]	208(2)	208(2)	218 (2)	218 (2)	203(2)	150(2)
Crystal system	monoclinic	monoclinic	monoclinic	orthorhombic	monoclinic	triclinic
Space group	*C*2/*c*	$P2_1/c$	$P2_1/n$	$Pna2_1$	$P2_1/c$	$P\bar{1}$
a [Å]	13.693(2)	19.379(4)	13.504(5)	16.021(5)	28.587(6)	12.544(3)
b [Å]	15.972(2)	19.040(4)	16.171(5)	25.135(5)	23.927(5	19.065(4)
c [Å]	21.196(2)	15.849(3)	19.307(5)	15.913(5)	33.789(7)	26.186(5)
α [°]	90	90	90	90	90	84.99(3)
β [°]	93.015(4)	113.679(4)	99.341(5)	90	105.98(3)	85.33(3)
γ [°]	90	90	90	90	90	89.51(3)
V [Å^3]	4629(1)	5356(2)	4160(2)	6408(3)	22219(8)	6218(2)
Z	4	4	4	4	4	2
Crystal size [cm]	0.4 × 0.4 × 0.4	0.4 × 0.4 × 0.1	0.2 × 0.2 × 0.1	0.2 × 0.1 × 0.1	0.2 × 0.2 × 0.4	0.15 × 0.15 × 0.10
ρ_{calcd} [Mg·m^{-3}]	1.204	1.160	1.096	1.152	1.086	1.083
F(000)	1784	2008	1496	2392	7728	2173
μ(Mo-K_α) [cm^{-1}]	0.223	0.198	0.232	0.292	0.323	0.315
hkl range	−10/17, −19/19, −24/26	11/26, −26/25, −21/20	−18/14, −21/20, −17/25	−19/19, −23/31, −19/19	−30/30, −25/25, −36/36	−14/14, −22/22, −29/31
$2\theta_{max.}$ (°)	52.74	58.76	58.76	52.12	45.00	50.16
Reflections collected/unique	14873/4730	32430/13365	25852/10112	34204/12380	95913/29035	54949/20231
R(int.)	0.0346	0.0485	0.0235	0.0651	0.0470	0.0830
Data/restraints/ parameters	4730/10/347	13365/0/768	10112/0/654	12380/7/658	29035/6/2225	20231/47/1215
Goodness of Fit on F^2	1.011	1.007	0.960	1.046	0.939	1.039
$R1/wR2$ [$I > 2\sigma(I)$]	0.0657/0.1616	0.0594/0.1259	0.0352/0.0883	0.0739/0.1432	0.0728/0.2037	0.0805/0.2076
$R1/wR2$ (all data)	0.1112/0.1922	0.1247/0.1492	0.0592/0.0996	0.1315/0.1632	0.1126/0.2234	0.1203/ 0.2333
Absolute structure parameter	/	/	/	0.49(7)	/	/
Largest diff. Peak/hole [e·Å^{-3}]	0.581/0.656	0.330/0.251	0.345/-0.186	0.213/−0.254	1.258/ −0.445	1.371/−0.564

 © 2004 Wiley-VCH Verlag GmbH & Co. KGaA, Weinheim

moved under reduced pressure, and **1** and **2** were characterized by ^{31}P NMR spectroscopy (cf. Table 1).

$[Na_2(THF)_5(P_4Ph_4)]$ (3): $PhPCl_2$ (3.83 g, 21.4 mmol) was dissolved in THF (ca. 50 mL), and added to freshly prepared sodium sand (1.23 g, 53.5 mmol, prepared from Na in boiling toluene). The mixture was heated to reflux for 3 days. An orange suspension was formed that contained ca. 75% of **4**. Filtration and concentration of the THF solution to ca. 30 mL gave yellow crystals upon storage at −20 °C overnight. The yellow crystals were isolated and dried in vacuo for 45 min. Yield 1.97 g (48% ref. to **3**-THF); m.p. 101−103 °C. ^1H NMR (C_7D_8): δ = 1.32 (m, 16 H, THF), 3.36 (m, 16 H, THF), 6.38 (br., 2 H, *p*-H), 6.62 (br., 4 H, *m*-H), 6.78 (br., 2 H, *p*-H), 6.91 (br., 4 H, *o*-H), 7.29 (br., 4 H, *m*-H), 7.86 (br., 4 H, *o*-H). $^{13}C\{^1H,^{31}P\}$ NMR (C_6D_6): δ = 25.27 (THF), 67.55 (THF), 120.69 (4-C in Ph), 125.89 (4-C in Ph), 130.54 (2,6-C in Ph), 132.42 (2,6-C in Ph), 146.1 (1-C in Ph), 151.60 (1-C in Ph) (no P−C coupling observed, signals of 3,5-C overlap with solvent resonances at ca. 127 ppm). $^{31}P\{^1H\}$ NMR (C_7D_8, +25 °C): δ ≈ −23.0 (br), −74.6 (br), −88.0 (br). $^{31}P\{^1H\}$ NMR (C_7D_8, −83 °C): δ ≈ −25 to −30 (m, 2P), −26.5 (B part of an AA′BB′ spin system, 8P), ca. −70 (m, 2P), −90.7 (A part of an AA′BB′ spin system), cf. Table 2. $C_{40}H_{52}Na_2O_4P_4$ (766.72): calcd. C 62.7, H 6.80, P 16.2; found C 60.0, H 6.55, P 16.5.

$[Na_2(THF)_4(P_4Mes_4)]$ (4): $MesPCl_2$ (1.31 g, 5.9 mmol) was dissolved in THF (ca. 50 mL) and added to freshly prepared sodium sand (0.33 g, 14.5 mmol, prepared from Na in boiling toluene). The mixture was heated to reflux for 2.5 days. A red suspension was formed which was filtered. The solvent was completely removed, and the remaining yellow solid recrystallized from THF/hexane, 1:2. Yield 0.31 g (27% ref. to **4**−2THF); m.p. 238 °C decomp. to a brown solid. ^1H NMR (C_6D_6): δ = 1.51 (m, 8 H, THF), 2.04 (s, 6 H, *p*-CH_3 in Mes), 2.16 (s, 6 H, *p*-CH_3 in Mes), 2.47 (br., 6 H, *o*-CH_3 in Mes), 2.70 (s, 12 H, *o*-CH_3 in Mes), 3.31 (br., 6 H, *o*-CH_3 in Mes), 3.57 (m, 8 H, THF), 6.61 (br., 4 H, 3,5-H in Mes), 6.81 (br., 4 H, 3,5-H in Mes). $^{13}C\{^1H,^{31}P\}$ NMR (C_6D_6): δ = 20.43 (*p*-CH_3 in Mes), 20.56 (*p*-CH_3 in Mes), 23.56 (*o*-CH_3 in Mes), 24.47 (THF), 26.17 (*o*-CH_3 in Mes), 66.60 (THF), 128.13 (3,5-C in Mes at P_B), 129.41 (3,5-C in Mes at P_A), 135.03 (4-C in Mes at P_A), 137.34 (1-C in Mes at P_A), 141.43 (4-C in Mes at P_B), 141.89 (2,6-C in Mes at P_A), 145.09 (2,6-C in Mes at P_B), 150.40 (1-C in Mes at P_B) (no P−C coupling observed). $^{31}P\{^1H\}$ NMR (C_6D_6): cf. Table 2. $C_{52}H_{76}Na_2O_4P_4$ (935.05): calcd. C 66.80, H 8.20, O 6.80; found C 65.50, H 6.69, O 7.01.

$[Na_2(THF)_4(P_4tBu_4)]$ (5): $tBuPCl_2$ (5.71 g, 35.9 mmol) was dissolved in THF (ca. 50 mL), and added to freshly prepared sodium sand (2.10 g, 90.0 mmol, prepared from Na in boiling toluene). The mixture was heated to reflux for 5 days. A dark-green suspension formed, which contained ca. 53% of **5**. This was filtered, the filtrate reduced to ca. 10 mL, and layered with 20 mL of pentane. Light yellow crystals formed on storage at −20 °C and were isolated. The crystals still contained ca. 15% *cyclo*-$[Na(THF)_4(P_5tBu_4)]$ and were recrystallized from THF/hexane, 1:2 to give **5** in 95% purity. Yield 1.23 g (40% ref. to **5**-4THF); m.p. 240 °C decomp. to a brown solid. ^1H NMR (C_7D_8/[D_8]THF, 2:1): δ = 1.51 (br., 36 H, *t*Bu). $^{13}C\{^1H,^{31}P\}$ NMR (C_7D_8/[D_8]THF, 2:1): δ = 28.64 [2 $C(CH_3)_3$], 29.06 [2 $C(CH_3)_3$], 30.84 (6 CH_3 in *t*Bu), 37.81 (6 CH_3 in *t*Bu). $^{31}P\{^1H\}$ NMR (C_7D_8/[D_8]THF, 2:1): cf. Table 2.

$[K_2(THF)_6(P_4Mes_4)]$ (6): Potassium (1.12 g, 28.30 mmol) was added to a solution of $MesPCl_2$ (2.55 g, 11.51 mmol) in THF (40 mL). The mixture was heated to reflux for 3 h. The resultant dark red suspension was filtered, and the filtrate reduced to ca. 5 mL. A yellow precipitate formed, which redissolved on heating the solution. Dark-orange crystals formed on storing the saturated solution of **6** at ambient temperature. The orange-red, crystalline solid was isolated and dried in vacuo for 2 h. Yield 0.84 g (43% ref. to **6**−6THF); m.p. 200−201 °C. ^1H NMR (C_7D_8/[D_8]THF, 2:1): δ = 2.06 (s, 6 H, *p*-CH_3 in Mes), 2.11 (s, 6 H, *p*-CH_3 in Mes), 2.36 (s, 6 H, *o*-CH_3 in Mes), 2.62 (s, 12 H, *o*-CH_3 in Mes), 3.22 (s, 6 H, *o*-CH_3 in Mes), 6.41 (br., 4 H, 3,5-H in Mes), ca. 6.7 (br., 4 H, 3,5-H in Mes). $^{13}C\{^1H,^{31}P\}$ NMR (C_7D_8/[D_8]THF, 2:1): δ = 19.8 (*p*-CH_3 in Mes), 20.0 (*p*-CH_3 in Mes), 23.15 (*o*-CH_3 in Mes), 25.41 (*o*-CH_3 in Mes), 26.30 (*o*-CH_3 in Mes), 127.6 (3,5-C in Mes at P_A), 128.6 (3,5-C in Mes at P_B), 134.31 (4-C in Mes at P_A), 138.6 (1-C in Mes at P_A), 141.48 (2,6-C in Mes at P_A), ca. 141.4 (4-C in Mes at P_B), 144.68 (2,6-C in Mes at P_B), 153.5 (1-C in Mes at P_B) (no P−C coupling observed). $^{31}P\{^1H\}$ NMR (C_7D_8/[D_8]THF, 2:1): cf. Table 2.

$[\{K(L)_2\}_2\{K(L)\}_6(P_4Mes_4)_4\cdot 0.5THF]_\infty$ (L = 1,4-Dioxane) (7): A solution of **6** (0.21 g, 0.31 mmol) in 1,4-dioxane (5 mL) was layered with *n*-pentane (15 mL) and stored for 2 weeks at room temperature. Large orange crystalline plates formed, which were isolated and dried in vacuo for 1 h. Yield 0.15 g; m.p. 175−177 °C; the compound is insoluble in hydrocarbon solvents, but shows signs of decomposition when dissolved in THF (cf. ^{31}P NMR spectroscopic data). ^{31}P NMR ([D_8]THF): δ = −10.3 (br. m, 2P), −14.4 (B part of an AA′BB′ spin system of $(P_4Mes_4)^{2-}$, 4P), −83.6 (br., 4P), −85.3 [dd, 2P, $^1J_{P,P}$ = 376.3, $^1J_{P,H}$ = 204.4 Hz, MesPH of $K(HP_2Mes_2)$], −106.2 (br. m, 4P), −109.7 [A part of an AA′BB′ spin system of $(P_4Mes_4)^{2-}$, 4 P], −136.2 [d, 2 P, $^1J_{P,P}$ = 376.3 Hz, $MesP^-$ of $K(HP_2Mes_2)$], −143.2 [d, 1 P, $^1J_{P,H}$ = 163 Hz, K(HPMes)[28]].

Acknowledgments

Financial support from the Graduiertenförderung des Landes Sachsen (PhD grant for A. S.), the Studienstiftung des Deutschen Volkes (PhD grant for R. W.), and the German Academic Exchange Service (313-ARC-XVI-02/10) is gratefully acknowledged. We thank Dipl.-Chem. S. Gerber and Prof. Dr. H. Krautscheid for the data collection on compound **7**.

[1] M. Baudler, K. Glinka, *Chem. Rev.* **1993**, *93*, 1623−1667.
[2] H. Köhler, A. Michaelis, *Ber. Dtsch. Chem. Ges.* **1877**, *10*, 807−814.
[3] M. Baudler, C. Gruner, G. Fürstenberg, B. Kloth, F. Saykowski, U. Özer, *Z. Anorg. Allg. Chem.* **1978**, *446*, 169−176.
[4] M. Baudler, B. Makowka, *Z. Anorg. Allg. Chem.* **1985**, *528*, 7−21.
[5] A. Schmidpeter, G. Burget, *Phosphorus Sulfur* **1985**, *22*, 323−336.
[6] G. Fritz, K. Stoll, *Z. Anorg. Allg. Chem.* **1986**, *538*, 78−112.
[7] G. Fritz, R. Biastoch, K. Stoll, T. Vaahs, D. Hanke, H. W. Schneider, *Phosphorus Sulfur* **1987**, *30*, 385−388.
[8] A. Schisler, U. Huniar, P. Lönnecke, R. Ahlrichs, E. Hey-Hawkins, *Angew. Chem.* **2001**, *113*, 4345−4348, *Angew. Chem. Int. Ed.* **2001**, *40*, 4217−4219.
[9] K. Izod, *Adv. Inorg. Chem.* **2000**, *50*, 33−107.
[10] [10a] K. Issleib, K. Krech, *Chem. Ber.* **1965**, *98*, 2545−2550. [10b] K. Issleib, E. Fluck, *Z. Anorg. Allg. Chem.* **1965**, *339*, 274−280. [10c] K. Issleib, K. Krech, *Chem. Ber.* **1966**, *99*, 1310−1315. [10d] K. Issleib, M. Hoffmann, *Chem. Ber.* **1966**, *99*, 1320−1324; K. Issleib, C. Rockstroh, I. Duchek, E. Fluck, *Z. Anorg. Allg. Chem.* **1968**, *360*, 77−87. [10e] K. Issleib, K. Krech, *J. Prakt. Chem.* **1969**, *311*, 463−471.
[11] [11a] M. Baudler, D. Koch, E. Tolls, K. M. Diederich, B. Kloth, *Z. Anorg. Allg. Chem.* **1976**, *420*, 146−145. [11b] P. R. Hoffmann, K. G. Caulton, *J. Am. Chem. Soc.* **1975**,

 © 2004 Wiley-VCH Verlag GmbH & Co. KGaA, Weinheim

6370−6374. [11c] M. Baudler, D. Koch, *Z. Anorg. Allg. Chem.* **1976**, *425*, 227−235.
[12] J. Geier, H. Rüegger, M. Wörle, H. Grützmacher, *Angew. Chem.* **2003**, *113*, 4081−4085; *Angew. Chem. Int. Ed.* **2003**, *42*, 3951−3945.
[13] H. Köpf, R. Voigtländer, *Chem. Ber.* **1981**, *114*, 2731−2743.
[14] R. A. Jones, M. H. Seeberger, B. R. Whittlesey, *J. Am. Chem. Soc.* **1985**, *107*, 6424−6426.
[15] [15a] M. Baudler, H. Suchomel, *Z. Anorg. Allg. Chem.* **1983**, *503*, 7−14. [15b] H. Binder, B. Schuster, W. Schwarz, K. W. Klinkhammer, *Z. Anorg. Allg. Chem.* **1999**, *625*, 699−701. [15c] M. Baudler, L. Riese-Meyer, U. Schings, *Z. Anorg. Allg. Chem.* **1984**, *519*, 24−30.
[16] [16a] M. Baudler, H. Suchomel, *Z. Anorg. Allg. Chem.* **1983**, *505*, 39−47. [16b] D. Bongert, G. Heckmann, W. Schwarz, H.-D. Hausen, H. Binder, *Z. Anorg. Allg. Chem.* **1995**, *621*, 1358−1364. [16c] D. Bongert, H.-D. Hausen, W. Schwarz, G. Heckmann, H. Binder, *Z. Anorg. Allg. Chem.* **1996**, *622*, 1167−1172.
[17] A. Schisler, Dissertation, University of Leipzig, **2003**.
[18] [18a] M. Baudler, B. Carlsohn, W. Böhm, G. Reuschenbach, *Z. Naturforsch., Teil B* **1976**, *31*, 558−564. [18b] M. Baudler, G. Reuschenbach, *Z. Anorg. Allg. Chem.* **1980**, *464*, 9−16. [18c] L. R. Smith, J. L. Mills, *J. Am. Chem. Soc.* **1976**, *98*, 3852−3857.
[19] M. C. J. M. van Hooijdonk, G. Gerritsen, L. Brandsma, *Phosphorus, Sulfur, Silicon* **2000**, *162*, 39−49.
[20] M. Baudler, H. Tschäbunin, H. Suchomel, J. Hasenbach, *Z. Naturforsch., Teil B* **1994**, *49*, 773−777.
[21] A negative sign was generally used for the coupling constants $^1J_{P,P}$, and the remaining signs and coupling constants were calculated with the program *SPINWORKS* (K. Marat, *SPINWORKS*, version 2000 05 10, University of Manitoba).
[22] M. Baudler, W. Driehsen, S. Klautke, *Z. Anorg. Allg. Chem.* **1979**, *459*, 48−58.
[23] [23a] Z. Hou, X. Jia, A. Fujita, H. Tezuka, H. Yamazaki, Y. Wakatsuki, *Chem. Eur. J.* **2000**, *6*, 2994−3005. [23b] Z. Hou, A. Fujita, H. Yamazaki, Y. Wakatsuki, *Chem. Commun.* **1998**, 669−670: [23c] S. Brooker, F. T. Edelmann, T. Kottke, H. W. Roesky, G. M. Sheldrick, D. Stalke, K. H. Whitmire, *J. Chem. Soc., Chem. Commun.* **1991**, 144−146. [23d] Q. Shen, M. Qi, Y. Lin, *J. Organomet. Chem.* **1990**, *399*, 247−254.
[24] [24a] G. W. Rabe, H. Heise, G. P. A. Yap, L. M. Liable-Sands, I. A. Guzei, A. L. Rheingold, *Inorg. Chem.* **1998**, *37*, 4235−4236. [24b] C. Frenzel, D. Somoza Jr., S. Blaurock, E. Hey-Hawkins, *J. Chem. Soc., Dalton Trans.* **2001**, 3115−3118.
[25] R. Blom, A. Haaland, *J. Mol. Struc.* **1985**, *128*, 21−27.
[26] G. W. Rabe, G. P. A. Yap, A. L. Rheingold, *Inorg. Chem.* **1997**, *36*, 1990−1991.
[27] G. W. Rabe, S. Kehradmandan, H. Heise, I. A. Guzei, L. M. Liable-Sands, A. L. Rheingold, *Main Group Chem.* **1998**, *2*, 221−228.
[28] C. Frenzel, P. Jörchel, E. Hey-Hawkins, *Chem. Commun.* **1998**, 1363−1364.
[29] H.-J. Gosink, F. Nief, L. Ricard, F. Mathey, *Inorg. Chem.* **1995**, *34*, 1306−1307.
[30] C. J. Schaverien, J. B. Van Mechelen, *Organometallics* **1991**, *10*, 1704−1709.
[31] B. Werner, T. Kräuter, B. Neumüller, *Organometallics* **1996**, *15*, 3746−3851 (and ref. therein).
[32] J. D. Smith, *Adv. Organomet. Chem.* **1998**, *43*, 267−348.
[33] B. Riegel, A. Pfitzner, G. Heckmann, H. Binder, E. Fluck, *Z. Anorg. Allg. Chem.* **1995**, *621*, 1989−1996.
[34] W. Vokusil, J. F. Arens, *Recl. Trav. Chim. Pays-Bas* **1963**, *82*, 302−304.
[35] F. Nief, F. Mathey, *Tetrahedron* **1991**, *47*, 6673−6680.
[36] G. M. Sheldrick, *SADABS − A Program for Empirical Absorption Correction,* Göttingen, Germany, **1998**.
[37] [37a] *SHELXTL PLUS, Siemens Analyt. X-ray Inst. Inc.* **1990**, XS: *Program for Crystal Structure Solution*, XL: Program for Crystal Structure Determination, XP: Interactive Molecular Graphics. [37b] G. M. Sheldrick, *SHELXL-97*, University of Göttingen, **1997**.

Received February 23, 2004
Early View Article
Published Online June 1, 2004

 © 2004 Wiley-VCH Verlag GmbH & Co. KGaA, Weinheim

Tris(pyrazolyl)methane Ligands: Syntheses and Structures of Monometallic and Metallodendritic Complexes

Alberto Sánchez-Méndez,[a] Gustavo F. Silvestri,[a] Ernesto de Jesús,[a] F. Javier de la Mata,[a] Juan C. Flores,*[a] Rafael Gómez,[a] and Pilar Gómez-Sal[a]

Keywords: N ligands / Titanium / Palladium / Molybdenum / Dendrimers

The substituted ligands $Me_3SiC(pz)_3$ (**1**) and $Me_3SiOCH_2C(pz)_3$ (**2**) have been prepared starting from $HC(pz)_3$ and $HOCH_2C(pz)_3$. The molecular structure of compound **1** has been determined by X-ray diffraction studies, which show a propeller-like conformation of the pyrazolyl rings. Compound **2** has been found to be useful for the synthesis of $[Mo(CO)_3\{Me_3SiOCH_2C(pz)_3\}]$ (**3**), $[TiCl_2(N\mathit{t}Bu)\{Me_3SiOCH_2C(pz)_3\}]$ (**4**), and $[PdCl_2\{Me_3SiOCH_2C(pz)_3\}]$ (**5**), through ligand exchange reactions. The characterization of the new complexes is compatible with a tridentate coordination of the ligands in complexes **3** and **4**, and a bidentate coordination in **5** as confirmed by an X-ray analysis carried out with the palladium complex. The procedure has been extended for the synthesis of the carbosilane G1–$[OCH_2C(pz)_3]_4$ (**6**) and the tetrametallic compound G1–$[OCH_2C(pz)_3Mo(CO)_3]_4$ (**7**) (G1 = $Si(CH_2CH_2CH_2Me_2Si)_4$–).
(© Wiley-VCH Verlag GmbH & Co. KGaA, 69451 Weinheim, Germany, 2004)

Introduction

Since their introduction by Trofimenko's pioneering work,[1] tris(pyrazolyl)-borates, or scorpionates, have become a very important class of tripodal nitrogen-donating ligands in modern coordination chemistry. These versatile family of substituted and non substituted ligands have been used to synthesize complexes of most metals of the periodic table, some of which have useful applications in a wide range of areas.[2] The isoelectronic and isosteric tris(pyrazolyl)methane ligands have received much less attention until the significant improvement of their synthetic procedures.[3] Subsequently, this area of chemistry has rapidly developed new modified ligands and complexes, including those functionalized at the methine central carbon atom of tris(pyrazoly)methane[4–7] and related systems.[5] The substitution of the reactive methine proton by other functional groups have led, for instance, to the preparation of ligands and complexes soluble and stable in water,[6] and offered the opportunity to synthesize multitopic ligands and polynuclear compounds by linking tris(pyrazolyl)methane units in a molecular core.[7]

In the last few years we have focused our research work into the chemistry of carbosilane dendrimers containing early transition metal complexes, located at the dendritic periphery or at the focal point, and usually bonded through O- or N-donor anchoring ligands.[8] Since poly(pyrazolyl)-methanes can be functionalized with different groups at the central carbon atom while coordinated to metallic moieties at the other side, we decided to evaluate the possible application of this type of neutral ligands in the field of carbosilane metallodendritic chemistry.

This paper describes our results using silyl and siloxy derivatives of tris(1-pyrazolyl)methane and -ethane for the synthesis of early and late transition metal complexes. In addition, the preparation and characterization of a molybdenum tetranuclear compound with a carbosilane core is presented.

Results and Discussion

Synthesis of Ligands

$Me_3SiC(pz)_3$ (**1**) was prepared by the deprotonation reaction of tris(pyrazolyl)methane with LiMe in THF, followed by the addition of chlorotrimethylsilane in the same solvent (Scheme 1). The preparation of compound **1** with *n*-butyllithium as a base has been reported during the course of this work; **1** was described as an orange yellow solid, which was characterized by ^1H NMR spectroscopy, and the molecular peak observed by MS.[4] The procedure used here, including the isolation and purification of the intermediate $LiC(pz)_3$ (**I**, see Scheme 1 and the Exp. Sect.), allows for the synthesis of **1** in 75% yield as an analytically pure white solid. The product is stable in air and soluble in all common organic solvents. Single crystal of **1** suitable for X-ray structure determinations were obtained by recrystallization from pentane.

[a] Departamento de Química Inorgánica, Universidad de Alcalá, Campus Universitario, 28871 Alcalá de Henares (Madrid), Spain
Fax: (internat.) + 34-91-8854683
E-mail: juanc.flores@uah.es

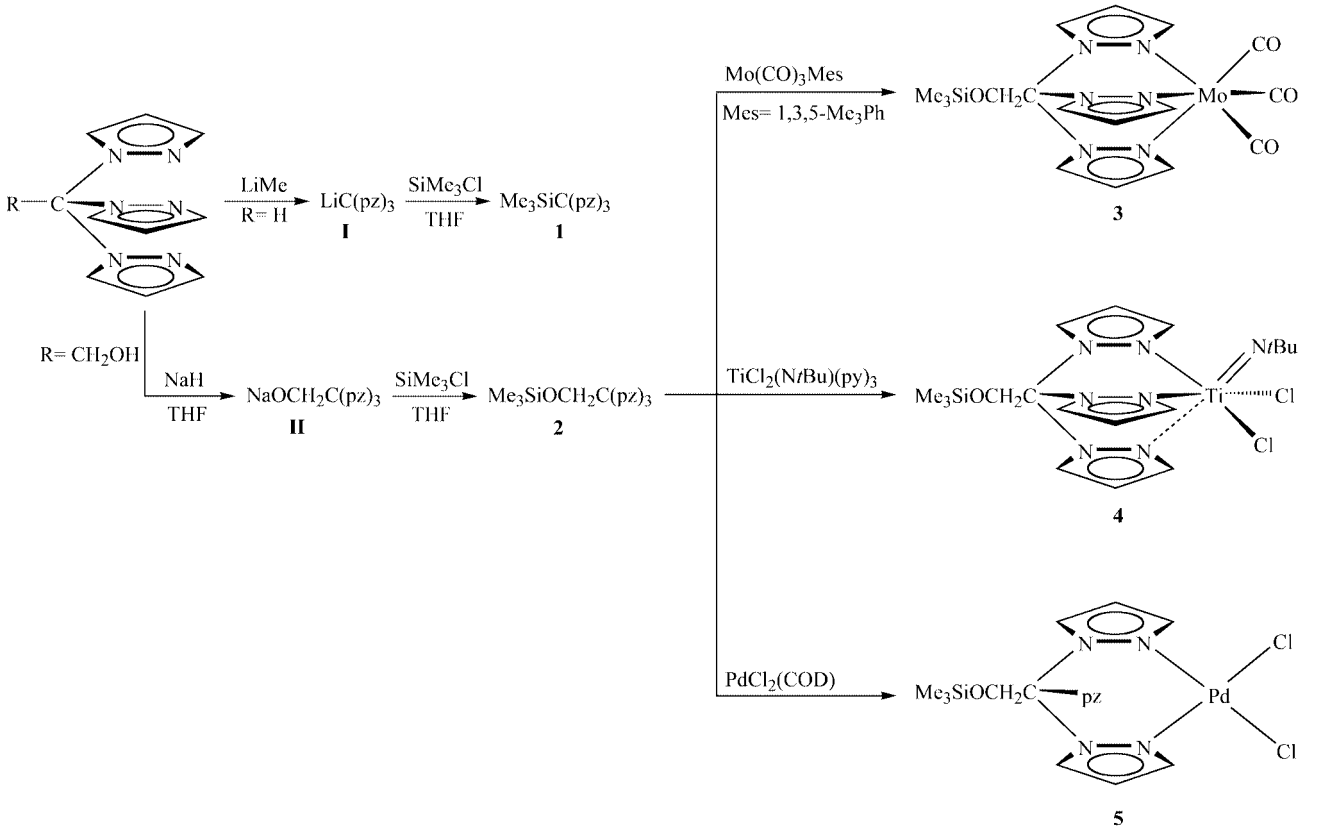

Scheme 1

A computer molecular modeling study of this compound shows several close contacts between the atoms in the 5-position of the pyrazolyl rings (C and H) and the $SiMe_3$ fragment. Maximum interaction occurs when the three rings are parallel to the C_3 axis (Figure 1a) in the tripodal arrangement expected in coordination complexes, and this steric hindrance minimizes by rotation of the pyrazolyl rings about the N−C(methine) bond (Figure 1b). These results are confirmed in the solid-state structure determined by X-ray diffraction studies, and in solution by the chemical behavior found for compound **1** (vide infra). At this point it is worth mentioning that our attempts to functionalize the central carbon atom of $HC(3,5\text{-}Me_2pz)_3$ failed, as was also noted by Reger who explained that the methyl groups in the 5-position block the reaction at that carbon atom.[4]

The reaction of 2,2,2-tris(pyrazolyl)ethanol with NaH in THF at room temperature resulted in the quantitative formation of the alkoxide **II** as an intermediate (Scheme 1), which was isolated as a hygroscopic white solid and characterized spectroscopically.[9] Subsequent addition of $SiMe_3Cl$ in THF gave $Me_3SiOCH_2C(pz)_3$ (**2**) in 80% yield after workup. Compound **2** was isolated as a colorless oil, which is stable in air and very soluble in all common organic solvents. Molecular modeling of the siloxy derivative **2** reveals a much more relaxed structure. Only some close contacts are observed between the 5-position atoms and the CH_2O-$SiMe_3$ moiety, if the tripodal arrangement is in the eclipsed conformation along the $(pz)_3C-CH_2O$ bond (Figure 1c).

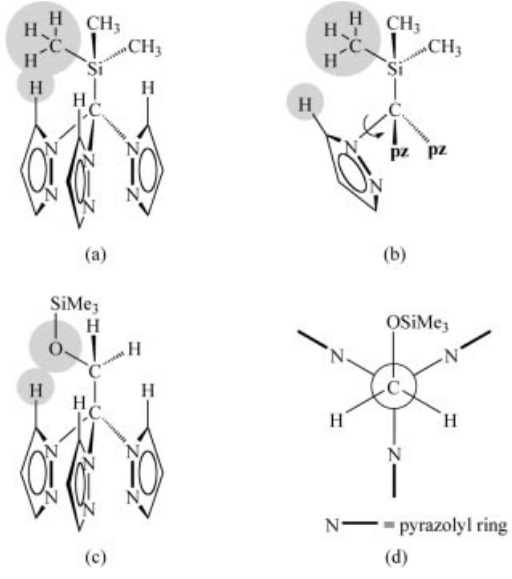

Figure 1. Representations of close contacts in compound **1** (a) and a more relaxed disposition (b); representations of close contacts in compound **2** (c) and the staggered conformation (d)

These interactions become negligible for the staggered conformation (Figure 1d) or by rotation of the pyrazolyl ring. The latter is in agreement with the small rotation barrier along the central $C-CH_2OR$ bond proposed by Reger in related rhenium compounds.[7b]

 © 2004 Wiley-VCH Verlag GmbH & Co. KGaA, Weinheim

The NMR spectra of compounds **1** and **2** confirm the presence of three equivalent pyrazolyl rings in each molecule. The ^1H and $^{13}C\{^1H\}$ NMR spectroscopic data for both compounds are almost the same for the atoms in the 3- and 4-position of the rings. However, those in the 5-position are assigned more up field for compound **1** (δ = 6.63 and 128.5 ppm, proton and carbon, respectively) than for **2** (δ = 7.44 and 131.0 ppm), an effect probably related to the significant steric hindrance discussed above between the pyrazolyl rings and the $SiMe_3$ group in compound **1**. Both derivatives show an IR band $\nu_{C=N}$ around 1515 cm^{-1} in the usual range for free pyrazolyl rings.

Complexes Syntheses

The labile ligand substitution in $[Mo(CO)_3\{1,3,5\text{-}(CH_3)_3C_6H_3\}]$, $[TiCl_2(NtBu)(py)_3]$, and $[PdCl_2(COD)]$ by ligand **2**, leads to the formation of $[Mo(CO)_3\{Me_3SiOCH_2C(pz)_3\}]$ (**3**), $[TiCl_2(NtBu)\{Me_3SiOCH_2C(pz)_3\}]$ (**4**), and $[PdCl_2\{Me_3SiOCH_2C(pz)_3\}]$ (**5**), respectively, in high yields (see Scheme 1, and the Exp. Sect.). The formation of the molybdenum compound **3** required the use of a polar solvent such as THF or acetonitrile, whereas no reaction was observed in toluene. Instead, compounds **4** and **5** were readily prepared in toluene under reflux conditions. They are found to be stable (**5**), or moderately sensitive as a solid (**3**), or very sensitive to air (**4**). They are insoluble in alkanes, complex **3** is only soluble in polar solvents (THF, CH_3CN, acetone), compound **4** in chlorinated solvents, and complex **5** in aromatic solvents.

Similar attempts that use compound **1** as the entering ligand resulted in a mixture of the starting materials for the titanium and palladium compounds, and an untreatable insoluble greenish solid for the reaction with $[Mo(CO)_3$(mesitylene)]. The different chemical behavior showed by compounds **1** and **2** in these reactions can arise as a result of the important steric interaction between the $SiMe_3$ fragment and the pyrazolyl rings in compound **1**. Its tripodal arrangement to form complexes analogous to **3** or **4**, or the bidentate coordination as in **5** are hindered probably because the molecule minimizes the steric hindrance, thus positioning the three pyrazolyl rings in a three-bladed propeller conformation similar to that observed in the solid state (vide infra).

A number of tricarbonyl tris(pyrazolyl)methane metal complexes have been described,[3a,7] including molybdenum compounds[10] with tris(pyrazolyl)silane ligands.[11] The titanium examples are much more limited,[12] although some interesting heteroscorpionate-like complexes have recently been reported.[13] In the case of palladium(II), bis(pyrazolyl)methane as well as tris(pyrazolyl)methane compounds have been described.[14,15]

Complexes **3**–**5** were characterized by NMR and IR spectroscopy and elemental analysis, and the molecular structure of compound **5** has been determined by X-ray diffraction studies.

The ^1H NMR spectrum of complex **3** at room temperature exhibits one set of three multiplets for the pyrazolyl protons, whereas at lower temperature each type of pyrazolyl proton gives two resonances in the ratio 2:1. This finding is consistent with a staggered conformation of the ligand, as represented in Figure 1d, with a small rotation barrier along the central C–CH_2OR bond, as earlier proposed by Reger for dinuclear rhenium compounds.[7b]

The ^1H NMR spectra of complexes **4** and **5** are simple at 50 °C because at this temperature their different conformers rapidly interconvert on the NMR time-scale. Only one type of pyrazolyl ring is observed for compound **4**, and two are observed for **5** in a 2:1 ratio due to the bidentate coordination of ligand **2** to the palladium atom. On cooling the NMR samples, the spectra become more complicated, indicating the presence of conformational isomers in both complexes.

Thus, the spectra for the imide complex **4** at −80 °C in CD_2Cl_2 exhibits ten resonances in the range δ = 7.60–8.40 ppm assigned to the pyrazolyl protons H^3 and H^5, and two singlets assigned to the Me_3Si- (δ = 0.36 and 0.41 ppm) and to the Me_3C groups (δ = 0.90 and 0.97 ppm), indicating the presence of two conformers in a 1:1.25 ratio, with a total of five different pyrazolyl environments. Mixtures of conformers have also been described for related titanium compounds with tridentate N-donor ligands.[16] For the current case (**4**), the observation of two conformers can be attributed to the presence of the *tert*-butyl imide group with an important *trans* influence and to the presumable rotation barrier for the Me_3SiOCH_2 moiety (see conformers A and B in Figure 2).

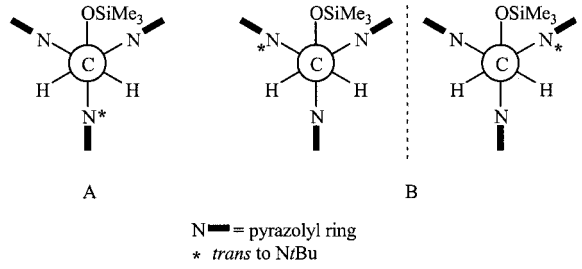

Figure 2. Conformer projections for compound **4**

The ^1H NMR spectra of derivative **5** at −50 °C in $CDCl_3$ shows twelve resonances for the pyrazolyl protons (δ = 6.40–8.40 ppm) and two singlets for the Me_3Si group (δ = 0.06 and 0.28 ppm). The splitting of these resonances and their relative intensities are in agreement with the presence of two conformers in an approximate ratio of 1:3, each with two equivalent pyrazolyl rings. These data are interpreted as the result of a boat-to-boat conformational exchange between the isomers depicted in Scheme 2,[14,15] which are observable at low temperature in an unequal population because of the different natures of the substituents in the axial position on the methine carbon (pz or Me_3SiOCH_2). It is worth noting that the exchange process between the non-coordinated and the coordinated pyrazolyl rings, a feature described as a "tumbling" process[1a] and commonly found in related complexes,[15,17] was not observed for compound **5** below 50 °C. A similar result has been reported for some

 © 2004 Wiley-VCH Verlag GmbH & Co. KGaA, Weinheim

palladium(II) complexes containing the rigid ligand 2-pyridyl-bis(3,5-dimethylpyrazolyl)methane, in which the pyridine group remains uncoordinated.[14a] However, the tris(pyrazolyl)methane ligand in compound **5** is flexible as demonstrated by the observation of the boat-to-boat inversion. The effect, nevertheless, could be ascribed to the presence of the Me_3SiOCH_2 substituent, which might hinder the ability of the free-pyrazolyl ring to coordinate to the metal center and, therefore, preclude the formation of the pentacoordinate intermediate involved during the tumbling process.

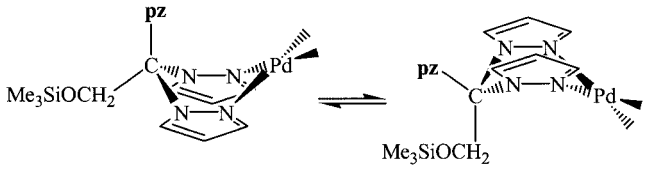

Scheme 2

The $^{13}C\{^1H\}$ NMR spectroscopic data for derivatives **3**–**5** are in agreement with a tripodal coordination of the tris(pyrazolyl)methane ligand in compounds **3** and **4**, and a bidentate *cis* coordination in a square-planar geometry for **5**. The spectra for **3** and **4** show one set of pyrazolyl resonances, whereas the spectrum for **5** shows the presence of nonequivalent rings in a 2:1 ratio; no mixtures of conformers are detected by $^{13}C\{^1H\}$ NMR spectroscopy at room temperature.

The IR spectra of compounds **3** and **5**, obtained as KBr pellets, show a band $\nu_{C=N}$ at around 1519 cm^{-1} not far from the absorption observed in the free ligand. In addition, the spectrum for the molybdenum complex shows two strong absorptions in the carbonyl region at 1901 cm^{-1} (a_1 mode) and 1764 cm^{-1} (e mode), as expected for a C_{3v} symmetry in an octahedral tricarbonyl complex. The observed ν_{CO} values are similar to those reported for related group 6 metal complexes.[11]

Synthesis of Dendritic Molecules

The methodology described above for the preparation of ligand **2** and compound **3** was extended to synthesize $G1-[OCH_2C(pz)_3]_4$ (**6**) and $G1-[OCH_2C(pz)_3Mo(CO)_3]_4$ (**7**) (Scheme 3), whereas attempts to prepare the corresponding tetrametallic analogues of compounds **4** and **5** yielded untreatable mixtures of insoluble solids. Thus, the reaction of chloro-containing carbosilane $G1-Cl_4$[18] with the sodium salt **II** in THF results in the formation of $G1-[OCH_2C(pz)_3]_4$ (**6**) as a colorless oil in a 76% yield. Subsequent treatment with $[Mo(CO)_3(mesitylene)]$ in refluxing THF leads to the dendritic compound **7**. Compounds **6** and **7** are found to be fairly stable in air. The

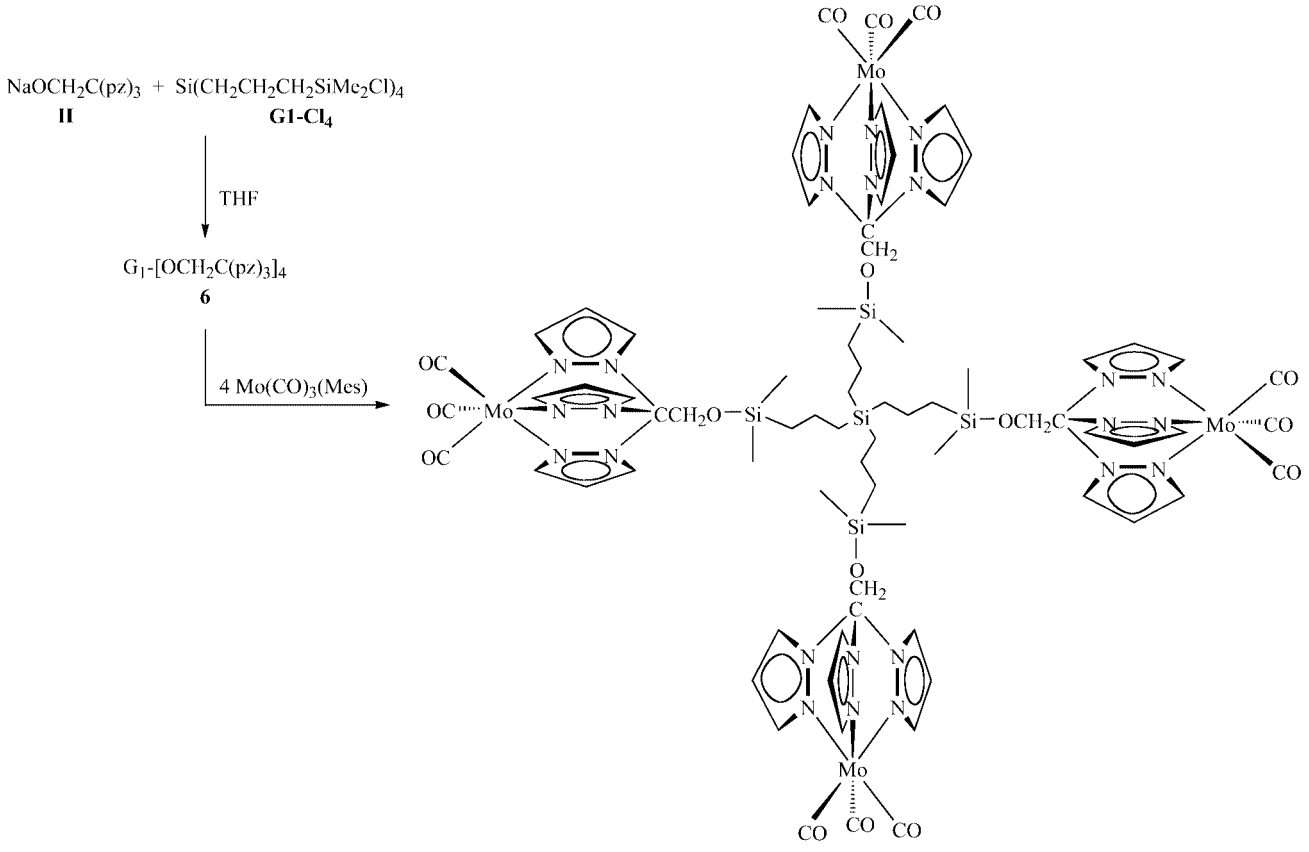

Scheme 3

 © 2004 Wiley-VCH Verlag GmbH & Co. KGaA, Weinheim

organic compound is soluble in all common organic solvent, whereas the tetra-molybdenum complex is only slightly soluble in polar solvents such us acetone. The latter fact is relevant since it severely limits the preparation of higher generations of this type of metallodendrimers.

^1H and $^{13}C\{^1H\}$ NMR chemical shifts of the terminal $-OCH_2C(pz)_3$ groups for **6** are similar to those for **2**; the spectra are also quite similar, with additional signals for the methylene groups of the $SiCH_2CH_2CH_2Si$ chains in **6**. The most significant difference in the NMR spectroscopic data of **6** relative to that of the starting material G1−Cl_4, is the shift of the $SiMe_2$ resonances form $\delta = 0.38$ (^1H) and 0.2 (^{13}C) to 0.00 (^1H) and −2.4 (^{13}C) for **6**. The ^1H and $^{13}C\{^1H\}$ NMR spectra for compound **7** are consistent with the structure depicted in Scheme 3, and the peripheral organometallic units are in an electronic environment like that described for the mononuclear complex **3**.

The IR spectra of compounds **6** and **7** show a band $\nu_{C=N}$ at around 1518 cm^{-1}, and two strong ν_{CO} bands at 1906 cm^{-1} and 1757 cm^{-1} in the case of **7**.

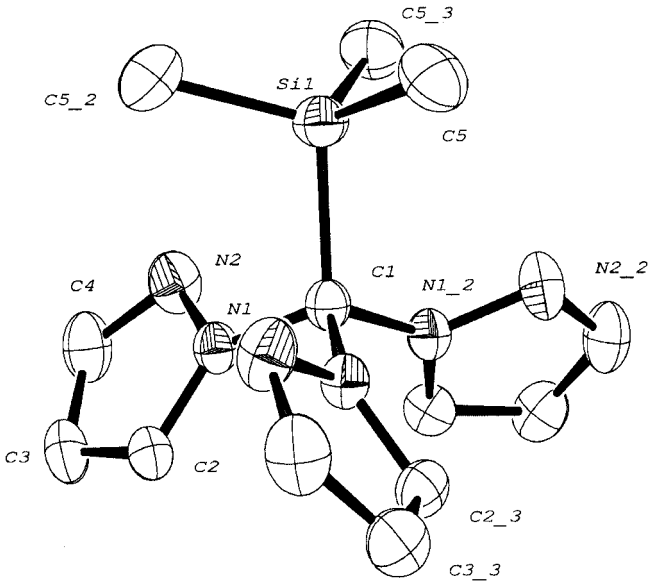

Figure 3. Molecular structure of compound **1**

Structures of $Me_3SiC(pz)_3$ (1) and $[PdCl_2\{Me_3SiOCH_2C(pz)_3\}]$ (5)

The molecular structures of both compounds have been determined by single-crystal X-ray diffraction studies. Figure 3 and Figure 4 show ORTEP representations of them, and Table 1 and Table 2 summarize their relevant structural data.

The molecular structure of **1** consists of discrete molecules and provides the first reported structure containing a tris(pyrazolyl)methane−Si linkage. The C−Si bond lies on a threefold axis in the *R*-3 space group, and only one third of the molecule appears in the asymmetric part of the unit cell. The geometry around the silicon atom is tetrahedral, but the Si(1)−C(1) bond length is clearly longer [1.968(3) Å] than the other Si−C bond lengths [1.858(3) Å]. The geometry around C(1) is distorted tetrahedral as shown by the Si(1)−C(1)−N(1) angle [111.5(1)°]. The three methyl groups bonded to the Si atom are located in a staggered configuration with respect to the C−N(pyrazolyl) bonds. The pyrazolyl rings are tilted with respect to the threefold axis to give the molecule a propeller-like shape. The Si−C−N−N torsion angle [46.4(2)°] provides a measure of this twist.

This shape is similar to that found in other molecules such as tris(3,5-dimethylpyrazol-1-yl)methane[19] and tris(3,5-dimethylpyrazol-1-yl)silane.[20] However, it is worth mentioning that only one of the possible conformers is present in the crystal of **1**; the isomer with the N(2) and the Si

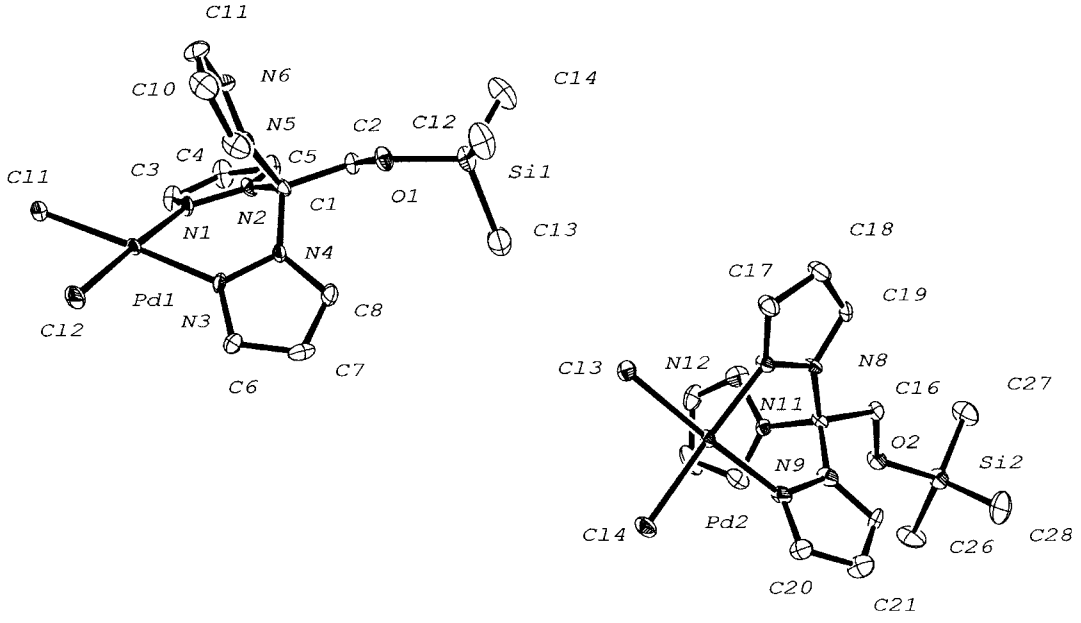

Figure 4. Molecular structure of the palladium complex **5**

 © 2004 Wiley-VCH Verlag GmbH & Co. KGaA, Weinheim

Table 1. Bond lengths (Å) and angles (°) for compound **1**; symmetry transformations used to generate equivalent atoms: #1: $-x + y + 1$, $-x + 1$, z

Si(1)−C(5)	1.858(3)	N(1)−C(1)	1.460(2)
Si(1)−C(1)	1.968(3)	N(2)−C(4)	1.328(3)
N(1)−C(2)	1.357(2)	C(2)−C(3)	1.358(3)
N(1)−N(2)	1.354(2)	C(3)−C(4)	1.382(3)
C(5)#1−Si(1)−C(5)	111.2(1)	N(1)−C(2)−C(3)	106.9(2)
C(5)−Si(1)−C(1)	107.7(1)	N(1)#1−C(1)−N(1)	107.4(1)
C(2)−N(1)−N(2)	111.7(2)	N(1)−C(1)−Si(1)	111.5(1)
C(2)−N(1)−C(1)	129.5(2)	C(2)−C(3)−C(4)	104.9(2)
N(2)−N(1)−C(1)	118.6(2)	N(2)−C(4)−C(3)	112.6(2)
C(4)−N(2)−N(1)	103.7(2)		

Table 2. Bond lengths (Å) and angles (°) for compound **5**

Molecule 1		Molecule 2	
Pd(1)−N(3)	2.003(4)	Pd(2)−N(9)	2.005(5)
Pd(1)−N(1)	2.027(4)	Pd(2)−N(7)	2.016(4)
Pd(1)−Cl(2)	2.2841(12)	Pd(2)−Cl(4)	2.2778(13)
Pd(1)−Cl(1)	2.2845(14)	Pd(2)−Cl(3)	2.2842(14)
Si(1)−O(1)	1.671(4)	Si(2)−O(2)	1.678(4)
Si(1)−C(12)	1.850(6)	Si(2)−C(26)	1.853(6)
Si(1)−C(13)	1.854(7)	Si(2)−C(27)	1.862(6)
Si(1)−C(14)	1.858(6)	Si(2)−C(28)	1.863(7)
N(1)−C(3)	1.321(7)	N(7)−C(17)	1.330(7)
N(1)−N(2)	1.358(6)	N(7)−N(8)	1.363(6)
N(2)−C(5)	1.366(7)	N(8)−C(19)	1.355(6)
N(2)−C(1)	1.478(6)	N(8)−C(15)	1.461(6)
N(3)−C(6)	1.332(7)	N(9)−C(20)	1.319(7)
N(3)−N(4)	1.363(5)	N(9)−N(10)	1.361(6)
N(4)−C(8)	1.362(7)	N(10)−C(22)	1.359(7)
N(4)−C(1)	1.437(6)	N(10)−C(15)	1.457(6)
N(5)−N(6)	1.351(7)	N(11)−C(23)	1.352(7)
N(5)−C(9)	1.371(7)	N(11)−N(12)	1.353(7)
N(5)−C(1)	1.465(6)	N(11)−C(15)	1.456(6)
N(6)−C(11)	1.315(8)	N(12)−C(25)	1.330(7)
O(1)−C(2)	1.415(6)	O(2)−C(16)	1.410(6)
C(1)−C(2)	1.523(7)	C(15)−C(16)	1.548(6)
C(3)−C(4)	1.397(8)	C(17)−C(18)	1.394(7)
C(4)−C(5)	1.382(8)	C(18)−C(19)	1.371(8)
C(6)−C(7)	1.379(9)	C(20)−C(21)	1.389(9)
C(7)−C(8)	1.350(8)	C(21)−C(22)	1.357(8)
C(9)−C(10)	1.360(9)	C(23)−C(24)	1.379(9)
C(10)−C(11)	1.389(10)	C(24)−C(25)	1.390(9)
N(3)−Pd(1)−N(1)	87.41(17)	N(9)−Pd(2)−N(7)	87.37(18)
N(3)−Pd(1)−Cl(2)	89.94(12)	N(9)−Pd(2)−Cl(4)	90.07(12)
N(1)−Pd(1)−Cl(2)	177.34(13)	N(7)−Pd(2)−Cl(4)	177.44(14)
N(3)−Pd(1)−Cl(1)	175.64(12)	N(9)−Pd(2)−Cl(3)	175.39(13)
N(1)−Pd(1)−Cl(1)	90.72(13)	N(7)−Pd(2)−Cl(3)	90.85(13)
Cl(2)−Pd(1)−Cl(1)	91.90(5)	Cl(4)−Pd(2)−Cl(3)	91.70(5)
O(1)−C(2)−C(1)	107.9(4)	O(2)−C(16)−C(15)	107.6(4)
C(2)−O(1)−Si(1)	123.9(3)	C(16)−O(2)−Si(2)	122.8(3)
N(4)−C(1)−N(5)	107.8(4)	N(11)−C(15)−N(10)	108.1(4)
N(4)−C(1)−N(2)	109.1(4)	N(11)−C(15)−N(8)	108.7(4)
N(5)−C(1)−N(2)	107.4(4)	N(10)−C(15)−N(8)	108.9(4)
N(4)−C(1)−C(2)	112.6(4)	N(11)−C(15)−C(16)	110.8(4)
N(5)−C(1)−C(2)	110.7(4)	N(10)−C(15)−C(16)	111.2(4)
N(2)−C(1)−C(2)	109.1(4)	N(8)−C(15)−C(16)	109.1(4)
Pd(1)−C(1)−C(2)−O(1)	−143.1	Pd(2)−C(15)−C(16)−O(2)	133.0
C(1)−C(2)−O(1)−Si(1)	159.4	C(15)−C(16)−O(2)−Si(2)	−159.9

 © 2004 Wiley-VCH Verlag GmbH & Co. KGaA, Weinheim

atom located on the same side of the plane defined by the three nitrogen atoms bonded to the central carbon atom. Obviously, this arrangement found in the solid state is incompatible with a bi- or tridentate coordination of compound **1** to a metal center.

The molecular structure of compound **5** consists of discrete molecules with one Pd atom with a *cis* configuration in a square-planar environment. The metal atom is bonded to two chlorine and two nitrogen atoms from the tris(pyrazolyl)methane ligand, whereas one of the pyrazolyl rings remains uncoordinated. The asymmetric part of the unit cell comprises two molecules. Both molecules are very similar, except for the position of the Me_3SiOCH_2 moiety, whose orientations differ with respect to the rest of the structure in such a way that the two molecules are enantiomers.

Two examples of palladium complexes containing the tris(pyrazolyl)methane ligand have been described and structurally characterized. The octahedral palladium(IV) complex $[PdMe_3\{HC(pz)_3\}]I$[21] and the square-planar Pd^{II} species $[Pd\{HC(pz)_3\}_2][BF_4]_2$,[15a] both cationic compounds, show the κ^3-and the κ^2-mode of coordination of the ligand, respectively. The neutral compound **5** is also a Pd^{II} square-planar complex, with Pd−N bond lengths [ranging from 2.003(4) Å to 2.027(4) Å] and N−Pd−N angle [87.41(1)°] very similar to those found in $[Pd\{HC(pz)_3\}_2][BF_4]_2$.[15a]

In contrast with the other examples, the two coordinated rings in both molecules of the asymmetric unit have different inclinations with respect to the coordination plane of the metal. The dihedral angle of this plane with the pyrazolyl ring closer to the Me_3SiOCH_2 moiety is 36.0(1)° [rings with N(3)−N(4) and N(9)−N(10)], whereas the angle with the other pyrazolyl ring is 29.3(1)° [rings with N(1)−N(2) and N(7)−N(8)]. This structural feature is probably caused by the orientation of the siloxy group and the different steric interactions over the coordinated pyrazolyl rings in the solid state.

In both molecules, the non-coordinated pyrazolyl ring is oriented towards the palladium coordination plane with an angle between the planes of 57.1°. The distances between the N apical and Pd atoms are 3.180 Å in Pd(1)−N(5) and 3.195 Å in Pd(2)−N(11), and the Pd(1)−N(6) and Pd(2)−N(12) distances are 3.738 Å and 3.762 Å, respectively. The donor nitrogen atoms N(6) and N(12) are pointing to the opposite side of the Me_3SiOCH_2 moieties.

Conclusion

Tris(pyrazolyl)methane compounds substituted at the methine carbon atom have been prepared and characterized. Their ability as coordination ligands is greatly affected by the substituent. Thus, $Me_3SiOCH_2C(pz)_3$ (**2**) allows the straightforward preparation of transition metal complexes **3**−**5**, whereas similar attempts using $Me_3SiC(pz)_3$ (**1**) all failed. The result is interpreted as a consequence of the "steric pressure" of the Me_3Si group over the pyrazolyl rings in **1**, which blocks their ability to coordinate. Ligand **2** is tridentately coordinated in $[Mo(CO)_3\{Me_3SiOCH_2C(pz)_3\}]$ (**3**) and $[TiCl_2(NtBu)\{Me_3SiOCH_2C(pz)_3\}]$ (**4**), and bidentately coordinated in $[PdCl_2\{Me_3SiOCH_2C(pz)_3\}]$ (**5**). The dynamic behavior of these complexes in solution is consistent with a staggered conformation of ligand **2** in complexes **3** and **4** at low temperature. In addition, the absence of chemical exchange between the free and the coordinated pyrazolyl rings in compound **5** is explained in terms of the steric effect exerted by the Me_3SiOCH_2 group over the tris(pyrazolyl)methane ligand. The preparation of poly(pyrazolyl)methane complexes can be readily extended to polymetallic systems as demonstrated by the synthesis of the carbosilane precursor **6**, and the tetramolybdenum complex **7**. However, modification of the ligand will be required to reduce its steric crowding and to obtain more soluble compounds, in order to apply this methodology in dendrimer chemistry. Further work along these lines is currently underway.

Experimental Section

General Remarks: All operations were performed under an argon atmosphere using Schlenk or dry-box techniques. Unless otherwise stated, reagents were obtained from commercial sources and used as received. $[TiCl_2(NtBu)(py)_3]$,[22] $[PdCl_2(COD)]$,[23] $[Mo(CO)_3\{1,3,5\text{-}(CH_3)_3C_6H_3\}]$,[24] carbosilane $G1\text{−}Cl_4$,[18] $HC(pz)_3$, and $HOCH_2C(pz)_3$[3a] were prepared according to literature procedures. Solvents were previously dried and distilled under argon as described elsewhere.[25] NMR spectra were recorded on Varian Unity 500+, VR-300 or 200 NMR spectrometers. Chemical shifts (δ) are reported in ppm referenced to $SiMe_4$ for ^1H and ^{13}C. IR spectra were recorded on a Perkin−Elmer FT-IR Spectrum-2000 spectrophotometer. Elemental analyses were performed by Microanalytical Laboratories of the University of Alcalá on a Heraeus CHN-O-Rapid mycroanalyzer. Molecular modeling was carried out using CambridgeSoft Chem. 3D Pro 5.0 for Mac and MM2 force field computations.

Preparation of (Trimethylsilyl)tris(1-pyrazolyl)methane (1): LiMe (3.0 mL, 1.6 M in diethyl ether, 4.80 mmol) was slowly added with a funnel equipped with a bubbler to a solution of $HC(pz)_3$ (1.00 g, 4.67 mmol) in THF (20 mL) at −78 °C, and the reaction mixture was stirred overnight and allowed to warm up to room temperature. Removal of the solvent under vacuum led to intermediate **I** as an off-white solid that was washed with pentane (10 mL). Solid **I** was dissolved in THF (20 mL), treated with an excess of $SiMe_3Cl$ (1.0 mL, 7.88 mmol) at 0 °C, and the resulting solution stirred for 4 h. The volatiles were removed in vacuo and the residue extracted into hexane (2 × 10 mL). Compound **1** was isolated as a white solid by evaporation of the filtrates under vacuum to dryness, and recrystallized from pentane. Yield: 1.00 g (75%). $C_{13}H_{18}N_6Si$ (286.41): calcd. C 54.52, H 6.33, N 29.34; found C 54.65, H 6.64, N 29.73%. ^1H NMR ($CDCl_3$): δ = 0.29 (s, 9 H, $SiMe_3$), 6.28 (dd, 3 H, $J_{H,H}$ = 1.5, 2.6 Hz, pz−H^4), 6.63 (d, $J_{H,H}$ = 2.6 Hz, 3 H, pz−H^5), 7.65 (d, $J_{H,H}$ = 1.5 Hz, 3 H, pz−H^3) ppm. $^{13}C\{^1H\}$ NMR ($CDCl_3$): δ = −0.6 ($SiMe_3$), 105.9 (pz−C^4), 128.5 (pz−C^5), 140.6 (pz−C^3) ppm, $C(pz)_3$ not observed. IR (KBr): $\tilde{\nu}$ = 1510 cm^{-1} (s, C=N).

Preparation of 1-(Trimethylsiloxy)tris-2,2,2-(1-pyrazolyl)ethane (2): A solution of $HOCH_2C(pz)_3$ (1.00 g, 4.09 mmol) in THF (15 mL)

 © 2004 Wiley-VCH Verlag GmbH & Co. KGaA, Weinheim

was added to NaH (0.17 g, 60% dispersion in mineral oil, 4.25 mmol) previously washed with hexane and suspended in THF (15 mL). When the evolution of H_2 ceased, the solvent was removed under vacuum to lead to intermediate **II** as a white solid, which was washed with pentane (10 mL).[9] The solid was then dissolved in THF (20 mL), $SiMe_3Cl$ (0.6 mL, 4.73 mmol) was added at 0 °C, and the resulting solution stirred for 2 h at room temperature. The volatiles were removed in vacuo, and the residue extracted into hexane (2 × 10 mL) to give **2** as a colorless oil. Yield: 1.03 g (80%). $C_{14}H_{20}N_6OSi$ (316.44): calcd. C 53.14, H 6.37, N 26.56; found C 53.64, H 6.33, N 26.05%. ^1H NMR ($CDCl_3$): δ = 0.02 (s, 9 H, $SiMe_3$), 5.19 (s, 2 H, CH_2O), 6.29 (dd, 3 H, $J_{H,H}$ = 1.7, 2.7 Hz, pz−H^4), 7.44 (d, $J_{H,H}$ = 2.7 Hz, 3 H, pz−H^5), 7.62 (d, $J_{H,H}$ = 1.7 Hz, 3 H, pz−H^3) ppm. $^{13}C\{^1H\}$ NMR ($CDCl_3$): δ = −0.7 ($SiMe_3$), 66.9 (CH_2O), 90.3 [$C(pz)_3$], 106.2 (pz−C^4), 131.0 (pz−C^5), 141.1 (pz−C^3) ppm. IR (CsI/Nujol): $\tilde{\nu}$ = 1518 cm^{-1} (s, C=N).

Preparation of $[Mo(CO)_3\{Me_3SiOCH_2C(pz)_3\}]$ (3): In a Schlenk, $[Mo(CO)_3\{1,3,5\text{-}(CH_3)_3C_6H_3\}]$ (95 mg, 0.32 mmol) was added to a solution of **2** (100 mg, 0.32 mmol) in acetonitrile or THF (15 mL) at room temperature. The yellow solution was stirred overnight and evaporated to dryness, and the yellow solid was washed with hexane and recrystallized form THF. Yield: 143 mg (90%). $C_{17}H_{20}N_6O_4SiMo$ (496.41): calcd. C 41.13, H 4.06, N 16.93; found C 41.27, H 3.89, N 16.46%. ^1H NMR ([D_6]acetone): δ = 0.44 (s, 9 H, $SiMe_3$), 5.99 (s, 2 H, CH_2O), 6.49 (m, 3 H, pz−H^4), 8.02 (m, 3 H, pz−H^5), 8.33 (m, 3 H, pz−H^3) ppm. $^{13}C\{^1H\}$ NMR ([D_6]acetone): δ = −0.7 ($SiMe_3$), 63.0 (CH_2O), 85.6 [$C(pz)_3$], 107.5 (pz−C^4), 133.3 (pz−C^5), 146.0 (pz−C^3), 229.8 (CO)ppm. IR (KBr): $\tilde{\nu}$ = 1901 and 1764 cm^{-1} (s, CO), 1518 cm^{-1} (m, C=N).

Preparation of $[TiCl_2(N\mathit{t}Bu)\{Me_3SiOCH_2C(pz)_3\}]$ (4): $[TiCl_2(N\mathit{t}Bu)(py)_3]$ (452 mg, 1.06 mmol), **2** (335 mg, 1.06 mmol), and toluene (15 mL) were placed into a glass ampoule equipped with a high vacuum greaseless stopcock. The mixture was kept at reduced pressure, evacuating the vapors regularly through the stopcock, and heated at 100 °C for 24 h. The resulting salmon-color solid was filtered and washed with pentane (2 × 10 mL). Yield: 385 mg (72%). $C_{18}H_{29}N_7OSiTiCl_2$ (506.33): calcd. C 42.70, H 5.77, N 19.36; found C 43.17, H 5.36, N 18.82%. ^1H NMR ($CDCl_3$, 50 °C): δ = 0.47 (s, 9 H, $SiMe_3$), 1.06 (s, 9 H, NtBu), 5.45 (s, 2 H, CH_2O), 6.28 (m, 3 H, pz−H^4), 7.85 (m, 3 H, pz−H^5), 8.19 (m, 3 H, pz−H^3) ppm. $^{13}C\{^1H\}$ NMR ($CDCl_3$): δ = −0.3 ($SiMe_3$), 30.6 (CMe_3), 62.2 (CH_2O), 69.4 (CMe_3), 83.3 [$C(pz)_3$], 106.8 (pz−C^4), 129.8 (pz−C^5), 145.9 (pz−C^3) ppm.

Preparation of $[PdCl_2\{Me_3SiOCH_2C(pz)_3\}]$ (5): $[PdCl_2(COD)]$ (81 mg, 0.28 mmol) was added to a solution of compound **2** (90 mg, 0.28 mmol) in toluene (15 mL), and the mixture was refluxed for 1.5 h. The solvent was evaporated, and the yellow-orange residue was washed with hexane (2 × 10 mL) and recrystallized from acetone to afford **5** as orange crystals suitable for X-ray analysis. Yield: 130 mg (94%). $C_{14}H_{20}N_6OSiPdCl_2$ (493.76): calcd. C 34.06, H 4.08, N 17.02; found C 34.42, H 4.05, N 16.58%. ^1H NMR ($CDCl_3$, 50 °C): δ = 0.15 (s, 9 H, $SiMe_3$), 5.48 (s, 2 H, CH_2O), 6.40, 6.63 (m, m, 2 H, 1 H, pz−H^4), 6.96, 7.89 (m, m, 2 H, 1 H,

Table 3. Crystal data and structure refinement for compounds **1** and **5**

	1	**5**
Empirical formula	$C_{13}H_{18}N_6Si$	$C_{14}H_{20}Cl_2N_6OPdSi$
Molecular weight	286.42	493.77
Color	colorless	yellow
Temperature, K	293(2)	150(2)
Wavelength (Å)	0.71073	0.71073
Crystal system, space group	trigonal, $R\bar{3}$	triclinic, $P\bar{1}$
a (Å)	13.293(1)	7.8816(13)
b (Å)	13.293(1)	14.796(3)
c (Å)	15.364(1)	17.1711(14)
α (°)	90	90.14(1)
β (°)	90	98.99(1)
γ (°)	120	90.24(1)
Volume [(Å)^3]	2351.2(3)	1977.8(5)
Z (g cm^{-3})	6, 1.214	4, 1.658
Absorption coefficient (mm^{-1})	0.150	1.284
F(000)	912	992
Crystal size, mm	0.40 × 0.35 × 0.20	0.50 × 0.45 × 0.30
θ ranges (°)	5.03−27.52	5.01−27.50
Limiting indices	$-17 \le h \le 17$, $-16 \le k \le 17$, $-19 \le l \le 19$	$-10 \le h \le 10$, $-19 \le k \le 19$, $-22 \le l \le 22$
Reflections collected/unique	12700/1197 [*R*(int) = 0.1416]	67152/8994 [*R*(int) = 0.3110]
Reflections observed	883 [$I > 2\sigma(I)$]	7161 [$I > 2\sigma(I)$]
Completeness to θ (%)	99.3	99.0
Absorption correction	none	analytical
Max. and min. transmission		0.7486 and 0.5459
Refinement method	full-matrix least-squares on F^2	full-matrix least-squares on F^2
Data/restraints/parameters	1197/0/85	8994/0/508
Goodness of fit on F^2	1.062	1.092
Final *R*[a] indices [$I > 2\sigma(I)$]	R_1 = 0.0432, wR_2 = 0.0994	R_1 = 0.0509, wR_2 = 0.1238
R int (all data)	R_1 = 0.0654, wR_2 = 0.1127	R_1 = 0.0709, wR_2 = 0.1513
Largest diff. peak and hole, e/Å^3	0.140, −0.219	1.417, −1.881

[a] $R_1 = \Sigma||F_o| - |F_c||/\Sigma|F_o|$; $wR_2 = \{[\Sigma\omega(F_o^2 - F_c^2)]/[\Sigma\omega(F_o^2)^2]\}^{1/2}$.

 © 2004 Wiley-VCH Verlag GmbH & Co. KGaA, Weinheim

pz−H^5), 8.01, 8.49 (m, m, 1 H, 2 H, pz−H^3) ppm. $^{13}C\{^1H\}$ NMR ($CDCl_3$): δ = −0.5 ($SiMe_3$), 66.5 (CH_2O), 107.4, 108.9 and 146.0 (coord. pz−C^{4,5,3}) 109.1, 134.1 and 144.0 (non coord. pz−C^{4,5,3}) ppm. IR (KBr): $\tilde{\nu}$ = 1519 cm^{-1} (m, C=N).

Preparation of G1−[OCH$_2$C(pz)$_3$]$_4$ (6): This compound was prepared according to the procedure described above for **2**, from NaOCH$_2$C(pz)$_3$ (**II**, 1.288 g, 4.84 mmol) and carbosilane G1−Cl$_4$ (0.690 g, 1.21 mmol) in THF (20 mL). The resulting oil was dissolved in pentane (20 mL), washed with water, and the organic layer dried with $MgSO_4$. The solvent was removed under vacuum giving compound **6** as a colorless oil. Yield: 1.29 g (76%). $C_{64}H_{92}N_{24}O_4Si_5$ (1402.02): calcd. C 54.83, H 6.61, N 23.98; found C 53.89, H 6.82, N 23.57%. ^1H NMR ($CDCl_3$): δ = 0.00 (s, 6 H, $SiMe_2$), 0.44 (m, 2 H, Si*CH*$_2$), 0.56 (m, 2 H, *CH*$_2$SiMe$_2$), 1.24 (m, 2 H,CH$_2$*CH*$_2$CH$_2$), 5.19 (s, 2 H, CH_2O), 6.29 (dd, 3 H, $J_{H,H}$ = 1.4, 2.3 Hz, pz−H^4), 7.43 (d, $J_{H,H}$ = 2.3 Hz, 3 H, pz−H^5), 7.61 (d, $J_{H,H}$ = 1.4 Hz, 3 H, pz−H^3) ppm. $^{13}C\{^1H\}$ NMR ($CDCl_3$): δ = −2.4 ($SiMe_2$), 16.8 (CH_2), 17.5 (CH_2), 20.8 (CH_2), 66.8 (CH_2O), 90.1 [C(pz)$_3$], 106.1 (pz−C^4), 130.8 (pz−C^5), 140.9 (pz−C^3) ppm. IR (CsI/Nujol): $\tilde{\nu}$ = 1517 cm^{-1} (m, C=N).

Preparation of G1−[OCH$_2$C(pz)$_3$Mo(CO)$_3$]$_4$ (7): A yellow solution of [Mo(CO)$_3${1,3,5-(CH$_3$)$_3$C$_6$H$_3$}] (137 mg, 0.46 mmol) and compound **6** (160 mg, 0.11 mmol) in THF (20 mL) was refluxed for 1.5 h. At room temperature, a greenish precipitate was filtered, washed with hexane (2 × 5 mL), and recrystallized from acetone to afford **7** as a mustard-yellow solid. Yield: 143 mg (61%). $C_{76}H_{92}N_{24}O_{16}Si_5Mo_4$ (2121.91): calcd. C 43.02, H 4.37, N 15.84; found C 42.62, H 4.72, N 15.75%. ^1H NMR ([D$_6$]acetone): δ = 0.41 (s, 6 H, $SiMe_2$), 0.58 (m, 2 H, Si*CH*$_2$), 0.89 (m, 2 H, *CH*$_2$SiMe$_2$), 1.35 (m, 2 H, CH$_2$*CH*$_2$CH$_2$), 5.98 (s, 2 H, CH_2O), 6.46 (m, 3 H, pz−H^4), 8.01 (m, 3 H, pz−H^3), 8.27 (m, 3 H, pz−H^5) ppm. $^{13}C\{^1H\}$ NMR ([D$_6$]acetone): δ = −1.9 ($SiMe_2$), 17.6 (CH_2), 18.6 (CH_2), 27.7 (CH_2), 63.5 (CH_2O), 107.0 (pz−C^4), 131.7 (pz−C^5), 146.0 (pz−C^3) ppm, C(pz)$_3$ and CO not observed. IR (KBr): $\tilde{\nu}$ = 1906 and 1757 cm^{-1} (s, CO), 1519 cm^{-1} (m, C=N).

X-ray Crystallography Studies: Suitable monocrystals of **1** and **5** were obtained from a saturated solution in pentane at −30 °C, and by slow evaporation of acetone at room temperature. A summary of crystal data, data collection, and refinement parameters for the structure analysis of both compounds is given in Table 3. A colorless (**1**) or yellow (**5**) crystal was glued to a glass fiber and mounted on Kappa-CCD Bruker-Nonius diffractometer with area detector, and data were collected with graphite monochromated Mo-K_α radiation (λ = 0.71073 Å). For compound **1**, data were collected at room temperature, with an exposure time of 30 s per frame (five sets; 224 frames; phi and omega scans 2° scan-width). For compound, **5** data collection was performed at 150 K, with an exposure time of 10 s per frame (12 sets; 510 frames; phi and omega scans 2° scan-width). Raw data were corrected for Lorenz and polarization effects.

Structures were solved by direct methods, completed by subsequent difference Fourier techniques, and refined by full-matrix least-squares on F^2(SHELXL-97).[26] Anisotropic thermal parameters were used in the last cycles of refinement for the non hydrogen atoms in both structures. Hydrogen atoms were found in the final Fourier maps and were refined with isotropic thermal displacement parameters.

All the calculations were made with the WINGX system.[27]

CCDC-232262 and -232263 contains the supplementary crystallographic data for compounds **1** and **5**, respectively. These data can be obtained free of charge at www.ccdc.cam.ac.uk/conts/retrieving.html [or from the Cambridge Crystallographic Data Centre, 12 Union Road, Cambridge CB2 1EZ, UK; Fax: (internat.) + 44-1223-336-033; E-mail: deposit@ccdc.cam.ac.uk].

Acknowledgments

We gratefully acknowledge Prof. Reger for the useful information related to the synthesis and purification of the pyrazolylmethane precursors. We also thank the DGI-Ministerio de Ciencia y Tecnología (project BQU2001−1160) for financial support.

[1] [1a] S. Trofimenko, *J. Am. Chem. Soc.* **1966**, *88*, 1842. [1b] S. Trofimenko, *J. Am. Chem. Soc.* **1967**, *89*, 3170. [1c] S. Trofimenko, *J. Am. Chem. Soc.* **1969**, *91*, 588. [1d] S. Trofimenko, *J. Am. Chem. Soc.* **1969**, *91*, 3183.

[2] S. Trofimenko, *Scorpionates: The Coordination Chemistry of Polypyrazolylborate Ligands*, Imperial College Press, London, **1999**.

[3] [3a] D. L. Reger, T. C. Grattan, K. J. Brown, C. A. Little, J. J. S. Lamba, A. L. Rheingold, R. D. Sommer, *J. Organomet. Chem.* **2000**, *607*, 120. [3b] S. Julia, J. M. del Mazo, L. Avila, J. Elguero, *Org. Prep. Proced. Int.* **1984**, *16*, 299.

[4] D. L. Reger, T. C. Grattan, *Synthesis* **2003**, 350.

[5] [5a] A. Otero, J. Fernández-Baeza, J. Tejeda, A. Antiñolo, F. Carrillo-Hermosilla, E. Díaz-Barra, A. Lara-Sánchez, M. Fernández-López, *J. Chem. Soc., Dalton Trans.* **2000**, 2367. [5b] B. S. Hammes, M. T. Kieber-Emmons, J. A. Letizia, Z. Shirin, C. J. Carrano, L. N. Zakharov, A. L. Rheingold, *Inorg. Chim. Acta* **2003**, *346*, 227.

[6] [6a] W. Kläui, M. Berghahn, G. Rheinwald, H. Lang, *Angew. Chem. Int. Ed.* **2000**, *39*, 2464; *Angew. Chem.* **2000**, *112*, 2590. [6b] C. Santini, M. Pellei, G. Gioia Lobbia, A. Cingolani, R. Spagna, M. Camalli, *Inorg. Chem. Commun.* **2002**, *5*, 430.

[7] [7a] D. L. Reger, R. F. Semeniuc, M. D. Smith, *J. Organomet. Chem.* **2003**, *666*, 87. [7b] D. L. Reger, K. J. Brown, M. D. Smith, *J. Organomet. Chem.* **2002**, *658*, 50. [7c] D. L. Reger, R. F. Semeniuc, M. D. Smith, *J. Chem. Soc., Dalton Trans.* **2002**, 476.

[8] [8a] S. Arévalo, J. M. Benito, E. de Jesús, F. J. de la Mata, J. C. Flores, R. Gómez, *J. Organomet. Chem.* **2000**, *602*, 208. [8b] J.M. Benito, S. Arévalo, E. de Jesús, F. J. de la Mata, J. C. Flores, R. Gómez, *J. Organomet. Chem.* **2000**, *610*, 42. [8c] S. Arévalo, E. de Jesús, F. J. de la Mata, J. C. Flores, R. Gómez, *Organometallics* **2001**, *20*, 2583. [8d] R. Andrés, E. de Jesús, F. J. de la Mata, J. C. Flores, R. Gómez, *Eur. J. Inor. Chem.* **2002**, 2281. [8e] J.M. Benito, E. de Jesús, F. J. de la Mata, J. C. Flores, R. Gómez, P. Gómez-Sal, *J. Organomet. Chem.* **2002**, *664*, 258. [8f] S. Arévalo, E. de Jesús, F. J. de la Mata, J. C. Flores, R. Gómez, P. Gómez-Sal, P. Ortega, S. Vigo, *Organometallics* **2003**, *22*, 5109.

[9] Intermediate **II** was obtained free of THF. ^1H NMR ($CDCl_3$): δ = 5.06 (s, 2 H, CH_2O), 6.34 (narrow m, 3 H, pz−H^4), 7.06 (*p*s, 3 H, pz−H^5), 7.70 (*p*s, 3 H, pz−H^3) ppm.

[10] S. Trofimenko, *J. Am. Chem. Soc.* **1970**, *92*, 5118.

[11] E. E. Pullen, D. Rabinovich, C. D. Incarvito, T. E. Concolino, A. L. Rheingold, *Inorg. Chem.* **2000**, *39*, 1561.

[12] S. C. Lawrence, M. E. G. Skinner, J. C. Green, P. Mountford, *Chem. Commun.* **2001**, 705.

[13] A. Otero, J. Fernández-Baeza, A. Antiñolo, F. Carrillo-Hermosilla, J. Tejeda, A. Lara-Sánchez, L. Sánchez-Barba, M. Fernández-López, A. M. Rodríguez, I. López-Solera, *Inorg. Chem.* **2002**, *41*, 5193.

[14] [14a] N. Arroyo, F. Gómez-de la Torre, F. A. Jalón, B. R. Manzano, B. Moreno-Lara, A. M. Rodríguez, *J. Organomet. Chem.* **2000**, *603*, 174. [14b] J. Ruiz, M. T. Martínez, F. Florenciano, V. Rodríguez, G. López, J. Pérez, P. A. Chaloner, P. B. Hitchcock, *Inorg. Chem.* **2003**, *42*, 3650. [14c] S. Tsuji, D. C. Swenson, R. F. Jordan, *Organometallics* **1999**, *18*, 4758.

 © 2004 Wiley-VCH Verlag GmbH & Co. KGaA, Weinheim

[15] [15a] A.J. Canty, N. J. Minchin, L. M. Engelhardt, B. W. Skelton, A. H. White, *J. Chem. Soc., Dalton Trans.* **1986**, 645. [15b] P. E. Byers, A.J. Canty, R. T. Honeyman, *Adv. Organomet. Chem.* **1992**, *34*, 1. [15c] F. A. Jalón, B. R. Manzano, A. Otero, M. C. Rodríguez-Pérez, *J. Organomet. Chem.* **1995**, *494*, 179.

[16] A. J. Blake, P. E. Collier, S. C. Dunn, W.-S. Li, P. Mountford, O. V. Shishkin, *J. Chem. Soc., Dalton Trans.* **1997**, 1549.

[17] E. Gutiérrez, S. A. Hudson, A. Monge, M. C. Nicasio, M. Paneque, C. Ruiz, *J. Organomet. Chem.* **1998**, *551*, 215.

[18] [18a] A. W. van der Made, P. W. N. M. van Leeuwen, *J. Chem. Soc., Chem. Commun.* **1992**, 1400. [18b] B. Alonso, I. Cuadrado, M. Morán, J. Losada, *J. Chem. Soc., Chem. Commun.* **1994**, 2575. [18c] D. Seyferth, T. Kugita, A. L. Rheinglod, G. P. A. Yap, *Organometallics* **1995**, *14*, 5362.

[19] [19a] J. P. Declercq, M. Van Meerssche, *Acta Crystallogr., Sect. C* **1984**, *40*, 1098. [19b] L. E. Ochando, J. Rius, D. Louër, R. M. Claramunt, C. Lopez, J. Elguero, J. M. Amigó, *Acta Crystallogr., Sect. B* **1997**, *53*, 939.

[20] S. Vepachedu, R. T. Stibrany, S. Knapp, J. A. Potenza, H. J. Schugar, *Acta Crystallogr., Sect. C* **1995**, *51*, 423.

[21] [21a] P. K. Byers, A. J. Canty, B. W. Skelton, A. H. White, *J. Chem. Soc., Chem. Commun.* **1987**, 1093. [21b] P. K. Byers, A. J. Canty, B. W. Skelton, A. H. White, *Organometallics* **1990**, *9*, 826.

[22] A. J. Blake, P. E. Collier, S. C. Dunn, W. S. Li, P. Mountford, O. V. Shishkin, *J. Chem. Soc., Dalton Trans.* **1997**, 1549.

[23] D. Drew, J. R. Doyle, in *Inorganic Syntheses* (Ed.: F. A. Cotton), McGraw-Hill Book Company, New York, **1972**, vol. 13, pp. 47.

[24] R. J Angelici, *Synthesis and Techniques in Inorganic Chemistry* (Ed.: W. B. Saunders), Philadelphia, **1977**, pp. 237.

[25] D. P. Perrin, W. L. F. Armarego, *Purification of Laboratory Chemicals*, 3rd ed., Pergamon Press, Oxford, **1988**.

[26] G. M. Sheldrick, *SHELXL 97, Program for Crystal Structure Refinement*, University of Göttingen, Göttingen, Germany, **1997**.

[27] WinGX System: L. J. Farrugia, *J. Appl. Crystallogr.* **1999**, *32*, 837.

Received February 26, 2004
Early View Article
Published Online June 7, 2004

 © 2004 Wiley-VCH Verlag GmbH & Co. KGaA, Weinheim

Lithium and Potassium Amides of Sterically Demanding Aminopyridines

Natalie M. Scott,[a] Thomas Schareina,[b] Oleg Tok,[a] and Rhett Kempe*[a]

Keywords: Amido ligands / Coordination polymers / Lithium / N ligands / Potassium

The reaction of Grignard compounds of 1-bromo-2,4,6-diisopropylbenzene (**1**) or 1-bromo-2,6-dimethylbenzene (**2**), formed in situ, with 2,6-dibromopyridine in the presence of a catalytic amount of [(dme)$NiBr_2$] (dme = 1,2-dimethoxyethane) and tricyclohexylphosphane (1:2 ratio) leads to the corresponding monoarylated bromopyridines. These bromopyridines undergo Pd-catalysed aryl amination (Buchwald–Hartwig amination) with 2,6-diisopropylaniline giving rise to (2,6-diisopropylphenyl)[6-(2,4,6-triisopropylphenyl)pyridin-2-yl]amine (Ap*H) and (2,6-diisopropylphenyl)[6-(2,6-dimethylphenyl)pyridin-2-yl]amine (Ap′H) (Ap = aminopyridinate). Deprotonation of Ap*H in diethyl ether using BuLi results (after workup in hexane) in a colourless crystalline material. X-ray structural analysis reveals it to be a monomeric three-coordinate lithium aminopyridinate. In toluene solution, an equilibrium between [$(Ap^*Li)_2$] (in excess at room temperature) and [$Ap^*Li(OEt_2)$] (prominent at low temperature) is observed. Reaction of Ap′H with BuLi in diethyl ether gives rise to [Ap*LiAp*$Li(OEt_2)$]. Deprotonation of Ap*H and Ap′H using KH leads to $[Ap^*K]_n$ and $[Ap'K]_\infty$, respectively. $[Ap'K]_\infty$ is a rare example of a crystalline organometallic polymer, as determined by X-ray analysis.
(© Wiley-VCH Verlag GmbH & Co. KGaA, 69451 Weinheim, Germany, 2004)

Introduction

During the renaissance[1] of (amido)metal[2] chemistry, aminopyridinato ligands[3] have been used extensively to stabilise early transition metal and lanthanide ions (Scheme 1).

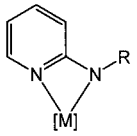

Scheme 1. Aminopyridinato ligand ([M] = early transition metal moiety; R = aryl, silyl or alkyl substituent)

The aminopyridinato ligands used thus far have exhibited a relatively low steric demand, especially in the plane perpendicular to the pyridine moiety. This characteristic has restricted the chemistry of the corresponding metal complexes so far, leading to the formation of "ate" species, for example.[3,4] In order to minimise this feature, we became interested in designing bulkier aminopyridinato ligands by the introduction of 2,6-alkylphenyl (alkyl = methyl or isopropyl) substituents at the amido N atom as well as the 6-position of the pyridine ring. Here, we report on the synthesis and structure of the lithium and potassium amides of Ap*H and Ap′H (Scheme 2).

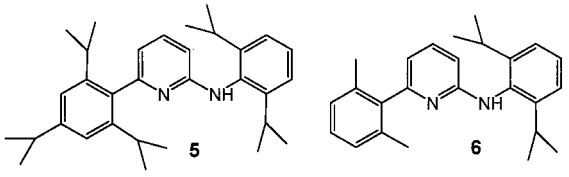

Scheme 2. Ap*H (**5**) and Ap′H (**6**)

The syntheses and structures of alkali metal aminopyridinates were described first by Clegg and Snaith et al.[5] These compounds are remarkable examples of the diversity metal amides can show in terms of binding and aggregation modes.[6] One of the most common structures observed is a dimer containing two coordinated solvent molecules (Scheme 3).[7]

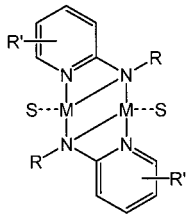

Scheme 3. The dimeric bis(solvent)-coordinated structure motive (M = alkali metal; R, R′ = alkyl, aryl or silyl substituent; S = mono- or bidentate donor solvent molecule)

Furthermore, structurally diverse alkali metal aminopyridinates have been found in aminopyridinato "ate" complexes[8] and in main group amides.[9]

[a] Lehrstuhl für Anorganische Chemie II, Universität Bayreuth, 95440 Bayreuth, Germany
E-mail: kempe@uni-bayreuth.de
[b] Leibniz-Institut für Organische Katalyse, Buchbinderstrasse 5–6, 18055 Rostock, Germany

Results and Discussion

Synthesis of the Ligands

The reaction of in situ formed Grignard compounds of 1-bromo-2,4,6-diisopropylphenyl or 1-bromo-2,6-dimethylphenyl (**1**, **2**) with 2,6-dibromopyridine in the presence of a catalytic amount of [(dme)$NiBr_2$] and tricyclohexylphosphane (1:2 ratio) leads to the bromopyridines **3** and **4** (Scheme 4). The catalyst system was chosen on the basis of results of parallel screening experiments with various phosphane/group 10 metal combinations. The best combination also turned out to be optimal in terms of material availability (both components can be obtained commercially), selectivity and activity.[10]

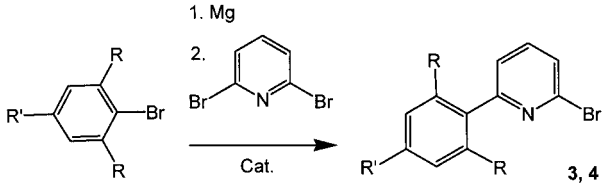

Scheme 4. Synthesis of **3** and **4** (**3** with R, R′ = *i*Pr; **4** with R = CH_3, R′ = H)

Compounds **3** and **4** undergo Pd-catalysed aryl amination (Buchwald–Hartwig amination) with 2,6-diisopropylaniline giving rise to **5** and **6**, respectively.[11] Despite the steric demands of the reactants, good yields have been observed for these two reactions.

Synthesis, Structure and Dynamic Behaviour of the Aminopyridinates

Deprotonation of **5** in diethyl ether using BuLi gave rise (after workup in hexane) to a colourless crystalline material (compound **7**) in about 80% yield (Scheme 5). X-ray crystal structure analysis of **7** revealed it to be a monomeric three-coordinated lithium aminopyridinate in the solid state (Figure 1).

The nearly equivalent Li–N distances [Li–N1 1.987(5), Li–N2 2.020(5) Å] indicate a delocalised binding mode.[12] The coordination of the lithium ion is approximately trigonal-planar (sum of angles = 353°; deviation of Li out of the plane N1–N2–O = 0.26 Å). The steric demand of deprotonated **5** is large. The maximum atom–atom distances of deprotonated **5** in **7** are a = 15 Å (Scheme 6) and, approximately perpendicular to it, b = 8 Å (Scheme 6). Comparison of these distances with those of the bulky, η^5-coordinated Cp* ligand[13] (Cp* = pentamethylcyclopentadienyl), which has a distance of $a = b$ = 6.2 Å for both directions, indicates that deprotonated **5** should be effective for the protection of large metal ions.

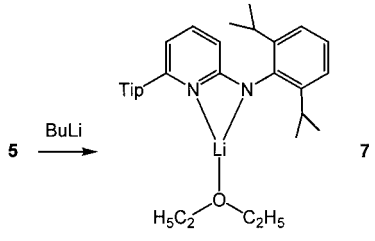

Scheme 5. Synthesis of **7** (Tip = 2,4,6-triisopropylphenyl)

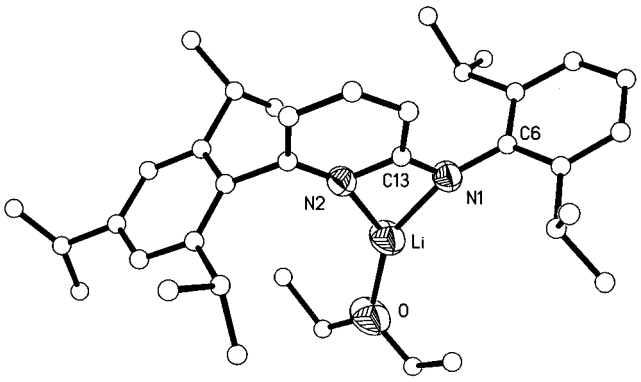

Figure 1. Molecular structure of **7** (ellipsoids correspond to the 50% probability level); selected bond lengths [Å] and angles [°]: Li–O 1.903(5), Li–N1 1.987(5), Li–N2 2.020(5); O–Li–N1 150.4(3), O–Li–N2 132.9(3), N1–Li–N2 69.28(16)

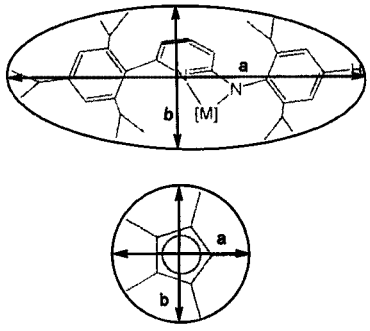

Scheme 6. Description of the steric demand of deprotonated **5**

^{1}H NMR spectroscopy of **7** at room temperature revealed it to be dynamic (Figure 2). One possibility is that the isopropyl groups of the aniline moiety and the pyridine substituent have restricted rotation due to the strained η^2-coordination mode [angle N1–Li–N2 = 69.28(16)°]. Alternatively, two different compounds (e.g. isomers) could exist in solution. Cooling of the NMR sample resulted in the formation of signals from a second compound (Figure 2). A characteristic of this "room-temperature compound" (**7a**) is that ether coordination is not observed as evidenced by the matching of the well-resolved ether signals to those of "free ether" in C_7D_8. In accordance with the structure of **8** (see discussion below) we propose a "solvent-free" dimeric structure for **7a** (Scheme 7)

Cooling down to −30 °C results in a change in the ratio of **7**/**7a** from 2:1 to 3:1. Precipitation of **7** starts at −50 °C (broad signals). Signal resolution occurs with the addition

 © 2004 Wiley-VCH Verlag GmbH & Co. KGaA, Weinheim

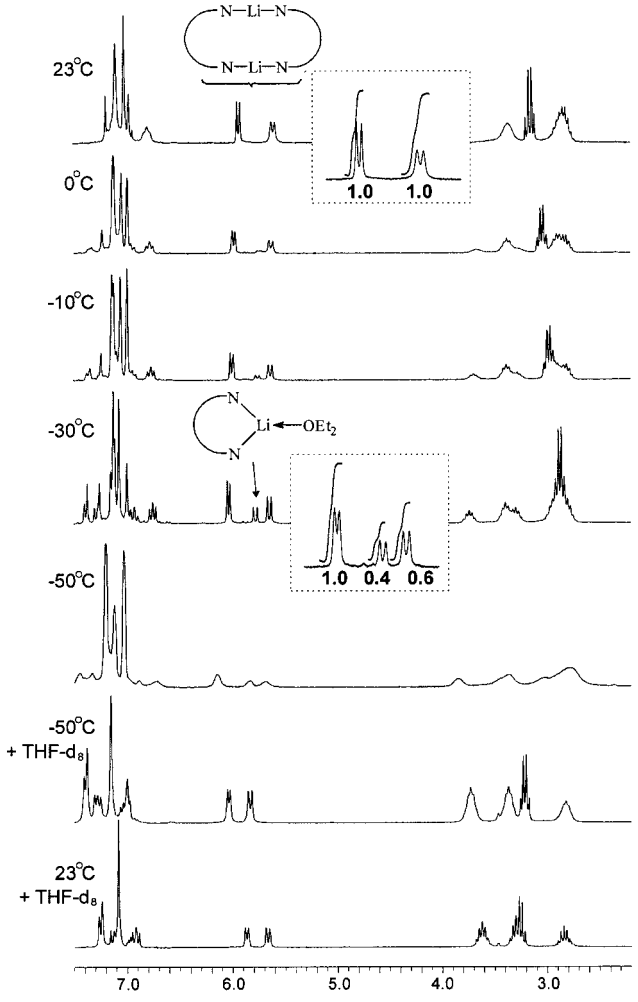

Figure 2. ^{1}H NMR of **7** in C_7D_8 at different temperatures; the two last spectra show signals after addition of $[D_8]$THF

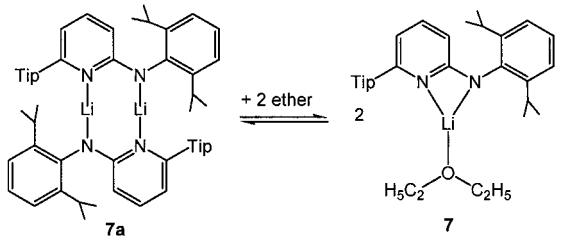

Scheme 7. Equilibrium between **7a** (dominant at room temperature) and **7** (low-temperature ether adduct)

of an excess of $[D_8]$THF at this temperature with the formation of a THF adduct analogous to **7**. This is indicated by a new, third signal set accompanied by the signals of "free ether". Raising the temperature to 25 °C causes only marginal changes of the signal set, which is in accordance with the expected temperature dependence. Furthermore, the signals observed for the pyridine protons suggest a delocalised binding mode in solution for both **7** and **7a**.[12]

Reaction of **6** with BuLi in diethyl ether gave (after work up in hexane) a crystalline material (**8**) in good yield (Scheme 8).

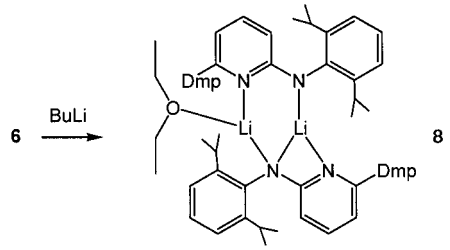

Scheme 8. Synthesis of **8** (Dmp = 2,6-dimethylphenyl)

X-ray crystal structure analysis of **8** revealed a dimeric structure in the solid state (Figure 3). Both Li atoms are coordinated in an almost trigonal-planar manner. The deviations of the lithium atoms out of the coordination planes are 0.43 Å (Li1) and 0.23 Å (Li2). One of the two Ap′ ligands acts as a bridge (bridging binding mode) with a significantly longer $N_{pyridine}-Li$ than $N_{amido}-Li$ bond, indicative of a localisation of the anionic charge of this ligand at the amido nitrogen atom. The second Ap′ ligand binds one of the lithium atoms in the strained η^2-binding mode [N4−Li2−N3 65.82(14)°] whereas the N_{amido} lone pair acts as a bridge to the second lithium atom. The steric demands of this new ligand can be described as mentioned above for Ap* (Scheme 6). The maximum atom−atom distances are a = 13 Å and, perpendicular to it, b = 8 Å. NMR studies reveal a similar dimeric structure in toluene solution as found in the solid state.

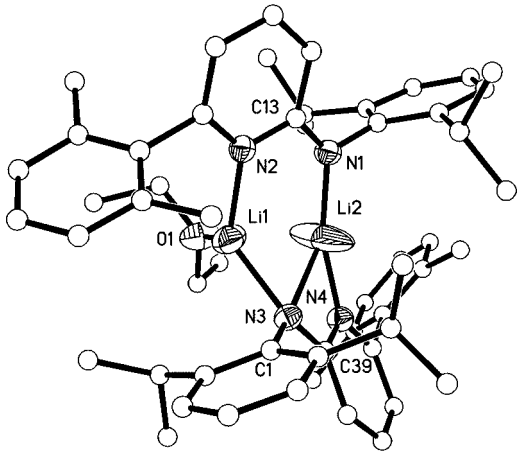

Figure 3. Molecular structure of **8** (ellipsoids correspond to the 50% probability level); selected bond lengths [A] and angles [°]: N4−Li2 1.922(4), N3−Li1 2.023(3), N3−Li2 2.271(5), N2−Li1 2.005(3), O1−Li1 2.013(4), N1−Li2 1.907(4); N2−Li1−O1 112.85(15), N2−Li1−N3 129.09(16), O1−Li1−N3 104.09(14), N1−Li2−N4 164.4(5), N1−Li2−N3 119.1(3), N4−Li2−N3 65.82(14)

The reactions of **5** and **6** with KH lead to crystalline **9** and **10**, respectively, according to Scheme 9. Crystals of **10**

 © 2004 Wiley-VCH Verlag GmbH & Co. KGaA, Weinheim

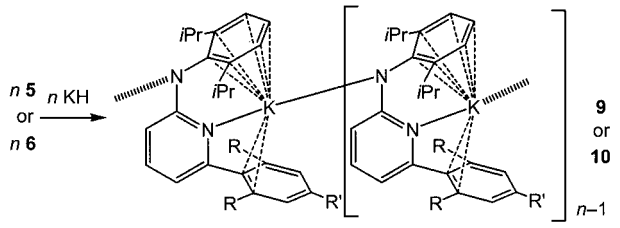

Scheme 9. Synthesis of **9** (R, R′ = *i*Pr) and **10** (R = CH_3, R′ = H)

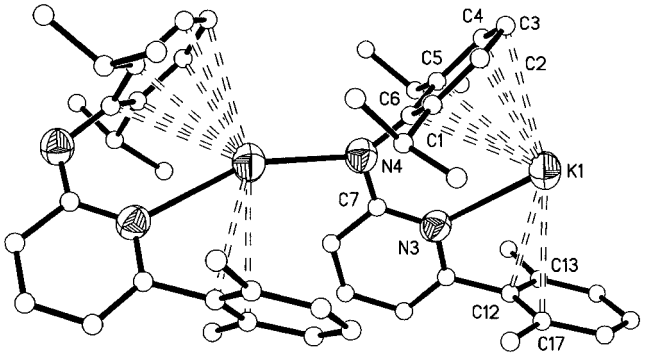

Figure 4. Part of the molecular structure of **10** (ellipsoids correspond to the 50% probability level); selected bond lengths [Å] and angles [°]: C1−K1 3.125(9), C2−K1 3.218(10), C3−K1 3.260(10), C4−K1 3.260(10), C5−K1 3.187(9), C6−K1 3.137(9), C12−K1 3.292(9), C17−K1 3.341(9), N3−K1 2.815(7), N4−K1 2.739(7); N4−K1−N3 157.2(2)

suitable for X-ray analysis were grown from diethyl ether (crystal structure: Figure 4).

The structure of **10** is best described as a coordinative one-dimensional polymer. (The amidoaryl groups appear on the same side in successive "monomer residues" − pseudo-isotactic.) The amido N atom coordinates one potassium atom and the pyridine function binds the next. The coordination thus can be described as a *transoid*-bridging binding mode (Scheme 10).

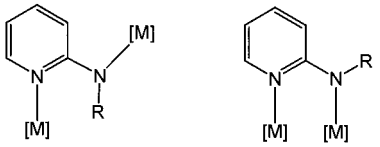

Scheme 10. *transoid*- (left) and *cisoid*-bridging binding (right) mode of aminopyridinato ligands ([M] metal moiety)

The binding situation observed for **10** might be helpful in explaining the mechanism of polymeric by-product formation found during aminopyridinato early transition metal complex syntheses.[3] The *transoid*-bridging binding mode formed by a two-coordinate potassium ion would be unstable without the π-coordination of the electron-rich phenyl substituents which coordinatively saturate the system. From an alternative viewpoint it could be said that the electron-rich arene functions of **5** and **6** are ideal for coordinatively saturating the potassium atoms and owing to geometric restrictions, the *transoid*-bridging binding mode is favoured. A detailed discussion of bond lengths and angles of **10** is precluded by the high disorder in the X-ray structure and grown-together twinned crystals. Despite the fact that a potassium−arene interaction is a common phenomenon, polymeric structures based on these are rarely observed[14] and homoleptic systems are almost unknown.[15]

Conclusions

Grignard coupling and palladium-catalysed aryl amination are efficient methods for the preparation of sterically encumbered aminopyridines. The steric coverage of deprotonated aminopyridines (aminopyridinato ligands) approaches the nanometer range and the cover area is about 3.3 and 2.8 times larger for deprotonated **5** and deprotonated **6**, respectively, than for Cp*. The structural and dynamic behaviour of the lithium and potassium amides in solution differ significantly. Compound **10** is a rare example of an Ap complex exhibiting the *transoid*-bridging binding mode.

Experimental Section

General Procedures: All reactions and manipulations with air-sensitive compounds were performed under dry argon, using standard Schlenk and drybox techniques. Solvents were distilled from sodium benzophenone ketyl. Deuterated solvents were obtained from Cambridge Isotope Laboratories and were degassed, dried (CaH_2) and distilled prior to use. NMR spectra were obtained using either a Bruker ARX 250 or Bruker DRX 500 spectrometer. Chemical shifts are reported in ppm relative to the deuterated solvent. *n*BuLi, KH, 1-bromo-2,4,6-triisopropylbenzene, 1-bromo-2,6-dimethylbenzene, $NiBr_2$(dme), tricyclohexylphosphane, 2,6-diisopropylaniline, 3-bis(diphenylphosphanyl)propane, sodium *tert*-butoxide, 1,2-dibromoethane and tris(dibenzylideneacetone)dipalladium(0) were purchased from commercial suppliers. X-ray crystal structure analyses were performed by using a STOE-IPDS I or II equipped with an Oxford Cryostream low-temperature unit. Structure solution and refinement were accomplished using SIR97,[16] SHELXL-97[17] and WinGX.[18] Crystallographic details are summarised in Table 1. CCDC-231858 (for **10**), -231859 (for **8**) and -231860 (for **7**) contain the supplementary crystallographic data for this paper. These data can be obtained free of charge at www.ccdc.cam.ac.uk/conts/retrieving.html [or from the Cambridge Crystallographic Data Centre, 12 Union Road, Cambridge CB2 1EZ, UK; Fax: + 44-1223-336-033; E-mail: deposit@ccdc.cam.ac.uk]

Preparation of 1-MgBr-[2,4,6-(*i*Pr)$_3$C$_6$H$_2$] (1): THF (30 mL) was added to magnesium turnings (0.94 g, 38.7 mmol). 1-Br-2,4,6-(*i*Pr)$_3$C$_6$H$_2$ (35.2 mmol, 9.97 g, 8.86 mL) was then added and the resulting suspension stirred and activated using 1,2-dibromoethane. An exothermic reaction took place and an ice bath was used to cool the reaction mixture when the reaction became too vigorous. After 1 h, the cooled reaction mixture was stirred at 50 °C overnight. The reaction mixture was filtered and the filtrate directly used in the preparation of **3**.

 © 2004 Wiley-VCH Verlag GmbH & Co. KGaA, Weinheim

Table 1. Details of the X-ray crystal structure analyses

	7	**8**	**10**
Crystal system	monoclinic	monoclinic	orthorhombic
Space group	$P2_1/c$	$P2_1/n$	*Pbca*
a [Å]	18.235(4)	10.780(5)	12.669(1)
b [Å]	19.007(4)	17.869(5)	37.704(5)
c [Å]	10.013(2)	25.205(5)	18.694(1)
β [°]	95.70(3)	91.49(5)	–
V [Å^3]	3453.2(5)	4854(3)	8929.6(15)
Z	4	4	8
Crystal size [mm]	0.18 × 0.16 × 0.08	0.5 × 0.4 × 0.3	0.4 × 0.2 × 0.2
$\rho_{calcd.}$ [g cm^{-3}]	1.592	1.099	1.180
μ [mm^{-1}] (Mo-K_α)	0.060	0.064	0.250
T [K]	193(2)	193(2)	193(2)
θ range [°]	2.14–26.07	1.40–26.03	1.08–20.56
No. of unique reflections	6405	9521	4511
No. of reflections observed [$I > 2\sigma(I)$]	3076	7740	3477
No. of parameters	361	551	489
wR^2 (all data)	0.170	0.149	0.242
R value [$I > 2\sigma(I)$]	0.059	0.050	0.097

Preparation of 1-MgBr-[2,6-(Me)$_2$C$_6$H$_3$] (2): THF (30 mL) was added to magnesium turnings (0.94 g, 38.7 mmol). 1-Br-2,6-Me$_2$C$_6$H$_3$ (35.2 mmol, 6.50 g, 4.69 mL) was then added and the resulting suspension stirred. The reaction mixture was activated using 1,2-dibromoethane (approx. 0.4 mL). An exothermic reaction took place and an ice bath was used to cool the reaction mixture when the reaction became too vigorous. After 2 h, the cooled reaction mixture was stirred at 50 °C for 12 h. The reaction mixture was filtered and the filtrate directly used in the preparation of **4**.

Preparation of 3: 2,6-Dibromopyridine (7.91 g, 33.4 mmol), dioxane (35 mL), tricyclohexylphosphane [0.075 mmol, 1.5 mL (0.05 M in THF)] and [NiBr$_2$(dme)] (0.012 g, 0.0375 mmol) were added together in a Schlenk flask under argon; **1** was then added to the stirred suspension resulting in a beige precipitate. The reaction mixture was warmed to 50 °C and stirred for 72 h. Water and $CHCl_3$ were added and the resulting suspension transferred to a 2-L separating funnel. The organic phase was collected and the inorganic phase washed with $CHCl_3$ and extracted. The combined organic phases were washed with a saturated sodium chloride solution and dried with Na_2SO_4. The solvent was removed to afford a white precipitate. The precipitate was recrystallised from hot *n*-octane and washed with *n*-pentane (20 mL). Yield 7.05 g (58%). M.p. 232–233 °C $C_{20}H_{26}BrN$ (360.3): calcd. C 66.67, H 7.27, N 3.89; found C 67.56, H 7.48, N 3.78. ^{1}H NMR (250 MHz, $CDCl_3$, 298 K): δ = 1.00–1.30 [m, 18 H, CH(C*H*$_3$)$_2$], 2.44 [sept, 2 H, C*H*(CH$_3$)$_2$], 2.88 [sept, 1 H, C*H*(CH$_3$)$_2$], 7.02 (s, 2 H, 9,11-H), 7.21 (d, 1 H, 3-H), 7.45 (d, 1 H, 5-H), 7.59 (br. dd, 1 H, 4-H) ppm. ^{13}C NMR (250 MHz, $CDCl_3$, 298 K): δ = 23.85 [2 CH$_3$, (*C*H$_3$)$_2$CH], 24.06 [2 CH$_3$, (*C*H$_3$)$_2$CH], 24.17 [2 CH$_3$, (*C*H$_3$)$_2$CH], 30.41 [*C*H(CH$_3$)$_2$, C-13,-15], 34.44 [*C*H(CH$_3$)$_2$, C-14], 120.76 (CH, C-9,11), 123.94 (CH, C-3/5), 125.90 (CH, C-3/5), 134.88 (C, C-7), 137.93 (CH, C-4), 141.46 (C, C-2), 146.12 (C, C-8,12), 149.29 (C, C-10), 161.30 (C, C-6) ppm.

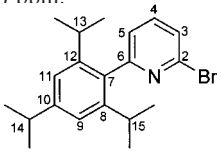

Preparation of 4: 2,6-Dibromopyridine (7.91 g, 33.4 mmol), dioxane (35 mL), tricyclohexylphosphane (0.075 mmol, 1.5 mL (0.05 M in THF) and [NiBr$_2$(dme)] (0.012 g, 0.0375 mmol) were combined in a Schlenk flask and cooled to 0 °C. Compound **2** was then slowly added dropwise to the cooled, stirred suspension. A beige precipitate resulted and the resulting mixture was then warmed to room temperature where a moderate exothermic reaction took place. Once the reaction mixture was cooled to room temperature, it was stirred and after 1 h heated to 50 °C for 72 h. Water (50 mL) and CH_2Cl_2 (50 mL) were added and the resulting suspension transferred to a 2-L separating funnel. The organic phase was collected and the inorganic phase washed with CH_2Cl_2 and extracted. The combined organic phases were washed with a saturated sodium chloride solution and dried with Na_2SO_4. The organic phase was concentrated to dryness under vacuum resulting in a red-orange oily product. The reddish oil was purified using silica chromatography (dichloromethane) and then crystallised from pentane at –20 °C. Yield 7.80 g (89%). M.p. 62–63 °C. $C_{13}H_{12}BrN$ (262.1): calcd. C 59.56, H 4.61, N 5.34; found C 60.30, H 4.74, N 5.28. ^{1}H NMR (250 MHz, $CDCl_3$, 298 K): δ = 1.91 (s, 6 H, CH$_3$), 6.92 (s, 2 H, 9,11-H), 6.86–7.35 (m, 3 H, Ar, 3,5,10-H), 7.44 (br. dd, 1 H, 4-H) ppm. ^{13}C NMR (250 MHz, $CDCl_3$, 298 K): δ = 20.17 (2 CH$_3$, C-13,14), 123.41 (CH, C-3/5), 126.03 (CH, C-3/5), 127.52 (CH, C-9,11), 128.21 (C, C-10), 135.64 (C, C-8,12), 138.91 (CH, C-4), 140.73 (C, C-2/7), 141.71 (C, C-2/7), 160.88 (C, C-6) ppm.

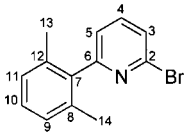

Preparation of Ap*H (5): In a drybox the solids **3** (4.00 g, 11.12 mmol), 1,3-bis(diphenylphosphanyl)propane (0.115 g, 0.279 mmol), tris(dibenzylideneacetone)dipalladium(0) (0.126 g, 0.139 mmol) and sodium *tert*-butoxide (0.90 g, 3.10 mmol) were combined in a Schlenk flask. 2,6-Diisopropylaniline (11.12 mmol, 1.97 g, 2.10 mL) and toluene (40 mL) were added to the flask. The

 © 2004 Wiley-VCH Verlag GmbH & Co. KGaA, Weinheim

resulting mixture was heated at 95 °C for 48 h. The reaction mixture was cooled to room temperature, and water (50 mL) and diethyl ether (50 mL) were added. The organic phase was extracted and the remaining inorganic phase was washed with diethyl ether (3 × 20 mL). The combined organic phases were washed with a saturated sodium chloride solution and the organic phase was dried with sodium sulfate. The solvent was removed under reduced pressure and the resulting red-orange solid was purified using silica chromatography (dichloromethane). Yield 5.00 g (89%). M.p. 162−163 °C. $C_{32}H_{44}N_2$ (456.7): calcd. C 84.16, H 9.71, N 6.13; found C 83.94, H 9.75, N 5.71. ^{1}H NMR (250 MHz, $CDCl_3$, 298 K): δ = 1.00−1.27 [m, 30 H, CH(CH_3)$_2$], 2.70 [sept, 2 H, CH(CH$_3$)$_2$], 2.90 [sept, 1 H, CH(CH$_3$)$_2$], 3.25 [sept, 2 H, CH(CH$_3$)$_2$], 3.72 (br. s, 1 H, NH), 5.91 (br. d, ^1J = 8.30 Hz, 1 H, 3-H), 5.97 (br. s, 1 H, 4-H), 6.61 (br. d, ^1J = 7.2 Hz, 1 H, 5-H), 7.03−7.40 (m, Ar, 5 H, 9,11,18,19,20-H) ppm. ^{13}C NMR (250 MHz, $CDCl_3$, 298 K): δ = 22.43 [CH(CH$_3$)$_2$, C-22,23], 23.95 [2 CH(CH$_3$)$_2$, C-32,33/28,29/30,31], 24.14 [2 CH(CH$_3$)$_2$, C-32,33/28,29/30,31], 24.51 [2 CH(CH$_3$)$_2$, C-32,33/28,29/30,31], 28.47 [CH(CH$_3$)$_2$, C-24,25,26,27], 30.33 [CH(CH$_3$)$_2$, C-13,14], 34.47 [CH(CH$_3$)$_2$, C-15], 103.64 (CH, C-3), 114.89 (CH, C-5), 120.74 (CH, C-9,11), 123.92 (CH, C-18,20), 127.90 (CH, C-19), 134.51 (C, C-16), 136.61 (C, C-7), 137.35 (CH, C-4), 146.01 (C, C-8,12), 148.01 (C, C-17,21), 148.45 (C, C-10), 158.54 (C, C-2/6), 159.08 (C, C-2/6) ppm.

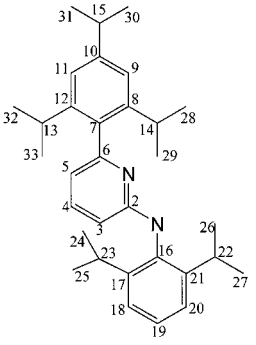

Preparation of Ap′H (6): In a drybox the solids **4** (2.00 g, 7.63 mmol), 1,3-bis(diphenylphosphanyl)propane (0.115 g, 0.279 mmol), tris(dibenzylideneacetone)dipalladium(0) (0.126 g, 0.139 mmol) and sodium *tert*-butoxide (0.83 g, 8.6 mmol) were combined in a Schlenk flask. 2,6-Diisopropylaniline (7.63 mmol, 1.35 g, 1.43 mL) and toluene (30 mL) were added to the flask. The resulting mixture was heated at 95 °C for 72 h. The reaction mixture was cooled to room temperature, and water (50 mL) and diethyl ether (50 mL) were added. The organic phase was extracted and the remaining inorganic phase washed with diethyl ether (3 × 20 mL). The combined organic phases were washed with a saturated sodium chloride solution and the organic phase was dried with sodium sulfate. The solvent was removed under reduced pressure and the resulting red solid was then purified using column chromatography (dichloromethane) and crystallised at −20 °C from pentane to afford a white crystalline material. Yield 2.10 g (77%). M.p. 106−107 °C. $C_{25}H_{30}N_2$ (358.5): calcd. C 83.75, H 8.43, N 7.81; found C 83.37, H 8.54, N 7.72. ^{1}H NMR (250 MHz, $CDCl_3$, 298 K): δ = 0.88−1.20 [m, 12 H, CH(CH_3)$_2$], 2.09 (s, 6 H, CH_3), 3.25 [sept, 2 H, CH(CH$_3$)$_2$], 3.76 (v. br. s, 1 H, NH), 5.86 (br. d, ^1J = 8.30 Hz, 1 H, 3-H), 5.98 (br. s, 1 H, 4-H), 6.49 (br. d, ^1J = 7.2 Hz, 1 H, 5-H), 7.03−7.35 (m, Ar, 6 H, 9,10,11,17,18,19-H) ppm. ^{13}C NMR (250 MHz, $CDCl_3$, 298 K): δ = 20.10 (CH$_3$, C-13,14), 23.75 [CH(CH$_3$)$_2$, C-21,22], 28.44 [CH(CH$_3$)$_2$, C-23,24,25,26], 103.73 (CH, C-3), 114.08 (CH, C-5), 124.06 (CH, C-17,19), 127.56 (CH, C-9,11), 127.70 (CH, C-10/18), 128.00 (CH, C-10/18), 134.18 (C, C-15), 135.75 (C, C-8,12), 138.04 (CH, C-4), 140.74 (C, C-7), 148.01 (C, C-16,20), 158.43 (C, C-2/6), 159.37 (C, C-2/6) ppm.

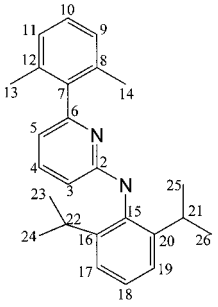

Preparation of 7: *n*BuLi (1.38 mL, 1.6 M, 2.20 mmol) was slowly added to a stirred solution of Ap*H (1.00 g, 2.20 mmol) in diethyl ether (40 mL) at 0 °C. After complete addition, the mixture was stirred and warmed to room temperature (ca. 1 h). The reaction mixture was concentrated to dryness and hexane (20 mL) added. The solvent volume was reduced to ca. 2 mL in vacuo, and on standing colourless crystals of the title complex formed. Yield 0.96 g (82%). $C_{36}H_{53}LiN_2O$ (536.8): calcd. C 80.56, H 9.95, N 5.22; found C 79.85, H 9.66, N 4.90. ^{1}H NMR (250 MHz, C_7D_8, 298 K): δ = 0.89 (br. m, 6 H, CH$_3$, OEt$_2$), 0.98−1.40 [m, 30 H, CH(CH_3)$_2$], 2.83 [br. m, 3 H, CH(CH$_3$)$_2$] 3.11 (m, 4 H, CH$_2$, OEt$_2$), 3.25 [br. m, 2 H, CH(CH$_3$)$_2$], 5.61 (br. d, ^1J = 8.05 Hz, 1 H, 3-H), 5.92 (d, ^1J = 6.90 Hz, 1 H, 5-H), 6.95 (br. dd, 1 H, 4-H), 6.98−7.32 (m, Ar, 5 H, 9,11,18,19,20-H) ppm. ^{13}C NMR (250 MHz, C_7D_8, 298 K): δ = 14.99 (2 CH$_3$, Et$_2$O), 24.37 [CH(CH$_3$)$_2$, C-22,23], 24.47 [CH(CH$_3$)$_2$, C-28,29,32,33], 24.88 [CH(CH$_3$)$_2$, C-30,31], 28.42 [CH(CH$_3$)$_2$, C-24,25,26,27], 30.66 [br., CH(CH$_3$)$_2$, C-13,14], 34.94 [br., CH(CH$_3$)$_2$, C-15], 66.17 (2 CH$_2$, Et$_2$O), 107.15 (br. CH, C-3), 108.58 (br., CH, C-5), 120.76, 120.97, 124.47, 137.88, 145.18 (br., CH, C-4), 146.70, 148.52, 157.32 (br., C, C-6), 169.56 (br., C, C-2) ppm. ^{1}H NMR (250 MHz, C_7D_8, 273 K): δ = 0.92 (m, 6 H, CH$_3$, OEt$_2$), 0.98−1.38 [m, 30 H, CH(CH_3)$_2$], 2.88 [v. br. m, 3 H, CH(CH$_3$)$_2$], 3.05 (m, 4 H, CH$_2$, OEt$_2$), 3.36 [v. br. m, 1 H, CH(CH$_3$)$_2$], 3.76 [v. br. m, 1 H, CH(CH$_3$)$_2$], 5.62 (br. d, ^1J = 8.50 Hz, 1 H, 3-H), 6.69 (v. br. d, 3-H*), 5.98 (d, ^1J = 6.80 Hz, 1 H, 5-H), 6.77 (br. dd, 1 H, 4-H), 6.90−7.32 (m, Ar, 5 H, 9,11,18,19,20-H) ppm. ^{13}C NMR (250 MHz, C_7D_8, 273 K): δ = 14.45 (2 CH$_3$, Et$_2$O), 24.43 [CH(CH$_3$)$_2$, C-22,23], 24.62 [CH(CH$_3$)$_2$, C-28,29,32,33], 24.97 [CH(CH$_3$)$_2$, C-30,31], 28.36 [CH(CH$_3$)$_2$, C-24,25,26,27], 30.67 [br., CH(CH$_3$)$_2$, C-13,14], 37.00 [br., CH(CH$_3$)$_2$, C-15], 66.24 (2 CH$_2$, Et$_2$O), 107.29 (br., CH, C-3), 108.59 (br., CH, C-5), 120.43, 121.06, 123.63, 124.59, 137.25, 137.09, 144.63 (br., CH, C-4), 145.23, 146.64, 148.65, 157.36 (br., C, C-6), 169.51 (br., C, C-2) ppm. ^{1}H NMR (250 MHz, C_7D_8, 243 K): δ = 0.86 (m, 6 H, CH$_3$, OEt$_2$), 0.95−1.40 [m, 30 H, CH(CH_3)$_2$], 2.89 [m, 3 H, CH(CH$_3$)$_2$], 3.25 [br. m, 1 H, CH(CH$_3$)$_2$], 3.39 (m, 4 H, CH$_2$, OEt$_2$), 3.70 [br. m, 1 H, CH(CH$_3$)$_2$], 5.64 (br. d, ^1J = 8.50 Hz, 3-H), 5.69 (v. br. d, ^1J = 8.30 Hz, 3-H*), 6.04 (d, ^1J = 6.90 Hz, 1 H, 5-H), 6.75 (br. dd, 1 H, 4-H), 6.98−7.40 (m, Ar, 5 H, 9,11,18,19,20-H) ppm. ^{13}C NMR (250 MHz, C_7D_8, 243 K): δ = 14.44 (2 CH$_3$, Et$_2$O), 24.53 [CH(CH$_3$)$_2$, C-22,23], 24.64 [CH(CH$_3$)$_2$, C-28,29,32,33], 24.88 [CH(CH$_3$)$_2$, C-30,31], 28.46 [br., CH(CH$_3$)$_2$, C-24,25,26,27], 30.86 [br., CH(CH$_3$)$_2$, C-13,14], 35.29 [CH(CH$_3$)$_2$, C-15], 66.20 (2 CH$_2$, Et$_2$O), 104.72 (br., CH, C-3*), 104.98 (br., CH, C-5*), 107.29 (br., CH, C-3), 108.59 (br., CH, C-5), 120.53 (br.*), 121.06, 122.47 (br.*), 123.88 (br.*), 124.75, 137.37, 138.36 (*),

 © 2004 Wiley-VCH Verlag GmbH & Co. KGaA, Weinheim

139.49 (*), 143.40 (CH, C-4), 144.79 (CH, C-4*), 145.28, 146.64 (*), 146.78 (br.), 147.96 (*), 148.60 (*), 148.84, 157.01 (C, C-6*), 157.47 (C, C-6), 169.64 (C, C-2), 169.92 (C, C-2*) ppm. ^{1}H NMR (250 MHz, C_7D_8, 223 K): δ = 0.69 (v. br. s, 6 H, CH_3, OEt_2), 0.95−1.50 [v. br. m, 30 H, CH(CH_3)$_2$], 2.77 [v. br. m, 3 H, CH(CH$_3$)$_2$], 3.15 [v. br. m, 1 H, CH(CH$_3$)$_2$], 3.36 (v. br. m, 4 H, CH_2, OEt_2), 3.79 [v. br. m, 1 H, CH(CH$_3$)$_2$], 5.64 (v. br. d, 3-H), 5.69 (v. br. d, 3-H*), 6.14 (v. br. s, 1 H, 5-H), 6.85 (v. br. s, 1 H, 4-H), 6.98−7.45 (v. br. m, Ar, 5 H, 9,11,18,19,20-H) ppm. ^{1}H NMR (250 MHz, C_7D_8 {addition of two drops of C_4D_8O} 298 K): δ = 1.07 (m, 6 H, CH_3, OEt_2), 1.20−1.40 [m, 30 H, CH(CH_3)$_2$], 2.84 [m, 1 H, CH(CH$_3$)$_2$], 3.23 (m, 4 H, CH_2, OEt_2), 3.35 [m, 2 H, CH(CH$_3$)$_2$], 3.65 [m, 2 H, CH(CH$_3$)$_2$], 5.66 (br. d, ^1J = 8.60 Hz, 1 H, 3-H), 5.86 (d, ^1J = 6.90 Hz, 1 H, 5-H), 6.91 (br. dd, 1 H, 4-H), 6.98−7.26 (m, Ar, 5 H, 9,11,18,19,20-H) ppm. ^{13}C NMR (250 MHz, C_7D_8 {addition of two drops of C_4D_8O}, 298 K): δ = 15.45 (2 CH_3, Et_2O), 23.99 [CH(CH$_3$)$_2$, C-22*,23*], 24.31 [CH(CH$_3$)$_2$, C-28*,29*,32*,33*], 24.94 [CH(CH$_3$)$_2$, C-30*,31*], 28.20 [CH(CH$_3$)$_2$, C-24*,25*,26*,27*], 30.38 [CH(CH$_3$)$_2$, C-13*,14*], 34.88 [CH(CH$_3$)$_2$, C-15*], 65.91 (2 CH_2, Et_2O), 104.71 (CH, C-3*/5*), 104.82 (CH, C-3*/5*), 120.20 (CH, C-9*,11*), 121.40 (CH, C-19*), 123.44 (CH, C-18*,20*), 136.44 (CH, C-4*), 140.00 (C, C-10*), 143.10 (C, C-8*,12*), 146.61 (C, C-17*,21*), 147.40 (C, C-7*), 149.75 (C, C-16*), 156.95 (C, C-6*), 169.10 (C, C-2*) ppm. ^{1}H NMR (250 MHz, C_7D_8 {addition of two drops of C_4D_8O}, 223 K): δ = 1.06 (m, 6 H, CH_3, OEt_2), 1.16−1.33 [m, 30 H, CH(CH_3)$_2$], 2.84 [br. m, 1 H, CH(CH$_3$)$_2$], 3.26 (m, 4 H, CH_2, OEt_2), 3.35 [br. m, 2 H, CH(CH$_3$)$_2$], 3.65 [br. m, 2 H, CH(CH$_3$)$_2$], 5.67 (d, ^1J = 8.60 Hz, 1 H, 3-H), 5.87 (d, ^1J = 6.90 Hz, 1 H, 5-H), 6.91 (br. dd, 1 H, 4-H), 6.98−7.26 (m, Ar, 5 H, 9,11,18,19,20-H) ppm. ^{13}C NMR (250 MHz, C_7D_8 {addition of two drops of C_4D_8O}, 223 K): δ = 15.46 (2 CH_3, Et_2O), 23.99 [CH(CH$_3$)$_2$, C-22*,23*], 24.18 [CH(CH$_3$)$_2$, C-28*,29*,32*,33*], 24.94 [CH(CH$_3$)$_2$, C-30*,31*], 28.20 [CH(CH$_3$)$_2$, C-24*,25*,26*,27*], 30.38 [CH(CH$_3$)$_2$, C-13*,14*], 34.88 [CH(CH$_3$)$_2$, C-15*], 65.91 (2 CH_2, Et_2O), 104.18 (CH, C-3*,5*), 120.12 (CH, C-9*,11*), 121.21 (CH, C-19*), 123.36 (CH*, C-18,20*), 136.56 (CH, C-4*), 139.67 (C, C-10*), 142.74 (C, C-8*,12*), 146.24 (C, C-17*,21*), 147.25 (C, C-7*), 149.39 (C, C-16*), 156.78 (C, C-6*), 168.40 (C, C-2*) ppm. * = monomeric isomer.

Preparation of 8: *n*BuLi (0.63 mL, 1.6 M, 1.00 mmol) was slowly added to a stirred solution of Ap′H (0.36 g, 1.00 mmol) in diethyl ether (40 mL) at 0 °C. After complete addition, the mixture was stirred and warmed to room temperature (ca. 1 h). The reaction mixture was reduced to dryness and hexane (20 mL) added. The solvent volume was reduced to ca. 10 mL in vacuo, and on standing colourless crystals of the title complex formed. Yield 0.35 g (88%). $C_{54}H_{68}Li_2N_4O$ (803.0): calcd. C 80.76, H 8.53, N 6.98; found C 79.18, H 8.20, N 6.95; the slightly too low C value is due to removal of the coordinated ether during the drying process. ^{1}H NMR (500 MHz, C_7D_8, 298 K): δ = 0.99 (br. m, 6 H, CH_3, OEt_2), 0.92−1.10 [m, 24 H, CH(CH_3)$_2$], 1.92 (s, 12 H, CH_3), 3.19 (m, 4 H, CH_2, OEt_2), 3.27 [sept, 4 H, CH(CH$_3$)$_2$], 5.58 (br. d, ^1J = 8.05 Hz, 2 H, 3-H), 5.76 (d, ^1J = 6.90 Hz, 2 H, 5-H), 6.83 (br. dd, 2 H, 4-H), 6.98−7.10 (m, Ar, 12 H, 9,10,11,17,18,19-H) ppm. ^{13}C NMR (250 MHz, C_7D_8, 298 K): δ = 15.32 (2 CH_3, Et_2O), 20.08 (2 CH_3, C-13,14), 24.18 [2 CH$_3$, CH(CH$_3$)$_2$, C-23,25/24,26], 24.58 [2 CH_3, CH(CH$_3$)$_2$, C-23,25/24,26], 28.44 [2 CH_3, CH(CH$_3$)$_2$, C-23,25/24,26], 65.88 (2 CH_2, Et_2O), 106.19 (CH, C-3/5), 107.46 (CH, C-3/5), 124.90 (CH, C-17,19), 127.30−128.40 (CH, C-9,10,11,18), 135.78 (C, C-8,12), 138.53 (CH, C-4), 141.13 (C, C-7), 143.86 (C, C-15), 144.89 (C, C-16,20), 157.16 (C, C-6), 169.19 (C, C-2) ppm.

Preparation of 9: Diethyl ether (50 mL) was added to the solids KH (0.09 g 2.19 mmol) and Ap*H (1.00 g, 2.19 mmol) and the reaction mixture stirred for 12 h. The mixture was filtered and the filtrate concentrated to dryness under vacuum. The resulting off-white residue was washed with hexane (30 mL) and the resulting white precipitate dried under vacuum. Yield 0.86 g (79%). $[C_{32}H_{43}KN_2]_n$: calcd. C 77.68, H 8.76, N 5.66; found C 77.39, H 8.94, N 5.34. ^{1}H NMR (250 MHz, C_6D_6, 298 K): δ = 1.10−1.30 [m, 30 H, CH(CH_3)$_2$], 2.85 [sept, 1 H, CH(CH$_3$)$_2$], 3.18 [sept, 2 H, CH(CH$_3$)$_2$], 3.33 [sept, 2 H, CH(CH$_3$)$_2$], 5.76 (v. br. d, 1 H, 3-H), 5.92 (br. d, ^1J = 6.80 Hz, 1 H, 5-H), 6.93 (br. dd, 1 H, 4-H), 6.90−7.21 (m, Ar, 5 H, 9,11,18,19,20-H) ppm. ^{13}C NMR (250 MHz, C_6D_6, 298 K): δ = 24.15 [CH(CH$_3$)$_2$, C-28,29,32,33], 24.46 [CH(CH$_3$)$_2$, C-30,31], 25.11 [CH(CH$_3$)$_2$, C-22,23], 28.38 [CH(CH$_3$)$_2$, C-13,14], 30.44 [CH(CH$_3$)$_2$, C-24,25,26,27], 34.93 [CH(CH$_3$)$_2$, C-15], 106.58 (CH, C-3), 120.73 (CH, C-9,11), 121.93 (CH, C-5), 123.82 (CH, C-18,20), 125.84 (CH, C-19), 136.26 (CH, C-4), 139.96 (C, C-7), 143.49 (C, C-16), 146.54 (C, C-8,12), 146.77 (C, C-10), 147.99 (C, C-17,21), 154.05 (C, C-6), 157.81 (C, C-2) ppm.

Preparation of 10: Diethyl ether (50 mL) was added to the solids KH (0.09 g 2.19 mmol) and Ap′H (1.00 g, 2.19 mmol) and the reaction mixture stirred for 12 h. The mixture was filtered and the filtrate concentrated to dryness under vacuum. The resulting off-white residue was washed with hexane (30 mL) and the resulting white precipitate dried under vacuum. Yield 0.86 (79%). Crystals of **6** were grown from diethyl ether. $C_{25}H_{29}KN_2$ (396.6): calcd. C 75.71, H 7.37, N 7.06; found C 75.45, H 7.63, N 6.63. ^{1}H NMR (250 MHz, C_6D_6, 298 K): δ = 1.11−1.16 [m, 12 H, CH(CH_3)$_2$], 2.25 (s, 6 H, CH_3), 3.32 [m, 2 H, CH(CH$_3$)$_2$], 5.85 (v. br. d, 1 H, 3-H), 6.23 (br. d, 1 H, 5-H), 7.00−7.45 (m, Ar, 7 H, 4,9,10,11,17,18,19-H) ppm. ^{13}C NMR (250 MHz, C_6D_6, 298 K): δ = 20.47 (CH_3, C-13,14), 24.11 [CH(CH$_3$)$_2$, C-23,24,25,26], 28.53 [CH, CH(CH$_3$)$_2$, C-21,22], 121.42 (1 CH, C-3/4/5), 123.09, 123.97 (CH, C-17,19), 124.40, 127.26 (CH, C-9,11), 135.65, 135.83 (C, C-8,12), 137.07 (1 CH, C-3/4/5), 150.07 (C, C-16,20) ppm. ^{1}H NMR (250 MHz, C_4D_8O, 298 K): δ = 1.08−1.12 [m, 12 H, CH(CH_3)$_2$], 2.20 (s, 6 H, CH_3), 3.39 [m, 2 H, CH(CH$_3$)$_2$], 5.34 (v. br. d, 1 H, 3-H), 5.51 (br. d, 1 H, 5-H), 6.76 (br. dd, 1 H, 4-H), 6.95−7.02 (m, Ar, 6 H, 9,10,11,17,18,19-H) ppm. ^{13}C NMR (250 MHz, C_4D_8O, 298 K): δ = 20.45 (CH_3, C-13,14), 24.51 [CH(CH$_3$)$_2$, C-23,24,25,26], 28.90 [CH, CH(CH$_3$)$_2$, C-21,22,], 101.92 (v. br., 1 CH, C-3/4/5), 104.21 (1 CH, C-3/4/5), 119.77 (v. br., 1 CH, C-3/4/5), 122.58 (CH, C-17,19), 126.29 (CH, C-10), 126.79 (CH, C-9,11), 135.03 (CH, C-18), 135.50 (C, C-8,12), 142.82 (v. br., C, C-16,20), 144.82 (br., C, C-7), 157.74 (C, C-6), 165.71 (v. br., C, C-2) ppm; C-15 signal could not be observed.

Acknowledgments

We thank Wolfgang Milius for his support in the X-ray laboratory and Elena Klimkina for her help with the assignment of the NMR spectroscopic data. Financial support from the Alexander von Humboldt Stiftung (N. M. S.), the Deutsche Forschungsgemeinschaft (Schwerpunktprogramm 1166 "Lanthanoidspezifische Funktionalitäten in Molekül und Material") and the Fonds der Chemischen Industrie is gratefully acknowledged.

[1] R. Kempe, *Angew. Chem.* **2000**, *112*, 478−504; *Angew. Chem. Int. Ed.* **2000**, *39*, 468−493.
[2] M. F. Lappert, P. P. Power, A. R. Sanger, R. C. Srivastava,

 © 2004 Wiley-VCH Verlag GmbH & Co. KGaA, Weinheim

Metal and Metalloid Amides, Ellis Horwood Ltd., Chichester, **1980**.
[3] R. Kempe, *Eur. J. Inorg. Chem.* **2003**, 791−803.
[4] For review, see: R. Kempe, H. Noss, T. Irrgang, *J. Organomet. Chem.* **2002**, *647*, 12−20.
[5] [5a] D. Barr, W. Clegg, R. E. Mulvey, R. Snaith, *J. Chem. Soc., Chem. Commun.* **1984**, 469−470. [5b] D. Barr, W. Clegg, R. E. Mulvey, R. Snaith, *J. Chem. Soc., Chem. Commun.* **1984**, 700−701.
[6] [6a] A. Bashall, A. D. Bond, A. D. Hopkins, S. J. Kidd, M. McPartlin, A. Steiner, R. Wolf, A. D. Woods, D. S. Wright, *J. Chem. Soc., Dalton Trans.* **2002**, 343−351. [6b] S. T. Liddle, W. Clegg, *J. Chem. Soc., Dalton Trans.* **2001**, 3549−3550. [6c] D. R. Armstrong, W. Clegg, R. P. Davies, S. T. Liddle, D. J. Linton, P. R. Raithby, R. Snaith, A. E. H. Wheatley, *Angew. Chem. Int. Ed.* **1999**, *38*, 3367−3370. [6d] R. E. Marsh, A. L. Spek, *Acta Crystallogr., Sect. B: Struct. Sci.* **2001**, *57*, 800−805. [6e] P. C. Andrews, W. Clegg, R. E. Mulvey, *Angew. Chem. Int. Ed. Engl.* **1990**, *29*, 1440−1441. [6f] C. Jones, P. C. Junk, S. G. Leary, N. A. Smithies, *J. Chem. Soc., Dalton Trans.* **2000**, 3186−3190. [6g] S. T. Liddle, W. Clegg, *J. Chem. Soc., Dalton Trans.* **2001**, 402−408. [6h] F. A. Cotton, Hong-Cai Zhou, *Inorg. Chim. Acta* **2000**, *298*, 216−220. [6i] F. A. Cotton, L. M. Daniels, C. A. Murillo, Hong-Cai Zhou, *C. R. Acad. Sci., Ser. IIc: Chim.* **1999**, *2*, 579−582.
[7] [7a] L. M. Engelhardt, G. E. Jacobsen, P. C. Junk, C. L. Raston, B. W. Skelton, A. H. White, *J. Chem. Soc., Dalton Trans.* **1988**, 1011−1020. [7b] P. C. Andrews, D. R. Baker, R. E. Mulvey, W. Clegg, P. A. O'Neil, *Polyhedron* **1991**, *10*, 1839−1841. [7c] N. Feeder, R. Snaith, A. E. H. Wheatley, *Eur. J. Inorg. Chem.* **1998**, 879−883. [7d] M. Polamo, M. Leskela, *J. Chem. Soc., Dalton Trans.* **1996**, 4345−4349. [7e] R. Kempe, A. Spannenberg, S. Brenner, *Z. Kristallogr.* **1996**, *211*, 567−568. [7f] S. T. Liddle, W. Clegg, *Polyhedron* **2002**, *21*, 2451−2455. [7g] J. Baldamus, M. L. Cole, U. Helmstedt, E.-M. Hey-Hawkins, C. Jones, P. C. Junk, F. Lange, N. A. Smithies, *J. Organomet. Chem.* **2003**, *665*, 33−42.
[8] [8a] M. Tayebani, S. Gambarotta, G. Yap, *Organometallics* **1998**, *17*, 3639−3641. [8b] M. S. Hill, P. B. Hitchcock, *Angew. Chem. Int. Ed.* **2001**, *40*, 4089−4092. [8c] S. R. Boss, R. Haigh, D. J. Linton, A. E. H. Wheatley, *J. Chem. Soc., Dalton Trans.* **2002**, 3129−3134. [8d] A. Spannenberg, P. Arndt, R. Kempe, *Angew. Chem. Int. Ed.* **1998**, *37*, 832−835. [8e] D. J. Darensbourg, B. J. Frost, D. L. Larkins, *Inorg. Chem.* **2001**, *40*, 1993−1999. [8f] R. P. Davies, D. J. Linton, R. Snaith, A. E. H. Wheatley, *Chem. Commun.* **2000**, 1819−1820.
[9] [9a] S. J. Coles, M. B. Hursthouse, J. S. Joy, M. A. Paver, *J. Chem. Soc., Dalton Trans.* **2000**, 3239−3241. [9b] A. D. Bond, E. L. Doyle, S. J. Kidd, A. D. Woods, D. S. Wright, *Chem. Commun.* **2001**, 777−778. [9c] U. Braun, T. Habereder, H. Noth, J. Piotrowski, M. Warchhold, *Eur. J. Inorg. Chem.* **2002**, 1132−1145.
[10] T. Schareina, R. Kempe, *Angew. Chem.* **2002**, *114*, 1591−1594; *Angew. Chem. Int. Ed.* **2002**, *41*, 1521−1523.
[11] For examples of 2-aminopyridine syntheses using Pd-catalyzed aryl amination, see: [11a] S. Wagaw, S. L. Buchwald, *J. Org. Chem.* **1996**, *61*, 7240−7241. [11b] J. F. Hartwig, *Synlett* **1996**, 329−340. [11c] J. Silberg, T. Schareina, R. Kempe, K. Wurst, M. R. Buchmeiser, *J. Organomet. Chem.* **2001**, *622*, 6−18. [11d] T. Schareina, G. Hillebrand, R. Kempe, *Eur. J. Inorg. Chem.* **2001**, 2421−2426. [11e] M. R. Buchmeiser, T. Schareina, R. Kempe, K. Wurst, *J. Organomet. Chem.* **2001**, *634*, 39−46.
[12] The anionic function of the ligand is not localised at the amido N atom.
[13] R. Beckhaus, J. Oster, R. Kempe, A. Spannenberg, *Angew. Chem.* **1996**, *108*, 1636−1638; *Angew. Chem. Int. Ed. Engl.* **1996**, *35*, 1565−1567.
[14] [14a] C. Nather, H. Bock, Z. Havlas, T. Hauck, *Organometallics* **1998**, *17*, 4707−4715. [14b] Yuxia Liu, D. Ballweg, T. Muller, I. A. Guzei, R. W. Clark, R. West, *J. Am. Chem. Soc.* **2002**, *124*, 12174−12181. [14c] C. Janiak, *Chem. Ber.* **1993**, *126*, 1603−1607. [14d] P. C. Andrews, G. D. Fallon, M. Maguire, A. C. Peatt, *Angew. Chem.* **2000**, *112*, 4690−4692; *Angew. Chem. Int. Ed.* **2000**, *39*, 4516−4518. [14e] G. Solari, E. Solari, C. Floriani, A. Chiesi-Villa, C. Rizzoli, *Organometallics* **1997**, *16*, 508−510. [14f] C. Frenzel, P. Jorchel, E. Hey-Hawkins, *Chem. Commun.* **1998**, 1363−1364. [14g] A. Mandel, J. Magull, *Z. Anorg. Allg. Chem.* **1996**, *622*, 1913−1919. [14h] I. Korobkov, S. Gambarotta, G. P. A. Yap, *Angew. Chem.* **2003**, *115*, 838−842; *Angew. Chem. Int. Ed.* **2003**, *42*, 814−818. [14i] S. Neander, J. Kornich, F. Olbrich, *J. Organomet. Chem.* **2002**, *656*, 89−96. [14j] H. Bock, K. Gharagozloo-Hubmann, S. Holl, M. Sievert, *Z. Naturforsch., Teil B* **2000**, *55*, 1163−1178. [14k] C. Kayser, R. Fischer, J. Baumgartner, C. Marschner, *Organometallics* **2002**, *21*, 1023−1030. [14l] M. L. Cole, P. C. Junk, *J. Organomet. Chem.* **2003**, *666*, 55−62. [14m] H.-J. Gosink, F. Nief, L. Ricard, F. Mathey, *Inorg. Chem.* **1995**, *34*, 1306−1307. [14n] H. Viebrock, T. Panther, U. Behrens, E. Weiss, *J. Organomet. Chem.* **1995**, *491*, 19−25.
[15] [15a] D. L. Clark, J. C. Gordon, J. C. Huffman, R. L. Vincent-Hollis, J. G. Watkin, B. D. Zwick, *Inorg. Chem.* **1994**, *33*, 5903−5911. [15b] C. Eaborn, P. B. Hitchcock, K. Izod, A. J. Jaggar, J. D. Smith, *Organometallics* **1994**, *13*, 753−754.
[16] A. Altomare, M.C. Burla, M. Camalli, G.L. Cascarano, C. Giacovazzo, A. Guagliardi, A. G. G. Moliterni, G. Polidori, R. Spagna, *J. Appl. Crystallogr.* **1999**, *32*, 115−119.
[17] G. M. Sheldrick, *SHELX97 Programs for Crystal Structure Analysis*, Release 97-2, Institut für Anorganische Chemie der Universität, Tammannstraße 4, 37077 Göttingen, Germany, **1998**.
[18] L. J. Farrugia, *J. Appl. Crystallogr.* **1999**, *32*, 837−838.

Received March 22, 2004
Early View Article
Published Online June 1, 2004

 © 2004 Wiley-VCH Verlag GmbH & Co. KGaA, Weinheim

Synthesis and Structural Characterization of Novel Oxorhenium(v) Complexes Containing N-Heterocyclic Carbenes

Beatriz Royo,*[a] Eberhardt Herdtweck,[b] and Carlos C. Romão[a]

Keywords: Carbene ligands / Oxo ligands / Rhenium

Reaction of $[ReOCl_3(PPh_3)_2]$ with 2 equiv. of 1,3-diisopropylimidazol-2-ylidene (*i*Pr-carbene) affords $[ReOCl_3(i\text{Pr-carbene})_2]$ (**1**). When an excess of free carbene is used, the dicationic species $[ReOCl(i\text{Pr-carbene})_4][Cl]_2$ (**2**) is isolated. The cationic dioxorhenium complex $[ReO_2(i\text{Pr-carbene})_4]^+$ has been isolated as its I^- (**3**) and ReO_4^- (**4**) salts by different reactions. Treatment of $[ReO_2I(PPh_3)_2]$ with an excess of 1,3-diisopropylimidazol-2-ylidene yields compound **3** in quantitative yield. The cationic species is also isolated as an ReO_4^- salt from the reaction of $[ReO_2Me(PhCCPh)]$ with 1,3-diisopropylimidazol-2-ylidene. The molecular structures of $[ReOCl_3(i\text{Pr-carbene})_2]$ (**1**) and $[ReO_2(i\text{Pr-carbene})_4][ReO_4]$ (**4**) have been determined by single-crystal X-ray diffraction.

(© Wiley-VCH Verlag GmbH & Co. KGaA, 69451 Weinheim, Germany, 2004)

Introduction

Since the first isolation and X-ray structural characterization of free stable Wanzlick carbenes[1] by Arduengo,[2] a new area of transition metal complexes with these imidazolylidene-type carbenes as ligands has developed.[3]

Acting as strong Lewis bases, N-heterocyclic carbenes (NHC) are promising alternatives for the well-established phosphane ligands in organometallic catalysis. A rich variety of transition metal complexes with this type of ligand is known. However, few examples of oxometal complexes containing N-heterocyclic carbenes have been reported. Indeed, the first example of an oxometal−NHC derivative $[ReO_3Me{\cdot}NHC]$ was published in 1994 by Herrmann et al., although no structural characterization was possible.[5] To the best of our knowledge, the X-ray diffraction studies of $[TiCl_3(1,3\text{-diisopropyl-4,5-dimethylimidazol-2-ylidene})(\mu\text{-}O)]_2$,[6] $[VOCl_3(1,3\text{-dimesitylimidazol-2-ylidene})]$[7] and $[UO_2Cl_2(1,3\text{-dimesitylimidazol-2-ylidene})_2]$[8] are the only examples of oxo transition metal and actinide derivatives containing NHCs that have been reported in the literature. During the preparation of this manuscript the X-ray diffraction studies of the cationic dioxorhenium(v) and -technetium(v) complexes $[ReO_2(1,3\text{-diisopropyl-4,5-dimethylimidazol-2-ylidene})_4][PF_6]$ and $[TcO_2(1,3\text{-diisopropyl-4,5-dimethylimidazol-2-ylidene})_4][TcO_4]{\cdot}2.5THF$ were reported.[9]

[a] Instituto de Tecnologia Química e Biológica da Universidade Nova de Lisboa,
Quinta do Marquês, EAN, Apt. 127, 2781-901 Oeiras, Portugal
Fax: (internat.) + 351-21-4411-277
E-mail: broyo@itqb.unl.pt
[b] Anorganisch-chemisches Institut der Technischen Universität München,
Lichtenbergstraβe 4, 85747 Garching bei München, Germany

In the present study we describe the synthesis of oxorhenium derivatives containing an NHC ligand and the first X-ray molecular structure of a chlorooxorhenium(v)−NHC complex.

Results and Discussion

Reaction of $[ReOCl_3(PPh_3)_2]$ with 2 equiv. of 1,3-diisopropylimidazol-2-ylidene in toluene at room temperature affords $[ReOCl_3(i\text{Pr-carbene})_2]$ (**1**; *i*Pr-carbene = 1,3-diisopropylimidazol-2-ylidene), which was isolated as a green

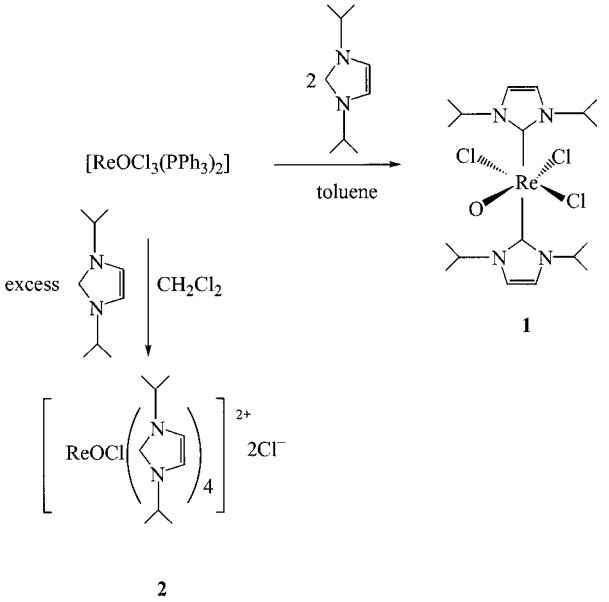

Scheme 1. Synthesis of $[ReOCl_3(i\text{Pr-carbene})_2]$ (**1**) and $[ReOCl(i\text{Pr-carbene})_4][Cl]_2$ (**2**)

crystalline solid. Double substitution of the triphenylphosphane is preferred since treatment of $[ReOCl_3(PPh_3)_2]$ with 1 equiv. of 1,3-diisopropylimidazol-2-ylidene yields a mixture of compound **1** and unchanged starting material. The reaction of $[ReOCl_3(PPh_3)_2]$ with an excess of free carbene in dichloromethane gives the green dicationic complex $[ReOCl(i\text{Pr-carbene})_4][Cl]_2$ (**2**). Compound **2** is the result of the displacement of two chloride ions and both triphenylphosphane ligands by the imidazol-2-ylidene ligand (Scheme 1).

The ^{1}H NMR spectrum of **1** displays a doublet at δ = 1.40 ppm for the methyl protons of the isopropyl group, a multiplet at δ = 5.75 ppm for the CH proton of the isopropyl group and a singlet at δ = 7.10 ppm for the olefinic protons of the carbene ligand. In contrast, two signal groups of the carbene ligands can be observed for **2**, indicating two inequivalent sets of *i*Pr substituents. This is in agreement with an approximate octahedral environment for the rhenium atom in **2**, with the oxygen and chlorine atoms *trans* to each other. The ^{1}H NMR spectrum of **2** shows two doublets at δ = 2.63 and 2.94 ppm for the methyl protons of the isopropyl group, two multiplets at δ = 4.92 and 5.35 ppm for the CH proton of the isopropyl group and two multiplets at δ = 8.52 and 8.43 ppm for the olefinic protons of the carbene ligand. The ^{13}C NMR signal of the metal-coordinated carbene C atom is shifted by about 85 ppm to higher field upon complexation of the ligand to the metal atom (δ = 175 ppm for **1** compared with δ = 260 ppm for the free ligand). The IR spectra of **1** and **2** show strong ν(ReO) absorptions at 972 and 989 cm^{-1}, respectively. The mass spectrum of **2** gives the molecular ion *m*/*z* (%) = 423 (100). The main fragment corresponds to the loss of one carbene ligand.

Solid samples of compounds **1** and **2** showed no decomposition in air when exposed for shorts periods of time, but solutions of **1** and **2** are moisture-sensitive; traces of water lead to formation of $[ReO_2(i\text{Pr-carbene})_4][ReO_4]$.[9] Compound **1** is soluble in aromatic hydrocarbons such as benzene or toluene, while compound **2** is insoluble in toluene, dichloromethane, tetrahydrofuran or diethyl ether, and slightly soluble in acetonitrile.

Crystals of **1** suitable for an X-ray structure analysis were grown from toluene at −20 °C and its molecular structure was determined by single-crystal X-ray diffraction.

The reaction of $[ReO_2I(PPh_3)_2]$ with excess of 1,3-diisopropylimidazol-2-ylidene in dichloromethane at −20 °C affords $[ReO_2(i\text{Pr-carbene})_4][I]$ (**3**) [Equation (1)]. The displacement of the iodine atom and both triphenylphosphane ligands in $[ReO_2I(PPh_3)_2]$ by a carbene affords the monocationic species **3**. A similar displacement has been observed previously upon treatment of $[ReO_2I(PPh_3)_2]$ with 2 equiv. of dppe yielding $[ReO_2(dppe)_2][I]$.[10] Compound **3** was isolated as a brown solid, soluble in dichloromethane and insoluble in hexane or diethyl ether. Its ^{1}H NMR spectrum shows two resonances for the methyl protons of the isopropyl group, a doublet at δ = 0.70 ppm and a doublet at δ = 1.18 ppm, indicating a hindered rotation of the isopropyl groups, a multiplet for the CH proton of the isopropyl group at δ = 5.74 ppm, and a singlet at δ = 7.09 ppm for the olefinic protons of the carbene. The resonance of the metal-coordinated C atom appears at δ = 172.6 ppm which compares well with other rhenium−carbene complexes such as $[Re(1,3\text{-dimethylimidazol-2-ylidene})_2I(CO)_3]$ (δ = 175.1 ppm)[11] and $[ReO_3Me(1,3\text{-dimethylimidazol-2-ylidene})_2]$ (δ = 176.7 ppm).[5] The mass spectrum of $\mathbf{3}^+$ gives the molecular ion *m*/*z* (%) = 827 (100). The Re=O vibration of the central dioxorhenium(v) unit appears at 782 cm^{-1}. Similar values have been reported for the Re=O vibration in $[ReO_2(1,3\text{-diisopropyl-4,5-dimethylimidazol-2-ylidene})_4][PF_6]$,[9] and in $[ReO_2(dppe)_2][I]$.[10]

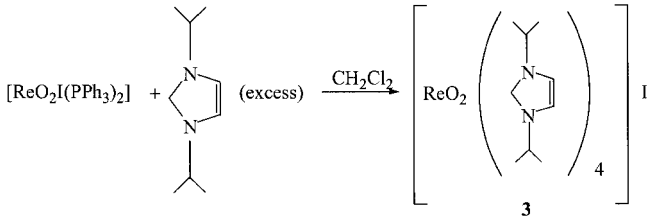

(1)

The $[ReO_2(i\text{Pr-carbene})_4]^+$ cation is also formed by reaction of $[ReO_2Me(PhCCPh)]$ with an excess of 1,3-diisopropylimidazol-2-ylidene in tetrahydrofuran [Equation (2)]. When a solution of $[ReO_2Me(PhCCPh)]$ in THF was treated with an excess of 1,3-diisopropylimidazol-2-ylidene, a brown solution was obtained. After removal of the solvent, the residue was extracted into toluene and the solution was cooled to −20 °C. Light-yellow crystals separated from the solution. On the basis of elemental analysis, spectroscopic evidence and X-ray crystallography, the yellow crystals were formulated as $[ReO_2(i\text{Pr-carbene})_4][ReO_4]$ (**4**). The ^{1}H NMR spectrum of the toluene-insoluble brown residue shows a mixture of complexes which could not be separated by recrystallisation. It seems reasonable to explain the formation of **4** as the result of the reaction of adventitious water.

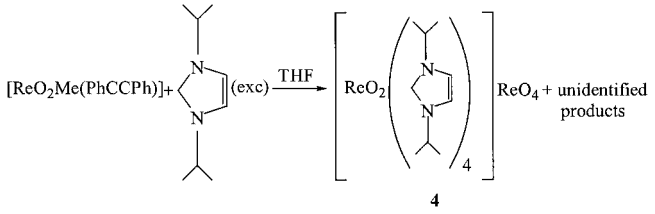

(2)

Crystallographic Studies

A single crystal of the carbene complex **1** was obtained from toluene by standard cooling techniques and its molecular structure was determined by single-crystal X-ray diffraction. Figure 1 shows an ORTEP-style plot of the monomeric neutral molecule. Selected bond lengths and bond angles are reported in Table 1. The asymmetric unit shows two crystallographically independent molecules A and B,

 © 2004 Wiley-VCH Verlag GmbH & Co. KGaA, Weinheim

each of which is located around a center of inversion, and one solvent molecule (toluene). The intrinsic symmetry of the carbene moiety implies a 50:50 disorder of one chlorine atom and of the oxo ligand. As expected from NMR and IR spectroscopic data, the rhenium atom is coordinated by two carbene ligands in the apical positions of the octahedral coordination sphere. Three chloro and one oxo ligand complete the octahedron in the equatorial plane.

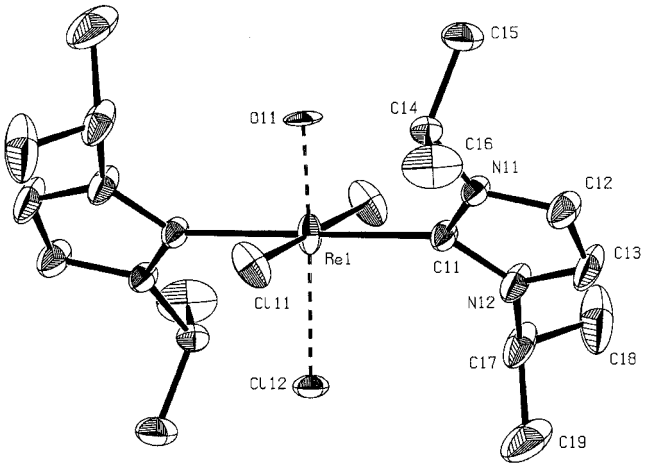

Figure 1. ORTEP representation of compound **1**·toluene (molecule A) in the solid state; thermal ellipsoids are at the 50% probability level; hydrogen atoms are omitted for clarity; dashed lines indicate a disorder (see Exp. Sect.)

Table 1. Selected interatomic distances [Å] and angles [°] for [$ReOCl_3$(*i*Pr-carbene)$_2$(toluene)] (**1**·toluene) and [ReO_2(*i*Pr-carbene)$_4$][ReO_4] (THF) (**4**·THF)

	1·toluene	**4**·THF
Re1−Cl11	2.3943(12)	
Re1−Cl12	2.298(3)	
Re1−O1/O11	1.770(8)	1.796(4)
Re1−O2		1.798(4)
Re1−C11	2.181(4)	2.185(5)
Re1−C21		2.184(3)
Re1−C31		2.208(5)
Re1−C41		2.207(5)
Cl11−Re1−Cl12	83.83(10)	
Cl11−Re1−O11	90.1(3)	
Cl11−Re1−C11	89.63(11)	
O1−Re1−O2		178.92(15)
C11−Re1−C21		89.9(2)
C11−Re1−C41		89.5(2)
C21−Re1−C31		89.9(2)
C31−Re1−C41		90.7(2)

All bond lengths and bond angles of the N-heterocyclic carbene ligand lie within the typical ranges. The very short Re1−Cl12 distance [2.298(3) Å] and the very long Re1=O11 double bond [1.770(8) Å] in comparison to the statistical range given by the CCDC[12a] are caused by the disorder, and therefore have to be regarded as artificial effects. With 2.3943(12) Å, the Re−Cl11 distance fits the mean value of 2.376[12a] Å very well. The dihedral angles N11−C11−Re1−Cl11 and N11−C11−Re1−O11 are −50.5(4)° and 39.4(5)°, respectively. Thus, the carbene moiety defined by N11−C11−N12 is staggered with respect to the planar $ReCl_3O$ unit.

Cooling of a saturated THF solution of **4** to −20 °C for several days yielded clear yellow crystals suitable for X-ray analysis. Figure 2 shows an ORTEP-style plot of the monomeric cationic part of compound **4**. Selected bond lengths and bond angles are reported in Table 1. The asymmetric unit shows one cationic tetrakis(carbene)dioxorhenium moiety, one perrhenate anion, and one solvent molecule (THF). As expected from NMR and IR spectroscopic data, the rhenium atom is coordinated by two oxo ligands in the apical positions and four carbene groups in the basal plane of the octahedral coordination sphere. All bond lengths and bond angles of the N-heterocyclic carbene ligand lie within the typical ranges. The Re1=O11 double-bond lengths [1.796(4) Å and 1.798(4) Å] represent the upper end in the statistical range given by the CCDC.[12b] The dihedral angles N11−C11−Re1−O1, N21−C21−Re1−O1, N31−C31−Re1−O1, and N41−C41−Re1−O1 are 143.6(4)°, 147.5(4)°, 142.0(4)°, and 149.5(5)°, respectively. Thus, the four carbene species are arranged in a propeller mode around the central linear O=Re=O moiety fitting an approximate D_4 symmetry in the solid state.

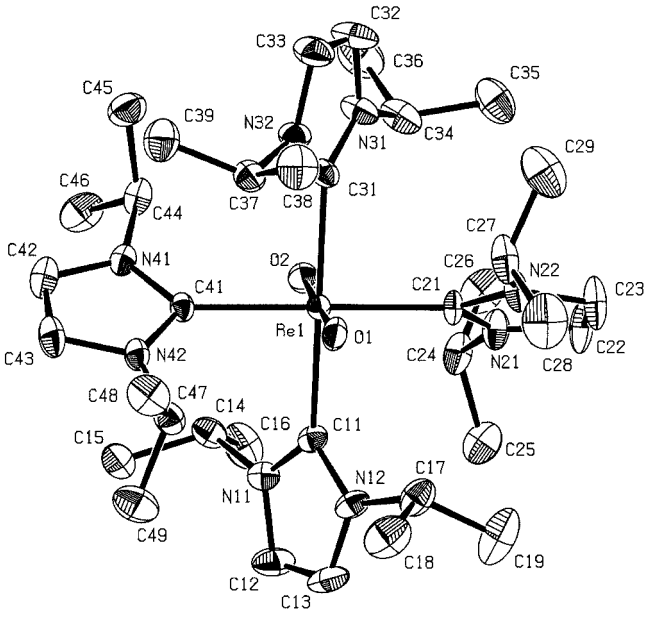

Figure 2. ORTEP representation of the cationic part of compound **4**·THF in the solid state; thermal ellipsoids are at the 50% probability level; hydrogen atoms omitted for clarity

Conclusions

A series of oxorhenium(v) derivatives containing the N-heterocyclic carbene 1,3-diisopropylimidazol-2-ylidene have been prepared. The strong Lewis base carbene easily re-

 © 2004 Wiley-VCH Verlag GmbH & Co. KGaA, Weinheim

places the triphenylphosphane and halide ligands to give neutral and cationic oxorhenium−carbene complexes.

Experimental Section

General Remarks: All manipulations were carried out under dinitrogen using standard Schlenk-line and glovebox techniques. Solvents were purified by conventional methods and distilled under nitrogen prior to use. NMR spectra were recorded with a Bruker AMX 300 spectrometer. Infrared spectra were recorded with a Unicam Mattson Model 7000 FTIR spectrophotometer using KBr pellets. Electrospray mass spectrometric experiments were performed with a Bruker Daltonic esquire 3000 plus spectrometer. Elemental analyses were performed in our laboratories (ITQB). 1,3-Diisopropylimidazolin-2-ylidene,[13] $[ReOCl_3(PPh_3)_2]$,[14] $[ReO_2I(PPh_3)_2]$,[15] and $[ReO_2Me(PhCCPh)]$[16] were prepared according to literature procedures.

Trichlorobis(1,3-diisopropylimidazol-2-ylidene)oxorhenium(v) (1): 1,3-Diisopropylimidazolin-2-ylidene (4.82 mL of a 0.34 M solution in THF, 1.64 mmol) was added to a suspension of $[ReOCl_3(PPh_3)_2]$ (0.68 g, 0.80 mmol) in toluene (0.40 mL) at −20 °C and the reaction mixture was stirred for 30 min. The mixture was then allowed to warm up to room temperature and was stirred for a further 16 h. The toluene solution was filtered and the volume of the filtrate was reduced in vacuo to about 10 mL. Cooling to −20 °C yielded green crystals of **1**. Yield: 0.30 g (65%). $C_{18}H_{32}Cl_3N_4ORe$ (613.05): calcd. C 35.27, H 5.26, N 9.14; found C 35.37, H 5.32, N 9.25. Selected IR data (KBr): ν(ReO) = 972 vs cm^{-1}. ^1H NMR (300 MHz, CD_2Cl_2): δ = 7.10 (s, 2 H, C*H*C*H*), 5.75 (m, 2 H, C*H*Me$_2$), 1.40 (d, $J_{H,H}$ = 6 Hz, 12 H, CH*Me*) ppm. ^{13}C NMR (75 MHz, CD_2Cl_2): δ = 174.9 (Re*C*$_{carbene}$), 119 (*CH*C*H*), 49 (*C*HMe$_2$), 23 (CH*Me*$_2$) ppm.

Chlorotetrakis(1,3-diisopropylimidazol-2-ylidene)oxorhenium(v) Dichloride (2): 1,3-Diisopropylimidazolin-2-ylidene (15.23 mL of a 0.34 M solution in THF, 5.18 mmol) was added at −20 °C to a suspension of $[ReOCl_3(PPh_3)_2]$ (1 g, 1.29 mmol) in dichloromethane (30 mL). When the addition was completed, the mixture was allowed to warm up to room temperature and was then stirred for a further 20 h. The dichloromethane solution was then filtered, the filtrate was concentrated in vacuo to about 10 mL and was cooled to −20 °C, giving deep-green crystals of **2**. Yield: 0.82 g (72%). $C_{36}H_{64}Cl_3N_8ORe$ (917.53): calcd. C 47.13, H 7.03, N 12.21; found C 46.98, H 6.82, N 12.02. Selected IR data (KBr): ν(ReO) = 989 vs cm^{-1}. ^1H NMR (300 MHz, NCMe): δ = 8.52 (m, 2 H, C*H*C*H*), 8.43 (m, 2 H, C*H*C), 5.35 (q, $J_{H,H}$ = 6 Hz, 2 H, C*H*Me$_2$), 4.92 (q, $J_{H,H}$ = 6 Hz, 2 H, C*H*Me$_2$), 2.94 (d, $J_{H,H}$ = 6 Hz, 12 H, CH*Me*$_2$), 2.63 (d, $J_{H,H}$ = 6 Hz, 12 H, CH*Me*$_2$) ppm. MS (ES): *m*/*z* (%) = 423/422 (100) [M^+].

Tetrakis(1,3-diisopropylimidazol-2-ylidene)dioxorhenium(v) Iodide (3): 1,3-Diisopropylimidazolin-2-ylidene (14.70 mL of a 0.34 M solution in THF, 5 mmol) was added at room temperature to a solution of $[ReO_2I(PPh_3)_2]$ (1 g, 1.14 mmol) in dichloromethane (20 mL). The reaction mixture was stirred for 16 h and was then concentrated in vacuo to about 8 mL. Cooling of the dichloromethane solution to −20 °C afforded the title compound **3**, which was isolated as a brown solid. Yield: 0.84 g (78%). $C_{36}H_{64}IN_8O_2Re$ (954.07): calcd.C 45.32, H 6.76, N 11.74; found C 45.03, H 6.69, N 11.65. Selected IR data (KBr): ν(ReO) = 782 vs cm^{-1}. ^1H NMR (300 MHz, $CDCl_3$): δ = 7.09 (s, 2 H, C*H*C*H*), 5.74 (m, 2 H, C*H*Me$_2$), 1.18 (d, $J_{H,H}$ = 6 Hz, 12 H, CH*Me*$_2$), 0.70 (d, $J_{H,H}$ = 6 Hz, 12 H, CH*Me*$_2$) ppm. ^{13}C NMR (75 MHz, $CDCl_3$): δ = 172.6 (Re-C$_{carbene}$), 117.9 (*CH*C*H*), 49.8 (*C*HMe$_2$), 23.2(CH*Me*$_2$) ppm.

Tetrakis(1,3-diisopropylimidazol-2-ylidene)dioxorhenium(v) Perrhenate (4): 1,3-Diisopropylimidazolin-2-ylidene (5.5 mL of a 0.14 M solution in THF, 0.77 mmol) was added to a solution of $[ReO_2Me(PhCCPh)]$ (0.32 g, 0.77 mmol) in tetrahydrofuran (20 mL) at −30 °C. The mixture was stirred at low temperature for 20 min and at room temperature for 2 h. All the volatiles were removed under vacuum and the residue was extracted into toluene. The volume of the toluene solution was reduced in vacuo to about 10 mL and was kept in a refrigerator at −20 °C to yield the title compound **4** as light-yellow crystals. Yield: 0.28 g (47%). $C_{36}H_{64}N_8O_6Re_2$ (1077.4): calcd. C 40.13, H 5.99, N 10.40; found C 39.89, H 5.86, N 10.35. Selected IR (KBr): ν(ReO) = 910vs cm^{-1}. ^1H NMR (300 MHz, $CDCl_3$): δ = 7.09 (s, 2 H, C*H*C*H*), 5.74 (m, 2 H, C*H*Me$_2$), 1.18 (d, $J_{H,H}$ = 6 Hz, 12 H, CH*Me*$_2$), 0.70 (d, $J_{H,H}$ = 6 Hz,12 H, CH*Me*$_2$) ppm. ^{13}C NMR (75 MHz, $CDCl_3$): δ = 172.6 (Re-C$_{carbene}$), 117.9 (*CH*C*H*), 49.8 (*C*HMe$_2$), 23.2(CH*Me*$_2$) ppm. MS (ES): *m*/*z* (%) = 827/825 (100) [M^+].

Table 2. Summary of the crystallographic data for $[ReOCl_3(i$Pr-carbene$)_2$(toluene)] (**1**·toluene) and $[ReO_2(i$Pr-carbene$)_4][ReO_4]$ (THF) (**4**·THF)

	1·toluene	**4**·THF
Empirical formula	$C_{25}H_{40}Cl_3N_4ORe$	$C_{40}H_{72}N_8O_7Re_2$
Formula mass	705.17	1149.48
Crystal system	monoclinic	monoclinic
Space group	$P2_1/c$ (no. 14)	Cc (no. 92)
a [Å]	18.7146(2)	16.3702(1)
b [Å]	11.0958(2)	16.2740(1)
c [Å]	14.5390(2)	18.6526(1)
β [°]	102.468(1)	106.0127(3)
V [Å^3]	2947.87(7)	4776.41(5)
Z	4	4
ρ_{calcd} [g·cm^{-3}]	1.589	1.599
μ [mm^{-1}]	4.418	5.116
T [K]	123	153
F(000)	1408	2296
Crystal size [mm]	0.61 × 0.18 × 0.15	0.35 × 0.27 × 0.14
Θ range [°]	2.45/25.35	2.50/25.35
Index ranges $h/k/l$	±22/±13/±17	±19/±19/±22
Reflections collected	66812	48058
Independent reflections [$I_o > 2\sigma(I_o)$/all data/R_{int}]	5391/4598/0.037	8550/8209/0.053
Data/restraints/parameters	5391/0/340	8550/2/531
$R1$ [$I_o > 2\sigma(I_o)$/all data]	0.0325/0.0391	0.0213/0.0235
$wR2$ [$I_o > 2\sigma(I_o)$/all data]	0.0590/0.06615	0.0499/0.0510
GOF	1.136	1.024
Weights a/b	0.0000/12.8838	0.0213/11.5906
$\Delta\rho_{max/min}$ [e·Å^{-3}]	0.87/−0.78	0.69/−0.78

Crystal Structure Determination of 1 and 4: Details of the X-ray experiment, data reduction, and final structure refinement calculations are summarized in Table 2. Crystals of complex **1** (or **4**) suitable for X-ray structure determination were grown from a toluene (THF) solution, fixed with perfluorinated ether in a glass capillary and transferred to the diffractometer. Preliminary examination and data collection were carried out on a Kappa-CCD device (Nonius Mach3) at the window of a rotating anode (Nonius Fr591; 50 kV; 60 mA; 3.0 kW) and graphite-monochromated Mo-K_α radiation (λ = 0.71073 Å). Data collection was performed at 123 (153) K with an exposure time of 30 (15) s per frame [φ- and ω-scans, rotation modus, Δφ/Δω = 2.0° (1.0°)]. A total number of 66812

 © 2004 Wiley-VCH Verlag GmbH & Co. KGaA, Weinheim

(48058) reflections were collected.[17a] After merging, a sum of 5391 (8550) independent reflections remained and was used for all calculations. Data were corrected for Lorentz and polarization effects. Corrections for absorption and/or decay effects were applied during the scaling procedure. The unit-cell parameters were obtained by full-matrix least-squares refinements of 5725 (4535) reflections with the program SCALEPACK.[17b] The structures were solved by a combination of direct methods and difference-Fourier syntheses.[17c] All non-hydrogen atoms of the asymmetric unit were refined with anisotropic thermal displacement parameters. All hydrogen atoms were calculated in ideal positions riding on the parent carbon atom. Full-matrix least-squares refinements were carried out by minimizing $\Sigma w(F_o^2 - F_c^2)^2$ with the SHELXL-97 weighting scheme and stopped at a maximum shift/err value < 0.001.[17d] Neutral-atom scattering factors for all atoms and anomalous dispersion corrections for the non-hydrogen atoms were taken from the International Tables for Crystallography.[17e] All other calculations (including ORTEP graphics) were done with the program PLATON.[17f] Compound **1**·toluene crystallizes with two crystallographically independent molecules A and B in the asymmetric unit. Each of them is located around a center of inversion. This implies a 50:50 disorder of one chlorine ligand and the oxygen atom. Compound **4**·THF appears to be a twin. Twin refinement ends with Flack's parameter at $\varepsilon = 0.443(6)$. Despite the virtual symmetry of the molecule there is no way to transform the coordinates into the centrosymmetric space group *C*2/*c*. Attempts to solve and to refine the experimental data in *C*2/*c* failed. CCDC-229836 (**1**) and -229837 (**4**) contain the supplementary crystallographic data for this paper. These data can be obtained free of charge at www.ccdc.cam.ac.uk/conts/retrieving.html [or from the Cambridge Crystallographic Data Centre, 12 Union Road, Cambridge CB2 1EZ, UK; Fax: (internat.) + 44-1223-336033; E-mail: deposit@ccdc.cam.ac.uk].

Acknowledgments

This work was supported by FCT through project POCTI 37726/QUI/01. We wish to acknowledge Maria da Conceição Almeida for providing data from the Elemental Analyses Service and Dr. Ana Coelho for providing data from the Mass Spectrometry Laboratory at the Instituto de Tecnologia Química e Biolgica (ITQB), Universidade Nova de Lisboa, Oeiras, Portugal.

[1] [1a] K. Öfele, *J. Organomet. Chem.* **1968**, *12*, 42. [1b] H. W. Wanzlick, H. T. Schönherr, *Angew. Chem. Int. Ed. Engl.* **1968**, *7*, 141.
[2] A. J. Arduengo, R. L. Harlow, M. Kline, *J. Am. Chem. Soc.* **1991**, *113*, 361.
[3] D. Bourissou, O. Guerret, F. P. Gabbaï, G. Bertrand, *Chem. Rev.* **2000**, *100*, 39.
[4] W. A. Herrmann, *Angew. Chem. Int. Ed.* **2002**, *41*, 1290.
[5] W. A. Herrmann, K. Öfele, M. Elison, F. E. Kühn, P. W. Roesky, *J. Organomet. Chem.* **1994**, *480*, C7.
[6] N. Kuhn, T. Kratz, D. Bläser, R. Boese, *Inorg. Chim. Acta* **1995**, *238*, 179.
[7] C. D. Abernethy, G. M. Codd, M. D. Spicer, M. K. Taylor, *J. Am. Chem. Soc.* **2003**, *125*, 1128.
[8] W. J. Oldham Jr, S. M. Oldham, B. L. Scott, K. D. Abney, W. H. Smith, D. A. Costa, *Chem. Commun.* **2001**, 1384.
[9] H. Braband, T. I. Zahn, U. Abram, *Inorg. Chem.* **2003**, *42*, 6160.
[10] M. Freni, D. Giusto, P. Romiti, G. Minghetti, *Gazz. Chim. Ital.* **1969**, *99*, 286.
[11] D. Mihalios, PhD Thesis, Technische Universität München, **1992**.
[12] [12a] A search for hexacoordinate trichlorooxorhenium compounds gives 45 hits within a range for the Re−Cl bond lengths of 2.315−2.481 Å and for the Re=O double bond of 1.605−1.755 Å. [12b] A search for hexacoordinate *trans*-dioxorhenium compounds gives 54 hits within a range for the Re=O double bonds of 1.729−1807 Å. [12c] The Cambridge Structural Database: a quarter of a million crystal structures and rising: F. H. Allen, *Acta Crystallogr., Sect. B* **2002**, *58*, 380−388. [12d] New Software for searching the Cambridge Structural Database and visualizing crystal structures: I. J. Bruno, J. C. Cole, P. R. Edgington, M. Kessler, C. F. Macrae, P. McCabe, J. Pearson, R. Taylor, *Acta Crystallogr., Sect. B* **2002**, *58*, 389−397.
[13] W. A. Herrmann, C. Köcher, L. J. Gooßen, R. J. Artus, *Chem. Eur. J.* **1996**, *2*, 1627.
[14] N. P. Johnson, C. J. L. Lock, G. Wilkinson, *Inorg. Synth.* **1967**, *9*, 145.
[15] G. F. Ciani, G. D′Alfonso, P. F. Romiti, A. Sironi, M. Freni, *Inorg. Chim. Acta* **1983**, *72*, 29.
[16] J. K. Felixberger, J. G. Kuchler, E. Herdtweck, R. A. Paciello, W. A. Herrmann, *Angew. Chem. Int. Ed. Engl.* **1988**, *27*, 946.
[17] [17a] Data Collection Software for Nonius Kappa-CCD Devices, Delft, The Netherlands, **2001**. [17b]Processing of X-ray Diffraction Data Collected in Oscillation Mode: Z. Otwinowski, W. Minor, *Methods Enzymol.* **1996**, *276*, 307. [17c] SIR92: A. Altomare, G. Cascarano, C. Giacovazzo, A. Guagliardi, M. C. Burla, G. Polidori, M. Camalli, *J. Appl. Cryst.* **1994**, *27*, 435−436. [17d] G. M. Sheldrick, *SHELXL-97*, University of Göttingen, Göttingen, Germany, **1988**. [17e] *International Tables for Crystallography*, vol. C (Ed.: A. C. J. Wilson), Kluwer Academic Publishers, Dordrecht, The Netherlands, **1992**; Tables 6.1.1.4 (pp. 500−502), 4.2.6.8 (pp. 219−222), and 4.2.4.2 (pp. 193−199). [17f] A. L. Speck, *PLATON, A Multipurpose Crystallographic Tool*, Utrecht University, Utrecht, The Netherlands, **2001**.

Received January 28, 2004
Early View Article
Published Online June 11, 2004

 © 2004 Wiley-VCH Verlag GmbH & Co. KGaA, Weinheim

Structural and Dynamic Studies of Zinc, Gallium, and Cadmium Complexes of a Dicarboxylate Pendant-Armed Cross-Bridged Cyclen

Weijun Niu,[a] Edward H. Wong,*[a] Gary R. Weisman,*[a] Yijie Peng,[a] Carolyn J. Anderson,[b] Lev N. Zakharov,[c] James A. Golen,[c][‡] and Arnold L. Rheingold[c]

Keywords: Zinc / Gallium / Cadmium / Cyclen / Cross-bridged ligand / Pendant arms

Zn^{II}, Ga^{III}, and Cd^{II} complexes of a dicarboxylate pendant-armed derivative of an important new cross-bridged cyclen ligand were prepared and characterized spectrally. Crystal structures of the Zn^{II} and Ga^{III} complexes both feature pseudo-octahedral metal centers, fully enveloped by the ligand's *cis*-N_4O_2 donor set with the zinc coordination sphere less distorted. All Ga–N and Ga–O bonds are significantly shorter than the corresponding values in the zinc structure. Solution NMR spectral studies revealed dynamic enantiomerization for the Zn^{II} complex with $\Delta G^{\neq}$ = 12.3(1) kcal/mol (24 °C). By contrast, the Ga^{III} complex gave only slow-exchange limit spectra up to the highest temperature measured [87(2) °C; $\Delta G^{\neq} > 21.1(2)$ kcal/mol].

(© Wiley-VCH Verlag GmbH & Co. KGaA, 69451 Weinheim, Germany, 2004)

Introduction

The enhanced kinetic inertness imparted to metal complexes formed by cross-bridged cyclam and cyclen ligands has generated interest in the catalytic as well as radiopharmaceutical potentials of these ligands.[1−4] This superior inertness towards decomplexation even under highly acidic or oxidizing conditions, which discourages common decomplexation pathways, is a consequence of our ligand design.[5−7] While the importance of accessible, ancillary *cis*-coordination sites for catalytic or biomimetic applications has been noted[8−10] for carriers of radiometals such as ^{64}Cu, ^{67}Ga, and ^{111}In, complete envelopment of such cations within the chelator is desirable to ensure even more inert complexes.[11−13] *N*-Functionalization of the parent ligands with pendant arms containing additional donor sites is an effective way to attain this goal. We have already reported a dicarboxylate-armed cyclam ligand, CB-H_2TE2A, and its copper(II) complex, Cu-CB-TE2A, as well as its cyclen analogue, Cu-CB-DO2A.[2,7] Their in vivo behavior using ^{64}Cu labelling has also been investigated.[1,2] Herein, we report the syntheses and spectral characterizations of the zinc(II), gallium(III), and cadmium(II) complexes of the dicarboxylate pendant-armed cross-bridged cyclen CB-H_2DO2A (ligand H_2 **1**).[14,15] Their diamagnetic nature makes solution NMR spectral studies possible. X-ray structures of both the Zn^{II} and Ga^{III} complexes were determined. These d^{10}-cations are without ligand-field stabilization factors and offer the opportunity to compare charge and size effects on coordination preferences.

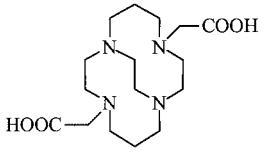

CB-H_2TE2A

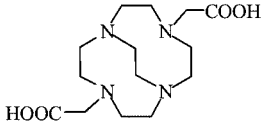

CB-H_2**1**DO2A

Results and Discussion

Synthesis

In the presence of a stoichiometric amount of aqueous NaOH, cross-bridged ligand H_2 **1** and hydrated $Zn(ClO_4)_2$ or $Cd(ClO_4)_2$ formed a cloudy solution in methanol after refluxing. Upon filtration to remove a small amount of white precipitate and ether diffusion into the supernatant,

[a] Department of Chemistry, University of New Hampshire, Durham, New Hampshire 03824, USA
Fax: (internat.) + 1-603-862-4278
E-mail: ehw@cisunix.unh.edu
gary.weisman@unh.edu
[b] Mallinckrodt Institute of Radiology, Washington University School of Medicine,
St. Louis, MO 63110, USA
Fax: (internat.) + 1-314-362-9940
E-mail: AndersonCJ@mir.wustl.edu
[c] Department of Chemistry and Biochemistry, University of California,
San Diego, La Jolla, California 92093, USA
E-mail: arnrhein@chem.ucsd.edu
[‡] On leave from the Department of Chemistry and Biochemistry, University of Massachusetts Dartmouth, North Dartmouth, Massachusetts 02747, USA

 © 2004 Wiley-VCH Verlag GmbH & Co. KGaA, Weinheim **DOI: 10.1002/ejic.200400075**

in each case, pure crystals of the neutral complexes co-crystallized with sodium perchlorate, [Zn·**1**]$(NaClO_4)_{1.5}$ and [Cd·**1**]$(NaClO_4)$, were obtained as revealed by both IR spectral and analytical data. To synthesize the gallium complex, equivalent amounts of the ligand and $Ga(NO_3)_3$ with sodium acetate as the base were refluxed in methanol. The resulting white precipitate was redissolved in aqueous methanol and diffusion of a mixture of diethyl ether and methanol into this solution yielded clear crystals of the complex [Ga·**1**]NO_3.

Infrared Data

The solid-state IR spectra of all isolated complexes contained strong carboxylate stretches and those of the Zn^{II} and Cd^{II} complexes occur between 1595 and 1645 cm^{-1}. By contrast, the Ga^{III} complex has its carboxylate bands at significantly higher frequencies (1672 and 1692 cm^{-1}). In addition, strong stretching bands are also observed for the nitrate (1284−1363 cm^{-1}) or perchlorate (1091−1107 cm^{-1}) anion in the respective complex.

NMR Spectral Data

The ^1H NMR spectrum of Zn·**1** in CD_3OD (or D_2O) is indicative of time-averaged C_{2v} symmetry. This is most clearly shown by the downfield singlet resonance of the pendant-arm methylene protons (see Figure 1, top).

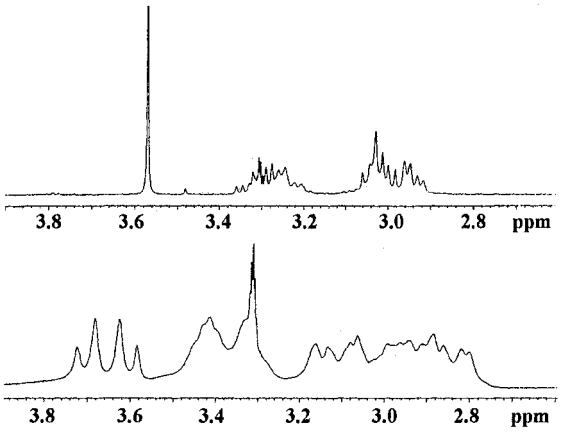

Figure 1. Variable-temperature 400 MHz ^1H NMR spectra of Zn-CB-DO2A in CD_3OD at 24 °C (top) and at −80 °C (bottom)

Likewise, the $^{13}C\{^1H\}$ NMR spectrum exhibits only four methylene ^{13}C resonances (two broad), in keeping with C_{2v} symmetry (see Figure 2, top). These data are in contrast to the solid-state X-ray structure, which approximates C_2 symmetry (vide infra) and suggest onset of a dynamic solution enantiomerization (see Figure 3). This was confirmed by the low-temperature NMR spectra in CD_3OD at −80 °C. While this proton spectrum contains broad and poorly resolved resonances in the upfield region, the pendant-arm CH_2 signal is clearly resolved into the AB pattern of diastereotopic methylene protons expected for C_2 symmetry (see Figure 1, bottom). Similarly, two of the four methylene ^{13}C resonances are resolved into two separate signals each at low temperature (see Figure 2, bottom). Complete lineshape analysis of the broadest carbon resonance at 24(2) °C (see Exp. Sect.), which is in intermediate fast exchange, allows us to calculate a free energy of activation of 12.3(1) kcal/mol for the enantiomerization. Either a dissociative process involving detachment of pendant arms or a nondissociative pseudorotation mechanism is consistent with the observed dynamic behavior.

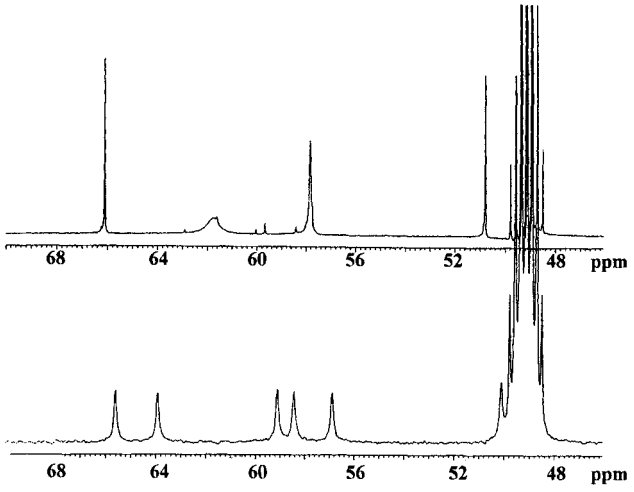

Figure 2. Variable-temperature 100 MHz $^{13}C\{^1H\}$ NMR spectra of Zn-CB-DO2A in CD_3OD at 24 °C (top) and at −80 °C (bottom)

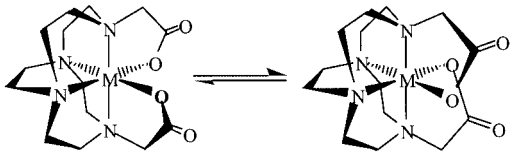

Figure 3. Enantiomerization of the zinc(II) complex of CB-DO2A

Both the proton and $^{13}C\{^1H\}$ NMR spectra of [Cd·**1**] at room temperature in D_2O (see Exp. Sect.) are similar to the Zn^{II} complex data, again indicative of averaged C_{2v} solution symmetry on the NMR timescale. In addition, satellites due to $^{111,113}Cd$ coupling can also be observed in several of the ^1H as well as ^{13}C resonances. These attest to the integrity of the complex in solution since such couplings would be lost upon facile ligand exchange.

Unlike the zinc and cadmium complexes, at ambient temperature [Ga·**1**]NO_3 in D_2O gave proton and $^{13}C\{^1H\}$ NMR spectra consistent with a solution structure of C_2 symmetry (see Figure 4 and Exp. Sect.) in agreement with its X-ray structure (vide infra). The pendant-arm CH_2 protons exhibit an AB pattern with an additional W-long-range doublet coupling to the B portion of the subspectrum (apparent AB of ABX, although even this is an oversimplification since the X proton must be further coupled as well). Six signals having no dynamic broadening are observed in the methylene region of the $^{13}C\{^1H\}$ spectrum. Thus, enantiomerization is in the slow exchange limit on

 © 2004 Wiley-VCH Verlag GmbH & Co. KGaA, Weinheim

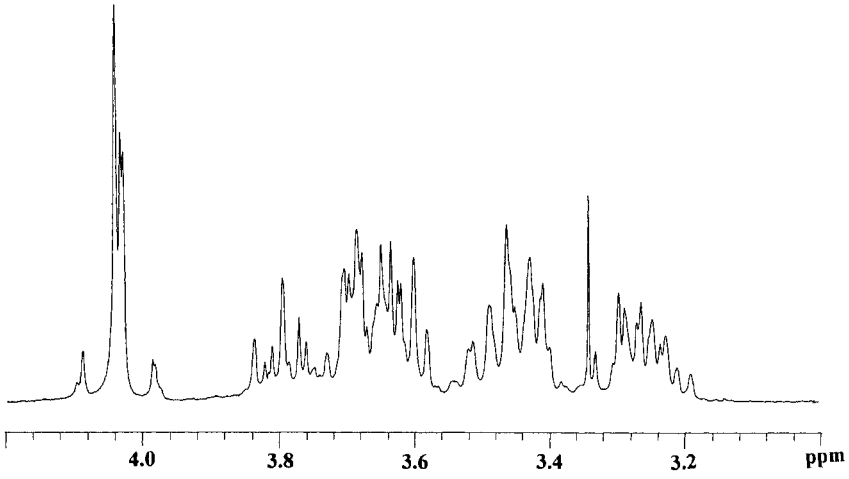

Figure 4. 360 MHz ^{1}H NMR spectrum of [Ga-CB-DO2A]NO_3 in D_2O

the ^{1}H and ^{13}C NMR timescales in solution at room temperature. High-temperature ^{1}H NMR spectra up to 87(2) °C show no dynamic broadening of the AB portion of the pendant-arm *AB*X multiplet. (Interestingly, the integration of this multiplet decreases over time, indicating significant H/D exchange.) Complete lineshape simulations of AB → BA dynamic exchange of the apparent *AB*X subspectrum of the pendant-arm CH_2 protons allow us to place a lower limit of 21.0(2) kcal/mol on the enantiomerization barrier at 87(2) °C. This dramatic increase in going from Zn·**1** to [Ga·**1**]$^+$ may be attributed to the higher cationic charge at the Ga^{III} center and stronger metal−ligand bonds, which may inhibit any dissociative process involving the coordinated carboxylate pendant arms. The X-ray solid-state structural comparison between [Zn·**1**] and [Ga·**1**]$^+$ in the next section lends support to this premise. Since this gallium complex does not rapidly enantiomerize, we can further conjecture that pendant-arm dissociation rather than non-dissociative pseudorotation is most likely the relevant dynamic process.

X-ray Structural Data

The core structure of the zinc complex [Zn·**1**] is shown in Figure 5. The Zn^{II} cation is fully enveloped within the *cis*-N_4O_2 donor set of the cross-bridged ligand in a near-octahedral geometry. The axial N(2)−Zn(1)−N(4) angle of 178.32(6) [176.07(6)]° (structural data for a second independent molecule are given in brackets) is close to linearity, showing an unusually good fit for Zn^{II} within the cross-bridged cyclen cavity. Previous structural data of zinc complexes of the cross-bridged cyclen and its derivatives have shown the cation significantly distended from the ligand cavity with much more distorted axial N−Zn−N angles of between 148 and 159°.[16−18] Another manifestation of these distortions can also be seen in their longer axial N−Zn bonds (2.17−2.26 Å) compared to the average of 2.12 Å found in Zn·**1**. The near-octahedral coordination geometry around Zn(1) here can also be seen in the N(1)−Zn(1)−O(3) angle of 172.30(6) [170.20(6)]° and the N(3)−Zn(1)−O(1) angle of 173.95(6) [174.18(6)]°. Indeed, all Zn−N and Zn−O bond lengths are within a relatively narrow range of 2.067−2.177 Å. Selected bond lengths and angles are shown in Table 1. An X-ray structure of a DOTA complex of zinc(II) featuring a related *cis*-N_4O_2 ligand coordination mode has been reported.[19] This has an axial N−Zn−N angle of 153.9°, an axial Zn−N distance of 2.232 Å, an equatorial Zn−N distance of 2.171Å, and a shorter Zn−O distance of 2.037 Å. However, without the cross-bridging ethylene, the equatorial N−Zn−N angle is opened up to 107.8° [compared to the 83.84(6)° for N(1)−Zn(1)−N(3) here]. Also, in the reported structure the coordinated carboxylate pendant arms are on the equatorial macrocyclic nitrogen atoms rather than the axial ones and the DOTA structure is thus close to C_{2v} symmetry.

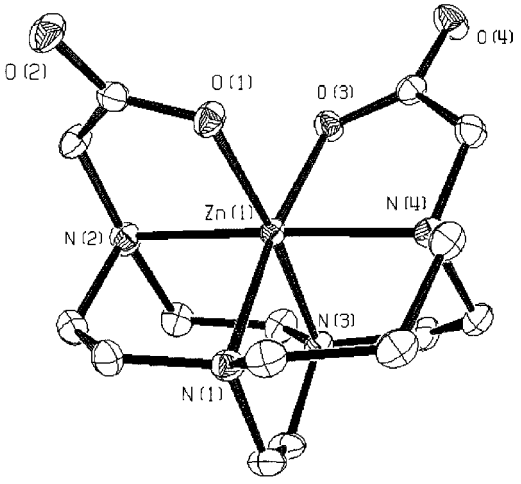

Figure 5. Molecular structure of Zn-CB-DO2A·$NaClO_4$; hydrogen atoms and sodium perchlorate have been omitted for clarity

The X-ray structure of [Ga·**1**]NO_3 also reveals a fully enveloped Ga^{III} cation within the ligand's cleft (see Figure 6). The distortion from an idealized octahedral geometry is more pronounced here with an axial N(2)−Ga(1)−N(2A)

 © 2004 Wiley-VCH Verlag GmbH & Co. KGaA, Weinheim

Table 1. Selected bond lengths [Å] and bond angles [°] for [Zn·**1**]($NaClO_4$) (values for two symmetry-independent molecules are given)

Zn(1)−O(1)	2.0839(14), 2.0665(4)	O(1)−Zn(1)−O(3)	94.70(6), 93.79(6)
Zn(1)−O(3)	2.1106(13), 2.1255(4)	O(1)−Zn(1)−N(1)	91.79(6), 93.10(6)
Zn(1)−N(1)	2.1555(17), 2.1766(17)	O(1)−Zn(1)−N(2)	83.21(6), 82.06(6)
Zn(1)−N(2)	2.1168(17), 2.1342(17)	O(1)−Zn(1)−N(3)	173.95(6),174.18(6)
Zn(1)−N(3)	2.1600(17), 2.1477(17)	O(1)−Zn(1)−N(4)	97.88(6), 98.28(6)
Zn(1)−N(4)	2.1159(17), 2.1415(17)	O(3)−Zn(1)−N(1)	172.30(6), 170.20(6)
		O(3)−Zn(1)−N(2)	98.46(6), 102.32(6)
		O(3)−Zn(1)−N(3)	90.00(6),89.91(6)
		O(3)−Zn(1)−N(4)	82.74(6), 81.57(6)
		N(1)−Zn(1)−N(2)	86.44(6), 85.52(6)
		N(1)−Zn(1)−N(3)	83.84(6), 83.80(6)
		N(1)−Zn(1)−N(4)	92.25(6), 90.55(6)
		N(2)−Zn(1)−N(3)	92.34(6), 92.76(6)
		N(2)−Zn(1)−N(4)	178.32(6), 176.07(6)
		N(3)−Zn(1)−N(4)	86.48(7), 86.70(7)

angle of 164.6(1)°. In accord with the higher charge of this cation, all Ga−N and Ga−O bonds are significantly shorter than the corresponding ones in the zinc(II) structure, with Ga(1)−N(1) at 2.046(2) Å, Ga(1)−N(2) at 2.078(2) Å, and especially Ga(1)−O(1) at 1.942(1) Å. Another noteworthy difference is the disparate carboxylate C−O distances here: 1.298(2) Å for the Ga-coordinated C(7)−O(1) versus 1.227(2) Å for the uncoordinated C(7)−O(2). In the zinc structure, these average to very similar values of 1.26 Å and 1.25 Å, respectively, most likely due to further coordination of the carbonyl oxygen atoms to sodium cations in the crystal lattice. Selected bond lengths and angles for this structure are listed in Table 2. The X-ray structure of a related gallium(III) complex of a DOTA derivative is in the published literature.[13] A *cis*-N_4O_2 donor set is also found here with an axial N−Ga−N angle of 156.3°, Ga−N distances of 2.12−2.16 Å, and short Ga−O distances of 1.90−1.93 Å. Again, the coordinated carboxylate pendant arms are attached to the equatorial instead of axial cyclen nitrogen atoms. In the absence of the ethylene cross-bridge, the equatorial N−Ga−N angle opens up to 105.6°.

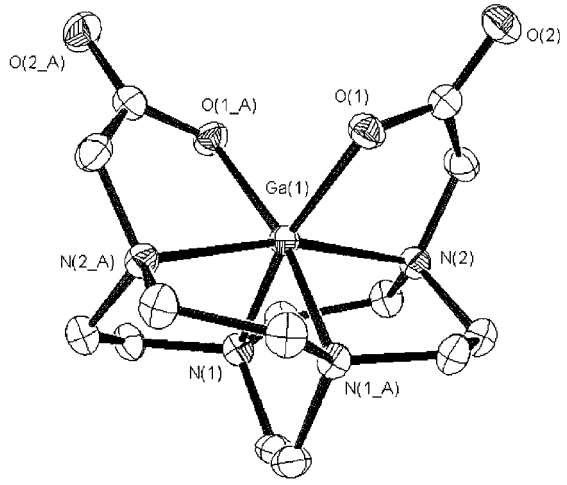

Figure 6. Molecular structure of [Ga-CB-DO2A]NO_3; hydrogen atoms and nitrate have been omitted for clarity

Table 2. Selected bond lengths [Å] and bond angles [°] for [Ga·**1**]NO_3

Ga(1)−O(1)	1.9421(13)	O(1)−Ga(1)−O(1A)	90.28(8)
Ga(1)−N(1)	2.0461(15)	O(1)−Ga(1)−N(1)	165.20(5)
Ga(1)−N(2)	2.0780(15)	O(1)−Ga(1)−N(1A)	93.60(6)
		O(1)−Ga(1)−N(2)	83.23(6)
		O(1)−Ga(1)−N(2A)	107.90(6)
		N(1)−Ga(1)−N(1A)	86.24(9)
		N(1)−Ga(1)−N(2)	81.99(6)
		N(1)−Ga(1)−N(2A)	86.75(6)
		N(2)−Ga(1)−N(2A)	164.56(9)

Conclusion

Under basic conditions, Zn^{II}, Ga^{III}, and Cd^{II} complexes of the dicarboxylate pendant-armed cross-bridged cyclen H_2**1** were prepared. In solution, both the Zn^{II} and Cd^{II} complexes were found by NMR spectroscopy to exhibit fast dynamic enantiomerization at room temperature; the Zn^{II} complex has a $\Delta G^{\neq}$ barrier of 12.3(1) kcal/mol at 24(2) °C. In contrast, the Ga^{III} complex exhibits C_2 symmetry consistent with its solid-state structure with no dynamic broadening on either the ^1H or ^{13}C NMR timescales. X-ray structures confirm full ligand envelopment of both the Zn^{II} and Ga^{III} cations with significantly shorter Ga−N and Ga−O bonds. A dissociative enantiomerization mechanism is in agreement with the dramatically higher barrier of the Ga complex. These data, taken as a whole, infer that such pendant-armed ligand complexes of Ga^{III} will exhibit even greater kinetic stability than the parent cross-bridged complexes. Future kinetic inertness studies are clearly warranted.

Experimental Section

CAUTION: *Although we did not encounter any problems, perchlorate salts of metal complexes containing organic ligands and solvents are potentially explosive and should be handled only in small quantities and with great caution!*

 © 2004 Wiley-VCH Verlag GmbH & Co. KGaA, Weinheim

General Methods and Materials: ^{1}H and ^{13}C{^{1}H} NMR spectra were recorded with a Bruker AM-360 or Varian Inova-400 instrument and referenced to TMS. Acetonitrile was used as an internal reference in D_2O with the methyl proton resonance set at δ = 2.06 ppm and ^{13}C resonance at δ = 1.70 ppm. Low-temperature ^{1}H and ^{13}C NMR spectral studies were carried out with the Varian Inova-400. A methanol chemical shift thermometer (0.03% concd. HCl in MeOH) was used to monitor the probe temperature.[20] High-temperature spectra were recorded with the Bruker AM-360 and the probe temperature calculated from the chemical shift difference between the proton signals of neat ethylene glycol.[21] Complete lineshape analysis of the two-site mutual exchange broadening exhibited by the δ = 61.77 ppm room temperature [24(2) °C] ^{13}C{^{1}H} resonance of [Zn·**1**] in CD_3OD (fast intermediate exchange) was carried out using the program WINDNMR-Pro version 7.1.5 (Hans J. Reich, University of Wisconsin, Madison, WI, USA, **2001**),[22] which is based on the modified Bloch equations as expressed by Rogers and Woodbrey;[23] Δν (484 Hz) was determined from the anisotropically broadened, slow-exchange limit spectrum (CD_3OD at −80 °C). The simulations gave a rate constant k (forward = reverse) of 6.0(5) × 10^3 s^{-1}. The $\Delta G^{\neq}$ at 24(2) °C was calculated using the Eyring equation with K = 1. A lower limit was placed upon the enantiomerization barrier of [Ga·**1**]$^+$ in D_2O through comparison of the experimental proton *AB*X subspectrum of the pendant-arm CH_2 protons with simulated spectra (WINDNMR-Pro) allowing exchange of A and B nuclei. For k = 1.5 s^{-1}, calculated broadening is significantly greater than that observed experimentally at 87(2) °C.

IR spectra were recorded as KBr pellets with a Nicolet MX-1 FT Spectrophotometer. Elemental analyses were obtained from Atlantic Microlab. Inc., Norcross, GA, USA. Reactions were run under nitrogen with magnetic stirring in standard Schlenk glassware. Bulk solvent removal was by rotary evaporation under reduced pressure and trace volatile removal from solids was by vacuum pump. Solvents were used as purchased. Cross-bridged ligand **1**[14,15] was prepared as a trifluoroacetate salt by a modification of published methods.[6]

[Zn·1](NaClO$_4$)$_{1.5}$: An aqueous solution of NaOH (0.970 N) (0.818 mL) was added to a MeOH solution (10 mL) of H_2**1**·(CF_3COOH)·(H_2O) (113 mg, 0.265 mmol) to form a clear solution. A MeOH solution (6 mL) of $Zn(ClO_4)_2$·$6H_2O$ (100 mg, 0.270 mmol) was then added into this solution. After refluxing for 2 d and cooling to room termperature, this MeOH solution was centrifuged off from a small amount of precipitate. Et_2O vapor diffusion into the supernatant yielded 106 mg (71.2%) of a white crystalline solid. IR (KBr): $\tilde{\nu}$ = 1617 cm^{-1} (broad) (ν_{COO}). ^{1}H NMR (360.13 MHz, D_2O): δ = 3.63 (s, 4 H, CH_2COO), 3.20−3.37 (m, 8 H), 3.03 (s, 4 H, cross-bridging CH_2CH_2), 2.89−3.08 (m, 8 H) ppm. ^{1}H NMR (400 MHz, CD_3OD): δ = 3.61 (s, 4 H, CH_2COO), 3.20−3.41 (m, 8 H), 3.07 (s, 4 H, cross-bridging CH_2CH_2), 2.91−3.15 (m, 8 H) ppm. ^{1}H NMR (400 MHz, CD_3OD, −80 °C): δ = 3.72 (AB, CH_2COO, J = 16.4 Hz, 4 H), 3.24−3.48 (m, 8 H), 2.72−3.19 (m, 12 H) ppm. ^{13}C{^{1}H} (D_2O): δ = 179.03, 64.94, 61.10, 56.83, 49.95 ppm. ^{13}C{^{1}H} NMR (100 MHz, CD_3OD): δ = 177.85, 66.11, 61.77 (br.), 57.85, 50.80 ppm. ^{13}C{^{1}H} NMR (100 MHz, CD_3OD, −80 °C): δ = 178.59, 65.62, 63.93, 59.12, 58.44, 56.89, 50.12 ppm. $C_{14}H_{24}Cl_{1.5}N_4Na_{1.5}O_{10}Zn$ (561.41): calcd. C 29.95, H 4.31, N 9.98; found C 30.05, H 4.68, N 9.81. X-ray quality crystals were grown by ether diffusion into a sample dissolved in 95% ethanol solution. These have a composition of [Zn·**1**](NaClO$_4$)(C_2H_5OH)(H_2O)$_{0.5}$.

[Cd·1](NaClO$_4$)(H$_2$O)$_{1.5}$: An aqueous solution of NaOH (0.970 N) (0.64 mL) was added to a clear solution of H_2**1**·(CF_3COOH)·(H_2O) (89.0 mg, 0.208 mmol) and $Cd(ClO_4)_2$·$6H_2O$ (94.8 mg, 0.226 mmol) in 15 mL MeOH to form a cloudy solution. The reaction mixture was refluxed for 7 h, cooled, and some white precipitate was centrifuged off. Et_2O vapor diffusion into the supernatant yielded 73.0 mg (61.1%) of a white crystalline solid. IR (KBr): $\tilde{\nu}$ = 1615, 1595 cm^{-1} (ν_{COO}). ^{1}H NMR (360.13 MHz, D_2O):

Table 3. Crystallographic data for [Zn·**1**](NaClO$_4$) and [Ga·**1**]NO_3

	[Zn·**1**](NaClO$_4$)	[Ga·**1**]NO_3
Empirical formula	$C_{16}H_{31}ClN_4NaO_{9.50}Zn$	$C_{14}H_{24}GaN_5O_7$
Formula mass	555.26	444.10
Crystal system, space group	monoclinic, $P2_1/c$	orthorhombic, $P2_12_12$
a [Å]	16.2288(10)	8.7107(7)
b [Å]	9.3084(6)	12.5119(10)
c [Å]	29.0705(18)	7.5586(6)
α [°]	90.0	90.0
β [°]	95.564(1)	90.0
γ [°]	90.0	90.0
V [Å^3]	4370.8(5)	823.79(11)
Z	8	2
T [K]	150(2)	218(2)
λ [Å]	0.71073 (Mo-K_α)	0.71073 (Mo-K_α)
$\rho_{calcd.}$ [g·cm^{-3}]	1.688	1.790
μ [mm^{-1}]	1.326	1.724
Measured reflections	27282	6004
Independent reflections	10255 (R_{int} = 0.028)	1967 (R_{int} = 0.0260)
Independent reflections	9175	1872
$R^{[a]}$, $R^{[b]}$(ωF^2) (obsd. data)	0.0347; 0.0853	0.0231; 0.0553
$R^{[a]}$, $R^{[b]}$(ωF^2) (all data)	0.0412; 0.0853	0.0244; 0.0557
GOF	1.143	1.006

[a] $R = \Sigma||F_o| - |F_c||/\Sigma|F_o|$. [b] $R(\omega F^2) = \{\Sigma[\omega(F_o^2 - F_c^2)^2]/\Sigma[\omega(F_o^2)^2]\}^{1/2}$; $\omega = 1/[\sigma^2(F_o^2) + (aP)^2 + bP]$, $P = [2F_c^2 + \max(F_o,0)]/3$.

 © 2004 Wiley-VCH Verlag GmbH & Co. KGaA, Weinheim

δ = 3.48 (s, 4 H, CH_2COO, ^{111}Cd, ^{113}Cd satellites, J = 11.6 Hz), 2.94−3.26 (m, 12 H), 2.89 (s, 4 H, cross-bridging CH_2CH_2, ^{111}Cd, ^{113}Cd satellites, J = 13.7 Hz), 2.81 (br. dd, 4 H, J = 12.1, 4.4 Hz) ppm. $^{13}C\{^1H\}$ NMR (90.55 MHz, D_2O): δ = 179.23 (^{111}Cd,^{113}Cd satellites, J = 11.3 Hz), 64.95 (^{111}Cd, ^{113}Cd satellites, J = 6.0 Hz), 60.58, 57.32, 47.63 (^{111}Cd, ^{113}Cd satellites, J = 15.3 Hz) ppm. $C_{14}H_{27}CdClN_4NaO_{9.5}$ (574.24): calcd. C 29.28, H 4.74, N 9.76, Cl 6.17; found C 29.31, H 4.70, N 9.65, Cl 5.96.

[Ga·1](NO$_3$)$_3$: A solution of $Ga(NO_3)$ hydrate (38.6 mg, ca. 0.15 mmol) in MeOH (6 mL) was added to an MeOH solution (14 mL) of H_2**1**·(CF_3COOH)·(H_2O) (66.4 mg, 0.155 mmol) to form a clear solution. Anhydrous NaOAc (46.3 mg, 0.564 mmol) in MeOH (7 mL) was then added in two portions. The reaction mixture was refluxed for 2 d, after which time a white precipitate was isolated by centrifugation. The resulting white precipitate was dried to give the product complex (41.9 mg, 62.9%). This was redissolved in a H_2O (2.6 mL)/MeOH (3.2 mL) mixture followed by Et_2O/MeOH (1:1) vapor diffusion into this solution to yield crystals suitable for X-ray analyses. IR (KBr): $\tilde{\nu}$ = 1692 (s), 1672 (s) cm^{-1} (ν_{COO}), 1363 (s), 1351 (s), 1339 (s), 1299 (s), 1284 (s) cm^{-1} (broad) (ν_{NO3}). ^1H NMR (360.13 MHz, D_2O): δ = 4.03 and 4.06 (AB of apparent ABX, CH_2COO, J_{AB} = 16.8, $J_{BX} \approx$ 1.5 Hz, 4 H), 3.57−3.85 (m, 10 H), 3.38−3.54 (m, 6 H), 3.18−3.31 (m, 4 H, cross-bridging CH_2CH_2) ppm. $^{13}C\{^1H\}$ NMR (90.55 MHz, D_2O): δ = 174.89, 64.07, 63.67, 57.11, 57.09, 54.87, 51.78 ppm. $^{13}C\{^1H\}$ NMR (90.55 MHz, [D_6]DMSO): δ = 169.92, 63.65, 61.92, 56.21, 55.35, 54.06, 50.25 ppm. $C_{14}H_{24}GaN_5O_7$ (444.10): calcd. C 37.86, H 5.45, N 15.77; found C 37.82, H 5.45, N 15.75.

X-ray Crystallography: Diffraction intensity data were collected with Bruker Smart Apex CCD {[Zn·**1**]($NaClO_4$)} and Siemens P4 CCD ([Ga·**1**]NO_3) diffractometers. Crystal data collection, and refinement parameters are given in Table 3. The structures were solved using direct methods, completed by subsequent difference Fourier syntheses, and refined by full-matrix least-squares procedures on F^2. SADABS absorption corrections were applied to both sets of data {$T_{min.}/T_{max.}$= 0.917 and 0.724 for [Zn·**1**]($NaClO_4$) and [Ga·**1**]NO_3, respectively}. In both structures all non-hydrogen atoms were refined with anisotropic displacement coefficients. Hydrogen atoms were treated as idealized contributions except the H atoms of solvent water molecules in [Zn·**1**]($NaClO_4$) involved in H-bonds which were located on the F-map and refined with isotropic thermal parameters. The Flack parameter for [Ga·**1**]NO_3 is 0.014(11). All software and sources of scattering factors are contained in the SHELXTL (5.10) program package (G. Sheldrick, Bruker XRD, Madison, WI, USA). CCDC-229393 {[Zn·**1**]($NaClO_4$)} and -229394 ([Ga·**1**]NO_3) contain the supplementary crystallographic data for this paper. These data can be obtained free of charge at www.ccdc.cam.ac.uk/conts/retrieving.html [or from the Cambridge Crystallographic Data Centre, 12 Union Road, Cambridge CB2 1EZ, UK; Fax: (internat.) + 44-1223-336-033; E-mail: deposit@ccdc.cam.ac.uk].

Acknowledgments

Financial support of this research was from NIH grants CA93375 and GM55916-01 at UNH and an NSF instrumentation grant at the University of California, San Diego.

[1] X. Sun, M. Wuest, G. R. Weisman, E. H. Wong, D. P. Reed, R. J. Motekaitis, A. E. Martell, M. J. Welch, C. J. Anderson, *J. Med. Chem.* **2002**, *45*, 469−477.
[2] C. A. Boswell, X. Sun, W. Niu, G. R. Weisman, E. H. Wong, A. L. Rheingold, C. J. Anderson, *J. Med. Chem.* **2004**, *47*, 1465−1474.
[3] J. Springborg, *Dalton Trans.* **2003**, 1653−1665.
[4] T. J. Hubin, *Coord. Chem. Rev.* **2003**, *241*, 27−46.
[5] G. R. Weisman, M. E. Rogers, E. H. Wong, J. P. Jasinski, E. S. Paight, *J. Am. Chem. Soc.* **1990**, *112*, 8604−8605.
[6] G. R. Weisman, E. H. Wong, D. C. Hill, M. E. Rogers, D. P. Reed, J. C. Calabrese, *Chem. Commun.* **1996**, 947−948.
[7] E. H. Wong, G. R. Weisman, D. C. Hill, D. P. Reed, M. E. Rogers, J. P. Condon, M. A. Fagan, J. C. Calabrese, K.-C. Lam, I. A. Guzei, A. L. Rheingold, *J. Am. Chem. Soc.* **2000**, *122*, 10561−10572.
[8] J. Chin, M. Banaszczyk, V. Jubian, X. Zou, *J. Am. Chem. Soc.* **1989**, *111*, 186−90.
[9] R. Hettich, H.-J. Schneider, *J. Am. Chem. Soc.* **1997**, *119*, 5638−5647.
[10] J. A. Halfen, S. Mahapatra, E. C. Wilkinson, S. Kaderli, V. G. Young Jr., L. Que Jr., A. D. Zuberbuehler, W. B. Tolman, *Science (Washington, D. C.)* **1996**, *271*, 1397−1400.
[11] C. J. Anderson, M. J. Welch, *Chem. Rev.* **1999**, *99*, 2219−2234.
[12] D. E. Reichert, J. S. Lewis, C. J. Anderson, *Coord. Chem. Rev.* **1999**, *184*, 3−66.
[13] A. Heppeler, S. Froidevaux, H. R. Macke, E. Jermann, M. Behe, P. Powell, M. Hennig, *Chem. Eur. J.* **1999**, *5*, 1974−1981.
[14] D. A. Moore (Mallinckrodt Medical, Inc., USA), in *PCT Int. Appl.* Wo, **1994**, pp. 58ff.
[15] H. S. Winchell, J. Y. Klein, E. D. Simhon, R. L. Cyjon, O. Klein, H. Zaklad (Concat, Inc., USA), in *U.S.*, **1999**, pp. 41ff, Cont.-in-part of U.S. Ser. No. 560,626.
[16] W. Niu, E. H. Wong, G. R. Weisman, L. N. Zakharov, C. D. Incarvito, A. L. Rheingold, *Polyhedron* **2004**, *23*, 1019−1025.
[17] W. Niu, E. H. Wong, G. R. Weisman, D. C. Hill, K.-C. Lam, R. D. Sommer, L. N. Zakharov, A. L. Rheingold, manuscript in preparation.
[18] T. J. Hubin, N. W. Alcock, M. D. Morton, D. H. Busch, *Inorg. Chim. Acta* **2003**, *348*, 33−40.
[19] A. Riesen, M. Zehnder, T. A. Kaden, *Acta Crystallogr., Sect. C: Cryst. Struct. Commun.* **1991**, *47*, 531−533.
[20] A. L. Van Geet, *Anal. Chem.* **1970**, *42*, 679−680.
[21] M. L. Kaplan, F. A. Bovey, H. N. Cheng, *Anal. Chem.* **1975**, *47*, 1703.
[22] H. J. Reich, *J. Chem. Educ.: Software, Ser. D* **1996**, *3*, 17−19, 27−33, 56−66.
[23] J. Sandström, in *Dynamic NMR Spectroscopy*, Academic Press, NewYork, **1982**, p. 14.

Received January 29, 2004
Early View Article
Published Online June 11, 2004

 © 2004 Wiley-VCH Verlag GmbH & Co. KGaA, Weinheim

Synthesis, Structure and Magnetic Properties of a Series of Novel Isophthalate-Bridged Manganese(II) Polymers with Double-Layer or Double-Chain Structures

Chengbing Ma,[a,d] Changneng Chen,[a] Qiutian Liu,*[a] Feng Chen,[a] Daizheng Liao,[b] Licun Li,[b] and Licheng Sun[c]

Keywords: Manganese / Crystal structure / Isophthalic acid / Magnetic properties / Structural topology

Four isophthalate-bridged manganese(II) coordination polymers, $[Mn_4(ip)_4(H_2O)_2(Him)_4]_n$ (**1**), $[Mn(ip)(Him)_2]_n$ (**2**), $[Mn(ip)(dpe)]_n{\cdot}0.5ndpe\cdot n H_2O$ (**3**) and $[Mn_2(ip)_2(bpy)_2]_n$ (**4**) [ip = isophthalate, Him = imidazole, bpy = 2,2′-bipyridine and dpe = (*E*)-1,2-bis(4-pyridyl)ethene], have been rationally synthesized and characterized by single-crystal X-ray structure determinations and magnetic studies. Both **1** and **3** are two-dimensional (2D) double-layer polymers. In **1**, novel Mn_4 entities are linked by ip ligands, while **3** is made of $[Mn(ip)]_n$ parallel double chains cross-linked by the μ-dpe ligands. Both **2** and **4** are one-dimensional (1D) double-chain polymers, where **2** is composed of $[Mn(ip)]_n$ parallel double chains capped by the Him ligands, while **4** is made of $[Mn_2(ip)_2]_n$ helical double chains capped by the chelating bpy ligands. Variable-temperature magnetic susceptibility measurements revealed weak antiferromagnetic exchange interactions between the adjacent Mn^{II} ions of the four coordination polymers. The data of **2**–**4** were fitted to the homonuclear alternating chain model to give magnetic coupling parameters of $J_1 = -0.71(4)$ to $-1.01(3)$ cm^{-1} and $J_2 = -0.02(2)$ to $-0.46(2)$ cm^{-1}. In the case of **1**, the fitting of magnetic data considering only the interactions within the Mn_4 moiety led to $J = -2.17(1)$ cm^{-1} and $zJ' = -0.01(5)$ cm^{-1}, using a combination of a dimeric model and a mean molecular field approximation model.

(© Wiley-VCH Verlag GmbH & Co. KGaA, 69451 Weinheim, Germany, 2004)

Introduction

Currently, there is great interest in metal-organic hybrid materials containing paramagnetic metal ions within extended structures. This is driven to a large extent by their fascinating network topologies and potential application in the field of molecular magnetism.[1,2] The low-dimensional (1D chain-like or 2D layer-like) extended structures have attracted special interest on account of their specific structural features and unusual nonlinear optical and magnetic properties.[3] Therefore, rational design and construction of new materials with specific network structures and investigation of their properties have become a particularly important and topical subject. One commonly used strategy to construct such extended networks is to select appropriate bridging ligands which can transmit magnetic interactions in addition to binding several metal ions in a specific coordination geometry. Accordingly, polycarboxylic acid ligands are good candidates for this purpose. The three isomeric benzenedicarboxylic acids, i.e. phthalic acid, isopthalic acid and terephthalic acid, are especially suitable since they can bind metal ions in a variety of modes and can provide various superexchange pathways, which transmit magnetic interactions between metal ions through either the carboxylate group or the benzene ring of the ligand. Among these three isomeric dicarboxylates, major studies performed using terephthalate resulted in a rich variety of complexes with interesting structures and various magnetic properties.[4] The other two isomers have not been studied extensively for this purpose.[5,6]

On the other hand, the manganese(II) carboxylate complexes have long been of special interest since they are known to exist at the active sites of some metalloenzymes.[7] As part of our ongoing work on manganese complexation by dicarboxylic acids,[8] we have explored the reaction systems containing the Mn^{2+} ion and the isomeric benzenedicarboxylic acids as primary bridging ligand, paying par-

[a] State Key Laboratory of Structural Chemistry, Fujian Institute of Research on the Structure of Matter, Chinese Academy of Sciences,
Fuzhou 350002, China
Fax: (internat.) + 86-591-3714946
E-mail: lqt@ms.fjirsm.ac.cn
[b] Department of Chemistry, Nankai University,
Tianjin, China
[c] State Key Laboratory of Fine Chemicals, Dalian University of Technology,
Dalian, China
[d] Graduate School of the Chinese Academy of Sciences,
Beijing, China

 © 2004 Wiley-VCH Verlag GmbH & Co. KGaA, Weinheim **DOI: 10.1002/ejic.200400095**

ticular attention to rational design of the magnetically coupled complexes with specific polymeric frameworks. Concurrently, introduction into the reaction systems of diimine chelating ligands, such as 2,2′-bipyridine and 1,10-phenanthroline, imidazole or linear ditopic ligands, such as 4,4′-bipyridine and (*E*)-1,2-bis(4-pyridyl)ethene, as ancillary ligands, was expected to inhibit the expansion of polymeric frameworks in order to obtain the desired low-dimensional polymers, or to induce the evolution of novel structures.

In this work, we report a novel family of Mn^{2+} coordination polymers **1**−**4**. They were isolated by treatment of an Mn^{2+} salt with isophthalic acid in the presence of selected ancillary ligands − imidazole, (*E*)-1,2-bis(4-pyridyl)ethene and 2,2′-bipyridine, under different crystallization conditions (Scheme 1). Single-crystal X-ray diffraction analyses revealed either double-chain structures or double-layer structures, which differ substantially from those of several metal isophthalate polymeric compounds reported previously.[5,9] The isophthalate ligands display various coordination modes (Scheme 2) and mediate overall antiferromagnetic exchange interactions between Mn^{2+} ions in these coordination polymers.

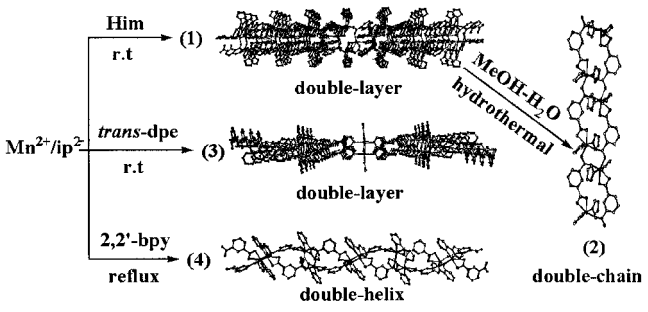

Scheme 1

Results and Discussion

Preparation of the Complexes and IR Spectroscopy

When compared with the manganese complexes containing monocarboxylate ligands such as acetate, benzoate and their derivatives, the structural information for manganese dicarboxylate complexes is relatively scarce. This is mainly because of the insolubility of the polymeric materials resulted from the reaction of a dicarboxylate with an Mn^{2+} salt under ambient conditions. The reaction of isophthalate with Mn^{2+} salts in the presence of imidazole is an exception, resulting in a clear solution. Cosolvent methanol was added in order to promote crystallization of **1**. As indicated in the structural description of **1** given below, only three of the four carboxyl O atoms in the isophthalate ligand (see b in Scheme 2) are coordinated and there is a relatively rare aqua coordination to the metal ion. The unexpected ancillary ligation by water often results in poor control over the framework of the final product. The fact that hydrothermal reaction can enhance metal−ligand interactions rather than metal−water coordination has been clearly demonstrated in several cases.[10] Further study of the reaction of **1** in an H_2O/CH_3OH solvent mixture under hydrothermal conditions led to deposition of **2**, in which metal−water coordination was blocked and all of the carboxyl O atoms take part in coordination (see c in Scheme 2). Taking into account that formation of higher dimensionality systems is prevented by the axially capping imidazole ligands in the 1D chain structure of **2**, the coordination polymer **3**, possessing a 2D layer structure, was expected with confidence when the linear *exo*-bidentate (*E*)-1,2-bis(4-pyridyl)ethene ligand was used in place of the axial imidazole ligands. The near parallel double-chain of $[Mn(ip)]_n$ in **2** was modified to a distorted double-helical chain of $[Mn_2(ip)_2]_n$ in **4** by means of *cis* chelation of the rigid 2,2′-bipyridine ligand used in place of the imidazole ligand.

IR spectra of the coordination polymers offer some valuable information about both the presence of isophthalate and the coordination modes of the carboxylates. The absence of any strong absorptions around 1700 cm^{-1} indicates that all carboxyl groups in **1**−**4** are deprotonated. Of three strong characteristic peaks at 1566, 1448 and 1394 cm^{-1} for **1**, the one at 1566 cm^{-1} is attributed to $\nu_{as}(COO)$ of all the carboxylate groups, while the peaks at 1448 cm^{-1} and 1394 cm^{-1} may be assigned to $\nu_s(COO)$ of the bidentate carboxylate group and the monodentate carboxylate group, respectively, since it is known that the difference $\Delta = \nu_{as} - \nu_s$ is smaller in the former (118 cm^{-1}) than in the latter (172

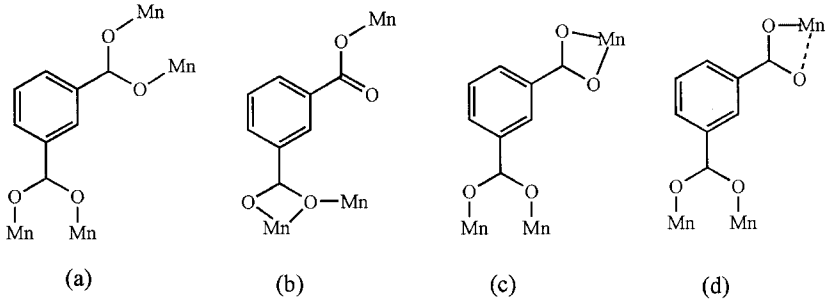

Scheme 2. Coordination modes of isophthalate found in this work: (a) bridging bis(bidentate) μ_4-mode, (b) bridging/chelating bidentate and monodentate μ_3-mode, (c) bridging and chelating bis(bidentate) μ_3-mode, and (d) bridging bidentate and monodentate μ_3-mode

 © 2004 Wiley-VCH Verlag GmbH & Co. KGaA, Weinheim

cm^{-1}).[11] Amongst the four strong absorptions at 1557, 1541, 1444, 1390 cm^{-1} for **2** (1568, 1547, 1429 and 1394 cm^{-1} for **3**, and 1572, 1556, 1439 and 1394 cm^{-1} for **4**), the peaks at 1557 and 1541 cm $^{-1}$ for **2** (1568 and 1547 cm^{-1} for **3**, and 1572 and 1556 cm^{-1} for **4**) are attributed to ν_{as}(COO) of the three complexes. The splitting of the ν_{as}(COO) peak indicates that both carboxylate groups of the ip ligand are in two different coordination modes,[11b] which is consistent with their respective crystal structures. The other two peaks at 1444 and 1390 cm^{-1} for **2** (1429 and 1394 cm^{-1} for **3**, and 1439 and 1394 cm^{-1} for **4**) correspond to ν_s(COO) of the bidentate chelating carboxylate group and the bidentate bridging carboxylate group, respectively.

Description of the Crystal Structures

The X-ray structure determination revealed a novel and complex covalently bonded 2D network for **1**, containing two crystallographically independent manganese(II) ions of different octahedral geometry. As shown in Figure 1 for compound **1**, the ip ligands are of two types: A and B [as shown in Scheme 2 (a) and (b), respectively]. The two crystallographically independent Mn atoms (Mn1 and Mn2), with an interatomic distance of 3.476(2) Å, are bridged by one μ-aqua (Ow), one $\mu_{1,3}$-OCO and one $\mu_{1,1}$-OCO bridge. To the best of our knowledge, this type of triply bridged Mn dimeric core is unique, although three examples containing one μ-aqua and two $\mu_{1,3}$-OCO bridges were previously reported.[12] The bond valence sum (BVS) calculations[13] give the values of 2.00 and 2.11 for Mn1 and Mn2, respectively, indicating that the Mn centers are of +2 oxidation state. In order to maintain the electroneutrality of the compound, the Ow is assigned as a neutral water ligand. Additionally, the absence of characteristic IR absorptions around 1700 cm^{-1} expected for the vibration of protonated carboxyl groups (COOH), indicates that all carboxyl groups in **1** are deprotonated. Furthermore, the Mn−Ow distances of 2.229(2) and 2.331(2) Å fall in the normal range found in other Mn complexes,[12,14] which also suggests that the bridging ligand is water. The Mn1 and Mn2 atoms are coordinated by one N atom of Him, one bridging Ow atom, and two bridging O atoms from the μ_4-ip ligands. Two O atoms of the μ_3-ip ligand chelate to Mn1 and coordinate monodentately to Mn2, respectively, completing the distorted octahedral geometries (Table 1) of the two Mn ions. The Mn_2 unit is further dimerized through two *syn*/*anti*-carboxylate bridges from symmetry-related μ_4-ip ligands to form a novel nonplanar cyclic Mn tetramer containing four Mn octahedra and two carboxylate groups with Mn1···Mn2A = 5.309(2) Å. The most remarkable structural feature of **1** is that each Mn tetramer connects eight ip ligands to form an infinite 2D coordination framework featuring an unprecedented puckered rhombic grid-like $[Mn_{16}(ip)_8(H_2O)_8(Him)_{16}]$ as the basic building block (Figure 2). Each apex of the grid is occupied by a Mn_4 clus-

Table 1. Selected bond lengths [Å] and angles [°] for **1** (symmetry codes: A: $-x + 1, -y + 1, -z + 1$; B: $x + 1, y + 1, z$, C $x, y + 1, z$)

Mn1−O5A	2.090(2)	O5A−Mn1−O1	137.13(8)
Mn1−O7B	2.139(2)	O7B−Mn1−O1	96.64(9)
Mn1−N1	2.196(3)	N1−Mn1−O1	103.58(1)
Mn1−Ow	2.229(2)	Ow−Mn1−O1	78.44(8)
Mn1−O2	2.267(2)	O2−Mn1−O1	55.46(8)
Mn1−O1	2.425(2)	O6−Mn2−O8B	176.91(1)
Mn2−O6	2.082(2)	O6−Mn2−O4C	95.94(1)
Mn2−O8B	2.127(2)	O8B−Mn2−O4C	86.77(1)
Mn2−O4C	2.143(2)	O6−Mn2−N3	91.29(1)
Mn2−N3	2.197(3)	O8B−Mn2−N3	89.63(1)
Mn2−O1	2.312(2)	O4C−Mn2−N3	101.43(1)
Mn2−Ow	2.331(2)	O6−Mn2−O1	96.24(1)
O5A−Mn1−O7B	121.58(1)	O8B−Mn2−O1	80.77(9)
O5A−Mn1−N1	100.13(1)	O4C−Mn2−O1	161.06(9)
O7B−Mn1−N1	82.68(1)	N3−Mn2−O1	92.75(1)
O5A−Mn1−Ow	87.39(9)	O6−Mn2−Ow	90.79(9)
O7B−Mn1−Ow	82.57(9)	O8B−Mn2−Ow	87.88(9)
N1−Mn1−Ow	165.25(1)	O4C−Mn2−Ow	86.58(9)
O5A−Mn1−O2	87.64(9)	N3−Mn2−Ow	171.46(1)
O7B−Mn1−O2	150.72(9)	O1−Mn2−Ow	78.80(8)
N1−Mn1−O2	94.71(1)	Mn2−O1−Mn1	94.36(8)
Ow−Mn1−O2	98.29(9)	Mn1−Ow−Mn2	99.27(9)

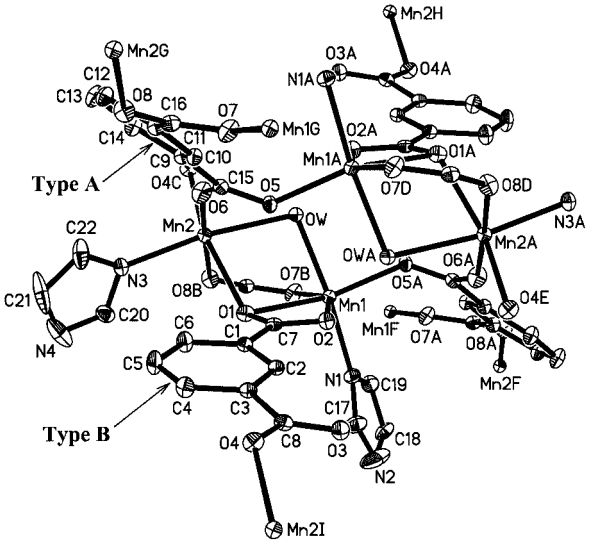

Figure 1. The local coordination environments of the Mn^{2+} centers in **1** (ellipsoids at 30% probability); types A and B indicate two independent ip ligands with different coordination modes

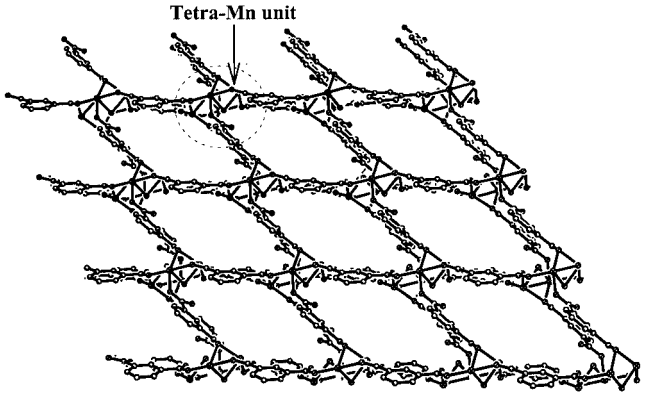

Figure 2. A view of the 2D layer showing rhombic grids in **1**, with the imidazole ligands excluded for clarity

 © 2004 Wiley-VCH Verlag GmbH & Co. KGaA, Weinheim

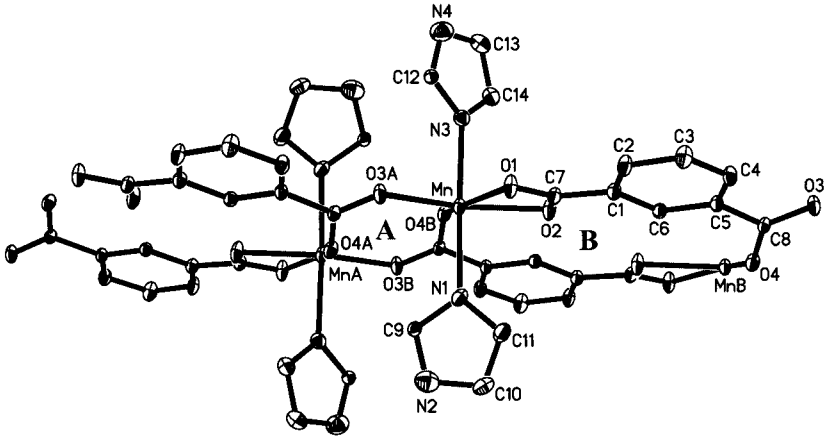

Figure 3. The local coordination environment of the Mn^{2+} center in **2** (ellipsoids at 30% probability); **A** and **B** denote the two subrings contained in the $[Mn_2(\mu\text{-}OCO)_2]$ and $[Mn_2(\mu\text{-}ip)_2]$ moieties, respectively

ter which is surrounded by ip ligands in bridging bis(bidentate) μ_4, bridging/chelating bidentate and monodentate μ_3 modes.

The structure of **2** differs from the structure of **1** since the coordination of water to Mn was completely precluded. Each ip ligand coordinates to three Mn atoms through two carboxylate groups in an interesting bridging and chelating bis(bidentate) μ_3 mode [Scheme 2 (c)] resulting in an infinite 1D polymer. Figure 3 illustrates the distorted octahedral geometry of the Mn^{2+} center (Table 2) with four O atoms from three ip ligands in the equatorial plane, and with two Him N atoms occupying the *trans*-axial positions. One pair of symmetry-related Mn atoms (Mn and MnA) with an interatomic distance of 4.480(2) Å is bridged by two carboxylate groups to produce a four-membered (two octahedra and two carboxylate groups) ring (**A**), whereas the other pair of symmetry-related Mn atoms (Mn and MnB) with an interatomic distance of 7.098(2) Å are bridged by two extended ip ligands to produce another four-membered (two octahedra and two isophthalate groups) ring (**B**). The two types of subrings, **A** and **B**, alternately interlock through Mn−O−C edge-sharing to produce a 1D parallel double chain of $[Mn(ip)]_n$ (with respect to the Mn atoms) in the *c* direction. Interestingly, the capping Him ligands are located at both sides of the double chain (Figure 4), thus preventing a 2D structure for **2**. It is reasonable to expect that a 2D double-layer framework will be created if the Him ligands are replaced by bidentate linear linkers such as 4,4′-bipyridine or (*E*)-1,2-bis(4-pyridyl)ethene.

Table 2. Selected bond lengths [Å] and angles [°] for **2** (symmetry codes: A: $x, y, z - 1$; B: $-x + 1, -y + 2, -z + 2$)

Mn−O3A	2.118(2)	O2−Mn−N1	87.99(1)
Mn−O4B	2.170(2)	O3A−Mn−N3	88.01(1)
Mn−O2	2.181(2)	O4A−Mn−N3	83.76(1)
Mn−N1	2.234(3)	O7B−Mn2−O3	85.96(18)
Mn−N3	2.244(3)	O2−Mn−N3	90.71(1)
Mn−O1	2.342(3)	N1−Mn−N3	171.70(1)
O3A−Mn−O4B	105.41(9)	O3A−Mn−O1	94.42(9)
O1−Mn1−O2A	118.66(2)	O4B−Mn−O1	158.00(1)
O3A−Mn−O2	152.19(1)	O2−Mn−O1	57.77(9)
O4B−Mn−O2	102.05(9)	N1−Mn−O1	98.62(11)
O3A−Mn−N1	96.95(1)	N3−Mn−O1	87.58(11)
O4B−Mn−N1	88.50(1)	N4−Mn2−O4	130.48(18)

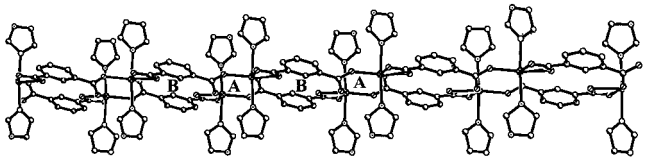

Figure 4. A view of the double-chain framework of **2** showing alternate interlocking of the two types of subrings (**A** and **B**) into parallel double chains of $[Mn(ip)]_n$

Complex **3** was obtained when (*E*)-1,2-bis(4-pyridyl)-ethene (dpe) was used instead of Him in the reaction. As expected, the structure of **3** is an infinite 2D double-layer polymer. The solvate dpe molecule is distorted within the crystal lattice but its presence was confirmed by elemental analysis. However, the neutral polymeric framework is clearly defined. As shown in Figure 5, the coordination mode of the ip ligand is identical to that found in **2**. Again, three ip ligands coordinate equatorially to one Mn atom through four carboxyl O atoms [Mn−O = 2.113(5)−2.329(5) Å] (Table 3), forming a 1D parallel double chain of $[Mn(ip)]_n$ almost the same as that contained in **2**. One remarkable structural feature of **3** is that the adjacent double chains of $[Mn(ip)]_n$ are cross-linked by linear μ-dpe ligands in the axial directions of the Mn octahedra [Mn−N1 = 2.263(5), Mn−N2C = 2.266(6) Å] giving a novel 2D double-layer framework with large open rectangular cavities (Figure 6). The intracavity Mn···Mn separation, bridged through the dpe, the ip and the μ_2-bridging carboxylate group, is 13.919 × 10.178 × 4.028 Å. These layers stack along the crystallographic *a* axis, generating large rectangular channels, which in turn accommodate solvate dpe and water molecules in the crystal lattice (Figure 7).

 © 2004 Wiley-VCH Verlag GmbH & Co. KGaA, Weinheim

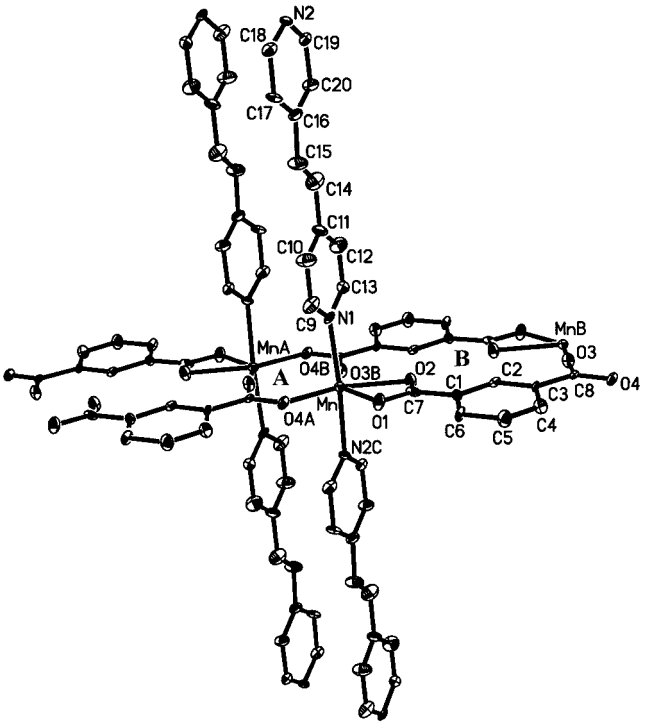

Figure 5. The local coordination environment of the Mn^{2+} center in **3** (ellipsoids at 25% probability); **A** and **B** denote the two subrings similarly to those found in **2**

Table 3. Selected bond lengths [Å] and angles [°] for **3** (symmetry codes: A: $-x + 3, -y - 2, -z - 1$; B: $x, y - 1, z$, C $x + 1, y, z - 1$)

Mn−O4A	2.113(5)	O2−Mn−N1	92.2(2)
Mn−O3B	2.145(5)	O4A−Mn−N2C	87.9(2)
Mn−O2	2.245(4)	O3B−Mn−N2C	87.7(2)
Mn−N1	2.263(5)	O2−Mn−N2C	92.0(2)
Mn−N2C	2.266(6)	N1−Mn−N2C	174.8(2)
Mn−O1	2.329(5)	O4A−Mn−O1	147.76(18)
O4A−Mn−O3B	123.72(19)	O3B−Mn−O1	88.36(17)
O4A−Mn−O2	91.06(18)	O2−Mn−O1	56.80(17)
O3B−Mn−O2	145.16(19)	N1−Mn−O1	94.3(2)
O4A−Mn−N1	89.1(2)	N2C−Mn−O1	90.5(2)
O3B−Mn−N1	90.5(2)		

When 2,2′-bipyridine (bpy) was used instead of Him, complex **4** was obtained. The X-ray structure determination reveals that **4** is a 1D chain-like polymer constructed from $[Mn_2(ip)_2(bpy)_2]$ units. As shown in Figure 8, two symmetry-unrelated ip ligands exhibit two types of coordination mode [shown in Scheme 2 (c) and (d)]. The latter is a bridging bidentate and monodentate μ_3 mode. Several differences in the coordination environments of the two crystallographically distinct Mn^{2+} atoms can be observed (Table 4). The Mn2 atom has a distorted octahedral geometry coordinated by two N and four O atoms, whereas the Mn1 atom is in distorted trigonal-bipyramidal geometry, being coordinated by two N and three O atoms. However, the Mn1···O6 distance of 2.528(5) Å indicates a

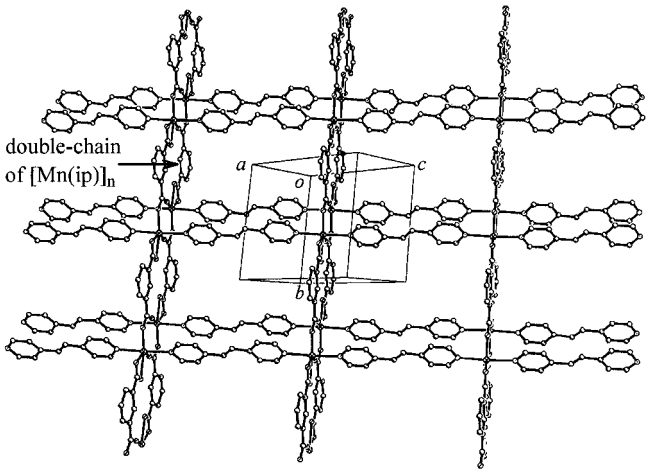

Figure 6. A view of the double-layer framework of **3** showing the μ-dpe bridges between the double-chain of $[Mn(ip)]_n$ and the formation of a rectangular cavity

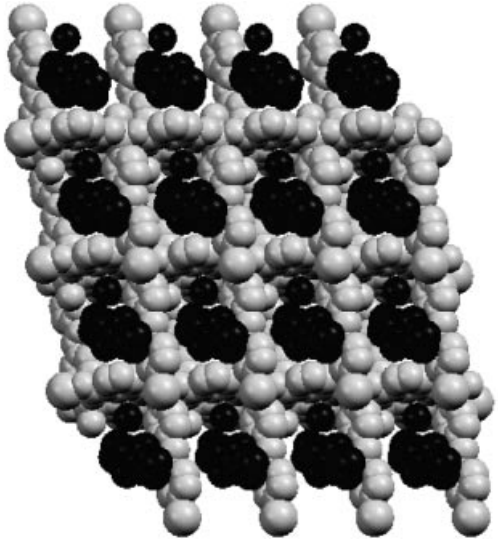

Figure 7. Space-filling diagram of **3** showing solvate molecules (black) contained in the rectangular channels in the *a* direction

weak interaction, which may be described as a semichelating coordination mode of the monodentate carboxylate group.[15] Similarly to **2** and **3**, every three ip ligands coordinate to one Mn atom to produce a 1D double chain of $[Mn_2(ip)_2]_n$ (Figure 9). It is worth noting that the $[Mn_2(ip)_2]_n$ motif, featuring a double-helix chain with a long pitch of about 10 Å, is more distorted than those of $[Mn(ip)]_n$ in **2** and **3** due to *cis* chelation of the rigid bpy ligand to an Mn center. The double chain also differs structurally from that reported previously in an isomeric complex containing an $[Mn(ip)(bpy)]_n$ core,[16] where all Mn atoms were symmetry-dependent, and all carboxyl O atoms were coordinated to Mn centers with all of the Mn−O bond lengths in the usual range [2.111(2)−2.284(3) Å]. Interestingly, the adjacent double-helical chains of **4** were intercalated in a zipper style to form 2D supramolecular layers through the π-π stacking interactions between the

 © 2004 Wiley-VCH Verlag GmbH & Co. KGaA, Weinheim

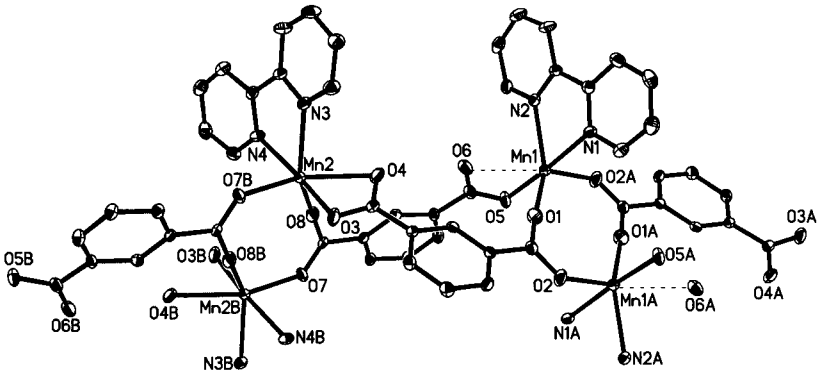

Figure 8. The local coordination environments of the Mn^{2+} centers in **4** (ellipsoids at 30% probability)

Table 4. Selected bond lengths [Å] and angles [°] for **4** (symmetry codes: A: $-x + 1, -y + 1, -z + 1$; B: $-x + 2, -y, -z + 2$)

Mn1−O1	2.101(5)	O2A−Mn1−N1	88.6(2)
Mn1−O2A	2.123(4)	O5−Mn1−N1	174.74(19)
Mn1−O5	2.145(5)	N2−Mn1−N1	72.24(19)
Mn1−N2	2.245(5)	O8−Mn2−O7B	113.05(18)
Mn1−N1	2.273(5)	O8−Mn2−O3	102.2(2)
Mn2−O8	2.094(5)	O7B−Mn2−O3	85.96(18)
Mn2−O7B	2.121(4)	O8−Mn2−N3	136.7(2)
Mn2−O3	2.224(5)	O7B−Mn2−N3	100.57(18)
Mn2−N3	2.276(5)	O3−Mn2−N3	106.8(2)
Mn2−N4	2.322(5)	O8−Mn2−N4	85.02(19)
Mn2−O4	2.393(5)	O7B−Mn2−N4	86.10(19)
O1−Mn1−O2A	118.66(19)	O3−Mn2−N4	170.89(19)
O1−Mn1−O5	96.8(2)	N3−Mn2−N4	70.36(18)
O2A−Mn1−O5	89.63(19)	O8−Mn2−O4	87.41(18)
O1−Mn1−N2	137.7(2)	O7B−Mn2−O4	140.72(18)
O2A−Mn1−N2	98.57(19)	O3−Mn2−O4	56.20(17)
O5−Mn1−N2	103.1(2)	N3−Mn2−O4	82.87(18)
O1−Mn1−N1	88.4(2)	N4−Mn2−O4	130.48(18)

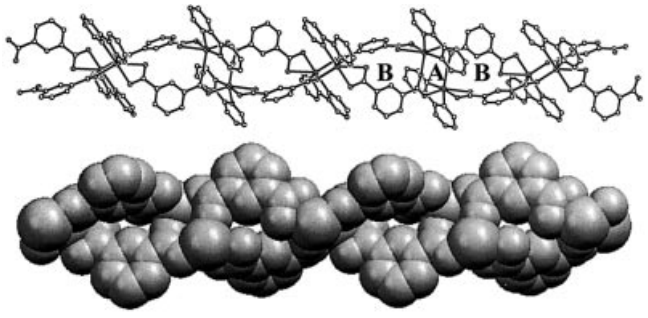

Figure 9. A view of the double-chain structure of **4** (top), **A** and **B** denote the two subrings within the $[Mn_2(\mu\text{-}OCO)_2]$ and $[Mn_2(\mu\text{-}ip)_2]$ moieties, respectively; space-filling diagram of the double-helix structure of **4** with the capping bpy ligands omitted (bottom)

bpy ring planes with face-to-face distances of ca. 3.55−3.68 Å (Figure 10).

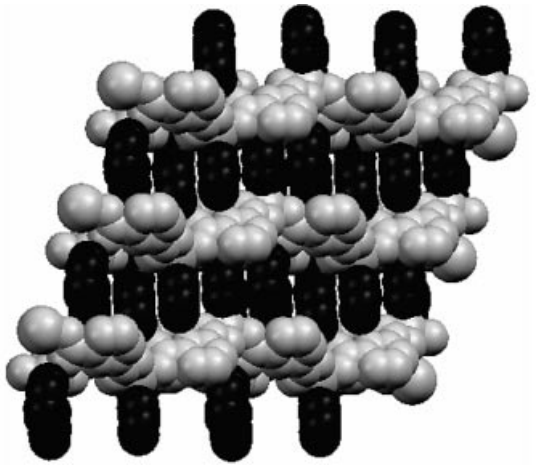

Figure 10. Space-filling diagram of a supramolecular layer in **4** showing the zipper-like intercalation of bpy ligands (black) from adjacent double-chains

Magnetic Susceptibility Study of Compounds

The magnetic behavior of complex **1** is plotted in Figure 11. At room temperature, the experimental effective magnetic moment (μ_{eff}) is 7.93μ_B, which is slightly smaller than the value of 8.37μ_B expected for two uncoupled Mn^{2+} ions (S1 = S2 = 5/2). Upon cooling from room temperature to 80 K, the value of μ_{eff} remains essentially constant, then gradually decreases to 4.24 μ_B at 5 K, indicative of an overall antiferromagnetic coupling between the Mn^{2+} centers.

As indicated in the structure description, **1** is a 2D double-layer polymer built from Mn_4 entities linked by ip ligands. No appropriate analytical expressions were available for calculation of the interaction parameters for this double-layer system. However, magnetic coupling between Mn tetramers through the extended ip bridging ligands and between the mixed water/carboxyl-bridged Mn dimers through the *syn*/*anti*-bridging carboxylate groups are all expected to be very weak. Thus, a simplified analysis of this coupling system can be accomplished by either of two approaches:

(i) The first approach neglects the Mn intertetramer magnetic interactions through the extended ip-bridging ligands. The observed magnetic behavior was simulated using modified Equation (1), which was obtained by combining the dimer model of $S = 5/2$ spins ($\boldsymbol{H} = -2J\boldsymbol{S}_1\boldsymbol{S}_2$)[17] with the Mn interdimeric interactions (zJ') under the molecular field approximation[18] [see inset of Figure 11 (a)].

 © 2004 Wiley-VCH Verlag GmbH & Co. KGaA, Weinheim

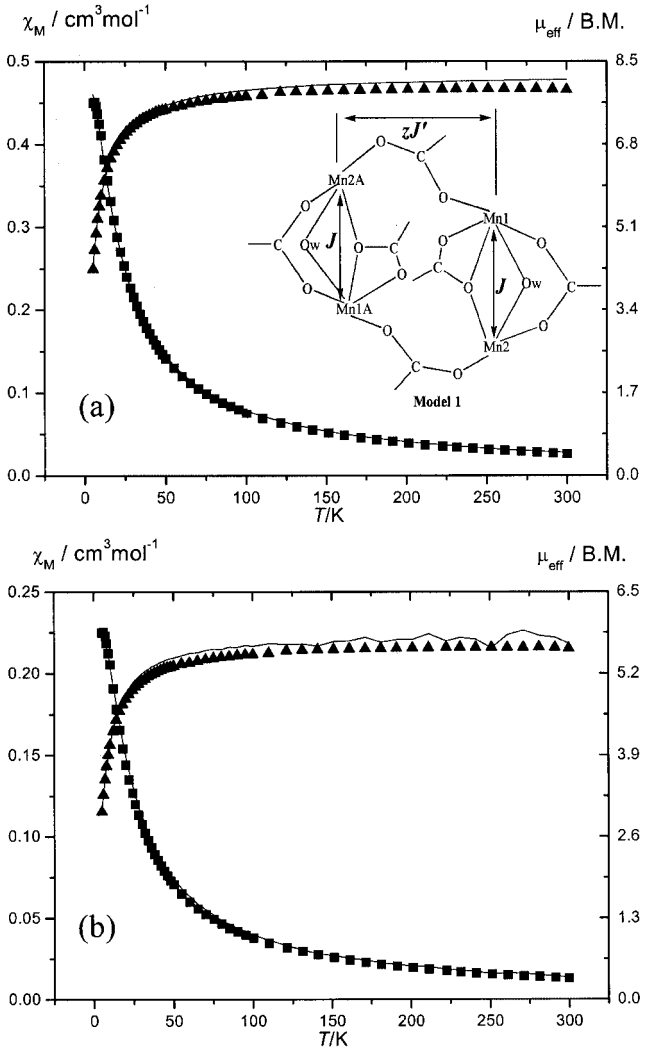

Figure 11. Experimental magnetic susceptibilities (χ_M, marked as square) and effective magnetic moment (μ_{eff}, marked as triangle) as a function of temperature for complex **1**; the solid lines represent the calculated values

$$\chi_M = \chi_{bi}/\left(1 - zJ'\chi_{bi}/Ng^2\beta^2\right)$$

where

$$\chi_{bi} = \frac{2Ng^2\beta^2}{kT}\left[\frac{55+30\exp(-10J/kT)+14\exp(-18J/kT)+5\exp(-24J/kT)+\exp(-28J/kT)}{11+9\exp(-10J/kT)+7\exp(-18J/kT)+5\exp(-24J/kT)+3\exp(-28J/kT)+\exp(-30J/kT)}\right] \quad (1)$$

A best-fit result with parameters $J = -2.16(8)$ cm^{-1}, $zJ' = -0.01(4)$ cm^{-1}, $g = 1.96(9)$, and the agreement factor R [defined as $R = \Sigma[(\chi_M T)_{calcd.} - (\chi_M T)_{obsd.}]^2/[\Sigma(\chi_M T)_{obsd.}]^2 = 1.73 \times 10^{-4}$ was obtained over the temperature range studied.

The small negative zJ' value agrees well with the notion that the *syn*/*anti*-carboxylate bridge always mediates very weak magnetic couplings due to the expanded metallic core and the mismatch in the orientation of magnetic orbitals.[19] The small zJ'/J ratio (ca. 0.006) validates the use of the mean molecular field approximation model.[20]

(ii) In the second approach the magnetic interactions through the *syn*/*anti*-carboxylate bridges were ignored, and the magnetic behavior of **1** was simulated using the analytical expression according to Equation (2) based on the homonuclear alternating chain structure,[21] where $u_i = \coth[J_iS(S+1)/kT] - kT/[J_iS(S+1)]$ $(i = 1, 2)$.

$$\chi = \frac{Ng^2S(S+1)\mu_B^2}{3kT}\left(\frac{1+u_1+u_2+u_1u_2}{1-u_1u_2}\right) \quad (2)$$

The best fit gives the parameters $J_1 = -1.48(4)$ cm^{-1}, $J_2 = -0.01(9)$ cm^{-1}, $g = 1.96(5)$ and $R = 7.99 \times 10^{-4}$ over the temperature range studied.

Although the latter simulation is mathematically logical, the theoretical curve is not smooth in the high-temperature range (100−300 K), which can be seen from Figure 11 (b). On the basis of this, the result derived from the first simulation seems to be more exact for compound **1**.

Complexes **2**, **3** and **4** have similar magnetic properties and the plots of the effective magnetic moment (μ_{eff}) vs. T are shown in Figure 12. At room temperature, the values of μ_{eff} were 5.90 μ_B, 5.88 μ_B and 5.83 μ_B per one Mn^{2+} ion for **2**, **3** and **4**, respectively. These values are close to, or slightly lower than, the value of 5.91 μ_B expected for an "isolated" Mn^{2+} ion ($S = 5/2$). As the temperature is lowered, the μ_{eff} values remain essentially constant in the regions 300−60 K, 300−80 K, and 300−100 K for **2**, **3**, and **4**, respectively. When the temperature is further lowered, the μ_{eff} values decrease continuously down to 4.15 μ_B, 3.54 μ_B and 3.67 μ_B at 5 K for **2**, **3** and **4**, respectively, indicating overall antiferromagnetic couplings between Mn^{2+} centers for the three complexes. Considering that the magnetic interaction between two Mn centers separated by > 14 Å through μ-dpe in **3** is very weak, the analytical expression according to

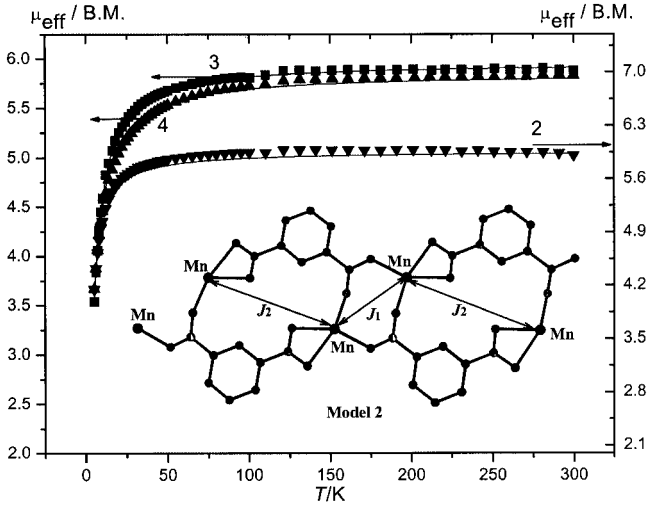

Figure 12. Experimental effective magnetic moment (μ_{eff}) as a function of temperature for complexes **2**−**4**; the solid lines represent the calculated values

 © 2004 Wiley-VCH Verlag GmbH & Co. KGaA, Weinheim

Equation (2) for the homonuclear alternating chain structure (see inset of Figure 12) can be adopted to simulate the magnetic behavior of the three complexes.

The least-squares fitting of the experimental data over the full temperature range led to $J_1 = -0.71(4)$ cm^{-1}, $J_2 = -0.02(2)$ cm^{-1}, $g = 2.02(2)$ and the agreement factor $R = 2.10 \times 10^{-4}$ for **2**, $J_1 = -1.01(3)$ cm^{-1}, $J_2 = -0.09(1)$ cm^{-1}, $g = 2.01(1)$ and $R = 6.0 \times 10^{-5}$ for **3**, and $J_1 = -0.80(1)$ cm^{-1}, $J_2 = -0.46(2)$ cm^{-1}, $g = 1.98(2)$ and $R = 8.1 \times 10^{-4}$ for **4**.

All these negative J_1 values fall in the range (-0.7 to -1.84 cm^{-1}) expected for doubly bridged Mn^{2+} carboxylate compounds,[22] and the differences in them [J_1(**3**) > J_1(**4**) > J_1(**2**)] agree well with the inter-Mn distance (4.028 Å for **3**, 4.322 Å for **4** and 4.480 Å for **2**). Shorter separation of paramagnetic centers allows more effective magnetic coupling. For all of the complexes, the smaller negative J_2 value can be attributed to a very weak antiferromagnetic interaction through the extended bridging ip ligand pathway. Its low magnitude can be associated with the excessive span (> 7 Å) of the ip ligand bridge, and is logically smaller than the J_1 value mediated by double carboxylate bridges presenting short pathways.

Conclusion

In this paper, four low-dimensional coordination polymers **1**−**4** have been synthesized by treatment of an Mn^{2+} salt with isophthalic acid and with the participation of selected ancillary ligands − Him, dpe and bpy − under different crystallization conditions. The evolution of structure of these compounds was as expected. Under ambient conditions, the spontaneous assembly of ip and Mn^{2+} salt with the participation of Him ligand yielded the novel 2D double-layer framework **1**. Hydrothermal conditions inhibited coordination of water to the metal atom, as expected, and led to the formation of **2**, which consists of an interesting double-chain framework. Polymer **3**, with a 2D double-layer framework, was rationally induced by the use of secondary μ-dpe ligands as axial connectors of Mn octahedra in double chains of $[Mn(ip)]_n$. The parallel $[Mn(ip)]_n$ double-chain moiety was further modified to the helical double-chain framework in **4** by introduction of the steric constraint caused by *cis* chelation of the rigid bpy ligand. The results show that metal-organic coordination polymers with a specific architecture may be elaborated by the judicious choice of the organic spacer and ancillary ligand, along with careful manipulation of various reaction conditions such as the reaction temperature and solvent. The magnetic properties of these compounds revealed overall weak antiferromagnetic exchange interactions between Mn^{2+} ions through the bridging carboxylate group of the ip ligand or through the extended ip ligand bridge. The coupling interactions, as well as the differences in them, were explained briefly according to the structural parameters and their variations.

Experimental Section

General Remarks: All chemicals were of reagent grade and used as received. Elemental analyses were performed with a Vario EL-III element analyzer. IR spectra of KBr pellets (4000−400 cm^{-1}) were recorded with an FTS-40 spectrophotometer. Variable-temperature magnetic susceptibilities were measured over the temperature range 5−300 K on crystalline samples mounted in a capsule using a model CF-1 superconducting magnetometer. Diamagnetic corrections were estimated with Pascal's constants for all the complexes: -2.50×10^{-4} c.g.s. for **1**, -1.68×10^{-4} c.g.s. for **2**, -2.56×10^{-4} c.g.s. for **3** and -3.55×10^{-4} c.g.s. for **4**.

Synthesis of $[Mn_4(ip)_4(H_2O)_2(Him)_4]_n$ (1): Solid $Mn(OAc)_2{\cdot}4H_2O$ (0.50 g, 2 mmol) was added to an H_2O/MeOH (ca. 4:1, v/v, 20 mL) solvent mixture containing isophthalic acid (H_2ip) (0.34 g, 2 mmol), KOH (0.23 g, 4 mmol) and imidazole (Him) (0.14 g, 2 mmol) with continuous stirring. The solution was stirred at room temperature for 2 h, then filtered. The filtrate was left in a $CaCl_2$ desiccator for approximately one month to produce colorless crystals of **1** in 68% yield (0.41 g). $C_{44}H_{36}Mn_4N_8O_{18}$ (1184.57): calcd. C 44.61, H 3.06, N 9.46; found C 44.69, H 3.14, N 9.44. IR (KBr): $\tilde{\nu}$ = 3320 (br., s), 3080 (m), 1612 (s), 1566 (s), 1520 (m), 1477 (m), 1448 (s), 1394 (s), 1325 (m), 1271(w), 1255 (w), 1157 (w), 1126 (w), 1092 (w), 1070 (m), 1061(s), 935 (w), 906 (w), 856 (w), 837 (w), 820 (m), 744 (s), 712 (s), 704 (s), 658 (s), 619 (m), 538 (w), 459 (w), 434 (m) cm^{-1}.

Synthesis of $[Mn(ip)(Him)_2]_n$ (2): Complex **1** (1.2 g, 1 mmol) was dissolved in an H_2O/MeOH (ca. 4:1, v/v, 15 mL) solvent mixture and was heated at 140 °C in a 20-mL sealed Teflon-lined stainless vessel for 4 d, then cooled to room temperature over a period of 5 h. This gave colorless crystals of **2** in 54% yield (0.77 g). $C_{14}H_{12}MnN_4O_4$ (355.22): calcd. C 47.34, H 3.41, N 15.77; found C 47.37, H 3.49, N 15.72. IR (KBr): $\tilde{\nu}$ = 3064 (m), 1605 (s), 1557 (s), 1541 (s), 1477 (m), 1446 (s), 1444 (s), 1390 (s), 1352 (m), 1311 (w), 1277 (w), 1250 (w), 1178 (w), 1157 (m), 1134 (m), 1119 (s), 1076 (w), 1057 (s), 1041 (s), 939 (m), 908 (m), 877 (m), 827 (w), 816 (w), 780 (s), 746 (s), 715 (s), 658 (w), 611 (m), 573 (w), 532 (w), 451 (w), 432 (m), 408 (m) cm^{-1}.

Synthesis of $[Mn(ip)(dpe)]_n{\cdot}0.5ndpe\cdot nH_2$O (3): $Mn(OAc)_2{\cdot}4H_2O$ (0.25 g, 1 mmol), dissolved in water (10 mL), was mixed with an H_2O/EtOH (ca. 1:1, v/v, 10 mL) solvent mixture containing H_2ip (0.17 g, 1 mmol), KOH (0.11 g, 2 mmol) and dpe (0.28 g, 1.5 mmol) leading to the immediate precipitation of a yellow powder which was filtered. Small yellow crystals of **3**, suitable for X-ray diffraction, were grown from the filtrate upon standing at room temperature for three weeks. Yield: 11% (0.06 g). $C_{26}H_{21}MnN_3O_5$ (510.40): calcd. C 61.18, H 4.15, N 8.23; found C 61.25, H 4.16, N 8.21. IR (KBr): $\tilde{\nu}$ = 3442 (br., s), 3037 (m), 1608 (s), 1568 (s), 1547 (s), 1479 (m), 1429 (s), 1394 (s), 1254 (w), 1217 (m), 1105 (w), 1074 (w), 1014 (s), 972 (m), 912 (w), 827 (s), 746 (s), 719 (s), 660 (w), 552 (s), 509 (w), 424 (m) cm^{-1}.

Synthesis of $[Mn_2(ip)_2(bpy)_2]_n$ (4): 2,2′-bipyridine (bpy) (0.31 g, 2 mmol) in DMF (10 mL) was slowly added to a solution of $Mn(OAc)_2{\cdot}4H_2O$ (0.50 g, 2 mmol), H_2ip (0.34 g, 2 mmol) and NaOH (0.16 g, 4 mmol) in water (25 mL) with continuous stirring, resulting in a yellow suspension. The suspension was transferred into a 50-mL round-bottomed flask and heated to reflux for about a week during which time yellow crystals of **4** deposited in 17% yield (0.13 g). $C_{36}H_{24}Mn_2N_4O_8$ (750.47): calcd. C 57.62, H 3.22, N 7.47; found C 57.69, H 3.17, N 7.38. IR (KBr): $\tilde{\nu}$ = 3053 (m), 1610 (s), 1572 (s), 1556 (s), 1473 (m), 1439 (s), 1394 (s), 1313 (w), 1244

 © 2004 Wiley-VCH Verlag GmbH & Co. KGaA, Weinheim

Table 5. Crystallographic data summary for complexes **1**−**4**

	1	**2**	**3**	**4**
Empirical formula	$C_{44}H_{36}Mn_4N_8O_{18}$	$C_{14}H_{12}MnN_4O_4$	$C_{26}H_{21}MnN_3O_5$	$C_{36}H_{24}Mn_2N_4O_8$
Formular mass	1184.57	355.22	510.40	750.47
Space group	$P\bar{1}$	$P\bar{1}$	$P\bar{1}$	$P\bar{1}$
a [Å]	10.4583(4)	8.5166(3)	8.9571(3)	9.4704(2)
b [Å]	10.7926(5)	9.2897(3)	10.1785(5)	10.3376(3)
c [Å]	12.4562(5)	10.2230(3)	13.9174(7)	18.5433(6)
α [°]	91.296(1)	73.463(2)	77.395(2)	74.079(1)
β [°]	109.401(1)	74.541(1)	71.240(2)	86.539(2)
γ [°]	116.898(1)	79.782(1)	77.657(2)	63.571(1)
V [Å^3]	1157.40(8)	742.78(4)	1158.24(9)	1559.30(8)
Z	1	2	2	2
T [K]	293(2)	293(2)	293(2)	293(2)
$D_{calcd.}$ [g cm^{-3}]	1.700	1.588	1.463	1.598
μ [mm^{-1}]	1.153	0.915	0.614	0.873
R[a]/wR[b]	0.0387/0.0935	0.0468/0.1308	0.0878/0.1928	0.0782/0.1484

[a] $R = \|\|F_o| - |F_c\|\|/|F_o|$. [b] $Rw = [w(|F_o| - |F_c|)^2/wF_o^2]^{1/2}$.

(m), 1155 (w), 1103 (w), 1076 (w), 1059 (w), 1016 (m), 827 (w), 756 (s), 737 (m), 715 (s), 687 (w), 650 (w), 627 (w), 521 (w), 415 (m) cm^{-1}.

X-ray Crystallographic Study: Intensity data were collected at 293 K with a Siemens SMART CCD diffractometer equipped with a graphite-monochromated Mo-K_α radiation source (λ = 0.71073 Å). Data were corrected for LP factors and empirical absorption correction was applied. Structures were solved by direct methods and refined by full-matrix least-squares refinement on F^2 using the SHELXTL-97 program package.[23] All non-hydrogen atoms were refined anisotropically, and hydrogen atoms were introduced geometrically with the exception of the water hydrogen atoms which were located from the difference Fourier syntheses. The free solvate dpe molecule in **3** was distorted in the lattice because of relatively poor crystal quality and so no attempt was made to refine the hydrogen atoms contained in it. Crystallographic data of **1**−**4** are outlined in Table 5. CCDC-220080 to -220083 contain the supplementary crystallographic data of **1**−**4** for this paper. These data can be obtained free of charge at www.ccdc.cam.ac.uk/conts/retrieving.html [or from the Cambridge Crystallographic Data Centre, 12 Union Road, Cambridge CB2 1EZ, UK; Fax: (internat.) + 44-1223-336-033; E-mail: deposit@ccdc.cam.ac.uk].

Acknowledgments

This work was supported by the NNSFC (No. 30170229), the State Key Basic Research and Development Plan of China (G1998010100, 001CB108906), and the Special Project of the Ministry of Science and Technology of China (2001CCA02500).

[1] [1a] *Magnetism: Molecules to Materials* (Eds.: J. S. Miller, M. Drillon), Wiley-VCH, Weinheim, **2002**, vol. 3. [1b] D. Gatteschi, O. Kahn, J. S. Miller, F. Palacio, *Magnetic Molecular Materials*, NATO ASI Series, Series E, Kluwer Academic Publishers, Dordrecht, The Netherlands, **1991**, vol. 198.

[2] [2a] H. O. Stumpf, L. Ouahab, Y. Pei, D. Grandjean, O. Kahn, *Science* **1993**, *261*, 447−449. [2b] S. Konar, P. S. Mukherjee, E. Zangrando, F. Lloret, R. N. Chaudhuri, *Angew. Chem. Int. Ed.* **2002**, *41*, 1561−1563. [2c] H. Miyasaka, N. Matsumoto, H. Okawa, N. Re, E. Gallo, C. Floriani, *J. Am. Chem. Soc.* **1996**, *118*, 981−994. [2d] E. W. Lee, Y. Kim, D.-Y. Jung, *Inorg. Chem.* **2002**, *41*, 501−506. [2e] J. S. Miller, A. J. Epstein, *Angew. Chem. Int. Ed. Engl.* **1994**, *33*, 385−415. [2f] J. Kim, J. M. Lim, Y. K. Choi, Y. K. Do, *Angew. Chem. Int. Ed. Engl.* **1996**, *35*, 998−1000. [2g] N. Guillou, S. Pastre, C. Livage, G. Férey, *Chem. Commun.* **2002**, 2358−2359.

[3] [3a] C. T. Chen, K. S. Suslick, *Coord. Chem. Rev.* **1993**, *128*, 293−322. [3b] S. D. Cox, T. E. Gier, G. D. Stucky, J. Bierlein, *J. Am. Chem. Soc.* **1998**, *110*, 2986−2987. [3c] M. Monfort, I. Resino, J. Ribas, X. Solans, M. Font-Bardia, P. Rabu, M. Drillon, *Inorg. Chem.* **2000**, *39*, 2572−2576. [3d] G. S. Matouzenko, G. Molnar, N. Brefuel, M. Perrin, A. Bousseksou, S. A. Borshch, *Chem. Mater.* **2003**, *15*, 550−556. [3e] *Extended Linear chain compounds* (Ed.: J. S. Miller), Plenum, New York, **1982**, vol. 3.

[4] [4a] J. Cano, G. D. Munno, J. L. Sanz, R. Ruiz, J. Faus, F. Lloret, M. Julve, A. Caneschi, *J. Chem. Soc., Dalton Trans.* **1997**, 1915−1523, and references cited therein. [4b] D.-F. Sun, R. Cao, Y.-C. Liang, Q. Shi, W.-P. Su, M.-C. Hong, *J. Chem. Soc., Dalton Trans.* **2001**, 2335−2340. [4c] C. S. Hong, Y. Do, *Inorg. Chem.* **1997**, *36*, 5684−5685. [4d] J. Cano, G. Demunno, J. Sanz, R. Ruiz, F. Lloret, J. Faus, M. Julve, *J. Chem. Soc., Dalton Trans.* **1994**, 3465−3469. [4e] D.-F. Xiang, X.-S. Tan, Q.-W. Hang, W.-X. Tang, B.-M. Wu, T. C. W. Mak, *Inorg. Chim. Acta* **1998**, *277*, 21−25. [4f] L.-C. Li, D.-Z. Liao, Z.-H. Jiang, S.-P. Yan, *Inorg. Chem.* **2002**, *41*, 421−424. [4g] K. S. Bürger, P. Chaudhuri, K. Wieghardt, B. Nuber, *Chem. Eur. J.* **1995**, *1*, 583−593.

[5] [5a] X.-S. Tan, J. Sun, D.-F. Xiang, W.-X. Tang, *Inorg. Chim. Acta* **1997**, *255*, 157−161. [5b] X.-S. Tan, D.-F. Xiang, W.-X. Tang, K.-B. Yu, *Polyhedron* **1997**, *16*, 1411−1415. [5c] H.-X. Zhang, B.-S. Kang, A.-W. Xu, Z.-N. Chen, Z.-Y. Zhou, A. S. C. Chan, K.-B. Yu, C. Chen, *J. Chem. Soc., Dalton Trans.* **2001**, 2559−2566.

[6] [6a] E. K. Shakhatreh, E. G. Bakalbassis, I. Brudgam, H. Hartl, J. Mrozinski, C. A. Tsipis, *Inorg. Chem.* **1991**, *30*, 2801−2806. [6b] Z.-N. Chen, H.-X. Zhang, K.-B. Yu, B.-S. Kang, H. Cai, C.-Y. Su, T.-W. Wang, Z.-L. Lu, *Inorg. Chem.* **1998**, *37*, 4775−4781.

[7] [7a] K. Wieghardt, *Angew. Chem. Int. Ed. Engl.* **1989**, *28*, 1153−1172. [7b] N. A. Law, M. T. Caudle, V. L. Pecoraro, *Adv. Inorg. Chem.* **1999**, *46*, 305−440.

[8] [8a] C.-B. Ma, C.-N. Chen, Q.-T. Liu, F. Chen, D.-Z. Liao, L.-C. Li, L.-C. Sun, *Eur. J. Inorg. Chem.* **2003**, 2872−2879. [8b] C.-B. Ma, C.-N. Chen, Q.-T. Liu, D.-Z. Liao, L.-C. Li, L.-C. Sun, *New J. Chem.* **2003**, *27*, 890−894. [8c] C.-B. Ma, C.-N. Chen, Q.-T. Liu, D.-Z. Liao, L.-C. Li, *Eur. J. Inorg. Chem.* **2003**, 1227−1231.

 © 2004 Wiley-VCH Verlag GmbH & Co. KGaA, Weinheim

[9] [9a] M. Devereux, M. McCann, V. Leon, M. Geraghty, V. McKee, J. Wikaira, *Met.-Based Drugs* **2000**, *7*, 275−278. [9b] S. A. Bourne, J. J. Lu, A. Mondal, B. Moulton, M. J. Zaworotko, *Angew. Chem. Int. Ed.* **2001**, *40*, 2111−2113. [9c] S. A. Bourne, A. Mondal, M. J. Zaworotko, *Cryst. Eng.* **2001**, *4*, 25−36.

[10] [10a] Y. Kim, D.-Y. Jung, *Inorg. Chem.* **2000**, *39*, 1470−1475. [10b] S. O. H. Gutschke, M. Molinier, A. K. Powell, R. E. P. Winpenny, P. T. Wood, *Chem. Commun.* **1996**, 823−824. [10c] O. M. Yaghi, H. Li, T. L. Groy, *J. Am. Chem. Soc.* **1996**, *118*, 9096−9097. [10d] R. Kuhlman, G. L. Schimek, J. W. Kolis, *Inorg. Chem.* **1999**, *38*, 194−196. [10e] C. Livage, C. Egger, G. Ferey, *Chem. Mater.* **1999**, *11*, 1546−1550.

[11] [11a] G. B. Deacon, R. J. Philips, *Coord. Chem. Rev.* **1980**, *33*, 227−250. [11b] K. Nakamoto, *Infrared and Raman Spectra of Inorganic and Coordination Compounds*, John Wiley & Sons, New York, **1986**.

[12] [12a] S.-B. Yu, S. J. Lippard, I. Shweky, A. Bino, *Inorg. Chem.* **1992**, *31*, 3502−3504. [12b] A. Caneschi, F. Ferraro, D. Gatteschi, M. C. Melandri, P. Rey, R. Sessoli, *Angew. Chem. Int. Ed. Engl.* **1989**, *28*, 1365−1367.

[13] [13a] H. H. Thorp, *Inorg. Chem.* **1992**, *31*, 1585−1588. [13b] I. D. Brown, D. Altermatt, *Acta Crystallogr., Sect. B* **1985**, *41*, 244−247.

[14] [14a] T. Lis, *Acta Crystallogr., Sect. B* **1977**, *33*, 2964−2967. [14b] B.-H. Ye, T. Mak, I. D. Williams, X.-Y. Li, *Chem. Commun.* **1997**, 1813−1814. [14c] B. Paluchowska, J. K. Maurin, J. Leciejewicz, *J. Coord. Chem.* **2000**, *51*, 335−347.

[15] [15a] G. Guilera, J. W. Steed, *Chem. Commun.* **1999**, 1563−1564. [15b] J. Tao, M.-L. Tong, X.-M. Chen, *J. Chem. Soc., Dalton Trans.* **2000**, 3669−3674.

[16] M.-L. Hu, D.-J. Xu, D.-P. Cheng, *J. Coord. Chem.* **2002**, *55*, 11−16.

[17] O. Kahn, *Molecular Magnetism*, VCH Publishers Inc., New York, **1993**.

[18] [18a] R. L. Carlin, *Magnetochemistry*, Spinger-Verlag, Berlin, **1986**. [18b]B. E. Myers, L. Berger, S. A. Friedberg, *J. Appl. Phys.* **1969**, *40*, 1149−1151.

[19] [19a] T. K. Maji, S. Sain, G. Mostafa, T.-H. Lu, J. Ribas, M. Monfort, N. R. Chaudhuri, *Inorg. Chem.* **2003**, *42*, 709−716. [19b] D. K. Towle, S. K. Hoffmann, W. E. Hatfield, P. Singh, P. Chaudhuri, *Inorg. Chem.* **1988**, *27*, 394−399. [19c] E. Colacio, J. M. Dominguez-Vera, J.-P. Costés, R. Kivekäs, J. P. Laurent, J. Ruiz, M. Sundberg, *Inorg. Chem.* **1992**, *31*, 774−778. [19d] C. Policar, F. Lambert, M. Cesario, I. Morgenstern-Badarau, *Eur. J. Inorg. Chem.* **1999**, 2201−2207. [19e] R. L. Carlin, K. Kopinga, O. Kahn, M. Verdaguer, *Inorg. Chem.* **1985**, *25*, 1786−1789.

[20] [20a] D. K. Towle, S. K. Hoffmann, W. E. Hatfield, P. Singh, P. Chaudhuri, *Inorg. Chem.* **1988**, *27*, 394−399. [20b] B. Chiari, A. Cinti, L. David, F. Ferraro, D. Gatteschi, O. Piovesana, P. F. Zanazzi, *Inorg. Chem.* **1996**, *35*, 7413−7418.

[21] R. Cortés, M. Drillon, X. Solans, L. Lezama, T. Rojo, *Inorg. Chem.* **1997**, *36*, 677−683.

[22] [22a] P. S. Mukherjee, S. Konar, E. Zangrando, T. Mallah, J. Ribas, N. R. Chaudhuri, *Inorg. Chem.* **2003**, *42*, 2695−2703. [22b] J. Cano, G. D. Munno, J. L. Sanz, R. Ruiz, J. Faus, F. Lloret, M. Julve, A. Caneschi, *J. Chem. Soc., Dalton Trans.* **1997**, 1915−1923. [22c] H. Oshio, E. Ino, I. Mogi, T. Ito, *Inorg. Chem.* **1993**, *32*, 5697−5703. [22d] W.-B. Lin, M. E. Chapman, Z.-Y. Wang, G. T. Yee, *Inorg. Chem.* **2000**, *39*, 4169−4173. [22e] B. Albela, M. Corbella, J. Ribas, I. Castro, J. Sletten, H. Stoeckli-Evans, *Inorg. Chem.* **1998**, *37*, 788−798. [22f] G. Fernández, M. Corbella, J. Mahia, M. A. Maestro, *Eur. J. Inorg. Chem.* **2002**, 2502−2510, and references cited therein.

[23] G. M. Sheldrick, *SHELXL-97*, University of Göttingen, **1997**.

Received February 6, 2004
Early View Article
Published Online June 11, 2004

 © 2004 Wiley-VCH Verlag GmbH & Co. KGaA, Weinheim

NMR Evidence for Major Groove Binding of Both Λ- and Δ-[Ru(bpy)$_2$(pqx)](PF$_6$)$_2$ to the Oligonucleotide d(CGCGAATTCGCG)$_2$

Achilleas Garoufis,*[a] Gerasimos Malandrinos,[a] and Nick Hadjiliadis*[a]

Keywords: Major groove / N ligands / NMR spectroscopy / Oligonucleotides / Ruthenium

The enantiomeric complexes Λ- and Δ-[Ru(bpy)$_2$(pqx)](PF$_6$)$_2$ [pqx = 2-(2′-pyridyl)quinoxaline] were synthesized and characterized by various spectroscopic techniques. Their binding properties to the oligonucleotide duplex d(CGCGAATTCGCG)$_2$ were subsequently studied by NMR spectroscopy. 1D and 2D NMR techniques provided evidence for major-groove binding of both enantiomers with the oligonucleotide. The Δ-[Ru(bpy)$_2$(pqx)](PF$_6$)$_2$ enantiomer binds more deeply enantiomer to the oligonucleotide than the Λone. The quinoxalinic moiety of the pqx ligand faces the major groove in the Δ complex and is oriented at the external side of the adduct in the Λ complex. Both complexes show some affinity for the T8C9 base sequence of the dodecanucleotide helix.
(© Wiley-VCH Verlag GmbH & Co. KGaA, 69451 Weinheim, Germany, 2004)

Indroduction

The binding properties of transition metal tris-chelate complexes with DNA have been extensively studied in recent years.[1,2] One of the pioneering works was the report by Barton et al. pointing out the remarkable difference in the binding strength of the enantiomers of [Zn(phen)$_3$]$^{2+}$ with DNA.[3] The interactions between CT-DNA and the enantiomeric ruthenium complexes Λ- and Δ-[Ru(phen)$_3$]$^{2+}$ have been studied by several methods, with controversial conclusions. Several studies led to the conclusion that the Δ-isomer either intercalates between the base pairs,[4−7] or is partially inserted,[8−10] or it binds to DNA in various ways[11,12] (e.g. in the major[8,10] or in the minor groove[13,14]). On the other hand Λ-[Ru(phen)$_3$]$^{2+}$ binds to DNA either by electrostatic forces,[4,5] or surface-bound interactions,[6,12] and with weak binding in the minor[13,14] or the major groove.[8,10] 2,2′-Bipyridine has been used as a ligand less often than 1,10-phenanthroline in tris-chelate complexes of Ru^{II} in studies of interactions with DNA due to the lower affinity of this ligand to bind to the DNA helix. Based on photophysical results, it has been suggested that Δ-[Ru(bpy)$_3$]$^{2+}$ binds weakly with DNA either by intercalation or electrostatic interactions.[4,5,15] It has also been reported that no enantiomeric discrimination is apparent between the binding of Λ- and Δ-[Ru(bpy)$_3$]$^{2+}$ with DNA.[16]

The interaction of the mixed-ligand complex [Ru(bpy)$_2$(phen)]$^{2+}$ with DNA has been studied by linear dichroism spectroscopy with the aim of investigating the role of each ligand involved in the complex. The results indicate that the complex shows a similar binding geometry to [Ru(phen)$_3$]$^{2+}$ in which one phen ligand faces the DNA base pairs, almost as if it were intercalated nearly parallel to them.[9] A similar mixed-ligand complex, [Ru(bpy)$_2$(ppz)]$^{2+}$ (ppz = 4,7-phenanthrolino[6,5-*b*]pyrazine, a non-classical intercalative ligand), which is longer than phen by a six-membered fused ring, shows that both Λ- and Δ-enantiomers bind in the major groove of DNA by partial intercalation of the ppz ligand. The bpy ligands are not capable of inducing intercalation and the enantioselectivity is maintained by the different interactions of the Δ- and Λ-enantiomers with the DNA major groove.[17] In an attempt to contribute to the better understanding of how these mixed-ligand complexes bind to DNA, we have synthesized, characterized and studied the binding properties of the enantiomeric complexes Λ- and Δ-[Ru(bpy)$_2$(pqx)]$^{2+}$ [pqx = 2-(2′-pyridyl)quinoxaline], to the oligonucleotide duplex d(5′-CGCGAATTCGCG-3′)$_2$ mainly by NMR spectroscopy. The ligand pqx was chosen based on the following criteria: (i) it has an asymmetric nature that could be extended to the two bpy ligands of the complex, making them magnetically distinct; (ii) it is more similar to the structure of bpy than phen, even though it contains a six-membered fused aromatic ring on one side of the molecule.

[a] Laboratory of Inorganic Chemistry, Dept. Chemistry, University of Ioannina,
Ioannina 45210 Greece
Fax: +30-265-104-4831
E-mail nhadjis@cc.uoi.gr

 © 2004 Wiley-VCH Verlag GmbH & Co. KGaA, Weinheim **DOI: 10.1002/ejic.200400270**

Results and Discussion

Synthesis, Characterization and Solution Structure of the Enantiomers

rac-[Ru(bpy)$_2$(pqx)](PF$_6$)$_2$ has been synthesized previously by a one-step reaction between *cis*-[RuCl$_2$(bpy)$_2$] and pqx,[18] although the enantiomeric resolution by chromatographic techniques was unsuccessful. This is the reason our synthesis of the enantiomers was based on the optically pure precursors Δ- and Λ-[Ru(bpy)$_2$(py)$_2$]A·12H$_2$O (A = *O*,*O*′-dibenzoyltartaric acid), by replacing the two pyridine molecules by the bidentate ligand 2-(2′-pyridyl)quinoxaline (pqx) in ethylene glycol/DMSO (9:1). Since the substitution of the pyridines by pqx requires high temperature (ca. 160 °C), a stream of argon was used to prevent the oxidation of Ru^{II}. Isolation of the final products was achieved after addition of NH_4PF_6.

The CD spectra of Λ- and Δ-[Ru(bpy)$_2$(pqx)](PF$_6$)$_2$ are mirror images of each other and exhibit absorptions at λ_{max} ($\Delta\varepsilon$) = 463.7 nm (−1.6 м$^{-1}$cm^{-1}), 419.2 (+ 9.5), 402.3 (+9.1), 376.2 (−4.2) and 361.6 (-4.8) for the Δ-enantiomer and at 464.2 (+1.6), 419. 5 (−9.4), 403.8 (−9.0), 377.0 (+ 4.2) and 362.4 (+ 4.8) for the Λ-enantiomer (Figure 1). These assignments were made by comparison with similar complexes of known configuration.[19,20]

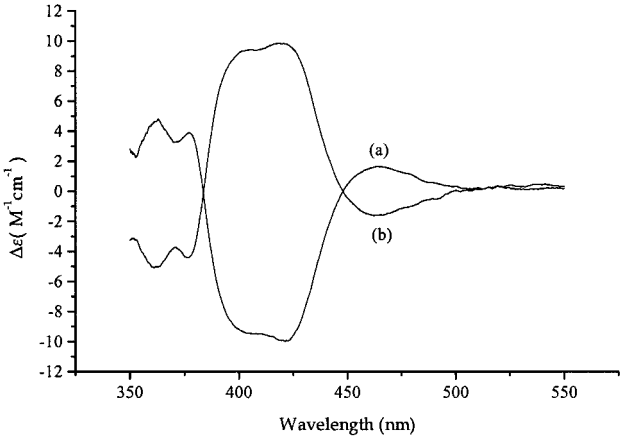

Figure 1. The CD spectra of: (a) Λ-[Ru(bpy)$_2$(pqx)](PF$_6$)$_2$ and (b) Δ-[Ru(bpy)$_2$(pqx)](PF$_6$)$_2$ in the region 350−550 nm

The ^{1}H and ^{13}C NMR resonances of the enantiomers were assigned assisted by 2D [^{1}H,^{1}H] DQF-COSY and 2D [^{1}H,^{13}C] HMBC/HMQC experiments. Figure 2 shows the structures of Λ- and Δ-[Ru(bpy)$_2$(pqx)](PF$_6$)$_2$ with atom labeling. Table 1 and 2 present chemical shift data for the enantiomeric complexes.

The ^{1}H and ^{13}C NMR spectra of both enantiomers show resolved signals for each of the bpy ligands, indicating that they are magnetically inequivalent. In addition, separate signals for the constituents of the bpy ligands (i.e. the pyridine rings) were observed. Sixteen proton and twenty carbon signals were observed in total, corresponding to all the proton and carbon nuclei of the two bpy ligands of each

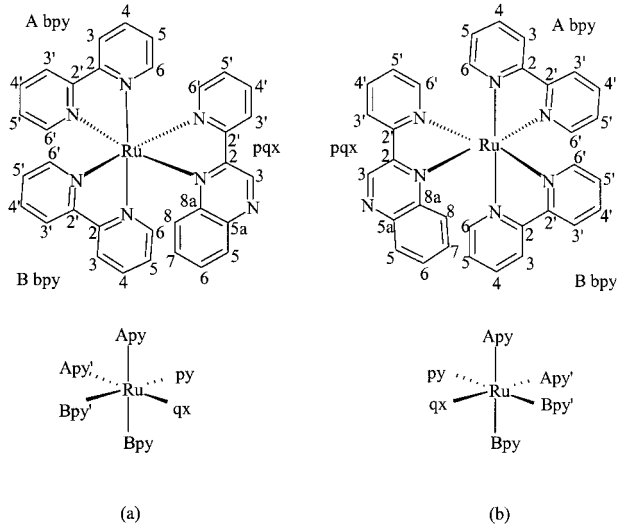

Figure 2. Structures of the enantiomeric complexes Λ- and Δ-[Ru(bpy)$_2$(pqx)]$^{2+}$, including atom numbering

enantiomer, which were fully assigned. This observation shows that the influence of the asymmetric nature of the pqx ligand on the magnetic environment of the two bpy molecules is important, in contrast to what was suggested for other similar complexes.[20−22] Since in the cases of Λ- and Δ-[Ru(bpy)$_2$(pqx)]$^{2+}$ the bpy ligands are magnetically discernible (probably due to the high magnetic field), it is necessary to define the relative location of the two bpy molecules towards pqx. In an attempt to determine the complete assignments of the enantiomers ^{13}C NMR spectroscopy was used to evaluate the Coordination Induced Shifts (CIS = $\delta_{complexed} - \delta_{free}$) and 2D [^{1}H^{1}H] ROE spectroscopy to investigate internuclear distances of less than 5 Å between the ligand protons. In general, the major effects affecting the CIS are: (i) the σ-withdrawal of electron density of the carbon nuclei through the nitrogen lone-pair upon coordination, causing downfield shifts, (ii) the π-back donation from the metal back-bonding to the π* orbitals of the ligand, causing downfield shifts, and (iii) the location of a carbon nucleus close to a high-electron-density area, such as an aromatic ring, causing dramatic upfield shifts. Figure 3 presents the CIS for all carbon atoms of the pyridine rings (py) of the complex Ru(bpy)$_3^{2+}$ together with the CIS of the pyridine rings of the two bpy (Abpy and Bbpy) and the pqx ligand of the complex Δ-[Ru(bpy)$_2$(pqx)]$^{2+}$ (see Figure 2). In the case of Ru(bpy)$_3^{2+}$ all six pyridine rings are magnetically equivalent, with the planes of the bipyridine rings perpendicular to each other. Also, the six pyridine rings are opposite to each other in the coordination sphere of the ruthenium.

As seen in Figure 2, the planes of the pyridine rings of Apy and Bpy, which occupy the axial sites of the complex, are perpendicular to the py and qx moieties of the pqx respectively. Since the quinoxalinic part of pqx is a more extended aromatic system (two fused six-membered aromatic rings) than a single pyridine ring, it is expected to provide a lower electron density to the C$_6$ atom of the per-

 © 2004 Wiley-VCH Verlag GmbH & Co. KGaA, Weinheim

Table 1. ^{13}C NMR[a] chemical shifts in ppm for the complex $[Ru(bpy)_2(pqx)](PF_6)_2$ in $CDCl_3$ at 298 K; CIS indicates the Coordination Induced Shifts ($CIS = \delta_{complexed} - \delta_{free}$)

Carbon[a]	$[Ru(bpy)_2(pqx)](PF_6)_2$	CIS
A bpy C2	157.24	+1.79
A bpy C3	125.75	+5.24
A bpy C4	139.29	+2.56
A bpy C5	128.72	+4.99
A bpy C6	151.86	+2.94
A bpy C2′	157.20	+1.75
A bpy C3′	125.76	+5.25
A bpy C4′	139.71	+2.98
A bpy C5′	129.17	+5.44
A bpy C6′	151.99	+3.07
B bpy C2	157.35	+1.90
B bpy C3	125.51	+5.00
B bpy C4	138.88	+2.15
B bpy C5	129.16	+5.43
B bpy C6	154.50	+5.58
B bpy C2′	157.16	+1.71
B bpy C3′	125.12	+4.61
B bpy C4′	139.17	+2.44
B bpy C5′	128.95	+5.22
B bpy C6′	151.89	+2.97
pqx C2	154.81	+5.37
pqx C3	144.93	+0.70
pqx C5a	144.55	+2.71
pqx C5	125.18	−4.53
pqx C6	132.57	+2.47
pqx C7	133.15	+3.10
pqx C8	131.50	+2.17
pqx C8a	143.71	+1.17
pqx C2′	157.45	+2.94
pqx C3′	128.15	+6.02
pqx C4′	139.56	+2.46
pqx C5′	129.27	+4.67
pqx C6′	152.70	+2.58

[a] NMR spectroscopic data at 600 MHz in $CDCl_3$ at 298 K (in ppm): (i) 2,2′-bipyridine: C2 = 155.45, C3 = 120.51, C4 = 136.73, C5 = 123.73, C6 = 148.92; (ii) ligand pqx: C2 = 149.44, C3 = 144.23, C5a= 141.84, C5 = 129.71, C6 = 130.10, C7 = 130.05, C8 = 129.33, C8a = 142.54, C2′ = 154.51, C3′ = 122.13, C4′ = 137.10, C5′ = 124.60, C6′ = 150.12; (iii) $[Ru(bpy)_3]^{2+}$: C2 = 156.50, C3 = 124.80, C4 = 138.00, C5 = 127.80, C6 = 150.80.

pendicularly located pyridine ring. Consequently, the CIS value of this nucleus differs from those of the other five C_6 and $C_{6'}$ atoms because it is less shielded, causing the higher downfield shift. Indeed, the C_6 of the Bpy ring shifts downfield by 5.60 ppm, about two times more than the C_6 of the other pyridine rings, indicating that Bpy is the one located vertically with respect to the quinoxaline ring system.

The σ- and π-back donations are two factors related to the bond strength that may also affect the CIS of the carbon nuclei of the pyridine rings. For both enantiomers the pyridine rings Apy′ and Bpy′ are located opposite the quinoxaline (qx) and pyridine (py) moieties of pqx, respectively, while the pyridine rings Apy and Bpy are opposite to each other (see Figure 2). Thus, only one of the five (py) rings seems to differ (slightly) from the others with respect to the σ- and π-back donation to the ruthenium coordination sphere. This is the Apy′ opposite to the (qx) moiety of the

Table 2. ^1H NMR chemical shifts in ppm of the free $[Ru(bpy)_2(pqx)](PF_6)_2$ complexes, identical in both Δ- and Λ-enantiomers and in the presence of the oligonucleotide duplex $[d(CGCGAATTCGCG)_2]$ in D_2O (100 mM buffer phosphate pH 7.01) at 298 K in a 1:1 molar ratio; all shifts are referred to HOD at $\delta = 4.69$ ppm

Complex proton	$[Ru(bpy)_2(pqx)](PF_6)_2$	Δ-Isomer	Λ-Isomer
A bpy H3	8.47	−0.06	−0.05
A bpy H3′	8.46	−0.06	−0.05
A bpy H4	7.97	−0.05	−0.03
A bpy H4′	7.98	−0.02	−0.02
A bpy H5	7.25	−0.07	−0.14
A bpy H5′	7.21	−0.15	−0.13
A bpy H6	7.54	−0.38	−0.38
A bpy H6′	7.57	−0.32	−0.35
B bpy H3	8.28	−0.07	−0.05
B bpy H3′	8.19	−0.07	−0.07
B bpy H4	7.95	−0.14	−0.14
B bpy H4′	7.81	−0.02	−0.03
B bpy H5	7.16	−0.04	−0.01
B bpy H5′	7.16	−0.02	−0.01
B bpy H6	7.53	−0.08	−0.08
B bpy H6′	7.28	−0.11	−0.07
pqx H3	9.51	−0.20	−0.15
pqx H3′	8.66	−0.15	−0.10
pqx H4′	8.03	−0.03	−0.03
pqx H5′	7.31	+0.04	+0.04
pqx H6′	7.64	−0.07	−0.05
pqx H5	7.85	−0.14	−0.14
pqx H8	7.57	−0.17	−0.17
pqx H6	7.32	−0.01	−0.01
pqx H7	7.17	−0.15	−0.19

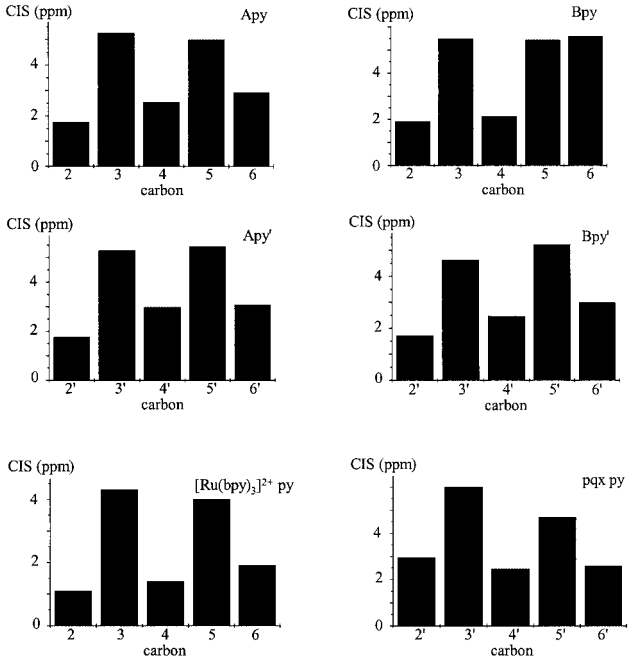

Figure 3. The patterns of CIS of the carbons for all the pyridine rings of the complex and the pyridine ring (all equivalent) of the complex $[Ru(bpy)_3]^{2+}$.

 © 2004 Wiley-VCH Verlag GmbH & Co. KGaA, Weinheim

pqx. Supposing that the Ru−N(py) bond strength differs from that of Ru−N(qx), the bond opposite to them will also differ. Consequently, the Apy′ with the higher downfield shifts of its carbon atoms (see Table 1) is probably located opposite the qx in the meridian plane of the ruthenium octahedron.

2D (^{1}H,^{1}H) ROESY spectroscopy was also used to confirm the above structure. Figure 4 shows the aromatic region of the ROESY spectrum of Δ-[Ru(bpy)$_2$(pqx)]$^{2+}$ at τ_m = 80 ms at a concentration of 5 mM and a temperature of 298 K. Note that three ROESY spectra were acquired with different mixing times of 60, 80 and 120 ms to select the optimum value for the intramolecular (^{1}H,^{1}H) correlation (r = 5 Å). The low concentration was necessary to avoid intermolecular contacts due to π-π stacking effects between the aromatic rings of the ligands of neighboring ions of the complex Δ-[Ru(bpy)$_2$(pqx)]$^{2+}$.[21]

Many intramolecular cross peaks were observed and were assigned to internuclei spin-spin interactions between the neighboring protons of the aromatic rings of the ligands, together with cross-peaks between the ring protons. A very clear cross-peak appears between H4′ of the pqx ligand and H6 of the Bbpy ligand, showing that these protons are close to each other. Additionally, the observation of an interligand cross-peak between H6 of Abpy and H6 of pqx confirms the structure shown in Figure 2. In this structure the plane of the Bpy′ ring is located perpendicular to the pyridine moiety of the pqx ligand and the Apy ring is also vertically located to the quinoxalinic ring system of the pqx ligand.

Interactions of the Enantiomers with d(CGCGAATTCGCG)$_2$

The addition of the Λ- or Δ-[Ru(bpy)$_2$(pqx)]$^{2+}$ enantiomer to the oligonucleotide duplex d(CGCGAATTCGCG)$_2$ causes changes in the proton chemical shifts of both enantiomers and the oligonucleotide; these are listed in Table 2 and 3.

The ^{1}H NMR spectra of the adduct of the Δ- or Λ-enantiomer to the oligonucleotide duplex at a 0.5:1 and 1:1 molar ratio at 298 K show only one set of resonances, indicating a fast exchange.[22]

A good indicator of which groove of the oligonucleotide the enantiomer binds to is the observed change in the chemical shifts of specific protons of the oligonucleotide duplex. The protons AH8 and GH8, CH6/H5, sugar H2′and H2′′ located in the major groove and AH2 and sugar H1′in the minor groove are mostly affected by this binding. The influence of the high electron density of the ligand aromatic protons causes upfield shifts of these protons. For both the Λ- and the Δ-enantiomer, only very small changes for all these protons (−0.02 to +0.02 ppm) were observed, showing that the stacking between the DNA base rings remains intact keeping the B-DNA structure. A π-type stacking interaction between the bases and the aromatic ligands of the enantiomers has to be excluded due to the

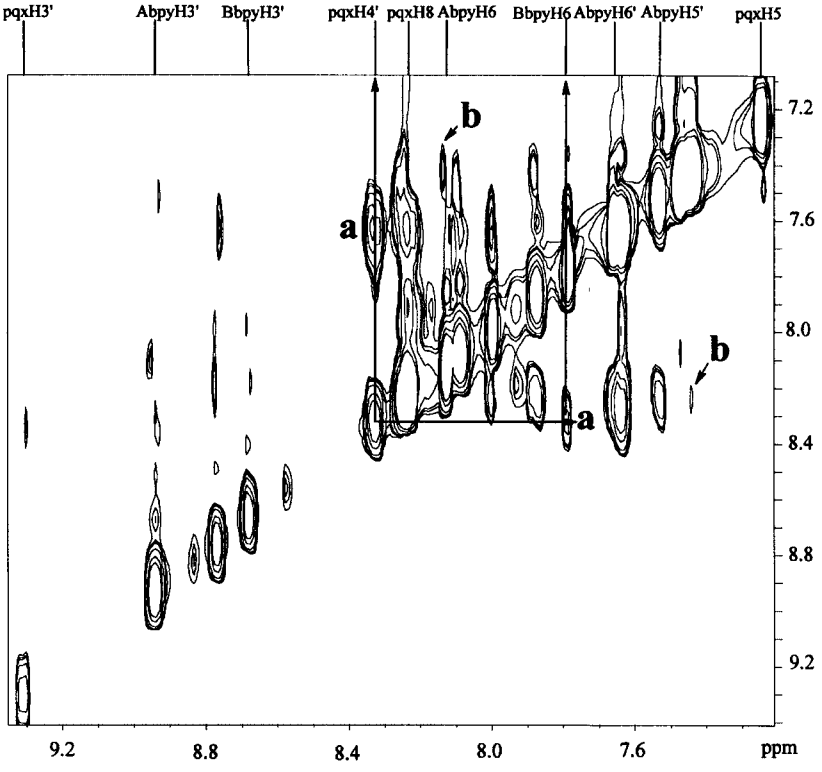

Figure 4. Part of the ROESY spectrum (τ_m = 80 ms) of Δ-[Ru(bpy)$_2$(pqx)](PF$_6$)$_2$; the labelled cross peaks correspond to ROE conducts assigned to the protons pqxH4′ and BbpyH6 (a) and pqxH6 and AbpyH6 (b), confirming the suggested structure of Figure 2

 © 2004 Wiley-VCH Verlag GmbH & Co. KGaA, Weinheim

Table 3. Chemical shift changes of the oligonucleotide protons upon addition of the Ru enantiomers under the same conditions; the changes indicate the difference between the bound and free DNA ($\delta_B - \delta_F$); all shifts are referred to HOD at $\delta = 4.69$ ppm

	H6/H8	H2/H5/CH3	H1′	H2′	H2′′
C1	7.49	5.76	5.62	1.83	2.27
Δ-	−0.01	−0.04	−0.03	−0.04	−0.01
Λ-	−0.02	−0.02	−0.04	−0.07	−0.01
G2	7.82		5.75	2.52	2.58
Δ-	−0.02		0.00	0.00	+0.01
Λ-	−003		−0.05	−0.01	+0.02
C3	7.20	5.23	5.46	1.77	2.20
Δ-	−0.00	0.00	0.00	−0.05	−0.06
Λ-	−0.02	+0.01	+0.01	−0.05	−0.07
G4	7.72		5.31	2.61	2.63
Δ-	0.00		−0.01	−0.05	−0.10
Λ-	−0.01		−0.02	−0.05	−0.10
A5	7.98	7.10	5.87	2.62	2.80
Δ-	0.00	−0.01	−0.01	−0.01	0.00
Λ-	−0.01	−0.01	−0.01	−0.01	0.00
A6	7.98	7.49	6.03	2.44	2.81
Δ-	0.00	−0.01	0.00	−0.01	−0.02
Λ-	−0.01	−0.01	0.00	−0.01	−0.02
T7	6.98	1.13	5.78	1.85	2.44
Δ-	0.00	+0.01	0.00	0.00	0.00
Λ-	0.00	+0.01	+0.01	0.00	+0.10
T8	7.24	1.39	5.97	2.04	2.42
Δ-	−0.02	−0.01	0.00	0.00	−0.01
Λ-	+0.02	0.00	−0.02	0.00	0.00
C9	7.33	5.49	5.53	1.93	2.29
Δ-	0.01	+0.01	0.00	0.00	−0.01
Λ-	−0.01	0.00	−0.03	−0.01	0.00
G10	7.78		5.72	2.51	2.57
Δ-	0.00		+0.01	0.00	+0.01
Λ-	0.00		0.00	0.00	+0.01
C11	7.14	5.30	5.62	1.76	2.14
Δ-	0.00	+0.01	−0.03	+0.03	+0.02
Λ-	0.00	0.00	−0.03	0.00	+0.02
G12	7.80		6.01	2.25	2.49
Δ-	−0.02		−0.04	−0.04	−0.02
Λ-	−0.02		−0.05	−0.02	0.00

small upfield shifts of the protons of the oligonucleotide bases. Even though the environment of the bases in DNA is already rich in electron density, since they are stacked over the *z* axis itself with a separation of 3.4 Å, intercalators cause upfield shifts of about −0.2 ppm in the base protons by increasing their electron density still further.[23]

Small changes in the chemical shifts for the pqx ligand protons in both the Δ- and Λ-$Ru(bpy)_2(pqx)]^{2+}$ enantiomers, ranging from +0.04 to −0.20 ppm, were also observed, thus excluding any possibility for intercalation. It is known that for an intercalating aromatic ring, which stacks above and below the ring planes of a DNA base-pair, a dramatic upfield shift of −0.5 to −1.0 ppm typically occurs.[24] The magnitude of the upfield shift depends on the relative position of the protons of the intercalating ligand and the center of the base plane. Classical intercalators, like dppz, cause higher upfield shifts of the protons that are located between the DNA bases, by about −0.80 ppm[22] in the complex Δ-$[Ru(phen)_2(dppz)]^{2+}$ and by -0.67 ppm in the complex Δ-$[Ru(Me_2phen)_2(dppz)]^{2+}$.[23] As for the other two bipyridine ligands (Abpy and Bbpy), the most affected protons are H6 and H6′ of Abpy, which shift upfield by -0.32 and -0.38 ppm, respectively, for both the Δ- and the Λ-enantiomer. These values are not large enough to allow us to conclude that this ligand intercalates between the base pairs. Upfield shifts of the order of −0.2 to −0.4 ppm have been observed for the proton signals of ligands that are either partially inserted between the DNA bases,[25,26] or associate to the DNA grooves (e.g. 1,10-phenanthroline). Both Λ- and Δ-$[Ru(phen)_3]^{2+}$ bind to the minor groove of the oligonucleotide[13,14] $d(CGCGATCGCG)_2$ and cause upfield changes of about −0.3 ppm in some of the phen proton signals.[14] It is worth mentioning that in both enantiomers the influence of the binding causes similar changes to the proton chemical shifts.

The intermolecular NOEs observed between the Λ- or Δ-enantiomer and $d(CGCGAATTCGCG)_2$ are listed in Table 4. Figure 5 and 6 show portions of the NOESY spectra of the Λ- or Δ-$[Ru(bpy)_2(pqx)]^{2+}$/$d(CGCGAATTCGCG)_2$ adduct at 298 K.

Table 4. Intermolecular NOEs observed between Δ- and Λ-$[Ru(bpy)_2(pqx)]^{2+}$ and the oligonucleotide duplex $d(CGCGAATTCGCG)_2$ at molar ratio 1:1 and temperature 298 K

Λ-$[Ru(bpy)_2(pqx)]^{2+}$	Δ-$[Ru(bpy)_2(pqx)]^{2+}$
T8H6 AbpyH3′	T8H6 AbpyH3′
T8H6 BbpyH3	T8H6 BbpyH4
T8H6 pqxH6′	T8H6 BbpyH6
H5pqx C9H2′′	T8H6 pqxH8
H5pqx G10H2′′	C9H6 pqxH8
	C9H6 BbpyH4
	G10H2′′ pqxH5
	C9H6 BbpyH3

In both NOE maps of the adducts the sequential NOEs arising from the inter- and intramolecular contacts between the oligonucleotide protons remain intact, indicating that the B-type conformation is kept upon interaction with Λ- or Δ-$[Ru(bpy)_2(pqx)]^{2+}$. This observation is consistent with a groove or a weak type of binding rather than with an intercalation, as this would cause significant perturbation in the DNA helix. Small differences in the cross-peak intensities of the duplex indicate insignificant changes of the oligonucleotide structure following interaction with the Ru enantiomers.

In the case of the Λ-isomer, a few cross-peaks with weak to medium intensities are observed. In the aromatic region, three intramolecular NOEs appear between the complex protons AbpyH3, BbpyH3 and pqxH6′, and T8H6. Since additional cross-peaks between the aromatic protons of bases C9 and T7 (neighboring to T8) and the enantiomer are not detected, the binding with intercalation above or below the T8 plane must be excluded. Taking into account that two more intermolecular cross-peaks between C9H2′′ and G10H2′′ and pqxH5 are observed, we can propose that

 © 2004 Wiley-VCH Verlag GmbH & Co. KGaA, Weinheim

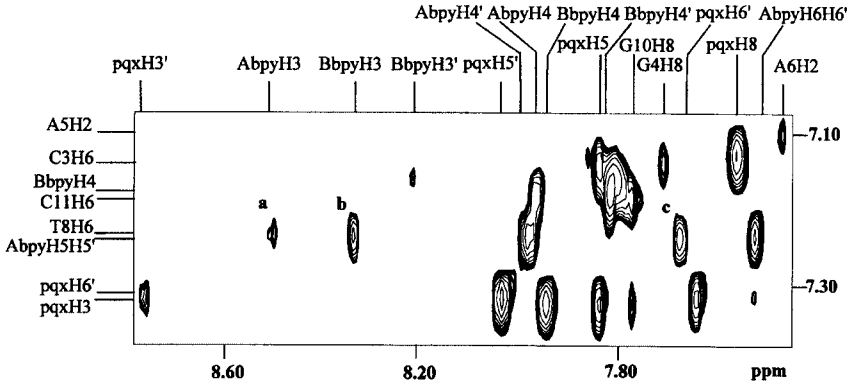

Figure 5. Part of the ^{1}H NOESY spectrum (τ_m = 350 ms) of the Λ-[Ru(bpy)$_2$(pqx)](PF$_6$)$_2$·[d(CGCGAATTCGCG)$_2$] adduct (1:1 molar ratio) at 298 K with the assignments of the aromatic protons; the labelled cross-peaks correspond to NOE conducts between the protons T8H6 and AbpyH3′ (a), T8H6 and BbpyH3 (b), and T8H6 and pqxH6′ (c)

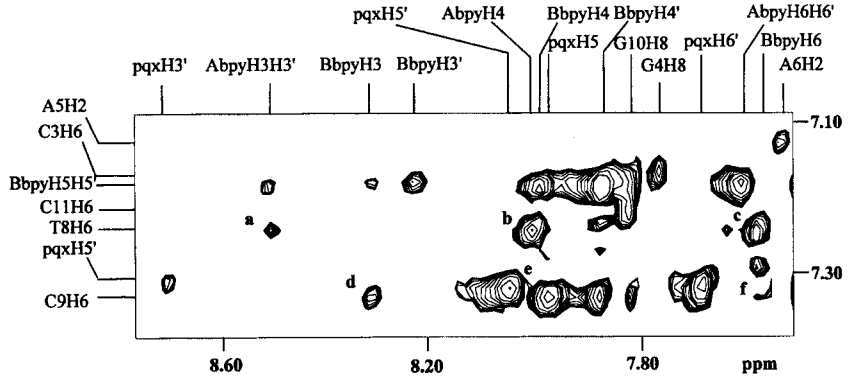

Figure 6. Part of the ^{1}H NOESY spectrum (τ_m = 350 ms) of the Δ-[Ru(bpy)$_2$(m-bpy-GHK)]Cl$_2$·[d(CGCGAATTCGCG)$_2$] adduct (1:1 molar ratio) at 298 K with the assignments of the aromatic protons; the labelled cross-peaks correspond to NOEs between the protons T8H6 and AbpyH3 (a), T8H6 and BbpyH4 (b), T8H6 and BbpyH6 (c), C9H6 and BbpyH3 (d), C9H6 and BbpyH4 (e), and C9H6 and pqxH8 (f)

the complex binds in the major groove of the oligonucleotide where all these protons are located. The absence of cross-peaks between the complex protons and the sugar H1′ proton, or the adenine ring protons H2, located in the minor groove support the suggestion of binding in the major groove, close to the base T8. All five observed intermolecular NOEs cannot arise from the same binding state of the complex to the oligonucleotide due to the fast exchange kinetics of the system but, fortunately, they are located in the same part of the oligonucleotide duplex. While binding is unambiguous for the region -T8-C9- of the d(CGCGAATTCGCG)$_2$ complex, it is difficult to suggest which of the three ligands (Abpy, Bbpy, or pqx) binds to the oligonucleotide. All five observed NOEs should belong to different binding states (different ligands) — T8H6 pqxH6 and T8H6 BbpyH3. In an attempt to understand how the enantiomer binds to the oligonucleotide, a binding model generated by manually docking the complex close to the T8 of the major groove of the helix was obtained. Rotation of the complex in the range of ±15° in its *x*, *y*, *z* axis, produced a superimposed structure that satisfied all the observed NOE cross-peaks. In general, the obtained structures show that the complex binds mainly through the ligand Abpy in the major groove of the helix while the pyridine rings Bpy of the ligand Bbpy and py of the ligand pqx, are oriented along the DNA *z* axis. The quinoxaline moiety of the pqx ligand occupies the external side of the Λ- [Ru(bpy)$_2$(pqx)]$^{2+}$/d(CGCGAATTCGCG)$_2$ adduct (Figure 7).

Moreover, with this orientation the complex has an approximate height along the *z* DNA axis of approximately 11.5 Å. This is defined as the distance between the Bbpy H4 and the H4 of the pyridine ring of the pqx ligand, which is closer to the dimensions of the major groove (11.6 Å width × 8.5 Å depth), than those of the minor (6.0 Å width × 8.2 Å depth) in the B-DNA structure.[27] In this way the depth of the insertion is also defined. A ligand (L) with an extended aromatic fused rings' system in its Ru^{II} complexes of general formulae [Ru(phen)$_2$(L)]$^{2+}$, intercalates between the DNA bases with significant perturbation of the DNA structure, thereby affecting the dimentions of the grooves. Such complexes (e.g. Δ-[Ru(Me$_2$phen)$_2$(dppz)]$^{2+}$,[23] Δ-[Ru(phen)$_2$(L)]$^{2+}$ L = dipyrido[3,2-*a*:2′,3′-*c*][6,7,8,9]tetrahydrophenazine,[28] etc.) bind to the minor groove following

 © 2004 Wiley-VCH Verlag GmbH & Co. KGaA, Weinheim

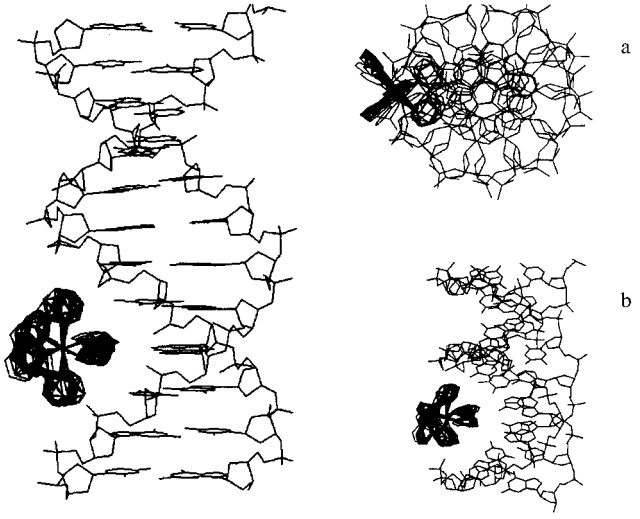

Figure 7. A molecular model of the interactions between Λ-$[Ru(bpy)_2(pqx)]^{2+}$ and $d(CGCGAATTCGCG)_2$ reflects qualitatively the binding of the complex to the oligonucleotide; inset: (a) top view along the *z*-axis showing the complex orientation with only the Abpy ligand facing the oligonucleotide; (b) a view across the major groove showing the complex orientation

the intercalating ligand which prefers the narrow minor groove and is stabilized by van der Waals interactions. On the other hand, complexes without a "leader" intercalative ligand such as $[Ru(bpy)_3]^{2+}$ or $[Ru(phen)_3]^{2+}$ bind without intercalation. Based on photophysical results it has been suggested that $[Ru(bpy)_3]^{2+}$ binds to DNA weakly[15] without intercalation and its electrostatic interactions with the DNA phosphates are ambiguous. Minor-[13,14] or major-groove[8,10] binding has been found for the related complex $[Ru(phen)_3]^{2+}$ for both Λ- and Δ-enantiomers by spectroscopic techniques. Λ-$[Ru(phen)_3]^{2+}$ was found to interact with the DNA minor groove only with one phenanthroline molecule such as in the case of Λ-$[Ru(bpy)_2(pqx)]^{2+}$ that interact only with the Abpy. Hiort et al. have suggested a major-groove binding for both enantiomers of the complex $[Ru(phen)_3]^{2+}$ based on LD studies.[10] Major-groove binding was also observed for both enantiomers of the complex $[Ru(bpy)_2(ppz)]^{2+}$, where the ligand ppz was deeply inserted between the base pairs.[17] In the case of Λ-$[Ru(bpy)_2(pqx)]^{2+}$, which clearly prefers the major groove, the 2,2′-bipyridine ligand seems to have a lower affinity than 1,10-phenanthroline, with van der Waals interactions with the DNA mainly taking place from the minor groove. On the other hand, electrostatic interactions that probably coexist in our case take place through the phosphates in the major groove. Additionally, the bpy ligands provide less steric hindrance than phenanthroline. These are probably the reasons why Λ-$[Ru(bpy)_2(pqx)]^{2+}$ prefers the major groove.

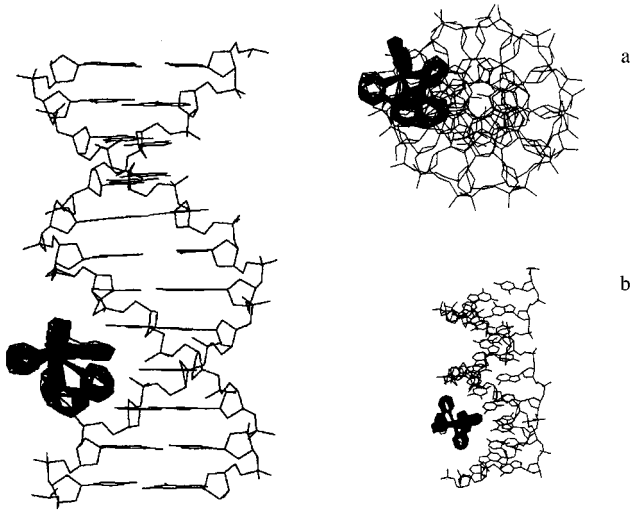

Figure 8. A molecular model of the interactions between Δ-$[Ru(bpy)_2(pqx)]^{2+}$ and $d(CGCGAATTCGCG)_2$ reflects qualitatively the binding of the complex to the oligonucleotide; inset: (a) top view along the *z*-axis showing that the complex inserts both the Bbpy and the pqx ligands into the major groove of the helix; (b) a view across the major groove showing the complex orientation

In the case of the Δ-isomer many more cross-peaks are observed, all of which are located at the same part of the oligonucleotide close to the bases T8 and C9, as in the case of the Λ- isomer. The protons that are involved in these intramolecular NOEs are all located in the major groove of the helix. This observation is in agreement with the results of 1D ^1H NMR spectra where the chemical-shift changes are very similar for both enanatiomers. However, some specific cross-peaks between the Δ-enantiomeric protons and the base ring protons, particularly in neighboring bases (e.g. the pqxH8 with T8H6 and C9H6), indicate that the complex is inserted deeply into the major groove. Due to the fast kinetics of the binding it is not possible to assign all the observed cross-peaks to one binding state, but, as shown in Figure 8, all the generated structures (according to the binding model procedure) place the Bpy of Bbpy and the quinoxalinic part of the pqx ligand close to the bases in the depth of the major groove. The Abpy ligand is located on the external part of the adduct without being in contact with the oligonucleotide helix.

To be consistent with the groove dimentions, this deeper insertion of the Δ- than the Λ-isomer means that the internal *z* axis of the complex is not parallel to the *z* axis of the helix but is slightly bent. In this orientation the complex interacts with the major groove of the oligonucleotide with the two ligands without causing a significant distortion of the DNA structure. Based on intramolecular NOE contacts, it has been suggested that the complex Δ-$[Ru(phen)_3]^{2+}$ binds to $d(CGCGATCGCG)_2$ by insertion of two phenanthroline molecules into the minor groove of the central AT part of the oligonucleotide.[13,14] This suggestion seems to be in contrast with our observation that the complex binds to the major groove. However, the complex $[Ru(bpy)_2(pqx)]^{2+}$ shows an affinity for the oligonucleotide T8C9 base sequence and not for the central AATT region, and this is probably the reason why the approach of the helix is from the major groove. In general, the central AATT region of $d(CGCGAATTCGCG)_2$ is preferred by molecules that bind from the minor groove.[29,30]

 © 2004 Wiley-VCH Verlag GmbH & Co. KGaA, Weinheim

Conclusions

In both enantiomers Λ- and Δ-[Ru(bpy)$_2$(pqx)]$^{2+}$ the asymmetric nature of the pqx ligand causes different magnetic environments of the two bpy ligands and allows the distinction of Abpy and Bbpy. The pqx ligand is not a classical intercalator and its DNA binding properties were previously unexplored. The determination of the complete assignment of these complexes allows us to understand better their binding properties with the oligonucleotide d(CGCGAATTCGCG)$_2$. The main conclusions are summarized below:

(i) As indicated by NMR spectroscopy, both enantiomers bind non-intercalatively in the d(CGCGAATTCGCG)$_2$ major groove close to the T8C9 sequence without significant perturbation of the helix structure. Evidence for a similar binding of the enantiomers comes from the similar changes in the proton chemical shifts of the adducts, and the NOE results.

(ii) Δ-[Ru(bpy)$_2$(pqx)]$^{2+}$ binds more deeply than Λ-[Ru(bpy)$_2$(pqx)]$^{2+}$, with two ligands (pqx and Bbpy) facing the DNA groove while the Λ isomer only has one (Abpy).

(iii) The quinoxalinic moiety of the pqx ligand in the case of Δ-[Ru(bpy)$_2$(pqx)]$^{2+}$ contributes to the interaction with the oligonucleotide while in the case of the Λ-enantiomer it is located in the external part of the adduct.

Experimental Section

Materials: All chemicals and solvents were of reagent grade and were used without further purification. The deoxynucleotide d(5′-CGCGAATTCGCG-3′) was purchased from OSWEL DNA Service (University of Southampton, UK) and purified by chromatography on a 120 × 2.5 cm Sephadex G-25 superfine column, using distilled water as eluent and lyophilized to dryness. The complexes *cis*-[RuCl$_2$(bpy)$_2$][31] and Λ- and Δ-[Ru(bpy)$_2$(py)$_2$]A·12H$_2$O (where A = *O*,*O*′-dibenzoyltartaric acid),[32,33] and the ligand 2-(2′-pyridyl)quinoxaline (pqx) were synthesised according to literature procedures.[34]

Instrumentation: Elemental analyses for C, H and N were performed using a Carlo−Erba 1108 apparatus. CD spectra were recorded on a Jasco J-720 spectropolarimeter. A 2-cm path length cuvette was used for the region 350−500 nm. All NMR spectroscopic data were acquired at 150.92 and 201.21 MHz for ^{13}C and 600.13 and 800.13 MHz for ^{1}H transmitter frequencies on AVANCE 600 and 800 MHz Bruker spectrometers. 1D (^{1}H and ^{13}C) spectra for both enantiomers were recorded at 298 K in either $CDCl_3$ or D_2O. In addition 2D (^{1}H,^{1}H) DQF-COSY, 2D (^{1}H,^{13}C) HMBC/HMQC and 2D (^{1}H,^{1}H) ROESY spectra were acquired in $CDCl_3$ on the AVANCE 600 and (^{1}H,^{1}H) DQF-COSY in D_2O on the 800 MHz instrument, at 298 K. In the case of (^{1}H,^{13}C) HMBC/HMQC spectra, a total of 2048 complex points in t_2 were collected for each of 320 t_1 increments. (^{1}H,^{1}H) ROESY spectra were collected at mixing times (τ_m) between 60 and 120 ms with the pulse program roesyetgp.[35,36] 2D (^{1}H,^{13}C) HMBC spectra were obtained using the inv4gplplrnd pulse sequence, optimized for long-range couplings, with a low-pass J-filter to suppress one-bond correlation. The AVANCE 800 instrument was used mainly to acquire the spectra of the [d(CGCGAATTCGCG)$_2$]/[Ru(bpy)$_2$(pqx)]$^{2+}$ adducts in D_2O at 298 K. (^{1}H,^{1}H) DQF-COSY spectra were recorded using the cosydfesgpph26 pulse programe, while the water suppression was achieved using excitation sculpting with gradients allowing for presaturation during relaxation delay in cases of radiation damping phasecycle.[37] The (^{1}H,^{1}H) NOESY spectra were collected in 4096 complex points in t_2 for each of 512 t_1 increments at two mixing times (τ_m) of 350 and 400 ms with the noesyesgpph26 phase-sensitive pulse programme using the TPPI method.[38] Finally the (^{1}H,^{13}C) HMQC spectra were collected in 2048 complex points in t_2 for each of 128 t_1 increments with the pulse sequence inv4prtp with decoupling during acquisition.[39] The NMR spectroscopic data were processed using the Bruker Xwin NMR Ver. 2.6 software.

Sample Preparation: In each oligonucleotide sample the amounts were estimated by weighing and the concentrations were determined from the absorption at 260 nm.[40] In all NMR experiments a 100 mM Na_2HPO_4/NaH_2PO_4, pH 7.00 (uncorrected for isotope effects) buffer was used. The lyophilized samples were dissolved in D_2O (99.9%) and lyophilized again to dryness. These samples were finally dissolved in 0.4 mL of D_2O (99.96%) and transferred to 5 mm NMR tubes. The 1D ^{1}H NMR spectra were recorded on samples with a concentration of about 50 OD_{260} units while the 2D NOE experiments were performed with more-concentrated samples (ca. 200 OD_{260}). No internal chemical-shift reference was added to the samples.

Molecular Modeling: Both Λ- and Δ-[Ru(bpy)$_2$(pqx)](PF$_6$)$_2$ were constructed manually from the X-ray atomic coordinates of the closely related complexes [Ru(bpy)$_2$(py)$_2$]$^{2+}$.[33] Each of the above complexes was docked manually at the major groove of the dodecanucleotide close to bases T8C9. The enantiomers were rotated along the axis *x*, *y*, *z*, to produce superimposed structures. This average structure satisfied all the observed NOE interatomic distances between the protons of the complex and the dodecanucleotide. The DNA helix was in the B-type configuration and was produced by the database of the molecular software program HyperChem. v. 6.0. Graphical outputs were obtained with the RasMol v2.6 software.

Δ-[Ru(bpy)$_2$(pqx)](PF$_6$)$_2$: Δ-[Ru(bpy)$_2$(py)$_2$]A·12H$_2$O (0.1 mmol, 105 mg) was dissolved in 10 mL of a 9:1 mixture of ethylene glycol and DMSO and a solution of pqx (0.4 mmol, 83 mg) in the same solvent (5 mL) was added. The mixture was refluxed for 24 hours under argon (99.999%). After cooling to room temperature, 5 mL of water was added and the mixture filtered to remove the excess of pqx. A saturated solution of NH_4PF_6 (5 mL) was added to the remaining clear solution. A deep-red precipitate was obtained by cooling the solution to 4 °C overnight, and this was filtered and washed with cold water (2 × 5 mL) and diethyl ether (2 × 5 mL). The crude solid was dissolved in MeCN and purified on an activated aluminum oxide column (20 × 1 cm) using MeCN as eluent. The solvent (MeCN) was evaporated from the collected brown-orange band to yield orange needles of Δ-[Ru(bpy)$_2$(pqx)](PF$_6$)$_2$ (yield 65%). $C_{33}H_{25}F_{12}N_7P_2Ru$: calcd. C 43.5, H 2.7, N 10.8; found C 42.9, H 2.9, N 10.7. ^{1}H NMR ($CDCl_3$, 600 MHz, 298 K): δ = 10.19 (s, pqxH$_3$), 9.31 (d, $^{3}J_{H,H}$ = 8.3 Hz, pqxH$_{3'}$), 8.95 (d, $^{3}J_{H,H}$ = 6.7 Hz, AbpyH$_3$), 8.94 (d, $^{3}J_{H,H}$ = 6.7 Hz, AbpyH$_{3'}$), 8.77 (d, $^{3}J_{H,H}$ = 8.1 Hz, BbpyH$_3$), 8.68 (d, $^{3}J_{H,H}$ = 8.1 Hz, BbpyH$_{3'}$), 8.33 (t, $^{3}J_{H,H}$ = 7.8 Hz pqxH$_{4'}$), 8.26 (t, $^{3}J_{H,H}$ = 7.5 Hz, AbpyH$_{4'}$), 8.23 (t, $^{3}J_{H,H}$ = 7.8 Hz, BbpyH$_4$), 8.24 (d, $^{3}J_{H,H}$ = 8.1 Hz pqxH$_8$), 8.23 (t, $^{3}J_{H,H}$ = 7.8 Hz, AbpyH$_4$), 8.13 (d, $^{3}J_{H,H}$ = 5.3 Hz, AbpyH$_6$), 8.09 (t, $^{3}J_{H,H}$ = 7.5 Hz, BbpyH$_{4'}$), 8.00 (d, $^{3}J_{H,H}$ = 5.3 Hz pqxH$_{6'}$), 7.88 (t, $^{3}J_{H,H}$ = 7.5 Hz pqxH$_7$), 7.79 (d, $^{3}J_{H,H}$ = 5.3 Hz, BbpyH$_6$),

 © 2004 Wiley-VCH Verlag GmbH & Co. KGaA, Weinheim

7.66 (d, $^3J_{H,H}$ = 5.3 Hz, AbpyH$_{6'}$), 7.64 (t, $^3J_{H,H}$ = 6.7 Hz, BbpyH$_5$), 7.64 (t, $^3J_{H,H}$ = 6.7 Hz, pqxH$_{5'}$), 7.54 (t, $^3J_{H,H}$ = 6.7 Hz, AbpyH$_{5'}$), 7.47 (t, $^3J_{H,H}$ = 6.7 Hz, BbpyH$_{5'}$), 7.45 (t, $^3J_{H,H}$ = 7.5 Hz AbpyH$_5$), 7.45 (d, $^3J_{H,H}$ = 5.3 Hz, BbpyH$_{6'}$), 7.44 (t, $^3J_{H,H}$ = 9.0 Hz, pqxH$_{6'}$), 7.25 (d, $^3J_{H,H}$ = 8.5 Hz, pqxH$_5$) ppm.

Λ-[Ru(bpy)$_2$(pqx)](PF$_6$)$_2$: A similar procedure was followed for this enantiomer starting with Λ-[Ru(bpy)$_2$(py)$_2$]A·12H$_2$O. $C_{33}H_{25}F_{12}N_7P_2Ru$: calcd. C 43.5, H 2.7, N 10.8; found C 43.4, H 2.6, N 10.7. ^{1}H NMR (CDCl$_3$, 600 MHz, 298 K): δ = 10.17 (s, pqxH$_3$), 9.31 (d, $^3J_{H,H}$ = 8.3 Hz pqxH$_{3'}$), 8.96 (d, $^3J_{H,H}$ = 6.7 Hz, AbpyH$_3$), 8.94 (d, $^3J_{H,H}$ = 6.7 Hz, AbpyH$_{3'}$), 8.78 (d, $^3J_{H,H}$ = 8.0 Hz, BbpyH$_3$), 8.69 (d, $^3J_{H,H}$ = 8.0 Hz, BbpyH$_{3'}$), 8.32 (t, $^3J_{H,H}$ = 7.8 Hz pqxH$_{4'}$), 8.27 (t, $^3J_{H,H}$ = 7.5 Hz, AbpyH$_{4'}$), 8.24 (d, $^3J_{H,H}$ = 8.0 Hz, pqxH$_8$), 8.24 (t, $^3J_{H,H}$ = 7.8 Hz, BbpyH$_4$), 8.22 (t, $^3J_{H,H}$ = 7.8 Hz, AbpyH$_4$), 8.12 (d, $^3J_{H,H}$ = 5.3 Hz, AbpyH$_6$), 8.09 (t, $^3J_{H,H}$ = 7.5 Hz BbpyH$_{4'}$), 8.00 (d, $^3J_{H,H}$ = 5.3 Hz, pqxH$_{6'}$), 7.88 (t, $^3J_{H,H}$ = 7.5 Hz, pqxH$_7$), 7.79 (d, $^3J_{H,H}$ = 5.3 Hz, BbpyH$_6$), 7.67 (d, $^3J_{H,H}$ = 5.2 Hz, AbpyH$_{6'}$), 7.64 (t, $^3J_{H,H}$ = 6.7 Hz, pqxH$_{5'}$), 7.64 (t, $^3J_{H,H}$ = 6.7 Hz, BbpyH$_5$), 7.54 (t, $^3J_{H,H}$ = 6.7 Hz, AbpyH$_{5'}$),7.46 (t, $^3J_{H,H}$ = 6.7 Hz, BbpyH$_{5'}$), 7.46 (d, $^3J_{H,H}$ = 5.3 Hz, BbpyH$_{6'}$), 7.45 (t, $^3J_{H,H}$ = 7.5 Hz, AbpyH$_5$), 7.43 (t, $^3J_{H,H}$ = 9.0 Hz, pqxH$_{6'}$), 7.25 (d, $^3J_{H,H}$ = 8.5 Hz, pqxH$_5$) ppm.

Acknowledgments

Financial support from the G.S.R.T. (PENED 99) is gratefully acknowledged. The NMR spectroscopic data were collected at the Large Scale Facility of Florence PARABIO supported by the E.U.

[1] B. Norden, P. Lincoln, B. Akerman, E. Tuite, *Met. Ions Biol. Sys.* **1996**, *33*, 177−252.
[2] E. D. A. Stemp, J. K Barton, *Met. Ions Biol. Sys.* **1996**, *33*, 325−365.
[3] J. K Barton, J. J. Dannenberg, A. L. Raphael, *J. Am. Chem. Soc.* **1982**, *104*, 4967−4969.
[4] A. Yamagishi, *J. Phys. Chem.* **1984**, *88*, 5709−5713.
[5] A. Yamagishi, *J. Chem. Soc., Chem. Commun.* **1983**, 572−573.
[6] J. P. Rehman, J. K. Barton, *Biochemistry* **1990**, *29*, 1701−1709.
[7] J. K. Barton, J. M. Goldberg, C. V. Kumar, N. J. Turro, *J. Am. Chem. Soc.* **1984**, *106*, 2081−2088.
[8] I. S. Haworth, A. H. Elock, J. Freeman, A. Rodger, W. G. Richards, *J. Biomol. Struct. Dyn.* **1991**, *9*, O23−O44.
[9] P. Lincoln, B. Norden, *J. Phys. Chem. B* **1998**, *102*, 9583−9594.
[10] C. Hiort, B. Norden, A. Rodger, *J. Am. Chem. Soc.* **1990**, *112*, 1971−1982.
[11] J. E. Coury, J. R. Anderson, L. McFail-Isom, L. D. Williams, L. A. Bottomley, *J. Am. Chem. Soc.* **1997**, *119*, 3792−3796.
[12] S. Satyanarayana, J. C. Dabrowiak, J. B. Chairs, *Biochemistry* **1993**, *32*, 2573−2584.
[13] M. Erikson, M. Leijon, C. Hiort, B. Nordèn, A. Graslünd, *Biochemistry* **1994**, *33*, 5031−5040.
[14] M. Erikson, M. Leijon, C. Hiort, B. Nordèn, A. Graslünd, *J. Am. Chem. Soc.* **1992**, *114*, 4933−4934.
[15] C. V. Kumar, J. K. Barton, N. J. Turro, *J. Am. Chem. Soc.* **1985**, *107*, 5518−5523.
[16] A. M. Pyle, J. P. Rehman, R. R. Meshoyerer, C. V. Kumar, N. J. Turro, J. K. Barton, *J. Am. Chem. Soc.* **1989**, *111*, 3051−3058.
[17] S. A Tysoe, R. J. Morgan, A. D. Baker, T. C. Sterkas, *J. Phys. Chem.* **1993**, *97*, 1707−1711.
[18] A. Garoufis, A. Koutsodimou, N. Katsaros, C. A. Mitsopoulou, N. Hadjiliadis, *Polyhedron* **1999**, *18*, 361−369.
[19] T. J. Rutherford, O. V. Gijte, A. Kirsch-De Mesmaeker, F. R. Keene, *Inorg. Chem.* **1997**, *36*, 4465−4474.
[20] J. G. Liu, B. H. Ye, Q. L. Zhang, X. H. Zou, Q. X. Zhen, X. Tian, L. N Ji, *J. Biol. Inorg. Chem.* **2000**, *5*, 119−128.
[21] E. M. Proudfoot, J. P. Mackay, P. Karuso, *Dalton Trans.* **2003**, 165−170.
[22] C. M. Dupureur, J. K. Barton, *Biochemistry* **1997**, *36*, 33−43.
[23] A. Greguric, I. D. Greguric, W. T. Hambley, J. R. Aldrich-Wright, J. G. Collins, *J. Chem. Soc., Dalton Trans.* **2002**, 849−855.
[24] S. Chndrasekaran, S. Kusuma, S. W. Boykin, W. D. Wilson, *Magn. Reson. Chem.* **1986**, *24*, 630−637.
[25] F. M. Foley, F. R. Keene, J. G. Collins, *J. Chem. Soc., Dalton Trans.* **2001**, 2968−2974.
[26] E. M. Proudfoot, J. P. Mackay, P. Karuso, *Biochemistry* **2001**, *40*, 4867−4878.
[27] S. Neidle, *DNA Structure and Recognition*, IRL Press, Oxford, **1994**.
[28] J. G. Collins, A. D. Sleeman, J. R. Aldrich-Wright, I. D. Greguric, W. T. Hambley, *Inorg. Chem.* **1998**, *37*, 3133−3141.
[29] R. E. Klevit, D. E. Wemmer, B. R. Reid, *Biochemistry* **1986**, *25*, 3296−3303.
[30] P. F. Fagan, H. P. Spielmann, S. T. Sigurdsson, S. M. Rink, P. B. Hopkins, D. E. Wemmer, *Nucleic Acids Res.* **1996**, *24*, 1566−1573.
[31] B. P. Sullivan, D. J. Salmon, T. J. Meyer, *Inorg. Chem.* **1978**, *17*, 3334−3341.
[32] O. Morgan, S. Wang, S. A. Bac, R. J. Morgen, R. D. Baker, T. C. Strekas, R. Engel, *J. Chem. Soc., Dalton Trans.* **1977**, 3773−3776.
[33] B. Kolp, H. Viebrock, A. von Zelewsky, D. Abelnm, *Inorg. Chem.* **2001**, *40*, 1196−1198.
[34] S. Kasselouri, A. Garoufis, G. Kalkanis, S. Perlepes, N. Hadjiliadis, *Inorg. Chim. Acta* **1993**, *207*, 255−257.
[35] T. L. Hwang, A.J. Shaka, *J. Am. Chem. Soc.* **1992**, *114*, 3157−3159.
[36] A. Bax, D. G. Davis, *J. Magn. Reson.* **1985**, *63*, 207−213.
[37] A. Derome, M. Williamson, *J. Magn. Reson.* **1990**, *88*, 177−185.
[38] T. L. Hwang, A. J. Shaka, *J. Magn. Reson. Series A* **1995**, *112*, 275−279.
[39] A. Bax, R. H. Griffey, B. L. Hawkins, *J. Magn. Reson.* **1983**, *55*, 301.
[40] P. N. Borer in *Handbook of Biochemistry and Molecular Biology* (Ed.: G. D. Fasman), CRC Cleveland, **1975**, pp. 589−590.

Received March 3, 2004
Early View Article
Published Online June 1, 2004

 © 2004 Wiley-VCH Verlag GmbH & Co. KGaA, Weinheim

Synthesis, Structure and Binding Properties of Nickel and Copper [14]Cyclidene Complexes with Appended Aza Crown Ethers

Bohdan Korybut-Daszkiewicz,*[a] Joanna Taraszewska,*[b] Katarzyna Zięba,[b] Anna Makal,[c] and Krzysztof Woźniak*[c]

Keywords: Cyclidene complexes / Crown ether compounds / Copper / Nickel / Electrochemistry

Copper(II) and nickel(II) cyclidenes linked with one or two 15-azacrown-5 ethers (**3Ni**, **4Ni** and **4Cu**) as well as similar model morpholine-substituted derivatives (**2Cu**, **2Ni**) have been synthesized and characterized using ESI mass-spectrometry, X-ray diffraction, spectroscopic methods and elemental analysis. Cyclic voltammetry of the copper complexes exhibits two reversible redox couples $Cu^{II/III}$ and $Cu^{II/I}$, whereas the nickel complexes show reversible $Ni^{II/III}$ and irreversible $Ni^{II/I}$ redox processes. Cyclic and differential pulse voltammetry have been used to study interactions of metal cations and amino acids with the above complexes. Na^+ and Li^+ interact weakly with the **3Ni** complex. In the presence of Mg^{2+}, the ligand isomerizes from aldehyde to enolate ion, which interacts strongly with Mg^{2+}. The presence of lysine caused a more pronounced shift of the $Cu^{II/III}$ potential in **4Cu** than did leucyne. This suggests that there are interactions between the NH_3^+ group and the crown ether moiety and between the carboxylic group and the Cu^{III} center of the former guest.

(© Wiley-VCH Verlag GmbH & Co. KGaA, 69451 Weinheim, Germany, 2004)

Introduction

Redox-active molecular receptors designed to complex and electrochemically recognize charged and neutral guest species have attracted great attention.[1−4] Compounds possessing such properties consist of a redox-active component and a macrocyclic ligand well suited for the complexation of guest species. The redox center in such systems can easily be switched between its oxidized and reduced forms, thus giving two different states with different charges. Each state is expected to behave differently in the binding process with some substrates. Ferrocene crown ethers[1−6] and ferrocene cryptands[7−11] have been the most extensively studied species. However, such electro-active components as cobaltocene[6] quinone, nitrobenzene, and others have also been used.[4] Plenio et al.[8,9] found that efficient electronic communication between the guest coordinated in the macrocyclic cavity and the redox active unit is crucial for the optimum performance of such molecular devices. Some redox switchable host−guest systems have frequently been proposed as the key components of potential molecular devices and sensors.[12,13]

Azamacrocyclic ligands can stabilize unusual oxidation states of coordinated transition metal ions, making them a promising tool for the construction of supramolecular sensors and switches. Rybak-Akimova et al.[14−16] have synthesized a ditopic molecule consisting of 4-formylbenzo-15-crown-5 and a redox-active tetraazamacrocyclic nickel(II) complex as a receptor for $MeNH_3^+$ and β-$AlaH^+$.[14] They also proposed a ditopic receptor for dicarboxylic acids based on a 15-membered tetraazamacrocyclic (cyclidene)-nickel(II) complex conjugated with two cyclic tetraamines (cyclene),[15] and another for the molecular recognition of diammonium cations based on a cyclidene nickel(II) complex bearing two benzocrown ethers.[16] Bernhardt and Hayes[17] applied benzocrown ethers with appended cobalt cyclam as receptors for alkali cations. Fabbrizzi et al.[18] have synthesized luminescent molecular sensors operating through a metal-center redox couple, combining nickel(II) cyclam-like macrocycles or a copper 14-ane-S4 complex with organic fluorophores (mainly anthracene). Previously,[19] we have studied tetraazamacrocyclic nickel(II) complexes functionalized with benzo-15-crown 5 ethers as receptors for group I and II metal cations.

In this paper we describe the synthesis and characterization of 14-member copper(II) and nickel(II) cyclidenes linked with one or two 15-aza-crown-5 ethers (Scheme 1, complexes **3Ni**, **4Ni** and **4Cu**), as potential receptors for alkali, alkaline-earth metal cations and zwitterionic species such as amino acids. Ligands containing binding sites for

[a] Institute of Organic Chemistry, Polish Academy of Sciences, Kasprzaka 44/52, 01-224 Warszawa, Poland
Fax: (internat.) + 48-22-632-6681
E-mail: bkd@icho.edu.pl
[b] Institute of Physical Chemistry, Polish Academy of Sciences, Kasprzaka 44/52, 01-224 Warszawa, Poland
Fax: (internat.) + 48-22-632-5276
E-mail: jota@ichf.edu.pl
[c] Department of Chemistry, University of Warsaw, Pasteura 1, 02-093 Warszawa, Poland

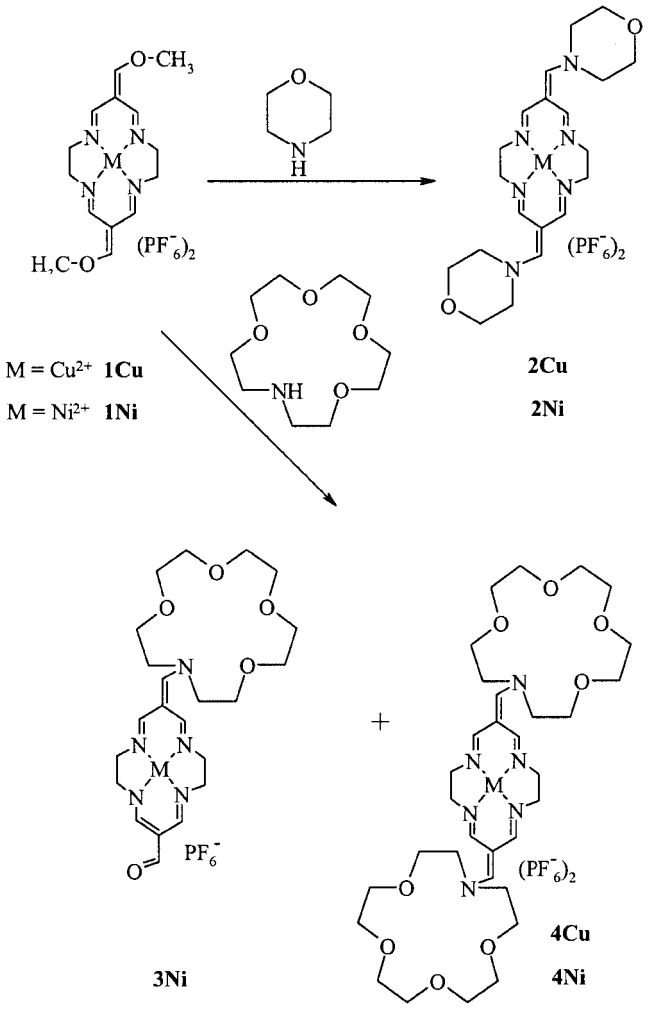

Scheme 1

both cations and anions should be suitable for studying the recognition of such species. This may be important in understanding many biological and communication processes at the molecular level. Transition metal porphyrins[20] and phthalocyanines[21] bearing crown ethers substituents are among several known ditopic macrocyclic molecules containing transition metal and ammonium ion binding sites. Kimura et al.[22] have shown that a molecule composed of a macrocyclic polyamine covalently linked with benzo-15-crown-5 ether forms stable 1:1 complexes with zwitterionic substrates such as amino acids.

Results and Discussion

Synthesis and Structure

Copper(II) and nickel(II) *O*-methylated [14]cylidene complexes **1Cu** and **1Ni** (Scheme 1) reacted with morpholine as well as with 1-aza-15-crown-5 to form amino-substituted cyclidenes **2Cu, 2Ni** or **4Cu, 4Ni**. When complex **1Ni** was used in excess, the monosubstituted product **3Ni** was isolated by chromatography on an SP Sephadex C25 column. Complexes **3Ni** and **4Cu** gave crystals suitable for X-ray analysis.

Structural Details

Complex **4Cu** (Figure 1) crystallizes in the triclinic $P\bar{1}$ space group, as a salt in which two PF_6^- ions interact with one complexed Cu^{II} cation. The complex occupies a special position, with the central Cu atom located exactly on the crystallographic symmetry center. Therefore, the inner symmetry of the molecule becomes a crystallographic feature and, crystallographically, only half of the molecule is independent. Together with one PF_6^- ion the independent half of the **4Cu** molecule defines the crystallographic asymmetric unit.

The macrocyclic fragment of **4Cu** is nearly planar, except for the part including C(1) and C(2), which is an aliphatic part of the ring. The C(1)−C(2) bond length is 1.519 Å and the carbon atoms are above and below the macrocycle plane accordingly. The valence angles C(2)−N(1)−C(3) and C(1)−N(2)−C(5) are close to 120° − a characteristic of such macrocyclic compounds. The bond lengths between other atoms of the macrocyclic moiety reveal their partial double bond character, thus confirming the aromatic character of the tetraazamacrocyclic compound. N(1) and N(2) bind the Cu^{II} cation at the center of the macrocycle with a bond length that is characteristic of N−Cu^{II} interactions (ca. 1.90 Å). C(6) and N(3) are coplanar with the Cu^{II} cation and the coordinating N(1) and N(2) atoms and both C(4)−C(6) and C(6)−N(3) bonds show partial double character, indicating that the lone electron pair of N(3) contributes to the electron density of the aromatic macrocycle. Important bond lengths and angles are given in Table 1. N(3) is nearly coplanar with C(5) and C(3); the rest of the crown ether is forced to be located at close to 100° with respect to the azamacrocyclic moiety. The conformation of the crown ether in this structure is not the most preferable for the coordination of the cations, with the oxygen atoms O(2) and O(4) directed outside the crown and the carbons C(10) and C(15) pointing inwards. Some weak interactions appear to occur between O(1) and O(3) and the hydrogen atoms connected to C(10) and C(15), although the interatomic distances are too long to be classified as regular hydrogen bonds (Table 1). Some reorganization of the crown must occur prior to, or simultaneously with, the process of possible cation complexation. The average C−C and C−O distances in the crown ether are slightly shorter than the average expected C−C and C−O bond lengths (Table 1) but are consistent with the distances reported in crystallographic databases.

The PF_6^- ion shows standard octahedral geometry (Table 1) and is localized close to the macrocycle ring. F(14) interacts with the Cu^{2+} ion (the two atoms are 3.027 Å apart). Together with the macrocyclic nitrogen atoms, F(14) completes the coordination sphere of the Cu^{2+}, making it roughly octahedral, with N(1)−Cu−F(14) and N(2)−Cu−F(14) of 78.92° and 77.68°, respectively. There

 © 2004 Wiley-VCH Verlag GmbH & Co. KGaA, Weinheim

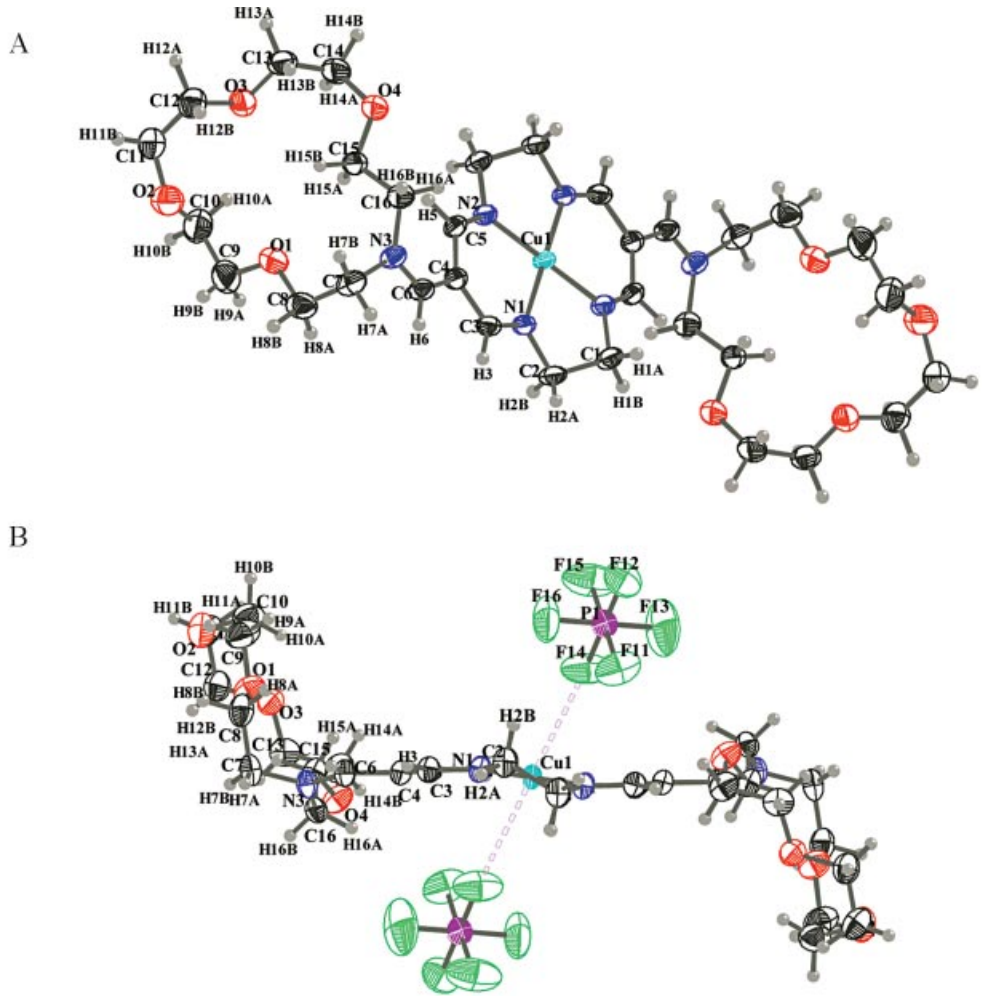

Figure 1. Structure of **4Cu**: (A) with atom labeling, (B) including coordinating PF_6^- molecules

are no other significant interactions between the PF_6^- ion and the macrocyclic Cu complex.

There are also no special intermolecular interactions such as hydrogen bonds that would stabilize the crystal structure of **4Cu**. The packing is rather close and reveals a two-layered structure (Figure 2). The first layer consists of parallel packed macrocyclic moieties and PF_6^- ions while the crown ether compounds build the second layer, forming cages.

3Ni crystallizes in the monoclinic $P2_1/c$ space group, as a salt of one PF_6^- ion interacting with the Ni cation complexed by the macrocyclic compound (Figure 3). The complex occupies a general crystallographic position and together with the PF_6^- ion constitutes the crystallographic asymmetric unit. There are four symmetry related **3Ni** molecules in the unit cell.

The overall structure of the macrocyclic Ni^{II} complex is similar to that in **4Cu**, although there are some differences. The inter-atomic distances between the Ni^{II} ion and the four coordinating nitrogen atoms are slightly shorter than in the **4Cu** structure. This length is characteristic for this type of coordination. The presence of an extra negative charge within the macrocycle ring also has a significant influence. The bonds connecting C(9) with C(8) and C(10)

Table 1. Important structural parameters for **4Cu** (distances in Å)

Parameter definition	
Cu(1)−N(2)	1.913(2)
Cu(1)−N(1)	1.918(2)
C(1)−N(2)#1	1.464(4)
C(1)−C(2)	1.519(4)
C(2)−N(1)	1.465(4)
C(3)−N(1)	1.282(4)
C(3)−C(4)	1.439(4)
C(4)−C(6)	1.399(4)
C(4)−C(5)	1.436(4)
C(5)−N(2)	1.281(4)
C(6)−N(3)	1.313(4)
C(7)−N(3)	1.482(4)
C(16)−N(3)	1.472(4)
Average interatomic distances in the crown ether	
C−C	1.50(3)
C−O	1.41(2)
Average P−F distance	
P−F	1.570(9)

 © 2004 Wiley-VCH Verlag GmbH & Co. KGaA, Weinheim

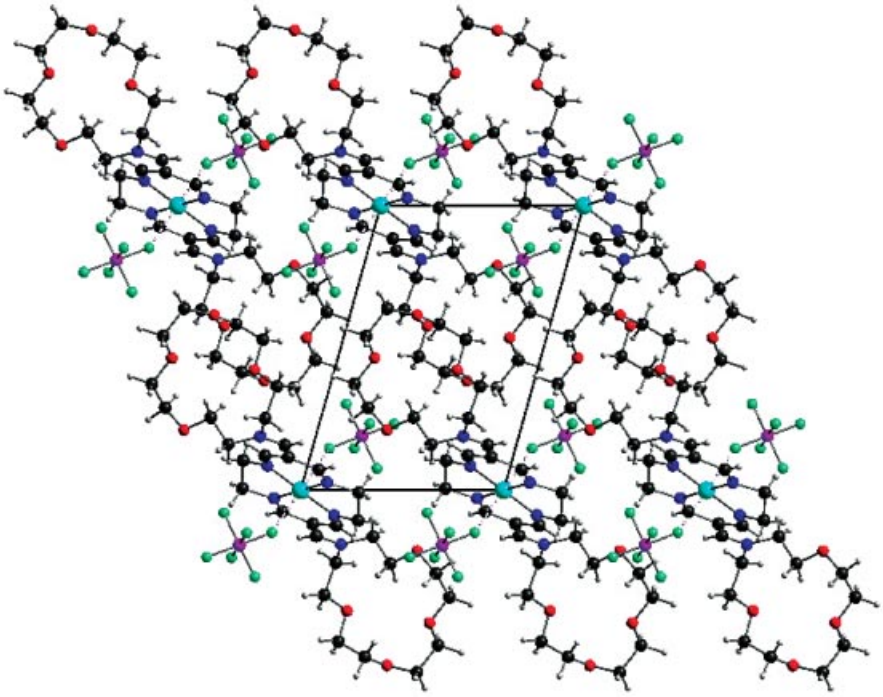

Figure 2. Packing of the **4Cu** molecules in the crystal lattice − view along the *y*-axis

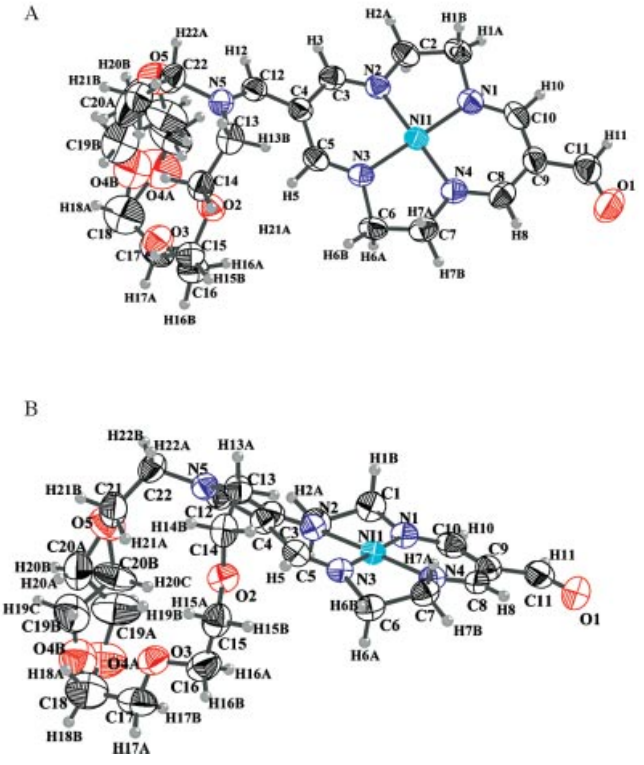

Figure 3. Structure of **3Ni**: (A) view of the macrocyclic compound and (B) presentation of the disorder in the crown ether part

are of equal length and shorter than expected for a typical C−C single bond. This confirms that most of the negative charge is located around C(9), close to the aldehyde group connected with the macrocycle. The exocyclic bond length C(9)−C(11) is typical for a C=C double bond, and the effect is due to both the negative charge on C(9) and the conjugation of the double bond of the carbonyl group with the double bonds of the macrocycle; This is confirmed by the coplanarity of O(1) with C(8) and C(10) (with torsion angles of 1.7° and 179.6°, respectively). The opposite part of the macrocycle is not exactly parallel to the first one, although the atoms that comprise it all lay in one plane and the aromatic character of the compound is confirmed by the bond lengths (Table 2). Similarly to the **4Cu** structure, the lone electron pair of N(5) of the crown ether joins the aromatic system of the macrocycle and, therefore, fixes the location of the crown at the angle with respect to the macrocycle plane. Probably due to the negative charge on C(9), the crown moiety is closer to the macrocycle ring than in **4Cu**, with an angle between the average crown ether plane and the macrocycle of less than 90°. The conformation of the crown is close to that preferable for cation complexation, with only O(5) pointing somewhat outside the ring. The fragment including O(4), C(19) and C(20) atoms proved to be disordered. There are two possible conformations that share nearly the same occupation, designated as A and B. The disorder causes quite large thermal ellipsoids in the structure. The more important bond lengths and angles are reported in Table 2.

The PF_6^- ion does not appear to form close contacts with the complexed Ni^{II} ion or **3Ni** moiety and, not being stabilized in the crystal structure by any well-defined interaction, it seems to rotate freely in the space among the **3Ni** molecules. This may explain the severe disorder in the ion's

 © 2004 Wiley-VCH Verlag GmbH & Co. KGaA, Weinheim

Table 2. Important structural parameters for **3Ni** (distances in Å)

Parameter definition	
Ni(1)−N(1)	1.837(3)
Ni(1)−N(3)	1.847(3)
Ni(1)−N(4)	1.851(3)
Ni(1)−N(2)	1.851(3)
C(1)−N(1)	1.472(5)
C(1)−C(2)	1.505(6)
C(2)−N(2)	1.469(5)
C(3)−N(2)	1.277(4)
C(3)−C(4)	1.419(5)
C(4)−C(12)	1.401(5)
C(4)−C(5)	1.422(5)
C(5)−N(3)	1.292(5)
C(6)−N(3)	1.476(4)
C(6)−C(7)	1.489(5)
C(7)−N(4)	1.477(5)
C(8)−N(4)	1.297(5)
C(8)−C(9)	1.396(6)
C(9)−C(10)	1.394(6)
C(9)−C(11)	1.427(6)
C(10)−N(1)	1.293(5)
C(11)−O(1)	1.215(5)
C(12)−N(5)	1.305(5)
C(13)−N(5)	1.466(5)
C(18)−O(4B)	1.27(2)
C(18)−O(4A)	1.56(1)
C(19A)−O(4A)	1.392(9)
C(19A)−C(20A)	1.43(2)
C(20A)−O(5)	1.44(2)
C(19B)−O(4B)	1.28(2)
C(19B)−C(20B)	1.56(3)
C(20B)−O(5)	1.42(2)
C(22)−N(5)	1.463(5)
Average interatomic distances in the crown ether	
C−C	1.48(1)
C−O	1.42(1)
Average P−F bond length	
P−F	1.49(4)

structure. At least four possible conformations for the ion may appear.

The packing of the **3Ni** and PF_6^- ions resembles that observed in **4Cu**. Again, there are two different layers, one consisting of the parallel placed macrocycle moieties and another built up by the crown ethers, forming cages of each pair of crown moieties (Figure 4). The PF_6^- ions are located in tunnels formed in bends of the **3Ni** moieties. Again, there are no significant interactions such as hydrogen bond that would stabilize the structure.

Electrochemical Characteristics of Cu and Ni Complexes

Cyclic voltammograms (CV) of the studied complexes recorded in ACN containing 0.1 M $[Bu_4N]BF_4$ are presented in Figure 5. The CV of complexes **2Cu** and **4Cu** exhibit two reversible redox couples, $Cu^{II/I}$ and $Cu^{II/III}$, respectively. Comparison of the corresponding E_fs (Table 3) indicates that the aza crowns facilitate the $Cu^{II/III}$ redox process and

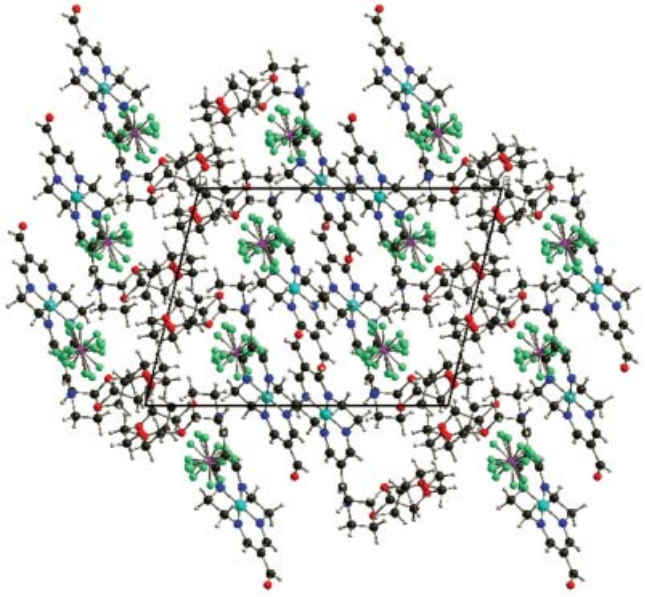

Figure 4. Packing of **3Ni** molecules in the crystal lattice − view along the *y*-axis

make the $Cu^{II/I}$ process more difficult. **3Ni** exhibits a reversible $Ni^{II/III}$ redox process, similar to complex **4Ni**, and an irreversible $Ni^{II/I}$ process.

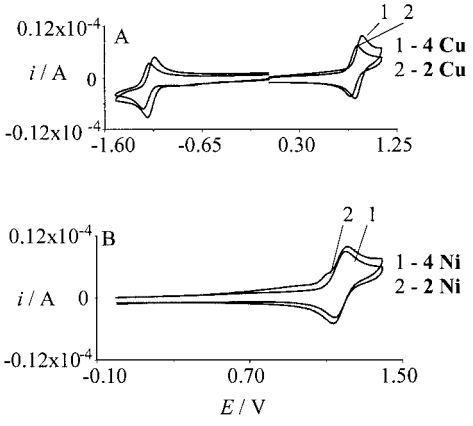

Figure 5. Cyclic voltammograms of the studied complexes (5×10^{-4} M): (A) 1 − **4Cu**, 2 − **2Cu**; (B) 1 − **4Ni**, 2 − **2Ni**

Table 3. Formal potentials of $Cu^{II/I}$, $Cu^{II/III}$ and $Ni^{II/III}$ redox couples in Cu and Ni complexes

Complex	E_f [V] vs. MCE M^{II}/M^{I}	E_f [V] vs. MCE M^{II}/M^{III}
2Cu	−1.150	0.880
2Ni	−1.510[a]	1.179
3Ni	−1.700[a]	1.000
4Cu	−1.200	0.830
4Ni	−1.590[a]	1.170

[a] Potential of irreversible cathodic peak.

Complexation of Cations

The addition of increasing amounts of Li^+ and Na^+ cations to a solution of **3Ni** resulted in a weak positive poten-

 © 2004 Wiley-VCH Verlag GmbH & Co. KGaA, Weinheim

Table 4. Shifts of the formal potential of $Ni^{II/III}$ in complex **3Ni** upon addition of metal cations

	Na^+ (1 equiv.)	Li^+ (1 equiv.)	K^+ (1 equiv.)	Mg^{2+} (0.25 equiv.)	Ba^{2+} (0.25 equiv.)	Mg^{2+} (0.5 equiv.)	Ba^{2+} (5 equiv.)
ΔE/mV	10	5	–	10	6	E_a/V = 1.21[a]	E_a/V = 1.21[a]
ΔE/mV	−28	−18	−5	E_c/V = −1.50[b]	E_c/V = −1.70	E_c/V = −1.50	

[a] New anodic peak. [b] New cathodic peak.

tial shift of the $Ni^{II/III}$ redox couple and a more pronounced anodic shift of the $Ni^{II/I}$ cathodic wave (Table 4). With further addition of Li^+ and Na^+ cations the $Ni^{II/III}$ redox potential did not change; however, the $Ni^{II/I}$ potential shifted by 70 mV and by about 100 mV in the presence of 10 equiv. of Li^+ and Na^+, respectively. These results indicate that the binding ability of Li^+ and Na^+ cations to the crown ether moiety is significant when Ni^{II} in the azamacrocycle is reduced to Ni^{I}. With Ni^{III} the complexation of both cations is very weak. The addition of K^+ did not change the $Ni^{II/III}$ potential, and changed only slightly (5 mV) the $Ni^{II/I}$ potential.

The addition of 0.25 equiv. of Mg^{2+} cation to the solution of **3Ni** resulted in an anodic shift of the $Ni^{II/III}$ redox potential by 10 mV and the appearance of a new irreversible $Ni^{II/I}$ peak at the potential 200 mV less negative (Table 4). After addition of 0.5 equiv. of Mg^{2+} a new anodic peak *a* appeared at 170 mV more positive (see A in Figure 6). With increasing Mg^{2+} the current of the new anodic peak increased at the expense of the anodic current of the original peak. At higher concentrations of Mg^{2+} two peaks could be still observed on the differential pulse voltammograms. The currents of both peaks vs. the equivalents of Mg^{2+} added are plotted in Figure 7. However, the reduction current corresponding to the first process remained unchanged. In the cathodic region, with increasing Mg^{2+} the height of the new peak at −1.500 V increased at the expense of the original peak

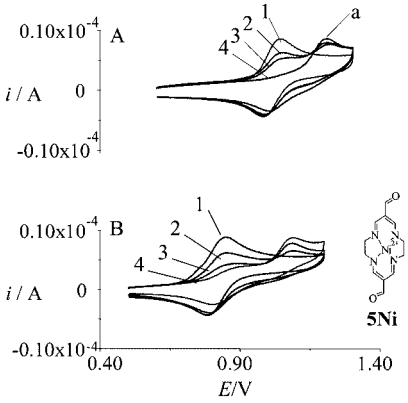

Figure 6. Cyclic voltammograms of 5×10^{-4} M of complexes **3Ni** (A) and **5Ni** (B) upon addition of Mg^{2+} (equiv.): (1) 0; (2) 0.5; (3) 1; (4) 2; inset: structure of **5Ni**

The above effects are explained in Scheme 2.

The small anodic potential shift of E_f after the addition of 0.25 equiv. of Mg^{2+} indicates complexation of this guest

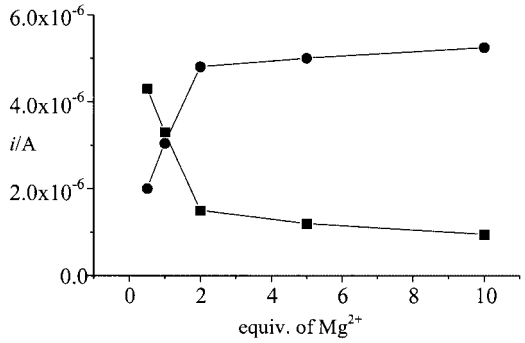

Figure 7. Currents corresponding to the oxidation of Ni^{II} from the aldehyde form of **3Ni** (squares) and from the enolate form (circles) vs. Mg^{2+} added (equiv.)

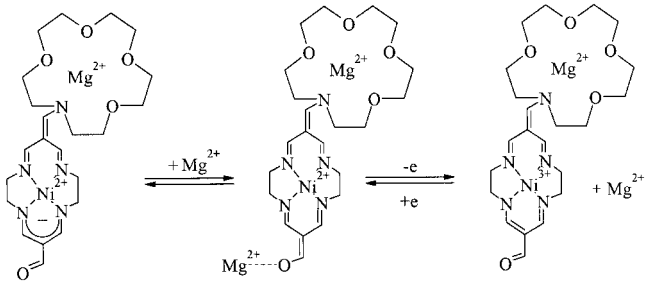

Scheme 2

cation in the crown ether moiety. Further addition of Mg^{2+} forces the charge to shift from the macrocyclic ring to the oxygen of the aldehyde group. This results in the formation of an enolate anion, which interacts with a second Mg^{2+} cation. The second anodic peak corresponds to the oxidation of Ni^{II} from this complex. The so-produced Ni^{III} forces the negative charge to shift again to the macrocyclic ring, with formation of the original complex, which is reduced at about 0.985 V.

To verify the above explanation complex **5Ni** was synthesized.[23] After the addition of Mg^{2+} its electrochemical behavior (Figure 6, B) was similar to that of the **3Ni**. Interaction of an enolate anion with Mg^{2+} was also confirmed by UV/Vis spectroscopy (Figure 8). For both complexes, the absorption band corresponding to Ni^{II} shifts to shorter wavelengths with increasing equivalents of Mg^{2+} cations.

After the addition of 0.25 equiv. of Ba^{2+} the $Ni^{II/III}$ redox potential is shifted towards positive values by 6 mV; however, the second anodic peak at 1.21 V began to appear after the addition of 5 equiv. and increased with the addition of further amounts of Ba^{2+}.

 © 2004 Wiley-VCH Verlag GmbH & Co. KGaA, Weinheim

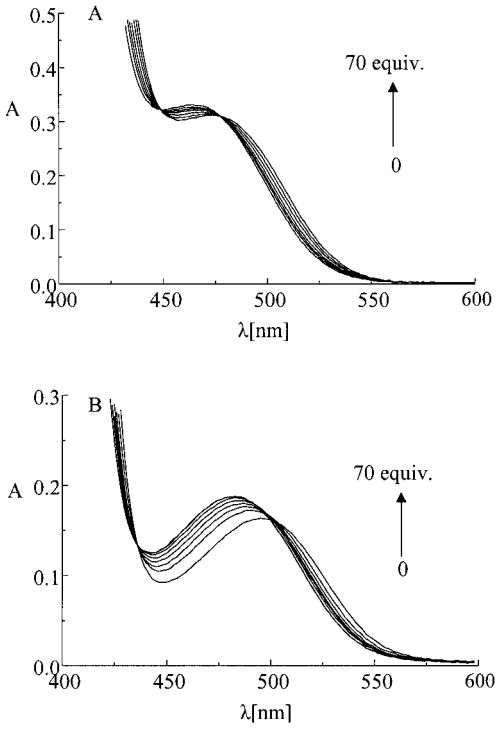

Figure 8. Spectrophotometric titration curves of solutions of **3Ni** (A) and of **5Ni** (B) with $Mg(ClO_4)_2$

The addition of alkali and alkaline earth metal cations to solutions of **4Cu** and **4Ni** had no influence on the E_fs of $Cu^{II/III}$ and $Ni^{II/III}$ redox systems. However, the presence of NH_4^+ exerted a significant influence on the $Cu^{II/I}$ redox process in complex **4Cu**. Figure 9, A, shows the CV of **4Cu** after the addition of 1 equiv. of NH_4^+ cation. The reduction peak *a* at about 200 mV less negative than that of peak *b*, corresponding to the reduction of $Cu^{II/I}$ from complex **4Cu**, is due to the $Cu^{II/I}$ reduction from the part of complex **4Cu** with NH_4^+ cation complexed in the crown ether moiety.

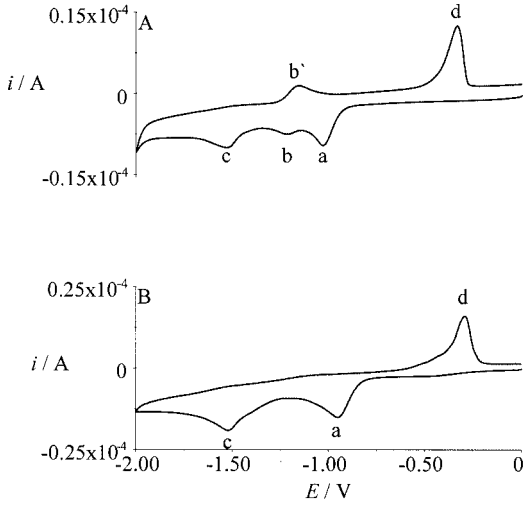

Figure 9. Cyclic voltammograms of complex **4Cu** (5×10^{-4} M) upon addition of (A) 1 equiv. of NH_4^+ and (B) 1 equiv. of Mg^{2+}; scan rate 0.05 Vs^{-1}

Peak *c*, at ca. −1.520 V, corresponds to the $Cu^{I/0}$ reduction in this complex. The proximity of the positively charged cation to the positive copper center can destabilize the complex (which is usually less stable in the case of Cu^+). The anodic peak *d* at ca. −0.300 V corresponds to the oxidation of copper deposited on the electrode surface (which was confirmed by the experiment with CuCl). Peaks *bb′* correspond to the reversible $Cu^{II/I}$ redox process from the original **4Cu** complex. They disappeared at higher concentrations of NH_4^+.

The addition of Na^+ cation had no influence on the $Cu^{II/I}$ redox potential in complex **4Cu**; however, the irreversible $Ni^{II/I}$ potential in complex **4Ni** is shifted anodically by 25 mV after the addition of 20 equiv. of this cation, suggesting that after formation of Ni^I the Na^+ cation is complexed in the crown ether moiety of complex **4Ni**. After the addition of Mg^{2+} cations to the solution of **4Cu** (Figure 9, B) the $Cu^{II/I}$ reduction peak is shifted anodically by about 280 mV (Figure 9, B; peak *a*) versus the original peak *b*. Peaks *c* and *d* were also recorded. A significant increase in both reduction currents (peaks *a* and *c*) indicates that the proximity of Mg^{2+} in the crown ether moiety to the positive copper center can destabilize the complex on the level of Cu^{II}. Such behavior may also be connected with a relatively high concentration of Mg^{2+} in the double layer region. In such a case, Mg^{2+} may influence the electrochemical behavior of the copper center in the azamacrocycle. The CV curves of complex **4Cu** in the presence of Ca^{2+} were similar.

Recognition of Amino Acids

The two α-amino acids (leucine and glycine), β-alanine and lysine (Scheme 3) were chosen as substrate molecules that might interact with complexes **4Cu** and **4 Ni**. Leucine and glycine may interact only with the crown ether moiety (NH_3^+ group) or with the metal cation in the macrocyclic ring through the formation of a coordination bond with the COO^- group. β-Alanine and, especially, lysine, due to the carboxylic and NH_3^+ groups at C-ω, are expected to undergo two-centered fixation. Studies were carried out in acetonitrile/water, 4:1, due to the insolubility of amino acids in pure aprotic solvent.

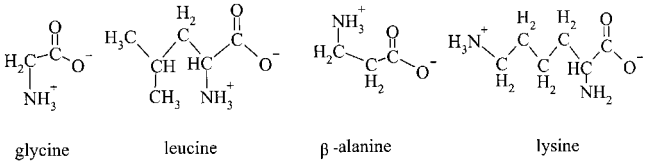

Scheme 3

Unfortunately, electrospray ionization mass spectrometry revealed the decomposition of complexes **4Cu** and **4Ni** (more rapidly) in the presence of leucine and lysine. The peak at *m/z* = 220.2 (Figure 10) corresponds to the free, protonated aza crown ether. The decomposition rate in the presence of lysine (pH of the medium 9.3) was faster than in the presence of leucine (pH of the medium 6.2). Therefore, electrochemical measurements were carried over a short time (3 min after addition of amino acids). Figure 11 shows

 © 2004 Wiley-VCH Verlag GmbH & Co. KGaA, Weinheim

the differential pulse voltammogram (DPV) of the **4Cu** complex recorded after the addition of 2 equiv. of leucine or lysine. In both cases the $Cu^{II/III}$ redox peak diminishes and starts to be irreversible. In the presence of leucine, the $Cu^{II/III}$ peak potential is shifted cathodically by 7 mV, and in the presence of lysine by 40 mV. A potential shift of 10 mV was observed after the addition of 2 equiv. of glycine, and of 30 mV after addition of 2 equiv. of β-alanine. A slight cathodic potential shift with leucine and glycine may be due to the interaction of Cu^{III} with the carboxylic group. The presence of the positively charged NH_3^+ group in the immediate vicinity of the COO^- group and of a highly charged Cu^{III} ion may explain the small potential shift and destabilization of the Cu^{III} complex. The more substantial potential shift observed for β-alanine is consistent with a stronger interaction of the carboxylic group with the Cu^{III} center due to the presence of the charged ammonium group at C-β. For lysine, one can expect the two-center interactions − of the carboxylic group with the Cu^{III} center and of the NH_3^+ group at C-ω with the crown ether moiety. In this case the potential shift (40 mV) may be the result of these two effects − the cathodic shift due to the coordination of the carboxylic group, and the anodic potential shift due to complexation of the charged ammonium group. We found that after the addition of 2 equiv. of acetate anion to a solution of complex **6Cu**[24] (Scheme 4) the $Cu^{II/III}$ potential shifted 80 mV towards less positive values.

Crystallographic data indicate that the lone-pair electrons of the crown ether nitrogen atom contribute to the electron density of the cyclidene macrocycle. This may diminish the binding properties of the crown ether moiety towards cat-

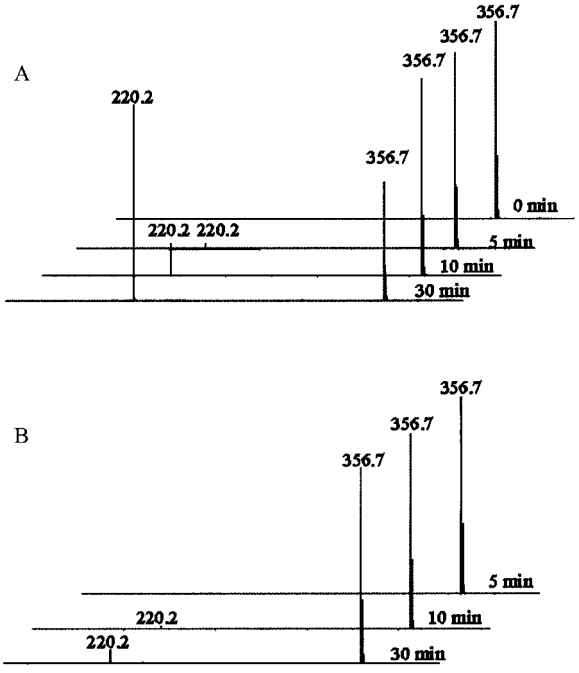

Figure 10. Electrospray ionization mass spectra as a function of time in acetonitrile/H_2O, 4:1, solutions containing 10^{-5} M of complex **4Cu** + 10^{-4} M of the corresponding amino acid: (A) lysine and (B) leucine

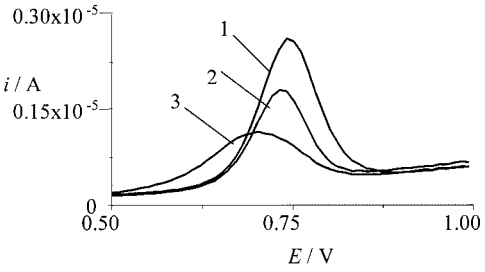

Figure 11. Differential pulse voltammograms of complex **4Cu** recorded in acetonitrile/H_2O, 4:1, containing 0.1 M $[Bu_4N]BF_4$ as supporting electrolyte: (1) 5×10^{-4} M **4Cu**, (2) with 2 equiv. of leucine, and (3) with 2 equiv. of lysine

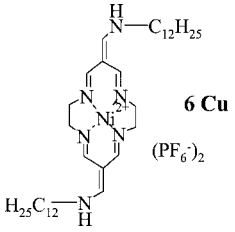

Scheme 4

ions. Conversely, the interaction of the carboxylic group with the central copper ion should reverse this effect and facilitate complexation of the ammonium group in the presence of lysine. Simultaneous binding of carboxylic and ammonium groups with leucine is not possible due to the short distance between them.

Conclusion

Comparison of the E_fs for complexes **4Cu** and **2Cu** indicates that the presence of aza crowns facilitates the $Cu^{II/III}$ redox process and makes the $Cu^{II/I}$ process more difficult.

The interaction of Na^+ and Li^+ with the **3Ni** complex was quite weak. In the presence of Mg^{2+}, the ligand aldehyde isomerizes to enolate ion. Crystallographic data indicate that the lone-pair electrons on the crown ether nitrogen atom contribute to the electron density of the cyclidene macrocycle. This may be one of the reasons why the addition of alkali and alkaline earth metal cations to the solutions of **4Cu** and **4Ni** has no influence on the E_fs of $Cu^{II/III}$ and $Ni^{II/III}$ redox systems. However, the presence of NH_4^+, Mg^{2+} and Ca^{2+} cations influences significantly the $Cu^{II/I}$ redox process in complex **4Cu**.

A more pronounced shift of the $Cu^{II/III}$ potential in **4Cu** in the presence of lysine than with leucine suggests that there is, in the first case, a simultaneous interaction between the NH_3^+ group and the crown ether moiety and between the carboxylic group and the Cu^{III} center.

Experimental Section

Chemicals: All solvents (Merck) were used without further purification. Deionized water from a Milli-Q system (Millipore, Bedford,

 © 2004 Wiley-VCH Verlag GmbH & Co. KGaA, Weinheim

MA, USA), distilled additionally from a quartz still, was used. As supporting electrolyte, electrochemical grade $[Bu_4N]BF_4$ (Fluka) was used. Cations were added as their perchlorate salts.

Instrumentation: Cyclic and differential pulse voltammograms were measured at a glassy carbon (GC-20) electrode with a Pt plate as the counter electrode and an Ag/Ag^+ reference electrode. This was connected to the electrolytic cell via an intermediate vessel filled with the solution under investigation. The Ag/Ag^+ reference electrode contained an internal solution of 0.001 M $AgNO_3$ + 0.10 M $[Bu_4N]BF_4$ in acetonitrile. The potential of this reference electrode was 200 mV vs. 1 M NaCl aqueous calomel electrode (MCE). All potentials in this paper are expressed vs. this reference electrode. Solutions were deaerated by flushing with pure argon. The measuring system was an Autolab (EcoChemie, Netherlands). Electronic spectra were recorded using a Cary 1 (Varian) spectrophotometer. NMR spectra were obtained on a Varian Mercury 400 spectrometer. Signals are reported in ppm relative to residual solvent signal. IR spectra (paraffin oil mulls) were recorded with a Perkin−Elmer Spectrum 2000 FT-IR spectrometer. ESI mass spectra were measured on a Mariner Perseptive Biosystem mass spectrometer.

Synthesis

Syntheses of 5,12-dimethyl-1,4,8,11-tetraazacyclotetradeca-4,11-diene diperchlorate and of complexes **1Cu** and **1Ni** have been described elsewhere.[24]

[6,13-Bis(morpholinomethylidene)-1,4,8,11-tetrazacyclotetradeca-4,7,11,14-tetraene]nickel(II) Bis(hexafluorophosphate) (2Ni): Morpholine (0.18 cm^3, 1 mmol) was added to a solution of complex **1Ni** (0.32 g, 0.5 mmol) in dry acetonitrile (25 mL). The mixture was then stirred for 4 h at room temperature, and the resulting solution was applied to a 2 × 20 cm acidic alumina column. The column was then washed with acetonitrile. A fast-moving orange band was collected, evaporated and dissolved in acetonitrile/H_2O, 1:1. Solid NH_4PF_6 (0.2 g) was then added to the solution and the resultant orange crystalline product that precipitated upon evaporation of acetonitrile was filtered off and dried under reduced pressure. Yield 0.29 g, 79%. $C_{20}H_{30}N_6NiO_2{\cdot}(PF_6)_2$ (735.1): calcd. C 32.7, H 4.1, N 11.4; found C 32.9, H 4.1, N 11.4. ^1H NMR (CD_3CN, 400 MHz): δ = 3.54 (s, 8 H, NCH_2CH_2N), 3.69 (b. m, 4 H, morpholine CH_2 groups), 3.70 (b. m, 4 H, morpholine CH_2 groups), 3.82 (b. m, 8 H, morpholine CH_2 groups), 7.58 (s, 2 H, exoc. =CH−N), 7.74 (b. s, 4 H, N=C−H). ^{13}C NMR (CD_3CN, 100 MHz): 51.7, 57.1, 66.1 and 67.2 (morpholine CH_2), 60.1 (b, NCH_2CH_2N), 103.6 (ring-C=), 162.9 (exoc. =CH−N, ring H−C=N signals were not observed due to dynamic line broadening). IR (Nujol): $\tilde{\nu}$ = 1600 and 1568 (ν C=N and C=C), 840 and 558 (PF_6^-) cm^{-1}. UV/Vis (CH_3CN, nm): λ_{max} (ε) = 267 (28980), 380 (52360), 459 (1400). ESI MS: *m*/*z* = 444.2 $[C_{20}H_{30}N_6NiO_2]^{2+}$.

[6,13-Bis(morpholinomethylidene)-1,4,8,11-tetraazacyclotetradeca-4,7,11,14-tetraene]copper(II) Bis(hexafluorophosphate) (2Cu): Complex was synthesized from copper(II) complex **1Cu** following the same procedure as for **2Ni**. Yield 75%. $C_{20}H_{30}CuN_6O_2{\cdot}(PF_6)_2$ (740.0): calcd. C 32.5, H 4.1, N 11.4; found C 32.6, H 4.2, N 11.5. IR (Nujol): $\tilde{\nu}$ = 1599 (ν C=N and C=C), 833 and 533 (PF_6^-) cm^{-1}. UV/Vis (CH_3CN, nm): λ_{max} (ε) = 294 (27370), 347 (65900), 507 (301). ESI MS: *m*/*z* = 224.6 $[C_{20}H_{30}CuN_6O_2]^{2+}$.

{6,13-Bis[(1,4,7,10-tetraoxa-13-azacyclooctadecano-13-yl)methylidene]-1,4,8,11-tetraazacyclotetradeca-4,7,11,14-tetraene}nickel(II) Bis(hexafluorophosphate) (4Ni): 1,4,7,10-Tetraoxa-13-azacyclooctadecane (0.22 g, 1 mmol) was added to a solution of complex **1Ni** (0.315 g, 0.5 mmol) in dry acetonitrile (25 mL). The mixture was then stirred for 4 h at room temperature, and the resulting solution was applied to a 2 × 20 cm acidic alumina column. The column was subsequently washed with acetonitrile. A fast-moving orange band was then collected, evaporated and crystallized from acetonitrile/water. The orange crystalline product that precipitated upon evaporation of acetonitrile was filtered off and dried under reduced pressure. Yield 0.39 g, 78%. $C_{32}H_{54}N_6NiO_8{\cdot}(PF_6)_2$ (999.4): calcd. C 38.5, H 5.5, N 8.4; found C 38.4, H 5.5, N 8.5. ^1H NMR (CD_3CN, 400 MHz): δ = 3.60−3.90(m, 48 H, NCH_2CH_2N and crown ether CH_2 groups), 7.66 (s, 2 H, exocyclic =CH−N), 7.99 (v.b. s, 4 H, ring N=C−H). ^{13}C NMR (CD_3CN, 100 MHz): 55.7, 61.6, 68.0, 69.8, 70.7, 70.8, 70.9, 71.1, 71.2, 71.3 (crown ether CH_2), 60.1 (broad, ring NCH_2-CH_2N), 104.7 (ring =C; ring H−C=N signals were not observed due to dynamic line broadening), 165.3 (exocyclic = CH−N). IR (Nujol): $\tilde{\nu}$ = 1594 vs, 1559 w (ν C=N and C=C), 842 vs and 559 s (PF_6^-) cm^{-1}. UV/Vis (CH_3CN): λ_{max} (ε) = 267 (28980), 380 (52360), 459 (1400) nm. ESI MS (CH_3CN, *m*/*z*): 354.2$[C_{32}H_{54}O_8N_6Ni]^{2+}$.

{6-Formyl-13-[(1,4,7,10-tetraoxa-13-azacyclooctadecano-13-yl)methylidene]-1,4,8,11-tetraazacyclotetradeca-4,7,11,14-tetraen}-nickel(II) Hexafluorophosphate (3Ni): 1,4,7,10-Tetraoxa-13-azacyclooctadecane (0.11 g, 0.5 mmol) was added to a solution of complex **1Ni** (0.315 g, 0.5 mmol) in dry acetonitrile (25 mL). The mixture was then stirred for 2 h at room temperature. The resulting solution was diluted with water (25 mL) and applied to the SP Sephadex C25 cation exchange column (25 × 2 cm). The column was then washed with water and eluted with 0.2 M Na_2SO_4 solution. Two resultant orange bands were separated and the products precipitated with an excess NH_4PF_6. After filtration the isolated solid products were dissolved in acetonitrile, diluted with water/ethanol, 1:1, and crystallized upon slow evaporation of solvents. The first fraction contained complex **3Ni** (yield 30%), and the previously described complex **4Ni** was isolated from the second fraction. $C_{22}H_{34}N_5NiO_5{\cdot}PF_6$ (652.2): calcd. C 40.5, H 5.3, N 10.7; found C 40.4, H 5.3, N 10.5. ^1H NMR (CD_3CN, 400 MHz): δ = 3.60−3.90 (m, 28 H, NCH_2CH_2N and crown ether CH_2 groups), 7.57 (s, 1 H, exocyclic =CH−N), 7.50 (v.b. s, 1 H) and 8.37 (v.b. s, 1 H, ring N=C−H crown ether site), 7.50 (b. s, 1 H) and 7.86 (b. s, 1 H, ring N=C−H formyl site), 9.20 (s, 1 H, O=C−H). ^{13}C NMR (CD_3CN, 100 MHz): δ = 55.5, 61.5, 68.2, 70.0, 70.7, 70.8, 71.0, 71.2, 71.2, 71.2 (crown ether CH_2), 58.6, 59.0, 59.3, 60.8 (broad, ring NCH_2-CH_2N), 104.8 (ring =C−CHN), 114.2 (ring =C−CHO, ring H−C=N not observed), 164.5 (=CH−N), 187.3 C=O. IR (Nujol): $\tilde{\nu}$ = 1656 m,1594 vs, 1569 m, 1541 (ν C=O, C=N and C=C), 841 vs and 558 s (PF_6^-) cm^{-1}. UV/Vis (CH_3CN, nm): λ_{max} (ε) = 247 (15900), 281 (26880), 357 (28140), 371 (29040), 474 sh (636). ESI MS (CH_3CN): *m*/*z* = 506.2 $[C_{22}H_{34}N_5NiO_5]^+$.

{6,13-Bis[(1,4,7,10-tetraoxa-13-azacyclooctadecano-13-yl)methylidene]1,4,8,11-tetraazacyclotetradeca-4,7,11,14-tetraene}copper(II) Hexafluorophosphate (4Cu): This complex was synthesized from copper(II) complex **1Cu** following the same procedure as with **4Ni**. Yield 85%, red crystals. $C_{32}H_{54}CuN_6O_8{\cdot}(PF_6)_2$ (1004.3): calcd. C 38.3, H 5.4, N 8.4; found C 38.3, H 5.5, N 8.5. IR (Nujol): $\tilde{\nu}$ = 1646 w, 1599 s, 1587 s (PF_6^-), 841 vs and 558 s (PF_6^-) cm^{-1}. UV/Vis (CH_3CN, nm): λ_{max} (ε) = 290 (17050), 345 (43050), 492 (306). ESI MS (CH_3CN) *m*/*z* =356.7 $[C_{32}H_{54}CuN_6O_8]^{2+}$.

X-ray Crystallographic Study: The structures of **3Ni** and **4Cu** complexes were determined in single-crystal X-ray diffraction experiments. Both measurements were performed on a Kuma KM4CCD κ-axis diffractometer with graphite-monochromated Mo-K_α radi-

 © 2004 Wiley-VCH Verlag GmbH & Co. KGaA, Weinheim

ation (λ = 0.71073 A, 45.0 kV, 40.0 mA) at room temperature (293 K). In each experiment the crystal was positioned 62 mm from the KM4CCD camera. Some 600 frames were measured for each crystal at 1.0° intervals with counting times of 33 s for the **3Ni** crystal and 27 s for **4Cu**. A numeric absorption correction was applied to the collected datasets. Data reduction and analysis were carried out with the Kuma Diffraction programs.

The structures were solved by direct methods using the SHELXS-97[25] program and subsequent refinement was also carried out with SHELXL-97.[26] Refinement was based on F^2 for all reflections except those with negative intensities. Weighted R factors, wR and all goodness-of-fit S values were based on F^2, whereas conventional R factors were based on the amplitudes, with F set to zero for negative F^2. The $F_o^2 > 2\sigma(F_o^2)$ criterion was applied only in calculating R factors and was not relevant to the choice of reflections for the refinement. The R factors based on F^2 are, for both structures, about twice as large as those based on F. For the **3Ni** structure some hydrogen atoms were located in idealized geometrical positions. Also, some special constraints were applied to the anisotropic displacement parameters of some atoms; the constraints were necessary due to disorder in the crown-ether compound and PF_6^- ion. Scattering factors were taken from Table 4.2.6.8 and 6.1.1.4 of International Crystallographic Tables Vol. C.[27]

3Ni: $C_{22}H_{34}NiN_5O_5{\cdot}PF_6$, M = 652.22, T = 293(2) K, λ = 0.71073 Å; crystal system, monoclinic; space group, $P2_1/c$; unit cell dimensions, a = 18.454(4) Å, b = 11.406(2) Å, c = 13.642(3) Å, α = 90°, β = 103.93(3)°, γ = 90°; V = 2787.0(10) Å^3; Z = 4; calculated density = 1.554 Mg m^{-3}; absorption coefficient = 0.836 mm^{-1}; F(000) = 1352; crystal size: 0.34 × 0.16 × 0.07 mm; θ range for data collection: 3.41 to 22.50°; index range: $-19 \le h \le 19$, $-12 \le k \le 12$, $-12 \le l \le 14$; reflections collected = 16239; unique reflections = 3637 [R_{int}= 0.0632]; completeness to θ = 22.50°: 99.7%; refinement method, full-matrix least-squares on F^2, data/restraints/parameters: 3637/51/460; goodness-of-fit on F^2 = 1.148; final R int [$I > 2\sigma(I)$]: $R1$ = 0.0445, $wR2$ = 0.1170; R int (all data): $R1$ = 0.0589, $wR2$ = 0.1273; extinction coefficient = 0.0020(7); weight = $1/[\sigma^2(F_o^2) + (0.0712P)^2 + 0.00P]$ where $P = [\max(F_o^2, 0) + 2F_c^2]/3$; largest diffraction peak and hole: 0.604 and −0.348 e·Å^{-3}.

4Cu: $C_{32}H_{54}CuF_{12}N_6O_8P_2$, M = 1004.29, T = 293 K, λ = 0.71073 Å; crystal system, triclinic; space group, $P\bar{1}$; unit cell dimensions, a = 8.7793(18) Å, b = 9.783(2) Å, c = 13.301(3) Å, α = 106.50(3)°, β = 103.90(3)°, γ = 93.88(3)°; V = 1051.9(4) Å^3; Z = 1; calculated density = 1.585 Mg m^{-3}; absorption coefficient = 0.703 mm^{-1}, F(000) = 51, crystal size = 0.30 × 0.20 × 0.10 mm, θ range for data collection = 3.32 to 22.50°; index ranges: $-8 \le h \le 9$, $-10 \le k \le 10$, $-14 \le l \le 14$; reflections collected = 6301, unique reflections = 2740 [R_{int} = 0.0443]; completeness to θ = 22.50°: 99.5%; refinement method, full-matrix least-squares on F^2; data/restraints/parameters: 2740/0/386; goodness-of-fit on F^2 = 1.056; final Rint [$I > 2\sigma(I)$]: $R1$ = 0.0374, $wR2$ = 0.0989; R int (all data): $R1$ = 0.0437, $wR2$ = 0.1047; extinction coefficient = 0.004(2); weight = $1/[\sigma^2(F_o^2) + (0.0671P)^2 + 0.2486P]$ where $P = [\max(F_o^2, 0) + 2F_c^2]/3$; largest diffraction peak and hole: 0.413 and −0.287 e·Å^{-3}.

CCDC-227140 and -227141 (for **3Ni** and **4Cu**, respectively) contain the supplementary crystallographic data for this paper. These data can be obtained free of charge at www.ccdc.cam.ac.uk/conts/retrieving.html [or from the Cambridge Crystallographic Data Centre, 12 Union Road, Cambridge CB2 1EZ, UK; Fax: (internat.) +44-1223-336-033; E-mail: deposit@ccdc.cam.ac.uk].

Acknowledgments

Financial support for B. K. D. and K. W. by the State Committee for Scientific Research (project 4 T09A 048 23) is gratefully acknowledged. The authors are grateful to Mrs. S. Pawłowska for technical help. X-ray measurements were undertaken in the Crystallographic Unit of the Physical Chemistry Laboratory at the Chemistry Department of the University of Warsaw.

[1] P. D. Beer, *Adv. Inorg. Chem.* **1992**, *39*, 79−154.
[2] P. D. Beer, P. A. Gale, Z. Chen, *Adv. Phys. Org. Chem.* **1998**, *31*, 1−84.
[3] P. D. Beer, P. A. Gale, G. Z. Chen, *Coord. Chem. Rev.* **1999**, 185−186, 3−36.
[4] P. L. Boulas, M. Gómez-Kaifer, L. Echengoyen, *Angew. Chem. Int. Ed.* **1998**, *37*, 216−247.
[5] I. Ion, J. C. Moutet, A. Popescu, E. Saint-Aman, L. Tomazeswski, I. Gautier-Luneau, *J. Electroanal. Chem.* **1997**, *440*, 145−152.
[6] H. Plenio, D. Burth, *Organometallics* **1996**, *15*, 4054−4062.
[7] C. D. Hall, S. Y. Chu, *J. Organomet. Chem.* **1995**, *498*, 221−228.
[8] H. Plenio, R. Diodone, *J. Organomet. Chem.* **1995**, *492*, 73−80.
[9] H. Plenio, C. Aberle, *Organometallics* **1997**, *16*, 5950−5957.
[10] H. Plenio, J. Yang, R. Diodone, J. Heinze, *Inorg. Chem.* **1994**, *33*, 4098−4104.
[11] J. C. Medina, T. T. Goodnow, S. Bott, J. L. Atwood, A. E. Kaifer, G. W. Gokel, *J. Chem. Soc., Chem. Commun.* **1991**, 290−292.
[12] V. Balzani, M. Gómez-López, J. F. Stoddart, *Acc. Chem. Res.* **1998**, *31*, 405−416.
[13] A. P. de Silva, H. Q. N. Gunarante, C. P. McCoy, *Nature* **1993**, *346*, 42−44.
[14] E. V. Rybak-Akimova, Y. D. Lampeka, *Supramol. Chem.* **1995**, *4*, 297−304.
[15] O. P. Kryatova, A. G. Kolchinski, E. V. Rybak-Akimova, *Tetrahedron* **2003**, *59*, 231−239.
[16] O. P. Kryatova, A. G. Kolchinski, E. V. Rybak-Akimova, *J. Inclus. Phenom.* **2002**, *42*, 251−260.
[17] P. V. Bernhardt, E. J. Hayes, *Inorg. Chem.* **2002**, *41*, 2892−2902.
[18] L. Fabbrizzi, M. Licchelli, P. Pallavicini, *Acc. Chem. Res.* **1999**, *32*, 846−853.
[19] J. Taraszewska, K. Zięba, B. Korybut-Daszkiewicz, *Electrochim. Acta* **2001**, *46*, 3219−3225.
[20] V. Thanabal, V. Krishnan, *J. Am. Chem. Soc.* **1982**, *104*, 3643−3650.
[21] O. E. Sielcken, M. M. Tilborg, M. F. M. Roks, R. Hendriks, W. Drenth, R. J. M. Nolte, *J. Am. Chem. Soc.* **1987**, *109*, 4261−4265.
[22] E. Kimura, H. Fujioka, M. Kodama, *J. Chem. Soc., Chem. Commun.* **1986**, 1158−1159.
[23] W. Grochala, A. Jagielska, K. Woźniak, A. Więckowska, R. Bilewicz, B. Korybut-Daszkiewicz, J. Bukowska, L. Piela, *J. Phys. Org. Chem.* **2001**, *14*, 63−73.
[24] B. Korybut-Daszkiewicz, A. Więckowska, R. Bilewicz, S. Domagała, K. Woźniak, *J. Am. Chem. Soc.* **2001**, *123*, 9356−9366.
[25] G. M. Sheldrick, *Acta Crystallogr., Sect. A* **1990**, *46*, 467−473.
[26] M. Sheldrick, *SHELXL-97. Program for the Refinement of Crystal Structures; University of Göttingen, Germany.*
[27] *International Tables of Crystallography* (Ed.: A. J. C. Wilson), Kluwer, Dordrecht, **1992**, vol. C, 19.

Received December 9, 2003
Early View Article
Published Online June 11, 2004

 © 2004 Wiley-VCH Verlag GmbH & Co. KGaA, Weinheim

A Study of the Electronic Spin-State Crossover in $\{Fe[HC(3,4,5\text{-}Me_3pz)_3]_2\}(BF_4)_2$

Daniel L. Reger,*[a] J. Derek Elgin,[a] Mark D. Smith,[a] Fernande Grandjean,[b] Leila Rebbouh,[b] and Gary J. Long*[c]

Keywords: Iron / N ligands / Spin crossover / Magnetic properties / Mössbauer spectroscopy

The synthesis, structural, magnetic, and Mössbauer spectroscopic properties of $\{Fe[HC(3,4,5\text{-}Me_3pz)_3]_2\}(BF_4)_2$ are reported. The single-crystal X-ray structure results indicate that at 150 K $\{Fe[HC(3,4,5\text{-}Me_3pz)_3]_2\}(BF_4)_2$ has a structure which is very similar to that observed at 220 K for the trigonally distorted octahedral, high-spin $\{Fe[HC(3,5\text{-}Me_2pz)_3]_2\}(BF_4)_2$ complex. Both the magnetic and Mössbauer spectroscopic results indicate that $\{Fe[HC(3,4,5\text{-}Me_3pz)_3]_2\}(BF_4)_2$ is high spin between 160 and 296 K. Upon cooling, $\{Fe[HC(3,4,5\text{-}Me_3pz)_3]_2\}(BF_4)_2$ exhibits a complete electronic spin-state crossover from the high-spin to the low-spin state at approximately 110 K and remains completely low spin down to 4.2 K; upon subsequent warming from 4.2 K, the transition from the low-spin to the high-spin state occurs at 148 to 150 K. $\{Fe[HC(3,4,5\text{-}Me_3pz)_3]_2\}(BF_4)_2$ exhibits a rather large thermal hysteresis of 38 K in its spin-state crossover. Thus, $\{Fe[HC(3,4,5\text{-}Me_3pz)_3]_2\}(BF_4)_2$ behaves differently from both $\{Fe[HC(3,5\text{-}Me_2pz)_3]_2\}(BF_4)_2$, which is known to show a unique spin-state crossover of one-half of its iron(II) ions associated with a phase transition, and $Fe[HB(3,4,5\text{-}Me_3pz)_3]_2$, which is known to remain high-spin even upon cooling to 1.7 K.
(© Wiley-VCH Verlag GmbH & Co. KGaA, 69451 Weinheim, Germany, 2004)

Introduction

The various unsubstituted and methyl-substituted tris(pyrazolyl)borate anionic ligands[1] have become very important in coordination chemistry and are known to sometimes provide a crystal-field potential that leads to a spin-state crossover in nominally octahedral high-spin iron(II) complexes.[2−4] This crossover, which involves a change from the paramagnetic $^5T_{2g}$ high-spin state to the diamagnetic $^1A_{1g}$ low-spin state, can be induced by cooling, by optical excitation, or by the application of pressure.[5−9]

The ubiquity of the tris(pyrazolyl)borate ligands in yielding a variety of electronic spin-state behaviors in iron(II) complexes led us to undertake an extensive investigation of the iron(II) complexes formed with the related unsubstituted and methyl-substituted tris(pyrazolyl)methane neutral ligands.[10−17] This work showed different behaviors for $\{Fe[HC(3,5\text{-}Me_2pz)_3]_2\}(BF_4)_2$ and $\{Fe[HC(3,5\text{-}Me_2pz)_3]_2\}I_2$: the first complex exhibits[10−13] a unique structural phase transition upon cooling, a phase transition that induces a spin-state crossover to the low-spin state of only one-half of the initially identical high-spin iron(II) ions; in contrast, the second complex exhibits[14−15] the more usual complete spin-state crossover upon cooling and at high-pressure. Interestingly, the low-spin complex, $\{Fe[HC(pz)_3]_2\}(BF_4)_2$, undergoes a gradual spin-state transition[11] to the high-spin state upon heating above 295 K, a transition which is very similar to that observed[7] in the analogous borate complex, $Fe[HB(pz)_3]_2$.

We have undertaken an investigation of $\{Fe[HC(3,4,5\text{-}Me_3pz)_3]_2\}(BF_4)_2$ (**1**) for two reasons: because $Fe[HB(3,4,5\text{-}Me_3pz)_3]_2$ is known[7] to remain high-spin even upon cooling to 1.7 K and to show a spin-state crossover to the low-spin state at high pressure,[7] and because $\{Fe[HC(3,5\text{-}Me_2pz)_3]_2\}(BF_4)_2$ has a unique spin-state crossover behavior. Herein we report the synthesis, the single-crystal X-ray structure and magnetic analysis, and Mössbauer spectroscopic studies of this new complex, a complex that does show a complete spin-state crossover from the high-spin to the low-spin state upon cooling.

Results and Discussion

Synthesis

The reaction of $Fe(BF_4)_2\cdot 6H_2O$ and two equivalents of $HC(3,4,5\text{-}Me_3pz)_3$ prepared according to a modified literature procedure[18] in tetrahydrofuran leads to the formation of $\{Fe[HC(3,4,5\text{-}Me_3pz)_3]_2\}(BF_4)_2$ (**1**), see Scheme 1.

[a] Department of Chemistry and Biochemistry, University of South Carolina, Columbia, SC 29208, USA
[b] Institute of Physics, B5, University of Liège, 4000 Sart-Tilman, Belgium
[c] Department of Chemistry, University of Missouri-Rolla, Rolla, MO 65409-0010, USA

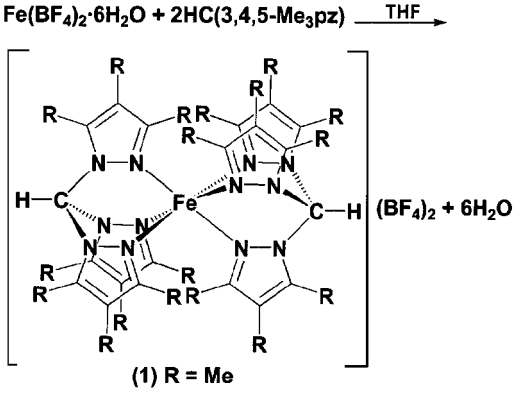

Scheme 1

$\{Fe[HC(3,4,5\text{-}Me_3pz)_3]_2\}(BF_4)_2$ in powder form is white, and its single crystals are colorless indicating that the iron(II) is high-spin at room temperature.[8,11] The solution phase ^1H NMR spectrum is broad with chemical shifts ranging from 41 to −43 ppm, a range that is indicative of a paramagnetic high-spin iron(II) complex.

X-ray Structure

The single-crystal X-ray structure of the iron(II) cation in **1** is shown in Figure 1 and a view down the H−C−Fe−C−H pseudo-threefold axis of the cation is shown in Figure 2. Crystallographic information and selected bond lengths and angles are given in Table 1 and Table 2. The structure of the N_6 coordination environment is that of a distorted octahedron in which the largest structural deviation results from the restrictions imposed by the chelate rings; the intraligand N−Fe−N angles average 84.1°. The average Fe−N bond length is 2.162 Å, a value that is clearly indicative of a high-spin iron(II) complex. In contrast, an average Fe−N bond length of about 1.97 Å is typical of a low-spin iron(II) complex with an N_6 coordination environment.[3] The structure of the cation in **1** is very similar to that in $\{Fe[HC(3,5\text{-}Me_2pz)_3]_2\}(BF_4)_2$. In this complex the average Fe−N bond length is 2.17 Å and the chelate rings restrict the intraligand N−Fe−N angles to an average of 84.3°.[11]

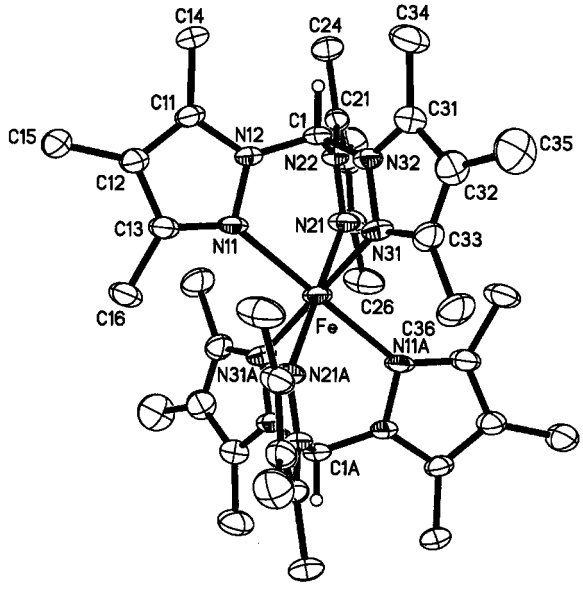

Figure 1. The structure of the cation in $\{Fe[HC(3,4,5\text{-}Me_3pz)_3]_2\}(BF_4)_2$ (**1**) with atom numbering

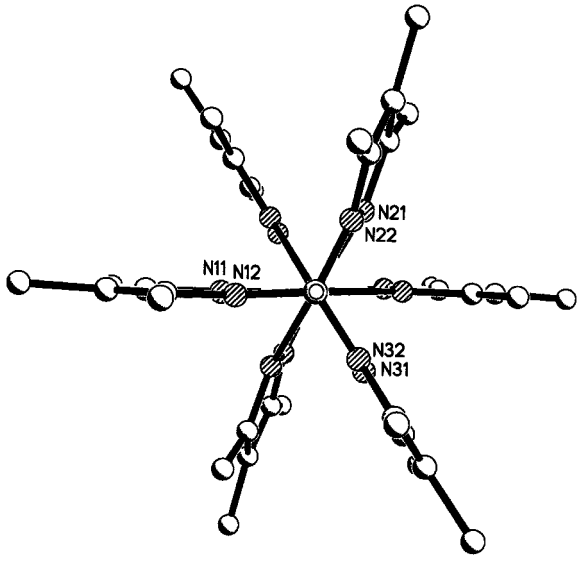

Figure 2. A view down the H−C−Fe−C−H pseudo-threefold axis of the cation in $\{Fe[HC(3,4,5\text{-}Me_3pz)_3]_2\}(BF_4)_2$ (**1**)

Table 1. Crystallographic data for $\{Fe[HC(3,4,5\text{-}Me_3pz)_3]_2\}(BF_4)_2$ (**1**)

Formula	$C_{38}H_{56.7}B_2F_8FeN_{12}O_{0.35}$
Molecular mass (g mol^{-1})	916.72
Space group	$P-1$
Crystal system	triclinic
a (Å)	10.5451(5)
b (Å)	10.8148(6)
c (Å)	11.0021(6)
α (deg)	83.4960(10)
β (deg)	88.5220(10)
γ (deg)	63.4790(10)
V (Å^3)	1115.02(10)
Z	1
Crystal color, habit	colorless, block
$D_{calcd.}$ (g cm^{-3})	1.364
Temperature (K)	150(1)
Diffractometer	Bruker SMART APEX CCD
Radiation	Mo-K_α (λ = 0.71073 Å)
$R(F)$ (%)[a]	4.75
$R(wF^2)$ (%)[a]	12.17

[a] Quantity minimized: $R(F) = \Sigma[F_o - F_c]/\Sigma[F_o]$; $R(wF2) = \Sigma[w(F_o^2 - F_c^2)^2]/\Sigma[(wF_o^2)]^{1/2}$.

One interesting difference between the two structures involves the "tilting" of the pyrazolyl rings away from an ideal C_{3v} arrangement. In the absence of tilting the FeN(n1)−N(n2)−C(n1) torsion angles (where n denotes the ring number) would be 180° and the iron(II) ion would reside in the planes defined by the pyrazolyl rings. In general, this torsion angle decreases as the size of the metal ion in-

 © 2004 Wiley-VCH Verlag GmbH & Co. KGaA, Weinheim

Table 2. Selected bond lengths and angles in {Fe[HC(3,4,5-Me$_3$pz)$_3$]$_2$}(BF$_4$)$_2$ (**1**)

Bond lengths (Å)	
Fe−N(31)	2.150(2)
Fe−N(21)	2.159(2)
Fe−N(11)	2.1784(19)
C1−N(32)	1.436(3)
C1−N(12)	1.439(3)
C1−N(22)	1.445(3)
Bond angles (°)	
N(31)−Fe−N(21)	83.25(8)
N(31)−Fe−N(21)	96.75(8)
N(31)−Fe−N(11)	84.54(8)
N(21)−Fe−N(11)	84.64(8)
N(31)−Fe−N(11)	95.46(8)
N(21)−Fe−N(11)	95.36(8)
N(32)−C1−N(12)	111.75(19)
N(32)−C1−N(22)	111.75(19)
N(12)−C1−N(22)	111.38(19)

creases, because the bite size of these ligands is largely fixed, and increasing the tilting is an important way to accommodate larger metal ions.[10] In the fully high-spin structure[11] of {Fe[HC(3,5-Me$_2$pz)$_3$]$_2$}(BF$_4$)$_2$ this torsion angle averages 168°, with the range from 167.3 to 172.4°. In contrast, as is shown in Figure 2, in **1** two of the angles [178.92(16) and 179.74(16)°] suggest very little tilting, whereas the third ring shows substantial tilting with an angle of 164.55(15)°; the average value is 174.4°. The size of these angles is important: the angles are approximately 180° in these complexes when the iron(II) is low spin, and the Fe−N bond lengths are about 0.2 Å shorter.[10,13] Unfortunately, we have been unable to obtain the low-temperature crystal structure of **1** in order to follow how these angles change upon spin-state crossover, because the crystals shatter upon cooling to low temperature.

Magnetic Results

The temperature dependence of the molar magnetic susceptibility and the effective magnetic moment, μ_{eff}, of **1** is shown in Figure 3. This figure includes magnetic results for two full cycles of cooling and heating and reveals that the results for the second cooling and heating cycle are identical to those of the first cycle. Between 150 and 295 K the complex is paramagnetic and exhibits Curie law behavior with a Curie constant of 3.136 K/(emu/mol) and a small Weiss temperature of 1.85 K. These values correspond to an effective magnetic moment, μ_{eff}, of 5.01 μ_B between 150 and 295 K, a moment which is typical of high-spin iron(II) with a nominal octahedral $^5T_{2g}$ electronic ground state. Thus, above 150 K **1** is fully high spin.

As is shown in Figure 3, upon cooling below 150 K **1** exhibits a sharp decrease in its molar magnetic susceptibility beginning at about 110 K such that at 100 K and below the complex is essentially diamagnetic as would be expected of a low-spin iron(II) complex with a nominal octahedral $^1A_{1g}$ electronic ground state. Upon subsequent heating from 5 K, the complex remains low spin until, at 138 K, the magnetic susceptibility increases sharply such that at 148 K it is the same as that of the high-spin state. This behavior is typical of an iron(II) spin-state crossover, albeit with a rather large magnetic hysteresis of about 38 K.

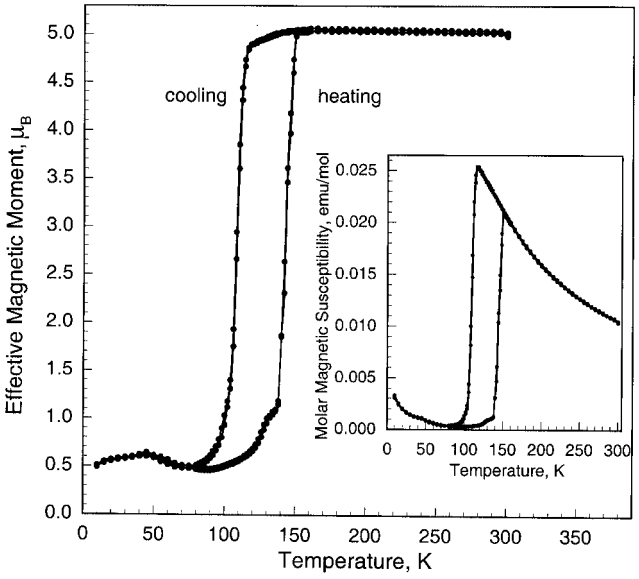

Figure 3. The temperature dependence of the effective magnetic moment of {Fe[HC(3,4,5-Me$_3$pz)$_3$]$_2$}(BF$_4$)$_2$ (**1**); inset: the temperature dependence of the molar magnetic susceptibility of **1**

Below about 60 K the molar magnetic susceptibility of **1** (see Figure 3) shows a small increase, which would be typical of an approximate 0.01 weight percent trace of either a high-spin iron(II) or a high-spin iron(III) impurity. Again, this behavior is typical of a diamagnetic complex whose low temperature magnetic properties are extremely sensitive to the presence of any paramagnetic impurities. Further, as is shown in Figure 3, below about 80 K the effective magnetic moment of **1** is essentially constant at 0.5 μ_B, a value which results partly from the trace impurity and predominately from a second-order Zeeman contribution to the molar magnetic susceptibility, i.e. the temperature-independent paramagnetic contribution to the moment of a diamagnetic complex that has a low-lying excited magnetic state; in this case the $^5T_{2g}$ state is the low-lying excited state at temperatures below the spin-state crossover.

Mössbauer Spectroscopic Results

The Mössbauer spectra of **1** obtained upon cooling from 296 K are shown in Figure 4, and the corresponding spectra obtained upon heating from 4.2 K are shown in Figure 5. In all cases the spectra have been fit with one or two symmetric quadrupole doublets, and selected hyperfine parameters are given in Table 3. The temperature dependence of the observed isomer shifts and quadrupole splittings is shown in Figure 6. The hyperfine parameters of the single quadrupole doublet observed at 160 K and above clearly indicate that **1** is high spin above this temperature.[2,7,11] Further, the hyperfine parameters of the single quadrupole

 © 2004 Wiley-VCH Verlag GmbH & Co. KGaA, Weinheim

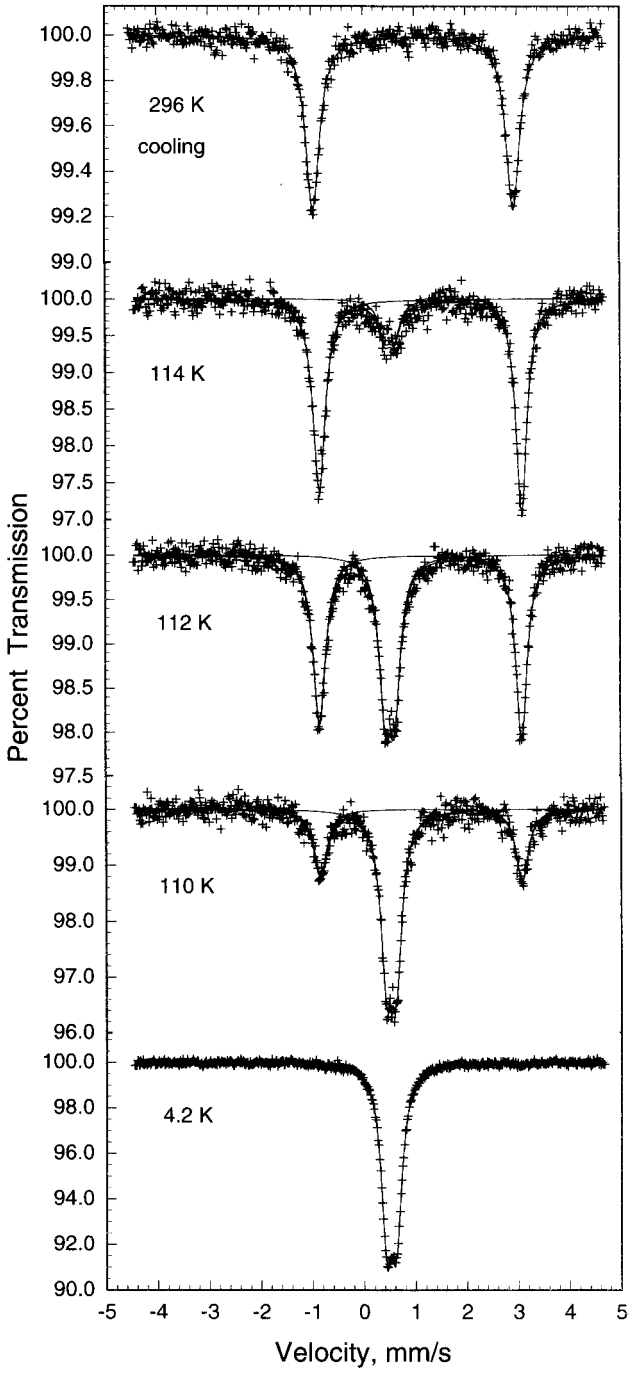

Figure 4. The Mössbauer spectra of {Fe[HC(3,4,5-$Me_3pz)_3]_2$}$(BF_4)_2$ (**1**) obtained at the indicated temperatures upon cooling from 296 K

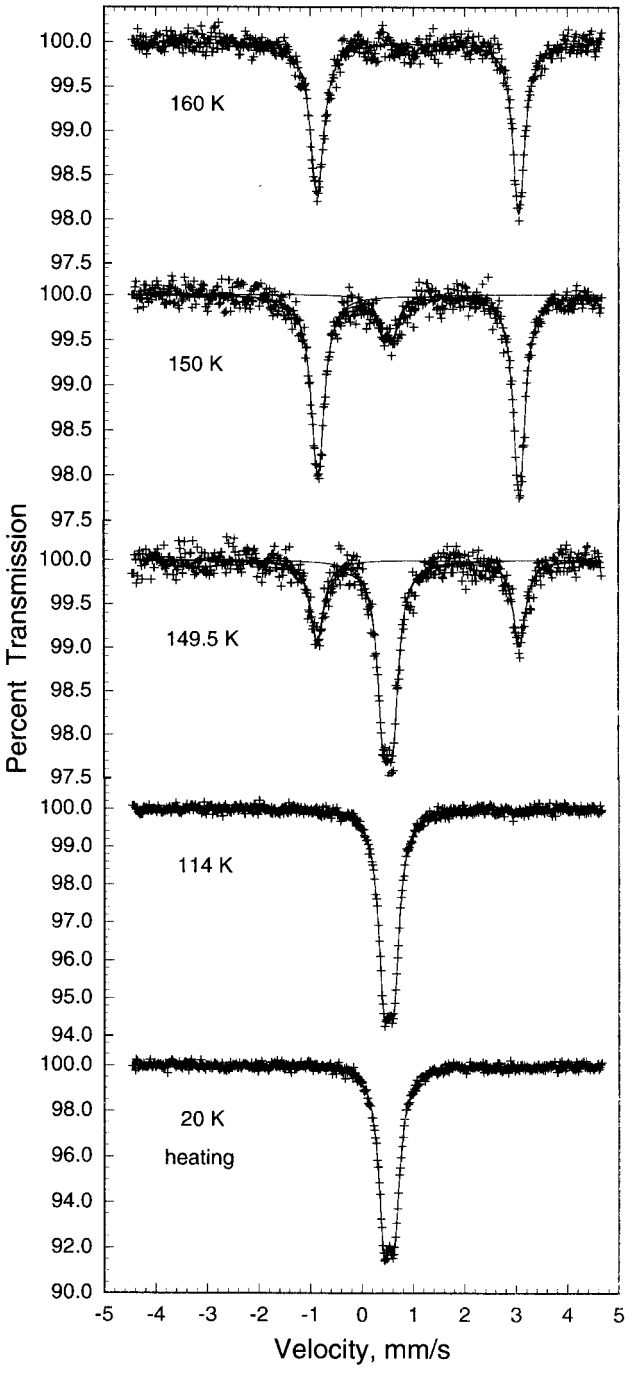

Figure 5. The Mössbauer spectra of {Fe[HC(3,4,5-$Me_3pz)_3]_2$}$(BF_4)_2$ (**1**) obtained at the indicated temperatures upon heating from 4.2 K

doublet observed between 4.2 and 100 K suggest that **1** is low spin at these temperatures. The linear temperature dependence of the high-spin isomer shift observed between 110 and 300 K is expected and, within the high-temperature limit, leads to an effective vibrating mass[19] of 64 g mol^{-1}. In the low-temperature limit, between 4 and 100 K, where the low-spin isomer shift is obtained, almost no temperature dependence of the isomer shift is observed, as expected.

The quadrupole splitting of approximately 3.9 mm s^{-1} observed for high-spin iron(II) is close to the maximum 4 mm s^{-1} expected[20] valence contribution to the quadrupole splitting, whereas the small quadrupole splitting of about 0.2 mm s^{-1} observed for the low-spin iron(II) results from the lattice contribution. The lattice contribution is usually opposite in sign to the valence contribution, and explains the reduction of the high-spin iron(II) quadrupole splitting from 4 to 3.9 mm s^{-1}. As expected, the low-spin quadrupole splitting resulting from the lattice contribution is virtually independent of temperature. Between 110 and 300 K the quadrupole splitting of the high-spin iron(II) does

 © 2004 Wiley-VCH Verlag GmbH & Co. KGaA, Weinheim

Table 3. Selected Mössbauer spectroscopic hyperfine parameters

Complex	T (K)	δ[a] (mm s^{-1})	ΔE_Q (mm s^{-1})	Γ (mm s^{-1})	Area (%)	ε (%ε)/(mm s^{-1})	Assignment
{Fe[HC(3,4,5-Me$_3$pz)$_3$]$_2$}(BF$_4$)$_2$ (**1**)	296	1.002	3.89	0.28	100	0.662	HS
	114[b]	1.113	3.93	0.28	85.9	2.320	HS
		0.516	0.19	0.27	14.1	0.381	LS
	112[b]	1.113	3.93	0.28	57.6	1.695	HS
		0.516	0.19	0.27	42.4	1.245	LS
	110[b]]	1.112	3.92	0.30	34.2	1.132	HS
		0.523	0.19	0.27	65.8	2.178	LS
	100[b]	0.516	0.19	0.27	100	3.707	LS
	60[b]	0.522	0.20	0.27	100	4.506	LS
	20[b]	0.521	0.20	0.27	100	5.140	LS
	4.2	0.521	0.20	0.26	100	5.353	LS
	106[c]	0.516	0.19	0.26	100	3.419	LS
	114[c]	0.516	0.19	0.26	100	3.357	LS
	149.5[c]	1.100	3.93	0.30	38.7	0.870	HS
		0.513	0.18	0.27	61.3	1.381	LS
	150[c]	1.103	3.92	0.29	86.4	1.871	HS
	160[c]	1.093	3.92	0.28	100	1.662	HS
	220[c]	1.058	3.92	0.31	100	1.064	HS
{Fe[HC(3,5-Me$_2$pz)$_3$]$_2$}(BF$_4$)$_2$ (**2**)	295[d]	1.004	3.87	0.27	100	–	HS
	85[d]	1.131	3.88	0.26	50	–	HS
		0.529	0.20	0.26	50	–	LS
Fe[HB(3,5-Me$_2$pz)$_3$]$_2$ (**4**)	300[e]	1.03	3.65	0.33	100	–	HS
	78[e]	0.55	0.11	0.26	100	–	LS
Fe[HB(3,4,5-Me$_3$pz)$_3$]$_2$ (**3**)	293[e]	1.04	3.70	0.26	100	–	HS
	78[e]	1.13	3.72	0.26	100	–	HS
	4.2[e]	1.17	3.70	0.25	100	–	HS
	1.7[e]	1.20	3.71	0.29	100	–	HS

[a] The isomer shifts are given relative to room temperature α-iron foil. [b] Data obtained upon cooling from 296 K. [c] Data obtained upon heating from 4.2 K. [d] The average values obtained from Ref. 11. [e] Data obtained from Ref. 7.

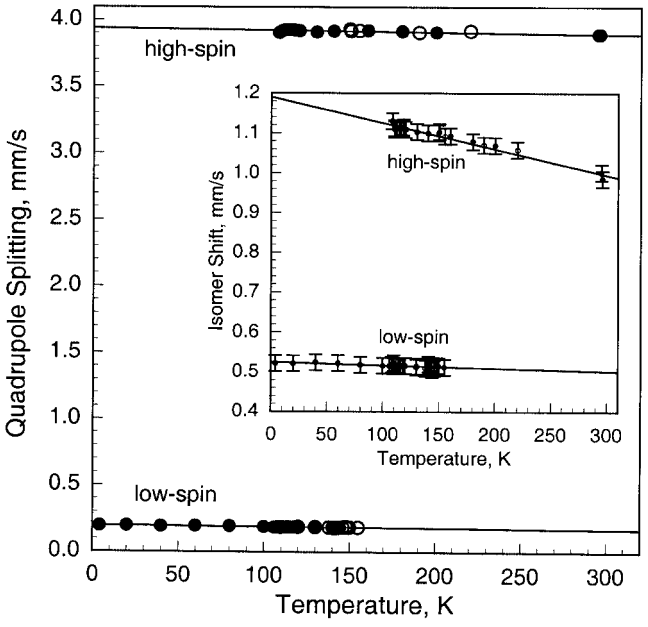

Figure 6. The temperature dependence of the Mössbauer spectroscopic quadrupole splitting of {Fe[HC(3,4,5-Me$_3$pz)$_3$]$_2$}(BF$_4$)$_2$ (**1**); inset: the temperature dependence of the isomer shift of **1**

not vary with temperature. Hence, the excited orbital states must lie at relatively high energy and are not thermally populated.

The population of the iron(II) high-spin state in **1** is shown in Figure 7 as a function of cooling from 295 to 4.2 K and subsequent heating from 4.2 to 240 K. Between 160 and 100 K the Mössbauer spectra of **1** exhibit two quadrupole doublets, which indicate the coexistence of the two electronic spin states at these temperatures. This spin-state coexistence is typical of a complex undergoing a spin-state crossover with a large thermal hysteresis; in this case a hysteresis of about 39 K is obtained, which agrees well with that (38 K) obtained from the magnetic studies (see above). It should be noted that there are both strong similarities and differences between the Mössbauer spectroscopic results for **1** and several related compounds. Although the hyperfine parameters of **1** are virtually identical to those of {Fe[HC(3,5-Me$_2$pz)$_3$]$_2$}(BF$_4$)$_2$ **2** (see Table 3), as would be expected on the basis of their very similar crystal structures at 150 and 220 K, respectively (see above), **1** undergoes a complete spin-state crossover with a distinct thermal hysteresis, whereas **2** shows no thermal hysteresis and is only 50 percent converted into the low-spin state, a conversion that is induced by the low-temperature phase transition.

 © 2004 Wiley-VCH Verlag GmbH & Co. KGaA, Weinheim

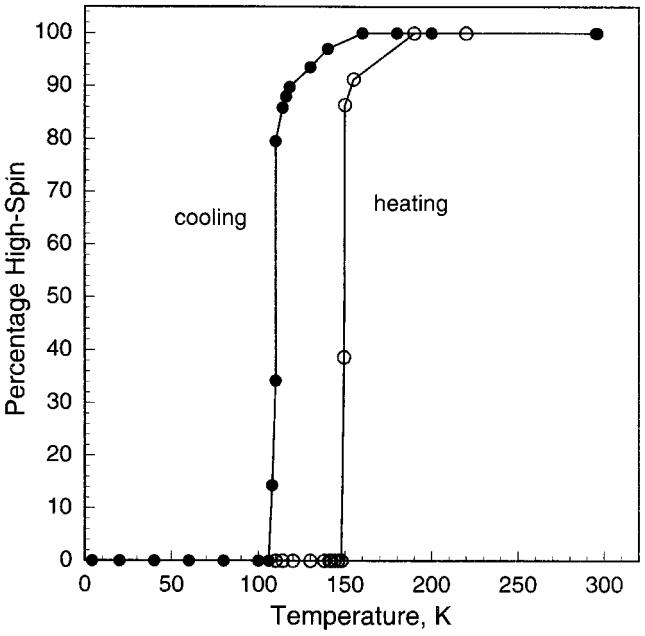

Figure 7. The percentage of high-spin iron(II) observed in the Mössbauer spectra of $\{Fe[HC(3,4,5\text{-}Me_3pz)_3]_2\}(BF_4)_2$ (**1**) as a function of temperature

Further, the structure of **1** is different from its analogous tris(pyrazolyl)borate complex, $Fe[HB(3,4,5\text{-}Me_3pz)_3]_2$ (**3**); the former shows a complete spin-state crossover upon cooling, whereas the latter does not exhibit any spin-state crossover and remains high-spin[7] even upon cooling to 1.7 K (see Table 3). The single-crystal X-ray structure of **3** has recently been determined,[21] and its structure has been found to be very similar to that of **1**, except that its average Fe−N bond length is 2.19 Å, i.e. it is 0.02 Å longer than that in **1**. This increase in the Fe−N bond length, which reduces the σ-electron density at the iron(II) in **3** relative to that in **1**, accounts for the significantly lower 295 K isomer shift observed in **1** than in $Fe[HB(3,4,5\text{-}Me_3pz)_3]_2$ (**3**) (see Table 3). Further, the distortion of the iron(II) coordination environment in **1** is found to be substantially larger[22,23] than that in **3**. The larger distortion accounts for the substantially larger quadrupole splitting observed in **1** relative to **3**. Finally, it should be noted that the spin-state crossover observed in **1** is similar to that observed in $Fe[HB(3,5\text{-}Me_2pz)_3]_2$ (**4**),[2,6,7] which shows a gradual spin-state crossover between 150 and 220 K, but again, the hyperfine parameters of **1** and **4** are somewhat different.

Because the temperature dependence of the Mössbauer spectra has been measured under identical conditions, i.e. a constant geometry and with a constant energy window, the changes in the spectroscopic absorption area as a function of temperature are directly related to the changes in the iron-57 recoil-free fraction. The logarithm of the total spectral absorption area observed in the Mössbauer spectra of **1** as a function of temperature is shown in Figure 8. The general decrease in ln(area) with increasing temperature is expected, but the jumps and hysteresis at approximately 110 K are unusual and are related to the spin-state crossover. The solid lines shown in Figure 8 correspond to a fit with the Debye model[19] between 4.2 and 100 K and between 150 and 296 K. These fits assume an effective vibrating mass of 57 g mol^{-1} and yield effective Mössbauer temperatures of 156 K for the low-spin state and 139 K for the high-spin state. The accuracy of these temperatures is estimated to be ± 10 K.

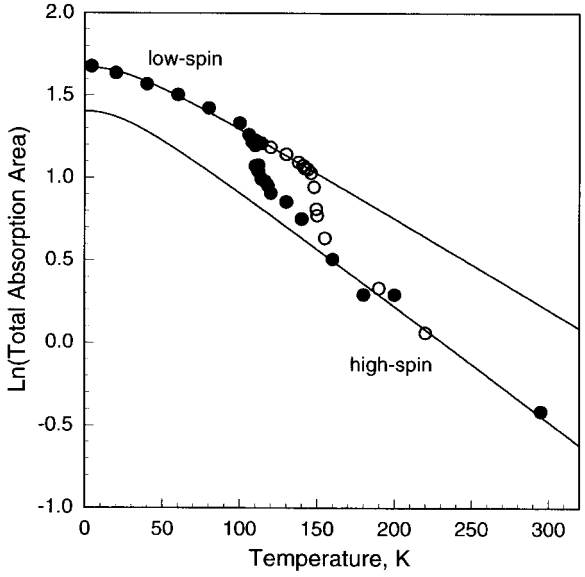

Figure 8. The logarithm of the total spectral absorption area observed in the Mössbauer spectra of $\{Fe[HC(3,4,5\text{-}Me_3pz)_3]_2\}(BF_4)_2$ (**1**) as a function of temperature; the straight lines correspond to the slope associated with the low-spin data obtained between 4.2 and 100 K and the high-spin data obtained between 160 and 296 K

The high-spin iron(II) ion in **1** has an average iron−nitrogen bond length of 2.162 Å, which is substantially larger than the typical value of 1.97 Å observed[9] for low-spin iron(II) complexes. The shorter average bond length leads to stronger bonding, more effective binding of the iron(II) ion into the lattice site, a higher recoil-free fraction, and a higher effective Mössbauer temperature for the low-spin iron(II) than for the high-spin iron(II) state.

Conclusions

The solid-state structure and color of $\{Fe[HC(3,4,5\text{-}Me_3pz)_3]_2\}(BF_4)_2$ clearly show that the complex contains high-spin iron(II) at ambient temperature. Both magnetic and Mössbauer studies show that the complex rapidly and completely changes to the low-spin state below 100 K. This behavior shows significant hysteresis upon heating where the change back to high spin does not begin until 138 K. This magnetic behavior is very different from the closely related complex $\{Fe[HC(3,5\text{-}Me_2pz)_3]_2\}(BF_4)_2$ that exhibits a spin-state crossover to the low-spin state of only one-half of the initially identical high-spin iron(II) ions and shows no hysteresis effects.[10−13] This very different behavior of $\{Fe[HC(3,4,5\text{-}Me_3pz)_3]_2\}(BF_4)_2$ is further evidence to sup-

 © 2004 Wiley-VCH Verlag GmbH & Co. KGaA, Weinheim

port our earlier contention that the unusual spin-state crossover behavior of {Fe[HC(3,5-$Me_2pz)_3]_2$}$(BF_4)_2$ is completely controlled by the phase transition, one which prevents one-half of the initially identical high-spin iron(II) ions from changing to the low-spin form.

Experimental Section

Synthesis and Characterization: All operations were carried out under a nitrogen atmosphere using either standard Schlenk techniques or a dry box. All solvents were dried, degassed, and distilled prior to use. $Fe(BF_4)_2 \cdot 6H_2O$ was purchased from Aldrich. The synthesis of 3,4,5-trimethylpyrazole was performed according to a published method.[24]

Synthesis of tris(3,4,5-trimethylpyrazol-1-yl)methane: A 100 mL round-bottom flask was charged with 3,4,5-trimethylpyrazole (2.2 g, 20 mmol), tetra-*N*-butylammonium bromide (0.32 g, 1.0 mmol) and distilled H_2O (40 mL). Once the materials were dissolved, sodium carbonate (12.7 g, 120 mmol) was slowly added (*Caution: mildly exothermic reaction on addition*). Once the aqueous solution had cooled to near room temperature, chloroform (20 mL) was added to the flask. The flask was equipped with a reflux condenser and heated at a gentle reflux for 3 days, to give in a golden brown emulsion. The mixture was allowed to cool to room temperature, filtered through a Büchner funnel to remove the excess base, and the organic layer separated from the aqueous layer. The organic layer was washed with distilled water (2 × 10 mL) and dried over sodium sulfate. The drying agent was removed by filtration, and the solvent removed by rotary evaporation. The resulting oily, brown solid was flushed through a plug of silica with chloroform (2 × 100 mL) to afford a pale yellow solid (1.4 g, 62%). M.p. 156−157 °C (literature[18]: 156−157 °C). ^{1}H NMR ($CDCl_3$): δ = 186, 1.92 (3,5-CH_3, s, s; 9 H, 9 H,), 2.12 (4-CH_3, s, 9 H), 8.03 (C*H*, s, 1 H) ppm.

Synthesis of {Fe[HC(3,4,5-$Me_3pz)_3]_2$}$(BF_4)_2$: A 50 mL round-bottom Schlenk flask was charged with $Fe(BF_4)_2 \cdot 6H_2O$ (0.200 g, 0.60 mmol) and distilled THF (3 mL) was added with the use of a syringe. A second 50 mL round-bottom Schlenk flask was charged with tris(3,4,5-trimethylpyrazol-1-yl)methane (0.500 g, 1.5 mmol) and distilled THF (6 mL) was added by a syringe. Once the starting materials were dissolved, the ligand/THF solution was added to the metal/THF solution by cannula transfer. The resulting mixture was left to stir overnight, yielding a white powder precipitate. The solvent was removed by cannula filtration, and the solid was washed with distilled hexane and dried under vacuum (0.47 g, 85% yield). M.p.: decomposes above 318 °C. ^{1}H NMR ([D_6]acetone): δ = 41.2, 20.9, 7.4 (18, 18, 18, v. br., br., br., Me_3), −42.8 (2, v. br., *H*−C). TOF MS ES+: *m*/*z* calcd. for {Fe[HC(3,4,5-$Me_3pz)_3]_2$}$(BF_4)^+$: 823.4129; found: 823.4132. Elemental Analysis: calcd. C 49.79, H 6.19, N 18.34; found C 49.21, H 6.21, N 18.43. Crystals for X-ray crystallographic and magnetic analysis, and Mössbauer spectroscopy were grown by layering a saturated acetone solution with hexane.

X-ray Structure Determination of {Fe[HC(3,4,5-$Me_3pz)_3]_2$}$(BF_4)_2 \cdot 0.35H_2O$: A colorless block crystal was mounted onto the end of a thin glass fiber using inert oil. X-ray intensity data covering the full sphere of reciprocal space were obtained at 150(1) K on a Bruker SMART APEX CCD-based diffractometer with Mo-K_α radiation, λ = 0.71073 Å.[25] The raw data frames were integrated with SAINT+,[25] which also corrected for Lorentz polarization effects. The final unit cell parameters are based on the least-squares refinement of 6654 reflections from the data set with $I > 5(\sigma)I$. Analysis of the data showed negligible crystal decay during data collection. An empirical absorption correction, based on the multiple measurement of equivalent reflections, was applied with the program SADABS.[25]

{Fe[HC(3,4,5-$Me_3pz)_3]_2$}$(BF_4)_2 \cdot 0.35H_2O$ crystallizes in the triclinic system and the structure was solved in the $P-1$ space group through a combination of direct methods and difference Fourier syntheses and refined by full-matrix least-squares against F^2 by using the SHELXTL software package.[26] The {Fe[HC(3,4,5-$Me_3pz)_3]_2$}$^{2+}$ cation resides on a center of symmetry and the BF_4^- counterion is rotationally disordered; a model incorporating four distinct orientations of the BF_4^- anion was used in the refinement. A total of 68 restraints were employed to maintain a chemically reasonable geometry for the disordered components. Initially, the site occupation factors for the four components were allowed to refine freely, but were subsequently fixed at the refined values and then adjusted slightly to sum to unity (0.38, 0.39, 0.14, 0.09). Atoms of the two minor components were refined with only isotropic displacement parameters. A significant, isolated electron-density peak present near the end of the refinement was assumed to be a partially occupied water molecule, which refined to a 35% occupancy; its hydrogen atoms were not located or calculated. All non-hydrogen atoms, except for the BF_4^- atoms mentioned above, were refined with anisotropic displacement parameters. Hydrogen atoms were placed in geometrically idealized positions and refined as standard riding atoms.

It was not possible to obtain the single-crystal X-ray structure of {Fe[HC(3,4,5-$Me_3pz)_3]_2$}$(BF_4)_2$ (**1**) in the low-spin state, because the crystals always shattered upon cooling through the spin-state crossover. Further, changes in the magnetic behavior of the compound upon grinding prevented the measurement of the powder diffraction pattern of the complex at low temperature in the low-spin state.

Magnetic Measurements: Magnetic susceptibilities were measured on crystalline samples at 0.5 T by using a Quantum Design MPMS XL SQUID magnetometer. Clear gelatine capsules were used as sample containers for measurements between 5 and 350 K. The very small diamagnetic contribution of the gelatine capsule had a negligible contribution to the overall magnetization which was dominated by the sample. The molar magnetic susceptibilities were corrected for the diamagnetic susceptibility of {Fe[HC(3,4,5-$Me_3pz)_3]_2$}$(BF_4)_2$ by using the value of −0.0004632 emu/mol that was obtained from Pascal's constants.

Mössbauer Spectroscopic Measurements: The Mössbauer spectroscopic absorber contained 50 mg/cm^2 of powder mixed with boron nitride, and the spectra were measured between 4.2 and 295 K on a constant-acceleration spectrometer which utilized a room-temperature rhodium-matrix cobalt-57 source and was calibrated at room temperature with α-iron foil. The estimated absolute errors are ± 0.005 mm/s for the isomer shifts, ± 0.01 mm/s for the quadrupole splittings and line widths, and ± 0.2 percent for the relative spectral absorption areas.

Acknowledgments

G. J. L. thanks the Francqui Foundation of Belgium for his appointment as a "Chaire Francqui Interuniversitaire au titre étranger" during the 2002−2003 academic year. The authors also acknowledge with thanks the financial support of the US National Science Foundation through grant CHE-0110493 for D. L. R. and

 © 2004 Wiley-VCH Verlag GmbH & Co. KGaA, Weinheim

DMR-9521739 for G. J. L. and the Fonds National de la Recherche Scientifique, Belgium, through grant 9.456595, and the Fonds de la Recherche Fondamentale Collective, Belgium, through grants 2.4531.00F and 2.4522.01. L. R. and F. G. thank the Ministère de la Région Wallonne for grant RW/115012.

[1] S. Trofimenko, *Scorpionates: The Coordination Chemistry of Polypyrazolylborate Ligands*, Imperial College Press, London, **1999**.
[2] G. J. Long, F. Grandjean, D. L. Reger, in *Spin Crossover in Transition Metal Compounds* (Eds.: P. Gütlich, H. A. Goodwin), Springer, Berlin, **2004**, in press.
[3] P. Gütlich, A. Hauser, H. Spiering, *Angew. Chem. Int. Ed. Engl.* **1994**, *33*, 2024−2054 and references cited therein.
[4] F. A. Cotton, J. Wilkinson, C. A. Murillo, M. Bochmann, *Advanced Inorganic Chemistry* (6th ed.), John Wiley & Sons, New York, **1999**, pp. 785−786.
[5] J. P. Jesson, S. Trofimenko, D. R. Eaton, *J. Am. Chem. Soc.* **1967**, *89*, 3158−3164.
[6] J. P. Jesson, J. F. Weiher, S. Trofimenko, *J. Chem. Phys.* **1968**, *48*, 2058−2066.
[7] G. J. Long, B. B. Hutchinson, *Inorg. Chem.* **1987**, *26*, 608−613.
[8] F. Grandjean, G. J. Long, B. B. Hutchinson, I. Ohlhausen, P. Neill, J. D. Holcomb, *Inorg. Chem.* **1989**, *28*, 4406−4414.
[9] C. Hannay, M.-J. Hubin-Franskin, F. Grandjean, V. Briois, J.-P. Itié, A. Polian, S. Trofimenko, G. J. Long, *Inorg. Chem.* **1997**, *36*, 5580−5588.
[10] D. L. Reger, C. A. Little, A. L. Rheingold, M. Lam, T. Concolino, A. Mohan, G. J. Long, *Inorg. Chem.* **2000**, *39*, 4674−4675.
[11] D. L. Reger, C. A. Little, A. L. Rheingold, M. Lam, L. M. Liable-Sands, B. Rhagitan, T. Concolino, A. Mohan, G. J. Long, V. Briois, F. Grandjean, *Inorg. Chem.* **2001**, *40*, 1508−1520.
[12] D. L. Reger, C. A. Little, V. G. Young Jr., M. Pink, *Inorg. Chem.* **2001**, *40*, 2870−2874.
[13] D. L. Reger, C. A. Little, M. D. Smith, G. J. Long, *Inorg. Chem.* **2002**, *41*, 4453−4460.
[14] D. L. Reger, C. A. Little, M. D. Smith, A. L. Rheingold, K.-C. Lam, T. L. Concolino, G. J. Long, R. P. Hermann, F. Grandjean, *Eur. J. Inorg. Chem.* **2002**, 1190−1197.
[15] C. Piquer, F. Grandjean, O. Mathon, S. Pascarelli, D. L. Reger, C. Little, G. J. Long, *Inorg. Chem.* **2003**, *42*, 982−985.
[16] V. Briois, P. Sainctavit, G. J. Long, F. Grandjean, *Inorg. Chem.* **2001**, *40*, 912−918.
[17] D. L. Reger, C. A. Little, A. L. Rheingold, R. Sommer, G. J. Long, *Inorg. Chim. Acta* **2001**, *316*, 65−70.
[18] C. Pettinari, M. Pellei, A. Cingolani, D. Martini, A. Drozdov, S. Troyanov, W. Panzeri, A. Mele, *Inorg. Chem.* **1999**, *38*, 5777−5787.
[19] R. H. Herber, in *Chemical Mössbauer Spectroscopy* (Ed.: R. H. Herber), Plenum; New York, **1984**, pp. 199−216.
[20] D. C. Price, F. Varret, *Studies Physical Theoretical Chem.: Adv. Mössbauer Spectroscopy* **1983**, *25*, 316−397.
[21] D. L. Reger, J. R. Gardinier, M. D. Smith, unpublished results.
[22] The Fe−N bond and N−Fe−N angular distortion parameters[23] are 0.491 and 6.51 percent for **1** and 0.107 and 4.25 percent for **2**.
[23] B. Renner, G. Lehmann, *Z. Krist.* **1986**, *175*, 43−59.
[24] A. Wlodarczyk, R. M. Richardson, M. D. Ward, J. A. McCleverty, *Polyhedron* **1996**, *15*, 27−35.
[25] SMART Version 5.625, SAINT+ Version 6.02a and SADABS. Bruker Analytical X-ray Systems Inc., Madison, Wisconsin, USA, **1998**.
[26] Sheldrick, G. M., SHELXTL Version 5.1, Bruker Analytical X-ray Systems Inc., Madison, Wisconsin, USA, **1997**.

Received December 30, 2003
Early View Article
Published Online June 1, 2004

 © 2004 Wiley-VCH Verlag GmbH & Co. KGaA, Weinheim

Ruthenium Nitrosyl Complexes of Bis(3,5-dimethylpyrazol-1-yl)methane Oxyanions

Mayreli Ortiz,[a] Alicia Díaz,[a] Roberto Cao,*[a] Reynier Suardíaz,[b] Antonio Otero,[c] Antonio Antiñolo,[c] and Juan Fernández-Baeza[c]

Keywords: Ruthenium nitrosyl complexes / Nitric oxide / NNO Scorpionates / Bis(pyrazolic) ligands

New ruthenium(II) mononitrosyl complexes of general composition $[Ru(NO)LCl_2]$, $[Ru(NO)L(en)]Cl_2$ and $[Ru(NO)L_2]Cl$ have been obtained upon treating $Ru(NO)Cl_3$ with potential κ^3-*N*,*N*,O ligands bis(3,5-dimethylpyrazol-1-yl)methanesulfonate (bdmpzsa) and bis(3,5-dimethylpyrazol-1-yl)acetate (bdmpza) in 1:1 and 1:2 molar ratios. These mononitrosyl complexes have a sharp, intense νNO band in the IR spectra within 1874–1851 cm^{-1}, indicating a linear Ru–NO^+ coordination. For both $[Ru(NO)L_2]Cl$ compounds, a dynamic switch on-off process occurs between the oxyanionic moieties on the apical position *trans* to NO^+ and the pyrazolic ligands on the equatorial plane. A dynamic ^1H NMR experiment of this process gave $\Delta G^{\#}$= 46–48 kJ·mol^{-1} at 218–228 K for the acetate derivative.
(© Wiley-VCH Verlag GmbH & Co. KGaA, 69451 Weinheim, Germany, 2004)

Introduction

In the past decade nitric oxide, NO, has been widely studied since it was found to be an essential component in many physiological processes. The physiological functions of NO are various: a killer of invading microorganisms, primary messenger in regulating blood pressure and neurotransmitter. Dysfunction in NO metabolism has been associated with several disease states, such as epilepsy, arthritis, hypertension and septic shock.[1]

Ruthenium(III) complexes coordinate nitric oxide, NO, to form stable Ru^{II} mononitrosyl complexes. This reaction can occur rapidly in aqueous solution.[1b] It is assumed that, generally, a $Ru^{II}-NO^+$ linear bond is formed. The νNO bands (IR) lie within the range 1789−1960 cm^{-1}.[2,3]

However, when a linear Ru^{II} mononitrosyl complex is submitted to a chemical (or electrochemical) one-electron reduction,[4] the stable low-spin d^6 configuration of Ru^{II} apparently remains unaffected while the electron transferred in the reduction process is accepted by NO, by which it is transformed into a radical, NO·. This radical is ESR active with g_x = 1.995; g_y = 2.035, and g_z = 1.883. Under such conditions the NO· radical can easily be released.[4a] The NO· signal can be observed in the ESR spectrum of these Ru^{II} mononitrosyl complexes at 77 K. Some Ru^{II} nitrosyl complexes photochemically dissociate NO·.[5]

Different Ru^{III} complexes with polyaminocarboxylic acids have been studied as NO scavengers.[6] Complexes of Ru^{II} coordinated to NO^+, NO· and NO^- have been obtained by the interaction of NO with $[Ru(hedta)Cl]^-$ [hedta: *N*-(hydroxyethyl)ethylenediaminetriacetate] and further electrochemical reduction.[6b]

The first report on ruthenium nitrosyl complexes with pyrazol-1-yl derivatives included the study of $[TpRuNOCl_2]$, $[pzTpRuNOCl_2]$ and $[Tp^*RuNOCl_2]$ (Tp: trispyrazol-1yl borate; Tp*: 3,5-substituted Tp).[7] Ruthenium nitrosyl complexes with 3,5-dimethylpyrazole have also been reported.[8] These complexes were structurally characterized by single-crystal X-ray diffraction and in all cases the Ru−N−O angle lies between 176.2 and 179.6°, while the νNO band (IR) appears within 1894−1790 cm^{-1}.

Recently, we reported different ruthenium(II) complexes with bis(3,5-dimethylpyrazol-1-yl)methane derivatives: Bis(3,5-dimethylpyrazol-1-yl)methanesulfonate (bdmpzsa, **1**), and bis(3,5-dimethylpyrazol-1-yl)acetate (bdmpza, **2**) (Figure 1).[9] Both ligands lie on the equatorial plane and coordinate as κ^3-*N*,*N*,O scorpionates, but with a weak interaction through the oxyanionic moiety.

[a] Laboratorio de Bioinorgánica, Facultad de Química, Universidad de La Habana,
La Habana 10400, Cuba
Fax: (internat.) +537-8733502
E-mail: cao@fq.uh.cu
[b] Departamento de Química Física, Facultad de Química, Universidad de La Habana,
La Habana 10400, Cuba
[c] Departamento de Química Inorgánica, Orgánica y Bioquímica, Facultad de Ciencias Químicas, Universidad de Castilla-La Mancha,
13071 Ciudad Real, Spain
Supporting information for this article is available on the WWW under http://www.eurjic.org or from the author.

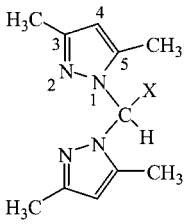

Figure 1. Schematic representation of the studied ligands bis(3,5-dimethylpyrazol-1-yl)methanesulfonate (bdmpzsa, **1**) (X = SO_3^-), and bis(3,5-dimethylpyrazol-1-yl)acetate (bdmpza, **2**) (X = COO^-)

In this paper, we report on Ru^{II} mononitrosyl complexes with ligands **1** and **2**, prepared by the interaction of the ligands with $Ru(NO)Cl_3$.

Results and Discussion

In the synthesized complexes reported previously,[9] the bis(pyrazolic) ligands lie on the equatorial plane − only one set of signals appear in the NMR spectra. Conversely, NO is assumed to be coordinated on an apical position. In compounds **3** and **4**, one bis(pyrazolic) ligand and the two chloride anions lie on the equatorial plane (Figure 2 for **4**). In **5** and **6** both bis(pyrazolic) ligands lie on the equatorial plane, while in **7** and **8** ethylenediamine (en) and the bis(pyrazolic) ligand lie in this plane.

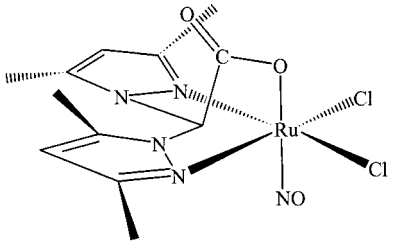

Figure 2. Representation of compound **4**

Very small shifts appear in the NMR signals of the pyrazolic rings upon coordination, as reported previously.[9]

To confirm the earlier ^1H and ^{13}C NMR assignments of the pyrazolic rings the ^1H,^{15}N gs-HMBC (NMR) two-dimensional spectrum of $[Ru(bdmpza)_2(NO)]Cl$ (**6**) was recorded (Figure 3).

This technique permits the correlation of coupling of ^1H and ^{15}N signals of atoms 2−3 bonds apart. Two signals of ^{15}N coupled to ^1H occur: one at δ = 127.5 ppm (N^1) and another at δ = 212.5 ppm (N^2). The former couples through three bonds to the protons of the $CH_3{}^5$, through two bonds to the methylenic (CH) proton, and through three bonds to the protons of the CH group of the pyrazolic ring. The ^{15}N signal at δ = 212.5 ppm (N^2) ppm couples through three bonds to the protons of $CH_3{}^3$, through three bonds to the proton of the methylenic (CH) and through

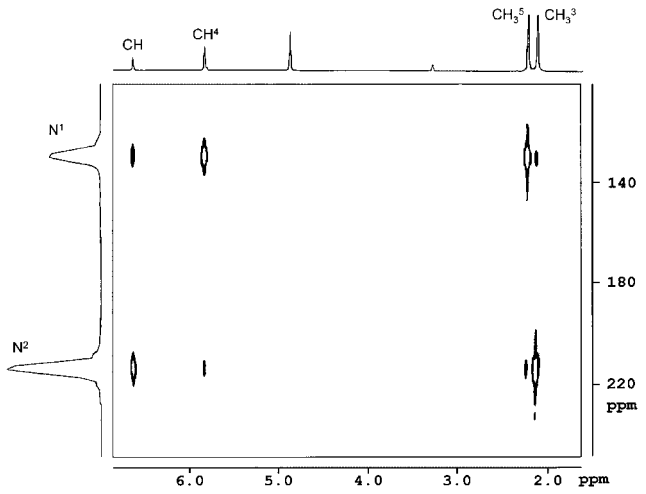

Figure 3. ^1H, ^{15}N gs-HMBC spectrum of $[Ru(bdmpza)_2NO]Cl$ in CD_3OD

three bonds to the proton of the CH group of the pyrazolic ring. Small shifts (Δδ = 2 ppm) were now observed for ^{15}N of N^1 and N^2 of the pyrazolic ring upon coordination. These results confirm the previous assignments.

Coordinated NO could not be detected by this technique since the neighboring protons are too distal. Nevertheless, the small chemical shifts in the spectra of the obtained Ru^{II} nitrosyl complexes indicate that coordinated NO, with a significant *trans* effect, is on an apical position. Only one set of ^{15}N signals are observed, confirming that the bis(pyrazolic) ligands lie on the equatorial plane.

IR stretching bands of the oxyanionic moieties and the methylenic CH signals (^1H and ^{13}C NMR) of the pyrazolic rings shift very slightly upon coordination. This indicates that the oxyanionic moiety is weakly coordinated. In addition, the IR spectra of both $[Ru(NO)L_2]Cl$ complexes (**5** and **6**) present only one asymmetric stretching band for the oxyanionic groups: 1647 [$\nu_{as}(COO^-)$] and 1249 cm^{-1} [$\nu_{as}(SO_3^-)$] respectively, indicating that they are equivalent. Conversely, in the ^1H NMR spectra, δ_H of methylenic CH at room temperature broadens when two bis(pyrazolic) ligands (**1** or **2**) are coordinated. This can be interpreted as a dynamic switch on-off exchange between both oxyanionic groups to coordinate to Ru^{II} at the only vacant site left, since the four positions on the equatorial plane are occupied by the four N atoms of both bis(pyrazolic) rings, plus NO on an apical position.

A dynamic-^1H NMR technique was used to confirm a switch on-off exchange between both groups in $[Ru(NO)L_2]Cl$ (**5**, **6**). With decreasing temperature the proton signal of the methylenic groups of **6** initially broadened further and then, finally, decoalesced into two broad singlets at 193 K (Figure 4).

This latter effect should be because the dynamic exchange is "frozen", such that one oxyanionic group remains near Ru^{II} and the other more distant. From the difference in chemical shifts and the approximately estimated coalescence temperature (218−228 K), the free energy of acti-

 © 2004 Wiley-VCH Verlag GmbH & Co. KGaA, Weinheim

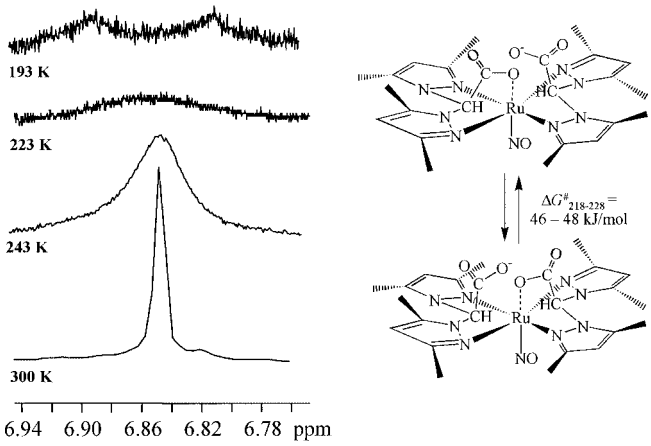

Figure 4. Switch on-off process of carboxylate groups in compound **6** studied by dynamic ^{1}H NMR spectroscopy

vation ($\Delta G^{\#}$) of the process could be evaluated,[10] corresponding to 46−48 kJ·mol^{-1} for [Ru(NO)(bdmpza)$_2$]Cl (**6**). This low value supports the proposed room-temperature dynamic process that causes the observed equivalency between both methylenic groups. For compound **5**, decoalescence takes place below 193 K, indicating an even weaker coordination of the sulfonate group with respect to the carboxylate.

The switch on-off process was modeled by molecular dynamics for complex **6**. Movement of the bonding oxygen atom of one of the carboxylate groups, as time function, indicates a fast motion to and from the proximity of Ru^{II} (Figure 5, a). The steric effect of the CH_3[3] groups in the pyrazolic rings is important in this dynamic process since it restricts the complete approach of the carboxylate groups to Ru^{II} (Figure 5, b).

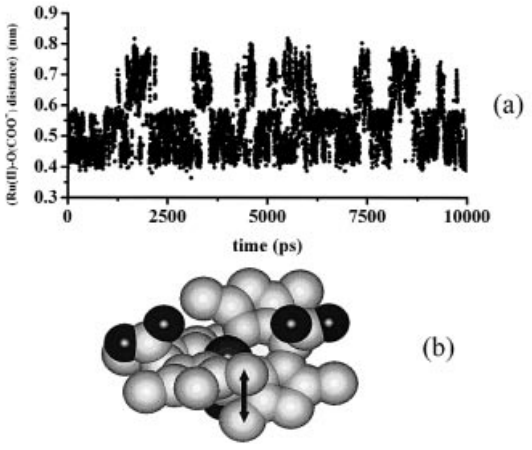

Figure 5. (a) Ru^{II}−OOC− distance as time function obtained by molecular dynamics; (b) schematic representation of complex **6** where both switching oxygen atoms of the carboxylate groups are in black, as is Ru^{II} (a larger sphere); steric repulsion between both CH_3[3] groups is indicated by a double arrow

This prediction agrees with both the low $\Delta G^{\#}$ obtained from ^{1}H NMR studies and the very similar chemical shifts (^{13}C NMR) of the carboxylate group in the free ligand (**2**) and in complex **6**.

We earlier reported that for the complex [Ru(NEt$_3$)(bdmpza)$_2$], formed by treating [Ru(bdmpza)$_2$] with NEt$_3$, the COO$^-$ and CH signals in the ^{13}C NMR spectrum are two well-defined singlets, while the ν_{as}(COO$^-$) band (IR) appears as two peaks at 1660 and 1647 cm^{-1}. A similar result occurs in the ^{13}C NMR spectrum of [Ru(NEt$_3$)(bdmpzsa)$_2$].[9] Comparing these results with those obtained for **5** and **6**, where the switch on-off process is observed, shows that NO$^+$ evidently weakens the *trans* position much more than NEt$_3$. This can be explained by the strong *trans* effect of NO$^+$, which provokes the observed switch on-off process of the oxyanionic groups.

Coordination of NEt$_3$ was also used here to "freeze" the dynamic exchange of both oxyanionic groups in the obtained nitrosyl complexes. For this, the reaction products of [Ru(NO)L$_2$]Cl (**5**, **6**) and NEt$_3$ (1:1 molar ratio) in methanol were isolated and purified. Once NEt$_3$ was coordinated to Ru^{II} *trans* to NO, leaving both oxyanionic groups free, the methylenic protonic signals became sharp and the ^{13}C NMR spectra gave only one set of signals (Supporting Information, Figure S1; for Supporting Informations see also the footnote on the first page of this article).

As expected, the obtained mononitrosyl complexes are ESR silent and completely diamagnetic according to SQUID determinations, which excludes any possible Ru^{III} impurity.

All IR spectra of the mononitrosyl complexes gave a sharp, intense band at 1874−1851 cm^{-1}, and only very slight differences (0−4 cm^{-1}) were observed between the spectra of samples prepared as KBr tablets and those recorded in CH_2Cl_2 solutions. The band, assigned as νNO, indicates a linear coordination to Ru^{II}.

Heating KBr tablets of different samples from 200 up to 400 K resulted in no significant loss in intensity and only slight, reversible, shifts to higher frequencies (3−17 cm^{-1}) in the νNO band. These results indicate that NO is characterized by a stable coordination to Ru^{II} in the studied complexes.

Conclusion

Stable Ru^{II} complexes with a typical Ru^{II}−NO$^+$ bond have been obtained by reacting ligands **1** and **2** with Ru(NO)Cl$_3$. Compounds **5** and **6**, with two pyrazolic ligands, are characterized by a switch on-off process between both oxyanionic groups. This process has been studied by dynamic ^{1}H NMR for complex **6**, for which $\Delta G^{\#}_{218-228K}$ = 46−48 kJ·mol^{-1} was obtained. This process, modeled by molecular dynamics studies, should be enhanced by the *trans* effect of NO over the oxyanionic groups in **5** and **6**.

Experimental Section

Reagents: All chemicals used, including Ru(NO)Cl$_3$, were of high quality and purchased from Aldrich. Solvents were dried and distilled before use.

 © 2004 Wiley-VCH Verlag GmbH & Co. KGaA, Weinheim

Spectroscopy: Electronic spectra were recorded with an Ultrospec III spectrophotometer (Pharmacia-LKB) interfaced with a microcomputer for data acquisition. IR spectra were recorded with a Perkin-Elmer 883 FT-IR spectrometer, with samples prepared as KBr tablets and as CH_2Cl_2 solutions in CaF_2 cells. ESR spectra at room temperature were carried out at X-band with a Bruker ESP 300 spectrometer, operating at 100 kHz field modulation. The frequency was measured with a Hewlett−Packard 5352B frequency counter. NMR spectra were obtained with a Bruker AC 250 (62.89 MHz for ^{13}C) equipped with an ASPECT 3000 computer. All samples were dissolved in [D_4]methanol (30 mg/0.4 mL) and recorded at 300 K. Chemical shifts (δ) are expressed in ppm and referred to tetramethylsilane (TMS). The nature of each carbon atom was determined using the DEPT technique with proton pulses at θ = 135°. Quantitative measurements were carried out by recording the ^{13}C NMR spectra using the inverse-gated decoupled technique with a relaxation D_1 = 10 s, to fulfill the condition $D_1 > 5T_1$ (maximum) for hydrogenated carbon atoms. The ^1H NMR dynamic experiment was carried out with a Varian FT-300, using an Oxford Instruments VTC 4 unit, measured by a thermocouple and calibrated with [D_4]methanol, within 300 and 193 K, using [D_6]acetone as solvent. ^1H, ^{15}N gs-HMBC spectra were obtained with a Bruker AV 400 (40.53 MHz for ^{15}N) equipped with a GRASP accessory, using [D_4]methanol as solvent. The chemical shifts (δ, ppm)/CH_3NO_2 of the ^{15}N signals have been converted into the liquid ammonia reference scale. Resonances observed upfield of nitromethane were assigned as negative chemical shifts and those downfield as positive chemical shift for the conversion.

Molecular Dynamics: Molecular dynamics calculations were performed using the Gromos 96 program with additional parameters of ab initio calculus and crystallographic data of similar compounds.[11] One solute molecule and 168 solvent molecules of methanol made up the studied system, confined in a truncate octahedral box of 2.8 nm (300 K, 1 atm). Periodic frontier conditions were used; simulation time of 10 ns with a path of 0.002 ps.

Magnetic Susceptibility Determinations: Magnetic susceptibility measurements (1.8−300 K) were carried out with a Quantum Design SQUID magnetometer under an applied magnetic field of 1 T at high temperature and 100 G at low temperature to avoid any problem of magnetic saturation. The device was calibrated with $(NH_4)_2Mn(SO_4)_2{\cdot}6H_2O$. Corrections for the diamagnetism were estimated from Pascal constants. Experimental susceptibilities were also corrected for the temperature-independent paramagnetism [60 × 106 $cm^3{\cdot}mol^{-1}$ per copper(II) ion] and the magnetization of the sample holder.

The ligand [{Li(bdmpzsa)(H_2O)}$_4$] (**1**) (and, alternatively, the potassium salt) was prepared as reported previously.[9]

[{Li(bdmpza)(H_2O)}$_4$] (2): This ligand was prepared as reported previously.[12]

[Ru(NO)(bdmpzsa)($Cl)_2$] (3): $Ru(NO)Cl_3$ (50 mg, 0.21 mmol) was dissolved in methanol (20 mL) containing ligand **1** (61 mg, 0.21 mmol) and stirred for 12 h in an inert atmosphere. The soformed brownish-red suspension was roto-evaporated and the product dissolved in dichloromethane to separate LiCl by filtration. The solution was then evaporated to dryness under vacuum, and a brownish red hygroscopic solid was obtained. Yield: 75 mg (73.5%). $C_{11}H_{15}Cl_2N_5O_4RuS$ (485.3): calcd. C 27.21, H 3.09, N 14.43; found C 27.18, H 3.12, N 14.41. IR (KBr): $\tilde{\nu}$ = 1874 ν(NO), 1562 ν(C=N), 1175 $\nu_{as}(SO_3^-)$, 1114 $\nu_s(SO_3^-)$, 334 ν(Ru−Cl) cm^{-1}. IR (CH_2Cl_2): $\tilde{\nu}$ = 1874 ν(NO) cm^{-1}. UV/Vis: λ (log ε) = 230 (sh) (π → π*), 457 (2.95, d-d) nm. ^1H NMR (250 MHz, CD_3OD, 298 K): δ = 2.11 (s, 6 H, Me^3), 2.42 (s, 6 H, Me^5), 5.85 (s, 2 H, H^4), 6.82 (s, 1 H, CH) ppm. $^{13}C\{^1H\}$ NMR/DEPT-135° (62.89 MHz, CD_3OD, 298 K): δ = 10.9 (+, Me^5), 13.3 (+, Me^3), 75.2 (+, CH), 105.8 (+, C^4), 141.3 (0, C^5), 147.5 (0, C^3) ppm.

[Ru(NO)(bdmpza)($Cl)_2$] (4): A procedure similar to that described for **3** was used, but with $Ru(NO)Cl_3$ (50.0 mg, 0.21 mmol) and ligand **2** (53.3 mg, 0.21 mmol) to afford a brownish-red hygroscopic solid. Yield: 0.080 g (84.7%). $C_{12}H_{15}Cl_2N_5O_3Ru$ (449.3): calcd. C 32.07, H 3.34, N 15.59; found C 32.04, H 3.37, N 15.61. IR/KBr: $\tilde{\nu}$ = 1872 ν(NO), 1645 $\nu_{as}(CO_2^-)$, 1562 ν(C=N), 1387 $\nu_s(CO_2^-)$, 336 ν(Ru−Cl) cm^{-1}. IR (CH_2Cl_2): $\tilde{\nu}$ = 1868 ν(NO) cm^{-1}. UV/Vis: λ (log ε) = 234 (sh, π → π*), 400 (2.96, d-d) nm. ^1H NMR (250 MHz, CD_3OD, 298 K): δ = 2.15 (s, 6 H, Me^3), 2.24 (s, 6 H, Me^5), 5.86 (s, 2 H, H^4), 6.62 (s, 1 H, CH) ppm. $^{13}C\{^1H\}$ NMR / DEPT-135° (62.89 MHz, CD_3OD, 298 K): δ = 11.2 (+, Me^5) 13.3 (+, $M3^5$), 73.9 (+, CH), 107.3 (+, C^4), 142.4 (0, C^5), 149.5 (0, C^3), 169.7 (0, C=O) ppm.

[Ru(NO)(bdmpzsa)$_2$]Cl (5): A procedure similar to that for **3** was used, but with $Ru(NO)Cl_3$ (50.0 mg, 0.21 mmol) and ligand **1** (122.0 mg, 0.42 mmol) to furnish a brownish red crystalline solid. Yield: 140 mg (91.0%). $C_{22}H_{30}ClN_9O_7RuS_2$ (733.2): calcd. C 36.03, H 4.09, N 17.20; found C 35.99, H 4.12, N 17.18. IR (KBr): $\tilde{\nu}$ = 1865 ν(NO), 1564 ν(C=N), 1249 $\nu_{as}(SO_3^-)$, 1049 $\nu_s(SO_3^-)$ cm^{-1}. IR (CH_2Cl_2): $\tilde{\nu}$ = 1868 ν(NO) cm^{-1}. UV/Vis: λ (log ε) = 251 (sh, π → π*), 374 (sh, MLCT), 455 (2.59, d-d) nm. ^1H NMR (250 MHz, CD_3OD, 298 K): δ = 2.12 (s, 12 H, Me^3), 2.22 (s, 12 H, Me^5), 5.86 (s, 4 H, H^4), 6.67 (s, 2 H, CH) ppm. $^{13}C\{^1H\}$ NMR/ DEPT 135° (62.89 MHz, CD_3OD, 298 K): δ = 11.3 (+, Me^5), 13.2 (+, Me^3), 75.2 (+, CH), 107.4 (+, C^4), 143.0 (0, C^5), 150.1 (0, C^3) ppm.

[Ru(NO)(bdmpza)$_2$]Cl (6): A procedure similar to that for **3** was used, but with $Ru(NO)Cl_3$ (50.0 mg, 0.21 mmol) and ligand **2** (106.6 mg, 0.42 mmol) to give a brownish red crystalline solid. Yield: 134 mg (96.4%). $C_{24}H_{30}ClN_9O_5Ru$ (661.1): calcd. C 43.60, H 4.54, N19.07; found C 43.58, H 4.57, N 19.04. IR (KBr): $\tilde{\nu}$ = 1860 ν(NO), 1647 $\nu_{as}(CO_2^-)$, 1562 ν(C=N), 1385 $\nu_s(CO_2^-)$ cm^{-1}. IR (CH_2Cl_2): $\tilde{\nu}$ = 1862 ν(NO) cm^{-1}. UV/Vis: λ (log ε) = 250 (sh, π → π*), 376 (3.52, MLCT), 564 (2.84, d-d) nm. ^1H NMR (250 MHz, CD_3OD, 298 K): δ = 2.15 (s, 12 H, Me^3), 2.24 (s, 12 H, Me^5), 5.85 (s, 4 H, H^4), 6.61 (s, 2 H, CH) ppm. $^{13}C\{^1H\}$ NMR/DEPT 135° (62.89 MHz, CD_3OD, 298 K): δ = 11.2 (+, Me^5), 13.4 (+, Me^3), 73.9 (+, CH), 107.1 (+, C^4), 142.6 (0, C^5), 149.6 (0, C^3), 169.6 (0, C=O) ppm.

[Ru(NO)(bdmpzsa)(en)]Cl_2 (7): A procedure similar to that for **3** was used, but with $Ru(NO)Cl_3$ (50.0 mg, 0.21 mmol), ligand **1** (61.0 mg 0.21 mmol) and ethylenediamine (14 μL, 0.21 mmol) to afford a brownish red crystalline solid. Yield: 105.0 mg (91.3%). $C_{13}H_{23}Cl_2N_7O_4RuS$ (545.4): calcd. C 28.62, H 4.22, N 17.98; found C 28.60, H 4.25, N17.96. IR (KBr): $\tilde{\nu}$ = 3234 $\nu_{as}(NH_2)$, 3135 $\nu_s(NH_2)$, 1855 (1818, sh) ν(NO), 1557 ν(C=N), 1178 $\nu_{as}(SO_3^-)$, 1113 $\nu_s(SO_3^-)$, 328 ν(Ru−Cl) cm^{-1}. IR (CH_2Cl_2): $\tilde{\nu}$ = 1851 ν(NO) cm^{-1}. UV/Vis: λ (log ε) = 252 (sh, π → π*), 308 (sh, MLCT), 455 (2.88, d-d) nm. ^1H NMR (250 MHz, CD_3OD, 298 K): δ = 2.16 (s, 6 H, Me^3), 2.44 (s, 6 H, Me^5), 2.24 /2.63 [t, 4 H, CH_2(en)], 5.95 (s, 2 H, H^4), 6.80 (s, 1 H, CH) ppm. $^{13}C\{^1H\}$ NMR/NOE suppression, DEPT 135° (62.89 MHz, CD_3OD, 298 K): δ = 10.8 (+, 2 C, Me^5), 13.1 (+, 2 C, Me^3), 45.6/45.5 [−, 2 C, CH_2(en)], 75.3 (+, 1 C, CH), 106.9 (+, 2 C, C^4), 142.5 (0, 2 C, C^5), 151.3 (0, 2 C, C^3) ppm.

[Ru(NO)(bdmpza)(en)]Cl_2 (8): A procedure similar to that for **3** was used, but with $Ru(NO)Cl_3$ (50.0 mg, 0.21 mmol), ligand **2** (53.3 mg, 0.21 mmol) and ethylenediamine (14 μL, 0.21 mmol) to furnish a brownish red crystalline solid. Yield: 97 mg (90.6%).

 © 2004 Wiley-VCH Verlag GmbH & Co. KGaA, Weinheim

$C_{14}H_{23}Cl_2N_7O_3Ru$ (509.4): calcd. C 33.00, H 4.52, N 19.25; found C 33.03, H 4.55, N 19.21. IR (KBr): $\tilde{\nu}$ = 3233 $\nu_{as}(NH_2)$, 3130 $\nu_s(NH_2)$, 1867 (1822, sh) ν(NO), 1637 $\nu_{as}(CO_2^-)$, 1560 ν(C=N), 1386 $\nu_s(CO_2^-)$ cm^{-1}. IR (CH_2Cl_2): $\tilde{\nu}$ = 1863 ν(NO) cm^{-1}. UV/Vis: λ (log ε) = 252 (sh, $\pi\rightarrow\pi^*$), 300 (sh, MLCT), 464 (2.96, d-d) nm. ^{1}H NMR (250 MHz, CD_3OD, 298 K): δ = 2.13 (s, 6 H, Me^3), 2.27 (s, 6 H, Me^5), 2.31 /2.65 (t, 4 H, CH_2(en)), 5.86 (s, 2 H, H^4), 6.62 (s, 1 H, CH) ppm. $^{13}C\{^1H\}$ NMR/NOE suppression, DEPT-135° (62.89 MHz, CD_3OD, 298 K): δ = 11.6 (+, 2 C, Me^5), 13.5 (+, 2 C, Me^3), 46.5/46.4 [−, 2 C, CH_2(en)], 74.8 (+, 1 C, CH), 107.5 (+, 2 C, C^4), 142.8 (0, 2 C, C^5), 149.1 (0, 1 C, C^3), 170.03 (0, 1 C, C=O) ppm.

Supporting Information Available (see also footnote on the first page of this article): ^{13}C NMR spectrum with suppressed NOE of $[Ru(NO)(bdmpza)_2(NEt_3]$ (Figure S1).

Acknowledgments

This research was supported by a grant from the Universidad de Castilla-La Mancha, Spain. The authors acknowledge Professor Teófilo Rojo and Dr. Luis Lezama (University of the Basque Country, Bilbao, Spain) for ESR facilities and Professor Francisco Lloret (University of Valencia, (Spain) for SQUID determinations.

[1] [1a] S. Moncada, R. M. J. Palmer, E. A. Higgs, *Biochem. Pharmacol.* **1989**, *38*, 1709−1715. [1b] A. R. Buttler, D. L. H. Williams, *Chem. Soc. Rev.* **1993**, *22*, 233−241.
[2] B. Mondal, H. Paul, V. G. Puranik, G. K. Lahiri, *J. Chem. Soc., Dalton Trans.* **2001**, 481−487.
[3] G. B. Yi, M. A. Khan, D. R. Powell, G. B. Richter-Addo, *Inorg. Chem.* **1998**, *37*, 208−214.
[4] [4a] D. R. Lang, J. A. Davis, L. G. F. Lopes, A. A. Ferro, L. C. G. Vasconcellos, D. W. Franco, E. Tfouni, A. Wieraszko, M. J. Clarke, *Inorg. Chem.* **2000**, *39*, 2294−2300. [4b] B. R. McGarvey, A. A. Ferro, E. Tfouni, C. W. B. Bezaerra, I. Bagatin, D. W. Franco, *Inorg. Chem.* **2000**, *39*, 3577−3581. [4c] M. Wanner, T. Schreiring, W. Kaim, *Inorg. Chem.* **2001**, *40*, 5704−5707.
[5] [5a] A. K. Patra, P. K. Mascharak, *Inorg. Chem.* **2003**, *42*, 7363−7365. [5b] C. F. Works, C. J. Jocher, G. D. Bart, X. Bu, P. C. Ford, *Inorg. Chem.* **2002**, *41*, 3728−3739. [5c] C. F. Works, P. C. Ford, *J. Am. Chem. Soc.* **2000**, *122*, 7592−7593.
[6] [6a] S. P. Fricker, E. Salde, N. A. Powell, O. J. Vaughan, G. R. Henderson, S. A. Murrer, I. C. Megson, S. K. Bisland, F. W. Flitney, *Br. J. Pharmacol.* **1997**, *122*, 1441. [6b] Y. Chen, F.-T. Lin, R. E. Shepherd, *Inorg. Chem.* **1999**, *38*, 973−983. [6c] J. M. Slocik, M. S. Ward, K. V. Somayajula, R. E. Shepherd, *Trans. Metal Chem.* **2001**, *26*, 351−364.
[7] M. Onishi, *Bull. Chem. Soc. Jpn.* **1991**, *64*, 3039−3045.
[8] D. S. Bohle, E. S. Sagan, *Eur. J. Inorg. Chem.* **2000**, 1609−1616.
[9] M. Ortiz, A. Díaz, R. Cao, A. Otero, J. Fernández-Baeza, *Inorg. Chim. Acta* **2003**, *357*, 19−24.
[10] J. Sandström, *Dynamic NMR Spectroscopy*, Academic Press, New York, **1982**.
[11] A. López-Hernández, R. Müller, H. Kopf, N. Burzlaff, *Eur. J. Inorg. Chem.* **2002**, 671−677.
[12] A. Otero, J. Fernández-Baeza, J. Tejeda, A. Antiñolo, F. Carrillo-Hermosilla, E. Díez-Barra, A. Lara-Sánchez, M. Fernández-López, *J. Chem. Soc., Dalton Trans.* **2000**, 2367−2374.

Received January 23, 2004
Early View Article
Published Online June 17, 2004

 © 2004 Wiley-VCH Verlag GmbH & Co. KGaA, Weinheim

Restricted Phenyl Rotation in Pyridyl Thioether Ligands N,S-Chelated to Congested Diiminoruthenium Cores

Laura Baradello,[a] Sandra Lo Schiavo,[a] Francesco Nicolò,[a] Santo Lanza,[a] Giuseppe Alibrandi,[a] and Giuseppe Tresoldi*[a]

Keywords: Activation barriers / N,S ligands / Restricted rotation / Ruthenium

The thioethers 2-pyridylmethyl *p*-tolyl sulfide (**a**) and *p*-chlorophenyl 2-pyridylmethyl sulfide (**b**) react with the precursors *cis*-[$RuCl_2$(*N*,*N*-diimine)$_2$] [diimine = di-2-pyridyl sulfide (dps), **1**; 2,2′-bis(4-methylpyridyl) sulfide (4mdps), **2**; 2,2′-bis(5-methylpyridyl) sulfide (5mdps), **3**; di-2-pyrimidyl sulfide (dprs), **4**; and 2,2′-bis(5-ethylpyrimidyl) sulfide (5edprs), **5**] in the presence of NH_4PF_6 to give the complexes [Ru(*N*,*N*-diimine)$_2$(*N*,*S*-**a**)][PF_6]$_2$ and [Ru(*N*,*N*-diimine)$_2$(*N*,*S*-**b**)][PF_6]$_2$, respectively. As a consequence of the *N*,*S* chelation all the complexes contain a five-membered RuSCCN(*Ru*–*N*) ring, the sulfur and ruthenium atoms of which are stereogenic centres, with (*R*) and (*S*) and Δ and Λ configurations, respectively. Furthermore, the coordinated thioethers contain anisochronous methylene protons and phenyl protons which are sensor nuclei for pyramidal sulfur inversion and rotation of the pendant phenyl ring, respectively. In the low-temperature ^{1}H NMR spectra of the complexes a single AB system for the methylene protons, in agreement with a fast sulfur inversion, is observed. Well-separated signals of the two *ortho*- as well as the *meta*-phenyl protons, indicating restricted phenyl rotation, are also observed. At higher temperatures the fast exchange of the two halves of the phenyl ring leads to averaged signals for the phenyl protons. The rates and activation energies of this fluxional process were measured by one-dimensional band-shape analysis. Certain trends were immediately apparent. The rotation barrier values ($\Delta G^{\#}_{298}$) of the dps, 4mdps and 5mdps complexes were ca. 4.0 kJ·mol^{-1} lower than those of the dprs and 5edprs complexes. On the contrary, substitution of H^4 or H^5 dps protons with methyl groups and H^5 dprs protons with ethyl groups, as well as substitution of **a** with **b**, leaves the rotation-barrier values practically unchanged. This effect can be correlated to the steric hindrance produced by the two ligands *cis* to the rotating group. The crystal structure of the enantiomeric couple Δ*S*/Λ*R* of [Ru(dps)$_2$(2-pyridymethyl 2-pyridyl sulfide)][PF_6]$_2$ (**1c**), in which the 2-pyrimidylmethyl 2-pyridyl sulfide (**c**) ligand acts in an *N*,*S*-bidentate mode forming a five-membered RuSCCN(*Ru*–*N*) chelate ring, is also reported.

(© Wiley-VCH Verlag GmbH & Co. KGaA, 69451 Weinheim, Germany, 2004)

Introduction

The chemistry of di-2-pyridyl sulfide (dps) is of interest in that the ligand, which usually adopts an *N*,*N*-bidentate coordination,[1−13] can exhibit a variety of bonding modes to metal atoms, for example monodentate,[10−12] and bridging.[11−14] Consequently, dps complexes can exhibit interconversion between different coordination species or fluxional processes.[10−12] The *N*,*N* chelation[15−20] of dps, and similar thioether compounds containing heterocycles, to the ruthenium(II) ion, and a *cis* arrangement[15−17,19,20] around the metal atom, are usually observed, although complexes with a *trans* configuration[18] or which contain a four-membered RuSCN(*Ru*−*N*)[19] ring have also been obtained. As a consequence of the *N*,*S* coordination, the thioether ligand contains a stereogenic sulfur centre [(*R*) and (*S*) configurations] and a pendant ring. The ^{1}H and ^{13}C NMR spectra of the complexes containing *cis*-Ru(*N*,*N*-dprs)$_2$ or *cis*-Ru(*N*,*N*-dps)$_2$ fragments (dprs = di-2-pyrimidyl sulfide) and the *N*,*S*-chelated thioether ligand phpys (phenyl pyridyl sulfide) below 240 K are temperature-dependent due to the restricted rotation of the pendant ring.

The NMR investigation of [Ru(*N*,*N*-diimine)$_2$(*N*,*S*-thioether)][PF_6]$_2$ [20] (diimine = dps or dprs; thioether = pySCH_2R or prSCH_2R, where py = pyridyl, pr = pyrimidyl and R = phenyl derivative) shows the presence of two invertomers as pairs of enantiomers (Δ*R*, Λ*S* and Δ*S*, Λ*R*) due to the Δ and Λ configurations of the ruthenium atom and the (*R*) and (*S*) configurations of the sulfur atom. The sulfur inversion produces the exchange [(*R*) ⇄ (*S*)] whereas the racemization process (Δ ⇄ Λ) was absent and the rotation of the pendant ring fast.

In order to study the effect of the steric hindrance of the Ru(diimine)$_2$ fragment on the phenyl rotation and the effect of the ring size on the sulfur inversion we have selected a series of [$RuCl_2$(diimine)$_2$] precursors and thioethers suitable for *N*,*S* chelation. We report on the dynamic behaviour

[a] Dipartimento di Chimica Inorganica, Chimica Analitica e Chimica Fisica, Università di Messina,
Salita Sperone 31, 98166 Messina, Italy
Fax: + 39-090-393756
E-mail: Tresoldi@chem.unime.it

 © 2004 Wiley-VCH Verlag GmbH & Co. KGaA, Weinheim **DOI: 10.1002/ejic.200400120**

of the compounds obtained from 2-pyridylmethyl *p*-tolyl sulfide (**a**) and *p*-chlorophenyl 2-pyridylmethyl sulfide (**b**) with *cis*-[$RuCl_2$(*N*,*N*-diimine)$_2$] compounds [diimine = dps, **1**; 2,2′-bis(4-methylpyridyl) sulfide (4mdps), **2**; 2,2′-bis(5-methylpyridyl) sulfide (5mdps), **3**; dprs, **4** and 2,2′-bis(5-ethylpyrimidyl) sulfide (5edprs) **5**]. The crystal structure of the couple $\Delta S/\Lambda R$ of [Ru(dps)$_2$(2-pyridymethyl 2-pyridyl sulfide)][PF_6]$_2$ (**1c**) is also reported.

Results

Synthesis of the Compounds Containing an N,S-Chelate Ligand

The air-stable compounds **1a**, **3a**−**5a**, **1b**−**5b** and **1c** were obtained by the reactions depicted in Scheme 1. The new precursors [$RuCl_2$(*N*,*N*-4mdps)$_2$] (**2**), [$RuCl_2$(*N*,*N*-5mdps)$_2$] (**3**) and [$RuCl_2$(*N*,*N*-5edprs)$_2$] (**5**) were prepared from $RuCl_3 \cdot 3H_2O$ and 4mdps,[21] 5mdps[21] or the new ligand 5edprs; see Exp. Sect.).

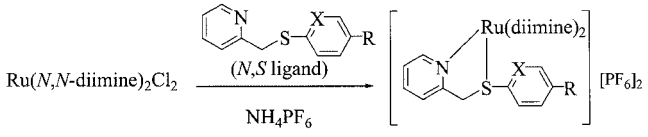

	Ru(*N*,*N*-diimine)$_2$Cl$_2$	*N*,*S* ligand	Complex
1	Ru(dps)$_2$Cl$_2$	**a** (X = CH, R = Me)	**1a**
3	Ru(5mdps)$_2$Cl$_2$	**a**	**3a**
4	Ru(dprs)$_2$Cl$_2$	**a**	**4a**
5	Ru(5edprs)$_2$Cl$_2$	**a**	**5a**
1	Ru(dps)$_2$Cl$_2$	**b** (X = CH, R = Cl)	**1b**
2	Ru(4mdps)$_2$Cl$_2$	**b**	**2b**
3	Ru(5mdps)$_2$Cl$_2$	**b**	**3b**
4	Ru(5edprs)$_2$Cl$_2$	**b**	**4b**
5	Ru(dps)$_2$Cl$_2$	**c** (X = N, R = H)	**1c**

Scheme 1

The complexes are yellow or orange solids that are soluble in acetone or acetonitrile and slightly soluble in methanol, ethanol and water. They were characterised by elemental analysis, conductivity measurements in acetonitrile solution with values characteristic of 1:2 electrolytes (330−300 $S \cdot cm^2 \cdot mol^{-1}$), IR spectroscopy, which shows the bands of PF_6^- (ca. 842 and 558 cm^{-1}) and those characteristic of thioether ligands in the range 1630−1540 cm^{-1}. This indicates that the ligands dps, 4mdps, 5mdps, dprs and 5edprs act as bidentate *N*,*N*-chelate ligands,[8−20] whereas **a**, **b** and **c** are *N*,*S*-chelate ligands.[19,20] These findings were confirmed by subsequent ^1H and ^{13}C NMR spectroscopic studies.

Low-Temperature ^1H NMR Spectra

At low temperatures the NMR spectra of these complexes show well-separated signals of the two *ortho*- (as well as the *meta*-) phenyl protons. The spectrum of **4b** at 218 K in the δ = 8.2−3.7 ppm range is shown in Figure 1; the data are listed in Table 1. Because of the slow phenyl rotation two doublets of doublets are observed in the phenyl region for the *ortho*-protons at δ = 8.09 (partially overlapped with the signal of the H^5 pyrimidine proton) and 5.38 ppm, labelled **M** and **N**, respectively. Furthermore, two doublets of doublets for the *meta*-protons are observed at δ = 7.60 and 6.75 ppm, labelled **O** and **P**, respectively. The coupling constants between **M** and **O** and **N** and **P** are 8.6 Hz and between **M** and **N** and **O** and **P** 2.3 Hz. In the methylene region two doublets appear at δ = 4.65 and 3.87 ppm ($^2J_{H,H}$ = 17.4 Hz).

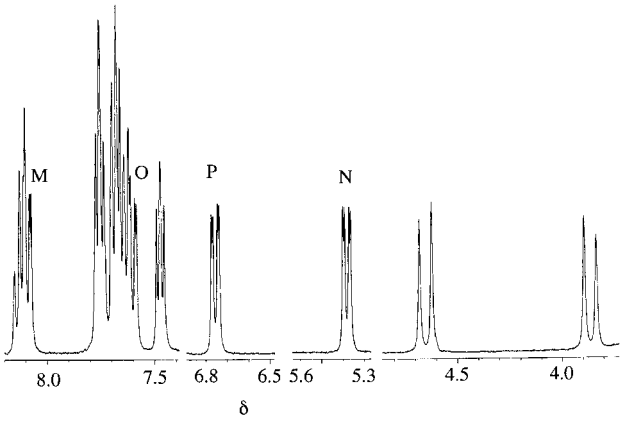

Figure 1. ^1H NMR spectrum of [Ru(*N*,*N*-dprs)$_2$(*N*,*S*-**b**)][PF_6]$_2$ (**4b**) at 218 K in $(CD_3)_2CO$ (range δ = 8.2−3.7 ppm)

The full assignment of the signals and the solution structure was based on 2D COSY, phase-sensitive 2D NOESY, decoupling experiments and one-dimensional ^1H NMR spectra at variable temperatures. In this way the twelve signals, as doublets of doublets due to the protons of the four pyrimidine rings with the coupling constants $J_{4,5} \approx 4.6$, $J_{4,6} \approx 2.1$, $J_{5,6} \approx 6.0$ Hz and the ten signals due to the protons of the pyridine, the phenyl and methylene groups of the **b** ligand, were assigned.

Dynamic NMR Studies

The dynamic behaviour of the complexes was preliminarily examined by phase-sensitive 2D NOESY spectroscopy, which shows the interchanges (positive cross-peaks) and the interactions (negative cross-peaks) between the protons. The phase-sensitive 2D NOESY spectra of the dprs and 5edprs complexes were recorded almost at the same temperature (245−250 K) whereas those of the dps, 4mdps and 5mdps complexes were recorded at lower temperatures as the dynamic process is faster than for the dprs and 5edprs complexes (vide infra).

The spectrum for **4b**, at 248 K, is shown in Figure 2. At this temperature the *ortho*-phenyl signals as well as the *meta* signals are split as the fluxional process that exchanges the two halves of the phenyl ring is slow. Positive cross-peaks, due to chemical exchange of magnetization, are detected between the phenyl protons **M** and **N** (at δ = 8.09 and 5.38

 © 2004 Wiley-VCH Verlag GmbH & Co. KGaA, Weinheim

Table 1. Low-temperature ^{1}H NMR spectroscopic data

Complex[a]	*N,S*-ligand positions						*N,N*-ligand positions				
T [K]	2	3	4	5	6	CH_2	ring	3	4	5	6
1a		7.60[b]	7.84[b]	7.58[b]	9.40[b]	4.38[b]	C	7.62	8.14	7.63	9.35
218	7.80[c]	7.29[c]	2.12[d]	6.38[c]	5.07[c]	3.60[b]	D	8.19	8.03	7.17	7.60
	$J_{2,3} = J_{5,6} = 7.7$			$J_{2,6} = J_{3,5} = 1.7$		$J = 16.7$	E	8.16	8.23	7.36	8.03
							F	7.62	8.11	7.64	9.16
3a		7.56[b]	8.03[b]	7.63[b]	9.49[b]	4.28[b]	C	7.38	7.76	2.35[e]	9.24
213	7.76[c]	7.28[c]	2.11[d]	6.40[c]	5.04[c]	3.48[b]	D	7.88	7.84	1.89[e]	7.84
	$J_{2,3} = J_{5,6} = 8.2$			$J_{2,6} = J_{3,5} = 1.8$		$J = 16.9$	E	8.09	8.01	2.03[e]	7.92
							F	7.67	8.01	2.35[e]	8.99
4a		7.68[b]	8.12[b]	7.75[b]	9.40[b]	4.52[b]	C		8.54	7.60	9.42
223	7.90[c]	7.34[c]	2.14[d]	6.49[c]	5.10[c]	3.79[b]	D		8.97	7.45	8.79
	$J_{2,3} = J_{5,6} = 8.2$			$J_{2,6} = J_{3,5} = 2.1$		$J = 17.5$	E		9.13	7.65	9.04
							F		8.93	7.74	9.63
5a		7.65[b]	8.10[b]	7.73[b]	9.51[b]	4.47[b]	C	1.07[e]	8.52	2.66[f]	9.36
228	7.87[c]	7.33[c]	2.14[d]	6.48[c]	4.97[c]	3.77[b]	D	0.85[e]	8.95	2.34[f]	8.74
	$J_{2,3} = J_{5,6} = 8.0$			$J_{2,6} = J_{3,5} = 2.2$		$J = 17.2$	E	0.92[e]	9.07	2.41[f]	8.92
							F	1.14[e]	8.91	2.69[f]	9.62
1b		7.61[b]	8.08[b]	7.65[b]	9.38[b]	4.50[b]	C	7.57	7.89	7.59	9.43
208	7.98[c]	7.58[c]		6.73[c]	5.26[c]	3.67[b]	D	8.26	8.04	7.18	7.60
	$J_{2,3} = J_{5,6} = 8.5$			$J_{2,6} = J_{3,5} = 1.8$		$J = 16.9$	E	8.16	8.22	7.37	8.07
							F	7.60	8.03	7.58	9.18
2b		7.62[b]	8.00[b]	7.58[b]	9.29[b]	4.49[b]	C	7.46	2.28[e]	7.36	9.15
207	7.95[c]	7.56[c]		6.79[c]	5.18[c]	3.66[b]	D	8.05	2.39[e]	7.02	7.46
	$J_{2,3} = J_{5,6} = 8.6$			$J_{2,6} = J_{3,5} = 2.4$		$J = 17.0$	E	8.12	2.47[e]	7.22	8.05
							F	7.90	2.43[e]	7.49	8.96
3b		7.57[b]	8.02[b]	7.64[b]	9.48[b]	4.40[b]	C	7.48	7.84	2.33[e]	9.25
217	7.94[c]	7.54[c]		6.71[c]	5.25[c]	3.55[b]	D	8.04	7.93	1.89[e]	7.48
	$J_{2,3} = J_{5,6} = 8.5$			$J_{2,6} = J_{3,5} = 2.1$		$J = 16.9$	E	8.09	8.04	2.01[e]	7.89
							F	7.88	8.04	2.31[e]	8.99
4b		7.63[b]	8.13[b]	7.75[b]	9.41[b]	4.65[b]	C		8.61	7.67	9.46
218	8.09[c]	7.60[c]		6.75[c]	5.38[c]	3.87[b]	D		8.98	7.47	8.81
	$J_{2,3} = J_{5,6} = 8.6$			$J_{2,6} = J_{3,5} = 2.3$		$J = 17.4$	E		9.14	7.67	9.05
							F		8.94	7.75	9.66
5b		7.63[b]	8.08[b]	7.71[b]	9.49[b]	4.57[b]	C	1.07[e]	8.60	2.68[f]	9.35
218	8.04[c]	7.58[c]		6.73[c]	5.25[c]	3.81[b]	D	0.91[e]	8.92	2.31[f]	8.72
	$J_{2,3} = J_{5,6} = 8.6$			$J_{2,6} = J_{3,5} = 2.5$		$J = 17.4$	E	0.84[e]	9.07	2.40[f]	8.91
							F	1.37[e]	8.90	2.68[f]	9.61
1c		7.40[b]	7.72[b]	7.43[b]	9.25[b]	4.55[b]	C	7.50	7.90	7.49	9.15
223		7.93[g]	7.82[g]	7.19[g]	7.48[g]	3.69[b]	D	8.17	8.02	7.17	7.58
						$J = 16.9$	E	8.23	8.16	7.34	8.03
							F	8.00	8.09	7.62	9.17

[a] At 300.13 MHz, in [D$_6$]acetone; δ in ppm with respect to TMS, *J* in Hz. [b] Picolyl fragment. [c] Phenyl fragment. [d] Methyl of **a**. [e] Methyl of the *N,N* ligand. [f] Methylene of 5edprs. [g] Pyridyl fragment.

ppm, respectively) and **O** and **P** (at $\delta = 7.60$ and 6.75 ppm, respectively) while the strong NOEs (negative cross peaks) include interactions between the methylene protons, intra-ring interactions in the phenyl ring (**M/O** and **N/P**) and in the pyrimidine ring (H^6/H^5) and, most significantly, the following interactions: methylene proton at $\delta = 4.65$ ppm/H^3 pyridine proton at $\delta = 7.63$ ppm, methylene proton at $\delta = 3.87$ ppm/H^6 pyrimidine proton at $\delta = 9.66$ ppm, H^6 pyrimidine proton at $\delta = 9.46$ ppm/H^6 pyridine proton at $\delta = 9.41$ ppm, H^6 pyrimidine proton at $\delta = 9.46$ ppm and that at $\delta = 9.05$ ppm, H^6 pyrimidine proton at $\delta = 9.66$ ppm and that at $\delta = 8.81$ ppm. If we assume that the sulfur inversion is fast at low temperatures and that the phenyl rotation is slow, the *ortho*-phenyl protons (**M** and **N**) are anisochronous as are the *meta*-protons (**O** and **P**), and the phenyl rotation exchanges protons **M** and **N** and **O** and **P**. Furthermore the negative cross-peaks found in the 2D NOESY spectrum suggest that in the invertomer depicted (Figure 3) the pyrimidine ring labelled C is *cis* to the phenyl ring B and the ring F is *cis* to the pyridine ring A, while ring E is *trans* to the sulfur atom. In the other invertomer (not shown) the phenyl ring should be *cis* to the ring F.

Similar structures for the other complexes at low temperature can be deduced from the data listed in Table 1. The ring and the position of the protons were assigned by the one- and two-dimensional experiments mentioned previously and by comparison of the spectra. In particular, the solution structure depicted in Figure 4 is proposed for an invertomer of **1a**.

Upon warming the solutions, the spectral lines of the phenyl protons broaden and coalesce in the range 255−295 K. At 330 K, the highest temperature reached, averaged signals are observed for the *ortho*- as well the *meta*-phenyl protons of all the complexes (Table 2). For instance,

 © 2004 Wiley-VCH Verlag GmbH & Co. KGaA, Weinheim

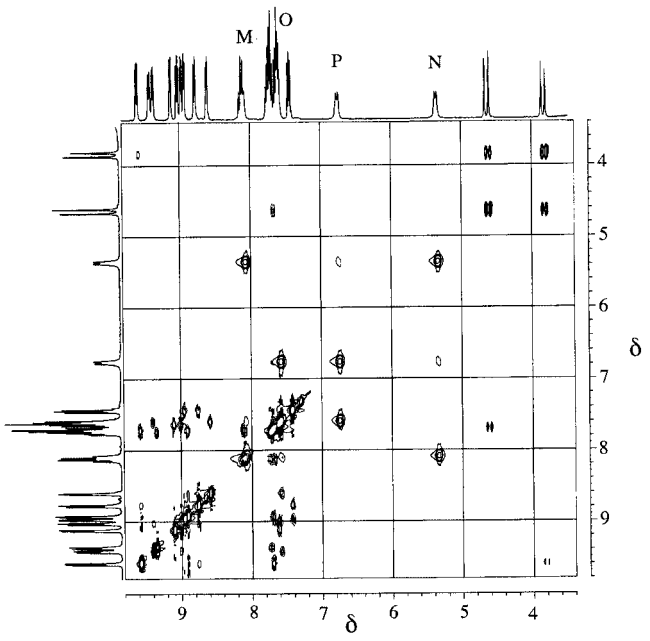

Figure 2. Phase-sensitive 2D NOESY spectrum of **4b** at 248 K in $(CD_3)_2CO$ (range δ = 9.8−3.4 ppm)

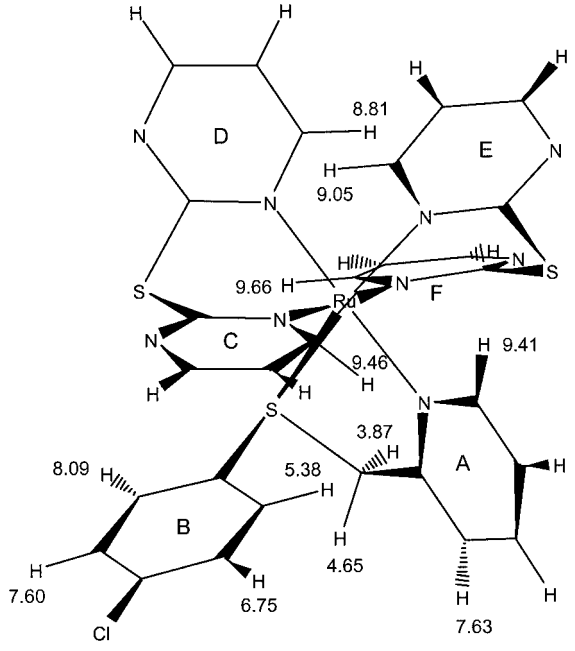

Figure 3. Proposed solution structure of **4b**; the rings are labelled A−F; the following signal assignments, based on 2D NOESY spectra at low temperatures, show vicinal protons at δ = 8.09−7.60, 6.75−5.38, 7.63−4.65, 9.66−3.87, 9.46−9.41, 9.46−9.05, 9.66−8.81 ppm

the *meta*- and the *ortho*-phenyl proton signals of **1a** are observed at δ = 6.83 and 6.50 ppm, respectively, near the statistical average of δ = 6.84 and 6.44 ppm, respectively, as expected for a single dynamic process. Furthermore, the *meta*- and the *ortho*-phenyl proton signals of **4b** are observed at δ = 7.12 and 6.67 ppm, respectively. The last signal in this complex, as well as in other dprs and 5edprs

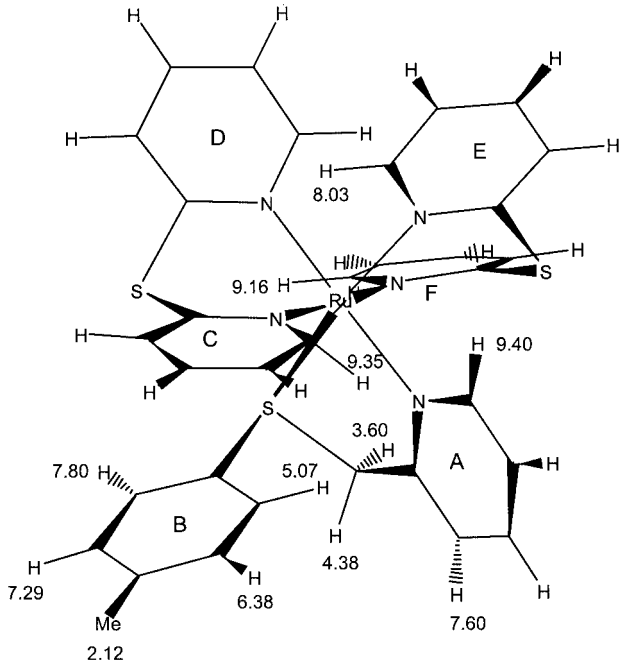

Figure 4. Proposed solution structure of **1a**; the rings are labelled A−F; the following signal assignments, based on 2D NOESY spectra at low temperatures, show vicinal protons at δ = 7.80−7.29, 6.38−5.07, 7.60−4.38, 9.16−3.60, 9.40−9.35, 6.38−2.12, 7.29−2.12, 9.40−8.03 ppm

complexes, is rather broad due to the great chemical-shift differences of the exchanging protons (ca. 2.7 ppm) and the energy-barrier values ($\Delta G^{\#}_{298} \approx$ 54.3 kJ·mol^{-1}, vide infra and Table 3). Although the dynamic behaviour of the complexes in CD_3CN parallels that observed in acetone, decomposition above 340 K is observed. Furthermore solubility problems in other solvents prevent detailed NMR studies at higher temperatures. It is worth noting that this process has a negligible effect on the methylene protons which appear, at all the temperatures, as a single AB system.

COSY and NOESY experiments were also performed at high temperatures allowing the complete assignment of the proton signals. In particular the signals of **4b** at δ = 9.20, 7.71, 8.06 and 7.64 ppm were assigned to the pyridine protons H^6, H^5, H^4 and H^3, respectively, of the *N*,*S*-coordinated ligand (Table 2).

The rates of the process were deduced by band-shape analysis of the phenyl signals. Some experimental and computer-simulated spectra are shown in Figure 5. Activation energy data were calculated from fifteen independent fittings in the temperature range 210−330 K. The activation energy data for the other complexes were obtained by a similar method and are collected in Table 3.

The ^{13}C NMR spectra of the complexes were interpreted easily, at least for the carbon signals of the *N*,*S*-chelate ligand, by comparison of the spectra of the present complexes with those of the free ligands and other complexes containing *N*,*S*-chelate ligands,[19,20] with the help of the jmod pulse sequence. The variable-temperature ^{13}C NMR spectra of **4b** in the range δ = 142−124 ppm are shown in

 © 2004 Wiley-VCH Verlag GmbH & Co. KGaA, Weinheim

Table 2. ^{1}H NMR spectroscopic data

Complex[a]	*N*,*S*-ligand positions					*N*,*N*-ligand positions				
	3	4	5	6	CH_2	ring	3	4	5	6
a	7.37[b]	7.67[b]	7.19[b]	8.46[b]	4.24[b]					
	7.08[c]	7.25[d]	2.26[e]							
b	7.36[b]	7.68[b]	7.20[b]	8.45[b]	4.31[b]					
	7.06[c]	7.41[d]								
c	7.49[b]	7.67[b]	7.19[b]	8.48[b]	4.60[b]					
	7.28[f]	7.59[f]	7.07[f]	8.44[f]						
1a[g]	7.64[b]	7.98[b]	7.60[b]	9.23[b]	4.34[b]	C	7.97	8.08	7.56	9.10
	6.50[c]	6.83[d]	2.17[e]		3.59[b]	D	8.09	7.99	7.15	7.39
					J = 16.9	E	8.16	8.17	7.34	7.85
						F	7.49	7.83	7.56	9.30
3a[g]	7.55[b]	7.95[b]	7.65[b]	9.30[b]	4.29[b]	C	7.34	7.66	2.36[e]	9.12
	6.50[c]	6.83[d]	2.17[e]		3.60[b]	D	7.95	7.82	1.90[e]	7.03
					J = 16.9	E	8.04	7.96	2.03[e]	7.65
						F	7.85	7.92	2.35[e]	8.88
4a[g]	7.67[b]	8.09[b]	7.74[b]	9.23[b]	4.46[b]	C		8.51	7.51	9.28
	6.50[c]	6.93[d]	2.19[e]		3.70[b]	D		8.92	7.37	8.63
					J = 17.4	E		9.05	7.54	8.91
						F		8.87	7.65	9.40
5a[g]	7.63[b]	8.08[b]	7.77[b]	9.32[b]	4.40[b]	C	1.16[e]	8.45	2.74[h]	9.11
	6.48[c]	6.92[d]	2.20[e]		3.63[b]	D	1.03[e]	8.96	2.49[h]	8.75
					J = 17.3	E	0.96[e]	8.85	2.43[h]	8.45
						F	1.23[e]	8.80	2.78[h]	9.23
1b[g]	7.64[b]	7.98[b]	7.61[b]	9.23[b]	4.42[b]	C	7.58	7.87	7.58	9.31
	6.65[c]	7.06[d]			3.64[b]	D	8.09	7.99	7.15	7.38
					J = 17.0	E	8.17	8.15	7.34	7.84
						F	7.97	8.08	7.58	9.09
2b[g]	7.60[b]	7.97[b]	7.58[b]	9.15[b]	4.39[b]	C	7.39	2.34[e]	7.40	9.04
	6.63[c]	7.07[d]			3.63[b]	D	7.93	2.41[e]	6.98	7.12
					J = 17.0	E	7.99	2.50[e]	7.16	7.60
						F	7.80	2.47[e]	7.42	8.85
3b[g]	7.56[b]	7.97[b]	7.65[b]	9.31[b]	4.37[b]	C	7.45	7.71	2.38[e]	9.15
	6.66[c]	7.06[d]			3.64[b]	D	7.97	7.83	1.90[e]	7.03
					J = 16.9	E	8.05	7.97	2.02[e]	7.67
						F	7.85	7.92	2.35[e]	8.87
4b[g]	7.64[b]	8.06[b]	7.71[b]	9.20[b]	4.52[b]	C		8.53	7.51	9.26
	6.67[c]	7.12[d]			3.71[b]	D		8.89	7.34	8.60
					J = 17.5	E		9.02	7.51	8.87
						F		8.84	7.61	9.36
5b[g]	7.64[b]	8.08[b]	7.76[b]	9.34[b]	4.49[b]	C	1.15[e]	8.52	2.73[h]	9.15
	6.65[c]	7.14[d]			3.68[b]	D	1.02[e]	8.98	2.49[h]	8.78
					J = 17.4	E	0.94[e]	8.87	2.43[h]	8.50
						F	1.21[e]	8.80	2.76[h]	9.26
1c[g]	7.48[b]	7.89[b]	7.52[b]	9.05[b]	4.47[b]	C	7.40	7.75	7.42	9.18
	7.90[f]	7.80[f]	7.16[f]	7.40[f]	3.66[b]	D	8.10	8.00	7.18	7.59
					J = 16.7	E	8.10	8.16	7.33	7.83
						F	7.90	8.08	7.57	9.09

[a] At 300.13 MHz, in [D_6]acetone, at 298 K unless stated otherwise; δ in ppm with respect to TMS, J in Hz. [b] Picolyl fragment. [c] *ortho*-Phenyl proton. [d] *meta*-Phenyl proton. [e] Methyl proton. [f] Pyridyl fragment. [g] At 330 K. [h] Methylene of 5edprs.

Figure 6. In the ^{13}C NMR spectrum at 208 K the signals of the more deshielded carbon atoms appear at δ = 169.5, 169.2, 168.9 and 168.3 ppm (quaternary pyrimidine carbon atoms), while two overlapped signals for the C^6 pyrimidine carbon atoms appear at δ = 164.6 ppm, the others being well separated (δ = 164.5 and 163.0 ppm). The signal of the more deshielded carbon atom of **b** is observed at δ = 162.40 ppm (quaternary pyridine carbon atoms) while the C^6 pyridine carbon atom (δ = 155.5 ppm) is shielded with respect to the C^4 pyrimidine carbon atoms (δ = 158.6, 158.2, 158.1 and 156.8 ppm). Figure 6 shows the C^4 pyridine signal (δ = 138.6 ppm), the *ortho*-phenyl carbon signals (δ = 135.6 and 128.5 ppm), the *meta*-phenyl carbon signals (δ = 129.4 and 129.3 ppm), the CS signal (δ = 135.5 ppm), the CCl signal (δ = 128.5 ppm) and the signals of the C^3 and C^5 pyridine carbon atoms of **b** at δ = 124.3 and 124.1 ppm. The signals of the C^5 pyrimidine carbon atoms (not shown in Figure 6) are observed at δ = 122.2, 121.6 ppm, with two overlapping signals at δ = 121.3 ppm.

Upon warming the solutions, the signals of the *ortho*- and *meta*-phenyl carbon atoms broadened and then coalesced. The coalescence temperature (T_c) for the *meta*-phe-

 © 2004 Wiley-VCH Verlag GmbH & Co. KGaA, Weinheim

Table 3. Activation energy data

	$\Delta G^{\#}_{298}$ [kJ·mol^{-1}]	$\Delta H^{\#}$ [kJ·mol^{-1}]	$\Delta S^{\#}$ [J·K^{-1}·mol^{-1}]
1a	50.0 ± 0.2	43.9 ± 1.2	−20.6 ± 4.9
1b	49.7 ± 0.1	50.5 ± 0.7	+2.8 ± 2.7
2b	50.1 ± 0.2	55.4 ± 1.8	+17.6 ± 6.6
3a	49.1 ± 0.1	50.7 ± 1.1	+5.4 ± 4.0
3b	49.7 ± 0.1	55.1 ± 1.0	+18.0 ± 3.5
4a	53.5 ± 0.2	49.6 ± 2.0	−13.0 ± 7.5
4b	54.3 ± 0.1	60.5 ± 1.1	+20.8 ± 4.2
5a	55.4 ± 0.6	73.6 ± 2.8	+61.1 ± 9.6
5b	55.2 ± 0.1	61.6 ± 0.7	+21.4 ± 2.5

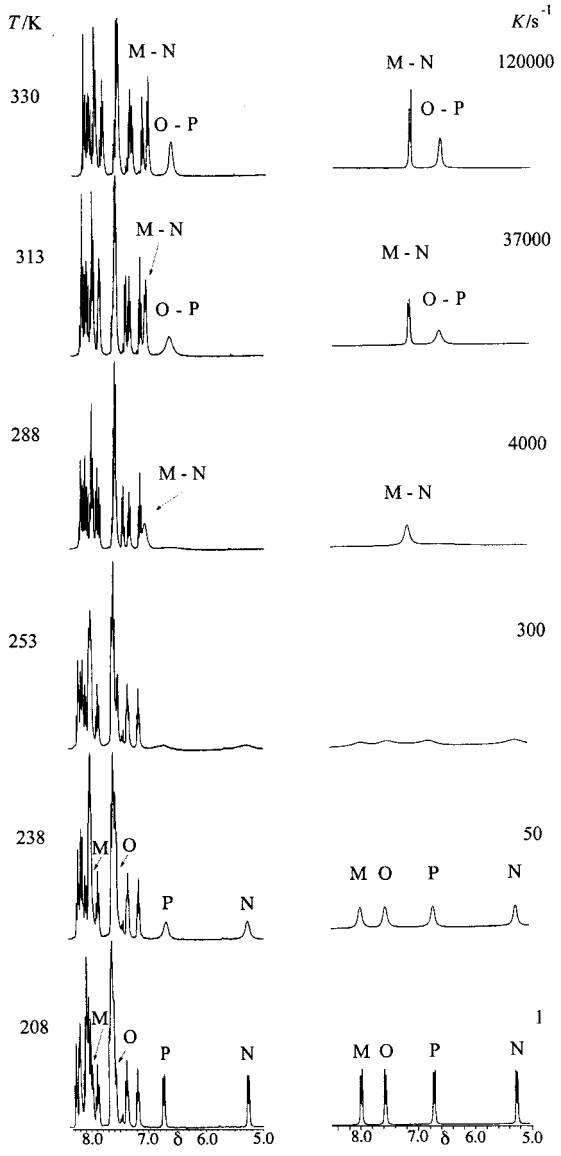

Figure 5. Selected variable-temperature ^{1}H NMR spectra of [Ru(*N*,*N*-dps)$_2$(*N*,*S*-**b**)][PF$_6$]$_2$ (**1b**) in (CD$_3$)$_2$CO (range δ = 8.4−4.8 ppm); simulated spectra on the right

nyl carbon atoms is 255 K. Their chemical-shift difference at 208 K is 12.09 Hz. The value of $\Delta G^{\#}_{255}$ (55.2 kJ·mol^{-1}), calculated from $\Delta G^{\#}_{T_c}$ = 19.14 T_c 10^{-3} (9.97 + logT_c/$\Delta\nu$),

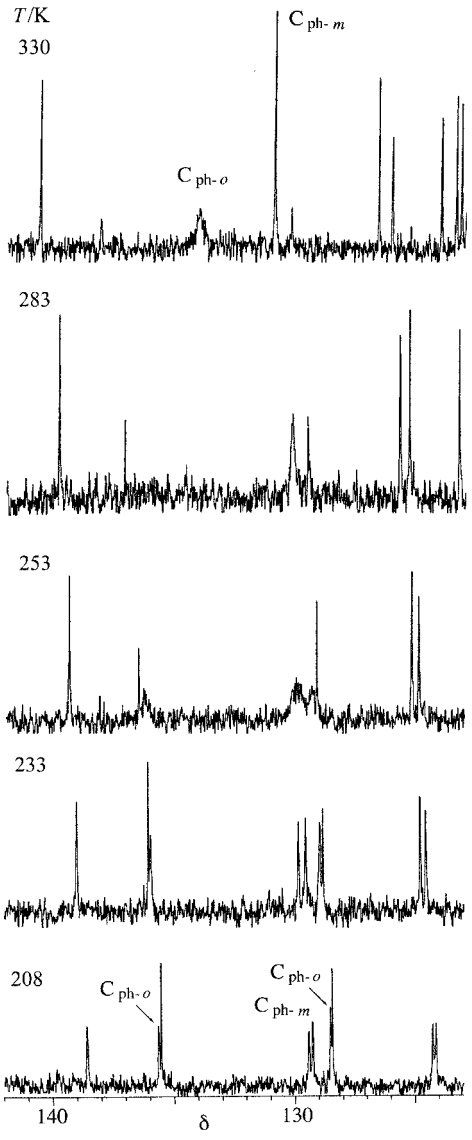

Figure 6. Selected variable-temperature ^{13}C NMR spectra of **4b** in (CD$_3$)$_2$CO (range δ = 141−124 ppm)

is in good agreement with the activation-energy barriers ($\Delta H^{\#}$ = 60.5 kJ·mol^{-1} and $\Delta S^{\#}$ = 20.8 J·K^{-1}·mol^{-1}) listed in Table 3.

In the fast-exchange regime (330 K) averaged signals of the *ortho*-phenyl (δ = 134.1 ppm) and *meta*-phenyl carbon atoms (δ = 131.0 ppm) are observed. Selected ^{13}C NMR spectroscopic data at low and high temperatures are listed in Table 4.

Molecular Structure of [Ru(dps)$_2$(2-pyridyl 2-pyridylmethyl sulfide)][PF$_6$]$_2$·(CH$_3$)$_2$CO (1c·C$_3$H$_6$O)

The complex cation of Ru^{2+} crystallizes in a 1:2 ratio with the hexafluorophosphate anions (both affected by a noticeable rotational disorder) for charge balance and in a 1:1 ratio with a disordered acetone molecule of the solvent. The crystal packing is stabilized by several hydrogen-bond interactions involving the fluorine atoms of the PF_6^-

 © 2004 Wiley-VCH Verlag GmbH & Co. KGaA, Weinheim

Table 4. Selected ^{13}C NMR spectroscopic data[a]

Complex	T [K]	*N,S* ligand										
		Pyridyl ring							Other signals			
		C−CH_2	C^3	C^4	C^5	C^6	C^{ortho}	C^{meta}	CH_2	C−S	C−CH_3	CH_3
1a	228	163.2	124.2	139.2	124.1	156.1	132.1	130.0	46.7	140.8	127.6	20.0
		158.4[b]	157.5[b]	157.5[b]	157.2[b]		127.4	129.6				
	318	164.5	125.6	140.6	125.3	157.3	132.1	131.0	48.3	142.4	129.0	21.2
		159.0[b]	158.7[b]	158.5[b]	158.4[b]							
3a	218	162.8	123.5	137.7	123.4	154.8	131.4	129.8	46.2	140.1	127.6	19.7
		157.1[b]	156.9[b]	156.2[b]	156.1[b]		127.5	128.8	16.5[c]	16.3[c]	16.0[c]	16.0[c]
	328	163.0	123.7	137.8	123.7	154.8	130.4	129.2	49.2	140.5		20.0
		156.4[b]	156.2[b]	155.6[b]	154.9[b]				16.5[c]	16.3[c]	16.1[c]	16.0[c]
4a	228	163.5	125.1	139.3	124.9	156.3	134.1	130.0	46.7	141.5	126.8	20.2
		165.4[b]	165.4[b]	165.3[b]	163.4[b]		132.0	129.2				
	318	164.6	126.4	140.4	125.9	157.5	132.8	131.4	48.2	142.9	127.8	21.1
		166.3[b]	166.2[b]	166.2[b]	164.5[b]							
5a	228	163.9	124.3	138.7	124.0	156.0	133.9	130.3	46.1[d]	140.9	126.5	19.7
		167.6[b]	167.0[b]	166.9[b]	166.0[b]		127.2	129.2	15.5[c]	15.5[c]	15.1[c]	15.0[c]
	329	165.0	126.6	140.8	126.3	158.3	132.5	131.8	48.8[e]	143.4		21.5
		165.2[b]	165.2[b]	165.0[b]	164.9[b]				16.3[c]	16.1[c]	15.6[c]	15.5[c]
1b	228	162.6	124.1	138.2	124.0	155.4	135.4	129.7	46.2	135.6	127.8[f]	
		157.8[b]	157.2[b]	156.9[b]	156.0[b]		128.9	129.3				
	328	164.1	125.8	139.8	125.5	157.6	133.9	131.0	48.2	138.2	128.6[f]	
		159.0[b]	158.7[b]	158.6[b]	158.3[b]							
2b	228	162.6	127.3	138.0	127.3	154.5	135.4	130.0	46.1	135.5	127.4[f]	
		157.7[b]	156.5[b]	155.8[b]	154.8[b]		128.1	128.9	19.4[c]	19.3[c]	19.2[c]	18.9[c]
	330	164.4	128.6	139.8	128.4	156.6	134.2	130.6	48.5	138.0	128.6[f]	
		158.9[b]	157.9[b]	157.9[b]	157.4[b]				21.1[c]	21.0[c]	20.9[c]	20.6[c]
3b	228	162.8	124.0	138.2	124.0	155.4	135.4	129.8	46.4	135.6	128.0[f]	
		157.4[b]	157.3[b]	156.5[b]	156.3[b]		128.6	129.6	16.8[c]	16.7[c]	16.4[c]	16.3[c]
	328	164.5	125.8	139.9	125.5	157.5	134.1	130.7	48.6	138.1	128.5[f]	
		158.9[b]	158.8[b]	158.4[b]	158.3[b]				18.2[c]	18.1[c]	18.0[c]	17.9[c]
4b	208	162.4	124.3	138.6	124.1	155.5	135.6	129.4	45.4	135.5	128.5[f]	
		164.6[b]	164.6[b]	164.5[b]	163.0[b]		128.5	129.3				
	330	164.1	126.6	140.6	126.1	157.6	134.1	131.0	48.1	138.2	130.3[f]	
		166.3[b]	166.2[b]	166.2[b]	164.7[b]							
5b	223	162.8	124.4	138.8	124.3	156.1	135.9	129.9	45.9[g]	136.0	129.2[f]	
		163.9[b]	163.9[b]	163.7[b]	162.0[b]		128.7	129.3	15.5[c]	15.2[c]	15.1[c]	15.0[c]
	328	164.4	126.5	140.7	126.2	158.9	134.0	131.0	48.3[h]	138.3	130.7[f]	
		165.1[b]	165.0[b]	164.7[b]	163.3[b]				16.0[c]	16.0[c]	15.6[c]	15.5[c]

[a] At 75.56 MHz, in [D_6]acetone; δ in ppm with respect to TMS. [b] C^6 carbon atoms of the *N,N* ligand. [c] Methyl signals of the *N,N* ligand. [d] CH_2 signals of the ethyl group at δ = 21.9, 21.9, 21.6 and 21.4 ppm. [e] CH_2 signals of the ethyl group at δ = 23.8, 23.7, 23.6 and 23.5 ppm. [f] CCl signal. [g] CH_2 signals of the ethyl group at δ = 21.0, 21.9, 21.7 and 21.5 ppm. [h] CH_2 signals of the ethyl group at δ = 23.6, 23.5, 23.4 and 23.2 ppm.

anions and the oxygen atom of the acetone with the hydrogen atoms of the dps ligands [at a distance of 2.443(5) Å]. The geometry about the ruthenium(II) ion is distorted octahedral (Figure 7), with the coordination polyhedron defined by five nitrogen atoms and one sulfur atom: two *N,N*-chelate dps ligands are *cis* to each other while the molecule of 2-pyridyl 2-pyridylmethyl sulfide is bidentate through S(3) and N(5). The distortion of the geometry is mainly caused by the sulfur atom, with a significantly longer Ru−S(3) distance [2.370(1) Å] than the five similar Ru−N bonds [mean 2.104(5) Å, with a slightly shorter bond to N(2) due to the sulfur *trans* effect]. Despite the different size of the chelating rings (6 atoms for dps and 5 for the 2-pyridylmethyl sulfide), the bite angles of the three bidentate ligands are almost equal and N(5)−Ru−S(3) is only slightly narrower than the other two equal chelating angles corresponding to dps molecules [81.39(9)° vs. 89.3(1)°]. The same Ru^{II} coordination has already been observed in our previous work[19] for the $[Ru(N,N'\text{-dps})_2(N,S\text{-dps})]^{2+}$ cation, where the distortion is more important due to the significantly shorter N···S bite of one dps, which closes the corresponding chelating angle up to 67.8(2)°. The larger steric hindrance for the bigger bite and bulk of 2-pyridyl 2-pyridylmethyl sulfide with respect to the *N,S*-dps chelating ligand might be related to the significant elongation of the Ru−N bonds in the corresponding complex [mean value 2.104(5) vs. 2.078(5) Å, respectively]. Moreover, the elongation of the distance to the N atom in the *trans* position causes a contraction the Ru−S(3) bond [2.370(1) vs. 2.424(2) Å, respectively]. However, the Ru−N bonds are still significantly longer than the analogous distances in the known Ru(bipy) complexes due to the reduction in back bonding when dps replaces bipy ligands, as evidenced in the previous work. The dps ligand adopts a twisted *N,N*-inside "butterfly-like" arrangement and the resulting six-membered chelate rings show the usual boat conformation, as evidenced by the

 © 2004 Wiley-VCH Verlag GmbH & Co. KGaA, Weinheim

puckering analysis[22] on the Ru/N1/C1/S1/C6/N2 [Ru/N3/C16/S2/C11/N4] ring: θ = 90.8(2)° [92.4(2)]°, φ = 0.7(7)° [4.6(2)]°, QT = 0.847(5) [0.920(2)] Å and Δ_S(Ru) = 0.008(2) [0.045(2)]. The C and N atoms lie on a plane from which the Ru and S atoms deviate by 0.7516(3) [0.8584(3)] Å and 0.718(1) [0.741(1)] Å on the same side, respectively. The two chiral atoms [Ru and S(3)] in the cation might generate two possible couples of enantiomers of the complex and, due to the presence of a crystallographic centre of symmetry, the crystal packing is a racemic mixture corresponding to the couple $\Delta S/\Lambda R$ (one arbitrary enantiomer of which is represented in Figure 7).

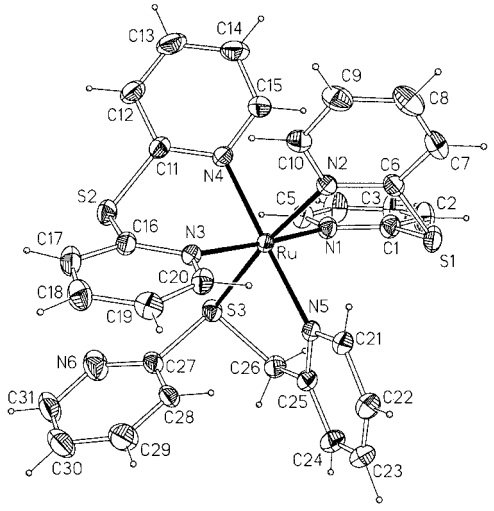

Figure 7. View of the cation **1c**·C_3H_6O showing the labelling scheme; anions and co-crystallized acetone moieties have been omitted for clarity; thermal ellipsoids are drawn at 50% probability while the size of the hydrogen atoms is arbitrary

Discussion

Our previous studies[19] on the dynamic behaviour of [Ru(*N*,*N*-dprs)$_2$(*N*,*S*-phpys)][PF_6]$_2$ and [Ru(*N*,*N*-dps)$_2$(*N*,*S*-phpys)][PF_6]$_2$ (phpys = phenyl pyridyl sulfide), containing a four-membered RuSCN(*Ru*−*N*) ring, showed that, in the range 180−240 K, a restricted rotation of the pendant phenyl ring was operative, affecting only the phenyl proton signals. Above 240 K extensive internal arrangements were invoked to explain the changes in the aromatic region of the ^{1}H NMR spectra at higher temperature.

The ^{1}H NMR spectra of the complexes containing a four-membered RuSCN(*Ru*−*N*) ring — [Ru(*N*,*N*-diimine)(*N*,*S*-pySCH_2R)][PF_6]$_2$ or [Ru(*N*,*N*-diimine)$_2$(*N*,*S*-prSCH_2R)][PF_6]$_2$ [20] — at the lowest temperature reached (190 K) clearly show the presence of two slowly exchanging invertomers, and restricted rotation is not observed. It is likely that restricted rotation of the phenyl group occurs below 190 K but experimental difficulties ruled out the possibility of confirming this proposal. Furthermore, for these complexes, which contain a chiral ruthenium atom (configurations Δ and Λ) and a chiral sulfur atom [configurations (*S*) and (*R*)] the possibility of racemisation ($\Delta \rightleftarrows \Lambda$) was discarded and only the sulfur inversion [(*R*) $\rightleftarrows$ (*S*)] occurred.

In this work owing to the *N*,*S* chelation of the thioethers **a** and **b** and the consequent formation of a five-membered metallacycle, two invertomers, as the enantiomeric couples $\Delta R/\Lambda S$ and $\Delta S/\Lambda R$, are expected and, consequently, two AB systems for the methylene protons in the ^{1}H NMR spectra. However, the spectra only show a single AB system. This can indicate the presence of: (i) only one invertomer, (ii) two invertomers that give superimposed signals, or (iii) two rapidly exchanging invertomers at low temperatures. The presence of only one invertomer or two invertomers that give superimposed signals, should eliminate the possibility of a rotation process exchanging the *ortho*- as well as the *meta*-phenyl protons, whereas the NOESY experiments indicate the exchange of the phenyl protons.

It is important to note at this point that the splitting patterns of the methylene protons (single AB system) and phenyl protons (coupling constants between **M** and **N** as well as **O** and **P)** rule out the possibility of a slow sulfur inversion at low temperatures, while the splitting patterns of the methylene protons at higher temperatures (single AB system) also rule out the possibility of racemisation ($\Delta \rightleftarrows \Lambda$) which should average the environments of the methylene protons. In other words, due to the very fast sulfur inversion even at low temperatures, averaged methylene proton signals as well as averaged phenyl proton signals of the two invertomers were observed, whereas due to the restricted phenyl rotation the two *ortho*- (and *meta*-) phenyl protons are anisochronous. The fast rotation of the phenyl ring at high temperatures makes the averaged environments of the two *ortho*- (and *meta*-) protons equivalent, whereas the methylene protons are practically unaffected.

On the other hand, from literature precedents it is unlikely that the two invertomers have similar resonances. In particular, the methylene proton signals are very sensitive to the sulfur configurations and four doublets are observed in the methylene region when two slowly exchanging invertomers are present.[20,23,24] Furthermore, the H^3 pyridine proton of the *N*,*S*-chelate ligand and the other pyridine and pyrimidine protons gave well-separated signals for the two invertomers at low temperature,[20] whereas for the present compounds only a single signal is present. Thus, two rapidly exchanging invertomers are present. In order to firmly establish this point and other structural features we attempted several crystallizations of the present compounds. None of the complexes containing ligands **a** or **b** gave crystals suitable for X-ray crystallography; however, the reaction of 2-pyridyl 2-pyridylmethyl sulfide (**c**) and [$RuCl_2$(dps)$_2$] in the presence of NH_4PF_6 gave [Ru(*N*,*N*-dps)$_2$(*N*,*S*-**c**)][PF_6]$_2$ (**1c**) which easily formed crystals. The X-ray analysis revealed the enantiomeric couple $\Delta S/\Lambda R$. Moreover, the ^{1}H NMR spectra of this complex are compatible with the presence of two rapidly exchanging invertomers: a single AB system is observed for the methylene protons at low temperatures (Table 1).

 © 2004 Wiley-VCH Verlag GmbH & Co. KGaA, Weinheim

For the complexes [*cis*-Ru(*N*,*N*-diimine)(*N*,*S*-pySCH$_2$R)][PF$_6$]$_2$ and [*cis*-Ru(*N*,*N*-diimine)$_2$(*N*,*S*-prSCH$_2$R)][PF$_6$]$_2$ [20] the access to the transition state of sulfur inversion is difficult due to the four-membered chelate ring. However, the relatively high-energy ground state, due to the simultaneous presence of the congested Ru(diimine)$_2$ fragment and the sterically demanding four-membered *N*,*S*-chelate ring, explains the low energy-barrier of the process. In the present complexes the steric demand of the Ru(diimine)$_2$ fragments is similar, whereas the increase of the chelate ring-size decreases the transition-state energy of the inversion, which consequently is fast. Therefore, the only fluxional process observed which exchanges the *ortho*- and *meta*-protons (whereas other protons are practically unchanged) is a phenyl rotation. The possible mechanisms that need to be considered are: (i) a dissociative mechanism with formation of five-coordinate species in which exchange of the two halves of the phenyl ring is operative, (ii) an associative mechanism involving solvent, anion or free ligand with formation of a seven-coordinate species in which restricted rotation of phenyl ring occurs, or (iii) phenyl rotation in the octahedral complexes without any bond rupture. The dissociative mechanism can be discarded on the basis of the following findings: (i) the NMR spectra are temperature-reversible and concentration-independent, (ii) the exchange rates are similar in acetone and acetonitrile, (iii) the steric hindrance to phenyl rotation can be very much diminished by dissociation of the Ru−S or Ru−N bond; and (iv) in the presence of a Ru−S bond dissociation the sulfur inversion and phenyl rotation would occur at the same rate. On the contrary, at low temperatures, sulfur inversion is fast whereas phenyl rotation is slow. An associative mechanism involving solvent, anion or free ligand is also unlikely. In fact, when the free ligand is added, separate signals are observed and the exchange rates are not affected. Addition of chloride or hexafluorophosphate anion does not affect the rate of the process. Therefore, the only mechanism consistent with all the experimental results appears to be the phenyl rotation in the octahedral complexes. This phenyl rotation occurs at higher rates in the complexes containing Ru(dprs)$_2$ or Ru(5edprs)$_2$ fragments than in those containing Ru(dps)$_2$, Ru(4mdps)$_2$ or Ru(5mdps)$_2$ fragments, the differences in the averaged $\Delta G^{\#}_{298}$ values being 4 kJ·mol^{-1} (Table 3); the substitution of dps with 4mdps or 5mdps leaves the magnitude of $\Delta G^{\#}_{298}$ practically unchanged. Similarly, substitution of dprs with 5edprs or **a** with **b** does not affect the values of $\Delta G^{\#}_{298}$. On this basis we suggest that the contribution of electronic effects to the restricted phenyl rotation is negligible while the parameters observed are correlated to the hindrance produced by the two ligands *cis* to the rotating group. Crystallographic data of [Ru(*N*,*N*-dps)$_2$(*N*,*S*-**c**)][PF$_6$]$_2$ and similar complexes[15,18,19] indicate that *N*,*N* chelation is favoured by the combination of the boat conformation for the six-membered metallacycle and a twisted *N*,*N*-inside conformation of dps which corresponds to the best pyridine dihedral angle for chelation to the metal atom. We have no crystallographic data of dprs complexes containing **a** or **b** or other *N*,*S* ligands; however, it is very likely that the conformation of the *N*,*N* chelate dprs is similar. Since the pyridine or pyrimidine rings are inclined the hindrance to rotation is mainly determined by the size of the N atom and, to a lesser extent, by the CH[6] group. In other words, the inclined pyrimidine ring of dprs is somewhat "bulkier" than the inclined pyridine ring of dps, producing enhanced hindrance to the phenyl rotation.

Conclusion

The reactions of a series of thioethers bearing CH$_2$Py groups has allowed us to extend the chemistry of polypyridylruthenium(II) compounds containing *N*,*S*-coordinated ligands with a five-membered chelate ring. The NMR experiments clearly show that the phenyl rotation in the octahedral complexes is the fluxional process that produces the exchange of the *ortho*- and *meta*-phenyl protons. The steric hindrance of the ruthenium substrates appears to play a determinant role for the phenyl rotation which, in the complexes containing dps ligands or methyl derivatives, occurs at lower rates than in those containing dprs or 5edprs; the difference in the averaged $\Delta G^{\#}$ values being 4 kJ·mol^{-1}. The ring size of the *N*,*S*-coordinated thioether ligand plays a determinant role for the sulfur inversion. When the inverting sulfur atom is present in a five-membered *N*,*S*-chelated ring, the process is fast even at low temperatures, whereas in a four-membered ring[20] it is much slower. Further experiments are in progress with the aim of studying the effect of the nature of congested Ru(*N*,*N*-diimine)$_2$ cores and sterically demanding thioethers on the energy barrier of the dynamic processes.

Experimental Section

General Remarks: Di-2-pyridyl sulfide,[25] di-2-pyrimidyl sulfide,[19] 2-pyridylmethyl *p*-tolyl sulfide,[26] *p*-chlorophenyl 2-pyridylmethyl sulfide,[26] 2-pyridyl 2-pyridylmethyl sulfide,[26] [RuCl$_2$(dps)$_2$]·2H$_2$O[15] and [RuCl$_2$(dprs)$_2$]·2H$_2$O[19] were prepared by published methods. Other reagents and solvents were used as received. Conductivity measurements were done with a Radiometer CDM 3 conductivity meter. Infrared spectra were recorded with an FT-IR 1720X spectrophotometer with samples as Nujol mulls placed between KBr plates and the ^{1}H and ^{13}C NMR spectra with a Bruker AMX 300 spectrometer. The following Bruker programs were used: zg, homodecnew, zgpg, jmod, cosy, noesy.pt, invb. Simulations of static and dynamic spectra were performed with the G NMR program. Selected ^{1}H NMR spectroscopic data for the complexes are given in Tables 1 and 2, activation energy data are given in Table 3 and ^{13}C NMR spectroscopic data are given in Table 4.

2,2′-Bis(5-ethylpyrimidyl) Sulfide (5edprs): 2-Chloro-5-ethylpyrimidine (4.85 g, 34.0 mmol) was dissolved in *N*,*N*-dimethylformamide (30 mL), under N$_2$. Na$_2$S (1.37 g, 17.5 mmol) was added. The resulting mixture was heated to reflux with stirring for 4 h. The initial pale-yellow solution gradually turned green, then deep yellow. The solvent was distilled off under reduced pressure and the residue extracted with CH$_2$Cl$_2$. Evaporation of the solvent gave a pale-yellow solid, which was crystallized from CH$_2$Cl$_2$ (30 mL) by care-

 © 2004 Wiley-VCH Verlag GmbH & Co. KGaA, Weinheim

ful addition of heptane, washed with pentane and dried in vacuo. Yield 1.26 g (30%). Selected IR data (KBr): $\tilde{\nu}$ = 1607 ms, 1574 s, 1538 vs, 1267 s, 1230 vs, 1142 vs, 1068 s, 938 vs, 820 vs, 790 s, 767 vs, 653 vs, 646 vs 638 vs, 499 vs cm^{-1}. ^1H NMR ([D$_6$]acetone, 298 K): δ = 1.25 (t, $^3J_{H,H}$ = 7.6 Hz, 6 H, CH_3), 2.67 (q, 4 H, CH_2), 8.56 (s, 4 H, H^3 and H^6) ppm. $^{13}C\{^1H\}$ NMR ([D$_6$]acetone, 298 K): δ = 15.05 (CH_3), 23.45 (CH_2), 158.25 (C^3 and C^6) ppm. $C_{12}H_{14}N_4S$ (246.33): calcd. C 58.51, H 5.73, N 22.74, S 13.01; found C 58.40, H 5.80, N 22.60, S 13.00.

2,2′-Bis(4-methylpyridyl) Sulfide (4mdps):[21] 2-Bromo-4-methylpyridine (9.70 g, 56.4 mmol) was dissolved in *N*,*N*-dimethylformamide (30 mL) under N_2. Na_2S (2.28 g, 29.2 mmol) was added. The resulting mixture was heated to reflux with stirring for 6 h. The initial pale-yellow solution gradually turned green, then yellow. Distillation under reduced pressure gave the solvent at 30−50 °C and the compound as a yellow oil at 150 °C. The oil was kept at −24 °C until it solidified. Selected IR data (KBr): $\tilde{\nu}$ = 1625 s, 1590 vs, 1556 s, 1539 s, 1282 ms, 1233 s, 1221 s, 1119 vs, 1079 vs, 986 s, 869 ms, 849 vs, 823 vs, 700 vs, 539 s, 517 s cm^{-1}. ^1H NMR ([D$_6$]acetone, 298 K): δ = 2.30 (s, 6 H, CH_3), 7.09 (dd, $J_{6,5}$ = 5.0 Hz, $J_{5,3}$ = 1.3 Hz, 2 H, H^5), 7.31 (d, 2 H, H^3), 8.33 (d, 2 H, H^6) ppm. $^{13}C\{^1H\}$ NMR ([D$_6$]acetone, 298 K): δ = 20.60 (CH_3), 123.50 (C^5), 126.70 (C^3), 150.30 (C^6) ppm.

2,2′-Bis(5-methylpyridyl) Sulfide (5mdps):[21] The compound was obtained in the same way as above starting from 2-bromo-5-methylpyridine (9.70 g, 56.4 mmol) and Na_2S (1.37 g, 17.5 mmol). Selected IR data (KBr): $\tilde{\nu}$ = 1667 vs, 1586 vs, 1557 vs, 1504 s, 1221 vs, 1102 vs, 1084 s, 1025 vs, 828 vs, 724 s cm^{-1}. ^1H NMR ([D$_6$]acetone, 298 K): δ = 2.30 (s, 6 H, CH_3), 7.32 (d, $J_{4,3}$ = 8.1 Hz, 2 H, H^3), 7.54 (dd, $J_{6,4}$ = 2.2 Hz, 2 H, H^4), 8.33 (d, 2 H, H^6) ppm. $^{13}C\{^1H\}$ NMR ([D$_6$]acetone, 298 K): δ = 17.80 (CH_3), 125.90 (C^3), 138.40 (C^4), 151.05 (C^6) ppm.

[RuCl$_2$(*N*,*N*-4mdps)$_2$] (2): $RuCl_3 \cdot 3H_2O$ (1 g, 3.8 mmol), LiCl (1 g, 23.6 mmol) and 4mdps (1.65 g, 7.63 mmol) were refluxed in DMF (30 mL) under N_2 for 4 h. After cooling to room temperature and addition of acetone (30 mL), the mixture was allowed to stand at 4 °C overnight giving a dark-red solid which was filtered and washed with acetone. The compound was dried over P_4O_{10} in vacuo. Yield 0.92 g (40%). Selected IR data (KBr): $\tilde{\nu}$ = 1650 br, 1599 vs, 1282 s, 1140 s, 1082 s, 820 vs, 720 s cm^{-1}. ^1H NMR ($CDCl_3$, 298 K): δ = 2.23 (s, 6 H, CH_3), 2.34 (s, 6 H, CH_3), 6.62 (dd, $J_{6,5}$ = 6.0 Hz, $J_{5,3}$ = 1.9 Hz, 2 H, H^5), 7.13 (dd, $J_{6,5}$ = 6.0 Hz, $J_{5,3}$ = 1.9 Hz, H^5), 2 H, 7.14 (d, 2 H, H^3),7.31 (d, 2 H, H^3),8.30 (d, 2 H, H^6), 10.04 (d, 2 H, H^6) ppm. $C_{24}H_{24}Cl_2N_4RuS_2$ (604.58): calcd. C 47.68, H 4.00, N 9.27, S 10.61; found C 47.80, H 4.00, N 9.35, S 10.60.

[RuCl$_2$(*N*,*N*-5mdps)$_2$] (3): $RuCl_3 \cdot 3H_2O$ (1 g, 3.8 mmol), LiCl (1 g, 23.6 mmol) and 5mdps (1.65 g, 7.63 mmol) were refluxed in DMF (20 mL) under N_2 for 5 h. The solution was cooled to room temperature and 40 mL of acetone added. The mixture was allowed to stand at −24 °C overnight. An orange-red solid had formed which was filtered, washed with acetone/diethyl ether mixtures [2:1 (21 mL), 1:1 (30 mL) and 1:3 (40 mL)] and dried over P_4O_{10} in vacuo. Yield 1.03 g (45%). Selected IR data (KBr): $\tilde{\nu}$ = 1630 br, 1589 s, 1284 s, 1234 s, 1136 vs, 1101 vs, 822 vs, 722 s, 532 s cm^{-1}. ^1H NMR ([D$_6$]acetone, 298 K): δ = 2.01 (s, 6 H, CH_3), 2.41 (s, 6 H, CH_3), 7.33 (dd, $J_{4,3}$ = 7.9 Hz, $J_{6,3}$ = 0.8 Hz, 2 H, H^3), 7.38 (dd, $J_{4,3}$ = 7.9 Hz, $J_{6,4}$ = 2.5 Hz, 2 H, H^4), 7.53 (dd, $J_{4,3}$ = 7.9 Hz, $J_{6,3}$ = 0.8 Hz, 2 H, H^3), 7.62 (dd, $J_{4,3}$ = 7.9 Hz, $J_{6,4}$ = 2.5 Hz, 2 H, H^4), 8.30 (dd, 2 H, H^6), 10.04 (dd, 2 H, H^6) ppm. $C_{24}H_{24}Cl_2N_4RuS_2$ (604.58): calcd. C 47.68, H 4.00, N 9.27, S 10.61; found C 47.60, H 4.10, N 9.30, S 10.70.

[Ru(*N*,*N*-5edprs)$_2$Cl$_2$] (4): This red compound was obtained in the same way as above, starting from $RuCl_3 \cdot 3H_2O$ (1 g, 3.8 mmol), LiCl (1 g, 23.6 mmol) and 5etdprs (1.94 g, 7.63 mmol). Yield 0.88 g (35%). Selected IR data (KBr): $\tilde{\nu}$ = 1675 vs, 1540 vs, 1220 s, 1182 vs, 1136 vs, 1058 vs, 910 vs, 822 vs, 752vs, 740 vs 720 s, 662 s cm^{-1}. ^1H NMR ([D$_6$]acetone, 298 K): δ = 1.02 (t, $^3J_{H,H}$ = 7.6 Hz, 6 H, CH_3), 1.34 (t, $^3J_{H,H}$ = 7.6 Hz, 6 H, CH_3), 2.48 (q, 4 H, CH_2), 2.78 (q, 4 H, CH_2), 8.34 (dd, $J_{4,3}$ = 7.9 Hz, $J_{6,4}$ = 2.6 Hz, 2 H, H^4), 8.49 (dd, $J_{6,4}$ = 2.6 Hz, 2 H, H^6), 8.59 (d, $J_{6,4}$ = 2.8 Hz, 2 H, H^4), 10.01 (d, $J_{6,4}$ = 2.8 Hz, 2 H, H^6). $C_{24}H_{28}Cl_2N_8RuS_2$ (664.64): calcd. C 43.37, H 4.24, N 16.86, S 9.65; found C 43.50, H 4.30, N 17.00, S 9.70.

[Ru(*N*,*N*-dps)$_2$(*N*,*S*-a)][PF$_6$]$_2$ (1a): $[RuCl_2(dps)_2] \cdot 2H_2O$ (0.195 g, 0.33 mmol) and 2-pyridylmethyl *p*-tolyl sulfide (0.286 g, 1.33 mmol) were refluxed in 50 mL of ethanol/water (3:2) under N_2 for 4 h. After filtration of the solution into 80 mL of water containing NH_4PF_6 (0.49 g, 3 mmol), a yellow precipitate was obtained, filtered, washed with cold water (30 mL) and dried overnight. The solid was then dissolved in acetone (15 mL), precipitated with diethyl ether (100 mL), washed with diethyl ether (70 mL) and dried over P_4O_{10} under vacuum. Yield 0.165 g (50%). Selected IR data (KBr): $\tilde{\nu}$ = 1589 vs, 1561 ms, 1284 s, 1165 s, 878 vs, 843 br, 770 vs, 741 ms, 727 s, 558 vs cm^{-1}. $C_{33}H_{29}F_{12}N_5P_2RuS_3$ (982.81): calcd. C 40.33, H 2.97, N 7.12; found C 40.15, H 3.05, N 7.10. Conductivity: Λ_M (MeCN, 2 × 10^{-4} mol·dm^{-3}, 25 °C) = 316 S·cm^2·mol^{-1}.

[Ru(*N*,*N*-5mdps)$_2$(*N*,*S*-a)][PF$_6$]$_2$ (3a): The compound was obtained in the same way as **1a**, starting from $[RuCl_2(5mdps)_2]$ (0.201 g, 0.33 mmol) and 2-pyridylmethyl *p*-tolyl sulfide (0.286 g, 1.33 mmol). Yield 0.220 g (64%). Selected IR data (KBr): $\tilde{\nu}$ = 1667 s, 1597 s, 1565 ms, 1494 vs, 1283 vs, 1240 vs, 1120 vs, 1106 s, 877 vs, 840 br, 775 vs, 740 s, 725 ms, 557 vs, 530 vs cm^{-1}. $C_{37}H_{37}F_{12}N_5P_2RuS_3$ (1038.9): calcd. C 42.78, H 3.59, N 6.74; found C 42.90, H 3.60, N 6.80. Conductivity: Λ_M (MeCN, 2 × 10^{-4} mol·dm^{-3}, 25 °C) = 328 S·cm^2·mol^{-1}.

[Ru(*N*,*N*-dprs)$_2$(*N*,*S*-a)][PF$_6$]$_2$ (4a): $[RuCl_2(dprs)_2] \cdot 2H_2O$ (0.196 g, 0.33 mmol) and 2-pyridylmethyl *p*-tolyl sulfide (0.286 g, 1.33 mmol) were heated to reflux in 50 mL of ethanol/water (3:2). After 3 h, the solution was filtered and 50 mL of water containing NH_4PF_6 (0.65 g, 4 mmol) was added. The mixture was heated for 2 h. The solution obtained was allowed to stand until a brown precipitate was formed, which was filtered, washed with water, and dried overnight. The solid was then dissolved in acetone (10 mL) and added to the top of a chromatography column (diameter 2 cm) packed with aluminium oxide (50 g; Aldrich, neutral, 150 mesh, deactivated with water 0.15 g). Elution with CH_2Cl_2/acetone (3:2) gave a yellow-orange band which was collected, concentrated (10 mL) and precipitated with diethyl ether (50 mL). The solid obtained was washed with diethyl ether (50 mL) and dried over P_4O_{10} under vacuum. Yield 0.130 g (40%). Selected IR data (KBr): $\tilde{\nu}$ = 1604 ms, 1561 s, 1547 s, 1164 s, 1084 ms, 1014 ms, 876vs, 842 br, 762 vs, 751 ms, 722 ms, 649 ms, 597 ms, 558 vs cm^{-1}. $C_{29}H_{25}F_{12}N_9P_2RuS_3$ (986.76): calcd. C 35.30, H 2.55, N 12.78; found C 35.20, H 2.60, N 12.80. Conductivity: Λ_M (MeCN, 2 × 10^{-4} mol·dm^{-3}, 25 °C) = 305 S·cm^2·mol^{-1}.

[Ru(*N*,*N*-5edprs)$_2$(*N*,*S*-a)][PF$_6$]$_2$ (5a): This compound was prepared by refluxing a mixture of $[RuCl_2(5edprs)_2]$ (0.332 g, 0.50 mmol) and 2-pyridylmethyl *p*-tolyl sulfide (0.646 g, 3.0 mmol) in 50 mL of ethanol/water (3:2) under N_2 for 5 h. After filtration of the solution into 80 mL of water containing NH_4PF_6 (0.49 g, 3 mmol) an orange precipitate was obtained, which was filtered and dried overnight. The crude product was dissolved in acetone (10 mL) and

 © 2004 Wiley-VCH Verlag GmbH & Co. KGaA, Weinheim

added to the top of a chromatography column (diameter 2 cm) packed with aluminium oxide (50 g; Aldrich, neutral, 150 mesh, deactivated with water 0.15 g). Elution with CH_2Cl_2/acetone (3:2) gave a yellow-orange band which was collected, concentrated (10 mL) and the product precipitated with diethyl ether (50 mL). The solid obtained was washed with diethyl ether (50 mL) and dried over P_4O_{10} under vacuum. Yield 0.220 g (40%). Selected IR data (KBr): $\tilde{\nu}$ = 1667 s, 1581 s, 1544 vs, 1234 s, 1187s, 1142 s, 1060 s, 880 vs, 843 br, 755 vs, 740 vs, 727 s, 663 s, 557 cm^{-1}. $C_{37}H_{41}F_{12}N_9P_2RuS_3$ (1099.0): calcd. C 40.44, H 3.76, N 11.47; found C 44.50, H 3.80, N 11.40. Conductivity: Λ_M (MeCN, 2×10^{-4} mol·dm^{-3}, 25 °C) = 310 S·cm^2·mol^{-1}.

[Ru(*N*,*N*-dps)$_2$(*N*,*S*-b)][PF$_6$]$_2$ (1b): This yellow compound was prepared in the same way as **1a**, starting from [$RuCl_2$(dps)$_2$]·$2H_2O$ (0.195 g, 0.33 mmol) and *p*-chlorophenyl 2-pyridylmethyl sulfide (0.313 g, 1.33 mmol). Yield 0.160 g (48%). Selected IR data (KBr): $\tilde{\nu}$ = 1589 s, 1284 s, 1164 s, 1094 vs, 1011 s, 879 vs, 847 br, 770 vs, 744 ms, 726 ms, 558 vs, 508 ms cm^{-1}. $C_{32}H_{26}ClF_{12}N_5P_2RuS_3$ (1003.2): calcd. C 38.31, H 2.61, N 6.98; found C 38.10, H 2.65, N 7.00. Conductivity: Λ_M (MeCN, 2×10^{-4} mol·dm^{-3}, 25 °C) = 307 S·cm^2·mol^{-1}.

[Ru(*N*,*N*-4mdps)$_2$(*N*,*S*-b)][PF$_6$]$_2$ (2b): This yellow compound was prepared in a similar fashion to **1a**, starting from [$RuCl_2$(4mdps)$_2$] (0.201 g, 0.33 mmol) and *p*-chlorophenyl 2-pyridylmethyl sulfide (0.313 g, 1.33 mmol). Yield 0.180 g (51%). Selected IR data (KBr): $\tilde{\nu}$ = 1674 s, 1605 vs, 1288 s, 1093 vs, 1011 vs, 878 vs, 843 br, 776 vs, 740 vs, 720 s, 557 vs, 508 s, 499 s cm^{-1}. $C_{32}H_{26}ClF_{12}N_5P_2RuS_3$ (1059.3): calcd. C 40.82, H 3.24, N 6.61; found C 40.90, H 3.30, N 6.60. Conductivity: Λ_M (MeCN, 2×10^{-4} mol·dm^{-3}, 25 °C) = 318 S·cm^2·mol^{-1}.

[Ru(*N*,*N*-5mdps)$_2$(*N*,*S*-b)][PF$_6$]$_2$ (3b): This yellow compound was prepared in the same way as **1a**, starting from [$RuCl_2$(5mdps)$_2$] (0.201 g, 0.33 mmol) and *p*-chlorophenyl 2-pyridylmethyl sulfide (0.313 g, 1.33 mmol). Yield 0.200 g (56%). Selected IR data (KBr): $\tilde{\nu}$ = 1678 vs, 1605 s, 1598 s, 1568 s, 1283 s, 1241 s, 1119 vs, 1092 vs, 1009 vs, 876 vs, 836 br, 764 vs, 741 s, 725 ms, 558 vs, 530 s, 512 s cm^{-1}. $C_{36}H_{34}ClF_{12}N_5P_2RuS_3$ (1059.3): calcd. C 40.82, H 3.24, N 6.61, S 9.08; found C 40.80, H 3.30, N 6.70, S 9.10. Conductivity: Λ_M (MeCN, 2×10^{-4} mol·dm^{-3}, 25 °C) = 307 S·cm^2·mol^{-1}.

[Ru(*N*,*N*-dprs)$_2$(*N*,*S*-b)][PF$_6$]$_2$ (4b): This orange compound was obtained in the same way as **1a**, starting from [$RuCl_2$(dprs)$_2$]·$2H_2O$ (0.196 g, 0.33 mmol) and *p*-chlorophenyl 2-pyridylmethyl sulfide (0.313 g, 1.33 mmol). Yield 0.151 g (45%). Selected IR data (KBr): $\tilde{\nu}$ = 1579 vs, 1575 vs, 1548 vs, 1167 vs, 1096 s, 1011 s, 874 vs, 846 br, 767 s, 753 vs, 742 ms, 558 vs, 509 ms cm^{-1}. $C_{28}H_{22}ClF_{12}N_9P_2RuS_3$ (1007.2): calcd. C 33.37, H 2.20, N 12.52; found C 33.30, H 2.30, N 12.50. Conductivity: Λ_M (MeCN, 2×10^{-4} mol·dm^{-3}, 25 °C) = 309 S·cm^2·mol^{-1}.

[Ru(*N*,*N*-5edprs)$_2$(*N*,*S*-b)][PF$_6$]$_2$ (5b): This orange compound was prepared and purified in the same way as **5a**, starting from [$RuCl_2$(5edprs)$_2$] (0.332 g, 0.50 mmol) and *p*-chlorophenyl 2-pyridylmethyl sulfide (0.707 g, 3.0 mmol). Yield 0.252 g (45%). Selected IR data (KBr): $\tilde{\nu}$ = 1667 vs, 1580 s, 1548 vs, 1243 s, 1143 s, 1095 s, 1061 s, 1011 s, 880 vs, 846 br, 762 s, 757 s, 558 vs cm^{-1}. $C_{36}H_{38}ClF_{12}N_9P_2RuS_3$ (1119.4): calcd. C 38.63, H 3.42, N 11.26, S 8.59; found C 38.60, H 3.55, N 11.20, S 8.60. Conductivity: Λ_M (MeCN, 2×10^{-4} mol·dm^{-3}, 25 °C) = 284 S·cm^2·mol^{-1}.

[Ru(*N*,*N*-dps)$_2$(*N*,*S*-c)][PF$_6$]$_2$ (1c): This yellow compound was obtained in the same way as **4a**, starting from [$RuCl_2$(dps)$_2$]·$2H_2O$ (0.195 g, 0.33 mmol) and 2′-pyridyl 2-pyridylmethyl sulfide (0.178 g, 0.882 mmol) Yield 0.226 g (70%). Selected IR data (KBr): $\tilde{\nu}$ = 1610 ms, 1588 s, 1571 s, 1561 ms, 1284 s, 1165 s, 1130 ms, 1089 ms, 878 s, 845 br, 769 vs, 741 s, 727 ms, 558 vs, 528 ms cm^{-1}. $^{13}C\{^1H\}$ NMR ([D_6]acetone, 298 K): δ = 45.9 (CH_2), 123.6 (C^5_c), 124.0, 125.4, 126.0, 126.7 (4 C^5_{dps}), 127.2 (C^5_c), 127.5 (C^3_c), 128.7, 128.8, 129.6, 130.2 (4 C^3_{dps}), 130.4 (C^3_c), 138.4 (C^4_c), 138.6, 139.3, 139.7, 140.0 (4 C^4_{dps}), 140.4 (C^4_c), 150.1 (C^6_c), 153.8 (C^2_c), 156.6 (C^2_{dps}), 157.1 (C^6_c), 157.1 (C^6_{dps}), 157.5 (C^2_{dps}), 157.9 (C^6_{dps}), 158.1 (C^2_{dps}), 158.4, 158.7 (2 C^6_{dps}), 159.2 (C^2_{dps}), 165.0 (C^2_c). $C_{31}H_{26}F_{12}N_6P_2RuS_3$ (969.77): calcd. C 38.40, H 2.70, N 8.67, S 9.92; found C 38.35, H 2.80, N 8.60, S 9.90. Conductivity: Λ_M (MeCN, 2×10^{-4} mol·dm^{-3}, 25 °C) = 327 S·cm^2·mol^{-1}.

Single-Crystal X-ray Diffraction Study of 1c: Suitable crystals of complex **1c** were obtained by slow evaporation of solvent from a diethyl ether/acetone (1:1) solution. Diffraction data were collected with a Siemens P4 automatic four-circle diffractometer. Lattice parameters were obtained from least-squares refinement of the setting angles of 42 reflections within the 2θ range 6−30°. A summary of the crystallographic data and the structure refinement is reported in Table 5. Monitoring of three standard reflection measurements evidenced no crystal deterioration. The reflection intensities were evaluated by a learnt-profile procedure[27] among 2θ shells and then corrected for Lorentz-polarization effects. Absorption correction was applied by fitting a pseudo-ellipsoid to the azimuthal scan data (0−360% range by a 10% step) of 15 high χ reflections.[28] Data collection and reduction were performed with the XSCANS[29] and SHELXTL[30] package. The structure was solved by a combination of standard Direct Methods[31] and Fourier synthesis, and refined by minimising the function $\Sigma w(F_o^2 - F_c^2)^2$ with the full-matrix least-squares technique based on all independent *F*, using SHELXL-97.[32] All non-hydrogen atoms were refined anisotropically. Hydrogen atoms were included in the model refinement with the "riding

Table 5. Crystallographic data for **1c**·C_3H_6O

Empirical formula	$[C_{31}H_{26}N_6S_3Ru][PF_6]_2$·$(CH_3)_2CO$
Formula mass	1027.85
Crystal dimensions	0.37 × 0.27 × 0.20 mm
Crystal colour and form	yellow, irregular
Crystal system	monoclinic
Space group	$P2_1/c$ (no. 14)
Unit cell dimensions	a = 11.760(1) Å
	b = 13.792(1) Å
	c = 25.883(2) Å
	β = 90.051(8)°
V	4197.8(6) Å^3
Z	4
F(000)	2064
$\rho_{calcd.}$	1.626 g/cm^3
μ	0.689 mm^{-1}
λ (graphite-monochromated)	0.71073 Å (Mo-K_α)
2θ range	4.3−50°
Data collected (2θ-ω)	8597
Data independent (refined)	7369 (R_{int} = 0.0240)
Data observed	5938 [$I \geq 2\sigma(I)$]
Variables	532
Completeness to 2θ = 50°	0.995
$R1$[a] (observed/refined data)	0.0462/0.0617
$wR2$[b] (observed/refined data)	0.1110/0.1210
GOF[c] (observed/refined data)	1.040/1.040
Max. diff. peak and hole	0.588/−0.547 e·Å^{-3}
Max. and mean shift/esd	0.002/0.001

[a] $R = (\Sigma||F_o| - |F_c||)/\Sigma|F_o|$. [b] $Rw = \{\Sigma[w(F_o^2 - F_c^2)^2]/[\Sigma w(F_o^2)^2]\}^{1/2}$. [c] GOF= $\{\Sigma[w(F_o^2 - F_c^2)^2/(N_{obs.} - N_{var.})]\}^{1/2}$.

 © 2004 Wiley-VCH Verlag GmbH & Co. KGaA, Weinheim

model'' method with the X−H bond geometry and isotropic displacement parameter depending on the parent X atom. The co-crystallized acetone molecules and hexafluorophosphate anions show large atomic thermal ellipsoids due to the expected rotational disorder of their spherical moieties. Any attempt to represent the biggest ellipsoids as adjacent atomic partial occupancies was unsuccessful. The final geometrical calculations and drawings were carried out with the PARST program[33] and the XPW utility of the Siemens package, respectively. Selected bond lengths and bond angles are reported in Table 6 while Figure 7 represents the complex cation with its atomic labelling scheme. CCDC-226905 contains the supplementary crystallographic data for this paper. These data can be obtained free of charge at www.ccdc.cam.ac.uk/conts/retrieving.html [or from the Cambridge Crystallographic Data Centre, 12 Union Road, Cambridge CB2 1EZ, UK; Fax: + 44-1223-336033; E-mail: deposit@ccdc.cam.ac.uk].

Table 6. Selected bond lengths [Å] and angles [°] for **1c**·C_3H_6O

Ru−N(2)	2.096(3)	Ru−N(1)	2.102(3)
Ru−N(4)	2.103(3)	Ru−N(5)	2.108(3)
Ru−N(3)	2.112(3)	Ru−S(3)	2.370(1)
N(1)−C(5)	1.352(6)	N(1)−C(1)	1.354(6)
C(1)−S(1)	1.768(5)	S(1)−C(6)	1.772(5)
C(6)−N(2)	1.350(5)	C(10)−N(2)	1.352(5)
N(3)−C(20)	1.317(5)	N(3)−C(16)	1.362(5)
S(2)−C(16)	1.769(5)	C(11)−S(2)	1.771(5)
C(11)−N(4)	1.340(5)	C(15)−N(4)	1.355(6)
N(5)−C(21)	1.346(5)	N(5)−C(25)	1.358(5)
C(25)−C(26)	1.478(7)	C(26)−S(3)	1.829(5)
C(27)−S(3)	1.822(5)	C(27)−N(6)	1.404(7)
C(31)−N(6)	1.407(8)		
N(2)−Ru−N(1)	89.3(1)	N(2)−Ru−N(4)	86.1(19
N(1)−Ru−N(4)	86.6(1)	N(2)−Ru−N(5)	92.9(1)
N(1)−Ru−N(5)	92.9(1)	N(2)−Ru−N(3)	93.1(1)
N(4)−Ru−N(3)	89.3(1)	N(5)−Ru−N(3)	91.2(1)
N(1)−Ru−S(3)	86.6(1)	N(4)−Ru−S(3)	99.6(1)
N(5)−Ru−S(3)	81.39(9)	N(3)−Ru−S(3)	91.4(1)
C(1)−S(1)−C(6)	103.5(2)	C(16)−S(2)−C(11)	103.5(2)
C(25)−C(26)−S(3)	111.7(3)	C(27)−S(3)−C(26)	97.6(2)

Acknowledgments

This work was supported by the Università of Messina, Italy (PRA, **2001**).

[1] D. C. Black, *Aust. J. Chem.* **1967**, *20*, 2101−2107.
[2] R. Driver, W. R. Walker, *Aust. J. Chem.* **1968**, *21*, 331−337.
[3] M. E. Bridson, W. R. Walker, *Aust. J. Chem.* **1970**, *23*, 1191−1197.
[4] G. C. Pappalardo, A. Seminara, *J. Inorg. Nucl. Chem.* **1976**, *38*, 1993−1995.
[5] A. Forchioni, V. Librando, G. C. Pappalardo, *J. Chem. Soc., Dalton Trans.* **1977**, 638−641.
[6] M. Kondo, S. Kawata, S. Kitagawa, H. Kiso, M. Munukata, *Acta Crystallogr., Sect. C* **1995**, *51*, 567−569.
[7] O. S. Jung, D. H. Jo, Y. A. Lee, B. J. Conklin, C. G. Pierpoint, *Inorg. Chem.* **1997**, *36*, 19−24.
[8] F. Nicolò, G. Bruno, G. Tresoldi, *Acta Crystallogr., Sect. C* **1996**, *52*, 2188−2191.
[9] G. Tresoldi, S. Lo Schiavo, P. Piraino, *Inorg. Chim. Acta* **1997**, *254*, 381−385.
[10] G. Tresoldi, E. Rotondo, P. Piraino, M. Lanfranchi, A. Tiripicchio, *Inorg. Chim. Acta* **1992**, *194*, 233−241.
[11] G. De Munno, G. Bruno, E. Rotondo, G. Giordano, S. Lo Schiavo, P. Piraino, G. Tresoldi, *Inorg. Chim. Acta* **1993**, *208*, 67−75.
[12] G. Tresoldi, P. Piraino, E. Rotondo, F. Faraone, *J. Chem. Soc., Dalton Trans.* **1991**, 425−430.
[13] W. M. Teles, N. G. Fernandes, A. Abras, C. A. L. Filgueiras, *Trans. Met. Chem.* **1999**, *24*, 321−325.
[14] R. J. Andersen, P. J. Steel, *Acta Crystallogr., Sect. C* **1998**, *54*, 2188−2191.
[15] G. Bruno, F. Nicolò, S. Lo Schiavo, M. S. Sinicropi, G. Tresoldi, *J. Chem. Soc., Dalton Trans.* **1995**, 17−24.
[16] G. Tresoldi, S. Lo Schiavo, P. Piraino, P. Zanello, *J. Chem. Soc., Dalton Trans.* **1996**, 885−892.
[17] G. Bruno, F. Nicolò, G. Tresoldi, *Acta Crystallogr., Sect. C* **2000**, *56*, 282−283.
[18] G. Bruno, F. Nicolò, G. Tresoldi, S. Lanza, *Acta Crystallogr., Sect. C* **2002**, *58*, M56−M58.
[19] R. Scopelliti, G. Bruno, C. Donato, G. Tresoldi, *Inorg. Chim. Acta* **2001**, *313*, 43−55.
[20] G. Tresoldi, S. Lo Schiavo, S. Lanza, P. Cardiano, *Eur. J. Inorg. Chem.* **2002**, 181−191.
[21] Z. Wolnicka-Rutkowska, Z. Talik, *Pr. Nauk. Akad. Ekon. im. Oskara Langego Wroclawiu* **1982**, *191*, 151−161; *Chem. Abstr.* **1983**, *98*, 1258316.
[22] D. Cremer, J. A. Pople, *J. Am. Chem. Soc.* **1975**, *97*, 1354−1358.
[23] E. W. Abel, D. Ellis, K. G. Orrell, *J. Chem. Soc., Dalton Trans.* **1992**, 2243−2249.
[24] E. W. Abel, P. J. Heard, K. G. Orrell, M. B. Hursthouse, M. A. Mazid, *J. Chem. Soc., Dalton Trans.* **1993**, 3795−3801.
[25] C. Chachaty, C. Pappalardo, C. G. Scarlata, *J. Chem. Soc., Perkin Trans. 2* **1976**, 1234−1238.
[26] F. Haviv, R. W. DeNet, R. J. Michaels, J. D. Ratajczyk, G. W. Carter, P. R. Young, *J. Med. Chem.* **1983**, *26*, 218−222.
[27] R. Diamond, *Acta Crystallogr., Sect. A* **1969**, *25*, 43−55.
[28] G. Kopfmann, R. Huber, *Acta Crystallogr., Sect. A* **1968**, *24*, 348−351.
[29] *XSCANS*, release 2.31, Bruker AXS Inc., Madison, Wisconsin, USA, **1999**.
[30] G. M. Sheldrick, *SHELXTL*, VMS version 5.05, Siemens Analytical X-ray Instruments Inc., Madison, Wisconsin, USA, **1991**.
[31] A. Altomare, O. Cascarano, C. Giacovazzo, A. Guagliardi, M. C. Burla, G. Polidori, M. Camalli, *J. Appl. Crystallogr.* **1994**, *27*, 435−436.
[32] G. M. Sheldrick, *SHELXL-97, Program for Crystal Structure Refinement*, University of Göttingen, Germany, **1997**.
[33] M. Nardelli, *J. Appl. Chem.* **1995**, *28*, 659; locally modified version.

Received February 13, 2004
Early View Article
Published Online June 7, 2004

 © 2004 Wiley-VCH Verlag GmbH & Co. KGaA, Weinheim

Zwitterionic Phosphorus Ylide Adducts of Boron-Bridged *ansa*-Zirconocene Complexes as Precatalysts for Olefin Polymerization

Pamela J. Shapiro,*[a] Feilong Jiang,[a] Xiaoping Jin,[a] Brendan Twamley,[a] Jasson T. Patton,[b] and Arnold L. Rheingold[c]

Keywords: Zirconium / Metallocenes / Boron / Ylides / Catalysis

Methylenetriphenylphosphorane was coordinated to the boron of phenylborylidene-bridged bis(cyclopentadienyl)- and bis(2-Me,4-Ph-indenyl)zirconium dichloride to form zwitterionic *ansa*-zirconocene complexes. The cyclopentadienyl complex **2**, when activated with MAO, exhibits remarkable polymerization activity that is more than an order of magnitude greater than that of a related amidoborylidene-bridged complex as well as the commercially important pre-catalyst [Cp′–$SiMe_2$–*N*–*t*Bu]$TiCl_2$ (Cp′ = C_5Me_4). The zwitterionic bis(2-Me,4-Ph-indenyl)zirconium dichloride species is isolated as a mixture of *rac* and *meso* isomers **4**–**6**. The propylene polymerization efficiency of the isomer mixture activated by MAO is greater than that of a related silylene bridged system at 70 and 85 °C; however, the activity of the zwitterionic system decreased with further increase in temperature. The high level of isotactic triads (63.6%) and pentads (52.4%) in the polypropylene formed by **4**–**6** indicates that the *rac* isomer is the most active precatalyst of the mixture. The molecular structures of **2** and the *rac* bis-indenylzirconium isomer **4** and one of the *meso* isomers **5** are described.

(© Wiley-VCH Verlag GmbH & Co. KGaA, 69451 Weinheim, Germany, 2004)

Introduction

Carbon and silicon are the most common constituents of the bridges connecting the two ancillary ligands in *ansa*-metallocene olefin polymerization catalysts. Bridges based on P,[1−4] As,[5] B,[6−12] and B−P[13] are also reported. Unique to these heteroatom bridges is the potential to vary their coordination environment and hybridization while the ligand is attached to the metal.

In developing boron-bridged metallocene complexes,[10−12] one of our objectives is to use the bridging atom as a noncoordinating counteranion for the cationic metal center. Work from our group[10] and from Bochmann's group[14] has demonstrated that, in some cases, the boron bridge coordinates anionic moieties such as Cl^-, CH_3^-, and $C_6F_5^-$ to form stable, isolable salts. The nature of the countercation and the alkyl anion appear to be crucial in these cases because reactions between complex **1** (Equation 1) and alkyllithium, Grignard, dialkylzinc, and alkylaluminum reagents generally lead to decomposition of the complex,[11] presumably as a result of alkyl anion attack at the boron. When we replaced the weakly bound dimethyl sulfide ligand in **1** with more strongly coordinating trimethylphosphane, we were able to alkylate the zirconium center using alkyllithium and Grignard reagents.[15] The trimethylphosphane adduct and the stable borate bridged complexes exhibit ethylene polymerization activity when activated with MAO, but complex **1** does not.[10]

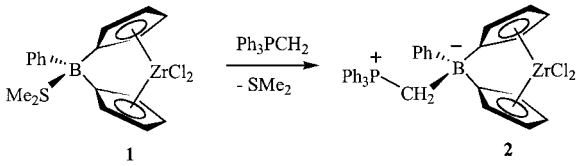

(1)

Since phosphorus ylides have been shown to have a high affinity for Lewis acidic boron centers,[16−18] we introduced Ph_3PCH_2 onto the boron bridge of the *ansa*-zirconocene complex in order to protect the boron bridge from attack by organometallic alkylating reagents and activators such as MAO. The ylide conferred remarkable ethylene polymerization activity to the complex, prompting us to explore the effectiveness of this adduct in related boron-bridged bis(indenyl)zirconium systems in the context of propylene polymerization catalysis.

[a] Dept. of Chemistry, University of Idaho, Moscow, ID 83844-2343, USA
Fax: (internat.) +01-208-885-6173
E-mail: shapiro@uidaho.edu
[b] The Dow Chemical Company, Catalysis Laboratory, Midland, Michigan 48674, USA
[c] Dept. of Chemistry and Biochemistry, University of California, San Diego, La Jolla, CA 92039-0332, USA

 © 2004 Wiley-VCH Verlag GmbH & Co. KGaA, Weinheim **DOI: 10.1002/ejic.200300932**

Results and Discussion

Synthesis and Structural Characterization of $[(Ph_3CH_2)PhB(\eta^5\text{-}C_5H_4)_2ZrCl_2]$

As shown in Equation 1, Ph_3PCH_2 readily displaces the Me_2S adduct on the boron in **1** to form complex **2**. Single crystals of **2** suitable for an X-ray structure determination were grown from dichloromethane solution. The molecular structure is shown in Figure 1, where pertinent bond lengths and angles are also listed. Crystallographic data is listed in Table 1. The most important geometrical parameters of the molecular structure are the angles about the boron bridge and the tilt of the cyclopentadienyl rings on zirconium. The centroid−Zr−centroid angle (120.2°) and dihedral angle between the cyclopentadienyl rings (66°) are within the range of the other boron-bridged dicyclopentadienylzirconium dichloride complexes.[10−12] Boron-bridged complexes exhibit greater distortion than silicon-bridged complexes and less distortion than carbon-bridged complexes relative to $(\eta^5\text{-}C_5H_5)_2ZrCl_2$.[12] The Cp−B−Cp angle of 97.1(4)° is close to that of $[Me(Ph)BCp_2ZrCl_2]^-$ [97.2(4)°],[10] and narrower than that of $[Cl(Ph)BCp_2ZrCl_2]^-$ [99.4(4)°][10] and the neutral complexes {(L)PhBCp$_2$ZrCl$_2$; L = SMe_2 [101.1(2)°], PMe_3 [100.1(3)°]}.[11] This indicates that the Lewis basicity of the ylide is similar to that of a methyl anion. The angle about the ylide carbon P(1)−C(17)−B(1) [121.7(3)°] is similar to that of $Ph_3CH_2B(C_6F_5)_3$ [123.38(10)°].[18] The P(1)−C(17) [1.788(5) Å] and C(17)−B(1) [1.666(7) Å] bond lengths are also similar to those of $Ph_3CH_2B(C_6F_5)_3$ [1.7919(14) Å and 1.675(2) Å, respectively], which has been characterized as a methylene-bridged phosphonium-borate betaine with bond lengths in the range of C(sp^3)−X bonds.[18]

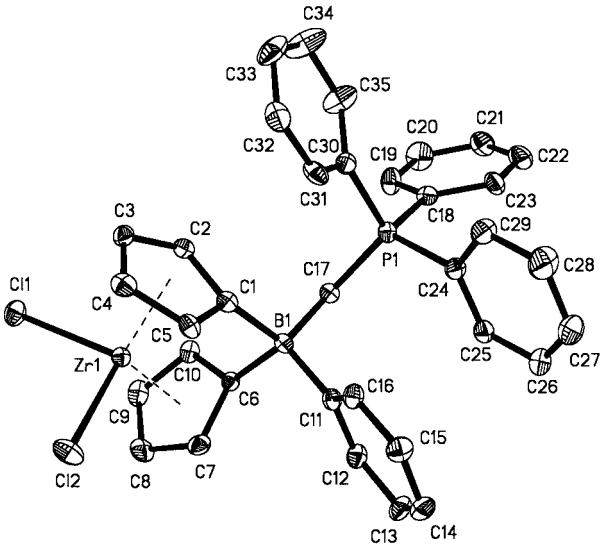

Figure 1. Thermal ellipsoid (30%) drawing of **2**; hydrogen atoms are omitted for clarity; selected bond lengths (Å) and angles (°): B(1)−C(17) 1.666(7), P(1)−C(17) 1.788(5), Zr−cent(1−5) 2.171, Zr−cent(6−10) 2.169, C(1)−B(1)−C(6) 97.1(4), cent−Zr−cent 120.2

Table 1. Crystallographic Data for **2**, **4**, and **5**

	2	**4** +2C_6H_6	**5**
Formula	$C_{36}H_{31}BC_{15}PZr$	$C_{69}H_{58}BCl_2PZr$	$C_{57}H_{46}BCl_2PZr$
Formula mass	773.86	1091.05	934.84
Crystal system	Triclinic	Triclinic	Triclinic
Space group	$P\bar{1}$	$P\bar{1}$	$P\bar{1}$
a (Å)	10.6014(2)	11.8486(7)	13.2315(13)
b (Å)	14.3862	14.6255(9)	13.4195(14)
c (Å)	23.1797(3)	17.1894(11)	16.18550(17)
α (°)	97.2838	81.11(1)	92.515(2)
β (°)	92.0132(7)	72.04(10	106.197(2)
γ (°)	98.0542(7)	75.36(1)	116.865(2)
V (Å^3)	3467.07(7)	2732.1(3)	2512.9(4)
Z	4	2	2
$\rho_{calcd.}$ (Mg/m^3)	1.483	1.326	1.236
μ (mm^{-1})	0.774	0.371	0.392
F_{000}	1568	1132	964
Crystal size (mm)	0.50 × 0.20 × 0.08	0.15 × 0.14 × 0.04	0.27 × 0.26 × 0.07
θ range (°)	0.89 to 25.00	1.83 to 25.00	1.74 to 25.00?
Index ranges	$-12 \le h \le 14$, $-19 \le k \le 18$, $-30 \le l \le 30$	$-14 \le h \le 14$, $-17 \le k \le 17$, $-20 \le l \le 20$	$-15 \le h \le 15$,$-15 \le k \le 15$, $-20 \le l \le 20$
No. reflections collected	33309	27158	23167
No. independent reflections	15906[*R*(int) = 0.0385	9617 [*R*(int) = 0.0766]	8810 [*R*(int) = 0.0603]
Data/restraints/parameters	15906/0/793	9617/0/669	8810/0/561
GOF on F^2	1.187	1.054	1.069
$R(F_o)$ [$I>2\sigma(I)$]	0.0682	0.0682	0.0720
$wR(F_o^2)$ [$I>2\sigma(I)$]	0.2436	0.1319	0.1581
Largest diff. peak/hole e·Å^{-3}	1.694/−1.516	1.038/−0.605	0.949/−1.043

 © 2004 Wiley-VCH Verlag GmbH & Co. KGaA, Weinheim

Table 2. Polymerization results for **2** compared with other metallocene systems

Complex	Alkene	Efficiency gP/gM	MW (PDI)
2	ethylene/octene[a]	6835920	17200 (2.30)
	propylene[b]	27186	ND
[Cp′-$SiMe_2$-*N*-*t*Bu]$TiCl_2$ (CGC)	ethylene/octene[a]	441729	86300 (3.65)
(*i*Pr)$_2$N−BCp_2ZrCl_2	ethylene/octene[a]	346400	8400 (3.93)
	propylene[b]	20984	ND
$Me_2SiCp_2ZrCl_2$	ethylene/octene[a]	93725	8800 (2.42)
	propylene[b]	34421	ND
Cp_2ZrCl_2	ethylene/octene[a]	199509	22100 (2.90)
	propylene[b]	10962	ND

[a] 140 °C, 1000 equiv. MAO, 3.4 Mpa ethylene. [b] 70 °C, 1000 equiv. MAO, 150 g propylene.

Olefin Polymerization Studies with 2

Complex **2** exhibits exceptionally high ethylene polymerization activity when activated with 1000 equiv. of MAO (Table 2). Although the experiment was run in the presence of 1-octene, the high density of the polymer product (>>0.92 g/mL) indicated that little, if any, octene was incorporated. The polymerization efficiency of precatalyst **2** is more than an order of magnitude greater than that of a related amidoborane-bridged system[6] and the commercially successful precatalyst [Cp′−$SiMe_2$−*N*−*t*Bu]$TiCl_2$[19] (Cp′ = C_5Me_4). Although less impressive, the propylene polymerization efficiency of **2** is comparable with other boron- and silicon-bridged precatalysts.

Bis(indenyl)Zr Analogs of 2

The favorable performance of **2** as a precatalyst for ethylene and propylene polymerization prompted us to examine boron-bridged bis(indenyl)zirconocene complexes for their propylene polymerization activity. A small number of boron-bridged bis(indenyl)zirconium complexes have been reported.[6−9] A couple of these exhibit propylene polymerization activities that are comparable with the most active silicon- and carbon-bridged systems.[6,7] Further, in one case, very high isospecificity from a *rac* isomer was observed.[7]

To prepare indenyl analogs of **2**, we made some minor modifications to the original synthetic approach to phenylborylidene-bridged bis(indenyl)zirconium dichloride reported by Reetz et al.[7] (Scheme 1). With the use of $ZrCl_4(SMe_2)_2$[20] as a starting material, we obtained SMe_2 adducts of the boron-bridged complexes instead of ethyl ether adducts. In general, the SMe_2 adducts reacted more cleanly with the phosphane ylides than the ether adducts and afforded higher yields of our target complexes. Initially, we pursued the synthesis of the simple, unsubstituted bis(indenyl) analog of **2**. The poor solubility of this species in toluene and its poor stability in $CHCl_3$ and CH_2Cl_2 made it difficult to purify. Coordinating solvents such as THF and DMSO were avoided because they competed with the ylide group for coordination to the boron. Furthermore, the ^1H, ^{13}C and 2-D NMR spectra of these complexes were of little use for structure identification because of difficulties with sorting indenyl ring resonances from the overlapping arene resonances of the phenyl rings on the ylide and the boron. We attempted to rectify these problems by replacing Ph_3PCH_2 with Me_3PCH_2. We hoped that Me_3PCH_2 would improve the solubility of the complex, simplify its NMR spectroscopic characterization, and form a more stable adduct with the boron bridge. Unfortunately, the PMe_3CH_2 adduct was even more sensitive to decomposition than the Ph_3PCH_2 adduct, and preliminary screenings of the polymerization activities of the *ansa*-zirconocene complexes indicated that the Ph_3PCH_2 adduct was by far the best candidate.

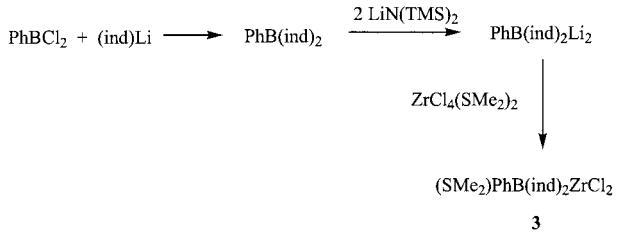

Scheme 1

The propylene polymerization activity of a sample of the ylide adduct of the boron-bridged bis(indenyl)zirconium complex and the molecular weight of the polymer were promising enough to convince us to modify the indenyl rings in order to form a more soluble system that would be easier to purify. Replacing the indenyl (ind) rings with 2-methyl,4-phenylindenyl[21] (2-Me,4-Ph-ind) rings gave us a ^1H NMR signal from the 2-Me group that was useful for evaluating the number and ratio of the three *ansa*-zirconocene diastereomers **4**−**6** (Figure 2) that constituted the product.

The ligand (2-Me,4-Ph-ind)$_2$BPh was prepared in a manner similar to Reetz's (ind)$_2$BPh.[7] In Reetz's synthesis, (ind)$_2$BPh was treated with the base P(*i*Pr)$_3$ in order to promote double bond isomerization within the indenyl rings and convert the bridgehead carbon atoms attached to boron from sp^3 to sp^2 so as to reduce the amount of boron−carbon bond cleavage during metallation of the ligand. Since this base-treatment step had no apparent effect on the isomer composition of (2-Me,4-Ph-ind)$_2$BPh, it was eliminated from our procedure. In addition, harsher conditions were necessary to doubly deprotonate (2-Me,4-Ph-

 © 2004 Wiley-VCH Verlag GmbH & Co. KGaA, Weinheim

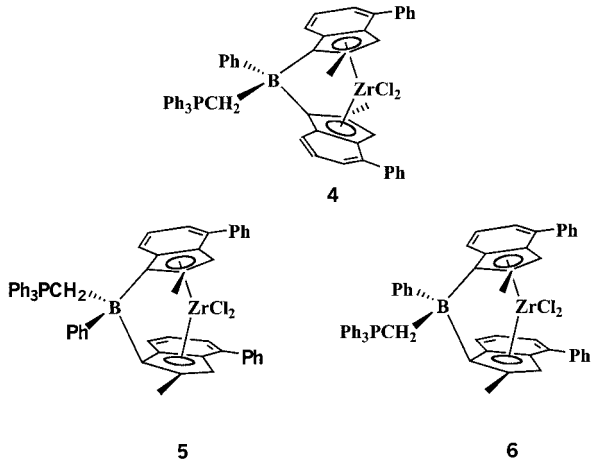

Figure 2. Three diastereomers of $(Ph_3PCH_2)B(2\text{-Me},4\text{-Ph-ind})_2ZrCl_2$

ind)$_2$BPh with Li[N(SiMe$_3$)$_2$] (48 h. at 75 °C) than were required for (ind)$_2$BPh. The increased solubility of the *ansa*-zirconocene complexes in hydrocarbon solvents such as benzene and toluene aided in their purification, crystallization, and NMR spectroscopic characterization.

NMR Characterization of Indenyl Complexes 3−6

The presence of two sets of methyl, phenyl, and indenyl resonances in the ^{1}H NMR spectrum of **3** reveals the presence of two isomers in a 2:1 ratio. Judging from the ratio of diastereomers obtained from the synthesis of **4**−**6** (vide infra), the predominant species corresponds to the *meso* isomers, and the less abundant isomer is the *rac* species. The appearance of only once set of signals for the *meso* isomers can probably be attributed to rapid exchange of SMe$_2$ between the diastereotopic sites on the borylidene bridge.[11]

A representative ^{1}H NMR spectrum of a mixture of **4**−**6**, isolated by crystallization from the bulk reaction product, is shown in Figure 3. With the exception of two olefinic resonances above δ = 6 ppm, the region between 6.5−8.1 ppm containing indenyl and arenyl resonances is quite complex. The methyl and methylene regions (2−4 ppm) of the ^{1}H spectrum are the most useful for evaluating the isomer composition of the material. A persistent unidentified impurity with ^{1}H NMR signals upfield of δ = 2 ppm was invariably present in recrystallized samples of the ylide adducts dissolved in CD_2Cl_2. Since the intensity of the peaks due to this impurity increased over time, and the solvent was predried over molecular sieves, we attribute the impurity to decomposition promoted by the solvent.

The ^{31}P spectrum of the mixture shows three distinct resonances, one for each isomer. The ^{31}P signals were correlated with methylene ^{1}H NMR resonances by selective phosphorus decoupling (Figure 4). The diastereotopic protons of the methylene group in the *rac* isomer **4** appear as two doublet of doublets (dd) at δ = 3.9 and 3.3 ppm. Saturation of the ^{31}P signal at δ = 32.2 ppm results in their collapse to two doublets. The other ^{31}P resonances at δ = 31.8 and 33.0 ppm must therefore be assigned to the *meso* isomers **5** and **6**. Notably, only one broad ^{11}B resonance at δ = −5 ppm is observed for the isomer mixture. Assignments of the 2-Me peaks of the indenyl rings were based on their intensities relative to the ylide methylene resonances. One of the two inequivalent methyl resonances of **4** is obscured by the methyl resonance of one of the *meso* isomers. We were not successful in purifying the *rac* isomers of either **3** or **4** from their *meso* isomers; however, we did isolate X-ray quality crystals of isomers **4** and **5**, allowing their molecular structures to be determined (vide infra).

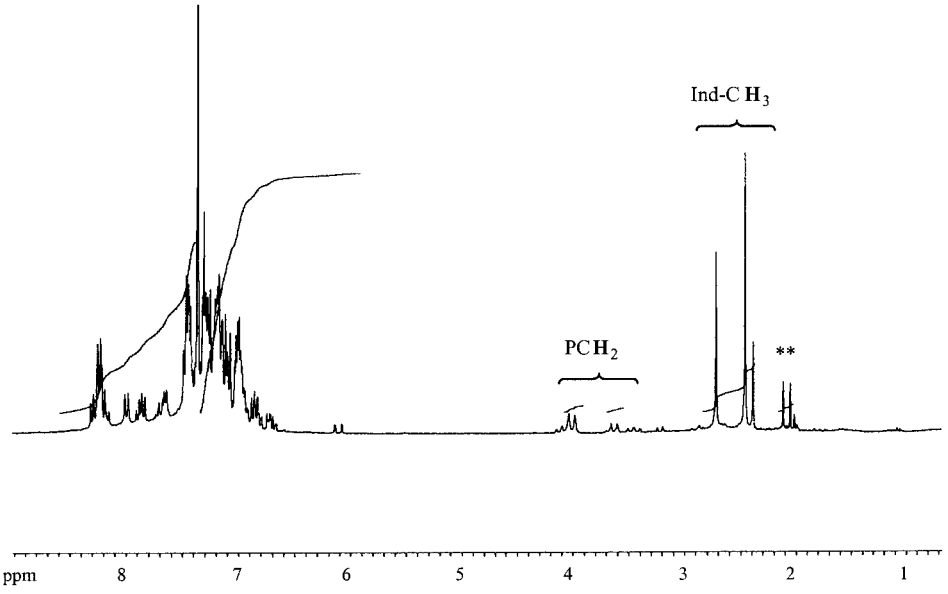

Figure 3. A representative ^{1}H NMR spectrum of a mixture of **4**−**6** (* = unidentified impurity); a 3:1 ratio of *meso*:*rac* isomers is observed

 © 2004 Wiley-VCH Verlag GmbH & Co. KGaA, Weinheim

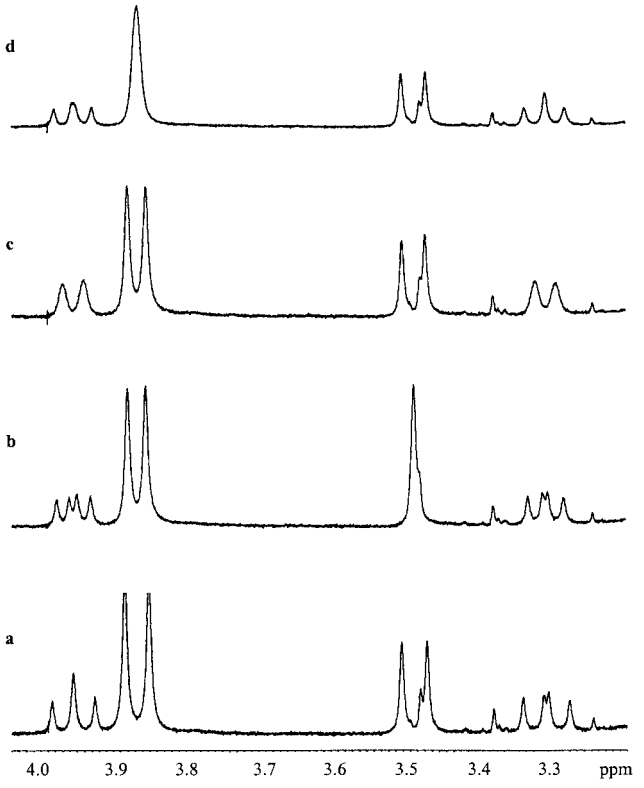

Figure 4. ^{1}H spectra of ylide CH_2 region of isomer mixture **4**−**6** with a) no ^{31}P decouplingand selective decoupling of ^{31}P signal at: b) 33.0 ppm, c) δ = 32.2 ppm, d) δ = 31.8 ppm

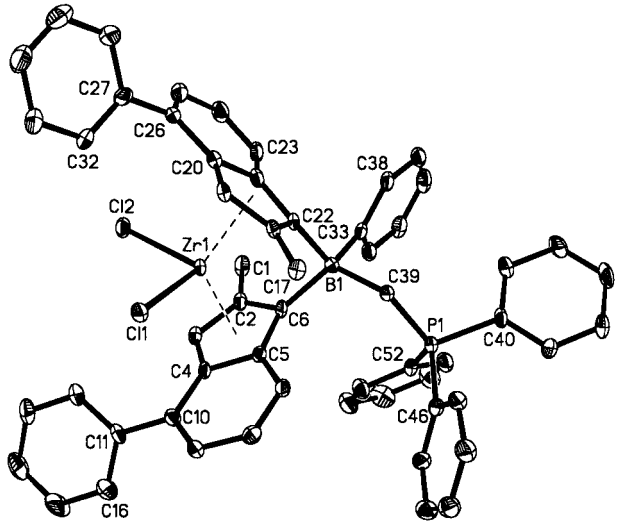

Figure 5. Molecular structure of complex **4**; hydrogen atoms are omitted for clarity

Crystallographic Characterization of Isomers 4 and 5

The molecular structures of **4** and **5** are shown in Figure 5 and Figure 6, respectively. Crystallographic data for both isomers are included with data for **2** in Table 1. Selected bond lengths and angles for **4** and **5** are listed in Table 3 and Table 4, respectively.

There are three other molecular structures of *rac* boron-bridged bis(indenyl)zirconium complexes in the literature: (L)PhB(ind)$_2$ZrCl$_2$ (L = THF, PMe$_3$) published by Reetz,[7] and the structure of *i*Pr$_2$NB(ind)ZrCl$_2$ published by Ashe.[6] Of the four structures, **4** has the smallest angle between the boron and the indenyl bridgehead carbon atoms; 97.6(3)° for **4** vs. 101.5 (L=THF) and 99.4 (L=PMe$_3$) for (L)PhB(Ind)$_2$ZrCl$_2$, and 104.9° for *i*Pr$_2$NB(ind)$_2$ZrCl$_2$. Nevertheless, the centroid−Zr−centroid angle for **4** (123.2°) is slightly larger than those of (L)PhB(Ind)$_2$ZrCl$_2$ (122.3, L=THF; 121.5, L=PMe$_3$), and the dihedral angle between the indenyl ring planes of **4** (65.7°) is slightly smaller than that of *i*Pr$_2$NB(Ind)$_2$ZrCl$_2$ (66.8°). Thus, small changes in the bite angle at boron has little effect on the geometry between the indenyl rings on the zirconium. On the other hand, changing the size of the bridging atom does influence the geometry of the metallocene, with silicon affording a more relaxed structure with a dihedral angle of 62° between the rings and carbon causing a more open structure with an angle of 71° between the ring planes.[12]

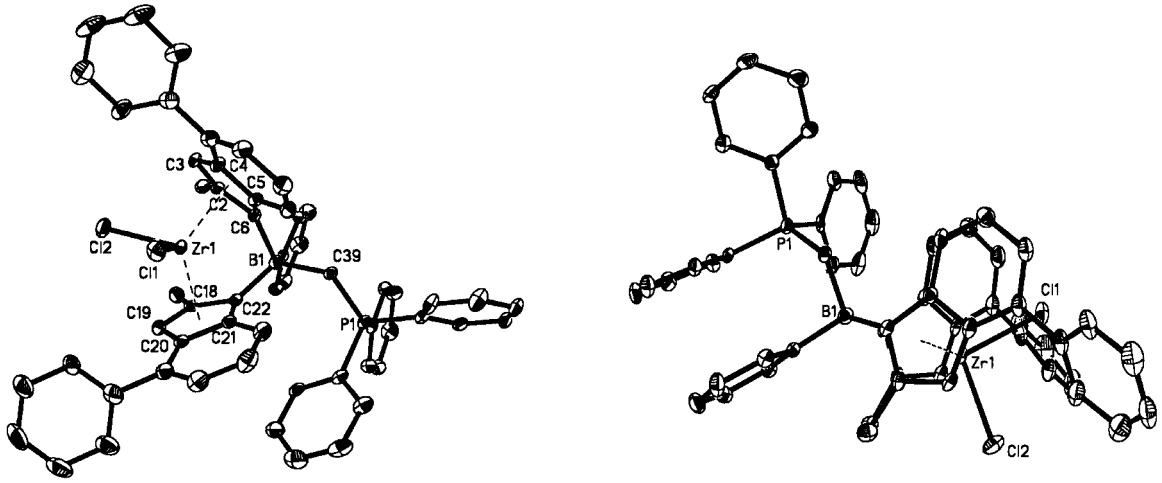

Figure 6. Thermal ellipsoid (30%) drawing of **5** [side (a) and top (b) views]; hydrogen atoms are omitted for clarity

 © 2004 Wiley-VCH Verlag GmbH & Co. KGaA, Weinheim

Table 3. Selected bond lengths (Å) and angles (°) for **4**

Zr(1)−Cl(2)	2.4285(13)	C(5)−C(6)	1.454(6)
Zr(1)−Cl(1)	2.4491(12)	C(18)−C(19)	1.395(6)
B(1)−C(33)	1.630(7)	C(18)−C(22)	1.431(6)
B(1)−C(39)	1.662(7)	C(2)−C(3)	1.404(6)
B(1)−C(6)	1.667(7)	C(2)−C(6)	1.434(6)
B(1)−C(22)	1.679(7	C(19)−C(20)	1.398(6)
P(1)−C(39)	1.807(5)	C(20)−C(21)	1.433(7)
Zr(1)−C(22)	2.440(4)	C(21)−C(22)	1.460(6)
Zr(1)−C(6)	2.449(4)	C(21)−C(23)	1.419(7)
Zr(1)−C(18)	2.482(4)		
Zr(1)−C(2)	2.489(5)	C(33)−B(1)−C(39)	102.1(4)
Zr(1)−C(5)	2.501(4)	C(33)−B(1)−C(6)	118.7(4)
Zr(1)−C(21)	2.508(4)	C(39)−B(1)−C(6)	115.5(4)
Zr(1)−C(19)	2.546(5)	C(33)−B(1)−C(22)	111.9(4)
Zr(1)−C(3)	2.549(5)	C(39)−B(1)−C(22)	111.3(4)
Zr(1)−C(4)	2.590(4	C(6)−B(1)−C(22)	97.6(3)
Zr(1)−C(20)	2.597(5)	Cl(2)−Zr(1)−Cl(1)	96.96(4)
cent(2−6)−Zr	2.203	B(1)−C(39)−P(1)	123.2(4)
cent(18−22)−Zr	2.205	cent−Zr−cent	123.2
C(3)−C(4)	1.407(6)	ind/ind	65.7
C(4)−C(5)	1.452(6)		

Table 4. Selected bond lengths (Å) and angles (°) for **5**

Zr(1)−Cl(1)	2.4038(14)	C(3)−C(4)	1.401(7)
Zr(1)−Cl(2)	2.4547(14)	C(4)−C(5)	1.441(6)
B(1)−C(33)	1.623(7)	C(5)−C(6)	1.447(7)
B(1)−C(22)	1.660(8)	C(18)−C(19)	1.390(7)
B(1)−C(6)	1.660(7)	C(18)−C(22)	1.457(7)
B(1)−C(39)	1.695(7)	C(19)−C(20)	1.401(7)
P(1)−C(39)	1.793(4)	C(20)−C(21)	1.433(7)
Zr(1)−C(2)	2.499(5)	C(21)−C(22)	1.461(7)
Zr(1)−C(3)	2.559(5)		
Zr(1)−C(5)	2.502(5)	C(6)−B(1)−C(39)	110.3(4)
Zr(1)−C(6)	2.445(4)	C(33)−B(1)−C(39)	104.0(4)
Zr(1)−C(4)	2.604(5)	C(33)−B(1)−C(6)	113.4(4)
Zr(1)−C(18)	2.491(5)	C(33)−B(1)−C(22)	116.2(4)
Zr(1)−C(19)	2.546(5)	C(22)−B(1)−C(6)	98.2(4)
Zr(1)−C(20)	2.626(5)	C(22)−B(1)−C(39)	115.1(4)
Zr(1)−C(21)	2.482(5)	B(1)−C(39)−P(1)	125.7(3)
Zr(1)−C(22)	2.455(4)	Cl(1)−Zr−Cl(2)	97.49(5)
C(1)−C(2)	1.501(7)	cent−Zr−cent	123.2
C(2)−C(3)	1.411(6)	ind/ind	68.3
C(2)−C(6)	1.445(6)		

The geometric features of the boron-ylide adduct in **4** are very similar to those of **2**, even though chemically, the interaction appears to be weaker in **4**. The bond lengths B(1)−C(39) [1.662(7) Å] and P(1)−C(39) [1.807(5) Å] are very similar to the corresponding distances in **2**, as is the bond angle B(1)−C(39)−P(31) [123.2(4)°].

The molecular structure of **5** is the first structure of a *meso* isomer of a borylidene-bridged bis(indenyl)zirconium complex and is one of very few reported structures of *meso* *ansa*-bis(indenyl)zirconocene complexes of any kind reported in the literature.[22,23] The noticeable influence of the span of the bridge on the tilt of the indenyl rings is evident by comparing the cent−Zr-cent angle and of **5** (123.2°) and the dihedral angle between the ring planes (68.3°) with the corresponding angles of ethandiyl-bridged *meso*-C_2H_4[4,4′-(2,7-dimethylindenyl)$_2$]$ZrCl_2$ (131.8° and 52.9°, respectively).[22] The bond lengths and angles of the boron-ylide portion of the structure are, within statistical error, similar to the values for **2** and **4**.

Polymerization Activity of (Ph_3pch_2)PhB(2-Me,4-Ph-Ind)$_2ZrCl_2$ (4−6) as a Mixture of Isomers

The propylene polymerization activity of the mixture of *meso* and *rac* diastereomers **4**−**6** activated with MAO is compared with that of the silicon-bridged complex *rac*-$SiMe_2$(2-Me,4-Ph-Ind)$_2Zr$(1,4-Ph_2-butadiene)[24,25] (**7**) in Table 5. The activity of the mixture of boron-bridged species is more than twice that of the silicon-bridged complex at 70 °C and 85 °C; however, the activity of **4**−**5** drops substantially at ≥100 °C, while the activity of **7** increases at higher temperatures. The molecular weight of the polymer product starts out higher for **4**−**6** than for **7** and drops with increasing temperature for both systems. The polydispersity indexes are close to 2 for both systems, at least at the lower temperatures of 70 °C and 85 °C, signifying the homogeneity of the active catalyst centers. The narrow polydispersity and relatively high melting temperature of the polymer produced by **4**−**6** suggests that the *rac* isomer **4** is the most active species in the mixture of isomers. Indeed, ^{13}C NMR analysis of the microstructure of the polypropylene product formed by **4**−**6** reveals a 63.6:26.5:9.8 ratio of mm:mr:rr triads and a mmmm pentad composition of 52.4%.

Table 5. Propylene polymerization results for isomer mixture **4**−**6** and **7**

Complex	*T*p (°C)	Efficiency gP/gZr	MW (PDI)	T_m (°C)
4−**6**	70	1081024	373000 (1.96)	156.2
4−**6**	85	1020311	196000 (2.24)	155.3
4−**6**	100	713375	132000 (2.14)	154.5
4−**6**	115	333920	31900 (2.89)	152.7
7	70	450108	513000 (1.80)	158.8
7	85	502987	309000 (2.00)	156.8
7	100	834442	184400 (3.30)	153.7
7	115	900218	79800 (2.81)	153.7

Conclusion

The exceptionally high ethylene polymerization activity of MAO-activated **2** is a result that we do not yet understand. We are currently preparing alkyl derivatives of this system in order to examine their reactivity with various Lewis-acid activators to elucidate the nature of the active catalyst.[26]

Complex **2** is considerably more stable than its indenyl analogs **4**−**6**. Whereas **2** is stable indefinitely in chloroform or dichloromethane solution, the indenyl complexes decompose in these solvents. In addition, the indenyl compounds decompose over weeks in the solid state if they are not refrigerated (−30 °C).

Although at 70 °C and 85 °C the performance of **4**−**6** as precatalysts for propylene polymerization was significantly

 © 2004 Wiley-VCH Verlag GmbH & Co. KGaA, Weinheim

better than that of a silicon-bridged species used as a benchmark in industry, the poor thermal stability of the boron-bridged system and our inability to isolate the *rac* isomer **4** from the mixture diminishes its utility.

The fairly high percentage of isotactic triads (63.6%) and pentads (52.4%) in the polypropylene formed with **4**−**6** is interesting because it indicates that *rac* isomer **4** is the most active species among the three diastereomers, since it constitutes only about 25% of the mixture. A more dramatic effect of the higher activity of a *rac* isomer on the isotacticity of polypropylene produced by a mixture of *rac* and *meso* *ansa*-zirconocene species has been reported by Collins et al.[22]

Alternative synthetic methods designed to increase selectivity for *rac* isomer **4** were explored, such as the reaction between (Ph)B(2-CH_3-4-Ph-ind)$_2$and $Zr(NMe_2)_4$[27,28] and the reaction of (Ph)B(2-CH_3-4-Ph-ind)$_2Li_2$ with either $Cl_2(PEt_3)_2Zr(\eta^2-1,4\text{-}Ph_2-C_4H_4)$[24,25] or Cl$_2$(THF)Zr[PhN-$(CH_2)_3$NPh];[29] these methods have been used successfully for the *rac*-selective synthesis of other bridged bis(indenyl)-zirconium complexes. Unfortunately, these approaches did not afford isolable *ansa*-zirconocene products.

The preparation of other ylide-like adducts of these boron-bridged *ansa*-zirconocene complexes is currently being explored in order to generate more stable species from which the pure *rac* isomer can be isolated.

Experimental Section

General Remarks: All manipulations were carried out under argon atmosphere using Schlenk and glovebox techniques. Argon and nitrogen were purified by passage over an oxy tower BASF catalyst (Aldrich) and molecular sieves (4 Å). ^{1}H, ^{13}C, ^{11}B, and ^{31}P NMR spectra were recorded on Varian Unit Plus 400 MHz NMR (100 MHz ^{13}C) IBM NR-300 (300 MHz ^{1}H; 75 MHz ^{13}C) and Bruker AVANCE 500 spectrometers (500 MHz ^{1}H; 125 MHz ^{13}C). ^{1}H and ^{13}C spectra were referenced to residual protons in the solvent. ^{11}B and ^{31}P were referenced to external standards (BF_3·OEt_2 and 80% H_3PO_4). Deuterated solvents were dried over molecular sieves (4 Å). $PhBCl_2$ (Aldrich) was used as received. Toluene, benzene, pentane, petroleum ether, and dichloromethane solvents were dried over alumina and stored in line pots over Na/benzophenone or CaH_2 in the case of dichloromethane. $Me_2S(Ph)B(\eta^5\text{-}C_5H_4)_2ZrCl_2$[11] and Ph_3PCH_2[30] were prepared according to literature procedures. 2-Methyl-4-phenylindene was prepared as described in the literature[21] and was also purchased from Boulder Scientific and used as received. Elemental analyses were performed by Desert Analytics (Tuscon, Az).

$Ph_3PCH_2(Ph)B(\eta^5\text{-}C_5H_4)_2ZrCl_2$ (2): Toluene (80 mL) was transferred to a mixture of Ph_3PCH_2 (1.71 g, 6.2 mmol) and **1** (3.30 g, 6.2 mmol) in a flask cooled to −78 °C. The reaction solution was warmed to room temperature and stirred for 18 h to give a grey suspension. The precipitate was isolated by filtration and washed with toluene (30 mL × 2), and dried under vacuum. The resulting yellow-grey solid was redissolved in dichloromethane (20 mL) and layered with pentane. Slow diffusion of the pentane into the dichloromethane caused the precipitation of crystalline product, which was washed with pentane (30 mL × 2) and dried under vacuum (yield: 3.05 g, 75%). ^{1}H NMR (300 K, $CDCl_3$): δ = 7.57 (m, 3 H, C_6H_5), 7.38 (m, 14 H, C_6H_5), 6.97 (m, 3 H, C_6H_5), 6.60 (m, 4 H, C_5H_4), 5.51 (m, 4 H, C_5H_4), 2.67 (d, $^2J_{PH}$ = 16.5 Hz, 2 H, PCH_2) ppm. ^{13}C{^{1}H} NMR (300 K, $CDCl_3$): δ = 135, 133.3 (BC_6H_5), 133.4, 133.3, 129.2, 129.1 (PC_6H_5), 127.112, 125.0, 124.8 (C_5H_4), 122.9 (d, $^1J_{P,C}$ = 84 Hz, PCH_2) ppm. ^{31}P{^{1}H} NMR (300 K, $CDCl_3$): δ = 37.1 ppm. ^{11}B NMR (300 K, $CDCl_3$): δ = −9.1 ppm. $C_{35}H_{30}BCl_2PZr$ (654.5): calcd. C 64.22, H 4.62; found C 64.03, H 4.71.

(Ph)(2-CH_3-4-Ph-ind)$_2$B: $PhBCl_2$ (1.3 mL, 1.58 g, 10 mmol) was added to a solution of (2-Me,4-Ph-ind)Li (4.2 g, 20 mmol) in Et_2O (70 mL) at −78 °C. The reaction mixture turned from red to yellow as it warmed to room temperature. After stirring for 15 h, the reaction was filtered, and the filtrate was dried under vacuum, to give a yellow solid that consisted of (Ph)(2-CH_3-4-Ph-ind)$_2$B as a mixture of double bond isomers complexed by 0.5 equiv. Et_2O (yield: 4.8 g, 91%). ^{1}H NMR (300 K, C_6D_6): δ = 7.60−7.50 (m, 6 H, C_6H_5), 7.30−7.01 (m, 30 H, C_6H_5 + PhC_6H_3), 6.50 (d, PhC_6H_3), 4.18, 4.11(s, 2 H, MeC_5H_2), 3.01 (m, 2 H, Et_2O), 1.84, 1.81, 1.73 (s, 6 H, CH_3), 0.90 (3 H, Et_2O) ppm.

(Ph)B(2-CH_3-4-Ph-Ind)$_2Li_2$: Lithium bis(trimethylsilyl)amide (2.88 g, 17.20 mmol) was added to a solution of (Ph)B(2-CH_3-4-Ph-ind)$_2$ (4.20 g, 7.93 mmol) in toluene (150 mL) cooled to −78 °C. The reaction mixture was allowed to warm to room temperature and then heated at 75 °C with stirring for 48 h to give a suspension. The precipitate was isolated by filtration and washed with toluene (30 mL × 2) and petroleum ether (50 mL), and dried under vacuum, to give a grey-orange solid (yield: 2.30 g, 54%). ^{1}H NMR (300 K, [D$_6$]DMSO): δ = 7.73 (d, $^3J_{H,H}$ = 7.4 Hz, 6 H, C_6H_5), 7.34 (t, $^3J_{H,H}$ = 7.5 Hz, 9 H, C_6H_5), 7.13 (t, $^3J_{H,H}$ = 7.0 Hz, 2 H, indenyl), 6.78 (d, $^3J_{H,H}$ = 7.8 Hz, 2 H, 6.29 (m, 2 H, indenyl), 6.06 (m, 2 H, indenyl), 1.89 (s, 6 H, CH_3) ppm.

$Me_2S(Ph)B(2\text{-}CH_3\text{-}4\text{-}Ph\text{-}ind)_2ZrCl_2$ (3): $Zr(SMe_2)_2Cl_4$ solid (0.98 g, 2.74 mmol) was added to a suspension of (Ph)B(2-CH_3,4-Ph-ind)$_2Li_2$ (1.40 g, 2.74 mmol) in toluene (120 mL) cooled to −78 °C. The mixture was allowed to warm to room temperature and stirred for 18 h. After filtration to remove LiCl, the volatiles were removed from the filtrate under vacuum. The filtrate residue was washed with petroleum ether (30 mL × 2) and dried under vacuum (yield: 1.70 g, 86%). Recrystallization of **3** from benzene/pentane gave a red-brown, crystalline product with the formula **3**·4C_6H_6. ^{1}H NMR (300 K, C_6D_6): minor isomer (*rac*): δ = 7.91 (d, $^3J_{H,H}$ = 7.2 Hz, 6 H, C_6H_5) 6.46, 6.77 (m, 6 H, C_6H_5), 2.11 (s, 6 H, CH_3) ppm; major isomer (*meso*): δ = 7.90 (d, $^3J_{H,H}$ = 7.2 Hz, 6 H, C_6H_5), 6.61 (m, 6 H, C_6H_5), 2.09 (s, 6 H, CH_3) ppm; both isomers: δ = 7.55−7.0 (m, 22 H, indenyl and C_6H_5), 2.24 (s, 12 H, SCH_3) ppm. ^{13}C{^{1}H} NMR (300 K, C_6D_6): δ 140.23, 139.97, 138.82, 137.54, 137.51, 134.30, 133.64, 131.19, 129.81, 128.84, 128.81, 128.76, 128.65, 128.62, 128.58, 128.55, 128.23, 125.49, 125.17, 123.41, 119.06, 117.86, 108.11, 106.89, 104.88, 19.30, 12.29, 19.14, 17.33, 16.45, 16.36. No ^{11}B signal was detected, possibly due to extreme broadening caused by rapid exchange of the Me_2S adduct. $C_{46}H_{41}ZrCl_2B$ (766.8): calcd. C 74.69, H 5.39; found C 74.67, H 5.13.

$Ph_3PCH_2(Ph)B(2\text{-}CH_3\text{-}4\text{-}Ph\text{-}Ind)_2ZrCl_2$ (4−6): Ph_3PCH_2 (511 mg, 1.85 mmol) was added to a solution of **3** (1.21 g, 1.85 mmol) in toluene (120 mL) at −78 °C, and the reaction was warmed to room temperature with stirring. The reaction solution was dark red in color after it was stirred at room temperature for 18 h. After filtration, the volatiles were removed from the filtrate under reduced pressure, and the residue was washed with pentane (50 mL × 2) and dried under vacuum to give a red solid. Recrystallization of the

 © 2004 Wiley-VCH Verlag GmbH & Co. KGaA, Weinheim

red solid from a benzene solution over which pentane was layered afforded red crystals that were suitable for X-ray diffraction studies. The crystals were washed with pentane and dried under vacuum (yield: 795 mg, 46%). ^{1}H NMR (300 K, C_6D_6): all isomers: δ 8.2−8.0 (m, C_6H_5), 7.88 (d, C_6H_5), 7.71 (m, C_6H_5), 7.59 (d, C_6H_5), 7.4−6.5 (large m) ppm; **4**: 3.96 (dd, $^2J_{PH}$ = 17.5, $^2J_{H,H}$ = 15 Hz, 1 H, PCH_2), 2.25 (s, 3 H, CH_3), 2.18 (s, 3 H, CH_3) ppm; **5** and **6**: 3.87 (d, $^2J_{PH}$ = 16.6 Hz, 1 H, PCH_2), 3.49 (d, $^2J_{PH}$ = 16.5 Hz,1 H, PCH_2), 3.30 (dd, $^2J_{PH}$ = 17.5, $^2J_{H,H}$ = 15 Hz, 1 H, PCH_2), 2.52 (s, 3 H, CH_3). 2.26 (s, 3 H, CH_3) ppm. ^{13}C NMR (300 K, C_6D_6): δ = 141.42, 136.48, 133.81, 130.65, 130.04, 129.19, 129.10, 129.19, 128.95, 128.72, 128.45, 128.34, 128.10, 126.98, 125.62, 124.48, 124.44, 123.78, 122.88, 122.06, 121.62, 118.87, 118.48, 108.37, 107.09, 104.89, 102.89, 42.75, 42.64, 21.51, 21.22, 21.04, 20.91 ppm. ^{31}P NMR (300 K, C_6D_6): **4**: δ = 32.21 ppm; **5** and **6**: δ = 31.8, 33.0 ppm. ^{11}B NMR (300 K, C_6D_6): δ = −5 ppm. $C_{57}H_{46}BCl_2PZr$ (934.9): calcd. C 73.23, H 4.96; found C 68.30, H 4.85. Carbon was repeatedly low when reanalyzed. We attribute this to impurities that we were unable to remove from the sample.

Ethylene/Octene Copolymerizations: All feeds were passed through columns of activated alumina and Q-5™ catalyst prior to introduction to the reactor. A stirred 2-L Parr reactor was charged with Isopar-E solvent (about 740 g) and 1-octene comonomer (118 g). Hydrogen was added as a molecular weight control agent by differential pressure expansion from a 75 mL addition tank at 25 psi (2070 kPa). The reactor contents were then heated to the polymerization temperature of 140 °C and saturated with ethylene at 500 psig (3.4 Mpa). The metal complex and activators were mixed as dilute toluene solutions, transferred to a catalyst addition tank and injected into the reactor through a stainless steel transfer line. The polymerization conditions were maintained for 15 minutes with ethylene added on demand to keep the pressure constant. Heat was continually removed from the reaction with an internal cooling coil. The resulting solution was removed from the reactor, quenched with isopropyl alcohol, and stabilized by the addition of a toluene solution (10 mL) containing a hindered phenol antioxidant (approximately 67 mg, Irganox™ 1010 from Ciba Geigy Corporation) and a phosphorus stabilizer (approximately 133 mg, Irgafos™ 168 from Ciba Geigy Corporation). Between polymerization runs, a wash cycle was conducted in which mixed alkanes were added (850 g) to the reactor that was then heated to 150 °C. The reactor was then emptied of the heated solvent immediately prior to a new polymerization run.

Propylene Polymerizations: All feeds were passed though columns of activated alumina and Q-5™ catalyst prior to introduction to the reactor. A stirred 2-L jacketed Autoclave Engineers Zipper-Clave™ reactor was charged with Isopar-E solvent (about 625 g) and propylene (about 150 g). Hydrogen was added as a molecular weight control agent by differential pressure expansion from a 75 mL addition tank (Δ350 kPa). The reactor was heated to 70 °C and allowed to equilibrate. The metal complex and activators were mixed as dilute toluene solutions, transferred to a catalyst addition tank and injected into the reactor through a stainless steel transfer line. Heat was continually removed from the reaction with a cooling coil in the jacket. The resulting mixture was removed from the reactor.

Polymers were recovered by drying for about 20 h in a vacuum oven set at 140 °C. High temperature gel permeation chromatography (GPC) analysis of polymer samples were carried out in 1,2,4-trichlorobenzene at 135 °C on a Waters 150C high temperature instrument. A polystyrene/polyethylene or polypropylene universal calibration was carried out on the isolated polyethylene or polypropylene polymer samples using narrow molecular weight distribution polystyrene standards from Polymer Laboratories.

^{13}C{^{1}H} NMR Analysis of Polypropylene: The solution ^{13}C analysis was performed on a Varian Unit Plus 400 MHz NMR spectrometer. The sample was prepared by heating the polymer (0.4 g) to 150 °C in a mixture of [D_2]tetrachloroethane/orthodichlorobenzene (3.0 g of 50:50 wt. mixture) containing 0.025 M chromium acetylacetonate until homogenized. The data were acquired at 120 °C using continuous ^{1}H decoupling, 4000 transients per data file, and a 0.7 s pulse repetition delay.

X-ray Crystallographic Study: Yellow crystals of **2** obtained by recrystallization from chloroform were sealed in capillaries under N_2. A suitable crystal was selected, and data were collected at 173 K on a Siemens P4/CCD instrument (Mo-*Kα* radiation, λ = 0.71073 Å). Crystals of **4** and **5** obtained by recrystallization from benzene/petroleum ether were covered with a layer of hydrocarbon oil. Suitable crystals of each were selected, attached to glass fibers, and placed in a low-temperature nitrogen stream. Data for both **4** and **5** were collected at 203(2) K on a Bruker/Siemens SMART APEX instrument (Mo-*Kα* radiation, λ = 0.71073 Å) equipped with a Siemens LT-2A low temperature device. Data were measured using omega scans of 0.3° per frame for 10 s, and a half sphere of data was collected. A total of 1471 frames were collected for each crystal with a final resolution of 0.84 Å. The first 50 frames were recollected at the end of data collection to monitor for decay. Cell parameters were retrieved with SMART software and refined with SAINTPlus on all observed reflections (SMART: v. 5.625 and SAINTPlus: v. 6.22, Bruker AXS, Madison, WI). Data reduction and correction for Lorentz polarization and decay were performed using the SAINTPlus software. Absorption corrections were applied to **2**, **4** and **5** with SADABS (SADABS: v. 2.01, Sheldrick, G.M., Bruker AXS Inc., Madison, WI).

All three structures were solved by direct methods and all refined by the least-squares method on F^2 with the SHELXTL program package (SHELXTL v. 5.10, Bruker AXS Inc., Madison, WI). All three structures were solved in the space group $P\bar{1}$ (# 2) by analysis of systematic absences. Non-hydrogen atoms were refined anisotropically. Hydrogen atoms were added geometrically and refined with a riding model with their parameters constrained to the parent atom site.

The structure of **2** contains two crystallographically independent molecules along with two molecules of chloroform in the asymmetric unit. The structure of **5** contains large voids in the asymmetric unit (ca. 446 Å^3). An irresolvable mixture of the solvent of crystallization, petroleum ether, occupied these voids. The solvent contribution to the scattering was removed using the SQUEEZE routine in PLATON,[31] and approximately 76 electrons were removed. No decomposition was observed during the collection for any of the crystals.

CCDC-226719 to -226721 contains the supplementary crystallographic data for this paper. These data can be obtained free of charge at www.ccdc.cam.ac.uk/conts/retrieving.html [or from the Cambridge Crystallographic Data Centre, 12 Union Road, Cambridge CB2 1EZ, UK; Fax: +44 1223/336-033; E-mail: deposit@ccdc.cam.ac.uk].

Acknowledgments

Financial support for this work was provided by The Dow Chemical Company. P. J. S. thanks the referees for this manuscript for their helpful suggestions.

 © 2004 Wiley-VCH Verlag GmbH & Co. KGaA, Weinheim

[1] H. Köpf, N. Klouras, *Monatsh. Chem.* **1983**, *114*, 243−247.
[2] J. H. Shin, T. Hascall, G. Parkin, *Organometallics* **1999**, *18*, 6−9.
[3] J. H. Shin, B. M. Bridgewater, G. Parkin, *Organometallics* **2000**, *19*, 5155−5159.
[4] N. Leyser, K. Schmidt, H.-H. Brintzinger, *Organometallics* **1998**, *17*, 2155−2161.
[5] N. Klouras, *Z. Naturforsch., Teil B* **1991**, *46*, 647−649.
[6] A. J. Ashe, X. Fang, J. W. Kampf, *Organometallics* **1999**, *18*, 2288−2290.
[7] M. T. Reetz, M. Willuhn, C. Psiorz, R. Goddard, *Chem. Commun.* **1999**, 1105−1106.
[8] K. A. Rufanov, V. V. Kotov, N. B. Kazennova, D. A. Lemenovskii, E. V. Avtomonov, J. Lorberth, *J. Organomet. Chem.* **1996**, *525*, 287−289.
[9] K. Rufanov, E. Avtomonov, N. Kazennova, V. Kotov, A. Khvorost, D. Lemenovskii, J. Lorberth, *J. Organomet. Chem.* **1997**, *536−537*, 361−373.
[10] C. T. Burns, D. S. Stelck, P. J. Shapiro, A. Vij, *Organometallics* **1999**, *18*, 5432−5434.
[11] D. S. Stelck, P. J. Shapiro, N. Basickes, *Organometallics* **1997**, *16*, 4546−4550.
[12] P. J. Shapiro, *Eur. J. Inorg. Chem.* **2001**, 321−326.
[13] K. Aleksander, O. Starzewski, W. M. Kelly, A. Stumpf, D. Freitag, *Angew. Chem. Int. Ed.* **1999**, *38*, 2439−2442.
[14] S. J. Lancaster, M. Bochmann, *Organometallics* **2001**, *20*, 2093−2101.
[15] D. S. Stelck, PhD Thesis, University of Idaho, **2001**.
[16] H. Schmidbaur, G. Mueller, G. Blaschke, *Chem. Ber.* **1980**, *113*, 1480−6.
[17] H. J. Bestmann, K. Suehs, T. Roeder, *Angew. Chem.* **1981**, *93*, 1098−1100.
[18] S. Doering, G. Erker, R. Froehlich, O. Meyer, K. Bergander, *Organometallics* **1998**, *17*, 2183−2187.
[19] A. L. McNight, R. M. Waymouth, *Chem. Rev.* **1998**, *98*, 2587−2598, and references cited therein.
[20] E. C. Lund, T. Livinghouse, *Organometallics* **1990**, *9*, 2426−2427.
[21] W. Spaleck, F. Küber, A. Winter, J. Rohrmann, B. Bachmann, M. Antberg, V. Dolle, E. Paulus, *Organometallics* **1994**, *13*, 954−963.
[22] S. Collins, W. J. Gauthier, D. A. Holden, B. A. Kuntz, N. J. Taylor, D. G. Ward, *Organometallics* **1991**, *10*, 2061−2068.
[23] T. Kato, H. Uchin, N. Iwama, K. Imaeda, M. Kashimoto, in *Metalorganic Catalysts for Synthesis and Polymerization* (Ed.: W. Kaminsky), Springer-Verlag, Berlin, **1999**, pp. 195.
[24] E. Y. Chen, D. D. Devore, R. E. Campbell, D. P. Green, J. T. Patton, J. Soto, D. R. Wilson, US Patent 6,127,563, (Dow Chemical Co.), **2000**.
[25] F. J. Timmers, J. C. Stevens, D. D. Devore, R. K. Rosen, J. T. Patton, D. R. Neithamer, US Patent 6,465,384 B1, (Dow Chemical Co.), **2002**.
[26] Note added in proof: Per the suggestion of a referee, we examined an NMR scale reaction between **2** and two molar equivalents of $AlMe_3$ in C_6D_6 in order to determine if MAO is possibly destructive to the complex. One major new species was observed, which we tentatively assign as the dimethylzirconium analog of **2**, along with two minor zirconocene species. Some decomposition was also apparent. There is no evidence of methane production, nor is there any evidence of ylide abstraction from the zirconocene by $AlMe_3$. We verified this by comparing the ^{31}P and ^{1}H NMR spectroscopic data for the reaction with that of a direct reaction between the ylide and $AlMe_3$.
[27] G. M. Diamond, S. Rodewald, R. F. Jordan, *Organometallics* **1995**, *14*, 5−7.
[28] G. M. Diamond, R. F. Jordan, J. L. Petersen, *J. Am. Chem. Soc.* **1996**, *118*, 8024−8033.
[29] X. Zhang, Q. Zhu, I. A. Guzei, R. F. Jordan, *J. Am. Chem. Soc.* **2000**, *122*, 8093−8094.
[30] H. Schmidbaur, H. Stuhler, W. Vornberger, *Chem. Ber.* **1972**, *105*, 1084−1086.
[31] A. L. Spek, *Acta Crystallogr., Sect. A* **1990**, *46*, C-34.

Received December 14, 2003
Early View Article
Published Online June 7, 2004

 © 2004 Wiley-VCH Verlag GmbH & Co. KGaA, Weinheim

EurJIC
European Journal of Inorganic Chemistry

Issue 17/2004

Pages 3379–3570

Papers available ahead of print in Early View at www.interscience.wiley.com

Earliest available Table of Contents:
Automatically, free of charge by e-mail through
www.interscience.wiley.com/alerts

COVER PICTURE

The cover picture shows a stereoselective mononuclear triple-stranded helicate complex. Three chiral binaphthol *N*-oxide derivative ligands are coordinated to a trivalent ytterbium metal atom. This very stable and symmetrical structure was obtained by spontaneous self-assembly. NMR spectroscopy and X-ray crystallography were used for unambiguous characterisation. In the picture, the greenish sphere indicates the ytterbium atom and the larger spheres indicate the oxygen atoms. All those ligands, depicted in different shades to highlight the helical effect, are identical. Details are discussed in the article by M. Capó et al. on p. 3405 ff.

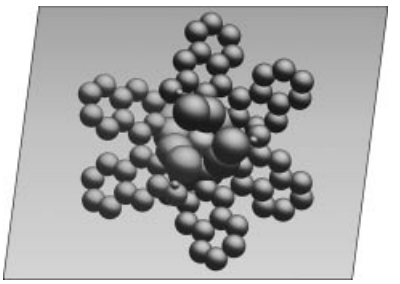

MICROREVIEW

Contents

3393 **A. Dahlén, G. Hilmersson***

Samarium(II) Iodide Mediated Reductions – Influence of Various Additives

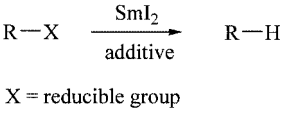

Keywords: Samarium / Samarium iodide / Reduction / Additives / Co-solvent

 © 2004 Wiley-VCH Verlag GmbH & Co. KGaA, Weinheim

FULL PAPERS

3405 **M. Capó,* J. Gonzalez, H. Adams**

Self-Assembly of Stereoselective, Mononuclear, Triple-Stranded Helicate Complexes ML_3 with Trivalent Scandium and Lanthanide Metal Ions − Quantitative Transmetallation of the Lanthanide(III) Ion by Sodium(I) Ions

Keywords: Helical structures / Lanthanides / Self-assembly / Stereoselective / Transmetallation

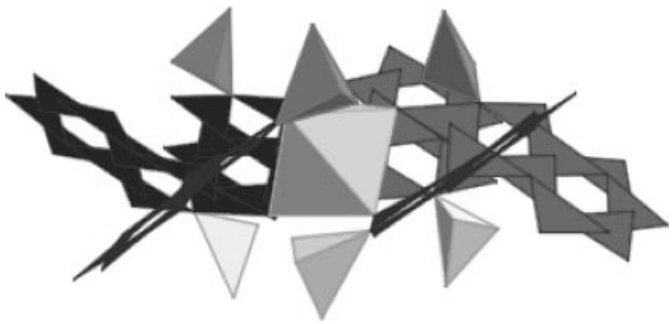

3409 **N. Avarvari, M. Fourmigué,* E. Canadell**

Electron-Rich Organoantimony(III) Dithiolate Complexes

Keywords: Antimony / Noncovalent interactions / S ligands / X-ray diffraction

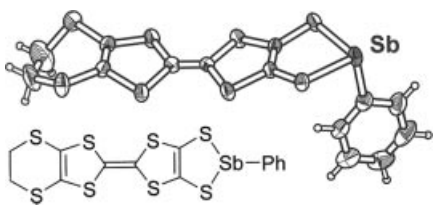

3415 **S. Jung, Y. Kang,* H.-S. Kim, Y.-H. Kim, C.-L. Lee, J.-J. Kim, S.-K. Lee, S.-K. Kwon***

Effect of Substitution of Methyl Groups on the Luminescence Performance of Ir^{III} Complexes: Preparation, Structures, Electrochemistry, Photophysical Properties and Their Applications in Organic Light-Emitting Diodes (OLEDs)

Keywords: Electrochemistry / Electrophosphorescence / Iridium / Luminescence / N ligands

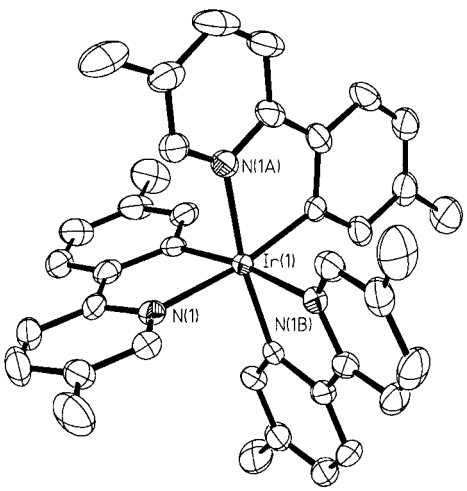

3424 **B. Siggelkow, M. B. Meder, C. H. Galka, L. H. Gade***

Synthesis, Structures and Catalytic Properties of Bis(2-pyridylimino)isoindolatopalladium Complexes

Keywords: Hydrogenation / N ligands / Palladium

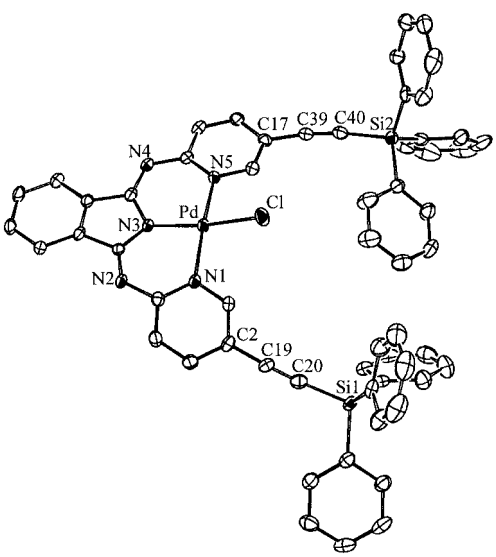

© 2004 Wiley-VCH Verlag GmbH & Co. KGaA, Weinheim

3436 **V. César, S. Bellemin-Laponnaz,* L. H. Gade***

Cationic and Neutral Rhodium(I) Oxazolinylcarbene Complexes

Keywords: Carbenes / N ligands / Oxazolines / Rhodium / X-ray diffraction

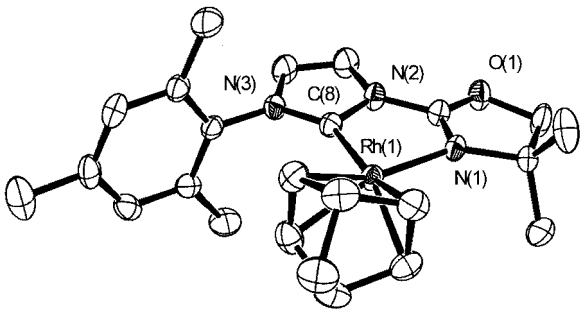

3445 **M. Laforgia, L. Cerasino, N. Margiotta, M. A. M. Capozzi, C. Cardellicchio, F. Naso, G. Natile***

Synthesis and Characterization of Platinum(II) Complexes of Diethyl [(Methylsulfinyl)methyl]-phosphonate: Potential Drugs against Bone Tumors

Keywords: Antitumor agents / NMR spectroscopy / O ligands / Platinum / S ligands

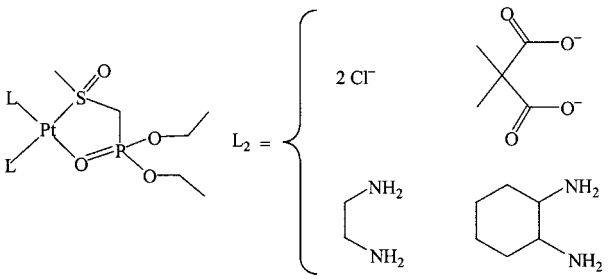

3453 **N. V. Belkova, O. A. Filippov, A. M. Filin, L. N. Teplitskaya, Y. V. Shmyrova, V. V. Gavrilenko, L. M. Golubinskaya, V. I. Bregadze, L. M. Epstein,* E. S. Shubina***

Interaction of the $[GaH_4]^-$ Anion with Weak XH Acids − A Spectroscopic and Theoretical Study

Keywords: Hydrides / Hydrogen bonding / IR spectroscopy / Theoretical methods / Boron / Gallium

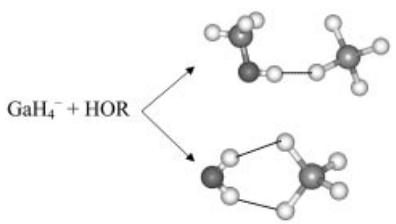

3462 **B. Keita, I. M. Mbomekalle, Y. W. Lu, L. Nadjo,* P. Berthet, T. M. Anderson, C. L. Hill***

Electron Transfer Behavior of Multi-Iron Sandwich-Type Polyoxometalates and Electrocatalytic Reduction Reactions

Keywords: Polyoxometalates / Sandwich complexes / Iron / Cyclic voltammetry

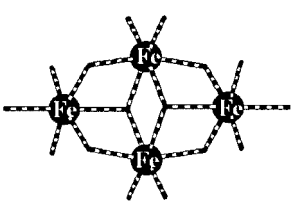

3476 **R. H. Herber,* I. Nowik, D. A. Loginov, Z. A. Starikova, A. R. Kudinov**

Bonding, Metal-Atom Dynamics and Hyperfine Interactions of η-Phospholyl- and η-Pentaphospholyliron Complexes

Keywords: Iron / Mössbauer spectroscopy / P ligands / Sandwich compounds / Spin−lattice relaxation

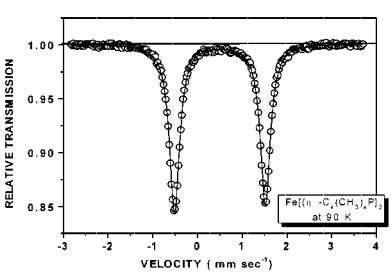

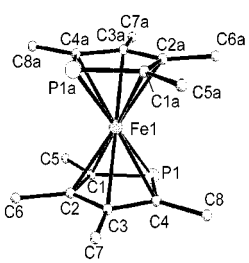

 © 2004 Wiley-VCH Verlag GmbH & Co. KGaA, Weinheim

3484 **C. Pettinari,* F. Marchetti, R. Pettinari, A. Cingolani, E. Rivarola, C. Phillips, J. Tanski, M. Rossi, F. Caruso***

Tin(II) and Lead(II) 4-Acyl-5-pyrazolonates: Synthesis, Spectroscopic and X-ray Structural Characterization

Keywords: Lead / Mössbauer spectroscopy / N ligands / NMR spectroscopy / Tin

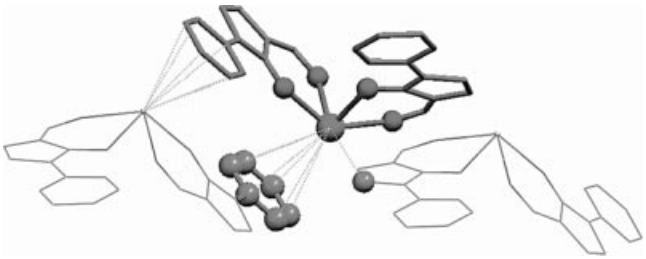

3498 **K. Heinze,* J. D. Bueno Toro**

Solid- and Solution-Phase Synthesis of a Library of Mixed-Metal Complexes

Keywords: Bridging ligands / Heterometallic complexes / Isomers / Group 6 elements / Solid-phase synthesis

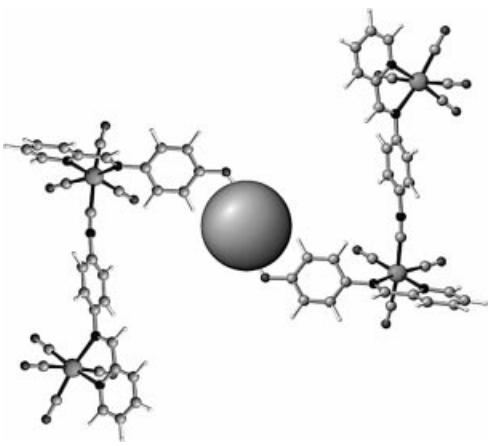

3508 **V. Jancik, M. M. M. Cabrera, H. W. Roesky,* R. Herbst-Irmer, D. Neculai, A. M. Neculai, M. Noltemeyer, H.-G. Schmidt**

Phosphane-Catalyzed Reactions of $LAlH_2$ with Elemental Chalcogens; Preparation of $[LAl(\mu\text{-}E)_2AlL]$ [E = S, Se, Te, L = $HC\{C(Me)N(Ar)\}_2$, Ar = 2,6-iPr$_2$C$_6$H$_3$]

Keywords: Aluminum / Catalysis / Chalcogens / Phosphanes / Reaction mechanisms

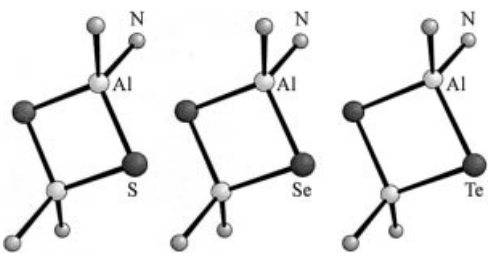

3513 **R. Steudel,* Y. Steudel**

The Thermal Decomposition of S_2O Forming SO_2, S_3, S_4 and S_5O − An ab initio MO Study

Keywords: Cycloaddition / Disproportionation / Sulfur / Sulfur heterocycles / Thermodynamics / Transition states

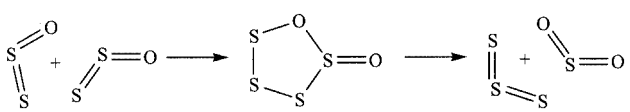

3522 **C. Ma, W. Wang, X. Zhang, C. Chen, Q. Liu,* H. Zhu, D. Liao, L. Li**

Molecular, One- and Two-Dimensional Systems Built from Manganese(II) and Phthalate/Diimine Ligands: Syntheses, Crystal Structures and Magnetic Properties

Keywords: Manganese / N ligands / Magnetic properties / Structure elucidation

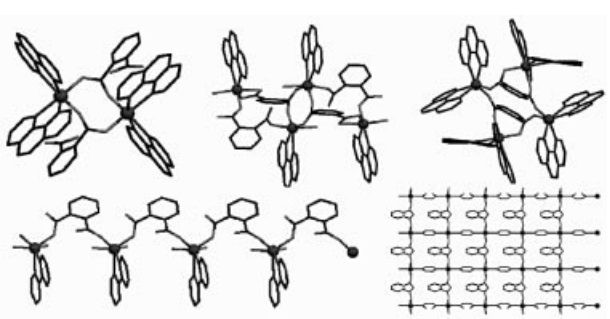

 © 2004 Wiley-VCH Verlag GmbH & Co. KGaA, Weinheim

3533 **D. Martin, A. Baceiredo,* G. Bertrand***

Synthesis of a Persistent $1\sigma^3,3\sigma^3$-Diphosphaallyl Cation Featuring a Localized Phosphorus–Carbon Double Bond

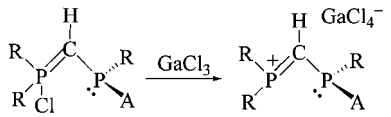

Keywords: Allylic cations / Phosphorus / Phosphaalkenes / Phosphacumulenes / Phosphorus ylides

3538 **T. N. Parac-Vogt, K. Kimpe, S. Laurent, C. Piérart, L. Vander Elst, R. N. Muller, K. Binnemans***

Gadolinium DTPA-Monoamide Complexes Incorporated into Mixed Micelles as Possible MRI Contrast Agents

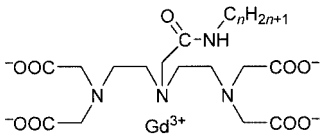

Keywords: MRI contrast agents / Lanthanides / DTPA-monoamide derivatives / Micelles

3544 **S. Kheradmandan, T. Fox, H. W. Schmalle, K. Venkatesan, H. Berke***

Mono- and Dinuclear High-Spin Half-Sandwich Manganese(II) Complexes Containing Acetylide and TMEDA Ligands

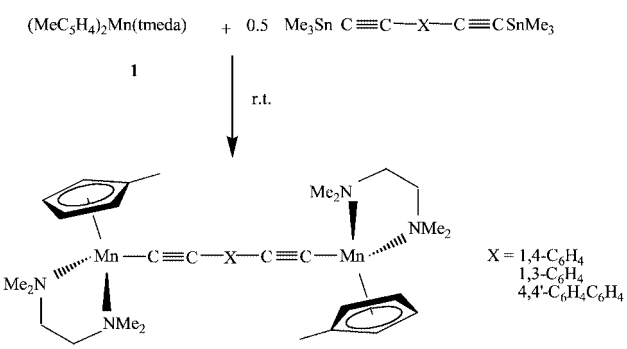

Keywords: Alkyne ligands / Cyclopentadienyl ligands / Half-sandwich complexes / Molecular devices / N ligands

3555 **S. Sharma, M. Chandra, D. S. Pandey***

New Multifunctional Complexes $[Ru(\kappa^3\text{-L})(EPh_3)_2Cl]^+$ [E = P, As; L = 2,4,6-Tris(2-pyridyl)-1,3,5-triazine] Containing both Group V and Polypyridyl Ligands

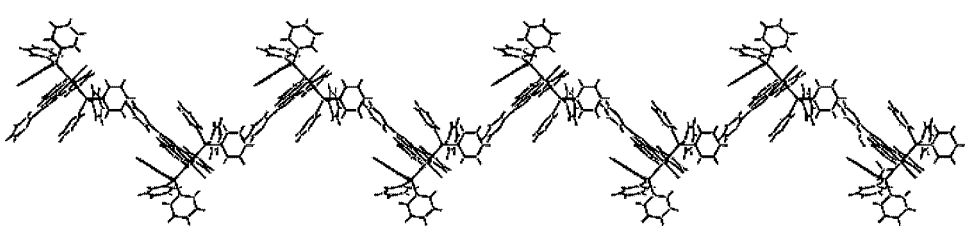

Keywords: Ruthenium / Tertiary phosphanes / 2,4,6-Tris(2-pyridyl)-1,3,5-triazine / DNA / Topoisomerase II

 © 2004 Wiley-VCH Verlag GmbH & Co. KGaA, Weinheim

3564 **D. Belletti, C. Graiff, R. Pattacini,* G. Predieri, A. Tiripicchio**

Polynuclear Rhenium and Manganese Selenido-Carbonyl Complexes − Reversible Square to Butterfly Conversion of the Re_4Se_2 Core by CO Loss in $[Re_4(\mu_3\text{-}Se)_2(CO)_{16}(PPh_3)_2]$, and the Crystal Structure of $[Mn_2(\mu_2\text{-}Se_2)(CO)_5(PPh_3)_2]$

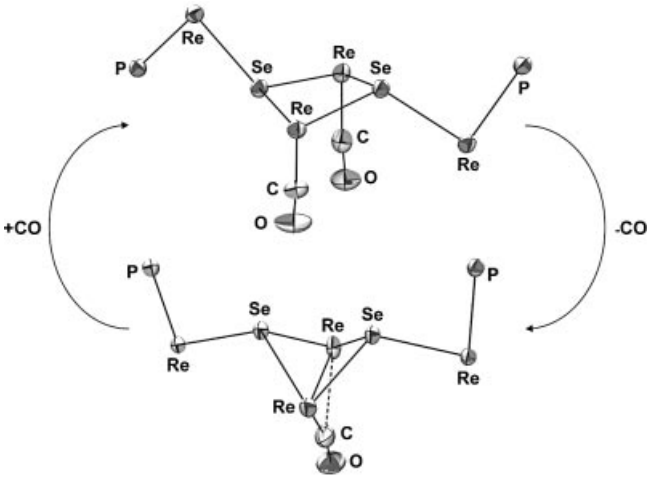

Keywords: Cluster compounds / Manganese / Rhenium / Selenium

 © 2004 Wiley-VCH Verlag GmbH & Co. KGaA, Weinheim

Samarium(II) Iodide Mediated Reductions – Influence of Various Additives

Anders Dahlén[a] and Göran Hilmersson*[a]

Keywords: Samarium / Samarium iodide / Reduction / Additives / Co-solvent

Samarium(II) iodide is a one-electron transfer reagent that has become highly appreciated as a mild and selective reducing agent in recent years. It has been found experimentally that various additives and co-solvents largely control the reactivity of SmI_2. This microreview provides an overview of the current knowledge of the reagent SmI_2 as a reducing agent, in particular with additives that increase its reactivity. The use of various proton sources is covered, as well as the effect of co-solvents. Furthermore, the very powerful reagent mixture SmI_2/H_2O/amine is also described.
(© Wiley-VCH Verlag GmbH & Co. KGaA, 69451 Weinheim, Germany, 2004)

Introduction

Reductions constitute a fundamental class of reactions in synthetic organic chemistry, the most common reducing agents are hydrogen gas in combination with Pd/C or active catalysts, alkali metals and hydrides. However, the chemoselectivity of these reagents is often low, which prevents effective synthesis of new more complex target molecules. It is in this respect that the mild reducing agent SmI_2, introduced by Kagan and co-workers in the late 1970s, is receiving much interest today. Kagan showed that SmI_2 promotes reduction of halides, aldehydes, ketones and carboxylic acids, and reductive eliminations and deoxygenations.[1] Since then, a number of SmI_2-based reductive couplings and sequenced reactions have been developed,[2] and new applications are steadily being discovered. SmI_2 is generally considered a selective single-electron transfer reagent that generates carbon-centred radicals from halides or related species. Therefore, it is particularly useful for ketone-olefin coupling reactions, pinacol coupling reactions and radical addition to alkenes and alkynes. SmI_2 has even begun to appear frequently in natural product and multi-step synthesis.[3] Due to the intense interest in this reagent, SmI_2 is now commercially available as a 0.1 M solution in THF.

Over the years, several reviews have been published on the use of SmI_2 in various reduction and coupling reactions.[4] However, recently there has been considerable progress in the use of SmI_2 as a simple reducing agent. SmI_2 represents an important reagent, but it is often necessary to enhance the reactivity by adding various salts and co-solvents. Due to limited knowledge of the active species in these mixtures, the emphasis in this review is not on the

[a] Organic Chemistry, Department of Chemistry, Kemivagen 10, 41296 Göteborg, Sweden

Anders Dahlén was born in Trollhättan (Sweden) in 1977. He received his M. Sc. degree in 2001. The Diploma work was made at the Department of Chemistry, Göteborg University, with the title "Complexation of Lanthanide(II) iodide using Chiral Polyethers and Studies of the Rates of SmI_2-mediated Reductions". Since 2001, he is a PhD student at the Department of Chemistry at the Göteborg University under the supervision of Associate Professor Göran Hilmersson. His current research interests are mechanistic investigations and development of new synthetic methods mediated by lanthanide(II) reagents.

Göran Hilmersson was born in Alingsås (Sweden) in 1966. He studied chemistry at Göteborg University, and obtained his B. Sc. degree in 1991, followed by his PhD degree in 1996 under the supervision of Professor Per Ahlberg. He was a Research Associate for 14 months at The Scripps Research Institute, La Jolla, CA, USA with Professor Julius Rebek, Jr., a postdoc funded by the Knut and Alice Wallenberg Foundation. In 1997, he returned to Göteborg University as Assistant Professor and in 2000 he became Associate Professor of Organic Chemistry. His research is focused on structure and dynamics of chiral alkali metal complexes used in asymmetric addition reactions and development of lanthanide(II)-mediated reduction reactions.

MICROREVIEWS: This feature introduces the readers to the author's research through a concise overview of the selected topic. Reference to important work from others in the field is included.

structures, but on the effect of various additives. The possibility to perform coupling reactions catalytically on SmI_2, with the aid of, for example, mischmetal has also been reported. However, this will not be discussed any further since a recent review is available,[5] in addition, the focus here will be on SmI_2-mediated reductions. Our intention is to deliver an updated summary of SmI_2-mediated reductions that may inspire further studies on structures and mechanisms of this highly interesting reducing agent.

Preparation of SmI_2

The compound SmI_2 has been known for more than seventy years,[6] but it did not receive much attention until Kagan and co-workers published their pioneering work.[1] They discovered the mild reducing properties of SmI_2 and a simple method for its preparation. A number of reports of SmI_2 prepared in THF from excess samarium metal and an iodine source, such as diiodoethane, diiodomethane, iodine or iodoform, have been published.[1,7] SmI_2 in THF is often obtained quantitatively as a deep blue solution with a concentration of 0.1 M. If excess iodine is used in the preparation, SmI_3 is formed, and the solution does not reach the intense dark blue, almost black, colour associated with SmI_2. Few reports describe the use of bulk solvents other than THF; however, SmI_2 can be readily produced in tetrahydropyran, acetonitrile, pivalonitrile and DME.[8] Kagan and co-workers concluded that addition of HMPA to SmI_2 in acetonitrile neither enhances the reactivity nor improves the amount of pinacol coupling, and that the maximum concentration of SmI_2 is generally lower in solvents other than THF.[8a] However, a thorough investigation into the reaction rates of various reductions and couplings with SmI_2 in different solvents is unfortunately not yet available.

Addition of Alcohols and Water

Ever since the introduction of SmI_2 in synthetic applications, it has been realised that various proton sources may be used to alter the product composition. By far the most commonly used alcohols in SmI_2-mediated reductions are methanol and *tert*-butyl alcohol (Scheme 1).[1b,9]

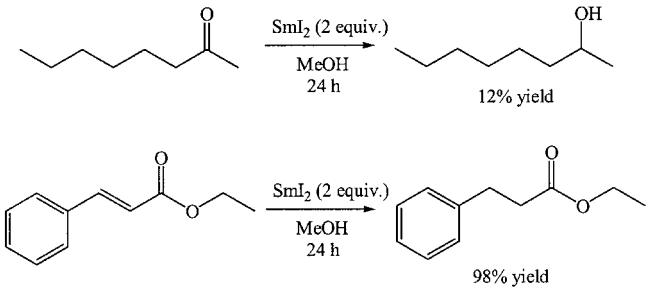

Scheme 1. Reduction of ketones and α,β-unsaturated esters with SmI_2 and methanol

The reductions of α,β-unsaturated esters proceed smoothly with either methanol or *tert*-butyl alcohol, but it appears that both of these alcohols are poor proton donors in the reduction of ketones, thus resulting in low yields.[1b]

The modification of the proton source has been investigated in the reduction of propargylic esters, in which a very high regioselectivity was obtained merely by changing the proton source from *t*BuOH to dimethyl L-tartrate (L-DMT). The allene isomer was obtained with *t*BuOH, while in the case of L-DMT an excess of the acetylene isomer was formed (Scheme 2).[10]

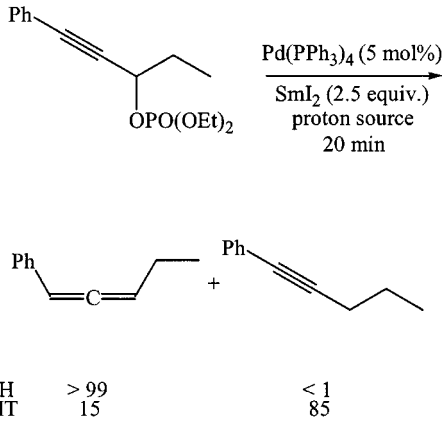

Scheme 2. Reduction of a propargylic ester with *t*BuOH and L-DMT

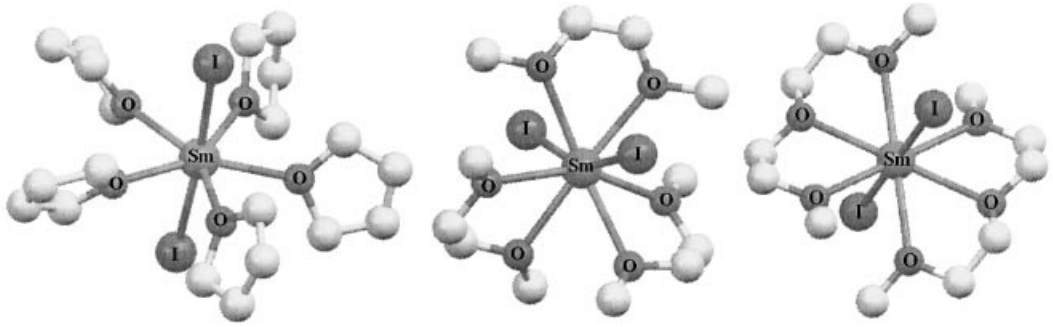

Figure 1. Ball-and-stick representation of the solid-state structures of $SmI_2(THF)_5$, $SmI_2(glyme)_3$ and $SmI_2(diglyme)_2$; hydrogen atoms have been omitted

 © 2004 Wiley-VCH Verlag GmbH & Co. KGaA, Weinheim

Keck and co-workers have shown that the presence of nearby chelating groups has a remarkable impact on the rates of reduction.[11] They concluded that methanol is the additive of choice to obtain high yields without loss of diastereoselectivity in the reduction of, for example, β-hydroxy ketones (Scheme 3).

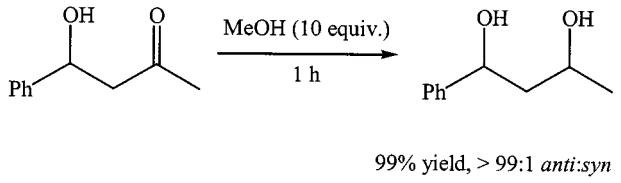

Scheme 3. SmI_2/MeOH-mediated reduction of β-hydroxy ketones

Previous studies on solid-state structures of SmI_2, crystallised from ether solutions, have shown that ethers are excellent coordinating groups to SmI_2 (Figure 1).[8c,12]

As chelating ethers are known to coordinate to SmI_2, we wanted to explore the use of alcohols with coordinating groups as alternatives to other simple alcohols. The initial rate of reduction of a ketone (3-heptanone) with various alcohols was investigated, and chelating ether groups on the alcohol were used since they were expected to coordinate to Sm^{II}, thus placing the proton source close to the source of electrons (Figure 2).[13] This should, therefore, produce a strong reducing agent, resembling hydrogen radicals or hydride reagents.

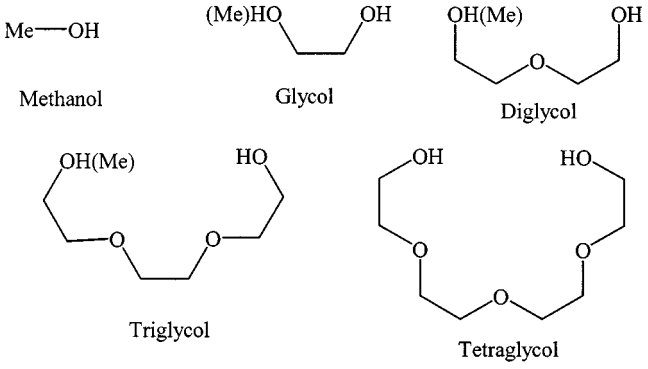

Figure 2. Chelating alcohols/glycols

The introduction of coordinating ether functions to the alcohol revealed a correlation between the rate and the number of coordinating groups. Monomethyl glycols gave higher rates of reduction for each extension of the ethereal group chain. SmI_2/tri(ethylene glycol) monomethyl ether resulted in a rate enhancement of approximately 5 times relative to that of SmI_2/MeOH. Further rate enhancements were noticed when glycols were used; the fastest rate for the glycols appeared to be with di(ethylene glycol) which was more than 70 faster than that with methanol, or 255 times faster than the rate with THF. The significant increase in rate with diglycol suggests that a dimeric transition state is present (Scheme 4). The presence of a primary kinetic isotope effect proved that the rate-limiting step in this reduction is the transfer of at least one proton. It was also shown that full occupancy of the coordination sphere, as with the tetradentate ligand tetra(ethylene glycol), resulted in a decrease in the rate. The coordination plays an important role in SmI_2-mediated reductions.

It has been found that steric hindrance around the substrate also affects the rate of reduction.[14] The less sterically crowded 4-phenyl-2-butanone was reduced approximately 130 times faster than 2-methyl-3-heptanone with the reagent mixture SmI_2/diglycol.

Recently, Flowers and co-workers investigated the role of the acidity constant (pK_a) of the alcohol in the reduction of acetophenone and found a linear correlation for the reaction rate vs. pK_a.[15] The more acidic alcohols resulted in higher reduction rates. However, water did not fit into this correlation, most likely due to unique, unexplained reactivity and complexation properties (Figure 3).[16]

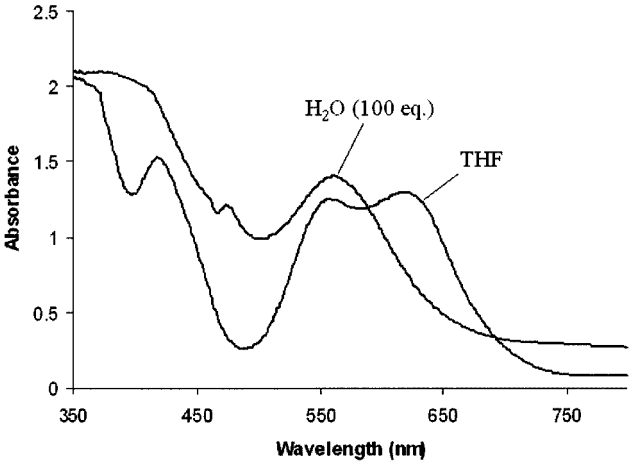

Figure 3. Comparison of SmI_2 in THF and SmI_2 in water

Nakamura and co-workers developed an enantioselective reduction of α-halo- and α-methoxy ketones with C_2-symmetric chiral diols, e.g. (*R*)-2,2′-bis[(*S*)-2-hydroxy-2-phenylethoxy]-1,1′-binaphthyl [(*R*,*S*)-DHPEB].[17] High yields were obtained with up to 94% *ee* within 2 h at −45 °C (Scheme 5). These diols contain four or five coordinating functional groups and, therefore, bind tightly to SmI_2, providing a transition state that facilitates the asymmetric protonation of the enolate.

Alcohols have been the dominating proton sources in SmI_2-mediated reductions, while water, even though it is also a good proton source, has not been employed to the same extent. Some of the previously mentioned studies confirm that the use of water leads to different product compositions and occasionally higher yields.[10,11a] Good to excellent yields were reported in the conversion of aromatic carboxylic acids to alcohols with a SmI_2/H_2O system (Scheme 6).[18]

Kamochi and Kudo have extensively studied the use of Brönsted acids and bases as additives in SmI_2-mediated reduction of carboxylic acids, amides, nitriles, pyridines and phenol derivatives. In particular aromatic compounds were reduced in high yields, and the use of acids and bases in

 © 2004 Wiley-VCH Verlag GmbH & Co. KGaA, Weinheim

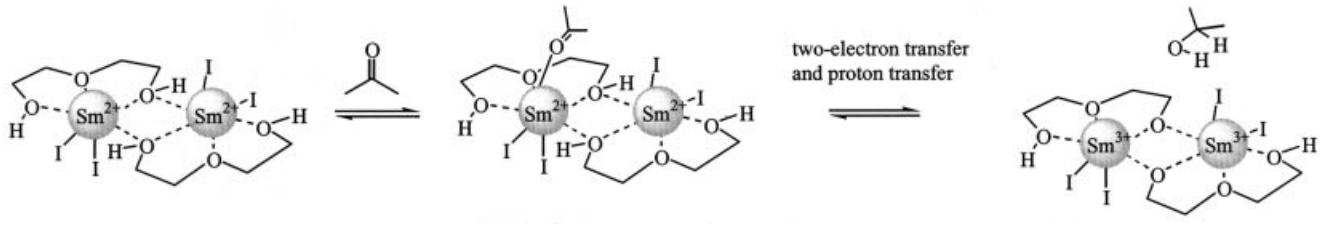

Scheme 4. SmI_2/diglycol-mediated reduction of a ketone

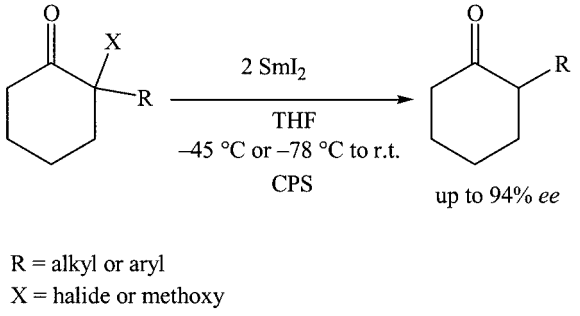

Scheme 5. Enantioselective reduction mediated by a chiral proton source (CPS)

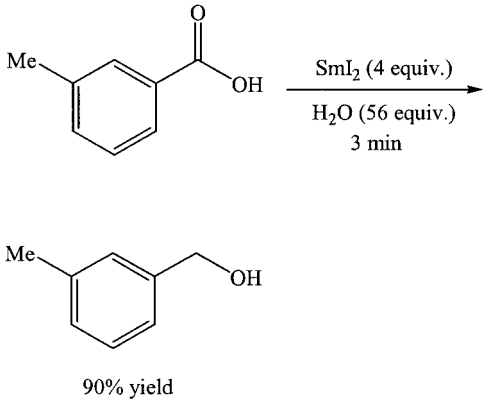

Scheme 6. Reduction of aromatic carboxylic acids with SmI_2/H_2O

SmI_2-mediated reductions indicates that certain reactions are dependent on pH.[19]

Curran and co-workers reported on the SmI_2-mediated reduction of various functional groups in the presence of water (Scheme 7).[20] The reduction rate of ketones, α,β-unsaturated esters, sulfoxides and alkyl iodides was significantly accelerated by the addition of water. The results indicated that the accelerating role of water may be more intricate than simply acting as a proton donor, i.e. it may both accelerate the reduction by enhancing the reducing power as well as acting as a proton donor.

Only a few examples of high diastereoselectivity have been reported for SmI_2/H_2O-mediated reductions of ketones. One example of such a reduction is a step in the total synthesis of Atractyligenin (Scheme 8), which gave selectivity for the α-isomer.[21]

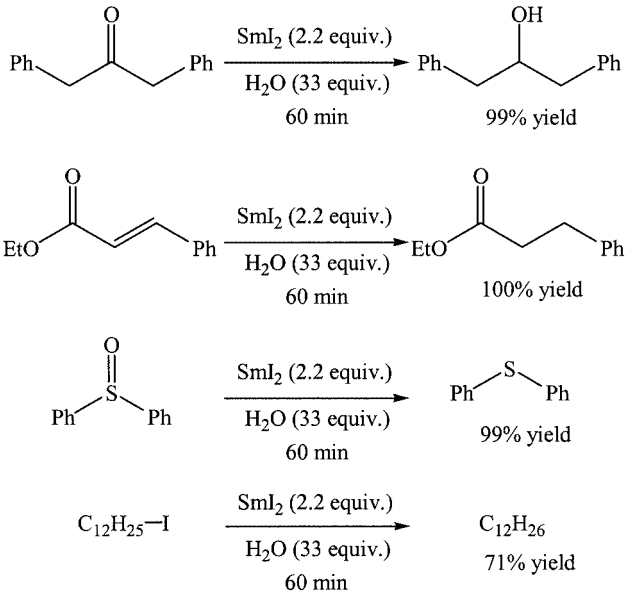

Scheme 7. Various SmI_2/H_2O-mediated reductions

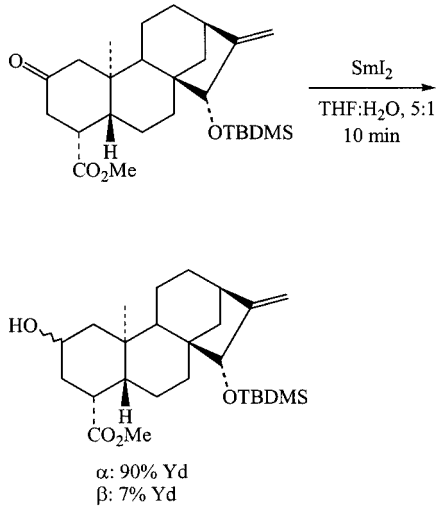

Scheme 8. Diastereoselective reduction of Atractyligenin with SmI_2/H_2O

Selective isotopic labelling with deuterium is an important feature, since it can be used to establish mechanistic pathways. This can be readily accomplished using deuterium oxide instead of water in SmI_2-mediated reductions. Deuterium oxide is one of the most inexpensive available sources of deuterium; in addition, it is a nonhazardous

 © 2004 Wiley-VCH Verlag GmbH & Co. KGaA, Weinheim

compound. Dideuterated carboxylic acids have been successfully synthesised from unsaturated acids in high yields and diastereoselectivities (Scheme 9).[22]

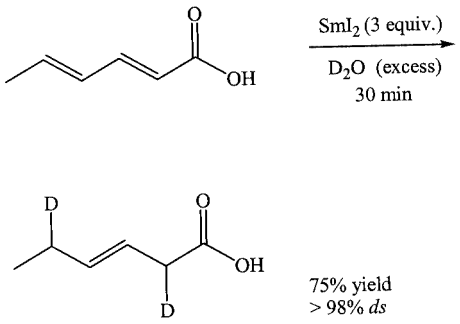

Scheme 9. SmI_2/D_2O reduction of unsaturated carboxylic acid

Studer and Curran have reported on the reductive demethoxylation of aromatic dimethylacetals in the presence of SmI_2/H_2O with excellent yields. Comparison was also made with TFA and $BF_3{\cdot}Et_2O$ in this study, which gave pinacol as the major product, while addition of water gave mostly reduction (Scheme 10).[23]

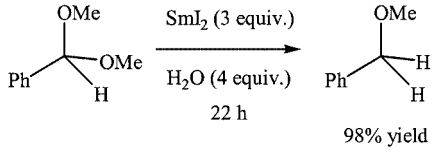

Scheme 10. Reductive demethoxylation with SmI_2/H_2O

SmI_2-HMPA-Mediated Reductions

The Effect of HMPA on Various Simple Reductions

In 1987, Inanaga and co-workers reported that the addition of hexamethylphosphoramide (HMPA) to THF solutions of SmI_2 resulted in a substantial enhancement of the rate of reduction and reductive coupling.[24] Carbon–halogen bonds were effectively and quantitatively reduced to C–H bonds by a mixture of SmI_2-HMPA in THF (Scheme 11). Alkyl, vinyl and aryl halides were rapidly reduced, with approximately 5% HMPA as co-solvent in THF. Upon the addition of HMPA to the SmI_2 solution in THF, the colour changed from blue to purple.

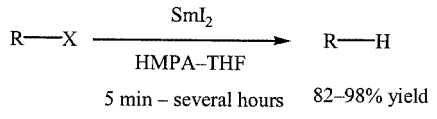

Scheme 11. General SmI_2-HMPA-mediated reduction of alkyl halides

The mixture of SmI_2-HMPA was reported to promote reductive dimerisations of, for example, unsaturated carbonyl compounds.[25] Cabrera and Alper reported that SmI_2-HMPA was also efficient for selective reduction of α,β-unsaturated carbonyl compounds (the compounds investigated were esters, acids, amides and anhydrides).[26]

The reactive SmI_2-HMPA mixture was later proven to be useful for desulfonylation of various phenyl sulfones, as reported by Künzer and co-workers (Scheme 12).[27]

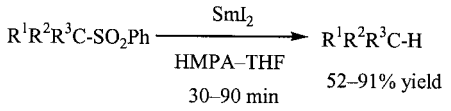

Scheme 12. SmI_2-HMPA-mediated reduction of phenyl sulfones

Fuh and co-workers have studied the kinetics of the SmI_2-mediated reduction of an aliphatic ketone to an alcohol. In the absence of HMPA, the reduction of 2-heptanone to 2-heptanol is very slow, only 28% of the ketone is reduced after 16 days. However, with only one equivalent of HMPA added, the reactions are reported to be complete in less than one hour.[28]

The Structure and Mechanism of the SmI_2-HMPA Reagent

The reduction of a simple functional group with a single electron transfer reagent must involve the formation of a radical intermediate. If there are several functional groups in the compound, there is a chance that this radical rearranges or undergoes an intramolecular reaction. Curran has utilised the radical clock technique to investigate the kinetics of reductions in the presence of HMPA.[29] The amount of directly reduced product was observed to increase upon addition of HMPA. They also predicted the presence of an alkylsamarium intermediate, which could either be coupled with an aldehyde or reduced in the presence of an alcohol, directly or through rearrangement, depending on the ratio of the rate constants k_{Sm}/k_C (Scheme 13).

It was not until Hou and Wakatsuki reported on the solid-state structure of $SmI_2(HMPA)_4$ that mechanistic details for the increased reactivity of the SmI_2-HMPA mixture could be rationalised (Figure 4).[30] The square-planar arrangement with four HMPA molecules coordinating to Sm^{II} could be the key for the selectivity of these reactions. The substrates can either approach the metal centre from above or below.

Interestingly, when 10 equivalents of HMPA were added to the SmI_2 solution, purple crystals of $Sm(HMPA)_6I_2$ were formed.[31] It was suggested that the six bulky HMPA molecules, coordinated to the samarium centre, block the approaching substrate, thereby giving rise to a lowering of selectivity through an outer-sphere mechanism. Flowers and co-workers reported, based on linear sweep voltammetric studies,[32] that the oxidation potential of SmI_2 in THF increases from −1.33 V to −2.05 V (vs. $Ag/AgNO_3$ in THF) when four equivalents of HMPA was added. Further addition of HMPA did not affect the oxidation potential. They also determined the standard potentials $E°(SmI_2^+/SmI_2)$ and $E°(SmI_2^+$-HMPA/SmI_2-HMPA) in THF to be -0.98 ± 0.04 and -1.75 ± 0.06 V vs. SCE, respectively.[33] Accordingly, the change in reducing power for SmI_2 upon

 © 2004 Wiley-VCH Verlag GmbH & Co. KGaA, Weinheim

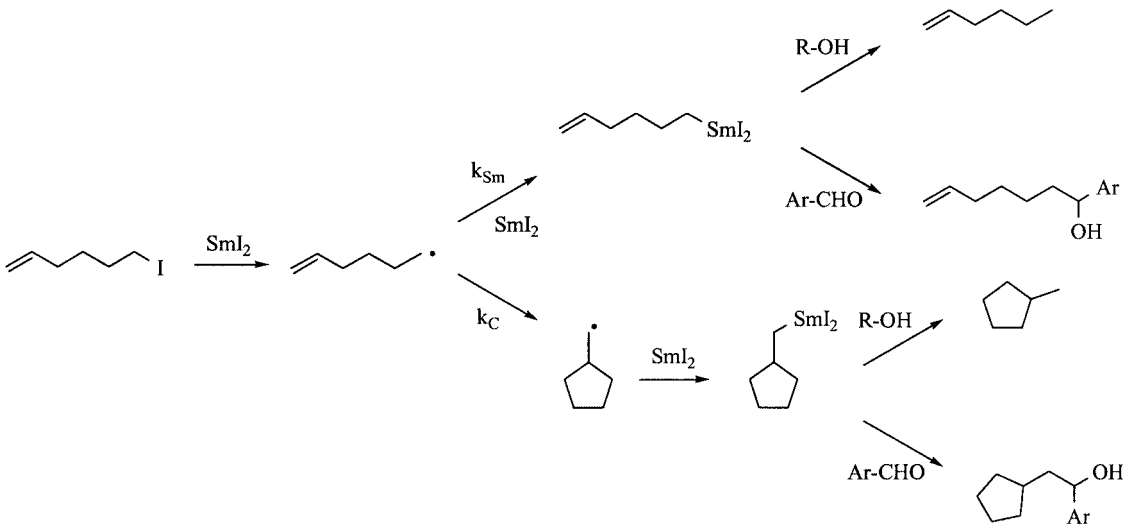

Scheme 13. Suggested pathways of the alkylsamarium intermediate

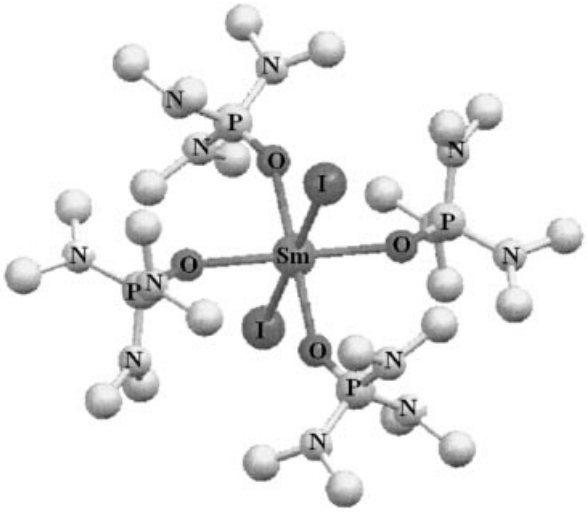

Figure 4. Ball-and-stick representation of the solid-state structure of $SmI_2(HMPA)_4$; hydrogen atoms have been omitted

addition of HMPA was 0.8 V (corresponding to a decrease in free energy of 18 kcal mol^{-1}). Skrydstrup and co-workers also determined the standard potential $E°$ of SmI_2^+/SmI_2 by cyclic voltammetry, which was -1.41 ± 0.08 V vs. Fe^+/Fe.[34]

Further work on the SmI_2-HMPA reagent proved, by vapour pressure osmometry (VPO), that SmI_2 is a monomer in HMPA-THF.[35] Based on UV/Vis studies it was also concluded that there are four HMPA molecules coordinated to SmI_2 in solution. Moreover, the strength of the bonds between Sm and O in SmI_2-HMPA was investigated by detailed VPO analysis. It was concluded that the fourth HMPA molecule is not very tightly bonded, indicating that some reduction may occur through an inner-sphere electron transfer after dissociation of one HMPA molecule (Scheme 14).

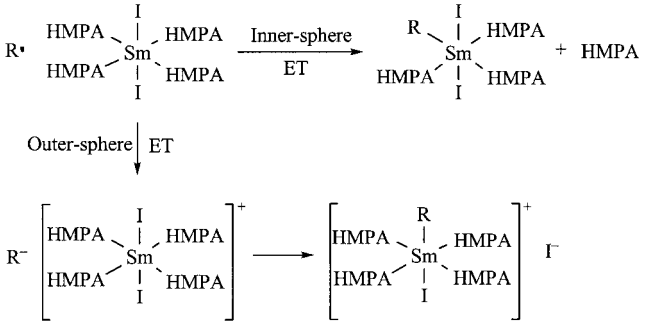

Scheme 14. Inner- and outer-sphere mechanistic pathways

Addition of HMPA to SmI_2 in THF was reported by Daasbjerg and co-workers to result in a strong increase in conductivity, which strongly indicates that HMPA induces ionic cluster formation.[36] In addition, cyclic voltammetry, conductivity measurements, UV spectroscopy and kinetic measurements were performed. The equilibria shown in Equation (1) and Equation (2) are suggested.

$$Sm(THF)_5I_2 + 4\ HMPA \rightleftharpoons [Sm(HMPA)_4(THF)_2]^{2+}\ 2I^- + 3\ THF \quad (1)$$

$$[Sm(HMPA)_4(THF)_2]^{2+}\ 2I^- + 2\ HMPA \rightleftharpoons [Sm(HMPA)_6]^{2+}\ 2I^- + 2\ THF \quad (2)$$

With four equivalents of HMPA, almost all Sm^{2+} exists in the complex $[Sm(HMPA)_4(THF)_2]^{2+}2I^-$, while approximately 10 equivalents of HMPA are necessary to drive the equilibrium towards $[Sm(HMPA)_6]^{2+}2I^-$. The redox couple

 © 2004 Wiley-VCH Verlag GmbH & Co. KGaA, Weinheim

$[Sm(HMPA)_4(THF)_2]^{3+}2I^-/[Sm(HMPA)_4(THF)_2]^{2+}2I^-$ was determined to be -1.79 ± 0.08 V vs. SCE (or 0.9 V larger than that of Sm^{3+}/Sm^{2+} in THF). The degree of outer-sphere character of the reduction of alkyl halides is smallest for chlorides and increases with increasing atomic number (Cl < Br < I). Altogether, the rate of reduction was observed to increase by a factor of up to 15 000 with four equivalents of HMPA per SmI_2 in THF.

The knowledge of Sm^{II}-HMPA complexes was expanded with additional kinetic and mechanistic studies by Flowers and co-workers.[37] The reduction of a series of halides and ketones were investigated again, and it was suggested that the halides are reduced by $[Sm(HMPA)_4(THF)_2]I_2$ through an outer-sphere electron transfer, while the ketones are reduced by $[Sm(HMPA)_4(THF)_2]I_2$ through an inner-sphere electron transfer. The activation parameters for ketone reductions were almost identical using either $[Sm(HMPA)_4(THF)_2]I_2$ or $[Sm(HMPA)_6]I_2$, indicating that the reduction proceeds via the same or a similar transition state regardless of the amount of HMPA.

Other Co-Solvents

The addition of HMPA to SmI_2 has been found to give a very reactive, yet selective, reducing agent. However, its toxicity has encouraged several research groups to search for viable nontoxic co-solvents or additives as replacements for HMPA. Hasegawa and Curran reported that DMPU (1,3-dimethyl-3,4,5,6-tetrahydro-2(1*H*)-pyrimidinone) could be used as an alternative to HMPA (Figure 5).[20] However, in order to obtain similar results they had to use acetonitrile as solvent instead of THF, as the effect of DMPU was too small. Later, Flowers and co-workers studied the reducing power of SmI_2 in THF in the presence of various additives, for example, trimethyl phosphate (TMP), pentamethylphosphoramidate (PMP) and DMPU.[38] It was necessary to use a large excess (30 equiv.) of DMPU to attain the maximum increase of 0.9 V in the oxidation potential. It was also found that the reduction potential for SmI_2-DMPU in acetonitrile was between that of SmI_2 in THF and that of SmI_2-HMPA in THF.[39] Cabri and co-workers reported promising results using nitrogen additives [Et_3N, 1,8-diazabicyclo[5.4.0]undec-7-ene (DBU) or 1,1,3,3-tetramethylguanidine (TMG)] in a SmI_2-mediated cyclisation reaction.[40]

Addition of Metal Salts and Other Counterions

Beside the extensive use of co-solvents and various proton donors, a few reports also describe the addition of metal salts and the use of different counterions. However, these methods often provide coupling in the absence of a proton source.

Flowers and co-workers reported on the addition of LiBr and LiCl to SmI_2. A large rate enhancement was observed in the pinacol coupling of cyclohexanone when adding LiBr or LiCl. Undried salts resulted in reduction of the ketone

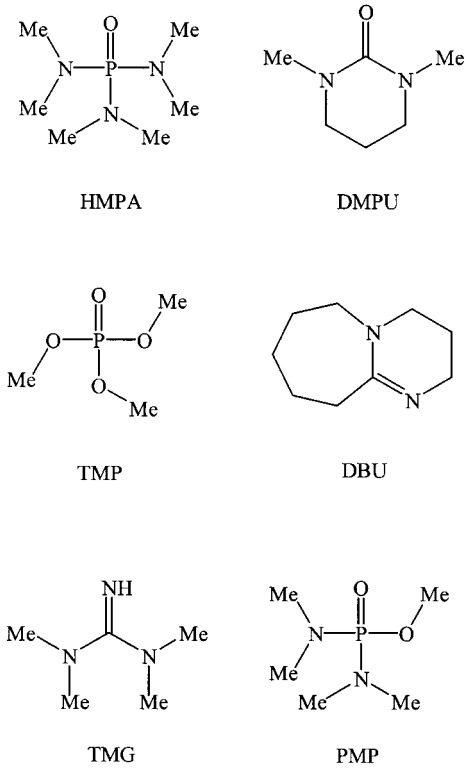

Figure 5. Various co-solvents

to the corresponding alcohol.[41] An extended study of the SmI_2/LiBr mixture showed that the redox potential had increased to -2.07 V vs. $Ag/AgNO_3$ (relative to SmI_2 with a redox potential of -1.58 V).[42] This suggests that $SmBr_2$ and LiI are formed, since $SmBr_2$ is known to be a stronger reductant than SmI_2. Addition of HMPA to the mixture of SmI_2 and LiBr made led to a more powerful mixture with a redox potential of -2.63 V vs. $Ag/AgNO_3$ and, as expected, a significant rate enhancement was observed in the reduction of various functional groups. Samarium(II) bromide is also readily prepared from Sm metal and tetrabromoethane, as recently reported by Namy and co-workers.[43] They used the black suspension of $SmBr_2$ in THF in combination with mischmetal in various pinacol couplings of ketones.

Another fascinating counterion for Sm^{II} is the silylamide. Samarium(II) disilylamide [$Sm(HMDS)_2$] has been prepared from sodium hexamethyldisilazane (Na-HMDS) and SmI_2 (Scheme 15).[44]

The samarium disilylamide has a redox potential of -2.1 V vs. $Ag/AgNO_3$, and is thus a stronger alternative to SmI_2. In addition, the $Sm(HMDS)_2$ provides a somewhat higher rate of reaction than $[Sm(HMPA)_6]I_2$, is less carcinogenic and has better solubility properties than SmI_2, especially in solvents other than THF.[45] However, this reagent has so far not seen any widespread use. The solid-state structure of $Sm(HMDS)_2$ has the shape of a distorted tetrahedron (Figure 6).[44]

Addition of catalytic amounts (1%) of, for example, $ZrCl_4$, VCl_3 and NiI_2 to SmI_2 have been reported to improve the reaction rates to the extent that HMPA can be

 © 2004 Wiley-VCH Verlag GmbH & Co. KGaA, Weinheim

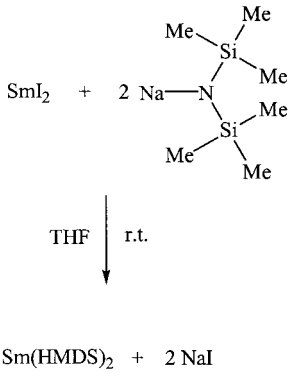

Scheme 15. Preparation of $Sm(HMDS)_2$ from SmI_2 and Na-HMDS in THF

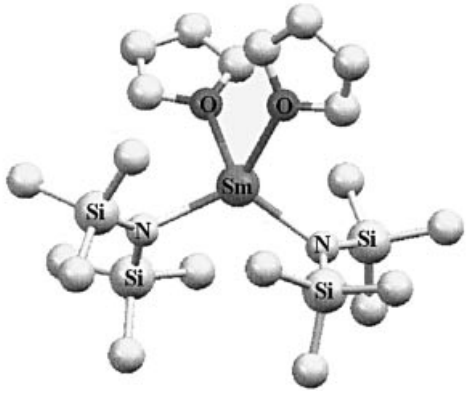

Figure 6. Ball-and-stick representation of the solid-state structure of $Sm(HMDS)_2$; hydrogen atoms have been omitted

avoided in several reactions.[46] Especially, reduction of epoxides to alkenes is considerably accelerated with NiI_2 (the reaction time is 20 minutes, while the uncatalysed reaction requires 12 h). Furthermore, reduction of dodecyl phenyl sulfone to dodecane occurs in good yield after 2 h at reflux. Several couplings and reductions are completed in less than 30 minutes. In addition, hetero couplings between ketones and imines are obtained in high yields by the SmI_2/NiI_2 mixture within five minutes.[47] However, the details regarding the high reactivity of this catalytic system is not yet available preventing full utilisation of this interesting additive.

SmI_2/H_2O/Amine-Mediated Reductions

With the aim of finding a nontoxic replacement for HMPA in SmI_2-mediated reductions, a number of ligands were screened in a simple reduction of a ketone, in combination with methanol or water as proton source. The rate of reduction was not affected by mono or polyethers. However, addition of triethylamine and water had a dramatic effect on the reduction rate.[48] Other amines (e.g. TMEDA and PMDTA) were employed in the reduction and showed similar results. With one or two equivalents of amine, there is a very fast initial reduction, but the reaction stops with a low chemical yield. This reaction requires water as a proton source, while methanol can be used, it is considerably less powerful. Incremental addition of amine and water proved that the reduction of ketones requires two equivalents of SmI_2, four equivalents of amine and six equivalents of water in order to obtain a quantitative yield of the alcohol. The product in the reaction is often very simple to purify since all water, amine, samarium and iodide precipitates as $Sm(OH)_3$ and $R_3N{\cdot}HI$. The by-products can be removed by filtration, which leaves the THF solution of the reduced alcohol. The balanced reduction reaction is given in Equation (3).

$$R_2C{=}O + 2\,SmI_2 + 6\,H_2O + 4\,R_3N \rightleftharpoons R_2CHOH + 2\,Sm(OH)_3 + 4\,R_3N{\cdot}HI \quad (3)$$

The combination of SmI_2, amine and water gives significantly increased rates of reduction relative to the commonly used SmI_2-HMPA mixtures. The rates of reduction of ketones using the combination of water and amine is more than 100 000 times higher than those without proton sources (Scheme 16).[48] Recently, we showed that this instantaneous and quantitative reduction of ketones also constitutes a simple and accurate quantitative determination of [SmI_2], [$SmBr_2$] and [YbI_2].[7f]

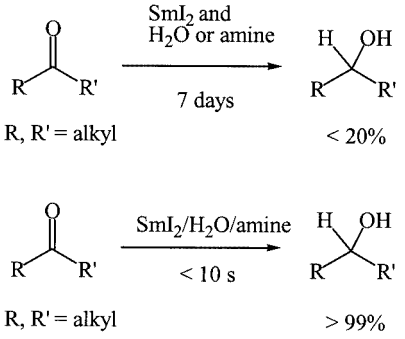

Scheme 16. The rate of reduction of ketones mediated by SmI_2/H_2O/amine is more than 100 000 times faster than with SmI_2 and H_2O or amine

During our continuing study on the reactivity of the SmI_2/H_2O/amine mixtures, we observed that not only ketones but also imines and α,β-unsaturated esters were reduced instantaneously, i.e. reactions were complete in less than 10 seconds.[14] The SmI_2/H_2O/amine mixture is particularly useful for the reductive imino-pinacol coupling of hindered imines and iminium perchlorates, since these are difficult to couple by other methods.[49]

UV/Vis studies have revealed that water is a very good ligand for samarium(II), i.e. it readily replaces THF. The amine Et_3N, however, does not compete with the bulk THF for coordination to samarium. Unfortunately, the reduction

 © 2004 Wiley-VCH Verlag GmbH & Co. KGaA, Weinheim

of ketones with SmI_2/H_2O/amine is too fast for kinetic investigations. Phosphor ligands, on the other hand, also form hydrohalide salts. We found that the reductions of ketones indeed are accelerated using a phosphorus ligand, i.e. $Me_2PCH_2CH_2PMe_2$. Since the rate of reduction using this ligand was much lower, we could determine that there is a kinetic isotope effect, $k^{H2O}/k^{D2O} = 4.5$, indicating a rate determining hydrogen-transfer in the reduction of ketones. The driving force for the reaction has been suggested to be the precipitation of the by-products.[14]

When conjugated double and triple bonds were found to be rapidly reduced to simple alkenes or alkanes, it was concluded that the SmI_2/H_2O/amine mixture is a very powerful reductant (Scheme 17).[50]

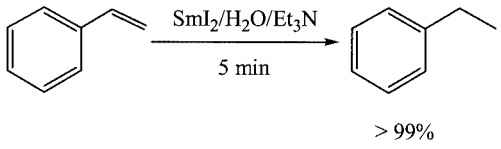

Scheme 17. Reduction of conjugated olefins

The reagent mixture SmI_2/H_2O/amine is also superior for the reduction of halides relative to various other additives (Scheme 18). The reduction of bromides, which takes hours with SmI_2-HMPA, proceeds in minutes with SmI_2/H_2O/amine. Alkyl and aryl iodides are reduced in less than one minute with SmI_2/H_2O/amine.[51]

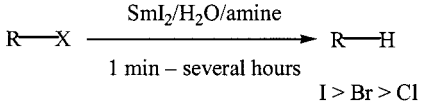

Scheme 18. Reduction of alkyl and aryl halides mediated by SmI_2/H_2O/amine

Kinetic studies have proven that there is a first-order dependence on amine, indicating that the amine is part of the rate-limiting step of the reduction. There is no observed kinetic isotope effect on addition of water. Electrochemical investigations were also carried out on the SmI_2/H_2O/amine mixture. The addition of only amine had no effect on the oxidation potential. Addition of both water and amine to a THF solution of SmI_2 resulted in an irreversible oxidation, and the redox potential could not be determined. The oxidized Sm^{3+} precipitates rapidly from the solution, preventing the measurement of the redox potential of the Sm^{2+}/Sm^{3+} couple.[51]

Recently, we discovered that SmI_2/H_2O/amine mixtures also mediate deallylation reactions (Scheme 19).[52]

This novel deprotection reaction was employed in the cleavage of various allyl ether-protected carbohydrates. The high yields observed with this method makes it particularly useful for the simultaneous deprotection of several allyl groups. There is an unusual chemoselectivity for deprotection. The allyl group on the anomeric carbon does not undergo any deprotection when SmI_2/H_2O/amine is used (Scheme 20), while the other allyl groups are rapidly deprotected.

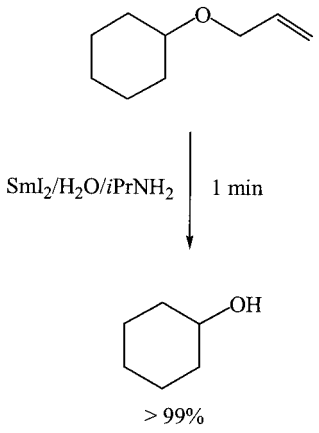

Scheme 19. Allyl ether cleavage

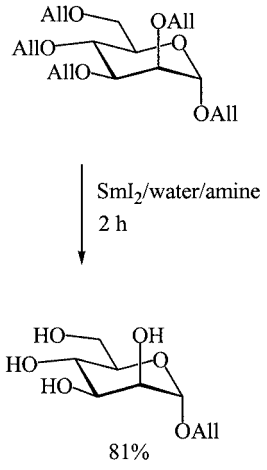

Scheme 20. Selective deallylation of allylmannoside with SmI_2/water/amine

The use of SmI_2/H_2O/amine is particularly advantageous for reductions, since it does not react violently with moisture or oxygen, in strong contrast to most other strong reducing agents, for example alkali metals, hydrogen gas or different hydrides.

Photoinduced Reduction System

The very reactive $SmI_2/h\nu$ system developed by Ogawa and co-workers deserves to be mentioned in this review even though it is not strictly an additive. Ogawa and coworkers discovered in 1997 that alkyl halides, and in particular chlorides that are generally difficult to reduce with SmI_2 (even with SmI_2-HMPA), are efficiently reduced by SmI_2 in THF upon irradiation with visible light ($700 > h\nu > 300$ nm).[53] Irradiation with light of higher or lower wavelengths has no effect on the reactions. Interestingly, the optimum wavelength is similar to the absorption maxima for SmI_2 in THF at 565 and 617 nm, respectively, indicating that SmI_2 is activated by light irradiation.

Additionally, it was found that $SmI_2/h\nu$ also gives excellent results for the cleavage of C−Se, C−Te and C−OTs

 © 2004 Wiley-VCH Verlag GmbH & Co. KGaA, Weinheim

bonds (Scheme 21).[54] Organic selenides cannot be reduced by SmI_2-HMPA.

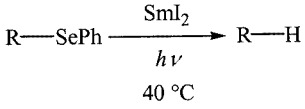

Scheme 21. Photoinduced reduction of selenides by SmI_2 in the presence of visible light

Conclusion

Herein we have summarised that the reactivity of SmI_2 can be significantly adjusted using various additives and or co-solvents. The addition of various additives to SmI_2 clearly gives the working chemist tools to modify and control the reducing properties, which is important for selective reduction of one particular group of several similar groups within the same substrate. SmI_2 is beginning to be appreciated as a mild and selective reducing agent in synthetic organic chemistry, but the reaction mechanisms through which the addition of various additives and co-solvents act are far from understood. The current mechanistic knowledge is mainly based on the initial suggestion made by Kagan some 25 years ago, and since then only small achievements have been reported. New applications for SmI_2 and for other lanthanide(II) reagents will most likely emerge from detailed structural and mechanistic studies of SmI_2 and other lanthanide(II) reagents. SmI_2 is attractive as a general reducing agent, since it is considered nontoxic and its handling procedures are nonhazardous, in contrast to most other reducing agents.

[1] [1a] J. L. Namy, P. Girard, H. Kagan, *Nouv. J. Chim.* **1977**, *1*, 5−7. [1b] P. Girard, J. L. Namy, H. B. Kagan, *J. Am. Chem. Soc.* **1980**, *102*, 2693−2698. [1c] H. B. Kagan, J. L. Namy, P. Girard, *Tetrahedron Suppl.* **1981**, *9*, 175−180.

[2] [2a] S. Fukuzawa, H. Matsuzawa, S. Yoshimitsu, *J. Org. Chem.* **2000**, *65*, 1702−1706. [2b] M. Sono, Y. Nakashiba, K. Nakashima, M. Tori, *J. Org. Chem.* **2000**, *65*, 3099−3106. [2c] G. A. Molander, D. J. St. Jean Jr., *J. Org. Chem.* **2002**, *67*, 3861−3865. [2d] T. K. Hutton, K. Muir, D. J. Procter, *Organic Lett.* **2002**, *4*, 2345−2347. [2e] G. A. Molander, G. A. Brown, I. S. de Gracia, *J. Org. Chem.* **2002**, *67*, 3459−3463.

[3] [3a] R. Nomura, T. Endo, *Chem. Eur. J.* **1998**, *4*, 1605−1610. [3b] G. A. Molander, K. M. George, L. G. Monovich, *J. Org. Chem.* **2003**, *68*, 9533−9540. [3c] M. Sono, A. Hashimoto, K. Nakashima, M. Tori, *Tetrahedron Lett.* **2000**, *41*, 5115−5118. [3d] H. Miyaoka, A. Nishiyama, H. Nagaoka, Y. Yamada, *Synlett* **2003**, *5*, 717−719. [3e] T. L. Fevig, R. L. Elliott, D. P. Curran, *J. Am. Chem. Soc.* **1988**, *110*, 5064−5067.

[4] [4a] G. A. Molander, *Chem. Rev.* **1992**, *92*, 29−68. [4b] G. A. Molander, in Organic Reactions, vol. 46, *Reductions with Samarium(II) Iodide* (L. A. Paquette et al., Eds.), John Wiley & Sons, **1994**, pp. 211−367. [4c]G. A. Molander, C. R. Harris, *Chem. Rev.* **1996**, *96*, 307−338. [4d] A. Krief, A.-M. Laval, *Chem. Rev.* **1999**, *99*, 745−777. [4e] G. A. Molander, *Radicals in Organic Synthesis* (P. Renaud, M. P. Sibi, Eds.), Wiley-VCH: Weinheim, **2001**, vol. 1, pp. 153−182. [4f]P. G. Steel, *J. Chem. Soc., Perkin Trans. 1* **2001**, *21*, 2727−2751. [4g] H. B. Kagan, *Tetrahedron* **2003**, *59*, 10351−10372.

[5] M.-I. Lannou, F. Hélion, J.-L. Namy, *Tetrahedron* **2003**, *59*, 10551−10565.

[6] [6a] G. Jantsch, N. Skalla, *Z. Anorg. Chem.* **1930**, *193*, 391−405. [6b] G. Jantsch, N. Skalla, L. Jawure, *Z. Anorg. Chem.* **1931**, *201*, 207−220.

[7] [7a] J. L. Namy, P. Girard, H. B. Kagan, *Nouv. J. Chem.* **1981**, *5*, 479−484. [7b] G. A. Molander, C. Kenny, *J. Org. Chem.* **1991**, *56*, 1439−1445. [7c] T. Imamoto, M. Ono, *Chem. Lett.* **1987**, *3*, 501−502. [7d] N. Akane, Y. Kanagawa, Y. Nishiyama, Y. Ishii, *Chem. Lett.* **1992**, *12*, 2431−2434. [7e] J. M. Concellon, H. Rodriguez-Solla, E. Bardales, M. Huerta, *Eur. J. Org. Chem.* **2003**, *9*, 1775−1778. [7f] A. Dahlén, G. Hilmersson, *Eur. J. Inorg. Chem.* **2004**, 3020−3024.

[8] [8a] B. Hamann, J. L. Namy, H. B. Kagan, *Tetrahedron* **1996**, *52*, 14225−14234. [8b] J. L. Namy, M. Colomb, H. B. Kagan, *Tetrahedron Lett.* **1994**, *35*, 1723−1726. [8c] W. J. Evans, T. S. Gummersheimer, J. W. Ziller, *J. Am. Chem. Soc.* **1995**, *117*, 8999−9002. [8d] J. M. Concellón, P. L. Bernad, M. Huerta, S. García-Granda, M. R. Díaz, *Chem. Eur. J.* **2003**, *9*, 5343−5347.

[9] J. Inanaga, S. Sakai, Y. Handa, M. Yamaguchi, Y. Yokoyama, *Chem. Lett.* **1991**, *12*, 2117−2118.

[10] A. Yoshida, K. Mikami, *Synlett* **1997**, *12*, 1375−1376.

[11] [11a] G. E. Keck, C. A. Wager, T. Sell, T. T. Wager, *J. Org. Chem.* **1999**, *64*, 2172−2173. [11b] G. E. Keck, C. A. Wager, *Org. Lett.* **2000**, *2*, 2307−2309. [11c] G. E. Keck, A. P. Truong, *Org. Lett.* **2000**, *4*, 3131−3134.

[12] [12a] A. L. Rheingold, A. Sen, V. Chebolu, *Inorg. Chem.* **1987**, *26*, 1821−1823. [12b] M. Håkansson, M. Vestergren, B. Gustafsson, G. Hilmersson, *Angew. Chem. Int. Ed.* **1999**, *38*, 2199−2201. [12c] W. J. Evans, R. N. R. Broomhall-Dillard, J. W. Ziller, *Polyhedron* **1998**, *17*, 3361−3370.

[13] A. Dahlén, G. Hilmersson, *Tetrahedron Lett.* **2001**, *42*, 5565−5569.

[14] A. Dahlén, G. Hilmersson, *Chem. Eur. J.* **2003**, *9*, 1123−1128.

[15] P. R. Chopade, E. Prasad, R. A. Flowers II, *J. Am. Chem. Soc.* **2004**, *126*, 44−45.

[16] A. Dahlén, G. Hilmersson, B. W. Knettle, R. A. Flowers II, *J. Org. Chem.* **2003**, *68*, 4870−4875.

[17] Y. Nakamura, S. Takeuchi, Y. Ohgo, M. Yamaoka, A. Yoshida, K. Mikami, *Tetrahedron* **1999**, *55*, 4595−4620.

[18] Y. Kamochi, T. Kudo, *Chem. Lett.* **1993**, *9*, 1495−1498.

[19] [19a] Y. Kamochi, T. Kudo, *Tetrahedron Lett.* **1994**, *35*, 4169−4172. [19b] Y. Kamochi, T. Kudo, *Tetrahedron* **1992**, *48*, 4301−4312. [19c] Y. Kamochi, T. Kudo, *Tetrahedron Lett.* **1991**, *32*, 3511−3514.

[20] E. Hasegawa, D. P. Curran, *J. Org. Chem.* **1993**, *58*, 5008−5010.

[21] A. K. Singh, R. K. Bakshi, E. J. Corey, *J. Am. Chem. Soc.* **1987**, *109*, 6187−6189.

[22] J. M. Concellon, H. Rodríguez-Solla, *Chem. Eur. J.* **2002**, *8*, 4493−4497.

[23] A. Studer, D. P. Curran, *Synlett* **1996**, *3*, 255−257.

[24] J. Inanaga, M. Ishikawa, M. Yamaguchi, *Chem. Lett.* **1987**, *7*, 1485−1486.

[25] J. Inanaga, Y. Handa, T. Tabuchi, K. Otsubo, M. Yamaguchi, T. Hanamoto, *Tetrahedron Lett.* **1991**, *32*, 6557−6558.

[26] A. Cabrera, H. Alper, *Tetrahedron Lett.* **1992**, *33*, 5007−5008.

[27] H. Künzer, M. Stahnke, G. Sauer, R. Wiechert, *Tetrahedron Lett.* **1991**, *32*, 1949−1952.

[28] M.-R. S. Fuh, T.-Y. Lin, S.-C. Chang, *Talanta* **1998**, *46*, 861−866.

[29] E. Hasegawa, D. P. Curran, *Tetrahedron Lett.* **1993**, *34*, 1717−1720.

[30] Z. Hou, Y. Wakatsuki, *J. Chem. Soc., Chem. Commun.* **1994**, *10*, 1205−1206.

[31] Z. Hou, Y. Zang, Y. Wakatsuki, *Bull. Chem. Soc. Jpn.* **1997**, *70*, 149−153.

[32] M. Shabangi, R. A. Flowers II, *Tetrahedron Lett.* **1997**, *38*, 1137−1140.

[33] M. Shabangi, M. L. Kuhlman, R. A. Flowers II, *Organic Lett.* **1999**, *1*, 2133−2135.

 © 2004 Wiley-VCH Verlag GmbH & Co. KGaA, Weinheim

[34] R. J. Enemaerke, K. Daasbjerg, T. Skrydstrup, *Chem. Commun.* **1999**, *4*, 343−344.
[35] J. B. Shotwell, J. M. Sealy, R. A. Flowers II, *J. Org. Chem.* **1999**, *64*, 5251−5255.
[36] R. J. Enemarke, T. Hertz, T. Skrydstrup, K. Daasbjerg, *Chem. Eur. J.* **2000**, *6*, 3747−3754.
[37] E. Prasad, R. A. Flowers II, *J. Am. Chem. Soc.* **2002**, *124*, 6895−6899.
[38] M. Shabangi, J. M. Sealy, J. R. Fuchs, R. A. Flowers II, *Tetrahedron Lett.* **1998**, *39*, 4429−4432.
[39] M. L. Kuhlman, R. A. Flowers II, *Tetrahedron Lett.* **2000**, *41*, 8049−8052.
[40] W. Cabri, I. Candiani, M. Colombo, L. Franzoi, A. Bedeschi, *Tetrahedron Lett.* **1995**, *36*, 949−952.
[41] J. R. Fuchs, M. L. Mitchell, M. Shabangi, R. A. Flowers II, *Tetrahedron Lett.* **1997**, *38*, 8157−8158.
[42] B. W. Knettle, R. A. Flowers II, *Organic Lett.* **2001**, *3*, 2321−2324.
[43] F. Helion, M.-I. Lannou, J.-L. Namy, *Tetrahedron Lett.* **2003**, *44*, 5507−5510.
[44] W. J. Evans, D. K. Drummond, H. Zhang, J. L. Atwood, *Inorg. Chem.* **1988**, *27*, 575−579.
[45] E. Prasad, B. W. Knettle, R. A. Flowers II, *J. Am. Chem. Soc.* **2002**, *124*, 14663−14667.
[46] F. Machrouhi, B. Hamann, J.-L. Namy, H. B. Kagan, *Synlett* **1996**, *7*, 633−634.
[47] F. Machrouhi, J.-L. Namy, *Tetrahedron Lett.* **1999**, *40*, 1315−1318.
[48] A. Dahlén, G. Hilmersson, *Tetrahedron Lett.* **2002**, *43*, 7197−7200.
[49] M. Kim, B. W. Knettle, A. Dahlén, G. Hilmersson, R. A. Flowers II, *Tetrahedron* **2003**, *59*, 10397−10402.
[50] A. Dahlén, G. Hilmersson, *Tetrahedron Lett.* **2003**, *44*, 2661−2664.
[51] A. Dahlén, G. Hilmersson, B. W. Knettle, R. A. Flowers II, *J. Org. Chem.* **2003**, *68*, 4870−4875.
[52] A. Dahlén, A. Sundgren, M. Lahmann, S. Oscarson, G. Hilmersson, *Organic Lett.* **2003**, *5*, 4085−4088.
[53] A. Ogawa, Y. Sumino, T. Nanke, S. Ohya, N. Sonoda, T. Hirao, *J. Am. Chem. Soc.* **1997**, *119*, 2745−2746.
[54] A. Ogawa, S. Ohya, M. Doi, Y. Sumino, N. Sonoda, T. Hirao, *Tetrahedron Lett.* **1998**, *39*, 6341−6342.

Received May 26, 2004

 © 2004 Wiley-VCH Verlag GmbH & Co. KGaA, Weinheim

Self-Assembly of Stereoselective, Mononuclear, Triple-Stranded Helicate Complexes ML_3 with Trivalent Scandium and Lanthanide Metal Ions – Quantitative Transmetallation of the Lanthanide(III) Ion by Sodium(I) Ions

Magdalena Capó,*[a] José Gonzalez,[a] and Harry Adams[b]

Keywords: Helical structures / Lanthanides / Self-assembly / Stereoselective / Transmetallation

Mononuclear triple-stranded helicate complexes ML_3 (M = Sc^{3+}, La^{3+}, Sm^{3+}, Yb^{3+}) were self-assembled and structurally characterized by NMR spectroscopy and high-resolution mass spectrometry. The solid-state structure of the ytterbium complex was determined by X-ray crystallography. The core lanthanide metal ion was replaced quantitatively by three sodium ions. Homo- and heterotrinuclear complexes containing the alkali metal ions Li^+ and Na^+ were obtained from the mononuclear lanthanide complexes.

(© Wiley-VCH Verlag GmbH & Co. KGaA, 69451 Weinheim, Germany, 2004)

Introduction

Helicate derivatives by self-assembly of multidentate organic ligands and metal ions have been a subject of current interest during the last two decades.[1] A tetradentate chiral ligand unit **1**[2] has been designed that self-assembles with lanthanide ions of different sizes to yield mononuclear triple-stranded helicates. The chiral ligand **1** in solution is able to form trinuclear helicates by self-assembly in the presence of sodium or lithium triflates[3] and mononuclear helicates in the presence of trivalent scandium or lanthanide triflates.

Here we report the formation of four stereoselective triple helices obtained quantitatively from the enantiomerically pure ligand (*S*)-**1**[4] and $M(OTf)_3$ (Scheme 1). The stoichiometry of the complexes has been determined by NMR titration experiments and mass spectrometry.

Results and Discussion

Treatment of $Sc(OTf)_3$ in acetonitrile with racemic or enantiopure (*S*)-**1** in the ratio 1:3 led to the formation of a single highly symmetrical metal complex, as demonstrated by the ^1H NMR spectrum, which contains a single set of resonances[5] (Figure 1).

A ^{45}Sc NMR spectrum was recorded to study the interaction between the ligand and the scandium ion. After

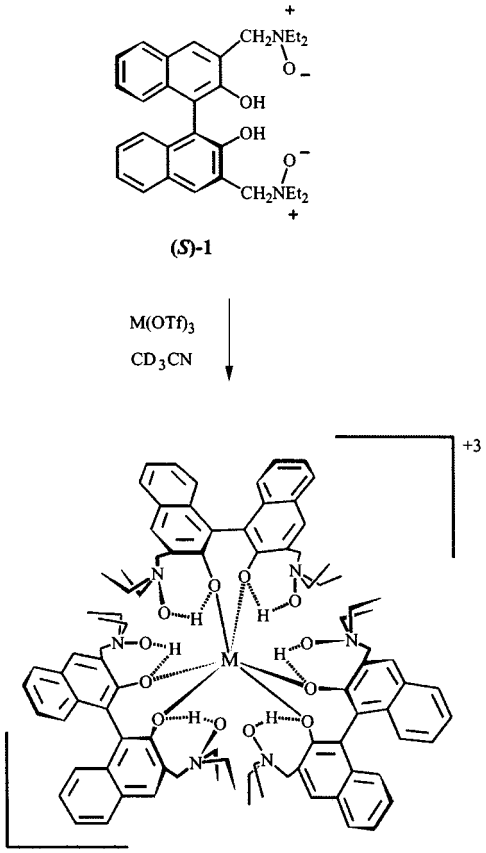

2 M = Sc^{+3}
3 M = La^{+3}
4 M = Sm^{+3}
5 M = Yb^{+3}

Scheme 1

[a] Departament de Química, Universitat de les Illes Balears, 07071 Palma de Mallorca, Spain
Fax: (internat.) + 34-97-117-3426
E-mail: magdalena.capo@uib.es
[b] Department of Chemistry, University of Sheffield, Sheffield, S3 7HT, UK

Supporting information for this article is available on the WWW under http://www.eurjic.org or from the author.

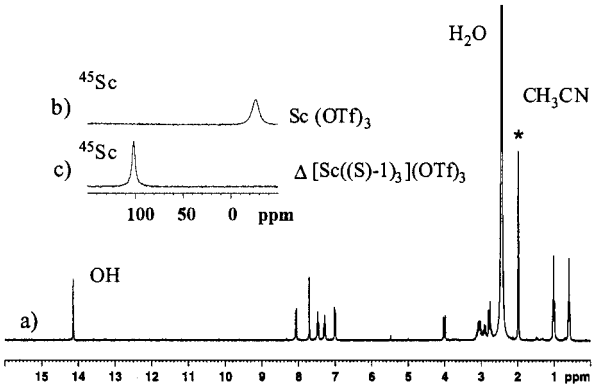

Figure 1. a) The ^{1}H NMR spectra of Δ-[Sc{(*S*)-**1**}$_3$](OTf)$_3$ (**2**) in CD_3CN solution; b) ^{45}Sc NMR spectra of scandium triflate; c) ^{45}Sc NMR spectra of complex Δ-[Sc{(*S*)-**1**}$_3$](OTf)$_3$ (**2**)

addition of 3 equiv. of the ligand (*S*)-**1** to a solution of $Sc(OTf)_3$ in acetonitrile, the ^{45}Sc NMR resonance of the bound cation undergoes a downfield shift to δ = 106 ppm. The presence of a sharp singlet evidences a magnetically equivalent arrangement around the scandium cation (Figure 1c). The ^{45}Sc NMR spectrum of free $Sc(OTf)_3$ shows a broad singlet at δ = −30 ppm. The diastereotopic benzilic protons were used as probe for the ^{1}H NMR analysis of the complexes **2**−**5**. The signals of the benzilic protons are largely split into two AB patterns, except for the ytterbium complex **5**, where they appear as a broad doublet at δ = 1.2−1.11 ppm (Figure 2). A characteristic NMR property of a paramagnetic lanthanide ion, such as Yb^{III}, is the large chemical-shift range usually shown by the ligand resonances.[6] These paramagnetically shifted resonances are highly sensitive to slight structural and electronic variations.

The appearance of ^{1}H NMR resonances with a large downfield shift [δ(OH) = 31.53 ppm], and aromatic and benzilic protons with large upfield shifts (δ = 4.53 and 1.2−1.01 ppm, respectively) is consistent with complexation of the ligand (*S*)-**1** by the paramagnetic ytterbium ion (Figure 2).

Due to the fact that the chemical shift in paramagnetic complexes is strongly temperature-dependent, significant changes in the proton resonances can be observed with small temperature variations for complex **5** (Figure 2). A 2D ^{1}H-^{1}H DQF-COSY (ESI) NMR experiment allowed the assignment of all peaks of complex **5**.

Single crystals of the ytterbium complex **5** suitable for an X-ray diffraction study could be obtained.[7] The crystal structure shows **5** to be mononuclear in the solid state[8] (Figure 3a). Each (*S*)-**1** ligand wraps around the metal ion. All the oxygen atoms are distributed in a tubular maner. In the center of the cavity the ytterbium ion is surrounded by six oxygen atoms, with Yb−O distances ranging from 2.208 to 2.248 Å (Figure 3b).

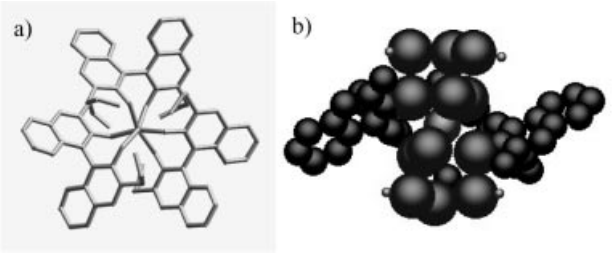

Figure 3. a) Molecular structure of Δ-[Yb{(*S*)-**1**}$_3$] (OTf)$_3$ (**5**) (top view); ethyl chains and triflates are omitted for clarity; b) space-filling representation; selected bond lengths [Å]: Yb(1)−O(1) 2.208, Yb(1)−O(2) 2.212, Yb(1)−O(3) 2.237, Yb(1)−O(4) 2.244, Yb(1)−O(5) 2.250, Yb(1)−O(6) 2.248, Yb(1)−O(7) 4.103, Yb(1)−O(8) 4.180, Yb(1)−O(9) 4.215, Yb(1)−O(10) 4.136, Yb(1)−O(11) 4.240, Yb(1)−O(12) 4.251

The selectivity of the ligand (*S*)-**1** with Ln^{III} ions in acetonitrile was monitored by ^{1}H NMR spectroscopy by adding a solution containing La/Sm/Yb in a 1:1:1 ratio to 3 equiv. of the ligand. The ^{1}H NMR spectrum shows the presence of a single metal complex corresponding to the ytterbium complex **5**.

The characterization of heteronuclear complexes bearing lanthanides is interesting because magnetic superexchange interactions between the bridged metal atoms may exist.[9] Further studies to obtain trinuclear dimetallic complexes $Ln^{III}/2Na^{I}$ or $Ln^{III}/2Li^{I}$ (Scheme 2) were therefore performed. Unfortunately, the addition of 2 equiv. of sodium or lithium triflate to the lanthanide complexes **3**−**5** to synthesize heterotrinuclear complexes failed, probably due to the repulsion between the lanthanide and the alkali ions. However, treatment of complexes LnL_3 with sodium acetate

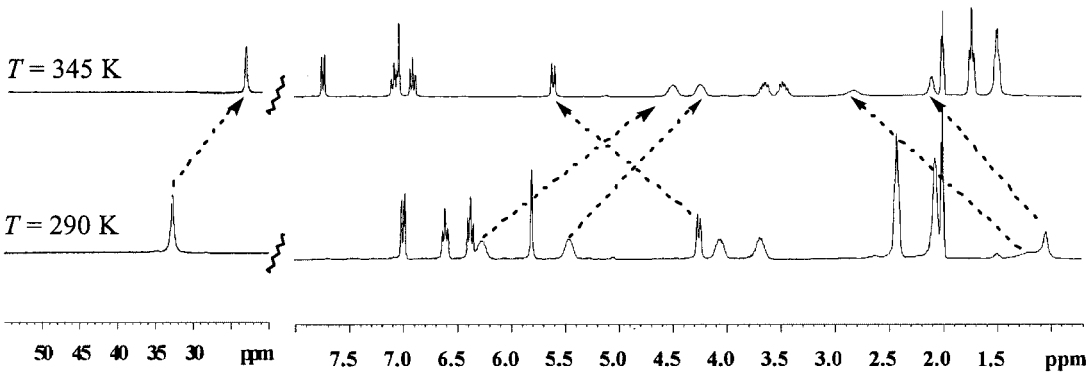

Figure 2. ^{1}H NMR spectra of complex **5**

 © 2004 Wiley-VCH Verlag GmbH & Co. KGaA, Weinheim

resulted in spectral changes, completed by the addition of 3 equiv. of sodium acetate. As a result, the central Ln^{III} ion of the homonuclear complexes **3**−**5** was replaced quantitatively by the alkali metal ion, and ytterbium acetate was isolated by filtration as a white microcrystalline powder. Interestingly, the addition of sodium acetate to complexes **3**−**5** gave identical spectra to the trinuclear helicate **6** obtained from the ligand (*S*)-**1** and 3 equiv. of sodium triflate.[3] Finally, a heterotrinuclear complex **7** was obtained by substitution of the two external sodium ions by addition of 2 equiv. of lithium triflate to complex **6**.

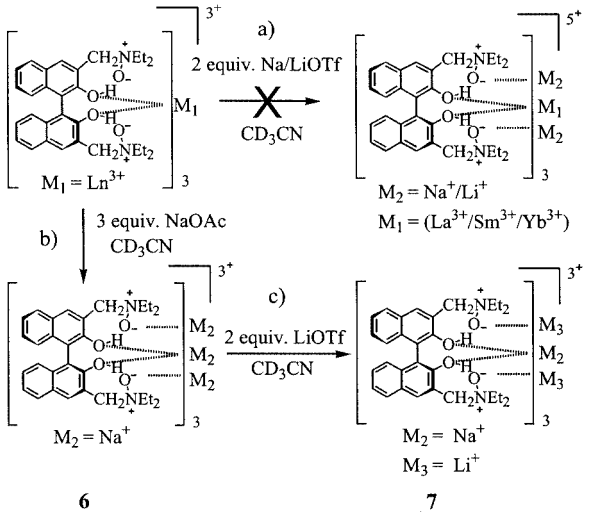

Scheme 2

The exchange process was observed by ^{7}Li NMR spectroscopic studies in CD_3CN (Figure 4) where, if we compare the lithium spectrum of complex **7** with that of complex **8**, we can observe a signal at δ = 1.35 ppm corresponding to the lithium ions placed at the external positions. The selective exchange of the two sodium ions at the apical positions by two lithium ions can be attributed to the fact that the size and shape of the sites are more suitable for the ionic radius and the coordination geometry of this ion. Evidence for this substitution was also observed in a ^{7}Li-^{1}H 2D HOESY NMR spectrum.

The formation of the homo- and heterotrinuclear complexes Δ-[Na_3{(*S*)-**1**}$_3$](OTf)$_3$ (**6**) and Δ-[$LiNa_2${(*S*)-**1**}$_3$](OTf)$_3$ (**7**) was further confirmed by ESI mass spectrometry {ESI-MS: *m*/*z* = 1832.6791 (calcd. for $C_{92}H_{108}F_6N_6Na_3O_{18}S_2$ [M − OTf]$^+$), found 1832.6344; MS (FAB$^+$): *m*/*z* = 1972 [MNa^+], 1956 [MLi^+], 1950 [MH^+], 1800 [M − OTf]}.

In summary, we have presented our efforts to prepare and characterize different stereoselective triple helical lanthanide complexes in solution and the solid state by the choice of a large La^{III}, a medium-sized Sm^{III} and a small Yb^{III} lanthanide ion. The recognition of one specific lanthanide ion (ytterbium) in the presence of others (lanthanum and samarium) is of great interest due to the minimal size differences of these ions and their similar chemical properties.

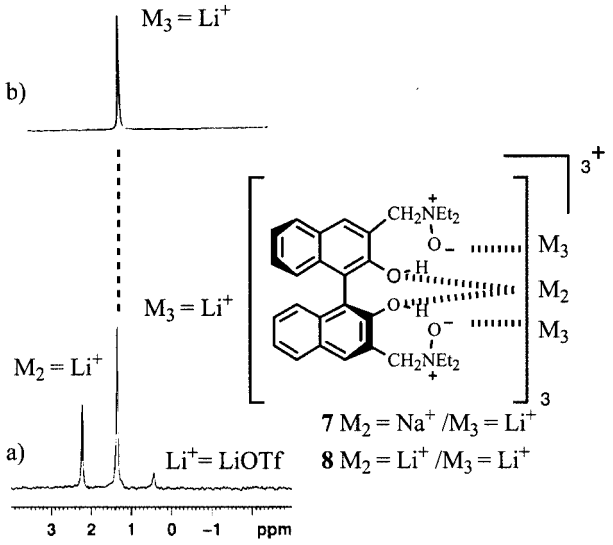

Figure 4. a) ^{7}Li NMR soectrum of complex **8** in CD_3CN solution; b) ^{7}Li NMR of complex **7** where there is only one signal corresponding to the lithium ions at the symmetrical external positions M_3

The homo- and heterotrinuclear complexes containing alkali atoms were obtained from the mononuclear lanthanide complexes. To the best of our knowledge this is the first case where a lanthanide(III) ion is replaced quantitatively by an alkali metal ion.

Experimental Section

General: The 1:3 complexes were prepared by mixing the ligand (*S*)-**1** with stoichiometric amounts of M(OTf)$_3$ in acetonitrile. The complexes were directly isolated in 70−80% yield by removing the solvent.

(*S*)-1: $[\alpha]_{589}^{25}$ = −186 (*c* = 0.010, CH_3CN). ^{1}H NMR (CD_3CN, 300 MHz): δ = 16.40 (br. s, 2 H, OH), 7.90−788 (m, 2 H), 7.28−7.26 (m, 4 H), 7.14−7.12 (m, 2 H), 4.73 (m, 4 H), 3.39 (m, 8 H), 1.4 (t, *J* = 7.2 Hz, 12 H) ppm. ^{13}C NMR (CD_2Cl_2, 75 MHz) 156.5, 136.4, 132.8, 128.7, 127.8, 127.3, 125.3, 122.9, 122.0, 119.6, 69.5, 60.7, 60.3, 9.5, 9.2 ppm. MS (FAB$^+$): *m*/*z* = 489 [MH^+]. HRMS (FAB+): *m*/*z* = 489.2753 (calcd. for $C_{30}H_{37}N_2O_4$), found 489.2741.

Δ-[Sc{(*S*)-1}$_3$](OTf)$_3$ (2): M.p. 256−257 °C. $[\alpha]_{589}^{25}$ = +190.8 (*c* = 0.24, CH_2Cl_2). ^{1}H NMR (CD_3CN): δ = 14.16 (s, 6 H), 8.10 (d, *J* = 8.0 Hz, 6 H), 7.74 (s, 6 H), 7.50 (t, *J* = 7.5 Hz, 6 H), 7.31 (t, *J* = 7.7 Hz, 6 H), 7.03 (d, *J* = 8.4 Hz, 6 H), 4.03 (d, *J* = 13.5 Hz, 6 H), 3.13−2.76 (m, 24 H), 2.81 (d, *J* = 13.5 Hz, 6 H), 1.03 (t, *J* = 7.1 Hz, 18 H), 0.61 (t, *J* = 7.2 Hz, 18 H) ppm. ^{13}C NMR (CD_3CN, 75 MHz): δ = 156.6, 135.9, 134.7, 128.8, 128.3, 127.5, 125.9, 123.7, 121.9, 119.8, 63.5, 60.8, 57.5, 7.4, 7.2 ppm. ^{45}Sc NMR (CD_3CN, 72 MHz): δ = 106 ppm. MS (FAB$^+$): *m*/*z* = 1980 [MNa^+], 1958 [MH^+], 1808 [M − OTf].

Δ-[La{(*S*)-1}$_3$](OTf)$_3$ (3): M.p. 243−244 °C. $[\alpha]_{589}^{25}$ = +79.2 (*c* = 0.24, CH_2Cl_2). ^{1}H NMR (CD_3CN): δ = 14.64 (s, 6 H), 8.17 (d, *J* = 8.0 Hz, 6 H), 7.85 (s, 6 H), 7.52 (t, *J* = 7.4 Hz, 6 H), 7.34 (t, *J* = 7.6 Hz, 6 H), 6.93 (d, *J* = 8.4 Hz, 6 H), 3.92 (d, *J* = 13.7 Hz, 6 H),

 © 2004 Wiley-VCH Verlag GmbH & Co. KGaA, Weinheim

3.14−2.88 (m, 24 H), 2.98 (d, J = 13.7 Hz, 6 H), 1.07 (t, J = 7.1 Hz, 18 H), 0.59 (t, J = 7.2 Hz, 18 H) ppm. ^{13}C NMR (CD_3CN, 75 MHz): δ = 153.8, 135.8, 135.0, 128.7, 127.9, 124.8, 123.7, 121.5, 119.9, 64.0, 60.3, 58.8, 7.0, 6.8 ppm. MS (FAB$^+$): m/z = 2073 [MNa^+], 2051 [MH^+], 1902 [M − OTf].

Δ-[Sm{(*S*)-1}$_3$](OTf)$_3$ (4): M.p. 238−239 °C. $[\alpha]_{589}^{25}$ = +159 (c = 0.024, CD_3CN). ^{1}H NMR (CD_3CN): δ = 18.03 (s, 6 H), 7.86 (d, J = 6.9 Hz, 6 H), 7.38 (t, J = 7.3 Hz, 6 H),7.31(s, 6 H), 7.16 (t, J = 7.2 Hz, 6 H), 6.59 (d, J = 8.4 Hz, 6 H), 3.57 (d, J = 13.7 Hz, 6 H), 3.38−3.16 (m, 24 H), 2.65 (d, J = 13.7 Hz, 6 H), 1.27 (t, J = 6.9 Hz, 18 H), 0.86 (t, J = 6.9 Hz, 18 H) ppm. ^{13}C NMR (CD_3CN, 75 MHz): δ = 155.5, 135.38, 134.36, 128.75, 127.81, 127.04, 124.65, 123.33, 119.75, 117.85, 64.02, 61.00, 58.94, 7.40, 7.28 ppm. ESI-MS: m/z = 1916.4758 [M − OTf].

Δ-[Yb{(*S*)-1}$_3$](OTf)$_3$ (5): M.p. 254−255 °C. $[\alpha]_{589}^{25}$ = +200.8 (c = 0.12, CH_2Cl_2). ^{1}H NMR (CD_3CN): δ = 31.53 (br. s, 6 H), 7.05 (d, J = 8.1 Hz, 6 H), 6.65 (t, J = 7.5 Hz, 6 H), 6.42 (t, J = 7.4 Hz, 6 H), 6.12 (br. s, 6 H), 5.89 (s, 6 H), 5.39 (br. s, 6 H), 4.35 (d, J = 8.4 Hz, 6 H), 4.07−4.01 (m, 6 H), 3.69−3.62 (m, 6 H), 2.36 (s, 18 H), 2.03 (s, 18 H), 1.38 (br. s, 6 H), 1.11 (s, 6 H) ppm. ^{13}C NMR (CD_3CN, 75 MHz): δ = 132.5, 129.8, 127.9, 127.3, 125.9, 125.7, 125.0, 124.0, 123.5, 119.9, 63.3, 61.4, 59.4, 8.8, 8.3 ppm. MS (FAB$^+$): m/z = 2109 [MNa^+], 2087 [MH^+], 1936 [M − OTf]. HRMS (FAB$^+$): m/z = 1936.64543 (calcd. for $C_{92}H_{108}F_6N_6O_{18}S_2Yb$ [M − HOTf + H^+]), found 1936.65769. Pale-yellow single crystals of **5** were obtained by the slow evaporation of the solvent from a CH_3CN solution.

Δ-[Na$_3${(*S*)-1}$_3$](OTf)$_3$ (6): $[\alpha]_{589}^{25}$ = +299 (c = 0.014, CH_3CN). ^{1}H NMR (CD_3CN, 300 MHz): δ = 16.01 (s, 6 H, OH), 8.14 (d, J = 5 Hz, 6 H), 7.68 (s, 6 H), 7.49 (t, J = 7 Hz, 6 H), 7.33 (t, J = 7 Hz, 6 H), 7.03 (d, J = 8.4 Hz, 6 H), 3.86 (d, J = 13.2 Hz, 6 H), 2.94 (m, 24 H), 2.72 (d, J = 13.2 Hz, 6 H), 1.02 (t, J = 6.9 Hz, 18 H), 0.5 (t, J = 6.9 Hz, 18 H) ppm. ^{13}C NMR (CD_3CN, 75 MHz): δ = 154.05, 135.07, 133.64, 128.39, 128.06, 127.20, 124.93, 123.27, 122.25, 118.97, 65.62, 60.91, 58.00, 7.98, 7.21 ppm. ^{23}Na NMR (CD_3CN, 79 MHz): δ = 5.69, −1.06 ppm. ESI-MS: m/z = 1832.6791 (calcd. for $C_{92}H_{108}F_6N_6Na_3O_{18}S_2$ [M − OTf]$^+$); found 1832.6344.

Δ-[Li$_2$Na{(*S*)-1]$_3$}(OTf)$_3$ (7): ^{1}H NMR (CD_3CN, 300 MHz): δ = 15.66 (s, 6 H, OH), 8.08 (d, J = 5 Hz, 6 H), 7.53 (s, 6 H), 7.48 (t, J = 7 Hz, 6 H), 7.36(t, J = 7 Hz, 6 H), 7.08 (d, J = 8.4 Hz, 6 H), 4.11 (d, J = 13 Hz, 6 H), 3.03−2.83 (m, 24 H), 2.82 (d, J = 13 Hz, 6 H), 1.02 (t, J = 6.9 Hz, 18 H), 0.57 (t, J = 6.9 Hz, 18 H) ppm. ^{13}C NMR (CD_3CN, 75 MHz): δ = 153.89, 135.91, 134.55, 129.41, 129.06, 128.39, 125.45, 124.39, 122.47, 119.70, 66.95, 61.72, 58.75, 9.46, 7.85 ppm. ^{7}Li NMR (CD_3CN, 116 MHz): δ = 1.32 ppm. MS (FAB$^+$): m/z = 1972 [MNa^+], 1956 (MLi^+), 1950 [MH^+], 1800 [M − OTf] ESI-MS: m/z = 1799.7284 (calcd. for $C_{92}H_{108}F_6Li_2N_6NaO_{18}S_2$ [M − OTf]$^+$); found 1799.7358.

Δ-[Li$_3${(*S*)-1}$_3$](OTf)$_3$ (8): $[\alpha]_{589}^{25}$ = +329 (c = 0.012, CH_3CN). ^{1}H NMR (CD_3CN, 300 MHz): δ = 15.36 (s, 6 H, OH), 8.08 (d, J = 5 Hz, 6 H), 7.50 (s, 6 H), 7.48 (t, J = 7 Hz, 6 H), 7.35(t, J = 7 Hz, 6 H), 7.08 (d, J = 8.4 Hz, 6 H), 3.89 (d, J = 13 Hz, 6 H), 3.05−2.87 (m, 24 H), 2.72 (d, J = 13 Hz, 6 H), 1.01 (t, J = 6.9 Hz, 18 H), 0.52 (t, J = 6.9 Hz, 18 H) ppm. ^{13}C NMR (CD_3CN, 75 MHz): δ = 153.25, 134.85, 133.88, 128.50, 128.37, 127.33, 125.18, 123.57, 122.18, 119.16, 65.35, 60.87, 57.26, 8.58, 6.88 ppm. ^{7}Li NMR (CD_3CN, 116 MHz): δ = 2.23, 1.35 ppm. HRMS (ES): m/z = 1783.7546 (calcd. for $C_{92}H_{108}F_6Li_3N_6O_{18}S_2$ [M − OTf]$^+$), found 1783.7593.

Acknowledgments

We thank the DGICYT (PB96-0203) for financial support.

[1] [1a] D. L. Caulder, K. N. Raymond, *J. Chem. Soc., Dalton Trans.* **1999**, 1185−1200. [1b] S. Leininger, B. Olenyuk, P. J. Stang, *Chem. Rev.* **2000**, *100*, 853−907. [1c] U. Knof, A. von Zelewsky, *Angew. Chem. Int. Ed.* **1999**, *38*, 302−322. [1d] M. Albrecht, *Chem. Rev.* **2001**, *101*, 3457−3497. [1e] B. Bocquet, G. Benardinelli, N. Ouali, S. Floquet, F. Renaud, G. Hopfgartner, C. Piguet, *Chem. Commun.* **2002**, 930−931. [1f] J.-C. G. Bünzi, C. Piguet, *Chem. Rev.* **2002**, *102*, 1897−1928. [1g] J. M. Lehn, *Proc. Nat. Acad. Sci.* **2002**, *99*, 4763−4768. [1h] R. W. Saalfrank, N. Loew, S. Trummer, G. M. Sheldrick, M. Teichert, D. Stalke, *Eur. J. Inorg. Chem.* **1998**, *5*, 559−563.

[2] J. Gonzalez, PhD Dissertation, Universitat de les Illes Balears, **1999**.

[3] M. Capó, J. M. Saá, A. Alvarez, *Chem. Commun.* **2002**, 1982−1983.

[4] Both (*R*)- and (*S*)-**1** ligands can be obtained in enantiomerically pure form: D. J. Cram, R. C. Helgeson, S. C. Peacock, L. J. Klapan, P. Domeir, L. A. Moreau, K. Koga, J. M. Mayer, Y. Chao, M. G. Siegel, D. H. Hoffman, G. D. Y. Sogah, *J. Org. Chem.* **1978**, *43*, 1930−1946.

[5] The NMR spectra of complexes **2**−**5** from racemic **1** or from enantiomerically pure (*S*)-**1**/(*R*)-**1** are identical; this means that only sterospecific homochiral Λ-*RRR* or Δ-*SSS* complexes are formed. [5a] M. A. Masood, E. J. Enemark, T. D. P. Stack, *Angew. Chem. Int. Ed.* **1998**, *37*, 928−932. [5b] A. Lützen, M. Hapke, J. Griep-Raming, D. Haase, W. Saak, *Angew. Chem. Int. Ed.* **2002**, *41*, 2086−2089. [5c] P. Baret, V. Beaujolais, D. Gaude, Ch. Coulombeau, J.-L. Pierre, *Chem. Eur. J.* **1997**, *3*, 969−973. [5d] Y. Cui, H. L. Ngo, W. Lin, *Chem. Commun.* **2003**, 1388−1389.

[6] [6a] S. Aime, M. Botta, M. Fasano, E. Terreno, *Chem. Soc. Rev.* **1998**, *27*, 19−29. [6b] N. Ouali, B. Bocquet, S. Rigault, P.-Y. Morgantini, J. Weber, C. Piguet, *Inorg. Chem.* **2002**, *41*, 1436−1445.

[7] G. M. Sheldrick, *SHELX97, Program for Crystal Structure determination*, University of Göttingen, Göttingen, Germany, **1997**.

[8] Crystal data for **5**: $C_{93}H_{108}F_9N_6O_{21}S_3Yb$, M = 2086.7, monoclinic, space group, a = 19.3176(4), b = 24.6970(5), c = 24.6970(5) Å, V = 10927.23 Å^3, T = 196 K, space group $P2_1/n$, Z = 4, μ(Mo-K_α) = 0.99 mm^{-1}, 69857 reflections measured, 26360 unique, R_{int} = 0.0843. The final $wR2$ was 0.1545 (all data).

[9] [9a] S. Akine, T. Taniguchi, T. Nabeshima, *Angew. Chem. Int. Ed.* **2002**, *41*, 4670−4673. [9b] M. Botta, U. Casellato, C. Scalco, S. Tamburini, P. Tomasin, P. A. Vigato, S. Aime, A. Barge, *Chem. Eur. J.* **2002**, *8*, 3917−3926.

Received March 26, 2004
Early View Article
Published Online July 14, 2004

 © 2004 Wiley-VCH Verlag GmbH & Co. KGaA, Weinheim

Electron-Rich Organoantimony(III) Dithiolate Complexes

Narcis Avarvari,[a] Marc Fourmigué,*[a] and Enric Canadell[b]

Keywords: Antimony / Noncovalent interactions / S ligands / X-ray diffraction

Electron-rich dithiolene complexes of the antimony(III) PhSb moiety, formulated as [SbPh(dddt)] (**1**) (dddt: 5,6-dihydro-1,4-ditthine-2,3-dithiolate) and [SbPh(EDT-TTFS$_2$)] (**2**) (EDT-TTFS$_2$: 4,5-ethylenedithio-tetrathiafulvalene-4′,5′-dithiolate), have been prepared by deprotection of the corresponding precursors and trapping of the intermediate dithiolates with $PhSbCl_2$. Both complexes have been structurally characterized. The analysis of their single-crystal X-ray structures shows original supramolecular organizations governed by secondary Sb···S contacts, with distorted octahedral coordination geometries around the Sb center. Band-structure calculations for complex **2** reveal only weak dispersion of the valence and conduction bands, with an energy gap of 1.68 eV.
(© Wiley-VCH Verlag GmbH & Co. KGaA, 69451 Weinheim, Germany, 2004)

Introduction

Following their discovery in the 1960s,[1] homoleptic dithiolene complexes,[2] and particularly the square-planar complexes of d^8 metal cations (Ni, Pt, Pd), became the subject of extensive investigations,[3] mainly oriented toward the preparation and understanding of their magnetic[4] and conducting (eventually superconducting) salts.[5] In that respect, heteroleptic complexes, which involve one or more dithiolate ligands together with other ligands (bipy, dppe, Cp, CN,....) in the metal coordination sphere, have been much less investigated,[6,7] despite a wide variety of possible applications, for example as luminescent[8] or magnetic systems.[9] More recently, the dithiolate ligand built directly on a tetrathiafulvalene core ($TTFS_2^{2-}$) ($TTFS_2^{2-}$: tetrathiafulvalene-4,5-dithiolate) became available[10,11] and prompted the preparation of a wealth of novel dithiolene complexes, such as the homoleptic ones — the square-planar metallic Ni, Pt or Pd complexes described by Kobayashi and co-workers[12,13] or the tris(dithiolene) vanadium complexes[14] — or heteroleptic ones of general formula [$ML_n(TTFS_2)$] [ML_n = $TiCp_2$,[15] $Ni(CN)_2$,[16] Pt(bipy),[17,18] CoCp,[19] Pt(dppe),[20] Au(py-Ph),[21] M(dppf),[22]...]. These tetrathiafulvalene-4,5-dithiolate complexes are particularly attractive since they combine the properties of the TTF core with those of the dithiolene complex moiety.

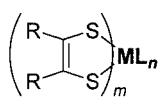

$(dt)_mML_n$ complexes

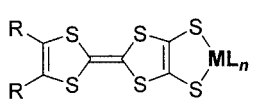

$(TTFS_2)ML_n$ complexes

We recently became interested in main-group derivatives of such heteroleptic dithiolene complexes and concentrated on the antimony moiety SbPh as the ML_n group in order to take advantage of both the diffuse lone pair of the Sb^{III} and its capacity to exhibit secondary coordination.[23] Indeed, in [SbPh(dmit)]·(THF) (dmit: 1,3-dithiole-2-thione-4,5-dithiolate),[24] the oxygen atom of the THF molecule and the outer sulfur atom of the C=S fragment enter the antimony coordination sphere of neighboring molecules, affording dimerized infinite chains stabilized by these Sb···O and Sb···S interactions. The flexibility of the coordination around antimony is further demonstrated by the observation of two successive single-crystal structural phase-transitions. On the other hand, in [SbPh(dmid)],[25] secondary Sb···S contacts lead to the formation of a centrosymmetric cyclic octagonal "Sb_4S_4" motif as a result of a formal tetramerization of the [SbPh(dmid)] molecule. Such motifs are also encountered in open-framework antimony sulfides.[26]

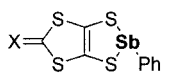

X = S PhSb(dmit)
X = O PhSb(dmid)

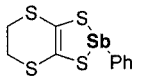

PhSb(dddt)

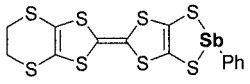

(EDT-TTFS$_2$)SbPh

Although [SbPh(dmit)] and [SbPh(dmid)] differ only in the terminal chalcogen C=X (X = O, S) atom, they have rather distinct structures, demonstrating a very high structural flexibility in the solid state thanks to secondary Sb···S and Sb···O contacts in which the terminal chalcogen is always involved. This prompted us to investigate Sb^{III}-based dithiolene complexes with a completely different backbone

[a] Laboratoire Chimie, Ingénierie Moléculaire et Matériaux (CIMMA), UMR 6200 CNRS-Université d'Angers,
2 Bd. Lavoisier, 49045 Angers cedex, France
Fax: (internat.) +33-2-41735090
E-mail: marc.fourmigue@univ-angers.fr
[b] Institut de Ciència de Materials de Barcelona (CSIC), Campus de la UAB,
08193 Bellaterra, Spain

in order to study the structural adaptability of the system, and we focused on more electron-rich dithiolate ligands, thus keeping an eye on the possibility of accessing open-shell species upon oxidation. Therefore, complexes derived from $dddt^{2-}$ and EDT-$TTFS_2^{2-}$ have been prepared. Their solid-state crystalline structures along with the band-structure calculation for the TTF-based compound are reported here.

Results and Discussion

Syntheses

Deprotection of 5,6-dihydro-[1,3]dithiolo[4,5-*b*][1,4]dithiin-2-one[27] with two equivalents of (Me_4N·OH) in THF leads to the formation of the corresponding dithiolate $dddt^{2-}$. Subsequent fast addition of $PhSbCl_2$,[28] followed by purification workup, afforded **1** as an orange solid (Scheme 1). The elemental analysis and ^1H NMR spectroscopic data are in agreement with the proposed formulation. Suitable single crystals for an X-ray analysis (vide infra) were grown by slow evaporation of the solvent from a CH_2Cl_2 solution of the complex. Similarly, deprotection of 4,5-bis[(2-cyanoethyl)thio]-4′,5′-ethylenedithiotetrathiafulvalene[29,30] with two equivalents of (Me_4N·OH) in THF afforded the highly air sensitive TTF dithiolate. This was quenched with $PhSbCl_2$ to give complex **2**, which was analyzed by ^1H and ^{13}C NMR spectroscopy, mass spectrometry and elemental analysis. Red crystals of **2**, suitable for an X-ray analysis, were obtained by recrystallization from toluene. The complex is readily soluble in THF and only sparingly soluble in other organic solvents. As described in our previous study,[25] the addition rate of $PhSbCl_2$ is a crucial parameter in order to reach an optimum yield of the dithiolene complex. This is related to the reactivity of **1** or **2**, once formed, towards a second equivalent of dithiolate to give a highly reactive dianionic species. A fast addition of $PhSbCl_2$ to the dithiolate suspension ensures a good yield of the desired product.

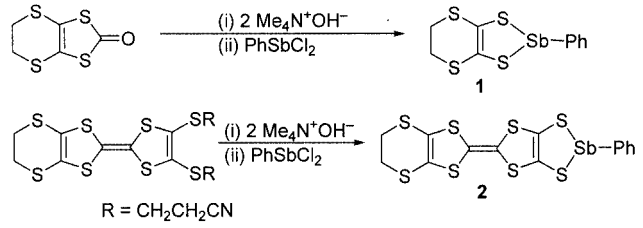

Scheme 1

Structure of [SbPh(dddt)]

The complex crystallizes in the triclinic system, space group $P\bar{1}$, with three crystallographically independent molecules (noted A, B and C in the following) in the unit cell, together with one CH_2Cl_2 molecule (Figure 1). Selected intramolecular bond lengths and bond angles for each of the molecules are listed in Table 1 and 2, respectively. They are similar to those observed in [SbPh(dmit)] and [SbPh(dmid)], with a primary coordination pattern around the antimony atom consisting, as expected, of two S (dithiolate) atoms and one C(*ipso*) atom, with the phenyl group almost perpendicular to the S−Sb−S plane. The folding angle of the SbS_2C_2 metallacycle along the S···S hinge, a characteristic of coordinated dithiolene complexes, amounts to 31.89(23)°, 24.23(27)° and 26.98(18)° in molecules A−C, respectively. The differences between the three molecules are not so important if one takes into account that the rotation barrier of such metallacycles is rather low.[9] Every molecule completes its coordination sphere by a complex set of secondary Sb···S interactions (Figure 2). Both Sb1A and Sb1B exhibit two short Sb···S contacts with sulfur atoms of neighboring molecules located in the least-square equatorial plane along with the two dithiolene sulfur atoms (see Table 1). The intermolecular Sb···S distances lie between 3.31 and 3.61 Å, well below the sum of the van der Waals radii (3.80 Å).[31] Altogether, the coordination around Sb1A and Sb1B is of distorted octahedral type if one takes into account the $5s^2$ lone pair, probably lying *trans* to the phenyl group. On the other hand, Sb1C engages in only one such Sb···S secondary interaction and appears, from that point of view, coordinatively unsaturated. These secondary interactions around Sb1A and Sb1B give rise to the formation of an eight-membered ring with alternating Sb and S atoms. The resulting tetramolecular Sb_4S_4 units

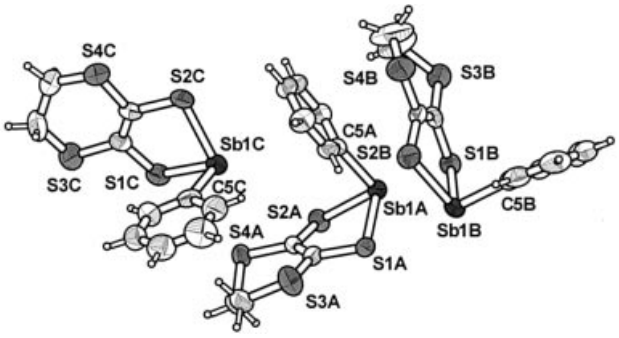

Figure 1. ORTEP drawing of the three crystallographically independent PhSb(dddt) molecules along with their numbering scheme

Table 1. Selected bond lengths (Å) for [SbPh(dddt)]; symmetry transformations used to generate equivalent atoms: (a) x, y, z; (b) $1-x, -y, 1-z$; (c) $2-x, -y, 1-z$; (d) $1+x, y, z$

Molecule A			
Sb1A−S1A	2.458(2)	Sb1A−C5A	2.149(8)
Sb1A−S2A	2.475(2)		
Sb1A···S1B[a]	3.31(2)	Sb1A···S1C[b]	3.42(2)
Molecule B			
Sb1B−S2B	2.451(3)	Sb1B−C5B	2.133(9)
Sb1B−S1B	2.468(2)		
Sb1B···S2A[c]	3.43(4)	Sb1B···S2C[d]	3.61(2)
Molecule C			
Sb1C−S1C	2.435(3)	Sb1C−C5C	2.156(8)
Sb1C−S2C	2.463(3)		
Sb1C···S4A[a]	3.36(5)		

 © 2004 Wiley-VCH Verlag GmbH & Co. KGaA, Weinheim

are connected together by two molecules C, affording infinite chains running along the *a*-axis. These chains are well separated from each other by: (i) the phenyl and ethylene groups of the constituting molecules, which point toward the outside of the columns, and (ii) by disordered CH_2Cl_2 molecules included into the channels formed between the columns. These Sb_4S_4 cyclic patterns have also been identified in the structure of [SbPh(dmid)], while Sb_2S_2 motifs are found in [SbPh(dmit)]. They are also frequently observed in the open-framework antimony sulfides based on the primary Sb−S bonds.

Table 2. Selected bond angles (°) for [SbPh(dddt)] (**1**)

Molecule A			
C5A−Sb1A−S1A	95.9(2)	S1A−Sb1A−S2A	84.40(7)
C5A−Sb1A−S2A	93.2(2)		
Molecule B			
C5B−Sb1B−S2B	94.1(2)	S2B−Sb1B−S1B	85.30(8)
C5B−Sb1B−S1B	96.0(2)		
Molecule C			
C5C−Sb1C−S1C	94.9(3)	S1C−Sb1C−S2C	85.04(8)
C5C−Sb1C−S2C	95.0(2)		

Structure of [SbPh(EDT-TTFS$_2$)]

The complex crystallizes in the orthorhombic system, space group $Pca2_1$ with one molecule in a general position in the unit cell (Figure 3). Intramolecular bond lengths and angles are in the usual range (Table 3). The EDT-TTF moieties stack on top of each other along the *b*-axis. As often observed with neutral tetrathiafulvalene derivatives, the dithiole rings are folded along the S···S hinge, by 19.97(69)° on the ethylenedithio side and by 13.30(63)° on the metallacycle side. On the other hand, the metallacycle itself is also distorted, with a folding along the S···S hinge of 19.09(32)°, weaker than that observed in [SbPh(dddt)]. The antimony coordination sphere (Figure 4) is completed by four Sb···S secondary interactions, two of them with sulfur atoms (S7, S8) located in the least-square equatorial plane along with the two dithiolene sulfur atoms (Sb···S7: 3.85 Å; Sb···S8: 3.47 Å) and two with sulfur atoms (S3, S4) of a neighboring molecule in the stack along the *b*-axis (Sb···S3: 3.83 Å, Sb···S4: 3.89 Å). Note that these distances, excluding the shortest Sb···S8 one, are close to or above the van der Waals Sb···S (3.80 Å) distance, indicating weaker interactions than in [SbPh(dddt)].

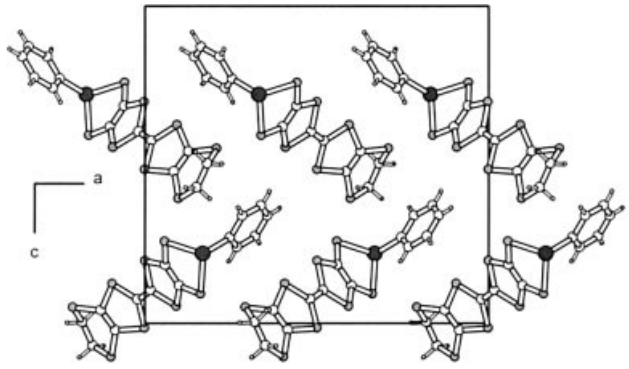

Figure 3. A view of the unit cell of (EDT-TTFS$_2$)SbPh

Table 3. Selected bond lengths (Å) and angles (°) in [SbPh(EDT-TTFS$_2$)] (**2**); symmetry transformations used to generate equivalent atoms: (a) 0.5 + *x*, 2 − *y*, *z*; (b) 1 − *x*, 2 − *y*, −0.5 + *z*; (c) *x*, −1 + *y*, *z*

Sb1−S1	2.450(2)	Sb1−C9	2.136(9)
Sb1−S2	2.458(2)		
Sb1···S7^a	3.852(7)	Sb1···S8^b	3.467(2)
Sb1···S3^c	3.826(2)	Sb1···S4^c	3.895(2)
C9−Sb1−S1	98.0(2)	C9−Sb1−S2	95.9(2)
S1−Sb1−S2	87.98(7)		

Electrochemical and Theoretical Studies

Cyclic voltammetry measurements were performed on complex **2** in order to determine its electrochemical behav-

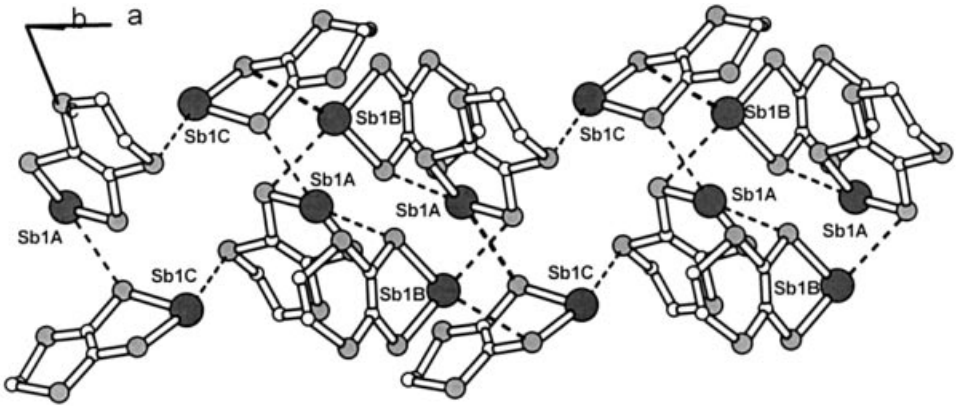

Figure 2. A view of the columns with the tetramolecular motif built on two Sb1A and two Sb1B molecules, connected together by Sb1C molecules; phenyl groups and hydrogen atoms have been omitted for clarity; Sb atoms are in dark grey, sulfur atoms in light grey

 © 2004 Wiley-VCH Verlag GmbH & Co. KGaA, Weinheim

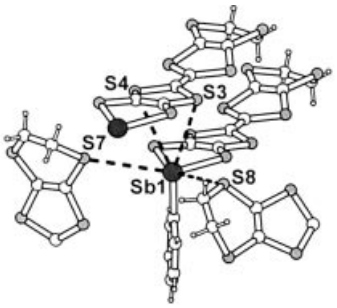

Figure 4. Detail of the coordination sphere of antimony in (EDT-$TTFS_2$)SbPh

iour and hence its potential utilization as a donor in electrocrystallization experiments. Although the two characteristic oxidation peaks, corresponding to the formation of the $[\mathbf{2}]^{+\cdot}$ radical cation at $E = 0.69$ V (SCE) and the $[\mathbf{2}]^{2+}$ dication at $E = 0.89$ V (SCE), are observed as expected, the overall process is only partially reversible, showing that the oxidized species of **2** is not stable in solution. This kinetic instability can be related to the flexibility of the antimony coordination sphere, leading to a multitude of ligand-scrambling reactions in solution.[25] Solutions of the neutral complex **2** in THF are also unstable, since a deposit of unidentified compounds precipitated out of the solution within one day. These observations show that the complex **2** is probably not a suitable donor for electrocrystallization experiments.

However, the complex set of intermolecular contacts identified within the crystalline structure of **2** prompted us to undertake a band-structure calculation in order to evaluate the energy gap between the valence and the conduction band of **2** along with the dispersion of these bands, thus envisaging the eventuality of an intrinsic semiconducting behavior for this compound. Indeed, previous studies dealing with the tetrakis(telluromethyl)tetrathiafulvalene (MeTe)$_4$TTF reported interesting results concerning the semiconducting properties of the compound in neutral state, very likely due to zigzag chains formed by Te···Te contacts.[32] The calculated band structure for complex **2**, represented in Figure 5, shows a valence-band built up from the HOMO of the EDT fragment, with a dispersion of about 0.2 eV.

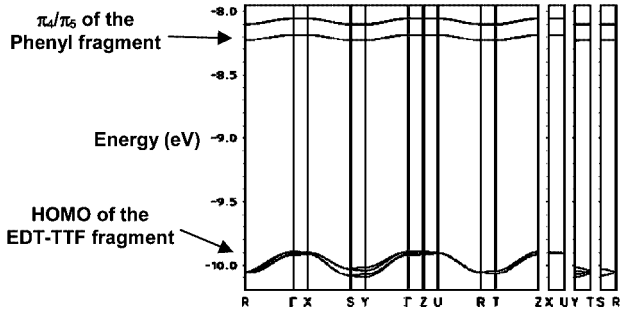

Figure 5. Calculated band structure for **2**; Γ = (0, 0, 0), R = (0.5, 0.5, 0.5), X = (0.5, 0, 0), S = (0.5, 0.5, 0), Y = (0, 0.5, 0), Z = (0, 0, 0.5), U = (0.5, 0, 0.5), T = (0, 0.5, 0.5) in units of the reciprocal lattice vectors

This rather weak value for the valence-band dispersion is very likely due to the absence of an antimony contribution to the HOMO of the molecule. An Sb-based HOMO would probably have led to a larger dispersion band when taking into account the numerous Sb···S intermolecular contacts. The conduction band, the dispersion of which is even weaker, also has no Sb contribution, but is exclusively formed from the empty π_4 and π_5 orbitals of the phenyl rings. Although these dispersions are somewhat slightly underestimated because of the single-ζ basis-set employed in the calculation, the bands still remain rather flat. This result, along with the gap-energy value of 1.68 eV, allows us to assess that complex **2** should be a modest semiconductor. Preliminary conductivity measurements on compressed pellets gave a σ value of about 10^{-5} S·cm^{-1}.

Experimental Section

General: The syntheses of the complexes were carried out under nitrogen, using standard Schlenk techniques. Dry toluene and hexane were obtained by distillation over Na and dry CH_2Cl_2 and CH_3CN by distillation over P_2O_5; THF was distilled from sodium/benzophenone. NMR spectra were recorded on a Bruker ARX 500 spectrometer operating at 500.04 MHz for ^{1}H and 125.75 MHz for ^{13}C. Mass spectrometry was performed on an HP 5989A spectrometer in the EI mode, with an ionization energy of 70 eV. Elemental analyses were performed by the "Service d′Analyse du CNRS" at Gif/Yvette, France. 5,6-Dihydro-[1,3]dithiolo[4,5-*b*][1,4]dithiin-2-one,[27] EDT-TTF(SCH_2-CH_2CN)$_2$,[29,30] and phenyldichlorostibane[28] were prepared according to literature methods.

[SbPh(dddt)] (2): A solution of Me_4NOH (3.5 g 25 wt % in MeOH, 9.6 mmol) in 5 mL of THF was added to a Schlenk tube containing 5,6-dihydro-[1,3]dithiolo[4,5-*b*][1,4]dithiin-2-one (1 g, 4.8 mmol) in 30 mL of THF under magnetic stirring. A yellow precipitate appeared immediately corresponding to the formation of dddt^{2-}. After 10 min of stirring at room temperature, dichlorophenylstibane (1.3 g, 4.8 mmol) in 10 mL of THF was rapidly added. The solution became orange and a cream precipitate of tetramethylammonium chloride was formed. The suspension was stirred for 2 h and then filtered through Celite. After evaporation of the solvent, the resulting oil was dissolved in a minimum amount of toluene and then rapidly chromatographed with toluene through a short silica-gel column. After removal of solvent under vacuum, addition of a small volume of THF, precipitation with pentane, filtration and drying on a vacuum line, complex **2** was recovered as a yellow solid. Yield 0.6 g (33%). Single crystals for X-ray analysis were grown by slow evaporation of the solvent from a solution of **2** in CH_2Cl_2. ^{1}H NMR ($CDCl_3$): δ = 2.97−3.02 (m, 2 H, CH_2), 3.18−3.21 (m, 2 H, CH_2), 7.36−7.43 (m, 3 H, H *para* and *meta*), 7.60 (dd, $^3J_{H,H}$ = 8.1, $^4J_{H,H}$ = 1.4 Hz, 2 H, H *ortho*) ppm. $C_{10}H_9S_4Sb$·THF: calcd. C 37.26, H 3.80; found C 37.11, H 3.71.

[SbPh(EDT-$TTFS_2$)] (2): A solution of EDT-TTF(SCH_2-CH_2CN)$_2$ (1 g, 2.15 mmol) in 40 mL of THF was treated with a solution of Me_4NOH (1.57 g, 25 wt % in MeOH, 4.3 mmol) in 10 mL of THF. An orange precipitate of EDT-TTF-S_2^{2-} was formed within a few minutes and after 30 min of stirring dichlorophenylstibane (0.58 g, 2.15 mmol) in 10 mL of THF was added rapidly. The reaction mixture was stirred for 2 h, then the solvent was evaporated, the residue washed with methanol, dissolved in THF and filtered through Celite. After evaporation of THF to a small volume, MeCN was ad-

 © 2004 Wiley-VCH Verlag GmbH & Co. KGaA, Weinheim

Table 4. Crystallographic data for **1** and **2**

	1	**2**
Empirical formula	$C_{10.33}H_{9.67}Cl_{0.67}S_4Sb$	$C_{14}H_9S_8Sb$
Formula mass	407.47	555.44
Crystal size (mm)	0.6 × 0.15 × 0.015	0.12 × 0.08 × 0.04
Crystal system	triclinic	orthorhombic
Space group	$P\bar{1}$	$Pca2_1$
a (Å)	12.4692(14)	18.320(4)
b (Å)	12.8323(17)	6.0582(12)
c (Å)	15.573(2)	16.983(3)
α (°)	86.452(16)	90.
β (°)	68.424(14)	90.
γ (°)	67.680(14)	90.
V (Å^3)	2134.9(5)	1884.9(7)
Z	6	4
T (K)	293(2)	293(2)
$D_{calcd.}$ (g·cm^{-3})	1.902	1.957
μ (mm^{-1})	2.343	2.343
Measured refl.	21615	10932
Unique refl.	7680	1886
Obs. refl.[a]	3510	1466
Abs. correction	numerical	multi-scan
T_{min}, T_{max}	0.623, 0.960	0.834, 0.889
R_{int}	0.125	0.0575
R_1 [a]	0.0446	0.031
wR_2	0.0871	0.0531
Res. density (e·Å^{-3})	+0.62, −0.54	+0.58, −0.38

The values were calculated for data with $I > 2\sigma(I)$.

ded, and then the resulting precipitate was filtered through a glass frit and dried under vacuum to yield complex **2** as a red-brown powder. Yield 0.58 g (49%). ^{1}H NMR ([D$_8$]THF): δ = 3.31 (s, 4 H, CH$_2$), 7.33 (tt, $^3J_{H,H}$ = 7.2, $^4J_{H,H}$ = 1.3 Hz, 1 H, H *para*), 7.40 (t, $^3J_{H,H}$ = 7.2 Hz, 2 H, H *meta*), 7.84 (dd, $^3J_{H,H}$ = 7.2, $^4J_{H,H}$ = 1.4 Hz, 2 H, H *ortho*) ppm. ^{13}C NMR ([D$_8$]THF): δ = 30.2 (CH$_2$), 107.7 (C=C), 113.8 (C=C), 121.4 (C=C), 128.9 (CH-*meta*), 129.8 (CH-*para*), 133.8 (CH-*ortho*), 149.0 (C-*ipso*) ppm. MS (EI): *m*/*z* (%) = 553, 555 (60) [M$^+$]. $C_{14}H_9S_8Sb$: calcd. C 30.27, H 1.63; found C 30.07, H 1.61.

Electrochemistry: Cyclic voltammetry experiments were performed on a VPM potentiostat in dry-THF solutions of 0.05 M nBu$_4$NPF$_6$ as electrolyte at room temperature, at a scan rate of 100 mV·s^{-1}. A Pt working electrode (diameter 1 mm), a Pt counter electrode and an SCE reference electrode were used.

Band-Structure Calculations: The tight-binding band-structure calculations were based upon the effective one-electron Hamiltonian of the extended Hückel method.[33] The off-diagonal matrix elements of the Hamiltonian were calculated according to the modified Wolfsberg−Helmholz formula.[34] All valence electrons were explicitly taken into account in the calculations, and the basis set consisted of single-ζ Slater-type orbitals, because of the higher reliability in the case of atoms with very diffuse orbitals such as antimony when compared with the double-ζ basis set.[35]

X-ray Crystallography: Crystals of [SbPh(dddt)] or [SbPh(EDT-TTFS$_2$)] were mounted on top of a thin glass fiber. Data were collected on a Stoe Imaging Plate Diffraction System (IPDS) with graphite monochromated Mo-K_α radiation (λ = 0.71073 Å). The crystal data are summarized in Table 4. Structures were solved by direct methods (SHELXS-97) and refined (SHELXL-97) by full-matrix least-squares methods. Absorption corrections were applied for both structures. Hydrogen atoms were introduced at calculated positions (riding model), included in structure factor calculations, and not refined.

CCDC-233353 (for **1**) and -233354 (for **2**) contain the supplementary crystallographic data for this paper. These data can be obtained free of charge at www.ccdc.cam.ac.uk/conts/retrieving.html [or from the Cambridge Crystallographic Data Centre, 12 Union Road, Cambridge CB2 1EZ, UK; Fax: +44-1223-336033; E-mail: deposit@ccdc.cam.ac.uk].

[1] [1a] R. Williams, E. Billig, J. H. Waters, H. B. Gray, *J. Am. Chem. Soc.* **1966**, *88*, 43. [1b] G. N. Schrauzer, V. Mayweg, *J. Am. Chem. Soc.* **1962**, *84*, 3221. [1c] A. Davison, N. Edelstein, R. H. Holm, A. H. Maki, *J. Am. Chem. Soc.* **1963**, *85*, 2029.
[2] U. T. Mueller-Westerhoff, B. Vance, in *Comprehensive Coordination Chemistry* (Ed.: G. Wilkinson), Pergamon Press, Oxford, **1987**, Ch. 16.5, 595−631.
[3] T. B. Rauchfuss, *Progr. Inorg. Chem.* **2003**, *52*, 1.
[4] P. I. Clemenson, *Coord. Chem. Rev.* **1990**, *106*, 171.
[5] P. Cassoux, L. Valade, H. Kobayashi, A. Kobayashi, R. A. Clark, A. E. Underhill, *Coord. Chem. Rev.* **1991**, *110*, 115.
[6] A. E. Pullen, R.-M. Olk, *Coord. Chem. Rev.* **1999**, *188*, 211.
[7] M. Fourmigué, *Coord. Chem. Rev.* **1998**, *178-180*, 823.
[8] M. Hissler, J. E. McGarrah, W. B. Connick, D. K. Geiger, S. D. Cummings, R. Eisenberg, *Coord. Chem. Rev.* **2000**, *208*, 115.
[9] M. Fourmigué, *Acc. Chem. Res.* **2004**, *37*, 179.
[10] N. Le Narvor, N. Robertson, T. Weyland, J. D. Kilburn, A. E. Underhill, M. Webster, N. Svenstrup, J. Becher, *Chem. Commun.* **1996**, 1363.
[11] N. Le Narvor, N. Robertson, E. Wallace, J. D. Kilburn, A. E. Underhill, P. N. Bartlett, M. Webster, *J. Chem. Soc., Dalton Trans.* **1996**, 823.
[12] A. Kobayashi, H. Tanaka, M. Kumasaki, H. Torii, B. Narymbetov, T. Adachi, *J. Am. Chem. Soc.* **1999**, *121*, 10763.
[13] H. Tanaka, Y. Okano, H. Kobayashi, W. Suzuki, A. Kobayashi, *Science* **2001**, *291*, 285.
[14] T. Yoneda, Y. Kamata, K. Ueda, T. Sugimoto, T. Tada, M. Shiro, H. Yoshino, K. Murata, *Synth. Met.* **2003**, *135-136*, 573.
[15] [15a] R. D. McCullough, J. A. Belot, J. Seth, A. L. Rheingold, G. P. A. Yap, D. O. Cowan, *J. Mater. Chem.* **1995**, *5*, 1581. [15b] R. D. McCullough, J. A. Belot, A. L. Rheingold, G. P. A. Yap, *J. Am. Chem. Soc.* **1995**, *117*, 9913.
[16] [16a] T. Naito, N. Kobayashi, T. Inabe, *Synth. Met.* **1999**, *102*, 1687. [16b] T. Naito, N. Kobayashi, T. Inabe, *Chem. Lett.* **1998**, 723.
[17] K. Kubo, M. Nakano, H. Tamura, G.-E. Matsubayashi, *Inorg. Chim. Acta* **2002**, *336*, 120.
[18] Y. Misaki, Y. Tani, K. Takahashi, K. Tanaka, *Mol. Cryst. Liquid Cryst. Sect. A* **2002**, *379*, 71.
[19] H. Mori, M. Nakano, H. Tamura, G.-E. Matsubayashi, *J. Organomet. Chem.* **1999**, *574*, 77.
[20] R. D. McCullough, J. A. Belot, *Chem. Mater.* **1994**, *6*, 1396.
[21] K. Kubo, M. Nakano, H. Tamura, G.-E. Matsubayashi, M. Nakamoto, *J. Organomet. Chem.* **2003**, *669*, 141.
[22] K.-S. Shin, Y.-K. Han, D.-Y. Noh, *Bull. Korean Chem. Soc.* **2003**, *24*, 235.
[23] N. W. Alcock, *Adv. Inorg. Chem. Radiochem.* **1972**, *15*, 1.
[24] N. Avarvari, E. Faulques, M. Fourmigué, *Inorg. Chem.* **2001**, *40*, 2570.
[25] N. Avarvari, M. Fourmigué, *Organometallics* **2003**, *22*, 2042.
[26] A. V. Powell, S. Boissière, A. M. Chippindale, *Chem. Mater.* **2000**, *12*, 182.
[27] J. Larsen, C. Lenoir, *Synthesis* **1989**, 134.
[28] M. Nunn, D. B. Sowerby, D. M. Wesolek, *J. Organomet. Chem.* **1983**, *251*, C45.
[29] N. Svenstrup, K. M. Rasmussen, T. K. Hansen, J. Becher, *Synthesis* **1994**, 809.
[30] L. Binet, J.-M. Fabre, C. Montginoul, K. B. Simonsen, J. Becher, *J. Chem. Soc., Perkin Trans. 1* **1996**, 783.

 © 2004 Wiley-VCH Verlag GmbH & Co. KGaA, Weinheim

[31] A. Bondi, *J. Phys. Chem.* **1964**, *68*, 441.
[32] [32a] H. Inokuchi, K. Imaeda, T. Enoki, T. Mori, Y. Maruyama, G. Saito, N. Okada, H. Yamochi, K. Seki, Y. Higuchi, N. Yasuoka, *Nature* **1987**, *329*, 39. [32b] J. D. Martin, E. Canadell, J. Y. Becker, J. Bernstein, *Chem. Mater.* **1993**, *5*, 1199.
[33] M. H. Whangbo, R. Hoffmann, *J. Am. Chem. Soc.* **1978**, *100*, 6093.
[34] J. H. Ammeter, H.-B. Bürgi, J. Thibeault, R. Hoffmann, *J. Am. Chem. Soc.* **1978**, *100*, 3686.
[35] T. Hughbanks, R. Hoffmann, M.-H. Whangbo, K. R. Stewart, O. Eisenstein, E. Canadell, *J. Am. Chem. Soc.* **1982**, *104*, 3876.
Received March 9, 2004
Early View Article
Published Online June 23, 2004

 © 2004 Wiley-VCH Verlag GmbH & Co. KGaA, Weinheim

Effect of Substitution of Methyl Groups on the Luminescence Performance of Ir^{III} Complexes: Preparation, Structures, Electrochemistry, Photophysical Properties and Their Applications in Organic Light-Emitting Diodes (OLEDs)

Sungouk Jung,[a] Youngjin Kang,*[b] Hyung-Sun Kim,[a] Yun-Hi Kim,[a] Chang-Lyoul Lee,[c] Jang-Joo Kim,[c] Sung-Koo Lee,[d] and Soon-Ki Kwon*[a]

Keywords: Electrochemistry / Electrophosphorescence / Iridium / Luminescence / N ligands

A series of dimethyl-substituted tris(pyridylphenyl)iridium(III) derivatives [(*n*-MePy–*n*′-MePh)$_3$Ir] [*n* = 3, *n*′ = 4 (**1**); *n* = 4, *n*′ = 4 (**2**); *n* = 4, *n*′ = 5 (**3**); *n* = 5, *n*′ = 4 (**4**); *n* = 5, *n*′ = 5 (**5**)] have been synthesized and characterized to investigate the effect of the substitution of methyl groups on the solid-state structure and photo- and electroluminescence. The absorption, emission, cyclic voltammetry and electroluminescent performance of **1**–**5** have also been systematically evaluated. The structures of **2** and **4** have been determined by a single-crystal X-ray diffraction analysis. Under reflux (> 200 °C) in glycerol solution, *fac*-type complexes with a distorted octahedral geometry are predominantly formed as the major components in all cases. Electrochemical studies showed much smaller oxidation potentials relative to Ir(ppy)$_3$ (Hppy = 2-phenylpyridine). All complexes exhibit intense green photoluminescence (PL), which has been attributed to metal-to-ligand charge transfer (MLCT) triplet emission. The maximum emission wavelengths of thin films of **1**, **3**, **4** and **5** at room temperature are in the range 529–536 nm, while **2** displays a blue-shifted emission band (λ_{max} = 512 nm) with a higher PL quantum efficiency (Φ_{PL} = 0.52) than those of complexes **1** and **3**–**5**; this is attributed to a decrease of the intermolecular interactions. Multilayered organic light-emitting diodes (OLEDs) were fabricated by using three (**2**, **3** and **4**) of these Ir^{III} derivatives as dopant materials. The electroluminescence (EL) spectra of the devices, which have the maximum peaks at 509–522 nm, with shoulder peaks near 552 nm, are consistent with the PL spectra in solution at 298 K. The devices show operating voltages at 1 mA/cm^2 of 4.9, 5.6, 5.1, and 4.6 V for Ir(ppy)$_3$, **2**, **3**, and **4**, respectively. In particular, the device with **2** shows a higher external quantum efficiency (η_{ext} = 11% at 1 mA/cm^2) and brightness (4543 cd/m^2 at 20 mA/cm^2) than Ir(ppy)$_3$ (η_{ext} = 6.0% at 1 mA/cm^2; 3156 cd/m^2 at 20 mA/cm^2) and other Ir(dmppy)$_3$ derivatives, (dmppy = dimethyl-substituted ppy), under the same conditions. The methyl groups at the *meta* (Ph) and *para* (Py) positions to the Ir metal atom have a great influence on absorption, emission, redox potentials and electroluminescence.
(© Wiley-VCH Verlag GmbH & Co. KGaA, 69451 Weinheim, Germany, 2004)

Introduction

Luminescent transition metal complexes, such as those of groups 9 or 10, are currently of great interest due to their various applications in photochemistry, organic light-emitting diodes (OLEDs), and chemical sensors for small molecules.[1] Among these transition metal complexes, Ir^{III} complexes have been regarded as excellent phosphorescent materials because of their ability to achieve maximum internal quantum efficiency, nearly 100%, as well as high external quantum efficiency in OLEDs.[2] Based on previous reports, a promising phosphorescent metal complex in OLEDs should have a short lifetime in the excited state and high phosphorescent efficiency. Based on these considerations, a number of researchers have focused recently on the development of cyclometallated (C^N)Ir^{III} complexes.[2] In particlar, luminescent Ir(ppy)$_3$ (Hppy = 2-phenylpyridine) derivatives have been described where adjustment of the band gap between the HOMO and LUMO energy levels could be achieved by modification of the substituents on the ppy rings.[3] Accordingly, to control the energy of the Ir(ppy)$_3$ system from blue light emission to red, a judicious incorporation of electron donors/acceptors as substituents on the ppy frameworks is an essential prerequisite.[4,5] For example, introduction of electron-donating groups to the pyridine ring and electron-withdrawing groups to the phenyl ring can cause a decrease of the HOMO level and an increase of the LUMO level, respectively, inducing a larger

[a] School of Applied Chemical Engineering and Engineering Research Institute, Gyeongsang National University
Chinju 660-701, South Korea
Fax: (internat.) + 82-55-753-6311
E-mail: skwon@nongae.gsnu.ac.kr
[b] Division of Science Education, Kangwon National University
Chuncheon 200-701, South Korea
kangy@kangwon.ac.kr
[c] School of Materials Science and Engineering, Seoul National University
Seoul 151-744, South Korea
[d] LG Electronic Institute of Technology
16 Woomyeon-Dong, Seocho-Gu, Seoul 137-724, South Korea
Supporting information for this article is available on the WWW under http://www.eurjic.org or from the author.

band gap than that of $Ir(ppy)_3$. Although extensive research on the investigation of luminescent properties of Ir^{III} derivatives containing two *ortho*-chelating (C^N) ligands and a bidentate ancillary LX (e.g. monoanionic chelating ligands, acac = acetylacetonate, pic = picolinate, sal = salicyliminate), and their use and performance as triplet emitters in EL devices has been well documented over several years, the illustration of the effect of substituents, such as simple functional groups, and the dependence on their positions on the phenyl or pyridine rings in the ppy backbone, still remains virtually unexplored.[1e,5] During our ongoing investigation of phosphorescent $Ir(ppy)_3$ derivatives, we have observed that attached methyl groups as substituents on the ppy ligand have a remarkable influence on the electrochemical and photophysical properties.[6] Our interest in the development of highly efficient phosphors for application in OLEDs has prompted us to synthesize $Ir(ppy)_3$ derivatives and investigate their photophysical and electroluminescent characteristics. The methyl moiety was chosen for the following reasons: (i) The emissions of $Ir(ppy)_3$ derivatives come from phosphorescence with triplet character of both ligand-centered ($\pi-\pi^*$) and MLCT (metal-to-ligand charge transfer) transitions. This phosphorescence is strongly affected by the triplet energy of the *ortho*-chelating C∧N ligands. Therefore substituents, even methyl groups, on the ppy rings could play a key role in the alteration of the triplet energy. (ii) Although a methyl group is a weaker electron-donating group than other functional groups (e.g. OMe, NR_2 etc.), incorporating the methyl group as a substituent on the ppy rings has an influence on the HOMO and/or the LUMO level, as well as the ^{3}MLCT state of the complex. Herein we describe the results of our systematic investigation on the preparation, structural characterization, electrochemical behavior, photophysical properties and the fabrication of multiplayer phosphorescent light-emitting devices of a series of *fac*-[Ir^{III}(dmppy)$_3$] complexes [Hdmppy = *n*-methyl-2-(*n′*-methylphenyl)pyridine].

Results and Discussion

Syntheses and Structures

The methyl-substituted ppy ligands were synthesized by the Suzuki coupling[7] reaction of 2-bromo-*n*-methylpyridine with the corresponding *n′*-methylphenylboronic acid in the presence of K_2CO_3 and [$Pd(PPh_3)_4$] catalyst (Scheme 1).

These ligands were obtained in good yields (70−90%). Complexes **1**−**5** were synthesized by a slight modification of the previous synthetic methodology reported by Watt et al.[8b] The reaction of [$Ir(acac)_3$] with the corresponding methyl-substituted ppy ligands at high temperature (> 200 °C), gave **1**−**5** in moderate yields. Even though the ligands methylated at the 6- or 3′-position were synthesized successfully in moderate yields, the complexation of these ligands with the Ir^{III} starting material hardly occurs under the same reaction conditions. We attribute this mainly to steric factors.

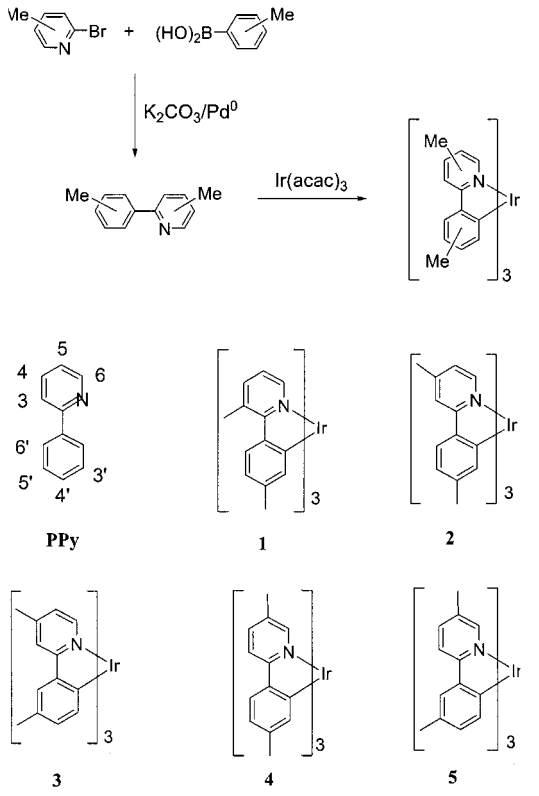

Scheme 1

There is a possibility of the formation of two isomers (*fac* and *mer*) during the reaction of $Ir(acac)_3$ and the Hdmppy ligands.[8a] However, we found that the *fac* isomer was formed as the major component, although some *mer* isomer was also formed. The formed *mer* isomers were not isolated because of their extremely low yields. All complexes are very stable up to 300 °C without degradation in air. In the ^{1}H NMR spectra, complexes **1**−**5** exhibit six well-resolved peaks due to the ppy rings, indicating that all complexes

Table 1. Selected bond lengths [Å] and angles [°] for **2** and **4**

Compound **2**			
Ir(1)−C(12)	2.015(8)	Ir(1)−C(38)	2.016(9)
Ir(1)−C(25)	2.034(8)	Ir(1)−N(1)	2.131(6)
Ir(1)−N(2)	2.114(7)	Ir(1)−N(3)	2.125(7)
C(12)−Ir(1)−N(1)	80.1(3)	C(38)−Ir(1)−N(3)	79.3(3)
C(25)−Ir(1)−N(2)	78.5(3)	C(12)−Ir(1)−C(38)	95.3(3)
C(38)−Ir(1)−N(1)	86.4(3)	C(38)−Ir(1)−C(25)	97.7(3)
C(38)−Ir(1)−N(2)	174.0(3)	C(12)−Ir(1)−C(25)	95.5(3)
Compound **4**[a]			
Ir(1)−C(12)	2.002(5)	Ir(1)−N(1)	2.111(5)
C(12)−Ir(1)−N(1)	79.3(2)	C(12A)^{i}−Ir(1)−C(12)	95.2(3)
C(12A)^{i}−Ir(1)−N(1B)^{ii}	171.6(2)	C(12)−Ir(1)−N(1B)^{ii}	91.6(2)
N(1B)^{ii}−Ir(1)−N(1)	94.48(19)		

[a] Symmetry transformations used to generate equivalent atoms: i: *z*, *x*, *y*; ii: *y*, *z*, *x*.

 © 2004 Wiley-VCH Verlag GmbH & Co. KGaA, Weinheim

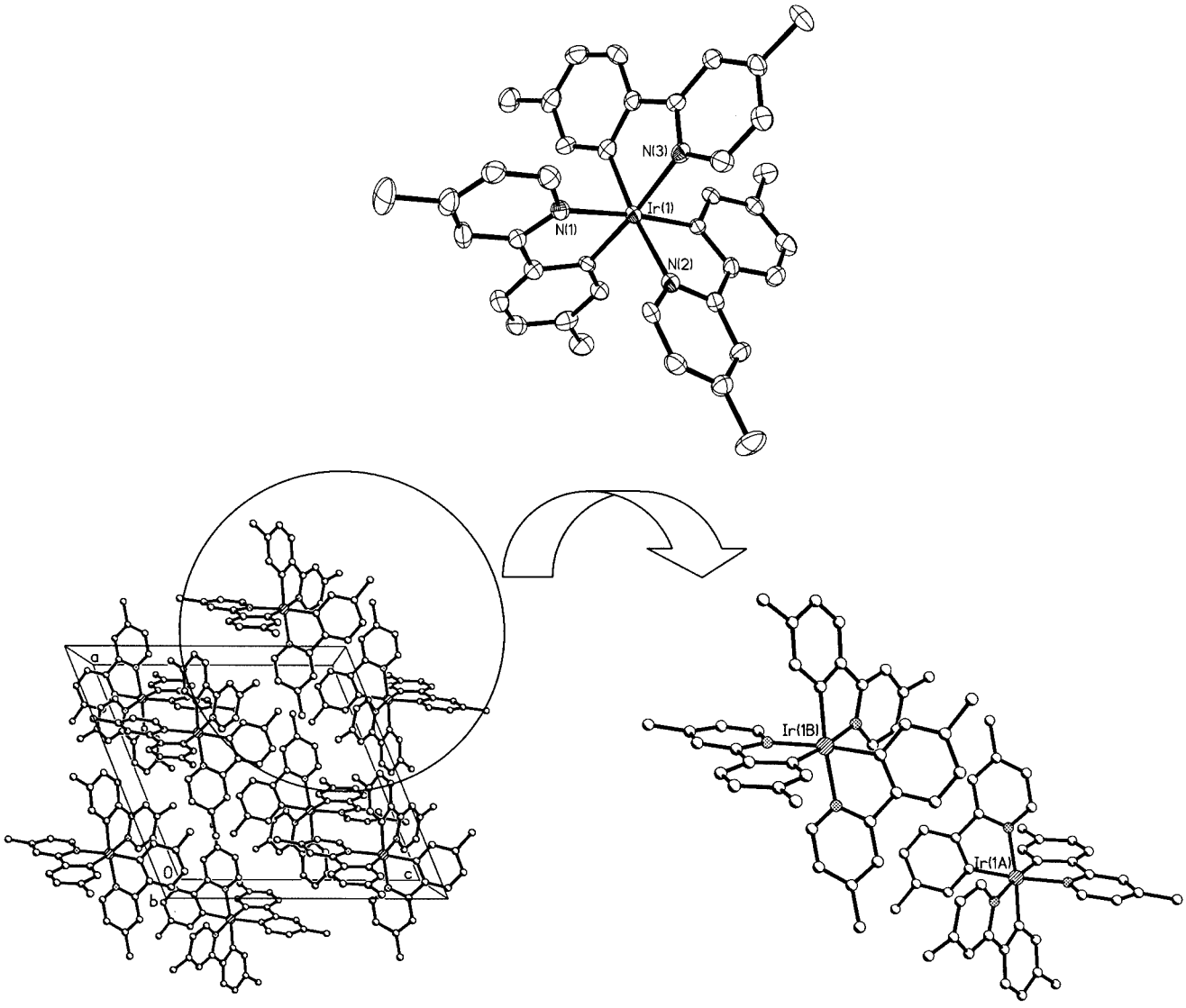

Figure 1. Top: Molecular structure of **2** with atom labeling schemes and 50% thermal ellipsoids; all hydrogen atoms have been omitted for clarity; bottom: crystal packing diagram between two adjacent molecules of **2** showing the lack of a π−π stacking interaction in the solid state

have a facial geometry around the Ir atom. Complexes **1**−**5** were fully characterized by mass spectrometry and elemental analyses, and crystal structures of **2** and **4** were obtained. Selected bond lengths and angles are presented in Table 1; refinement and structure-solution data can be found in the Exp. Sect. Complexes **2** and **4** exhibit only the *fac* configuration, with a distorted octahedral geometry around the Ir atom, as shown in Figures 1 and 2, respectively. The dihedral angle between the phenyl and pyridine rings in **2** (8.81°) is approximately three times larger than that of **4** (3.4°), indicating a decreased conjugation of the 4,4′-ppy ligands. The Ir−C bond lengths, ranging from 2.002(5) to 2.034 Å, are within the range reported for other mononuclear complexes with the $Ir(ppy)_2$ moiety [1.97(2)−2.13(6) Å],[9] and are also close to values reported for $[(tpy)_2Ir(\mu\text{-}Cl)_2Ir(tpy)_2]$ [Htpy = 2-(*p*-tolyl)pyridine] and other substituted *fac*-$[Ir(ppy)_3]$ derivatives.[8a,10] The σ-donor C atoms in the dmppy ligand arrange in a *trans* disposition to the dative N atoms of adjacent ppy ligands. The Ir−N bonds [2.111(5)−2.131 (6) Å] observed in **2** and **4** are slightly longer than those of $[Ir(acac)(tpy)_2]$ [2.040(5) Å] and $[Ir(acac)(ppy)_2]$ [2.010(9) Å].[5b] These observed elongations imply a stronger *trans* influence of the phenyl ring in comparison to the pyridyl groups having a *trans*-*N*,*N*′ configuration. In the crystal packing, **4** displays an effective overlap of the pyridine rings between two adjacent molecules (Figure 2). The shortest separation distance is about 3.22 Å, which is sufficiently short to suggest π−π stacking interactions. Complex **2** does not exhibit an effective overlap in the crystal packing, as shown in Figure 1. Recently, many reports have described that intermolecular π−π interactions have a direct influence on luminescent properties.[2c,5] The influence of this intermolecular interaction on the luminescence of the Ir^{III} complexes in this work is discussed below.

 © 2004 Wiley-VCH Verlag GmbH & Co. KGaA, Weinheim

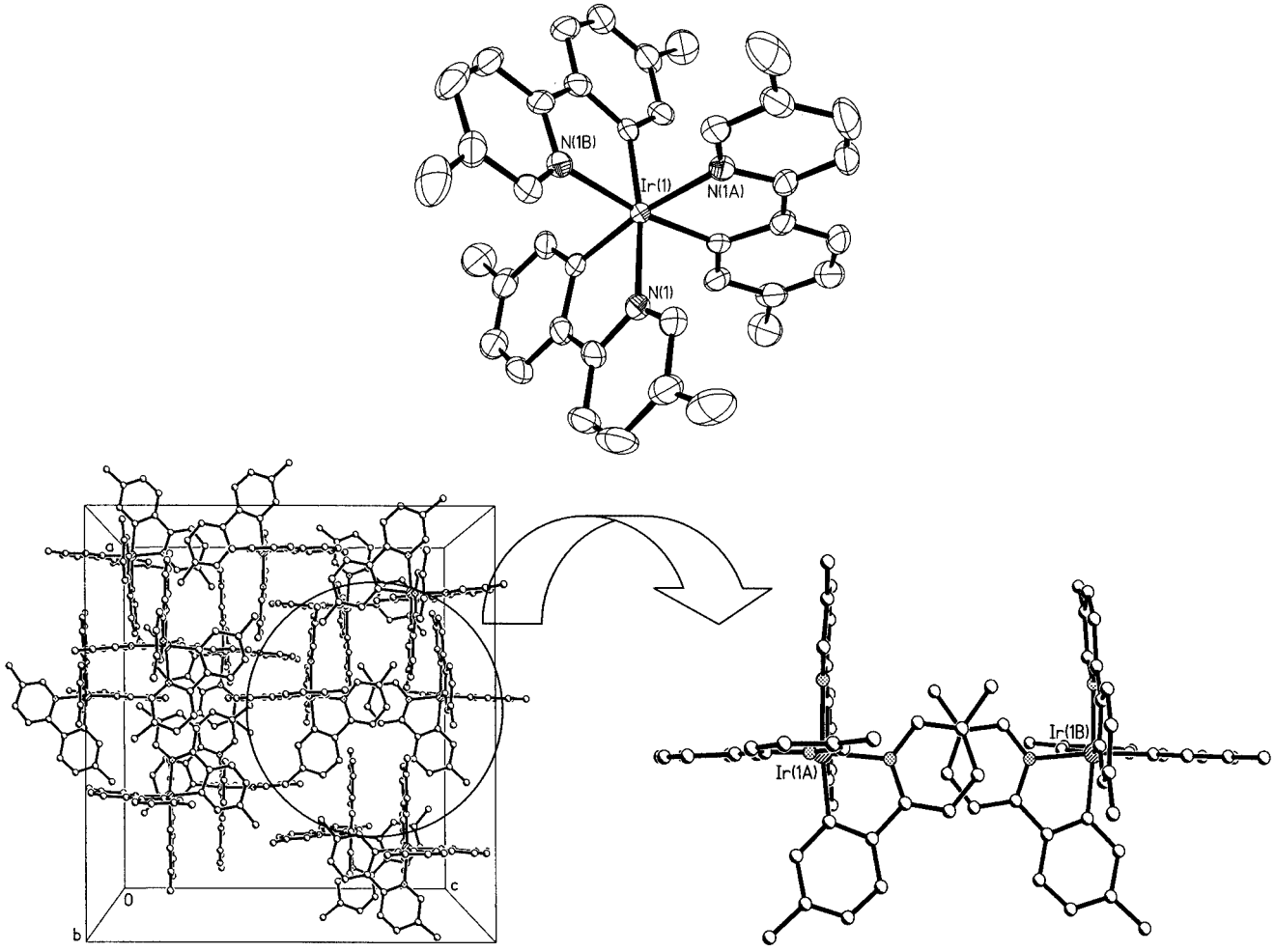

Figure 2. Top: Molecular structure of **4** with atom labeling schemes and 50% thermal ellipsoids; all hydrogen atoms have been omitted for clarity; bottom: crystal packing diagram between two adjacent molecules of **4** showing the intermolecular interaction in the solid state

Photoluminescent and Electrochemical Properties

Table 2 summarizes the photophysical data of **1**−**5**. The UV/Vis spectra of all compounds exhibit intense absorption bands between 250 and 310 nm ($\varepsilon > 10^4$ $mol^{-1}{\cdot}dm^3{\cdot}cm^{-1}$), indicating that the electronic transitions are mostly ligand-centered (LC) π−π * transitions (Figure 3). The absorption patterns of **1**−**5** and [Ir(ppy)$_3$] are similar in the 250−550 nm region.[11] However, the ^{1}MLCT and ^{3}MLCT peaks in **1**, **3**, **4** and **5** appear at lower energies than in [Ir(ppy)$_3$], while those of **2** occur at much higher energy with larger extinction coefficients. These observed blue- or red-shifted MLCT bands show that the methyl groups on the dmppy rings have a significant effect on the electronic

Table 2. Photophysical and electrochemical data of **1**−**5**[a] and [Ir(ppy)$_3$]

	UV (ε [10^3 $L{\cdot}mol^{-1}{\cdot}cm^{-1}$])	E_m (λ_{max}) Solution	Film	Φ_{PL}	Redox $E_{1/2}^{[ox]}$ [V]
[Ir(ppy)$_3$]	283(4.9), 380(4.1), 405(4.0), 455(3.5), 490(3.1)	514	516	0.40[b]	0.71
1	284(4.9), 384(4.1), 408(4.0), 455(3.6), 493(3.2)	522	529	0.41	0.51
2	278(4.9), 374(4.2), 407(4.0), 452(3.6), 484(3.3)	509	512	0.52	0.54
3	284(4.9), 391(4.1), 414(4.0), 456(3.6), 493(3.2)	524	534	0.32	0.49
4	284(4.9), 383(4.1), 412(4.0), 459(3.5), 493(3.2)	524	536	0.34	0.52
5	284(4.9), 384(4.0), 414(3.9), 458(3.4), 497(3.0)	524	532	0.29	0.47

[a] All the data were obtained in CH_2Cl_2 at ambient temperature with the same concentration. [b] Ref.[8a]

 © 2004 Wiley-VCH Verlag GmbH & Co. KGaA, Weinheim

transition energies. The emission spectra of all complexes in solution and as thin films at room temperature are dominated by phosphorescence in the region 509−534 nm. Interestingly, both the absorption and emission spectra of **2** are blue-shifted relative to the other complexes and [Ir(ppy)$_3$]. This result can be explained by correlating the electronic and steric effects due to the methyl substituents. As reported previously,[5] the emission energy of [Ir(ppy)$_3$] can be controlled readily by adding substituents to the rings. To investigate the electronic effects caused by the addition of methyl groups, cyclic voltammetry experiments were carried out for all complexes, including [Ir(ppy)$_3$]. Due to the limited range available in CH_2Cl_2 and the inability of our instrument to measure the reduction potentials in the range −2.7 to −3.5 V, we obtained only the oxidation potentials for complexes **1**−**5** (Table 2). For the electrochemical behavior of Ir(ppy)$_3$ analogues it has been proposed that the oxidative and reductive processes involve the Ir−phenyl and −pyridine moiety of the C^N ligand, respectively. DFT calculations on a similar methyl-substituted Ir(ppy)$_3$ derivative, tris[2-(3-methylpyrid-2-yl)phenyl]iridium(III), provide evidence that the HOMO levels are mostly due to the Ir d_{z^2} orbital with some π-orbital contributions from the phenyl rings, while the LUMO levels in this complex are mostly due to the pyridine π* orbital.[8c] The same description complex has also been reported theoretically for the parent [Ir(ppy)$_3$] complex by Hay.[12] Reversible oxidation waves are observed for all complexes between 0.47 and 0.54 V. It is noteworthy that all of the complexes show lower oxidative potentials than [Ir(ppy)$_3$], indicating the relative ease of oxidation (see Figure 4). This can be ascribed to the great electron-donating ability of the methyl group. Complexes **3** and **5**, in particular, exhibit lower oxidation potentials than those of the other methyl-substituted complexes **1**, **2**, and **4**. Based on our DFT calculations, there are nodes at the 4′- and 6′-positions in the HOMO. In the HOMO, the electron density is mostly dispersed at the 3′- and 5′-positions, and also involves the 1′- and 2′-positions in the phenyl ring. Therefore, the donating effect from the methyl groups at either the 4′- or the 6′-position does not have a significant influence on the HOMO energy levels, while methyl groups at the 3′- or 5′-positions effectively donate electron density to the dmppy moiety, leading to a decrease in the oxidation potentials. The reduction process of the Ir(ppy)$_3$ derivatives was also shown to be due to the C^N ligand and is also affected by the various substituents.[8a] However, one of the key factors that affect the reduction potential in these systems is the degree of conjugation between the phenyl and pyridine rings. More effective conjugation stabilizes the LUMO, leading to a decreased reduction potential. Although we could not observe the reductive process, the reduction potential of **2** should be higher than that of complex **4**, as supported by the structural data.

Another fact affecting the nature of the luminescence in [Ir(ppy)$_3$] is the degree of steric hindrance. Lee et al. have demonstrated that higher photoluminescence quantum efficiencies (Φ_{PL}) and shorter lifetimes in [Ir(ppy)$_3$] derivatives can be achieved by the introduction of sterically hindered spacers, such as pinene.[2c] Although the effect on luminescence, such as excimer formation and from intermolecular π−π interactions, is less demonstrated in octahedral complexes than in square-planar Pt^{II} complexes,[13] these blue-shifted absorption and emission maxima for **2** could be attributed to a reduction of π-orbital conjugation between the phenyl and pyridine rings as well as the lack of intermolecular interactions in the solid state.[16] Therefore, we believe that the observed blue-shifted absorption and emission spectra of complex **2** are probably due to steric factors with a contribution from the strong electron-donating effect of the methyl group.

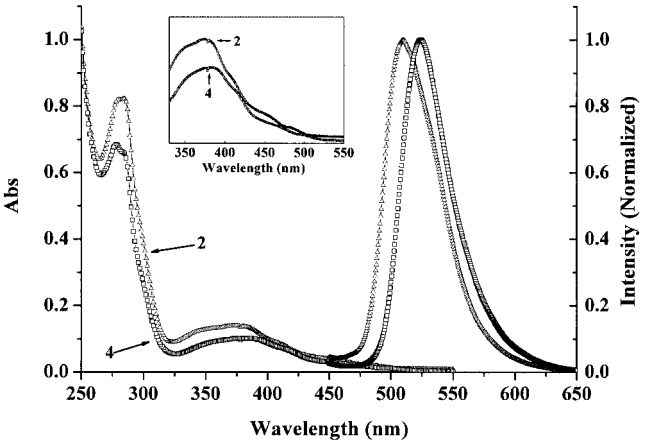

Figure 3. Absorption and emission spectra of **2** (triangles) and **4** (squares) in CH_2Cl_2 at room temperature; inset: MLCT bands of **2** and **4** in the UV/Vis region

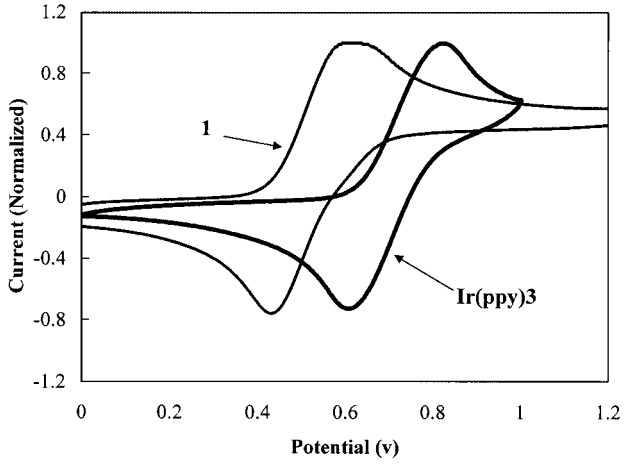

Figure 4. Cyclic voltammograms of **1** and [Ir(ppy)$_3$] in 0.1 M nBu$_4$NPF$_6$ at a scan rate of 50 mV/s

The PL quantum yields were obtained relative to [Ir(ppy)$_3$] (Φ_{PL} = 0.4) and increase in the order [Ir(4,4′dmppy)$_3$] (**2**) > [Ir(3,4′dmppy)$_3$] (**1**) > [Ir(5,4′dmppy)$_3$] (**4**) > [Ir(4,5′dmppy)$_3$] (**3**) > [Ir(5,5′dmppy)$_3$] (**5**). The observed high Φ_{PL} value for **2** can

 © 2004 Wiley-VCH Verlag GmbH & Co. KGaA, Weinheim

be attributed partially to the reduction of intermolecular interactions. The lifetimes of the excited state in all complexes at room temperature are longer (> 1 μs) than that of [Ir(ppy)$_3$], indicating that the substituents generate a number of vibronic modes in the excited state of [Ir(dmppy)$_3$] (see Supporting Information).[15]

Based on our observation with respect to **2**, the blue-shifted emission energy, high PL efficiency and absence of intermolecular interactions are due to the incorporation of methyl groups at the *para* position of the pyridine and the *meta* position of the phenyl rings relative to the Ir atom. This phenomenon shows that the position of the substitution on the pyridine or phenyl rings as well as the electronic effect of the substituent have an influence on the phosphorescence of [Ir(ppy)$_3$] and related systems. When compared to the other positions, the 4- and 4′-positions are quite sensitive to both the photophysical and structural aspects.

Electroluminescent Properties

The electroluminescent properties of compounds **2**, **3** and **4** were investigated. Devices with the Ir phosphor doped into the emissive layer were fabricated. EL-device performance was conducted using complexes **2**, **3** or **4** as dopant and 4,4′-bis(9-carbazolyl)-1,1′-biphenyl (CBP) as host in all cases. In addition, to compare with previous works, EL devices with a similar structure were also fabricated with [Ir(ppy)$_3$], except for the cathode, as reported by Thompson et al.,[1b] by vacuum-deposition techniques. The device structure used in this work is a typical multi-layer, employing indium tin oxide (ITO) as the anode, copper-phthalocyanine (CuPc: 10 nm) as the hole injection material, 4,4′-bis[(1-naphthyl)(phenyl)amino]-1,1′-biphenyl (NPD: 40 nm) as the hole-transport material, **2**, **3**, or **4** as the dopant material, CBP as the host material (20 nm), 2,9-dimethyl-4,7-diphenyl-1,10-phenanthroline (BCP: 10 nm) as the hole-blocking material, aluminium tris(8-quinolinolate) (Alq$_3$: 40 nm) as the electron-transport material, LiF as the electron-injection layer, (1 nm) and Al (100 nm) as the cathode, as shown in Figure 5. All complexes display green emission in the range of 508−520 nm in the EL spectra, which are well matched to those of the PL spectra in solution. There are no characteristic emission peaks from CBP or Alq$_3$, indicating that the emission originates mostly from the dopant (Figure 6). Furthermore, these results support the proposal that effective energy transfer from the host (CBP) to the dopant (Ir complex) occurs in the emissive layer. More detailed EL characteristics are shown in Table 3. The turn-on voltages (defined as 1 mA/cm^2) of [Ir(ppy)$_3$], **2**, **3** and **4** are 3.4, 5.6, 5.1 and 4.6 V, respectively (Figure 7). The intermolecular interactions (e.g. π−π stacks in molecular crystals) in the solid state and the ability to trap charges in the emissive layer are considered the most important factors in determining the operating voltage. The strong electronic coupling and intermolecular interactions in the molecular crystals contribute to effective injection and transport of charges, leading to lower operating voltages.[16] On the other hand, effective charge-trapping by the dopants gives rise to increasing driving voltages in OLEDs.[17] If the dopant material functions as a hole trap, the HOMO level of the dopant could be above that of the host material. In other words, materials having a lower oxidation potential can function as effective hole traps in OLEDs. Therefore, the observed higher operating voltages for **2** and **4**, relative to [Ir(ppy)$_3$], are predominantly caused by effective hole trapping.[18] These results are consistent with the electrochemical behaviors of **1**−**5** and [Ir(ppy)$_3$]. The brightness of the devices at 20 mA/cm^2 are 4543 cd/m^2, 4470 cd/m^2, 3551 cd/m^2 and 3235 cd/m^2, for **2**, **3**, **4** and [Ir(ppy)$_3$], respectively. With increasing current density, the external quantum efficiency of devices containing **2**, **3**, **4** and [Ir(ppy)$_3$] gradually decreased. Similar results have been reported previously, and are attributed to the increase of triplet-triplet annihilation of the exciton at high voltage levels. As expected, the device fabricated using complex **2** exhibits higher brightness and external quantum efficiency, as well as stronger EL intensity, than those of the other complexes or [Ir(ppy)$_3$] (see Figures 8 and 9). In contrast, the device efficiencies of **1** and **4** are lower than that of [Ir(ppy)$_3$] under the same conditions. The positions of the substituents as well as the nature of the substituents on the ppy rings could be important factors in achieving high electroluminescent efficiency in substituted Ir(ppy)$_3$ systems.

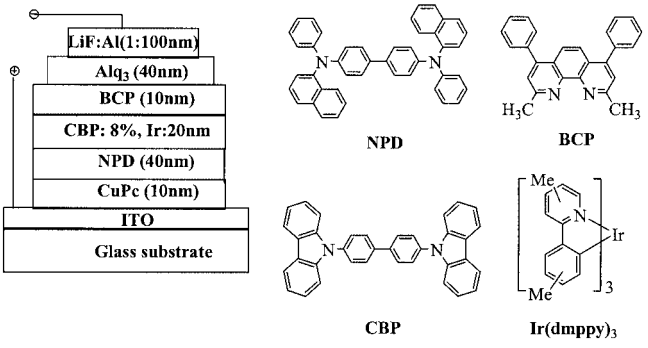

Figure 5. Device structures and molecular structure used in this study

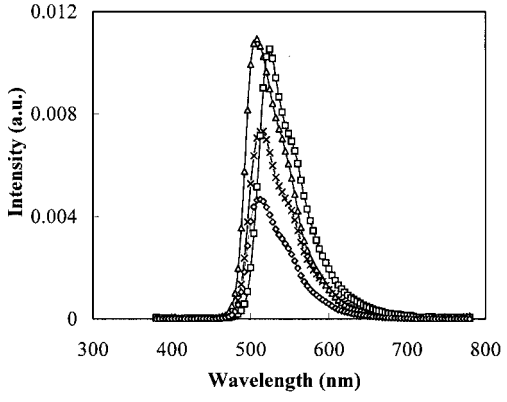

Figure 6. EL spectra of [Ir(ppy)$_3$], (X), **2** (triangles), **3** (squares) and **4** (diamonds) device structure: ITO/NPD/CBP-Ir(dmppy)$_3$/BCP/Alq$_3$/LiF-Al)

 © 2004 Wiley-VCH Verlag GmbH & Co. KGaA, Weinheim

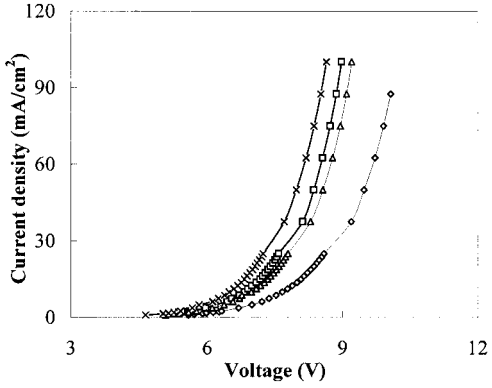

Figure 7. Voltage versus current-density characteristics of $[Ir(ppy)_3]$- (X), **2**- (triangles), **3**- (squares), and **4**-doped (diamonds) devices

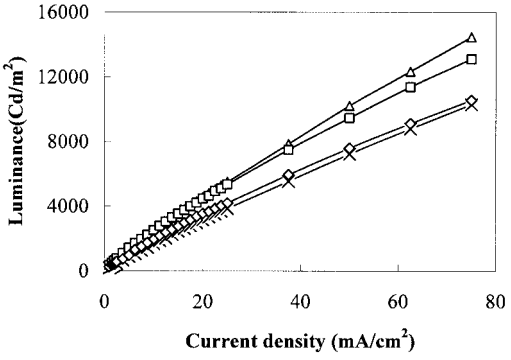

Figure 8. Luminance versus current-density characteristics of $[Ir(ppy)_3]$- (X), **2**- (triangles), **3**- (squares), and **4**-doped (diamonds) devices

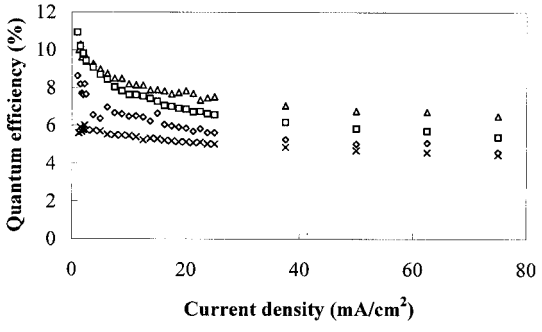

Figure 9. External quantum efficiency versus current-density characteristics of of $[Ir(ppy)_3]$- (X), **2**- (triangles), **3**- (squares), and **4**-doped (diamonds) devices

Conclusion

A series of dimethyl-substituted $[Ir(dmppy)_3]$ derivatives have been synthesized and characterized, including their photo-electroluminescent and electrochemical properties. The nature of their solid-state structures depends on the position of the methyl groups on the phenyl and pyridine rings. These methyl groups give rise to several distinct triplet states, affecting the electrochemical behavior and electroluminescence of the Ir^{III} complexes. As expected, they also considerably perturb the absorption, redox potentials, and photo- and electroluminescent efficiency. Lower oxidation potentials than that of $[Ir(ppy)_3]$ were observed in all cases, indicating that the methyl group induces a relatively easy oxidation and leads to effective hole trapping. Complex **2**, which has methyl groups at the 4′- and 4-positions exhibits a brighter green emission and higher Φ_{PL} than $[Ir(ppy)_3]$. In addition, a significant improvement of the external quantum efficiency (η_{ext} = 11%), which is nearly 200% higher than that of $[Ir(ppy)_3]$, is also observed in OLEDs. Further investigation on the effects on luminescent properties depending on other bulky functional groups into various positions of the ppy ligand is currently in progress.

Experimental Section

General Considerations. All experiments were performed under dry N_2 using standard Schlenk techniques. All solvents were freshly distilled from appropriate drying reagents prior to use. All starting materials were purchased from either Aldrich or Strem and used without further purification. Methyl-substituted phenyl or pyridine compounds were synthesized by slight modification of previous reports.[8]

Measurements: ^1H NMR and mass spectra were recorded with a Bruker DRX 500 MHz spectrometer and JEOL-JMS 700 instrument, respectively. UV/Vis and photoluminescent spectra for all samples with concentrations in the range of 10−50 μM were obtained with a Lambda 900 UV/Vis spectrometer and a Perkin−Elmer Luminescence spectrometer LS 50B. All solutions for photophysical experiments were degassed with more than three repeated freeze-pump-thaw cycles in a vacuum line. Melting points were determined with an Electrothermal 9100 apparatus. Emission lifetimes were measured with the fourth harmonic of a Q-switched Nd-YAG laser using the upper excited state energy transfer with a pulse duration of 6 ns and a repetition rate of 10 Hz. The laser beam had a diameter of 5 mm and an optical power of about 50 mJ. The emission from the film was recorded by a gated intensified diode array detector through a monochromator. The system allows for an integration time (gate width) of detection from 100 ns to 10

Table 3. Electroluminescent data of $[Ir(ppy)_3]$ and **2**-, **3**- and **4**-doped OLEDs

	Luminance [Cd/m²] at 20 mA/cm²	Operating voltage [V][a]	External quantum efficiency (%) at 1 mA/cm²	at 10 mA/cm²	at 50 mA/cm²
$Ir(ppy)_3$	3156	4.9	6.0	5.4	4.7
2	4543	5.6	11	8.2	6.8
3	4470	5.1	10.9	7.6	5.8
4	3551	4.6	8.6	6.5	5.0

[a] The operating voltages in all cases were defined as 1 mA/cm².

 © 2004 Wiley-VCH Verlag GmbH & Co. KGaA, Weinheim

ms and a variable delay after excitation. Cyclic voltammetry was performed with an Autolab potentiostat from Echochemie under nitrogen in a one-compartment electrolysis cell consisting of a platinum wire working electrode, a platinum wire counter electrode, and a quasi Ag/AgCl reference electrode. Cyclic voltammograms were monitored at scan rates of either 100 $mV \cdot s^{-1}$ or 50 $mV \cdot s^{-1}$ and recorded in distilled dichloromethane. The concentration of the complex was maintained at 0.5 mM or less and each solution contained 0.1 M of tetrabutylammonium hexafluorophosphate (TBAP) as the electrolyte. The ferrocenium/ferrocene couple (0.40V) was used as the internal standard.

X-ray Crystallographic Analysis: Suitable crystals of **2** and **4** were obtained from slow vapor diffusion of toluene/benzene/hexane (2:1:1) into a solution of **2** or **4** in CH_2Cl_2. The crystal of **2** or **4** was attached to a glass fiber and mounted on a Bruker SMART diffractometer equipped with a graphite-monochromated Mo-K_α (λ = 0.71073 Å) radiation, operating at 50 kV and 30 mA and a CCD detector; 45 frames of two-dimensional diffraction images were collected and processed to obtain the cell parameters and orientation matrix. All data collections were performed at 173 K. The data collection 2θ ranges were 3.1−56.62° for **2** and 4.26−56.56° for **4**. No significant decay was observed during the data collection. The raw data were processed to give structure factors using the SAINT program. Each structure was solved by direction methods and refined by full-matrix least squares against F^2 for all data using the SHELXTL software (version 5.10).[19] All non-hydrogen atoms in compounds **2** and **4** were anisotropically refined. All other hydrogen atoms were included in the calculated positions and their contributions in structural factor calculations were included. Compound **2** cocrystallizes with benzene in the monoclinic crystal system with space group $P2_1/n$. The disordered benzene molecule was not modeled successfully. However, hydrogen atoms in benzene were included in the calculated positions and their contributions included in the structure factor. Compound **4** belongs to the cubic crystal system ($I\bar{4}3d$ space group). Crystal data for **2** and **4** are summarized in Table 4. Selected bond lengths and angles for **2** and **4** are given in Table 1. In the case of **2**, since the large positive (3.236 $e/Å^{-3}$) and negative (−3.306 $e/Å^{-3}$) difference Fourier peaks are located at short distances from Ir (0.84 Å and 0.90 Å, respectively), these peaks can be attributed to ghosts of the heavy Ir atom.[20] CCDC-220262 (**2**) and -220263 (**4**) contain the supplementary crystallographic data for this paper. These data can be obtained free of charge at www.ccdc.cam.ac.uk/conts/retrieving.html [or from the Cambridge Crystallographic Data Centre, 12 Union Road, Cambridge CB2 1EZ, UK; Fax: (internat.) + 44-1223-336 033; E-mail: deposit@ccdc.cam.ac.uk].

Fabrication of Electroluminescent Devices: A glass substrate precoated with indium tin oxide (ITO) was cleaned in an ultrasonic bath of acetone, followed by 2-propanol. Surface treatment was carried out by exposing ITO to a UV ozone plasma. OLEDs withg CBP as host material were fabricated as follows. The hole-injecting layer, a 10 nm thick film of CuPc was deposited on the ITO surface by high-vacuum thermal evaporation and a 40 nm thickness α-NPD as hole-transporting layer was deposited onto the CuPc. An [Ir(dmppy)$_3$]-doped (dmppy = dimethyl-substituted ppy) host CBP layer was thermally co-evaporated onto the α-NPD layer. The [Ir(dmppy)$_3$] doping concentration was 8% in CBP. A 10 nm thick BCP (2,9-dimethyl-4,7-diphenyl-1,10-phenanthroline) layer was then deposited as the exciton-blocking layer, followed by a 40 nm thick Alq_3 layer as an electron-transporting layer. Finally, LiF (1 nm) and Al (100 nm) were deposited on top of the organic layers by thermal evaporation. The fabricated multilayer organic light-emitting devices have the structure of ITO/CuPc (10 nm)/α-NPD (40 nm)/CBP-Ir(dmppy)$_3$ (20 nm)/BCP (10 nm)/Alq_3 (40 nm)/LiF (1 nm)/Al (100 nm).

Table 4. Crystallographic data for **2** and **4**

	2	**4**
Empirical formula	$C_{39}H_{36}IrN_3 \cdot 0.5C_6H_6$	$C_{39}H_{36}IrN_3$
Formula mass	777.96	738.91
Space group	$P2_1/n$	$I\bar{4}3d$
a [Å]	15.5695(9)	23.4008(10)
b [Å]	14.6261(8)	23.4008(10)
c [Å]	16.1088(9)	23.4008(10)
β [°]	111.8840(10)	90
V [Å^3]	3403.0(3)	12814.2(9)
Z	4	16
$D_{calcd.}$ [$Mg \cdot cm^{-3}$]	1.518	1.532
μ [cm^{-1}]	39.56	41.99
$2\theta_{max}$ [°]	56.62	56.64
No. of refections measured	21580	39294
No. of refections used	7996	2650
R_{int}	0.1391	0.1027
No. of parameters	415	130
Final R [$I > 2\sigma(I)$]		
$R1$[a]	0.0525	0.0341
$wR2$[b]	0.1182	0.0755
R (all data)		
$R1$[a]	0.0950	0.0429
$wR2$[b]	0.1582	0.0800
Goodness of fit on F^2	1.006	1.253

General Preparation of [Ir(n,n'-dmppy)$_3$]: The corresponding complexes were synthesized by a slight modification of Watt's procedures.[8b] A solution of the corresponding methyl-substituted phenylpyridine ligand (6 equiv., 2.64 mmol) in glycerol was added at ambient temperature under N_2 to a stirred anhydrous degassed glycerol solution (20 mL) of [Ir(acac)$_3$] (0.217 g, 0.44 mmol). The reaction mixture was refluxed for 24−48 h. The reaction mixture was then cooled to room temperature, 1 N HCl was added, and the mixture filtered to give a crude product. The pure complexes were obtained by chromatographic workup on silica gel using ethyl acetate/hexane as eluent.

[Ir(3,4′dmppy)$_3$] (1): ^{1}H NMR (CD_2Cl_2, 25 °C): δ = 7.86 (d, J = 8.4 Hz, 3 H), 7.46 (dd, J = 7.5, 0.9 Hz, 3 H), 7.36 (dd, J = 5.4, 1.5 Hz, 3 H), 6.67−6.78 (m, overlap, 9 H), 2.82 (s, 9 H, CH_3), 2.12 (s, 9 H, CH_3) ppm. MS (EI): m/z = 739 [M^+]. $C_{39}H_{36}IrN_3$ (739.25): calcd. C 63.39, H 4.91, N 5.69; found C 63.31, H 4.89, N 5.67.

[Ir(4,4′dmppy)$_3$] (2): ^{1}H NMR (CD_2Cl_2, 25 °C): δ = 7.71 (s, 3 H), 7.56 (d, J = 8.1 Hz,, 3 H), 7.36 (d, J = 5.47 Hz, 3 H), 6.71−6.74 (m, overlap, 6 H), 6.61 (dd, J = 1.2, 0.3 Hz, 3 H), 2.44 (s, 9 H, CH_3), 2.12 (s, 9 H, CH_3) ppm. MS (EI): m/z = 739 [M^+]. $C_{39}H_{36}IrN_3$ (739.25): calcd. C 63.39, H 4.91, N 5.69; found C 63.38, H 4.95, N 5.71.

[Ir(4,5′dmppy)$_3$] (3): ^{1}H NMR (CD_2Cl_2, 25 °C): δ = 7.74 (s, 3 H), 7.50 (s, 3 H), 7.42 (d, J = 5.7 Hz, 3 H), 6.75 (dd, J = 1.5, 0.9 Hz, 3 H), 6.64 (d, J = 0.6 Hz, 6 H), 2.44 (s, 9 H, CH_3), 2.27 (s, 9 H, CH_3) ppm. MS (EI): m/z = 739 [M^+]. $C_{39}H_{36}IrN_3$ (739.25): calcd. C 63.39, H 4.91, N 5.69; found C 63.40, H 4.86, N 5.61.

[Ir(5,4′dmppy)$_3$] (4): ^{1}H NMR (CD_2Cl_2, 25 °C): δ = 7.80 (d, J = 8.4 Hz, 3 H), 7.55 (d, J = 7.8 Hz, 3 H), 7.47 (ddd, J = 7.8, 2.1, 0.6 Hz, 3 H), 7.31 (dd, J = 1.2, 0.9 Hz, 3 H), 6.72 (dd, J = 7.8, 1.2 Hz, 6 H), 6.58 (d, J = 0.9 Hz, 3 H), 2.15 (s, 9 H, CH_3), 2.12 (s, 9 H, CH_3) ppm. MS (EI): m/z = 739 [M^+]. $C_{39}H_{36}IrN_3$ (739.25): calcd. C 63.39, H 4.91, N 5.69; found C 63.30, H 4.84, N 5.62.

 © 2004 Wiley-VCH Verlag GmbH & Co. KGaA, Weinheim

[Ir(5,5′dmppy)$_3$] (5): ^{1}H NMR (CD_2Cl_2, 25 °C): δ = 7.83 (d, J = 8.4 Hz, 3 H), 7.50 (m, overlap, 6 H), 7.37 (dd, J = 1.2, 0.6 Hz, 3 H), 6.59−6.67 (m, overlap, 6 H), 2.27 (s, 9 H, CH_3), 2.17 (s, 9 H, CH_3) ppm. MS (EI): m/z = 739 [M^+]. $C_{39}H_{36}IrN_3$ (739.25): calcd. C 63.39, H 4.91, N 5.69; found C 63.43, H 4.85, N 5.67.

Supporting Information: Spectroscopic data (^{1}H NMR, mass, and absorption/emission spectra), lifetime determination, electrochemical data and crystal-packing diagrams.

Acknowledgments

This work was supported by LG Electronics' national program funded by the Ministry of Commerce, Industry and Energy (project code: 00014756), the Information Technology Research Center (ITRC) under the Ministry of Information & Communications and the Korea Research Foundation Grant (KRF-2002-050-C00010).

[1] [1a] M. A. Baldo, M. E. Thompson, S. R. Forrest, *Nature* **2000**, *403*, 750. [1b] M. A. Baldo, S. Lamansky, P. E. Burrows, M. E. Thompson, S. R. Forrest, *Appl. Phys. Lett.* **1999**, *75*, 4. [1c] C. Adachi, M. A. Baldo, S. R. Forrest, M. E. Thompson, *Appl. Phys. Lett.* **2000**, *77*, 904. [1d] R. Gao, D. G. Ho, H. Hernandez, M. Selke, D. Murphy, P. I. Djurovich, M. E. Thompson, *J. Am. Chem. Soc.* **2002**, *124*, 14828. [1e] S. Lamansky, P. I. Djurovich, D. Murphy, F. Abdel-Razzaq, H.-E. Lee, C. Adachi, P. E. Burrows, S. R. Forrest, M. E. Thompson, *J. Am. Chem. Soc.* **2001**, *123*, 4304. [1f] S. Lamansky, R. C. Kwong, M. Nugent, P. I. Djurovich, M. E. Thompson, *Org. Electrochem.* **2001**, *2*, 53. [1g] M. Ikai, S. Tokito, Y. Sakamoto, T. Suzuki, Y. Taga, *Appl. Phys. Lett.* **2001**, *79*, 156. [1h] C. Adachi, M. A. Baldo, S. R. Forrest, M. E. Thompson, *J. Appl. Phys.* **2001**, *90*, 5048. [1i] M-J. Yang, T. Tsutsui, *Jpn. J. Appl. Phys.* **2000**, *39*, L828. [1j] E. Vander Donckt, B. Camerman, F. Hendrick, R. Herne, R. Vandeloise, *Bull. Soc. Chim. Belg.* **1994**, *103*, 207. [1k] Y. Amao, Y. Ishikawa, I. Okura, *Anal. Chim. Acta* **2001**, *445*, 177. [1l] D. Song, S. Wang, *Eur. J. Inorg. Chem.* **2003**, *20*, 3744.

[2] [2a] D. F. O'Brien, M. A. Baldo, M. E. Thompson, S. R. Forrest, *Appl. Phys. Lett.* **1999**, *74*, 442. [2b] J.-P. Duan, P.-P. Sun, C.-H. Cheng, *Adv. Mater.* **2003**, *15*, 224. [2c] H. Z. Xie, M. W. Liu, O. Y. Wang, X. H. Zhang, C. S. Lee, L. S. Hung, S. T. Lee, P. F. Teng, H. L. Kwong, H. Zheng, C. M. Che, *Adv. Mater.* **2001**, *13*, 1245. [2d] Y.-Y. Noh, C.-L. Lee, J.-J. Kim, K. Yase, *J. Chem. Phys.* **2003**, *118*, 2853. [2e] Y. Wang, N. Herron, V. V. Grushin, D. LeCloux, V. Petrov, *Appl. Phys. Lett.* **2001**, *79*, 449. [2f] F. Neve, A. Crispini, S. Serroni, F. Loiseau, S. Campagna, *Inorg. Chem.* **2001**, *40*, 1093. [2g] G. Calogero, G. Giuffrida, S. Serroni, V. Ricevuto, S. Campagna, *Inorg. Chem.* **1995**, *34*, 541. [2h] F. Neve, A. Crispini, S. Campagna, S. Serroni, *Inorg. Chem.* **1999**, *38*, 2250. [2i] S. M. Zakeeruddin, M. K. Nazeeruddin, P. Pechy, F. P. Rotzinger, R. Humphry-Baker, K. Kalyanasundaram, M. Grätzel, V. Shklover, T. Haibach, *Inorg. Chem.* **1997**, *36*, 5937.

[3] [3a] C. Adachi, R. C. Kwong, P. Djurovich, V. Adamovich, M. A. Baldo, M. E. Thompson, S. R. Forrest, *Appl. Phys. Lett.* **2001**, *79*, 2082. [3b] Y. Kawamuura, S. Yanagida, S. R. Forrest, *J. Appl. Phys.* **2002**, *92*, 87. [3c] F.-C. Chen, Y. Yang, M. E. Thompson, J. Kido, *Appl. Phys. Lett.* **2002**, *80*, 2308.

[4] [4a] B. D. Alleyne, V. adamovich, J. Brooks, P. I. Djurovich, M. E. Thompson, *224th ACS National Meeting, USA* **2002**, INOR-204. [4b] M. E. Thompson, *4th ICEL (International Conference on Electroluminescence of Molecular Materials and Related Phenomena), Korea* **2003**, O-41.

[5] [5a] V. V. Grushin, N. Herron, D. D. LeCloux, W. J. Marshall, V. A. Petrov, Y. Wang, *Chem. Commun.* **2001**, 1494. [5b] S. Lamansky, P. Djurovich, D. Murphy, F. Abdel-Razzaq, R. Kwong, I. Tsyba, M. Bortz, B. Mui, R. Bau, M. E. Thompson, *Inorg. Chem.* **2001**, *40*, 1704.

[6] [6a] S. O. Jung, Q. H. Zhao, H.-S. Kim, Y.-H. Kim, J.-S. Kim, C.-L. Lee, J.-J. Kim, B.-K. An, S. Y. Park, S.-K. Kwon, *224th ACS National Meeting, Boston, USA* **2002**, 18−22. [6b] S. O. Jung, Y.-H. Kim, Y.-H. Kim, Y. Kang, H.-Y. Oh, S.-K. Kwon, *226th ACS National Meeting, New York, USA* **2003**, 7−11. [6c]S. O. Jung, Y. Kang, H.-S. Kim, Y.-H. Kim, K. Yang, S.-K. Kwon, *Bull. Korean Chem. Soc.* **2003**, *24*, 1521. [6d] C.-L. Lee, K. B. Lee, J.-J. Kim, *Appl. Phys. Lett.* **2000**, *77*, 2280. [6e] R. R. Das, C.-L. Lee, Y.-Y. Noh, J.-J. Kim, *Opt. Mater.* **2002**, *21*, 143.

[7] Recent review: [7a] J. Hassan, M. Sévignon, C. Gozzi, E. Schulz, M. Lemaire, *Chem. Rev.* **2002**, *102*, 1359. [7b] A. Suzuki, *J. Organomet. Chem.* **1999**, *576*, 147.

[8] [8a] For a recent report, see: A. B. Tamayo, B. D. Alleyne, P. I. Djurovich, S. Lamansky, I. Tsyba, N. N. Ho, R. Bau, M. E. Thompson, *J. Am. Chem. Soc.* **2003**, *125*, 7377. [8b] K. Dedeian, P. I. Djurovich, F. O. Garces, G. Carlson, R. J. Watts, *Inorg. Chem.* **1991**, *30*, 1685. [8c] M. G. Colombo, T. C. Brunold, T. Riedener, H. U. Guedel, M. Fortsch, H.-B. Buergi, *Inorg. Chem.* **1994**, *33*, 545.

[9] [9a] R. Urban, R. Krämer, S. Mihan, K. Polborn, B. Wagner, W. Beck, *J. Organomet. Chem.* **1996**, *517*, 191. [9b] F. Neve, A. Crispini, *Eur. J. Inorg. Chem.* **2000**, 1039.

[10] F. O. Garces, K. Dedeian, N. L. Keder, R. J. Watts, *Acta Crystallogr., Sect. C* **1993**, *49*, 1117.

[11] [11a] K. Ichimura, T. Kobayashi, K. A. King, R. J. Watts, *J. Phys. Chem.* **1987**, *91*, 6104. [11b] K. A. King, P. J. Spellane, R. J. Watts, *J. Am. Chem. Soc.* **1985**, *107*, 1431.

[12] P. J. Hay, *J. Phys. Chem. A* **2002**, *106*, 1634.

[13] [13a] S.-C. Chan, M. C. W. Chan, Y. Wang, C.-M. Che, K.-K. Cheung, N. Zhu, *Chem. Eur. J.* **2001**, *7*, 4180 and references cited therein. [13b] J. Brook, Y. Babayan, S. Lamansky, P. I. Djurovich, I. Tsyba, R. Bau, M. E. Thompson, *Inorg. Chem.* **2002**, *41*, 3055.

[14] The emission spectra of all complexes, except **2**, in the solid state exhibit red-shifted and broader bands with similar maximum emission wavelengths to those of the corresponding spectra in solution under the same conditions. In contrast, complex **2** still shows a blue-shifted emission in the solid state relative to [Ir(ppy)$_3$].

[15] J. R. Lakowicz, *Principles of Fluorescence Spectroscopy*, Kluwer Academic, New York, **1999**.

[16] L. S. Sapochak, A. Padmaperuma, N. Washton, F. Endrino, G. T. Schmett, J. Marshall, D. Fogarty, P. E. Burrows, S. R. Forrest, *J. Am. Chem. Soc.* **2001**, *123*, 6300.

[17] [17a] P. A. Lane, L. C. Palilis, D. F. O'Brien, C. Giebeler, A. J. Cadby, D. G. Lidzey, A. J. Campbell, W. Blau, D. D. C. Bradley, *Phys. Rev. B.* **2001**, *63*, 235206. [17b] D. F. O'Brien, C. Giebeler, R. B. Fletcher, A. J. Cadby, L. C. Palilis, D. G. Lidzey, P. A. Lane, D. D. C. Bradley, W. Blau, *Synth. Met.* **2001**, *116*, 379. [17c] X. Gong, J. C. Ostrowski, D. Moses, G. C. Bazan, A. J. Heeger, *Adv. Funct. Mater.* **2003**, *13*, 439.

[18] The emission bands originating from CBP (host) or NPD at a lower concentration (0.1 wt.-%) of dopant (Ir complexes) in EL devices were not observed in all cases.

[19] *SHELXTL NT Crystal Structure Analysis Package*, version 5.14, Bruker AXS, Analytical X-ray System, Madison, WI, USA, **1999**.

[20] K.-M. Park, I. Yoon, B. S. Yoo, J. B. Choi, S. S. Lee, B. G. Kim, *Acta Crystallogr., Sect. C* **2000**, *56*, 1191.

Received February 12, 2004
Early View Article
Published Online June 15, 2004

 © 2004 Wiley-VCH Verlag GmbH & Co. KGaA, Weinheim

Synthesis, Structures and Catalytic Properties of Bis(2-pyridylimino)-isoindolatopalladium Complexes

Bettina Siggelkow,[a] Markus B. Meder,[a] Christian H. Galka,[a] and Lutz H. Gade*[a]

Keywords: Hydrogenation / N ligands / Palladium

Reaction of the bis(2-pyridylimino)isoindole derivatives (10-Me)-BPI (**1a**), (11-Me)-BPI (**1b**), (11-Br)-BPI (**1c**), (4-Me)-BPI (**1d**) and 4-Me-10-*t*BuBPI (**1e**) with $[PdCl_2(PhCN)_2]$ and triethylamine in benzene gave the square-planar palladium(II) complexes [PdCl{(10-Me)-BPI}] (**2a**), [PdCl{(11-Me)-BPI}] (**2b**), [PdCl{(11-Br)-BPI}] (**2c**), [PdCl(4-MeBPI)] (**2d**) and [PdCl(4-Me-10-*t*BuBPI)] (**2e**), respectively. Extraction of the crude product **2b** with aqueous sodium carbonate solution led to the formation of the dinuclear carbonato-bridged complex $[\{(11\text{-Me-BPI})Pd\}_2(\mu\text{-}CO_3)]$ (**3**) which was characterized by an X-ray structure analysis. Reaction of 11-Br-BPI (**1c**) with a large excess (6 equiv.) of the acetylenes Me_3SiCCH, Ph_3SiCCH and PhCCH under Sonogashira conditions gave the alkynylated derivatives 11-(Me_3SiCC)-BPI (**4a**), 11-(Ph_3SiCC)-BPI (**4b**) and 11-(PhCC)-BPI (**4c**), which were metallated with bis(benzonitrile)dichloropalladium(II) to yield the Pd^{II} complexes [PdCl{11-(Me_3SiCC)-BPI}] (**5a**), [PdCl{11-(Ph_3SiCC)-BPI}] (**5b**) and [PdCl{11-(PhCC)-BPI}] (**5c**), respectively. The activity of **2b** in the catalytic hydrogenation of C=C double bonds was tested for the reaction with styrene, 1-octene and cyclohexene. The stability of the palladium complex, the reproducibility of the reaction kinetics, the different behaviour towards the three olefins chosen as substrates, as well as the possibility of isolating the non-decomposed catalyst after several catalytic runs, provides circumstantial evidence for molecular catalysis with the BPI-palladium complexes.

(© Wiley-VCH Verlag GmbH & Co. KGaA, 69451 Weinheim, Germany, 2004)

Introduction

Polydentate ligands have been widely used in the development of homogeneous hydrogenation catalysts.[1] In most cases phosphane or phosphane-heterodonor ligands have been chosen due to the well-established capacity of the soft phosphane ligators to stabilize the low-valent intermediates in the catalytic cycle.[2] A practical disadvantage in the use of phosphorus-based ligands is their propensity to be oxidized if exposed to air over extended periods of time. This has encouraged research into non-phosphorus-containing hydrogenation catalysts which combine molecular stability with sufficient activity to allow the catalytic hydrogenation of alkenes at atmospheric dihydrogen pressure.[3]

Costa, Pelagatti et al. have recently studied the hydrogenation activity of palladium(II) complexes stabilized by polydentate P∩N∩O,[4,5] N∩N∩S,[6] and N∩N∩N ligands.[7] In particular, the use of tridentate nitrogen donor ligands gave rise to relatively efficient Pd^{II} hydrogenation catalysts. The activation of dihydrogen is thought to involve the protonation of a basic site in the polydentate N-ligand and this formally protonated site is subsequently involved in the elimination of the saturated reaction product.

In view of this work on palladium-catalyzed homogeneous hydrogenations we have studied the catalytic activity of Pd complexes containing derivatives of the well-established bis(2-pyridylimino)isoindolate (BPI) ligands (**A**).[8–10] These ligands have been extensively studied in oxidation catalysis;[11] however, there is as yet no report of their application to other catalytic reactions. This class of formally anionic ligands appeared to be promising for the development of new palladium-based hydrogenation catalysts due to their tendency to tautomerise and act as neutral ligands **A′**, as has been recently established for the free ligand in solution and for the Cd complex **B** by X-ray diffraction.[12] Given the work by Costa, Pelagatti and coworkers,[4–7] this capacity of the BPI ligands was thought to favour homogeneous hydrogenation activity of their palladium(II) complexes.

There are only two previous reports in the literature of the coordination of BPI ligands to divalent palladium,[13,14] although with no further investigation of their reactivity. In this work we report the synthesis and structural characterization of several new BPI-Pd complexes, the first results of the integration of the BPI-ligand unit into more elaborate molecular architectures and, finally, a first study of the hydrogenation activity of a BPI-Pd derivative towards several alkenes.

[a] Anorganisch-Chemisches Institut, Universität Heidelberg, Im Neuenheimer Feld 270, 69120 Heidelberg, Germany
E-mail: lutz.gade@uni-hd.de

 © 2004 Wiley-VCH Verlag GmbH & Co. KGaA, Weinheim **DOI: 10.1002/ejic.200400179**

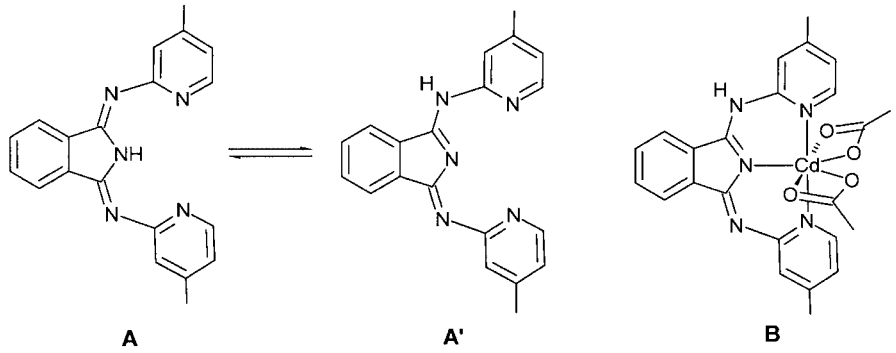

Results and Discussion

Synthesis and Structural Characterization of the BPI-Palladium Complexes

The bis(2-pyridylimino)isoindole derivatives **1a**−**1e** were prepared according to the synthetic route first described by Siegl et al. by reaction of a 2-aminopyridine derivative with an *ortho*-phthalodinitrile (Scheme 1).[9] A slight modification of the reaction conditions — the replacement of *n*-butanol by *n*-hexanol as the solvent — gave significantly better yields of the ligand precursors than those reported in the literature.

The preparation of the corresponding square-planar palladium(II) complexes **2a**−**2e** was carried out in benzene using $[PdCl_2(PhCN)_2]$ as the Pd^{II} precursor and triethylamine as auxiliary base (Scheme 1). The coordination of the BPI ligands to palladium(II) can be conveniently monitored by ^1H NMR spectroscopy. The most characteristic change in the NMR spectra is the coordination shift of the 6-pyridyl protons from ca. $\delta = 8.4$ ppm in the free ligand to ca. $\delta = 9.5$ ppm in the palladium complexes, and the disappearance of the NH resonance of the isoindole unit.

Since there is no previous example of an X-ray structure analysis of a BPI-Pd complex, and in order to establish the structural details of these compounds, single-crystal X-ray diffraction studies of compounds [PdCl(11-Br-BPI)] (**2c**) and [PdCl(4-Me-10-*t*Bu-BPI)] (**2e**) were carried out. Their molecular structures are displayed in Figure 1 and 2, respectively, and their principal bond lengths and angles are compared in Table 1.

Both complexes are mononuclear and possess the expected square-planar coordination geometry. The central palladium atom is coordinated to the three ligating nitrogen atoms of the BPI ligand (N1, N3 and N5) as well as to the chloro ligand. The chloropalladium units are slightly displaced from the molecular plane defined by the three N atoms, as is evident from the N1−Pd−N5 angles of 172.0(1)° and 171.0(2)° for **2c** and **2e**, respectively. This distortion is reflected in an even more pronounced way by the N3−Pd−Cl angles [**2c**: 167.75(9)°; **2e**: 166.3(2)°] and may be due to the repulsive interaction of the chloro ligand with the *ortho*-hydrogen atoms of the pyridyl groups. The Pd−N bond lengths to the pyridyl units are in the range of 2.053−2.071 Å, whereas the amide-type central Pd−N3 bond length is contracted to 1.962(3) Å for **2c** and 1.957 Å for **2e**. This pattern is consistent with the previously reported structural data of BPI-transition metal complexes.[9,10] The Pd−Cl bond lengths of 2.333(1) Å (**2c**) and 2.332(3) Å (**2e**) are similar to those found for other chloropalladium complexes bearing tridentate ligands.[15]

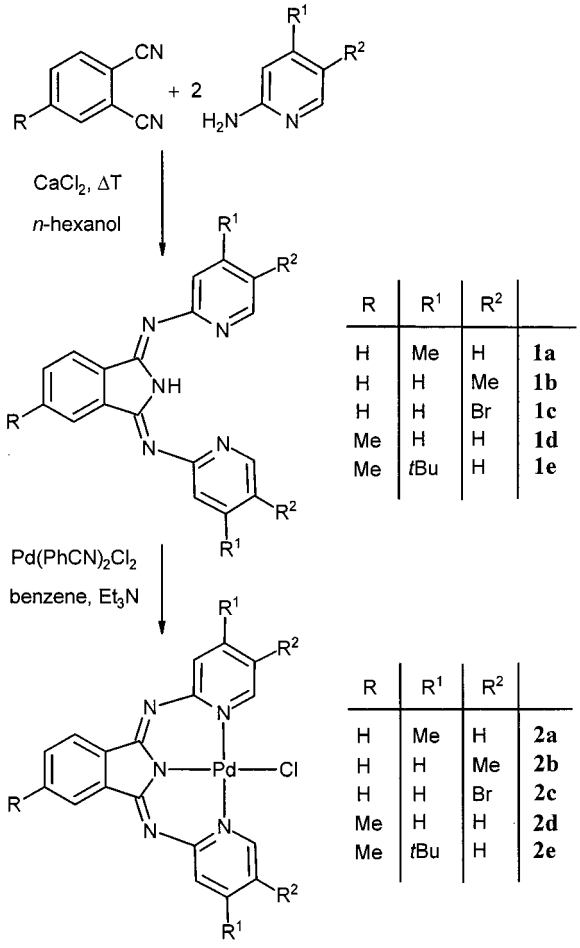

R	R¹	R²	
H	Me	H	**1a**
H	H	Me	**1b**
H	H	Br	**1c**
Me	H	H	**1d**
Me	*t*Bu	H	**1e**

R	R¹	R²	
H	Me	H	**2a**
H	H	Me	**2b**
H	H	Br	**2c**
Me	H	H	**2d**
Me	*t*Bu	H	**2e**

Scheme 1. Synthesis of the BPI-ligands **1a**−**1e** and their palladation to give the Pd^{II} complexes **2a**−**2e**

In the metallation of the BPI ligand-precursors stoichiometric amounts of triethylammonium chloride are formed, which are usually extracted with water after the complete conversion into the complexes. In the synthesis of **2b** the

 © 2004 Wiley-VCH Verlag GmbH & Co. KGaA, Weinheim

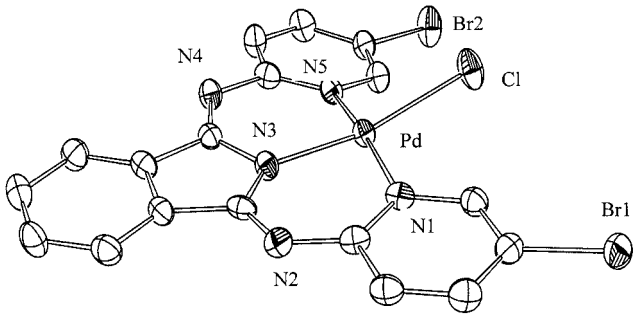

Figure 1. Molecular structure of complex **2c**; selected bond lengths and angles are listed in Table 1

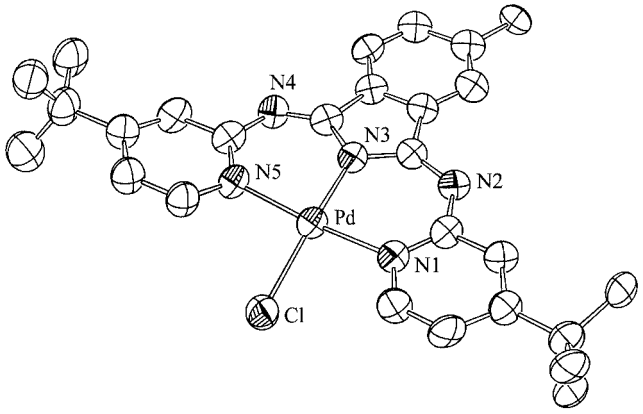

Figure 2. Molecular structure of complex **2e**; selected bond lengths and angles are listed in Table 1

Table 1. Selected bond lengths (Å) and angles (°) of complexes **2c** and **2e**

	2c	**2e**
Pd−N1	2.068(3)	2.071(7)
Pd−Cl	2.333(1)	2.332(3)
Pd−N5:	2.053(3)	2.058(7)
C2−Br1	1.895(4)	–
Pd−N3	1.962(3)	1.957(6)
C16−Br2	1.884(4)	–
Cl−Pd−N1	92.85(9)	92.2(2)
Cl−Pd−N3	167.75(9)	166.31(19)
Cl−Pd−N5	89.95(8)	91.1(2)
N1−Pd−N5	172.0(1)	171.0(2)

crude product was extracted with an aqueous sodium carbonate solution on one occasion, which led to a partial exchange of the chloro ligand by the carbonate dianion. From this mixture the dinuclear carbonato-bridged complex [{(11-Me-BPI)Pd}$_2$(μ-CO_3)] crystallized and its structure was established by a single-crystal X-ray structure analysis. Its molecular structure is displayed in Figure 3 along with the principal bond lengths and angles.

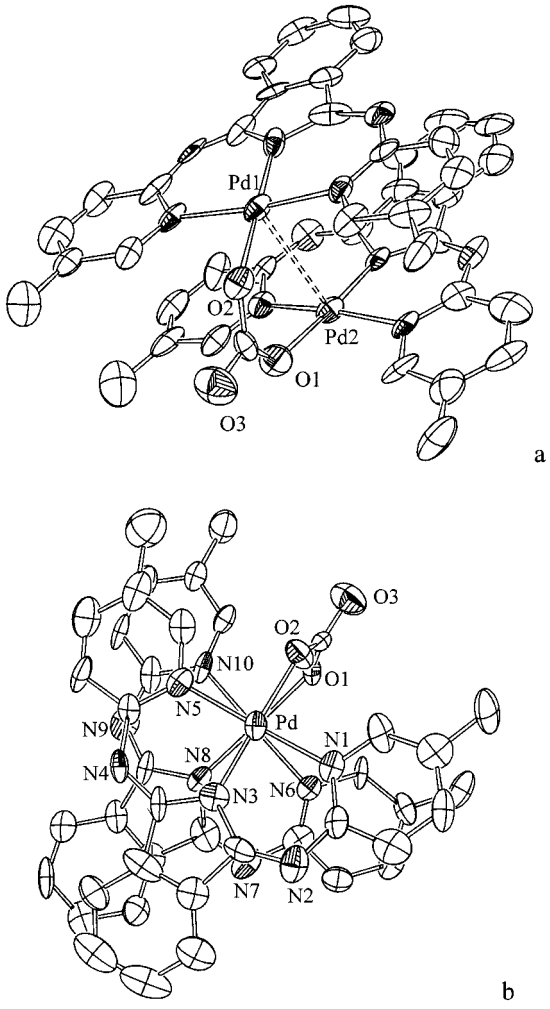

Figure 3. a) Molecular structure of complex **3**; selected bond lengths (Å) and angles (°): Pd1−N1 2.05(1), Pd2−N6 2.07(1), C41−O1 1.23(2), Pd1−N3 1.93(2), Pd2−N8 1.94(1), C41−O2 1.34(2), Pd1−N5 2.05(1), Pd2−N10 2.06(2), C41−O3 1.22(2), Pd1−O2 2.04(1), Pd2−O1 2.03(1); N1−Pd1−N5 172.5(5), N1−Pd1−O2 89.7(6), N6−Pd2−O1 90.4(7), N6−Pd2−N10 73.4(5), N3−Pd1−O2 178.3(5), N8−Pd2−O1 175.7(6); b) view along the Pd−Pd axis

As is evident from the structure represented in Figure 3, the exchange of the chloro ligands in two of the Pd complexes by a bridging carbonato ligand gives a dinuclear complex with a stacked arrangement of the two complex fragments. The relative disposition of the two molecular halves and their parallel orientation may be due to the combination of a weakly attractive Pd−Pd contact and π-stacking interactions between the aromatic rings in the ligands. The Pd−Pd distance of 3.031 Å is in the range of previously established d^8-metal-metal contacts.[16] The view along the Pd−Pd axis in Figure 3b reveals the slight twist in the orientation of the two planar metal-ligand units (N5−Pd1−Pd2−N10 = 16.5°).

We note that Gagné et al. have reported the crystal structure of a dinuclear BPI-copper complex containing a bridging carbonato ligand.[9c] In contrast to the Pd complex presented in this work, the CO_3^{2-} ligand in their Cu complex

 © 2004 Wiley-VCH Verlag GmbH & Co. KGaA, Weinheim

connects two orthogonally oriented BPI-metal units. Both Pd atoms in compound **3** possess an almost ideal square-planar coordination geometry and the two halves of the molecule are structurally almost identical and very similar to **2c** and **2e**. The carbonato ligand is almost planar, with similar metric parameters to the copper complex mentioned above. It is interesting to note the difference in the C−O bond lengths [C41−O1 1.23(2), C41−O3 1.22(2) Å, C41−O2 1.34(2) Å] in the bridging ligand.

Synthesis of Alkynyl-Substituted BPI Ligands

The bis(2-pyridylimino)isoindole ligands give well-defined complex structures and may thus be used as building blocks in more complex molecular architectures. In order to test whether the ligand periphery of the BPI ligands may be modified a posteriori, we studied the alkynylation of the ligand **1c** by the Sonogashira method.[17] The reaction of 11-Br-BPI (**1c**) with a large excess (6 equiv.) of the acetylenes Me_3SiCCH, Ph_3SiCCH and PhCCH in Et_3N using 10 mol % of $[Pd(PPh_3)_4]$/CuI gave the alkynylated derivatives 11-(Me_3SiCC)-BPI (**4a**), 11-(Ph_3SiCC)-BPI (**4b**) and 11-(PhCC)-BPI (**4c**) as yellow solids in good yields (Scheme 2).

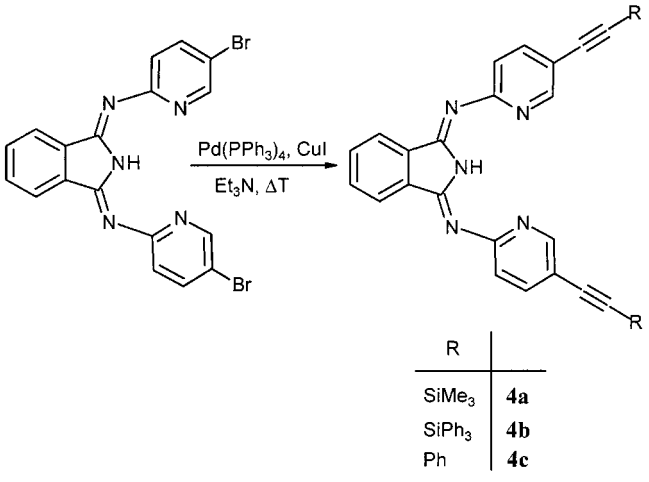

Scheme 2. Synthesis of the alkynyl-substituted BPI ligands **4a**−**4c**

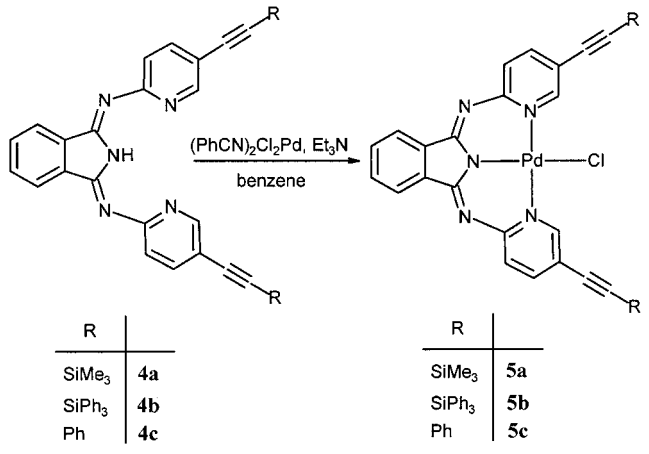

Scheme 3. Synthesis of the alkynyl-substituted BPI-palladium(II) complexes **5a**−**5c**

Synthesis and Structural Characterization of the Alkynyl-Substituted BPI-Palladium Complexes

The synthesis of the corresponding palladium(II) complexes was carried out as described above for complexes **2a**−**2e**, by reaction of the ligands **4a**−**4c** with bis(benzonitrile)dichloropalladium(II) and triethylamine in benzene. After workup, the orange complexes [PdCl{11-(Me_3SiCC)-BPI}] (**5a**) and [PdCl{11-(Ph_3SiCC)-BPI}] (**5b**) as well as the dark-red compound [{11-(PhCC)-BPI}PdCl] (**5c**), respectively, were isolated in good yields (Scheme 3).

The metallation of the BPI ligands **4a** and **4b** may be conveniently monitored by ^{29}Si NMR spectroscopy. The resonances of the Me_3Si-substituted ligand are shifted from $\delta = -17.4$ ppm in **4a** to $\delta = -22.0$ ppm in [PdCl{11-(Me_3SiCC)-BPI}] (**5a**) and from $\delta = -28.5$ ppm in **4b** to $\delta = -22.1$ ppm in [PdCl{11-(Ph_3SiCC)-BPI}] (**5b**). The formation of the alkynyl-substituted complexes **5a**−**5c** was confirmed by their FAB mass spectra, in which the $[M - Cl]^+$ cation was found as the principal fragment.

Single crystals of **5a** and **5b** which were suitable for X-ray diffraction were obtained from solutions of the compounds in CH_2Cl_2 (**5a**) and CH_2Cl_2/pentane (**5b**) at ambient temperature. In order to establish the details of the influence that the alkynyl substitution exerts upon the molecular structures of the BPI-palladium complexes, X-ray structure analyses of both complexes **5a** and **5b** were carried out. Their molecular structures are displayed in Figure 4 and 5, respectively, and their principal bond lengths and angles are compared in Table 2.

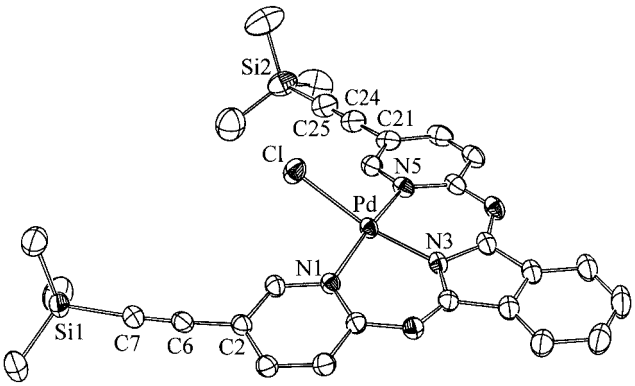

Figure 4. Molecular structure of complex **5a**; selected bond lengths and angles are listed in Table 2

The general features of the metal complex structures of **5a** and **5b** are similar to those of **2c** and **2e**. As in the case of the latter, the palladium atom is slightly displaced from the plane defined by the N-donors, as can be inferred from the N5−Pd−N1 angles [**5a**: 168.41(6)°; **5b**: 167.4(1)°]. The "bending" of the chloro ligands out of the plane of the BPI-Pd unit is even more pronounced than in **2c** and **2e** [N3−Pd−Cl = 165.30(5)° (**5a**) and 163.75(8)°(**5b**)]. This decrease of the N3−Pd−Cl angle may be attributed to increased steric crowding at the 11-position in the series Br < Me_3Si < Ph_3Si, along with the *ortho*-H···Cl repulsion, thus

 © 2004 Wiley-VCH Verlag GmbH & Co. KGaA, Weinheim

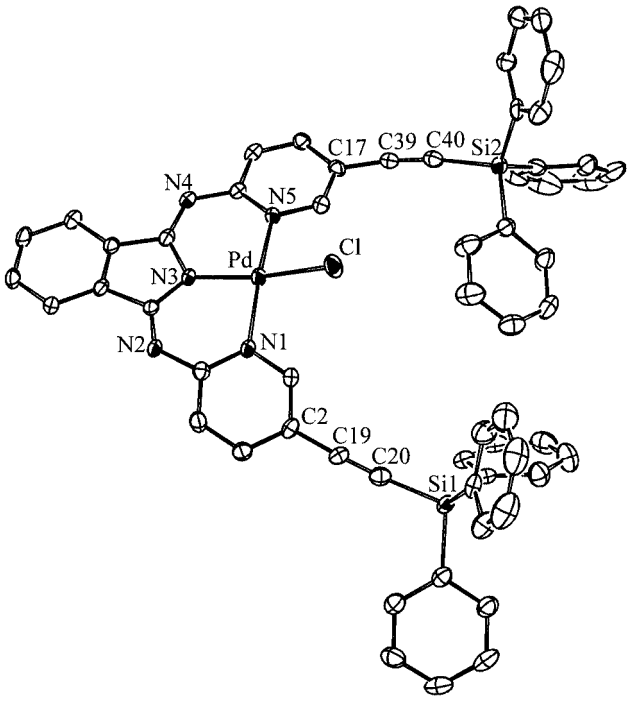

Figure 5. Molecular structure of complex **5b**; selected bond lengths and angles are listed in Table 2

Table 2. Selected bond lengths (Å) and angles (°) of complexes **5a** and **5b**

	5a	5b
Pd−N1	2.052(2)	2.034(3)
Pd−N3	1.958(2)	1.952(2)
Pd−N5	2.046(2)	2.027(2)
Pd−Cl	2.3350(6)	2.3353(8)
C6−C7	1.203(3)	
C24−C25	1.203(4)	
C19−C20		1.190(4)
C39−C40		1.192(4)
N1−Pd−N5	168.41(6)	167.4(1)
Cl−Pd−N3	165.30(5)	163.75(8)
C2−C6−C7	176.8(2)	
C17−C39−C40		171.1(3)
C6−C7−Si1	176.6(2)	
C39−C40−Si2		175.3(3)
C21−C24−C25	179.9(2)	
C2−C19−C20		177.2(3)
C24−C25−Si2	178.7(2)	
C19−C20−Si1		164.2(3)

pushing the Cl ligands out of the plane. The Pd−N bond-length pattern is again similar to that observed in **2c** and **2e**, with greater Pd−N distances for the pyridyl groups [Pd−N5 = 2.046(2) Å (**5a**), 2.027(2) Å (**5b**) and Pd−N1 = 2.052(2) Å (**5a**), 2.034(3) Å (**5b**)] and contracted bond lengths for the central formally anionic donor [Pd−N3 = 1.958(2) Å (**5a**) 1.952(2) Å (**5b**)].

Catalytic Hydrogenation of Olefins with [PdCl(4-Me-BPI)] (2b)

As indicated in the introduction, there is a substantial interest in the development of molecular non-phosphane-containing palladium catalysts for homogeneous hydrogenations. A limiting factor is the propensity of many palladium complexes of that type to undergo degradation under the conditions of the catalytic reaction. Given the stability of the BPI-Pd complexes and the capacity of the imino units in the ligand framework to act as sites of intermediate protonation, we hoped that they might hydrogenate alkenes without decomposition. As a first test system we chose the complex [PdCl(4-Me-BPI)] (**2b**) which is significantly more soluble in polar organic solvents than the unsubstituted parent complex. In order to test its activity towards hydrogenation of C=C double bonds in different chemical environments, the hydrogenation of three substrates — styrene, 1-octene and cyclohexene — was investigated.

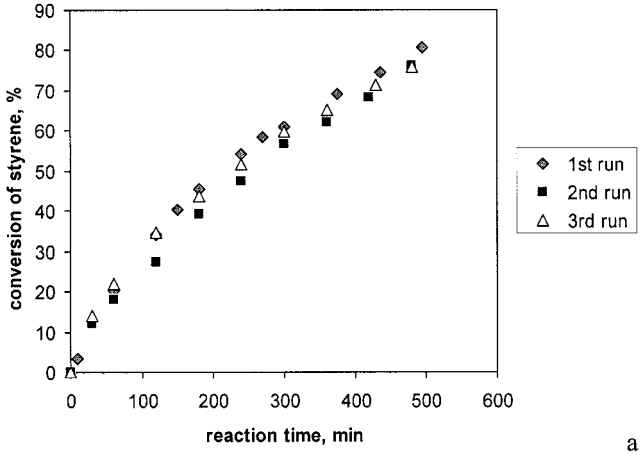

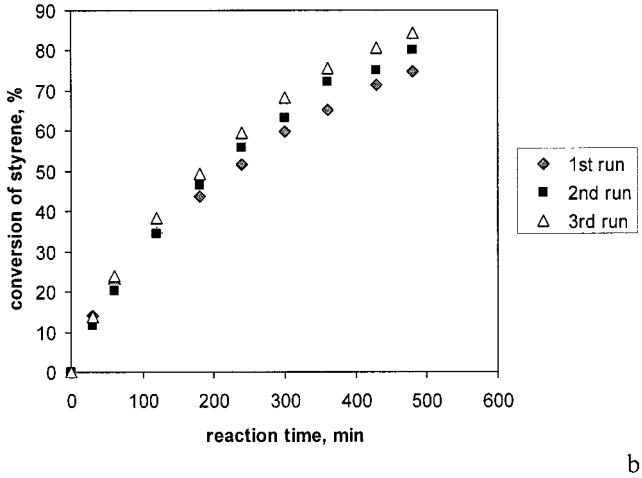

Figure 6. Hydrogenation of styrene at 25 ± 1 °C in THF at a hydrogen pressure of 1 bar using 2 mol % of the catalyst **2b**: a) the conversion curves for three independent catalytic runs; b) isolation of the catalyst that had been used in the third run and re-used in two further catalytic runs

 © 2004 Wiley-VCH Verlag GmbH & Co. KGaA, Weinheim

All reactions were carried out at 25 ± 1 °C in THF at a hydrogen pressure of 1 bar using 2 mol % of the catalyst **2b**. We first studied the hydrogenation of styrene to ethylbenzene. The conversion curves for three independent catalytic runs are displayed in part a of Figure 6 which were carried out under the specified standard conditions and the same substrate and catalyst concentrations; in all three cases the catalyst **2b** was isolated without detectible decomposition after the conversion. In view of this apparent stability of the catalyst, the sample which had been used in the third run and had subsequently been isolated, was employed in two further catalytic runs, again under identical conditions. As can be seen in part b of Figure 6, this procedure also did not lead to a significant change in the catalytic activity of **2b**. After each of the three catalytic runs, the solvent and reaction product were removed in vacuo, the solid residue characterized by ^{1}H NMR spectroscopy and then used in the subsequent catalytic conversion. It is evident from the absence of a signal at δ = 8.5 ppm, which would be due to the demetallated BPI ligand, that there was no decomposition even after three cycles. The stability of the system is shown by comparison of the ^{1}H NMR spectra of **2b** before the catalysis (Figure 7, top) with that recorded after the three cycles of catalysis, isolation of the catalyst and re-use of the catalyst (Figure 7, bottom). We were not able to detect hydridopalladium intermediates by ^{1}H NMR spectroscopy during the course of the catalytic reaction.

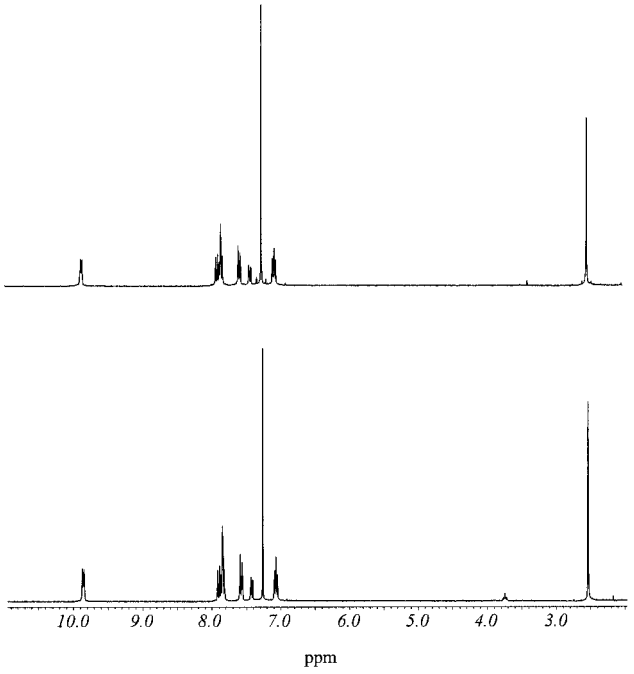

Figure 7. Top: ^{1}H NMR spectrum of **2b** before the catalysis; bottom: ^{1}H NMR spectrum of the catalyst recorded after three cycles of catalysis, isolation of the catalyst, and re-use of the catalyst

We found that if the hydrogenation is carried out in methanol instead of THF as solvent, the palladium complex decomposes during the course of the reaction leading to the precipitation of palladium black, which is inactive under the reaction conditions. This catalyst degradation is evidenced by ^{1}H NMR spectroscopy and the observation of the proton signal of the free ligand at δ = 8.5 ppm.

As a second substrate, and as an example of a long-chain terminal alkene, the hydrogenation of 1-octene catalyzed by **2b** was investigated. Of particular interest was the competing reaction in this transformation, the isomerization of the alkene to a mixture of *E*- and *Z*-2-octene. The course of this reaction, as followed by GC-MS, is represented in Figure 8.

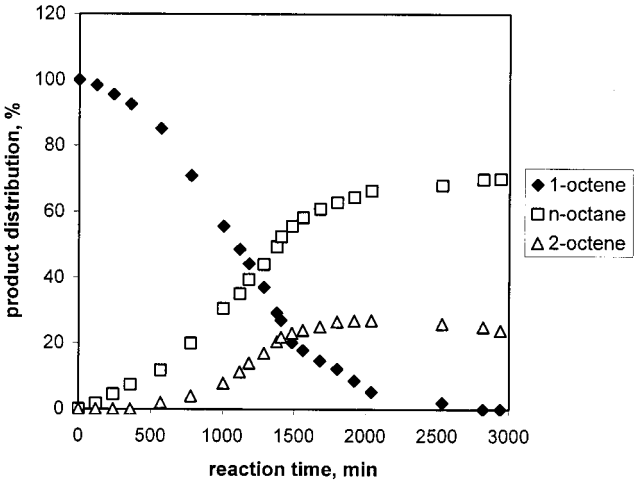

Figure 8. Hydrogenation of 1-octene catalyzed by **2b** and the concomitant isomerization of the alkene to a mixture of *E*- and *Z*-2-octene, as followed by GC-MS

After a short induction period, during which the catalytically active species is generated, the conversion of 1-octene sets in, giving n-octane and a mixture of *Z*-2-octene and *E*-2-octene. After the complete consumption of 1-octene, the conversion into n-octane was around 70%, while 27% of the starting material were converted into the mixture of 2-octenes. The hydrogenation of the latter is extremely slow and practically insignificant within the timeframe represented in Figure 8.

The lack of activity in the hydrogenation of internal C=C double bonds was also apparent from the reaction with cyclohexene. Whereas this substrate is readily hydrogenated by colloidal or heterogeneous Pd catalysts, it is known to be converted only very slowly by molecular Pd catalysts.[18] After 1500 minutes only 5% of the alkene had been converted and even after 9000 minutes the conversion was only at about 12%. A comparison of the conversion curves for the hydrogenation of the three alkenes investigated in this study is given in Figure 9.

As previously noted by Elsevier et al. for N-ligand Pd catalysts, the "mercury test"[19] for potential colloidal metal catalysis is not applicable to palladium compounds such as **2b**.[3d,18] However, the stability of complex **2b** that we observed in the catalytic hydrogenations, the reproducibility of the reaction kinetics, the different behaviour towards the three olefins chosen as substrates and, finally, the possibility of isolating the non-decomposed catalyst after several cata-

 © 2004 Wiley-VCH Verlag GmbH & Co. KGaA, Weinheim

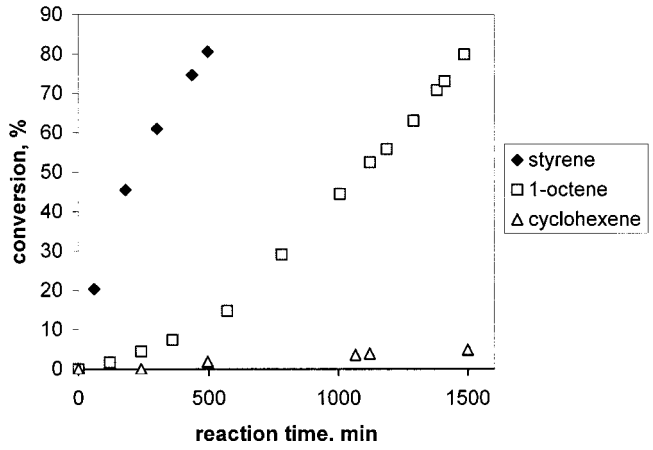

Figure 9. A comparison of the conversion curves for the hydrogenation of styrene, 1-octene and cyclohexene

lytic runs, provides strong circumstantial evidence for molecular catalysis with the BPI-palladium complex.

Although the mechanistic details of the catalytic cycle remain to be established, and no reaction intermediates could be detected to date, a reaction sequence based on the mechanistic proposal by Costa, Pelagatti and co-workers,[4−7] is put forward in Scheme 4. It takes the previously observed possibility of imino-N protonation in the ligand framework into account.[12] Preliminary studies with the other BPI derivatives reported in this work indicate an essentially similar behaviour.

Conclusion

In this paper we have reported the first detailed synthetic and structural study of bis(2-pyridylimino)isoindolatopalladium(II) complexes. The possibility of modifying the peripheral ligand structure after the assembly of the BPI unit has been demonstrated by the Sonogashira alkynylation of a bromopyridyl derivative. This provides the first example of a possible modular variation of these ligands which is of particular interest in catalyst design based on these systems. A detailed study into the hydrogenation activity of one of the Pd complexes has established a novel active molecular catalyst for alkene hydrogenation. Current and future work is aimed towards the elucidation of the mechanism of this catalytic reaction.

Experimental Section

All manipulations were performed under nitrogen. Solvents were dried according to standard methods and saturated with nitrogen. The deuterated solvents used for the NMR spectroscopic measurements were degassed by three successive "freeze-pump-thaw" cycles and stored over 4 Å molecular sieves. Solids were separated from suspensions by filtration through dried Celite or by centrifugation. The ^{1}H, ^{13}C and ^{29}Si NMR spectra were recorded on Bruker AC 200, Bruker Avance 250 and Bruker AMX 400 FT NMR spectrometers, respectively [reference: tetramethylsilane, using the residual protonated solvent peak (^{1}H) or the carbon resonance (^{13}C)]. Infrared spectra were recorded on a Nicolet Magna IRTM 750 spectrometer. Elemental analyses were carried out by the microanalytical service at the Chemistry Department of the University of Strasbourg. (10-Me)-BPI (**1a**), (11-Me)-BPI (**1b**), (11-Br)-BPI (**1c**), (4-Me)-BPI (**1d**)[9] and $[PdCl_2(PhCN)_2]$[20] were prepared according to published procedures. All other chemicals used as starting materials were obtained commercially and used without further purification.

Preparation of 4-Me-10-*t*BuBPI (1e): 4-Methylphthalodinitrile (1.50 g, 10.6 mmol) and 2-amino-4-(*tert*-butyl)pyridine (3.96 *g* = 26.1 mmol) were heated unter reflux in hexanol in the presence of a catalytic amount of $CaCl_2$ (0.16 g, 1.36 mmol) for 18 h. After

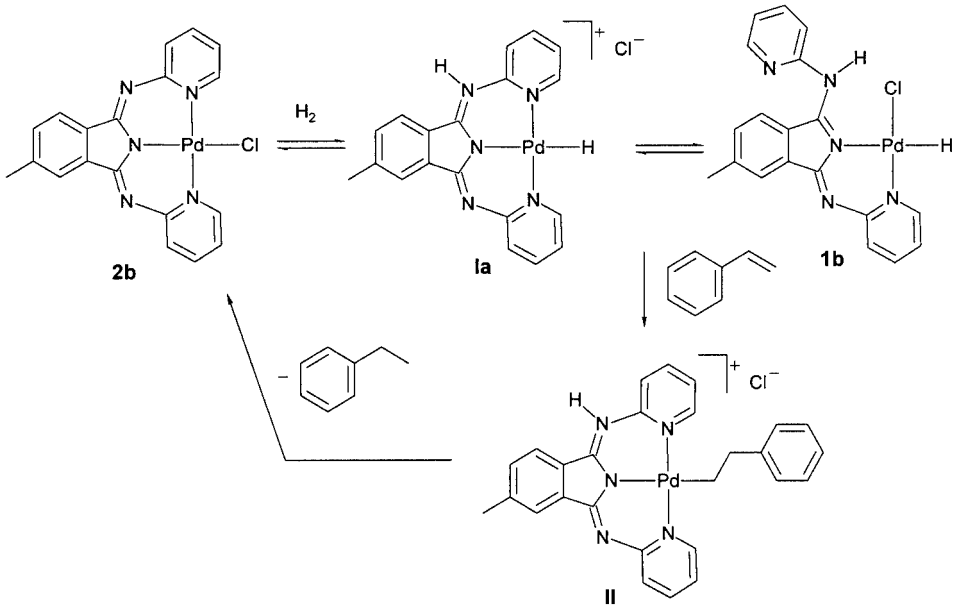

Scheme 4. Proposed mechanism of the Pd-catalyzed hydrogenation

 © 2004 Wiley-VCH Verlag GmbH & Co. KGaA, Weinheim

cooling to room temperature, the solid reaction product was isolated by filtration washed three times with 50 mL of water and then dried in a dessiccator over P_4O_{10} to give compound **1e** as a crystalline yellow solid. Yield: 2.53 g (5.94 mmol, 56%). M.p. 204 °C. ^{1}H NMR (400.16 MHz, C_6D_6): δ = 1.1, 1.2 (each s, each 9 H, 10-*t*Bu), 2.05 (s, 3 H, 4-CH_3), 6.84 (m, 2 H, 11-H), 6.94 (br. d, $^3J_{H,H}$ = 7.9 Hz, 1 H, 5-H), 7.72 (m, 2 H, 9-H), 8.02 (br. s, 1 H, 3-H), 8.12 (d, $^3J_{H,H}$ = 7.9 Hz, 1 H, 6-H), 8.60 (d, $^3J_{H,H}$ = 5.3 Hz, 2 H, 12-H), 11.91 (br. s, 1 H, N−H) ppm. $^{13}C\{^1H\}$ NMR (100.6 MHz, C_6D_6): δ = 21.6 (4-*C*H_3), 30.4 [10-C(*C*H_3)$_3$], 34.5 [10-*C*(CH$_3$)$_3$], 117.7 (C-11), 121.1 (C-9), 122.9 (C-5), 123.6 (C-6), 132.8 (C-3), 137.2 (C-1, C-2), 141.9 (C-4), 148.1 (C-12), 154.1 (C-7), 161.8 (C-8, C-10) ppm. IR (KBr): $\tilde{\nu}$ = 3237 (m, br), 2962 (m), 2867 (w), 1633 (m), 1590 (s), 1534 (w), 1477 (w), 1401 (w), 1365 (w), 1354 (w), 1310 (vw), 1285 (w), 1265 (w), 1219 (w), 1201 (vw), 1180 (vw), 1108 (vw), 1037 (vw), 928 (m), 890 (m), 826 (m), 716 (m) cm^{-1}. $C_{27}H_{31}N_5$ (425.57): calcd. C 76.20, H 7.34, N 16.46; found C 76.48, H 7.36, N 16.25.

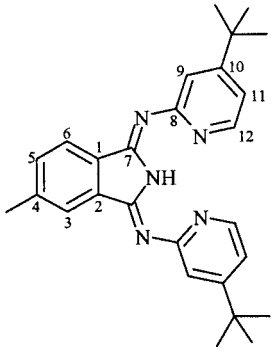

General Procedure for the Preparation of the Palladium(II) Complexes 2a−2e: The bis(2-pyridyl)isoindole (BPI) derivative (in general 0.3 mmol) together with 1.1 molar equivalents of $[PdCl_2(PhCN)_2]$ and 1.1 molar equivalents of NEt_3 were dissolved in benzene and stirred at room temperature for two days. Depending on the substitution pattern of the ligand, the palladium complex either precipitated directly from the reaction mixture or remained in solution. For compounds **2a−2d** direct precipitation of the reaction product was observed and the resulting solid was separated by filtration. The co-product NEt_3HCl was extracted from the solid by extraction three times with 50 mL of water and the crude product thus obtained was recrystallized from CH_2Cl_2/*n*-hexane. In the case of complex **2e** the reaction product remained in solution. After removal of the solvent and the volatiles in vacuo, the solid residue was extracted with 10 mL of benzene and the solvent of the extract evaporated in vacuo. After washing three times with 50 mL of water and 10 mL of hexane, the crude product thus obtained was recrystallized from CH_2Cl_2/*n*-hexane. Compounds **2a−2e** are deep yellow-ochre crystalline solids.

[PdCl{(10-Me)-BPI}] (2a): Yield: 45%. M.p. 287 °C (dec.). ^{1}H NMR (300.17 MHz, $CDCl_3$, 295 K): δ = 2.41 (s, 6 H, CH_3), 6.88 (d, $^3J_{H,H}$ = 6.6 Hz, 2 H, H-11), 7.40 (s, 2 H, H-9), 7.60 (m, 2 H, H-5), 8.01 (m, 2 H, H-6), 9.67 (d, $^3J_{H,H}$ = 6.6 Hz, 2 H, H-12) ppm. $^{13}C\{^1H\}$ NMR (100.61 MHz, $CDCl_3$, 295 K): δ = 20.6 (CH_3), 121.3 (C-11), 122.2 (C-9), 126.6 (C-5), 131.3 (C-6), 137.9 (C-1,2), 149.9 (C-7/8/10/12), 151.2 (C-7/8/10/12), 152.7 (C-7/8/10/12), 153.8 (C-7/8/10/12) ppm. IR (KBr): $\tilde{\nu}$ = 1581 (vs), 1517 (s), 1466 (s), 1402 (vw), 1376 (w), 1295 (s), 1315 (w), 1180 (s), 1098 (vs), 944 (w) cm^{-1}. $C_{20}H_{16}ClN_5Pd$ (468.25): calcd. C 51.30, H 3.44, N 14.96; found C 50.97, H 2.89, N 15.38.

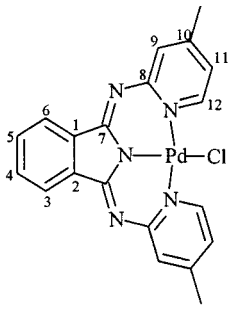

[PdCl{(11-Me)-BPI}] (2b): Yield: 98%. M.p.: 280 °C. ^{1}H NMR (300.17 MHz, CD_2Cl_2, 295 K): δ = 2.38 (s, 6 H, CH_3), 7.43 (d, $^3J_{H,H}$ = 8.2 Hz, 2 H, H-9), 7.61 (dd, $^3J_{H,H}$ = 5.5, $^4J_{H,H}$ = 2.9 Hz, 2 H, H-5), 7.68 (dd, $^3J_{H,H}$ = 8.2, $^4J_{H,H}$ = 2.2 Hz, 2 H, H-10), 7.95 (dd, $^3J_{H,H}$ = 5.5, $^4J_{H,H}$ = 2.9 Hz, 2 H, H-6), 9.64 (d, $^4J_{H,H}$ = 2.2 Hz, 2 H, H-12) ppm. $^{13}C\{^1H\}$ NMR (75.48 MHz, CD_2Cl_2, 295 K): δ = 18.1 (CH_3), 122.0 (C-5), 125.8 (C-9), 129.8 (C-11), 131.2 (C-6), 137.9 (C-1,2), 140.5 (C-10), 150.2 (C-12), 152.7 (C-7/8), 152.9 (C-7/8) ppm. IR (KBr): $\tilde{\nu}$ = 2920 (br), 1620 (w), 1587 (s), 1576 (s), 1482 (w), 1473 (s), 1375 (s), 1302 (w), 1243 (w), 1189 (w), 1143 (vw), 1100 (s), 912 (w), 832 (w), 692 (s) cm^{-1}. $C_{20}H_{16}ClN_5Pd$ (468.25): calcd. C 51.30, H 3.44, N 14.96; found C 51.75, H 3.30, N 14.46.

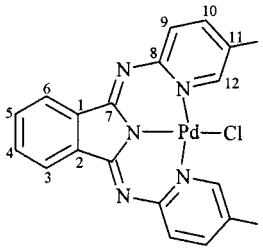

[PdCl{(11-Br)-BPI}] (2c): Yield: 34%. M.p.: 202 °C. ^{1}H NMR (400.13 MHz, $CDCl_3$, 295 K): δ = 7.47 (d, $^3J_{H,H}$ = 8.7 Hz, 2 H, H-9), 7.64 (dd, $^3J_{H,H}$ = 8.7, $^4J_{H,H}$ = 2.2 Hz, 2 H, H-10), 8.06−8.09 (m, 4 H, H-5,6), 10.07 (d, $^4J_{H,H}$ = 2.2 Hz, 2 H, H-12) ppm. $^{13}C\{^1H\}$ NMR (75.5 MHz, CD_2Cl_2, 295 K): δ = 114.9 (C-11), 122.7 (C-5), 127.4 (C-9), 131.6 (C-6), 137.4 (C-1,2), 141.9 (C-10), 148.6 (C-12), 150.7 (C-8), 153.7 (C-7) ppm. FAB-MS: *m*/*z* = 562 [M − Cl]$^+$. IR (KBr): $\tilde{\nu}$ = 3450 (br), 3110 (vw), 2962 (w), 2924 (vw), 2361 (vw), 1640 (w), 1598 (w), 1563 (s), 1518 (s), 1454 (s), 1361 (m), 1320 (vw), 1290 (vw), 1261 (m), 1232 (vw), 1185 (s), 1098 (s), 1020 (s), 915 (w), 860 (w), 839 (w), 801 (s), 702 (w), 684 (w) cm^{-1}. $C_{18}H_{10}Br_2ClN_5Pd$ (597.99): calcd. C 36.15, H 1.68, N 11.71; found C 36.74, H 2.01, N 11.60.

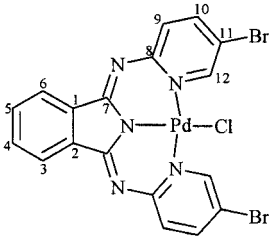

[PdCl(4-MeBPI)] (2d): Yield: 63%. M.p.: >165 °C (dec.). ^{1}H NMR (200.14 MHz, CD_2Cl_2, 298 K): δ = 2.37 (s, 3 H, 4-CH_3), 6.92 (m,

 © 2004 Wiley-VCH Verlag GmbH & Co. KGaA, Weinheim

2 H, 11-H), 7.25 (d, $^3J_{H,H}$ = 7.7 Hz, 1 H, 5-H), 7.36 (d, $^3J_{H,H}$ = 7.5 Hz, 2 H, 9-H), 7.60 (br. s, 1 H, 3-H), 7.65 (d, $^3J_{H,H}$ = 7.7 Hz, 1 H, 6-H), 7.71 (m, 2 H, 10-H), 9.63 (d, $^3J_{H,H}$ = 6.2 Hz, 2 H, 12-H) ppm. $^{13}C\{^1H\}$ NMR (75.5 MHz, [D$_6$]DMSO, 353 K): δ = 21.3 (4-CH_3), 121.2 (C-11), 123.5 (C-9), 124.2 (C-5), 128.0 (C-6), 133.8 (C-3), 136.8 (C-1), 139.6 (C-2), 140.9 (C-10), 144.0 (C-4), 153.6 (C-8), 155.4 (C-7 u. C-12) ppm. IR (KBr): $\tilde{\nu}$ = 2917 (w), 1644 (w), 1579 (s), 1530 (s), 1487 (vw), 1461 (s), 1427 (m), 1367 (m), 1320 (w), 1289 (m), 1215 (vw), 1182 (w), 1135 (m), 1079 (w), 1016 (w), 873 (vw), 826 (vw), 770 (m), 708 (vw) cm^{-1}. $C_{19}H_{14}ClN_5Pd$ (454.04): calcd. 50.22, H 3.11, N 15.42; found C 49.84, H 3.21, N 15.23.

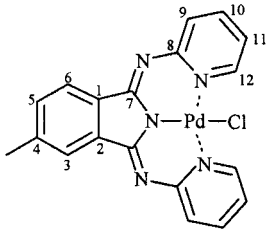

[PdCl(4-Me-10-*t*BuBPI)] (2e): Yield: 73%. M.p.: 192 °C (dec.). ^1H NMR (400.16 MHz, CD_2Cl_2, 298 K): δ = 1.27 (s, 18 H, 10-*tBu*), 2.39 (s, 3 H, 4-CH_3), 6.93 (m, 2 H, 11-H), 7.25 (br. d, $^3J_{H,H}$ = 7.6 Hz, 1 H, 5-H), 7.35 (m, 2 H, 9-H), 7.57 (br. s, 1 H, 3-H), 7.61 (d, $^3J_{H,H}$ = 7.6 Hz, 1 H, 6-H), 9.51 (m, 2 H, 12-H) ppm. $^{13}C\{^1H\}$ NMR (100.6 MHz, CD_2Cl_2, 298 K): δ = 22.3 (4-*C*H$_3$), 30.5 [10-C(*C*H$_3$)$_3$], 35.4 [10-*C*(CH$_3$)$_3$], 118.2 (C-11), 122.4 (C-5), 123.0 (C-6), 123.6 (C-9), 132.6 (C-3), 135.9 (C-1), 138.7 (C-2), 142.6 (C-4), 152.4 (C-7/C-8), 153.5 (C-12), 154.1 (C-7/C-8), 164.4 (C-10) ppm. IR (KBr): $\tilde{\nu}$ = 2962 (m), 2867 (w), 1577 (s), 1559 (w), 1521 (w), 1507 (m), 1477 (m), 1402 (w), 1368 (w), 1319 (vw), 1296 (w), 1262 (w), 1214 (vw), 1181 (m), 1145 (w), 1114 (m), 1048 (m), 1022 (w), 949 (vw), 920 (vw), 890 (vw), 797 (w), 714 (w) cm^{-1}. $C_{27}H_{30}ClN_5Pd$ (566.44): calcd. C 57.25, H 5.34, N 12.36; found C 57.08, H 5.50, N 12.16.

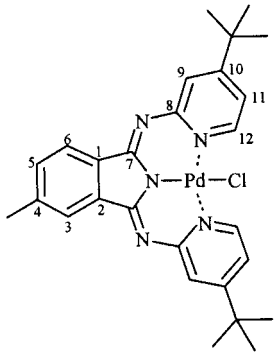

General Procedure for the Preparation of the Alkynyl-Substituted Ligands 4a−4c: The BPI derivative **1c** (0.7 mmol), six molar equivalents of the substituted acetylene, 0.2 molar equivalents of CuI and 0.2 molar equivalents of tetrakis(triphenylphosphane)palladium(0) were stirred in 10 mL of triethylamine at 60 °C. The reaction time was 6 d for **4a**, 4 d for **4b** and 24 h for **4c**. After cooling the reaction mixture to ambient temperature, the solvent was removed in vacuo. The residue was redissolved in 10 mL of CH_2Cl_2, the solution extracted with 10 mL of water and then dried over magnesium sulfate. The evaporation of the solvent in vacuo yielded the reaction products as pure yellow microcrystalline solids.

(11-TMS-ethynyl)-BPI (4a): Yield: 50%. M.p.: 168 °C. ^1H NMR (300.17 MHz, $CDCl_3$, 295 K): δ = 0.29 (s, 18 H, CH_3), 7.32 (d, $^3J_{H,H}$ = 7.4 Hz, 2 H, H-9), 7.58 (s, 2 H, H-5), 7.77 (dd, $^3J_{H,H}$ = 7.4, $^4J_{H,H}$ = 3.6 Hz, 2 H, H-10), 7.97 (s, 2 H, H-6), 8.66 (d, $^3J_{H,H}$ = 3.6 Hz, 2 H, H-12), 13.72 (s, 1 H, N−H) ppm. $^{13}C\{^1H\}$ NMR (75.48 MHz, $CDCl_3$, 295 K): δ = 0.9 (CH_3), 98.2 (C-Si), 102.2 (*C*-C$_{aryle}$), 116.3 (C-11), 122.6 (C-9), 128.3 (C-5), 131.7 (C-6), 135.5 (C-1,2), 140.8 (C-10), 150.9 (C-12), 153.8 (C-7), 159.2 (C-8) ppm. ^{29}Si NMR (79.5 MHz, $CDCl_3$, 295 K): δ = −17.4 ppm. IR (KBr): $\tilde{\nu}$ = 2959 (s), 2155 (s), 1624 (s), 1566 (s), 1465 (s), 1360 (w), 1307 (vw), 1251 (w), 1220 (s), 1096 (w), 1036 (w), 925 (vw), 872 (s), 843 (s), 758 (w), 695 (w) cm^{-1}. $C_{28}H_{29}N_5Si_2$ (491.74): calcd. C 68.39, H 5.94, N 14.24; found C 68.52, H 6.51, N 13.63.

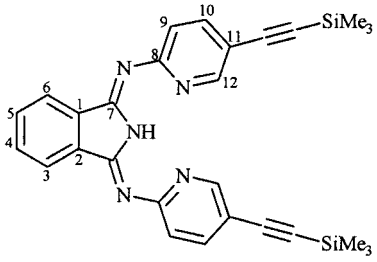

(11-Ph$_3$Si-ethynyl)-BPI (4b): Yield: 69%. M.p.: 198 °C. ^1H NMR (300.17 MHz, $CDCl_3$, 295 K): δ = 7.37−7.72 (m, 34 H, Ph−H, H-5, H-9), 7.91 (d, $^3J_{H,H}$ = 7.0 Hz, 2 H, H-10), 8.07 (s, 2 H, H-6), 8.82 (s, 2 H, H-12), 13.77 (s, 1 H, N−H) ppm. $^{13}C\{^1H\}$ NMR (100.61 MHz, $CDCl_3$, 295 K): δ = 82.0 (C≡*C*Si), 91.7 (*C*≡CSi), 106.0 (C-Ph), 116.1 (C-11), 122.5 (C-5/9), 123.0 (C-5/9), 127.9 (C-Ph), 129.8 (C-Ph), 130.1 (C-Ph), 131.9 (C-6), 135.5 (C-1,2), 141.1 (C-10), 151.0 (C-12), 153.7 (C-7), 158.4 (C-8) ppm. ^{29}Si NMR (79.5 MHz, $CDCl_3$, 295 K): δ = −28.5 ppm. FAB-MS: *m*/*z* = 864 [M + H]$^+$. IR (KBr): $\tilde{\nu}$ = 3304 (br), 2935 (w), 2676 (s), 2070 (s), 1623 (vs), 1565 (vs), 1459 (s), 1428 (vs), 1185 (w), 1113 (vs), 1035 (w) cm^{-1}. $C_{58}H_{41}N_5Si_2$ (864.17): calcd. C 80.61, H 4.78, N 8.10; found C 80.36, H 4.33, N 7.72.

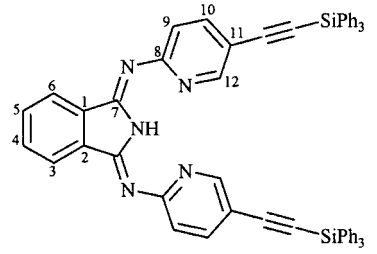

(11-Ph-ethynyl)-BPI (4c): Yield: 77%. M.p.: 246 °C. ^1H NMR (300.17 MHz, CD_2Cl_2, 295 K): δ = 7.39−7.45 (m, 10 H, Ph−H), 7.60 (d, $^3J_{H,H}$ = 7.9 Hz, 2 H, H-9), 7.68−7.70 (dd, $^3J_{H,H}$ = 5.5, $^4J_{H,H}$ = 3.0 Hz, 2 H, H-5), 7.89−7.93 (dd, $^3J_{H,H}$ = 7.9, $^4J_{H,H}$ = 2.2 Hz, 2 H, H-10), 8.05 (dd, $^3J_{H,H}$ = 5.5, $^4J_{H,H}$ = 2.9 Hz, 2 H, H-6), 8.84 (d, $^4J_{H,H}$ = 2.2 Hz, 2 H, H-12), 14.07 (s, 1 H, N−H) ppm. $^{13}C\{^1H\}$ NMR (75.48 MHz, $CDCl_3$, 295 K): δ = 86.5 (C≡C), 92.8 (C≡C), 107.2 (C-Ph), 116.6 (C-11), 122.6 (C-9), 127.6 (C-5), 128.4 (C-Ph), 128.6 (C-Ph), 129.5 (C-Ph), 131.6 (C-6), 135.3 (C-1,2), 140.4 (C-10), 150.5 (C-12), 153.8 (C-7), 158.9 (C-8) ppm. IR (KBr): $\tilde{\nu}$ = 3278 (br), 2962 (s), 2145 (vw), 1638 (s), 1571 (s), 1492 (w), 1463 (w), 1457 (vw), 1261 (s), 1220 (vw), 1095 (s), 1019 (s), 800 (s),

 © 2004 Wiley-VCH Verlag GmbH & Co. KGaA, Weinheim

693 (vw) cm^{-1}. $C_{34}H_{21}N_5$ (499.57): calcd. C 81.74, H 4.23, N 14.02; found C 82.33, H 4.87, N 14.59.

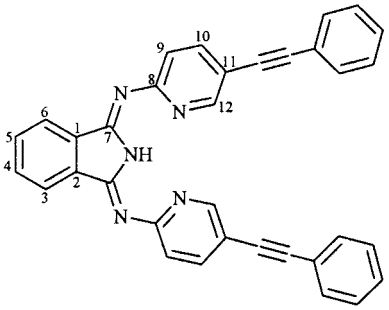

Preparation of Complexes 5a−5c: The preparation of complexes **5a** and **5c** was carried out using 0.3 mmol of the ligand precursors **4a** and **4c** following the procedure described for **2e**. Complex **5b** was prepared on the same scale as described above for **2a−2d**. The alkynyl-substituted complexes were obtained as orange or orange-red crystalline solids.

[PdCl{(11-TMS-ethynyl)-BPI}](5a): Yield: 49%. M.p.: 197 °C (dec.). ^1H NMR (300.17 MHz, $CDCl_3$, 295 K): $\delta = -0.26$ (s, 18 H, CH_3), 7.45 (d, $^3J_{H,H} = 9.0$ Hz,, 2 H H-9), 7.58 (m, 2 H, H-5), 7.82 (dd, $^3J_{H,H} = 9.0$, $^4J_{H,H} = 2.2$ Hz, 2 H, H-10), 7.96 (m, 2 H, H-6), 9.91 (d, $^4J_{H,H} = 2.2$ Hz, 2 H, H-12) ppm. $^{13}C\{^1H\}$ NMR (100.61 MHz, $CDCl_3$, 295 K): $\delta = 99.9$ (*C*≡CSi), 100.2 (C≡*C*Si), 116.4 (C-11), 122.4 (C-9), 125.9 (C-5), 131.5 (C-6), 137.5 (C-1,2), 141.4 (C-10), 150.7 (C-12), 153.9 (C-7), 156.6 (C-8) ppm. ^{29}Si NMR (79.5 MHz, $CDCl_3$, 295 K): $\delta = -22.0$ ppm. FAB-MS: $m/z = 596$ $[M - Cl]^+$. IR (KBr): $\tilde{\nu} = 2959$ (w), 2145 (w), 1560 (s), 1474 (s), 1459 (vs), 1364 (w), 1288 (w), 1248 (w), 1185 (w), 1099 (s) cm^{-1}. $C_{28}H_{28}ClN_5PdSi_2$ (632.61): calcd. C 53.16, H 4.46, N 11.07; found C 53.02, H 4.18, N 10.89.

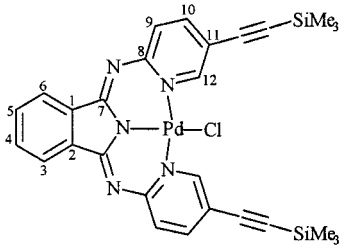

[PdCl{(11-Ph_3Si-ethynyl)-BPI}] (5b): Yield: 42%. M.p.: 202 °C. ^1H NMR (300.18 MHz, $CDCl_3$, 295 K): $\delta = 7.37-7.71$ (m, 34 H, H−Ph, H-5,9), 7.92 (d, $^3J_{H,H} = 8.8$ Hz, 2 H, H-10), 8.04 (m, 2 H, H-6), 10.11 (s, 2 H, H-12) ppm. $^{13}C\{^1H\}$ NMR (75.48 MHz, $CDCl_3$, 295 K): $\delta = 82.2$ (C≡C), 95.1 (C≡C), 104.5 (C-Ph), 115.9 (C-11), 122.6 (C-9), 126.1 (C-5), 128.1 (C-Ph), 130.1 (C-Ph), 131.8 (C−Ph, C-6), 132.2 (C−Ph, C-8), 132.8 (C-Ph), 137.6 (C-1,2), 141.6 (C-10), 151.2 (C-12), 154.3 (C-7), 157.1 (C-8) ppm. ^{29}Si NMR (79.5 MHz, $CDCl_3$, 295 K): $\delta = -22.1$ ppm. FAB-MS: $m/z = 968$ $[M - Cl]^+$. IR (KBr): $\tilde{\nu} = 3065$ (s), 2155 (s), 2070 (s), 1624 (s), 1566 (vs), 1483 (w), 1459 (s), 1425 (s), 1359 (vw), 1304 (vw), 1262 (vw), 1218 (w), 1185 (w), 1113 (s), 1028 (w), 997 (w), 846 (vw), 818 (w) cm^{-1}. $C_{58}H_{40}ClN_5PdSi_2$ (1003.0): calcd. C 69.31, H 4.01, N 6.97; found C 69.83, H 4.55, N 6.35.

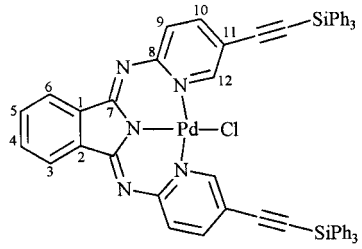

[PdCl{(11-Ph-ethynyl)-BPI}] (5c): Yield: 136 mg (212 μmol, 53%). M.p.: 150 °C. ^1H NMR (300.17 MHz, $CDCl_3$, 295 K): $\delta = 7.35$ (m, 8 H, Ph−H), 7.46 (d, $^3J_{H,H} = 7.0$ Hz, 2 H, H-9), 7.54 (m, 4 H, Ph−H, H-5), 7.85 (d, $^3J_{H,H} = 7.0$ Hz, 2 H, H-10), 7.92 (s, 2 H, H-6), 10.07 (s, 2 H, H-12) ppm. $^{13}C\{^1H\}$ NMR (100.61 MHz, $CDCl_3$, 295 K): $\delta = 85.2$ (C≡C), 94.0 (C≡C), 116.6 (C-11), 122.4 (C-5), 126.0 (C-9), 128.4 (C-Ph), 128.9 (C-Ph), 131.4 (C-Ph), 131.8 (C-Ph), 132.1 (C-6), 137.4 (C-1,2), 140.9 (C-10), 150.4 (C-12), 153.7 (C-7), 156.2 (C-8) ppm. FAB: $m/z = 604$ $[M - Cl]^+$. IR (KBr): $\tilde{\nu} = 2963$ (s), 2217 (w), 1560 (s), 1491 (w), 1459 (s), 1364 (w), 1261 (s), 1185 (w), 1097 (vs), 1022 (vs) cm^{-1}. $C_{34}H_{20}ClN_5Pd$ (640.44). calcd.: calcd. C 63.76, H 3.15, N 10.94; found C 63.32, H 2.99, N 10.63.

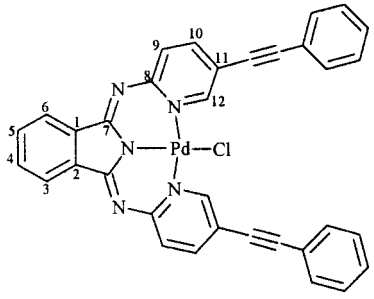

Catalyst Testing: The catalyst tests were carried out in THF at 1 bar H_2 pressure using 2 mol % of palladium catalyst (the catalyst concentration being ca. 1.5 μmol·mL^{-1}). The course of the catalytic hydrogenations was monitored by GC/MS performed with a Shimadzu GC-17A/GCMS-QP5050A. Column: SGE BPX5, 5% phenyl, polysilylphenylene-siloxane, nonpolar, 30 m, 0.22 mm, carrier gas He. The products were analyzed by comparison of the recorded mass spectra and retention times with those of authentic samples. The measured relative ratio of the products was calibrated by comparative measurements with known substance ratios using pure substances.

GC/MS Parameters for Styrene Hydrogenation: T (start) = 50 °C, T (injector) = 250 °C, T (interface) = 280 °C, 30.0 m (0.22 mm), 0.7 mL/min He (flow rate), 66.3 kPa (column pressure), temperature program: 5.0 min, 50 °C; 2 °C/min, 80 °C; 20 °C/min, 250 °C; retention times: t_R (ethylbenzene) = 7.84 min, t_R (styrene) = 9.12 min,

GC/MS Parameters for 1-Octene Hydrogenation: T (start) = 35 °C, T (injector) = 250 °C, T (interface) = 280 °C, 30.0 m (0.22 mm), 1.5 mL/min He (flow rate), 133.2 kPa (column pressure), temperature program: 8.0 min, 35 °C; 30 °C/min, 250 °C; t_R (1-octene) = 5.62 min, t_R (*n*-octane) = 5.93 min, t_R [(*cis*/*trans*)-2-octene] = 6.35 min.

GC/MS Parameters for Cyclohexene Hydrogenation: T (start) = 35 °C, T (injector) = 250 °C, T (interface) = 280 °C, 30.0 m (0.22 mm), 1.5 mL/min He (flow rate), 133.2 kPa (column press-

 © 2004 Wiley-VCH Verlag GmbH & Co. KGaA, Weinheim

Table 3. X-ray experimental data of compounds **2c**, **2e**, **3**, **5a**, and **5b**

	2c	**2e**	**3**	**5a**	**5b**
Formula	$C_{39}H_{26}Br_4Cl_8N_{10}Pd_2$	$C_{31.5}H_{40}Cl_5N_5Pd$	$C_{87}H_{82}Cl_{10}N_{20}O_{10}Pd_4$	$C_{29}H_{30}Cl_3N_5PdSi_2$	$C_{58}H_{40}ClN_5PdSi_2$
Formula mass	1450.77	772.34	2347.88	717.53	1005.02
Crystal system	monoclinic	triclinic	orthorhombic	triclinic	triclinic
Space group	*C*2/*c*	$P\bar{1}$	*Pbcn*	$P\bar{1}$	$P\bar{1}$
a (Å)	12.8115(3)	7.6784(15)	27.7458(5)	8.3844(1)	9.0527(2)
b (Å)	13.4458(3)	14.752(3)	14.4426(6)	12.8717(3)	14.2176(2)
c (Å)	26.3815(7)	15.751(3)	23.158(1)	15.9248(4)	19.3151(4)
α (°)	–	74.79(3)	–	77.111(5)	74.634(5)
β (°)	91.723(5)	85.90(3)	–	84.970(5)	88.341(5)
γ (°)	–	88.83(3)	–	80.587(5)	82.949(5)
V (Å^3)	4542.4(2)	1717.2(6)	9279.9(6)	1650.42(6)	2378.99(8)
Z	4	2	4	2	2
$\rho_{calcd.}$ (g·cm^{-3})	2.12	1.49	1.68	1.44	1.40
*F*000	2792	790	4712	728	1028
μ (mm^{-1})	4.826	0.959	1.120	0.905	0.542
Temperature (K)	173	193	173	173	173
Wavelength (Å)	0.71073	0.71073	0.71073	0.71073	0.71073
Radiation		Mo-K_α graphite monochromated			
Number of data meas.	8979	5053	19840	10278	16796
Number of data with $I > 3\sigma(I)$	3684	3435 ($I > 2\ \sigma(I)$]	3886	5878	7055
Number of variables	285	494	589	361	604
R	0.029	0.072	0.081	0.027	0.036
Rw	0.039	–	0.100	0.034	0.046
wR_2	–	0.186	–	–	–
GOF	1.006	1.081	1.006	1.030	1.039
Largest peak in final difference (e·Å^{-3})	0.301	1.204	1.450	0.308	0.669

ure), temperature program: 8.0 min, 35 °C; 30 °C/min, 250 °C; t_R (cyclohexane) = 2.49 min, t_R (cyclohexene) = 2.74 min.

X-ray Crystallographic Study of 2c, 2e, 3, 5a and 5b: Suitable crystals of the complexes **2c**, **2e**, **3**, **5a** and **5b** were obtained by layering concentrated solutions of the compounds in dichloromethane or chloroform with hexanes and allowing slow diffusion at room temperature. The crystal data for **2c**, **3**, **5a** and **5b** were collected on a Nonius Kappa CCD diffractometer at −100 °C and transferred to a DEC Alpha workstation; for all subsequent calculations the Nonius OpenMoleN package was used.[21] The data for **2e** were collected on a CAD4 (Enraf−Nonius) four-circle diffractometer at −80 °C and the structure solution was carried out using the SHELX-97 structure-solution package.

All structures were solved by direct methods with absorption corrections being part of the scaling procedure of the data reductions. After refinement of the heavy atoms, difference Fourier maps revealed the maxima of residual electron density close to the positions expected for the hydrogen atoms; they were introduced as fixed contributors in the structure-factor calculations with fixed coordinates (C−H: 0.95 Å) and isotropic temerature factors [B(H) = 1.3 B_{eqv}(C) Å^2] but not refined. The hydrogen atoms of the solvents were not refined. Full least-square refinements on F^2. A final difference map revealed no significant maxima of electron density. The scattering factor coefficients and the anomalous dispersion coefficients were taken from the literature.[22] Crystal data and experimental details for the crystals of **2c**, **2e**, **3**, **5a** and **5b** are given in Table 3.

CCDC-232252 to -232256 (for **2c**, **2e**, **3**, **5a** and **5b**, respectively) contain the supplementary crystallographic data for this paper. These data can be obtained free of charge at www.ccdc.cam.ac.uk/conts/retrieving.html [or from the Cambridge Crystallographic Data Centre, 12 Union Road, Cambridge CB2 1EZ, UK; Fax: +44-1223-336033; E-mail: deposit@ccdc.cam.ac.uk].

Acknowledgments

We thank the Deutsche Forschungsgemeinschaft, the CNRS, and the Institut Universitaire de France for funding. We are grateful to Dr. André DeCian and Natalie Gruber for carrying out the X-ray diffraction studies.

[1] Early work: [1a] T. P. Dang, H. B. Kagan, *J. Chem. Soc., Chem. Commun.* **1968**, 481. [1b] W. S. Knowles, M. J. Sabacky, B. D. Vineyard, *J. Chem. Soc., Chem. Commun.* **1972**, 10−11. [1c] H. B. Kagan, T. P. Dang, *J. Am. Chem. Soc.* **1972**, *94*, 6429−6433. [1d] M. D. Fryzuk, B. Bosnich, *J. Am. Chem. Soc.* **1977**, *99*, 6262−6267. [1e] M. D. Fryzuk, B. Bosnich, *J. Am. Chem. Soc.* **1978**, *100*, 5491−5494. [1f] H. Brunner, W. Pieronczyk, *Angew. Chem.* **1979**, *91*, 655−656; *Angew. Chem. Int. Ed. Engl.* **1979**, *18*, 620−621. [1g] W. S. Knowles, *Acc. Chem. Res.* **1983**, *16*, 106−112. [1h] H. Takaya, K. Massima, K. Koyano, M. Yagi, H. Kumobayashi, T. Taketomi, S. Akutagawa, R. Noyori, *J. Org. Chem.* **1986**, *51*, 629−635.

[2] [2a] J. Halpern, in *Organotransition Metal Chemistry* (Eds.: Y. Ishida, M. Tsutsui), Pergamon Press, New York, **1975**, p. 106. [2b] J. Halpern, T. Okamoto, A. Zakhariev, *J. Mol. Catal.* **1977**, *2*, 65−68. [2c] B. R. James, in *Comprehensive Organometallic Chemistry*, vol. 8 (Eds.: G. Wilkinson, F. G. A. Stone, E. W. Abel), Pergamon Press, Oxford, **1982**, p. 285−370. [2d] H. Brunner, in *Applied Homogeneous Catalysis with Organometallic Compounds*, vol. 1 (Eds.: B. Cornils, W. A. Herrmann), VCH, Weinheim, **1996**, p. 201−219.

[3] [3a] B. C. Y. Hui, W. K. Teo, G. L. Rempel, *Inorg. Chem.* **1973**,

 © 2004 Wiley-VCH Verlag GmbH & Co. KGaA, Weinheim

12, 757−762. [3b] M. Cais, *Chim. Ind. (Milan)* **1979**, *61*, 365−398. [3c] M. Sodeoka, M. Shibasaki, *J. Org. Chem.* **1985**, *50*, 1147−1149. [3d] R. van Asselt, C. J. Elsevier, *J. Mol. Catal.* **1991**, *65*, L13−L19.
[4] A. Bacchi, M. Carcelli, M. Costa, A. Leporati, E. Leporati, P. Pelagatti, C. Pelizzi, G. Pelizzi, *J. Organomet. Chem.* **1997**, *535*, 107−120.
[5] P. Pelagatti, A. Bacchi, M. Carcelli, M. Costa, A. Fochi, P. Ghiaini, E. Leporati, M. Masi, C. Pelizzi, G. Pelizzi, *J. Organomet. Chem.* **1999**, *583*, 94−105.
[6] P. Pelagatti, A. Venturini, A. Leporati, M. Carcelli, M. Costa, A. Bacchi, G. Pelizzi, C. Pelizzi, *J. Chem. Soc., Dalton Trans.* **1998**, 2715−2721.
[7] M. Costa, P. Pelagatti, C. Pellizi, D. Rogolino, *J. Mol. Catal. A: Chemical* **2002**, *178*, 21−26.
[8] J. A. Elvidge, R. P. Linsted, *J. Chem. Soc.* **1952**, 5008−5012.
[9] [9a] W. O. Siegl, *J. Org. Chem.* **1977**, *42*, 1872−1878. [9b] W. O. Siegl, *Inorg. Nucl. Chem. Lett.* **1974**, *10*, 825−829. [9c] R. R. Gagné, W. A. Marritt, D. N. Marks, W. O. Siegl, *Inorg. Chem.* **1981**, *20*, 3260−3267. [9d] W. O. Siegl, F. C. Ferris, P. A. Mucci, *J. Org. Chem.* **1977**, *42*, 3442−3443. [9e] R. D. Bereman, G. D. Shields, J. R. Dorfman, J. Bordner, *J. Inorg. Biochem.* **1983**, *19*, 75−93.
[10] [10a] D. M. Baird, W. P. Maehlmann, R. D. Bereman, P. Singh, *J. Coord. Chem.* **1997**, *42*, 107−126. [10b] A. W. Addison, P. J. Burke, K. Henrick, *Inorg. Chem.* **1982**, *21*, 60−63. [10c] E. Balogh-Hergovich, J. Kaiser, G. Speier, G. Huttner, A. Jacobi, *Inorg. Chem.* **2000**, *39*, 4224−4229. [10d] P. J. Domaille, R. L. Harlow, S. D. Ittel, W. G. Peet, *Inorg. Chem.* **1983**, *22*, 3944−3952.
[11] [11a] J. D. Druliner, S. D. Ittel, P. J. Krusic, C. A. Tolman, US Patent 4326084, **1982**. [11b]L. Saussine, E. Brazi, A. Robine, H. Mimoun, J. Fischer, R. Weiss, *J. Am. Chem. Soc.* **1985**, *107*, 3534−3540. [11c] E. Balogh-Hergovich, G. Speier, M. Réglier, M. Giorgi, E. Kuzmann, A. Vértes, *Eur. J. Inorg. Chem.* **2003**, 1735−1740.
[12] O. P. Anderson, A. la Cour, A. Dodd, A. D. Garrett, M. Wicholas, *Inorg. Chem.* **2003**, *42*, 4513−4515.
[13] R. J. Letcher, W. Zhang, C. Bensimon, R. J. Crutchley, *Inorg. Chim. Acta* **1993**, *210*, 183−191.
[14] D. N. Marks, W. O. Siegl, R. P. Gagné, *Inorg. Chem.* **1982**, *21*, 3140−3141.
[15] See for example: [15a] A. W. Kleij, H. Klijn, J. T. B. H. Jastrzebski, A. L. Spek, G. van Koten, *Organometallics* **1999**, *18*, 277−285. [15b] J. Andrieu, J.-M. Camus, J. Dietz, P. Richard, R. Poli, *Inorg. Chem.* **2001**, *40*, 1597−1605.
[16] [16a] P. Pyykkö, *Chem. Rev.* **1997**, *97*, 597−636. [16b] A. Dedieu, *Chem. Rev.* **2000**, *100*, 543−600.
[17] [17a] K. Sonogashira, Y. Tohda, N. Hagihara, *Tetrahedron Lett.* **1975**, 4467−4470. [17b] I. B. Campbell, in *Organocopper Reagents* (Ed.: R. J. K. Taylor), Oxford University Press, Oxford, **1994**, p. 217−235. [17c] *Metal-Catalyzed Cross-Coupling Reactions* (Eds.: F. Diederich, P. J. Stang), Wiley-VCH, Weinheim, **1998**.
[18] M. W. van Laren, C. J. Elsevier, *Angew. Chem.* **1999**, *111*, 3926−3929; *Angew. Chem. Int. Ed.* **1999**, *38*, 3715−3717.
[19] [19a] G. M. Whitesides, M. Hackett, R. L. Brainard, J.-P. Lavalleye, A. F. Sowinski, A. N. Izumi, S. S. Moore, D. W. Brown, E. M. Staudt, *Organometallics* **1985**, *4*, 1819−1830. [19b] R. H. Crabtree, M. F. Mellea, J. M. Mihelcic, J. M. Quirk, *J. Am. Chem. Soc.* **1982**, *104*, 107−113.
[20] [20a] M. S. Kharasch, R. C. Seyler, F. R. Mayo, *J. Am. Chem. Soc.* **1938**, *60*, 882−884. [20b] J. R. Doyle, P. E. Slade, H. B. Jonassen, *Inorg. Synth.* **1960**, *6*, 216−219. [20c] E. Kuljian, H. Frye, *Z. Naturforsch., Teil B* **1964**, *19*, 651.
[21] Nonius *OpenMoleN, Interactive Structure Solution*, Delft, **1997**.
[22] D. T. Cromer, J. T. Waber, *International Tables for X-ray Crystallography*, The Kynoch Press, Birmingham, **1974**.

Received March 4, 2004
Early View Article
Published Online June 23, 2004

 © 2004 Wiley-VCH Verlag GmbH & Co. KGaA, Weinheim

Cationic and Neutral Rhodium(I) Oxazolinylcarbene Complexes

Vincent César,[a] Stéphane Bellemin-Laponnaz,*[a] and Lutz H. Gade*[a,b]

Keywords: Carbenes / N ligands / Oxazolines / Rhodium / X-ray diffraction

Reaction of $[Rh(\mu\text{-}O\textit{t}Bu)(diene)]_2$ [diene = 1,5-cyclooctadiene (COD) or bicyclo[2.2.1]hepta-2,5-diene (NBD)] with the oxazolinylcarbene ligand precursor 2-(4,4-dimethyl)oxazolinylimidazolium bromide ("$Me_2carboxH^+Br^-$", **2**) yielded the five-coordinate complexes [RhBr(Me_2carbox)(diene)] [diene = COD (**3**), NBD (**4**)]. Single-crystal X-ray structure analyses established a distorted trigonal bipyramidal configuration for **3**, whereas the molecular structure of **4** is distorted square pyramidal. The dynamic properties of these five-coordinate complexes have been investigated by variable temperature ^1H NMR spectroscopy, indicating polytopal rearrangements of the five-coordinate complexes. The two compounds were converted into the square-planar cationic complexes $[Rh(Me_2carbox)(diene)]^+$ (**5** and **6**, respectively), which have been isolated and fully characterised. The rhodium complex [RhBr(Me_2carbox)(CO)] (**7**) was obtained in high yield in a one-step reaction of the ligand precursor **2** and [Rh(acac)-$(CO)_2$] (acac = acetylacetonate).
(© Wiley-VCH Verlag GmbH & Co. KGaA, 69451 Weinheim, Germany, 2004)

Introduction

The combination of ligand donor units with very different coordination properties in a di- or polydentate spectator ligand ("hetero-donor ligands") may permit a stereoelectronic control of the reactivity at the remaining coordination sites in a transition metal complex. This has been an underlying principle in the development of many phosphane-heteroatom-based polydentate ligands employed in molecular catalysts.[1]

In recent years, *N*-heterocyclic carbenes have emerged as a new class of spectator ligands in transition metal complexes with ever increasing potential in homogeneous catalysis.[2] They are strong σ-donors and in many respects resemble phosphorus-donor ligands rather than classical Fischer- or Schrock-type carbenes.[3] In this regard, they may replace phosphane units in heterodonor ligands in combination with more "classical" ligand functionalities.[4,5] Among these novel chelating ligand systems, *N*-functionalised carbene complexes have recently received much attention and have given rise to exciting results in homogeneous catalysis.[5,6]

We previously reported the direct coupling of oxazolines and *N*-heterocyclic carbenes, and this new class of C,N-donor ligands (**A**) has been successfully employed in various catalytic reactions.[6] The ligand synthesis is modular, assembling both units in a single coupling step, which was thought to be an efficient strategy in the development of novel catalysts.

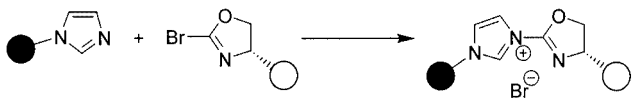

(A)

The rigidity of the bidentate ligand **A** allows for the modeling of a well-defined active space in its molecular catalysts. In this paper we report a number of new complexes of rhodium(I) containing a type **A** ligand which is derived from a 2-(4,4-dimethyl)oxazolinylimidazolium salt. A detailed structural study was intended to provide insight into the nature of precursors and active rhodium catalysts based on these systems.[6b]

Results and Discussion

Synthesis and Structural Characterization of the Bromo{1-(4,4-dimethyl-4,5-dihydrooxazol-2-yl)-3-mesitylimidazol-2-ylidene}rhodium(I) Complexes 3 and 4

As described in a previous paper,[6a] the imidazolium salt **2** is readily obtained from 1-mesityl-1*H*-imidazole and commercially available 4,5-dihydro-4,4-dimethyloxazole. Following the procedure reported by Meyers and Novachek, the reaction of the lithiated oxazole (*t*BuLi, THF, −78 °C) with 1,2-dibromotetrafluoroethane gave the corresponding

[a] Laboratoire de Chimie Organométallique et de Catalyse (UMR 7513), Institut Le Bel, Université Louis Pasteur,
4, rue Blaise Pascal, 67070 Strasbourg, France
Fax: + 33-390-241531
E-mail: gade@chimie.u-strasbg.fr
bellemin@chimie.u-strasbg.fr
[b] Anorganisch-Chemisches Institut, Universität Heidelberg,
Im Neuenheimer Feld 270, 69120 Heidelberg, Germany
Fax: + 49-6221-545609
E-mail: lutz.gade@uni-hd.de

 © 2004 Wiley-VCH Verlag GmbH & Co. KGaA, Weinheim DOI: 10.1002/ejic.200400182

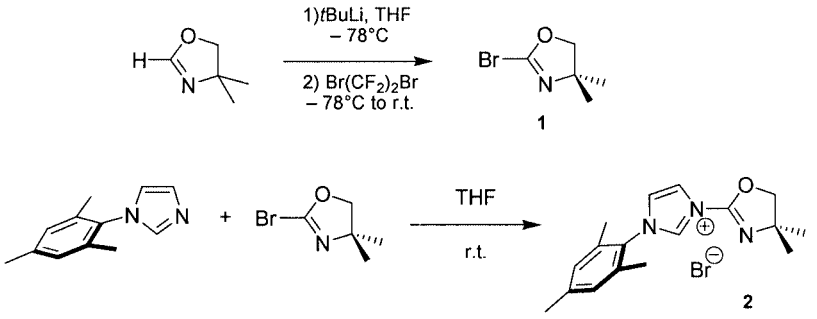

Scheme 1. Synthesis of the 2-bromooxazoline **1** and the oxazolinyl imidazolium salt **2** as ligand precursor

2-bromo-4,5-dihydro-4,4-dimethyloxazole **1** in 65−70% yield (Scheme 1).[7] Treatment of **1** with 1-mesityl-1*H*-imidazole in THF at 50 °C gave the ligand precursor, the 2-(4,4-dimethyloxazolinyl)imidazolium salt (Me_2oxcarb-H^+Br^-) **2**, in about 80% yield (Scheme 1).[6a]

All attempts to generate the free carbene Me_2oxcarb by reaction of **2** with an external base were unsuccessful and led to the nonspecific degradation of the compound. We therefore chose to generate the corresponding rhodium complexes by using precursors that already contain an anionic ligand with sufficient basicity and are capable of in situ deprotonation of the imidazolium salt. Following a general procedure first reported by Herrmann and co-workers,[8] we prepared the rhodium(I) alkoxide precursor [Rh(μ-O*t*Bu)(diene)]$_2$ in situ by reaction of [Rh(COD)Cl]$_2$ or [Rh(NBD)Cl]$_2$ with potassium *tert*-butoxide at room temperature in THF. The resulting solution was then slowly added to a suspension of the imidazolium salt **2** at −78 °C and the mixture was allowed to warm slowly to room temperature overnight. Using this procedure, we obtained the rhodium complexes [Rh(Me_2oxcarb)(COD)Br] (**3**) and [Rh(Me_2oxcarb)(NBD)Br] (**4**) as orange, air-stable solids in 86% and 84% yield, respectively (Scheme 2).

The formation of the carbene complexes was confirmed by ^{13}C NMR spectroscopy. Signals characteristic of N-heterocyclic carbene carbon nuclei[4,5] at δ = 177.2 ppm ($J_{Rh,C}$ = 53 Hz) and at δ = 183.6 ppm ($J_{Rh,C}$ = 55 Hz) were observed for complexes **3** and **4**, respectively Furthermore, a significant coordination shift of the *C*(=N)O ^{13}C NMR resonances in both cases (**3**: δ = 158.8 ppm; **4**: δ = 155.6 ppm) in comparison with the ligand precursor **2** (δ = 148.8 ppm) indicates the coordination of the oxazoline ring. The latter is also supported by the oxazoline ν(C=N) vibrational band which is shifted to lower wavenumbers (**3**: 1677 cm^{-1}; **4**: 1664 cm^{-1}) compared to the free oxazoline in **2** (1691 cm^{-1}). The details of the molecular structure of both complexes were determined by single-crystal X-ray

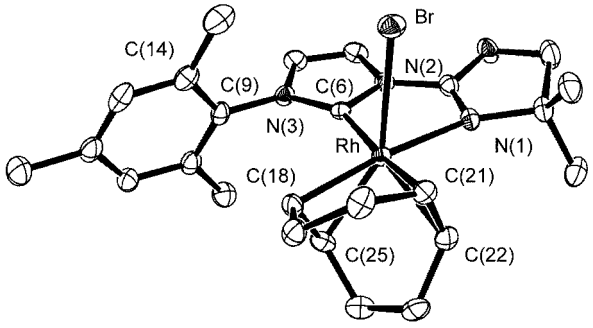

Figure 1. Molecular structure of **3**; selected bond lengths (Å) and angles (°): Rh−Br 2.7545(3), Rh−N(1) 2.255(2), Rh−C(6) 2.022(2), Rh−C(18) 2.090(3), Rh−C(25) 2.096(3), Rh−C(21) 2.223(2), Rh−C(22) 2.251(2), C(21)−C(22) 1.371(4), C(18)−C(25) 1.428(4); C(6)−Rh−N(1) 77.47(9), C(6)−Rh−Br 86.98(7), N(1)−Rh−Br 81.89(6)(4)

diffraction studies and are depicted in Figure 1 and 2, along with the principal bond lengths and interbond angles.

The X-ray structure analyses confirm the bidentate nature of the oxazolinylcarbene ligand in these rhodium complexes. The coordination geometry of **3** around the metal center is best approximated by a distorted trigonal bipyramidal arrangement with C(6), C(21) and C(22) occupying the apical positions whereas the coordination geometry of **4** is essentially square pyramidal. A steric interaction between the COD ligand and the mesityl ring seems to be the origin of the trigonal bipyramidal arrangement of **3**. The mesityl rings are oriented almost orthogonally to the imidazolyl rings [dihedral angle for **3**: C(14)−C(9)−N(3)−C(6) 80.0°; dihedral angle for **4**: C(10)−C(9)−N(2)−C(1) 78.6°].

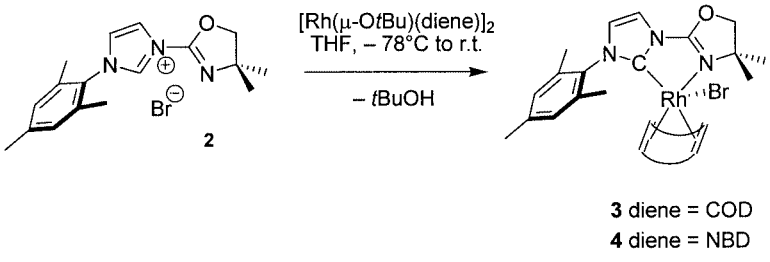

Scheme 2. Synthesis of the five-coordinate complexes [RhBr(ligand)(diene)] **3** and **4**

 © 2004 Wiley-VCH Verlag GmbH & Co. KGaA, Weinheim

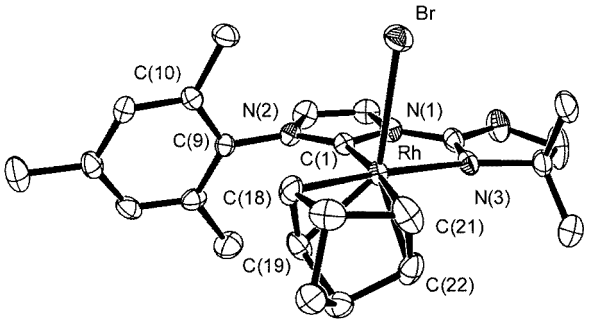

Figure 2. Molecular structure of **4**; selected bond lengths (Å) and angles (°): Rh−Br 2.7615(3), Rh−N(3) 2.178(2), Rh−C(1) 2.016(2), Rh−C(18) 2.070(2), Rh−C(19) 2.105(3), Rh−C(21) 2.192(2), Rh−C(22) 2.177(2), C(21)−C(22) 1.357(5), C(18)−C(19) 1.401(4); C(1)−Rh−Br 95.13(7), C(1)−Rh−N(3) 77.49(8), N(3)−Rh−Br 89.12(5)

As expected, the $Rh-C_{COD}$ distances in **3**, which are *trans* to the carbene carbon atom, are longer than the $Rh-C_{COD}$ bond lengths *trans* to the oxazoline [2.223(2)−2.251(2) Å versus 2.090(3)−2.096(3) Å]. This pronounced *trans* influence[5j,9] is also reflected in the difference in the C=C double bond distances of the coordinated COD ligand. For the double bond *trans* to the carbene a C=C bond length of 1.371(4) Å is found, in comparison with the value of 1.428(4) Å for the double bond *trans* to the oxazoline *N*-atom. In contrast, due to the more rigid conformation and smaller bite angle of the NBD ligand in complex **4**, compared to COD, the *trans* influence of the *N*-heterocyclic carbene in **4** on the Rh−C bond lengths of the diolefin is less pronounced [2.192(2)−2.178(2) Å versus 2.105(3)−2.070(2) Å *trans* to the oxazoline unit]. The distances between the rhodium and the carbene carbon atoms are 2.022(2) Å and 2.016(2) Å for **3** and **4**, respectively, and are similar to those found in related structures.[4b,10]

Signals attributable to the COD ligand are not observed in the ^{1}H NMR spectrum (recorded at 300 MHz) of **3** at 25 °C, indicating a coalescence phenomenon and thus a dynamic process. Upon lowering the temperature to −60 °C, four broad signals between δ = 1.5 and 2.5 ppm appear, which correspond to the -CH_2- groups, while two resonances for the olefin protons are observed at δ = 3.6 and 5.3 ppm. This exchange process has a free activation enthalpy $\Delta G^{\ddagger}$ of about 54 kJ/mol. The fact that only two signals of the four olefin protons are observed at low temperature, in spite of their chemical inequivalence, suggests that a second fast-exchange process takes place which has a low activation barrier (vide infra).

In the ^{1}H NMR spectrum of complex **4**, recorded at 25 °C, only one signal for the olefin protons is observed (δ = 3.59 ppm) indicating fast exchange at that temperature.[11] At −22 °C, this resonance coalesces, and two signals at δ = 4.67 ppm and at δ = 2.67 ppm are detected at −70 °C, as shown in Figure 3. The estimated $\Delta G^{\ddagger}$ of the exchange process associated with this coalescence is ca. 46 kJ/mol. The mechanism operating in the dynamic processes observed for **3** and **4** has to explain the rapid exchange of the two inequivalent C=C double-bond positions in the molecular structures of both complexes. In line with the ubiquitous dynamic processes observed for pentacoordinate molecules, we propose a sequence of Berry pseudorotations as displayed in Scheme 3.

One possible pathway interconverting the two square-pyramidal complexes **A** and **B** (each with a "marked" C=C double bond) involves the intermediates **I**−**III**, which are connected by Berry-type polytopal rearrangements. However, in the low-temperature-limit spectra of both **3** and **4** the (four inequivalent) olefin hydrogen atoms give rise to two signals and not four, as expected. This may be due to fast Br^- exchange even at these low temperatures. Dissociation and the subsequent reassociation of the anion to the ionic planar intermediate, combined with the Berry rearrangements of the pentacoordinate complexes, would indeed lead to the equilibration of the four olefin protons in both complexes. This rapid bromide dissociation and association mechanism is supported by the observed fast intermolecular bromide exchange between **3** and **4** and the respective square-planar complex cations, as discussed in the following section

Synthesis and Structural Characterization of the Cationic {1-(4,4-Dimethyl-4,5-dihydrooxazol-2-yl)-3-mesitylimidazol-2-ylidene}(diolefin)rhodium(I) Complexes 5 and 6

The bromo ligand in the pentacoordinate complex **3** can be removed by the addition of an excess of KPF_6 in dichloromethane (Scheme 4). The cationic complex [Rh(Me_2-carbox)(COD)](PF_6) (**5**) was isolated in nearly quantitative yield as a red solid. In the same fashion, the analogous cationic complex [Rh(Me_2carbox)(NBD)](BF_4) (**6**) derived from **4** was obtained by addition of an excess of $NaBF_4$ in a dichloromethane/water solvent system.

The formulation of compounds **5** and **6** was substantiated by their analytical data, and the molecular structures displayed in Scheme 4 are consistent with the resonance patterns in the NMR spectra. The ^{1}H NMR spectra of complexes **5** and **6**, recorded at room temperature, display two signals for the olefin protons since both square-planar complexes possess C_s symmetry. In the ^{13}C NMR spectra of **5** and **6** the carbene signals are observed at δ = 174.2 ppm ($J_{C,Rh}$ = 54 Hz) and δ = 175.3 ppm ($J_{C,Rh}$ = 59 Hz), respectively.

In order to establish the details of their molecular structures, both compounds were characterized by single-crystal X-ray diffraction which confirmed the expected square-planar arrangement of the ligands around the metal centre (Figure 4 and 5). As for complexes **3** and **4**, the mesityl ring is oriented almost orthogonally to the imidazolyl ring [dihedral angle for **5**: C(10)−C(9)−N(3)−C(8) 99.3°; dihedral angle for **6**: C(14)−C(9)−N(3)−C(8) 87.4°]. Both the Rh−C distances [Rh−C(8) = 2.037(7) Å for **5** and Rh−C(8) = 2.039(6) Å for **6**] and the nitrogen to rhodium distances [Rh−N(1) = 2.136(3) Å and Rh−N(1) = 2.120(5) Å] are within the expected range.[5a][5l][5m] A *trans* influence of the carbene ligand is also found, but appears to be less pronounced than for the pentacoordinate neutral complexes. This is also reflected in the C=C double-bond

 © 2004 Wiley-VCH Verlag GmbH & Co. KGaA, Weinheim

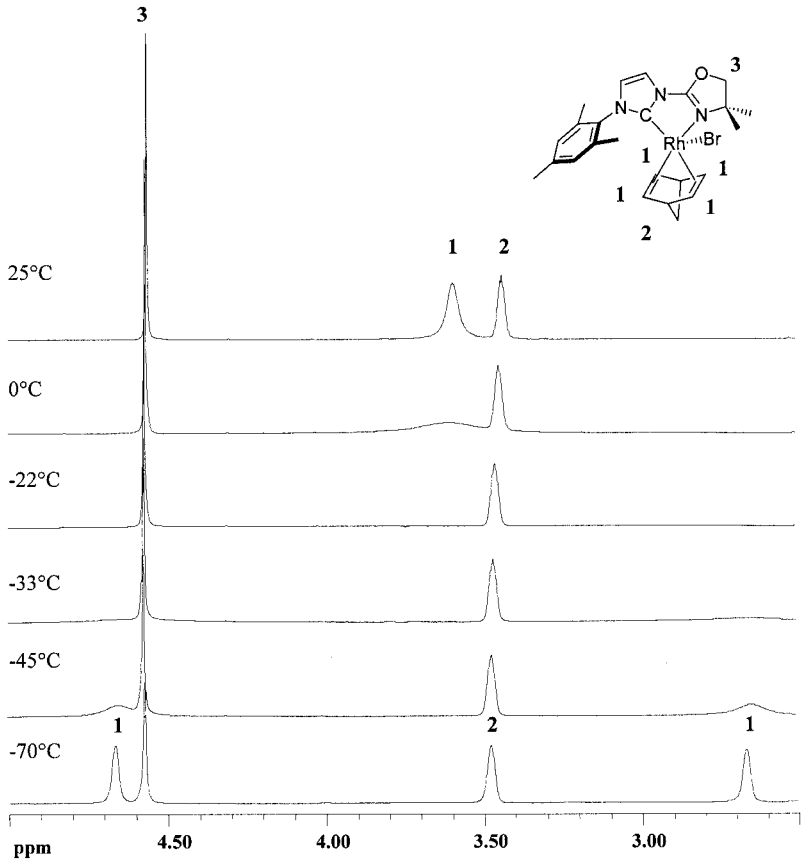

Figure 3. Variable temperature ^{1}H NMR spectra of **4** in the region δ = 2.5−5.0 ppm (recorded in CD_2Cl_2)

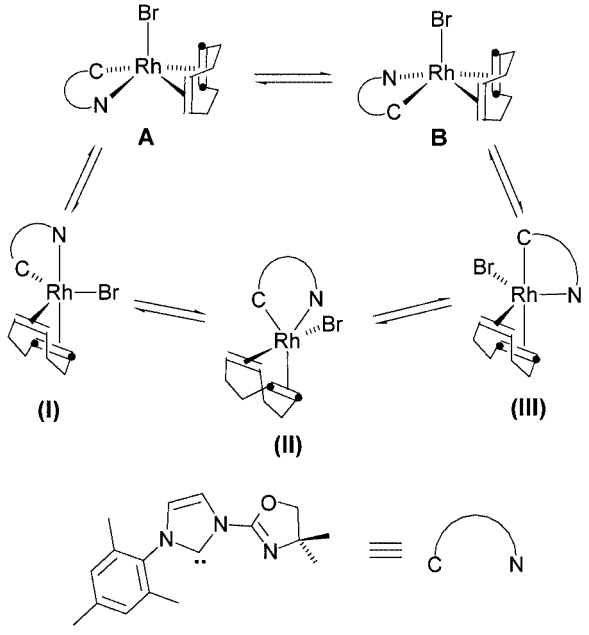

Scheme 3. A sequence of Berry pseudo-rotations leading to the exchange of the positions of the C=C double bonds in the chelating diolefin ligands relative to the C,N bidentate ligand. This process, together with the dissociation and re-association of Br^-, explains the exchange pattern observed in the variable temperature ^{1}H NMR spectra of **3** and **4**

lengths. In complex **5**, for instance, the bond length of the double bond *trans* to the carbene is 1.357(8) Å, compared with the value of 1.371(7) Å for the double bond *trans* to the oxazoline N-atom [1.371(4) Å and 1.428(4) Å in the neutral compound **3**].

The rapid dissociative Br^- exchange postulated for compounds **3** and **4** is supported by the observation of rapid intermolecular bromide exchange between these pentacoordinate complexes and their corresponding square-planar cations **5** and **6**. The ^{1}H NMR spectrum of a 1:1 mixture of the neutral complex **4** and the ionic complex **6**, dissolved in CD_2Cl_2, shows an average resonance pattern of those of **4** and **6**, instead of the spectra of separate species. The same average resonance is observed at −70 °C and is compared in Figure 6 with those of **4** and **6** recorded at the same temperature. This implies fast intermolecular exchange at low temperature (Scheme 5) and indicates that such a dissociative mechanism is probably at the origin of the low energy fluxional process in the neutral pentacoordinate complexes.

Synthesis and Structural Characterization of the Square-Planar Complex Bromo{1-(4,4-dimethyl-4,5-dihydrooxazol-2-yl)-3-mesitylimidazol-2-ylidene}(carbonyl)rhodium(I) (7)

Both the square-planar complexes **5** and **6** are cations. As a neutral analogue we synthesized a rhodium carbonyl derivative by direct reaction of the imidazolium precursor **2** with [Rh(acac)(CO)$_2$] (Scheme 6).[12] The complex

 © 2004 Wiley-VCH Verlag GmbH & Co. KGaA, Weinheim

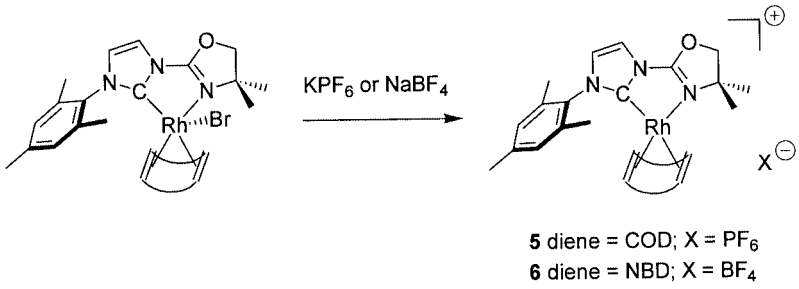

Scheme 4. Synthesis of the cationic four-coordinate complexes [Rh(ligand)(diene)]$^+$ **5** and **6**

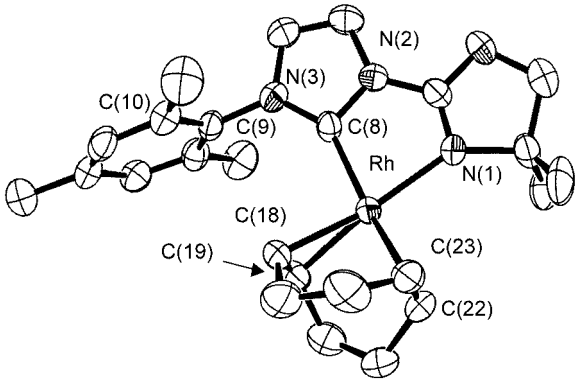

Figure 4. Molecular structure of **5**; selected bond lengths (Å) and angles (°): Rh−N(1) 2.136(3), Rh−C(8) 2.037(7), Rh−C(18) 2.122(4), Rh−C(19) 2.116(4), Rh−C(22) 2.226(5), Rh−C(23) 2.206(5), C(18)−C(19) 1.371(7), C(22)−C(23) 1.357(8); C(8)−Rh−N(1) 78.7(2), C(18)−Rh−C(23) 81.5(2)

[RhBr(Me$_2$carbox)(CO)] (**7**) was obtained in high yield by reacting the two components in THF at room temperature. The synthesis is based on the protonation of the acetylacetonate by the imidazolium precursor and trapping the resulting carbene by coordination to the rhodium(I) centre. The $\nu_{(C=O)}$ band of the carbonyl ligand is observed in the IR spectrum at 1974 cm^{-1} and the detection of a signal at δ = 184.0 ppm in the ^{13}C NMR spectrum, with a characteristic $J_{C,Rh}$ coupling constant of 60 Hz, established the formation of the carbene complex.

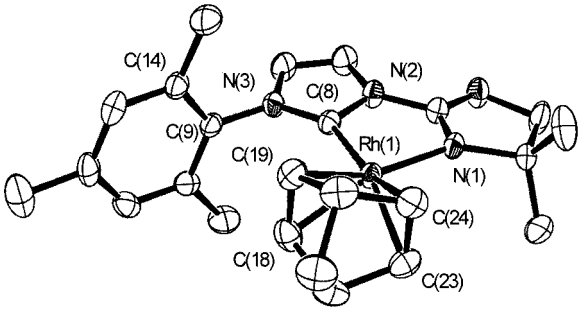

Figure 5. Molecular structure of **6**; selected bond lengths (Å) and angles (°): Rh(1)−C(8) 2.039(6), Rh(1)−N(1) 2.120(5), Rh(1)−C(18) 2.098(7), Rh(1)−C(19) 2.106(7), Rh(1)−C(23) 2.196(7), Rh(1)−C(24) 2.189(7), C(18)−C(19) 1.38(1), C(23)−C(24) 1.35(1); C(8)−Rh−N(1) 78.2(2), C(19)−Rh−C(24) 67.1(3)

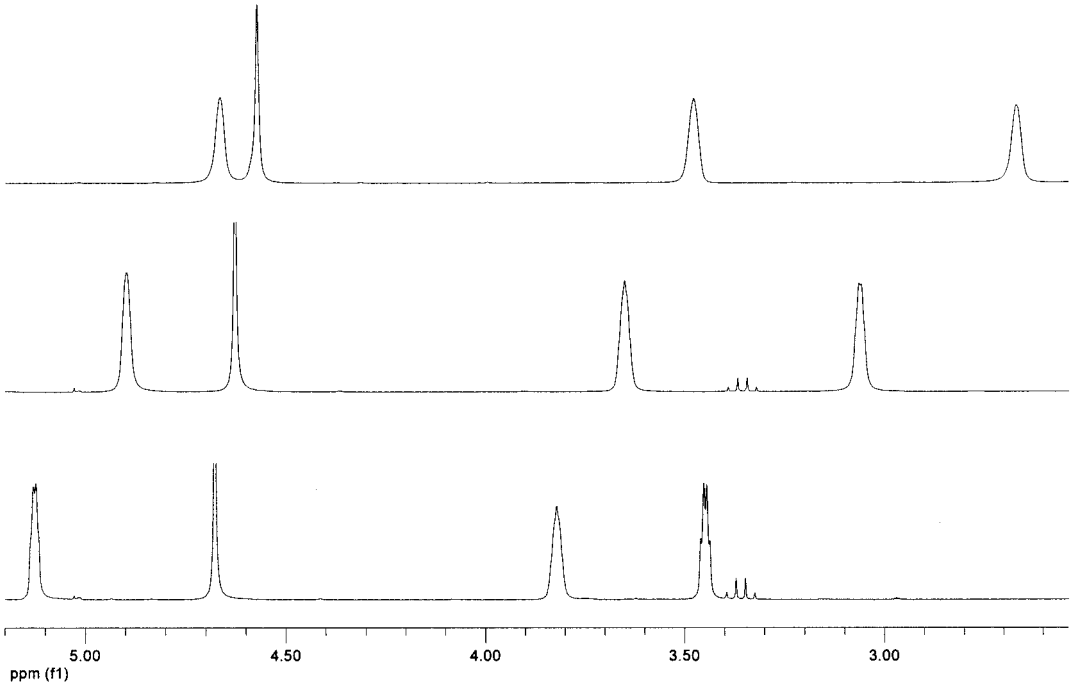

Figure 6. ^{1}H NMR spectra of complex **4** (top), a 1:1 mixture of **4** and **6** (middle) and **6** (bottom) recorded in CD_2Cl_2 at 203 K

 © 2004 Wiley-VCH Verlag GmbH & Co. KGaA, Weinheim

Scheme 5. Rapid intermolecular Br^- exchange between complexes **4** and **6**

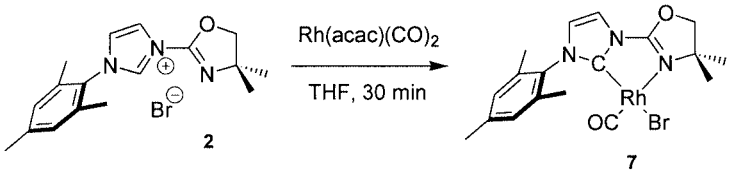

Scheme 6. Synthesis of the neutral four-coordinate complexes [RhBr(ligand)(CO)] (**7**)

The single-crystal X-ray diffraction study of compound **7** confirmed the square-planar coordination geometry (Figure 7). The carbonyl ligand is disposed *trans* to the oxazoline unit whereas the bromide is coordinated *trans* to the carbene. The rhodium−carbene distance [Rh−C(2) = 1.950(4) Å] and the rhodium−nitrogen distance [Rh−N(3) = 2.143(3) Å]) are within the expected range.[13]

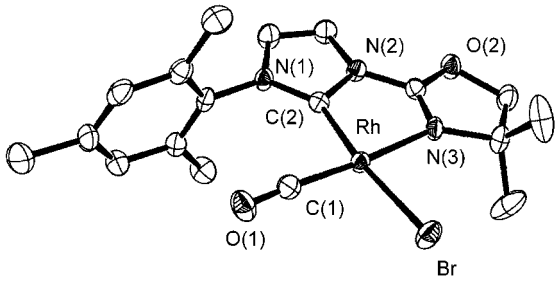

Figure 7. Molecular structure of **7**; selected bond lengths (Å) and angles (deg): Rh−Br 2.5072(5), Rh−C(1) 1.807(4), Rh−C(2) 1.950(4), Rh−N(3) 2.143(3), C(1)−O(1) 1.152(4); Br−Rh−C(1) 90.1(1), Br−Rh−C(2) 173.0(1), C(2)−Rh−N(3) 78.4(1).

It is interesting to compare the C−Rh−N bite angles of the chelating oxazolinylcarbene ligand in the molecular structures of compounds **3**−**7**. The values found for the five-coordinate complexes **3** and **4** are 77.47(9)° and 77.49(8)°, respectively, while the corresponding data of the square-planar cations **5** and **6** are 78.7(2)° and 78.2(2)°, respectively. In the neutral complex **7** this value is 78.4(1)°. The rigidity of the ligand upon coordination to a metal centre thus imposes very well defined metric data, with little variation, regardless of the coordination number or charge of the complex.

Conclusion

The direct condensation of a 2-bromooxazoline derivative with an imidazole provides a modular bidentate ligand precursor which readily coordinates to rhodium(I) complex fragments. The rigidity of the ligand allows for only small variations of the metal−ligand bond lengths and angles, regardless of the coordination number or charge of the complex. The structural details concerning the binding of this class of oxazolinylcarbene ligands have been established in this work. They provide the basis for a systematic use of these functionalised *N*-heterocyclic carbene ligands in catalysis. The first results in catalysis, which we obtained recently, indicate their considerable potential.[6]

Experimental Section

All manipulations were performed under an inert atmosphere of dry nitrogen using standard Schlenk techniques or by working in a glove box. THF and diethyl ether were distilled from sodium/benzophenone. Pentane was distilled from a sodium/potassium alloy, dichloromethane was dried over CaH_2 and subsequently distilled. ^1H and ^{13}C NMR spectra were recorded on a Bruker Avance 300 NMR spectrometer at 300 MHz and 75 MHz and were referenced to the residual proton solvent peak. Infrared spectra were obtained on a FT-IR Perkin−Elmer 1600 spectrometer and the mass spectra were recorded by the "service de spectrométrie de masse de l'Université Louis Pasteur" on an Autospec HF mass spectrometer. The elemental analyses were performed by the analytical services of the Strasbourg and Heidelberg Chemistry Departments. $[RhCl(COD)]_2$ and $[RhCl(nbd)]_2$ were prepared according to literature procedures.[14] $[Rh(acac)(CO)_2]$ was synthesized by reacting $[RhCl(CO)_2]_2$ with Na(acac) in THF. Potassium *tert*-butoxide was sublimed prior to use. $RhCl_3{\cdot}3H_2O$ was provided by BASF AG (Ludwigshafen). All other reagents were commercially available and used as received.

2-Bromo-4,5-dihydro-4,4-dimethyloxazole (1): *t*BuLi (17.7 mL, 1.7 M in pentane, 30.0 mmol) was added dropwise to a solution of 4,5-dihydro-4,4-dimethyloxazole (3.0 mL, 27.3 mmol) in anhydrous THF (80 mL) at −78 °C over a period of 5 min. The resulting yellow solution was stirred for an additional 15 min prior to the addition of 1,2-dibromo-1,1,2,2-tetrafluoroethane (4.84 mL, 36.8 mmol). The solution was allowed to warm to ambient temperature overnight and was subsequently concentrated to about 15 mL. The brown crude product was purified by a short bulb-to-

 © 2004 Wiley-VCH Verlag GmbH & Co. KGaA, Weinheim

bulb distillation to yield a colorless solution of the expected bromo-oxazoline in THF (concentration of about 18% w/w) (2.58 g of pure compound, 53%). ^{1}H NMR ($CDCl_3$): δ = 4.12 (s, 2 H, oxa CH_2), 1.34 (s, 6 H, CH_3) ppm. ^{13}C{^{1}H} NMR ($CDCl_3$): δ = 141.4 (N*C*O), 76.3 (*C*H), 71.6 (*C*H_2), 25.5 (*C*H_3) ppm.

1-(4,5-Dihydro-4,4-dimethyloxazol-2-yl)-3-mesitylimidazolium Bromide (2): 1-Mesityl-1*H*-imidazole (1.11 g, 5.96 mmol) was added to a solution of **1** (1.11 g, 6.23 mmol) in THF (ca. 1.0 M) and the mixture was heated at 50 °C for 2 hours. A white solid precipitated during this period of time. After cooling, diethyl ether (10 mL) was added to complete the precipitation. The product was filtered, washed with diethyl ether (2 × 10 mL) and dried in vacuo to yield 1.80 g (82%) of **2** as a white powder. ^{1}H NMR ($CDCl_3$): δ = 10.57 (t, ^4J = 1.5 Hz, 1 H, NC*H*N), 8.14 (dd, ^3J = 2.1, ^4J = 1.5 Hz, 1 H, 4,5-imidazolium C*H*), 7.60 (dd, ^3J = 2.1, ^4J = 1.5 Hz, 1 H, 4,5-imidazolium C*H*), 7.00 (s, 2 H, mesityl C*H*), 4.53 (s, 2 H, CH_2), 2.32 (s, 3 H, *para* CH_3), 2.16 (s, 6 H, *ortho* CH_3), 1.45 (s, 6 H, oxazoline CH_3) ppm. ^{13}C{^{1}H} NMR ($CDCl_3$): δ = 148.8 (*C*NO), 142.2 (mesityl *C*), 138.3 (N$_2$*C*), 134.4, 130.5 (mesityl *C*), 130.4 (mesityl *C*H), 125.8, 121.3 (imidazolium *C*H), 83.2 (*C*H_2), 68.7 (oxazoline *C*^{4}), 28.4 (*ortho* *C*H_3), 21.5 (*para* *C*H_3), 18.4 (oxazoline *C*H_3) ppm. MS (FAB): *m*/*z* (%) = 284.0 [M]$^+$ (100), 187.0 [M − C_5H_8NO]$^+$ (22). FT-IR (KBr): $\tilde{\nu}$ = 1691 cm^{-1} (s, $\nu_{C=N}$). $C_{17}H_{22}BrN_3O$ (364.29): calcd. C 56.05, H 6.09, N 11.54; found C 55.66, H 6.08, N 11.49.

Bromo(η^4-1,5-cyclooctadiene){1-(4,5-dihydro-4,4-dimethyloxazol-2-yl)-3-mesitylimidazol-2-ylidene}rhodium(I) (3): [RhCl(1,5-COD)]$_2$ (48 mg, 0.098 mmol) and KO*t*Bu (24 mg, 2.2 equiv.) were stirred in THF (5 mL) for 30 min at room temperature. The resulting dark yellow solution was then slowly added to a suspension of the imidazolium salt **2** (72 mg, 2.0 equiv.) in THF (10 mL) at −78 °C. The mixture was allowed to warm to room temperature overnight. The bright yellow solution was centrifuged, the supernatant was separated and the solvents evaporated to give a yellow powder which was washed with pentane (2−3 mL) and dried in vacuo to yield compound **3** (97 mg, 86%). Suitable crystals for an X-ray diffraction studies were obtained by slow diffusion of Et_2O into a solution of **3** in CH_2Cl_2. ^{1}H NMR ($CDCl_3$, 298 K): δ = 7.69 (d, ^3J = 2.1 Hz, 1 H, 4/5-im C*H*), 6.96 (s, 2 H, mes C*H*), 6.82 (d, ^3J = 2.1 Hz, 1 H, 5/4-im C*H*), 4.66 (s, 2 H, oxa CH_3), 2.29 (s, 3 H, *para* CH_3), 2.12 (br, 4 H, COD CH_2), 2.08 (s, 6 H, *ortho* CH_3), 1.74 (br, 4 H, COD CH_2), 1.49 (s, 6 H, oxa CH_3) ppm. ^{13}C{^{1}H} NMR ($CDCl_3$, 298 K): δ = 177.2 (d, $^1J^{103}_{Rh,}{}^{13}_{C}$ = 53 Hz, N$_2$*C*), 158.8 (N*C*O), 140.4 (*C*$_{mes}$), 134.5 (*C*$_{mes}$), 133.6 (*C*$_{mes}$), 129.5 (*C*H$_{mes}$), 125.2 (*C*H$_{im}$), 118.8 (*C*H$_{im}$), 84.3 (oxa *C*H$_2$), 67.8 (oxa *C*^{4}), 30.5 (br, COD *C*H$_2$), 27.8 (oxa *C*H$_3$), 21.2 (*para* *C*H$_3$), 18.1 (*ortho* *C*H$_3$) ppm. MS (ESI): *m*/*z* (%) = 486.09 (22) [M − Br − COD + 2CH$_3$CN + H$_2$O]$^+$, 527.12 (100) [M − Br − COD + 3CH$_3$CN + H$_2$O]$^+$. FT-IR (KBr): $\tilde{\nu}$ = 1677 cm^{-1} (s, $\nu_{C=N}$). $C_{25}H_{33}BrN_3ORh$ (574.36): calcd. C 52.28, H 5.79, N 7.32; found C 51.82, H 5.66, N 7.38.

Bromo{1-(4,5-dihydro-4,4-dimethyloxazol-2-yl)-3-mesitylimidazol-2-ylidene}(η^4-2,5-norbornadiene)rhodium(I) (4): Solid [RhCl(nbd)]$_2$ (86 mg, 0.186 mmol) and KO*t*Bu (46 mg, 0.41 mmol, 2.2 equiv.) were weighed and placed in a Schlenk tube. THF (6 mL) was then added and the reaction mixture was stirred for 30 minutes at ambient temperature. The solution thus obtained was slowly added to a suspension of the imidazolium salt **2** (136 mg, 0.373 mmol, 2.0 equiv.) in THF (12 mL) at −78 °C. The mixture was allowed to warm to ambient temperature overnight and was centrifuged. The resulting orange-red supernatant was separated and the solvents evaporated in vacuo. The crude solid was washed two or three times with pentane (5 mL). Complex **4** was obtained as an orange powder (175 mg, 84%). Crystallization from CH_2Cl_2/Et_2O gave small orange crystals suitable for an X-ray diffraction study. ^{1}H NMR ($CDCl_3$): δ = 7.30 (d, ^3J = 2.1 Hz, 1 H, 4/5-im C*H*), 6.95 (s, 2 H, C*H*$_{mes}$), 6.62 (d, ^3J = 2.1 Hz, 1 H, 4/5-im C*H*), 4.52 (s, 2 H, oxa CH_2), 3.58 (br. m, 4 H, 2/3/5/6-nbd C*H*), 3.45 (m, 2 H, 1/4-nbd C*H*), 2.30 (s, 3 H, *para* CH_3), 2.20 (s, 6 H, *ortho* CH_3), 1.45 (s, 6 H, oxa CH_3), 0.98 (s, 2 H, CH_{2nbd}) ppm. ^{13}C{^{1}H} NMR ($CDCl_3$): δ = 183.6 (d, $^1J^{103}_{Rh,}{}^{13}_{C}$ = 55 Hz, N$_2$*C*), 155.6 (N*C*O), 139.5 (*C*$_{mes}$), 135.6 (*C*$_{mes}$), 133.6 (*C*$_{mes}$), 128.8 (*C*H$_{mes}$), 123.5 (*C*H$_{im}$), 115.6 (*C*H$_{im}$), 84.6 (oxa *C*H$_2$), 67.3 (oxa *C*^{4}), 60.1 (nbd *C*H$_2$), 49.2 (1/4-*n*bd *C*H), 28.5 (oxa *C*H$_3$), 21.1 (*para* *C*H$_3$), 18.6 (*ortho* *C*H$_3$) ppm. MS (ESI): *m*/*z* (%) = 478.13 (100) [M − Br]$^+$. FT-IR (KBr): $\tilde{\nu}$ = 1664 cm^{-1} (s, $\nu_{C=N}$). $C_{24}H_{29}BrN_3ORh$ (558.32): calcd. C 51.63, H 5.23, N 7.53; found C 51.11, H 5.19, N 7.34.

(η^4-1,5-Cyclooctadiene){1-(4,5-dihydro-4,4-dimethyloxazol-2-yl)-3-mesitylimidazol-2-ylidene}rhodium(I) Hexafluorophosphate (5): Solid KPF_6 (34 mg, 0.185 mmol, 1.5 equiv.) was added to an orange solution of **3** (70 mg, 0.122 mmol) in CH_2Cl_2 (5 mL). Degassed water (5 mL) was subsequently added and the mixture was stirred vigorously for 30 minutes. The organic layer was decanted and the aqueous layer was washed with an additional 5 mL of CH_2Cl_2. The organic layers were combined, dried over Na_2SO_4 and the volatiles were removed in vacuo. After washing with Et_2O (5 mL) and drying, an orange powder was isolated (76 mg, 98%). Suitable crystals for an X-ray diffraction study were obtained by slow diffusion of Et_2O into a saturated solution of **5** in CH_2Cl_2/Et_2O. ^{1}H NMR ($CDCl_3$): δ = 7.50 (d, ^3J = 2.1 Hz, 1 H, 4/5-im CH), 6.96 (s, 2 H, C*H*$_{mes}$), 6.75 (d, ^3J = 2.1 Hz, 1 H, 4/5-im C*H*), 5.32−5.29 (m, 2 H, COD C*H*), 4.70 (s, 2 H, oxa CH_2), 3.66−3.64 (m, 2 H, COD C*H*), 2.33 (s, 3 H, *para* CH_3), 2.33−2.10 (m, 4 H, COD CH_2), 2.10 (s, 6 H, *ortho* CH_3), 1.98−1.92 (m, 2 H, COD CH_2), 1.82−1.76 (m, 2 H, COD CH_2), 1.49 (s, 6 H, oxa CH_3) ppm. ^{13}C{^{1}H} NMR ($CDCl_3$, 298 K): δ = 174.2 (d, $^1J^{103}_{Rh,}{}^{13}_{C}$ = 54 Hz, N$_2$*C*), 160.2 (N*C*O), 140.8, 134.2, 133.0 (*C*$_{mes}$), 129.7 (*C*H$_{mes}$), 125.3 (*C*H$_{im}$), 118.2 (*C*H$_{im}$), 97.6 (d, $J^{103}_{Rh,}{}^{13}_{C}$ = 7.5 Hz, COD *C*H), 85.1 (oxa *C*H$_2$), 74.4 (d, $J^{103}_{Rh,}{}^{13}_{C}$ = 13 Hz, COD *C*H), 67.9 (oxa *C*^{4}), 31.8, 29.1 (COD *C*H$_2$), 27.4 (oxa *C*H$_3$), 21.2 (*para* *C*H$_3$), 17.6 (*ortho* *C*H$_3$) ppm. MS (ESI): *m*/*z* (%) = 486.09 (100) [RhL(CH$_3$CN)$_2$(H$_2$O)]$^+$, 527.12 (46) [RhL(CH$_3$CN)$_3$(H$_2$O)]$^+$. FT-IR (KBr): $\tilde{\nu}$ = 1664 cm^{-1} (s, $\nu_{C=N}$). $C_{25}H_{33}F_6N_3OPRh$ (639.42): calcd. C 46.96, H 5.20, N 6.57; found C 46.9, H 5.35, N 6.65.

{1-(4,5-Dihydro-4,4-dimethyloxazol-2-yl)-3-mesitylimidazol-2-ylidene}(η^4-2,5-norbornadiene)rhodium(I) Tetrafluoroborate (6): Solid $NaBF_4$ (37 mg, 0.340 mmol, 2 equiv.) was added to an orange solution of **4** (95 mg, 0.170 mmol) in CH_2Cl_2 (5 mL). Degassed water (5 mL) was then added and the resulting red mixture was stirred vigorously for 30 min. The organic layer was removed and the aqueous layer was washed with an additional 5 mL of CH_2Cl_2. The organic layers were combined, dried over Na_2SO_4 and the volatiles were removed in vacuo. Crystallization of the crude material from CH_2Cl_2/Et_2O gave reaction product **6** in the form of long, red needles (77 mg, 80%). Suitable crystals for an X-ray diffraction study were obtained by slow diffusion of Et_2O into a saturated solution of **4** in CH_2Cl_2/Et_2O. ^{1}H NMR ($CDCl_3$): δ = 7.52 (d, ^3J = 2.1 Hz, 1 H, 4/5-im C*H*), 6.81 (s, 2 H, C*H*$_{mes}$), 6.67 (d, ^3J = 2.1 Hz, 1 H, 4/5-im C*H*), 5.13 (br, 2 H, nbd C*H*), 4.76 (s, 2 H, oxa CH_2), 3.87 (br, 2 H, nbd C*H*), 3.52 (br, 2 H, 1/4nbd C*H*), 2.26 (s, 3 H, *para* CH_3), 2.07 (s, 6 H, *ortho* CH_3), 1.33 (s, 6 H, oxa CH_3), 1.31 (s, 2 H, nbd CH_2) ppm. ^{13}C{^{1}H} NMR ($CDCl_3$): δ = 175.3 (d, $^1J^{103}_{Rh,}{}^{13}_{C}$ = 59 Hz, N$_2$*C*), 161.8 (N*C*O), 140.5, 134.4, 132.5 (*C*$_{mes}$), 129.2 (*C*H$_{mes}$), 124.7 (*C*H$_{im}$), 117.4 (*C*H$_{im}$), 85.8 (oxa *C*H$_2$), 82.2 (oxa *C*^{4}), 66.3, 65.8 (nbd *C*H), 59.0 (nbd *C*H$_2$), 53.9, 53.5 (1/4-nbd

 © 2004 Wiley-VCH Verlag GmbH & Co. KGaA, Weinheim

Table 1. X-ray experimental data of compounds **3**−**7**

	3	**4**	**5**	**6**	**7**
Formula	$C_{25}H_{33}BrN_3ORh$	$C_{24}H_{29}BrN_3ORh$	$C_{25}H_{33}BrN_3ORhPF_6$	$C_{72}H_{87}N_9O_3Rh_3{\cdot}3BF_4{\cdot}2CH_2Cl_2{\cdot}H_2O$	$C_{18}H_{21}BrN_3O_2Rh$
Mol. mass	574.38	558.33	639.43	1883.57	494.20
Crystal system	orthorhombic	monoclinic	monoclinic	monoclinic	monoclinic
Space group	*Pbca*	$P12_1/n$ (no. 1)	$C1c$ (no. 1)	$P12_1/c$ (no. 1)	$P12_1/c$ (no. 1)
a (Å)	13.3030(2)	10.8649(1)	11.6730(2)	26.2844(2)	10.6735(3)
b (Å)	18.9492(2)	9.2177(1)	23.2279(5)	11.5110(1)	11.6164(3)
c (Å)	18.6447(3)	22.4762(3)	10.1204(3)	28.0873(2)	16.3699(4)
β (°)		91.557(5)	97.450(5)	97.268(5)	103.738(5)
V (Å^3)	4700.0(1)	2250.15(4)	2720.9(1)	8429.8(1)	1971.60(9)
Z	8	4	4	4	4
$\rho_{calcd.}$ (g·cm^{-3})	1.62	1.65	1.56	1.48	1.66
$F000$	2336	1128	1304	3832	984
μ (mm^{-1})	2.449	2.555	0.751	0.785	2.908
Temperature (K)	173	173	293	294	173
Wavelength (Å)	0.71073	0.71073	0.71073	0.71073	0.71073
Number of data meas.	13757	11954	7090	25736	9055
Number of data with $I > 3\sigma(I)$	4481	5853	5347	16749	3680
Number of variables	280	271	332	1039	226
R	0.029	0.030	0.036	0.069	0.029
Rw	0.036	0.054	0.047	0.089	0.049
GOF	1.032	1.028	1.012	1.209	1.026
Largest peak in final difference (e·Å^{-3})	0.509	2.088	0.405	1.482	0.402

*C*H), 27.7 (oxa *C*H$_3$), 21.1 (*para* *C*H$_3$), 17.7 (*ortho* *C*H$_3$) ppm. MS (ESI): *m/z* (%) = 478.12 (24) [M − BF$_4$]$^+$, 510.11 (64) [M − BF$_4$ − nbd + 3CH$_3$CN]$^+$, 537.12 (100). FT-IR (KBr): $\tilde{\nu}$ = 1662 cm^{-1} (s, $\nu_{C=N}$).

Bromo(carbonyl){1-(4,5-dihydro-4,4-dimethyloxazol-2-yl)-3-mesityl-imidazol-2-ylidene}rhodium(I) (7): [Rh(acac)(CO)$_2$] (75 mg, 0.290 mmol) and the imidazolium salt **2** (106 mg, 1.0 equiv.) were placed in a Schlenk tube and dissolved in THF (8 mL). A rapid evolution of a gas (CO) was observed and the solution color immediately turned bright yellow. After stirring for 50 minutes at ambient temperature, the reaction mixture was centrifuged, the supernatant was separated and the solvents evaporated to dryness. The crude product was washed with pentane (2 × 4 mL) to yield the analytically pure compound **7** as a yellow microcrystalline solid (122 mg, 85%). Crystallization from CH_2Cl_2/pentane gave yellow crystals suitable for X-ray diffraction. ^{1}H NMR ($CDCl_3$): δ = 7.28 (d, ^3J = 2.3 Hz, 1 H, 4/5-im C*H*), 7.04 (s, 2 H, C*H*$_{mes}$), 6.70 (d, ^3J = 2.3 Hz, 1 H, 4/5-im C*H*), 4.62 (s, 2 H, oxa C*H*$_2$), 2.32 (s, 3 H, *para* C*H*$_3$), 2.10 (s, 6 H, *ortho* C*H*$_3$), 1.72 (s, 6 H, oxa C*H*$_3$) ppm. ^{13}C{^{1}H} NMR ($CDCl_3$): δ = 187.4 (d, $^1J^{103}_{Rh,}{}^{13}_{C}$ = 78 Hz, *C*O), 184.0 (d, $^1J^{103}_{Rh,}{}^{13}_{C}$ = 60 Hz, N$_2$*C*), 158.5 (N*C*O), 140.4 (*C*$_{mes}$), 135.0 (*C*$_{mes}$), 134.0 (*C*$_{mes}$), 129.4 (*C*H$_{mes}$), 123.5 (*C*H$_{im}$), 114.7 (*C*H$_{im}$), 86.4 (oxa *C*H$_2$), 67.4 (oxa *C*^{4}), 28.2 (oxa *C*H$_3$), 21.2 (*para* *C*H$_3$), 18.0 (*ortho* *C*H$_3$) ppm. FT-IR (KBr): $\tilde{\nu}$ = 1974 cm^{-1} (s, $\nu_{C=O}$), 1670 cm^{-1} (s, $\nu_{C=N}$). $C_{17}H_{21}BrN_3O_2Rh$ (494.19): calcd. C 43.75, H 4.28, N 8.50; found C 42.93, H 4.05, N 8.14.

Intermolecular Br$^-$ Exchange between Complexes 4 and 6: Equal amounts of compounds **4** and **6** (20 μmol) were weighed, placed into an NMR tube and dissolved in CD_2Cl_2 (0.5 mL). In an ^{1}H NMR spectrum, which was recorded at 203 K, the signals of complexes **4** and **6** were not observed separately but a set of resonances at the weighted mean chemical shift indicated a fast intermolecular exchange of bromide between **4** and **6**.

X-ray Crystallographic Study of Compounds 3−7: Suitable crystals of complexes **3**, **4**, **5**, **6** and **7** were obtained by layering concentrated solutions of the compounds in dichloromethane with pentane, hexane or diethyl ether (vide supra) and allowing slow diffusion at room temperature. The crystal data were collected at −100 °C on a Nonius KappaCCD diffractometer and transferred to a DEC Alpha workstation; for all subsequent calculations the Nonius OpenMoleN package was used.[15] The structures were solved by direct methods with absorption corrections being part of the scaling procedure of the data reductions. After refinement of the heavy atoms, difference Fourier maps revealed the maxima of residual electron density close to the positions expected for the hydrogen atoms; they were introduced as fixed contributors in the structure factor calculations with fixed coordinates (C−H: 0.95 Å) and isotropic temperature factors [B(H) = 1.3 B_{eqv}(C) Å^2] but not refined. Full least-square refinements on F^2. A final difference map revealed no significant maxima of electron density. The scattering factor coefficients and the anomalous dispersion coefficients were taken from the literature.[16] Crystal data and experimental details for the crystals of compounds **3**−**7** are given in Table 1.

CCDC-229779 ... -229783 (for **3**−**7**, respectively) contain the supplementary crystallographic data for this paper. These data can be obtained free of charge at www.ccdc.cam.ac.uk/conts/retrieving.html [or from the Cambridge Crystallographic Data Centre, 12 Union Road, Cambridge CB2 1EZ, UK; Fax: +44-1223-336033; E-mail: deposit@ccdc.cam.ac.uk].

[1] [1a] G. Helmchem, A. Pfaltz, *Acc. Chem. Res.* **2000**, *33*, 326. [1b] For a general review, covering phosphinooxazoline ligands in catalysis, see: P. Braunstein, F. Naud, *Angew. Chem.* **2001**, *113*, 702; *Angew. Chem. Int. Ed.* **2001**, *40*, 681.

[2] Reviews: [2a] W. A. Herrmann, *Angew. Chem.* **2002**, *114*, 1342−1363; *Angew. Chem. Int. Ed.* **2002**, *41*, 1290−1309. [2b] D. Bourissou, O. Guerret, F. Gabbaï, G. Bertrand, *Chem. Rev.*

 © 2004 Wiley-VCH Verlag GmbH & Co. KGaA, Weinheim

2000, *100*, 39−92. [2c] W. A. Herrmann, C. Köcher, *Angew. Chem.* **1997**, *109*, 2257−2282; *Angew. Chem. Int. Ed. Engl.* **1997**, *36*, 2162−2187. Review on *N*-heterocyclic carbene-transition metal complexes in asymmetric catalysis: M. C. Perry, K. Burgess, *Tetrahedron: Asymmetry* **2003**, *14*, 951−961.

[3] K. H. Dötz, H. Fischer, P. Hofmann, F. R. Kreissl, U. Schubert, K. Weiss, *Transition Metal Carbene Complexes*, Verlag Chemie, Weinheim, **1983**.

[4] [4a] J. A. Chamizo, P. B. Hitchcock, H. A. Jasim, M. F. Lappert, *J. Organomet. Chem.* **1993**, *451*, 89−96. [4b] W. A. Herrmann, C. Köcher, L. J. Goossen, G. R. J. Artus, *Chem. Eur. J.* **1996**, *2*, 1627−1636. [4c] D. S. McGuinness, K. J. Cavell, *Organometallics* **2000**, *19*, 741−748. [4d] C. Yang, H. M. Lee, S. P. Nolan, *Org. Lett.* **2001**, *3*, 1511−1514. [4e] P. L. Arnold, A. C. Scarisbrick, A. J. Blake, C. Wilson, *Chem. Commun.* **2001**, 2340−2341. [4f] A. A. Danopoulos, S. Winston, T. Gelbrich, M. B. Hursthouse, R. P. Tooze, *Chem. Commun.* **2002**, 482−483. [4g] A. A. Danopoulos, S. Winston, M. B. Hursthouse, *J. Chem. Soc., Dalton Trans.* **2002**, 3090−3091.

[5] [5a] W. A. Herrmann, L. J. Goossen, M. Spiegler, *Organometallics* **1998**, *17*, 2162−2168. [5b] J. C. C. Chen, I. J. B. Lin, *Organometallics* **2000**, *19*, 5113−5121. [5c] A. A. D. Tulloch, A. A. Danopoulos, R. P. Tooze, S. M. Cafferkey, S. Kleinhenz, M. B. Hursthouse, *Chem. Commun.* **2000**, 1247−1248. [5d] E. Peris, J. A. Loch, J. Mata, R. H. Crabtree, *Chem. Commun.* **2001**, 201−202. [5e] S. Gründemann, A. Kovacevic, M. Albrecht, J. W. Faller, R. H. Crabtree, *Chem. Commun.* **2001**, 2274−2275. [5f] S. Gründemann, M. Albrecht, J. A. Loch, J. W. Faller, R. H. Crabtree, *Organometallics* **2001**, *20*, 5485−5488. [5g] A. A. D. Tulloch, A. A. Danopoulos, G. J. Tizzard, S. J. Coles, M. B. Hursthouse, R. S. Hay-Motherwell, W. B. Motherwell, *Chem. Commun.* **2001**, 1270−1271. [5h] S. Gründemann, A. Kovacevic, M. Albrecht, J. W. Faller, R. H. Crabtree, *J. Am. Chem. Soc.* **2002**, *124*, 10473−10481. [5i] A. A. Danopoulos, S. Winston, W. B. Motherwell, *Chem. Commun.* **2002**, 1376−1377. [5j] J. A. Loch, M. Albrecht, E. Peris, J. Mata, J. W. Faller, R. H. Crabtree, *Organometallics* **2002**, *21*, 700−706. [5k] J. J. Van Veldhuizen, S. B. Garber, J. S. Kingsbury, A. H. Hoveyda, *J. Am. Chem. Soc.* **2002**, *124*, 4954−4955. [5l] A. A. Danopoulos, S. Winston, M. B. Hursthouse, *J. Chem. Soc., Dalton Trans.* **2002**, 3090−3091. [5m] A. A. D. Tulloch, S. Winston, A. A. Danopoulos, G. Eastham, M. B. Hursthouse, *Dalton Trans.* **2003**, 699−708. [5n] M. C. Perry, X. Cui, M. T. Powell, D.-R. Hou, J. H. Reibenspies, K. Burgess, *J. Am. Chem. Soc.* **2003**, *125*, 113−123. [5o] H. Seo, H.-J. Park, B. Y. Kim, J. H. Lee, S. U. Son, Y. K. Chung, *Organometallics* **2003**, *22*, 618−620. [5p] L. G. Bonnet, R. E. Douthwaite, B. M. Kariuki, *Organometallics* **2003**, *22*, 4187−4189.

[6] [6a] V. César, S. Bellemin-Laponnaz, L. H. Gade, *Organometallics* **2002**, *21*, 5204−5208. [6b] V. César, S. Bellemin-Laponnaz, L. H. Gade, *Angew. Chem.* **2004**, *116*, 1036−1039; *Angew. Chem. Int. Ed.* **2004**, *43*, 1014−1017.

[7] A. I. Meyers, K. A. Novachek, *Tetrahedron Lett.* **1996**, *37*, 1747−1748.

[8] C. Köcher, W. A. Herrmann, *J. Organomet. Chem.* **1997**, *532*, 261−265.

[9] [9a] A. R. Chianese, X. Li, M. C. Janzen, J. W. Faller, R. H. Crabtree, *Organometallics* **2003**, *22*, 1663. [9b] A. C. Hillier, H. M. Lee, E. D. Stevens, S. P. Nolan, *Organometallics* **2001**, *20*, 4246.

[10] H. Seo, B. Y. Kim, J. H. Lee, H.-J. Park, S. U. Son, Y. K. Chung, *Organometallics* **2003**, *22*, 4783−4791.

[11] The ^{1}H NMR chemical shift is consistent with a square-pyramidal arrangement of **4**, see: [11a] M. A. Garralda, E. Pinilla, M. A. Monge, *J. Organomet. Chem.* **1992**, *427*, 193−200. [11b] For the ^{1}H NMR chemical shift of NBD in a trigonal-bipyramidal arrangement, see: D. P. Rice, J. A. Osborn, *J. Organomet. Chem.* **1971**, *30*, C84−89.

[12] W. A. Herrmann, M. Elison, J. Fischer, C. Köcher, G. R. J. Artus, *Chem. Eur. J.* **1996**, *2*, 772−780.

[13] For NHC−Rh−CO complexes, see reference 9 and: S. Burling, L. D. Field, H. L. Li, B. A. Messerle, P. Turner, *Eur. J. Inorg. Chem.* **2003**, 3179−3184. For NHC−Ir−CO complexes, see ref.[5m]

[14] [14a] E. W. Abel, M. A. Bennet, G. Wilkinson, *J. Chem. Soc.* **1959**, 3178−3182. [14b] J. Chatt, L. M. Venanzi, *J. Chem. Soc.* **1957**, 4735−4741.

[15] Nonius *OpenMoleN, Interactive Structure Solution*, Delft, **1997**.

[16] D. T. Cromer, J. T. Waber, *International Tables for X-ray Crystallography*, The Kynoch Press, Birmingham, **1974**.

Received February 5, 2004
Early View Article
Published Online June 23, 2004

 © 2004 Wiley-VCH Verlag GmbH & Co. KGaA, Weinheim

Synthesis and Characterization of Platinum(II) Complexes of Diethyl [(Methylsulfinyl)methyl]phosphonate: Potential Drugs against Bone Tumors

Mariarita Laforgia,[a,b] Leonardo Cerasino,[a] Nicola Margiotta,[a] Maria A. M. Capozzi,[c] Cosimo Cardellicchio,[d] Francesco Naso,[d,e] and Giovanni Natile*[a,b]

Keywords: Antitumor agents / NMR spectroscopy / O ligands / Platinum / S ligands

Cisplatin is the most important metal-based drug used in tumor therapy; however, it suffers from severe side effects and a limited spectrum of activity. Since phosphonates are known to have a selective tropism for bones and calcified tissues, we have carried on the synthesis of different platinum complexes with a phosphonate ligand. The ligand used is diethyl [(methylsulfinyl)methyl]phosphonate (SMP), which can act as an O,S-donor towards Pt. Moreover, since the sulfur atom is a stable stereogenic center, the ligand is obtained in two enantiomeric forms. The synthesised complexes have the general formula $[PtL_2(SMP)]$, in which L_2 stands for a bidentate (dimethylmalonate, 1,2-diaminocyclohexane, ethylenediamine) or two monodentate (chloride) ligands. The formation of a five-membered chelate ring contributes to the chemical stability of complexes with SMP, and 2D NMR experiments have allowed determination of the ring puckering, which is dependent upon the chirality of the sulfur stereocenter. For the (*S*) configuration at the sulfur center (free ligand), the δ puckering of the chelate ring is favoured. Preliminary studies have shown that these compounds are stable under physiological conditions.

(© Wiley-VCH Verlag GmbH & Co. KGaA, 69451 Weinheim, Germany, 2004)

Introduction

Modern anticancer chemotherapy makes use of a variety of drugs having very different chemical structures and mechanisms of action. Among them, cisplatin is still one of the most frequently prescribed drugs for the treatment of several solid tumors, particularly testicular, ovarian, and bladder carcinomas.[1] In spite of its simple chemical structure, the mechanism of action of cisplatin is rather complex. The biological effect probably stems from covalent binding of platinum to two adjacent purine bases on the same strand of DNA.[2−6] This event causes remarkable changes in the natural DNA conformation and from there a cascade of biological alterations finally leading to cell death. The clinical use of cisplatin is limited by toxic side effects and by a narrow spectrum of activity.[7] In order to overcome these limitations, thousands of platinum compounds have been synthesised and tested with the aim of increasing either the activity or the selectivity against the great variety of tumors.

The replacement in the cisplatin molecule of either the two ammine or the two chlorine ligands by other ligands has represented a very general procedure for the synthesis of new potential drugs. Moreover, this methodology gives the possibility of targeting the drug to a particular organ or tissue by coordinating ligands that have a particular affinity for specific receptors (drug targeting approach).[8−10] To this end, Keppler has proposed a class of platinum compounds containing aminobis(phosphonate) ligands, which are expected to have a selective tropism for bones and other calcified tissues because of the affinity of the phosphonate group for Ca^{2+} ions (Scheme 1, A).[11,12] This expectation is justified by the clinical use of bis(phosphonates) (such as Etidronate, Clodronate, Pamidronate and Alendronate[13]) in the treatment of hypercalcaemia. Pharmacological studies performed on platinum complexes with aminobis(phosphonates) have confirmed the activity towards bone tumors and other forms of tumors involving an anomalous balance of Ca^{2+} ions and which are resistant to cisplatin.[14]

One limitation of the compounds with aminobis(phosphonates) is their chemical instability. The oxygen atom of

[a] Dipartimento Farmaco-Chimico, Università degli Studi di Bari, Via E. Orabona 4, 70125 Bari, Italy
E-mail: natile@farmchim.uniba.it
[b] Consorzio Interuniversitario di Ricerca in Chimica dei Metalli nei Sistemi Biologici, Via C. Ulpiani 27, 70125 Bari, Italy
[c] Dipartimento di Scienze Agro-Ambientali, Chimica e Difesa Vegetale, Facoltà di Agraria, Università degli Studi di Foggia, Via Napoli 25, 71100 Foggia, Italy
[d] Consiglio Nazionale delle Ricerche, Istituto di Chimica dei Composti Organometallici (ICCOM), Sezione di Bari, Via E. Orabona 4, 70125 Bari, Italy
[e] Dipartimento di Chimica, Università di Bari, Via E. Orabona 4, 70125 Bari, Italy

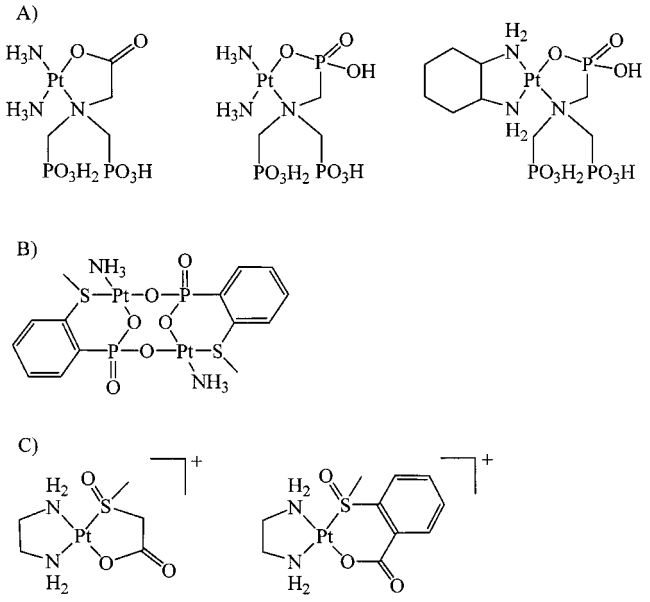

Scheme 1. Structures of platinum complexes with: A) aminobis(phosphonate) ligands, B) [2-(methylsulfanyl)phenyl]phosphonate, and C) (methylsulfinyl)acetate and 2-(methylsulfinyl)benzoate

the phosphonate group and the nitrogen atom of a tertiary amine are weak donors for platinum and the aminobis(phosphonates) can be easily displaced by stronger nucleophiles, in spite of the stabilization stemming from the formation of a five-membered chelate ring.[15,16] However, the stability of this class of compounds can be increased by introducing in the molecule of the phosphonate a group with a higher coordination affinity for platinum, such as a sulfoxide. The use of sulfoxides as ligands in platinum drugs was already proposed by Farrell some years ago.[17] A series of compounds having the general formula [Pt(diamine)Cl(R^1R^2SO)]$^+$ showed interesting biological activity[18,19] in spite of their being positively charged (for years neutrality was considered a prerequisite for activity of cisplatin analogues).

Other O,S-donor ligands have been used in the past for the synthesis of cisplatin analogues. In particular, [2-(methylsulfanyl)phenyl]phosphonate has been used by Kozelka et al.[20] In that case, reaction with aquated cisplatin led to the loss of one ammine ligand and formation of a dimeric species with bridging phosphonate groups, which was practically insoluble in any solvent (Scheme 1, B). (Methylsulfinyl)-acetate and 2-(methylsulfinyl)benzoate have been used by Pasini and co-workers.[21] They used chelated diamines such as ethylenediamine (en) and 1,2-diaminocyclohexane (dach) in order to prevent dissociation of the amine group *trans* to the sulfur atom (Scheme 1, C). The obtained compounds were found to be moderately cytotoxic towards L1210 leukaemia cells; however, no selective tropism for particular tissues was investigated.

In the present study we report on the synthesis and spectroscopic characterization of platinum complexes with the new ligand diethyl [(methylsulfinyl)methyl]phosphonate (SMP; Scheme 2). Apart from the substitution of a sulfoxide for a tertiary amine, another major difference between Keppler's aminobis(phosphonates) and SMP is the presence in the latter ligand of phosphonic groups blocked as diethyl esters. This chemical change could be critical for modulating the hydrophobic/hydrophilic balance of the compounds.

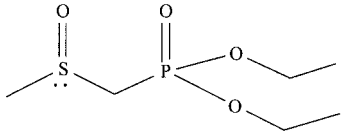

Scheme 2. Shorthand drawing of the diethyl [(methylsulfinyl)methyl]phosphonate ligand, SMP

Results and Discussion

Characterization of the Complexes

Two types of complexes have been synthesised and characterized in this work: neutral complexes (**1** and **2**; Scheme 3) containing, besides SMP, two chloride ions or a dimethylmalonate ligand (dmm), and cationic species (**3** and **4**; Scheme 3) in which a diamine (en or dach) and an SMP molecule saturate the four coordination positions of the platinum(II) center.

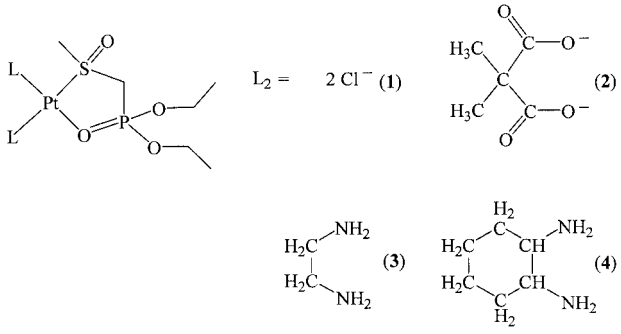

Scheme 3. Shorthand drawing of the synthesised complexes with the SMP ligand

The synthesis of the complexes is straightforward. The dichloro species **1** was prepared by direct reaction of potassium tetrachloroplatinate with SMP and is soluble both in aqueous and in organic solvents. Removal of the chloride ligands by reaction with silver sulfate and addition of potassium dimethylmalonate affords complex **2**, which is rather soluble both in water and in organic solvents such as methanol and ethanol. The cationic species **3** and **4** were prepared from **1** by addition of the selected diamine, which displaces the two chloride ions. Compounds **3** and **4** can also be prepared by reaction of SMP with a platinum complex already containing the diamine; however, in this case the two leaving ligands must be very labile (solvent molecules).

The stereochemical characterization of the complexes was performed essentially by NMR spectroscopy (Table 1).

 © 2004 Wiley-VCH Verlag GmbH & Co. KGaA, Weinheim

Table 1. NMR spectroscopic data for the SMP ligand and the [PtL_2(SMP)] complexes; coupling constants [Hz], are given as ($J_{H,H}$), {$J_{H,P}$}, and [$J_{H,Pt}$]; multiplicity stemming from coupling with Pt is not considered

Compd.	Solvent	^{1}H					^{31}P{^{1}H}	^{13}C{^{1}H}			
		CH_3SO	$SOCH_2P$	$POCH_2CH_3$	OCH_2CH_3	L_2	CH_2PO	H_3CSO	$SOCH_2P$	$POCH_2C$	OCH_2CH_3
SMP	D_2O	2.86 d {2}	3.59 dd[a]; 3.56 dd[a] (14.9) {11.5}	4.26 dq[a]; 4.25 dq[a] {8} (7.5)	1.35 t (7.5)		19.8	39.8 s	49.0 d $^1J_{C,P}$ = 140	65.5 s; 65.4 s	16.0 s
	[D_6]-acetone	2.83 s	3.44 dd[a]; 3.32 dd[a] (15) {11.5}	4.13 dq; 4.12 dq {8} (7.5)	1.28 t (7.5)		20.7	42.0 d $^3J_{C,P}$ = 5.8	51.9 s $^1J_{C,P}$ = 126	63.8 s; 63.7 s	17.3 s; 17.2 s
1	D_2O	3.69 d {2} [18]	4.72−4.50 m[b]	4.46−4.28 m	1.43 t; 1.40 t (7.5)		14.8 $^2J_{P,Pt}$ = 46	46.2 d $^3J_{C,P}$ = 6.8	50.1 d[b] $^1J_{C,P}$ = 113	66.5 d; 66.4 d $^2J_{C,P}$ = 6.0;6.3	16.9 s; 16.8 s
	[D_6]-acetone	3.57 s [18]	4.72 dd[a]; 4.05 dd[a] (15.2) {11.5} [15.6, 13.3]	4.31−4.15 m	1.32 t; 1.30 t (7.5)		15.5 $^2J_{P,Pt}$ = 90	43.0 d $^3J_{C,P}$ = 6.8	49.8 d $^1J_{C,P}$ = 136	63.5 d; 62.8 d $^2J_{C,P}$ = 5.8	16.0 s; 15.9 s
2	D_2O	3.67 d {2} [18]	4.62−4.40 m[b]	4.40−4.25 m	1.39 t; 1.33 t (7.5)	1.75 s; 1.72 s	15.8 $^2J_{P,Pt}$ = 46	44.5 d $^3J_{C,P}$ = 6.8		65.3 d; 65.2 d $^2J_{C,P}$ = 6.0;6.3	15.8 s; 15.7 s
3·SO_4	D_2O	3.62 d {2} [18]	4.60−4.40 m[b]	4.38−4.24 m	1.40 t; 1.38 t (7.5)	2.84 s [40]	16.2 $^2J_{P,Pt}$ = 48	45.0 d $^3J_{C,P}$ = 6.8		65.3 d; 65.2 d $^2J_{C,P}$ = 5.7;6.0	15.7 s; 15.6 s
4·SO_4	D_2O	3.70 d {2} [18]	4.60−4.40 m[b]	4.40−4.25 m	1.41 t; 1.36 t (7.5)	2.70−2.50 m[c]	16.3 $^2J_{P,Pt}$ = 48	44.9 d $^3J_{C,P}$ = 6.8		65.3 d; 65.2 d $^2J_{C,P}$ = 5.7;6.0	15.7 s; 15.6 s

[a] Precise chemical shifts and coupling constants of protons in multiplets have been calculated, when possible, through NMR decoupling experiments. [b] The signals of the central methylene protons in D_2O are detectable only soon after dissolution; exchange with deuterium then occurs and the signals disappear. [c] Only the chemical shift of the methylidene protons is reported for the (*R*,*R*)-dach ligand.

The SMP Ligand

Coordination of the SMP ligand through the sulfoxide functionality was clearly evident from the downfield shift (ca. 0.8 ppm) of the SMe protons. The coupling constant between the methyl protons and the platinum atom (18 Hz) is also in the normal range for sulfoxides *S*-coordinated to the platinum atom.[22] In D_2O, it is also possible to observe a long-range coupling between the methyl protons and the phosphorus atom ($^4J_{H,P} \approx 2$ Hz).

The protons of the methylene group bridging the sulfur and the phosphorus atoms are relatively acidic, and in D_2O or CD_3OD undergo rapid exchange with the deuterium of the solvent. Such a behavior resembles that of chelated amino acids.[23,24] The methylene proton signals, however, are nicely observable when [D_6]acetone solutions are measured (Figure 1) and in the following discussion we will refer to spectra taken in this solvent (apart from the free ligand, only compound **1** is soluble in acetone). The two methylene protons are magnetically non-equivalent, both in the free SMP ligand and in the complex, because of the diastereotopic splitting caused by the chiral sulfur center. Upon complexation, the signal of one proton of the methylene group undergoes a downfield shift similar to that observed for the SMe protons (δ = 4.05 ppm; $\Delta\delta$ = 0.73 ppm). In contrast, the second methylene proton signal undergoes a downfield shift which is almost twice as large (δ = 4.72 ppm; $\Delta\delta$ = 1.28 ppm). Each methylene proton shows couplings with the phosphorus atom ($^2J_{H,P}$ = 11.5 Hz), the geminal proton ($^2J_{H,H}$ = 15.2 Hz) and the platinum atom ($^3J_{H,Pt}$ = 15.6 and 13.3 Hz for the δ = 4.72 and 4.05 ppm resonances, respectively). The less-shielded proton has a higher coupling constant with platinum than the more shielded proton. The different values of the coupling constants with platinum are indicative of a different H−C−S−Pt torsion angle (higher coupling constant for torsion angles closer to 180° according to Karplus's rule).[25]

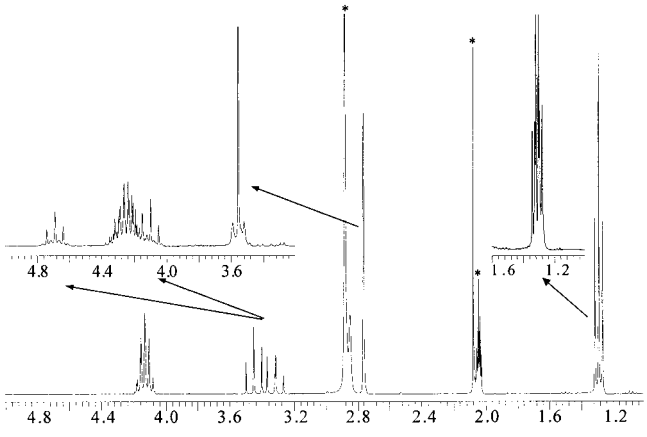

Figure 1. ^{1}H NMR spectra (300 MHz, [D_6]acetone) of the free ligand diethyl [(methylsulfinyl)methyl]phosphonate (SMP, bottom) in comparison with its platinum complex *cis*-[$PtCl_2$(SMP)] (top); asterisks indicate solvent peaks

A 2D NOE experiment has shown the presence of cross-peaks between both methylene protons and the SMe group (Figure 2). This is in agreement with a "quasi equatorial" disposition of the SMe group which, in a staggered confor-

 © 2004 Wiley-VCH Verlag GmbH & Co. KGaA, Weinheim

mation, comes in between the two methylene protons. In contrast, a "quasi axial" disposition of the SMe group would be in agreement with the SMe group having NOE cross-peaks with only one methylene proton. A "quasi equatorial" SMe group implies that, starting with a free ligand having an (*S*) configuration at the sulfur center, in the complexed molecule the chelate ring assumes a δ puckering (Scheme 4). It should be noted that, upon coordination to the platinum atom, the priorities of the groups bound to the sulfur atom change; however, we have chosen to refer to the chirality of the free ligand also for the complexed sulfoxide. One NOE cross-peak is stronger than the other and involves the methylene proton less coupled with the platinum atom (and having more axial character); conversely, the NOE is weaker for the proton more coupled with the platinum atom (and having more equatorial character). This is the expected trend for a reduced puckering of the five-membered chelate ring and a conformation around the S−C(methylene) bond that is intermediate between staggered and eclipsed, with the consequence that the "quasi equatorial" SMe group is brought closer to the "quasi axial" methylene proton and farther from the "quasi equatorial" methylene proton.

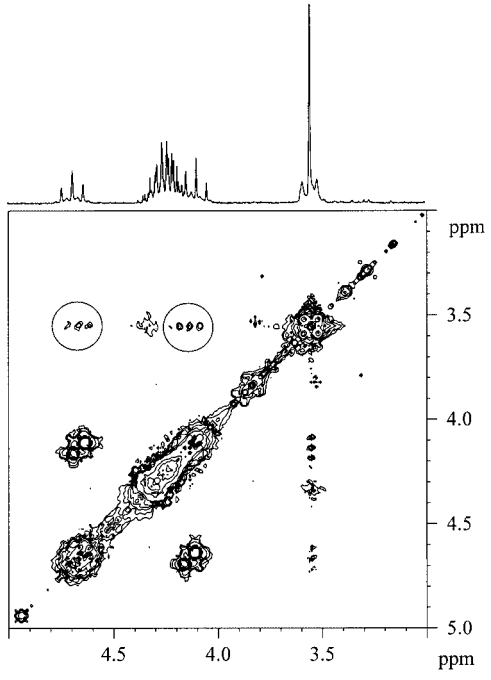

Figure 2. 2D-NOESY contour plot (300 MHz, [D_6]acetone) of complex **1**; cross-peaks between the SMe protons and the central methylene protons are in circles

The deshielding effect of the S=O double bond of the sulfoxide is probably responsible for the greater shift to low field of the "quasi equatorial" methylene proton signal. The positioning of the SMe group in a "quasi equatorial" conformation is also in agreement with the smaller steric interaction between diaxial substituents in the 1,3-positions of the chelate ring [OEt and (S)O instead of OEt and (S)Me].

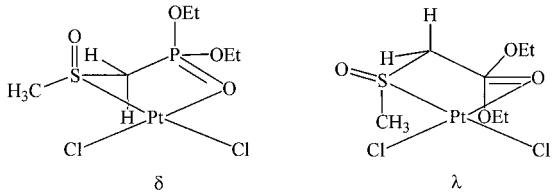

Scheme 4. δ and λ puckering of the five-membered chelate ring of coordinated SMP for an (*S*) configuration at the sulfur center of the free ligand; δ puckering is favoured

It is worth mentioning that for the analogous complex with (methylsulfinyl)acetate,[21] the correlation between the configuration of the sulfoxide and the puckering of the chelate ring is opposite to that observed in the present case [δ conformation of the chelate ring for an (*R*) configuration of the sulfoxide as deduced from crystallographic data]. Steric repulsions between "quasi axial" substituents in positions 1 and 3 of the ring are critical for the puckering of the chelate ring. Thus, diethyl [(methylsulfinyl)methyl]phosphonate prefers to place the methyl group in a "quasi equatorial" position and the oxygen in a "quasi axial" position because of a smaller repulsion between the axial substituents in positions 1 and 3 of the ring. This corresponds to a δ puckering of the chelate ring for an (*S*) configuration of the starting sulfoxide (Scheme 4). In contrast, in the case of (methylsulfinyl)acetate, there are no axial substituents in position 3 of the chelate ring with respect to the coordinated sulfur atom (the noncoordinated oxygen atom of the carbonyl group being nearly coplanar with the coordination plane). Therefore, it is most likely that the δ conformation of the ring for the (*R*) configuration of the sulfoxide, observed in the solid state of the latter complex, is not determined by intraligand steric constraints (practically absent), but by crystal lattice interactions.

Upon coordination to the platinum atom, the two ethoxy residues of the phosphonate group undergo a small downfield shift with respect to the free SMP ligand ($\Delta\delta \approx$ 0.1 ppm for the methylene protons and 0.04−0.02 ppm for the methyl protons). The phosphorus signal undergoes an upfield shift of ca. 5 ppm; moreover, it exhibits a coupling constant with Pt of ca. 90 Hz. Such a value for $^2J_{Pt,P}$ is perfectly compatible with tabulated values for classical Pt−O−P couplings (Figure 3, A).[26] It is worth noting that the $^2J_{Pt,P}$ coupling constant decreases from 90 to 46 Hz upon changing the solvent from [D_6]acetone to D_2O (Figure 3, B). We believe that such a dramatic change is correlated with the acidity of the methylene group bridging the sulfur and phosphorus atoms which, in water, are likely to undergo partial proton dissociation.

The acidity of the methylene group is revealed by the low pH (ca. 4.6) observed in solutions of compounds **1**, **2**, **3**, and **4** in water. This implies that the methylene group bridging the sulfur and the phosphorus atoms can dissociate one proton, becoming a carbanion. Because of the fast exchange with the solvent, it is only possible to detect the central methylene protons by performing the NMR experiments in H_2O/D_2O (90:10) (Figure 4).

 © 2004 Wiley-VCH Verlag GmbH & Co. KGaA, Weinheim

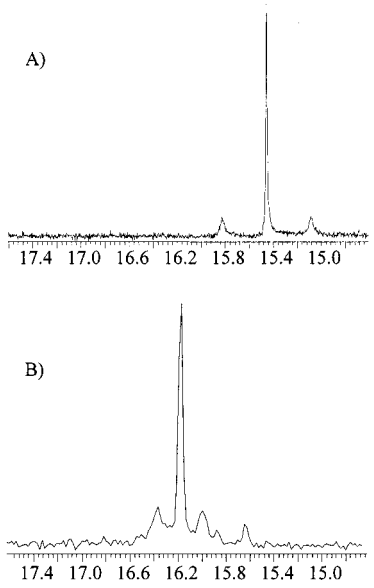

Figure 3. ^{31}P (121.5 MHz) NMR spectra of complex **1**: in [D_6]acetone (A) and in D_2O (B)

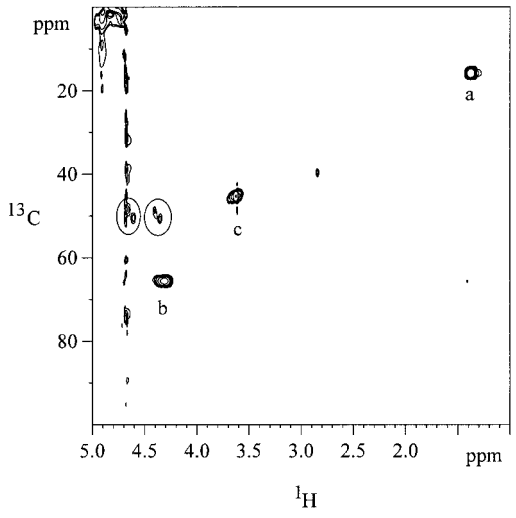

Figure 4. ^{13}C,^{1}H-2D-HETCOR contour plot of complex **1** in H_2O/D_2O (90:10, v/v) showing the cross-peaks (in circles) between ^{1}H and ^{13}C of the rather acidic methylene group bridging the sulfur and phosphorus atoms of the coordinated SMP ligand; cross-peaks a, b, and c are related to the ethoxy methyl and methylene groups and to the sulfoxide methyl group, respectively

The Malonato Ligand (Complex 2)

The ^{1}H NMR spectrum of compound **2**, besides the signals of the SMP ligand, which are very similar to those of the parent dichloro complex, exhibits two singlets at δ = 1.75 and 1.72 ppm assignable to the methyl groups of the dimethylmalonato ligand. The two methyl signals are shifted by 0.47 and 0.44 ppm with respect to those of free dimethylmalonato and are indicative of its bidentate coordination. The non-equivalence of the two methyl groups stems from the lack of symmetry of the coordination plane generated by the asymmetric sulfoxide.

The Diamine Ligands (Complexes 3 and 4)

The NMR signals of the SMP ligand of compounds **3** and **4** are also very similar to those of the parent dichloro complex. In compound **3**, the coordination of the ethylenediamine ligand is supported by the ^{1}H NMR signals of the two methylene groups bridging the two coordinated nitrogen atoms. In D_2O, the two methylene groups give a unique sharp singlet at $\delta \approx 2.84$ ppm (0.2 ppm downfield from the signal of free ethylenediamine) with a coupling with Pt of ca. 40 Hz (the usual value for $^{3}J_{Pt,H}$). The coordination of the 1,2-diaminocyclohexane ligand to Pt in compound **4** is supported by the downfield shifts of the proton signals of the cyclohexane ring. The shift is particularly relevant for the protons of the asymmetric carbon centers adjacent to the amine groups ($\Delta\delta \approx 0.7$ ppm).

Stability of the Complexes

The dichloro complex **1** in aqueous solution undergoes a slow process of solvolysis, as revealed by the appearance of new signals. Particularly diagnostic are the two new signals belonging to the CH_3SO protons which, however, are very close to that of the starting complex and still show similar couplings with Pt. This implies that in the new species the sulfoxide group is still bound to the platinum atom. Moreover, the ^{31}P NMR spectra also show the appearance, with time, of two new signals which, again, are very close to that of the starting complex and still show similar couplings with Pt. Therefore, in the newly formed solvato species the phosphonate group is still bound to the platinum atom. All the new peaks disappear if LiCl (0.1 M concentration) is added to the solution. Therefore, it could be concluded that the new species are solvato species in which one or both chloride ligands of the starting substrate have been displaced by water molecules. It can be noted, however, that, due to the asymmetry of the SMP ligand, two monosolvato species can be formed, one with the solvent molecule *trans* to the sulfoxide and the other with the solvent molecule *trans* to the phosphonate group. Therefore, it is most likely that the observed new species are monosolvated.

The stability of the dimethylmalonato compound **2** was investigated in water solution containing a 0.1 M chloride concentration. Formation of a small amount of species containing a monodentate dmm ligand was observed soon after dissolution at room temperature. This was immediately followed by the appearance of the peak of free dmm. After 7 h at 25 °C, the intensities of bidentate and free dmm were ca. 1:1. After 3 d at 25 °C and pH = 6.3, the ratio of bidentate and free dmm was 1:3.8.

The stability of compounds **3** and **4** was also investigated. In water solution both compounds are stable in the absence of coordinating ligands. However, if chloride ions are present, ready replacement of the SMP ligand and precipitation of insoluble [$PtCl_2$(en)] or [$PtCl_2$(dach)] is observed. This behavior is in agreement with previous observations on the reactivity of platinum complexes containing chelated O,S ligands and bidentate amines.[20,21] In the case of bidentate amines the reaction with extra ligands (such as Cl^-)

 © 2004 Wiley-VCH Verlag GmbH & Co. KGaA, Weinheim

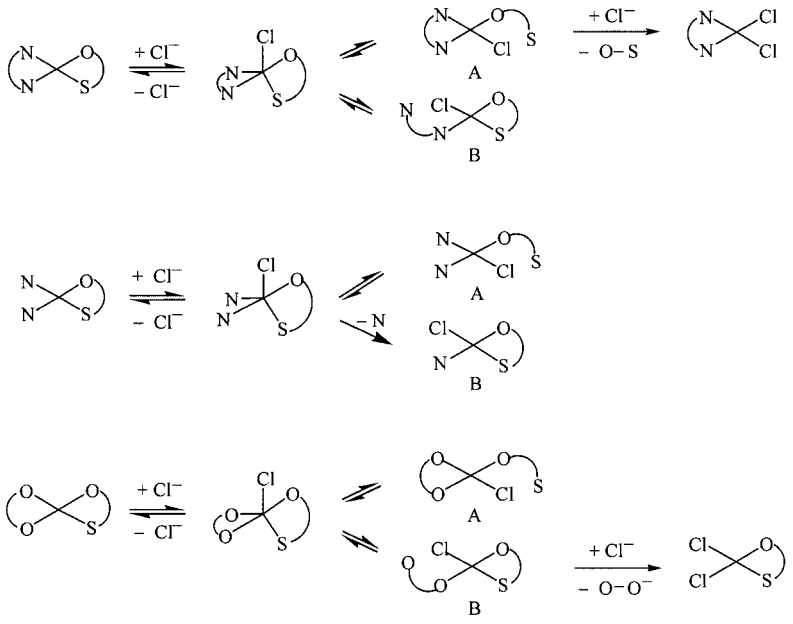

Scheme 5. Different behavior of ancillary ligands in the displacement reaction with chloride ions

leads to displacement of the O,S ligand in preference to the bidentate diamine. In contrast, when the platinum complex contains, besides the O,S ligand, two monodentate amines, the reaction with extra ligands leads to displacement of the amine group *trans* to the sulfur atom.

The different behavior of compounds with monodentate and bidentate amines can be rationalized in the following way. In substitution reactions involving four-coordinate square-planar complexes, the trigonal-bipyramidal transition state is stabilized by electron-acceptor ligands lying in the trigonal plane (sulfur is a good acceptor having empty 3d orbitals, and in the case of sulfoxide there is also an unfilled π^* orbital). In the case of a bidentate amine (top row of Scheme 5), the entering of the first chloride ion can lead to two intermediate species, each of them having a monocoordinated bidentate ligand (species A and B); A will be more reactive than B because it contains a singly bonded O-donor ligand which is more labile than a singly bonded N-donor ligand. Therefore, A will react in preference to B with a second molecule of incoming nucleophile (the Cl^- anion) leading to the complete displacement of the O,S ligand. In contrast, in the case of monoamines (middle row of Scheme 5), the reaction path leading to B will be favoured with respect to that leading to A since in the case of B the back reaction is disfavoured (it requires the attack by a molecule of N which has already left).

By a similar reasoning we can explain the different reactivity with chloride of compound **2** (the malonato ligand displaced in preference to the SMP ligand) with respect to compounds **3** and **4** (the SMP ligand displaced in preference to the diamine). In the former case (bottom row of Scheme 5) the intermediate species A and B formed after the entering of the first chloride ion both contain an equally labile singly bonded O-donor ligand (oxygen is not a good donor for platinum). However, the equilibrium between A and B will be shifted in favour of B because the latter contains a better set of donor atoms (Cl, S, 2 O) than the former (Cl, 3 O). Therefore, the loss of the O,O ligand from the most abundant intermediate B will be the preferred reaction path.

Conclusions

In conclusion, diethyl [(methylsulfinyl)methyl]phosphonate (SMP) has proven to be a versatile ligand for platinum allowing the synthesis of different complexes in which SMP acts invariably as an O,S-donor ligand. Unlike the vast majority of metal phosphonate complexes reported in the literature, the present ligand is in the form of a dialkyl ester, coordinating the metal atom by the oxygen atom formally doubly bonded to the phosphorus atom.

It has been shown that the puckering of the O,S chelate ring depends upon the chirality at the sulfur center [δ puckering for an (*S*) configuration of the free ligand]. Moreover, for coordinated SMP, the protons of the methylene group bridging the sulfur and phosphorus atoms are rather acidic as revealed by the rather low pH of aqueous solutions of the complexes. Depending upon the nature of the ancillary ligands, the SMP can behave as a leaving ligand (ancillary diamines) or as a non-leaving ligand (ancillary monoamine, malonato or chloro ligands). The two possibilities are likely to influence in a different way the antitumor activities of these compounds.

We hope that some of these new platinum complexes might follow the promising route marked by Keppler's complexes with aminobis(phosphonates), which show selective

 © 2004 Wiley-VCH Verlag GmbH & Co. KGaA, Weinheim

activity against bone tumors and those forms of tumors involving an anomalous balance of calcium ions.

Experimental Section

General Methods: NMR spectra were recorded with a Bruker AVANCE DPX-WB 300 MHz instrument. Standard Bruker automation programs were used for 2D NMR experiments. ^{1}H chemical shifts are referenced to TMS by using the residual protic peak of the solvent as internal reference (δ = 2.04 ppm for [D$_6$]acetone and δ = 4.80 ppm for deuterium oxide). ^{13}C NMR chemical shifts are also referenced to TMS. ^{31}P NMR chemical shifts are referenced to 85% H_3PO_4. IR spectra were obtained with a Perkin−Elmer Spectrum One Infrared Spectrophotometer using KBr as solid support for pellets. Elemental analyses were performed with a Carlo Erba Elemental Analyzer mod. 1106 instrument.

Starting Materials: The diethyl [(methylsulfinyl)methyl]phosphonate ligand (SMP) was prepared by a reported procedure.[27] The ligand contains a chiral sulfur atom and can be prepared either as the pure (*S*) or (*R*) enantiomer or as a racemic mixture. In our investigation we have used both the (*S*) enantiomer and the racemic mixture. The preparation of the (*R*) enantiomer is under way.

[PtCl$_2$(SMP)] (1): A solution of SMP (250 mg, 1.17 mmol) in water (10 mL) was added dropwise to a solution of potassium tetrachloroplatinate (510 mg, 1.23 mmol) in the same solvent (10 mL). Within a few minutes, the reaction mixture turned from red to yellow-orange. The solution was stirred at room temperature for 24 h, then the solvent was removed by lyophilization and the orange solid residue extracted with acetone in order to remove insoluble KCl and unchanged potassium tetrachloroplatinate. Concentration of the acetone solution to dryness under reduced pressure gave an oily residue which, after trituration with diethyl ether, afforded a yellow-orange solid which proved to be the pure complex [PtCl$_2$(SMP)]. Yield: 95% (533 mg). $C_6H_{15}Cl_2O_4PPtS$ (480.20): calcd. C 15.00, H 3.15; found C 15.04, H 3.15. IR: $\tilde{\nu}$ = 2913 (ν_{C-H}), 1253 ($\nu_{P=O}$), 1048 ($\nu_{S=O}$), 1013 (ν_{P-O-R}), 321 (ν_{Pt-Cl}) cm^{-1}. See Table 1 for NMR spectroscopic data.

[Pt(dmm)(SMP)] (2): A solution of potassium dimethylmalonate (dmm, 43 mg, 0.206 mmol) in water (2 mL) was added dropwise to a solution of [PtCl$_2$(SMP)] (99 mg, 0.206 mmol) in water (10 mL). After stirring at room temperature for 12 h, a stoichiometric amount of Ag_2SO_4 (64 mg, 0.206 mmol) was added to the solution and stirring was resumed for an additional 12 h. The suspension was filtered to remove AgCl and the solution concentrated to dryness by lyophilization. The yellow solid was extracted with methanol, to remove insoluble K_2SO_4, and the organic solution concentrated to dryness under reduced pressure. The resulting yellow solid proved to be the desired complex of composition [Pt(dmm)(SMP)]·H_2O. Yield: 69% (79 mg). $C_{11}H_{23}O_9PPtS$ (557.42): calcd. C 23.70, H 4.16; found C 23.48, H 4.54. IR: $\tilde{\nu}$ = 2935 (ν_{C-H}), 1633 ($\nu_{C=O}$), 1251 ($\nu_{P=O}$), 1050 ($\nu_{S=O}$), 1021 (ν_{P-O-R}) cm^{-1}. See Table 1 for NMR spectroscopic data.

[Pt(en)(SMP)]Cl$_2$ (3·2Cl) and [Pt{(*R*,*R*)-dach}(SMP)]Cl$_2$ (4·2Cl): A solution of ethylendiamine (en, 13.7 mg, 0.228 mmol) or (*R*,*R*)-1,2-diaminocyclohexane (*R*,*R*-dach, 26 mg, 0.228 mmol) in water (2 mL) was added dropwise to a solution of the chloro complex [PtCl$_2$(SMP)] (110 mg, 0.228 mmol) in the same solvent (10 mL). The reaction mixture turned immediately from yellow to colourless. Evaporation of the solvent under reduced pressure left a pale-yellow oily residue which, after trituration with diethyl ether, afforded a pale-yellow solid product, which proved to be the desired complex. Compounds **3**·2Cl and **4**·2Cl are highly hygroscopic materials and were characterized only by NMR spectroscopy (see Table 1).

[Pt(en)(SMP)](SO$_4$) (3·SO$_4$) and [Pt{(*R*,*R*)-dach}(SMP)](SO$_4$) (4·SO$_4$): The reaction was performed as described in the previous preparation. The resulting colourless solution was treated with a stoichiometric amount of Ag_2SO_4 (71 mg, 0.228 mmol) which caused precipitation of AgCl which was removed by filtration. Lyophilization of the solution left a white solid which proved to be the desired complex. Yield: 60%.

3·SO$_4$: $C_8H_{23}N_2O_8PPtS_2$ (565.46): calcd. C 17.00, H 4.10, N 4.95; found C 17.30, H 4.48, N 5.34. IR: $\tilde{\nu}$ = 3207 (ν_{N-H}), 2988 (ν_{C-H}), 1245 ($\nu_{P=O}$), 1127 (ν_{SO4}), 1052 ($\nu_{S=O}$), 1021 (ν_{P-O-R}) cm^{-1}. See Table 1 for NMR spectroscopic data.

4·SO$_4$: $C_{12}H_{29}N_2O_8PPtS_2$ (619.56): calcd. C 23.26, H 4.72, N 4.52; found C 23.16, H 5.10, N 4.88. IR: $\tilde{\nu}$ = 3205 (ν_{N-H}), 2988−2937 (ν_{C-H}), 1250 ($\nu_{P=O}$), 1117 (ν_{SO4}), 1049 ($\nu_{S=O}$), 1023 (ν_{P-O-R}) cm^{-1}. See Table 1 for NMR spectroscopic data.

Acknowledgments

The authors thank the Ministero dell'Istruzione, Università e Ricerca (MIUR), Rome (Cofin N. 2001053898 and 2000 N. MMO3027791 and National Project "Stereoselezione in Sintesi Organica, Metodologie e Applicazioni"), the EC (COST Chemistry projects D20/0001/2000 and D20/0003/01), Consiglio Nazionale delle Ricerche (CNR-Agenzia 2000), the University of Bari and the FIRB project "Progettazione, preparazione e valutazione biologica e farmacologica di nuove molecole organiche quali potenziali farmaci innovativi" for financial support.

[1] P. J. Loehrer, L. H. Einhorn, *Ann. Intern. Med.* **1984**, *100*, 704−713.
[2] J. Reedijk, A. M. J. Fichtinger-Shepman, A. T. Van Oosterom, *Struct. Bonding (Berlin)* **1987**, *67*, 53−89.
[3] W. I. Sundquist, S. J. Lippard, *Coord. Chem. Rev.* **1990**, *100*, 293−322.
[4] J. Reedijk, *Inorg. Chim. Acta* **1992**, *873*, 198−200.
[5] A. M. J. Fichtinger-Shepman, J. L. Van der Veer, J. H. J. Den Hartog, P. H. M. Lohman, J. Reedijk, *Biochemistry* **1985**, *24*, 707−713.
[6] A. M. Fuertes, C. Alonso, J. M. Pérez, *Chem. Rev.* **2002**, *103*, 645−662.
[7] D. D. Von Hoff, R. Schilsky, C. M. Reichert, R. L. Reddick, M. Rozencweig, R. C. Young, F. M. Muggia, *Cancer Treat. Rep.* **1979**, *63*, 1527−1531.
[8] P. J. Bednarski, R. Gust, T. Spruss, N. Knebel, A. Otto, M. Farbel, R. Koop, E. Holler, E. von Angerer, H. Schonenberger, *Cancer Treat. Rev.* **1990**, *17*, 221−231.
[9] H. H. Lee, B. D. Palmer, B. C. Baguley, M. Chin, W. D. McFadyen, G. Wickham, D. Thorsbourne-Palmer, L. P. G. Wakelin, W. A. Denny, *J. Med. Chem.* **1992**, *35*, 2983−2987.
[10] A. Rosenfeld, J. Blum, D. Gibson, A. Ramu, *Inorg. Chim. Acta* **1992**, *201*, 219−221.
[11] T. Klenner, P. Valenzuela-Paz, F. Amelung, H. Munch, H. Zahn, B. K. Keppler, H. Blum, in *Metal Complexes in Cancer Chemotherapy* (Ed.: B. K. Keppler), VCH Weinheim, **1993**, p. 85−127.
[12] F. Wingen, D. Scmahl, *Arzneim.-Forsch./Drug Res.* **1985**, *35*, 1565−1571.

 © 2004 Wiley-VCH Verlag GmbH & Co. KGaA, Weinheim

[13] J. H. Lin, *Bone* **1996**, *18*, 75−85.
[14] B. K. Keppler, M. R. Berger, T. Klenner, M. E. Heim, *Adv. Drug Res.* **1990**, *19*, 243−310.
[15] S. S. G. E. Van Boom, J. Reedijk, *J. Chem. Soc., Chem. Commun.* **1993**, *18*, 1397−1398.
[16] K. J. Barnham, M. I. Djuran, P. del Socorro, P. J. Sadler, *J. Chem. Soc., Chem. Commun.* **1994**, *6*, 721−722.
[17] N. Farrell, *J. Chem. Soc., Chem. Commun.* **1982**, *6*, 331−332.
[18] N. Farrell, D. M. Kiley, W. Schmidt, M. P. Hacker, *Inorg. Chem.* **1990**, *29*, 397−403.
[19] J. Landi, M. P. Hacker, N. Farrell, *Inorg. Chim. Acta* **1992**, *202*, 79−83.
[20] C. Mauger, M. Vazeux, A. Albinati, J. Kozelka, *Inorg. Chem. Commun.* **2000**, *3*, 704−707.
[21] A. Pasini, G. D'Alfonso, C. Manzotti, M. Moret, S. Spinelli, M. Valsecchi, *Inorg. Chem.* **1994**, *33*, 4140−4148.
[22] F. P. Fanizzi, G. Natile, M. Lanfranchi, A. Tiripicchio, *Inorg. Chim. Acta* **1997**, *264*, 11−18.
[23] P. A. Sutton, D. A. Buckingham, *Acc. Chem. Res.* **1987**, *20*, 357−364.
[24] E. C. Constable, *Metals and Ligands Reactivity*, Ellis Horwood, London **1990**.
[25] M. Karplus, *J. Chem. Phys.* **1959**, *30*, 11−15.
[26] T. G. Appleton, J. R. Hall, D. W. Neale, *Inorg. Chim. Acta* **1985**, *104*, 19−31.
[27] M. A.M. Capozzi, C. Cardellicchio, G. Fracchiolla, P. Tortorella, F. Naso, *J. Am. Chem. Soc.* **1999**, *121*, 4708−4709.

Received March 10, 2004
Early View Article
Published Online June 24, 2004

 © 2004 Wiley-VCH Verlag GmbH & Co. KGaA, Weinheim

Interaction of the $[GaH_4]^-$ Anion with Weak XH Acids − A Spectroscopic and Theoretical Study

Natalia V. Belkova,[a] Oleg A. Filippov,[a] Andrey M. Filin,[a] Liliya N. Teplitskaya,[a] Yulia V. Shmyrova,[a] Vyacheslav V. Gavrilenko,[a] Ludmila M. Golubinskaya,[a] Vladimir I. Bregadze,[a] Lina M. Epstein,*[a] and Elena S. Shubina*[a]

Keywords: Hydrides / Hydrogen bonding / IR spectroscopy / Theoretical methods / Boron / Gallium

The dihydrogen bonding (DHB) between the hydride atom of the $[Bu_4N][GaH_4]$ salt and different XH acids, namely CF_3CH_2OH, FCH_2CH_2OH, *i*PrOH, MeOH, indole and 4-$O_2NC_6H_4NH_2$, has been investigated for the first time by low-temperature IR spectroscopy. The DHB spectroscopic and thermodynamic parameters in solvents of low polarity and high basicity (E_j = 1.37) were obtained. The nature, structures, energies and electron distributions of the model DHB complexes of GaH_4^- with H_2O, MeOH, CF_3OH, H_2NCF_3 or $NO_2C_6H_4NH_2$ were studied by DFT calculations and compared with those of the analogous complexes of BH_4^- with H_2O, MeOH or CF_3OH. Two types of DHB structures with monodentate and symmetric chelate coordination were found. The lengthening of the X–H and Ga–H bonds, electron polarization and overlap population of the H···H bond are greater in the first type of structure. A comparative analysis of experimental data demonstrates that the spectroscopic and thermodynamic characteristics, e.g. ν(XH) and ν(GaH) band shifts, $\nu(XH)_{bonded}$ integral intensities, formation enthalpies and E_j of all the DHB complexes increase down the group (BH_4^-·HX < GaH_4^-·HX).

(© Wiley-VCH Verlag GmbH & Co. KGaA, 69451 Weinheim, Germany, 2004)

Introduction

The unconventional intermolecular hydrogen bond between XH proton donors and the hydride ligands of transition metal hydride complexes ($XH^{\delta+}\cdots{}^{-\delta}HM$) were discovered between 1995 and 1996 and have been actively investigated since this time with several reviews appearing on the topic.[1−6] The formation conditions, structural and energetic characteristics of these unusual hydrogen bonds were determined by low-temperature IR and NMR spectroscopy in solution and by X-ray and neutron diffraction in the solid state. A variety of theoretical methods were devoted to the nature and structure of this dihydrogen bond (DHB) formed by transition metal hydrides in the gas phase.[1,5,7,8] It has been shown that these H···H complexes are important intermediates in proton transfer reactions leading to transition metal dihydrogen complexes.[1,6,9−11] In very recent DFT work,[11] the solvent was introduced by a polarizable continuum model and its stabilising effect on the protonation process was studied.

The ability of main group element hydrides to form DHBs was studied for the first time using boron hydrides.[12−17] An analysis of the structures from the Cambridge Structural Database and theoretical calculations on the dimer $(BH_3NH_3)_2$ led to the conclusion that the DHB moiety is significantly bent.[12,13] Later, our IR investigations in solution combined with theoretical studies of the $(H_3NBH_3)_2$ dimer as well as the DHB of BH_4^- and BH_3NH_3 with proton donors (H_2O, MeOH and HCN) led to the conclusion that substantial deviations from linearity in the solid state are caused by the crystalline packing.[14,15] The linearity of the (B)H···HX moiety and reasonable electron density changes have been demonstrated by theoretical calculations of $(H_3NBH_3)_2$ using the RHF/6-31G[15] and A1M[16] methods, though the nonlinear bifurcated DHB (of C_{2v} symmetry) was reported in previous works (HF, DFT, MP2 methods).[17] Recently, neutron diffraction measurements corrected the "heavy" atom assignments for $(H_3NBH_3)_2$ leading to the structure with practically linear NH···H(B) DHBs and bent BH···H(N) moieties.[18] The similarity between BH···HX, MH···HX and classical H bonds in the structure was established.[1,6,15] Recently, some reports have been devoted to theoretical DHB calculations of the other main group hydride complexes EH···HX.[19−21] A theoretical study of DHB complexes between some simple hydrides (for example, BeH_2, MgH_2, SiH_4, GeH_4 and SnH_4) and HF showed a correlation between H···H distances and the energies of the DHB.[22] Cyclotriallumozane $(NH_2AlH_2)_3$ was found theoretically to have a favourable twist-boat conformation in the gas phase with two H···H interactions.[23] A comparison of the calculated structures and energies of NH···HE (E = B, Al, Ga) for $(NH_3EH_3)_2$ predicted C_2 symmetry for the dimers of the Al and Ga

[a] A. N. Nesmeyanov Institute of Organoelement Compounds, Russian Academy of Sciences,
Vavilov str. 28, 119991 Moscow, Russia
Fax: (internat.) + 7-095-135-5085
E-mail: shu@ineos.ac.ru

hydrides and the DHB energy was shown to decrease down the group.[17]

It is noteworthy that experimental studies of Al and Ga hydrides have considered only the structures of the crystalline adducts.[20] An intramolecular NH···HAl hydrogen bond was determined from an X-ray diffraction study of the alane−piperidine complex[24] and six short H···H contacts were found in the structure of the $[(NH_2AlH_2)_3]_2$ dimer.[23] The neutron diffraction crystal structure of cyclotrigallozane $(NH_2GaH_2)_3$ indicated self-assembly from four NH···HGa dihydrogen bonds.[23] To date, there is no evidence for the existence of GaH···HX interactions in solution. However, DHB interactions are very important allowing control over reactivity and selectivity in solution. This has potential implications in catalysis and promises an important role in the creation of supramolecular assemblies and new covalent materials.[1,20]

In this work we present the results of a VT-IR investigation (190−290 K) including spectroscopic and thermodynamic characteristics of DHB formed in low-polarity solvents between GaH_4^- (**1**) and proton donors of different strength, i.e. CF_3CH_2OH, FCH_2CH_2OH, *i*PrOH, MeOH, indole and 4-$O_2NC_6H_4NH_2$. VT-IR spectroscopy, as has been previously shown, is a very convenient method for studying DHB complexes providing not only evidence of the formation of DHB, but also allowing the detection of the separate bands of the initial and H-bonded complexes. The technique also enables determination of the formation energy.[6,15]

The nature, structures, energies and electron distributions of the model DHB complexes formed between **1** and H_2O, MeOH, CF_3OH, H_2NCF_3 or 4-$O_2NC_6H_4NH_2$ are discussed on the basis of ab initio calculations and compared with those of analogous complexes of BH_4^- with H_2O, MeOH, or CF_3OH.

Results and Discussion

Spectroscopic Evidence for Hydrogen Bonding in Solution

The IR spectra of OH and NH acids (in the concentration range of 10^{-2} to 10^{-3} M in order to exclude self-association) were measured in dichloromethane with an excess of gallohydride **1**. The intensities of the ν(XH) stretching vibrations decrease in the presence of **1** and new, lower frequency broad bands (3392−3224 cm^{-1}) of H-bonded XH groups [$\nu(XH)_{bonded}$] appear (e.g. Figure 1). This pattern demonstrates formation of hydrogen bonds between proton donors and the gallium hydride. The intensities of the $\nu(XH)_{bonded}$ bands increase as the temperature decreases as illustrated in Figure 1 for MeOH. This indicates the right shift for the H-bonding equilibrium upon cooling.

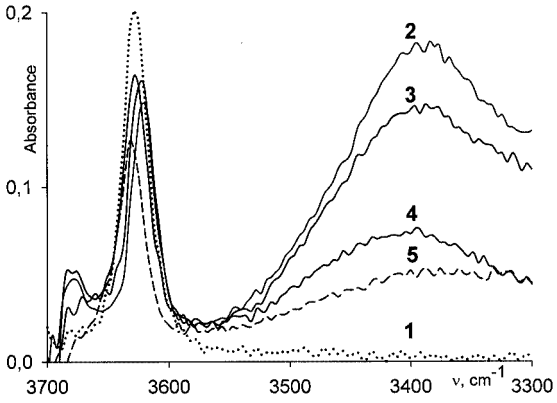

Figure 1. IR spectra in the ν(OH) range of MeOH (c = 0.015 M, CH_2Cl_2) at 260 K (1); in the presence of $[Bu_4N]GaH_4^-$ (0.09 M): at 200 K (2); 220 K (3); 260 K (4); 290 K (5)

All spectroscopic parameters, i.e. frequency shifts [$\Delta\nu(XH) = \nu(XH)_{free} - \nu(XH)_{bonded}$], half-widths of the $\nu(XH)_{bonded}$ bands ($\Delta\nu_{1/2}$) and integral intensities [$A(XH)_{bonded}$] increase with the increase of the proton-donating ability of XH in the following sequence: 4-$O_2NC_6H_4NH_2$ < *i*PrOH < MeOH < $FCH_2CH_2OH \approx C_8H_6NH$ < CF_3CH_2OH. The values of Δν(XH) increase along this series from 144 to 250 cm^{-1}, $A(XH)_{bonded}$ increases from 5.12×10^4 to 9.52×10^4 $L \cdot cm^{-2} \cdot mol^{-1}$ and $\Delta\nu_{1/2}$ increases from 97 to 287 cm^{-1} (Table 1).

Interesting results were obtained from the study of the GaH_4^-/4-$O_2NC_6H_4NH_2$ system in CH_2Cl_2 solution. Two bands of the NH_2 group of 4-$O_2NC_6H_4NH_2$ in the IR spectra can be assigned to asymmetrical (ν^{as} = 3509 cm^{-1}) and symmetrical (ν^{s} = 3411 cm^{-1}) stretching vibrations. In the presence of the anion **1**, two new bands (3481 and 3337

Table 1. Spectroscopic characteristics of the hydrogen-bonded complexes of XH acids to GaH_4^-

HX	$\nu(XH)_{free}$ [cm^{-1}]	$\nu(XH)_{bond}$ [cm^{-1}]	$\Delta\nu(XH)$ [cm^{-1}]	$\Delta\nu_{1/2}$ [cm^{-1}]	$A(XH)_{bond} \times 10^4$ [$L \cdot cm^{-2} \cdot mol^{-1}$]
4-$NO_2C_6H_4NH_2$	3509(as)	3481[a]	123[b]		
	3411(s)	3337[a]		68[c]	5.12[c]
Indole	3473	3224	249	132	7.33
*i*PrOH	3604	3392	212	219	–
CH_3OH	3619	3393	226	189	6.23
FCH_2CH_2OH	3605	3369	236	235	7.67
CF_3CH_2OH	3600	3350	250	287	9.52

[a] New bands, assignments are discussed in the text. [b] Mean of ν^{as} and ν^{s} bands of free 4-nitroaniline was used as $\nu(XH)_{free}$ for ν(XH) calculation. [c] For the band at 3337 nm^{-1}.

 © 2004 Wiley-VCH Verlag GmbH & Co. KGaA, Weinheim

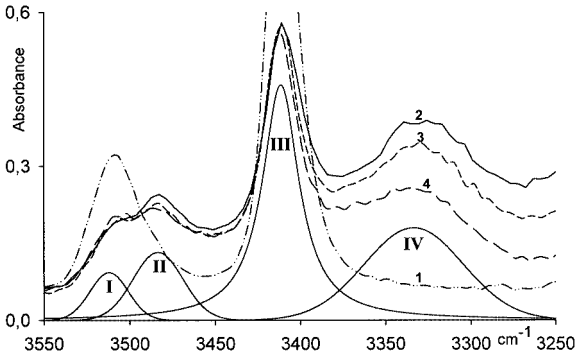

Figure 2. IR spectra in the ν(NH) range of 4-$O_2NC_6H_4NH_2$ (c = 0.02 M, CH_2Cl_2) at 200 K (1); in the presence of $[Bu_4N]GaH_4^-$ (0.09 M): at 200 K (2); 230 K (3); 250 K (4) and separation of the band (2) on the four components: $\nu(NH)^{as}$ (I), $\nu(NH)^{as}$ (III) and II, IV (see text for assignment)

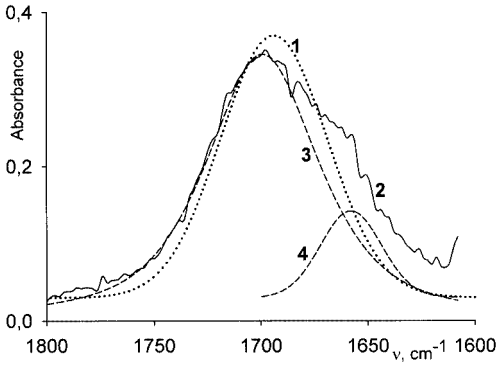

Figure 3. IR spectra in the ν(GaH) range of $[Bu_4N]GaH_4^-$ (c = 0.03 M, THF) at 200 K (1); in the presence of 4-$O_2NC_6H_4NH_2$ (0.08 M) at 200 K (2); separation of the band (2) on the two components: $\nu(GaH)_{free}$ (3) and $\nu(GaH)_{bonded}$ (4)

cm^{-1}) appear and grow upon cooling (Figure 2). There are two possibilities for the assignments of these two bands. In the case of monodentate coordination, these bands could be attributed to the free and bonded species, respectively. In the case of bidentate coordination, these bands would correspond to the ν^{as} and ν^{s} bands of the bonded species. Analysis of the IR spectra and band separation enables us to suggest the first type of assignment.[25] The new high-frequency band ν(NH) at 3481 cm^{-1} is narrow ($\Delta\nu_{1/2}$ = 34 cm^{-1}) and the second new band at 3337 cm^{-1} is much broader ($\Delta\nu_{1/2}$ = 68 cm^{-1}). Shifts of these bands corresponding to $[\nu(NH)^{as} + \nu(NH)^{s}]/2$ are −21 and 123 cm^{-1}, respectively. Taking into account both factors, we can assign these bands as $\nu(NH)_{free}$ = 3481 cm^{-1} and $\nu(NH)_{bond}$ = 3337 cm^{-1}. The results of theoretical calculations (see below) confirm both the monodentate coordination and this assignment.

Spectroscopic evidence for the hydride ligand being the site of DHB formation was obtained from a range of Ga−H stretching vibrations studied in THF at 180−290 K. It was shown earlier that DHB formation results in a low-frequency shift of the M−H or B−H stretches for the groups participating in H-bonding, whereas the bands corresponding to the groups that do not participate in H-bonding shift to the high-frequency region.[6,15] Thus, the formation of GaH···HX bonds, leads to some broadening of the ν(GaH) band accompanied by the appearance of low-frequency and high-frequency shoulders assignable to stretching vibrations of the one bonded and three free GaH bonds, respectively. Such changes were observed in the interaction with the weakest proton donor used, i.e. 4-$O_2NC_6H_4NH_2$ (Figure 3). The band intensity of **1**, ν(GaH) = 1700 cm^{-1}, decreases and the stretching vibrations of the free GaH groups in the DHB complex are displaced to the high-frequency range. Those of the GaH-bonded group appear as the low-frequency shoulder.

One could expect more pronounced changes for stronger XH acids, as in the case of the $BH_4^-/(CF_3)_2CHOH$ system.[15] However, less pronounced changes were observed in the IR spectra of **1** in the presence of FCH_2CH_2OH and indole at 200 K. Moreover, the ν(GaH) band intensity decreases as the temperature increases (> 240 K) probably due to proton transfer with subsequent H_2 gas evolution and formation of covalent Ga−O/Ga−N bonds. We have not yet studied this process in more detail, but there are many examples of boron hydride alcoholysis/hydrolysis studies in the literature, e.g. the BH_4^-/R^fOH[26] and GaH_4^-/ROH[27] systems. However, the H···H bonding was not considered as an intermediate along the reaction pathway. By analogy with transition metal hydrides,[6] we suggest Scheme 1 for the reaction with alcohols where the proton transfer from DHB complexes leads to nonclassical (η^2-H_2) complex formation followed by hydrogen elimination yielding alkoxy derivatives. Evidently, the (η^2-H_2) complexes of **1** should be very unstable as for other main group element hydrides, but the data concerning the theoretical and experimental evidence of the boron analogue[28] (IR spectra in cryogenic matrices at 13−27 K) support our hypothesis.

$$\underset{\mathbf{1}}{GaH_4^- + ROH} \rightleftharpoons \underset{\mathbf{2}}{[H_3Ga(H\cdots HOR)]^-} \rightleftharpoons \underset{\mathbf{3}}{[H_3Ga(\eta^2\text{-}H)\cdot OR]^-} \longrightarrow \underset{\mathbf{4}}{H_3GaOR^- + H_2}$$

Scheme 1

The participation of more alcohol molecules in the reaction generates alkoxy products of different compositions, $[H_{4-n}Ga(OR)_n]^-$.[27] The same is true of the aminolysis reactions. The reaction can stop at the first step of DHB intermediate formation, depending on temperature and the amount and strength of the proton donor. The interaction with weakest XH acid used (4-nitroaniline), as mentioned above, does not lead to proton transfer and H_2 evolution in the temperature range of 180−250 K. IR spectroscopic changes demonstrate only DHB formation (equilibrium **1** ⇆ **2**; Scheme 1). The temperature dependence is reversible. The interaction with the stronger FCH_2CH_2OH or indole leads to the reduction of the ν(GaH) intensity at 230 K and to practically full disappearance of this band at ambient temperature. At the same time, a very broad and high frequency absorbance (1800−1850 cm^{-1}) appears which probably corresponds to the Ga−H stretching of different al-

 © 2004 Wiley-VCH Verlag GmbH & Co. KGaA, Weinheim

coholysis or aminolysis products (**4** in Scheme 1). The same spectroscopic changes were observed in the interaction with the stronger OH acid F_3CCH_2OH (Figure 4, line 2). In this case, some decrease in the $\nu(GaH)_{free}$ band intensity (1700 cm^{-1}) of the DHB complex took place even at low temperature (200 K) with the simultaneous appearance of the broad high-frequency absorbance. Upon a temperature change from 200 to 290 K, broad overlapping bands (1763 cm^{-1} at 200 K and 1810 cm^{-1} at 290 K) increased irreversibly (Figure 4). Moreover, the intensity of these bands increased concomitantly with the decrease of the $\nu(GaH)_{free}$ band (Figure 4). These can be tentatively assigned to the ν(GaH) vibrations of $[GaH_{4-n}(OCH_2CF_3)_n]^-$.[27] However, a special study is necessary in order to obtain the data corresponding to the spectroscopic changes during the alcoholysis/aminolysis reactions and definite assignment of each band.

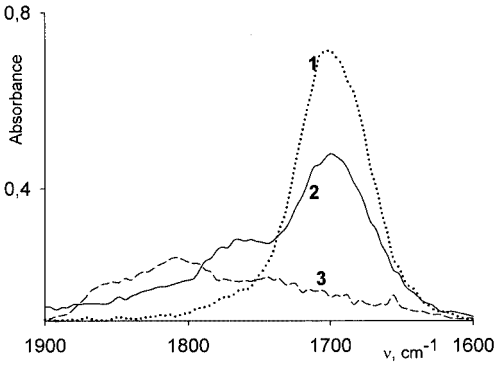

Figure 4. IR spectra in the ν(GaH) range of $[Bu_4N]GaH_4^-$ (c = 0.04 M, THF) at 200 K (1); in the presence of TFE (0.10 M): at 200 K (2); at 290 K (3)

It should be noted that the Δν(GaH) values of the DHB complexes of **1** with weak proton donors are 10−30 cm^{-1} larger than the Δν(BH) values for the analogous DHB complexes of BH_4^-.[15] The changes in the spectroscopic characteristics of the XH acids in the presence of **1**, such as ν(XH) band shifts, $\nu(XH)_{bonded}$ band half-widths ($\Delta\nu_{1/2}$) and integral intensities (A), are also higher than those in the presence of BH_4^-.

Strength of GaH···HX Bonds

The enthalpies ($-\Delta H$) of the GaH···HX bond formations were determined from the empirical correlation Equations (1) and (2). These were proposed by Iogansen for classical H-bonded systems[29−31] but have also proved to be valid for dihydrogen bonds to transition metal [6] and boron hydrides.[15]

$$-\Delta H^\circ = 18 \times \Delta\nu/720 + \Delta\nu \quad (1)$$

$$-\Delta H^\circ = 2.9(\Delta A)^{1/2} \quad (2)$$

The enthalpy values of dihydrogen-bonded complex formation obtained from frequency shifts [Equation (1)] and integral intensity changes [Equation (2)] have similar values as is apparent from Table 2. The GaH···HX bond energies correspond to medium-strength H bonds: $-\Delta H^0$ values of the DHB complexes change from 4.0 to 5.4 kcal·mol^{-1} with the exception of the weak DHB to 4-$O_2NC_6H_4NH_2$ (2.6 kcal·mol^{-1}).

Table 2. The enthalpy values of DHB complexes [kcal·mol^{-1}] of GaH_4^- (**1**) and P_i factors of proton donors[29]

HX	$-\Delta H^0$ [a]	$-\Delta H^0$[b]	P_i [29]
4-$O_2NC_6H_4NH_2$	2.6	–	0.41
Indole	4.4	4.5	0.75
*i*PrOH	4.0	–	0.58
CH_3OH	4.3	4.1	0.63
FCH_2CH_2OH	4.4	4.7	0.74
CF_3CH_2OH	5.4	5.2	0.89

[a] $-\Delta H^0$ calculated using Equation (1). [b] $-\Delta H^0$ calculated using Equation (2).

The proton accepting ability of the hydride hydrogen of **1** was determined using the "rule of factors" proposed by Iogansen [29] for organic systems [Equation (3)], where P_i is the proton-donating ability from Table 2,[29] i.e. $-\Delta H_{11}$ = 4.6 kcal·mol^{-1} for the phenol/ethyl ether pair in CH_2Cl_2, with $P_1 = E_1 = 1.0$.

$$-\Delta H_{ij} = -\Delta H_{11} P_i E_j \quad (3)$$

The basicity factor (E_j) is independent of the proton donor and solvent and for **1** is equal to 1.37±0.09. Thus, it is possible to compare the proton-accepting ability of **1** with those of boron complexes, some transition metal hydrides and even with organic bases (Table 3).

Table 3. Basicity factors of hydride ligands of GaH_4, boron and transition metal hydrides and some organic bases

Compound	E_j	Ref.	Compound	E_j	Ref.
GaH_4^-	1.37	this work	$[(CH_2CH_2PPh_2)_3FeH_2]$	1.0	[9]
BH_4^-	1.25	[15]	$[(CH_2CH_2PPh_2)_3RuH_2]$	1.33	[9]
$[B_{12}H_{12}]^{2-}$	0.61	[32]	$[MeC(CH_2PPh_2)_3(CO)RuH_2]$	1.39	[33]
$[B_{10}H_{10}]^{2-}$	0.78	[32]	$[(CH_2CH_2PPh_2)_3OsH_2]$	1.66	[9]
Et_3NBH_3	0.53	[15]	DMSO	1.27	[29]
$P(OEt)_3BH_3$	0.41	[15]	Py	1.67	[29]

The E_j value of **1**, as one can see from Table 3, is significantly larger than those of the neutral boron hydrides and even of BH_4^- (E_j = 1.25), i.e. the proton-accepting ability of hydride ligands increases down the group (B)−H < (Ga)−H. The proton-accepting ability of **1** is close to that of the strongest transition metal hydrides (and organic bases) known to date.[1,6,15] The transition metal hydrides with larger basicity factors ($E_j > 1.5$) undergo complete proton transfer from weak XH acids (fluorinated alcohols) to the hydride ligand.[1,6,9] Thus, the ease of proton transfer and alcoholysis during the interaction of **1** with

 © 2004 Wiley-VCH Verlag GmbH & Co. KGaA, Weinheim

FCH_2CH_2OH and especially F_3CCH_2OH, in contrast to BH_4^-, could be due to the larger proton accepting ability of GaH_4^- compared with that of BH_4^-.

Computational Study

A theoretical investigation of the model complexes $GaH_4^-\cdot H_2O$ (**5**), $GaH_4^-\cdot 2H_2O$ (**5′**), $GaH_4^-\cdot CH_3OH$ (**6**), $GaH_4^-\cdot CF_3OH$(**7**), $GaH_4^-\cdot CF_3NH_2$(**8**) and $GaH_4^-\cdot O_2NC_6H_4NH_2$ (**9**) was performed using the B3LYP approximation with the standard basis set 6-311G(d,p) (see Exp. Sect.). In order to establish the role of the central atom, the model complexes $BH_4^-\cdot H_2O$ (**10**), $BH_4^-\cdot CH_3OH$ (**11**) and $BH_4^-\cdot CF_3OH$ (**12**) were calculated with the 6-311++G(d,p) basis set. This basis set was chosen because of better agreement between the calculated and experimental ν(BH) frequencies.

Structures of DHB Complexes

The results from the theoretical studies are in agreement with the experimental results, showing that the hydride ligand is a proton-accepting site in all cases. There are two types of XH acids. The first type involves the XH acids with only one proton available for donation (CH_3OH, CF_3OH). The XH acids of the second group possesses two H atoms (H_2O, CF_3NH_2, 4-$O_2NC_6H_4NH_2$). Therefore, the possibility of mono- or bidentate coordination for the last proton donor group was considered.

A linear arrangement of the triatomic HX···H(Ga) moiety for the first proton donor group was found (Table 4). The X−H···H angles are close to 180° (170.6°, 174.6° and 165.8° for **6**, **7** and **9**, respectively) and, as was shown earlier, this is typical for classical H-bonding and DHB complexes MH···HX and BH···HX.[1,6,15] The H···H distances are smaller than the sum of van der Waals radii (2.4 Å) and decrease for stronger alcohols (from 1.639 Å for **6** to 1.328 Å for **7**) (Table 4, Figure 5). Experimentally obtained H···H distances for MH···HX are in the range of 1.65−2.1 Å.[1,6] In the case of the neutral dimer ($NH_2HGaH\cdots HNHGaH_2$), this distance in the crystal is equal to 1.9 Å.[2] Therefore, the H···H distance obtained for **7** (1.328 Å) is probably too short.

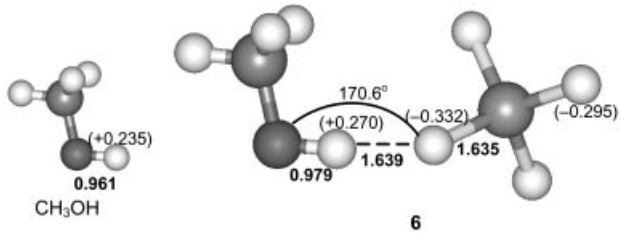

Figure 5. The geometries [Å and °] and Mulliken charges (in parentheses) of the model complex $GaH_4^-\cdot CH_3OH$ (**6**)

The formation of the H···H hydrogen bond leads to the elongation of the Ga−H and O−H bond lengths from their values in the isolated molecules. For example, r(Ga−H) = 1.622 Å in **1** and 1.635 Å in complex **6**, r(O−H) = 0.961 Å in CH_3OH and 0.979 Å in **6**. These changes are close to those previously reported for MH···HX and BH···HX complexes.[1,6,15] However, the H···H distance in **6** (1.639 Å) is shorter and the value of Δr(Ga−H) = 0.013 Å is larger than the corresponding values in complex **11** [r(H···H) = 1.654 Å and Δr(B−H) = 0.005 Å]. The increase in the elongations of the OH bonds is dependent of the OH acid strength (about three times when the CH_3 group (**6**, **11**) is substituted by CF_3 (**7**, **12**), Table 4).

Interesting results were obtained for the second group of XH acids. The minima on the potential energy surfaces for H_2O and CF_3NH_2 are achieved for bidentate coordination when the two hydride atoms of **1** interact with both hydrogen atoms of the XH_2 groups forming a symmetrical chelated structure (Figure 6). The interaction between these species leads to nonlinear OH···H and NH···H moieties and

Table 4. The characteristics of DHB complexes calculated by the DFT method

	Model complex	Angle H···HX [°]	r(H···H) [Å]	Δr (EH) [Å]	Δr (XH) [Å]	ΔqH (EH)	ΔqH (XH)	$-\Delta H$ [kcal·mol^{-1}]	$-\Delta H$ per H bond [kcal·mol^{-1}]
5	$GaH_4^-\cdot H_2O$	147.5	2.005 *0.028*	0.007	0.006	0.019	0.010	10.7	5.4
5′	$GaH_4^-\cdot 2H_2O$	147.2	2.032 *0.024*	0.003	0.006	0.001	0.010	20.4	5.1
6	$GaH_4^-\cdot CH_3OH$	170.6	1.639 *0.074*	0.013	0.018	0.018	0.035	9.1	
7	$GaH_4^-\cdot CF_3OH$	174.6	1.328 *0.190*	0.034	0.064	0.020	0.022	19.6	
8	$GaH_4^-\cdot CF_3NH_2$	140.8	2.047 *0.044*	0.011	0.008	0.018	0.010	12.6	6.3
9	$GaH_4^-\cdot O_2NC_6H_4NH_2$	165.8	1.755 *0.098*	0.021	0.021	0.019	0.034	17.9	
10	$BH_4^-\cdot H_2O$	174.5	1.690 *0.152*	0.006	0.019	0.044	0.038	11.6	
11	$BH_4^-\cdot CH_3OH$	172.8	1.654 *0.174*	0.005	0.021	0.032	0.014	11.13	
12	$BH_4^-\cdot CF_3OH$	164.6	1.350	0.014	0.072	0.075	0.049	24.02	

 © 2004 Wiley-VCH Verlag GmbH & Co. KGaA, Weinheim

induces less bond elongation. The H···H distances are longer than in the complexes of the first group (Table 4).

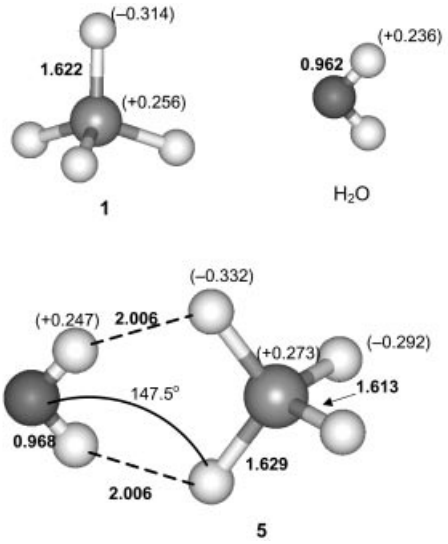

Figure 6. The geometries [Å and °] and Mulliken charges (in parentheses) of the model complex $GaH_4^-\cdot H_2O$ (**5**)

Thus, the DHB complexes **5** (Figure 6) and **8** exhibit longer H···H distances (2.005 and 2.047 Å) than for **6** and **7**, smaller elongations (0.007−0.011Å) and more acute O−H···H and N−H···H angles (147.5° and 140.8°, respectively). Interaction with the second water molecule leads to complex **5′** with a second symmetrical chelated ring and practically the same OH···H angle. Only the Ga−H elongations are less (in 0.004 Å) and the H···H distance is a little larger (in 0.027 Å) compared with that in **5**.

It was found that the differences in the structures of the $EH_4^-\cdot H_2O$ complexes depend on the central atom. The monodentate coordination of H_2O is characteristic for $BH_4^-\cdot H_2O$ (**10**) instead of the symmetrical chelate structure of **5** (Figure 6). The O−H···H angle of **10** (174.5°) is larger than in **5** and is close to 180°. The additional interaction between the free hydride atoms of BH_4^- and the free hydrogen atom in the water molecule[15] should not be regarded as the second H bond because the H···H distance is equal to 2.48 Å. This is larger than the sum of the van der Waals radii.

Reducing the proton donor strength by substitution of R in RNH_2 from CF_3 in **8** to 4-$O_2NC_6H_4$ in **9** also leads to monodentate coordination of the proton donor with an additional interaction of the second acidic hydrogen atom similar to the situation in **10**. This additional interaction can also not be regarded as a DHB bond (H···H distance = 2.449 Å; Figure 7).

The increase of the N−H···H angle (165.8°), the additional lengthening of the Ga−H and O−H bonds (0.021, 0.021 Å) and the shortening of the H···H distance (1.755 Å) are characteristic for **9** when compared with **8**.

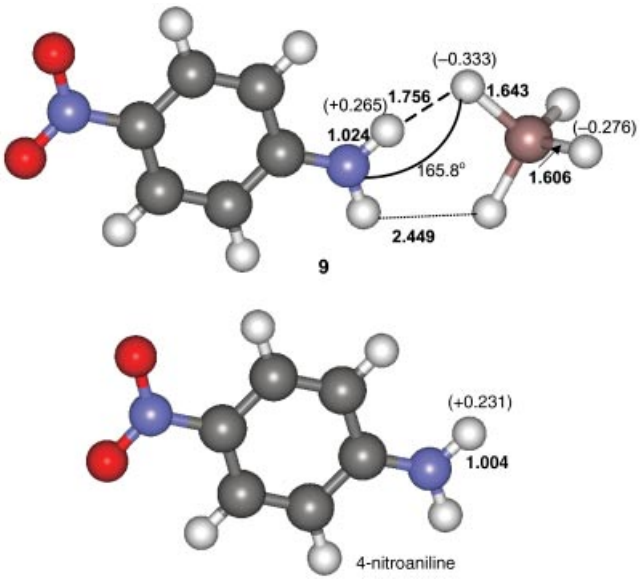

Figure 7. The geometries [Å and °] and Mulliken charges (in parentheses) of the model complex $GaH_4^-\cdot O_2NC_6H_4NH_2$ (**9**)

Energies of DHB Complexes and Electron Density Changes

The calculated energy values of the complexes (Table 4) are larger than those obtained experimentally. For example, the energy of $GaH_4^-\cdot CH_3OH$ (**6**) is about twice as high as the enthalpy value obtained from Equations (2) and (3) from IR spectroscopic data (Table 2). The probable cause of such overestimation may be the decrease of the DHB energy on going from the gas phase (calculations) to solution (experimental measurements).[6,15] As was indicated previously, the significant solvation effects are related to ion-molecular H bonds due to the significantly larger solvation energies for anions over hydrogen-bonded complexes.[34] Note, however, that the energy overestimation is more for $BH_4^-\cdot HOR$ complexes. This could be explained by the smaller dimension and greater solvation effect of BH_4^- in comparison with GaH_4^-.[34] It is remarkable that the calculated energy values for the linear monodentate complexes (9.1−19.6 kcal·mol^{-1}) are higher than for the bidentate nonlinear DHBs (5.35−6.3 kcal·mol^{-1} per bond). The energy increase is dependent on the XH acid strength, for example, **6** < **7** (Table 4).

The overlap populations (*o.p.*) of the H···H bonds and the electron redistribution upon DHB formation also depend on the type of coordination and the acid strength. The *o.p.* of the H···H bonds vary in the range of 0.016−0.095 and their values are larger in the case of linear monodentate coordination. Small but positive overlap populations indicative of the covalent component of DHB increase upon going from **6** to **7**. The electrostatic attraction between the partial negative charge of the hydrogen atom of GaH_4^- (−0.314) and partial positive charge of the proton donors (from 0.22 to 0.27 dependent on their strength) is the driving force for dihydrogen bonding $GaH^{\delta-}\cdots{}^{+\delta}HX$ as was previously determined for $MH^{\delta-}\cdots{}^{+\delta}HX$.[1,6] DHB formation leads to an increase of the charges which is a little

 © 2004 Wiley-VCH Verlag GmbH & Co. KGaA, Weinheim

more substantial in the case of the monodentate complexes, especially for the hydrogen atom of the XH acids [for example, ΔqH(OH) = 0.035 for **6** and ΔqH(OH) = 0.010 for **5**] (Table 4).

The calculation of the interaction of **1** with a strong acid shows the proton transfer reaction leading to the dihydrogen complex formation [Equation (4)].

$$GaH_4^- + H_3O^+ \rightarrow GaH_3\text{-}(\eta^2\text{-}H_2) + H_2O \quad (4)$$

Upon proton transfer to a hydride ligand, the tetrahedron of **1** transforms in to the planar gallium trihydride with the side on (η^2-H_2) ligand (Figure 8). The H−H distance is equal to 0.756 Å which is a little longer than in the H_2 molecule (0.74 Å) and shorter than in transition metal dihydrogen complexes (0.8−1.1 Å).[1,4,6] The large energy calculated (167.16 kcal·mol^{-1}) is in agreement with Equation (4) which demands significant electron and structural reorganization. Such an unstable dihydrogen complex was predicted theoretically and observed experimentally by IR matrix isolation in the case of boron.[28]

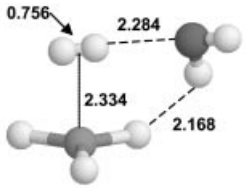

Figure 8. The geometries [Å] of the unstable products of the proton transfer reaction (4)

Spectroscopic Characteristics of DHB Complexes

The calculated spectroscopic characteristics of the complexes (stretching vibrations of X−H and Ga−H bonds) are presented in Table 5. The $\nu(XH)_{bonded}$ bands are shifted to the low-frequency range in agreement with the experimental observations. The values of the shifts depend on the strength of the XH acid and the linearity of the X−H···H moiety. Linear bonds result in larger ν values. The value of ν(OH) in complex **6** is about twice as large as in nonlinear **5**, although the acidity of methanol and water are similar ($pK_a \approx 15.5$). The ν(OH) value depends on the proton-donating ability in the sequence: $F_3COH > CH_3OH > NO_2C_6H_4NH_2 > H_2O \geq CF_3NH_2$.

The bands of the free Ga−H groups in the complexes increase in agreement with the experimental IR spectroscopic changes observed for DHB complexes with **1**, the boron analogue [15] and transition metal hydrides.[6]

Hence, the calculations reproduced the main structural features and the charge redistribution occurring as a result of hydrogen-bond formation as a function of the proton-donor strength and the type of coordination.

Conclusion

The present variable-temperature IR investigation of the interaction between GaH_4^- and different XH acids shows for the fist time the GaH···HX dihydrogen-bond formation in solution. The spectroscopic characteristics, DHB formation enthalpies with different XH acids and the E_j factors of GaH_4^- were determined and appear to be greater than those of the boron analogue DHB, demonstrating an increase in the proton-accepting ability down the group. Two types of DHB model complexes were determined from DFT calculations: the linear monodentate with XH acids or 4-nitroaniline and the nonlinear bidentate with XH_2 acids containing symmetrical chelate hydrogen bonds to two hydride atoms of **1**. This last type of DHB was not found for BH_4 and is specific to the GaH_4^- anion. It was shown that the elongation of the bonds of the GaH···HX moiety, polarisation of the partners and the energy depend on the type of coordination and the strength of the X−H acids.

A study of a number of group 13 hydride DHB complexes would be of great interest for determining the EH···HX energies and structures as a function of the position of the group 13 element, as well as the mechanisms of aminolysis and alcoholysis through DHB. We are currently investigating these issues.

Experimental Section

The $[Bu_4N][GaH_4]$ salt (**1**) was prepared as described in the literature.[36] Fluorinated alcohols were provided by P&M (Moscow, Russia). The solutions for IR studies were prepared under argon by standard Schlenk technique. Tetrahydrofuran (THF) was freshly distilled from $LiAlH_4$ and CH_2Cl_2 was purified by distillation from CaH_2 before use. The anhydrous solvents were thoroughly degassed prior to use.

Table 5. Calculated ν(XH) and ν(GaH) frequencies for the model complexes [cm^{-1}]

	Model complex	$\nu(XH)_{free}$[a]	$\nu(XH)_{bond}$[a]	$\Delta\nu(XH)$[a]	$\nu(GaH)_{free}$	$\nu(GaH)_{bond}$	$\Delta\nu(GaH)$[b]
5	$GaH_4^-\cdot H_2O$	3672 (as)	3532	140	1739	1656	37
6	$GaH_4^-\cdot CH_3OH$	3607	3278	329	1719	1669	24
7	$GaH_4^-\cdot CF_3OH$	3591	2486	1105	1766	1688	5
8	$GaH_4^-\cdot CF_3NH_2$	3415 (as)	3281	134	1739	1636	57
9	$GaH_4^-\cdot O_2NC_6H_4NH_2$	3409 (s) 3521 (as)	3124	285	1757	1677	16

[a] The values are presented by a scaling factor 0.94.[35] [b] $\Delta\nu(GaH) = \nu(GaH)_{initial} - \nu(GaH)_{bond} = 1693 - \nu(GaH)_{bond}$.

 © 2004 Wiley-VCH Verlag GmbH & Co. KGaA, Weinheim

Table 6. Comparative analysis of the frequencies [cm^{-1}], energy [$kcal \cdot mol^{-1}$], Mulliken charges and overlap population of GaH_4^-, calculated with different basis sets

B3LYP/ basis set	6-31G(d,p)	6-31++G(d,p)	6-311G(d,p)	6-311+G(d,p)	6-311++G(d,p)	ν(exp)[a]
ν_i (calcd.)	737.1	744.2	731.9	731.6	729.7	733
	800.1	802.5	786.3	785.7	781.4	(780)
	1795.3	1780.8	1693.6	1690.1	1685.2	1700[b]
	1847.5	1846.6	1766.7	1765.9	1762.7	1770
E_{termal}	17.855	17.823	17.251	17.233	17.19	
qGa	−0.516	0.095	0.256	0.252	0.408	
qH	−0.121	−0.274	−0.314	−0.313	−0.352	
Overlap population	0.800	0.707	0.716	0.716	0.695	

[a] IR, Raman frequencies of $CsGaH_4$ in diglyme solution.[39] [b] IR frequency of ν(GaH) Bu_4NGaH_4 in THF solution: 1696 cm^{-1}.

The IR spectra of THF or CH_2Cl_2, solutions (cells CaF_2, $d = 0.012 - 0.120$ cm) were measured with a Specord M-82 (Carl Zeiss Jena) spectrometer with a 2−4 cm^{-1} resolution. The low-temperature IR studies were carried out in the OH and GaH stretching regions using a Carl Zeiss Jena cryostat in the temperature range of 200−300 K with the accuracy of the temperature setting being ±0.5 K. Concentrations of $[Bu_4N][GaH_4]$ were varied from 10^{-1} to 10^{-2} M in the range of ν(XH) to 10^{-2} to 10^{-3} M in the range of ν(GaH). The concentrations of the XH acids in the first range were between 10^{-2} and 10^{-3} M or between 10^{-1} to 10^{-2} M in the range of ν(GaH).

The theoretical calculations of the model complexes $GaH_4^- \cdot H_2O$, $GaH_4^- \cdot CH_3OH$, $GaH_4^- \cdot CF_3OH$, $GaH_4^- \cdot CF_3NH_2$, and $GaH_4^- \cdot NO_2C_6H_4NH_2$ were performed by the hybrid density functional method[37] with the Gaussian 98 series of programs.[38] Firstly, several basis sets were used to perform the GaH_4^- calculations (Table 6).

Finally, the choice of the basis set was made based on good agreement between the calculated and experimental ν(GaH) frequencies. For the first two basis sets [6-31G(d,p) and 6-31++G(d,p)] $\Delta\nu(GaH) = \nu(GaH)_{exp} - \nu(GaH)_{calcd.}$ values were too large (101.7 and 87.2 cm^{-1}, respectively), while for the 6-311G(d,p) basis set they were equal to 6.4[39] or 2.6 cm^{-1} (this work). The basis set chosen [6-311G(d,p)] is also better for the electron-density description, giving the positive charge on Ga (as for B in the boron analogue)[15,16] though the Ga atom has either negative, or near to zero charge with the first two poorer basis sets. The higher computational levels increased the time of computations but practically did not improve the results. Therefore, the basis set 6-311G(d,p) was chosen for further calculations of the above-mentioned complexes **1**·HX.

Acknowledgments

This work was supported by European Commission's RTN Programme "HYDROCHEM" (HPRN-CT-2002-00176), the Russian Foundation for Basic Research (02-03-32068, 03-03-06277, 04-03-32456) and the Fundamental Research Program of the RAS Presidium.

[1] L. M. Epstein, E. S. Shubina, *Coord. Chem. Rev.* **2002**, *231*, 165.
[2] E. S. Shubina, N. V. Belkova, L. M. Epstein, *J. Organomet. Chem.* **1997**, *17*, 536−537.
[3] J. C. M. Rivas, L. Brammer, *Coord. Chem. Rev.* **1999**, *43*, 183.
[4] R. H. Morris, in *Recent Advances in Hydride Chemistry*, Elsevier, Amsterdam, **2001**, p. 3.
[5] E. Clot, O. Eisenstein, D.-H. Lee, R. H. Crabtree, in *Recent Advances in Hydride Chemistry*, Elsevier, Amsterdam, **2001**, p. 75.
[6] L. M. Epstein, N. V. Belkova, E. S. Shubina, in *Recent Advances in Hydride Chemistry*, Elsevier, Amsterdam, **2001**, p. 391.
[7] I. Alcorta, I. Rozas, J. Elguero, *J. Mol. Struct.* **2001**, *537*, 139.
[8] F. Maseras, A. Lledos, E. Clot, O. Eisenstein, *Chem. Rev.* **2000**, *100*, 615.
[9] E. I. Gutsul, N. V. Belkova, M. S. Sverdlov, L. M. Epstein, E. S. Shubina, V. I. Bakhmutov, T. N. Gribanova, R. M. Minyaev, C. Bianchini, M. Peruzzini, F. Zanobini, *Chem. Eur. J.* **2003**, 2219.
[10] N. V. Belkova, A. V. Ionidis, L. M. Epstein, E. S. Shubina, St. Gruendemann, N. S. Golubev, H.-H. Limbach, *Eur. J. Inorg. Chem.* **2001**, 1753.
[11] N. V. Belkova, L. M. Epstein, A. Lledos, F. Maseras, E. S. Shubina, *J. Am. Chem. Soc.* **2003**, *125*, 7715.
[12] T. B. Richardson, S. de Gala, R. H. Crabtree, P. E. M. Siegbahn, *J. Am. Chem. Soc.* **1995**, *117*, 12875.
[13] R. H. Crabtree, P. E. M. Siegbahn, O. Eisenstein, A. L. Rheingold, T. F. Koetzle, *Acc. Chem. Res.* **1996**, *29*, 348.
[14] E. S. Shubina, E. V. Bakhmutova, L. M. Epstein, *Mendeleev Commun.* **1997**, 87.
[15] L. M. Epstein, E. S. Shubina, E. V. Bakhmutova, L. N. Saitkulova, V. I. Bakhmutov, A. L. Chistyakov, I. V. Stankevich, *Inorg. Chem.* **1998**, *37*, 3013.
[16] P. L. A. Popelier, *J. Phys. Chem. A.* **1998**, *102*, 1873.
[17] C. J. Cramer, W. L. Gladfelter, *Inorg. Chem.* **1997**, *36*, 5358.
[18] W. T. Kloster, T. F. Koetzle, P. E. M. Siegbahn, T. B. Richardson, R. H. Crabtree, *J. Am. Chem. Soc.* **1999**, *121*, 6337.
[19] I. Alcorta, I. Rozas, J. Elguero, *Chem. Soc. Rev.* **1998**, *27*, 163.
[20] R. Coustecean, J. E. Jackson, *Chem. Rev.* **2001**, *101*, 1963.
[21] S. Aldridge, A. J. Downs, *Chem. Rev.* **2001**, *101*, 3305.
[22] S. J. Grabowski, *Chem. Phys. Lett.* **1999**, *312*, 542.
[23] J. P. Campbell, J. W. Hwang, W. G. Young, R. B. Dreele, C. J. Cramer, W. L. Gladfelter, *J. Am. Chem. Soc.* **1998**, *120*, 521.
[24] J. L. Atwood, G. A. Koutsantonis, G. A. Lee, C. L. Raston, *J. Chem. Soc., Chem. Commun.* **1994**, 91.
[25] G. N. Patwari, T. Ebata, N. Mikami, *Chem. Phys.* **2002**, *283*, 193.
[26] J. Golden, C. Schreier, B. Singaram, S. Williamson, *Inorg. Chem.* **1992**, *31*, 1533.
[27] V. V. Gavrilenko, V. S. Kolesov, L. I. Zakharkin, *Russ. Chem. Bull.* **1984**, 2766.
[28] P. R. Schreiner, H. F. Schaefer, P. v. R. Schleyer, *J. Chem. Phys.* **1994**, *101*, 7625.
[29] A. V. Iogansen, *Theor. Experim. Khim.* **1971**, *7*, 302 and 314.
[30] A. V. Iogansen, *The Hydrogen Bond*, Nauka, Moscow, **1981**, p. 134.
[31] A. V. Iogansen, *Spectrochim. Acta A.* **1999**, *55*, 1585.
[32] E. S. Shubina, E. V. Bakhmutova, A. M. Filin, I. B. Sivaev, L. N. Teplitskaya, A. L. Chistyakov, I. V. Stankevich, V. I.

 © 2004 Wiley-VCH Verlag GmbH & Co. KGaA, Weinheim

Bakhmutov, V. I. Bregadze, L. M. Epstein, *J. Organomet. Chem.* **2002**, *657*, 155.

[33] V. I. Bakhmutov, E. V. Bakhmutova, N. V. Belkova, C. Bianchini, L. M. Epstein, M. Peruzzini, E. S. Shubina, E. V. Vorontsov, F. Zanobini, *Can. J. Chem.* **2001**, *79*, 479.

[34] L. M. Epstein, L. N. Saitkulova, E. S. Shubina, *J. Mol. Struct.* **1992**, *270*, 325.

[35] G. Rauhut, P. Pulay, *J. Phys. Chem.* **1995**, *99*, 3093.

[36] L. I. Zakharkin, V. V. Gavrilenko, Yu. N. Karaksin, *Synt. Inorg. Metal-Org. Chem.* **1971**, *1*, 37.

[37] A. D. Becke, *J. Chem. Phys.* **1993**, *98*, 5648.

[38] M. J. Frisch, G. W. Trucks, H. B. Schlegel, G. E. Scuseria, M. A. Robb, J. R. Cheeseman, V. G. Zakrzewski, J. A. Montgomery, Jr., R. E. Stratmann, J. C. Burant, S. Dapprich, J. M. Millam, A. D. Daniels, K. N. Kudin, M. C. Strain, O. Farkas, J. Tomasi, V. Barone, M. Cossi, R. Cammi, B. Mennucci, C. Pomelli, C. Adamo, S. Clifford, J. Ochterski, G. A. Petersson, P. Y. Ayala, Q. Cui, K. Morokuma, D. K. Malick, A. D. Rabuck, K. Raghavachari, J. B. Foresman, J. Cioslowski, J. V. Ortiz, A. G. Baboul, B. B. Stefanov, G. Liu, A. Liashenko, P. Piskorz, I. Komaromi, R. Gomperts, R. L. Martin, D. J. Fox, T. Keith, M. A. Al-Laham, C. Y. Peng, A. Nanayakkara, M. Challacombe, P. M. W. Gill, B. Johnson, W. Chen, M. W. Wong, J. L. Andres, C. Gonzalez, M. Head-Gordon, E. S. Replogle, and J. A. Pople, *Gaussian 98, Revision A.9*, Gaussian, Inc., Pittsburgh PA, **1998**.

[39] A. P. Kurbakova, L. A. Leites, V. V. Gavrilenko, Yu. N. Karaksin, L. I. Zakharkin, *Spectrochim. Acta, Sect. A* **1975**, *31*, 281.

Received February 2, 2004
Early View Article
Published Online June 23, 2004

 © 2004 Wiley-VCH Verlag GmbH & Co. KGaA, Weinheim

Electron Transfer Behavior of Multi-Iron Sandwich-Type Polyoxometalates and Electrocatalytic Reduction Reactions

Bineta Keita,[a] Israel Martyr Mbomekalle,[a] Yu Wei Lu,[a] Louis Nadjo,*[a] Patrick Berthet,[b] Travis M. Anderson,[c] and Craig L. Hill*[c]

Keywords: Polyoxometalates / Sandwich complexes / Iron / Cyclic voltammetry

The physicochemical and electrocatalytic behaviors of eight multi-iron Wells–Dawson sandwich-type polyoxometalates were studied with specific emphasis on the Fe^{III} centers. Magnetization measurements were used to identify and quantify the antiferromagnetic interactions between the edge-sharing Fe^{III} units. Electrochemical studies show the stepwise reduction of the Fe^{III} centers, in complete agreement with magnetization conclusions. The location of the potential of each wave depends on the pH of the solution, as well as the concentration and composition of the electrolyte. In addition, ion-pairing studies show there is a positive shift of the Fe^{III} centers with an increase in ion pairing (i.e. $K^+ > Na^+ > Li^+$). The electrocatalytic reduction of dioxygen and hydrogen peroxide is efficient for all the complexes. However, there is a pronounced increase in efficiency as the number of Fe^{III} centers in the complex increases (i.e. 4 $Fe^{III} > 3$ $Fe^{III} > 2$ Fe^{III}). The mixed-metal complexes [αββα-Na_{14}-$(Mn^{II}OH_2)_2(Fe^{III})_2(As_2W_{15}O_{56})_2$ and αββα-$Na_{14}(Mn^{II}OH_2)_2$-$(Fe^{III})_2(P_2W_{15}O_{56})_2$] are also efficient catalysts for the reduction of NO and HNO_2.
(© Wiley-VCH Verlag GmbH & Co. KGaA, 69451 Weinheim, Germany, 2004)

Introduction

Fundamental and applied studies on polyoxometalates (POMs for convenience) continue to grow unabated.[1−6] This is due, in part, to their proven value in catalysis and other areas, as well as their highly modifiable nature. Redox potentials, acidity, size, shape, polarity, and other properties can all readily be altered synthetically. Symmetries in the structures of the POMs result in the equivalence of several metal centers that are detectable, for example, by NMR spectroscopy on fully oxidized species, and by EPR and/or NMR spectroscopy on their reduced analogues.[7−13] This equivalence of the metal centers raises the following question about the molecular electrochemistry of these compounds: in the absence of other possible mechanistic complications, related usually to pH or ion pairing of the countercations, can it be expected that symmetry-equivalent metal centers will be reduced simultaneously, or will the interactions between adjacent metal centers induce a stepwise reduction?[14]

Despite the structural equivalence of the twelve metal centers in the α-$PW_{12}O_{40}^{3-}$ Keggin anion (Figure 1A), a stepwise reduction of the tungsten centers is observed.[8] EPR experiments on this species show that the added electron is delocalized (type II in the scheme proposed by Robin

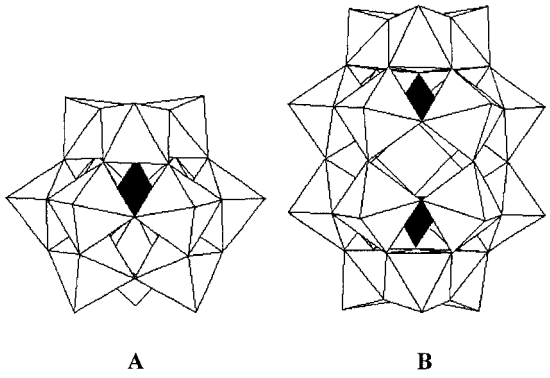

A B

Figure 1. Polyhedral representations of prototypical (A) Keggin (α-$XW_{12}O_{40}^{n-}$) and (B) Wells−Dawson (α-$X_2W_{18}O_{62}^{n-}$) anions

[a] Laboratoire de Chimie Physique, UMR 8000, CNRS, Université Paris-Sud,
Bâtiment 420, 91405 Orsay Cedex, France
Fax: (internat.) + 33-169154328
E-mail: nadjo@lcp.u-psud.fr
[b] Laboratoire de Physico-Chimie de l'Etat Solide, UMR 8648, CNRS, Université Paris-Sud,
Bâtiment 410, 91405 Orsay Cedex, France
[c] Department of Chemistry, Emory University,
Atlanta, Georgia, 30322, U.S.A.
Fax: (404) 727-6611
E-mail: chill@emory.edu
Supporting information for this article is available on the WWW under http://www.eurjic.org or from the author.

 © 2004 Wiley-VCH Verlag GmbH & Co. KGaA, Weinheim **DOI: 10.1002/ejic.200400099**

and Day)[1,15] over all twelve tungsten centers suggesting that there is communication between the metal centers. In general, complete delocalization of the added electrons over all twelve metal centers appears to be the rule for all unsubstituted, highly symmetrical α-Keggin anions. Introduction of lower symmetry results in a variation in the degree of valence trapping.[10,11,13] Unlike the spherical α-Keggin anion, the Wells−Dawson structure (Figure 1B) is shaped like a prolate ellipsoid,[16] consisting of six "cap" tungsten centers and twelve "belt" tungsten centers. The non-equivalence of the "cap" and "belt" tungsten sites raises the issue of the initial site of the electron transfer. All the evidence supports the fact that the added electrons are first introduced into the "belt" tungsten sites.[9−13,17−23] Extended Hückel calculations provide a qualitative understanding of the initial electron transfer site in these compounds. In complete analogy with the Keggin model, a stepwise reduction of the equivalent metal centers is also seen in the Wells−Dawson POMs, with various degrees of valence trapping observed upon the introduction of other substituents such as d-electron-containing metal species.

Recently we reported the synthesis and electrochemical properties of the sandwich-type POM, αββα-$Na_{12}(Fe^{III}OH_2)_2(Fe^{III})_2(As_2W_{15}O_{56})_2$ (**Fe4As4**).[24] The accumulation of adjacent edge-sharing Fe^{III} centers in **Fe4As4** gives more favorable electrocatalytic properties to the complex than those observed in the monosubstituted complex, α_2-$As_2(FeOH_2)W_{17}O_{61}^{7-}$. Analogous complexes containing phosphorus heteroatoms (instead of arsenic) are known,[25−30] but the presence of arsenic facilitates the reduction of both Fe^{III} and W^{VI} centers. Preliminary studies of **Fe4As4** and its phosphorus analogue, αββα-$Na_{12}(Fe^{III}OH_2)_2(Fe^{III})_2(P_2W_{15}O_{56})_2$ (**Fe4P4**), indicate that both complexes show the stepwise reduction of the four antiferromagnetically coupled Fe^{III} centers in the central unit.[25] However, a comprehensive investigation of the equivalence of the heterometallic centers in the sandwich-type derivatives, highlighting their eventual interactions and rationalizing their electrochemistry, is lacking. We now report such a study. In the present work, magnetic measurements on several recently reported multi-iron Wells−Dawson sandwich-type POMs [including **Fe4As4**, **Fe4P4**, αααα-$Na_{16}(NaOH_2)_2(Fe^{III})_2(X_2W_{15}O_{56})_2$ [X = As^V (**Fe2As4**) or P^V (**Fe2P4**)], ααβα-$Na_{14}(NaOH_2)$-$(Fe^{III}OH_2)(Fe^{III})_2(X_2W_{15}O_{56})_2$ [X = As^V (**Fe3As4**) or P^V (**Fe3P4**)] and the mixed-metal complexes, αββα-Na_{14}-$(Mn^{II}OH_2)_2(Fe^{III})_2(X_2W_{15}O_{56})_2$ [X = As^V (**Fe2Mn2As4**) or As^V (**Fe2Mn2P4**)], see Figure 2 for structures] are used to identify and quantify the interactions between adjacent Fe^{III} (or Mn^{II}) centers, and electrochemical measurements illustrate how ion pairing, pH, and electrolyte compositions influence the redox properties of the complexes. In addition, these results show how the redox properties of the sandwich-type POMs are affected by the metal population of the central unit.[31] Specifically, the tetraferric complexes **Fe4As4** and **Fe4P4** are better than the diferric complexes **Fe2As4** and **Fe2P4** for the electrocatalytic reduction of dioxygen and hydrogen peroxide.

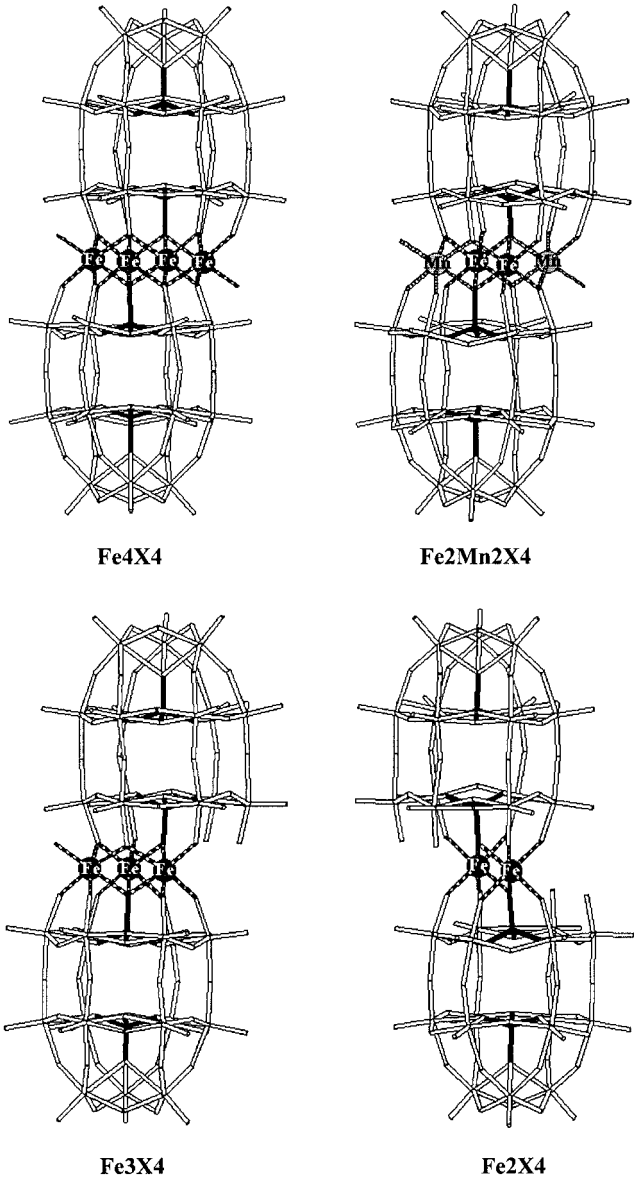

Figure 2. Combination wireframe/ball-and-stick representations of the eight multi-iron Wells−Dawson sandwich-type complexes studied here

Results and Discussion

Magnetic Studies

The crystallographic results of the present multi-iron sandwich-type complexes suggest that the arrangement of the Fe^{III} centers in edge-sharing octahedra will lead to electronic coupling between these metals.[24−27,29] Recently, we reported a detailed study of the magnetic properties of the arsenic complex, αββα-$Na_{12}(Fe^{III}OH_2)_2(Fe^{III})_2$-$(As_2W_{15}O_{56})_2$ (**Fe4As4**).[24] Here we report on the magnetic properties of the remaining complexes, which were all studied in a 0.1 T field. At 2 K, the magnetic moments per formula unit (for complexes **Fe4P4**, **Fe2As4**, **Fe2P4**, **Fe3As4**, **Fe3P4**, **Fe2Mn2As4**, and **Fe2Mn2P4**) are from three to seventy times lower than those expected for samples containing

 © 2004 Wiley-VCH Verlag GmbH & Co. KGaA, Weinheim

the same number of non-interacting Fe^{III} or Mn^{II} ions. This is the first indication that antiferromagnetic interactions are present between the magnetic ions that form the central cluster. The magnetic moments decrease regularly with temperature for the trinuclear clusters (**Fe3As4** and **Fe3P4**), while shoulders or bumps are observed for the dinuclear (**Fe2As4** and **Fe2P4**) and tetranuclear (**Fe4P4**, **Fe2Mn2As4**, and **Fe2Mn2P4**) clusters. Plots of χT versus T were calculated from the experimental data in order to carry out a quantitative analysis of the magnetic interactions (Figure 3). For that purpose, the experimental susceptibility was written as shown in Equation (1), where χ_0 represents the temperature independent contributions due mainly to the diamagnetism of the ligands, and $\chi_{cluster}$ represents the intrinsic susceptibility of the cluster. The latter is given by Equation (2), in which the mean value $<S_T(S_T + 1)>$ depends on the temperature, which in turn determines the population of the energy levels resulting from individual spin coupling. These energy levels are eigenvalues of the magnetic Hamiltonian of the cluster. For the POMs under study here, the more general Hamiltonian is that describing the tetranuclear clusters (**Fe4As4**, **Fe4P4**, **Fe2Mn2As4**, and **Fe2Mn2P4**), while the related trinuclear (**Fe3As4** and **Fe3P4**) and dinuclear (**Fe2As4** and **Fe2P4**) clusters may easily be deduced from the former by setting the spin value of one or two of the metal ions to zero. Since the magnetic ions of the central tetranuclear clusters are found at the corners of an almost regular rhomboid, the magnetic interactions may be represented by two exchange constants, J_1 and J_2, which describe the interactions along the sides of the rhomboid and along its shortest diagonal, respectively (Scheme 1).

$$\chi_{mol} = \chi_{cluster} + \chi_0 \quad (1)$$

$$\chi_{cluster} = g^2 N\beta^2 <S_T(S_T + 1)> /3k\ T \quad (2)$$

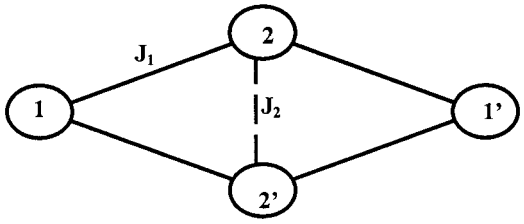

Scheme 1. Exchange pathways for the Fe_4 clusters

These interactions are of the superexchange type, and they are mediated by the two bridging oxygen atoms forming an edge shared by two neighboring FeO_6 or MnO_6 octahedra. Therefore, the magnetic energy of the cluster can be described by the following Heisenberg-type Hamiltonian [Equation (3)]. The eigenvalues of this Hamiltonian operator are obtained by the vector-coupling method of Kambe [Equation (4)],[32a] where S_{13}, S_{24}, and S_T are related with the spin operators $S_{13} = S_1 + S_3$, $S_{24} = S_2 + S_4$, and $S_T = S_{13} + S_{24}$. For a system of four ions with spin $S_i = 5/2$, there are 146 (S_T, S_{13}, S_{24}) combinations of energy E_i, whereas there are 27 and 6 combinations for systems with

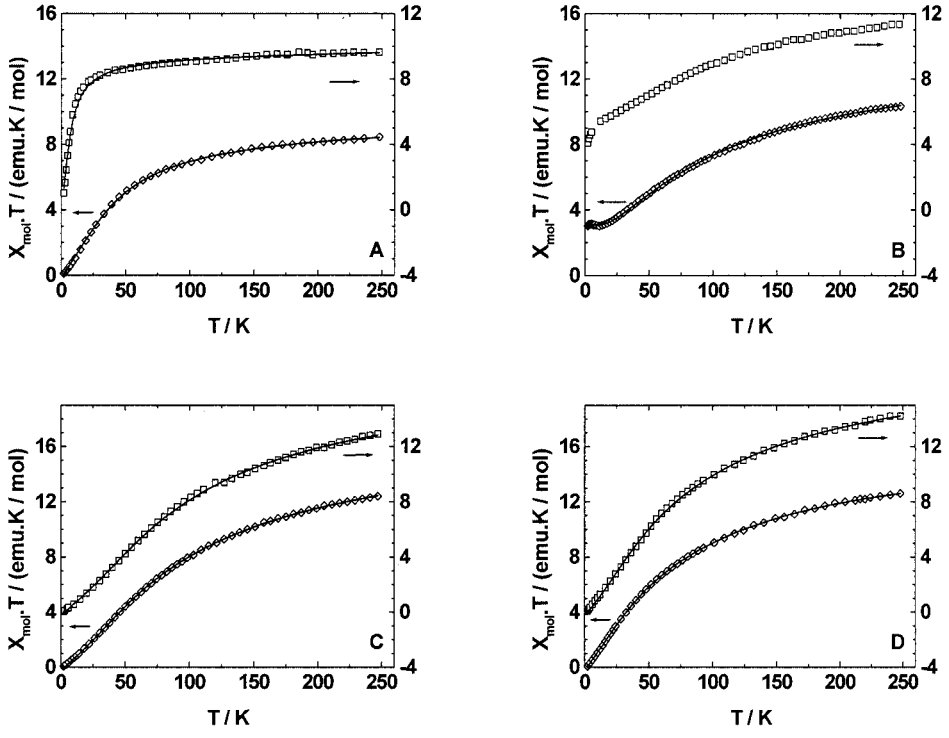

Figure 3. $\chi_{mol}T$ versus T plots for (A) **Fe2As4** and **Fe2P4**, (B) **Fe3As4** and **Fe3P4**, (C) **Fe4As4** and **Fe4P4**, and (D) **Fe2Mn2As4** and **Fe2Mn2P4**; the data corresponding to the phosphorus-based compounds are represented by squares, and the arsenic analogues are represented by diamonds; the continuous line represents the least-squares fit to the data using the parameters given in Table 1

 © 2004 Wiley-VCH Verlag GmbH & Co. KGaA, Weinheim

three or two ions, respectively. After the calculation of these energies, the mean value of $<S_T(S_T + 1)>$ is obtained using Equation (5), with $b_i = 2S_T(E_i) + 1$ and $a_i = b_iS_T(Ei)$-$[S_T(E_i) + 1]$.

$$H = -2J_1(S_1S_2 + S_2S_3 + S_3S_4 + S_4S_1) - 2J_2S_1S_3 \quad (3)$$

$$E(S_T, S_{13}, S_{24}) = -J_1[S_T(S_T + 1) - S_{13}(S_{13} + 1) - S_{24}(S_{24} + 1)] - J_2[S_{13}(S_{13} + 1) - S_1(S_1 + 1) - S_3(S_3 + 1)] \quad (4)$$

$$<S_T(S_T + 1)> = \Sigma a_i \exp(-E_i/kT)/\Sigma b_i \exp(-E_i/kT) \quad (5)$$

The $\chi_M T$ versus T plots for all of the compounds are shown in Figure 3. It is possible to determine the magnetic parameters (g, J_1, J_2, $\chi_M T_{free}$, χ_0, E_0, and E_1) for each compound by fitting the calculated $\chi_{mol}T$ values to the experimental ones (Table 1). For **Fe4As4**, **Fe4P4**, **Fe2As4**, **Fe2P4**, **Fe2Mn2As4**, and **Fe2Mn2P4**, a small constant contribution $\chi_M T_{free}$ was subtracted from the experimental data before calculation. These contributions correspond to free Fe^{III} or Mn^{II} ions acting as countercations, or to fragments that occur as a result of some decomposition process taking place upon drying. Such a decomposition was reported by Coronado and co-workers for the closely related compound $\alpha\beta\beta\alpha$-$[(Mn^{II}OH_2)_2(Mn^{II})_2(P_2W_{15}O_{56})_2]^{16-}$.[32b] For most of the complexes under study here, the subtracted contributions represent less than 3% of the magnetic ions. However, for **Fe2P4**, this contribution represents nearly 17% of the magnetic ions, suggesting there is significantly more decomposition of this complex.

Examination of the values given in Table 1 confirms the antiferromagnetic nature of the interactions between the ions of spin $S_i = 5/2$. The ground states of complexes **Fe4As4**, **Fe4P4**, **Fe2As4**, **Fe2P4**, **Fe2Mn2As4**, and **Fe2Mn2P4** have a total spin of $S = 0$, whereas the ground state of **Fe3As4** is $S = 3/2$. For most complexes, the ground state is well separated (more than 5 cm^{-1}) from the first excited state. In complex **Fe3As4**, three antiferromagnetic interactions take place along the sides of a triangle; two of these interactions are described by J_1, and the third one by J_2. The orientations of the individual spins cannot simultaneously satisfy the constraints resulting from these interactions, and the system appears frustrated. Consequently, several configurations have close energies: the gap between $E_0(S_T = 3/2)$ and $E_1(S_T = 5/2)$ is 0.9 cm^{-1}, and that between E_0 and $E_2(S_T = 1/2)$ is 4.0 cm^{-1}. The values of the temperature-independent susceptibilities χ_0 are quite different from one complex to another and are sometimes positive. In addition, the Landé g-factors are close to 2 for all of the samples. A comparison of the interaction constants J_1 and J_2 shows that the interactions along an edge of the rhomboids are stronger than those interactions along the short diagonal. The structural data indicates first that the longest Fe−O distances are found along the diagonal bridges corresponding to J_2, and second, the lateral bridges corresponding to J_1 have longer Mn−O distances than Fe−O distances. Therefore, the differences between J_1(Mn−Fe), J_1(Fe−Fe), and J_2(Fe−Fe) may partially be explained by the M−O distances. However, the strength of these interactions also depends on the M−O−M bridging angles as well. The absolute value of J_2 determined for **Fe2P4** is lower than those obtained for the other complexes.[33] This low value accounts for the fast increase in $\chi_{mol}T$ at low temperature. This particular behavior was confirmed on a second sample from another batch, but it cannot be explained from the structural characteristics of the dinuclear unit, which are very close to those of **Fe2As4**. This suggests that some prominent modifications may have taken place when the product was dried, which is also consistent with the high value of χT_{free}. Attempts to fit the magnetic parameters of **Fe3P4** were unsuccessful. This is most likely due to the presence of a small amount of **Fe2P4** in the measured sample, which could explain the difference observed at low temperature between the $\chi_{mol}T$ product of **Fe3P4** and that of **Fe3As4**. However, this difference disap-

Table 1. Magnetic parameters and first energy levels of the compounds under study

Compound	**Fe2P4**	**Fe2As4**	**Fe3As4**	
g	2.07	2.03	2.04	
J_1/cm^{-1}	−	−	−4.76	
J_2/cm^{-1}	−0.50	−2.95	−2.47	
χT_{free} /emu K mol^{-1}	1.50	0.25	0.	
χ_0/emu mol^{-1}	1.48 10^{-3}	1.31 10^{-3}	−1.30 10^{-4}	
E_0/cm^{-1} [S_T]	−8.7 [0]	−51.6 [0]	−112.8 [1.5]	
$E_1 - E_0/cm^{-1}$	1.0	5.9	0.9	
Compound	**Fe4P4**	**Fe4As4**	**Fe2Mn2P4**	**Fe2Mn2As4**
g	2.05	2.03	2.07	1.99
J_1/cm^{-1}	−4.76	−4.70	−3.63	−3.54
J_2/cm^{-1}	−2.04	−2.98	−2.51	−3.37
χT_{free} /emu K mol^{-1}	0.50	0.19	0.53	0.58
χ_0/emu mol^{-1}	−4.4 10^{-4}	−9.7 10^{-4}	−5.6 10^{-8}	−1.9 10^{-3}
E_0/cm^{-1} [S_T]	−260.1 [0]	−244.7 [0]	−185.9 [0]	−170.3 [0]
$E_1 - E_0/cm^{-1}$ [S_T]	9.5	9.3	7.2	7.1

 © 2004 Wiley-VCH Verlag GmbH & Co. KGaA, Weinheim

pears at higher temperature, suggesting that the magnetic interactions in both complexes are rather similar.

The susceptibilities of the tetranuclear clusters (**Fe4As4**, **Fe4P4**, **Fe2Mn2As4**, and **Fe2Mn2P4**) are very close to one another. With the use of the fitted parameters, the susceptibilities of **Fe4As4** and **Fe4P4** were extrapolated to 300 K, which gives 13.6 and 13.1 emu K mol^{-1}, respectively, for the $\chi_{mol}T$ products. These values are close to the calculated value of 13.3 emu K mol^{-1}, determined from the effective moment of **Fe4P4**, 10.3 μ_B, measured at 300 K by Zhang et al.[25]

pK_a Studies

To assess the stability of each of these complexes over a relatively large pH domain, we first determined their apparent pK_a values. In addition to the potential proton mobility of the water molecules fixed on the external $Fe^{III}-OH_2$ sites, protonatable sites might exist on the α-$X_2W_{15}O_{56}^{12-}$ (where X = As^V or P^V) unit itself. Measurements were performed with a 0.025 M solution of LiOH. The presence of Li^+ also helps to ensure the complete solubility of the samples. Experimental curves for all of the complexes are provided in the Supporting Information.[34]

Table 2 summarizes the results for complexes **Fe4As4**, **Fe4P4**, **Fe2As4**, **Fe2P4**, **Fe3As4**, and **Fe3P4**. The pK_a values are consistent with values reported for other similar sandwich-type complexes. Titration of the POMs without previous addition of acid gives similar results, and the results suggest that the number of mobile protons corresponds to the number of water molecules on the external Fe^{III} centers. Specifically, there are two, one, and zero mobile protons for complexes **Fe4As4** (and **Fe4P4**), **Fe3As4** (and **Fe3P4**), and **Fe2As4** (and **Fe2P4**), respectively. The pK_a values for the ionizable protons are comparable for similar complexes.[35−37] The number of protonatable sites on the POM framework itself seems to depend critically on the structure and, presumably, on the electronic interactions within the sandwich-type complexes. However, this behavior was not examined in more acidic solutions (less than pH = 2.5). It is also worth noting that the pK_a values do not smoothly increase as the pH of the solution is increased (and the POM deprotonated); in addition, the increase in the negative charge on the POM as a result of deprotonation causes an inversion in the observed pK_a values between the multi-iron sandwich complexes. This behavior has previously been observed in other POMs.[38−40] Finally, we note that the same acid−base properties are observed for both P and As heteroatoms.[41]

Electrochemical Studies

All of the compounds studied here are stable, at least in the timescale of the voltammetric studies, in the pH = 5 buffer medium (1 M CH_3COOLi and CH_3COOH) selected for these studies. The electrochemistry of the lacunary species (α-$P_2W_{15}O_{56}^{12-}$ and α-$As_2W_{15}O_{56}^{12-}$) were previously described.[24,42−44] There are positive potential shifts of the waves of α-$As_2W_{15}O_{56}^{12-}$ relative to those of α-$P_2W_{15}O_{56}^{12-}$ (20 mV and 54 mV for the first and second waves, respectively).[45] In contrast with the voltammograms of α-$As_2W_{15}O_{56}^{12-}$ and α-$P_2W_{15}O_{56}^{12-}$, those of **Fe4As4** and **Fe4P4** show four new waves in the potential domain +0.2 to −0.5 V. Figure 4A shows the CVs of α-$P_2W_{15}O_{56}^{12-}$ and **Fe4P4**. The four new waves are attributed to the reduction of the four Fe^{III} centers within the sandwich complex. At pH 3 (2 M NaCl + HCl), the formal potentials for the Fe^{III}/Fe^{II} redox couples are: 0.227, 0.124, −0.016 and − 0.093 V (vs. SCE), respectively. These potentials are distinctly more positive than the first W wave of α-$P_2W_{15}O_{56}^{12-}$ and **Fe4P4** (Figure 4A). This is consistent with the fact that Fe^{III} is known to reduce more easily than W^{VI} centers within substituted heteropolytungstates.[46] Corresponding data for the other complexes are included in the Supporting Information. The reduction of the W^{VI} centers is also influenced by the presence of the Fe^{III} centers in the sandwich molecule. The first wave of α-$P_2W_{15}O_{56}^{12-}$, which is slightly composite, splits into two waves in **Fe4P4**. This behavior is related to differences in the acid−base properties of the two POMs. Analogous to the CVs of α-$As_2W_{15}O_{56}^{12-}$ and α-$P_2W_{15}O_{56}^{12-}$, those of **Fe4As4** and **Fe4P4** are also very similar to each other. The presence of the arsenic heteroatom facilitates the reduction of both the Fe^{III} and W^{VI} centers (Figure 4B). The number of W^{VI} waves observed for **Fe4As4** or **Fe4P4**, and hence, the electron number for each wave, depends on the pH of the electrolyte. Rather classical electrochemical behaviors were observed for the W^{VI} centers in these complexes. Therefore, the focus of these studies will remain exclusively on the Fe^{III} centers. Figure 4C shows the stepwise reduction of the Fe^{III} centers in **Fe4P4**, with the potential domain restricted to that of the Fe^{III} redox processes. The X-ray crystal structures of **Fe4As4** and **Fe4P4** suggest that there are two types of symmetry-equivalent Fe^{III} centers.[24,25] There are two "external" Fe^{III} sites, which share two oxygen atoms with one α-$X_2W_{15}O_{56}^{12-}$ unit and three oxygen atoms with the other α-$X_2W_{15}O_{56}^{12-}$ unit. The sixth vertex of the octahedra is occupied by a water molecule. The sixth vertex of the two "internal" Fe^{III} sites is occupied by an additional

Table 2. Apparent pK_a values in 1 M LiCl at 25 °C for the multi-iron sandwich-type complexes

Heteroatom	X = As		X = P	
POM	Without added acid	With added acid	Without added acid	With added acid
Fe4X4 (X = As or P)	5.22, 5.42	5.32, 5.40	5.28, 5.80	5.17, 5.64
Fe3X4 (X = As or P)	5.62	2.54, 5.37	5.83	3.99, 5.86
Fe2X4 (X = As or P)	no titratable proton	2.76, 4.51, 3.58, 4.50	no titratable proton	2.19, 4.49, 3.82, 4.29

 © 2004 Wiley-VCH Verlag GmbH & Co. KGaA, Weinheim

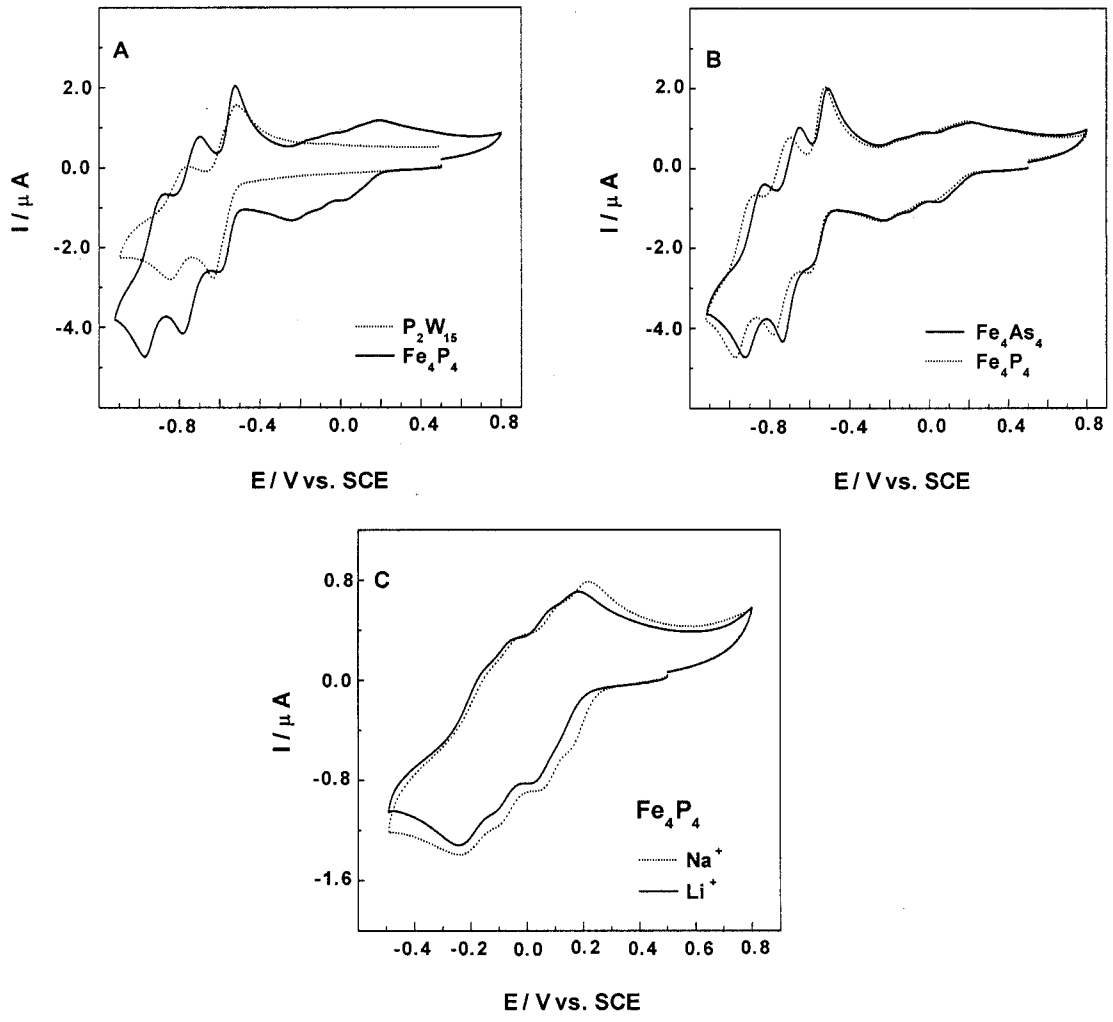

Figure 4. Cyclic voltammograms of **Fe4As4** and **Fe4P4** (2×10^{-4} M); the scan rate was 10 mV s^{-1}, the working electrode was glassy carbon, and the reference electrode was SCE; all measurements were performed in a 1 M CH_3COOLi + 1 M CH_3COOH (pH = 5) buffer solution except in (C), where the dotted line represents a measurement taken in a 0.5 M Na_2SO_4 + NaOH (pH = 5) buffer solution

oxygen atom from one of the two α-$X_2W_{15}O_{56}^{12-}$ units (rather than a water ligand). The structural data alone would suggest that there would be two groups of redox processes rather than four. The complete splitting into four distinct one-electron reduction processes suggests that there is some type of electronic communication involving the Fe^{III} centers.[47] This interaction must generate and/or reinforce inequivalence among the sites, especially in the reduced state; this is also consistent with the magnetic measurements. Finally, it is worth noting that all of the voltammetric patterns of **Fe4As4** and **Fe4P4** are perfectly well-defined and well-behaved at pH = 5. This observation is in contrast with the report that **Fe4P4** shows ill-defined waves with very small current intensities in media of pH > 4.[35] These differences may be due to differences in the media used to collect these measurements: this point was examined by running the CV in the same electrolyte (0.5 M Na_2SO_4 and NaOH, pH = 5) as that used in reference 35. The results in Figure 4C show that the waves remain perfectly well-defined (dotted line curve), and no decreased current is observed relative to the voltammogram recorded in acetate medium (solid line curve).

Ion Pairing

Although ion-pairing, pH, and ionic strength effects all exist simultaneously and act in competition, the data presented in Figure 4C allows the opportunity to discuss the first of these phenomena. In this system, an overall positive shift is observed for the Fe^{III} centers when a Na_2SO_4-based medium is used instead of CH_3COOLi. Since the two systems have the same ionic strength and pH (even though the buffer capacity is greater for CH_3COOLi), this positive shift must be due, in part, to the nature of the cation. It was previously shown that Na^+ engages in more intimate ion pairing with POMs than Li^+ since the hydrodynamic radius of Li^+ is greater than that of Na^+.[48,49] The positive shift of the potential for the Fe^{III} centers increases with increased ion pairing (i.e. $K^+ > Na^+ > Li^+$). For example, with both the pH and ionic strength kept constant, the formal potential measured for the Fe^{III}/Fe^{II} couple in

 © 2004 Wiley-VCH Verlag GmbH & Co. KGaA, Weinheim

$Ge(FeOH_2)W_{11}O_{39}^{5-}$ is more positive with a Na^+ countercation than with Li^+. Complexes **Fe4As4** and **Fe4P4**, however, contain four Fe^{III} centers and could display more complex ion-pairing behavior. In addition, the two Fe^{III} sites with ionizable terminal water ligands further complicate the matter since ion-pairing and protonation can compete.[37] Figure 4C illustrates this complexity by showing that effects of the cation differ from one wave to the next. For example, the second and fourth redox couples (which are better behaved) experience a 35 mV shift and a negligibly small shift, respectively, with a change in medium from Na^+ to Li^+. The shift due to cation effects is larger for the first two redox couples. To further illustrate the competition between ion-pairing and protonation of the terminal water ligands, the pH of the system was lowered from five to three (prepared with 0.5 M Li_2SO_4 and H_2SO_4 or 0.5 M Na_2SO_4 and H_2SO_4). The results suggest that protonation supersedes ion-pairing with decreasing pH. These general trends are in good agreement with the apparent pK_a values measured previously. Complex **Fe4As4** gave results similar to **Fe4P4** under the same experimental conditions. The nature of the cation of the supporting electrolyte has a similar effect on the W^{VI} waves as described previously for monosubstituted Keggin derivatives.[37] For the remaining electrochemical studies, Na^+ is the countercation used since most of the POMs studied here were originally synthesized as the Na^+ salts.

pH Effects

The behavior of the W^{VI} waves of the POMs as a function of pH was the subject of several previous investigations.[1,4,37,43,46,50–52] Similar variations were observed within the present multi-iron sandwich-type derivatives, but they were not the focus of this particular study. We wished to determine how changes in pH affect the formal potentials of the Fe^{III} waves. Provisionally, it is worth noting that changes in pH might cause two or more of these waves to merge, although that phenomenon was not observed in these studies. For the present purpose, pH effects (from pH = 2 to pH = 7) were studied by adding an appropriate amount of concentrated mineral acid or base to a 2 M solution of NaCl. The high concentration of NaCl was used to minimize any effect induced by small ionic strength variations.

Figure 5 represents the variation in the formal potential between pH 2 and pH 7 for each of the Fe^{III} centers in **Fe4As4** and **Fe4P4**. The four Fe^{III} centers are numbered according to their formal potentials from the least negative (Fe1) to the most negative (Fe4). The formal potentials of the Fe^{III}/Fe^{II} redox couples do not vary smoothly with pH. Such an intricate pH dependence was described previously in the case of a single Fe^{III} center within monosubstituted Keggin derivatives.[37] Electronic communication between Fe^{III} centers in the sandwich-type derivatives might render the changes in their formal potentials pH interdependent, and possibly, might also render them more complex. Nevertheless, some new trends do appear in Figure 5. Focusing first on **Fe4As4**, the Fe1 and Fe2 centers show almost parallel formal potential changes; however, between pH 2–3 and pH 4–5 quasi-independent behavior is seen. The variation is almost linear above pH 5, with a slope of 55 mV/pH. In contrast, the formal potential for Fe3 is nearly independent for pH values up to 6, after which the potential begins to vary slightly. For Fe4, a linear dependence is observed from pH 3 to 5, with a slope of 26 mV/pH. At higher pH values, the potential is almost independent of pH. Although the present observations specifically concern the Fe^{III}/Fe^{II} redox couples and not only the Fe^{III} redox states, the variation in the formal potentials follow the trends expected based on the apparent pK_a values. In particular, the regions in which the formal potential is independent of pH are consistent with the possibility that ion pairing supersedes protonation. Furthermore, the formal potentials of the two internal Fe^{III} centers are not expected to depend directly on pH. The observed dependence must therefore be because of

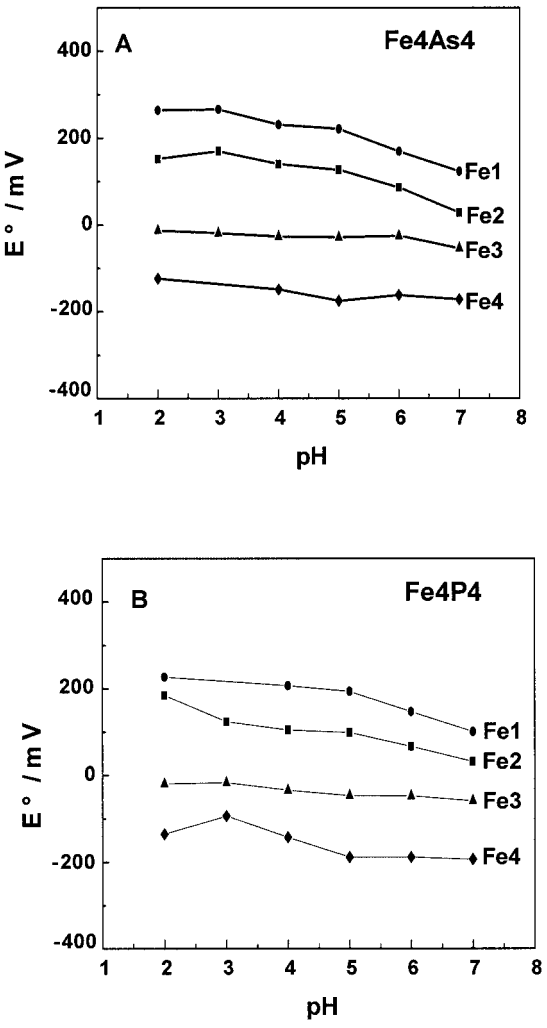

Figure 5. Plot of the formal potentials of **Fe4As4** (A) and **Fe4P4** (B) as function of pH for the four one-electron Fe^{III}-centered redox processes; the Fe^{III} centers are labeled FeX (with X = 1, 2, 3, or 4) from the most positive to the least positive reduction potential; the pH 2–3 solutions are comprised of 2 M NaCl + HCl, the pH 4–5 solutions are comprised of 2 M NaCl + 0.1 M CH_3COONa + 0.1 M CH_3COOH, and the pH 6–7 solutions are comprised of 2 M NaCl + 0.05 M NaH_2PO_4 + 0.05 M NaOH

 © 2004 Wiley-VCH Verlag GmbH & Co. KGaA, Weinheim

the electronic communication between all of the Fe^{III} centers. The same trends were observed for **Fe4P4** as well, albeit small differences, which are presumably linked to differences induced by the different heteroatoms (As versus P) within these complexes. Finally, ion-pairing and pH effects converge during the reduction processes to suggest that the external Fe^{III} centers are reduced first. This is consistent with Pope's report on $(MnOH_2)_2(Mn)_2(PW_9O_{34})_2^{10-}$, in which it was discovered that oxidation first occurs at the Mn centers with water ligands.[53] However, due to the low intensity of the observed effects and to the fact that oxidation and reduction might involve different molecular orbitals, support (or invalidation) for the present hypothesis will be sought from complementary theoretical calculations.

Diferric and Triferric Sandwich-Type Complexes

Figure 6 shows the voltammograms of **Fe4As4**, **Fe3As4**, and **Fe2As4**, restricted to the waves attributed to the reduction of the Fe^{III} centers only. Several conclusions emerge from these patterns. For each CV, the number of waves corresponds to the number of Fe^{III} atoms in each complex. These observations suggest there are sufficiently strong interactions between the Fe^{III} centers in each of the complexes to induce complete splitting of their redox processes into separate steps. Qualitatively, the overall current intensities are also consistent with the number of Fe^{III} atoms in each complex. The number of Fe^{III} centers was also investigated by controlled potential coulometry measurements, which give three electrons per molecule for **Fe3As4** and **Fe3P4** and two electrons per molecule for **Fe2As4** and **Fe2P4** for the exhaustive reduction of these centers. At pH 3, the following values were determined: 3.95 ± 0.05 electrons per molecule for **Fe4As4** and **Fe4P4** at − 0.250 V (vs. SCE); 2.95 ± 0.06 electrons per molecule for **Fe3As4** and **Fe3P4** with the potential set at − 0.300 V (vs. SCE); 1.95 ± 0.07 electrons per molecule for **Fe2As4** and **Fe2P4** at − 0.360 V (vs. SCE). The CV patterns shift in the negative potential direction with a decrease in the number of Fe^{III} atoms. This is most likely related to the overall increase in the negative charge of the POM due to the decrease in the number of Fe^{III} atoms, and it is probably also related to the differences in pK_a in the reduced forms. The formal potentials measured from the CVs of the Fe^{III}/Fe^{II} centers within the complexes are included in the Supporting Information.

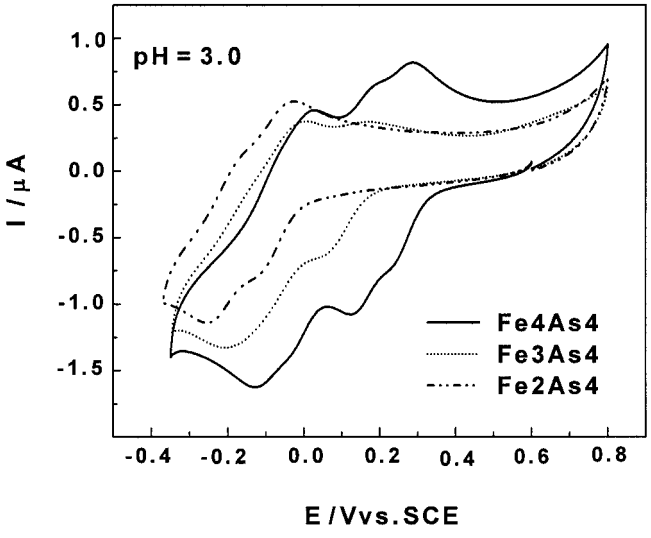

Figure 6. Cyclic voltammograms of **Fe4As4**, **Fe3As4**, and **Fe2As4** in 2×10^{-4} M, pH = 3 (2 M NaCl + HCl) buffer solution; the scan rate was 10 mV s^{-1}, the working electrode was glassy carbon, and the reference electrode was SCE

The relative potential shifts of the waves also seem to support the distinction between the external $Fe^{III}O_5(OH_2)$ centers and the internal $Fe^{III}O_6$ centers within the present complexes. Previously, we concluded that the external $Fe^{III}O_5(OH_2)$ centers are likely to be reduced before the internal $Fe^{III}O_6$ centers. Indeed, the CVs of **Fe3As4** and **Fe3P4** show the disappearance of a wave that can be attributed to an external $Fe^{III}O_5(OH_2)$ center in **Fe4As4** and **Fe4P4**. The CVs of **Fe2As4** and **Fe2P4**, which have no external $Fe^{III}O_5(OH_2)$ centers, also agree with this hypothesis since only two waves assigned to internal $Fe^{III}O_6$ centers are observed. These conclusions are also supported by the apparent pK_a values.

Mixed-Metal Sandwich-Type Complexes

Preliminary characterization of the mixed-metal multi-iron sandwich complexes indicated that they are stable from pH 0 to 7. In **Fe2Mn2P4**, the presence of Mn^{II} modifies the characteristics of the Fe^{III} and W^{VI} waves, which are observed at slightly more positive potentials than in **Fe2P4**. Figure 7 compares the Fe^{III}-based redox processes of complexes **Fe2P4** and **Fe2Mn2P4**. Controlled potential coulometry confirms that exhaustive reduction of these centers consumes 2.00 ± 0.05 electrons per molecule. Examination of Figure 7A shows that the first wave of **Fe2P4** is larger than that of **Fe2Mn2P4**, and that the first wave tends to merge with the second wave. Thus an ECE- or EEC-type process seems to be favored in the former complex. This observation leads to the conclusion that the reduced form of **Fe2Mn2P4** is less basic than the corresponding form of **Fe2P4**. The important influence of basicity is illustrated in Figure 7B. At pH 5, the two Fe^{III}-based waves merge in both complexes with coalescence being somewhat incomplete for **Fe2Mn2P4**, which shows a slightly composite wave.[54] The differences in the behavior of the arsenic analogues (complexes **Fe2As4** and **Fe2Mn2As4**) are less clear than those of the corresponding phosphorus analogues. The results indicate a clear influence of the central heteroatom, P or As, that consists (at pH 3) of an overall positive shift of the Fe^{III} waves without a current increase when P is replaced by As (see Supporting Information). A tentative explanation for this lack of change in the current is that the relevant pK_a values in the reduced forms of the As derivatives are very close from one complex to another.

A detailed study of the Mn^{II} wave in complex **Fe2Mn2P4** reveals, as expected, that the oxidation process becomes more difficult (i.e. moves towards more positive potentials) when the pH of the supporting electrolyte decreases. This point is illustrated for pH = 1 in Figure 7C where this process is kinetically sluggish. However, pre-treatment of the

 © 2004 Wiley-VCH Verlag GmbH & Co. KGaA, Weinheim

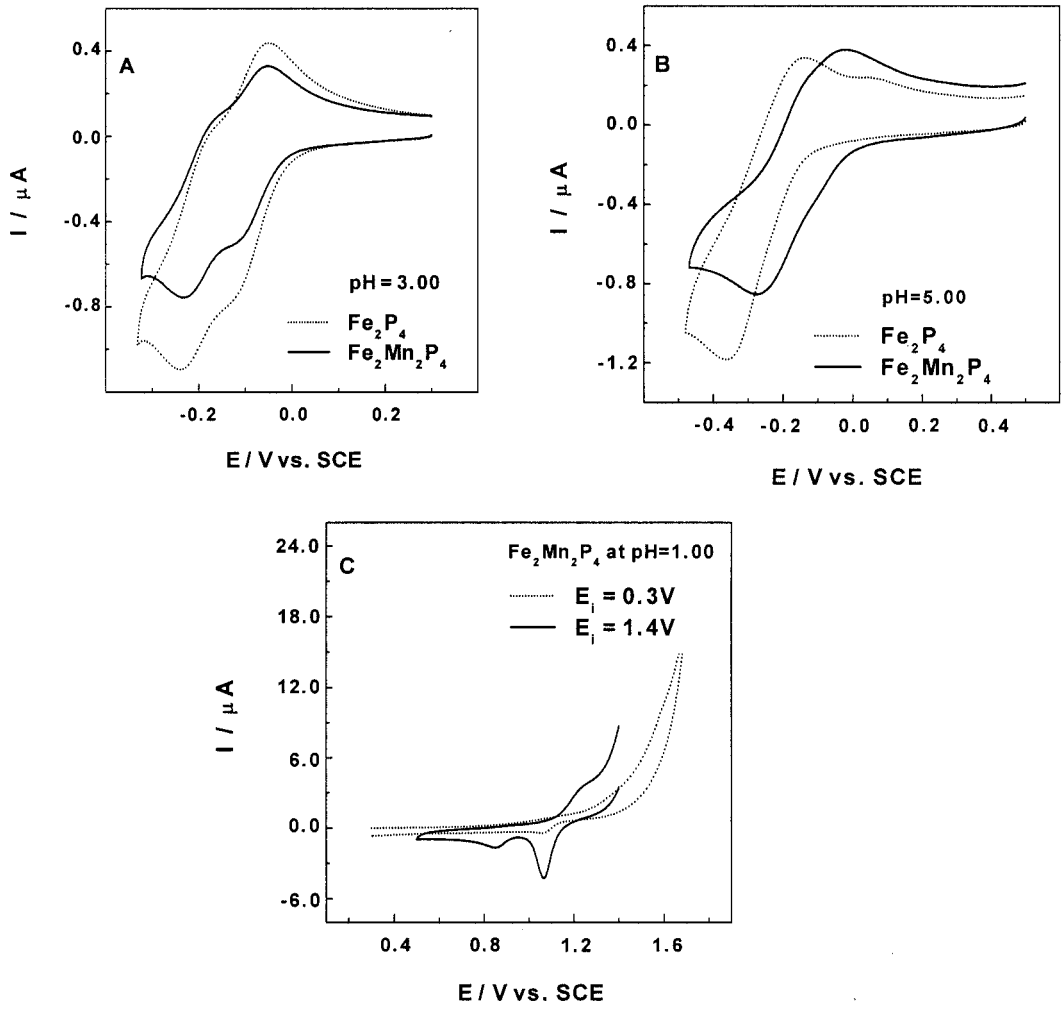

Figure 7. Cyclic voltammograms of **Fe2P4** and **Fe2Mn2P4** in different buffer solutions; the concentration of the POM was 2×10^{-4} M in all the solutions; the scan rate was 10 mV s^{-1}, the working electrode was glassy carbon, and the reference electrode was SCE; (A) comparison of **Fe2P4** and **Fe2Mn2P4** in a pH = 3 buffer (0.5 M Na_2SO_4 + H_2SO_4); (B) comparison of **Fe2P4** and **Fe2Mn2P4** in a pH = 5 medium (1 M CH_3COOLi +1 M CH_3COOH); (C) study of the Mn^{II} centers in **Fe2Mn2P4** in a pH = 1 medium (0.5 M Na_2SO_4 + H_2SO_4); E_i = initial potential; see the text for more details

electrode surface by pausing its potential at +1.4 V for a short time (120 s) prior to scanning the potential in the negative direction clearly reveals the presence of Mn^{II}. Under these conditions two reduction waves are observed, which are accompanied by a fairly well-behaved oxidation wave for the Mn^{II} centers on reversing the potential. This result is also shown in Figure 7C. Separation of the reduction into two steps is less pronounced in a pH 3 medium, where only a shoulder is observed. Examination of all these results together suggests that, for the two pH values we have explored (pH 3 and 5), the oxidation of Mn^{II} to Mn^{IV} is followed by the stepwise reduction of Mn^{IV} on reversing the potential. In addition, holding the potential at a selected positive value activates the electrode surface faster than continuous potential cycling. Continuous potential cycling of the electrode through the region in which the oxidation of interest is expected constitutes another technique in the activation of the glassy carbon surface electrode in the study of POM-based Mn^{II} centers. Steckhan and Sadakane found that this procedure gradually revealed the presence of the two waves of α-$Si(MnOH_2)W_{11}O_{39}^{6-}$ in a pH 6 phosphate buffer.[55] In contrast, we have previously shown that the merging of the two redox systems of Mn^{II} in α_2-$P_2(MnOH_2)Mo_2W_{15}O_{61}^{8-}$ results in a composite broad wave while cycling in a pH 6 phosphate medium (with concomitant deposition of an electroactive film on the electrode surface).[56]

Electrocatalysis

A pH 3 medium was selected for the studies on the electrocatalytic reductions of O_2 and H_2O_2. The efficiency of the catalytic process is evaluated by an excess parameter γ, which is defined as C° (O_2)/C° (POM) for dioxygen and C° (H_2O_2)/C° (POM) for hydrogen peroxide (C° = concen-

 © 2004 Wiley-VCH Verlag GmbH & Co. KGaA, Weinheim

tration of the relevant species indicated in parentheses).[57] The catalytic efficiency (CAT) is defined as follows: CAT = [I (POM + O_2 or H_2O_2) − I^d (POM)]/I^d (POM), where I (POM + O_2 or H_2O_2) is the current for the reduction of the POM in the presence of O_2 or H_2O_2 and I^d is the corresponding diffusion current for the POM alone.

Figure 8A shows the CVs for **Fe4As4** in the absence and presence of dioxygen. The electrocatalytic reduction of O_2 starts after the second Fe^{III} reduction wave and precludes the possibility of observing other Fe^{III} reduction waves. This is consistent with the formation of an iron-dioxygen adduct upon reduction of the first two Fe^{III} centers. This adduct is subsequently reduced to give water with regeneration of the catalyst; an inner-sphere mechanism is likely to be operating. Water was confirmed to be the final product in the reduction of hydrogen peroxide by the same catalytic system. It is interesting that the final reduction process starts after the second Fe^{III} wave. Since the naked electrode does not reduce dioxygen in the potential region explored here, the reduced forms of the POM must drive the electrocatalytic process.[58] At the potential location of the second Fe^{III} wave, the number of electrons accumulated in the POM framework is not sufficient to carry out the overall process. Figure 8B compares the CVs of **Fe4As4**, **Fe3As4**, and **Fe2As4** in the presence of the same excess of dioxygen. The onset of the electrocatalytic process shifts in the negative potential direction when the number of Fe^{III} atoms decreases. Qualitatively, the catalytic efficiency follows the same trend. The reasons given before, which postulate an overall inner-sphere process remains valid here, even though an obvious binding site for dioxygen on **Fe2As4** is difficult to assign.

The electrocatalytic reduction of hydrogen peroxide by **Fe4As4** is shown in Figure 8C and compared with the reduction of dioxygen by the same system. The catalytic reduction of H_2O_2 is facile and occurs on the first Fe^{III} wave

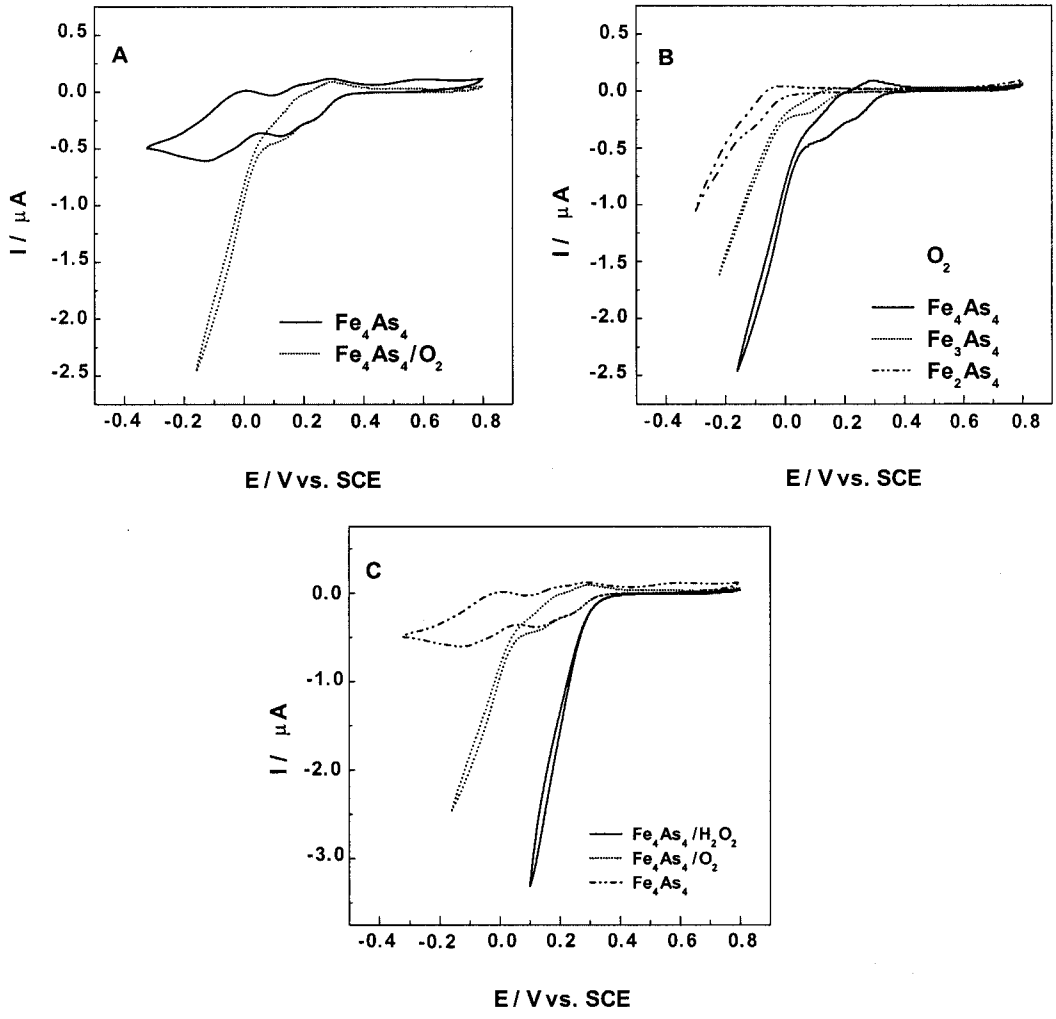

Figure 8. Cyclic voltammograms for the electrocatalytic reduction of dioxygen and hydrogen peroxide; the excess parameter for dioxygen or hydrogen peroxide was $\gamma = 5$, the scan rate was 2 mV s^{-1}, the working electrode was glassy carbon, the reference electrode was SCE, the concentration of the POM was 2×10^{-4} M, and the buffer had a pH of 3 (2 M NaCl + HCl); (A) electrocatalytic reduction with **Fe4As4**; (B) comparison of **Fe4As4**, **Fe3As4**, and **Fe2As4**; (C) comparison of the catalytic activity of **Fe4As4** towards dioxygen and hydrogen peroxide reduction

 © 2004 Wiley-VCH Verlag GmbH & Co. KGaA, Weinheim

of **Fe4As4** at a potential much more positive than that observed for the electrocatalytic reduction of O_2. This observation indicates that the final reduction product of dioxygen is water. Complexes **Fe2As4** and **Fe3As4** give similar results, and the onset of the electrocatalytic process is seen to strictly follow the order of reduction of the three complexes.

Selected values of catalytic efficiencies (CAT) for the reduction of dioxygen and hydrogen peroxide are included in the Supporting Information. The general trends from Figure 8 are confirmed and quantified. Focusing specifically on complexes **Fe4As4** and **Fe4P4**, it appears that under the same experimental conditions, the phosphorus-containing complex **Fe4P4** is slightly more efficient than the arsenic analogue **Fe4As4** for the reduction of dioxygen, while the opposite is true for the reduction of hydrogen peroxide. This observation underscores the impossibility of anticipating which electrocatalyst would be more efficient when an inner-sphere pathway is operative. Three points deserve special emphasis. First, the electrocatalytic processes observed here remain efficient in other media. For example, at pH = 5, a CAT value of 523% was measured for the electrocatalytic reduction of O_2 by **Fe4P4** at a potential of −240 mV. This observation, and others not specifically described here, are important in that they establish the utility of the Fe^{III} centers within these multi-iron sandwich complexes in media of low proton availability. Second, we found that there is still ample room for optimization of the selected media for efficient electrocatalytic processes within these compounds. Third, despite the apparent superiority of **Fe4As4** and **Fe4P4** in the present voltammetric study, **Fe3As4** and **Fe3P4** might ultimately be the most useful long term catalysts, in part, due to their better stability under a wide range of conditions.[27,29]

Examination of these two electrocatalytic processes sheds some light on the reaction pathways. Dioxygen does not coordinate to Fe^{III} but it does coordinate to Fe^{II}. In the presence of only one Fe center [as in α_2-$As_2(FeOH_2)W_{17}O_{61}^{7-}$], no electron source is available immediately after the reduction potential of Fe^{III} to drive the catalytic process to completion. This observation underscores the importance of the accumulation of Fe^{III} centers, which carry out immediate further reduction of the adduct. It is also important to note that the accumulation of these catalytic centers decreases the overall negative charge of the POM, rendering its reduction more facile, and ultimately, saving energy during the electrocatalytic process. If H_2O_2 complexes with the Fe^{III} centers, then this might result in a favorable process for the electrocatalytic reaction. In support of this, complexes **Fe3As4** and **Fe3P4**, which have only one such exchangeable center, have approximately the same efficiency as α_2-$As_2(FeOH_2)W_{17}O_{61}^{7-}$ for the electrocatalytic reduction of H_2O_2.

Cooperativity Effects In Electrocatalytic NO_x Reduction

It is well established that Fe^{III}-substituted POMs catalyze the reduction of NO and/or NO_2^-.[58−60] The first step in this process is the formation of a complex with the Fe^{II} form of the POM and nitrogen oxide.[31,58] The actual catalytic reduction of this complex takes place with remarkable enhancement of the current intensity at more negative potentials where a large number of supplementary electrons accumulate in the W framework. With the goal of saving energy by moving the electron reservoir closer to the Fe^{III}-reduction potential, we have previously synthesized several Wells−Dawson-type monosubstituted derivatives, including α_1-$P_2(FeOH_2)W_{17}O_{61}^{7-}$ and α_2-$P_2(FeOH_2)Mo_2W_{15}O_{61}^{7-}$ in which the Fe- and W-waves or Fe- and Mo-waves merge in an appropriate pH media.[31,56] This strategy is favorable, and the entire catalytic process occurs at the reduction potential of the Fe^{III} center, which is now observed concomitantly with the Mo^{VI} or W^{VI} reduction waves. The same phenomenon is observed here. These results are illustrated briefly with **Fe2Mn2P4** in Figure 9, with $NaNO_2$ as the starting substrate. An important current intensity increase is observed with increasing γ values [γ is the excess parameter defined as γ = C° (NO_x)/C° (POM)] at the reduction potential of the Fe^{III} centers in a pH 1 solution.[61] In this potential region, no reduction is observed for NO or HNO_2 present in the solution.[62][63] Figure 9 shows unambiguously that the catalytic process begins simultaneously with the reduction of the Fe^{III} centers. Furthermore, it is worth noting the high efficiency of the electrocatalytic process, even though modest γ values were used. Finally, in the timescale of cyclic voltammetry, **Fe2P4** shows the same phenomenon as **Fe2Mn2P4** with regard to the electrocatalytic reduction of NO and NO_2^-. However, the latter complex might be a better choice for this catalytic process due to the greater stability of its Fe^{II} forms.[29] Under the same experimental conditions, **Fe2Mn2As4** also shows good catalytic efficiency for the reduction of nitrite. In addition, its activity at 0 V is 25% higher than that of **Fe2Mn2P4** as seen by the positive potential shift of the Fe^{III} waves in the former complex relative to the latter due to the different heteroatoms (i.e. As vs. P).

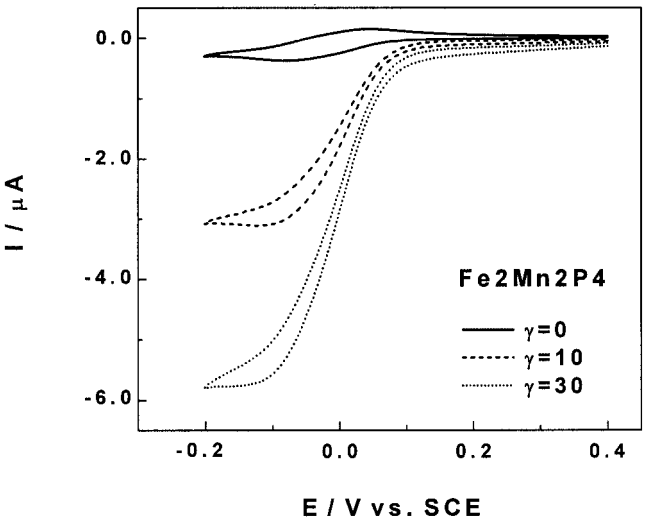

Figure 9. Cyclic voltammetric study of the electrocatalytic reduction of nitrite with a 2×10^{-4} M solution of **Fe2Mn2P4** in a pH = 1 medium (0.5 M Na_2SO_4 + H_2SO_4); the scan rate was 2 mV s^{-1}, the working electrode was glassy carbon, and the reference electrode was SCE

 © 2004 Wiley-VCH Verlag GmbH & Co. KGaA, Weinheim

However, in a pH = 5 medium, the catalytic process (obtained with $NaNO_2$ as the starting substrate) is no longer observed in the iron reduction potential region, but rather it occurs in the reduction potential region of the first W wave. This observation is in full agreement with the expected absence of NO and HNO_2 in this medium. In contrast, experiments with pure NO[62,63] at pH = 5 show that the catalytic process starts directly in the potential region in which reduction of iron takes place . We have also examined the catalytic reduction of NO at pH = 1. All these results confirm that NO is the species that is electrocatalytically reduced by the present complexes throughout the evaluated pH region.

Conclusion

The X-ray crystallographic studies of **Fe4As4**, **Fe4P4**, **Fe2As4**, **Fe2P4**, **Fe3As4**, **Fe3P4**, and **Fe2Mn2P4** strongly suggest that electronic coupling exists between the Fe^{III} centers in this large class of multi-iron sandwich-type POMs. Magnetic studies corroborate this prediction and quantify these interactions in the oxidized states of the POMs. Electrochemical studies further indicate there is a stepwise reduction of the Fe^{III} centers. Ion-pairing studies show there is a positive shift of the Fe^{III} centers with increased ion pairing (i.e. $K^+ > Na^+ > Li^+$). Furthermore, ion-pairing and pH effects converge during the reduction processes to suggest that the external Fe^{III} centers of **Fe4As4** and **Fe4P4** are reduced before the internal Fe^{III} sites. Finally, electrocatalytic results show that the accumulation of Fe^{III} centers within a sandwich-type complex yield more favorable catalytic properties. This is attributable to the fact that there is a positive potential shift of the Fe^{III}-based redox processes associated with the accumulation of Fe^{III} centers, and in the case of the catalytic reductions of O_2, NO, or HNO_2, it also suggests that the presence of sites on the POM, which are likely to anchor the relevant molecule during its reduction, may also help to facilitate inner-sphere electron transfer.

Experimental Section

General Remarks: Samples of **Fe4As4**, **Fe4P4**, **Fe2As4**, **Fe2P4**, **Fe3As4**, **Fe3P4, Fe2Mn2As4**, and **Fe2Mn2P4** were obtained by published procedures,[25−27,29−30] and purity was confirmed by IR, elemental analysis, and cyclic voltammetry. Infrared spectra (1% by weight of POM in KBr) were recorded on a Perkin−Elmer Spectrum One FT-IR spectrometer. Measurements of pH and pK_a were performed with a Tacussel MVN 83 millivoltmeter-pH meter. Magnetic measurements were performed on a SQUID magnetometer, Quantum Design MPMS-5. The water content of the samples was measured by thermogravimetric analyses (TGA). All chemicals used were high purity grade and were used without further purification.

pK_a Studies: Measurements were carried out twice using LiOH (0.025 M) under the following conditions: after calibration of the experimental set-up, and standardization of the different reagent solutions, the initial 10 mL solution contained 5×10^{-4} M of the relevant POM dissolved in either pure 1.00 M LiCl or 1.00 M LiCl/3×10^{-3} M HCl. The measurement cell was thermostatted to 25 °C. The solutions were thoroughly deaerated with pure Ar, and the cell was kept under positive pressure at all times during the experiments.

Electrochemical Experiments: The pH values of the buffer solutions range from pH 2 to pH 7. Buffers between pH 2−3 are comprised of 2 M NaCl and HCl. Buffers between pH 4−5 are comprised of 2 M NaCl, 0.1 M CH_3COONa, and CH_3COOH, and buffers between pH 6−7 are made up of 2 M NaCl, 0.05 M NaH_2PO_4, and NaOH. Certain experiments required the use of more specialized buffer solutions. These buffer solutions are described in the text of the Results and Discussion. Solutions were deaerated with Ar for 30 min prior to measurements and kept under positive pressure at all times. Pure NO (N_2O grade) was purchased from Air Liquide (France). The concentration of POM in solution was 2×10^{-4} M, unless otherwise stated. The source, mounting, and polishing of the glassy carbon electrodes (GC, Tokai, Japan, 3 mm diameter) has been described in previous work.[31] The counter electrode was a platinum gauze of large surface area. The electrochemical apparatus was an EG and G 273A under computer control (M270 software). All experiments were performed at ambient temperature, and potentials are quoted against a saturated calomel electrode (SCE).

Acknowledgments

This work was supported in part by the University Paris XI and the CNRS (UMR, 8000 and 8648). We also thank the NSF (Grant CHE-0236686) for the research and Véronique Barra for running several experiments.

[1] M. T. Pope, *Heteropoly and Isopoly Oxometalates*, Springer-Verlag, Berlin, **1983**.
[2] M. T. Pope, A. Müller, *Angew. Chem. Int. Ed., Engl.* **1991**, *30*, 34−48.
[3] M. T. Pope, A. Müller, Eds., *Polyoxometalates: from Platonic Solids to Anti-Retroviral Activity*, Kluwer, Dordrecht, The Netherlands, **1994**.
[4] Topical issues on polyoxometalates: C. L. Hill (Editorial), *Chem. Rev.* **1998**, *98*, 1−389.
[5] M. T. Pope, A. Müller, Eds., *Polyoxometalate Chemistry: From Topology via Self-Assembly to Applications*, Kluwer, Dordrecht, The Netherlands, **2001**.
[6] T. Yamase, M. T. Pope, Eds., *Polyoxometalate Chemistry for Nano-Composite Design*, Nanostructure Science and Technology, Kluwer, Academic/Plenum Publishing, New York, **2002**.
[7] J. F. Keggin, *Proc. Roy. Soc.* **1934**, *A144*, 75−77.
[8] G. M. Varga Jr., E. Papaconstantinou, M. T. Pope, *Inorg. Chem.* **1970**, *9*, 662−667.
[9] C. Sanchez, J. Livage, J. P. Launay, M. Fournier, *J. Am. Chem. Soc.* **1983**, *105*, 6817−6823.
[10] M. Kozik, C. F. Hammer, L. C. W. Baker, *J. Am. Chem. Soc.* **1986**, *108*, 2748−2749.
[11] M. Kozik, C. F. Hammer, L. C. W. Baker, *J. Am. Chem. Soc.* **1986**, *108*, 7627−7630.
[12] M. Kozik, L. C. W. Baker, *J. Am. Chem. Soc.* **1990**, *112*, 7604−7611.
[13] N. Casañ-Pastor, L. C. W. Baker, *J. Am. Chem. Soc.* **1992**, *114*, 10384−10394.
[14] The problem of pure electron transfer reactions to and from molecules containing at least two identical redox centers has received appropriate attention in several studies. Two main classes are described: the first class of compounds are those cases in which non-interacting redox centers are present and for which successive electron transfers are expected to follow

 © 2004 Wiley-VCH Verlag GmbH & Co. KGaA, Weinheim

simple statistics in the absence of coupled chemical steps. For example, see F. Ammar, J. M. Savéant, *J. Electroanal. Chem.* **1973**, *47*, 115−125; F. Ammar, J. M. Savéant, *J. Electroanal. Chem.* **1973**, *47*, 215−221; J. B. Flanagan, S. Margel, A. J. Bard, F. C. Anson, *J. Am. Chem. Soc.* **1978**, *100*, 4248−4253. The second group includes molecules in which various phenomena (including conjugation, ion pairing, solvation changes, and structural variations) induce or reveal interactions between the sites, and correlatively, differences between their half reaction potentials. These constitute the majority of published examples. For example, see A. J. Bard, *Pure Appl. Chem.* **1971**, *25*, 379−393; A. J. Bard, J. Phelps, *J. Electroanal. Chem.* **1970**, *25*, A2−A5; J. M. Fritsch, H. Weingarten, *J. Am. Chem. Soc.* **1968**, *90*, 793−795; C. P. Andrieux, J. M. Savéant, *J. Electroanal. Chem.* **1970**, *28*, 339−348; V. D. Parker, K. Nyberg, L. Eberson, *J. Electroanal. Chem.* **1969**, *22*, 150−152.

[15] The delocalized electron undergoes localization at low temperatures, otherwise the mixed valence compound is classified as type III under the scheme of Robin and Day.

[16] [16a] B. Dawson, *Acta Crystallogr.* **1953**, *6*, 113−126. [16b] H. D′Amour, *Acta Crystallogr., Sect. B* **1976**, *32*, 729−740.

[17] R. A. Prados, M. T. Pope, *Inorg. Chem.* **1976**, *15*, 2547−2553.

[18] J. L. Altenau, M. T. Pope, R. A. Prados, H. So, *Inorg. Chem.* **1975**, *14*, 417−421.

[19] R. Acerete, S. Harmalker, C. F. Hammer, M. T. Pope, L. C. W. Baker, *J. Chem. Soc., Chem. Commun.* **1979**, 777−779.

[20] L. Kazansky, M. Fedotov, *J. Chem. Soc., Chem. Commun.* **1980**, 644−646.

[21] A. Chemseddine, C. Sanchez, J. Livage, J. P. Launay, M. Fournier, *Inorg. Chem.* **1984**, *23*, 2609−2613.

[22] J. N. Barrows, M. T. Pope, *Inorg. Chim. Acta* **1993**, *213*, 91−98.

[23] B. Keita, Y. Jean, B. Lévy, L. Nadjo, R. Contant, *New J. Chem.* **2002**, *26*, 1314−1319.

[24] I. M. Mbomekalle, B. Keita, L. Nadjo, P. Berthet, K. I. Hardcastle, C. L. Hill, T. M. Anderson, *Inorg. Chem.* **2003**, *42*, 1163−1169.

[25] X. Zhang, Q. Chen, D. C. Duncan, C. Campana, C. L. Hill, *Inorg. Chem.* **1997**, *36*, 4208−4215.

[26] X. Zhang, T. M. Anderson, Q. Chen, C. L. Hill, *Inorg. Chem.* **2001**, *40*, 418−419.

[27] T. M. Anderson, X. Zhang, K. I. Hardcastle, C. L. Hill, *Inorg. Chem.* **2002**, *41*, 2477−2488.

[28] I. M. Mbomekalle, B. Keita, L. Nadjo, P. Berthet, W. A. Neiwert, C. L. Hill, M. D. Ritorto, T. M. Anderson, *Dalton Trans.* **2003**, 2646−2650.

[29] I. M. Mbomekalle, B. Keita, L. Nadjo, W. A. Neiwert, L. Zhang, K. I. Hardcastle, C. L. Hill, T. M. Anderson, *Eur. J. Inorg. Chem.* **2003**, 3924−3928.

[30] Dong and co-workers have also recently published the synthesis and characterization of **Fe4As4**, see: [30a] L. H. Bi, J. Y. Liu, Y. Shen, J. G. Jiang, E. K. Wang, S. J. Dong, *Gaodeng Xuexiao Huaxue Xuebao* **2002**, *23*, 472−474. [30b] L. Bi, J. Liu, Y. Shen, J. Jiang, S. Dong, *New. J. Chem.* **2003**, *27*, 756−764.

[31] B. Keita, F. Girard, L. Nadjo, R. Contant, R. Belghiche, M. Abbessi, *J. Electroanal. Chem.* **2001**, *508*, 70−80.

[32] [32a] K. Kambe, *J. Phys. Soc., Jpn.* **1950**, *5*, 48−51. [32b] C. J. Gómez-García, J. J. Borrás-Almenar, E. Coronado, L. Ouahab, *Inorg. Chem.* **1994**, *33*, 4016−4022.

[33] Recent calculations on the electronic transfer parameters in reduced phosphotungstates have given J values of 4000 cm^{-1}, while those observed in the eight complexes studied here are of the order of 2−5 cm^{-1}. For more information, see: N. Suaud, A. Gaita-Ariño, J. M. Clemente-Juan, J. Sánchez-Marín, E. Coronado, *J. Am. Chem. Soc.* **2002**, *124*, 15134−15140.

[34] For more information on general procedures for handling pK_a data, see [34a] A. E. Martell, R. J. Motekaitis, *Determination and Use of Stability Constants*, 2nd ed., VCH Publishers, Inc., New York, **1992**. [34b]M. T. Caudle, C. D. Caldwell, A. L. Crumbliss, *Inorg. Chim. Acta* **1995**, *240*, 519−525.

[35] L. Ruhlmann, L. Nadjo, J. Canny, R. Contant, R. Thouvenot, *Eur. J. Inorg. Chem.* **2002**, 975−986.

[36] R. Contant, M. Abbessi, J. Canny, A. Belhouari, B. Keita, L. Nadjo, *Inorg. Chem.* **1997**, *36*, 4961−4967.

[37] J. E. Toth, F. C. Anson, *J. Electroanal. Chem.* **1988**, *256*, 361−370.

[38] E. Papaconstantinou, M. T. Pope, *Inorg. Chem.* **1967**, *6*, 1152−1155.

[39] R. Contant, J.-M. Fruchart, *Rev. Chim. Miner.* **1974**, *11*, 123−140.

[40] B. Keita, Y. W. Lu, L. Nadjo, R. Contant, *Electrochem. Commun.* **2000**, *2*, 720−726.

[41] The present results differ substantially for at least one of the two pK_a values attributed by Ruhlmann and co-workers (ref.[35]) to the successive deprotonation of the two water molecules attached to the external metal atoms in αββα-$(MOH_2)_2(M)_2(P_2W_{15}O_{56})_2$ (M = Mn, Fe, Co, Cu, Zn, or Cd). In addition, the two pK_a values for **Fe2P4** are identical to those found for **Fe4P4**. However, the numbers for **Fe2P4** (even accounting for some experimental uncertainty) could only feature pK_a values for the protonable sites within the molecule.

[42] W. Song, X. Wang, Y. Liu, H. Xu, *J. Electroanal. Chem.* **1999**, *476*, 85−89.

[43] B. Keita, I. M. Mbomekalle, L. Nadjo, R. Contant, *Electrochem. Commun.* **2001**, *3*, 267−273.

[44] R. Contant, R. Thouvenot, *Can. J. Chem.* **1991**, *69*, 1498−1506.

[45] This observation is in agreement with the remark drawn from the study of α-$As_2W_{15}O_{56}^{12-}$ and α-$P_2W_{15}O_{56}^{12-}$ that the former species is easier to reduce than the latter, see B. Keita, I. M. Mbomekalle, L. Nadjo, R. Contant, *Eur. J. Inorg. Chem.* **2002**, 473−479.

[46] B. Keita, A. Belhouari, L. Nadjo, R. Contant, *J. Electroanal. Chem.* **1998**, *442*, 49−57.

[47] Although coupling between the Fe centers is invoked as an explanation for the separation (or lack thereof) of the various reduction waves, reduction of these centers (whether clearly sequential or not) may also depend simply on the effect of the extra negative charge taken on by the POM each time a Fe^{III} center is reduced to Fe^{II}. Literature has solved the case of the first reduction potentials of several Keggin species under conditions of no protonation. The correlation line has a slope of −0.18 V/unit charge (see ref.[1,18]). The same correlation was also suggested for select examples of second reduction potentials (see M. T. Pope, G. M. Varga Jr., *Inorg. Chem.* **1966**, *5*, 1249−1254). In the latter case, only highly symmetrical POMs with little or no ion pairing were addressed and the reduced centers were all W-based. In the multi-iron compounds we address here, electrons are localized essentially in the Fe_4 central unit where ion pairing is extensively operative and in competition with protonation. In addition, we have to consider the Wells-Dawson trivacant species as the precursors in the synthesis of the present sandwich complexes. Therefore only a semi-quantitative evaluation of this phenomenon can be made at best. However, the observation of a broad, single large cathodic current featuring the combined series of one-electron reduction processes of the four Fe centers made on $[Fe_4(OH_2)_{10}(β\text{-}XW_9O_{33})_2]^{n-}$ (n = 6, X = As^{III}, Sb^{III}; n = 4, X = Se^{IV}, Te^{IV}) in which Fe centers are not directly connected (ref.[51]) supports the idea of electronic communication between Fe centers. It can therefore be concluded that the stepwise addition of electrons required in molecular electrochemistry and the subsequent stepwise increase in the overall negative charge of the POM are not sufficient to split the waves measurably in a case where direct influence between structurally equivalent centers does not exist.

[48] Anson et al. (ref.[37]) have also shown that reduced forms of Fe^{III}-monosubstituted Keggin anions engage in ion-pairing with alkali metal cations.

[49] [49a] V. A. Grigoriev, C. L. Hill, I. A. Weinstock, *J. Am. Chem.*

 © 2004 Wiley-VCH Verlag GmbH & Co. KGaA, Weinheim

Soc. **2000**, *122*, 3544−3545. [49b] V. A. Grigoriev, D. Cheng, C. L. Hill, I. A. Weinstock, *J. Am. Chem. Soc.* **2001**, *123*, 5292−5307.
[50] B. Keita, L. Nadjo, *Mater. Chem. Phys.* **1989**, *22*, 77−103.
[51] U. Kortz, M. G. Savelieff, B. S. Bassil, B. Keita, L. Nadjo, *Inorg. Chem.* **2002**, *41*, 783−789.
[52] L. Cheng, H. Sun; B. Liu, J. Lin, S. Dong, *Electrochem. Commun.* **1999**, *1*, 155−158.
[53] X. Zhang, G. B. Jameson, C. J. O′Connor, M. T. Pope, *Polyhedron* **1996**, *15*, 917−922.
[54] Such differences in the pK_a values of the two complexes might be explained by considering that **Fe2Mn2P4** should behave much like a saturated complex, while **Fe2P4** is more lacunary in nature.
[55] M. Sadakane, E. Steckhan, *J. Mol. Catal. A: Chem.* **1996**, *114*, 221−228.
[56] B. Keita, Y. W. Lu, L. Nadjo, R. Contant, M. Abbessi, J. Canny, M. Richet, *J. Electroanal. Chem.* **1999**, *477*, 146−157.
[57] B. Keita, M. Benaïssa, L. Nadjo, R. Contant, *Electrochem. Commun.* **2002**, *4*, 663−668.
[58] J. E. Toth, F. C. Anson, *J. Am. Chem. Soc.* **1989**, *111*, 2444−2451.
[59] B. Keita, L. Nadjo, R. Contant, M. Fournier, G. Hervé, (CNRS), *French Patent 89l1,728*, **1989**.
[60] B. Keita, L. Nadjo, R. Contant, M. Fournier, G. Hervé, (CNRS), *Eur. Patent Appl. EP 382,644*, **1990**; *Chem. Abst.* **1991**, *114*, 191882u.
[61] At pH = 1, the actual active species should be HNO_2 and/or NO. In fact, the following sequence is known: $HNO_2 \rightarrow H^+ + NO_2^-$ pK_a = 3.3 at 18 °C and HNO_2 disproportionates in fairly acidic solution: 3 $HNO_2 \rightarrow HNO_3$ +2 NO + H_2O. The rate of this reaction is known to be low.
[62] A. Belhouari, B. Keita, L. Nadjo, R. Contant, *New J. Chem.* **1998**, 83−86.
[63] B. Keita, A. Belhouari, L. Nadjo, R. Contant, *J. Electroanal Chem.* **1995**, *381*, 243−250.

Received February 6, 2004
Early View Article
Published Online June 17, 2004

 © 2004 Wiley-VCH Verlag GmbH & Co. KGaA, Weinheim

Bonding, Metal-Atom Dynamics and Hyperfine Interactions of η-Phospholyl- and η-Pentaphospholyliron Complexes

Rolfe H. Herber,*[a] Israel Nowik,[a] Dmitry A. Loginov,[b] Zoya A. Starikova,[b] and Alexander R. Kudinov[b]

Keywords: Iron / Mössbauer spectroscopy / P ligands / Sandwich compounds / Spin−lattice relaxation

A number of structurally related sandwich compounds of iron, in which the central metal atom is ligated to rings containing one or five phosphorus atoms, have been investigated by temperature-dependent ^{57}Fe Mössbauer spectroscopy, differential scanning calorimetry and single-crystal X-ray diffraction. The quadrupole hyperfine interaction at 90 K evidences a linear dependence on the number of ring phosphorus atoms, decreasing by about 0.35 mm·s^{-1} for each ring carbon atom replaced by P. This effect is directly related to the change in the overlap between metal atom d-orbitals and ligand 3s,3p or 2s,2p orbitals due to an increase in the respective bond lengths. Several one-electron oxidation products of these compounds, which are paramagnetic, have also been examined and show spin–lattice relaxation rates which are fast compared to the characteristic Mössbauer timescale of 98 ns at all temperatures above 90 K.
(© Wiley-VCH Verlag GmbH & Co. KGaA, 69451 Weinheim, Germany, 2004)

Introduction

In a recent detailed study, Kudinov et al.[1] have discussed the synthesis, electrochemistry, and chemical reactivity of η-pentaphospholyl complexes of iron and ruthenium, including a number of double- and triple-decker sandwich compounds. In a continuation of previous research[2] in which temperature-dependent ^{57}Fe Mössbauer spectroscopy was used, in the present study the metal-atom lattice dynamics and hyperfine interactions of the central atom in the phosphorus-containing ferrocene-like complexes of Kudinov et al.[1] have been examined in detail over the temperature range 90 to 350 K (where appropriate). In addition, as needed, differential scanning calorimetry and magnetic susceptibility measurements have been carried out to extend these spectroscopic results. Such studies can shed light not only on the relationship between the dynamic properties of the iron atom and the details of the local molecular architecture, but also on the spin−lattice dynamics of such systems.

Among the complexes included in this study are [Cp*Fe(η-C_4Me_4P)] (**1**) (Cp* = η-C_5Me_5), [Cp*Fe(μ-η:η-C_4Me_4P)FeCp]PF_6 (**2**) (Cp = η-C_5H_5), [Fe(η-$C_4Me_4P)_2$] (**3**), [Cp*Fe(μ-η:η-P_5)FeCp]PF_6 (**4**), [Cp*Fe(μ-η:η-P_5)FeCp*]-BF_4 (**5**), [Cp*Fe(μ-η:η-Cp*)FeCp]PF_6 (**6**), [Cp*Fe(η-P_5)] (**7**), and [FeCp^*_2] (**8**) (the anions are omitted in the chart given below).

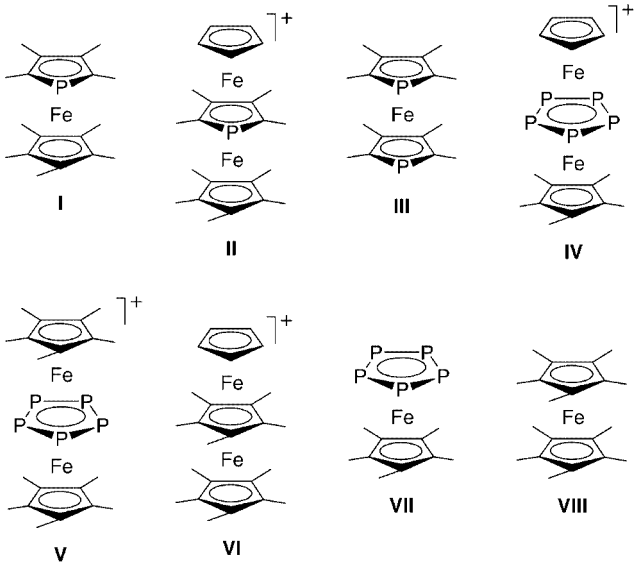

Single crystal X-ray diffraction data for **3** have also been acquired in the present study and are reported herein.

Results and Discussion

The Mössbauer spectra of all the compounds examined in this study consist of well-resolved doublets, and a typical spectrum (of **5**) is shown in Figure 1. The hyperfine parameters at 90 K — the isomer shift (IS), the quadrupole split-

[a] Racah Institute of Physics, The Hebrew University of Jerusalem,
91904 Jerusalem, Israel
E-mail: herber@vms.huji.ac.il
[b] A. N. Nesmeyanov Institute of Organoelement Compounds,
28 ul. Vavilova, 119991 Moscow, GSP-1, Russian Federation
E-mail: arkudinov@ineos.ac.ru

 © 2004 Wiley-VCH Verlag GmbH & Co. KGaA, Weinheim **DOI: 10.1002/ejic.200400210**

Table 1. ^{57}Fe Mössbauer parameters of the compounds discussed in the text; the parenthetical numbers accompanying the parameters are the experimental errors in the last significant figure(s)

	1	**2**	**3**	**4**	**5**	**6**	**7**	**8**	Units
IS(90)	0.500(4)	0.492(5)	0.501(4)	0.469	0.477(4)	0.515(4)	0.461(3)	0.502(2)	$mm{\cdot}s^{-1}$
QS(90)	2.202(4)	2.248(5)	2.027(4)	0.880	0.830(4)	2.541(4)	0.639(3)	2.479(2)	$mm{\cdot}s^{-1}$
$-dIS/dT$	4.70(6)	3.82(15)	5.08	4.84(13)	4.85(11)	4.78(4)	6.05	5.06(9)	$mm{\cdot}s^{-1}{\cdot}K^{-1} \times 10^4$
M_{eff}	89	109	82	86	86 ± 2	86 ± 6	69 ± 2		dalton
$-d\ \ln A/dT$	4.64(4)	16.2(4)	7.56	12.89(4)	4.43	6.81(5)	10.6(6)	15.5(3)	$K^{-1} \times 10^3$
Θ_M	137	66	112	84	143	115	103	78	K

ting, (QS) — as well as the temperature dependence of the logarithm of the recoil-free fraction (*f*) and of the IS, and the parameters derived therefrom, are summarized in Table 1. All IS's are referred to the center of a room temperature α-Fe absorber spectrum. In several cases, as will be noted below, the spectra also revealed the presence of a small quantity of an impurity which is the unavoidable consequence of the synthetic procedures. In these cases, appropriate corrections, especially to the spectral area calculations, were applied as needed.

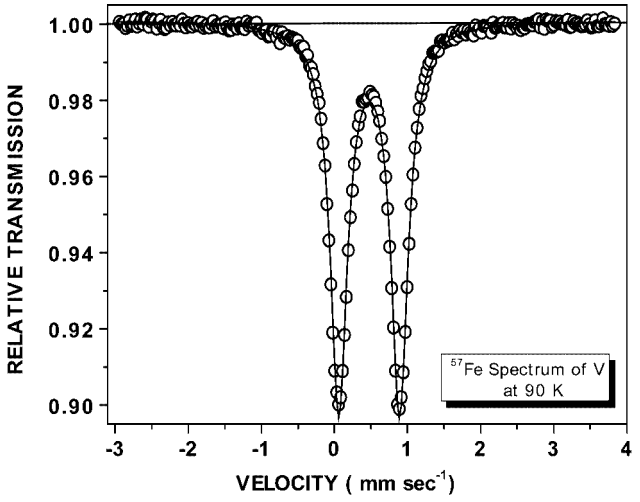

Figure 1. Mössbauer spectrum of **5** at 90 K; the velocity scale is with respect to the centroid of a room temperature α-Fe absorber spectrum

Compound 1

As will be noted from Table 1, the IS at 90 K is very similar to that of decamethylferrocene (**8**),[3] but somewhat smaller than that of the parent ferrocene itself ($0.537\ mm{\cdot}s^{-1}$), in agreement with the earlier conclusion[4] that ring substitution of H by CH_3 influences the s-electron density at the iron atom in only a very minor way. In contrast, the difference in the QS is smaller in **1** than in **8** by $0.277\ mm{\cdot}s^{-1}$, indicating a significant change in the details of the metal-ligand overlap when one of the ring CH groups is replaced by a phosphorus atom, an observation which will be further developed below. The temperature dependence of the IS in the high temperature limit (190−330 K) is well fitted by a linear regression, $[(4.70 \pm 0.06) \times 10^{-4}$ $mm{\cdot}s^{-1}{\cdot}K^{-1}]$ with a correlation coefficient (*R*) of 0.998 for 10 data points. The effective vibrating mass, M_{eff}, calculated from these data is 88 ± 2 daltons. The difference between this value and the "bare" iron atom value of 57 daltons is, of course, a reflection of the covalency of the metal−ring interaction, and is similar to the values reported for other ferrocene-related solids. Rayon and Frenking[5] have estimated the bonding interaction in ferrocene to be 45% coulombic and 55% covalent, and it is reasonable to assume that a comparable partitioning occurs in the present case.

The temperature dependence of the logarithm of the recoil-free fraction, $f = e^{-k^2x^2}$, which is given by the temperature dependence of the logarithm of the area, *A*, under the resonance curve for an optically "thin" absorber of **1**, is summarized graphically in Figure 2.

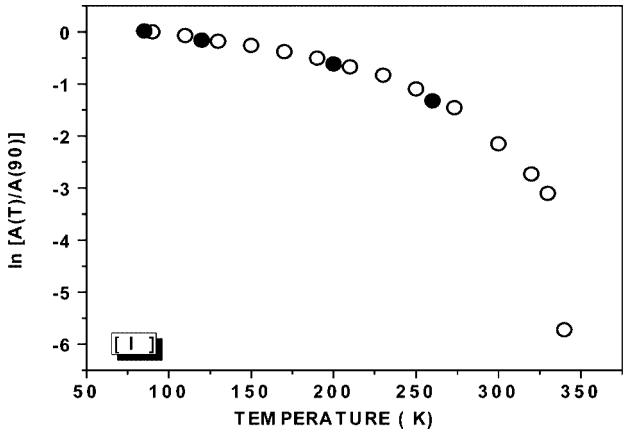

Figure 2. Temperature dependence of ln *A* for **1**; the open circles represent data acquired in a warming mode from 90 K, the full circles data acquired in a cooling mode following the measurement at 340 K

It is seen that although the data are completely reversible (filled versus open data points), the results are not at all well fitted by a linear regression, and, in fact, *f* becomes vanishingly small at temperatures above about 340 K. It should be noted that this temperature is significantly smaller than the melting point of the neat solid. These results have been associated[2,6] with the onset of ring rotation which, in the case of two five-membered rings, one of which has five methyl substituents and the other one (or more) ring substituents of very different steric requirements, such as an H or a ring P atom, leads to a librational motion of

 © 2004 Wiley-VCH Verlag GmbH & Co. KGaA, Weinheim

the two rings relative to each other. This librational motion, in turn, results in the presence of low-frequency optical modes which can take up the recoil of the gamma absorption, and hence significantly reduce the *f* value of the iron atom, as has been observed in a number of octamethyl ferrocene complexes.

Finally, it is worth noting that the resonance spectra of **1** do not show any significant motional anisotropy of the iron atom of the kind noted[7] in other ferrocene-related solids, over the entire temperature range noted above.

Compound 2

As before, the hyperfine parameters at 90 K are included in Table 1. The IS is, as expected, very similar to that observed in **1** and in this context it is clear that the presence of an additional FeCp entity does not change this parameter (or the QS) significantly. However, it is worth noting that while the presence of two different Fe atoms in the structure cannot be resolved from the hyperfine parameters, the line widths in such compounds are invariably significantly larger than in compounds with only one kind of metal atom in the structure. In the case of **1** and **2** at the same temperature, this difference corresponds to a line width increase of about 0.050 mm·s^{-1}. A fit of the data for **2** with two equally intense doublets of natural line width yields a somewhat better χ^2 than that with one doublet of broad lines. The difference in QS between the two doublets is about 0.17 mm·s^{-1}. The QS is similar to that observed in **1** as a necessary consequence that both iron atoms "see" a single phospholyl ring in one direction, and a hydrocarbon ring in the opposite direction.

The temperature-dependence of ln *f* is linear above 170 K, and in this case does not show the sharp decrease observed in **1**, although this may be due to the fact that the maximum temperature used in this case was below the point where ring librational motion becomes significant. On the other hand, the temperature dependence of the area ratio in **2** evidences a significant motional anisotropy, as summarized graphically in Figure 3. It should also be noted that the temperature dependence of ln *f* is exceptionally large, leading to a rather "soft" covalent lattice as "seen" by the metal atom in this structure.

Compound 3

The Mössbauer parameters of this complex (Table 1) show, as expected, almost the same IS, but again a twofold decrease in the QS relative to compound **1**. The temperature dependence of the IS is linear over almost the entire range, except at the higher limit, for reasons that will be discussed below. The temperature dependence of the QS as well is nearly negligible over the entire range except at the highest temperatures. What is most remarkable about **3** is the temperature-dependence of ln *f*, which is summarized graphically in Figure 4. It will be immediately apparent that ln *f* is only moderately temperature dependent to about 338 K, and then drops sharply, becoming experimentally unobservable at temperatures above 340 K. It should be noted that

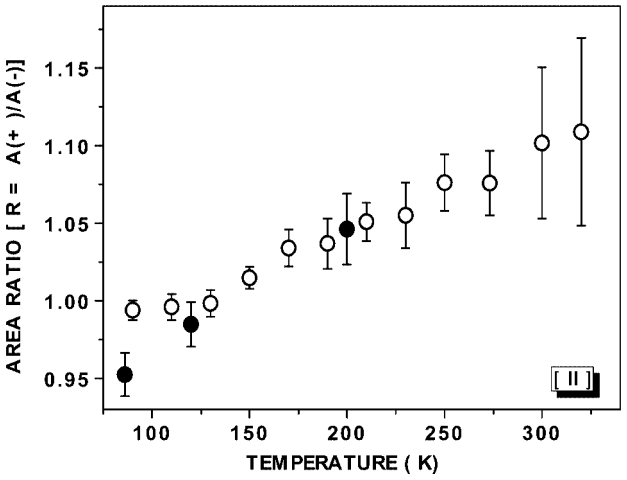

Figure 3. The temperature dependence of the area ratio for **2**; the non-unity value in the low temperature limit is presumed to arise from the temperature-independent texture effect of preferential crystallite orientation in the sample holder

the melting point of this compound is about 464 K, and has not been reported earlier in the literature.[8] Again, this *f* anomaly, *which occurs some 123 °C below the melting point*, is associated with the onset of librational motion of the two rings relative to each other. Strong supporting evidence for this interpretation is provided by the differential scanning calorimetry data summarized in Figure 5. The DSC data show a very sharp endothermic peak, starting at about 339 K and reaching a maximum at 341.8 K. On cooling, the exotherm is similarly sharp, with a maximum at 329 K. The 12.8 K hysteresis is also evident in the ln *f* data summarized in Figure 4, in which the cooling data, represented by the filled circles, do not evidence an experimentally observable resonance effect until a temperature of about 310 K is reached in this regime.

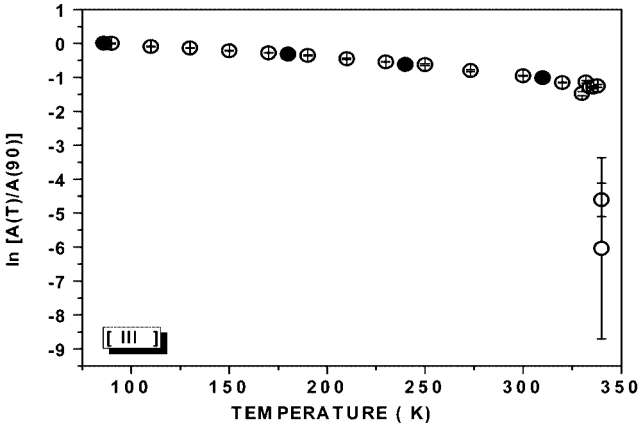

Figure 4. Temperature-dependence of ln *A* for **3**; the open circles pertain to data acquired in a warming mode, while the full circles represent data acquired in a cooling mode after the highest temperature point had been obtained

 © 2004 Wiley-VCH Verlag GmbH & Co. KGaA, Weinheim

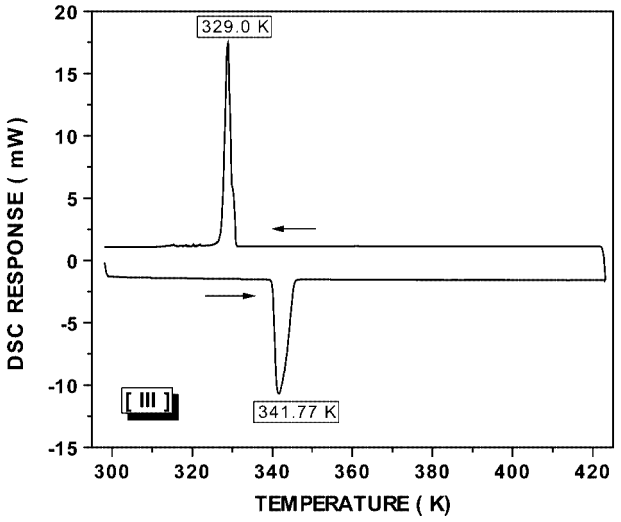

Figure 5. Differential scanning calorimetry data for **3** showing both the warming and cooling data; the approximate 12 degree hysteresis is also evident in the Mössbauer data, as discussed in the text

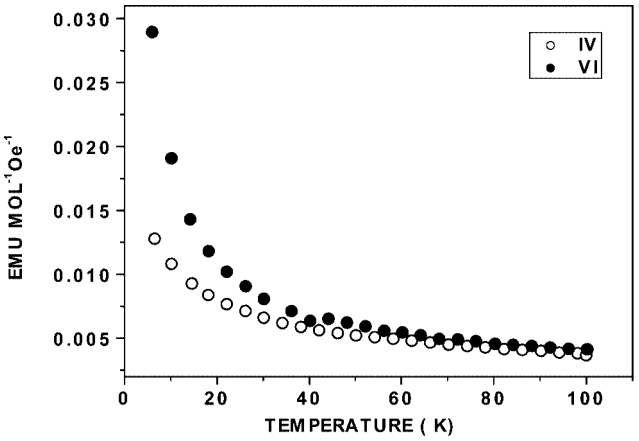

Figure 6. Magnetic susceptibility data for **4** and **6** consistent with paramagnetic behavior above 6 K

Compound 4

This compound is closely related to the pentaphospholyliron complex **7** described earlier,[9,10] with two significant differences: there is an additional FeCp group attached to the phosphorus ring, and the whole complex carries a positive charge, which is balanced by a PF_6^- counterion. The hyperfine interactions at 90 K and the derived parameters are included in Table 1. As noted above, despite the differences in the ligands attached to the two iron atoms, the Mössbauer parameters of the two metal atoms are sufficiently similar that they cannot be distinguished from each other. The IS (90 K) values of **4** and **7** are essentially identical, while the QS (90 K) values differ by about 0.24 mm·s^{-1}. It should be kept in mind, however, that the QS value for **4** reflects an average of the two different metal centers. Moreover, this parameter is nearly temperature independent in the range 90−300 K, and on further warming shows a pronounced negative slope to 350 K, while the temperature dependence of ln f is well fitted by a linear regression [$-(11.52 \pm 0.07) \times 10^{-3}$ K^{-1}; correlation coefficient: 0.993 for 21 data points] over the temperature range 90−350 K, and shows no discontinuity at about 300 K.

The spectra of **4** show two well-resolved maxima over the entire temperature range rather than the broadened collapsed spectrum characteristic of one-electron oxidized ferrocenoids, as reported earlier.[6,11] To substantiate the expected paramagnetic nature of **4**, the magnetic susceptibility of the compound (as well as of **6**) was determined over the temperature range 6−100 K under a field of 39 Oe; the results are summarized in Figure 6.

The experimental data were fitted by using the Curie−Weiss law $\chi = \chi_0 + C/(T - \Theta)$, where χ_0 is the temperature-independent susceptibility, C is the Curie constant and Θ is the Curie−Weiss temperature. For **4** the Curie constant is 0.167 emu·mol^{-1}·Oe^{-1} and the Curie−Weiss temperature is −0.09 K, showing clearly that **4** is paramagnetic over the entire temperature range. These results and those of the Mossbauer data provide clear evidence that the spin−lattice relaxation rate in this compound is fast with respect to the characteristic Mössbauer time scale (ca. 100 ns) at all temperatures above 90 K, while spin−spin relaxation can be ruled out in view of the local structure surrounding the iron atoms in next-neighbor molecules. There is no persuasive evidence for iron atom motional anisotropy over the range 90−350 K and the hyperfine parameters are completely reversible in cooling from the upper to the lower temperature of this range. It might be conjectured that the difference in the resonance spectra of compounds such as **4** (as compared to its neutral analogue) and that of ferrocenium ions and ferrocene might be related in some way to the presence of the five methyl groups in the Cp* ring. However, as will be discussed more fully below, resonance spectroscopic data for **8** and its one-electron oxidation product show clearly that the presence of the ring methyl substituents does not play a role in this difference of behavior.

Compound 5

The structure of **5** is very similar to that of **4** except that the second Cp ring is fully methyl substituted in the latter. The Mössbauer parameters, included in Table 1, are very similar to those of **4** and require no further elaboration except as noted below. Since the spectra of **5** again consist of two well-separated resonance maxima over the whole temperature range, the conclusions reached above for **4** relative to the spin−lattice relaxation rate are equally valid in this case.

The temperature dependence of ln f is shown graphically in Figure 7, from which it is seen that there is a significant change in slope on warming at about 170 K, and a second change in slope (of much smaller magnitude) between 190 and 200 K. To elucidate the origin of these changes a DSC scan was obtained over the temperature range 150−260 K. This scan shows two endotherms, one at about 170 K, the other at 193.5 K. The ΔH and ΔJ values for the latter transition are 1.19 kJ·mol^{-1} and 6.16 J·mol^{-1}·K^{-1}, respectively, in reasonable agreement with the barriers to internal rotation of the rings in polyene-metal complexes reported in

 © 2004 Wiley-VCH Verlag GmbH & Co. KGaA, Weinheim

the literature.[12] Thus it is inferred that the discontinuity observed in the ln *f* data shown in Figure 7 can be associated with the onset of ring rotation/libration of the two Cp* rings relative to the central η^5-P_5 ring in the molecular center. As in the case of the structurally closely related **4** there is no significant motional anisotropy of the iron atom observable over the entire temperature range.

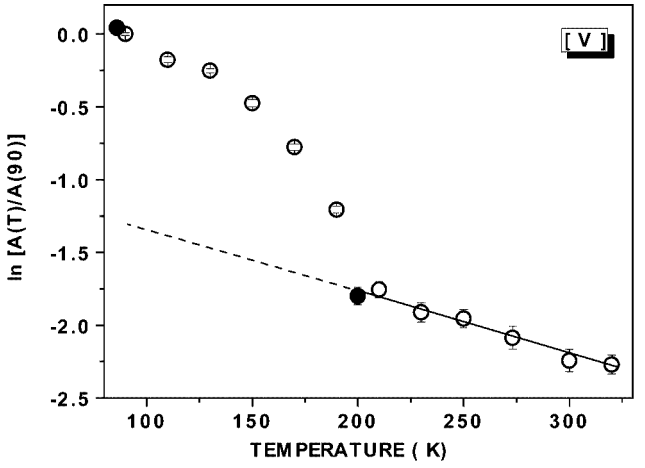

Figure 7. Temperature dependence of ln *A* for **5**; the two cooling regime data points (filled circles) were acquired after the 320 K data had been obtained

Compound 6

Finally, the Mössbauer spectra of **6** have been examined in considerable detail, although this molecule does not involve a phospholyl ring atom in its structure. The hyperfine parameters and associated constants are included in Table 1 and are not otherwise remarkable. As noted above, while the two different iron atoms are not resolvable on the basis of their hyperfine interactions, the linewidths (fwhm) in these spectra are again discernably broader than those observed in di-iron compounds in which the two metal atoms are located in identical environments.

The temperature dependence of the IS shows a small amount of curvature at low temperatures, but is reasonably well fitted by a linear regression in the high temperature regime (210−350 K) with a correlation coefficient of 0.997 for 10 data points. The QS is essentially temperature independent, but the area-ratio parameter shows evidence for a significant metal atom motional anisotropy. The temperature dependence of ln *f* is linear over the entire temperature range with a correlation coefficient of 0.997 for 19 data points.

As was noted for **4** and **5**, the resonance spectra of **6** consist of well-resolved doublets over the entire range. Since the susceptibility data included in Figure 6 (Curie constant 0.176 emu·mol^{-1}·Oe^{-1} and Weiss constant −10.4 K) again show this compound to be paramagnetic over the entire temperature range, it is concluded that above 86 K, the spin−lattice relaxation rate is again fast compared to the characteristic Mössbauer timescale.

Compound 8 and its One-Electron Oxidation Product

The MS parameters of decamethylferrocene (**8**) are included in Table 1 and have been published previously.[3] They are included in the present discussion due to the obvious structural relationship of this compound to those of the "double decker" compounds discussed above. In addition, a detailed MS study of the relaxation spectra of its one-electron oxidation product (as both the BF_4^- and PF_6^- salts) has been carried out, and will be reported separately.[13] Suffice it to say in the context of the present discussion that the presence of the ring methyl groups plays little role in the rate of the spin−lattice relaxation and the conclusions reached above for this rate in **4**, **5**, and **6** are not related to this ring substitution, but to the presence of two iron atoms in the structure, separated by a η^5 ring moiety which gives rise to the fast relaxation rates observed in these solids.

Systematics of the QS Hyperfine Interaction

The present data set includes structurally very similar compounds with, however, a variable number of ring phosphorus atoms as part of the sandwich architecture. The parameter most influenced by this number is the QS, and the change in the QS as a function of the number of ring phosphorus atoms is summarized graphically in Figure 8 in which the correlation coefficient of the linear regression is 0.994 for eight data points. Clearly, in these structurally closely related compounds the concept of the "partial quadrupole splitting" parameter[14] appears well justified, with each ring phosphorus atom diminishing the QS by 0.35 mm·s^{-1}. The relationship summarized in Figure 8 can be accounted for in terms of the molecular orbital treatment of the metal−ligand interactions in ferrocene-like complexes. The fundamental treatment for ferrocene has been well dealt with in the 1965 paper by Collins,[15] who showed that the Dahl and Ballhausen[16] treatment (as well as the slightly different scheme of Shustorovich and Dyatkina[17]) accounts for both the magnitude of the quadrupole interaction in ferrocene, as well as the large reduction in this parameter observed in the one-electron oxidation product. A major contribution to the QS is from the overlap of the e_{2g} and $3d_2$ orbitals, and the decrease in the QS on one-electron oxidation arises from the removal of electron density from the $3d_0$ orbital in the HOMO of the combination. A detailed representation of the MO correlation diagram for the interactions between Fe^{2+} and five-membered cyclic ligands has been given by Frenking.[18] The corresponding MO-level scheme for P_5-containing systems has been published by von Schleyer et al.[19] as applied to a titanium complex. In particular, from the Cp-metal-P5 MO diagram[19] it is seen that the HOMO has contributions from metal e_2', a′, and e1′′ levels as well as the e_2' π-orbitals of the cyclic P_5 ligand. It is clear from a comparison of these two schemes that the nature of the HOMO in these complexes changes significantly when the 2s2p orbitals of carbon are replaced successively by the 3s3p orbitals of phosphorus, and it is this change which can account qualitatively for the experimental data summarized in Figure 8.

 © 2004 Wiley-VCH Verlag GmbH & Co. KGaA, Weinheim

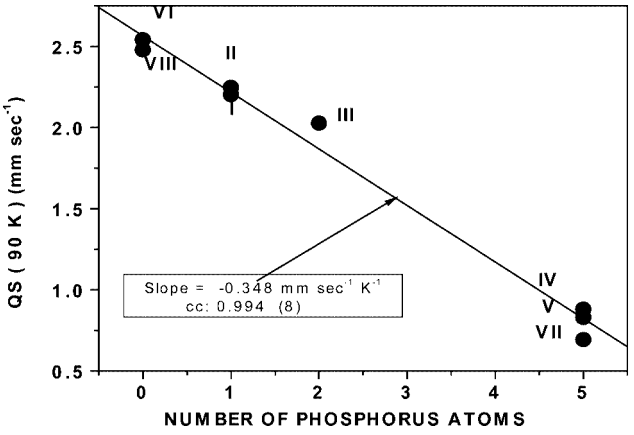

Figure 8. Dependence of the quadrupole hyperfine interaction at 90 K as a function of the number of ring phosphorus atoms in the compounds discussed in the text

Spin Relaxation in Triple-Decker Cations

As noted above, one-electron oxidation of ferrocene, decamethylferrocene (**8**) and related compounds, gives rise to relaxation spectra consisting of an asymmetric broadened resonance envelope, the temperature dependence of which is characteristic of a spin−lattice Raman relaxation process. In contrast, the triple-decker cations examined in the present study (**4**, **5**, and **6**) give rise to well-resolved doublet spectra, albeit with the quadrupole interactions given in Table 1. Since magnetic-susceptibility measurements have shown (in the case of **4** and **6**) that these compounds are paramagnetic at temperatures above 6 K, it is clear that the doublet spectra arise because the spin−lattice relaxation rate is rapid with respect to the characteristic Mössbauer time scale (ca. 10^{-9} s). Thus, at all temperatures of the present study, the resonant (scattering) nucleus sees an average zero hyperfine field, giving rise to narrow resonance lines in the spectra.

X-ray Diffraction Study

The structure of complex **3** was investigated by single-crystal X-ray diffraction. It has the expected sandwich structure (Figure 9). Selected bond lengths and angles are given in Table 2. These values are similar to those for other diphosphaferrocenes.[20−22] The conformation of the phospholyl rings corresponds to C_{2h} symmetry — the two P atoms are located in opposite directions (α = 180°). An analogous conformation was observed for one of two molecules in the unit cell of octaethyldiphosphaferrocene.[20] Other conformations reported for diphosphaferrocenes include C_{2v}, in which the two phosphorus atoms are eclipsed (α = 0°)[21] and C_1, in which the P atoms are superposed with the β-carbon of the other ring (α = 140−145°).[22]

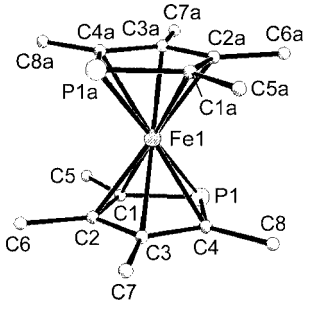

Figure 9. Structure of complex **3** (hydrogen atoms are omitted for clarity)

Table 2. Selected bond lengths (Å) and angles (°) for complex **3**

Fe(1)−P(1)	2.2909(4)	C(1)−P(1)	1.7790(14)
Fe(1)−C(1)	2.0991(13)	C(4)−P(1)	1.7783(15)
Fe(1)−C(2)	2.0674(14)	C(1)−C(2)	1.4241(18)
Fe(1)−C(3)	2.0726(13)	C(2)−C(3)	1.4356(18)
Fe(1)−C(4)	2.0953(14)	C(3)−C(4)	1.422(2)
C(1)−P(1)−C(4)	89.86(7)	C(2)−C(3)−C(4)	111.91(12)
C(2)−C(1)−P(1)	112.61(9)	C(3)−C(4)−P(1)	113.06(10)
C(1)−C(2)−C(3)	112.54(12)		

Cowley et al.[23] have reported the X-ray structure of the complex $[Ag\{(\eta\text{-}C_4Me_4P)_2Fe\}_2]^+$ in which Ag^+ is coordinated to the lone pairs of phosphorus atoms of **3**. The metal-to-ring distances Δ(Fe···C_4Me_4P) (1.6851−1.7026 Å, average 1.694 Å) in the $[Ag\{(\eta\text{-}C_4Me_4P)_2Fe\}_2]^+$ cationare longer than the corresponding value in **3** (1.6578 Å). An analogous elongation of Δ in $[Pd\{(\eta\text{-}C_4Et_4P)_2Fe\}_2]$ as compared with $[Fe(\eta\text{-}C_4Et_4P)_2]$ was also observed.[20] This elongation is apparently connected with a weakening of direct donation due to a decrease of the donor ability of the ring ligand. Moreover, the phospholyl rings coordinated with the metal atom are in a staggered conformation leading to steric repulsion.

Summary and Conclusions

Eight organometallic compounds of iron, having a variable number of ring-phosphorus-containing ligands, have been examined by temperature-dependent ^{57}Fe Mössbauer spectroscopy, differental-scanning calorimetry, and single-crystal X-ray diffraction. The quadrupole splitting (QS) hyperfine interaction is sensitive to the number of ring P-atoms, and decreases as this number increases. The paramagnetic species produced by one-electron oxidation of the neutral precursors show slow spin−lattice relaxation which increases, as expected, with increasing temperature. Compound **3**, the bis-cyclopentadienylphospholyl complex, shows both from Mössbauer recoil-free fraction data and the DSC results that onset of ring rotation gives rise to librational motion affecting the dynamics of the metal atom.

Experimental Section

Complexes **1**,[24] **2**,[25] **3**,[8] **4**,[26] **5**,[1] **6**,[27] **7**[1] and **8**,[27] were prepared as described in the literature. All of the compounds examined in this study were rapidly transferred from sealed ampoules to

 © 2004 Wiley-VCH Verlag GmbH & Co. KGaA, Weinheim

screw-cap perspex sample holders, sealed with Teflon tape and rapidly cooled to 78 K. Mössbauer spectra were recorded at increasing temperatures (in 20 K steps) to the maximum temperature, and then in a cooling mode to ascertain the reversibility of the data. The details of spectrometer calibration, temperature control and data reduction have been reported previously.[2] All isomer shifts are reported with respect to the centroid of a room temperature α-Fe absorber spectrum which was also used for spectrometer calibration.

Differential scanning calorimetry data (DSC) were acquired with a Mettler Toledo Star System at warming and cooling rates of 5 K per minute.

Magnetic susceptibility data were acquired in the temperature range 6 to 100 K using a commercial (Quantum Design MPMS-5S) super-conducting interference device (SQUID) magnetometer.

X-ray Crystal Structure Determination: The red plate-like crystals of **3** were grown by slow evaporation of the solvent from a pentane solution. Crystal data: $C_{16}H_{24}FeP_2$ (M = 334.14), monoclinic, space group $C2/c$ (no. 15), a = 14.298(2), b = 12.839(2), c = 8.849(1) Å, β = 104.369(3), V = 1573.6(4) Å^3, Z = 4, $d_{calcd.}$ = 1.410 g·cm^{-3}, μ = 1.146 mm^{-1}, $F(000)$ = 704, crystal size 0.20 × 0.40 × 0.60 mm.

Single-crystal X-ray diffraction experiments were carried out with a Bruker SMART 1000 CCD area detector, using graphite monochromated Mo-K_α radiation (λ = 0.71073 Å, ω-scans with a 0.3° step in ω and 10 s per frame exposure, $2\theta < 60°$) at 120 K. Reflection intensities were integrated using SAINT software,[28] the absorption correction was applied by semi-empirical method SADABS,[29] T_{max}/T_{min} = 0.802/0.391. A total of 6332 reflections were measured, 2075 (R_{int} = 0.0179) independent reflections were used in further calculations and refinement. The structures were solved by direct methods and refined by the full-matrix least-squares method against F^2 in anisotropic (for non-hydrogen atoms) approximation. All hydrogen atoms were located from the difference Fourier syntheses and were included in the final refinement using a rigid motion model in isotropic approximation. The final refinements converged to R_1 = 0.0377 [from 1868 unique reflections with $I > 2\sigma(I)$] and wR_2 = 0.1055 (from all 2075 unique reflections); the number of refined parameters was 88, GOOF = 0.943, largest diff. peak and hole 1.891 and −0.641 eA^{-3}. All calculations were performed on an IBM PC/AT using the SHELXTL software.[30]

CCDC-232591 contains the supplementary crystallographic data for this paper. These data can be obtained free of charge at www.ccdc.cam.ac.uk/conts/retrieving.html [or from the Cambridge Crystallographic Data Centre, 12, Union Road, Cambridge CB2 1EZ, UK; Fax: +44-1223-336033; E-mail: deposit@ccdc.cam.ac.uk].

Acknowledgments

The authors are indebted to Ms. Janet Zoldan of the Technion-Israel Institute of Technology for the careful DSC scans reported herein, Mr. E. Galstyan for the SQUID susceptibility measurements, and Prof. I. Felner for numerous helpful discussions. This research was supported in part by the Israel Academy of Sciences. Z. A. Starikova gratefully acknowledges the financial support of the Russian Foundation for Basic Research (Grant No. 03-03-32214).

[1] A. R. Kudinov, D. A. Loginov, Z. A. Starikova, P. V. Petrovskii, M. Corsini, P. Zanello, *Eur. J. Inorg. Chem.* **2002**, 3018−3027.
[2] R. H. Herber, I. Nowik, H. Schottenberger, K. Wurst, N. Schuler, A. G. Müller, *J. Organomet. Chem.* **2003**, *682*, 163−171, and references cited therein.
[3] R. H. Herber, in *Unusual Structures and Physical Properties in Organometallic Chemistry* (Eds.: M. Gielen, R. Willem, B. Wrackmeyer), Wiley, Chichester, **2002**, 207−218.
[4] R. H. Herber, B. Bildstein, P. Denifl, H. Schottenberger, *Inorg. Chem.* **1997**, *36*, 3586−3594, and references cited therein.
[5] V. M. Rayón, G. Frenking, *Organometallics* **2003**, *22*, 3304−3308.
[6] I. Nowik, R. H. Herber, *Inorg. Chim. Acta* **2000**, *310*, 191−195.
[7] [7a] I. Nowik, R. H. Herber, *J. Phys. Chem. Solids* **2003**, *64*, 313−317. [7b] I. Nowik, R. H. Herber, *J. Phys. Chem. Solids* **2003**, *64*, 1225.
[8] F. Nief, F. Mathey, L. Ricard, F. Robert, *Organometallics* **1988**, *7*, 921−926; G. de Lauzon, B. Deschamps, J. Fischer, F. Mathey, A. Mitschler, *J. Am. Chem. Soc.* **1980**,*102*, 994−1000.
[9] O. J. Scherer, T. Brück, *Angew. Chem. Int. Ed. Engl.* **1987**, *26*, 59, and references cited therein.
[10] R. H. Herber, O. J. Scherer, *Inorg. Chim. Acta* **2000**, *308*, 116−120.
[11] R. H. Herber, T. P. Hanusa, *Hyperfine Interact.* **1997**, *108*, 563−575.
[12] [12a] C. A. Morrison, S. F. Bone, D. W. H. Rankin, H. E. Robertson, J. A. S. Howell, P. C. Yates, N. Fey, *Organometallics* **2001**, *20*, 2309−2320. [12b] P. Comba, T. Gyr, *Eur. J. Inorg. Chem.* **1999**, 1787−1792. [12c] A. Almenningen, A. Haaland, S. Samdal, J. Brunvoll, J. L. Robbins, J. C. Smart, *J. Organomet. Chem.* **1979**, *173*, 293−299. [12d] A. Kubo, R. Ikeda, D. Nakamura, *J. Chem. Soc., Faraday Trans. 2* **1986**, *82*, 1543−1562. [12e] R. B. Woodward, M. Rosenblum, M. C. Whiting, *J. Am. Chem. Soc.* **1952**, *74*, 3458−3459. [12f] M. Rosenblum, R. B. Woodward, *J. Am. Chem. Soc.* **1958**, *80*, 5443−5449.
[13] R. H. Herber, I. Nowik, manuscript to be published.
[14] G. M. Bancroft, in *Mössbauer Spectroscopy*, J. Wiley & Sons, New York, **1973**, 121−145.
[15] R. L. Collins, *J. Chem. Phys.* **1965**, *42*, 1072−1080.
[16] J. P. Dahl, C. F. Ballhausen, *Mat. Fys. Medd. Dan. Vid., Selsk.* **1961**, 33; *Chem. Abstr.* **1964**, *61*, 1379g.
[17] E. M. Shustorovich, M. E. Dyatkina, *Dokl. Akad. Nauk* **1959**, *128*, 1234−1237; *Chem. Abstr.* **1962**, *57*, 1747f; *Chem. Abstr.* **1963**, *58*, 7386f, *Chem. Abstr.* **1966**, *64*, 18431b.
[18] G. Frenking, *J. Organomet. Chem.* **2001**, *636*, 9−23.
[19] E. Urnezius, W. W. Brennessel, C. J. Cramer, J. E. Ellis, P. von Ragué Schleyer, *Inorg. Chem.* **2003**, *16*, 290−294; see also R. Poli, *ChemTracts* **2003** (*16*) 290−94.
[20] X. Sava, L. Ricard, F. Mathey, P. Le Floch, *Organometallics* **2000**, *19*, 4899−4903.
[21] [21a] P. B. Hitchcock, G. A. Lawless, I. Marriano, *J. Organomet. Chem.* **1997**, *527*, 305−308. [21b] J. Zakrzewski, A. Klys, M. Bukowska-Strzyzewska, A. Tosik, *Organometallics* **1998**, *17*, 5880−5886.
[22] [22a] G. De Lauzon, B. Deschamps, J. Fescher, F. Mathey, A. Mitschler, *J. Am. Chem. Soc.* **1980**, *102*, 994−1000. [22b] S. Qiao, D. A. Hoic, G. C. Fu, *Organometallics* **1998**, *17*, 773−774.
[23] D. A. Atwood, A. H. Cowley, S. M. Dennis, *Inorg. Chem.* **1993**, *32*, 1527−1528.
[24] G. E. Herberich, B. Ganter, *Organometallics* **1997**, *16*, 522−524.
[25] A. R. Kudinov, D. A. Loginov, S. N. Ashikhmin, A. A. Fil′chikov, L. S. Shul′pina, P. V. Petrovskii, *Izv. Akad. Nauk, Ser. Khim.* **2000**, 1647−1649 [*Russ. Chem. Bull.* **2000**, *49*, 1637−1639 (Engl. Transl.)].
[26] O. J. Scherer, T. Brück, G. Wolmershäuser, *Chem. Ber.* **1989**, *122*, 2049−2054.
[27] A. R. Kudinov, M. I. Rybinskaya, Yu. T. Struchkov, A. I.

 © 2004 Wiley-VCH Verlag GmbH & Co. KGaA, Weinheim

Yanovskii, P. V. Petrovskii, *J. Organomet. Chem.* **1987**, *336*, 187−197.
[28] *SMART v. 5.051 and SAINT v. 5.00, Area detector control and integration software*, **1998**, Bruker AXS Inc., Madison, WI 53719, USA.
[29] G. M. Sheldrick, *SADABS*, **1997**, Bruker AXS Inc., Madison, WI 53719, USA.
[30] G. M. Sheldrick, *SHELXTL-97, v. 5.10*, Bruker AXS Inc., Madison, WI 53719, USA.

Received March 15, 2004
Early View Article
Published Online June 23, 2004

 © 2004 Wiley-VCH Verlag GmbH & Co. KGaA, Weinheim

Tin(II) and Lead(II) 4-Acyl-5-pyrazolonates: Synthesis, Spectroscopic and X-ray Structural Characterization

Claudio Pettinari,*[a] Fabio Marchetti,[a] Riccardo Pettinari,[a] Augusto Cingolani,[a] Eleonora Rivarola,[b] Christine Phillips,[c] Joseph Tanski,[c] Miriam Rossi,[c] and Francesco Caruso*[d]

Keywords: Lead / Mössbauer spectroscopy / N ligands / NMR spectroscopy / Tin

Novel tin(II) β-diketonate $Sn(Q)_2$ complexes [HQ = 1-R^1-3-R^3-4-R^4(C=O)-pyrazol-5-one; HQ^C: R^1 = Ph, R^3 = Me, R^4 = Cy; HQ^S: R^1 = Ph, R^3 = Me, R^4 = $CHPh_2$; HQ^L: R^1 = Ph, R^3 = Me, R^4 = CH_2Ph; HQ^T: R^1 = Ph, R^3 = Me, R^4 = CH_2tBu; HQ^E: R^1 = Ph, R^3 = Me, R^4 = Et; HQ^B: R^1 = Ph, R^3 = Me, R^4 = *t*Bu; HQ^W: R^1 = Ph, R^3 = Me, R^4 = *p*-(*t*Bu)Ph; HQ^R: R^1 = Ph, R^3 = Me, R^4 = *p*-[$(CH_2)_5CH_3$]Ph; HQ^N: R^1 = *p*-NO_2Ph, R^3 = Me, R^4 = Ph; HQ^M: R^1 = Me, R^3 = Me, R^4 = Ph; HQ^D: R^1 = Me, R^3 = Me, R^4 = Me; HQ^P: R^1 = Ph, R^3 = Ph, R^4 = Ph; HQ^G: R^1 = Ph, R^3 = Ph, R^4 = Me; HQ^F: R^1 = *p*-CF_3Ph, R^3 = Me, R^4 = Ph; HQ^H: R^1 = *p*-CF_3Ph, R^3 = Me, R^4 = Me] have been isolated and characterized by single-crystal X-ray diffraction analyses, IR, ^{1}H, ^{13}C, ^{119}Sn NMR and ^{119}Sn Mössbauer spectroscopy, ESI mass spectrometry, conductivity and molecular weight measurements. The tin complexes SnQ_2 are air-stable, contrary to equivalent compounds of classical β-diketones, and adopt mononuclear pseudo-trigonal-bipyramidal structures ($pSnO_4$, where p is a stereochemically active lone electron pair) in which both ligands chelate a single metal center, as confirmed in the X-ray crystal structure of $Sn(Q^L)_2$. This structure fits a trend for all "SnO_4" compounds: Sn–O(primary) and Sn–O(secondary) bonds are associated with small O(primary)–Sn–O(primary) and wide O(secondary)–Sn–O(secondary) bond angles. The reactivity of $Sn(Q^T)_2$ toward RI (R = Me or Et) and $CrCO_6$ has been investigated. The compounds PbQ_2 (HQ = HQ^T, HQ^B, HQ^W, HQ^D) have been also synthesized and the X-ray structures of $Pb(Q^B)_2$ and $Pb(Q^T)_2$ in the solid state determined. These are different from SnQ_2 and are composed of "PbO_4" moieties with additional interactions from neighboring units to produce polymeric forms. Compound $Pb(Q^T)_2$ is unusual in having the metal–O(pyrazolonato) bond longer than the metal–O(acyl) one, probably due to a Pb–arene interaction with a neighboring phenyl ring. The sterically less hindered $Pb(Q^D)_2$ reacts with phen (1,10-phenanthroline) yielding the mixed ligand complex [$Pb(Q^D)_2$(phen)]. In this work, in addition to the different coordination numbers expressed by Sn and Pb, associated with the larger covalent radius of the latter, the binding mode of 4-acyl-5-pyrazolonates to Pb is *syn* whereas for Sn it is *anti*.
(© Wiley-VCH Verlag GmbH & Co. KGaA, 69451 Weinheim, Germany, 2004)

Introduction

The discovery of several important new applications has led to renewed interest in tin(II) and lead(II) compounds containing chelating ligands. For example, SnF_2 has been incorporated into toothpaste for over two decades,[1] primarily as a convenient fluoride source, but more recently the inherent antimicrobial activity of the tin itself has also been claimed.[2–4] As a result, orally viable Sn^{II} derivatives are greatly desired and a number of researchers are involved in this field.[5] Moreover, new molecular precursors for MOCVD techniques are required to prepare suitable thin films of SnO_2, which is a semiconductor highly transparent in the visible region and highly reflective in the IR region,[6] adhesive to many substrates and with good chemical and mechanical stability. SnO_2 has a number of specific properties that make it useful as a transparent and conducting coating on glass,[7] in gas-sensing devices[8,9] and in transparent electrodes in photovoltaic devices.[10–12] β-Diketonates of tin(IV)[13–15] and tin(II)[16] seem to be good sources of SnO_2. Lead chelates are the basis for thin films of Pb-containing ferromagnetic ceramics such as [$PbTiO_3$], [$Pb(Zr,Ti)O_3$] and [$(Pb,La)(Zr,Ti)O_3$] that have important applications in nonvolatile ferroelectric memories, infrared detectors, electro-optic devices, sensors and micro-actuators.[17–26] Finally, the design and synthesis of new,

[a] Università di Camerino, Dipartimento di Scienze Chimiche, Via S. Agostino 1, 62032 Camerino MC, Italy
Fax: (internat.) + 39-0737-637345
E-mail: claudio.pettinari@unicam.it
[b] Università di Palermo, Dipartimento di Chimica Inorganica e Analitica Stanislao Cannizzaro, Parco d'Orleans II, 90128, Palermo, Italy
Fax: (internat.) + 39-091-427584
E-mail: rivarola@unipa.it
[c] Vassar College, Department of Chemistry, Poughkeepsie, NY 12604-0484, USA
Fax: (internat.) + 1-845-437-5732
E-mail: rossi@vassar.edu
[d] Istituto di Chimica Biomolecolare, CNR, Piazzale Aldo Moro 5, 00185, Rome, Italy
Fax: (internat.) + 39-06-49913628
E-mail: francesco.caruso@icb.cnr.it

 © 2004 Wiley-VCH Verlag GmbH & Co. KGaA, Weinheim **DOI: 10.1002/ejic.200400225**

volatile and thermally stable lead(II) complexes has received increased attention.[27−29]

In the last decade we have reported on the interaction between 4-acyl-5-pyrazolones, an interesting family of asymmetric β-diketones (Figure 1), and several metal acceptors such as Sn,[30] Rh,[31] Ba,[32] Sr,[33] Cu,[34] Cd,[35] and Ag.[36] We have demonstrated that it is possible to tune the chemical properties by appropriate choice of the substituents in the R^1 and R^4 positions of the ligand. Sometimes the complexes obtained show unusual structural and physicochemical features such as good solubility in polar protic solvents.[37] More recently we have described antitumor titanium acylpyrazolonates,[38] and volatile copper acylpyrazolonates.[39]

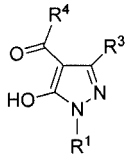

Q^CH: R^1 = Ph, R^3 = Me, R^4 = Cy
Q^SH: R^1 = Ph, R^3 = Me, R^4 = $CHPh_2$
Q^LH: R^1 = Ph, R^3 = Me, R^4 = CH_2Ph
Q^TH: R^1 = Ph, R^3 = Me, R^4 = CH_2tBu
Q^EH: R^1 = Ph, R^3 = Me, R^4 = Et
Q^BH: R^1 = Ph, R^3 = Me, R^4 = *t*Bu
Q^WH: R^1 = Ph, R^3 = Me, R^4 = *p*-*t*BuPh
Q^RH: R^1 = Ph, R^3 = Me, R^4 = *p*-[$(CH_2)_5$Me]Ph
Q^NH: R^1 = *p*-NO_2Ph, R^3 = Me, R^4 = Ph
Q^MH: R^1 = Me, R^3 = Me, R^4 = Ph
Q^DH: R^1 = Me, R^3 = Me, R^4 = Me
Q^PH: R^1 = Ph, R^3 = Ph, R^4 = Ph
Q^GH: R^1 = Ph, R^3 = Ph, R^4 = Me
Q^FH: R^1 = *p*-CF_3Ph, R^3 = Me, R^4 = Ph
Q^HH: R^1 = *p*-CF_3Ph, R^3 = Me, R^4 = Me

Figure 1. Q proligands used in this work

In 1994 we synthesized some tin(II) acylpyrazolonates[40] and found that these compounds are more stable than analogous tin(II) derivatives of classical β-diketonates.[16,41−43] Here we report a systematic investigation of the interaction of tin(II) with acylpyrazolonates to determine if variation of steric and electronic features of acylpyrazolones can affect the solid-state and solution structures of tin(II) compounds. The reactivity of the species obtained was also tested toward carbonylmetal compounds and alkyl halides. In addition, the structural properties and reactivities of new Pb^{II} acylpyrazolonates are compared.

Results and Discussion

Interaction of the acylpyrazolone proligands HQ with tin(II) dichloride in methanol, in the presence of sodium methoxide, yielded SnQ_2 derivatives **1**−**15** as precipitates (Scheme 1). In contrast to classical bis(β-diketonato)tin(II) complexes, Sn^{II} derivatives of the asymmetric Q^- ligands are quite stable to air and moisture. They are pale-yellow solids with sharp melting points. The solubility of **1**−**15** varies widely depending on the R^1, R^3 and R^4 substituents. When R^1 is a Ph or 4-$O_2NC_6H_4$ group and R^4 is an Me group (**1**−**9**), the compounds are soluble in DMSO, acetone and chlorohydrocarbon solvents, where they are not electrolytes. When R^1 = R^3 = Me (**10**, **11**), and when R^1 = *p*-$F_3CC_6H_4$ (**14**, **15**) higher solubility in acetonitrile, alcohols and aromatic solvents was found. Moreover, derivatives **12**−**15** are partially dissociated in DMSO, similar to diorganotin(IV) complexes of $(Q^P)^-$, $(Q^G)^-$, $(Q^F)^-$ and $(Q^H)^-$.[30,44,45] Compounds **1**−**15** do not undergo hydrolysis in chloroform or acetone solution. Molecular weight determinations carried out for all derivatives in chloroform suggest monomeric structures in solution.

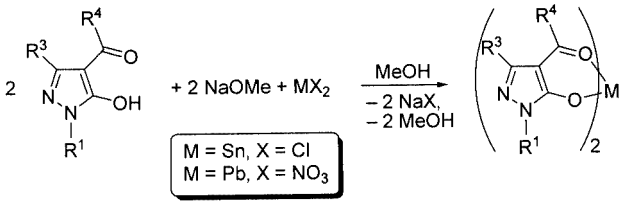

Scheme 1

The infrared spectra of **1**−**15** show the disappearance of the broad band due to intramolecular O−H···O stretching vibration, which is observed in the free HQ proligands in the range 2300−2800 cm^{-1}. Only a small shift to lower frequencies (from about 1620 to about 1600 cm^{-1}) was found for the carbonyl band ν(C=O). In addition, new absorptions were identified in the region 300−500 cm^{-1}, likely due to ν(Sn−O).[30,37,44,45] These features are in accordance with deprotonation of acylpyrazolones and coordination to the tin atom through both oxygen atoms.[46,47]

In the case of derivatives **1**, **2**, **4** and **7**−**15** ^1H and ^{13}C NMR spectra carried out at room temperature show one set of resonances for each magnetically equivalent group of H or C, whereas the ^1H and ^{13}C NMR spectra of **3**, **5** and **6** show three sets of signals due to the three isomers depicted in Figure 2, assuming the tin atom exists in a trigonal-bipyramidal coordination environment. This different behavior is probably due to the steric bulk of Q in derivatives **3**, **5** and **6**, which increases the energetic barrier to interconversion among the three isomers. To confirm this hypothesis we recorded the ^1H NMR spectrum of compound **2** in dichloromethane at 183 K: two broad resonances for each equivalent group of protons emerged, in accordance with a lack of fluxionality at this temperature.

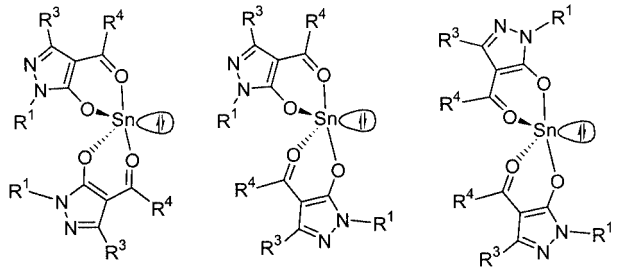

Figure 2. SnQ_2 stereoisomers found in chloroform solution of derivatives **3**, **5** and **6**

The ^{119}Sn NMR spectra of derivatives **1**−**15** show a single resonance in the range from δ = −700 to −775 ppm, typical of tin(II) derivatives with an SnO_4 core.[40,48−50] The presence of only one ^{119}Sn resonance in the case of deriva-

 © 2004 Wiley-VCH Verlag GmbH & Co. KGaA, Weinheim

tives **3**, **5** and **6** seems to indicate that the tin center is not sensitive to changes in the configurational arrangement of the acylpyrazolonate donors. As previously observed, electron-withdrawing groups in the periphery of the acylpyrazolonato donors cause an upfield shift compared to those of electron-releasing ones, because of an increase in the ionic character of Sn−O bonds or, alternatively, to a greater contribution of the tin 5p atomic orbital to the Sn−O molecular orbital. An example is $Sn(Q^F)_2$ (δ = −775.2 ppm) with respect to $Sn(Q^D)_2$ (δ = −701.6 ppm). This allows the tin lone pair to became more concentrated in an orbital having increased 5s character.

We recorded ^{119m}Sn Mössbauer spectra of representative derivatives **1**−**6**, **8**−**12**, **14** and **15** and of six other similar complexes to verify this hypothesis in the solid state (Table 1). Systems containing divalent tin are readily recognized by their high δ values of 3−4 mm·s^{-1}. In fact, the lone pair of the Sn^{2+} ion retains a high 5s character; Sn^{II}−ligand covalent bonds induce a hybridization process having a partial p character leading to the decrease of isomer shift δ value and to moderate quadrupole splitting Δ values, typically 1−2 mm·s^{-1}.[51] The complexes examined by Mössbauer spectroscopy have 1:2 Sn^{II}/ligand stoichiometries and the tin atom, possessing a lone pair, is coordinated to four oxygen atoms from Q^- with formation of a six-membered chelate ring of the type Sn^{II}−O−C=C−C=O→Sn^{II}.[52]

Table 1. Mössbauer data of Sn^{II} complexes

Compound	δ [a][b] [mm·s^{-1}]	Δ [b] [mm·s^{-1}]	$\Gamma\pm$ [b] [mm·s^{-1}]
$Sn(Q^C)_2$ (**1**)	3.14	1.86	0.82
$Sn(Q^T)_2$ (**2**)	3.19	1.85	0.87
$Sn(Q^B)_2$ (**3**)	3.07	1.94	0.80
$Sn(Q^E)_2$ (**4**)	3.33	1.78	0.93
$Sn(Q^W)_2$ (**5**)	3.17	1.83	0.99
$Sn(Q^L)_2$ (**6**)	3.17	1.98	0.77
$Sn(Q^S)_2$ (**8**)	3.24	1.78	0.83
$Sn(Q^N)_2$ (**9**)	3.07	1.87	0.89
$Sn(Q^M)_2$ (**10**)	2.99	1.98	0.81
$Sn(Q^D)_2$ (**11**)	3.29	1.68	0.86
$Sn(Q^P)_2$ (**12**)	3.22	1.94	0.98
$Sn(Q^F)_2$ (**14**)	3.26	1.89	0.87
$Sn(Q^H)_2$ (**15**)	3.36	1.96	0.83
$Sn(Q^{Br})_2$ [c]	3.00	1.85	0.81
$Sn(Q^{R'})_2$ [d]	3.06	1.77	0.77
$Sn(Q^{Me})_2$ [e]	3.13	1.98	0.86
$Sn(Q^{CCl3})_2$ [f]	3.13	1.97	0.95
$Sn(Q^{Ph})_2$ [g]	3.15	1.83	0.89
$Sn(Q^{F'})_2$ [h]	3.26	1.69	0.92

[a] With respect to room-temperature spectrum of $CaSnO_3$. [b] ±0.01 mm·s^{-1}. [c] HQ^{Br} = 4-(*p*-bromophenyl)-3-methyl-1-phenylpyrazol-5-one. [d] $HQ^{R'}$ = 3-methyl-1-phenyl-4-(*p*-tolyl)pyrazol-5-one. [e] HQ^{Me} = 3,4-dimethyl-1-phenylpyrazol-5-one. [f] HQ^{CCl3} = 3-methyl-1-phenyl-4-(trichloroacetyl)pyrazol-5-one. [g] HQ^{Ph} = 3-methyl-1,4-diphenylpyrazol-5-one. [h] $HQ^{F'}$ = 3-methyl-1-phenyl-4-(trifluoroacetyl)pyrazol-5-one.

The variation of the Mössbauer parameter values of isomer shift, δ, and quadrupole splitting, Δ, (Tables 1 and 2) is around 0.37 mm·s^{-1} and 0.30 mm·s^{-1}, respectively, and the $\Gamma\pm$ values indicate that a unique Sn^{II} site is present in the complexes examined. The different R groups in the ligand may cause variations in the δ and Δ parameters: the electron-withdrawing nature of the R groups can influence the polarity of the Sn−O bond and the 5s electron density at the tin nucleus. Moreover, the R substituents can affect steric hindrance giving rise to a greater degree of distortion in the coordination sphere of the tin atom. In any case, the small variation observed may be indicative of the same type of coordination to the Sn^{II} atom. In any case, the small variation observed in the δ values may be indicative of a poor influence of electron-withdrawing groups of acylpyrazolonate donors.

Table 2. δ and Δ ranges in β-oxo enolates of Sn^{II}

Complex	δ	Δ	Ref.
Sn^{II}−Q ligand	2.99−3.36 (0.37)	1.68−1.98 (0.30)	this work
Sn^{II}−acac	2.92−3.60 (0.68)	1.66−2.21 (0.55)	[42]
Sn^{II}−β-oxo enolate	2.91−3.31 (0.40)	1.80−2.25 (0.45)	[43]

By comparing the Mössbauer parameter values with those of parent β-oxo enolates of Sn^{II} [42,43,53] and adopting the fingerprint method as a criterion of inferring structural arrangements (Table 2), a tin complex having four oxygen atoms from two molecules of the ligand in a trigonal-bipyramidal geometry can be assigned, with the lone pair occupying an equatorial site.

Selected positive electrospray MS data of complexes **2**, **5**, **6** and **9** are reported in Table 3. In our case, since only charged species are transferred from solution to the gas phase, quantitative ESI-MS results do not represent the real relative distribution of the species in solution. However, the data seem to indicate that, in solution, these derivatives can undergo loss of the anionic pyrazolonate ligands, which immediately interact with protons or sodium ions, yielding mono-charged species such as $[H_2Q]^+$ or $[Na(HQ)]^+$. The presence of Na adducts is typical of ESI mass spectra, due to the fact that the O-donor immediately interacts and aggregates with the small quantity of alkali metal ions present in the solvents. The possibility of interaction in solution is strongly dependent on the nature of the ligands. In some cases aggregation of Sn and Q in acetonitrile is significant even at 10^{-3} M, with smaller aggregates such as $[Sn(Q)]^+$, $[NaSn(Q)_2]^+$, $[Sn_2(Q)_3]^+$ being dominant over larger adducts. Some minor peaks present in the spectra of **2** and **5** are due to the interaction of the SnQ_2 species with K^+ or H^+. The isotopic distribution of these species is in agreement with the calculated composition.

The absence of ions containing MeCN indicates no binding between the solvent and Sn. In the ESI mass spectra of the same complexes, recorded in the negative detection mode, the predominant peak is always that due to the anionic ligand $[Q]^-$. In some cases, peaks due to association of two $(Q)^-$ ligands with one Na^+ cation were also identified. Interestingly, all spectra exhibit peaks due to $SnCl_3^-$, $Sn(Q)Cl_2^-$, $KSn(Q)Cl_3^-$, and $Sn(Q)_2Cl^-$: all species containing Cl from the solvent.

 © 2004 Wiley-VCH Verlag GmbH & Co. KGaA, Weinheim

Table 3. Selected ESI-MS data for the compounds **2**, **5**, **6**, **9** and **21**−**23**

Compound[a]	FW	H_2Q^+	HQ + Na^+	$(Q)_2M$ + H^+	$(Q)_2M$ + Na^+	$[(Q)_3M_2]^+$	$[SnCl_3]^-$	$(Q)^-$	$SnO(Q)^-$	$SnCl_2Q^-$	$[KSnCl_3Q]^-$
$Sn(Q^T)_2$ (**2**)	661.37	273 [5]	295 [3]	662 [20]	685 [100]	1049 [18]	225 [15]	271 [100]	406 [5]	461 [18]	
$Sn(Q^B)_2$ (**3**)	633.31		281 [100]	634 [15]	656[50]			257 [100]	392 [5]		
$Sn(Q^W)_2$ (**5**)	785.51	334 [5]			786 [60]		225 [75]	333 [100]	467 [60]	523 [60]	592 [50]
$Sn(Q^L)_2$ (**6**)[b]	701.35		315 [10]		724 [5]			291 [100]			
$Sn(Q^S)_2$ (**8**)	853.54	369 [10]	391[100]	854 [10]	876 [5]			367 [100]	502 [45]	557 [15]	
$Sn(Q^N)_2$ (**9**)	763.29		356 [100]		764 [5]			322 [100]	457 [10]		
$Sn(Q^P)_2$ (**12**)	797.44		363 [100]	798 [10]	820 [30]	916 [50]		339 [100]			
$Pb(Q^w)_2$ (**21**)[c]	874.02		357 [100]					333 [100]			
$Pb(Q^D)_2$ (**22**)[d]	513.52					873 [100]		153 [100]			
$Pb(Q^D)_2$(phen) (**23**)[e]	665.72		186 [5]					153 [100]			

[a] Relative intensity in square brackets; FW = calculated molecular weight. [b] A peak at *m/z* = 605 is assigned to the species $[(Q)_2Na]^-$. [c] Other peaks: 691 [20] $[(HQ)_2Na]^+$, 1119 [10] $[(Q)_2Pb_2Cl]^+$, 1771 [100] $[(Q)_4Pb_2Na]^+$. [d] A peak at *m/z* = 360 [30] is assigned to the species $[(Q)Pb]^+$. [e] A peak at *m/z* = 542 [100] is assigned to the species $[(Q)Pb(Phen)]^+$.

The crystal structure of bis{3-methyl-1-phenyl-4-(phenylacetyl)pyrazolon-5-ato}tin(II) (**6**) consists of discrete molecules with no additional interactions besides those due to van der Waals forces. The tin atom lies on a crystallographic twofold axis. Table 4 shows selected bond lengths and angles for this molecule. Each tin atom is bound to four oxygen atoms from the two 4-acyl-5-pyrazolonato ligands (Figure 3). These four oxygen atoms are located on one side of the tin atom due to the presence of a stereochemically active lone pair on the opposite side. Generally, the 4-acyl-5-pyrazolonato ligands form a short metal−O(pyrazolonato) bond compared to the longer metal−O(acyl) bond. This is also the case here as the Sn1−O1 distance is 2.125(7) Å and the Sn1−O2 distance is 2.334(7) Å. The geometry at the tin atom is a distorted trigonal bipyramid with an axial O2−Sn−O52 bond angle of 146.2(3)°; such distortion from 180° is due to the presence of a lone pair and the chelating features of the ligand. The O1−Sn−O51 angle of 89.2(3)° also shows significant deviation from the ideal value of 120° due to the lone pair. This structure is similar to that of bis(4-acetyl-3-methyl-1-phenylpyrazolon-5-ato)tin(II), which has been determined crystallographically both as the pure complex[40] and as a methanol solvate,[54] although neither shows a twofold axis as for **6**. The structural parameters in the coordination sphere of all three structures are similar, as shown in Table 5.

Table 4. Selected bond lengths [Å] and angles [°] for $Sn(Q^L)_2$

Bond lengths	
Sn−O1	2.125(7)
Sn−O2	2.334(7)
O1−C5	1.27(1)
O2−C6	1.25(1)
N1−C5	1.36(1)
N1−C7	1.43(1)
Bond angles	
O2−Sn−O1	80.4(3)
O1−Sn−O1′	89.2(3)
O1−Sn−O2′	75.9(3)
O2−Sn−O2′	146.2(3)
C5−O1−Sn	128.7(5)
C6−O2−Sn	130.3(5)
Torsion angles	
O5−N1−C7−C8	−13.8

The existence of two very different sets of Sn−O bond lengths in "SnO_4" compounds is also observed in other Sn^{II} β-diketonates and is not limited to compounds with asymmetric ligands. An analysis of compounds found in the Cambridge Database is shown in Figure 4. The lower left side of the graph shows the Sn−O(primary) bond and the upper right side shows the Sn−O(secondary) bond. For each "SnO_4" compound the Sn−O(primary) and Sn−O(secondary) bonds are associated with small O(primary)−Sn−O(primary) and wide O(secondary)−Sn−O(secondary) bond angles. The title compound is circled in Figure 4 and fits the trend as well. It is of interest to note the unique species located at the center of the graph — pentane-1,5-diaminium bis(oxalato)tin(II) — the only one showing four equal Sn−O bonds (2.21 Å) and four equal O−Sn−O bond angles (120°).[55]

$Sn(Q^T)_2$ (**2**) reacts with methyl iodide or ethyl iodide to afford $[SnMeI(Q^T)_2]$ (**16**) and $[SnEtI(Q^T)_2]$ (**17**), respectively (Scheme 2). Compounds **16** and **17** are air- and moisture-stable, and soluble in DMSO, acetone, aromatic and chlorohydrocarbon solvents, where they are non-electrolytes. Their IR spectra exhibit new bands in the range 500−600 cm^{-1} due to ν(Sn−C) and below 250 cm^{-1} caused by ν(Sn−I). Their ^1H NMR spectra show a multiplicity of broad resonances in accordance with the presence of several isomers in solution, as previously found for $SnRCl(Q)_2$-type derivatives.[52,56,57] Accordingly, the resonances in the ^{13}C NMR spectra are very broad and in the ^{119}Sn NMR spectra four (**17**) and five absorptions (**16**) are found in the range $\delta = -400$ to -700 ppm.[52,56,57]

 © 2004 Wiley-VCH Verlag GmbH & Co. KGaA, Weinheim

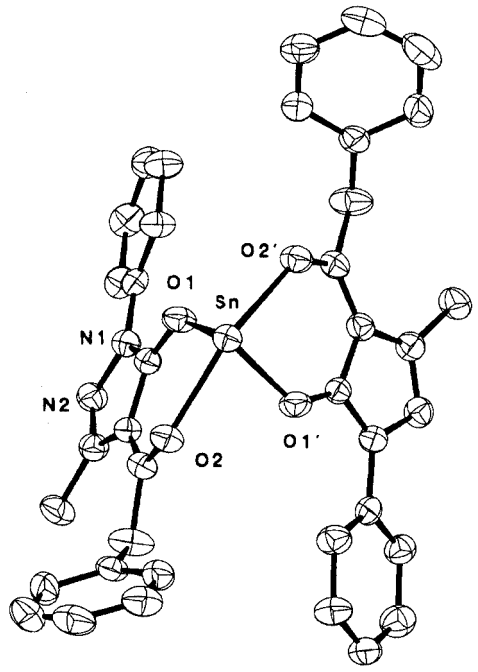

Figure 3. X-ray molecular structure of $Sn(Q^L)_2$ (**6**)

Compound **2** also reacts with $Cr(CO)_6$ in toluene to afford, upon irradiation, the novel derivative $[Cr(CO)_5Sn(Q^T)_2]$ (**18**; Scheme 2). Derivative **18** is the first example of a bis(acylpyrazolonato)tin(II) fragment acting as a Lewis base able to replace a CO ligand by donation of the lone pair to a $Cr(CO)_5$ fragment. This compound is stable in air and soluble in several organic solvents like DMSO, acetone, alcohols, aromatics and chlorohydrocarbons.

The IR spectrum of **18** shows several absorption bands in the metal−carbonyl stretching region at $\tilde{\nu}$ = 2059, 1947 and 1880 cm^{-1}. The second band is more intense than the others, in accordance with "local" C_{4v} symmetry for the $Cr(CO)_5$ fragment.[58] The ν(C=O) band of the acylpyrazolonato undergoes an upfield shift from $\tilde{\nu}$ = 1605 to 1610 cm^{-1} and in the far-IR region the ν(Sn−O) band shows a small downfield shift, indicating a lowering of the Sn−O bond strength.

The ^1H and ^{13}C NMR spectra of derivative **18** show one set of broad resonances, where the acyl fragment is shielded with respect to starting derivative **2**. The observed NMR and IR trends can be ascribed to the presence of back-donation Cr→Sn (*d*→*d*) π-bonding, as previously hypothesized for similar compounds.[59]

Table 5. X-ray structural parameters in the coordination sphere of bis(4-acyl-5-pyrazolon-5-ato)tin(II)

	R^1 = Ph, R^3 = R^4 = Me[40]	R^1 = Ph, R^3 = R^4 = Me; methanol solvate[54]	R^1 = Ph, R^3 = Me, R^4 = CH_2−Ph $Sn(Q^L)_2$ **6** [this work]
Sn−O1	2.141(5)	2.144(6)	2.125(7)
Sn−O2	2.296(6)	2.260(6)	2.334(7)
Sn−O1′	2.133(5)	2.149(7)	2.125(7)
Sn−O2′	2.313(6)	2.365(7)	2.334(7)
O1−Sn−O1′	86.7(2)	91.1(2)	89.2(3)
O2−Sn−O2′	149.8(2)	145.3(2)	146.2(3)

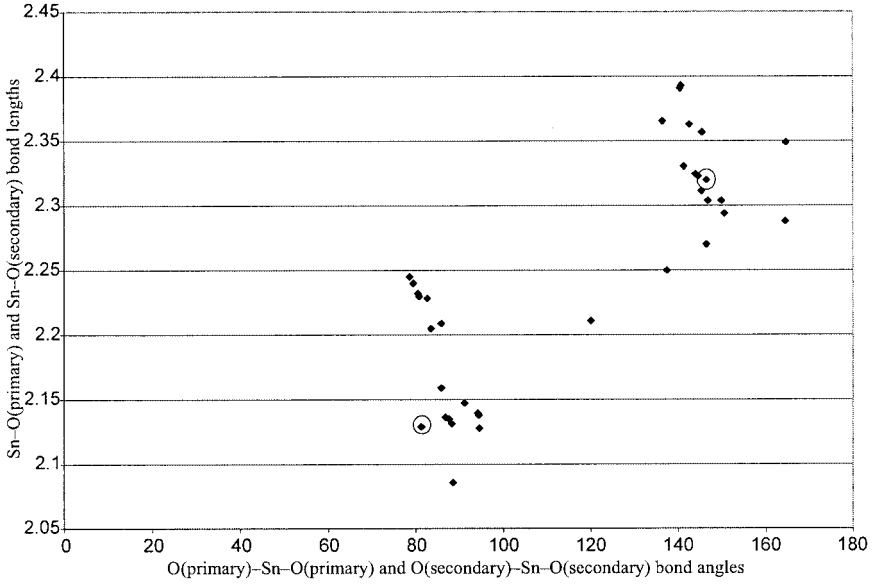

Figure 4. Selected structural parameters in "SnO_4" compounds

 © 2004 Wiley-VCH Verlag GmbH & Co. KGaA, Weinheim

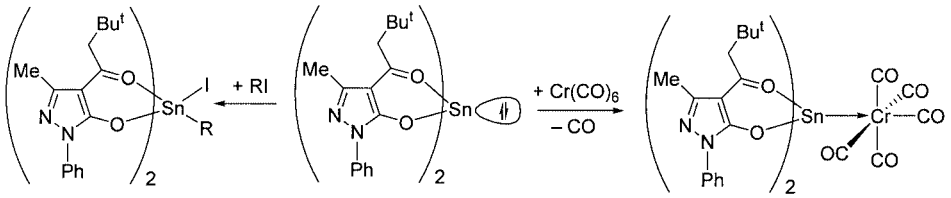

16 R = Me
17 R = Et

18

Scheme 2

By interaction of selected HQ proligands (HQ = HQ^B, HQ^T, HQ^W, HQ^D) with lead(II) nitrate in methanol, and in the presence of sodium methoxide, the air- and moisture-stable derivatives PbQ_2 **19**–**22** formed as precipitates (Scheme 1). They are pale-yellow solids with sharp melting points, soluble in DMSO, acetone and chlorohydrocarbon solvents, where they are non-electrolytes. Molecular weight determinations carried out in chloroform suggest aggregation in solution, as the experimental molecular weight is always higher than that expected for monomeric compounds. This observation is supported by the crystallographic results described below.

The IR and NMR spectra have features similar to those found in the tin(II) species. Interestingly, the number of signals and the chemical shift at room temperature do not seem to depend on the nature of the metal. However the low-temperature ^{1}H NMR spectrum of **20** suggests that there is no fluxionality at 183 K, as three sharp signals are seen for each equivalent group of protons.

The reactivity of derivative Pb(Q^D)$_2$ (**22**) was tested toward 1,10-phenanthroline, giving **23**. The ^{1}H NMR spectrum of **23** shows all the expected resonances for phen and for the pyrazolone protons in a 1:2 ratio. The ^{13}C NMR spectrum further confirms the existence and stability of compound **23** in chlorohydrocarbon solution, with no evidence of dissociation for either Q^D and phen ligands. However, the crystalline stability of **23** is lower than that of **19**–**22**. In fact, it has no sharp melting point and its decomposition starts at 156 °C, in accordance with a weak interaction of the {Pb(Q^D)$_2$} moiety with phen, probably due to the presence of the lead(II) lone pair.

Attempts to synthesize phen derivatives of lead(II) and tin(II) with other acylpyrazolonates failed, even under extreme reaction conditions, such as prolonged stirring and warming. Since these acylpyrazolonates contain bulky R^1 and R^4 groups (different from methyl in Q^D) we conclude that steric factors explain such a difference.

The ESI mass spectra of **21** and **22** exhibit peaks not only due to [H$_2$Q]$^+$ and [Na(HQ)]$^+$, but also due to [Pb(HQ)$_2$Cl]$^+$ and [NaPb$_2$(Q)$_4$]$^+$ species. The latter is particularly interesting since it suggests the possibility of aggregation between two different mononuclear lead species in solution. More surprisingly, the ESI mass spectrum of **23** exhibits a peak due to [Pb(Q)(phen)]$^+$, which is indicative of a strong interaction between Pb(Q)$_2$ and phen.

Table 6. Selected bond lengths [Å] and angles [°] for Pb(Q^B)$_2$

Bond lengths	
Pb–O1	2.274(6)
Pb–O2	2.56(1)
Pb–O51	2.324(7)
Pb–O52	2.38(1)
Pb–N2′	2.961(8)
Pb–O51′′	3.055(7)
O1–C5	1.29(1)
O2–C6	1.23(1)
O51–C55	1.27(1)
O52–C56	1.23(1)
N1–C5	1.37(1)
N1–C7	1.42(1)
N51–C55	1.36(1)
N51–C57	1.42(2)
Bond angles	
O2–Pb–O1	72.1(3)
O51–Pb–O1	82.1(2)
O51–Pb–O2	143.7(4)
O52–Pb–O1	86.6(3)
O52–Pb–O2	80.8(3)
O52–Pb–O51	72.4(3)
O1–Pb–O51′′	157.8(2)
O2–Pb–O51′′	112.1(4)
O51–Pb–O51′′	83.4(3)
O1–Pb–N2′	81.4(2)
O2–Pb–N2′	107.3(2)
O51–Pb–N2′	72.4(2)
O51′′–Pb–N2′	116.1(2)
O52–Pb–N2′	162.4(3)
C5–O1–Pb	118.6(5)
C6–O2–Pb	131.3(7)
C55–O51–Pb	127.5(7)
C56–O52–Pb	137.6(6)
Torsion angles	
O1–N1–C7–C12	–23.4.
O51–N51–C57–C62	48.9

A crystallographic study of bis(3-methyl-1-phenyl-4-pivaloylpyrazolon-5-ato)lead(II), Pb(Q^B)$_2$ (**19**), shows no imposed symmetry (Figure 5). Table 6 shows selected structural data for this species. Similar to the tin compound **6**, each metal atom is bound to four oxygen atoms from the two Q^B ligands. The general pattern seen in metal 4-acyl-5-pyrazolonate compounds is also followed as the

 © 2004 Wiley-VCH Verlag GmbH & Co. KGaA, Weinheim

Pb1−O1[O51](pyrazolonato) bond length is 2.274(6) Å [2.324(7) Å] and the Pb1−O2[O52](acyl) bond length is 2.56(1) Å [2.38(1) Å]; that is, the former is shorter. Both Q^B ligands are in a *syn* configuration — equivalent ligand substituents (for instance R^1 = Ph) are on the same side, whereas in the tin compound **6** they are opposite (*anti* configuration).

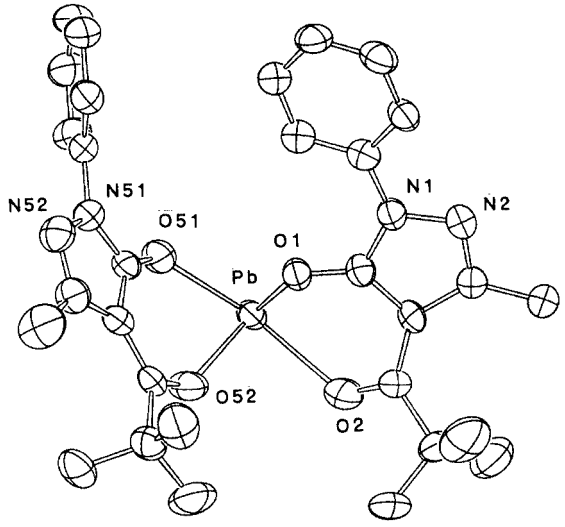

Figure 5. Atomic arrangement of the moiety $Pb(Q^B)_2$ (**19**)

The four oxygen atoms are located on one side of the lead atom, suggesting the presence of a stereochemically active lone pair as for **6**. However, unlike compound **6**, there are two additional atoms bound to the metal atom: N2′ [Pb1−N2′ = 2.961(8) Å], which belongs to the neighboring crystallographic unit (−*x*, −*y* + 2, −*z* + 1), and O51′′ [Pb1−O51′′ = 3.055(7) Å] of the unit (−*x* + 1, −*y* + 2, −*z* + 1; see Figure 6). These lead interactions suggest the metal coordination number to be six with a distorted octahedral geometry, because of departure from ideal *cis* angles of 90° [range from 72.1(3)° (O1−Pb1−O2) to 116.1(2)° (N2′−Pb1−O51′′)]. The latter wide *cis* bond angle and the corresponding long Pb−N2′ and Pb−O51′′ lengths indicate the presence of a stereochemically active lone pair in that area. Another factor contributing to octahedral distortion is the bent chelate ring (containing O1 and O2) that allows its attached pyrazole ring to stack with the pyrazole ring linked to another unit (of O1′ and O2′) at about 3.6 Å.

The linear polymeric structure propagates along the *a* axis in *anti*-parallel chains, and the hydrophobic region is located near the central area of the unit cell.

Bis(4-*tert*-butyl-3-methyl-1-phenylacetylpyrazolon-5-ato)lead(II), $Pb(Q^T)_2$ (**20**), was also studied using X-ray crystallographic methods (Figure 7) and shows no imposed symmetry on the molecular structure. Selected bond lengths and angles can be found in Table 7. As in compound **19**, a number of intermolecular interactions contribute to make the geometry of the lead atom distorted octahedral (Figure 8). They are different than in **19** and involve the nitrogen atom of one unit [Pb−N2′ = 3.121(6) Å] and a phenyl ring of another unit, with Pb−C bond lengths in the range 3.57−3.70 Å. The latter interaction is similar to that of bis(tetraphenyldithioimidodiphosphinato)lead(II), where the Pb−phenyl ring distances are in the range 3.07−3.31 Å.[60]

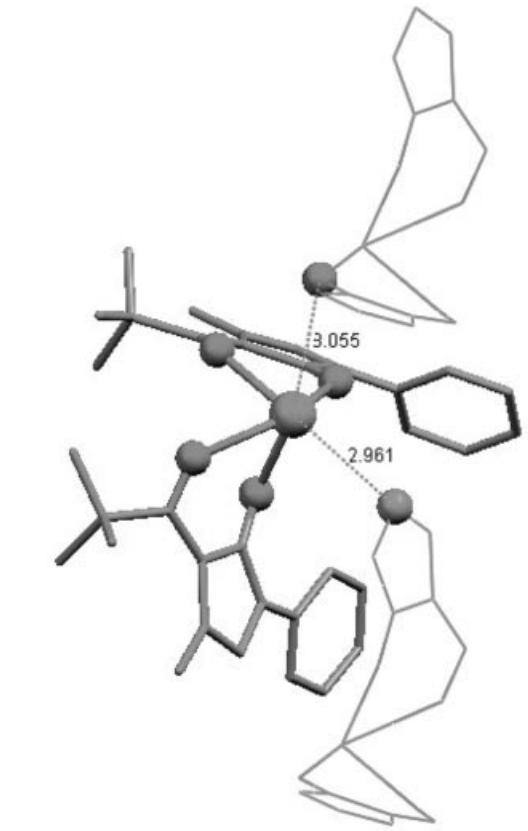

Figure 6. Whole coordination sphere for the polymeric chain of $Pb(Q^B)_2$ (**19**); Pb and its 6 bound atoms are depicted in ball-and-stick style, the 2 Q^B ligands bound at short distances as capped stick (shown also in Figure 5), and the 2 ligands bound at longer distances as wire frame [Pb−N2′ = 2.961(8) Å and Pb−O51′′ = 3.055(7) Å]

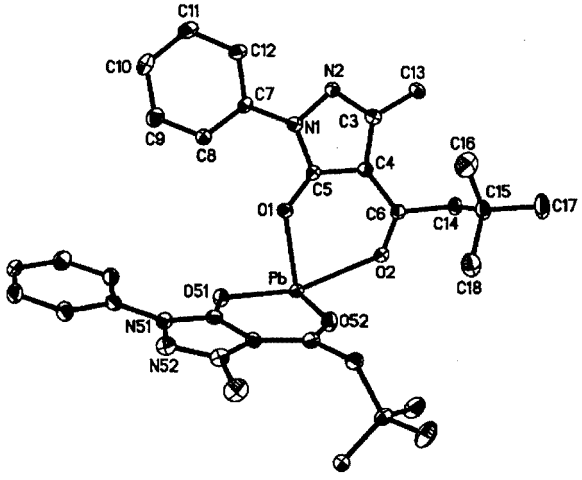

Figure 7. Atomic arrangement of the moiety $Pb(Q^T)_2$ (**20**)

 © 2004 Wiley-VCH Verlag GmbH & Co. KGaA, Weinheim

A similar interaction is present in $[Pb(1,2\text{-}C_6H_4Me_2)_2\text{-}(AlCl_4)_2]$ where the Pb−C(phenyl) distances are in the range 3.30−4.48 Å.[61] Therefore, compound **20** shows the best η^6-Pb−phenyl interaction.

Tsble 7. Selected bond lengths [Å] and angles [°] for $Pb(Q^T)_2$

Bond lengths	
Pb−O1	2.379(9)
Pb−O2	2.360(8)
Pb−O51	2.280(7)
Pb−O52	2.458(7)
Pb−N2′	3.121(6)
Pb−C7′′	3.698(7)
Pb−C8′′	3.656(8)
Pb−C9′′	3.595(8)
Pb−C10′′	3.573(8)
Pb−C11′′	3.599(8)
Pb−C12′′	3.665(8)
O1−C5	1.26(1)
O2−C6	1.25(2)
O51−C55	1.28(1)
O52−C56	1.24(1)
N1−C5	1.36(2)
N1−C7	1.40(1)
N2−C3	1.30(1)
N51−C55	1.37(1)
N51−C57	1.41(1)
N52−C53	1.32(1)
Bond angles	
O2−Pb−O1	76.2(3)
O51−Pb−O1	139.7(3)
O51−Pb−O2	77.2(3)
O52−Pb−O1	76.6(3)
O52−Pb−O2	93.3(3)
O52−Pb−O51	75.3(2)
C5−O1−Pb	128.6(5)
C6−O2−Pb	137.1(5)
C55−O51−Pb	126.4(6)
C56−O52−Pb	133.4(5)
Torsion angles	
C5−N1−C7−C8	−0.5.
C55−N51−C57−C62	−7.2

As mentioned previously, 4-acyl-5-pyrazolonato ligands typically form a short metal−O(pyrazolonato) bond and a long metal−O(acyl) bond. In $Pb(Q^T)_2$ one ligand is consistent with this pattern as the Pb−O51(pyrazolonato) bond is 2.280(7) Å and the Pb−O52(acyl) bond is 2.458(7) Å. However, the other ligand is not since the Pb−O1(pyrazolonato) bond of 2.379(9) Å is longer than the Pb−O2(acyl) bond of 2.360(8) Å. This longer Pb−O(pyrazolonato) bond can be explained as this ligand contains the phenyl ring that interacts with the lead atom in a neighboring unit.

An investigation of "PbO_4" complexes in the CSD database shows that they have different packing arrangements with neighboring molecules in the solid. Only one "PbO_4" species, bis(dipivaloylmethanato)lead(II), has no interactions with the neighboring units, much like the "SnO_4" compounds described above, with both chelating ligands on the lead atom bent away from the stereochemically active lone pair.[62][63] The two bulky *t*Bu substituents on the symmetrical β-diketonato ligand probably prevent Pb from having a high coordination number. In general, the intermolecular interactions seen in other "PbO_4" compounds are not found in the similar "SnO_4" species. This is presumably due to the larger covalent radius of Pb allowing for a higher coordination number. Lead commonly interacts with nitrogen and oxygen ligands. For instance, the lead atom in bis(4-butanoyl-3-methyl-1-phenylpyrazolonato)lead(II), besides covalent bonds to the four oxygen atoms of the two chelating ligands, shows intermolecular interactions with lone pairs from two N atoms of neighboring units.[64] This interaction gives the lead atom a distorted octahedral geometry and allows for the molecules in the crystal to arrange in a polymeric chain. Another example is in *catena*-[bis(μ_2-1,1,1-trifluoro-5,5-dimethylhexane-2,4-dionato-*O*,*O*′)lead(II), where each Pb atom interacts with two oxygen atoms from neighboring units,[65] leading to a "PbO_6" system. The structure of bis(4-acetyl-3-methyl-1-phenylpyrazolon-5-ato)lead(II) is a trinuclear species that contains intermolecular interactions with two nitrogen atoms from a second ligand, and one oxygen atom from a third ligand.[64] Another variation is the formation of dinuclear compounds instead of polynuclear chains, as in bis(2,2-dimethyl-6,6,7,7,8,8-heptafluorooctane-3,5-dionato)lead(II) where the lead atoms stabilize a skewed geometry.[63]

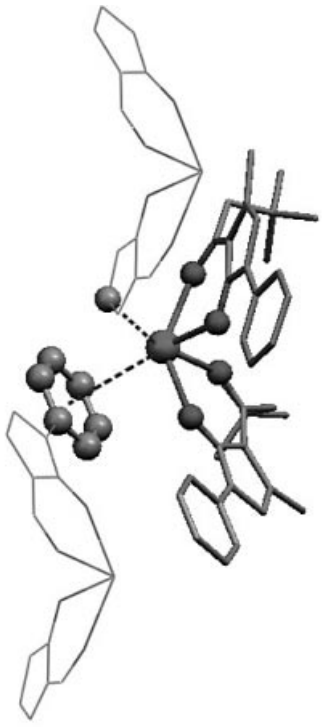

Figure 8. Whole coordination sphere for the polymeric chain of $Pb(Q^T)_2$ (**20**); Pb and its bound atoms are depicted in ball-and-stick style, the 2 Q^T ligands bound at short distances as capped stick (also shown in Figure 7), and the 2 ligands bound at longer distances as wire frame [Pb−N2′ = 3.121(6) Å and Pb−Ph′′ range = 3.55−3.70 Å]

 © 2004 Wiley-VCH Verlag GmbH & Co. KGaA, Weinheim

In summary, Pb compounds **19** and **20** both contain a lead atom having coordination number 6 and interacting with atoms in neighboring units. Compound **19** is novel because this chain-like structure has a central PbQ_2 unit interacting on one side with a nitrogen atom from a second unit, and on the other side with an oxygen atom from a third unit; compound **20** shows an intermolecular interaction between the lead atom and all six C atoms of a phenyl ring.

Conclusion

4-Acyl-5-pyrazolones, HQ, form MQ_2 compounds for M = Sn^{II} and Pb^{II} that differ markedly in their structural features. Both Q ligands have an *anti* configuration on the tin atom and *syn* configuration on the lead atom. The tin compounds are mononuclear and have a trigonal-bipyramidal metal geometry, distorted by the metal lone pair located in the equatorial plane. The lead compounds show an increased coordination number, forming polynuclear compounds of varied structure. In this work a Pb−arene interaction has been found in $Pb(Q^T)_2$, whereas there is no such interaction in $Pb(Q^B)_2$. Such a dramatic structural change probably arises due to steric reasons, as the addition of a CH_2 moiety in the peripheral area of the Q^B acyl group makes this ligand equal to Q^T.

Ligand substitution is important if additional ligands are to be included in the coordination sphere of lead(II). Thus, the only PbQ_2 derivative able to react with phen is with Q = Q^D, a ligand containing R^1 = Me, in contrast with those that are not reactive and having R^1 = Ph.

The lone pair in SnQ_2 derivatives can be donated to, for instance, carbonylchromium derivatives stabilizing a Cr−Sn bond.

Experimental Section

General Remarks: 3-Methyl-1-phenylpyrazolon-5-one, *N*-methylhydrazine, *N*-(4-nitrophenyl)hydrazine, ethyl acetoacetate, ethyl benzoyl acetate, potassium hydroxide, sodium methoxide, tin(II) dichloride and the acyl chlorides employed (benzoyl chloride, acetyl chloride, cyclohexanecarbonyl chloride, pivaloyl chloride, *tert*-butylacetyl chloride, phenylacetyl chloride, diphenylacetyl chloride, propionyl chloride, ethanoyl chloride, 4-*tert*-butylbenzoyl chloride) were purchased from Aldrich (Milwaukee) and used as received. Solvent evaporations were always carried out under vacuum by using a rotary evaporator. The samples for microanalysis were dried in vacuo to constant weight (20 °C, ca. 0.1 Torr). All syntheses were carried out under nitrogen. Hydrocarbon solvents were dried by distillation from sodium/potassium; dichloromethane was distilled from calcium hydride. All solvents were degassed with dry nitrogen prior to use. Elemental analyses (C, H, N) were performed in-house with a Fisons Instruments 1108 CHNS-O Elemental Analyser. IR spectra were recorded from 4000 to 200 cm^{-1} with a Perkin−Elmer System 2000 FT-IR instrument. ^1H, $^{13}C\{^1H\}$, $^{19}F\{^1H\}$ and $^{119}Sn\{^1H\}$ NMR spectra were recorded with a VXR-300 Varian instrument (300 MHz for ^1H, 75 MHz for ^{13}C, 282.2 MHz for ^{19}F and 111.8 MHz for ^{119}Sn). The chemical shifts (δ) are reported in parts per million (ppm) from $SiMe_4$ (^1H and ^{13}C), $CFCl_3$ (^{19}F) or $SnMe_4$ (^{119}Sn); relative intensity (%) in square brackets. Melting points are uncorrected and were measured with an SMP3 Stuart scientific instrument and with a capillary apparatus. The electrical conductivity measurements (Λ_m, reported as $\Omega^{-1}\cdot cm^2\cdot mol^{-1}$) of dichloromethane or DMSO solutions of complexes **1**−**23** were recorded with a Crison CDTM 522 conductimeter at room temperature. Molecular weight determinations (MW) were performed at 40 °C with a Knauer KNA0280 vapour pressure osmometer calibrated with benzil; the solvent was Baker Analysed Spectrophotometric grade chloroform. The results were reproducible to ±2%. ^{119m}Sn Mössbauer spectra were recorded on solid samples at liquid nitrogen temperature by using a conventional constant acceleration spectrometer, coupled with a multichannel analyser [a.e.n., Ponteranica (BG), Italy] equipped with a cryostat Cryo (RIAL, Parma, Italy). A $Ca^{119}SnO_3$ Mössbauer source, 10 mCi (from Ritverc, St. Petersburg, Russia) moving at room temperature with constant acceleration in a triangular waveform was used. The velocity calibration was made using a ^{57}Co Mössbauer source, 10 mCi, and an iron foil as absorber (from Ritverc, St. Petersburg, Russia). The 4-acyl-5-pyrazolones (here indicated as QH) were synthesized by the procedure reported by Jensen[66] or by our previous methods.[30−40]

$Sn(Q^C)_2$ (1): Potassium hydroxide (0.112 g, 2.0 mmol) and tin(II) dichloride (0.190 g, 1 mmol) were added to a methanol solution (30 mL) of Q^CH (0.566 g, 2 mmol). A colorless precipitate formed immediately. After 1 h, it was filtered off, washed with methanol (10 mL) and recrystallized from chloroform/methanol. Yield 0.603 g (88%). M.p. 166−169 °C. $C_{34}H_{38}N_4O_4Sn$ (685.4): calcd. C 59.58, H 5.59, N 8.17; found C 59.33, H 5.83, N 8.23. Λ_m (CH_2Cl_2, 1 × 10^{-3} M) = 0.1. MW ($CHCl_3$, c = 1.5 × 10^{-3} mol/L): 668. IR (nujol): $\tilde{\nu}$ = 1604 vs, 1593 vs ν(C=O), 451 s, 399 s ν(Sn−O) cm^{-1}. ^1H NMR ($CDCl_3$): δ = 1.20−1.90 (m), 2.78 [t, 11 H, C(=O)-C_6H_{11}], 2.28 (s, 3 H, 3-CH_3), 7.15 (t), 7.38 (t), 7.72 (d, 5 H, NC_6H_5) ppm. ^{13}C NMR ($CDCl_3$): δ = 17.1 (s, 3-CH_3), 26.0, 26.1, 29.7, 46.6 [s, C(=O)C_6H_{11}], 103.9 (s, C-4), 121.5, 125.8, 128.7, 138.2 (s, C_{arom}), 148.1 (s, C-3), 161.6 (s, C-5), 199.9 (s, CO) ppm. ^{119}Sn NMR ($CDCl_3$): δ = −727.5 ppm.

$Sn(Q^T)_2$ (2): Compound **2** was synthesized as described for compound **1**. Yield 0.622 g (94%). M.p. 140−142 °C. $C_{32}H_{38}N_4O_4Sn$ (661.4): calcd. C 58.11, H 5.79, N 8.47; found C 58.25, H 5.65, N 8.49. Λ_m (CH_2Cl_2, 1 × 10^{-3} M) = 0.2. MW ($CHCl_3$, c = 1.6 × 10^{-3} mol/L): 659. IR (nujol): $\tilde{\nu}$ = 1605 vs, 1593 vs ν(C=O), 452 s, 439 s, 391 s ν(Sn−O) cm^{-1}. ^1H NMR ($CDCl_3$, 293 K): δ = 1.05 [s, 9 H, C(=O)$CH_2C(CH_3)_3$], 2.27 (s, 3 H, 3-CH_3), 2.50 [s, 2 H, C(=O)$CH_2C(CH_3)_3$], 7.18 (t), 7.33 (t), 7.75 (d, 5 H, NC_6H_5) ppm. ^1H NMR (CD_2Cl_2, 183 K): δ = 0.93 [br. s, 9 H, C(=O)-$CH_2C(CH_3)_3$], 1.92 (br. s), 2.21 (br. s, 3 H, 3-CH_3), 2.40 (br. s), 2.56 [br. s, 2 H, C(=O)$CH_2C(CH_3)_3$], 7.15 (br. t), 7.33 (br. t), 7.67 (br. d, 5 H, NC_6H_5) ppm. ^{13}C NMR ($CDCl_3$): δ = 17.8 (s, 3-CH_3), 30.2 [s, C(=O)$CH_2C(CH_3)_3$], 32.1 [s, C(=O)$CH_2C(CH_3)_3$], 50.6 [s, C(=O)$CH_2C(CH_3)_3$], 106.4, (s, C-4), 121.1, 125.6, 128.6, 138.0 (s, C_{arom}), 148.2 (s, C-3), 161.2 (s, C-5), 195.8 (s, CO) ppm. ^{119}Sn NMR ($CDCl_3$): δ = −726.9 ppm.

$Sn(Q^B)_2$ (3): Compound **3** was synthesized as described for compound **1**. Yield 0.430 g (68%). M.p. 198−200 °C. $C_{30}H_{34}N_4O_4Sn$ (633.3): calcd. C 56.90, H 5.41, N 8.85; found C 56.58, H 5.50, N 8.61. Λ_m (CH_2Cl_2, 1 × 10^{-3} M) = 0.6. MW ($CHCl_3$, c = 1.6 × 10^{-3} mol/L): 594. IR (nujol): $\tilde{\nu}$ = 1602 vs, 1595 vs ν(C=O), 475 vs, 446 s, 411 m ν(Sn−O) cm^{-1}. ^1H NMR ($CDCl_3$): δ = 1.25 (s) [24], 1.39 (s) [2], 1.58 (s) [1] [9 H, C(=O)C(CH_3)$_3$], 2.40 (s) [24], 2.65 (s) [2], 2.72 (s) [1] (3 H, 3-CH_3), 7.16 (t), 7.30 (t), 7.45 (t), 7.73 (d), 7.85 (d, 5 H, NC_6H_5) ppm. ^{13}C NMR ($CDCl_3$): δ = 20.2 (s, 3-

CH_3), 26.9 [s, C(=O)*C*(CH_3)$_3$], 27.9 [s, C(=O)C(*C*H_3)$_3$], 104.0, (s, C-4), 121.0 (*), 121.3, 125.6, 126.6 (*), 128.5, 129.0 (*), 135.8 (*), 138.1 (s, C_{arom}), 145.7 (s, C-3), 162.1 (s, C-5), 195.7 (s, CO) ppm. ^{119}Sn NMR ($CDCl_3$): δ = −754.4 ppm.

Sn(Q^E)$_2$ (4): Compound **4** was synthesized as described for compound **1**. Yield 0.500 g (87%). M.p. 152−154 °C. $C_{26}H_{24}N_4O_4Sn$ (575.2): calcd. C 54.29, H 4.21, N 9.74; found C 54.10, H 4.15, N 9.63. Λ_m (CH_2Cl_2, 1 × 10^{-3} M) = 0.1. MW ($CHCl_3$, c = 1.9 × 10^{-3} mol/L): 560. IR (nujol): $\tilde{\nu}$ = 1601 vs ν(C=O), 445 m, 426 s, 387 s ν(Sn−O) cm^{-1}. ^{1}H NMR ($CDCl_3$): δ = 1.20 [t, 3 H, C(=O)-CH_2CH_3], 2.51 [q, 2 H, C(=O)CH_2CH$_3$), 2.16 (s, 3 H, 3-CH_3), 7.16 (t), 7.31 (t), 7.69 (d, 5 H, NC_6H_5) ppm. ^{13}C NMR ($CDCl_3$): δ = 8.63 [s, C(=O)CH_2CH_3], 17.1 (s, 3-CH_3), 32.6 [s, C(=O)-*C*H_2CH_3], 104.4, (s, C-4), 121.0, 125.6, 128.5, 138.0 (s, C_{arom}), 148.2 (s, C-3), 160.7 (s, C-5), 197.1 (s, CO) ppm. ^{119}Sn NMR ($CDCl_3$): δ = −723.4 ppm.

Sn(Q^W)$_2$ (5): Compound **5** was synthesized as described for compound **1**. Yield 0.495 g (63%). M.p. 229−231 °C. $C_{42}H_{42}N_4O_4Sn$ (785.5): calcd. C 64.22, H 5.39, N 7.13; found C 63.91, H 5.53, N 7.06. Λ_m (CH_2Cl_2, 1 × 10^{-3} M) = 0.4. MW ($CHCl_3$, c = 1.4 × 10^{-3} mol/L): 743. IR (nujol): $\tilde{\nu}$ = 1599 vs, 1592 vs ν(C=O), 436 m, 383 s ν(Sn−O) cm^{-1}. ^{1}H NMR ($CDCl_3$): δ = 1.32 (s) [2], 1.38 (s) [10], 1.40 (s) [1] [9 H, C(=O)C_6H_5C(CH_3)$_3$], 1.72 (s) [10], 1.96 (s) [2], 2.05 (s) [1] (3 H, 3-CH_3), 7.14 (t), 7.18 (t), 7.35−7.60 (m), 7.75 (d), 7.79 (d), 7.97 [d, 9 H, NC_6H_5 and C(=O)C_6H_5C(CH_3)$_3$] ppm. ^{13}C NMR ($CDCl_3$): δ = 16.3, 16.5 (s, 3-CH_3), 31.1, 31.2 [s, C(=O)C_6H_5C(*C*H_3)$_3$], 35.1 [s, C(=O)C_6H_5*C*(CH$_3$)$_3$], 120.7, 120.8, 121.7, 121.8, 125.1, 125.3, 125.4, 126.5, 127.2, 128.0, 128.3, 128.6, 128.7, 128.8, 128.9, 129.1, 129.5, 136.2, 137.9 (s, C_{arom}), 149.0 (s, C-3), 155.2 (s, C-5) ppm; C-4 and CO signals not observed. ^{119}Sn NMR ($CDCl_3$): δ = −759.4 ppm.

Sn(Q^L)$_2$ (6): Compound **6** was synthesized as described for compound **1**. Yield 0.687 g (98%). M.p. 185−187 °C. $C_{36}H_{30}N_4O_4Sn$ (701.3): calcd. C 61.65, H 4.31, N 7.99; found C 61.45, H 4.42, N 7.82. Λ_m (CH_2Cl_2, 1 × 10^{-3} M) = 0.2. MW ($CHCl_3$, c = 1.5 × 10^{-3} mol/L): 688. IR (nujol): $\tilde{\nu}$ = 1604 vs, 1590 vs ν(C=O), 441 m, 433 m, 390 m ν(Sn−O) cm^{-1}. ^{1}H NMR ($CDCl_3$): δ = 2.18 (s) [1], 2.24 (s) [6], 2.51 (s) [2] (3 H, 3-CH_3), 3.50 (s) [1], 3.78 (s) [6], 4.05 (s) [1] [2 H, C(=O)C$H_2C_6H_5$], 6.95 (t), 7.02−7.45 (m), 7.48 (t), 7.75 (d), 7.83 [d, 10 H, NC_6H_5 and C(=O)$CH_2C_6H_5$] ppm. ^{13}C NMR ($CDCl_3$): δ = 15.8, 16.9, 17.1 (s, 3-CH_3), 43.9, 44.2, 45.0 [s, C(=O)C$H_2C_6H_5$], 103.8, 104.8 (s, C-4), 120.6, 120.9, 121.3, 121.5, 125.5, 126.6, 126.9, 127.1, 128.1, 128.3, 128.4, 128.8, 129.0, 129.1, 132.5, 133.1, 134.2, 136.3, 137.7 (s, C_{arom}), 148.0, 148.8 (s, C-3), 161.1 (s, C-5), 192.9, 193.1 (s, CO) ppm. ^{119}Sn NMR ($CDCl_3$): δ = −738.6 ppm.

Sn(Q^R)$_2$ (7): Compound **7** was synthesized as described for compound **1**. Yield 0.678 g (78%). M.p. 157−160 °C. $C_{48}H_{54}N_4O_4Sn$ (869.7): calcd. C 66.29, H 6.26, N 6.44; found C 65.96, H 6.33, N 6.37. Λ_m (CH_2Cl_2, 1 × 10^{-3} M) = 0.4. MW ($CHCl_3$, c = 1.5 × 10^{-3} mol/L): 855. IR (nujol): $\tilde{\nu}$ = 1605 vs, 1583 s ν(C=O), 447 vs, 409 w, 387 m ν(Sn−O) cm^{-1}. ^{1}H NMR ($CDCl_3$): δ = 0.88 [t, 3 H, C(=O)C_6H_4(CH$_2$)$_6$CH_3], 1.25−1.40 (m), 1.60 (m), 2.67 [t, 12 H, C(=O)C_6H_4(CH_2)$_6$CH$_3$], 1.65 (s, 3 H, 3-CH_3), 7.08 (t), 7.17 (t), 7.23 (d), 7.37 (d), 7.75 [d, 10 H, NC_6H_5 and C(=O)-C_6H_4(CH$_2$)$_6$CH$_3$] ppm. ^{13}C NMR ($CDCl_3$): δ = 14.1 [s, C(=O)-C_6H_4(CH$_2$)$_6$*C*H$_3$], 16.2 (s, 3-CH_3), 22.6, 29.1, 29.2, 31.2, 31.8, 36.0 [s, C(=O)C_6H_4(*C*H$_2$)$_6$CH$_3$], 105.5 (s, C-4), 120.8, 125.5, 128.2, 128.4, 128.6, 136.4, 138.0, 147.0 (s, C_{arom}), 149.1 (s, C-3), 161.8 (s, C-5), 191.2 (s, CO) ppm. ^{119}Sn NMR ($CDCl_3$): δ = −757.6 ppm.

Sn(Q^S)$_2$ (8): Compound **8** was synthesized as described for compound **1**. Yield 0.495 g (58%). M.p. 78−79 °C. $C_{48}H_{38}N_4O_4Sn$ (853.5): calcd. C 67.55, H 4.49, N 6.56; found C 67.12, H 4.50, N 6.48. Λ_m (CH_2Cl_2, 1 × 10^{-3} M) = 0.8. MW ($CHCl_3$, c = 1.5 × 10^{-3} mol/L): 812. IR (nujol): $\tilde{\nu}$ = 1610 vs, 1595 vs ν(C=O), 435 m, 426 m, 397 m ν(Sn−O) cm^{-1}. ^{1}H NMR ($CDCl_3$): δ = 2.40 (s, 3 H, 3-CH_3), 5.63 [s, 1 H, C(=O)C*H*(C_6H_5)$_2$], 7.10−7.32 (m), 7.74 [d, 15 H, NC_6H_5 and C(=O)CH(C_6H_5)$_2$] ppm. ^{13}C NMR ($CDCl_3$): δ = 17.5 (s, 3-CH_3), 58.4 [s, C(=O)*C*H(C_6H_5)$_2$], 105.9 (s, C-4), 121.2, 125.8, 127.0, 127.5, 127.7, 127.9, 128.5, 128.7, 129.2, 129.7, 129.8, 137.9, 139.1 (s, C_{arom}), 148.0 (s, C-3), 162.2 (s, C-5), 193.2 (s, CO) ppm. ^{119}Sn NMR ($CDCl_3$): δ = −747.0 ppm.

Sn(Q^N)$_2$ (9): Compound **9** was synthesized as described for compound **1**. Yield 0.580 g (76%). M.p. > 350 °C. $C_{34}H_{24}N_6O_8Sn$ (763.2): calcd. C 53.50, H 3.17, N 11.01; found C 53.09, H 3.10, N 10.72. Λ_m (CH_2Cl_2, 1 × 10^{-3} M) = 0.2. MW ($CHCl_3$, c = 0.8 × 10^{-3} mol/L): 725. IR (nujol): $\tilde{\nu}$ = 1606 vs, 1589 s ν(C=O), 446 m, 433 m, 408 m ν(Sn−O) cm^{-1}. ^{1}H NMR ($CDCl_3$): δ = 21.72 (s, 3 H, 3-CH_3), 7.51 (d), 7.63 (m), 7.96−8.15 [m, 9 H, $NC_6H_4NO_2$ and C(=O)C_6H_5] ppm. ^{13}C NMR ($CDCl_3$): δ = 16.3 (s, 3-CH_3), 103.4, (s, C-4), 119.4, 119.7, 124.4, 124.9, 128.2, 128.4, 128.5, 132.4 (s, C_{arom}) ppm; signals of C-3, C-5 and CO not observed. ^{119}Sn NMR ($CDCl_3$): δ = −789.5 ppm.

Sn(Q^M)$_2$ (10): Compound **10** was synthesized as described for compound **1**. Yield 0.351 g (64%). M.p. 165−168 °C. $C_{24}H_{22}N_4O_4Sn$ (549.1): calcd. C 52.49, H 4.04, N 10.20; found C 52.07, H 4.08, N 10.02. Λ_m (CH_2Cl_2, 1 × 10^{-3} M) = 0.2. MW ($CHCl_3$, c = 1.5 × 10^{-3} mol/L): 542. IR (nujol): $\tilde{\nu}$ = 1582 vs ν(C=O), 432 w, 411 m, 399 m ν(Sn−O) cm^{-1}. ^{1}H NMR ($CDCl_3$): δ = 1.76 (s, 3 H, 3-CH_3), 3.33 (s, 3 H, NCH_3), 7.40−7.60 [m, 5 H, C(=O)C_6H_5] ppm. ^{13}C NMR ($CDCl_3$): δ = 16.3 (s, 3-CH_3), 31.7 (s, NCH_3), 104.3, (s, C-4), 120.7, 128.1, 128.5, 131.4, 139.5 (s, C_{arom}), 148.1 (s, C-3), 161.9 (s, C-5), 190.6 (s, CO) ppm. ^{119}Sn NMR ($CDCl_3$): δ = −734.7 ppm.

Sn(Q^D)$_2$ (11): Compound **11** was synthesized as described for compound **1**, with water as solvent. Yield 0.234 g (55%). M.p. 154−155 °C. $C_{14}H_{18}N_4O_4Sn$ (425.0): calcd. C 39.56, H 4.27, N 13.18; found C 39.88, H 4.16, N 12.78. Λ_m (CH_2Cl_2, 1 × 10^{-3} M) = 0.1. MW ($CHCl_3$, c = 1.8 × 10^{-3} mol/L): 412. IR (nujol): $\tilde{\nu}$ = 1578 vs ν(C=O), 454 m, 414 s, 396 s ν(Sn−O) cm^{-1}. ^{1}H NMR ($CDCl_3$): δ = 2.31 (s, 3 H, 3-CH_3), 2.38 [s, 3 H, C(=O)CH_3], 3.27 (s, 3 H, NCH_3) ppm. ^{13}C NMR ($CDCl_3$): δ = 16.9 (s, 3-*C*H$_3$), 27.5 [s, C(=O)*C*H$_3$], 31.5 (s, NCH_3), 104.1 (s, C-4), 147.4 (s, C-3), 160.7 (s, C-5), 192.6 (s, CO) ppm. ^{119}Sn NMR ($CDCl_3$): δ = −701.6 ppm.

Sn(Q^P)$_2$ (12): Compound **12** was synthesized as described for compound **1**. Yield 0.598 g (75%). M.p. 245−248 °C. $C_{44}H_{30}N_4O_4Sn$ (797.4): calcd. C 66.27, H 3.79, N 7.03; found C 65.98, H 3.81, N 6.93. Λ_m (CH_2Cl_2, 1 × 10^{-3} M) = 0.4. MW ($CHCl_3$, c = 1.5 × 10^{-3} mol/L): 790. IR (nujol): $\tilde{\nu}$ = 1608 s, 1595 vs ν(C=O), 440 m, 399 m ν(Sn−O) cm^{-1}. ^{1}H NMR ($CDCl_3$): δ = 6.88−7.22 (m), 7.33 (d), 7.51 (t), 7.78 (t), 7.90 (d), 7.95 (d), 8.12 [d, 15 H, NC_6H_5, C(=O)C_6H_5 and 3-C_6H_5] ppm. ^{13}C NMR ($CDCl_3$): δ = 103.6, (s, C-4), 121.2, 122.1, 126.1, 127.6, 127.7, 127.9, 128.8, 129.1, 129.4, 129.8, 130.3, 131.7, 133.3, 137.9, 138.3 (s, C_{arom}), 152.7 (s, C-3), 162.2 (s, C-5), 191.2 (s, CO) ppm. ^{119}Sn NMR ($CDCl_3$): δ = −768.8 ppm.

Sn(Q^G)$_2$ (13): Compound **13** was synthesized as described for compound **1**. Yield 0.444 g (66%). M.p. 207−209 °C. $C_{44}H_{30}N_4O_4Sn$ (673.3): calcd. C 60.65, H 3.89, N 8.32; found C 60.50, H 3.92, N 8.10. Λ_m (CH_2Cl_2, 1 × 10^{-3} M) = 0.2. MW ($CHCl_3$, c = 1.5 × 10^{-3} mol/L): 642. IR (nujol): $\tilde{\nu}$ = 1617 s, 1611 s ν(C=O), 452 m, 430 m, 416 m ν(Sn−O) cm^{-1}. ^{1}H NMR ($CDCl_3$): δ = 1.96 (s), 2.18 [s, 3 H, C(=O)CH_3), 7.05−7.58 (m), 7.90 (d, 10 H, NC_6H_5 and 3-

 © 2004 Wiley-VCH Verlag GmbH & Co. KGaA, Weinheim

C_6H_5) ppm. ^{13}C NMR ($CDCl_3$): δ = 28.0 [s, C(=O)CH_3], 105.3, (s, C-4), 121.2, 126.1, 128.5, 128.9, 129.0, 129.5, 134.2, 138.4 (s, C_{arom}), 152.8 (s, C-3), 160.6 (s, C-5), 194.9 (s, CO) ppm. ^{119}Sn NMR ($CDCl_3$): δ = −743.5 ppm.

Sn(Q^F)$_2$ (14): Compound **14** was synthesized as described for compound **1**. Yield 0.558 g (69%). M.p. 240−242 °C. $C_{36}H_{24}F_6N_4O_4Sn$ (809.3): calcd. C 53.43, H 2.99, N 6.92; found C 53.15, H 3.08, N 6.62. Λ_m (CH_2Cl_2, 1×10^{-3} M) = 0.1. Λ_m (DMSO, 1×10^{-3} M) = 13.0. MW ($CHCl_3$, $c = 1.7 \times 10^{-3}$ mol/L): 775. IR (nujol): $\tilde{\nu}$ = 1598 vs ν(C=O), 436 m, 428 m, 403 m ν(Sn−O) cm^{-1}. ^{1}H NMR ($CDCl_3$): δ = 1.63 (s, 3 H, 3-CH_3), 7.40 (d), 7.45−7.65 (d), 7.98 [d, 9 H, $NC_6H_4CF_3$ and C(=O)C_6H_5] ppm. ^{13}C NMR ($CDCl_3$): δ = 15.9 (s, 3-CH_3), 104.9 (s, C-4), 119.8, 125.5, 125.6, 127.9, 128.1, 131.7, 132.4, 138.4, 140.3 (s, C_{arom}), 149.4 (s, C-3), 162.1 (s, C-5), 191.8 (s, CO) ppm; CF_3 signal not observed. ^{19}F NMR ($CDCl_3$): δ = −62.8 ppm. ^{119}Sn NMR ($CDCl_3$): δ = −775.2 ppm.

Sn(Q^H)$_2$ (15): Compound **15** was synthesized as described for compound **1**. Yield 0.562 g (82%). M.p. 267−270 °C. $C_{26}H_{10}F_6N_4O_4Sn$ (685.1): calcd. C 45.58, H 2.94, N 8.18; found C 45.45, H 2.88, N 8.18. Λ_m (CH_2Cl_2, 1×10^{-3} M) = 0.1. Λ_m (DMSO, 1×10^{-3} M) = 11.1. MW ($CHCl_3$, $c = 1.8 \times 10^{-3}$ mol/L): 670. IR (nujol): $\tilde{\nu}$ = 1620 s, 1607 s ν(C=O), 444 s, 438 m, 404 m ν(Sn−O) cm^{-1}. ^{1}H NMR ($CDCl_3$): δ = 2.15 (s, 3 H, 3-CH_3), 2.31 [s, 3 H, C(=O)CH_3] 7.58 (d), 7.95 (d, 4 H, $NC_6H_4CF_3$) ppm. ^{13}C NMR ($CDCl_3$): δ = 16.8 (s, 3-CH_3), 27.7 [s, C(=O)CH_3], 104.5 (s, C-4), 120.2, 125.7, 125.8, 138.2 (s, C_{arom}), 148.2 (s, C-3), 162.4 (s, C-5), 192.2 (s, CO) ppm; CF_3 signal not observed. ^{19}F NMR ($CDCl_3$): δ = −62.7 ppm. ^{119}Sn NMR ($CDCl_3$): δ = −741.9 ppm.

SnMeI(Q^T)$_2$ (16): Compound **2** (0.661 g, 1 mmol) was dissolved in an excess of methyl iodide (30 mL). The mixture was stirred under reflux for 4 d. Removal of the unconverted methyl iodide under reduced pressure left a solid residue, which was recrystallized from chloroform/*n*-hexane and shown to be compound **16**. Yield 0.755 g (94%). M.p. 123−125 °C. $C_{33}H_{41}IN_4O_4Sn$ (803.3): calcd. C 49.34, H 5.14, N 6.97; found C 49.68, H 5.25, N 7.06. Λ_m (CH_2Cl_2, 1×10^{-3} M) = 0.3. IR (nujol): $\tilde{\nu}$ = 1600 vs, 1581 vs ν(C=O), 552 sh, 542 m ν(Sn−C), 470 s, 392 m ν(Sn−O), 225 s br. ν(Sn−I) cm^{-1}. ^{1}H NMR ($CDCl_3$): δ = 0.95 (s), 1.00 (s), 1.14 (s), 1.18 [s, 18 H, C(=O)$CH_2C(CH_3)_3$], 1.35 (s, $^2J_{Sn,H}$ = 116.8 Hz), 1.48 (s, $^2J_{Sn,H}$ = 118.0 Hz), (s, 3 H, $SnCH_3$), 2.45 (s), 2.49 (s), 2.55 (s, 6 H, -3CH_3), 2.64 (s), 2.67 (s), 2.68 [s, 4 H, C(=O)$CH_2C(CH_3)_3$], 7.09 (br. m), 7.30 (br. m), 7.49 (br. t), 7.57 (br. m), 7.86 (br. d), 8.04 (br. d, 10 H, NC_6H_5) ppm. ^{13}C NMR ($CDCl_3$): δ = 9.9 (br. s, $SnCH_3$), 17.9 (br. s, 3-CH_3), 30.3 [br. s, C(=O)$CH_2C(CH_3)_3$], 33.0 [br. s, C(=O)-$CH_2C(CH_3)_3$], 50.5 [br. s, C(=O)$CH_2C(CH_3)_3$], 106.9 (br. s, C-4), 120.5, 121.3, 121.8, 126.5, 129.0, 137.3 (br. s, C_{arom}), 149.2 (br. s, C-3), 162.2 (br. s, C-5), 196.3 (br. s, CO) ppm. ^{119}Sn NMR ($CDCl_3$): δ = −496.4, −652.2, −663.3, −668.5, −677.2 ppm.

SnEtI(Q^T)$_2$ (17): Compound **17** was synthesized as for compound **16**, but with ethyl iodide. Yield 0.719 g (88%). M.p. 134−137 °C. $C_{34}H_{43}IN_4O_4Sn$ (817.3): calcd. C 49.96, H 5.30, N 6.85; found C 50.03, H 5.45, N 6.90. Λ_m (CH_2Cl_2, 1×10^{-3} M) = 0.5. IR (nujol): $\tilde{\nu}$ = 1600 vs, 1583 vs ν(C=O), 555 m ν(Sn−C), 465 m, 396 w ν(Sn−O), 220 s br. ν(Sn−I) cm^{-1}. ^{1}H NMR ($CDCl_3$): δ = 0.94 (s), 1.00 (s), 1.02 (s), 1.16 [s, 18 H, C(=O)$CH_2C(CH_3)_3$], 1.24 (t), 1.28 (t), 2.62 (m), 2.67 (m, 5 H, $SnCH_2CH_3$), 2.37 (br. s, 6 H, 3-CH_3), 2.49 (br. s, 4 H, C(=O)$CH_2C(CH_3)_3$], 7.12 (br. m), 7.30 (br. m), 7.45 (br. t), 7.60 (br. m), 7.88 (br. d), 8.04 (br. d, 10 H, NC_6H_5) ppm. ^{13}C NMR ($CDCl_3$): δ = 10.5, 32.9 (br. s, $SnCH_2CH_3$), 17.9 (br. s, 3-CH_3), 30.4 [br. s, C(=O)$CH_2C(CH_3)_3$], 32.1 [br. s, C(=O)-$CH_2C(CH_3)_3$], 50.6 [br. s, C(=O)$CH_2C(CH_3)_3$], 107.0 (br. s, C-4), 120.5, 121.2, 121.8, 126.4, 129.0, 137.4 (br. s, C_{arom}), 149.1 (br. s, C-3), 162.5 (br. s, C-5), 196.5 (br. s, CO) ppm. ^{119}Sn NMR ($CDCl_3$): δ = −614.1, −626.1, −631.0, −639.5 ppm.

Cr(CO)$_5$Sn(Q^T)$_2$ (18): Compound **2** (0.661 g, 1 mmol) was dissolved in a toluene solution (30 mL) of hexacarbonylchromium (0.220 g, 1 mmol). The mixture was irradiated and stirred under reflux for 4 d. Removal of the solvent under reduced pressure left a solid residue, which was recrystallized from chloroform/*n*-hexane and shown to be compound **18**. Yield 0.751 g (88%). M.p. 73−76 °C. $C_{37}H_{38}CrN_4O_9Sn$ (853.4): calcd. C 52.07, H 4.49, N 6.57; found C 52.45, H 4.61, N 6.88. Λ_m (CH_2Cl_2, 1×10^{-3} M) = 0.4. IR (nujol): $\tilde{\nu}$ = 2059 m, 1947 s, 1880 m ν(Cr−C≡O), 1610 vs, 1595 vs ν(C=O), 440 m, 433 m, 392 w ν(Sn−O) cm^{-1}. ^{1}H NMR ([D$_6$]benzene): δ = 1.05 [s, 9 H, C(=O)$CH_2C(CH_3)_3$], 2.20 (s, 3 H, 3-CH_3), 2.30 [s, 2 H, C(=O)$CH_2C(CH_3)_3$], 7.02 (t), 7.21 (t), 8.25 (d, 5 H, NC_6H_5) ppm. ^{13}C NMR ([D$_6$]benzene): δ = 16.1 (s, 3-CH_3), 30.0 [s, C(=O)$CH_2C(CH_3)_3$], 31.9 [s, C(=O)$CH_2C(CH_3)_3$], 49.6 [s, C(=O)$CH_2C(CH_3)_3$], 105.8 (s, C-4), 120.1, 126.1, 129.2, 138.3 (s, C_{arom}), 147.0 (s, C-3), 194.4 (s, CO) ppm; C-5 and Cr(*C*O) signals not observed. ^{119}Sn NMR ([D$_6$]benzene): δ = −377.2 ppm.

Pb(Q^B)$_2$ (19): Compound **19** was synthesized as described for compound **20** (see below). Yield 0.567 g (76%). M.p. 248−250 °C. $C_{30}H_{34}N_4O_4Pb$ (721.8): calcd. C 49.92, H 4.75, N 7.76; found C 49.62, H 4.90, N 7.77. Λ_m (CH_2Cl_2, 1×10^{-3} M) = 0.5. MW ($CHCl_3$, $c = 1.6 \times 10^{-3}$ mol/L): 950. IR (nujol): $\tilde{\nu}$ = 1600 vs, 1595 vs ν(C=O), 469 s, 434 m 412 vs, 386s ν(Pb−O) cm^{-1}. ^{1}H NMR ($CDCl_3$): δ = 1.23 [s, 9 H, C(=O)$C(CH_3)_3$], 2.36 (3 H, 3-CH_3), 7.13 (t), 7.30 (t), 7.74 (d, 5 H, NC_6H_5) ppm. ^{13}C NMR ($CDCl_3$): δ = 20.4 (s, 3-CH_3), 28.3 [s, C(=O)$C(CH_3)_3$], 33.4 [s, C(=O)$C(CH_3)_3$], 104.8 (s, C-4), 121.9, 125.8, 128.9, 138.6 (s, C_{arom}), 145.5 (s, C-3), 163.6 (s, C-5), 204.6 (s, CO) ppm.

Pb(Q^T)$_2$ (20): Potassium hydroxide (0.112 g, 2.0 mmol) and $Pb(NO_3)_2$ (0.331 g, 1 mmol) were added to a methanol solution (30 mL) of Q^{T}H (0.566 g, 2 mmol). A colourless precipitate formed immediately. After 1 h, it was filtered off, washed with methanol (10 mL) and recrystallized from chloroform/methanol. Yield 0.562 g (75%). M.p. 224−227 °C. $C_{32}H_{38}N_4O_4Pb$ (749.9): calcd. C 51.26, H 5.18, N 7.47; found C 51.05, H 5.35, N 7.46. Λ_m (CH_2Cl_2, 1×10^{-3} M) = 0.4. MW ($CHCl_3$, $c = 1.8 \times 10^{-3}$ mol/L): 842. IR (nujol): $\tilde{\nu}$ = 1600 vs, 1592 vs ν(C=O), 441 vs, 411 w, 397 m ν(Pb−O) cm^{-1}. ^{1}H NMR ($CDCl_3$, 293 K): δ = 1.02 [s, 9 H, C(=O)$CH_2C(CH_3)_3$], 2.27 (s, 3 H, 3-CH_3), 2.53 [s, 2 H, C(=O)-$CH_2C(CH_3)_3$], 7.14 (t), 7.30 (t), 7.77 (d, 5 H, NC_6H_5) ppm. ^{1}H NMR (CD_2Cl_2, 293 K): δ = 1.05 [s, 9 H, C(=O)$CH_2C(CH_3)_3$], 2.32 (s, 3 H, 3-CH_3), 2.57 [s, 2 H, C(=O)$CH_2C(CH_3)_3$], 7.16 (t), 7.29 (t), 7.81 (d, 5 H, NC_6H_5) ppm. ^{1}H NMR (CD_2Cl_2, 193 K): δ = 0.93 (s). 1.05 [s, 9 H, C(=O)$CH_2C(CH_3)_3$], 1.62 (s), 1.75 (s), 1.87 (s, 3 H, 3-CH_3), 2.36 (s), 2.42 (s), 2.58 [s, 2 H, C(=O)$CH_2C(CH_3)_3$], 7.12 (t), 7.26 (t), 7.44 (t), 7.78 (d), 7.81 (d, 5 H, NC_6H_5) ppm. ^{13}C NMR ($CDCl_3$): δ = 18.4 (s, 3-CH_3), 30.4 [s, C(=O)$CH_2C(CH_3)_3$], 32.2 [s, C(=O)$CH_2C(CH_3)_3$], 51.0 [s, C(=O)$CH_2C(CH_3)_3$], 108.1 (s, C-4), 121.7, 125.7, 129.0, 138.5 (s, C_{arom}), 148.0 (s, C-3), 162.3 (s, C-5), 196.0 (s, CO) ppm.

Pb(Q^W)$_2$ (21): Compound **21** was synthesized as described for compound **20**. Yield 0.769 g (88%). M.p. 251−253 °C. $C_{42}H_{42}N_4O_4Pb$ (874.0): calcd. C 57.72, H 4.84, N 6.41; found C 57.43, H 5.01, N 6.47. Λ_m (CH_2Cl_2, 1×10^{-3} M) = 0.7. MW ($CHCl_3$, $c = 1.4 \times 10^{-3}$ mol/L): 1042. IR (nujol): $\tilde{\nu}$ = 1605 vs, 1595 vs ν(C=O), 473 m, 469 m, 412 m, 382 vs ν(Pb−O) cm^{-1}. ^{1}H NMR ($CDCl_3$): δ = 1.35 [s, 9 H, C(=O)$C_6H_5C(CH_3)_3$], 1.64 (s, 3 H, 3-CH_3), 7.10 (t), 7.18 (t), 7.30 (d), 7.42 (d), 7.76 [d, 9 H, NC_6H_5 and C(=O)-

 © 2004 Wiley-VCH Verlag GmbH & Co. KGaA, Weinheim

$C_6H_5C(CH_3)_3$] ppm. ^{13}C NMR ($CDCl_3$): δ = 16.6 (s, 3-CH_3), 31.4 [s, C(=O)$C_6H_5C(CH_3)_3$], 35.2 [s, C(=O)$C_6H_5C(CH_3)_3$], 106.2 (s, C-4),121.3, 125.3, 125.6, 128.4, 128.9, 138.5 (s, C_{arom}), 149.1 (s, C-3), 163.0 (s, C-5), 191.7 (s, CO) ppm.

$Pb(Q^D)_2$ (22): Compound **22** can be synthesized as described for compound **20**, but also as follows: $Pb(OOCCH_3)_2 \cdot 3H_2O$ (0.379 g, 1 mmol) was added to a water solution (30 mL) of Q^DH (0.308 g, 2 mmol). A colorless precipitate formed immediately and this was filtered, washed with methanol (10 mL), dried to constant weight under reduced pressure and recrystallized from chloroform/diethyl ether. Yield 0.345 g (65%). M.p. 214−216 °C. $C_{14}H_{18}N_4O_4Pb$ (531.7): calcd. C 32.75, H 3.52, N 10.91; found C 32.43, H 3.66, N 10.72. Λ_m (CH_2Cl_2, 1 × 10^{-3} M) = 0.4. MW ($CHCl_3$, c = 1.8 × 10^{-3} mol/L): 763. IR (nujol): $\tilde{\nu}$ = 1586 vs ν(C=O), 454 vs, 388 vs, 373 s ν(Pb−O) cm^{-1}. ^1H NMR ($CDCl_3$): δ = 2.30 (s, 3 H, 3-CH_3), 2.40 [s, 3 H, C(=O)CH_3], 3.28 (s, 3 H, NCH_3) ppm. ^{13}C NMR ($CDCl_3$): δ = 17.4 (s, 3-CH_3), 28.1 (s, NCH_3), 31.5 [s, C(=O)CH_3], 105.9 (s, C-4), 147.1 (s, C-3), 161.8 (s, C-5), 192.8 (s, CO) ppm.

$Pb(Q^D)_2$(phen) (23): Compound **22** (0.532 g, 1 mmol) and phen (0.180 g, 1 mmol) were dissolved in benzene (30 mL) and the clear solution stirred at room temperature for 2 h. The solvent was then removed and the residue treated with diethyl ether (20 mL), affording a colorless precipitate, which was filtered off, dried to constant weight under reduced pressure and recrystallized from chloroform/*n*-hexane. Yield 0.541 g (78%). M.p. 156 °C (dec.). $C_{26}H_{26}N_4O_4Pb$ (693.7): calcd. C 45.02, H 3.78, N 12.11; found C 44.82, H 3.96, N 11.87. Λ_m (CH_2Cl_2, 1 × 10^{-3} M) = 0.3. MW ($CHCl_3$, c = 1.8 × 10^{-3} mol/L): 640. IR (nujol): $\tilde{\nu}$ = 1590 vs ν(C=O), 446 vs, 393 m, 374 s ν(Pb−O), 291 m ν(Pb−N) cm^{-1}. ^1H NMR ($CDCl_3$): δ = 2.29 (s, 6 H, 3-CH_3), 2.32 [s, 6 H, C(=O)CH_3], 3.21 (s, 6 H, NCH_3), 7.73 (dd), 7.85 (s), 8.33 (dd), 9.38 (dd, 8 H, CH_{phen}) ppm. ^{13}C NMR ($CDCl_3$): δ = 17.3 (s, 3-CH_3), 28.2 (s, NCH_3), 31.0 [s, C(=O)CH_3], 105.5 (s, C-4), 123.7, 126.7, 129.3, 136.8, 146.5, 150.2 (s, C_{phen}), 145.8 (s, C-3), 162.6 (s, C-5), 191.8 (s, CO) ppm.

X-ray Crystallographic Study: Experimental data for compounds **6**, **19** and **20** can be found in Table 8. The crystal of bis(3-methyl-4-phenyl-1-phenylacetylpyrazolon-5-ato)tin(II) (**6**) decayed slightly but no decay correction was applied to the data. For crystals of bis(3-methyl-1-phenyl-4-pivaloylpyrazolon-5-ato)lead(II) (**19**) and bis(4-*tert*-butyl-3-methyl-1-phenylacetylpyrazolon-5-ato)lead(II) (**20**) no decay was seen. The data for compounds **6** and **19** were collected with a Syntex $P2_1$ diffractometer equipped with a graphite-monochromated beam at 298 K. The heavy-atom method in CAOS was used to solve both structures.[67] Once the heavy-atom peak had been located in the Patterson map, a Fourier synthesis was performed to locate the other non-hydrogen atoms until all atoms were found. All non-hydrogen atoms were refined anisotropically until convergence. The hydrogen atoms were then placed at a fixed C−H bond length of 0.96 Å using a subroutine of CAOS, further refinement was applied with the H atoms riding on their attached atoms until convergence. Data were refined by full-matrix least-squares

Table 8. Crystal and refinement data

	6	**19**	**20**
Empirical formula	$C_{38}H_{30}N_4O_4Sn$	$C_{30}H_{34}N_4O_4Pb$	$C_{32}H_{38}N_4O_4Pb$
Formula mass	701.35	721.82	749.97
Crystal habit	Plate	Block	Block
Crystal size [mm]	0.30 × 0.25 × 0.10	0.20 × 0.15 × 0.15	0.25 × 0.20 × 0.20
Crystal system	monoclinic	triclinic	triclinic
Space group	$A2$	$P\bar{1}$	$P\bar{1}$
Crystal color	colorless	colorless	colorless
a [Å]	14.388(8)	10.693(7)	10.614(2)
b [Å]	5.801(3)	11.307(8)	12.278(2)
c [Å]	19.958(12)	13.473(9)	13.462(3)
α [°]	90	70.07(2)	95.311(4)
β [°]	110.67(2)	89.66(2)	111.434(3)
γ [°]	90	70.92(2)	104.811(3)
V [Å^3]	1558.6	1437.035	1544.74(5)
Z	4	2	2
T [K]	293	293	243
$D_{calcd.}$ [Mg m^{-3}]	1.37	1.61	1.61
$2\theta_{max}$ [°]	56	60	56.5
μ [mm^{-1}]	0.86	5.83	5.50
Wavelength (graphite- monochromated) [Å]	Mo (0.71069)	Mo (0.71069)	Mo (0.71069)
Transmission factors	1.00, 0.94	1.00, 0.78	0.609, 0.406
Measured reflections	4223	8357	9794
Unique reflections	2071	8088	6669
R (merged)	0.040	0.052	0.026
F(000)	652	688	744
h_{min}, h_{max}	0, 19	0, 14	−13, 13
k_{min}, k_{max}	0, 7	−14, 15	−15, 12
l_{min}, l_{max}	−26, 24	−18, 18	−17, 11
Refined reflections [$F > n\sigma(F)$]	1887 (n = 6)	6443 (n = 7)	5657 (n = 6)
Refined parameters	204	352	370
R, R_w	0.046, 0.064	0.061, 0.076	0.029, 0.038
S	0.86	0.89	0.94
Equivalent reflections	77	17	3125
Scan mode	2θ-θ	2θ-θ	ω

 © 2004 Wiley-VCH Verlag GmbH & Co. KGaA, Weinheim

procedures on *F*. The data for compound **20** were collected with a Bruker P4 diffractometer equipped with a SMART CCD detector at 243 K. Absorption correction was applied with SADABS. The structure was solved by direct methods and standard difference-map techniques, and was refined by full-matrix least-squares procedures on F^2 with SHELXTL (Version 6.10).[68] Hydrogen atoms were included in calculated positions. Difference electron density measurements showed no important residual electron density for all three structures. CCDC-233990 to -233992 (for **6**, **19**, and **20**, respectively) contain the supplementary crystallographic data for this paper. These data can be obtained free of charge at www.ccdc.cam.ac.uk/conts/retrieving.html [or from the Cambridge Crystallographic Data Centre, 12 Union Road, Cambridge CB2 1EZ, UK; Fax: (internat.) + 44-1223-336033; E-mail: deposit@ccdc.cam.ac.uk].

Acknowledgments

Our thanks go to the University of Camerino, University of Palermo, CNR, Rome, Fondazione CARIMA, Vassar College URSI program, for financial support, and Dr. Ged Parkin for use of the diffractometer.

[1] N. Tinanoff, *J. Clin. Dent.* **1990**, *6*, 22−37.
[2] M. Addy, *J. Clin. Periodontol.* **1986**, *13*, 957−964.
[3] B. B. Beiswanger, P. M. Doyle, R. D. Jackson, M. E. Mallatt, M. S. Mau, B. W. Bollmer, M. M. Crisanti, C. B. Guay, A. C. Lanzalaco, M. F. Lucacovic, S. Majeti, L. K. McClanaghan, *J. Clin. Dent.* **1995**, *6*, 46−53.
[4] M. A. Perlich, L. A. Bacca, B. W. Bollmer, A. C. Lanzalaco, L. K. McClanaghan, L. K. Sewak, B. B. Beiswanger, W. A. Eichold, J. R. Hull, R. D. Jackson, M. S. Mau, *J. Clin. Dent.* **1995**, *6*, 54−58.
[5] M. C. Barret, M. F. Mahon, K. C. Molloy, J. W. Steed, P. Wright, *Inorg. Chem.* **2001**, *40*, 4384−4388.
[6] Z. M. Jarzebski, J. P. Marton, *J. Electrochem. Soc.* **1976**, *123*, 199C−205C. Z. M. Jarzebski, J. P. Marton, *J. Electrochem. Soc.* **1976**, *123*, 299C−310C. Z. M. Jarzebski, J. P. Marton, *J. Electrochem. Soc.* **1976**, *123*, 333C−346C.
[7] J. M. Blocher, Jr., *Thin Solid Films* **1981**, *77*, 51−63.
[8] M. J. Madou, S. R. Morrison, *Chemical Sensing with Solid Devices*, Academic Press, San Diego, **1989**, chapter 5, pp. 159−196.
[9] K. Ihokura, J. Watson, *The Stannic Oxide Gas Sensor − Principles and Applications*, CRC Press, Boca Raton, FL, **1994**.
[10] J. H. Burroughes, D. D. Bradley, A. R. Brown, Q. N. Marks, K. Mackay, R. H. Friend, P. L. Burns, A. B. Holmes, *Nature* **1990**, *347*, 539−541.
[11] A. R. Schlatmann, D. Wilms Floet, A. Hilberer, F. Garten, P. J. M. Smulders, T. M. Klapwijk, G. Hadziioannou, *Appl. Phys. Lett.* **1996**, *69*, 1764−1766.
[12] A. C. Arias, J. R. de Lama, I. A. Hummenlgem, *Adv. Mater.* **1998**, *10*, 392−394.
[13] A. Gamard, O. Babot, B. Jousseaume, M.-C. Rascle, T. Toupance, G. Campet, *Chem. Mater.* **2000**, *12*, 3419−3426.
[14] H. Cachet, A. Gamard, G. Campet, B. Jousseaume, T. Toupance, *Thin Solid Films* **2001**, *388*, 41−49.
[15] D. Boegeat, B. Jousseaume, T. Toupance, G. Campet, L. Fournes, *Inorg. Chem.* **2000**, *39*, 3924−3927.
[16] K.-M. Chi, C.-C. Lin, Y.-H. Lu, J.-H. Liao, *J. Chin. Chem. Soc.* **2000**, *47*, 425−431.
[17] O. Auciello, R. Ramesh, *MRS Bull.* **1996**, *21*, 21−21.
[18] O. Auciello, R. Ramesh, *MRS Bull.* **1996**, *21*, 29−29.
[19] S. K. Dey, P. V. Alluri, *MRS Bull.* **1996**, *21*, 44−48.
[20] B. A. Tuttle, R. W. Schwartz, *MRS Bull.* **1996**, *21*, 49−54.
[21] R. E. Jones Jr., S. B. Desu, *MRS Bull.* **1996**, *21*, 55−58.
[22] J. F. Scott, F. M. Ross, C. A. Paz de Aranjo, M. C. Scott, M. Huffman, *MRS Bull.* **1996**, *21*, 33−39.
[23] W. R. Warren, D. Dimos, R. M. Waser, *MRS Bull.* **1996**, *21*, 40−45.
[24] A. I. Kingon, S. K. Steiffer, C. Basceri, S. R. Summerfelt, *MRS Bull.* **1996**, *21*, 46−52.
[25] D. K. Fork, F. A. Leplingard, J. J. Kingston, *MRS Bull.* **1996**, *21*, 53−58.
[26] D. L. Polla, L. F. Francis, *MRS Bull.* **1996**, *21*, 59−65.
[27] K. Nagashima, N. Funakubo, S. Seki, Y. Sadawa, Y. Miura, N. Higuchi, H. Matchida, *Chem. Vap. Depos.* **2000**, *6*, 311−314.
[28] M. A. Malik, P. O'Brien, M. Motevalli, A. C. Jones, T. Leedham, *Polyhedron* **1999**, *18*, 1641−1646.
[29] V. V. Krisyuk, A. E. Turgambaeva, I. K. Igumenov, *Chem. Vap. Depos.* **1998**, *4*, 43−46.
[30] C. Pettinari, F. Marchetti, A. Cingolani, A. Gindulyte, L. Massa, M. Rossi, F. Caruso, *Eur. J. Inorg. Chem.* **2001**, 2171−2180.
[31] C. Pettinari, F. Marchetti, A. Cingolani, G. Bianchini, A. Drozdov, V. Vertlib, S. Troyanov, *J. Organomet. Chem.* **2001**, *651*, 5−14.
[32] C. Pettinari, F. Marchetti, A. Cingolani, D. Leonesi, S. Troyanov, A. Drozdov, *J. Chem. Soc., Dalton Trans.* **1999**, 1555−1562.
[33] F. Marchetti, C. Pettinari, R. Pettinari, A. Cingolani, A. Drozdov, S. Troyanov, *J. Chem. Soc., Dalton Trans.* **2002**, 2616−2623.
[34] F. Marchetti, C. Pettinari, A. Cingolani, D. Leonesi, A. Drozdov, S. Troyanov, *J. Chem. Soc., Dalton Trans.* **1998**, 3325−3333.
[35] C. Pettinari, F. Marchetti, A. Cingolani, R. Pettinari, S. Troyanov, A. Drozdov, *J. Chem. Soc., Dalton Trans.* **2000**, 831−836.
[36] A. Cingolani, Effendy, F. Marchetti, C. Pettinari, R. Pettinari, B. W. Skelton, A. H. White, *Inorg. Chem.* **2002**, *41*, 1151−1161.
[37] C. Pettinari, F. Marchetti, A. Cingolani, D. Leonesi, E. Mundorff, M. Rossi, F. Caruso, *J. Organomet. Chem.* **1998**, *557*, 187−205.
[38] F. Caruso, M. Rossi, J. Tanski, R. Sartori, R. Sariego, S. Moya, S. Diez, E. Navarrete, A. Cingolani, F. Marchetti, C. Pettinari, *J. Med. Chem.* **2000**, *43*, 3665−3670.
[39] C. Pettinari, F. Marchetti, C. Santini, R. Pettinari, A. Drozdov, S. Troyanov, G. A. Battiston, R. Gerbasi, *Inorg. Chim. Acta* **2001**, *315*, 88−95.
[40] C. Pettinari, F. Marchetti, A. Cingolani, C. Marciante, R. Spagna, M. Colapietro, *Polyhedron* **1994**, *13*, 939−950.
[41] K. D. Bos, H. A. Budding, E. J. Bulten, J. G. Noltes, *Inorg. Nucl. Chem. Lett.* **1973**, *9*, 961−964.
[42] P. F. R. Ewings, P. G. Harrison, D. E. Fenton, *J. Chem. Soc., Dalton Trans.* **1975**, 821−826.
[43] A. B. Cornwell, P. G. Harrison, *J. Chem. Soc., Dalton Trans.* **1975**, 1722−1726.
[44] F. Caruso, M. Rossi, F. Marchetti, C. Pettinari, *Organometallics* **1999**, *18*, 2398−2400.
[45] F. Marchetti, C. Pettinari, A. Cingolani, R. Pettinari, M. Rossi, F. Caruso, *J. Organomet. Chem.* **2001**, *645*, 134−145.
[46] K. Nakamoto, C. Udovich, J. Takemoto, *J. Am. Chem. Soc.* **1970**, *92*, 3973−3976.
[47] R. C. Mehrotra, R. Bohra, D. P. Gaur, *Metal β-Diketonates and Allied Derivatives*, Academic Press, London, **1978**, chapter 2 and references cited therein.
[48] D. L. Reger, S. J. Knox, M. F. Huff, A. L. Rheingold, B. S. Haggerty, *Inorg. Chem.* **1991**, *30*, 1754−1759.
[49] M. N. Hansen, K. Niedenzu, J. Serwatowska, J. Serwatowski, K. R. Woodrum, *Inorg. Chem.* **1991**, *30*, 866−868.
[50] J. Christoph, H. Schumann, C. Stader, *Chem. Ber.* **1988**, *121*, 1745−1751.
[51] R.V. Parish, *Mössbauer Spectroscopy Applied to Inorganic*

 © 2004 Wiley-VCH Verlag GmbH & Co. KGaA, Weinheim

Chemistry (Ed.: G. J. Long), Plenum, New York, **1984**, chapter 16, p. 558−575.
[52] F. Caruso, D. Leonesi, F. Marchetti, E. Rivarola, M. Rossi, V. Tomov, C. Pettinari, *J. Organomet. Chem.* **1996**, *519*, 29−44.
[53] P. F. R. Ewings, P. G. Harrison, T.J. King, *J. Chem. Soc., Dalton Trans.* **1975**, 1455−1458.
[54] A. Jain, S. Saxena, R. Bohra, A. K. Rai, *Main Group Met. Chem.* **1995**, *18*, 661−667.
[55] S. Ayyappan, A. K. Cheetham, S. Natarajan, C. N. R. Rao, *Chem. Mater.* **1998**, *10*, 3746−3755.
[56] C. Pettinari, F. Marchetti, D. Leonesi, M. Rossi, F. Caruso, *J. Organomet. Chem.* **1994**, *483*, 123−137.
[57] B. Bovio, A. Cingolani, F. Marchetti, C. Pettinari, *J. Organomet. Chem.* **1993**, *458*, 39−48.
[58] A. B. Cornwell, P. G. Harrison, *J. Chem. Soc., Dalton Trans.* **1975**, 1486− 1490 and references cited therein.
[59] A. B. Cornwell, P. G. Harrison, *J. Chem. Soc., Dalton Trans.* **1975**, 2017−2022 and references cited therein.
[60] J. S. Casas, A. Castineiras, I. Haiduc, A. Sanchez, J. Sordo, E. M. Vazquez-Lopez, *Polyhedron* **1994**, *13*, 2873−2879.
[61] W. Frank, F. G. Wittmer, *Chem. Ber./Recueil* **1997**, *130*, 1731−1732.
[62] V. V. Krisyuk, I. A. Baidina, S. A. Gromilov, V. I. Alekseev, S. A. Prokhorova, *Zh. Strukt. Khim.* **1997**, *38*, 434−439; *Chem. Abstr.* **1997**, *128*, 108817.
[63] M. A. Malik, P. O′Brien, M. Motevalli, A. C. Jones, T. Leedham, *Polyhedron* **1999**, *18*, 1641−1646.
[64] B. A. Uzoukwu, P. U. Adiukwu, S. S. Al-Juaid, P. B. Hitchcock, J. D. Smith, *Inorg. Chim. Acta* **1996**, *250*, 173−176.
[65] V. V. Krisyuk, I. A. Baidina, S. A. Gromilov, E. V. Bol'shakova, *Zh. Strukt. Khim.* **1994**, *35*, 197−201; *Chem. Abstr.* **1994**, *122*, 252588.
[66] B. S. Jensen, *Acta Chem. Scand.* **1959**, *13*, 1347−1357.
[67] CAOS Program: M. Camalli, R. Spagna, *J. Appl. Crystallogr.* **1994**, *27*, 861−862.
[68] G. M. Sheldrick, SHELXTL*, An Integrated System for Solving, Refining and Displaying Crystal Structures from Diffraction Data*, University of Göttingen, Göttingen, Germany, **1981**.

Received March 19, 2004
Early View Article
Published Online July 6, 2004

 © 2004 Wiley-VCH Verlag GmbH & Co. KGaA, Weinheim

Solid- and Solution-Phase Synthesis of a Library of Mixed-Metal Complexes

Katja Heinze*[a] and Juan D. Bueno Toro[a]

Keywords: Bridging ligands / Heterometallic complexes / Isomers / Group 6 elements / Solid-phase synthesis

A solid-phase synthesis protocol has been developed for the stepwise assembly of mixed-metal dinuclear complexes built from chromium, molybdenum and tungsten and a directional bridging ligand. Complexes with all nine possible metal combinations have been prepared on polystyrene/divinylbenzene copolymer employing a metal-complex-compatible silyl ether linker. Release of the metal complexes from the polymeric support is accomplished by fluoridolysis under mild conditions. The metal sequence in these complexes is precisely determined by the reaction sequence and is retained under the applied reaction conditions as shown by IR, NMR and UV/Vis spectroscopic analysis of the cleaved soluble products. Additionally, the same complex library has been prepared by conventional solution-phase synthesis to allow evaluation of the advantages and disadvantages of the solid-phase synthesis method.
(© Wiley-VCH Verlag GmbH & Co. KGaA, 69451 Weinheim, Germany, 2004)

Introduction

Monodisperse oligomers are essential for understanding the chemistry and the physics of polymeric organic and inorganic materials.[1] Several synthetic strategies have been developed for their synthesis — self-organisation processes, random syntheses followed by separation processes or step-by-step syntheses — all of which have advantages and disadvantages. Full control over chain length, end groups and building-block sequence can be achieved using a stepwise assembly of building blocks.

Although the step-by-step synthesis is straightforward, it becomes increasingly difficult for higher oligomers due to the purification steps needed. An elegant solution to this problem is synthesis on a solid support (solid-phase synthesis[2]). This synthetic method, introduced by R. B. Merrifield for the synthesis of peptides,[3] allows the purification of all intermediates by simple filtration. The development of new synthetic sequences which enable the (preferably combinatorial) solid-phase synthesis of non-natural, functionalised oligomeric compounds might aid the identification of synthetic oligomers with the capability of performing functions similar to those of peptides and proteins, for example catalysis, molecular recognition, signal transduction or conversion of chemical into mechanical energy.[2]

Organometallic compounds, however, have only recently been synthesised by this method,[4−17] and the solid-phase synthesis of oligometallic complexes, in particular, remains a challenge.[5,17] This is probably due to the fact that the metal−ligand bonds of organometallic building blocks are much more labile than typical bonds of organic molecules, and thus the required orthogonal stability and reactivity of the polymer−molecule bond and the connections between the building blocks is much more difficult to achieve for organometallic complexes than for organic molecules.

A system satisfying the above criteria consists of a silyl ether linker between the molecule and the polymer support, which is cleavable by fluoride ions,[18] and inert metal−isocyanide bonds between the organometallic building blocks.[19]

The solution and solid-phase synthesis of homometallic di- and trinuclear complexes with carbonylmolybdenum complexes as building blocks has been reported recently.[5] The extension of this synthetic strategy to assembling mixed-metal dinuclear complexes is reported in this contribution.

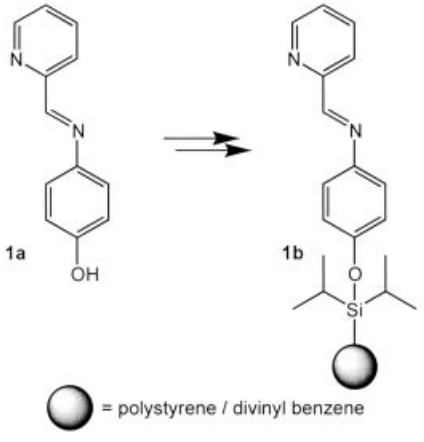

Scheme 1

[a] Anorganisch-Chemisches Institut der Universität Heidelberg
Im Neuenheimer Feld 270, 69120 Heidelberg, Germany
Fax.: (internat.) + 49-6221-545707
E-mail: katja.heinze@urz.uni-heidelberg.de
Supporting information for this article is available on the WWW under http://www.eurjic.org or from the author.

 © 2004 Wiley-VCH Verlag GmbH & Co. KGaA, Weinheim **DOI: 10.1002/ejic.200400244**

Results and Discussion

General Solution- and Solid-Phase Synthesis

The hydroxy-functionalised Schiff-base ligand **1a** was used as starting point for the stepwise assembly of mixed-metal complexes. For the solid-phase synthesis approach **1a** was attached to polystyrene/divinylbenzene copolymer by a silyl ether linker to give the immobilised ligand **1b** (Scheme 1).[4] The silyl ether allows the release of the final products of the solid-phase synthesis from the support by mild fluoridolysis.[4,5,18]

Addition of a suitable $\{M^1(CO)_3\}$ source (M^1 = Cr, Mo, W) to **1a** or **1b** furnished the reactive soluble or polymer-bound complexes **2a**−**4a** and **2b**−**4b**,[4], respectively (Scheme 2). These THF-containing complexes were subsequently treated with the bridging ligand (4-isocyanophenyl)(pyridin-2-ylmethylene)amine C≡N−(N∩N′)[19] to give the stable tricarbonyl isocyanide complexes **5a**−**7a** and **5b**−**7b**, respectively (Scheme 2). The potentially chelating diimine moiety of C≡N−(N∩N′) was finally coordinated to an $\{M^2(CO)_4\}$ fragment (M^2 = Cr, Mo, W) to give the dinuclear mixed-metal complexes **8a**−**16a** and **8b**−**16b**, respectively (Scheme 2). Each member of this "3 × 3 library" of mixed-metal complexes has been prepared by both solution- and solid-phase synthesis according to Scheme 2.

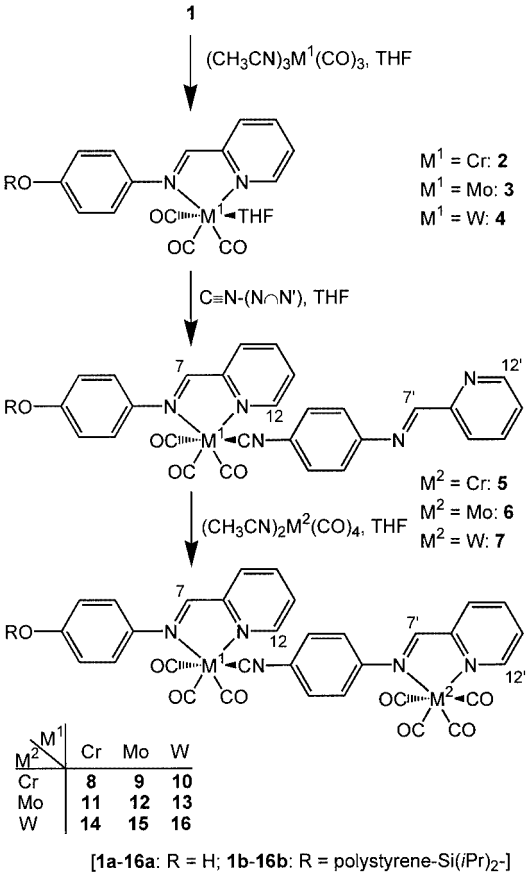

M^2 \ M^1	Cr	Mo	W
Cr	**8**	**9**	**10**
Mo	**11**	**12**	**13**
W	**14**	**15**	**16**

Scheme 2

All reactions in solution had to be performed under exact stoichiometric conditions to reduce the formation of side products such as X−(N∩N′)M(CO)$_4$ (X = CN, OH) or C≡N−(N∩N′)M(CO)$_3$C≡N−(N∩N′) which are difficult to remove after the synthesis of the dinuclear complexes (see Exp. Sect.).

Properties of the Soluble Complexes 5a−16a

The two Schiff-base ligands present in the mononuclear complexes **5a**−**7a** give rise to several overlapping signals in the aromatic region of the ^{1}H NMR spectra (see Exp. Sect.). Pronounced chemical-shift differences are observed for the two imine protons $H^7/H^{7'}$ and the two protons α to the pyridine nitrogen atom ($H^{12}/H^{12'}$) due to the presence (H^7: δ = 8.58−8.89 ppm; H^{12}: δ = 9.30−9.41 ppm) and absence ($H^{7'}$: δ = 8.73−8.74 ppm; $H^{12'}$: δ = 8.53−8.59 ppm) of a coordinated metal centre (see Scheme 2 and Exp. Sect. for atom numbering).

Complexes **5a**−**7a** display the typical ν_{CO} absorption pattern of a facially coordinated $\{M^1(CO)_3\}$ fragment with disturbed local C_{3v} symmetry[4,19−21] and an absorption band due to the coordinated isocyanide group of the C≡N−(N∩N′) ligand in their IR spectra (see Exp. Sect.). The absorption bands of **5a**−**7a** in the UV/Vis spectra between 613−655 nm can be assigned to a metal-to-ligand charge transfer transition of the $\{(diimine)M^1(CO)_3\}$ chromophore (see Exp. Sect.).[4,19−21] The MLCT bands show negative solvatochromism as expected (see Supporting Information).[22] A linear solvation-energy relationship analysis reveals that the most dominant term influencing the charge transfer is the polarity of the solvent, followed by the hydrogen-acceptor ability of the solvent (see Supporting Information).[23]

The IR spectra of the dinuclear complexes are superpositions of the spectra of the corresponding tricarbonyl and tetracarbonyl complexes [disturbed local C_{3v} and C_{2v} symmetry of the $M(CO)_n$ moieties, respectively];[4,19−21] one ν_{CN} absorption and five ν_{CO} absorptions (two absorptions are not resolved) are observed in each case (Table 1). This finding was corroborated by DFT calculations of complexes **8a**−**16a** (see Supporting Information): the ν_{CO} and ν_{CN} absorptions of the $M^1(CO)_3(CNR)$ moieties are independent of the metal in the $M^2(CO)_4$ fragment and vice versa (Figure 1; all standard deviations are below 2 cm^{-1}).

The ^{1}H NMR spectra of **8a**−**16a** consist of overlapping signals in the aromatic region. Particularly informative is the chemical shift of the two imine protons ($H^7/H^{7'}$: δ = 8.35−8.90 ppm) and the two protons α to the pyridine nitrogen atom ($H^{12}/H^{12'}$: δ = 9.14−9.40 ppm) which are influenced by metal coordination (cf. complexes **5a**−**7a**, Table 1, Exp. Sect.).

In the UV/Vis spectra of **8a**−**16a** two absorptions are observed in the visible region. These two absorptions arise from MLCT transitions of the $\{(diimine)M^1(CO)_3\}$ chromophore at lower energy and of the $\{(diimine)M^2(CO)_4\}$ chromophore at higher energy (Table 1).[4,19−21]

A thorough examination of the spectroscopic data reveals that all dinuclear complexes exhibit similar but distinguish-

 © 2004 Wiley-VCH Verlag GmbH & Co. KGaA, Weinheim

Table 1. Selected IR, UV/Vis and ^{1}H NMR spectroscopic data of **8a**−**16a** in THF

M^2/M^1	[a]	Cr	Mo	W
Cr	$\tilde{\nu}^1_{CO}$	1830	1826	1827
	$\tilde{\nu}^2_{CO}$	1849	1850	1849
	$\tilde{\nu}^3_{CO}$	1904	1906 (sh)	1903 (sh)
	$\tilde{\nu}^4_{CO}$	1912	1917	1911
	$\tilde{\nu}^5_{CO}$	2007	2007	2006
	$\tilde{\nu}_{CN}$	2073	2077	2073
	λ_{max} (ε)	574 (4240)	585 (7480)	600 (6070)
	δ_H(imine)	8.51 (2 H)	8.35, 8.47	8.49, 8.90
Mo	$\tilde{\nu}^1_{CO}$	1827	1824	1827
	$\tilde{\nu}^2_{CO}$	1849	1848	1848
	$\tilde{\nu}^3_{CO}$	1910	1904	1909 (br)
	$\tilde{\nu}^4_{CO}$	1913	1917	
	$\tilde{\nu}^5_{CO}$	2013	2012	2013
	$\tilde{\nu}_{CN}$	2070	2078	2067
	λ_{max} (ε)	546 (6925)	536 (5575)	547 (5290)
		628 (5205)	600 (4545)	608 (4860)
	δ_H(imine)	8.54, 8.57	8.57, 8.61	8.57, 8.90
W	$\tilde{\nu}^1_{CO}$	1825	1824	1826
	$\tilde{\nu}^2_{CO}$	1847	1849	1848
	$\tilde{\nu}^3_{CO}$	1894	1894	1895
	$\tilde{\nu}^4_{CO}$	1915	1918	1912
	$\tilde{\nu}^5_{CO}$	2006	2006	2006
$\tilde{\nu}^5_{CO}$	$\tilde{\nu}_{CN}$	2072	2075	2071
	λ_{max} (ε)	551 (6000)	554 (7425)	561 (8580)
		643 (5210)	605 (5515)	606 (6860)
	δ_H(imine)	8.53, 8.87	8.57, 8.90	8.87, 8.90

[a] IR values given in cm^{-1}; λ_{max} in nm, ε in $M^{-1}\cdot cm^{-1}$; δ in ppm.

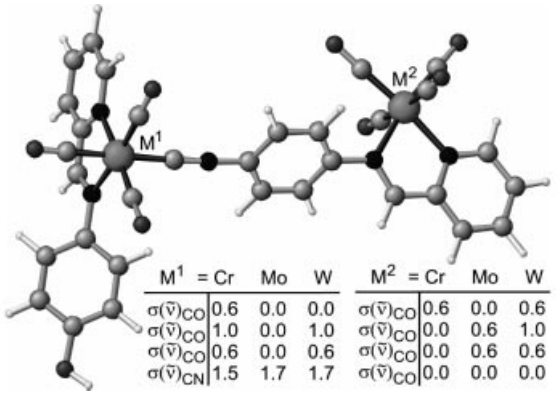

Figure 1. DFT (B3LYP, LANL2DZ) optimised geometry of complex **8a** ($M^1 = M^2 = Cr$) and standard deviations of the calculated average IR wavenumbers [cm^{-1}] of the $M(CO)_n$ fragments of complexes **8a**−**16a**

able features. This allows the determination of the metal sequence of the complexes simply by a combination of IR (Figure 2), ^{1}H NMR and UV/Vis spectroscopic data (Table 1, Supporting Information).[19]

There are five obvious criteria to distinguish complexes **8a**−**16a**:

(i):$\tilde{\nu}_{CN} \geq 2075$ cm^{-1}: M^1 = Mo (**9a**, **12a**, **15a**) (Figure 2);

(ii): $\tilde{\nu}^5_{CO} \geq 2012$ cm^{-1}: M^2 = Mo (**11a**, **12a**, **13a**) (Figure 2);

(iii): (i) and (ii): $M^1 = M^2$ = Mo (**12a**) (Figure 2);

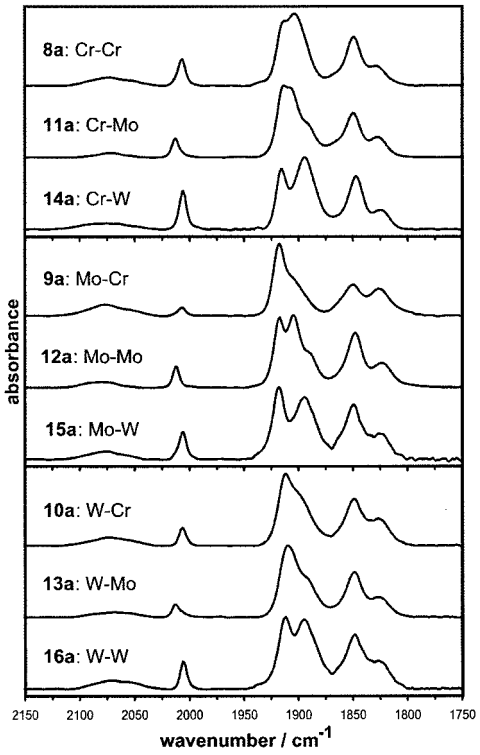

Figure 2. IR spectra of complexes **8a**−**16a** in THF

(iv): one $\delta_{H(imine)} \geq 8.87$ ppm: M^1 or M^2 = W (**10a**, **13a**, **14a**, **15a**);

(v): two $\delta_{H(imine)} \geq 8.87$ ppm: $M^1 = M^2$ = W (**16a**).

With these criteria the sequences of all complexes, except the Cr/W isomers **10a** and **14a**, can be unambiguously determined, for example (i) and (iv) describe complex **15a**. The two isomeric complexes **10a** and **14a** can be distinguished either by their IR spectroscopic pattern around 1900 cm^{-1}, as the difference between $\tilde{\nu}^3_{CO}$ and $\tilde{\nu}^4_{CO}$ amounts to 8 cm^{-1} for **10a** and 21 cm^{-1} for **14a** (Figure 2, Table 1), or by their MLCT absorptions in the UV/Vis spectra (Figure 3, Table 1). The energetic difference between the two MLCT absorptions is smaller for **10a** (2240 cm^{-1}) than for **14a** (3080 cm^{-1}) as expected from the MLCT absorptions of the corresponding mononuclear complexes (see Exp. Sect. and refs.[4,21]).

Thus, all complexes can be distinguished by their spectroscopic signatures. These findings also imply that the complexes retain their metal sequence under the applied reaction conditions — there is no rearrangement, polymerisation or carbonyl scrambling.

In the solid state the IR data of **8a**−**16a** show that hydrogen bonds from the hydroxy group of the ligand **1a** are present ($\tilde{\nu}_{OH}$ = 3340−3469 cm^{-1}, see Exp. Sect.). These energies are compatible with the formation of OH···O hydrogen bonds between OH groups of different complexes or between the OH group and carbonyl ligands of different complexes.[20,21]

For ligand **1a** and complexes **5a**−**7a** broad, structured absorption bands are observed in the region 3000−3455

 © 2004 Wiley-VCH Verlag GmbH & Co. KGaA, Weinheim

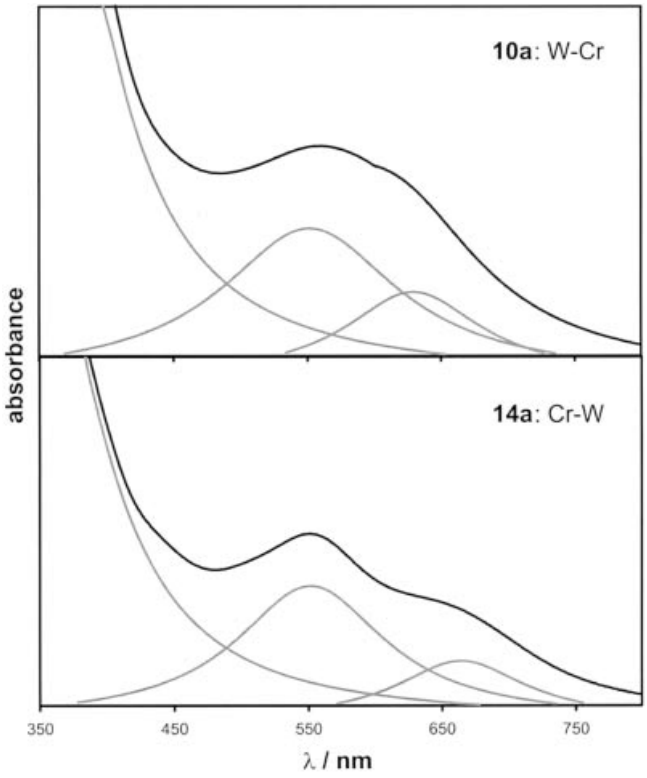

Figure 3. UV/Vis spectra of **10a** and **14a** in THF and deconvolution of the MLCT bands (Lorenz profiles)[24]

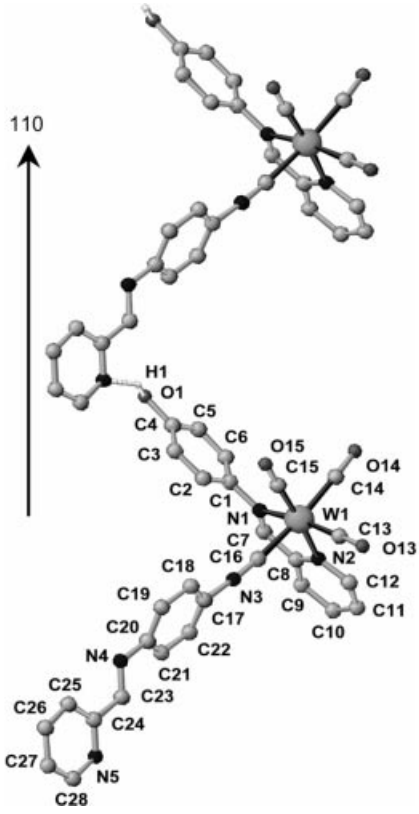

Figure 5. Structure of **7a** in the solid state

cm^{-1}, which again suggests hydrogen-bonded structures. This has been confirmed by determination of the crystal structures of **1a** and **7a** (Figures 4 and 5). Intramolecular bond lengths and angles are unremarkable for both structures (Table 2), although the intermolecular connectivity is noticeable.

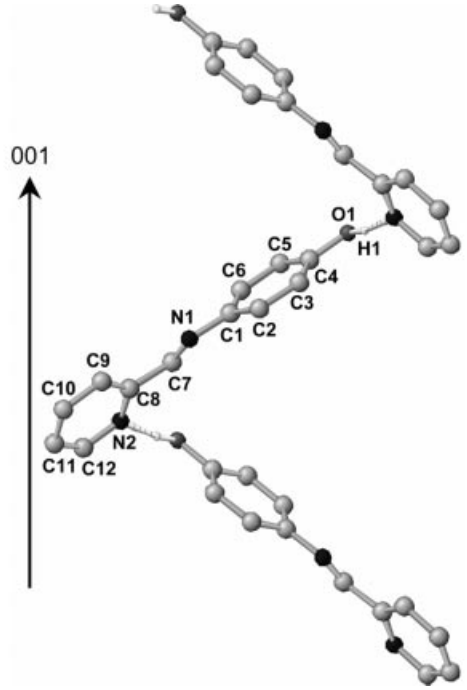

Figure 4. Structure of **1a** in the solid state

In both solid-state structures the OH group of the ligand forms hydrogen bonds to the nitrogen atom of a pyridine ring of a neighbouring molecule (**1a**: O1···N2; **7a**: O1···N5; Table 3, Figures 4 and 5). The molecules of **1a** form a zigzag chain along the 001 direction (a glide plane of the space group *Pbca*; repeat distance $c/2 = 6.8$ Å), while the molecules of **7a** form a linear chain along the 110 direction (repeat distance 13.9 Å). The repeat distance for **7a** is more than twice as large as for **1a**. Thus, **7a** can be viewed as a higher homologue of **1a** with a $W(CO)_3-C\equiv N-(N^{\cap}N')$ fragment inserted between the hydrogen donor and acceptor groups. In addition, this insertion introduces a directional change and thus straightens the zigzag chain of **1a** (angle between OH vectors of adjacent molecules ±61°) to a linear chain of **7a** (angle between OH vectors of adjacent molecules 0°).

Properties of 5b−16b

All polymer-bound complexes **5b**−**16b** were directly characterised on the solid support by IR and diffuse-reflectance UV/Vis spectroscopy, as well as thermogravimetric analyses (Table 4, Exp. Sect. and Supporting Information). The progress of the heterogeneous reactions can be monitored by IR spectroscopy due to the intense characteristic carbonyl and isocyanide absorption bands in this otherwise empty spectral region 1800−2100 cm^{-1}.[5,25,26] These characteristic patterns allow the detection of $\{M(CO)_3\}$ and

 © 2004 Wiley-VCH Verlag GmbH & Co. KGaA, Weinheim

Table 2. Selected bond lengths [Å] and angles [°] for **1a** and **7a**

1a		**7a**	
		W1−N1	2.212(8)
		W1−N2	2.236(8)
		W1−C13	1.968(11)
		W1−C14	2.000(12)
		W1−C15	1.940(10)
		W1−C16	2.095(11)
		C13−O13	1.159(11)
		C14−O14	1.153(12)
		C15−O15	1.179(12)
		C16−N3	1.167(12)
		N1−C7	1.281(12)
		N2−C8	1.360(12)
		C7−C8	1.475(14)
C4−O1	1.3593(13)	C4−O1	1.376(12)
O1−H1	0.980(19)	O1−H1	1.12(11)
N1−C7	1.2743(14)	N4−C23	1.281(13)
N2−C8	1.3505(15)	N5−C24	1.322(13)
C7−C8	1.4709(16)	C23−C24	1.453(14)
		N1−W1−N2	72.2(3)
		N1−W1−C13	166.9(3)
		N1−W1−C14	94.0(4)
		N1−W1−C15	103.7(4)
		N1−W1−C16	87.0(3)
		N2−W1−C13	94.7(4)
		N2−W1−C14	96.8(4)
		N2−W1−C15	175.1(4)
		N2−W1−C16	89.8(3)
		C13−W1−C14	88.2(4)
		C13−W1−C15	89.3(4)
		C13−W1−C16	92.3(4)
		C14−W1−C15	86.2(4)
		C14−W1−C16	173.4(4)
		C15−W1−C16	87.3(4)
		N1−C7−C8−N2	−2.6(13)
N1−C7−C8−N2	−163.06(10)	N4−C23−C24−N5	174.8(11)
		C7−N1−C1−C2	131.3(11)
C7−N1−C1−C2	−148.66(11)	C23−N4−C20−C21	32.8(17)

Table 3. Hydrogen-bonding geometry (distances in Å, angles in °)

D−H···A	D−H	D···A	H···A	D−H···A
1a: O1−H1···N2[a]	0.980(19)	2.7450(13)	1.772(20)	171.8(17)
7a: O1−H1···N5[b]	1.12(11)	2.757(12)	1.74(11)	148(9)

[a] Symmetry code $-x + 1/2, y, z + 1/2$. [b] Symmetry code $x + 1, y + 1, z$.

$\{M(CO)_4\}$ fragments on the polymer support. The intensity of these absorption bands can be compared to the intensity of the ν_{CH} absorption bands of the polymer backbone as internal standard, thus allowing a semi-quantitative reaction control.[5] The final immobilised dinuclear complexes display signals due to the $\{M(CO)_3\}$ and $\{M(CO)_4\}$ fragments and due to the isocyanide functional group (Table 4). The IR criteria (see above) for the different metal−metal sequences apply for the immobilised complexes as well, allowing the confirmation of the correct chain-growth even on a solid support:

Table 4. Analytical data of **8b**−**16b**

M^2/M^1 [a]		Cr	Mo	W
Cr	$\tilde{\nu}^1_{CO}$ [b]	1846	1826 (sh)	1850
	$\tilde{\nu}^2_{CO}$ [b]	1890	1853	
	$\tilde{\nu}^{3,4}_{CO}$ [b]	1917	1922	1914
	$\tilde{\nu}^5_{CO}$ [b]	2008	2007	2008
	$\tilde{\nu}_{CN}$ [b]	2072	2081	2070
	λ_{max} [c]	420, 850	420, 730	420, 800
	$\Delta m/m_{exp}$ ($\Delta m/m_{calcd.}$ [d])	10.9 (11.7)	11.5 (11.5)	9.0 (10.9)
Mo	$\tilde{\nu}^1_{CO}$ [b]	1848	1822	1848
	$\tilde{\nu}^2_{CO}$ [b]	1888 (sh)	1851	1890 (sh)
	$\tilde{\nu}^{3,4}_{CO}$ [b]	1914	1921	1911
	$\tilde{\nu}^5_{CO}$ [b]	2015	2013	2013
	$\tilde{\nu}_{CN}$ [b]	2071	2086	2077
	λ_{max} [c]	420, 850	420, 800	420, 790
	$\Delta m/m_{exp}$ ($\Delta m/m_{calcd.}$ [d])	11.7 (11.5)	11.0 (11.2)	10.9 (10.6)
W	$\tilde{\nu}^1_{CO}$ [b]	1847	1824	1853
	$\tilde{\nu}^2_{CO}$ [b]	1904	1903	
	$\tilde{\nu}^{3,4}_{CO}$ [b]	1918 (sh)	1918	1918
	$\tilde{\nu}^5_{CO}$ [b]	2007	2007	2007
	$\tilde{\nu}_{CN}$ [b]	2073	2083	2075
	λ_{max} [c]	420, 890	420, 670	420, 940
	$\Delta m/m_{exp}$ ($\Delta m/m_{calcd.}$ [d])	11.2 (10.9)	11.5 (10.6)	10.4 (10.2)

[a] IR values given in cm^{-1}; λ_{max} in nm, ε in $M^{-1}\cdot cm^{-1}$; δ in ppm; $\Delta m/m$ in %. [b] In CsI. [c] In polytetrafluoroethylene. [d] $\Delta m/m_{exp}$ at 200 °C; $\Delta m/m_{calcd.} = 100 \times (7 \times M_{CO})/[M_{resin} + M_{ligand} + (7 \times M_{CO}) + M_{M1} + M_{M2}]$ with $M_{CO} = 28$ g·mol^{-1}, $M_{resin} = 1160$ g·mol^{-1} (resin loading 0.9 mmol·g^{-1}), $M_{ligand} = 207$ g·mol^{-1}, M_{M1}, $M_{M2} = 52$ (Cr), 96 (Mo), 184 (W) g·mol^{-1}.

(i): $\tilde{\nu}_{CN} \geq 2081$ cm^{-1}: M^1 = Mo (**9b**, **12b**, **15b**) (Table 4);

(ii): $\tilde{\nu}^5_{CO} \geq 2012$ cm^{-1}: M^2 = Mo (**11b**, **12b**, **13b**) (Table 4);

(iii): (i) and (ii): $M^1 = M^2$ = Mo (**12b**) (Table 4).

The diffuse-reflectance spectra of the polymer-bound dinuclear complexes **8b**−**16b** show broad absorptions in the visible spectral region which can be assigned to the MLCT transitions of the two $\{(diimine)M(CO)_n\}$ chromophores ($n = 3$ at lower energy; $n = 4$ at higher energy; Table 4).[4,6]

These absorption bands are considerably shifted to lower energy relative to the MLCT bands of the soluble complexes as previously observed for similar immobilised complexes[4−6] (Tables 1 and 4). As the energy of the MLCT absorptions is dominated by the solvent polarity (see above and ref.[22]) the shift of the absorption bands of the immobilised complexes towards lower energy should be due to lower polarity of the polymer matrix. Even the degree of cross-linking influences the energy of the MLCT absorption bands. Resins with lower cross-linking (1% vs. 2% divinylbenzene) induce an even more pronounced bathochromic shift of the MLCT bands (Figure 6, Table 4 and ref.[5]). Obviously, the resin polarity decreases with decreasing cross-linking. This lower polarity of the 1% cross-linked resin might be induced by the lower internal pressure due to the pressure dependence of the polarity.[22] Thus, the MLCT absorption bands of the carbonyl complexes can be used to measure the resin polarity of different polymeric supports.

 © 2004 Wiley-VCH Verlag GmbH & Co. KGaA, Weinheim

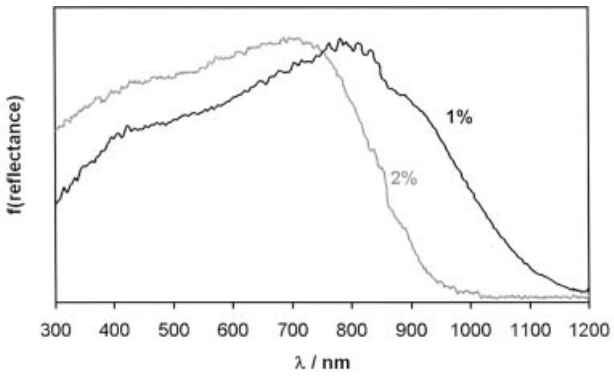

Figure 6. DRS UV/Vis spectra of **12b** (polystyrene with 1% and 2% divinylbenzene)

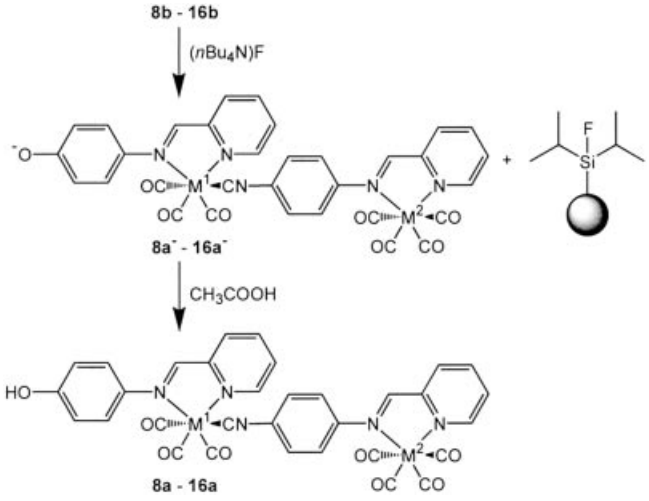

Scheme 3

Thermogravimetric analyses of resins **8b**−**16b** show that carbon monoxide is released up to 200 °C, as detected from the IR spectrum of the gas above heated samples.[5] The weight losses $\Delta m/m$ up to 200 °C of around 11% correspond well to the calculated weight losses (seven carbon monoxide molecules per immobilised complex) based on the initial ligand loading of the polymer (Figure 7, Table 4 and Supporting Information). This finding confirms the quantitative formation of the dinuclear complexes on the polymer, as the corresponding tricarbonyl complexes **5b**−**7b** show a weight loss, $\Delta m/m$, of around 6% (three carbon monoxide molecules per immobilised complex, Figure 7).

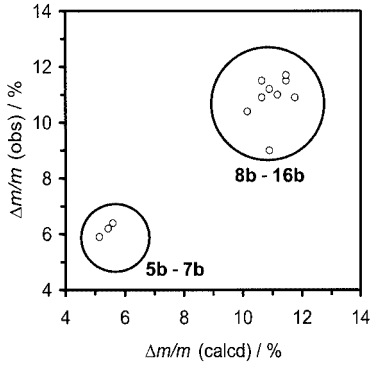

Figure 7. Correlation of experimental and calculated weight losses of resins **5b**−**16b**

In the final step of the solid-phase synthesis the dinuclear complexes were released from the support by cleavage of the Si−O bond with fluoride ions (Scheme 3).[4,5,18] The soluble anionic complexes **8a**$^-$−**16a**$^-$ can be detected in the IR and UV/Vis spectra of the cleavage solution (Table 5). All ν_{CO} absorption bands of **8a**$^-$−**16a**$^-$ are shifted to lower energy, while the MLCT absorption bands are hypsochromically shifted, due to the negatively charged ligand, relative to the neutral parent complexes **8a**−**16a**.

Protonation of **8a**$^-$−**16a**$^-$ with acetic acid yields the neutral complexes **8a**−**16a**, which were characterised as above. In all cases no spectroscopic evidence was observed for the formation of side products, thus confirming the identity and stability of the polymer-bound complexes.

Advantages/Disadvantages of the Synthetic Methods

The obvious drawback of the solution synthesis is the difficulty of obtaining pure samples. The solution synthesis requires exact stoichiometric reaction conditions to avoid formation of side products (mainly monomeric tetracarbonyl complexes) and tedious purification procedures of the products.

In the solid-phase synthesis approach, however, excess reagents can be used, driving the reactions to completion and thus avoiding the formation of polymer-bound side products. The reaction progress on the solid phase can be monitored by IR spectroscopy.[5,25,26] On the other hand the solid-phase synthesis requires adaptation of all reaction conditions and optimisation of the solid support. For the synthesis of the soluble complexes **8a**−**16a** identical reaction conditions can be applied irrespective of the metal centre to be incorporated (see Exp. Sect.). The synthesis of the polymer-bound complexes **8b**−**16b**, however, requires different reaction conditions depending on the metal fragment $\{M(CO)_3\}$ (M = Cr, Mo, W) to be attached. The highly reactive chromium derivatives must be handled at low temperatures (−30 °C) to avoid formation of tetracarbonyl complexes, which seems to be promoted by the polymer support, while the less reactive carbonyltungsten complexes must be activated at higher temperatures (60 °C); the solution reactions all proceed at room temperature (see Exp. Sect.). In addition, for reactions involving $\{M(CO)_n\}$ (M = Cr and W; n = 3, 4) the properties of the polymer support have to be optimised. The degree of cross-linking (2% divinylbenzene in the initial experiments with molybdenum[4,5]) has to be reduced to 1% divinylbenzene giving polymers

 © 2004 Wiley-VCH Verlag GmbH & Co. KGaA, Weinheim

Table 5. IR and UV/Vis spectroscopic data of **8a**$^-$−**16a**$^-$ in THF

M^2/M^1	[a]	Cr	Mo	W
Cr	$\tilde{\nu}^1_{CO}$	1805	1805	1814
	$\tilde{\nu}^2_{CO}$	1830	1833	1841
	$\tilde{\nu}^3_{CO}$	1892	1894	
	$\tilde{\nu}^4_{CO}$	1905	1908	1897
	$\tilde{\nu}^5_{CO}$	2000	2002	2002
	$\tilde{\nu}_{CN}$	2088	2087	2084
	λ_{max}	460, 535, 600 (sh)	465, 540, 590 (sh)	433, 530, 600 (sh)
Mo	$\tilde{\nu}^1_{CO}$	1810	1808	1803
	$\tilde{\nu}^2_{CO}$	1832	1835	1832
	$\tilde{\nu}^3_{CO}$		1897	1880 (sh)
	$\tilde{\nu}^4_{CO}$	1897	1912	1897
	$\tilde{\nu}^5_{CO}$	2006	2009	2006
	$\tilde{\nu}_{CN}$	2071	2094	2084
	λ_{max}	470, 560, 600 (sh)	475, 544, 600 (sh)	468, 565, 600 (sh)
W	$\tilde{\nu}^1_{CO}$	1810	1804	1809
	$\tilde{\nu}^2_{CO}$	1830	1831	1831
	$\tilde{\nu}^3_{CO}$	1885	1884	1885
	$\tilde{\nu}^4_{CO}$	1905	1909	1903
	$\tilde{\nu}^5_{CO}$	2000	2000	2000
	$\tilde{\nu}_{CN}$	2084	2084	2079
	λ_{max}	468, 550, 600 (sh)	467, 550 (sh), 600 (sh)	450 (sh), 500 (sh), 600 (sh)

[a] IR values given in cm^{-1}; λ_{max} in nm.

with better swelling properties and larger effective pore-sizes. The better swelling properties of the low cross-linked resins impart a lower internal pressure (as shown by the "solvent" dependence of the MLCT absorption bands) and thus render the heterogeneous reactions faster and more selective.

Conclusion

Dinuclear mixed-metal complexes with different metal centres at well-defined positions have been synthesised in solution and on a polymer support. The metal sequence of the soluble complexes can be determined by a combination of standard spectroscopic techniques and is retained under the applied reaction conditions. The solution synthesis is straightforward; however, the purification of the products is rather difficult, making this approach less suitable for longer-chain complexes. The solid-phase synthesis, although requiring more reaction steps (ligand immobilisation and product release) and differently optimised reaction conditions for each different reaction step, is much easier to accomplish. Furthermore, the solid-phase synthesis approach can easily be extended to longer-chain complexes by repeating the chain-growth reaction steps before the capping reaction without having to worry about solubility and purification of intermediates. This demonstrates the use of solid-phase synthesis methods in organometallic combinatorial chemistry.

Experimental Section

General: Unless noted otherwise, all manipulations were carried out under argon by means of standard Schlenk techniques. All solvents were dried by standard methods and distilled under argon prior to use. **1a**[4,5], **1b**[4,5] and C≡N−(N∩N′)[19] were prepared by literature methods. Polystyrene resins cross-linked with 1% divinylbenzene and with a ligand loading of 0.9 mmol·g^{-1} were used unless noted otherwise. The acetonitrile complexes were prepared from (cycloheptatriene)$M(CO)_3$ and (norbonadiene)$M(CO)_4$,[27,28] respectively, by reaction with CH_3CN (M = Cr, Mo, W). All other reagents were used as received from commercial sources. NMR spectra were recorded with a Bruker Avance DPX 200 at 200.15 MHz (^1H) at 303 K; chemical shifts are quoted in ppm with respect to residual solvent peaks as internal standards (CD_2Cl_2: δ = 5.32 ppm). IR spectra were recorded with a BioRad Excalibur FTS 3000 spectrometer using CaF_2 cells or CsI disks. UV/Vis/NIR spectra were recorded with a Perkin−Elmer Lambda 19, 0.2-cm cells (Hellma, Suprasil). DRS-UV/Vis spectra were measured with the same instrument using the Perkin−Elmer integrating sphere and poly(tetrafluoroethylene) as reference. Mass spectra were recorded with a Finnigan MAT 8400 spectrometer with a 4-nitrobenzyl alcohol matrix (FAB). Elemental analyses were performed by the microanalytical laboratory of the Organic Chemistry Department, University of Heidelberg. Thermogravimetric measurements were carried out with a Mettler TC 50, heating rate 10 K·min^{-1} under argon from 30−800 °C.

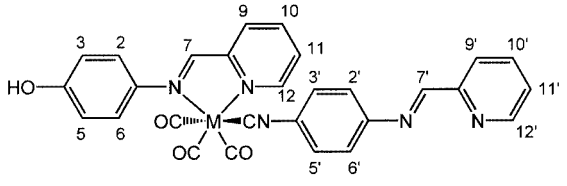

Solution Syntheses of 5a−7a: Freshly prepared $[M(CO)_3(CH_3CN)_3]$ (M = Cr, Mo, W) was added to a solution of **1a** (198 mg, 1 mmol) in THF (40 mL). The blue solution was stirred until IR control indicated complete formation of the THF complexes **2a**, **3a** or **4a**. C≡N−(N∩N′) (207 mg, 1 mmol) was added as a solid and the

 © 2004 Wiley-VCH Verlag GmbH & Co. KGaA, Weinheim

solution turned green immediately. The green solution was stirred until IR control indicated complete formation of the isocyanide complexes **5a**, **6a** or **7a**. The complexes were either isolated by addition of petroleum ether (boiling range 40−60 °C) and filtration of the precipitate or the solutions were used directly for the preparations of **8a−16a**.

5a: MS (FAB): *m/z* (%) = 541 (8) [M^+], 457 (48) [$M^+ - 3$ CO]. UV/Vis (THF): λ_{max} (ε) = 655 nm (6330 $M^{-1}\cdot cm^{-1}$). IR (THF): $\tilde{\nu}$ = 2071 (m, CN), 1915 (vs, CO), 1861 (s, CO), 1826 (s, CO) cm^{-1}. IR (CsI): $\tilde{\nu}$ = 3455 (br., OH), 2085 (m, CN), 1907 (vs, CO), 1838 (s, CO), 1811 (s, CO) cm^{-1}. ^{1}H NMR (CD_2Cl_2): δ = 7.0−7.6 (m, 10 H, $H^{2,6}$, $H^{2',6'}$, $H^{3,5}$, $H^{3',5'}$, H^{11}, $H^{11'}$), 7.8−8.0 (m, 3 H, H^9, H^{10}, $H^{10'}$), 8.23 (d, $^3J_{H,H}$ = 7.0 Hz, 1 H, $H^{9'}$), 8.53 (br. s, 1 H, $H^{12'}$), 8.58 (br. s, 1 H, H^7), 8.74 (br. s, 1 H, $H^{7'}$), 9.41 (d, $^3J_{H,H}$ = 5.2 Hz, 1 H, H^{12}) ppm. Satisfactory elemental analyses could not be obtained due to the inclusion of variable amounts of solvent molecules.

6a: MS (FAB): *m/z* (%) = 587 (31) [M^+], 559 (100) [$M^+ - CO$], 380 (95) [$M^+ - CN-(N\cap N')$]. UV/Vis (THF): λ_{max} (ε) = 613 nm (3475 $M^{-1}\cdot cm^{-1}$). IR (THF): $\tilde{\nu}$ = 2076 (m, CN), 1918 (vs, CO), 1855 (s, CO), 1824 (s, CO) cm^{-1}. IR (CsI): $\tilde{\nu}$ = 3388 (br., OH), 2089 (m, CN), 1911 (vs, CO), 1833 (s, CO), 1808 (s, CO) cm^{-1}. ^{1}H NMR (CD_2Cl_2): δ = 6.97 (d, $^3J_{H,H}$ = 8.8 Hz, 2 H, $H^{3,5}$), 7.3−7.7 (m, 8 H, $H^{2,6}$, $H^{2',6'}$, $H^{3',5'}$, H^{11}, $H^{11'}$), 7.8−8.0 (m, 3 H, H^9, H^{10}, $H^{10'}$), 8.2−8.3 (m, 1 H, $H^{9'}$), 8.59 (d, $^3J_{H,H}$ = 5.4 Hz, 1 H, $H^{12'}$), 8.66 (s, 1 H, H^7), 8.73 (br. s, 1 H, $H^{7'}$), 9.30 (d, $^3J_{H,H}$ = 5.2 Hz, 1 H, H^{12}) ppm. Satisfactory elemental analyses could not be obtained due to the inclusion of variable amounts of solvent molecules.

7a: UV/Vis (THF): λ_{max} (ε) = 627 nm (3225 $M^{-1}\cdot cm^{-1}$). IR (THF): $\tilde{\nu}$ = 2071 (m, CN), 1913 (vs, CO), 1848 (s, CO), 1825 (s, CO) cm^{-1}. IR (CsI): $\tilde{\nu}$ = 3412 (br., OH), 2087 (m, CN), 1906 (vs, CO), 1831 (s, CO), 1807 (s, CO) cm^{-1}. ^{1}H NMR (CD_2Cl_2): δ = 7.01 (d, $^3J_{H,H}$ = 8.8 Hz, 2 H, $H^{3,5}$), 7.3−7.7 (m, 8 H, $H^{2,6}$, $H^{2',6'}$, $H^{3',5'}$, H^{11}, $H^{11'}$), 7.8−8.0 (m, 3 H, H^9, H^{10}, $H^{10'}$), 8.2−8.3 (m, 1 H, $H^{9'}$), 8.58 (br. s, 1 H, $H^{12'}$), 8.74 (br. s, 1 H, $H^{7'}$), 8.89 (br. s, 1 H, H^7), 9.40 (d, $^3J_{H,H}$ = 5.2 Hz, 1 H, H^{12}) ppm. Satisfactory elemental analyses could not be obtained due to the inclusion of variable amounts of solvent molecules.

Solution Syntheses of 8a−16a: Freshly prepared [$(CH_3CN)_2M(CO)_4$] (M = Cr, Mo, W) (1 mmol) was added to a solution of **5a**, **6a** or **7a** (1 mmol) in THF. The dark solution was stirred until IR control indicated complete formation of the dinuclear complex. Addition of petroleum ether (boiling range 40−60 °C) precipitated the product complexes, which were purified by repeated washings with diethyl ether (removal of mononuclear complexes) and recrystallisation from THF/diethyl ether.

8a: $C_{32}H_{19}Cr_2N_5O_8$ (705.5): calcd. C 54.48, H 2.71, N 9.93; found C 53.32, H 3.98, N 9.38. MS (FAB): *m/z* (%) = 705 (5) [M^+]. IR (CsI): $\tilde{\nu}$ = 3469 (br., OH), 2082 (m, CN), 2008 (m, CO), 1906 (vs, CO), 1833 (br., s, CO) cm^{-1}. ^{1}H NMR (CD_2Cl_2): δ = 7.1−7.7 (m, 10 H, $H^{2,6}$, $H^{2',6'}$, $H^{3,5}$, $H^{3',5'}$, H^{11}, $H^{11'}$), 7.7−8.0 (m, 4 H, H^9, $H^{9'}$, H^{10}, $H^{10'}$), 8.51 (br. s, 2 H, H^7, $H^{7'}$), 9.29 (d, $^3J_{H,H}$ = 3.6 Hz, 1 H, $H^{12/12'}$), 9.40 (d, $^3J_{H,H}$ = 3.8 Hz, 1 H, $H^{12/12'}$) ppm.

9a: $C_{32}H_{19}CrMoN_5O_8$ (749.5): calcd. C 51.28, H 2.56, N 9.34; found C 51.46, H 3.49, N 9.36. IR (CsI): $\tilde{\nu}$ = 3449 (br., OH), 2091 (m, CN), 2009 (m, CO), 1910 (vs, CO), 1831 (br., s, CO) cm^{-1}. ^{1}H NMR (CD_2Cl_2): δ = 6.88 (br. d, 2 H, $H^{3,5}$), 7.1−7.5 (m, 8 H, $H^{2,6}$, $H^{2',6'}$, $H^{3',5'}$, H^{11}, $H^{11'}$), 7.7−7.9 (m, 4 H, H^9, $H^{9'}$, H^{10}, $H^{10'}$), 8.35, 8.47 (s, 1 H, H^7, $H^{7'}$), 9.14 (m, 2 H, $H^{12,12'}$) ppm.

10a: $C_{32}H_{19}CrN_5O_8W$ (837.4): calcd. C 45.90, H 2.29, N 8.36; found C 45.49, H 3.43, N 7.90. IR (CsI): $\tilde{\nu}$ = 3399 (br., OH), 2088 (m, CN), 2009 (m, CO), 1904 (vs, CO), 1831 (br., s, CO) cm^{-1}. ^{1}H NMR (CD_2Cl_2): δ = 6.9−7.1 (m, 2 H, $H^{3,5}$), 7.3−7.7 (m, 8 H, $H^{2,6}$, $H^{2',6'}$, $H^{3',5'}$, H^{11}, $H^{11'}$), 7.9−8.1 (m, 4 H, H^9, $H^{9'}$, H^{10}, $H^{10'}$), 8.49 (s, 1 H, $H^{7'}$), 8.90 (s, 1 H, H^7), 9.29 (d, $^3J_{H,H}$ = 5.4 Hz, 1 H, $H^{12,12'}$), 9.40 (d, $^3J_{H,H}$ = 5.8 Hz, 1 H, $H^{12,12'}$) ppm.

11a: $C_{32}H_{19}CrMoN_5O_8$ (749.5): calcd. C 51.28, H 2.56, N 9.34; found C 51.43, H 3.53, N 9.62. MS (FAB): *m/z* (%) = 749 (5) [M^+], 665 (10) [$M^+ - 3$ CO]. IR (CsI): $\tilde{\nu}$ = 3449 (br., OH), 2091 (m, CN), 2014 (m, CO), 1909 (vs, CO), 1833 (br., s, CO) cm^{-1}. ^{1}H NMR (CD_2Cl_2): δ = 7.0−7.1 (m, 2 H, $H^{3,5}$), 7.2−7.7 (m, 8 H, $H^{2,6}$, $H^{2',6'}$, $H^{3',5'}$, H^{11}, $H^{11'}$), 7.8−8.1 (m, 4 H, H^9, $H^{9'}$, H^{10}, $H^{10'}$), 8.54, 8.57 (s, 1 H, H^7, $H^{7'}$), 9.20 (d, $^3J_{H,H}$ = 5.8 Hz, 1 H, $H^{12,12'}$), 9.40 (d, $^3J_{H,H}$ = 5.0 Hz, 1 H, $H^{12,12'}$) ppm.

12a: $C_{32}H_{19}Mo_2N_5O_8$ (793.4): calcd. C 48.44, H 2.41, N 8.83; found C 48.17, H 3.55, N 8.47. MS (FAB): *m/z* = 792 (5) [$M^+ - H$], 380 (100) [$M^+ - CN-(N\cap N') - Mo - 4$ CO]. IR (CsI): $\tilde{\nu}$ = 3340 (br., OH), 2088 (m, CN), 2013 (m, CO), 1913 (vs, CO), 1908 (vs, CO), 1833 (br., s, CO) cm^{-1}. ^{1}H NMR (CD_2Cl_2): δ = 6.99 (d, $^3J_{H,H}$ = 8.8 Hz, 2 H, $H^{3,5}$), 7.3−7.8 (m, 8 H, $H^{2,6}$, $H^{2',6'}$, $H^{3',5'}$, H^{11}, $H^{11'}$), 7.8−8.1 (m, 4 H, H^9, $H^{9'}$, H^{10}, $H^{10'}$), 8.57 (s, 1 H, $H^{7'}$), 8.61 (s, 1 H, H^7), 9.20 (d, $^3J_{H,H}$ = 4.8 Hz, 1 H, $H^{12,12'}$), 9.30 (d, $^3J_{H,H}$ = 4.8 Hz, 1 H, $H^{12,12'}$) ppm.

13a: $C_{32}H_{19}MoN_5O_8W$ (881.3): calcd. C 43.61, H 2.17, N 7.95; found C 42.45, H 2.93, N 7.92. MS (FAB): *m/z* = 881 (30) [M^+], 853 (38) [$M^+ - CO$], 741 (45) [$M^+ - 5$ CO]. IR (CsI): $\tilde{\nu}$ = 3396 (br., OH), 2085 (m, CN), 2013 (m, CO), 1904 (vs, CO), 1830 (br., s, CO) cm^{-1}. ^{1}H NMR (CD_2Cl_2): δ = 6.9−7.1 (m, 2 H, $H^{3,5}$), 7.3−7.7 (m, 8 H, $H^{2,6}$, $H^{2',6'}$, $H^{3',5'}$, H^{11}, $H^{11'}$), 7.9−8.1 (m, 4 H, H^9, $H^{9'}$, H^{10}, $H^{10'}$), 8.57 (s, 1 H, $H^{7'}$), 8.90 (s, 1 H, H^7), 9.20 (d, $^3J_{H,H}$ = 5.4 Hz, 1 H, $H^{12,12'}$), 9.40 (d, $^3J_{H,H}$ = 5.6 Hz, 1 H, $H^{12,12'}$) ppm.

14a: $C_{32}H_{19}CrN_5O_8W$ (837.4): calcd. C 45.90, H 2.29, N 8.36; found C 44.78, H 3.32, N 7.71. MS (FAB): *m/z* = 725 (15) [$M^+ - 4$ CO], 669 (8) [$M^+ - 6$ CO], 641 (10) [$M^+ - 7$ CO]. IR (CsI): $\tilde{\nu}$ = 3450 (br., OH), 2084 (m, CN), 2007 (m, CO), 1906 (vs, CO), 1831 (br., s, CO) cm^{-1}. ^{1}H NMR (CD_2Cl_2): δ = 6.9−7.1 (m, 2 H, $H^{3,5}$), 7.2−7.7 (m, 8 H, $H^{2,6}$, $H^{2',6'}$, $H^{3',5'}$, H^{11}, $H^{11'}$), 7.8−8.1 (m, 4 H, H^9, $H^{9'}$, H^{10}, $H^{10'}$), 8.53 (s, 1 H, H^7), 8.87 (s, 1 H, $H^{7'}$), 9.31 (br. s, 1 H, $H^{12,12'}$), 9.40 (br. s, 1 H, $H^{12,12'}$) ppm.

15a: $C_{32}H_{19}MoN_5O_8W$ (881.3): calcd. C 43.61, H 2.17, N 7.95; found C 44.38, H 3.32, N 8.02. MS (FAB): *m/z* = 853 (5) [$M^+ - CO$], 797 (4) [$M^+ - 3$ CO], 685 (5) [$M^+ - 7$ CO]. IR (CsI): $\tilde{\nu}$ = 3393 (br., OH), 2093 (m, CN), 2009 (m, CO), 1910 (vs, CO), 1829 (br., s, CO) cm^{-1}. ^{1}H NMR (CD_2Cl_2): δ = 7.02 (d, $^3J_{H,H}$ = 8.6 Hz, 2 H, $H^{3,5}$), 7.2−7.7 (m, 8 H, $H^{2,6}$, $H^{2',6'}$, $H^{3',5'}$, H^{11}, $H^{11'}$), 7.7−8.0 (m, 4 H, H^9, $H^{9'}$, H^{10}, $H^{10'}$), 8.57 (s, 1 H, H^7), 8.90 (s, 1 H, $H^{7'}$), 9.20 (d, $^3J_{H,H}$ = 5.2 Hz), 1 H, $H^{12,12'}$, 9.40 (d, $^3J_{H,H}$ = 5.2 Hz, 1 H, $H^{12,12'}$) ppm.

16a: $C_{32}H_{19}N_5O_8W_2$ (969.2): calcd. C 39.66, H 1.98, N 7.23; found C 40.77, H 2.69, N 7.98. MS (FAB): *m/z* = 969 (15) [M^+]. IR (CsI): $\tilde{\nu}$ = 3464 (br., OH), 2085 (m, CN), 2007 (m, CO), 1900 (vs, CO), 1831 (br., s, CO) cm^{-1}. ^{1}H NMR (CD_2Cl_2): δ = 7.02 (m, 2 H, $H^{3,5}$, $^3J_{H,H}$ = 7.2 Hz), 7.2−7.7 (m, 8 H, $H^{2,6}$, $H^{2',6'}$, $H^{3',5'}$, H^{11}, $H^{11'}$), 7.9−8.1 (m, 4 H, H^9, $H^{9'}$, H^{10}, $H^{10'}$), 8.87, 8.90 (s, 1 H, H^7, $H^{7'}$), 9.32 (d, $^3J_{H,H}$ = 5.2 Hz, 1 H, $H^{12,12'}$), 9.40 (d, $^3J_{H,H}$ = 5.8 Hz, 1 H, $H^{12,12'}$).

Solid-Phase Synthesis of 5b−7b: Freshly prepared [$M(CO)_3(CH_3CN)_3$] (M = Cr, Mo, W) (0.5 mmol), dissolved in

 © 2004 Wiley-VCH Verlag GmbH & Co. KGaA, Weinheim

CH_3CN (15 mL), was added to resin **1b** (ca. 0.25 mmol), swollen in toluene (15 mL). The suspension was stirred (M = Cr: 20 min, −30 °C; M = Mo: 20 min, 20 °C; M = W: 60 min, 60 °C) and the resin turned from yellow to blue. The solvents were removed by filtration and the polymer was quickly washed with toluene/CH_3CN (1:1) until IR spectroscopy of the solution indicated complete removal of the excess $[M(CO)_3(CH_3CN)_3]$. Due to the sensitivity of the immobilised complex, the resin swollen in toluene was immediately treated with the ligand C≡N−(N∩N′) (104 mg, 0.5 mmol), dissolved in THF (5 mL). The polymer turned green immediately, and after 30 min, the resin was washed with THF until IR spectroscopy indicated complete removal of the excess C≡N−(N∩N′). The resin was dried under reduced pressure giving a dark green powder or used directly for further reactions. No soluble (diimine)$Mo(CO)_x$ complexes were observed by IR spectroscopy at any stage of the reaction.

5b: IR (CsI): $\tilde{\nu}$ = 2074 (m, CN), 1919 (s, CO), 1863 (m, CO), 1833 (m, CO) cm^{-1}. UV/Vis: λ_{max} = 420 (sh), 880 (br.) nm. TG (200 °C): $\Delta m/m$ = 6.4% (calcd. 5.8%).

6b: IR (CsI): $\tilde{\nu}$ = 2084 (m, CN), 1922 (s, CO), 1857 (m, CO), 1826 (m, CO) cm^{-1}. UV/Vis: λ_{max} = 420 (sh), 810 (br.) nm. TG (200 °C): $\Delta m/m$ = 6.2% (calcd. 5.4%).

7b: IR (CsI): $\tilde{\nu}$ = 2072 (m, CN), 1913 (s, CO), 1850 (m, CO), 1822 (m, CO) cm^{-1}. UV/Vis: λ_{max} = 420 (sh), 830 (br.) nm. TG (200 °C): $\Delta m/m$ = 5.9% (calcd. 5.1%).

Solid-Phase Synthesis of 8b−16b: Freshly prepared $[M(CO)_4(CH_3CN)_2]$ (0.5 mmol) dissolved in THF (15 mL) was added to resin **5b**, **6b** or **7b** (ca. 0.25 mmol), swollen in THF (5 mL). After stirring at 20 °C for 2 h, the resin was washed with THF until IR spectroscopy indicated complete removal of the excess $[M(CO)_4(CH_3CN)_2]$. The resin was dried under reduced pressure giving a black powder. No soluble (diimine)$M(CO)_x$ complexes were observed by IR spectroscopy at any stage of the reaction.

Cleavage Procedure: A solution of tetra-*n*-butylammonium fluoride TBAF·$3H_2O$ (2 equiv.) in THF was added to a suspension of the appropriate resin in THF (10 mL). The suspension was stirred at ambient temperature for 6 h. IR spectroscopy indicated the formation of the anionic complexes **8a**$^-$−**16a**$^-$. The polymer was filtered and washed with THF until the wash solutions were colourless. The combined filtrates were acidified with acetic acid, concentrated under reduced pressure and the complexes were precipitated by addition of diethyl ether. Recrystallisation as above yielded the complexes **8a**−**16a**. After cleavage, mass spectrometry of the remaining silyl fluoride polymer indicated complete removal of the complexes.[18]

Crystallographic Structure Determinations: The measurements were carried out with an Enraf−Nonius Kappa CCD diffractometer using graphite monochromated Mo-K_α radiation. The data were processed using the standard Nonius software.[29] All calculations were performed using the SHELXT PLUS software package. Structures were solved using direct or Patterson methods with the SHELXS-97 program and refined with the SHELXL-97 program.[30] Graphical handling of the structural data during refinement was performed using XMPA[31] and WinRay.[32] Atomic coordinates and anisotropic thermal parameters of the non-hydrogen atoms were refined by full-matrix least-squares calculations. Data relating to the structure determinations are collected in Table 6. CCDC-233938 (**1a**) and -233939 (**7a**) contain the supplementary crystallographic data for this paper. These data can be obtained free of charge at www.ccdc.cam.ac.uk/conts/retrieving.html [or from the Cambridge Crystallographic Data Centre, 12 Union Road, Cambridge CB2 1EZ, UK; Fax: (internat.) + 44-1223-336033; E-mail: deposit@ccdc.cam.ac.uk].

Computational Methods: Density functional calculations were carried out with the Gaussian03/DFT[33] program series. The B3LYP formulation of density functional theory was used employing the LanL2DZ basis set.[33] Harmonic vibrational frequencies and IR

Table 6. X-ray crystallographic data of **1a** and **7a**

	1a	**7a**
Empirical formula	$C_{12}H_{10}N_2O$	$C_{28}H_{19}WN_5O_4$·1.6THF
Formula mass	198.22	673.34·1.6THF
Crystal dimension [mm]	0.50 × 0.20 × 0.20	0.15 × 0.10 × 0.08
Crystal system	orthorhombic	triclinic
Space group (no.)	*Pbca* (61)	$P\bar{1}$ (2)
a [Å]	15.611(3)	9.2510(19)
b [Å]	9.285(2)	9.4420(19)
c [Å]	13.678(3)	21.324(4)
α [°]	90	84.46(3)
β [°]	90	87.01(3)
γ [°]	90	83.45(3)
Cell volume [Å^3]	1982.6(7)	1840.2(6)
Molecular units per cell	8	2
μ [mm^{-1}]	0.087	3.184
Density (calcd.) [g cm^{-3}]	1.328	1.420
T [K]	200	200
Scan range (2Θ) [°]	5.2−60.1	4.4−55.2
Scan speed [s·$frame^{-1}$]	10	20
Measured reflections	22451	11662
Unique reflections	2902	8162
Obs. reflections [$I \geq 2\sigma(I)$]	2119	4691
Parameters refined	176	424
Max./min. of residual electron density [e·Å^{-3}]	0.24/−0.19	3.00/−1.21
Agreement factors	R_1 = 4.2%	R_1 = 7.6%
(F^2 refinement)	R_w = 10.9%	R_w = 18.1%

 © 2004 Wiley-VCH Verlag GmbH & Co. KGaA, Weinheim

intensities were calculated by numerical second derivatives using analytically calculated first derivatives. Frequencies are not scaled.

Acknowledgments

This work was supported by the Deutsche Forschungsgemeinschaft and the Fonds der Chemischen Industrie. The permanent, generous support from Prof. Dr. G. Huttner is gratefully acknowledged.

[1] *Electronic Materials: The Oligomer Approach* (Eds.: K. Müllen, G. Wegner), Wiley-VCH Weinheim, **1998**.
[2] F. Zaragoza Dörwald, *Organic Synthesis on Solid Phase*, Wiley-VCH Weinheim, **2000**.
[3] R. B. Merrifield, *J. Am. Chem. Soc.* **1963**, *85*, 2149−2154.
[4] K. Heinze, *Chem. Eur. J.* **2001**, *7*, 2922−2932.
[5] K. Heinze, J. B. Toro, *Angew. Chem.* **2003**, *115*, 4671−4674; *Angew. Chem. Int. Ed.* **2003**, *42*, 4533−4536.
[6] K. Heinze, V. Jacob, C. Feige, *Eur. J. Inorg. Chem.*, in press.
[7] M. S. Robillard, A. R. P. M. Valentijn, N. J. Meeuwenoord, G. A. van der Marel, J. H. van Boom, J. Reedijk, *Angew. Chem.* **2000**, *112*, 3226−3229; *Angew. Chem. Int. Ed.* **2000**, *39*, 3096−3099.
[8] K. S. Schmidt, M. Boudvillain, A. Schwartz, G. A. van der Marel, J. H. van Boom, J. Reedijk, B. Lippert, *Chem. Eur. J.* **2002**, *8*, 5566−5570.
[9] M. S. Robillard, J. S. Leith, G. A. van der Marel, J. H. van Boom, J. Reedijk, *Eur. J. Inorg. Chem.* **2003**, 1529−1532.
[10] D. R. van Staveren, N. Metzler-Nolte, *Chem. Commun.* **2002**, 1406−1407.
[11] K. S. Schmidt, D. V. Filippov, N. J. Meeuwenoord, G. A. van der Marel, J. H. van Boom, B. Lippert, J. Reedijk, *Angew. Chem.* **2000**, *112*, 383−385; *Angew. Chem. Int. Ed.* **2000**, *39*, 375−377.
[12] N. E. Landbeater, E. L. Sharp, *Organometallics* **2003**, *22*, 4167−4169.
[13] S. I. Khan, A. E. Beilstein, M. Sykora, G. D. Smith, X. Hu, M. W. Grinstaff, *Inorg. Chem.* **1999**, *38*, 3922−3925.
[14] A. E. Beilstein, M. W. Grinstaff, *Chem. Commun.* **2000**, 509−510.
[15] I. Vargas-Baca, D. Mitra, H. J. Zulyniak, J. Banerjee, H. F. Sleiman, *Angew. Chem.* **2001**, *113*, 4765−4768, *Angew. Chem. Int. Ed.* **2001**, *40*, 4629−4632.
[16] J. F. Valliant, R. W. Riddoch, D. W. Hughes, D. G. Roe, T. K. Fauconnier, J. R. Thornback, *Inorg. Chim. Acta* **2001**, *325*, 155−163.
[17] S. van Zutphen, M. S. Robillard, G. A. van der Marel, H. S. Overkleeft, H. den Dulk, J. Brouwer, J. Reedijk, *Chem. Commun.* **2003**, 634−635.
[18] K. Heinze, U. Winterhalter, T. Jannack, *Chem. Eur. J.* **2000**, *6*, 4203−4210.
[19] K. Heinze, V. Jacob, *Eur. J. Inorg. Chem.* **2003**, 3918−3923.
[20] K. Heinze, *J. Chem. Soc., Dalton Trans.* **2002**, 540−547.
[21] K. Heinze, V. Jacob, *J. Chem. Soc., Dalton Trans.* **2002**, 2379−2385.
[22] A. Vlček, Jr., *Coord. Chem. Rev.* **2002**, *230*, 225−242.
[23] M. J. Kamlet, J.-L. M. Abboud, M. H. Abraham, R. W. Taft, *J. Org. Chem.* **1983**, *48*, 2877−2887.
[24] Lorenz profiles $y = 2A/\pi[w/(4(x - x_c)^2 + w^2)]$. For **10a**: x_{c1} = 342.1, w_1 = 108.7, A_1 = 434.8; x_{c2} = 551.5, w_2 = 161.4, A_2 = 122.4; x_{c3} = 629.2, w_3 = 122.9, A_3 = 53.5; R^2 = 0.99964; for **14a**: x_{c1} = 342.4, w_1 = 113.3, A_1 = 272.0; x_{c2} = 551.5, w_2 = 136.6, A_2 = 79.4; x_{c3} = 664.2, w_3 = 116.6, A_3 = 30.0; R^2 = 0.99952.
[25] B. Yan, *Acc. Chem. Res.* **1998**, *31*, 621−630.
[26] B. Yan, H.-U. Gremlich, S. Moss, G. M. Coppola, Q. Sun, L. Liu, *J. Comb. Chem.* **1999**, *1*, 46−54.
[27] M. A. Bennett, L. Pratt, G. Wilkinson, *J. Chem. Soc.* **1961**, 2037−2044.
[28] E. W. Abel, M. A. Bennett, R. Burton, G. Wilkinson, *J. Chem. Soc.* **1958**, 4559−4563.
[29] R. Hooft, Collect, *Data Collection Software*, Nonius, The Netherlands, **1998**; http://www.nonius.com
[30] G. M. Sheldrick, *SHELXS-97, Program for Crystal Structure Solution*, University of Göttingen, Germany, **1997**; http://www.shelx.uni-ac.gwdg.de/shelx/index.html; G. M. Sheldrick, *SHELXL-97, Program for Crystal Structure Refinement*, University of Göttingen, Germany, **1997**; http://www.shelx.uni-ac.gwdg.de/shelx/index.html; *International Tables for X-ray Crystallography*, Kynoch Press, Birmingham, U. K., **1974**, vol. 4.
[31] L. Zsolnai, G. Huttner, *XPMA*, University of Heidelberg, Germany, **1998**; http://www.rzuser.uni-heidelberg.de/~il1/laszlo/xpm.html
[32] R. Soltek, G. Huttner, *WinRay*, University of Heidelberg, Germany, **1999**; http://www.uni-heidelberg.de/institute/fak12/AC/huttner/frame/frame_soft.html
[33] M. J. Frisch, G. W. Trucks, H. B. Schlegel, G. E. Scuseria, M. A. Robb, J. R. Cheeseman, J. A. Montgomery, Jr., T. Vreven, K. N. Kudin, J. C. Burant, J. M. Millam, S. S. Iyengar, J. Tomasi, V. Barone, B. Mennucci, M. Cossi, G. Scalmani, N. Rega, G. A. Petersson, H. Nakatsuji, M. Hada, M. Ehara, K. Toyota, R. Fukuda, J. Hasegawa, M. Ishida, T. Nakajima, Y. Honda, O. Kitao, H. Nakai, M. Klene, X. Li, J. E. Knox, H. P. Hratchian, J. B. Cross, C. Adamo, J. Jaramillo, R. Gomperts, R. E. Stratmann, O. Yazyev, A. J. Austin, R. Cammi, C. Pomelli, J. W. Ochterski, P. Y. Ayala, K. Morokuma, G. A. Voth, P. Salvador, J. J. Dannenberg, V. G. Zakrzewski, S. Dapprich, A. D. Daniels, M. C. Strain, O. Farkas, D. K. Malick, A. D. Rabuck, K. Raghavachari, J. B. Foresman, J. V. Ortiz, Q. Cui, A. G. Baboul, S. Clifford, J. Cioslowski, B. B. Stefanov, G. Liu, A. Liashenko, P. Piskorz, I. Komaromi, R. L. Martin, D. J. Fox, T. Keith, M. A. Al-Laham, C. Y. Peng, A. Nanayakkara, M. Challacombe, P. M. W. Gill, B. Johnson, W. Chen, M. W. Wong, C. Gonzalez, J. A. Pople, *Gaussian 03*, Revision B.03, Gaussian, Inc., Pittsburgh, PA, **2003**.

Received March 26, 2004
Early View Article
Published Online June 18, 2004

 © 2004 Wiley-VCH Verlag GmbH & Co. KGaA, Weinheim

Phosphane-Catalyzed Reactions of $LAlH_2$ with Elemental Chalcogens; Preparation of [LAl(μ-E)$_2$AlL] [E = S, Se, Te, L = HC{C(Me)N(Ar)}$_2$, Ar = 2,6-*i*Pr$_2$C$_6$H$_3$]

Vojtech Jancik,[a] Monica M. Moya Cabrera,[b] Herbert W. Roesky,*[a] Regine Herbst-Irmer,[a] Dante Neculai,[a] Ana M. Neculai,[a] Mathias Noltemeyer,[a] and Hans-Georg Schmidt[a]

Dedicated to Professor Raymundo Cea Olivares

Keywords: Aluminum / Catalysis / Chalcogens / Phosphanes / Reaction mechanisms

Addition of catalytic amounts of a phosphane to a reaction mixture containing $LAlH_2$ [**2**; L = HC{C(Me)N(Ar)}$_2$, Ar = 2,6-*i*Pr$_2$C$_6$H$_3$] and elemental Se or Te resulted in the formation of poorly soluble [LAl(μ-Se)$_2$AlL] (**3**) and [LAl(μ-Te)$_2$AlL] (**4**), respectively. The sulfur analogue [LAl(μ-S)$_2$AlL] (**5**) could not be obtained from the direct reaction of **2** with elemental sulfur; consequently, its synthesis was successfully achieved from the reaction of [$LAlH_2$] and [LAl(SH)$_2$]. A possible mechanism for the formation of [LAl(μ-Se)$_2$AlL] and [LAl(μ-Te)$_2$AlL] is discussed. The molecular structures of compounds **3**–**5** were determined by X-ray structure analyses.

(© Wiley-VCH Verlag GmbH & Co. KGaA, 69451 Weinheim, Germany, 2004)

Introduction

Aluminum compounds containing heavier Group 16 elements have been comparatively less-well studied than those containing Al−O bonds, mainly due to the thermodynamic stability of the latter species. Recently, we have reported the preparation of unusual species of composition [LAl(EH)$_2$] [L = HC{C(Me)N(Ar)}$_2$, Ar = 2,6-*i*Pr$_2$C$_6$H$_3$, E = O, S, Se],[1−3] as well as the catalytic role of P(NMe$_2$)$_3$ in the synthesis of [LAl(SH)$_2$] (**1**).[2] As an extension of our interest in this type of compounds, we explored the influence of phosphanes on the $LAlH_2$/Se(Te) system. So far, there are only a few examples of compounds containing Al−E moieties in which the chalcogen atom is not directly bonded to any alkyl, aryl or trialkylsilyl group.[4−25] Three different aggregation modes have been observed for species containing Al and chalcogen atoms in a 1:1 molar ratio, mainly depending on the hapticity of the chalcogen atom. In these systems, the chalcogens can act either as a μ- or μ$_3$-bridging ligand as a consequence of the steric hindrance of the substituents present on the aluminum. Thus, the [AlE]$_n$ core can be either square planar (n = 2),[4−13,17] cubic (n = 4)[13−17] or adopt a hexagonal drum structure (n = 6).[14] Other examples containing Al and E in a ratio that deviates from 1:1 have also been reported to exhibit a bent Al−E−Al moiety, adamantane-like Al_4E_6 or more complex structures.[3,20−24] We have recently shown that [$LAlH_2$] (**2**), prepared from LH and AlH_3·NMe$_3$, reacts with elemental selenium[3] and, in the presence of a phosphane as catalyst, also with elemental sulfur,[2] to give species of the general formula [LAl(EH)$_2$] (E = Se, S). The selenium derivative is thermodynamically unstable and decomposes to yield [{LAl(SeH)}$_2$Se] with elimination of H_2Se.[3] Nevertheless, no product formation was observed from the reaction of $LAlH_2$ with elemental Te, although extreme reaction conditions were used. Herein, we report on the significant influence of catalytic amounts of phosphane in the reaction of **2** and Se and Te leading to [LAl(μ-Se)$_2$AlL] (**3**) and [LAl(μ-Te)$_2$AlL] (**4**), respectively. [LAl(μ-S)$_2$AlL] (**5**) could not be obtained using this protocol, therefore **5** was synthesized by the direct reaction of [LAl(SH)$_2$] with [$LAlH_2$].

[a] Institute of Inorganic Chemistry, University of Göttingen, Tammannstrasse 4, 37077 Göttingen, Germany
Fax: +49-551-393-373
E-mail: hroesky@gwdg.de
[b] Instituto de Química, UNAM, Circuito Exterior Cd. Universitaria,
Coyoacán, D. F. 04510, Mexico
Fax: +52-55-6162203 or -6162217
E-mail: monica.moya@correo.unam.mx

Results and Discussion

Addition of catalytic amounts of P(NMe$_2$)$_3$ or PMe_3 to a suspension of **2** and Se or Te resulted in the formation of [LAl(μ-E)$_2$AlL] (**3** E = Se; **4** E = Te) in high yields at ambi-

 © 2004 Wiley-VCH Verlag GmbH & Co. KGaA, Weinheim DOI: 10.1002/ejic.200400062

ent temperature. Compounds **3** and **4** are sparingly soluble in common organic solvents such as toluene, dichloromethane and tetrahydrofuran. In order to gain further insight regarding the role of the phosphane in this system, we investigated the reaction mechanism and possible by-products involved in this reaction. All attempts to follow the kinetics of these reactions by means of ^1H NMR spectroscopy failed due to the poor solubility of the elemental chalcogens and resulting products. However, previous experimental data revealed that the formation of **1** proceeds via the reactive intermediate [LAlH(SH)].[2] In order to obtain further insight into the reaction mechanism, we carried out several experiments varying the stoichiometry of the starting materials. The most striking finding was that, in the presence of phosphane, [LAl(μ-E)$_2$AlL]. analogous to the [LGa(μ-E)$_2$GaL] (E = O, S) derivatives prepared recently by Power et al.,[26] was the only product formed, regardless of the stoichiometry of the reagents employed; the direct reaction of **2** with elemental Se (in absence of the phosphane) led entirely to the formation of [LAl(SeH)$_2$].[3] In the latter case, another type of reaction mechanism involving a higher coordinated aluminum center formed by complexation of Se_2 to the aluminum has been suggested.[3,27–29] Finally, due to the fact that $TePR_3$ compounds are known to be good sources of soluble and reactive Te,[30–32] we carried out the direct reaction of **2** with $TePEt_3$ in an equimolar ratio. The reaction leads to pure **4** and free PEt_3 in almost quantitative yield, indicating that the gas evolved during the reaction is H_2 instead of H_2Te. All the experimental results outlined here are highly supportive of the proposed reaction mechanism. Therefore, we assume that Se and Te initially react with the corresponding phosphanes to yield $SeP(NMe_2)_3$ and $TePMe_3$, respectively. These compounds are unstable[30–32] and react in the following steps with **2** to yield [LAlH(EH)] (E = Se, Te), with elimination of phosphane. The last step corresponds to the formation of [LAl(μ-E)$_2$AlL] (E = Se, Te) by an elimination of two molecules of H_2. The splitting of the species into monomer units LAlE in the gas phase can indicate an intramolecular elimination followed by dimerisation, but we were not able to isolate such intermediates. Scheme 1 shows the steps involved in this reaction.

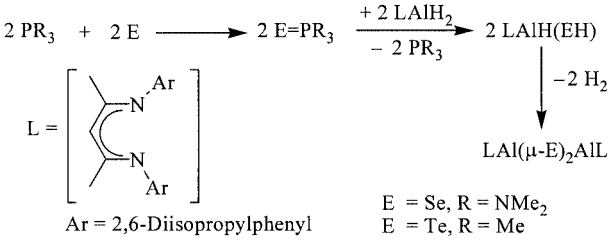

Scheme 1

As mentioned above, the reaction between [LAlH$_2$] (**2**) and elemental sulfur catalyzed by phosphane leads to [LAl(SH)$_2$] (**1**) and not to the desired [LAl(μ-S)$_2$AlL] (**5**).[2] Therefore we used the latent protic character of the hydrogen atoms from the SH groups of **1** and reacted the latter species in refluxing toluene with **2**. After 15 h we obtained **5** as a white insoluble microcrystalline solid in 92% yield. Scheme 2 summarizes the preparation of the three compounds.

Compounds **3**–**5** are insoluble in common organic solvents, and the powders obtained after the syntheses yielded nicely shaped monocrystals from a mixture of toluene/trichloromethane (10:1). The crystallization was achieved by solvation of [LAl(μ-E)$_2$AlL] with 2.32 equivalents of trichloromethane and 0.68 equivalents of toluene (**5**; E = S), two molecules of trichloromethane and one molecule of toluene (**3**; E = Se), or 2.73 molecules of trichloromethane and 0.27 molecules of toluene (**4**; E = Te) sharing the same spatial position in the crystal lattice, as shown by single-crystal X-ray structural analysis (Figures 1–3).[19]

The three isostructural compounds crystallize in the monoclinic space group *C*2/*m* and possess almost identical cell parameters (see Table 1). Taking into account the covalent radii (1.02 S, 1.17 Se and 1.35 Å Te),[33] the Al–S (2.237, 2.245 Å), Al–Se (2.359, 2.370 Å) and Al–Te bonds (2.575, 2.581 Å) are similar to one another. Furthermore, the E(1)–Al–E(1A) angles vary from 96.5° in **5** to 97.9° in

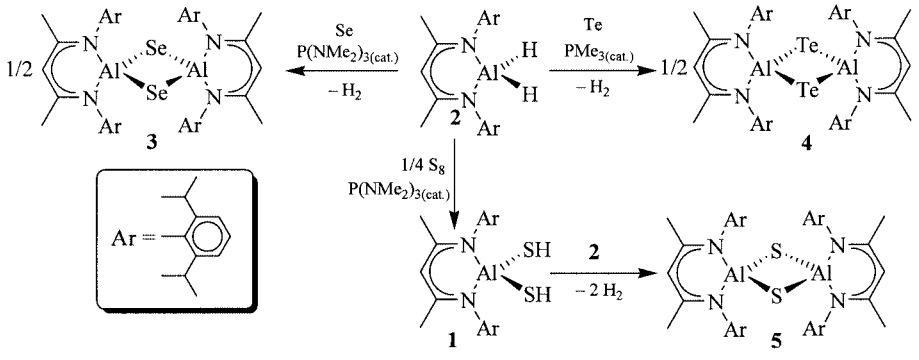

Scheme 2

 © 2004 Wiley-VCH Verlag GmbH & Co. KGaA, Weinheim

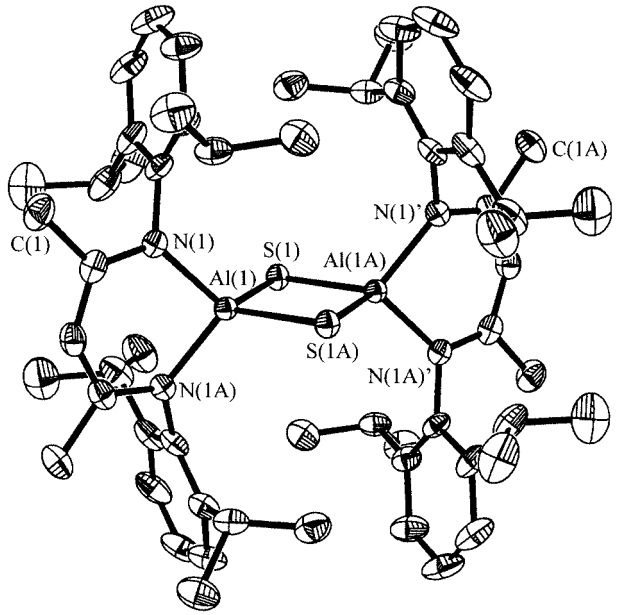

Figure 1. Molecular structure of LAl(μ-S)$_2$AlL (**5**) with 50% thermal ellipsoids; hydrogen atoms and solvent molecules are omitted for clarity; selected bond lengths [Å] and angles [°]: Al(1)−N(1)[N(1A)] 1.928(2), Al(1)−S(1) 2.237(1), Al(1)−S(1A) 2.245(1), S(1)−Al(1)−S(1A) 96.5(1), Al(1)−S(1)−Al(1A) 83.5(1), N(1)−Al(1)−N(1A) 94.9(1)

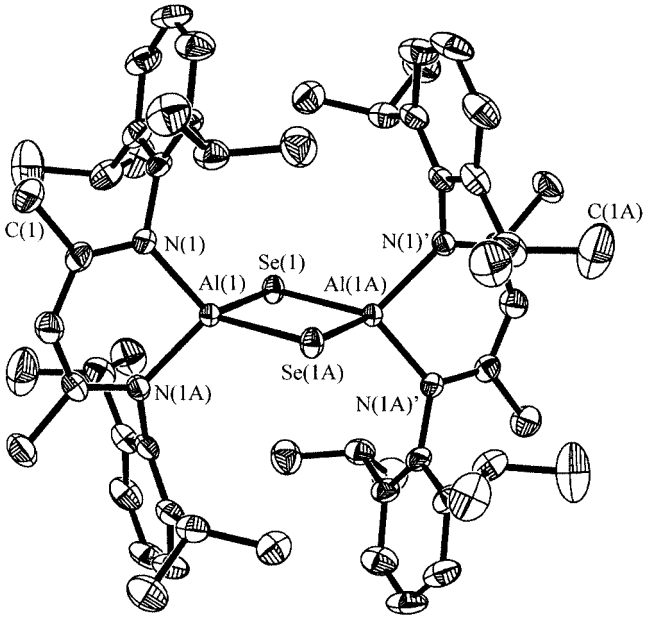

Figure 2. Molecular structure of LAl(μ-Se)$_2$AlL (**3**) with 50% thermal ellipsoids; hydrogen atoms and solvent molecules are omitted for clarity; selected bond lengths [Å] and angles [°]: Al(1)−N(1)[N(1A)] 1.924(3), Al(1)−Se(1) 2.359(1), Al(1)−Se(1A) 2.370(1), Se(1)−Al(1)−Se(1A) 97.5(1), Al(1)−Se(1)−Al(1A) 82.5(1), N(1)−Al(1)−N(1A) 95.2(2)

4 due to the larger radii of the chalcogen atom. All Al_2E_2 rings are, due to their symmetry, essentially planar, and the Al−E bond lengths are analogous to those of similar Al_2E_2 species (2.208−2.248 Å for S, 2.221−2.381 Å for Se, and 2.562−2.588 Å for Te), but the E(1)−Al−E(1A) (E = Se,

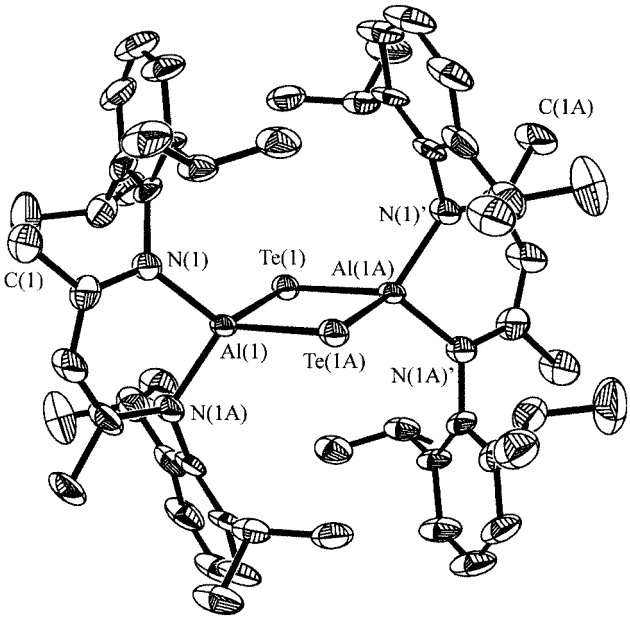

Figure 3. Molecular structure of LAl(μ-Te)$_2$AlL (**4**) with 50% thermal ellipsoids; hydrogen atoms and solvent molecules are omitted for clarity; selected bond lengths [Å] and angles [°]: Al(1)−N(1)[N(1A)] 1.908(5), Al(1)−Te(1) 2.575(3), Al(1)−Te(1A) 2.581(2), Te(1)−Al(1)−Te(1A) 97.9(1), Al(1)−Te(1)−Al(1A) 82.1(1), N(1)−Al(1)−N(1A) 96.0(3)

Te) angle is significantly more obtuse than those reported in the literature (99.9−103.6° for Se and 102.8−103.8° for Te)[4−12] due to the steric bulk of the β-diketiminato ligand. The latter values are similar to those of Al_4E_4 clusters (94.2−99.2° for Se and 94.1−96.3° for Te),[14,15] where the chalcogen atoms are always coordinated to three aluminum atoms. The S(1)−Al−S(1A) angle fits within the range of similar compounds (95.9−101.9°).[9−11] Selected bond lengths and angles for **3**−**5** are listed in Table 2.

All three compounds decompose without melting at temperatures above 200 °C, indicating their high thermal stability. The high stability of compounds **3**−**5** is further supported by the EI-mass spectra, which exhibit [M^+] ions for all three molecules: *m*/*z* = 952 (100%) for S, 1048 (48%) for Se and 1144 (25%) for Te. Unfortunately, due to the low solubility of **3**−**5** we were not able to record NMR spectra.

Conclusion

In summary, we have prepared and structurally characterized three new thermally stable aluminum chalcogenides [LAl(μ-E)AlL] (E = S, Se, Te). Furthermore, the significant influence of the phosphane on the product formation has been demonstrated and a possible mechanism for the conversion of aluminum hydrides to aluminum selenides and tellurides outlined.

Experimental Section

General: All the reactions and handling of reagents were performed under an atmosphere of dry nitrogen using Schlenk techniques or a

 © 2004 Wiley-VCH Verlag GmbH & Co. KGaA, Weinheim

Table 1. X-ray crystallographic data for **3**−**5**

	3·C_7H_8·2$CHCl_3$	**4**·0.27C_7H_8·2.73$CHCl_3$	**5**·0.68C_7H_8·2.32$CHCl_3$
Empirical formula	$C_{67}H_{92}Al_2Cl_6N_4Se_2$	$C_{62.63}H_{86.9}Al_2Cl_{8.18}N_4Te_2$	$C_{65.08}H_{89.78}Al_2Cl_{6.97}N_4S_2$
Molecular mass	1378.03	1495.14	1293.08
Temperature (K)	200(2)	100 (2)	100 (2)
Crystal system	monoclinic	monoclinic	monoclinic
Space group	*C*2/*m*	*C*2/*m*	*C*2/*m*
a (Å)	18.329 (4)	17.972 (2)	18.021 (3)
b (Å)	19.161 (5)	19.125 (2)	19.107 (3)
c (Å)	11.984 (3)	11.923 (2)	11.920 (2)
β (°)	125.54 (2)	124.84 (2)	125.22 (2)
V (Å^3)	3424.7(14)	3363.5 (8)	3353.0 (10)
Z	2	2	2
$D_{calcd.}$ (Mg·m^{-3})	1.336	1.476	1.281
Wavelength (Å)	0.71073	1.54178	1.54178
Absorption coefficient (mm^{-1})	1.38	10.40	3.84
F(000)	1436	1520	1369
θ range (°)	3.51−24.99	3.78−58.10	3.79−57.76
	$-21 \le h \le 21$	$-19 \le h \le 19$	$-19 \le h \le 19$
	$-4 \le k \le 22$	$-18 \le k \le 20$	$-20 \le k \le 15$
	$-14 \le l \le 14$	$-12 \le l \le 12$	$-13 \le l \le 13$
Reflections collected	4065	6352	7081
Independent reflections	3111 (R_{int} = 0.0307)	2314 (R_{int} = 0.0356)	2370 (R_{int} = 0.0224)
Data/restraints/parameters	3111/111/258	2314/405/332	2370/285/295
Goodness-on-fit on F^2	1.076	1.126	1.146
Final R_{int} [$I > 2\sigma(I)$]	R_1 = 0.0435	R_1 = 0.0510	R_1 = 0.0398
	wR_2 = 0.1083	wR_2 = 0.1174	wR_2 = 0.0989
R_{int} (all data)	R_1 = 0.0546	R_1 = 0.0535	R_1 = 0.0451
	wR_2 = 0.1171	wR_2 = 0.1187	wR_2 = 0.1017
Largest different peak and hole (e·Å^{-3})	0.881, −0.614	1.661, −0.878	0.436, −0.416

Table 2. Selected bond lengths (Å) and angles (°) for **3**−**5**

	3·1 C_7H_8·2 $CHCl_3$ (E = Se)	**4**·0.27 C_7H_8·2.73 $CHCl_3$ (E = Te)	**5**·0.68 C_7H_8·2.32 $CHCl_3$ (E = S)
Al−N	1.924 (3)	1.908 (5)	1.928 (2)
Al−E(1)	2.359 (2)	2.575 (3)	2.237 (1)
Al−E(1A)	2.370 (2)	2.581 (2)	2.245 (1)
E(1)−Al−E(1A)	97.5 (1)	97.9 (1)	96.5 (1)
Al(1)−E−Al(1A)	82.5 (1)	82.1 (1)	83.5 (1)

glovebox. Toluene was dried (Na/benzophenone ketyl) and distilled prior to use. Tellurium (99.5%; Aldrich) and PMe_3 (1 M solution in toluene; Fluka) were used as received. $P(NMe_2)_3$ (97%; Aldrich) was freshly distilled prior to use. Elemental red selenium,[34] $[LAlH_2]$,[3] $[LAl(SH)_2]$[2] and $TePEt_3$ [35] were prepared by literature procedures.

Infrared spectra were recorded as KBr pellets on a Bio-Rad Digilab FTS-7 spectrometer in the range 4000−350 cm^{-1}. Mass spectra were obtained with a Finnigan MAT 8230 or a Varian MAT CH5 instrument (70 eV). Elemental analyses were performed by the Analytical Laboratory, Institute of Inorganic Chemistry, University of Goettingen. Melting points were measured in sealed glass tubes and are uncorrected.

[LAl(μ-Se)$_2$AlL] (3): Toluene (20 mL) was added to a mixture of **2** (1.000 g, 2.239 mmol) and red selenium (0.176 g, 2.239 mmol) and after dissolution of **2**, freshly distilled $P(NMe_2)_3$ (0.03 mL, 0.055 mmol) was added. The reaction mixture was stirred for an additional 16 h and the white insoluble product was filtered off, washed with toluene (5 mL) and dried in vacuo. Yield: 1.07 g (91%). Decomp. without melting above 260 °C. IR (KBr pellet): $\tilde{\nu}$ = 3061 vw, 2959 st, 2927 w, 2868 w, 1588 vw, 1544 vst, 1462 w, 1438 m, 1392 vst, 1317 m, 1291 vw, 1249 w, 1177 w, 1101 w, 1058 vw, 1024 w, 937 vw, 867 w, 801 m, 775 vw, 763 w, 539 vw, 463 vw, 435 w, 411 vw cm^{-1}. EI-MS: *m*/*z* (%) = 1048 (48) $[M]^+$, 523 (28) $[M/2]^+$. $C_{58}H_{82}Al_2N_4Se_2$ (1047.2): calcd. C 66.52, H 7.89, N 5.35; found C 67.10, H 8.03, N 5.33.

[LAl(μ-Te)$_2$AlL] (4). Method 1: Toluene (20 mL) was added to a mixture of **2** (1.000 g, 2.239 mmol) and tellurium (0.285 g, 2.230 mmol) and after complete dissolution of **2**, PMe_3 (0.03 mL, 1 M solution in toluene, 0.030 mmol) was added. The reaction mixture was stirred for an additional 15 h, the pale yellow insoluble product was filtered off, washed with toluene (5 mL) and dried in vacuo. Yield: 1.15 g (90% based on Te). Decomp. without melting above 260 °C. IR (KBr pellet): $\tilde{\nu}$ = 3061 w, 3024 vw, 2990 w, 2968 vs, 2956 vs, 2930 st, 2866 m, 1587 w, 1543 vs, 1462 vs, 1440 vs, 1394 vs, 1365 sh, 1300 m, 1251 s, 1176 m, 1100 m, 1057 m, 1024 m, 937 m, 942 w, 868 st, 798 vs, 780 m, 761 st, 708 vw, 648 w, 595 vw, 537 w, 447 vw, 417 vst cm^{-1}. EI-MS: *m*/*z* (%) = 1144 (25) $[M]^+$, 574 (60) $[M/2]^+$, 443 (100) $[M/2 - Te - H]^+$. $C_{58}H_{82}Al_2N_4Te_2$ (1144.5): calcd. C 60.87, H 7.22, N 4.90; found C 60.50, H 7.15, N 4.82.

 © 2004 Wiley-VCH Verlag GmbH & Co. KGaA, Weinheim

Method 2: Toluene (20 mL) was added to a mixture of **2** (1.000 g, 2.239 mmol) and $TePEt_3$ (0.550 g, 2.239 mmol) and the reaction mixture was stirred for an additional 2 h. The pale-yellow insoluble product was filtered off, washed with toluene (5 mL) and dried in vacuo. Yield: 1.22 g (95%).

[LAl(μ-S)$_2$AlL] (5): Toluene (20 mL) was added to a mixture of **1** (1.144 g, 2.239 mmol) and **2** (1.000 g, 2.239 mmol) and the reaction mixture was refluxed over a period of 15 h. After this time, the mixture was cooled to ambient temperature and a white insoluble product was filtered off, washed with toluene (5 mL) and dried in vacuo. Yield: 1.96 g (92%). Decomp. without melting above 200 °C. IR (KBr pellet): $\tilde{\nu}$ = 3062 vw, 2959 st, 2924 m, 2866 w, 1589 vw, 1547 vst, 1529 sh, 1462 m, 1437 m, 1390 vst, 1317 st, 1291 vw, 1249 m, 1176 w, 1100 vw, 1058 vw, 1024 w, 937 vw, 868 w, 801 m, 775 w, 763 w, 652 vw, 541 w, 516 m, 472 w, 454 m cm^{-1}. EI-MS: *m*/*z* (%) = 952 (100) $[M]^+$, 937 (64) $[M - CH_3]^+$, 909 (21) $[M - C_3H_7]^+$, 477 (58) $[M/2]^+$. $C_{58}H_{82}Al_2N_4S_2$ (953.40): calcd. C 73.07, H 8.67, N 5.88; found C 72.63, H 8.53, N 5.88.

X-ray Crystallographic Study: Data for the X-ray structures of [LAl(μ-S)$_2$AlL] and [LAl(μ-Te)$_2$AlL] were collected on a Bruker three-circle diffractometer equipped with a SMART 6000 CCD area-detector, whereas data for the X-ray structural analysis of [LAl(μ-Se)$_2$AlL] were collected on a Stoe-AED 2 four-circle diffractometer. Structures were solved by direct methods (SHELXS-97)[36] and refined by full-matrix least-squares methods on F^2 with SHELXL-97.[37] The non-hydrogen atoms were refined anisotropically; hydrogen atoms were included at geometrically idealized positions and refined with the riding model.
CCDC-228825 (for **5**), -228826 (for **3**), -228827 (for **4**) contain the supplementary crystallographic data for this paper. These data can be obtained free of charge at www.ccdc.cam.ac.uk/conts/retrieving.html [or from the Cambridge Crystallographic Data Centre, 12 Union Road, Cambridge CB2 1EZ, UK; Fax: + 44-1223-336033; E-mail: deposit@ccdc.cam.ac.uk].

Acknowledgments

We thank the Deutsche Forschungsgemeinschaft, the Göttinger Akademie der Wissenschaften and the Fonds der Chemischen Industrie (predoctoral fellowship to V. J.) for funding.

[1] G. Bai, Y. Peng, H. W. Roesky, J. Li, H.-G. Schmidt, M. Noltemeyer, *Angew. Chem.* **2003**, *115*, 1164−1167; *Angew. Chem. Int. Ed.* **2003**, *42*, 1132−1135.
[2] V. Jancik, Y. Peng, H. W. Roesky, J. Li, D. Neculai, A. M. Neculai, R. Herbst-Irmer, *J. Am. Chem. Soc.* **2003**, *125*, 1452−1453.
[3] C. Cui, H. W. Roesky, H. Hao, H.-G. Schmidt, M. Noltemeyer, *Angew. Chem.* **2000**, *112*, 1885−1887; *Angew. Chem. Int. Ed.* **2000**, *39*, 1815−1817.
[4] C. Cui, H. W. Roesky, H.-G. Schmidt, M. Noltemeyer, *Organometallics* **1999**, *18*, 5120−5123.
[5] C. Cui, H. W. Roesky, H.-G. Schmidt, M. Noltemeyer, *Inorg. Chem.* **2000**, *39*, 3678−3681.
[6] W. J. Grigsby, C. L. Raston, V.-A. Tolhurst, B. W. Skelton, A. H. White, *J. Chem. Soc., Dalton Trans.* **1998**, 2547−2556.
[7] M. G. Gardiner, C. L. Raston, V.-A. Tolhurst, *J. Chem. Soc., Chem. Commun.* **1995**, 2501−2502.
[8] P. D. Godfrey, C. L. Raston, B. W. Skelton, V.-A. Tolhurst, A. H. White, *Chem. Commun.* **1997**, 2235−2236.
[9] C. Schnitter, A. Klemp, H. W. Roesky, H.-G. Schmidt, C. Röpken, R. Herbst-Irmer, M. Noltemeyer, *Eur. J. Inorg. Chem.* **1998**, 2033−2039.
[10] A. Ecker, R. Köppe, C. Üffing, H. Schnöckel, *Z. Anorg. Allg. Chem.* **1998**, *624*, 817−822.
[11] R. J. Wehmschulte, P. P. Power, *Chem. Commun.* **1998**, 335−336.
[12] H. Zhu, J. Chai, H. W. Roesky, M. Noltemeyer, H.-G. Schmidt, D. Vidovic, J. Magull, *Eur. J. Inorg. Chem.* **2003**, 3113−3119.
[13] K. S. Klimek, J. Prust, H. W. Roesky, M. Noltemeyer, H.-G. Schmidt, *Organometallics* **2001**, *20*, 2047−2051.
[14] C. F. Harlan, E. G. Gillan, S. G. Bott, A. R. Barron, *Organometallics* **1996**, *15*, 5479−5488.
[15] S. Schulz, H. W. Roesky, H. J. Koch, G. M. Sheldrick, D. Stalke, A. Kuhn, *Angew. Chem.* **1993**, *105*, 1828−1830; *Angew. Chem. Int. Ed. Engl.* **1993**, *32*, 1729−1731.
[16] A. H. Cowley, R. A. Jones, P. R. Harris, D. A. Atwood, L. Contreras, C. J. Burek, *Angew. Chem.* **1991**, *103*, 1164−1166; *Angew. Chem. Int. Ed. Engl.* **1991**, *30*, 1143−1146.
[17] T. Hirabayashi, K. Inoue, K. Yokota, Y. Ishii, *J. Organomet. Chem.* **1975**, *92*, 139−145.
[18] G. H. Robinson, M. F. Self, W. T. Pennington, S. A. Sangokoya, *Organometallics* **1988**, *7*, 2424−2426.
[19] R. J. Wehmschulte, P. P. Power, *J. Am. Chem. Soc.* **1997**, *119*, 9566−9567.
[20] W. Uhl, A. Vester, *J. Organomet. Chem.* **1993**, *443*, 9−17.
[21] W. Uhl, R. Gerding, I. Hahn, S. Pohl, W. Saak, H. Reuter, *Polyhedron* **1996**, *15*, 3987−3992.
[22] W. Uhl, U. Schuetz, *Z. Naturforsch., Teil B* **1994**, *49*, 931−934.
[23] W. Zheng, H. Hohmeister, N. C. Mösch-Zanetti, H. W. Roesky, M. Noltemeyer, H.-G. Schmidt, *Inorg. Chem.* **2001**, *40*, 2363−2367.
[24] W. Zheng, N. C. Mösch-Zanetti, H. W. Roesky, M. Noltemeyer, M. Hewitt, H.-G. Schmidt, T. R. Schneider, *Angew. Chem.* **2000**, *112*, 4446−4449; *Angew. Chem. Int. Ed.* **2000**, *39*, 4276−4279.
[25] M. Witt, H. W. Roesky, *Curr. Sci.* **2000**, *78*, 410−430.
[26] N. J. Hardman, P. P. Power, *Inorg. Chem.* **2001**, *40*, 2474−2475.
[27] C. Jones, G. A. Koutsantonis, C. L. Raston, *Polyhedron* **1993**, *12*, 1829−1848.
[28] C. L. Raston, *J. Organomet. Chem.* **1994**, *475*, 15−24.
[29] M. G. Gardiner, C. L. Raston, V.-A. Tolhurst, *J. Chem. Soc., Chem. Commun.* **1995**, 1457−1458.
[30] M. L. Steigerwald, C. R. Sprinkle, *Organometallics* **1988**, *7*, 245−246.
[31] L.-B. Han, F. Mirzaei, M. Tanaka, *Organometallics* **2000**, *19*, 722−724.
[32] N. Kuhn, G. Henkel, H. Schumann, R. Fröhlich, *Z. Naturforsch., Teil B* **1990**, *45*, 1010−1018.
[33] J. E. Huheey, *Inorganic Chemistry: Principles of Structure and Reactivity*, Harper Collins College Publishers, New York, **1993**, p. 292.
[34] J. Meyer, *Ber.* **1913**, *46*, 3089−3091.
[35] R. A. Zingaro, B. H. Steeves, K. Irgolic, *J. Organomet. Chem.* **1965**, *4*, 320−323.
[36] G. M. Sheldrick, SHELXS-97, Program for Structure Solution, *Acta Crystallogr., Sect. A* **1990**, *46*, 467−473.
[37] G. M. Sheldrick, SHELXL-97, *Program for Crystal Structure Refinement*, University of Göttingen, Göttingen, Germany, **1997**.

Received January 23, 2004
Early View Article
Published Online June 23, 2004

 © 2004 Wiley-VCH Verlag GmbH & Co. KGaA, Weinheim

The Thermal Decomposition of S_2O Forming SO_2, S_3, S_4 and S_5O − An ab initio MO Study

Ralf Steudel*[a] and Yana Steudel[a]

Keywords: Cycloaddition / Disproportionation / Sulfur / Sulfur heterocycles / Thermodynamics / Transition states

All chemically reasonable [2+2] and [2+3] dipolar addition reactions between two S_2O molecules forming heterocyclic intermediates of composition S_4O_2, as well as the decomposition of these species to generate the observed products S_3 and SO_2, have been studied by gas-phase ab initio MO calculations at the G3X(MP2) level of theory. The reaction enthalpies, Gibbs energies and, partly, activation enthalpies of 17 reactions have been calculated. The [2+2] cycloadditions of S_2O are all endothermic and are characterized by high barriers. The reaction of lowest activation enthalpy ($\Delta H^{\#}_{298}$ = 11 kJ·mol^{-1}) is the exothermic [2+3] cycloaddition of two S_2O molecules resulting in the five-membered heterocycle oxatetrathiolane 2-oxide S_4O_2 (**7**), which is predicted to decompose at 298 K exothermally and without any activation enthalpy to SO_2 plus S_3. The S_3 molecule is predicted to add exothermally to S_2O to give the five-membered homocycle S_5O which has, in fact, been prepared in this way before. The bimolecular decomposition of S_5O to SO_2, S_4 and S_5 is also exothermic and may explain the formation of the red S_4 molecule on condensation of S_2O at temperatures below –130 °C. The implications of these results for the understanding of the chemistry on Jupiter's moon Io are discussed.
(© Wiley-VCH Verlag GmbH & Co. KGaA, 69451 Weinheim, Germany, 2004)

Introduction

Disulfur monoxide is a combustion product of elemental sulfur under special reaction conditions, along with SO_2 and SO_3. S_2O is also formed in numerous redox reactions between reduced sulfur compounds and oxidizing agents as well as in thermal decomposition reactions of sulfur-rich sulfane oxides and sulfur oxides.[1] S_2O can be obtained in a practically pure form by the heterogeneous reaction of thionyl chloride vapor with solid silver sulfide at 160 °C and low pressures, see Equation (1).[2]

$$SOCl_2 + Ag_2S \rightarrow S_2O + 2AgCl \quad (1)$$

More recently, S_2O has seemingly been generated in solution by thermal decomposition of suitable organic precursors (e.g., sulfane oxides) or of S_8O, and the S_2O unit[3−5] and its decomposition product S_3 [5] have been trapped in situ by addition reactions with either unsaturated transition metal complexes[3] or with olefins, dienes or diazoalkanes.[4,5] These fascinating developments may result in a renaissance of S_2O chemistry in solution, although it must be stressed that this molecule has never been observed directly (e.g., spectroscopically) in liquid solutions.

The molecule S_2O is bent (C_s symmetry) in a similar fashion to its more symmetrical triatomic relatives O_3, SO_2 and S_3 (C_{2v} symmetry in each case). The most accurate experimental geometrical parameters of S_2O are d_{SO} = 145.6 pm, d_{SS} = 188.5 pm and a_{SSO} = 117.9°.[6]

The reactivity of S_2O has not been studied systematically, probably due to its thermal instability.[1] On condensation of gaseous S_2O at low temperatures, by dissolution in cold inert solvents or by increasing its partial pressure in the gas-phase at room temperature to values above 1 mbar, S_2O decomposes rapidly.[1] The final decomposition products of S_2O are elemental sulfur (S_8) and sulfur dioxide but the following intermediates have been observed under differing reaction conditions (in chronological order):

Deep-yellow amorphous polysulfur oxides of composition S_xO ($x > 3$) are formed on condensation of gaseous S_2O at −196 °C and subsequent warming of the condensate to 20 °C; at temperatures below −130 °C the initial condensates are cherry-red but after warming to near room temperature they turn yellow and on subsequent cooling they remain yellow.[2,7] The red color is as more intense with higher S_2O concentrations in the original gas.

Sulfur radicals have been detected by low-temperature ESR spectroscopy (−150 °C) in condensates formed from gaseous S_2O.[2]

The probably homocyclic oxide S_5O has been obtained in solution when a gaseous S_2O/SO_2 mixture was bubbled into inert solvents at low temperatures (e.g., $CHCl_3$ at −60 °C) followed by removal of the excess SO_2 under vacuum.[8] At temperatures above −20 °C the intensely yellow-colored dissolved S_5O decomposes with formation of SO_2 and elemental sulfur.

[a] Institut für Chemie, Technische Universität Berlin, Sekr. C2, 10623 Berlin, Germany
Fax (internat.) +49-30-3142-6519
E-mail: steudel@schwefel.chem.tu-berlin.de

The yellow-green molecule S_3 has been detected by low-temperature Raman spectroscopy in matrix-isolation experiments with gaseous S_2O,[9] as well as by UV/Vis spectroscopy of condensates of from gaseous S_2O (absorption at 420 nm).[10]

The red molecule S_4 has been detected by UV/Vis spectroscopy (absorption at 530 nm) in the aforementioned low-temperature condensates of S_2O,[10] although the Raman spectra of matrix-isolated and then thermally decomposed S_2O (by controlled diffusion) did not show any evidence for S_4.[9]

The mechanisms by which these intermediates and products are formed are unknown. Therefore, we have calculated by ab initio MO methods the most likely initial products of the thermal S_2O decomposition as well as some of the relevant transition states using the high-level G3X(MP2) method which is known to produce reliable thermodynamic data for sulfur-rich molecules.[11,12] Bimolecular reactions have been assumed for the initial stages. Our results shed a new light on the interpretation of the colors observed on Jupiter's moon Io, the surface of which is partly covered by elemental sulfur and sulfur oxides.

Results and Discussion

According to the above discussion the primary decomposition reactions of S_2O are expected to be the following [Equations (2) and (3)].

$$2\,S_2O \rightarrow S_3 + SO_2;\quad \Delta H^\circ_{298} = -49\ \text{kJ·mol}^{-1},\ \Delta G^\circ_{298} = -50\ \text{kJ·mol}^{-1} \qquad (2)$$

$$S_2O + S_3 \rightarrow \textit{cyclo}\text{-}S_5O;\quad \Delta H^\circ_{298} = -87\ \text{kJ·mol}^{-1},\ \Delta G^\circ_{298} = -34\ \text{kJ·mol}^{-1} \qquad (3)$$

Our calculated energies, enthalpies as well as the Gibbs energies of the species mentioned in Equations (2)−(18) are listed in Table 1. These data show that the reactions according to Equations (2) and (3) are strongly exothermic as well as exergonic. This then also holds for the overall reaction [Equation (4)].

$$3\,S_2O \rightarrow S_5O + SO_2;\quad \Delta H^\circ_{298} = -136\ \text{kJ·mol}^{-1},\ \Delta G^\circ_{298} = -83\ \text{kJ·mol}^{-1} \qquad (4)$$

The homocyclic S_5O molecule (pentathiolane oxide) may be considered as the simplest representative of the so-called polysulfur oxides (mentioned in the Introduction), which probably consist of cyclic and chain-like sulfur-rich species of unknown molecular mass and with the oxygen atoms mainly present as sulfoxide groups.[1]

The calculated NBO atomic charges of the S_2O molecule are −0.78 for oxygen, +1.00 for the central and −0.23 for the terminal sulfur atom. Therefore, the molecule is expected to undergo dipolar addition reactions. In the following sections we investigate the most reasonable [2+2] and [2+3] cycloaddition reactions between two S_2O molecules. Any [3+3] cycloaddition, on the other hand, seems to be unlikely since atoms of equal charge would have to combine to form covalent bonds. The calculated geometrical parameters of S_2O are d_{SO} = 146.5 pm d_{SS} = 190.8 pm and α_{SSO} = 118.2°.

[2+2] Additions

The most likely first step of the reaction shown in Equation (2) is an intermolecular S···O attraction between the

Table 1. Absolute negative energies (E°_{298}), enthalpies (H°_{298}) and Gibbs energies (G°_{298}) of S_2O and of some molecules derived from S_2O and related species as well as some transition states (in atomic units, a.u.); the energies E (second column) apply to the potential minimum

Species	E [B3LYP/6-31G(2df)]	E°_{298} [G3X(MP2)]	H°_{298} [G3X(MP2)]	G°_{298} [G3X(MP2)]
$^1S_2$	796.3385956	795.4702525	795.4664757	795.4913546
^1SO	473.3218595	472.8212909	472.8175141	472.8416794
S_3	1194.5686550	1193.2629065	1193.2582631	1193.2901174
SO_2	548.6258870	548.0552118	548.0511341	548.0799803
S_2O	871.5880695	870.6496178	870.6452823	870.6756205
S_4	1592.7706551	1591.0340368	1591.0277978	1591.0640979
S_5	1990.9860366	1988.8133239	1988.8055877	1988.8449648
S_4O_2 (**1**)	1743.1399635	1741.2603185	1741.2520547	1741.2926215
S_4O_2 (**2**)	1743.1597292	1741.2805680	1741.2721372	1741.3131003
S_4O_2 (**3**)	1743.1689558	1741.2919627	1741.2833581	1741.3247626
S_4O_2 (**4**)	1743.1758703	1741.3017985	1741.2935166	1741.3336862
S_2O_2 (**5**)	946.7883751	945.7796616	945.7746033	945.8070334
S_3O (**6**)	1269.7580733	1268.3837243	1268.3782365	1268.4122013
S_4O_2 (**7**)	1743.1842906	1741.3031432	1741.2948781	1741.3349394
S_5O (**8**)	2066.1868312	2063.9455664	2063.9366570	2063.9785408
TS1	1743.1366089	1741.2562897	1741.2483141	1741.2888809
TS2	1743.1482802	1741.2685296	1741.2603229	1741.3016585
TS3	1743.1543248	1741.2788239	1741.2704678	1741.3123835
TS4	1743.1554147	1741.2762517	1741.2681896	1741.3087797
TS5	1743.1692604	1741.2945684	1741.2864885	1741.3267559
TS6	1743.1810069	1741.3033498	1741.2954840	1741.3351048

 © 2004 Wiley-VCH Verlag GmbH & Co. KGaA, Weinheim

positively charged central sulfur atom of molecule 1 and the negatively charged oxygen atom of molecule 2. Two such configurations — configurations A and B — are possible, as shown in Figure 1.

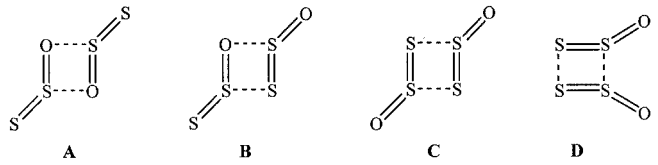

Figure 1. Four possible configurations for the [2+2] cycloaddition between two S_2O molecules

If the subsequent dipolar cycloaddition occurs according to the [2+2] type the four-membered heterocycles **1** or **2** of composition S_4O_2 shown in Figure 2 will result. However, the corresponding reactions given in Equations (5) and (6) are predicted to be strongly endothermic.

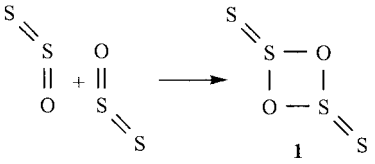

$\Delta H°_{298} = 101$ kJ mol^{-1}
$\Delta G°_{298} = 154$ kJ mol^{-1} (5)

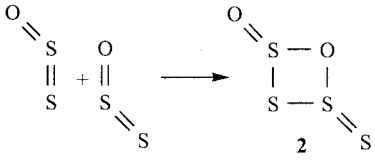

$\Delta H°_{298} = 48$ kJ mol^{-1}
$\Delta G°_{298} = 100$ kJ mol^{-1} (6)

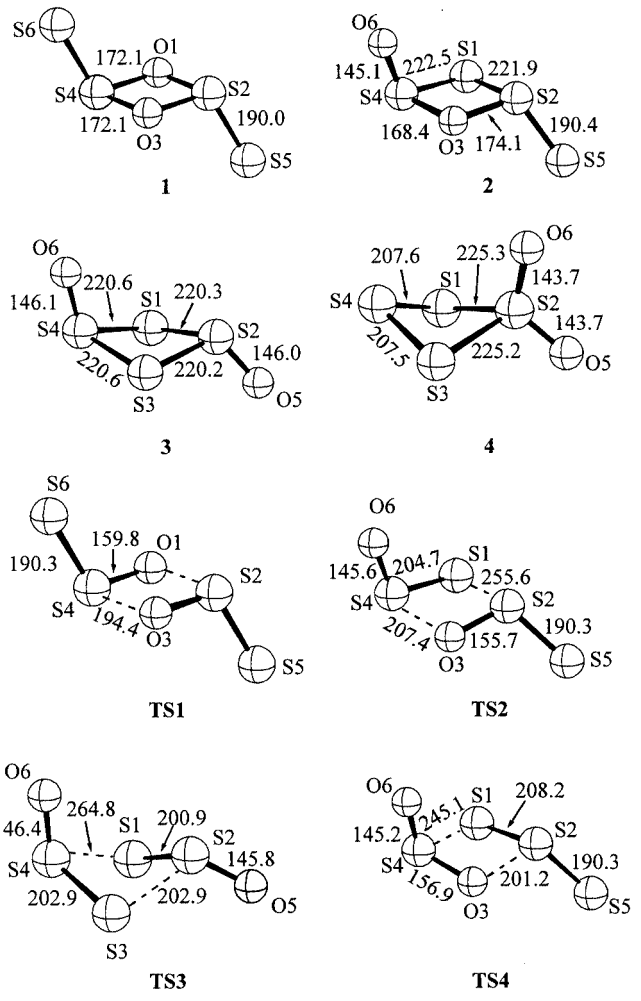

Figure 2. Geometries of four isomers of the four-membered heterocycles S_4O_2 (**1**−**4**) and of the transition states for their formation (**TS1**−**4**); the structures of **1** and **TS1** have C_{2h} symmetry, whereas all others have C_1 symmetry; bond lengths in pm (for more details see Tables 2 and 4)

The pseudo-heterocycle **1** (1,3,2,4-dioxadithiethane 2,4-disulfide) is of C_{2h} symmetry. The four-membered ring is planar and the two exocyclic sulfur atoms are located *trans* to each other (torsion angles S−S−O−S: ±108.3°). All bond lengths show normal values and the bond angles are in the expected range of 82−110° (Table 2). Compared to the S_2O molecule the charges on all atoms of **1** have increased ($S_{terminal}$: −0.25; $S_{central}$: +1.13; O: −0.88).

The transition state for the formation of **1** from S_2O (**TS1**) has been located on the potential-energy surface (PES) of S_4O_2; its structure is given in Figure 2. This structure is also of C_{2h} symmetry and rather similar to that of **1**, although the S−O bond lengths (159.8 and 194.4 pm) are different from those in **1** (172.1 pm; 146.5 pm in S_2O). Additional geometrical data are listed in Table 2. The formation of **TS1** from two molecules of S_2O requires an activation enthalpy of 111 kJ·mol^{-1} rendering this reaction rather unlikely.

The heterocycle **2** (oxatrithiethane 2-oxide 4-sulfide) has no symmetry at all. The maximum charge separation between the S and O atoms in **2** (2.3 electrostatic units) is even larger than in the case of **1** (see Table 3). Consequently, there is a relatively large dipole moment of 1.60 D. The four-membered ring of **2** is not planar (torsion angles in the ring: ±12−16°), and the two exocyclic atoms are in a *trans* position to each other as in the case of **1**.

The structure of the transition state for the formation of **2** from S_2O is also shown in Figure 2 (**TS2**, symmetry C_1). As expected, two of the bonds within the four-membered ring are extremely long (S1−S2: 255.6 pm; S4−O3: 207.4 pm). Bond angles and torsion angles are listed in Tables 2 and 4. The formation of **TS2** from two molecules of S_2O requires an activation enthalpy of 79 kJ·mol^{-1}.

If the dipolar addition of two S_2O molecules took place between the four sulfur atoms the homocyclic tetrathiethane 1,3-dioxide **3**, with two exocyclic oxygen atoms (Figure 1, configuration C), would result [Equation (7)].

 © 2004 Wiley-VCH Verlag GmbH & Co. KGaA, Weinheim

Table 2. Bond angles (°) of the species **1**−**4**, **7**, **8** and **TS1**−**6**; for numbering of atoms see Figure 2 and 4

Angle	**1**	**2**	**3**	**4**	**7**	**8**	**TS1**	**TS2**	**TS3**	**TS4**	**TS5**	**TS6**
123	82.2	84.7	87.7	82.6	98.2	97.5	83.4	85.7	92.7	86.5	106.9	95.2
234	97.8	108.7	88.7	82.9	123.6	104.8	96.6	101.8	79.6	103.5	111.2	120.4
341	82.2	85.8	87.5	91.5			83.4	89.2	90.0	85.5		
412	97.8	77.6	88.7	82.9			96.6	75.2	78.0	76.6		
125	109.8	112.5	110.0	110.5			109.9	117.6	112.8	110.8		
325	109.8	108.5	110.0	110.5			109.9	109.6	116.6	114.0		
146	109.8	110.2	110.7				109.9	112.1	110.8	110.3		
346	109.8	109.1	110.7		109.4	101.9	109.9	107.9	112.3	111.2	96.3	113.2
126				112.5								
345					94.5	96.2					94.4	95.2
526				121.5								
546					106.6	114.8					116.1	104.7
451					87.8	103.3					98.4	84.6
512					96.3	95.1					87.2	103.0

Table 3. Atomic charges (NBO) of the atoms in the various cyclic isomers of composition S_4O_2 (**1**−**4**, **7**) and in S_5O (**8**) as well as in the transition states **TS1**−**6**; for numbering of atoms see Figure 2 and 4

Atom	S_4O_2 (**1**)	S_4O_2 (**2**)	S_4O_2 (**3**)	S_4O_2 (**4**)	S_4O_2 (**7**)	S_5O (**8**)	**TS1**	**TS2**	**TS3**	**TS4**	**TS5**	**TS6**
1	−0.88	−0.23	−0.22	−0.09	+0.05	+0.03	−0.90	−0.35	−0.24	−0.26	−0.11	+0.18
2	+1.13	+0.75	+1.08	+1.83	+0.38	+0.06	+1.09	+0.92	+1.08	+0.58	+0.83	+0.19
3	−0.88	−0.89	−0.22	−0.09	−0.87	−0.13	−0.90	−0.14	−0.32	−0.90	−0.82	−0.84
4	+1.13	+1.44	+1.05	+0.06	+1.46	+1.01	+1.09	+1.25	+1.05	+1.53	+1.10	+1.54
5	−0.25	−0.22	−0.83	−0.85	−0.16	−0.12	−0.20	−0.87	−0.77	−0.12	−0.19	−0.20
6	−0.25	−0.85	−0.84	−0.85	−0.86	−0.85	−0.20	−0.79	−0.79	−0.84	−0.80	−0.86

Table 4. Torsion angles (°) of the species **2**−**4**, **7**, **8** and **TS2**−**6**; for numbering of atoms see Figure 2 and 4

Angle	**2**	**3**	**4**	**7**	**8**	**TS2**	**TS3**	**TS4**	**TS5**	**TS6**
1234	−15.6	−20.5	−31.5	8.7	46.7	−21.3	−38.4	−25.9	50.1	3.5
2341	15.9	20.5	34.3			27.0	28.1	21.8		
3412	−12.0	−20.5	−34.3			−16.2	−37.2	−21.0		
4123	11.6	20.5	31.5			21.9	28.6	16.2		
4125	119.5	130.9				131.8	149.1	130.7		
4325	−127.9	−130.9	−140.8			−139.2	−155.7	−137.2		
2146	96.8	90.7				92.8	76.7	90.0		
2346	−94.0	−90.7		−81.1	−128.5	−86.1	−84.5	−88.3	−122.5	−77.5
4326			79.8							
2345				28.2	−11.6				−5.7	30.9
1546				60.4	78.7				70.0	62.2
3215				−46.5	−63.4				−62.3	−48.1
1543				−51.3	−27.5				−29.1	−53.5
2154				55.6	57.3				53.4	57.8

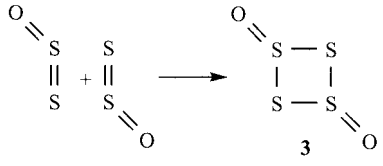

3 (7)

$\Delta H°_{298}$ = 19 kJ mol^{-1}
$\Delta G°_{298}$ = 70 kJ mol^{-1}

Surprisingly, the structure of **3** is not of C_{2h} symmetry (in analogy to that of **1**) but approximately of C_s symmetry (see Figure 2; enforcing C_s symmetry results in one imaginary vibrational wavenumber). The S−S bond lengths within the homocycle are only pairwise equivalent but almost identical (220.2 and 220.6 pm). The absolute values of the four S−S−S−O torsion angles are also pairwise identical but the two pairs are quite different from each other (±90.7°

 © 2004 Wiley-VCH Verlag GmbH & Co. KGaA, Weinheim

and ±130.9°). The four S−S−S−S torsion angles are all ±20.5°. For further bond and torsion angles, see Tables 2 and 4.

The symmetrical structure of **3** (C_{2h} symmetry) is only 1 kJ·mol^{-1} less stable than the global minimum structure. However, this C_{2h} structure corresponds to a first-order transition state with one imaginary vibrational wavenumber and connects two equivalent structures of C_s symmetry that have dipole moments of 0.60 D.

The generation of **3** from S_2O requires an activation enthalpy of 53 kJ·mol^{-1}. The structure of the corresponding transition state **TS3** is shown in Figure 2. This structure is even less symmetrical than the structure of **3**, with S−S bond lengths in the range 200.9−264.8 pm and S−S−S−S torsion angles of ca. 28° and −38° (two each). For additional parameters, see Tables 2 and 4.

The formation of an isomeric tetrathiethane 1,2-dioxide from S_2O seems to be rather unlikely since atoms of equal charge would have to form bonds with each other (Figure 1, configuration D). Interestingly, the homocyclic S_4O_2 isomer **4** with a sulfone group (tetrathiethane 1,1-dioxide; see Figure 2) is also a stationary point on the PES of S_4O_2. This species is approximately of C_s symmetry (μ = 2.20 D) and exhibits the expected bond length pattern with two long S−S bonds (225.2 pm) and two S−S bonds of normal length (207.5 pm). The formation of **4** from S_2O is slightly exothermic. However, this transformation cannot be an elementary reaction but must be a multistep process [Equation (8)].

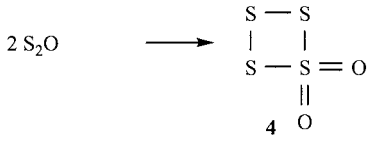

(8)

$\Delta H°_{298}$ = −8 kJ mol^{-1}
$\Delta G°_{298}$ = +46 kJ mol^{-1}

The hypothetical isomerization reactions of the heterocycles **1** or **2** to give **4** are exothermic by −109 and −56 kJ·mol^{-1}, respectively, but there is no simple mechanism either for these transformations. The decomposition of **4** to SO_2 and S_3 is exothermic, as expected [Equation (9)].

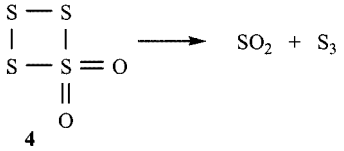

(9)

$\Delta H°_{298}$ = −42 kJ mol^{-1}
$\Delta G°_{298}$ = −96 kJ mol^{-1}

Other reactions of **1** and **2** may be possible besides isomerizations. In principle, isomer **1** could split into singlet S_2 ($^1\Delta_g$; $^1S_2$) and the hypothetical S_2O_2 isomer **5**, which is known to be the global minimum on the PES of singlet S_2O_2 [Equation (10)].[13]

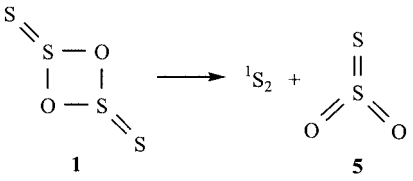

(10)

$\Delta H°_{298}$ = +29 kJ mol^{-1}
$\Delta G°_{298}$ = −15 kJ mol^{-1}

The planar molecule S_2O_2 is of C_{2v} symmetry with two equivalent S−O bonds of length 143.9 pm and an S−S bond of 189.7 pm (a_{OSO} = 119.5°; β_{OSS} = 120.3°; μ = 0.97 D). The S_2 molecule formed in Equation (10) would most probably return to is triplet ground state and either dimerize to give the spectroscopically observed S_4 molecule or trigger a radical-chain polymerization which would explain the sulfur radicals observed by ESR spectroscopy in condensates of S_2O at low temperatures.[2] The latter behavior of S_2 is well-known.

In a similar fashion, the S_4O_2 isomer **2** could theoretically split off singlet SO ($^1\Delta$) with formation of the hypothetical planar S_3O molecule **6** [Equation (11)] but this reaction is strongly endothermic.

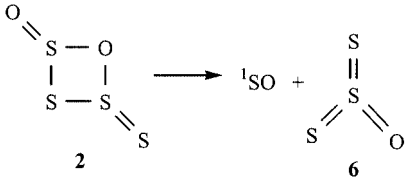

(11)

$\Delta H°_{298}$ = 201 kJ mol^{-1}
$\Delta G°_{298}$ = 155 kJ mol^{-1}

The planar star-like molecule S_3O is also of C_{2v} symmetry with the geometrical parameters d_{SS} = 190.7, d_{SO} = 145.2 pm and a_{SSS} = 121.4° (μ = 0.99 D). Sulfur monoxide (^{1}SO and ^{3}SO) is known to rapidly disproportionate to S_2O and SO_2.[1] The further fate of the species **5** and **6** cannot be predicted with certainty but disproportionation, with formation of elemental sulfur and either S_2O or SO_2, are most likely to occur.

The reactions shown in Equations (5) and (6) as well as Equations (10) and (11) are all highly unlikely at low temperatures due to their endothermic nature and, as far as is known, due to their high activation enthalpies. Nevertheless, it should be pointed out that isomer **2** could easily split into SO_2 and S_3 and thus explain these observed products by a cycloreversion reaction which was first proposed by Tang and Brown [Equation (12)].[9] This reaction is, in fact, strongly exothermic.

 © 2004 Wiley-VCH Verlag GmbH & Co. KGaA, Weinheim

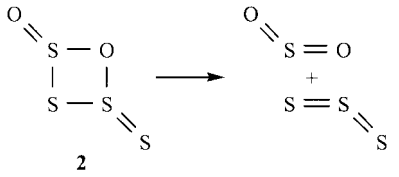

2 (12)

$\Delta H°_{298} = -98$ kJ mol^{-1}
$\Delta G°_{298} = -150$ kJ mol^{-1}

The structure of the transition state for the reaction shown in Equation (12) is also shown in Figure 2 (**TS4**); its formation from **2** requires only 10 kJ·mol^{-1}. The molecules S_3 and SO_2 are preformed in **TS4** and are connected by a very long S−O bond (201.2 pm) and a similarly long S−S bond (245.1 pm). For further data on **TS4**, see Tables 2−4.

[2+3] Additions

Since the hypothetical [2+2] cycloadditions of two S_2O molecules cannot explain the thermal decomposition of this compound at low temperatures we have investigated the alternative [2+3] mechanism for which two approaches (A and B) are possible, as shown in Figure 3. In the case of A the two most highly charged atoms (O and $S_{central}$) of neighboring molecules would combine due to their opposite atomic charges. This interaction is more likely than configuration B, in which the highly negatively charged oxygen atom would combine with the slightly negatively charged terminal sulfur atom of the neighboring molecule resulting in 1-oxatetrathiolane 3-oxide. In addition, the latter molecule would not help to explain the formation of SO_2 and S_3. The product expected from configuration B (**7a**) was found to be much less stable than **7** and this also holds for the six-membered ring 1,4,2,3,5,6-dioxatetrathiane (**7b**) which would be the expected product of a [3+3] cycloaddition of two S_2O molecules.[14] For these reasons, we have only investigated in detail the formation of the 1-oxatetrathiolane 2-oxide **7** (configuration A in Figure 3).

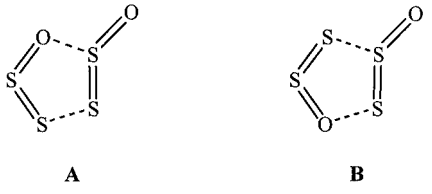

A **B**

Figure 3. Two possible configurations for the [2+3] cycloaddition between two S_2O molecules

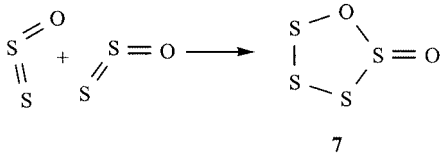

7 (13)

$\Delta H°_{298} = -11$ kJ mol^{-1}
$\Delta G°_{298} = +43$ kJ mol^{-1}

We predict that the reaction shown in Equation (13) is exothermic and therefore more likely than all alternative bimolecular reactions of S_2O discussed above.

The structure of **7** is shown in Figure 4. It is characterized by two normal S−S bonds and, neighboring the exocyclic oxygen atom, one rather long S−S bond (231.9 pm). The SO_2 structural unit is already close in geometry to the free SO_2 molecule, which is a well-known leaving group. This view is supported by the rather long S2−O3 single bond (176.5 pm) between the SO_2 and S_3 units. The second S−O single bond of **7** is of normal length (162.5 pm). The absolute values of the torsion angles within the ring are between 9° and 56° (Table 4). The exocyclic atom is in an axial position (μ = 2.26 D).

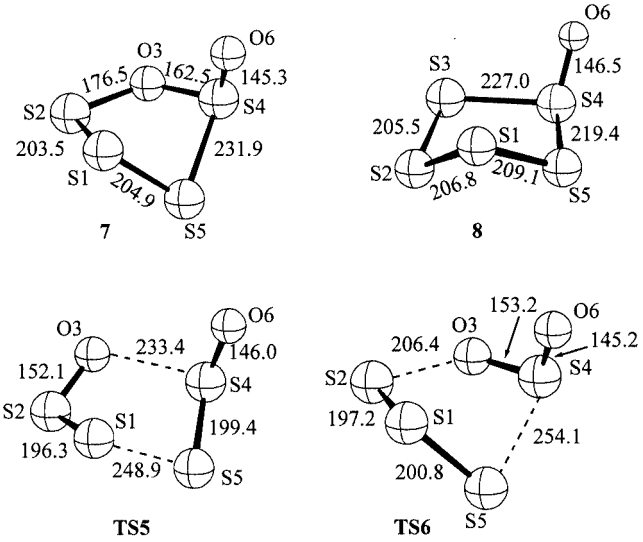

Figure 4. Geometries of the five-membered heterocycles S_4O_2 (**7**) and S_5O (**8**) and of the transition states for their formation (**TS5** and **6**); bond lengths in pm (for more details see Tables 2 and 4.)

The formation of **7** from S_2O proceeds via the transition state TS5, the structure of which is also shown in Figure 4. This species is of C_1 symmetry and the two S_2O units are connected by an S−O bond of length 233.4 pm and an S−S bond of length 248.9 pm. The torsion angles within the five-membered ring range from 6° to 62° (absolute values). All bond angles have normal values (see Tables 2 and 4). The enthalpy of **TS5** is just 11 kJ·mol^{-1} above that of two S_2O molecules. Therefore, Equation (13) describes the reaction channel of lowest activation enthalpy of all reactions between two S_2O molecules studied in this work.

The thermal dissociation of **7** into S_3 and SO_2 [Equation (14)] is exothermic.

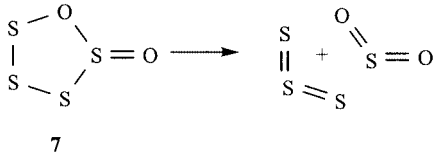

7 (14)

$\Delta H°_{298} = -38$ kJ mol^{-1}
$\Delta G°_{298} = -92$ kJ mol^{-1}

 © 2004 Wiley-VCH Verlag GmbH & Co. KGaA, Weinheim

The transition state for this reaction has been located on the PES (**TS6**). Its geometry is depicted in Figure 4, with more details in Tables 2 and 4. On the potential energy surface (E_o) **TS6** is 9 kJ·mol^{-1} less stable than oxatetrathiolane oxide **7** [B3LYP/6-31G(2df,p) data] but the G3X(MP2) enthalpies and Gibbs energies of **TS6** and **7** at 298 K are practically identical, with slightly lower values calculated for the **TS6** geometry (Table 1). Therefore, we assume that the dissociation of **7** proceeds spontaneously at 298 K and the reactions given in Equations (13) and (14) perfectly explain the initial stages of the thermal decomposition of S_2O at low and moderate temperatures.

The structure of S_3 calculated in this work (d_{SS} = 193.3 pm; α_{SSS} = 118.2°) agrees fairly well with the recently determined experimental gas-phase structure [d_{SS} = 191.7(1) pm, α_{SSS} = 117.36(6)°].[15] The calculated NBO atomic charges of the S_3 molecule are +0.32 for the central atom and −0.16 for the two terminal atoms. This molecule may therefore interact with S_2O with formation of the homocyclic S_5O molecule (**8**) by a [2+3] dipolar addition [Equation (3)]. The calculated structure of **8** is shown in Figure 4. The molecule contains the oxygen atom in an axial position with regard to the nonplanar S_5 ring. The S−S bond lengths vary between 205.5 and 227.0 pm (μ = 1.73 D). These structural data are in accordance with those of the related homocyclic oxides S_7O[16] and S_8O,[17] which have both been characterized by single-crystal X-ray diffraction analyses. The very long S3−S4 bond is probably the main reason for the thermal instability of S_5O, which decomposes on attempts to isolate it from solutions in which it has been prepared by dissolution of gaseous S_2O.[8] Since the torsion angle at this particular bond is only 11.6°, far from the optimum value of 90°, a large bond length is to be expected. We have previously shown that torsion angles and bond lengths in sulfur rings are related to each other.[18] All other torsion angles within the five-membered homocycle have absolute values of between 28° and 64°, mainly caused by the small ring size.

The IR spectrum of S_5O in CS_2 at −65 °C is characterized by a strong absorption at 1138 cm^{-1} in agreement with our calculated value for the S=O stretching vibration of 1131 cm^{-1} (scaled by 0.95). The remaining fundamentals of **8** are located at 490, 457, 398, 379, 305, 287, 260, 238, 212, 191 and 67 cm^{-1} [B3LYP/6-31G(2df,p) data, scaled by 0.95].

The formation of S_5O according to Equation (3) seems to proceed without any activation enthalpy. We have scanned the reaction coordinate of the reverse reaction — the dissociation of S_5O into S_2O and S_3 — by increasing the bond lengths S1−S5 and S3−S4 of **8** in steps of 0.5 pm up to 270 pm and optimizing all other parameters. The energy increased continuously to higher values but no maximum could be found.

The further fate of S_3 and S_5O in the decomposing S_2O/S_3 mixture can be discussed only in a somewhat speculative manner. If S_3 should attack S_5O the well-known S_8O[1] may be formed, although radicals may also originate from the head-to-tail polymerization of S_3. On the other hand, if two S_3 molecules undergo a cycloaddition reaction of the [2+3] type, the hypothetical S_5=S molecule will result, while a [3+3] addition would give the well-known *cyclo*-S_6. These cycloaddition reactions are both strongly exothermic.[19] However, so far no experimental evidence for the possible formation of either S_8O or S_6 from S_2O is available.

The reported formation of S_4 from S_2O has not been explained yet since no elementary reactions are known to generate this molecule directly from S_2O at low temperatures in an exothermic reaction. In principle, S_4 could originate from S_2 by dimerization but the direct formation of S_2 from S_2O is strongly endothermic even if the S_2 molecule is formed in its triplet ground state [Equation (15)].

$$2\,S_2O \rightarrow {}^3S_2 + S_2O_2\,(\mathbf{5});\quad \Delta H^\circ_{298} = +84\ \text{kJ·mol}^{-1},\ \Delta G^\circ_{298} = +90\ \text{kJ·mol}^{-1} \tag{15}$$

The red S_4 molecule is probably responsible for the cherry-red color of condensates made from pure or almost pure S_2O at liquid nitrogen temperature.[20] It seems that S_4 and the sulfur radicals detected by ESR spectroscopy are formed only if the concentration of S_2O is very high since no S_4 has been detected in matrix-isolation experiments with diffusion-controlled decomposition of S_2O.[9] Therefore, more complex reactions may be responsible for the formation of S_4. While the reaction in Equation (16) is spin-forbidden and endothermic[21] the bimolecular decomposition of S_5O is exothermic and might produce S_4 even at low temperatures [Equation (17)].

$$S_5O + S_2O \rightarrow SO_2 + S_4 + {}^3S_2;\quad \Delta H^\circ_{298} = +50\ \text{kJ·mol}^{-1},\ \Delta G^\circ_{298} = +1\ \text{kJ·mol}^{-1} \tag{16}$$

$$2\,S_5O \rightarrow SO_2 + S_4 + \textit{cyclo}\text{-}S_5;\quad \Delta H^\circ_{298} = -29\ \text{kJ·mol}^{-1},\ \Delta G^\circ_{298} = -84\ \text{kJ·mol}^{-1} \tag{17}$$

The observation that S_5O, dissolved in $CHCl_3$ or CS_2, decomposes at temperatures above −20 °C with formation of SO_2 and elemental sulfur[8] indicates that the reaction according to Equation (17) has a rather small activation enthalpy. In this context it is interesting to mention that S_2O, if condensed very slowly on a cold finger at −196 °C, produces a condensate that is transparent and just slightly pink colored but turns intensely red on warming to ca. −150 °C.[7]

Theoretically, S_4 could also be formed from S_3, as shown in Equation (18), but this reaction is slightly endothermic and spin-forbidden and therefore may require a substantial activation enthalpy.

$$2\,S_3 \rightarrow {}^3S_2 + S_4;\quad \Delta H^\circ_{298} = +13\ \text{kJ·mol}^{-1},\ \Delta G^\circ_{298} = +17\ \text{kJ·mol}^{-1} \tag{18}$$

Thus, the reactions shown in Equations (13), (14), (3) and (17) are most likely responsible for the formation of S_4 from

 © 2004 Wiley-VCH Verlag GmbH & Co. KGaA, Weinheim

S_2O on condensation. However, S_4 will play a role only if the S_2O concentration and therefore the concentrations of S_3 and consequently of S_5O are not too low.

Implications for the Chemistry on Jupiter's Moon Io

Large parts of Jupiter's satellite Io are covered by elemental sulfur and solid sulfur dioxide ("SO_2 frost").[22] The surface temperature varies between 80 and 1400 K, not only due to day-and-night changes but also due to the presence of several "hot spots". There are a number of active volcanoes on Io, the most prominent of which is named Pele. The plume of Pele reaches a height of 350 km since both the gravitational force and the atmospheric pressure (ca. 10^{-7} bar) are much lower on Io than on Earth. Spectroscopic measurements have shown that Pele's plume contains SO_2, SO as well as S_2 and it is widely believed that this volcano is powered by hot silicate magma which heats underground deposits of SO_2 and elemental sulfur; if the pressure is high enough eruptions will occur.[23] Equilibrated hot mixtures of elemental sulfur and sulfur dioxide always contain a few percent of SO and S_2O, depending on temperature, total pressure and S:O ratio.[24] S_3 is also expected to be a prominent constituent of the hot sulfur/SO_2 mixture ejected from the magma chamber.[24] During the volcanic eruptions the unstable (highly reactive) species sprayed into the Ionian atmosphere experience both a sharp drop in total pressure and a steep temperature gradient but they are now also exposed to the UV radiation of the Sun. In addition, S_2O may also be formed within the plume from SO and S_3 by the following spin-allowed reaction [Equation (19), which we found to be exothermic and exergonic.[25]

$$^3SO + S_3 \rightarrow S_2O + {}^3S_2;\quad \Delta H^\circ_{298} = -70\ kJ{\cdot}mol^{-1},\ \Delta G^\circ_{298} = -68\ kJ{\cdot}mol^{-1} \qquad (19)$$

The question is then: What will be the lifetime and the sink for the S_2O molecules?

The present results indicate that S_2O will most probably react with S_3 to give S_5O as soon as the temperature within the volcanic plume drops below a certain limit and the chemical equilibrium is no longer established. Due to the low S_2O concentration a reaction between two S_2O molecules as in Equation (13) is less probable. The S_5O molecules may then be deposited on the surface of Io, but on exposure to UV radiation they will eventually decompose to elemental sulfur and SO_2. On the other hand, S_2O may also be decomposed photolytically into SO and sulfur atoms.

S_4 has been thought to be responsible for the orange or red deposits on the surface of Io which have been detected in particular in the vicinity of volcanoes, and S_2O has been suggested as the precursor of this S_4.[23] Our results and discussions show that S_2O is not likely to produce S_4 under the temperature and pressure conditions of the Ionian atmosphere since the concentrations of S_2O and its decomposition products S_3 and S_5O within the volcanic plumes will simply be too low to allow a series of bimolecular reactions like $S_2O \rightarrow S_3 \rightarrow S_5O \rightarrow S_4$. In addition, it should be mentioned that the published color pictures of Io's surface often use artificially enhanced colors ("false colors") to enhance the contrast of the color variations, in which case orange may look red, while the true colors of the sulfur deposits on Io's surface are more yellowish.[26]

Conclusion

The most likely initial step of the thermal decomposition of pure disulfur monoxide is a [2+3] cycloaddition between two S_2O molecules to give the five-membered ring oxatetrathiolane 2-oxide **7**. This reaction is exothermic and the activation enthalpy is small. The heterocycle **7** is predicted to spontaneously dissociate at 298 K into SO_2 and S_3, a reaction which is also exothermic and which has no barrier. Therefore, pure S_2O is not stable in the gas phase at partial pressures above 1 mbar, in solid condensates at temperatures above −130 °C, or in liquid solutions above −70 °C. The S_3 molecule can add exothermally to another S_2O molecule with formation of the homocyclic sulfoxide S_5O (pentathiolane oxide, **8**) which has previously been prepared in this way. However, at higher concentrations, as in condensates of pure or almost pure S_2O, the S_3 and S_2O molecules may also undergo radical-chain polymerization reactions since ESR spectra have shown the presence of sulfur radicals. The result of all of these reactions are polysulfur oxides of varying and partly unknown molecular size and, finally, especially at higher temperatures, elemental sulfur and sulfur dioxide. The most reasonable [2+2] cycloaddition reactions between two S_2O molecules resulting in various isomers of S_4O_2 are all strongly endothermic and therefore unlikely at low temperatures.

Computational Details

Standard ab initio calculations were carried out with the GAUSSIAN 98 series of programs[27] at the G3X(MP2) level of theory.[28] This theory corresponds effectively to QCISD(T)/G3XL//B3LYP/6-31G(2df,p) energy together with zero-point vibrational and isogyric corrections. The G3X(MP2) theory represents a modification of the G3(MP2) theory[29] with three important changes: (1) B3LYP/6-31G(2df,p) geometry, (2) B3LYP/6-31G(2df,p) zero-point energy, and (3) addition of a *g* polarization function to the G3Large basis set for the second-row atoms at the Hartree−Fock level. All three features are particularly important for the proper description of the sulfur-containing compounds examined in this work. For instance, the geometries of several cluster species are poorly predicted by the MP2 theory.

For all investigated molecules a charge-density analysis, at the B3LYP/6-31G(2df,p) level, was performed using the natural bond orbital (NBO) approach.[30] NBO atomic charges of small molecules have recently been demonstrated to agree well with experimental values obtained from X-ray diffraction data.[31] Unless otherwise noted, all relative enthalpies reported in this publication are given as ΔH°_{298} and correspond to the G3X(MP2) level.

 © 2004 Wiley-VCH Verlag GmbH & Co. KGaA, Weinheim

The harmonic fundamental vibrations were calculated at the B3LYP/6-31G(2df,p) level. The corresponding eigenvalues were all positive for the minimum-energy structures reported below while transition states had one negative eigenvalue. Dipole moments (μ) are given in D (1 D = 3.336×10^{-30} Cm).

Acknowledgments

This work was supported by the Deutsche Forschungsgemeinschaft, the Konrad-Zuse-Zentrum für Informationstechnik, Berlin, and the Verband der Chemischen Industrie.

[1] Reviews: P. W. Schenk, R. Steudel, *Angew. Chem.* **1965**, *77*, 437−445; *Angew. Chem. Int. Ed. Engl.* **1965**, *4*, 402−409. P. W. Schenk, R. Steudel, in *Inorganic Sulfur Chemistry* (Ed.: G. Nickless), Elsevier, Amsterdam, **1968**, p. 367−418. R. Steudel, in *Gmelin Handbuch der Anorganischen Chemie*, 8. Auflage, Schwefel, Ergänzungsband 3, Springer, Berlin, **1980**, pp. 1−69. R. Steudel, *Top. Curr. Chem.* **2003**, *231*, 203−230.

[2] P. W. Schenk, R. Steudel, *Z. Anorg. Allg. Chem.* **1966**, *342*, 253−262. P. W. Schenk, R. Steudel, *Angew. Chem.* **1964**, *76*, 97; *Angew. Chem. Int. Ed. Engl.* **1964**, *3*, 61.

[3] G. A. Urove, M. E. Welker, *Organometallics* **1988**, *7*, 1013−1014. A. Ishii, M. Murata, H. Oshida, K. Matsumoto, J. Nakayama, *Eur. J. Inorg. Chem.* **2003**, 3716−3721.

[4] B. L. Hayes, M. E. Welker, *Organometallics* **1998**, *17*, 5534−5539. A. Ishii, T. Kawai, K. Tekura, H. Oshida, J. Nakayama, *Angew. Chem.* **2001**, *113*, 1978−1980; *Angew. Chem. Int. Ed.* **2001**, *40*, 1924−1926.

[5] A. Ishii, M. Nakabayashi, J. Nakayama, *J. Am. Chem. Soc.* **1999**, *121*, 7959−7960. A. Ishii, M. Nakabayashi, Y.-N. Jin, J. Nakayama, *J. Organomet. Chem.* **2000**, *611*, 127−135.

[6] C. J. Marsden, B. J. Smith, *Chem. Phys.* **1990**, *141*, 325−334.

[7] R. Steudel, P. W. Schenk, J. Bilal, *Z. Anorg. Allg. Chem.* **1967**, *353*, 250−258.

[8] W. Genz, P. W. Schenk, *Z. Anorg. Allg. Chem.* **1970**, *379*, 300−311. W. Genz, *Doctoral Dissertation*, Techn. Univ. Berlin, **1969**.

[9] S.-Y. Tang, C. W. Brown, *Inorg. Chem.* **1975**, *14*, 2856−2858.

[10] B. Hapke, F. Graham, *Icarus* **1989**, *79*, 47−55.

[11] R. Steudel, Y. Steudel, M. W. Wong, *Top. Curr. Chem.* **2003**, *230*, 117−134.

[12] M. W. Wong, *Top. Curr. Chem.* **2003**, *231*, 1−29.

[13] C. J. Marsden, B. J. Smith, *Chem. Phys.* **1990**, *141*, 335−353. Y. Murakami, S. Onishi, T. Kobayashi, N. Fujii, N. Isshiki, K. Tsuchiya, A. Tezaki, H. Matsui, *J. Chem. Phys. A* **2003**, *107*, 10996−11000.

[14] B3LYP/6-31G(2df,p) energies (E_o): **7a** −1743.15974; **7b** −1743.15247 a.u.

[15] M. C. McCarthy, S. Thorwirth, C. A. Gottlieb, P. Thaddeus, *J. Am. Chem. Soc.* **2004**, *126*, 4096−4097.

[16] R. Steudel, R. Reinhardt, T. Sandow, *Angew. Chem.* **1977**, *89*, 757−758; *Angew. Chem. Int. Ed. Engl.* **1977**, *16*, 716−717.

[17] R. Steudel, P. Luger, H. Bradaczek, M. Rebsch, *Angew. Chem.* **1973**, *85*, 452−453; *Angew. Chem. Int. Ed. Engl.* **1973**, *12*, 423−424. P. Luger, H. Bradaczek, R. Steudel, M. Rebsch, *Chem. Ber.* **1976**, *109*, 180−184.

[18] R. Steudel, *Top. Curr. Chem.* **1982**, *102*, 149−176. R. Steudel, B. Eckert, *Top. Curr. Chem.* **2003**, *230*, 1−80.

[19] Statement based on reaction enthalpies at 298 K calculated from the novel thermodynamic data reported in: R. Steudel, Y. Steudel, M. W. Wong, *Top. Curr. Chem.* **2003**, *230*, 117−134.

[20] For color photographs of this condensate and of the yellow polysulfur oxide obtained on warming to 20 °C, see: R. Steudel, *Bild der Wissenschaft* **1969**, 206−215.

[21] The minimum energy structure of S_4 is of C_{2v} symmetry; see M. W. Wong, R. Steudel, *Chem. Phys. Lett.* **2003**, *379*, 162−169.

[22] *Satellites of Jupiter* (Ed.: D. Morrison), University of Arizona Press, Tucson, **1982**. *Satellites* (Eds.: J. A. Burns, M. S. Matthews), University of Arizona Press, Tucson, **1986**. See also: http://www.wappswelt.de/tnp/nineplanets/io.html, http://seds.lpl.arizona.edu/nineplanets/nineplanets/io. html and http://www.solarviews.com/eng/io.htm

[23] For a recent review on the sulfur chemistry on Io, see: J. I. Moses, M. Yu. Zolotov, B. Fegley, *Icarus* **2002**, *156*, 76−106.

[24] M. Yu. Zolotov, B. Fegley, *Icarus* **1998**, *132*, 431−434 and *133*, 293−297.

[25] Calculated from the following G3X(MP2) data of triplet SO ($^3\Sigma^-$) and triplet S_2 ($^3\Sigma^-_g$). ^{3}SO: $H°_{298}$ = −472.844326, $G°_{298}$ = −472.869528; $^3S_2$: $H°_{298}$ = −795. 483873, $G°_{298}$ = −795. 509785.

[26] R. Steudel, G. Holdt, A. T. Young, *J. Geophys. Res.* **1986**, *91*, 4971−4977. See also: http://galileo.jpl.nasa.gov/images/io/ioimages.html

[27] M. J. Frisch, G. W. Trucks, H. B. Schlegel, G. E. Scuseria, M. A. Robb, J. R. Cheeseman,V. G. Zakrzewski, J. A. Montgomery, Jr., R. E. Stratmann, J. C. Burant, S. Dapprich, J. M. Millam, A. D. Daniels, K. N. Kudin, M. C. Strain, O. Farkas, J. Tomasi, V. Barone, M. Cossi, R. Cammi, B. Mennucci, C. Pomelli, C. Adamo, S. Clifford, J. Ochterski, G. A. Petersson, P. Y. Ayala, Q. Cui, K. Morokuma, D. K. Malick, A. D. Rabuck, K. Raghavachari, J. B. Foresman, J. Cioslowski, J. V. Ortiz, A. G. Baboul, B. B. Stefanov, G. Liu, A. Liashenko, P. Piskorz, I. Komaromi, R. Gomperts, R. L. Martin, D. J. Fox, T. Keith, M. A. Al-Laham, C. Y. Peng, A. Nanayakkara, C. Gonzalez, M. Challacombe, P. M. W. Gill, B. Johnson, W. Chen, M. W. Wong, J. L. Andres, C. Gonzalez, M. Head-Gordon, E. S. Replogle, J. A. Pople, *GAUSSIAN 98*, Gaussian Inc., Pittsburgh, PA, **1998**.

[28] L. A. Curtiss, P. C. Redfern, K. Raghavachari, J. A. Pople, *J. Chem. Phys.* **2000**, *114*, 108−117.

[29] L. A. Curtiss, P. C. Redfern, K. Raghavachari, V. Rassolov, J. Pople, *J. Chem. Phys.* **1999**, *110*, 4703−4709.

[30] A. E. Reed, L. A. Curtiss, F. Weinhold, *Chem. Rev.* **1988**, *88*, 899−926.

[31] M. Messerschmidt, A. Wagner, M. W. Wong, P. Luger, *J. Am. Chem. Soc.* **2002**, *124*, 732−733.

Received February 18, 2004
Early View Article
Published Online June 24, 2004

 © 2004 Wiley-VCH Verlag GmbH & Co. KGaA, Weinheim

Molecular, One- and Two-Dimensional Systems Built from Manganese(II) and Phthalate/Diimine Ligands: Syntheses, Crystal Structures and Magnetic Properties

Chengbing Ma,[a] Wenguo Wang,[a] Xiaofeng Zhang,[a] Changneng Chen,[a] Qiutian Liu,*[a] Hongping Zhu,[a] Daizheng Liao,[b] and Licun Li[b]

Keywords: Manganese / N ligands / Magnetic properties / Structure elucidation

Several new Mn^{II} compounds, $[Mn_2(Hphth)_2(phen)_4](Hphth)_2{\cdot}2H_2O$ (**1**; H_2phth = phthalic acid, phen = 1,10-phenanthroline), $[Mn_2(Hphth)_2(phen)_4](ClO_4)_2{\cdot}2H_2O$ (**2**), $[Mn_4(phth)_4(phen)_4(H_2O)_4]{\cdot}2EtOH$ (**3**), $\{[Mn_4(phth)_2(phen)_8](PF_6)_4\}_2$ (**4**), $[Mn_4(phth)_2(bipy)_8](ClO_4)_4{\cdot}2EtOH$ (**5**; bipy = 2,2′-bipyridine), $[Mn(phth)(bipy)(H_2O)_2]_n$ (**6**), and $[Mn(phth)(pyz)(H_2O)_2]_n$ (**7**; pyz = pyrazine), have been synthesized by treatment of the appropriate Mn^{2+} salt and H_2phth with different diimine ligands. They were characterized by X-ray diffraction and show a variety of nuclearities, ranging from dinuclear (**1** and **2**) to tetranuclear (**3**–**5**), and dimensionalities, ranging from a 1D chain (**6**) to a 2D layer network (**7**), in which the phthalates act as primary bridging ligands coordinating to Mn atoms through their carboxylate groups in various bonding modes. Variable-temperature magnetic susceptibility measurements reveal weak anti-ferromagnetic coupling interactions in **1**, **3**, **4** and **6**.

(© Wiley-VCH Verlag GmbH & Co. KGaA, 69451 Weinheim, Germany, 2004)

Introduction

There has been increasing interest in the study and synthesis of discrete polynuclear or low-dimensional systems of paramagnetic metal ions, driven to a large extent by their specific structural features, their promising application in diverse areas of technology, such as magnetic recording and magnetic optics in the field of molecular magnetism,[1,2] and their unique properties,[3] as well as their potential as model compounds for the study of the active sites of the metalloenzymes with interacting paramagnetic centers.[4–6] A commonly used strategy to obtain such systems is to select appropriate extended bridging ligands which can transmit magnetic interactions and bind several metal centers through various bonding modes. In this sense, the terephthalate ligand has been used in many synthetic systems, and has generated a great variety of complexes whose magnetic behaviors have been extensively studied.[7–17] However, phthalate, an *o*-isomer of terephthalate, has been used only sparingly for this purpose,[18–20] in spite of the fact that it exhibits versatile bonding modes in metal complexes,[21] and that the neighboring carboxyls are noncoplanar with themselves and with the benzene ring. This could make the phthalate a promising candidate to produce new cluster topologies and to transmit various magnetic interactions.

Special attention has been paid to the structure and properties of manganese carboxylate cluster complexes due to their biological significance.[4,5,22] The Mn^{2+} ion usually plays a structural and/or hydrolytic role;[23] it is also found in some redox enzymes in the reduced form. Dinuclear manganese centers exist in manganese catalase, catalytically disproportionating H_2O_2,[24] and in ribonucleotide reductase, facilitating the reduction of RNA to DNA.[25] A tetranuclear manganese cluster in the oxygen-evolving center (OEC) of photosystem II successfully oxidizes H_2O to O_2,[26,27] though its structure is still a mystery. Recently, it has been shown that one pyrophosphatase needs three Mn^{2+} ions for catalytic activity.[28] To date, the chemistry of manganese cluster complexes with simple acetate and benzoate ligands has been fully developed,[29] but the use of dicarboxylate ligands for this purpose is relatively uncommon.[30–32] In the course of our ongoing work on manganese complexation by dicarboxylates, we have reported a trivalent dinuclear manganese complex with a (μ-oxo)bis(μ-Hphth) bridging core,[33] and have explored the structural transformation mediated by *o*-, *m*- and *p*-phthalate.[34] In this paper, keeping in mind that the number of the manganese complexes derived from phthalate is still low,[31,33–37] we have further explored the reaction of phthalic acid and a manganese(II) salt, with the introduc-

[a] State Key Laboratory of Structural Chemistry, Fujian Institute of Research on the Structure of Matter, Chinese Academy of Sciences,
Fuzhou 350002, China
Fax: (internat.) +86-591-3714946
E-mail: lqt@ms.fjirsm.ac.cn
[b] Department of Chemistry, Nankai University,
Tianjin 300071, China

Supporting information for this article is available on the WWW under http://www.eurjic.org or from the author.

 © 2004 Wiley-VCH Verlag GmbH & Co. KGaA, Weinheim **DOI: 10.1002/ejic.200400166**

tion of the chelating 2,2′-bipyridine (bipy) and 1,10-phenanthroline (phen) ligands and the *exo*-bidentate μ-pyrazine (pyz) ligand as ancillary ligands, with the aim of inhibiting the expansion of the polymeric frameworks in order to obtain the desired polynuclear and low-dimensional complexes, or to induce the evolution of a novel structure, and obtained a new series of compounds (**1**−**7**). Various coordination modes of the phthalate to the Mn ion (Scheme 1) and a wide variety of structural topologies for these complexes are found. The magnetic properties of selected compounds are also discussed.

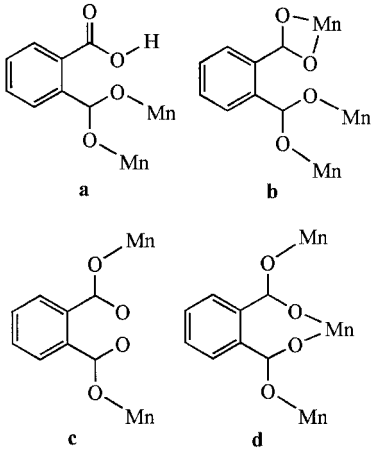

Scheme 1. Coordination modes of phthalate: (a) mono-bidentate; (b) bridging and chelating bis-bidentate; (c) bis-monodentate; (d) chelating/bridging bis-bidentate

Results and Discussion

Synthesis

Treatment of a mixture of H_2phth and an Mn^{2+} salt in the presence of various diimines gave compounds **1**−**7**, which were successfully isolated under different crystallization conditions. Partial deprotonation of H_2phth (H_2phth/KOH = 1:1) avoids the immediate precipitate derived from the direct reaction of $phth^{2-}$, Mn^{2+} and phen in EtOH/H_2O, leading to the formation of dinuclear compounds **1** and **2** with double μ-Hphth bridges; the use of H_2phth in the absence of KOH gave a known inclusion complex $[Mn(phen)_2(H_2O)Cl]Cl·0.5H_2phth$.[38] In general, increasing the KOH/H_2phth molar ratio is favorable to the complete deprotonation of H_2phth and leads to Mn complexes **3**, **4**, **6** and **7** containing completely deprotonated phthalate. Complex **5** contains a partially deprotonated Hphth ligand, probably due to the higher basicity of bipy. The use of neutral H_2phth and bipy resulted in the formation of a known Hphth compound with an $[Mn_2(\mu\text{-}O)(\mu\text{-}Hphth)_2]$ core.[33] The cyclic tetramanganese cluster **5** was isolated in the presence of bipy, while under similar conditions we only isolated the dinuclear complex **2** in the presence of phen. However, refluxing the reaction mixture containing $phth^{2-}$, Mn^{2+} and phen in EtOH/H_2O for several days caused the above-mentioned precipitate to dissolve, and led to the serendipitous formation of **3** and **4** from a one-pot reaction process. Here, PF_6^- as a specific counterion is crucial for the crystallization of both the compounds, even though there is no PF_6^- in compound **3**. When other counterions such as ClO_4^- was used instead of PF_6^-, we only isolated compound **2**. We also tried to omit the counterion from the reaction system, but either compound **1** or a known polymeric compound $[Mn(phth)(phen)(H_2O)_2]_n$ [35] was obtained depending on the degree of deprotonation of H_2phth. Attempts to prepare a bipy complex structurally analogous to **3** failed, even when varying counterion, solvent and starting Mn^{2+} salt. As expected, complex **7**, with a 2D layer framework, was isolated when the *exo*-bidentate μ-pyz ligand was used as the secondary linker instead of the chelating bipy ligand, as it is the end-capping bipy ligand that blocks the way towards higher dimensionality and maintains the 1D chain-like structure of **6**.

Structure Descriptions of Complexes 1−7

Both **1** and **2** contain the $[Mn_2(Hphth)_2(phen)_4]^{2+}$ cation, counterions and solvate water molecules in a molar ratio of 1:2:2 in the unit cell. The cations in **1** and **2** possess similar structural parameters, as listed in Table 1. Two equivalent Mn atoms related by a crystallographic inversion center are bridged by two carboxylate groups of Hphth ligands (Figure 1) in a *syn-anti* mode. The metal−metal distance of 4.786 Å for **1** (4.836 Å for **2**) is the largest amongst analogous dinuclear Mn^{2+} complexes with only two *syn-anti* bridging carboxylate groups: $[Mn_2(PhCOO)_2(bipy)_4]^{2+}$ (4.509 Å),[39] $[Mn_2(MeCOO)_2(bipy)_4]^{2+}$ (4.583 Å)[40] and $[Mn_2(ClCH_2COO)_2(phen)_4]^{2+}$ (4.613 Å).[41] The Mn atom

Table 1. Selected bond lengths (Å) and angles (°) for **1** and **2**

	Complex **1**	Complex **2**
Mn−O1	2.1176(16)	2.117(2)
Mn−O2A	2.1342(14)	2.127(2)
Mn−N3	2.2557(19)	2.260(3)
Mn−N2	2.265(2)	2.247(3)
Mn−N1	2.269(2)	2.271(3)
Mn−N4	2.3088(18)	2.286(3)
O1−Mn−O2A[a]	94.71(6)	92.94(9)
O1−Mn−N3	92.24(7)	92.14(10)
O2A−Mn−N3	89.56(6)	89.59(10)
O1−Mn−N2	97.32(8)	96.20(11)
O2A−Mn−N2	101.32(7)	100.50(11)
N2−Mn−N3	164.82(7)	166.53(11)
O1−Mn−N1	169.50(7)	168.65(12)
O2A−Mn−N1	92.25(6)	93.71(10)
N3−Mn−N1	95.67(8)	97.10(11)
N2−Mn−N1	73.57(8)	73.54(12)
O1−Mn−N4	85.42(6)	83.45(10)
O2A−Mn−N4	162.77(7)	162.50(10)
N3−Mn−N4	73.23(7)	73.50(11)
N2−Mn−N4	95.73(7)	96.92(11)
N1−Mn−N4	90.25(7)	92.83(10)

[a] Symmetry codes: (**1**) A: $-x, -y + 1, -z + 2$; (**2**) A: $-x + 2, -y + 2, -z$.

 © 2004 Wiley-VCH Verlag GmbH & Co. KGaA, Weinheim

is in a distorted octahedral geometry, coordinated by four N atoms [Mn−N = 2.2557(19)−2.3088(18) Å for **1**, and 2.247(3)−2.286(3) Å for **2**] from two chelating phen ligands and two O atoms [Mn−O = 2.1176(16) Å and 2.1342(14) Å for **1**, and 2.117(2) Å and 2.127(2) Å for **2**] from bridging carboxylate groups. The Hphth, which acts as a mono-bidentate ligand (see a in Scheme 1), employs just one μ_2-carboxylate group to bridge two Mn atoms, with the other protonated one free. The characteristic IR absorptions for the stretching vibration of the protonated carboxylic group of Hphth appear at 1689 cm^{-1} for **1** (1701 cm^{-1} for **2**). The bond-valence sum (BVS) calculations based on the equation $s = \exp[(r_0 - r)/B]$[42] (r is the observed bond length and r_0 and B are empirically determined parameters[43]) give values of 1.97 and 1.99 for **1** and **2**, respectively, indicating that the Mn centers in both compounds are in the +2 oxidation state, and that the ligand is a partially deprotonated phthalate anion. The other complexes in this work gave similar values and are therefore not discussed further.

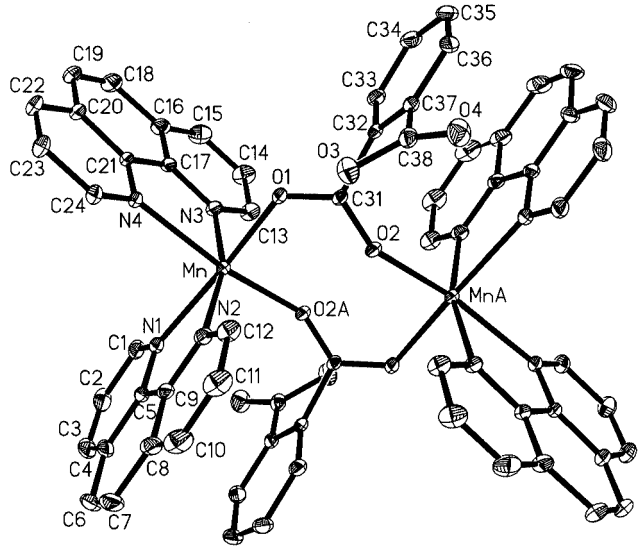

Figure 1. The structural view of the cation in **1** and **2** (ellipsoids at 20% probability)

Some differences were observed between the hydrogen-bonding networks of compounds **1** and **2**. Besides a short intramolecular hydrogen bond with an O6···O7 distance of 2.376 Å found in the uncoordinated Hphth ions, three intermolecular hydrogen bonds also exist in the structure of **1**. The water molecule (O9) bridges the coordinated Hphth ions of the adjacent cations through two hydrogen bonds to produce 1D chains [O9···O4$^{\#}$ 2.763 Å; O3···O9$^{\&}$ 2.544 Å; &: $-x - 1, -y + 1, -z + 1$; #: $x, y, z - 1$] (see a in Figure 2); the uncoordinated Hphth ions link to the hydrogen-bonded chain through a third intermolecular hydrogen bond with an O9···O8 distance of 2.725 Å. As for compound **2**, besides a hydrogen bond between the solvate water molecules, with an O9···O9 distance of 2.502 Å, a second intermolecular hydrogen bond between the protonated carboxylic groups of the adjacent cations links together the cations of **2** to form 1D hydrogen-bonded chains [O3···O4$^{\#}$ 2.634 Å; #: $-x + 3, -y + 2, -z$] (see b in Figure 2); no hydrogen-bonding interaction with the ClO_4^- counterion was observed.

The crystal structure of **3** contains one neutral discrete tetramanganese cluster and two solvate ethanol molecules in each independent crystallographic unit. The whole molecule lies on a crystallographic inversion center implying that only two Mn atoms (Mn1 and Mn2) are crystallographically independent. As shown in Figure 3, the four coplanar Mn^{2+} ions arrayed at the four corners of an approximate rhombus (sides 6.069−6.301Å and angles 140.65° and

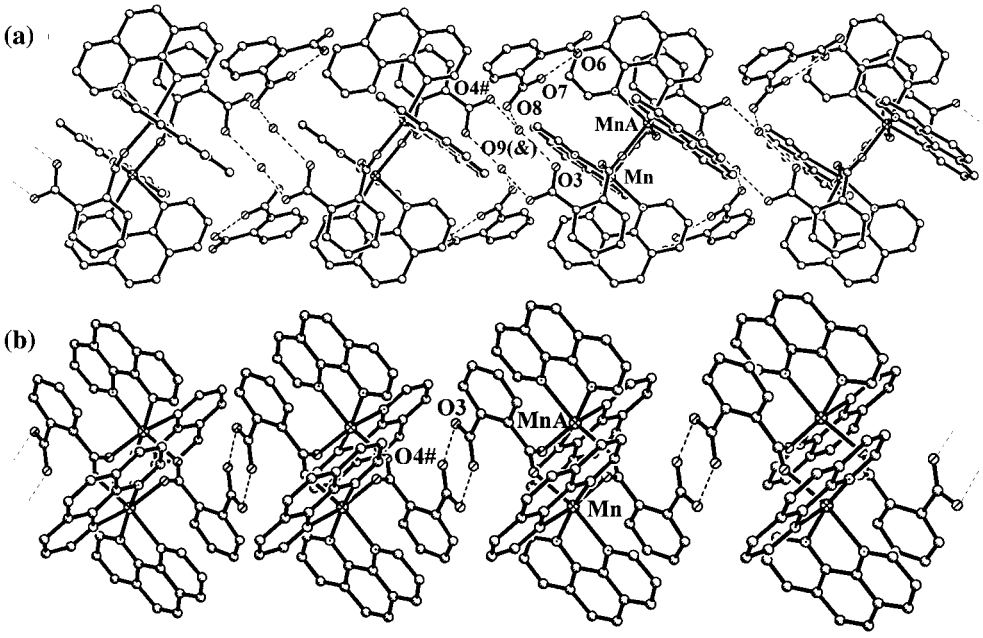

Figure 2. A view of the 1D hydrogen-bonded chains in **1** (a), and **2** (b)

 © 2004 Wiley-VCH Verlag GmbH & Co. KGaA, Weinheim

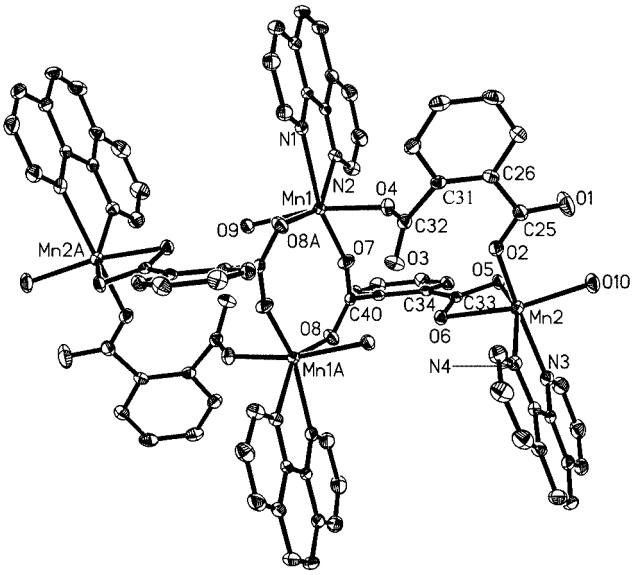

Figure 3. The structural view of the neutral tetranuclear cluster in **3** (ellipsoids at 30% probability)

39.35°), are bridged by two symmetry-related μ_3-phth ligands, one above and one below the Mn_4 rhombic plane. It is noteworthy that the phth ligand displays a unique bridging and chelating bis-bidentate mode, coordinating to three metal atoms through its one bridging carboxylate group and one chelating carboxylate group (see b in Scheme 1). To the best of our knowledge, this type of coordination mode for the phth ligand has not been found in other metal complexes.[21] In the Mn_4 rhombus, the two central Mn atoms (Mn1 and Mn1A, Mn1···Mn1A = 4.170 Å) are bridged by two bridging carboxylate groups of μ_3-phth ligands, and further linked to the two outer Mn atoms (Mn2 and Mn2A) through another chelating end of the same μ_3-phth ligands. Two bis-monodentate μ_2-phth ligands (see c in Scheme 1), four chelating phen ligands and four terminal water ligands complete the peripheral ligation, meaning that the Mn centers have distorted octahedral geometries (Table 2). All the phen-ring planes are nearly parallel with each other.

Table 2. Selected bond bengths (Å) and angles (°) in **3**

Mn1−O7	2.106(2)	O9−Mn1−N2	90.46(9)
Mn1−O4	2.110(2)	O7−Mn1−N1	156.93(10)
Mn1−O8A[a]	2.139(2)	O4−Mn1−N1	91.11(9)
Mn1−O9	2.289(2)	O8A−Mn1−N1	80.18(9)
Mn1−N2	2.324(3)	O9−Mn1−N1	97.64(9)
Mn1−N1	2.359(3)	N2−Mn1−N1	70.43(9)
Mn2−O2	2.099(2)	O2−Mn2−O10	87.32(10)
Mn2−O10	2.155(3)	O2−Mn2−O5	102.86(9)
Mn2−O5	2.200(2)	O10−Mn2−O5	102.97(10)
Mn2−N4	2.218(3)	O2−Mn2−N4	92.84(10)
Mn2−N3	2.287(3)	O10−Mn2−N4	98.97(11)
Mn2−O6	2.323(2)	O5−Mn2−N4	153.45(9)
O7−Mn1−O4	89.81(9)	O2−Mn2−N3	165.12(10)
O7−Mn1−O8A	122.84(9)	O10−Mn2−N3	88.09(11)
O4−Mn1−O8A	91.47(9)	O5−Mn2−N3	91.96(9)
O7−Mn1−O9	85.49(9)	N4−Mn2−N3	73.91(10)
O4−Mn1−O9	167.77(9)	O2−Mn2−O6	94.24(8)
O8A−Mn1−O9	81.67(9)	O10−Mn2−O6	160.57(10)
O7−Mn1−N2	86.75(9)	O5−Mn2−O6	57.78(7)
O4−Mn1−N2	100.57(9)	N4−Mn2−O6	100.29(9)
O8A−Mn1−N2	148.28(9)	N3−Mn2−O6	94.79(9)

[a] Symmetry code: A: $-x + 1, -y + 1, -z + 1$.

It is worth noting that the rhombic Mn_4 cluster in **3**, with an unprecedented [$Mn_4(\mu_3$-phth$)_2$] core, provides an important addition to the available Mn_4 aggregate database, although several rhombic or "butterfly-like" Mn_4 carboxylate clusters with an [Mn_4{μ-carboxilic-O(H)}] core have been reported.[29,44−49]

Some interesting supramolecular contacts are observed in the solid-state structure of **3**. One hydrogen bond links the coordinated water molecule (O10) and the carboxyl O atom (O5) of the symmetry-related Mn-tetramer to generate 1D hydrogen-bonded ribbons [O10···O5& 2.723 Å; &:

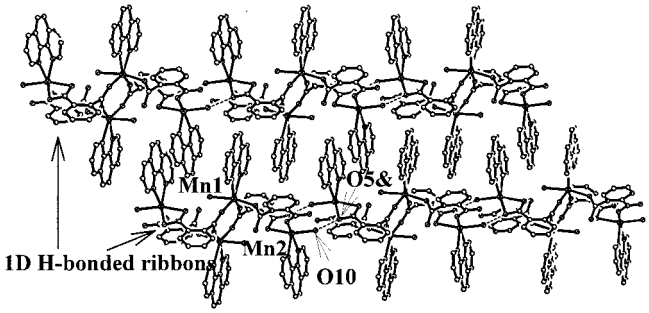

Figure 4. A view of the 2D supramolecular layer in **3**, showing the zipper-like intercalation of adjacent 1D hydrogen-bonded ribbons through face-to-face π-π interactions between the phen ligands; only two 1D hydrogen-bonded ribbons are displayed for clarity

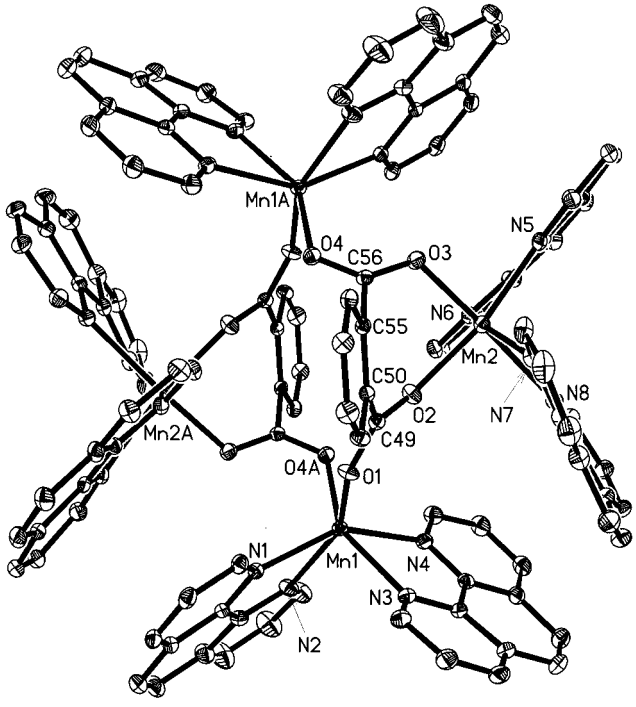

Figure 5. The structural view of one of the tetranuclear cluster cations in **4** (ellipsoids at 20% probability)

 © 2004 Wiley-VCH Verlag GmbH & Co. KGaA, Weinheim

$-x, -y, -z$]; the adjacent ribbons are further intercalated in a zipper fashion into a 2D supramolecular layer through inter-ribbon π-π stacking interactions between the phen ligands, with face-to-face distances of 3.212−3.338 Å (Figure 4).

Each independent crystallographic unit of **4** contains two distinct, but very similar, discrete tetramanganese cluster cations, $[Mn_4(phth)_2(phen)_8]^{4+}$, and eight PF_6^- anions. The structure of one of these cations is shown in Figure 5. The cation possesses a crystallographically imposed center of symmetry implying that only two Mn atoms (Mn1 and Mn2) are crystallographically independent. The four coplanar Mn^{2+} ions are singly bridged by four *syn-anti* carboxylate groups from two phth ligands, each of which adopts a chelating/bridging bis-bidentate mode (Scheme 1d) to coordinate to three Mn atoms, forming a 16-membered nonplanar macrocyclic structure $(-Mn-O-C-O)_4$, with four Mn atoms located at the four corners of an approximate molecular rectangle of sides 4.941 Å and 5.456 Å. Each Mn center exhibits a strongly distorted octahedral geometry (Table 3), being coordinated by four N atoms [Mn−N = 2.288(5)−2.317(5) Å for Mn1; 2.222(5)−2.336(5) Å for Mn2] of two chelating phen ligands, and two O atoms [Mn−O = 2.100(4) Å for Mn1; 2.110(4) Å for Mn2] of carboxylate groups of phth ligand (s). The difference between the coordination environments around Mn1 and Mn2 is that the two O atoms coordinated to Mn1 belong to two phth ligands, whereas the two O atoms coordinated to Mn2 are from two ends of one phth ligand. There are no close intermolecular contacts in the structure, and the tetramanganese cluster units are well isolated, with a shortest intermolecular Mn···Mn distance of 8.573 Å.

Table 3. Selected bond lengths (Å) and angles (°) in **4** and **5**

Complex **4**			
Mn1−O1	2.100(4)	N3−Mn1−N4	71.13(19)
Mn1−O4A[a]	2.100(4)	N2−Mn1−N4	88.89(19)
Mn1−N1	2.288(5)	O3−Mn2−O2	87.78(17)
Mn1−N3	2.301(5)	O3−Mn2−N6	105.20(17)
Mn1−N2	2.306(5)	O2−Mn2−N6	91.14(17)
Mn1−N4	2.317(5)	O3−Mn2−N7	97.79(19)
Mn2−O3	2.110(4)	O2−Mn2−N7	94.24(18)
Mn2−O2	2.110(4)	N6−Mn2−N7	156.57(18)
Mn2−N6	2.222(5)	O3−Mn2−N5	88.61(16)
Mn2−N7	2.242(5)	O2−Mn2−N5	163.39(17)
Mn2−N5	2.250(5)	N6−Mn2−N5	74.19(18)
Mn2−N8	2.336(5)	N7−Mn2−N5	102.32(19)
O1−Mn1−O4A	94.97(16)	O3−Mn2−N8	169.53(17)
O1−Mn1−N1	84.30(17)	O2−Mn2−N8	89.62(17)
O4A−Mn1−N1	118.59(16)	N6−Mn2−N8	84.99(17)
O1−Mn1−N3	84.18(18)	N7−Mn2−N8	72.28(18)
O4A−Mn1−N3	149.89(17)	N5−Mn2−N8	96.67(17)
N1−Mn1−N3	91.34(17)	N1−Mn1−N4	149.63(17)
O1−Mn1−N2	154.08(19)	N3−Mn1−N4	71.13(19)
O4A−Mn1−N2	88.27(18)	N2−Mn1−N4	88.89(19)
N1−Mn1−N2	71.71(18)	O3−Mn2−O2	87.78(17)
N3−Mn1−N2	105.52(19)	O3−Mn2−N6	105.20(17)
O1−Mn1−N4	117.03(18)	O2−Mn2−N6	91.14(17)
O4A−Mn1−N4	82.77(17)	O3−Mn2−N7	97.79(19)
N1−Mn1−N4	149.63(17)	O2−Mn2−N7	94.24(18)
Complex **5**			
Mn1−O1	2.101(3)	N2−Mn1−N1	71.50(15)
Mn1−O4A[a]	2.113(3)	O1−Mn1−N4	85.83(12)
Mn1−N3	2.262(4)	O4A−Mn1−N4	158.02(13)
Mn1−N2	2.271(4)	N3−Mn1−N4	71.09(12)
Mn1−N1	2.305(4)	N2−Mn1−N4	97.72(13)
Mn1−N4	2.393(3)	N1−Mn1−N4	85.20(13)
Mn2−O2	2.127(3)	O2−Mn2−O3	84.67(12)
Mn2−O3	2.159(3)	O2−Mn2−N8	99.54(13)
Mn2−N8	2.230(3)	O3−Mn2−N8	89.74(12)
Mn2−N7	2.248(4)	O2−Mn2−N7	99.31(13)
Mn2−N5	2.266(3)	O3−Mn2−N7	162.44(12)
Mn2−N6	2.276(4)	N8−Mn2−N7	72.75(13)
O1−Mn1−O4A	97.52(12)	O2−Mn2−N5	91.49(13)
O1−Mn1−N3	107.58(12)	O3−Mn2−N5	101.87(12)
O4A−Mn1−N3	87.27(12)	N8−Mn2−N5	164.71(14)
O1−Mn1−N2	155.93(15)	N7−Mn2−N5	95.14(13)
O4A−Mn1−N2	88.05(14)	O2−Mn2−N6	156.63(13)
N3−Mn1−N2	96.03(14)	O3−Mn2−N6	83.26(13)
O1−Mn1−N1	85.17(14)	N8−Mn2−N6	100.33(14)
O4A−Mn1−N1	116.67(13)	N7−Mn2−N6	98.22(14)
N3−Mn1−N1	151.71(14)	N5−Mn2−N6	71.62(14)

[a] Symmetry code: A: $-x + 1, -y + 1, -z + 1$.

In each independent crystallographic unit of **5**, there is one discrete tetramanganese cluster cation, $[Mn_4(phth)_2(bipy)_8]^{4+}$, four ClO_4^- anions and two solvate ethanol molecules. The composition of the cation is similar to that in **4**, except that the chelating ligand is bipy in **5** rather than phen. In the structure of the cation (Figure 6), the phth ligand adopts the same coordination mode to that found in **4**, and the four Mn^{2+} ions also form a cyclic structure. Similarly to those found in **4**, the coordination environments around Mn1 and Mn2 are strongly distorted octahedral (Table 3), with four N atoms [Mn−N = 2.262(4)−2.393(3) Å for Mn1; 2.230(3)−2.276(4) Å for Mn2] of two chelating bipy ligands and two O atoms

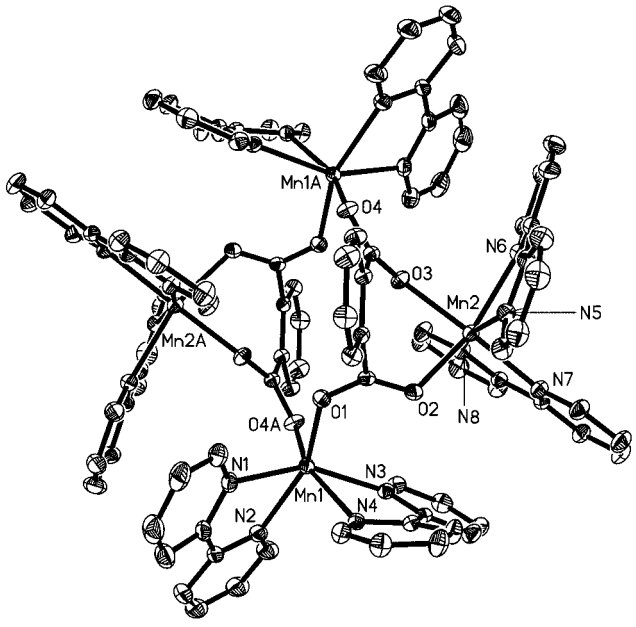

Figure 6. The structural view of the tetranuclear cluster cation in **5** (ellipsoids at 20% probability); Mn···Mn2A = 5.199 Å and Mn···Mn2 = 5.416 Å

 © 2004 Wiley-VCH Verlag GmbH & Co. KGaA, Weinheim

[Mn−O = 2.101(3) and 2.113(3) Å for Mn1; 2.127(3) and 2.159(3) Å for Mn2] of carboxylate groups of the phth ligand (s) at the six apexes of the Mn octahedron. A similar complex with the same cationic core has been reported previously.[31]

Compound **6** consists of infinite 1D chains in which adjacent Mn atoms, with an interatomic distance of 7.131 Å, are bridged by one phth ligand (Figure 7a). The Mn atom is in a distorted octahedral geometry (Table 4), being coordinated by two N atoms [Mn−N1 = 2.312(2) Å, Mn−N2 = 2.289(2) Å] of one chelating bipy ligand, two O atoms [Mn−O5 = 2.193(2) Å, Mn−O6 = 2.285(2) Å] of water molecules and two O atoms [Mn−O1 = 2.128(2) Å, Mn−O4A = 2.135(2) Å] from bis-monodentate phth ligands (Scheme 1c). All bipy ligands parallel to each other are located on one side of the chain, with a dihedral angle of 105.4° between the bipy ligand plane and the benzene ring plane of the phth ligand, forming an unsymmetric chain structure. It should be noted that the coordination mode for the phth ligand exhibited in **6** differs greatly from

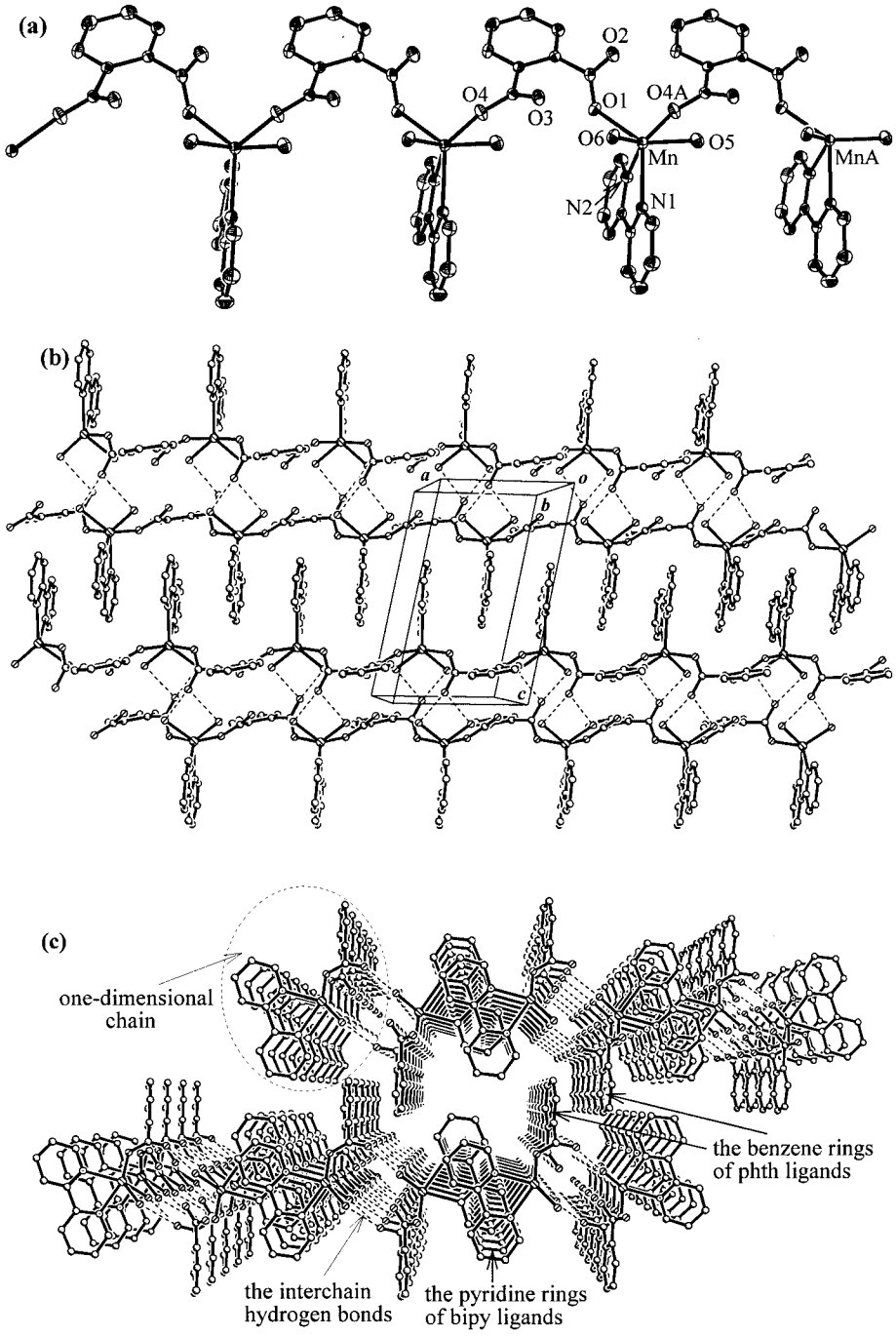

Figure 7. (a) The 1D chain structure of **6** (ellipsoids at 30% probability); (b) a view of the 2D supramolecular layer in **6**; (c) the packing diagram of **6**, showing the 3D supramolecular network sustained by complicated supramolecular contacts

 © 2004 Wiley-VCH Verlag GmbH & Co. KGaA, Weinheim

that found in the known complex [Mn(phth)(phen)-$(H_2O)_2]_n$,[35] in which the phth dianion employs just one carboxylate group to bridge two Mn atoms, with the other free. Interestingly, in compound **6** two neighboring chains connect to each other by a hydrogen-bonding interactions [O5···O2# 2.884 Å; O6···O2# 2.712 Å; #: $-x + 1, -y, -z$] to form a set of 1D hydrogen-bonded double-chains with the bipy ligands growing outwards at both sides of the double-chain (Figure 7b). Meanwhile, the adjacent two sets of the double-chains are correlated through π-π stacking interactions between the bipy ligands, with face-to-face distances of about 3.512 Å and 3.535 Å (Figure 7b) to construct a 2D layer, which is further packed into a 3D supramolecular network (Figure 7c) through inter-layer π-π stacking interactions between the benzene rings of the phth ligands with a face-to-face distance of about 3.450 Å.

Table 4. Selected bond lengths (Å) and angles (°) in **6** and **7**

Complex **6**			
Mn−O1	2.128(2)	O5−Mn−O6	83.37(8)
Mn−O4A[a]	2.135(2)	O1−Mn−N2	83.99(8)
Mn−O5	2.193(2)	O4A−Mn−N2	82.81(9)
Mn−O6	2.285(2)	O5−Mn−N2	131.01(9)
Mn−N2	2.289(2)	O6−Mn−N2	132.14(9)
Mn−N1	2.312(2)	O1−Mn−N1	126.47(9)
O1−Mn−O4A	86.99(9)	O4A−Mn−N1	132.12(9)
O1−Mn−O5	141.72(8)	O5−Mn−N1	85.62(8)
O4A−Mn−O5	83.57(8)	O6−Mn−N1	83.46(8)
O1−Mn−O6	80.82(8)	N2−Mn−N1	70.04(9)
O4A−Mn−O6	140.66(9)		
Complex **7**			
Mn−O1	2.132(3)	O3A−Mn−O3	178.6(2)
Mn−O3	2.166(3)	O1−Mn−N2B	93.30(9)
Mn−N2B[a]	2.330(5)	O3−Mn−N2B	89.32(10)
Mn−N1	2.377(5)	O1−Mn−N1	86.70(9)
O1−Mn−O1A[a]	173.40(18)	O3−Mn−N1	90.68(10)
O1−Mn−O3A	86.32(12)	N2B−Mn−N1	180.000(1)
O1−Mn−O3	93.76(12)		

[a] Symmetry codes: (**6**) A: $x - 1, y, z$; (**7**) A: $-x + 1/2, -y + 3/2, z$; B: $x, -y + 3/2, z + 1/2$.

In the structure of **7**, as shown in Figure 8, the Mn atom is in a slightly distorted octahedral geometry (Table 4), being *trans*-coordinated by two N atoms [Mn−N1 = 2.377(5) Å, Mn−N2B = 2.330(5) Å] of μ-pyz ligands, two O atoms [Mn−O3 = 2.166(3) Å] of water molecules and two O atoms [Mn−O1 = 2.132(3) Å] from phth ligands. The phth ligand, in a coordination mode similar to that found in **6**, is coordinated to two Mn atoms through two O atoms from two carboxylate groups, resulting in a 1D $[Mn(phth)]_n$ chain in the *a* direction. The μ-pyz ligands link adjacent $[Mn(phth)]_n$ chains to generate an infinite 2D layer consisting of rectangular grids with dimensions of 7.511 × 7.630 Å measured through the μ-phth ligands and μ-pyz ligands, respectively. The adjacent layers parallel to each other are further inter-connected into a stacked multi-layer 3D supramolecular network through an inter-layer hydrogen bond between the water ligand and the carboxylate O atom [O3···O2# 2.762 Å; #: $-x, y + 1/2, -z + 1/2$] (Figure 9). Compound **7** is the first example of a Mn complex with both carboxylate and pyrazine ligands.

Magnetic Properties

The variable-temperature (5−300 K) magnetic behaviors of complexes **1** and **6**, and **3** and **4**, in the form of μ_{eff} vs. T plots are shown in Figure 10 and 11, respectively.

As shown in these figures, at room temperature the experimental effective magnetic moments (μ_{eff}) of 5.94 and 6.04 μ_B of **1** and **6**, respectively, are close to the value (5.92 μ_B) expected for one isolated Mn ion ($S = 5/2$); while the μ_{eff} value (11.75 μ_B or so) of **3** and **4** per Mn_4 unit is also close

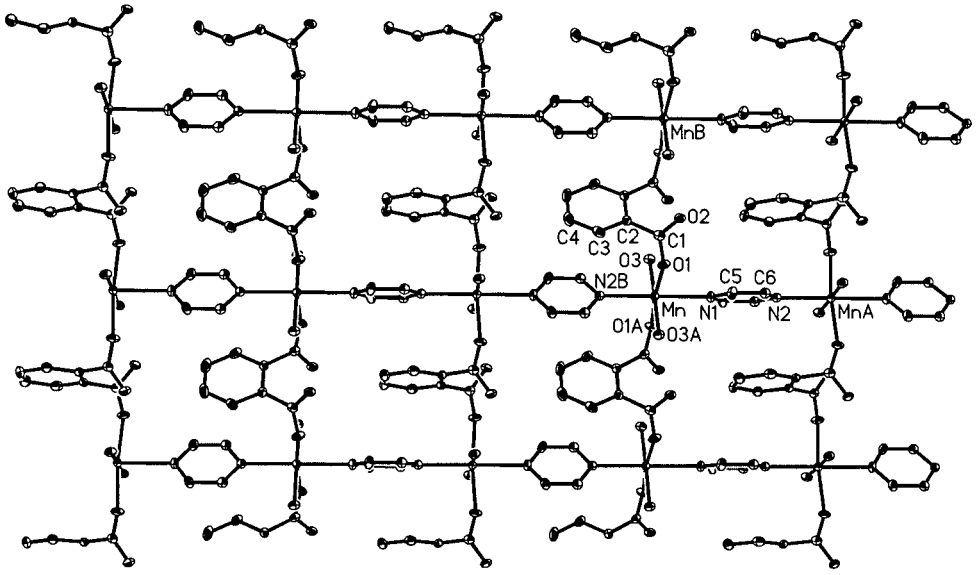

Figure 8. The 2D layer structure of **7** (ellipsoids at 30% probability)

 © 2004 Wiley-VCH Verlag GmbH & Co. KGaA, Weinheim

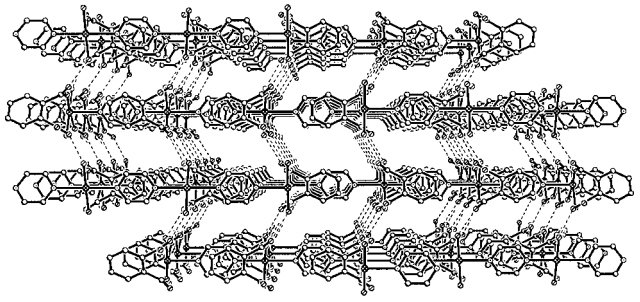

Figure 9. The packing diagram of **7**, showing the multi-layer-stacked 3D hydrogen-bonded network; the inter-layer hydrogen bonds are indicated by dotted lines

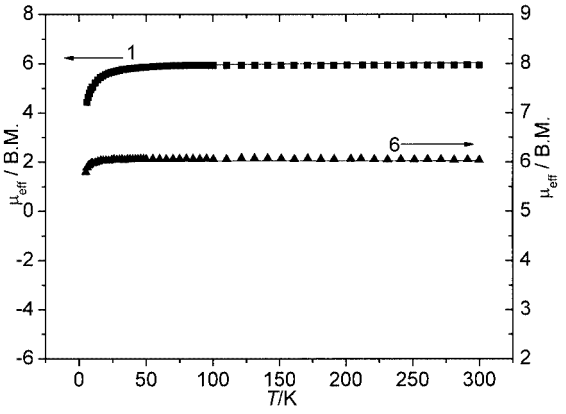

Figure 10. Effective magnetic moment (μ_{eff}) as function of temperature for **1** (■) and **6** (▲); the solid lines represent the calculated values

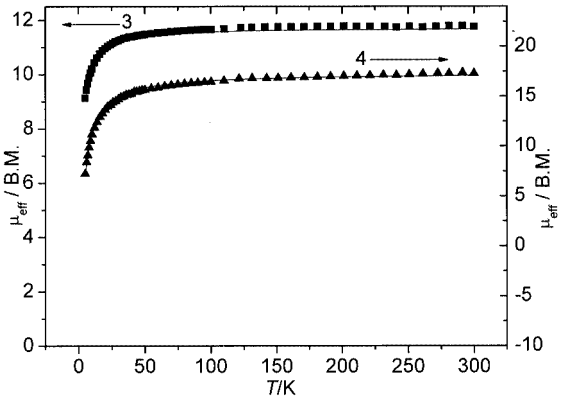

Figure 11. Effective magnetic moment (μ_{eff}) as function of temperature for **3** (■) and **4** (▲); the solid lines represent the calculated values

to the expected value of 11.83 μ_B. As the temperature is lowered to 75 K or lower, the μ_{eff} values remain essentially constant and then decrease gradually, indicative of an overall antiferromagnetic coupling between Mn^{2+} ions for these complexes. A dinuclear Heisenberg model ($H = -JS_1 \cdot S_2$) and a uniform chain model[50] ($\boldsymbol{H} = -2J \cdot \Sigma \boldsymbol{S}_i \cdot \boldsymbol{S}_{i+1}$) were used to fit the experimental data of **1** and **6**, respectively. The best-fit parameters over the full temperature range are as follows: $J = -0.34(4)$ cm^{-1}, $g = 2.04(9)$ and $R = 1.91 \times 10^{-4}$ for **1**; $J = -0.01(4)$ cm^{-1}, $g = 2.03$ and $R = 3.33 \times 10^{-4}$ for **6**, with the agreement factor, R, defined as $\Sigma[(\chi_M T)_{calcd.} - (\chi_M T)_{obsd.}]^2/[\Sigma(\chi_M T)_{obsd.}]^2$.

In either rhombic Mn_4 entity of **3** or rectangular Mn_4 entity of **4**, there are two possible exchange pathways: one through the μ-OCO bridge, and the other through both carboxylate moieties involving the benzene ring (Mn1−O4−C32−C31−C26−C25−O2−Mn2 in **3** and the similar path in **4**). The latter transmission of the coupling can be considered very small and negligible, therefore dinuclear and tetranuclear rectangular Heisenberg models were used for **3** [$H = -J(S_1 \cdot S_2)$] and **4** [$H = -2J(S_1 \cdot S_2 + S_2 \cdot S_3 + S_3 \cdot S_4 + S_4 \cdot S_1)$] to fit their experimental data, based on the consideration that all the coupling parameters (J) between adjacent pairs of Mn^{2+} ions are equal. The best-fit parameters over the full temperature range are as follows: $J = -1.09$ cm^{-1}, $g = 1.97$ and $R = 6.59 \times 10^{-4}$ for **3**; $J = -0.26$ cm^{-1}, $g = 2.00$ and $R = 2.25 \times 10^{-4}$ for **4**.

For complex **3**, the superexchange constant J (-1.09 cm^{-1}), corresponding to the coupling interaction between Mn1 and Mn1A doubly bridged by carboxylates of phth ligands (Figure 3), is similar to those previously reported between Mn^{2+} ions with a similar bridging network (J between -0.96 and -1.84 cm^{-1}),[9,12,51−54] and indicates the presence of a weak antiferromagnetic coupling through the short pathway of the carboxylate bridge of phth. A larger J value than that found in compound **1** [$-0.34(4)$ cm^{-1}] agrees well with the shorter metal−metal separation of 4.170 Å in **3** (4.786 Å in **1**).

For complex **4**, the small value of the superexchange constant ($J = -0.26$ cm^{-1}), corresponding to the coupling interaction transmitted by a single *syn-anti* carboxylate of a phth ligand (Figure 5), can be considered as normal, taking into account the nature of the bridging carboxylate. The exchange coupling through the carboxylato moiety is largely determined by the conformation of the bridge between two interacting metal centers.[55] Of three most common carboxylato bridging conformations (*syn-syn*, *anti-anti* and *syn-anti*), the *syn-anti* carboxylato bridge induces a much smaller J value than the other two types of conformations because of the expanded metallic core and the mismatch in the orientation of magnetic orbitals related to the high asymmetry of the *syn-anti* bridging network.[56] The non-planarity of the Mn−OCO−Mn bridging network accounts for the small value of the magnetic coupling interactions.

Conclusion

The phthalate-Mn^{2+}-diimine(bipy/phen/pyz) reaction system has been explored, and the ability of phthalate to act as a bridging ligand has been confirmed by synthesizing a new series of compounds (**1**−**7**), which show a variety of nuclearities and dimensionalities. Two singly deprotonated Hphth ligands bridging two Mn atoms in both dinuclear compounds **1** and **2** in a *syn-anti* conformation give the largest $Mn^{2+} \cdots Mn^{2+}$ distance among analogous dinuclear Mn^{2+} complexes. The coordination mode shown in

 © 2004 Wiley-VCH Verlag GmbH & Co. KGaA, Weinheim

Scheme 1b is found for the first time in metal phthalate complexes, and compound **3** represents a novel structural type of Mn_4 clusters, with unique μ_3-phthalates supporting a rhombic Mn_4 unit. Two new tetranuclear compounds **4** and **5** crystallise as different salts, with the four Mn atoms located at the four corners of an approximate rectangle bridged by four *syn-anti* carboxylates of two phth ligands. The novel 2D layer network of compound **7** is reasonably formed from the novel 1D singly phth-bridged chain of compound **6** when the secondary bridging μ-pyz ligand is used in place of the end-capping bipy ligand. Although the Mn-acetate/benzoate-diimine(bipy/phen) system has given several compounds before, the new series of compounds reported in this work provides an important addition to the family of still poorly developed manganese dicarboxylate complexes, especially those in a discrete form.

Variable-temperature magnetic susceptibility measurements of compounds **1**, **3**, **4** and **6** reveal weak antiferromagnetic coupling interactions in all cases mediated through either the carboxylate group of the phth ligand or the whole extended phth ligand. The result indicates that, although magnetic interactions transmitted through the phth, as expected, are weak, the magnitude and nature of the coupling interactions can be influenced by various factors, such as the metal−metal separation, the carboxylate bridging modes and the degree of coplanarity of the bridging network.

Experimental Section

General Remarks: All chemicals were of reagent grade and used as received. Elemental analyses were performed with a Vario EL III CHNOS element analyzer. IR spectra of KBr pellets (4000−400 cm^{-1}) were recorded with a Magna-75 FT-IR spectrophotometer. The variable-temperature susceptibility (5−300 K) was measured with a model CF-1 superconducting extraction sample magnetometer in a 10 kG applied field with the crystalline sample kept in a capsule for weighing. Diamagnetic corrections were estimated with Pascal's table.[57]

$[Mn_2(Hphth)_2(phen)_4](Hphth)_2·2H_2O$ (1): A solution of 1,10-phenanthroline (phen) (0.40 g, 2 mmol) in EtOH (10 mL) was slowly addded with continuous stirring to an aqueous solution (20 mL) containing $Mn(OAC)_2·4H_2O$ (0.25 g, 1 mmol), phthalic acid (H_2phth; 0.17 g, 1 mmol) and KOH (0.056 g. 1 mmol). The mixture was stirred for five minutes at room temperature, then filtered. The filtrate was left to stand at room temperature for one week or so to deposit yellow crystals of **1** in 47% yield (0.72 g). $C_{80}H_{56}Mn_2N_8O_{18}$ (1527.2): calcd. C 62.91, H 3.70, N 7.34; found C 62.88, H 3.74, N 7.39. IR (KBr): $\tilde{\nu}$ = 3438 (m), 3068 (m), 1689 (s), 1591 (vs), 1558 (m), 1516 (s), 1497 (m), 1448 (m), 1425 (s), 1410 (vs), 1356 (m), 1342 (m), 1284 (m), 1254 (m), 1221 (m), 1159 (m), 1140 (m), 1101 (m), 1043 (m), 964 (m), 897 (w), 866 (m), 852 (s), 845 (s), 810 (m), 789 (m), 771 (m) 758 (m), 739 (m), 729 (vs), 681 (w), 638 (m), 627 (m), 584 (m), 555 (w), 434 (w), 420 (m) cm^{-1}.

$[Mn_2(Hphth)_2(phen)_4](ClO_4)_2·2H_2O$ (2): Compound **2** was prepared using a procedure similar to that used for preparing **1**, except that $Mn(ClO_4)_2·6H_2O$ was used as the starting Mn^{2+} source. Yellow crystals of **2** were obtained in 33% yield (0.46 g). $C_{64}H_{46}Cl_2Mn_2N_8O_{18}$ (1395.9): calcd. C 55.07, H 3.32, N 8.03; found C 55.02, H 3.34, N 8.07. IR (KBr): $\tilde{\nu}$ = 3427 (br. m), 3088 (m), 1701 (s), 1587 (vs), 1544 (m), 1493 (m), 1441 (m), 1411 (vs), 1367 (m),1348 (w), 1258 (w), 1142 (m), 1089 (s), 1043 (m), 1011 (m), 841 (m), 817 (m), 769 (m), 728 (s), 661 (m), 628 (m), 561 (m), 452 (w), 419 (m) cm^{-1}.

$[Mn_4(phth)_4(phen)_4(H_2O)_4]·2EtOH$ (3) and $\{[Mn_4(phth)_2(phen)_8](PF_6)_4\}_2$ (4): Compounds **3** and **4** were obtained from a one-pot synthetic procedure: A yellow suspension containing H_2phth (0.68 g, 4 mmol), KOH (0.46 g, 8 mmol), $Mn(OAc)_2·4H_2O$ (1.00 g, 4 mmol), phen (0.80 g, 4 mmol) and $(NMe_4)PF_6·6H_2O$ (1.31 g, 4 mmol) in H_2O/EtOH (1:1, 40 mL) was heated to reflux in a 50 mL round-bottomed flask for 10 days, during which time the yellow suspension turned tclear, and a large yellow cube-like crystal of **3** formed. Heating at lower temperature than before for an additional 2 d, during which time many soft and flimsy sheet crystals of **4** were deposited on the surface of the crystal of **3**. Crystals of **3** and **4** were mechanically collected in 27% yield (0.48 g) and 19% yield (0.49 g), respectively (based on Mn).

3: $C_{84}H_{68}Mn_4N_8O_{22}$ (1761.2): calcd. C 57.29, H 3.89, N 6.36; found C 57.33, H 3.81, N 6.43. IR (KBr): $\tilde{\nu}$ = 3450 (s), 3331 (br. s), 3062 (m), 1626 (s), 1547 (vs), 1516 (vs), 1495 (m), 1448 (m), 1423 (vs), 1402 (vs), 1342 (m), 1292 (w), 1219 (w), 1142 (w), 1101 (m), 1090 (m), 1043 (m), 995 (w), 941 (w), 864 (m), 850 (s), 812 (w), 781 (m), 758 (m), 729 (s), 702 (m), 648 (m), 636 (w), 592 (w), 557 (w), 451 (m), 420 (m) cm^{-1}.

4: $C_{224}H_{144}F_{48}Mn_8N_{32}O_{16}P_8$ (5139.0): calcd. C 52.35, H 2.82, N 8.72; found C 52.41, H 2.90, N 8.69. IR (KBr): $\tilde{\nu}$ = 3421 (w), 3079 (w), 1608 (s), 1591 (vs), 1566 (vs), 1497 (m), 1444 (m), 1425 (vs), 1407 (w), 1342 (m), 1317 (w), 1301 (w), 1223 (m), 1145 (m), 1103 (m), 1090 (w), 1049 (w), 953 (w), 841 (vs), 773 (w), 729 (s), 773 (m), 729 (s), 698 (w), 649 (w), 640 (w), 559 (s), 472 (w), 445 (w), 420 (m) cm^{-1}.

$[Mn_4(phth)_2(bipy)_8](ClO_4)_4·2EtOH$ (5): Compound **5** was obtained using a procedure similar to that used for preparing **2**, except that 2,2′-bipyridine (bipy) was used as the starting diimine species. Large yellow crystals of **5** were obtained in 56.5% yield (0.32 g). $C_{100}H_{84}Cl_4Mn_4N_{16}O_{26}$ (2287.4): calcd. C 52.51, H 3.70, N 9.80; found C 52.49, H 3.75, N 9.84. IR (KBr): $\tilde{\nu}$ = 3481 (br. m), 3070 (m), 1606 (m), 1593 (vs), 1564 (vs), 1489 (w), 1473 (m), 1439 (vs), 1417 (m), 1400 (m),1315 (w), 1248 (w), 1176 (w), 1142 (m), 1090 (vs), 1043 (w), 1014 (s), 862 (w), 833 (w), 814 (w), 764 (s), 739 (s), 727 (m), 696 (w), 652 (m), 623 (s), 558 (w), 567 (w), 449 (w), 415 (m) cm^{-1}.

$[Mn(phth)(bipy)(H_2O)_2]_n$ (6): A mixture containing $Mn(OAc)_2·4H_2O$ (0.50 g, 2 mmol), H_2phth (0.34 g, 2 mmol), KOH (0.22 g, 4 mmol) and bipy (0.31 g, 2 mmol) in EtOH/H_2O (1:5, 60 mL) was heated to reflux for 4 hours in a 100 mL round-bottomed flask, then filtered. The filtrate was left undisturbed at 4 °C for one month or so, resulting in the deposition of light-yellow crystals of **6** in 21.3% yield (0.18 g). $C_{18}H_{16}MnN_2O_6$ (411.27): calcd. C 52.56, H 3.92, N 6.81; found C 52.61, H 3.96, N 6.84. IR (KBr): $\tilde{\nu}$ = 3450 (br. m), 1603 (s), 1581 (vs), 1494 (m), 1414 (vs), 1389 (m), 1233 (m), 1250 (m), 1239 (m), 1111 (w), 884 (w), 826 (m), 756 (s), 690 (m), 645 (m), 589 (w), 525 (m), 411 (m) cm^{-1}.

$[Mn(phth)(pyz)(H_2O)_2]_n$ (7): A suspension containing $Mn(OAc)_2·4H_2O$ (0.50 g, 2 mmol), H_2phth (0.34 g, 2 mmol), KOH (0.22 g, 4 mmol) and pyrazine (pyz; 0.16 g, 2 mmol) in MeOH/H_2O (1:4, 20 mL) was heated at 140 °C for 4 days under autogenous pressure in a 25 mL sealed Teflon-lined stainless-steel vessel, then allowed to cool to room temperature, to give pale-yellow crystals

 © 2004 Wiley-VCH Verlag GmbH & Co. KGaA, Weinheim

Table 5. Crystallographic data for complexes **1**−**3**

	1	**2**	**3**
Empirical formula	$C_{80}H_{56}Mn_2N_8O_{18}$	$C_{64}H_{46}Cl_2Mn_2N_8O_{18}$	$C_{84}H_{68}Mn_4N_8O_{22}$
Molecular mass	1527.21	1395.87	1761.22
Space group	$P\bar{1}$	$P\bar{1}$	$P\bar{1}$
a (Å)	11.8388(2)	10.6882(3)	12.3449(2)
b (Å)	12.26390(10)	12.1634(3)	12.5268(2)
c (Å)	13.6053(2)	13.6195(3)	14.77880(10)
α (°)	110.6900(10)	108.48	115.0320(10)
β (°)	97.6450(10)	96.3030(10)	93.6410(10)
γ (°)	93.5350(10)	105.0000(10)	109.1450(10)
V (Å^3)	1818.91(4)	1586.10(7)	1900.82(5)
Z	1	1	1
T (°C)	20	20	20
λ (Mo-K_α) (Å)	0.71037	0.71037	0.71037
ρ_{calcd}.(g·cm^{-3})	1.394	1.461	1.539
μ (mm^{-1})	0.425	0.561	0.734
R[a]	0.0421	0.0496	0.0442
wR[b]	0.1127	0.1246	0.0948

[a] $R = \Sigma||F_o| - |F_c||/\Sigma|F_o|$. [b] $wR = [\Sigma w(|F_o| - |F_c|)^2/\Sigma wF_o^2]^{1/2}$.

Table 6. Crystallographic data for complexes **4**−**7**

	4	**5**	**6**	**7**
Empirical formula	$C_{224}H_{144}F_{48}Mn_8N_{32}O_{16}P_8$	$C_{100}H_{84}Cl_4Mn_4N_{16}O_{26}$	$C_{18}H_{16}MnN_2O_6$	$C_{12}H_{12}MnN_2O_6$
Molecular mass	5138.99	2287.39	411.27	335.18
Space group	$P\bar{1}$	$P\bar{1}$	$P\bar{1}$	$Pccn$
a (Å)	14.52200(10)	14.2703(4)	7.1312(5)	7.6296(11)
b (Å)	18.6579(3)	14.3887(4)	10.1622(8)	11.4509(14)
c (Å)	21.2235(3)	15.3922(4)	11.9270(9)	15.021(2)
α (°)	83.7010(10)	88.5840(10)	88.758(2)	90
β (°)	83.4490(10)	63.2820(10)	79.0820(10)	90
γ (°)	81.4470(10)	66.6120(10)	89.269(2)	90
V (Å^3)	5624.19(13)	2545.13(12)	848.46(11)	1312.3(3)
Z	1	1	2	4
T (°C)	20	20	20	20
λ (Mo-K_α) (Å)	0.71037	0.71037	0.71037	0.71037
ρ_{calcd}.(g·cm^{-3})	1.517	1.492	1.610	1.696
μ (mm^{-1})	0.600	0.674	0.818	1.036
R[a]	0.0796	0.0595	0.0441	0.0455
wR[b]	0.1759	0.1445	0.1089	0.0885

[a] $R = \Sigma||F_o| - |F_c||/\Sigma|F_o|$. [b] $wR = [\Sigma w(|F_o| - |F_c|)^2/\Sigma wF_o^2]^{1/2}$.

of **7** in 12.4% yield (0.08 g). $C_{12}H_{12}MnN_2O_6$ (335.18): calcd. C 43.00, H 3.61, N 8.36; found C 43.03, H 3.67, N 8.33. IR (KBr): $\tilde{\nu}$ = 3405 (m), 3218 (br. m), 1608 (s), 1547 (vs), 1486 (m), 1419 (vs), 1329 (m), 1088 (m), 1007 (m), 831 (m), 800 (w), 764 (s), 731 (w), 696 (w), 637 (m), 528 (m), 420 (m) cm^{-1}.

X-ray Crystallographic Study: Intensity data for complexes **1**−**7** were collected at 293 K with a Siemens SMART CCD diffractometer equipped with graphite-monochromated Mo-K_α radiation (λ = 0.71073 Å). An empirical absorption correction was applied by using the SADABS program, and the structures were solved by direct methods and refined on F^2 by a full-matrix least-squares procedure with the SHELXTL-97 program package.[58] Non-hydrogen atoms were refined anisotropically, with the exceptions of F22, F23 and F24 in one of the PF_6^- ions in **4**, which were refined isotropically. Hydrogen atoms were introduced geometrically except for those on the water molecules and the solvate ethanol molecules, which were located from the difference Fourier syntheses and refined isotropically. Crystallographic data of **1**−**7** are outlined in Table 5 and 6.

CCDC-231921 to -231927 (for **1**−**7**, respectively) contain the supplementary crystallographic data for this paper. These data can be obtained free of charge at www.ccdc.cam.ac.uk/conts/retrieving.html [or from the Cambridge Crystallographic Data Centre, 12 Union Road, Cambridge CB2 1EZ, UK; Fax: +44-1223-336033; E-mail: deposit@ccdc.cam.ac.uk].

Acknowledgments

This work was supported by NNSFC (No. 30170229), the 973 Project of China (G1998010100, G001CB108906), and the State Expert Project of Key Basic Research (2001CCA02500).

[1] J. S. Miller, A. J. Epstein, *Angew. Chem. Int. Ed. Engl.* **1994**, *33*, 385−415.
[2] C. P. Landee, M. Melville, J. S. Miller, *Magnetic Molecular Ma-*

 © 2004 Wiley-VCH Verlag GmbH & Co. KGaA, Weinheim

terials (Eds.: D. Gatteschi, O. Kahn, J. S. Miller, F. Palacio), Kluwer, Dordrecht, The Netherlands, **1991**.
[3] C. T. Chen, K. S. Suslick, *Coord. Chem. Rev.* **1993**, *128*, 293−322.
[4] K. Wieghardt, *Angew. Chem. Int. Ed. Engl.* **1989**, *28*, 1153−1172.
[5] N. A. Law, M. T. Caudle, V. L. Pecoraro, *Adv. Inorg. Chem.* **1999**, *46*, 305−440.
[6] L. Que Jr., A. True, *Prog. Inorg. Chem.* **1990**, *38*, 97−200.
[7] E. G. Bakalbassis, A. P. Bozopoulos, J. Mrozinski, P. J. Rentzeperis, C. A. Tripis, *Inorg. Chem.* **1988**, *27*, 529−532.
[8] P. Chaudhuri, K. Oder, K. Weighardt, S. Ghering, W. Haase, B. Nuber, J. Weiss, *J. Am. Chem. Soc.* **1988**, *110*, 3657−3658.
[9] J. Cano, G. Demunno, J. Sanz, R. Ruiz, F. Lloret, J. Faus, M. Julve, *J. Chem. Soc., Dalton Trans.* **1994**, 3465−3469, and references cited therein.
[10] K. S. Bürger, P. Chaudhuri, K. Wieghardt, B. Nuber, *Chem. Eur. J.* **1995**, *1*, 583−593.
[11] J. Cano, G. D. Munno, J. L. Sanz, R. Ruiz, J. Faus, F. Lloret, M. Julve, A. Caneschi, *J. Chem. Soc., Dalton Trans.* **1997**, 1915−1523, and references cited therein.
[12] C. S. Hong, Y. Do, *Inorg. Chem.* **1997**, *36*, 5684−5685.
[13] D.-F. Xiang, X.-S. Tan, Q.-W. Hang, W.-X. Tang, B.-M. Wu, T. C. W. Mak, *Inorg. Chim. Acta* **1998**, *277*, 21−25.
[14] L. Deakin, A. M. Arif, J. S. Miller, *Inorg. Chem.* **1999**, *38*, 5072−5077.
[15] E. G. Bakalbassis, P. Bergerat, O. Kahn, S. Jeannin, Y. Jeannin, Y. Dromzee, M. Guillot, *Inorg. Chem.* **1992**, *31*, 625−631.
[16] D.-F. Sun, R. Cao, Y.-C. Liang, Q. Shi, W.-P. Su, M.-C. Hong, *J. Chem. Soc., Dalton Trans.* **2001**, 2335−2340.
[17] L.-C. Li, D.-Z. Liao, Z.-H. Jiang, S.-P. Yan, *Inorg. Chem.* **2002**, *41*, 421−424.
[18] E. K. Shakhatreh, E. G. Bakalbassis, I. Brudgam, H. Hartl, J. Mrozinski, C. A. Tsipis, *Inorg. Chem.* **1991**, *30*, 2801−2806.
[19] A. Escuer, R. Vicente, F. A. Mautner, A. S. M. Goher, *Inorg. Chem.* **1997**, *36*, 1233−1236.
[20] E. G. Bakalbassis, D. G. Paschalidis, C. P. Raptopoulou, V. Tangoulis, *Inorg. Chem.* **1998**, *37*, 4735−4737.
[21] H.-X. Zhang, B.-S. Kang, A.-W. Xu, Z.-N. Chen, Z.-Y. Zhou, A. S. C. Chan, K.-B. Yu, C. Chen, *J. Chem. Soc., Dalton Trans.* **2001**, 2559−2566, and references cited therein.
[22] V. L. Pecoraro, *Manganese Redox Enzymes*, VCH Publishers, New York, **1992**.
[23] F. C. Wedler, *Manganese in Health and Disease* (Ed.: D. J. Klimis-Tavantzis), CRC Press, Inc., Ann Arbor, **1994**.
[24] S. V. Antonyuk, V. R. Melikadamyan, A. N. Popov, V. S. Lamzin, P. D. Hempstead, P. M. Harrison, P. J. Artymyuk, V. V. Barynin, *Crystallogr. Rep.* **2000**, *45*, 105−116.
[25] A. Willing, H. Follmann, G. Auling, *Eur. J. Biochem.* **1988**, *170*, 603−611.
[26] R. J. Debus, *Biochim. Biophys. Acta* **1992**, *1102*, 269−271.
[27] A. Zouni, H. T. Witt, J. Kern, P. Fromme, N. Krauß, W. Saenger, P. Orth, *Nature* **2001**, *409*, 739−743.
[28] G. B. Conyers, G. Wu, M. J. Bessman, A. S. Mildvan, *Biochemistry* **2000**, *39*, 2347−2354.
[29] G. Christou, *Acc. Chem. Res.* **1989**, *22*, 328−335, and references cited therein.
[30] M. W. Wemple, H. L. Tsai, S. Wang, J. P. Clude, W. E. Streib, J. C. Huffman, D. N. Hendrickson, G. Christou, *Inorg. Chem.* **1996**, *35*, 6437−6449.
[31] Z.-H. Jiang, S.-L. Ma, D.-Z. Liao, S.-P. Yan, G.-L. Wang, X.-K. Yao, R.-J. Wang, *J. Chem. Soc., Chem. Commun.* **1993**, 745−747.
[32] C. Canada-Vilalta, W. E. Streib, J. C. Huffman, T. A. O′Brien, E. R. Davidson, G. Christou, *Inorg. Chem.* **2004**, *43*, 101−115.
[33] C.-N. Chen, H.-P. Zhu, D.-G. Huang, T.-B. Wen, Q.-T. Liu, D.-Z. Liao, J.-Z. Cui, *Inorg. Chim. Acta* **2001**, *320*, 159−166.
[34] C.-B. Ma, C.-N. Chen, Q.-T. Liu, D.-Z. Liao, L.-C. Li, L.-C. Sun, *New J. Chem.* **2003**, *27*, 890−894.
[35] Y.-G. Zhang, J.-M. Li, M. Zhu, Q.-M. Wang, X.-T. Wu, *Chem. Lett.* **1998**, 1051−1052.
[36] R. Bermejo, M. Fondo, A. García-Deibe, A. M. González, A. Sousa, J. Sanmartín, C. A. McAuliffe, R. G. Pritchard, M. Watkinson, V. Lukov, *Inorg. Chim. Acta* **1999**, *293*, 210−217.
[37] C. Cañada-Vilalta, M. Pink, G. Christou, *Dalton Trans.* **2003**, 1121−1125.
[38] C.-B. Ma, W.-G. Wang, H.-P. Zhu, C.-N. Chen, Q.-T. Liu, *Inorg. Chem. Commun.* **2001**, *4*, 730−733.
[39] B. Albela, M. Corbella, J. Ribas, I. Castro, J. Sletten, H. Stoeckli-Evans, *Inorg. Chem.* **1998**, *37*, 788−798.
[40] R. L. Rardin, W. B. Tolman, S. J. Lippard, *New J. Chem.* **1991**, *15*, 417−430.
[41] G. Fernández, M. Corbella, J. Mahía, M. A. Maestro, *Eur. J. Inorg. Chem.* **2002**, 2502−2510.
[42] H. H. Thorp, *Inorg. Chem.* **1992**, *31*, 1585−1588.
[43] I. D. Brown, D. Altermatt, *Acta Crystallogr., Sect. B* **1985**, *41*, 244−247.
[44] G. Aromi, S. M. J. Aubin, M. A. Bolcar, G. Christou, H. J. Eppley, K. Folting, D. N. Hendrickson, J. C. Huffman, R. C. Squire, H.-L. Tsai, S. Wang, M. W. Wemple, *Polyhedron* **1998**, *17*, 3005−3020, and references cited therein.
[45] G. Aromi, M. W. Wemple, S. M. J. Aubin, K. Folting, D. N. Hendrickson, G. Christou, *J. Am. Chem. Soc.* **1998**, *120*, 5850−5851.
[46] R. J. Kulawiec, R. H. Crabtree, G. W. Brudvig, G. K. Schulte, G. K, *Inorg. Chem.* **1988**, *27*, 1309−1311.
[47] E. Libby, J. K. McCusker, E. A. Schmitt, K. Folting, D. N. Hendrickson, G. Christou, *Inorg. Chem.* **1991**, *30*, 3486−3495.
[48] S. Wang, K. Folting, W. E. Streib, E. A. Schmitt, J. K. McCusker, D. N. Hendrickson, G. Christou, *Angew. Chem. Int. Ed. Engl.* **1991**, *30*, 304−306.
[49] C. Gedye, C. Harding, V. Mckee, J. Nelson, J. Patterson, *J. Chem. Soc., Chem. Commun.* **1992**, 392−393.
[50] W. Hiller, J. Strahle, A. Datz, M. Hanack, W. E. Hatfield, L. W. TerHaar, P. Gutlich, *J. Am. Chem. Soc.* **1984**, *106*, 329−335.
[51] H. Oshio, E. Ino, I. Mogi, T. Ito, *Inorg. Chem.* **1993**, *32*, 5697−5703.
[52] B. Albela, M. Corbella, J. Ribas, I. Castro, J. Sletten, H. Stoeckli-Evans, *Inorg. Chem.* **1998**, *37*, 788−798.
[53] C. S. Hong, S.-K. Son, Y. S. Lee, M.-J. Jun, Y. Do, *Inorg. Chem.* **1999**, *38*, 5602−5610.
[54] P. S. Mukherjee, S. Konar, E. Zangrando, T. Mallah, J. Ribas, N. R. Chaudhuri, *Inorg. Chem.* **2003**, *42*, 2695−2703.
[55] O. Kahn, *Molecular Magnetism*, VCH, Weinheim (Germany), **1993**.
[56] C. Policar, F. Lambert, M. Cesario, I. Morgenstern-Badarau, *Eur. J. Inorg. Chem.* **1999**, 2201−2207, and references cited therein.
[57] P. Pascal, *Ann. Chim. Phys.* **1910**, *19*, 5−70.
[58] G. M. Sheldrick, *SHELXL-97*, University of Göttingen, **1997**.

Received February 28, 2004
Early View Article
Published Online June 23, 2004

 © 2004 Wiley-VCH Verlag GmbH & Co. KGaA, Weinheim

Synthesis of a Persistent $1\sigma^3,3\sigma^3$-Diphosphaallyl Cation Featuring a Localized Phosphorus−Carbon Double Bond

David Martin,[a,b] Antoine Baceiredo,*[a] and Guy Bertrand*[a,b]

Keywords: Allylic cations / Phosphorus / Phosphaalkenes / Phosphacumulenes / Phosphorus ylides

tert-Butyl thiol, 2,6-dimethylthiophenol, 2,6-dimethylphenol, and 2,6-bis(*tert*-butyl)-4-methylphenol cleanly add to the $1\sigma^4,3\sigma^2$-diphosphacumulene **1** to afford the corresponding *C*-phosphanyl phosphorus ylides **2a–d**. Treatment of **2a** with gallium trichloride quantitatively leads to the *C*-phosphonio phosphaalkene **3**, resulting from the1,3-migration of the sulfido group. Under the same experimental conditions, cleavage of the arylthio and aryloxy groups of **2b** and **2c** leading to the *C*-phosphonio phosphaalkene **4** is observed. In the case of the sterically most crowded derivative, **2d**, abstraction of the chloride ion affords the $1\sigma^3,3\sigma^3$-diphosphaallyl cation **5**, which is stable for several weeks in dichloromethane at –20 °C, but decomposes after a few minutes at above 0 °C. Compound **5** reacts at low temperatures with an excess of acetonitrile or benzaldehyde to afford quantitatively and regioselectively the corresponding five-membered heterocycles **6** and **7**. The NMR spectroscopy data and reactivity suggest that **5** features a localized double bond with a planar diamino-substituted phosphorus center, and a single bond with a pyramidalized (amino)(aryloxy)phosphanyl group.
(© Wiley-VCH Verlag GmbH & Co. KGaA, 69451 Weinheim, Germany, 2004)

Introduction

The stability of the 1,3-diphosphaallylic cations **A**−**D** is strongly dependent on the coordination number of the phosphorus atoms. Compounds **A**[1] and **B**,[2] featuring one or two σ^4-P atoms, have been isolated, whereas cations of type **C**[1a,3] and **D**,[4] which feature two σ^2-P and two σ^3-P atoms, respectively, have only been postulated as transient intermediates. Interestingly, derivatives **D** are the phosphorus analogues of the well-known and highly stable amidinium salts.[5] This striking difference between nitrogen and phosphorus chemistry lies in the superior ability of nitrogen to achieve a planar configuration and therefore to act as a π-donor.[6] In the case of diaminocarbocations, both amino substituents are involved in the stabilization of the positive charge, while calculations[6b−6d] predict that for **D** only one phosphorus atom acts as a π-donor, while the second one remains pyramidal. Therefore **D** is best described as (phosphanylmethylene)phosphonium ion **D′** that bears simultaneously a nucleophilic and an electrophilic center. This ambivalence underlines the synthetic potential of this species, but it also explains their apparent instability, especially with respect to ring-closure reactions. Indeed, a theoretical study by Schoeller[4] demonstrated that, depending on the nature of the phosphorus and carbon substituents, the energy-minimum structure could either be the open form **D** or the cyclic three-membered heterocycle valence isomer **E**. We have already reported the isolation of the cyclic isomer $\mathbf{E_b}$,[4] and here we report the synthesis and characterization of the first persistent $1\sigma^3,3\sigma^3$-diphosphaallyl cation of type **D**, as well as its reactivity towards dipolarophiles.

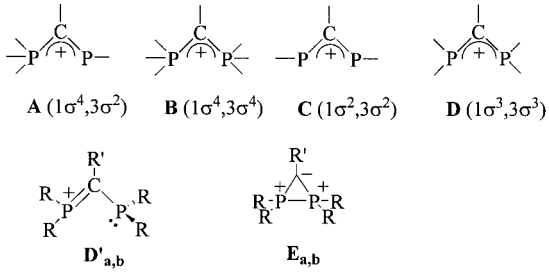

a: R = NH_2, R′ = SiH_3: $\varepsilon_{(D)} - \varepsilon_{(E)} = 5.8$ kcal·mol^{-1}
b: R = N(*i*Pr)$_2$, R′ = $SiMe_3$: $\varepsilon_{(D)} - \varepsilon_{(E)} = -6.1$ kcal·mol^{-1}

Results and Discussion

According to the theoretical study, a decrease of the steric hindrance should favor the open cation **D** over its cyclic isomer **E**. However, our previous experimental work[4b] demonstrated that in order to observe **D**, it is not

[a] Laboratoire Hétérochimie Fondamentale et Appliquée (UMR, 5069), Université Paul Sabatier,
118 Route de Narbonne, 31062 Toulouse Cedex 04, France,
[b] UCR-CNRS Joint Research Chemistry Laboratory (UMR, 2282),
Department of Chemistry, University of California,
Riverside, CA 92521-0403, USA
Fax: (internat.) + 1-909-787-2725
E-mail: gbertran@mail.ucr.edu

only necessary to avoid the ring closure to **E**, but also to prevent the 1,3-migration of a phosphorus substituent, which gives the far more stable phosphoniophosphaalkene isomer **F** (see Scheme 1). Since small substituents at phosphorus atoms favor the 1,3-migration process, we decided to keep bulky substituents on both phosphorus atoms and to decrease the size of the C substituent (R′); H was the best candidate.

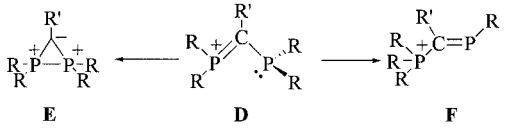

E **D** **F**

Scheme 1

Abstraction of chloride from *P*-chloro phosphorus ylides is a known method to obtain the corresponding methylenephosphonium salts;[7] thus, *P*-chloro-*C*-phosphanyl phosphorus ylides **2** appeared to be potential precursors for the desired $1\sigma^3,3\sigma^3$-diphosphaallyl cation **D**. However, the classical routes to ylides are not applicable for the synthesis of **2a**−**d** and therefore we investigated several original approaches. We found that the recently discovered $1\sigma^4,3\sigma^2$-diphosphacumulene **1**[8] cleanly reacts with acidic compounds of type A−H to afford the desired ylides **2a**−**d** (see Scheme 2). Reactions take place at low temperatures except in the case of the very crowded 2,6-di-*tert*-butyl-4-methylphenol, which requires an additional hour at room temperature. All compounds were obtained as orange oils, and were unequivocally characterized by multinuclear NMR spectroscopy. In the ^{31}P NMR spectra, the addition of A−H resulted in the disappearance of the characteristic low-field signal for the σ^2-phosphorus atom of cumulene **1**, and ylides **2a**−**d** appeared as AX systems with a rather large phosphorus−phosphorus coupling constant ($^2J_{P,P} \approx$ 200 Hz). The PCP carbon atoms give doublet of doublets, with chemical shifts in the range δ = 30−50 ppm, as expected for ylides of this type.

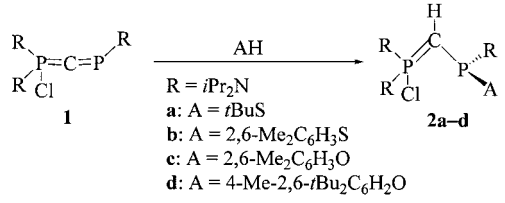

1 **2a–d**

Scheme 2

Addition at −78 °C of 1 equiv. of gallium trichloride to the sterically least hindered ylide, **2a**, quantitatively afforded the (*E*)-*C*-phosphoniophosphaalkene **3**,[9] resulting from the 1,3-migration of the sulfido group. This compound displays an AX system at δ = 305 and 67 ppm ($^2J_{P,P}$ = 137 Hz), the low-field ^{31}P signal being characteristic of the phosphaalkene moiety. Therefore, it can be concluded that the steric demand of the *t*BuS group is not large enough and the σ^4,λ^4-phosphorus atom in **3** is able to accommodate two diisopropylamino and the alkylthio groups.

Taking this result into account, the *tert*-butylthio group was replaced by a larger 2,6-dimethylphenylthio substituent, and ylide **2b** was treated with 1 equiv. of $GaCl_3$ at low temperature. Here again, the expected diphosphaallyl cation was not observed. We obtained in near-quantitative yield the phosphonio phosphaalkene **4**,[9] resulting from the cleavage of the phenylthio group. The cation **4** (X = CF_3SO_3) can also be synthesized by simply adding at low temperature 1 equiv. of trifluoromethanesulfonic acid to a dichloromethane solution of **1** and therefore was unequivocally identified. In the same way, when ylide **2c**, featuring the 2,6-dimethylphenyloxy instead of the -phenylthio group, was treated with 1 equiv. of $GaCl_3$ at low temperature, the phosphonio phosphaalkene **4** was obtained in nearly quantitative yield.

These results might be rationalized by the complexation of the oxygen and sulfur atom by the Lewis acid that enhances their leaving-group ability. In an attempt to protect these heteroatom centers and favor the abstraction of chloride, the steric hindrance at the *ortho* positions of the phenyloxy substituent was increased by using *tert*-butyl instead of methyl groups; 1 equiv. of $GaCl_3$ was added at low temperature to a dichloromethane solution of ylide **2d**. The formation of a mixture of **4** and a new compound **5** was observed in a 20:80 ratio. The ^{31}P NMR spectrum of **5** displays an AX system at δ = 134 and 122 ppm ($^2J_{P,P}$ = 134 Hz). These signals are by far at too low a field for a cyclic structure of type **E**, and at too high a field for the phosphaalkene structure of type **F**. In the ^{13}C NMR spectrum, a CH signal appears as a doublet of doublets at δ = 91.4 ppm ($^1J_{P,C}$ = 146 and 84 Hz) and in the ^{1}H NMR spectrum, the signal for the corresponding proton is also a doublet of doublets at δ = 5.58 ppm ($^2J_{PH}$ = 11 and 4 Hz), demonstrating that the PCHP sequence is preserved. ^{1}H and ^{13}C NMR spectra, obtained while selectively irradiating one phosphorus center, demonstrated that two diisopropylamino groups are linked to the phosphorus atom with signal at δ = 134 ppm, and one amino and the phenoxide group are linked to the phosphorus center with signal at δ = 122 ppm. Clearly, derivative **5** is the desired cation, featuring two σ^3-phosphorus centers. The ^{31}P NMR chemical shifts are in the range for a bis(diisopropylamino)(methylene)phosphonium salt[10] and an (alkyl)(amino)(phenyloxy)phosphane; therefore, as predicted by the calculations, this "$1\sigma^3,3\sigma^3$-diphosphaallylic cation" features a localized double bond involving the diamino-substituted phosphorus atom and a single bond. In other words, the molecule is probably highly unsymmetrical, the phenyloxy-substituted phosphorus atom remains pyramidal. Although **5** is stable in dichloromethane at −20 °C for several weeks, it decomposes above 0 °C after a few minutes, preventing its isolation and an X-ray diffraction study.

As transient $1\sigma^3,3\sigma^3$-diphosphaallylic cations are known to undergo 1,3-dipolar cycloaddition,[4b] we tested the reactivity of **5** with two different dipolarophiles. Compound **5** reacts at low temperature with an excess of acetonitrile or

 © 2004 Wiley-VCH Verlag GmbH & Co. KGaA, Weinheim

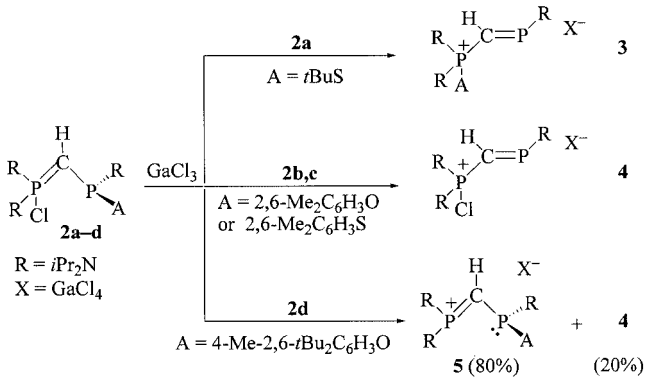

Scheme 3

benzaldehyde to afford quantitatively and regioselectively the five-membered heterocycles **6** and **7**, respectively.[11] The observed regioselectivity reinforced the hypothesis of the diamino-substituted P center acting as the electrophilic part of the molecule. Indeed, it is quite likely that the reaction proceeds stepwise: complexation of the heteroatom of the dipolarophile to the planar phosphorus atom, followed by nucleophilic attack of the phosphane center at the activated carbon atom of the nitrile and aldehyde groups.

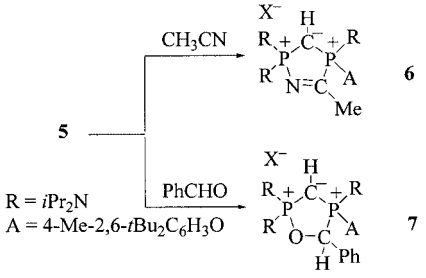

Scheme 4

Conclusion

$1\sigma^3,3\sigma^3$-diphosphaallylic cations are thermodynamically stable species but they are highly reactive. The presence of bulky substituents at both phosphorus centers is required in order to prevent 1,3-shift, and the presence of a small substituent on the carbon atom is necessary to favor the open form and to therefore prevent the ring closure that leads to the three-membered heterocyclic isomer. At least for nonsymmetrically substituted compounds, there is no delocalization of the π system. We are currently investigating the possibility of preparing symmetrical, isolable $1\sigma^3,3\sigma^3$-diphosphaallylic cations, by including such species in a cyclic system.

Experimental Section

General Remarks: All manipulations were performed under argon using standard Schlenk techniques. Dry, oxygen-free solvents, freshly distilled thiol, thiophenol and freshly sublimed phenols were employed. ^{1}H, ^{13}C and ^{31}P NMR spectra were recorded with Bruker AC80, AC200, WM250 or AMX400 spectrometers. ^{1}H and ^{13}C chemical shifts are reported in ppm relative to Me_4Si as external standard. ^{31}P NMR downfield chemical shifts are expressed with a positive sign, in ppm, relative to external 85% H_3PO_4.

Preparation of *P*-Chloro-*C*-Phosphanyl Phosphorus Ylides 2a−d: In a typical experiment, a toluene solution (0.6 mL) of 1 equiv. of thiol, thiophenol or phenols was added to a toluene solution (1 mL) of cumulene **1** (0.11 mmol) at −78 °C. The reaction was monitored by ^{31}P NMR spectroscopy. Ylides **2a−c** were readily obtained after the solution mixture was warmed to room temperature. In the case of the more crowded ylide **2d**, the reaction was complete after 1 h at room temperature. After removal of the solvent under vacuum, derivatives **2a−d** were obtained as orange oils. They are formed in nearly quantitative yields and are used without further purification.

2a: $^{31}P\{^1H\}$ NMR (C_6D_6): δ = 58.5 and 57.5 ($^2J_{P,P}$ = 200 Hz) ppm. ^{1}H NMR (C_6D_6): δ = 1.20 (d, $^3J_{H,H}$ = 7 Hz, 6 H, CHCH_3), 1.23 (d, $^3J_{H,H}$ = 7 Hz, 6 H, CHCH_3), 1.31 (d, $^3J_{H,H}$ = 6 Hz, 12 H, CHCH_3), 1.36 (d, $^3J_{H,H}$ = 7 Hz, 6 H, CHCH_3), 1.39 (d, $^3J_{H,H}$ = 7 Hz, 6 H, CHCH_3), 1.60 (s, 9 H, SCCH_3), 2.6 (pseudo t, $^2J_{PH}$ = 6 Hz, 1 H, PCHP), 3.68 (m, 2 H, NCH), 3.80 (m, 2 H, NCH), 4.07 (m, 2 H, NCH) ppm. $^{13}C\{^1H\}$ NMR (C_6D_6): δ = 23.0 (d, $J_{P,C}$ = 2 Hz, SCCH_3), 24.0 (d, $J_{P,C}$ = 3 Hz, CHCH_3), 24.2 (d, $J_{P,C}$ = 3 Hz, CHCH_3), 24.7 (d, $J_{P,C}$ = 3 Hz, CHCH_3), 33.9 (pseudo t, $J_{P,C}$ = 140 Hz, P*C*P), 44.4 (d, $J_{P,C}$ = 6 Hz, S*C*CH$_3$), 46.9 (br., NCH), 47.0 (br., NCH), 47.6 (br., NCH), 48.7 (br., NCH) ppm.

2b: $^{31}P\{^1H\}$ NMR (C_6D_6): δ = 79.0 and 62.0 ($^2J_{P,P}$ = 196 Hz) ppm. ^{1}H NMR (C_6D_6): δ = 1.16 (d, $^3J_{H,H}$ = 5 Hz, 12 H, CHCH_3), 1.22 (d, $^3J_{H,H}$ = 4 Hz, 12 H, CHCH_3), 1.25 (d, $^3J_{H,H}$ = 5 Hz, CHCH_3), 12 H, 2.86 (s, 6 H, $C_{arom.}CH_3$), 3.22 (septd, $^3J_{H,H}$ = 4, $^3J_{PH}$ = 7 Hz, 2 H, NCH), 3.66 (septd, $^3J_{H,H}$ = 5, $^3J_{PH}$ = 7 Hz, 4 H, NCH), 6.9 (m, 3 H, $H_{arom.}$) ppm. $^{13}C\{^1H\}$ NMR (C_6D_6): δ = 22.7 (d, $J_{P,C}$ = 11 Hz, CHCH_3), 23.4 (s, $C_{arom.}CH_3$), 23.5 (m, CHCH_3), 23.9 (d, $J_{P,C}$ = 9 Hz, CHCH_3), 44.8 (dd, $J_{P,C}$ = 160 and 34 Hz, PCP), 48.2 (d, $J_{P,C}$ = 8 Hz, NCH), 48.4 (d, $J_{P,C}$ = 8 Hz, NCH), 45.9 (d, $J_{P,C}$ = 6 Hz, NCH), 126.2 (s, $C_{arom.}H$), 128.3 (d, $J_{P,C}$ = 5 Hz, $C_{arom.}H$), 143.3 (s, $C_{arom.}$), 144.0 (d, $J_{P,C}$ = 9 Hz, $C_{arom.}$) ppm.

2c: $^{31}P\{^1H\}$ NMR (C_6D_6): δ = 128 and 67 ($^2J_{P,P}$ = 187 Hz) ppm. ^{1}H NMR (C_6D_6): δ = 1.05 (d, $^3J_{H,H}$ = 6 Hz, 6 H, CHCH_3), 1.16 (d, $^3J_{H,H}$ = 6 Hz, 12 H, CHCH_3), 1.18 (d, $^3J_{H,H}$ = 6 Hz, 6 H, CHCH_3), 1.33 (d, $^3J_{H,H}$ = 8 Hz, 6 H, CHCH_3), 1.54 (d, $^3J_{H,H}$ = 8 Hz, 6 H, CHCH_3), 2.27 (s, 6 H, $C_{arom.}CH_3$), 2.77 (dd, $^2J_{PH}$ = 3 and 4 Hz, 1 H, PCHP), 3.55 (septd, $^3J_{H,H}$ = 6, $^3J_{PH}$ = 16 Hz, 4 H, NCH), 3.65 (m, 2 H, NCH), 6.79 (t, $^2J_{H,H}$ = 10 Hz, 1 H, $H_{arom.}$), 6.94 (d, $^2J_{H,H}$ = 10 Hz, 2 H, $H_{arom.}$) ppm. $^{13}C\{^1H\}$ NMR (C_6D_6): δ = 16.8 (s, $C_{arom.}CH_3$), 22.9 (d, $J_{P,C}$ = 6 Hz, CHCH_3), 23.9 (d, $J_{P,C}$ = 6 Hz, CHCH_3), 24.6 (d, $J_{P,C}$ = 4 Hz, CHCH_3), 46.0 (d, $J_{P,C}$ = 11 Hz, NCH), 46.2 (dd, $J_{P,C}$ = 127 and 35 Hz, PCP), 48.0 (d, $J_{P,C}$ = 8 Hz, NCH), 48.6 (d, $J_{P,C}$ = 11 Hz, NCH), 121.7 (d, $J_{P,C}$ = 2 Hz, $C_{arom.}H$), 124.3 (s, $C_{arom.}$), 128.9 (d, $J_{P,C}$ < 1 Hz, $C_{arom.}H$), 131.9 (d, $J_{P,C}$ = 2 Hz, $C_{arom.}$) ppm.

2d: $^{31}P\{^1H\}$ NMR (C_6D_6): δ = 140 and 68 ($^2J_{P,P}$ = 180 Hz) ppm. ^{1}H NMR (C_6D_6): δ = 1.11 (d, $^3J_{H,H}$ = 7 Hz, 6 H, CHCH_3), 1.17 (d, $^3J_{H,H}$ = 5 Hz, 6 H, CHCH_3), 1.19 (d, $^3J_{H,H}$ = 5 Hz, 6 H, CHCH_3), 1.37 (d, $^3J_{H,H}$ = 6 Hz, 12 H, CHCH_3), 1.46 (d, $^3J_{H,H}$ = 7 Hz, 6 H, CHCH_3), 1.74 (s, 18 H, CCH_3), 2.30 (s, 3 H, $C_{arom.}CH_3$), 3.65 (sept d, $^3J_{H,H}$ = 6, $^3J_{PH}$ = 16 Hz, 2 H, NCH), 3.79 (septd, $^3J_{H,H}$ = 7, $^3J_{PH}$ = 16 Hz, 2 H, NCH), 4.02 (septd, $^3J_{H,H}$ = 5,

 © 2004 Wiley-VCH Verlag GmbH & Co. KGaA, Weinheim

$^3J_{PH}$ = 12 Hz, 2 H, NCH), 7.11 (s, 2 H, $H_{arom.}$) ppm. $^{13}C\{^1H\}$ NMR (C_6D_6): δ = 21.3 (s, $C_{arom.}CH_3$), 23.9 (br., $CHCH_3$), 24.6 (d, $J_{P,C}$ = 6.3 Hz, $CHCH_3$), 25.1 (d, $J_{P,C}$ = 4.2 Hz, $CHCH_3$), 30.2 (s, CCH_3), 34.3 (s, CCH_3), 42.5 (dd, $J_{P,C}$ = 161 and 44 Hz, PCP), 47.3 (d, $J_{P,C}$ = 11.6 Hz, NCH), 48.0 (d, $J_{P,C}$ = 5.2 Hz, NCH), 48.3 (d, $J_{P,C}$ = 9.1 Hz, NCH), 48.4 (d, $J_{P,C}$ = 4 Hz, NCH), 125.8 (s, $C_{arom.}H$), 136 (s, $C_{arom.}$), 142 (d, $J_{P,C}$ = 2 Hz, $C_{arom.}$), 152 (d, $J_{P,C}$ = 40 Hz, $C_{arom.}$) ppm.

Abstraction of Chloride from Ylides 2a−d: In a typical experiment, a CH_2Cl_2 solution (0.8 mL) of ylide **2** (0.1 mmol) was added to a CH_2Cl_2 solution (0.3 mL) of 1 equiv. of $GaCl_3$ at −78 °C. The solution mixture was warmed to room temperature. The solvent was removed under vacuum and the residue was characterized without further purification. In the case of **5**, which is not stable above 0 °C, $CDCl_3$ was used as the solvent and the solution mixture was spectroscopically characterized at −40 °C.

3: $^{31}P\{^1H\}$ NMR ($CDCl_3$): δ = 305 and 67 ($^2J_{P,P}$ = 137 Hz) ppm. ^1H NMR ($CDCl_3$): δ = 1.40 (d, $^3J_{H,H}$ = 7 Hz, 24 H, $CHCH_3$), 1.45 (d, $^3J_{H,H}$ = 6 Hz, 12 H, $CHCH_3$), 1.59 (d, $^3J_{H,H}$ = 1 Hz, 9 H, $SCCH_3$), 3.9 (septd, $^3J_{H,H}$ = 7, $^3J_{PH}$ = 14 Hz, 4 H, NCH), 4.2 (br., 2 H, NCH), 6.0 (dd, $^2J_{PH}$ = 12 and 7 Hz, 1 H, PCHP) ppm. $^{13}C\{^1H\}$ NMR ($CDCl_3$): δ = 23.4 (d, $J_{P,C}$ = 2 Hz, $CHCH_3$), 24.6 (d, $J_{P,C}$ = 2 Hz, $CHCH_3$), 33.7 (d, $J_{P,C}$ = 6 Hz, $SCCH_3$), 49.6 (d, $J_{P,C}$ = 6 Hz, NCH), 50.2 (d, $J_{P,C}$ = 4 Hz, NCH), 56.7 (d, $J_{P,C}$ = 6 Hz, $SCCH_3$), 100.0 (dd, $J_{P,C}$ = 118 and 55 Hz, PCP) ppm.

4: $^{31}P\{^1H\}$ NMR ($CDCl_3$): δ = 309 and 60 ($^2J_{P,P}$ = 161 Hz) ppm. ^1H NMR ($CDCl_3$): δ = 1.37 (d, $^3J_{H,H}$ = 7 Hz, 12 H, $CHCH_3$), 1.38 (d, $^3J_{H,H}$ = 6 Hz, 12 H, $CHCH_3$), 1.42 (d, $^3J_{H,H}$ = 7 Hz, 12 H, $CHCH_3$), 3.9 (septd, $^3J_{H,H}$ = 7, $^3J_{PH}$ = 21 Hz, 4 H, NCH), 4.4 (m, 2 H, NCH), 6.4 (dd, $^2J_{PH}$ = 11 and 4 Hz, 1 H, PCHP) ppm. $^{13}C\{^1H\}$ NMR ($CDCl_3$): δ = 22.5 (d, $J_{P,C}$ = 12 Hz, $CHCH_3$), 26.6 (br., $CHCH_3$), 49.5 (d, $J_{P,C}$ = 4 Hz, NCH), 54 (d, $J_{P,C}$ = 13 Hz, NCH), 101 (dd, $J_{P,C}$ = 142 and 57 Hz, PCP) ppm.

5: $^{31}P\{^1H\}$ NMR ($CDCl_3$, 233 K): δ_A = 134 and δ_B = 122 ($^2J_{P,P}$ = 134 Hz) ppm. ^1H NMR ($CDCl_3$, 233 K): δ = 1.19 (d, $^3J_{H,H}$ = 6 Hz, $CHCH_3$), 6 H, 1.22 (d, $^3J_{H,H}$ = 7 Hz, 6 H, $CHCH_3$), 1.28 (d, $^3J_{H,H}$ = 6 Hz, 12 H, $CHCH_3$), 1.39 (d, $^3J_{H,H}$ = 6 Hz, 12 H, $CHCH_3$), 1.45 (s, 18 H, CCH_3), 2.31 (s, 3 H, $C_{arom.}CH_3$), 3.41 (septd, $^3J_{H,H}$ = 6, $^3J_{PAH}$ = 7 Hz, 2 H, NCH), 3.94 (br., coupled with P_A, 2 H, NCH), 4.0 (br., coupled with P_B, 2 H, NCH), 5.58 (dd, $^2J_{PAH}$ = 11 Hz and $^2J_{PBH}$ = 4 Hz, 1 H, PCHP), 7.06 (s, 2 H, $H_{arom.}$) ppm. $^{13}C\{^1H\}$ NMR ($CDCl_3$, 233 K): δ = 21.6 (s, $C_{arom.}CH_3$), 22.3 (br., coupled with P_A, $CHCH_3$), 23.3 (d, J_{PAC} = 4 Hz, $CHCH_3$), 24.5 (br., coupled with P_B, $CHCH_3$), 24.7 (br., coupled with P_A, $CHCH_3$), 30.6 (s, CCH_3), 31.8 (s, $C_{arom.}CCH_3$), 46 (br., NCH), 48 (br., NCH), 49 (br., NCH), 91.4 (dd, J_{PAC} = 146 Hz and J_{PBC} = 84 Hz, PCP), 125.9 (s, $C_{arom.}H$), 135.7 (s, $C_{arom.}$), 131.2 (d, J_{PBC} = 2 Hz, $C_{arom.}$), 148.4 (d, J_{PBC} = 10 Hz, $C_{arom.}$) ppm.

Five-Membered Heterocycles 6 and 7: A CH_2Cl_2 solution (0.8 mL) of ylide **2d** (0.1 mmol) was added to a CH_2Cl_2 solution (0.3 mL) of 1 equiv. of $GaCl_3$ at −78 °C. The formation of **5** was monitored by ^{31}P NMR spectroscopy at −40 °C. Then an excess of dried acetonitrile or benzaldehyde was added and the reaction mixture was warmed to room temperature. The solvent was removed under vacuum. The residue was washed with Et_2O and the resulting yellow powder was dried under vacuum.

6: $^{31}P\{^1H\}$ NMR ($CDCl_3$): δ = 63 and 55 (AB system, $^2J_{P,P}$ = 229 Hz) ppm. ^1H NMR ($CDCl_3$): δ = 1.02 (dd, $^2J_{PH}$ = 9, 7 Hz, 1 H, PC*H*P), 1.22 (d, $^3J_{H,H}$ = 7 Hz, 6 H, $CHCH_3$), 1.29 (d, $^3J_{H,H}$ = 7 Hz, 12 H, $CHCH_3$), 1.39 (d, $^3J_{H,H}$ = 7 Hz, 6 H, $CHCH_3$), 1.43 (d, $^3J_{H,H}$ = 5 Hz, 6 H, $CHCH_3$), 1.43 (s, 18 H, CCH_3), 1.45 (d, $^3J_{H,H}$ = 5 Hz, 6 H, $CHCH_3$), 2.26 (s, 3 H, $C_{arom.}CH_3$), 2.82 (d, $^2J_{PH}$ = 6 Hz, 3 H, N=CCH_3), 3.37 (septd, $^3J_{H,H}$ = 5, $^3J_{P\tilde{H}}$ 1 Hz, 2 H, NCH), 3.70 (septd, $^3J_{H,H}$ = 7, $^3J_{P\tilde{H}}$ 1 Hz, 2 H, NCH), 3.90 (septd, $^3J_{H,H}$ = 7, $^3J_{PH}$ = 15 Hz, 2 H, NCH), 6.97 (s, 2 H, $H_{arom.}$) ppm. $^{13}C\{^1H\}$ NMR ($CDCl_3$): δ = 16.8 (dd, $J_{P,C}$ = 163 and 167 Hz, PCP), 20.9 (s, $C_{arom.}CH_3$), 21.7 (d, $J_{P,C}$ = 5 Hz, $CHCH_3$), 22.8 (d, $J_{P,C}$ = 5 Hz, $CHCH_3$), 23.0 (d, $J_{P,C}$ = 5 Hz, $CHCH_3$), 23.3 (d, $J_{P,C}$ = 4 Hz, $CHCH_3$), 23.4 (d, $J_{P,C}$ = 6 Hz, $CHCH_3$), 29.7 (s, CCH_3), 30.3 (s, CCH_3), 48.1 (d, $J_{P,C}$ = 7 Hz, NCH), 48.6 (d, $J_{P,C}$ = 5 Hz, NCH), 49.6 (d, $J_{P,C}$ = 5 Hz, NCH), 125.5 (s, $C_{arom.}H$), 134.0 (s, $C_{arom.}$), 135.7 (s, $C_{arom.}$), 141.8 (d, $J_{P,C}$ = 9 Hz, $C_{arom.}$), 187 (d, $J_{P,C}$ = 64 Hz, C=N) ppm.

7: $^{31}P\{^1H\}$ NMR ($CDCl_3$): δ = 72 and 66 (AB system, $^2J_{P,P}$ = 142 Hz) ppm. ^1H NMR ($CDCl_3$): δ = 0.76 (d, $^3J_{H,H}$ = 7 Hz, 6 H, $CHCH_3$), 1.10 (d, $^3J_{H,H}$ = 7 Hz, 6 H, $CHCH_3$), 1.23 (d, $^3J_{H,H}$ = 7 Hz, 6 H, $CHCH_3$), 1.40 (d, $^3J_{H,H}$ = 7 Hz, 12 H, $CHCH_3$), 1.43 (s, 18 H, CCH_3), 1.54 (d, $^3J_{H,H}$ = 7 Hz, 6 H, $CHCH_3$), 2.34 (s, 3 H, $C_{arom.}CH_3$), 3.26 (septd, $^3J_{H,H}$ = 7, $^3J_{PH}$ < 1 Hz, 2 H, NCH), 3.88 (septd, $^3J_{H,H}$ = 7, $^3J_{PH}$ < 1 Hz, 4 H, NCH), 5.9 (dd, $^2J_{H,P}$ = 7, 9 Hz, 1 H, PCHO), 7.2 (m, 3 H, $H_{arom.}$), 7.53 (s, 2 H, $H_{arom.}$), 7.7 (m, 2 H, $H_{arom.}$) ppm. $^{13}C\{^1H\}$ NMR ($CDCl_3$): δ = 15.7 (dd, $J_{P,C}$ = 173 and 152 Hz, PCHP), 20.8 (s, $C_{arom.}CH_3$), 22.8 (br., $CHCH_3$), 23.2 (br., $CHCH_3$), 23.8 (d, $J_{P,C}$ = 5 Hz, $CHCH_3$), 25.6 (br., $CHCH_3$), 29.7 (s, CCH_3), 30.3 (s, CCH_3), 47.6 (d, $J_{P,C}$ = 7 Hz, N*C*H), 49.2 (d, $J_{P,C}$ = 5 Hz, N*C*H), 49.6 (d, $J_{P,C}$ = 5 Hz, NCH), 50.7 (d, $J_{P,C}$ = 5 Hz, NCH), 80.3 (dd, $J_{P,C}$ = 80 and 3 Hz, PCHO), 125.6 (s, $C_{arom.}H$), 128.6 (d, $J_{P,C}$ = 5 Hz, $C_{arom.}H$), 129.3 (d, $J_{P,C}$ = 1 Hz, $C_{arom.}H$), 133.0 (s, $C_{arom.}$), 134.0 (d, $J_{P,C}$ = 2 Hz, $C_{arom.}$), 135.2 (s, $C_{arom.}H$), 141.1 (d, $J_{P,C}$ = 5 Hz, $C_{arom.}$), 142.5 (s, $C_{arom.}$) ppm.

Acknowledgments

Thanks are due to the ACS/PRF (38192-AC4) and the CNRS for financial support of this work.

[1] [1a] H. H. Karsch, H. U. Reisacher, G. Müller, *Angew. Chem. Int. Ed. Engl.* **1986**, *25*, 454. [1b] G. Becker, W. Becker, R. Knebl, H. Schmidt, U. Hildembrand, M. Westerhausen, *Phosphorus Sulfur* **1987**, *30*, 349. [1c] H. Grützmacher, H. Pritzkow, *Angew. Chem. Int. Ed. Engl.* **1989**, *28*, 740.

[2] [2a] F. Ramirez, N. B. Desai, B. Hansen, N. McKelvie, *J. Am. Chem. Soc.* **1961**, *83*, 3539. [2b] O. I. Kolodiazhnyi, in *Phosphorus Ylides* (Ed.: O. I. Kolodiazhnyi), Wiley-VCH, Weinheim, **1999**, p. 186.

[3] [3a] F. Castan, A. Baceiredo, J. Fischer, A. De Cian, G. Commenges, G. Bertrand, *J. Am. Chem. Soc.* **1991**, *113*, 8160. [3b] M. Soleilhavoup, Y. Canac, A. Polozov, A. Baceiredo, G. Bertrand, *J. Am. Chem. Soc.* **1994**, *116*, 6149. [3c] Y. Canac, A. Baceiredo, W. W. Schoeller, D. Gigmes, G. Bertrand, *J. Am. Chem. Soc.* **1997**, *119*, 7579.

[4] [4a] T. Kato, H. Gornitzka, A. Baceiredo, W. W. Schoeller, G. Bertrand, *Science* **2000**, *289*, 754. [4b] T. Kato, H. Gornitzka, A. Baceiredo, W. W. Schoeller, G. Bertrand, *J. Am. Chem. Soc.* **2002**, *124*, 2506.

[5] [5a] G. A. Olah, P. v R. Schleyer, in *Carbonium Ions* (Ed.: P. v. R. Schleyer), Wiley, New York, **1976**. [5b] R. A. Volkmann, in *Comprehensive Organic Synthesis* (Ed.: B. M. Trost), Pergamon Press, Oxford, **1991**, vol. 1, p. 355.

[6] [6a] J. Kapp, C. Schade, A. M. El-Nahasa, P. v. R. Schleyer, *Angew. Chem. Int. Ed. Engl.* **1996**, *35*, 2236. [6b] H. Grützmacher, C. M. Marchand, *Coord. Chem. Rev.* **1997**, *163*,

 © 2004 Wiley-VCH Verlag GmbH & Co. KGaA, Weinheim

287. [6c] W. W. Schoeller, U. Tubbesing, *Inorg. Chem.* **1998**, *37*, 3183. [6d] J. Rissler, M. Hartmann, C. M. Marchand, H. Grützmacher, G. Frenking, *Chem. Eur. J.* **2001**, *7*, 2834. [6e] S. Loss, C. Widauer, H. Ruegger, U. Fleischer, C. M. Marchand, H. Grützmacher, G. Frenking, *Dalton Trans.* **2003**, 85.

[7] [7a] H. Grützmacher, H. Pritzkow, *Angew. Chem. Int. Ed. Engl.* **1991**, *30*, 709. [7b] H. Grützmacher, H. Pritzkow, *Angew. Chem. Int. Ed. Engl.* **1992**, *31*, 99.

[8] T. Kato, H. Gornitzka, A. Baceiredo, G. Bertrand, *Angew. Chem. Int. Ed.* **2000**, *39*, 3319.

[9] The (*E*) configuration of phosphaalkenes **3** and **4** was assigned by comparing the J_{PP} values with that observed in a similar compound[1b] which was crystallographically characterized.

[10] O. Guerret, G. Bertrand, *Acc. Chem. Res.* **1997**, *30*, 486.

[11] Derivative **4** does not react with benzaldehyde and acetonitrile. The regiochemistry of products **6** and **7** was assigned by comparing the NMR spectroscopy data with that observed in similar compounds.[4b]

Received March 5, 2004
Early View Article
Published Online June 23, 2004

 © 2004 Wiley-VCH Verlag GmbH & Co. KGaA, Weinheim

Gadolinium DTPA-Monoamide Complexes Incorporated into Mixed Micelles as Possible MRI Contrast Agents

Tatjana N. Parac-Vogt,[a] Kristof Kimpe,[a] Sophie Laurent,[b] Corinne Piérart,[b] Luce Vander Elst,[b] Robert N. Muller,[b] and Koen Binnemans*[a]

Keywords: MRI contrast agents / Lanthanides / DTPA-monoamide derivatives / Micelles

Four monoamide derivatives of Gd–DTPA with alkyl chains consisting of 12, 14, 16, or 18 carbon atoms were synthesized. The gadolinium(III) complexes with chain lengths of 14, 16 or 18 carbon atoms were efficiently incorporated into mixed micelles whereas the complex with a chain length of 12 carbon atoms was not incorporated into a micellar structure. The size distribution of the micelles was measured by photon correlation spectroscopy. The mean sizes of the micelles for all the complexes lay within a narrow range, typically between 11 and 20 nm. The NMRD curves of the gadolinium(III) DTPA-monoamide complexes incorporated into mixed micelles display higher relaxivity values than the commercially available Gd–DTPA contrast agent. Moreover, micelles with gadolinium DTPA-monoamide complexes showed higher relaxivities than micelles containing the corresponding gadolinium DTPA-bis(amide) complexes, most likely because of a more efficient exchange of the coordinated water molecule.

(© Wiley-VCH Verlag GmbH & Co. KGaA, 69451 Weinheim, Germany, 2004)

Introduction

MRI (magnetic resonance imaging) contrast agents are routinely used in medicine because they provide reliable results that assist in the rapid clinical interpretation of MRI images. Most of the commonly used contrast agents achieve their effect by enhancing the relaxation rate of water protons in tissues. In general, contrast agents consist of a paramagnetic metal centre, typically gadolinium(III), which must be complexed to a strong chelating ligand, since the free metal ions are toxic at the concentrations needed for diagnosis. Water-soluble, anionic $[Gd(DTPA)(H_2O)]^{2-}$ was the first contrast agent approved for use in humans and is currently in routine use as a clinical magnetic resonance imaging agent under the name Magnevist® (Schering, Berlin, Germany). This complex contains one inner-sphere water molecule[1–4] that exchanges rapidly with bulk water,[5] providing an efficient relaxation of the surrounding water protons. However, $[Gd(DTPA)(H_2O)]^{2-}$ is a nonspecific contrast agent since its hydrophilicity results in an efficient enhancement of contrast only through its preferential distribution in the bloodstream. In recent years, contrast agents with improved characteristics, such as increased efficacy and organ specificity, have been sought.

Several different approaches to slow the rotational motion of gadolinium-based contrast agents, and thus to improve their relaxation efficiency, have been reported in the literature. These include synthesis of covalently or noncovalently bound macromolecular gadolinium(III) chelates such as dendrimers,[6] linear polymers[7–9] or proteins.[10,11] Some of these strategies proved to be rather disappointing since the relaxivity gain obtained by increasing the molecular size was often far less than expected as a result of some internal flexibility or the nonrigid attachment of the chelate to the macromolecule.[6–11]

An increase in the relaxivity could also be achieved by the synthesis of molecules with an efficient targeting system that is able to provide interactions between the agent and specific macromolecular receptors. For these purposes various hydrophobic groups have been introduced into the DTPA molecule through amidation of monoacid tetraester DTPA derivatives. The paramagnetic complexes of these compounds were investigated for the detection of tumors and myocardial infections.[12–14] In addition, incorporation of certain amphipathic gadolinium(III) complexes into liposomal membranes yielded paramagnetically labeled liposomes which significantly enhanced proton relaxivity.[15–21] Liposomes bearing gadolinium(III) complexes with long alkyl chains are expected to be less toxic and more tissue-specific, and their potential to deliver various MRI contrast

[a] Katholieke Universiteit Leuven, Department of Chemistry, Celestijnenlaan 200F, 3001 Leuven, Belgium
Fax: (internat.) + 32-16-327992
E-mail: Koen.Binnemans@chem.kuleuven.ac.be
[b] NMR laboratory, Department of Organic Chemistry, University of Mons-Hainaut, 7000 Mons, Belgium
Fax: (internat.) + 32-65-373520
E-mail: Robert.Muller@umh.ac.be

Supporting information for this article is available on the WWW under http://www.eurjic.org or from the author.

 © 2004 Wiley-VCH Verlag GmbH & Co. KGaA, Weinheim **DOI: 10.1002/ejic.200400187**

enhancement agents to selective sites has also been investigated.[15−21]

Another interesting strategy for the development of new types of contrast reagents is the synthesis of amphiphilic gadolinium(III) complexes which can self-assemble to form micelles.[22,23] One example of this is the Gd−DOTA derivative (DOTA = 1,4,7,10-tetraazacyclododecane-1,4,7,10-tetraacetic acid) with a long alkyl chain, which was reported by André et al.[24] This compound displayed high relaxation rates because of an increase in the rotational correlation time. Alternatively, the lipophilic gadolinium(III) complexes can be incorporated into mixed micelles in order to obtain supramolecular systems with a better control of the size.[25] We recently described the synthesis of amphiphilic bis(amide) derivatives of DTPA with alkyl chains consisting of 12, 14, 16, and 18 carbon atoms, whose gadolinium(III) complexes were incorporated into mixed micelles.[26] The resulting supramolecular structures showed an increase in relaxivity relative to Gd−DTPA, because of the lower mobility of the paramagnetic complex inside the micelle. In order to investigate the effects of the structure of the lipophilic gadolinium(III) complex on the overall relaxivity of the micelles, we have now synthesized amphiphilic monoamide derivatives of DTPA with alkyl chains of various lengths. The gadolinium complexes of these ligands were incorporated into mixed micelles and the NMRD profiles of these paramagnetic micelles are reported.

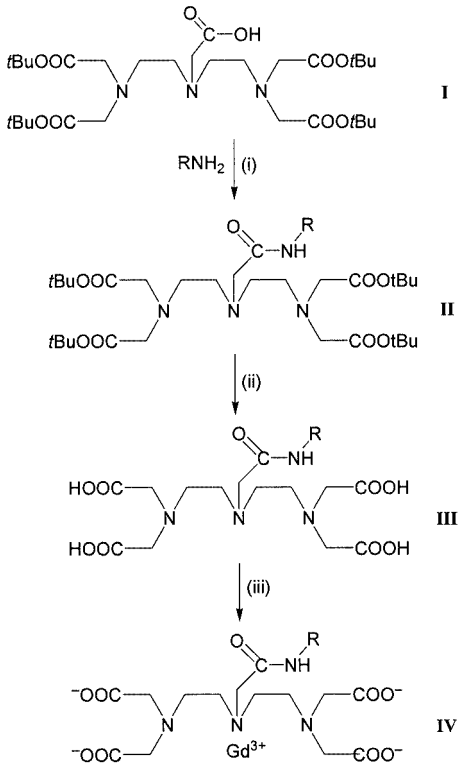

Scheme 1. Synthesis of DTPA monoamide derivatives; reaction conditions: (i) DEPC, TEA, DMF; (ii) 6 M HCl; (iii) pyridine, $GdCl_3$

Results and Discussion

Ligands and Complexes

The ligands DTPA-monolaurylamide (DTPA−MC12), DTPA-monomyristylamide (DTPA−MC14), DTPA-monopalmitylamide (DTPA−MC16) and DTPA-monostearylamide (DTPA−MC18) were synthesized according to Scheme 1.

Infrared spectroscopic data of all the ligands showed strong absorptions in the regions around 3410 and 1745−1670 cm^{-1}, corresponding to NH and CO stretching modes, respectively.[27] Upon complexation with gadolinium(III), the CO stretching vibrations of the free acid groups disappear, while the CO stretching mode of the amide shifts ca. 40 cm^{-1}, indicating amide oxygen coordination to the lanthanide ion. Although the negative-mode electron-spray mass spectra were not very informative, the positive-mode electron-spray mass spectra of Gd−DTPA−MC12, Gd−DTPA−MC14, Gd−DTPA−MC16 and Gd−DTPA−MC18 in chloroform/methanol solutions showed cluster peaks at *m*/*z* values of 716, 744, 772, and 800, respectively, which indicate coordination of gadolinium(III) to the ligand. These results are consistent with the formation of complexes in which DTPA−MC12, DTPA−MC14, DTPA−MC16 and DTPA−MC18 act as octadentate ligands, and where the ninth coordination site of gadolinium(III) is occupied by a water molecule (Figure 1). Initially, it might seem unusual that these negatively charged complexes were detected in the positive-mode electron-spray mass spectra. However, we used the positive ESI-MS for the best sensibility of the technique. In the ESI spectra, we observed protonated molecular ions or adducts of sodium. This can be explained by the fact that the molecules contain basic groups (carboxylate and amine groups) that can be protonated readily. Moreover, these groups can exhibit Lewis basicity, forming adducts with sodium ions.

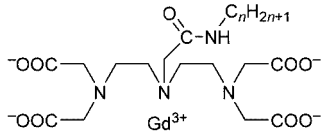

Figure 1. Schematic representation of the Gd−DTPA-monoamide complex; the ligand coordinates to the gadolinium(III) ion through four acetate oxygen atoms, three nitrogen atoms and one carbonyl oxygen atom of the amide group, while a water molecule occupies the ninth coordination site

^{1}H NMR Studies of the Complexes

The low solubility of the lanthanide(III) complexes of DTPA−MC14, DTPA−MC16 and DTPA−MC18 limited the scope of solution studies. A range of deuterated solvents including D_2O, $CDCl_3$, CD_2Cl_2, [D_6]DMSO, CD_3OH, CD_3CN, $(CD_3)_2CO$, and various combinations of these solvents, were used in attempts to obtain solutions of the complexes suitable for NMR measurements. Unfortunately, the concentration of most of the solutions was too low to obtain good-quality NMR spectra. However, in the case of

 © 2004 Wiley-VCH Verlag GmbH & Co. KGaA, Weinheim

the La−DTPA−MC18 complex, it was possible to obtain a relatively well-resolved proton NMR spectrum in $[D_6]DMSO/CD_3OH$ solution. This spectrum showed that the DTPA resonances of the complex are significantly broadened compared to the free ligand. As previously described for the bis(amide)-DTPA complexes, the broadening of DTPA resonances indicates the presence of several interconverting isomers in solution.[26] Variable-temperature NMR studies on this complex did not provide more information about the exchange process since the strong solvent peaks at δ = 2.61 ppm ($[D_6]DMSO$) and 3.28 ppm (CD_3OH) obscured some of the DTPA resonances.

Mixed Micelle Formation and Size Distribution

A phospholipid (DPPC) and a surfactant (Tween 80), whose structures are given in the Supporting Information, together with the gadolinium(III) complexes of DTPA−MC12, DTPA−MC14, DTPA−MC16, and DTPA−MC18 ligands were used to prepare mixed micelles. The micelle size was determined at room temperature by photon correlation spectroscopy. All micelles were monodisperse. The mean diameters of the micelles were all within a narrow range (11−20 nm, see Supporting Information), indicating that their size is virtually independent of the length of the monoamide chain, and that the phospholipid DPPC determines micelle size. A schematic representation of a mixed micelle incorporating a gadolinium(III) complex is shown in Figure 2.

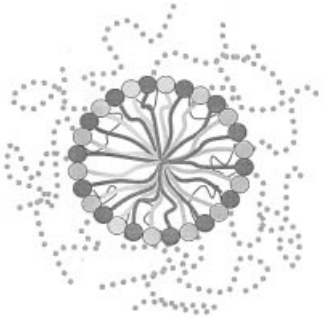

Figure 2. Schematic representation of the amphiphilic gadolinium(III) complex incorporated into a mixed micelle: gadolinium(III) complex (black circles and lines), DPPC phospholipid (gray circles and lines), Tween® 80 (gray dots)

Nuclear Magnetic Relaxation Dispersion (NMRD) Measurements

Figure 3 shows the proton NMRD profiles of the relaxivity of Gd−DTPA−MC12, Gd−DTPA−MC14, Gd−DTPA−MC16 and Gd−DTPA−MC18 in micellar solution at 37 °C. As expected, the inclusion of the gadolinium(III) complexes Gd−DTPA−MC14, Gd−DTPA−MC16 and Gd−DTPA−MC18 into micelles results in an increased relaxivity when compared with the parent complex Gd−DTPA. The hump at higher field strengths (20−60 MHz), which is typical for supramolecular structures, is also seen here. As explained previously, this is caused by a decrease in the rotational mobility of the paramagnetic complex.[26] On the other hand, the proton NMRD profile of Gd−DTPA−MC12 in micellar solution is much less intense and does not reach a maximum at high magnetic fields. This behaviour is typical of a hydrophilic gadolinium(III) complex of low molecular weight and suggests that this complex is very loosely bound or not incorporated at all into the micellar structure.

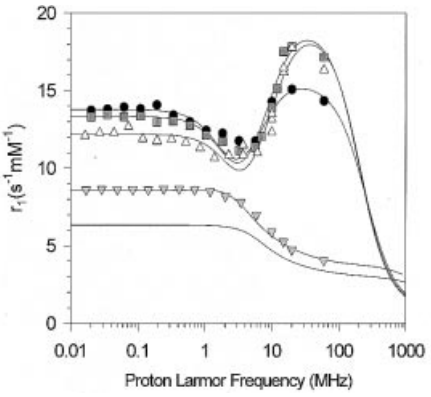

Figure 3. NMRD profiles of micellar solutions of Gd−DTPA−MC12 (triangles down), Gd−DTPA−MC14 (circles), Gd−DTPA−MC16 (squares) and Gd−DTPA−MC18 (triangles up), at 37 °C; the NMRD profile of Gd−DTPA (line underneath) has been added for comparison[32]

The data were analysed using the classical inner-sphere[28−29] and outer-sphere[30] theories. The distance of closest approach was set at 0.36 nm, the relative diffusion constant was fixed at 3.3×10^{-9} m^2s^{-1} and the distance for the inner-sphere interaction was set at 0.31 nm. The number of coordinated water molecules was assumed to be equal to one by analogy with other derivatives of Gd−DTPA.[31−33] The parameters describing the electronic relaxation of Gd (the electronic relaxation time at very low magnetic field, τ_{SO}, and the correlation time modulating the electronic relaxation, τ_V) as well as the "global" rotational correlation time, τ_R, and the residence time of the coordinated water molecule, τ_M, were simultaneously fitted. The results are shown in Table 1.

Table 1. Parameters obtained from the theoretical fitting of the proton NMRD data (T = 37 °C)

Compound	τ_R [ns]	τ_M [ns]	τ_{SO} [ps]	τ_V [ps]
Gd−DTPA−MC12	0.105	310	210	40
Gd−DTPA−MC14	0.91	680	194	41
Gd−DTPA−MC16	1.12	510	154	39
Gd−DTPA−MC18	1.07	500	127	38
Gd−DTPA[a]	0.059	143	82	23
Gd−DTPA−BMA[b]	0.064	967	76	23

[a] From ref.[32]: τ_R, τ_{SO} and τ_V obtained from the fitting of the proton NMRD data, τ_M obtained from the fitting of the ^{17}O transverse relaxation rates. [b] From ref.[33]

The parameters obtained for Gd−DTPA−MC14, Gd−DTPA−MC16 and Gd−DTPA−MC18 are quite similar, having a rotational correlation time of about 1 ns.

 © 2004 Wiley-VCH Verlag GmbH & Co. KGaA, Weinheim

This value is at least two orders of magnitude lower than the rotational correlation time calculated by the Stokes−Einstein theory for a rigid sphere (τ_R ranging between 112 and 673 ns depending on the micelle size). The observed difference can be related to the local motion of the gadolinium(III) complex within the micellar structure. The values of τ_M are in the same range for the three complexes, and are larger than for the parent compound Gd−DTPA but smaller than that of Gd−DTPA−BMA [a hydrophilic bis(amide) derivative of Gd−DTPA]. Indeed it is well known that Gd−DTPA derivatives with amide groups are characterized by a decreased exchange rate of the coordinated water molecule and that τ_M is related to the number of amide functions and their substituents.[34]

The values for τ_R are smaller than the ones reported for the corresponding bis(amide) derivatives incorporated into the same micellar structure. This is probably related to a more efficient immobilisation of the paramagnetic part of the bis(amide) derivatives caused by the incorporation of both hydrophobic chains into the micellar membrane. These smaller τ_R values are not reflected by a subsequent decrease but by an increase in relaxivity because of the smaller τ_M values, which induce an opposing effect. Moreover, the relaxivity of the micellar solution of the Gd−DTPA−MC18 complex bearing an amide chain of 18 carbon atoms, and thus longer than the DPPC chains, is similar to that of its analogue with 16 carbon atoms, at the magnetic field strengths used for imaging.

The τ_R value obtained for the complex Gd−DTPA−MC12 in the micellar solution is much lower than those of the other complexes, which indicates that this complex is either very loosely incorporated inside the micellar membrane or not incorporated at all. It seems that the aliphatic chain of this complex is too short and the hydrophobic character of the complex too low to allow efficient incorporation into the micellar structures.

Conclusion

While it appears that the gadolinium(III) complex of Gd−DTPA−MC12 does not form mixed micelles with DPPC and Tween 80, the gadolinium(III) complexes of DTPA−MC14, DTPA−MC16, and DTPA−MC18 ligands were successfully incorporated into mixed micelles to obtain supramolecular structures with a decreased mobility. The relaxivities of solutions containing these micelles are significantly higher than of solutions of Gd−DTPA as a result of the reduced mobility of the gadolinium(III) complexes. At imaging fields (20−60 MHz), all micellar solutions show similar relaxivities, which is in contrast to the bis(amide) complexes in which the lowest relaxivities were observed for the complex containing the longest side chains.[26] This observation suggests that the insertion of the monoamide compound Gd−DTPA−MC18 is similar to that of the homologues with shorter chain length despite being inserted into micelles composed of DPPC, whose alkyl chain is shorter. By a comparison of the relaxivity data of the monoamide compounds with those of the previously reported bis(amide) compounds, we can conclude that the relaxivity gain, relative to Gd−DTPA, is higher for mixed micelles in which monoamide complexes are inserted than for the micelles in which bis(amide) compounds of the same chain length are inserted.

Experimental Section

Chemicals: Reagents were obtained from Aldrich Chemical Co. Inc., Acros Organics, or Fluka, and used without further purification. 1,2-Dipalmitoyl-*sn*-glycero-3-phosphatidylcholine (DPPC) was obtained from Genzyme Pharmaceuticals (Switzerland). Gadolinium(III) chloride hexahydrate was purchased from GFS chemicals (USA).

Instruments: ^{1}H NMR spectra were obtained using a Bruker Avance 300 operating at 300 MHz. IR spectra (KBr pellets) were measured with a Bruker IFS66 FTIR spectrometer. Mass spectra were obtained using a Q-tof 2 (Micromass, Manchester UK). Samples (0.1 g) were dissolved in methanol/water (50:50) and infused at a rate of 5 μL/min.

Synthesis of the Ligands

***N*,*N*-Bis(2-{bis[2-(1,1-dimethylethoxy)-2-oxoethyl]amino}ethyl)-glycine (Product I in Scheme 1):** This compound was prepared according to a published procedure.[35] Yield 45%. IR: $\tilde{\nu}$ = 2977, 2935 (C−H alkyl stretch); 1733 (CO, ester); 1646 (COOH) cm^{-1}. ^{1}H NMR ([D$_6$]DMSO): δ = 1.45 (s, 36 H, 12 × CH_3), 2.98 (t, 4 H, 2 × CH_2), 3.10 (br., 4 H, 2 × CH_2), 3.36 (s, 8 H, 4 × CH_2), 3.58 (s, 2 H, CH_2) ppm. ES-MS$^+$: *m*/*z* = 618 [M + H]$^+$ ($C_{30}H_{55}N_3O_{10}$, $M_{calcd.}$ = 617).

DTPA-Monoamides: The alkylamine (4.72 mmol) was added to a solution of *N*,*N*-bis(2-{bis[2-(1,1-dimethylethoxy)-2-oxoethyl]-amino}ethyl)glycine (4.72 mmol) in DMF (80 mL). After the dropwise addition of DEPC [$(EtO)_2P(O)CN$] (0.8 mL, 5.28 mmol), the reaction mixture was kept at 3 °C by cooling in an ice bath. Triethylamine (5.92 mmol) was then added slowly to the solution. After 10 min, the amine had fully reacted and the solution was warmed to room temperature and allowed to stand for 30 min. DMF was then removed by evaporation under reduced pressure. The crude product dissolved in ethyl acetate (132 mL) and washed with saturated aqueous sodium hydrogen carbonate (2 × 100 mL) then saturated aqueous sodium chloride solution (2 × 80 mL) to obtain product **II** in Scheme 1. Product **II** (838 mg, 1.05 mmol) was dissolved in 6 N HCl (8 mL). The mixture was stirred at room temperature for 1 h and then washed with dichloromethane (2 × 10 mL). The aqueous phase was concentrated to give DTPA-monamide (product **III** in Scheme 1).

Analytical Data for the Ligands

DTPA−MC12: Yield 73% (1.93 g). IR: $\tilde{\nu}$ = 3422 (N−H stretch), 2938, 2851 (C−H alkyl stretch), 1745 (CO acid), 1674 (CO, amide I) cm^{-1}. ^{1}H NMR ($CDCl_3$): δ = 0.80 (t, 3 H, CH_3), 1.1−1.3 (m, 20 H, 10 × CH_2), 2.7 (t, 4 H, 2 × CH_2), 2.8 (t, 4 H, 2 × CH_2), 3.35 (t, 2 H, CH_2), 3.4 (s, 2 H, CH_2), 3.9 (s, 8 H, 4 × CH_2), 4.4 (s, 4 H, 4 × OH) ppm. ES-MS$^+$: 561 [M + H]$^+$ ($C_{26}H_{48}N_4O_9$, $M_{calcd.}$ = 560).

DTPA−MC14: Yield 14% (390 mg). IR: $\tilde{\nu}$ = 3422 (N−H stretch), 2941, 2851 (C−H alkyl stretch), 1745 (CO acid), 1674 (CO, amide I) cm^{-1}. ^{1}H NMR (MeOD, $CDCl_3$): δ = 0.89 (t, 3 H, CH_3), 1.27

 © 2004 Wiley-VCH Verlag GmbH & Co. KGaA, Weinheim

(s, 22 H, 11 × CH_2), 1.55 (m, 2 H, CH_2), 2.89 and 3.02 (m, 8 H, 4 × CH_2), 3.45 (m, 4 H, 2 × CH_2), 3.92 (s, 8 H, 4 × CH_2) ppm. ES-MS$^+$: 589 $[M + H]^+$ ($C_{28}H_{52}N_4O_9$, $M_{calcd.}$ = 588).

DTPA−MC16: Yield (PA) 12% (349 mg). IR: $\tilde{\nu}$ = 3424 (N−H stretch), 2932, 2851 (C−H alkyl stretch), 1745 (CO acid), 1674 (CO, amide I) cm^{-1}. ^{1}H NMR (MeOD, $CDCl_3$): δ = 0.83 (t, 3 H, CH_3), 1.27 (s, 26 H, 13 × CH_2), 1.39 (m, 2 H, CH_2), 2.70 and 3.05 (m, 8 H, 4 × CH_2), 4.12 (s, 8 H, 4 × CH_2) ppm. ES-MS$^+$: 617 $[M + H]^+$ ($C_{30}H_{56}N_4O_9$, $M_{calcd.}$ = 616).

DTPA−MC18: Yield (SA) 22% (669 mg). IR: $\tilde{\nu}$ = 3432 (N−H stretch), 2921, 2843 (C−H alkyl stretch), 1745 (CO acid), 1671 (CO, amide I) cm^{-1}. ^{1}H NMR (MeOD/$CDCl_3$): δ = 0.89 (t, 3 H, CH_3), 1.27 (s, 30 H, 15 × CH_2), 1.55 (m, 2 H, CH_2), 2.89 and 3.02 (m, 8 H, 4 × CH_2), 3.45 (m, 4 H, 2 × CH_2), 3.92 (s, 8 H, 4 × CH_2) ppm. ES-MS$^+$: 667 $[M + Na]^+$, 645 $[M + H]^+$ ($C_{32}H_{60}N_4O_9$, $M_{calcd.}$ = 644).

Synthesis of the Gadolinium(III) Complexes (Product IV in Scheme 1): The complexes were synthesized according to the general procedure as follows: A solution of the hydrated $GdCl_3$ salt (1.1 mmol) in H_2O (1 mL) was added to the ligand (1 mmol) dissolved in pyridine (30 mL), and the mixture was heated at 70 °C for 3 h. The solvents were evaporated under reduced pressure and the crude product was then refluxed in ethanol for 1 h. After cooling to room temperature, the complex was filtered off and dried in vacuo. The absence of free gadolinium was confirmed using a xylenol orange indicator.[36]

Analytical Data for the Complexes

Gd−DTPA−MC12: Yield 74% (529 mg). IR: $\tilde{\nu}$ = 3408 (N−H stretch), 3092 (N−H amide), 2930, 2850 (C−H alkyl stretch), 1634 (CO, amide I/COO^- assym. stretch) cm^{-1}. ES-MS$^+$: 716 $[M + H]^+$ ($C_{26}H_{45}GdN_4O_9$, $M_{calcd.}$ = 715).

Gd−DTPA−MC14: Yield 85% (631 mg). IR: $\tilde{\nu}$ = 3410 (N−H stretch), 3090 (N−H amide), 2931, 2856 (C−H alkyl stretch), 1632 (CO, amide I/COO^- assym. stretch) cm^{-1}. ES-MS$^+$: 744 $[M + H]^+$($C_{28}H_{49}GdN_4O_9$, $M_{calcd.}$ = 743).

Gd−DTPA−MC16: Yield 61% (470 mg). IR: $\tilde{\nu}$ = 3410 (N−H stretch), 3094 (N−H amide), 2922, 2849 (C−H alkyl stretch); 1630 (CO, amide I/COO^- assym stretch) cm^{-1}. ES-MS$^+$: 772 $[M + H]^+$ ($C_{30}H_{53}GdN_4O_9$, $M_{calcd.}$ = 771).

Gd−DTPA−MC18: Yield 67% (535 mg). IR: $\tilde{\nu}$ = 3401 (N−H stretch), 3094 (N−H amide), 2926, 2848 (C−H alkyl stretch), 1630 (CO, amide I/COO^- assym. stretch) cm^{-1}. ES-MS$^+$: 800 $[M + H]^+$ ($C_{32}H_{57}GdN_4O_9$, $M_{calcd.}$ = 799).

Sodium/Potassium Content: Prior to incorporation into micelles, the potassium and sodium ion contents of the compounds were checked by flame photometry (IL, 943, Instrumentation Laboratories, Massachusetts, USA). The Na^+ and K^+ ion contents were measured using a sample that had been obtained by extracting a solution of complex (1.6 mg) in chloroform/methanol (10:1) with 2 mL of water. Na^+ content (mmol/mol of the complex): Gd−DTPA−MC12: 3.0; Gd−DTPA−MC18: 0.4; Gd−DTPA−MC16: 0.1; Gd−DTPA−MC14: 0.4. K^+ content: no K^+ was found in any of the complexes.

Preparation of Micelles: 1,2-Dipalmitoyl-*sn*-glycero-3 phosphatidylcholine (DPPC) (225 mg) and the complex (25 mg) were dissolved in chloroform/methanol (1:1) (50 mL). Concentration under reduced pressure yielded a thin film, which was then rehydrated with hot water (5 mL, 70 °C). This solution was sonicated for 15 min using a 70-W sonicator while maintaining the temperature at 65 °C with a thermostatic bath. After sonication, 75 mg of a surfactant was added (Tween 80®, polyoxyethylene sorbitan monooleate), followed by another 15 min of sonication.

Determination of Micelle Size: The mean micelle sizes were determined by photon correlation spectroscopy performed with a BIC multiangle laser light scattering system at room temperature and with a 90° scattering angle (Brookhaven Instruments Corporation, Holtsville, USA). The intensity-weighted micelle diameter was measured on diluted suspensions and calculated by a nonnegatively constrained least-squares (multiple pass) routine. The error is of the order of 20%. The diameters obtained are as follows: micellar solutions with Gd−DTPA−MC12: 20 nm, with Gd−DTPA−MC14: 13 nm, with Gd−DTPA−MC16: 18 nm, with Gd−DTPA−MC18: 11 nm.

***T_1* Measurements:** Proton Nuclear Magnetic Relaxation Dispersion (NMRD) profiles were recorded between 0.24 mT and 1.2 T with a Field Cycling instrument (Stelar Spinmaster FFC-2000, Stelar S.R.L., Mede, Italy) on 0.6 mL solutions in 10-mm (o.d.) tubes. Proton relaxation rates were also measured at 0.47 T, and 1.5 T with Minispec PC-120, and mq-60 (Bruker, Karlsruhe, Germany). All samples were diluted 10 times and the temperature was maintained at 37 °C. ^{1}H NMRD data were fitted according to the theoretical inner-sphere model described by Solomon[28] and Bloembergen[29] and to the outer-sphere contribution described by Freed.[30] Calculations were performed with a previously described software package.[37,38]

Acknowledgments

K. K., T. N. P. V. and K. B. thank the K. U. Leuven for financial support (VIS/01/006.01/20002-06/2004 and GOA 03/03). K. B. acknowledges the F.W.O.−Flanders (Belgium) for a Postdoctoral Fellowship. S. L., C. P., L. V. E. and R. N. M. thank the ARC Program 00/05-258 of the French Community of Belgium and kindly acknowledge the support and sponsorship concerted by COST Action D18 "Lanthanide Chemistry for Diagnosis and Therapy".

[1] C. C. Bryden, C. N. Reilley, *Anal. Chem.* **1982**, *54*, 610−615.
[2] J. A. Peters, *Inorg. Chem.* **1988**, *27*, 4686−4691.
[3] C. F. G. C. Geraldes, A. D. Sherry, W. P. Cacheris, K. T. Kuan, R.D. Brown III, S. H. Koenig, M. Spiller, *Magn. Reson. Med.* **1988**, *8*, 191−199.
[4] C. A. Chang, H. G. Brittain, J. Telser, M. F. Tweedle, *Inorg. Chem.* **1990**, *29*, 4468−4473.
[5] K. Micskei, L. Helm, E. Brucher, A. E. Merbach, *Inorg. Chem.* **1993**, *32*, 3844−3850.
[6] É. Tóth, D. Pubanz, S. Vauthey, L. Helm, A. E. Merbach, *Chem. Eur. J.* **1996**, *2*, 1607−1615.
[7] M. Spanoghe, D. Lanens, R. Dommisse, A. Van der Linden, F. Alderweireldt, *J. Magn. Reson. Imaging* **1992**, *10*, 913−917.
[8] V. S. Vexler, O. Clement, H. Schmitt-Willich, R. C. Brasch, *J. Magn. Res. Imaging* **1994**, *4*, 381−388.
[9] T. S. Desser, D. L. Rubin, H. H. Muller, F. Qing, S. Khodor, G. Zanazzi, S. U. Young, D. L. Ladd, J. A. Wellons, K. E. Kellar, J. L. Toner, R. A. Snow, *J. Magn. Res. Imaging* **1994**, *4*, 467−472.
[10] É. Tóth, F. Connac, L. Helm, K. Adzamli, A. E. Merbach, *J. Biol. Inorg. Chem.* **1998**, *3*, 606−613.
[11] S. Aime, M. Botta, M. Fasano, E. Terreno, *Chem. Soc. Rev.* **1998**, *27*, 19−29.
[12] J. Platzek, U. Niedballa, B. Radüchel, P. Mareski, H.-J. Weinmann, A. Mühler, B. Misselwitz, PCT Int. Appl. WO 96 26 182, **1996**; *Chem. Abstr.* **1996**, *125*, 275257j.

 © 2004 Wiley-VCH Verlag GmbH & Co. KGaA, Weinheim

[13] J. Platzek, U. Niedballa, P. Mareski, B. Raduchel, H.-J. Weinmann, A. Muhler, B. Misselwitz, US Patent No. 5,676,923, **1997**.
[14] J. Platzek, U. Speck, U. Niedballa, B. Raduchel, H.-J. Weinmann, W. Ebert; US Patent No. 6,495,118, **2002**.
[15] G. W. Kabalka, E. Buonocore, K. Hubner, T. Moss, N. Norley, L. Huang, *Radiology* **1987**, *163*, 255.
[16] G. W. Kabalka, E. Buonocore, K. Hubner, M. Davis, L. Huang, *Magn. Reson. Med.* **1988**, *8*, 89.
[17] C. W. M. Grant, S. Karlik, E. Florio, *Magn. Reson. Med.* **1989**, *11*, 236.
[18] V. J. Caride, H. D. Sostman, R. J. Winchell, J. C. Gore, *Magn. Reson. Imaging* **1984**, *2*, 107.
[19] E. C. Unger, P. Macdougall, P. Cullis, C. Tilcock, *Magn. Reson. Imaging* **1989**, *7*, 417.
[20] R. A. Schwendener, R. Wuthrich, S. Dverwell, G. Westera, G. K. Von Schulthess, *Int. J. Pharm.* **1989**, *49*, 249.
[21] G. W. Kabalka, M. A. Davis, T. H. Moss, E. Buonocore, K. Hubner, E. Holmberg, K. Maruyama, L. Huang, *Magn. Reson. Med.* **1991**, *19*, 406−415.
[22] E. Toth, L. Helm, K. E. Kellar, A. E. Merbach, *Chem. Eur. J.* **1999**, *5*, 1202−1211.
[23] K. Binnemans, C. G. Görller-Walrand, *Chem. Rev.* **2002**, *102*, 2303−2345.
[24] J. P. André, E. Toth, H. Fischer, A. Seelig, H. R. Mäcke, A. E. Merbach, *Chem. Eur. J.* **1999**, *5*, 2977−2983.
[25] P. L. Anelli, L. Lattuada, V. Lorusso, M. Schneider, H. Tourner, F. Uggeri, *Magn. Reson. Mater. Phys., Biol. Med.* **2001**, *12*, 114; H. Tournier, R. Hyacinthe, M. Schneider, *Acad. Radiol.* **2002**, *9* (suppl. 1), S20−S28.
[26] [26a] K. Kimpe, T. N. Parac-Vogt, S. Laurent, C. Piérart, L. Vander Elst, R. N. Muller, K. Binnemans, *Eur. J. Inorg. Chem.* **2003**, 3021−3027. [26b] S. Laurent, S. Ergot, C. Piérart, L. Vander Elst, R. N. Muller, *Proceedings of the Annual Meeting of the Royal Society of Chemistry of Belgium*, **2003**.
[27] E. Pretsch, T. Clerc, J. Seibl, W. Simon in *Tabellen zur Strukturaufklärung organischer Verbindungen mit spektroskopischen Methoden*, Springer, Berlin, **1976**.
[28] I. Solomon, *Phys. Rev.* **1955**, *99*, 559−565.
[29] N. Bloembergen, *J. Chem. Phys.* **1957**, *27*, 572−573.
[30] J. H. Freed, *J. Chem. Phys.* **1978**, *68*, 4034−4037.
[31] M. C. Alpoim, A. M. Urbano, C. F. G. C. Geraldes, J. A. Peters, *J. Chem. Soc., Dalton Trans.* **1992**, 463−467.
[32] S. Laurent, L. Vander Elst, S. Houzé, N. Guérit, R. N. Muller, *Helv. Chim. Acta* **2000**, *83*, 394−406.
[33] S. Laurent, F. Botteman, L. Vander Elst, R. N. Muller, *Eur. J. Inorg. Chem.* **2004**, 463−468.
[34] F. Botteman, G. N. Nicolle, L. Vander Elst, S. Laurent, A. E. Merbach, R. N. Muller, *Eur. J. Inorg. Chem.* **2002**, 2686−2693.
[35] P. L. Anelli, F. Fedeli, O. Gazzotti, L. Lattuada, G. Lux, F. Rebasti, *Bioconjugate Chem.* **1999**, *10*, 137−140.
[36] G. Brunisholz, M. Randin, *Helv. Chim. Acta* **1959**, *42*, 1927.
[37] R. N. Muller, D. Declercq, P. Vallet, F. Giberto, B. Daminet, H. W. Fischer, F. Maton, Y. Van Haverbeke, in *Proc., ESMRMB, 7th Annual Congress, Strasbourg, France*, **1990**, p. 394.
[38] P. Vallet, PhD Dissertation, University of Mons-Hainaut, Belgium, **1992**.

Received March 8, 2004
Early View Article
Published Online June 23, 2004

 © 2004 Wiley-VCH Verlag GmbH & Co. KGaA, Weinheim

Mono- and Dinuclear High-Spin Half-Sandwich Manganese(II) Complexes Containing Acetylide and TMEDA Ligands

Sohrab Kheradmandan,[a] Thomas Fox,[a] Helmut W. Schmalle,[a] Koushik Venkatesan,[a] and Heinz Berke*[a]

Keywords: Alkyne ligands / Cyclopentadienyl ligands / Half-sandwich complexes / Molecular devices / N ligands

The d^5 high-spin Mn^{II} half-sandwich complexes [Mn(C≡CR)(MeC_5H_4)(tmeda)] (R = $SiMe_3$ **2**; Ph **3**; *t*Bu **4**; C≡C$SiMe_3$ **5**; C≡CPh **6**; tmeda = *N*,*N*,*N*′,*N*′-tetramethylethylenediamine) were prepared by the reaction of [Mn(MeC_5H_4)$_2$(tmeda)] (**1**) with 1 equiv. of the corresponding acetylene or the trimethyltin acetylide. The dinuclear complexes [Mn(C≡C–C≡C$SiMe_3$)$_2$(tmeda)]$_2$ (**7**) and [Mn_2($MeCp$)$_2$(μ_1-*t*BuC≡C)$_2$(μ_1-tmeda)] (**8**), which contain Mn–Mn bonds, were synthesized by treating **1** with an excess of HC≡C–C≡C$SiMe_3$ or HC≡C*t*Bu, respectively. Dinuclear complexes of the type [(MeC_5H_4)(tmeda)MnC≡C–X–C≡CMn(tmeda)(C_5H_4Me)] [X = 1,3-C_6H_4 **9**; 1,4-C_6H_4 **10**; 4,4′-(C_6H_4)$_2$ **11**] were obtained by treatment of **1** with 0.5 equiv. of the corresponding acetylides 1,3-C_6H_4-(C≡C$SnMe_3$)$_2$, 1,4-C_6H_4(C≡C$SnMe_3$)$_2$ and 4,4′-(C_6H_4)$_2$-(C≡C$SnMe_3$)$_2$ in benzene for 24 h to yield the corresponding dinuclear complexes in very good yields. All the mono- and dinuclear compounds have been characterized by NMR, IR, Raman spectroscopy and elemental analyses. X-ray diffraction studies have been performed on complexes **3** and **5**–**11**.
(© Wiley-VCH Verlag GmbH & Co. KGaA, 69451 Weinheim, Germany, 2004)

Introduction

Mono- and dinuclear transition metal acetylide complexes offer an interesting perspective for the construction of organometallic systems as molecular-level single-electron devices and the bottom-up construction of miniaturized components capable of performing specific electronic functions. This is an important challenge for many facets of modern chemistry.[1−15] During the last decade several organometallic research groups have focused on the development of facile synthetic routes to $L_mMC_xM'L'_{m'}$ rigid rod transition metal complexes.[2,16−91] Our ongoing interest in such building blocks is devoted to the synthesis and physical properties of molecular species that might function as wires. Specifically, they should consist of an all-carbon chain capped by two redox-active metal termini.[36,46,57,63,74,75] We have sought to explore reactions to prepare mono- and dinuclear precursors containing polyyne ligands. We have already reported some of the results involving manganese centers with strong-field ligands such as phosphanes.[36,46,57,63,74,75] We subsequently decided to synthesize and study the properties of molecules with weak-field ligands, such as tmeda, expecting high-spin configurations of the metal centers.[92−100] In addition to the above reasons, the $L_mMn-C_4-MnL_m$ systems were selected as target molecules because a build-up of di- and oligonuclear Mn complexes seemed not only to be synthetically feasible by acetylide substitution processes, but also by coupling of $Mn-C_2$ units, such as Mn−alkynyl and Mn−vinylidene moieties. These possibilities have been corroborated by recent studies in our group.[36,46,57,74,75,101] For instance, we have published the synthesis of redox-active dinuclear complexes of the type [{Mn(dmpe)$_2$(X)}$_2$(μ-C_4)]$^{n+}$ (X = C≡CH, C≡C−C≡C$SiMe_3$ and n = 0−2), which were obtained by an in situ C−C coupling of [Mn^{III}-(dmpe)$_2$(C≡CH)(C≡C)] units.[74,75,101] We have also previously reported the synthesis and characterization of [I(dmpe)$_2$MnC≡C−C≡CMn(dmpe)$_2$I]$^{n+}$ [57] in a preliminary communication and report herein the mononuclear half-sandwich complexes of the type [(MeC_5H_4)(tmeda)MnC≡CR] (R = $SiMe_3$, Ph, *t*Bu, C≡C$SiMe_3$, C≡CPh) and dinuclear half-sandwich complexes of the type [(MeC_5H_4)(tmeda)Mn−X−Mn(tmeda)(MeC_5H_4)] [X = 1,4-C_6H_4(C≡C)$_2$, 1,3-C_6H_4(C≡C)$_2$, 4,4′-$C_6H_4C_6H_4$-(C≡C)$_2$].

The first representatives of the manganocene family — [$MnCp_2$] and [Mn(MeC_5H_4)$_2$][102,103] — have been known for around 40 years and their electronic and structural properties have been studied extensively; however, their synthetic potential, in particular with regard to Cp or MeC_5H_4 replacement by other organometallic units, has not been exploited appropriately except for earlier work from our group.[63,104] The mononuclear complexes were obtained by the reaction of [(MeC_5H_4)$_2$Mn(tmeda)][105,106] with RC≡CR′ (R′ = H, $SnMe_3$, R = $SiMe_3$, Ph, *t*Bu,

[a] Anorganisch-Chemisches Institut der Universität Zürich, Winterthurerstrasse 190, 8057 Zürich, Switzerland
E-mail: hberke@aci.unizh.ch
Supporting information for this article is available on the WWW under http://www.eurjic.org or from the author.

 © 2004 Wiley-VCH Verlag GmbH & Co. KGaA, Weinheim **DOI: 10.1002/ejic.200400006**

C≡CSiMe$_3$, C≡CPh) and the corresponding dinuclear systems by treatment of 0.5 equiv. of the bifunctional acetylenes Me$_3$SnC≡C−R"−C≡CSnMe$_3$ [R′′ = 1,4-C$_6$H$_4$(C≡C)$_2$,[107−109] 1,3-C$_6$H$_4$(C≡C)$_2$,[107−109] or 4,4′-C$_6$H$_4$C$_6$H$_4$(C≡C)$_2$ [107−109] with [Mn(MeC$_5$H$_4$)$_2$(tmeda)].

Results and Discussion

On the basis of known, facile methylcyclopentadienyl replacements in [Mn(MeC$_5$H$_4$)$_2$(dmpe)],[63,103,105] where one of the methylcyclopentadienyl rings is bound to the manganese center in an η^5 fashion and the other in an η^2 fashion,[103,105] we thought that it should be even easier to replace one of the methylcyclopentadienyl rings in [Mn(MeC$_5$H$_4$)$_2$(tmeda)][106] (**1**), which comprises two η^1-methylcyclopentadienyl rings bound to the manganese center, by an acetylide ligand. Reaction of **1** with 1 equiv. of various acetylenes HC≡CSiMe$_3$ or Me$_3$SnC≡CSiMe$_3$, PhC≡CH or PhC≡CSnMe$_3$, *t*BuC≡CH or *t*BuC≡CSnMe$_3$, Me$_3$SiC≡C−C≡CH, Me$_3$SiC≡C−C≡CSnMe$_3$ or PhC≡C−C≡CSnMe$_3$ yielded, in THF at room temperature for 3 d, the corresponding high-spin d^5 Mn^{II} mononuclear complexes of the type [(MeC$_5$H$_4$)(tmeda)MnC≡CR] (R = SiMe$_3$ **2**; Ph **3**; *t*Bu **4**; C≡CSiMe$_3$ **5**; C≡CPh **6**) quantitatively (Scheme 1). The ^{1}H NMR spectra of complexes **3**, **4** and **6** at 20 °C contain proton resonances for the ring protons of the MeC$_5$H$_4$ group in the high-field region, while for **2** and **5** similar resonances are not present. The only proton resonances that are observed for complexes **2** and **5** are for the SiMe$_3$ protons at δ = 7.3 and 4.8 ppm, respectively. The signals of the methyl and the methylene protons of the tmeda ligand of these complexes are observed between δ = 60 and 110 ppm. The paramagnetic behavior of these complexes apparently influences the relaxation of the ^{15}N nucleus, so that ^{15}N resonances can be observed. The ^{15}N NMR spectra of **3**, **4** and **6** reveal resonances for the tmeda ligand at higher field, at $\delta \approx -75$ to −90 ppm. The proton resonances for the methyl and the methylene protons of the tmeda ligand are absent. The ^{1}H and ^{15}N NMR spectroscopic data for complexes **2**−**6** are summarized in Table 1.

Table 1. ^{1}H and ^{15}N NMR spectroscopic data (δ [ppm]) for complexes **2**−**6**

	^{15}N NMR	^{1}H NMR		
		$CH_3C_5H_4$	$CH_3C_5H_4$	CH_2 or CH_3
2	−75.6 (br.)	–[a]	–[a]	–[a]
3	−85.9 (br.)	−27.7	106.5	62.1 (br.)
4	−90.7 (br.)	−19.8	151.0	62.6, 102.1
5	−79.8 (br.)	–[a]	–[a]	–[a]
6	−81.7 (br.)	−10.2	−9.0	–[a]

[a] Not observed.

Raman spectroscopy showed characteristic bands for the ν(C≡C) vibrations for these complexes between 2000 and 2100 cm^{-1}.

The structure of **3** was additionally confirmed by an X-ray diffraction study (Figure 1). A pseudo-tetrahedral coordination of the manganese center was found. The bond

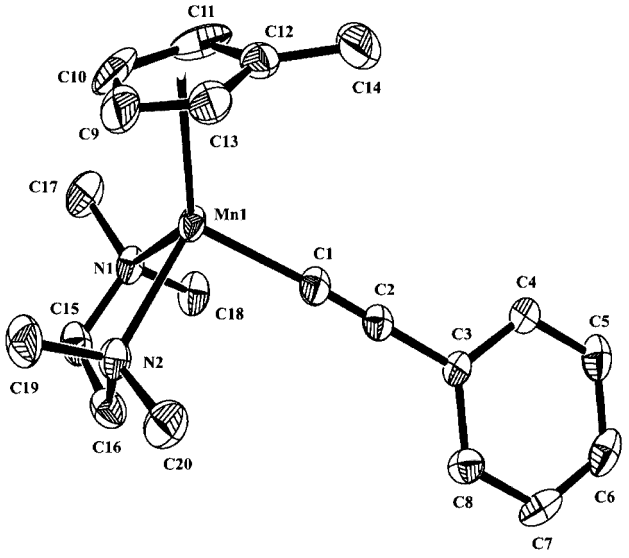

Figure 1. Molecular structure of **3** (30% probability displacement ellipsoids); hydrogen atoms are omitted for clarity; selected bond lengths [Å] and angles [°]: Mn−C1 2.142(2), C1−C2 1.158(3), C2−C3 1.473(3), Mn−MeCp (centroid) 2.5144(2); Mn−C1−C2 176.76(19), C1−C2−C3 179.5(2)

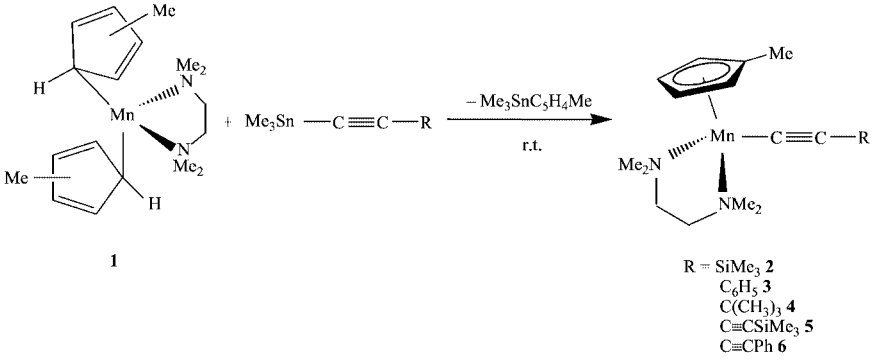

Scheme 1

 © 2004 Wiley-VCH Verlag GmbH & Co. KGaA, Weinheim

lengths of 1.158(3) Å and 2.142(2) Å for C1−C2 and Mn−C1, respectively, fall into the range observed for similar kinds of complexes.[63]

The structure of **5** was also confirmed by a single-crystal X-ray diffraction study (Figure 2). The crystals were obtained by cooling the compound in a mixture of pentane and benzene to −30 °C. The solid-state structure reveals a pseudo-tetrahedral coordination of the manganese center. The bond lengths of 1.109(3) Å and 1.203(3) Å for C1−C2 and C3−C4, respectively, confirm the triple-bond nature of these bonds. An X-ray diffraction analysis also confirmed the spectroscopically derived structure of **6** which is related

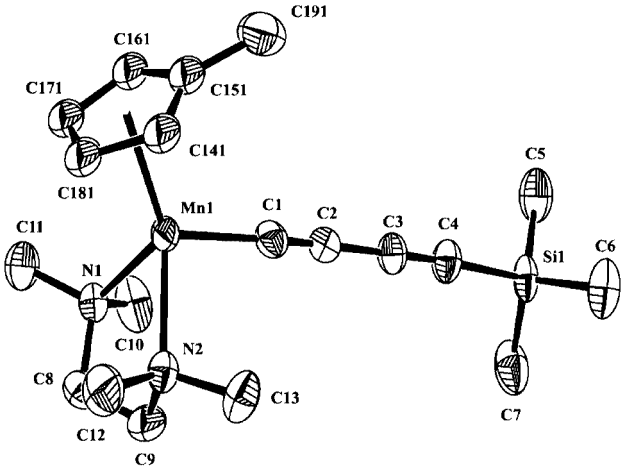

Figure 2. Molecular structure of **5** (30% probability displacement ellipsoids); hydrogen atoms are omitted for clarity; selected bond lengths [Å] and angles [°]: Mn−C1 2.160(2), C1−C2 1.109(3), C2−C3 1.473(3), C3−C4 1.203(3), Mn−MeCp (centroid) 2.4805(5); Mn−C1−C2 176.5(2), C1−C2−C3 178.9(2), C2−C3−C4 179.3(2), C3−C4−Si 176.7(2)

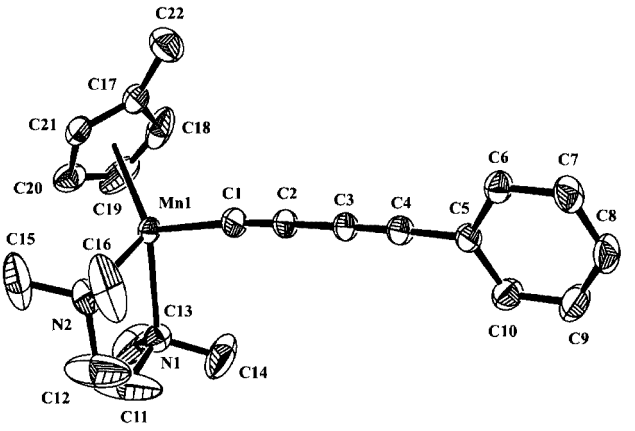

Figure 3. Molecular structure of **6** (30% probability displacement ellipsoids); hydrogen atoms are omitted for clarity; selected bond lengths [Å] and angles [°]: Mn−C1 2.1222(19), C1−C2 1.220(3), C2−C3 1.397(3), C3−C4 1.206(3), Mn−MeCp (centroid) 2.4914(5); Mn−C1−C2 174.98(17), C1−C2−C3 178.3(2), C2−C3−C4 178.7(2), C3−C4−C5 176.0(2)

to **5** (Figure 3). The solid-state structure revealed the C1−C2 and C3−C4 bond lengths to be 1.220(3) Å and 1.206(3) Å, respectively.

Both methylcyclopentadienyl rings in **1** could be replaced by using an excess of the acetylene component. Stirring of **1** with $Me_3SiC{\equiv}C{-}C{\equiv}CH$ at room temperature for 5 d yielded the dinuclear complex **7** (Scheme 2). The ^1H NMR spectrum of **7** in [D_8]toluene at 25 °C shows only a signal for the $SiMe_3$ protons. In the ^{15}N NMR spectrum, the nitrogen atoms of the tmeda ligands are observed as a broad resonance at $\delta = -93.4$ ppm. Characteristic ν(C≡C) vibrations appear in the Raman spectrum at 2154, 2115 and 2001 cm^{-1}. The structure of **7** was confirmed by an X-ray

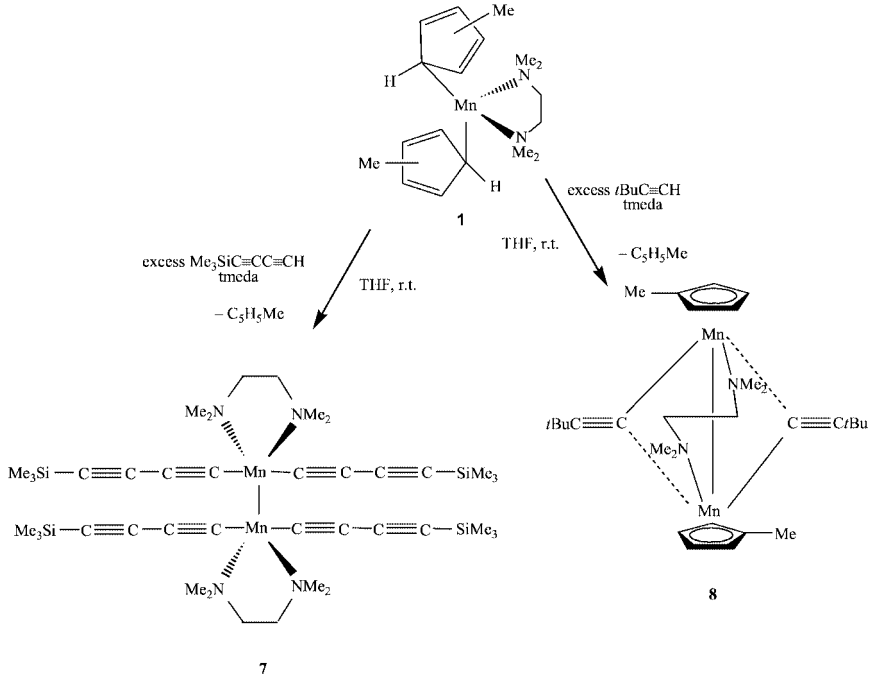

Scheme 2

 © 2004 Wiley-VCH Verlag GmbH & Co. KGaA, Weinheim

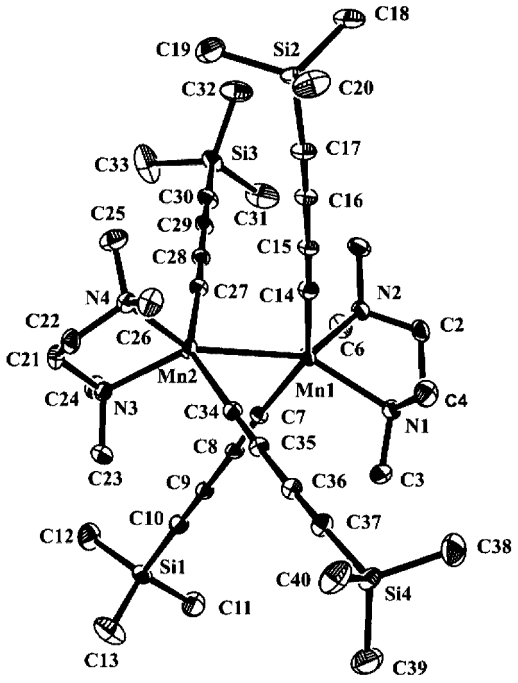

Figure 4. Molecular structure of **7** (30% probability displacement ellipsoids); hydrogen atoms are omitted for clarity; selected bond lengths [Å] and angles [°]: Mn1−Mn2 2.8059(4), Mn1−C7 2.095(2), Mn1−C14 2.088(2), C7−C8 1.212(3), Mn2−C27 2.103(2), Mn2−C34 2.099(2), C27−C28 1.210(3), C8−C9 1.387(3), C9−C10 1.208(3), C14−C15 1.208(3), C15−C16 1.385(3), C16−C17 1.214(3), C28−C29 1.392(3), C29−C30 1.204(3), C34−C35 1.205(3), C35−C36 1.394(3), C36−C37 1.209(3); C7−Mn1−C14 147.43(8), Mn1−C7−C8 175.50(18), Mn1−C14−C15 176.57(19), C27−Mn2−C34 146.09(8), Mn2−C27−C28 173.18(19), Mn2−C34−C35 178.69(19), C7−C8−C9 177.5(2), C8−C9−C10 179.4(3), C27−C28−C29 178.3(2), C28−C29−C30 178.5(2), C9−C10−Si1 178.3(2), C14−C15−C16 177.7(2), C15−C16−C17 179.3(2), C16−C17−Si2 173.2(2), C29−C30−Si3 178.8(2), C34−C35−C36 178.2(2), C35−C36−C37 178.7(2), C36−C37−Si4 176.8(2), C27−Mn2−Mn1 76.11(6), C14−Mn1−Mn2 76.37(2), Mn1−Mn2−C34 70.11(6), Mn2−Mn1−C7 71.08(6)

diffraction analysis (Figure 4). In the solid-state structure a bond length of 2.8059(4) Å was found between the two manganese centers Mn1−Mn2, which is similar to compounds with Mn−Mn single bonds reported earlier, for instance $Mn_2(CO)_{10}$.[110−114] However, we should note that the electron counts for both complexes are different, so that the character of the unique single bond of **7** might also be different. The C7−C8 bond length was observed to be 1.212(3) Å, which is expected for a C≡C bond. The Mn1−C7−C8 unit possesses a bond angle of 175.50(18)°, which shows that this butadiynyl chain is slightly bent, as are the other three C_4 units. The coordination geometry of the Mn centers may thus be derived from a trigonal bipyramid with the tmeda ligand and the neighbouring manganese atom in the equatorial plane and the acetylide moieties in the axial positions [the angle between the planes (Mn2, N3, N4) (Mn2, Mn1, C4) is 84.48(7)°; other related angles between planes have similar values]. The rather acute C7−Mn1−C14 bond angle of 147.43(18)° stresses the fact that the two acetylide units at an Mn center are quite far away from the ideal *trans* position; the reason for this deviation could not be determined. It is supposed that there is an electronic driving force, and one possibility could be a secondary-type interaction between the manganese centers and the metal-adjacent triple bonds. For example, the Mn1−C34 distance of 2.877(2) Å is within the sum of the van der Waals radii and the Mn1−C35 distance of 3.531(2) Å is just about the sum of the van der Waals radii. When an excess of *t*BuC≡CH was used in the reaction with **1**, the unexpected dinuclear complex **8** was obtained (Scheme 2), with η^5-methylcyclopentadienyl rings at each Mn atom. The two manganese centers are bridged by one tmeda ligand and are connected by a presumably ligand-enforced Mn−Mn bond, which was confirmed by an X-ray diffraction study on **8** (Figure 5).

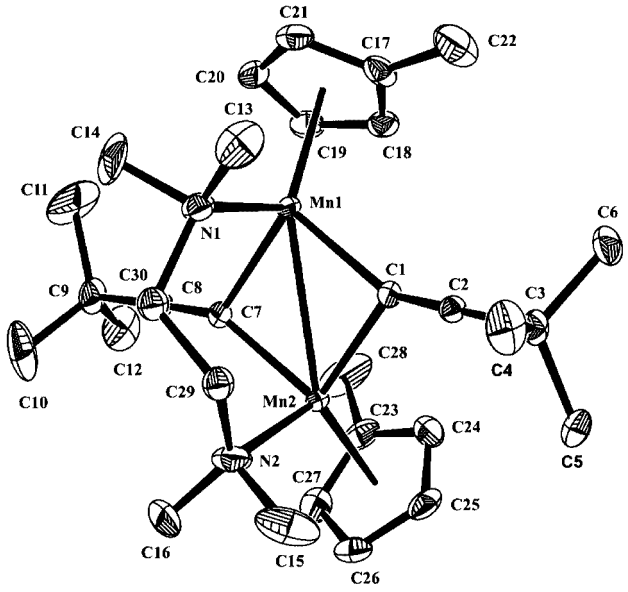

Figure 5. Molecular structure of **8** (30% probability displacement ellipsoids); hydrogen atoms are omitted for clarity; selected bond lengths [Å] and angles [°]: Mn1−Mn2 2.8738(5), Mn1−C1 2.192(2), Mn1−C7 2.220(3), Mn2−C1 2.179(13), Mn2−C7 2.234(3), C1−C2 1.204(3), C2−C3 1.795(3), Mn1−MeCp1 (centroid) 2.491(3), Mn2−MeCp2 (centroid) 2.496(3); C1−Mn1−C7 98.58(9), C1−Mn2−C7 98.69(9), Mn1−C1−C2 152.8(2), Mn2−C7−C8 151.6(2), C1−C2−C3 179.5(3), C7−C8−C9 176.6(3), Mn1−C1−Mn2 80.98(7), C1−Mn1−Mn2 48.49(5), C1−Mn2−Mn1 48.89(5) Mn2−C7−Mn1 81.66(7), C7−Mn1−Mn2 50.14(7), C7−Mn2−Mn1 89.85(7)

The acetylide moiety also bridges the two manganese centers. The ^{1}H NMR spectrum of **8** in [D_8]toluene at 30 °C reveals a broad resonance for the methylcyclopentadienyl ring at $\delta = -11.4$ ppm and the corresponding resonances for the *tert*-butyl groups and the methyl and methylene groups of the tmeda ligand, which are observed at low field ($\delta = 14.2$, 34.6 and 65.5 ppm, respectively). The ^{15}N NMR spectrum shows a broad resonance at $\delta = -73.8$ ppm. In the Raman spectrum a band attributed to a ν(C≡C) vibration is observed at 2052 cm^{-1}.

The [Mn(MeC_5H_4)$_2$(tmeda)] complex **1** is a valuable starting material and allows access to dinuclear complexes

 © 2004 Wiley-VCH Verlag GmbH & Co. KGaA, Weinheim

bridged by sp-carbon units. Complexes of this type have been widely studied in conjunction with potential molecular-wire applications.[32−35,43−45,50,52,55,56,66,69,70,72,87,115,127a] Complexes **9**, **10** and **11** were obtained by treatment of **1** with 0.5 equiv. of the corresponding acetylenes 1,3-$C_6H_4(C{\equiv}CSnMe_3)_2$, 1,4-$C_6H_4(C{\equiv}CSnMe_3)_2$ or 4,4′-$(C_6H_4)_2(C{\equiv}CSnMe_3)_2$ in benzene for 24 h to afford the corresponding dinuclear complexes in very good yields (Scheme 3). The ^{1}H NMR spectrum of **9** in [D$_8$]THF at 22 °C reveals two signals for the protons of the cyclopentadienyl rings, both paramagnetically shifted to high field at $\delta = -63.7$ and -45.9 ppm, and a broad resonance in the downfield region at $\delta = 163.3$ ppm. The proton resonance for the tmeda moieties appears at $\delta = 74.2$ ppm, while the aromatic protons are observed as two broad signals at $\delta =$ 38.6 and 41.6 ppm. The resonance of the tmeda ligands appears in the ^{15}N NMR spectrum (20 °C) as a broad signal at $\delta \approx -100.4$ ppm. The ^{1}H NMR spectra of complexes **10** and **11** show significant differences in comparison with that of complex **9**, since only the proton resonances corresponding to the methylcyclopentadienyl rings [$\delta = -8.1$ (**10**) and -24.9 ppm (**11**)] and the aromatic protons [$\delta = 27.2$ (**10**) and 20.7 ppm (**11**)] could be observed.

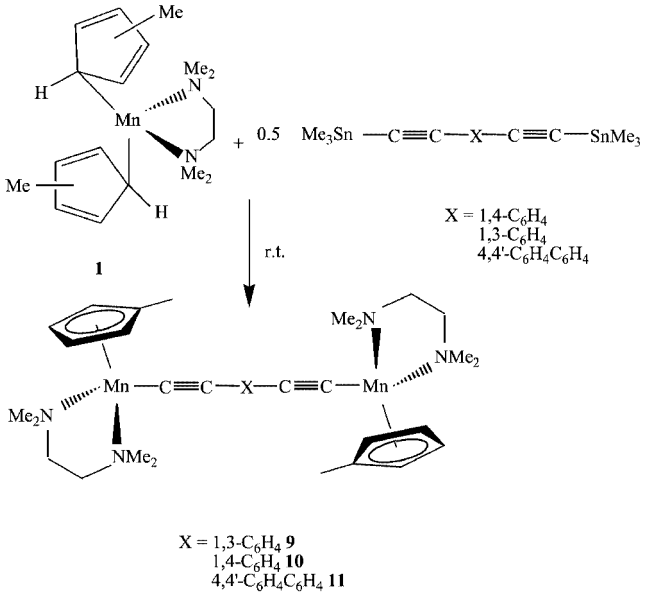

Scheme 3

The structures of complexes **9**, **10** and **11** were characterized by X-ray diffraction analyses. The solid-state structures of these complexes reveal different types of bonding of the methylcyclopentadienyl groups to the manganese centers. In complex **9** the methylcyclopentadienyl rings are η^3- and η^3-bound (see Supporting Information), whereas in **10** both possess η^2 hapticity (Figure 6); the maximum hapticity of the MeC_5H_4 rings (η^5,η^5) is observed in **11** (Figure 7). These different bonding situations might arise from the fact that the interaction between the methylcyclopentadienyl ring and the manganese center is quite ionic in nature and can therefore not be expressed by localized covalent interactions, but rather by partly localized ionic interactions of the ion-pair type.[100] Based on the ionic bonding, the energetic differences between the various binding modes are expected to be relatively small. Hence, simple packing forces on the order of 1 kcal·mol^{-1} might be just enough to induce different ring slippage modes in otherwise quite related structures. The C≡C bond lengths found in these complexes are similar to compounds already reported in the literature. CV experiments (ca. 0 to +1.5 V) failed to oxidize the complexes **9**, **10** and **11** possessing high-spin d^5-metal centers further.

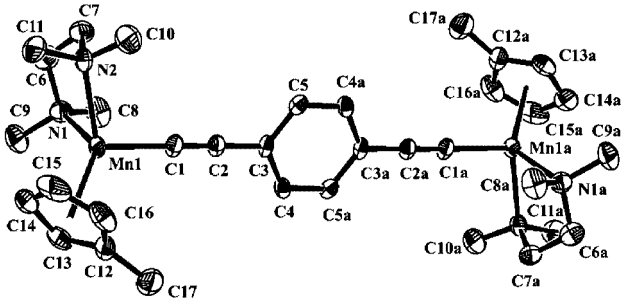

Figure 6. Molecular structure of **10** (30% probability displacement ellipsoids); hydrogen atoms are omitted for clarity; selected bond lengths [Å] and angles [°]: Mn1−C1 2.109(3), C1−C2 1.203(4), C2−C3 1.438(4), Mn1−N1 2.333(3), Mn1−N2 2.269(3); Mn1−C1−C2 177.3(3), C1−C2−C3 179.0(4)

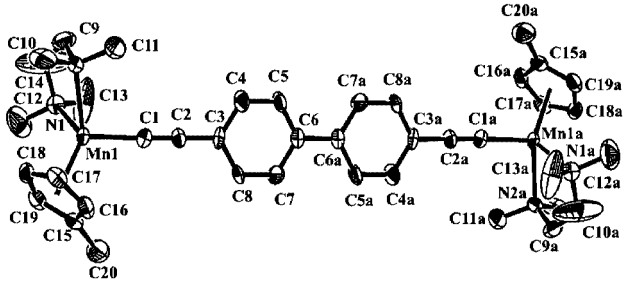

Figure 7. Molecular structure of **11** (30% probability displacement ellipsoids); hydrogen atoms are omitted for clarity; selected bond lengths [Å] and angles [°]: Mn1−C1 2.096(6), C1−C2 1.212(6), C2−C3 1.436(6), C3−C8 1.370(6), C8−C7 1.365(6), C4−C5 1.375(6), C5−C6 1.372(6), C6−C6a 1.488(8), Mn1−Cp (centroid) 2.1524(5); Mn1−C1−C2 177.2(5), C1−C2−C3 178.8(6)

Conclusions

Mono- and dinuclear complexes of polyynes capped by Mn^{II} half-sandwich units were synthesized. A series of these complexes has been structurally characterized showing a variety of different hapticities of the cyclopentadienyl rings. This observation witnesses quite ionic bonding of these rings as would indeed be expected for d^5 high-spin complexes. The manganese centers have a stable electron configuration additionally indicated by the inability to further oxidize them. Based on this we might conclude that the d electrons in the dinuclear complexes **9**−**11** are contracted, which also prevents strong electronic communication of the

 © 2004 Wiley-VCH Verlag GmbH & Co. KGaA, Weinheim

metal centers. It is therefore suggested that these complexes belong to class I or to the weaker interaction side of class II compounds according to the Robin/Day classification.[127b]

Experimental Section

General: Reagent-grade benzene, toluene, hexane, pentane, diethyl ether and tetrahydrofuran were dried and distilled from sodium benzophenone ketyl prior to use. Dichloromethane was distilled first from P_2O_5, and then prior to use from CaH_2. Literature procedures were used to prepare the following compounds: 1,2-bis(dimethylphosphanyl)ethane (dmpe),[128] $[Mn(MeC_5H_4)_2]$,[102,103] $[Mn(MeC_5H_4)_2(tmeda)]$,[105,106] $Me_3SnC{\equiv}CSiMe_3$,[129] $Me_3SiC{\equiv}C{-}C{\equiv}CH$,[130] $PhC{\equiv}CSnMe_3$, $tBuC{\equiv}CSnMe_3$,[128] $PhC{\equiv}C{-}C{\equiv}CSnMe_3$,[131] and $Me_3SnC{\equiv}C{-}R''{-}C{\equiv}CSnMe_3$ [R'' = 1,4-$C_6H_4(C{\equiv}C)_2$, 1,3-$C_6H_4(C{\equiv}C)_2$, 4,4′-$C_6H_4C_6H_4(C{\equiv}C)_2$].[107–109] *n*BuLi (1.6 M in hexane) and Me_3SnCl were used as received. All the manipulations were carried out under nitrogen using Schlenk techniques or in a drybox. IR spectra were obtained with a Bio-Rad FTS-45 instrument and the Raman spectra with a Renishaw Ramanscope spectrometer (514 nm). ^1H NMR spectra were measured with a Varian Gemini-2000 at 300 MHz and ^{15}N NMR spectra at 50.70 MHz with a Bruker DRX 500 spectrometer. All NMR spectra of paramagnetic compounds were obtained from concentrated solutions of analytically pure samples. The assignment of the ^1H NMR signals for paramagnetic signals is principally based on the investigations of Köhler et al.[132–134] Chemical shifts for ^1H are given in ppm with respect to the signals for residual solvent protons (^1H) of the deuterated solvents and for ^{15}N related to nitromethane.

Synthesis of $[Mn(\eta^1\text{-}MeC_5H_4)_2(tmeda)]$ (1): A diethyl ether solution (5 mL) of tmeda (116.2 mg, 1.0 mmol) was added to a diethyl ether solution (5 mL) of $[Mn(MeCp)_2]$ (213 mg, 1.0 mmol), and the mixture stirred at room temperature for 15 min. The solvent was then evaporated in vacuo and the solid residue was washed with pentane (3 × 5 mL). Colorless crystals of **1** were obtained by crystallizing from a mixture of THF (2 mL) and pentane (20 mL) at −40 °C. Yield 313 mg, 95%. $C_{18}H_{30}MnN_2$ (329.39): calcd. C 65.64, H 9.18, N 8.50; found C 65.36, H 9.41, N 8.45. ^1H NMR ([D$_8$]THF, 300 MHz, 30 °C): δ = −39.1 (br., 8 H, $CH_3C_5H_4$), −3.5 (br., 6 H, $CH_3C_5H_4$), 30.6 (br., 16 H, tmeda) ppm. $^{15}N\{^1H\}$ NMR ([D$_8$]THF, 50.70 MHz, 20 °C): δ = −75.7 (br., tmeda) ppm.

Synthesis of $[Mn(C{\equiv}CSiMe_3)(\eta^5\text{-}MeCp)(tmeda)]$ (2): A THF solution (5 mL) of $Me_3SiC{\equiv}CH$ (98.2 mg, 1.0 mmol) or $Me_3SiC{\equiv}CSnMe_3$ (261 mg, 1.0 mmol) was added to a THF solution (10 mL) of $[Mn(\eta^1\text{-}MeC_5H_4)_2(tmeda)]$, and the mixture stirred at room temperature for 3 d. The solvent was evaporated in vacuo and the solid residue was extracted with 10 mL of pentane. The pentane solution was concentrated to 5 mL, filtered through Celite and crystallized to give pure colorless crystals of **2** at −40 °C (330 mg, 95% yield). $C_{18}H_{30}MnN_2$ (347.48): calcd. C 65.64, H 9.18, N 8.50; found C 65.36, H 9.41, N 8.45. ^1H NMR ([D$_8$]THF, 300 MHz, 30 °C): δ = 7.3 (br., 9 H, $SiMe_3$) ppm. $^{15}N\{^1H\}$ NMR ([D$_8$]THF, 50.70 MHz, 7 °C): δ = −75.6 (br., tmeda) ppm. Raman: $\tilde{\nu}$ = 2021 [s, ν(C=C)] cm^{-1}.

Synthesis of $[Mn(C{\equiv}CPh)(\eta^5\text{-}MeCp)(tmeda)]$ (3): A THF solution (5 mL) of $PhC{\equiv}CH$ (102.1 mg, 1.0 mmol) or $PhC{\equiv}CSnMe_3$ (265 mg, 1.0 mmol) was added to a THF solution (10 mL) of $[Mn(\eta^1\text{-}MeC_5H_4)_2(tmeda)]$, and the mixture stirred at room temperature for 3 d. The solvent was evaporated in vacuo and the solid residue was extracted with 5 mL of benzene. The benzene solution was filtered through Celite and crystallized from a mixture of benzene (5 mL) and pentane (20 mL) to give pure yellow crystals of the title compound at −40 °C (341 mg, 97% yield). $C_{20}H_{28}MnN_2$ (351.40): calcd. C 68.36, H 8.03, N 7.97; found C 68.63, H 7.88, N 7.74. ^1H NMR ([D$_8$]THF, 300 MHz, 20 °C): δ = −27.7 (br., 4 H, $CH_3C_5H_4$), 24.9 (br., 5 H, C_6H_5), 62.1 (br., 16 H, tmeda), 106.5 (br., 3 H, $CH_3C_5H_4$) ppm. $^{15}N\{^1H\}$ NMR ([D$_8$]THF, 50.70 MHz, 10 °C): δ = −85.9 (br., tmeda) ppm. Raman: $\tilde{\nu}$ = 2074 [s, ν(C=C)] cm^{-1}.

Synthesis of $[Mn(C{\equiv}C\text{t}Bu)(\eta^5\text{-}MeCp)(tmeda)]$ (4): A THF solution (5 mL) of $tBuC{\equiv}CH$ (82.1 mg, 1.0 mmol) or $tBuC{\equiv}CSnMe_3$ (245 mg, 1.0 mmol) was added to a THF solution (10 mL) of $[Mn(\eta^1\text{-}MeC_5H_4)_2(tmeda)]$, and the mixture stirred at room temperature for 3 d. The solvent was evaporated in vacuo and the solid residue was extracted with 10 mL of pentane. The pentane solution was concentrated to 5 mL, filtered through Celite and crystallized to give pure light-blue crystals of **4** at −40 °C (265 mg, 80% yield). $C_{18}H_{32}MnN_2$ (331.41): calcd. C 65.24, H 9.73, N 8.45; found C 65.60, H 9.70, N 8.56. ^1H NMR ([D$_8$]toluene, 300 MHz, 20 °C): δ = −19.8 (br., 4 H, $CH_3C_5H_4$), 14.5 (br., 9 H, *t*Bu), 62.6, 102.1 (br., 16 H, tmeda), 151.0 (br., 3 H, $CH_3C_5H_4$) ppm. $^{15}N\{^1H\}$ NMR ([D$_8$]THF, 50.70 MHz, 10 °C): δ = −90.7 (br., tmeda) ppm. Raman: $\tilde{\nu}$ = 2075 [s, ν(C=C)] cm^{-1}.

Synthesis of $[Mn(C{\equiv}C{-}C{\equiv}CSiMe_3)(\eta^5\text{-}MeCp)(tmeda)]$ (5): A THF solution (5 mL) of $Me_3SiC{\equiv}C{-}C{\equiv}CH$ (122.2 mg, 1.0 mmol) or $Me_3SiC{\equiv}C{-}C{\equiv}CSnMe_3$ (285 mg, 1.0 mmol) was added to a THF solution (10 mL) of $[Mn(\eta^1\text{-}MeC_5H_4)_2(tmeda)]$ (329.4 mg, 1.0 mmol), and the mixture stirred at room temperature for 3 d. The solvent was evaporated in vacuo and the solid residue was washed with pentane (3 × 5 mL). Benzene (5 mL) was added to the pentane solution (5 mL) and the resulting mixture was filtered through Celite and crystallized to give pure light-yellow crystals of complex **5** at −40 °C (357 mg, 96% yield). $C_{19}H_{32}MnN_2Si$ (371.50): calcd. C 65.24, H 9.73, N 8.45; found C 65.60, H 9.70, N 8.56. ^1H NMR ([D$_8$]toluene, 300 MHz, 20 °C): δ = 4.8 (br., 9 H, $SiMe_3$) ppm. $^{15}N\{^1H\}$ NMR ([D$_8$]THF, 50.70 MHz, 10 °C): δ = −90.7 (br., tmeda) ppm. Raman: $\tilde{\nu}$ = 2075 [s, ν(C=C)] cm^{-1}.

Synthesis of $[Mn(C{\equiv}C{-}C{\equiv}C{-}Ph)(\eta^5\text{-}MeCp)(tmeda)]$ (6): A THF solution (5 mL) of $PhC{\equiv}C{-}C{\equiv}CSnMe_3$ (290 mg, 1.0 mmol) was added to a THF solution (10 mL) of $[Mn(\eta^1\text{-}MeC_5H_4)_2(tmeda)]$ (329.4 mg, 1.0 mmol), and the mixture stirred at room temperature for 3 d. The solvent was evaporated in vacuo and the solid residue was washed with pentane (3 × 5 mL). THF (5 mL) was added and the mixture filtered through Celite. Diethyl ether (30 mL) was added and light yellow brown crystals of complex **6** were obtained at −40 °C (353 mg, 92% yield). $C_{22}H_{28}MnN_2$ (375.42): calcd. C 70.39, H 7.52, N 7.46; found C 70.52, H 7.46, N 7.13. ^1H NMR ([D$_8$]toluene, 300 MHz, 20 °C): δ = −10.2, −9.0 (br., 4 H, $CH_3C_5H_4$), 15.5 (br., 5 H, C_6H_5) ppm. $^{15}N\{^1H\}$ NMR ([D$_8$]THF, 50.70 MHz, 10 °C): δ = −81.7 (br., tmeda) ppm. Raman: $\tilde{\nu}$ = 2174 (s), 2022 [s, ν(C=C)] cm^{-1}.

Synthesis of $[Mn(C{\equiv}C{-}C{\equiv}CSiMe_3)_2(tmeda)]_2$ (7): A THF solution (5 mL) containing an excess of $Me_3SiC{\equiv}C{-}C{\equiv}CH$ (1.22 g, 10 mmol) was added to a THF solution (10 mL) of $[Mn(\eta^1\text{-}MeC_5H_4)_2(tmeda)]$ (329.4 mg, 1.0 mmol), and the mixture stirred at room temperature for 5 d. The solvent was evaporated in vacuo and the solid residue was washed with pentane (3 × 5 mL). The olive-green solid was dissolved in toluene (5 mL) and pentane (30 mL) was added to obtain olive-green crystals of complex **7** at −40 °C (871 mg, 95% yield). $C_{40}H_{68}Mn_2N_2Si_2$ (827.23): calcd. C

 © 2004 Wiley-VCH Verlag GmbH & Co. KGaA, Weinheim

58.08, H 8.29, N 6.77; found C 58.26, H 8.35, N 6.89. ^{1}H NMR ([D$_8$]toluene, 300 MHz, 25 °C): δ = 3.0 (s, 18 H, SiMe$_3$) ppm. ^{15}N{^{1}H} NMR ([D$_8$]toluene, 50.70 MHz, 10 °C): δ = −93.4 (br., tmeda) ppm. Raman: $\tilde{\nu}$ = 2154 (s), 2115 (s), 2001 [s, ν(C≡C)] cm^{-1}.

Synthesis of [Mn$_2$(MeCp)$_2$(μ$_1$-tmeda)(μ$_1$-*t*BuC≡C)$_2$] (8): A THF solution (5 mL) containing an excess of *t*BuC≡CH (821.5 mg, 10 mmol) was added to a THF solution (10 mL) of [Mn(η^1-MeC$_5$H$_4$)$_2$(tmeda)] (659 mg, 2.0 mmol), and the mixture stirred at room temperature for 5 d. The solvent was evaporated in vacuo and the solid residue was washed with pentane (3 × 5 mL). The olive-green solid was dissolved in benzene (5 mL) and pentane (30 mL) was added to obtain olive-green crystals of complex **8** at −40 °C (383 mg, 70% yield). C$_{30}$H$_{48}$Mn$_2$N$_2$ (546.60): calcd. C 65.92, H 8.85, N 5.13; found C 66.21, H 8.64, N 5.03. ^{1}H NMR ([D$_8$]toluene, 300 MHz, 30 °C): δ = −11.4 (br., 8 H, CH$_3$C$_5$*H*$_4$), 14.2 (s, 18 H, *t*Bu), 34.6, 65.5 (br., 16 H, tmeda) ppm. ^{15}N{^{1}H} NMR ([D$_8$]toluene, 50.70 MHz, 20 °C): δ = −73.8 (br., tmeda) ppm. Raman: $\tilde{\nu}$ = 2052 [s, ν(C≡C)] cm^{-1}.

Synthesis of [{(η^3-MeCp)(tmeda)Mn}$_2$(μ-1,3-C$_6$H$_4$(C≡C)$_2$] (9): A benzene solution (10 mL) of 1,3-C$_6$H$_4$(C≡CSnMe$_3$)$_2$ (452 mg, 1.0 mmol) was added to a benzene solution (20 mL) of [Mn(η^1-MeC$_5$H$_4$)$_2$(tmeda)] (659 mg, 2.0 mmol), and the mixture stirred at room temperature for 24 h. The solvent was evaporated in vacuo and the solid residue was washed with pentane (3 × 5 mL). The olive-green solid was dissolved in toluene (5 mL) and pentane (30 mL) was added to obtain light-orange crystals of complex **9** at −30 °C (469 mg, 75% yield). C$_{34}$H$_{50}$Mn$_2$N$_4$ (624.68): calcd. C 65.37, H 8.07, N 8.97; found C 65.08, H 8.44, N 8.68. ^{1}H NMR ([D$_8$]THF, 300 MHz, 30 °C): δ = −62.9 (br., 4 H, CH$_3$C$_5$*H*$_4$), −44.9 (br., 4 H, CH$_3$C$_5$*H*$_4$), 34.5 (br., 2 H, C$_6$H$_4$), 41.3 (br., 2 H, C$_6$H$_4$), 77.0 (br., 16 H, tmeda), 161.5 (br., 3 H, C*H*$_3$C$_5$H$_4$) ppm. ^{15}N{^{1}H} NMR ([D$_8$]THF, 50.70 MHz, 20 °C): δ = −100.4 (br., tmeda) ppm. Raman: $\tilde{\nu}$ = 2067 [s, ν(C≡C)] cm^{-1}.

Synthesis of [{(η^1-MeCp)(tmeda)Mn}$_2$(μ-1,4-C$_6$H$_4$(C≡C)$_2$] (10): A benzene solution (10 mL) of 1,4-C$_6$H$_4$(C≡CSnMe$_3$)$_2$ (452 mg, 1.0 mmol) was added to a benzene solution (20 mL) of [Mn(η^1-MeC$_5$H$_4$)$_2$(tmeda)] (659 mg, 2.0 mmol), and the mixture stirred at room temperature for 24 h. The solvent was evaporated in vacuo and the solid residue was washed with pentane (3 × 5 mL). The olive-green solid was redissolved in toluene (5 mL) and pentane (30 mL) was added to obtain light-orange crystals of the title compound at −30 °C (500 mg, 80% yield). C$_{34}$H$_{50}$Mn$_2$N$_4$ (624.68): calcd. C 65.37, H 8.07, N 8.97; found C 65.51, H 8.11, N 8.61. ^{1}H NMR ([D$_8$]THF, 300 MHz, 30 °C): δ = −8.8 (br., 8 H, CH$_3$C$_5$*H*$_4$), 27.2 (br., 4 H, C$_6$H$_4$) ppm. ^{15}N{^{1}H} NMR ([D$_8$]THF, 50.70, 20 °C): δ = −71.3 (br., tmeda) ppm. Raman: $\tilde{\nu}$ = 2071 [s, ν(C≡C)] cm^{-1}.

Synthesis of [{(η^5-MeCp)(tmeda)Mn}$_2${μ-4,4′-(C$_6$H$_4$)$_2$(C≡C)$_2$}] (11): A benzene solution (10 mL) of 4,4-(C$_6$H$_4$)$_2$(C≡CSnMe$_3$)$_2$ (528 mg, 1.0 mmol) was added to a benzene solution (20 mL) of [Mn(η^1-MeC$_5$H$_4$)$_2$(tmeda)] (659 mg, 2.0 mmol), and the mixture stirred at room temperature for 24 h. The solvent was evaporated in vacuo and the solid residue was washed with pentane (3 × 5 mL). The olive-green solid was redissolved in toluene (5 mL) and pentane (30 mL) was added to obtain light-orange crystals of complex **11** at −30 °C (500 mg, 80% yield). C$_{34}$H$_{50}$Mn$_2$N$_4$ (624.68): calcd. C 65.37, H 8.07, N 8.97; found C 65.51, H 8.11, N 8.61. ^{1}H NMR ([D$_8$]THF, 300 MHz, 30 °C): δ = −8.8 (br., 8 H, CH$_3$C$_5$*H*$_4$), 27.2 (br., 4 H, C$_6$H$_4$) ppm. ^{15}N{^{1}H} NMR ([D$_8$]THF, 50.70 MHz,

Table 2. Crystallograhic details for **3** and **5**−**7**

	3	**5**	**6**	**7**
Empirical formula	$C_{20}H_{28}MnN_2$	$C_{19}H_{32}MnN_2Si$	$C_{22}H_{28}MnN_2$	$C_{20}H_{34}MnN_2Si_2$
Formula mass	351.38	371.50	375.40	413.61
Color	yellow block	pale yellow block	yellow block	olive-green plate
Crystal size [mm]	0.30 × 0.52 × 0.51	0.53 × 0.58 × 0.73	0.28 × 0.40 × 0.72	0.26 × 0.41 × 0.52
T [K]	183(2)	183(2)	183(2)	183(2)
λ(Mo-K_α) [Å]	0.71073	0.71073	0.71073	0.71073
Crystal system	monoclinic	orthorhombic	monoclinic	monoclinic
Space group	$P2_1/a$	$P2_12_12_1$	$P2_1/c$	$P2_1/c$
a [Å]	13.0770(9)	10.0023(10)	11.4503(8)	12.9613(4)
b [Å]	11.4899(9)	11.8147(7)	16.0633(10)	29.8420(11)
c [Å]	13.6328(10)	19.0675(12)	12.0656(8)	12.9613(4)
β [°]	102.489(8)	90	112.112(8)	90.056(7)
V [Å^3]	1999.9(3)	2253.3(3)	2056.0(2)	5013.3(3)
Z	4	4	4	8
$\rho_{calcd.}$ [g·cm^{-3}]	1.167	1.095	1.213	1.096
μ [mm^{-1}]	0.661	0.640	0.648	0.627
F(000)	748	796	796	1768
Transmission range	0.8471−0.7555	0.7794−0.7135	0.8412−0.6702	0.8560−0.7807
θ range [°]	6.02 ≤ 2θ ≤ 60.92	5.74 ≤ 2θ ≤ 60.68	6.24 ≤ 2θ ≤ 60.66	4.44 ≤ 2θ ≤ 56.04
Measured reflections	20820	25415	21358	39994
Unique reflections	5973	6693	6116	11802
$I > 2\sigma(I)$ reflections	2985	4339	4120	9231
Parameters	213	219	231	472
Gof (for F^2)	1.026	1.140	1.096	1.078
R_1 [$I > 2\sigma(I)$],[a] R_1 (all data)	0.0410, 0.0898	0.0367, 0.0667	0.0426, 0.0682	0.0344, 0.0472
wR_2 [$I > 2\sigma(I)$],[b] wR_2 (all data)	0.0730, 0.0784	0.0573, 0.0598	0.1040, 0.1101	0.0637, 0.0653
$\Delta\rho_{max/min}$	0.548/−0.448	0.455/−0.458	0.569/−0.588	0.423/−0.263

[a] $R1 = \Sigma(F_o - F_c)/\Sigma F_o$; $I > 2\sigma(I)$. [b] $wR2 = [\Sigma w(F_o^2 - F_c^2)^2/\Sigma w(F_o^2)^2]^{1/2}$.

 © 2004 Wiley-VCH Verlag GmbH & Co. KGaA, Weinheim

Table 3. Crystallographic details of **8**−**11**

	8	**9**	**10**	**11**
Empirical formula	$C_{30}H_{48}Mn_2N_2$	$C_{171}H_{240}Mn_8N_{16}$	$C_{34}H_{50}Mn_2N_4$	$C_{40}H_{54}Mn_2N_4$
Molecular mass	546.58	2959.31	624.66	700.75
Color	olive-green block	olive-green block	yellow plate	yellow plate
Crystal size [mm]	0.22 × 0.25 × 0.26	0.26 × 0.45 × 0.57	0.05 × 0.30 × 0.39	0.06 × 0.13 × 0.25
T [K]	183(2)	183(2)	173(2)	173(2)
λ(Mo-K_α) [Å]	0.71073	0.71073	0.71073	0.71073
Crystal system	monoclinic	monoclinic	monoclinic	monoclinic
Space group	$P2_1/n$	$P2_1/c$	$P2_1/n$	$P2_1/c$
a [Å]	14.1396(11)	14.4364(10)	7.7597(7)	7.9877(6)
b [Å]	14.0700(7)	18.3976(14)	15.2611(11)	11.9903(9)
c [Å]	15.6110(10)	16.2726(16)	14.5355(13)	20.5803(18)
β [°]	95.988(9)	90.573(10)	98.399(10)	100.599(10)
V [Å^3]	3088.8(3)	4321.7(6)	1702.9(2)	1937.4(3)
Z	4	1	2	2
$\rho_{calcd.}$ [g·cm^{-3}]	1.175	1.137	1.218	1.201
μ [mm^{-1}]	0.836	0.615	0.768	0.683
F(000)	1168	1578	664	744
Transmission range	0.8635−0.8027	0.7707−0.6799	0.9641−0.7524	0.9660−0.8194
θ range [°]	6.00 ≤ 2θ ≤ 60.70	4.36 ≤ 2θ ≤ 51.94	5.34 ≤ 2θ ≤ 55.78	3.94 ≤ 2θ ≤ 51.82
Measured reflections	36111	36990	14209	11833
Unique reflections	8653	7999	4045	3604
$I > 2\sigma(I)$ reflections	4263	2050	1920	1464
Parameters	303	262	186	213
Gof (for F^2)	0.908	1.302	1.024	0.840
R_1 [$I > 2\sigma(I)$],[a] $R1$ (all data)	0.0378, 0.0913	0.1503, 0.2700	0.0383, 0.0981	0.0559, 0.1380
wR_2 [$I > 2\sigma(I)$],[b] wR_2 (all data)	0.0539, 0.0577	0.3464, 0.3728	0.0567, 0.0596	0.0760, 0.0837
$\Delta\rho_{max/min}$	0.531/−0.540	0.890/−0.619	0.288/−0.707	0.665/−0.686

[a] $R1 = \Sigma(F_o - F_c)/\Sigma F_o$; $I > 2\sigma(I)$. [b] $wR2 = [\Sigma w(F_o^2 - F_c^2)^2/\Sigma w(F_o^2)^2]^{1/2}$.

20 °C): δ = −71.3 (br., tmeda) ppm. Raman: $\tilde{\nu}$ = 2071 [s, ν(C≡C)] cm^{-1}.

X-ray Diffraction Studies on 3 and 5−11: Crystals of **3** and **5**−**11**, protected in hydrocarbon oil, were selected for the X-ray experiments using a polarizing microscope. They were mounted on the tip of a glass fibre and immediately transferred to the goniometer of an imaging plate detector system (Stoe IPDS diffractometer), where they were cooled to 183(2) K [**10** and **11** 173(2) K] using an Oxford Cryogenic System. The crystal−image distances were set to 50 mm (**3**, **5**, **6**, and **8**), 60 mm (**7** and **10**), and 70 mm (**9** and **11**) (θ_{max} = 30.46, 30.34, 30.33, 30.35, 28.02, 27.89, 25.97 and 25.91° for **3** and **5**−**11**, respectively). The φ-rotation (**3**, **6**) or φ-oscillation (**5**, **7**−**11**) scan modes were applied according to the diffraction power of the measured crystals. For the cell-parameter refinements 7998 (**5**), 8000 (**3**, **6**−**10**) or 4287 (**11**) reflections were selected out of the whole limiting spheres. A total of 20820 (**3**), 25415 (**5**), 21358 (**6**), 39994 (**7**), 36111 (**8**), 36990 (**9**), 14209 (**10**), and 11833 (**11**) diffraction intensities were collected,[135] of which 5973, 6693, 6116, 11802, 8653, 7999, 4045, and 3604, respectively, were unique (R_{int} = 0.0618, 0.0504, 0.0524, 0.0424, 0.0762, 0.1014, 0.0932, and 0.1190 for **3** and **5**−**11**, respectively) after data reduction. Numerical absorption corrections[136] based on 16, 20, 12, 19, 15, 22, 6, and 6 crystal faces, respectively, were applied with FACEitVIDEO and XRED.[135] The structures were solved by direct methods (**5**) and by the Patterson method (for the other seven compounds) using the program SHELXS-97.[137] Interpretation of the difference Fourier maps, preliminary plot generations and checking for higher symmetry were performed with PLATON[138] and the implemented program LEPAGE.[139] All heavy atoms were refined (SHELXL-97)[140] using anisotropic displacement parameters, except for disordered atoms in the structures of **5**, **8**, and **9**, which were refined isotropically. The positions of the H atoms were calculated after each refinement cycle (riding model). Structural plots (Figures 1−7) were generated using ORTEP. Further crystallographic data and refinement results are presented in Tables 2 and 3, and Table S1 in the Supporting Information (see also the footnote on the first page of this article). It is noteworthy to mention the difficulties in performing a rapid preparation of the crystals in the protecting oil. Some crystals deteriorated relatively fast at room temperature, and in these cases a Peltier element was used at 253 K to save the crystals during the preparation under polarized light. For the intensity measurements of crystals of **5** and **6** a collimator with 0.80 mm diameter had to be used (see Table 2). For compound **7** two measurements were necessary (the last measurement with 37 h measuring time) to determine that the metrically tetragonal unit cell belongs to the Laue class $P2/m$ (space group $P2_1/c$). Furthermore, a twin refinement with ratio 1:3 was successfully performed using the twin matrix (001, 0−10, −100) for this structure. A detailed description of structure solution and refinement is given in the CIF file of **7**. Compound **9** most probably belongs to a modulated structure type: four very weak intensity peaks were observed between the strong reflection intensities in one reciprocal direction (modulo5). The weak reflections were not used for the unit-cell determination. Application of programmes DISPLA, XYZ, RECIPE, INDEX and CELL[135] resulted in space group $P21/c$. The structure was solved without difficulties; however, anisotropic refinement showed many non-hydrogen atoms to have non-positive definite displacement parameters or indicated many split atomic positions. Thus, most of the atoms were refined with

 © 2004 Wiley-VCH Verlag GmbH & Co. KGaA, Weinheim

isotropic displacement parameters. It should be noted that only about 25% of the intensity data were observed [$I > 2\sigma(I)$]. Additionally, for a disordered toluene solvent molecule with very large isotropic displacement parameters the site occupation factors were fixed at estimated values of 1/4. For this reason compound **9** has a Z value of 1 and the enlarged chemical formula as given in Table 3. Finally, 45 distance restraints had to be used to stabilize the refinement. The structures of **10** and **11** possess centres of inversion that coincide with crystallographic inversion centres, thus only one half of each complex needed to be refined, resulting in Z values of 2 ($Z' = 1/2$). The crystals of compound **11** were very sensitive to mechanical touch. Due to the thin plate-like crystal (0.25 × 0.13 × 0.06 mm) and the necessity to seal the susceptible crystal of fair quality into a thin-walled glass capillary including protecting oil, the background intensities increased drastically. The centering procedure introduced systematic errors that were probably added to the measured intensity data. Only about 40% of these data were considered observed, which explains the relatively high R_{int} (11.9%) and $R\sigma(I)$ (21.65%) values. The reliability factors of the final refinement [$R1 = 5.59\%$ and $wR2 = 8.37\%$ (all data)] are acceptable, and the standard uncertainties for C−C bond lengths range between 0.005 Å and 0.009 Å, which can be considered as an acceptable result. CCDC-226222 to -226229 (**3**, **5**−**11**, respectively) contain the supplementary crystallographic data for this paper. These data can be obtained free of charge at www.ccdc.cam.ac.uk/conts/retrieving.html [or from the Cambridge Crystallographic Data Centre, 12 Union Road, Cambridge CB2 1EZ, UK; Fax: (internat.) + 44-1223-336033; E-mail: deposit@ccdc.cam.ac.uk].

Acknowledgments

Funding from the Swiss National Science Foundation (SNSF) and from the University of Zürich is gratefully acknowledged.

[1] M. I. Bruce, *Chem. Rev.* **1998**, *98*, 2797.
[2] U. H. F. Bunz, *Angew. Chem. Int. Ed. Engl.* **1996**, *35*, 969.
[3] R. L. Carroll, C. B. Gorman, *Angew. Chem. Int. Ed.* **2002**, *41*, 4378.
[4] C. L. Carter, R. E. Siatkowsky, H. Woltjien, *Molecular Electronic Devices*, Elsevier, Amsterdam, **1988**.
[5] C. P. Collier, J. O. Jeppesen, Y. Luo, J. Perkins, E. W. Wong, J. R. Heath, J. F. Stoddart, *J. Am. Chem. Soc.* **2001**, *123*, 12632.
[6] D. Gust, *Nature* **1994**, *372*, 133.
[7] A. Harriman, R. Ziessel, *Coord. Chem. Rev.* **1998**, *171*, 331.
[8] A. Harriman, R. Ziessel, *Chem. Commun.* **1996**, 1707.
[9] J. R. Heath, *Acc. Chem. Res.* **1999**, *32*, 388.
[10] J. Jortner, M. Ratner, *Molecular Electronics*, Blackwell Science, Oxford, United Kingdom, **1997**.
[11] D. L. Pearson, L. Jones, J. S. Schumm, J. M. Tour, *Synth. Met.* **1997**, *84*, 303.
[12] P. F. H. Schwab, M. D. Levin, J. Michl, *Chem. Rev.* **1999**, *99*, 1863.
[13] M. D. Ward, *Chem. Ind.* **1997**, 640.
[14] M. D. Ward, *Chem. Ind.* **1996**, 568.
[15] V. Balzani, M. Venturi, A. Credi, *Molecular Devices and Machines − A Journey into the Nanoworld*, Wiley-VCH Verlag GmbH & Co., Weinheim, **2003**.
[16] C. Joachim, *New J. Chem.* **1991**, *15*, 223.
[17] M. H. Chisholm, *Angew. Chem. Int. Ed. Engl.* **1991**, *30*, 673.
[18] J. M. Tour, R. Wu, J. S. Schumm, *J. Am. Chem. Soc.* **1991**, *113*, 7064.
[19] G. M. Whitesides, J. P. Mathias, C. T. Seto, *Science* **1991**, *254*, 1312.
[20] P. J. Stang, R. Tykwinski, *J. Am. Chem. Soc.* **1992**, *114*, 4411.
[21] T. Yamamoto, A. Morita, Y. Miyazaki, T. Maruyama, H. Wakayama, Z. Zhou, Y. Nakamura, T. Kanbara, S. Sasaki, K. Kubota, *Macromolecules* **1992**, *25*, 1214.
[22] N. G. Connelly, M. P. Gamasa, J. Gimeno, C. Lapinte, E. Lastra, J. P. Maher, N. Lenarvor, A. L. Rieger, P. H. Rieger, *J. Chem. Soc., Dalton Trans.* **1993**, 2575.
[23] G. Frapper, M. Kertesz, *Inorg. Chem.* **1993**, *32*, 732.
[24] T. Rappert, O. Nurnberg, H. Werner, *Organometallics* **1993**, *12*, 1359.
[25] A. C. Benniston, V. Goulle, A. Harriman, J. M. Lehn, B. Marczinke, *J. Phys. Chem.* **1994**, *98*, 7798.
[26] U. H. F. Bunz, *Angew. Chem. Int. Ed. Engl.* **1994**, *33*, 1073.
[27] R. W. Wagner, J. S. Lindsey, *J. Am. Chem. Soc.* **1994**, *116*, 9759.
[28] T. Yamamoto, T. Maruyama, Z. H. Zhou, T. Ito, T. Fukuda, Y. Yoneda, F. Begum, T. Ikeda, S. Sasaki, H. Takezoe, A. Fukuda, K. Kubota, *J. Am. Chem. Soc.* **1994**, *116*, 4832.
[29] V. Grosshenny, A. Harriman, R. Ziessel, *Angew. Chem. Int. Ed. Engl.* **1995**, *34*, 1100.
[30] M. Sato, E. Mogi, M. Katada, *Organometallics* **1995**, *14*, 4837.
[31] L. M. Tolbert, X. D. Zhao, Y. Z. Ding, L. A. Bottomley, *J. Am. Chem. Soc.* **1995**, *117*, 12891.
[32] M. D. Ward, *Chem. Soc. Rev.* **1995**, *24*, 121.
[33] R. Dagani, *Chem. Eng. News* **1996**, *74*, 22.
[34] F. Coat, C. Lapinte, *Organometallics* **1996**, *15*, 477.
[35] V. Grosshenny, A. Harriman, R. Ziessel, *Angew. Chem. Int. Ed. Engl.* **1996**, *34*, 2705.
[36] V. V. Krivykh, I. L. Eremenko, D. Veghini, I. A. Petrunenko, D. L. Pountney, D. Unseld, H. Berke, *J. Organomet. Chem.* **1996**, *511*, 111.
[37] O. Lavastre, L. Ollivier, P. H. Dixneuf, S. Sibandhit, *Tetrahedron* **1996**, *52*, 5495.
[38] V. Mahias, S. Cron, L. Toupet, C. Lapinte, *Organometallics* **1996**, *15*, 5399.
[39] M. Sato, Y. Hayashi, S. Kumakura, N. Shimizu, M. Katada, S. Kawata, *Organometallics* **1996**, *15*, 721.
[40] M. Akita, M. C. Chung, A. Sakurai, S. Sugimoto, M. Terada, M. Tanaka, Y. Morooka, *Organometallics* **1997**, *16*, 4882.
[41] D. Astruc, *Acc. Chem. Res.* **1997**, *30*, 383.
[42] A. C. Benniston, A. Harriman, V. Grosshenny, R. Ziessel, *New J. Chem.* **1997**, *21*, 405.
[43] M. Brady, W. Q. Weng, Y. L. Zhou, J. W. Seyler, A. J. Amoroso, A. M. Arif, M. Bohme, G. Frenking, J. A. Gladysz, *J. Am. Chem. Soc.* **1997**, *119*, 775.
[44] F. Coat, M. A. Guillevic, L. Toupet, F. Paul, C. Lapinte, *Organometallics* **1997**, *16*, 5988.
[45] N. D. Jones, M. O. Wolf, D. M. Giaquinta, *Organometallics* **1997**, *16*, 1352.
[46] V. V. Krivykh, H. Berke, *Abstr. Pap. Am. Chem. Soc.* **1997**, *213*, 103.
[47] O. Lavastre, M. Even, C. Troccon, P. H. Dixneuf, A. Pacreau, J. P. Vairon, *Macromol. Symp.* **1997**, *122*, 71.
[48] T. Weyland, C. Lapinte, G. Frapper, M. J. Calhorda, J. F. Halet, L. Toupet, *Organometallics* **1997**, *16*, 2024.
[49] M. Guillemot, L. Toupet, C. Lapinte, *Organometallics* **1998**, *17*, 1928.
[50] F. Paul, C. Lapinte, *Coord. Chem. Rev.* **1998**, *180*, 431.
[51] A. von Zelewsky, P. Belser, *Chimia* **1998**, *52*, 620.
[52] T. Weyland, K. Costuas, A. Mari, J. F. Halet, C. Lapinte, *Organometallics* **1998**, *17*, 5569.
[53] M. Younus, N. J. Long, P. R. Raithby, J. Lewis, *J. Organomet. Chem.* **1998**, *570*, 55.
[54] F. Coat, M. Guillemot, F. Paul, C. Lapinte, *J. Organomet. Chem.* **1999**, *578*, 76.
[55] R. Dembinski, T. Lis, S. Szafert, C. L. Mayne, T. Bartik, J. A. Gladysz, *J. Organomet. Chem.* **1999**, *578*, 229.
[56] R. Dembinski, S. Szafert, P. Haquette, T. Lis, J. A. Gladysz, *Organometallics* **1999**, *18*, 5438.
[57] S. Kheradmandan, K. Heinze, H. W. Schmalle, H. Berke, *Angew. Chem. Int. Ed.* **1999**, *38*, 2270.
[58] O. Lavastre, S. Cabioch, P. H. Dixneuf, J. Sedlacek, J. Vohlidal, *Macromolecules* **1999**, *32*, 4477.

 © 2004 Wiley-VCH Verlag GmbH & Co. KGaA, Weinheim

[59] S. Le Stang, F. Paul, C. Lapinte, *Inorg. Chim. Acta* **1999**, *291*, 403.
[60] A. M. McDonagh, M. G. Humphrey, M. Samoc, B. Luther-Davies, *Organometallics* **1999**, *18*, 5195.
[61] A. M. McDonagh, M. G. Humphrey, M. Samoc, B. Luther-Davies, S. Houbrechts, T. Wada, H. Sasabe, A. Persoons, *J. Am. Chem. Soc.* **1999**, *121*, 1405.
[62] K. Oyaizu, K. Yamamoto, Y. Ishii, E. Tsuchida, *Chem. Eur. J.* **1999**, *5*, 3193.
[63] D. Unseld, V. V. Krivykh, K. Heinze, F. Wild, G. Artus, H. Schmalle, H. Berke, *Organometallics* **1999**, *18*, 1525.
[64] M. I. Bruce, B. D. Kelly, B. W. Skelton, A. H. White, *J. Organomet. Chem.* **2000**, *604*, 150.
[65] M. I. Bruce, P. J. Low, K. Costuas, J. F. Halet, S. P. Best, G. A. Heath, *J. Am. Chem. Soc.* **2000**, *122*, 1949.
[66] R. Dembinski, T. Bartik, B. Bartik, M. Jaeger, J. A. Gladysz, *J. Am. Chem. Soc.* **2000**, *122*, 810.
[67] F. Franceschi, E. Solari, R. Scopelliti, C. Floriani, *Angew. Chem. Int. Ed.* **2000**, *39*, 1685.
[68] J. Gil-Rubio, M. Laubender, H. Werner, *Organometallics* **2000**, *19*, 1365.
[69] S. Le Stang, F. Paul, C. Lapinte, *Organometallics* **2000**, *19*, 1035.
[70] F. Paul, W. E. Meyer, L. Toupet, H. J. Jiao, J. A. Gladysz, C. Lapinte, *J. Am. Chem. Soc.* **2000**, *122*, 9405.
[71] T. Ren, G. Zou, J. C. Alvarez, *Chem. Commun.* **2000**, 1197.
[72] M. Carano, M. Careri, F. Cicogna, I. D'Ambra, J. L. Houben, G. Ingrosso, M. Marcaccio, F. Paolucci, C. Pinzino, S. Roffia, *Organometallics* **2001**, *20*, 3478.
[73] R. D'Amato, A. Furlani, M. Colapietro, G. Portalone, M. Casalboni, M. Falconieri, M. V. Russo, *J. Organomet. Chem.* **2001**, *627*, 13.
[74] F. J. Fernandez, M. Alfonso, H. W. Schmalle, H. Berke, *Organometallics* **2001**, *20*, 3122.
[75] F. J. Fernandez, O. Blacque, M. Alfonso, H. Berke, *Chem. Commun.* **2001**, 1266.
[76] W. Y. Wong, G. L. Lu, K. F. Ng, C. K. Wong, K. H. Choi, *J. Organomet. Chem.* **2001**, *637*, 159.
[77] W. Y. Wong, G. L. Lu, K. F. Ng, K. H. Choi, Z. Y. Lin, *J. Chem. Soc., Dalton Trans.* **2001**, 3250.
[78] S. Chakraborty, R. H. Laye, P. Munshi, R. L. Paul, M. D. Ward, G. K. Lahiri, *J. Chem. Soc., Dalton Trans.* **2002**, 2348.
[79] N. Chanda, R. H. Laye, S. Chakraborty, R. L. Paul, J. C. Jeffrey, M. D. Ward, G. K. Lahiri, *J. Chem. Soc., Dalton Trans.* **2002**, 3496.
[80] M. Freemantle, *Chem. Eng. News* **2002**, *80*, 17.
[81] M. H. Garcia, M. P. Robalo, A. R. Dias, M. T. Duarte, W. Wenseleers, G. Aerts, E. Goovaerts, M. P. Cifuentes, S. Hurst, M. G. Humphrey, M. Samoc, B. Luther-Davies, *Organometallics* **2002**, *21*, 2107.
[82] W. Y. Wong, K. Y. Ho, K. H. Choi, *J. Organomet. Chem.* **2003**, *670*, 17.
[83] W. Y. Wong, K. Y. Ho, S. L. Ho, Z. Y. Lin, *J. Organomet. Chem.* **2003**, *683*, 341.
[84] P. Leoni, F. Marchetti, L. Marchetti, M. Pasquali, *Chem. Commun.* **2003**, 2372.
[85] M. C. Chung, X. H. Gu, B. A. Etzenhouser, A. M. Spuches, P. T. Rye, S. K. Seetharaman, D. J. Rose, J. Zubieta, M. B. Sponsler, *Organometallics* **2003**, *22*, 3485.
[86] J. N. Anderson, N. J. Brookes, B. J. Coe, S. J. Coles, M. E. Light, M. B. Hursthouse, *Acta Crystallogr., Sect. C* **2003**, *59*, M215.
[87] J. Stahl, J. C. Bohling, E. B. Bauer, T. B. Peters, W. Mohr, J. M. Martin-Alvarez, F. Hampel, J. A. Gladysz, *Angew. Chem. Int. Ed.* **2002**, *41*, 1872.
[88] T. Ren, G. L. Xu, *Comments Inorg. Chem.* **2002**, *23*, 355.
[89] F. Paul, J. Y. Mevellec, C. Lapinte, *J. Chem. Soc., Dalton Trans.* **2002**, 1783.
[90] S. Rigaut, F. Monnier, F. Mousset, D. Touchard, P. H. Dixneuf, *Organometallics* **2002**, *21*, 2654.
[91] S. Rigaut, J. Massue, D. Touchard, J. L. Fillaut, S. Golhen, P. H. Dixneuf, *Angew. Chem. Int. Ed.* **2002**, *41*, 4513.
[92] J. P. Barbier, R. Hugel, *Inorg. Chim. Acta* **1974**, *10*, 93.
[93] J. P. Barbier, R. Hugel, *J. Inorg. Nucl. Chem.* **1973**, *35*, 781.
[94] P. Chaudhuri, *Coord. Chem. Rev.* **2003**, *243*, 143.
[95] C. Mantel, A. K. Hassan, J. Pecaut, A. Deronzier, M. N. Collomb, C. Duboc-Toia, *J. Am. Chem. Soc.* **2003**, *125*, 12337.
[96] S. Blanchard, G. Blain, E. Riviere, M. Nierlich, G. Blondin, *Chem. Eur. J.* **2003**, *9*, 4260.
[97] C. Dendrinou-Samara, M. Alexiou, C. M. Zaleski, J. W. Kampf, M. L. Kirk, D. P. Kessissoglou, V. L. Pecoraro, *Angew. Chem. Int. Ed.* **2003**, *42*, 3763.
[98] G. S. Papaefstathiou, S. P. Perlepes, *Comments Inorg. Chem.* **2002**, *23*, 249.
[99] J. T. Brockman, J. C. Huffman, G. Christou, *Angew. Chem. Int. Ed.* **2002**, *41*, 2506.
[100] S. Kheradmandan, H. W. Schmalle, H. Jacobsen, O. Blacque, T. Fox, H. Berke, M. Gross, S. Decurtins, *Chem. Eur. J.* **2002**, *8*, 2526.
[101] F. J. Fernandez, K. Venkatesan, O. Blacque, H. W. Schmalle, H. Berke, *Chem. Eur. J.* **2003**, *9*, 6192.
[102] E. O. Fischer, H. Leipfinger, *Z. Naturforsch., Teil B* **1955**, *10*, 353.
[103] G. Wilkinson, F. A. Cotton, J. M. Birmingham, *J. Inorg. Nucl. Chem.* **1956**, *2*, 95.
[104] D. Unseld, PhD thesis, University of Zürich, **1999**.
[105] C. G. Howard, G. S. Girolami, G. Wilkinson, M. Thornton-Pett, M. B. Hursthouse, *J. Am. Chem. Soc.* **1984**, *106*, 2033.
[106] J. Heck, W. Massa, P. Weinig, *Angew. Chem. Int. Ed. Engl.* **1984**, *23*, 722.
[107] S. Takahashi, Y. Kuroyama, K. Sonogashira, N. Hagihara, *Synthesis* **1980**, 627.
[108] W. B. Austin, N. Bilow, W. J. Kelleghan, K. S. Y. Lau, *J. Org. Chem.* **1981**, *46*, 2280.
[109] R. Nast, H. Grouhi, *J. Organomet. Chem.* **1979**, *182*, 197.
[110] G. S. Girolami, C. G. Howard, G. Wilkinson, H. M. Dawes, M. Thorntonpett, M. Motevalli, M. B. Hursthouse, *J. Chem. Soc., Dalton Trans.* **1985**, 921.
[111] C. G. Howard, G. Wilkinson, M. Thorntonpett, M. B. Hursthouse, *J. Chem. Soc., Dalton Trans.* **1983**, 2025.
[112] J. I. Davies, C. G. Howard, A. C. Skapski, G. Wilkinson, *J. Chem. Soc., Chem. Commun.* **1982**, 1077.
[113] H. J. Haupt, C. Heinekamp, U. Florke, U. Juptner, *Z. Anorg. Allg. Chem.* **1992**, *608*, 100.
[114] P. M. N. Low, A. L. Tan, T. S. A. Hor, Y. S. Wen, L. K. Liu, *Organometallics* **1996**, *15*, 2595.
[115] N. Robertson, C. A. McGowan, *Chem. Soc. Rev.* **2003**, *32*, 96.
[116] L. Jones, J. S. Schumm, J. M. Tour, *J. Org. Chem.* **1997**, *62*, 1388.
[117] T. Bartik, B. Bartik, M. Brady, R. Dembinski, J. A. Gladysz, *Angew. Chem. Int. Ed. Engl.* **1996**, *35*, 414.
[118] T. Bartik, W. Q. Weng, J. A. Ramsden, S. Szafert, S. B. Falloon, A. M. Arif, J. A. Gladysz, *J. Am. Chem. Soc.* **1998**, *120*, 11071.
[119] S. B. Falloon, S. Szafert, A. M. Arif, J. A. Gladysz, *Chem. Eur. J.* **1998**, *4*, 1033.
[120] C. R. Horn, J. M. Martin-Alvarez, J. A. Gladysz, *Organometallics* **2002**, *21*, 5386.
[121] C. R. Horn, J. A. Gladysz, *Eur. J. Inorg. Chem.* **2003**, 2211.
[122] H. J. Jiao, K. Costuas, J. A. Gladysz, J. F. Halet, M. Guillemot, L. Toupet, F. Paul, C. Lapinte, *J. Am. Chem. Soc.* **2003**, *125*, 9511.
[123] W. Mohr, J. Stahl, F. Hampel, J. A. Gladysz, *Chem. Eur. J.* **2003**, *9*, 3324.
[124] J. A. Ramsden, W. Q. Weng, A. M. Arif, J. A. Gladysz, *J. Am. Chem. Soc.* **1992**, *114*, 5890.
[125] D. R. Senn, A. Wong, A. T. Patton, M. Marsi, C. E. Strouse, J. A. Gladysz, *J. Am. Chem. Soc.* **1988**, *110*, 6096.
[126] W. Q. Weng, T. Bartik, M. Brady, B. Bartik, J. A. Ramsden, A. M. Arif, J. A. Gladysz, *J. Am. Chem. Soc.* **1995**, *117*, 11922.
[127][127a] A. Wong, J. A. Gladysz, *J. Am. Chem. Soc.* **1982**, *104*,

 © 2004 Wiley-VCH Verlag GmbH & Co. KGaA, Weinheim

4948. [127b] M. B. Robin, P. Day, *Adv. Inorg. Chem. Radiochem.* **1967**, *10*, 247.
[128] R. J. Burt, J. Chatt, W. Hussain, G. J. Leigh, *J. Organomet. Chem.* **1979**, *182*, 203.
[129] J. L. Brefort, R. J. P. Corriu, P. Gerbier, C. Guerin, B. J. L. Henner, A. Jean, T. Kuhlmann, F. Garnier, A. Yassar, *Organometallics* **1992**, *11*, 2500.
[130] G. Zweifel, S. Rajagopalan, *J. Am. Chem. Soc.* **1985**, *107*, 700.
[131] G. Himbert, H. Umbach, M. Barz, *Z. Naturforsch., Teil B* **1984**, *39*, 661.
[132] N. Hebendanz, F. H. Köhler, G. Muller, J. Riede, *J. Am. Chem. Soc.* **1986**, *108*, 3281.
[133] F. H. Köhler, N. Hebendanz, G. Muller, U. Thewalt, B. Kanellakopulos, R. Klenze, *Organometallics* **1987**, *6*, 115.
[134] F. H. Köhler, B. Schlesinger, *Inorg. Chem.* **1992**, *31*, 2853.
[135] *STOE-IPDS*, Software package, version 2.87 5/1998, STOE & Cie, GmbH, Darmstadt, Germany, 1998.
[136] P. Coppens, L. Leiserow, D. Rabinovi, *Acta Crystallogr.* **1965**, *18*, 1035.
[137] G. M. Sheldrick, *Acta Crystallogr., Sect. A* **1990**, *46*, 467.
[138] A. L. Spek, *Acta Crystallogr., Sect. A* **1990**, *46*, 34.
[139] Y. Lepage, *J. Appl. Crystallogr.* **1987**, *20*, 264.
[140] G. M. Sheldrick, *Program for refinement of crystal structure*, University of Göttingen, Germany **1997**.

Received January 6, 2004
Early View Article
Published Online June 17, 2004

 © 2004 Wiley-VCH Verlag GmbH & Co. KGaA, Weinheim

New Multifunctional Complexes $[Ru(\kappa^3\text{-}L)(EPh_3)_2Cl]^+$ [E = P, As; L = 2,4,6-Tris(2-pyridyl)-1,3,5-triazine] Containing both Group V and Polypyridyl Ligands

Sanjeev Sharma,[a] Manish Chandra,[a] and Daya Shankar Pandey*[a]

Keywords: Ruthenium / Tertiary phosphanes / 2,4,6-Tris(2-pyridyl)-1,3,5-triazine / DNA / Topoisomerase II

Synthesis, structure, reactivity and enzyme inhibitory activity of the new cationic ruthenium complexes $[Ru(\kappa^3\text{-}L)(EPh_3)_2Cl]BF_4$ [L = 2,4,6-tris(2-pyridyl)-1,3,5-triazine (tptz); E = P (**1**), As (**2**)] and their substitution products $[Ru(\kappa^3\text{-}tptz)(PPh_3)(dtc)]Cl$ (**3**), $[Ru(\kappa^3\text{-}tptz)(PPh_3)(CN)_2]$ (**4**), $[Ru(\kappa^3\text{-}tptz)(AsPh_3)(dtc)]BF_4$ (**5**), and $[Ru(\kappa^3\text{-}tptz)(AsPh_3)(CN)_2]$ (**6**) are reported. The complexes were characterized by analytical and spectroscopic methods and the structures of the complexes **1**, **2** and **3** determined by X-ray diffraction studies. C–H···X (X = Cl, F and S), C–H···π and π–π interactions were observed in these complexes. Further studies indicated that the complexes $[Ru(\kappa^3\text{-}L)(EPh_3)_2Cl]^+$ could find application as precursors in the synthesis of other ruthenium complexes or as metallo-ligands. The complexes also interact with DNA, which was illustrated by absorption titration studies with CT-DNA and inhibition of topoisomerase II of the filarial parasite *Setaria cervi*.

(© Wiley-VCH Verlag GmbH & Co. KGaA, 69451 Weinheim, Germany, 2004)

Introduction

Recently, (polypyridyl)Ru^{II} complexes have received considerable attention owing to their possible application in conversion of solar energy to electrical energy,[1] in long-range electron and energy transfer,[2] molecular electronic devices,[3] self-assembly processes[4] and as photoprobes for DNA.[5] Polypyridyl bridging ligands containing a delocalized π-electron system have drawn special attention in this regard. Using such ligands, many luminescent and redox-active compounds have been synthesized and studied extensively.[6] During the past few years, we have been interested in the synthesis and characterization of metallo-ligands/synthons based on organometallic systems containing organonitriles and polypyridyl ligands.[7] During our studies on the reactivity of hydrated Ru^{III} chloride in the presence of excess EPh_3 or $[RuCl_2(PPh_3)_3]$ with 2,4,6-tris(2-pyridyl)-1,3,5-triazine (tptz), we have isolated a completely new series of cationic complexes $[Ru(\kappa^3\text{-}L)(EPh_3)_2Cl]^+$. These compounds are examples of ruthenium complexes containing both Group V and polypyridyl ligands, which are associated with classical coordination chemistry.

The new cationic complexes $[Ru(\kappa^3\text{-}L)(EPh_3)_2]Cl]^+$ all possess κ^3-bonded tptz, two tertiary phosphane or arsane ligands, a labile chloro group, and have the potential to exhibit rich chemistry. The ligand tptz primarily acts as a tridentate ligand similar to terpyridine (tpy), but is more versatile than tpy. The complexes under study offer a unique opportunity to behave as metallo-ligands because of the presence of vacant donor sites at the tptz ligand and, thus, could find applications in the synthesis of homo-, hetero di- or polynuclear systems. Furthermore, DNA binding studies have shown that ruthenium complexes containing polypyridyl ligands are of significant importance.[5] It was felt that the new complexes of the series $[Ru(\kappa^3\text{-}L)(EPh_3)_2Cl]^+$ could be used as DNA probes. Although, a number of reports dealing with DNA binding and inhibition activity of (polypyridyl)Ru^{II} complexes are available in the literature, activity of the complexes incorporating triphenylphosphane or triphenylarsane and a polypyridyl ligand have yet to be examined. We report herein, on the reactivity, absorption titration studies and inhibitory activity against DNA topo II of the filarial parasite *Setaria cervi* of the new, air-stable mononuclear complexes $[Ru(\kappa^3\text{-}tptz)(L_2)Cl]^+$.

Results and Discussion

The air-stable cationic complexes **1**, **2** and their representative substitution products $[Ru(\kappa^3\text{-}tptz)(PPh_3)(dtc)]Cl$ (**3**), $[Ru(\kappa^3\text{-}tptz)(PPh_3)(CN)_2]$ (**4**), $[Ru(\kappa^3\text{-}tptz)(AsPh_3)(dtc)]BF_4$ (**5**), and $[Ru(\kappa^3\text{-}tptz)(AsPh_3)(CN)_2]$ (**6**) were obtained in excellent yield as shown in Scheme 1. The compounds were characterized spectroscopically and gave satisfactory elemental analyses. The microanalyses, FAB-MS and NMR (^1H and ^{31}P) data of the complexes correspond to their respective formulas.

^1H NMR spectroscopic data of the complexes are given in the Exp. Sect. The positions and integrated intensities of

[a] Department of Chemistry, Awadhesh Pratap Singh University, Rewa 486003 (M.P.), India
E-mail: dsprewa@yahoo.com

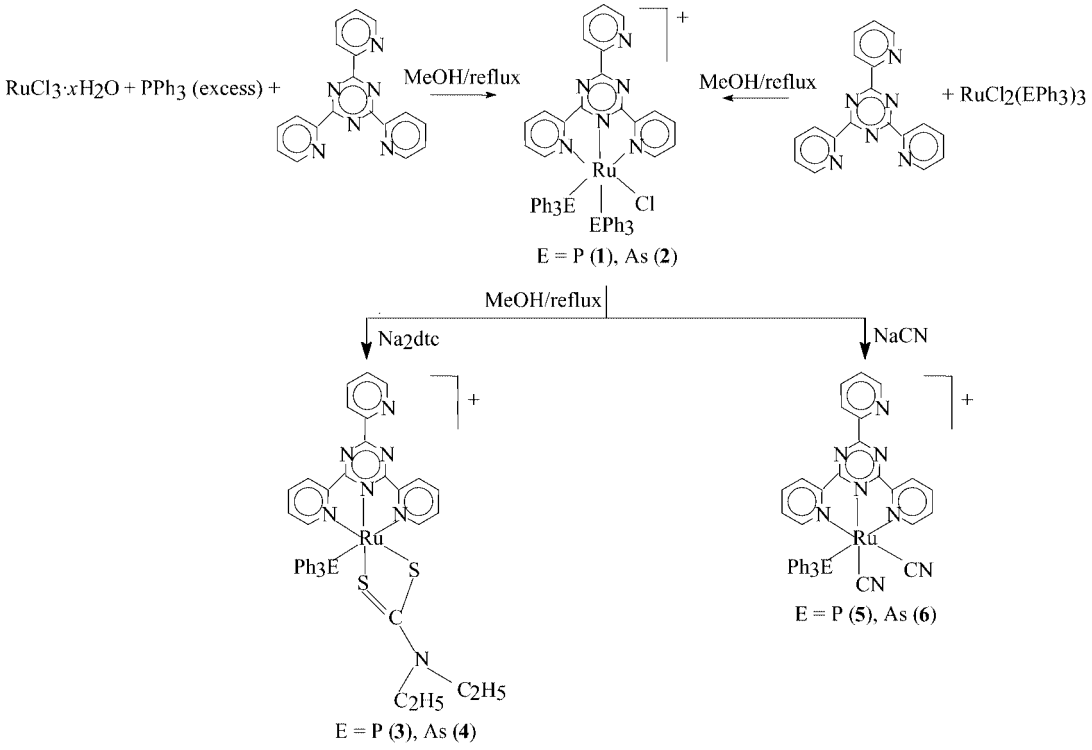

Scheme 1

the signals corresponding to tptz corroborated well with a system containing two magnetically equivalent coordinated pyridyl rings and one uncoordinated pyridyl ring. This observation indicated coordination of the tptz to Ru in a κ^3-manner. The aromatic protons of the PPh_3 and $AsPh_3$ ligands gave a broad multiplet in the usual region with δ = 7.26−7.07 ppm. Integrated intensities and positions of the signals were consistent with the respective formulas of the complexes. The main feature of the ^1H NMR spectra of the diethyl dithiocarbamate containing complexes **3** and **4** is the presence of multiplet signals at high field with chemical shifts characteristic of methyl and methylene protons. In the complexes **3** and **4**, these appeared at δ = 4.10 (q, J = 7.2 Hz, 2 H), 3.62 (q, J = 6.9 Hz, 2 H), 1.52 (t, J = 7.2 Hz, 3 H), 1.13 (t, J = 6 Hz, 3 H) and 4.03 (q, J = 7.2 Hz, 2 H), 3.55 (q, J = 7.2 Hz, 2 H), 1.50 (t, J = 7.2 Hz, 3 H), 1.10 (t, J = 6.1 Hz, 3 H) ppm, respectively. The presence of signals in this region strongly suggests coordination of the diethyl dithiocarbamate to the metal center. In the $^{31}P\{^1H\}$ NMR spectra of the complexes **1**, **3** and **5**, single sharp resonances were observable at δ = 16.24, 37.81 and 32.89 ppm, respectively. The presence of a single sharp peak in the $^{31}P\{^1H\}$ NMR spectrum of complex **1** suggests that both the ^{31}P nuclei are chemically equivalent and that the triphenylphosphane ligands are *trans*-disposed in this complex.

Electrochemical properties of the new complexes were observed by cyclic voltammetry. The cyclic voltammogram of complex $[Ru(\kappa^3\text{-tptz})(AsPh_3)_2Cl]BF_4$ (**2**) is shown in Figure 1. The ruthenium complexes with the tptz ligand $[Ru(\kappa^3\text{-tptz})(PPh_3)_2Cl]BF_4$ and $[Ru(\kappa^3\text{-tptz})(AsPh_3)_2Cl]BF_4$ exhibited reversible ($Ru^{II/III}$) metal-based oxidation couples at 1.05 (70) V and 1.02 (50) V, respectively.[8] In the cathodic potential window, three ligand-based reversible and quasi-reversible reduction couples were observed in the range 0.89−1.50 V for the tptz ligand.

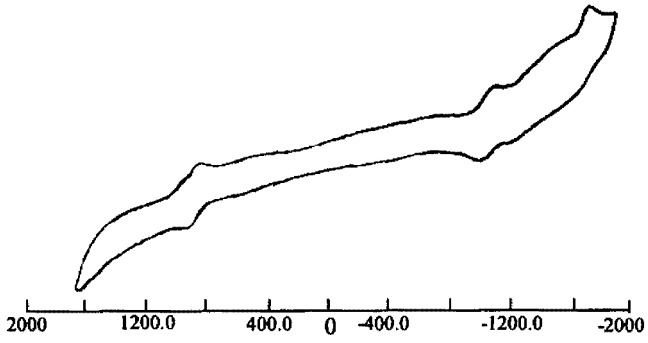

Figure 1. Cyclic voltammogram of the complex **2**

In the electronic absorption spectra of complexes **1** and **2**, the MLCT transitions appeared in the visible region at λ (ε) = 472 (24022) and 489 (6930) nm, respectively, while the ligand-centered transitions were observed at λ (ε) = 309 (63759), 273 (149195) (for **1**) and 342 (7250), 271.5 (21355) (for **2**) nm. Complexes **3**−**6** exhibited red-shifted absorptions when compared with complexes **1** and **2**. The complexes do not luminesce in air at room temperature.

Molecular structures of complexes **1**−**3** were established crystallographically.[9] Both complexes **1** and **2** crystallize in the $P2_1/c$ space group, while complex **3** crystallizes in a very rare $F2dd$ space group (Table 3). In all the complexes, Ru is

 © 2004 Wiley-VCH Verlag GmbH & Co. KGaA, Weinheim

bonded covalently within the major coordination sites of tptz in a κ^3-manner by two phosphorus or arsenic atoms from the triphenylphosphane or arsane ligand and a chloro group in complex **1** and **2** and one phosphorus atom from the triphenylphosphane ligand and a dithiolato group in complex **3**. There is a distorted octahedral coordination geometry about the ruthenium center. The N(1)−Ru(1)−N(2) and N(2)−Ru(1)−N(3) angles in complex **1** are essentially equal with 78.77(12) and 78.47(11)°, while in complexes **2** and **3** these angles are 78.91(13) and 78.44(12)° and 76.9(5) and 77.1(5)°, respectively. This suggests some inward bending of the coordinated pyridyl group and may be the reason for the observed distortion. The bond length of Ru(1) to the central triazine nitrogen atom Ru(1)−N(2) in complex **1** is 1.936(3) Å, which is shorter than the bond of Ru(1) to the coordinated pyridyl nitrogen atom Ru(1)−N(1) [2.110(3) Å] and Ru(1)−N(3) [2.103(3) Å]. Similarly, in complexes **2** and **3** Ru(1)−N(2) is 1.931(3) and 1.968(13) Å, and the Ru(1)−N(1) and Ru(1)−N(3) distances are 2.098(3), 2.099(3) Å and 2.099(17), 2.076(13) Å, respectively. The Ru−N bond lengths are consistent with a κ^3-coordination of tptz and similar to those reported for other $(tptz)Ru^{II}$ complexes.[10] The triphenylphosphane ligands in complex **1** and the triphenylarsane ligands in complex **2** are *trans*-disposed as indicated by the P(1)−Ru(1)−P(2) angle of 178.52(3)° and As(1)−Ru(1)−As(2) angle of 178.26(2)°. The Ru(1)−P(1) and Ru(1)−P(2) distances are 2.4130(11) and 2.4264(11) Å in complex **1**, while in complex **2** the Ru(1)−As(1) and Ru(1)−As(2) distances are 2.481(6) and 2.491(6) Å, respectively. In complex **3**, the Ru1−S1 and Ru1−S2 distances are 2.427(4) and 2.407(4) Å, respectively. These are essentially equivalent or similar to those in related complexes.[11] The Ru−Cl distances in both complexes **1** and **2** are normal and are similar to Ru−Cl distances in other complexes (Table 1).[12]

The triazine ring from tptz and the coordinated pyridyl rings are almost coplanar. In complexes **1** and **2**, the uncoordinated pyridyl ring is inclined from the coordinated part of the ligand tptz by 25.9 and 23.3°, respectively. In complex **3**, which is obtained by replacement of one PPh_3 ligand and the chloro group of complex **1** by a dithiocarbamate ligand, the tptz ligand has regained its planarity. This is suggested by the angle of inclination (2.4°).

Selection of ligands plays an important role amongst the factors that induce the self-assembly processes. The ligands EPh_3 and triazine are expected to show different propensities for molecular arrangement based on the stacking arrangement of phenyl or triazine rings. The X-ray structure for complexes **1**−**3** revealed intermolecular C−H···X (X =

Table 2. Selected hydrogen bond lengths [Å] and angles [°] for the complex **1**−**3**

D−H−A	*d*(D−H)	*d*(H−A)	*d*(D−A)	∠(DHA)
1				
C(8)−H(8)−Cl(1)	0.93	2.69	3.536(4)	151.9
C(14)−H(14)−Cl(1)	0.93	2.72	3.566(4)	152.3
C(24)−H(24)−Cl(1)	0.93	2.71	3.411(5)	132.7
C(26)−H(26)−Cl(1)	0.93	2.81	3.669(4)	153.7
C(39)−H(39)−F(3)[a]	0.93	2.51	3.041(8)	116.1
C(43)−H(43)−F(2)[b]	0.93	2.53	3.443(7)	165.7
2				
C(39)−H(39)−F(1)[a]	0.84(7)	2.44(7)	3.084(9)	134(6)
C(8)−H(8)−Cl(1)	0.93	2.82	3.671(5)	151.8
3				
C(15)−H(15)−N(4)	0.93	2.47	2.79(2)	100.4
C(20)−H(20A)−S(1)	0.97	2.53	3.10(2)	117.3
C(22)−H(22B)−S(2)	0.97	2.61	2.98(2)	103.0
C(25)−H(25)−S(2)	0.93	2.70	3.477(19)	142.0
C(37)−H(37)−S(2)	0.93	2.77	3.615(19)	151.0

[a] x, y, z. [b] $x, y, z + 1$.

Table 1. Selected bond lengths [Å] and angles [°] for complexes **1**−**3**

1		**2**		**3**	
Ru(1)−Cl(1)	2.4473(11)	Ru(1)−Cl(1)	2.443(11)	Ru(1)−N(1)	2.099(17)
Ru(1)−P(1)	2.4130(11)	Ru(1)−As(1)	2.481(6)	Ru(1)−N(2)	1.968(13)
Ru(1)−P(2)	2.4264(11)	Ru(1)−As(2)	2.491(6)	Ru(1)−N(3)	2.076(13)
Ru(1)−N(1)	2.110(3)	Ru(1)−N(1)	2.098(3)	Ru(1)−P(1)	2.323(4)
Ru(1)−N(2)	1.936(3)	Ru(1)−N(2)	1.931(3)	Ru(1)−S(1)	2.427(4)
Ru(1)−N(3)	2.103(3)	Ru(1)−N(3)	2.099(3)	Ru(1)−S(2)	2.407(4)
N(2)−Ru(1)−N(1)	78.77(12)	N(2)−Ru(1)−N(1)	78.91(13)	S(1)−C(19)	1.758(18)
N(3)−Ru(1)−N(2)	78.47(11)	N(3)−Ru(1)−N(2)	78.44(12)	S(2)−C(19)	1.66(2)
N(1)−Ru(1)−Cl(1)	103.31(9)	N(1)−Ru(1)−Cl(1)	102.45(10)	N(7)−C(19)	1.37(2)
N(2)−Ru(1)−Cl(1)	177.16(9)	N(2)−Ru(1)−Cl(1)	178.15(9)	N(1)−Ru(1)−N(2)	76.9(5)
N(3)−Ru(1)−Cl(1)	99.48(8)	N(3)−Ru(1)−Cl(1)	100.21(9)	N(2)−Ru(1)−N(3)	77.1(5)
P(1)−Ru(1)−Cl(1)	91.21(4)	As(1)−Ru(1)−Cl(1)	91.14(3)	N(2)−Ru(1)−P(1)	94.4(4)
P(2)−Ru(1)−Cl(1)	89.44(4)	As(2)−Ru(1)−Cl(1)	90.40(3)	S(1)−Ru(1)−S(2)	72.54(15)
P(2)−Ru(1)−P(1)	178.52(3)	As(2)−Ru(1)−As(1)	178.26(2)	P(1)−Ru(1)−S(2)	94.09(14)
N(4)−C(49)−C(50)−N(6)	154.1(4)	N(4)−C(49)−C(50)−N(6)	−156.7(4)	S(1)−Ru(1)−N(2)	98.9(4)
				S(2)−C(19)−S(1)	113.6(11)
				C(22)−N(7)−C(19)−S(2)	−3(3)
				N(4)−C(13)−C(14)−N(6)	177.6(15)

 © 2004 Wiley-VCH Verlag GmbH & Co. KGaA, Weinheim

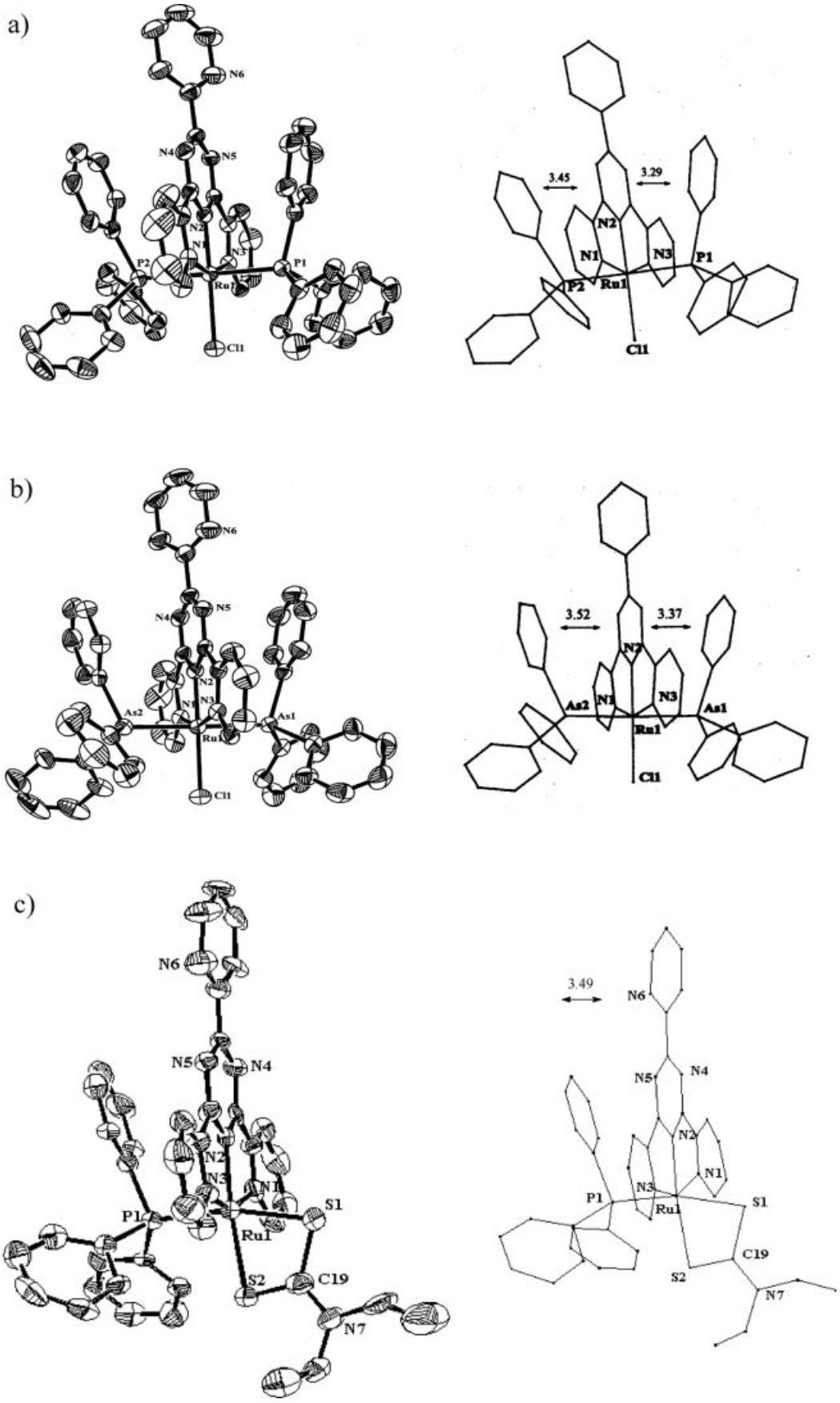

Figure 2. (a) Molecular structure of $[Ru(\kappa^3\text{-tptz})(PPh_3)_2]Cl]^+$ (**1**); (b) molecular structure of $[Ru(\kappa^3\text{-tptz})(AsPh_3)_2]Cl]^+$ (**2**); (c) molecular structure of $[Ru(\kappa^3\text{-tptz})(PPh_3)(dtc)]^+$ (**3**)

 © 2004 Wiley-VCH Verlag GmbH & Co. KGaA, Weinheim

F, N, S and Cl) and π−π interactions. (Table 2) Complex **1** shows C−H···Cl intramolecular interactions, which involve Cl and an adjacent hydrogen atom attached to the phenyl (PPh_3) rings. However, this type of interaction is not apparent in complex **2** which has an analogous structure. The absence of a C−H···Cl type interaction is probably due to the longer Ru−As bond in complex **2** when compared with the Ru−P distance in complex **1**. The importance of π−π stacking interactions between aromatic rings, which lie in the range 3.4−3.5 Å, has widely been recognized in the intercalation of drugs with DNA[13] in biological systems. In all the complexes **1**−**3**, intramolecular π−π interactions have been found with the interaction distances in the range 3.29−3.52 Å (see a, b and c in Figure 2). In complexes **1** and **2**, the intermolecular π−π stacking interaction [distance 3.42 Å (**1**) and 3.67 Å (**2**)] results in a single helical motif (see a in Figure 3), while C−H···π, C−H···S−C and π−π stacking (3.39 Å) interactions in complex **3** lead to a double helical network (b in Figure 3).[13]

Interaction of the complexes with DNA is supported by the results from absorption titration studies with calf thymus DNA and inhibition studies (gel electrophoresis) of topoisomerase II of the filarial parasite *S. cervi*. Chloride salts of the complexes were used for DNA binding and inhibition studies. It is well documented that nonplanar octahedral complexes can partially intercalate with the DNA helix or they can show groove binding interactions with the major or minor groove of the helix.[14] Fixed amounts of metal complexes [13.3 μM (**1**) and 40 μM (**2**)] were titrated with an increasing amount of CT-DNA over a range of DNA concentrations from 0 to 112 μM.[15] Absorption spectra were measured after equilibration and the binding constants of the complexes with CT-DNA were determined by monitoring the decay in absorbance with increasing DNA concentration. The model of Bard and Thorp for noncooperative and nonspecific binding was used.[16] Figure 4 depicts the UV/Vis spectra of complex **1** for a solution buffered at pH = 7.1 in the presence of increasing quantities of CT-DNA. Absorption spectra exhibited an average decrease in absorption (hypochromism) of 29% and 42% and bathochromic shifts of 7.5 and 6.5 nm for complexes **1** and **2**, respectively. These observations are consistent with the values reported for other polypyridyl transition metal complexes.[17,18] Binding constants for complexes **1** and **2** are 2.5×10^4 M^{-1} ($s = 0.25$) and 2.1×10^4 M^{-1} ($s = 0.21$), respectively. The value for $s < 1$ is similar to other re-

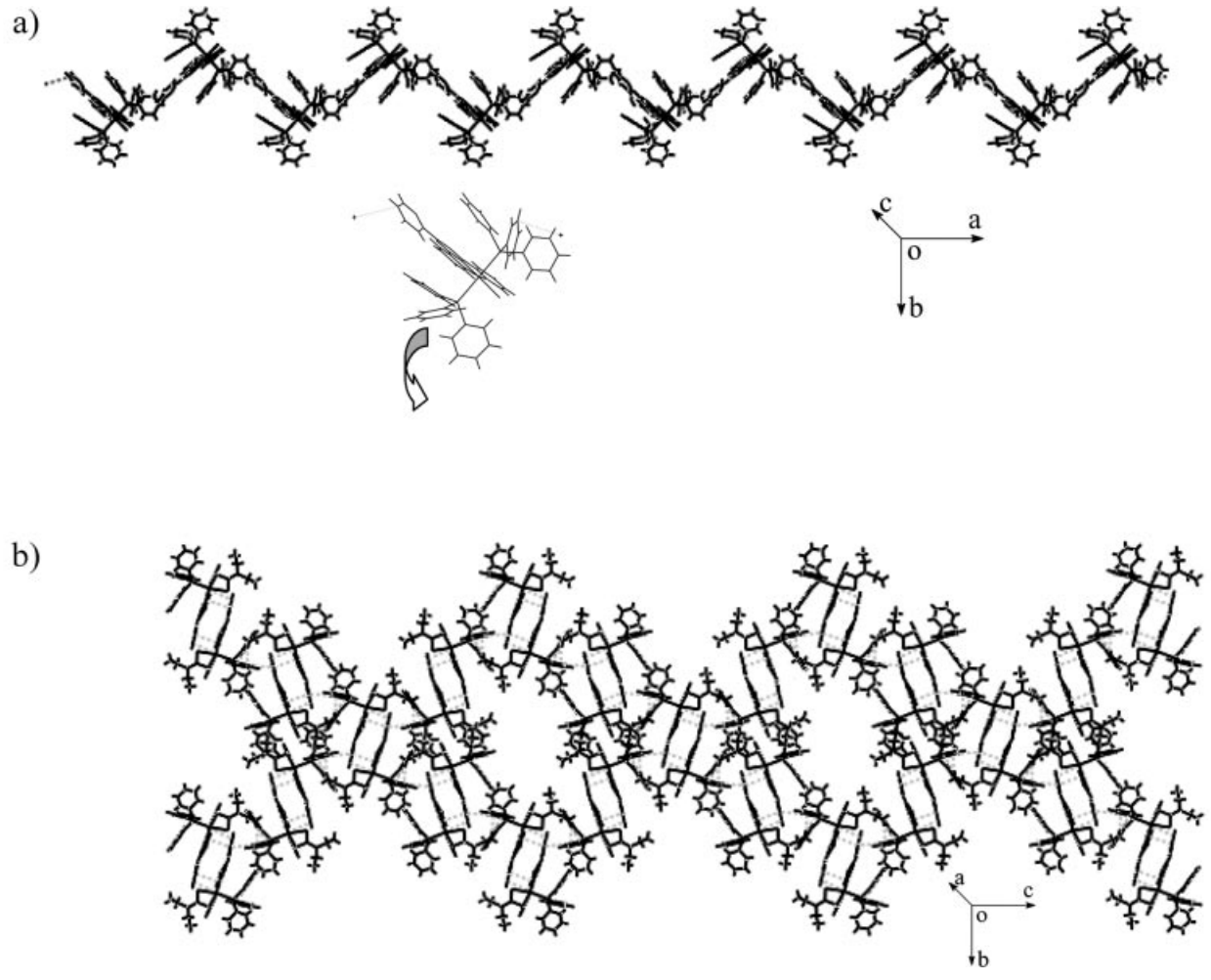

Figure 3. (a) An intermolecular π−π stacking interaction results in a single helical network for complex **1**; (b) intermolecular C−H···π, C−H···S−C and π−π stacking interactions result in a double helical network for complex **3**

 © 2004 Wiley-VCH Verlag GmbH & Co. KGaA, Weinheim

ports.[17] The binding strength of the compounds **1** and **2** to nucleotides is relatively poor. This may be due to the presence of the bulky EPh_3 groups *trans* to each other, which causes steric hindrance. Also, the phenyl rings of EPh_3 restrict further the intercalating properties of the complexes. The six-coordinate ruthenium center does not intercalate with the nucleotide and the absorption titration data supports that tptz is stacking with other tptz ligands of nearby complexes bound on the surface of the DNA.[17] Further addition of a 12-fold excess of CT-DNA after saturation of a 13.3 μM solution of complex **1** or addition of a 16-fold excess of CT-DNA to a 40 μM solution of complex **2** caused no changes in the absorption spectra of the final equilibrium mixtures over a period of 48 h. This indicates a strong interactive binding mode of (κ^3- tptz)Ru^{II} complexes.

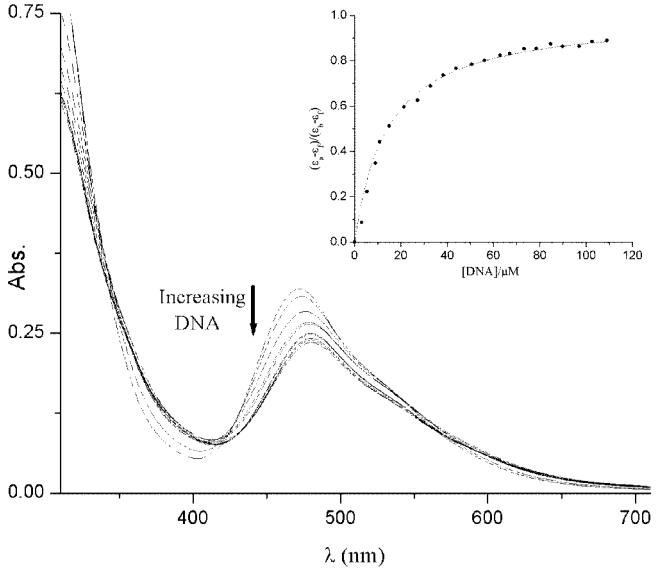

Figure 4. Absorption spectra of $[Ru(\kappa^3\text{-tptz})Cl(PPh_3)_2]^+$ (13.3 μM), in buffer A in the presence of an increasing amount of CT DNA (0−112 μM); inset represents a plot of $(\varepsilon_a - \varepsilon_f)/(\varepsilon_b - \varepsilon_f)$ vs. [DNA] in μM for $[Ru(\kappa^3\text{-tptz})Cl(PPh_3)_2]^+$; the best-fit line is superimposed on the data according to the model of Bard and Thorp[17] for the absorption titration [$K_b = 2.5 \times 10^4$ M^{-1} ($s = 0.25$)]

Efficacy of complexes **1** and **2** against DNA topoisomerase II (topo-II) of the filarial parasite *S. cervi* was examined. The interaction behavior is supported by the inhibitory effect of the metal complexes on DNA topoisomerase II of the filarial parasite. Potential antifilarial agents act either on membrane receptors or on metabolic enzymes. DNA topoisomerases are cellular enzymes that are intricately involved in the topographic structure of DNA transcription and mitosis.[18] In general, inhibition depends upon the availability of binding sites for the enzyme on DNA. Topoisomerase has been identified as an important biochemical target in chemotherapy and microbial infections. Complexes **1** and **2** are potential inhibitors of DNA topo-II of the filarial parasite *S. cervi* with 86% and 93% inhibition at a 10 μM concentration (Figure 5).

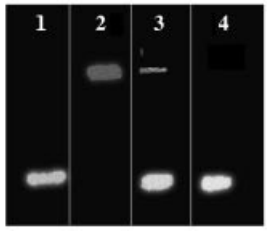

Figure 5. Inhibition of *S. cervi* topoisomerase II by complexes **1** and **2**; lane 1: pBR322 alone; lane 2: DNA + *S. cervi* topo II; lanes 3 and 4 correspond to complex $[Ru(\kappa^3\text{-tptz})Cl(PPh_3)_2]^+$ and $[Ru(\kappa^3\text{-tptz})Cl(AsPh_3)_2]^+$ (10 μM) and the inhibition percentage is 86% and 93%, respectively

Conclusions

In this work, we have presented the synthesis of the (polypyridyl)Ru^{II} complexes $[Ru(\kappa^3\text{-tptz})(PPh_3)_2Cl]^+$, which have many potential uses. We have shown that they can be employed as precursors of other Ru^{II} complexes, as metalloligands or as biocatalysts. Detailed studies of the structure, reactivity and assembling capability of the substituted complexes is in progress in our laboratory.

Experimental Section

General: All reactions were carried out under nitrogen and in deaerated solvents. The solvents were of AR grade and were purified rigorously by standard procedures[19] prior to use. Triply distilled and deionized water was used for the preparation of the various buffers. 2,4,6-Tris(2-pyridyl)-1,3,5-triazine (tptz), ammonium tetrafluoroborate, ruthenium(III) chloride hydrate (all Aldrich) and tetrabutylammonium perchlorate (Fluka) were used as received. Calf thymus (CT) DNA, supercoiled pBR322 DNA, bovine serum albumin (BSA), ATP, dithiothreitol (DTT), agarose, ethidium bromide, sodium dodecyl sulfate (SDS) and proteinase were procured from Sigma Chem. Topoisomersase II from filarial parasite *Setaria cervi* was partially purified according to the method by Pandeya et al.[20] The complex $RuCl_2(PPh_3)_3$ was prepared by a literature method.[21]

Physical Measurements

Spectroscopy and Electrochemistry: Microanalyses were performed by the microanalytical section of the Sophisticated Analytical Instrumentation Centre, Central Drug Research Institute, Lucknow. IR and electronic spectra were recorded with Shimadzu 8201PC and Shimadzu UV-1601 spectrophotometers, respectively. Electronic absorption spectra were measured in a quartz cuvette with a path length of 1 cm. ^1H, ^1H-^1H COSY, ^{13}C and ^{31}P NMR spectra were recorded with a Bruker DRX-300 NMR instrument. FAB mass spectra were recorded with a JEOL SX 102/DA 6000 mass spectrometer using Xenon (6 kV, 10 mA) as the FAB gas. The accelerating voltage was 10 kV and the spectra were recorded at room temperature with *m*-nitrobenzyl alcohol as the matrix. Thermal denaturation analyses were conducted with a DU-640 spectrophotometer. Electrochemical data were acquired with a PAR model 273A electrochemistry system at a scan rate of 50 mVs^{-1}. The sample solutions (10^{-3} M) were prepared in purified acetonitrile containing $Et_4N^+ClO_4^-$ (0.1 M) as the supporting electrolyte. Solutions were

 © 2004 Wiley-VCH Verlag GmbH & Co. KGaA, Weinheim

deoxygenated by bubbling dinitrogen for about 20 min before each experiment. The platinum wire working and auxiliary electrodes, and an aqueous saturated calomel reference electrode were used in a three-electrode configuration.

X-ray Crystallography: Suitable crystals for X-ray crystallographic studies for the complexes **1**−**3** were obtained from CH_2Cl_2/petroleum ether (60−80°C) at room temperature over a period of 3 d. All the pertinent crystallographic data are recorded in Table 3. Intensity data were collected at 293(2) K with an Enraf−Nonius CAD 4 diffractometer using graphite-monochromated Mo-K_α radiation (λ = 0.70930) from plate-like crystals with dimensions 0.22 × 0.22 × 0.17 (**1**), 0.4 × 0.35 × 0.35 (**2**) and 0.25 × 0.35 × 0.41 mm (**3**) in the ω-2θ scan mode in the range from 1.51 to 24.92°. Intensities of these reflections were measured periodically to monitor crystal decay. The structures were solved by direct methods and refined by full-matrix least squares on F^2 (SHELX-97).[10] In the final cycles of refinement all the non-H atoms were treated anisotropically. The contribution due to H atoms attached to carbon atoms was included as a fixed contribution. Final residual values and goodness-of-fit were $R1$ = 0.0405, $wR2$ = 0.1132, GOF = 1.104 (**1**), $R1$ = 0.0343, $wR2$ = 0.0803, GOF = 1.063 (**2**) and $R1$ = 0.0673, $wR2$ = 0.1968, GOF = 1.066 (**3**). CCDC-229719 (**1**), -229720 (**2**) and -233890 (**3**) contain the supplementary crystallographic data for this paper. These data can be obtained free of charge at www.ccdc.cam.ac.uk/conts/retrieving.html [or from the Cambridge Crystallographic Data Centre, 12 Union Road, Cambridge CB2 1EZ, UK; Fax: (internat.) + 44-1223-336-033; E-mail: deposit@ccdc.cam.ac.uk].

DNA Binding and Cleavage Studies

DNA Topoisomerase II Estimation: For activity measurements, the reaction was carried out (10 μL) in a mixture containing buffer B, 10 mM $MgCl_2$, 1 mM ATP, 0.1 mM EDTA, 0.5 mM DTT, 30 μg/mL BSA and enzyme protein. The reaction was started by incubation at 37 °C for 30 min and stopped by addition of 5 μL of loading dye. The samples were electrophoresed on 1% agarose gel in tris-acetate buffer at 20 V for 18 h. Gels were stained with ethidium bromide (0.5 μg/mL) visualized and photographed on a UVP GDS 7500 UV trans-illuminator. The percentage relaxation was measured by micro densitometry of gel using the Gel base/Gel blot Pro Gel analysis software programme. ^{1}H-NMR and UV/Vis spectral analyses were used to check the stability of the complexes towards the solvent (water and DMSO) and no change was observed. Buffer A (5 mM Tris-HCl, pH = 7.1, 50 mM NaCl) was used for absorption titration and buffer B (50 mM tris-HCl, pH = 7.5, 50 mM KCl) was used for inhibition studies.

Preparation of $[Ru(\kappa^3\text{-tptz})(PPh_3)_2]Cl]BF_4\cdot H_2O$ (1): Complex **1** was prepared by either of the following two methods.

Method (a): Hydrated ruthenium trichloride $RuCl_3\cdot xH_2O$ (0.260 g, 1.0 mmol), dissolved in hot methanol (10 mL), was added to a refluxing solution of triphenylphosphane (PPh_3; 1.578 g, 6.0 mmol) in methanol (50 mL) and the solution was heated under reflux for 1 h. Ligand tptz (0.312 g, 1.0 mmol) was added to the resulting suspension and the contents of the flask were heated under reflux for 8−10 h. After the resulting purple solution was cooled to room temperature, any solid residue was filtered and the filtrate was concentrated under reduced pressure to one fourth of its volume. A saturated solution of ammonium tetrafluoroborate, dissolved in methanol, was added to the concentrated solution and the mixture left for slow crystallization in a refrigerator at 8 °C. The microcrystalline product, which slowly deposited, was separated by filtration and washed repeatedly with methanol and diethyl ether and then dried in vacuo. Yield 73% (0.786 g). $C_{54}H_{44}BClF_4N_6OP_2Ru$ (1078.3): calcd. C 60.11, H 4.08, N 7.79; found C 60.08, H 4.12, N 7.74. FAB-MS: *m/z* obsd. (calcd.), rel. int., [assignm.]: 973 (973), 29, $[Ru(\kappa^3\text{-tptz})(PPh_3)_2Cl]^+$; 711 (711), 69, $[Ru(\kappa^3\text{-tptz})(PPh_3)Cl]^+$; 675 (675), 25, $[Ru(\kappa^3\text{-tptz})(PPh_3)]^{+2}$; 413 (414), 12, $[Ru(\kappa^3\text{-tptz})]^{+2}$. ^{1}H NMR: δ = 9.12 (d, J = 4.80 Hz, 2 H), 8.92 (d, J = 3.00 Hz), 1 H, 8.74 (d, J = 7.8 Hz, 1 H), 8.57 (d, J = 6.5 Hz, 1 H), 8.12 (t,

Table 3. Crystal data for complexes **1**−**3**

	1	**2**	**3**
Empirical formula	$C_{54}H_{44}BClF_4N_6OP_2Ru$	$C_{54}H_{44}As_2BClF_4N_6ORu$	$C_{41}H_{43}ClN_7O_{2.50}PRuS_2$
Formula mass	1078.22	1166.12	905.43
Color and habit	purple-black block	violet-black block	black plate
Crystal size [mm]	0.22 × 0.22 × 0.17	0.4 × 0.35 × 0.35	0.25 × 0.35 × 0.41
Space group	$P2_1/c$	$P2_1/c$	$F2dd$
System	monoclinic	monoclinic	orthorhombic
Unit cell dimensions			
a [Å]	12.338(3)	12.439(8)	13.9940(13)
b [Å]	24.823(5)	25.127(3)	30.5770(19)
c [Å]	16.291(4)	16.399(13)	40.295(3)
β [Å]	101.16(2)	101.27	90.00
V [Å^3]	2532.4(4)	3753.0(12)	17242(2)
Z	4	4	16
$d_{calcd.}$ [mg/m^3]	1.463	1.541	1.395
μ [mm^{-1}]	0.502	1.732	0.604
Temperature [K]	293(2)	293(2)	293(2)
No.of reflections	7469	7220	3157
No. of refined parameters	639	807	505
R factor all	0.0515	0.0496	0.0907
R factor [$I > 2\sigma(I)$]	0.0405	0.0343	0.0673
$wR2$	0.1132	0.0803	0.1968
$wR2$ [$I > 2\sigma(I)$]	0.1045	0.0727	0.1716
Goodness of fit	1.104	1.063	1.066

 © 2004 Wiley-VCH Verlag GmbH & Co. KGaA, Weinheim

J = 7.5 Hz, 2 H), 8.00 (t, J = 7.8 Hz, 2 H), 7.58 (t, J = 5.1 Hz, 1 H), 7.38 (t, J = 6.3 Hz, 2 H) and 7.26−7.07 (br. m, aromatic protons of PPh_3) ppm. $^{31}P\{^1H\}$ NMR: δ = 16.24 (s) ppm. UV/Vis: λ_{max} (ε [dm^3 $mol^{-1}cm^{-1}$]) = 472 (24022), 309(63759), 273 (149195) nm.

Method (b): A suspension of $[RuCl_2(PPh_3)]$ (0.982 g, 1.0 mmol) in methanol (50 mL) was treated with tptz (0.312 g, 1.0 mmol) and the resulting solution was heated under reflux for 8.0 h resulting in a purple solution. After cooling to room temperature, the resulting solution was filtered through Celite to remove any solid impurities. A saturated solution of ammonium tetrafluoroborate, dissolved in methanol, was added to the filtrate and it was left in the refrigerator for slow crystallization. After several days, a purple-black crystalline product had separated. Analytical and spectroscopic data were identical to those of the previous method but the yield was higher.

Preparation of $[Ru(\kappa^3\text{-tptz})(AsPh_3)_2Cl]BF_4\cdot H_2O$ (2): This complex was prepared by a similar method (complex **1**) except that $AsPh_3$ (1.836 g, 6.0 mmol) was used in place of PPh_3. A violet-black complex was obtained. Yield 71% (0.827 g). $C_{54}H_{44}As_2BClF_4N_6ORu$ (1166.1): calcd. C 55.57, H 3.77, N 7.20; found C 55.62, H 3.68, N 7.12. FAB-MS: *m*/*z* obsd. (calcd.), rel. int., [assignm.]: 1061 (1061), 19, $[Ru(\kappa^3\text{-tptz})(AsPh_3)_2Cl]^+$; 755 (755), 54, $[Ru(\kappa^3\text{-tptz})(AsPh_3)Cl]^+$; 449 (449), 35, $Ru(\kappa^3\text{-tptz})Cl]^+$. ^1H NMR: δ = 9.26 (d, J = 5.1 Hz, 2 H), 8.93 (d, J = 3.6 Hz, 1 H), 8.69 (d,, J = 8.1 Hz 1 H), 8.65 (d, J = 7.8 Hz, 1 H), 8.11 (m, J = 7.5 Hz, 4 H), 7.59 (t, J = 5.1 Hz, 1 H), 7.51 (t, J = 6.3 Hz, 2 H) and 7.23−7.03 (br. m, aromatic protons of $AsPh_3$) ppm. UV/Vis: λ_{max} (ε [dm^3 $mol^{-1}cm^{-1}$]) = 489 (6930), 342 (7250), 271.5 (21355) nm.

Preparation of $[Ru(\kappa^3\text{-tptz})(PPh_3)(dtc)]Cl$ (3): Complex **3** was prepared by the reaction of $[Ru(\kappa^3\text{-tptz})(PPh_3)_2Cl]Cl$ (0.501 g, 0.5 mmol) with sodium diethyldithiocarbamate (0.112 g, 0.5 mmol) in methanol in the same way as Method (b) for complex **1**. Yield 75% (0.322 g). $C_{41}H_{37}ClN_7PRuS_2$ (859.4): calcd. C 57.24, H 4.30, N 11.40; found C 57.46, H 4.17, N 11.21. FAB-MS: *m*/*z* obsd. (calcd.), rel. int., [assignm.]: 824 (823), 100, $[Ru(\kappa^3\text{-tptz})(PPh_3)dtc]^+$; 561 (562), 94, $[Ru(\kappa^3\text{-tptz})(dtc)]^+$; 414 (413), 38, $[Ru(\kappa^3\text{-tptz})]^{+2}$. ^1H NMR: δ = 9.00 (d, J = 5.4 Hz, 2 H), 8.94 (d, J = 3.9 Hz, 1 H), 8.80 (d, J = 7.8 Hz, 1 H), 8.73 (t, J = 7.5 Hz, 2 H), 8.09 (m), 7.77 (t, J = 6 Hz, 2 H) 7.60 (t, J = 2.7 Hz, 1 H) 7.16 (m), 7.003 (t, J = 7.5 Hz, 6 H), 4.10 (q, J = 7.2 Hz, 2 H), 3.62 (q, J = 6.9 Hz, 2 H), 1.52 (t, J = 7.2 Hz, 3 H), 1.13 (t, J = 6 Hz, 3 H) ppm. $^{31}P\{^1H\}$ NMR: δ = 37.81 (s) ppm. UV/Vis: λ_{max} (ε [dm^3 $mol^{-1}cm^{-1}$]) = 245 (60488), 289 (49367), 387 (16805), 485 (13173) nm.

Preparation of $[Ru(\kappa^3\text{-tptz})(PPh_3)(CN)_2]$ (4): Complex **4** was prepared by the reaction of $[Ru(\kappa^3\text{-tptz})(PPh_3)_2(Cl)]BF_4$ (0.539 g, 0.5 mmol) with a slight excess of sodium cyanide according to the procedure of Method (b) for complex **1**. Yield 63% (0.229 g). $C_{38}H_{27}N_8PRu$ (727.7): calcd. C 62.72, H 3.71, N 15.40; found C 62.69, H 3.65, N 15.38. FAB-MS: *m*/*z* obsd. (calcdd), rel. int., [assignm.]: 701 (702), 31, $[Ru(\kappa^3\text{-tptz})(PPh_3)(CN)]^+$; 675 (676), 33, $[Ru(\kappa^3\text{-tptz})(PPh_3)]^{2+}$; 413 (414), 35, $Ru(\kappa^3\text{-tptz})]^{2+}$. ^1H NMR: δ = 9.04 (d, J = 3.0 Hz, 1 H), 8.92 (d, J = 3.9 Hz, 1 H), 8.71 (d, J = 7.5 Hz, 1 H), 8.63 (t, J = 7.5 Hz, 1 H), 8.16 (m, 4 H), 7.75 (m, 2 H), 7.22 (m), 7.09 (t, J = 5 Hz, 1 H) ppm. $^{31}P\{^1H\}$ NMR: δ = 32.89 (s) ppm. UV/Vis: λ_{max} (ε [dm^3 $mol^{-1}cm^{-1}$]) = 233 (31663), 247 (35003), 372 (1489), 522 (1722) nm.

Preparation of $[Ru(\kappa^3\text{-tptz})(AsPh_3)(dtc)]BF_4$ (5): Complex **5** was prepared by the reaction of $[Ru(\kappa^3\text{-tptz})(AsPh_3)_2(Cl)]BF_4$ (0.583 g, 0.5 mmol) with sodium diethyldithiocarbamate (0.112 g, 0.5 mmol) in methanol according to the procedure for complex **2**. Yield 70% (0.334 g). $C_{41}H_{38}AsBF_4N_7Ru$ (891.6): calcd. C 51.51, H 3.97, N 10.26; found C 59.20, H 3.49, N 14.53. FAB- MS: *m*/*z* obsd. (calcd.), rel. int., [assignm.]: 868 (867), 60, $[Ru(\kappa^3\text{-tptz})(AsPh_3)(dtc)]^+$; 562 (561), 100, $[Ru(\kappa^3\text{-tptz})(dtc)]^+$; 413 (414), 36, $Ru(\kappa^3\text{-tptz})]^{2+}$. ^1H NMR: δ = 9.26 (d, J = 5.1 Hz, 1 H), 9.05 (d, J = 5.4 Hz, 2 H), 8.94 (t, J = 4.2 Hz, 1 H), 8.80 (dd, J = 5.4 Hz, 3 H), 8.66 (d), 8.09 (t, J = 7.8 Hz, 4 H) 7.79 (t, J = 6.3 Hz, 2 H) 7.58 (m), 7.17 (m), 6.83 (d, J = 7.1 Hz, 3 H), 4.10 (q, J = 7.2 Hz, 2 H), 3.55 (q, J = 7.2 Hz, 2 H), 1.50 (t, J = 7.2 Hz, 3 H), 1.10 (t, J = 6.1 Hz, 3 H) ppm. UV/Vis: λ_{max} (ε [dm^3 $mol^{-1}cm^{-1}$]) = 229 (11600), 277 (11500), 343 (2500), 493 (2100) nm.

Preparation of $[Ru(\kappa^3\text{-tptz})(AsPh_3)(CN)_2]$ (6): Complex **6** was prepared by the reaction of $[Ru(\kappa^3\text{-tptz})(AsPh_3)_2(Cl)]BF_4$ (0.583 g, 0.5 mmol) with a slight excess of sodium cyanide according to the procedure for complex **2**. Yield 62% (0.239 g). $C_{38}H_{27}AsN_8Ru$ (771.7): calcd. C 59.14, H 3.50, N 14.52; found C 59.20, H 3.49, N 14.53. FAB-MS: *m*/*z* obsd. (calcd.), rel. int., [assignm.]: 745 (745), 43, $[Ru(\kappa^3\text{-tptz})(AsPh_3)(CN)]^+$; 719 (720), 35, $[Ru(\kappa^3\text{-tptz})(AsPh_3)]^{2+}$; 413 (414), 41, $[Ru(\kappa^3\text{-tptz})]^{2+}$. ^1H NMR: δ = 9.21 (d, J = 4.6 Hz, 2 H), 9.05 (d, J = 3.9 Hz, 1 H), 8.79 (d, J = 6.5 Hz, 1 H), 8.43 (t, J = 7.5 Hz, 2 H), 8.25 (m, 4 H), 7.86 (m, 2 H), 7.27 (m), 7.13 (t, J = 5.3 Hz, 2 H) ppm. UV/Vis: λ_{max} (ε [dm^3 $mol^{-1}cm^{-1}$]) = 231 (12786), 320 (11607), 504 (1982) nm.

Acknowledgments

Thanks are due to the Department of Science and Technology, Ministry of Science and Technology, New Delhi for providing financial assistance [SP/S1/F-04/2000] and the National Single Crystal X-ray Diffraction Laboratory, Indian Institute of Technology, Mumbai, for providing single-crystal X-ray data.

[1] [1a] J.-M. Lehn, *Supramolecular Chemistry*, VCH, Weinheim, **1995**. [1b]E. Amouyal, *Sol. Energy Matter. Sol. Cells* **1995**, *38*, 249. [1c] V. Balzani, P. Ceroni, A. Juris, M. Venturi, F. Puntariero, S. Campagna, S. Serroni, *Coord. Chem. Rev.* **2001**, *545*, 219. [1d] A. Beyeler, P. Belser, *Coord. Chem. Rev.* **2002**, *230*, 29. [1e] S. Campagna, P. D. Pietro, F. Loiseau, B. Maubert, N. McClenaghan, R. Passalacqua, F. Puntoriero, V. Ricevuto, S. Serroni, *Coord. Chem. Rev.* **2002**, *229*, 67.

[2] [2a] K. D. Demadis, C. M. Hartshorn, T. J. Meyer, *Chem. Rev.* **2001**, *101*, 2655. [2b] B. S. Brunschwig, C. Creutz, N. Sutin, *Chem. Soc. Rev.* **2002**, *31*, 168.

[3] [3a] N. H. Dam-Rauer, G. Cerullo, A. Yeh, T. R. Boussie, C. V. Shank, J. K. McCusker, *Science* **1997**, *275*, 54. [3b] F. L. Carter, R. E. Siatkowski, *Molecular Electronics Devices* (Ed.: H. Wohltjn), North Holland, Amsterdam, The Netherlands, **1998**.

[4] [4a] F. Bargiletti, L. Flamigni, *Chem. Soc. Rev.* **2000**, *29*, 1. [4b] S. S. Sun, A. J. Lees, *Inorg. Chem.* **2001**, *41*, 3154. [4c] K. Chichak, U. Jacquremard, N. R. Branda, *Eur. J. Inorg. Chem.* **2002**, 357. [4d] T. Steiner, *Angew. Chem. Int. Ed.* **2002**, *41*, 48 and refrences therein.

[5] [5a] N. Gupta, N. Grover, G. A. Neyhart, P. Singh, H. H. Thorp, *Inorg. Chem.* **1993**, *32*, 310. [5b] K. E. Erkkila, D. T. Odom, J. K. Barton, *Chem. Rev.* **1999**, *29*, 2777. [5c] J. Kelly, A. Tossi, D. McConnel, C. Ohuigin, *Nucleic Acids Res.* **1985**, *13*, 6017. [5d] A. Ambroise, B. G. Maiya, *Inorg. Chem.* **2000**, *39*, 4264.

[6] [6a] S. W. Keller, S. A. Johnson, E. S. Brigham, E. T. Yonemoto, T. E. Mallouk, *J. Am. Chem. Soc.* **1995**, *117*, 12879. [6b] B. E. Buchanan, R. Wang, G.V. Johannes, R. Hage, J. G. Hassnoot, J. Reedijk, *Inorg. Chem.* **1995**, *34*, 3358. [6c] E. Brauns, W. Sumner, J. A. Clark, S. M. Molnar, Y. Kawanishi, K. J. Brewer, *Inorg. Chem.* **1997**, *36*, 2861. [6d] J. -D. Lee, L. M. Vrana, E. R. Bullock, K.J. Brewer, *Inorg. Chem.* **1998**, *37*, 3575. [6e] C. Ceroni, F. Paolucci, S. Roffia, S. Serroni, S. Campagna, A. J.

 © 2004 Wiley-VCH Verlag GmbH & Co. KGaA, Weinheim

Bard, *Inorg. Chem.* **1998**, *37*, 2829. [6f] D. J. Chesnut, A. Kusnetzow, R. R. Birgeard, J. Zubieta, *Inorg. Chem.* **1999**, *38*, 2663. [6g] G. Albano, P. Belser, C. Dual, *Inorg. Chem.* **2001**, *40*, 1408. [6h] C. Metcalfe, S. Spey, H. Adams, J. A. Thomas, *J. Chem. Soc., Dalton Trans.* **2002**, 4732.

[7] [7a] A. Singh, A. N. Sahay, D. S. Pandey, M. C. Puerta, P. Valerga, *J. Organomet. Chem.* **2000**, *613*, 250. [7b] A. N. Sahay, D. S. Pandey, M. G. Walwalkar, *J. Organomet. Chem.* **2000**, *605*, 74. [7c] A. Singh, N. Singh, D. S. Pandey, *J. Organomet. Chem.* **2002**, *642*, 48. [7d] M. Chandra, A. N. Sahay, S. M. Mobin, D. S. Pandey, *J. Organomet. Chem.* **2002**, *658*, 43−49.

[8] B. P. Sullivan, D. J. Salmon, T. J. Meyer, *Inorg. Chem.* **1978**, *17*, 3334.

[9] [9a] S. Mackay, W. Dong, C. Edwards, A. Henderson, C. Gilmox, N. Stewart, K. Shankland, A. Donald, University of Glasgow, Scotland, **1999**. [9b] G. M. Sheldrick, *SHELXS-97: Program for structure solution and refinement of crystal structures*, University of Göttingen, Germany, **1997**. [9c] G. M. Sheldrick, *SHELXL-97: Program for structure refinement*, University of Göttingen, Germany, **1997**. [9d] C. K. Johnson, *ORTEP III*, Report ORNL-5138, Oak Ridge National Laboratory, Oak Ridge, TN, **1976**. [9e]*PLATON:* A. L. Spek, *Acta Crystallogr., Sect. A* **1990**, *46*, C31.

[10] [10a] P. Paul, B. Tyagi, A. K. Bilakhia, D. Parthsarthi, E. Suresh, *Inorg. Chem.* **2000**, *39*, 14 and references cited therein. [10b] M. Chandra, A. N. Sahay, D. S. Pandey, M. C. Puerta, P. Valerga, *J. Organomet. Chem.* **2002**, *648*, 39.

[11] [11a] M. R. Churchill, K. M. Keil, F. V. Bright, S. Pandey, G. A. Baker, J. B. Keister, *Inorg. Chem.* **2000**, *39*, 5807. [11b] P. Ghosh, A. Chakravorty, *Inorg. Chem.* **1997**, *36*, 64. [11c] H. Sugimoto, K. Tsuge, K. Tanaka, *J. Chem. Soc., Dalton Trans.* **2001**, 57.

[12] [12a] M. I. Bruce, F. S. Wong, B. W. Skelton, A. H. White, *J. Chem. Soc., Dalton Trans.* **1981**, 1398. [12b] R. O. Gould, C. L. Jones, R. D. Robertson, T. A. Stephenson, *J. Chem. Soc., Dalton Trans.* **1981**, 129. [12c] T. Hayashida, H. Nagashima, *Organometallics* **2002**, *21*, 3884. [12d] H. Nishiyama, M. Konno, K. Aoki, H. M. L. Davies, M. L. Huw, *Organometallics* **2002**, *21*, 2536.

[13] [13a] E. A. Meyer, R. K. Castellano, F. Diederich, *Angew. Chem. Int. Ed.* **2003**, *11*, 42. [13b] D. Braga, P. J. Dyson, F. Grepioni, B. F. G. Johnson, *Chem. Rev.* **1994**, *94*, 1585.

[14] [14a] J. K. Barton, *Science* **1986**, *233*, 727. [14b] J. K. Barton, J. J. Dannesberg, A. L. Raphael, *J. Am. Chem. Soc.* **1982**, *104*, 4967. [14c] J. K. Barton, A. T. Danishefsky, J. M. Goldberg, *J. Am. Chem. Soc.* **1984**, *106*, 2172.

[15] The concentration of CT DNA was determined spectroscopically by using the molar extinction coefficient $\varepsilon(\lambda = 260\ nm) = 6600\ M^{-1}\cdot cm^{-1}$. [15a] M. E. Reichmann, S. A. Rice, C. A. Thomas, P. Doty, *J. Am. Chem. Soc.* **1954**, *76*, 3074. Solutions of DNA in an appropriate buffer A gave a ratio of UV absorption at 260 and 280 nm of $A_{260/280} \approx 1.8-1.9$, indicating that the DNA was sufficiently free of protein. [15b] J. Marmur, *J. Mol. Biol.* **1961**, *3*, 208.

[16] [16a] M. T. Carter, M. Rodriguez, A. J. Bard, *J. Am. Chem. Soc.* **1989**, *111*, 8901. [16b] S. R. Smith, G. A. Neyhart, W. A. Kalsbeck, H. H. Thorp, *New J. Chem.* **1994**, *18*, 397.

[17] Setting the value of $s > 1$ makes our fit unusual. It is consistent with other reports and suggests that it may be due to stacking of intercalculator molecules on the DNA surface. [17a] A. M. Pyle, J. P. Rehmann, R. Meshoyrer, C. V. Kumar, N. J. Turro, J. K. Barton, *J. Am. Chem. Soc.* **1989**, *111*, 3051. [17b] R. B. Nair, E. S. Teng, S. L. Kirkland, C. J. Murphy, *Inorg. Chem.* **1998**, *37*, 139. [17c] J.-G. Liu, Q.-L. Zhang, X.-F. Shi, L.-N. Ji, *Inorg. Chem.* **2001**, *40*, 5045. [17d] A. Frodl, D. Herebian, W. S. Sheldrick, *J. Chem. Soc., Dalton Trans.* **2002**, 3664.

[18] J. C. Wang, *J. Biol. Chem.* **1991**, *266*, 6659.

[19] D. D. Perrin, W. L. F. Armango, D. R. Perrin, *Purification of Laboratory Chemicals*, Pergamon, Oxford, U. K., **1986**.

[20] [20a] U. Pandya, J. K. Saxena, S. M. Kaul, P. K. Murthy, R. K. Chatterjee, R. P. Tripathi, A. P. Bhaduri, O. P. Shukla, *Med. Sci. Res.* **1999**, *27*, 103−106. [20b] R. P. Tripathi, S. K. Rastogi, B. Kundu, J. K. Saxena, V. J. M. Reddy, S. Shrivastav, S. Chandra, A. P. Bhaduri, *Comb. Chem. High Throughput Screening* **2001**, *4*, 237.

[21] P. S. Hallman, T. A. Stephenson, G. Wilkinson, *Inorg. Synth.* **1970**, *12*, 238.

Received January 28. 2004
Early View Article
Published Online July 7, 2004

 © 2004 Wiley-VCH Verlag GmbH & Co. KGaA, Weinheim

Polynuclear Rhenium and Manganese Selenido-Carbonyl Complexes − Reversible Square to Butterfly Conversion of the Re_4Se_2 Core by CO Loss in $[Re_4(\mu_3\text{-}Se)_2(CO)_{16}(PPh_3)_2]$, and the Crystal Structure of $[Mn_2(\mu_2\text{-}Se_2)(CO)_5(PPh_3)_2]$

Daniele Belletti,[a] Claudia Graiff,[a] Roberto Pattacini,*[a] Giovanni Predieri,[a] and Antonio Tiripicchio[a]

Keywords: Cluster compounds / Manganese / Rhenium / Selenium

The reaction of Ph_3PSe with $[Mn_2(CO)_{10}]$ leads to the formation of $[Mn_4(\mu_3\text{-}Se)_2(\mu\text{-}CO)(CO)_{14}(PPh_3)_2]$, which contains a butterfly "Mn_2Se_2 core", along with traces of $[Mn_2(\mu_2\text{-}Se_2)(CO)_5(PPh_3)_2]$ (**1**), which contains a tetrahedral Mn_2Se_2 core. The reaction of Ph_3PSe with $[Re_2(CO)_8(NCMe)_2]$ affords two new complexes, $[Re_4(\mu_3\text{-}Se)_2(CO)_{16}(PPh_3)_2]$ (**2**) and $[Re_4(\mu_3\text{-}Se)_2(\mu\text{-}CO)(CO)_{14}(PPh_3)_2]$ (**3**). Their molecular structures, determined by X-ray diffraction methods, exhibit a nearly square-planar Re_2Se_2 and a butterfly Re_2Se_2 core, respectively. These air-stable tetrarhenium selenido-carbonyl species display a reversible loss/addition of a CO molecule, which is accompanied by the formation/cleavage of a Re–Re bond and the consequent rearrangement of the Re_2Se_2 core, from square to butterfly and vice versa.
(© Wiley-VCH Verlag GmbH & Co. KGaA, 69451 Weinheim, Germany, 2004)

Introduction

The chemistry of polynuclear transition-metal chalcogenide complexes is a continuously expanding research area, as pointed out in recent reviews.[1] Apart from their fundamental significance as a class of complexes with peculiar chemical and structural properties, the growing interest in these species stems from their potential applications as catalysts, electrocatalysts and precursors for semiconductors.[2] The presence of chalcogenide ligands often appears decisive in facilitating cluster-growth reactions,[3] and in this regard sulfur atoms have been shown to be highly effective,[4] as are selenium and tellurium atoms, although these have been much less studied.[2a,5,6]In this context, systematic investigations carried out by our group on the reactivity of tertiary phosphane and diphosphane selenides towards $[M_3(CO)_{12}]$ (M = Fe or Ru) have shown that these reactions provide simple, sometimes selective, synthetic routes to phosphane-substituted, selenido-carbonyl metal clusters.[6]

In recent years Adams and co-workers have described the reaction between thiirane and $[Mn_2(CO)_9(MeCN)]$, which gives the simplest sulfido-carbonyl manganese cluster $[Mn_2S_2(CO)_7]$ whose reactivity towards different metal fragments has been widely investigated.[7a,7c−7g] Moreover, the synthesis of the dimetallic selenido-carbonyl Mo−Mn complex $[CpMoMn(CO)_5(\mu\text{-}S_2)]$ has been achieved by treating $[CpMnMo(CO)_8]$ with elemental selenium.[7b,7h,7i]

Manganese clusters and complexes bearing selenide ligands have been scarcely investigated.[7a,7b] In particular, in the syntheses reported in the literature polyselenide anions,[8] diorganyl diselenides[9] and elemental selenium[10] have been used as starting materials.

Recently,[11] we have reacted different phosphane selenides with three manganese carbonyl complexes, namely $[Cp'Mn(CO)_2(THF)]$, $[CpMn(CO)_2(THF)]$ (Cp = η^5-C_5H_5, Cp′ = η^5-C_5H_4Me, THF = tetrahydrofuran) and $[Mn_2(CO)_8(NCMe)_2]$ in order to produce new phosphane-substituted selenido-carbonyl manganese derivatives. In particular, the reactions of tertiary phosphanes R_3PSe with $[Mn_2(CO)_8(NCMe)_2]$ in an equimolar ratio resulted in the formation of the bis-selenido tetramanganese clusters $[Mn_4(\mu_3\text{-}Se)_2(\mu\text{-}CO)(CO)_{14}(PR_3)_2]$, the structures of two of which, $[Mn_4(\mu_3\text{-}Se)_2(\mu\text{-}CO)(CO)_{14}(PPh_3)_2]$[7a] and $[Mn_4(\mu_3\text{-}Se)_2(\mu\text{-}CO)(CO)_{14}(PMePh_2)_2]$,[11] having been determined by X-ray diffraction methods.

In this paper, the synthesis and crystal-structure characterization of the first tetrahedral Mn_2Se_2 carbonyl complex, $[Mn_2(\mu_2\text{-}Se_2)(CO)_5(PPh_3)_2]$, obtained by reacting two equivalents of phosphane selenide with $[Mn_2(CO)_{10}]$ in the presence of Me_3NO is described. Moreover, the reaction of Ph_3PSe with the analogous Re carbonyl derivative $[Re_2(CO)_8(NCMe)_2]$ yielded two new tetrarhenium selenido-carbonyl compounds, namely $[Re_4(\mu_3\text{-}Se)_2(CO)_{16}(PPh_3)_2]$ and $[Re_4(\mu_3\text{-}Se)_2(\mu\text{-}CO)(CO)_{14}(PPh_3)_2]$, whose crystal structures were determined by X-ray diffraction methods. These com-

[a] Dipartimento di Chimica Generale e Inorganica, Chimica Analitica, Chimica Fisica, Università di Parma,
Parco Area delle Scienze 17/A, 43100 Parma, Italy
E-mail: rpatacci@nemo.unipr.it

 © 2004 Wiley-VCH Verlag GmbH & Co. KGaA, Weinheim **DOI: 10.1002/ejic.200400090**

pounds show interesting reversible loss/addition of a CO molecule together with the formation/cleavage of a Re−Re bond and the consequent rearrangement of the Re_4Se_2 core.

Results and Discussion

Reaction of $Mn_2(CO)_{10}$ with Ph_3PSe; Crystal Structure of $[Mn_2(\mu_2\text{-}Se_2)(CO)_5(PPh_3)_2]$ (1)

The availability of sulfur-containing starting compounds such as thiirane allows for the efficient synthesis of the simplest tetrahedral Mn_2S_2 complex $[Mn_2(\mu_2\text{-}S_2)(CO)_7]$.[7c] However, the absence of analogous selenium compounds does not permit the easy synthesis of compounds containing an $Mn_2(\mu_2\text{-}Se_2)$ core. As has already been described,[11] the reaction of equimolar amounts of $[Mn_2(CO)_8(CH_3CN)_2]$ and Ph_2MePSe at 50 °C gives $[Mn_4(\mu_3\text{-}Se)_2(\mu\text{-}CO)(CO)_{14}(PMePh_2)_2]$ as the unique product (80% yield). The same compound is also obtained when $Mn_2(CO)_{10}$ is treated with Ph_3PSe in a 1:2 molar ratio and in the presence of Me_3NO. In this case, however, the yield of the $[Mn_4(\mu_3\text{-}Se)_2(\mu\text{-}CO)(CO)_{14}(PMePh_2)_2]$ cluster decreases to 70% while another complex, namely $[Mn_2(\mu_2\text{-}Se_2)(CO)_5(PPh_3)_2]$ (**1**), is also formed. Although only traces of compound **1** were isolated, suitable crystals for X-ray analysis were obtained.

The $^{31}P\{^1H\}$ NMR spectrum of **1** recorded at room temperature shows a broad peak at δ = 13.6 ppm, indicating the equivalence of the two phosphane ligands in solution. In addition, in the carbonyl region of the IR spectrum recorded in the solid state, a band at 1789 cm^{-1} is observed and attributed to a bridging carbonyl group. An ORTEP view of compound **1** is shown in Figure 1, together with the atom numbering scheme; selected bond lengths and angles are listed in Table 1.

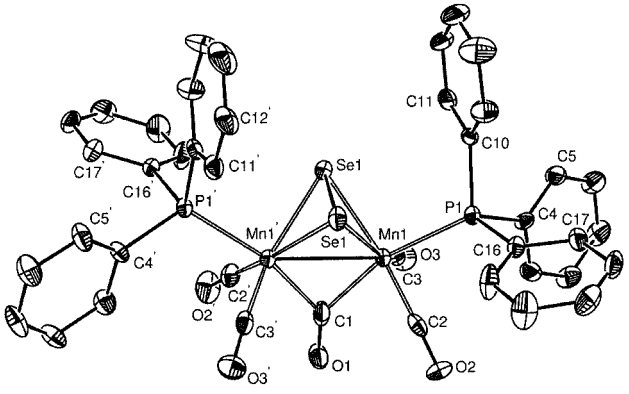

Figure 1. View (ORTEP, 30% probability level) of the molecular structure of **1** with the atom numbering scheme.

Complex **1** has a crystallographically imposed C_2 symmetry, with the twofold axis passing through the C1 and O1 atoms and the midpoints of the Mn1−Mn1′ and Se1−Se1′ bonds. The structure of this compound is very similar to that of the phosphane-unsubstituted and -monosubstituted sulfur derivatives $[Mn_2(\mu_2\text{-}S_2)(CO)_{7-n}(PPh_3)_n]$ (n = 0, 1)[7c,7d,7f] and the iron diselenide compounds $[Fe_2(\mu_2\text{-}Se_2)(CO)_{6-n}(PPh_3)_n]$ (n = 1, 2).[12] The complex possesses a tetrahedral Mn_2Se_2 core in which the Mn−Mn bond length is 2.702(2) Å, slightly longer than that observed in the sulfur derivatives [2.6745(5) and 2.6747(5) Å for n = 0 and n = 1, respectively]. The Se−Se bond length [2.311(2) Å] is in good agreement with those observed in $[Fe_2(\mu_2\text{-}Se_2)(CO)_{6-n}(PPh_3)_n]$ [2.297(2) and 2.296(1) Å for n = 1 and n = 2, respectively]. Moreover, each manganese atom is coordinated by two terminal carbonyls and by a posphane molecule [P1−Mn1 = 2.308(2) Å], while a CO group symmetrically bridges the Mn−Mn edge, with an Mn−C1 bond length of 2.01(1) Å.

Table 1. Selected bond lengths (Å) and angles (°) for **1**[a]

Mn(1)−Se(1′)[a]	2.4461(13)	Mn(1)−Se(1)	2.4478(13)
Mn(1)−Mn(1′)	2.702(2)	Se(1)−Se(1′)	2.3105(16)
Mn(1)−P(1)	2.308(2)		
P(1)−Mn(1)−Se(1′)	98.46(7)	P(1)−Mn(1)−Se(1)	92.99(7)
Se(1′)−Mn(1)−Se(1)	56.34(4)	P(1)−Mn(1)−Mn(1′)	147.28(6)
Se(1′)−Mn(1)−Mn(1)	56.52(3)	Se(1)−Mn(1)−Mn(1′)	56.46(3)
Se(1′)−Se(1)−Mn(1)	61.87(3)	Se(1′)−Se(1)−Mn(1)	61.79(4)
Mn(1′)−Se(1)−Mn(1)	67.02(5)		

[a] Symmetry transformations used to generate equivalent atoms: $-x, y, -z + 1/2$.

Reaction of $[Re_2(CO)_8(CH_3CN)_2]$ with Ph_3PSe; Crystal Structures of $[Re_4(\mu_3\text{-}Se)_2(CO)_{16}(PPh_3)_2]$ (2) and $[Re_4(\mu_3\text{-}Se)_2(\mu\text{-}CO)(CO)_{14}(PPh_3)_2]$ (3)

The reaction of $[Re_2(CO)_8(CH_3CN)_2]$ with Ph_3PSe, carried out under the same experimental conditions used for the synthesis of $[Mn_4(\mu_3\text{-}Se)_2(\mu\text{-}CO)(CO)_{14}(PMePh_2)_2]$,[11] led to the formation of two new tetrarhenium diselenide phosphane-substituted carbonyl compounds, namely $[Re_4(\mu_3\text{-}Se)_2(CO)_{16}(PPh_3)_2]$ (**2**) and $[Re_4(\mu_3\text{-}Se)_2(\mu\text{-}CO)(CO)_{14}(PPh_3)_2]$ (**3**), whose structures were determined by X-ray diffraction methods.

ORTEP views of compounds **2** and **3** are shown in Figures 2 and 3, respectively, together with the atom numbering scheme; selected bond lengths and angles are listed in Tables 2 and 3.

Complex **2** displays a nearly planar Re_4Se_2 core [the dihedral angle between the Re1Re2Se1 and Re1Re2Se planes is 21.7° and the non-bonding Re1···Re2 and Se1···Se2 separ-

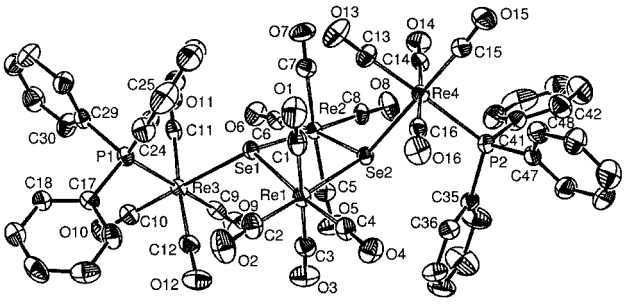

Figure 2. View (ORTEP, 30% probability level) of the molecular structure of **2** with the atom numbering scheme

 © 2004 Wiley-VCH Verlag GmbH & Co. KGaA, Weinheim

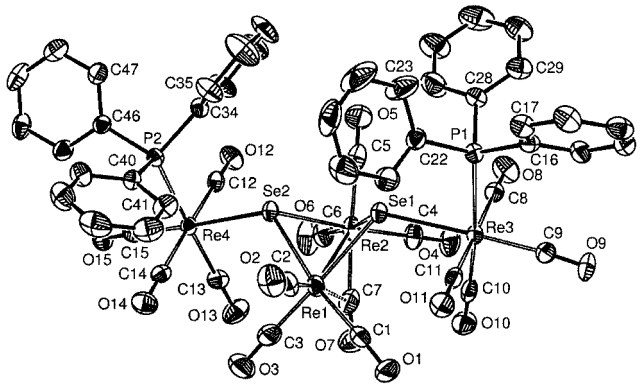

Figure 3. View (ORTEP, 30% probability level) of the molecular structure of **3** with the atom numbering scheme

Table 2. Selected bond lengths (Å) and angles (°) for **2**

Re(1)−Se(1)	2.6610(9)	Re(1)−Se(2)	2.6680(9)
Re(2)−Se(2)	2.6462(9)	Re(2)−Se(1)	2.6675(9)
Re(3)−Se(1)	2.6666(9)	Re(4)−Se(2)	2.6505(9)
Re(4)−P(2)	2.503(2)	Re(3)−P(1)	2.511(2)
Se(1)−Re(1)−Se(2)	79.74(3)	Se(2)−Re(2)−Se(1)	80.02(3)
P(1)−Re(3)−Se(1)	92.27(6)	P(2)−Re(4)−Se(2)	88.00(6)
Re(1)−Se(1)−Re(2)	98.19(3)	Re(1)−Se(1)−Re(3)	119.84(3)
Re(2)−Se(1)−Re(3)	115.35(3)	Re(2)−Se(2)−Re(4)	118.49(3)
Re(2)−Se(2)−Re(1)	98.54(3)	Re(4)−Se(2)−Re(1)	118.32(3)

Table 3. Selected bond lengths (Å) and angles (°) for **3**

Re(1)−Se(1)	2.5701(8)	Re(1)−Se(2)	2.5759(10)
Re(2)−Se(1)	2.6364(9)	Re(1)−Re(2)	2.9978(15)
Re(3)−Se(1)	2.6507(8)	Re(2)−Se(2)	2.6278(8)
Re(4)−Se(2)	2.6445(8)	Re(3)−P(1)	2.5009(17)
Re(1)−C(7)	2.618(8)	Re(4)−P(2)	2.5090(17)
Re(2)−C(7)	2.025(8)	O(7)−C(7)	1.144(10)
Se(1)−Re(1)−Se(2)	75.89(3)	Se(2)−Re(2)−Se(1)	73.90(2)
P(1)−Re(3)−Se(1)	85.31(4)	P(2)−Re(4)−Se(2)	83.44(4)
Re(1)−Se(1)−Re(2)	70.29(3)	Re(1)−Se(1)−Re(3)	117.73(3)
Re(2)−Se(1)−Re(3)	117.73(3)	Re(2)−Se(2)−Re(4)	117.81(3)
Re(1)−Se(2)−Re(2)	70.34(3)	Re(1)−Se(2)−Re(4)	120.09(3)
Se(1)−Re(1)−Re(2)	55.89(2)	Se(1)−Re(2)−Re(1)	53.82(2)
Se(2)−Re(1)−Re(2)	55.64(3)	Se(2)−Re(2)−Re(1)	54.016(16)
Re(2)−C(7)−Re(1)	79.3(3)	Re(2)−C(7)−O(7)	159.5(8)

ations are 4.027(3) and 3.416(1) Å respectively]. Both Re1 and Re2 are bound to four terminal carbonyl groups and to two selenium atoms in a slightly distorted octahedral environment. Each of the two Se atoms is also bound to another Re atom from the $Re(CO)_4(PPh_3)$ group in which the P atom from the phosphane is coordinated to the Re atom [Re3−P1 and Re4−P2 = 2.511(2) and 2.503(2) Å respectively]. The two selenium atoms triply bridge three nonbonded rhenium atoms, with the six Se−Re bond lengths being almost equal [2.646(1)−2.668(1) Å].

The crystal structure of complex **3** compares well with that of the manganese derivative $[Mn_4(\mu_3\text{-}Se)_2(\mu\text{-}CO)(CO)_{14}(PMePh_2)_2]$.[11] In contrast to compound **2**, in which the Re_4Se_2 group contains a nearly planar Re_2Se_2 array, in complex **3** a butterfly Re_2Se_2 core is observed. Thus, the two Re atoms occupy the hinge [Re1−Re2 bond length of 2.998(1) Å] and the two Se atoms the wing sites [the nonbonding Se1···Se2 separation is 3.164(1) Å and the dihedral angle between the Re1Re2Se1 and Re1Re2Se2 wings is 96.1°]. Both Re1 and Re2 atoms are bound to three terminal carbonyl ligands, while a fourth carbonyl group is involved in an incipient bridging interaction with Re1 [the Re(1)−C(7) and Re(2)−C(7) distances are 2.618(8) and 2.025(8) Å, respectively, and the O(7)−C(7)−Re(2) angle is 159.5(8)°]. The Re1−Re2 distance is in agreement with that expected for a metal−metal bond. Only one example of a carbonyl ligand bridging two Re atoms with a longer M−M distance [3.0391(6) Å] has been reported in the literature.[13] The butterfly Re_2Se_2 array is slightly asymmetrical, with the Re1−Se1 and Re1−Se2 bond lengths [2.5701(8) and 2.5759(10) Å, respectively] being shorter than the Re2−Se1 and Re2−Se2 ones [2.6364(9) and 2.6278(8) Å]. Analogously to compound **2**, each of the two Se atoms is also bound to another Re centre of a $Re(CO)_4(PPh_3)$ group in such a way that the Se atoms triply bridge three Re metal centres. In both complexes the atoms Re3, Se1, Se2, Re4 lie in a nearly planar array [maximum deviation for Se1 in **2** and Se2 in **3** of 0.078(2) and 0.0120(7) Å, respectively]. Regarding the position of the $Re(CO)_4PPh_3$ groups, a *trans* configuration is present in **3** with an Re3−Se1−Se2−Re4 torsion of 175.09° and a *cis* configuration in **2** with the corresponding torsion angle of 6.67°; in both cases the phosphane ligands point in the directions which minimize the steric hindrance. In particular, the disposition of the two phosphane molecules could be described as *cis* in compound **2** and *trans* in compound **3**.

Thermal Treatment of 2; Reversible Conversion to 3 by CO Loss

Stirring a solution of **2** in THF at room temperature leads slowly to the formation of **3**, in quantitative yield, by loss of a carbonyl molecule. This process is found to be faster in polar solvents and under moderate heating. This conversion can be monitored by IR spectroscopy. As shown in Figure 4, the IR absorption bands of the terminal CO group display distinct changes in the regions 1980−2040 (typical of a $Re(CO)_4L$ type of structure), and 2050−2100 cm^{-1}. Finally, the formation of an incipient bridging CO group is observed at 1896 cm^{-1}.

The loss of the carbonyl ligand induces a structural modification. A Re−Re bond is formed and the Re_2Se_2 conformation changes from nearly planar to butterfly. It is not possible to determine which carbonyl leaves the Re_2Se_2 core, although the longer C−Re distances involving the axial carbonyls [spanning from 1.98(1) to 2.01(1) Å] than the equatorial ones [spanning from 1.90(1) to 1.93(1) Å] suggest a higher lability. The subsequent rearrangement of the core carbonyls allows the rotation of the $Re(CO)_4P$ moiety around the Re−Se bond and the inversion of the selenium atom.

 © 2004 Wiley-VCH Verlag GmbH & Co. KGaA, Weinheim

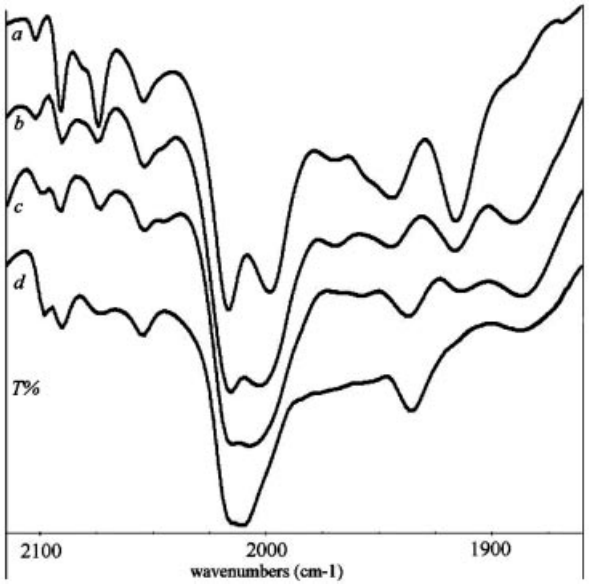

Figure 4. Conversion of **2** into **3** in THF/CH_2Cl_2 (1:1) at 50 °C monitored by FT-IR spectroscopy by sampling the mixture, drying *in vacuo* and redissolving the sample in CH_2Cl_2: (a) pure **2** (t = 0 min); (b) t = 15 min; (c) t = 30 min; (d) pure **3** (t = 45 min)

The process can be reversed by placing **3** under moderate CO pressure, obtaining complex **2** in quantitative yields. There are only a few known examples of reversible CO addition to transition metal compounds, mainly those supported on inorganic matrices or in high-nuclearity clusters.[14a,14b] Some examples of M−M bond cleavage due to reversible CO addition are knwon in the literature,[15] but very few involve two stable species.[16]

As pointed out for the synthesis of $[Mn_4(\mu_3\text{-}Se)_2(\mu\text{-}CO)(CO)_{14}(PMePh_2)_2]$,[11] the reaction mechanism leading to the synthesis of M_4Se_2 core compounds (M = Mn, Re) is believed to proceed via the formation of intermediates of the type $[M_2(\mu\text{-}Se)(CO)_8(PR_3)]$ (PR_3 = tertiary phosphane ligand). This product results from the initial attack of the phosphane selenide on the dinuclear compound and can, in turn, undergo a dimerization, leading to the formation of $[M_4(\mu_3\text{-}Se)_2(CO)_{16}(PR_3)_2]$ complexes. Finally, the loss of a carbonyl ligand from the aforementioned structures can give rise to novel $[M_4(\mu_3\text{-}Se)_2(\mu\text{-}CO)(CO)_{14}(PR_3)_2]$ complexes. In the case of rhenium, both final products were isolated, and seem to have similar thermodynamic stabilities. On the other hand, the manganese compound $[Mn_4(\mu_3\text{-}Se)_2(CO)_{16}(PR_3)_2]$ could not be isolated, probably because

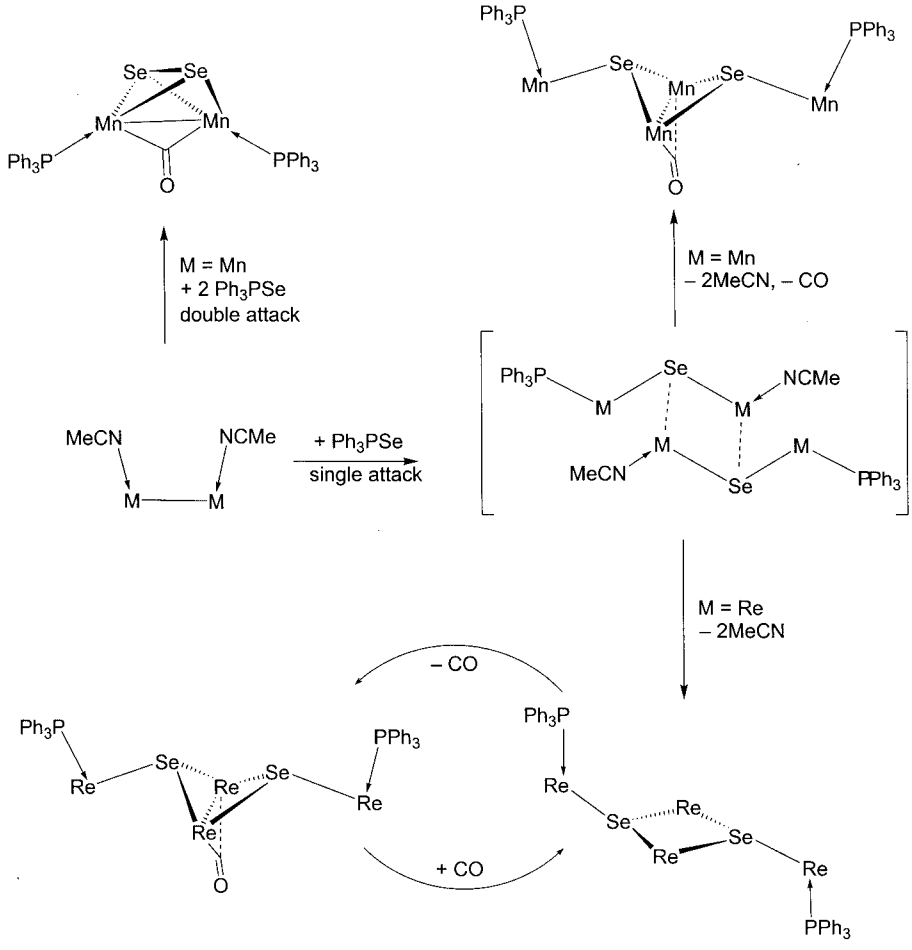

Scheme 1. (terminal carbonyl groups omitted for clarity)

 © 2004 Wiley-VCH Verlag GmbH & Co. KGaA, Weinheim

of the greater stability of the related decarbonylated compound (see Scheme 1).

Experimental Section

General Remarks: The starting reagents triphenylphosphane selenide, $[Re_2(CO)_{10}]$ and $[Mn_2(CO)_{10}]$ were pure commercial products (Aldrich and Fluka) and were used as received. The solvents (C. Erba) were dried and distilled by standard techniques before use. Preparative TLC was carried out on silica (Merck, 60 PF_{254}, 20 × 20 cm glass plates). After the chromatographic workup, the products were extracted with dichloromethane. Purity was checked by elemental analysis and ^{31}P NMR spectroscopy. Elemental (C, H) analyses were performed with a Carlo Erba EA 1108 automated analyzer. IR spectra (CH_2Cl_2 solutions) were recorded on a Nexus FT spectrometer. ^1H (300 MHz) and $^{31}P\{^1H\}$ (161.90 MHz, 85% H_3PO_4 as external reference) NMR spectra ($CDCl_3$ solutions) were recorded on a Bruker AC 300 and a Bruker AMX 400 instrument, respectively.

Synthesis of $[Mn_2(\mu_2\text{-}Se)_2(\mu\text{-}CO)(CO)_4(PPh_3)_2]$ (1): Ph_3PSe (350 mg, 1.03 mmol) and Me_3NO (23 mg, 1.03 mmol) were dissolved in toluene (60 mL) and the resulting solution brought to 45 °C. A 15 mL toluene solution of $[Mn_2(CO)_{10}]$ (200 mg, 0.52 mmol) was then added dropwise. A progressive colour change from yellow to deep brown was observed. The reaction was stopped after 30 min, the solvents removed in vacuo and the brown solid redissolved in a small amount of dichloromethane. Two products were isolated by preparative TLC (CH_2Cl_2/hexane, 2:1), namely brownish red $[Mn_4(\mu_3\text{-}Se)_2(\mu\text{-}CO)(CO)_{14}(PPh_3)_2]$ (yield 70%), identified by comparison of the spectroscopic data with those observed previously,[11] and $[Mn_2(\mu_2\text{-}Se)_2(\mu\text{-}CO)(CO)_4(PPh_3)_2]$ (**1**) (yield 5%) as a brown crystalline solid.
1: FTIR (CH_2Cl_2): ν(CO) = 1979 vs, 1944 vs, 1890 vs, 1865 m, 1789 vs. $^{31}P\{^1H\}$ NMR: δ = 13.6 ppm. $C_{41}H_{30}Mn_2O_5P_2Se_2$: calcd. C 52.81, H 3.24; found C 52.84, H 3.25.

Reaction of $[Re_2(CO)_8(MeCN)_2]$ with Ph_3PSe: CH_3CN (41 mg, 1 mmol) and Me_3NO (68 mg, 0.61 mmol) were added to a dichloromethane solution of $[Re_2(CO)_{10}]$ (200 mg, 0.31 mmol in 40 mL) and the resulting reaction mixture stirred at room temperature for 2 h. Evaporation of the solvent gave $[Re_2(CO)_8(MeCN)_2]$ as a yellow solid, which was redissolved in 50 mL of toluene. Ph_3PSe (105 mg, 0.31 mmol) was added and the reaction mixture warmed to 70 °C for 2 h. A colour change from yellow to intense red was observed after 30 mins. Evaporation of the solvent yielded the crude product as an orange solid. Cromatography (preparative TLC; CH_2Cl_2/hexane, 1:1) gave red $[Re_4(\mu_3\text{-}Se)_2(CO)_{16}(PPh_3)_2]$ (**2**) and orange-yellow $[Re_4(\mu_3\text{-}Se)_2(\mu\text{-}CO)(CO)_{14}(PPh_3)_2]$ (**3**) bands together with some decomposition material and small amounts of unchanged reagents. Compound **2** is more soluble than **3** in all common laboratory solvents.
2: FT-IR (CH_2Cl_2): ν(CO) = 2090 w, 2074 w, 2016 vs, 1998 vs, 1954 sh, 1943 m, 1916 m. $^{31}P\{^1H\}$ NMR: δ = 1.0 (br) ppm. $C_{52}H_{30}O_{16}P_2Re_4Se_2$: calcd. C 33.30, H 1.64; found C 33.29, H 1.62.
3: FT-IR (CH_2Cl_2): ν(CO) = 2098 w, 2091 w, 2016 vs, 2011 vs (sh), 1936 m, 1895 m. $^{31}P\{^1H\}$ NMR: δ = 0.8 (br) ppm. $C_{51}H_{30}O_{15}P_2Re_4Se_2$: calcd. C 33.16, H 1.64; found C 33.14, H 1.61.

Thermal Treatment of 2; Conversion into 3: A solution of compound **2** (100 mg, 0.051 mmol) in 10 mL of THF was stirred for 40 minutes at 50 °C. The quantitative formation of **3** was monitored by FT-IR spectroscopy.

Reaction of 3 with CO; Conversion into 2: A suspension of **3** (100 mg, 0.054 mmol) in 5 mL of CH_2Cl_2 was stirred under 5 atm. of CO. After 5 h an orange solution was formed. Cluster **3** was quantitatively converted into **2**, as confirmed by FT-IR spectroscopy in CH_2Cl_2.

X-ray Data Collection, Structure Solution and Refinement for Complexes 1, 2·CH_2Cl_2 and 3: Crystals suitable for X-ray analysis were obtained by layering methanol on dichloromethane solutions (**1** and **2·CH_2Cl_2**) or by slow evaporation of solvent from a THF solution (**3**). The intensity data were collected at room temperature on a Philips PW 1100 (**1**) or on a Bruker area detector AXS Smart 1000 (**2·CH_2Cl_2** and **3**) diffractometer (both using graphite-monochromated Mo-K_α radiation, λ = 0.71073 Å). Crystallographic and experimental details for the structures are summarized in

Table 4. Crystal data and structure refinement for compounds **1**, **2·CH_2Cl_2** and **3**

	1	**2·CH_2Cl_2**	**3**
Empirical formula	$C_{41}H_{30}Mn_2O_5P_2Se_2$	$C_{52}H_{30}O_{16}P_2Re_4Se_2\ CH_2Cl_2$	$C_{51}H_{30}O_{15}P_2Re_4Se_2$
Mol. mass	932.39	1960.35	1847.41
Cryst system	monoclinic	monoclinic	monoclinic
Space group	*C*2/*c*	*C*2/*c*	$P2_1/n$
a (Å)	19.387(1)	47.584(2)	9.613(5)
b (Å)	10.328(1)	10.154(2)	21.859(5)
c (Å)	19.723(1)	32.376(2)	25.998(5)
β (°)	101.69(1)	128.25(1)	98.84(1)
V (Å^3)	3867(1)	12285(3)	5398(3)
Z	4	8	4
$D_{calcd.}$ (g·cm^{-3})	1.601	2.120	2.273
F(000)	1856	7280	3416
Crystal size	0.11 × 0.12 × 0.14	0.14 × 0.12 × 0.15	0.10 × 0.13 × 0.50
μ (cm^{-1})	26.62	92.44	104.14
Reflns. coll.	4802	67151	60529
Reflns. unique	4678 (R_{int} = 0.0984)	14263 (R_{int} = 0.0766)	12606 (R_{int} = 0.0432)
Obsd. reflns. [$I > 2\sigma(I)$]	1757	8391	6866
Parameters	236	727	668
R_{int} [$I > 2\sigma(I)$]	$R1$ = 0.0633,[a] $wR2$ = 0.1010[b]	$R1$ = 0.0400, $wR2$ = 0.0846	$R1$ = 0.0344, $wR2$= 0.0387
R_{int} (all data)	$R1$ = 0.2033, $wR2$ = 0.1361	$R1$ = 0.0896, $wR2$ = 0.0970	$R1$ = 0.0908, $wR2$= 0.0442

[a] $R1 = \Sigma||F_o| - |F_c||/\Sigma|F_o|$. [b] $wR2 = \{\Sigma[w(F_o^2 - F_c^2)^2]/\Sigma[w(F_o^2)^2]\}^{1/2}$.

 © 2004 Wiley-VCH Verlag GmbH & Co. KGaA, Weinheim

Table 4. An empirical absorption correction was made for **1** (maximum and minimum value for the transmission coefficient 1.000 and 0.625).[17a,17b] For complexes **2·CH_2Cl_2** and **3** (maximum and minimum effective transmission value 1.000 and 0.405, 1.000 and 0.534. respectively) the raw frame data were processed using SAINT and SADABS to yield the reflection data file and the Bruker software was used for the absorption correction.[17c−17e] The structures were solved by Patterson and Fourier methods and refined by full-matrix least-squares procedures (based on F_o^2) (SHELX-97),[18] first with isotropic thermal parameters and then with anisotropic thermal parameters in the last cycles of refinement for all the non-hydrogen atoms**.** In the crystals of **2·CH_2Cl_2** dichloromethane molecules of solvation were found. The hydrogen atoms in **1**, **2·CH_2Cl_2** and **3** were introduced into their geometrically calculated positions and refined as riding on the corresponding parent atoms, except the hydrogen atoms of the solvent molecule.

CCDC-230259 (for **1**), -230260 (for **2·CH_2Cl_2**) and -230261 (for **3**) contain the supplementary crystallographic data for this paper. These data can be obtained free of charge at www.ccdc.cam.ac.uk/conts/retrieving.html [or from the Cambridge Crystallographic Data Centre, 12 Union Road, Cambridge CB2 1EZ, UK; Fax: +44-1223-336033; E-mail: deposit@ccdc.cam.ac.uk].

Acknowledgments

Financial support from Ministero dell'Università e della Ricerca Scientifica e Tecnologica (Cofin 2000) is gratefully acknowledged. The facilities of the Centro Interfacoltà di Misure "G. Casnati" (Università di Parma) were used to record the NMR spectra.

[1] [1a] L. C. Roof, J. W. Kolis, *Chem. Rev.* **1993**, *93*, 1037. [1b] D. Fenske, G. Longoni, G. Schmid, in *Clusters and Colloids* (Ed.: G. Schmid), VCH, Weinheim, **1994**, chapter 3, p. 89.

[2] [2a] S. Dehnen, A. Eichhofer, D. Fenske, *Eur. J. Inorg. Chem.* **2002**, *2*, 279. [2b] M. L. Steigerwald, *Polyhedron* **1994**, *13*, 1245. [2c] G. Henkel, S. Weissgräber in, *Metal Clusters in Chemistry* (Eds.: P. Braunstein, L. Oro, P. Raithby), VCH, Weinheim, **1999**, vol. 1, p. 163.

[3] [3a] M. L. Steigerwald, T. Siegrist, E. M. Gyorgy, B. Hessen, Y.-U. Kwon, S. M. Tanzler, *Inorg. Chem.* **1994**, *33*, 3389. [3b] S. Ulvenlund, A. Bengtsson-Kloo, in *Metal Clusters in Chemistry* (Eds.: P. Braunstein, L. Oro, P. Raithby), VCH, Weinheim, **1999**, vol. 1, 561−602. [3c] D. Fenske, J. F. Corrigan, in *Metal Clusters in Chemistry* (Eds.: P. Braunstein, L. Oro, P. Raithby), VCH, Weinheim, **1999**, vol. 3, 1302−1324.

[4] [4a] H. Ogino, S. Inomata, H. Tobita, *Chem. Rev.* **1998**, *98*, 2093. [4b] R. D. Adams, *Polyhedron* **1985**, *4*, 2003. [4c] R. D. Adams, *J. Cluster Sci.* **1990**, *1*, 249.

[5] [5a] P. Mathur, *Adv Organomet. Chem.* **1997**, *41*, 243. [5b] P. Braunstein, C. Graiff, C. Massera, G. Predieri, J. Rosé, A. Tiripicchio, *Inorg. Chem.* **2002**, *41*, 1372.

[6] [6a] D. Cauzzi, C. Graiff, G. Predieri, A. Tiripicchio, in *Metal Cluster in Chemistry* (Eds.: P. Braunstein, L. Oro, P. Raithby), vol. 1, VCH, Weinheim, **1999**, p. 193. [6b]C. Graiff, G. Predieri, A. Tiripicchio, *Eur. J. Inorg. Chem.* **2003**, *9*, 1659. [6c] D. Cauzzi, D. Belletti, C. Graiff, A. Minarelli, R. Pattacini, G. Predieri, A. Tiripicchio, *J. Chem. Soc., Dalton Trans.* **2002**, 3160. [6d] D. Belletti, C. Graiff, C. Massera, A. Minarelli, G. Predieri, A. Tiripicchio, D. Acquotti, *Inorg. Chem.* **2003**, *42*, 850.

[7] [7a] R. D. Adams, O.-S. Kwon, S. Sanyal, *J. Organomet. Chem.* **2003**, *681*, 256. [7b] R. D. Adams, O.-S. Kwon, *Inorg. Chem.* **2003**, *42*, 6175. [7c] R. D. Adams, O.-S. Kwon, M. D. Smith, *Inorg. Chem.* **2001**, *40*, 5322. [7d] R. D. Adams, O.-S. Kwon, M. D. Smith, *Inorg. Chem.* **2002**, *41*, 6281. [7e] R. D. Adams, O.-S. Kwon, M. D. Smith, *Inorg. Chem.* **2002**, *41*, 1658. [7f] R. D. Adams, O.-S. Kwon, M. D. Smith, *Organometallics* **2002**, *21*, 1960. [7g] R. D. Adams, S. Miao, *J. Organomet. Chem.* **2003**, *665*, 43. [7h] R. D. Adams, S. Miao, *Organometallics* **2003**, *22*, 2492. [7i] R. D. Adams, B. Captain, O.-S. Kwon, S. Miao, *Inorg. Chem.* **2003**, *42*, 3356.

[8] S. C. O'Neal, W. T. Pennington, J. W. Kolis, *Inorg. Chem.* **1990**, *29*, 3134.

[9] W.-F. Liaw, C.-Y. Chuang, W.-Z. Lee, C.-K. Lee, G.-H. Lee, S.-M. Peng, *Inorg. Chem.* **1996**, *35*, 2530.

[10] W. Eikens, S. Jäger, P. G. Jones, C. Thörne, *J. Organomet. Chem.* **1996**, *511*, 67.

[11] D. Belletti, C. Graiff, C. Massera, R. Pattacini, G. Predieri, A. Tiripicchio, *Inorg. Chim. Acta* **2003**, *356*, 187.

[12] P. Baistrocchi, M. Careri, C. Graiff, M. Lanfranchi, P. Manini, G. Predieri, A. Tiripicchio, *Inorg. Chim. Acta* **1996**, *252*, 367.

[13] D. A. Kort, K.-Y. Shih, W. Wu, P. E. Fanwick, R. A. Walton, *Organometallics* **1995**, *14*, 448.

[14] [14a] Y. Izumi, T. Chihara, H. Yamazaki, Y. Iwasawa, *J. Phys. Chem.* **1994**, *98*, 594. [14b] Y. Izumi, T. Chihara, H. Yamazaki, Y. Iwasawa, *J. Am. Chem. Soc.* **1993**, *115*, 462.

[15] [15a] H. Vahrenkamp, *Adv. Organomet. Chem.* **1983**, *22*, 169. [15b] R. D. Adams, L.-W. Yang, *J. Am. Chem. Soc.* **1983**, *105*, 235. [15c] R. D. Adams, O.-S. Kwon, M. D. Smith, *Inorg. Chem.* **2002**, *41*, 1658.

[16] D. Nucciarone, N. J. Taylor, A. J. Carty, *Organometallics* **1988**, *7*, 127.

[17] [17a] N. Walker, D. Stuart, *Acta Crystallogr., Sect. A* **1983**, *39*, 158. [17b] F. Ugozzoli, *J. Comput. Chem.* **1987**, *11*, 109. [17c] *SMART Software Users Guide, Version 5.0*; Bruker Analytical X-ray Systems, Madison, WI, **1999**. [17d] *SAINT Software Users Guide*; Bruker Analytical X-ray Systems: Madison, WI, **1999**. [17e] G. M. Sheldrick, *SADABS*; Bruker Analytical X-ray Systems, Madison, WI, **1999**.

[18] [18a] G. M. Sheldrick, *SHELXL-93, a program for crystal structure determination*; University of Göttingen: Germany, **1993**. [18b] G. M. Sheldrick, *SHELXL-97, a program for crystal structure refinement*; University of Göttingen: Germany, **1997.**

Received February 3, 2004
Early View Article
Published Online July 6, 2004

 © 2004 Wiley-VCH Verlag GmbH & Co. KGaA, Weinheim

EurJIC
European Journal of Inorganic Chemistry

Issue 18/2004

Pages 3571–3764

Papers available ahead of print in Early View at www.interscience.wiley.com

Earliest available Table of Contents:
Automatically, free of charge by e-mail through
www.interscience.wiley.com/alerts

COVER PICTURE

The cover picture shows a butterfly mimicking the main features of compounds $[L_2Pt(\mu\text{-}S)_2PtL_2]$ (L_2 = phosphane). Its flight simulates the flexibility of the $\{Pt(\mu\text{-}S)_2Pt\}$ core about the S–S axis; its body represents the strongly nucleophilic sulfide ligands and the wings the $\{PtL_2\}$ fragments. Exploration of the reactivity of the butterfly compounds has revealed an exceptionally rich and diverse chemistry. Details are discussed in the Microreview by P. González-Duarte et al. on p. 3585ff., who acknowledge Victor Sarto i Monteys for the butterfly picture (V. S. i M. holds the copyright).

MICROREVIEW

Contents

3585 **P. González-Duarte,* A. Lledós, R. Mas-Ballesté**

Extending The Reaction Landscape of the $\{Pt(\mu\text{-}S)_2Pt\}$ Core: From Metal Centers to Non-Metallic Electrophiles

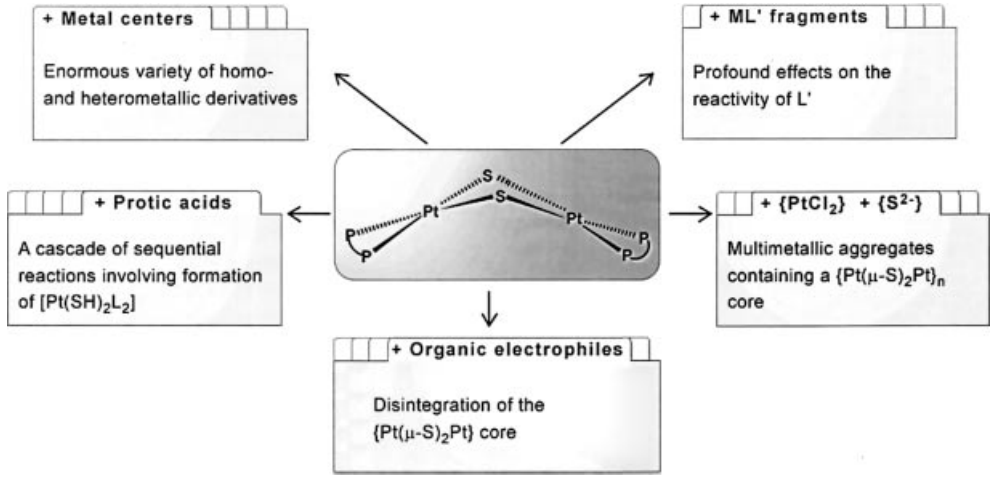

Keywords: Platinum / Sulfur / Metalloligand / Nucleophile / Building block

 © 2004 Wiley-VCH Verlag GmbH & Co. KGaA, Weinheim

FULL PAPERS

3601 **B. Štíbr,* J. Holub, M. Bakardjiev, W. Milius, B. Wrackmeyer**

Monocarbaborane Chemistry: Cage Opening of *nido*-1-CB_8H_{12} by Tertiary Bases − an Example of a Straightforward *nido* → *arachno* Transformation; Isolation of a New Series of 4-L-*arachno*-5-CB_8H_{12} Compounds (L = NMe_3, NEt_3, and Quinoline)

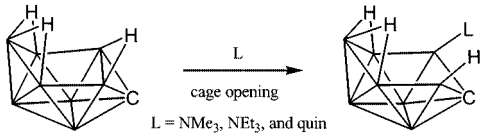

Keywords: Boranes / Carboranes / Monocarbaboranes / NMR spectroscopy / X-ray diffraction

3605 **B. Brellochs, J. Bačkovský, B. Štíbr,* T. Jelínek, J. Holub, M. Bakardjiev, D. Hnyk, M. Hofmann, I. Císařová, B. Wrackmeyer**

New Ways to a Series of Parent Representatives of the Eight-, Nine-, and Ten-Vertex Monocarbaborane Family

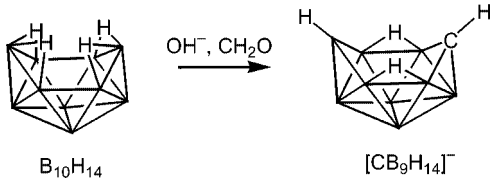

Keywords: Boranes / Carboranes / Geometry optimization / GIAO calculations / Monocarbaboranes

3612 **U. Braun, B. Böck, H. Nöth,* I. Schwab, M. Schwartz, S. Weber, U. Wietelmann**

Reactions of Group 13 and 14 Hydrides and Group 1, 2, 13 and 14 Organyl Compounds with (*tert*-Butylimino)(2,2,6,6-tetramethylpiperidino)-borane

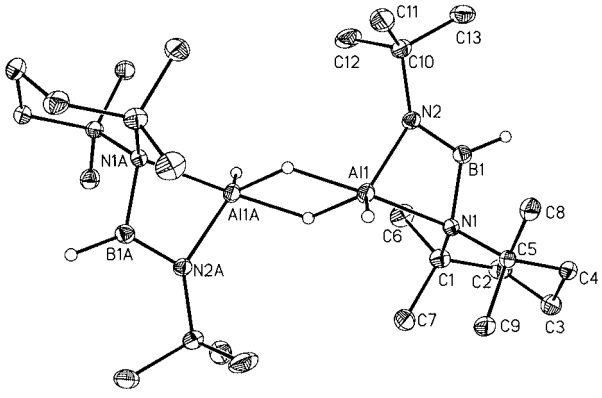

Keywords: BN triple bonds / Insertion reactions / (*N*-Metal-*tert*-butylamino)(2,2,6,6-tetramethylpiperidino)boranes / Multinuclear NMR / X-ray structures

3629 **U. Braun, T. Habereder, H. Nöth***

Lithium *tert*-Butyl[phenyl(2,2,6,6-tetramethylpiperidino)boryl]amide: A Versatile Reagent

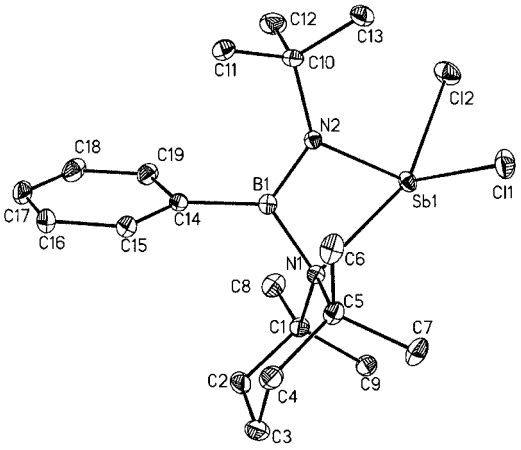

Keywords: Lithium *tert*-butyl[phenyl(2,2,6,6-tetramethylpiperidino)boryl]amide / *N*−Metal borylamides

 © 2004 Wiley-VCH Verlag GmbH & Co. KGaA, Weinheim

3644 **C. Wippert Rodrigues, C. Limberg,* H. Pritzkow**

Metalation of 2-Propenylphenol

Keywords: Molybdenum / Oxo complexes / Alkoxides / Lithium / Metalation

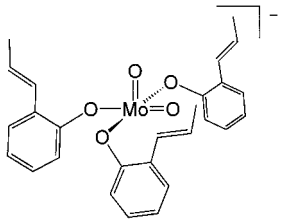

3651 **Y. Yamamoto,* Y. Miyabe, K. Itoh**

Synthesis of a Dinuclear Ruthenabicyclic Complex and Its Ligand-Substitution Reactions

Keywords: Alkyne ligands / Carbonyl ligands / Metallacycles / Phosphane ligands / Ruthenium

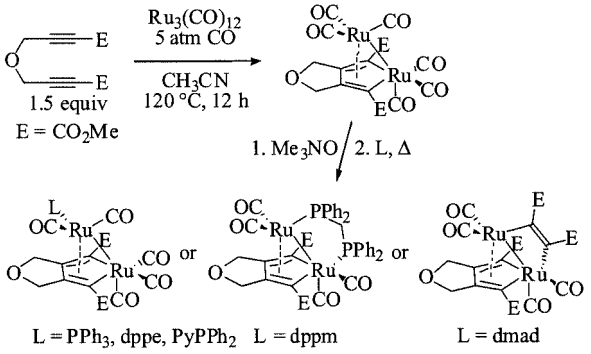

3662 **C. Jiang, Z. Yu, S. Wang, C. Jiao, J. Li, Z. Wang,* Y. Cui***

Rational Design of Metal-Organic Frameworks Based on 5-(4-Pyridyl)tetrazolate: From 2D Grids to 3D Porous Networks

Keywords: Coordination polymers / Fluorescence / Hydrothermal synthesis / N ligands / Self-assembly

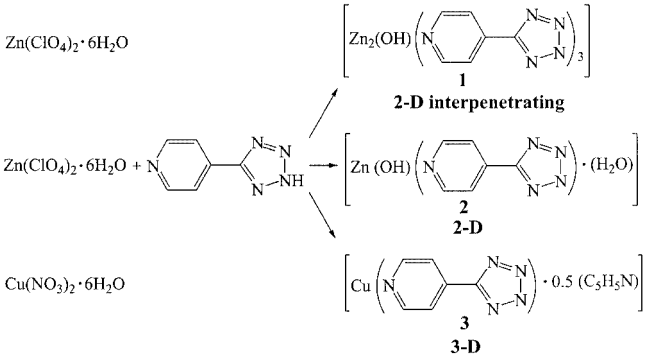

3668 **G. A. Carriedo,* P. Crochet, F. J. García Alonso, J. Gimeno,* A. Presa-Soto**

Synthesis and Catalytic Activity of (η^6-*p*-Cymene)(phosphane)ruthenium(II) Complexes Supported on Poly(biphenoxyphosphazene) or Chiral Poly(binaphthoxyphosphazene) Copolymers

Keywords: Phosphazenes / Polymers / Immobilization / Arene ligands / Hydrogen transfer / Ruthenium

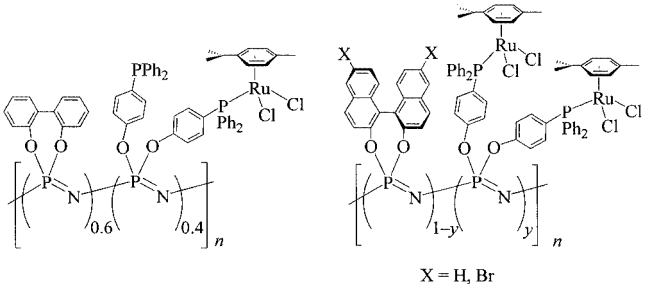

3675 **A. Burg, E. Lozinsky, H. Cohen, D. Meyerstein***

Mechanism of Reduction of the Nitrite Ion by Cu^{I} Complexes

Keywords: Nitrite / Copper(I) / Reduction / NO

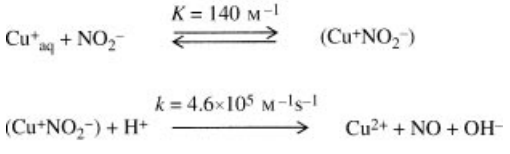

 © 2004 Wiley-VCH Verlag GmbH & Co. KGaA, Weinheim

3681 **S. Wang, J.-L. Zuo,* H.-C. Zhou, Y. Song, S. Gao, X.-Z. You***

Heterobimetallic Complexes Based on $[(Tp)Fe(CN)_3]^-$: Syntheses, Crystal Structures and Magnetic Properties

Keywords: Chain structures / Cyanide ligands / Iron / Magnetic properties / Polynuclear complexes

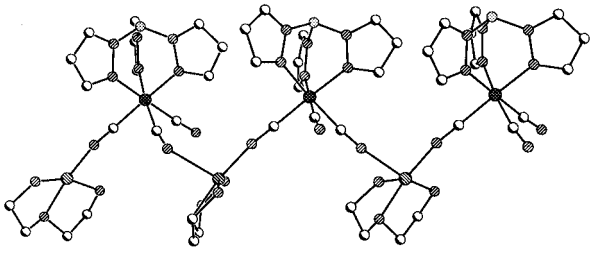

3688 **R. Bronisz**

Synthesis and Characterisation of Coordination Polymers of Cu^{II} and Zn^{II} with 1,3-Bis(1,2,3,4-tetrazol-2-yl)propane − Rotational Freedom of the Donor Group Favours Structural Diversification

Keywords: Coordination polymers / Copper / Flexibility / N ligands / Zinc

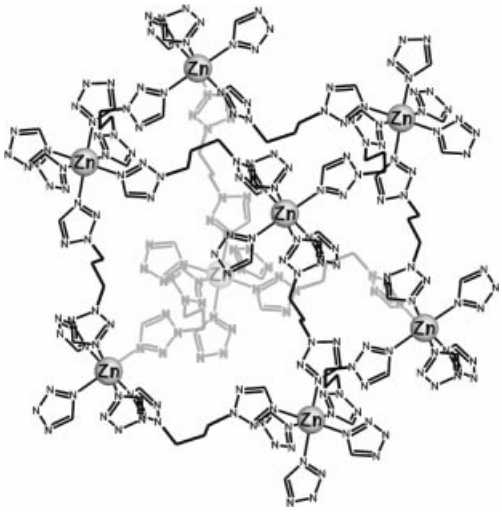

3696 **M. R. Bermejo,* A. M. González-Noya, V. Abad, M. I. Fernández, M. Maneiro, R. Pedrido, M. Vázquez**

Formation of Novel 1-D Chains by μ-Amido Bridging of Dinuclear Manganese(III)-Schiff Base Complexes

Keywords: Amides / Manganese / Schiff bases / 1-D chains

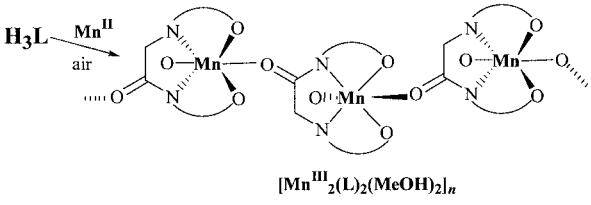

3706 **J.-L. Song, A. V. Prosvirin, H.-H. Zhao, J.-G. Mao***

Syntheses and Crystal Structures of Two Cobalt Carboxylate−Phosphonates with 4,4′-Bipyridine as a Secondary Metal Linker

Keywords: Hydrothermal synthesis / Crystal structure / Cobalt phosphonates / Inorganic-organic hybrids / Open frameworks

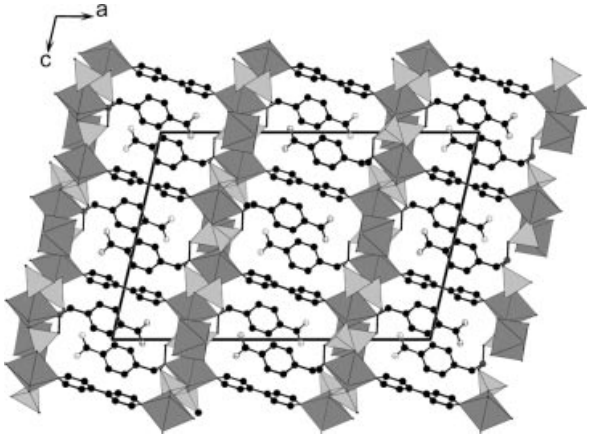

 © 2004 Wiley-VCH Verlag GmbH & Co. KGaA, Weinheim

3712 **M.-L. Feng, J.-G. Mao***

Three New Organically Templated Polyoxomolybdates with Capping Selenite Anions

Keywords: Hydrothermal synthesis / Inorganic-organic hybrid composites / Molybdenum / Polyoxometalates / Selenium

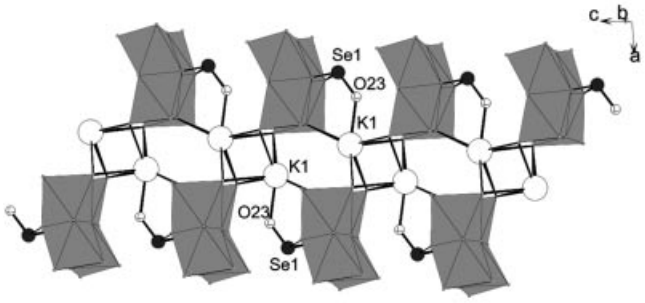

3718 **Y. Song, J. Yu,* Y. Li, M. Zhang, R. Xu***

A New 3-D Open-Framework Zinc Phosphate $[C_6H_{16}N_2]\cdot[Zn_2(HPO_4)_3]$ Synthesized by a Solvothermal Combinatorial Approach

Keywords: Solvothermal synthesis / Structure / Combinatorial approach / Host-guest systems / Zinc phosphate

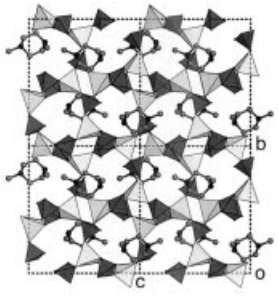

3724 **L. S. Natrajan, C. Wilson, J. Okuda, P. L. Arnold***

Group 4 Complexes of Chelating Dianionic [OSO] Binaphtholate Ligands; Synthesis and Alkene Polymerisation Catalysis

Keywords: Binaphthol ligands / Polymerisation catalysis / Organometallic / Group 4 elements / Zirconium / Titanium

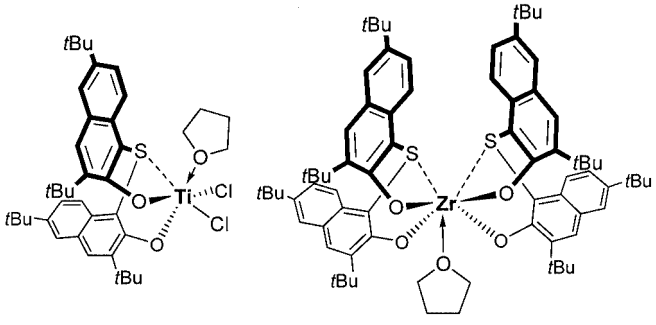

3733 **G. A. van Albada, A. Mohamadou, I. Mutikainen, U. Turpeinen, J. Reedijk***

Synthesis, Characterisation, Properties and X-ray Structures of Cu^{II} Coordination Compounds with 5,5′-Dimethylbipyridine and Various Anions: Control of Stoichiometry and Structure by the Counterions

Keywords: Copper / EPR spectroscopy / Infrared spectroscopy / Magnetic properties / N ligands

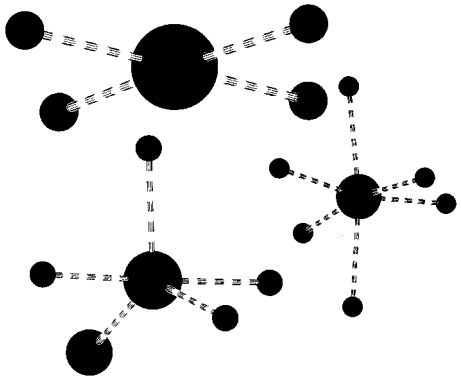

 © 2004 Wiley-VCH Verlag GmbH & Co. KGaA, Weinheim

3743 **V. Montiel-Palma, E. Huitrón-Rattinger, S. Cortés-Llamas, M.-Á. Muñoz-Hernández,* V. García-Montalvo, E. López-Honorato, C. Silverstru**

Towards Cationic Gallium Derivatives: Metallacycles from the Reactions of Organogallium Compounds with Tetraorganodichalcogenoimidodiphosphinates and a New *N*-(Diphenylthiophosphinyl)thioureato Ligand

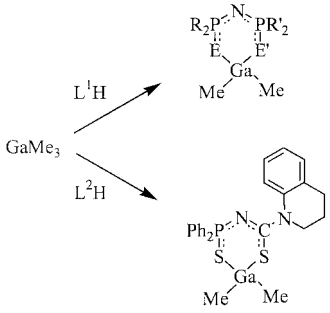

Keywords: Cationic catalysts / Chelating ligands / Gallium / Metallacycles / Phosphorus

3751 **R. Wang, L. Han, L. Xu, Y. Gong, Y. Zhou, M. Hong,* A. S. C. Chan**

Syntheses and Characterizations of Metal-Organic Frameworks with Unusual Topologies Derived from Flexible Dipyridyl Ligands

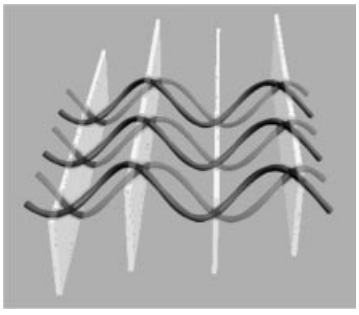

Keywords: Bridging ligands / Cadmium / Coordination polymers / X-ray diffraction / Zinc

 © 2004 Wiley-VCH Verlag GmbH & Co. KGaA, Weinheim

Extending The Reaction Landscape of the {Pt(μ-S)$_2$Pt} Core: From Metal Centers to Non-Metallic Electrophiles

Pilar González-Duarte,*[a] Agustí Lledós,[a] and Rubén Mas-Ballesté[a]

Keywords: Platinum / Sulfur / Metalloligand / Nucleophile / Building block

The outstanding nucleophilicity of the {Pt(μ-S)$_2$Pt} core in compounds [L$_2$Pt(μ-S)$_2$PtL$_2$] (L$_2$ = phosphane) accounts for their ability to act as metalloligands towards main group and transition metals, and thus for the high number of [{L$_2$Pt(μ$_3$-S)$_2$PtL$_2$}$_x$ML′$_y$]^z aggregates already described. However, the electronic and molecular features underpinning this behavior anticipate a landscape of comparable richness for the reactions of [L$_2$Pt(μ-S)$_2$PtL$_2$] with non-metal electrophiles. Exploration of the chemistry of [L$_2$Pt(μ-S)$_2$PtL$_2$] (L$_2$ = chelating diphosphane) towards various electron-acceptor species has been the aim of our research for the past years. In this microreview we survey the synthetic strategies of [L$_2$Pt(μ-S)$_2$PtL$_2$] compounds, their distinguishing electronic and molecular features, the dynamic processes and electron-donor properties of the {Pt(μ-S)$_2$Pt} core, and its binding ability towards metal centers. Moreover, particular attention is given to the reaction chemistry of [L$_2$Pt(μ-S)$_2$PtL$_2$] with organic electrophiles and protic acids, as well as to the influence of the {Pt(μ-S)$_2$Pt} core on the reactivity of inorganic or organic L′ ligands in [{L$_2$Pt(μ$_3$-S)$_2$PtL$_2$}$_x$ML′$_y$]^z aggregates.
(© Wiley-VCH Verlag GmbH & Co. KGaA, 69451 Weinheim, Germany, 2004)

Introduction

The outstanding ability of sulfur to bind heavy metals is not only evidenced by the enormous variety of metal sulfide minerals found in nature, but also by the occurrence of platinum group metals in mineral ores different from native deposits. One of these examples is cooperite, a platinum-bearing sulfide with the general formula $Pt_{0.6}Pd_{0.3}Ni_{0.1}S$, in which platinum(II) ions are coordinated by sulfide anions in a square-planar arrangement and these are tetrahedrally coordinated by four platinum ions.[1] In parallel to their

[a] Departament de Química, Universitat Autònoma de Barcelona, 08193 Bellaterra, Barcelona, Spain
Fax (internat.): +34-935-813-101
E-mail: Pilar.Gonzalez.Duarte@uab.es

Pilar González-Duarte (center) was born in Barcelona (Spain). She studied Chemistry at the Universitat de Barcelona and obtained a Master Degree in Chemistry at the University of Michigan (Ann Arbor, US). She received her Ph.D. at the Universitat Autònoma of Barcelona in 1975 with Prof. E. Casassas, in the area of analytical chemistry. After holding several positions at the Universitat Autònoma de Barcelona she became full professor of Inorganic Chemistry in 1990. Following her initial studies on metal thiolates in the solid phase and in solution she has, since 1990, been studying the coordination ability of recombinant metallothioneins and the reactivity of metal complexes with sulfur containing ligands.
Rubén Mas-Ballesté (right) was born in Barcelona (Catalonia, Spain) in October of 1975. He studied Chemistry at the Universitat Autònoma de Barcelona where he obtained his BSc. degree in Chemistry in June of 1998, and his Ph.D. in February of 2004 under the supervision of Prof. Pilar González-Duarte and Prof. Agustí Lledós. From June 2004 he is doing a postdoctoral stay in the Lawrence Que's group at the University of Minnesota (USA). His research interests are the reactivity of metal chalcogenides and the synthesis and reactivity of structural and functional models of non-heme iron proteins.
Agustí Lledós (left) was born in 1955 in Barcelona. He received his BSc degree in Chemistry from the Universitat Autònoma de Barcelona in 1979, and his Ph.D. in 1984 at the same university, under the supervision of Juan Bertrán. After a postdoctoral stay at the Université de Paris-Sud (Orsay) with Yves Jean, he returned to the Universitat Autònoma in 1987 and created a research group devoted to the computational study of transition metal complexes. He was appointed Professor of Physical Chemistry in 1994. His research interests concern the computational modeling of transition metal systems, with focus on hydride complexes, σ-bond activation, bimetallic compounds and homogeneous catalysis.

MICROREVIEWS: This feature introduces the readers to the author's research through a concise overview of the selected topic. Reference to important work from others in the field is included.

abundance, the chemistry of metal sulfides has also been the object of extensive studies and still attracts great attention, mainly because of their structural diversity,[2] essential role in catalysis,[3] and rich solid-state and bioinorganic chemistry.[4] In contrast, platinum sulfide chemistry has received much less attention for many decades of the past century despite the fact that the first platinum-sulfur complex, $(NH_4)_2[Pt(\eta^2\text{-}S_5)_3]$, was isolated in 1903.[5]

A main hallmark in the field of platinum(II)−sulfur chemistry was established by Chatt and Mingos in 1970, who obtained several complexes of various nuclearities and structures.[6] Among them, $[(PMe_2Ph)_2Pt(\mu\text{-}S)_2Pt(PMe_2Ph)_2]$, followed by $[(PPh_3)_2Pt(\mu\text{-}S)_2Pt(PPh_3)_2]$[7] reported by Ugo et al. one year later, constitute the first examples of platinum(II) sulfide complexes containing the $\{Pt(\mu\text{-}S)_2Pt\}$ core. As a result of these studies, they also described the corresponding monoalkylated species $[L_2Pt(\mu\text{-}S)(\mu\text{-}SR)PtL_2]^+$ (L = PMe_2Ph, R = $PhCH_2$ [6] and L = PPh_3, R = CH_3 [7]) and the trinuclear $[Pt_3(PMe_2Ph)_6(\mu_3\text{-}S)_2]Cl_2$ complex,[6] whose formation provided the first evidence for the nucleophilicity of the bridging sulfido ligands in the $\{Pt(\mu\text{-}S)_2Pt\}$ core.

The evolution of the chemistry of $[L_2Pt(\mu\text{-}S)_2PtL_2]$ (L = phosphane) has proceeded very rapidly over the past two decades. Thus, the significant number of known homo- and heterometallic derivatives of $[L_2Pt(\mu\text{-}S)_2PtL_2]$ shows that this species is one of the most effective metalloligands identified to date. A summary of the historical milestones in platinum-sulfur chemistry leading to sulfide-bridged aggregates with the $\{Pt(\mu\text{-}S)_2Pt\}$ core, as well as the main developments in their synthesis, structure, and reactivity were excellently reviewed by Fong and Hor, who have made important contributions to this field.[8] Overall, the ability of the sulfido ligands in the $\{Pt(\mu\text{-}S)_2Pt\}$ core to extend their coordination mode from μ-S to μ_3-S accounts for the behavior of $[L_2Pt(\mu\text{-}S)_2PtL_2]$ as building blocks for higher nuclearity complexes, and the flexible hinge angle between the two $Pt^{II}S_2$ planes for the varied coordination geometries at the heterometal M in the corresponding $[\{L_2Pt(\mu_3\text{-}S)_2PtL_2\}_xML'_y]^z$ aggregates.

Remarkably, the reaction chemistry of $[L_2Pt(\mu\text{-}S)_2PtL_2]$ compounds towards nonmetallic electrophiles was not the object of systematic studies until much more recently. Combination of experimental results and theoretical calculations has allowed for a detailed knowledge of the cascade of reactions of $[L_2Pt(\mu\text{-}S)_2PtL_2]$ in the presence of either organic electrophiles, such as CH_2Cl_2,[9] or the simplest electron-acceptor species, the proton.[10] In addition, the influence of $\{Pt(\mu\text{-}S)_2Pt\}$ core on the reactivity of L′ in $[\{L_2Pt(\mu_3\text{-}S)_2PtL_2\}_xML'_y]^z$ aggregates has been explored.[11] All these results promise to inspire new approaches that contribute towards the unveiling of the potential of $[L_2Pt(\mu\text{-}S)_2PtL_2]$ compounds as nucleophilic agents.

Understanding the rich and diverse chemistry of the $\{Pt(\mu\text{-}S)_2Pt\}$ core has been the aim of our research for the past several years. Our approach has focused on the use of chelating diphosphanes as terminal L ligands,[12] with an emphasis on the chemistry of $[L_2Pt(\mu\text{-}S)_2PtL_2]$ with nonmetal electrophiles[9,10] and ML'_y fragments.[11] This report surveys the present knowledge on the nucleophilicity of the $\{Pt(\mu\text{-}S)_2Pt\}$ core in $[L_2Pt(\mu\text{-}S)_2PtL_2]$ compounds; the previous review by Fong and Hor is our starting point.[8] Thus, the peculiarities concerning the synthesis of $[L_2Pt(\mu\text{-}S)_2PtL_2]$ compounds, their distinguishing electronic and molecular features, the dynamic processes and electron-donor properties of the $\{Pt(\mu\text{-}S)_2Pt\}$ core, and the reactivity of $[L_2Pt(\mu\text{-}S)_2PtL_2]$ towards metallic and nonmetallic electrophiles will be summarized.

Synthesis, and Molecular and Electronic Structures of $[L_2Pt(\mu\text{-}S)_2PtL_2]$ Complexes

Synthetic Procedures

Despite their apparent simplicity, the synthetic routes reported for complexes with the formula $[L_2Pt(\mu\text{-}S)_2PtL_2]$ (Scheme 1) are not straightforward, often leading to mixture of products.[8] The most common procedure is based on the metathesis reaction between $[PtCl_2L_2]$ and $Na_2S{\cdot}9H_2O$,[6] for which only monometallic precursors with L = phosphane ligands have been used. These have generally been obtained by replacing 1,5-cyclooctadiene (cod) in $[PtCl_2(cod)]$ by the corresponding phosphane.[13] Other less direct routes entail the oxidation of $[PtL_4]$ with S_8, which affords phosphane sulfide as secondary product,[7] or, the reaction between $[PtCl_2L_2]$ and NaSH.[14] The latter involves the formation of $[Pt(SH)_2L_2]$ first and then its subsequent reaction with a second equivalent of $[PtCl_2L_2]$, thus yielding $[L_2Pt(\mu\text{-}S)_2PtL_2]$ plus two equivalents of HCl. However, as commented below, the presence of HCl is inconvenient as it can cause disintegration of the $\{Pt(\mu\text{-}S)_2Pt\}$ core.[10] Overall, the first pathway offers more advantages and becomes particularly adequate when the solubility of $[L_2Pt(\mu\text{-}S)_2PtL_2]$ in the organic solvent used is high, and thus its separation from unreacted $Na_2S{\cdot}9H_2O$ and formed NaCl is feasible. This requirement is best accomplished by the chelating diphosphanes 1,2-bis(diphenylphosphanyl)ethane (dppe) or 1,3-bis(diphenylphosphanyl)propane (dppp) than by PPh_3.[9,15]

Our studies on the reactivity of $[L_2Pt(\mu\text{-}S)_2PtL_2]$ (L_2 = dppe or dppp) towards nonmetal electrophiles[9,10] have provided information about the appropriate reaction conditions to obtain $[L_2Pt(\mu\text{-}S)_2PtL_2]$ from $[PtCl_2L_2]$ and $Na_2S{\cdot}9H_2O$ with maximum yield and purity (Scheme 2). To this end, the use of nonchlorinated solvents, the absence of protic acids in the reaction medium, and the purity of the reagent $Na_2S{\cdot}9H_2O$ are the main requirements. The choice of solvent is relevant so as to circumvent its reaction with $[L_2Pt(\mu\text{-}S)_2PtL_2]$, which occurs for L = PMe_2Ph, PPh_2py, PPh_3 and L_2 = dppf, dppe, dppp in the presence of CH_2Cl_2, as explained below. For the same reason, traces of CH_2Cl_2 that may be present in the $[PtCl_2L_2]$ starting complex should be eliminated. Similarly, the presence of protic acids should be avoided as they may cause protonation and subsequent disintegration of the $\{Pt(\mu\text{-}S)_2Pt\}$ core in the final $[L_2Pt(\mu\text{-}S)_2PtL_2]$ product.[10] Concern for the quality of the

 © 2004 Wiley-VCH Verlag GmbH & Co. KGaA, Weinheim

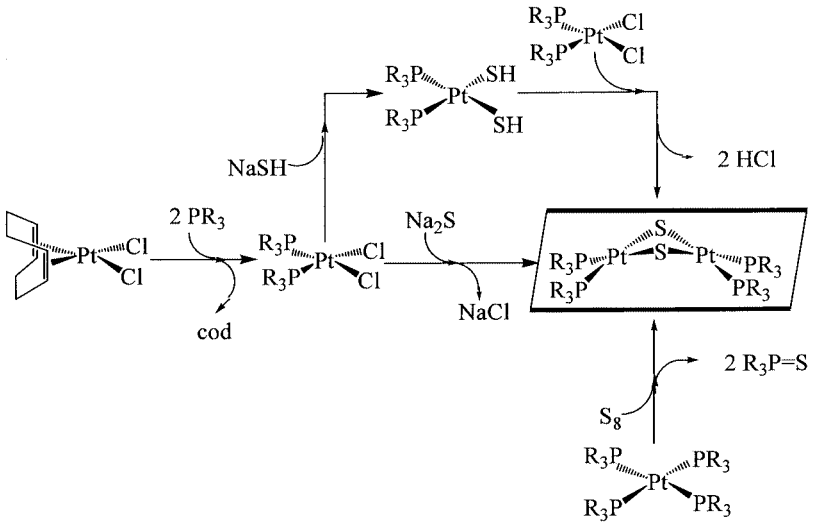

Scheme 1. Common synthetic procedures for [$L_2Pt(\mu\text{-}S)_2PtL_2$] complexes with unidentate or bidentate terminal phosphane ligands

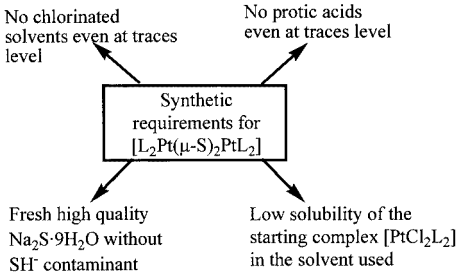

Scheme 2. Optimum reaction conditions for obtaining [$L_2Pt(\mu\text{-}S)_2PtL_2$] complexes from [$PtCl_2L_2$] and $Na_2S{\cdot}9H_2O$

reagent $Na_2S{\cdot}9H_2O$ arises from the observation that [$Pt(SH)_2L_2$], whose formation requires the presence of hydrogen sulfide anions, is not an uncommon by-product in the synthesis of [$L_2Pt(\mu\text{-}S)_2PtL_2$]. Finally, an additional factor that may hamper the synthesis of pure [$L_2Pt(\mu\text{-}S)_2PtL_2$] is the formation of the trimetallic complex [{$L_2Pt(\mu_3\text{-}S)_2PtL_2$}$PtL_2$]$Cl_2$ as a consequence of the coexistence in solution of the final product, [$L_2Pt(\mu\text{-}S)_2PtL_2$], with one of the reagents, [$PtCl_2L_2$]. This undesirable process is minimized with the use of solvents in which [$PtCl_2L_2$] is very slightly soluble and, consequently, the [$PtCl_2L_2$]/[$L_2Pt(\mu\text{-}S)_2PtL_2$] concentration ratio in solution during the reaction is very low.

All previous conclusions regarding the synthesis of [$L_2Pt(\mu\text{-}S)_2PtL_2$] from [$PtCl_2L_2$] and $Na_2S{\cdot}9H_2O$ have been obtained by monitoring the reactions with L_2 = dppe or dppp over time by ^{31}P-NMR spectroscopy.[12] This technique is revealed to be very useful for the monitoring of the evolution of the products from the reagents, as well as for the determination of the reaction time that corresponds to the maximum yield.

Molecular and Electronic Structures

The core of [$L_2Pt(\mu\text{-}S)_2PtL_2$] compounds consists of a four-membered {$Pt(\mu\text{-}S)_2Pt$} ring, with the platinum(II) atoms in a square-planar arrangement. The main geometric parameters for complexes structurally characterized by X-ray diffraction are shown in Table 1.[9,14–17] A distinguishing structural feature within this family of compounds is the degree of hinging of the {Pt_2S_2} core, which is measured by the dihedral angle θ between the two PtS_2 planes. According to reported data, this angle is highly dependent on the nature of the terminal L ligands. Similar features have been found for complexes containing {M_2S_2}

Table 1. Main geometric parameters of the {$Pt(\mu\text{-}S)_2Pt$} core in structurally characterized complexes; distances in angstroms and angles in degrees

Complex	Pt–S	Pt–P	Pt···Pt	S···S	Pt–S–Pt	S–Pt–S	P–Pt–P	θ[a]	Ref.
[$Pt_2(PPh_2Py)_4(\mu\text{-}S)_2$]	2.33	2.28	3.55	3.01	99.6	80.4	102.9	180.0	[14]
[$Pt_2(PPh_3)_4(\mu\text{-}S)_2$]	2.11[b]	2.22	3.17	2.69[b]	99.0	80.3	98.7	168.2	[16]
[$Pt_2(dppe)_2(\mu\text{-}S)_2$]	2.35	2.24	3.29	3.13	88.9	83.7	86.2	140.2	[15]
[$Pt_2(dppp)_2(\mu\text{-}S)_2$]	2.34	2.25	3.23	3.10	87.4	83.0	94.6	134.8	[9]
[$Pt_2(PMe_2Ph)_4(\mu\text{-}S)_2$]	2.34	2.26	3.17	–	85.5	81.6	–	121.0	[17]

[a] Dihedral angle between the two PtS_2 planes. [b] Values of Pt–S and S···S distances could be indicative of experimental inaccuracy on localization of sulfur atoms in the structure.

 © 2004 Wiley-VCH Verlag GmbH & Co. KGaA, Weinheim

cores, in which M = Ni[18] or Pd.[19] According to a theoretical and structural analysis on $[L_2M(\mu\text{-}X)_2ML_2]$ complexes, in which M has a d^8 electronic configuration, the driving force for the hinging of the $\{M_2S_2\}$ core arises from attractive metal···metal interactions between an occupied d_{z^2} orbital and an empty p_z orbital (Figure 1).[20] This interaction is modulated by the nature of the metal center, the terminal ligands, and the bridging atoms. Thus, the tendency to form bent structures increases with the diffuseness of the metal orbitals (i.e. going down the group of the periodic table), with the σ-donor ability of the terminal L ligands, and with decreasing electronegativity of the bridging X atoms. On the basis of these general rules it is clear that complexes with the formula [(phosphane)Pt(μ-S)$_2$Pt(phosphane)] are very well suited to adopt bent structures. However, steric interactions between terminal ligands can prevent the folding of the $\{M_2S_2\}$ core, as observed for M = Pt and L = PPh_2py[14] or PPh_3,[16] where the resulting core is planar or almost planar, respectively. Moreover, the increase in the Pt−X distances from X = S to Te could account for the planar structures observed for the $\{Pt(\mu\text{-}X)_2Pt\}$ core with Se^{2-} or Te^{2-} bridging ligands (Table 2).[21−24] This increase involves elongation of the Pt···Pt distance, which thus becomes too long to allow for the attractive interactions that underlie the folding of the $\{Pt(\mu\text{-}X)_2Pt\}$ core.

The electronic structure of complexes containing the $\{Pt(\mu\text{-}X)_2Pt\}$ (X = S, Se or Te) core has been analyzed from a theoretical point of view in recent works.[25,26] Thus, DFT calculations for model complexes using simplified terminal phosphane ligands have revealed that in all cases the highest energy occupied molecular orbital (HOMO) consists of an antibonding combination of the chalcogen p_π orbitals (p_z). A 3-D plot of this molecular orbital calculated for the model compound $[(PH_3)_2Pt(\mu\text{-}S)_2Pt(PH_3)_2]$ is shown in Figure 2. In addition, the orbital HOMO-1 consists essentially of a bonding combination of the same atomic orbitals. From this orbital analysis it can be inferred that a high electron density is located on the bridging chalcogenide ligand, which will thus be responsible for the nucleophilic character of $[L_2Pt(\mu\text{-}X)_2PtL_2]$ compounds. The energy of the HOMO is a good criterion for the comparison of the relative Lewis basicity of complexes containing the $\{Pt(\mu\text{-}X)_2Pt\}$ core. The energy of the HOMO in $[Pt_2(\mu\text{-}Te)_2(PMe_3)_4]$ (−3.46 eV) is considerably higher than that calculated for $[Pt_2(\mu\text{-}S)_2(H_2P(CH_2)_nPPH_2)_2]$ (n = 2, 3) (−3.89 eV), indicating that the lone electron pairs in the $\{Pt_2Te_2\}$ core are more accessible than those in the sulfur analogue.[25] These energy values are consistent with the lower oxidation potentials found for $\{Pt_2Te_2\}$ than for $\{Pt_2S_2\}$ containing complexes.

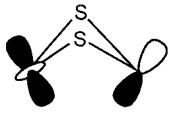

Figure 1. The driving force underlying the hinging of the $\{Pt(\mu\text{-}S)_2Pt\}$ core: $d_{z^2}-p_z$ metal to metal interactions

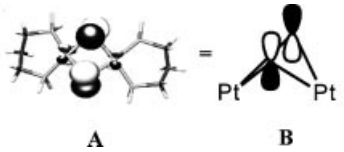

Figure 2. (A) 3D plot of the HOMO orbital in the model complex $[\{PH_2(CH_2)_3PH_2\}Pt(\mu\text{-}S)_2Pt\{PH_2(CH_2)_3PH_2\}]$; (B) corresponding schematic drawing

The structural and electronic features of complexes $[L_2Pt(\mu\text{-}S)_2PtL_2]$ reveal new perspectives for further studies. On the one hand, the different values found for the dihedral angle between the two PtS_2 planes in related $[L_2Pt(\mu\text{-}S)_2PtL_2]$ compounds show the flexibility of the $\{Pt_2S_2\}$ core and anticipate its involvement in dynamic processes. On the other hand, the high electron-density on the sulfide ligands in the above-mentioned core accounts for the electron-donor behavior of this family of complexes, which should be explored by means of electrochemical measurements. Both issues are considered in the following sections.

Dynamic Processes: The Flight of the Butterfly

Structural data on $[L_2Pt(\mu\text{-}S)_2PtL_2]$ complexes show a wide range for the folding degree of the $\{Pt_2S_2\}$ core, from strongly bent (θ = 121°, L = PMe_2Ph)[17] to planar (θ = 180°, L = PPh_2py)[14] rings (Table 1). In addition, theoretical calculations indicate that the energy cost for the hinging movement is low; the energy difference between bent and planar geometries is about 4−8 kcal/mol.[20,27] Interestingly, in theoretically studied model systems the planar geometry is not a minimum in the potential energy surface but, instead, it constitutes the transition state from a folded geometry to the corresponding reverse folding, as depicted

Table 2. Main geometric parameters of the $\{Pt(\mu\text{-}X)_2Pt\}$ (X = Se^{2-} or Te^{2-}) core in structurally characterized complexes; distances in angstroms and angles in degrees

Complex	Pt−X	Pt−P	Pt···Pt	X···X	Pt−X−Pt	X−Pt−X	P−Pt−P	θ[a]	Ref.
$[Pt_2(PPh_3)_4(\mu\text{-}Se)_2]$	2.46	2.27	3.76	3.13	100.4	79.6	99.5	180.0	[21]
$[Pt_2(PPh_3)_4(\mu\text{-}Te)_2]$	2.62	2.30	4.10	3.25	102.7	76.9	100.4	180.0	[22]
$[Pt_2(PEt_3)_4(\mu\text{-}Te)_2]$	2.61	2.28	4.10	3.26	102.9	77.1	106.1	180.0	[23]
$[Pt_2(dppe)_2(\mu\text{-}Te)_2]$	2.63	2.25	3.96	3.46	97.7	82.3	86.0	180.0	[24]

[a] Dihedral angle between the two PtS_2 planes.

 © 2004 Wiley-VCH Verlag GmbH & Co. KGaA, Weinheim

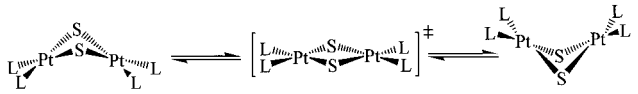

Scheme 3. Dynamic process arising from the flexibility of the {Pt(μ-S)$_2$Pt} core; the sign ‡ denotes a transition state

in Scheme 3. The low energy of the transition state is consistent with the hinging process that occurs at room temperature. Experimental evidence was obtained from ^{13}C NMR spectroscopic data on [L$_2$Pt(μ-S)$_2$PtL$_2$] complexes with the chelating phosphanes dppe or dppp as terminal ligands that showed the equivalence of all phenyl groups at room temperature in solution (Scheme 4). However, the hinged geometry of the {Pt$_2$S$_2$} core in the corresponding X-ray structures[9,15] was inconsistent with NMR data unless a dynamic process enabled the phenyl rings to become symmetry-equivalent in solution. The fact that this equivalence is maintained even at low temperature is indicative of the low energy barrier of the bending process. In addition, it is worth noting that [L$_2$Pt(μ-S)$_2$PtL$_2$] complexes containing unidentate phosphane PR$_3$ do not allow for the distinguishing of the hinging process and the fast rotation along the Pt−P bond, which could account for the observed equivalence of all R groups in ^{13}C NMR measurements. Overall, the well-established term butterfly to designate [L$_2$Pt(μ-S)$_2$PtL$_2$] complexes appears particularly adequate on the basis of the dynamic properties of the {Pt$_2$S$_2$} core.

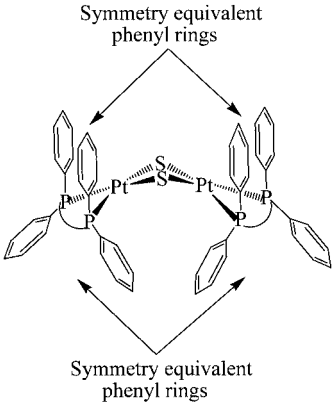

Scheme 4. Asymmetry of the phenyl rings in a chelating phosphane considering a hinged geometry for the {Pt(μ-S)$_2$Pt} core

Other fast reversible intramolecular dynamic processes involving the {Pt$_2$S$_2$} core have also been observed. One of them, consisting of the intramolecular S−H···S proton exchange in the complexes [L$_2$Pt(μ-S)(μ-SH)PtL$_2$]$^+$ (L$_2$ = dppe or dppp),[28] provided the first example of a fast S−H···S proton exchange in a metal complex. Experimental evidence came from VT-^{31}P{^{1}H} NMR spectroscopic data (Figure 3), which showed the equivalence of the four phosphorus nuclei at 300 K in solution. However, the proton transfer between both sulfur atoms is frozen at 200 K and, consequently, the phosphorus nuclei in the *trans* and *cis* dispositions with respect to the bridging SH group show different chemical shift values. From the NMR data, $\Delta G^{\ddagger}$ of about 11 kcal/mol was estimated for the S−H···S proton-transfer process. Theoretical studies corroborated the feasibility of the S−H···S proton transfer process as well as its corresponding experimental energy. They also showed that the transition state involves a trigonal S−H−S arrangement, in which the partial rupture of the S−H bond is compensated by the partial formation of the new S−H bond (Scheme 5).

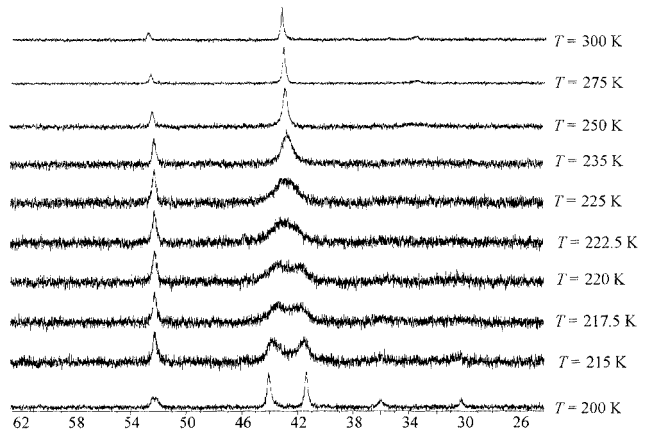

Figure 3. VT-^{31}P{^{1}H} NMR spectra of complex [Pt$_2$(dppe)$_2$(μ-S)(μ-SH)]ClO$_4$

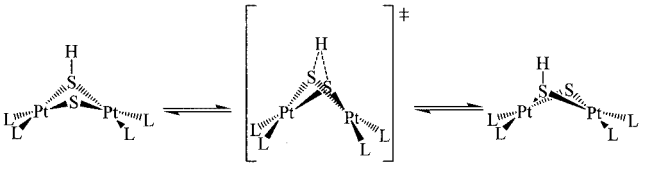

Scheme 5. Fast intramolecular S−H···S proton transfer in [L$_2$Pt(μ-S)(μ-SH)PtL$_2$]$^+$

It is worth mentioning the role played by the flexibility of the {Pt$_2$S$_2$} ring in the process. Thus, the S···S distance is notably shorter in the transition sate (2.98 Å) than in the reactants (3.24 Å), the shortening of this distance is attained by increasing the degree of folding of the {Pt$_2$S$_2$} ring ($\theta > 130°$ in the reactants and about 109° in the transition sate).

Remarkably, no proton transfer processes have been observed for [L$_2$Pt(μ-S)(μ-SH)PtL$_2$]$^+$ complexes in which PPh$_3$ replaces dppe or dppp.[29,30] One possible factor to account for these differences is the bulkiness of PPh$_3$ that could prevent the hinging of the {Pt(μ-S)$_2$Pt} fragment, thus disfavoring the folded transition state required for the intramolecular S−H···S proton transfer. Another explanation is the possible interaction of the S−H proton with a phenyl ring of PPh$_3$, thus stabilizing the [L$_2$Pt(μ-S)(μ-SH)PtL$_2$]$^+$ cation in relation to the transition state.

A similar transfer process has been observed in [(PPh$_3$)$_2$Pt(μ-S){μ-S-Au(PPh$_3$)}Pt(PPh$_3$)$_2$]$^+$, closely related to [L$_2$Pt(μ-S)(μ-SH)PtL$_2$]$^+$, on the basis of the isolobal analogy of [H]$^+$ and [AuPPh$_3$]$^+$ fragments (Scheme 6).[31] It is noteworthy that in the former cation, the intramolecular exchange is observed even if the terminal ligand is PPh$_3$. Probably, the larger size of the gold atom, which in the transition state interacts with the two sulfur atoms of the {Pt(μ-S)$_2$Pt} core, provokes less important geometric constraints

 © 2004 Wiley-VCH Verlag GmbH & Co. KGaA, Weinheim

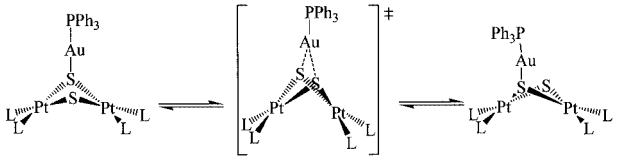

Scheme 6. Fast intramolecular exchange of the $[AuPPh_3]^+$ group in the $[L_2Pt(\mu\text{-}S)\{\mu\text{-}S\text{-}(AuPPh_3)\}PtL_2]^+$ cation

in this core than the proton. In all, the lower flexibility of the $\{Pt_2S_2\}$ ring in $[(PPh_3)_2Pt(\mu\text{-}S)\{\mu\text{-}S\text{-}Au(PPh_3)\}\text{-}Pt(PPh_3)_2]^+$ is not an impediment for the observation of intramolecular exchange of the $[AuPPh_3]^+$ fragment.

The $\{Pt(\mu\text{-}S)_2Pt\}$ Core as Electron-Donor in Redox Processes

An immediate consequence arising from the electronic structure of the $\{Pt(\mu\text{-}S)_2Pt\}$ core is its ability to act as an electron-donor. The more direct way to observe this property is the study of the possible oxidation processes of the $[L_2Pt(\mu\text{-}S)_2PtL_2]$ complexes. Despite the potential interest of the redox properties of $[L_2M(\mu\text{-}X)_2ML_2]$ systems in the field of bioinorganic chemistry,[32−34] this feature had not been considered in the study of $[L_2Pt(\mu\text{-}S)_2PtL_2]$ complexes until very recently. On the other hand, theoretical analysis has allowed to establish that bonding between antipodal atoms in binuclear complexes depends on the total number of electrons in the framework. Thus, qualitative rules anticipate that electrochemical oxidation of the $\{M_2X_2\}$ (M = d^8-metal) core induces formation of X−X or M−M bonds as a result of changing the number of electrons in the framework molecular orbitals.[20,27,32,35] However, experimental evidence showing variations in the connectivity of the atoms in the $\{M(\mu\text{-}X)_2M\}$ rings as a consequence of the redox processes are very scarce.

Recently, the energetic and structural consequences of the successive removal of two electrons from the $\{Pt(\mu\text{-}S)_2Pt\}$ core in $[L_2Pt(\mu\text{-}S)_2PtL_2]$ (L_2 = dppe or dppp) complexes have been studied by combining electrochemical measurements and DFT calculations. Assignment of the structure corresponding to the species involved in the cyclic voltammogram peaks relied on the theoretical calculations.[25] The cyclic voltammetric measurements were indicative of two consecutive monoelectronic oxidations. In addition, cyclic voltammetric data showed that the radical cation $[L_2Pt(\mu\text{-}S)_2PtL_2]^+$ is unstable and gives rise to the disintegration of the $\{Pt(\mu\text{-}S)_2Pt\}$ core. The stability of the oxidized $[L_2Pt(\mu\text{-}S)_2PtL_2]^+$ form is highly dependent on the nature of the terminal ligand, and is greater for dppp than for dppe.

Structural data obtained from theoretical calculations on the species $[L_2Pt(\mu\text{-}S)_2PtL_2]^{n+}$ (n = 0, 1, 2; L_2 = $H_2P(CH_2)_2PH_2$ or $H_2P(CH_2)_3PH_2$) show differences between neutral and monocationic species, the latter having slightly shorter S···S distances and smaller S−Pt−S angles, as well as longer Pt···Pt distances. These changes involve the formation of an incipient S−S bond. The abstraction of a second electron from the $\{Pt(\mu\text{-}S)_2Pt\}$ core enhances the structural tendencies found in the monoxidized complexes. These variations eventually lead to the formation of a S−S bond (S−S = 2.11 Å), with the concomitant lengthening of the Pt···Pt distance (Pt···Pt approximately 3.50 Å) and the larger folding along the S−S axis to give a highly bent geometry (θ = 104 °). In all, the oxidation of the $\{Pt(\mu\text{-}S)_2Pt\}$ core consists of two subsequent one-electron removals, thus giving rise to the bridging of the two metal centers by a disulfide S_2^{2-} ligand. The redox behavior of $[L_2Pt(\mu\text{-}S)_2PtL_2]$ (L_2 = dppe or dppp) together with the main calculated structural features for neutral and oxidized forms in the model compound $[\{H_2P(CH_2)_2PH_2\}Pt(\mu\text{-}S)_2Pt\{H_2P(CH_2)_2PH_2\}]$ are depicted in Scheme 7. The evolution of the NPA (Natural Population Analysis) charges throughout the oxidation process agrees with the oxidation of the sulfur ligands.

With the aim of verifying that theoretical and experimental data were fully consistent, the redox potentials of the oxidation processes were calculated. The accurate calculation of redox potentials is still a very demanding problem, and only very recently the reduction potentials for some small organic molecules have been reported.[36] In large systems, with transition metal atoms, only semi-quantitative results can be expected. The methodology used for the theoretical estimation of the redox potentials involving the oxidation of $[L_2Pt(\mu\text{-}S)_2PtL_2]$ compounds requires calculation of the Gibbs energy of the oxidation reaction in solution, $(\Delta G_{ox})_{sol}$, following the approach based on continuum solvent models.[37] The absolute redox potential can be calculated according to the following expression: $E_{ox} = (\Delta G_{ox})_{sol}/nF$.

To obtain the electrode potential value referenced with respect to a reference electrode it is necessary to calculate the difference between the calculated absolute potential and the absolute potential of the reference electrode. For this purpose, we used the value of +4.43 V assigned to the absolute reduction potential of the hydrogen electrode.[38] The closeness between the electrochemical data and DFT calculations confirmed that the experimentally observed abstraction of two electrons from $[L_2Pt(\mu\text{-}S)_2PtL_2]$ results in the formation of a S−S bond to give the disulfide containing complexes $[L_2Pt(\mu\text{-}S_2)PtL_2]^{2+}$.

Studies devoted to the redox behavior of complexes $[L_2Pt(\mu\text{-}X)_2PtL_2]$ (X = S, Se, Te) are very scarce in the literature. From a theoretical perspective, an early work demonstrated the ability of the $\{Pt(\mu\text{-}Se)_2Pt\}$ core to present a redox behavior similar to that observed for the $\{Pt(\mu\text{-}S)_2Pt\}$ core. Thus, Hartree−Fock calculations on $[(PH_3)_2Pt(\mu\text{-}Se)_2Pt(PH_3)_2]^{n+}$ (n = 0, 2) provided evidence for the formation of a Se−Se bond as a result of the oxidation of the $\{Pt(\mu\text{-}Se)_2Pt\}$ core.[21] The closest work to the study of the redox properties of $[L_2Pt(\mu\text{-}S)_2PtL_2]$ complexes consists of the isolation and characterization of $[(PEt_3)_2Pt(\mu\text{-}Te)_2Pt(PEt_3)_2]$ and $[(PEt_3)_2Pt(\mu\text{-}Te_2)Pt(PEt_3)_2]^{2+}$.[23] Analogously to the $\{Pt(\mu\text{-}S)_2Pt\}$ core, chemical oxidation of $[(PEt_3)_2Pt(\mu\text{-}Te)_2Pt(PEt_3)_2]$ causes a decrease in the Te−Te distance from a nonbonding (3.263 Å) to a bonding dis-

 © 2004 Wiley-VCH Verlag GmbH & Co. KGaA, Weinheim

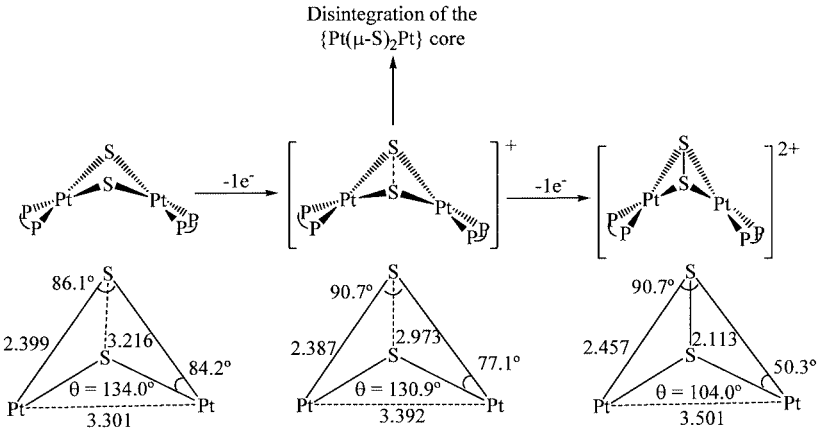

Scheme 7. Redox behavior of [L_2Pt(μ-S)$_2$PtL_2] (L_2 = dppe or dppp); calculated main structural parameters for [Pt_2{$H_2P(CH_2)_2PH_2$}$_2$(μ-S)$_2$]$^{n+}$ (n = 0, 1 or 2) are included

tance (2.695 Å), indicating the formation of a Te−Te bond in the dication.

According to the experimental CV data, the difficulties found in determining all the species involved in the oxidation of the {Pt_2S_2} core arise from the disintegration of the monocationic species, which leads to the well-known trimetallic [{L_2Pt(μ$_3$-S)$_2$PtL_2}PtL_2]$^{2+}$ complex as the main product. Calculations of the thermodynamics of possible processes following disintegration of [L_2Pt(μ-S)$_2$PtL_2]$^+$ show that the most favorable process involves the recombination of two [L_2Pt(μ-S)$_2$PtL_2]$^+$ species to give the cited trimetallic complex and the neutral mononuclear [L_2Pt(S_2)] complex.

Complexes with functionalized {Pt(μ-S)$_2$Pt} cores are also able to show redox properties. In [(PPh_3)$_2$Pt(μ-S)(μ-SHgR))Pt(PPh_3)$_2$]$^+$, the observed process consists of the monoelectronic oxidation of the sulfide ligand that is not coordinated to the mercury atom.[39] However, the poor solubility of [(PPh_3)$_2$Pt(μ-S)$_2$Pt(PPh_3)$_2$] hampered comparison between the redox properties of the {Pt(μ-S)$_2$Pt} and {Pt(μ-S)(μ-SHg)Pt}$^+$ cores. Notwithstanding this, results obtained with the highly soluble [L_2Pt(μ-S)$_2$PtL_2] (L_2 = dppe or dppp) are consistent with the hypothesis presented by Hor et al., indicating that the sulfide ligands in the {Pt(μ-S)$_2$Pt} fragment are electroactive.

When the two sulfur atoms of the {Pt(μ-S)$_2$Pt} core act as electron-donors towards a metal center, a different redox activity is observed. Thus, electrochemical studies on the trimetallic clusters [{L_2Pt(μ$_3$-S)$_2$PtL_2}PtL_2]$^{2+}$ (L_2 = dppm, dppe, dppp, dppb) have shown that the cationic core {Pt_3(μ$_3$-S)$_2$}$^{2+}$ is able to accept one electron, as observed by means of cyclic voltammetric measurements.[40] These data indicate that the electron-donor properties of the {Pt(μ-S)$_2$Pt} core can be reversed, thus becoming an electron-acceptor, after coordination to a metal center. The electrochemical features of this family of trimetallic complexes are also highly dependent on the chelate ring size of the phosphane ligands.

Compounds [L_2Pt(μ-S)$_2$PtL_2] as Metalloligands to Metal Centers

Homo- and Heterometallic Derivatives of [L_2Pt(μ-S)$_2$PtL_2]

The behavior of [L_2Pt(μ-S)$_2$PtL_2] (L = phosphane) as a metalloligand to metal centers has prompted most of the research undertaken in this field of chemistry. The electronic and dynamic properties of the {Pt(μ-S)$_2$Pt} core, already explained, account for the outstanding ability of [L_2Pt(μ-S)$_2$PtL_2] compounds to act as building blocks for higher nuclearity aggregates with the general formula [{L_2Pt(μ$_3$-S)$_2$$L_2$}$_xML'_y$]^z. At the same time, the wide coordination environments offered by main group or transition metals together with the nature of their accompanying L′ species, either ligands or counter ions, enhance the structural diversity of this family of derivatives. As depicted in Scheme 8, aggregates of known structure include those with varied coordination geometries about the heterometal: linear,[41,42] angular,[43] T-shaped,[42,44] Y-shaped,[45] tetrahedral,[12,15,46] square planar,[12,47] square pyramidal,[48] distorted trigonal prismatic,[49] trigonal bipyramidal,[50] hexagonal bipyramidal,[51] "piano stool"[52] and others.[53,54] These aggregates also display the ability of the [L_2Pt(μ-S)$_2$PtL_2] metalloligand to function as a unidentate,[41] bridging,[53] or chelating ligand.[52] Concerning the nature of the heterometal M, a wide range of p- and d-block elements have been studied. Those included in [{L_2Pt(μ$_3$-S)$_2$$L_2$}$_xML'_y$]^z aggregates described subsequently to the earlier report by Fong and Hor,[8] are the following: V^V,[51] Mo^{VI},[51] Re^I,[50] Os^{II},[52] Rh^{III},[52] Ir^{III},[52] Zn^{II},[12,48] Cd^{II},[12,48] U^{VI},[51] and Sn^{IV}.[29] Moreover, it is remarkable that [L_2Pt(μ-S)$_2$PtL_2] metalloligands allow stabilization of oxidation states that are unstable in sulfur-thiolate environments as it occurs in tetrahedral {M^{II}(SR)$_4$}$^{2-}$, M = Co[55] or Cu,[15] complexes. Overall, on the basis of this formidable body of information, it seems that current knowledge on the wide family of the homo- and heterometallic deriva-

 © 2004 Wiley-VCH Verlag GmbH & Co. KGaA, Weinheim

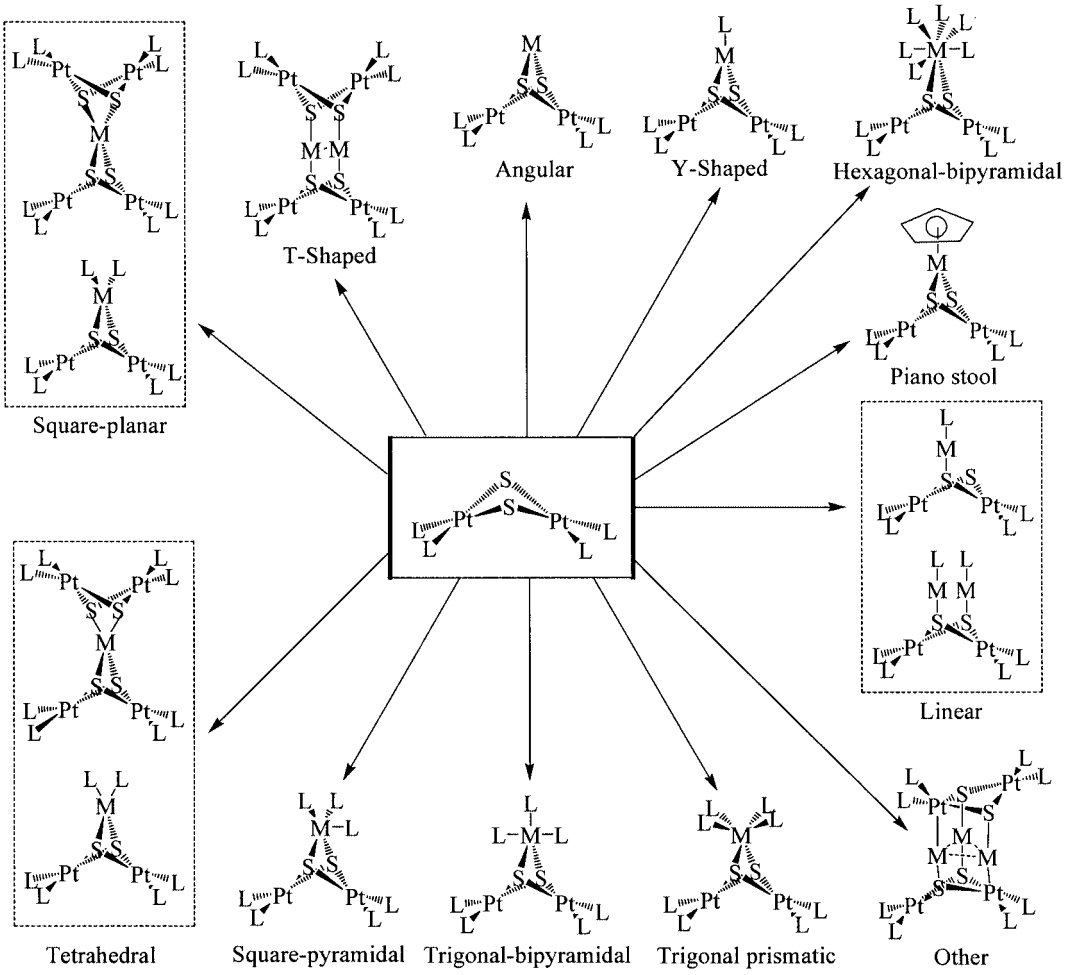

Scheme 8. Coordination environments at M in $[\{L_2Pt(\mu\text{-}S)_2PtL_2\}_xML'_y]^z$ aggregates

tives of $[L_2Pt(\mu\text{-}S)_2PtL_2]$ compounds has achieved a considerable degree of maturity.

The suitability of electrospray mass spectrometry (ESI MS) to characterize charged inorganic species in solution has allowed its use for probing the reactivity of the $\{Pt(\mu\text{-}S)_2Pt\}$ core towards metal ions. This technique has proved very effective in providing a preliminary detection and characterization of the heterometallic aggregates predominant in solution as a result of a particular reaction. On the basis of the good correlation found between the ESI mass spectra and synthesis-scale reactions, the synthetic strategies can thus be focused on the synthesis of those aggregates that are supported by ESI MS evidence.[29,30]

Influence of $[L_2Pt(\mu\text{-}S)_2PtL_2]$ on the Reactivity of ML′ Fragments

Significantly, despite the widespread attention devoted to the synthesis and characterization of $[\{L_2Pt(\mu_3\text{-}S)_2L_2\}_xML'_y]^z$ aggregates, studies on the influence of the $[L_2Pt(\mu\text{-}S)_2PtL_2]$ metalloligand on the reactivity of L′ remained unreported. In order to fill this gap, we recently described the synthesis and structural characterization of complexes $[\{(dppp)Pt(\mu\text{-}S)_2Pt(dppp)\}PtL']^z$ (L′ = cod,[11] $z = 2+$ or L′ = 2Cl, $z = 0$[56]), and studied the substitution reactions of cod and chloride ligands. Experimental results showed that cod was substitutionally inert towards dppp while chloride was easily replaced by dmso or phosphane ligands. These features were inconsistent with the common procedure used to obtain $[PtCl_2(dppp)]$ from $[PtCl_2(cod)]$ and dppp, and with the usual stability of $[PtCl_2(dppp)]$ in dmso solvent. Within this context, the influence of $[(dppp)Pt(\mu\text{-}S)_2Pt(dppp)]$ on the reactivity of the $\{Pt(cod)\}^{II}$ or $\{PtCl_2\}$ fragments deserved further consideration. Results obtained on the unusual reactivity observed for $[\{(dppp)Pt(\mu\text{-}S)_2Pt(dppp)\}Pt(cod)]^{2+}$ in the presence of $NaCH_3O$ are described below. Those concerning the substitution of chloride ligands in $[\{(dppp)Pt(\mu\text{-}S)_2Pt(dppp)\}PtCl_2]$ are given in the next section.

With the aim of exploring the influence of the $\{Pt(\mu\text{-}S)_2Pt\}$ core on the reactivity of the $\{Pt(cod)\}^{II}$ fragment, we obtained complexes $[\{Pt_2(\mu_3\text{-}S)_2(dppp)_2\}Pt(cod)]Cl_2$ and $[\{Pt_2(\mu_3\text{-}S)_2(cod)_2\}Pt(dppp)]Cl_2$ by reacting $[Pt_2(\mu\text{-}S)_2(dppp)_2]$ and $[PtCl_2(cod)]$ (1:1), and $[Pt(SH)_2(dppp)]$ and $[PtCl_2(cod)]$ (1:2), respectively.[11] In contrast with the general behavior of cationic olefin complexes of platinum,[57,58] the synthesized complexes did not undergo spontaneous loss of the unsaturated ligand and thus allowed exploration of their reactivity towards a strong nucleophile such as so-

 © 2004 Wiley-VCH Verlag GmbH & Co. KGaA, Weinheim

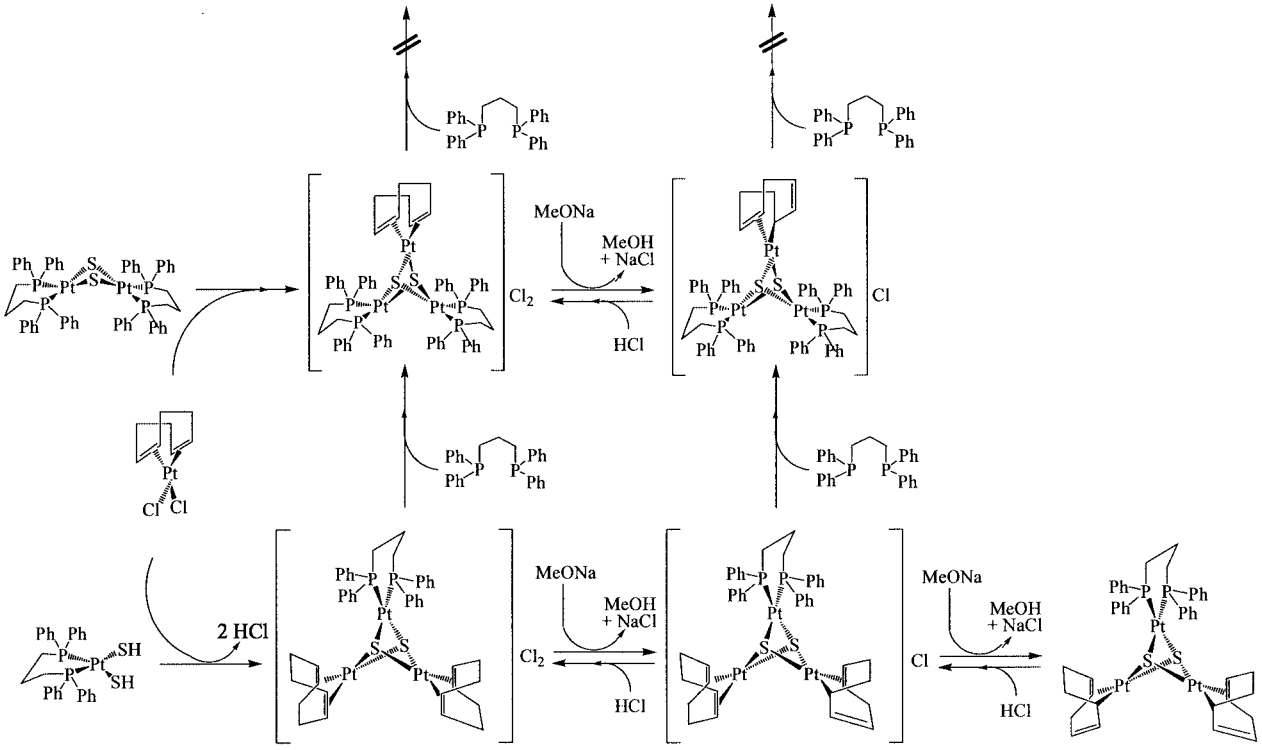

Scheme 9. Reactivity of cod containing derivatives of $[L_2Pt(\mu\text{-}S)_2PtL_2]$

dium methoxide (Scheme 9). Remarkably, unlike previous reports on the attack of $NaCH_3O$ on the $\{Pt(cod)\}^{II}$ fragment,[59][60] the above reactions did not promote the nucleophilic attack of the methoxide anion, but only deprotonation of cod, thus leading to $[\{Pt_2(\mu_3\text{-}S)_2(dppp)_2\}Pt(C_8H_{11})]Cl$, $[\{Pt_2(\mu_3\text{-}S)_2(cod)(C_8H_{11})\}Pt(dppp)]Cl$ and $[\{Pt_2(\mu_3\text{-}S)_2(C_8H_{11})_2\}Pt(dppp)]$. Concerning the substitution of cod, in neutral or anionic form, by dppp, the five complexes obtained behaved differently. Those containing the $\{Pt_2(\mu_2\text{-}S)_2(dppp)_2\}$ moiety were substitutionally inert. By contrast, those based on the $\{Pt_2(\mu_2\text{-}S)_2(dppp)L\}$ moiety with $L = C_8H_{12}$ or $C_8H_{11}^-$ underwent the substitution reaction readily. However, DFT calculations indicated that thermodynamic factors were not responsible for the observed differences. Consequently, kinetic effects should account for the reluctance of the ligand cod to be replaced by dppp in $[\{Pt_2(\mu_3\text{-}S)_2(dppp)_2\}Pt(cod)]^{2+}$ and $[\{Pt_2(\mu_3\text{-}S)_2(dppp)_2\}Pt(C_8H_{11})]^+$, where the steric hindrance imposed by $\{Pt_2(\mu_2\text{-}S)_2(dppp)_2\}$ disfavors an associative pathway for the corresponding exchange reactions.

An interesting example to test the influence of $[L_2Pt(\mu\text{-}S)_2PtL_2]$ on the properties of a $\{ML'_y\}$ fragment has recently been provided by Brunner et al.,[61] who synthesized the heterometallic trinuclear complex $[\{Pt_2(\mu\text{-}S)_2[\{(-)\text{-diop}\}]Rh(cod)]Cl$ by reacting the chiral $[Pt_2(\mu\text{-}S)_2\{(-)\text{-diop}\}]$ metalloligand with $[Rh(cod)Cl]_2$. However, its further use as a catalyst in enantioselective transformations afforded moderate results, which are mainly attributed to the reluctance of cod to be displaced from the trinuclear complex. This observation is consistent with the low tendency of cod in $[\{(PPh_3)_2Pt(\mu\text{-}S)_2Pt(PPh_3)_2\}Rh(cod)]^+$ to be substituted by H_2, CO, SO_2, and dppe, as reported by Briant et al. in 1985.[62] Overall, reported results fully confirm that the binding of the $[L_2Pt(\mu\text{-}S)_2PtL_2]$ metalloligand to $\{Pt(cod)\}^{2+}$ or $\{Rh(cod)\}^+$ causes profound alterations in the chemistry of such fragments. Extension of these findings to other fragments and studies on the influence of terminal L ligands on their properties may provide new perspectives within the area of organometallic chemistry.

$[L_2Pt(\mu\text{-}S)_2PtL_2]$ Compounds as Building Blocks

Further evidence of the influence of the $\{Pt(\mu\text{-}S)_2Pt\}$ core on the reactivity of bonded ML'_y fragments was recently provided by the lability of chloride ligands in $[\{(dppp)Pt(\mu\text{-}S)_2Pt(dppp)\}PtCl_2]$.[56] This became apparent through independent experimental data: (i) the partial or total loss of chloride ligands in some of the species identified in the characterization of this compound by ESI MS; (ii) the isolation of $[\{(dppp)Pt(\mu\text{-}S)_2Pt(dppp)\}PtCl(dmso)]Cl$ when the former complex is dissolved in dmso; and (iii) the displacement of chloride ligands by formation of $[\{(dppp)Pt(\mu\text{-}S)_2Pt(dppp)\}Pt(dppp)]Cl_2$ after addition of an stoichiometric amount of dppp. All these findings were in good agreement with previous reports on the lability of chloride ligand in the $[\{(PPh_3)_2Pt(\mu\text{-}S)_2Pt(PPh_3)_2\}PtCl(PPh_3)]^+$ complex.[63]

On the basis of the ability of the $\{Pt(\mu\text{-}S)_2Pt\}$ core to facilitate substitution of chloride ligands in $[\{Pt_2S_2\}PtCl_2]$ fragments, we designed a novel route to obtain multimetallic aggregates containing a $\{Pt_2S_2\}_n$ core (Scheme 10). The synthetic strategy involves first the expansion of the $\{Pt_2S_2\}$ ring to a $[\{Pt_2S_2\}PtCl_2]$ moiety. Replacement of chloride ligands by sulfide then causes the $\{PtCl_2\}$ fragment to form a $\{Pt_2S_2\}$ linking unit between two $\{Pt_2S_2\}$ rings, thus af-

 © 2004 Wiley-VCH Verlag GmbH & Co. KGaA, Weinheim

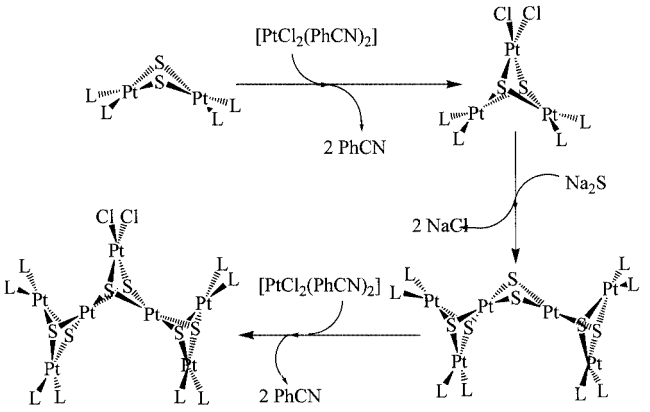

Scheme 10. Synthetic strategy to obtain multimetallic complexes containing the $\{Pt(\mu\text{-}S)_2Pt\}_n$ core

fording a new $[\{Pt_2S_2\}_2\{Pt_2S_2\}]$ core. Its subsequent evolution into $[\{Pt_2S_2\}_3PtCl_2]$ lays the foundation for a new cycle.

According to the first step in Scheme 10, the reaction between $[(dppp)Pt(\mu\text{-}S)_2Pt(dppp)]$ and $[PtCl_2(PhCN)_2]$ afforded the unprecedented trinuclear $[\{(dppp)Pt(\mu\text{-}S)_2Pt(dppp)\}PtCl_2]$ complex, in spite of the fact that other nuclearities had been proposed for related complexes obtained under similar reaction conditions.[47,64] Another interesting feature as a result of the reactions depicted in Scheme 10 is that the characterization of the high nuclearity complexes $[\{Pt_2(\mu_3\text{-}S)_2(dppp)_2\}_2\{Pt_2(\mu\text{-}S)_2\}]$ and $[\{Pt_2(\mu_3\text{-}S)_2(dppp)_2\}Pt_2(\mu_3\text{-}S)_2PtCl_2\{Pt_2(\mu_3\text{-}S)_2(dppp)_2\}]$ was mainly achieved by means of MALDI-TOF mass spectrometry, which thus revealed its potential use in further studies.

In all, while high nuclearity heterometallic derivatives of $[L_2Pt(\mu\text{-}S)_2PtL_2]$ had been reported,[42,53] the systematic approach described above to obtain multimetallic derivatives is unprecedented. In fact, it demonstrates that the nucleophilicity of the $\{Pt(\mu\text{-}S)_2Pt\}$ core can be driven to build nuclearity-controlled multinuclear aggregates containing a $\{Pt_2S_2\}_n$ core. Extension of the same strategy to other metals with square-planar coordination may allow control of the size of metal chalcogenide compounds and thus of their properties and potential applications.

Reactivity towards Non-Metallic Electrophiles

Organic Electrophiles

The nucleophilicity of the sulfide bridges in the $\{Pt(\mu\text{-}S)_2Pt\}$ core towards organic electrophiles was established as a result of the reaction of $[L_2Pt(\mu\text{-}S)_2PtL_2]$ (L = PMe_2Ph, PPh_3) compounds with $PhCH_2Br$[6] or CH_3I.[7] These reactions led to the corresponding monoalkylated cation $[L_2Pt(\mu\text{-}S)(\mu\text{-}SR)PtL_2]^+$ (R = Me or CH_2Ph), even if stoichiometric excess of the alkyl halide was present. Very recently, extension of the previous reaction to organic dihal-

Table 3. Complexes obtained upon exposure of $[L_2Pt(\mu\text{-}S)_2PtL_2]$ in CH_2Cl_2

Complex	Terminal ligand	Experimental evidences	Ref.
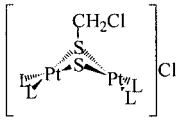	L = PPh_3 L_2 = dppf [a] L_2 = dppe [b] L_2 = dppp [c]	NMR	[68] [69] [9] [9]
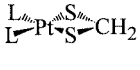	L = PMe_2Ph L = dppy [d] L_2 = dppe[b] L_2 = dppp[c]	NMR and X-ray diffraction	[70] [14] [9] [9]
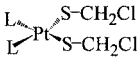	L_2 = dppf [a] L = PPh_3	NMR	[69] [71]
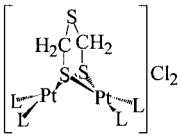	L_2 = dppp[c]	NMR and X-ray diffraction	[9]
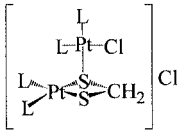	L = PPh_3	NMR and X-ray diffraction	[46]

[a] dppf = $[Fe(C_5H_4PPh_2)_2]$. [b] dppe = $Ph_2P(CH_2)_2PPh_2$. [c] dppp = $Ph_2P(CH_2)_3PPh_2$. [d] dppy = $PPh_2(C_5H_4N)$.

 © 2004 Wiley-VCH Verlag GmbH & Co. KGaA, Weinheim

ides has allowed isolation of the dialkylated derivative $[(PPh_3)_2Pt(\mu\text{-}(SC_2H_4S)\text{-}S,S')Pt(PPh_3)_2]$ by reacting $[(PPh_3)_2Pt(\mu\text{-}S)_2Pt(PPh_3)_2]$ with 100-fold excess of 1,2-dichloroethane.[65] Similar double alkylations have been achieved in complexes containing the $\{Pt(\mu\text{-}Se)_2Pt\}$[66,67] or $\{Ni(\mu\text{-}S)_2Ni\}$[18] core.

A particular case of the previous reaction involving organic halides is the surprising progression of $[L_2Pt(\mu\text{-}S)_2PtL_2]$ compounds when they are dissolved in chlorinated solvents, mainly CH_2Cl_2. Thus, in recent years, several different species have been characterized as a result of often unexpected reactions in this solvent (Table 3).[9,14,46,68−71] The first attempt to account for the apparent dispersion of the compounds obtained is due to Fong and Hor, who proposed a possible mechanism for the formation of various thiolato complexes from the disintegration of the $\{Pt(\mu\text{-}S)_2Pt\}$ core in CH_2Cl_2.[8] However, the lack of a systematic study prompted us to monitor the reaction of $[L_2Pt(\mu\text{-}S)_2PtL_2]$ (L_2 = dppe, dppp) with CH_2Cl_2 by means of ^{31}P, ^1H, and ^{13}C NMR spectroscopy, electrospray mass spectrometry, and X-ray data.[9] DFT calculations were also performed to obtain an energetic picture of the process. It is worth noting that the main information on both reactions was obtained by a series of $^{31}P\{^1H\}$ NMR spectra recorded as a function of time, as shown in Figure 4. These results allowed us not only to formulate all the steps involved from the initial to the final products (Scheme 11), but also to account for the nature and diversity of the compounds reported in closely related systems (Table 3).

The evolution of $[L_2Pt(\mu\text{-}S)_2PtL_2]$ compounds with various phosphanes as terminal ligands (L = PMe_2Ph, PPh_2py, PPh_3; L_2 = dppf, dppe, dppp) upon exposure to the weak alkylating agent CH_2Cl_2 is depicted in Scheme 11. Thus, the first step of the reaction involves monoalkylation of the corresponding $\{Pt(\mu\text{-}S)_2Pt\}$ core to yield spectroscopically identifiable intermediates with the formula $[L_2\{Pt(\mu\text{-}S)(\mu\text{-}SCH_2Cl)Pt\}L_2]^+$,[9,68,69] whose energy is only slightly higher than that of the reactants. The monoalkylated intermediates subsequently undergo an internal self-alkylation process to afford $[L_2\{Pt(\mu\text{-}S_2CH_2)Pt\}L_2]^{2+}$ species, of elusive nature, but fully consistent with the double alkylation reported as a result of the reaction between $[(PPh_3)_2Pt(\mu\text{-}S)_2Pt(PPh_3)_2]$ and 1,2-dichloroethane. Calculations indicate that $[L_2\{Pt(\mu\text{-}S_2CH_2)Pt\}L_2]^{2+}$ are highly unstable species, that should decompose to give the monometallic complexes $[L_2PtCl_2]$ and $[L_2Pt(S_2CH_2)]$. Consistently, further pro-

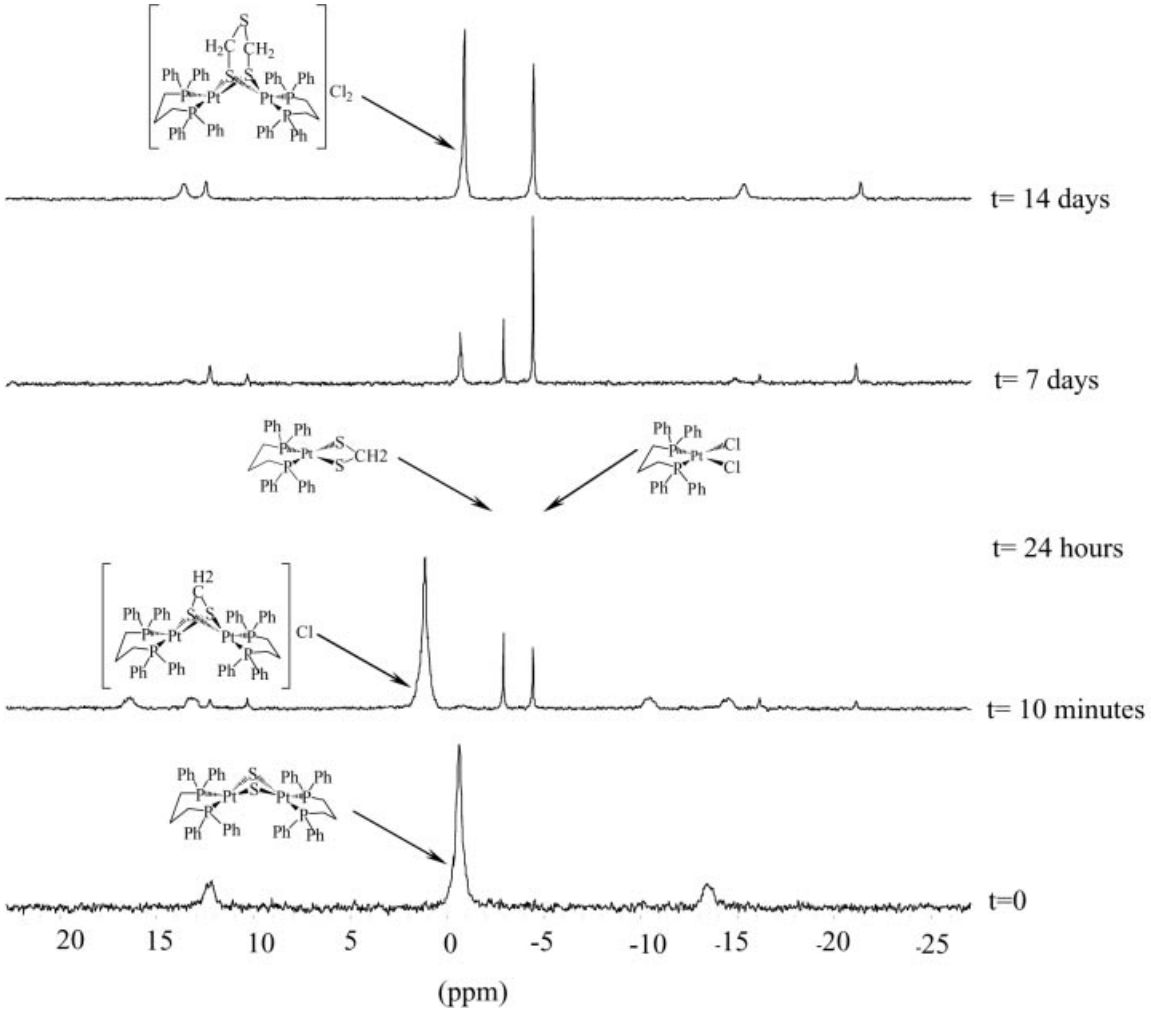

Figure 4. Progression of $[Pt_2(dppp)_2(\mu\text{-}S)_2]$ in CH_2Cl_2 as a function of time monitored by $^{31}P\{^1H\}$ NMR spectroscopy

 © 2004 Wiley-VCH Verlag GmbH & Co. KGaA, Weinheim

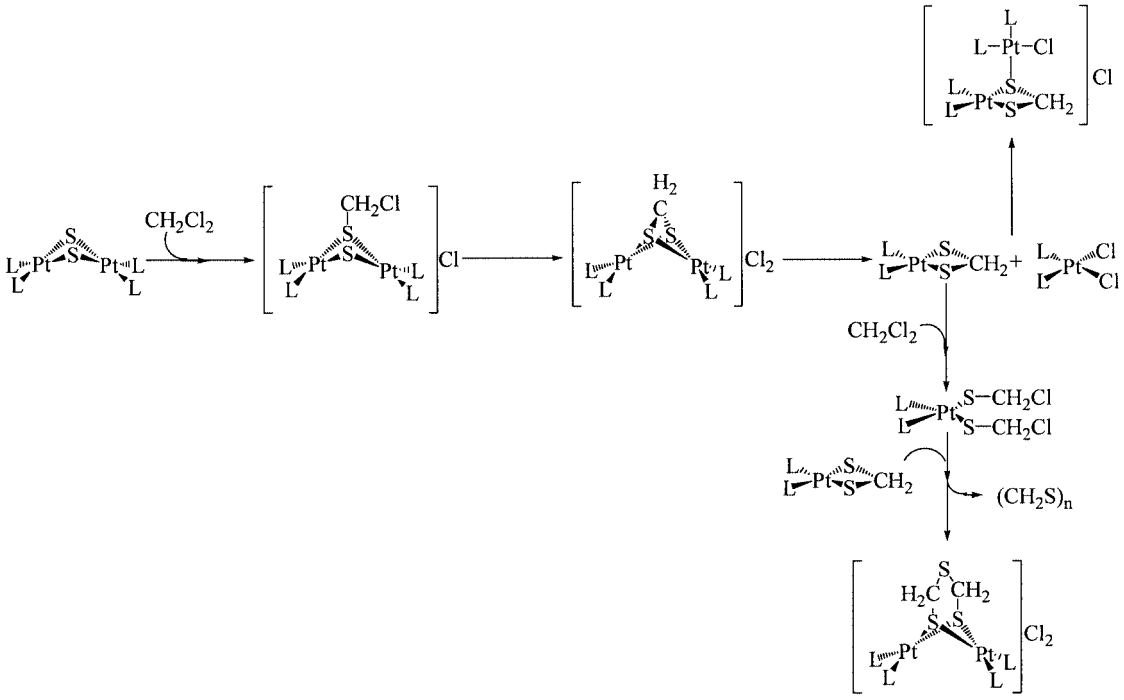

Scheme 11. Reaction pathway corresponding to the evolution of compounds $[L_2Pt(\mu\text{-}S)_2PtL_2]$ in CH_2Cl_2; the nature of phosphane L ligands is given in the text

gression of $[L_2\{Pt(\mu\text{-}S_2CH_2)Pt\}L_2]^{2+}$ leads to a mixture of the above monometallic products. Compound $[L_2PtCl_2]$ is well-established in the literature for a wide range of terminal ligands, and $[L_2Pt(S_2CH_2)]$ has been fully characterized for L = PMe_2Ph,[70] dppy,[14] dppe,[9] and dppp[9] (Table 3). Remarkably, up to this stage, the reaction pathway is common for all $[L_2Pt(\mu\text{-}S)_2PtL_2]$ compounds (L = PMe_2Ph, PPh_2py, PPh_3; L_2 = dppf, dppe, dppp); further evolution is dependent on the nature of the terminal ligands. Thus, for PMe_2Ph, PPh_2py and dppe, the reaction of $[L_2Pt(\mu\text{-}S)_2PtL_2]$ with CH_2Cl_2 does not progress any further after formation of the corresponding $[L_2PtCl_2]$ and $[L_2Pt(S_2CH_2)]$ compounds. Significantly, the latter species form faster for dppe- than for dppp-containing complexes.

Further evolution of the reaction mixture of $[L_2PtCl_2]$ and $[L_2Pt(S_2CH_2)]$ in CH_2Cl_2 depends on the nucleophilicity of the sulfur atoms in the latter compound. Hence, activation of a second molecule of CH_2Cl_2 yields complex $[L_2Pt(SCH_2Cl)_2]$, as observed for L_2 = dppf.[69] Subsequent activation of the C−Cl bonds in the latter compound by reaction with an additional molecule of $[L_2Pt(S_2CH_2)]$ leads to the bimetallic complex $[L_2Pt\{\mu\text{-}(SCH_2SCH_2S)\text{-}S,S'\}PtL_2]Cl_2$, by means of the mechanism depicted in Scheme 12, as observed for L_2 = dppp.[9] Surprisingly, the evolution of $[L_2PtCl_2]$ and $[L_2Pt(S_2CH_2)]$ for L = PPh_3 has shown two different alternatives. On the one hand, analogously to that observed for L_2 = dppf, complex $[(PPh_3)_2Pt(SCH_2Cl)_2]$ was isolated.[71] However, in addition, the condensation reaction between $[(PPh_3)_2PtCl_2]$ and $[(PPh_3)_2Pt(S_2CH_2)]$ to afford $[(PPh_3)_2Pt(S_2CH_2)Pt(PPh_3)_2Cl]Cl$ has recently been described.[46]

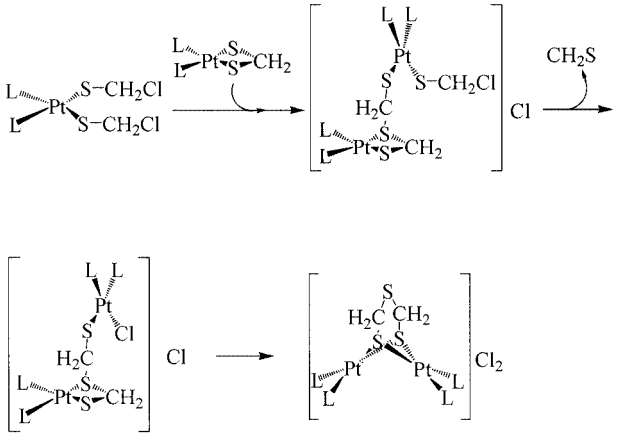

Scheme 12. Mechanism of the evolution from $[L_2Pt(SCH_2Cl)_2]$ to $[L_2Pt\{\mu\text{-}[S_3(CH_2)_2]\}PtL_2]Cl_2$ as observed for L_2 = dppp

Overall, the reactivity of $[L_2Pt(\mu\text{-}S)_2PtL_2]$ towards CH_2Cl_2 provides evidence for the complex sequence of reactions triggered by the nucleophilicity of the sulfur atoms in the $\{Pt_2S_2\}$ core and shows the ability of the terminal phosphane ligands to tune such reactions. On the basis of the high number and different natures of the isolated species, it seems that the reaction of $[L_2Pt(\mu\text{-}S)_2PtL_2]$ with organic electrophilic agents deserves further attention.

Protic Acids

A nice demonstration of the nucleophilicity of the sulfur atoms in the $\{Pt(\mu\text{-}S)_2Pt\}$ ring should be provided by the reaction of $[L_2Pt(\mu\text{-}S)_2PtL_2]$ compounds with the simplest

 © 2004 Wiley-VCH Verlag GmbH & Co. KGaA, Weinheim

electron-acceptor species, i.e. the proton. In other words, the well-established reactivity of [L_2Pt(μ-S)$_2$PtL_2] towards metal centers and organic electrophiles assures the basic character of such compounds in the presence of protic acids. Notwithstanding this, the systematic study of these properties had not been undertaken until very recently. As a result, the whole set of reactions ensuing the protonation of the {Pt(μ-S)$_2$Pt} core has been established for L_2 = dppe and dppp.[10]

The first evidence of the protonation of [L_2Pt(μ-S)$_2$PtL_2] compounds were provided by Hor et al. who fully characterized the [(PPh$_3$)$_2$Pt(μ-S)(μ-SH)Pt(PPh$_3$)$_2$]$^+$ cation following its previous identification by ESI MS measurements.[29,30] However, consistently with the results obtained for L_2 = dppe and dppp,[10] the corresponding diprotonated [(PPh$_3$)$_2$Pt(μ-SH)$_2$Pt(PPh$_3$)$_2$]$^{2+}$ complex was not isolated. Remarkably, the only example of a {Pt(μ-SH)$_2$Pt} core was found for L = $C_6F_5^-$, although in this case neither the monoprotonated nor the totally deprotonated precursors were described.[72] As opposed to the reluctance of the {Pt(μ-S)$_2$Pt} core to afford complexes [L_2Pt(μ-SH)$_2$PtL_2]$^{2+}$ (L = phosphane), its [(PPh$_3$)$_2$Pt(μ-SeH)$_2$Pt(PPh$_3$)$_2$]$^{2+}$ analog is the only species reported as a result of the protonation of the {Pt(μ-Se)$_2$Pt} core.[73]

The reaction pathways by which compounds [L_2Pt(μ-S)$_2$PtL_2] (L_2 = dppe, dppp) react with protic acids were obtained by monitoring their titration with HCl (Scheme 13) or $HClO_4$ by ^{31}P{H} NMR spectroscopy and mass spectrometric techniques.[10] Characterization of all the species involved required previous isolation and structural characterization of [Pt(SH)$_2$$L_2$] and [{$L_2$Pt(μ-S)$_2PtL_2$}Pt$L_2$]$^{2+}$, for both dppe and dppp ligands. DFT calculations corroborated the thermodynamic feasibility of the reactions proposed on the basis of the experimental data. The first protonation step leads to the structurally characterized [L_2Pt(μ-S)(μ-SH)PtL_2]$^+$ cations, but the second step implies disintegration of the platinum-sulfur ring, thus giving rise to various mononuclear species. The subsequent evolution of some of these species allows regeneration of [L_2Pt(μ-S)(μ-SH)PtL_2]$^+$, while formation of complexes [Pt$Cl_2$$L_2$] and [{$L_2$Pt(μ-S)$_2PtL_2$}Pt$L_2$]$^{2+}$ is responsible for the cycles' dead end. Whereas the reaction pathway is essentially common for both phosphane ligands, dppe and dppp, the different coordinating ability of Cl^- or ClO_4^- determines the nature of the final products, a mixture of [Pt$Cl_2$$L_2$] and [{$L_2$Pt(μ-S)$_2PtL_2$}Pt$L_2$]$Cl_2$ or only [{L_2Pt(μ-S)$_2$PtL_2}PtL_2](ClO_4)$_2$.

The previous results show that the evolution of complexes [L_2Pt(μ-S)$_2$PtL_2] (L_2 = dppe or dppp) in the presence of protic acids depends on several factors: (i) the concentration and nature of the protic acid, i.e. the coordinative features of the conjugate anion; (ii) the nature of the ter-

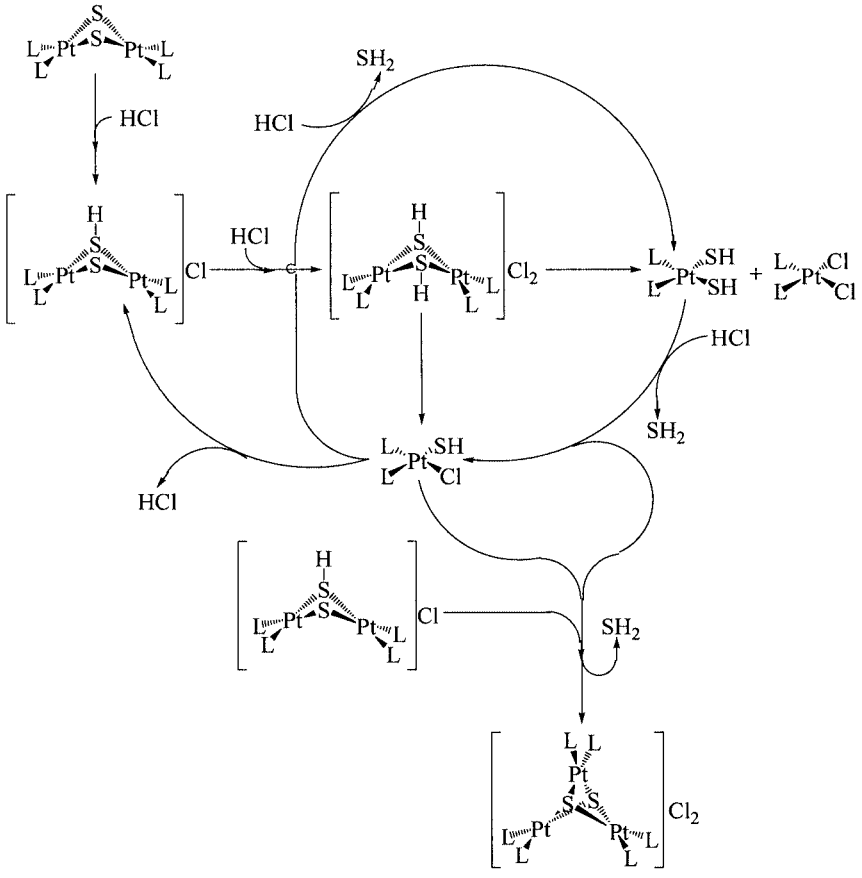

Scheme 13. Reaction pathway corresponding to the evolution of [L_2Pt(μ-S)$_2$PtL_2] upon exposure to HCl as observed for L_2 = dppe or dppp

 © 2004 Wiley-VCH Verlag GmbH & Co. KGaA, Weinheim

minal phosphane ligand, dppe containing species are more reactive than those with dppp; and (iii) the reaction medium used, the amount of $[Pt_3(\mu_3\text{-}S)_2(L_2)_3]^{2+}$ formed is directly related to the polarity of the solvent.

In summary, the reaction of compounds $[L_2Pt(\mu\text{-}S)_2PtL_2]$ (L_2 = dppe or dppp) with protic acids provides a new insight into the exceptionally rich chemistry arising from the nucleophilicity of the $\{Pt_2S_2\}$ core. On the one hand, protonation of the stable monoprotonated $[L_2Pt(\mu\text{-}S)(\mu\text{-}SH)PtL_2]^+$ complexes triggers a cascade of sequential reactions by which compounds $[Pt(SH)_2L_2]$ are formed. These are the keystone species for regenerating $[L_2Pt(\mu\text{-}S)(\mu\text{-}SH)PtL_2]^+$ complexes, and thus for the cyclical nature of the overall process. Remarkably, complex species containing the Pt−SH fragment, which is present in the above complexes, have been proposed as intermediates in the removal of sulfur as SH_2 from petroleum feedstock, known as hydrodesulfurization (HDS).[74−76] Both the cyclical nature of the processes described and the relevance of complexes containing the Pt−SH fragment in HDS provide additional interest to the results obtained with respect to their potential catalytic applications.

Concluding Remarks and Perspectives

The chemistry of compounds $[L_2Pt(\mu\text{-}S)_2PtL_2]$ (L = phosphane) is becoming increasingly important because of the exceptional ability of the $\{Pt_2S_2\}$ core to act as a powerful nucleophile towards virtually any electron-acceptor species. While its behavior as a metalloligand to metal centers has attracted unceasing attention, exploration of the chemistry involved in the reaction with nonmetal electrophiles has emerged in the recent years. The outstanding richness of this chemistry is witnessed by the cascade of reactions that the $\{Pt_2S_2\}$ core undergoes upon exposure to organic electrophiles and protic acids. The cyclical nature of some of these reactions as well as some of the intermediate species involved are promising for possible catalytic applications. In addition, the unusual reactivity of $\{ML'_y\}$ fragments in $[\{L_2Pt(\mu\text{-}S)_2PtL_2\}ML'_y]^z$ compounds has allowed taking advantage of the influence of the $\{Pt(\mu\text{-}S)_2Pt\}$ core to substantially modify the chemistry of either organic or inorganic L′ ligands. Because of this influence, an atypical C−H allylic activation for cod and an enhanced lability for chloride ligands have been established. The former allows envisaging further developments in organometallic chemistry. The latter has led to a novel route for the building of nuclearity-controlled multimetallic aggregates containing a $\{Pt_2S_2\}_n$ core that may be of use to obtain metal chalcogenide compounds of definite size and thus specific properties.

Our interest in exploring the chemistry of $[L_2Pt(\mu\text{-}S)_2PtL_2]$ compounds has been widely rewarded by its exceptional richness and diversity. Further developments will contribute to establish the still undefined limits of the nucleophilicity of the $\{Pt_2S_2\}$ core, as well as to find applications of this reactivity in main areas of chemistry. The potential of the $\{Pt_2S_2\}$ core to activate slightly polarized bonds involving carbon atom is the aim of our research for future studies.

Acknowledgments

We wish to thank our coworkers, who are cited in the literature section, for their numerous contributions and Prof. William Clegg for his extremely valuable crystallographic studies. We are also grateful to the Ministerio de Educación y Ciencia of Spain (projects CTQ2004-01463/BQ4 and BQU2002-04110-CO2-02) for financial support.

[1] A. F. Wells, *Structural Inorganic Chemistry*, 5th edition; Clarendon Press, Oxford, **1984**.
[2] I. Dance, K. Fisher, *Prog. Inorg. Chem.* **1994**, *41*, 637.
[3] T. B. Rauchfuss, *Inorg. Chem.* **2004**, *43*, 14.
[4] E. I. Stiefel, *ACS Symp. Ser.* **1996**, *653*, 2.
[5] K. A. Hofmann, F. Höchlen, *Ber. Dtsch. Chem. Ges.* **1903**, *36*, 3090.
[6] J. Chatt, D. M. P. Mingos, *J. Chem. Soc. A* **1970**, 1243.
[7] R. Ugo, G. La Monica, S. Cenini, A. Segre, F. Conti, *J. Chem. Soc. A* **1971**, 522.
[8] S.-W. A. Fong, T. S. A. Hor, *J. Chem. Soc., Dalton Trans.* **1999**, 639.
[9] R. Mas-Ballesté, M. Capdevila, P. A. Champkin, W. Clegg, R. A. Coxall, A. Lledós, C. Mégret, P. González-Duarte, *Inorg. Chem.* **2002**, *41*, 3218.
[10] R. Mas-Ballesté, G. Aullón, P. A. Champkin, W. Clegg, C. Mégret, P. González-Duarte, A. Lledós, *Chem. Eur. J.* **2003**, *9*, 5023.
[11] R. Mas-Ballesté, P. A. Champkin, W. Clegg, P. González-Duarte, A. Lledós, G. Ujaque, *Organometallics* **2004**, *23*, 2522−2532.
[12] M. Capdevila, Y. Carrasco, W. Clegg, R. A. Coxall, P. González-Duarte, A. Lledós, J. A. Ramírez, *J. Chem. Soc., Dalton Trans.* **1999**, 3103.
[13] M. P. Brown, R. J. Puddephatt, M. Rashidi, K. R. Seddon, *J. Chem. Soc., Dalton Trans.* **1977**, 951.
[14] V. W.-W. Yam, P. K.-Y. Yeung, K.-K. Cheung, *J. Chem. Soc., Chem. Commun.* **1995**, 267.
[15] M. Capdevila, Y. Carrasco, W. Clegg, R. A. Coxall, P. González-Duarte, A. Lledós, J. Sola, G. Ujaque, *J. Chem. Soc., Chem. Commun.* **1998**, 597.
[16] H. Li, G. B. Carpenter, D. A. Sweigart, *Organometallics* **2000**, *19*, 1823.
[17] C. E. Briant, C. J. Gardner, T. S. A. Hor, N. D. Howells, D.M.P. Mingos, *J. Chem. Soc., Dalton Trans.* **1984**, 2645.
[18] S. S. Oster, R. J. Lachicotte, W. D. Jones, *Inorg. Chim. Acta* **2002**, *330*, 118.
[19] M. Capdevila, W. Clegg, R. A. Coxall, P. González-Duarte, M. Hamidi, A. Lledós, J. Sola, G. Ujaque, *Inorg. Chem. Commun.* **1998**, *12*, 466.
[20] G. Aullón, G. Ujaque, A. Lledós, S. Alvarez, P. Alemany, *Inorg. Chem.* **1998**, *37*, 804.
[21] A. Bencini, M. di Varia, R. Morassi, P. Stoppioni, F. Mele, *Polyhedron* **1996**, *15*, 2079.
[22] R. D. Adams, T. A. Wolfe, B. W. Eichhorn, R. C. Haushalter, *Polyhedron* **1989**, *8*, 701.
[23] A. L. Ma, J. B. Thoden, L. F. Dahl, *J. Chem. Soc., Chem. Commun.* **1992**, 1516.
[24] H. Wolkers, K. Dehnike, D. Fenske, A. Kassanov, S. S. Hafner, *Acta Crystallogr., Sect. C* **1991**, *47*, 1627.
[25] R. Mas-Ballesté, M. Capdevila, P. González-Duarte, M. Hamidi, A. Lledós, C. Mégret, D. de Montauzon, *Dalton Trans.* **2004**, 706.
[26] G. Aullón, M. Hamidi, A. Lledós, S. Alvarez, *Inorg. Chem.* **2004**, *43*, 3702.

 © 2004 Wiley-VCH Verlag GmbH & Co. KGaA, Weinheim

[27] M. Capdevila, W. Clegg, P. González-Duarte, A. Jarid, A. Lledós, *Inorg. Chem.* **1996**, *35*, 490.
[28] G. Aullón, M. Capdevila, W. Clegg, P. González-Duarte, A. Lledós, R. Mas-Ballesté, *Angew. Chem. Int. Ed.* **2002**, *41*, 2776.
[29] S.-W. A. Fong, W. T. Yap, J. J. Vittal, T. S. A. Hor, W. Henderson, A. G. Oliver, C. E. F. Rickard, *J. Chem. Soc., Dalton Trans.* **2001**, 1986.
[30] S.-W. A. Fong, J. J. Vittal, W. Henderson, T. S. A. Hor, A. G. Oliver, C. E. F. Rickard, *Chem. Commun.* **2001**, 421.
[31] Z. Li, Z.-H. Loh, K. F. Mok, T. S. A. Hor, *Inorg. Chem.* **2000**, *39*, 5299.
[32] G. Aullón, E. Ruiz, S. Alvarez, *Chem. Eur. J.* **2002**, *8*, 2508.
[33] E. I. Solomon, T. C. Brunold, M. I. Davis, J. N. Kemsley, S.-K. Lee, F. Lehnert, F. R. Neese, A. J. Skulan, Y.-S. Yang, J. Zhou, *Chem. Rev.* **2000**, *100*, 235.
[34] L. Que Jr., W. B. Tollman, *Angew. Chem. Int. Ed.* **2002**, *41*, 1114.
[35] S. Alvarez, A. A. Palacios, G. Aullón, *Coord. Chem. Rev.* **1999**, *185-186*, 431.
[36] M.-H. Baik, C. K. Schauer, T. Ziegler, *J. Am. Chem. Soc.* **2002**, *124*, 11167.
[37] S. Blasco, I. Demachy, Y. Jean, A. Lledós, *New J. Chem.* **2001**, *25*, 611.
[38] H. Reiss, A. Heller, *J. Phys. Chem.* **1985**, *89*, 4207.
[39] X. Xu, S.-W. A. Fong, Z. Li, Z.-H. Loh, J. J. Vittal, W. Henderson, S.-B. Khoo, T. S. A. Hor, *Inorg. Chem.* **2002**, *41*, 6838.
[40] K. Matsumoto, K. Takahashi, M. Ikuzawa, H. Kimoto, S. Okeya, *Inorg. Chim. Acta* **1998**, *281*, 174.
[41] W. Bos, J. J. Bour, P. P. J. Schlebos, P. Hageman, W. P. Bosman, J. M. M. Smits, J. A. C. van Wietmarschen, P. T. Beurskens, *Inorg. Chim. Acta* **1986**, *119*, 141.
[42] Z. Li, K. F. Mok, T. S. A. Hor, *J. Organomet. Chem.* **2003**, *682*, 73.
[43] M. Zhou, Y. Xu, A.-M. Tan, P.-H. Leung, K. F. Mok, L.-L. Koh, T. S. A. Hor, *Inorg. Chem.* **1995**, *34*, 6425.
[44] C. E. Briant, T. S. A. Hor, N. D. Howells, D. M. P. Mingos, *J. Organomet. Chem.* **1983**, *256*, C15.
[45] H. Liu, A. L. Tan, Y. Xu, K. F. Mok, T. S. A. Hor, *Polyhedron* **1997**, *16*, 377.
[46] Z. Li, W. Zheng, H. Liu, K. F. Mok, T. S. A. Hor, *Inorg. Chem.* **2003**, *42*, 8481.
[47] C. E. Briant, T. S. A. Hor, N. D. Howells, D. M. P. Mingos, *J. Chem. Soc., Chem. Commun.* **1983**, 1118.
[48] Z. Li, Z.-H. Loh, S.-W. A. Fong, Y.-K. Yan, W. Henderson, K. F. Mok, T. S. A. Hor, *J. Chem. Soc., Dalton Trans.* **2002**, 1027.
[49] M. Zhou, Y. Xu, C.-F. Lam, L.-L. Koh, K. F. Mok, P.-H. Leung, T. S. A. Hor, *Inorg. Chem.* **1993**, *32*, 4660.
[50] H. Liu, C. Jiang, J. S. L. Yeo, K. F. Mok, L. K. Liu, T. S. A. Hor, Y. K. Yan, *J. Organomet. Chem.* **2000**, *595*, 276.
[51] S.-W. A. Fong, W. T. Yap, J. J. Vittal, W. Henderson, T. S. A. Hor, *J. Chem. Soc., Dalton Trans.* **2002**, 1826.
[52] S.-W. A. Fong, T. S. A. Hor, W. Henderson, B. K. Nicholson, S. Gardyne, S. M. Devoy, *J. Organomet. Chem.* **2003**, *679*, 24.
[53] V. W.-W. Yam, P. K.-Y. Yeung, K.-K. Cheung, *Angew. Chem. Int. Ed. Engl.* **1996**, *35*, 739.
[54] V. W.-W. Yam, K.-L. Yu, E. C.-C. Cheng, P. K.-Y. Yeung, K.-K. Cheung, N. Zhu, *Chem. Eur. J.* **2002**, *8*, 4122.
[55] H. Liu, A. L. Tan, K. F. Mok, T. S. A. Hor, *J. Chem. Soc., Dalton Trans.* **1996**, 4023.
[56] R. Mas-Ballesté, W. Clegg, A. Lledós, P. González-Duarte, *Eur. J. Inorg. Chem.* **2004**, 3223.
[57] P. J. Albietz, K. Yang, R. J. Lachicotte, R. Eisenberg, *Organometallics* **2000**, *19*, 3543.
[58] M. Fusto, F. Giordano, I. Orabona, F. Ruffo, A. Panunzi, *Organometallics* **1997**, *16*, 5981.
[59] A. Macchioni, G. Bellachioma, G. Cardaci, M. Travaglia, C. Zuccacia, B. Milani, G. Corso, E. Zangrado, G. Mestroni, C. Carfagna, M. Formica, *Organometallics* **1999**, *18*, 2677.
[60] G. R. Hoel, R. A. Stockland, G. K. Anderson, F. T. Ladipo, J. Braddock-Wilking, N. P. Rath, J. C. Mareque-Rivas, *Organometallics* **1998**, *17*, 1155.
[61] H. Brunner, M. Weber, M. Zabel, *J. Organomet. Chem.* **2003**, *684*, 6.
[62] C. E. Briant, D. I. Gilmour, M. A. Luke, D. M. P. Mingos, *J. Chem. Soc., Dalton Trans.* **1985**, 851.
[63] Z. Li, H. Liu, K. F. Mok, A. S. Batsanov, J. A. K. Howard, T. S. A. Hor, *J. Organomet. Chem.* **1999**, *575*, 223.
[64] S. Narayan, V. K. Jain, *Transition Met. Chem.* **2000**, *25*, 400.
[65] S. H. Chong, A. Tjindrawan, T. S. A. Hor, *J. Mol. Cat. A* **2003**, *204-205*, 267.
[66] J. S. L. Yeo, J. J. Vittal, W. Henderson, T. S. A. Hor, *Organometallics* **2002**, *21*, 2944.
[67] J. S. L. Yeo, J. J. Vittal, W. Henderson, T. S. A. Hor, *Eur. J. Inorg. Chem.* **2003**, 277.
[68] R. R. Gukathasan, R. H. Morris, A. Walker, *Can. J. Chem.* **1983**, *61*, 2490.
[69] M. Zhou, C.F. Lam, K. F. Mok, P.-H. Leung, T. S. A. Hor, *J. Organomet. Chem.* **1994**, *476*, C32.
[70] A. Shaver, R. D. Lai, P. H. Bird, W. Wickramasinghe, *Can. J. Chem.* **1985**, *63*, 2555.
[71] M. Zhou, P.-H. Leung, K. F. Mok, T. S. A Hor, *Polyhedron* **1996**, *15*, 1737.
[72] J. Ruiz, V. Rodríguez, C. Vicente, J. M. Martí, G. López, J. Pérez, *Inorg. Chem.* **2000**, *39*, 5299.
[73] J. S. L. Yeo, J. J. Vittal, W. Henderson, T. S. A. Hor, *J. Chem. Soc., Dalton Trans.* **2002**, 328.
[74] S. Kuwata, M. Hidai, *Coord. Chem. Rev.* **2001**, *213*, 211.
[75] A. Shaver, M. El-Khateeb, A.-M. Lebuis, *Angew. Chem. Int. Ed. Engl.* **1996**, *35*, 2362.
[76] R. J. Angelici, *Acc. Chem. Res.* **1988**, *21*, 387.

Received May 20, 2004

 © 2004 Wiley-VCH Verlag GmbH & Co. KGaA, Weinheim

Monocarbaborane Chemistry: Cage Opening of *nido*-1-CB_8H_{12} by Tertiary Bases − an Example of a Straightforward *nido* → *arachno* Transformation; Isolation of a New Series of 4-L-*arachno*-5-CB_8H_{12} Compounds (L = NMe_3, NEt_3, and Quinoline)

Bohumil Štíbr,*[a,b] Josef Holub,[a] Mario Bakardjiev,[a] Wolfgang Milius,[b] and Bernd Wrackmeyer[b]

Keywords: Boranes / Carboranes / Monocarbaboranes / NMR spectroscopy / X-ray diffraction

Room-temperature reactions between the carborane *nido*-1-CB_8H_{12} (**1**) and selected tertiary Lewis bases [L = NMe_3, NEt_3, and quinoline (quin)] in CH_2Cl_2 at room temperature for 24 h resulted in the isolation of a series of 4-L-*arachno*-5-CB_8H_{12} compounds (**2**; L = NMe_3, **2a**, L = NEt_3, **2b** and L = quin, **2c**). This main reaction mode can be classified as a straightforward *nido* → *arachno* transformation and was characterized by a cage opening of the original pentagonal face in **1** by L at the bridging site adjacent to the carbon apex with the formation of a hexagonal open face. The formation of **2a** was clean, whereas that of **2c** was accompanied by formation of the *closo*-[4-CB_8H_9]$^-$ (**3**) anion as a side-product. The first representative of the zwitterionic 1-L-*closo*-4-CB_8H_8 (**4**) series, 1-quin-*closo*-4-CB_8H_8 (**4c**), was isolated as another side product from the quinoline reaction. The structure of compound **2b** was determined by an X-ray diffraction analysis and the constitution of all compounds is consistent with the results of mass spectrometry. Multinuclear (^1H, ^{11}B, and ^{13}C), two-dimensional [^{11}B-^{11}B]-COSY, and $^1H\{^{11}B$(selective)$\}$ magnetic resonance measurements lead to complete assignments of all resonances and are in excellent agreement with the structures proposed.
(© Wiley-VCH Verlag GmbH & Co. KGaA, 69451 Weinheim, Germany, 2004)

Introduction

Although the *nido*-1-CB_8H_{12} (**1**) carborane has been known since 1977,[1] not much chemistry of this interesting compound has so far been reported. Carborane **1** was employed as a starting material for the preparation of the smaller monocarbaborane anions [2-CB_6H_7]$^-$, [1-CB_7H_8]$^-$, and [4-CB_8H_9]$^-$ (**3**), completing a series of the parent seven,[2] eight,[2,3] and nine-vertex[4] *closo* monocarbaboranes. The sole example of metallacarborane chemistry based on carborane **1** so far, has been the synthesis of the platinacarborane [6,6-$(PPh_3)_2$-*arachno*-6,4-$PtCB_7H_{11}$].[5] In the present work, we have extended the rather undeveloped chemistry of carborane **1** by its room-temperature reactions with selected tertiary amines (L = NMe_3, NEt_3, and quin). We would like to demonstrate that these reactions lead to a simple opening of the *nido* cage in **1** and the formation of a series of corresponding 4-L-*arachno*-5-CB_8H_{12} compounds. Numbering systems for the nine-vertex *closo*, *nido*, and *arachno* skeletons used in this work are given in Scheme 1. Structures are presented in a simplified manner; unmarked vertices in Scheme 1 stand for cluster BH units, while C denotes the CH vertex.

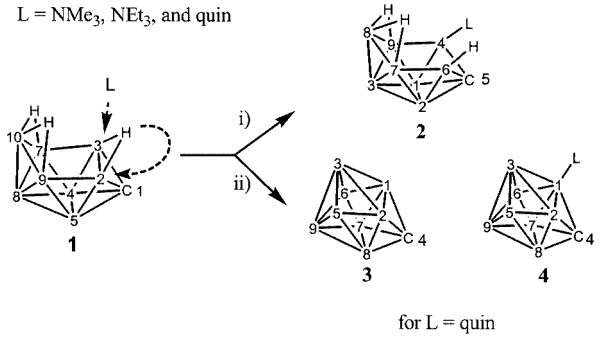

Scheme 1. Simplified scheme for the cluster opening in *nido*-1-CB_8H_{12} (**1**) by selected tertiary Lewis bases (L = NMe_3, NEt_3, and quinoline) and the formation of side products; i) L, ambient temperature, main reaction mode; ii) side reaction mode

Results and Discussion

As shown in path i) of Scheme 1, room-temperature reactions of the *nido*-1-CB_8H_{12} (**1**) monocarbaborane with

[a] Institute of Inorganic Chemistry, Academy of Sciences of the Czech Republic (Research Center for New Inorganic Compounds and Advanced Materials, University of Pardubice)
250 68 Řež, The Czech Republic
Fax: (internat.) +420-2209-40161
E-mail: stibr@iic.cas.cz
[b] Laboratorium für Anorganische Chemie der Universität Bayreuth
Postfach 101251, 95440 Bayreuth, Germany
Fax: (internat.) +49-(0)6221-487-672
E-mail: B.Wrack@uni-bayreuth.de

selected tertiary amines (L = Me_3N, Et_3N, and quin) in dichloromethane afforded a series of Lewis-base adducts of general formula 4-L-*arachno*-5-CB_8H_{12} (**2**) (**2a** for L = Me_3N, **2b** for L = Et_3N, and **2c** for L = quin) as the main reaction products in yields of 96, 36, and 35 %, respectively.

The formation of compounds of type **2** in this reaction can be classified as a clean *nido* → *arachno* transformation, in which the base L adds two more cluster electrons to the original 22-electron *nido* system of **1** to form 24-electron *arachno* ligand derivatives of structure **2**. As also outlined in Scheme 1, the most likely mechanism of this reaction involves an attack by L at the B4 site in **1**, followed by transfer of the 4,6-μ-H bridging hydrogen onto the B6 vertex with the formation of the cage BH_2 group. The reaction with Me_3N is very clean, while in the case of quinoline the formation of the *closo*-[4-CB_8H_9]$^-$ (**3**) anion in small yields was also observed. As shown in path ii) of Scheme 1, the quinoline reaction also produced small amounts of anion **3** (yield 12%) and 1-quin-*closo*-4-CB_8H_8 (**4c**) (yield 15%), compound **4c** being the first representative of the zwitterionic L-*closo*-CB_8H_8 series. The anion **3** and compound **4c** are most probably formed by air oxidation of compound **2c** during chromatography on silica gel.

The structure of **2b** was determined by an X-ray diffraction analysis and is depicted in Figure 1.

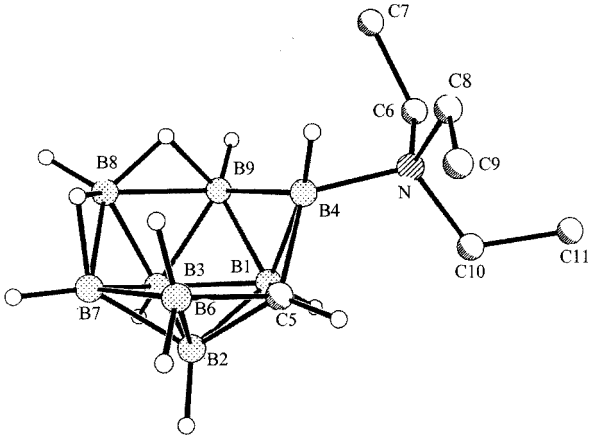

Figure 1. ORTEP representation of the molecular structure of 4-Et_3N-*arachno*-5-CB_8H_{12} (**2b**); selected bond lengths (Å) and angles (°): B1−B2 1.768(6), B1−B3 1.795(7), B1−B4 1.795(6), B1−C5 1.660(6), B1−B9 1.715(7), B2−B3 1.794(7), B2−C5 1.644(6), B2−B6 1.762(8), B2−B7 1.716(8), B3−B7 1.781(8), B3−B8 1.699(8), B3−B9 1.767(7), B4−C5 1.632(6), B4−B9 2.074(7), B4−N 1.639(5), C5−B6 1.673(7), B6−B7 1.991(8), B7−B8 1.805(8), B8−B9 1.789(8), C5−B4−B9 99.6(3), B4−C5−B6 111.8(4), B7−B6−C5 99.8(3), B7−B8−B9 104.6(4), and B8−B9−B4 112.0(4)

The molecule contains one BH_2 and one LBH group, one CH vertex and two non-equivalent BHB bridges within an open hexagonal face. A significant feature is that the cage CH group does not occupy the position of lowest connectivity 4, but the vertex of connectivity 5. The Et_3N substituent is attached at the B4 site in an asymmetric manner. The compounds are thus isomeric with the 6-L-*arachno*-4-CB_8H_{12} species reported previously by one of our groups.[6,7] The longest B−B separations (in Å) can be found in the open face for B4−B9 [2.074(7)] and B6−B7 [1.991(8)], followed by the "bridging" B7−B8 [1.805(8)] and B8−B9 [1.789(8)] distances. The shortest B−B distance can be seen for B3−B8 [1.699(8)], and all other B−B distances fall within the usual limits. In the open-face, the C5−B4 bond [1.632(6)] is shorter than C5−B6 [1.673(7)], and the other two C−B cage distances are in the usual range.

The constitutions of the *arachno* compounds of type **2** and that of the *closo* compound **4c** are in agreement with the results of NMR spectroscopy. All ^{11}B resonances were interrelated by [^{11}B-^{11}B]-COSY spectroscopy,[8] which, in combination with $^1H\{^{11}B(selective)\}$ measurements,[9] led to complete assignments of the resonances to individual cluster BH vertices for all compounds. Simplified stick diagrams interrelating the ^{11}B chemical shifts are given in Figure 2.

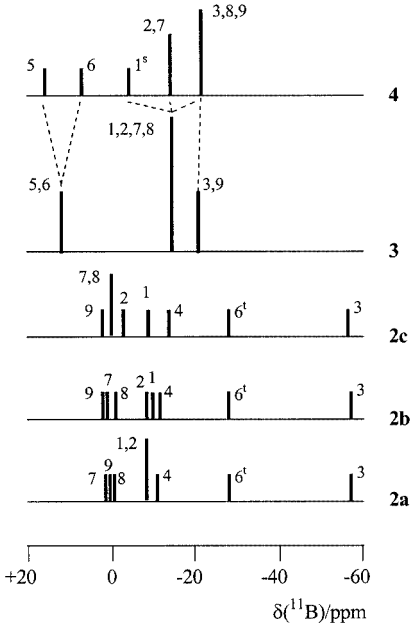

Figure 2. Simplified stick diagrams showing comparison of the ^{11}B NMR shifts and relative intensities for the 4-L-*arachno*-5-CB_8H_{12} compounds (**2**) (**2a** for L = NMe_3, **2b** for L = NEt_3, and **2c** for L = quin) (bottom traces), *closo*-[4-CB_8H_9]$^-$ (**3**) anion (data from reference[4]), and 1-quin-*closo*-4-CB_8H_8 (**4c**) (upper diagrams)

In accord with the crystallographic structure of **2b**, the ^{11}B NMR spectra of all compounds of type **2** (see bottom traces in Figure 2) consist of seven different doublets for BH vertices and one triplet due to the $B(6)H_2$ unit. Apart from resonances of the ligand L, the $^1H\{^{11}B\}$ NMR spectra of these compounds consist of thirteen singlets attributable to eight different *exo*-BH units, one *endo*-BH group, two signals of the *exo* and *endo* components of the cage CH_2 vertex, and to two different B−H−B bridges. The $^{13}C\{^1H\}$ NMR spectra of compounds of type **2** contain a broad singlet assigned to the cluster CH_2 group, the shifts for **2a** and **2b** being essentially the same. The mass spectrum of **2c** shows the expected molecular cut-off, whereas the spectra of **2a** and **2b** indicate fragmentation to [CB_8H_{10}] and L un-

 © 2004 Wiley-VCH Verlag GmbH & Co. KGaA, Weinheim

der the conditions of the MS experiment as the main fragmentation mode.

Although crystals of 1-quin-*closo*-4-CB_8H_8 (**4c**) were not suitable for an X-ray diffraction analysis, its structure in solution can be elucidated on the basis of NMR spectroscopy. As demonstrated in Figure 2 (upper traces), the ^{11}B NMR spectrum of **4c** shows straightforward similarities to that of the parent *closo*-[4-CB_8H_9]$^-$ anion (**3**).[4] It consists of seven different doublets, of which those assigned to B2,7 and B3,8,9 overlap, and one singlet assigned to the ligand-substituted boron B1. The $^1H\{^{11}B\}$ NMR spectrum of **4c** shows a set of low-field quinoline resonances of integral intensity 7 and seven resonances (integral intensity 9) due to the cage BH units, of which those attributed to 3-H, 8-H, and 9-H overlap. Moreover, the mass spectrum of **4c** shows the expected molecular cut-off, and the 1-quin-*closo*-4-CB_8H_8 constitution is the only asymmetric possibility among the 1-, 3- and 5-substituted isomers of the L-*closo*-4-CB_8H_8 series.

Conclusion

The room-temperature reactions between tertiary amines and compound **1** discussed in this work, especially that with trimethylamine, represent a straightforward *nido* → *arachno* transformation in the nine-vertex series of monocarbaboranes. Of similar character is the previously reported[10] conversion of the *nido*-[B_9H_{12}]$^-$ anion into 4-C_5H_5N-*arachno*-4-B_9H_{13} by treatment with C_5H_5N·HCl in the nine-vertex borane series. It is highly probable that compound **2b** acts as an intermediate in the formation of the *closo* anions [1-CB_7H_8]$^-$ and [1-CB_8H_9]$^-$,[4] and we are currently investigating this assumption in more detail together with the possibility of heteroatom insertion into the open face of compounds of type **2**. The 1-quin-*closo*-4-CB_8H_8 (**4c**) is the first representative of the zwitterionic 1-L-*closo*-4-CB_8H_8 (**4**) series and work aimed at a more effective preparation of these or similar compounds is in progress.

Experimental Section

General Remarks: All reactions were carried out with use of standard vacuum or inert-atmosphere techniques as described by Shriver[11] although some operations, such as column LC, were carried out in air. The starting carborane **1** was prepared according to the literature.[1] Dichloromethane and hexane (Fluka) were dried with CaH_2 and freshly distilled before use. Other chemicals were reagent or analytical grade and were used as purchased. The analytical TLC and column chromatography, melting points, mass spectrometry, and NMR spectroscopy were essentially carried out as described in other work from our laboratories.[12]

4-(Me_3N)-*arachno*-5-CB_8H_{12} (2a): A stream of anhydrous Me_3N was bubbled through a solution of compound **1** (111 mg, 1 mmol) in CH_2Cl_2 (20 mL) for 10 min at 0 °C and the mixture was then left stirring for 24 h at ambient temperature. Volatiles were then evaporated and the residue was subjected to chromatography on a silica gel column (30 × 2.5 cm) yielding a pure fraction of R_f (CH_2Cl_2) 0.64 which was identified by NMR spectroscopy as **2a** (162 mg, 96%). An analytical sample of **2a** was obtained by crystallization from a saturated CH_2Cl_2 solution, which was carefully covered by the same volume of hexane. **For 2a:** R_f (CH_2Cl_2) 0.64; m.p. >350 °C (dec.). ^{11}B NMR ($CDCl_3$): δ = 2.4 (d, $^1J_{B,H}$ ≈145 Hz, 1 B, B7), 1.6 (d, $^1J_{B,H}$ = 147 Hz, 1 B, B9), 0.15 (d, $^1J_{B,H}$ ≈150 Hz, 1 B, B8), −8.5 (d, $^1J_{B,H}$ ≈160 Hz, 2 B, B1,2), −10.6 (d, $^1J_{B,H}$ = 149 Hz, 1 B, B4), −27.6 (t, $^1J_{B,H}$ = 122/119 Hz,1 B, B6), −58.4 (d, $^1J_{B,H}$ = 150 Hz, 1 B, B3) ppm, all theoretical [^{11}B-^{11}B]-COSY cross-peaks observed, except for B6-B7, B7-B8, and B8-B9. $^1H\{^{11}B\}$ NMR ($CDCl_3$): δ = 3.35 (s, 1 H, 8-H), 3.22 (s, 1 H, 9-H), 3.12 (s, 1 H, 7-H), 2.86 (s, 9 H, Me_3N), 2.43 (s, 1 H, 1-H or 2-H), 2.38 (s, 1 H, 1-H or 2-H), 1.32 (s, 1 H, *endo*-4-H), 1.23 (s, 1 H, *exo*-6-H), 0.80 (s, 1 H, 5-H), 0.60 (s, 1 H, *endo*-6-H), −0.72 (s, 1 H, 3-H), −1.96 (s, 1 H, 7,8-μ-H), −2.06 (s, 1 H, 8,9-μ-H,) ppm. $^{13}C\{^1H\}$ NMR ($CDCl_3$): δ = 10.6 (br. s, 1 C, C5) ppm. MS (70 eV, EI): *m*/*z* (%) = 110 (9) [M − Me_3N − 2H]$^+$, 107 (100) [M − Me_3N − 5H]$^+$, 59 (48) [M − CB_8H_{12}]$^+$. $C_4H_{21}B_8N$ (169.76): calcd. C 28.29, H 12.47; found C 30.15, H 11.80.

4-(Et_3N)-*arachno*-5-CB_8H_{12} (2b): A solution of compound **1** (111 mg, 1 mmol) in CH_2Cl_2 (20 mL) was treated with triethylamine (303 mg, 3 mmol) and the mixture was then left stirring for 24 h at ambient temperature. Volatiles were then evaporated and the residue was subjected to chromatography on a silica gel column (30 × 2.5 cm) yielding a pure fraction of R_f (CH_2Cl_2) 0.5 which was identified by NMR spectroscopy as **2b** (76 mg, 36%). An analytical sample of **2b** was obtained by crystallization from a saturated CH_2Cl_2 solution that was covered by the same volume of hexane. **For 2b:** R_f (CH_2Cl_2) 0.5; m.p. >350 °C (dec.). ^{11}B NMR ($CDCl_3$): δ = 3.1 (d, $^1J_{B,H}$ ≈ 140 Hz, 1 B, B9), 2.2 (d, $^1J_{B,H}$ ≈ 145 Hz, 1 B, B7), −0.1 (d, $^1J_{B,H}$ = 155 Hz, 1 B, B8), −7.9 (d, $^1J_{B,H}$ = 155 Hz, 1 B, B2), −9.7 (d, $^1J_{B,H}$ = 158 Hz, 1 B, B1), −11.4 (d, $^1J_{B,H}$ = 156 Hz, 1 B, B4), −27.3 (t, $^1J_{B,H}$ = 116/119 Hz,1 B, B6), −58.2 (d, $^1J_{B,H}$ = 149 Hz, 1 B, B3) ppm, all theoretical [^{11}B-^{11}B]-COSY cross-peaks observed, except for B6-B7, B7-B8, and B8-B9. $^1H\{^{11}B\}$ NMR ($CDCl_3$): δ = 3.31 (s, 2 H, 8,9-H), 3.06 (s, 1 H, 7-H), 3.06 (s, 6 H, CH_3CH_2N), 2.39 (s, 1 H, 2-H), 2.30 (s, 1 H, 1-H), 1.34 (s, 9 H, CH_3CH_2N), 1.15 (s, 1 H, *exo*-6-H), 1.04 (s, 1 H, *endo*-4-H), 0.80 (s, 1 H, 5-H), 0.63 (s, 1 H, *endo*-6-H), −0.72 (s, 1 H, 3-H), −1.94 (s, 1 H, 7,8-μ-H), −2.04 (s, 1 H, 8,9-μ-H) ppm. $^{13}C\{^1H\}$ NMR ($CDCl_3$): δ = 10.6 (br. s, 1 C, C5) ppm. MS (70 eV, EI): *m*/*z* (%) = 213 (0.1) [M]$^+$, 110 (5) [M − Et_3N − 2H]$^+$, 101 (10) [M − CB_8H_{12}]$^+$. $C_7H_{27}B_8N$ (211.85): calcd. C 39.68, H 12.85; found C 40.25, H 11.92.

4-quin-*arachno*-5-CB_8H_{12} (2c), (quinH)$^+$*closo*-[4-CB_8H_9]$^-$ (3), and 1-quin-*closo*-4-CB_8H_8 (4c): A solution of compound **1** (111 mg, 1 mmol) in CH_2Cl_2 (20 mL) was treated with quinoline (303 mg, 3 mmol) and the mixture was then left stirring for 24 h at ambient temperature. Volatiles were then evaporated and the residue was subjected to chromatography on a silica gel column (30 × 2.5 cm) using CH_2Cl_2 as the mobile phase yielding pure fractions of R_f (CH_2Cl_2) 0.71 and 0.20 which were identified by NMR spectroscopy as **2c** (83 mg, 35%) and **4c** (35 mg, 15%). Further elution with MeCN/CH_2Cl_2 (1:2, v/v) gave a fraction of R_f = 0.23, which was identified by NMR spectroscopy[4] as **3** (28 mg, 12%). **For 2c:** R_f (CH_2Cl_2) 0.71; m.p. 245 °C. ^{11}B NMR ($CDCl_3$): δ = 3.5 (d, $^1J_{B,H}$ = 157 Hz, 1 B, B9), 0.5 (d, $^1J_{B,H}$ ≈ 150 Hz, 2 B, B7,8), −3.4 (d, $^1J_{B,H}$ = 147 Hz, 1 B, B2), −7.9 (d, $^1J_{B,H}$ = 151 Hz, 1 B, B1), −14.6 (d, $^1J_{B,H}$ = 150 Hz, 1 B, B4), −27.4 (t, $^1J_{B,H}$ = ≈115 Hz, 1 B, B6), −57.3 (d, $^1J_{B,H}$ = 151 Hz, 1 B, B3) ppm, all theoretical [^{11}B-^{11}B]-COSY cross-peaks observed, except for B3-B9, B6-B7, B4-B9, B7-B8, and B8-B9. $^1H\{^{11}B\}$ NMR ($CDCl_3$): δ = 3.45 (s, 2 H, 7-

 © 2004 Wiley-VCH Verlag GmbH & Co. KGaA, Weinheim

H,8), 3.30 (s, 1 H, 9-H), 2.76 (s, 1 H, 2-H), 2.45 (s, 2 H, 1-H, *endo*-4-H), 1.41 (s, 1 H, *exo*-6-H), 1.18 (s, 1 H, 5-H), 0.50 (s, 1 H, 3-H), 0.80 (s, 1 H, C*H*5), 0.63 (s, 1 H, *endo*-6-H), −0.72 (s, 1 H, 3-H), −1.69 (s, 1 H, 7,8-μ-H), −1.73 (s, 1 H, 8,9-μ-H) ppm. $^{13}C\{^1H\}$ NMR ($CDCl_3$): δ = 30.0 (br. s, 1 C, C5) ppm. MS (70 eV, EI): *m*/*z* (%) = 241 (32) $[M]^+$, 239 (100) $[M - 2H]^+$. $C_{10}H_{19}B_8N$ (239.82): calcd. C 50.08, H 7.99; found C 52.10, H 8.32. **For 4c:** R_f (CH_2Cl_2) 0.20; m.p. > 350 °C. ^{11}B NMR ($CDCl_3$): δ = 16.5 (d, $^1J_{B,H}$ = 141 Hz, 1 B, B5), 7.2 (d, $^1J_{B,H}$ = 140 Hz, 1 B, B6), −6.5 (s, 1 B, B1), −15.7 (d, $^1J_{B,H} \approx$ 135 Hz, 2 B, B2,7), −21.0 (d, *J* = 150 Hz, 3 B, B3,8,9) ppm, all theoretical [^{11}B-^{11}B]-COSY cross-peaks observed, except for B1-B2, B1-B7, B3-B5, B5-B8, and B5-B9. $^1H\{^{11}B\}$ NMR ($CDCl_3$): δ = 9.65−7.06 (m, 7 H, quin-H), 5.90 (s, 1 H, 4-H), 4.83 (s, 1 H, 5-H), 4.32 (s, 1 H, 6-H), 1.99 (s, 1 H, 2-H or 7-H), 1.47 (s, 1 H, 2-H or 7-H), 0.87 (s, 3 H, 3,8,9-H,) ppm. MS (70 eV, EI): *m*/*z* (%) = 237 (40) $[M]^+$, 236 (48) $[M - H]^+$.

X-ray Crystallographic Study: Crystals of **2b** were grown by slow diffusion of hexane vapors into a CH_2Cl_2 solution. The reflection intensities for compound **2b** were collected on a Siemens P4 diffractometer (graphite-monochromated Mo-K_α radiation, λ = 71.073 pm). The structure solution and refinement was carried out with the program package SHELXTL-PLUS V.5.1. The collection temperature for the structure determination was 296 K. All non-hydrogen atoms were refined with anisotropic temperature factors. The hydrogen atoms in **2b** were located by difference Fourier maps and the remaining hydrogen atoms were placed in calculated positions. All hydrogen atoms were refined applying the riding model with fixed isotropic temperature factors. Crystal data: $C_7H_{27}B_8N$, a colorless irregular block with dimensions 0.22 × 0.18 × 0.16 mm crystallizes in the monoclinic space group $P2_1/c$ with the lattice parameters *a* = 1119.06(19), *b* = 765.84(8), *c* = 1723.10(18) pm, β = 97.576(9)°, *V* = 1463.8(3) 10^6 pm^3, *Z* = 4, μ = 0.046 mm^{-1}; 3447 reflections collected in the range 2° ≤ 2ϑ ≤ 50°, 2554 reflections independent, 1238 assigned to be observed [$I > 2\sigma(I)$], full-matrix least-squares refinement against F^2 with 161 parameters converged at *R*1/*wR*2-values of 0.084/0.225; the max./min. residual electron density was 0.38/−0.39 10^{-6} e·pm^{-3}. CCDC-223376 contains the supplementary crystallographic data for this paper. These data can be obtained free of charge at www.ccdc.cam.ac.uk/conts/retrieving.html [or from the Cambridge Crystallographic Data Center, 12, Union Road, Cambridge CB2 1EZ, UK; fax: (internat.) +44-1223-336-033; E-mail: deposit@ccdc.cam.ac.uk].

Acknowledgments

This work was supported by Alexander von Humboldt Stiftung (FRG) (B. Š.), Die Deutsche Forschungsgemeinschaft (B. W.), Fonds der Chemischen Industrie (B.W.) and the Ministry of Education of Czech Republic (project no. LN00A028). We also thank Drs J. Fusek and Z. Plzák for some of the NMR measurements and mass spectra.

[1] K. Baše, S. Heřmánek, B. Štíbr, *Chem. Ind. (London)* **1977**, 951−952; K. Baše, B. Štíbr, J. Dolanský, J. Duben, *Collect. Czech. Chem. Commun.* **1981**, *46*, 2345−2353; S. Heřmánek, J. Fusek, B. Štíbr, J. Plešek, T. Jelínek, *Polyhedron* **1986**, *5*, 1873−1879.
[2] B. Štíbr, O. L. Tok, W. Milius, M. Bakardjiev, J. Holub, D. Hnyk, B. Wrackmeyer, *Angew. Chem. Int. Ed.* **2002**, *41*, 2126−2128.
[3] T. Jelínek, B. Štíbr, J. Plešek, J. D. Kennedy, M. Thornton-Pett, *J. Chem. Soc., Dalton Trans.* **1995**, 431−437.
[4] T. Jelínek, B. Štíbr, J. Holub, M. Bakardjiev, D. Hnyk, D. L. Ormsby, C. A. Kilner, M. Thornton-Pett, H.-J. Schanz, B. Wrackmeyer, J. D. Kennedy, *Chem. Commun.* **2001**, 1756−1757.
[5] J. H. Jones, B. Štíbr, J. D. Kennedy, A. D. Lawrence, M. Thornton-Pett, *J. Chem. Soc., Dalton Trans.* **1993**, 1269−1274.
[6] J. Plešek, B. Štíbr, X. L. R Fontaine, T. Jelínek, M. Thornton-Pett, S. Heřmánek, J. D. Kennedy, *Inorg. Chem.* **1994**, *13*, 2994−3002.
[7] J. Holub, B. Štíbr, J. D. Kennedy, M. Thornton-Pett, T. Jelínek, J. Plešek, *Inorg. Chem.* **1994**, *33*, 4545−4552.
[8] J. D. Kennedy, in *Multinuclear N. M. R.* (Ed.: J. Mason), Plenum Press, New York, **1987**, p. 221; W. C. Hutton, T. L. Venable, R. N. Grimes, *J. Am. Chem. Soc.* **1984**, *106*, 29−37; J. Schraml, J. M. Bellama, *Two-Dimensional NMR Spectroscopy*, John Wiley & Sons, New York, **1982**.
[9] X. L. R. Fontaine, J. D. Kennedy, *J. Chem. Soc., Dalton Trans.* **1987**, 1573−1575.
[10] B. M. Grabill, A. R. Pitochelli, M. F. Hawthorne, *Inorg. Chem.* **1962**, *1*, 626−631.
[11] D. F. Shriver, M. A. Drezdon, *Manipulation of Air Sensitive compounds*, 2nd ed., John Wiley & Sons, New York, **1986**.
[12] B. Štíbr, J. Holub, M. I. Bakardjiev, I. Pavlík, O. L. Tok, I. Císařová, B. Wrackmeyer, M. Herberhold, *Chem. Eur. J.* **2003**, *9*, 2239−2244.

Received November 4, 2003
Early View Article
Published Online July 12, 2004

 © 2004 Wiley-VCH Verlag GmbH & Co. KGaA, Weinheim

New Ways to a Series of Parent Representatives of the Eight-, Nine-, and Ten-Vertex Monocarbaborane Family

Bernd Brellochs,[a] Jaroslav Bačkovský,[b] Bohumil Štíbr,*[b] Tomáš Jelínek,[b] Josef Holub,[b] Mario Bakardjiev,[b] Drahomír Hnyk,[b] Mathias Hofmann,[c] Ivana Císarová,[d] and Berndt Wrackmeyer[e]

Keywords: Boranes / Carboranes / Geometry optimization / GIAO calculations / Monocarbaboranes

The conditions for a reaction between *nido*-$B_{10}H_{14}$ (**1**) and aqueous formaldehyde in an alkaline solution have been optimized, which resulted in the isolation of the [*arachno*-6-CB_9H_{14}]$^-$ anion (**2**) in 52% yield. Anion **2** was used as a convenient source for the synthesis of a series of basic monocarbaborane compounds. Thus, oxidation of **2** (Et_4N^+ salt) with I_2 in CH_2Cl_2 in the presence of Et_3N at room temperature afforded the [*nido*-6-CB_9H_{12}]$^-$ anion (**3**). Acidification of anion **2** (generated in situ from borane **1**) with hydrochloric acid, in the presence of both $FeCl_3 \cdot 6H_2O$ and CH_2O, led to the formation of *arachno*-4-CB_8H_{14} (**4**), from which *nido*-1-CB_8H_{12} (**5**) was obtained by dehydrogenation at 200 °C in quantitative yield. Compound **4** can easily be converted into the [*closo*-1-CB_7H_8]$^-$ anion (**6**) in 71% yield via reaction with Et_3N and I_2 in THF at –78 °C. Anion **6** is also formed in 75% yield by treatment of carborane **5** with Et_3N in refluxing toluene. The [*closo*-1-CB_8H_9]$^-$ anion (**7**) was isolated by iodination of carborane **5** in the presence of Et_3N (yield 81%) or by the heating of the PPh_4^+ salt of anion **2** at 220 °C (yield 95%). The structure of anion **2** was determined by an X-ray diffraction study and the structures of compounds **2**, **4**, **5**, and **7** were geometry optimized at the RMP2(fc)/6-31G* level. The NMR spectroscopic measurements are in some cases complemented by unpublished ^{13}C NMR spectroscopic data. (© Wiley-VCH Verlag GmbH & Co. KGaA, 69451 Weinheim, Germany, 2004)

Introduction

Until recently, the syntheses of the eight-, nine- and ten-vertex monocarbaboranes have been a rather difficult task[1] as the procedures for the preparation of the parent (unsubstituted) representatives of these families were based on multistep reaction sequences starting from *nido*-decaborane(14), $B_{10}H_{14}$. A new, simple synthesis of the previously reported[2] [*arachno*-6-CB_9H_{14}]$^-$ anion and some of its C-substituted derivatives is a straightforward breakthrough into the area of monocarbaborane chemistry. The work also includes facile routes to the isomeric *closo* anions [2-CB_9H_{10}]$^-$ and [1-CB_9H_{10}]$^-$ developed by one of the authors.[3] Based on these results, experimental details of the synthesis of [*arachno*-6-CB_9H_{14}]$^-$ and *arachno*-4-CB_8H_{14} have been communicated in a preliminary fashion[4] and a few of the authors immediately started investigating further consequences of this chemistry, especially those relating to the C-phenyl and other substituted monocarbaborane derivatives of designed cluster shapes.[5] We report here on the optimization of the new synthesis of the [*arachno*-6-CB_9H_{14}]$^-$ anion[2] together with new routes to the basic parent monocarbaboranes [*nido*-6-CB_9H_{12}]$^-$,[6] *arachno*-4-CB_8H_{14},[6,7] *nido*-1-CB_8H_{12},[6b,8] [*closo*-1-CB_7H_8]$^-$,[9] and [*closo*-4-CB_8H_9]$^-$.[4] Even though most of these compounds have been previously reported, the methods outlined in this paper dramatically improve access to most of these monocarbaborane species and make them generally available. The numbering systems used for compounds discussed in this work are in Scheme 1.

[a] LMU-München, Department Chemie und Pharmazie, Butenandtstrasse 5–13, 81377 München, Germany
Fax: (internat.) +49-(0)218077366
E-mail: b.brellochs@gmx.net
[b] Institute of Inorganic Chemistry, Academy of Sciences of the Czech Republic (Research Center for New Inorganic Compounds and Advanced Materials, University of Pardubice) 25068 Řež, Czech Republic
Fax: (internat.) +420-220940161
E-mail: stibr@iic.cas.cz
[c] Anorganisch-chemisches Institut der Universität, Im Neuenheimer Feld 270, 69120 Heidelberg, Germany
E-mail: matthias.hofmann@urz.uni-heidelberg.de
[d] Faculty of Natural Sciences of Charles University, Hlavova 2030, 12842 Prague 2, Czech Republic
Fax: (internat.) +420-221952378
E-mail: cisarova@natur.cuni.cz
[e] Laboratorium für Anorganische Chemie der Universität Bayreuth
Postfach 101251, 95440 Bayreuth, Germany
Fax: (internat.) +49-6221487-672
E-mail: B.Wrack@uni-bayreuth.de

Results and Discussion

Syntheses

It has previously been communicated[3,4] that the reaction of *nido*-decaborane(14), $B_{10}H_{14}$ (**1**), with an aqueous NaOH solution, followed by the addition of aqueous formal-

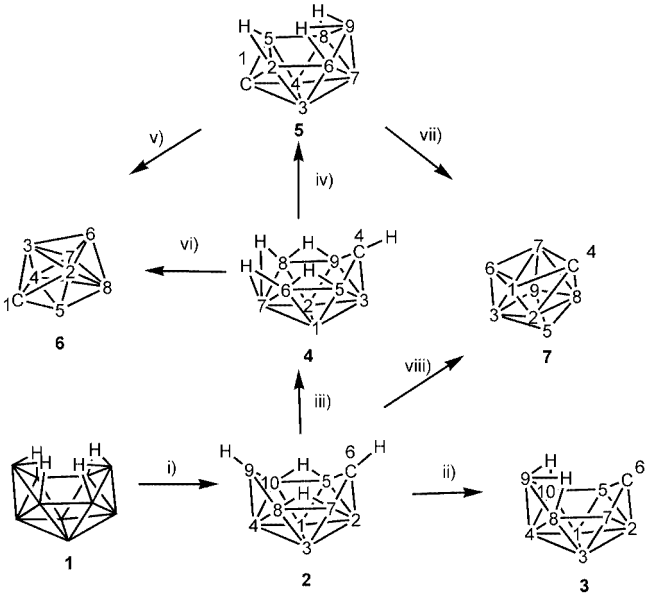

Scheme 1. Syntheses of carboranes from the [*arachno*-6-CB_9H_{14}]$^-$ (**2**) anion. i) aq. NaOH, CH_2O, r.t., 6 h. ii) I_2/Et_3N, CH_2Cl_2, room temp. iii) aq. HCl, aq. $FeCl_3$, hexane or aq. HCl, aq. CH_2O, hexane. iv) heating at 200 °C. v) Et_3N, toluene, reflux 6 h. vi) I_2/Et_3N, THF, −78 °C. vii) I_2/Et_3N, THF, −78 °C. viii) PPh_4^+ salt, 220 °C (the structures in schemes are presented in a simplified manner: calcd. C=CH and unmarked vertices of individual polyhedra stand for BH cluster units)

dehyde, generates the [*arachno*-6-CB_9H_{14}]$^-$ anion (**2**) (see path i) of Scheme 1]. The reaction may reasonably be predicted to proceed via the long-known[10] [*arachno*-6-$B_{10}H_{13}OH$]$^{2-}$ anion as in Equation (1) and Equation (2) and the overall reaction is then represented by Equation (3).

$$B_{10}H_{14} + 2\,OH^- \rightarrow [6\text{-}B_{10}H_{13}OH]^{2-} + H_2O \quad (1)$$

$$[6\text{-}B_{10}H_{13}OH]^{2-} + CH_2O + 2\,H_2O \rightarrow [6\text{-}CB_9H_{14}]^- + B(OH)_4^- + H_2 \quad (2)$$

$$B_{10}H_{14} + 2\,OH^- + CH_2O + H_2O \rightarrow [6\text{-}CB_9H_{14}]^- + B(OH)_4^- + H_2 \quad (3)$$

It was found, however, that the reaction of Equation (3) did not give the best yields of anion **2** using a 1:1 molar ratio of **1**/CH_2O. The reaction was in fact accompanied by a side formation of the previously reported[6] [*nido*-6-CB_9H_{12}]$^-$ anion (**3**) as in Equation (4).

$$[6\text{-}CB_9H_{14}]^- + CH_2O \rightarrow [6\text{-}CB_9H_{12}]^- + CH_3OH \quad (4)$$

Reaction 3 was therefore examined at variable **1**/CH_2O ratios, using 10% NaOH as the reaction medium at room temperature. The reaction was quenched after 5 h by precipitation with NEt_4Cl and the reaction products were analyzed by ^{11}B NMR spectroscopy. The results are shown in Table 1, from which it can be inferred that excess CH_2O promotes the side formation of anion **3**. Optimum reaction conditions for the formation of anion **2**, given in the Exp. Sect., are at molar ratios of 1:3.05. Anion **2** is then removed from the reaction mixture by extraction with Et_2O, followed by precipitation with a suitable countercation in water. The yield of **2,** prepared in this manner in several experiments, is approximately 50%; this one-pot procedure surpasses the previously reported method[2] in all aspects. Mechanistically, the formation of anion **2** is consistent with a unique subrogation of the B6H(OH) vertex in [*arachno*-6-$B_{10}H_{13}OH]^{2-}$ with the formaldehyde CH_2 unit.

Table 1. Products and yields of reactions 3 and 4

Molar ratio **1**/CH_2O[a]	Overall yield (%)[b]	**2**[c]	**3**[c]
1:1.05	43	90	10
1:2.05	45	90	10
1:3.05	58	95	–
1:4.5	76	67	33
1:6.5	68	72	20

[a] In 10% NaOH, room temp., 5 h, then precipitated with NEt_4Cl. [b] Sum of yields of NEt_4^+**2** and NEt_4^+**3**. [c] Content of anions **2** and **3** (in molar%) in the anionic mixture isolated (estimated from ^{11}B NMR spectra).

Anion **2** has become a multipurpose reagent for the preparation of the whole series of monocarbaborane compounds (see Scheme 1). As outlined in path ii) of Scheme 1, a room temperature reaction between Et_4N^+[*arachno*-6-$CB_9H_{14}]^-$ (Et_4N^+**2**) and elemental I_2 in CH_2Cl_2 in the presence of NEt_3 (proton scavenger) resulted in the oxidation of **2** and quantitative formation of the [*nido*-6-$CB_9H_{12}]^-$ anion,[6] which was isolated as its Et_4N^+ salt, Et_4N^+[*nido*-6-$CB_9H_{12}]^-$ (Et_4N^+**3**). The reaction is consistent with the stoichiometry as in Equation (5).

$$[6\text{-}CB_9H_{14}]^- + 2\,Et_3N + I_2 \rightarrow [6\text{-}CB_9H_{12}]^- + 2\,Et_3N{\cdot}HI \quad (5)$$

Anion **2** has also been found to be a very convenient source of the nine-vertex carborane *arachno*-4-CB_8H_{14} (**4**). A room temperature reaction of Na^+**2** with hydrochloric acid and $FeCl_3{\cdot}6H_2O$ in an aqueous medium in the presence of hexane (extraction medium) results in almost

$$6\text{-}CB_9H_{14}^- + Fe^{3+} + 3\,H_2O \rightarrow 4\text{-}CB_8H_{14} + Fe^{2+} + B(OH)_3 + 3/2\,H_2 \quad (6)$$

$$6\text{-}CB_9H_{14}^- + CH_2O + H_3O^+ + 2\,H_2O \rightarrow 4\text{-}CB_8H_{14} + CH_3OH + B(OH)_3 + H_2 \quad (7)$$

quantitative isolation of carborane **4** [see path iii) of Scheme 1 and Equation (6)]. Another, equally effective alternative, is the use of CH_2O in place of the iron trichloride as in Equation (7). Both reactions are carried out more conveniently in one pot from decaborane via in situ generation of anion **2** with typical yields in the range of 45−50% (based on the use of **1**). The formation of carborane **4** is obviously associated with a hydrolytic removal of the B9 vertex in **2**.

 © 2004 Wiley-VCH Verlag GmbH & Co. KGaA, Weinheim

Carborane **4** was converted quantitatively into *nido*-1-CB_8H_{12} (**5**) by heating in vacuo for 6 h at 200 °C (path iv) of Scheme 1) via lower-temperature modification of the previously reported method (sublimation through a hot tube at 350 °C).[6b] Compound **5** was then conveniently used for generating other important compounds of the eight- and nine-vertex monocarbaborane family. As shown in path v) of Scheme 1, treatment of carborane **5** with Et_3N in refluxing toluene led to the isolation of the [*closo*-1-$CB_7H_8]^-$ anion (**6**),[9] the reaction being consistent with the stoichiometry of Equation (8).

$$1\text{-}CB_8H_{12} + 2\,Et_3N \rightarrow Et_3NH^+[1\text{-}CB_7H_8]^- + Et_3N{\cdot}BH_3 \quad (8)$$

The anion **6** was then isolated in 75% yield as its PBu_4^+ salt, PBu_4^+**6**, upon treatment with aqueous NaOH and precipitation with PBu_4Cl. Salts of anion **6,** with any arbitrary countercation, may be similarly prepared. The reaction is consistent with the elimination of the B9 vertex in **5**, followed by closure of the rest of the carborane cage (see Scheme 2). As shown in path vi) of Scheme 1 [see also Equation (9)], anion **6** can also be generated in 71% yield via reaction between the *arachno* carborane **4** and I_2 in the presence of Et_3N in THF at −78 °C.

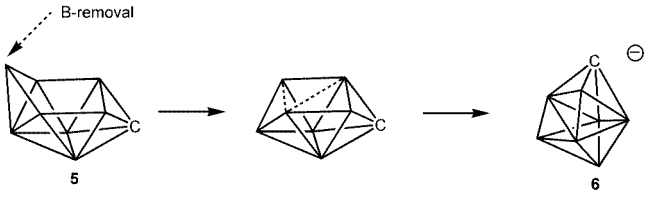

Scheme 2. Proposed formation of the [*closo*-1-$CB_7H_8]^-$ (**6**) anion via removal of the B9 vertex from *nido*-1-CB_8H_{12} (**7**); extra hydrogen atoms omitted for clarity

$$4\text{-}CB_8H_{14} + 4\,Et_3N + I_2 \rightarrow Et_3NH^+[1\text{-}CB_7H_8]^- + Et_3N{\cdot}BH_3 + 2\,Et_3N{\cdot}HI \quad (9)$$

The reaction may be explained by removing the B6 vertex in **4**, followed by oxidative closure of the remaining CB7 skeleton. A similar mechanism was proposed earlier for the formation of anion **6** from 6-Me_3N-*arachno*-4-CB_8H_{12}.[9] The Et_3NH^+ salt was again converted into PBu_4^+**6** as in the preceding case. Both procedures of Equations (8) and (9) are very simple and anion **6** now becomes one of the best available compounds of monocarbaborane chemistry. The same applies to the nine-vertex anion [*closo*-4-$CB_8H_9]^-$ (**7**) which was reported in a preliminary communication.[4] One method for the preparation of **7** is based on treatment of compound **5** with I_2 in the presence of Et_3N in THF at −78 °C [Equation (10) and path vii) of Scheme 1].

$$1\text{-}CB_8H_{12} + 3\,Et_3N + I_2 \rightarrow Et_3NH^+[4\text{-}CB_8H_9]^- + 2\,Et_3N{\cdot}HI \quad (10)$$

$$[6\text{-}CB_9H_{14}]^- \rightarrow [4\text{-}CB_8H_9]^- + [BH_3] + H_2 \quad (11)$$

The Et_3NH^+ salt was again converted in situ into PBu_4^+**7** (yield 81%) in an alkaline solution by precipitation with PBu_4Br. Other salts with suitable countercations can be isolated in a similar manner. The formation of **7** can be classified as a clean *nido* → *closo* conversion in which the original B2, B5 and B9 vertices in **5** are interconnected via oxidation to **7**. A very simple access to anion **7** is also the heating of PPh_4^+**2** at 220 °C [see Equation (11) and path viii) of Scheme 1]. The reaction provides PPh_4^+**7** in 95% yield as a single product and is associated with a clean elimination of the B9 vertex from anion **2** followed by cage closure. The process is probably associated with the rearrangement of one of the boron vertices as suggested in Scheme 3. This method is much more convenient than a similar heating of Cs^+**2**[4] (maximum yield of **7** 60%), which is associated with the side formation of other anions.

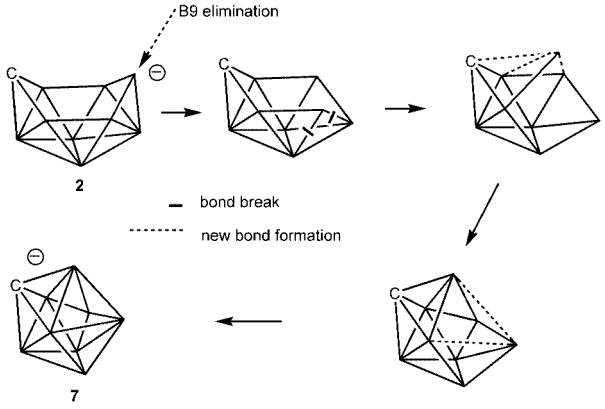

Scheme 3. Proposed formation of the [*closo*-1-$CB_8H_9]^-$ (**7**) anion via removal of the B9 vertex from the [*arachno*-6-$CB_9H_{14}]^-$ (**2**) cage; extra hydrogen atoms omitted for clarity

Structural Studies

The structures of anions **6** (I_2 and 1-Ph derivatives)[5b][5e,9] and **7**[4] have already been determined crystallographically and those of anions **6**,[11] and **7**[4,11] have been geometry-optimized. In this work these studies are complemented by an X-ray diffraction study of anion **2** (see Figure 1) and the geometries of compounds **2**, **3**, **4**, and **5** optimized at the RMP2(fc)/6-31G* level (see Figure 2).

The crystallographic structure of PPh_3Me^+**2**, depicted in Figure 1, is in agreement with the earlier proposed structure.[2] The anionic part contains one CH_2 and one BH_2 unit in the apical positions and two hydrogen bonds in the open hexagonal face. The longest bond lengths in the open face are those attached to B9, followed by the "bridging" B−B distances and C−B separations. The B8−B9−B10 angle is significantly (10.7°) smaller than B5−C6−B7. Other intracluster C−B and B−B distances are within usual limits. Comparisons between experimental and calculated bond lengths for anion **2** show good agreement, which reflects the accuracy of the calculations.

In the *nido* anion **3**, the calculated B5−B10 distance is 0.068 Å longer than the corresponding "bridged" B5−B10 separation in its *arachno* counterpart **2**. The B5−B10 dis-

 © 2004 Wiley-VCH Verlag GmbH & Co. KGaA, Weinheim

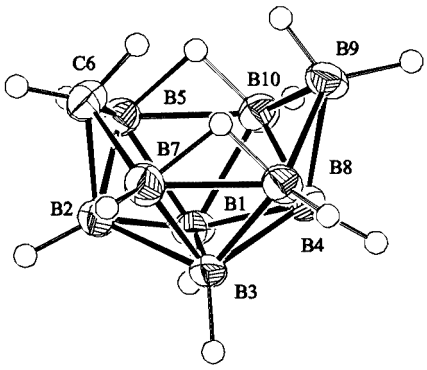

Figure 1. ORTEP representation of the crystallographically determined molecular structure of $PMePh_3^+[arachno\text{-}6\text{-}CB_9H_{14}]^-$ ($PMePh_3^+$**2**) (cationic part omitted); displacement ellipsoids are drawn at 50% probability level; selected bond lengths (Å) and angles (°): B1−B2 1.736(2), B1−B3 1.809(2), B1−B4 1.787(2), B1−B5 1.779(2), B1−B10 1.768(2), B2−B3 1.746(2), B2−B5 1.782(2), B2−C6 1.668(2), B2−B7 1.775(2), B3−B4 1.792(2), B4−B8 1.747(2), B4−B9 1.731(2), B4−B10 1.741(2), B5−C6 1.729(2), B5−B10 1.850(2), C6−B7 1.728(2), B7−B8 1.877(2), B8−B9 1.894(2), B9−B10 1.915(2), B5−C6−B7 112.66(10), B8−B9−B10 102.24(9)

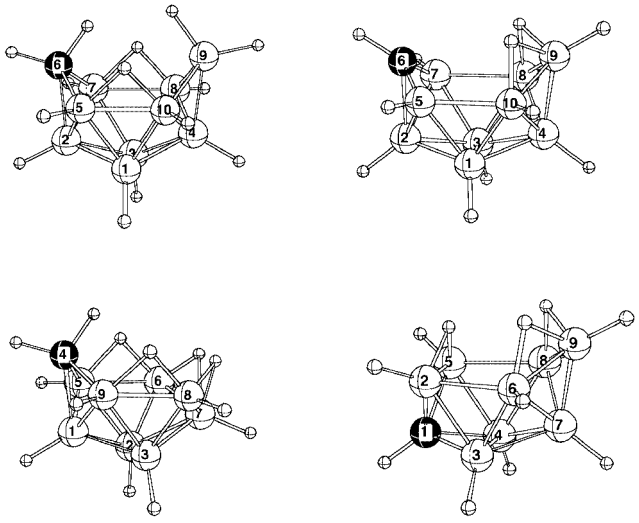

Figure 2. Geometry-optimized structures of $[arachno\text{-}6\text{-}CB_9H_{14}]^-$ (**2**), $[nido\text{-}6\text{-}CB_9H_{12}]^-$ (**3**), $arachno\text{-}4\text{-}CB_8H_{14}$ (**4**), and $nido\text{-}1\text{-}CB_8H_{12}$ (**5**) at the RMP2(fc)/6-31G* level; selected bond lengths (Å) and angles (°): **2** B1−B2 1.734, B1−B3 1.810, B1−B4 1.788, B1−B5 1.772, B1−B10 1.770, B2−B5 1.774, B2−C6 1.671, B4−B9 1.735, B4−B10 1.737, B5−C6 1.7233, B5−B10 1.849, B8−B9 1.913, B−H (mean) 1.199, B5-μH5,10 1.358, B10-μH5,10 1.284, C6−H (mean) 1.088, B5−C6−B7 112.2, B8−B9−B10 101.5; **3** B1−B2 1.749, B1−B3 1.809, B1−B4 1.804, B1−B5 1.765, B1−B10 1.765, B2−B5 1.793, B2−C6 1.696, B4−B9 1.710, B4−B10 1.777, B5−C6 1.539, B5−B10 1.917, B8−B9 1.762, B−H (mean) 1.198, B8-μH8,9 1.315, B9-μH8,9 1.338, C6−H 1.093, B5−C6−B7 118.1, B8−B9−B10 104.1; **4** B1−B2 1.798, B1−B3 1.733, B1−B5 1.799, B1−B6 1.720, B1−B7 1.816, B3−B4 1.669, B3−B5 1.762, B4−B9 1.720, B5−B6 1.827, B9−B7 1.837, B8−B9 1.827, B−H (mean) 1.189, B5-μH5,6 1.368, B6-μH5,6 1.290, C4−H (mean) 1.087, B6-μH6,7 1.246, B7-μH6,7 1.526, B5−C4−B9 114.6, B6−B7−B8 127.3; **5** C1−B2 1.592, C1−B3 1.608, B2−B5 1.891, B2−B6 1.937, B3−B4 1.817, B6−B7 1.799, B7−B9 1.696, B8−B9 1.775, B−H (mean) 1.189, B2-μH2,5 1.331, B6-μH6,9 1.315, B9-μH6,9 1.337, C1−H 1.087, B8−B9−B6 100.5

tance in **3** is also 0.155 Å longer than the "bridged" B8−B9 bond length. Further comparisons suggest that the B5−C6−B7 and B8−B9−B10 angles in **3** are 5.9 and 2.6° larger, respectively, than those in **2** and the B5−C6−B7 angle in **3** is also 14° larger than B8−B9−B10. This means than the open hexagonal faces in both anions **2** and **3** are rather irregular and more open in the area around the carbon vertices.

Calculations on the neutral carborane **4** at both the MP2/6-31G* and B3LYP/6-31G* levels characterized the C_s structure shown in Figure 2 as a minimum. Comparison of computed chemical shifts for this structure to experimental data leaves no doubt that the solution spectra are due to a static structure (C_s symmetric) and not time averaging of rapidly rearranging C_1 structures shown in Scheme 4. The *C*s structure contains two pairs of asymmetrical hydrogen bonds; the B5-μH5,6 distance is 0.078 Å longer than B6-μH5,6 and the B6-μH6,7 separation is 0.28 Å shorter than B7-μH6,7, which at 1.526 Å is extremely long. Comparison of the calculated open-face C−B (1.720/1.733 Å) and the bridging B−B (1.827/1.849 Å) distances and the B−C−B angles (114.6/112.2°) in anions **4** and **2**, respectively, suggests that the C4−B5−B6−B8−B9 section in **4** is very similar to the corresponding B5−C6−B7−B8−B10 part of the molecule of **2**. This corresponds to the fact that the two molecules are related by removing one boron vertex. Comparison of the bridging B−B distances in **4** shows that the B6−B7 separation is only slightly (0.01 Å) longer than the B5−B6 distance. In the *nido* compound **5**, the B2−B6 separation is significantly (0.162 Å) longer than the bridging B6−B9 distance and the other bridging B2−B5 separation is 0.116 Å longer than B6−B9. The B6−B9−B8 angle is at 100.5°, which is similar to the B8−B9−B10 angle in the *nido* anion **3** (cf. 104°) (Scheme 4).

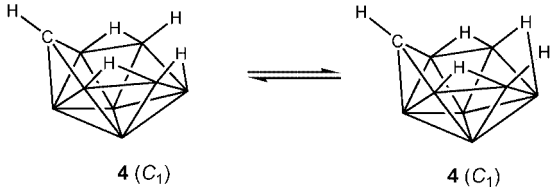

Scheme 4. Time averaging between two C_1 structures for compound **4**; averaged ^{11}B NMR shifts computed for this process at the IGLO-HF/DZ level are: 4.3 (B1), −39.8 (B2,3), 9.2 (C4), −9.6 (B5,9), −25.8 (B6,8), 26.8 (B7)

The ^{11}B and ^{1}H NMR spectroscopic data for all compounds encountered in this work have mostly been reported previously, in some cases we have added the data for anions with different countercations. The work is supplemented by the unpublished ^{13}C NMR shifts of the cage CH or CH_2 units for selected compounds. The optimized geometries have been used as a basis for the calculation of theoretical ^{11}B and ^{13}C NMR chemical shifts. A comparison between calculated and experimental shifts (see Exp. Sect.) is generally in good agreement.

 © 2004 Wiley-VCH Verlag GmbH & Co. KGaA, Weinheim

Conclusions

The efficient route from $B_{10}H_{14}$ to the starting monocarbaborane anion **2** has improved the yield of this anion by about five times, in comparison with the original procedure.[2] This means that the eight-, nine- and ten-vertex species prepared in this work are now one of the most readily accessible monocarbaboranes. Their chemistry should now contribute substantially to the development of carborane science. For example, the *closo* anions **6** and **7**, together with the recently reported [*closo*-$CB_6H_7]^-$ anion,[12] could act as "weakly coordinating anions" to complement $[CB_9H_{10}]^-$ and $[CB_{11}H_{12}]^-$, and their derivatives.[13] The compounds are also likely to be amenable to extensive substitution and metallacarborane chemistries. We are currently developing these areas with the aim of extending the knowledge of the chemistry of monocarbaboranes with less than ten cluster atoms.

Experimental Section

General Procedures: All reactions were carried out with the use of standard vacuum or inert-atmosphere techniques as described by Shriver,[14] although some operations, such as column LC, were carried out in air. The starting compound **1** was sublimed in vacuo at 80 °C using an apparatus equipped with a water-cooled sublimation finger. THF was distilled from sodium diphenyl ketyl, dichloromethane and hexane were dried over CaH_2 and freshly distilled before use. Other chemicals were reagent or analytical grade and were used as purchased. The purity of the individual compounds was checked by analytical TLC on Silufol (silica gel on aluminum foil; detection by iodine vapors, followed by 2% aqueous $AgNO_3$ spray). Melting points were measured in sealed capillaries under argon and are uncorrected. Multinuclear (^1H, ^{11}B, and ^{13}C) NMR spectroscopy was performed essentially with the instrumentation described in other related papers from our laboratories.[15] The ^{11}B and ^{13}C chemical shifts are given in the following manner: δ(exp.)/δ(calcd., IGLO-HF/DZ), δ(calcd., GIAO-HFII), δ(calcd., GIAO-B3LYP/II).

Salts of [*arachno*-6-$CB_9H_{14}]^-$ (2) (Optimized Procedure): A solution of compound **1** (1.24 g, 10 mmol) in 20 mL of hexane was treated with 10% aqueous NaOH (70 mL) whilst stirring and cooling at 0 °C. The cooling was continued and 2.5 g of an aqueous CH_2O solution (37%, w/w, stabilized with methanol) (ca. 31 mmol of CH_2O) diluted with 10 mL of water was added over a period of 1 h. The stirring was continued at ambient temperature for 12 h. The hexane layer was separated and the aqueous solution was extracted by three 10-ml portions of Et_2O and the combined extracts were evaporated with water (30 mL) to remove the diethyl ether. The remaining aqueous solution (solution A) was precipitated alternatively with solid $Et_4N^+Cl^-$ (1.7 g, 10 mmol), $PPh_4^+Cl^-$ (3.75 g, 10 mmol), and $Ph_3PMe^+Cl^-$ (3.15 g, 10 mmol). The white precipitates were isolated by filtration, the solids were washed with cold water (2 × 10 mL) and vacuum dried for 12 h to give pure Et_4N^+ (1.3 g, 51%), PPh_4^+ (2.6 g, 56%), and Ph_3PMe^+ (2.1 g, 52%) salts of anion **2**, respectively. The salts were recrystallized by diffusion of hexane vapors into solutions of CH_2Cl_2. M.p. 348 °C (decomp.). ^{11}B NMR (128.3 MHz, CD_3CN, 295 K): δ = −1.4/ 3.2, 5.4, −2.7 [d, ^1J(B,H) = 129 Hz, 1 B, B4], −10.3/−8.3, −5.6, −13.2 (d, ^1J(B,H) ≈160 Hz, 1 B, B2), −12.9/−14.2, −11.2, −17.3 [d, ^1J(B,H) = 154 Hz, 2 B, B5,7], −23.3/−21.1, −21.4, −25.5 [t, ^1J(B,H) = 106 Hz, 1 B, B9], −28.8/−28.6, −26.9, −32.1 [d, ^1J(B,H) = 128 Hz, 2 B, B8,10], −39.8/−41.4, −38.9, −44.4 [d, ^1J(B,H) = 138 Hz, 2 B, B1,3]. $^{13}C\{^1H\}$ NMR [100.6 MHz, $(CD_3)_2SO$, 295 K]: δ = −4.8/−1.4, −12.5, −2.0 (s br., 1 C, C6). $C_9H_{42}B_9N$ (253.75): calcd. C 42.60, H 16.68; found C 43.20, H 15.62.

Et_4N^+[*nido*-6-$CB_9H_{12}]^-$ (Et_4N^+3): Triethylamine (0.5 mL) was added to a solution of Et_4N^+**2** (381 mg, 1.5 mmol) in CH_2Cl_2 (20 mL) and the mixture was treated with solid I_2 (381 mg, 1.5 mmol) in several portions over a period of 2 h whilst stirring at room temperature. The mixture was then shaken with 5% aqueous $Na_2S_2O_3$ (20 mL) and water (20 mL). The bottom layer was separated, evaporated and the residual solid was vacuum dried at ambient temperature for 12 h to give pure Et_4N^+**3**. M.p. 298 °C (decomp.). ^{11}B NMR (128.3 MHz, CD_2Cl_2, 295 K): δ = 1.7/2.5.4.7, −1.1 [d, ^1J(B,H) = 135 Hz, 2 B, B5,7], −1.8/−3.0, −0.9, −10.0 [d, ^1J(B,H) ≈ 150 Hz, 1 B, B9], −4.6/−3.1, 1.7, −5.7 [d, ^1J(B,H) = 134 Hz, 2 B, B1,3], −12.5/−13.5, −9.6, −15.0 [d, ^1J(B,H) = 140 Hz, 2 B, B8,10], −30.7/−34.5, −31.2, −33.8 [d, ^1J(B,H) = 147 Hz, 1 B, B2], −37.9/−41.4, −38.4, −43.4 [d, ^1J(B,H) = 142 Hz, 1 B, B4]. ^{13}C NMR [100.6 MHz, $(CD_3)_2SO$, 295 K]: δ = 126.4/129.9, 124.7, 140 (d, $^1J_{C,H}$ = 144 Hz, 1 C, C6). $C_9H_{40}B_9N$ (251.73): calcd. C 42.94, H 16.02; found C 41.15, H 15.38.

***arachno*-4-CB_8H_{14} (4):** a) Solution A from the preparation of anion **2** (containing ca. 5.2 mmol of Na^+**2**) was added dropwise to a stirred mixture of aqueous HCl (ca. 4.5 M, 35 mL), $FeCl_3{\cdot}6H_2O$ (6.5 g) and hexane (30 mL) and the stirring was continued for 6 h (hydrogen evolution). The hexane layer was separated, evaporated and the residue sublimed at 50 °C (bath temperature) to obtain compound **4** (540 mg, 48%, based on **1** used), which was identified by NMR spectroscopy. ^{11}B NMR: δ = 17.0/16.3, 18.8, 12.6 (B7), −3.7/−2.9, 1.3, −6.5 (B1), −6.3/−7.8, −4.7, −9.7 (B5,9), −34.9/−36.4, −34.5, −42.8 (B6,8), −41.1/−47.1, −44.4/−49.6 (B2,3), experimental data from ref.[6a] ^{13}C NMR (125.8 MHz, $CDCl_3$, 295 K): δ = −10.8/−13.1, −16.4, −10.0 (t, $^1J_{C,H}$ = 134 and 162 Hz, 1 C, C4). b) Hexane (40 mL) and an aqueous solution of CH_2O (37%, w/v, stabilized with methanol) (1.6 g, ca. 20 mmol of CH_2O) were added to solution A from the preparation of anion **2** whilst stirring and cooling to 0 °C (bath temperature). The mixture was then treated dropwise with aqueous HCl (ca. 4.5 M, 35 mL) at 0 °C for 1 h, and the stirring was then continued for 6 h at room temperature (hydrogen evolution). The hexane layer was separated and pure compound **4** (563 mg, 50% based on **1**) was isolated as in the preceding experiment.

***nido*-1-CB_8H_{12} (5):** Freshly sublimed compound **4** (500 mg, 4.44 mmol) was placed in a 250-mL Pyrex tube equipped by a break seal and sealed in vacuo under cooling liquid nitrogen. The tube was then heated at 200 °C for 6 h and opened into a vacuum manifold under cooling with liquid nitrogen. The solid residue was then sublimed into a −78 °C trap to obtain pure compound **7** (495 mg, 99%), which was identified by spectroscopy. ^{11}B NMR: δ = 7.6/6.4, 8.9, 2.0 (B9), −3.3/−0.3, 0.2, −5.4 (B3,4), −11.5/−12.6, −9.3, −14.2 (B6,8), −26.5/−26.0, −24.7, −31.2 (B2,5), −53.3/−54.4, −52.6, −58.8 (B7), experimental data from ref.[16] ^{13}C NMR (125.8 MHz, $CDCl_3$, 295 K): δ = 31.1/29.5, 19.6, 35.7 (d, $^1J_{C,H}$ = 199 Hz, 1 C, C1).

[*closo*-1-$CB_7H_8]^-$ Anion (6): a) NEt_3 (1.6 mL) was added to a solution of compound **4** (260 mg, 2.31 mmol) in THF (20 mL) and the mixture was treated with a solution of I_2 (1175 mg, 4.62 mmol) in THF (30 mL) under vigorous stirring and cooled to −78 °C over

 © 2004 Wiley-VCH Verlag GmbH & Co. KGaA, Weinheim

a period of 1 h. The volatiles were then evaporated, the residual materials dried in vacuo for 1 h and then treated with a mixture of 5% KOH (20 mL) and CH_2Cl_2 (20 mL) under shaking. The CH_2Cl_2 layer, containing $NEt_3{\cdot}BH_3$ (identified via ^{11}B NMR), was discarded and the aqueous layer treated with solid PBu_4Cl (681 mg, 2.31 mmol). The precipitate was isolated by filtration and dried under vacuum for 2 h at room temperature. Crystallization by diffusion of hexane vapors into a CH_2Cl_2 solution gave white crystals (586 mg, 71%) which were identified by ^{11}B NMR spectroscopy[9] as PBu_4^+**6**. $^{13}C\{^{11}B\}$ NMR [100.6 MHz, $(CD_3)_2CO$, 295 K]: δ = 60.1 (s, 1 C, C1). b) Under strictly anaerobic conditions (deoxygenated Ar), a solution of compound **5** (300 mg, 2.71 mmol) in toluene (30 mL) was treated with NEt_3 (1 mL) and then heated at reflux for 6 h. The mixture was then cooled to ambient temperature and extracted with two 10-ml portions of 5% KOH. The aqueous layer was treated with solid PBu_4Cl (800 mg, 2.71 mmol) and then extracted with CH_2Cl_2 (20 mL). The organic layer was placed onto a silica gel column (2.5 × 20 cm) and elution with 5% MeCN in CH_2Cl_2 gave the main fraction of R_f = 0.23. This was evaporated to dryness and the residue crystallized by diffusion of hexane vapors into a CH_2Cl_2 solution to isolate white crystals of PBu_4^+**6** (681 mg, 75%).

[*closo*-4-CB_8H_9]$^-$ Anion (7): a) A solution of freshly sublimed compound **5** (150 mg, 1.36 mmol) in THF (10 mL) was treated with Et_3N (0.5 mL) whilst stirring and cooling to −78 °C and solid I_2 (346 mg, 1.36 mmol) was then added in several portions over a period of 1 h. The THF was evaporated and the residual solid treated with 5% aqueous KOH while shaking and cooling. The Et_3N thus evolved was evaporated and the residual solution filtered. The filtrate was treated with PBu_4Br (462 mg, 1.36 mmol) and extracted with CH_2Cl_2 (20 mL). The CH_2Cl_2 extract was mounted onto a silica gel column (2.5 × 20 cm) and elution with 5% MeCN in CH_2Cl_2 gave a pure fraction of R_f = 0.2. This was evaporated and the residual solid crystallized by diffusion of hexane vapors into a CH_2Cl_2 solution to isolate the white crystals of PBu_4^+**7** (405 mg, 81%). Other salts of anion **7** can be obtained by precipitation of the aqueous filtrate with a suitable countercation. ^{11}B NMR (160.4 MHz, $CDCl_3$, 25 °C): δ = 12.8 [d, ^1J(B,H) = 145 Hz, 2 B, B5,6], −14.3 [d, ^1J(B,H) = 148 Hz, 4 B, B1,2,7,8], −20.3 [d, ^1J(B,H) = 136 Hz, 1 B, B3,9], all theoretical [^{11}B-^{11}B]-COSY cross-peaks observed. $^1H\{^{11}B\}$ NMR (500 MHz, $CDCl_3$, 25 °C): δ = 4.37 (s, 2 H, H5,6), 4.13 (s, 1 H, H4), 1.47 (s, 4 H, H1,2,7,8), 0.64 (s, 2 H, H3,9). ^{13}C NMR (125.8 MHz, $CDCl_3$, 25 °C): δ = 44.5 (br.d, $^1J_{C,H}$ = 182 Hz, 1 C, C4). b) Solid PPh_4^+**2** (926 mg, 2 mmol) was heated for 2 h at 220 °C. The residual solid was dissolved in CH_2Cl_2 (10 mL) and the solution was carefully covered by hexane (20 mL). The white crystals that separated on standing for 3 days were identified by NMR spectroscopy as pure PPh_4^+**9** (849 mg, 95%).

Computational Details: The GAUSSIAN94 program package[17] was used for calculations, which were performed on the Power Challenge XL computer of the Supercomputing Center of the Charles University in Prague. The structures proposed on the basis of experimental ^{11}B and ^1H NMR spectroscopy were optimized first at RHF/6-31G* within the given symmetry restriction. Frequency calculations, carried out at the same level, determined the nature of the stationary points. Minima are characterized by zero imaginary frequency (NIMAG = 0). Further optimizations at RMP2(fc)/6-31G* included the effect of electron correlation. Selected geometry parameters are given in Figure 2. For MP2/6-31G* optimized geometries the chemical shieldings were calculated at a SCF level using both the IGLO (invariant gauge for localized orbitals) and GIAO (gauge-invariant atomic orbital) method. In addition the B3LYP density functional theory level was applied using GIAO, the latter being incorporated in the GAUSSIAN94. NMR shift calculations employed Huzinaga basis sets:[18] DZ (double zeta) and II well-designed for magnetic properties calculations.[19]

X-ray Crystallographic Study: Crystals of PPh_3Me^+**2** were grown by slow diffusion of hexane vapors into a CH_2Cl_2 solution. The crystal was mounted on a glass fiber with epoxy cement and measured on a four-circle diffractometer Nonius KappaCCD equipped with a CCD area detector at 150(2)K with Mo-K_α radiation (λ = 0.71073 Å, graphite-monochromated). The structure was solved by the direct method (SIR97)[20] and refined by a full-matrix least-squares procedure based on F^2 (SHELXL-97).[21] All non-hydrogen atoms were refined with anisotropic temperature factors. The hydrogen atoms of the carborane cage were located on difference Fourier maps and refined isotropically; remaining hydrogen atoms of PPh_3Me^+ were on calculated positions and refined applying the riding model with assigned temperature factors either $H_{iso}(H)$ = 1.2 U_{eq}(pivot atom) or $H_{iso}(H)$ = 1.5 U_{eq}(pivot atom) for the methyl moiety.

Crystal data: $C_{20}H_{32}B_9P$, a colorless block of dimensions 0.70 × 0.45 × 0.4 mm crystallizes in the monoclinic space group $P2_1/c$ with the lattice parameters a = 11.7370(2), b = 15.0650(2), c = 14.0740(2) Å, β = 107.8960(8)°, V = 2368.13(6) Å^3, Z = 4, μ = 0.122 mm^{-1}; 39627 reflections collected in the range 2° ≤ 2θ ≤ 55°, 5417 reflections independent (R_{int} = 0.029), 4824 assigned to be observed [$I > 2\sigma(I)$], full-matrix least-squares refinement against F^2 with 328 parameters converged at $wR(F^2)$ = 0.0990 ($R[F^2 > 2\sigma(F^2)]$ = 0.0356, $w = 1/[\sigma^2(F_o^2) + (0.0519P)^2 + 0.6888P]$ where $P = F_o^2 + 2F_c^2)/3$) and the max./min. residual electron density was 0.309/−0.303 e·Å^{-3}. CCDC-230897 contains the supplementary crystallographic data for this paper. These data can be obtained free of charge at www.ccdc.cam.ac.uk/conts/retrieving.html [or from the Cambridge Crystallographic Data Centre, 12 Union Road, Cambridge CB2 1EZ, UK; Fax: (internat.) +44-1223-336-033; E-mail: deposit@ccdc.cam.ac.uk].

Acknowledgments

This work was supported by Alexander von Humboldt Stiftung (FRG) (B. Š.), Deutsche Forschungsgemeinschaft (B. W.), Fonds der Chemischen Industrie (B. W.), the Ministry of Education of the Czech Republic (project no. LN00A028), and the Czech Academy of Sciences (grant no. S4032007). We also thank Dr. J. Fusek and O. L. Tok for partial NMR measurements, and I. Kanerová for experimental help.

[1] B. Štíbr, *Chem. Rev.* **1992**, *92*, 225−250.
[2] [2a] B. Štíbr, T. Jelínek, J. Plešek, S. Heřmánek, *J. Chem. Soc., Chem. Commun.* **1987**, 963−964. [2b] K. Nestor, T. Jelínek, X. L. R. Fontaine, J. D. Kennedy, M. Thornton-Pett, K. Baše, B. Štíbr, *J. Chem. Soc., Dalton Trans.* **1990**, 2887−2894.
[3] B. Brellochs in *Contemporary Boron Chemistry* (Eds.: M. G. Davidson, A. K. Hughes, K. Wade), Royal Society of Chemistry, Cambridge, UK, **2000**, pp. 212−214.
[4] T. Jelínek, B. Štíbr, J. Holub, M. Bakardjiev, D. Hnyk, D. L. Ormsby, C. A. Killner, M. Thornton-Pett, H.-J. Schanz, B. Wrackmeyer, J. D. Kennedy, *Chem. Commun.* **2001**, 1756−1757; B. Štíbr, B. Wrackmeyer. *J. Organomet. Chem.* **2002**, *657*, 3−8.
[5] [5a] T. Jelinek, C. A. Kilner, M. Thornton-Pett, J. D. Kennedy, *Chem. Commun.* **2001**, 1790−1791. [5b] A. Franken, C. A.

 © 2004 Wiley-VCH Verlag GmbH & Co. KGaA, Weinheim

Kilner, M. Thornton-Pett, J. D. Kennedy, *Collect. Czech. Chem. Commun.* **2002**, *67*, 869−912. [5c] T. Jelinek, M. Thornton-Pett, J. D. Kennedy, *Collect. Czech. Chem. Commun.* **2002**, *67*, 1035−1050. [5d] A. Franken, C. A. Kilner, M. Thornton-Pett, J. D. Kennedy, *J. Organomet. Chem.* **2002**, *657*, 176−179. [5e] A. Franken, C. A. Kilner, M. Thornton-Pett, J. D. Kennedy, *J. Organomet. Chem.* **2002**, *657*, 180−186. [5f] A. Franken, C. A. Kilner, M. Thornton-Pett, J. D. Kennedy, *Inorg. Chem. Commun.* **2002**, *5*, 581−584. [5g] A. Franken, C. A. Kilner, M. Thornton-Pett, J. D. Kennedy, *Chem. Commun.* **2002**, 2048−2049. [5h] N. J. Bullen, A. Franken, C. A. Kilner, J. D. Kennedy, *Chem. Commun.* **2003**, 1684−1685. [5i] A. Franken, C. A. Kilner, J. D. Kennedy, *Inorg. Chem. Commun.* **2003**, *6*, 1104−1108. [5j] S. L. Renard, A. Franken, C. A. Kilner, J. D. Kennedy, M. A. Halcrow, *New. J. Chem.* **2003**, *26*, 1634−1637.

[6] [6a] B. Štíbr, K. Baše, S. Heřmánek, J. Plešek, *J. Chem. Soc., Chem. Commun.* **1976**, 150−151. [6b] K. Baše, B. Štíbr, J. Dolanský, J. Duben, *Collect. Czech. Chem. Commun.* **1981**, *46*, 2345−2353.

[7] A. E. Wille, J. Plešek, J. Holub, B. Štíbr, P. J. Carroll, L. G. Sneddon, *Inorg. Chem.* **1996**, *35*, 5342−5346.

[8] [8a] K. Baše, S. Heřmánek, B. Štíbr, *Chem. Ind. (London)* **1977**, 951−952. [8b] S. Heřmánek, J. Fusek, B. Štíbr, J. Plešek, T. Jelínek, *Polyhedron* **1986**, *5*, 1873−1879.

[9] [9a] J. Plešek, T. Jelínek, B. Štíbr, S. Heřmánek, *J. Chem. Soc., Chem. Commun.* **1988**, 348−349. [9b] T. Jelínek, B. Štíbr, J. Plešek, J. D. Kennedy, M. Thornton-Pett, *J. Chem. Soc., Dalton Trans.* **1995**, 431−437.

[10] E. L. Muetterties, F. Klanberg, *Inorg. Chem.* **1966**, *5*, 315−316.

[11] P. v. R. Schleyer, K. Najafian, *Inorg. Chem.* **1998**, *7*, 3454−3470.

[12] B. Štíbr, O. L Tok, W. Milius, M. Bakardjiev, J. Holub, D. Hnyk, B. Wrackmeyer, *Angew. Chem. Int. Ed.* **2002**, *41*, 2126−2128.

[13] [13a] C. Reed, *Acc. Chem. Res.* **1998**, *31*, 133−139. [13b] S. Strauss, *Chem. Rev.* **1993**, *93*, 927−942.

[14] D. F. Shriver, M. A. Drezdon, *Manipulation of Air Sensitive Compounds*, 2nd ed., Wiley, New York, **1986**.

[15] B. Štibr, J. Holub, M. Bakardjiev, I. Pavlík, O. L. Tok, I. Císarová, B. Wrackmeyer, M. Herberhold, *Chem. Eur. J.* **2003**, *9*, 2239−2244.

[16] J. H. Jones, B. Štíbr, J. D. Kennedy, A. D. Lawrence, M. Thornton-Pett, *J. Chem. Soc., Dalton Trans.* **1993**, 1269−1274.

[17] M. J. Frisch, G. W. Trucks, H. B. Schlegel, P. M. W. Gill, B. G. Johnson, M. A. Robb, J. R. Cheeseman, T. Keith, G. A. Petterson, J. A. Montgomery, K. Raghavachari, M. A. Al-Laham, V. G. Zahrzewski, J. V. Ortiz, J. B. Foresman, J. Cioslowski, B. B. Stefanov, A. Nanayakkra, M. Challacombe, C. Y. Peng, P. Y. Ayala, Y. Chen, M. W. Wong, J. L. Andres, E. S. Replogle, R. Gomprets, R. L. Martin, D. J. Fox, J. S. Binkley, D. J. Defrees, L. Baker, J. P. Stewart, M. Head-Gordon, C. Gonzales, J. A. Pople, *GAUSSIAN94*, Revision B.2. Gaussian Inc., Pittsburg, PA, **1995**.

[18] S. Huzinaga, *Approximate Atomic Wave Functions*, University of Alberta, Edmonton, Canada, **1971**.

[19] W. Kutzelnigg, M. Schindler, U. Fleischer, *NMR*, *Basic Principles and Progress*, Springer-Verlag, Berlin, New York, **1990**; Vol. 23.

[20] A. Altomore, M. C. Burla, M. Camalli, G. Cascarano, C. Giacovazzo, A. Guagliardi, A. G. G. Molinerni, G. Polidori, R. Spagna, *J. Appl. Crystalogr.* **1999**, *32*, 115−119.

[21] G. M. Sheldrick, *SHELX97*, *Program for Crystal Structure Refinement* from Diffraction Data, University of Göttingen, Germany, **1997**.

Received February 16, 2004
Early View Article
Published Online July 12, 2004

 © 2004 Wiley-VCH Verlag GmbH & Co. KGaA, Weinheim

Reactions of Group 13 and 14 Hydrides and Group 1, 2, 13 and 14 Organyl Compounds with (*tert*-Butylimino)(2,2,6,6-tetramethylpiperidino)borane

Ulrike Braun,[a] Barbara Böck,[a] Heinrich Nöth,*[a] Ingo Schwab,[a] Manfred Schwartz,[a] Siegfried Weber,[a] and Ulrich Wietelmann[a]

Dedicated to Professor Dr. Dr. h. c. mult. Ernst Otto Fischer on the occasion of his 85th birthday

Keywords: BN triple bonds / Insertion reactions / (*N*-Metal-*tert*-butylamino)(2,2,6,6-tetramethylpiperidino)boranes / Multinuclear NMR / X-ray structures

(*tert*-Butylimino)(2,2,6,6-tetramethylpiperidino)borane (**1**) is a highly reactive species. Its B≡N triple bond inserts into the B–H bond of boranes, R_2BH, generating diborylamines of the type tmp–BH–N*t*Bu–BR_2 (tmp = 2,2,6,6-tetramethylpiperidino; R = H, Cl, Br, or organyl). Thexylborane reacts analogously, but only one of its two B–H bonds is used for the hydroboration of **1**. However, dihaloboranes $HB(Hal)_2$–SMe_2 (Hal = Cl, Br) give *B*-haloboration products tmp–B(Hal)–N*t*Bu–BH(Hal), while reactions with $H_2B(Hal)$–SMe_2 produce a mixture of two isomers by competing hydroboration and haloboration reactions. Tmp–BH–N*t*Bu–AlH_2 was obtained from **1** and AlH_3–NMe_3. It is a dimer in the solid state with pentacoordinate Al atoms and AlH_2Al bridges. Hydrosilylation of **1** was achieved with Me_2SiHCl, $SiHCl_3$ or Ph_2SiH_2 to give the *N*-silyl-substituted diaminoboranes tmp-BH-N*t*Bu–$SiX_{3-n}R_n$. Me_3SnH and Bu_3SnH behave similarly, giving the corresponding *N*-stannylated diaminoboranes. However, when Ph_3SnH was treated with **1**, the stannylborane tmp–B($SnPh_3$)–NH*t*Bu was formed showing an umpolung of the hydrostannylation. Organyllithium compounds provide access to *N*-lithiodiaminoboranes of the type tmp–BR–N*t*Bu–Li. The stability of these compounds depends on the substituent R. The least stable compound was the B–*t*Bu derivative followed by the *B*-methyl compound. However, in the presence of TMEDA tmp–BMe–N*t*Bu–Li is sufficiently stable to allow reactions, e.g. with *B*-chlorocatecholborane, to produce tmp–BMe–N*t*Bu–$BO_2C_6H_4$. The most stable lithium compound so far is tmp–BPh–N*t*Bu–Li–OEt_2, whose structure has been determined by X-ray crystallography. $MgBu_2$ behaves like LiR and both of its Mg–C bonds can be used for the insertion reaction. The same is also true of $ZnMe_2$. In contrast, at ambient temperature, only one of the E–C bonds of triorganylalanes, triorganylgallanes and $InPh_3$ is used for the insertion reaction. In the solid state, most of the new compounds show a weak to strong coordinate bond between the electrophilic centre (Li, Mg, Zn, Cd, B, Al, Ga and In) and the nitrogen atom of the tmp group which generates a four-membered ring.
(© Wiley-VCH Verlag GmbH & Co. KGaA, 69451 Weinheim, Germany, 2004)

Introduction

Iminoboranes, RN=BR′, featuring a B≡N triple bond are highly reactive chemical species due to their unsaturated character. Their reactivity exceeds that of the corresponding isolobal alkynes, a consequence of the higher polarity of the B≡N bond compared with the less polar C≡C bond of alkynes. The chemistry of iminoboranes has been reviewed in two comprehensive articles.[1,2] Iminoboranes have a high tendency to dimerize to 1,3-diaza-2,3-diboretidines or trimerize to borazine derivatives.[3,4] In the case of the (*tert*-butylimino)(2,2,6,6-tetramethylpiperidino)borane (tmp−B=N−*t*Bu, **1**) the rate of dimerization is retarded for steric and electronic reasons.[4] Besides this and related cycloaddition reactions, the (amino)(imino)boranes add to carbonylmetal fragments at the imino nitrogen atom of **1**. They also add protic acids HX or an E−X bond of sufficiently strong Lewis acids EX_n across the B≡N triple bond.[1,2] Here we

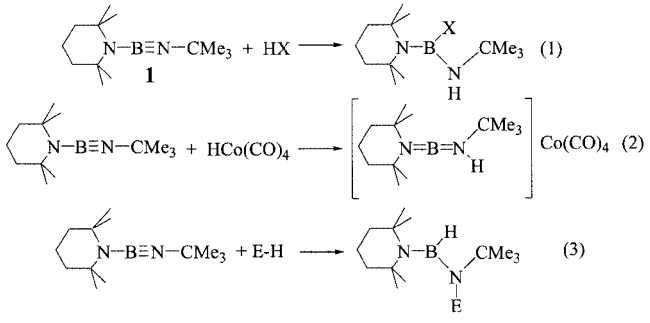

[a] Department of Chemistry, University of Munich, Butenandtstr. 5−13, 81377 Munich, Germany
E-mail: H.Noeth@lrz.uni-muenchen.de

 © 2004 Wiley-VCH Verlag GmbH & Co. KGaA, Weinheim **DOI: 10.1002/ejic.200300820**

report a systematic study of the behaviour of **1** towards hydrides of group 13 and 14 as well as organyl derivatives of the group 1, 2, 13 and 14 elements. Several hydroboration reactions of iminoboranes are already known,[1,2,5] but these and (amino)(imino)boranes offer even more interesting scopes.[6,7]

Usually, acidic polar hydrogen compounds HX [X = halogen, OR, SR, NHR, NR_2, $Co(CO)_4$] react with **1** by protonation of the *tert*-butylimino nitrogen atom according to Equation (1). In the case of bulky X groups, for instance $Co(CO)_4$,[8] diaminoborinium salts are formed as shown in Equation (2). This indicates that the first step in reaction (1) is the protonation of the imino nitrogen atom. On the other hand, when hydrides of electropositive elements, $ER_{rn-n}H_n$, are allowed to react with **1**, then the hydrogen atom of an E−H bond attacks at the boron atom.[2] This finally results in the formation of *N*-substituted diaminoboranes tmp−BH−N*t*Bu−$ER_{m-n}H_{n-1}$ as shown in Equation (3). Reaction (3) starts with an electrophilic attack at the N atom of the $NCMe_3$ group by the Lewis acidic centre of the element hydride $ER_{m-n}H_n$, followed by a hydride transfer to the boron atom. This kind of reaction will not occur if the central E atom is too weak a Lewis acid.

In this work we report on the behaviour of various hydrides of boron, aluminium, silicon and tin as well as of organyl compounds of lithium, magnesium, zinc, cadmium, boron, aluminium, gallium and indium.

Results

Reactions with Hydrides of Boron and Aluminium

We have already recently reported on the reaction of BH_3−THF with **1**.[5] When diborane is used as the source of BH_3 in the presence of hexane as a solvent, four compounds, **2**−**5**, besides the dimer of **1**, can be detected. After warming the reaction mixture from −196 °C to ambient temperature, ^{11}B NMR signals were found at δ = 28.7 and −4.4 (for **2**), 37.2 (for **3**), −20.8 (for **4**), and −26.2 ppm (for **5**). However, when BH_3−THF was used, the product distribution depended both on the concentration and the temperature of the solutions. At −60 °C, dilute solutions favoured the formation of **2**. Yields up to 82% can be achieved.

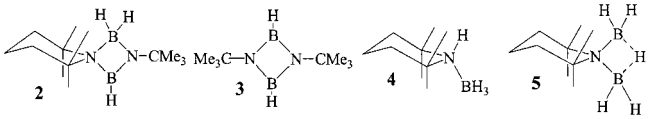

An almost quantitative conversion of **1** to **2** can be achieved, however, by employing H_3B−SMe_2 as the hydroborating reagent. In this case, it is important to add a hexane solution of **1** slowly at ambient temperature to a solution of H_3B−SMe_2 in hexane. Under these conditions the dimerization of **1** is prevented due to the presence of a local excess of the borane reagent.

On the other hand, no hydroboration of **1** was observed when employing the aminoboranes H_3B−NEt_3 or H_3B−$NHiPr_2$ at ambient temperature. However, when a solution of **1** and H_3B−$NHiPr_2$ was kept at reflux in hexane, hydrogen gas was formed besides the diborylamine **6** as shown in Equation (4). Hydroboration of **1** can also be achieved with catecholborane, dicyclohexylborane, diisoamylborane or 9-borabicyclo[3.3.1]nonane (9-BBN) as shown in Equations (5) and (6).

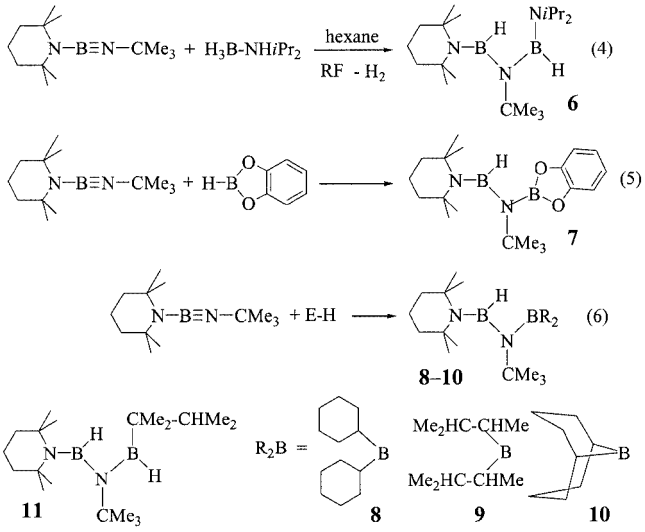

Because the B≡N triple bond of **1** also inserts into the B−C bond of triorganylboranes (vide infra), there might be competition between the insertion of the B−C bond and the B−H bond if both are present in the molecule. The results with the diorganylboranes indicate convincingly that the B−H bond is more reactive than the B−C bond, although thermodynamically there should be no strong difference between the two since the number of B−C and B−H bonds does not change. Kinetic investigations into the hydroboration of alkynes have shown that the rate of hydroboration depends on the equilibrium between the dimeric borane and the monomeric borane.[9,10] In spite of the high steric requirements of the diorganylboranes used in this study, all three compounds reacted chemoselectively. However, the rates of the reactions were quite different. 9-BBN reacted fastest and the reaction was complete within 2 h. Disiamylborane required 24 h and dicyclohexylborane needed 96 h. Amongst these, the dicylohexylborane is certainly the least bulky. Nevertheless, it showed the lowest rate. This is because the concentration of its monomeric unit is very low compared with those of the other species.[9] One factor that governs the monomer/dimer equilibrium is the strength of the BHB bridge bond as demonstrated by the corresponding BHB bridge frequencies in the IR spectra. These frequencies are 1590 cm^{-1} for dicyclohexylborane,[11] 1551 cm^{-1} for disiamylborane[12] and 1560 cm^{-1} for 9-BBN.[13] In contrast to these diorganylboranes, the symmetric dithexyldiborane shows a BHB band at 1565 cm^{-1} which is very close to that of the dimeric disiamylborane.[14] However, 8 d are required for a quantitative conversion of

 © 2004 Wiley-VCH Verlag GmbH & Co. KGaA, Weinheim

1 into **11**. In contrast to the hydroboration of organic substrates with thexylborane,[14–16] only one of its two B–H hydrogen atoms is used for the hydroboration of **1**.

In contrast, the haloboranes $H_{3-n}B(Hal)_n$ in the form of their Me_2S adducts react with **1** by hydroboration and/or haloboration. The dihaloboranes $HBCl_2$ and $HBBr_2$ show high positive charges at the boron atoms, e.g. +0.976 in $HBCl_2$ (see Table 1) which is almost the same as for BCl_3 but less than in BH_2Cl. Bond dissociation energies may also play a role and should favour the hydroboration route.[17] Both $HBCl_2$–SMe_2 and $HBBr_2$–SMe_2 exclusively give, however, the haloboration products **12** and **13** [Equation (7)]**.** This can be readily demonstrated by the absence of a doublet in the ^{11}B NMR spectrum for the tricoordinate B atom but the presence of a doublet for the tetracoordinate boron atom. This also confirms that compounds **12** and **13** have cyclic structures.

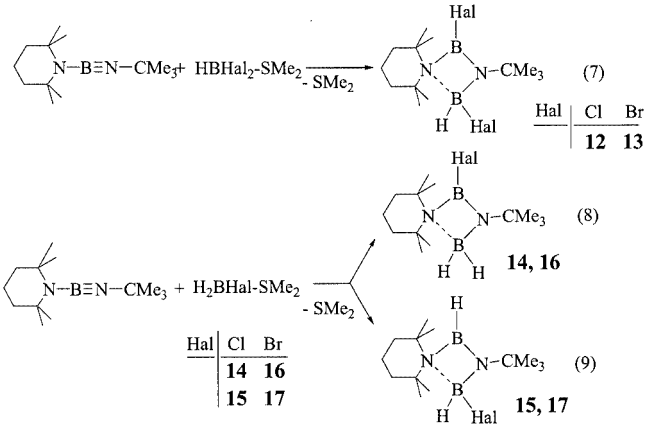

Table 1. Calculated charge densities for the series of chloroboranes $BH_{3-n}Cl_n$

	BH_3	H_2BCl	$HBCl_2$	BCl_3
q_B	0.495	0.724	0.976	0.9995
q_H	−0.165	−0.209	−0.149	
q_{Cl}	–	−0.307	−0.414	−0.3332

On the other hand, reactions of H_2BCl–SMe_2 and H_2BBr–SMe_2 with **1** lead to a mixture of the hydroboration products **15** and **17** with the haloboration products **14** and **16**. The product ratio of **14/15** was 33:66 while it was 50:50 for **16/17**. Therefore, there is a statistical preference for the hydroboration product **15** but not for **17**.

In order to obtain an insight into the formation of compounds **14** and **15**, we performed calculations at the B3LYP/6-311g and B3LYP/8-311+g(2d,f) levels for the model system $ClBH_2/H_2N–B=N–Me$. The results are summarised in Table 2 and shown in Figure 1. The two B–N bonds of the (amino)(imino)borane are in agreement with a higher bond order for the imino nitrogen atom, but also the B–N bond of the amino group NH_2 reveals π-bonding. Thus, the electronic structure of $H_2N–B=N–Me$ is best described by the two formulae **A** and **B**.

$$\underset{\mathbf{A}}{H_2N–B{\equiv}N–Me} \leftrightarrow \underset{\mathbf{B}}{H_2N{=}B{=}N–Me}$$

The adduct **C**, which is considered to be the first step in the hydro/haloboration of $H_2N–B=N–Me$, is more stable by 110.68 kJ/mol compared with the reagents. The adduct shows an allene-type configuration with a torsion angle H–N–N–C of −95.7°. The B–N bond lengths for the $H_2N–B$ and $B–NMe(BH_2Cl)$ groups were calculated as 1.357 and 1.309 Å while the B–N bond to the monochloroborane unit is 1.606 Å. This type of structure has been deduced from NMR spectroscopic data for **1**–ECl_3 (E = Al, Ga)[18] or **1**–$M(CO)_5$ (M = Cr, W)[19] and determined by X-ray crystallography for tmp=B=N*t*Bu(ECl_3) [E = Ga, and In with 1.345(2) and 1.316(2) Å, respectively].[20] These data are in agreement with B=N double bonding between the dicoordinate B atom and the tricoordinate N atoms (see Figure 1).

The adduct **C** is, however, less stable than the chloroboration/hydroboration compounds **D** and **E**. The hydroboration product **E** is more stable by 154.46 kJ/mol than **C**, while the chloroboration product **D** is more stable by178.76 kJ/mol. As expected, the energy difference between **D** and **E** of 24.21 kJ/mol is not large. In each case, the "open chain" structures are energetically favoured over the ring structures **F** and **G**. The energy difference between **D** and **F** is 65.47 kJ/mol in favour of **D**, while **E** is 65.62 kJ/mol more stable than the ring compound **G**. Thus, chloroboration to **D** is the thermodynamically more favourable reaction. This is in contrast to the observed preferred hydroboration of **1** with BH_2Cl. Thus, the model system does not mirror the experimental system.

The calculated B–N bond lengths in **E** are in agreement with B=N double bonding. The shortest B–N bond (1.395 Å) was calculated for an $H_2N–B$ bond while those to the BH_2 group are longest at 1.417 Å. However, the "central" B–N bond is also short at 1.449 Å. This indicates a bonding situation also found in 1,3-butadienes. In the case of **D** and **E**, the *cis* conformations were found to be energy minima. As can be seen from the B–N bond lengths of the ring structure **F** (see Table 2), there is only one N bond with double bond character. The $H_2N\cdots BH_2$ bond is rather long at 1.701 Å and the N and B atoms now exhibit tetracoordination. Although compound **F** shows three B–N single bonds and one B–N π-bond, one B–N bond in particular is quite weak and this is certainly the reason why the chain compound **D** with three B–N π-bonds is more stable. On the other hand, although the chloroboration chain compound **D** is favoured over the hydroboration product **E**, the ring isomer **G** is definitely more stable than the ring **F**. One of the reasons for this is that the B–N bond of the group $H_2N–BHCl$ is much shorter than in **F** which leads to its stabilisation. However, as shown experimentally for compound **14** and **15**, only the ring structures were experimentally observed and not the open-chain compounds as the

 © 2004 Wiley-VCH Verlag GmbH & Co. KGaA, Weinheim

Table 2. Model compounds optimised at the B3LYP level of theory; all structures are without imaginary frequencies, i.e. they are real minima; relative energies refer to $E(BH_2Cl)$ + E(iminoborane) = 0. 1 Hartree = 627.5095 kcal/mol = 2627.2568 kJ/mol

	B3LYP/6-311g				B3LYP/b3lyp/6-311+g(2df,p)			
	$-E$ [a.u.]	$-E$ [kJ/mol]	*zpe* [kJ/mol]	B−N [Å]	$-E$ [a.u.]	$-E$ [kJ/mol]	*zpe* [kJ/mol]	B−N [Å]
BH_2Cl	−486.28		55.36	−	−486.31	0	55.37	
Iminoborane	−175.51		19.00	1.24723	−175.57	0	18.56	
				1.39743				
Adduct1		−110.6829	26.10	1.30918		−89.1037	25.64	
				1.35696				
				1.60588				
Adduct2		−265.1378	26.50	1.39564		−253.5101	26.23	
				1.41705				
				1.44942				
iso-Adduct2		−289.3429	26.70	1.39874		−275.8459	26.24	
				1.40058				
				1.46438				
Ring		−199.6628	26.70	1.35622		−192.7342	26.49	1.67613
				1.53900				
				1.57649				
				1.70103				
iso-Ring		−223.7185	26.76	1.37194		−204.2356	26.52	1.64624
				1.53374				
				1.57333				
				1.65177				

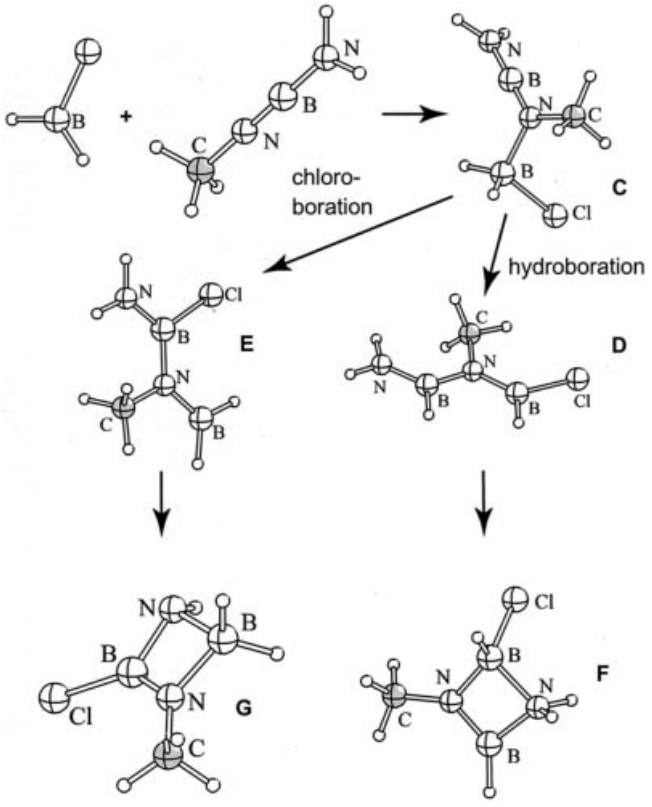

Figure 1. Optimised structures in the $BH_2Cl/H_2N-B=N-Me$ system

calculations suggest and this may be due to the fact that the amino nitrogen atom of the tmp unit is more basic than the NH_2 group of the model system.

For this reason we also performed calculations on tmp−BPh−N*t*Bu−BH_2 whose ring structure was determined by X-ray crystallography.[21] Indeed, optimization of the open-chain structure leads to the ring as the most stable species (Figure 2). The calculated B−N bond lengths compare favourably with the experimental values [experimental: PhB−N 1.594(3), PhB−N*t*Bu 1.367(3), *t*BuN−BH_2 1.555(3), H_2B−N(tmp) 1.665(3) Å, calcd. 1.618, 1.377, 1.561, 1.691 Å]. Clearly, a sufficiently basic N atom of the amino group is needed to favour the ring structure over the open-chain isomer.

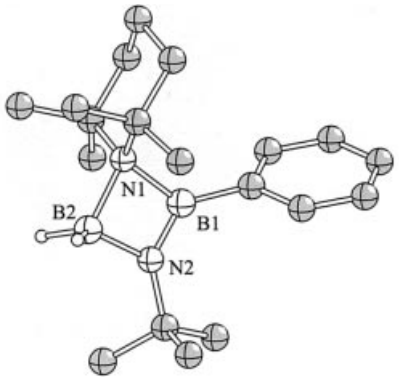

Figure 2. Optimised structure for tmp−BPh−N*t*Bu−BH_2 at the B3LYP/6-311G level of theory

Compound **1** forms adducts of type **C** with $AlCl_3$, $AlBr_3$, $GaCl_3$ and $InCl_3$[18,20] and no insertion reactions have so far been observed for these trihalide adducts in contrast with halosilanes.[22] It was, therefore, of interest to study the

 © 2004 Wiley-VCH Verlag GmbH & Co. KGaA, Weinheim

behaviour of AlH_3. This hydride was employed as AlH_3-NMe_3 [see Equation (10)].

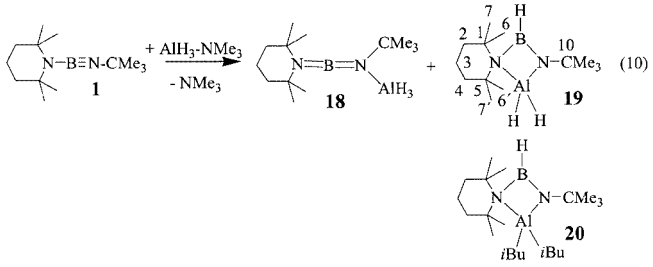

The reaction was followed in hexane solution by ^{11}B NMR spectroscopy which showed that two products were formed. Two new ^{11}B NMR signals appeared at $\delta = 33$ and 27 ppm in a ratio of 1:4. In the proton coupled ^{11}B NMR spectrum, the signal at $\delta = 27$ ppm was a doublet showing that this boron atom carries one hydrogen atom as expected for a hydroalumination product. Two ^{27}Al NMR signals at $\delta = 115$ and 80 ppm in an intensity ratio of 1:4 support the formation of two products. While the low-field signal points to the presence of a tetracoordinate Al atom, the other represents a pentacoordinate Al centre. The intensities of the ^{11}B and ^{27}Al signals change with time. The two high-field signals gain intensity and the low-field signals decrease correspondingly. Moreover, the IR spectrum contains a strong band at 1806 cm^{-1} which is typical for an antisymmetric NBN vibration. These latter data are in agreement with the formation of compound **18**.

Attempts to separate the two compounds by fractional crystallisation from toluene were unsuccessful. The solid obtained showed the same NMR signals as the original reaction mixture. However, well-formed single crystals of dimeric **19** (vide infra) could be selected from the solid material which separated from a hexane solution.

Diisobutylalane reacted chemoselectively with **1** by hydroalumination to the cyclic compound **20**. No transfer of the organyl group was observed. Thus, this reaction corresponds to the hydroalumination of C−C multiple bonds.[23] Nevertheless, compound **20** could not be obtained in a pure form. The reaction of $[(t\text{BuO})_2\text{AlH}]_2$ [24] produced a mixture of three compounds according to the ^{11}B NMR spectrum. We were unable to separate these compounds.

NMR and IR Spectra

Table 3 summarises the NMR spectroscopic data of the hydroboration/haloboration products of the (amino)-(imino)borane **1**. For the diborylamines of the type tmp−BH−N*t*Bu−BX_2, one would expect two ^{11}B NMR signals. This is, however, not the case for **8**, **9**, **10** and **11**. Only one broad signal was observed which showed a barely resolved doublet structure, indicating the presence of a BH group. In the proton-decoupled spectra the doublet vanished but the signal was still broad. Chemical shifts which can be compared with those of **8** to **11** occur in (amino)(organyl)boranes $R_2N-B(H)-R$ ($\delta^{11}B = 41-43$ ppm), monomeric aminoboranes R_2N-BH_2 ($\delta^{11}B = 37-39$ ppm) as well as diborylamines of the type $(R_2N)_2B-NMe-BMe_2$ ($\delta^{11}B = 44-46$ ppm) for the Me_2B group.[25] Thus, the observed chemical shifts for **8**−**10**, which show a better shielding than for any of these aminoboranes, indicate not only that B−N π-bonding is present for the BH group but also that there is a weak interaction of the R_2B group with the tmp nitrogen atom. This is in agreement with a bonding description provided by the formulae **H**−**K**.

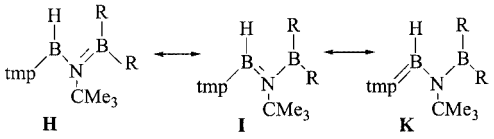

The contribution of **K** cannot be significant because there are only single ^1H and ^{13}C resonance signals for the methyl groups at positions 6/7 of the tmp unit in compounds **9** and **10** which indicates free rotation about the B−N bond of the tmp group. However, for the disiamylborane **8**, there are two signals for these hydrogen atoms and four ^{13}C resonances. This can be rationalised by the presence of a nonplanar NBNB skeleton or by a slow interconversion between a cyclic and a noncyclic species. In contrast to these diborylamines, those bearing hydrogen and halogen atoms at the boron atoms are of a cyclic nature as evidenced by two ^{11}B NMR signals as well as two ^1H and ^{13}C resonances for the tmp methyl groups. Those of the tricoordinate boron atoms can be found between $\delta = 20.0$ and 28.8 ppm, whereas those of the tetracoordinate boron atoms are in the range of $\delta = 2.8$ to -5.9 ppm. There are six ^1H NMR signals for the NMe_2 groups of tmp in the mixture of the monohalogen derivatives **14**−**17**. One may expect that compounds **14** and **16** should give rise to two signals for the methyl groups of the tmp ligand and four for compounds **15** and **17**. For the cyclic diborylamines one can expect four signals for these methyl groups provided that the ring is not planar. This is the case for the cyclic diborylamine $Cl_2B-Nt\text{Bu}-\text{BCl}-\text{tmp}$.[26] The C-1/5 carbon atoms of the tmp unit in the dichloro derivative **12** are more deshielded than in the monochloro isomers **14** and **15**, an effect of the stronger Lewis acidic character of the Cl_2B group compared with BHCl. Unfortunately, the corresponding ^{13}C NMR spectroscopic data for the bromo compounds are not available. Conversely, the parent cyclic diborylamine **2** shows only two signals for the methyl groups at positions 6 and 7 both in the ^1H and ^{13}C NMR spectra.[5]

Compounds **19** and **20** give two ^1H and ^{13}C NMR signals for the methyl groups of the tmp substituent in agreement with its cyclic structure. However, the proton resonance for **19** is not well resolved and appears as a broad signal. While the ^{11}B NMR signal for **19** at $\delta = 26.8$ ppm is a doublet in the proton-coupled spectrum [$^1J(^{11}B^1H) = 130$ Hz] no Al−H coupling was observed for the broad ^{27}Al signal at $\delta = 80$ ppm ($h_{1/2} = 9670$ Hz) or for that in **18** [$\delta^{27}Al = 32.6$ ($h_{1/2} = 5170$ Hz]. A strong band at 2468 cm^{-1} in the IR spectrum is typical for a terminal ^{11}BH group of a tricoordinate boron atom. Only a broad and unresolved band centred at 1830 cm^{-1} was observed for the AlH_n vibrations.

 © 2004 Wiley-VCH Verlag GmbH & Co. KGaA, Weinheim

Table 3. Selected NMR spectroscopic data of compounds tmp−BX−NCMe$_3$−BYY′; chemical shifts in ppm; coupling constants in Hz

	X	Y	Y′	δ^{11}B	δ^1H			δ^{13}C					
					2-H/4 3-H	6/7-H	C*Me*$_3$C-1/5		C-2/4	C-3	C-6/7	C-10	C*Me*$_3$
2	H	H	H	28.8 (d),[a] −4.4 (t)[b]				56.6	37.5	17.2	25.8, 30.1	49.6	30.3
8	H	C_5H_{11}	C_5H_{11}	35.5 (d)[c]	1.59−1.80 (m)	1.47, 1.50	1.44	54.1	36.8	15.7	30.7, 31.2, 34.3, 35.0	574	33.0
9	H	C_6H_{13}	C_6H_{13}	36.1[d]	1.60−1.88 (m)	1.42	1.51	55.9	37.6	15.8	32.9	53.4	34.1
10	H	9-BBN		35.3 (d)[e]	(br. m)	1.38	1.49	55.9	37.2	15.9	32.2	53.6	33.9
11	H	Thex	H	35.9 (d)[f]	(br. m)	1.32	1.36	56.4	37.4	16.2	33.8, 34.6	55.0	33.1
14	Cl	H	H	25.1, −5.9 (t)[g]	0.93−1.28 (m)	1.29, 1.31, 1.51	1.47	55.1	37.7	16.7	30.1, 30.3	54.9	33.6
15	H	Cl	H	30.6 (d),[h] 3.8 (d)[i]	0.93−1.28 (m)	1.32, 1.37, 1.55	1.50	55.1	36.7, 40.6	16.1	30.7, 30.8	51.1	32.9
12	Cl	Cl	H	25.1, 3.5 (d)[k]	0.98−1.41 (m)	1.23, 1.31,	1.37	59.8, 60.2	37.1	16.6	25.3, 26.7 30.5, 31.7	51.6	30.7
16	Br	H	H	30.8, 2.4 (t)[k] [l]	0.98−1.41 (m)	1.24, 1.26	1.59		38.7				
17	H	Br	H	32.3,[m] 1.0 (d)[n]	0.8−1.15 (m)	1.28, 1.29 1.35, 1.36	1.40						
13	Br	Br	H	22.6, 0.8 (d)[q]	0.8−1.15 (m)	1.20, 1.24, 1.63, 1.78	1.40						

[a] $^1J(^1H^{11}B)$ = 1.56. [b] $^1J(^1H^{11}B)$ = 111. [c] $^1J(^1H^{11}B)$ = 112. [d] $^1J(^1H^{11}B)$ = 119. [e] $^1J(^1H^{11}B)$ = 82. [f] $^1J(^1H^{11}B)$ = 108. [g] $^1J(^1H^{11}B)$ = 125. [h] $^1J(^1H^{11}B)$ = 142. [i] $^1J(^1H^{11}B)$ = 155. [k] $^1J(^1H^{11}B)$ = 148. [l] $^1J(^1H^{11}B)$ = 75. [m] $^1J(^1H^{11}B)$ = 105. [n] $^1J(^1H^{11}B)$ = 50. [q] $^1J(^1H^{11}B)$ = 105.

Crystal Structure of 19

The cyclic (tmp)borylaminoalane **19** crystallises in the triclinic space group $P\bar{1}$ with $Z = 4$. Therefore, there are two independent monomeric molecules in the unit cell. As shown in Figure 3, the monomers are connected to dimeric molecules via Al−H−Al bridges. The dimeric molecules possess crystallographic inversion centres making each Al atom pentacoordinate. The Al1−N1 bond is 0.242 Å longer than the Al1−N2 bond to the tricoordinate nitrogen atom N2. Also the B1−N1 bond is considerably longer [1.546(5) Å] than the B1−N2 bond [1.369(5) Å] which is typical for B−N π-bonding in monoaminoboranes. The hydrogen bonds between the two Al atoms are asymmetric as shown by the Al(1)−H1 and Al(1A)−H1 bond lengths of 1.65 and 1.46 Å, respectively, while the terminal Al−H bond has a length of 1.48 Å. The four-membered N1−B1−N2−Al1 ring is almost planar, the largest deviation from the mean plane is 0.012(3) Å. The geometry around Al1 is strongly distorted tetragonal-pyramidal. This is of course due to the sharp bond angles N1−Al1−N2 of 72.6(1)° and B1−N1−Al1 of 82.2(1)°. The bond angle N1−Al1−H1 to the apical atoms is 156.7°. As expected, the tmp ring adopts a chair conformation.

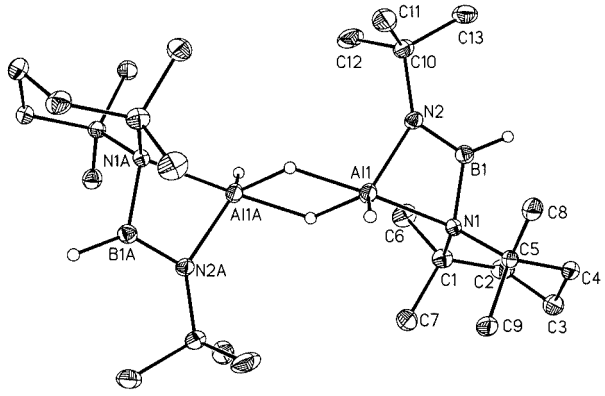

Figure 3. ORTEP representation of the molecular structure of **19**; selected bond lengths [Å]: Al1−N1 2.115(3), Al1−N2 1.873(1), Al1···B1 2.445(4), Al···Al1A 2.813(1), B1−N1 1.546(5), B1−N1 1.369(5), N1−C1 1.534(5), N1−C5 1.582(4), N2−C10 1.483(5), Al1−H1 1.65, Al1−H1A 1.46, Al1−H2 1.48, B1−H1B 1.18; selected bond angles [°]: N1−Al1−N2 72.6(1), N1−B1−N2 108.5(3), Al1−N1−B1 82.2(2), B1−N2−Al1 96.7(2), Al1−N1−C5 116.2(2), Al1−N1−C1 117.2(1), Al1−N2−C10 135.6(2), H1−Al1−H1A 121(1), H1−Al1−H1C 111, Al1−H1−Al1A 130, N1−Al1−H1A 103, N1−Al1−H1 157, H1B−B1−N2 130, H1B−B1−N1 121

Reactions with Hydrides of Silicon, Germanium and Tin

Within the series of hydrides of the heavier group 14 elements, the bond polarity of the E−H bond changes considerably. Moreover, the hydrides are only weak Lewis acids. Therefore, one may surmise that these hydrides will either not react with **1** or do so only very sluggishly and the hydrogen atom will either move to the boron atom or the nitrogen atom depending on the polarity of the E−H bond. The latter can, of course, be influenced by substituents.

No reaction was observed between Me_3SiH or Ph_3SiH and **1**. However, Ph_2SiH_2 did hydrosilylate **1** according to Equation (11) to yield tmp−BH−N*t*Bu−$SiPh_2H$ (**21**). Moreover, when **1** was treated with Me_2SiHCl or $SiHCl_3$ the corresponding hydrosilylation products **22** and **23** were formed and isolated as viscous oils in good yields.

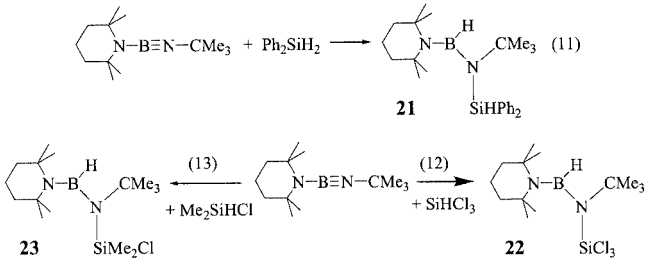

 © 2004 Wiley-VCH Verlag GmbH & Co. KGaA, Weinheim

Me_3GeH and Ph_3GeH did not react with **1** at ambient temperature. At elevated temperature only the dimerization of **1** to its corresponding 1,3,2,4-diazadiboretidine occurred.[4] However, Me_3SnH and Bu_3SnH hydrostannylated **1** as shown in Equation (14) while Ph_3SnH reacted according to Equation (15).

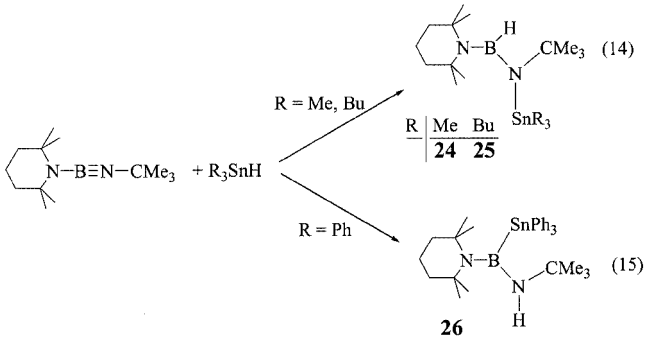

NMR Spectra

In the ^{11}B NMR spectrum of **26** [$\delta^{11}B$ = 44.6 ppm (br., $h_{1/2}$ = 700 Hz)], no $^{11}B^{119}Sn$ coupling could be observed. This is not unusual because of the rapid relaxation due to the quadrupole moment of the ^{11}B nucleus. Also, no ^{119}Sn resonance was found for the same reason. However, a broad ^1H NMR signal at δ = 5.13 ppm indicates the presence of an NH group. Moreover, the IR spectrum of **26** contains a strong band at 3383 cm^{-1} due to the NH vibration.[27] In addition, the ^1H and ^{13}C NMR spectra show three sets of signals for the phenyl groups. Clearly, the vicinity of the bulky tmp substituent induces hindered rotation about the Sn−C bonds. Furthermore, there is only one broad ^1H NMR signal for the methyl group at the tmp substituent and there was no sharpening of the signal at −60 °C. There are, however, two ^{13}C resonances for the methyl groups showing that rotation about the B−N bond is hindered. Most likely, the tmp group stands perpendicular to the N1−B1−Sn1−N2 plane. The final proof of the structure of **26** came from an X-ray diffraction study.

Table 4 shows that the boron nuclei of the two stannylation products of **1** are better shielded than they are in the hydrosilylation products. Moreover, the ^1H and ^{13}C resonances for the tmp methyl groups are at higher field than those of the silyl compounds **21** and **22**. Compounds **21** to **24** all show two ^1H and ^{13}C resonances for these methyl groups indicating hindered rotation. Therefore, one can assume that all these compounds most likely have cyclic structures.

X-ray Structure Analysis of 26

Crystals of **26** are orthorhombic. The space group is $P2_12_12_1$ with Z = 4. Figure 4 depicts the molecular structure of this molecule. It supports the conclusions deduced from the spectroscopic data.

The B−Sn bond length in **26** of 2.295(2) Å corresponds to a single bond as found, for example, in $Me_3Sn(Me_2N)B-B(NMe_2)SnMe_3$ [2.276(2) Å].[28] The two B1−N bonds differ by 0.087(3) Å, the longer bond involves the B−N bond to the tmp group which shows a crown configuration and whose C1−N1−C5 plane includes a twist angle with the N1−B1−N2 plane of 85.2°. The sum of the bond angles at N1 is 354.2° which shows that the N1 atom is almost sp^2-hybridised. There is a strong steric interaction between one of the phenyl groups with the *tert*-butyl group as seen by a B1−N2−C10 bond angle of 137.2(2)°. The torsion angle for the atoms Sn1−B1−N2−C10 is 13.5°, and the tmp substituent (C1−N1−C5) stands almost vertical (91.7°) to the N1−B1−Sn1 plane.

Reactions of Main Group Elements with Organyl Compounds MR_n (n = 1−3)

Reactions with Organyllithium Compounds

Some reactions of organylmetal compounds MR_n with **1** have so far only been described for M = Li and Mg in a review article.[3] In principle, organyllithium compounds should add to **1** according to Equation (16) but the stability of the resultant *N*-lithiodiaminoboranes depends on the nature of R.

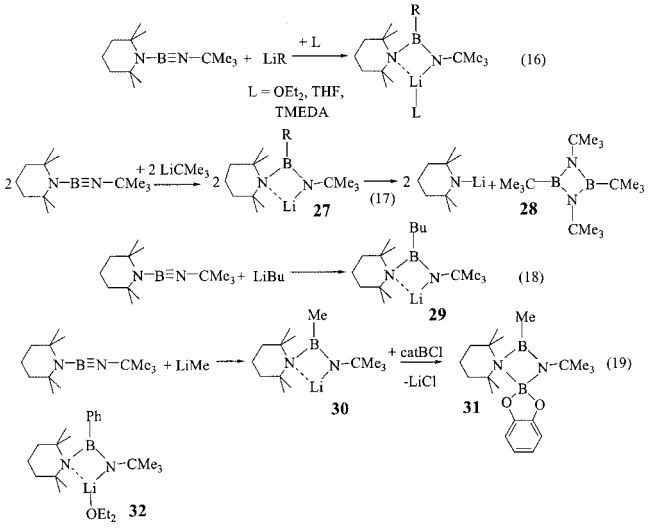

For instance, *tert*-butyllithium reacts according to Equation (16) but the product **27** is unstable and decomposes into Li(tmp) and the 1,3,2,4-diazadiboretidine **28** [Equation (17)]**.** In contrast, *n*-butyllithium leads to the stable *N*-lithiodiaminoborane **29**. Methyllithium yields compound **30** which, like **27**, decomposes. However, when the reaction (19) is performed in the presence of tetramethylethylenediamine then **30** can be treated with *B*-chlorocatecholborane to produce the cyclic diborylamine **31**. No reaction occurred between fluorenyllithium and **1**, but phenyllithium reacted smoothly in diethyl ether to give compound **32** which could be isolated as single crystals from a hexane/diethyl ether solution.

X-ray Structural Analyses of 32 and 31

Figure 5 shows the molecular structure of **32**. It features a four-membered LiN_2B ring with a tricoordinate Li atom. The Li1−N2 bond is 0.21 Å shorter than the coordinate Li1−N1 bond. Atom N2 has a planar geometry which al-

 © 2004 Wiley-VCH Verlag GmbH & Co. KGaA, Weinheim

Table 4. Selected NMR spectroscopic data of compounds **19**−**25**; chemical shifts δ in ppm; additional data can be found in the Exp. Sect.

	δ^{11}B	δE	δ^{1}H			δ^{13}C					
			2-H/4 3-H	6/7-H	C*Me*$_3$	C-1/5	C-2/4	C-3	C-6/7	C-10	C*Me*$_3$
19	26.8(d)[a]	80[b]	1.49−1.58 m	1.22 1.36	1.06	52.8	38.4	17.1	22.7 31.8	49.3	33.5
20	33.5 (d)[c]	109.5	1.35 1.53	1.23 br.	1.29	55.5	37.4	17.0	26.9, 29.2	50.5	33.8
21	37.7(d)[d]	−21.9	1.5 m, vbr	1.46 br	1.35	54.5	37.2	15.9	33.5 br	54.7	32.9
22	34.6[e]		1.3−1.7 m	1.37 1.40	1.38	55.6	36.7	15.4	32.7 34.8	56.7	31.6
23	35.9[f]		1.2−1.6 m	1.35 1.37	1.38	53.3	37.9	15.4	32.1 35.7	54.9	32.4
24	39.4[g]	−	1.1−1.5 n	1.17 1.28	1.34	52.6	40.4	18.5	26.9 36.1	55.4	34.9
25	39.2	−	1.1−1.5 m	1.18 1.28	1.34	52.6	40.4	18.6	27.3 35.5	55.2	34.0
26	44.6	−	1.40 m br.	1.26	1.13	52.9	39.7	18.7	29.1, 33.4	51.0	32.6

[a] $^{1}J(^{11}B^{1}H)$ = 52. [b] Line width 9670 Hz. [c] $^{1}J(^{11}B^{1}H)$ = 111. [d] $^{1}J(^{11}B^{1}H)$ = 114. [e] $^{1}J(^{11}B^{1}H)$ = 126. [f] $^{1}J(^{11}B^{1}H)$ = 111. [g] $^{1}J(^{11}B^{1}H)$ = 111.

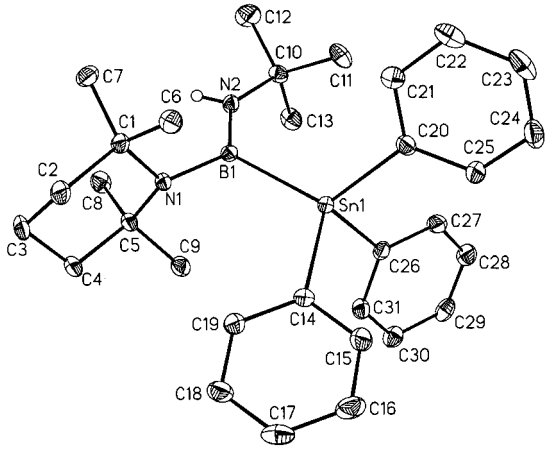

Figure 4. The molecular structure of (*tert*-butylamino)(tetramethylpiperidino)(triphenylstannyl)borane (**26**); selected bond lengths [A]: B1−Sn1 2.295(2), B1−N1 1.476(3), B1−N2 1.389(3), N1−C1 1.496(2), N1−C5 1.492(2), N2−C10 1.485(2), Sn1−C14 2.166(2), Sn1−C20 2.166(2), Sn1−C26 2.166(2); selected bond angles [°]: N1−B1−N2 119.4(2), N1−B1−Sn1 116.4(1), N2−B1Sn1 140.0(2), B1−N1−C1 117.2(1), B1−N1−C5 116.7(1), C1−N1−C5 120.3(2), B1−N2 C10 137.2(2), H2−N2−B1 109(1), H2−N2−C10 112(1), C14−Sn1−C20 104.44(7), C14−Sn1−C26 99.79(7), C20−Sn1−C26 102.74(8)

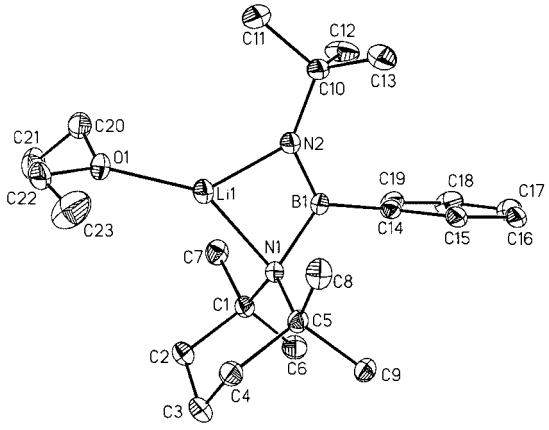

Figure 5. Molecular structure of **32**, ORTEP diagram; selected bond lengths [A]: Li1−N1 2.085(6), Li1−N2 1.884(5), Li1−O1 1.929(5), N1−B1 1.564(4), N2−B1 1.361(4), N2−C10 1.467(4), N1−C1 1.495(4), N1−C5 1.485(4), B1−C14 1.617(4); selected bond angles [°]: N1−Li1−N2 75.70(2), Li1−N1−B1 78.9(2), N1−B1−N2 112.9(2), B1−N2−Li1 91.6(2), N1−B1−C14 126.2(3), N2−B1−C14 120.9(3), N1−Li1−O1 136.2(3), N2−Li1−O1 142.5(3), C1−N1−C5 116.2(2)

lows good B−N π-bonding. The phenyl group stands almost perpendicular to the N1−B1−N2 plane (τ = 89.5°). This prevents B−C π-bonding. The four-membered ring has a flat butterfly structure as shown by an interplanar angle τ = 9.1° for the planes B1−N2−Li1 and B1−N1−Li1. As usual, the tmp ring has a chair conformation. Its N1 atom adopts a distorted tetrahedral geometry with bond angles ranging from 78.9(2) to 118.0(2)°. Although the ring structure of **32** is certain in the solid state, it is very likely that this structure is not retained in solution since only a single signal was observed for the methyl groups at the tmp substituent, both in the ^{1}H and ^{13}C NMR spectra.

An ORTEP plot of the molecular structure of the cyclic diborylamine **31** is shown in Figure 6. It features a planar four-membered B_2N_2 ring. The B1−N1 bond is 0.262 Å longer than the B1−N2 bond [1.378(3) Å]. The B−N bonds to B2 are 1.753(3) Å (N1) and 1.495(3) Å (N2), respectively. The latter is typical for a single bond between an sp^3-hybridised boron atom and an sp^2-hybridised N atom. The long B2−N1 distance corresponds to a weak bond which is in agreement with the NMR spectra which show only one signal for the tmp methyl groups indicating rotation about its B−N bond in solution. Although one might have expected the two B−O bonds to be equal in length, this is not the case and they differ by 0.04 Å. Their lengths are similar to those found for the bis(catecholato)borate anion.[29] The planes N1−C1−C5 and B2−O1−O2 stand almost perpendicular to the B1−N1−B2−N2 ring plane by 92.5 and 89.8°, respectively.

Reactions with Diorganylmagnesium, -zinc, -cadmium and -mercury Compounds

In order to test the possibility of a double insertion of **1** into metal−carbon bonds of dialkylmetal compounds ER_2 (E = Mg, Zn, Cd, Hg), we studied the reaction of **1** with

 © 2004 Wiley-VCH Verlag GmbH & Co. KGaA, Weinheim

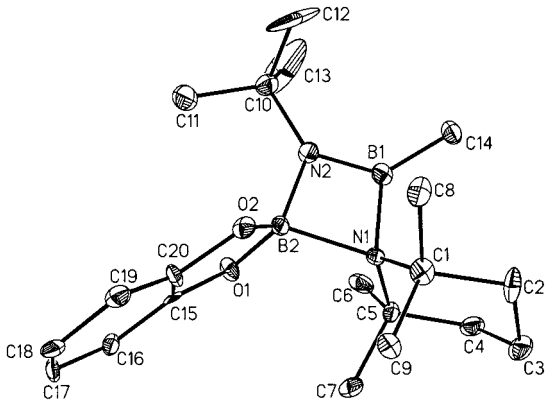

Figure 6. Molecular structure of tmp−BMe−N*t*Bu−Bcat (**31**); selected bond lengths [A]: B1−N1 1.756(4), B1−N2 1.377(4), B1−C14 1.578(5), N1−B2 1.561(4), B2−N2 1.494(4), B2−O1 1.503(6), B2−O2 1.423(6), N1−C1 1.559(6), N1−C5 1.534(6). O1−C15 1.347(5), O2−C20 1.395(5); selected bond angles [°]: B1−N1−B2 79.8(2), N1−B2−N2 86.0(2), B2−N2−B1 95.9(2), N1−B1−N2 98.3(2), B1−N2−C10 134.6(3), B2−N1−C10 129.5(2), C14−B1−N1 129.4(3), C1−N1−C5 114.7(3), O1−B2−O2 105.9(2), O1−B2−N1 112.7(3), O2−B2−N1 115.5(4)

dibutylmagnesium. Reactions (20) and (21) proceeded rapidly at −78 °C. Only a single ^{11}B NMR signal was found at $\delta^{11}B = 37.6$ ppm. This value is typical for metallated diaminoboranes. Compound **33** was obtained as a viscous oil and attempts at crystallisation were unsuccessful. Because the NMR spectroscopic data for **33** and **34** are rather similar to those of the lithium compound **30**, we assume that the magnesium atom is coordinated to the tmp nitrogen atom. Dibutylmagnesium reacts with **1** not only in a 1:1 stoichiometry but also in a 1:2 ratio to produce **34**. This product is also a viscous oil with $\delta^{11}B = 39.0$ ppm.

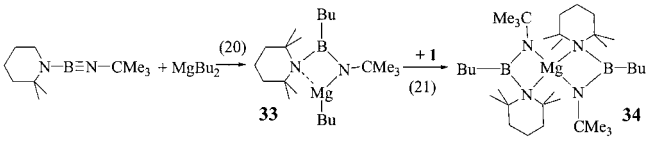

Dialkylzinc compounds are less reactive than dialkylmagnesium compounds. Nevertheless, **1** reacted with dimethylzinc in toluene to produce a solid 1:1 insertion product **35**, $\delta^{11}B = 39.4$ ppm, as shown in Equation (22). The compound was obtained as single crystals. A reaction in a 1:2 ratio to give **36** was also successful.

As a representative of organylcadmium compounds we studied the reaction of diphenylcadmium with **1** in toluene. Reaction (24) proceeded smoothly to give compound **37**. In contrast, diphenylmercury did not react with **1** either at ambient temperature or in refluxing toluene.

From the solutions of **37**, a few well-shaped crystals separated within several days. These, however, proved not to be compound **37** but rather $CdPh_2$. As far as we know, the structure of this compound has not yet been determined. Therefore, some data for this linear compound are listed in the references.[30] **37** is isostructural with $HgPh_2$.[31]

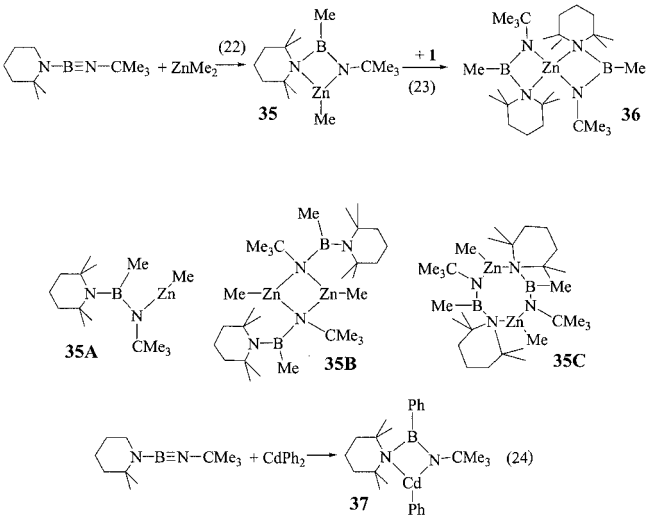

NMR Spectra

An overview of relevant NMR spectroscopic data of the lithium, magnesium, zinc and cadmium compounds is given in Table 5. The magnesium compound **33** exhibits only single ^1H and ^{13}C NMR signals for the methyl groups at the piperidino ring. This suggests a weak interaction of the Mg atom with the tmp nitrogen atom allowing rotation of the tmp group in solution. A similar situation is, therefore, expected for **34** which shows a broad low-field proton NMR signal for the C-6/7 group but two ^{13}C NMR signals. This can be explained by a hindered rotation about the B−N bond of the $BNCMe_3$ group where the *t*Bu group attached to the boron atom can be oriented either *cis* or *trans* to the *tert*-butyl group. This suggestion is supported by the strong deshielding of the protons of the CMe_3 group in **34**. The ^{11}B NMR signals of the two Mg compounds are rather similar, and the shielding of the boron nuclei are similar to those of the Li and Zn compounds.

The ^1H NMR spectrum of **35** reveals two sharp singlets for the BMe and ZnMe groups in a 1:1 ratio. Also, two ^{13}C NMR signals were observed for these groups. These are sharp for ZnMe ($\delta^{13}C = 11.3$ ppm) and broad for BMe ($\delta^{13}C = 1.0$ ppm). A single resonance represents the methyl groups at tmp and two signals in a 2:1 ratio were found for the CH_2 groups of the piperidino ring. Thus, in solution, the structure of compound **35** may either be monomeric or dimeric. However, in the case of the dimer (**35B**) one would expect a low-field shift of the protons of the CMe_3 group, due to the tetracoordination of the respective nitrogen atom. Because monomeric organylzinc amides are scarce, the alternative **35A** is not very likely. Another possibility might be the dimeric structure **35C** which we regard as unlikely because two sets of NMe_2 group are to be expected. However, the molecular structure of **35** has been shown to be a cyclic *N*-(methylzinc)diaminoborane in the solid state. For this reason we suggest that the structure of **36** is also spirocyclic in solution as found for **35** in the solid state.

 © 2004 Wiley-VCH Verlag GmbH & Co. KGaA, Weinheim

Table 5. Selected NMR spectroscopic data of compounds **30** and **32**−**37**; additional data can be found in the Exp. Sect.

	δ^{11}B	δ^{1}H				δ^{13}C					
		2,4-H	3-H	6,7-H	C*Me*$_3$	C-1,5	C-2,4	C-3	C-10	C-11−13	C-6,7
30	39.1	1.41 (t)	1.66 (m)	1.24 (br.)	1.13	51.05	40.83	18.14	8.49	32.26	31.9
32	34.0	1.54 (t)	1.62 (m)	1.30	1.02	52.67	37.89	19.14	49.91	3.86	36.64
33	37.6	0.95	1.68 (m)	1.26	1.18	51.3	39.9	18.0	48.8	32.7	32.3
34	39.0	0.72 (−)	1.59 (br.)	1.23	0.87	53.8	35.7	17.8	52.0	32.0	31.0, 32.5
35	39.5	1.38 (m)	1.66 (m)	1.26	1.13	50.9	40.8	18.1	53.2	32.1	31.8
36	39.1	1.15 (−)	1.64 (br. m)	1.13, 1.24	1.26	51.2	41.0	18.4	53.4	32.1	32.4, 38.6
37	35.4	1.32 (t)	1.54 (m)	1.06, 1.38	1.08	53.2	43.5	17.8	50.6	35.6	25.3, 38.6

The chemical shift $\delta^{11}B = 35.4$ ppm for **37** is compatible with the suggested $PhBN_2$ unit as found in $PhB(NMe_2)_2$ ($\delta = 32.4$ ppm) or $PhB(NEt_2)_2$ ($\delta = 34.1$ ppm).[25] As for **34**, only one ^{1}H NMR signal but two ^{13}C resonances were observed for the methyl groups at tmp in the ^{1}H and ^{13}C NMR spectra. The presence of the Cd atom follows from the satellites observed on the methyl carbon resonance which indicates a $^3J(^{111/113}Cd^{13}C)$ coupling.

Molecular Structure of 35

The zinc compound **35** crystallises in the monoclinic space group $P2_1/c$. Figure 7 shows the ORTEP plot. In the solid state, the methyl[*N*-(methylzinc)-*tert*-butylamino](tetramethylpiperidino)borane is present as a four-membered almost planar ring. Its shape, however, is a strongly distorted trapezoid due to four different endocyclic bond lengths. Endocyclic bond angles range from 70.43(8)° (N1−Zn1−N2) to 98.7(2)° (B1−N2−Zn1). The interplanar angle, τ, between the planes N1−Zn1−N2 and N1−B1−N2 is 2.9°. Notable is the tricoordinate zinc atom (sum of the bond angles = 360°). The B1−N2 bond is quite short at 1.350(4) Å, implying the presence of a B−N π-bond. As in many of the other structures presented here, the B1−N1 bond is long [1.555(3) Å], typical for a single bond. Analogously, the Zn1−N1 bond [2.222(2) Å] is much longer than the Zn1−N2 bond (1.908 Å). The tmp group adopts a chair conformation.

As far as we are aware, the structure of compound **35** is unique since alkylzinc amides $RZnNR_2$ are usually dimeric, containing a four-membered Zn_2N_2 ring.[31,32] The X-ray structure of $(MeZnNPh_2)_2$[33] shows Zn−N bond lengths of 2.080 and 2.066 Å to the tetracoordinate nitrogen atoms. These are much shorter than in compound **35** but longer than the Zn1−N2 bond to the tricoordinate N atom. Dimers of the type $(RZnNR_2)_2$ can be broken up with donors such as pyridine, but no adducts of the type $RZnNR_2(py)$ have yet been characterised in contrast to $RZnNR_2(py)_2$, in which the zinc atom is tetracoordinate.[33]

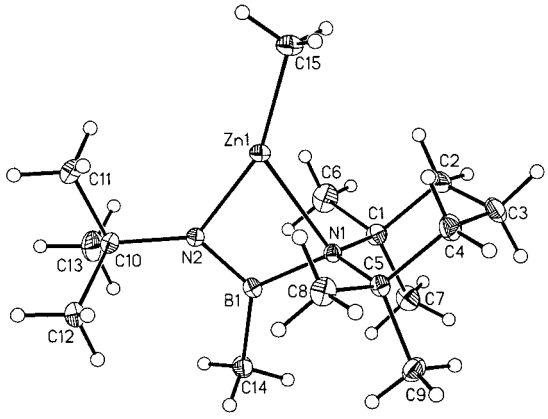

Figure 7. Molecular structure of **35** in the solid state; selected bond lengths [Å]: Zn1−N1 2.222(2), Zn1−N2 1.908(2), Zn1−C15 1.944(3), N1−C1 1.514(3), N1−C5 1.514(3), B1−N1 1.555(3), B1−N2 1.380(4), B1−C14 1.597(4), N2- C10 1.481(3); selected bond angles [°]: Zn1−N1−B1 81.59(2), Zn1−N1−C1 110.9(2), Zn1−N1−C5 110.2(2), N1−B1−N2 109.2(2), N1−B1−C14 122.8(2), N2−Zn1−N1 70.43(8); angles between planes [°]: Zn1N1nB1/Zn1N2B1 2.9, C1N1C5/Zn1N2B1N2 90.0

Reactions with Triorganylboranes, -alanes, -gallanes, and -indanes

The triorganyl compounds of the group 13 elements are medium to strong Lewis acids, the acidity being determined principally by the steric requirements of the organyl group. It was, therefore, expected that no 1:1 adducts would be observed in reactions with **1** because the (amino)(imino)-borane is only a moderate base. Indeed, no evidence for a stable 1:1 coordination compound with triorganylboranes was observed by NMR spectroscopy. However, organoboration of **1** occurs easily, but the rate depends strongly on the steric requirements of the organyl group. This is shown by the data for reaction (25).

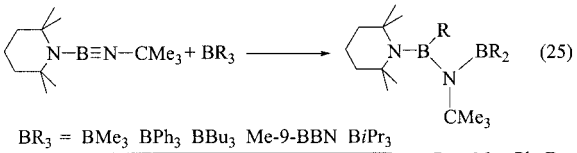

BR_3 =	BMe_3	BPh_3	BBu_3	Me-9-BBN	$BiPr_3$
rate (h)	1[a]	16	24	96	336

R = Me, Ph Bu [b] *i*Pr
38 **39** **40** **41** **42**

[a] at -78°C

[b] R = Me, BR_2 = 9-BBN

To rationalise these results we assume that there is a pre-equilibrium **1** + BR_3 ⇄ **1**·BR_3. The position of this equilibrium lies more on the side of the individual components the more bulky the R group becomes. Thus, the lower the concentration of the adduct, the slower the reaction rate. In the case of *B*-methyl-9-borabicyclo[3.3.1]nonane, it is the methyl group which moves to the boron atom. Most of

 © 2004 Wiley-VCH Verlag GmbH & Co. KGaA, Weinheim

these new asymmetrically substituted diborylamines (**38**−**42**) are liquids.

Although the triorganyl compounds of the heavier group 13 element are all dimeric, they react rapidly with **1** according to Equation (26). Most of the resultant compounds are viscous liquids. Some are solids, however, but single crystals of these could not be obtained.

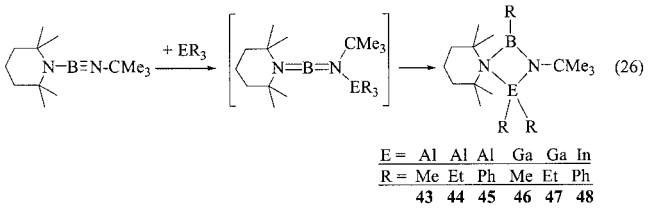

(26)

E =	Al	Al	Al	Ga	Ga	In
R =	Me	Et	Ph	Me	Et	Ph
	43	**44**	**45**	**46**	**47**	**48**

NMR Spectra

The NMR spectroscopic data of compounds **38**−**41** and **43**−**48** are summarised in Table 6 (ignoring the data for the substituents at element E which are found in the Exp. Sect.). The dialkyl[*N*-(tetramethylpiperidinoboryl)-*tert*-butylamino]boranes **38**−**41** exhibit two ^{11}B NMR signals. In case of **39**, only a single signal was observed. This is not totally surprising since resonances of CBN_2 and C_2BN groups can be close together [Ph_2BNR_2: δ = 40−43 ppm; $PhB(NR)_2$: δ = 33−36 ppm; $(Ph_2B)_2NH$: δ = 41 ppm].[25] In general, for the two groups, those of the C_2BN type are less well shielded than those for CBN_2. In general, boron atoms of diborylamines are less well shielded than boron atoms of aminoboranes. In all cases, two resonances were observed for the C-6/7 atoms revealing hindered rotation about the tmp group. No systematic influence on the $\delta^{11}B$ shifts by the group 13 element atoms in compounds **39**−**48** could be observed. Because all show two ^1H and ^{13}C signals for the C-6/7 methyl groups, it follows that these compounds most likely have ring structures with E−N1 bonds. This is supported by a ^{27}Al NMR signal at δ = 105 ppm for **43** which is consistent with a tetracoordinate Al atom. On the other hand, the rather broad ^{27}Al NMR signal at δ = 150 ppm for **44** points to a noncyclic structure with hindered rotation about the B−N bond of the tmp group. This conclusion for **43** as well as for **46** is supported by the X-ray structures of tmp−BPh−N*t*Bu−EMe_2 (E = Al, Ga) which will be discussed shortly.[21]

Discussion

The B≡N triple bond of iminoboranes is highly reactive and this has been further demonstrated by results described here for the (amino)(imino)borane **1**. The reaction with diborane is not selective because four different compounds were observed in addition to the hydroboration product **2**. The by-products result from B−N bond cleavages. However, **2** can be formed in high yield by employing $H_3B{-}SMe_2$ as the borane source. On the other hand, only hydroboration of **1** occurs with diorganylboranes and thexylborane (employed as its dimer). Hence, this reaction is faster than the organoboration of **1** which can be achieved by using triorganoboranes. This can be rationalised by the higher negative charge at the hydrogen atom compared with the organyl group, as well as of the ability of the hydridic hydrogen atom to form hydrogen bonds between two electropositive atoms. The competition between hydroboration and haloboration is chemoselective for the former in the case of the dihaloboranes $HB(Hal)_2{-}SMe_2$, while in case of monohaloboranes both reactions compete with each other. In this case, the hydroboration should be statistically more favourable. This is indeed observed for $H_2BCl{-}SMe_2$ but not for $H_2BBr{-}SMe_2$. In the latter case the observed 1:1 product ratio of the two isomers shows that bromoboration is favoured. If the determining factor were the partial negative charges at the hydrogen and halogen atoms, then the haloboration should win the competition as observed for $HB(Hal)_2$. From this point of view it was most surprising to find that $HSiCl_3$ reacts with **1** exclusively by hydrosilylation, although statistically the chlorosilylation of **1** should be favoured and this is indeed observed when em-

Table 6. Selected NMR spectroscopic data of compounds **38**−**48**; chemical shifts δ in ppm; additional data can be found in the Exp. Sect.

	$\delta^{11}B$	$\delta^{11}B/^{27}Al$	δ^1H				$\delta^{13}C$					
			2,4-H	3-H	C*Me*$_2$	C*Me*$_3$	C-1/5	C-2/4	C-3	C-6/7	C-10	C-11−13
38	40.7	45.7	1.53 (br.)		1.37, 1.44	1.41	56.4	38.3	15.2	32.3, 33.1	53.1	32.7
39	43.1	43.1	1.55 (br. m)		1.49	1.37	56.8	41.3	17.4	33.0, 37.0	56.4	33.7
40	40.9	46.1	1.6 (br. m)		1.43	1.9	56.9	38.9	15.5	27.2, 33.5	53.3	33.3
41	40.6	49.4	1.6 (br. m)		1.49	1.43	53.3	28.2				
43	38.5	105[a]	1.63−1.89		1.48, 1.61	1.25	57.1	36.8	16.2	30.1, 32.1	50.6	32.2
44	37.9	150[b]	1.62 (m)	1.52 (t)	1.48, 1.61	1.25	55.0	37.0	16.9	30.7, 32.4	50.6	33.6
45	42.1	−	1.83 (m)	1.34 (t)	1.50, 1.71	1.28	57.5	36.4	14.7	31.3, 33.2	51.9	33.6
46	36.3	−	1.40−1.8 (m)		1.32, 1.24	1.15	54.8	36.9	17.0	30.5, 32.1	50.7	32.8
47	36.9	−	1.45−1.80 (m)		1.27, 1.37	1.19	54.6	36.9	18.0	31.3, 32.4	50.8	33.6
48	35.5	−	1.78 (m)	(br.)	1.64	1.26	54.0	36.4	17.8	33.0, 33.5	51.6	33.4
49	37.6	−	1.77 (m)	(br.)	1.62	1.30	56.4	36.5	17.6	32.1, 33.0	51.3	34.7

[a] Line width 780 Hz. [b] Line width 2600 Hz.

 © 2004 Wiley-VCH Verlag GmbH & Co. KGaA, Weinheim

ploying diorganyldichorosilanes, trichloro(organyl)silanes or silicon tetrahalides.[8,22] The silanes must be sufficiently Lewis acidic. Thus, Me_3SiH and Ph_3SiH do not react with **1** in contrast to Me_2SiHCl and Ph_2SiH_2, although both are not strong Lewis acids but obviously of sufficient strength to induce the hydrosilylation of **1**. On the other hand, the hydrides Ph_3EH (E = Si, Ge) did not react with **1** in contrast to Me_3SnH, Bu_3SnH and Ph_3SnH. This indicates that steric factors also influence the hydrometallation of **1**. However, it was most surprising that with Ph_3SnH an umpolung of the insertion occurs. The imino nitrogen atom of **1** is protonated with formation of a B−Sn bond.

The organylmetal compounds LiR, MgR_2, ZnR_2, CdR_2, BR_3, AlR_3, GaR_3 and $InPh_3$ all react with **1** by organometallation. This is a new route to compounds of the type tmp−BR−N*t*Bu−ER_{n-1}. Paetzold et al. have studied the reactions of LiR compounds with the iminoboranes X−B=N−CMe_3 (X = Me, Et, Bu). These react in a 1:2 ratio and provided *N*-lithioazaborazoniaborate compounds.[34] However, with iminoboranes X−B≡N−CMe_3 [X = CMe_3, $N(SiMe_3)CMe_3$] *N*-lithioaminoboranes $LiN(CMe_3)$−BXR were obtained of which (TMEDA)$LiN(CMe_3)$−$B(CMe_3)_2$ was crystallographically characterised.[34] Usually, *N*-lithioaminoboranes are prepared by deprotonation of aminoboranes R_2B−NHR′, $RB(NHR')_2$ or $B(NHR)_3$.[35−40] Deprotonation of the diborylamine mes_2B−NH−$Bmes_2$ with LiR in diethyl ether leads to ionic $[(Et_2O)_3Li][N(Bmes_2)_2]$ with a linear BNB unit of an allenic type and short B−N bonds [1.343(5), 1.348(5) Å] due to the dicoordinate N atom,[36] while deprotonation of mes_2B−NH_2 gives dimeric $[(Et_2O)LiNHBmes_2]_2$.[37] In both cases the Li atoms are tricoordinate. In the latter case, the nitrogen atoms are tetracoordinate. Consequently, the B−N bond of the dimeric molecule is longer [1.386(4) Å] than in mes_2BNH_2. Association of *N*-lithioaminoboranes can be prevented by using multidentate bases as ligands as has been demonstrated for 9-*N*-lithio(trimethylstannylamino)borabicyclo-[3.3.1]nonane−pentamethylethylenetriamine.[39] The monomeric *N*-lithiodiaminoborane **32** is unique because in the solid state the intramolecular coordinative Li−N bond stabilises the tricoordination of the Li atom and the bulkiness of the groups at the two nitrogen atoms hinders association. The B2−N2 bond of **32** is at the shorter end for B−N bonds [1.361(4) Å] between tricoordinate B and N atoms indicating a high degree of π-bonding. However, the Li1−N1 bond is weak and is 0.2 Å longer than the Li1−N2 bond. This is a general observation for all the *N*-metallated diaminoboranes reported here (**19**, **32** and **35**) and many others of a similar type.[21] In solution, however, the coordinate Li1−N1 bond (also Mg−N, B−N, Al−N, Ga−N and In−N bonds) is opened as shown by only one ^1H or ^{13}C NMR signal for the methyl groups attached to the piperidino ring. For those where two or more signals were observed, one can assume that the ring structure with a coordinate N1−E bond is retained in solution as shown, for instance, for compounds **12**−**17**. In particular, the lithium compound **32** proved to be a versatile reagent and we will report on its chemistry in a forthcoming paper.[21]

Experimental Section

General: All experiments were performed under anhydrous conditions using Schlenk or vacuum-line techniques. Solvents were dried by conventional methods. Commercial chemicals were purified either by distillation, crystallisation or were used as supplied (solutions of LiR compounds). Several compounds were already available in our laboratory. The following compounds were prepared by literature methods: **1**,[4] $AlMe_3$−OEt_2,[40] Ph_3In−1,4-dioxane,[41] Ph_3Al,[42] thexylborane,[12] disiamylborane,[43,44] $HBCl_2$−SMe_2 and H_2BCl−SMe_2,[45] $HBBr_2$−SMe_2 and H_2BBr−SMe_2,[46] 9-BBN.[47] NMR: Bruker AC 200 (^7Li, ^{11}B, ^{119}Sn), Jeol GS270 (^1H, ^7Li, ^{11}B, ^{13}C, ^{14}N, ^{119}Sn), Jeol EX400 (^1H, ^{13}C) instruments. If not otherwise stated all NMR spectra were recorded in C_6D_6. References: $SiMe_4$ (int.), BF_3−OEt_2 (ext.), 1 M aqueous LiCl (ext.), C_6D_6 (int.), aqueous 1 M $NaNO_3$ (^{14}N), $SnMe_4$ (ext.). IR: Nicolet FT-IR spectrometer (liquids as capillary films, solids as nujol mulls). MS: Atlas CH7 instrument, 70 eV; reported data: mass, relative intensity, assignment. X-ray: Siemens P4 diffractometer equipped either with a scintillation counter or a CCD detector. Low-temperature device LT2, Mo-K_α radiation, graphite monochromator.

[(*tert*-Butyl)(2,2,6,6-tetramethylpiperidinoboryl)amino]-borane (2): A solution of H_3B−SMe_2 (0.39 mL, 7.0 M solution in hexane, 2.8 mmol) was added to a solution of **1** (2.9 mL of a 0.96 M solution, 2.8 mmol) in hexane. The reaction was slightly exothermic. After 24 h of stirring, all volatile components were removed at ambient temperature in vacuo. **2** remained as a colourless oil. ^1H (^{11}B-decoupled) NMR: δ = 3.91 (br., 2 H, BH_2), 4.77 (br., 1 H, BH) ppm. $C_{13}H_{30}B_2N_2$ (236.0): calcd. C 66.16, H 17.94, N 11.87; found C 64.76, H 17.25, N 11.67.

[(*tert*-Butyl)(2,2,6,6-tetramethylpiperidinoboryl)amino]diisopropylaminoborane (6): To a solution of freshly distilled diisopropylamine (0.42 mL, 3.0 mmol) in hexane (20 mL) was added at 0 °C a solution of BH_3−THF in hexane (1.0 M, 3.0 mL). After warming to ambient temperature, all volatile components were removed in vacuo leaving behind 0.44 g of H_3B−NH(*i*Pr)$_2$ {$\delta^{11}B$ = −20.58 [quat., $^1J(^1H^{11}B)$ = 96 Hz] ppm}. A solution of **1** in hexane (0.96 M, 3.10 mL, 3.0 mmol) was then added at −78 °C. No reaction occurred at room temperature. On heating to reflux overnight, the formation of **6** was noted by its ^{11}B NMR signal at δ = 50.6 ppm. The compound was isolated as a solid after removal of all volatile components in vacuo. Yield 0.82 g of **6** (98%). The ^1H NMR spectrum was not very informative as the signals were strongly overlapping.

[(*tert*-Butyl)(2,2,6,6-tetramethylpiperidinoboryl)amino]dicyclohexylborane (8): A solution of **1** (7.9 mL, 0.462 M, 3.6 mmol) in hexane was added with stirring to tetracyclohexyldiborane (0.65 g, 1.8 mmol). The diborane derivative dissolved slowly. About 2 h later, a precipitate formed. According to ^{11}B NMR spectroscopy the reaction was complete after 4 d. After removal of the solvent in vacuo, a colourless powder remained which proved to be pure **8**. Yield 1.4 g of **8** (98%), m.p. 122−124 °C. ^1H NMR: δ = 1.78 (br., 22 H, C_6H_{11}), 2.15 (br., 1 H, BH) ppm. ^{13}C NMR: δ = 24.1 (br., BC), 27.7 (*p*-C of C_6H_{11}), 28.7 (*m*-C), 28.9 (*o*-C) ppm. MS (70 eV): *m*/*z* (%) = 400 (75) [M^+], 385 (15) [M^+ − Me], 317 (100) [M^+ − C_6H_{11}] and others. $C_{25}H_{50}B_2N_2$ (400.31): calcd. C 75.01, H 12.59, N 7.00; found C 74.54, H 11.25, N 6.77.

[(*tert*-Butyl)(2,2,6,6-tetramethylpiperidinoboryl)amino]diisoamylborane (9): A solution of **1** (8.65 mL, 0.462 M, 4.0 mmol) in hexane was added with stirring to a hexane solution of freshly prepared

 © 2004 Wiley-VCH Verlag GmbH & Co. KGaA, Weinheim

dimeric disiamylborane (4.0 mmol). ^{11}B NMR spectroscopic analysis showed that the hydroboration of **1** was complete after 24 h. Removal of volatile material in vacuo left an oily residue which turned out to be pure **9**. Yield 1.47 g (97%). ^{1}H NMR: δ = 3.78 (br., 1 H, BH), 1.36, 1.35 [each 3 H, B(CH*Me*)], 1.01, 1.08 (each 6 H, CH*Me*$_2$) ppm. ^{13}C NMR: δ = 16.6 (br., BC), 23.0 (CH*Me*$_2$), 22.7 (BCH*Me*), 55.7 (CH*Me*$_2$) ppm. MS (70 eV): *m*/*z* (%) = 376 (28) [M$^+$], 361 (14) [M$^+$ − Me], 319 (40) [M$^+$ − C$_4$H$_9$], 305 (100) [M$^+$ − C$_5$H$_{11}$], 235 (100) [305 − C$_5$H$_{10}$]$^+$, 222 (24) [235 − CH$_2$]$^+$ and fragments of lower mass. $C_{23}H_{50}B_2N_2$ (376.29): calcd. C 73.42, H 13.39, N 7.44; found C 74.25, H 13.66, N 7.80.

9-[(*tert*-Butyl)(2,2,6,6-tetramethylpiperidinoboryl)amino]-9-borabicyclo[3.3.1]nonane (10): A solution of dimeric 9-borabicyclo[3.3.1]nonane (0.30 g, 1.4 mmol) in pentane (30 mL) was cooled to −78 °C. A solution of **1** (12.3 mL, 0.277 M, 2.8 mmol) in pentane was then slowly added. After stirring for 2 h at ambient temperature, the reaction was complete. A light yellow oil remained after removal of the pentane in vacuo (50 Torr). After addition of hexane (1 mL) and cooling of the solution to −50 °C, a colourless powder of **10** precipitated. Yield 0.91 g (95%), m.p. 65−67 °C. ^{1}H NMR: δ = 1.05 (2 H, CH), 1.90 (br., 12 H, 6 CH$_2$) ppm. ^{13}C NMR: δ = 12.1 (br., BMe), 23.5 (C$_a$), 26.5 (C$_d$), 33.0 (C$_c$) 33.2 (C$_b$) ppm. ^{14}N NMR: δ = −231 ppm. MS (70 eV): *m*/*z* (%) = 344 (95) [M$^+$], 329 (90) [M$^+$ − Me], 288 (15) [M$^+$ − C$_4$H$_8$], 261 (93) [M$^+$ − C$_6$H$_9$], and fragments of lower mass. $C_{21}H_{42}B_2N_2$ (344.20): calcd. C 73.28, H 12.30, N 8.14; found C 75.43, H 12.75, N 7.83.

[(*tert*-Butyl)(2,2,6,6-tetramethylpiperidinoboryl)amino](1,1,2-trimethylpropyl)borane (11): To freshly prepared *sym*-dithexyldiborane(6) (2.5 mmol) was added, with stirring, a solution of **1** (10.8 mL, 0.462 M, 5.0 mmol) in hexane. After stirring for 8 d. the reaction was complete as shown by ^{11}B NMR spectroscopy. After removal of the hexane in vacuo, a colourless, mobile liquid was left. Yield 1.19 g of **11** (98%). The compound decomposed on attempted distillation at 130 °C/10^{-2} Torr with formation of 2,3-dimethyl-2-butene (trapped at −196 °C and identified by NMR spectroscopy). ^{1}H NMR: δ = 0.91 [d, ^3J(^{1}H^{1}H) = 6.6 Hz, 6 H, CHMe$_2$], 0.94 (6 H, C*Me*$_2$) ppm. ^{13}C NMR: δ = 18.6 (CH$_2$), 22.5 (C*Me*$_2$), 29.0, (br., CB), 37.3 (*C*HMe$_2$) ppm. MS (70 eV): *m*/*z* (%) = 236 (32) [M$^+$ − C$_6$H$_{12}$], 180 (9) [236 − C$_4$H$_8$]$^+$, no M$^{\cdot+}$. $C_{19}H_{42}B_2N_2$ (320.18): calcd. C 71.28, H 13.23, N 8.75; found C 72.14, H 13.11, N 9.21.

{(*tert*-Butyl)[chloro(2,2,6,6-tetramethylpiperidino)boryl]amino}borane (14) and [(*tert*-Butyl)(2,2,6,6-tetramethylpiperidinoboryl)amino]chloroborane (15): To an emulsion of BH$_2$Cl−SMe$_2$ in hexane (2.7 mmol in 1.60 mL) was added dropwise a hexane solution of **1** (10.3 mL, 0.267 M, 2.7 mmol). After stirring for 5 h, a clear solution resulted. All volatile materials were removed in vacuo leaving behind a colourless viscous oil. In C$_6$D$_6$, this solution showed the presence of two isomers. **14:** ^{11}B NMR: δ = −5.9 [t, ^1J(^{11}B^{1}H) = 125 Hz], 25.1 ppm (ratio 1:1). **15:** ^{11}B NMR: δ = 3.8 [d, ^1J(^{11}B^{1}H) = 125 Hz], 30.6 [d, ^1J(^{11}B^{1}H) = 142 Hz] ppm (ratio 1:1). In addition a signal for (tmpB−NCMe$_3$)$_2$ (δ^{11}B = 34.6 ppm) was observed. The mixture could not be separated by fractional distillation.

{[Bromo(2,2,6,6-tetramethylpiperidino)boryl](*tert*-butyl)amino}borane (16) and Bromo[(*tert*-butyl)(2,2,6,6-tetramethylpiperidinoboryl)amino]borane (17): In analogy to **15** the components H$_2$BBr−SMe$_2$ (1.50 mL, 1.5 M, 2.2 mmol) and **1** (4.87 mL, 0.462 M, 2.2 mmol) were allowed to react in hexane. After 24 h, neither of the two starting materials could be detected by ^{11}B NMR spectroscopy. Four new signals were present, both as pairs in a 1:1 ratio. **16:** ^{11}B NMR: δ = 2.4 [t, ^1J(^{11}B^{1}H) = 75 Hz], 30.8 (s) ppm. **17:** ^{11}B NMR: δ = 1.0 [d, ^1J(^{11}B^{1}H) = 50 Hz], 32.3 [d, ^1J(^{11}B^{1}H) = 105 Hz] ppm. The mixture of isomers was not characterised by elemental analysis.

{(*tert*-Butyl)[chloro(2,2,6,6-tetramethylpiperidino)boryl]amino}chloroborane (12): To a stirred solution of HBCl$_2$−SMe$_2$ (1.50 mL, 1.30 M, 1.9 mmol) was added dropwise a hexane solution of **1** (7.28 mL, 0.267 M, 1.9 mmol). After 48 h, the reaction was quantitative. Removal of the volatile material left behind a colourless oil. Yield 0.55 g of **12** (93%). IR: ṽ = 2480 (νBH), 1480, 1450 (νBN$_2$), 660 (νBCl) cm^{-1}. $C_{13}H_{28}B_2Cl_2N_2$ (304.9): calcd. C 51.21, H 9.26, N 9.89; found C 51.11, H 9.39, N 9.34.

Bromo{[bromo(2,2,6,6-tetramethylpiperidino)boryl](*tert*-butyl)amino}borane (13): In analogy to **12** a hexane solution of HBBr$_2$−SMe$_2$ (19 mL, 0.23 M, 4.4 mmol) was allowed to react with **1** (7.33 mL, 0.23 M, 4.4 mmol). The reaction was slightly exothermic. After heating for several minutes to reflux, all volatile materials were removed in vacuo. **13** was obtained as a colourless viscous oil. Yield 1.69 g of **13** (97%). $C_{13}H_{28}B_2Br_2N_2$ (313.89): calcd. C 49.70, H 8.92, N 8.92; found C 48.98, H 8.97, N 8.76.

Dimeric [(*tert*-Butyl)(2,2,6,6-tetramethylpiperidinoboryl)amino]alane (19): A solution of **1** in hexane (18.7 mL, 0.186 M, 3.5 mmol) was diluted further with hexane (15 mL), cooled to −78 °C, and a solution of AlH$_3$−NMe$_3$ (0.31 g, 3.5 mmol in 25 mL of diethyl ether) was added dropwise with stirring. After warming the mixture to ambient temperature, the ^{11}B NMR spectrum showed a broad signal at δ = 34.7 ppm and doublet at δ = 27.1 ppm. The volume of the solution was then reduced by about 50%. After 1 d at −20 °C, crystals had separated. The majority of the crystals were well-developed prisms which proved to be **19**. The compound is very moisture-sensitive. Selected IR bands: ṽ = 2515, 2468 (ν$^{10/11}$BH), 1831 (νAlH), 1460 (νBN$_2$) cm^{-1}. $C_{25}H_{60}Al_2B_2N_4$ (504.37): calcd. C 61.92, H 11.99, N 11.11; found C 57.05, H 11.78, N 9.45.

[(*tert*-Butyl)(2,2,6,6-tetramethylpiperidinoboryl)amino]diisobutylalane (20): To a stirred solution of **1** (3.0 mL, 0.96 M, 2.9 mmol) in hexane was added a hexane solution of *i*Bu$_2$AlH (2.9 mL, 1.0 M diluted with 10 mL of hexane). After 24 h, the hexane was removed in vacuo leaving behind **20** as a colourless air- and moisture-sensitive liquid (1.05 g, 99%). ^{1}H NMR: δ = 0.46 [d, ^3J(^{1}H^{1}H) = 6.3 Hz, 4 H, AlC*H*$_2$], 1.22 [d, ^3J(^{1}H^{1}H) = 6.3 Hz, 12 H, CH(C*H*$_3$)$_2$], 2.20 [m, 2 H, C*H*(CH$_3$)$_2$] ppm. ^{13}C NMR: δ = 28.8, 29.2 [CH(*C*H$_3$)$_2$], 32.7 ppm; *C*H(CH$_3$)$_2$, Al*C* not observed. ^{27}Al NMR: δ = 109.5 ($h_{1/2}$ = 1960 Hz) ppm. IR: ṽ = 2460 cm^{-1} (νBH). $C_{21}H_{46}AlBN_2$ (364.41): calcd. C 69.22, H 12.72, N 7.69; found C 68.21, H 12.08, N 8.12.

[(*tert*-Butyl)(2,2,6,6-tetramethylpiperidinoboryl)amino]diphenylsilane (21): To a solution of Ph$_2$SiH$_2$ (0.415 g, 2.25 mmol) in toluene (10 mL) was added a solution of **1** (4.6 mL, 0.5 M) in hexane diluted with toluene (10 mL). The mixture was stirred for 2 weeks. After this time, the ^{11}B NMR signal of **1** could no longer be detected. Removal of the solvents left behind a colourless oil. Attempts at crystallisation were unsuccessful. Because the NMR spectroscopic data showed no impurities, no further purification attempts were deemed necessary. ^{1}H NMR: δ = 0.57 (SiMe$_2$), 7.10−9.0 (m, Ph) ppm. ^{13}C NMR: δ = 129.01, 129.53, 130.17, 136.17, 17.71 (Ph) ppm. ^{29}Si NMR: δ = −21.87 [^1J(^{1}H^{29}Si) = 21 Hz] ppm. Selected IR bands: ṽ = 2490, 2395 (νBH), 2120 (νSiH) cm^{-1}. $C_{25}H_{39}BN_2Si$ (406.2): calcd. C 73.96, H 9.68, N 6.89; found C 72.63, H 9.77, N 7.08.

[(*tert*-Butyl)(2,2,6,6-tetramethylpiperidinobory)amino]trichlorosilane (22): To a toluene solution of **1** (0.67 g, 3.0 mmol in 4.6 mL) was

 © 2004 Wiley-VCH Verlag GmbH & Co. KGaA, Weinheim

added at 0 °C a solution of $SiHCl_3$ (0.4 mL, 0.54 g, 4.0 mmol) in toluene (6 mL). After stirring for 30 min, all volatile material was removed in vacuo. Distillation afforded 0.66 g of **22** (62%), b.p. 110−115 °C/0.005 Torr, m.p. 40 °C. ^{14}N NMR: δ = −235, −298 ppm. IR: $\tilde{\nu}$ = 2492, 2460 st (νBH) cm^{-1}. $C_{13}H_{28}BCl_3N_2Si$ (357.64): calcd. C 43.66, H 7.89, N 7.83; found C 43.06, H 8.04, N 7.93.

[(*tert*-Butyl)(2,2,6,6-tetramethylpiperidinoboryl)amino]chlorodimethylsilane (23): Me_2SiHCl (300 mg, 3.2 mmol) was cooled to −78 °C. A solution of **1** (0.71 g, 3.2 mmol) in toluene (4.9 mL) was then added. The solution was then allowed to warm to room temperature with stirring. All volatile materials were removed in vacuo and the remaining liquid distilled at 70 °C/10^{-3} Torr. Yield 0.96 g of **23** (95%), m.p. 25−26 °C. ^1H NMR: δ = 0.57 ($SiMe_2$), 5.3 (BH, at −54 °C) ppm. ^{13}C NMR: δ = 8.75 (SiC) ppm. ^{14}N NMR: δ = −248, −307 ppm. IR: $\tilde{\nu}$ = 2460 (sh), 2420 m (νBH) cm^{-1}. $C_{15}H_{34}BClN_2Si$ (316.80): calcd. C 56.87, H 10.82, N 8.84; found C 54.07, H 10.79, N 9.28. The same result was achieved in the presence of a small amount of hydroquinone as a catalyst.

[(*tert*-Butyl)(2,2,6,6-tetramethylpiperidinoboryl)amino]trimethylstannane (24): To a solution of **1** (0.44 g, 2.0 mmol) in hexane (14 mL) was added Me_3SnH (1 mL). After heating the mixture to 50 °C, the reaction was complete (^{11}B NMR). All volatile materials were removed in vacuo. The residue, a colourless oil, proved to be sufficiently pure. However, on distillation only **1** could be isolated, b.p. 100−130 °C/0.1 Torr. Yield (before distillation) 0.40 g of **24** (93%). ^1H NMR: δ = 0.4 [$^2J(^1H^{119}Sn)$ = 55.1 Hz), $SnMe_3$] ppm. ^{13}C NMR: δ = 2.11 [$^1J(^{13}C^{119}Sn)$ = 388 Hz, $SnMe_3$] ppm. IR: $\tilde{\nu}$ = 2413, 2385 m (νBH) cm^{-1}. $C_{16}H_{37}BN_2Sn$ (386.99): calcd. C 49.66, H 9.64, N 7.24; found C 49.43, H 9.31, N 7.21.

Tributyl[(*tert*-butyl)(2,2,6,6-tetramethylpiperidinoboryl)amino]stannane (25): A solution containing **1** (0.89 g, 4.0 mmol) and Bu_3SnH (1.32 mL, 5.0 mmol) in toluene (10 mL) was heated to 60 °C for 2 h. The ^{11}B NMR spectrum showed the absence of **1** and a new signal at δ = 39.6 ppm. Volatile materials were removed from the solution in vacuo (0.001 Torr). The remaining colourless oil was distilled. The fraction of b.p. 120−135 °C/0.001 Torr consisted of 90% **25** and 10% Bu_3SnH according to NMR spectroscopic data. ^1H NMR (only main component): δ = 0.8−1.5 (m, Bu) ppm. ^{13}C NMR: δ = 18.75 [$^1J(^{13}C^{119}Sn)$ = 360 Hz, C_α], 29.09 [$^2J(^{13}C^{119}Sn)$ = 16 Hz, C_β], 27.79 [$^3J(^{13}C^{119}Sn)$ = 76 Hz, C_γ], 13.79 (C_δ) ppm. IR: $\tilde{\nu}$ = 2415 sh, 2388 m (νBH) cm^{-1}.

(*tert*-Butyl)[(2,2,6,6-tetramethylpiperidino)(triphenylstannyl)boryl]amine (26): Ph_3SnH (0.53 g, 1.5 mmol) was dissolved in toluene (50 mL). A solution of **1** in hexane (5.6 mL, 0.27 M, 1.5 mmol) was then added with stirring. After stirring for 1 d, a single ^{11}B NMR resonance at δ = 44.6 ppm was observed. A solid residue was left after removing all volatile components in vacuo. The solid was crystallised from hexane (40 mL) at −80 °C. Yield 0.44 g of **26** (75%), m.p. 106 °C. ^1H NMR: δ = 7.19 (m, 9 H, *o*-Ph and *p*-Ph), 7.81(m, 6 H, *m*-Ph) ppm. ^{13}C NMR: δ = 128.1, 128., 138.2, 144.6 ppm. ^{119}Sn NMR signal not detectable. $C_{31}H_{43}BN_2Sn$ (573.17): calcd. C 64.90, H 7.50, N 4.98; found C 64.74, H 7.41, N 4.62.

Lithium (*tert*-Butyl)(2,2,6,6-tetramethylpiperidinophenylboryl)amide−Diethyl Ether (32): A hexane solution of **1** (0.89 M, 5.59 mL, 5.0 mmol) was cooled to −78 °C. A solution of PhLi in cyclohexane/diethyl ether (2.0 M, 2.8 mL, 5.0 mmol) was then added dropwise with stirring. After the clear solution had reached room temperature, a light yellow precipitate appeared which redissolved on continued stirring. The solution showed a ^{11}B NMR signal at δ = 33.3 ppm. The brownish solid that remained after evaporation of the solvents in vacuo was crystallised from toluene at −78 °C. Yield 1.55 g of **32** (61%), m.p. 162 °C. ^{13}C NMR: δ = 125.14, 126.44, 134.13 (Ph) ppm; BC not found. ^7Li NMR (hexane): δ = 2.3 ($h_{1/2}$ = 9.7 Hz) ppm. $C_{23}H_{42}BLiN_2O$ (380.34): calcd. C 72.63, H 11.13, N 7.37; found C 64.75, H 10.04, N 7.41.

Lithium (*tert*-Butyl)[methyl(2,2,6,6-tetramethylpiperidino)boryl]amide−Tetramethylethylenediamine (30-TMEDA): To a solution of **1** (13.6 mL, 0.22 M, 3.0 mmol) in hexane at −78 °C was added tetramethylethylenediamine (0.45 mL, 3.0 mmol). A solution of LiMe in diethyl ether was then added (1.88 mL, 1.6 M, diluted with 25 mL of diethyl ether). After the addition, the solution became a bluish colour but at room temperature the solution was colourless. Some solid had formed which was removed by filtration. Dissolved in C_6D_6, this solid proved to be tmp−BMe−$NCMe_3$Li. Two ^{11}B NMR signals were observed for the filtrate at δ = 35.3 (90%) and 39.6 ppm (10%). The signal at δ = 39.6 ppm increased in intensity with time.

(*tert*-Butyl)[methyl(2,2,6,6-tetramethylpiperidinoboryl)amino]catecholborane (31): A solution of **30−TMEDA** (3.0 mmol, 16 mL) was allowed to quickly reach room temperature. A solution of *B*-chlorocatecholborane (0.6 g, 3.0 mmol) in diethyl ether (15 mL) was then added with stirring. A white precipitated rapidly formed. The suspension was stirred for 3 h and the solid was then removed by filtration and the filtrate reduced in volume to about 20 mL in vacuo and kept at −20 °C. Crystals of **31** separated within 2 d. Yield 0.75 g (73%), m.p. 158 °C. ^1H NMR: δ = 0.78 (s, BMe), 6.69−1.76 (m, 5 H) ppm. ^{13}C NMR: δ = 110.0, 119.27, 150.55 (C_{arom}) ppm. $C_{20}H_{34}BN_2O_2$ (356.11): calcd. C 67.45, H 9.62, N 7.87; found C 67.42, H 9.51, N 7.83.

Reaction of 1 with Butyllithium: BuLi (7.46 mL of a 0.670 M hexane solution, 5 mmol) was stirred and cooled to −78 °C followed by addition of a hexane solution of **1** (3.2 mL, 1.57 M). After warming to room temperature, a yellow solution formed. Evaporation of the solvent in vacuo gave a yellow solid, m.p. 74−75 °C. It showed a ^{11}B NMR signal at δ = 33.6 ppm (about 70%) and two other signals in toluene solution. The ^1H and ^{13}C NMR spectra indicated that the product was not pure. Attempts at purification by sublimation or crystallisation were unsuccessful.

Reaction of 1 with *tert*-Butyllithium. Formation of 1,2,3,4-*tert*-Butyl-1,3,2,4-diazadiboretidine (28): To a stirred solution of **1** (7.46 mL, 0.670 M) in hexane at −78 °C was added a hexane solution of $LiCMe_3$ (3.13 mL, 1.60 M, 5 mmol). The mixture was then allowed to warm to room temperature with stirring to give a yellow solution. After removal of all volatile components in vacuo, a yellow solid remained which on sublimation at 40 °C/0.001 Torr yielded colourless crystals of the diazadiboretidine **28**, m.p. 58−60 °C. ^1H NMR: δ = 1.23 (s, $BCMe_3$), 1.32 ($NCMe_3$) ppm (ratio 1:1). ^{13}C NMR: δ = 30.5 ($BCMe_3$), 33.8 ($NCMe_3$), 49.5 ($NCMe_3$) ppm; BC not detected. ^{11}B NMR: δ = 41.1 ppm.

Butylmagnesium (*tert*-Butyl)[butyl(2,2,6,6-tetramethylpiperidino)boryl]amide (33): A hexane solution of **1** (17.5 mL, 0.114 M, 2.0 mmol) was further diluted with hexane (20 mL). To the stirred solution at −78 °C was added a hexane solution of $MgBu_2$ (2.0 mL, 1 M). At room temperature the solution showed only one ^{11}B NMR signal at δ = 37.5 ppm indicating a quantitative reaction. Removal of the volatile materials gave an oily, non-volatile, moisture-sensitive residue. Attempted crystallisation from pentane at low temperature afforded no crystals. Attempted distillation in vacuo led to decomposition. ^1H NMR: δ = 0.95, 1.04, 1.11, 1.91, 1.27, 1.38, 1.51, 1.59 (Bu groups) ppm. ^{13}C NMR: δ = 14.3, 19.2, 27.0,

 © 2004 Wiley-VCH Verlag GmbH & Co. KGaA, Weinheim

27.8, 32.7, 38.6 (Bu) ppm. $C_{21}H_{45}BMgN_2$ (360.72): calcd. C 69.98, H 12.50, 7.76; found C 63.65, H 11.90, N 7.30.

Magnesium Bis{(*tert*-butyl)[butyl(2,2,6,6-tetramethylpiperidino)-boryl]amide} (34): Prepared in analogy to **33** from **1** (0.114 M solution, 22.0 mL, 2.4 mmol) and $MgBu_2$ (1.25 mL, 1 M, 1.25 mmol). Colourless oil, yield 0.7 g (95%). ^{11}B NMR: δ = 39.0 ppm. ^1H NMR: δ = 0.72−1.59 ppm (br. m, 2/4-H, 3-H, Bu). ^{13}C NMR: δ = 14.0, 27.5, 29.5, 31.8, 38.1 ppm (main signals). $C_{24}H_{72}B_2MgN_4$ (582.90): calcd. C 70.06, H 12.45, N 9.61; found C 67.61, H 12.02, N 8.74.

Methylzinc (*tert*-Butyl)[methyl(2,2,6,6-tetramethylpiperidino)boryl]-amide (35): To a stirred solution of **1** (0.27 M, 7.4 mL, 2.0 mmol), diluted with hexane (20 mL) at −78 °C, was added a solution of $ZnMe_2$ (0.09 M, 2.9 mL, 2.0 mmol), dissolved in toluene (10 mL). After the solution had attained ambient temperature, the volume of the solution was reduced to about 20 mL. At −78 °C, crystals appeared within a week. These were highly sensitive towards moisture. Recrystallisation at −40 °C from hexane yielded single crystals. The yield was not determined. ^1H NMR: δ = −0.09 (ZnMe), 0.62 (BMe) ppm. ^{13}C NMR: δ = −11.3 (ZnMe), 1.0 (br., BMe) ppm. $C_{15}H_{33}BN_2Zn$ (317.61): calcd. C 56.67, H 10.39, N 8.52; found C 52.44, H 9.75, N 8.49.

Zinc Bis{(*tert*-butyl)[methyl(2,2,6,6-tetramethylpiperidino)boryl]-amide} (36): Prepared in analogy to **35** from **1** (2.5 mmol) in hexane (40 mL) and $ZnMe_2$ (1.8 mL, 0.69 M, 1.25 mmol), dissolved in toluene (10 mL).**36** is a sticky oil from which no crystals could be obtained. Yield 0.64 g (96%). ^{11}B NMR: δ= 39.1 ppm. ^1H NMR: δ = 0.62 (BMe) ppm. ^{13}C NMR: δ = 1.32 (br., BMe) ppm. $C_{28}H_{60}B_2N_4Zn$ (539.81): calcd. C 62.40, H 11.13, N 10.04; found C 62.95, H 11.41, N 10.12.

Phenylcadmium (*tert*-Butyl)[phenyl(2,2,6,6-tetramethylpiperidino)-boryl]amide (37): A solution of **1** (3.2 mmol) in hexane (49 mL) was cooled to −78 °C. A solution of $CdPh_2$ (0.16 g, 3.2 mmol) in $CHCl_3$ (30 mL) was then added with stirring. At room temperature, all volatile materials were removed in vacuo and the oily residue treated with small quantities of toluene. From the resultant solution appeared some well-shaped crystals which proved to be $CdPh_2$. Concentration of the solution yielded **37** as a microcrystalline powder. Yield 1.19 g of **37** (76%), m.p. 160 °C (dec.). ^1H NMR: δ = 7.13, 7.21, 7.27, 7.53, 7.50, 7.71 (m, Ph) ppm. ^{13}C NMR: δ = 126.0, 126.8, 128.3, 132.9, 139.5 (Ph) ppm. $C_{25}H_{37}BCdN_2$ (488.36): calcd. C 61.43, H 7.63, N 5.73; found C 59.00, H 7.60, N 5.52.

{(*tert*-Butyl)[methyl(2,2,6,6-tetramethylpiperidino)boryl]amino}-dimethylborane (38): A solution of **1** in hexane (11.0 mL, 0.362 M,) was frozen at −196 °C and BMe_3 (4.1 mmol) condensed onto it. The mixture was allowed to slowly thaw. After 4 h of stirring, all volatile material was evaporated in vacuo at 50 Torr. A colourless oil remained. Yield 1.07 g of **38** (97%), m.p. 18−20 °C. ^1H NMR: δ = 0.58 (6 H, BMe_2), 0.82 (3 H, BMe) ppm. ^{13}C NMR: δ = 12.1 (br., BMe, BMe_2) ppm. ^{14}N NMR: δ = −230.6 ($h_{1/2}$ = 500 Hz) ppm. MS (70 eV): *m*/*z* (%) = 263 (1) [M^+ − Me], 222 (100) [$tmpBNCMe_3^+$]. $C_{16}H_{36}B_2N_2$ (278.10): calcd. C 69.10, H 13.05, N 10.07; found C 69.02, H 12.85, N 10.32.

{(*tert*-Butyl)[phenyl(2,2,6,6-tetramethylpiperidino)boryl]amino}-diphenylborane (39): To a suspension of BPh_3 (1.00 g, 4.1 mmol) in hexane (20 mL) was added a solution of **1** in hexane (14.7 mL, 0.283 M, 4.1 mmol). After stirring for 16 h, the ^{11}B NMR spectrum showed the absence of **1**. When the solvent was removed in vacuo a precipitate appeared which was isolated by filtration. A second crop was obtained from the filtrate. Yield 1.65 g of **39** (86%), m.p. 107−110 °C. ^1H NMR: δ = 7.25−8.04 ppm (m, 15 H, Ph). ^{13}C NMR: δ = 149.6 (br., BC), 125.9, 126.8, 127.4 130.8, 135.9, 138.8 (Ph), 149.6 (BC) ppm. MS (70 eV): *m*/*z* (%) = 464 (5) [M^+], 449 (15) [M^+ − Me], 387 (35) [M^+ − Ph], 299 (25) [M^+ − BPh_2], 222 (47) [**1**$^+$]. $C_{31}H_{42}B_2N_2$ (464.2): calcd. C 80.19, H 9.12, N 6.03; found C 78.02, H 9.05, N 5.80.

Dibutyl{(*tert*-butyl)[butyl(2,2,6,6-tetramethylpiperidino)boryl]-amino}borane (40): To a hexane solution of **1** (8.80 mL, 0.283 M, 2.5 mmol) at room temperature was added BBu_3 (0.40 g, 2.5 mmol) with a syringe. After stirring for 2 d, the reaction was complete. Volatile materials were then removed in vacuo. The remaining colourless oil of **40** solidified at −78 °C. Yield 0.95 g (94%). ^1H NMR: δ = 0.87−1.24 (several m, Bu) ppm. ^{13}C NMR: δ = 14.4 (Me of Bu), 20.1 (br., BC), 24.0 (br., N_2BC), 26.6, 27.0, 27., 30.2, 34.2 ($BCH_2CH_2CH_2Me$) ppm. $C_{25}H_{54}B_2N_2$ (404.34): calcd. C 74.26, H 13.46, N 6.93; found C 72.97, H 13.03, N 6.77.

9-{(*tert*-Butyl)[methyl(2,2,6,6-tetramethylpiperidino)boryl]-amino}-9-borabicyclo[3.3.1]nonane (41): A solution of **1** (2.5 mmol in 8.9 mL of hexane) at −78 °C was added to 9-methyl-9-borabicyclo[3.3.1]nonane (0.34 g, 2.5 mmol). Within 4 d, a clear solution had formed. Most of the solvent was then removed in vacuo and the solid material isolated by filtration. Yield 0.8 g of **41** (93%), m.p. 82 °C. The product was pure as shown by the NMR spectroscopic data. ^1H NMR: δ = 1.95 (br., 12 H) ppm. ^{13}C NMR: δ = 22.9 (C-α), 23.1 (C-β), 32.5 (C-γ) ppm.

{(*tert*-Butyl)[methyl(2,2,6,6-tetramethylpiperidino)boryl]amino}-dimethylalane (43): A hexane solution of $(AlMe_3)_2$ (0.95 mL, 2.19 M, 1.05 mmol) at −78 °C was added to a stirred solution of **1** in hexane (3.5 mL, 0.586 M, 2.1 mmol). At room temperature, the mixture was stirred for 24 h. The hexane was then removed. The remaining oil could not be distilled without decomposition. Yield 0.58 g of **43** (96%). Due to the high sensitivity of the oil towards moisture and air only an approximate elemental analysis was obtained, while the ^1H NMR spectrum showed the correct intensities for the CMe_3, $AlMe_2$ and BMe groups. The same compound was obtained by using $AlMe_3{\cdot}OEt_2$ instead of Al_2Me_6. Elemental analysis was performed without sufficient protection against the atmosphere. ^1H NMR: δ = −0.11 ($AlMe_2$), 0.78 (BMe) ppm. ^{13}C NMR: δ = 7.0 ($AlMe_2$), 18.9 (br., BMe) ppm. ^{27}Al NMR: δ = 105.9 ($h_{1/2}$ = 780 Hz) ppm. $C_{16}H_{30}AlBN_2$ (294.27): calcd. C 63.11, H 15.53, N 9.53; found C 51.82, H 9.04, N 7.93 (ratio C/H/N = 15:31:2).

{(*tert*-Butyl)[ethyl(2,2,6,6-tetramethylpiperidino)boryl]amino}-diethylalane (44): Prepared in analogy to **43**. $AlEt_3$ (0.38 g, 0.33 mmol) in hexane (3.3 mL), 10.9 mL of a hexane solution of **1** (0.306 mmol). Mobile, air- and moisture-sensitive liquid. Yield 1.11 g of **44** (98%). ^1H NMR: δ = 0.40 [q, $^3J(^1H^1H)$ = 7.3 Hz, 4 H, $AlCH_2$], 0.81−1.19 (m, 5 H, BEt), 1.42 [t, $^3J(^1H^1H)$ = 7.3 Hz, 6 H, $AlCH_2CH_3$] ppm. ^{13}C NMR: δ = 7.9 (br., $AlCH_2$), 10.7 ($AlCH_2CH_3$), 11.5 (BCH_2CH_3), 14.2 (br., BCH_2) ppm. MS (70 eV): *m*/*z* (%) = 336 (2) [M^+] and others. $C_{19}H_{42}AlBN_2$ (336.35): calcd. C 67.85, H 12.59, N 8.33; found C 62.97, H 11.84, N 7.69.

{(*tert*-Butyl)[phenyl(2,2,6,6-tetramethylpiperidino)boryl]amino}-diphenylalane (45): Obtained in analogy to **43**. To $AlPh_3$ (0.26 g, 1.0 mmol, 5 mL hexane) was added a solution of **1** in hexane (4.0 mL, 0.252 M, 1.0 mmol). The mixture was stirred for 4 d and the solid isolated by filtration (0.38 g). From the solution another crop of 0.08 g was obtained by partially removing the hexane. Yield: 0.46 g of **45** (95%), m.p. 168−170 °C (dec.). ^1H NMR ($CDCl_3$):δ = 7.22−8.11 (m, 15 H, Ph) ppm. ^{13}C NMR ($CDCl_3$): δ = 126.8, 126.9, 127.1, 128.7, 134.1, 17.6, 139.2 (Ph) ppm.

 © 2004 Wiley-VCH Verlag GmbH & Co. KGaA, Weinheim

$C_{31}H_{42}AlBN_2$ (480.49): calcd. C 77.49, H 8.81, N 5.83; found C 75.87, H 8.88, N 5.33.

{(*tert*-Butyl)[methyl(2,2,6,6-tetramethylpiperidino)boryl]amino}-dimethylgallane (46): At −78 °C a solution of **1** (10.9 mL, 0.306 M, 3.3 mmol) was slowly added to $GaMe_3$ (0.38 g, 3.3 mmol) with stirring. The mixture was stirred at ambient temperature for 5 d. Removal of the hexane left a colourless, highly air-sensitive mobile oil which proved to be pure **46** by NMR spectroscopy. ^{1}H NMR ($CDCl_3$): δ = −0.12 (6 H, $GaMe_2$), 0.58 (3 H, BMe) ppm. ^{13}C NMR ($CDCl_3$): δ= 3.3 (br., $GaMe_2$), 14.2 (br., BMe) ppm. IR: $\tilde{\nu}$ = 1370 ($\delta_{as}GaMe_2$), 1210 ($\delta_{sym}GaMe_2$) cm^{-1}. MS (70 eV): *m*/*z* (%) = 336 (1) [M$^+$], 321 (100) [M$^+$ − Me]. $C_{16}H_{36}BGaN_2$ (337.01): calcd. C 57.02, H 10.74, N 8.31; found C 61.52, H 10.96, N 7.87.

{(*tert*-Butyl)[ethyl(2,2,6,6-tetramethylpiperidino)boryl]amino}-diethylgallane (47): Obtained from $GaEt_3$ (0.34 g, 2.2 mmol) and **1** (7.2 mL, 0.306 M, 2.2 mmol); 24 h of stirring at ambient temperature. Colourless, mobile liquid, very moisture-sensitive. Due to the high sensitivity of the compound only an unsatisfactory C,H analysis was obtained. ^{13}C NMR ($CDCl_3$): δ = 10.8 (BCH_2CH_3), 11.4, 11.5 (GaEt), 14.0 (br., BCH_2CH_3) ppm. MS (70 eV, ^{11}B, ^{69}Ga): *m*/*z* (%) = 349 (7) [M$^+$ − Et], 239 (5) [tmpGaEt$^+$], 126 (100) [tmp$^+$ − Me]. $C_{19}H_{42}BGaN_2$ (379.09): calcd. C 60.20, H 11.17, N 7.39; found C 59.07, H 7.45, N 7.03.

{(*tert*-Butyl)[phenyl(2,2,6,6-tetramethylpiperidino)boryl]amino}-diphenylindane (48): Triphenylindium−1,4-dioxane (0.95 g, 2.2 mmol) in hexane (15 mL) was treated for 15 min with a hexane solution of **1** (7.2 mL, 0.306 M, 2.2 mmol). After 24 h of stirring, all volatile components were removed in vacuo and the solid **48** crystallised from a minimum amount of hexane. Yield 1.12 g (89%), m.p. 133−135 °C. ^{1}H NMR ($CDCl_3$): δ = 7.37−8.07 (m, Ph) ppm. ^{13}C NMR ($CDCl_3$): δ = 126.5 (*p*-C), 126.9, 127.3 (*p*-, *m*-, *o*-C of BPh); 127.9, 134.0, 138.6 (*p*-, *m*-, *o*-Ph of $InPh_2$), 144.0 (br., *i*-C of BPh), 156.5 (br., *i*-C of $InPh_2$) ppm. MS (70 eV): *m*/*z* (%) = 568 (2) [M$^{\cdot+}$], 491 (5) [M$^+$ − Ph], and many others. $C_{31}H_{42}BInN_2$ (568.32): calcd. C 65.52, H 7.45, N 4.93; found C 53.37, H 7.30, N 4.93.

X-ray Structural Determinations: Single crystals were placed in perfluoro ether oil under a blanket of nitrogen in the case of very sensitive crystals at −40 °C and a suitable crystal was selected. It was mounted on the tip of a glass fibre which was placed on the goniometer head while cooling with a stream of nitrogen, generally held at −80 °C. After alignment, data were collected on five sets of 15 frames each, which were used to determine the unit cell (Program SMART).[48] Data collection was then started (in case of data collection with a CCD device, data on 1200 frames were collected). After data reduction (Program SAINT),[48] the cell parameters were determined with a larger set of data. No absorption correction was applied except in the case of compound **24**. All structures were solved by direct methods (SHELX97).[49] Non-hydrogen atoms were refined anisotropically. In most cases, the hydrogen atoms were placed in calculated positions using the riding-model approach. However, NH, BH and AlH hydrogen positions were taken from the difference Fourier maps and refined isotropically. Relevant data can be found in Table 7. CCDC-221516 to -221520 contain the supplementary crystallographic data for this paper. These data

Table 7. Crystallographic data and information regarding the data collection and structure solutions for compounds **19**, **26**, **31**, **32** and **35**

	19	**26**	**32**	**31**	**35**
Empirical formula	$C_{26}H_{59}N_4Al_2B_2$	$C_{31}H_{43}B_2BSn$	$C_{23}H_{42}N_2OBLi$	$C_{20}H_{34}N_2O_2B_2$	$C_{15}H_{33}N_2BZn$
Formula mass	503.35	573.17	380.34	356.11	317.61
Crystal size [mm]	0.1 × 0.2 × 0.25	0.20 × 0.30 × 0.30	0.21 × 0.10 × 0.30	0.5 × 0.5 × 0.6	0.15 × 0.15 × 0.1
Crystal system	triclinic	orthorhombic	monoclinic	orthorhombic	monoclinic
Space group	$P\bar{1}$	$P2_12_12_1$	$P2_1/n$	$P2_12_12_1$	$P2_1/n$
a [Å]	10.499(4)	9.6974(1)	9.772(8)	19.799(1)	9.5172(2)
b [Å]	11 016(4)	16.0246(1)	13.187(8)	11.4759(1)	17.1486(1)
c [Å]	14.822(8)	18.9810(2)	19.02(1)	9.044(1)	10.8449(1)
α [°]	89.82(2)	90	90	90	90
β [°]	71.75(2)	90	96.40(2)	90	91.459(1)
γ [°]	80.28(1)	90	90	90	90
V [Å]	1603(1)	2949.59(6)	2436(3)	2052.87(2)	1769.39(4)
Z	2	4	4	4	4
ρ (calcd.) [Mg/m^3]		1.291	1.037	1.152	1.192
μ [mm^{-1}]	0.111	0.0887	0.061	0.072	1.379
F(000)	558	1192	840	776	688
Index range	$-12 \le h \le 12$	$-12 \le h \le 12$	$-12 \le h \le 7$	$-22 \le h \le 22$	$-12 \le h \le 11$
	$-12 \le k \le 12$	$-20 \le k \le 20$	$-14 \le k \le 16$	$-13 \le k \le 13$	$-20 \le k \le 19$
	$-16 \le l \le 16$	$-22 \le l \le 24$	$-24 \le l \le 17$	$-9 \le l \le 10$	$-13 \le l \le 13$
2θ [°]	49.42	58.22	57.94	48.80	58.72
T [K]	183(2)	183(2)	183(2)	183(2)	183(2)
Reflections (collected)	7885	17229	6400	9728	10100
Reflections (unique)	4152	6204	4141	3181	3540
Reflections (observed) (4σ)	3482	5962	2646	2973	2969
R (int.)	0.0366	0.0201	0.0548	0.0370	0.0281
Variables	345	324	262	243	181
Weighting scheme *x*/*y*	0.0376/2.4969	0.0166/0.4828	0.0308/1.7488	0.0325/1.5867	0.03550/1.4932
GOOF	1.170	1.056	1.221	1.157	1.137
Final *R* (4σ)	0.0713	0.0193	0.0807	0.0615	0.0414
Final *wR*2	0.1497	0.0413	0.1422	0.1264	0.0879
Largest residual peak [e/Å^3]	0.492	0.220	0.166	0.234	0.466

 © 2004 Wiley-VCH Verlag GmbH & Co. KGaA, Weinheim

can be obtained free of charge at www.ccdc.cam.ac.uk/conts/retrieving.html [or from the Cambridge Crystallographic Data Centre, 12 Union Road, Cambridge CB2 1EZ, UK; Fax: (internat.) + 44-1223-336-033; E-mail: deposit@ccdc.cam.ac.uk].

[1] P. Paetzold, *Adv. Inorg. Chem. Radiochem.* **1987**, *31*, 123−170.
[2] H. Nöth, *Angew. Chem.* **1988**, *100*, 1664−1684, *Angew. Chem. Int. Ed. Engl.* **1988**, *7*, 1603−1623.
[3] P. Paetzold, A. Richter, T. Thijssen, S. Würtemberg, *Chem. Ber.* **1979**, *112*, 3811−3827.
[4] H. Nöth, S. Weber, *Z. Naturforsch., Teil B* **1983**, *38*, 1460−1465.
[5] D. Männig, H. Nöth, M. Schwartz, S. Weber, U. Wietelmann, *Angew. Chem.* **1985**, *99*, 979−981, *Angew. Chem. Int. Ed. Engl.* **1985**, *24*, 998−999.
[6] E. Bulak, T. Varnah, P. Paetzold, U. Englert, *Z. Allg. Anorg. Chem.* **1999**, *625*, 3−15.
[7] H. Braunschweig, I. Manners, P. Paetzold, *Z. Naturforsch., Teil B* **1990**, *5*, 1453−1454.
[8] U. Wietelmann, PhD Thesis, University of Munich, **1986**.
[9] J. Chandrasekharan, H. C. Brown, *J. Org. Chem.* **1985**, *50*, 5181−5187.
[10] H. C. Brown, J. Chandrasekharan, D. J. Nelson, *J. Am. Chem. Soc.* **1984**, *106*, 3768−3771.
[11] H. C. Brown, S. H. Gupta, *J. Organomet. Chem.* **1971**, *32*, C1−C3.
[12] H. C. Brown, G. J. Klender, *Inorg. Chem.* **1962**, *1*, 204−214.
[13] H. C. Brown, E. F. Knights, *J. Am. Chem. Soc.* **1968**, *90*, 5281−5283.
[14] H. C. Brown, J. J. Katz, E. Negishi, *J. Am. Chem. Soc.* **1972**, *94*, 4025−4027.
[15] E. Negishi, H. C. Brown, *Synthesis* **1972**, 196−197.
[16] H. C. Brown, E. Negishi, *J. Am. Chem. Soc.* **1967**, *89*, 5285−5287.
[17] Bond dissociation energies could be a reason for the 50:50 ratio for **15/17**: Δ_{diss} [kJ/mol]: B−H 380.4, B−Cl 443.0, B−Br 367.8; see W. L. Jolly, *Modern Inorganic Chemistry*, McGraw Hill, New York, **1984**.
[18] H. Nöth, S. Weber, *Chem. Ber.* **1985**, *118*, 2554−2556.
[19] H. Nöth, W. Rattay, U. Wietelmann, *Chem. Ber.* **1987**, *120*, 859−861.
[20] U. Braun, T. Habereder, H. Nöth. *Z. Naturforsch.*, manuscript accepted.
[21] U. Braun, T. Habereder, H. Nöth, *Eur. J. Inorg. Chem.*, manuscript submitted.
[22] B. Böck, PhD Thesis, University of Munich, **1989**.
[23] N. M. Yoon, Y. S. Gyoung, *J. Org. Chem.* **1985**, *50*, 2443−2450.
[24] H. Nöth, H. Suchy, *Z. Anorg. Allg. Chem.* **1966**, *344*, 44−66.
[25] H. Nöth, B. Wrackmeyer, "Nuclear Magnetic Resonance Spectroscopy of Boron Compounds", vol. 14 of *NMR, Basic Principles and Progress* (Eds.: P. Diehl, E. Fluck, R. Kosfeld), Springer Publishers, Berlin, Heidelberg, New York, **1978.**
[26] H. Nöth, S. Weber, *Z. Naturforsch., Teil B* **1983**, *38*, 1460−1464.
[27] M. Hesse, H. Meier, B. Zeeh, *Spektrokopische Methoden in der Organischen Chemie*, 3rd ed., Thieme Verlag, Stuttgart, New York, **1987**.
[28] T. Habereder, H. Nöth, *Eur. J. Inorg. Chem.* **2001**, 1665−1669.
[29] H. Strasdeit, I. Büsching, A.-K. Duhme, S. Pohl, *Acta Crystallogr., Sect. C* **1993**, *49*, 567−578.
[30] X-ray structural data of $C_{12}H_{10}Cd$ (266.60), colourless prism, monoclinic, space group $P2_1/n$, cell axes and angles: a = 5.6664(7), b = 8.8080(7), c = 10.492(1) Å, β = 96.163(2)°, V = 477.5(1) Å^3, Z = 2, μ = 2.230 mm^{-1}, d = 1.854 Mg/m^3, F(000) = 260, T = 193 K, Index ranges: $-6 \le h \le 6$, $-10 \le k \le 10$, $-12 \le l \le 12$, reflections (collected) 2682, reflections (independent) 940 (4σ), max./min. transmission 0.746/0.589, variables 61, data/parameter ratio = 15.4:1, $R1$ = 0.0285, $wR2$ = 0.0719, largest difference peak 0.439 e/Å^3. Bond lengths [Å] and bond angles [°]: Cd1−C1 2.124(3), C1−C2 1.381(5), C2−C3 1.400(5), C3−C4 1.377(5), C4- C5 1.382(5), C5−C6 1.387(5), C6−C1 1.401(6). C1−Cd1−C1A 180, C2−C1−C6 116.4(3), Cd1−C1−C2 123.2(3), Cd1−C1−C6 120.2(3).
[31] D. Grdenič, B. Kamenar, A. Nagl, *Acta Crystallogr., Sect. B* **1977**, *33*, 587−589.
[32] N. A. Bell, H. M. Shearer, C. D. Spencer, *Acta Crystallogr., Sect. C* **1983**, *39*, 1182−1185.
[33] G. D. Coates, D. Ridley, *J. Chem. Soc.* **1965**, 1870−1877.
[34] P. Paetzold, C. Pelzer, R. Boese, *Chem. Ber.* **1988**, *121*, 51−59.
[35] U. Braun, T. Habereder, H. Nöth, H. Piotrowsky, M. Warchhold, *Eur. J. Inorg. Chem.* **2001**, 1132−1145.
[36] H. Chen, R. A. Bartlett, M. M. Olmstead, P. P. Power, S. C. Shone, *J. Am. Chem. Soc.* **1990**, *112*, 1049−1055.
[37] R. A. Bartlett, H. Chen, H. V. Rasika Dias, M. M. Olmstead, P. P. Power, *J. Am. Chem. Soc.* **1988**, *110*, 446−449.
[38] H. Chen, R. A. Bartlett, M. M. Olmstead, P. P. Power, S. C. Shoner, *J. Am. Chem. Soc.* **1990**, *112*, 1048−1955.
[39] T. Seifert, W. Storch, M. Vosteen, *Eur. J. Inorg. Chem.* **1998**, 1343−1349.
[40] F. Schindler, H. Schmidbaur, G. Jonas, *Chem. Ber.* **1965**, *98*, 3345−3352.
[41] Houben-Weyl, *Methoden der Organischen Chemie*, Thieme Verlag, Stuttgart, **1978**, vol. 13/14.
[42] M. Martin, Diploma Thesis, University of Munich, **1956**.
[43] H. C. Brown, D. B. Bigley, S. K. Arora, N. M. Yoon, *J. Am. Chem. Soc.* **1970**, *92*, 7161−7167.
[44] H. C. Brown, A. K. Mandal, S. U. Kalkarni, *J. Org. Chem.* **1972**, *42*, 1392−1398.
[45] H. C. Brown, N. Ravindran, S. U. Kulkarni, *J. Org. Chem.* **1979**, *44*, 2417 −2421.
[46] H. C. Brown, N. Ravindran, *Inorg. Chem.* **1977**, *16*, 2938−2940.
[47] H. C. Brown, *Boranes in Organic Chemistry*, Cornell University Press, Ithaca, New York, **1972**.
[48] *SMART*, *SAINT*, Siemens Analytical Instruments, Madison, Version 4.1.
[49] G. W. Sheldrick, University of Göttingen, **1997**.

Received November 5, 2003
Early View Article
Published Online July 6, 2004

 © 2004 Wiley-VCH Verlag GmbH & Co. KGaA, Weinheim

Lithium *tert*-Butyl[phenyl(2,2,6,6-tetramethylpiperidino)boryl]amide: A Versatile Reagent[‡]

Ulrike Braun,[a] Tassilo Habereder,[a] and Heinrich Nöth*[a]

Dedicated to Professor Nils Wiberg on the occasion of his 70th birthday

Keywords: Lithium *tert*-butyl[phenyl(2,2,6,6-tetramethylpiperidino)boryl]amide / *N*−Metal borylamides

A new synthesis of tmp(PhB)N(*t*BuNLi) (**1**, tmp = 2,2,6,6-tetramethylpiperidino) is presented. Compound **1** reacts with many group 13–15 halides, as well as with BH_3·THF, to afford, in most cases, compounds of the type tmp(PhB)N*t*Bu–ER_{n-1} (E = B, Al, Ga, In, Ge, Sn, P, As, Sb, and R = H, Me, Hal). The borane, alane, gallane and indane derivatives have cyclic structures, as shown by X-ray structure determinations, whereas ER_{n-1} = $GeCl_3$, $SnMe_3$, $SnMe_2Cl$, SnCl, catecholatophosphanyl, $AsCl_2$ and $SbCl_2$ are noncyclic, although the arsane and stibane derivatives show weak intramolecular E–N coordination to the tmp–N atom.

(© Wiley-VCH Verlag GmbH & Co. KGaA, 69451 Weinheim, Germany, 2004)

Introduction

Although *N*-lithioaminoboranes are well known and have been used in the synthesis of various types of aminoboranes, those of type **B** can be compared with amidines (**A**) and amidates (**C**); solid-state structures of their alkali metal salts of the latter are available.[2−5] The first structurally characterized amidine was the trimethylsilyl derivative $PhC(=NSiMe_3)N(SiMe_3)_2$.[6] Since then, the chemistry of amidines and amidinates has been extended into transition metals chemistry.[7,8] It is, therefore, of interest to compare the chemistry of alkali metal compounds containing type **B** anions with that of the carbon analogs. The former can also be seen as a special type of N−metal borylamides.

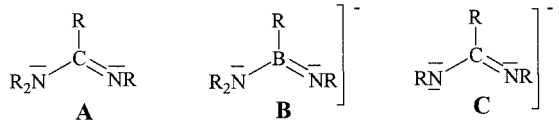

The structures of *N*-lithioborylamides[9−13] have been determined relatively recently, although some were used as reagents much earlier. The first reaction of an *N*-lithioaminoborane was reported by Dewar at al.[14] [Equation (1)]. Borazinylborazines have been obtained from N-lithioborazines and chloroborazines by Wagner and Bradford,[15] while both symmetrically and asymmetrically substituted diborylamines resulted from reactions of $R_2B-NR'Li$ and R''_2BCl.[16] Moreover, by using $PhB(NRLi)_2$ [17] a series of four-membered rings containing metal atoms, $M(NR)_2BPh$, as well as spirocyclic compounds, $M[(NR)_2BPh]_n$, have been obtained.[18] As reported in the preceding paper, many asymmetrically substituted diborylamines and metallated diaminoboranes of the type tmp−BX−$NCMe_3$−EX_{n-1} (tmp = 2,2,6,6-tetramethylpiperidino, E = B, Al, Ga, In, Si, Sn, Li, Mg, Zn, Cd; X = H, Me, Bu, Ph, Cl, Br) are accessible.[1] Among these is the stable lithium borylamide tmp−BPh−$NCMe_3Li$·OEt_2 (**1**), which offered itself as a reagent for further synthesis. The anion **B** of this compound is isoelectronic and isolobal with **A**.

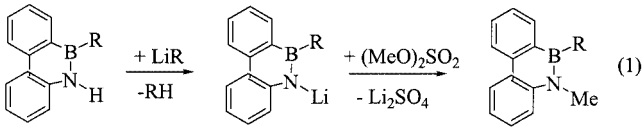

Results

Reactions of tmp−BPh−N(CMe$_3$)Li with Group 13 Compounds

Although the lithium compound **1** can be readily prepared by the addition of LiPh to the aminoiminoborane tmp−B=N−CMe_3 [1] we were looking for a more convenient synthesis, circumventing the isolation of the amino-

[‡] Contribution to the Chemistry of Boron, 254. Part 253: Ref.[1]

[a] Department of Chemistry, University of Munich, Butenandtstr. 5−13, 81377 München, Germany
E-mail: H.Noeth@lrz.uni-muenchen.de

iminoborane. Consequently, we developed a one-pot synthesis of **1** according to Equation (2). Yields are almost quantitative, and the resulting suspension of LiCl in the solution of **1** can be used directly for further synthesis.

The reaction of **1** with BH_3·THF in THF requires 2 equivalents of the borane reagent as the LiH formed as an intermediate reacts with the borane component to produce $LiBH_4$ [Equation (3)].[19] A 1:2 stoichiometry is also necessary for the quantitative conversion of **1** into the difluoroborane derivative **3**. The cyclic nature of **2** and **3** is proven by two ^{11}B NMR signals for a tricoordinate and a tetracoordinate boron atom as well as by X-ray structure determinations (see below).

Although boron halides cleave the CO bonds of ethers, no ether cleavage was observed in the reaction of **1** with *B*-(chloro)catecholborane, see Equation (4). The resulting borylated diaminoborane **4** is cyclic, as evidenced by ^{11}B NMR spectroscopy and the determination of its molecular structure. However, **1** did not react at ambient temperature with $tmpBCl_2$, tBuNHBCl_2, 2,4,6-trichloroborazine, and tB$uBCl_2$ in non-polar solvents.

Dimethylchloroalane, -gallane and -indane are dimeric in nonpolar solvents and may, therefore, be less likely to be attacked by **1** as a nucleophile. However, in the presence of diethyl ether, mononuclear species $Me_2ECl\ OEt_2$ form that may react with **1**. Indeed, reactions according to Equation (**7**) proceed readily to yield compounds **7**–**9**, all of which were shown to be cyclic by NMR spectroscopic data and X-ray structure determinations.

To synthesize noncyclic tmp–BPh–$NCMe_3$–AlX_2 compounds we treated the bulky monomeric bis(amino)chloroalane tmp_2AlCl [20] with **1**. The reaction was expected to proceed according to Equation (5). However, the only product we could isolate, in very low yield, was compound **8**, the tmpH solvate of tmp–BPh–$NCMe_3Li$. No LiCl precipitated.

After refluxing the mixture, the ^{11}B NMR spectrum exhibits a new signal at $\delta = 35.7$ ppm in addition to that of **1** in a 1:1 ratio, and a new broad ^{27}Al signal at $\delta = 82$ ppm. The isolated compound **6** shows practically the same NMR spectroscopic data as **1**, with additional signals for tmpH in the ^1H NMR spectrum.

Because the reaction was performed under strictly anhydrous conditions, we exclude the formation of tmpH by hydrolysis of tmp_2AlCl. Therefore, we assume that tmpH is formed by ether cleavage, as suggested in Equation (6). To test this hypothesis we kept an ether solution of tmp_2AlCl under reflux. While tmp_2AlCl shows a ^{27}Al NMR signal in

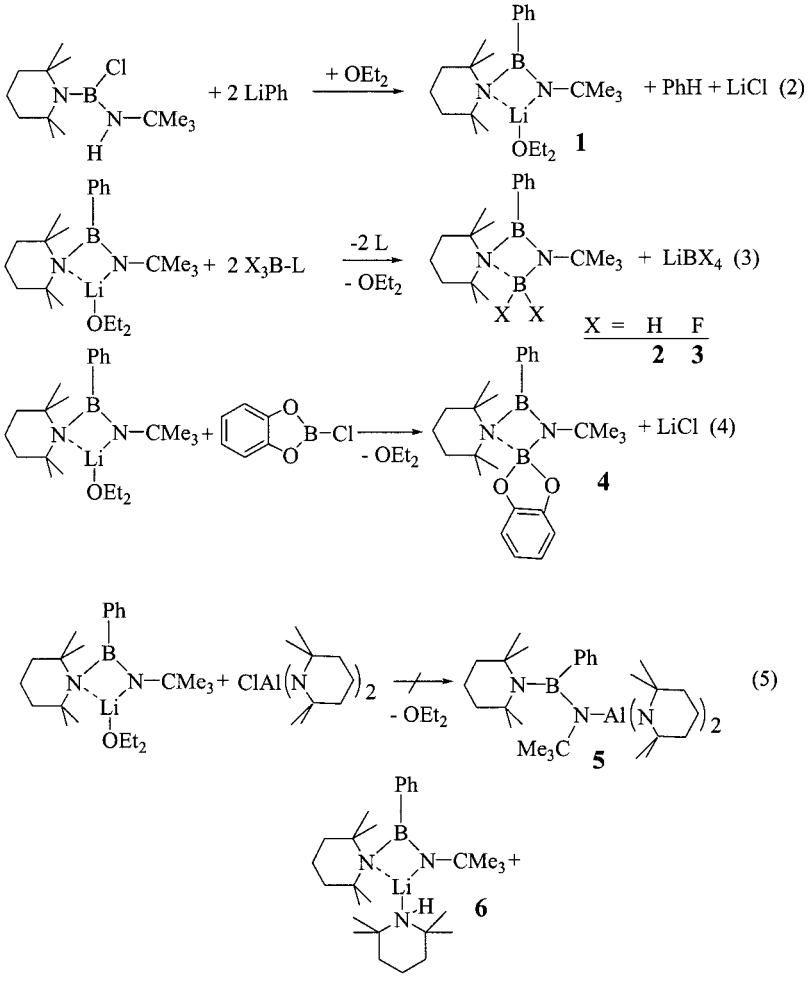

$$(tmp)_2AlCl + OEt_2 \longrightarrow tmpAl(Cl)OEt + tmpH + C_2H_4 \quad (6)$$

 © 2004 Wiley-VCH Verlag GmbH & Co. KGaA, Weinheim

hexane at δ = 134 ppm, ($h_{1/2}$ = 13 700 Hz), the ether solution, after heating for some time, exhibits two additional signals at δ = 112.8 and 82 ppm. The first of these results from $tmp_2AlCl{\cdot}OEt_2$,[21] while the second corresponds with dimeric tmpAl(OEt)Cl.[22] Although pure compounds could not be isolated, the data indicate that the assumption of ether cleavage by tmp_2AlCl is not unjustified.

We have not yet studied the interaction of **1** with $AlBr_3$, $GaCl_3$ and $InCl_3$ to see whether more than one halogen atom can be replaced by the anion of **1** in the formation of chelates where the coordination number of the metal atom could increase up to six.

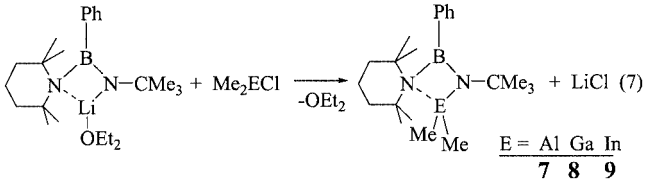

Spectra

Table 1 summarizes the ^1H, ^{11}B and ^{13}C NMR spectroscopic data of compounds **2**–**4** and **6**–**9**. Compound **6**, which is akin to **1**, shows a sharper ^{11}B signal than **1**, and a somewhat deshielded boron nucleus. Protons of the CMe_2 groups of the tmp substituent are better shielded than those of the coordinated tmpH molecule, although both nitrogen atoms are tetracoordinate. Proton signals of the CH_2 groups overlap (H2,3,4), while in **1** the protons at C2/4 and C3 are nicely separated triplets and multiplets.[1] Moreover, there is only one set of ^{13}C resonance each for the two tmp units in **6**. Thus, in solution the molecule is fluxional.

^{11}B resonances of the tricoordinate boron atom of **2**–**4** are shifted to lower field compared with **1**. This mirrors the influence of the charge withdrawal from the BN bonds as the substituents at the tetracoordinate B atom become more electronegative. The coupling constants $^1J(^{11}B^1H)$ and $^1J(^{19}F^{11}B)$ are similar to those in the corresponding 1,3,2,4-diazadiboretines.[23] Moreover, the difference in chemical shifts for the two ^1H and ^{13}C resonance of atoms H6,7 and C6,7 increases from **2** via **3** to **4**. The data confirm that the cyclic nature of these compounds is retained in solution.

Conversely, the ^{11}B shielding for the PhB boron atom is almost uninfluenced by the heteroatoms Al, Ga, and In in **7**–**9**. For the indium compound **9**, only a single resonance appears in the ^1H and ^{13}C NMR spectrum for H6,7 and C6,7, respectively. This indicates that, in solution, the In1–N1 bond is opened, while it is present in the solid state. That its structure in solution differs from that of **7** and **8** becomes apparent from the low field ^{13}C resonance of atoms C1,5. This deshielding is still noticeable for C2/4 and C3.

The fragmentation of compounds **2** and **3** in the mass spectrum starts from the molecular ion, which has a 100% relative intensity for the boron hydrogen compound **2**, but only 4.5% for the fluoroborane derivative **3**. In both cases, a methyl group is lost in a first step, which most likely comes from breaking the respective bond at the tmp unit (62 and 100% relative intensity, respectively). Strong peaks appear for ions ($M^+ - CMe_3$) (28 and 82%). Moreover, ions derived from the imino borane are also readily detected, as shown by fragments $tmp{-}B{=}NCMe_3^{+\cdot}$, $tmpB{-}Ph^+$, and $PhB{=}NCMe_3^+$. Loss of a tmp radical from $M^{\cdot+}$ can also be noted.

Fragmentation of the Al and Ga compounds **7** and **8** is characterized by strong peaks for the [M^+ − Me] ions (100 and 43%, respectively) where the E–C bonds of Al and Ga are broken. In addition, a [$M^+ - CMe_3$] peak appears for **7** (21.5%) but not for **8**. Also, fragments [$tmp{-}EMe^+$] are observed (100%, 42%), showing the preferred formation of $Me_3C{-}N{=}B{-}Ph$ in the fragmentation process, which is a stable leaving group. In contrast, fragmentation to give [$tmp{-}B{-}Ph^{\cdot+}$] is less favored because this would generate molecules $MeE{=}NCMe_3$, which are, most likely, not as stable as an imino borane unit.

Molecular Structures

The molecular structures of **2**–**4** and **6**–**9** were determined by X-ray structure analysis. Table 2 contains selected and relevant structural parameters. The molecular structures of **2**–**4** and **6**–**8** are depicted in Figure 1–6, respectively; data for compound **1** are added for comparison with **1·tmpH** (= **6**). In all cases, these compounds feature a four-membered ring.

Table 1. NMR spectroscopic data of compounds **2**–**4** and **6**–**9;** δ in ppm, coupling constants and line widths in Hz

	$\delta^{11}B$	δ^1H H2,4,3	H6,7	CMe_3	$\delta^{13}C$ C1,5	C2,4	C3	C6,7	C10	C11–13
BH_2, **2**	32.7, −4.3 t[a]	1.25–1.50 m	1.39, 1.70	1.23	57.5	37.0	17.1	27.0, 30.4	50.6	31.0
BF_2, **3**	35.7, 4.8 t[b]	1.28–1.56 m	1.49, 1.70	1.26	58.3	38.2	16.9	26.9, 31.9	51.5	32.0
CatB, **4**	35.9, 13.4	1.08–1.52 m	1.21, 1.91	1.17	57.7	38.1	16.9	27.2, 38.1	51.3	31.8
LitmpH, **6**	35.5	1.18–1.68 m	1.06, 1.29,	1.00	58.2, 59.3	38.1, 38.4	16.1, 18.6	33.3, 33.4	49.4	31.8
$AlMe_2$, **7**	36.5[c]	1.30–1.53 m	1.29, 1. 69	1.11	56.3	36.3	17.0	30.5, 32.8	51.1	33.6
$GaMe_2$, **8**	36.7[d]	1.28–1.57 m	1.25, 1.69	1.10	56.2	36.2	17.3	30.9, 32.8	51.7	33.7
$InMe_2$, **9**	35.0[e]	1.55 t, 1.69 m	1.20	1.00	65.9	38.1	18.9	37.5	52.4	33.4

[a] $^1J(^{11}B^1H)$ = 107. [b] $^1J(^{19}F^{11}B)$ = 48. [c] $h_{1/2}$ = 183. [d] $h_{1/2}$ = 137. [e] $h_{1/2}$ = 234.

 © 2004 Wiley-VCH Verlag GmbH & Co. KGaA, Weinheim

Table 2. Selected bond lengths (Å) and bond angles (°) of **2**−**4** and **6**−**9**

Compound	**1**·OEt_2	**1**·tmpH (**6**)	**2**	**3**	**4**	**7**	**8**	**9**
B1−N1 (Å)	1.564(4)	1.571(4)	1.593(4)	1.588(4)	1.584(2)	1.600(4)	1.593(3)	1.580(4)
B1−N2	1.361(4)	1.371(4)	1.370(3)	1.376(3)	1.369(2)	1.380(4)	1.377(3)	1.375(3)
B1−C14	1.617(4)	1.617(3)	1.586(3)	1.587(4)	1.583(2)	1.597(5)	1.596(4)	1.606(4)
N1−C1	1.528(3)	1.503(3)	1.539(2)	1.551(2)	1.547(2)	1.539(3)	1.544(3)	1.528(3)
N1−C5	1.526(3)	1.496(3)	1.539(2)	1.551(3)	1.552(2)	1.551(3)	1.532(3)	1.526(3)
N2−E	1.884(5)	1.883(5)	1.555(3)	1.523(4)	1.512(2)	1.869(2)	1.935(2)	2.137(2)
N1−E	2.085(6)	2.157(4)	1.665(3)	1.689(3)	1.741(3)	2.078(2)	2.175(2)	2.376(2)
N2−C10	1.467(4)	1.460(3)	1.463(3)	1.475(3)	1.483(2)	1.483(3)	1.474(3)	1.476(4)
X−E (X=O, C)	1.929(5)	2.155(5)	1.15(2)	1.383(2)	1.460(2)	1.977(3)	1.990(3)	2.170(3)
N1−B1−N2 (°)	112.9(2)	113.6(2)	96.8(2)	97.2(2)	86.2(1)	105.7(2)	106.6(2)	109.3(2)
N1−B1−C14	120.9(3)	124.7(2)	130.3(2)	130.7(2)	130.3(1)	126.0(2)	125.7(2)	125.1(2)
N2−B1−C14	126.1(3)	124.8(3)	132.8(2)	132.2(2)	131.8(2)	128.3(2)	127.6(2)	125.6(3)
B1−N2−E	91.6(2)	93.4(2)	93.9(2)	94.2(2)	95.8(1)	97.2(2)	98.9(2)	100.7(2)
B1−N1−E	78.9(2)	78.2(2)	82.1(2)	80.9(2)	80.0(1)	82.8(2)	83.3(2)	85.5(1)
N1−E−N2	75.7(2)	74.9(2)	87.2(2)	87.7(2)	86.2(1)	73.92(9)	70.8(1)	64.39(7)
B1−N2−C10	129.7(2)	129.2(2)	137.3(2)	136.2(2)	135.4(1)	131.4(2)	132.6(2)	131.9(2)
E−N2−C10	138.5(3)	137.3(2)	128.8(2)	129.6(2)	128.7(1)	131.1(2)	128.1(2)	127.3(2)
C1−N1−C5	116.2(2)	115.0(2)	114.5(2)	114.2(4)	114.2(1)	113.0(2)	113.3(2)	114.2(2)
X−E−X			112.6(2)	107.3(2)	105.7(1)	105.9(4)	109.6(3)	114.0(1)

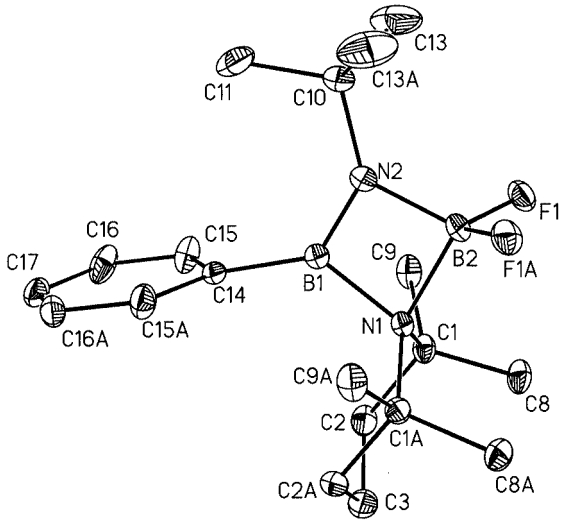

Figure 1. Molecular structure of compound **2**

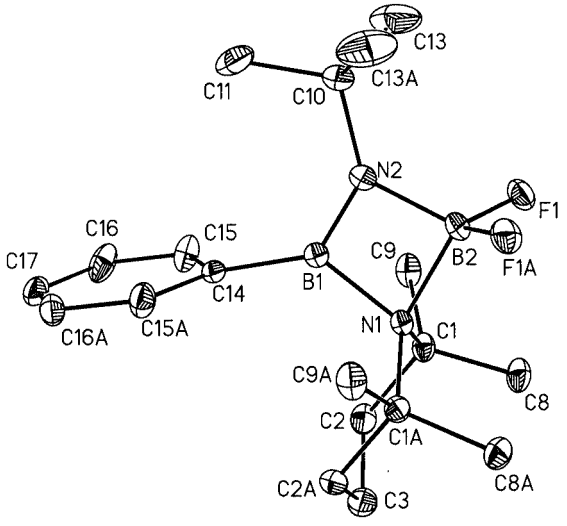

Figure 2. Molecular structure of compound **3**

B1, B2, N1, N2, C14, C17, C10 and C13 of compounds **2** and **3** sit on a mirror plane in the orthorhombic unit cell. The four-membered ring is planar and the phenyl group as well as the C1−N1−C1A unit of the chair-shaped tmp ring stand orthogonal to the ring plane. The B2−N1 bond length of the tetracoordinate atoms increase in the order $BH_2 < BF_2 <$ Bcat. This can be attributed to inductive effects, which are also mirrored in the B2−N2 bond length (H > F > OR). As expected, the B1−N2 bond is shorter, by about 0.2 Å, than the B1−N1 bond because the bond to N1 is a single bond to a tricoordinate boron atom. Moreover, the B2−N1 bond is even longer in both compounds [1.665(3) and 1.689(3) Å, respectively]. Compound **3** is isostructural with **2**; its B1−N1 bond is shorter than in **2** by

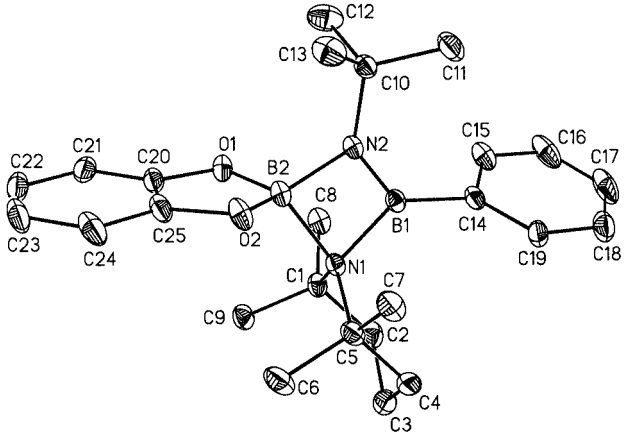

Figure 3. Molecular structure of compound **4**

 © 2004 Wiley-VCH Verlag GmbH & Co. KGaA, Weinheim

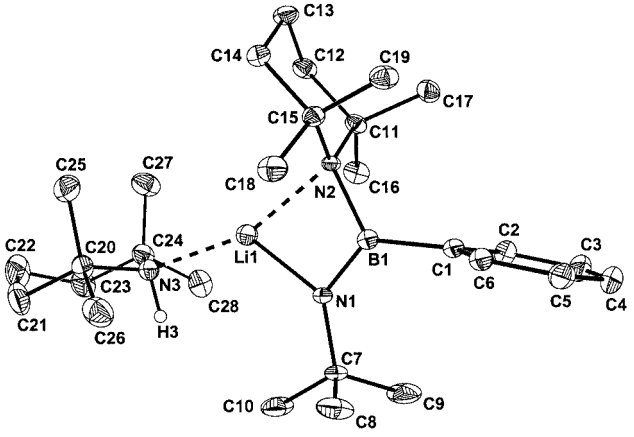

Figure 4. Molecular structure of compound **6**

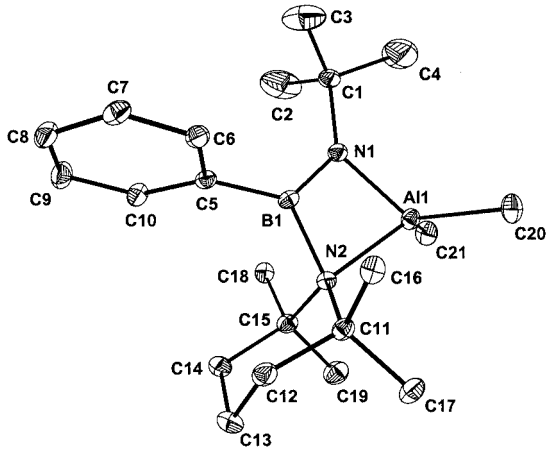

Figure 5. Molecular structure of compound **7**

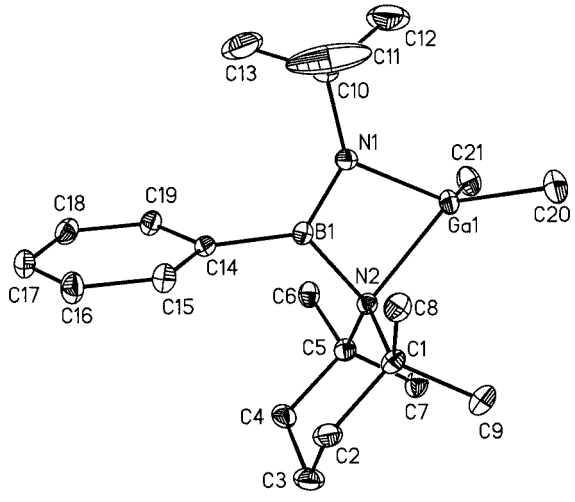

Figure 6. Molecular structure of compound **8**

0.006 Å but the B1−N2 bond is 0.009 Å longer. The B2−N2 bond is significantly shorter [1.523(4) Å] in **3** than in **2** [1.555(3) Å]. Bond angles at the boron atoms in these two compounds are more open than at the nitrogen atoms, and the N−B−N bond angle at the tetracoordinate boron atom is almost 10° smaller than at the tricoordinate boron atoms B1.

While the B1−N1 bond lengths decrease by 0.019 Å when moving from the aluminium compound **7** to the indium compound **9**, the B1−N2 bond lengths remain unaffected by the heavy group 13 atoms. However, the effect of these atoms leads to a shrinking of the N1−C1/5 bonds on moving from Al to In. There is a wider N1−B1−N2 bond angle for the indium compound [109.3(2)°] than in the aluminum derivative [105.9(3)°]; this can be attributed to the lengthening of the E−N1 bond from 2.079(3) Å in **7** to 2.376(2) Å in **9**.

As expected, the E−N2 bond lengths for the pair **7**/**9** also increase, but the difference is larger (0.298 Å) than for E−N1 (0.268 Å).

The four-membered ring of **7** is not planar. The molecule shows an interplanar N1−B1−N2/N1−Al1−N2 angle of 6.3°. In contrast, the ring of **8** is planar; nevertheless, its phenyl group is not perpendicular to the N1B1N2 plane but is twisted about the B1−C14 bond by 74.3°. The same twisting is found for the indium compound **9**. While the C_2E (E = Al, Ga, In) units stand orthogonal or almost perpendicular to the N1−E−N2 plane the C1−N1−C5 planes deviate from orthogonality with respect to the B1−N1−E plane by 4° for **7** and by 3.4° for **9**.

Reactions of tmp−BPh−N(CMe$_3$)Li with Group 14 Compounds

Particularly for steric reasons, the reactions of **1** with halides of group 14 should be less favored than with group 13 halides. Indeed, neither Me_3SiCl nor Ph_3SiCl reacted with **1**. However, $SiCl_4$, a stronger Lewis acid than the R_3SiCl compounds, reacts according to Equation (8) with the formation of tmp−BPh−N*t*Bu−$SiCl_3$. Such compounds can also be obtained from tmp−BPh(Cl) and LiN(CMe$_3$)(SiMe$_3$) in the presence of toluene [Equation (9)]. However, in addition to **10**, tmpBPh(Tol) is formed [Equation (10)]. The two compounds could not be separated by crystallization. Obviously, Li(tol) results from the solvent toluene that is metallated by the lithium amide, a not uncommon reaction.[24]

Like Me_3SiCl, the methylhalogermanes Me_3GeCl and Me_3GeBr are unreactive towards **1**, but $GeCl_4$, like $SiCl_4$, afforded the trichlorogermyl derivative **11** [Equation (11)], but reflux conditions in hexane are required. In contrast, **1** and Me_3SnCl interact easily to produce the trimethylstannyl derivative **12**, and reaction with Me_2SnCl_2 afforded compound **13**. However, an attempt to use Me_2SnCl_2 to attach two diaminoborane units to the Me_2Sn fragment [Equation (13)] was not successful − only monosubstitution was observed. In addition, on heating, decomposition occurred to give the diazadiboretidine (tmpB−N*t*Bu)$_2$, which was detected by ^{11}B NMR spectroscopy.[23] All these metallated diaminoboranes of type tmp−BPh−N*t*Bu−EX_n (E = Ge, Sn), **11**−**13**, are noncyclic (see below). No reactions were noted between **1** and Ph_3GeCl, Ph_3SnCl, and Ph_3PbCl in the presence of hexane, most likely due to steric reasons.

 © 2004 Wiley-VCH Verlag GmbH & Co. KGaA, Weinheim

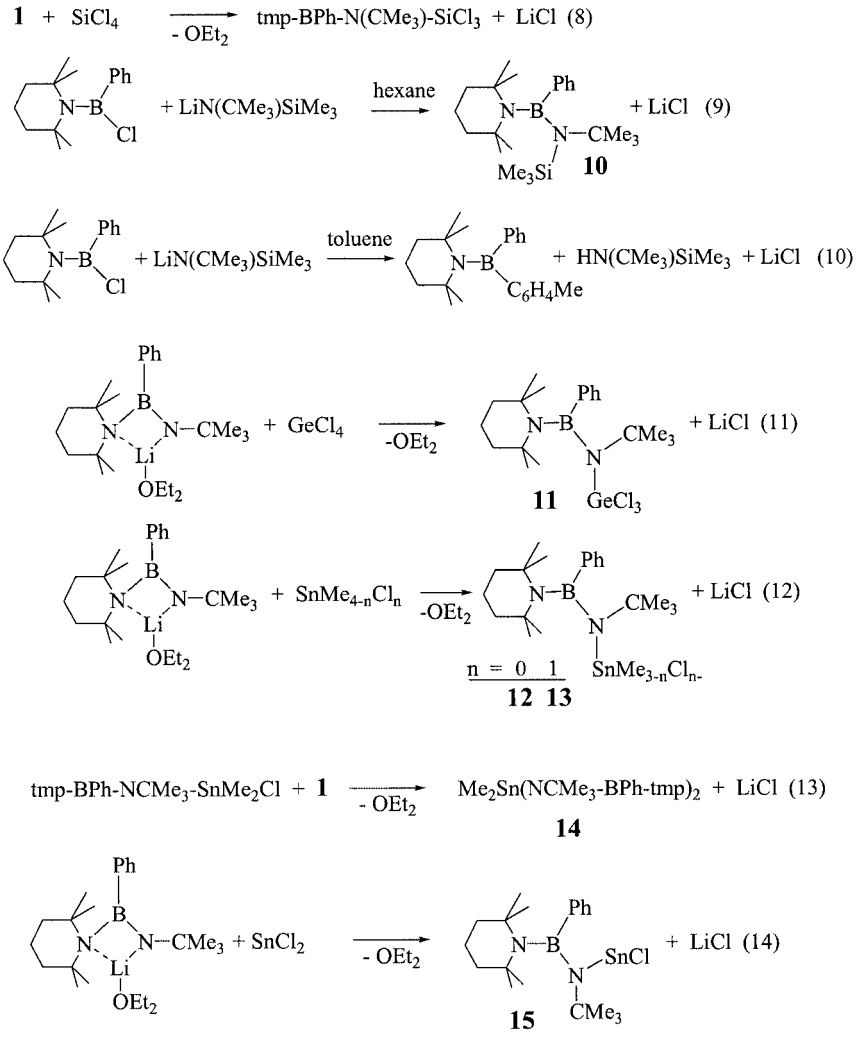

Similarly, only a single Cl atom of $SnCl_2$ could be replaced by the tmpBPh−N*t*Bu group [Equation (14)]. No ^{119}Sn resonance signal was detected for **15**, but $\delta^{11}B = 38.0$ ppm agrees with a metallated diaminoborane. In the gas phase, no mass higher than M^+ was found for **15**, suggesting that the compound is most likely monomeric in solution. No single crystals could be obtained, and, therefore, it was not possible to determine its solid-state structure.

NMR Spectra

In the NMR data of **11**−**13** and **15** (Table 3) the shielding of the ^{11}B nuclei is practically identical and at lower field than with the cyclic species **2**−**9**. In contrast to the latter, the N1 atoms reside in a planar environment and, therefore, can be considered to be sp^2 (see below). Since there are two NMR signals for the CMe_2 groups in the ^1H and ^{13}C NMR spectra there must be a hindered rotation about the B1−N1 bond. Indeed, the interplanar angle CN1C5/N1B1N2 is only 30° for the $GeCl_3$ compound; these angles are 118.3° and 117.7° for the tin compounds **12** and **13**. Therefore, B1−N1 π-bonding should not be pronounced in **12** and **13**. For **11** there may be hindered rotation about the B1−N1 bond due to steric hindrance. Cl substitution at Ge and Sn leads to a deshielding of the protons of the *t*Bu groups but this is not reflected in the ^{13}C resonances of either C10 or C11 to C13. In particular, the ^{13}C resonances for C1 and C5 fall in the same range as those for the cyclic species; however, those of C6/7 seem to be less well shielded. Thus, these data do not allow us to decide whether these compounds are cyclic or noncyclic. However, $\delta^{119}Sn$ for **12** and **13** are $\delta = 17.9$ and 93.1 ppm, indicating the presence of a tetracoordinate tin atom.[25] In particular, the tin resonance of **13** falls well within the range found for similar compounds [13,25] while the ^{119}Sn resonance of **12** corresponds well with that of $Me_3Sn(tBu)N-BH-tmp$ ($\delta^{119}Sn$ = 27.4),[21] 2-[trimethylsilyl(trimethylstannyl)amino]pyridine ($\delta^{119}Sn$ = 10.2 ppm),[26] and 8-[bis(trimethylstannyl)amino]-quinoline ($\delta^{119}Sn$ = 26.4).[27] Unfortunately, we were unable to record a ^{119}Sn spectrum for the tin(II) compound **15**. Since its ^1H, ^{11}B and ^{13}C NMR spectroscopic data are rather similar to those of the other two tin compounds we assume that this molecule is not associated (e.g. dimeric or trimeric). In accord with this, its mass spectrum shows the parent peak as the highest mass.

 © 2004 Wiley-VCH Verlag GmbH & Co. KGaA, Weinheim

Table 3. NMR spectroscopic data of **11**−**13** and **15**−**18**; δ (ppm), line widths $h_{1/2}$ (Hz)

	$\delta^{11}B$	$\delta^{1}H$ H2,4,3	H6,7	CMe_3	$\delta^{13}C$ C1,5	C2,4	C3	C6,7	C10	C11−13
$GeCl_3$,**11**	39.4 [a]	1.46−1.58 m	1.35, 1.41	1.21	56.8	38.8	15.9	34.2, 35.1	51.6	33.8
$SnMe_3$, **12**	39.8 [b]	1.39−1.64 m	1.17, 1.43	1.51	56.2	41.1	18.4	30.1, 35.1	52.4	34.9
$SnMe_2Cl$, **13**	39.8 [c]	1.39−1.64 m	1.02, 1.06	1.30	56.0	41.0	18.0	30.9, 36.3	52.1	35.6
SnCl, **15**	38.0 [d]	1.36−1.58 m	1.13, 1.29	1.13	53.4	38.9	17.6	31.9, 33.8	53.4	33.6
Pcat, **16**	40.5 [e]	1.42−1.66 m	1.37, 1.51	1.13	55.9	38.2	16.1	34.1, 34.6	58.7	33.3
$AsCl_2$, **17**	41.3 [f]	1.15−1.44 m	1.10, 1.48	1.53	55.3	38.8	17.7	30.8, 33.7	62.7	33.5
$SbCl_2$, **18**	42.7 [g]	1.12−1.33 m	1.05, 1.11	1.54	55.4	38.0	17.6	29.0, 33.7	60.6	34.3

Line widths: [a] 209. [b] 209. [c] 260. [d] 330. [e] 358. [f] 220. [g] 222.

Molecular Structures

Selected structural parameters for **11**−**13** are summarized in Table 4, and the structures of these compounds are depicted in Figures 7−9, respectively. In all these compounds the sum of bond angles at N1 is close to 360°, demonstrating that the atoms N1 are of sp^2 type. Therefore, this atom may form BN π-bonds with atom B1 in addition to atom N2.

Surprisingly, the B1−N1 bond of the trichlorogermyl compound **11** is significantly shorter than the B1−N2 bond [1.422(4) vs. 1.510(4) Å]. Inspection of the respective interplanar angles gives a value of 30.3° for C1N1C5/N1B1N2 and 60.5° for GeN2C10/N2B1N1. Therefore, the tmp group is better suited for BN π-bonding. The N1−B1−N2 bond angle of 123.3(3)° accords with the noncyclic structure. Another feature of interest is that one of the three Ge−Cl bond lengths is about 1% shorter than the other two. However, there is no apparent significant H···Cl interaction (all distances are longer than 3.35 Å) that would explain this deviation. The arrangement of the Ge1−N2−B2−N1 chain is *cisoid* in the solid state.

In contrast, the methylstannyl compounds **12** and **13** show a *transoid* arrangement for the Sn1−N2−B1−N1 chain. In **12** the B1−N1 bond is longer [1.475(5) Å] than the B1−N2 bond [1.430(4) Å], in agreement with interplanar angles of C1N1C5/N1B1N2 (116.4°) and C10N2Sn1/N2B1N1 (32.2°). The phenyl group is twisted against the N1B1N2 plane by 44.1°. B1 and N2 reside in a planar environment, as is also found for the chlorodimethylstannyl compound **13**. The B1−N1 bond in **13** is 0.01 Å shorter than in **12**, while the B1−N2 bond in **13** is 0.008 Å longer than in **12**. Such differences arise from the differ-

Table 4. Selected bond lengths (Å) and bond angles (°) of **11**−**13** and **16**−**18**

	$GeCl_3$, **11**	$SnMe_3$, **12**	$SnMe_2Cl$, **13**	Pcat, **16**	$AsCl_2$, **17**	$SbCl_2$, **18**
B1−N1	1.422(4)	1.475(5)	1.465(4)	1.431(4)	1.496(5)	1.527(2)
B1−N2	1.510(4)	1.430(4)	1.438(4)	1.530(5)	1.428(4)	1.411(2)
B1−C14	1.587(5)	1.601(5)	1.613(4)	1.596(5)	1.591(6)	1.595(3)
N2−C10	1.513(4)	1.505(3)	1.511(3)	1.535(5)	1.526(4)	1.516(2)
N1−C1	1.539(4)	1.498(4)	1.506(3)	1.539(5)	1.527(4)	1.534(2)
N1−C5	1.531(4)	1.501(4)	1.505(3)	1.531(5)	1.526(4)	1.535(2)
N2−E	1.796(2)	2.103(3)	2.081(2)	1.760(3)	1.872(3)	2.072(2)
E1−X1 (O, Cl)	2.1203(9)	2.140(3)	2.4016(8)	1.715(3)	2.292(1)	2.3899(6)
E1−X2 (O, Cl)	2.1312(9)	2.145(5)	2.122(3)	1.704(3)	2.234(1)	2.4809(7)
E1−N1	3.507	4.373	4.328	3.174	2.516(3)	2.539(1)
N1−B1−N2	123.3(3)	126.8(3)	128.1(2)	121.4(3)	111.3(3)	110.3(2)
N2−B1−C14	111.9(3)	113.1(3)	113.3(2)	114.7(3)	122.4(3)	123.8(2)
N1−B1−C14	124.7(3)	119.0(3)	118.5(2)	123.8(3)	126.2(3)	125.8(2)
B1−N2−E1	117.2(2)	116.2(2)	113.0(2)	106.0(2)	103.0(2)	102.4(1)
B1−N2−C10	121.3(2)	127.9(3)	128.8(2)	122.5(3)	128.3(3)	128.6(2)
C10−N2−E1	118.1(2)	115.8(2)	118.2(2)	128.6(2)	128.6(2)	128.9(1)
C1−N1−C5	114.8(2)	117.1(3)	116.8(2)	115.4(3)	115.6(3)	114.9(1)
B1−N1−C1	119.7(2)	119.4(2)	121.6(2)	120.6(3)	117.8(3)	117.3(1)
B1−N1−C5	124.8(2)	121.1(3)	119.8(2)	123.9(3)	115.6(3)	114.1(1)
N2−E1−X1	113.76(8)	113.2(1)	107.22(6)	108.0(2)	100.63(9)	101.62(4)
B1−E1−X2		−		105.6(2)	104.84(9)	98.72(4)
X1−E1−X2	102.37(3)	110.2(1)[a]	116.7(1)[b]	91.2(2)	93.00(5)	90.56(2)

[a] Other C−Sn−C angles 103.1(2) and 112.8(1). [b] Cl1−Sn1−C20 96.0(1), Cl1−Sn1−C21 101.2(1)

 © 2004 Wiley-VCH Verlag GmbH & Co. KGaA, Weinheim

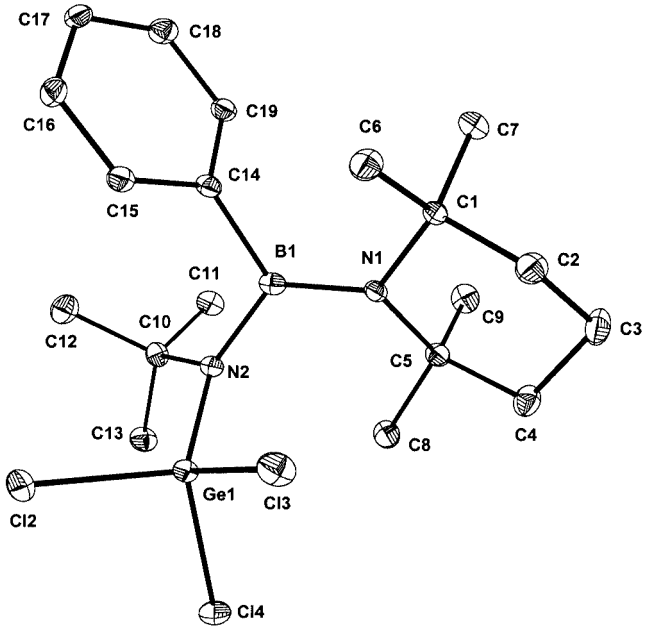

Figure 7. Molecular structure of **11**

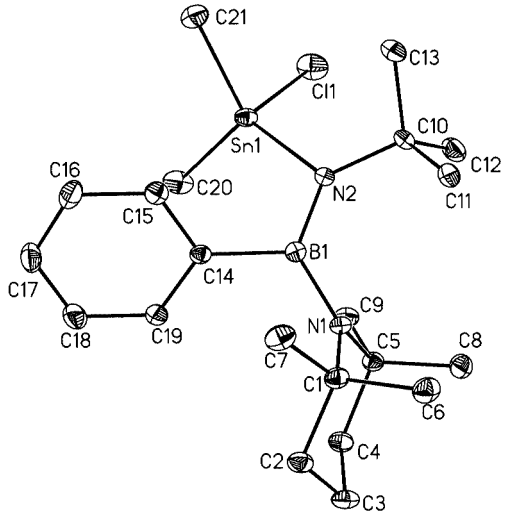

Figure 9. Molecular structure of **13**

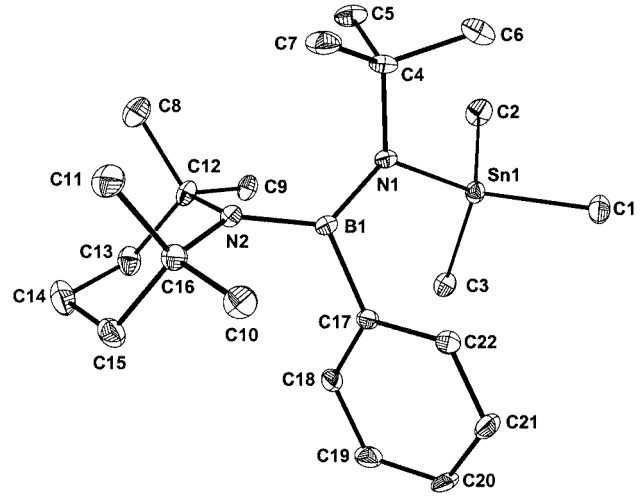

Figure 8. Molecular structure of **12**

ent interplanar angles of 30.9° for N1B1N2/B1N2Sn1 and 117.7° for N1B1N2/C1N1C5. The phenyl group is twisted against the N1B1N2 plane by 43.7°. Thus, the shortening is not a π-bonding effect but is rather due to the stronger electron-withdrawing $SnClMe_2$ substituent. This is also visible in the shorter SnC and SnN bonds in **13** although the differences are small. Notably, the C−Sn−C bond angles in **12** vary from 103.1(2) to 112.8(1)° and for **13** the Cl−Sn−C bond angles are 96.0 and 101.2(1)°, with a wide bond angle of 116.7(1)° for C20−Sn−C21.

Reactions with Halides of Group 15

While **1** reacted with PCl_3 in a 1:1 molar ratio to give an inseparable mixture of products, Ph_2PCl proved unreactive towards **1**. Ph_2PCl is not a strong electrophile, and its behavior corresponds with that of Ph_3GeCl and Ph_3SnCl. In contrast, 1,3,2-benzodioxaphosphorus chloride reacted smoothly with **1** according to Equation (15) to produce the borylated aminophosphane **16**. Its ^{31}P resonance at δ = 163.5 ppm for the tricoordinate P atom lies on the deshielded side for compounds with a PO_2N core.[28] The coupling constant $^2P(^{31}P^{13}C)$ is 23.3 Hz. Its sign, which has not been determined, would allow the determination of the configuration at the P atom. However, the compound is quite clearly noncyclic.

In contrast to PCl_3, both $AsCl_3$ and $SbCl_3$ reacted smoothly in the presence of diethyl ether to give the borylamino-dichloroarsane **17** and the borylamino-dichlorostibane **18**, respectively [Equation (16)]. However, $BiCl_3$ did not react in the nonpolar solvent hexane.

NMR Spectra

NMR spectroscopic data of **16**−**18** are summarized in Table 3. The ^{11}B NMR signals are typical for tricoordinate boron atoms and are slightly deshielded in comparison with the trichlorogermyl and methylstannyl derivatives tmp−BPh−N*t*Bu−EX_2. The protons of the *t*Bu groups are significantly deshielded compared with the compounds listed in Table 1. This seems to be due to the inductive effect of the chlorine atoms that, however, do not affect the protons of the CMe_2 groups, although a particularly large difference is noted for the arsenic compound **17**. In line with this is the deshielding of the ^{13}C nucleus of C10 in **16**, which is also noticeable for **17** and **18**.

 © 2004 Wiley-VCH Verlag GmbH & Co. KGaA, Weinheim

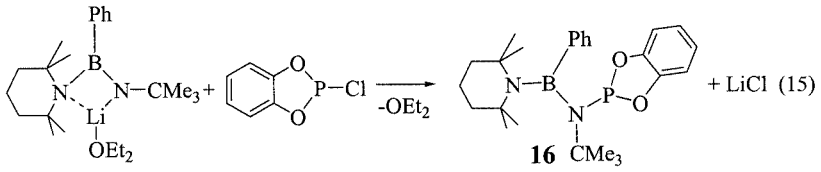

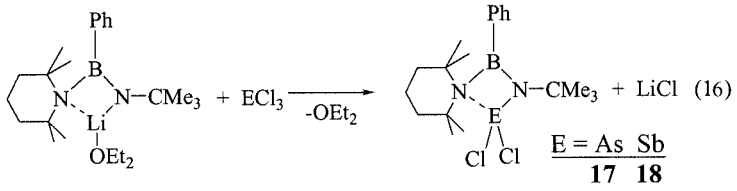

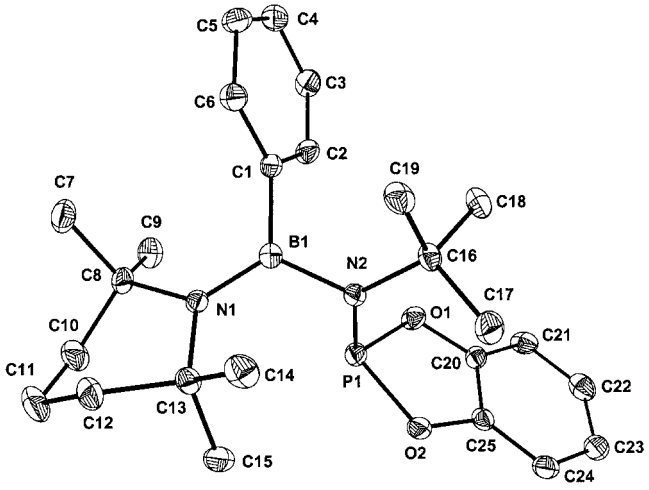

Figure 10. Molecular structure of **16**

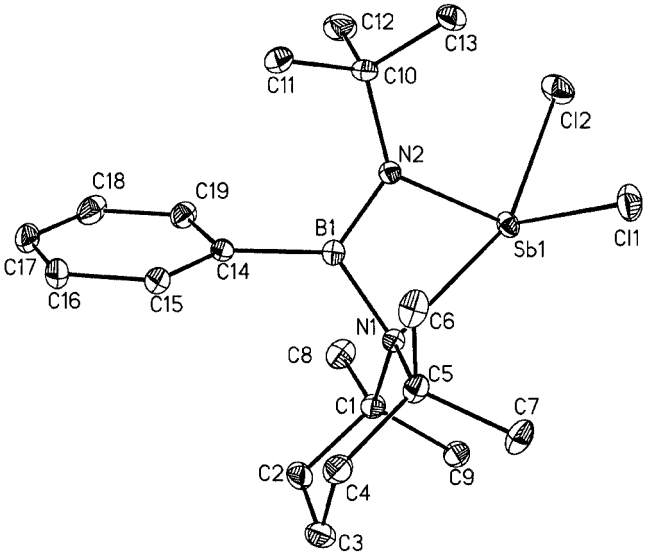

Figure 12. Molecular structure of **18**

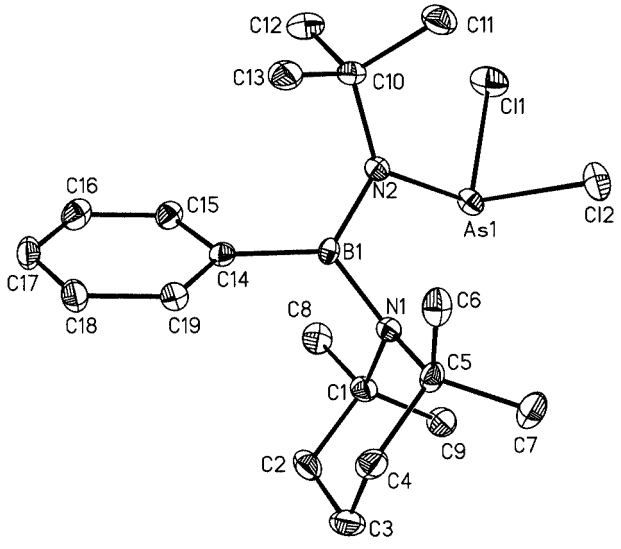

Figure 11. Molecular structure of **17**

Since there are two resonances each for these three compounds for the CMe_2 groups, hindered rotation about the B1–N1 bond is indicated. However, the NMR spectroscopic data are not conclusive as to whether **17** and **18** are cyclic or noncyclic in solution, while the ^{31}P resonance for **16** proves its noncyclic nature in solution. It was, therefore of interest to determine the solid-state structures of these compounds.

Molecular Structures

In analogy to the trichlorogermyl compound **11** there is also a shorter B–N bond in **16** to N1 [1.431(4) Å] than to N2 [1.528(3) Å]. This is due to a more planar arrangement of plane C1–N1–C5 with respect to the plane N1–B–N2 compared with the P1–N2–B1 plane (28.9° and 67.6°, respectively). Thus, there is stronger BN π-bonding to the N1 atom of the tmp unit, which possess not the usual chair conformation but rather the unusual skew conformation. The molecular conformation is, moreover, determined by a sterically most favored conformation; in this the C1N1C5 and C10N2P10 units are practically perpendicular (87.7°). This also allows a sterically favorable arrangement of the *t*Bu and the catecholatophosphorus units by opening the P1–N2–C10 bond angle to 128.5°. Notably, P1 points in the direction of N1 although there is no bonding interaction between these two atoms as the P1···N1 distance is as large as 3.174 Å.

 © 2004 Wiley-VCH Verlag GmbH & Co. KGaA, Weinheim

Conversely, the P1−N2 bond is short [1.670(3) Å]. Usually, P−N distances between tricoordinate P atoms and N atom are of the order of 1.80 Å [29]

The arsenic compound **17** shows a *cisoidal* arrangement of the N1B1N2As1 skeleton (Figure 11). B1−N1 π-bonding is excluded as the N1−B1 bond is longer than the B1−N2 bond and, in addition, N1 is not sp^2 as the sum of its bond angles is 349.0°. While the Cl1−As1−Cl2 angle is sharp [93.00(5)°] the N2−As1−Cl bond angle is 104.8(2)° and As1−N2−C10 is as wide as 128.6(2)°. However, the B1−N2−As1 bond angle is only 103.0°, pointing to preformation of a four-membered N1B1N2As1 ring. This, however, seems to be a steric effect exerted by the bulky *t*Bu group, as almost the same situation holds for the antimony compound **18**. Here, the Sb1−N2 bond is 2.072(2) Å and the Sb1−N1 atom distance is 2.539(1) Å. The N1−E and N2−E bond lengths differ by 0.644 Å in **17** and by 0.467 Å in **18**. All bond angles about E1 deviate strongly even for an approximate ψ-trigonal bipyramidal arrangement of atoms about the As and Sb centers, as the N1−As1−Cl1 and N1−Sb1−Cl2 bond angles of 158.4° and 157.6°, respectively, show. No doubt there is a weak E−N1 interaction, which is probably not retained in solution.

Discussion

The results described above demonstrate that **1** is a versatile reagent, leading to noncyclic and cyclic metallated diaminoboranes. The new compounds show structural features that are also present in metallo amidines.[2−8] However, the high steric requirement of the anion of **1** makes it less reactive than several lithium diorganylborylamides $R_2B-NR'Li$.[17,18,31]

Cyclic compounds **2**−**4** are readily accessible, while the cyclic compounds tmp−BX−N*t*Bu−BX_2 (X = Cl, Br) are better obtained by insertion of the BN triple bond of the amino iminoborane tmpB≡N*t*Bu into a boron halogen bond of BX_3.[32] These, like **2**−**4**, exhibit four different B−N bond lengths that depend on the combination of sp^2- and sp^3-type boron and nitrogen atoms; the shortest bonds involve tricoordinate B and N atoms, the longest tetracoordinate B and N atoms. These examples add to the arguments given by Power et al. on the influence of hybridization and multiple bonding in BN systems.[33]

While the catecholatoborane **4** as well as the analogous methyl derivative [1] are cyclic the liquid parent compound tmp−BH−N*t*Bu−Bcat[34] is considered to be noncyclic. This conclusion was based on NMR spectroscopic data. Thus, in contrast to **4**, only one set of ^1H and ^{13}C resonances occurs for the two CMe_2 groups, implying free rotation about the B1−N1 bond, while there are two for **4**. Moreover, even for **4** the B2−N1 bond may break at higher temperatures as it is rather long at 1.741(3) Å, which is close to the longest B−N bond of 1.756 Å found for $B_2Cl_4{\cdot}2NMe_3$.[35]

Halides of Al, Ga, and In react with alkali metal amidinates to give various analogs of the amindinato complexes of these element, all of which have chelate structures with either tetra-, penta- or hexacoordinate metal atoms.[36−39] In this study only one type has been characterized: compounds **6**−**8** are all four-membered chelates with tetracoordinate metal atoms. As expected, the coordinate E1−N1 bond is much longer than the single bond between atoms E1 and N2 (Table 2). Actually, this bond [2.078(2) Å] is longer than in most other amine adducts of $AlR_{3-n}X_n$, for which a range of 1.96−2.04 Å has been reported.[40,41] The Al1−N2 bond in **6** [1.869(2) Å] is longer than the terminal Al−N bonds in $[Al(N{=}CPh_2)_3]_2$ (av. 1.78 Å)[42] and several others,[43] but a better value for comparison is the Al−N bond in $[tmp_2AlF]_2$ [1.832(2) Å] where the fluorine atoms bridge the Al atoms.[20] Its Al−N bonds comprise tetracoordinate Al atoms and a tricoordinate N atom, as observed for **6**. Lesser differences in the two bond lengths are found for cyclic $Me_2Al(N\mathit{t}Bu)_2SMe(N\mathit{t}Bu)$ [1.908(2) and 1.918(2) Å][44] and cyclic $Me_2Al(NC_6H_2\mathit{t}Bu_3)_2P$ [1.974(3) and 1.981(4) Å] although the shorter bonds are longer than in **6**.[45] The same features are observed for **7** and **8**. With **7** the two Ga−N bonds can be compared with those of $[Ga(NMe_2)_3]_2$.[46] In this compound the bridging N atoms show Ga−N bond lengths of 1.964 and 1.974 Å while the Ga−N bonds to the terminal NMe_2 groups are, on average, 2.01 Å. Thus, the Ga1−N1 distance of 2.175(2) Å exceeds those of the bridging NMe_2 groups significantly while the Ga1−N2 bond length of 1.935(2) Å is considerably longer than the Ga−N bond to the terminal NMe_2 groups. The opening of the C−E−C bond angle from **6** to **8** suggests that the weakening of the E1−N1 bond is responsible for this change in structure, and that the In1−N1 bond is the easiest to break. Indeed, in solution this bond opens, as shown by the free rotation of the tmp unit about the B1−N1 bond. Most In−N bond lengths to tetracoordinate In lie in the range 2.196−2.246 Å.[47−50] Consequently, the In1−N1 bond [2.376(2) Å] is weak.

In contrast to the rich chemistry of silylamidines and silylamidinato complexes,[5,51,52] which allows even the synthesis of hexacoordinate Si chelates, no reactions of **1** with either trimethylhalosilanes or triphenylhalosilanes were observed, and even the reaction with $SiCl_4$ was not straightforward − the expected product tmp−BPh−N*t*Bu−$SiCl_3$ could not be isolated. In fact, in the synthesis of silylamidines the products formed are not only dependent on the stoichiometry of the reagents as *trans*-silylation reactions were also observed.[51] From the results obtained, the electrophilic character of element halides clearly plays a decisive role as well as steric factors. While Me_3SiCl and Me_3GeCl do not react with **1**, the more Lewis acidic Me_3SnCl readily did so. However, double substitution of halogen atoms in Me_2SnCl_2 and $SnCl_2$ were unsuccessful. This, we assume, is due to the bulkiness of **13** and **15**.

In line with these observations concerning reactivity, Ph_2PCl does not react with **1** while PCl_3 leads to an inseparable mixture of products. Conversely, the reactions with $AsCl_3$ and $SbCl_3$ produced the well-characterized compounds **17** and **18**. In **17**, the As1−N1 bond is 0.744 Å longer than the As1−N2 bond, indicating only a very

 © 2004 Wiley-VCH Verlag GmbH & Co. KGaA, Weinheim

weak interaction. In the analogous compound tmp−BCl−N*t*Bu−$AsCl_2$, As1−N1 is 2.619(4) Å and As1−N2 is 1.869(4) Å.[53] The latter is not significantly shorter than in **17** [1.872(3) Å]. As−N bonds to tricoordinate As and tricoordinate N atoms span the range 1.79−1.95 Å.[53−55] The compound closest in structure to **17** is the cyclic $ClAs(NPPh_3)_2SbCl_4$,[53] with As−N bond lengths of 1.843 and 1.946 Å; compound **19** is even more closely related.[54] The difference in Sb−N bonds lengths in **18** is 0.467 Å, and in tmp−BCl−N*t*Bu−$SbCl_2$ 0.471 Å.[55] Comparable Sb−N bond lengths in $Cl_2Sb(NSiMe_3)_2CPh$ are 3.262 and 2.122 Å [56] or 4.144 and 2.097 Å for $Cl_2Sb(NSMe_2NSiMe_3)SbCl_2$.[57] Therefore, these latter two compounds exhibit much weaker Sb−N interactions than Sb1−N1 in **18**.

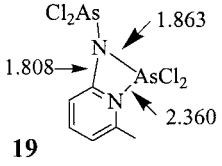

19

In conclusion, there are many analogies between the aminoborylamides and amidates, although **1** seems to be not as efficient a reagent as $R_2NCR-NR$ anions. This, however, is due to the large steric requirements of the anion of **1**. Thus, alkali metal salts with an anion $R_2N-BR'-NR''^-$ with R, R′, R″ = Me or R, R′ = Me and R″ = *i*Pr will be closer in reactivity to smaller amidates. However, *N*-metallated amino-, diamino- and triaminoboranes undoubtedly offer a wide new field for research and application.

Experimental Section

General Remarks: All experiments were conducted under anhydrous conditions using the Schlenk technique. Element halides or methyl element halides were commercial products of high quality. Compound **1** was prepared as described previously[1] or by the alternative procedure described below.

Elemental analyses were performed at the department's microanalytical laboratory. NMR: Bruker ACP-200 (^{7}Li, ^{11}B, ^{31}P, ^{119}Sn) or Jeol EX 400 (^{1}H, ^{13}C, ^{19}F); internal standards: C_6D_6, $CDCl_3$; external standards (1 M aqueous LiCl, H_3PO_4, $SnMe_4$) for all other nuclei. Mass spectra: VARIAN Atlas CH7; the mass numbers given refer to the most abundant isotope, and mass, relative intensity and assignment are reported. X-ray diffraction: Siemens P4 four circle diffractometer with a CCD area detector and LT2 device, Mo-K_α radiation, graphite monochromator. Data collection was performed with the programs implemented in SMART.[59]

(*tert*-Butylamino)[phenyl(2,2,6,6-tetramethylpiperidino)boryl]-lithium−Diethyl Ether (1): A solution of $tmpBCl_2$ (3.8 mL, 18 mmol) in hexane (20 mL) was added to a suspension of $LiHNCMe_3$ (1.44 g, 18.0 mmol) in hexane (30 mL). After stirring for 1 h the resultant precipitate was filtered off. All volatile material from the filtrate was then removed by distillation and the resultant oily residue of tmp−BCl−$NHCMe_3$ subjected to vacuum distillation (b.p. of 63 °C/0.001 Torr). Some $tmpB(NHCMe_3)_2$ was also obtained (higher boiling fraction). A 2 M solution of LiPh in cyclohexane/diethyl ether (8:2, 10.0 mL) was added dropwise while stirring to this bis(amino)chloroborane dissolved in hexane (100 mL). The resulting precipitate (LiCl) was filtered off, and the solvents were removed from the filtrate in vacuo. The so-obtained residue was then dissolved in hexane (30 mL) and the solution cooled to −20 °C. Within a few days colorless crystals separated. Yield: 3.4 g of **1** (95%). For further reactions, the suspension containing LiCl can be used directly.

General Procedure: A solution of the element halide compound was added to a freshly prepared and stirred solution of **1** in hexane at −78 °C. The insoluble material that formed in most of the reactions was removed by filtration (glass frit), and the solvents from the filtrate in vacuo. The residue was then crystallized from a suitable solvent.

2-*tert*-Butyl-5,5,9,9-tetramethyl-1-phenyl-2-aza-4-azonia-1-bora-3-borataspiro[3.5]nonane (2): A solution of BH_3·THF (1.77 mL, 3.4 M, 6.0 mmol) diluted with THF (100 mL) was added to **1** (3.0 mmol) in hexane (25 mL) at −78 °C. After warming to ambient temperature the ^{11}B NMR spectrum (^{1}H coupled) of the turbid solution shows a quintuplet at δ = −40.7 ppm ($LiBH_4$), a singlet at δ = 32.7 ppm (BPh), and a triplet at δ = −4.4 ppm (BH_2). All solvents were then removed and the residue extracted with hexane (about 25 mL) to leave behind white $LiBH_4$. The filtrate was subsequently reduced to about 15 mL. At −20 °C colorless crystals of **2** separated within a few days. Yield: 0.73 g (79%); m.p. 113 °C. $C_{19}H_{34}B_2N_2$ (312.09): calcd. C 73.29, H 10.61, N 9.00; found C 72.04, H 11.21, N 8.66. MS: (70 eV): *m*/*z* (%) = 312 (100) [M^+], 297 (62) [M^+ − Me], 255 (18) [M^+ − Bu], 240 (13) [M^+ − Me − Bu], 227 (43) [M^+ − H_2B − NBu], 187 (46) [M^+ − 125], 171 (35) [M^+ − tmpH], 144 (47) [M^+ − $tmpBH_2$ − Me], 126 (78) [tmp − Me^+].

2-*tert*-Butyl-3,3-difluoro-5,5,9,9-tetramethyl-1-phenyl-2-aza-4-azonia-3-borataspiro[3.5]nonane (3): A solution of BF_3·OEt_2 (0.75 mL, 6.0 mmol) in diethyl ether (10 mL) was slowly added, with stirring, to a solution of **1** (3.0 mmol) in hexane (30 mL). The solution showed at ambient temperature two ^{11}B singlet signals of almost equal intensity at 35.7 (BPh) and δ = 1.6 ppm ($LiBF_4$) (broad) and a triplet at δ = 4.8 ppm (BF_2). All volatile components were then removed in vacuo and the residue extracted with several portions of hexane. Subsequently, the insoluble $LiBF_4$ was removed from the last portion of the extracting hexane solution. The combined filtrates were then reduced to about 15 mL and kept at −20 °C. Within a few days, clear crystals of **3** separated. Yield: 0.7 g (72%), m.p. 121 °C. $C_{19}H_{32}B_2F_2N_2$ (348.08): calcd. C 65.50, H 9.19, N 8.04; found C 67.41, H 9.14, N 7.78. MS (70 eV): *m*/*z* (%) = 348 (4.5) [M^+], 333 (100) [M^+ − Me], 277 (82) [M^+ − Bu], 228 (15) [$tmpBPh^+$], 222 (16) [$tmpBNtBu^+$], 126 (23) [tmp − Me^+].

3-(Benzodioxo)-2-*tert*-butyl-5,5,9,9-tetramethyl-1-phenyl-2-aza-4-azonia-1-bora-3-borataspiro[3.5]nonane (4): A solution of *B*-chlorocatecholborane (0.46 g, 3.0 mmol) in diethyl ether (10 mL) was added at room temperature to a hexane solution of **1** (3.0 mmol). A white precipitate formed immediately. After stirring overnight the precipitate was separated by filtration and the filtrate reduced to 15 mL in vacuo. At −78 °C colorless crystals of **4** formed. Yield: 0.92 g (76%), m.p. 185 °C. $C_{25}H_{36}B_2N_2O_2$ (417.6): calcd. C 71.80, H 8.68, N 6.70; found C 71.83, H 8.97, N 6.69. MS (40 °C, 70 eV): *m*/*z* = 417 [M^+], 403 [M^+ − Me], 347 [M^+ − Me − Bu], 318 [$PhBNBu^+$], 277 [M^+ − tmp], 222 [$tmpBNBu^+$], m* = 298.8.

(2,2,6,6-Tetramethylpiperidine)lithium *tert*-Butyl[phenyl(2,2,6,6-tetramethylpiperidino)boryl]amide (6): A solution of **1** (3.0 mmol) in hexane (25 mL) was allowed to react at ambient temperature with

 © 2004 Wiley-VCH Verlag GmbH & Co. KGaA, Weinheim

a solution of tmp_2AlCl (3.0 mmol, 12.6 mL of a 0.238 M solution in hexane). The turbid mixture was then maintained at reflux for 1 d; 50% of **1** had reacted to a new compounds with $\delta^{11}B = 35.7$ ppm. Additional heating afforded no change in the ^{11}B NMR spectrum. The precipitate that had formed was filtered off. The yellow filtrate was then kept at −20 °C, providing a small amount of crystals of **6** that showed an ^{11}B NMR signal at δ = 35.5 ppm but no ^{27}Al NMR signal; m.p. 210 °C (dec.). $C_{28}H_{51}BLiN_3$ (447.47): calcd. C 75.16, H 11.49, N 9.39; found C 72.93, H 10.65, N 8.98. MS (70 eV): *m*/*z* (%) = 299 (100) [M^+ − tmpH − Li], 284 (100) [299 − Me^+], 243 (12) [299 − Bu^+], 126 (100) [tmp − Me^+].

2-*tert*-Butyl-3,3,5,5,9,9-hexamethyl-1-phenyl-2-aza-4-azonia-1-bora-3-aluminataspiro[3.5]nonane (7): A 1 M solution of Me_2AlCl in hexane (3 mL) was added to a suspension of **1** with LiCl (3.0 mmol **1** in 30 mL of hexane/diethyl ether) at room temperature. After stirring for 1 h the insoluble material was filtered off and the so-obtained colorless solution reduced to 15 mL. At −20 °C, colorless, moisture and air-sensitive crystals separated. Yield: 0.92 g of **7** (86%), m.p. 160 °C. $C_{21}H_{38}AlBN_2$ (356.32): calcd. C 70.72, H 10.66, N 7.88; found C 63.81, H 9.17, N 6.70. ^1H NMR (C_6D_6): δ = −0.06 (s, 6 H, $AlMe_2$) ppm. ^{13}C NMR ((C_6D_6): δ = 0.24 (br., $AlMe_2$) ppm. ^{27}Al NMR (C_6D_6): δ = 164, ($h_{1/2}$ = 1800 Hz) ppm. MS (70 eV): *m*/*z* (%) = 356 (8.5) [M^+], 341 (100) [M^+ − Me], 300 (21.5) [M^+ − Bu], 284 (100) [M^+ − Me − Bu], 269 (64) [284 − Me^+], 256 (32) [Me_2NBu^+], 228 (36.5) [tmpBPh$^+$], 216 (100) [M^+ − tmp], 183 (100) [tmpAlMe$^+$], 159 (100) [PhBNBu$^+$].

2-*tert*-Butyl-3,3,5,5,9,9-hexamethyl-1-phenyl-2-aza-4-azonia-1-bora-3-gallataspiro[3.5]nonane (8): Prepared in analogy to **7** by using Me_2GaCl (0.45 g, 3.0 mmol) dissolved in hexane (30 mL) to furnish very moisture- and air-sensitive crystals of **8**. Yield: 1.05 g (88%). $C_{21}H_{38}BGaN_2$ (399.06): calcd. C 63.1, H 9.52, N 7.02; found C 58.18, H 8.43, N 6.29. ^1H NMR (C_6D_6): δ = 0.32 (s, GaMe ppm.^{13}C NMR (C_6D_6): δ = 1.13 ($GaMe_2$) ppm. MS (70 eV): *m*/*z* (%) = 399 (0.5) [M^+], 384 (43) [M^+ − Me], 297 (9.5) [$GaMe_2^+$?], 224 (42) [tmpGaMe$^+$], 126 (11.5) [tmp − Me^+].

2-*tert*-Butyl-3,3,5,5,9,9-hexamethyl-1-phenyl-2-aza-4-azonia-1-bora-3-indataspiro[3.5]nonane (9): Prepared in analogy to **7** by using Me_2InCl (0.54 g, 3.0 mmol) dissolved in hexane (20 mL), with workup after stirring for 5 h. The filtrate was then reduced to ca. 20 mL. Crystals of **9** separated from the solution at −78 °C. Yield: 0.90 g (68%), m.p. > 200 °C. $C_{21}H_{38}BInN_2$ (444.16): calcd. C 56.74, H 8.56, N 6.30; found C 51.04, H 7.96, N 5.78. ^1H NMR (C_6D_6): δ = 0.06 (s, $InMe_2$) ppm. ^{13}C NMR ($CDCl_3$): δ = 1.0 ($InMe_2$) ppm.

Insufficient protection against air for **7**−**9** is responsible for the large deviation between calculated and found values in the elemental analysis.

[(*tert*-Butyl)(trimethylsilyl)amino](phenyl)(2,2,6,6-tetramethylpiperidino)borane (10): Li(tmp) (0.87 g, 5.9 mmol) was suspended in hexane (30 mL). After cooling the suspension to −78 °C, a solution of $PhBCl_2$ (0.78 mL, 5.9 mmol) in hexane (5 mL) was added with stirring. At room temperature only a single signal at $\delta^{11}B$ = 41.8 ppm was present, showing the complete conversion of $PhBCl_2$. The solid was filtered off and the filtrate treated with a freshly prepared solution of Li*N*t*Bu*($SiMe_3$) (5.9 mmol) in hexane (20 mL). The mixture was then kept under reflux for 5 d. Three ^{11}B NMR signals, at δ = 34.2 (60%), 23.4 (15%) and at 28.0 (25%) ppm, were detected, the first of which corresponds to **10**. In addition, three ^{27}Si NMR signals were found at δ = 9.1 (main signal), 17.6 and δ = 8.0 ppm. After removal of the hexane in vacuo the residue was treated with hexane (10 mL), the solid was removed by filtration and the so-obtained yellow solution kept at −20 °C. No crystals separated. Also, distillation did not allow **10** to be separated from the by-products.

[(*tert*-Butyl)(trichlorogermyl)amino](phenyl)(2,2,6,6-tetramethylpiperidino)borane (11): The solvent from a freshly prepared solution of **1** (1.77 mmol) in hexane (30 mL) was removed and the residue dissolved in diethyl ether (40 mL). $GeCl_4$ (0.3 mL) was then added to this solution, and the resultant suspension kept at reflux for 2 h. Since no complete conversion was noted the mixture was maintained at reflux for 5 days, after which only a single ^{11}B NMR signal was seen. The ether was then removed and the resultant oily residue treated with hexane (40 mL). On reducing the filtrate's volume to about 50%, crystals of **11** separated at −20 °C. Yield: 0.63 g (75%), m.p. 205 °C. $C_{19}H_{32}BCl_3GeN_2$ (478.22): calcd. C 47.68, H 6.69, N 5.85, Cl 22.24; found C 47.45, H 6.73, N 5.75, Cl 20.91.

[(*tert*-Butyl)(trimethylstannyl)amino](phenyl)(2,2,6,6-tetramethylpiperidino)borane (12): Prepared in analogy to **11** from **1** in hexane (3.0 mmol, 20 mL) and Me_3SnCl (0.76 g, 2.8 mmol) in hexane (15 mL). The suspension was then stirred for 2 days. Although only the ^{11}B NMR signal of **12** (δ = 39.8 ppm) was noted, the first crystals that separated from the filtrate at −20 °C proved to be Me_3SnCl. These were removed and the filtrate kept at −78 °C to afford crystals of **12**. Yield: 0.97 g (70%), m.p. 98 °C. $C_{22}H_{41}BN_2Sn$ (464.24): calcd. C 57.01, H 8.85, N 6.05; found C 54.80, H 8.68, N 5.68. ^1H NMR (C_6D_6): δ = 0.08 [t, $^2J(^{119}Sn^1H)$ = 56.3 Hz, 9 H] ppm. ^{13}C NMR (C_6D_6): δ = 1.4 [$^1J(^{119}Sn^{13}C)$ = 395.1 Hz] ppm. ^{119}Sn NMR (C_6D_6): δ = 17.9 ppm. MS (70 eV): *m*/*z* (%) = 464 (22) [M^+], 449 (100) [M^+ − Me], 324 (100) [M^+ − tmp], 165 (100) [$SnMe_3^+$].

[(*tert*-Butyl)(chlorodimethylstannyl)amino](phenyl)(2,2,6,6-tetramethylpiperidino)borane (13): A solution of Me_2SnCl_2 (0.44 g, 2.0 mmol) dissolved in boiling hexane (50 mL) was added to freshly prepared **1** (2.0 mmol) in hexane (30 mL) kept at −78 °C. The resulting suspension showed, at ambient temperature, only a single ^{11}B NMR signal at δ = 39.4 ppm. The filtrate was then reduced to 20 mL, and on cooling to −20 °C crystals of **13** separated. Yield: 0.71 g (73%), m.p. 145 °C (dec.). $C_{21}H_{38}BClN_2Sn$ (483.48): calcd. C 52.12, H 7.86, N 5.79; found C 45.67, H 7.51, N 5.74. ^1H NMR (C_6D_6): δ = 0.02 [d, $^2J(^{119}Sn^1H)$ = 52 Hz, 6 H, $SnMe_2$] ppm. ^{13}C NMR (C_6D_6): δ = −2.6 [$^1J(^{119}Sn^{13}C)$ = 390 Hz] ppm. ^{119}Sn NMR (C_6D_6): δ = 93.1 ppm.

Reaction of Me_2SnCl_2 with 1 in a 1:2: Ratio: In analogy to **13**, Me_2SnCl_2 (2.0 mmol) in hexane (50 mL) was reacted with **1** [4.0 mmol in hexane (40 mL)] at −78 °C. The ^{11}B NMR spectrum of the suspension showed, at ambient temperature, a signal at δ = 39.2 ppm in addition to that of the starting material. After 3 days, additional signals appeared at δ = 48.3 and δ = 5.4 ppm. A ^{119}Sn NMR spectrum revealed a signal at δ = 98.3 ppm, corresponding to $tmpMe_2SnCl$, while the ^{11}B NMR signal at δ = 39.2 ppm is typical for (tBuNBPh)$_2$.[23]

{(*tert*-Butyl)[chlorostannyl(II)]amino}(phenyl)(2,2,6,6-tetramethylpiperidino)borane (15): $SnCl_2$ (0.38 g, 2.0 mmol) was dissolved in THF (30 mL) and treated at 0 °C with a freshly prepared solution of **1** (4.0 mmol) in hexane (40 mL). A suspension formed, and the ^{11}B NMR spectrum shows a 50% conversion of **1**. On further stirring, no change was observed. After filtration and removal of solvent in vacuo a yellow oil remained that was dissolved in hexane (20 mL). At −20 °C compound **15** separated as a slightly yellow solid that is soluble in benzene, tetrahydrofuran or chloroform. No single crystals separated from these solutions. $C_{19}H_{32}BClN_2Sn$ (454.14): calcd. C 50.33, H 7.11, N 6.18; found C 48.75, H 7.05, N 5.51. MS (70 eV): *m*/*z* (%) = 454 (9) [M^+], 439 (25) [M^+ − Me],

 © 2004 Wiley-VCH Verlag GmbH & Co. KGaA, Weinheim

419 (9) [M^+ − Cl], 301 (60) [M^+ − MeSnCl], 278 (100) [M^+ − Cl − tmp], 126 (77)) [tmp − Me^+].

{(*tert*-Butyl)[(phenyl)(2,2,6,6-tetramethylpiperidino)boryl]amino}-1,3,2-benzodioxaphosphane (16): A solution of benzodioxaphosphorus chloride (0.35 g, 2.0 mmol) in toluene (20 mL) was added to a solution of **1** (2.0 mmol) in hexane (40 mL) with stirring to afford a white precipitate that dissolved on prolonged stirring. After 3 days, the reaction was complete (^{11}B NMR signal at δ = 41.1 ppm). Following removal of the solvents the resultant oily, semi-solid residue was treated with toluene (30 mL) and the insoluble material filtered off. From the filtrate, crystals of **16** separated at −20 °C. Yield: 0.59 g (67%), m.p. 177 °C. $C_{26}H_{36}BN_2O_2P$ (438.36): calcd. C 68.53, H 8.23, N 6.39; found C 64.88, H 8.32, N 6.30. ^{1}H NMR (C_6D_6): δ = 6.69 [dd, $^3J(^1H^1H)$ = 5.76, $^4J(^1H^1H)$ = 3.4 Hz], 6.95 [dd, $^3J(^1H^1H)$ = 5.76, $^4J(^1H^1H)$ = 3.2 Hz, cat H], 7.17, 7.18, 7.71

Table 5. Crystallographic data and data related to data collection and structure refinement

Compound	**2**	**3**	**4**	**6**	**7**	**8**
Chem. formula	$C_{19}H_{35}N_2B_2$	$C_{19}H_{33}N_2B_2F_2$	$C_{25}H_{36}N_2B_2O_2$	$C_{28}H_{51}N_3BLi$	$C_{21}H_{38}N_2AlB$	$C_{21}H_{38}N_2BGa$
Form. wght.	312.09	348.08	418.18	447.47	356.32	399.06
Cryst. size [mm]	0.30 x0.30 x0.40	0.15 x0.20 x0.20	0.5x0.5x0.6	0.2x0.3x0.4	0.09 x0.20 x0.30	0.30 x0.30 x0.40
Cryst. system	Orthorhombic	Orthorhombic	Monoclinic	Triclinic	Monoclinic	Monoclinic
Space group	Pnma	Pnma	P2(1)/n	P-1	P2(1)/c	P2(1)/c
a, [Å]	18.8488(4)	18.8134(2)	9.296	10.3038(7)	11.9770(5)	12.0288(3)
b, [Å]	11.3274(2)	11.400(1)	14.0167(2)	10.9388(8)	13.0568(7)	13.0359(1)
c, [Å]	8.9697(2)	8.9891(2)	18.1577(2)	14.6358(11)	13.9489(7)	13.9379(1)
α, [°]	90	90	90	70.850(1)	90	90
ß, [°]	90	90	93.505(1)	69.601(2)	92.143(2)	92.309(1)
γ, [°]	90	90	90	71.577(1)	90	90
V, [Å^3]	1915.10(7)	1927.88(5)	2361.51(4)	1422.3(2)	2179.82(18)	2183.78(6)
Z	4	8	4	2	4	4
ρ(calcd.), [Mg/m^3]	1.079	1.199	1.176	1.045	1.086	1.214
μ [mm^{-1}]	0.061	0.082	0.072	0.059	0.099	1.266
F(000)	684	752	904	496	784	856
Index range	-21<h<23	-25<h<21	-10<h<10	-11<h<14	-15<h<8	-11<h<16
	-14<k<14	-14<k<14	-15<k<13	-14<k<14	-15<k<16	-16<k<16
	-11<l<11	-11<ll<11	-21<l<21	-18<l<18	-17<l<17	-17<l<17
2 θ [°]	58.00	57.96	49.42	58.38	57.66	58.08
Temp, [K]	193	193	193	193	193	193
Refl. collected	10517	10715	11135	8389	12242	12131
Refl. unique	2115	2173	3661	4561	3703	3954
Refl. observed (4σ)	1730	1531	2795	3130	2455	3486
R (int.)	0.0403	0.0358	0.0400	0.0269	0.0526	0.0165
No. variables	127	141	280	302	226	227
Weight. Scheme x/y	0.0617/0.9314	0.0325/1.5867	0.0457/0-5923	0.0657/0.8623	0.0789/2.395	0.100/0
GOOF	1.265	1.024	1.156	1.101	1.014	1.036
Final R (4σ)	0.0665	0.0524	0.0465	0.0688	0.0637	0.0353
Final wR2	0.1650	0.1329	0.1131	0.1589	0.1470	0.0939
Larg. res. peak [e/Å^3]	0.543	0.334	0.274	0.279	0.396	0.675

Compound	**9**	**11**	**12**	**13**	**16**
Chem. formula	$C_{21}H_{38}BInN_2$	$C_{19}H_{32}BCl_3GeN_2$	$C_{22}H_{41}BN_2Sn$	$C_{21}H_{38}BClN_2Sn$	$C_{25}H_{36}BN_2O_2P$
Form. wght.	44.16	478.22	463.07	483.48	438.34
Cryst. size [mm]	0.2x0.3x0.3	0.2 x0.2 x0.3	0.1 x0.3 x0.3	0.20 x0.20 x0.30	0.10 x0.15 x0.20
Cryst. system	triclinic	Monoclinic	Triclinic	Monoclinic	Monoclinic
Space group	P-1	P2(1)/n	P-1	C2/c	P2(1)
a, [Å]	8.4799(1)	11.0513(6)	7.6774(1)	27.323(4)	12.765(5)
b, [Å]	10.7491(2)	14.7340(8)	9.9774(2)	9.1863(12)	7.837(3)
c, [Å]	12.5190(1)	13.9329(8)	16.7750(2)	19.328(3)	13.466(6)
α, [°]	97.582(1)	90	95.763(1)	90	90
ß, [°]	97.194(1)	106.0850(1	97.662(1)	106.896(2)	115.268(6)
γ [°]	93.232(1)	90	111.113(1)	90.	90
V, [Å^3]	1119.15(3)	2179.9(2)	1172.60(3)	4641.9(11)	1218.3(8)
Z	2	4	2	8	2
ρ(calcd.), [Mg/m^3]	1.318	1.457	1.312	1.384	1.195
μ [mm^{-1}]	1.062	1.780	1.097	1.223	0.136
F(000)	464	992	484	2000	472
Index range	-10<h<10	-14<h<14	-9<h<9	-33<h<31	-16<h<16
	-13<k<13	-19<k<16	-8<k<13	-11<k<11	-10<k<9
	-15<l<15	-17<l<17	-21<l<21	-24<l<24	-16<l<16
2 θ [°]	58.48	58.54	57.36	56.44	58.14
Temp, [K]	173(2)	183(2)	193	193	188(2)
Refl. collected	6735	12416	6804	11634	7003
Refl. unique	3596	4297	3697	4177	4680
Refl. observed (4σ)	3363	3278	3371	3549	3394
R (int.)	0.0108	0.0731	0.0161	0.0245	0.0319
No. variables	251	242	235	235	281
Weight scheme[1] x/y	0.0o789	0.35950.057/0.00	0.0216/6.3872	0.0532/0.4504	0.0643/0.1977
GOOF	1.148	1.045	1.097	1.145	1.017
Final R (4σ)	0.0224	0.0397	0.0263	0.0308	0.0602
Final wR2	0.619	0.0869	0.0677	0.0820	0.1288
Larg. res. peak [e/Å^3]	0.434	0.435	0.353	0.982	0.182

 © 2004 Wiley-VCH Verlag GmbH & Co. KGaA, Weinheim

Table 5 *(continued)*

Compound	**17**	**18**
Chem. formula	$C_{19}H_{32}AsBCl_2N_2$	$C_{19}H_{32}B\,Cl_2N_2Sb$
Form. wght.	445.10	491.93
Cryst. size [mm]	0.20 x0.20 x0.30	0.1 x0.2 x0.2
Cryst. system	Monoclinic	Monoclinic
Space group	P2(1)/c	P2(1)/c
a, [Å]	11.3035(6)	11.599(2)
b, [Å]	13.8516(8)	13.980(3)
c, [Å]	13.5671(7)	13.244(3)
α, [°]	90	90
β, [°]	90.903(1)	93.280(9)
γ, [°]	90	90
V, [Å3]	2124.0(2)	2144.1(8)
Z	4	4
ρ(calcd.), [Mg/m3]	1.392	1.524
μ [mm-1]	1.857	1.541
F(000)	928	1000
Index range	-7 <h<14	-15<h<15
	-16<k<16	-18<k<18
	-16<l<16	-17<l<17
2 θ [°]	57.84	57.38
Temp, [K]	193	193
Refl. collected	12031	31857
Refl. unique	3426	5318
Refl. observed (4σ)	2866	4291
R (int.)	0.0728	0.0316
No. variables	233	226
Weight scheme[1] x/y	0.1133/4.9651	0.0251/0.3618
GOOF	0.717	1.027
Final R (4σ)	0.0436	0.0219
Final wR2	0.1088	0.0497
Larg. res. peak [e/Å3]	0.537	0.397

[1] $w^{-1} = \sigma^2F_o^2 + (xP^2 + yP)$; $P = (F_o^2 + 2F_c^2)/3$.

(Ph) ppm. ^{13}C NMR (C_6D_6): δ = 112.3, 122.0 (cat C), 126.8, 128.9, 136.0 (Ph) ppm. ^{31}P NMR (C_6D_6): δ = 163.5 ppm.

{*tert*-Butyl[phenyl(2,2,6,6-tetramethylpiperidino)boryl]-amino}dichloroarsane (17): A solution of $AsCl_3$ (0.17 mL, 2.0 mmol) in hexane (10 mL) was added to a hexane solution of **1** (2.0 mmol in 30 mL). The mixture turned black and on continued stirring became a brownish suspension. After 3 h a ^{11}B NMR signal at δ = 41.3 ppm was detected. The solid was then removed and the yellow solution reduced to about 20 mL. At −20 °C an amorphous solid separated that was crystallized from hexane at ambient temperature. Yield: 0.58 g of **17** (65%), m.p. > 200 °C. $C_{19}H_{32}AsBCl_2N_2$ (445.10): calcd. C 51.22, H 7.19, N 6.29, Cl 15.93; found C 51.15, H 7.46, N 6.29, Cl 15.62.

{*tert*-Butyl[phenyl(2,2,6,6-tetramethylpiperidino)boryl]amino}-dichlorostibane (18): This was prepared from $SbCl_3$ (0.46 g, 2.0 mmol) and **1** (2.0 mmol) in hexane (30 mL). After 3 h the insoluble material was removed by filtration, and on cooling the filtrate (−20 °C) crystals of **18** separated. These crystals are highly sensitive to moisture. Yield: 0.65 g (66%), m.p. 144 °C. $C_{19}H_{32}N_2BCl_2Sb$ (491.93): calcd. C 46.35, H 6.50, N 5.69; found C 45.32, H 6.42, N 5.38. MS (79 eV): *m*/*z* (%) = 473 (25) [M^+ − Me], 456 (7) [M^+ − Cl], 332 (15) [tmpSbCl$_2^+$], 318 (33) [332 − Me^+].

X-ray Structure Determinations: Single crystals were covered with a polyfluoro ether oil and a specimen selected and mounted on the tip of a glass fiber. After cooling the crystal on the goniometer head to −80 °C with an LT2 device, the unit cell was determined from reflection collected on a total of 60 frames at five different settings of the ω and χ circles. Data collection was performed in the hemisphere mode (1264 frames). The program SAINT[59] was used for data reduction, and an absorption correction was applied using SADABS.[60] The structures were solved by direct methods (heavy atom methods for the Sb compound) using SHELX97.[61] This program was also applied for structure refinement. Non-hydrogen atoms were refined with anisotropic description. Most hydrogen atoms were visible after anisotropic refinement, but were placed in calculated positions and included in the refinement by applying a riding model. Data related to crystallography, data reduction and refinement are summarized in Table 5. CCDC-226743 to -226753 and -231319 (**9**) contain the supplementary crystallographic data for this paper. These data can be obtained free of charge at www.ccdc.cam.ac.uk/conts/retrieving.html [or from the Cambridge Crystallographic Data Centre, 12 Union Road, Cambridge CB2 1EZ, UK; Fax: +44-1223-336-033; E-mail: deposit@ccdc.cam.ac.uk].

[1] U. Braun, B. Böck, T. Habereder, H. Nöth, M. Schwartz, S. Weber, U. Wietelmann, *Eur. J. Inorg. Chem.*, in print.
[2] A. R. Sanger, *Inorg. Chem. Lett.* **1973**, *9*, 351−354.
[3] R. T. Boeré, R. T. Oakley, R. W. Reed, *J. Organomet. Chem.* **1987**, *331*, 161−167.
[4] K. Dehnicke, C. Ehrgeizinger, E. Hartmann, A. Binn, *J. Organomet. Chem.* **1988**, *352*, 161−167.
[5] K. Dehnicke, *Chemiker-Ztg.* **1990**, *114*, 295−304.
[6] G. Ehrgeizinger, F. Weller, K. Dehnicke, *Z. Naturforsch., Teil B* **1988**, *43*, 1119−1124.
[7] J. Barker, N. C. Blacker, P. R. Phillips, N. W. Alcock, W. Errington, M. G. H. Wallbridge, *J. Chem. Soc., Dalton Trans.* **1996**, 431−437.
[8] H. Roesky, B. Meller, M. Noltemeyer, H.-G. Schmidt, U. Scholz, G. M. Sheldrick, *Chem. Ber.* **1988**, *121*, 1403−1406.
[9] H. Chen, R. A. Bartlett, M. M. Olmstead, P. P. Power, S. C. Shoner, *J. Am. Chem. Soc.* **1990**, *112*, 1048−1055.
[10] R. A. Bartlett, H. Chen, H. V. R. Dias, M. M. Olmstead, P. P. Power, *J. Am. Chem. Soc.* **1988**, *110*, 446−449.
[11] R. A. Bartlett, X. Feng, M. M. Olmstead, P. P. Power, K. J. Weese, *J. Am. Chem. Soc.* **1988**, *110*, 4851−4854.
[12] B. Wrackmeyer, B. Schwarz, J. Weidinger, W. Milius, *Z. Naturforsch., Teil B* **1997**, *5*, 431−433.
[13] T. Seifert, W. Storch, M. Vosteen, *Eur. J. Inorg. Chem.* **1998**, 1343−1349.
[14] M. J. S. Dewar, P. M. Maitlis, *J. Am. Chem. Soc.* **1961**, *83*, 187−193.
[15] R. J. Wagner, J. L. Bradford, *Inorg. Chem.* **1962**, *1*, 99−106.
[16] H. Nöth, H. Vahrenkamp, *J. Organomet. Chem.* **1969**, *16*, 357−369.
[17] D. Fest, C. D. Habben, A. Meller, G. M. Sheldrick, D. Stalke, F. Pauer, *Chem. Ber.* **1990**, *123*, 703−706.
[18] C. D. Habben, A. Heine, G. M. Sheldrick, D. Stalke, *Z. Naturforsch., Teil B* **1992**, *47*, 1367−1369.
[19] Most likely the first reaction product is [tmp−PhB−N*t*BuBH$_3$]Li which will react with BH$_3$·THF to give LiBH$_4$ and *cyclo*-tmp−BPh−N*t*Bu−BH$_2$ (**2**).
[20] I. Krossing, H. Nöth, L. C. Tacke, M. Schmidt-Amelunxen, H. Schwenk-Kircher, *Chem. Ber./Receuil* **1997**, *130*, 1047−1052.
[21] The ^{27}Al resonance of tmp$_2$AlBr·OEt$_2$ was observed at δ = 125 ppm. I. Krossing, Ph.D. Thesis, University of Munich, **1997**.
[22] For [tmpAl(OEt)Cl]$_2$ a ^{27}Al resonance at δ = 89 ppm was observed. C. Tacke, PhD Thesis, University of Munich, **1994**.
[23] H. Nöth, B. Wrackmeyer, *Nuclear Magnetic Resonance Spectroscopy of Boron Compounds*, NMR Basic Principles and Progress (Eds.: P. Diehl, E. Fluck, R. Kosfeld), Springer Publishers, Heidelberg, Berlin, New York, **1973**.
[24] B. Glaser, PhD Thesis, University of Munich, **1985**.
[25] B. Wrackmeyer, *Annual Reports on NMR Spectroscopy* **1985**, *16*, 73−186.

 © 2004 Wiley-VCH Verlag GmbH & Co. KGaA, Weinheim

[26] B. Wrackmeyer, G. Kehr, H. Zhou, S. Ali, *Magn. Res. Chem.* **1996**, *34*, 921−928.
[27] M. Vosteen, PhD Thesis, University of Munich, **1999**.
[28] M. M. Crutchfield, C. M. Dungan, J. H. Letcher, V. Mark, J. R. van Wazer, *Topics in Phosphorus Chemistry* **1967**, *5*, 276.
[29] B. Eichhorn, H. Nöth, *Z. Naturforsch., Teil B* **2000**, *55*, 352−260.
[30] H. Nöth, I. Geisler, *Chem. Ber.* **1973**, *106*, 1943−1951.
[31] H. Fußstetter, G. Kopietz, H. Nöth, *Chem. Ber.* **1980**, *113*, 728−738.
[32] H. Nöth, S. Weber, *Z. Naturforsch., Teil B* **1983**, *38*, 1460−1465.
[33] A. Moezzi, M. M: Olmstead, P. P. Power, *J. Chem. Soc., Dalton Trans.* **1985,** 2949−234.
[34] D. Männig, H. Nöth, M. Schwartz, S. Weber, U. Wietelmann, *Angew. Chem.* **1985**, *97*, 979−980; *Angew. Chem. Int. Ed. Engl.* **1985**, *24*, 998−999.
[35] G. Johnson, J. Kane, R. Schaeffer, *J. Am. Chem. Soc.* **1970**, *92*, 7614−7615.
[36] M. P. Coles, D. C. Swenson, R. F. Jordan, V. G. Young Jr., *Oranometallics* **1997**, *16*, 5183−5194.
[37] J. Barker, N. C. Blacker, P. P. Phillips, N. N. Alcock, W. Errington, M. H. Wallbridge, *J. Chem. Soc., Dalton Trans.* **1996**, 431−437.
[38] S. Dagorne, R. F. Jordan, V. G. Young Jr., *Organometallics* **1999**, *18*, 4619−4623.
[39] Y. Zhou, D. S. Richeson, *Inorg. Chem.* **1996**, *35*, 2448−2451.
[40] A. Haaland, *Angew. Chem.* **1989**, *101*, 1017−1032; *Angew. Chem. Int. Ed. Engl.* **1989**, *28*, 992−1005.
[41] J. L. Atwood, G. A. Koutsantonis, F. C. Lee, C. L. Raston, *J. Chem. Soc., Chem. Commun.* **1994**, 91.
[42] S. J. Bryan, W. Clegg, R. Snaith, K. Wade, E. H. Wong, *J. Chem. Soc., Dalton Trans.* **1987**, 1223−1227.
[43] M. F. Lappert, P. P. Power, A. R. Sanger, R. C. Srivastava, *Metal and Metalloid Amides Synthesis − Structures, Physical and Chemical Properties*, Ellis Horwood Publ., New York, **1980**.
[44] B. Walfort, A. P. Leedham, Ch. A. Russell, *Inorg. Chem.* **2001**, *40*, 5668−5674.
[45] P. B. Hitchcock, H. A. Jasim, M. F. Lappert, H. D. Williams, *J. Chem. Soc., Chem. Commun.* **1986**, 1634−1636.
[46] K. M. Waggoner, M. M. Olmstead, P. P. Power, *Polyhedron* **1990**, *9*, 257−263.
[47] M. Mertz, W. Schwarz, D. Eberwein, J. Weidlein, H. Hess, H. P. Hausen, *Z. Anorg. Allg. Chem.* **1977**, *429*, 59−104.
[48] D. Arif, J. Bradley, *J. Chem. Soc., Chem. Commun.* **1985**, 783−784.
[49] K. Schmid, H. D. Hausen, K. W. Klinkhammer, J. Weidlein, *J. Organomet. Chem.* **1999**, *625*, 945−953.
[50] T. Gerstner, W. Schwarz, H. D. Hausen, *J. Organomet. Chem.* **1979**, *175*, 33−48.
[51] H. D. Hausen, K. Locher, J. Weidlein, *J. Organomet. Chem.* **1992**, *429*, C27−C32.
[52] H. H. Karsch, P. A. Schlüter, M. Reisky, *Eur. J. Inorg. Chem.* **1998**, 433−438.
[53] H. H. Karsch, P. A: Schlüter, F. Bienlein, M. Herke, E. Witt, A. Sladek, M. Heckel, *Z. Anorg. Allg. Chem.* **1990**, *583*, 7−16.
[54] A. Brandl, H. Nöth, *Chem. Ber.* **1988**, *121*, 1321−1328.
[55] R. Garbe, S. Wocadlo, H. C. Kang, W. Massa, K. Harms, K. Dehnicke, *Chem. Ber.* **1966**, *129*, 109−114.
[56] C. L. Raston, B. W. Shelton, V. H. Tolhurst, A. H. White, *J. Chem. Soc., Dalton Trans.* **2000**, 1279.
[57] C. Enzinger, F. Weller, K. Dehnicke, *Z. Naturforsch., Teil B* **1988**, *43*, 1119−1124.
[58] H. W. Roesky, K. Hübner, M. Noltemeyer, M. Schäfer, *Angew. Chem. Int. Ed. Engl.* **1991**, *103*, 856−857, *Angew. Chem. Int. Ed. Engl.* **1991**, *30*, 860−861.
[59] SMART and SAINT, Bruker Analytical Instruments, Madison, Version 5.1.
[60] SADABS, Absorption correction as implemented in SHELXTL, Bruker Analytical Instruments. Madison, Version 5.1.
[61] SHELX97, G. W. Sheldrick, University of Göttingen, **1997**.

Received February 13, 2004
Early View Article
Published Online July 21, 2004

 © 2004 Wiley-VCH Verlag GmbH & Co. KGaA, Weinheim

Metalation of 2-Propenylphenol

Cristina Wippert Rodrigues,[a] Christian Limberg,*[b] and Hans Pritzkow[a]

Keywords: Molybdenum / Oxo complexes / Alkoxides / Lithium / Metalation

In order to generate 2-propenylphenolate, **PO**$^-$, as a potential ligand for oxomolybdenum compounds, the lithiation of the parent phenol derivative, **POH**, was investigated. Treatment of **POH** with BuLi in THF yielded a tetramer of the corresponding alkoxide "**POLi**" with a heterocubane structure in which the coordination spheres of the Li centres are completed by THF molecules, i.e. $\{Li(THF)[\mu_3\text{-}OC_6H_4(CH{=}CH{-}CH_3)\text{-}2]\}_4$ (**1**). Compound **1** proved to be rather unreactive and unsuitable as a starting material for the introduction of the corresponding aryloxide ligands into the coordination sphere of molybdenum by salt metathesis. The latter did occur, however, when "**POLi**" was synthesised in the presence of 12-crown-4 and subsequently treated with molybdenyl chloride. This led to an unidentified aryloxide compound as well as to a hitherto unknown chlorooxomolybdate anion in the complexes [Li(12-crown-4)][MoO_2Cl_3(THF)] (**2**) and [{Li(12-crown-4)}$_2$Cl][MoO_2Cl_3(THF)] (**2′**) with an octahedral coordination sphere at the molybdenum centre in each case. An Mo(**PO**) complex was finally isolated for the first time when $MoO_2(OtBu)_2$ was employed as a starting material and treated with "**POLi**" prepared in situ in the presence of the crown ether. This led to the isolation of [Li(12-crown-4)$_2$][MoO_2(**PO**)$_3$] (**3**), which represents a rare example of a five-coordinate dioxomolybdenum(VI) complex as well as being the first example among these complexes with a square-pyramidal ligand arrangement. Comparison of **2** with **3** suggests that the low coordination number of the 14-electron compound **3** originates from the bulkiness of the **PO**$^-$ ligands. The crystal structures of all three compounds **1**–**3** are discussed.

(© Wiley-VCH Verlag GmbH & Co. KGaA, 69451 Weinheim, Germany, 2004)

Introduction

In order to establish a potential model of the surface intermediates during the SOHIO process, in which propene is oxidised with O_2 on bismuth molybdate catalysts to give acrolein,[1] we have been interested in the synthesis of high-valent (π-allyl)Mo complexes. Since the tendency of (π-allyl)Mo units to release allyl radicals increases with increasing oxidation state of the molybdenum centre, we decided to tether the allyl ligand through a donor function to the molybdenum atom thereby increasing the stability of the Mo−allyl bonding. By using phosphane donor functions, we succeeded in isolating a stable (allyl)Mo^{IV} compound (Scheme 1) which was prepared from an (olefin/phosphane)Mo chelate complex.[2] In order to obtain (allyl)molybdenum compounds in even higher oxidation states, ideally containing oxo ligands at the same time, it would be advantageous to replace the phosphane donor function by a "harder" oxo donor function. We thus decided to exploit the behaviour of the potential **PO**$^-$ ligand in contact with high valent molybdenum compounds.

[a] Anorganisch-Chemisches Institut, Universität Heidelberg, Im Neuenheimer Feld 270, 69120 Heidelberg, Germany
Fax: (internat.) + 49-6221-545707
[b] Institut für Chemie, Humboldt-Universität zu Berlin, Brook-Taylor-Str. 2, 12489 Berlin, Germany
Fax: (internat.) + 49-30-2093-6966
E-mail: Christian.limberg@chemie.hu-berlin.de

Results and Discussion

We envisioned that in-situ preparation of "**POLi**" as a source of **PO**$^-$ could be achieved simply by treatment of the parent phenol, **POH**, with BuLi in THF. Surprisingly, numerous attempted reactions between the corresponding reaction mixtures and high- or low-valent starting materials containing Mo−Cl units did not lead to LiCl salt metathesis. Since it has been shown in the past, that the structures and degree of aggregation of group 1 metal alkoxides can have a strong influence on their reactivity,[3] compound **1**, resulting from the lithiation reaction, was crystallised by cooling a concentrated solution in THF. A subsequent single-crystal X-ray diffraction study of **1** revealed the reason for its low reactivity; 4 equiv. of "**POLi**" assemble themselves in **1** to form an aggregate with an Li_4O_4 heterocubane core in the centre (see Figure 1 and Scheme 2). Each oxygen atom is thus connected to three Li cations as well as the aryl residue, while each Li ion is linked to three alkoxide oxygen atoms as well as to the O atom of a THF solvent molecule (selected bond lengths and angles are listed in Tables 1 and 2). While [Li(THF)(OPh)] forms a hexamer,[4] a heterocubane structure as shown in Scheme 2 was previously found for [Li(*N*-methylcaprolactam)(μ_3-OPh)]$_4$ [5] and, furthermore, it is reminiscent of the structure displayed by $[Li(THF)O_3SCF_3]_4$.[6] In this latter compound, the Li−O bonds are somewhat shorter than those observed for **1**

 © 2004 Wiley-VCH Verlag GmbH & Co. KGaA, Weinheim **DOI: 10.1002/ejic.200400209**

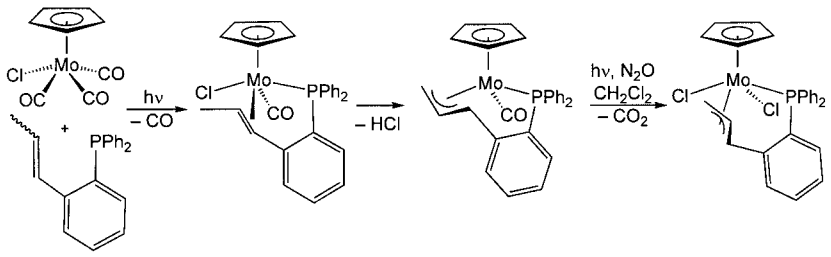

Scheme 1

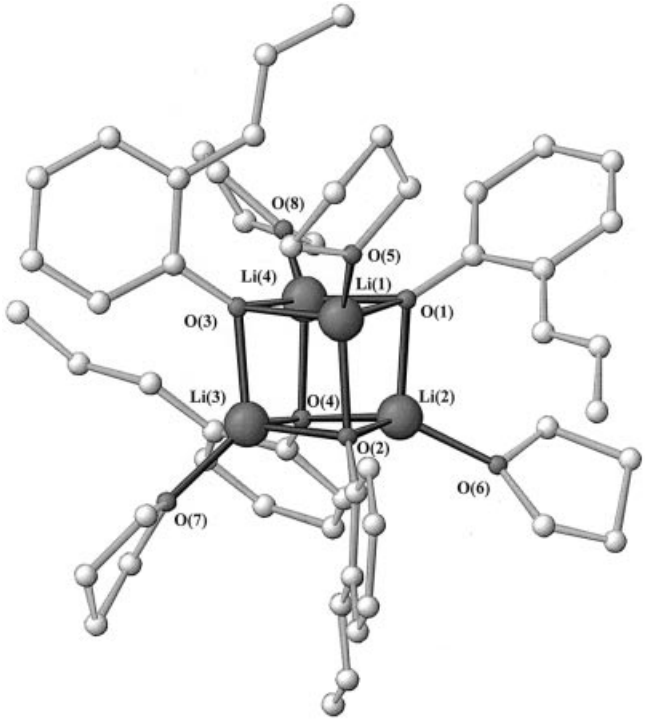

Figure 1. Molecular structure of **1** with partial atom labelling scheme; hydrogen atoms have been omitted for clarity

Table 1. Selected bond lengths [Å] for **1**

O(1)−Li(1)	1.928(5)	O(4)−Li(4)	1.996(5)
O(1)−Li(4)	1.953(4)	O(5)−Li(1)	1.917(5)
O(1)−Li(2)	1.960(5)	O(6)−Li(2)	1.913(5)
O(2)−Li(2)	1.931(5)	O(7)−Li(3)	1.925(5)
O(2)−Li(1)	1.949(5)	O(8)−Li(4)	1.906(4)
O(2)−Li(3)	1.980(5)	Li(1)−Li(3)	2.623(6)
O(3)−Li(3)	1.952(5)	Li(1)−Li(4)	2.629(6)
O(3)−Li(4)	1.952(5)	Li(1)−Li(2)	2.631(6)
O(3)−Li(1)	1.971(5)	Li(2)−Li(4)	2.604(6)
O(4)−Li(3)	1.930(5)	Li(2)−Li(3)	2.626(6)
O(4)−Li(2)	1.942(5)	Li(3)−Li(4)	2.652(6)

(1.928−1.996 Å) which in turn compare well with those found in [Li(*N*-methylcaprolactam)(μ_3-OPh)]$_4$ (1.88−2.00 Å). The Li−Li distances are all very similar (2.604−2.652 Å) and only somewhat longer than those in organolithium compounds with a heterocubane structure such as [Li(THF)*t*BuCH$_2$CH$_2$]$_4$ (2.479 Å in average).[7] The bond angles within the cubes amount to 90±8°, i.e. the cubic geometry is only slightly distorted. Even though a (*Z*)/(*E*) ligand mixture (1:5) was employed for the synthesis of **1**, only (*E*)- configured olefinic moieties were found in the molecular structure of **1** as shown by X-ray crystallography and there is no evidence for (*Z*)-configured groups in the crystalline bulk material on the basis of NMR spectroscopic investigations (signal assignments are supported by ^{1}H-^{1}H-COSY and ^{1}H-^{13}C-HSQC spectroscopic data and are thus unambiguous). Apparently, crystallisation proceeds only for the (all-*E*) arrangement and hence the yield of crystalline material is only 17%.

Table 2. Selected bond angles [°] for **1**

Li(1)−O(1)−Li(4)	85.3(3)	O(1)−Li(1)−O(2)	94.5(2)
Li(1)−O(1)−Li(2)	85.2(2)	O(1)−Li(1)−O(3)	95.1(2)
Li(4)−O(1)−Li(2)	83.5(3)	O(2)−Li(1)−O(3)	96.3(2)
Li(2)−O(2)−Li(1)	85.4(2)	O(2)−Li(2)−O(4)	95.3(2)
Li(2)−O(2)−Li(3)	84.4(3)	O(2)−Li(2)−O(1)	94.1(2)
Li(1)−O(2)−Li(3)	83.8(3)	O(4)−Li(2)−O(1)	97.6(2)
Li(3)−O(3)−Li(4)	85.6(3)	O(4)−Li(3)−O(3)	95.4(2)
Li(3)−O(3)−Li(1)	83.9(2)	O(4)−Li(3)−O(2)	94.2(2)
Li(4)−O(3)−Li(1)	84.1(3)	O(3)−Li(3)−O(2)	95.9(2)
Li(3)−O(4)−Li(2)	85.4(2)	O(3)−Li(4)−O(1)	94.9(3)
Li(3)−O(4)−Li(4)	85.0(3)	O(3)−Li(4)−O(4)	93.3(2)
Li(2)−O(4)−Li(4)	82.8(2)	O(1)−Li(4)−O(4)	96.1(3)

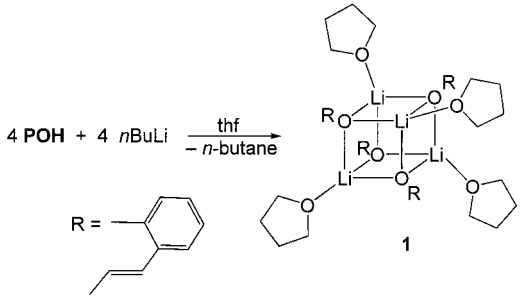

Scheme 2

It is also clear from Figure 1 that the Li_4O_4 core is effectively shielded by the large organic residues as well as the THF residues which altogether form a lipophilic-like layer around the alkoxide O atoms. Hence, a reaction with Mo−Cl units or even with water is indeed problematic. Accordingly, **1** proved to be stable to air whereas [Li(*N*-methylcaprolactam)(μ_3-OPh)]$_4$ was reported[5] to be air-sensitive.

To avoid formation of the stable tetrameric form of "**PO-Li**" in solution, i.e. **1**, and to thus obtain it in a more reac-

 © 2004 Wiley-VCH Verlag GmbH & Co. KGaA, Weinheim

tive state, 12-crown-4 was employed in subsequent experiments to separate the Li^+ ions. These potential ligands must be added to **POH** previous to the addition of BuLi and the resultant mixture has to be employed in situ since subsequent treatment of **1** with 12-crown-4 in THF does not enhance the reactivity.

Among other starting materials, MoO_2Cl_2 was chosen for treatment with 1 equiv. of "**POLi**" prepared by the above-mentioned route in the presence of 12-crown-4. Some of the MoO_2Cl_2 reacts to give a molybdenum aryloxide compound which, however, could neither be isolated in a pure state nor identified while the remainder apparently reacts with the Li(12-crown-4)Cl thus formed to give **2** with the hitherto unknown simple chlorooxo anion $[MoO_2Cl_3(THF)]^-$ (Scheme 3).

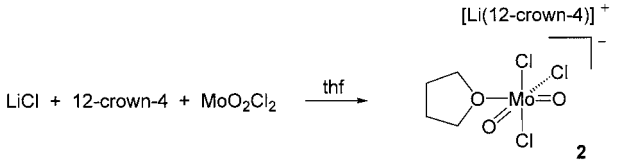

Scheme 3

Accordingly, for the formation of **2**, addition of **POH** is not necessary as shown by an analogous experiment performed without **POH** (1 equiv. of MoO_2Cl_2 then reacts to give LiCl and "MoO_2Bu_2" which decomposes while the other equiv. reacts with LiCl to give **2**). The chemistry of chlorooxomolybdenum compounds has been well explored and a large variety of such complexes (charged and uncharged) has been synthesised in the past.[8] The anion of **2** was unknown until now and while comparable anions of the type $[MoO_2Cl_3L]^-$ (with L = any donor) have been synthesised, for instance with L = H_2O,[9] their structures have so far eluded determination. Hence, attempts were made to crystallise **2** directly from the reaction mixture produced as described above. This led to crystals of **2′** where the $[Li(12\text{-crown-4})]^+$ cation is replaced by the novel cation $[\{Li(12\text{-crown-4})\}_2Cl]^+$. The molecular structure is shown in Figure 2 (selected bond lengths and angles are listed in Table 3). The cation is composed of two $[Li(12\text{-crown-4})]^+$ moieties which both coordinate to a chloride anion at almost identical distances [Li(1)−Cl(3) 2.305(9) Å; Li(2)−Cl(3) 2.310(8) Å]. One of the 12-crown-4 ligands is disordered with respect to both C and O atoms. The crystal structure of the neutral complex [Li(12-crown-4)Cl] has been determined previously.[10] A comparison with the corresponding $[\{Li(12\text{-crown-4})\}_2Cl]^+$ cation in **2′** revealed that, as expected in the absence of the second $[Li(12\text{-crown-4})]^+$ cation, the remaining Li−Cl bond is somewhat shorter [2.290(4) Å]. The difference is, however, not as large as might have been expected. In contrast to [Li(12-crown-4)Cl], in which all Li−O distances are equal, the Li−O bonds within each of the [Li(12-crown-4)] moieties in **2′** are all different, spanning a range of 1.976−2.210 Å. The Mo centre of the anion is surrounded by its ligands in a distorted octahedral geometry. The bond lengths of the two

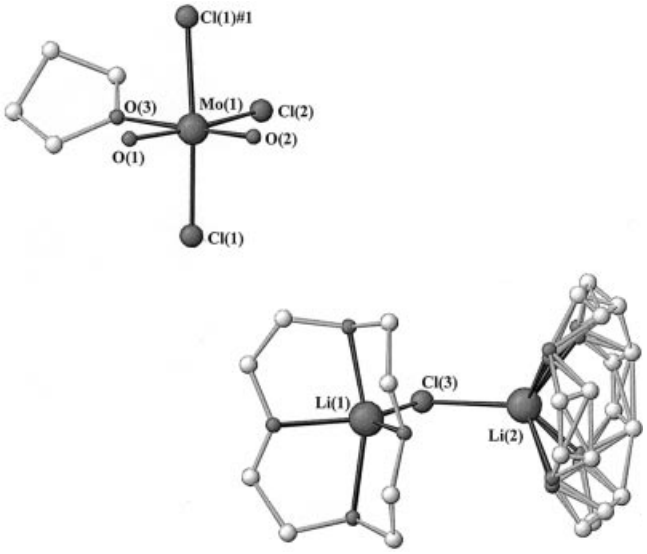

Figure 2. Molecular structure of **2′** with partial atom labelling scheme; hydrogen atoms have been omitted for clarity

Mo=O groups are significantly different since the comparatively weak THF donor is found in a *trans* position to O2 [→ strong bond to Mo; 1.670(5) Å] while a chloro ligand is bonded in a *trans* position to O1 [→ weaker bond to Mo; 1.704 Å]. The bond angle O2−Mo−O1 amounts to 102.9° and thus compares well with the angles found in other octahedral complexes containing the MoO_2^{2+} unit.

Table 3. Selected bond lengths [Å] and bond angles [°] for **2′**

Mo(1)−O(2)	1.670(5)	Mo(1)−Cl(1)	2.380(2)
Mo(1)−O(1)	1.704(4)	Mo(1)−Cl(2)	2.510(2)
Mo(1)−O(3)	2.293(3)	Li(1)−Cl(3)	2.305(9)
		Li(2)−Cl(3)	2.310(8)
O(2)−Mo(1)−O(1)	102.9(2)	O(3)−Mo(1)−Cl(1)	82.92(5)
O(2)−Mo(1)−O(3)	174.0(3)	O(2)−Mo(1)−Cl(2)	93.8(2)
O(1)−Mo(1)−O(3)	83.1(3)	O(1)−Mo(1)−Cl(2)	163.3(2)
O(2)−Mo(1)−Cl(1)	96.58(5)	O(3)−Mo(1)−Cl(2)	80.24(9)
O(1)−Mo(1)−Cl(1)	93.58(4)	Cl(1)−Mo(1)−Cl(2)	84.39(3)

Since the tendency of MoO_2^{2+} units to bind chloride is clearly very strong, $MoO_2(OtBu)_2$ was subsequently chosen as the starting material in order to finally obtain and isolate a $\mathbf{PO^-}$ complex by the synthetic route discussed above (direct treatment with **POH** leads to an air-sensitive brown oil which could not be purified sufficiently to allow its identification). After workup, a yellow, microcrystalline, very air-sensitive solid was obtained. IR spectroscopic measurements indicated the presence of an MoO_2 moiety whereas the ^1H NMR spectrum showed signals for (*E*)-configured **PO** residues [again there was no evidence for (*Z*) moieties] and 12-crown-4. Recrystallisation from 1,4-dioxane/hexane provided crystals suitable for a single-crystal X-ray diffraction study which indicated the composition [Li(12-crown-

 © 2004 Wiley-VCH Verlag GmbH & Co. KGaA, Weinheim

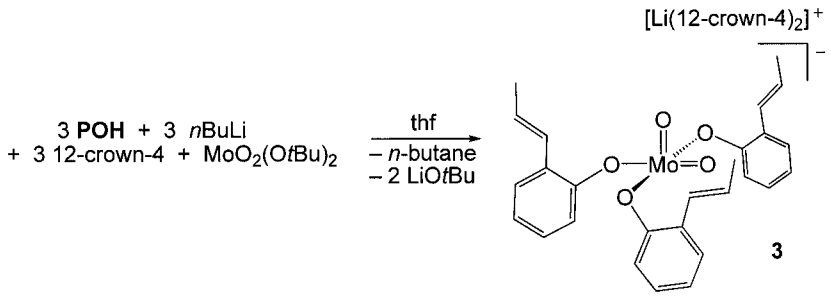

Scheme 4

4)$_2$][MoO_2(**PO**)$_3$] (**3**) (Scheme 4, Figure 3, selected bonds lengths and angles are listed in Table 4). The arrangement of the five oxygen atoms around the molybdenum centre represents a distorted square pyramid ($\tau^{[11]} = 0.1$) with O5 at the apical position. Five-coordinated dioxomolybdenum(VI) complexes such as the anion of **3** are rare. When formed, these 14-electron complexes are usually stabilised by additional donor molecules (e.g. solvent molecules such as here THF/dioxane) or aggregation. Accordingly, only five monomeric complexes displaying five-coordination in the solid state are known today[12–17] which uniformly exhibit trigonal-bipyramidal coordination geometries. The square-pyramidal arrangement of the ligands in **3** is thus unique. The successful isolation of the known compounds has been ascribed to the employment of bulky ligands and this hypothesis has very recently been confirmed in a systematic study.[16]

Table 4. Selected bond lengths [Å] and bond angles [°] for **3**

Mo(1)–O(5)	1.676(6)	Mo(1)–O(2)	1.977(4)
Mo(1)–O(4)	1.704(4)	O(1)–C(1)	1.357(6)
Mo(1)–O(1)	1.968(4)	O(2)–C(10)	1.332(7)
Mo(1)–O(3)	1.973(4)	O(3)–C(19)	1.342(7)
O(5)–Mo(1)–O(4)	105.8(2)	O(4)–Mo(1)–O(2)	144.0(2)
O(5)–Mo(1)–O(1)	104.1(2)	O(1)–Mo(1)–O(2)	80.5(2)
O(4)–Mo(1)–O(1)	90.3(2)	O(3)–Mo(1)–O(2)	80.1(2)
O(5)–Mo(1)–O(3)	103.8(2)	C(1)–O(1)–Mo(1)	128.5(3)
O(4)–Mo(1)–O(3)	92.3(2)	C(10)–O(2)–Mo(1)	136.1(4)
O(1)–Mo(1)–O(3)	150.2(2)	C(19)–O(3)–Mo(1)	126.4(3)
O(5)–Mo(1)–O(2)	110.2(2)		

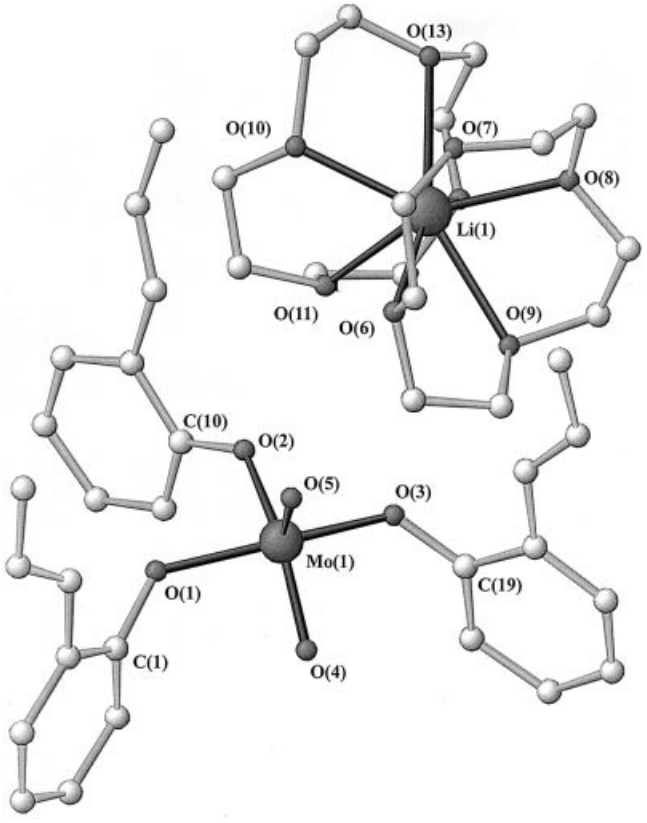

Figure 3. Molecular structure of **3** with partial atom labelling scheme; hydrogen atoms have been omitted for clarity

Along these lines, an explanation for the five-coordination of the molybdenum centre in **3** could also be based on the bulkiness of its aryl residues and the structural data support this assumption (see below).

Due to the square-pyramidal arrangement, the two terminal O atoms show quite different distances to Mo, i.e. the length of the bond between Mo and O5, lacking a *trans* ligand, amounts to 1.676(6) Å while the Mo–O4 bond is significantly longer [1.704(4) Å]. Atoms O1–O4 lie roughly in a plane (the deviations from the mean ideal plane amount to ±5.4 pm) and, as expected, the angles O5–Mo–O(1–4) are all somewhat larger than 90° (103.8–110.2°), the largest one occurring for O2 which is "clamped" by two bulky aryl residues so that C10 has to bend out of the basal plane. Furthermore, the small terminal oxo ligand O4 allows C1 and C19 to position themselves approximately within this plane. Accordingly, the O–Mo–O angles within the square base amount to 92.3–80.1°. In Figure 3 it can be seen that all aryl rings are arranged almost perpendicular to the basal plane to minimise steric crowding. All propenyl residues point in the same direction and an additional sixth ligand would have to approach from the other side where it would surely come into conflict with the aryl residues thus explaining the 5-coordination in the case of **3**. Due to the fact that three of these bulky aryloxide ligands were unexpectedly introduced at Mo in the course of the reaction shown in Scheme 4, an interaction between their olefinic functions and the Mo centre is clearly not possible either.

 © 2004 Wiley-VCH Verlag GmbH & Co. KGaA, Weinheim

The complex anions of **3** and **2/2′** both contain an MoO_2^{2+} moiety and three anionic ligands. In the case of **2/2′** these are chloride ligands whereas in **3** they are bulky aryloxide ligands. The latter prevent binding of an additional neutral donor leading to five-coordination in **3** while the "compact" chloride ligands in **2/2′** permit coordination of an additional THF molecule.

Conclusion

In summary, we have clarified the unusual behaviour of lithiated **POH** by elucidating the molecular structure of the corresponding lithium aryloxide. It displays a heterocubane arrangement in which the organic ligands and residues insulate the inorganic core and, with this in mind, precautions could be taken to avoid formation of this structure. These enabled the synthesis and characterisation of the first Mo/**PO** complex **3**. Compound **3** is a rare example of a five-coordinate MoO_2^{2+} complex which, at the same time, represents the first example of an MoO_2^{2+} compound with a square-pyramidal arrangement of its ligands. Moreover, the first structural characterisation of a compound with an anion of the type $[MoO_2Cl_3L]^-$ has been achieved. Compound **2** contains such an anion where L is THF. Exchange of bulky $\mathbf{PO}^-$ by Cl^- in the $[MoO_2X_3]^-$ moiety thus allows the additional coordination of a solvent molecule in **2** supporting the hypothesis that steric factors do indeed determine the coordination numbers observed in MoO_2^{2+} compounds.

Experimental Section

General Remarks: All manipulations were carried out with a vacuum line (at a background pressure $< 10^{-3}$ mbar), in a glovebox or by means of Schlenk-type techniques involving the use of dry argon. The $MoO_2(OtBu)_2$ complex was prepared as described in the literature.[18] All other starting materials were obtained commercially. Microanalyses were performed by the Analytische Laboratorien des Organisch-Chemischen Institutes der Universität Heidelberg using a Heraeus CHN-Analyser. All NMR spectra were recorded using a Bruker Avance-DPX 200 MHz spectrometer. Infrared (IR) spectra were recorded using samples prepared as KBr pellets with a Digilab Excalibur™ FTS 3000 FTIR spectrometer. Low-resolution mass spectra were recorded with a Finnigan MAT 8400 instrument. High-resolution mass spectra were performed at the Zentrum für Massenspektrometrie des Organisch-Chemischen Instituts der Universität Heidelberg using a JEOL JMS-700 spectrometer. The ions were generated by EI (70 eV).

[Li(THF){μ$_3$-OC$_6$H$_4$(CH=CH−CH$_3$)-2}]$_4$ (1): A solution of 2-propenylphenol (1.00 g, 7.45 mmol) in THF (10 mL) was cooled to −20 °C and a BuLi solution (1.6 M in hexane, 4.66 mL) was added slowly. After warming to room temp., all volatiles were removed yielding analytically pure **1** (1.30 g 1.53 mmol, 82%). Crystals were obtained by cooling a THF solution to −30 °C for 12 h. $C_{52}H_{68}Li_4O_8$ (848.9): calcd. C 73.58, H 8.07; found C 73.40, H 8.14. MS (EI/LR): *m/z* (%) = 707 (25) [(5 **POLi**)$^+$ + Li], 560 (8) [(4 **POLi**)$^+$], 427 (100) [(3 **POLi**)$^+$ + Li], 287 (19) [(2 **POLi**) + Li], 280 (12) [(2 **POLi**)$^+$], 147 (100) [**POLi**$^+$ + Li], 134 (100) [**POH**$^+$]. MS (EI/HR): *m/z* found (calcd.) = 707.4242 (707.4227, Δ*m* = 1.5 mmu) [$C_{45}H_{45}O_5{}^7Li_6$], 706.4225 (706.4219, Δ*m* = 0.6 mmu) [$C_{45}H_{45}O_5{}^6Li^7Li_5$], 560.3282 (560.3254, Δ*m* = 2.8 mmu) [$C_{36}H_{36}O_4{}^7Li_4$], 427.2577 (427.2600, Δ*m* = 2.3 mmu) [$C_{27}H_{27}O_3{}^7Li_4$], 426.2599 (426.2591, Δ*m* = 0.8 mmu) [$C_{27}H_{27}O_3{}^6Li^7Li_3$], 287.1790 (287.1787, Δ*m* = 0.3 mmu) [$C_{18}H_{18}O_2{}^7Li_3$], 280.1633 (280.1627, Δ*m* = 0.6 mmu) [$C_{18}H_{18}O_2{}^7Li_4$]. IR (KBr): $\tilde{\nu}$ = 3528 (w), 3054 (w), 3019 (w), 2976 (m), 2909 (w), 2876 (w), 2731 (w), 1589 (s), 1533 (m), 1476 (s),1447 (m), 1375 (w), 1304 (m), 1271 (m), 1184 (w), 1151 (m), 1105 (w), 1045 (m), 980 (m), 895 (w), 857 (m), 798 (m), 754 (s), 727 (m), 579 (m) cm^{-1}. ^{1}H NMR ($CDCl_3$): δ = 7.02 (m, 16 H, H_{Ar}), 6.87 (d, $^3J_{H,H}$ = 16.39 Hz, 4 H, $CH_3CH{=}CHC_6H_4$), 6.12 (m, 4 H, $CH_3CH{=}CHC_6H_4$), 3.53 (m, 16 H, THF), 1.70 (d, $^3J_{H,H}$ = 6.49 Hz, 12 H, $CH_3CH{=}CHC_6H_4$), 1.61 (m, 16 H, THF) ppm. ^{13}C{^{1}H} NMR ($CDCl_3$): δ = 164.15 (s, 4 C, C_{Ar}−O), 130−114 (m, 20 C, C_{Ar}), 128.57 (s, 4 C, $CH_3CH{=}CHC_6H_4$), 123.41 (s, 4 C, $CH_3CH{=}CHC_6H_4$), 68.46 (s, 8 C, THF), 25.64 (s, 8 C, THF), 18.84 (s, 4 C, $CH_3CH{=}CHC_6H_4$) ppm.

[Li(12-crown-4)][MoCl$_3$O$_2$(THF)] (2): A solution of MoO_2Cl_2 (0.55 g, 2.79 mmol) in THF (40 mL) was cooled to −20 °C and 12-crown-4 was added (0.49 g, 2.79 mmol). To the resultant solution, butyllithium was slowly added (1.11 mL of a 2.5 M toluene solution) resulting in a change of the original yellow colour to a dark brown. After warming to room temp., the solution was stirred for 0.5 h and a fine black solid precipitated which was filtered. All volatiles were removed from the filtrate and the residue extracted with acetone (40 mL). Removal of the solvent yielded the pure product **2** (0.55 g, 1.13 mmol, 40.5%). $C_{12}H_{24}Cl_3LiMoO_7$ (489.6): calcd. C 29.44, H 4.94; found C 29.54, H 4.97. IR (KBr): $\tilde{\nu}$ = 2935 (m), 2877 (w), 1705 (m), 1452 (m), 1362 (m), 1286 (m), 1243 (m), 1136 (m), 1086 (s), 1021 (m), 985 (s), 927 (s), 860 (s), 741 (s), 529 (w), 423 (w) cm^{-1}. ^{1}H NMR ([D$_8$]THF): δ = 3.84 (s, 16 H, 12-crown-4), 3.63 (m, THF), 2.10 (s, acetone), 1.78 (m, THF) ppm. ^{13}C{^{1}H} NMR ([D$_6$]acetone): δ = 68.93 (s, 16 C, 12-crown-4), 68.49 (s, 2 C, THF). Crystals of **2′** could be obtained by extraction of the residue mentioned above with THF rather than acetone and cooling the resultant solution for several weeks to −28 °C.

[Li(12-crown-4)$_2$][MoO$_2${OC$_6$H$_4$(CH=CHCH$_3$)-2}$_3$] (3): A solution of 2-propenylphenol (1.04 g, 7.45 mmol) and 12-crown-4 (1.33 g, 7.56 mmol) in THF (10 mL) was cooled to −20 °C and BuLi was slowly added (3.1 mL 2.5 M solution in toluene). After stirring for 5 min, the resultant mixture was added slowly to $MoO_2(OtBu)_2$ (0.70 g, 2.57 mmol), dissolved in THF (10 mL) held at −20 °C. After stirring for 2 h, the resultant yellow-brown solution was reduced to a volume of 5 mL. After 24 h at −28 °C, microcrystalline **3** had precipitated and, due to the high sensitivity of **3** in the solid state (almost any manipulation caused the formation of a white solid at the surface) and the varying amounts of crown ether complexed to the lithium cations (NMR spectroscopy shows that the Li/crown ether ratios varies between 1:1 and 1:2), we failed to obtain a correct elemental analysis. Yield 0.993 g, 1.120 mmol, 43.6%. IR (KBr): $\tilde{\nu}$ = 2974 (w), 2913 (w), 2879 (w), 1590 (s), 1555 (w), 1477 (s), 1447 (s), 1371 (w), 1304 (m), 1246 (w), 1184 (w), 1146 (w), 1090 (m), 1045 (s), 980 (s), 926 (w), 856 (s), 799 (m), 755 (s), 727 (m), 579 (m), 418 (m) cm^{-1}. ^{1}H NMR ([D$_8$]THF, *T* = 30 °C): δ = 7.33 (br, 3 H, H_{Ar}), 7.03 (d, $^3J_{H,H}$ = 16.04 Hz, 3 H, $CH_3CH{=}CHC_6H_4$), 6.9−6.7 (br, 6 H, H_{Ar}), 6.42 (br, 3 H, H_{Ar}), 6.00 (m, 3 H, $CH_3CH{=}CHC_6H_4$), 3.65 (s, 12-crown-4), 1.67 (br, 9 H, $CH_3CH{=}CHC_6H_4$). ^{1}H NMR ([D$_8$]THF, *T* = −30 °C): δ = 7.33 (d, $^3J_{H,H}$ = 7.51 Hz, 3 H, H_{Ar}), 7.03 (d, $^3J_{H,H}$ = 16.04 Hz, 3 H, $CH_3CH{=}CHC_6H_4$), 6.9−6.7 (m, 6 H, H_{Ar}), 6.42 (t, 3 H, H_{Ar}), 6.00 (m, 3 H, $CH_3CH{=}CHC_6H_4$), 3.65 (s, 12-crown-4), 1.67 (d, $^3J_{H,H}$ = 6.49 Hz,

 © 2004 Wiley-VCH Verlag GmbH & Co. KGaA, Weinheim

Table 5. Crystallographic data

	1	**2′**	**3**
Empirical formula	$C_{52}H_{68}Li_4O_8$	$C_4H_8Cl_3MoO_3$, $C_{16}H_{32}ClLi_2O_8$	$C_{27}H_{27}MoO_5$, $C_{16}H_{32}LiO_8$
Formula mass	848.82	708.14	886.78
Crystal size [mm]	0.38 × 0.30 × 0.23	0.20 × 0.16 × 0.10	0.25 × 0.25 × 0.20
Crystal system	triclinic	monoclinic	monoclinic
Space group	$P\bar{1}$	$P2_1/m$	$P2_1/c$
Z	4	2	4
a [Å]	13.8574(10)	7.3426(12)	15.9953(9)
b [Å]	18.6508(13)	11.878(4)	12.0367(7)
c [Å]	19.2746(14)	17.197(5)	23.3104(13)
α [°]	86.674(2)	90	90
β [°]	87.4470(10)	94.813(14)	106.5460(10)
γ [°]	79.6330(10)	90	90
V [Å^3]	4889.0(6)	1494.5(7)	4302.1(4)
d(calcd.) [g cm^{-3}]	1.153	1.574	1.369
T [K]	103(2)	293(2)	103(2)
Max./min. Transmission	1.0000 and 0.9723	1.0000 and 0.7061	1.0000 and 0.9137
Diffractometer	Nonius Kappa CCD		
Radiation	Mo-K_a, graphite-monochromated (λ = 0.71073 Å)		
Corrections	Lorentz polarisation factor		
Refinement	Full-matrix least-squares on F^2		
Absorption correction	Semi-empirical from equivalents		
Absorption coefficient [mm^{-1}]	0.074	0.847	0.368
F(000)	1824	728	1864
hkl range	h: −16 to 16	h: −10 to 9	h: −19 to 18
	k: −22 to 22	k: −17 to 17	k: 0 to 14
	l: 0 to 22	l: −25 to 25	l: 0 to 27
Θ range [°]	1.50 to 25.03	2.09 to 32.02	1.82 to 25.00
Measured reflections	53344	18492	25221
Independent reflections	17260	5346	7569
Observed reflections [$I > 2\sigma(I)$]	11563	4068	5591
Parameters	1506	270	531
R_1	0.0585	0.0662	0.0711
wR_2	0.1461	0.1304	0.1666
R (all)	0.0963	0.0919	0.0992
Residual electron density [eÅ^{-3}]	+0.942/−1.037	+2.932−2.868	+2.463−1.776

9 H, $CH_3CH{=}CHC_6H_4$) ppm. $^{13}C\{^1H\}$ NMR ([D$_8$]THF, T = 30 °C): δ = 164.77 (s, 3 C, C_{Ar}−O), 130−114 (m, 15 C, C_{Ar}), 128.77 (s, 3 C, $CH_3CH{=}CHC_6H_4$), 120.40 (s, 3 C, $CH_3CH{=}CHC_6H_4$), 71.25 (s, 12-crown-4), 18.23 (s, $CH_3CH{=}CHC_6H_4$) ppm. Recrystallisation of microcrystalline **3** from 1,4-dioxane/hexane at room temperature yielded crystals suitable for a single-crystal X-ray diffraction study.

X-ray Crystallographic Studies:[19] Crystals were obtained as described above. Diffraction data were recorded with a Bruker AXS Smart CCD diffractometer. Empirical absorption corrections were applied. The structures were solved using direct methods and refined anisotropically with the SHELXL-97[20] and SHELXS-97[21] programs. Hydrogen atoms were included with fixed distances and isotropic temperature factors 1.5 times those of the atoms to which they are attached. Parameters were refined against F^2. The R values are defined as $R_1 = \Sigma||F_o| - |F_o|/\Sigma|F_o|$, $R_w = [\Sigma(F_o^2 - F_c^2)^2/\Sigma w(F_o)^2]^{0.5}$. Table 5 lists the crystallographic data.

Acknowledgments

We are grateful to the Deutsche Forschungsgemeinschaft for a Heisenberg scholarship as well as funding. We would also like to thank the Fonds der Chemischen Industrie, the BMBF, the Karl-Winnacker-Stiftung and the Dr. Otto Röhm Gedächtnisstiftung for financial benefits.

[1] [1a] G. W. Keulks, L. D. Krenzke, T. M. Notermann, *Adv. Catal.* **1978**, *27*, 183. [1b] R. K. Grasselli, J. D. Burrington, *Adv. Catal.* **1981**, *30*, 133. [1c] R. K. Grasselli, J. D. Burrington, *Ind. Engl. Chem. Prod. Res. Dev.* **1984**, *23*, 394; J. Belgacem, J. A. Osborn, J. Kress, *J. Mol. Catal.* **1994**, *86*, 267. [1d] R. K. Grasselli, in *Handbook of Heterogeneous Catalysis* (Eds.: G. Ertl, H. Knözinger, J. Weitkamp), VCH Verlagsgesellschaft GmbH, Weinheim, **1997**, pp 2302; Y. H. Jang, W. A. Goddard III, *Top. Catal.* **2001**, *15*, 273.

[2] C. Wippert Rodrigues, B. Antelmann, C. Limberg, H. Pritzkow, *Organometallics* **2001**, *20*, 1825.

[3] D. C. Bradley, R. C. Mehrotra, I. P. Rothwell, A. Singh, *Alkoxo and Aryloxo Derivatives of Metals*, Academic Press, London, **2001**, p. 509.

[4] L. M. Jackman, D. Cizmeciyan, P. G. Williard, M. A. Nichols, *J. Am. Chem. Soc.* **1993**, *115*, 6262.

[5] D. Walther, U. Ritter, S. Gessler, J. Sieler, M. Kunert, *Z. Anorg. Allg. Chem.* **1994**, *620*, 101.

[6] H. Schumann, J. A. Meese-Marktscheffel, J. Loebel, *Z. Naturforsch., Teil B* **1990**, *45*, 1304.

[7] T. Kottke, R. J. Lagow, D. Hoffmann, R. D. Thomas, *Organometallics* **1997**, *16*, 789.

[8] *Gmelin Handbook of Inorganic Chemistry*, 8th ed., Springer, Berlin, **1990**, Syst. No. 53, Suppl. Vol. B6.

[9] M. J. Taylor, J. Michael, C. E. F. Rickard, L. A. Kloo, *J. Chem. Soc., Dalton Trans.* **1998**, 3195.

 © 2004 Wiley-VCH Verlag GmbH & Co. KGaA, Weinheim

[10] F. Gingl, W. Hiller, J. Strähle, H. Borgholte, K. Dehnicke, *Z. Anorg. Allg. Chem.* **1991**, *606*, 91.
[11] A. W. Addison, T. N. Rao, J. Reedijk, J. van Rijn, G. C. Verschor, *J. Chem. Soc., Dalton Trans.* **1984**, 1349.
[12] J. M. Berg, R. H. Holm, *J. Am. Chem. Soc.* **1985**, *107*, 917.
[13] M. Huang, C. W. DeKock, *Inorg. Chem.* **1993**, *32*, 2287.
[14] P. Barbaro, C. Blanchini, G. Scapacci, D. Masi, P. Zanello, *Inorg. Chem.* **1994**, *33*, 3180.
[15] J. M. Hawkins, J. C. Dewan, K. B. Sharpless, *Inorg. Chem.* **1986**, *25*, 1501.
[16] T. A. Hanna, A. K. Ghosh, C. Ibarra, M. A. Mendez-Rojas, A. L. Rheingold, W. H. Watson, *Inorg. Chem.* **2004**, *43*, 1511.
[17] A border case has been reported where two such molecules show a dimeric arrangement in the solid state with strong intermolecular Mo···O=Mo contacts (S. Bellemin-Laponnaz, K. S. Coleman, P. Dierkes, J.-P. Masson, J. A. Osborn, *Eur. J. Inorg. Chem.* **2000**, 1645). Moreover, the complex [(η^2-*t*Bu_2Pz)MoO_2Cl] (K. Most, S. Köpke, F. Dall'Antonia, N. C. Mösch-Zanetti, *Chem. Commun.* **2002**, *16*, 1676) can be described as showing 5-coordination if the η^2-pyrazolate ligand is regarded as occupying two coordination sites. However, such pyrazolate ligands are certainly special cases (both sterically and electronically) and are not comparable with "classical" charged or uncharged donor ligands.
[18] M. Jolly, J. P. Mitchell, V. C. Gibson, *J. Chem. Soc., Dalton Trans.* **1992**, *7*, 1331.
[19] CCDC-231744 (**1**), -231746 (**2′**) and -231745 (**3**) contain the supplementary crystallographic data for this paper. These data can be obtained free of charge at www.ccdc.cam.ac.uk/conts/retrieving.html [or from the Cambridge Crystallographic Data Centre, 12 Union Road, Cambridge CB2 1EZ, UK; Fax: (internat.) + 44-1223-336-033; E-mail: deposit@ccdc.cam.ac.uk].
[20] G. M. Sheldrick, *SHELXL-97, Program for Crystal Structure Refinement*, University of Göttingen, **1997**.
[21] G. M. Sheldrick, *SHELXS-97, Program for Crystal Structure Solution*, University of Göttingen, **1997**.

Received March 15, 2004
Early View Article
Published Online July 12, 2004

 © 2004 Wiley-VCH Verlag GmbH & Co. KGaA, Weinheim

Synthesis of a Dinuclear Ruthenabicyclic Complex and Its Ligand-Substitution Reactions

Yoshihiko Yamamoto,*[a] Yumiko Miyabe,[b] and Kenji Itoh[b]

Keywords: Alkyne ligands / Carbonyl ligands / Metallacycles / Phosphane ligands / Ruthenium

A trinuclear carbonylruthenium complex, $[Ru_3(CO)_{12}]$, was treated with diynes bearing ester, phenyl, or trimethylsilyl groups on the alkyne termini to give rise to various complexes. A diyne diester afforded a dinuclear ruthenacycle complex similar to known iron ferrole complexes and a mononuclear ruthenacyclopentadiene complex. The selectivity for the formation of these products varied depending on the ratio of the diyne diester toward $[Ru_3(CO)_{12}]$. When a phenyl-substituted diyne was employed, a cyclopentadienone complex was formed together with the expected dinuclear ruthenacycle complex. In contrast, a bis(trimethylsilyl)diyne gave the corresponding cyclopentadienone complex as the only product. Treatment of the obtained ruthenabicycle complex with trimethylamine oxide (Me_3NO) gave a mono(trimethylamine) complex, which was further converted into various phosphane complexes upon reaction with phosphanes in refluxing THF. The corresponding monophosphane complexes were obtained for all monodentate or bidentate phosphanes except for bis(diphenylphosphanyl)methane, which afforded a bridging bis(phosphane) complex. In contrast, when an isolated monodentate phosphane complex of 1,2-bis(diphenylphosphanyl)ethane and diphenyl(2-pyridyl)phosphane was treated with Me_3NO, P-P or P-N chelate complexes were formed, respectively. The dinuclear mono(amine)ruthenacycle complex also reacted with dimethyl butynedioate (dimethyl acetylenedicarboxylate, DMAD) in refluxing THF to afford a novel μ-η^2-alkyne complex together with the [2+2+2] cycloadduct between the diyne and DMAD. The highly electron-deficient character of DMAD is imperative for the formation of the μ-alkyne complex. Methyl propiolate and diphenylacetylene gave no corresponding μ-alkyne complexes.

(© Wiley-VCH Verlag GmbH & Co. KGaA, 69451 Weinheim, Germany, 2004)

Introduction

Metallacyclopentadienes have received considerable attention because of their close relevance to alkyne cyclooligomerization reactions.[1] The oxidative cyclization of two alkyne molecules with a low-valent transition-metal fragment gives rise to a metallacyclopentadiene. The diene moiety of a metallacyclopentadiene can be coordinated by another metal fragment to form a dinuclear complex.[2] Among such dinuclear metallacycle complexes, iron ferrole complexes, $[Fe_2(CO)_6(RC_2R')_2]$,[3,4] and their cobalt analogues[5] have been extensively explored as intermediates for the formation of a variety of organic molecules from alkynes and carbonyl transition-metal complexes. With respect to the ruthenium analogues, most examples have been obtained from the reaction of a trinuclear carbonyl cluster, $[Ru_3(CO)_{12}]$ (**1**), with monoalkynes and conjugated polyalkynes.[6,7] However, the reported yields of the dinuclear complexes were not high and generally below 50%. Therefore, further exploration of the dinuclear ruthenacycle complexes awaits an improved synthetic method.

We have recently developed ruthenium-catalyzed [2+2+2] cycloadditions of 1,6-diynes with unsaturated molecules, resulting in the formation of benzenes, cyclohexadienes, pyridines, pyridones, etc.[8] These cycloadditions essentially did not take place with monoalkynes, except for electron-deficient ones, indicating that the 1,6-diyne substrates play a critical role in the formation of the ruthenacycle key intermediate: the oxidative cyclization of the 1,6-diynes is entropically more favorable than that of monoalkynes. With these facts in mind, we further investigated the reaction of **1** with diynes to establish a highly efficient route to bicyclic analogues of the dinuclear ruthenacycle complexes.[9] Herein we report on the efficient synthesis of a dinuclear ruthenabicycle complex, using a diyne diester as an alkyne substrate, and its ligand-substitution reactions.

[a] Department of Applied Chemistry, Graduate School of Engineering, Nagoya University, Chikusa, Nagoya 464-8603, Japan
Fax: + 81-52-789-3209
E-mail: yamamoto@apchem.nagoya-u.ac.jp
[b] Department of Molecular Design and Engineering, Graduate School of Engineering, Nagoya University, Chikusa, Nagoya 464-8603, Japan

Results and Discussion

Reaction of $[Ru_3(CO)_{12}]$ with Diynes

At the outset, the diyne diester **2a** bearing methoxycarbonyl terminal substituents was examined as a diyne sub-

strate (Scheme 1) because the electron-deficient alkyne termini favor oxidative cyclization with a low-valent transition-metal fragment.[10] The trinuclear cluster $[Ru_3(CO)_{12}]$ (**1**) and **2a** were allowed to react under various reaction conditions (Table 1). In toluene, **1** and 2 equiv. of **2a** were heated at 110 °C under Ar for 0.5 h (run 1). The TLC analysis of the crude reaction mixture showed the complete consumption of **2a**. Separation by silica-gel chromatography gave pure **3a**. In the ^{1}H NMR spectrum of **3a**, the absorptions of the methylene protons adjacent to the ether oxygen atom appear at δ = 4.80 (dd, $J_{H,H}$ = 15.3, 2.4 Hz, 2 H) and 5.08 (dd, $J_{H,H}$ = 15.3, 2.4 Hz, 2 H) ppm, indicative of the diyne having undergone oxidative cyclization. This was also confirmed by the IR spectrum, which shows no alkyne absorption. Instead, strong absorptions corresponding to the CO ligands were observed around 2000 cm^{-1}. The ^{13}C NMR spectrum shows the resonance of the CO ligands at δ = 192.21, 193.60, and 194.37 ppm as well as three sp^2- and two sp^3-carbon signals. Finally, single-crystal X-ray crystallography unambiguously revealed that **3a** is a dinuclear ruthenacycle complex, as shown in Figure 1. The unit cell contains two crystallographically unique molecules **3a(A)** and **3a(B)**. Similar to known ferrole-type complexes,[6] the $[Ru_2(CO)_6]$ fragments of **3a** have a "non-sawhorse" geometry typified by a semi-bridging CO ligand and an Ru−Ru single bond of about 2.72 Å, which is within the range of Ru−Ru single bond lengths found previously.[6] In **3a(A)**, the Ru2−C2 and Ru2−C7 bond lengths are 2.071(9) and 2.105(8) Å, respectively, and the C2−C3 and C6−C7 bonds [1.467(11) and 1.478(10) Å] are longer than the C3−C6 bond [1.351(12) Å]. In contrast, the Ru2−C2 and Ru2−C7 bonds [2.096(7) and 2.114(8) Å] in **3a(B)** are longer than those in **3a(A)**, and the C3−C6 bond of 1.456(11) Å is longer than the C2−C3 and C6−C7 bonds [1.369(12) and 1.375(12) Å] in **3a(B)**. These data indicate that **3a(A)** and **3a(B)** are represented as structures **I** and **II**, respectively, in Scheme 2. These structural features are quite similar to the previously reported tetrakis(methoxycarbonyl) analogue.[6d]

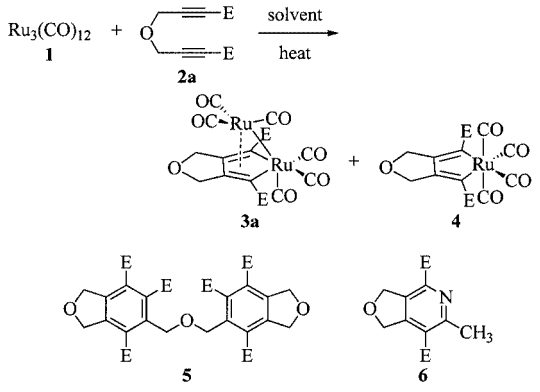

Scheme 1. Reaction of $[Ru_3(CO)_{12}]$ (**1**) with diyne diester **3a**

Together with **3a**, the diyne trimer **5** was also obtained in 13% yield as a result of the [2+2+2] cycloaddition of **2a**.[10c,10d] In addition, 51% of **1** was recovered intact. To improve the yield of **3a**, the reaction conditions were further optimized. Using acetonitrile instead of toluene as a solvent successfully suppressed the formation of **5**, although a trace amount of pyridine **6** was formed by [2+2+2] cycloaddition of **2a** with CH_3CN (Table 1, run 2). As a consequence, the yield of **3a** was raised to 56%. Although **1** was almost completely consumed, total recovery of ruthenium (**3a** and recovered **1**) was not more than 60%. This was probably because **1** decomposed under argon with concomitant extrusion of CO. Thus, the reaction was then conducted under 1 atm of CO in refluxing CH_3CN (run 3). The starting **2a** was totally consumed within 1 h. However, the yield of **3a** was not improved, and an additional product, **4**, was obtained as well as recovered **1**. The IR spectrum of **4** is very similar to that of **3a**. The absorptions of a conjugated carbonyl group and the CO ligands are observed at 1676 cm^{-1} and around 2000 cm^{-1}, respectively. In contrast to **3a**, only two singlet signals assigned to $-OCH_2-$ and $-OCH_3$ with a 2:3 integral ratio appear at δ = 4.65 and 3.75 ppm, respectively, in the ^{1}H NMR spectrum. Furthermore, in the ^{13}C NMR spectrum, five sp^2-carbon peaks are observed at δ = 171−190 and 133.66 ppm along with sp^3-carbon peaks assigned to $-OCH_2-$ and $-OCH_3$ at δ = 70.62 and 51.98 ppm, respectively. These data suggest that **4** is a highly symmetrical carbonylruthenium complex derived from **2a**. The detailed structural assignment was accomplished by X-ray crystallographic analysis. As shown in Figure 1, **4** is a mononuclear ruthenabicycle complex bearing four CO ligands. The unit cell contains two crystallographically unique molecules. The geometry of the ruthenium center is distorted octahedral with the basal plane consisting of the two CO ligands and the metallacycle carbon atoms C2 and C7; there are two apical CO ligands. The C13−Ru1−C14 angles are 164.5(3)° and 165.0(3)°. The ruthenacycle moieties present normal metallacyclopentadiene geometries with $C_\alpha-C_\beta$ bond lengths ranging from 1.307(13) to 1.388(12) Å, which are shorter than the $C_\beta-C_\beta$ bonds [1.471(12) and 1.432(12) Å]. The $Ru-C_\alpha$ distances, ranging from 2.110(10) to 2.172(8) Å, are similar to those of typical Ru−sp^2-C single bonds.[11]

Further optimization of the reaction conditions was carried out by performing the reaction under higher CO pressure in an autoclave. Under 5 atm of CO, **1** and 2 equiv. of **2a** were heated in CH_3CN at 120 °C for 12 h to afford **3a** in an improved isolated yield of 74% together with **4** in 20% yield (Table 1, run 4). Trace amounts of **6** and recovered **1** were also detected. Similar results were obtained from the reaction under 10 atm of CO (run 5). The reduced amounts of the diyne **2a** increased the product selectivity in favor of the dinuclear complex **3a**. The use of 1.5 equiv. of **2a** (**2a**/Ru = 1:2) gave predominantly **3a** in 87% yield (run 6). The reaction terminated after 1 h resulted in lower conversion of **1** (70%), and, interestingly, both **3a** and **4** were obtained in 43 and 21% yields, respectively (run 7). This result suggests that the initially formed mononuclear complex **4** might be converted into the dinuclear complex **3a**. In fact, the isolated **4** was treated with **1** (1 equiv. Ru) in CH_3CN at 120 °C under 5 atm of CO for 12 h to afford **3a** in 78% yield together with recovered **4** and **1** (18% and 23%, respec-

 © 2004 Wiley-VCH Verlag GmbH & Co. KGaA, Weinheim

Table 1. Reaction of $Ru_3(CO)_{12}$ (**1**) with diynes **2**

Run	**2**, R (equiv.)	Conditions	Products (yield [%])[a]	Recovered **1** [%]
1	**2a**, CO_2CH_3 (2)	Ar, toluene, reflux, 0.5 h	**3a** (27), **5** (13)	51
2	**2a**, CO_2CH_3 (2)	Ar, CH_3CN, reflux, 0.5 h	**3a** (56), **6** (trace)	4
3	**2a**, CO_2CH_3 (2)	CO (1 atm), CH_3CN, reflux, 1 h	**3a** (60), **4** (9), **6** (trace)	10
4	**2a**, CO_2CH_3 (2)	CO (5 atm), CH_3CN, 120 °C, 12 h	**3a** (74), **4** (20), **6** (trace)	trace
5	**2a**, CO_2CH_3 (2)	CO (10 atm), CH_3CN, 120 °C, 12 h	**3a** (62), **4** (24), **6** (trace)	9
6	**2a**, CO_2CH_3 (1.5)	CO (5 atm), CH_3CN, 120 °C, 12 h	**3a** (86), **6** (trace)	9
7	**2a**, CO_2CH_3 (1.5)	CO (5 atm), CH_3CN, 120 °C, 1 h	**3a** (43), **4** (21), **6** (trace)	30
8	**2b**, Ph (1.5)	CO (5 atm), CH_3CN, 120 °C, 12 h	**3b** (20), **7b** (8)	63
9	**2b**, Ph (3)	CO (5 atm), CH_3CN, 120 °C, 12 h	**3b** (25), **7b** (12)	37
10	**2c**, $Si(CH_3)_3$ (1.5)	CO (5 atm), CH_3CN, 120 °C, 12 h	**7c** (41)	43
11	**2c**, $Si(CH_3)_3$ (3)	CO (5 atm), CH_3CN, 120 °C, 12 h	**7c** (76)	8

[a] Isolated yield based on $Ru_3(CO)_{12}$.

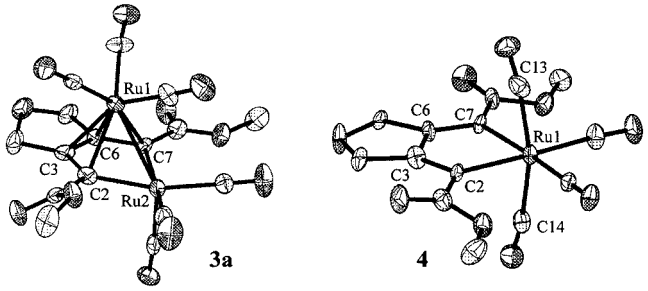

Figure 1. ORTEP diagrams of **3a** (left) and **4** (right), showing each one of two crystallographically unique molecules in the unit cell; all hydrogen atoms have been omitted for clarity

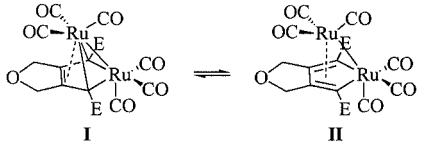

Scheme 2. Two unique structures of dinuclear ruthenabicycle complex **3a** (E = CO_2CH_3)

tively). In contrast, the reaction of **3a** with 1 equiv. of **2a** under the same conditions did not produce the mononuclear complex **4**. In this case, **3a** and **2a** were recovered in 98 and 96% yields, respectively. These facts clearly show that the use of exactly 1 equiv. of **2a** per 2 Ru atoms is essential for the selective formation of the desired dinuclear complex.

Next, diynes **2b**−**e** bearing other substituents were treated with **1** (Scheme 3). The phenyl-substituted diyne **2b** was found to be a less-efficient substrate under the reaction conditions optimized with respect to **2a**, resulting in a low conversion of **1** (Table 1, run 8). The expected dinuclear complex **3b** was obtained in 20% yield. In addition to **3b**, a small amount of new product **7b** was also obtained. In its IR spectrum, a weak absorption is observed at 1635 cm^{-1} as well as sharp and strong absorptions corresponding to the carbonyl ligands at 2086 and 2031 cm^{-1}. The former can be assigned to a conjugated ketone carbonyl group. In accordance with this assignment, a peak of the conjugated ketone carbon atom is observed at δ = 173.42 ppm in the ^{13}C NMR spectrum. The absorption of the CO ligands also appears as a single peak at δ = 193.53 ppm. On the basis of these spectroscopic data, **7b** was assigned to the cyclopentadienone complex depicted in Scheme 3.[12] This assignment was further confirmed by X-ray crystallography (Figure 2). The use of 3 equiv. of **2b** improved the conversion of **1**, while the yields of both products were only slightly increased (run 9).

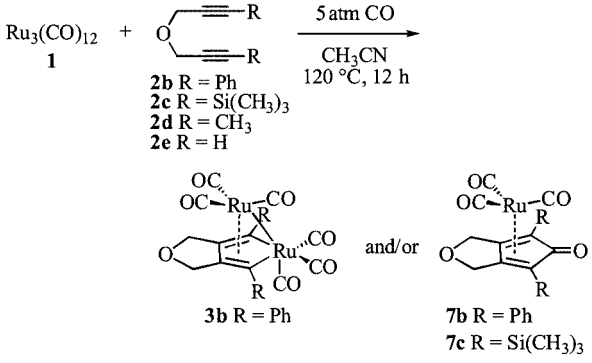

Scheme 3. Reactions of [$Ru_3(CO)_{12}$] (**1**) with diynes **2b**−**e**

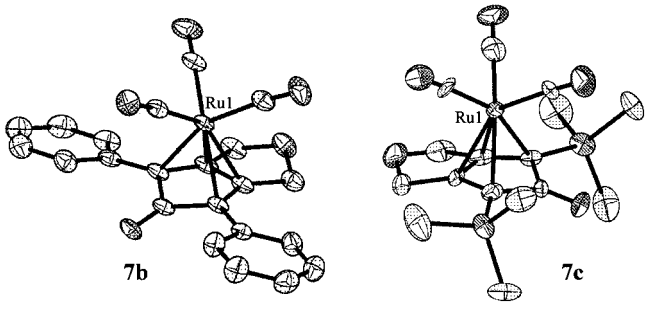

Figure 2. ORTEP diagrams of **7b** (left) and **7c** (right); all hydrogen atoms have been omitted for clarity

The reaction of the trimethylsilyl-substituted diyne **2c** with **1** gave rise to a sole product (Scheme 3). Its IR spectrum shows the presence of a conjugated carbonyl group (1623 cm^{-1}) and CO ligands (2136−2009 cm^{-1}), and the ^{13}C NMR spectral pattern is quite similar to that of **7b**, except for the upfield signal of the TMS-substituted sp^2-

 © 2004 Wiley-VCH Verlag GmbH & Co. KGaA, Weinheim

carbon atoms (δ = 65.78 ppm). These spectroscopic data allowed us to assign this product as the cyclopentadienone complex **7c**. This assignment was confirmed by X-ray crystallographic analysis (Figure 2). When 1.5 equiv. of **2c** (**2c**/Ru = 1:2) was employed, **7c** was isolated in 41% yield along with 43% recovered **1** (Table 1, run 10). The increased amount of **2c** (3 equiv., **2c**/Ru atom = 1:1) raised the yield of **7c** up to 76% yield (run 11).

In contrast to the diynes **2a**−**c**, the diynes bearing terminal methyl substituents (**2d**) or a propargyl ether (**2e**) gave intractable product mixtures. Therefore, the electron-withdrawing methoxycarbonyl group is the optimal terminal substituent for the formation of the dinuclear ruthenacycle framework.

Ligand-Substitution Reactions of Dinuclear Ruthenabicyclic Complex 3a

Having established the high-yield synthesis of the dinuclear ruthenacycle complex **3a**, we then explored its ligand-substitution reactions. Previously, Sappa, Tiripicchio, and co-workers have reported that a ferrole complex **8** reacts with various mono- and diphosphanes or nitriles in the presence of trimethylamine *N*-oxide (Me_3NO) to afford diferracycloheptadienones **10** together with simple ligand-substitution products **9** (Scheme 4).[3o] Such "flyover-bridged" complexes can be further converted into cyclopentadienone and *p*-benzoquinone derivatives. On the other hand, the reaction with phenylacetylene under the same reaction conditions resulted in the formation of a bicyclic complex **11**, probably via a "flyover" complex similar to **10**. In these cases, the ferracyclopentadiene moiety was singly cleaved at its $C_\beta-C_\beta$ bond, and subsequent CO insertion formed the "flyover-bridged" complexes. In contrast, we anticipated that such a metallacyclic ring cleavage cannot be viable for our bicyclic ruthenium complex **3a** because the ruthenacyclopentadiene moiety is stabilized by the fused dihydrofuran ring. In fact, the treatment of **3a** with 1 equiv. of Me_3NO in THF at room temperature for 1 h afforded a trimethylamine complex **12** in 93% isolated yield (Scheme 5). Its ^1H and ^{13}C NMR spectra are very similar to those of the parent **3a** except for the additional peaks of the trimethylamine ligand. The X-ray crystallographic analysis of **12** clearly showed that the amine ligand is located on the upper ruthenium(0) center (Ru1, Figure 3). This ligand substitution regioselectivity is in contrast to that observed for the iron ferrole complex **9**, in which the newly introduced ligands are uniformly found on the metallacycle iron(II) center. The Ru−Ru and Ru−N bond lengths are 2.70775(19) and 2.2468(13) Å, respectively. One of the two CO ligands on the Ru1 center occupies the semi-bridge position. The $C_\alpha-C_\beta$ bonds are only slightly longer than the $C_\beta-C_\beta$ bond, indicative of the ruthenacycle moiety behaving as a typical η^4-butadienyl ligand.

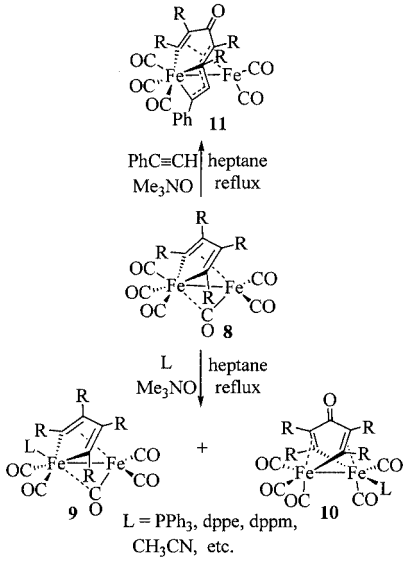

Scheme 4. Ligand-substitution reactions of iron ferrole complex **8** (R = C_2H_5)

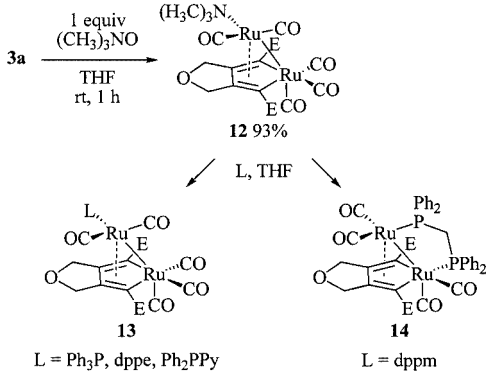

Scheme 5. Ligand-substitution reactions of dinuclear ruthenabicycle complex **3a** (E = CO_2CH_3)

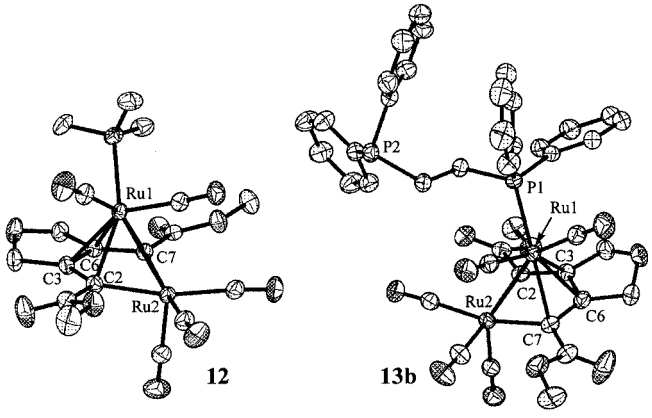

Figure 3. ORTEP diagrams of **12** (left) and **13b** (right); all hydrogen atoms have been omitted for clarity

Next, we carried out the substitutions of the amine ligand with various phosphanes, as outlined in Scheme 5 and Table 2. Upon treatment with 5 equiv. of triphenylphosphane in THF, **12** was completely consumed at room temperature after 96 h to give the expected phosphane complex **13a** (L = PPh_3) in 91% yield (run 1). Its ^1H NMR spectrum shows one singlet [δ = 3.41 (OCH_3) ppm] and a pair of doublets [δ = 3.94 and 4.65 ($-CH_2OCH_2-$) ppm] as well as the resonance of the aromatic protons (δ = 7.33−7.49

 © 2004 Wiley-VCH Verlag GmbH & Co. KGaA, Weinheim

ppm). The phosphorus resonance of **13a** is observed at lower field (δ = 41.87 ppm) than that of free PPh_3 (δ = −4.94 ppm) in the ^{31}P NMR spectrum. These facts clearly show the presence of the coordinated PPh_3 ligand in **13a**. Similarly, 1,2-bis(diphenylphosphanyl)ethane (dppe) was allowed to react with **12** at room temperature for 97 h (run 2). In the ^{31}P NMR spectrum of the obtained product both coordinated and free phosphorus peaks appear at δ = 40.77 and −11.57 ppm as doublets ($J_{P,P}$ = 42.3 Hz), indicative of dppe behaving as a two-electron donor ligand rather than a chelating one. This coordination mode was unambiguously confirmed by X-ray crystallography (Figure 3). The dppe ligand is located on the upper ruthenium center, and one of the remaining CO ligands occupies the semi-bridge position. The Ru1−P1 bond length is 2.3381(5) Å. At room temperature, the ligand exchange is slow and the yield of **13b** is moderate. In refluxing THF, however, the reaction is complete within 2 h, and the yield increases from 66% to 93% (run 3). Therefore, the amine complex **12** was subjected to the reaction with other phosphanes in refluxing THF.

Table 2. Reaction of trimethylamine complex **12** with phosphanes

Run	Phosphane (equiv.)	Conditions[a]	Product (yield [%])
1	Ph_3P (5)	room temp., 96 h	**13a** (91)
2	$Ph_2P(CH_2)_2PPh_2$ (5)	room temp., 97 h	**13b** (66)
3	$Ph_2P(CH_2)_2PPh_2$ (5)	reflux, 5 h	**13b** (88)
4	$Ph_2PCH_2PPh_2$ (5)	reflux, 2.5 h	**14** (91)
5	Ph_2PPy (5)	reflux, 2 h	**13c** (97)

[a] All reactions were carried out in THF under Ar.

Upon treatment with bis(diphenylphosphanyl)methane (dppm) under the same reaction conditions, **12** was consumed within 2.5 h (run 4). In contrast to the above complexes, the obtained product **14** turned out to have an unsymmetrical structure. In its ^1H NMR spectrum, the methoxy groups appear as two singlet peaks at δ = 3.00 and 3.82 ppm. Similarly, the dihydrofuran ring methylene groups in an unsymmetrical environment are observed as four doublets of doublets, and the methylene protons of the dppm ligand appear as a pair of doublets of doublets [δ = 4.95 ($J_{H,H}$ = 14, $J_{P,H}$ = 22.1 Hz) and 5.69 ($J_{H,H}$ = 14, $J_{P,H}$ = 26.9 Hz) ppm]. In the ^{31}P NMR spectrum, the two phosphorus atoms resonate at δ = 13.31 and 15.01 ppm ($J_{P,P}$ = 47.9 Hz). These data suggest that the dppm ligand forms an unsymmetrical ring. The structure of **14** was established by X-ray crystallography. As depicted in Figure 4, the dppm ligand bridges the two ruthenium centers to form a five-membered ring. The Ru2−P2 bond [2.3525(9) Å] is slightly longer than the Ru1−P1 bond [2.3276(8) Å]. The Ru−Ru bond of 2.7478(4) Å is slightly longer than those of **3a** [2.7156(7) Å] or **13b** [2.7208(2) Å].

As described above, the slight difference between dppe and dppm resulted in contrasting results. The former gave the monophosphane complex, whereas the latter directly formed the dppm-bridged complex with concomitant extrusion of 1 CO ligand. In this context, we further examined whether a similar dppe-bridged complex can be formed

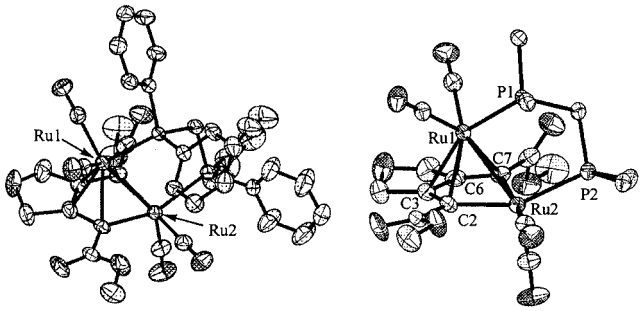

Figure 4. ORTEP diagrams of **14**; all hydrogen atoms and phenyl rings (right) have been omitted for clarity

when **13b** is treated with Me_3NO. The isolated **13b** was allowed to react with 1 equiv. of Me_3NO in THF at ambient temperature for 1 h to afford a new complex **15b** (Scheme 6). Its ^{31}P NMR spectrum, however, shows only one singlet signal at δ = 68.60 ppm, indicative of the dppe ligand forming a symmetrical chelate ring. The ^1H NMR spectrum also revealed its symmetrical structure: only one methoxy signal and a pair of doublets corresponding to the methylene protons on the dihydrofuran ring are observed together with the absorptions of the benzene rings and the ethylene tether of dppe. The detailed structure of **15b** was confirmed by an X-ray crystallographic analysis (Figure 5). In contrast to **14**, both phosphorus atoms of dppe are located on the Ru1 center, and the remaining CO ligand on Ru1 occupies the semi-bridge position. The Ru−P bonds of 2.3099(16) and 2.3125(7) Å are slightly shorter than that of the parent **13b**. Consequently, the difference in the P−P distances of these two bis(phosphane) ligands alters the coordination mode from the bridge-type for dppm to the chelating one for dppe.

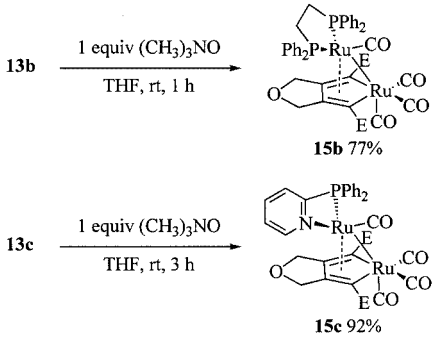

Scheme 6. Reactions of dinuclear ruthenabicycle phosphane complexes **13b** and **13c** with $(CH_3)_3NO$ (E = CO_2CH_3)

In addition to the above bis(phosphanes), a P-N ligand, Ph_2PPy (Py = 2-pyridyl), was also subjected to the ligand-substitution reaction with **12** (Table 3, run 5). As a result, Ph_2PPy behaved as a monophosphane ligand to give **13c** in 97% yield. In a similar manner to **15b**, a P-N chelate complex **15c** was obtained from **13c** in 92% yield (Scheme 6). The detailed structural data for these complexes were obtained by X-ray crystallography (Figure 6). The Ru−P bond is shortened from 2.3603(9) Å for **13c** to 2.3065(15)

 © 2004 Wiley-VCH Verlag GmbH & Co. KGaA, Weinheim

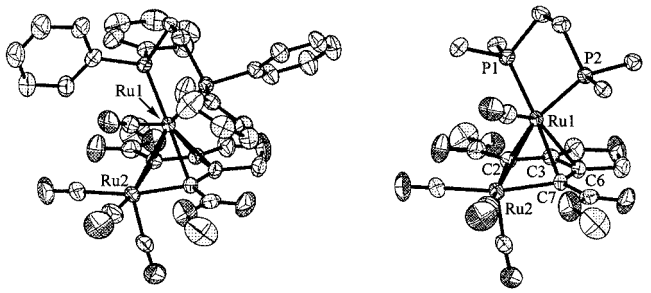

Figure 5. ORTEP diagrams of **15b**; all hydrogen atoms and phenyl rings (right) have been omitted for clarity

Å for **15c**. The Ru−Ru distance also decreases, from 2.7060(4) Å to 2.6774(6) Å, upon formation of the P-N chelate ring. The Ru1−N bond length is 2.152(5) Å.

Table 3. Comparison of average bond lengths [Å] of dinuclear ruthenacycle complexes

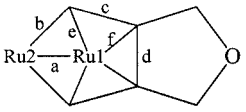

	3a(A)	3a(B)	12	13b	13c	14	15b	15c	16(A)	16(B)
a	2.716	2.718	2.708	2.721	2.706	2.748	2.704	2.677	2.729	2.729
b	2.088	2.105	2.105	2.099	2.103	2.102	2.086	2.106	2.171	2.135
c	1.473	1.372	1.424	1.414	1.418	1.418	1.427	1.431	1.380	1.416
d	1.351	1.456	1.402	1.428	1.451	1.413	1.400	1.397	1.473	1.397
e	2.246	2.227	2.209	2.274	2.249	2.249	2.230	2.198	2.198	2.187
f	2.239	2.264	2.304	2.278	2.291	2.248	2.311	2.259	2.298	2.297

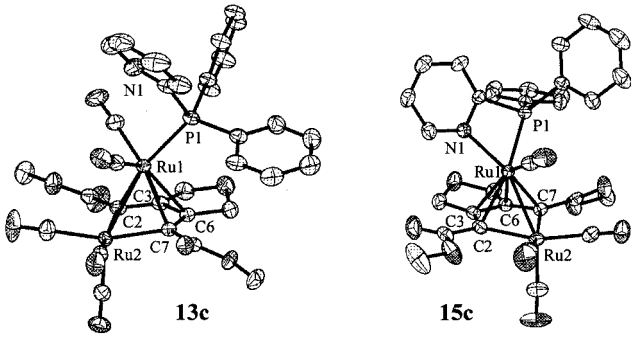

Figure 6. ORTEP diagrams of **13c** (left) and **15c** (right); all hydrogen atoms have been omitted for clarity

Reaction of Dinuclear (Amine)ruthenabicycle Complex 12 with Alkynes

As mentioned above, metallacyclopentadiene complexes have been investigated as intermediates in alkyne cyclotrimerizations.[1] Ferrole-type cobalt complexes have also been considered to be intermediates for $[Co_2(CO)_6]$-mediated alkyne cyclotrimerizations.[5f] In this respect, dicobalt complexes bearing a "flyover" hexatrienyl ligand have been obtained from the reaction of (cobaltacyclopentadiene)cobalt complexes with alkynes.[13] In addition, the reaction of a dinuclear cobaltacyclopentadiene complex derived from an amine-tethered diyne with phenylacetylene has been reported to give a fused benzene in high yield.[9a] With these facts in mind, we finally explored the reactivity of the amine complex **12** toward monoalkynes. At the outset, **12** was treated with 5 equiv. of dimethyl acetylenedicarboxylate (DMAD) in refluxing THF for 1 h (Scheme 7). As a result, a new ruthenacycle complex **16** was obtained together with trace amounts of the [2+2+2] cycloadduct **17** between the diyne **2a** and DMAD.[10c][10d] The ^{1}H NMR analysis of **16** disclosed that the complex consists of the symmetrical ruthenacycle moiety and the unsymmetrically coordinated DMAD fragment. The methoxy and methylene protons of the ruthenacycle appear as one singlet (δ = 3.68 ppm) and two doublet peaks [δ = 4.84 and 5.06 ($J_{H,H}$ = 14.7 Hz) ppm], respectively, whereas the methoxy protons of DMAD resonate at δ = 3.84 and 3.89 ppm. Similarly, the ^{13}C NMR spectrum shows 3 and 4 sp^2-carbon signals for the ruthenacycle (δ = 169.81, 155.07, and 147.95 ppm) and the DMAD ligand (δ = 171.58, 165.96, 127.31, and 88.77 ppm), respectively. The structure of **16** was finally determined by X-ray crystallography (Figure 7). The unit cell contains two crystallographically unique molecules **16(A)** and **16(B)**. DMAD bridges two ruthenium centers in a "parallel" μ-η^2 fashion. The μ-alkyne bond lengths are 1.337(12) and 1.294(12) Å, and the Ru−C_{alkyne} bond lengths range from 2.028(8) to 2.224(9) Å. These bond lengths are similar to those of previously reported (μ-alkyne)diruthenium complexes.[14] The Ru−Ru distances of 2.7289(7) Å and 2.7293(7) Å, similar to those of the above dinuclear ruthenacycle complexes [2.7039(7)−2.7478(4) Å], show the existence of a metal−metal bond. The lengths of the Ru−C_{alkyne} bonds as well as the Ru2−C2 or the Ru2−C7 bonds [2.082(8)−2.191(8) Å] are very similar to those of typical Ru−sp^2-C single bonds.[11] Thus, the formal oxidation state of the Ru1 and Ru2 centers can be regarded as +1 and +3, respectively. According to this analysis, we can conclude that the dinuclear (μ-alkyne)ruthenabicycle complex **16** is formed by a dinuclear oxidative addition of DMAD onto the ferrole-type dinuclear framework of **12**.

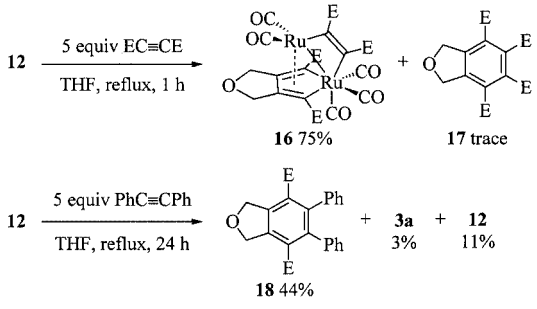

Scheme 7. Reactions of dinuclear (trimethylamine)ruthenacycle complex **12** with DMAD and diphenylacetylene (E = CO_2CH_3)

The novel (μ-alkyne)ruthenacycle complex **16** seemed to be an intermediate for the formation of **17**. Indeed, upon heating **16** in refluxing THF for 24 h, compound **17** was obtained in 11% yield, although 50% of starting **16** was recovered intact. A small amount of the hexacarbonyl complex **3a** was also detected (5%). The highly electron-de-

 © 2004 Wiley-VCH Verlag GmbH & Co. KGaA, Weinheim

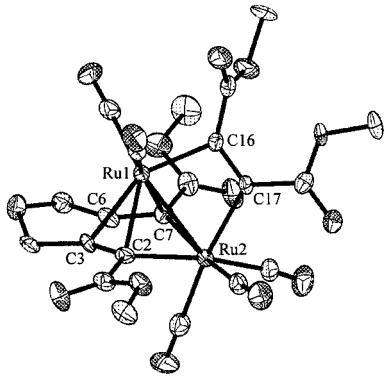

Figure 7. ORTEP diagrams of **16**, showing one of two crystallographically unique molecules in the unit cell; all hydrogen atoms have been omitted for clarity

ficient DMAD is essential for the formation of a μ-alkyne complex such as **16**. The reaction with electronically neutral diphenylacetylene afforded a coupling adduct **18** in 44% yield as well as the recovered **12** and trace amounts of **3a** (Scheme 7). Methyl propiolate never gave the corresponding complex because of its self-cyclotrimerization leading to 1,2,4- and 1,3,5-tris(methoxycarbonyl)benzenes. In contrast to our previous catalytic systems involving mononuclear ruthenacyclic intermediates,[8] the present dinuclear complex is less effective for the [2+2+2] cycloaddition due to the stabilization of the ruthenacycle moiety by coordination to the additional ruthenium center.

Conclusion

In conclusion, the diyne diester **2a** proved to be a suitable precursor for the synthesis of the dinuclear ruthenacyclic complex **3a**. The ratio of **2a**/Ru turned out to be critical as an excess of **2a** decreased the yield of **3a** because of the concomitant formation of the mononuclear ruthenacycle complex **4**, which is the precursor of **3a**. On the other hand, the diphenyldiyne **2b** gave the cyclopentadienone complex **7b** together with the desired ruthenacycle complex **3b**, and the disilyldiyne **2c** exclusively afforded the cyclopentadienone complex **7c** in good yield.

The treatment of the ruthenacycle complex **3a** with Me_3NO gave the mono(trimethylamine) complex **12**, which was further converted into various phosphane complexes upon reaction with phosphanes in refluxing THF. Among the bidentate phosphane ligands used, only dppm afforded the bridging diphosphane complex **14** directly. In contrast, the initially formed monodentate phosphane complexes of dppe and $PyPPh_2$ were treated with Me_3NO to give the P-P and P-N chelate complexes **15b** and **15c**, respectively.

The reaction of **12** with DMAD gave the novel μ-η^2-alkyne complex **16** together with the [2+2+2] cycloadduct **17**. The highly electron-deficient character of DMAD is imperative for the formation of the μ-alkyne complex; methyl propiolate and diphenylacetylene gave no corresponding μ-alkyne complexes.

Experimental Section

General Remarks: Flash chromatography was performed with a silica gel column (Merck Silica gel 60) eluting with a mixture of solvents (hexane/EtOAc). ^1H and ^{13}C NMR spectra were obtained for samples in $CDCl_3$ solution at 25 °C with a Varian Mercury 300 spectrometer. ^1H NMR chemical shifts are reported in δ units, in ppm relative to the singlet at $\delta = 7.26$ ppm for chloroform. ^{13}C and ^{31}P NMR spectra were fully decoupled and are reported in terms of chemical shift (δ, ppm) relative to the triplet at δ = 77.0 ppm for $CDCl_3$ or H_4PO_4 (85% in H_2O) as external standard, respectively. Coupling constants are reported in Hz. Infrared spectra were recorded for $CHCl_3$ sample solutions in 0.2-mm path-length sodium chloride cavity cells with a JASCO FT/IR-230 spectrometer. Elemental analyses were performed by the Microanalytical Center of Kyoto University. Melting points were obtained in capillary tubes and are uncorrected. Toluene and acetonitrile were dried with CaH_2 and distilled. THF was dried with benzophenone ketyl, and distilled.

Typical Procedure for the Reaction of $[Ru_3(CO)_{12}]$ with Diynes. Synthesis of Dinuclear Ruthenacycle Complex 3a from $[Ru_3(CO)_{12}]$ and Diyne 2a: A glass tube (28 mm o.d.) fitted with a stirring bar was charged with $[Ru_3(CO)_{12}]$ (128.0 mg, 0.20 mmol) and acetonitrile (2 mL) and saturated with CO. The tube was placed in a 100-mL stainless steel autoclave. The reactor was pressurized by CO to 5 atm. The contents were stirred at ambient temperature for 10 min, and then the pressurized CO was purged under a hood. A solution of diyne **2a** (63.4 mg, 0.30 mmol) in acetonitrile (3 mL) was added to this tube with a syringe, at ambient temperature. The reactor was pressurized again with CO to 5 atm. The contents were stirred at 120 °C for 12 h, and cooled to ambient temperature. After purging the excess CO under a fume hood, the reaction mixture was concentrated in vacuo. The residue was chromatographed on silica gel using hexane/EtOAc (10:1) as an eluent to give **3a** (151.1 mg, 87%) as a yellow solid: M.p. 110.0−111.0 °C. IR ($CHCl_3$, 25 °C): $\tilde{\nu}$ = 2096, 2068, 2062, 2029, 2011, 1689 cm^{-1}. ^1H NMR (300 MHz, $CDCl_3$, 25 °C): $\delta = 3.68$ (s, 6 H), 4.80 (dd, $J_{H,H} = 15.3$, 2.4 Hz, 2 H), 5.08 (dd, $J_{H,H} = 15.3$, 2.4 Hz, 2 H) ppm. ^{13}C NMR (75 MHz, $CDCl_3$, 25 °C): $\delta = 52.28$, 70.31, 127.62, 137.23, 172.38, 192.21, 193.60, 194.37 ppm. $C_{16}H_{10}O_{11}Ru_2$ (580.38): calcd. C 33.11, H 1.74; found C 33.11, H 1.91. Other reactions of $Ru_3(CO)_{12}$ with diynes **2a**−**c** were carried out in a similar way under the conditions summarized in Tables 1 and 2.

Mononuclear Ruthenacycle Complex 4: M.p. 128.5−130.0 °C. IR ($CHCl_3$, 25 °C): $\tilde{\nu}$ = 2145, 2073, 1676 cm^{-1}. ^1H NMR (300 MHz, $CDCl_3$, 25 °C): $\delta = 3.75$ (s, 6 H), 4.65 (s, 4 H) ppm. ^{13}C NMR (75 MHz, $CDCl_3$, 25 °C): $\delta = 51.98$, 70.62, 133.66, 171.08, 177.11, 186.32, 189.82 ppm. $C_{14}H_{10}O_9Ru$ (423.29): calcd. C 39.72, H 2.38; found C 39.69, H 2.48.

Dinuclear Ruthenacycle Complex 3b: M.p. 158.0−158.5 °C. IR ($CHCl_3$, 25 °C): $\tilde{\nu}$ = 2081, 2052, 2010 cm^{-1}. ^1H NMR (300 MHz, $CDCl_3$, 25 °C): $\delta = 4.43$ (dd, $J_{H,H} = 13.8$, 1.8 Hz, 2 H), 5.15 (dd, $J_{H,H} = 13.8$, 1.8 Hz, 2 H), 7.00−7.04 (m, 4 H), 7.11−7.17 (m, 2 H), 7.21−7.27 (m, 4 H) ppm. ^{13}C NMR (75 MHz, $CDCl_3$, 25 °C): $\delta = 69.50$, 126.57, 127.03, 128.13, 135.91, 147.15, 154.41, 193.49, 195.99, 198.52 ppm. $C_{24}H_{14}O_7Ru_2$ (616.50): calcd. C 46.76, H 2.29; found C 46.80, H 2.48.

Cyclopentadienone Complex 7b: M.p. 200 °C (decomp). IR ($CHCl_3$, 25 °C): $\tilde{\nu}$ = 2086, 2031, 1635 cm^{-1}. ^1H NMR (300 MHz, $CDCl_3$, 25 °C): $\delta = 5.11$ (dd, $J_{H,H} = 13.5$, 2.4 Hz, 2 H), 5.27 (dd, $J_{H,H} = 13.5$, 2.4 Hz, 2 H), 7.26−7.32 (m, 2 H), 7.35−7.41 (m, 4 H),

 © 2004 Wiley-VCH Verlag GmbH & Co. KGaA, Weinheim

7.80−7.85 (m, 4 H) ppm. ^{13}C NMR (75 MHz, $CDCl_3$, 25 °C): δ = 68.77, 75.26, 103.37, 126.96, 127.63, 128.76, 132.17, 173.42, 193.53 ppm. $C_{22}H_{14}O_5Ru$ (459.41): calcd. C 57.52, H 3.07; found C 57.37, H 3.35.

Cyclopentadienone Complex 7c: M.p. 143.5−144.5 °C. IR ($CHCl_3$, 25 °C): $\tilde{\nu}$ = 2136, 2084, 2064, 2028, 2009, 1623 cm^{-1}. ^{1}H NMR (300 MHz, $CDCl_3$, 25 °C): δ = 0.25 (s, 18 H), 4.77 (s, 4 H) ppm. ^{13}C NMR (75 MHz, $CDCl_3$, 25 °C): δ = −0.29, 65.78, 68.14, 114.07, 185.48, 193.67 ppm. $C_{16}H_{22}O_5RuSi_2$ (451.58): calcd. C 42.55, H 4.91; found C 42.39, H 4.83.

Synthesis of Trimethylamine Complex 12: $Me_3NO/2H_2O$ (24.6 mg, 0.22 mmol) was added to a degassed solution of **3a** (120.6 mg, 0.21 mmol) in THF (10 mL), and the reaction mixture was stirred for 1 h at ambient temperature under Ar. The solvent was removed in vacuo, and the residue was chromatographed on silica gel using hexane/EtOAc (2:1) as eluent to give **12** (117.8 mg, 93%) as a dark-red solid. M.p. 120 °C (decomp). IR ($CHCl_3$, 25 °C): $\tilde{\nu}$ = 2077, 2006, 1952, 1682 cm^{-1}. ^{1}H NMR (300 MHz, $CDCl_3$, 25 °C): δ = 2.69 (s, 9 H), 3.60 (s, 6 H), 4.76 (dd, $J_{H,H}$ = 15.9, 2.7 Hz, 2 H), 5.09 (dd, $J_{H,H}$ = 15.9, 2.7 Hz, 2 H) ppm. ^{13}C NMR (75 MHz, $CDCl_3$, 25 °C): δ = 51.62, 59.78, 70.43, 120.84, 137.03, 174.69, 194.33, 195.62, 201.48 ppm. $C_{18}H_{19}NO_{10}Ru_2$ (611.48): calcd. C 35.36, H 3.13, N 2.29; found C 35.28, H 3.10, N 2.24.

Typical Procedure for the Reaction of 12 with Phosphanes: Synthesis of dppe Complex 13b from 12: A degassed solution of **12** (122.4 mg, 0.20 mmol) and dppe (398.6 mg, 1.0 mmol) in THF (10 mL) was refluxed under N_2 for 5 h. The reaction mixture was concentrated in vacuo, and the residue was chromatographed on silica gel using hexane/EtOAc (8:1−4:1) as eluent to give **13b** (166.9 mg, 93%) as a yellow solid. M.p. 143.5−144.0 °C. IR ($CHCl_3$, 25 °C): $\tilde{\nu}$ = 2077, 2008, 1683 cm^{-1}. ^{1}H NMR (300 MHz, $CDCl_3$, 25 °C): δ = 1.92−2.04 (br. m, 2 H), 2.32−2.46 (br. m, 2 H), 3.47 (s, 6 H), 3.98 (d, $J_{H,H}$ = 13.2 Hz, 2 H), 4.67 (d, $J_{H,H}$ = 13.2 Hz, 2 H), 7.18−7.48 (m, 20 H) ppm. ^{13}C NMR (75 MHz, $CDCl_3$, 25 °C): δ = 22.13 (d, $J_{P,C}$ = 15.9 Hz), 28.03 (d, $J_{P,C}$ = 19.4 Hz), 51.73, 69.19, 128.39−128.74 (m), 130.68 (d, $J_{P,C}$ = 2.3 Hz), 131.54, 132.10 (d, $J_{P,C}$ = 10.2 Hz), 132.35 (d, $J_{P,C}$ = 18.2 Hz), 134.71, 136.99 (d, $J_{P,C}$ = 12 Hz), 173.14, 194.67, 195.36, 201.40 (d, $J_{P,C}$ = 13.1 Hz) ppm. ^{31}P NMR (121.5 MHz, $CDCl_3$, 25 °C): δ = −11.57 (d, $J_{P,P}$ = 42.3 Hz), 40.77 (d, $J_{P,P}$ = 42.3 Hz) ppm. $C_{41}H_{34}O_{10}P_2Ru_2$ (950.79): calcd. C 51.79, H 3.60; found C 51.91, H 3.50. The reactions of **12** with other phosphanes were carried out in a similar way under the conditions summarized in Table 3.

Complex 13a: M.p. 171.0−172.0 °C. IR ($CHCl_3$, 25 °C): $\tilde{\nu}$ = 2077, 2013, 1989, 1961, 1683 cm^{-1}. ^{1}H NMR (300 MHz, $CDCl_3$, 25 °C): δ = 3.41 (s, 6 H), 3.94 (d, $J_{H,H}$ = 13.4 Hz, 2 H), 4.65 (d, $J_{H,H}$ = 13.4 Hz, 2 H), 7.33−7.49 (m, 15 H) ppm. ^{13}C NMR (75 MHz, $CDCl_3$, 25 °C): δ = 51.62, 69.18, 127.85 (d, $J_{P,C}$ = 6.8 Hz), 128.39 (d, $J_{P,C}$ = 10.3 Hz), 130.64 (d, $J_{P,C}$ = 2.3 Hz), 132.26, 132.91, 133.07 (d, $J_{P,C}$ = 11.4 Hz), 135.56, 173.21, 194.70, 195.45, 200.95 (d, $J_{P,C}$ = 13.7 Hz) ppm. ^{31}P NMR (121.5 MHz, $CDCl_3$, 25 °C): δ = 41.87 ppm. $C_{33}H_{25}O_{10}PRu_2$ (814.66): calcd. C 48.65, H 3.09; found C 48.61, H 3.16.

Complex 13c: M.p. 153.5−154.0 °C. IR ($CHCl_3$, 25 °C): $\tilde{\nu}$ = 2075, 2014, 1987, 1682 cm^{-1}. ^{1}H NMR (300 MHz, $CDCl_3$, 25 °C): δ = 3.41 (s, 6 H), 4.06 (d, $J_{H,H}$ = 12.9 Hz, 2 H), 4.71 (dd, $J_{H,H}$ = 12.9, 1.5 Hz, 2 H), 7.20−7.30 (m, 2 H), 7.40−7.52 (m, 10 H), 7.63 (ddt, $J_{H,H}$ = 7.8, 3.6, 2.1 Hz, 1 H), 8.77−8.81 (m, 1 H) ppm. ^{13}C NMR (75 MHz, $CDCl_3$, 25 °C): δ = 51.55, 69.34, 123.91 (d, $J_{P,C}$ = 2.3 Hz), 126.85 (d, $J_{P,C}$ = 18.8 Hz), 128.38 (d, $J_{P,C}$ = 10.3 Hz), 130.71, 130.81 (d, $J_{P,C}$ = 2.9 Hz), 131.32, 133.62 (d, $J_{P,C}$ = 11.4 Hz), 134.57, 135.56 (d, $J_{P,C}$ = 6.8 Hz), 150.24 (d, $J_{P,C}$ = 18.2 Hz), 158.41, 159.42, 173.36, 195.07, 195.80, 200.18 (d, $J_{P,C}$ = 13.7 Hz) ppm. ^{31}P NMR (121.5 MHz, $CDCl_3$, 25 °C): δ = 46.12 ppm. $C_{32}H_{24}NO_{10}PRu_2$ (815.65): calcd. C 47.12, H 2.97, N 1.72; found C 46.99, H 3.13, N 1.69.

Complex 14: M.p. 235 °C (decomp). IR ($CHCl_3$, 25 °C): $\tilde{\nu}$ = 2032, 2010, 1977, 1941, 1682 cm^{-1}. ^{1}H NMR (300 MHz, $CDCl_3$, 25 °C): δ = 3.00 (s, 3 H), 3.82 (s, 3 H), 4.39 (d, $J_{H,H}$ = 13.2 Hz, 1 H), 4.69 (d, $J_{H,H}$ = 12.6 Hz, 1 H), 4.95 (dd, $J_{P,H}$ = 22.1, $J_{H,H}$ = 14 Hz, 1 H), 4.95 (d, $J_{H,H}$ = 13.2 Hz, 1 H), 5.18 (dd, $J_{H,H}$ = 12.6, 3.9 Hz, 1 H), 5.69 (dd, $J_{P,H}$ = 26.9, $J_{H,H}$ = 14 Hz, 1 H), 6.72−6.78 (m, 2 H), 6.95−7.11 (m, 3 H), 7.32−7.67 (m, 13 H), 7.94−8.02 (m, 2 H) ppm. ^{13}C NMR (75 MHz, $CDCl_3$, 25 °C): δ = 48.41 (dd, $J_{P,C}$ = 29, 18.2 Hz), 51.18, 51.66, 69.11, 71.07, 114.52 (dd, $J_{P,C}$ = 14.3, 5.2 Hz), 119.73 (d, $J_{P,C}$ = 5.7 Hz), 127.70−129.83 (m), 131.47 (d, $J_{P,C}$ = 2.3 Hz), 132.06 (d, $J_{P,C}$ = 13.1 Hz), 135.47−136.16 (m), 136.88, 137.22−137.45 (m), 140.89, 141.63, 143.39 (d, $J_{P,C}$ = 14.8 Hz), 143.99 (d, $J_{P,C}$ = 14.8 Hz), 174.80, 176.47, 176.52, 195.77 (d, $J_{P,C}$ = 9.7 Hz), 199.10 (d, $J_{P,C}$ = 12.5 Hz), 200.32 (d, $J_{P,C}$ = 9.1 Hz), 201.75 (dd, $J_{P,C}$ = 10.8, 9.1 Hz) ppm. ^{31}P NMR (121.5 MHz, $CDCl_3$, 25 °C): δ = 13.31 (d, $J_{P,P}$ = 47.9 Hz), 15.01 (d, $J_{P,P}$ = 47.9 Hz) ppm. $C_{39}H_{32}O_9P_2Ru_2$ (908.75): calcd. C 51.55, H 3.55; found C 51.27, H 3.62.

Typical Procedure for Reaction of Phosphane Complexes 13b,c with Me_3NO. Synthesis of dppe Chelate Complex 15b: $Me_3NO/2H_2O$ (12.4 mg, 0.11 mmol) was added to a degassed solution of **13b** (95.0 mg, 0.10 mmol) in THF (25 mL) and the reaction mixture was stirred at ambient temperature under Ar for 1 h. The solvent was removed in vacuo, and the residue was chromatographed on silica gel using hexane/EtOAc (2.5:1−1:1) as eluent to give **15b** (71.0 mg, 77%) as a yellow solid. M.p. 190 °C (decomp). IR ($CHCl_3$, 25 °C): $\tilde{\nu}$ = 2063, 1996, 1975, 1929, 1673 cm^{-1}. ^{1}H NMR (300 MHz, $CDCl_3$, 25 °C): δ = 2.40−2.65 (m, 4 H), 3.18 (s, 6 H), 3.47 (d, $J_{H,H}$ = 12.6 Hz, 2 H), 4.43 (dd, $J_{H,H}$ = 12.6, 2.4 Hz, 2 H), 7.19−7.26 (m, 4 H), 7.38−7.48 (m, 12 H), 7.64−7.72 (m, 4 H) ppm. ^{13}C NMR (75 MHz, $CDCl_3$, 25 °C): δ = 30.68 (dd, $J_{P,C}$ = 23.3, 22.2 Hz), 50.83, 68.75, 124.38 (t, $J_{P,C}$ = 8.5 Hz), 128.15 (t, $J_{P,C}$ = 6.8 Hz), 128.21 (t, $J_{P,C}$ = 6.8 Hz), 130.20, 130.52, 131.81 (t, $J_{P,C}$ = 5.7 Hz), 132.77 (d, $J_{P,C}$ = 3.5 Hz), 133.40 (t, $J_{P,C}$ = 5.1 Hz), 133.65, 133.95, 174.70, 196.34, 197.30, 203.98 (t, $J_{P,C}$ = 13.7 Hz) ppm. ^{31}P NMR (121.5 MHz, $CDCl_3$, 25 °C): δ = 68.60 ppm. $C_{40}H_{34}O_9P_2Ru_2$ (922.78): calcd. C 52.06, H 3.71; found C 51.96, H 3.71.

Complex 15c: M.p. 175.0−176.0 °C. IR ($CHCl_3$, 25 °C): $\tilde{\nu}$ = 2063, 1994, 1971, 1923, 1670 cm^{-1}. ^{1}H NMR (300 MHz, $CDCl_3$, 25 °C): δ = 3.21 (dt, $J_{H,H}$ = 12.5, 1.8 Hz, 1 H), 3.32 (s, 3 H), 3.69 (s, 3 H), 4.33 (dd, $J_{H,H}$ = 13.5, 2.1 Hz, 1 H), 4.51 (ddt, $J_{H,H}$ = 12.5, 3.6, 1.8 Hz, 1 H), 4.84 (dt, $J_{H,H}$ = 13.5, 1.8 Hz, 1 H), 6.94−7.02 (m, 2 H), 7.32−7.47 (m, 5 H), 7.55−7.61 (m, 3 H), 7.82−7.93 (m, 3 H), 8.04 (dd, $J_{H,H}$ = 5.4, 0.8 Hz, 1 H) ppm. ^{13}C NMR (75 MHz, $CDCl_3$, 25 °C): δ = 50.72, 51.56, 68.18, 70.13, 113.83 (d, $J_{P,C}$ = 19.9 Hz), 118.81 (d, $J_{P,C}$ = 3.4 Hz), 126.51 (d, $J_{P,C}$ = 2.3 Hz), 127.14, 127.99 (d, $J_{P,C}$ = 2.9 Hz), 128.34, 128.75 (d, $J_{P,C}$ = 10.8 Hz), 128.91, 129.07 (d, $J_{P,C}$ = 10.8 Hz), 129.21, 130.71 (d, $J_{P,C}$ = 2.3 Hz), 131.21 (d, $J_{P,C}$ = 11.3 Hz), 132.03 (d, $J_{P,C}$ = 2.3 Hz), 134.40 (d, $J_{P,C}$ = 13.1 Hz), 134.66, 137.26 (d, $J_{P,C}$ = 3.5 Hz), 152.19 (d, $J_{P,C}$ = 15.4 Hz), 172.40, 173.10, 177.13 (d, $J_{P,C}$ = 2.3 Hz), 177.39, 195.91, 197.08, 197.52, 205.02 (d, $J_{P,C}$ = 12.5 Hz) ppm. ^{31}P NMR (121.5 MHz, $CDCl_3$, 25 °C): δ = −2.60 ppm. $C_{31}H_{24}NO_9PRu_2$ (787.64): calcd. C 47.27, H 3.07, N 1.78; found C 47.19, H 3.23, N 1.70.

 © 2004 Wiley-VCH Verlag GmbH & Co. KGaA, Weinheim

Typical Procedure for the Reaction of 12 with Alkynes. Synthesis of DMAD Complex 16: A degassed solution of **12** (122.8 mg, 0.20 mmol) and DMAD (145.1 mg, 1.0 mmol) in THF (10 mL) was refluxed under N_2 for 1 h. The reaction mixture was concentrated in vacuo, and the residue was chromatographed on silica gel using hexane/EtOAc (8:1) as eluent to give **16** (104.7 mg, 75%) as a yellow solid. M.p. 119.0−120.0 °C. IR ($CHCl_3$, 25 °C): $\tilde{\nu}$ = 2113, 2056, 2009, 1704 cm^{-1}. ^1H NMR (300 MHz, $CDCl_3$, 25 °C): δ = 3.68 (s, 6 H), 3.84 (s, 3 H), 3.89 (s, 3 H), 4.84 (d, $J_{H,H}$ = 14.7 Hz, 2 H), 5.06 (d, $J_{H,H}$ = 14.7 Hz, 2 H) ppm. ^{13}C NMR (75 MHz, $CDCl_3$, 25 °C): δ = 52.73, 53.19, 71.64, 88.77, 127.31, 147.95, 155.07, 165.96, 169.81, 171.58, 187.87, 188.83, 194.10 ppm. $C_{21}H_{16}O_{14}Ru_2$ (694.48): calcd. C 36.32, H 2.32; found C 36.17, H 2.32. The reactions of **12** with other alkyes were carried out in a similar way.

Cycloadduct 18: M.p. 150.0−151.0 °C. IR ($CHCl_3$, 25 °C): $\tilde{\nu}$ = 1723 cm^{-1}. ^1H NMR (300 MHz, $CDCl_3$, 25 °C): δ = 3.49 (s, 6 H), 5.31 (s, 4 H), 6.90−6.96 (m, 4 H), 7.09−7.13 (m, 6 H). ^{13}C NMR (75 MHz, $CDCl_3$, 25 °C): δ = 52.01, 73.80, 126.65, 127.16, 128.28, 129.61, 138.39, 139.29, 141.07, 167.33 ppm. MS (EI): *m/z* (%) =

Table 4. Selected crystallographic data and collection parameters for **3a**, **4**, **7b**, **7c**, and **12**

	3a	**4**	**7b**	**7c**	**12**
Empirical formula	$C_{32}H_{20}O_{22}Ru_4$	$C_{28}H_{10}O_{18}Ru_2$	$C_{22}H_{14}O_5Ru$	$C_{16}H_{22}O_5RuSi_2$	$C_{18}H_{19}NO_{10}Ru_2$
Formula mass	1160.76	836.50	459.40	451.59	611.48
Crystal system	triclinic	triclinic	monoclinic	orthorhombic	orthorhombic
Space group	*P*1	*P*1	$P2_1/n$	$Pna2_1$	*Pbca*
a [Å]	7.2890(4)	7.4477(4)	12.5010(17)	13.5068(11)	14.5489(7)
b [Å]	8.4070(4)	7.6427(4)	11.1785(15)	7.7041(6)	16.5372(8)
c [Å]	15.6155(8)	13.9935(7)	13.5392(18)	19.7067(17)	18.0212(9)
α [°]	85.4440(10)	84.6270(10)	90	90	90
β [°]	79.6470(10)	78.4880(10)	96.956(3)	90	90
γ [°]	86.9670(10)	77.9490(10)	90	90	90
V [Å^3]	937.61(8)	762.17(7)	1878.1(4)	2050.6(3)	4335.9(4)
Z	1	1	4	4	8
$D_{calcd.}$ [Mg cm^{-3}]	4.111	3.645	1.625	1.463	1.873
μ [mm^{-1}]	3.339	2.150	0.866	0.901	1.447
F(000)	1128	820	920	920	2416
Crystal size [mm]	0.2 × 0.4 × 0.8	0.01 × 0.4 × 0.7	0.2 × 0.3 × 0.8	0.05 × 0.1 × 0.7	0.3 × 0.6 × 0.6
Reflections collected	7287	5879	14090	14810	32235
Independent reflections	5892	4759	4979	5170	5832
GOF on F^2	1.067	0.835	0.839	0.984	1.094
R[a]	0.0267,	0.0258,	0.0297,	0.0267,	0.0206,
wR[b]	0.0714	0.0686	0.0808	0.0678	0.0557
Largest diff. peak/hole [e·Å^{-3}]	0.448/−1.362	0.661/−1.076	0.710/−1.379	0.761/−0.335	0.693/−0.499

[a] $R_1 = \Sigma|(F_o - F_c)|/\Sigma(F_o)$. [b] $wR = \Sigma\{[w(F_o - F_c)^2]\}/\Sigma(wF_o^2)^{1/2}$.

Table 5. Selected crystallographic data and collection parameters for **13b**, **13c**, **14**, **15b**, **15c**, and **16**

	13b	**13c**	**14**	**15b**	**15c**	**16**
Empirical formula	$C_{41}H_{34}O_{10}P_2Ru_2$	$C_{32}H_{24}NO_{10}PRu_2$	$C_{39}H_{32}O_9P_2Ru_2$	$C_{40}H_{34}O_9P_2Ru_2$	$C_{31}H_{24}NO_9PRu_2$	$C_{42}H_{32}O_{28}P_2Ru_4$
Formula mass	950.76	815.63	908.73	922.75	787.62	1388.96
Crystal system	triclinic	triclinic	monoclinic	triclinic	monoclinic	triclinic
Space group	$P\bar{1}$	$P\bar{1}$	$P2_1/c$	$P\bar{1}$	$P2_1/c$	*P*1
a [Å]	11.4786(57)	11.2420(6)	16.9441(11)	10.5914(10)	14.3052(10)	8.1357(5)
b [Å]	11.9273(5)	11.9006(6)	12.7293(9)	10.7131(10)	20.8765(14)	9.2184(6)
c [Å]	15.0854(7)	13.4346(7)	20.2441(13)	17.0451(17)	11.4404(8)	17.9529(11)
α [°]	93.8670(10)	84.7860(10)	90	94.634(2)	90	95.7720(10)
β [°]	92.2860(10)	72.6960(10)	111.8660(10)	103.678(2)	96.981(2)	102.8400(10)
γ [°]	110.5380(10)	85.6630(10)	90	91.953(2)	90	109.9680(10)
V [Å^3]	1925.18(15)	1706.69(15)	4052.3(5)	1870.2(3)	3391.3(4)	1210.75(13)
Z	2	2	4	2	4	1
$D_{calcd.}$ [Mg cm^{-3}]	1.640	1.587	1.490	1.639	1.543	3.810
μ [mm^{-1}]	0.926	0.986	0.875	0.949	0.988	2.639
F(000)	956	812	1824	928	1568	1368
Crystal size [mm]	0.01 × 0.4 × 0.7	0.1 × 0.5 × 0.6	0.1 × 0.5 × 0.8	0.01 × 0.2 × 0.4	0.01 × 0.5 × 0.6	0.1 × 0.4 × 0.8
Reflections collected	15104	13218	30637	12716	25394	9402
Independent reflections	10090	8874	10862	9575	9036	7593
GOF on F^2	0.750	0.993	0.991	1.042	1.013	1.078
R[a]	0.0269,	0.0432,	0.0419,	0.0687,	0.0626,	0.0273,
wR[b]	0.0739	0.1572	0.1320	0.1641	0.2060	0.0735
Largest diff. peak/hole [e·Å^{-3}]	0.841/−0.443	4.212/−0.466	2.770/−0.699	3.386/−2.059	5.934/−0.584	0.570/−1.315

[a] $R_1 = \Sigma|(F_o - F_c)|/\Sigma(F_o)$. [b] $wR = \Sigma\{[w(F_o - F_c)^2]\}/\Sigma(wF_o^2)^{1/2}$.

 © 2004 Wiley-VCH Verlag GmbH & Co. KGaA, Weinheim

388 (100) [M^+], 373 (28) [$M^+ - CH_3$], 356 (82) [$M^+ - HOCH_3$]. $C_{24}H_{20}O_5$ (388.41): calcd. C 74.21, H 5.19; found C 73.97, H 5.43.

X-ray Crystallographic Determination: Single crystals suitable for X-ray analysis were obtained by recrystallization from hexane at −15 °C (**3a**), CH_2Cl_2/hexane at room temp. (**4**), EtOAc/hexane at room temp. (**7b**), EtOAc/hexane at −15 °C (**7c**), CH_2Cl_2/diethyl ether at −15 °C (**12**), diethyl ether/hexane at room temp. (**13b**), diethyl ether/hexane at room temp. (**13c**), $CHCl_3$/hexane at room temp. (**14**), CH_2Cl_2/hexane at room temp. (**15b**), CH_2Cl_2/diethyl ether at room temp. (**15c**), or CH_2Cl_2/hexane at 0 °C (**16**). Each crystal was mounted on a quartz fiber, and diffraction data were collected in θ ranges specified in Tables 4 and 5 at 173 K with a Bruker SMART APEX CCD diffractometer with graphite-monochromated Mo-K_α radiation (λ = 0.71073 Å). An absorption correction was applied using SADABS. The structure was solved by direct methods and refined by full-matrix least squares on F^2 with SHELXTL.[15] All non-hydrogen atoms were refined with anisotropic displacement parameters. All hydrogen atoms were placed in calculated positions. Final refinement details are compiled in Tables 4 and 5. CCDC-227166 (**3a**), -227167 (**4**), -227168 (**7b**), -227169 (**7c**), -227170 (**12**), -227171 (**13b**), -227172 (**13c**), -227173 (**14**), -227174 (**15b**), -227175 (**15c**), and -227176 (**16**) contain the supplementary crystallographic data for this paper. These data can be obtained free of charge at www.ccdc.cam.ac.uk/conts/retrieving.html [or from the Cambridge Crystallographic Data Centre, 12 Union Road, Cambridge CB2 1EZ, UK; Fax: + 44-1223-336033; E-mail: deposit@ccdc.cam.ac.uk].

Acknowledgments

We gratefully acknowledge financial support (14750677) from the Ministry of Education, Culture, Sports, Science and Technology, Japan.

[1] [1a] S. Otsuka, A. Nakamura, *Adv. Organomet. Chem.* **1976**, *14*, 245−283. [1b] N. E. Schore, *Chem. Rev.* **1988**, *88*, 1081−1119. [1c] N. E. Shore, in *Comprehensive Organic Synthesis*, vol. 5 (Eds.: B. M. Trost, I. Fleming, L. A. Paquette), Pergamon, Oxford, **1991**, p. 1129−1162. [1d] D. B. Grotjahn, in *Comprehensive Organometallic Chemistry II*, vol. 12 (Eds.: E. W. Abel, F. G. A. Stone, G. Wilkinson, L. S. Hegedus), Pergamon, Oxford, **1995**, p. 741−770. [1e] H. Bönnemann, W. Brijoux, in *Transition Metals for Organic Synthesis* (Eds.: M. Beller, C. Bolm), Wiley-VCH, Weinheim, **1998**, vol. 1, p. 114−135.

[2] [2a] L. R. Bateman, P. M. Maitlis, L. F. Dahl, *J. Am. Chem. Soc.* **1969**, *91*, 7292−7300. [2b] J. Levisalles, F. Rose-Munch, H. Rudler, *J. Chem. Soc., Chem. Commun.* **1981**, 1057−1059. [2c] H. Yamazaki, K. Yasufuku, Y. Wakatsuki, *Organometallics* **1983**, *2*, 726−732, and references cited therein. [2d] H. Yamazaki, Y. Wakatsuki, *J. Organomet. Chem.* **1984**, *272*, 251−263. [2e] S. B. Colbran, B. H. Robinson, J. Simpson, *Organometallics* **1985**, *4*, 1594−1601. [2f] K. Sünkel, *J. Organomet. Chem.* **1990**, *391*, 247−257. [2g] R. D. Adams, I. Arafa, G. Chen, J.-C. Lii, J.-G. Wang, *Organometallics* **1990**, *9*, 2350−2357. [2h] J. Müller, T. Akhnoukh, J. Pickardt, M. Siewing, B. Westphal, *J. Organomet. Chem.* **1993**, *459*, 325−333. [2i] F.-E. Hong, I.-R. Lue, S.-C. Lo, C.-C. Lin, *J. Organomet. Chem.* **1995**, *495*, 97−101. [2j] H. Matsuzaka, K. Ichikawa, T. Ishioka, H. Sato, T. Okubo, T. Ishii, M. Yamashita, M. Kondo, S. Kitagawa, *J. Organomet. Chem.* **2000**, *596*, 121−129.

[3] [3a] W. Hübel, E. H. Braye, *J. Inorg. Nucl. Chem.* **1959**, *10*, 250−268. [3b] E. Weiss, W. Hübel, R. Merényi, *Chem. Ber.* **1962**, *95*, 1155−1169. [3c] W. Hübel, R. Merényi, *Chem. Ber.* **1963**, *96*, 930−943. [3d] R. B. King, I. Haiduc, C. W. Eavenson, *J. Am. Chem. Soc.* **1973**, *95*, 2508−2516. [3e] G. Dettlaf, E. Weiss, *J. Organomet. Chem.* **1976**, *108*, 213−223. [3f] L. J. Todd, J. P. Hickey, J. R. Wilkinson, J. C. Huffman, K. Folting, *J. Organomet. Chem.* **1976**, *112*, 167−176. [3g] F. R. Young III, D. H. O'Brien, R. C. Pettersen, R. A. Levenson, D. L. von Minden, *J. Organomet. Chem.* **1976**, *114*, 157−164. [3h] M. Casarin, D. Ajò, G. Granozzi, E. Tondello, S. Aime, *Inorg. Chem.* **1985**, *24*, 1241−1246. [3i] S. Aime, E. Occhiello, *J. Chem. Soc., Dalton Trans.* **1986**, 1863−1865. [3j] M. Tasi, A. K. Powell, H. Vahrenkamp, *Angew. Chem.* **1989**, *101*, 327−328; *Angew. Chem. Int. Ed. Engl.* **1989**, *28*, 318−319. [3k] R. Giordano, E. Sappa, D. Cauzzi, G. Predieri, A. Tiripicchio, M. T. Camellini, *J. Organomet. Chem.* **1991**, *412*, C14−C18. [3l] A. Marzotto, M. B. Cingi, A. Ciccarese, D. A. Clemente, *Acta Crystallogr., Sect. C* **1991**, *47*, 96−99. [3m] D. Seyferth, C. M. Archer, J. C. Dewan, *Organometallics* **1991**, *10*, 3759−3763. [3n] S. A. R. Knox, B. R. Lloyd, D. A. V. Morton, A. G. Orpen, M. L. Turner, G. Hogarth, *Polyhedron* **1995**, *14*, 2723−2743. [3o] R. Giordano, E. Sappa, D. Cauzzi, G. Predieri, A. Tiripicchio, *J. Organomet. Chem.* **1996**, *511*, 263−271. [3p] D. Osella, G. Dutto, C. Nervi, M. J. McGlinchey, A. Vessières, G. Jaouen, *J. Organomet. Chem.* **1997**, *533*, 97−102. [3q] R. Calderón, H. Vahrenkamp, *J. Organomet. Chem.* **1998**, *555*, 113−118. [3r] M. Barrow, N. L. Cromhout, D. Cunningham, A. R. Manning, P. McArdle, *J. Organomet. Chem.* **2000**, *612*, 61−68.

[4] For examples of hydroxy ferrole complexes, see: [4a] A. A. Hock, O. S. Mills, *Proc. Chem. Soc. London* **1958**, 233−234. [4b] A. A. Hock, O. S. Mills, *Acta Crystallogr.* **1961**, *14*, 139−148. [4c] S. Aime, L. Milone, E. Sappa, A. Tiripicchio, A. M. M. Lanfredi, *J. Chem. Soc., Dalton Trans.* **1979**, 1664−1670. [4d] M. Periasamy, A. Mukkanti, D. S. Raj, *Organometallics* **2004**, *23*, 619−621.

[5] [5a] M. A. Bennett, P. B. Donaldson, *Inorg. Chem.* **1978**, *17*, 1995−2000. [5b] S. J. Tyler, J. M. Burlitch, *J. Organomet. Chem.* **1989**, *361*, 231−247. [5c] I. Moldes, T. Papworth, J. Ros, A. Alvarez-Larena, J. F. Piniella, *J. Organomet. Chem.* **1995**, *489*, C65−C67. [5d] T. Henkel, A. Klauck, K. Seppelt, *J. Organomet. Chem.* **1995**, *501*, 1−6. [5e] R. J. Baxter, G. R. Knox, P. L. Pauson, M. D. Spicer, *Organometallics* **1999**, *18*, 197−205. [5f] H. Lang, G. Rheinwald, U. Lay, L. Zsolnai, G. Huttner, *J. Organomet. Chem.* **2001**, *634*, 74−82.

[6] [6a] C. T. Sears Jr., F. G. A. Stone, *J. Organomet. Chem.* **1968**, *11*, 644−646. [6b] S. Aime, A. J. Deeming, *J. Chem. Soc., Dalton Trans.* **1981**, 828−832. [6c] A. Astier, J.-C. Daran, Y. Jeannin, C. Rigault, *J. Organomet. Chem.* **1983**, *241*, 53−68. [6d] M. I. Bruce, J. G. Matisons, B. W. Skelton, A. H. White, *J. Organomet. Chem.* **1983**, *251*, 249−260. [6e] A. A. Koridze, A. I. Yanovsky, Y. T. Struchkov, *J. Organomet. Chem.* **1992**, *1*, 277−284. [6f] M. I. Bruce, N. N. Zaitseva, B. W. Skelton, A. H. White, *Inorg. Chim. Acta* **1996**, *250*, 129−138. [6g] S. P. Tunik, E. V. Grachova, V. R. Denisov, G. L. Starova, A. B. Nikol'skii, F. M. Dolgushin, A. I. Yanovsky, Y. T. Struchkov, *J. Organomet. Chem.* **1997**, *536−537*, 339−343. [6h] M. I. Bruce, B. W. Skelton, A. H. White, N. N. Zaitseva, *J. Organomet. Chem.* **1998**, *558*, 197−207. [6i] P. J. Low, G. D. Enright, A. J. Carty, *J. Organomet. Chem.* **1998**, *565*, 279−282. [6j] P. J. Low, K. A. Udachin, G. D. Enright, A. J. Carty, *J. Organomet. Chem.* **1999**, *578*, 103−114.

[7] For other routes, see: [7a] I. Noda, H. Yasuda, A. Nakamura, *J. Organomet. Chem.* **1983**, *250*, 447−466. [7b] I. Noda, H. Yasuda, A. Nakamura, *Organometallics* **1983**, *2*, 1207−1214. [7c] H. Omori, H. Suzuki, Y. Moro-oka, *Organometallics* **1989**, *8*, 1576−1578. [7d] W. Krone-Schmidt, W. J. Sieber, N. M. Boag, C. B. Knobler, H. D. Kaesz, *J. Organomet. Chem.* **1990**, *394*, 433−454. [7e] B. K. Campion, R. H. Heyn, T. D. Tilley, *Organometallics* **1990**, *9*, 1106−1112. [7f] X. D. He, B. Chaudret, F. Dahan, Y.-S. Huang, *Organometallics* **1991**, *10*, 970−979. [7g] L. A. Brady, A. F. Dyke, S. E. Garner, S. A. R. Knox, A. Irving, S. M. Nicholls, A. G. Orpen, *J. Chem. Soc., Dalton Trans.* **1993**, 487−488. [7h] M. Nishio, H. Matsuzaka, Y. Mizobe, T. Tanase, M. Hidai, *Organometallics* **1994**, *13*, 4214−4226. [7i] J. A. Cabeza, I. del Río, F. Grepioni, M. Mor-

 © 2004 Wiley-VCH Verlag GmbH & Co. KGaA, Weinheim

eno, V. Riera, M. Suárez, *Organometallics* **2001**, *20*, 4190−4197.

[8] [8a] Y. Yamamoto, H. Kitahara, R. Ogawa, H. Kawaguchi, K. Tatsumi, K. Itoh, *J. Am. Chem. Soc.* **2000**, *122*, 4310−4319. [8b] Y. Yamamoto, R. Ogawa, K. Itoh, *J. Am. Chem. Soc.* **2001**, *123*, 6189−6190. [8c] Y. Yamamoto, S. Okuda, K. Itoh, *Chem. Commun.* **2001**, 1102−1103. [8d] Y. Yamamoto, H. Takagishi, K. Itoh, *Org. Lett.* **2001**, *3*, 2117−2119. [8e] Y. Yamamoto, H. Takagishi, K. Itoh, *J. Am. Chem. Soc.* **2002**, *124*, 28−29. [8f] Y. Yamamoto, H. Takagishi, K. Itoh, *J. Am. Chem. Soc.* **2002**, *124*, 6844−6845. [8g] Y. Yamamoto, K. Hata, T. Arakawa, K. Itoh, *Chem. Commun.* **2003**, 1290−1291. [8h] Y. Yamamoto, T. Arakawa, R. Ogawa, K. Itoh, *J. Am. Chem. Soc.* **2003**, *125*, 12143−12160. [8i] Y. Yamamoto, J. Ishii, H. Mishiyama, K. Itoh, *J. Am. Chem. Soc.* **2004**, *126*, 3712−3713. [8j] Y. Yamamoto, K. Kinpara, T. Saigoku, H. Nishiyama, K. Itoh, *Org. Biomol. Chem.* **2004**, *2*, 1287−1294.

[9] For examples of synthesis of dinuclear metallacycle complexes from α,ω-diynes, see: [9a] G. Predieri, A. Tiripicchio, M. T. Camellini, M. Costa, E. Sappa, *J. Organomet. Chem.* **1992**, *423*, 129−139. [9b] E. Boroni, M. Costa, G. Predieri, E. Sappa, A. Tiripicchio, *J. Chem. Soc., Dalton Trans.* **1992**, 2585−2590. [9c] K. Onitsuka, K. Miyaji, T. Adachi, T. Yoshida, K. Sonogashira, *Chem. Lett.* **1994**, 2279−2282. [9d] R. D. Adams, W. Fu, B. Qu, *J. Cluster Sci.* **2000**, *11*, 55−65.

[10] For examples of cyclotrimerization of diyne diesters, see: [10a] P. Bhatarah, E. H. Smith, *J. Chem. Soc., Chem. Commun.* **1991**, 277−278. [10b] P. Bhatarah, E. H. Smith, *J. Chem. Soc., Perkin Trans. 1* **1992**, 2163−2168. [10c] Y. Yamamoto, A. Nagata, K. Itoh, *Tetrahedron Lett.* **1999**, *40*, 5035−5038. [10d] Y. Yamamoto, A. Nagata, H. Nagata, Y. Ando, Y. Arikawa, K. Tatsumi, K. Itoh, *Chem. Eur. J.* **2003**, *9*, 2469−2483. [10e] A. Jeevanandam, R. P. Korivi, I. Huang, C.-H. Cheng, *Org. Lett.* **2002**, *4*, 807−810. [10f] M. Shanmugasundaram, M.-S. Wu, M. Jeganmohan, C.-W. Huang, C.-H. Cheng, *J. Org. Chem.* **2002**, *67*, 7724−7729. [10g] H. Nishiyama, E. Niwa, T. Inoue, Y. Ishima, K. Aoki, *Organometallics* **2002**, *21*, 2572−2574.

[11] A. F. Hill, in *Comprehensive Organometallic Chemistry II*, vol. 7 (Eds.: E. W. Abel, F. G. A. Stone, G. Wilkinson, D. F. Shriver, M. I. Bruce), Pergamon, Oxford, **1995**, p. 406.

[12] Similar (cyclopentadienone)ruthenium complexes have been reported, see: [12a] M. I. Bruce, J. R. Knight, *J. Organomet. Chem.* **1968**, *12*, 411−413. [12b] Y. Blum, Y. Shvo, D. F. Chodosh, *Inorg. Chim. Acta* **1985**, *97*, L25−L26. Also, see: [12c] E. Rüba, K. Mereiter, K. M. Soldouzi, C. Gemel, R. Schmid, K. Kirchner, E. Bustelo, M. C. Puerta, P. Valerga, *Organometallics* **2000**, *19*, 5384−5391, and references cited therin. [12d] A. F. Hill, A. D. Rae, M. Schultz, A. C. Willis, *Organometallics* **2004**, *23*, 81−85.

[13] [13a] O. S. Mills, G. Robinson, *Proc. Chem. Soc. London* **1964**, 187. [13b] J. Wessel, H. Hartl, K. Seppelt, *Chem. Ber.* **1986**, *119*, 453−463. [13c] G. Gervasio, E. Sappa, L. Markó, *J. Organomet. Chem.* **1993**, *444*, 203−209. [13d] R. J. Baxter, G. R. Knox, J. H. Moir, P. L. Pauson, M. D. Spicer, *Organometallics* **1999**, *18*, 206−214. [13e] F.-E. Hong, J.-Y. Wu, Y.-C. Huang, C.-K. Hung, H.-M. Gau, C.-C. Lin, *J. Organomet. Chem.* **1999**, *580*, 98−107.

[14] [14a] L. H. Staal, L. H. Polm, K. Vrieze, F. Ploeger, C. H. Stam, *J. Organomet. Chem.* **1980**, *199*, C13−C16. [14b] K. A. Johnson, W. L. Gladfelter, *Organometallics* **1989**, *8*, 2866−2871. [14c] K. A. Johnson, W. L. Gladfelter, *J. Am. Chem. Soc.* **1991**, *113*, 5097−5099. [14d] K. A. Johnson, W. L. Gladfelter, *Organometallics* **1992**, *11*, 2534−2542. [14e] J. S. Field, R. J. Haines, J. Sundermeyer, S. F. Woollam, *J. Chem. Soc., Dalton Trans.* **1993**, 3749−3757Å.

[15] G. M. Sheldrick, *SHELXTL 5.1*, Bruker AXS Inc., Madison, Wisconsin, **1997**.

Received February 14, 2004
Early View Article
Published Online June 24, 2004

 © 2004 Wiley-VCH Verlag GmbH & Co. KGaA, Weinheim

Rational Design of Metal-Organic Frameworks Based on 5-(4-Pyridyl)tetrazolate: From 2D Grids to 3D Porous Networks

Chao Jiang,[a] Zhaopeng Yu,[a] Sujing Wang,[a] Chao Jiao,[a] Jiaming Li,[a] Zhiyong Wang,*[a] and Yong Cui*[a]

Keywords: Coordination polymers / Fluorescence / Hydrothermal synthesis / N ligands / Self-assembly

The hydrothermal reactions of $Zn(ClO_4)_2·6H_2O$/$Cu(NO_3)_2·6H_2O$ with 5-(4-pyridyl)tetrazole in an ethanol/water or ethanol/water/pyridine medium yield one 2D and one 3D metal-organic coordination framework $[Zn_2(OH)(4\text{-ptz})_3]$ (**1**) and [Cu(4-ptz)·0.5(py)] (**3**) [4-ptz = 5-(4-pyridyl)-tetrazolate, py = pyridine], respectively. Complex **1** possesses two identical and independent rectangular grid sheets with twofold parallel interpenetration, in which the four-connected nodes of the net are provided by $Zn_2(OH)$ units connected to one another through 4-ptz and $(4\text{-ptz})_2$ bridges. These composite sheets are stacked one on top of another by hydrogen-bonding interactions to afford a 3D structure. There are many structural similarities between complex **1** and the recently reported 2D layered network [Zn(OH)(4-ptz)(H_2O)] (**2**), in particular the components of the network, the coordination mode of the 4-ptz ligand and the in situ formation of hydroxy groups. Complex **2** can be synthesized by the hydrothermal reaction of $Zn(ClO_4)_2·6H_2O$ and 5-(4-pyridyl)tetrazole in an ethanol/water/pyridine medium. The structural characterization of complex **3** shows a porous structure that contains the guest pyridine molecules. Additionally, compounds **1** and **2** exhibit strong fluorescence at room temperature in the solid state.

(© Wiley-VCH Verlag GmbH & Co. KGaA, 69451 Weinheim, Germany, 2004)

Introduction

The study of coordination frameworks has received increasing attention over recent years with a growing range of structural motifs being discovered. As far as is known, the functions of materials come from their structural features.[1] Many functional materials can be prepared by supramolecular self-assembly because the required structural variety and thermal stability can be obtained. For instance, the combination of organic spacers and transition-metal centers in coordination frameworks can affect the assembly of supramolecules, giving new types of electroluminescent materials, which have potential applications as light-emitting diodes (LEDs).[2] Also, a variety of NLO materials have been obtained by noncentrosymmetric organization of molecular building blocks,[3] while magnetic compounds have been synthesized by supramolecular chemistry dealing with open-shell units.[4] Therefore, the discovery of methods to control the assembly and solid-state structures in three dimensions has become one of the main challenges in crystal engineering. Many of these studies have heightened the awareness of the influence of the metal ion and ligand,[5] as well as the anion[6] and the solvent[7] on self-assembly. Recently, many chemists have focused on the control exerted by organic ligands on the supramolecular structure. Among them, N-donor bridging ligands,[1] in particular those with pyridyl[8] and nitrile[9] donor groups, have been used to construct coordination frameworks showing novel structural features. Due to the aromaticity and multiple N-donor atoms, tetrazolate is also an excellent donor group with potential applications in the construction of coordination frameworks.[10] Recently, three coordination frameworks, $[Zn_2(OH)(4\text{-ptz})_3]$ (**1**), [Zn(OH)(4-ptz)(H_2O)] (**2**), and [Cu(4-ptz)0.5(py)] (**3**), were prepared in our laboratory with 5-(4-pyridyl)tetrazolate (4-ptz) ligands. The present report is concerned with the syntheses, crystal structures and luminescent properties of these compounds.

Results and Discussion

Complex **1** was prepared by treating $Zn(ClO_4)_2·6H_2O$ with 5-(4-pyridyl)tetrazole in ethanol and water under hydrothermal conditions (Scheme 1). Addition of pyridine to the reaction solutions gave complex **2** under the same conditions as for complex **1**. The proportion of hydroxy groups in complex **2** is higher than that in complex **1**; they are presumably formed from water in situ. Complex **3** was prepared by the same method as complex **2** (Scheme 1), except that $Cu(NO_3)_2·6H_2O$ was used instead of $Zn(ClO_4)_2·6H_2O$; the Cu^+ ions are likely formed by the re-

[a] Department of Chemistry, University of Science and Technology of China,
Hefei, 230026 Anhui, P. R. China
Fax: (internat.) + 86-551-3631760
E-mail: zwang3@ustc.edu.cn

Supporting information for this article is available on the WWW under http://www.eurjic.org or from the author.

 © 2004 Wiley-VCH Verlag GmbH & Co. KGaA, Weinheim DOI: 10.1002/ejic.200400170

duction of Cu^{2+} by ethanol in situ.[11] The observed tetrazolate stretching frequencies (1624 and 1435 cm^{-1} in **1** and 1627 and 1439 cm^{-1} in **2** and 1616 and 1442 cm^{-1} in **3**) in the IR spectra of these compounds are consistent with those of other tetrazolate-based assemblies reported previously.[10]

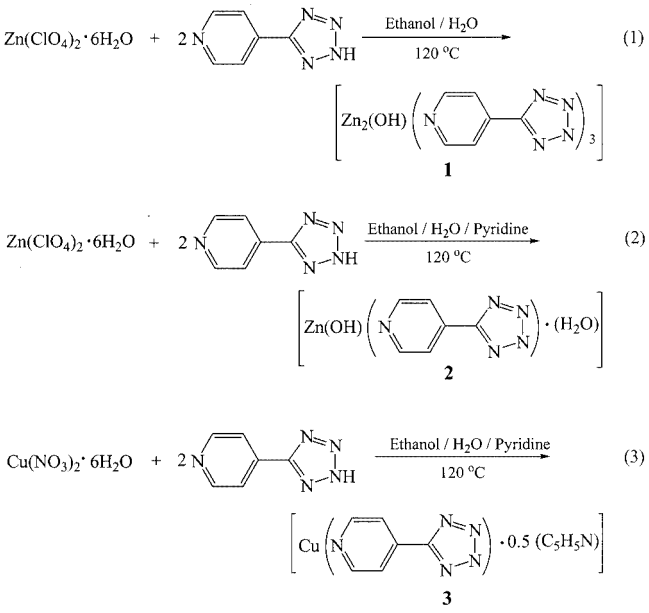

Scheme 1

Structural Description

$[Zn_2(OH)(4\text{-ptz})_3]$ (1) and $[Zn(OH)(4\text{-ptz})(H_2O)]$ (2)

The asymmetric unit of complex **1** comprises two Zn atoms, three 4-ptz ligands and a hydroxy group (Figure 1). Two crystallographically distinct zinc centers, Zn1 and Zn2, are linked by one hydroxy group with a Zn−O−Zn angle of 120.4(2)° [123.18(14)° in complex **2**]. Each doubly bridging 4-ptz ligand coordinates through the two nitrogen atoms of the tetrazolate and the pyridine moiety. Each zinc center is in a tetrahedral environment surrounded by one hydroxy group and three different 4-ptz ligands (in complex **2**, the zinc center is surrounded by two hydroxy groups and two different 4-ptz ligands) with the difference being that the Zn1 center is coordinated to two tetrazolate nitrogen atoms and one pyridine nitrogen atom, while the Zn2 center is coordinated to two pyridine nitrogen atoms and one tetrazolate nitrogen atom. The N−Zn−N(O) angles vary from 101.9(2) to 109.2(2)° [104.09(12) to 110.46(12)° in complex **2**], while O1−Zn1−N7 [127.0(2)°] and O1−Zn2−N10 [120.7(2)°] are much larger [O−Zn−O of 120.47(13)° in complex **2**]. All donor atoms form reasonably strong bonds with the zinc atom: the Zn−N bond lengths range from 1.991(5) to 2.048(6) Å [2.021(3) and 2.079(4) Å in complex **2**], and the Zn−O bond lengths of Zn1 and Zn2 are 1.902(4) and 1.908(5) Å, respectively [1.922(3) and 1.936(3) Å in complex **2**].

The structure of complex **1** consists of two identical and independent rectangular grid sheets, interpenetrating parallelly in the manner shown in Figures 2 and 3. This mode of interpenetration is topologically equivalent to that in [Cu(tcm)(bipy)], as can be appreciated from its topological essence.[12] The four-connected nodes of the net are provided by $Zn_2(OH)$ units, which are connected to one another through 4-ptz and $(4\text{-ptz})_2$ bridges, with grid lengths of 13.1 and 11.5 Å, respectively, and a grid angle of 91°. Individual sheets are corrugated so as to allow this interweaving. There are π−π interactions between the pyridyl or tetrazolate groups from two independent interpenetrat-

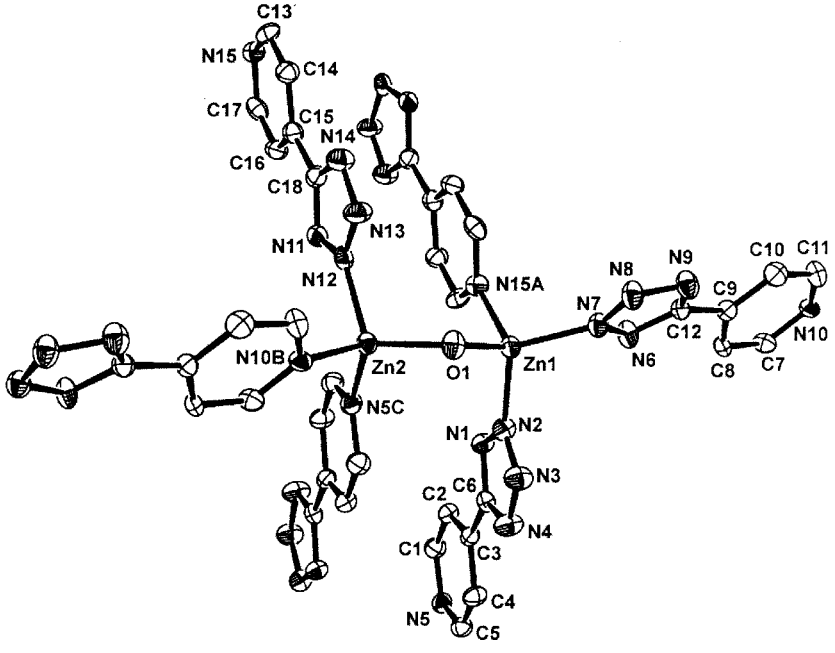

Figure 1. ORTEP drawing of **1** showing the local coordination environment of two crystallographically distinct Zn^{II} centers (thermal ellipsoids at 50% probability)

 © 2004 Wiley-VCH Verlag GmbH & Co. KGaA, Weinheim

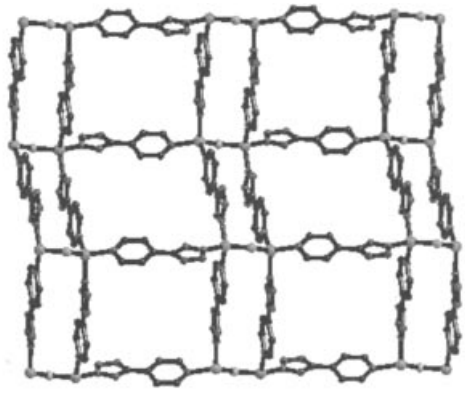

Figure 2. 2D rectangular grid net in **1**

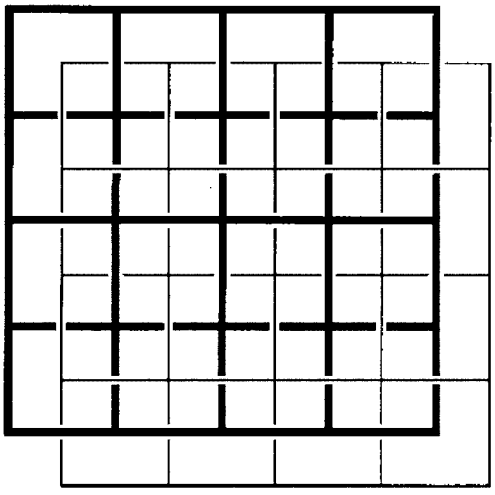

Figure 3. Schematic representation of the mode of interpenetration of two parallel rectangular grid nets; the four-connected nodes shown represent the centers of the $Zn_2(OH)$ aggregates

ing nets, which can be regarded as a stabilizing factor for the interpenetration. The composite structure resulting from this form of interpenetration is itself two-dimensional, and these composite sheets are stacked one on top of another by hydrogen-bonding interactions [O1···N3 (at $-x$, $-y$, $-z + 1$), 2.843 Å] forming a 3D structure (Figure 4).

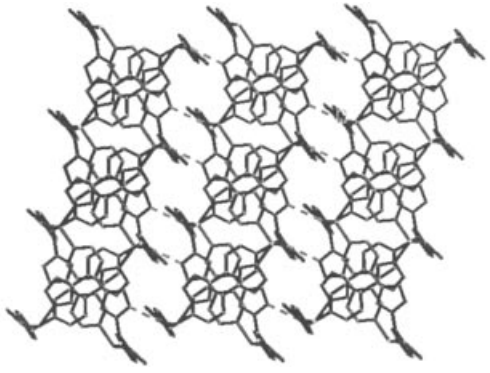

Figure 4. Three layers of the internally interwoven double sheets viewed approximately "edge-on"; the dashed lines represent the hydrogen bonding between layers in **1**

Comparing the structure of complex **1** with the recently reported 2D layered network [Zn(OH)(4-ptz)(H_2O)] (**2**),[10c] we can find many structural similarities involving the components of the network, the coordination mode of the 4-ptz ligand and in situ formation of the hydroxy groups. Complexes **1** and **2** differ mainly in their metal/ligand proportion, the presence of intercalated water molecules, and the topology and connectivity of their 2D coordination networks.[13] Comparing the 2D networks in complexes **1** and **2**, half of the hydroxy groups in complex **2** are replaced by 4-ptz ligands for complex **1**, which makes the grid sheets in complex **1** have bigger grid windows than in complex **2**. Thus, in complex **1** the grid sheets can undergo a twofold parallel interpenetration (see Supporting Information). The structural features exhibited by complexes **1** and **2** imply that the different pH values of the reaction solutions leads to different coordination environments of the metal ion and thus affects the self-assembly progress, resulting in a variety of coordination frameworks.

[Cu(4-ptz)·0.5(py)] (3)

The asymmetric unit of complex **3** comprises one Cu atom, one 4-ptz ligand and half a pyridine molecule (Figure 5). Each Cu atom coordinates to three tetrazolate nitrogen atoms and to one pyridyl nitrogen atom of four different 4-ptz ligands. Each Cu center adopts a highly distorted tetrahedral geometry. The bond angles vary from 90.41(14) to 123.57(14)°; this large range of bond angles is due to the large bulk of the tetrazolate and pyridyl groups compared with the radius of Cu^+. As such, each 4-ptz ligand is coordinated to four Cu atoms through the 1-, 2-, and 4-nitrogen atoms of tetrazolate, and the pyridyl nitrogen atom. The nitrogen donor atoms form strong bonds with the copper atom [from 1.985(3) to 2.130(3) Å]. The tetrazolate groups link the Cu atoms into a one-dimensional chain along the *a* axis (Figure 6). These chains are then interconnected by pyridyl groups from the 4-ptz ligands to give the resulting three-dimensional structure. Because of the bulkiness of the pyridyl groups of the 4-ptz ligands, channels form along the

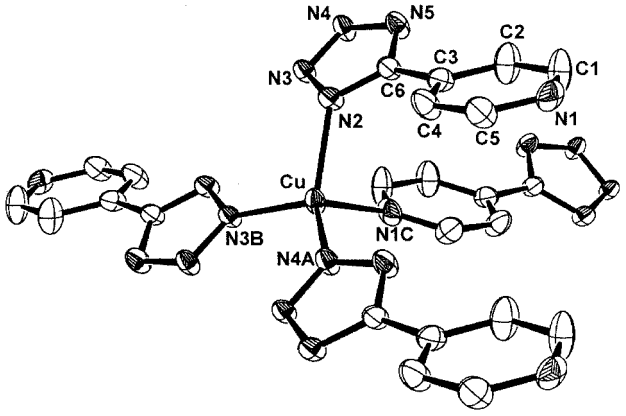

Figure 5. ORTEP drawing of **2** showing the local coordination environment of the Cu^I center (thermal ellipsoids at 50% probability)

 © 2004 Wiley-VCH Verlag GmbH & Co. KGaA, Weinheim

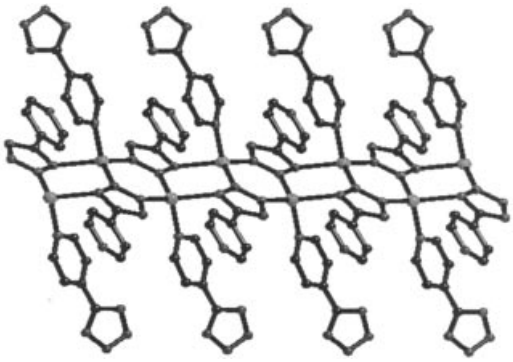

Figure 6. View of the one-dimensional copper chain linked by tetrazolate groups

a axis with an approximate cross-section of 4.4 × 4.4 Å (Figure 7). The solvent pyridine molecules reside in these channels (see Supporting Information). Thermogravimetric analysis showed that **3** loses 15.2% of its total weight in the 103−205 °C temperature range, which corresponds to the expected weight loss of half a pyridine molecule per formula unit (15.9%). Further details of the desolvation processes of complex **3** will form part of a future study.

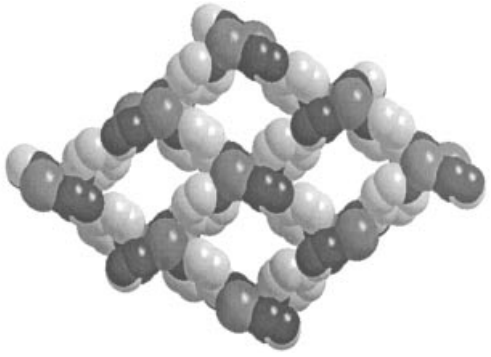

Figure 7. Space-filling view of the three-dimensional structure of **2** along the *a* axis

Structural Analysis

From the structures of complexes **1**, **2** and **3**, it can be seen that the metal ions in the three complexes all adopt a tetrahedral coordination environment, the difference being that Cu^{+} in complex **3** possesses a more distorted coordination geometry than Zn^{2+} in complexes **1** and **2**. Complex **1** has a bridging μ_2-OH group between two zinc ions and complex **2** possesses a Zn−OH−Zn−OH chain. As far as we know, the radius of Zn^{2+} (0.74 Å) is smaller than that of Cu^{+} (0.96 Å) so that there is a restriction of the coordination space around Zn^{2+} in comparison with Cu^{+}. As a result, Cu^{+} can tolerate a more congested tetrahedral coordination environment while Zn^{2+} has to employ bridging μ_2-OH ligands to extend its coordination space and thereby relax the crowded coordination sphere. On the other hand, the Pauling electronegativity of Cu is 1.90 while that of Zn is 1.65. As a result of this difference, copper has a stronger coordination capability than zinc. Due to this strong coordination capability and the larger coordination space of copper, three nitrogen atoms from the tetrazolate group of 4-ptz take part in the coordination in complex **3**, resulting in the three-dimensional framework. These observations confirm that different metals can affect or control the self-assembly process of a supramolecular coordination framework even when the ligands in the supramolecule are the same and the reaction conditions are similar.

Fluorescent Properties

The luminescent properties of complexes **1**, **2** and **3** were investigated in the solid state (Figure 8). Upon excitation at 296 nm, complex **1** shows a strong emission peak at 356 nm. The emission of complex **1** is neither MLCT (metal-to-ligand charge transfer) nor LMCT (ligand-to-metal charge transfer) in nature, and can probably be assigned to intraligand fluorescent emission since a similar emission (λ_{max} = 352 nm) is also observed for free 5-(4-pyridyl)tetrazole.

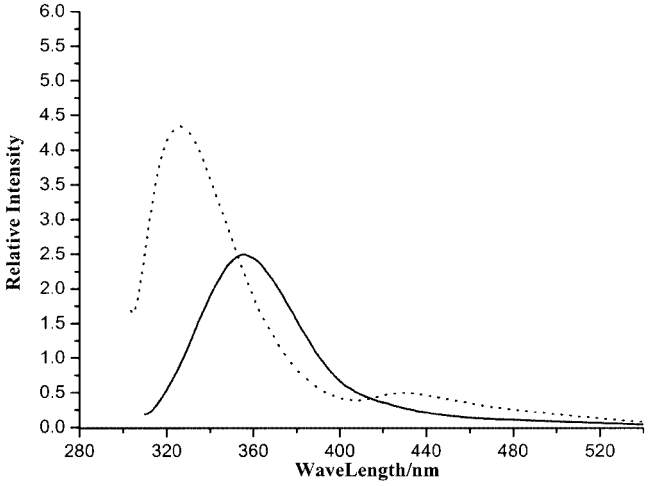

Figure 8. Excitation spectra and emission spectra of complex **1** (solid line) and complex **3** (dotted line) in the solid state at room temperature

Upon excitation at 294 nm, complex **2** displays a strong emission peak at 326 nm that can also be assigned to an intraligand fluorescent emission. Complex **2** shows an enhancement of the fluorescent intensity, which is almost twice that of free 5-(4-pyridyl)tetrazole. A relatively weak peak at 428 nm is also observed for **2**, and this peak may be tentatively assigned to phosphorescence.[10b] The Zn−OH−Zn−OH chain of complex **2** may be responsible for this phosphorescent emission since complex **1** only displays a strong emission peak at 352 nm. The exact phosphorescent-emission mechanism for complex **2** is unclear.

Complex **3** only displays a weak emission peak at 532 nm. The thermal stability of complexes **1** and **2** up to about 300 °C (TGA measurement) and their insolubility in common solvents make them good candidates for potential fluorescent materials.

 © 2004 Wiley-VCH Verlag GmbH & Co. KGaA, Weinheim

Conclusions

In summary, we have prepared two new coordination frameworks containing the 5-(4-pyridyl)tetrazolate ligand. The structural features exhibited by complexes **1**, **2** and **3** show the coordination flexibility of the tetrazolate group. The radius of the coordination metal ion also has a great influence on the self-assembly in a crystal, which provides a crucial clue for possible modification and tuning of the supramolecular framework. The luminescent results indicate that metal coordination and formation of coordination framework can affect the emission wavelength and intensity of the organic material. A more detailed study in this area is in progress in our laboratory.

Experimental Section

General Remarks: The ligand 5-(4-pyridyl)tetrazole was prepared from NaN_3 and 4-cyanopyridine according to a reported procedure.[14] Zinc perchlorate hexahydrate was prepared by the reaction of zinc hydroxide with perchloric acid.[15] ***Caution:*** *$Zn(ClO_4)_2{\cdot}6H_2O$ is potentially explosive and should be used with care!* All other chemicals were of AR grade. Elemental analyses (C, H, N) were performed using an Elementar Vario ELIII elemental analyser. IR spectra as KBr discs were recorded with a Bruker VECTOR-22 FT-IR spectrophotometer. Thermal gravimetric analysis was performed with a Shimadzu TGA-50H Thermal Gravimetric Analyzer at a heating rate of 5 °C·min^{-1}. Excitation and emission spectra were recorded with a Perkin−Elmer LS55 instruments luminescence spectrometer.

Preparation of 1: Hydrothermal treatment of $Zn(ClO_4)_2{\cdot}6H_2O$ (0.1 mmol, 0.037 g), 5-(4-pyridyl)tetrazole (0.2 mmol, 0.015 g), ethanol (0.6 mL), and water (0.2 mL) at 120 °C for 12 h yielded colorless plate crystals (0.015 g, only one pure phase) in 51% yield based on $Zn(ClO_4)_2{\cdot}6H_2O$. $C_{18}H_{13}N_{15}OZn_2$ (586.17): calcd. C 36.88, H 2.24, N 35.84; found C 37.02, H 2.19, N 35.97. IR (KBr): $\tilde{\nu}$ = 3444 (w), 1624 (s), 1556 (m), 1435 (s), 1374 (m), 1228 (m), 1176 (m), 1031 (s), 1011 (m), 976 (m), 850 (m), 756 (m), 719 (m), 556 (m), 532 (s), 496 (m) cm^{-1}.

Preparation of 2: Hydrothermal treatment of $Zn(ClO_4)_2{\cdot}6H_2O$ (0.1 mmol, 0.037 g), 5-(4-pyridyl)tetrazole (0.2 mmol, 0.015 g), ethanol (0.6 mL), water (0.2 mL) and pyridine (0.2 mL) at 120 °C for 12 h yielded colorless plate crystals (0.014 g, only one pure phase) in 57% yield based on $Zn(ClO_4)_2{\cdot}6H_2O$. $C_6H_7N_5O_2Zn$ (246.54): calcd. C 29.20, H 2.84, N 28.39; found C 29.33, H 2.94, N 28.54. IR (KBr): $\tilde{\nu}$ = 3250 (m), 3043 (w), 1626 (s), 1557 (w), 1453 (w), 1439 (s), 1382 (w), 1230 (m), 1172 (w), 1087 (w), 1049 (w), 1018 (m), 854 (m), 754 (w), 719 (m), 538 (w), 512 (m), 472 (w) cm^{-1}.

Preparation of 3: Hydrothermal treatment of $Cu(NO_3)_2{\cdot}6H_2O$ (0.1 mmol, 0.030 g), 5-(4-pyridyl)tetrazole (0.2 mmol, 0.015 g), ethanol (0.6 mL), water (0.2 mL), and pyridine (0.2 mL) at 120 °C for 48 h yielded yellow block crystals (0.011 g, only one pure phase) in 43% yield based on $Cu(NO_3)_2{\cdot}6H_2O$. $C_{17}H_{13}Cu_2N_{11}$ (498.46): calcd. C 40.96, H 2.63, N 30.91; found C 41.09, H 2.54, N 31.12. IR (KBr): $\tilde{\nu}$ = 3443 (w), 2919 (m), 1616 (s), 1442 (s), 1212 (m), 1059 (m), 1045 (m), 1007 (m), 840 (m), 754 (m), 708 (m), 530 (m), 470 (m) cm^{-1}.

X-ray Crystallographic Study: Crystal data and details of the structure refinements are presented in Table 1. Intensity data were collected with an R-AXIS-IV four-circle diffractometer using Mo-K_α radiation (λ = 0.71073 Å) at 291 K for compound **1**, and with a CCD area detector diffractometer at 293 K for compound **3**. The structure solutions and refinements were carried out using SHELXS-96[16] and SHELXL-97, respectively.[17] All hydrogen atoms were identified from difference maps and were included in the successive refinement cycles. All non-hydrogen atoms (including those of solvent water molecules) were refined anisotropically. CCDC-212430 (**1**) and -228746 (**3**) contain the supplementary crystallographic data for this paper. These data can be obtained free of charge at www.ccdc.cam.ac.uk/conts/retrieving.html [or from the Cambridge Crystallographic Data Centre, 12 Union Road, Cambridge CB2 1EZ, UK; Fax: (internat.) + 44-1223-336033; E-mail: deposit@ccdc.cam.ac.uk].

Table 1. Crystallographic data and refinement details for **1** and **3**

	1	3
Empirical formula	$C_{18}H_{13}N_{15}OZn_2$	$C_{17}H_{13}Cu_2N_{11}$
M	586.17	498.46
Crystal system	triclinic	monoclinic
Space group	$P\bar{1}$ (no. 2)	$P2_1/c$ (no. 14)
a [Å]	10.069(2)	5.726(7)
b [Å]	10.453(2)	16.474(2)
c [Å]	11.887(2)	9.941(2)
α [°]	71.16(3)	90
β [°]	67.16(3)	94.29(4)
γ [°]	79.14(3)	90
V [Å^3]	1088.4(4)	935.2(2)
Z	2	2
$D_{calcd.}$ [g cm^{-3}]	1.789	1.770
μ(Mo-K_α) [mm^{-1}]	2.253	2.305
F(000)	588	500
T [K]	291(2)	293(2)
Total data	3479	3847
Unique data	3479	1573
R_{int}	0.00	0.0320
Data [$I > 2\sigma(I)$[	2531	1324
$R1$[a] [$I > 2\sigma(I)$]	0.0497	0.0415
$wR2$[b] [$I > 2\sigma(I)$]	0.1205	0.1091
GOF[c]	1.124	0.979
Residuals [e·Å^{-3}]	0.633, −0.775	0.511, −0.680

GOF = $\{\Sigma[w(F_o^2 - F_c^2)2]/(n - p)\}^{1/2}$.

Acknowledgments

We acknowledge financial support from the National Natural Science Foundation of China (No. 50073021) and the Education Department of Anhui Province (2002kj330ZD).

[1] [1a] C. Janiak, *Dalton Trans.* **2003**, 2781−2804. [1b] B. Moulton, M. J. Zaworotko, *Chem. Rev.* **2001**, *101*, 1629−1658.
[2] [2a] M. Altmann, U. H. F. Bunz, *Angew. Chem. Int. Ed. Engl.* **1995**, *34*, 569−571. [2b] U. H. F. Bunz, *Chem. Rev.* **2000**, *100*, 1605−1644. [2c] Y.-B. Dong, G.-X. Jin, M. D. Smith, R.-Q. Huang, B. Tang, H.-C. zur Loye, *Inorg. Chem.* **2002**, *41*, 4909−4914. [2d] J. Zhanng, R.-G. Xiong, X.-T. Chen, Z.-L. Xue, S.-M. Peng, X.-Z. You, *Organometallics* **2002**, *21*,

 © 2004 Wiley-VCH Verlag GmbH & Co. KGaA, Weinheim

235−238. [2e] J. Zhanng, R.-G. Xiong, X.-T. Chen, C. M. Che, Z.-L. Xue, X.-Z. You, *Organometallics* **2001**, *20*, 4118−4121. [2f] J. Zhanng, R.-G. Xiong, J.-L. Zuo, X.-Z. You, *Chem. Commun.* **2000**, 1495−1496.
[3] O. R. Evanns, W. Lin, *Acc. Chem. Res.* **2002**, *35*, 511−522.
[4] O. Kahn, *Acc. Chem. Res.* **2002**, *33*, 647−657.
[5] [5a] B. F. Hoskins, R. Robson, D. A. Slizys, *Angew. Chem. Int. Ed. Engl.* **1997**, *36*, 2336−2338. [5b] A. J. Blake, N. R. Champness, S. S. M. Chung, W.-S. Li, M. Schröder, *Chem. Commun.* **1997**, 1005−1006. [5c] L. Carlucci, G. Ciani, P. Macchi, D. M. Proserpio, *Chem. Commun.* **1998**, 1837−1838.
[6] [6a] M. A. Withersby, A. J. Blake, N. R. Champness, P. Hubberstey, W.-S. Li, M. Schröder, *Angew. Chem. Int. Ed. Engl.* **1997**, *36*, 2327−2329. [6b] L. Ballester, I. Baxter, P. C. M. Duncan, D. M. L. Goodgame, D. A. Grachvogel, D. J. Williams, *Polyhedron* **1998**, *17*, 3613−3623.
[7] [7a] M. A. Withersby, A. J. Blake, N. R. Champness, P. A. Cooke, P. Hubberstey, M. Schröder, *J. Am. Chem. Soc.* **2000**, *122*, 4044. [7b] A. J. Blake, N. R. Champness, P. A. Cooke, J. E. B. Nicolson, C. Wilson, *J. Chem. Soc., Dalton Trans.* **2000**, 3811−3819. [7c] T. L. Hennigar, D. C. MacQuarrie, P. Losier, R. D. Rogers, M. J. Zaworotko, *Angew. Chem. Int. Ed. Engl.* **1997**, *36*, 972−973.
[8] [8a] R. W. Gable, B. F. Hoskins, R. Robson, *J. Chem. Soc., Chem. Commun.* **1990**, 1677−1678. [8b] B. F. Abrahams, B. F. Hoskins, D. M. Michail, R. Robson, *Nature* **1994**, *369*, 727−729. [8c] L. R. MacGillivray, S. Subramanian, M. J. Zaworotko, *J. Chem. Soc., Chem. Commun.* **1994**, 1325−1326. [8d] J. A. Real, E. Andres, M. C. Munoz, M. Julve, T. Granier, A. Bousseksou, F. Varret, *Science* **1995**, *268*, 265−267. [8e] J. S. Seo, D. Whang, H. Lee, S. I. Jun, J. Oh, Y. J. Jeon, K. Kim, *Nature* **2000**, *404*, 982−986.
[9] [9a] B. F. Abrahams, S. J. Egan, B. F. Hoskins, R. Robson, *Chem. Commun.* **1996**, 1099−1100. [9b] K. A. Hirsch, D. Venkataraman, S. R. Wilson, J. S. Moore, S. Lee, *J. Chem. Soc., Chem. Commun.* **1995**, 2199−2200.
[10] [10a] R.-G. Xiong, X. Xue, H. Zhao, X.-Z. You, B. F. Abrahams, Z. Xue, *Angew. Chem. Int. Ed.* **2002**, *41*, 3800−3803. [10b] X. Xue, X.-S. Wang, L.-Z. Wang, R.-G. Xiong, B. F. Abrahams, X.-Z. You, Z. Xue, C.-M. Che, *Inorg. Chem.* **2002**, *41*, 6544−6546. [10c] L.-Z. Wang, Z.-R. Qu, H. Zhao, X.-S. Wang, R.-G. Xiong, Z. Xue, *Inorg. Chem.* **2003**, *42*, 3969−3971. [10d] Z.-R. Qu, H. Zhano, X.-S. Wanng, Y.-H. Li, Y.-M. Song, Y.-J. Liu, Q.-O. Ye, R.-G. Xiong, B. F. Abrahams, Z.-L. Xue, X.-Z. You, *Inorg. Chem.* **2003**, *42*, 7710−7712. [10e] X. Xue, B. F. Abrahams, R.-G. Xiong, X.-Z. You, *Aust. J. Chem.* **2002**, *55*, 495−497. [10f] L.-Z. Wanng, X.-S. Wanng, Y.-H. Li, Z.-P. Bani, R.-G. Xiong, M. Xiong, G.-W. Li, *Chin. J. Inorg. Chem.* **2002**, *18*, 1191−1194.
[11] O. R. Evans, W. B. Lin, *Cryst. Growth Des.* **2001**, *1*, 9−11.
[12] S. R. Batten, R. Robson, *Angew. Chem. Int. Ed.* **1998**, *37*, 1461−1494.
[13] [13a] C. Jiang, Z. P. Yu, X. Zhu, Z. Y. Wang, *Inorg. Chem. Commun.* **2003**, *6*, 706−709. [13b] C. Jiang, Z. Y. Wang, *Polyhedron* **2003**, *22*, 2953−2959.
[14] H. Detert, D. Schollmeier, *Synthesis* **1999**, 999−1004.
[15] The Chemical Society of Japan, *Handbook of Inorganic Compounds Synthesis*, vol. 2, Chemical Industry Press, Beijing, **1986**, p. 480.
[16] G. M. Sheldrick, *SHELXS-96: Program for Crystal Structure Solution*, University of Göttingen, Germany, **1996**.
[17] G. M. Sheldrick, *SHELXL-97: Program for Crystal Structure Refinement*, University of Göttingen, Germany, **1997**.

Received March 1, 2004
Early View Article
Published Online July 12, 2004

 © 2004 Wiley-VCH Verlag GmbH & Co. KGaA, Weinheim

Synthesis and Catalytic Activity of (η^6-*p*-Cymene)(phosphane)ruthenium(II) Complexes Supported on Poly(biphenoxyphosphazene) or Chiral Poly(binaphthoxyphosphazene) Copolymers

Gabino A. Carriedo,*[a] Pascale Crochet,[a] Francisco J. García Alonso,[a] José Gimeno,*[a] and Alejandro Presa-Soto[a]

Keywords: Phosphazenes / Polymers / Immobilization / Arene ligands / Hydrogen transfer / Ruthenium

The polyphosphazene random copolymer containing diphenylphosphane ligands $\{[NP(OC_6H_4PPh_2)_2]_{0.4}[NP(O_2C_{12}H_8)]_{0.6}\}_n$ (**1a**) ($O_2C_{12}H_8$ = 2,2′-dioxy-1,1′-biphenyl), and the chiral binaphthoxy analogues $\{[NP(OC_6H_4PPh_2)_2]_{0.1}[NP(O_2C_{20}H_{12})]_{0.9}\}_n$ [$O_2C_{20}H_{12}$ = (*R*)-2,2′-dioxy-1,1′-binaphthyl] (**1b**) and $\{[NP(OC_6H_4PPh_2)_2]_{0.2}[NP(O_2C_{20}H_{10}Br_2)]_{0.8}\}_n$ [$O_2C_{20}H_{10}Br_2$ = (*R*)-2,2′-dioxy-6,6′-dibromo-1,1′-binaphthyl] (**1c**), reacted in dichloromethane at room temperature with appropriate amounts of the dimeric complex $[Ru(\eta^6\text{-}p\text{-cymene})Cl(\mu\text{-}Cl)]_2$ to give the corresponding polymeric (phosphane)Ru^{II} complexes $\{[NP(OC_6H_4PPh_2[RuCl_2(\eta^6\text{-}p\text{-cymene})]_x)_2]_{0.4}[NP(O_2C_{12}H_8)]_{0.6}\}_n$ [*x* = 0.5 (**2a**), 1 (**2b**)], $\{[NP(OC_6H_4PPh_2[RuCl_2(\eta^6\text{-}p\text{-cymene})])_2]_{0.1}[NP(O_2C_{20}H_{12})]_{0.9}\}_n$ (**3**) and $\{[NP(OC_6H_4PPh_2[RuCl_2(\eta^6\text{-}p\text{-cymene})])_2]_{0.2}[NP(O_2C_{20}H_{10}Br_2)]_{0.8}\}_n$ (**4**). The isolated products are soluble reddish solids, and are thermally very stable with very high glass transition temperatures. The reaction of **1b** or **1c** with the cationic precursor $[RuCl(PPh_3)_2(\eta^6\text{-}p\text{-cymene})][PF_6]$ in refluxing THF gave the crosslinked insoluble cationic polymeric complexes $\{[NP(OC_6H_4PPh_2)_2]_{0.1}[NP(O_2C_{20}H_{12})]_{0.9}[RuCl(\eta^6\text{-}p\text{-cymene})(PF_6)]_{0.05}\}_n$ (**5**) and $\{[NP(OC_6H_4PPh_2)_2]_{0.2}[NP(O_2C_{20}H_{10}Br_2)]_{0.8}[RuCl(\eta^6\text{-}p\text{-cymene})(PF_6)]_{0.08}\}_n$ (**6**). All the complexes were active catalysts in transfer hydrogenation of acetophenone by propan-2-ol, but the C_2-pockets containing the catalytic centers gave no enantioselectivity because of the conformational behavior of the chiral derivatives.

(© Wiley-VCH Verlag GmbH & Co. KGaA, 69451 Weinheim, Germany, 2004)

Introduction

Although many linear polyphosphazenes[1−5] $(N{=}PR_2)_n$, carrying ligands as lateral groups, can be used to form transition metal complexes,[6−12] the resulting materials have not been extensively characterized as polymer-supported catalysts.[13] Recently, according to the synthesis of the homopolymers $[NP(O_2C_{12}H_8)]_n$ ($O_2C_{12}H_8$ = 2,2′-dioxy-1,1′-biphenyl)[14] and the chiral analogue $[NP(O_2C_{20}H_{12})]_n$ [$O_2C_{20}H_{12}$ = (*R*)-2,2′-dioxy-1,1′-binaphthyl],[15] we reported the preparation of phosphazene random copolymers bearing diphenylphosphane groups (Scheme 1) $\{[NP(OC_6H_4PPh_2)_2]_x[NP(O_2C_{12}H_8)]_{1-x}\}_n$ (*x* = 0.4; **1a**),[16] $\{[NP(OC_6H_4\text{-}PPh_2)_2]_{0.1}[NP(O_2C_{20}H_{12})]_{0.9}\}_n$ [$O_2C_{20}H_{12}$ = (*R*)-2,2′-dioxy-1,1′-binaphthyl] (**1b**),[17] and $\{[NP(OC_6H_4\text{-}PPh_2)_2]_{0.2}[NP(O_2C_{20}H_{10}Br_2)]_{0.8}\}_n$ (**1c**) [$O_2C_{20}H_{10}Br_2$ = (*R*)-2,2′-dioxy-6,6′-dibromo-1,1′-binaphthyl].[17] The latter chiral polymers **1b**, **1c** were considered of potential interest in catalysis because they have the phosphane ligands located in the space (chiral pocket) defined by two consecutive

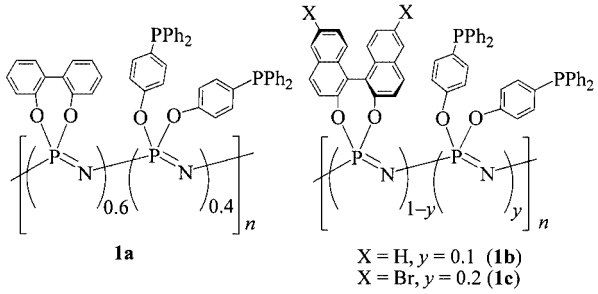

Scheme 1. Polyphosphazenes **1a**, **1b**, **1c**

$[NP(O_2C_{20}H_{10}X_2)]_n$ (X = H, Br) units,[18] and the very high glass transition temperatures of the polymers indicate their stereochemical rigidity.

(Arene)ruthenium(II) complexes have been widely used in homogeneous catalysis and have proven to be efficient precatalysts in a wide number of organic transformations of academic and industrial interest.[19] In particular, they have shown outstanding performance in catalytic transfer hydrogenations.[20] In order to explore the actual potential of the polyphosphazenes as supporting polymers, we considered the synthesis of well-defined complexes containing (arene)-ruthenium(II) fragments. It is well known that the development of cleaner and low-cost catalytic processes requires

[a] Departamento de Química Orgánica e Inorgánica, Instituto Universitario de Química Organometálica "Enrique Moles" (Unidad Asociada al CSIC), Facultad de Química, Universidad de Oviedo,
C/ Julián Clavería S/N, 33071 Oviedo, Spain
E-mail: gac@fq.uniovi.es

 © 2004 Wiley-VCH Verlag GmbH & Co. KGaA, Weinheim **DOI: 10.1002/ejic.200400194**

the immobilization of catalysts through coordination to functionalized polymers, and this immobilization has been revealed as one of the most reliable methodologies.[21]

Herein, we describe the synthesis and characterization of novel neutral or cationic polymeric (η^6-*p*-cymene)ruthenium(II) complexes supported by diphenylphosphane ligands in the achiral polyphosphazene **1a** and in the chiral polyphosphazenes **1b** and **1c**. They have proven to be active and recyclable catalysts in transfer hydrogenation of acetophenone by propan-2-ol although no enantiomeric excesses were observed when using the chiral derivatives. The stereochemical factors, which may determine this lack of selectivity by the chiral binaphthoxy derivatives, are also discussed.

Results and Discussion

Synthesis and Characterization of (Arene)(Linear and crosslinked polymeric phosphazene−phosphane)Ru^{II} Complexes

The reaction of the polyphosphazene−phosphane $\{[NP(OC_6H_4PPh_2)_2]_{0.4}[NP(O_2C_{12}H_8)]_{0.6}\}_n$ (**1a**) with $0.4x$ equiv. (x = 0.5, 1) of [Ru(η^6-*p*-cymene)Cl(μ-Cl)]$_2$ per polymeric unit in dichloromethane at room temperature gave the well-defined polymeric (phosphane)ruthenium(II) complexes $\{[NP(OC_6H_4PPh_2[RuCl_2(\eta^6\text{-}p\text{-cymene})]_x)_2]_{0.4}[NP(O_2C_{12}H_8)]_{0.6}\}_n$ [x = 0.5 (**2a**), 1 (**2b**)] (83 and 92% yield, respectively) (Scheme 2). The reaction was monitored by the decrease in intensity of the $^{31}P\{^1H\}$ singlet resonance due to the PPh_2 groups in **1a** ($\delta \approx -6$ ppm) and the appearance of a new singlet at δ = 23.7 ppm, arising from the coordinated PPh_2 groups in **2a**, **2b**. The final relative intensities of the phosphorus resonances were in agreement with the expected value for each polymer. Thus, all the diphenylphosphanyl groups available in complex **2b** were coordinated to ruthenium centers, while in **2a** 50% of the ligands remained free.

According to a similar procedure (Scheme 3), the ruthenium(II) polymeric complexes $\{[NP(OC_6H_4PPh_2[RuCl_2(\eta^6\text{-}p\text{-cymene})])_2]_{0.1}[NP(O_2C_{20}H_{12})]_{0.9}\}_n$ (**3**) and $\{[NP(OC_6H_4PPh_2[RuCl_2(\eta^6\text{-}p\text{-cymene})])_2]_{0.2}[NP(O_2C_{20}H_{10}Br_2)]_{0.8}\}_n$ (**4**) were obtained (90 and 88% yield) by treating the chiral polyphosphazenes **1b** and **1c** with 0.1 and 0.2 equiv., respectively, of [Ru(η^6-*p*-cymene)Cl(μ-Cl)]$_2$ per polymeric unit. The high ratio of binaphthoxy/diphenylphosphanyl groups of the polymers **1b**, **1c** ensured the location of the ruthenium fragments within the potentially chiral pocket formed by two consecutive binaphthoxy units.

Complexes **2a**, **2b, 3** and **4** were isolated as red, air-stable solids, which are soluble in dichloromethane but insoluble in hexane or propan-2-ol. Analytical and spectroscopic data (IR and ^1H, $^{31}P\{^1H\}$ and $^{13}C\{^1H\}$ NMR) supported the proposed formulations (see Exp. Sect. for details). As expected, the NMR signals of the polymers were broad to very broad and several of the weaker peaks could not be observed clearly.

The presence of the organometallic moiety [Ru(η^6-*p*-cymene)] was shown in the ^1H and $^{13}C\{^1H\}$ NMR spectra by the expected resonances for the nuclei of the aromatic ring, as well as for the methyl and isopropyl substituents. $^{31}P\{^1H\}$ NMR spectra contain resonances at $\delta \approx 23$ ppm corresponding to the coordinated diphenylphosphanyl groups, which compare well with those of the analogous

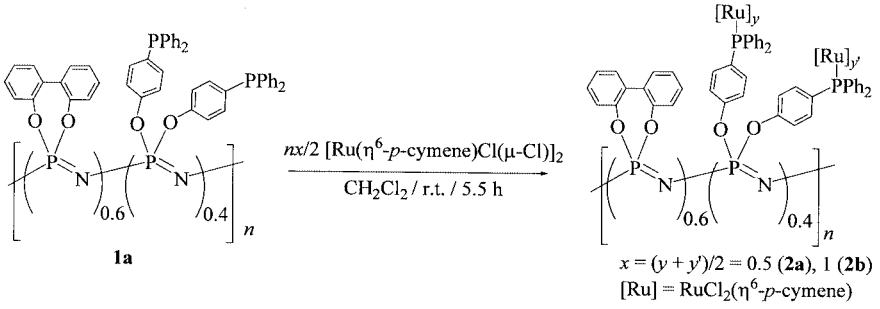

Scheme 2

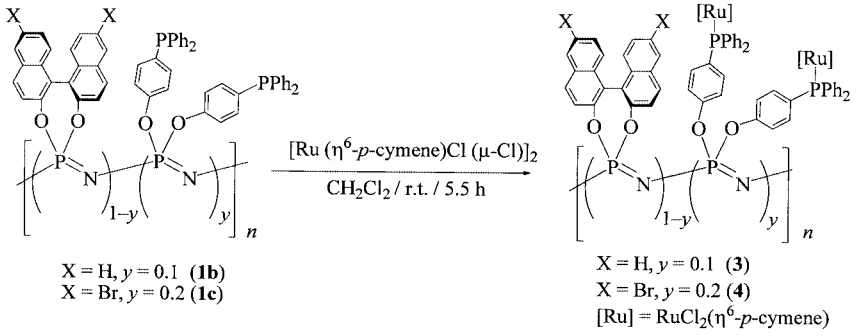

Scheme 3

 © 2004 Wiley-VCH Verlag GmbH & Co. KGaA, Weinheim

complex $[RuCl_2(PPh_3)(\eta^6\text{-}p\text{-cymene})]$ (δ = 23.1 ppm). In the case of **2a**, a signal corresponding to the uncoordinated PPh_2 groups (δ = −6.2 ppm) was also observed. The spectra also showed two broad signals corresponding to the distribution of chemical shifts of the two different phosphazene repeating units present in the polymeric chains, one at $\delta \approx -5$ ppm $[NP(O_2C_{12}H_8)]$ or $\delta = -3$ ppm $\{[NP(O_2C_{20}H_{12})]$ or $[NP(O_2C_{20}H_{10}Br_2)]\}$, and another at $\delta \approx -23$ ppm $[NP(OC_6H_4PPh_2)_2]$. In all cases, the relative intensities were in agreement with the chemical formulae proposed.

The DSC curves of the polymeric complexes **2a** and **2b** showed a well-defined glass transition. The measured T_g values (149 and 189 °C) were, as expected,[22] higher than that of the starting polymer **1a** (95 °C) and increased with increasing metal content. The glass transition could not be detected for the chiral binaphthoxy derivatives **4** and **5**, but they should be higher than those of the corresponding polymers **1b** (268 °C) and **1c** (256 °C). These values, and the very broad NMR spectra observed at room temperature, are clear indicators of the high stereochemical rigidity of the polymeric chains, a factor that should favor the stereochemical selectivity of the chiral sites in asymmetric processes.[23]

In order to investigate whether the inclusion of the Ru^{II} active centers inside a solid chiral matrix would result in the expected[24] enhanced enantiomeric induction, the crosslinked polymeric complexes $\{[NP(OC_6H_4PPh_2)_2]_{0.1}[NP(O_2C_{20}H_{12})]_{0.9}[RuCl(\eta^6\text{-}p\text{-cymene})(PF_6)]_{0.05}\}_n$ (**5**) and $\{[NP(OC_6H_4PPh_2)_2]_{0.2}[NP(O_2C_{20}H_{10}Br_2)]_{0.8}[RuCl(\eta^6\text{-}p\text{-cymene})(PF_6)]_{0.08}\}_n$ (**6**) were synthesized (Scheme 4) by treating the ligands $\{[NP(OC_6H_4PPh_2)_2]_{0.1}[NP(O_2C_{20}H_{12})]_{0.9}\}_n$ (**1b**) and $\{[NP(OC_6H_4PPh_2)_2]_{0.2}[NP(O_2C_{20}H_{10}Br_2)]_{0.8}\}_n$ (**1c**) with the appropriate amount of the cationic precursor $[RuCl(PPh_3)_2(\eta^6\text{-}p\text{-cymene})][PF_6]$ in refluxing THF. The displacement of the PPh_3 ligands in the cationic complex by the PPh_2 groups attached to the polymer was favored by the insolubility of the final products. Therefore, this substitution method is very convenient for the preparation of crosslinked polymeric complexes with controlled composition, as has been already observed in other cases with phosphazenes carrying pyridine ligands.[25]

Materials **5** and **6**, isolated (95 and 94 yield%) as air-stable, slightly red and green solids, respectively, were insoluble in common organic solvents. Microanalysis (including Ru and P) and spectroscopic data (IR and ^{31}P NMR) support the proposed formulation. Their ^{31}P NMR spectra in the solid state show broad signals at δ = 24.4, 23.2 (**5**) and 24 (**6**) ppm corresponding to the coordinated diphenylphosphanyl groups, and a very broad resonance at δ = −8.5 (**5**) and −9.3 (**6**) ppm for the phosphorus atoms of the polymeric chain. The composition and structure were also confirmed by the IR spectra that showed the absorptions (i) at $\tilde{\nu}$ = 2965 (m) and 2855 (w) cm^{-1} due to the *p*-cymene fragment, (ii) at $\tilde{\nu}$ = 838 cm^{-1} from the PF_6^- anion, and (iii) in the $\tilde{\nu}$ = 1200−1300 cm^{-1} region for the stretching ν(PN) modes of the phosphazene chain.

Catalytic Activity in the Transfer Hydrogenation of Ketones

In order to test the catalytic activity and enantioselectivity of the Ru^{II} complexes supported on the chiral phosphazenes, the transfer hydrogenation of acetophenone by propan-2-ol was investigated, in the presence of catalytic amounts of **2a**, **2b**, **3**, **4**, **5** and **6** (Scheme 5). For comparative purposes, the efficiencies of the analogous homogeneous ruthenium(II) catalysts, $[RuCl_2(\eta^6\text{-}p\text{-cymene})(PPh_3)]$ and $[RuCl(\eta^6\text{-}p\text{-cymene})(PPh_3)_2][PF_6]$, were also observed under the same reaction conditions. In a typical experiment, NaOH was added to either a suspension of the supported ruthenium catalyst precursor (**2a**, **2b**, **3**−**6**) or a solution of the respective mononuclear complex and acetophenone (0.25 M) in propan-2-ol (ketone/Ru/base = 500:1:24) at reflux. The reactions were monitored by gas chromatography. Table 1 shows the catalytic performances. Supported ruthenium(II) complexes **2a**, **2b, 3** and **4** afforded high conversions after ca. 24 h (TON = 450−475; Table 1, Entries 3−6). It is interesting to note that a fast initial rate is observed in the reduction of acetophenone by complex **4**, giving a yield of 53% after 1 h (TOF = 265 h^{-1}). As expected, complexes $[RuCl_2(\eta^6\text{-}p\text{-cymene})(PPh_3)]$ and $[RuCl(\eta^6\text{-}p\text{-cymene})(PPh_3)_2][PF_6]$ were active under homogeneous conditions, showing comparable efficiencies (TON = 475 and 480, respectively) to those of the supported catalysts, but with higher rates (4.5 h) (Table 1, En-

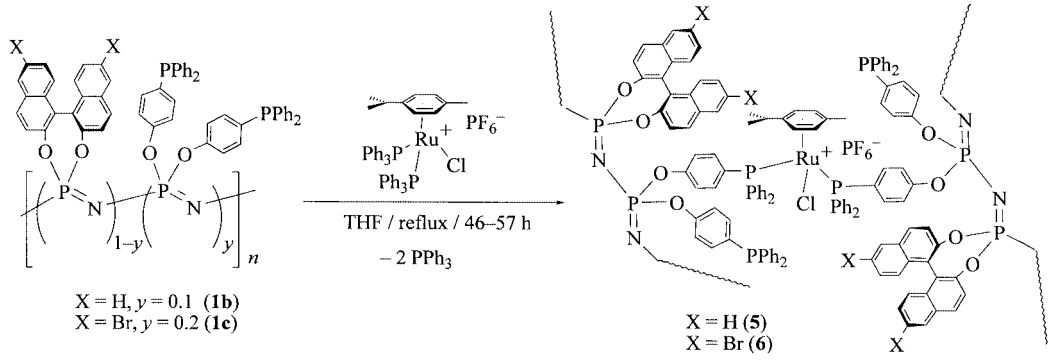

Scheme 4

 © 2004 Wiley-VCH Verlag GmbH & Co. KGaA, Weinheim

tries 1 and 2). The crosslinked supported complexes **5**−**6** were also active catalysts although they were less efficient than their linear analogues **3** and **4** (Table 1, Entries 7 and 8).

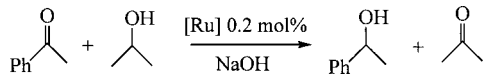

Scheme 5

Table 1. Transfer hydrogenation of acetophenone

Entry[a]	Catalyst	Yield [%][b]	Time [h]	TON[c]
1	$[RuCl_2(PPh_3)(p\text{-cymene})]$	95	4.5	475
2	$[RuCl(PPh_3)_2(p\text{-cymene})][PF_6]$	96	4.5	480
3	**2a**	90	24	450
4	**2b**	92	24	460
5	**3**	92	24	460
6	**4**	95	24	475
7	**5**	70	24	350
8	**6**	65	24	325

[a] Conditions: reactions were carried out at 82 °C using 5 mmol of acetophenone (0.25 M in propan-2-ol); ketone/Ru/NaOH = 500:1:24. [b] Yield in 1-phenylethanol, determined by GC. [c] Turnover number, TON = mol of 1-phenylethanol/mol of Ru.

In order to take advantage of the insolubility of the immobilized catalysts in propan-2-ol, the catalytic activity of the supported ruthenium(II) complexes was examined by successive runs after recycling by simple decantation (see Exp. Sect. for details). Catalysts **2b**, **3**−**6** were active in the second run (40−60% yields) but with a notable reduction in efficiency (Table 2). In contrast, catalyst **2a** showed only a slight loss of activity after six successive runs (Figure 1) with a cumulative turnover number of 2430.

Table 2. Transfer hydrogenation of acetophenone; second run for complexes **2b**, **3**−**6**

Entry[a]	Catalyst	Yield [%][b]	Time [h]	Cumulative TON[c]
1	**2b**	57	24	745
2	**3**	60	24	760
3	**4**	47	24	710
4	**5**	54	24	620
5	**6**	40	24	525

[a] Conditions: reactions were carried out at 82 °C using 5 mmol of acetophenone (0.25 M in propan-2-ol); ketone/Ru/NaOH = 500:1:24. [b] Yield in 1-phenylethanol, determined by GC. [c] Turnover number calculated over the two runs.

Although we made no attempt to characterize the recycled catalysts, it is apparent that the active catalytic species show a moderate to good stability after the first run has been completed. As is well established from a variety of mechanistic studies, transient ruthenium(II) hydride derivatives are the active species in this type of transfer hydrogenation.[26] These species are formed during the first catalytic

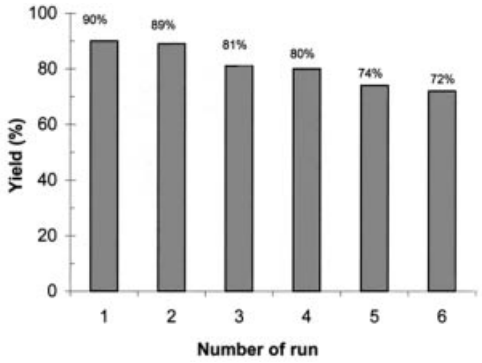

Figure 1. Transfer hydrogenation of acetophenone by **2a**; conditions: reaction carried out at 82 °C using 5 mmol of acetophenone (0.25 M in propan-2-ol); ketone/Ru/NaOH = 500:1:24; yield of 1-phenylethanol after 24 h determined by GC; global TON for six uses = 2430

cycle in which the supported pre-catalyst undergoes a chloride/isopropoxide ligand exchange followed by β-elimination. Although in the first run the required excess of NaOH (24 mol per mol of Ru) for the formation of the active species is used, we observed that better conversions are achieved by addition of NaOH in each run.[27]

In all cases, the leaching of ruthenium from the support during the catalytic experiments was determined by atomic absorption spectroscopy of the metal in solution, after removal of the polymer. When complex **2a** was used, the leaching never exceeded 5% of the initial quantity of ruthenium, in agreement with its recyclability. In contrast, the polymers **2b**, **3** and **4** suffered a greater loss of ruthenium during the first use (ca. 35−50%), which probably accounts for the large decrease in their catalytic activity. As expected in the case of the crosslinked polymers **5** and **6**, the ruthenium leaching is very low and their poor catalytic performances most likely reflect the low accessibility of the active center.

Unfortunately, enantiomeric excesses were observed with neither linear nor crosslinked chiral polymers. As the presence of the active centers within the chiral pockets is unquestionable, these results seem to indicate that in the overall average arrangement of the solid matrix, the local conformations of the polymer chains bearing the chiral sites are too open to induce enantioselectivity. However, another more subtle factor could be the helical secondary structure found for analogous phosphazene chains with binaphthoxy groups.[28] It is well known that the helical polymers form good enantioselective catalysts,[29] but the combination of the secondary helical structure and the centrochiralities present in the main chain may be counterproductive.[30] In this case, it might be better to use a catalyst with either one or another of these features.

Conclusions

This work shows that neutral $[Ru(\eta^6\text{-}p\text{-cymene})Cl_2]$ and cationic $[Ru(\eta^6\text{-}p\text{-cymene})Cl]^+$ fragments can be supported by chiral and achiral polyphosphazenes, giving rise to linear

 © 2004 Wiley-VCH Verlag GmbH & Co. KGaA, Weinheim

or crosslinked polymeric complexes (**2a**, **2b**, **3**−**6** in Schemes 2−4) in which the metal fragments are linked to the polymeric backbone through phosphane lateral groups.

These materials are active polymer-supported catalysts for the transfer hydrogenation of acetophenone with high conversions. Complex **2a** was also recyclable and, in contrast with its homogeneous counterparts which were active only in one run, it could be recovered without significant ruthenium leaching after various catalytic transformations (cumulative TON = 2430 after 6 runs). The activity of **2a** is similar to that of the previously described ruthenium(II) catalyst supported on commercially available R_2P-Merrifield-type polymers.[21f]

Although the active centers supported in polymers **3**−**6** are situated in the chiral pockets generated by two consecutive chiral binaphthoxyphosphazene units, no enantiomeric excess of the resulting secondary alcohol was observed. This may be due to the conformational characteristics of the polymeric chains with pockets that are too wide to induce enantioselectivity. Our observations may represent another experimental example of the combination of chiral polymeric units within a secondary helical structure being counterproductive in asymmetric induction.[30]

Experimental Section

General Comments: All reactions were carried out under nitrogen. The polymeric ligand $\{[NP(OC_6H_4PPh_2)_2]_{0.4}[NP(O_2C_{12}H_8)]_{0.6}\}_n$ (**1a**) was prepared by a method described elsewhere,[16] using $[NPCl_2]_n$ obtained by the procedure described by Magill et al.[31] The product had less than 0.14% of unchanged chlorine, a negligible fraction of oxidized phosphane sites (ca. 3.5%), and contained 0.7 units of polytetrahydrofuran (PTHF). Therefore, its actual degree of functionalization with PPh_2 groups was 1.87 mmol per gram of polymer $(FD)_P = 1.87$. As observed with the previously published analogue,[16] the GPC chromatogram was poorly defined indicating a very broad distribution with an estimated average M_w of 300000 ($M_w/M_n = 12.5$). The T_g (DSC) occurred at 95 °C ($\Delta C_p = 0.19\ Jg^{-1}K^{-1}$). In the polymers $\{[NP(OC_6H_4PPh_2)_2]_{0.1}[NP(O_2C_{20}H_{12})]_{0.9}\}_n$ [17] (**1b**) and $\{[NP(OC_6H_4PPh_2)_2]_{0.2}[NP(O_2C_{20}H_{10}Br_2)]_{0.8}\}_n$,[17] (**1c**) a fraction of the $-PPh_2$ sites had been oxidized to $-P(=O)Ph_2$ (20% and 12%, respectively) and their actual degrees of functionalization with active PPh_2 ligands (the values used to calculate the stoichiometric amounts of Ru complex below) were $(FD)_P = 0.45$ mmol/g and $(FD)_P = 0.69$ mmol/gram, respectively. The precursor complexes $[RuCl_2(PPh_3)(\eta^6\text{-}p\text{-cymene})]$[32] and $[Ru(\eta^6\text{-}p\text{-cymene})Cl(\mu\text{-}Cl)]_2$ [33] were prepared as described previously. $[RuCl(PPh_3)_2(\eta^6\text{-}p\text{-cymene})][PF_6]$ was prepared similarly to the analogous complexes described in the literature.[34] THF was treated with KOH and distilled twice from Na in the presence of benzophenone. The IR spectra were recorded with a Perkin−Elmer FT Paragon 1000 spectrometer. NMR spectra were recorded with Bruker AC-200, AC-300, DPX-300 and Avance 300 instruments, using $CDCl_3$ as solvent unless otherwise stated. ^{31}P NMR spectra of the insoluble polymers were obtained from $[D_6]$DMSO or $CDCl_3$ suspensions using a Varian Unity plus (300 MHz) instrument at the Universitat de Barcelona (Serveis Cientifico-Tècnics). ^1H and $^{13}C\{^1H\}$ NMR chemical shifts are given in δ relative to TMS. $^{31}P\{^1H\}$ NMR chemical shifts are given in δ relative to external 85% aqueous H_3PO_4. Coupling constants are in Hz. C, H, N analyses were performed with a Perkin−Elmer 240 microanalyzer. Ru analyses were performed by Galbraith Laboratories. T_g values were measured with a Mettler DSC 300 differential scanning calorimeter in the second heating cycle unless otherwise stated. Thermal gravimetric analyses were performed with a Mettler TA 4000 instrument. The polymer samples were heated at a rate of 10 °C/min from ambient temperature to 800 °C under a constant flow of nitrogen. Gas chromatographic measurements were carried out with a Hewlett Packard HP6890 instrument. HP-INNOWAX cross-linked polyethylene glycol (30 m, 250 μm) or Supelco Beta-Dex™ 120 (30 m, 250 μm) columns were used.

General Procedure for Catalytic Transfer Hydrogenation of Acetophenone: Under an inert gas, acetophenone (5 mmol), the ruthenium catalyst precursor (0.01 mmol of Ru, 0.2 mol %) and propan-2-ol (17.5 mL) were introduced into a Schlenk tube fitted with a condenser, and heated at 82 °C for 15 min. Then NaOH (2.5 mL of a 0.096 M solution in propan-2-ol, 4.8 mol %) was added and the reaction monitored by gas chromatography. Acetone and 1-phenylethanol were the only products detected in all cases. The recycling process was carried out as follows: After cooling the reaction mixture to room temperature, the insoluble polymer was decanted and washed twice with 10 mL of propan-2-ol. Then, propan-2-ol (17.5 mL), acetophenone (5 mmol) and NaOH (2.5 mL of a 0.096 M solution in propan-2-ol, 4.8 mol %) were added and the mixture heated at 82 °C.

$\{[NP(OC_6H_4PPh_2[RuCl_2(\eta^6\text{-}p\text{-cymene})]_x)_2]_{0.4}[NP(O_2C_{12}H_8)]_{0.6}\}_n$ [x = 0.5 (2a); 1 (2b)]: The dimer $[Ru(\eta^6\text{-}p\text{-cymene})Cl(\mu\text{-}Cl)]_2$ (0.043 g, 0.14 mmol of Ru) was added to a solution of $\{[NP(OC_6H_4PPh_2)_2]_{0.4}[NP(O_2C_{12}H_8)]_{0.6}\}_n$ (**1a**) (0.15 g, 0.28 mmol of PPh_2 groups) in CH_2Cl_2 (15 mL), and the mixture stirred at room temperature for 5.5 h. The resulting solution was concentrated to ca. 1 mL and poured dropwise into hexane (500 mL) to give **2a** as a slightly reddish solid that was dried in vacuo. Yield 0.16 g, (83%). The reddish complex **2b** was prepared similarly using $\{[NP(OC_6H_4\text{-}PPh_2)_2]_{0.4}[NP(O_2C_{12}H_8)]_{0.6}\}_n$ (**1**) (0.20 g, 0.37 mmol of PPh_2 groups) and the dimer $[Ru(\eta^6\text{-}p\text{-cymene})Cl(\mu\text{-}Cl)]_2$ (0.114 g, 0.37 mmol of Ru) and stirring for 5.5 h. The yield was 0.29 g (92%).

2a: $^{31}P\{^1H\}$ NMR (25 °C): δ = 23.7 (m, $C_6H_4PPh_2Ru$), −5.6 [m, $N{=}P(O_2C_{12}H_8)$], −6.2 ($C_6H_4PPh_2$), −22.5 [m, $N{=}P(OC_6H_4PPh_2)_2$] ppm. ^1H NMR (25 °C): δ = 7.5, 7.3, 7.1, 6.7 (aromatic rings); 4.9, 4.7 [$CH_3C_6H_4CH(CH_3)_2$]; 3.4, 1.6 (PTHF), 2.7 [$CH_3C_6H_4CH(CH_3)_2$], 1.5 [$CH_3C_6H_4CH(CH_3)_2$], 0.9 [$CH_3C_6H_4CH(CH_3)_2$] ppm. $^{13}C\{^1H\}$ NMR (25 °C): δ = 152.5, 135, 121.5 (PC_6H_4O), 138, 134, 129 [$P(C_6H_5)_2$], 149, 130.5, 129, 126, 123 ($PO_2C_{12}H_8$); 96, 89.5, 87, 30.5, 22 (*p*-cymene), 71, 27 (PTHF) ppm. FTIR (KBr): $\tilde{\nu}$ = 3054 (m, C−H str., arenes), 2937 (m, C−H str., PTHF), 2855(m, C−H str., PTHF), 1587 (w), 1491 (m), 1477 (m), 1435 (s, C=C str., *p*-cymene), 1374 (m), 1268(s, sh, PO−C str.), 1246 (vs, N−P str.), 1197 (vs, N−P str.), 1169 (vs), 1095 (vs, P−OC str.), 1015 (w), 931 (vs, br, POC def.), 834 (m), 785 (s, PNP def.), 749 (s), 717 (w), 696 (s), 609 (m), 586 (sh), 524 (m, br) cm^{-1}. $C_{28.4}H_{27.2}Cl_{0.8}NO_{2.7}P_{1.8}Ru_{0.4}$ (550.27): calcd. C 62.0, H 4.98, N 2.54; found C 61.1, H 5.35, N 2.54 (calcd. values include the 0.7 PTHF content). TGA: Continuous loss of mass from 170 °C, with maxima at 220 °C (6%), 340 °C (21%), 430 °C (16%). Residue at 800 °C: 41%. T_g (DSC) = 149 °C. $\Delta C_p = -0.113\ J[gK]^{-1}$. Only observed during the second cooling cycle.

2b: $^{31}P\{^1H\}$ NMR (25 °C): δ = 23.6 (m, $C_6H_4PPh_2Ru$), −5.4 [m, $N{=}P(O_2C_{12}H_8)$], −23.5 [m, $N{=}P(OC_6H_4PPh_2)_2$] ppm. ^1H NMR

 © 2004 Wiley-VCH Verlag GmbH & Co. KGaA, Weinheim

(25 °C): δ = 7.5, 7.3, 7.2, (br, aromatic rings); 5.0, 4.8 [$CH_3C_6H_4CH(CH_3)_2$], 3.4, 1.6 (PTHF); 2.7 [$CH_3C_6H_4CH(CH_3)_2$], 0.9 [$CH_3C_6H_4CH(CH_3)_2$] ppm. $^{13}C\{^1H\}$ NMR (CD_2Cl_2, 25 °C): δ = 134, 129 [$P(C_6H_5)_2$]; 98, 87, 30.5, 22 (*p*-cymene); 71, 27 (PTHF) ppm. FTIR (KBr): $\tilde{\nu}$ = 3057 (m, C−H str., arene), 2941 (m, C−H str., PTHF), 2864 (m, C−H str., PTHF), 1588 (w), 1492 (m), 1480 (m), 1435 (s, C=C str., *p*-cymene), 1376 (m), 1246 (vs, N−P str.), 1212 (vs, N−P str.), 1198 (vs, N−P str.), 1172 (vs), 1117 (m), 1094 (vs, P−OC str.), 1016 (w), 935 (v, br, POC def.), 840 (w), 786 (m, PNP def.), 752 (m), 717 (w), 696 (m), 609 (w), 524 (s, br) cm^{-1}. $C_{32.4}H_{32.8}Cl_{1.6}NO_{2.7}P_{1.8}Ru_{0.8}$ (672,74): calcd. C 57.8, H 4.91; N 2.08.; found C 56.9, H 4.38, N 2.18 (calcd. values include the 0.7 PTHF content). TGA: Continuous loss of mass from 180 °C, with maxima at 260 °C (24%), 480 °C (23%), 720 °C (10%). Residue at 800 °C: 43%. T_g (DSC) = 189 °C, ΔC_p= 0.139 J[gK]$^{-1}$.

{[NP(OC$_6$H$_4$PPh$_2$[RuCl$_2$(η^6-*p*-cymene)])$_2$]$_{0.1}$[NP(O$_2$C$_{20}$H$_{12}$)]$_{0.9}$}$_n$ (3): The reddish complex **3** was prepared by stirring a solution of {[NP(OC$_6$H$_4$PPh$_2$)$_2$]$_{0.1}$[NP(O$_2$C$_{20}$H$_{12}$)]$_{0.9}$}$_n$ (**1b**) (0.50 g, 0.225 mmol of PPh_2 groups) in CH_2Cl_2 (30 mL) with the dimer [Ru(η^6-*p*-cymene)Cl(μ-Cl)]$_2$ (0.0735 g, 0.24 mmol of Ru) at room temperature for 5.5 h. The polymer was isolated according to the procedure described previously for **2a**. The yield was 0.51 g (90%). $^{31}P\{^1H\}$ NMR (CD_2Cl_2, 25 °C): δ = 26.8 (m, Ph_2P=O), 23.0 (m, $C_6H_4PPh_2Ru$), −2.8 [m, N=$P(O_2C_{20}H_{12})$], −23.5 [m, N=$P(OC_6H_4PPh_2)_2$] ppm. ^1H NMR (CD_2Cl_2, 25 °C): δ = 7.3 (v br, aromatic rings); 5.0 [v br, $CH_3C_6H_4CH(CH_3)_2$], 2.6 [v br, $CH_3C_6H_4CH(CH_3)_2$], 0.9 [v br, $CH_3C_6H_4CH(CH_3)_2$] ppm. $^{13}C\{^1H\}$ NMR (CD_2Cl_2, 25 °C): δ = 149, (NPO*C* naphthalene ring), 136, 134, 130, 124 (v, br naphthalene and phosphane ring), 32, 24 (br, *p*-cymene) ppm. FTIR (KBr): $\tilde{\nu}$ = 3054 (m, C−H str., arenes), 2960 (m, C−H str., *p*-cymene), 2866 (m, C−H str., *p*-cymene), 1620 (w), 1592 (m), 1508 (m), 1465 (w), 1434 (m), 1398 (m), 1363 (m), 1317 (s), 1256 (sh, s, N−P str.), 1219 (vs, N−P str.), 1190 (sh, vs, N−P str.), 1154 (sh, m), 1095 (w), 1072 (s, P−OC str.), 1030 (w), 963 (vs, br, POC def.), 895 (m), 868 (s), 811(s, PNP def.), 772 (w), 746 (s), 713 (m), 694 (m), 655(m), 571 (s), 523 (m), 487 (m) cm^{-1}. $C_{23.2}H_{15.84}Cl_{0.32}NO_{2.04}P_{1.2}Ru_{0.16}$ (405.94): calcd. C 68.6, H 3.93, N 3.45 (calcd. values take into account the 20% of oxidized phosphane sites); found C 66.3, H 4.01, N 3.42. TGA: Continuous loss of mass from 180 °C, with maxima at 212 (6%), 500 (31%) and 790 °C (7%). Residue at 800 °C: 56%. No T_g was observed in the DSC thermogram up to 300 °C.

{[NP(OC$_6$H$_4$PPh$_2$[RuCl$_2$(η^6-*p*-cymene)])$_2$]$_{0.2}$[NP(O$_2$C$_{20}$H$_{10}$Br$_2$)]$_{0.8}$}$_n$ (4): The dimer [Ru(η^6-*p*-cymene)Cl(μ-Cl)]$_2$ (0.095 g, 0.31 mmol of Ru) was added to a solution of {[NP(OC$_6$H$_4$PPh$_2$)$_2$]$_{0.2}$[NP(O$_2$C$_{20}$H$_{10}$Br$_2$)]$_{0.8}$}$_n$ (**1c**) (0.50 g, 0.345 mmol of PPh_2 groups) in CH_2Cl_2 (30 mL), and the mixture was stirred at room temperature for 5.5 h. The resulting solution was concentrated to ca. 1 mL and poured dropwise into hexane (500 mL) to give **4** as an orange solid that was dried in vacuo. Subsequently, the product was reprecipitated from CH_2Cl_2/diethyl ether, washed with Et_2O (2 × 30 mL) and dried under vacuum at room temperature for 1 d. Yield 0.53 g (88%). $^{31}P\{^1H\}$ NMR (25 °C): δ = 27.5 (m, Ph_2P=O), 23.1 (m, $C_6H_4PPh_2Ru$), −4.3 [m, N=$P(O_2C_{20}H_{10}Br_2)$], −20.0 [m, N=$P(OC_6H_4PPh_2)_2$] ppm. ^1H NMR (25 °C): δ = 7.3 (v br, aromatic rings); 1.8 [br, $CH_3C_6H_4CH(CH_3)_2$], 1.3 [br, $CH_3C_6H_4CH(CH_3)_2$] ppm. FTIR (KBr): $\tilde{\nu}$ = 3055 (m, C−H str., arenes), 2958 (w, C−H str., *p*-cymene), 2865 (w, C−H str, *p*-cymene), 1585 (m), 1493 (m), 1436 (w), 1354 (m), 1317 (s), 1253 (sh, s, N−P str.), 1218 (vs, N−P str.), 1191 (sh, s, N−P str.), 1154 (s), 1117 (w), 1066 (m, P−OC str.), 959 (vs, br, POC def.), 943 (sh, s), 874 (m), 826 (m), 808 (m, PNP def.), 779 (w), 748 (w), 728 (w), 692 (m), 656(w), 602 (w), 570 (m), 521(m), 474 (w) cm^{-1}. $C_{26.7}H_{18.5}Br_{1.6}Cl_{0.70}NO_{2.05}P_{1.4}Ru_{0.35}$ (617.54): calcd. C 51.93, H 3.02, N 2.27 (calcd. values take into account the 12% of oxidized phosphane sites); found C 50.8, H 2.95, N 2.35. TGA: Continuous loss of mass from 180 °C, with maxima at 210 °C (7%), 490 (37%) and 780 (16%). Residue at 800 °C: 40%. No T_g was observed in the DSC thermogram up to 300 °C.

{[NP(OC$_6$H$_4$PPh$_2$)$_2$]$_{0.1}$[NP(O$_2$C$_{20}$H$_{12}$)]$_{0.9}$[RuCl(η^6-*p*-cymene)(PF$_6$)]$_{0.05}$}$_n$ (5): The complex [RuCl(η^6-*p*-cymene)(PPh_3)$_2$][PF_6] (0.061 g, 0.065 mmol) was added to a solution of {[NP(OC$_6$H$_4$PPh$_2$)$_2$]$_{0.1}$[NP(O$_2$C$_{20}$H$_{12}$)]$_{0.9}$}$_n$ (**1b**) (0.50 g, 0.225 mmol of PPh_2 groups) in THF (30 mL) and the resulting mixture was refluxed for 48 h. Then the solvent was evaporated and the free PPh_3 was extracted with diethyl ether (3 × 20 mL). The reddish solid residue was dried under vacuum at room temperature for 6 h. Yield 0.50 g (95%). $^{31}P\{^1H\}$ NMR ([D$_6$]DMSO suspension, 25 °C): δ = 24.4, 23.2 (m, $C_6H_4PPh_2Ru$), −8.5 [v br, N=$P(O_2C_{20}H_{12})$, N=$P(OC_6H_4PPh_2)_2$], −148 (m, PF_6^-) ppm. FT IR (KBr): $\tilde{\nu}$ = 3053 (m, C−H str., arenes), 2965 (m, C−H str, *p*-cymene), 2855 (w, C−H str., *p*-cymene), 1620 (w), 1591 (m), 1506 (w), 1436 (m), 1398 (m), 1362 (m), 1317 (s), 1258 (sh,s, N−P str.), 1218 (vs, N−P str.), 1186 (sh,vs, N−P str.), 1148 (sh, s), 1116 (m), 1069 (m, P−OC str.), 961 (s, br, POC def.), 943 (sh, s), 895 (m), 865 (s), 838 (m, P−F str., PF_6^-), 808 (s, PNP def.), 772 (w), 745 (s), 712 (m), 693 (s), 654 (m), 571 (s), 560 (sh,m, P−F str., PF_6^-), 538 (m), 486 (m), 472 (m), 450 (m) cm^{-1}. $C_{22.1}H_{14.3}Cl_{0.05}F_{0.3}NO_{2.02}P_{1.25}Ru_{0.05}$ (377.42): calcd. C 70.3, H 3.82, Cl, F 1.98, N 3.71, P 10.3, Ru 1.34 (calcd. values take into account the 20% of oxidized phosphane sites); found C 67.0, H 3.81, Cl, F 1.53, N 3.52, P 8.83, Ru 1.11. TGA: Continuous loss of mass from 60 °C, with maxima at 510 °C (42.6%). Residue at 800 °C: 57.4%. No T_g was observed in the DSC thermogram up to 300 °C.

{[NP(OC$_6$H$_4$PPh$_2$)$_2$]$_{0.2}$[NP(O$_2$C$_{20}$H$_{10}$Br$_2$)]$_{0.8}$[RuCl(η^6-*p*-cymene)(PF$_6$)]$_{0.08}$}$_n$ (6): The complex [RuCl(η^6-*p*-cymene)(PPh_3)$_2$][PF_6] (0.074 g, 0.079 mmol) was added to a solution of {[NP(OC$_6$H$_4$PPh$_2$)$_2$]$_{0.2}$[NP(O$_2$C$_{20}$H$_{10}$Br$_2$)]$_{0.8}$}$_n$ (**1c**) (0.50 g, 0.345 mmol of PPh_2 groups) in THF (30 mL) and the resulting mixture was refluxed for 57 h. Then the solvent was evaporated and the free PPh_3 was extracted with diethyl ether (5 × 20 mL). The green solid residue was dried under vacuum at room temperature for 12 h. Yield 0.50 g (94%). $^{31}P\{^1H\}$ NMR ($CDCl_3$ suspension, 25 °C): δ = 24 (m, $C_6H_4PPh_2Ru$), − 9.3 [v br, N=$P(O_2C_{20}H_{10}Br_2)$, N=$P(OC_6H_4PPh_2)_2$]. FT IR (KBr): $\tilde{\nu}$ = 3053 (m, C−H str., arenes), 2960 (m, C−H str., *p*-cymene), 2852 (m, C−H str., *p*-cymene), 1584 (m), 1492 (m), 1437 (m), 1393 (m), 1354 (m), 1317 (s), 1258 (s, N−P str.), 1216 (vs, N−P str.), 1187 (sh,vs, N−P str.), 1115 (s), 1065 (s, P−OC str.), 956 (s, br, POC def.), 942 (vs), 872 (s), 838 (sh, P−F str., PF_6^-), 826 (s), 805 (s, PNP def.), 777 (s), 748 (m), 726 (s), 690 (s), 654 (m), 601 (m), 568 (s), 560 (sh, P−F str., PF_6^-), 533 (s), 514 (s), 492 (s), 472 (s) cm^{-1}. $C_{24}H_{14.72}Br_{1.6}Cl_{0.08}F_{0.48}NO_{2.05}P_{1.48}Ru_{0.08}$ (543.63): calcd. C 53.0, H 2.73, N 2.58, P 8.43; Ru 1.49 (calcd. values take into account the 12% oxidized phosphane sites); found C 51.5, H 2.74, N 2.54, P 7.34, Ru 1.35. TGA: Continuous loss of mass from 160 °C, with maxima at 220 °C (9%), 470 °C (40%), and 770 °C (9%). Residue at 800 °C: 39%. No T_g was observed in the DSC thermogram up to 300 °C.

Acknowledgments

The authors thank the Ministerio de Ciencia y Tecnología (Projects BQU-2001-3676, BQU2000-0227 and CAJAL-01-03), the FICYT

 © 2004 Wiley-VCH Verlag GmbH & Co. KGaA, Weinheim

(Project PB-EXPO1-15 and Grant BP01-130) and the Gobierno Principado de Asturias (PR-01-GE-6) for financial support.

[1] [1a] C. W. Allen, *Coord. Chem. Rev.* **1994**, *130*, 137. [1b] I. Manners, *Angew. Chem. Int. Ed. Engl.* **1996**, *35*, 1602. [1c] R. De Jaeger, M. Gleria, *Prog. Polym. Sci.* **1998**, *23*, 179. [1d] R. De Jaeger, M. Gleria (Eds.), *Phosphazenes: A Worldwide Insight*, NOVA Science Publishers, New York, **2004**.

[2] [2a] H. R. Allcock, *Appl. Organomet. Chem.* **1998**, *12*, 659. [2b] H. R. Allcock, M. A. Hofmann, C. M. Ambler, R. V. Morford, *Macromolecules* **2002**, *35*, 3484. [2c] M. A. Hofmann, C. M. Ambler, A. E. Maher, E. Chalkova, X. Y. Zhou, S. N. Lvov, H. R. Allcock, *Macromolecules* **2002**, *35*, 6490.

[3] H. R. Allcock, *Chem. Mater.* **1994**, *6*, 1476.

[4] G. A. Carriedo, J. I. Fidalgo Martínez, F. J. García Alonso, E. Rodicio González, A. Presa Soto, *Eur. J. Inorg. Chem.* **2002**, 1502.

[5] G. A. Carriedo, F. J. García Alonso, P. A. González, *Macromol. Rapid Commun.* **1997**, *18*, 371.

[6] H. R. Allcock, J. L. Desorcie, G. H. Riding, *Polyhedron* **1987**, *6*, 119.

[7] K. B. Visscher, H. R. Allcock, *Chem. Mater.* **1994**, *6*, 2040.

[8] H. R. Allcock, A. A. Dembek, E. H. Klingenberg, *Macromolecules* **1991**, *24*, 5208.

[9] H. R. Allcock, E. N. Silverberg, C. J. Nelson, W. D. Coggio, *Chem. Mater.* **1993**, *5*, 1307.

[10] G. A. Carriedo, F. J. García Alonso, J. L. García Álvarez, C. Díaz Valenzuela, N. Yutronic Sáez, *Polyhedron* **2002**, *21*, 2587.

[11] G. A. Carriedo, F. J. García Alonso, P. A. González, C. Díaz Valenzuela, N. Yutronic Sáez, *Polyhedron* **2002**, *21*, 2579.

[12] C. Díaz, P. Castillo, G. A. Carriedo, P. Gómez Elipe, F. J. García Alonso, *Macromol. Chem. Phys.* **2002**, *203*, 1912.

[13] [13a] H. R. Allcock, K. D. Lavin, N. M. Tollefson, T. L. Evans, *Organometallics* **1983**, *2*, 267. [13b] R. A. Dubois, P. E. Garrou, K. D. Lavin, H. R. Allcock, *Organometallics* **1986**, *5*, 460. [13c] V. Chandrasekhar, A. Athimoolam, *Org. Lett.* **2002**, *4*, 2113. [13d] V. Janout, P. Cefelin, D. R. Tur, S. V. Vinogradova, *Polym. Bull.* **1986**, *15*, 303. [13e] B. Valter, B. Masar, V. Janout, H. Hrudkova, P. Cefelin, D. R. Tur, S. V. Vinogradova, *Makromol. Chem.* **1991**, *192*, 1549.

[14] G. A. Carriedo, L. Fernández-Catuxo, F. J. García Alonso, P. Gómez-Elipe, P. A. González, *Macromolecules* **1996**, *29*, 5320.

[15] G. A. Carriedo, F. J. García Alonso, P. A. González, J. L. García Álvarez, *Macromolecules* **1998**, *31*, 3189.

[16] G. A. Carriedo, F. J. García Alonso, P. A. González, P. Gómez Elipe, *Polyhedron* **1999**, *18*, 2853.

[17] G. A. Carriedo, F. J. García Alonso, A. Presa Soto, *Eur. J. Inorg. Chem.* **2003**, 4341.

[18] S. D. Dreher, T. J. Katz, K.-C. Lam, A. L. Rheingold, *J. Org. Chem.* **2000**, *65*, 815.

[19] [19a] T. Naota, H. Takaya, S.-I. Murahashi, *Chem. Rev.* **1998**, *98*, 2599. [19b] B. M. Trost, F. D. Toste, A. B. Pinkerton, *Chem. Rev.* **2001**, *101*, 2067.

[20] [20a] G. Zassinovich, G. Mestroni, S. Gladiali, *Chem. Rev.* **1992**, *92*, 1051. [20b] R. Noyori, S. Hashiguchi, *Acc. Chem. Res.* **1997**, *30*, 97. [20c] M. J. Palmer, M. Wills, *Tetrahedron: Asymmetry* **1999**, *10*, 2045. [20d] R. Noyori, M. Yamakawa, S. Hashiguchi, *J. Org. Chem.* **2001**, *66*, 7931. [20e] D. Carmona, M. P. Lamata, L. A. Oro, *Eur. J. Inorg. Chem.* **2002**, 2239. [20f] K. Everaere, A. Mortreux, J. F. Carpentier, *Adv. Synth. Catal.* **2003**, *345*, 67.

[21] [21a] D. J. Bayston, C. B. Travers, M. E. C. Polywka, *Tetrahedron: Asymmetry* **1998**, *9*, 2015. [21b] K. Polborn, K. Severin, *Eur. J. Inorg. Chem.* **2000**, 1687. [21c] K. Polborn, K. Severin, *Chem. Eur. J.* **2000**, *6*, 4604. [21d] A. J. Sandee, D. G. I. Petra, J. N. H. Reek, P. C. J. Kamer, P. W. N. M. van Leeuwen, *Chem. Eur. J.* **2001**, *7*, 1202. [21e] Y. C. Chen, T. F. Wu, J. G. Deng, H. Liu, Y. Z. Jiang, M. C. K. Choi, A. S. C. Chan, *Chem. Commun.* **2001**, 1488. [21f] N. E. Leadbeater, *J. Org. Chem.* **2001**, *66*, 2168. [21g] S. Laue, L. Greiner, J. Wöltinger, A. Liese, *Adv. Synth. Catal.* **2001**, *343*, 711. [21h] C. Saluzzo, M. Lemaire, *Adv. Synth. Catal.* **2002**, *344*, 915 and references cited herein. [21i] Y. C. Chen, T. F. Wu, J. G. Deng, H. Liu, X. Cui, J. Zhu, Y. Z. Jiang, M. C. K. Choi, A. S. C. Chan, *J. Org. Chem.* **2002**, *67*, 5301. [21j] R. Akiyama, S. Kobayashi, *Angew. Chem. Int. Ed.* **2002**, *41*, 2602. [21k] S. Kobayashi, R. Akiyama, *Chem. Commun.* **2003**, 449. [21l] E. Dulière, M. Devillers, J. Marchand-Brynaert, *Organometallics* **2003**, *22*, 804. [21m] J. Q. Yu, H. C. Wu, C. Ramarao, J. B. Specer, S. V. Ley, *Chem. Commun.* **2003**, 678. [21n] S. B. Wendicke, E. Burri, R. Scopelliti, K. Severin, *Organometallics* **2003**, *22*, 1894. [21o] P. N. Liu, Y. C. Chen, X. Q. Li, Y. Q. Tu, J. G. Deng, *Tetrahedron: Asymmetry* **2003**, *14*, 2481.

[22] H. R. Allcock, A. A. Dembek, E. H. Klingenberg, *Macromolecules* **1991**, *24*, 5208.

[23] L. Pu, *Chem. Rev.* **1998**, *98*, 2405.

[24] P. Hesemann, J. J. Moreau, *Tetrahedron: Asymmetry* **2000**, *11*, 2183.

[25] G. A. Carriedo, F. J. García Alonso, A. Presa Soto, *J. Inorg. Organomet. Polym.* **2004**, *14*, 29.

[26] J. E. Bäckvall, *J. Organomet. Chem.* **2002**, *652*, 105.

[27] In the case of catalyst **2b**, the second run in the absence of base leads to only 50% of 1-phenylethanol after 24 h.

[28] [28a] G. A. Carriedo, F. J. García Alonso, J. L. García Álvarez, G. M. Lombardo, G. C. Pappalardo, F. Punzo, *Chem. Eur. J.*, in press. [28b] G. A. Carriedo, J. L. García Álvarez, F. J. García Alonso, A. Presa Soto, M. P. Tarazona, F. mendicuti, G. Marcelo, *Macromolecules*, in press.

[29] L. Pu, *Tetrahedron: Asymmetry* **1998**, *9*, 1457.

[30] M. Reggelin, M. Schultz, M. Holbach, *Angew. Chem. Int. Ed.* **2002**, *41*, 1614.

[31] A. N. Mujumdar, S. G. Young, R. L. Merker, J. H. Magil, *Macromolecules* **1990**, *23*, 14.

[32] M. A. Bennett, A. K. Smith, *J. Chem. Soc., Dalton* **1974**, 233.

[33] M. A. Bennett, T.-N. Huang, T. W. Matheson, A. K. Smith, *Inorg. Synth.* **1982**, *21*, 75.

[34] H. Werner, R. Werner, *Angew. Chem. Int. Ed. Engl.* **1978**, *17*, 683.

Received March 10, 2004
Early View Article
Published Online July 12, 2004

 © 2004 Wiley-VCH Verlag GmbH & Co. KGaA, Weinheim

Mechanism of Reduction of the Nitrite Ion by Cu^{I} Complexes

Ariela Burg,[a] Evgenia Lozinsky,[a] Haim Cohen,[a,b] and Dan Meyerstein*[a,c]

Keywords: Nitrite / Copper(I) / Reduction / NO

The reaction of Cu^{+}_{aq} with NO_2^- was studied. The results are consistent with the mechanism: $Cu^{+}_{aq} + NO_2^- \leftrightarrows (Cu^{+}NO_2^-)$, $K = 140 \pm 30$ M^{-1}; $(Cu^{+}NO_2^-) + H^+ \rightarrow Cu^{2+} + NO + OH^-$, $k = 4.6 \times 10^5$ M^{-1}s^{-1}. It is proposed that the copper is bound to the nitrogen in the transient complex $(Cu^{+}NO_2^-)$. In addition, the reaction was studied with $(Cu^{I}L^{i})^{+}$ complexes. The results show that the ligands reduce the value of K and that their effect on k depends on the redox potential of the $(Cu^{II/I}L^{i})$ couple. This reaction is the simplest model for the CuNIR (NIR = Nitric reductase) enzymes.
(© Wiley-VCH Verlag GmbH & Co. KGaA, 69451 Weinheim, Germany, 2004)

Introduction

The one-electron reduction of nitrite to NO is of major importance in a variety of biological processes[1−3] and in waste water treatment.[4−6] The reducing agent, or the electro-catalytic active agent,[7−9] is usually a low valent transition metal complex, e.g. Fe^{II},[9−13] Co^{I},[14,15] Ru^{II},[8,16] Cu^{I}.[17−20] For example, one of the steps in the important nitrogen cycle is the reduction of nitrite to nitric oxide.[21] Dinitrogen is released into the atmosphere by the activity of denitrifying bacteria found in soils and sediments.[22−25] The enzyme nitrite reductase (NIR) is essential for these bacteria.[1,2] Several mechanistic studies on the reduction of NO_2^- by Cu^{I} complexes in organic solvents were performed in order to elucidate the reduction mechanism, and as plausible models for the enzymatic process.[26−35] In the present work, we decided to study the mechanism and kinetics of the reaction between $Cu^{+}_{aq}/(Cu^{I}L)^{+}$ complexes and NO_2^-. The results indicate that a transient complex, $(Cu^{+}NO_2^-)$, is formed initially, and that this complex reacts with H_3O^+ to yield the final products.

It is of interest to note that the oxidation of NO by $Fe^{III}L$ complexes proceeds via the reverse mechanism[35] [see reaction (1)].

$$[Fe^{III}L] + NO \rightleftarrows [Fe^{III}L{\cdot}NO] \xrightarrow{OH^-} [Fe^{II}L] + HNO_2 \quad (1)$$

[a] Chemistry Department, Ben-Gurion University of the Negev, Beer-Sheva, Israel
[b] Nuclear Research Centre Negev, Beer-Sheva, Israel
[c] Department of Biological Chemistry, The College of Judea and Samaria, Ariel, Israel
E-mail: danmeyer@bgumail.bgu.ac.il

Results and Discussion

When Cu^{+}_{aq} is introduced into a solution containing excess $NaNO_2$ $(2.5-100) \times 10^{-3}$ M in the pH range 4.15−5.45 (buffered by 0.10 M acetate, the results are independent of the acetate concentration in the range 0.10−0.50 M), a decrease in the absorption at 355 nm due to nitrite is observed. The kinetics of this process, followed using the stopped-flow technique, obey a first order rate law on Cu^{I}. The observed rate increases with increasing $[NO_2^-]$. However, the results indicate that a limiting rate is observed at high $[NO_2^-]$ (see Figure 1).

Analysis of the results assuming a mechanism involving the fast formation of an intermediate complex fits well with the experimental data [Figure 2, reaction (2)]. The value of k_2 (Table 1) derived from the intercepts of plots analogous to Figure 2 is pH-dependent. A plot of k_2 vs. $[H_3O^+]$ (Figure 3) yields a straight line ($k_2 = k_{*2}[H_3O^+]$). From the slope of the line in this figure one obtains $k_{*2} = (4.6 \pm 0.5) \times 10^5$ M^{-1} s^{-1}.

$$Cu^{+}_{aq} + NO_2^- \xrightleftharpoons{K_{2app}} [Cu^{+}NO_2^-] \xrightarrow[H^+]{k_2} Cu^{2+}_{aq} + NO + OH^- \quad (2)$$

$$-d[NO_2^-]/dt = (k_2K_{2app}[NO_2^-][Cu^{+}_{aq}])/(1 + K_{2app}[NO_2^-])$$

$$1/k_{obsd.} = 1/(k_2K_{2app}[NO_2^-]) + 1/k_2$$

The results indicate that a mechanism in which an unreactive $Cu^{I}-NO_2^-$ complex is formed [reactions (3) and (4)] could yield the same rate law. However, this would require that the reaction according to reaction (4) is a third order process. Thus, this mechanism seems unlikely.

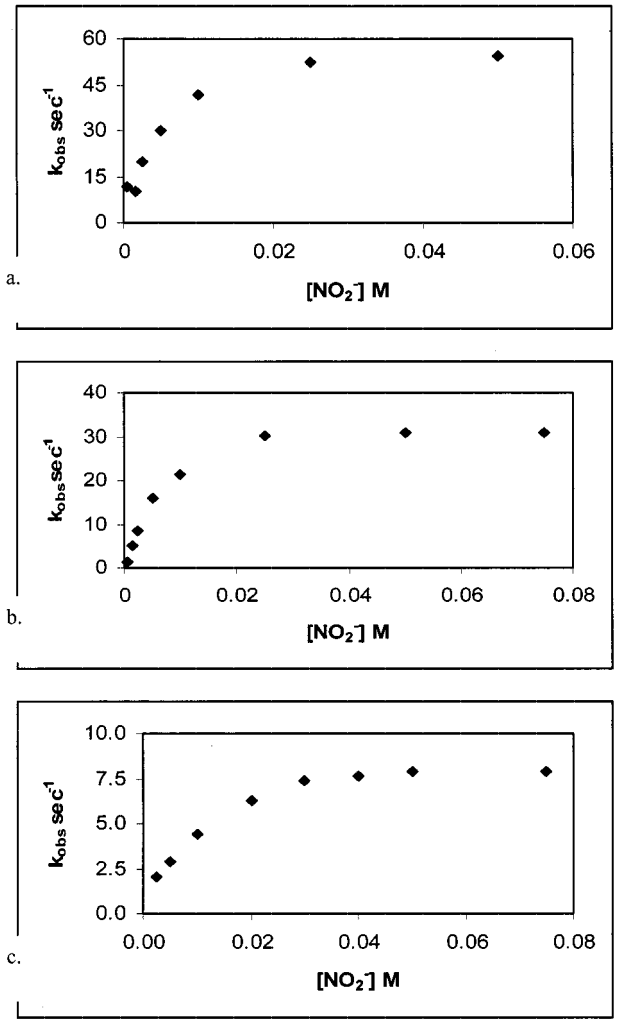

Figure 1. Dependence of $k_{obsd.}$ on the $[NO_2^-]$. The experiments were performed in solutions containing 5.0×10^{-4} M Cu^+_{aq}, 0.10 M $NaClO_4$, 0.10 M acetic acid, 0.023 M NH_4^+, helium saturated at a final pH of: a. 4.3, b. 4.65, c. 5.25.

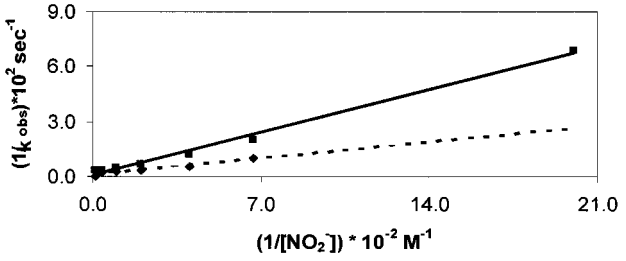

Figure 2. Dependence of $1/k_{obsd.}$ on $1/[NO_2^-]$. The experiments were performed in solutions containing 5.0×10^{-4} M Cu^+_{aq}, 0.10 M $NaClO_4$, 0.10 M acetic acid, 0.023 M NH_4^+, helium saturated, the final pH: 4.3 (-----), 4.65 (—)

$$Cu^+_{aq} + NO_2^- \rightarrow (Cu^+NO_2^-) \quad (3)$$

$$Cu^+_{aq} + NO_2^- \rightarrow P \quad (4)$$

$$Cu^+_{aq} + NO_2^- + H_3O^+ \rightarrow Cu^{2+}_{aq} + NO + OH^- \quad (5)$$

Table 1. The effect of $[H_3O^+]$ on k_2 and on the observed stability constant of the $(Cu^+NO_2^-)$ complex (the experiments were performed on helium-saturated solutions containing 5.0×10^{-4} M Cu^+_{aq}, 0.10 M $NaClO_4$, 0.10 M acetic acid, 0.023 M NH_4^+)

K_{2app} (M^{-1})	k_2 (M^{-1}s^{-1})	$[H_3O^+]$ (M)	pH
77	2.9	3.5×10^{-6}	5.45
62	3.4	4.0×10^{-6}	5.40
62	5.0	1.3×10^{-5}	4.90
152	8.2	2.0×10^{-5}	4.70
120	12	2.2×10^{-5}	4.60
132	12.7	4.0×10^{-5}	4.40
110	23	5.0×10^{-5}	4.30
154	33	7.1×10^{-5}	4.15

The value of k_2 (Table 1), derived from the intercepts of plots analogous to Figure 2, is pH dependent.

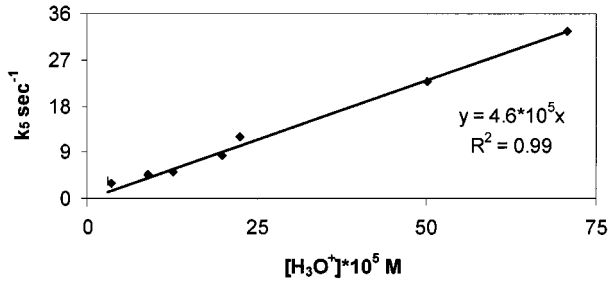

Figure 3. Dependence of k_5 on $[H_3O^+]$. The experiments were performed in solutions containing 5.0×10^{-4} M Cu^+_{aq}, 0.10 M $NaClO_4$, 0.10 M acetic acid, 0.023 M NH_4^+, helium saturated.

The apparent values of K_{2app}, derived from the slopes of the straight lines, e.g. from Figure 2 (at several pH's in this pH range) are presented in Table 1. The average of K_{2app} in the pH range 4.15−4.70 is 130 ±25 M^{-1} (Table 1). When the pH is increased, pH ≥ 4.7, the formation of CuOH [K_{sp}(CuOH) = 1×10^{-14} M^{-2} [36]] causes an apparent decrease in K_{2app}, (Table 1). The contribution of reaction (6)[37] to K_{2app} was examined, $K_2 = K_{2app}(1 + K_a[H^+])$.

$$HNO_2 \leftrightarrows NO_2^- + H^+; pK_a = 3.25 \quad (6)$$

This analysis indicates that reaction (6) has a minor effect on K_2, $K_2 = 140 \pm 30$ M^{-1}. From K_2, it can be calculated that when $[NO_2^-] = 7$ mM, the observed rate of reaction is ca. 50% of the maximum rate. Therefore, the binding of NO_2^- to Cu^+_{aq} is ca. 100 times weaker than that to CuNIR, in which $K_M = 0.074$ mM.[38]

Solutions of $NaNO_2$ were mixed with Cu^+_{aq} at a final pH of 2.20 (at this pH the nitrite is present mostly as HNO_2). Figure 4 describes $k_{obsd.}$ as a function of $[NaNO_2]$ at this acidic pH. It is apparent that there is no limiting rate (at higher pH's and the same NO_2^- concentrations a deviation from linearity is observed, as shown in Figure 1). Though

 © 2004 Wiley-VCH Verlag GmbH & Co. KGaA, Weinheim

HNO_2 is a stronger oxidant than NO_2^-,[37] there is no reason to suggest that reaction (7) occurs.

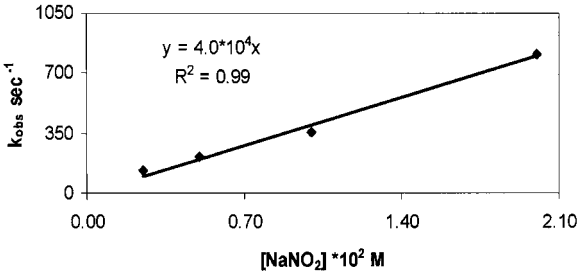

Figure 4. Dependence of $k_{obsd.}$ on $[NaNO_2]$. The experiments were performed in solutions containing 5.0×10^{-4} M Cu^+_{aq}, 0.10 M $NaClO_4$, 0.023 M NH_4^+, the final pH was 2.20, helium saturated

$$Cu^+_{aq} + HNO_2 \leftrightarrows (Cu^+HNO_2)^+ \quad (7)$$

Moreover, if $(Cu^+HNO_2)^+$ were formed its pK_a is expected to be lower than the pK_a of HNO_2. Therefore, when the pH $\geq$ 4.15, $(Cu^INO_2^-)$ is clearly the complex formed. At pH values lower than the pK_a of HNO_2, the NO_2^- concentration is low so that the apparent value for $k_{*5}K_5$ is expected to be lower at pH 2.20 than that observed at pH 4.15−5.45. The slope of the line in Figure 4 equals the apparent value of $k_{*2}K_2[H_3O^+] = 4.0 \times 10^4$, i.e. $k_{*2}K_2$ (at pH 2.20) $= 5.5 \times 10^6$ $M^{-2}sec^{-1}$ as compared to $k_{*2}K_2 = 4.6 \times 10^5 \times 140 = 6.4 \times 10^7$ $M^{-2}sec^{-1}$ at pH = 4.15−4.70. Thus, at pH 2.20 the apparent value of $k_{*2}K_2$ equals ca. 10% of that observed at pH 4.15−4.80. The nitrite concentration at pH 2.20 is ca. 10% of its concentration at pH $\geq$ 4.15. This result is in agreement with the suggested mechanism: It should be pointed out that if HNO_2 were the oxidant, a lower apparent rate is expected also at pH 2.20, as the concentration of HNO_2 is not proportional to $[H_3O^+]$ below the pK_a of HNO_2. However, the nonlinear dependence of the observed rate at pH $\geq$ 4.1 and the linear dependence at pH 2.20 on $[NO_2^-] + [HNO_2]$, proves that the active oxidant is NO_2^-.

The yield of NO from the reaction was measured by two techniques: 1. EPR, by measuring the effect of the addition of NO to 4,4,5,5-tetramethyl-2-(1-pyryl)-2-imidazoline-1-oxyl 3-oxide (PN) on the EPR spectrum. 2. Mass spectrometry. Both techniques revealed that [NO] $\geq$ 75% $[Cu^+_{aq}]$. This result demonstrates that the yield of NO is quantitative as some dioxygen always enters the samples during the handling of the solutions.

The mechanism observed here is in agreement with that observed for several other Cu^I complexes in methanol/acetonitrile.[26,28,29] However, the rate constant is considerably higher for Cu^+_{aq} than for those complexes. This observation is attributed to the stabilization of Cu^I by the ligands used in those studies, caused by an anodic shift of the redox potential of the $Cu^{II/I}$ couple. Therefore, it seemed of interest to study the mechanism and kinetics of reduction of NO_2^- by $(Cu^IL)^+$ complexes in aqueous solutions. Two complexes were studied:

1. A copper(I) complex which is a stronger reducing agent than Cu^+_{aq}. For this purpose, $(Cu^IL^1)^+$ (L^1 = 2,5,8,11-tetramethyl-2,5,8,11-tetraazadodecane, Figure 5) was chosen, $E^0(Cu^{II}L/Cu^IL^1) = 0.116$ V (vs. NHE),[39] at pH 5.0. At this pH $k[NO_2^- + (Cu^IL^1)^+] = 35 \pm 10$ $M^{-1}s^{-1}$ is obtained. The observed rate is nearly independent of $[H_3O^+]$ in the pH range 5.0−6.0. This rate is considerably higher than that obtained for Cu^+_{aq} over this pH range. The lack of dependence on $[H_3O^+]$ suggests that, in this case, H_2O acts as the proton donor, i.e. the general mechanism for the decomposition of the complex $[(Cu^IL^i)^+NO_2^-]$ is according to reaction (8).

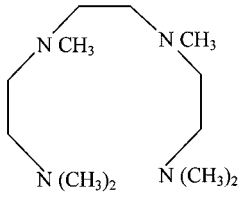

Figure 5. L^1 = 2,5,8,11-tetramethyl-2,5,8,11-tetraazadodecane

$$[(Cu^IL^i)^+NO_2^-] + H_3O^+/H_2O \rightarrow (Cu^{II}L^i)^{2+} + NO + (OH^- + H_2O)/2OH^- \quad (8)$$

From the results, which indicate that the observed rate increases linearly with $[NO_2^-]$, it can be estimated that $K = [(Cu^IL^1)^+NO_2^-)]/([(Cu^IL^1)^+][NO_2^-]) \leq 7$ M^{-1}, i.e. the ligation of NO_2^- to the complex is considerably weaker than to Cu^+_{aq}. This is probably due to steric hindrance caused by the ligand L^1, which is a very bulky ligand, or to the competition for a ligation site between a terminal tertiary amine group of L^1 and NO_2^-.

2. Copper(I) complexes which are weaker reducing agents[40,41] than Cu^+_{aq}. For this purpose, the complexes $[Cu^I(CH_3CN)_n]^+$ were chosen. These solutions contain a mixture of several species: $[Cu^+_{aq}$, $Cu^I(CH_3CN)]^+$, $[Cu^I(CH_3CN)_2]^+$, $[Cu^I(CH_3CN)_3]^+$, and the detailed composition of each solution can be calculated from the known stability constants of these complexes.[40,41] Solutions of $[Cu^I(CH_3CN)_n]^+$ 5.0×10^{-4} M were mixed with NO_2^- $[(2.5-100) \times 10^{-3}$ M) at different pH's (4.0−4.8) and different CH_3CN concentrations (0.048−0.96) M. The results demonstrate that:

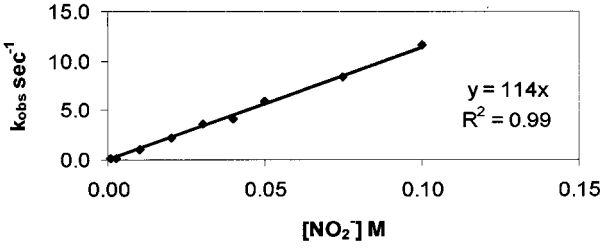

Figure 6. Dependence of $k_{obsd.}$ on $[NO_2^-]$. The experiments were performed in solutions containing 5.0×10^{-4} M Cu^+_{aq}, 0.10 M $NaClO_4$, 0.10 M acetic acid, 0.048 M CH_3CN, the final pH was 4.40, helium saturated.

 © 2004 Wiley-VCH Verlag GmbH & Co. KGaA, Weinheim

a) The observed rate depends linearly on $[NO_2^-]$ at all the CH_3CN concentrations studied (for example, see Figure 6). From these results, it can be calculated that $K_{10} = [(Cu^I(CH_3CN)_nNO_2^-)]/([Cu^I(CH_3CN)_n]^+[NO_2^-]) \leq 30$ M^{-1} [reaction (9)].

$$[Cu^I(CH_3CN)_n]^+ + NO_2^- \underset{}{\overset{K_9}{\rightleftharpoons}} [Cu^I(CH_3CN)_nNO_2^-] \quad (9)$$

$$\xrightarrow{k_9} \text{products}$$

The observation that $K_9 < K_2$ is probably due to one or more of the following facts:

I. Competition between one of the CH_3CN ligands and NO_2^- for the same ligation site. II. A change of hybridization from sp to sp^3 is required for the binding of NO_2^- to $[Cu^I(CH_3CN)_2]^+$, which is the major complex present in the solution.

b) The observed rate increases linearly with $[H_3O^+]$ at all the CH_3CN concentrations studied, e.g. Figure 7. The slope of the graph equals $k_9K_9 = 4.0 \times 10^5$ $M^{-2}sec^{-1}$. $k^*_2K_2$ for the Cu^+_{aq} system equals $140 \times 4.6 \times 10^5 = 6.4 \times 10^7$ $M^{-2}sec^{-1}$, i.e. at this CH_3CN concentration, acetonitrile reduces the rate of reaction by a factor of 150.

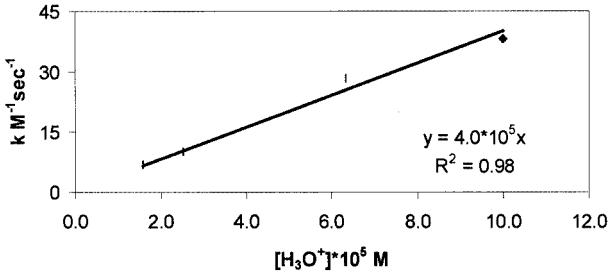

Figure 7. Dependence of k on $[H_3O^+]$. The experiments were performed in solutions containing 5.0×10^{-4} M $[Cu^I(CH_3CN)_n]^+$, 0.10 M $NaClO_4$, 0.10 M acetic acid, 0.96 M CH_3CN, helium saturated.

c) The observed rate at constant pH and $[NO_2^-]$ decreases with $[CH_3CN]$, (e.g. Figure 8).

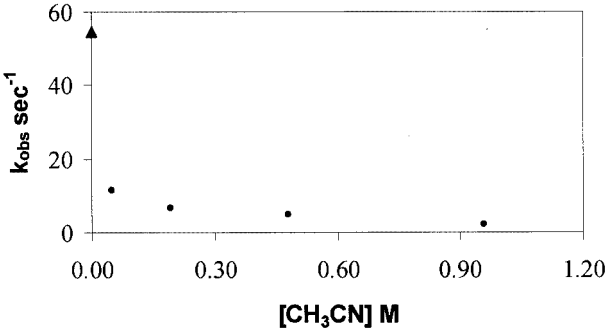

Figure 8. Dependence of k on $[CH_3CN]$. The experiments were performed in solutions containing 5.0×10^{-4} M $[Cu^I(CH_3CN)_n]^+$, 0.10 M $NaClO_4$, 0.10 M acetic acid, 0.10 M NO_2^-, helium saturated. solid triangle: result in the absence of CH_3CN, solid circles: results in presence of CH_3CN.

If Cu^+_{aq} were the only reacting species in solutions containing CH_3CN, i.e. if the rate of reaction of $[Cu^I(CH_3CN)_n]^+$ were negligible, then the expected observed rate in solutions containing 0.96 mol·dm^{-3} CH_3CN at pH 4.4 would be $k_{*2}K_2 \times [H_3O^+] \times ([Cu^+_{aq}]/[Cu^I]_T) = 140 \times 4.6 \times 10^5 \times 4 \times 10^{-5} \times (2.1 \times 10^{-9}/5.0 \times 10^{-4}) = 0.011$ $M^{-1}s^{-1}$. (Cu^+_{aq} concentration in this equation was calculated using the stability constants[40,41] of the $[Cu^I(CH_3CN)_n]^+$ complexes). However, $k_{obsd.} = 24$ $M^{-1}s^{-1}$ is obtained under these conditions. These results clearly demonstrate that the $[Cu^I(CH_3CN)_n]^+$ complexes react with NO_2^- and contribute to the observed rates of reaction. The results are not accurate enough to evaluate the rate constant of the reaction of each of the $[Cu^I(CH_3CN)_n]^+$ species accurately. However, the results (Figure 8) clearly demonstrate that the rate constants decrease with an increase in n.

Conclusions

The value of $K_2 = [(Cu^+NO_2)]/([Cu^+_{aq}][NO_2^-]) = 140 \pm 25$ M^{-1} is similar to values reported in the literature for Cu^I complexes with other ligands in organic solvents,[28,29] but higher than the values measured in this work for $[(Cu^IL^1)^+NO_2^-]$ $K \leq 7$ M^{-1} and for $[(Cu^I(CH_3CN)_n)^+NO_2^-]$, $K \leq 30$ M^{-1}. The stability constant of the $(Cu^+NO_2^-)$ complex suggests that nitrite binds to the copper via the nitrogen atom, as the stability constants of Cu^I complexes with oxo-anions are expected to be considerably lower.[42,43]

Experimental Section

Materials and Methods: $NaNO_2$, $CuSO_4$, Cu^0, NH_3, L^1 (L^1 = 2,5,8,11-tetramethyl-2,5,8,11-tetraazadodecane), acetonitrile, acetic acid, $NaClO_4$, and $HClO_4$ were purchased from Aldrich. PN [4,4,5,5-tetramethyl-2-(1-pyryl)-2-imidazoline-1-oxyl 3-oxide] was prepared according to modified procedures, along with small amounts of 4,4,5,5-tetramethyl-2-(1-pyryl)-2-imidazoline.[44] All solutions were prepared using A.R. grade chemicals and from distilled water further purified by passing through a Milli Q Millipore setup, final resistivity >10 mΩ/cm. The experiments were carried out at $[NaClO_4] = 0.1$ mol·dm^{-3}, at room temperature, 22±2 °C.

Solutions of $[Cu^I(NH_3)_2]^+$ and $(Cu^IL^i)^+$ were prepared via the conproportionation process, reaction (10). Solid copper metal was added to deaerated solutions containing $CuSO_4$ and an excess of NH_3, or L^i at the appropriate pH values.

$$Cu^0_s + (Cu^{II}L_n)^{2+}_{aq} + (2m - n)L \leftrightharpoons 2(Cu^IL_m)^+_{aq} \quad (10)$$

Cu^+_{aq} was obtained by injecting $[Cu^I(NH_3)_2]^+$ into an acetate buffer solution (acidic solution), or into an $HClO_4$ solution containing the nitrite. Under these conditions the following reactions (11) and (12) occur.

$$[Cu^I(NH_3)_2]^+ \underset{}{\overset{\text{fast}}{\rightleftharpoons}} Cu^+_{aq} + 2NH_3 \quad (11)$$

 © 2004 Wiley-VCH Verlag GmbH & Co. KGaA, Weinheim

$$NH_3 + H^+ \underset{}{\overset{\text{fast}}{\rightleftharpoons}} NH_4^+ \quad (12)$$

Thus, at pHs considerably lower than the pK_a of NH_4^+/NH_3 all the $[Cu^{I}(NH_3)_2]^+$ is transformed into Cu^{+}_{aq} (The ligand exchange of Cu^{I} is fast[45]).

Kinetic Measurements: Stopped-flow experiments were carried out using an SX.18 Applied PhotoPhysics stopped-flow instrument that enables kinetic measurements of reactions with lifetimes ≥ 2 msec. A 05−109 Spectra Kinetics Monochromator, which enables measurements in the range of 200−700 nm, was used. The optical path was 10 mm. All the kinetic runs are the average of at least a triplicate. The error limit for the rate constants and for the equilibria constants is ±10%.

The time-dependence of the absorbances at 355 nm was observed . This wavelength is the maximum of the absorption band of NO_2^- for the reactions of Cu^{+}_{aq} and $Cu^{I}(CH_3CN)_n^+$. Alternatively, the absorbance of the band at 635 nm, the maximum of the absorption band of $(Cu^{II}L^1)^{2+}$ for the reaction of $(Cu^{I}L^1)^+$, was observed.

Electron Paramagnetic Resonance (EPR) spectra were recorded using a Bruker EMX-220 digital X-band (ν = 9.4 GHz) spectrometer equipped with a Bruker EP 4241VT temperature control system. All spectra were recorded at room temperature (T = 297 K) with the following parameters: 20.12 mW nonsaturating microwave power, 100 kHz field modulation of 0.1 mT amplitude. EPR spectra were processed using the Bruker WIN-EPR and Microcalc™ Origin™ software.

Solutions of $(Cu^{I}L)^+$, nitrite and PN were mixed producing 4,4,5,5-tetramethyl-2-(1-pyryl)-2-imidazoline (PPN), which has a completely different EPR spectrum (Figure 9) from PN (PN reacts only with NO to produce PPN).
Mass Spectra: The mass spectrometer used in this study was a Balzers Quadrupole model QMG-421 instrument, with an SEM (secondary electron multiplier) detector.

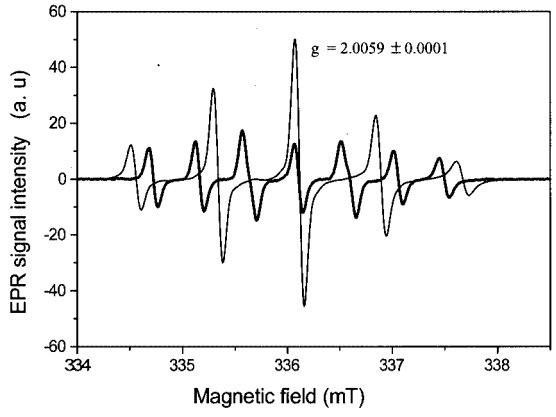

Figure 9. The EPR spectrum of PPN (bold line), formed by mixing 1:1 1.0 × 10^{-3} M $[Cu^{I}(NH_3)_2]^+$ with 5.0 × 10^{-2} M $NaNO_2$; this solution was mixed 4:1 with 1.55 × 10^{-3} M PN. The experiment was carried out in solutions containing also 0.08 M $NaClO_4$ and 0.08 M acetic acid. The EPR spectrum of PN (thin line) which does not change after mixing 1:1 2.0 × 10^{-4} M PN with 0.03 M $NaNO_2$, 0.10 M $NaClO_4$, 0.20 M acetic acid. The final pH was 4.7, the solutions were helium-saturated, ν = 9.424 GHz.

Acknowledgments

This study was supported in part by a grant from the Budgeting and Planning Committee of The Council of Higher Education. D. M. wishes to express his thanks to Mrs. Irene Evens for her ongoing interest and support.

[1] B. A. Averill, *Angew. Chem.* **1994**, *33*, 2057.
[2] B. A. Averill, *Chem. Rev.* **1996**, 2951.
[3] L. M. Murphy, F. E. Dodd, F. K. Yousafzai, R. R. Eady, S. S. Hasnain, *J. Mol. Biol.* **2002**, *315*, 859.
[4] D. Zhang, W. Verstraete, *Environ. Tech.* **2001**, *22*, 905.
[5] G. Gulis, M. Czompolyova, J. R. Cerhan, *Environ. Res.* **2002**, *88*, 182.
[6] P. D. Pedersen, K. Jensen, P. Lyngsie, N. H. Johansen, *Water Sci. Tech.* **2003**, *47*, 181.
[7] F. Armijo, E. Trollund, M. Reina, M. C. Arevalo, M. J. Aguirre, *Coll. Czechoslovak, Chem. Commun.* **2003**, *68*, 1723.
[8] G. H. Lu, D. W. Long, T. Zhan, H. Y. Zhao, *Chinese J. Anal. Chem.* **2002**, *30*, 1115.
[9] J. M. Rifkind, E. Nagababu, S. Ramasamy, L. B. Ravi, *Redox Report* **2003**, *8*, 234.
[10] R. Andrade, C. O. Viana, S. G. Guadagnin, F. G. R. Reyes, S. Rath, *Food Chem.* **2003**, *80*, 597.
[11] I. K. Choi, Y. Liu, D. W. Feng, K. J. Paeng, M. D. Ryan, *Inorg. Chem.* **1991**, *30*, 1832.
[12] Y. Liu, M. D. Ryan, *J. Electroanal. Chem.* **1994**, *368*, 209.
[13] O. Einsle, A. Messerschmidt, R. Huber, P. M. H. Kroneck, F. Neese, *J. Am. Chem. Soc.* **2002**, *124*, 11737.
[14] E. V. Kudrik, S. V. Makarov, A. Zahl, R. Van Eldik, *Inorg. Chem.* **2003**, *42*, 618.
[15] S. H. Cheng, Y. O. Su, *Inorg. Chem.* **1994**, *33*, 5847.
[16] M. R. Rhodes, M. H. Barley, T. J. Meyer, *Inorg. Chem.* **1991**, *30*, 629.
[17] S. Mahapatra, J. A. Halfen, W. B. Tolman, *J. Chem. Soc., Chem. Commun.* **1994**, 1625.
[18] C. E. Ruggiero, S. M. Carrier, W. B. Tolman, *Angew. Chem.* **1994**, *33*, 895.
[19] P. P. Paul, K. D. Karlin, *J. Am. Chem. Soc.* **1991**, *113*, 6331.
[20] F. Chun-Sing, W. Kwok-Yin, *J. Electroanal. Chem.* **1996**, *401*, 263.
[21] J. A. Cowan, *Inorganic Biochemistry, An Introduction*, VCH Publishers: New York, **1993**.
[22] N. Revsbech, B. Sorensen, *Denitrification in Soil and Sediment*; Plenum Press: New York, **1990**.
[23] B. C. Berks, S. J. Ferguson, J. W. B. Moir, D. J. Richardson, *Biochim. Biophys. Acta-Bioenergetics* **1995**, *1232*, 97.
[24] W. G. Zumft, *Microbiol. Biol. Rev.* **1997**, *61*, 533.
[25] I. M. Wasser, S. Vries, P. Moeenne-Loccoz, I. Schroeder, K. D. Karlin, *Chem. Rev.* **2002**, *102*, 1201.
[26] L. Casella, O. Carugo, *Inorg. Chem.* **1996**, *35*, 1101.
[27] E. T. Adman, M. E. Murphy, *Handbook of Metalloproteins*; Wiley, **2001**.
[28] M. Beretta, E. Bouwman, L. Casella, B. Douziech, W. L. Driessen, L. Gutierrez-Soto, E. Monzani, J. Reedijk, *Inorg. Chim. Acta* **2000**, *310*, 41.
[29] E. Monzani, G. J. A. A. Koolhaas, A. Spandre, E. Leggieri, L. Casella, M. Gullotti, G. Nardin, L. Randaccio, M. Fontani, P. Zanello, J. Reedijk, *JBIC* **2000**, *5*, 251.
[30] S. Suzki, K. Kataoka, K. Yamaguchi, *Acc. Chem. Res.* **2000**, *33*, 728.
[31] J. A. Halfen, A. J. Gengenbach, W. B. Tolman, *J. Am. Chem. Soc.* **1996**, *118*, 763.
[32] J. A. Halfen, W. B. Tolman, *J. Am. Chem. Soc.* **1994**, *116*, 5475.
[33] J. A. Halfen, S. Mahapatra, M. Olmstead, W. B. Tolman, *J. Am. Chem. Soc.* **2000**, *126*, 2173.
[34] W. B. Tolman, *Inorg. Chem.* **1991**, *30*, 4880.
[35] M. Hoshino, M. Maeda, R. Konishi, H. P. C. Ford, *J. Am. Chem. Soc.* **1996**, *118*, 5702.

 © 2004 Wiley-VCH Verlag GmbH & Co. KGaA, Weinheim

[36] J. A. Dean, *Lange's Handbook of Chemistry*; 14th ed.; McGraw-Hill, **1992**, section 8.
[37] *CRC Handbook of Chemistry and Physics*; 83rd ed.; CRC press, **2003**.
[38] T. Kakutani, H. Watanabe, K. Arima, T. Beppu, *J. Biochem.* **1981**, *80*, 453.
[39] G. Golub, H. Cohen, P. Paoletti, A. Bencini, L. Messori, I. Bertini, D. Meyerstein, *J. Am. Chem. Soc.* **1995**, *117*, 8353.
[40] A. Zuberbuhler, *Helv. Chim. Acta* **1970**, *53*, 473.
[41] P. Hemmerich, C. Sigwart, *Experientia* **1963**, *19*, 488.
[42] J. Bunting, K. Thong, *Can. J. Chem.* **1970**, *48*, 1654.
[43] M. Saphier, A. Burg, S. Sheps, H. Cohen, D. Meyerstein, *J. Chem. Soc., Dalton Trans.* **1999**, 1845.
[44] J. H. Osiecki, D. G. B. Boocock, R. Darcy, *J. Am. Chem. Soc.* **1972**, *94*, 7059.
[45] D. Meyerstein, *Inorg. Chem.* **1975**, *14*, 1716.

Received March 30, 2004
Early View Article
Published Online July 15, 2004

 © 2004 Wiley-VCH Verlag GmbH & Co. KGaA, Weinheim

Heterobimetallic Complexes Based on $[(Tp)Fe(CN)_3]^-$: Syntheses, Crystal Structures and Magnetic Properties

Shi Wang,[a] Jing-Lin Zuo,*[a] Hong-Cai Zhou,[b] You Song,[a] Song Gao,[c] and Xiao-Zeng You*[a]

Keywords: Chain structures / Cyanide ligands / Iron / Magnetic properties / Polynuclear complexes

With the anionic precursor $[(Tp)Fe^{III}(CN)_3]^-$ [**1**; Tp: hydrotris(pyrazolyl)borate] as a building block, two trinuclear complexes, $[(Tp)_2Fe^{III}{}_2(CN)_6Mn(CH_3OH)_4]\cdot 2CH_3OH$ (**2**), $[(Tp)_2Fe^{III}{}_2(CN)_6Ni(cyclam)]\cdot 2H_2O$ (**3**; cyclam: 1,4,8,11-tetraazacyclotetradecane) and a one-dimensional polymer, $[(Tp)Fe^{III}(CN)_3Cu(dien)]ClO_4\cdot H_2O$ (**4**; dien: diethylenetriamine), have been synthesized and structurally characterized. In complex **2**, each of the two $[(Tp)Fe(CN)_3]^-$ units binds through one of its three cyanide groups to a central $[Mn(CH_3OH)_4]^{2+}$ core. In complex **4**, a zigzag chain is formed by combining $[TpFe(CN)_3]^-$ and $[Cu(dien)]^{2+}$ fragments alternately through cyano bridges. The magnetic properties of complexes **2**–**4** have been investigated in the temperature range 2–300 K. A weak antiferromagnetic interaction between the Mn^{II} and Fe^{III} ions has been found in complex **2**. The magnetic data of **2** can be fitted with the isotropic Hamiltonian $\hat{H} = -2J(\hat{S}_1\cdot\hat{S}_2 + \hat{S}_2\cdot\hat{S}_3) - 2J'\hat{S}_1\cdot\hat{S}_3$, where J and J' are the intramolecular exchange coupling parameters between adjacent and peripheral spin carriers, respectively. This leads to values of $J = -2.19$ cm^{-1} and $g = 2.13$. The same fitting method was applied to complex **3** to give values of $J = 17.2$ cm^{-1} and $g = 2.37$, showing that there is a ferromagnetic interaction between the Fe^{III} and Ni^{II} ions. The 1-D chain of **4** is treated as alternating uniform Fe–Cu dimers with different intradimeric (J_d) and interdimeric (J_c) exchange constants, leading to $J_d = 10.9$ cm^{-1}, $J_c = 1.29$ cm^{-1} and $g = 2.54$.
(© Wiley-VCH Verlag GmbH & Co. KGaA, 69451 Weinheim, Germany, 2004)

Introduction

Tremendous effort has been devoted to the study of cyanide-containing metal complexes because of their unique magnetic properties, such as high-*Tc* magnetism and light- or pressure-tuning of magnetization.[1−4] Among those, low-dimensional as well as polynuclear clusters have attracted much attention since such systems can be used to investigate the intermetallic magnetic coupling quantitatively; there is no appropriate model for quantitative magnetic analysis to high-dimenisonal systems. Recently, synthetic strategies to prepare cyanide-bridged bimetallic systems by using modified cyanometalates as multidentate ligands and linkers have been developed. The following are representative examples: $[(tacn)M(CN)_3]$ ($M = Co^{3+}$, Cr^{3+}; tacn = 1,4,7-triazacyclononane),[5] $[(Me_3tacn)M(CN)_3]$ ($M = Cr^{3+}$, Mo^{3+}; Me_3tacn = *N*,*N*′,*N*′′-trimethyl-1,4,7-triazacyclononane),[6] $[(tach)M(CN)_3]$ ($M = Cr^{3+}$, Fe^{3+}, Co^{3+}; tach = 1,3,5-triaminocyclohexane),[7] $[Fe(bipy)(CN)_4]^-$, $[Fe(bipy)(CN)_4]^{2-}$ and $[Fe(phen)(CN)_4]^-$ (bipy = 2,2′-bipyridine; phen = 1,10-phenanthroline).[8,9] In an effort to extend this interesting chemistry, we chose the tailored cyanometalate precursor $(Bu_4N)[(Tp)Fe(CN)_3]$ [**1**; Tp = hydrotris(pyrazolyl)borate; Bu_4N^+ = tetrabutylammonium cation], which consists of three CN^- groups and a hydrotris(pyrazolyl)borate (Tp) ligand. The anion has recently been reported by Julve's group as its tetraphenylphosphonium salt.[10] Tp is a classical scorpionate ligand containing a C_3 axis. It has been used as a protecting group to prepare topological analogues of the P clusters of nitrogenase.[11] Compared to tacn-type ligands, Tp is sterically similar but bears a negative charge. Thus, it may direct the formation of new complexes with interesting structures and magnetic properties. Herein, we report the preparation, crystal structures and magnetic properties of two trinuclear complexes $[(Tp)_2Fe^{III}{}_2(CN)_6Mn(CH_3OH)_4]\cdot 2CH_3OH$ (**2**) and $[(Tp)_2Fe^{III}{}_2(CN)_6Ni(cyclam)]\cdot 2H_2O$ (**3**; cyclam: 1,4,8,11-tetraazacyclotetradecane), and a one-dimensional polymer $[(Tp)Fe^{III}(CN)_3Cu(dien)]ClO_4\cdot H_2O$ (**4**; dien: diethylenetriamine).

[a] Coordination Chemistry Institute, State Key Laboratory of Coordination Chemistry, Nanjing University, Nanjing 210093, China
[b] Department of Chemistry and Biochemistry, Miami University, Oxford, OH 45056-1465, USA
[c] State Key Laboratory of Rare Earth Materials Chemistry and Applications, College of Chemistry and Molecular Engineering, Peking University, Beijing 100871, China

Results and Discussion

Synthesis and Spectral Features

In this paper the anionic precursor $[(Tp)Fe(CN)_3]^-$ (**1**) is used as a building block to prepare cyanide-bridged multinuclear clusters and coordination polymers. The tetrabutylammonium salt of **1** was isolated as an orange crystalline solid in 78% yield. Only one C≡N stretching vibration (2117 cm^{-1}) is observed in its IR spectrum. It is soluble in most organic solvents such as acetonitrile, acetone, methanol and DMF.

Reaction of $Mn(ClO_4)_2$ with $(Bu_4N)[(Tp)Fe^{III}(CN)_3]$ (**1**) in methanol yields the trinuclear complex $[(Tp)_2Fe^{III}{}_2(CN)_6Mn(CH_3OH)_4]\cdot 2CH_3OH$ (**2**). The occurrence of two peaks of medium intensity in the C≡N stretching region of the IR spectrum is consistent with the presence of bridging (2151 cm^{-1}) and terminal (2129 cm^{-1}) cyanide ligands. Another trinuclear complex, $[(Tp)_2Fe^{III}{}_2(CN)_6Ni(cyclam)]\cdot 2H_2O$ (**3**), was formed from the reaction of $Ni(cyclam)(ClO_4)_2$ and $(Bu_4N)[(Tp)Fe(CN)_3]$ in ethanol and water. The C≡N stretching frequencies are located at 2119 and 2157 cm^{-1}. Both complexes are soluble in some organic solvents. The solvates in both **2** and **3** can easily lose solvent upon exposure to air.

The reaction of $Cu(ClO_4)_2\cdot 6H_2O$, dien and $(Bu_4N)[(Tp)Fe(CN)_3]$ in aqueous solution leads to the formation of brown, crystalline $[(Tp)Fe^{III}(CN)_3Cu(dien)]ClO_4\cdot H_2O$ (**4**). The C≡N stretching region of the IR spectrum of **4** is consistent with the presence of bridging (a peak of medium intensity at 2157 cm^{-1}) and terminal (a weak absorption at 2131 cm^{-1}) cyanide ligands.

Crystal Structures

Selected bond lengths and angles for complexes **2**−**4** are compiled in Table 1−3.

Table 1. Selected bond lengths and angles in complex **2**

Bond lengths (Å)			
Fe(1)−N(2)	1.975(2)	Fe(1)−N(4)	1.966(2)
Fe(1)−N(6)	1.977(3)	Fe(1)−C(10)	1.931(3)
Fe(1)−C(11)	1.928(3)	Fe(1)−C(12)	1.915(3)
C(12)−N(9)	1.149(4)	Mn(1)−N(9)	2.174(2)
Mn(1)−O(1)	2.198(2)	Mn(1)−O(2)	2.1906(19)
Bond angles (°)			
Fe(1)−C(10)−N(7)	177.9(3)	Fe(1)−C(11)−N(8)	175.9(3)
Fe(1)−C(12)−N(9)	176.1(3)	Mn(1)−N(9)- C(12)	167.2(2)
C(11)−Fe(1)−C(12)	86.98(13)	C(10)−Fe(1)−C(12)	87.06(12)
N(9)−Mn(1)−O(1)	89.72(9)	N(9)−Mn(1)−O(2)	90.63(8)

The ORTEP drawing for complex **2** is depicted in Figure 1. Complex **2** consists of a trinuclear $[\{(Tp)Fe(CN)_3\}_2Mn(CH_3OH)_4]$ cluster and two methanol solvate molecules. In this trinuclear cluster, the $[(Tp)Fe(CN)_3]^-$ unit acts as a monodentate ligand through one of its three cyanide groups toward a central $[Mn(CH_3OH)_4]^{2+}$ core. Each iron(III) ion is coordinated by three Tp nitrogen atoms and three cyanide carbon atoms, with a C_{3v} symmetry. The Fe(1)−C(cyano) bond lengths [1.915(3)−1.931(3) Å] are in good agreement with those observed in other low-spin iron(III) complexes.[8,9] The Fe−C≡N angles for both terminal [175.9(3)° and 177.9(3)°] and bridging [176.1(3)°] cyanide groups depart slightly from strict linearity. The manganese atom is six-coordinate in a

Table 2. Selected bond lengths and angles in complex **3**

Bond lengths (Å)			
Fe(1)−C(11)	1.928(4)	Fe(1)−C(12)	1.911(4)
Fe(1)−C(10)	1.938(4)	Fe(1)−N(4)	1.978(3)
Fe(1)−N(6)	1.989(3)	Fe(1)−N(2)	1.997(3)
C(11)−N(8)	1.144(5)	C(10)−N(7)	1.132(5)
C(12)−N(9)	1.143(5)	Ni(1)−N(9)	2.096(3)
Ni(1)−N(10)	2.052(3)	Ni(1)−N(11)	2.070(3)
Bond angles (°)			
Fe(1)−C(11)−N(8)	179.0(4)	Fe(1)−C(10)−N(7)	178.6(4)
Fe(1)−C(12)−N(9)	177.8(4)	Ni(1)−N(9)−C(12)	171.5(3)
C(11)−Fe(1)−C(12)	84.97(16)	C(10)−Fe(1)−C(12)	89.21(16)
N(9)−Ni(1)−N(10)	89.38(13)	N(9)−Ni(1)−N(11)	89.98(13)

Table 3. Selected bond lengths and angles in complex **4**

Bond lengths (Å)			
Fe(1)−N(5)	1.970(2)	Fe(1)−N(7)	1.978(2)
Fe(1)−N(9)	1.973(3)	Fe(1)−C(10)	1.924(3)
Fe(1)−C(15)	1.939(3)	Fe(1)−C(16)	1.928(3)
C(15)−N(11)	1.147(4)	C(16)−N(12)	1.140(4)
C(10)−N(4)	1.153(4)	Cu(1)−N(4)	1.978(3)
Cu(1)−N(1)	1.996(3)	Cu(1)−N(2)	2.010(3)
Cu(1)−N(3)	1.994(3)	N(11)−Cu(1)#2	2.443(3)
Bond angles (°)			
Fe(1)−C(10)−N(4)	178.9(3)	Cu(1)−N(4)−C(10)	170.4(3)
Fe(1)−C(15)−N(11)	170.7(3)	Fe(1)−C(16)−N(12)	176.0(3)
C(15)−Fe(1)−C(16)	86.12(13)	C(15)−Fe(1)−C(10)	90.19(13)
N(4)−Cu(1)−N(2)	171.60(11)	N(1)−Cu(1)−N(4)	96.52(11)
N(1)−Cu(1)−N(3)	160.38(12)	N(2)−Cu(1)−N(3)	84.26(11)
N(4)−Cu(1)−N(11)#1[a]	103.60(11)	Cu(1)#2−N(11)−C(15)	138.1(3)

[a] #1: $x, -y + 1/2, z + 1/2$; #2: $x, -y + 1/2, z - 1/2$.

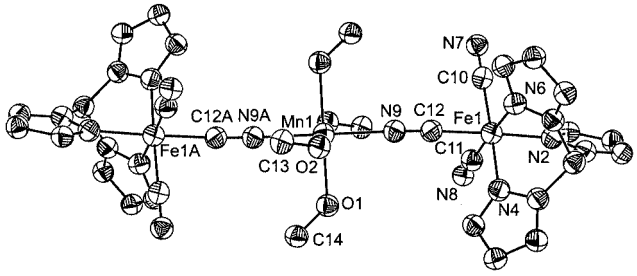

Figure 1. Molecular structure of $[(Tp)_2Fe^{III}{}_2(CN)_6Mn(CH_3OH)_4]\cdot 2CH_3OH$ (**2**); the solvate methanol molecules and hydrogen atoms have been omitted for clarity (ORTEP, 50% ellipsoids)

 © 2004 Wiley-VCH Verlag GmbH & Co. KGaA, Weinheim

squashed octahedral geometry. Four oxygen atoms from the methanol molecules form the equatorial plane. The Mn(1)−O distances [2.198(2) and 2.1906(19) Å] are almost equivalent. Two cyanide nitrogen atoms occupy the axial positions. The Mn(1)−N(9) distance is 2.174(2) Å. The Mn(1)−N(9)≡C(12) bond angle [167.2(2)°] deviates significantly from 180°. The O(1)−Mn(1)−N(9) and O(2)−Mn(1)−N(9) bond angles are 89.72(9)° and 90.63(8)°, respectively. Non-coordinated CH_3OH molecules are inserted into the crystal spaces.

The intramolecular Fe···Mn and Fe···Fe separations are 5.193(2) and 10.386(3) Å, respectively, and the shortest intermolecular Fe···Fe, Mn···Fe, and Mn···Mn distances are 10.056(3), 8.819(5) and 10.950(3) Å, respectively.

The structure of complex **3** is very similar to that of complex **2** (Figure 2) except for the central $[Ni(cyclam)]^{2+}$ core. The Fe(1)−C(12)≡N(9) and Ni(1)−N(9)≡C(12) bond angles are 177.8(4)° and 171.5(3)°, respectively, which depart somewhat from strict linearity. The nickel atom is in an elongated octahedral environment. Four nitrogen atoms from the cyclam ligand form the equatorial plane. Two cyanide nitrogen atoms occupy the axial positions. The Ni(1)−N(9) distance is 2.096(3) Å, which is slightly longer than the average Ni−N(cyclam) bond length [2.061(3) Å].

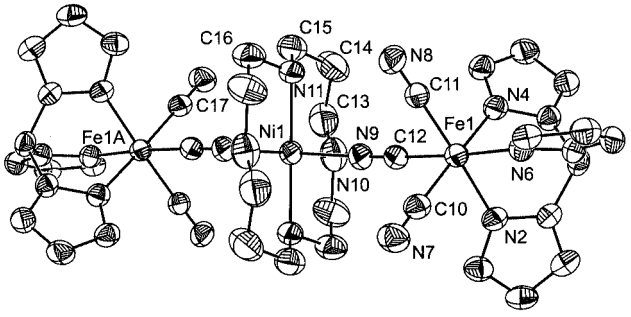

Figure 2. Molecular structure of $[(Tp)_2Fe^{III}{}_2(CN)_6Ni(cyclam)]\cdot 2H_2O$ (**3**); the solvate water molecules and hydrogen atoms have been omitted for clarity (ORTEP, 50% ellipsoids)

The intramolecular Fe···Ni and Fe···Fe separations through bridging cyanides are 5.132(2) and 10.265(5) Å, respectively. The shortest intermolecular Fe···Fe, Ni···Fe, and Ni···Ni distances are 7.622(4), 6.996(2) and 11.046(1) Å, respectively.

X-ray crystallography of **4** reveals that the structure consists of a one-dimensional cationic polymer $[\{TpFe(CN)_3\}\{Cu(dien)\}]_n^{n+}$, with free perchlorate counteranions (Figure 3 and 4). The zigzag chain is made up of a cyano-bridged alternating $[TpFe(CN)_3]^-$−$[Cu(dien)]^{2+}$ fragment. Within the chain, $[TpFe(CN)_3]^-$ uses two *cis*-CN groups to connect with two $[Cu(dien)]^{2+}$ units, while each $[Cu(dien)]^{2+}$ unit is linked to two $[TpFe(CN)_3]^-$ ions at *cis* positions. The central iron atom is six-coordinate with three Tp nitrogen atoms and three cyanide carbon atoms. The Fe(1)−N(Tp) bond lengths [1.970(2)−1.978(2) Å] are considerably shorter than those found in the high-spin iron(III) complex $[Fe(Tp)Cl_3]^-$ [2.152(4)−2.175(5) Å].[12] The Fe−C≡N angles of the bridging cyanide ligands [170.7(3)° and 178.9(3)°] and of the terminal cyanide groups [176.0(3)°] depart somewhat from strict linearity. The Cu^{II} center adopts a distorted square-pyramidal geometry, where one $[TpFe(CN)_3]^-$ unit is bound to the basal site [Cu(1)−N(4), 1.978(3) Å] and the other is bound to the elongated apical site [Cu(1)#2−N(11), 2.443(3) Å] [#2: x, $-y + 1/2$, $z - 1/2$]. The remaining three basal sites are occupied by the dien ligand, with an average Cu−N bond length of 2.000(3) Å. The value of the Cu(1)−N(4)≡C(10) bond angle is 170.4(3)°. However, the Cu(1)#2−N(11)≡C(15) bond angle is 138.1(3)°. The Fe···Cu separations within the chain are 5.040(2) Å for Fe(1)···Cu(1) and 5.062(2) Å for Fe(1)···Cu(1)#2. The shortest interchain Fe···Fe, Cu···Cu and Fe···Cu distances are 8.169(2), 13.345(2) and 11.062(4) Å, respectively.

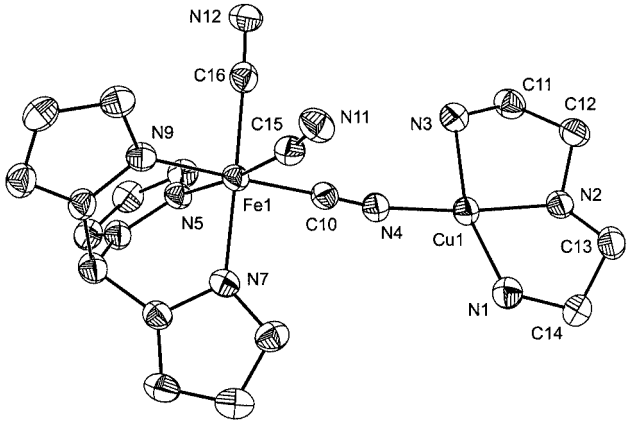

Figure 3. Molecular structure of $[(Tp)Fe^{III}(CN)_3Cu(dien)]ClO_4\cdot H_2O$ (**4**); the solvate water molecule, perchlorate and hydrogen atoms have been omitted for clarity (ORTEP, 50% ellipsoids)

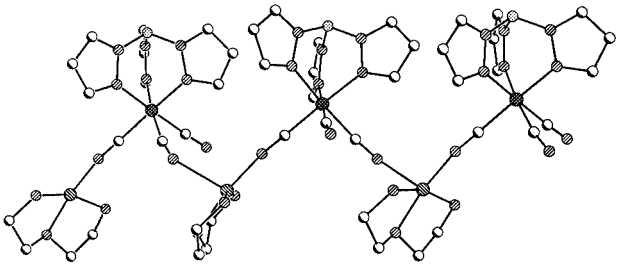

Figure 4. Structure of the one-dimensional chain of **4** running parallel to the *c* axis

Magnetic Properties

The temperature dependence of $\chi_M T$ for complex **2** (χ_M being the magnetic susceptibility per Fe_2Mn unit) is shown in Figure 5. The value of $\chi_M T$ at room temperature is 5.74 emu·K·mol^{-1} (6.78 μ_B). This value is consistent with the presence of a high-spin Mn^{II} atom and two low-spin Fe^{III} atoms magnetically isolated. As the temperature is lowered, $\chi_M T$ decreases steadily until it reaches a value of 1.03 emu·K·mol^{-1} at 2.0 K, indicating a weak antiferromagnetic interaction between the Mn^{II} and Fe^{III} ions.

 © 2004 Wiley-VCH Verlag GmbH & Co. KGaA, Weinheim

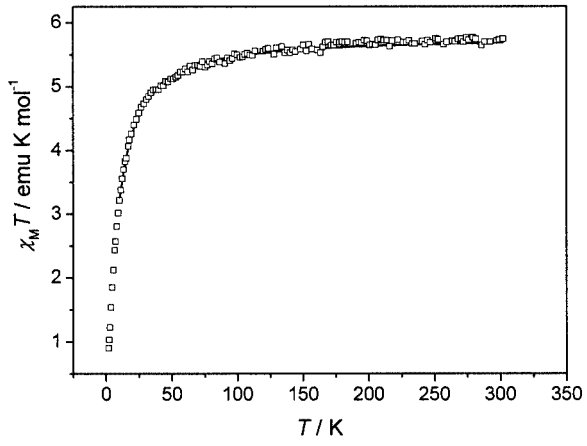

Figure 5. Plot of temperature dependence of $\chi_M T$ measured at 30 kOe field for **2**; the solid line represents the best-fit curve from 10 K to 300 K

The magnetic data has been fitted into the isotropic Hamiltonian:

$$\hat{H} = -2J\cdot(\hat{S}_1\cdot\hat{S}_2 + \hat{S}_2\cdot\hat{S}_3) - 2J'\cdot\hat{S}_1\cdot\hat{S}_3 \quad (1)$$

where $\hat{S}_1$, $\hat{S}_2$ and $\hat{S}_3$ are the spin operators of iron(III), manganese(II) and iron(III), respectively; J and J' are the intramolecular exchange coupling parameters between adjacent and peripheral spin carriers, respectively. Because the two iron(III) ions in the iron(III)-manganese(II)-iron(III) cluster are far apart, the quality of the fit does not depend on J', and hence the fit with $J' = 0$ has been used. The theoretical expression of the magnetic susceptibility of the Fe^{III}-Mn^{II}-Fe^{III} unit ($S_1 = S_3 = 1/2$, $S_2 = 5/2$) is:

$$\chi_M = Ng^2\beta^2/4kT(A/B) \quad (2)$$

where $A = 35 + 10\exp(-7J/kT) + 35\exp(-2J/kT) + 84\exp(5J/kT)$ and $B = 3 + 2\exp(-7J/kT) + 3\exp(-2J/kT) + 4\exp(5J/kT)$. The best fit to the experimental data above 10 K gives $J = -2.19$ cm^{-1} and $g = 2.13$. The agreement factor $R = \Sigma[(\chi_M T)_{obsd} - (\chi_M T)_{cald}]^2/\Sigma[(\chi_M T)_{obsd}]^2$ is 7.7×10^{-5}, which indicates a good agreement, as shown in Figure 5. The J value can be compared with the value of -0.9 cm^{-1} observed in another centrosymmetric Fe^{III}-Mn^{II}-Fe^{III} trinuclear complex.[9b]

The magnetic centers in complex **3** have similar linkages to complex **2**, but they show very different magnetic behaviors due to the replacement of the Mn^{II} ion in **2** by the Ni^{II} ion in **3** (Figure 6). For complex **3**, the value of $\chi_M T$ at room temperature is 2.70 emu·K·mol^{-1} (4.65 μ_B), which is higher than the expected spin-only value of 1.75 emu·K·mol^{-1} per Fe_2Ni unit ($g_{Fe} = g_{Ni} = 2$, $S_{Fe} = 1/2$ and $S_{Ni} = 1$), indicating a possible ferromagnetic coupling between the Fe^{III} and Ni^{II} centers. When the temperature is lowered, the $\chi_M T$ product increases up to a maximum value of 5.03 emu·K·mol^{-1} at 6.0 K and then decreases abruptly below this temperature. This indicates that the ferromagnetic interaction between the metal ions dominates the magnetic properties in this system, which is in agreement with the field dependence of the magnetization (the saturation magnetization $Ms = 4.65\ N\beta$, see Figure 7).

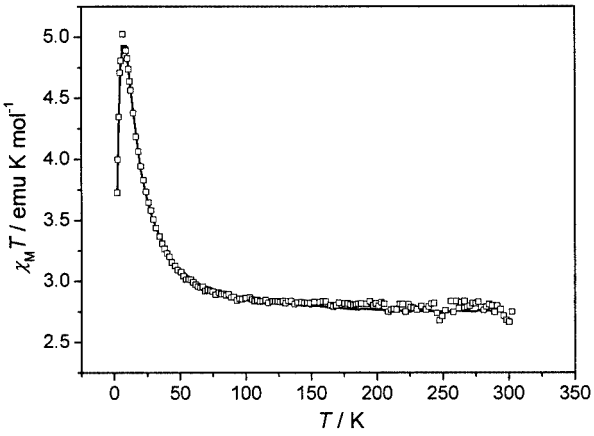

Figure 6. Plot of temperature dependence of $\chi_M T$ measured at 10 kOe field for **3**; the solid line represents the best-fit curve

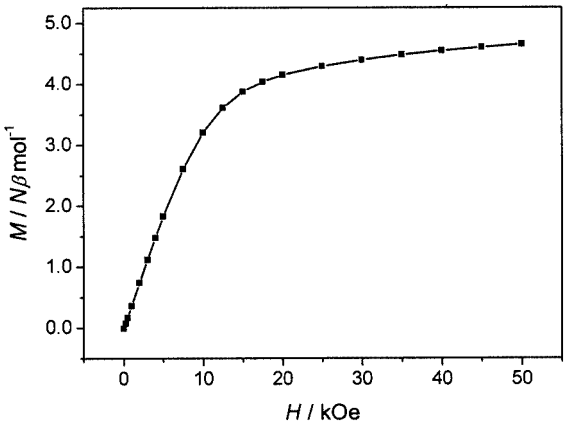

Figure 7. Field dependence of magnetization of complex **3** at 1.85 K

The same fitting method as complex **2** is suitable for the magnetic properties of complex **3**, except that $S_2 = 1$ (for Ni^{II} ion); the theoretical expression of the magnetic susceptibility is:

$$\chi_M = 2Ng^2\beta^2/kT(A/B) \quad (3)$$

where $A = 1 + 5\exp(2J/kT) + \exp(-2J/kT)$ and $B = 3 + 5\exp(2J/kT) + 3\exp(-2J/kT) + \exp(-4J/kT)$. The best fit to the experimental data in the whole temperature range gives $J = 17.2$ cm^{-1} and $g = 2.37$. The agreement factor $R = \Sigma[(\chi_M T)_{obsd} - (\chi_M T)_{cald}]^2/\Sigma[(\chi_M T)_{obsd}]^2$ is 9.2×10^{-4} (Figure 6).

 © 2004 Wiley-VCH Verlag GmbH & Co. KGaA, Weinheim

The magnetic behavior of complex **4** (χ_M being the magnetic susceptibility per FeCu unit) is shown in Figure 8. $\chi_M T$ at room temperature is 1.21 emu·K·mol^{-1} (3.11 μ_B), a value expected for a low-spin iron(III) atom and a copper(II) atom magnetically isolated. It increases continuously on cooling, reaching a maximum value of 2.62 emu·K·mol^{-1} at 3 K, and then decreases to 2.33 emu·K·mol^{-1} at 2 K. This curve is in agreement with a ferromagnetic coupling between the Fe^{III} (S = 1/2) and Cu^{II} (S = 1/2) ions. The susceptibility data per FeCu (unit) can be fitted by a Curie−Weiss law $\chi_M = C/(T - \theta)$ in the temperature range 50−300 K, giving a Curie constant C of 1.20 emu·K·mol^{-1}, and a Weiss constant θ, of +6.16 K. The C value corresponds to one Fe^{III} (S = 1/2) ion and one Cu^{II} (S = 1/2) ion magnetically isolated. The positive value of θ indicates a ferromagnetic interaction between the Fe^{III} and Cu^{II} ions. On the basis of the crystal data, complex **4** has a 1-D zigzag chain structure and, furthermore, the Fe−CN−Cu linkages are unequal. Therefore, when the Heisenberg−Dirac−Van Vleck dimer model ($H = -2JS_1S_2$) or the 1-D uniform chain model[13] was used in this magnetic system, no rational result was obtained. To get a set of useful fitting results to interpret the magnetic exchange between the magnetic centers, the theoretical approach and treatment reported by Rojo and Kou[14] are suitable here. Thus, the 1-D chain can be considered as alternating uniform Fe−Cu dimers with different intradimeric and interdimeric exchange constants. Therefore,

$$\chi_d = \frac{2Ng^2\beta^2}{kT}\frac{1}{3+\exp(-2J_d/kT)} \quad (4)$$

$$\chi_d = \frac{Ng^2\beta^2}{3kT}S_d(S_d+1) \quad (5)$$

$$\chi_M = \chi_{chain} = \frac{Ng^2\beta^2}{3kT}\frac{1+u}{1-u}S_d(S_d+1) \quad (6)$$

where $u = \coth[J_cS_d(S_d + 1)/kT] - kT/[J_cS_d(S_d + 1)]$ and J_d and J_c are intradimeric and interdimeric exchange constants, respectively.

The best fit to the experimental data above 5 K gives J_d = 10.9 cm^{-1}, J_c = 1.29 cm^{-1} and g = 2.54. The agreement factor $R = \Sigma[(\chi_M T)_{obsd} - (\chi_M T)_{cald}]^2/\Sigma[(\chi_M T)_{obsd}]^2$ is 6.3 × 10^{-4} (Figure 8). The Fe^{III}-Cu^{II} exchange coupling parameter is comparable to that of the cyano-bridged cyclic tetranuclear complex $[Fe^{III}_2Cu^{II}_2(\mu\text{-}CN)_4(bipy)_6](PF_6)_6\cdot 4CH_3CN\cdot 2CHCl_3$ (J = 6.3 cm^{-1}).[9a] The small J_c value might be attributed to the more bent Cu(1)#2−N(11)≡C(15) bond angle [138.1(3)°], which has an unfavorable effect on the magnetic coupling.

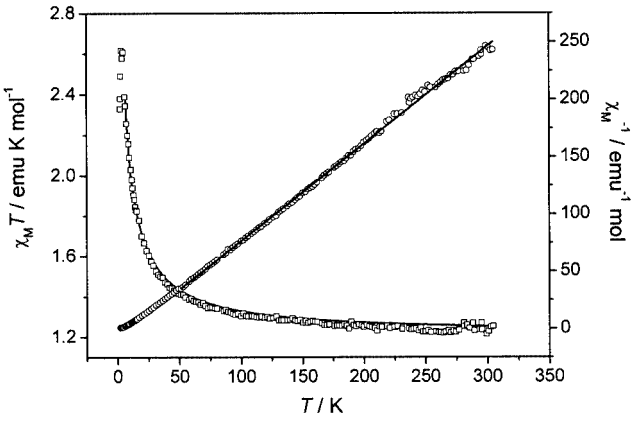

Figure 8. Plots of temperature dependence of $\chi_M T$ (open squares) and χ_M^{-1} (open circles) measured at 10 kOe field for **4**; the solid lines represent the best-fit curve from 5 K to 300 K for $\chi_M T$ and the best fit to the Curie−Weiss law from 50 K to 300 K for χ_M^{-1}

Experimental Section

Materials and Physical Measurements: $Ni(cyclam)(ClO_4)_2$ was synthesized as described previously.[15] The amine ligands diethylenetriamine (dien), 1,4,8,11-tetraazacyclotetradecane (cyclam) and all other reagents were purchased from standard sources and used as received. The IR spectra were recorded on a Nicolet-170SX FT-IR spectrophotometer with KBr pellets in the range 4000−400 cm^{-1}. Elemental analyses for C, H and N were performed on a Perkin-Elmer 240C analyzer. Variable-temperature magnetic susceptibility date were collected using a Quantum Design MPMS SQUID magnetometer. The experimental susceptibilities were corrected for the diamagnetism of the constituent atoms (Pascal's Tables).[16]

Safety Note: Although we have experienced no problem with the compounds reported in this work, perchlorate salts with organic ligands are often explosive and should be handled with great caution.

$[(Tp)_2Fe^{III}_2(CN)_6Mn(CH_3OH)_4]\cdot 2CH_3OH$ (2): Solid $Mn(ClO_4)_2\cdot 6H_2O$ (36 mg, 0.1 mmol) was added to a methanol solution (5 mL) of $(Bu_4N)[(Tp)Fe(CN)_3]$ (59 mg, 0.1 mmol). After slow evaporation of the resulting solution, red plate-like crystals **2** were formed and collected by filtration. Yield: 75%. $C_{28}H_{36}B_2Fe_2MnN_{18}O_4$: calcd. C 38.35, H 4.14, N 28.75; found C 38.61, H 4.45, N 28.64. IR (KBr): $\tilde{\nu}$ = 2129 (ν_{CN}) and 2151 cm^{-1} (ν_{CN}).

$[(Tp)_2Fe^{III}_2(CN)_6Ni(cyclam)]\cdot 2H_2O$ (3): A mixture of ethanol and water (1:1, 10 mL) was gently layered on top of a solution of $Ni(cyclam)(ClO_4)_2$ (91 mg, 0.2 mmol) in water (3 mL). A solution of $(Bu_4N)[(Tp)Fe(CN)_3]$ (118 mg, 0.2 mmol) in ethanol (2 mL) was added carefully as a third layer. Orange crystals of **3** were obtained after one week, washed with ethanol and diethyl ether, and dried in air. Yield: 60%. $C_{34}H_{46}B_2Fe_2N_{22}NiO$: calcd. C 42.06, H 4.78, N 31.74; found C 41.67, H 5.07, N 31.14. IR (KBr): $\tilde{\nu}$ = 2119 (ν_{CN}) and 2157 cm^{-1} (ν_{CN}).

$[(Tp)Fe^{III}(CN)_3Cu(dien)]ClO_4\cdot H_2O$ (4): A stock solution (0.075 M, 2 mL) of dien was added to an aqueous solution of

 © 2004 Wiley-VCH Verlag GmbH & Co. KGaA, Weinheim

Table 4. Crystal and refinement data for complexes **2**−**4**

	2	**3**	**4**
Formula	$C_{30}H_{44}B_2Fe_2MnN_{18}O_6$	$C_{34}H_{46}B_2Fe_2N_{22}NiO$	$C_{16}H_{25}BClCuFeN_{12}O_5$
Formula mass	941.09	970.96	631.13
Crystal system	monoclinic	monoclinic	monoclinic
Space group	$P2_1/c$	$P2_1/c$	$P2_1/c$
a (Å)	9.3221(5)	9.6157(9)	13.902(2)
b (Å)	16.4877(9)	17.0115(15)	13.345(2)
c (Å)	14.4151(8)	14.0948(12)	15.007(2)
α (°)	90	90	90
β (°)	94.7070(10)	95.787(2)	112.978(3)
γ (°)	90	90	90
Z	2	2	4
V (Å^3)	2208.1(2)	2293.8(4)	2563.3(6)
D_{calcd} (g cm^{-3})	1.415	1.406	1.635
T (K)	213(2)	293(2)	213(2)
λ (Å)	0.71073	0.71073	0.71073
μ (mm^{-1})	0.990	1.085	1.553
F(000)	970	1004	1288
$2\theta_{max}$ (°)	50.0	52.0	52.0
hkl range	$-5 \le h \le 11$ $-19 \le k \le 18$ $-17 \le l \le 12$	$-11 \le h \le 7$ $-20 \le k \le 18$ $-16 \le l \le 17$	$-17 \le h \le 16$ $-15 \le k \le 16$ $-15 \le l \le 18$
Collected	8504	12217	15377
Unique	3816	4490	5037
Parameters	274	286	334
GOF	1.018	1.088	1.041
R_1 [$I > 2\sigma(I)$]	0.0440	0.0536	0.0478
wR_2 [$I > 2\sigma(I)$]	0.1138	0.1147	0.1198
(D map) max./min. [e·Å^{-3}]	0.202/−0.241	0.668/−0.350	0.442/−0.493

$Cu(ClO_4)_2 \cdot 6H_2O$ (4 mL, 56 mg, 0.15 mmol). A methanol solution of $(Bu_4N)[(Tp)Fe(CN)_3]$ (5 mL, 89 mg, 0.15 mmol) was added to this dark blue solution. Slow evaporation of the resulting solution in air afforded brown crystals. Yield: 80%. $C_{16}H_{25}BClCuFeN_{12}O_5$: calcd. C 30.45, H 3.99, N 26.63; found C 30.74, H 4.06, N 26.35. IR: (KBr): $\tilde{\nu}$ = 2131 (ν_{CN}) and 2157 cm^{-1} (ν_{CN}).

X-ray Crystallography: The structures of complexes **2**−**4** were determined. Suitable crystals were obtained by slow evaporation of the preparative reaction solution. Crystals were mounted in Paratone oil and placed in the dinitrogen cold stream of a Bruker Apex D8 diffractometer equipped with a 4 K CCD area detector for complex **2** or a Bruker-AXS P3 diffractometer equipped with a 1 K CCD area detector for complex **4**. Cell parameters were retrieved using SMART software and refined using SAINT on all observed reflections. Data were collected using the following strategy: 606 frames of 0.3° in ω with φ = 0°, 435 frames of 0.3° in ω with φ = 90°, and 235 frames of 0.3° in ω with φ = 180°. An additional 50 frames of 0.3° in ω with φ = 0° were collected to allow for decay correction. The highly redundant data sets were reduced using SAINT and corrected for Lorentz and polarization effects. Absorption corrections were applied using SADABS supplied by Bruker. Structures were solved by direct methods using the program SHELXL-97. The positions of metal atoms and their first coordination spheres were located from direct-methods *E*-maps; other non-hydrogen atoms were found in alternating difference Fourier syntheses and least-squares refinement cycles and, during the final cycles, refined anisotropically. Hydrogen atoms were placed in calculated positions and refined as riding atoms with a uniform value of U_{iso}. Crystallographic parameters and agreement factors are contained in Table 4.

CCDC-231294 (for **2**), -231295 (for **3**) and -231296 (for **4**) contain the supplementary crystallographic data for this paper. These data can be obtained free of charge at www.ccdc.cam.ac.uk/conts/retrieving.html or from the Cambridge Crystallographic Data Centre, 12 Union Road, Cambridge CB2 1EZ, UK [Fax: +44-1223-336033; E-mail: deposit@ccdc.cam.ac.uk].

Acknowledgments

This work was supported by The Major State Basic Research Development Program (G2000077500) and the National Natural Science Foundation of China (NSF20201006, 90101028, 20125104 and 20221101). The X-ray diffractometer is supported by NSF grant EAR-0003201.

[1] [1a] S. Ferlay, T. Mallah, R. Quahès, P. Veillet, M. Verdaguer, *Nature* **1995**, *378*, 701−703. [1b] S. M. Holmes, G. Girolami, *J. Am. Chem. Soc.* **1999**, *121*, 5593−5594.

[2] [2a] O. Sato, T. Iyoda, A. Fujishima, K. Hashimoto, *Science* **1996**, *271*, 49−51. [2b] N. Shimamoto, S. I. Ohkoshi, O. Sato, K. Hashimoto, *Inorg. Chem.* **2002**, *41*, 678−684. [2c] V. Escax, A. Bleuzen, C. Cartier dit Moulin, F. Villain, A. Goujon, F. Varret, M. Verdaguer, *J. Am. Chem. Soc.* **2001**, *123*, 12536−12543.

[3] [3a] C. P. Berlinguette, D. Vaughn, C. Canada-Vilalta, J. R. Galán-Mascarós, K. R. Dunbar, *Angew. Chem. Int. Ed.* **2003**, *42*, 1523−1526. [3b] V. Marvaud, C. Decroix, A. Scuiller, C. Guyard-Duhayon, J. Vaissermann, F. Gonnet, M. Verdaguer, *Chem. Eur. J.* **2003**, *9*, 1677−1691. [3c] V. Marvaud, C. Decroix, A. Scuiller, F. Tuyèras, C. Guyard-Duhayon, J. Vaissermann, J. Marrot, F. Gonnet, M. Verdaguer, *Chem. Eur. J.* **2003**, *9*, 1692−1705.

 © 2004 Wiley-VCH Verlag GmbH & Co. KGaA, Weinheim

[4] [4a] K. R. Dunbar, R. A. Heintz, *Prog. Inorg. Chem.* **1997**, *45*, 283−391. [4b] M. Ohba, H. Ōkawa, *Coord. Chem. Rev.* **2000**, *198*, 313−328. [4c] H. Ōkawa, M. Ohba, *Bull. Chem. Soc. Jpn.* **2002**, *75*, 1191−1203. [4d] E. Coronado, F. Palacio, J. Veciana, *Angew. Chem. Int. Ed.* **2003**, *42*, 2570−2572.
[5] J. L. Heinrich, P. A. Berseth, J. R. Long, *Chem. Commun.* **1998**, 1231−1232.
[6] [6a] P. A. Berseth, J. J. Sokol, M. P. Shores, J. L. Heinrich, J. R. Long, *J. Am. Chem. Soc.* **2000**, *122*, 9655−9662. [6b] J. J. Sokol, M. P. Shores, J. R. Long, *Angew. Chem. Int. Ed.* **2001**, *40*, 236−239. [6c] M. P. Shores, J. J. Sokol, J. R. Long, *J. Am. Chem. Soc.* **2002**, *124*, 2279−2292.
[7] J. Y. Yang, M. P. Shores, J. J. Sokol, J. R. Long, *Inorg. Chem.* **2003**, *42*, 1403−1419.
[8] [8a] R. Lescouëzec, F. Lloret, M. Julve, J. Vaissermann, M. Verdaguer, R. Llusar, S. Uriel, *Inorg. Chem.* **2001**, *40*, 2065−2072. [8b] R. Lescouëzec, J. Vaissermann, C. Ruiz-Pérez, F. Lloret, R. Carrasco, M. Julve, M. Verdaguer, Y. Dromzee, D. Gatteschi, W. Wernsdorfer, *Angew. Chem. Int. Ed.* **2003**, *42*, 1483−1486.
[9] [9a] H. Oshio, O. Tamada, H. Onodera, T. Ito, T. Ikoma, S. Tero-Kubota, *Inorg. Chem.* **1999**, *38*, 5686−5689. [9b] R. Lescouëzec, F. Lloret, M. Julve, J. Vaissermann, M. Verdaguer, *Inorg. Chem.* **2002**, *41*, 818−826.
[10] R. Lescouëzec, J. Vaissermann, F. Lloret, M. Julve, M. Verdaguer, *Inorg. Chem.* **2002**, *41*, 5943−5945.
[11] [11a] Y. Zhang, J.-L. Zuo, H.-C. Zhou, R. H. Holm, *J. Am. Chem. Soc.* **2002**, *124*, 14292−14293. [11b] J.-L. Zuo, H.-C. Zhou, R. H. Holm, *Inorg. Chem.* **2003**, *42*, 4624−4631.
[12] H. Fukui, M. Ito, Y. Morooka, N. Kitajima, *Inorg. Chem.* **1990**, *29*, 2868−2870.
[13] J. C. Bonner, M. E. Fisher, *Phys. Rev. Sect. A* **1964**, *135*, 640−658.
[14] [14a] R. Cortés, M. Drillon, X. Solans, L. Lezama, T. Rojo, *Inorg. Chem.* **1997**, *36*, 677−683. [14b] H.-Z. Kou, B.-C. Zhou, D.-Z. Liao, R.-J. Wang, Y.-D. Li, *Inorg. Chem.* **2002**, *41*, 6887−6891.
[15] B. Bosnich, M. L. Tobe, G. A. Webb, *Inorg. Chem.* **1965**, *4*, 1109−1112.
[16] R. L. Carlin, *Magnetochemistry*, Springer-Verlag Publishers, Berlin, Heidelberg, **1986**.

Received February 14, 2004
Early View Article
Published Online July 6, 2004

 © 2004 Wiley-VCH Verlag GmbH & Co. KGaA, Weinheim

Synthesis and Characterisation of Coordination Polymers of Cu^{II} and Zn^{II} with 1,3-Bis(1,2,3,4-tetrazol-2-yl)propane − Rotational Freedom of the Donor Group Favours Structural Diversification

Robert Bronisz[a]

Keywords: Coordination polymers / Copper / Flexibility / N ligands / Zinc

The novel bidentate ligand 1,3-bis(1,2,3,4-tetrazol-2-yl)propane (pbtz), which possesses a flexible spacer, was synthesised in order to investigate the influence of the flexibility of ligand molecules on the architecture of coordination polymers. For that purpose the reactions between pbtz and $M(ClO_4)_2 \cdot 6H_2O$ salts (M = Cu^{II} and Zn^{II}) were performed. The complexes $[\{Cu(pbtz)_3\}(ClO_4)_2]_\infty$ and $[\{Zn(pbtz)_3\}(ClO_4)_2 \cdot 2EtOH]_\infty$ were characterised by IR and UV/Vis spectroscopy and their crystal structures were determined by single-crystal X-ray diffraction measurements. In both compounds the pbtz ligand molecules act as N4,N4′ connectors bridging the central atoms, and the 2-substituted tetrazole rings coordinate in a monodentate fashion to the central atoms forming M(tetrazole)$_6$ cores. $[\{Cu(pbtz)_3\}(ClO_4)_2]_\infty$ was isolated as a 1D coordination polymer. The copper(II) ions are triply bridged by ligand molecules, leading to the formation of infinite 1D chains. A highly unusual manner of bridging, with the tethering of two neighbouring central atoms by the same kind of ligand molecules, although possessing different conformations, is observed. In $[\{Zn(pbtz)_3\}(ClO_4)_2 \cdot 2EtOH]_\infty$ the six-coordinate zinc(II) ions, which are bridged by single ligand molecules, serve as topological nodes, leading to the formation of a 3D α-polonium-type network. The crystal structure of the Zn^{II} complex contains only one such net solvated by ethanol molecules. A conformational analysis of the ligand molecules in both compounds demonstrates that the flexibility of the pbtz and the ability of the tetrazole rings in particular to adopt various, relative orientations is responsible for the diversity of the architectures of the obtained complexes.
(© Wiley-VCH Verlag GmbH & Co. KGaA, 69451 Weinheim, Germany, 2004)

Introduction

The schematic method created by Wells[1] and developed further by Robson[2] for the description of coordination polymers characterises such materials as a self-repeating system of nodes (central atoms) and rods (ligand molecules). This approach assumes the presence of a coordination bond, which is much stronger than other contacts such as hydrogen bonds or π−π interactions, and points to the importance of the coordination geometry of the central atom. In effect, the presence of coordination bonds means that the coordination geometry of the central atom can be propagated throughout the network. This indicates the possibility of a more reasoned approach to the synthesis of new materials with a desired topology and dimensionality, especially in the case of the application of rigid rod-like molecules as ligands.[3,4] In reality, however, this simple way of forecasting the architecture of the coordination networks is strongly perturbed both by the ability of the metal ions to form complexes with heteroleptic surrounded central atoms and by the influence of the angularity of the rigid ligand molecules,[5−10] *cis*/*trans* isomerism,[11] and the conformational freedom of ligands possessing a flexible spacer.[12−16] The flexibility of the ligand molecules usually leads to great structural diversification of the products, including the formation of supramolecular isomers.[17]

The length of the ligand molecule affects the distance between the bridged central atoms. This separation implies either the formation of voids, which can be filled by solvent molecules, or interpenetrated structures.[18−20] In bis(4-pyridyl)alkanes the position of the nitrogen donor atom means that although various configurations can be adopted by the pyridyl rings in relation to the alkyl spacer, the intraligand N···N′ distance depends only on the conformation of the alkyl spacer.[14] A more complicated situation arises in the case of five-membered polyazole rings as the donor groups. Conjugated bis(polyazoles) can act as linear or angular connectors, and in such a situation the distance between the central atoms bridged by common ligand molecules depends on the relative orientation of the polyazole rings.[21−29] The incorporation of an alkyl spacer tethering imidazole,[30−34] pyrazole,[35] benzimidazole,[36,37] triazole,[38−45] benzotriazole,[37,46,47] or tetrazole[48−57] moieties causes a significant increase of the flexibility of the ligand molecule, thus allowing the formation of a wide range of coordination polymer architectures.

Among the five-membered polyazoles, the coordination chemistry of 2-substituted tetrazoles is very much under-

[a] Faculty of Chemistry, University of Wroclaw,
F. Joliot-Curie 14, 50-383 Wroclaw, Poland
Fax: (internat.) + 48-71-328-2348
E-mail: bron@wchuwr.chem.uni.wroc.pl

 © 2004 Wiley-VCH Verlag GmbH & Co. KGaA, Weinheim DOI: 10.1002/ejic.200400171

developed, especially in relation to their 1-substituted isomers.[47−54,58−63] In the majority of 2-substituted tetrazole complexes the polyazole ring coordinates to the metal ion in a monodentate fashion through the N4 nitrogen atom.[55,56,64,65] This ability to form a coordination bond through the *exo*-nitrogen atom of the tetrazole ring enables the use of this donor group for the preparation of nonchelating bi- and polypodal ligands appropriate for the construction of coordination polymers. Indeed, the results of recently started investigations of a new family of ligands, namely 1,ω-bis(1,2,3,4-tetrazol-2-yl)alkanes, point to their usefulness in the preparation of coordination networks with various dimensionalities and topologies. Thus, 1,2-bis(1,2,3,4-tetrazol-2-yl)ethane (ebtz) reacts with Zn^{II} to form a triple-stranded 1D linear chain,[55] whereas the complexes obtained from the reaction of Cu^{II} with 1,4-bis(1,2,3,4-tetrazol-2-yl)butane (bbtz) were isolated, depending on the reaction conditions, as either 2D or 3D networks.[56] Naturally, in such a situation an intriguing question arises concerning the architecture of the coordination polymers in the case of the application of an intermediate-length spacer tethering the tetrazole rings, namely 1,3-propylene; therefore a new flexible ligand 1,3-bis(1,2,3,4-tetrazol-2-yl)propane (pbtz; Scheme 1) was synthesised.

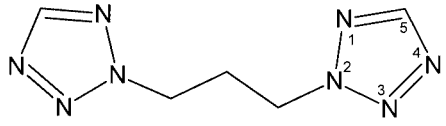

Scheme 1

Taking into account the tendency to structural diversification of the products in the case of the application of flexible ligand molecules, the investigation of the coordination abilities of pbtz was focused first of all on octahedrally coordinating metal ions, aiming especially at complexes with a homoleptic ligand environment. In this paper the synthesis of the pbtz ligand and the coordination polymers obtained from the reaction of pbtz with perchlorate salts of Cu^{II} and Zn^{II} is reported in detail. The results of spectroscopic investigations and single-crystal X-ray diffraction studies of 1D and 3D polynuclear complexes are also presented.

Results and Discussion

Synthesis, Properties and Spectroscopic Characterisation

The new flexible ligand 1,3-bis(1,2,3,4-tetrazol-2-yl)propane (**1**) was synthesised by alkylation of sodium tetrazolate with 1,3-dibromopropane, according to the method described previously for other members of this family of ligands.[55,56] Because of the competitive process of formation of 1-substituted tetrazoles in this synthetic route[66−68] a low yield of pbtz was also obtained in this case due to the formation of other bis(tetrazole) ligands, namely 1,3-bis(1,2,3,4-tetrazol-1-yl)propane and 1-(1,2,3,4-tetrazol-1-yl)-3-(1,2,3,4-tetrazol-2-yl)propane.[54] The pbtz ligand was isolated as a colourless liquid. It is completely miscible in polar solvents such as methanol, acetonitrile, and dichloromethane, although it is significantly less soluble in CCl_4 and is completely insoluble in aliphatic hydrocarbons; it is stable during storage at room temperature.

The results of elemental analysis indicated that the reactions between pbtz and $M(ClO_4)_2{\cdot}6H_2O$ salts (M = Cu^{II}, Zn^{II}), performed in a 3:1 ligand/metal stoichiometry, afforded complexes with formula $[\{Cu(pbtz)_3\}(ClO_4)_2]_\infty$ (**2**) and $[\{Zn(pbtz)_3\}(ClO_4)_2{\cdot}2EtOH]_\infty$ (**3**).

The synthesis of **2** leads first of all to the formation of small amounts of a light-blue polycrystalline solid. After about 10 d, crystals of **2** started to grow accompanied by the partial disappearance of the products precipitated during the first stage of the synthesis. Because only very small amounts of these polycrystalline products were formed, and due to their lack of homogeneity, it was not possible to characterise them. Therefore, only the light-blue crystals of complex **2** were isolated and characterised. The synthesis of the Cu^{II} complex depends strongly on the ethanol volume, the presence of water in the solvent, and the growing time of the crystals, and therefore this influences both the yield of product **2** and amount of the polycrystalline mixture formed.

The preparation of the zinc(II) complex was successful only in absolute ethanol; the addition of water prevents formation of the product. Under these reaction conditions only the formation of complex **3** was observed. In contrast to **2**, the zinc(II) complex is unstable during storage in air, and a few days after removal from the mother liquor crystals of **3** become cloudy.

The IR spectrum of pbtz is characteristic of 2-alkyltetrazoles.[69] The formation of a coordination bond through the N4 nitrogen atom of the tetrazole ring involves changes in the bands that are composed from combinations of the vibrations of the tetrazole ring components. The characteristic narrow band located at 3141 cm^{-1} and assigned to $\nu(C_{ring}-H)$ stretching vibrations in **1** is shifted to higher frequencies by 10 cm^{-1} and 6 cm^{-1} for complexes **2** and **3**, respectively. The bands attributed to the stretching vibrations of the N=N (1450 cm^{-1}), C=N (1360 cm^{-1}) and N−N (1290 cm^{-1}) bonds in the IR spectrum of the free pbtz ligand are also shifted to higher wavenumbers after complexation. These changes are in agreement with those observed for $[Cu(2\text{-alkyltetrazole})_2X_2]$ (X = Cl^-, SCN^-)[70] and complexes of Zn^{II} and Cu^{II} with ebtz[55] and bbtz[56] ligands. In contrast to **2**, the broad, intense band located at 3393 cm^{-1} observed for compound **3** confirms the presence of alcohol molecules in the crystal lattice of the Zn^{II} complex. The presence of nonsplit, strong absorption bands at 1094 and 624 cm^{-1} for **2** and 1090 and 626 cm^{-1} for **3** points to a lack of strong deviation of the perchlorate anions from tetrahedral symmetry.[71]

The electronic spectrum of complex **2** shows a d-d transition at 15400 cm^{-1} with a shoulder at 9800 cm^{-1}. These values are characteristic of square-planar CuN_4 or distorted octahedral CuN_4X_2 (X = N, O) chromophores[72] and are

 © 2004 Wiley-VCH Verlag GmbH & Co. KGaA, Weinheim

similar to those found for mononuclear complexes of 1-alkyltetrazoles, such as $[Cu(1\text{-alkyltetrazole})_6](BF_4)_2$.[73]

Structural Studies

Description of the Crystal Structure of 2

The structure of **2** is depicted in Figure 1 together with the labelling scheme of the atoms. The Cu^{II} ion environment is formed by six 2-substituted tetrazole rings coordinating monodentately through their N4 nitrogen atoms. The four nitrogen atoms forming an equatorial plane are placed at distances of 1.993(2) and 2.061(2) Å. The distance to both axially located nitrogen atoms is equal to 2.414(2) Å. The N−Cu−N angles are close to 90°, ranging from 88.36(6) to 91.64(6)°. This coordination geometry of the elongated octahedron is typical for CuN_6 chromophores distorted by the Jahn−Teller effect and is similar to those found for other complexes of both 2-substituted[56] and 1-substituted tetrazoles.[47,60]

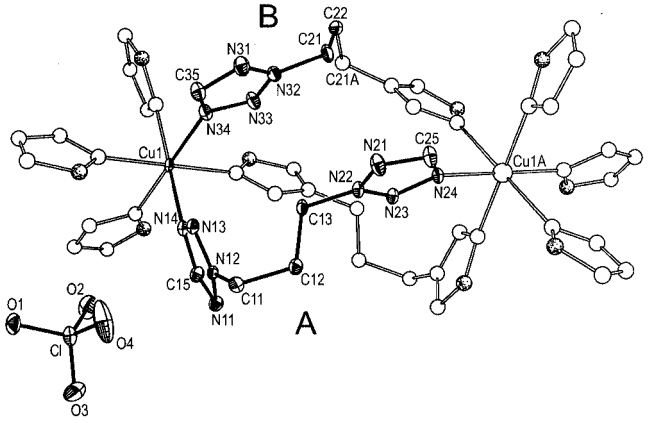

Figure 1. Coordination geometry around Cu^{II} in **2** and labelling scheme of atoms (50% probability displacement ellipsoids); hydrogen atoms are omitted for clarity; selected torsion angles [°] for ligand molecule **A**: N11−N12−C11−C12 86.0(2), N12−C11−C12−C13 54.2(2), C11−C12−C13−N22 172.6(2), N21−N22−C13−C12 −91.2(2) (*TG* conformation); for ligand molecule **B**: N31−N32−C21−C22 −132.6(2), N32−C21−C22−C21a −75.9(2) (*GG′* conformation); atom C21A generated by symmetry operation $-x, y, -z + 3/2$

Each molecule of pbtz acts as an N4,N4′ bridging ligand and three molecules of pbtz simultaneously link two neighbouring copper(II) ions. This bridging propagates along the *c* axis and leads to the formation of an infinite chain (Figure 2a). In the case of 1,3-bis(polyazolyl)propane ligands a similar motif of a triple-stranded infinite chain has been found for complexes of Fe^{II} and Cu^{II} with 1,3-bis(1,2,3,4-tetrazol-1-yl)propane.[54] Among polynuclear complexes based on 1,ω-bis(polyazolyl) ligands possessing an alkyl spacer other than 1,3-propylene, this type of bridging of the metal atoms has been observed for complexes of 1,1-bis(1,2,3,4-tetrazol-2-yl)methane,[74] 1,2-bis(1,2,3,4-tetrazol-2-yl)ethane,[55] 1,2-bis(1,2,3,4-tetrazol-1-yl)ethane[47,49] and 1,2-bis(1,2,3,4-tetrazol-1-yl)propane.[50] In **2** the copper atoms linked by common ligand molecules are separated by a distance of 9.001(1) Å while the shortest distance between the copper atoms from neighbouring chains is 8.950(1) Å. These data clearly show that in relation to 1D coordination polymers based on bis(tetrazolyl)ethane ligands[47,49,50,55] an elongation of the spacer in pbtz results in an increase of the metal−metal separation within the polymeric unit of **2** by 1.6−2.3 Å.

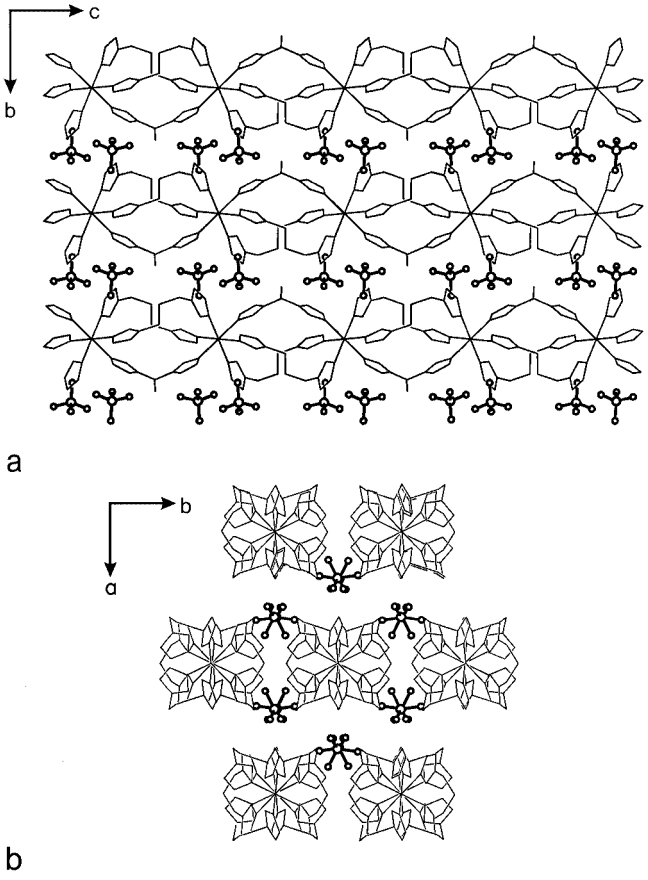

Figure 2. Projection of the structure of **2** (a) along the *a* axis and (b) along the *c* axis; hydrogen atoms are omitted for clarity

An unusual feature of the triple-stranded bridge in **2** is the presence of ligand molecules with two different conformations that simultaneously tether the same two central atoms. In this compound two crystallographically related ligand molecules adopt *TG* conformations whereas the third molecule of pbtz adopts a *GG′* conformation. A comparison of the torsion angles for both types of pbtz ligands shows that a change of the spacer conformation in ligand **A** is accompanied by rotation of the tetrazole ring, which leads to an adjustment of the intramolecular N4···N4′ distance relative to that in ligand **B**. Hence, despite differences between the conformations of the pbtz molecules the N4···N4′ distances are similar and are equal to 7.015(2) Å and 6.827(3) Å for molecules adopting the *TG* and *GG′* conformations, respectively. This behaviour, observed here for the first time for complexes based on alkylbis(polyazole) ligands, demonstrates a fundamental difference of the properties of the pbtz ligand in relation to those of 1,3-

 © 2004 Wiley-VCH Verlag GmbH & Co. KGaA, Weinheim

bis(pyridyl-4-yl)propane — the distance between the metal centers depends only on the alkyl spacer conformation.[14]

The architecture of **2** enforces a localisation of the perchlorate ions in the channels between the polymeric chains (Figure 2b). The perchlorate ions do not form any coordination bonds with the copper(II) ions. However, they are engaged in the formation of C15−H15···O2(Cl) ($-x$, $-y + 1$, $-z + 2$) and C25−H25···O4(Cl) ($-x + 1/2$, $y + 1/2$, $-z + 3/2$) contacts. Direct C25−H25···N13 (x, $-y + 2$, $z - 1/2$) contacts are also observed between the polymeric chains. As a result no voids are accessible for the incorporation of solvent molecules.

Description of the Crystal Structure of 3

In **3** there are two crystallographically independent zinc(II) ions. The coordination environments of both central atoms are similar and consist of six nitrogen atoms from monodentate 2-substituted tetrazole moieties (Figure 3). There are two sets of metal−ligand bond lengths for Zn1−N [2.150(3) and 2.172(3) Å], whereas for the second crystallographically independent zinc atom the Zn2−N distances are practically the same, ranging from 2.163(3) to 2.166(3) Å. The values of the N−Zn−N angles vary from 87.0(1) to 92.2(1)° for Zn1 and from 88.8(1) to 90.9(1)° for Zn2, indicating a significantly larger rhombic distortion of the coordination environment in the case of the Zn1 atom, consisting in this case of a compression of the coordination octahedron along the threefold axis in the c direction. The coordination geometry, especially in the case of the Zn1 atom, is similar to that found for Zn^{II} in the 1D coordination polymer $[\{Zn(ebtz)_3\}(ClO_4)_2]_\infty$.[55]

The pbtz molecule acts as an N4,N4′ bridging ligand. In this case, contrary to **2**, six pbtz molecules are coordinated to one central atom and two central atoms are bridged only by a single ligand molecule. This bridging fashion of the adjacent zinc atoms spreads in the three noncoplanar directions, leading to the formation of a 3D coordination polymer. In this way an octahedral network composed of distorted rhombohedral "boxes" is formed (Figure 4). The topology of the network in **3** originates from the coordination symmetry of the zinc atoms. However, differences in the relative orientations of the neighbouring octahedra mean that the coordination bond directions do not determine the direction of the propagation of the network. In spite of this the flexibility of the pbtz molecules enables a bridging of the central atoms, which are separated by distances of 10.666(1) and 10.706(1) Å. In comparison with octahedral networks based on butylbis(polyazole) ligands, this fitting of the geometry of the pbtz molecules to the localisation of the coordination sites of the neighbouring central atoms involves a significant shortening of the appropriate M···M distances by about 2.4−3.6 Å.[33,34,52,54] As a consequence, such a large decrease of the distances between the central atoms causes a lack of free space accessible for the interpenetration, leading, in the case of the 1,3-propylene spacer, to the formation of a coordination polymer composed from only one octahedral network. Known α-

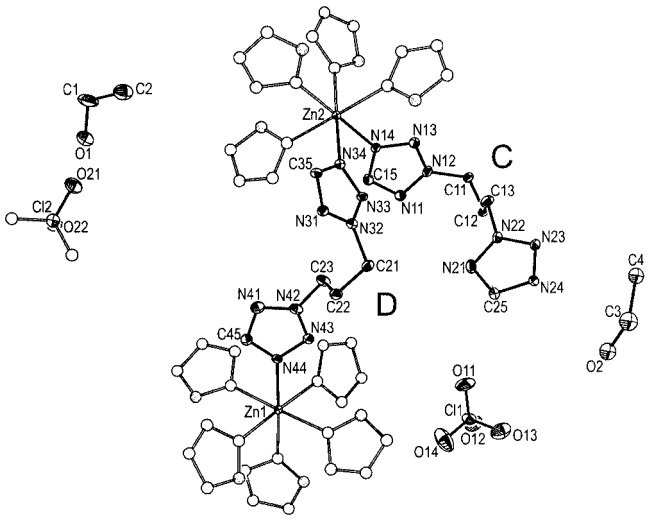

Figure 3. Coordination geometry around Zn^{II} in **3** and labelling scheme of atoms (30% probability displacement ellipsoids); hydrogen atoms are omitted for clarity; selected torsion angles [°] for ligand molecule **C**: N13−N12−C11−C12 104.6(4), N12−C11−C12−C13 −69.4(5), C11−C12−C13−N22 172.0(4), N21−N22−C13−C12 −76.4(5) (*TG* conformation); for ligand molecule **D**: N31−N32−C21−C22 70.4(5), N32−C21−C22−C23 57.9(5), C21−C22−C23−N42 176.2(4), N41−N42−C23−C22 87.0(5) (*TG* conformation)

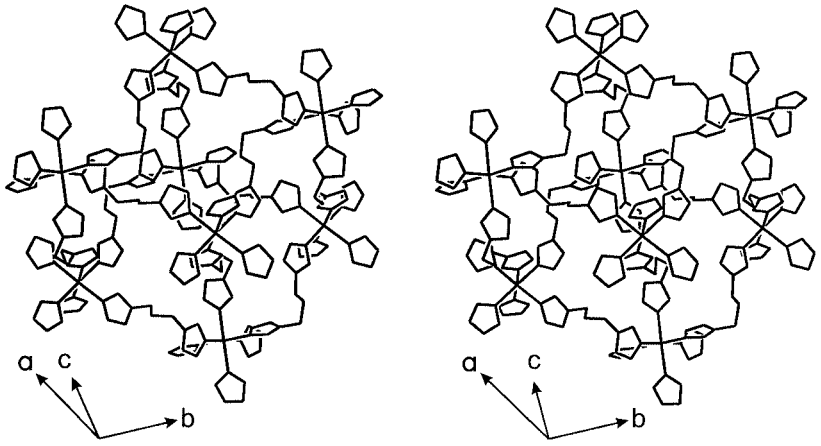

Figure 4. A stereoview of the 3D net in **3**; hydrogen atoms, ethanol molecules and perchlorate anions are omitted for clarity

 © 2004 Wiley-VCH Verlag GmbH & Co. KGaA, Weinheim

polonium-type 3D systems based on alkylbis(polyazole) ligands contain four or more methylene groups in the alkyl spacer and they are composed from two[33,34,51] or three[52,54] 3D interpenetrated nets. Compound **3** therefore represents the first example of a non-interpenetrated 3D α-polonium-type system based on a flexible bis(polyazole) ligand.

The transition from compound **2** (1D net) to compound **3** (3D net) involves an increase of the number of pbtz molecules possessing the opposite localisation of the nitrogen donor atoms. This is expressed by an increase of the angles between the nitrogen−metal bonds (for central atoms bridged by common ligand molecule) from about 60 to 110°. This corresponds to the change of character of the pbtz molecules from angular (in **2**) to more linear (in **3**) connectors. In consequence, the distances between the zinc atoms separated by common ligand molecules in **3** are about 1.7 Å greater than the analogous Cu···Cu distance in **2**. Naturally, this large separation of the metal atoms in **3** explains the lack of bridging ligand molecules possessing a *GG′* conformation. The differences between ligand molecules possessing a *TG* conformation of the spacers suggests that the increase of the intramolecular N4···N4′ distances in **3** relative to **2** is achieved in two ways. A comparison of ligands **A** (inverted structure) in **2** and **C** in **3** indicates that a combined effect both of the change of the spacer conformation and the relative orientation of the rings is responsible for the increase of the N4···N4′ distance. Surprisingly, the torsion angles for ligand **A** (compound **2**) and ligand **D** (compound **3**) suggest that the increase of the metal···metal separations in this case results from the change of the relative orientation of the tetrazole rings; the conformation of the alkyl spacers remains unchanged (see Figure 5). In contrast to ligands possessing axially symmetrical donor groups, (e.g. 4-pyridyl), a noncolinear orientation of the metal−nitrogen bond and the ring−alkyl bond (here N−C) enables the bridging of metal atoms separated by different distances despite the retention of the same conformation of the alkyl spacer. The conformational flexibility of the spacer observed in complexes **2** and **3**, and especially the rotational freedom of the tetrazole ring, is responsible for the adoption of various relative orientations by the donor groups and therefore by the N4 donor atoms, which leads to the difference in the metal−metal distances and the topology of the networks as well.

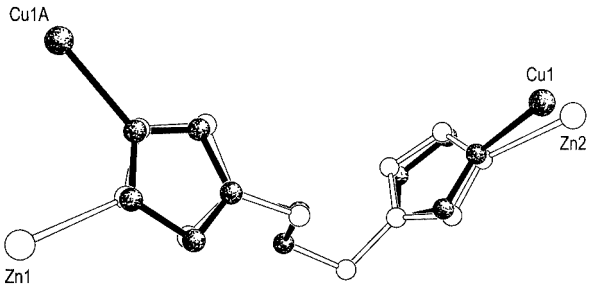

Figure 5. A superposition of the ligand molecules **A** (compound **2**) and **D** (compound **3**); hydrogen atoms are omitted for clarity; atom Cu1A generated by symmetry operation: $-x$, y, $-z + 3/2$

The perchlorates are noncoordinated and are gathered around the Zn(tetrazole)$_6$ cores. The remaining free space (943 Å^3; 17.1% of the unit cell volume) is composed of two kinds of voids with approximate volumes of 82 and 68 Å^3. The ethanol molecules that occupy the larger voids are arranged in pillars positioned parallel to the *c* axis (Figure 6). The space situated in the void of the rhombohedral boxes is occupied by ethanol molecules disordered about the threefold axis. The perchlorates are engaged in the formation of hydrogen bonds O2−H2···O21(Cl) ($-y + 2/3$, $x - y + 1/3$, $z + 1/3$) and O2−H2···O11(Cl) ($x + 1/3$, $y + 2/3$, $z + 2/3$) with both types of ethanol molecules.

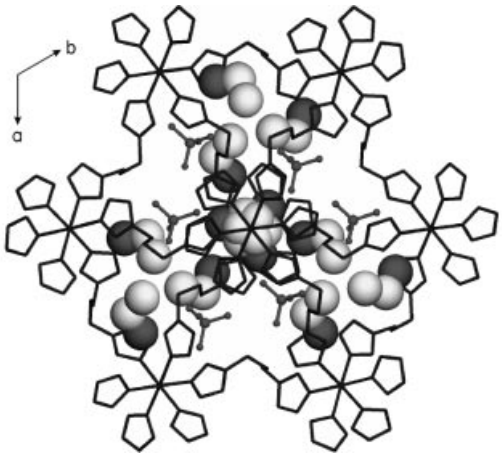

Figure 6. A view along the *c* axis showing channels filled by ethanol molecules in **3**; hydrogen atoms are omitted for clarity

Concluding Remarks

The new flexible ligand 1,3-bis(1,2,3,4-tetrazol-2-yl)propane and two coordination polymers of Cu^{II} and Zn^{II} have been synthesised. They were characterised spectroscopically and the crystal structures of both complexes were determined. The bidentate and nonchelating nature of the pbtz ligand is reflected in the polymeric structure of the complexes: $[\{Cu(pbtz)_3\}(ClO_4)_2]_\infty$ crystallises as a 1D triple-stranded infinite chain, whereas $[\{Zn(pbtz)_3\}(ClO_4)_2 \cdot 2EtOH]_\infty$ was isolated as a 3D network.

A strong influence of the spacer length on the architecture of the coordination polymers in this series of complexes based on 1,ω-bis(1,2,3,4-tetrazol-2-yl)alkanes is observed. Thus, use of pbtz rather than 1,2-bis(1,2,3,4-tetrazol-2-yl)ethane,[55] resulted not only in a 1D system but also in a coordination polymer of higher dimensionality (3D). In comparison with 1,4-bis(1,2,3,4-tetrazol-2-yl)butane,[56] a shortening of the alkyl spacer to 1,3-propylene resulted in the lowering of the degree of interpenetration and the formation of coordination polymers built up from only one octahedral network.

The coordination polymers described in this paper are based exclusively on octahedrally coordinated central atoms. Differences between the coordination properties of

 © 2004 Wiley-VCH Verlag GmbH & Co. KGaA, Weinheim

the Cu^{II} and Zn^{II} ions are reflected both in the course of the syntheses and in the diversification of the architectures of the isolated complexes. The flexibility of the ligand molecules, and especially the rotational freedom of the tetrazole rings, enable this structural diversification. The conformational analysis has shown that a rotation of the tetrazole rings around the ring−spacer bond ($C_{alkyl}-N2_{ring}$) can compensate a change of conformation of the alkyl spacer, leading to adjustment of the distances between the N4 and N4′ donor atoms. This peculiarity enables a bridging of the same two central atoms by the ligand molecules even though they possess different conformations. On the other hand the possibility of changing the relative orientation of the donor groups (tetrazole rings) by the simultaneous retention of the spacer conformation significantly influences the intrapolymer metal−metal distances. This leads, in consequence, to the formation of a coordination network with a different architecture. In summary, the rotational freedom of donor groups, especially their relative orientations, plays a similar role to the orientation effect of the donor group in the case of rigid ligands,[75,76] enabling here the formation of 1D and 3D networks.

Experimental Section

General Remarks: The infrared spectra of pbtz and its complexes were recorded with a Bruker IFS66 IR FTIR spectrometer in the range 50−4000 cm^{-1} as nujol mulls. ^1H and ^{13}C NMR spectra were obtained with an AMX Bruker NMR 300 MHz spectrometer at room temperature in CD_3CN solutions. The ligand-field spectra were measured on powdered, pure samples with the diffuse-reflectance technique using a Cary 500 SCAN UV/Vis/NIR spectrometer. Elemental analyses for C, H, N were performed with a Perkin−Elmer 240C elemental analyser. Ethanol was dried by distilling from magnesium ethanolate. 1*H*-tetrazole was prepared by a previously described procedure.[55,77] The degree of hydration of the $Cu(ClO_4)_2{\cdot}6H_2O$ and $Zn(ClO_4)_2{\cdot}6H_2O$ salts was determined with an ICP spectrometer. The other commercially available reagents were used without further purification. ***Caution:*** Even though no problems were encountered it is worth mentioning that complexes containing perchlorates are potentially explosive and should be synthesised on a milligram scale and handled with care!

Synthesis of 1,3-Bis(1,2,3,4-tetrazol-2-yl)propane (1): A solution of NaOH (0.15 mol, 6.0 g) in water (20 mL) was added in a few portions to 1*H*-tetrazole (0.15 mol, 10.5 g) dissolved in water (20 mL). After cooling, the resulting clear solution was concentrated to dryness in a rotary evaporator. The remaining solid matter was finally dehydrated by an azeotropic distillation with three portions (100 mL each) of absolute ethanol. 1,3-Dibrompropane (0.07 mol, 7.15 mL) was then added to the obtained sodium tetrazolate suspended in MeCN (300 mL). The reaction mixture was stirred and refluxed for 4 d. The NaBr formed was filtered off and solvents were evaporated under reduced pressure. The resulting yellow oil was dissolved in water (150 mL). The aqueous solution was extracted with pentane (3 × 100 mL) and then with CCl_4 (10 × 100 mL). The crude product was isolated by removal of the solvent from the CCl_4 phase and purified by column chromatography on silica gel (230 mesh) using dichloromethane/acetone (100:5, v/v) as eluent (R_f = 0.38). Yield: 1.81 g (12.8%). $C_5H_8N_8$ (180.17): calcd. C 33.3, H 4.48, N 62.2; found C 33.8, H 4.60, N 61.9. ESI-MS: *m*/*z* calcd. for $C_5H_9N_8$ [LH^+] 181.2; found 181.1. IR: $\tilde{\nu}$ = 3141 (m), 3012 (w), 2965 (w), 1773 (w), 1629 (w), 1450 (s), 1361 (s), 1284 (s), 1186 (m), 1167 (w, sh), 1135 (s), 1051 (w, sh), 1028 (s), 1009 (m), 986 (w), 887 (m), 803 (w), 757 (w), 727 (w), 709 (s), 689 (m), 661 (w), 640 (w), 475 (m), 370 (m) cm^{-1}. ^1H NMR (300 MHz, CD_3CN, 298 K): δ = 2.69 (q, $^3J_{H,H}$ = 6.7 Hz, 2 H, 2-H), 4.74 (t, $^3J_{H,H}$ = 6.7 Hz, 4 H, 1-H, 3-H), 8.58 (s, 2 H, 5-H) ppm. ^{13}C NMR (300 MHz, CD_3CN, 298 K): δ = 29.09, 50.83, 153.98 ppm.

Synthesis of $[\{Cu(pbtz)_3\}(ClO_4)_2]_\infty$ (2): A solution of $Cu(ClO_4)_2{\cdot}6H_2O$ (0.020 mmol, 7.4 mg) in EtOH (2.0 mL) was added to a solution of pbtz (0.060 mmol, 10.8 mg) in EtOH (2.0 mL). The reaction mixture was heated to 50 °C to give a clear solution. A few minutes after cooling, the solution became turbid and a small amount of precipitate appeared. The precipitate was left in the solution. The reaction mixture was kept in a closed tube at room temperature. Light-blue crystals were formed after 3 weeks. The crystals of **2** were separated manually under the microscope from the rest of the polycrystalline solids and then dried in air. Yield: 3.8 mg (24%). $C_{15}H_{24}Cl_2CuN_{24}O_8$ (802.95): calcd. C 22.4, H 3.01, N 41.9; found C 22.7, H 3.11, N 41.5. IR: $\tilde{\nu}$ = 3549 (w), 3151 (m), 3036 (w), 2980 (m, sh), 2923 (s), 2854 (s, sh), 1626 (w), 1468 (s, sh), 1460 (s), 1447 (sh), 1378 (m), 1367 (m), 1312 (m), 1292 (m), 1273 (w), 1211 (w), 1205 (w), 1185 (m), 1151 (s), 1139 (s), 1092 (vs), 1044 (w), 1044 (w), 1037 (w), 1029 (w), 1023 (w), 974 (w), 900 (w), 885 (m), 844 (m), 810 (w), 756 (w), 719 (w), 710 (w), 700 (m), 693 (m), 673 (w), 644 (w), 624 (s), 473 (w), 455 (w), 404 (m), 391 (w), 361 (w), 295 (w), 276 (w), 251 (w), 210 (w), 183 (w) cm^{-1}. UV/Vis: λ_{max} = 15400, 9800 cm^{-1}.

Synthesis of $[\{Zn(pbtz)_3\}(ClO_4)_2{\cdot}2EtOH]_\infty$ (3): A solution of pbtz (0.06 mmol, 11.6 mg) in absolute ethanol (0.4 mL) was added to a solution of $Zn(ClO_4)_2{\cdot}6H_2O$ (0.02 mmol, 7.4 mg) in ethanol (0.4 mL). The resulting clear solution was allowed to stand in a closed tube at room temperature for 1 week. After this time, colorless crystals were collected and dried in a stream of nitrogen. Yield: 10.3 mg (57.4%). $C_{15}H_{24}Cl_2N_{24}O_8Zn{\cdot}2EtOH$ (896.92): calcd. C 25.4, H 4.04, N 37.5; found C 25.0, H 3.89, N 37.6. IR: $\tilde{\nu}$ = 3396 (br. s), 3169 (w), 3146 (m), 2953 (s, sh), 2925 (s), 2854 (m), 1650 (w, br), 1466 (m), 1455 (m), 1374 (m), 1364 (w, sh), 1304 (w), 1285 (m), 1204 (w), 1181 (w), 1151 (s, sh), 1140 (s, sh), 1109 (vs), 1090 (s, sh), 1029 (m, sh), 991 (w), 940 (w), 929 (w), 877 (w), 818 (w), 708 (w), 689 (m), 637 (m, sh), 626 (s), 475 (w), 388 (w), 191 (w) cm^{-1}.

X-ray Crystallographic Study: Single crystals of complexes **2** and **3** were obtained directly from the synthesis. The crystals were coated with a layer of inert oil, mounted on a glass fiber and transferred to the cold nitrogen stream of the diffractometer. Measurements of crystals of both compounds were performed with a Kuma KM4CCD κ-axis diffractometer with graphite-monochromated Mo-K_α radiation, equipped with an Oxford Cryosystem device. Crystal data and refinement details for **2** and **3** are listed in Table 1. The data were corrected for Lorentz and polarisation effects. No absorption correction was applied. Data reduction and analysis were carried out with the Oxford Diffraction (Poland) Sp. z o.o (formerly Kuma Diffraction Wroclaw, Poland) programs. The structures were solved by direct methods (program SHELXS-97[78]) and refined by the full-matrix least-squares method on all F^2 data using the SHELXL-97[79] programs. An analysis of the holes was performed using the Platon program.[80] The visualisation of the extended structure depicted in Figure 6 was prepared using the OLEX[81] program. For **2** all non-hydrogen atoms were refined with anisotropic displacement parameters. Hydrogen atoms were located from the Fourier difference map and were refined with isotropic displacement parameters. For **3** the zinc atoms, the atoms of the

 © 2004 Wiley-VCH Verlag GmbH & Co. KGaA, Weinheim

Table 1. Crystal data and structure refinement parameters for **2** and **3**

	2	**3**
Empirical formula	$C_{15}H_{24}Cl_2CuN_{24}O_8$	$C_{15}H_{24}Cl_2ZnN_{24}O_8 \cdot 1.92C_2H_6O$
Formula mass	803.02	893.15
T [K]	293(2)	100(2)
λ [Å]	0.71073	0.71073
Crystal system	monoclinic	trigonal
Space group	$C2/c$	$R\bar{3}$
a [Å]	18.5212(11)	17.5080(9)
b [Å]	8.9503(5)	17.5080(9)
c [Å]	18.0019(9)	20.7888(16)
α [°]	90	90
β [°]	90.566(7)	90
γ [°]	90	120
V [Å^3]	2984.0(3)	5.518.7(6)
Z	4	6
D_c [Mg·m^{-3}]	1.787	1.612
μ [mm^{-1}]	0.999	0.894
$F(000)$	1636	2694
Crystal size [mm]	0.10 × 0.12 × 0.17	0.12 × 0.12 × 0.15
θ range for data collection [°]	3.39 to 28.47	3.69 to 28.43
Ranges of h,k,l	$-24 \le h \le 24$	$-22 \le h \le 22$
	$-11 \le k \le 11$	$-23 \le k \le 19$
	$-24 \le l \le 20$	$-27 \le l \le 27$
Reflections collected	14322	12692
Independent reflections	3552	5313
R_{int}	0.0429	0.0331
Data/restraints/parameters	3552/0/276	5313/4/341
GOF(F^2)	1.101	1.078
Final R_1/wR_2 indices [$I > 2\sigma(I)$]	0.0374/0.0868	0.0435/0.1161
Largest diff. peak/hole [e·Å^{-3}]	0.405/−0.999	0.798/−0.605

ligands, the perchlorate anions and one of the two ethanol molecules were refined with anisotropic displacement parameters. Hydrogen atoms were included from the geometry of the molecules and were then refined isotropically. The three residual density peaks positioned about a threefold axis were modelled as the second ethanol molecule. For refinement of the respective position of this EtOH molecule three distance restraints — C−C = 1.44(1), C−O = 1.42(1) and C···O = 2.38(1) Å — were applied.[82] The oxygen and carbon atoms were refined isotropically. A refinement with a freely established occupancy factor showed the partial occupation of this position. A consideration of the presence of these additional small amounts of ethanol molecules (ca. 0.4 ethanol molecules per formula unit) solvating the crystal lattice of **3** leads to agreement with the results of the elemental analysis. CCDC-232496 (**2**) and -232497 (**3**) contain the supplementary crystallographic data for this paper. These data can be obtained free of charge at www.ccdc.cam.ac.uk/conts/retrieving.html [or from the Cambridge Crystallographic Data Centre, 12 Union Road, Cambridge CB2 1EZ, UK; Fax: (internat.) + 44-1223-336-033; E-mail: deposit@ccdc.cam.ac.uk].

Acknowledgments

I would like to thank Prof. Zbigniew Ciunik and Dr. Andrzej Kochel for the single-crystal X-ray data collection and Dr. Krzysztof Drabent for his valuable comments. The author thanks the MENiS for financial support.

[1] A. F. Wells, *Structural Inorganic Chemistry*, Oxford University Press, Oxford, **1975**.
[2] R. Robson, *J. Chem. Soc., Dalton Trans.* **2000**, 3735−3744.
[3] M. J. Zaworotko, *Chem. Commun.* **2001**, 1−9.
[4] P. J. Hagrman, D. Hagrman, J. Zubieta, *Angew. Chem. Int. Ed.* **1999**, *38*, 2638−2684; *Angew. Chem.* **1999**, *18*, 2798−2848.
[5] J. A. R. Navarro, B. Lippert, *Coord. Chem. Rev.* **2001**, *222*, 219−250.
[6] C. V. K. Sharma, R. D. Rogers, *Cryst. Eng.* **1998**, *1*, 19−38.
[7] Z. Huang, H.-B. Song, M. Du, S.-T. Chen, X.-H. Bu, *Inorg. Chem.* **2004**, *43*, 931−944.
[8] D. M. Shin, I. S. Lee, Y. K. Chung, M. S. Lah, *Inorg. Chem.* **2003**, *42*, 5459−5461.
[9] D. M. Shin, I. S. Lee, Y. K. Chung, M. S. Lak, *Chem. Commun.* **2003**, 1036−1037.
[10] Y.-B. Dong, J.-P. Ma, F.-Z. Liang, M. D. Smith, *Dalton Trans.* **2003**, 1472−1479.
[11] J. M. Knaust, S. W. Keller, *Inorg. Chem.* **2002**, *41*, 5650−5652.
[12] L. Carlucci, G. Ciani, D. M. Proserpio, *Coord. Chem. Rev.* **2003**, *246*, 247−289.
[13] L. Carlucci, G. Ciani, D. M. Proserpio, S. Rizzato, *Cryst. Eng. Commun.* **2003**, *5*, 190−199.
[14] L. Carlucci, G. Ciani, D. M. Proserpio, S. Rizzato, *Cryst. Eng. Commun.* **2002**, *4*, 121−129.
[15] M. J. Plater, M. R. St. J. Foreman, T. Gelbrich, S. J. Coles, M. B. Hursthouse, *J. Chem. Soc., Dalton Trans.* **2000**, 3065−3073.
[16] M. J. Plater, M. R. St. J. Foreman, T. Gelbrich, S. J. Coles, M. B. Hursthouse, *J. Chem. Soc., Dalton Trans.* **2000**, 1995−2000.
[17] B. Moulton, M. J. Zaworotko, *Chem. Rev.* **2001**, *101*, 1629−1658.
[18] S. R. Batten, R. Robson, *Angew. Chem. Int. Ed.* **1998**, *37*, 1460−1494; *Angew. Chem.* **1998**, *11*, 1558−1595.
[19] S. R. Batten, *Cryst. Eng. Commun.* **2001**, *18*, 1−7.
[20] K. A. Hirsch, S. R. Wilson, J. S. Moore, *Chem. Eur. J.* **1997**, *3*, 765−771.
[21] E. B. Rusanov, V. V. Ponomarova, V. V. Komarchuk, H. Stoeckli-Evans, E. Fernandes-Ibañes, F. Stoeckli, J. Sieler, K.

 © 2004 Wiley-VCH Verlag GmbH & Co. KGaA, Weinheim

V. Domasevitch, *Angew. Chem. Int. Ed.* **2003**, *42*, 2499−2501; Angew. Chem. **2003**, *22*, 2603−2605.
[22] V. V. Ponomarova, V. V. Komarchuk, I. Boldog, A. N. Chernega, J. Sieler, K. V. Domasevitch, *Chem. Commun.* **2002**, 436−437.
[23] I. Boldog, E. B. Rusanov, A. N. Chernega, J. Sieler, K. V. Domasevitch, *J. Chem. Soc., Dalton Trans.* **2001**, 893−897.
[24] I. Boldog, E. B. Rusanov, A. N. Chernega, J. Sieler, K. V. Domasevitch, *Polyhedron* **2001**, *20*, 887−897.
[25] I. Boldog, J. Sieler, K. V. Domasevitch, *Inorg. Chem. Commun.* **2003**, *6*, 769−772.
[26] I. Boldog, J. Sieler, A. N. Chernega, K. V. Domasevitch, *Inorg. Chim. Acta* **2002**, *338*, 69−77.
[27] Y. Garcia, O. Kahn, L. Rabardel, B. Chansou, L. Salmon, J. P. Tuchagues, *Inorg. Chem.* **1999**, *38*, 4663−4670.
[28] W. Vreugdenhil, J. G. Haasnoot, R. A. G. De Graaff, H. A. Nieuwenhuis, D. Reefman, J. Reedijk, *Acta Crystallogr., Sect. C* **1987**, *43*, 1527−1530.
[29] C. L. Zilverentant, W. L. Driessen, J. G. Haasnoot, J. J. A. Kolnaar, J. Reedijk, *Inorg. Chim. Acta* **1998**, *282*, 257−260.
[30] L. P. Wu, Y. Yamagiwa, T. Kuroda-Sowa, T. Kamikawa, M. Munakata, *Inorg. Chim. Acta* **1997**, *256*, 155−159.
[31] J.-F. Ma, J.-F. Liu, Y. Xing, H.-Q. Jia, Y.-H. Lin, *J. Chem. Soc., Dalton Trans.* **2000**, 2403−2407.
[32] J.-F. Ma, J. Yang, G.-L. Zheng, L. Li, J.-F. Liu, *Inorg. Chem.* **2003**, *42*, 7531−7534.
[33] P. C. M. Duncan, D. M. L. Goodgame, S. Menzer, D. J. Williams, *Chem. Commun.* **1996**, 2127−2128.
[34] L. Ballester, I. Baxter, C. M. Duncan, D. M. L. Goodgame, D. A. Grachvogel, D. J. Williams, *Polyhedron* **1998**, *17*, 3613−3623.
[35] D. A. McMorran, S. Pfadenhauer, P. J. Steel, *Aust. J. Chem.* **2002**, *55*, 519−522.
[36] J.-F. Ma, J.-F. Liu, Y. Xing, H.-Q. Jia, Y.-H. Lin, *New J. Chem.* **2000**, *24*, 759−763.
[37] X. Meng, Y. Song, H. Hou, Y. Fan, G. Li, Y. Zhu, *Inorg. Chem.* **2003**, *42*, 1306−1315.
[38] L.-F. Tang, Z.-H. Wang, J.-F. Chai, W.-L. Jia, Y.-M. Xu, J.-T. Wang, *Polyhedron* **2000**, *19*, 1949−1954.
[39] L.-F. Tang, Z.-H. Wang, J.-F. Chai, X.-B. Leng, J.-T. Wang, H.-G. Wang, *J. Organomet. Chem.* **2002**, *642*, 179−185.
[40] Effendy, F. Marchetti, C. Pettinari, R. Pettinari, B. W. Skelton, A. H. White, *Inorg. Chem.* **2003**, *42*, 112−117.
[41] B. Li, B. Li, X. Zhu, L. Zhu, Y. Zhang, *Acta Crystallogr., Sect. C* **2003**, *59*, 350−351.
[42] B. Li, Z. Xu, Z. Cao, L. Zhu, K. Yu, *Trans. Met. Chem.* **1999**, *24*, 622−627.
[43] Q. Zhao, H. Li, X. Wang, Z. Chen, *New J. Chem.* **2002**, *26*, 1709−1710.
[44] G. A. van Albada, R. C. Guijt, J. G. Haasnoot, M. Lutz, A. L. Spek, J. Reedijk, *Eur. J. Inorg. Chem.* **2000**, 121−126.
[45] Y. Garcia, P. J. van Koningsbruggen, H. Kooijman, A. L. Spek, J. G. Haasnoot, O. Kahn, *Eur. J. Inorg. Chem.* **2000**, 307−314.
[46] H. Hou, X. Meng, Y. Song, Y. Fan, Y. Zhu, H. Lu, C. Du, W. Shao, *Inorg. Chem.* **2002**, *41*, 4068−4075.
[47] P. Børsting, J. J. Steel, *Eur. J. Inorg. Chem.* **2004**, 376−380.
[48] P. J. van Koningsbruggen, Y. Garcia, G. Bravic, D. Chasseau, O. Kahn, *Inorg. Chim. Acta* **2001**, *326*, 101−105.
[49] J. Schweifer, P. Weinberger, K. Mereiter, M. Boca, C. Reichl, G. Wiesinger, G. Hilscher, P. J. van Koningsbruggen, H. Kooijman, M. Grunert, W. Linert, *Inorg. Chim. Acta* **2002**, *339*, 297−306.
[50] P. J. van Koningsbruggen, Y. Garcia, L. Fournès, H. Kooijman, A. L. Spek, J. G. Haasnoot, J. Moscovici, K. Provost, A. Michalowicz, F. Renz, P. Gütlich, *Inorg. Chem.* **2000**, *39*, 1891−1900.
[51] P. J. van Koningsbruggen, Y. Garcia, H. Kooijman, A. L. Spek, J. G. Haasnoot, O. Kahn, J. Linares, E. Codjovi, F. Varret, *J. Chem. Soc., Dalton Trans.* **2001**, 466−471.
[52] C. M. Grunert, J. Schweifer, P. Weinberger, W. Linert, K. Mereiter, G. Hilscher, M. Müller, G. Wiesinger, P. J. van Koningsbruggen, *Inorg. Chem.* **2004**, *43*, 155−165.
[53] M. F. Rudolf, R. Bronisz, Z. Ciunik, *Proc. XXXIII ICCC*, Florence, Italy, August 30 to September 4, **1998**, p. 111.
[54] R. Bronisz, PhD Thesis, Wroclaw University, Poland, **1999**.
[55] R. Bronisz, *Inorg. Chim. Acta* **2002**, *340*, 215−220.
[56] R. Bronisz, *Inorg. Chim. Acta* **2004**, *357*, 396−404.
[57] L. Wiehl, *Acta Crystallogr., Sect. B* **1993**, *49*, 289−303.
[58] R. Hinek, H. Spiering, D. Shollmeyer, P. Gütlich, A. Hauser, *Chem. Eur. J.* **1996**, *11*, 1427−1434.
[59] A. Ozarowski, B. R. McGarvey, *Inorg. Chem.* **1989**, *28*, 2262−2266.
[60] P. E. M. Wijnands, J. S. Wood, J. Reedijk, W. J. A. Maaskant, *Inorg. Chem.* **1996**, *35*, 1214−1222.
[61] T. Buchen, D. Schollmeyer, P. Gütlich, *Inorg. Chem.* **1996**, *35*, 155−161.
[62] J. Jeftic, R. Hinek, S. C. Capelli, A. Hauser, *Inorg. Chem.* **1997**, *36*, 3080−3087.
[63] J.-T. Yamaura, R. Kato, Y. Hagai, H. Saito, T. Hyodo, *Phys. Rev. B: Condens. Mat.* **1998**, *58*, 14098−14101.
[64] E. J. van den Heuvel, P. L. Franke, G. C. Verschoor, A. P. Zuur, *Acta Crystallogr., Sect. C* **1983**, *39*, 337−339.
[65] A. S. Lyakhow, P. N. Gaponik, M. M. Degtyarik, L. S. Ivashkevich, *Acta Crystallogr.* **2003**, *E59*, m38−m40.
[66] G. I. Koldobskii, V. A. Ostrovskii, *Russ. Chem. Rev.* **1994**, *10*, 797−814.
[67] M. Begtrup, P. Larsen, *Acta Chem. Scand.* **1990**, *44*, 1050−1057.
[68] H. Gallardo, E. Meyer, A. J. Bortoluzzi, F. Molin, A. Mangrich, *Inorg. Chim. Acta* **2004**, *357*, 505−512.
[69] N. I. Sushko, N. I. Makarevich, N. A. Matveeva, O. A. Ivashkevich, P. N. Gaponik, *Zh. Prikl. Spektrosk.* **1991**, *54*, 923−933.
[70] M. M. Degtyarik, P. N. Gaponik, V. N. Naunenko, A. I. Lesnikovich, M. V. Nikanovich, *Spectrochim. Acta* **1987**, *A43*, 349−353.
[71] K. Nakamoto, *Infrared and Raman spectra of Inorganic and Coordination Compounds*, 4th ed., Wiley, New York, **1986**.
[72] A. B. P. Lever, *Inorganic Electronic Spectroscopy*, 2nd ed., Elsevier, Amsterdam **1984**.
[73] P. L. Franke, W. L. Groeneveld, *Trans. Met. Chem.* **1981**, *6*, 54−56.
[74] Unpublished results.
[75] M. B. Zaman, M. D. Smith, D. M. Ciurtin, H.-K. zur Loye, *Inorg. Chem.* **2002**, *41*, 4895−4903.
[76] M. B. Zaman, K. Udachin, M. Akhtaruzzaman, Y. Yamashita, J. A. Ripmeester, *Chem. Commun.* **2002**, 2322−2323.
[77] T. Kamiya, Y. Saito, *Ger. Offen.* 2147023, **1973**.
[78] G. M. Sheldrick, *SHELXS-97, Program for solution of crystal structures*, University of Göttingen, **1997**.
[79] G. M. Sheldrick, *SHELXL-97, Program for crystal structure refinement*, University of Göttingen, **1997**.
[80] L. Spek, *Acta Crystallogr., Sect. A* **1990**, *46*, C34.
[81] O. V. Dolomanov, A. J. Blake, N. R. Champness, M. Schröder, *J. Appl. Crystallogr.* **2003**, *36*, 1283−1284.
[82] C. J. Kepert, M. J. Rosseinsky, *Chem. Commun.* **1999**, 375−376.

Received March 2, 2004
Early View Article
Published Online July 22, 2004

 © 2004 Wiley-VCH Verlag GmbH & Co. KGaA, Weinheim

Formation of Novel 1-D Chains by μ-Amido Bridging of Dinuclear Manganese(III)-Schiff Base Complexes

Manuel R. Bermejo,*[a] Ana M. González-Noya,[b] Víctor Abad,[a] M. Isabel Fernández,[b] Marcelino Maneiro,[b] Rosa Pedrido,[a] and Miguel Vázquez[a]

Keywords: Amides / Manganese / Schiff bases / 1-D chains

Three novel neutral manganese(III) complexes of stoichiometry Mn(R-amsal-3,5-di-*t*Bu)$(H_2O)_n$ [H_3-R-amsal-3,5-di-*t*Bu = 3-aza-4-(2-hydroxyphenyl)-*N*-(2-hydroxyphenyl)but-3-enamide; (R = H, 4-Me, 5-*t*Bu)] have been synthesised using potentially trianionic and pentadentate Schiff-base ligands containing an amide group. Complexes were thoroughly characterised by elemental analysis, FAB mass spectrometry, infrared spectroscopy, magnetic susceptibility measurements and molar conductivities. Recrystallisation of these complexes from methanol yielded single crystals of [Mn_2(amsal-3,5-di-*t*Bu)$_2$(MeOH)$_2$]$_n$ **1**, [Mn_2(4-Me-amsal-3,5-di-*t*Bu)$_2$-(MeOH)$_2$]$_n$ **2** and [Mn_2(5-*t*Bu-amsal-3,5-di-*t*Bu)$_2$(MeOH)$_2$]$_n$ **3** with methanol as solvate. Their X-ray characterisation shows that these complexes consist of infinite one-dimensional chains with a repeating cyclic dimeric unit, where the amide oxygen atom is bridging two neighbouring manganese(III) ions. Paramagnetic ^{1}H NMR spectroscopy confirmed the presence of Mn^{III} in these complexes, while the cyclic voltammetry studies suggest the possibility of obtaining polynuclear Mn^{IV} complexes with this kind of ligand.
(© Wiley-VCH Verlag GmbH & Co. KGaA, 69451 Weinheim, Germany, 2004)

Introduction

In recent years, considerable efforts have been focused on the synthesis and characterisation of polynuclear manganese complexes.[1] This is mainly because di- or multi-nuclear manganese sites involving oxygen or nitrogen donor ligands are important in the function of enzymes such as alkaline phosphatase,[2] pseudocatalases,[3] manganese-based superoxide dismutase (MnSOD)[4] and the oxygen evolving complex (OEC) of photosystem II.[5] Moreover, the synthetic complexes have been shown to exhibit a variety of interesting structural and physical properties.[6]

Recently, we have directed our attention to the coordination chemistry of manganese with Schiff bases containing amide groups. Our interest in this kind of ligands derives from the known ability of ligands containing amide groups to stabilise high oxidation states of metal ions when coordinated with the deprotonated nitrogen atom.[7–9]

Previously, we succeeded in stabilising the neutral Mn^{III} complexes[10] with ligands derived from H_3-amsal [H_3-amsal = 3-aza-4-(2-hydroxyphenyl)-*N*-(2-hydroxyphenyl)but-3-enamide] by two methods (an electrochemical synthesis and the Boucher procedure[11]). Nevertheless, the low solubilities of these complexes in most common solvents have prevented, until now, their structural characterisation by X-ray diffraction. The knowledge of such structures should improve understanding of ligand design and the synthesis of high oxidation state polymeric manganese complexes.

In order to establish the structural make-up of these complexes, we decided to investigate whether the introduction of *tert*-butyl groups on the aromatic rings of the Schiff base ligands would improve the solubility of the resulting complexes and allow structural characterisation. We have designed some new amide-derived Schiff base ligands in order to prepare novel manganese(III) complexes, and in this paper we report the results.

Results and Discussion

Synthesis and Characterisation of the Ligands

The new unsymmetrical Schiff base ligands reported in this study were prepared in a manner analogous (Scheme 1) with the three-step method to similar ligands described by us previously.[10]

The first step involves a carbodiimide amide coupling[12] of *N*-benzyloxycarbonylglycine with 2-hydroxyaniline, 2-hydroxy-4-methylaniline or 2-hydroxy-5-*tert*-butylaniline in THF. This reaction proceeds in excellent yield (see Exp. Sect.) and large quantities of amides **1a**, **1b** or **1c** can be

[a] Departamento de Química Inorgánica, Facultade de Química, Universidade de Santiago de Compostela, 15782 Santiago de Compostela, Spain
[b] Departamento de Química Inorgánica, Facultade de Ciencias, Universidade de Santiago de Compostela, 27002 Lugo, Spain
Fax: (internat.) +34-981-597-525
E-mail: qimb45@usc.es

 © 2004 Wiley-VCH Verlag GmbH & Co. KGaA, Weinheim **DOI: 10.1002/ejic.200400198**

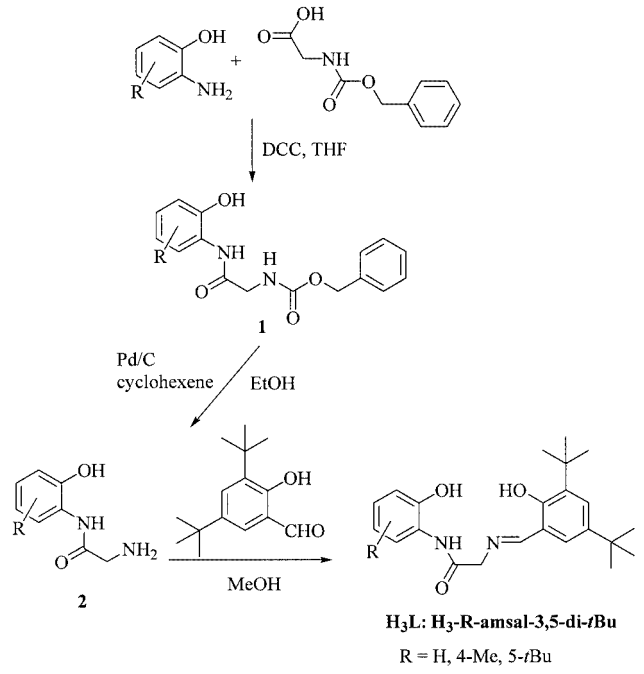

Scheme 1. Reaction diagram for the preparation of the Schiff−base ligands

prepared. The second step involves the removal of the *Z* protecting group from the amine functionality by sacrificial hydrogenation using cyclohexene and palladium on charcoal as the catalyst.[13] This methodology yielded the desired amines **2a**, **2b** or **2c** in high yield and with high purity. Amines **2a**, **2b** and **2c** were then employed as the precursors of the new ligands via conventional condensation reactions with a commercially available substituted salicylaldehyde. The obtained Schiff bases were satisfactorily characterised by elemental analysis, mass spectrometry (Table 1), ^{1}H NMR (Table 2), ^{13}C NMR and IR (Table 3) spectroscopy.

Mass Spectrometry, NMR and IR Spectroscopy

The mass spectra of the ligands each show the peak for H_3L^+ at 100% intensity (see Table 1), in accord with the proposed formulae.

The ^{1}H NMR spectroscopic data for the ligands are shown in Table 2. The spectra of H_3-R-amsal-3,5-di-*t*Bu, recorded using [D$_6$]DMSO as solvent, exhibit a singlet at $\delta \approx 8.6$ ppm assigned to the imine hydrogen atom, corroborating the formation of C=N bonds. The aromatic protons lie in the range $\delta = 6.50-8.03$, while the presence of a singlet at $\delta \approx 4.5$ indicates the presence of the methylene group. Furthermore, all spectra show three singlets in the region of 9.21−13.79 that disappear on deuteration. The peak at higher field was assigned to the NH proton while the two signals at lower field correspond to the OH protons. The spectra of these Schiff bases also show two singlets (for H_3-amsal-3,5-di-*t*Bu and H_3-4-Me-amsal-3,5-di-*t*Bu) or three singlets (for H_3-5-*t*Bu-amsal-3,5-di-*t*Bu) in the range $\delta = 1.2-1.4$, indicating the presence of two or three non-equivalent *tert*-butyl groups, respectively.

Table 1. Analytical and other selected data for the ligands

Ligand	Yield	Colour	M.p. (°C)	MS-EI (*m*/*z*)	Analysis (%)[a] C	H	N
H_3-amsal-3,5-di-*t*Bu	85%	pale yellow	176	382	72.0 (72.3)	8.0 (7.9)	7.2 (7.3)
H_3-4-Me-amsal-3,5-di-*t*Bu	84%	white	172	396	72.6 (72.7)	8.2 (8.1)	7.1 (7.1)
H_3-5-*t*Bu-amsal-3,5-di-*t*Bu	87%	white	240	438	73.9 (74.0)	8.8 (8.7)	6.4 (6.4)

[a] Found (calculated).

Table 2. ^{1}H NMR spectroscopic data for the ligands in [D$_6$]DMSO

Ligand[b]	Proton[a] (a)	(b)	(c)	(d)	(e)	H_{arom}
H_3-amsal-3,5-di-*t*Bu	9.91 (br)	9.30 (s)	4.51 (s)	8.63 (s)	13.70 (s)	6.71−8.03
H_3-4-Me-amsal-3,5-di-*t*Bu[c]	9.73 (br)	9.21 (s)	4.51 (s)	8.52 (s)	13.72 (s)	6.50−7.81
H_3-5-*t*Bu-amsal-3,5-di-*t*Bu[d]	9.71 (s)	9.30 (s)	4.52 (s)	8.64 (s)	13.79 (s)	6.73−7.92

[a] See Scheme 2 for atom labelling. [b] Ligands show two singlets at $\delta \approx 1.3$ and 1.4 assigned to the *tert*-butyl groups. [c] Includes a singlet at $\delta = 2.10$ assigned to the methyl group. [d] Includes a singlet at $\delta = 1.20$ assigned to the *tert*-butyl group.

Table 3. Selected IR bands (in cm^{-1}) for the ligands

Ligand	ν(OH)	ν(NH)	ν(amide I)	ν(CN)	ν(amide II)
H_3-amsal-3,5-di-*t*Bu	3369 (m)	3104 (br)	1657 (s, br)	1639 (sh)	1595 (m)
H_3-4-Me-amsal-3,5-di-*t*Bu	3381 (m)	3105 (br)	1662 (vs)	1633 (s)	1603 (m)
H_3-5-*t*Bu-amsal-3,5-di-*t*Bu	3385 (m)	3115 (br)	1661 (m)	1628 (vs)	1585 (m)

 © 2004 Wiley-VCH Verlag GmbH & Co. KGaA, Weinheim

The ^{13}C NMR spectra of the ligands in [D_6]DMSO show signals corresponding to the aromatic carbon atoms (between δ = 115 and 160 ppm), a signal due to the imine carbon atom (around 165 ppm) and a resonance assigned to the carbonyl carbon atom (around 168 ppm). Additionally, the methylene carbon and the methyl and *tert*-butyl groups, where appropriate, give signals below δ = 70 ppm.

The most significant IR bands for the ligands are recorded in Table 3. They have been assigned by comparison with the IR spectra of the amine precursors and on the basis of our knowledge in this field.[10a]

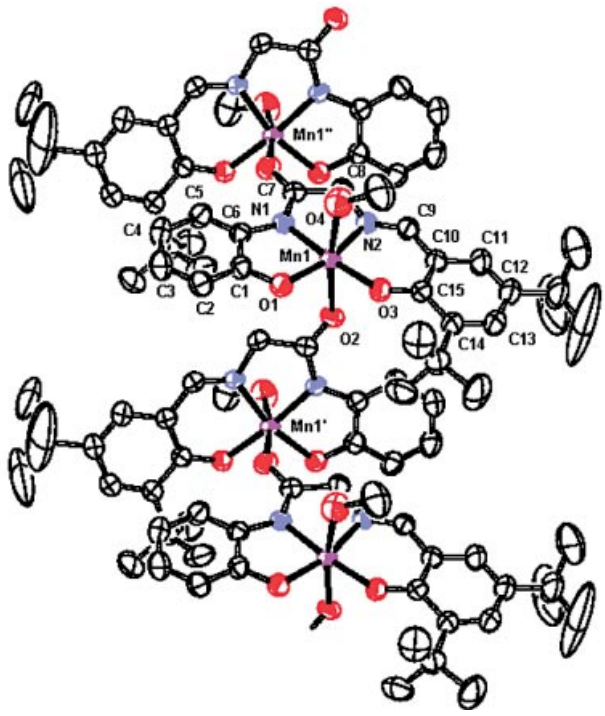

Figure 1. An ORTEP view of the crystal structure of [Mn_2(amsal-3,5-di-*t*Bu)$_2$(MeOH)$_2$]$_n$ **1**; ellipsoids are drawn at 50% probability; symmetry operations: ′: $-x + 1$, $y - 1/2$, $-z + 1/2$; ′′: $-x + 1$, $y + 1/2$, $-z + 1/2$

Synthesis and Characterisation of Manganese Complexes

The manganese complexes were prepared following a variation of the Boucher method reported by us.[10c,14]

The brown powdery solid compounds were obtained in high yield via this synthetic route, and appear to be stable in the solid state and in solution. They are moderately soluble in common organic solvents and soluble in polar aprotic coordinating solvents such as DMF and DMSO.

Elemental analyses indicate that these manganese complexes have the general stoichiometry Mn(R-amsal-3,5-di-*t*Bu)(H_2O)$_4$, suggesting that they are neutral manganese(III) species in which the ligands are tri-deprotonated. Molar conductivity measurements in 10^{-3} M DMF solutions, in the range 3−9 μS cm^{-1}, show the non-electrolytic behaviour of these complexes.[15]

Mass Spectrometry and IR Spectroscopy

Fast atom bombardment (FAB) mass spectra contain peaks relating to fragments of the form $[MnL]^+$, indicating ligand coordination to the metal centre. Furthermore, these

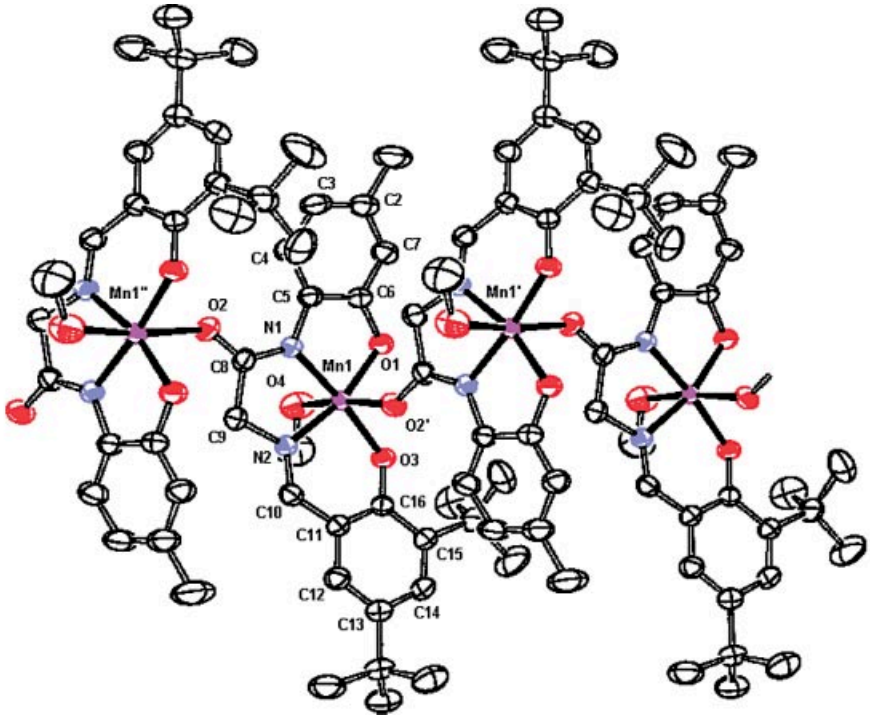

Figure 2. An ORTEP view of the crystal structure of [Mn_2(4-Me-amsal-3,5-di-*t*Bu)$_2$(MeOH)$_2$]$_n$ (**2**); ellipsoids are drawn at 50% probability; symmetry operations: ′: $-x + 1$, $y + 1/2$, $-z + 1/2$; ′′: $-x + 1$, $y - 1/2$, $-z + 1/2$

 © 2004 Wiley-VCH Verlag GmbH & Co. KGaA, Weinheim

spectra exhibit peaks due to the fragment $[Mn_2L_2]^+$, which can be attributed tentatively to the presence of dimeric/polymeric species in the solid state.

The ligand coordination to the metal centre is also supported by the IR spectra, which are very similar for all the complexes. Thus, a band at about 1620 cm^{-1}, attributable to ν(CN), shifted to lower energy compared with the free ligands values, indicating the coordination of the ligand to the metal through the imine nitrogen atom. This ν(CN) band is strong and broad and it obscures the amide I and amide II bands. Additionally, bands centred at ca. 3400 cm^{-1} can be observed in these spectra, in accordance with the presence of coordinated and/or lattice water or methanol.

Finally, the absence of a strong band at ca. 1100 cm^{-1} confirms the absence of perchlorate anions in these manganese complexes.

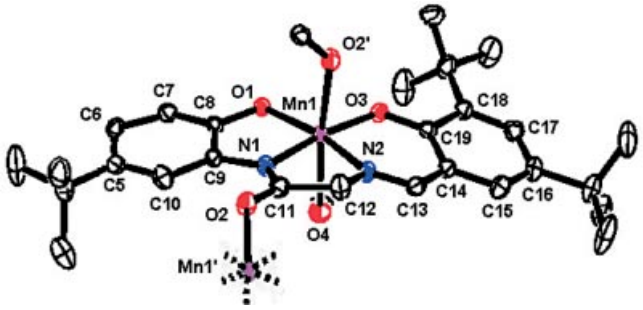

Figure 3. An ORTEP view of the environment around the manganese centre for $[Mn_2(5\text{-}t\text{Bu-amsal-3,5-di-}t\text{Bu})_2(MeOH)_2]_n$ (**3**); ellipsoids are drawn at 50% probability

X-Ray Diffraction Studies

Crystal Structures of Complexes 1, 2 and 3

Single crystals of $[Mn_2(amsal\text{-}3,5\text{-di-}t\text{Bu})_2(MeOH)_2]_n$ (**1**), $[Mn_2(4\text{-Me-amsal-}3,5\text{-di-}t\text{Bu})_2(MeOH)_2]_n$ (**2**) and $[Mn_2(5\text{-}t\text{Bu-amsal-}3,5\text{-di-}t\text{Bu})_2(MeOH)_2]_n$ (**3**) suitable for X-ray diffraction studies were grown as detailed in the Exp. Sect. These analyses show that **1**, **2** and **3** have similar structures that consist of a polymeric chain of repeating dimeric units. These dimeric units contain two ligand units, two manganese centres and two molecules of methanol. Furthermore, complexes **1**, **2** and **3** contain methanol as solvate. Complexes **1** and **2** crystallise in the orthorhombic space group *Pbca*, while complex **3** crystallises in the monoclinic space group *C*2/*c*. The ORTEP diagrams for **1** and **2** are shown in Figure 1 and Figure 2, respectively. The ORTEP view of the environment of the manganese atom for complex **3** is shown in Figure 3. Experimental details are given in Table 4 and selected bond lengths and angles in Table 5.

The geometry around each Mn atom can be described as distorted octahedral, where the trianionic and pentadentate ligand coordinates the Mn^{III} centre with the two phenol O-atoms [O(1), O(3)], the imine N-atom [N(2)] and the amide N-atom [N(1)] occupying the equatorial positions (see Figure 3). The coordination sphere around each manganese centre is then completed by a capping methanol molecule [O(4)] and an amide O-atom [O(2′)] from the neighbouring complex molecule. Thus, the amide oxygen atom [O(2)] of one ligand is coordinated to the manganese ion of the neighbouring molecule, acting as a bridge, which generates an infinite one-dimensional chain $Mn-O_{amide}(L)-Mn-O'_{amide}(L)$ resulting in a Mn···Mn distance of 6.064 Å for **1**, 6.120 Å for **2**, and 6.035 Å for **3**.

Table 4. Crystal data and details of refinement for the complexes **1**, **2** and **3**

	1	**2**	**3**
Empirical formula	$C_{25}H_{34}MnN_2O_5$	$C_{26}H_{36}MnN_2O_5$	$C_{29}H_{43}MnN_2O_5$
Molecular mass	497.49	511.52	554.59
Temperature [K]	293(2)	293(2)	110(2)
Wavelength [nm]	0.71073	0.71073	0.71073
Crystal system	orthorhombic	orthorhombic	monoclinic
Space group	*Pbca*	*Pbca*	*C*2/*c*
a [Å]	18.653(3)	19.572(3)	37.646(10)
b [Å]	8.8588(14)	8.8073(12)	7.2783(19)
c [Å]	32.470(6)	32.192(4)	23.023(6)
α [°]	90.00	90.00	90.00
β [°]	90.00	90.00	108.256(5)
γ [°]	90.00	90.00	90.00
Z	8	10	8
Absorption coefficient [mm^{-1}]	0.513	0.511	0.478
Crystal size [mm^3]	0.82 × 0.42 × 0.06	0.44× 0.33 × 0.18	0.13 × 0.17 × 0.13
Reflections collected	29618	34239	18487
Independent reflections	5928 [*R*(int) = 0.0577]	6310 [*R*(int) = 0.0537]	6759 [*R*(int) = 0.0344]
Final *R* int [$I > 2\sigma(I)$]	*R*1 = 0.0711	*R*1 = 0.0447	*R*1 = 0.0525
	*wR*2 = 0.1818	*wR*2 = 0.1225	*wR*2 = 0.1044
R int (all data)	*R*1 = 0.1302	*R*1 = 0.0910	*R*1 = 0.1173
	*wR*2 = 0.2237	*wR*2 = 0.1662	*wR*2 = 0.1299

 © 2004 Wiley-VCH Verlag GmbH & Co. KGaA, Weinheim

Table 5. Selected bond lengths [Å] and angles [°] for the complexes **1**, **2** and **3**

	1	**2**	**3**
$Mn1-O3_{phenol}$	1.881(3)	1.8913(18)	1.875(2)
$Mn1-O1_{phenol}$	1.916(3)	1.9198(19)	1.930(2)
$Mn1-N1_{amide}$	1.939(4)	1.942(2)	1.933(3)
$Mn1-N2_{imine}$	1.964(4)	1.963(2)	1.958(3)
$Mn1-O2'_{amide}$	2.321(3)	2.349(2)	2.242(3)
$Mn1-O4_{methanol}$	2.275(5)	2.281(2)	2.270(4)
$O2=C_{amide}$	1.247(6)	1.247(3)	1.248(4)
Mn1···Mn1′	6.064	6.120	6.035
O3−Mn1−O1	103.33(15)	104.01(8)	104.35(10)
O1−Mn1−N1	82.87(15)	83.31(9)	83.44(11)
O3−Mn1−N2	92.15(16)	91.21(9)	91.36(11)
N1−Mn1−N2	81.64(16)	81.48(9)	80.84(12)
O4−Mn1−O2′	171.60(17)	173.34(8)	173.93(9)

It is well known that Mn^{III} complexes are able to form dimeric or polymeric species through different coordinative bridges:[14,16] μ-Oxo, μ-phenoxo, μ-aquo, μ-carboxylate, μ-cyanide, μ-thiocyanate, etc. μ-oxo and μ-phenoxo bridges generate dimeric structures; μ-carboxylate, μ-cyanide and μ-thiocyanate usually yield polymeric species, while the μ-aquo ligand can generate both dimeric or polymeric structures. The distance Mn···Mn for the complexes reported herein are longer than the corresponding distances in μ-oxo, μ-phenoxo or μ-aquo Mn^{III} complexes, and shorter than the distances found for μ-carboxylate Mn^{III} complexes. On the other hand, ionic metal(II) complexes with amide ligands where oxygen amide atoms behave as bridges have been reported.[17] However, to the best of our knowledge, the type of compound reported in the present case, with Mn^{III}, has not been described previously in the literature.

The bond distances in the equatorial plane Mn−N [ranging from 1.933 to 1.964 Å] and Mn−O [in the range 1.875−1.930 Å] are typical of manganese(III) complexes[16,18] and corroborate complete deprotonation of the ligands. The distances $Mn-O4_{methanol}$ [2.270−2.281 Å] are in agreement with other previous results,[18] and are longer than the axial distances $Mn-O2'_{amide}$, except for complex **3**. The distances $O2=C_{amide}$ (ca. 1.247) are longer than those found for the related free ligands (ca. 1.235),[10a] as expected. The axial Mn−O distances are considerably longer than the equatorial Mn−O bond lengths quoted above, indicating that the Jahn−Teller elongation expected for a high-spin d^4 manganese(III) ion is present along the chain of these polymers.

The deviation from an ideal octahedral geometry is also revealed by the range of angles observed around the metal centre [from 80.84 to 104.35°], as well as by the interaxial angle O4−Mn1−O2′ of ca. 173°. The slight deviation of the equatorial plane from planarity further reinforces this distortion (maximum deviation from the calculated least-squares plane formed by O1, N1, N2 and O3 is ca. 0.004 Å for **1**, 0.009 Å for **2** and 0.025 Å for **3**, with the manganese atoms lying out of this plane by ca. 0.011 Å for **1**, 0.006 Å for **2** and 0.025 Å for **3**). These planes also present a gauche conformation.

These ligands are expected to show a high degree of planarity owing to the conjugation and presence of only one sp^3 atom in the chelate rings (named as C8 for **1**, C9 for **2** and C12 for **3** in Figures 1, 2 and 3, respectively). In fact, the angles between calculated chelate planes present values of 0.81° and 4.43° for **1**, 2.90° and 7.68° for **2**, and the highest values for **3** (10.87° and 14.91°).

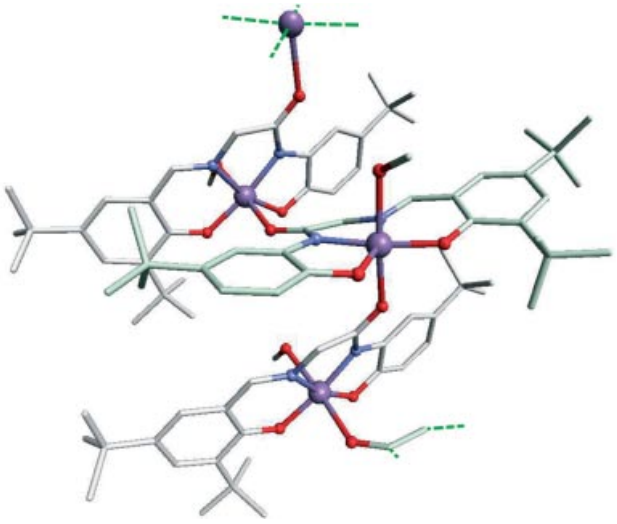

Figure 4. Part of the polymeric 1−D chain of **3**, showing the zigzag disposition of the manganese centres (in violet)

It is interesting to note that these infinite chains are not linear (see Figure 4), as the manganese atoms are situated in a zigzag arrangement. The angles between neighbouring manganese atoms (Mn1′−Mn1−Mn1′′) are 93.85° for **1**, 92.03° for **2** and 74.17° for **3**. The head-to-tail arrangement of the ligands allows coordination of the amide oxygen atom of each unit to the metal ion of the next unit in the chain.

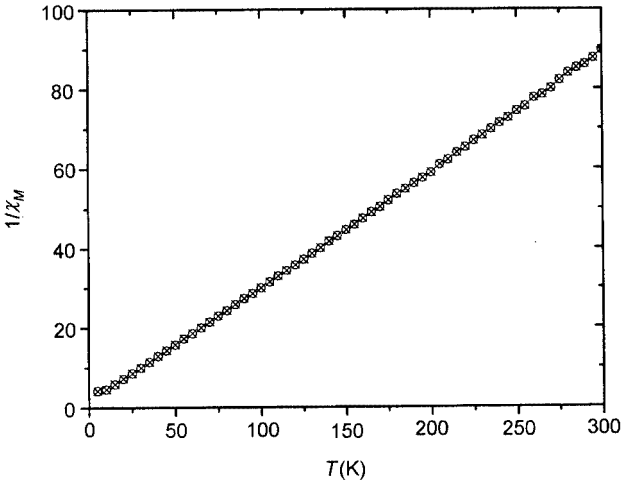

Figure 5. Thermal dependence of $1/\chi_M$ for **2**

 © 2004 Wiley-VCH Verlag GmbH & Co. KGaA, Weinheim

Magnetic Studies

The study of room temperature magnetic properties for the complexes shows that their magnetic moments (see Exp. Sect.) are all close to the spin-only value of 4.9 BM, expected for a magnetically dilute octahedral high-spin d^4 manganese(III) ion.

Variable temperature magnetic susceptibility of the complexes were measured in the temperature range 5−300 K using a small applied field of 5000 G. Plots of the reciprocals of the magnetic susceptibilities against absolute temperature are linear, so that all the complexes obey the Curie−Weiss law. An example is shown in Figure 5 for complex **2**.

The magnetic behaviours of complexes **1**, **2** and **3** are identical and can be illustrated by the thermal variation of the $\chi_M T$ versus T plot for complex **2** as in Figure 6. The $\chi_M T$ product is practically constant in the 300−100 K range with an observed value (3.34 ± 0.3 $cm^3\ mol^{-1}\ K$) corresponding to the value expected for an isolated high-spin Mn^{III} cation. On further reduction of the temperature, this value decreases smoothly down to 2.99 $cm^3\ mol^{-1}\ K$ at 30 K, and then more steeply to reach a value of 1.17 $cm^3\ mol^{-1}\ K$ at 5 K.

We attempted theoretical calculations to reproduce, and for comparison with, the experimental results. For an infinite chain of 4/2 local spins the simpler analytical expression that may be used to fit the experimental data derives from Fisher's expression:[19]

$\chi T = [Ng^2\beta^2 S(S + 1)/3k][(1 + u)/(1 - u)]$ where
$u = \coth[-2JS(S + 1)/kT] - [kT/-2JS(S + 1)]$

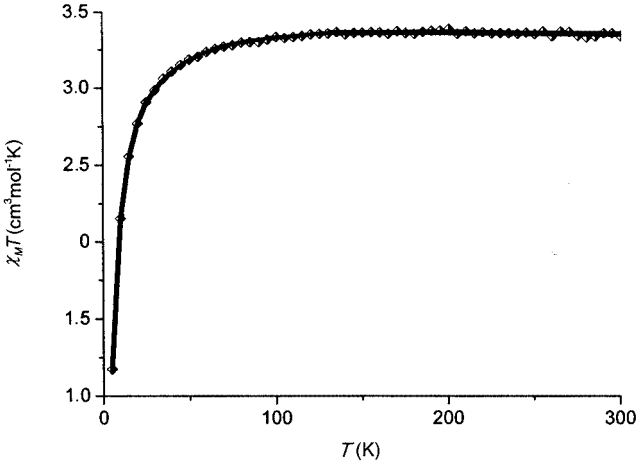

Figure 6. Thermal dependence of $\chi_M T$ for **2**; the full line (−) corresponds to the best data fit

The best agreement between experimental and calculated data from 300 to 5 K corresponds to $J = -0.3\ cm^{-1}$ and $g = 2.05$ with an agreement factor R ($= \Sigma[(\chi_M T)_{obsd.} - (\chi_M T)_{calcd.}]^2/\Sigma[(\chi_M T)_{obsd.}]^2$) of $3.4.10^{-4}$.

This study indicates little or no antiferromagnetic interaction between neighbouring metal centres in the solid state. Therefore, we can interpret the magnetic properties of these Mn^{III} polymer complexes as ordinary paramagnetic[19] and this is in agreement with the intermolecular Mn···Mn distances of about 6 Å.

^{1}H NMR Spectroscopy

Paramagnetic ^{1}H NMR spectra for the complexes were recorded in [D_6]DMSO at room temperature. The data are presented in Table 6.

The spectra obtained for these complexes contain three or four proton resonances that lie outside the diamagnetic region (δ = 0−14). The interpretation of these data is based on the findings of Pecoraro and co-workers[21] and also on our own results[10a,10b,22] for other Mn^{III} complexes with related Schiff base ligands. The protons *ortho* to the ring position occupied by a Mn-coordinated atom H3′, H6 and H6′ (see Scheme 2), were not observed.

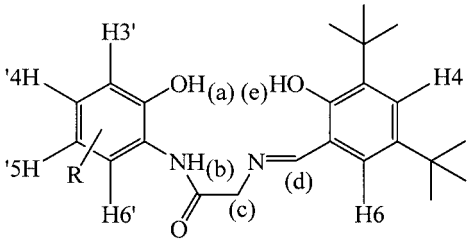

Scheme 2. Hydrogen atom labelling of the ligands for the ^{1}H NMR studies

Two or three relatively sharp peaks are observed upfield between δ = −14 and −32 ppm, which we have assigned to the H4 protons of the aldehyde and to H4′ and H5′ protons of the amine.[10a,10b,21,22] The comparison between the spec-

Table 6. ^{1}H NMR and electrochemical data for the complexes

Complex	^{1}H NMR H4	H4′	H5′	$-CH_2-$	Redox potentials[a] E_{ox}/V	E_{red}/V	Peak
1	−31.95	−14.80	−25.90	35.90	−	−0.278	R1
					0.778	−	O2
2	−31.50	na[b]	−27.08	34.46	−	−0.282	R1
					0.690	−	O2
3	−32.07	−18.42	na	30.42	−	−0.286	R1
					0.700	0.602	O2,R2

[a] Potentials *vs.* SCE. [b] na = not applicable.

 © 2004 Wiley-VCH Verlag GmbH & Co. KGaA, Weinheim

tra of these three complexes, with substitution of the H4′ and H5′ positions of the amine ring, provides an indication of the appropriate assignments. Clearly the upfield peaks at $\delta \approx -32$ correspond to the H4 protons. The features at $\delta = -14.80$ and -18.42 arise from H4′ protons, while the downfield resonances at $\delta = -25.90$ and -27.08 arise from H5′ protons.

Additionally, one broad peak observed downfield ($\delta = 30-36$) can be assigned to the aliphatic protons in the methylene bridge between the imine and amide nitrogen atoms.

It is well known that high-spin Mn^{III} complexes in an octahedral field show isotropically shifted ^1H NMR spectra arising from ligand protons.[23] Therefore, the data obtained from these NMR studies serve to corroborate the formation of these novel manganese(III) complexes.

Electrochemical Behaviour of the Complexes

Cyclic voltammograms of all the complexes were obtained from dimethylformamide solutions at slow scan rates of 0.02 V s^{-1} over a potential range from +1 to −1 V. The numerical data are given in Table 6 and a typical voltammogram is shown in Figure 7.

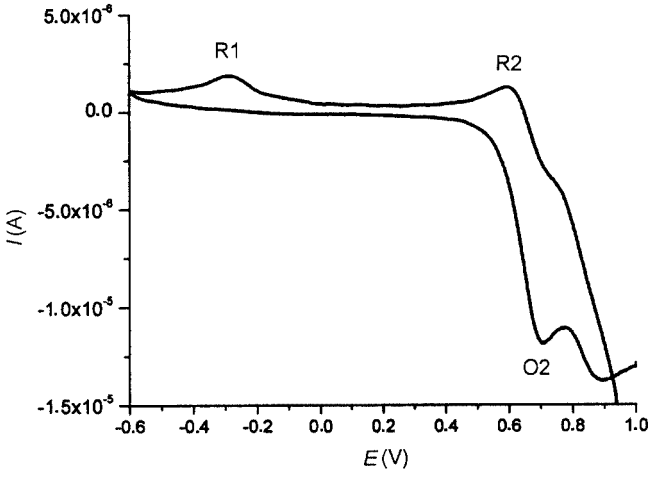

Figure 7. Cyclic voltammetry for **3**

All the complexes behave similarly. All voltammograms display an irreversible process at negative potentials (quoted as R1 in Table 6), which we assign to the reduction of manganese(III) to manganese(II).[14,24]

On the other hand, a second redox process assigned to the oxidation of manganese(III) to manganese(IV) is present at positive potentials for all the complexes (quoted as O2 in Table 6). This redox wave is irreversible for **1** and **2**, but for **3** presents an important rate of reversibility (R2, see Figure 7).

It is interesting to note that the presence of the methyl or *tert*-butyl groups on the aromatic ring of the amine precursor decreases this oxidation potential as it does with related ligands.[25] Hence, it seems obvious that manganese(IV) could be stabilised by this kind of ligand, containing hard donor atoms, especially if an electron-donating substituent were to be introduced.[7a,7b,8a,8b]

We found that the complexes exhibit low current intensities in their redox waves. This behaviour is attributed to the polymeric nature of these complexes, which results in a lower diffusion coefficient.[26]

Conclusion

Self-assembly of manganese ions with the novel unsymmetrical and potentially trianionic pentadentate amide group-containing Schiff base ligands, leads to neutral, polymeric manganese(III) complexes. The X-ray crystal structures of these complexes show that the oxygen amide atom of these ligands can act as a bridge between neighbouring manganese atoms and afford zigzag one-dimensional chains, previously unreported for manganese(III) ions. In addition, the observations reported here could be helpful for the study of biological systems, in which relatively weak but cooperative interactions between sets of metal ions and linked amide groups are present.

Finally, it seems that this kind of ligand is suitable for stabilization of Mn^{III} complexes, and could have potential in the synthesis of polynuclear Mn^{IV} complexes.

Experimental Section

General: Starting materials were purchased from Aldrich except manganese(II) perchlorate hexahydrate (Fluka) and cyclohexene (Panreac) and were used without further purification.
Elemental analyses were performed on a Carlo Erba EA 1108 analyser. NMR spectra were recorded on a Bruker WM-250 spectrometer using [D_6]DMSO as solvent; δ = chemical shift in ppm; s = singlet, d = doublet, t = triplet, m = multiplet, br = broad. Infrared spectra were recorded as KBr pellets on a Bruker UFS-66V spectrophotometer in the range 4000−600 cm^{-1}. The bands are reported as: vs = very strong, s = strong, m = medium, w = weak, sh = shoulder, and br = broad. Mass spectrometry (Electronic Impact) was performed on a Hewlett−Packard 5988A mass spectrometer, whilst fast atom bombardment (FAB) was done on a Micromass AutoSpec mass spectrometer, employing *m*-nitrobenzyl alcohol as the matrix. Magnetic susceptibility measurements in the 5−300 K temperature range were performed using a SQUID magnetometer operating at 5000 G. Room temperature magnetic susceptibilities were measured using a Digital Measurement system MSB-MKI, calibrated using tetrakis(isothiocyanato)cobaltate(II). Conductivities were obtained at 25 °C from 10^{-3} M solutions in DMF on a Philips PW9526 instrument. Cyclic voltammetry was performed by using an EG&G PAR model 273 potentiostat, controlled by the EG&G PAR model 270 software, in conjunction with a three-electrode cell, fitted with a purge gas inlet and outlet, consisting of a graphite disc working-electrode, a saturated calomel reference electrode and a platinum auxiliary electrode. Voltammograms were obtained from ca. 10^{-3} M dimethylformamide solutions of the metal complexes containing 0.1 M tetraethylammonium perchlorate as supporting electrolyte.

 © 2004 Wiley-VCH Verlag GmbH & Co. KGaA, Weinheim

Syntheses

Preparation of Schiff Base Ligands: Ligands were prepared according to a three-step method previously reported by us[10] and which is shown in Scheme 1.

First Step. Synthesis of Precursors 1a, 1b and 1c

***N*-(2-Hydroxyphenyl)-2-[(phenylmethoxy)carbonylamino]ethanamide (1a):** 2-Hydroxyaniline (2.61 g, 23.9 mmol) and a slight excess of *N*,*N*′-dicyclohexylcarbodiimide (5.3 g, 25.7 mmol) was added to a solution of *N*-benzyloxycarbonylglycine (5 g, 23.9 mmol) in THF (100 mL). This mixture was stirred at room temperature for four hours.[12] The insoluble *N*,*N*′-dicyclohexylurea was removed by filtration and the solvent replaced by ethyl acetate (100 mL). Addition of petroleum ether (b.p. 40−60 °C) afforded 6.46 g (90%) of the amine **1a**. M.p. 172 °C. ^{1}H NMR (250 MHz, [D$_6$]DMSO): δ = 4.06 (d, 2 H), 5.30 (s, 2 H), 6.96 (m, 1 H), 7.56 (m, 5 H), 7.91 (t, 1 H), 8.09 (d, 1 H), 9.31 (s, 1 H), 10.09 (s, 1 H) ppm. IR (KBr): $\tilde{\nu}$ = 3392 (s, OH), 3270 and 3075 (both s, NH), 1677 (vs, amide I), 1618 (s, amide II) cm^{-1}. EI-MS: *m*/*z* = 300.1. $C_{16}H_{16}N_2O_4$ (300.0): calcd. C 64.0, H 5.4, N 9.3; found C 64.1, H 5.5, N 9.4.

***N*-(2-Hydroxy-4-methylphenyl)-2-[(phenylmethoxy)carbonylamino]-ethanamide (1b):** Preparation as described above, using 2-hydroxy-4-methylaniline (2.95 g, 23.9 mmol). Yield 6.78 g (90%). M.p. 185 °C. ^{1}H NMR (250 MHz, [D$_6$]DMSO): δ = 2.43 (s, 3 H), 4.07 (d, 2 H), 5.30 (s, 2 H), 6.82 (d, 1 H), 6.92 (s, 1 H), 7.60 (m, 5 H), 7.94 (t, 1 H), 7.97 (s, 1 H), 9.30 (s, 1 H), 9.99 (s, 1 H) ppm. IR (KBr): $\tilde{\nu}$ = 3392 (s, OH), 3269 and 3076 (both s, NH), 1677 (vs, amide I), 1618 (s, amide II) cm^{-1}. EI-MS: *m*/*z* = 314.1. $C_{17}H_{18}N_2O_4$ (314.0): calcd. C 65.0, H 5.8, N 8.9; found C 65.1, H 6.0, N 9.1.

***N*-(2-Hydroxy-5-*tert*-butylphenyl)-2-[(phenylmethoxy)carbonylamino]ethanamide (1c):** Preparation as described above, using 2-hydroxy-5-*tert*-butylaniline (3.95 g, 23.9 mmol). Yield 6.4 g (75%). M.p. 185 °C. ^{1}H NMR (250 MHz, [D$_6$]DMSO): δ = 1.30 (s, 9 H), 3.88 (d, 2 H), 5.09 (s, 2 H), 6.80 (d,1 H), 6.96 (d, 1 H), 7.37 (m, 5 H), 7.71 (t, 1 H), 7.92 (s, 1 H), 9.15 (s, 1 H), 9.66 (s, 1 H) ppm. IR (KBr): $\tilde{\nu}$ = 3390 (s, OH), 3268 (s, NH), 3077 (m, NH), 1678 (vs, amide I), 1617 (s, amide II) cm^{-1}. EI-MS: *m*/*z* = 356.1. $C_{20}H_{24}N_2O_4$ (356.0): calcd. C 67.4, H 6.8, N 7.9; found C 67.5, H 6.9, N 7.8.

Second Step. Synthesis of precursors 2a, 2b and 2c

2-Amino-*N*-(2-hydroxyphenyl)ethanamide (2a): A solution of **1a** (2 g, 6.7 mmol) in ethanol (100 mL) was mixed with cyclohexene (5 mL, in excess to the molar proportion required) and commercial 10% Pd−C catalyst (0.50 g; catalyst:substrate ratio 1:4 by weight).[13] The mixture was refluxed for 15 min. The catalyst was removed by filtration and washed with ethanol, and the combined filtrates were evaporated under reduced pressure to give the deprotected amine **2a**. Yield 1.05 g (95%). M.p. 148 °C. ^{1}H NMR (250 MHz, [D$_6$]DMSO): δ = 3.26 (s, 2 H), 6.77 (m, 1 H), 6.88 (s, 1 H), 6.89 (s, 1 H), 8.18 (d, 1 H) ppm. IR (KBr): $\tilde{\nu}$ = 3431 (s, OH), 3420 and 3252 (both s, NH$_2$), 3083 (s, br, NH), 1649 (vs, amide I), 1614 (s, amide II) cm^{-1}. EI-MS: *m*/*z* = 166.0. $C_8H_{10}N_2O_2$ (166.0): calcd. C 57.8, H 6.1, N 16.9; found C 57.5, H 6.2, N 16.6.

2-Amino-*N*-(2-hydroxy-4-methylphenyl)ethanamide (2b): Preparation as described above, using **1b** (2 g, 6.36 mmol). Yield 1.09 g (95%). M.p. 175 °C. ^{1}H NMR (250 MHz, [D$_6$]DMSO): δ = 2.12 (s, 3 H), 3.17 (s, 2 H), 6.49 (d, 1 H), 6.61 (d, 1 H), 7.49 (d, 1 H) ppm. IR (KBr): $\tilde{\nu}$ = 3356 (s, OH), 3278 (s, NH$_2$), 3046 (s, br, NH), 1655 (vs, amide I), 1606 (s, amide II) cm^{-1}. EI-MS: *m*/*z* = 180.1. $C_9H_{12}N_2O_2$ (180.0): calcd. C 60.0, H 6.7, N 15.6; found C 60.3, H 6.9, N 15.5.

2-Amino-*N*-(2-hydroxy-5-*tert*-butylphenyl)ethanamide (2c): Preparation as described above, using **1c** (2 g, 5.61 mmol) Yield 1 g (80%). M.p. 210 °C. ^{1}H NMR (250 MHz, [D$_6$]DMSO): δ = 0.91 (s, 9 H), 3.12 (s, 2 H), 6.55 (d, 1 H), 6.69 (d, 1 H), 8.03 (s, 1 H) ppm. IR (KBr): $\tilde{\nu}$ = 3380 (vs, OH), 3270 (vs, NH$_2$), 3065 (m, NH), 1650 (vs, amide I), 1610 (s, amide II) cm^{-1}. EI-MS: *m*/*z* = 222.1. $C_{12}H_{18}N_2O_2$ (222.0): calcd. C 64.9, H 8.1, N 12.6; found C 64.6, H 8.1, N 12.7.

Third Step. Preparation of Schiff Base Ligands: The Schiff-base ligands were prepared in a standard manner by the reaction of equimolecular quantities of 3,5-di-*tert*-butyl-2-hydroxybenzaldehyde and the appropriate amines **2a**, **2b** or **2c**, which is typified by the preparation of H$_3$-5-*t*Bu-amsal-3,5-di-*t*Bu. The amine **2c** (0.5 g, 2.25 mmol) and the salicylaldehyde (0.53 g, 2.25 mmol) were dissolved in methanol (100 mL) and the solution was brought to reflux. The volume of the solution was reduced over a three hour period to ca. 50 mL, using a Dean−Stark trap and was then allowed to cool. The solid, which precipitated, was collected by filtration, washed with diethyl ether (3 mL) and dried in vacuo. The purity of the ligands was checked by elemental analysis, mass spectrometry (Table 1), ^{1}H NMR (Table 2), ^{13}C NMR and IR (Table 3) spectroscopy.

Synthesis of the Complexes

All of the manganese complexes were obtained using the same procedure. A typical preparation is outlined below.

Mn(amsal-3,5-di-*t*Bu)(H$_2$O)$_4$: A solution of NaOH (0.03 g, 0.78 mmol) in water (3 mL) was added to a solution of the ligand H$_3$-amsal-di-*t*Bu (0.1 g, 0.26 mmol) in methanol (15 mL). Manganese(II) perchlorate hexahydrate (0.15 g, 0.41 mmol) in 5 mL of methanol was then added and a rapid change of solution colour was observed, from yellow to brown. (***CAUTION:*** All perchlorates are potentially explosive. Although no problems have been encountered during this study, care should be taken in the handling and treatment of these materials). After stirring at room temperature in the presence of air for 12 h, the solid formed was collected by filtration, washed with hexane and dried in vacuo. Yield 80%. $C_{23}H_{35}MnN_2O_7$ (505.9): calcd. C 54.6, H 6.9, N 5.5; found C 54.8, H 6.7, N 5.3. MS(FAB): *m*/*z* (%) = 434 (100, MnL), 869 (12, Mn_2L_2). Magnetic moment μ_{eff} = 5.0 B. M. Conductivity (in DMF) Λ_M = 3 μS cm^{-1}.
Recrystallisation of the dark brown powder from methanol by slow evaporation afforded brown crystals of [Mn$_2$(amsal-3,5-di-*t*Bu)$_2$(MeOH)$_2$]$_n$ **1**, suitable for X-ray diffraction studies.

Mn(4-Me-amsal-3,5-di-*t*Bu)(H$_2$O)$_2$: Yield 65%. $C_{24}H_{33}MnN_2O_5$ (483.9): calcd. C 59.5, H 6.8, N 5.8; found C 60.1, H 6.6, N 5.5. MS(FAB): *m*/*z* (%) = 449 (100, MnL), 898.1 (16, Mn_2L_2). Magnetic moment μ_{eff} = 5.1 B. M. Conductivity (in DMF) Λ_M = 3 μS cm^{-1}. Recrystallisation of the brown powder in methanol yielded crystals of [Mn$_2$(4-Me-amsal-3,5-di-*t*Bu)$_2$(MeOH)$_2$]$_n$ **2**, suitable for X-ray analyses.

Mn(5-*t*Bu-amsal-3,5-di-*t*Bu)(H$_2$O)$_4$: Yield 70%. $C_{27}H_{43}MnN_2O_7$ (561.9): calcd. C 57.7, H 7.7, N 5.0; found C 58.1, H 7.5, N 5.0. MS(FAB): *m*/*z* (%) = 490.3 (100, MnL), 981.6 (18, Mn_2L_2). Magnetic moment μ_{eff} = 4.9 B. M. Conductivity (in DMF) Λ_M = 9 μS cm^{-1}.
Recrystallisation of the brown powder in methanol yielded crystals of [Mn$_2$(5-*t*Bu-amsal-3,5-di-*t*Bu)$_2$(MeOH)$_2$]$_n$ **3**, suitable for X-ray studies.

 © 2004 Wiley-VCH Verlag GmbH & Co. KGaA, Weinheim

Crystallographic Measurements

Crystals of **1, 2** and **3** suitable for single-crystal X-ray studies were obtained as described above. Data were collected at 293 K for **1** and **2**, and at 120 K for **3** on a Bruker SMART 1000 diffractometer, employing graphite-monochromated MoK_α (λ = 0.71073 Å) radiation. The structures were solved by direct methods[26] and finally refined by full-matrix least-squares based on F^2. An empirical absorption correction was applied using SADABS.[27] Non-hydrogen atoms were anisotropically refined. Hydrogen atoms were included in the structure factor calculation in idealised positions.

CCDC-228228 (for **1**), -228227 (for **2**) and -228226 (for **3**) contain the supplementary crystallographic data for this paper. These data can be obtained free of charge at www.ccdc.cam.ac.uk/conts/retrieving.html [or from the Cambridge Crystallographic Data Centre, 12 Union Road, Cambridge CB2 1EZ, UK; Fax: (internat.) +44-1223-336-033; E-mail: deposit@ccdc.cam.ac.uk].

Acknowledgments

We thank the Ministerio de Ciencia y Tecnología of Spain (BQU2003−00167) for financial support.

[1] [1a] J. D. Crowley, D. A. Traynor, D. C. Weatherburn in *Metal Ions in Biological Systems*, vol. 37 (Eds.: A. Sigel, H. Sigel); Marcel Dekker, New York, **2000**, p. 209−278. [1b]D. S. Marlin, E. Bill, T. Weyhermuller, E. Rentschler, K. Wieghardt, *Angew. Chem. Int. Ed.* **2002**, *41*, 4775−4779.

[2] D. Yang, J. Wang, Y. Bao, L. An, *Prep. Biochem. Biotech.* **2003**, *33*, 113−123.

[3] [3a] G. C. Dismukes, *Chem. Rev.* **1996**, *96*, 2909−2926. [3b] A. Gelasco, S. Bensiek, V. L. Pecoraro, *Inorg. Chem.* **1998**, *37*, 3301−3309.

[4] [4a] G. E. Borgstahl, H. E. Parge, M. J. Hickey, W. F. Beyer Jr., R. A. Hallewell, J. A. Trainer, *Cell* **1992**, *71*, 107−118. [4b] R. Kramer, *Angew. Chem. Int. Ed.* **2000**, *39*, 4469−4470.

[5] [5a] V. K. Yachandra, K. Sauer, M. P. Klein, *Chem. Rev.* **1996**, *96*, 2927−2950. [5b] W. Ruttinger, G. C. Dismukes, *Chem. Rev.* **1997**, *97*, 1−24. [5c] J. E. Penner-Hahn in *Metal Sites in Proteins and Models* (Eds.: H. A. O. Hill, P. J. Sadler, A. J. Thomson); Springer-Verlag, **1998**, p. 1−36. [5d]C. Tommos, G. T. Babcock, *Acc. Chem. Res.* **1998**, *31*, 18−25. [5e] N. A. Law, M. T. Caudle, V. L. Pecoraro, *Adv. in, Inorg. Chem.* **1998**, *46*, 305−440. [5f] T. M. Rajendiran, M. T. Caudle, M. L. Kirk, I. Setyawati, J. W. Kampf, V. L. Pecoraro, *J. Biol. Inorg. Chem.* **2003**, *8*, 283−293.

[6] [6a] C. E. Holloway, M. Melnik, *Rev. in Inorg. Chem.* **1996**, *16*, 101−314. [6b] J. L. Seela, M. J. Knapp, K. S. Kolack, H.-R. Chang, J. C. Huffman, D. N. Hendrickson, G. Christou, *Inorg. Chem.* **1998**, *37*, 516−525 and references cited therein. [6c] A. Cornia, A. Caneschi, P. Dapporto, A. C. Fabretti, D. Gatteschi, W. Malavasi, C. Sangregorio, R. Sessoli, *Angew. Chem. Int. Ed.* **1999**, *38*, 1780−1782 and references cited therein.

[7] [7a] E. Kimura, A. Sakonaka, R. Machida, M. Kodama, *J. Am. Chem. Soc.* **1982**, *104*, 4255−4257. [7b] L. L. Diaddario, W. R. Robinson, D. W. Margerum, *Inorg. Chem.* **1983**, *22*, 1021−1025. [7c] C. M. Che, W. K. Cheng, *J. Chem. Soc., Chem. Commun.* **1986**, 1443−1444. [7d] M. Koikawa, H. Ôkawa, Y. Maeda, S. Kida, *Inorg. Chim. Acta* **1992**, *194*, 75−79. [7e] M. Koikawa, H. Ôkawa, S. Kida, *J. Chem. Soc., Dalton Trans.* **1988**, 641−645.

[8] [8a] K. Bertoncello, G. D. Fallon, K. S. Murray, *Inorg. Chim. Acta* **1990**, *174*, 57−60. [8b] T. J. Collins, R. D. Powell, C. Slebodnick, E. S. Uffelman, *J. Am. Chem. Soc.* **1990**, *112*, 899−901. [8c] W. H. Leung, J. X. Ma, V. W. W. Yam, C. M. Che, C. K. Poon, *J. Chem. Soc., Dalton Trans.* **1991**, 1071−1076. [8d] S. K. Chandra, A. Chakravorty, *Inorg. Chem.* **1992**, *31*, 760−765.

[9] P.-H. Ko, T.-Y. Chen, J. Zhu, K.-F. Cheng, S.-M. Peng, C.-M. Che, *J. Chem. Soc., Dalton Trans.* **1995**, 2215−2219.

[10] [10a] M. R. Bermejo, A. M. González, M. Fondo, A. García-Deibe, M. Maneiro, J. Sanmartín, O. L. Hoyos, M. Watkinson, *New J. Chem.* **2000**, *24*, 235−241. [10b] M. R. Bermejo, A. M. González, M. Fondo, M. Maneiro, M. Rey, M. Vázquez, O. L. Hoyos, J. C. García-Monteagudo, *Inorg. Chim. Acta* **2000**, *307*, 106−114. [10c] M. R. Bermejo, A. M. González, M. Maneiro, M. Rey, M. Vázquez, O. L. Hoyos, *J. Coord. Chem.* **2001**, *54*, 25−34.

[11] L. J. Boucher, C. G. Coe, *Inorg. Chem.* **1975**, *14*, 1289−1294.

[12] J. C. Sheenan, G. P. Hess, *J. Am. Chem. Soc.* **1955**, *77*, 1067−1068.

[13] A. E. Jackson, R. A. W. Jonhstone, *Synthesis* **1976**, 685−687.

[14] M. R. Bermejo, A. Castiñeiras, J. C. García-Monteagudo, M. Rey, A. Sousa, M. Watkinson, C. A. McAuliffe, R. G. Pritchard, R. L. Beddoes, *J. Chem. Soc., Dalton Trans.* **1996**, 2935−2944.

[15] W. I. Geary, *Coord. Chem. Rev.* **1971**, *7*, 81.

[16] [16a] N. Aurangzeb, C. E. Hulme, C. A. McAuliffe, R. G. Pritchard, M. Watkinson, A. García-Deibe, M. R. Bermejo, A. Sousa, *J. Chem. Soc., Chem. Commun.* **1992**, 1524−1526. [16b] C. E. Hulme, M. Watkinson, M. Haynes, R. G. Pritchard, C. A. McAuliffe, N. Jaiboon, B. Beagley, A. Sousa, M. R. Bermejo, M. Fondo, *J. Chem. Soc., Dalton Trans.* **1997**, 1805−1814. [16c] H. Miyasaka, H. Ieda, N. Matsumoto, N. Re, R. Crescenzi, C. Floriani, *Inorg. Chem.* **1998**, *37*, 255−263. [16d] M. R. Bermejo, M. Fondo, A. García-Deibe, A. M. González, A. Sousa, J. Sanmartín, C. A. McAuliffe, R. G. Pritchard, M. Watkinson, V. Lukov, *Inorg. Chim. Acta* **1999**, *293*, 210−217. [16e] N. Matsumoto, Y. Sunatsuki, H. Miyasaka, Y. Hashimoto, D. Luneau, J.-P. Tuchagues, *Angew. Chem. Int. Ed.* **1999**, *38*, 171−173. [16f] S. Sailaja, K. Rajender Reddy, M. V. Rajasekharan, C. Hureau, E. Riviere, J. Cano, J.-J. Girerd, *Inorg. Chem.* **2003**, *42*, 180−186.

[17] D. M. L. Goodgame, D. A. Grachvogel, I. Hussain, A. J. P. White, D. J. Williams, *Inorg. Chem.* **1999**, *38*, 2057−2063.

[18] O. L. Hoyos, M. R. Bermejo, M. Fondo, A. García-Deibe, A. M. González, M. Maneiro, R. Pedrido, *J. Chem. Soc., Dalton Trans.* **2000**, 3122 and references cited therein.

[19] M. E. Fisher, *Am. J. Phys.* **1964**, *32*, 343.

[20] [20a] M. R. Bermejo, A. Sousa, A. García-Deibe, M. Maneiro, J. Sanmartín, M. Fondo, *Polyhedron* **1999**, *15*, 511−518. [20b] N. Aurangzeb, C. E. Hulme, C. A. McAuliffe, R. G. Pritchard, M. Watkinson, M. R. Bermejo, A. Sousa, *J. Chem. Soc., Chem. Commun.* **1994**, 2193−2195. [20c] A. García-Deibe, M. R. Bermejo, A. Sousa, C. A. McAuliffe, P. McGlynn, P. T. Ndifon, R. G. Pritchard, *J. Chem. Soc., Dalton Trans.* **1993**, 1605−1610.

[21] J. A. Bonadies, M. J. Maroney, V. L. Pecoraro, *Inorg. Chem.* **1989**, *28*, 2044−2051.

[22] M. R. Bermejo, M. Fondo, A. García-Deibe, M. Rey, J. Sanmartín, A. Sousa, M. Watkinson, C. A. McAuliffe, R. G. Pritchard, *Polyhedron* **1996**, *15*, 4185−4194.

[23] [23a] T. J. Swift in *NMR of Paramagnetic Molecules* (Eds.: G. N. Lamar, W. D. Horrocks Jr., R. H. Holm); Academic Press, New York, **1973**, p. 53−83. [23b]D. W. Wright, H. J. Mok, C. E. Dubé, W. H. Armstrong, *Inorg. Chem.* **1998**, *37*, 3714−3718.

[24] [24a] M. Watkinson, M. Fondo, M. R. Bermejo, A. Sousa, C. A. McAuliffe, R. G. Pritchard, N. Jaiboon, N. Aurangzeb, M. Naeem, *J. Chem. Soc., Dalton Trans.* **1999**, 31−41. [24b] M. Maneiro, M. R. Bermejo, A. Sousa, M. Fondo, A. M. González, A. Sousa-Pedrares, C. A. McAuliffe, *Polyhedron* **2000**, *19*, 47−54.

[25] M. Maneiro, M. R. Bermejo, M. I. Fernández, E. Gómez-Fórneas, A. M. González-Noya, A. M. Tyryshkin, *New J. Chem.* **2003**, *27*, 727−733.

 © 2004 Wiley-VCH Verlag GmbH & Co. KGaA, Weinheim

[26] R. C. Karpoor, B. S. Aggarwal, *Principles of Polarography*, J. Wiley, New York, **1991**.
[27] G. M. Sheldrick, *SHELX97, Programs for Crystal Structure Analysis*, University of Göttingen, Germany, **1998**.
[28] G. M. Sheldrick, *SADABS, Program for Scaling and Correction of Area Detector Data*, University of Göttingen, Germany, **1996**.

Received March 10, 2004
Early View Article
Published Online July 12, 2004

 © 2004 Wiley-VCH Verlag GmbH & Co. KGaA, Weinheim

Syntheses and Crystal Structures of Two Cobalt Carboxylate−Phosphonates with 4,4′-Bipyridine as a Secondary Metal Linker

Jun-Ling Song,[a] Andrey V. Prosvirin,[b] Han-Hua Zhao,[b] and Jiang-Gao Mao*[a]

Keywords: Hydrothermal synthesis / Crystal structure / Cobalt phosphonates / Inorganic-organic hybrids / Open frameworks

The hydrothermal syntheses and crystal structures of two novel cobalt carboxylate–phosphonates with 4,4′-bipyridine (4,4′-bipy) as the secondary metal linker are reported. Compound **1**, $[Co_3(H_2L)_2(H_2O)_4(4,4'\text{-bipy})]$, where H_5L = 4-$HO_2CC_6H_4CH_2N(CH_2PO_3H_2)_2$, crystallizes in the monoclinic space group $C2/c$ with a = 25.9281(5), b = 9.76310(10), c = 17.3671(5) Å, β = 103.290(2)°, V = 4278.6(2) Å^3, and Z = 4. Its structure contains a pillar-layered architecture in which Co^{II} octahedra are linked by carboxylate–phosphonate ligands to form a 2D layer and these layers are crosslinked further by 4,4′-bipy ligands to form a porous 3D network. Compound **2**, $[Co_2(PMIDA)(H_2O)_5(4,4'\text{-bipy})]\cdot 4H_2O$, where H_4PMIDA = $H_2O_3PCH_2N(CH_2CO_2H)_2$, crystallizes in the triclinic space group $P\bar{1}$ with a = 7.8009(7), b = 13.4560(12), c = 13.5453(12) Å, α = 65.207(2), β = 88.035(2), γ = 77.135(2)°, V = 1255.57(19) Å^3, and Z = 2. The crystal structure of compound **2** contains 1D zigzag chains in which two cobalt(II) ions are bridged by PMIDA ligand to form dimeric units, and these dimeric units are connected further by bridging 4,4′-bipy ligands.

(© Wiley-VCH Verlag GmbH & Co. KGaA, 69451 Weinheim, Germany, 2004)

Introduction

Recently, many research studies have been devoted to the synthesis of metal phosphonates with open-framework or microporous structures because of their potential applications in ion-exchange, catalysis and sensors.[1−6] Furthermore, interesting magnetic properties have been observed in some of these systems. For example, weak ferromagnetic or canted antiferromagnetic behavior has been observed in some Mn^{II}, Fe^{II}, Cu^{II} and Co^{II} compounds.[3,7−14] The strategy of attaching functional groups such as carboxylic acids, crown ethers and amines to the phosphonic acid molecule has been found to be an effective method for the preparation of metal phosphonates with open-framework and microporous structures. For example, a series of novel microporous materials has been synthesized by hydrothermal reactions of different metal salts with carboxylate-functionalised phosphonic acids $H_2O_3PCH_2CH_2CO_2H$ and $H_2O_3PCH_2CO_2H$.[15−17] The use of additional bidentate metal linkers, such as 1,10-phenanthroline, 2,2′-bipyridine, piperazine and 4,4′-bipyridine, results in various mixed-metal hybrids of V and Mo.[13,18] Reports regarding the corresponding divalent transition metal compounds are rare.[12,13] We selected two carboxylate−phosphonic acids, H_5L [H_5L = 4-$HOOCC_6H_5CH_2N(CH_2PO_3H_2)_2$] and H_4PMIDA [H_4PMIDA = $H_2O_3PCH_2N(CH_2COOH)_2$] (Scheme 1), in combination with 4,4′-bipyridine (4,4′-bipy) as the secondary metal linker. Zinc(II) and cobalt(II) compounds prepared from H_4PMIDA have been reported previously.[19] Hydrothermal reactions of the metal salts with the above phosphonic acids and 4,4′-bipy led to two new cobalt carboxylate−phosphonates, namely $[Co_3(H_2L)_2(H_2O)_4(4,4'\text{-bipy})]$ (**1**) and $[Co_2(PMIDA)(H_2O)_5(4,4'\text{-bipy})]\cdot 4H_2O$ (**2**). Herein we report their syntheses and crystal structures.

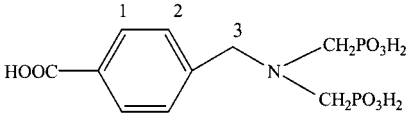

H_5L

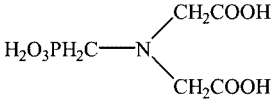

H_4PMIDA

Scheme 1. The structure of H_5L and H_4PMIDA

[a] State Key Laboratory of Structural Chemistry, Fujian Institute of Research on the Structure of Matter, The Chinese Academy of Sciences,
Fuzhou 350002, P. R. China
[b] Department of Chemistry, Texas A&M University,
P. O. Box 30012, College Station, TX 77843-3012, USA
E-mail: mjg@ms.fjirsm.ac.cn

 © 2004 Wiley-VCH Verlag GmbH & Co. KGaA, Weinheim **DOI: 10.1002/ejic.200400212**

Results and Discussion

Crystal Structure Descriptions for Compounds 1 and 2

As shown in Figure 1, the asymmetric unit of compound **1** contains two unique Co^{II} atoms. The Co(1) atom is octahedrally coordinated by the tridentate phosphonate ligand (1 N and 2 O), two phosphonate oxygen atoms from two other phosphonate ligands, and one nitrogen atom from a 4,4′-bipy ligand. The Co(1)−O bond lengths are in the range from 2.036(7) to 2.087(6) Å, and the Co(1)−N bond lengths are in the range from 2.154(8) to 2.348(8) Å. The O−Co−O and O−Co−N bond angles deviate from the values for an ideal octahedron (Table 1). The atom Co(2) lies on a twofold symmetry axis and is octahedrally coordinated to two phosphonate oxygen atoms from two Co(1)(H_2L) units, and four water ligands. The Co−O bond lengths fall between 2.049(6) and 2.152(7) Å, and the O−Co−O bond angles are in the range from 84.5(3) to 95.6(3)°. These bond lengths and angles are similar to those in $Co_2[PMIDA]_2(H_2O)_5{\cdot}H_2O$,[19] as well as for other cobalt(II) phosphonates.[13,14,20] The carboxylate−phosphonate ligand is hexadentate and occupies three coordination sites on one Co^{II} ion and also bridges three Co^{II} ions. The phosphonate group containing P(2) is tridentate, whereas the one containing the atom P(1) is bidentate. It should be noted that the benzoic acid moiety does not coordinate to metal ions and remains protonated (O2). The atom O(11) in the P(1)O_3 group is also noncoordinating. This PO_3 group is singly protonated based on P−O distances and charge balance. The noncoordinating carboxylate (O2) and phosphonate (O11) oxygen atoms are hydrogen-bonded to an aquo ligand (O1W) (Table 1). The [CoN_2O_4] and [CoO_6] octahedra are interconnected by bridging carboxylate−phosphonate ligands in the plane {400} (Figure 2). The interlayer distance is 12.9 Å (1/2*a*). The 2D layers are further crosslinked by 4,4′-bipy ligands

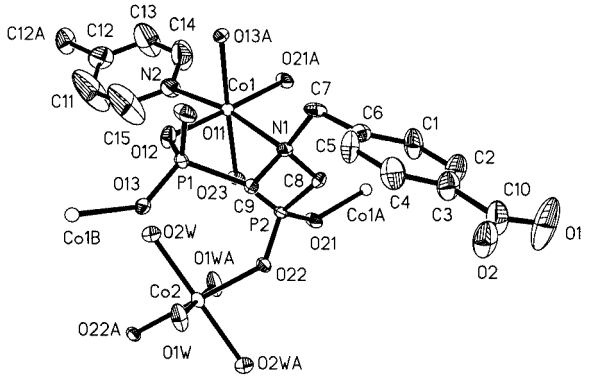

Figure 1. ORTEP representation of the asymmetric unit of compound **1**; thermal ellipsoids are drawn at the 50% probability level

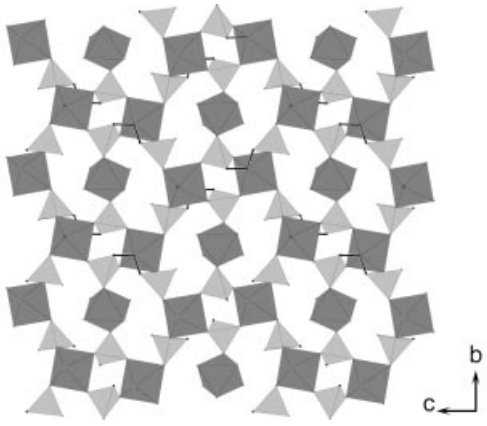

Figure 2. A <400> cobalt carboxylate−phosphonate layer in **1**; the CPO_3 tetrahedra and CoN_2O_4 octahedra are represented by medium and light gray, respectively; the $CH_2C_6H_5COOH$ moiety of the ligand has been omitted for clarity

Table 1. Selected bond lengths [Å] and angles [°] for compound **1**

Co(1)−O(12)	2.036(7)	Co(2)−O(22)#3	2.049(6)
Co(1)−O(23)	2.063(7)	Co(2)−O(2W)#3	2.121(7)
Co(1)−O(13)#1	2.082(6)	Co(2)−O(2W)	2.121(7)
Co(1)−O(21)#2	2.087(6)	Co(2)−O(1W)#3	2.152(7)
Co(1)−N(2)	2.154(8)	Co(2)−O(1W)	2.152(7)
Co(1)−N(1)	2.348(8)	C(10)−O(1)	1.209(15)
Co(2)−O(22)	2.049(6)	C(10)−O(2)	1.290(14)
Hydrogen bonds:			
O(1w)···O(1)#6	2.735(11)	O(1W)···O(11)#5	2.992(10)
O(12)−Co(1)−O(23)	92.2(3)	O(22)−Co(2)−O(22)#3	180.0(3)
O(12)−Co(1)−O(13)#1	90.0(3)	O(22)−Co(2)−O(2W)#3	84.5(3)
O(23)−Co(1)−O(13)#1	177.7(3)	O(22)#3−Co(2)−O(2W)#3	95.5(3)
O(12)−Co(1)−O(21)#2	178.0(3)	O(22)−Co(2)−O(2W)	95.5(3)
O(23)−Co(1)−O(21)#2	89.8(3)	O(22)#3−Co(2)−O(2W)	84.5(3)
O(13)#1−Co(1)−O(21)#2	88.0(3)	O(2W)#3−Co(2)−O(2W)	180.0(6)
O(12)−Co(1)−N(2)	87.9(3)	O(22)−Co(2)−O(1W)#3	91.8(3)
O(23)−Co(1)−N(2)	92.0(3)	O(22)#3−Co(2)−O(1W)#3	88.2(3)
O(13)#1−Co(1)−N(2)	88.7(3)	O(2W)#3−Co(2)−O(1W)#3	89.5(3)
O(21)#2−Co(1)−N(2)	92.0(3)	O(2W)−Co(2)−O(1W)#3	90.5(3)

Symmetry transformations used to generate equivalent atoms: #1: $-x + 1/2, y - 1/2, -z + 1/2$; #2: $-x + 1/2, -y - 3/2, -z$; #3: $-x + 1/2, -y - 1/2, -z$; #4: $-x + 1, y, -z + 1/2$; #5: $-x + 1/2, y + 1/2, -z + 1/2$; #6: $x, -y - 1, -z$.

 © 2004 Wiley-VCH Verlag GmbH & Co. KGaA, Weinheim

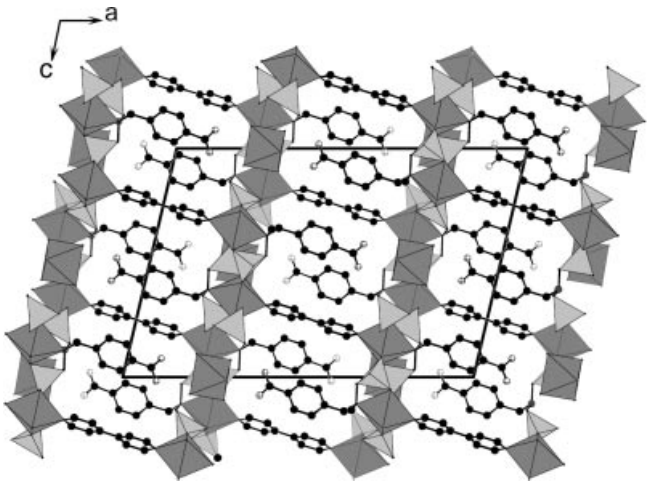

Figure 3. A view of the crystal structure of complex **1** along the *b* axis; the CPO_3 tetrahedra and CoN_2O_4 octahedra are represented by medium and light gray, respectively; C and O atoms are represented by black and crossed circles, respectively

to form a pillar-layered structure (Figure 3), which contains channels with a size of about 9 × 11 Å based on the crystal structure. The benzoic acid moieties are located in these channels.

Compound **2** features a 1D zigzag chain structure. There are two independent Co^{II} ions in the asymmetric unit of compound **2** (Figure 4). Co(1) is octahedrally coordinated to a tetradentate PMIDA ligand, an aquo ligand and a nitrogen atom from a 4,4′-bipy ligand, whereas Co(2) is octahedrally coordinated by one 4,4′-bipy N atom, one phosphonate oxygen atom from a neighboring Co(1)(PMIDA) chelating unit as well as four aquo ligands. The Co−O distances are in the range from 2.082(4) to 2.181(4) Å, and the Co−N distances fall in the range 2.115(3) to 2.156(4) Å. These bond lengths are similar to those in other Co^{II} complexes with O- and N-containing ligands.[13,14,19,20] The PMIDA ligand is pentadentate, occupying four sites on a Co^{II} ion (1 N, 3 O) and bridging to another Co^{II} ion. O(1) and O(3) atoms of the carboxylate groups remain noncoordinating. The phosphonate group adopts a bidentate and bridging coordination mode, with one oxygen atom (O11) not involved in metal coordination. This type of coordination mode is different from that for $Co_2[PMIDA]_2(H_2O)_5{\cdot}H_2O$,[19] in which the phosphonate group is tridentate and one carboxylate group is bidentate. The PMIDA ligand in compound **1** has been fully deprotonated based on charge balancing.

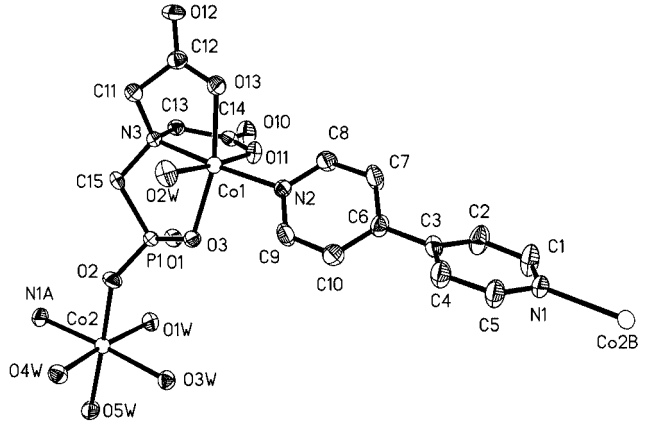

Figure 4. An ORTEP representation of the asymmetric unit of **2**; thermal ellipsoids are drawn at the 30% probability level

The two types of cobalt(II) octahedra are bridged by a PMIDA ligand to form a dimeric unit, and such dimeric units are further interconnected by bridging 4,4′-bipy ligands to form a 1D chain (Figure 5). These chains are held together by hydrogen bonds among noncoordinating carboxylate (O12 and O10) and phosphonate(O1) oxygen atoms as well as aquo ligands, resulting in a porous 3D network (Figure 6, Table 2). The lattice water molecules are located in the pores and are also involved in hydrogen bonding (Table 2, Figure 6).

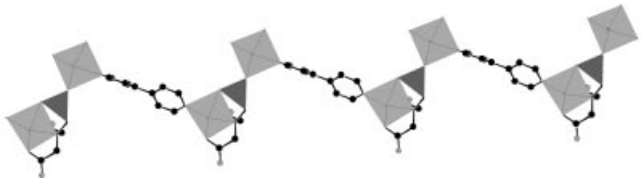

Figure 5. A 1D zigzag chain along the diagonal axis *b* and the −*c* axis in **2**; the CPO_3 tetrahedra and CoN_2O_4 octahedra are represented by medium and light gray, respectively

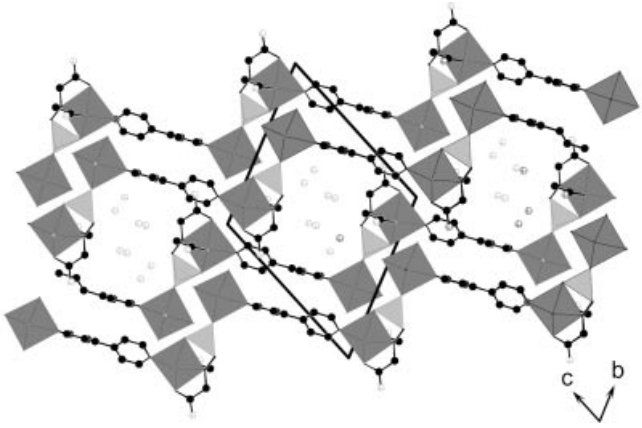

Figure 6. A view of the crystal structure of **2** along the *a* axis; the CPO_3 tetrahedra and CoN_2O_4 octahedra are represented by medium and light gray, respectively; C and O atoms are represented by black and crossed circles, respectively

TGA Studies

The TGA diagram of compound **1** shows three main stages of weight loss. The first stage begins at 138 °C and is complete at 342 °C, and corresponds to the loss of four water molecules. The observed weight loss of 6.4% is in good agreement with the calculated value of 6.7%. The second stage, occurring between 347 and 820 °C, corresponds to the combustion of 4,4′-bipy and diphosphonate ligands. The third stage, which overlaps with the second, continues up to 1000 °C and corresponds to further decomposition of the compound. Assuming the final product is a mixture

 © 2004 Wiley-VCH Verlag GmbH & Co. KGaA, Weinheim

Table 2. Selected bond lengths [Å] and angles [°] for compound **2**

Co(1)−O(11)	2.082(4)	Co(2)−N(1)#1	2.148(4)
Co(1)−O(13)	2.085(4)	Co(2)−O(3W)	2.181(4)
Co(1)−N(2)	2.099(4)	Co(2)−O(5W)	2.075(4)
Co(1)−O(3)	2.115(3)	Co(2)−O(2)	2.091(4)
Co(1)−O(2W)	2.125(4)	Co(2)−O(1W)	2.120(4)
Co(1)−N(3)	2.156(4)	Co(2)−O(4W)	2.122(4)
Hydrogen bonds:			
O(1W)···O(1)	2.675(5)	O(2W)···O(10)#5	2.789(6)
O(1W)···O(3W)	2.973(5)	O(3W)···O(4W)	2.927(5)
O(3W)···O(4W)#2	2.756(5)	O(3W)···O(10)#3	2.865(6)
O(3W)···O(1)#3	2.628(5)	O(3W)···O(5W)	2.953(5)
O(4W)···O(2)	2.910(5)	O(4W)···O(5W)	2.936(5)
O(5W)···O(12)#4	2.747(5)	O(6W)···O(6W)#6	2.655(12)
O(6W)···O(8W)#6	2.611(13)	O(6W)···O(9W)	2.633(2)
O(7W)···O(8W)#7	2.786(9)	O(7W)···O(9W)#6	2.904(16)
O(8W)···O(1)#6	2.851(7)		
O(13)−Co(1)−N(3)	79.75(15)	O(2)−Co(2)−O(3W)	91.57(14)
N(2)−Co(1)−N(3)	171.75(17)	O(1 W)−Co(2)−O(3W)	87.46(14)
O(3)−Co(1)−N(3)	86.69(15)	O(4 W)−Co(2)−O(3W)	85.73(14)
O(2W)−Co(1)−N(3)	96.13(16)		

Symmetry transformations used to generate equivalent atoms: #1: $x, y + 1, z - 1$; #2: $-x + 1, -y + 1, -z + 2$; #3: $-x, -y + 1, -z + 2$; #4: $x, y + 1, z$; #5: $x + 1, y, z$; #6: $-x, -y + 1, -z + 1$; #7: $x - 1, y, z$.

of $Co(PO_3)_2$ and $Co_2P_2O_7$ in a molar ratio of 1:1, the total weight loss should be 52.8%. On the other hand, if compound **1** completely decomposes to CoO, the total weight loss is calculated to be 79.2%. The observed weight loss (70.2%) is between these two theoretical values, and indicates the partial decomposition of $Co(PO_3)_2$ and $Co_2P_2O_7$ to CoO. The TGA weight loss curves of compound **2** also exhibit three stages. The first stage (24−269 °C) corresponds to loss of the four water molecules of crystallisation and five aquo ligands. The observed weight loss of 24.8% is in good agreement with the calculated value of 24.9% based on the loss of a total of nine H_2O molecules. The second loss occurs at 330−570 °C, and corresponds to the decomposition of the 4,4′-bipy and carboxylate−phosphonate ligand. The third stage, occurring between 620 and 1000 °C, corresponds to further decomposition of the organic groups. If the residue is assumed to be a mixture of CoO and $Co_2P_2O_7$ in a molar ratio of 2:1, the total weight loss is calculated to be 66.5%. On the other hand, if the final residue is CoO alone, the total weight loss is calculated to be 88.6%. The observed weight loss (74.8%) is between these two theoretical values, indicating that some $Co_2P_2O_7$ has decomposed to CoO.

Conclusion

In summary, the hydrothermal syntheses and crystal structures of two novel cobalt carboxylate−phosphonates containing 4,4′-bipy as the secondary metal linker have been described. The interconnection of the metal carboxylate−phosphonate layer in compound **1** by 4,4′-bipy leads to a pillar-layered architecture. In compound **2**, the dinuclear metal carboxylate−phosphonate units are crosslinked by 4,4′-bipy ligands resulting in a 1D chain. We believe that a wide range of new open-frameworks and microporous materials can be developed by self-assembly or by structure-directed synthesis of other metal phosphonate building blocks with secondary metal linkers such as 4,4′-bipy or acidic carboxylic acid. In the latter case, the carboxylate ligand may remain protonated and noncoordinated, in other words, it can act as an intercalated species between two metal phosphonate layers. Such compounds may have good ion-exchange properties and could exhibit proton conductivity.

Experimental Section

Materials and Instrumentation: All chemicals were obtained from commercial sources and used without further purification. Elemental analyses were performed with a Vario EL III elemental analyzer. Thermogravimetric analyses were carried out with a NETZSCH STA 449C unit at a heating rate of 15 °C/min under nitrogen. IR spectra were recorded with a Magna 750 FT-IR spectrophotometer on KBr pellets in the range 4000−400 cm^{-1}. ^1H and ^{31}P NMR spectra were recorded with a Varian Unity 500 NMR spectrometer using D_2O as solvent. H_3PO_4 (85%) was used as ^{31}P standard reference.

Preparation of H_5L and H_4PMIDA: H_5L was prepared by a Mannich-type reaction using 4-(aminomethyl)benzoic acid (15.1 g, 0.1 mol), hydrochloric acid (16 mL), deionized water (20 mL), phosphoric acid (32.8 g, 0.4 mol) and paraformaldehyde (9.0 g, 0.3 mol), according to known procedures.[16,21] The ^{31}P NMR spectrum shows a single peak at $\delta = 7.69$ ppm. ^1H NMR (D_2O) : $\delta = 3.50$ (d, $J_{H,P} = 12.5$ Hz, 4 H, NCH_2PO_3), 4.74 (s, 2 H, 3-H), 7.73 (d, $J_{H,H} = 5.5$ Hz, 2 H, 2-H), 8.13 (d, $J_{H,H} = 5.5$ Hz, 2 H, 1-H) ppm (see Scheme 1 for atomic labeling). IR (KBr): $\tilde{\nu} = 3423$ (w), 2995 (m), 2771 (m), 2657 (m), 1720 (s), 1618 (w), 1583 (w), 1458 (m), 1435 (w), 1417 (w), 1327 (m), 1232 (m), 1138 (s), 1107 (s), 1022 (s), 939 (s), 862 (w), 810 (w), 746 (m), 710 (m), 580 (s), 519 (w), 494 (m), 451 (m) cm^{-1}. H_5L: $C_{10}H_{15}NO_8P_2$ (339.18): calcd. C 35.53, H 4.34, N 4.22; found C 35.41, H 4.46, N 4.13. H_4PMIDA

 © 2004 Wiley-VCH Verlag GmbH & Co. KGaA, Weinheim

Table 3. Crystal data and structure refinements for compounds **1** and **2**

	1	**2**
Empirical formula	$C_{30}H_{40}Co_3N_4O_{20}P_4$	$C_{15}H_{32}Co_2N_3O_{16}P$
Formula mass	1077.33	659.27
Space group	*C*2/*c*	$P\bar{1}$
a [Å]	25.9281(5)	7.8009(7)
b [Å]	9.76310(10)	13.4560(12)
c [Å]	17.3671(5)	13.5453(12)
α [°]	90.0	65.207(2)
β [°]	103.290(2)	88.035(2)
γ [°]	90.0	77.135(2)
V [Å^3]	4278.55(15)	1255.57(19)
Z	4	2
$D_{calcd.}$ [g·cm^{-3}]	1.672	1.744
μ [mm^{-1}]	1.381	1.466
Measured reflections	6367	6417
Independent reflections	3699	4356
No. of parameters refined	279	335
GOF on F^2	1.214	1.066
R1, *wR*2 [$I > 2\sigma(I)$][a]	0.0728/0.1326	0.0533/0.1132
R1, *wR*2 (all data)	0.1326/0.2037	0.0828/0.1308

[a] $R1 = |F_o| - |F_c|/|F_o|$, $wR2 = \{w[(F_o)^2 - (F_c)^2]^2/w[(F_o)^2]^2\}^{1/2}$, $I > 4\sigma(I)$ for compound **1**.

was also synthesized by a Mannich-type reaction according to procedures described previously.[22]

Preparation of [$Co_3(H_2L)_2(H_2O)_4$(4,4′-bipy)] (1): A mixture of $CoCl_2·6H_2O$ (0.24 g, 1.0 mmol), H_5L (0.17 g, 0.5 mmol) and 4,4′-bipy (0.09 g, 0.5 mmol) in distilled water (10 mL) was placed in a sealed hydrothermal reaction vessel equipped with a Teflon liner (25 mL), and then heated to 170 °C for 5 d. Pink crystals of **1** were collected. Yield: 0.09 g (ca. 26% based on cobalt). The initial and final pH values of this solution were 4.0 and 3.5, respectively. $C_{30}H_{40}Co_3N_4O_{20}P_4$ (1077.33): calcd. C 33.45, H 3.74, N 5.20; found C 33.65, H 3.56, N 5.26.

Preparation of [Co_2(PMIDA)$(H_2O)_5$(4,4′-bipy)]·$4H_2O$ (2): A mixture of $Co(CH_3COO)_2·2H_2O$ (0.24 g, 1.0 mmol), H_4PMIDA (0.11 g 0.5 mmol) and 4,4′-bipyridine (0.09 g 0.5 mmol) in distilled water (10 mL) was placed in a sealed hydrothermal reaction vessel equipped with a Teflon liner (25 mL), and then heated to 80 °C for 5 d. The resulting orange-red solution was filtered and ethanol was allowed to diffuse slowly into the solution at room temperature. Orange-red crystals of **2** appeared after several days and were collected. Yield: 0.16 g (ca. 48% based on cobalt). The initial and final pH values of the solutions were 4.0 and 4.5, respectively. IR (KBr): $\tilde{\nu}$ = 3290 (s), 1668 (m), 1612 (s), 1578 (m), 1537 (m), 1433 (w), 1371 (m), 1335 (w), 1259 (w), 1119 (m), 1086 (s), 1070 (s), 960 (s), 814 (m), 769 (m), 735 (w), 636 (m), 575 (w), 515 (w), 488 (w). $C_{15}H_{32}Co_2N_3O_{16}P$ (659.27): calcd. C 27.33, H 4.89, N 6.37; found C 27.41, H 4.76, N 6.42.

X-ray Crystallographic Study: Single crystals of compounds **1** and **2** were mounted on a Siemens Smart CCD diffractometer equipped with a graphite-monochromated Mo-K_α radiation source (λ = 0.71073 Å). Intensity data were collected by the narrow-frame method at 293 K. A hemisphere of data (1271 frames at 5 cm detector distances) was collected with scan widths of 0.30° in ω and exposure time of 20 s per frame. The first 50 frames were collected again at the end of data collection to assess the stability of the crystal, and it was found that the decay in intensity was less than 1%. Both data sets were corrected for Lorentz and polarization factors as well as for absorption using the SADABS program.[23] Both structures were solved by direct methods and refined by full-matrix least-squares fitting on F^2 using SHELX-97.[23] All non-hydrogen atoms were refined with anisotropic thermal parameters. Hydrogen atoms were located at geometrically calculated positions and refined with isotropic thermal parameters. Crystallographic data and structural refinements for compounds **1** and **2** are summarized in Table 3. Selected bond lengths and angles are listed in Tables 1 and 2, respectively. CCDC-233617 (**1**) and -233618 (**2**) contain the supplementary crystallographic data for this paper. These data can be obtained free of charge at www.ccdc.cam.ac.uk/conts/retrieving.html [or from the Cambridge Crystallographic Data Centre, 12 Union Road, Cambridge CB2 1EZ, UK; Fax: (internat.) + 44-1223-336-033; E-mail: deposit@ccdc.cam.ac.uk].

Acknowledgments

This work was supported by the National Natural Science Foundation of China (20371047). We thank Prof. Kim Dunbar and John Bacsa for their great help with the manuscript. K. R. D. gratefully acknowledges the Department of Energy (DE-FG03-02ER45999), the National Science Foundation (NIRT-NSF DMR-0103455), the Welch Foundation A1449, and Texas A&M University (TITF) for funding of this research.

[1] [1a] A. K. Cheetham, G. Ferey, T. Loiseau, *Angew. Chem. Int. Ed.* **1999**, *38*, 3269. [1b] J. Zhu, X. Bu, P. Feng, G. D. Stucky, *J. Am. Chem. Soc.* **2000**, *122*, 11563.
[2] A. Clearfield, in *New Developments in Ion Exchange Materials* (Eds.: M. Abe, T. Kataoka, T. Suzuki), Kodansha, Ltd., Tokyo, **1991**.
[3] G. Cao, H.-G. Hong, T. E. Mallouk, *Acc. Chem. Res.* **1992**, *25*, 420.
[4] G. Alberti, *Comprehensive Supramolecular Chemistry* (Ed: J. M. Lehn), Pergamon/Elsevier Science, Ltd., Oxford, U. K., **1996**, vol. 7.
[5] A. Clearfield, in *Progress in Inorganic Chemistry* (Ed.: K. D. Karlin), John Wiley & Sons, New York, **1998**, vol. 47, pp. 371−510.
[6] L. A. Vermeulen, in *Progress in Inorganic Chemistry*, vol. 44 (“Molecular Level Artificial Photosynthetic Materials”) (Ed.: G. J. Meyer), John Wiley & Sons, New York, **1997**, p. 143.
[7] S. G. Carling, D. Visser, R. K. Kremer, *J. Solid State Chem.* **1993**, *106*, 111.
[8] B. Bujoli, O. Pena, P. Palvadeau, J. Le Bideau, C. Payen, J. Rouxel, *Chem. Mater.* **1993**, *5*, 583.
[9] C. Bellitto, F. Federici, A. Altomare, R. Rizzi, S. A. Ibrahim, *Inorg. Chem.* **2000**, *39*, 1803.
[10] P. Rabu, P. Janvier, B. Bujoli, *J. Mater. Chem.* **1999**, *9*, 1323.
[11] S. O. H Gutschke, D. J. Price, A. K. Powell, P. T. Wood, *Angew. Chem. Int. Ed.* **1999**, *38*, 1088.
[12] [12a] P. Yin, L.-M. Zheng, S. Gao, X.-Q. Xin, *Chem. Commun.* **2001**, 2346. [12b] L.-M. Zheng, S. Gao, H.-H. Song, S. Decurtins, A. J. Jacobson, X.-Q. Xin, *Chem. Mater.* **2002**, *14*, 3143. [12c] L.-M. Zheng, P. Yin, X.-Q. Xin, *Inorg. Chem.* **2002**, *41*, 4084.
[13] [13a] R.-B. Fu, X.-T. Wu, S-M. Hu, J.-J. Zhang, Z.-Y. Fu, W.-X. Du, *Inorg. Chem. Commun.* **2003**, *6*, 827. [13b] R.-B. Fu, X.-T. Wu, S-M. Hu, J.-J. Zhang, Z.-Y. Fu, W.-X. Du, S.-Q. Xia, *Eur. J. Inorg. Chem.* **2003**, 1798. [13c] R.-B. Fu, S-M. Hu, Z.-Y. Fu, J.-J. Zhang, W.-X. Du, X.-T. Wu,, *New J. Chem.* **2003**, *27*, 230.
[14] [14a] P. Yin, S. Gao, L.-M. Zheng, Z.-M. Wang, X.-Q. Xin, *Chem. Commun.* **2003**, 1076. [14b] S.-S. Bao, L.-M. Zheng, Y.-J.

 © 2004 Wiley-VCH Verlag GmbH & Co. KGaA, Weinheim

Liu, W. Xu, S.-H. Feng, *Inorg. Chem.* **2003**, *42*, 5037. [14c] P. Yin, S. Gao, L.-M. Zheng, Z.-M. Wang, X.-Q. Xin, *Chem. Mater.* **2003**, *15*, 3233.
[15] [15a] F. Fredoueil, M. Evain, D. Massiot, M. Bujoli-Doeuff, P. Janvier, A. Clearfield, B. Bujoli, *J. Chem. Soc., Dalton Trans.* **2002**, 1508. [15b] S. Drumel, P. Janiver, P. Barboux, M. Bujoli-Doeuff, B. Bujoli, *Inorg. Chem.* **1995**, *34*, 148.
[16] [16a] J.-G. Mao, Z. Wang, A. Clearfield, *Inorg. Chem.* **2002**, *41*, 2334. [16b] J.-G. Mao, Z. Wang, A. Clearfield, *J. Chem. Soc., Dalton Trans.* **2002**, 4541. [16c] J.-G. Mao, Z. Wang, A. Clearfield, *Inorg. Chem.* **2002**, *41*, 3713. [16d] C. Lei, J.-G. Mao, Y.-Q. Sun, H.-Y. Zeng, A. Clearfield, *Inorg. Chem.* **2003**, *42*, 6157.
[17] [17a] N. Stock, S. A. Frey, G. D. Stucky, A. K. Cheetham, *J. Chem. Soc., Dalton Trans.* **2000**, 4292. [17b] S. Ayyappan, G. D. Delgado, A. K. Cheetham, G. Ferey, C. N. R. Rao, *J. Chem. Soc., Dalton Trans.* **1999**, 2905. [17c] A. Distler, S. C. Sevov, *Chem. Commun.* **1998**, 959.
[18] [18a] E. Burkholder, V. Golub, C. J. O'Connor, J. Zubieta, *Chem. Commun.* **2003**, 2128. [18b] E. Finn, R. C. Burkholder, J. Zubieta, *Chem. Commun.* **2001**, 1852. [18c] R. C. Finn, J. Zubieta, *Inorg. Chem.* **2001**, *40*, 2466. [18d] R. C. Finn, E. Burkholder, J. Zubieta, *Inorg. Chem.* **2001**, *40*, 3745.
[19] J.-G. Mao, A. Clearfield, *Inorg. Chem.* **2002**, *41*, 2319.
[20] [20a] A. Turner, P. A. Jaffrès, E. J. MacLean, D. Villemin, V. McKee, G. B. Hix, *Dalton Trans.* **2003**, 1314. [20b] H. Jankovics, M. Daskalakis, C. P. Raptopoulou, A. Terzis, V. Tangoulis, J. Giapintzakis, T. Kiss, A. Salifoglou, *Inorg. Chem.* **2002**, *41*, 3366.
[21] K. Moedritzer, R. R. Irani, *J. Org. Chem.* **1966**, *31*, 1603.
[22] B. Zhang, D. M. Poojary, A. Clearfield, G.-Z. Peng, *Chem. Mater.* **1996**, *8*, 1333.
[23] [23a] G. M. Sheldrick, *Program SADABS*, University Göttingen, **1995**. [23b] G. M. Sheldrick, *SHELXTL − Crystallographic Software Package*, version 5.1, Bruker-AXS, Madison, WI, USA, **1998**.

Received March 16, 2004
Early View Article
Published Online July 14, 2004

 © 2004 Wiley-VCH Verlag GmbH & Co. KGaA, Weinheim

Three New Organically Templated Polyoxomolybdates with Capping Selenite Anions

Mei-Ling Feng[a] and Jiang-Gao Mao*[a]

Keywords: Hydrothermal synthesis / Inorganic-organic hybrid composites / Molybdenum / Polyoxometalates / Selenium

Three new organically templated polyoxomolybdates with selenite anions as capping groups have been synthesized by hydrothermal reactions and structurally characterized. The structure of $\{Hbipy\}_3\{KMo_4O_{13}(SeO_3)\}$ (**1**; bipy = 4,4′-bipyridine) features a 1D anionic double chain of $\{KMo_4O_{13}(SeO_3)\}^{3-}$ units. Four $Mo^{VI}O_6$ octahedra in compound **1** form a planar Mo_4O_{13} cluster unit through corner-, edge- and face-sharing. The Mo_4O_{13} cluster unit is further capped by an $Se^{IV}O_3$ group in a bidentate fashion. These monocapped cluster units are further interconnected by bridging K^+ cations into a 1D double chain. Both $\{H_2bipy\}_2\{Mo_5O_{15}(SeO_3)_2\}\cdot H_2O$ (**2**) and $\{H_2pip\}_2\{Mo_5O_{15}(SeO_3)_2\}\cdot 3H_2O$ (**3**; pip = piperazine) contain a bicapped Mo_5O_{15} cluster unit in which five $Mo^{VI}O_6$ octahedra form a planar Mo_5O_{15} cluster unit through edge- and corner-sharing, with the two $Se^{IV}O_3$ anions as tridentate capping groups on the two open sides of the cluster unit to form an $\{Mo_5O_{15}(SeO_3)_2\}^{4-}$ anion. The $\{Mo_5O_{15}(SeO_3)_2\}^{4-}$ cluster anions in compounds **2** and **3** are further inter-linked by the organic templates through hydrogen bonds to form a 2D layer.
(© Wiley-VCH Verlag GmbH & Co. KGaA, 69451 Weinheim, Germany, 2004)

Introduction

Polyoxometalates (POMs) are one of the most widely used inorganic components due to the extreme variability of their compositions, molecular characteristics, properties and applications.[1] Recently, a lot of research efforts have been focused on the functionalization of POMs with transition metal complex or lanthanide complex moieties — the coordinated transition metal or lanthanide metal complex cation serves to provide charge-compensation, space-filling, and structure-directing roles. In most cases, the transitional-metal and the rare-earth ions are found to be either sandwiched between two polymolybdate anions or as a capping atom on the cluster unit.[2−5] For polyoxomolybdates with a small cluster unit, such as Mo_4O_{13}, Mo_5O_{15} and Mo_6O_{18}, the cluster unit can be further capped by one or two tetrahedral groups such as PO_4, RPO_3, SO_4, AsO_4, $RAsO_3$, etc.[6−8] However, studies on polymolybdates with capping XO_3 groups (X = Se^{IV}, Te^{IV}, As^{III}, Sb^{III}, Bi^{III}) are rare.[9]

We are particularly interested in metal selenites. A few examples of open frameworks of metal selenites have been reported.[10−13] An organically templated 2D zinc selenite was first reported by Harrison et al.[10] Organically templated 3D iron(II), cobalt(II), nickel(II) and zinc(II) selenites have also been reported by Rao and co-workers.[11] Both organically templated and organically linked vanadium selenites have also been reported.[12,13] So far only polyoxomolybdates with an Mo_6O_{18} cluster unit capped by a selenite group have been reported.[9] We therefore decided to study systematically the syntheses and crystal structures of organically templated polyoxomolybdates containing capping selenite groups. Our research efforts led to three new organically templated polyoxomolybates with selenite anions as capping groups, namely $\{Hbipy\}_3\{KMo_4O_{13}(SeO_3)\}$ (**1**), with an $\{Mo_4O_{13}\}^{2-}$ cluster unit, and $\{H_2bipy\}_2\{Mo_5O_{15}(SeO_3)_2\}\cdot H_2O$ (**2**) and $\{H_2pip\}_2\{Mo_5O_{15}(SeO_3)_2\}\cdot 3H_2O$ (**3**) containing an Mo_5O_{15} cluster unit capped by two $Se^{IV}O_3$ anions. We report here their syntheses, characterizations and crystal structures.

Results and Discussion

The synthetic procedures for the formation of compounds **1**−**3** are interesting. Both compounds **1** and **2** were obtained from the same starting materials but in a different molar ratio: a higher Mo/Se ratio leads to compound **2** with an MO_5O_{15} cluster unit but without K^+ as an inter-cluster linker. For the synthesis of compound **3**, it is necessary to use $(NH_4)_6Mo_7O_{24}$ as the source of the Mo^{VI} ions as the use of K_2MoO_4 led to $\{H_2bipy\}_3\{Mo_8O_{27}\}$ with a known $\{Mo_8O_{27}\}^{6-}$ cluster unit.[14] Thus, the source of molybdenum, the Mo/Se ratio, the cation used and the pH value of the reaction have a strong effect on the compound formed.

The structure of compound **1** (Figure 1) features a 1D anionic double chain composed of $\{KMo_4O_{13}(SeO_3)\}^{3-}$ units in which the monocapped $Mo_4O_{13}(SeO_3)$ cluster units are interconnected by bridging K^+ cations. As shown in

[a] State Key Laboratory of Structural Chemistry, Fujian Institute of Research on the Structure of Matter, The Chinese Academy of Sciences,
Fuzhou 350002, P. R. China
E-mail: mjg@ms.fjirsm.ac.cn

 © 2004 Wiley-VCH Verlag GmbH & Co. KGaA, Weinheim DOI: 10.1002/ejic.200400246

Figure 1, there are four Mo and one Se atoms in an asymmetric unit. All four Mo atoms are octahedrally coordinated. The Mo−O bonds are in the range 1.689(4)−2.416(4) Å. The MoO_6 octahedra are severely distorted, two Mo−O bonds are significantly elongated and two Mo−O(terminal) bonds are much shorter than the remaining ones. The Se atom is three-coordinate, with Se−O distances ranging from 1.644(5) to 1.738(4) Å. These Mo−O and Se−O distances are similar to those reported in the literature.[6,9] Based on the results of bond-valence calculations, all Mo atoms are in the +6 oxidation state, and the Se atom has a +4 oxidation state: the calculated total bond valences for the Mo atoms are in the range of 5.945 to 6.062, and that for the Se atom is 4.03.[15] Thus, the polyhedron of Se^{IV} can be described as a ψ-SeO_3 tetrahedron with one corner of the tetrahedron occupied by the lone pair of electrons.

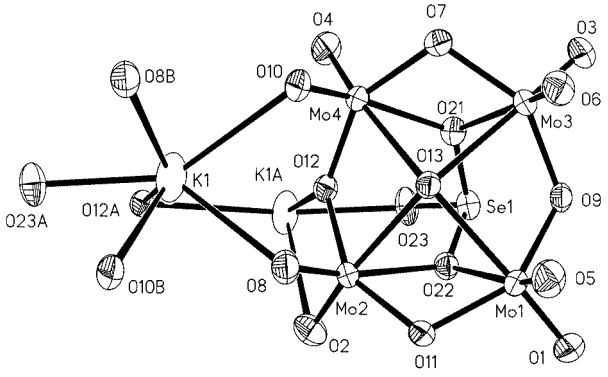

Figure 1. ORTEP representation of the asymmetric unit of compound **1**; thermal ellipsoids are drawn at 50% probability; the organic templates have been omitted for clarity; symmetry codes for the generated atoms: a: $-x + 1/2, -y + 1/2, -z + 1/2$; b: $-x + 1/2, -y + 1/2, -z + 2$

The four $Mo^{VI}O_6$ octahedra are interconnected by edge- and face-sharing to form a planar $Mo_4O_{13}(SeO_3)$ cluster unit. The mean deviation from the plane defined by Mo(1), Mo(2), Mo(3), and Mo(4) is 0.0104 Å. O(13) is a μ_4 metal linker, bridging all four Mo^{VI} centers and lies 0.734 Å out of the Mo_4 plane. The selenite group is capping on the opposite site of O(13) in a bidentate fashion. O(21) and O(22) each bridge two Mo^{VI} centers, whereas O(23) is not bonded to the Mo^{VI} center. Two $Mo^{VI}O_6$ octahedra [Mo(1) and Mo(2) or Mo(3) and Mo(4)] form a dimer by face-sharing, resulting in two relatively short Mo···Mo separations [3.1428(8) and 3.1543(8) Å]. These dimers are further interconnected by edge-sharing, although with larger Mo···Mo separations [3.304(1) and 3.329(1) Å]. The Mo−O(SeO_3) bond lengths are in the range 2.258(4)−2.289(4) Å (Table 1), and are similar to those reported in heteropolymolybdates of Se^{IV} functionalized by amino acids containing an $Mo_6O_{18}(SeO_3)$ cluster core.[9] To some extent, such a $Mo_4O_{13}(SeO_3)$ cluster unit resembles those reported in tetramolybdo complexes of dialkyl and diaryl arsinates.[6] However, this type of cluster unit differs significantly from the Mo_4O_{12} cluster in copper−Mo−$O_3PCH_2CH_2PO_3$ com-

Table 1. Selected bond lengths [Å] for compounds **1**−**3**

Compound **1**[a]			
Mo(1)−O(1)	1.697(4)	Mo(1)−O(5)	1.704(5)
Mo(1)−O(9)	1.929(4)	Mo(1)−O(11)	1.934(4)
Mo(1)−O(22)	2.289(4)	Mo(1)−O(13)	2.386(4)
Mo(1)−Mo(2)	3.1428(8)	Mo(2)−O(2)	1.689(4)
Mo(2)−O(8)	1.714(4)	Mo(2)−O(11)	1.912(4)
Mo(2)−O(12)	1.928(4)	Mo(2)−O(22)	2.258(4)
Mo(2)−O(13)	2.411(4)	Mo(3)−O(3)	1.705(4)
Mo(3)−O(6)	1.709(4)	Mo(3)−O(9)	1.910(4)
Mo(3)−O(7)	1.929(4)	Mo(3)−O(21)	2.287(4)
Mo(3)−O(13)	2.394(4)	Mo(3)−Mo(4)	3.1543(8)
Mo(4)−O(4)	1.705(4)	Mo(4)−O(10)	1.725(4)
Mo(4)−O(7)	1.909(4)	Mo(4)−O(12)	1.917(4)
Mo(4)−O(21)	2.282(4)	Mo(4)−O(13)	2.416(4)
K(1)−O(23)#1	2.564(5)	K(1)−O(12)#1	2.706(4)
K(1)−O(8)#2	2.831(5)	K(1)−O(8)	2.831(5)
K(1)−O(10)	2.949(5)	K(1)−O(10)#2	3.069(5)
Compound **2**[b]			
Mo(1)−O(8)	1.735(16)	Mo(1)−O(8)#1	1.735(16)
Mo(1)−O(6)#1	1.903(15)	Mo(1)−O(6)	1.903(15)
Mo(1)−O(10)	2.318(15)	Mo(1)−O(10)#1	2.318(15)
Mo(2)−O(1)	1.709(17)	Mo(2)−O(4)	1.710(16)
Mo(2)−O(2)	1.882(5)	Mo(2)−O(3)	1.945(16)
Mo(2)−O(9)#1	2.361(16)	Mo(2)−O(11)	2.380(14)
Mo(3)−O(5)	1.699(15)	Mo(3)−O(7)	1.726(15)
Mo(3)−O(6)	1.943(16)	Mo(3)−O(3)	1.968(16)
Mo(3)−O(11)	2.164(15)	Mo(3)−O(10)#1	2.360(14)
Hydrogen bonds:			
N(1)···O(3)#2	2.625(25)	N(2)···O(8)#3	2.743(28)
O(1W)···O(9)#1	2.820(24)	O(1W)···O(9)	2.820(24)
Compound **3**[c]			
Mo(1)−O(1)	1.711(5)	Mo(1)−O(2)	1.721(5)
Mo(1)−O(15)	1.911(5)	Mo(1)−O(11)	1.924(5)
Mo(1)−O(31)	2.318(5)	Mo(1)−O(22)	2.363(5)
Mo(2)−O(3)	1.711(5)	Mo(2)−O(4)	1.713(5)
Mo(2)−O(12)	1.900(5)	Mo(2)−O(11)	1.997(5)
Mo(2)−O(32)	2.194(5)	Mo(2)−O(22)	2.328(5)
Mo(3)−O(5)	1.700(5)	Mo(3)−O(6)	1.705(6)
Mo(3)−O(13)	1.938(5)	Mo(3)−O(12)	1.947(5)
Mo(3)−O(32)	2.327(5)	Mo(3)−O(23)	2.354(5)
Mo(4)−O(7)	1.699(5)	Mo(4)−O(8)	1.723(5)
Mo(4)−O(13)	1.882(5)	Mo(4)−O(14)	1.960(5)
Mo(4)−O(21)	2.272(5)	Mo(4)−O(33)	2.317(5)
Mo(5)−O(9)	1.696(5)	Mo(5)−O(10)	1.713(6)
Mo(5)−O(14)	1.956(5)	Mo(5)−O(15)	1.969(5)
Mo(5)−O(21)	2.202(5)	Mo(5)−O(31)	2.278(5)
Hydrogen bonds:			
N(1)···O(10)#3	2.710(10)	N(1)···O(14)#4	2.786(8)
N(2)···O(11)	2.768(8)	N(4)···O(2W)#5	2.783(9)
O(1W)···O(2W)#5	2.734(10)		

[a] Symmetry transformations used to generate equivalent atoms: #1: $-x + 1/2, -y + 1/2, -z + 1$; #2: $-x + 1/2, -y + 1/2, -z + 2$; #3: $-x, 1 - y, 1 - z$; #4: $-x, y, 1/2 - z$. [b] Symmetry transformations used to generate equivalent atoms: #1: $-x + 1, y, -z + 1$; #2: $1/2 - x, -1/2 + y, 1 - z$; #3: $1 - x, y, -z$. [c] Symmetry transformations used to generate equivalent atoms: #1: $-x + 1, -y, -z + 1$; #2: $-x, -y + 1, -z + 1$; #3: $x - 1, y, z$; #4: $-1/2 + x, 1/2 - y, 1/2 + z$; #5: $-1/2 + x, 1/2 - y, -1/2 + z$.

 © 2004 Wiley-VCH Verlag GmbH & Co. KGaA, Weinheim

pounds,[16] in that one Mo^{VI} ion in the latter cluster compounds is in a square-pyramidal geometry and the cluster units are noncyclic.

The $\{Mo_4O_{13}(SeO_3)\}^{4-}$ cluster units in compound **1** are bridged by K^+ ions through K−O(23) bonds to form a novel 1D double chain along the *c* axis (Figure 2). The K^+ ion is six-coordinate, with four terminal oxygen atoms from four cluster units, one bridging oxygen atom [O(12a)] from a cluster unit and one oxygen atom from a selenite group. The K−O distances are in the range 2.564(5)−3.069(5) Å (Table 1). The templates — the bipy ligands — are singly protonated. Packing of these templates forms cavities, which are occupied by $\{KMo_4O_{13}(SeO_3)\}^{3-}$ anionic chains (Figure 3).

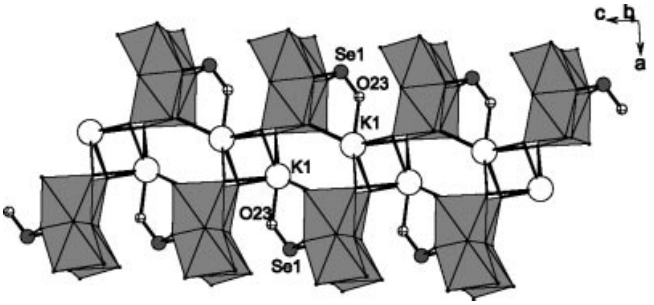

Figure 2. The 1D anionic chain of $\{KMo_4O_{13}(SeO_3)\}^{3-}$ moieties along the *c* axis in **1**; the MoO_6 octahedra are shaded in gray; the K, Se and O atoms are drawn as open, hatched and crossed circles, respectively

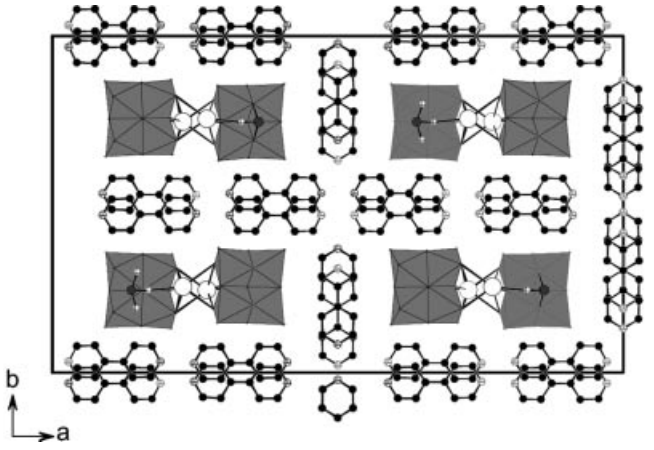

Figure 3. A view of the crystal structure of **1** along the *c* axis; the MoO_6 octahedra are shaded in gray; the K, Se, C, N and O atoms are drawn as open, hatched, black, octanded and crossed circles, respectively

Compounds **2** and **3** both contain a bicapped $\{Mo_5O_{15}(SeO_3)_2\}^{4-}$ anionic cluster unit (Figure 4). Five MoO_6 octahedra form a planar Mo_5O_{15} unit by sharing four edges and one corner. The corner-sharing occurs between two $Mo(2)O_6$ octahedra in compound **2**, and between $Mo(3)O_6$ and $Mo(4)O_6$ octahedra in compound **3.** The two opposite sides of the cluster unit are capped by two selenite groups (Figure 4). This type of bicapped Mo_5O_{15} cluster unit is similar to those reported previously in polymolybdophosphonates or -phosphates.[7] The Mo_5O_{15} cluster unit in compound **2** is less coplanar than the Mo_4O_{13} cluster unit in compound **1**. The mean deviation from the plane defined by Mo(1), Mo(2), Mo(3), and Mo(2a) and Mo(3a) is 0.1847 Å. The two Se^{IV} centers are 2.133 Å away from the Mo_5 plane. The Mo−O and Se−O distances are similar to those in compound **1** (Table 1). All Mo atoms are in the +6 oxidation state and the Se atoms are in the +4 oxidation state based on the results of bond-valence calculations.[15]

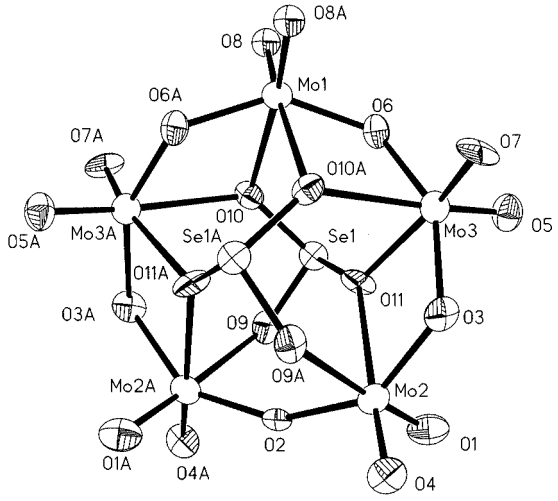

Figure 4. ORTEP representation of the $Mo_5O_{15}(SeO_3)_2^{4-}$ unit in **2**; the thermal ellipsoids are drawn at 50% probability; symmetry code for the generated atoms: a: $1 - x, y, 1 - z$

The bicapped $\{Mo_5O_{15}(SeO_3)_2\}^{4-}$ anionic cluster units in compounds **2** are hydrogen-bonded with the templates, which in this case are doubly protonated bipy ligands, $\{H_2bipy\}^{2+}$, resulting in a hydrogen-bonded <201> 2D layer (Figure 5). The hydrogen bonds are formed between the amine groups of bipy and the terminal oxygen atoms of the cluster unit (Figure 5, Table 1). The lattice water mol-

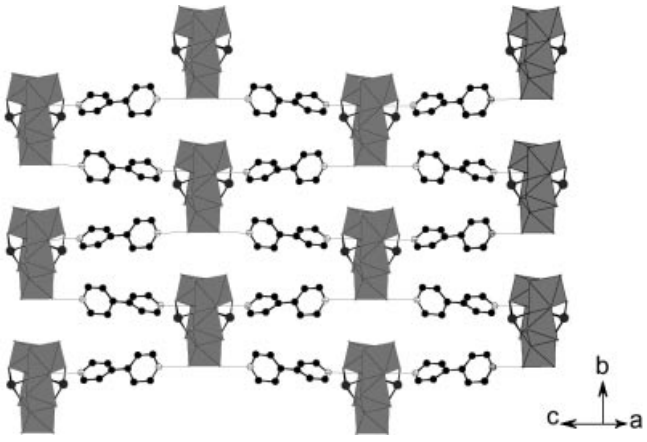

Figure 5. A <201> layer built from $Mo_5O_{15}(SeO_3)_2^{4-}$ units interconnected by $[H_2bipy]^{2+}$ cations through hydrogen bonding in **2**; the MoO_6 octahedra are shaded in gray; the Se, C, N and O atoms are drawn as open, black, octanded and crossed circles, respectively; hydrogen bonds are drawn as dotted lines

 © 2004 Wiley-VCH Verlag GmbH & Co. KGaA, Weinheim

ecules are located between the layers and are involved in hydrogen bonding with the oxygen atom [O(9)] of the selenite group (Table 1).

Similar to compound **2**, the bicapped $\{Mo_5O_{15}(SeO_3)_2\}^{4-}$ anionic cluster units of compounds **3** are also interlinked by hydrogen bonds, although in this case to doubly protonated piperazines, containing atoms N1 and N2, resulting in a <040> corrugated layer (Figure 6, Table 1). The other doubly protonated piperazine molecules, containing N3 and N4, are located in the cavities formed by packing of the 2D layers, as are the lattice water molecules. These lattice water molecules are also involved in hydrogen bonding (Table 1).

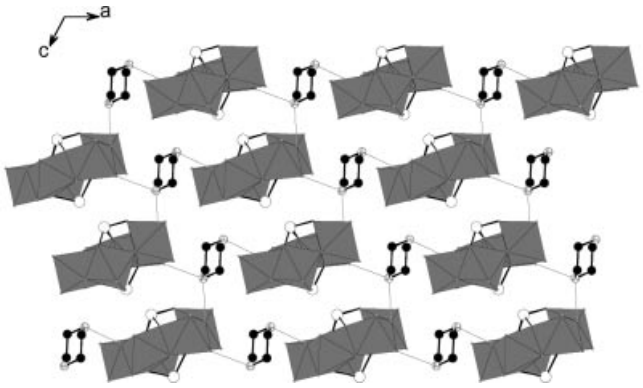

Figure 6. A <040> corrugated layer built from $Mo_5O_{15}(SeO_3)_2^{4-}$ units interconnected by $[H_2pip]^{2+}$ cations through hydrogen bonding in **3**; the MoO_6 octahedra are shaded in gray; the Se, C, N and O atoms are drawn as open, black, octanded and crossed circles, respectively; hydrogen bonds are drawn as dotted lines

The results of XRD powder-diffraction studies for compounds **1**−**3** indicate that all three compounds were isolated as single phases.

The IR spectra of compounds **1**−**3** all exhibit a strong band around 930−933 cm^{-1}, characteristic of ν(Mo=O). The bands around 720−730 and 438−457 cm^{-1} can be assigned to the vibrations of the selenite groups. The bands around 1614−1622 and 1403−1421 cm^{-1} originate from the templates — bipy in compounds **1** and **2**, and piperazine in compound **3**.

The TGA diagram of compound **1** indicates that it is stable up to 234 °C (Figure 7). The subsequent weight loss corresponds to the release of the template molecules and the decomposition of the cluster chain. The process is complete at 490 °C. Compound **2** starts to release its lattice water at 160 °C; the second weight loss corresponds to the release of the template bipy molecules and the decomposition of the cluster unit, which is complete at 487 °C. The TGA curves of compound **3** show two main weight losses (Figure 7). The first one starts at 143 °C and is complete at 202 °C, corresponding to the release of its three lattice water molecules. The unusually high temperature needed for the release of lattice water molecules may be due to the strong hydrogen bonds formed. The observed weight loss of 4.3% is in good agreement with the calculated value (4.5%). The

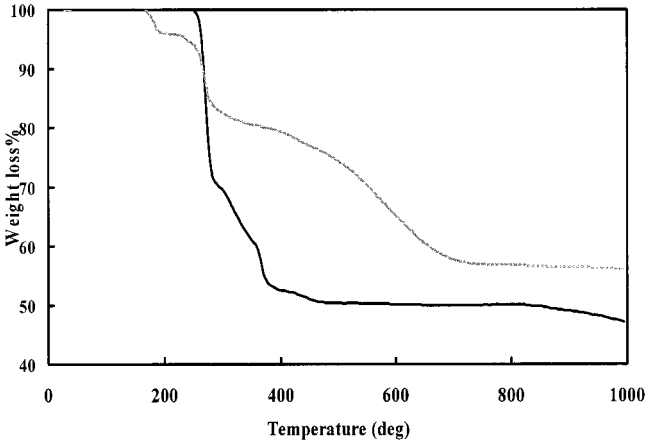

Figure 7. TGA curves for compounds **1** (black line) and **3** (grey line)

second weight loss, covering a temperature range from 235 to 843 °C, corresponds to the loss of the piperazine molecules and decomposition of the compound. The residual solids were not identified due to insufficient samples collected.

Conclusion

Three novel organically templated polymolybdates containing selenite groups as capping groups have been synthesized by hydrothermal reactions. These three examples demonstrate that the selenite group can be capped on many other polymolybdate cluster units in addition to the Mo_6O_{18} cluster reported previously.[9] Our future work will explore more organically templated selenite- or tellurite-containing polymolybdates.

Experimental Section

Materials and Methods: All chemicals were obtained from commercial sources and used without further purification. Mo, K and Se analyses were carried out with an ICPQ-100 spectrometer. IR spectra were recorded with a Magna 750 FT-IR spectrometer as KBr pellets in the range 4000−400 cm^{-1}. Thermogravimetric analyses were carried out with a NETZSCH STA 449C unit at a heating rate of 15 °C/min under nitrogen. The XRD powder patterns were collected with a Philips X'Pert-MPD diffractometer using graphite-monochromated Cu-K_α radiation in the angular range $2\theta = 5-70°$ with a step size of 0.02° and a counting time of 3 s per step.

Preparation of $\{Hbipy\}_3\{KMo_4O_{13}(SeO_3)\}$ (1): A mixture of K_2MoO_4 (0.270 g, 1.0 mmol), SeO_2 (0.221 g, 2.0 mmol) and 4,4′-bipyridine (0.0792 g, 0.5 mmol) in 10 mL of distilled water was sealed in an autoclave equipped with a Teflon liner (25 mL), and then heated at 160 °C for 6 d. The pH values before and after the reaction were 5.0 and 5.5, respectively. Colorless, needle-shaped crystals of **1** were collected in about 33% yield (0.101 g) (based on Mo). $C_{30}H_{27}KMo_4N_6O_{16}Se$ (1229.4): calcd. C 29.28, H 2.21, K 3.18, Mo 31.22, N 6.83, Se 6.42; found C 29.13, H 1.85, K 2.8, Mo 30.6, N 6.76, Se 6.7. IR (KBr): $\tilde{\nu}$ = 3435 br, 2047 m, 1614 s, 1595 s, 1567 m, 1526 m, 1489 s, 1407 m, 1326 m, 1213 s, 1065 m, 1009

 © 2004 Wiley-VCH Verlag GmbH & Co. KGaA, Weinheim

m, 995 m, 930 s, 907 s, 894 s, 870 s, 807 s, 723 s, 685 s, 568 s, 539 m, 457 m cm^{-1}.

Preparation of $\{H_2bipy\}_2\{Mo_5O_{15}(SeO_3)_2\}\cdot H_2O$ (2): A mixture of K_2MoO_4 (0.551 g, 2.0 mmol), SeO_2 (0.229 g, 2.0 mmol) and 4,4′-bipyridine (0.0792 g, 0.5 mmol) in 10 mL of distilled water was sealed in an autoclave equipped with a Teflon liner (25 mL), and then heated at 160 °C for 6 d. The initial and final pH values for the reaction solution were 5.0 and 6.0, respectively. Colorless, plate-shaped crystals of **2** were collected in about 48% yield (0.251 g) (based on Mo). $C_{20}H_{22}Mo_5N_4O_{22}Se_2$ (1308.4): calcd. C 18.34, H 1.69, Mo 36.55, N 4.28, Se 12.07; found C 18.09, H 1.8, Mo 36.1, N 4.56, Se 11.8. IR (KBr): $\tilde{\nu}$ = 3089 br, 2080 m, 1622 s, 1557 m, 1514 m, 1489 s, 1404 m, 1371 m, 1204 s, 1001 m, 932 s, 904 s, 847 m, 803 s, 723 s, 684 s, 584 s, 553 s, 442 m cm^{-1}.

Preparation of $\{H_2pip\}_2\{Mo_5O_{15}(SeO_3)_2\}\cdot 3H_2O$ (3): A mixture of $(NH_4)_6Mo_7O_{24}$ (0.355 g, 0.29 mmol), SeO_2 (0.339 g, 3.0 mmol) and piperazine (0.0896 g, 1.0 mmol) in 10 mL of distilled water was sealed in an autoclave equipped with a Teflon liner (25 mL), and then heated at 110 °C for 5 d. The pH values before and after the reaction were 5.0 and 5.5, respectively. Colorless, brick-shaped crystals of **3** were collected in about 53% yield (0.132 g) (based on Mo). $C_8H_{30}Mo_5N_4O_{24}Se_2$ (1204.0): calcd. C 7.97, H 2.51, Mo 39.84, N 4.65, Se 13.12; found C 7.819, H 2.38, Mo 39.2, N 4.39, Se 12.7. IR (KBr): $\tilde{\nu}$ = 3017 br, 1615 s, 1579 s, 1454 s, 1421 s, 1382 s, 1329 w, 1307 m, 1205 s, 1086 m, 1075 m, 1059 m, 1004 s, 932 s, 902 s, 780 w, 730 s, 651 s, 578 s, 480 m, 438 m cm^{-1}.

X-ray Single-Crystal Structure Determination: Single crystals of compounds **1**−**3** were mounted on a Siemens Smart CCD diffractometer equipped with graphite-monochromated Mo-K_α radiation (λ = 0.71073 Å). Intensity data were collected by the narrow-frame method at 293 K. All three data sets were corrected for Lorentz and polarization factors, as well as for absorption, with the SADABS program.[17a] The space groups of compounds **1** and **3** were determined uniquely to be *C*2/*c* and $P2_1/n$, respectively. For compound **2** the space group could be one *C*2, *C*2/*m*, or *Cm*. However, based on the E-value statistics, it is noncentrosymmetric, and furthermore, no reasonable solution was found for *C*2/*m* and *Cm*; thus, *C*2 was used for the subsequent refinements of compound **2**. All structures were solved by direct methods and refined by full-matrix least-squares fitting on F^2 with SHELX-97.[17b] All non-hydrogen atoms were refined with anisotropic thermal parameters. Hydrogen atoms attached to carbon atoms and of amine groups were located at geometrically calculated positions and refined with isotropic thermal parameters. The hydrogen positions for the singly protonated bipy ligands in compound **2** were difficult to determine accurately and were not refined; neither were the hydrogen atoms of the lattice water molecules. Crystallographic data and structural refinements for compounds **1**−**3** are summarized in Table 2. Selected bond lengths are listed in Table 1. CCDC-234093 (**1**), -234094 (**2**) and -234095 (**3**) contain the supplementary crystallographic data for this paper. These data can be obtained free of charge at www.ccdc.cam.ac.uk/conts/retrieving.html [or from the Cambridge Crystallographic Data Centre, 12 Union Road, Cambridge CB2 1EZ, UK; Fax: (internat.) + 44-1223-336-033; E-mail: deposit@ccdc.cam.ac.uk].

Acknowledgments

This work was supported by the National Natural Science Foundation of China (20371047).

[1] [1a] *Polyoxometalate Chemistry for Nanocomposite Design* (Eds.: M. T. Pope, T. Yamase), Kluwer, Dordrecht, **2002**. [1b] *Polyoxometalates: From Topology via Self-Assembly to Applications* (Eds.: M. T. Pope, A. Müller), Kluwer, Dordrecht, **2001**.

[2] [2a] D. Hagrman, P. J. Zapf, J. Zubieta, *Chem. Commun.* **1998**, 1283. [2b] Y.-S. Zhou, L.-J. Zhang, X.-Z. You, S. Natarajan, *J. Solid State Chem.* **2001**, *159*, 209. [2c] L. A. Meyer, R. C. Haushalter, *Inorg. Chem.* **1993**, *32*, 1579. [2d] R. S. Rarig Jr., J. Zubieta, *J. Solid State Chem.* **2002**, *167*, 370. [2e] R. S. Rarig Jr., L. Bewley, V. Golub, C. J. O'Connor, J. Zubieta, *Inorg. Chem. Commun.* **2003**, *6*, 539.

[3] [3a] C.-D. Wu, C.-Z. Lu, H.-H. Zhuang, J.-S. Huang, *Inorg. Chem.* **2002**, *41*, 5636. [3b] M. Yuan, E. Wang, Y. Lu, Y. Li, C. Hu, N. Hu, N. H. Jia, *Inorg. Chem. Commun.* **2002**, *5*, 505. [3c] C. du Peloux, A. Dolbecq, P. Mialane, J. Marrot, E. Rivière, F. Sécheresse, *Angew. Chem. Int. Ed.* **2001**, *40*, 2455. [3d] L. Xu, Y. Sun, E. Wang, E. Shen, Z. Liu, C. Hu, Y. Xing, Y. Lin, H. Jia, *New J. Chem.* **1999**, *23*, 1041. [3e] L. Xu, Y. Sun, E. Wang, E. Shen, Z. Liu, C. Hu, Y. Xing, Y. Lin, H. Jia, *J. Solid State Chem.* **1999**, *146*, 533.

[4] [4a] C.-D. Wu, C.-Z. Lu, H.-H. Zhuang, J.-S. Huang, *J. Am.*

Table 2. Crystal data and structure refinements for compounds **1**−**3**

	1	**2**	**3**
Empirical formula	$C_{30}H_{27}KMo_4N_6O_{16}Se$	$C_{20}H_{22}Mo_5N_4O_{22}Se_2$	$C_8H_{30}Mo_5N_4O_{24}Se_2$
Formula mass	1229.40	1308.4	1203.98
Space group	*C*2/*c*	*C*2	$P2_1/n$
a [Å]	42.480(3)	20.466(1)	12.0310(2)
b [Å]	24.841(2)	8.6581	21.5069(3)
c [Å]	7.040(1)	8.6581(6)	12.7401(1)
β [°]	98.476(3)	113.600(3)	117.723(1)
V [Å^3]	7347.5(8)	1754.3(2)	2918.08(7)
Z	8	2	4
$D_{calcd.}$ [g·cm^{-3}]	2.223	2.476	2.741
μ [mm^{-1}]	2.522	3.905	4.687
Reflections collected	22520	2700	8650
Independent reflections	6497 (R_{int} = 4.38%)	2420 (R_{int} = 5.34%)	5025 (R_{int} = 2.55%)
Observed data [$I > 2\sigma(I)$]	5112	2017	4506
GOF on F^2	1.123	1.212	1.101
*R*1, *wR*2 [$I > 2\sigma(I)$][a]	0.0490/0.1006	0.0722/0.1424	0.0401/0.0907
*R*1, *wR*2(all data)	0.0686/0.1087	0.0991/0.1640	0.0472/0.0956

[a] $R1 = \|F_o - F_c\|/|F_o|$; $wR2 = \{w(F_o^2 - F_c^2)^2/w(F_o^2)^2\}^{1/2}$.

 © 2004 Wiley-VCH Verlag GmbH & Co. KGaA, Weinheim

Chem. Soc. **2002**, *124*, 3836. [4b] C.-Z. Lu, C.-D. Wu, H.-H. Zhuang, J.-S. Huang, *Chem. Mater.* **2002**, *14*, 2649. [4c] C.-D. Wu, C.-Z. Lu, X. Lin, H.-H. Zhuang, J.-S. Huang, *Inorg. Chem. Commun.* **2002**, *5*, 664. [4d] D. Hagrman, J. Zubieta, *Chem. Commun.* **1998**, 2005; E. Brukholder, J. Zubieta, J. *Chem. Commun.* **2001**, 2056.

[5] [5a] L. A. Mundi, R. C. Haushalter, *Inorg. Chem.* **1992**, *31*, 3050. [5b] M. Yuan, E. Wang, Y. Lu, Y. Li, C. Hu, N. Hu, H. Jia, *J. Solid State Chem.* **2003**, *170*, 192. [5c] Y. Zhou, L. Zhang, X. You, S. Natarajan, *Inorg. Chem. Commun.* **2001**, *4*, 699.

[6] [6a] K. M. Barkigia, L. M. Rajkovic, M. T. Pope, E. Prince, C. O. Quicksall, *Inorg. Chem.* **1980**, *19*, 2531. [6b] K. M. Barkigia, L. M. Rajkovic, M. T. Pope, C. O. Quicksall, *J. Am. Chem. Soc.* **1975**, *97*, 4146. [6c] K. Y. Matsumoto, *Bull. Chem. Soc. Jpn.* **1979**, *52*, 3284.

[7] [7a] E. Burholder, V. Golub, C. J. O'Connor, J. Zubieta, *Chem. Commun.* **2003**, 2128. [7b] R. B. Fu, X. T. Wu, S. M. Hu, J. J. Zhang, Z. Y. Fu, W. X. Du, S. Q. Xia, *Eur. J. Inorg. Chem.* **2003**, 1798. [7c] U. Kortz, C. Marquer, R. Thouvenot, M. Nierlich, *Inorg. Chem.* **2003**, *42*, 1158. [7d] E. Burholder, V. Golub, C. J. O'Connor, J. Zubieta, *Inorg. Commun.* **2003**, *42*, 6729.

[8] [8a] U. Kortz, *Inorg. Chem.* **2000**, *39*, 625. [8b] D. G. Lyxell, D. Bostrom, M. Hashimoto, L. Pettersson, *Acta Crystallogr., Sect. B* **1998**, *54*, 424. [8c] K. F. Hsu, S. L. Wang, *Inorg. Chem.* **1998**, *37*, 3230. [8d] U. Kortz, M. T. Pope, *Inorg. Chem.* **1995**, *34*, 2160.

[9] U. Kortz, M. G. Savelieff, F. Y. A. Ghali, L. M. Khalil, S. M. Maalouf, D. I. Sinno, *Angew. Chem. Int. Ed.* **2002**, *41*, 4070.

[10] W. T. A. Harrison, M. L. F. Phillips, J. Stanchfield, T. M. Nenoff, *Angew. Chem. Int. Ed.* **2000**, *39*, 3808.

[11] [11a] A. Choudhury, D. Udaya Kumar, C. N. R. Rao, *Angew. Chem. Int. Ed.* **2002**, *41*, 158. [11b] D. Udayakumar, C. N. R. Rao, *J. Mater. Chem.* **2003**, *13*, 1635.

[12] I. Pasha, A. Choudhury, C. N. R. Rao, *Inorg. Chem.* **2003**, *42*, 410.

[13] Z. Shi, D. Zhang, S. Feng, G. Li, Z. Dai, W. Fu, X. Chen, J. Hua, *J. Chem. Soc., Dalton Trans.* **2002**, 1832.

[14] W. T. A. Harrison, L. L. Dussack, A. J. Jacobson, *Acta Crystallogr., Sect. C* **1996**, *52*, 1075.

[15] I. D. Brown, D. Altermatt, *Acta Crystallogr., Sect. B* **1985**, *41*, 244.

[16] [16a] R. C. Finn, J. Zubieta, *Inorg. Chem.* **2001**, *40*, 2466. [16b] R. C. Finn Jr., R. S. Rarig, J. Zubieta, *Inorg. Chem.* **2002**, *41*, 2109.

[17] [17a] G. M. Sheldrick, *Program SADABS*, Universität Göttingen, **1995**. [17b] G. M. Sheldrick, *SHELXTL, Crystallographic Software Package*, version 5.1, Bruker-AXS, Madison, WI, **1998**.

Received March 28, 2004
Early View Article
Published Online July 22, 2004

 © 2004 Wiley-VCH Verlag GmbH & Co. KGaA, Weinheim

A New 3-D Open-Framework Zinc Phosphate $[C_6H_{16}N_2]\cdot[Zn_2(HPO_4)_3]$ Synthesized by a Solvothermal Combinatorial Approach

Yu Song,[a] Jihong Yu,*[a] Yi Li,[a] Min Zhang,[a] and Ruren Xu*[a]

Keywords: Solvothermal synthesis / Structure / Combinatorial approach / Host-guest systems / Zinc phosphate

By application of a combinatorial approach, a new open-framework zinc phosphate $[C_6H_{16}N_2]\cdot[Zn_2(HPO_4)_3]$ (denoted as phase **D**) has been obtained in the $Zn(OAc)_2\cdot2H_2O/H_3PO_4/N,N'$-dimethylpiperazine/ethylene glycol solvothermal reaction system at 180 °C. The factors influencing formation of the reaction products, such as crystallization temperature, solvent, as well as gel compositions, have been systematically studied. Phase **D** was characterized by X-ray powder diffraction, ICP, and TG analyses, and its structure was determined by single-crystal X-ray diffraction analysis. It crystallizes in the monoclinic space group $P2_1/n$ (no.14), with a = 8.6931(3) Å, b = 14.4394(5) Å, c = 12.6492(3) Å, β = 96.418(2)°, and Z = 4. It is composed of ZnO_4, $PO_3(OH)$ and $PO_2(OH)(=O)$ tetrahedral units linked by Zn–O–P bonds, forming an open-framework with intersecting eight-membered ring channels along the [100], [010], and [101] directions.
(© Wiley-VCH Verlag GmbH & Co. KGaA, 69451 Weinheim, Germany, 2004)

Introduction

Since pioneering work on the preparation of aluminophosphate molecular sieves by Wilson et al. in 1982,[1] open-framework metal phosphates have received much attention because of their great importance in many current fields of applied chemistry. This results from their catalytic and adsorptive properties, as well as optical, electronic and magnetic properties.[2–5] These materials are generally prepared under hydrothermal or solvothermal conditions in the presence of an organic amine as a structure-directing agent. A large number of metal phosphates (MePOs) with interesting open-framework structures have been obtained (Me = Al, Ga, In, Mn, Fe, Co, Ni, Zn, Sn, Ti, Zr, V, and Mo, etc.), amongst which open-framework zinc phosphates exhibit a vast structural diversity. To date, a large number of zinc phosphates have been prepared with 0-D cluster, 1-D chain, 2-D layer and 3-D open-framework structures.[6–16] Notable examples are the extra-large microporous compounds, such as ND-1 with 24-membered ring channels,[13] and $[H_3N(CH_2)_6NH_3][Zn_4(PO_4)_2(HPO_4)_2]\cdot3H_2O$ with 20-membered ring channels,[15] and the helical channel compounds, such as $[NH_3(CH_2)_2NH_2(CH_2)_2NH_3][Zn(PO_4)_3(HPO_4)]$[14a] which contains intersecting helical channels, and $[Zn_2(HPO_4)_4][Co(dien)_2]H_3O$ (dien = diethylenetriamine) with multidirectional helical channels.[16] The structures of these compounds are typically built up from tetrahedral ZnO_4 and PO_4 units, although in some cases ZnO_5 and ZnO_6 polyhedra exist. The structural variety is greatly enriched by the employment of various templating agents or structure-directing agents, such as organic amines, alkali metal cations and metal complexes.

Compared to the traditional synthesis methods for materials, the combinatorial approach has been proven as a high-throughput technique for the discovery of new materials. Following their application in the discovery of new drugs, combinatorial methods have been employed in many research areas, such as organic and inorganic chemistry, and biochemistry.[17–20] In recent years, a hydrothermal combinatorial method has been applied successfully in the syntheses of zeolites and related open-framework materials.[21–25] Akporiaye and co-workers first reported the application of a combinatorial strategy to the hydrothermal synthesis of zeolites using a multiple autoclave to perform at least 100 crystallizations under hydrothermal conditions.[21] Maier and co-workers modified the multi-autoclave so that the microgram-scale hydrothermal synthesis of TS-1 could be conducted in an array format on an Si wafer.[22] Bein and co-workers developed this methodology by introducing automatic identification of the products within the autoclave blocks.[23] By applying a hydrothermal combinatorial approach we have obtained three open-framework zinc phosphates including phases **A** $\{[C_6H_{16}N_2]_{0.5}\cdot[C_5H_{14}N_2]\cdot[Zn_6(PO_4)_5(H_2O)]\cdot3H_2O\}$ with sixteen-, ten- and eight-membered ring channels, phase **B** $[Zn_3(PO_4)_2(H_2O)]$ with eight-membered ring channels, and phase **C** $\{[C_4H_{14}N_2]\cdot[Zn_5(PO_4)_4(H_2O)]\}$.[24] Zhang et al. reported application of the combinatorial method to the synthesis of SAPO-34 by a vapor-phase transport technique.[25]

[a] State Key Laboratory of Inorganic Synthesis and Preparative Chemistry, College of Chemistry, Jilin University, Changchun 130012, P. R. China
Fax: (internat.) + 86-431-5168608
E-mail: jihong@mail.jlu.edu.cn
Supporting information for this article is available on the WWW under http://www.eurjic.org or from the author.

 © 2004 Wiley-VCH Verlag GmbH & Co. KGaA, Weinheim DOI: 10.1002/ejic.200400216

Recently, we reported a new 2-D layered aluminophosphate $[C_2H_8N]_2{\cdot}[Al_2(HPO_4)(PO_4)_2]$ with a distinctive H-bonded helix formed by the organic amine templates and the inorganic network, prepared using a solvothermal combinatorial method.[26]

In this work, a new open-framework zinc phosphate $[C_6H_{16}N_2]{\cdot}[Zn_2(HPO_4)_3]$ from the $Zn(OAc)_2{\cdot}2H_2O/H_3PO_4$/*N*,*N*′-dimethylpiperazine/ethylene glycol reaction system has been obtained using the solvothermal combinatorial approach at 180 °C. The influence of various synthetic factors on the nature of the crystalline products, such as crystallization temperature, solvent type, as well as the gel compositions, has been systematically examined.

Results and Discussion

Using *N*,*N*′-dimethylpiperazine as the template and ethylene glycol as the solvent, a new phase **D** $\{[C_6H_{16}N_2]{\cdot}[Zn_2(HPO_4)_3]\}$ was crystallized from the $Zn(OAc)_2{\cdot}2H_2O/H_3PO_4$/*N*,*N*′-dimethylpiperazine/ethylene glycol system at 180 °C. Figure 1 shows its crystallization field. Pure phase **D** can be formed over a wide range at this temperature. Interestingly, if a certain amount of H_2O is added to the ethylene glycol, i.e., H_2O/ethylene glycol (1:4), phase **A** $\{[C_6H_{16}N_2]_{0.5}{\cdot}[C_5H_{14}N_2]{\cdot}[Zn_6(PO_4)_5(H_2O)]{\cdot}3H_2O\}$, with 16-membered ring main channels,[24] and phase **B** $[Zn_3(PO_4)_2(H_2O)]$, with eight-membered ring channels,[24] are formed. In addition, the range of formation for phase **D** becomes narrow. Furthermore, if 80% H_2O is added to the solvent mixture then no phase **D** is formed. Under this condition, the crystallization diagram is similar to that of the H_2O system at 180 °C, as reported previously.[24]

The powder X-ray diffraction pattern for phase **D** $\{[C_6H_{16}N_2]{\cdot}[Zn_2(HPO_4)_3]\}$ is shown in Figure 2, and is in agreement with the simulated XRD pattern generated from the single-crystal structural data of **D**, proving the phase purity.

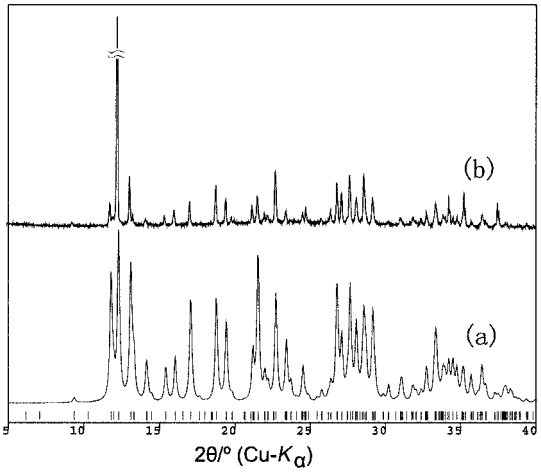

Figure 2. (a) Simulated and (b) experimental X-ray powder diffraction patterns of phase **D**

The influence of crystallization temperature was studied further. Upon reduction of the crystallization temperature to 140°C, phase **B** and an amine−phosphate cluster $([C_6H_{16}N_2]{\cdot}[H_2PO_4]_{0.5})$[28] (denoted as phase **E**), crystallize from the above system, and no phase **D** was obtained. As shown in Figure 3, phase **B** forms in the areas where $3 \leq P/Zn \leq 5$ and $3 \leq R/Zn \leq 7$ (R = *N*,*N*′-dimethylpiperazine), $4 \leq P/Zn \leq 5$ and $2 \leq R/Zn < 3$, with pH values of 7−9, while upon increase or decrease of the H_3PO_4 content, phase **E** begins to appear. Phases **B** and **E** coexist in the areas where $1 \leq P/Zn \leq 2$ and $1 \leq R/Zn \leq 7$, $6 \leq P/Zn \leq 7$ and $3 \leq R/Zn \leq 7$, and P/Zn = 3 and R/Zn = 3. Phase **E** forms in the areas where $3 \leq P/Zn \leq 5$ and $1 \leq R/Zn \leq 1.5$, and $6 \leq P/Zn \leq 7$ and $1 \leq R/Zn \leq 2$. On the other

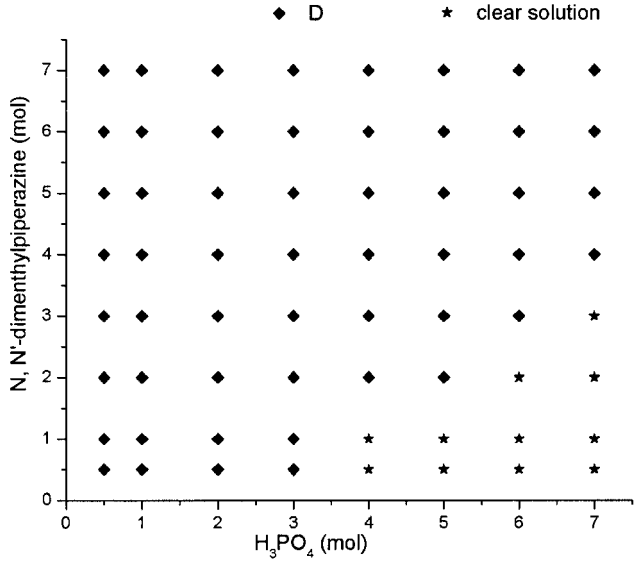

Figure 1. Crystallization field of phase **D** in the ethylene glycol system at 180 °C

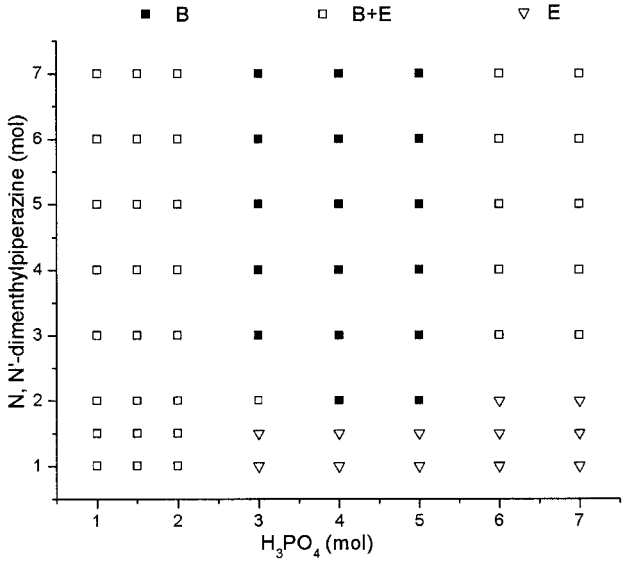

Figure 3. Crystallization field of phases **B** and **E** in the ethylene glycol system at 140°C

 © 2004 Wiley-VCH Verlag GmbH & Co. KGaA, Weinheim

hand, when the the temperature was increased to 200°C, no crystalline product was obtained in the ethylene glycol system. However, phases **B** and **C** $\{[C_4H_{14}N_2]\cdot[Zn_5(PO_4)_4(H_2O)]\}$[26] are formed in the H_2O system at this temperature. Figure 4 shows its formation diagram. Phase **C** was obtained previously at 180 °C in the presence of trace amounts of transition metal cations, in the H_2O system.[24]

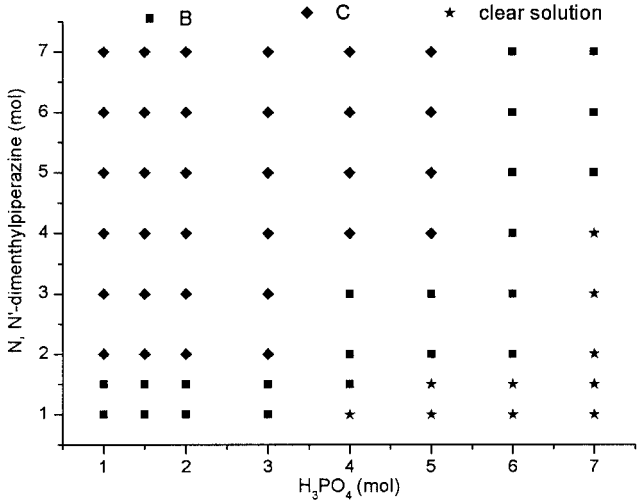

Figure 4. Crystallization field of phases **B** and **C** in the H_2O system at 200°C

Phase **D** $\{[C_6H_{16}N_2]\cdot[Zn_2(HPO_4)_3]\}$ crystallizes in the monoclinic space group $P2_1/n$ (no.14) with a = 8.6931(3) Å, b = 14.4394(5) Å, c = 12.6492(3) Å, β = 96.418(2)°, and Z = 4. As shown in Figure 5, each asymmetric unit contains 25 non-hydrogen atoms, of which 17 belong to the framework and eight to the guest molecules. There are two crystallographically independent zinc and three crystallographically independent phosphorus atoms. The Zn atoms are all tetrahedrally coordinated to oxygen atoms, and each makes four Zn−O−P bonds. The Zn−O bond lengths are in the range 1.922(2)−1.979(2) Å and the O−Zn−O bond angles are in the range 102.02(11)−114.99(11)°, which are typical for zinc phosphates.[6−16] The P atoms are tetrahedrally coordinated. P(1) and P(2) each share three oxygen atoms with adjacent Zn atoms. The $P-O_{bridging}$ bond lengths are in the range 1.509(3)−1.538(2) Å. The fourth P−O bond belongs to a P−OH group, with bond lengths of 1.574 (3) Å for P(1)−O(9)H and 1.572(3) Å for P(2)−O(10)H Å. The P(3) atom shares two oxygen atoms with adjacent Zn atoms. The P−O bond lengths are 1.504(3) Å for P(3)−O(3) and 1.499(3) Å for P(3)−O(8). The terminal O(11) and O(12) atoms are both disordered over two sites. P(3)−O(11) is a terminal P=O bond, while P(3)−O(12) is a terminal P−OH bond.

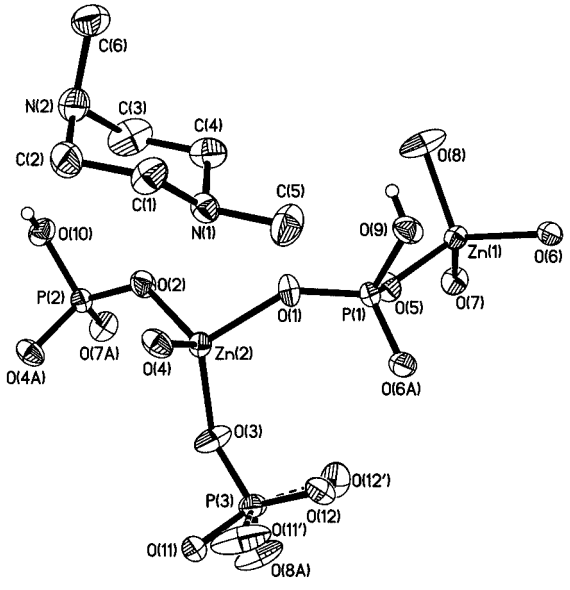

Figure 5. Thermal ellipsoid plot (50%) for **D** showing the atom labeling scheme

The alternation of ZnO_4, $PO_3(OH)$ and $PO_2(OH)(=O)$ tetrahedral units through Zn−O−P linkages forms an open-framework with eight-membered ring channels along the [100] direction (Figure 6), which are intersected with eight-membered ring channels along both the [010] and [101] directions. The 3-D open-framework can be viewed as a network of 4.8.12-net sheets parallel to the *ac* plane through O(7) atoms. This 4.8.12-net sheet is illustrated in Figure 7.

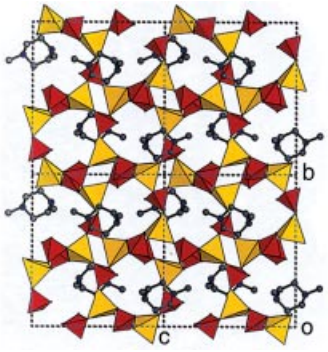

Figure 6. Polyhedral view of the framework structure of **D** viewed along the [100] direction showing the eight-membered ring channels (color code: Zn: yellow; P: red; C: grey; N: blue)

The balance of charge in the complex is achieved by diprotonation of *N*,*N*′-dimethylpiperazine. Each N atom of *N*,*N*′-dimethylpiperazine forms one H-bond to a framework oxygen atom. The N···O distances are in the range of 2.715(4)−3.015(5) Å.

Analysis of the structures of these phases gives some insight into the relative influence of various synthetic factors on the nature of the resulting crystalline products. In this work, the organic templating agent added to the initial reaction system for all the above compounds is *N*,*N*′-dimethylpiperazine. However, it was partially decomposed to *N*-methylpiperazine in phase **A**, which crystallized at 180°C in the H_2O system, and to *N*,*N*′-dimethylethylenediamine in phase **C**, which crystallized at 200°C in the H_2O system. It remained intact in phase **D** crystallized at 180°C in the ethylene glycol system and in phase **E** crystallized at 140

 © 2004 Wiley-VCH Verlag GmbH & Co. KGaA, Weinheim

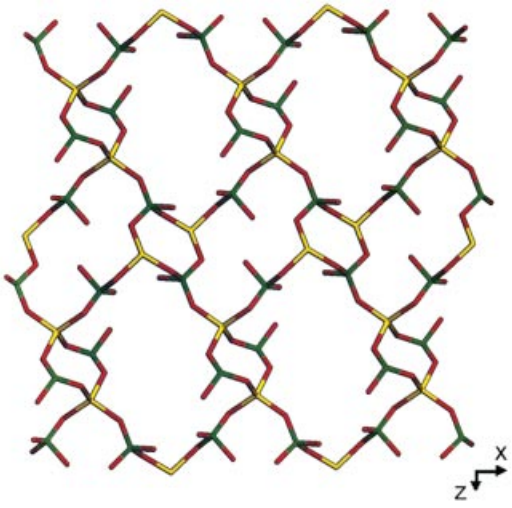

Figure 7. 4.8.12-net sheet parallel to the *ac* plane of **D** (color code: Zn: yellow; P: green; O: red)

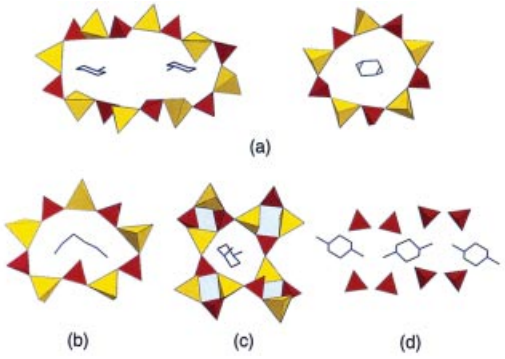

Figure 8. (a) The two diprotonated *N*-methylpiperazine molecules residing in the 16-membered ring channel viewed along the [100] direction and one diprotonated *N*,*N*′-dimethylpiperazine molecule residing in the 10-membered ring channel along [010] direction of **A**; (b) one diprotonated *N*,*N*′-dimethylethylenediamine molecule in the 10-membered ring channel of **C**; (c) one diprotonated *N*,*N*′-dimethylpiperazine molecule in the eight-membered ring channel of **D**; (d) structure of **E** containing a discrete zinc phosphate cluster and *N*,*N*′-dimethylpiperazine molecules (color code: Zn: yellow; P: red; C: grey; N: blue)

°C in the ethylene glycol system. Figure 8 (a−d) shows the templating molecules in the structures of phases **A**, **C**, **D** and **E**. It appears that *N*,*N*′-dimethylpiperazine is easily decomposed in the H_2O system at 180−200°C, but remains intact in the ethylene glycol system at 140−180°C. The above results indicate that the identities of crystallization products are strongly dependent on the organic amine species that are in turn affected by the crystallization temperature, as well as the solvent under solvothermal conditions.

Conclusions

A new open-framework zinc phosphate $[C_6H_{16}N_2]\cdot[Zn_2(HPO_4)_3]$ (phase **D**) with intersecting eight-membered ring channels has been obtained by applying a solvothermal combinatorial approach to the $Zn(OAc)_2\cdot 2H_2O/H_3PO_4/N,N'$-dimethylpiperazine/ethylene glycol system at 180°C. Factors such as gel composition, crystallization temperature and solvent, have significant influence on the resulting crystalline products. Four open-framework zinc phosphate phases **A** $\{[C_6H_{16}N_2]_{0.5}\cdot[C_5H_{14}N_2]\cdot[Zn_6(PO_4)_5(H_2O)]\cdot 3H_2O\}$, **B** $[Zn_3(PO_4)_2(H_2O)]$, **C** $\{[C_4H_{14}N_2]\cdot[Zn_5(PO_4)_4(H_2O)]\}$, **D** $\{[C_6H_{16}N_2]\cdot[Zn_2(HPO_4)_3]\}$, and an amine−phosphate cluster **E** $\{[C_6H_{16}N_2]\cdot[H_2PO_4]_{0.5}\}$, were obtained in the presence of the structure-directing agent *N*,*N*′-dimethylpiperazine in the H_2O or ethylene glycol systems. Our studies show that the state of the organic species, which is affected by the crystallization temperature and the solvent used, play an important role in the formation of the final crystalline products. This work further demonstrates that the combinatorial approach will assist greatly in the discovery of new open-framework materials and can improve our understanding of the factors that influence the crystallization of such materials.

Experimental Section

Synthesis and Characterization: The reactions were performed on the $Zn(OAc)_2\cdot 2H_2O/H_3PO_4/N,N'$-dimethylpiperazine/ethylene glycol or H_2O system in a multiautoclave with dimensions of 14 cm × 14 cm × 5.5 cm. The multiautoclave consists of a stainless steel block (3 cm in height) with 64 individual Teflon chambers (0.7 cm in diameter, 3.0 cm in depth, 800 μL in volume per chamber). Firstly, an aqueous or glycol solution of $Zn(OAc)_2$ was added to each Teflon chamber while they were mounted in a frame, using a Tecan CH Miniprep 75 pipette robot, followed by addition of *N*,*N*′-dimethylpiperazine (98.5%, ACROS) and H_3PO_4 (85 wt%). The reaction mixtures were shaken for homogenization using a vibration apparatus for 1 h. The 64 Teflon chambers were placed in the stainless steel block, then sealed by two stainless steel covers on top and bottom. Sixty-four individual Teflon covers (0.5 cm in thickness) were mounted on the top cover. The multiautoclave was heated in an oven at 140−200 °C for 60 h. After cooling, the arrays of Teflon chambers were put into a Hermle 2300 centrifuge apparatus for sample separation. The products were washed with deionized water followed by centrifugation several times. The products were dried at room temperature. The dried samples were transferred to a sample holder with 64 holes for automated X-ray analysis. Automated X-ray diffraction analysis was carried out with a computer-controlled *xyz* stage with a Bruker D8 Discover microdiffractometer with GADDS equipped with a CCD detector and using Cu-K_α radiation. Traditional X-ray diffraction analyses were performed with the X-ray diffraction (XRD) patterns collected with a Siemens D5005 diffractometer with Cu-K_α radiation (λ = 1.541 Å). Inductively coupled plasma (ICP) analyses were performed with a Perkin-Elmer Optima 3300DV spectrometer. Elemental analyses were conducted using a Perkin-Elmer 2400 elemental analyzer. Inductively coupled plasma (ICP) analysis showed that phase **D** contains 23.2 and 16.8 wt% of Zn and P, respectively (calcd. 24.3 and 17.4 wt%, respectively). The elemental analysis gave C, H and N contents of 13.8, 3.9 and 5.6 wt%, respectively (calcd. 13.5, 3.6 and 5.2 wt%, respectively). A NETZSCH STA 449C unit was used to carry out the thermogravimetric analysis (TGA) in air with a heating rate of 20°C/min. The occluded *N*,*N*′-dimethylpiperazine molecules decomposed at 200−450°C with a weight loss of 22.0 wt% (calcd. 22.2%).

 © 2004 Wiley-VCH Verlag GmbH & Co. KGaA, Weinheim

Structure Determination: A suitable single crystal of phase **D** with dimensions 0.15 × 0.10 × 0.10 mm, was carefully selected under a polarizing microscope and glued to a thin glass fiber with cyanoacrylate (superglue) adhesive. The intensity data were collected with a Siemens diffractometer fitted with a Bruker SMART CCD detector, using graphite-monochromated Mo-K_α radiation (λ = 0.71073 Å). Data processing was done using the SAINT processing program. The structure was solved by direct methods and refined on F^2 by full-matrix least squares using SHELXTL97.[27] The Zn and P atoms were located first, and then the oxygen, carbon, and nitrogen atoms were located in the Fourier difference maps. O(11) and O(12) are disordered over two sites. The diprotonation of *N*,*N*′-dimethylpiperazine is suggested for the balance of charge. The hydrogen atoms on the amine molecules and in the P−OH bond were located geometrically. All non-hydrogen atoms were refined with anisotropic thermal parameters. The details of data collection and refinement are given in Table 1. Selected bond lengths and bond angles are listed in Table 2. CCDC-228303 contains the supplementary crystallographic data for this paper. These data can be obtained free of charge at www.ccdc.cam.ac.uk/conts/retrieving.html [or from the Cambridge Crystallographic Data Centre, 12 Union Road, Cambridge CB2 1EZ, UK; Fax: (internat.) + 44-1223/336-033; E-mail: deposit@ccdc.cam.ac.uk].

Table 1. Crystal data and structure refinement for phase **D**

Empirical formula	$C_6H_{19}N_2O_{12}P_3Zn_2$
Formula mass	534.88
Temperature	293(2) K
Wavelength	0.71073 Å
Crystal system, space group	monoclinic, $P2_1/n$
Unit cell dimensions	a = 8.6931(3) Å, α = 90° b = 14.4394(5) Å, β = 96.418(2)° c = 12.6492(3) Å, γ = 90°
Volume	1577.82(9) Å^{-3}
Z, calculated density	4, 2.252 Mg/m^3
Absorption coefficient	3.412 mm^{-1}
F(000)	1080
Crystal size	0.15 × 0.10 × 0.10 mm
θ range for data collection	2.15−23.26°
Limiting indices	$-9 \le h \le 9$, $-9 \le k \le 16$, $-14 \le l \le 13$
Reflections collected/unique	7342/2255 (R_{int} = 0.0388)
Completeness to θ = 23.36°	99.9%
Refinement method	full-matrix least squares on F^2
Data/restraints/parameters	2255/0/244
Goodness-of-fit on F^2	1.058
Final R indices [$I > 2\sigma(I)$][a]	R_1 = 0.0240, wR_2 = 0.0633
R indices (all data)	R_1 = 0.0292, wR_2 = 0.0652
Largest diff. peak/hole	0.435/−0.297e·Å^{-3}

[a] $R_1 = [\Delta F/(F_o)]$; $wR_2 = ([w(F_o^2 - F_c^2)])/[w(F_o^2)^2]^{1/2}$, $w = 1/\sigma^2(F_o^2)$.

Table 2. Selected bond lengths and angles for phase **D**

Bond lengths [Å]			
Zn(1)−O(7)	1.945(2)	Zn(1)−O(5)	1.948(2)
Zn(1)−O(6)	1.965(2)	Zn(1)−O(8)	1.972(3)
Zn(2)−O(1)	1.922(2)	Zn(2)−O(3)	1.925(3)
Zn(2)−O(2)	1.929(2)	Zn(2)−O(4)	1.979(2)
P(1)−O(5)	1.510(3)	P(1)−O(1)	1.511(3)
P(1)−O(6)[a]	1.531(3)	P(1)−O(9)	1.574(3)
P(2)−O(7)[b]	1.509(3)	P(2)−O(2)	1.513(2)
P(2)−O(4)[c]	1.538(2)	P(2)−O(10)	1.572(3)
P(3)−O(11′)	1.417(7)	P(3)−O(8)[d]	1.499(3)
P(3)−O(3)	1.504(3)	P(3)−O(12)	1.567(5)
P(3)−O(11)	1.607(6)	P(3)−O(12′)	1.629(6)
O(4)−P(2)[c]	1.538(2)	O(6)−P(1)[a]	1.531(3)
O(7)−P(2)[e]	1.509(3)	O(8)−P(3)[f]	1.499(3)

Bond angles [°]			
O(7)−Zn(1)−O(5)	104.94(11)	O(7)−Zn(1)−O(6)	112.24(11)
O(5)−Zn(1)−O(6)	114.99(11)	O(7)−Zn(1)−O(8)	114.33(11)
O(5)−Zn(1)−O(8)	104.24(12)	O(6)−Zn(1)−O(8)	106.06(12)
O(1)−Zn(2)−O(3)	113.39(12)	O(1)−Zn(2)−O(2)	102.02(11)
O(3)−Zn(2)−O(2)	114.34(11)	O(1)−Zn(2)−O(4)	104.27(11)
O(3)−Zn(2)−O(4)	112.94(11)	O(2)−Zn(2)−O(4)	108.89(11)
O(5)−P(1)−O(1)	110.76(15)	O(5)−P(1)−O(6)[a]	112.78(15)
O(1)−P(1)−O(6)[a]	111.49(15)	O(5)−P(1)−O(9)	108.97(14)
O(1)−P(1)−O(9)	108.26(15)	O(6)[a]−P(1)−O(9)	104.26(14)
O(7)[b]−P(2)−O(2)	113.17(15)	O(7)[b]−P(2)−O(4)[c]	110.54(15)
O(2)−P(2)−O(4)[c]	110.08(14)	O(7)[b]−P(2)−O(10)	105.50(15)
O(2)−P(2)−O(10)	108.33(14)	O(4)[c]−P(2)−O(10	109.02(14)
O(11′)−P(3)−O(8)[d]	116.2(3)	O(11′)−P(3)−O(3)	120.0(3)
O(8)[d]−P(3)−O(3)	111.19(16)	O(11′)−P(3)−O(12)	69.5(5)
O(8)[d]−P(3)−O(12)	121.1(3)	O(3)−P(3)−O(12)	113.4(2)
O(8)[d]−P(3)−O(11)	102.0(3)	O(3)−P(3)−O(11)	102.6(2)
O(12)−P(3)−O(11)	103.7(3)	O(11′)−P(3)−O(12′)	111.9(5)
O(8)[d]−P(3)−O(12′)	91.2(3)	O(3)−P(3)−O(12′)	101.4(3)
O(11)−P(3)−O(12′)	146.1(4)	P(1)−O(1)−Zn(2)	145.01(18)
P(2)−O(2)−Zn(2)	131.32(15)	P(3)−O(3)−Zn(2)	133.56(17)
P(2)[c]−O(4)−Zn(2)	130.08(15)	P(1)−O(5)−Zn(1)	133.83(16)
P(1)[a]−O(6)−Zn(1)	120.26(14)	P(2)[e]−O(7)−Zn(1)	137.35(17)
P(3)[f]−O(8)−Zn(1)	132.09(18)		

Hydrogen bonds	[Å]	[°]
O(9)−H(9)···O(11)[f]	2.574(7)	169.0
O(9)−H(9)···O(11′)[f]	2.573(7)	145.6
O(10)−H(10)···O(11)[c]	2.520(7)	164.2
O(10)−H(10)···O(11′)[c]	2.577(7)	143.7
N(1)−H(1)···O(4)	2.715(4)	171.9
N(2)−H(2)···O(8)[g]	3.015(5)	162.9

[a] Symmetry transformations used to generate equivalent atoms: $-x + 2, -y - 1, -z$. [b] $x - 1/2, -y - 3/2, z - 1/2$. [c] $-x + 1, -y - 1, -z - 1$. [d] $x - 1, y,$. [e] $x + 1/2, -y - 3/2, z + 1/2$. [f] $x + 1, y, z$. [g] $-x + 2, -y - 1, -z - 1$.

Acknowledgments

We are grateful to the National Natural Science Foundation of China and the State Basic Research Project (G2000077507) for financial support.

[1] S. T. Wilson, B. M. Lok, C. A. Messina, T. R. Cannan, E. M. Flanigen, *J. Am. Chem. Soc.* **1982**, *104*, 1146.
[2] A. K. Cheetham, G. Férey, T. Loiseau, *Angew. Chem. Int. Ed.* **1999**, *38*, 3268, and references therein.
[3] [3a] J. M. Bennet, W. J. Dytrych, J. J. Pluth, J. W. Richardson, J. V. Smith, *Zeolites* **1986**, *6*, 349. [3b] M. E. Davis, C. Saldarriaga, C. Montes, J. Garces, C. Crowder, *Nature* **1988**, *331*, 698. [3c] J. Yu, R. Xu, *Acc. Chem. Res.* **2003**, *36*, 481, and references therein.
[4] [4a] G. Férey, *Chem. Mater.* **2001**, *13*, 3084, and references therein. [4b] J. Yu, R. Xu, J. Li, *Solid State Sci.* **2000**, *2*, 181, and references therein.
[5] [5a] C. N. R. Rao, S. Natarajan, S. Neeraj, *J. Am. Chem. Soc.* **2000**, *122*, 2810, and references therein. [5b] R. Raja, G. Sankar, J. M. Thomas, *J. Am. Chem. Soc.* **2001**, *123*, 8153. [5c] S. Natarajan, *Chem. Commun.* **2002**, 780.
[6] [6a] J. Yu, Y. Wang, Z. Shi, R. Xu, *Chem. Mater.* **2001**, *13*, 2972.

 © 2004 Wiley-VCH Verlag GmbH & Co. KGaA, Weinheim

[6b] W. Liu, Y. Liu, Z. Shi, W. Pang, *J. Mater. Chem.* **2000**, *10*, 1451.
[7] A. Choudhruy, S. Natarajan, C. N. R. Rao, *Inorg. Chem.* **2000**, *39*, 4295.
[8] S. B. Harmon, S. C. Sevov, *Chem. Mater.* **1998**, *10*, 3020.
[9] T. E. Gier, X. Bu, P. Feng, G. D. Stucky, *Nature* **1998**, *395*, 154.
[10] [10a] W. T. A. Harrison, M. L. Phillips, *Chem. Commun.* **1996**, 2771. [10b] W. T. A. Harrison, T. E. Gier, G. D. Stucky, R. W. Broach, R. A. Bedard, *Chem. Mater.* **1996**, *8*, 145.
[11] G. Alberti, M. Bartocci, M. Santarelli, R. Vivani, *Chem. Commmun.* **1996**, 2771.
[12] W. T. A. Harrison, M. L. F. Phillips, *Angew. Chem. Int. Ed. Engl.* **1995**, *34*, 1745.
[13] G. Yang, S. C. Sevov, *J. Am. Chem. Soc.* **1999**, *121*, 8389.
[14] [14a] S. Neeraj, S. Natarajan, C. N. R. Rao, *Chem. Commun.* **1999**, 165; *Chem. Mater.* **1999**, *11*, 1390; *New J. Mater.* **1999**, 23, 303; *J. Solid State Chem.* **2000**, *150*, 417. [14b] S. Ayyappan, X. Bu, A. K. Cheetham, S. Natarajan, C. N. R. Rao, *Chem. Commun.* **1998**, 2181. [14c] S. Ayyappan, A. K. Cheetham, S. Natarajan, C. N. R. Rao, *Chem. Mater.* **1998**, *10*, 3764. [14d] S. Natarajan, R. Vaidhanathan, C. N. R. Rao, S. Ayyappan, A. K. Cheetham, *Chem. Mater.* **1999**, *11*, 1633.
[15] A. R. Jennifer, T. A. H. William, *J. Mater. Chem.* **2000**, *10*, 2853.
[16] Y. Wang, J. Yu, M. Guo, R. Xu, *Angew. Chem. Int. Ed.* **2003**, *42*, 4089.
[17] Special issue: *Acc. Chem. Res.* **1996**, *29*, 112.
[18] G. Lowe, *Chem. Soc. Rev.* **1995**, *24*, 309.
[19] X. -D. Xiang, X. Sun, G. Briceno, Y. Lou, K. A. Wang, H. Chang, H. Chang, W. G. Wallace-Freedman, S. -W. Chen, P. G. Schultz, *Science* **1995**, *268*, 1738.
[20] J. N. Cawse, *Acc. Chem. Res.* **2001**, *34*, 213.
[21] [21a] D. E. Akporiaye, I. M. Dahl, A. Karlsson, R. Wendelbo, *Angew. Chem. Int. Ed.* **1998**, *37*, 609. [21b] D. Akporiaye, I. Dahl, A. Karlsson, M. Plassen, R. Wendelbo, D. S. Bem, R. W. Broach, G. J. Lewis, M. Miller, J. Moscoso, *Miroporous Mesoporous Mater.* **2001**, *48*, 367.
[22] [22a] J. Klein, C. W. Lehmann, H.-W. Schmidt, W. F. Maier, *Angew. Chem. Int. Ed.* **1998**, *37*, 3369. [22b] J. M. Newsam, T. Bein, J. Klein, W. F. Maier, W. Stichert, *Miroporous Mesoporous Mater.* **2001**, *48*, 355.
[23] K. Choi, D. Gardner, N. Hilbrandt, T. Bein, *Angew. Chem. Int. Ed.* **1999**, *38*, 2891.
[24] Y. Song, J. Yu, G. Li, Y. Li, Y. Wang, R. Xu, *Chem. Commun.* **2002**, 1720.
[25] L. Zhang, J. Yao, C. Zeng, N. Xu, *Chem. Commun.* **2003**, 2232.
[26] Y. Song, J. Yu, Y. Li, R. Xu, *Angew. Chem. Int. Ed.* **2004**, *43*, 2399.
[27] G. M. Sheldrick, *SHELXL Program*, version 5.1; Siemens Industrial Automation, Inc., Madison, WI, **1997**.
[28] A. Choudhury, S. Natarajan, C. N. R. Rao, *J. Chem. Soc., Dalton Trans.* **2000**, 2595.

Received March 18, 2004
Early View Article
Published Online July 12, 2004

 © 2004 Wiley-VCH Verlag GmbH & Co. KGaA, Weinheim

Group 4 Complexes of Chelating Dianionic [OSO] Binaphtholate Ligands; Synthesis and Alkene Polymerisation Catalysis

Louise S. Natrajan,[a] Claire Wilson,[a] Jun Okuda,[b] and Polly L. Arnold*[a]

Keywords: Binaphthol ligands / Polymerisation catalysis / Organometallic / Group 4 elements / Zirconium / Titanium

Mono- and bis(ligand)titanium and -zirconium complexes of a sulfur-bridged binaphtholate [1,1′-S(2-$HOC_{10}H_4$-*t*Bu_2-3,6)$_2$] ($H_2\mathbf{L^{SN}}$) have been synthesised and characterised. Complexes of the general form [M($\mathbf{L^{SN}}$)X_2] (X = Cl, CH_2Ph) are prepared by protonolysis or metathesis. X-ray crystallographic structural characterisation of the dibenzyl complex [Zr($\mathbf{L^{SN}}$)(CH_2Ph)$_2$] is reported, as well as the structure of its partially oxidised derivative [Zr($\mathbf{L^{SN}}$)(CH_2Ph)(OCH_2Ph)]$_2$. Complexes of the form [M($\mathbf{L^{SN}}$)$_2$] are readily formed; these can be converted by comproportionation reactions into the mono-$\mathbf{L^{SN}}$ derivatives above. The X-ray crystal structure of a bis(sulfur-bridged biphenolate) is presented. The representative complexes have been tested as alkene polymerisation catalysts, in conjunction with a methylalumoxane cocatalyst, and for the first time a zirconium complex of a sulfur-bridged biphenolate-type ligand has been found to be active in the polymerisation of ethene.

(© Wiley-VCH Verlag GmbH & Co. KGaA, 69451 Weinheim, Germany, 2004)

1 Introduction

The continuing search for alternatives to cyclopentadienyl-based ancillary ligand sets for Group 4 olefin polymerisation catalysts has produced a huge range of new polydentate ligand systems, of which biphenolates have been identified as good ligands.[1,2] However, aryloxides are not generally considered to contribute sufficient electron density to be isolobal with the cyclopentadienyl ligand.[3] Biphenol ligands in which the two phenol rings are joined in the *ortho* position by a potential donor group, such as sulfur, can provide an increased stabilisation of reactive, electron-deficient metal centres.[4] A diverse range of complexes that contain these atom-bridged biphenolates, where the coordinating ligand set is denoted [OXO] (X = S^5, $S_2{}^6$, SO^7, P^8 for example), have now been reported.

Group 4 complexes incorporating [OXO] ligands have been identified as promising alkene polymerisation systems in the form {M[OXO]$_2$$Cl_2$}/MAO (MAO = methylalumoxane).[9] The bridging heteroatom, if coordinated, helps provide the stereochemically rigid framework essential for stereoregular polymer formation.[4] Density functional calculations show that a bridging sulfur atom increases the polymerisation rate by destabilising the π-bound intermediate [Ti(tbmp)Me-(H_2C=CH_2)]$^+$ {tbmp = 2,2′-thiobis(6-*tert*-butyl-4-methylphenol), an [OSO] ligand} with respect to the reactants.[10] Additionally, the calculations suggest that the unsaturated backbone provided by the phenolate plays an important role in stabilising the transition states. The titanium complexes [Ti(tbmp)X_2] (X = Cl, O*i*Pr) exhibit high catalytic activities for the polymerisation of ethene,[9] styrene[11] and dienes[12] when activated with MAO, and can also co-polymerise ethene and styrene.[13]

There are very few reports of the analogous zirconium(IV) complexes. The zirconium derivatives are reportedly far more air- and moisture-sensitive than their titanium counterparts and react less cleanly.[2] In contrast with zirconocene α-olefin polymerisation catalysts,[14] the Zr[OSO] complexes reported so far exhibit no catalytic activity.[2] We have recently introduced the use of the larger naphtholate analogues of [OSO] biphenolates, [1,1′-S(2-$HOC_{10}H_4$-*t*Bu_2-3,6)$_2$] ($H_2\mathbf{L^{SN}}$), in order to stabilise the first sulfur-bridged bis(aryloxide) complexes of lanthanides;[15] the thionaphthol [$\mathbf{L^{SN}}$] thus seemed better suited as a supporting ancillary ligand for zirconium(IV).

Herein, we report the first structurally characterised zirconium(IV) complexes supported by an [OSO] ligand set. Comparative investigations between $H_2\mathbf{L^{SN}}$ and tbmp have led us to synthesise and characterise a new family of Group 4 complexes of the general formula [M($\mathbf{L^{SN}}$)X_2] (X = chloride, amide, alkyl; M = Ti, Zr). In addition, their stability and activity towards olefin polymerisation has been studied and compared with that of relevant tbmp analogues.

[a] School of Chemistry, The University of Nottingham, University Park, Nottingham NG7 2RD, UK
Fax: (internat.) + 44-115-951-3563
E-mail: Polly.Arnold@Nottingham.ac.uk
[b] Institute of Inorganic Chemistry, Aachen University of Technology (RWTH), Prof.-Pirlet-Strasse 1, 52074 Aachen, Germany

 © 2004 Wiley-VCH Verlag GmbH & Co. KGaA, Weinheim **DOI: 10.1002/ejic.200400174**

2 Results and Discussion

2.1 Halide Complexes Supported by L^{SN}

2.1.1 Reaction of K_2L^{SN} with $TiCl_4$·2THF

Treatment of the solvent-free dipotassium salt [$K_2\mathbf{L}^{SN}$] with [$TiCl_4$·2THF] in toluene results in the formation of the monomeric complex [Ti($\mathbf{L}^{SN}$)Cl_2·THF] (**1**), albeit in poor yield (18%). It is found that the bis(ligand) complex [Ti($\mathbf{L}^{SN}$)$_2$] (**2**) is consistently formed by over-reaction,[16] and is always initially present as one third of the product mixture irrespective of the reaction stoichiometry employed (Scheme 1).

The formation of the bis(ligand) complexes analogous to **2** in the reactions of chelating biphenols only becomes significant when the addition of ligand to metal is accelerated or conducted in the absence of a donating solvent.[16,17] Although single crystals of **2** were obtained from a diethyl ether solution at −30 °C, they were unsuitable for single-crystal X-ray diffraction analysis due to rapid loss of lattice solvent.

The ^{1}H NMR spectrum of **2** reveals the presence of two sets of aromatic signals for the ligand, indicating the presence of a single geometrical isomer out of the three possible ones. The *cis*-facial conformation of ligands in **2** (C_2), rather than a *trans*-facial (C_i) or *mer-trans* (D_{2d}) arrangement, affords two sets of ligand resonances. This has been observed previously in the bis[OOO]zirconium complex [Zr{(OC_6H_3*t*Bu-2-Me-4-CH_2-6)$_2$)O}$_2$] {[OOO] = 2-oxapropanediyl-1,3-bis(2-*tert*-butyl-4-methylphenol)},[17] and in the biphenolato bis[OCO]Zr complex {[OCO] = [2,2′-methylenebis(6-*tert*-butyl-4-methylphenol)}.[18] In **2**, this apparent C_2 symmetry is consistent with the coordination of both sulfur atoms. In contrast, the structurally characterised bis[ONO]titanium(IV) complex [Ti{($OC_6H_2Me_2$-2,4)$_2$NPr}$_2$] adopts the more familiar *trans-mer* conformation.[19]

High-temperature ^{1}H NMR spectroscopy of [D_8]toluene solutions of **2** do not show any processes that render the two aromatic rings of the ligands equivalent. Thus, besides the structural rigidity of **2** over an accessible temperature range, the thermal barrier to *fac-cis*/*fac-trans* isomerism is high.

2.1.2 Reaction of H_2L^{SN} with $TiCl_4$

The reaction of [$H_2\mathbf{L}^{SN}$] with neat $TiCl_4$ in hexane or toluene yields the THF-free complex **1a**, which is anticipated to be dimeric in solution[20] (Scheme 1). If triethylamine is added to precipitate the HCl by-product, only the bis(ligand) complex is isolated.[2] However, if THF is added, further conversion of **1** into **2** is slowed down but not eliminated completely, so that neither product is formed in good yield. Analytically pure **2** is most readily obtained in a synthetically useful yield of 70% by the protonolysis reaction of [$H_2\mathbf{L}^{SN}$] with [Ti($OEt)_4$] (vide infra).

As an alternative route to **1**, a stoichiometric reaction of $H_2\mathbf{L}^{SN}$ with [Ti($NMe_2)_2Cl_2$] was undertaken. Again, monitoring the reaction by ^{1}H NMR spectroscopy reveals the existence of a relatively short-lived species assigned as [Ti($\mathbf{L}^{SN}$)(Cl)NMe_2] (**3**) by comparison with related complexes, but its decomposition into **2** precludes further characterisation.

2.1.3 Preparation of 1 by Comproportionation

The synthesis of **1** is best achieved by comproportionation: Treatment of **2** with 1 equiv. of [$TiCl_4$·2THF] in a 4:1 mixture of dichloromethane/tetrahydrofuran at −60 °C (Scheme 1) affords, after warming to ambient temperature, a dark brown solution from which **1** may be isolated in 96% yield.

2.1.4 Reactions of [L^{SN}] with $ZrCl_4$·2THF

Treatment of stoichiometric solvent-free [$K_2\mathbf{L}^{SN}$] with [$ZrCl_4$·2THF] in toluene results in the formation of the colourless bis(ligand) complex [Zr($\mathbf{L}^{SN}$)$_2$·THF] (**5**) in an

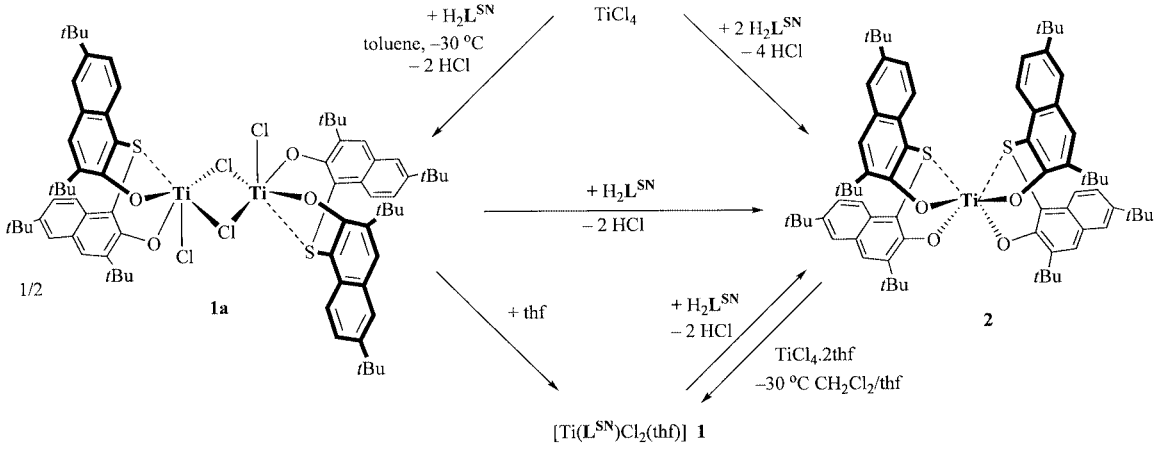

Scheme 1. Reactions of $H_2\mathbf{L}^{SN}$ with $TiCl_4$

 © 2004 Wiley-VCH Verlag GmbH & Co. KGaA, Weinheim

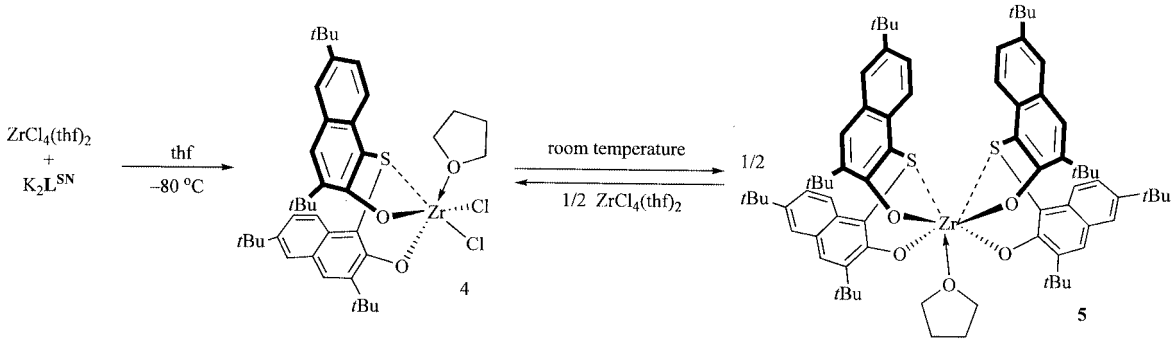

Scheme 2. Synthesis of $Zr^{IV}-\mathbf{L}^{SN}$ adducts

isolated yield of 34% (Scheme 2). Single crystals of **5** suitable for X-ray diffraction were grown by slow cooling of a saturated diethyl ether solution of **5** to −30 °C. The comproportionation of **5** and [$ZrCl_4$·2THF] in THF affords the desired complex [$Zr(\mathbf{L}^{SN})Cl_2$·THF] (**4**) in 53% yield.

$$Zr(NMe_2)_2Cl_2 + H_2\mathbf{L}^{SN} \xrightarrow[-80\ ^\circ C]{thf} Zr(\mathbf{L}^{SN})(NMe_2)Cl\ \mathbf{6} \xrightarrow{\text{room temp}} Zr(\mathbf{L}^{SN})_2(HNMe_2)\ \mathbf{7} \quad (1)$$

The protonolysis reaction of $H_2\mathbf{L}^{SN}$ with [$Zr(NMe_2)_2Cl_2$·2THF] yields the amido chloride **6** as an intermediate. Irrespective of the reaction solvent polarity, this rapidly undergoes a ligand redistribution reaction to form the amine-stabilised analogue of **5**, [$Zr(\mathbf{L}^{SN})_2(HNMe_2)$] (**7**), as the major product [Equation (1)]. The coordinated molecule of $HNMe_2$ is retained in the product even when the reaction solvent is THF.

2.2 Single-Crystal X-ray Analysis of [$Zr(\mathbf{L}^{SN})_2$·THF] (5)

Cooling of a concentrated diethyl ether solution of **5** to −30 °C affords single colourless blocks suitable for a X-ray diffraction study. The solid-state molecular structure (Figure 1) confirms the expected connectivity. Selected interatomic distances and angles are collected in Table 1.

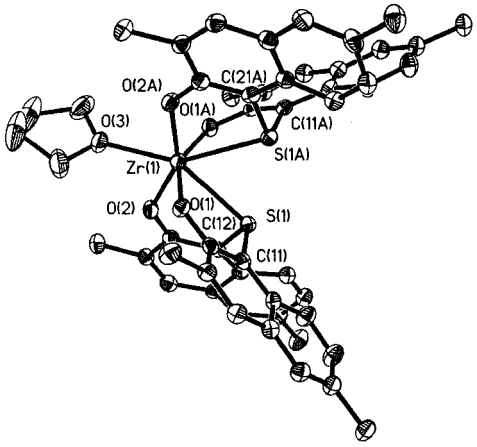

Figure 1. Thermal ellipsoid drawing of **5**·Et_2O (50% probability); methyl groups and solvent of crystallisation removed for clarity

The first significant feature of the molecular structure of **5** is the co-facial arrangement of the two binaphthol ligands, which imparts a distorted capped octahedral ge-

Table 1. Selected interatomic distances [Å] and angles [°] for **5**·Et_2O and **9** and **10**

5·Et_2O		**9**		**10**	
Zr(1)−O(1)	2.002(2)	Zr(1)−O(1)	1.981(2)	Zr(1)−O(1)	1.992(3)
Zr(1)−O(2)	2.087(2)	Zr(1)−O(2)	2.004(2)	Zr(1)−O(2)	1.986(3)
Zr(1)−O(3)	2.283(3)	Zr(1)−O(3)	2.259(2)	Zr(1)−O(5A)	2.136(3)
Zr(1)−S(1)	2.7657(8)	Zr(1)−S(1)	2.9248(7)	Zr(1)−S(1)	2.8881(13)
S(1)−C(21)	1.784(3)	Zr(1)−C(40)	2.296(3)	Zr(1)−O(5)	2.166(3)
S(1)−C(11)	1.799(3)	Zr(1)−C(50)	2.312(3)	Zr(1)−C(40)	2.228(5)
O(1)−C(12)	1.340(3)	Zr(1)−C(51)	2.850(3)	Zr(1)−Zr(1A)	3.4904(13)
O(2)−C(22)	1.331(3)	S(1)−C(21)	1.789(3)	S(1)−C(21)	1.790(5)
O(1)−Zr(1)−O(2)	93.71(8)	O(1)−Zr(1)−O(2)	92.94(8)	O(1)−Zr(1)−O(2)	95.10(14)
O(1)−Zr(1)−O(3)	104.94(6)	O(1)−Zr(1)−O(3)	166.14 (8)	O(2)−Zr(1)−O(5A)	91.63(14)
O(2)−Zr(1)−O(3)	75.59(5)	O(2)−Zr(1)−O(3)	83.54(8)	O(1)−Zr(1)−O(5A)	148.15(13)
O(1)−Zr(1)−S(1)	73.60(6)	O(1)−Zr(1)−C(40)	92.21(10)	O(2)−Zr(1)−C(40)	97.88(17)
O(2)−Zr(1)−S(1)	71.63(6)	O(2)−Zr(1)−C(40)	99.02(10)	O(2)−Zr(1)−S(1)	70.13(9)
O(3)−Zr(1)−S(1)	146.963(15)	O(1)−Zr(1)−C(50)	91.39(11)	O(1)−Zr(1)−S(1)	70.91(9)
O(2)−Zr(1)−S(1A)	137.09(6)	O(2)−Zr(1)−C(50)	140.56(10)	O(5A)−Zr(1)−S(1)	82.34(9)
O(3)−Zr(1)−S(1A)	146.963(15)	C(40)−Zr(1)−C(50)	119.96(12)	O(5)−Zr(1)−S(1)	91.14(9)
S(1)−Zr(1)−S(1A)	66.07(3)	O(1)−Zr(1)−S(1)	70.41(6)		
O(2A)−Zr(1)−S(1)	137.09(6)	O(2)−Zr(1)−S(1)	69.79(5)		
		O(3)−Zr(1)−S(1)	95.84(6)		

 © 2004 Wiley-VCH Verlag GmbH & Co. KGaA, Weinheim

ometry on the seven-coordinate zirconium centre. The four naphtholate oxygen atoms describe the equatorial plane, while S(1) and S(1A) occupy approximate axial positions. The bound THF molecule resides in the apical site, opposite and in between the two sulfur atoms. However, the O(1)−Zr(1)−O(1A) and O(2)−Zr(1)−O(2A) angles are not linear, and are 150° and 94°, respectively. Naphtholate−zirconium bond lengths are in the range expected for zirconium−oxygen single bonds (observed range: 1.89−2.06 Å).[21] The C(11)−S(1)−C(21) bond angle of each thionaphthol ligand [109.6(1)°] is relatively large, and the naphthol wings are opened out slightly, enabling the sulfur atom to come into close proximity to the metal ion. As a result, a sulfur−zirconium interaction with a distance of 2.7657(8) Å is established.[22]

The C−S−C dihedral angle between the two naphthol planes of each ligand is 57°, and notably, the intramolecular S−S distance is 3.015 Å which is considerably shorter than the sum of the van der Waals radii of two S atoms (3.6 Å), and shorter than 3.33 Å (a single S−S bond plus 1.50 Å) − it was suggested that this value indicates a nonbonding interaction between two atoms (Figure 2).[23] This implies a significant intramolecular sulfur interaction in the solid state. The nonlinearity of the O(1)−Zr(1)−O(1A) and O(2)−Zr(1)−O(2A) moieties also suggests an S−S interaction that bends both *fac* ligands towards each other.

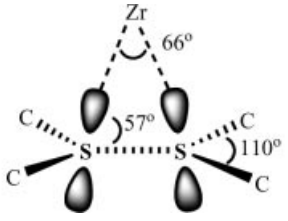

Figure 2. Suggested S−S (σ−π)-(π−π) interaction in **5** (for clarity, only the filled p orbital on each S atom is indicated); the dashed lines represent the Zr−S vector on the C_{2v} plane of each binaphthol ligand and the S−S interaction

Nonbonded intramolecular sulfur−sulfur interactions are relatively rare but can be energetically favourable. For example, the S_4 moiety in bis[8-(phenylthio)naphthyl] 1,1′-disulfide, which exhibits short nonbonded sulfur distances of 2.988(2) Å, is aligned in a linear fashion displaying two $n_p(S)$-σ*(S−S) 3-c-4-e bonds.[24] Nonbonding S interactions in this system are noted to have a greater influence on the solid-state geometry in the naphthalene complexes than in the corresponding phenyl disulfide. In the same way, the p-type lone pair orbital of Se in the R−Se−R′ fragments (R ≠ R′ = alkyl/aryl) has also been shown to play an important role in intramolecular nonbonding interactions.[25]

Ab initio calculations and statistical studies indicate that S···S close contacts in R−S−R fragments (R = H, alkyl, aryl) are attractive for a range of orientations (i.e. for a range of dihedral angles between the C_{2v} axis of each fragment), and there is a maximum probability for a colinear S···S arrangement.[26] Although calculations show that at short distances (3 Å) the interactions are mainly repulsive,[27,28] the dispersion contribution, which is substantial for the large, polarisable sulfur atom, provides an important attractive force that is able to compensate the repulsive electrostatic force. In **5**, the hard metal ion binds a molecule of THF, and the sulfur−sulfur dipole interaction is preferred over the formation of closer dative bonds between the metal and the soft sulfur atoms.

2.3 Alkyl Derivatives of L^{SN}

2.3.1 Dialkyltitanium Complexes

Attempts to prepare the dibenzyl complex [Ti(L^{SN})($CH_2Ph)_2$] by protonolysis of [Ti($CH_2Ph)_4$] with [H_2L^{SN}] resulted only in the recovery of starting materials. This contrasts with the facile preparation of the biphenolate complex [(tbmp)Ti($CH_2Ph)_2$].[2] ^{1}H NMR spectroscopy suggests the formation of [Ti(L^{SN})($CH_2Ph)_2$] (**8**) by metathesis between **1** and the Grignard reagent $PhCH_2MgCl$, but no tractable product could be isolated.

In an attempt to synthesise a dimethyl complex [Ti(L^{SN})Me_2], a hexane solution of **1** was treated with 2 equiv. of LiMe.[29] However, even at temperatures below −10 °C, the reaction mixture quickly became dark to yield an intractable mixture of products. A one-pot reaction at −80 °C of H_2L^{SN} with 4 equiv. of LiMe, followed by addition of $TiCl_4$, also yielded no tractable product.

2.3.2 Dibenzylzirconium Complexes

In contrast to the tetrabenzyltitanium reaction, treatment of 1 equiv. of [H_2L^{SN}] with tetrabenzylzirconium in THF results in the rapid formation of the bis(ligand) THF adduct **5**. No intermediates were detectable (by solution NMR spectroscopy) during the course of this reaction. This route to **5** gives higher yields than metathesis reactions with zirconium tetrachloride.

$$ZrBz_4 + H_2L^{SN} \xrightarrow[-80\ ^\circ C]{thf} \underset{\mathbf{9}}{Zr(L^{SN})(CH_2Ph)_2(thf)} \quad (2)$$

A synthetic scale-up of the reaction (about 2.0 g) sufficiently reduces the extent of ligand redistribution to permit the isolation of the dibenzyl complex **9** as a pale yellow solid in moderate yield (47%) [Equation (2)]. This complex is significantly less sensitive to light than the parent alkyl compound, and if the reaction is carried out in the absence of donating solvents, an intractable product mixture results. The ^{1}H NMR spectroscopic resonances ([D_6]benzene) for the methylene benzyl moieties appear as a singlet at δ = 2.67 ppm, rather than an AB quadruplet.[30] Low-temperature ^{1}H NMR studies in [D_8]toluene and CD_2Cl_2 reveal no fluxional process slower than the NMR timescale that would render the two methylene protons inequivalent.[31]

2.3.3 Single-Crystal X-ray Analysis of [Zr(L^{SN})($CH_2Ph)_2$·THF] (9)

The molecular structure of **9** is shown in Figure 3. It is evident that the metal atom maintains a mononuclear en-

 © 2004 Wiley-VCH Verlag GmbH & Co. KGaA, Weinheim

vironment, and the bound THF molecule occupies an apical coordination site of a distorted octahedron. The ligand facially caps the zirconium atom, with relatively short naphtholate oxygen−zirconium distances of 1.981(2) and 2.004(2) Å for O(1) and O(2), respectively. The sulfur atom is geometrically placed in a *trans* arrangement to C(40) of the η^1-benzyl group, with a correspondingly long sulfur−zirconium distance of 2.9248(7) Å. As a result, the mean planes of the two naphthalene rings of the ligands form a dihedral angle of 78.0°, with an associated C(11)−S(1)−C(21) bond angle of 106.3(1)°.

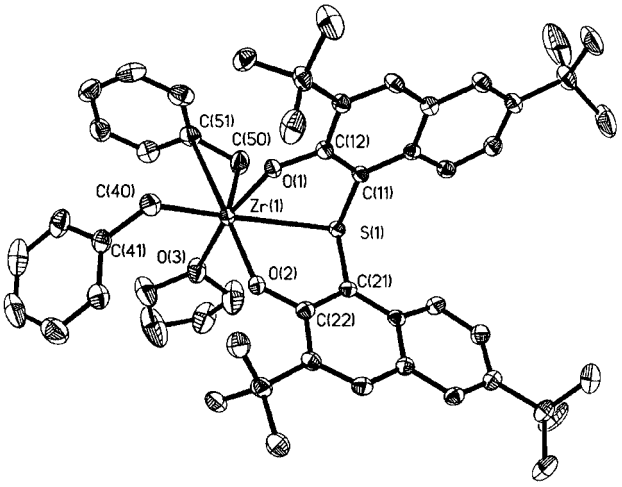

Figure 3. Molecular structure of **9**; view along the 100 plane; ellipsoids set at the 50% probability level; H atoms removed for clarity

The two coordinated benzyl groups are clearly distinguishable in the solid state, and display η^1- and η^2-bonding modes.[30] The η^2-bound benzyl ring [C(50), (C51)] has an acute Zr(1)−C(50)−C(51) angle of 95.3(2)°, in contrast to that of the η^1-benzyl group [Zr(1)−C(40)−C(41) 118.8(2)°]. The acuteness of this angle results in the close proximity of the phenyl ring to the zirconium atom, and in particular gives rise to a short Zr−C_{ipso} interaction of 2.850(3) Å.[30]

2.3.4 Reactivity of 9 with Air

Exposure of dibenzyl compound **9** to air affords three compounds, which can be identified by ^{1}H NMR spectroscopy [Equation (3)]. To date, we have been unable to isolate the analytically pure major product by recrystallisation, but were able to obtain single crystals suitable for structure analysis to confirm the identity. The complex is formally the product of the insertion of one oxygen atom per metal atom into the Zr−C bond of a benzyl group. The controlled O atom insertion into a bound alkyl group at an early transition metal is unusual,[32] and to the best of our knowledge, this is the first time a benzyl group has been selectively oxygenated. Usually, reaction with an oxygen atom source such as pyridine *N*-oxide or trimethylamine *N*-oxide, or air or water, forms oxo adducts containing the Zr−O−Zr unit.[33] Treatment of the dibenzyl complex **9** with trimethylamine *N*-oxide shows that the same product is formed, confirming that **10** derives from the reaction with air; but while the yield is greatly improved for this reaction, we were unable to obtain correct elemental analysis data for this complex. Work is in progress to identify whether the oxidisable sulfur bridge is involved in this oxygen atom insertion into the Zr−C bond.

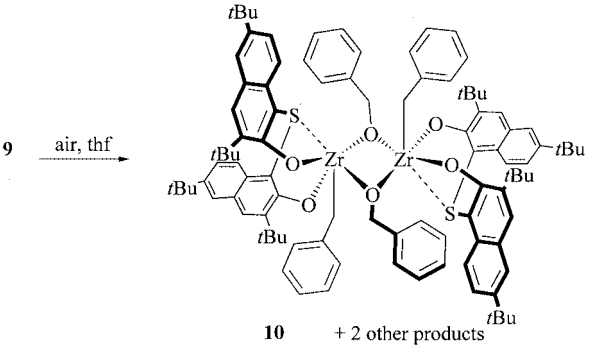

(3)

The molecular structure of **10** (Figure 4) is dinuclear and unsolvated. The geometry at Zr is essentially octahedral with a *fac*-$\mathbf{L^{SN}}$ ligand, a small cone angle of the [OSO] group and a relatively long Zr(1)−S(1) contact of 2.8881(13) Å. The remaining benzyl group shows no additional agostic interaction with the metal atom. The oxygenated benzyl group bridges the zirconium centre and its symmetry-related equivalent in a nearly symmetrical fashion with an average Zr−O distance of 2.15 Å, relative to an average Zr−$O_{naphtholate}$ distance of 1.99 Å, and a Zr−Zr′ distance of 3.490(1) Å.

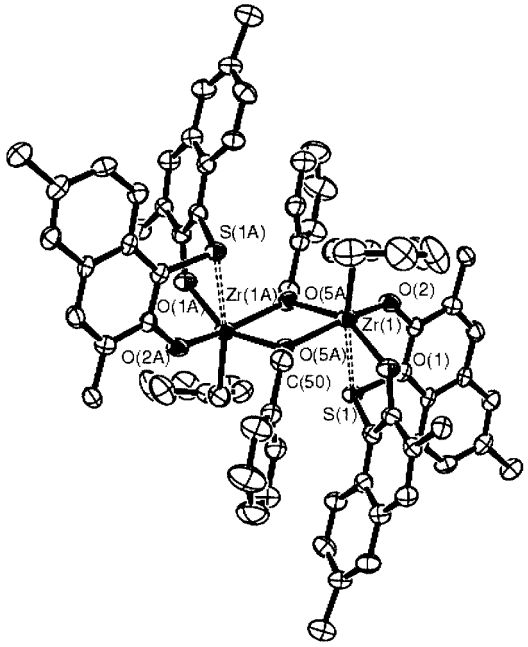

Figure 4. Molecular structure of **10**; ellipsoids set at the 50% probability level; solvent and Me groups removed for clarity

Interestingly, the Zr−S distances in both [Zr($\mathbf{L^{SN}}$)$_1$X$_2$] complexes are longer than those in the sterically more congested [Zr($\mathbf{L^{SN}}$)$_2$] complex, giving further weight to the at-

 © 2004 Wiley-VCH Verlag GmbH & Co. KGaA, Weinheim

Table 2. Results for the polymerisation of ethene and propene

Complex (mmol)	Yield [g]	Time [min]	Activity[a]	M_w[b] ($\times 10^5$)	M_n [b]	M_w/M_n [b]
1 [Ti($\mathbf{L^{SN}}$)Cl_2·THF] (0.027)[c]	7.92	60	29	2.04	46900	4.4
4 [Zr($\mathbf{L^{SN}}$)Cl_2·THF] (0.026)[c]	0.26	60	1	8.36	28000	30
9 [Zr($\mathbf{L^{SN}}$)$(CH_2Ph)_2$·THF] (0.023)[c]	5.95	60	26	0.22	4300	5.25
[(tbmp)$TiCl_2$] (0.02)[d]	7.90	5	1580	3.5	29000	11.9
[(tbmp)$TiCl_2]_2$ (0.0025)[e]	0.55	60	220	0.12	8000	2.2
[(tbmp)$ZrCl_2$] (0.02)[f]	inactive					
1 (0.027)[g]	4.22	60	15	0.02	510	4.1

[a] Activities quoted in kg PE mol^{-1}[catalyst] bar^{-1} h^{-1}. [b] PDI determined by GPC, results are an average of two runs. [c] Conditions used: 20 °C, 20 mg of catalyst, 1000 equiv. of MAO in 150 mL of toluene, 10 bar of ethene/propene, 1 h. [d] Results taken from ref.[2], run at 40 °C, 3 bar of ethene, 500 equiv. of MAO in 200 mL of toluene. [e] Result taken from ref.[20], run at 20 °C, 1 bar of ethene, 1000 equiv. of MAO in toluene. [f] Results taken from ref.[2], run at 20 °C, 3 bar of ethene, 500 equiv. of MAO in 200 mL of toluene. [g] 10 bar of propene.

tractive S−S interaction's dominance of the local geometry of the ligands in the bis(ligand) complex **5**.

2.4 Polymerisation of Ethene and Propene

Three suitable complexes were chosen for the polymerisation studies, [Ti($\mathbf{L^{SN}}$)Cl_2·THF] (**1**), [Zr($\mathbf{L^{SN}}$)Cl_2·THF] (**4**) and [Zr($\mathbf{L^{SN}}$)$(CH_2Ph)_2$·THF] (**9**). The results are collated in Table 2; for comparison, the analogous tbmp complexes have been included. A significant exotherm was observed during the first 10 min of each polymerisation run (except **4**/MAO), attaining a maximum temperature of 50 °C. For the remainder of each polymerisation run, the autoclave temperatures remained almost constant (within 5 °C).

The titanium dichloride system **1**/MAO and the bis(benzyl)zirconium complex **9**/MAO exhibit moderate activities for the polymerisation of ethene and produce polyethene with high molecular weights, whereas the corresponding zirconium chloride system **4**/MAO shows a much lower propensity to polymerise ethene. Under identical conditions, **1**/MAO also shows moderate activity for the polymerisation of propene. Theory suggests that the Ti-based catalysts are more active than their zirconium counterparts due to a slightly lower activation energy barrier;[10] the complete inactivity of the (tmbp)Zr species is therefore surprising.

The ethene polymerisation activity of **1**/MAO (28.94 kg PE mol^{-1}[Ti] bar^{-1} h^{-1}) compares well with the dimeric complex [(tbmp)$TiCl_2]_2$, which was tested at a lower catalyst concentration (220 kg PE mol[Ti]$^{-1}$ bar^{-1} h^{-1}).[20] However, the binaphthol-based catalyst remains an order of magnitude less active than the corresponding biphenol system. Theoretical studies also suggested that the catalyst activity is influenced by the extent of conjugation in the ligand backbone and that a C=C bridged system should be more active than a C−C system.[2,10] The naphthol bridge in these systems, which has a lower aromaticity than a phenol, supports this argument.

However, the Zr naphtholate systems are better catalysts than their phenolate counterparts. In view of the inactivity of the reported Zr-based biphenolates towards ethene polymerisation, these results are encouraging. Narrow molecular weight distributions and polydispersities for the sample isolated from the **1**/MAO/ethene run suggest that this a well-defined single-site catalyst. This is in contrast to the higher PDI reported for the [(tbmp)$TiCl_2$]/MAO system run for a brief period of time.[2] The polyolefin from the **1**/MAO/propene run was isolated as a viscous oil, with a low average molecular weight for the polymer. The molecular weight distribution appears bimodal, suggesting an ill-defined active catalyst species and/or the presence of more than one active site. Again, a bimodal distribution is apparent in the **4**/MAO/ethene system.

2.5 Conclusions

Titanium(IV) and zirconium(IV) complexes supported by the binaphtholate $\mathbf{L^{SN}}$ dianion have been synthesised and structurally characterised. The formation of bis($\mathbf{L^{SN}}$) complexes renders the direct syntheses of titanium(IV) and zirconium(IV) dichloride complexes difficult, with possible further stabilisation of the zbis($\mathbf{L^{SN}}$)irconium complex by an S−S interaction. However, unlike aminebis(phenolate) [ONO] derivatives of Group 4 metals, the bis[OSO] complexes undergo disproportionation reactions to form heteroleptic adducts.

The first crystallographically characterised Zr[OSO] complexes have been isolated. The bis(OSO)zirconium THF adduct exhibits a co-facial arrangement of the naphthol ligands, a distorted capped octahedral geometry at Zr and close S−S distances, which suggest an unusual noncovalent S···S interaction in the solid state. The zirconium [OSO] complexes are kinetically more labile than related aminebis(phenolate) [ONO] adducts, but less labile than their titanium counterparts, and heteroleptic complexes are easier to isolate. The dibenzylzirconium complex reacts with air to insert an O atom rather than decompose to a μ-oxodizirconium complex. Preliminary reactions with the oxygen atom source trimethylamine *N*-oxide show that the same product is formed. Structural studies of the complexes have shown that the smaller Group 4 metal cations accommodate the symmetrical *fac* conformation of the $\mathbf{L^{SN}}$ ligand much more readily than the twisted conformation observed in the corresponding lanthanide chemistry.[15,34]

 © 2004 Wiley-VCH Verlag GmbH & Co. KGaA, Weinheim

The complexes **1** and **9** are effective ethene polymerisation pre-catalysts, whereas the dichloride **4** displays a surprisingly low activity towards ethene polymerisation. The catalyst system **1**/MAO is also moderately active for the polymerisation of propene.

3. Experimental Section

General Procedures: All experimental procedures were performed under dry, oxygen-free argon or dinitrogen, with standard Schlenk techniques (mechanical pump for vacuum 10^{-4} mbar). Subsequent manipulations of isolated compounds were carried out in a glove box (MBraun Unilab) under dry dinitrogen. All ^{1}H and ^{13}C NMR spectra were recorded with a Bruker DPX 300 spectrometer, operating frequency variable temperature unit at 300 K, unless otherwise stated. Chemical shifts are reported in parts per million and referenced to residual proton resonances in [D_6]benzene calibrated against external TMS. Mass spectra (EI and FAB) were run by Dr. Ali Abdul-Sada with a Kratos MS80RF instrument. Elemental analyses were determined by Dr. Stephen Boyer at London Metropolitan University and by Mr. Trevor Spencer at the University of Nottingham. Polymerisation runs were conducted in a purpose-built rig in the laboratory of Professor F. G. N. Cloke, at the University of Sussex, and GPC analysis was performed by Rapra Technology Ltd. A glass autoclave with a magnetically coupled stirrer was charged with a toluene solution of each complex, 1000 equiv. of MAO, and the vessel pressurised at 20 °C with 10 bar of ethene or 10 bar of propene for 1 h. Samples from the **1**/MAO/ethene and **4**/MAO/ethene were found to contain a significant amount of insoluble (in 1,2,3-trichlorobenzene) material and were difficult to filter. The chromatogram peak area for **4**/MAO/ethene is less than 20% that of the **1**/MAO/ethene and **9**/MAO/ethene samples, suggesting that the bulk of this sample remained insoluble. The insolubility of the polymer could be due to an exceptionally high molecular weight or a high degree of cross-linking. All solvents used (toluene, THF, diethyl ether, hexane, dichloromethane) were either degassed and purified by passage through activated alumina towers prior to use, or were freshly distilled from the appropriate alkali metal under dinitrogen, and thoroughly degassed prior to use. NMR spectroscopic grade [D_6]benzene and [D_8]toluene were refluxed over potassium metal, and CD_2Cl_2 refluxed over CaH_2 and vacuum-distilled before use. All chemicals were either obtained from Aldrich Chemicals, except *n*BuLi and sulfur dichloride (Acros), or were synthesised according to standard literature procedures.[35] Literature procedures for the preparation of [1,1′-S(2-HO$C_{10}H_4t$Bu$_2$-3,6)$_2$] ($H_2\mathbf{L}^{SN}$)[15] and [1,1′-S(2-KO$C_{10}H_4t$Bu$_2$-3,6)$_2$(THF)$_2$] ($K_2\mathbf{L}^{SN}$)[36] have previously been described.

[($\mathbf{L}^{SN}$)TiCl$_2$·THF] (1): A solution of $TiCl_4$·2THF in THF (30 mg, 0.09 mmol, 10 mL) was added dropwise to a solution of **2** in a 1:1 mixture of THF/dichloromethane (0.1 g, 0.09 mmol, 30 mL) cooled to −78 °C. The reaction mixture was left to warm slowly to ambient temperature, upon which it changed colour from orange to dark brown. After 12 h, all volatiles were removed under reduced pressure. The crude product was extracted into hexane and cooled to −30 °C. Analytically pure **1** was isolated as a microcrystalline brown solid in 96% yield (62 mg). ^{1}H NMR (C_6D_6): δ = 8.66 (d, $^3J_{H,H}$ = 8.85 Hz, 1 H, 8-H), 7.51 (s, 3H 4-H, 5-H, 7-H), 3.81 (br., 2 H, CH_2 THF), 1.62 (s, 9 H, 3-*t*Bu), 1.32 (br., 2 H, CH_2 THF), 1.19 (s, 9 H, 6-*t*Bu) ppm. $C_{36}H_{44}Cl_2O_2STi$·THF (731.71): calcd. C 65.66, H 7.16; found C 65.67, H 7.39.

[($\mathbf{L}^{SN}$)Ti(μ-Cl)Cl]$_2$ (1a): ^{1}H NMR/C_6D_6: δ = 8.61 (br., 1 H, 8-H), 7.38 (m, 3H 4-H, 5-H, 7-H), 1.48 (s, 9 H, 3-*t*Bu), 1.18 (s, 9 H, 6-*t*Bu) ppm.

[($\mathbf{L}^{SN}$)$_2$Ti] (2): A solution of $\mathbf{H_2L^{SN}}$ in THF (0.2 g, 0.37 mmol, 15 mL) was added dropwise to a cooled solution of Ti(OEt)$_4$ in THF (19.0 μL, 0.185 mmol, 10 mL) at −30 °C over a period of 20 min, and the mixture was warmed to room temperature over 12 h, by which time **2** had precipitated from the reaction mixture. The supernatant was decanted from the precipitate, and the crude powder washed with 3 × 10 mL cold hexane to yield analytically pure **2** in 70% yield (0.146 g). ^{1}H NMR (C_6D_6): δ = 8.93 (br., 1 H, 8-H), 8.87 (br., 1 H, 8-H), 7.59 (m, 6 H, 4-H, 5-H, 7-H), 1.67 (s, 9 H, 3-*t*Bu), 1.59 (s, 9 H, 3-*t*Bu), 1.23 (s, 9 H, 6-*t*Bu) ppm. EI-MS: *m*/*z* (%)= 1128 (24) [M^+]. $C_{72}H_{88}O_4S_2Ti$ (1128): calcd. C 76.56, H 7.85; found C 76.48, H 7.80.

[($\mathbf{L}^{SN}$)Ti(μ-NMe$_2$)Cl]$_2$ (3a): ^{1}H NMR (C_6D_6): δ = 8.48 (d, $^3J_{H,H}$ = 8.82 Hz, 1 H, 8-H), 7.58 (m, 3H 4-H, 5-H, 7-H), 1.78 (s, 3 H, NMe_2), 1.16 (s, 9 H, 3-*t*Bu), 1.31 (s, 9 H, 6-*t*Bu) ppm.

[($\mathbf{L}^{SN}$)Ti(μ-Cl)NMe$_2$]$_2$ (3b): ^{1}H NMR: δ = 8.79 (d, $^3J_{H,H}$ = 8.70 Hz, 1 H, 8-H), 7.58 (m, 3H 4-H, 5-H, 7-H), 1.78 (s, 3 H, NMe_2), 1.26 (s, 9 H, 3-*t*Bu), 1.71 (s, 9 H, 6-*t*Bu) ppm.

[($\mathbf{L}^{SN}$)ZrCl$_2$·THF] (4): A slurry of $ZrCl_4$·2THF in toluene (21 mg, 0.056 mmol, 7 mL) was added dropwise over a period of 20 min to a solution of **5** in toluene (70 mg, 0.056 mmol, 7 mL),which was cooled to −60 °C. The resultant solution was allowed to slowly attain room temperature over 4 h and stirred at room temperature for a further 10 h. All volatiles were removed under reduced pressure, and the crude product extracted into hexane (15 mL). Cooling to −30 °C afforded a colourless precipitate that was isolated and washed with cold hexane (3 × 5 mL) to give analytically pure **4** in 53% yield (0.021 g). ^{1}H NMR (C_6D_6): δ = 8.83 (br., 1 H, 8-H), 7.58 (m, 3 H, 4-H, 5-H, 7-H), 3.70 (br., 4 H,CH_2 THF), 1.58 (br., 9 H,3-*t*Bu), 1.35 (br., 4 H, CH_2 THF), 1.23 (s, 9 H, 6-*t*Bu) ppm. $C_{36}H_{44}Cl_2O_2SZr$·THF (775.1): calcd. C 61.98, H 6.76; found C 61.47, H 7.03.

[($\mathbf{L}^{SN}$)$_2$Zr·THF] (5): In the absence of light, a solution of $H_2\mathbf{L}^{SN}$ in THF (500 mg, 0.92 mmol, 20 mL) was added dropwise to a solution of Zr(CH_2Ph)$_4$ in THF (210 mg, 0.46 mmol, 15 mL), which was cooled to −60 °C over 30 min. Upon completion of the addition of the ligand, the reaction mixture was slowly warmed to room temperature and stirred at ambient temperature for a further 10 h. All volatiles were removed under reduced pressure, and the crude solid extracted into 5 mL of diethyl ether. Subsequent cooling to −30 °C afforded single crystals suitable for X-ray diffraction analysis in 45% yield (258 mg). ^{1}H NMR (C_6D_6): δ = 8.80 (d, $^3J_{H,H}$ = 8.97 Hz, 1 H, 8-H), 7.64 (s, 1 H, 4-H), 7.57 (s, 1 H, 5-H), 7.11 (d, $^3J_{H,H}$ = 8.97 Hz, 1 H, 7-H), 4.10 (br., 2 H, CH_2 THF), 1.57 (s, 9 H, 3-*t*Bu), 1.36 (br., 2 H, CH_2 THF) 1.23 (s, 9 H, 6-*t*Bu) ppm. $C_{72}H_{88}O_4S_2Zr$·THF (1245.0): calcd. C 73.37, H 7.77; found C 73.19, H 7.54.

[($\mathbf{L}^{SN}$)Zr(μ-NMe$_2$)Cl]$_2$ (6a): ^{1}H NMR (C_6D_6): δ = 8.81 (br., 2 H, 8-H), 7.56 (m, 6 H, 4-H, 5-H, 7-H), 3.85 (s, 3 H, μ-NMe_2), 1.66 (s, 18 H, 3-*t*Bu), 1.23 (s, 18 H, 6-*t*Bu) ppm.

[($\mathbf{L}^{SN}$)Zr(μ-Cl)NMe$_2$]$_2$ (6b): ^{1}H NMR (C_6D_6): δ = 8.76 (d, $^3J_{H,H}$ = 8.76 Hz, 2 H, 8-H), 7.56 (m, 6 H, 4-H, 5-H, 7-H), 1.61 (s, 3 H, NMe_2), 1.58 (s, 18 H, 3-*t*Bu), 1.19 (s, 18 H, 6-*t*Bu) ppm.

[($\mathbf{L}^{SN}$)$_2$Zr·HNMe$_2$] (7): ^{1}H NMR (C_6D_6): δ = 8.67 (br., 2 H, 8-H,), 7.59 (s, 2 H, 4-H), 7.55 (br., 2 H, 7 H), 7.44 (d, $^3J_{H,H}$ = 8.74 Hz,

 © 2004 Wiley-VCH Verlag GmbH & Co. KGaA, Weinheim

2 H, 7-H), 2.66 (br., 3 H, $HNMe_2$) 1.53 (s, 18 H, 3-*t*Bu), 1.23 (s, 18 H, 6-*t*Bu) ppm.

[(L^{SN})Ti(CH_2Ph)$_2$] (8): ^{1}H NMR (C_6D_6): δ_H = 8.69 (d, $^3J_{H,H}$ = 9.03 Hz, 1 H, 8-H), 7.51 (m, 3H 4-H, 5-H, 7-H), 7.05 (m, 5 H, CH_2Ph) 2.10 (s, 2 H, CH_2Ph), 1.62 (s, 9 H, 3-*t*Bu), 1.17 (s, 9 H, 6-*t*Bu) ppm.

[(L^{SN})Zr(CH_2Ph)$_2$·thf] (9): A solution of H_2L^{SN} in THF (2.0 g, 3.69 mmol, 25 mL) was added dropwise to a solution of $Zr(CH_2Ph)_4$ in THF (1.68 g, 3.69 mmol, 15 mL), which was cooled to −60 °C over 45 min. Upon completion of addition of the ligand, the reaction mixture was slowly warmed to room temperature and stirred for a further 15 h. All volatiles were removed under reduced pressure, and the crude solid extracted into 25 mL of diethyl ether. Cooling of the solution to −30 °C resulted in the precipitation of analytically pure **10** as a yellow powder, which was washed with 3 × 5 mL cold diethyl ether, and isolated in 47% yield (1.54 g). Single crystals suitable for X-ray diffraction studies were grown from slow concentration of the supernatant at −30 °C. ^{1}H NMR (C_6D_6): δ = 8.94 (d, $^3J_{H,H}$ = 8.76 Hz, 1 H, 8-H), 7.62 (s, 1 H, 4-H), 7.60 (s, 1 H, 7-H), 7.57 (s, 1 H, 5-H), 7.55 (m, 2 H, CH_2Ph), 6.87 (m, 3 H, CH_2Ph), 3.53 (br., 2 H, CH_2 THF), 2.67 (s, 2 H, CH_2Ph), 1.56 (s, 9 H, 3-*t*Bu), 1.24 (s, 9 H, 6-*t*Bu), 1.01 (br., 2 H, CH_2 THF) ppm. ^{13}C NMR (C_6D_6): δ = 166.68, 130.00, 129.67, 129.28 (quaternary C), 145.49, 140.10, 137.85, 133.39, 127.68, 126.17, 125.65 (CH), 65.48 (CH_2Ph) 31.34, 30.08 (*t*Bu), 73.18, 25.05 (THF) ppm. $C_{50}H_{54}O_2SZr$·thf (882.4): calcd. C 73.22, H 7.46; found C 73.49, H 7.69.

[(L^{SN})Zr(OCH_2Ph)(CH_2Ph)$_2$] (10). a) A Schlenk tube containing powdered **9** was exposed to air for 2 min. The resulting colourless powder was recrystallised from diethyl ether, from which crystals of **10** suitable for single-crystal X-ray diffraction were isolated. **b)** Under N_2, a glass vial was charged with a [D_6]benzene solution of **9** (20 mg, 22.6 μmol), and a [D_6]benzene solution of Me_3NO (1.6 mg, 22.6 μmol). The resultant mixture was filtered through glass wool into a Young's PTFE tap equipped NMR tube, and a ^{1}H NMR spectrum recorded immediately. The reaction was further monitored by ^{1}H NMR spectroscopy. t = 0 h: The ^{1}H NMR spectroscopic resonances of **9** have completely given way to a new transient species (not identified) and **10** in a 1:1 ratio. ^{1}H NMR (C_6D_6) of **10**: δ = 8.98 (d, $^3J_{H,H}$ = 8.46 Hz, 1 H, 8-H), 7.61 (m, 9 H, Ar), 3.59 (br., 1 H, OCH_2), 3.25 (br., 1 H, CH_2), 1.73 (s, 9 H, 3-*t*Bu), 1.26 (s, 9 H, 6-*t*Bu) ppm. $C_{50}H_{58}O_3SZr$ (830.3): calcd. C 72.32, H 7.04; found C 67.01, H 7.96. Yield, isolated from a mixture with **9** (42 mg, 1.4%). ^{1}H NMR (C_6D_6) of transient: δ = 9.16 (d, $^3J_{H,H}$ = 8.94 Hz, 1 H, 8-H), 7.41 (m, 9 H, Ar), 2.94 (br., 1 H, CH_2), 1.68 (s, 9 H, 3-*t*Bu), 1.45 (s, 9 H, 6-*t*Bu) ppm. t = 1 h: The ^{1}H NMR spectroscopic resonances due to **10** have grown considerably, while those for the transient species have decreased to a ratio of 5:2. t = 24 h: ^{1}H NMR spectrum contains a few more resonances of insignificant integral value but is essentially unchanged. t = 168 h: No change in ^{1}H NMR spectrum.

Crystallographic Data: X-ray data (Table 3) were collected using Mo-K_α radiation (λ = 0.71073 Å) with a Bruker SMART1000 CCD area detector diffractometer using ω scans. Structure solution and refinement was carried out with the SHELX suite of programs.[37] CCDC-217721 (**5**), -217722 (**9**) and -217723 (**10**) contain the supplementary crystallographic data for this paper. These data can be obtained free of charge at www.ccdc.cam.ac.uk/conts/retrieving.html [or from the Cambridge Crystallographic Data Centre, 12 Union Road, Cambridge CB2 1EZ, UK; Fax: (internat.) + 44-1223-336-033; E-mail: deposit@ccdc.cam.ac.uk].

Table 3. Crystallographic data and structure refinement for **5**·Et_2O and **9** and **10**

Empirical formula	$C_{80}H_{106}O_6S_2Zr$ (**5**·Et_2O)	$C_{54}H_{66}O_3SZr$ (**9**)	$C_{54}H_{68}O_4SZr$ (**10**)
Formula mass	1319.07	886.35	1808.73
Temperature [K]	150(2)	293(2)	150(2)
Wavelength [Å]	0.71073	0.71073	0.71073
Crystal system	monoclinic	monoclinic	monoclinic
Space group	*C*2/*c*	$P2_1/n$	$P2_1/n$
Unit cell dimensions	a = 33.175(2) Å	a = 16.5541(11) Å	a = 14.815(3) Å
	b = 11.2138(8) Å	b = 11.1071(8) Å	b = 21.612(4) Å
	c = 21.746(2) Å	c = 25.9090(18) Å	c = 16.183(3) Å
	β = 105.1690(10)°	β = 91.2190(10)°	β = 108.630(4)°
Volume [Å^3]	7808.0(10)	4762.8(6)	4910.1(15)
Z	4	4	2
$D_{calcd.}$ [Mg/m^3]	1.137	1.236	1.223
Absorption coefficient [mm^{-1}]	0.242	0.316	0.309
F(000)	2856	1880	1920
Crystal size [mm]	0.27 × 0.20 × 0.12	0.4 × 0.15 × 0.10	0.22 × 0.20 × 0.14
θ range for data collection [°]	1.92−26.37	2.21−29.04	1.73−28.77
Index ranges	$-42 \le h \le 44$	$-22 \le h \le 22$	$-18 \le h \le 9$
	$-14 \le k \le 14$	$-13 \le k \le 15$	$-26 \le k \le 27$
	$-28 \le l \le 29$	$-34 \le l \le 35$	$-7 \le l \le 21$
Reflections collected	35011	31092	16297
Independent reflections	7969 [R(int) = 0.049]	11709 [R(int) = 0.053]	8782 [R(int) = 0.0691]
Completeness to θ = 26.37°	99.8%	99.2%	76.2%
Absorption correction	Semi-empirical from equivalents	Semi-empirical from equivalents	None
Max. and min. transmission	0.904 and 0.864	1.000 and 0.870	
Refinement method	Full-matrix least squares on F^2	Full-matrix least squares on F^2	Full-matrix least squares on F^2
Data/restraints/parameters	7969/38/419	11709/0/532	8782/0/486
Goodness-of-fit on F^2	1.016	1.054	0.895
Final R int [$I > 2\sigma(I)$]	$R1$ = 0.0476, $wR2$ = 0.1293	$R1$ = 0.0581, $wR2$ = 0.1142	$R1$ = 0.0570, $wR2$ = 0.1302

 © 2004 Wiley-VCH Verlag GmbH & Co. KGaA, Weinheim

Acknowledgments

The authors thank the EPSRC (studentship for L. S. N., Advanced Fellowship for P. L. A.) and the Royal Society for funding, Professor F. Geoffrey N. Cloke for use of a catalyst testing apparatus, and the Deutsche Forschungsgemeinschaft and the Fonds der Chemischen Industrie for financial support.

[1] V. C. Gibson, S. K. Spitzmesser, *Chem. Rev.* **2003**, *103*, 283.
[2] A. Van der Linden, C. J. Schavarien, N. Meijboom, C. Ganter, G. Orpen, *J. Am. Chem. Soc.* **1995**, *117*, 3008.
[3] V. C. Gibson, *J. Chem. Soc., Dalton Trans.* **1994**, 1607.
[4] G. J. P. Britosvek, V. C. Gibson, D. F. Wass, *Angew. Chem. Int. Ed.* **1999**, *38*, 428.
[5] S. Fokken, T. P. Spaniol, H.-C. Kang, W. Massa, J. Okuda, *Organometallics* **1999**, *15*, 5069; L. Porri, A. Ripa, P. Colombo, E. Miano, S. Capelli, S. V. Meille, *J. Organomet. Chem.* **1996**, *514*, 213; F. Amor, S. Fokken, T. Kleinheim, T. P. Spaniol, J. Okuda, *J. Organomet. Chem.* **2001**, *621*, 3; Y. Takashima, Y. Nakayama, H. Yasuda, A. Nakamura, A. Harada, *J. Organomet. Chem.* **2002**, *654*, 74.
[6] J. Okuda, S. Fokken, T. Kleinhenn, T. P. Spaniol, *Eur. J. Inorg. Chem.* **2000**, 1321; C. Capacchione, A. Proto, H. Ebeling, R. Muelhaupt, K. Moeller, T. P. Spaniol, J. Okuda, *J. Am. Chem. Soc.* **2003**, *125*, 4964.
[7] J. Okuda, S. Fokken, H.-C. Kang, W. Massa, *Polyhedron* **1998**, *17*, 943; C. R. Cornman, K. M. Geiser-Bush, J. W. Kampf, *Inorg. Chem.* **1999**, *38*, 4303.
[8] R. Siefert, T. Weyhermuller, P. Chaudhuri, *J. Chem. Soc., Dalton Trans.* **2000**, 4656.
[9] T. Miyatake, K. Mizunuma, Y. Seki, M. Kakugo, *Macromol. Chem. Rapid Commun.,* 1989, **10**, 349; T. Miyatake, K. Mizunuma, M. Kakugo, *Macromol. Chem. Macromol. Symp.,* 1993, **66**, 203; F. G. Sernetz, R. Muelhaupt, S. Fokken, J. Okuda, *Macromolecules* **1997**, *30*, 1562; M. Kakugo, T. Miyatake, K. Mizunuma, *Stud. Surf. Sci. Catal.,* 1999, **56**, 517; M. Kakugo, T. Miyatake, K. Mizunuma, Y. Yagi, Sumitomo Chemical Co. U.S. 5043, 408.
[10] R. D. J. Froese, D. G. Musaev, T. Matsubara, K. Morokuma, *J. Am. Chem. Soc.* **1997**, *119*, 7190; R. D. J. Froese, D. G. Musaev, K. Morokuma, *Organometallics* **1999**, *18*, 373.
[11] J. Okuda, E. Masoud, *Macromol. Chem. Phys.* **1998**, *199*, 543.
[12] Y. Takashima, Y. Nakayama, K. Watanabe, T. Itono, N. Ueyama, A. Nakamura, H. Yasuda, A. Harada, *Macromolecules* **2002**, *35*, 7538.
[13] F. G. Sernetz, R. Muelhaupt, S. Fokken, J. Okuda, *Macromolecules* **1997**, *30*, 1562.
[14] W. Kaminsky, *J. Chem. Soc., Dalton Trans.* **1998**, 1413; X. Yan, A. Chernega, M. L. H. Green, J. Sanders, J. Souter, T. Ushioda, *J. Mol. Catal. A: Chem.* **1998**, *128*, 119; G. W. Coates, *Chem. Rev.* **2000**, *100*, 1223.
[15] P. L. Arnold, L. S. Natrajan, J. J. Hall, S. J. Bird, C. Wilson, *J. Organomet. Chem.* **2002**, *647*, 205.
[16] M. C. W. Chan, K.-H. Tam, Y.-L. Pui, N. Zhu, *J. Chem. Soc., Dalton Trans.* **2002**, 3085.
[17] V. Reimer, T. P. Spaniol, J. Okuda, H. Ebeling, A. Tuchbreiter, R. Muelhaupt, *Inorg. Chim. Acta* **2003**, *345*, 221.
[18] J. Okuda, S. Fokken, H.-C. Kang, W. Massa, *Chem. Ber.* **1995**, *128*, 221.
[19] E. Y. Tshuva, I. Goldberg, M. Kol, Z. Goldschmidt, *Inorg. Chem.* **2001**, *40*, 4263.
[20] Y. Nakayama, K. Waatanabe, N. Ueyama, A. Nakamura, A. Harada, J. Okuda, *Organometallics* **2000**, *19*, 2498.
[21] E. Y. Tshuva, I. Goldberg, M. Kol, *Organometallics* **2001**, *20*, 3071; M. G. Thorn, Z. C. Etheridge, P. E. Fanwick, I. P. Rothwell, *J. Organomet. Chem.* **1999**, *591*, 148.
[22] D. W. Stephan, T. T. Nadasdi, *Coord. Chem. Rev.* **1996**, *147*, 147.
[23] A single S−S bond is 1.83 Å; A. Bondi, *J. Phys. Chem.* **1964**, *68*, 441; *International Tables of Crystallography*, Kluwer Academic, Dordrecht, **1992**, vol. C.
[24] W. Nakanishi, S. Hayashi, T. Arai, *Chem. Commun.* **2002**, 2416.
[25] W. Nakanishi, S. Hayashi, S. Toyota, *Chem. Commun.* **1996**, 371; W. Nakanishi, S. Hayashi, S. Toyota, *J. Org. Chem.* **1998**, *63*, 8790; S. Hayashi, W. Nakanishi, *J. Org. Chem.* **1999**, *64*, 6688.
[26] C. Rovira, J. J. Novoa, *Chem. Eur. J.* **1999**, *5*, 3689.
[27] T. N. Guru Row, R. Parthasarathy, *J. Am. Chem. Soc.* **1981**, *103*, 477.
[28] I. Dance, *New. J. Chem.* **2003**, *27*, 22.
[29] S. Fokken, F. Reichwald, T. P. Spaniol, J. Okuda, *J. Organomet. Chem.* **2002**, *663*, 158, for comparison, the activity of the dimethyltitanium complex [(tbmp)$TiMe_2$] towards ethene polymerisation is calculated to be 12.52 kg PE g $[Ti]^{-1}$ bar^{-1} h^{-1}.
[30] M. Bochmann, S. J. Lancaster, M. B. Hursthouse, K. M. Abdul Malik, *Organometallics* **1994**, *13*, 2235; S. J. Lancaster, M. Bochmann, *Organometallics* **1993**, *12*, 663.
[31] F. Guerin, D. H. McConville, J. J. Vittal, G. A. P. Yap, *Organometallics* **1998**, *17*, 5172; R. M. Gauvin, J. Kress, *J. Mol. Catal. A: Chem.* **2002**, *182/183*, 411.
[32] For an earlier example of oxygen insertion into a Ti−Me bond, see: G. J. Erskine, G. J. B. Hurst, E. L. Weinberg, B. K. Hunter, J. D. McCowan, *J. Organomet. Chem.* **1984**, *267*, 265.
[33] M. J. Carney, P. J. Walsh, F. J. Hollander, R. G. Bergman, *Organometallics* **1992**, *11*, 761; S. J. Kim, I. N. Jung, B. R. Yoo, S. Cho, J. Ko, S. H. Kim, S. O. Kang, *Organometallics* **2001**, *20*, 1501; J. Scholz, G. A. Hadi, K. H. Thiele, H. Gorls, R. Weimann, H. Schumann, J. Sieler, *J. Organomet. Chem.* **2001**, *626*, 243; Y. Wielstra, S. Gambarotta, A. L. Spek, W. J. J. Smeets, *Organometallics* **1990**, *9*, 2142; H. G. Helmut, C. E. Denner, *J. Organomet. Chem.* **1990**, *391*, 53.
[34] L. S. Natrajan, J. J. Hall, A. J. Blake, C. Wilson, P. L. Arnold, *J. Solid State Chem.* **2003**, *171*, 90.
[35] $TiCl_4$·2thf and $ZrCl_4$·2thf: L. E. Manzer, *Inorg. Synth.* **1985**, *21*, 135; [$Zr(CH_2Ph)_4$]: U. Zucchini, E. Albizzati, U. Giannini, *J. Organomet. Chem.* **1971**, 357; [$Ti(NMe_2)_4$]: A. A. Naiini, S. L. Ringrose, Y. Su, R. A. Jacobsen, J. G. Verkade, *Inorg. Chem.* **1993**, *32*, 1290; [$Zr(NMe_2)_4$]: H. Schreider, G. T. Puchta, F. A. Kaul, G. Raudaschl-Sieber, F. Lefebvre, *J. Mol. Catal. A, Chem.* **2001**, *170*, 127.
[36] P. L. Arnold, J. J. Hall, L. S. Natrajan, A. J. Blake, C. Wilson, *Dalton Trans.* **2003**, 1053.
[37] *SHELXTL 5.10*, Bruker AXS Inc., Madison, Wisconsin, USA, **1997**; G. M. Sheldrick, *Acta Crystallogr., Sect. A* **1990**, *46*, 467. G. M. Sheldrick, *SHELXL-97*, University of Goettingen, Germany, **1997**.

Received February 24, 2004
Early View Article
Published Online July 22, 2004

 © 2004 Wiley-VCH Verlag GmbH & Co. KGaA, Weinheim

Synthesis, Characterisation, Properties and X-ray Structures of Cu^{II} Coordination Compounds with 5,5′-Dimethylbipyridine and Various Anions: Control of Stoichiometry and Structure by the Counterions

Gerard A. van Albada,[a] Aminou Mohamadou,[a][‡] Ilpo Mutikainen,[b] Urho Turpeinen,[b] and Jan Reedijk*[a]

Keywords: Copper / EPR spectroscopy / Infrared spectroscopy / Magnetic properties / N ligands

The synthesis, crystal structures, and electronic and magnetic properties of eight new Cu^{II} compounds containing the ligand 5,5-dimethyl-2,2′-bipyridine (dmbpy) with the general formula $[Cu^{II}(dmbpy)_x(L)_2]$ (where L = BF_4^-, $CF_3SO_3^-$, NO_3^-, Br^-, NCS^-, N_3^-, $HCOO^-$, and x = 1–3) are reported. The geometries of the Cu^{II} ions include a four-coordinate square-planar polymeric compound $[Cu(dmbpy)(N_3)_2]_n$ (**7**), the five-coordinate compounds, $[Cu(dmbpy)_2(C_2H_6O)](CF_3SO_3)_2$ (**2**), $[Cu(dmbpy)_2(NO_3)](NO_3)$ (**3**), $[Cu(dmbpy)_2(Br)]Br$ (**5**), $[Cu(dmbpy)(NCS)_2]_n$ (**6**) and $[Cu(dmbpy)_2(HCOO)](CF_3SO_3)$ (**8**), which have geometries ranging from square pyramidal to trigonal bipyramidal, and the six-coordinate compounds $[Cu(dmbpy)_3](BF_4)_2(C_2H_6O)$ (**1**) and $[Cu(dmbpy)(NO_3)_2]$ (**4**), which adopt an octahedrally based geometry. Except for compounds **3** and **4**, with nitrate as the anion, a variation of the copper/ligand ratios in the synthesis has no influence on the stoichiometry. The compounds have been characterised in detail by infrared, ligand field and EPR spectroscopy; the data are consistent with the single-crystal X-ray structures.
(© Wiley-VCH Verlag GmbH & Co. KGaA, 69451 Weinheim, Germany, 2004)

Introduction

The flexible coordination sphere around the copper(II) ion, in combination with steric and packing forces, is one of the effects that give rise to an enormous structural diversity in Cu^{II} coordination chemistry.[1] Copper(II) is one of the most important transition metals, especially due to its relevance as the active-site structure of metalloproteins,[2] but also with respect to its magnetochemistry.[3]

In structural chemistry, hydrogen bonding and π-π stacking forces are known to be important in stabilising the lattice structure. The ligand 2,2′-bipyridine (bpy) is one which has been studied extensively due to its structural aspects[4] and magneto-chemical properties.[3a][3b] Ssubstituted bpy ligands are also known, but their complexes are far less common.

Only a few X-ray crystal structures with Cu^{II} and the ligand 4,4′-dimethyl-2,2′-bipyridine have been reported — two mononuclear structures[5a][5b] and three polynuclear structures with copper(II) halides.[5c–5e] Recently the first X-ray structures of di- tri- and tetranuclear Cu^{II} compounds with this ligand were reported.[5f–5h]

In the present study the ligand 5,5′-dimethyl-2,2′-bipyridine (dmbpy; Scheme 1) has been selected. Quite surprisingly this ligand has hardly been studied and, to the best of our knowledge, only one 3D structure of a Cu^{II} compound has been published.[6] We have now extended this study towards Cu^{II} coordination compounds of general formula $[Cu^{II}(dmbpy)_x(L)_2]$ (where L = BF_4^-, $CF_3SO_3^-$, NO_3^-, Br^-, NCS^-, N_3^-, $HCOO^-$, and x = 1–3). A variety of new structures of different stoichiometry and dimensionality are reported together with their spectroscopic and magnetic properties.

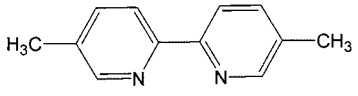

5,5′-dimethyl-2,2′-bipyridine (5,5′-dimethyl-2,2′-dipyridyl)

Scheme 1

Results and Discussion

Eight new Cu^{II} compounds containing the ligand 5,5-dimethyl-2,2′-bipyridine (dmbpy) with the general formula

[a] Leiden Institute of Chemistry, Gorlaeus Laboratories, Leiden University,
P. O. Box 9502, 2300 RA Leiden, The Netherlands
E-mail: reedijk@chem.leidenuniv.nl
[b] Laboratory of Inorganic Chemistry, Department of Chemistry, P. O. Box 55 (A.I.Virtasen aukio 1), 00014 University of Helsinki, Finland
[‡] On leave from: GRECI, Université de Reims Champagne-Ardenne, Faculté des Sciences, Reims, France

Table 1. Cu^{II} compounds with dmbpy

Compound[a]	Geometry Cu atom[b]	Colour	Diffuse reflectance (10^3 cm^{-1}), LF CT	EPR (solid at room temp.)	Elemental Analysis C, H, N obsd. (calcd.)%
1. $[Cu(dmbpy)_3](EtOH)(BF_4)_2$	oc (6)	blue-green	14.3 7.6 (br) 28.4	$g_\perp = 2.10$, $g_\parallel = 2.26$, $A_\parallel = 11.5$; (77 K: $A_\parallel = 13.3$)	53.7(54.7) 5.2 (5.1) 9.9 (10.1)
2. $[Cu(dmbpy)_2(EtOH)](CF_3SO_3)_2$	tbp (5), $\tau = 0.61$	green	13.5 10.7 (sh) 27.0	$g_1 = 2.03$, $g_2 = 2.12$, $g_3 = 2.28$	43.2 (43.3), 3.5 (3.9), 7.3 (7.2) [8.3(8.3) S]
3. $[Cu(dmbpy)_2(NO_3)](NO_3)$	sq.pyr. (5), $\tau = 0.34$	blue-green	13.9 10.1 (br) 26.5	$g = 2.14$	51.3 (51.8), 4.5 (4.4), 15.0 (15.1)
4. $[Cu(dmbpy)(NO_3)_2]$	oc. (6)	dark-blue	14.6 28.5 (br)	$g_\perp = 2.07$, $g_\parallel = 2.27$	38.6 (38.8), 3.1 (3.3), 15.0 (15.1)
5. [Cu(dmbpy)Br]Br	tbp (5), $\tau = 0.63$	blue	13.8 (br) 10.1 (br) 26.0	$g_x = 2.20$, $g_y = 2.15$, $g_z = 2.01$	48.3 (48.7), 4.2 (4.1), 9.6 (9.5)
6. $[Cu(dmbpy)(NCS)_2]_n$	sq.pyr. (5), $\tau = 0.19$	green	15.1 (br) 10.8 (sh) 21.5	$g_x = 2.05$, $g_y = 2.11$, $g_z = 2.23$	45.7 (46.2), 3.2 (3.3), 15.1 (15.4) [17.3 (17.6) S]
7. $[Cu(dmbpy)(N_3)_2]_n$	sq.pl. (4)	green	15.5 (br) 23.4 (s,br)	$g_\perp = 2.06$, $g_\parallel = 2.23$	42.8 (43.4), 3.5 (3.6), 33.2 (33.8)
8. $[Cu(dmbpy)_2(HCOO)](CF_3SO_3)$	tbp (5), $\tau = 0.49$	dark-blue	14.1 10.7 (sh) 24.0 (v br)	(77 K) $g_x = 2.24$, $g_y = 2.12$, $g_z = 2.02$	49.7 (49.9), 3.8 (4.0), 9.0 (9.1) [5.1 (5.1) S]

[a] Abbreviations: (v)br = (very)broad, sh = shoulder, s = strong. [b] Coordination number is given in brackets. Abbreviations: oc = octahedral; sq.pyr. = square pyramidal; sq.pl. = square planar; tbp = trigonal bipyramidal.

$[Cu^{II}(dmbpy)_x(L)_2]$ (where L = BF_4^-, $CF_3SO_3^-$, NO_3^-, Br^-, NCS^-, N_3^-, $HCOO^-$, and $x = 1-3$) have been synthesised (see Table 1). Except for compounds **3** and **4**, with nitrate as the anion, variation of the copper/ligand ratios in the synthesis has no influence on the stoichiometry. The crystal and molecular structures vary greatly, depending on the counterion, from case to case, as will be described below.

Description of the Crystal Structures

[Cu(dmbpy)$_3$](BF$_4$)$_2$(C$_2$H$_5$OH) (1)

The structure of **1** consists of a $[Cu(dmbpy)_3]^{2+}$ cation, two non-coordinating BF_4^- anions and an ethanol lattice molecule. The structure is depicted in Figure 1 together with the numbering scheme. Selected bond lengths and angles are listed in Table 2.

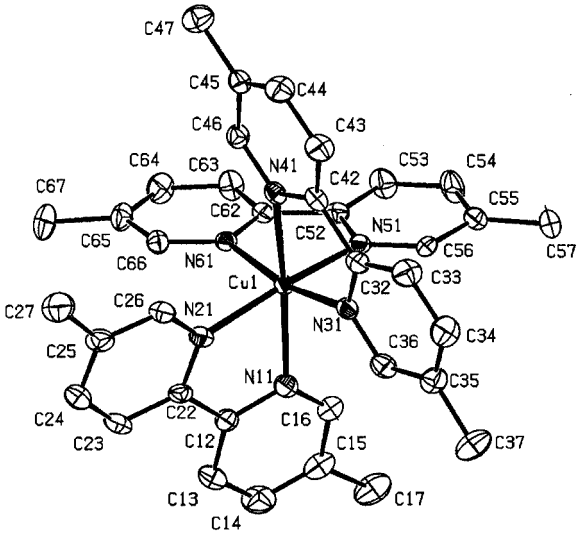

Figure 1. Thermal ellipsoid plot (50% probability) of $[Cu(dmbpy)_3](BF_4)_2(C_2H_5OH)$ (**1**) with atom-labelling scheme; non-coordinating tetrafluoroborate anions, ethanol molecule and H-atoms are omitted for clarity

Table 2. Selected bond lengths (Å) and angles (°) for $[Cu(dmbpy)_3](BF_4)_2(C_2H_6O)$ (**1**)

Cu1−N31	2.040(4)	Cu1−N21	2.050(4)
Cu1−N51	2.054(4)	Cu1−N61	2.056(4)
Cu1−N41	2.274(4)	Cu1−N11	2.281(4)
N31−Cu1−N21	95.03(15)	N31−Cu1−N51	94.13(14)
N21−Cu1−N51	166.73(15)	N31−Cu1−N61	168.52(15)
N21−Cu1−N61	92.54(14)	N51−Cu1−N61	79.97(14)
N31−Cu1−N41	76.56(15)	N21−Cu1−N41	96.67(14)
N51−Cu1−N41	94.78(14)	N61−Cu1−N41	94.02(14)
N31−Cu1−N11	99.42(15)	N21−Cu1−N11	76.37(14)
N51−Cu1−N11	92.67(14)	N61−Cu1−N11	90.74(14)
N41−Cu1−N11	171.76(13)		

The Cu atom has a distorted, elongated octahedral coordination with the basal plane comprised of four nitrogens from three chelating dmbpy ligands. The Cu−N distances vary from 2.040(4) to 2.056(4) Å with basal angles of 166.73(15)° and 168.52(15)°. The apical positions are occupied by nitrogen atoms of the two different bis-chelating dmbpy ligands [Cu−N distances of 2.274(4), 2.281(4) Å with an angle of 171.76(13)°].

The lattice structure is stabilised by weak stacking between the pyridine groups (shortest ring-ring distances of 4.29 Å) and by strong hydrogen bonding between the hydroxo group of the ethanol molecule and a fluorine atom of the tetrafluoroborate anion (O1···F12: 2.765 Å).

[Cu(dmbpy)$_2$(C$_2$H$_5$OH)](CF$_3$SO$_3$)$_2$ (2)

The structure of **2** consists of a $[Cu(dmbpy)_2(C_2H_6O)]^{2+}$ cation and two non-coordinating $CF_3SO_3^-$ anions. The structure is depicted in Figure 2 together with the number-

 © 2004 Wiley-VCH Verlag GmbH & Co. KGaA, Weinheim

ing scheme. Selected bond lengths and angles are listed in Table 3. The geometry around the copper(II) ion is distorted trigonal bipyramidal with the trigonal plane formed by the two nitrogens of two dmbpy ligands and an oxygen atom of a coordinating ethanol molecule, with a distance of 2.211(2) Å, which is in agreement with the few other structures with a $CuN_4O_{ethanol}$ chromophore.[4a,7]

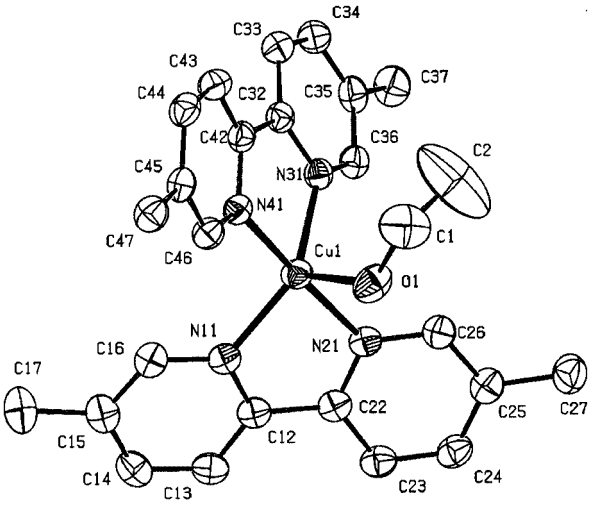

Figure 2. Thermal ellipsoid plot (50% probability) of $[Cu(dmbpy)_2(C_2H_5OH)](CF_3SO_3)_2$ (**2**) with atom-labelling scheme; non-coordinating triflate anions and H-atoms are omitted for clarity

Table 3. Bond lengths (Å) and angles (°) for $[Cu(dmbpy)_2(C_2H_6O)](CF_3SO_3)_2$ (**2**)

Cu1−N21	1.974(3)	Cu1−N41	1.976(3)
Cu1−N11	2.029(3)	Cu1−N31	2.036(3)
Cu1−O1	2.211(2)		
N21−Cu1−N41	171.08(10)	N21−Cu1−N11	81.53(10)
N41−Cu1−N11	101.63(10)	N21−Cu1−N31	102.34(10)
N41−Cu1−N31	81.37(10)	N11−Cu1−N31	135.43(10)
N21−Cu1−O1	87.21(10)	N41−Cu1−O1	83.94(9)
N11−Cu1−O1	117.99(10)	N31−Cu1−O1	106.57(10)

The Cu−N distances vary from 1.974(3) to 2.036(3) Å. The apical positions are occupied by two nitrogen atoms of the two dmbpy ligands with a *trans* angle of 135.43(10)°. The distortion from square pyramidal can be best described by the structural parameter τ (τ describes the relative amount of trigonality; $\tau = 0$ for square pyramid and $\tau = 1$ for trigonal bipyramidal), which in this case is 0.61. The structure can therefore be best described as distorted trigonal bipyramidal.[8] The lattice is stabilised by stacking of the pyridine rings, with a short ring-ring distance of 3.83 Å and a strong hydrogen bond between the ethanol oxygen hydrogen and the oxygen atom of one of the triflate anions (O1···O21: 2.6967 Å).

[Cu(dmbpy)$_2$(NO$_3$)](NO$_3$) (3)

The mononuclear structure **3** consists of a copper(II) ion, two dmbpy ligands, one monodentate coordinated nitrate anion and one uncoordinated nitrate anion. The structure is depicted in Figure 3 together with the numbering scheme. Selected bond lengths and angles are listed in Table 4.

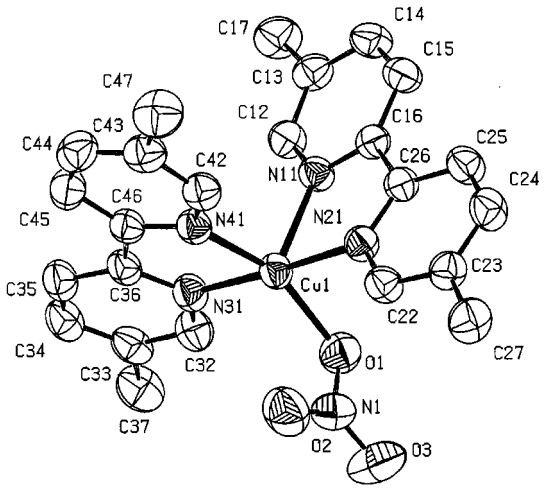

Figure 3. Thermal ellipsoid plot (50% probability) of $[Cu(dmbpy)_2(NO_3)](NO_3)$ (**3**) with atom-labelling scheme; the non-coordinating nitrate anion and H-atoms are omitted for clarity

Table 4. Bond lengths (Å) and angles (°) for $[Cu(dmbpy)_2(NO_3)](NO_3)$ (**3**)

Cu1−N31	1.974(2)	Cu1−N21	2.002(2)
Cu1−N41	2.034(2)	Cu1−O1	2.044(2)
Cu1−N11	2.156(2)	Cu1−O2	2.669(2)
N31−Cu1−N21	177.16(9)	N31−Cu1−N41	81.30(9)
N21−Cu1−N41	97.68(9)	N31−Cu1−O1	93.99(9)
N21−Cu1−O1	87.99(9)	N41−Cu1−O1	156.59(9)
N31−Cu1−N11	98.56(9)	N21−Cu1−N11	79.01(8)
N41−Cu1−N11	101.10(9)	O1−Cu1−N11	102.27(9)
O2−Cu1−N11	153.20(9)		

The geometry around the Cu^{II} atom is distorted square pyramidal with the basal plane formed by three nitrogen atoms of two ligands [distances vary from 1.974(2) to 2.034(2) Å] and one oxygen atom of the coordinated nitrate anion [Cu1−O1: 2.044(2) Å]. The apical position is occupied by a nitrogen atom of one ligand (Cu1−N11: 2.156 Å). A second oxygen atom of the coordinated nitrate anion is at a semi-coordination distance [Cu1−O2: 2.669(2) Å]. The angles of the basal plane are 177.16(9)° and 156.59(9)° and the distortion parameter τ in this case is 0.34. The lattice is stabilised by stacking of the pyridine rings, with a ring-ring distance of 3.74 Å.

[Cu(dmbpy)(NO$_3$)$_2$] (4)

The mononuclear structure **4** consists of a copper(II) ion, one dmbpy ligand, and two didentate-coordinated nitrate anions. The structure is depicted in Figure 4 together with the numbering scheme. Selected bond lengths and angles are listed in Table 5.

 © 2004 Wiley-VCH Verlag GmbH & Co. KGaA, Weinheim

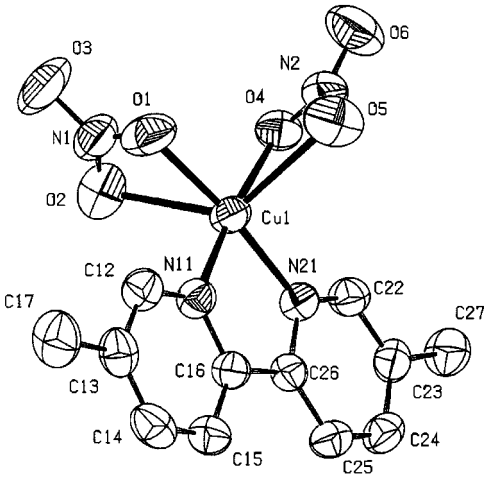

Figure 4. Thermal ellipsoid plot (50% probability) of $[Cu(dmbpy)(NO_3)_2]$ (**4**) with atom-labelling scheme; H-atoms are omitted for clarity

Table 5. Bond lengths (Å) and angles (°) for $[Cu(dmbpy)(NO_3)_2]$ (**4**)

Cu1−N11	1.966(3)	Cu1−N21	1.969(3)
Cu1−O4	1.979(3)	Cu1−O1	1.994(3)
Cu1−O2	2.484(4)	Cu1−O5	2.465(4)
N11−Cu1−N21	82.30(13)	N11−Cu1−O4	172.06(12)
N21−Cu1−O4	95.19(13)	N11−Cu1−O1	95.49(13)
N21−Cu1−O1	172.34(15)	O4−Cu1−O1	87.95(13)
O2- Cu1- O5	131.38(13)		

The geometry around the Cu^{II} atom is elongated octahedral with the basal plane formed by two nitrogen atoms of the dmbpy ligand [Cu−N distances 1.966(3), 1.969(3) Å] and two oxygen atoms of two different coordinated nitrate anions [Cu−O distances 1.979(3), 1.994(3) Å]. The apical positions are occupied by the other two oxygen atoms of two nitrate anions [Cu−O distances 2.484(4), 2.465(4) Å]. The angles of the basal plane deviate by only about 8° from linear [172.06(12)° and 172.34(15)°].

The lattice is stabilised by stacking of the pyridine rings, with a ring-ring distance of 3.70 Å. The nitrate anion is known to be a versatile anion, which in many cases gives rise to different coordinations. Also with the ligand bpy, a number of Cu^{II} compounds exists with different variations in the coordination of the nitrate anion.[6b,9]

[Cu(dmbpy)$_2$(Br)]Br (5)

The structure of **5** consists of a Cu^{II} ion, two dmbpy ligands, one coordinated bromide atom and one uncoordinated bromide atom. The structure is depicted in Figure 5 together with the numbering scheme. Selected bond lengths and angles are listed in Table 6. The geometry around the copper(II) ion is distorted trigonal bipyramidal with the trigonal plane formed by three nitrogens of the two dmbpy ligands. The apical positions are occupied by an N-atom and a bromide atom, with a *trans* angle of 135.32(8)°. The Cu−N distances vary from 1.979(3) to 2.113(3) Å, while the Cu−Br distance is 2.4256(6) Å.

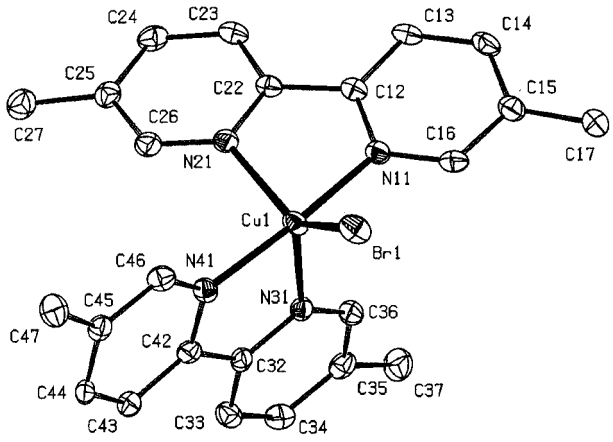

Figure 5. Thermal ellipsoid plot (50% probability) of $[Cu(dmbpy)_2(Br)]Br$ (**5**) with atom-labelling scheme; the non-coordinating bromide anion and H-atoms are omitted for clarity

Table 6. Bond lengths (Å) and angles (°) for $[Cu(dmbpy)_2(Br)]Br$ (**5**)

Cu1−N41	1.979(3)	Cu1−N11	1.985(3)
Cu1−N21	2.106(3)	Cu1−N31	2.113(3)
Cu1−Br1	2.4256(6)		
N41−Cu1−N11	173.31(11)	N41−Cu1−N21	94.79(11)
N11−Cu1−N21	79.40(11)	N41−Cu1−N31	80.29(11)
N11−Cu1−N31	97.07(11)	N21−Cu1−N31	97.65(10)
N41−Cu1−Br1	93.32(8)	N11−Cu1−Br1	93.17(8)
N21−Cu1−Br1	135.32(8)	N31−Cu1−Br1	127.03(8)

The distortion parameter τ in this case is 0.63. The lattice is stabilised by stacking of the pyridine rings, with a ring-ring distance of 3.60 Å. The parameters are in agreement with related structures with a $[Cu(N_4)Br]Br$ chromophore;[10] the parameters of $[Cu(bpy)_2(Br)]Br$[10c] are closest to those of compound **5**, with only a slight difference in the N11−Cu1−N31 bite angle of the bpy rings [106.7°; 97.07(11)° in **5**].

[Cu(dmbpy)(NCS)$_2$]$_n$ (6)

The structure of **6** is polymeric and consists of a Cu^{II} ion, one dmbpy ligand, one bridging and one monodentate coordinating thiocyanate anion. The structure is depicted in Figure 6 together with the numbering scheme. Selected bond lengths and angles are listed in Table 7. The geometry around the copper(II) ion is distorted square pyramidal with the basal plane formed by the two nitrogen atoms of the dmbpy ligand and two nitrogen atoms of two thiocyanate anions. The Cu−N distances vary from 1.950(3) to 2.014(3) Å. The apical position is occupied by a sulfur atom of the bridging thiocyanate anion with a Cu−S distance of 2.6335(12) Å, forming in this way a polynuclear compound in which the NCS^- anion forms a zigzag chain with the Cu

 © 2004 Wiley-VCH Verlag GmbH & Co. KGaA, Weinheim

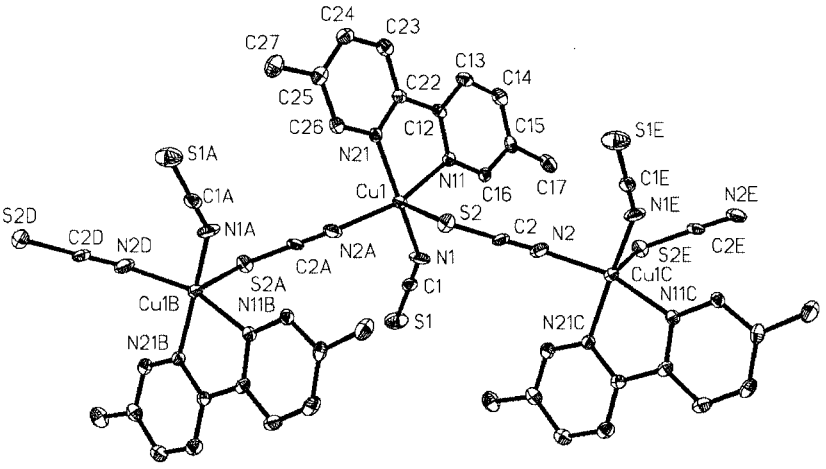

Figure 6. Thermal ellipsoid plot (50% probability) of $[Cu(dmbpy)(NCS)_2]_n$ (**6**) with atom-labelling scheme; H-atoms are omitted for clarity

Table 7. Bond lengths (Å) and angles (°) for $[Cu(dmbpy)(NCS)_2]_n$ (**6**)

Cu1−N11	950(3)	Cu1−N2a	1.989(4)
Cu1−N21	2.005(3)	Cu1−N11	2.014(3)
Cu1−S2	2.6335(12)		
N1−Cu1−N2a[a]	90.70(15)	N1−Cu1−N21	166.03(14)
N2a−Cu1−N21	91.10(14)	N1−Cu1−N11	91.76(14)
N2a−Cu1−N11	154.57(15)	N21−Cu1−N11	80.78(13)
N1−Cu1−S2	99.98(12)	N2A−Cu1−S2	103.22(12)
N21−Cu1−S2	93.09(9)	N11−Cu1−S2	101.27(9)
N1−C1−S1	179.0(4)	N2−C2−S2	178.4(4)

[a] a = $-x + 1$, $y + 1/2$, $-z + 1/2$.

ions. The angles of the square plane are 166.03(14)° and 154.57(15)°. The distortion parameter τ in this case is 0.19, and the two thiocyanate anions are almost linear (178.43° and 179.01°). The lattice is stabilised by stacking of the pyridine rings, with a ring-ring distance of 3.70 Å. The distances and angles are similar to the related compound $[Cu(bpy)(NCS)_2]_n$.[11a]

[Cu(dmbpy)(N$_3$)$_2$]$_n$ (7)

The structure of **7** is also polymeric and consists of a Cu^{II} ion coordinated by one dmbpy ligand and two bridging azide anions. The structure is depicted in Figure 7 together with the numbering scheme. Selected bond lengths and angles are listed in Table 8.

The geometry around the copper(II) ion is square-planar based with the basal plane formed by the two nitrogen atoms of the dmbpy ligand and two nitrogen atoms of two azide anions [Cu−N distances vary from 1.980(5) to 2.047(5) Å]. The basal planes are 171.1(2)° and 170.2(2)°. The two azide anions are almost linear [176.4° and 174.9(7)°]. The apical positions are occupied by nitrogen atoms of neighbouring azide anions at semi-coordination distances of 2.652(6) Å (Cu1−N31a, 1,1-azide bond) and 2.708(7) Å (Cu1−N43b, 1,3-azide bond), forming in this way a polymeric array (Figure 8). This array (--Cu--[(1,1-$N_3)_2$]--Cu--[(1,3-$N_3)_2$]--Cu--) is rather rare. So far, to the best of our knowledge, only one Cu^{II} compound, [Cu(3-picoline)$(N_3)_2]_n$,[12a] has been published with this alternating azide array. The lattice of the compound is further stabilised by stacking of the pyridine rings, with a ring−ring distance of 3.72 Å.

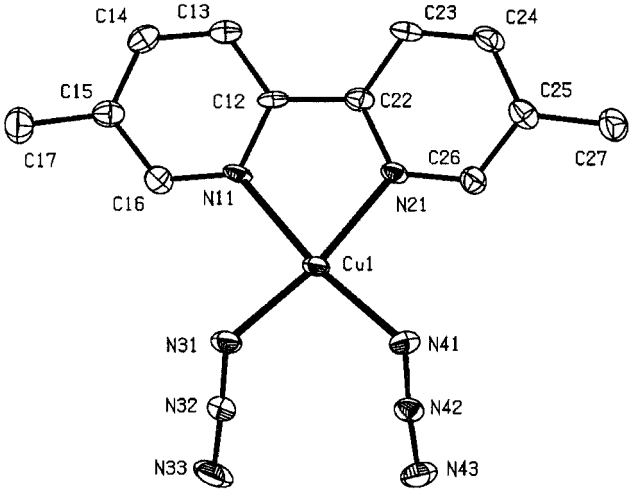

Figure 7. Thermal ellipsoid plot (50% probability) of $[Cu(dmbpy)(N_3)_2]_n$ (**7**) with atom-labelling scheme; H-atoms are omitted for clarity

Table 8. Bond lengths (Å) and angles (°) for $Cu(dmbpy)(N_3)_2$ (**7**)

Cu1−N31	1.980(5)	Cu1−N41	1.981(6)
Cu1−N11	2.039(5)	Cu1−N21	2.047(5)
Cu 1−N31a[a]	2.652(6)	Cu1−N43b[b]	2.708(7)
N31−Cu1−N41	98.2(2)	N31−Cu1−N11	90.5(2)
N41−Cu1−N11	171.1(2)	N31−Cu1−N21	170.2(2)
N41−Cu1−N21	90.9(2)	N11−Cu1−N21	80.3(2)
N33−N32−N31	176.4(7)	N43−N42−N41	174.9(7)

[a] a = $1 - x$, $-y$, $1 - z$. [b] b = $-x$, $-y$, $1 - z$.

 © 2004 Wiley-VCH Verlag GmbH & Co. KGaA, Weinheim

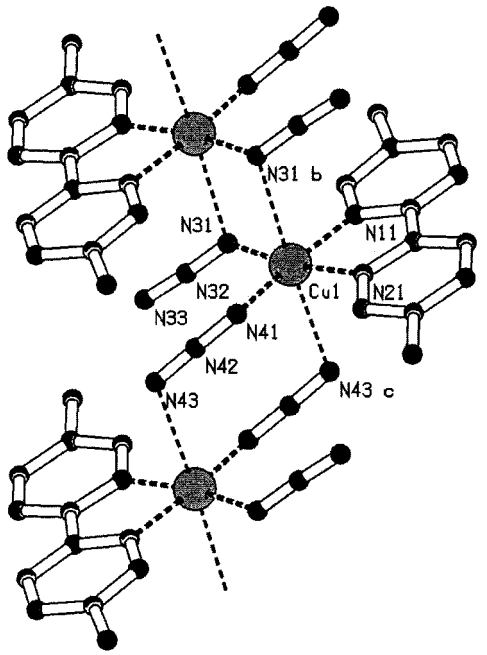

Figure 8. The polymeric structure of compound **7** with a bridging azide ligand

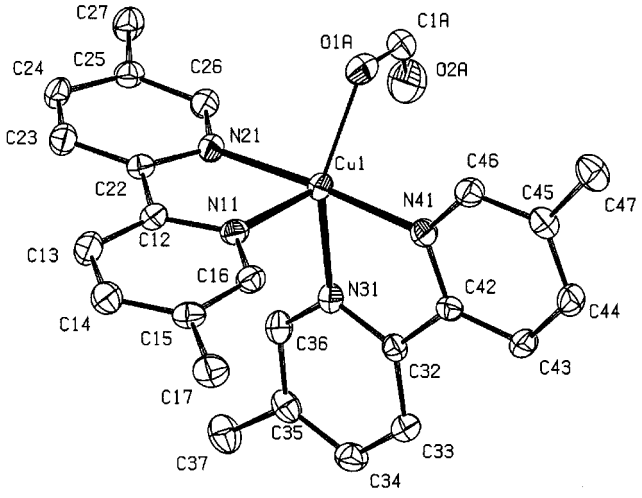

Figure 9. Thermal ellipsoid plot (50% probability) of $[Cu(dmbpy)_2(HCOO)](CF_3SO_3)$ (**8**) with atom-labelling scheme; the noncoordinating triflate anion and H-atoms are omitted for clarity; the formato anion shows only the major component (see text)

[Cu(dmbpy)$_2$(HCOO)](CF$_3$SO$_3$) (8)

The structure of **8** consists of a $[Cu(dmbpy)_2(HCOO^-)]^+$ cation and one non-coordinating $CF_3SO_3^-$ anion. The structure is depicted in Figure 9 together with the numbering scheme. Selected bond lengths and angles are listed in Table 9.

Table 9. Bond lengths (Å) and angles (°) for $[Cu(dmbpy)_2(HCOO)](CF_3SO_3)$ (**8**)[a]

Cu1−O1A	2.005(2)	Cu1−N41	1.9890(19)
Cu1−N21	1.9955(19)	Cu1−N11	2.1585(19)
Cu1−N31	2.084(2)	Cu1−O1B	1.923(9)
N41−Cu1−N21	175.56(8)	N41−Cu1−O1A	91.92(8)
N21−Cu1−O1A	92.08(8)	O1A−Cu1−N31	145.59(8)
N41−Cu1−N31	79.48(8)	N21−Cu1−N31	98.22(8)
N41−Cu1−N11	97.09(7)	N21−Cu1−N11	79.33(7)
O1A−Cu1−N11	117.68(8)	N31−Cu1−N11	96.53(7)
O1B−Cu1−N41	89.4(2)	O1B−Cu1−N21	94.8(2)
O1B−Cu1−N31	102.9(2)	O1B−Cu1−N11	160.3(2)

[a] O1A, O1B are the major and minor disordered components of the formato anion which were refined in two positions with ratio 0.8:0.2.

The geometry around the copper(II) ion is distorted trigonal bipyramidal with the trigonal plane formed by three nitrogens of the two dmbpy ligands [Cu-N distances vary from 1.9955(19) to 2.1585(19) Å]. The apical positions are occupied by an N-atom and an oxygen atom of the formato anion with a *trans* angle of 145.59(8)° (the *trans* angle of the major component of the disordered formato anion is chosen here). The second oxygen of the formato anion (O2A) is at a very long distance [2.912(2) Å]. All distances are in agreement with the few other known structures with the formato anion.[13] The distortion parameter τ for this compound is 0.49 (angle taken from the major component), and is therefore intermediate between trigonal pyramidal and square pyramidal. The lattice is stabilised by stacking of the pyridine rings, with a ring-ring distance of 3.672 Å.

Infrared Spectroscopy

In the infrared spectra the most important bands for characterisation of the compounds are those of the anions. In compound **1** the vibration of the tetrafluoroborate anion is observed at 1030 cm^{-1} as a single strong band. The most sensitive characteristic vibrations of the triflate anion is the $\nu_{as}S-O$, which is observed in compound **2** at 1245 cm^{-1} as a broad band with a weak, but sharp, peak at 1273 cm^{-1} and in compound **8** at 1263 cm^{-1}, in agreement with the literature for mononuclear or H-bonded triflate anions.[14]

The two related compounds **3** and **4** differ in composition (1:1 and 1:2, respectively). In compound **3** one nitrate anion is coordinating and one is non-coordinating, while in compound **4** both nitrate anions are coordinated. Most of the regions that are characteristic of nitrate vibrations[11b,15] are overlapped by strong ligand vibrations. However, in the region 1200−1300 cm^{-1} a clear difference in the infrared spectra is observed. In both compounds a broad strong band is observed at about 1270 cm^{-1}, which originates from the chelating nitrate anion.[11b,16] In addition, in compound **3**, which has two different types of nitrate coordination, a strong vibration is observed at about 1333 cm^{-1}. Although this value is slightly higher than expected for a free nitrate bond,[11b,15] this vibration must originate from the non-coordinated nitrate anion.

 © 2004 Wiley-VCH Verlag GmbH & Co. KGaA, Weinheim

In compound **6** the vibrations of the thiocyanate anion are observed as a strong split band at 2084 and 2047 cm^{-1} in agreement with the two types of thiocyanate (bridging and monodentate) present in the structure,[11] while in compound **7** the vibration of the azide anion is found as a split strong band at 2027 and 2070 cm^{-1}, in agreement with the two different types of bonding of the azide anions.[12]

The C=O stretching vibration of the formato anion in compound **8** is observed at 1597 cm^{-1} as a clear, strong, sharp band, in accordance with the literature[11b] and also with the fact that this band is absent in compounds **1**−**7**.

Electronic Spectroscopy

The diffuse-reflectance spectra of all compounds measured as solids are tabulated in Table 1. Compounds **1**, **4** and **7**, which have a square-planar based geometry exhibit bands at around 14.3−15.5 × 10^3 cm^{-1}, which is normal for planar-based (octahedral) geometries.[17] Compound **1** also displays a very broad shoulder at 7.6 × $10^3 cm^{-1}$, which is rather rare for distorted octahedral geometries and must originate from a small Jahn−Teller distortion.[17a]

The five-coordinate compounds **2**, **3**, **5**, **6** and **8**, which have trigonal bipyramidal or square-pyramidal geometries, all show bands at around 13.5−15.1 × $10^3 cm^{-1}$ and 10.1−10.8 × $10^3 cm^{-1}$, which are considered normal transitions for these geometries.[17]

All compounds have charge-transfer bands at around 26−28 × $10^3 cm^{-1}$, except the thiocyanate compound **6**, which has a band at 21.5 × 10^3 cm^{-1} of medium intensity that originates from a Cu^{II}−NCS charge transfer.[11] The azide compound **7** displays a very strong band at 23.4 × $10^3 cm^{-1}$, which originates from the strong Cu^{II}-azide charge transfer.[18]

Magnetic Properties

EPR Spectroscopy

The powder EPR spectrum of compound **1** at room temperature reveals an axial signal with $g_\perp$ = 2.10 and $g_\parallel$ = 2.26. A weak hyperfine splitting is observed with $A_\parallel$ = 11.5 mT. At 77 K the hyperfine splitting $A_\parallel$ becomes 13.3 mT, an indication that the geometry is changing at low temperature. The EPR values are in agreement with the distorted octahedral structure of this compound.

The spectrum of compound **2** at room temperature and at 77 K displays a rhombic signal with g_1 = 2.03, g_2 = 2.12 and g_3 = 2.28. This last value (g_3) is observed as a weak band. This spectrum agrees with the square-pyramidal geometry of the Cu^{II} atom.[17]

The EPR spectra of the nitrate compounds show a different pattern according to their different Cu^{II} geometry. Compound **3** at room temperature and at 77 K reveals an isotropic signal with g = 2.14, while compound **4** at room temperature and at 77 K shows the same axial signal with a $g_\perp$ of 2.07 and an unresolved $g_\parallel$ of 2.27.

The powder EPR spectra of compounds **5** and **6** (Figures 10 and 11) each display a rhombic pattern with three distinct g values. Compound **5** shows an inverted EPR signal with g_x = 2.20, g_y = 2.15 and g_z = 2.01. This pattern (with the lowest g value < 2.03) agrees with the fact that this compound has a compressed rhombic site and a predominant d_{z^2} ground state.[3b,17,19a] This value agrees with a trigonal bipyramidal geometry with an unpaired electron situated along the N11−N41 axis. For compound **6** the lowest g value is greater than 2.03, with g_x = 2.05, g_y = 2.11 and g_z = 2.23, which indicates a $d_{x^2-y^2}$ ground state.[3b,17,19b,19c]

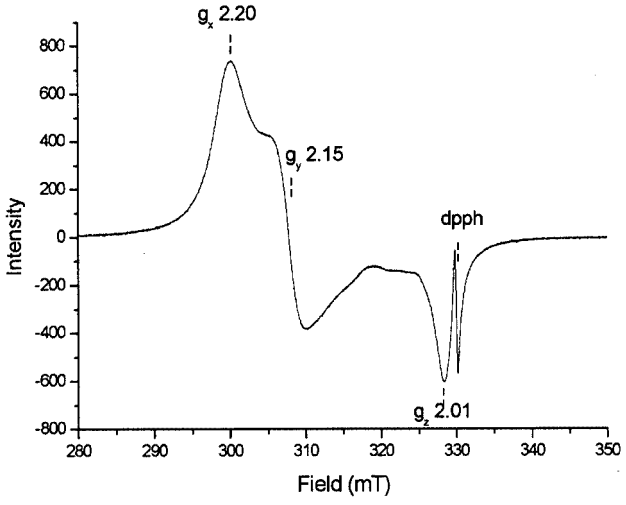

Figure 10. EPR spectrum (solid) of compound (**5**), see text

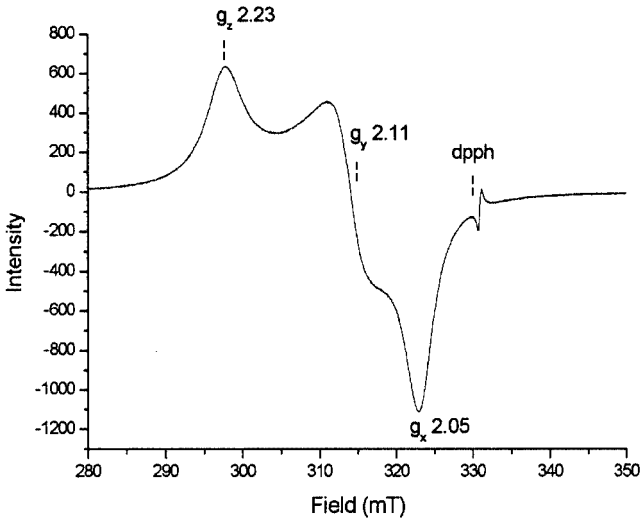

Figure 11. EPR spectrum (solid) of compound (**6**), see text

The EPR spectrum of compound **7** at room temperature and at 77 K reveals the same axial signal with a $g_\perp$ of 2.06 and an unresolved $g_\parallel$ of 2.23, which confirms the square-planar based structure of the compound.

The EPR spectrum of compound **8** at 77 K shows, like compound **5**, an inverted EPR signal with $g_x \approx 2.22$, g_y =

 © 2004 Wiley-VCH Verlag GmbH & Co. KGaA, Weinheim

2.12 and $g_z = 2.02$. The g_x appears as a broad band. This pattern (with lowest g value < 2.03) indicates a predominantly d_{z^2} ground state,[3b,17,19a] which is in agreement with the five-coordinate geometry.

For assigning the ground state in rhombic spectra the parameter $R = (g_2 - g_1)/(g_3 - g_2)$, with $g_3 > g_2 > g_1$, has been introduced.[3b,17c] This parameter is greater or smaller than 1 if the ground state is d_{z^2} or $d_{x^2-y^2}$, respectively. For the rhombic compounds **2**, **5**, **6** and **8** the R values are 0.56, 2.80, 0.50 and about 1.0, respectively, which confirms our conclusions.

Magnetic Susceptibility

For a few of the new compounds with potential magnetic exchange as a result of their structure and bridging anions, detailed variable-temperature magnetic susceptibility studies were performed. In the literature a number of Cu^{II} thiocyanate compounds exist which display a weak magnetic interaction even though the Cu−Cu distance is large (about 6 Å) and the magnetic orbitals are not co-planar. Examples are the compounds $[Cu(bpy)(NCS)_2]_n$ and $[Cu(pyrazine)(NCS)_2]_n$, with a weak antiferromagnetic interaction,[11a,11f] and two mixed-metal (Cu^{II}-Co^{II}) thiocyanide compounds,[11e] which give rise to a weak ferromagnetic interaction. In light of these results the magnetic susceptibility of a powdered sample of **6** was measured from 5 to 300 K. The spectrum of μ_{eff} versus T does not change significantly and stays within a range of 1.65−1.75 BM, which is close to the spin-only value of Cu (1.77 BM), so no significant interaction could be observed between neighbouring Cu atoms.

Similar results were obtained for compound **7**, which also gives no significant change between 5 and 300 K (μ_{eff} between 1.76−1.82 BM), so no magnetic interaction could be detected between neighbouring Cu atoms. This behaviour can be understood on the basis of the magnetic orbital orientation.[3a]

Conclusions

In this study eight new mononuclear Cu^{II} compounds with the ligand dmbpy have been synthesized and characterised. Depending on the selected anions, a great variety of geometries have been observed with Cu^{II}. In all cases the dmbpy ligand appears to be rather rigid, irrespective of whether one, two or three ligands bind to Cu^{II}. Five-coordinate structures, varying from square pyramidal to trigonal bipyramidal, are observed with triflate, nitrate, bromide, thiocyanate and formate as the anion. With tetrafluoroborate, nitrate and azide square-planar based (square planar to octahedron) complexes are obtained.

Comparing our results to Cu^{II} compounds with bpy as a ligand, we observe quite important differences: with bpy a very large number of mononuclear and anion-bridged dinuclear compounds has been reported with a similar set of anions,[4b] while the method of synthesis is similar to ours. Apparently the steric hindrance of the methyl groups of dmbpy prevents crystallisation of such dinuclear compounds.

In summary: the effect of the two methyl groups has resulted in a great variety of new compounds, which have no counterparts in bipyridine-containing complexes. Such dramatic differences resulting from apparently small ligand changes are as yet not fully understood.

Experimental Section

All chemicals were purchased from commercial sources and used as received.

General Synthesis of the Compounds: An equimolar amount of dmbpy and the copper(II) salt were dissolved separately in ethanol and were then slowly mixed together (Cu solution added to the ligand solution) and heated to about 40 °C. The solution was filtered to remove any solid particles and left to evaporate at room temperature. Crystals were obtained in a few days to a few weeks. Yields 43 to 72%. A difference in the ligand:copper ratio had no influence on the compounds, except for the nitrate compounds **3** and **4**, which are very sensitive to the exact ratio (1:1 and 1:2, respectively). The products were characterised by IR spectroscopy and elemental analysis (see Table 1).
Compounds **6** and **7** were prepared in the same way as above (using Cu^{II} triflate as the copper salt), but an equimolar amount of sodium thiocyanate or sodium azide, respectively, dissolved in a very small amount of water, was added slowly to the total solution. The solution was then filtered and left standing in the open air.
Compound **8** was initially obtained by using Cu^{II} triflate and the ligand dmbpy in methanol and adding a few drops of sodium hydroxide dissolved in water to the total solution. Within a few weeks dark-blue blocks of crystals appeared, which turned out to contain the formato anion. Apparently, the formato anion was formed in situ, a phenomenon observed earlier by using triethyl orthoformate.[13a,20] Subsequently, this compound was also synthesized in higher yield by adding sodium formate (dissolved in water) to the Cu/ligand solution in methanol.

Physical Techniques: C,H,N determinations were performed on a Perkin−Elmer 2400 Series II analyser. Ligand-field spectra were obtained on a Perkin−Elmer Lambda900 spectrophotometer using the diffuse-reflectance technique, with MgO as a reference. FT-IR spectra were obtained on a Perkin−Elmer Paragon 1000 FT-IR spectrophotometer equipped with a Golden Gate ATR device, using the reflectance technique (4000−300 cm^{-1}, resolution 4 cm^{-1}). X-band EPR spectra were recorded on polycrystalline samples at room temp. and at 77 K with a Jeol RE2X electron spin resonance spectrometer using DPPH ($g = 2.0036$) as a standard. Magnetic susceptibility measurements (5−300 K) were carried out using a Quantum Design MPMS-5 5T SQUID magnetometer (measurements carried out at 1000 Gauss). Data were corrected for magnetisation of the sample holder and for diamagnetic contributions, which were estimated from Pascal constants.

X-ray Crystallography. Compounds 1−4: A crystal was selected and mounted onto a glass fiber using the oil-drop method. Data were collected on a Rigaku AFC-7S diffractometer (graphite-monochromated Mo-K_α radiation, ω-2θ scans). The intensity data were corrected for Lorentz and polarisation effects, for absorption (psi-scan absorption correction) and extinction. The structures were solved by direct methods. The programs teXsan,[21a] SHELXS-97,[21b] and SHELXL-97[21c] were used for data reduction, structure solution

 © 2004 Wiley-VCH Verlag GmbH & Co. KGaA, Weinheim

Table 10. Crystallographic data

Crystal data	**1**	**2**	**3**	**4**	**5**	**6**	**7**	**8**
Formula	$C_{38}H_{42}B_2CuF_8N_6O$	$C_{28}H_{30}CuF_6N_4O_7S_2$	$C_{24}H_{24}CuN_8O_6$	$C_{12}H_{12}CuN_4O_6$	$C_{24}H_{24}Br_2CuN_4$	$C_{14}H_{12}CuN_4S_2$	$C_{12}H_{12}CuN_8$	$C_{26}H_{25}CuF_3N_4O_5S$
Molecular mass	835.94	776.22	556.03	371.79	591.83	363.94	331.84	626.10
Crystal system	orthorhombic	monoclinic	triclinic	monoclinic	monoclinic	monoclinic	monoclinic	triclinic
Space group	*Pbca* (no. 61)	$P2_1/n$ (no.14)	$P\bar{1}$ (no.2)	$P2_1/n$ (no.14)	$P2_1/c$ (no.14)	$P2_1/c$ (no.14)	$P2_1/n$ (no. 14)	$P\bar{1}$ (no.2)
a (Å)	14.162(2)	12.634(3)	8.1350(10	11.274(2)	7.9980(10)	9.0470(9)	7.6800	8.2240(6)
b (Å)	18.098(4)	17.073(4)	10.572(2)	10.349(2)	28.542(3)	10.9230(12)	17.620(4)	10.6900(9)
c (Å)	30.786(6)	15.252(3)	15.740(2)	12.849(3)	11.1440(10)	17.0520(16)	10.462(2)	15.3270(15)
α (°)	–	–	96.69(2)	–	–	–	–	92.024(8)
β (°)	–	100.03(3)	104.47(2)	100.61(3)	116.730(10)	118.985(8)	110.72(3)	99.527(7)
γ (°)	–	–	105.88(2)	–	–	–	–	90.056(7)
V (Å^3)	7891(3)	3239.6(13)	1235.6(3)	1473.5(5)	2272.1(4)	1474.0(3)	1324.2(5)	1328.0(2)
Z	8	4	2	2	4	4	4	2
$D_{calcd.}$ (g·cm^{-3})	1.407	1.591	1.494	1.676	1.730	1.640	1.665	1.566
F(000)	3448	1588	574	756	1180	740	676	642
μ (cm^{-1})	14.52	29.33	17.00	24.63	44.98	17.61	16.56	9.67
Crystal size (mm)	0.24 × 0.09 × 0.07	0.50 × 0.22 × 0.09	0.30 × 0.20 × 0.10	0.30 × 0.30 × 0.30	0.20 × 0.19 × 0.18	0.18 × 0.08 × 0.03	0.10 × 0.02 × 0.02	0.25 × 0.25 × 0.17
Colour	blue-green	green	blue-green	dark blue	blue	green	green	dark blue
Temperature (K)	193(2)	193(2)	293(2)	293(2)	173(2)	173(2)	173(2)	173(2)
θmin, θmax (°)	2.87–67.01	3.92–66.93	2.96–67.93	4.80–67.98	5.04–27.52	5.01–27.49	5.08–26.97	3.03–27.50
Total data	7024	5746	4821	2831	20518	16347	20508	20687
Total uniq. data (Rint)	7024 (0.0000)	5744 (0.0917)	4479 (0.0563)	2691 (0.0255)	5200 (0.500)	3356 (0.1133)	2737 (0.1019)	6034 (0.0374)
Observed data [$I > 2\sigma(I)$]	4694	4950	4051	1956	3730	2131	1989	4680
No. of ref. parameters	505	433	334	208	280	190	190	372
$wR2$ (all data)[a]	0.1672	0.1357	0.1443	0.1248	0.0859	0.1226	0.1935	0.0951
R[b]	0.0667	0.0511	0.0489	0.0476	0.0395	0.0528	0.0751	0.0386
S	1.029	1.068	1.023	1.032	1.022	1.029	1.073	1.025
Max. and min. Resd. dens. (e/Å^3)	0.0999;-0.037	0.840;-0.580	0.596; −0.347	0.415; −0.39	0.451; −0.530	0.695; −0.575	1.769; −1.067	0.458; −0.354

[a] $wR2 = \{\Sigma[w(F_o^2 - F_c^2)^2]/\Sigma[w(F_o^2)^2]\}^{1/2}$. [b] $R1 = \Sigma||F_o| - |F_c||/\Sigma|F_o|$.

and structure refinement, respectively. All non-hydrogen atoms were refined anisotropically. All H atoms, except the hydroxo atom of the ethanol molecule in compound **2**, were introduced in calculated positions and refined with fixed geometry with respect to their carrier atoms.

Compounds 5–8: Crystals suitable for structure determination were mounted in Lindemann-glass capillaries and transferred into the cold nitrogen stream of a Nonius KappaCCD diffractometer on a rotating anode (Mo-K_α radiation, graphite monochromator, λ = 0.71073). The intensity data were corrected for Lorentz and polarisation effects, and for absorption and extinction. The structures were solved by direct methods. The programs COLLECT,[21d] SHELXS-97,[21b] and SHELXL-97[21c] were used for data reduction, structure solution and structure refinement, respectively. All non-hydrogen atoms were refined anisotropically. All H atoms were introduced in calculated positions and refined with fixed geometry with respect to their carrier atoms. For compound **8** the formato anion was found to be disordered and was refined in two positions with ratio 0.8/0.2. Plots were obtained using the PLATON package.[21e] Crystallographic data of all compounds are listed in Table 10.

CCDC-228793–228800 (for compounds **1**–**8**, respectively) contain the supplementary crystallographic data for this paper. These data can be obtained free of charge at www.ccdc.cam.ac.uk/conts/retrieving.html [or from the Cambridge Crystallographic Data Centre, 12 Union Road, Cambridge CB2 1EZ, UK; Fax: + 44-1223-336033; E-mail: deposit@ccdc.cam.ac.uk].

Acknowledgments

The work described in this paper was supported by the Leiden University Study group WFMO (Werkgroep Fundamenteel Materialen Onderzoek) and the Council for Chemical Sciences of the Netherlands Organisation for Scientific Research (CW-NWO). Part of the work was supported financially by the Graduate Research School Combination "Catalysis".

[1] [1a] M. Melník, M. Kabešová, L. Macášková, C. E. Holloway, *J. Coord. Chem.* **1998**, *45*, 31–145. [1b] M. Melník, M. Kabešová, M. Koman, L. Macášková, J. Garaj, C. E. Holloway, A. Valent, *J. Coord. Chem.* **1998**, *45*, 147–359. [1c] M. Melník, M. Kabešová, M. Koman, L. Macášková, C. E. Holloway, *J. Coord. Chem.* **1999**, *48*, 271–374. [1d] M. Melník, M. Kabešová, M. Koman, L. Macášková, C. E. Holloway, *J. Coord. Chem.* **2000**, *50*, 177–322. [1e] B. P. Murphy, *Coord. Chem. Rev.* **1993**, *124*, 63–105. [1f] E. Bouwman, W. L. Driessen, J. Reedijk, *Coord. Chem. Rev.* **1990**, *104*, 143–172.

[2] [2a] K. D. Karlin, J. Zubieta, *Copper Coordination Chemistry*, Adenine Press, New York, **1983**. [2b]P. Comba, R. Remenyi, *Coord. Chem. Rev.* **2003**, *238*, 9–20, and references cited therein. [2c] E. I. Solomon, D. W. Randall, T. Glaser, *Coord. Chem. Rev.* **2000**, *200*, 595–632, and references cited therein.

 © 2004 Wiley-VCH Verlag GmbH & Co. KGaA, Weinheim

[3] [3a] O. Kahn, *Molecular Magnetism*, VCH Publishers, New York, **1993**, and references cited therein. [3b]E. Garribba, G. Micera, D. Sanna, L. Strinna-Erre, *Inorg. Chim. Acta* **2000**, *299*, 253−261. [3c] J. Černák, M. OrendÆč, I. Potočňák, J. Chomič, A. OrendÆčová, J. Skoršepa, A. Feher, *Coord. Chem. Rev.* **2002**, *224*, 51−66. [3d] J. G. Haasnoot, *Coord. Chem. Rev.* **2000**, *200*, 131−185. [3e] R. Mukherjee, *Coord. Chem. Rev.* **2000**, *203*, 151−218.

[4] [4a] L. Carlucci, G. Cianai, A. Gramaccioli, D. M. Proserpio, S. Rizzato, *Cryst. Eng. Commun.* **2000**, *29*, 1−10. [4b] CSD (Cambridge Structural Database), at time of writing, 260 X-ray structures were found with the ligand bipy.

[5] [5a] Z. Shen, J.-L. Zuo, Z. Yu, Y. Zhang, J.-F. Bai, C.-M. Che, H.-K. Fun, J. J. Vittal, X.-Z. You, *J. Chem. Soc., Dalton Trans.* **1999**, 3393−3397. [5b] L. Gasque, R. Moreno-Esparza, E. Mollins, J. L. Brianso-Penalva, L. Ruiz-Ramirez, G. Medina-Dickinson, *Acta Crystallogr., Sect. C* **1998**, *54*, 1848−1850. [5c] O. Gonzalez, A. M. Atria, E. Spodine, J. Manzur, M. T. Garland, *Acta Crystallogr., Sect. C* **1993**, *49*, 1589−1591. [5d] A. M. Atria, R. Baggio, M. T. Garland, O. Gonzalez, J. Manzur, O. Pena, E. Spodine, *J. Crystallogr. Spectrosc. Res.* **1993**, *23*, 943−947. [5e] A. Alvarez-Larena, J. L. Brianso-Penalva, J. F. Piniella, R. Moreno-Esparza, L. Ruiz-Ramirez, A. Tovar, *Z. Kristallogr.* **1995**, *210*, 543−544. [5f] G. A. van Albada, I. Mutikainen, U. Turpeinen, J. Reedijk, *Inorg. Chim. Acta* **2001**, *324*, 273−277. [5g] G. A. van Albada, I. Mutikainen, O. Roubeau, U. Turpeinen, J. Reedijk, *Inorg. Chim. Acta* **2002**, *331*, 208−215. [5h] J. R. Deschamps, C. M. Hartshorn, E. L. Chang, *Acta Crystallogr., Sect. E* **2002**, *58*, m606−m608.

[6] [6a] H. Kooijman, A. L. Spek, G. A. van Albada, J. Reedijk, *Acta Crystallogr., Sect. C* **2002**, *58*, m124−m126. [6b] In the Cambridge Structural Database (CSD) the structure with code ZEJQAA was obtained as containing the ligand dmbpy. However, in the original publication of ZEJQAA this structure was published as a note (K. J. Catalan, S. Jackson, J. D. Zubkowski, D. L. Perry, E. J. Valente, L. A. Feliu, A. Polanco, *Polyhedron* **1995**, *14*, 2165−2171) and should contain the ligand 4,4′-dimethyl-bpy. As no further details nor atomic coordinates are given, there is no proof that this structure actually contains the ligand dmbpy.

[7] [7a] G. Ferguson, J. N. Low, M. Quirás-Olozabal, J. M. Salas-Peregrín, F. Hueso-Ureña, M. N. Moreno-Carretero, *Polyhedron* **1996**, *15*, 3233−3239. [7b] B. Cervera, R. Ruiz, F. Lloret, M. Julve, J. Faus, M. C. Munoz, Y. Journaux, *Inorg. Chim. Acta* **1999**, *288*, 57−68.

[8] A. W. Addison, T. N. Rao, J. Reedijk, J. van Rijn, G. C. Verschoor, *J. Chem. Soc., Dalton Trans.* **1984**, 1349−1356.

[9] [9a] P. Y. Zavalij, B. L. Burton, W. E. Jones Jr., *Acta Crystallogr., Sect. C* **2002**, *58*, m330−m333. [9b] A. Tadsanaprasittipol, H.-B. Kraatz, G. D. Enright, *Inorg. Chim. Acta* **1998**, *278*, 143−149.

[10] [10a] G. Murphy, C. O′Sullivan, B. Murphy, B. Hathaway, *Inorg. Chem.* **1998**, *37*, 240−248. [10b] R. D. Willett, G. Pon, C. Nagy, *Inorg. Chem.* **2001**, *40*, 4342−4352. [10c] M. A. Khan, D. G. Tuck, *Acta Crystallogr., Sect. B* **1981**, *37*, 1409−1412.

[11] [11a] S. Ferlay, G. Francese, H. W. Schmalle, S. Decurtins, *Inorg. Chim. Acta* **1999**, *286*, 108−113. [11b] K. Nakamoto, *Infrared and Raman Spectra of Inorganic and Coordination Compounds*, John Wiley & Sons, 4th ed., New York, **1986**. [11c]T. Otieno, J. R. Blanton, K. J. Lanham, S. Parkin, *J. Chem. Cryst.* **2003**, *33*, 335−339. [11d] M. A. S. Goher, F. A. Mautner, *Polyhedron* **1999**, *18*, 1805−1810. [11e] A. Skorupa, B. Korybut-Daskiewicz, J. Mroziński, *Inorg. Chim. Acta* **2001**, *324*, 286− 292. [11f] H. N. Bordallo, L. Chapon, J. L. Manson, C. D. Ling, J. S. Qualls, D. Hall, D. N. Argyriou, *Polyhedron* **2003**, *22*, 2045−2049.

[12] [12a] F. A. Mautner, M. A. S. Goher, *Polyhedron* **1992**, *19*, 2537−2542. [12b] G. De Munno, M. G. Lombardi, M. Julve, F. Lloret, J. Faus, *Inorg. Chim. Acta* **1998**, *282*, 82−89. [12c] Z. Shen, J. L. Zuo, Z. Yu, Y. Zhang, J.-F. Bai, C.-M. Che, H.-K. Fun, J. J. Vittal, X.-Z. You, *J. Chem. Soc., Dalton Trans.* **1999**, 3393−3398.

[13] [13a] G. A. van Albada, S. Amani Komaei, H. Kooijman, A. L. Spek, J. Reedijk, *Inorg. Chim. Acta* **1999**, *287*, 226−231, and references cited therein. [13b] W. Fitzgerald, B. J. Hathaway, *J. Chem. Soc., Dalton Trans.* **1981**, 567−574. [13c] S. Aduldecha, M. E. Keniry, P. Akhter, S. Tyagi, B. J. Hathaway, *Acta Crystallogr., Sect. C* **1991**, *47*, 1378−1383. [13d] M. J. Scott, C. A. Goddard, R. H. Holm, *Inorg. Chem.* **1996**, *35*, 2558−2567.

[14] [14a] G. A. van Albada, W. J. J. Smeets, A. L. Spek, J. Reedijk, *Inorg. Chim. Acta* **1997**, *260*, 151−161. [14b] G. A. van Albada, W. J. J. Smeets, A. L. Spek, J. Reedijk, *J. Chem. Cryst.* **1998**, *28*, 427−432. [14c] G. A. van Albada, W. J. J. Smeets, A. L. Spek, J. Reedijk, *J. Chem. Cryst.* **2000**, *30*, 11−16.

[15] G. Díaz, S. Diez, L. López, R. Muñoz, M. Campos-Vallette, V. Manríquez, O. Wittke, *Vibr. Spectr.* **1993**, *6*, 37−42.

[16] [16a] A. M. Schuitema, M. Engelen, I. A. Koval, S. Gorter, W. L. Driessen, J. Reedijk, *Inorg. Chim. Acta* **2001**, *324*, 57−64. [16b] G. A. van Albada, I. Mutikainen, U. Turpeinen, J. Reedijk, *Acta Crystallogr., Sect. E* **2002**, *58*, m55−m57. [16c] T. X. Neenan, W. L. Driessen, J. G. Haasnoot, J. Reedijk, *Inorg. Chim. Acta* **1996**, *247*, 43−49.

[17] [17a] B. J. Hathaway, in *Comprehensive Coordination Chemistry* (Eds.: G. Wilkinson, R. D. Gill, J. A. McCleverty), Pergamon Press, Oxford, **1987**, vol. 5. [17b] A. B. P. Lever, *Inorganic Electronic Spectroscopy*, 2nd. ed., Elsevier, Amsterdam, **1984**. [17c]B. J. Hathaway, D. E. Billing, *Coord. Chem. Rev.* **1970**, *5*, 143−207.

[18] [18a] G. A. van Albada, M. T. Lakin, N. Veldman, A. L. Spek, J. Reedijk, *Inorg. Chem.* **1995**, *34*, 4910−4917. [18b] J. E. Pate, P. K. Ross, T. J. Thamann, C. A. Reed, K. D. Karlin, T. N. Sorrell, E. I. Solomon, *J. Am. Chem. Soc.* **1989**, *111*, 5198−5209.

[19] [19a] R. Gupta, T. K. Lal, R. Mukherjee, *Polyhedron* **2002**, *21*, 1245−1253. [19b] J. Fawcett, S. H. Laurie, C. Simpson, M. C. R. Symons, F. A. Taiwo, I. Hawkins, *Inorg. Chim. Acta* **2001**, *312*, 245−248. [19c] M. Koman, M. Melník, J. Moncol, *Inorg. Chem. Commun.* **2000**, *3*, 262−266. [19d] L. David, C. Crăciun, O. Cozar, V. Chiş, C. Agut, D. Rusu, M. Rusu, *J. Mol. Struct.* **2001**, *563*/*564*, 573−578.

[20] T. S. Schilperoort, F. J. Rietmeijer, R. A. G. de Graaff, J. Reedijk, *Acta Crystallogr., Sect. C* **1986**, *42*, 1491−1494.

[21] [21a] *teXsan. Single Crystal Structure Analysis Software*, Version 1.6, Molecular Structure Corporation, The Woodlands, TX 77381, USA, **1993**. [21b] G. M. Sheldrick, SHELXS-97, *Program for Crystal Structure Determination*, University of Göttingen, Germany, **1997**. [21c] G. M. Sheldrick, SHELXL-97. *Program for the Refinement of Crystal Structures*, University of Göttingen, Germany, **1997**. [21d] Nonius *COLLECT*. Nonius BV, Delft, The Netherlands, **2002**. [21e]A. L. Spek, *J. Appl. Cryst.* **2003**, *36*, 7−13.

Received February 18, 2004
Early View Article
Published Online July 6, 2004

 © 2004 Wiley-VCH Verlag GmbH & Co. KGaA, Weinheim

Towards Cationic Gallium Derivatives: Metallacycles from the Reactions of Organogallium Compounds with Tetraorganodichalcogenoimidodiphosphinates and a New *N*-(Diphenylthiophosphinyl)thioureato Ligand

Virginia Montiel-Palma,[a] Estefanía Huitrón-Rattinger,[a] Sara Cortés-Llamas,[a] Miguel-Ángel Muñoz-Hernández,*[a] Verónica García-Montalvo,[b] Eddie López-Honorato,[b] and Cristian Silvestru[c]

Keywords: Cationic catalysts / Chelating ligands / Gallium / Metallacycles / Phosphorus

The organometallic complexes of general formulae $[Me_2Ga\{\eta^2\text{-}E,E'\text{-}[R_2P(E)NP(E')R'_2]\}]$ [R = R′ = Ph, E = E′ = O (**1**); R = R′ = Ph, E = E′ = S (**2**); R = R′ = Ph, E = E′ = Se (**3**); R = R′ = Ph, E = O, E′ = S (**4**); R = Me, R′ = Ph, E = S, E′ = O (**5**)] and $[Me_2Ga\{\eta^2\text{-}S,S'\text{-}[Ph_2P(S)NC(S)(C_9H_{10}N)]\}]$ (**6**) were obtained by facile methane elimination reactions from $GaMe_3$ and the acidic ligands L^1H $[(XPPh_2)_2NH$ (X = O, S, Se), $(OPPh_2)(SPPh_2)NH$, and $(OPMe_2)(SPPh_2)NH]$ and L^2H $[Ph_2P(S)NHC(S)(C_9H_{10}N)]$ in toluene. Replacement of one phosphorus atom by a carbon atom in the ligand skeleton of L^1H gave the new ligand L^2H, which, upon reaction with $GaMe_3$, gave compound **6**, which shows no significant structural differences with respect to **1**–**5**. Therefore, L^2H does not induce partial planarity in the six-membered ring, indicating the necessity for replacing both phosphorus atoms of the ligand by carbon atoms, as in the β-diketonate-type derivatives, in order to impose ring planarity. Thus, despite originating from a variety of ligands with differing donor atoms and substituents at the phosphorus atoms, all complexes show little structural differences.

(© Wiley-VCH Verlag GmbH & Co. KGaA, 69451 Weinheim, Germany, 2004)

Introduction

Comparisons between the bonding in organic and inorganic (carbon-free) analogs are widely sought throughout chemistry and have led to a higher understanding of electronically related systems. In particular, the consequences of π-electron delocalization in planar chelate rings have been traditionally assessed by comparison of their properties with those of their nonplanar counterparts arising from atom substitution.[1,2]

In this light, tetraorganodichalcogenoimidodiphosphinato $\{[R_2P(E)NP(E')R'_2]^-$ (E = E′ = chalcogen) $(L^1)\}$ and *N*-(diorganothiophosphinyl)thioureato $\{[R_2P(S)NC(S)R''_2]^-$ $(L^2)\}$ ligands can be regarded as inorganic analogs of the much used β-diketonate ligands. It is the flexibility of the six-membered $M\{\eta^2\text{-}E,E'\text{-}(EPNPE')\}$ (M = main group or transition metal) ring derived from L^1 that has been credited for the variety of structural and coordination modes encountered, a number of which have even given rise to supramolecular structures or proved to be potential building blocks for the design of new materials; others have found prospective industrial use in catalytic systems or biological applications.[3,4] Accordingly, the last decade has seen a considerable growth in the investigations of complexes bearing this kind of ligands, yet surprisingly only a discrete number of organometallic gallium derivatives have been isolated.

From the first organogallium derivative of L^1, $[Et_2Ga\{\eta^2\text{-}Se,Se'\text{-}[Ph_2P(Se)NP(Se)Ph_2]\}]$[5] (**3**-Et), to Uhl's organodigallium(II) compounds, $[\{(Me_3Si)_2HC\}_2Ga\{\eta^2\text{-}O,O'\text{-}[Ph_2P(O)NP(O)Ph_2]\}]$, $[\{(Me_3Si)_2HC\}Ga\{\mu\text{-}\eta^2\text{-}O,O'\text{-}[Ph_2P(O)NP(O)Ph_2]\}]_2$, and $[\{(Me_3Si)_2HC\}Ga\{\eta^2\text{-}S,S'\text{-}[Ph_2P(S)NP(S)Ph_2]\}]_2$,[6] this class of compounds has given insights into the feasibility of preparation and stability towards ligand-redistribution reactions.

Perhaps more importantly, however, cationic gallium species with chelating ligands are desirable for applications in homogeneous catalytic reactions such as alkene polymerization to prevent undesirable ligand exchange/redistribution reactions. Amongst some of the most representative examples are those gallium cations supported by sal-

[a] Centro de Investigaciones Químicas, Universidad Autónoma del Estado de Morelos,
Av. Universidad 1001, Col. Chamilpa, Cuernavaca, Morelos 62210, Mexico
Fax: (internat.) + 52-777-329-7997
E-mail: mamund2@buzon.uaem.mx
[b] Instituto de Química, Universidad Nacional Autónoma de México. Circuito Exterior, Ciudad Universitaria, México 04510, D. F., Mexico
[c] Facultatea de Chimie si Inginerie Chimica, Universitatea Babes-Bolyai, 3400 Cluj-Napoca, Romania

omphen,[7] amidinate,[8,9] β-diketonate[10] and more recently terphenyl[11] ligands. In these systems, ligand bite angles and steric protection play a crucial role in the prevention of nucleophilic attack, besides allowing electronic and steric control. Indeed, Jordan has demonstrated that along the cationic amidinate series $[\{MeC(NiPr)_2\}_2Ga_2Me_3]^+$, $[\{tBuC(NiPr)_2\}GaMe_2\{tBuC(NiPr)_2\}GaMe]^+$ and $[\{tBuC(NtBu)_2\}GaMe]^+$, susceptibility to dimerization decreases, as does nucleophilic addition.[8,9]

In our search for new organogallium cations we recently started a program to systematically explore the incorporation of bulky wide-bite-angle tetraorganodichalcogenoimidodiphosphinato (L^1) and *N*-(diorganothiophosphinyl)thioureato (L^2) ligands at organogallium centers. The ligands in these complexes are closely related to the bis(iminophosphorano)methanide ligand system, which has been used to prepare the monomeric aluminum complexes [κ*N*,κ*N*′-$\{[Ph_2P(Me_3SiN)]_2CH\}AlR_2$] (R = Me, Bu) and [κ*N*,κ*N*′-$\{[Ph_2P(Me_3SiN)]_2CH\}Al(Cl)Et$], and the dimetallic complex [κ*C*,κ*C*′,κ*N*,κ*N*′-$\{[Ph_2P(Me_3SiN)]_2C\}(Me_2Al)_2$]. These complexes show catalytic activity towards ethylene polymerization when activated by trityl tetrafluoroborate, presumably due to formation of a cationic species.[12] Herein we report the facile synthesis and characterization of complexes of general formulae [$Me_2Ga\{\eta^2$-*E*,*E*′-$[R_2P(E)NP(E')R'_2]\}$] and [$Me_2Ga\{\eta^2$-*S*,*S*′-$[Ph_2P(S)NC(S)R'')]\}$] which were envisioned to be good precursors of organometallic cationic species.

Results and Discussion

The synthesis of the new proligand L^2H was carried out in two steps. First, diphenyl isothiocyanide was synthesized according to reported general procedures for the synthesis of similar types of ligands from $Ph_2P(S)Cl$ and KNCS.[13−15] The purified product was then treated with tetrahydroquinoline in CH_2Cl_2, yielding L^2H after treatment with hexane (Scheme 1). Crystals suitable for X-ray diffraction analysis were deposited from hexane at −20 °C. The molecular structure is shown in Figure 1 and the collection and crystal data are given in the Exp. Sect.

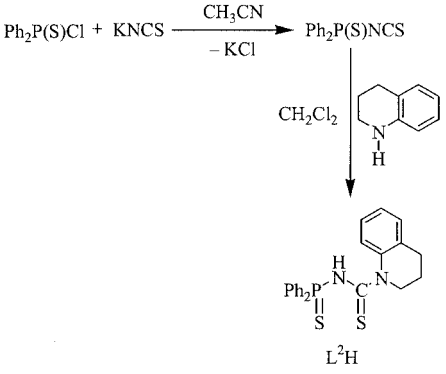

Scheme 1. The synthesis of the new ligand L^2H

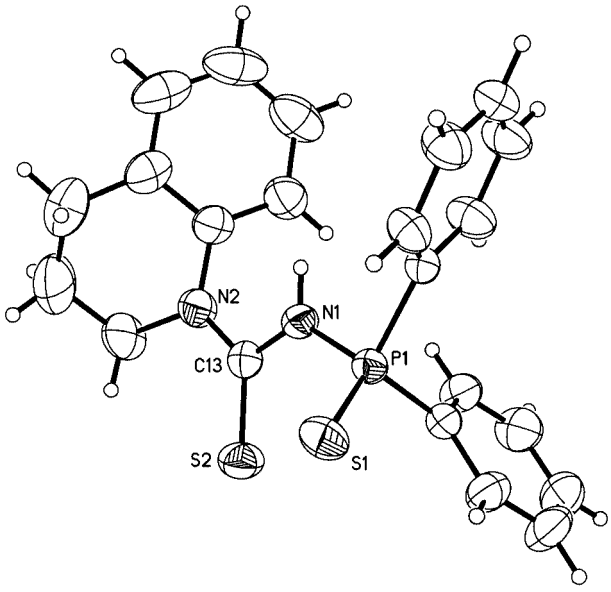

Figure 1. Molecular structure of L^2H with thermal ellipsoids at 50% probability level

The organogallium compounds of general formulae [$Me_2Ga\{\eta^2$-*E*,*E*′-$[R_2P(E)NP(E')R'_2]\}$] [R = R′ = Ph, E = E′ = O (**1**); R = R′ = Ph, E = E′ = S (**2**); R = R′ = Ph, E = E′ = Se (**3**); R =R′ = Ph, E = O, E′ = S (**4**); R = Me, R′ = Ph, E = S, E′ = O (**5**)] and [$Me_2Ga\{\eta^2$-*S*,*S*′-$[Ph_2P(S)NHC(S)(C_9H_{10}N)]\}$] (**6**) were obtained in good yields by room temperature methane elimination reactions between $GaMe_3$ and the ligands L^1H or L^2H in toluene, as depicted in Scheme 2.

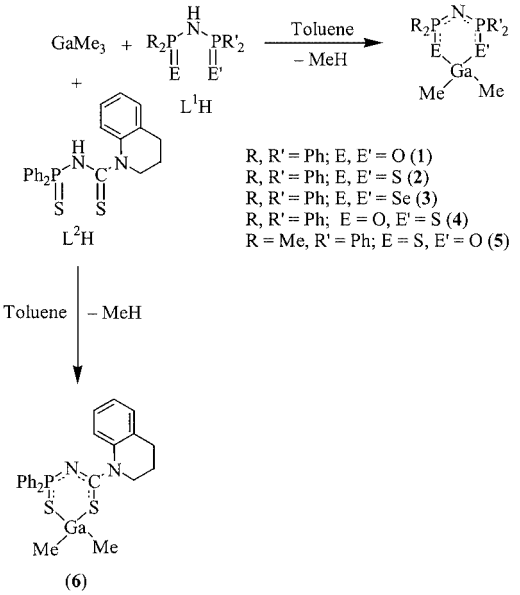

Scheme 2. General synthesis of complexes **1**−**6**

Apart from the organogallium complexes mentioned in the introduction, only one other Ga derivative bearing this

 © 2004 Wiley-VCH Verlag GmbH & Co. KGaA, Weinheim

type of ligand has been structurally characterized. The inorganic tris(chelate) [Ga{η²-*O*,*O*′-[$Ph_2P(O)NP(O)PPh_2$]$_3$}] exhibits a slightly distorted octahedral GaO_6 core as well as three six-membered Ga(OPNPO) rings.[16] On the other hand, the coordination chemistry with thiophosphorylthioureato (L^2) type ligands is much less developed. Only a few complexes of this kind have been reported and, to the best of our knowledge, no group-13 derivatives have been isolated. Interestingly, the formation of a cavity that would host an alkaline metal ion led to the X-ray diffraction study of cadmium and palladium dinuclear *N*-thiophosphorylated thiourea complexes from α,ω-diamines that allow the connection of two units of tetracoordinate transition metal centers.[15]

Complexes **1**−**6** were characterized by physical (m.p.), chemical (C, H and N analysis), and spectroscopic techniques (multinuclear NMR and IR spectroscopy). In addition, solid-state structures of **1**, **2**, **4**, **5** and **6** were obtained by single-crystal X-ray diffraction.

The first indications of the complexation of L^1 and L^2 were given by the absence of ν(NH) bands in the IR spectra and of the N*H* resonances in the ^{1}H NMR solution spectra of the products, particularly in complexes **2**−**6**.[3] Moreover, as expected for metal coordination, the $^{31}P\{^1H\}$ NMR spectra show a high-field shift of the resonance signals for the homoleptic complexes **2** and **3**, and for the P−O resonance of the mixed-chalcogen species. Furthermore, in the case of the selenium derivative **3** there is a considerable decrease in the $^1J_{P,Se}$ coupling constant with respect to the free ligand (Table 1). On the contrary, there is a small down-field change in the chemical shift of the $^{31}P\{^1H\}$ NMR resonance of **1**, although it should be noted that in the tetraphenylimidodiphosphinic acid (L^1H) used as precursor, the acidic hydrogen atom is probably located in an intermolecular O−H···O bridge[17] which does not permit straightforward deductions.

Table 1. Selected spectroscopic parameters of complexes **1**−**6** compared to acidic ligands L^1H and L^2H

	$^{31}P\{^1H\}$ NMR of complex	$^{31}P\{^1H\}$ NMR of acidic ligand
1	26.4 (s)[a]	19.4 (s)[3][b]
2	36.7 (s)[b]	55.7 (s)[18][c]
3	29.3 (s, $^1J_{P,Se}$ = 534 Hz)[c]	53.0 (s, $^1J_{P,Se}$ = 793 Hz)[19][b]
4	27.1 (d, $^2J_{P,P}$ = 3.6 Hz, PS)	56.1 (d, $^2J_{P,P}$ = 17.5 Hz, PS)
	34.8 (d, $^2J_{P,P}$ = 3.6 Hz, PO)[a]	23.1 (d, $^2J_{P,P}$ = 17.5 Hz, PO)[20][b]
5	39.2 (d, $^2J_{P,P}$ = 7.3 Hz, PS)	63.0 (d, $^2J_{P,P}$ = 19.5 Hz, PS)
	24.7 (d, $^2J_{P,P}$ = 7.3 Hz, PO)[a]	23.9 (d, $^2J_{P,P}$ = 19.5 Hz, PO)[21][b]
6	41.1 (s)[a]	56.9 (s)[b]

[a] C_6D_6. [b] $CDCl_3$. [c] [D_6]THF.

Crystals of complexes **1**−**6** (Figures 2−6, respectively) suitable for X-ray analysis were grown from saturated hexane solutions at −20 °C. The molecular structures of the five complexes show a six-membered metallacycle with the geometry around the gallium center being that of a distorted tetrahedron (see below). The dimethylgallium fragment is found to coordinate in a bidentate fashion to the L^1 or L^2 ligands (Tables 2 and 3). Although the crystals of **3** diffracted, we were unable to obtain an acceptable refinement of the data, which, however, show good similarities with those of the already reported diethyl analogue [Et_2Ga{η²-*Se*,*Se*′-[$Ph_2P(Se)NP(Se)Ph_2$]}] (**3-Et**).[5]

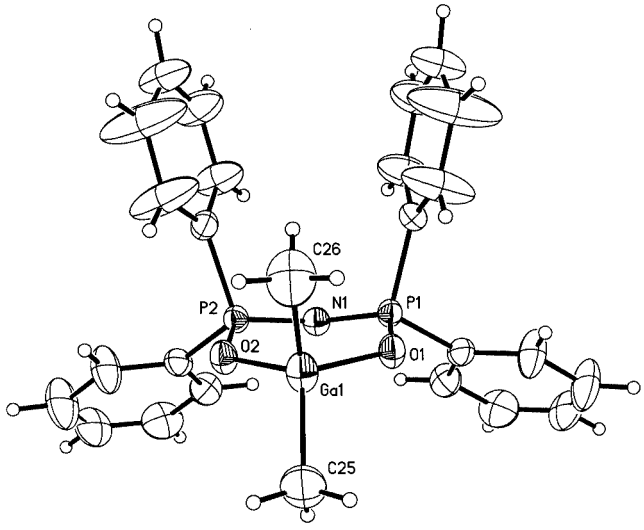

Figure 2. Molecular structure of **1** with thermal ellipsoids at 30% probability level

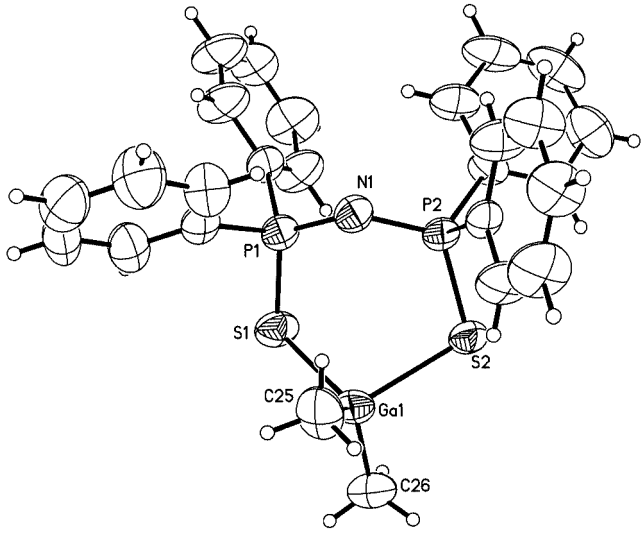

Figure 3. Molecular structure of **2** with thermal ellipsoids at 30% probability level

Compared to the free acidic ligands, the structural features of the complexes are as expected, with the P−E and P−E′ distances enlarged and the P−N distances shortened evidencing changes in bond orders. The P−O distances in the complexes — 1.526(3) and 1.527(3) Å (**1**), 1.530(3) (**4**) and 1.527(1) Å (**5**) — are longer than typical P=O distances [cf. $Ph_2P(O)OH$:[22] P−O 1.526(6), P=O 1.486(6) Å]. Accordingly, the P−S distances — 2.037(2) and 2.040(1) Å (**2**), 2.030(2) Å (**4**), and 2.011(1) Å (**6**) — are also longer than the distances of typical P=S bonds (1.89−1.96 Å). The

 © 2004 Wiley-VCH Verlag GmbH & Co. KGaA, Weinheim

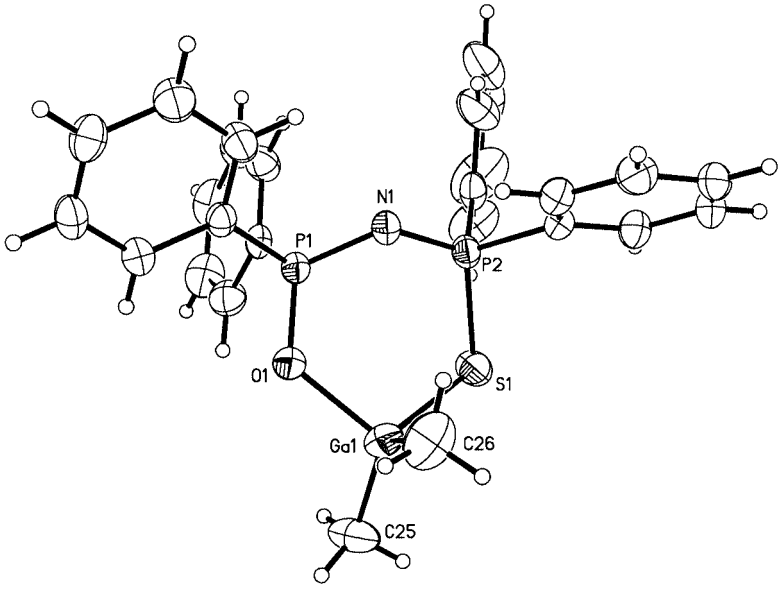

Figure 4. Molecular structure of **4** with thermal ellipsoids at 30% probability level

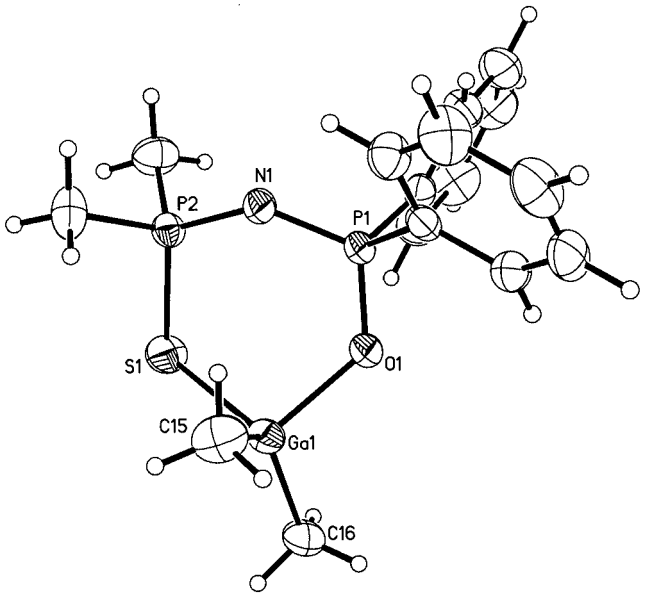

Figure 5. Molecular structure of **5** with thermal ellipsoids at 30% probability level

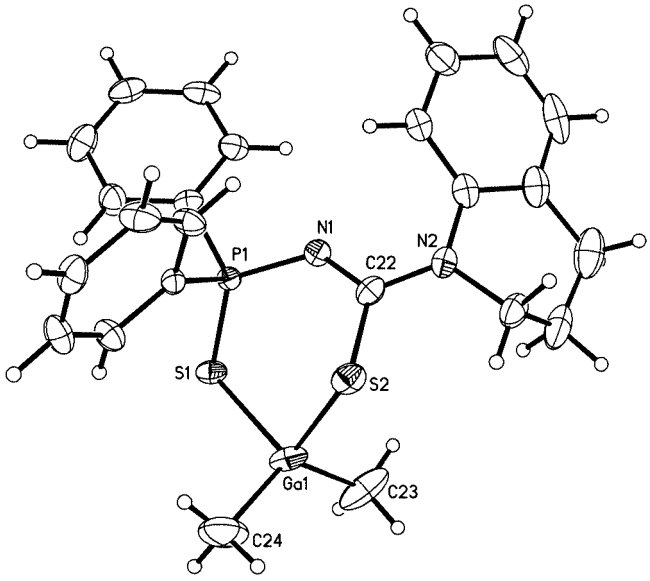

Figure 6. Molecular structure of **6** with thermal ellipsoids at 50% probability level

P−N bond lengths range from 1.59 to 1.61 Å and are somewhat shorter than typical P−N bond lengths {cf. [2-(Me_2NCH_2)C_6H_4]TeSPPh_2=NPPh_2=S:[23] P−S 2.057(1), P=S 1.945(1), P−N 1.612(3), P=N 1.557(3) Å} as expected due to a higher bond order.

In contrast, along the series, the C−Ga−C angles of the dimethylgallium fragments are practically the same, ranging from 125.3(2)° in **6** to 127.6(3)° in **4**. Additionally, apart from the dioxo derivative, comparisons of the P−N−P (or P−N−C) angles of the complexes with respect to those of the free ligands show little tendency to variation, with the largest difference being 6.4° in complex **2**. Amongst all the complexes, these angles differ very little as they range only from 123.4(1) Å in **1** to 138.1(2) Å in **2** (Table 3).

As demonstrated by the X-ray analysis, the conformations of the six-membered metallacycles are diverse: **1** is a chair with the Ga and N(1) atoms at the apices, **2** adopts an envelope conformation with Ga out of the plane, **4** has a twist-boat conformation also with Ga and N(1) at the apices, and **5** and **6** are both boats with Ga and N(1), and P(1) and S(2), respectively, at the apices. The closely related selenium derivative [Et_2Ga{η^2-*Se*,*Se*-[Ph_2P(Se)NP(Se)-Ph_2]}] (**3-Et**)[5] shows a distorted boat conformation with Se and P atoms at the apices. A nonplanar ring is a common feature of complexes derived from tetraorganodichalcogenoimidodiphosphinato ligands, as demonstrated by the variety of examples encountered in main-group and transition-metal chemistry. On the contrary, replacing phos-

 © 2004 Wiley-VCH Verlag GmbH & Co. KGaA, Weinheim

Table 2. Selected bond lengths [Å] and angles [°] for complexes **1**, **2**, **4**, **5** and **6**

1	Ga(1)−C(25)	1.938(5)	O(2)−Ga(1)−O(1)	97.9(1)
	Ga(1)−C(26)	1.994(7)	C(25)−Ga(1)−C(26)	126.0(4)
	Ga(1)−O(1)	1.951(3)	O(1)−Ga(1)−C(26)	107.7(3)
	Ga(1)−O(2)	1.953(3)	O(1)−Ga(1)−C(25)	107.7(3)
	O(1)−P(1)	1.527(3)	O(2)−Ga(1)−C(25)	107.7(3)
	O(2)−P(2)	1.526(3)	O(2)−Ga(1)−C(26)	106.9(3)
	P(1)−N(1)	1.590(3)		
	P(2)−N(1)	1.591(3)		
2	Ga(1)−C(25)	1.958(5)	S(2)−Ga(1)−S(1)	99.2(1)
	Ga(1)−C(26)	1.978(5)	C(25)−Ga(1)−C(26)	126.1(2)
	Ga(1)−S(1)	2.380(1)	S(1)−Ga(1)−C(26)	104.5(2)
	Ga(1)−S(2)	2.416(2)	S(1)−Ga(1)−C(25)	110.8(2)
	S(1)−P(1)	2.040(1)	S(2)−Ga(1)−C(25)	110.9(2)
	S(2)−P(2)	2.037(2)	S(2)−Ga(1)−C(26)	101.9(2)
	P(1)−N(1)	1.593(3)		
	P(2)−N(1)	1.588(3)		
4	Ga(1)−C(25)	1.957(5)	O(1)−Ga(1)−S(1)	99.1(1)
	Ga(1)−C(26)	1.963(5)	C(25)−Ga(1)−C(26)	127.6(3)
	Ga(1)−O(1)	1.945(3)	O(1)−Ga(1)−C(26)	107.3(2)
	Ga(1)−S(1)	2.389(1)	O(1)−Ga(1)−C(25)	106.8(2)
	O(1)−P(1)	1.530(3)	S(1)−Ga(1)−C(25)	102.1(2)
	S(1)−P(2)	2.030(2)	S(1)−Ga(1)−C(26)	110.3(2)
	P(1)−N(1)	1.596(3)		
	P(2)−N(1)	1.601(3)		
5	Ga(1)−C(15)	1.942(3)	O(1)−Ga(1)−S(1)	96.3(1)
	Ga(1)−C(16)	1.937(3)	C(15)−Ga(1)−C(16)	127.1(2)
	Ga(1)−O(1)	1.932(2)	O(1)−Ga(1)−C(15)	108.3(1)
	Ga(1)−S(1)	2.377(1)	O(1)−Ga(1)−C(16)	104.8(1)
	O(1)−P(1)	1.527(2)	S(1)−Ga(1)−C(15)	109.8(1)
	S(1)−P(2)	2.041(1)	S(1)−Ga(1)−C(16)	106.2(1)
	P(1)−N(1)	1.577(2)		
	P(2)−N(1)	1.612(2)		
6	Ga(1)−C(24)	1.960(4)	S(2)−Ga(1)−S(1)	103.4(1)
	Ga(1)−C(23)	1.961(4)	C(24)−Ga(1)−C(23)	125.3(3)
	Ga(1)−S(1)	2.3886(9)	S(1)−Ga(1)−C(24)	110.7(1)
	Ga(1)−S(2)	2.3535(9)	S(1)−Ga(1)−C(23)	104.8(1)
	S(1)−P(1)	2.011(1)	S(2)−Ga(1)−C(23)	109.3(1)
	S(2)−C(22)	1.758(3)	S(2)−Ga(1)−C(24)	101.4(1)
	P(1)−N(1)	1.614(2)		
	C(22)−N(1)	1.325(4)		

phorus with carbon in the ligand skeleton, as in the tetrahedral imidoylamidinato complex [$Me_2Ga\{\eta^2$-*N*,*N*′-$[HNC(CF_3)NC(CF_3)NH]\}$][27] leads to all atoms of the ring being coplanar. In addition, a small number of planar gallacycle rings have been structurally characterized as derivatives of β-diketonate ligands. For example, four-coordinate $[GaCl_2(bdk)]$[10] [bdk = (2,4-pentanedionato), acac and (2,2,6,6-tetramethylheptanedionato)], [GaMeCl(acac)][28] and $[GaCl\{N(SiMe_3)_2\}(acac)]$[28] all show planar six-membered GaO_2C_3 rings with O−Ga−O bite angles ranging from 96.1 to 99.3°. It is thus significant that in complex **6** replacement of one phosphorus atom by a carbon atom does not induce partial planarity in the ring.

Perhaps the most striking feature is the fact that along a series of chemically differing ligands, the structural variation is not as large as expected, despite the well-documented versatility of the PNP ligand.

The fact that the bite angles of the ligands in the complexes studied are in the range 96.3−108.4° (see Table 3) is indicative of their prospective good potential as cationic precursors. Steric protection for catalytically active metal centers can be provided by bulky multidentate ligands, and various examples have been reported with late transition metals[29] as well as aluminum.[30] Indeed, large bite angles in cationic, three-coordinate aluminum complexes have proved to be an effective approach to stabilize these highly reactive species. Bulky aluminum amidinate complexes $[\{RC(NR')_2\}AlMe]^+$ with small bite angles (N−Al−N angle of about 70° in neutral derivatives) are thermally unstable but the *N*,*N*′-diaryldiketiminate complex $[\{HC(CMeNAr)_2\}AlMe_2]$ (Ar = 2,6-*i*$Pr_2C_6H_3$) with a larger bite angle (N−Al−N angle of about 96°) and bulky *N*-aryl substituents yield a stable, three-coordinate cation upon abstraction of the alkyl group.[31] Moreover, in contrast to most precursors documented in the literature, the family of complexes reported herein is easily accessible and requires little purification. Current work in our laboratory is focused in this direction, treating complexes **1**−**6** and others with strong Lewis acids. The results of this work will be reported shortly.

Table 3. Selected structural features of organogallium metallacycles **1**, **2**, **4**, **5**, **6** and $[Et_2Ga\{\eta^2$-*Se*,*Se*′-$[Ph_2P(Se)NP(Se)Ph_2]\}]$ (**3-Et**)[5]

	P−N−P or P−N−C angle in ligand [°]	P−N−P or P−N−C angle in complex [°]	E−Ga−E′ angle [°]	Me−Ga−Me angle [°]	(PENPE′)Ga or (PSNCS)Ga ring conformation	Nonbonding E−E′ length [Å]	
1	180[17]	123.4(1)	97.9(1)	126.0(4)	chair	O(1)−O(2)	2.94
2	131.7(5)[24]	138.1(2)	99.2(1)	126.1(2)	envelope-	S(1)−S(2)	3.65
3-Et[5]	132.3(2)[25]	129.8(3)[5]	108.4(1)[5]	125.5(4)[5]	boat[5]	Se(1)−Se(2)	4.09
4	131.4(3)[26]	125.4(2)	99.1(1)	127.6(3)	twist boat	O(1)−S(1)	3.31
5	126.5[20]	131.1(1)	96.3(1)	127.1(2)	boat	O(1)−S(1)	3.22
6	128.8(1)	124.1(2)	103.4(1)	125.3(2)	boat	S(1)−S(2)	3.72

 © 2004 Wiley-VCH Verlag GmbH & Co. KGaA, Weinheim

Conclusion

Gallium metallacycles derived from dichalcogenoimidodiphosphinato ligands were obtained by facile methane elimination reactions. In the new complexes, the Ga center is in a distorted tetrahedral environment forming part of a six-membered metallacycle. The conformations of these rings do not correlate with the nature of the chalcogen nor with the substituents at the phosphorus or carbon atoms, but in all cases a nonplanar ring was observed. Exchanging a phosphorus atom by a carbon atom in the metallacycle ring does not result, even partially, in a planar structure of complex **6**.

Experimental Section

General Remarks: All glassware was rigorously dried in an oven at 130 °C for 24 h, assembled hot, and then allowed to cool under argon. All the manipulations of the air-sensitive compounds were conducted using standard inert-gas bench-top and glove-box techniques. Solvents were dried with sodium or potassium/benzophenone and freshly distilled prior to use. The L^1H ligands were synthesized according to literature methods: $(XPPh_2)_2NH$ (X = O,[32] S,[33] Se[33]), $(OPPh_2)(SPPh_2)NH$,[34] and $(OPMe_2)(SPPh_2)NH$.[35] NMR spectroscopic data (^1H, ^{13}C and ^{31}P) were obtained with Varian-Inova 400 MHz and Varian-Gemini-200 MHz instruments at 19 °C. Chemical shifts are reported relative to $SiMe_4$ for ^1H and ^{13}C, 85% H_3PO_4 for ^{31}P and are in ppm. Microanalyses were obtained with an Elementar Vario EL III instrument in the CHNS operation mode. Infrared spectra were recorded as KBr pellets with a Bruker Equinox 55 Spectrometer and are reported in cm^{-1}.

Synthesis of $Ph_2P(S)NHC(S)(C_9H_{10}N)$ (L^2H): Tetrahydroquinoline (0.65 mL, 5.1 mmol) was added to a stirred solution of $Ph_2P(S)NCS$ (1.42 g, 5.1 mmol) in CH_2Cl_2 (20 mL). After 4 h, the solvent was removed under vacuum, hexane (30 mL) was added and the mixture stirred for a further 2 h. The white solid deposited was filtered and dried under vacuum. Yield: 1.89 g (90%), m.p. 71−73 °C. Selected ^1H NMR data ($CDCl_3$, 300 MHz): δ = 3.97 (s, 1 H, NH) ppm. ^{13}C NMR ($CDCl_3$, 75.4 MHz): δ = 150.50 (C=S) ppm. ^{31}P NMR ($CDCl_3$, 121.4 MHz): δ = 56.89 (s) ppm. IR: $\tilde{\nu}$ = 3309 (νNH), 1445 (νCN), 1103 (νCS), 957, 882 (νPN), 647 (νPS) cm^{-1}. Crystals suitable for X-ray diffraction analysis were grown from hexane solution.

Synthesis of $[Me_2Ga\{\eta^2\text{-}O,O'\text{-}[Ph_2P(O)NP(O)Ph_2]\}]$ (1): A solution of trimethylgallium (0.08 g, 0.70 mmol) in toluene (10 mL) was added to a stirred suspension of $(OPPh_2)_2NH$ (0.3 g, 0.72 mmol) in toluene (20 mL), causing vigorous gas evolution and the formation of a clear colorless solution which was stirred for 4 h. Removal of the volatiles under reduced pressure produced a viscous substance, which was treated with hexane (5 mL) and stirred until the deposition of a white solid. The solid was separated from the solution by cannula filtration and dried under high vacuum. The remaining hexane solution at −20 °C deposited suitable crystals for X-ray analysis. Yield 0.27 g (87%), m.p. 77−78 °C. ^1H NMR ($CDCl_3$, 400 MHz): δ = −0.31 (s, 6 H, $GaCH_3$), 7.34−7.40 (m, 12 H, C_6H_5), 7.75 (m, 8 H, C_6H_5) ppm. ^{13}C NMR ($CDCl_3$, 100.6 MHz): δ = −4.52 (s, CH_3Ga), 128.30−131.26 (C_6H_5), 136.04 (d, $^1J_{C,P}$ = 140 Hz, *ipso*-C_6H_5) ppm. $^{31}P\{^1H\}$ NMR (C_6D_6, 161.8 MHz): δ = 26.43 (s) ppm. IR: $\tilde{\nu}$ = 3072 (m), 2960 (m), 2718 (w), 2365 (w), 2336 (w), 200.22 (w), 1959 (w), 1893 (w), 1814 (w), 1674 (w), 1590 (w), 1482 (m), 1436 (s), 1126 (s), 691 (s) 590 (s) cm^{-1}. $C_{26}H_{26}GaNO_2P_2$ (516.14): calcd. C 60.50, H 5.08, N 2.71; found C 60.43, H 5.03, N 2.72.

Compounds **2**−**6** were prepared in a similar manner to **1**.

$[Me_2Ga\{\eta^2\text{-}S,S\text{-}[Ph_2P(S)NP(S)Ph_2]\}]$ (2): $(SPPh_2)_2NH$ (0.30 g, 0.67 mmol) and trimethylgallium (0.08 g, 0.70 mmol) afforded **2** as a white solid. Yield 0.30 g (82%), m.p. 103−105 °C. ^1H NMR ($CDCl_3$, 400 MHz): δ = −0.25 (s, 6 H, CH_3Ga), 7.35 (m, 12 H, C_6H_5), 7.83 (m, 8 H, C_6H_5P) ppm. ^{13}C NMR ($CDCl_3$, 100.6 MHz): δ = −0.79 (s, $GaCH_3$), 128.41−131.36 (C_6H_5), 137.31 (d, $^1J_{C,P}$ = 140 Hz, *ipso*-C_6H_5) ppm. $^{31}P\{^1H\}$ NMR ($CDCl_3$, 161.8 MHz): δ = 36.71 (s) ppm. IR: $\tilde{\nu}$ = 3069.3 (w), 2962.3 (m), 2901.4 (w), 1999.5 (w), 1892.5 (w), 1809.7 (w), 1674 (w), 1582.8 (w), 1476.7 (m), 1433 (m),1258.9 (m), 1196.4 (s), 1104.7 (s), 1022.8 (s), 807.5 (s), 743.7 (s), 694.8 (s), 577.5 (s), 530.3 (s) cm^{-1}. $C_{26}H_{26}GaNP_2S_2$ (548.26): calcd. C 56.96, H 4.78, N 2.55, S 11.70; found C 57.01, H 4.79, N 2.60, S 11.87.

$[Me_2Ga\{\eta^2\text{-}Se,Se\text{-}[Ph_2P(Se)NP(Se)Ph_2]\}]$ (3): $(SePPh_2)_2NH$ (0.3 g, 0.55 mmol) and trimethylgallium (0.063 g, 0.55 mmol) generated **3** as a white solid. Yield 0.31 g (88%), m.p. 143 °C. ^1H NMR ($CDCl_3$, 400 MHz): δ = −0.11 (s, $^1J_{C,H}$ = 162, $^3J_{Se,H}$ = 4 Hz, 6 H, $GaCH_3$), 7.34−7.44 (m, 12 H, C_6H_5), 7.81 (m, 8 H, C_6H_5) ppm. $^{13}C\{^1H\}$ ($CDCl_3$, 100.6 MHz): δ = 0.20 ($GaCH_3$), 128.2−131.4 (C_6H_5), 136.8 (dd, $^1J_{P,C}$ = 98.49, $^2J_{C,Se}$ 4.19 Hz, *ipso*-C_6H_5) ppm. $^{31}P\{^1H\}$ NMR ($CDCl_3$, 81 MHz): δ = 29.3 (s, $^1J_{P,Se}$= 525 Hz) ppm. IR: $\tilde{\nu}$ = 3060 (w), 1583 (w), 1477 (w), 1433 (m), 1210 (s), 1108 (s), 1025 (w), 925 (w), 803 (m), 691 (s), 562 (s), 516 (m), 486 (m) cm^{-1}. $C_{26}H_{26}GaNP_2Se_2$ (642.08): calcd. C 48.64, H 4.08, N 2.18; found C 48.85, H 4.11, N 2.14.

$[Me_2Ga\{\eta^2\text{-}S,O\text{-}[Ph_2P(S)NP(O)Ph_2]\}]$ (4): Compound **4** was obtained as a white solid from $(SPPh_2)NH(OPPh_2)$ (0.3 g, 0.69 mmol) and trimethylgallium (0.08 g, 0.70 mmol). Yield 0.27 g, 73%, m.p. 83−85 °C. ^1H NMR (200 MHz, C_6D_6): δ = 0.22 (s, 6 H, $GaCH_3$), 6.98 (m, 12 H, C_6H_5), 7.96 (m, 8 H, C_6H_5) ppm. ^{13}C NMR (50.3 MHz, C_6D_6): δ = −1.50 (s, $GaCH_3$), 128.59 (m, and C_6H_5), 131.58 (m, C_6H_5), 136.23 (d, $^1J_{C,P}$ = 105 Hz, *ipso*-C_6H_5), 139.32 (d, $^1J_{C,P}$ = 83 Hz, *ipso*-C_6H_5) ppm. $^{31}P\{^1H\}$ NMR (161.8 Hz, C_6D_6): δ = 27.07 (d, $^2J_{P,P}$ = 3.56 Hz, $GaOPPh_2$), 34.78 (d, $^2J_{P,P}$ = 3.56 Hz, $GaSPPh_2$) ppm. IR: $\tilde{\nu}$ = 3053.2 (m), 2966 (s), 2909 (m), 2712 (w), 1968 (w), 1890 (w), 1825 (w), 1775 (m), 1674 (w), 1591 (m), 1482 (m), 1433 (s), 1410 (s), 1050 (s), 867 (s), 700 (s), 549 (s) cm^{-1}. $C_{26}H_{26}GaNOP_2S$ (532.20): calcd. C 58.67, H 4.92, N 2.63, S 6.03; found C 58.68, H 5.01, N 2.62, S 5.98.

$[Me_2Ga\{\eta^2\text{-}S,O\text{-}[Me_2P(S)NP(O)Ph_2]\}]$ (5): White compound **5** was synthesized from $(SPMe_2)(OPPh_2)NH$ (0.22 g, 0.71 mmol) and trimethylgallium (0.08 g, 0.70 mmol). Yield 0.25 g (87%), m.p. 116−118 °C. ^1H NMR (400 MHz, C_6D_6): δ = 0.35 (s, 6 H, $GaCH_3$), 1.39 (d, $^2J_{P,H}$ = 26.4 Hz, 6 H, $GaPCH_3$), 7.03 (m, 6 H, C_6H_5), 7.90 (m, 4 H, C_6H_5) ppm. ^{13}C NMR (50.3 Hz, C_6D_6): δ = −1.17 (s, $GaCH_3$), 26.37 (dd, $^1J_{C,P}$ = 122.56, $^3J_{C,P}$ = 5.01 Hz, PCH_3), 128.64 (m, C_6H_5), 131.63 (m, C_6H_5) ppm. $^{31}P\{^1H\}$ NMR (161.82 MHz, C_6D_6): δ = 25.61 (d, $^2J_{P,P}$ = 7.29 Hz, $GaOPPh_2$), 39.18 (d, $^2J_{P,P}$ = 7.29 Hz, $GaSPMe_2$) ppm. IR: $\tilde{\nu}$ = 3053 (m), 2966.0 (s), 2909 (m), 2712 (w), 1968 (w), 1890 (w), 1825 (w), 1755 (w), 1674 (w), 1591 (w), 1482 (m), 1433 (s), 1410 (s), 1050 (s), 867 (s), 700 (s), 549 (s) cm^{-1}. $C_{16}H_{22}GaNOP_2S$ (408.07): calcd. C 47.09, H 5.43, N 3.43, S 7.86; found C 47.13, H 5.51, N 3.39.

$[Me_2Ga\{\eta^2\text{-}S,S\text{-}[Ph_2P(S)N(C)NC_9H_{10}]\}]$ (6): White compound **6** was synthesized from $C_9H_{10}NC(S)NHP(S)(C_6H_5)_2$ (0.27 g,

 © 2004 Wiley-VCH Verlag GmbH & Co. KGaA, Weinheim

Table 4. Summary of crystallographic data for complexes L^2H, **1**, **2**, **4**, **5** and **6**

	L^2H	**1**	**2**	**4**	**5**	**6**
Empirical formula	$C_{22}H_{21}N_2PS_2$	$C_{26}H_{26}GaNO_2P_2$	$C_{26}H_{26}GaNP_2S_2$	$C_{26}H_{26}GaNOP_2S$	$C_{16}H_{22}GaNOP_2S$	$C_{24}H_{26}GaN_2PS_2$
Formula mass	408.50	516.14	548.26	532.20	408.07	507.28
Crystal system	monoclinic	orthorhombic	monoclinic	orthorhombic	triclinic	orthorhombic
Space group	$P2_1/c$	Cc	$P2_1/c$	$Pbca$	$P\bar{1}$	$P2_12_12_1$
a [Å]	10.4437(8)	9.645(1)	14.257(6)	16.687(4)	9.162(1)	8.481(2)
b [Å]	22.2312(16)	14.842(1)	8.852(4)	15.943(4)	9.308(1)	16.596(4)
c [Å]	9.1690(7)	17.743(2)	21.635(9)	19.526(5)	12.921(1)	17.078(4)
α [°]	90	90	90	90	106.216(1)	90
β [°]	106.6740(10)	90	101.881(7)	90	93.480(1)	90
γ [°]	90	90	90	90	111.178(1)	90
V [Å^3]	2039.3(3)	2539.8(6)	2671.9(19)	5195(2)	970.30(14)	2403.8(10)
Z	4	4	4	8	2	4
$D_{calcd.}$ ([g/cm^3]	1.331	1.350	1.363	1.361	1.397	1.402
F(000)	856	1064	1128	2192	420	1048
Crystal size [mm]	0.12 × 0.23 × 0.26	0.14 × 0.26 × 0.29	0.13 × 0.18 × 0.26	0.13 × 0.18 × 0.27	0.18 × 0.17 × 0.11	0.15 × 0.18 × 0.24
Temperature [K]	293	293	293	293	100	100
2θ range [°]	3.6−55	5.6−50	2.9−50	4.1−50	3.3−52	3.4−50
No. of reflections collected	22836	8938	12838	45930	10895	8640
No. of independent reflections	4662 (R_{int} = 0.0342)	4380 (R_{int} = 0.0209)	4645 (R_{int} = 0.0591)	4569 (R_{int} = 0.0569)	4199 (R_{int} = 0.0171)	4150 (R_{int} = 0.0330)
No. of observed reflections	3706 [$F > 4.0\sigma(F)$]	4225 [$F > 4.0\ \sigma(F)$]	3439 [$F > 4.0\ \sigma(F)$]	3978 [$F > 4.0\ \sigma(F)$]	3763 [$F > 4.0\ \sigma(F)$]	3687 [$F > 4.0\ \sigma(F)$]
No. of parameters	244	291	291	291	203	273
R	0.0442	0.0377	0.0631	0.0604	0.0368	0.0295
R_w	0.1138	0.0984	0.1559	0.1369	0.1032	0.0598
GOF	1.038	1.084	0.969	1.230	1.080	0.958
Largest difference electron density [e/Å^3]	0.449/−0.311	0.711/−0.496	1.056/−0.927	0.545/−0.244	0.667/−0.165	0.416 and −0.220

0.66 mmol) and trimethylgallium (0.076 g, 0.66 mmol). Yield 0.25 g (75%). Selected ^{1}H NMR data (80.96 MHz, C_6D_6): δ = 0.35 (s, 6 H, $GaCH_3$), 2.23 (m, 2 H, CH_2), 3.94 (m, 2 H, CH_2), 4.27 (m, 2 H, CH_2), 6.89−7.91 (m, 13 H, aromatic H) ppm. $^{31}P\{^1H\}$ NMR (80.96 MHz, C_6D_6): δ = 41.07 (s). $C_{24}H_{26}GaN_2PS_2$ (507.28): calcd. C 56.54, H 5.10, N 2.75, S 12.57; found C 56.81, H 5.21, N 2.64, S 12.43.

X-ray Crystallographic Study: Crystals suitable for X-ray diffraction for compounds L^2H, **1**, **2**, **4**, **5** and **6** were obtained from saturated hexane solutions as described above. X-ray data were collected with a Bruker APEX CCD diffractometer with Mo-K_α radiation. The structures were refined using the software package SHELXTL vers. 6.1.[36] All of the non-hydrogen atoms were refined anisotropically. The hydrogen atoms were put into calculated positions. Absorption correction in all cases was applied using SADABS.[37] Further details of the structure analyses are given in Table 4.[38]

Acknowledgments

We are indebted to CONACYT-México (Grant J30234-E) and UCMEXUS-CONACYT for generous support. We also thank CONACYT for a PhD grant to S. C.-L. and an undergraduate studentship to E. H.-R.

[1] J. E. Huheey, E. A. Keiter, R. L. Keiter, *Inorganic Chemistry*, 4th ed., Harper Collins College Publishers, New York, **1993**.
[2] I. Haiduc, *The Chemistry of Inorganic Ring Systems*, Wiley Interscience, New York, **1970**, vols. I and II.
[3] C. Silvestru, J. E. Drake, *Coord. Chem. Rev.* **2001**, *223*, 117−216 and references cited therein.
[4] P. Bhattacharyya, J. D. Woollins, *Polyhedron* **1995**, *14*, 3367−3388.
[5] M. A. Muñoz-Hernández, A. Singer, D. A. Atwood, R. Cea-Olivares, *J. Organomet. Chem.* **1998**, *571*, 15−19.
[6] W. Uhl, T. Spies, W. Saak, *Z. Anorg. Allg. Chem.* **1999**, *625*, 2095−2102.
[7] M. S. Hill, D. A. Atwood, *Eur. J. Inorg. Chem.* **1998**, 67−72.
[8] S. Dagorne, I. A. Guzei, M. P. Coles, R. F. Jordan, *J. Am. Chem. Soc.* **2000**, *122*, 274−289.
[9] A. V. Korolev, F. Delpech, S. Dagorne, I. A. Guzei, R. J. Jordan, *Organometallics* **2001**, *20*, 3367−3369.
[10] O. T. Beachley Jr., J. R. Gardinier, M. R. Churchill, *Organometallics* **2003**, *22*, 1145−1151.
[11] R. J. Wehmschulte, J. M. Steele, J. D. Young, M. A. Khan, *J. Am. Chem. Soc.* **2003**, *125*, 1470−1471.
[12] R. G. Cavell, K. Aparna, R. P. K. Babu, Q. Wang, *J. Mol. Catal. A: Chem.* **2002**, *189*, 137−143.
[13] A. Ziegler, V. P. Botha, I. Haiduc, *Inorg. Chim. Acta* **1975**, *15*, 123−128.
[14] R. A. Spence, J. M. Swan, S. H. B. Wright, *Aust. J. Chem.* **1969**, *22*, 2359−2370.
[15] N. G. Zabirov, V. V. Brus'ko, S. V. Kashevarov, F. D. Sokolov, V. A. Shcherbakova, A. Y. Verat, R. A. Cherkasov, *Russ. J. Gen. Chem.* **2000**, *70*, 1214−1221.
[16] V. García-Montalvo, R. Cea-Olivares, D. J. Williams, G. Espinosa-Pérez, *Inorg. Chem.* **1996**, *35*, 3948−3953.
[17] H. Nöth, *Z. Naturforsch., Teil B* **1982**, *37*, 1491.
[18] A. M. Z. Slawin, J. Ward, D. J. Williams, J. D. Woolins, *J. Chem. Soc., Chem. Commun.* **1994**, 421−422.
[19] P. Bahttacharyya, A. M. Z. Slawin, D. J. Williams, J. D. Woolins, *J. Chem. Soc., Dalton Trans.* **1995**, 2489−2495.
[20] R. Rösler, M. Stanciu, J. Yang, J. E. Drake, C. Silvestru, I. Haiduc, *Phosphorus, Sulfur Silicon* **1998**, *132*, 231.
[21] R. Rösler, M. Stanciu, J. Yang, I. Haiduc, *J. Chem. Soc., Dalton Trans.* **1996**, 391−399.
[22] D. Fenske, R. Mattes, J. Löns, K. F. Tebbe, *Chem. Ber.* **1973**, *106*, 1139−1144.
[23] J. E. Drake, M. B. Hursthouse, M. Kulcsar, M. E. Light, A. Silvestru, *J. Organomet. Chem.* **2001**, *623*, 153−160.

 © 2004 Wiley-VCH Verlag GmbH & Co. KGaA, Weinheim

[24] P. B. Hitchcock, J. F. Nixon, I. Silaghi-Dumitrescu, I. Haiduc, *Inorg. Chim. Acta* **1985**, *96*, 77.
[25] P. Bahttacharyya, J. Novasad, J. Phillips, A. M. Z. Slawin, D. J. Williams, J. D. Woolins, *J. Chem. Soc., Dalton Trans.* **1995**, 1607−1613.
[26] J. Yang, J. E. Drake, S. Hernandez-Ortega, R. Rösler, C. Silvestru, *Polyhedron* **1996**, *16*, 4061.
[27] D. R. Aris, J. Barker, P. R. Philips, N. W. Alcock, M. G. H. Wallbridge, *J. Chem. Soc., Dalton Trans.* **1997**, 909−910.
[28] O. T. Beachley Jr, J. R. Gardinier, M. R. Churchill, D. G. Churchill, K. M. Keil, *Organometallics* **2002**, *21*, 946−951.
[29] S. D. Ittel, L. K. Johnson, M. Brookhart, *Chem. Rev.* **2000**, *100*, 1169−1204.
[30] See for example: M. P. Coles, R. F. Jordan, *J. Am. Chem. Soc.* **1997**, *119*, 8125−8126.
[31] A. V. Korolev, E. Ihara, I. A. Guzei, V. G. Young Jr., R. F. Jordan, *J. Am. Chem. Soc.* **2001**, *123*, 8291−8309.
[32] F. T. Wang, J. Najdzionek, K. L. Leneker, H. Wasserman, D. M. Braitsch, *Synth. React. Inorg. Met.-Org. Chem.* **1978**, *8*, 119−125.
[33] P. Bahttacharyya, J. Novasad, J. Phillips, A. M. Z. Slawin, D. J. Williams, J. D. Woollins, *J. Chem. Soc., Dalton Trans.* **1995**, 1607−1613.
[34] J. Yang, J. E. Drake, S. Hernandez-Ortega, R. Rösler, C. Silvestru, *Polyhedron* **1997**, *16*, 4061−4071.
[35] R. Rösler, M. Stanciu, J. Yang, J. E. Drake, C. Silvestru, I. Haiduc, *Phosphorus, Sulfur Silicon* **1998**, *132*, 231−250.
[36] G. M. Sheldrick, *SHELXTL*, version 6.0, Bruker AXS, Inc., Madison, WI, USA, **2000**.
[37] G. M. Sheldrick, *SAINT-Plus*, version 6.0, Bruker AXS, Inc., Madison, WI, USA, **2000**.
[38] CCDC-236532 (**1**), -236533 (**2**), -236534 (**4**), -236535 (**5**), -236536 (**6**) and -236537 (L^2H) contain the supplementary crystallographic data for this paper. These data can be obtained free of charge at www.ccdc.cam.ac.uk/conts/retrieving.html [or from the Cambridge Crystallographic Data Centre, 12 Union Road, Cambridge CB2 1EZ, UK; Fax: (internat.) + 44-1223-336033; E-mail: deposit@ccdc.cam.ac.uk].

Received February 3, 2004
Early View Article
Published Online July 12, 2004

 © 2004 Wiley-VCH Verlag GmbH & Co. KGaA, Weinheim

Syntheses and Characterizations of Metal-Organic Frameworks with Unusual Topologies Derived from Flexible Dipyridyl Ligands

Ruihu Wang,[a] Lei Han,[a] Lijin Xu,[b] Yaqiong Gong,[a] Youfu Zhou,[a] Maochun Hong,*[a] and Albert S. C. Chan[b]

Keywords: Bridging ligands / Cadmium / Coordination polymers / X-ray diffraction / Zinc

Two flexible *exo*-bidentate ligands, 2,2′-bis(3-pyridylmethyleneoxy)-1,1′-biphenylene (3,3′-bpp) and 2,2′-bis(4-pyridylmethyleneoxy)-1,1′-biphenylene (4,4′-bpp), were synthesized and employed for the preparation of coordination polymers. Seven metal-organic complexes, $[Zn_2(3,3'\text{-bpp})_2Cl_4]$ (**1**), $[Zn_2(3,3'\text{-bpp})_2Br_4]$ (**2**), $[Zn(4,4'\text{-bpp})Cl_2]_n$ (**3**), $[Zn(4,4'\text{-bpp})Br_2]_n$ (**4**), $[Co(4,4'\text{-bpp})_2(SCN)_2]_n$ (**5**), $\{[Cd(4,4'\text{-bpp})_2(SCN)_2]\cdot 2H_2O\}_n$ (**6**) and $[Cd(4,4'\text{-bpp})(dca)_2]_n$ (**7**) (dca^- = dicyanamide), have been obtained through self-assembly reactions of 3,3′-bpp or 4,4′-bpp with the divalent metal ions Zn^{II}, Co^{II} and Cd^{II}. Crystal structure analyses reveal that **1** and **2** are dinuclear metallomacrocycles, are isomorphous and possess a layer network built from metallomacrocycles through π–π interactions. In drastic contrast, **3** and **4** exhibit a three-dimensional structure consisting of one-dimensional polymeric chains held together through π–π interactions between adjacent pyridyl rings. The metal-organic frameworks of **5**, **6**, and **7** possess unusual topologies: Complex **5** is a two-dimensional polymer based on folded rectangular boxes and zigzag chains, whereas **6** is a polycatenated species consisting of inclined interpenetrating two-dimensional layers, and each layer is constructed by the alternating assembly of left-hand (*M*) and right-hand (*P*) cylindrical 2_1 helices. In **7**, dca^- connects Cd^{II} centers forming a two-dimensional $\{Cd(dca)_2\}_n$ layer, which is fused with (*M*)- and (*P*)-Cd-(4,4′-bpp) helical chains into a three-dimensional structure. The results suggest that the nature of organic ligands and the coordination preferences of transitional metal ions have a great influence on the structures of metal-organic complexes.

(© Wiley-VCH Verlag GmbH & Co. KGaA, 69451 Weinheim, Germany, 2004)

Introduction

Metal-directed self-assembly of organic ligands and metal ions, or organometallic moieties, to form well-defined structures has been a very attractive field in recent years.[1−6] The increasing interest in this field is justified not only by the intellectual challenge in controlling and manipulating the self-assembly process,[3,4] but also by their fascinating structural diversities and potential application in functional materials, nanotechnology and biological recognition.[5,6] In this context, novel supramolecular topologies with various sizes and shapes of channels or cavities can be controlled and tuned through judiciously selecting assembly-influencing factors, such as structural characteristics of polydentate organic ligands,[7,8] the coordination nature of the metal ions,[9] counter anions,[10] the metal/ligand ratio,[11] and solvent system.[12] So far, of diverse elegant efforts to find the key factors in the course of the construction of metal-based supramolecules, the dominant and most efficient synthetic strategy is the employment of various organic ligands as molecular building blocks or tectons. Among these organic ligands, one of the most fruitful choices has been the use of neutral pyridyl-containing bidentate or multidentate organic building blocks, owing to their simple bridging mode and strong coordination ability to transition-metal ions. Rigid, rod-like, *exo*-bidentate ligands, such as 4,4′-bipyridine (4,4′-bipy),[13,14] are suitable examples of tectons that have been used often for the rational design of solid-state architectures of coordination polymers. Moreover, structures containing larger holes can potentially be built by using longer rigid connectors between the pyridyl rings. For example, Fujita et al. have reported a series of two-dimensional square frameworks with different sizes upon increasing the number of phenyl rings between the pyridyl rings.[15] Compared to rigid bridging ligands, flexible bridging tectons can produce some unique frameworks with beautiful aesthetics and useful properties because of their flexibility and conformational freedom.[16] However, owing to the difficulty in predicting the structures of the products, the rational design of coordination poly-

[a] State Key Laboratory of Structural Chemistry, Fujian Institute of the Research on the Structure of Matter, Chinese Academy of Sciences,
Fuzhou, Fujian 350002, China
Fax: (internat.) + 86-591-3714946
E-mail: hmc@ms.fjirsm.ac.cn
[b] Open Laboratory of Chirotechnology, Department of Applied Biology and Chemical Technology, The Hong Kong Polytechnic University,
Hong Hum, Hong Kong, China
Fax: (internat.) + 852-23649932
E-mail: bcachan@polyu.edu.hk

mers from flexible ligands is still a formidable challenge.[17]

In our previous studies we prepared a series of flexible organosulfur ligands by connecting (methylsulfanyl)pyridyl or -pyrimidyl groups to aromatic ring spacers.[18−21] Assembly of such flexible tectons and metal ions resulted in several unique structural motifs, such as a metallosupramolecular cube,[18] a one-dimensional nanotube,[19] square rings with guest molecules,[20] and two-dimensional crown-like structures.[20,21] Considering the geometric requirement of symmetry and stereochemistry, and with the aim of investigating the effects of distortion of the connector in the dipyridyl ligands on the assembly process and products, we have introduced a biphenyl connector into the reaction system and prepared two more flexible ligands, 2,2′-bis(3-pyridylmethyleneoxy)-1,1′-biphenylene (3,3′-bpp) and 2,2′-bis(4-pyridylmethyleneoxy)-1,1′-biphenylene (4,4′-bpp), in which the distortion of the biphenyl connector can endow the metal-organic frameworks with unique structural and functional properties.[22] Moreover, metal-organic complexes with a biphenyl connector can be used as simple probes for the investigation of chiral complexes derived from 1,1′-bi-2-naphthol.[23,24] Herein, we wish to report the syntheses and characterizations of two metallomacrocyclic complexes based on 3,3′-bpp — $[Zn_2(3,3'\text{-bpp})_2Cl_4]$ (**1**) and $[Zn_2(3,3'\text{-bpp})_2Br_4]$ (**2**) — and five novel coordination polymers based on 4,4′-bpp — $[Zn(4,4'\text{-bpp})Cl_2]_n$ (**3**), $[Zn(4,4'\text{-bpp})Br_2]_n$ (**4**), $[Co(4,4'\text{-bpp})_2(SCN)_2]_n$ (**5**), $[\{Cd(4,4'\text{-bpp})_2(SCN)_2\}\cdot 2H_2O]_n$ (**6**), and $[Cd(4,4'\text{-bpp})(dca)_2]_n$ (**7**) (dca^- = dicyanamide).

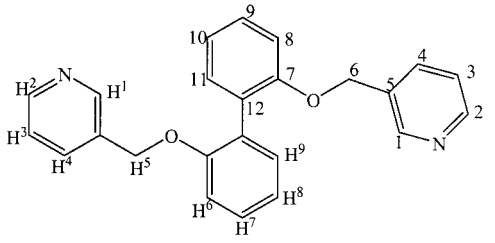

3,3'-bpp

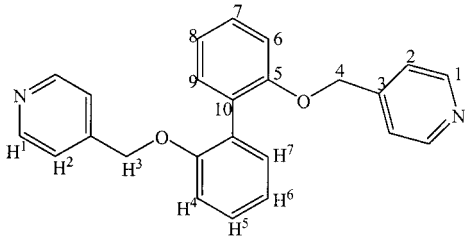

4,4'-bpp

Result and Discussion

Synthesis and Characterization

The ligands 3,3′-bpp and 4,4′-bpp are readily prepared from commercially available 2,2′-biphenol and 3-picolyl chloride hydrochloride or 4-picolyl chloride hydrochloride in the presence of NaOH by a convenient method. The ligands are soluble in most solvents, except for water. Treatment of 3,3′-bpp with $ZnCl_2$ or $ZnBr_2$ in a 1:1 molar ratio in $MeOH/H_2O$ for several hours produced large amounts of white precipitates of **1** and **2**, respectively, in quantitative yield. The elementary analysis results are consistent with dinuclear metallomacrocycles of formula $Zn_2(3,3'\text{-bpp})_2Cl_4$ and $Zn_2(3,3'\text{-bpp})_2Br_4$, respectively. Compounds **1** and **2** are poorly soluble in common solvents except for DMF and DMSO. Hence, ^1H NMR spectra were recorded in $[D_6]$DMSO; the results confirmed the proposed formula, displaying a symmetric pattern.

It is well known that the relative orientation of coordination sites in organic ligands is also one of the most important factors for controlling the construction of supramolecular architectures. Hence, it is expected that the relative different orientation of the nitrogen donors in the pyridyl rings might lead to unusual building blocks, whose assembly with metal ions can produce unique structural frameworks. Indeed, assembly of 4,4′-bpp with $ZnCl_2$ or $ZnBr_2$ in a 1:1 molar ratio generated the one-dimensional polymeric chain complexes **3** and **4**. The directed reaction of 4,4′-bpp and $ZnCl_2$ or $ZnBr_2$ in $MeOH/H_2O$ afforded precipitates that are not soluble in any solvents. The MeOH solution of 4,4′-bpp was layered on the top of an aqueous solution of $ZnCl_2$ or $ZnBr_2$, affording crystals suitable for X-ray single-crystal diffraction. Compounds **3** and **4** are insoluble in most common solvents. It is noteworthy that the Zn^{II} centers in **1**−**4** adopt a distorted tetrahedral coordination geometry, with two halide counteranions coordinating to a metal center as terminal ligands, preventing the formation of extended frameworks. This prompted us to choose either a metal ion with a high coordination number or bridging counteranions. Co^{II} and Cd^{II} are known to be usually six-coordinate with an octahedral geometry in their pyridyl-containing $Co(SCN)_2$ [25] and $Cd(SCN)_2$ [26] complexes. Reactions of 3,3′-bpp with Co^{II} and Cd^{II} with different counteranions failed to generate desirable single crystals, but we succeeded in the isolation of **5** and **6** by assembly of 4,4′-bpp with $Co(SCN)_2$ and $Cd(SCN)_2$ under the same reaction conditions. Interestingly, the metal centers demonstrate a similar coordination environment and the ligands possess the same coordination mode, although **5** and **6** represent two distinctly different structural motifs. Upon introducing the bridging dca^- ligand[27,28] into the reaction system, the three-dimensional complex **7**, consisting of dca−Cd layers and Cd-(4,4′-bpp) helical chains, was successfully isolated.

In the IR spectra of complexes **1**−**7**, the absorption bands of the skeletal vibrations of the aromatic rings appear in the 1420−1630 cm^{-1} region. The C≡N stretching vibration of the thiocyanate group in **5** and **6** appears as a single and very strong peak at 2075 and 2030 cm^{-1}, respectively, similar to those found in thiocyanate-*N* coordination.[24,25] The IR spectrum in complex **7** displays strong absorption bands in the 2170−1305 cm^{-1} region, indicating the presence of C≡N of dca^-.[27,28]

 © 2004 Wiley-VCH Verlag GmbH & Co. KGaA, Weinheim

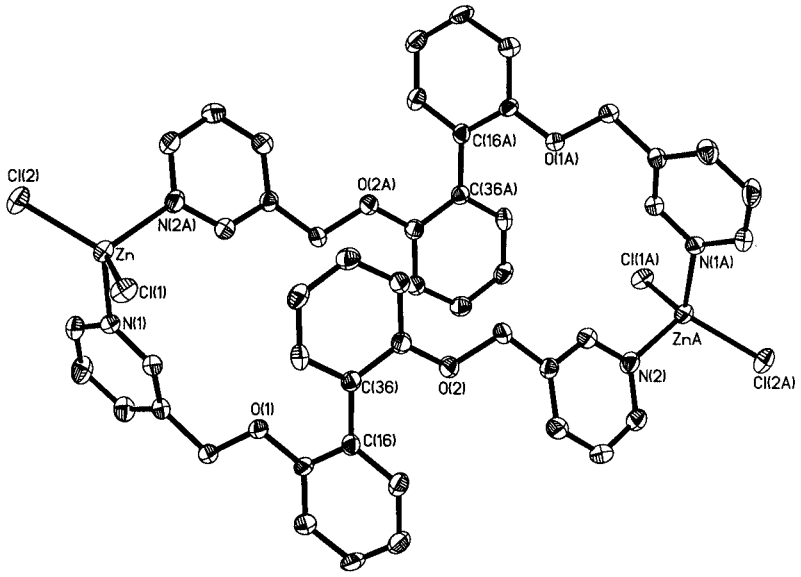

Figure 1. Molecular structure of complex **1** with the thermal ellipsoids at 30% probability level

Structural Description

$[Zn_2(3,3'\text{-bpp})_2Cl_4]$ (1)

The single-crystal X-ray diffraction analysis of **1** shows a neutral, dinuclear, metallacyclic structural motif with the Zn^{II} having a distorted tetrahedral geometry. As shown in Figure 1, each Zn^{II} is coordinated by two nitrogen atoms from different 3,3′-bpp and two terminal Cl^- ions. The Zn−N bond lengths are in the range 2.061(4)−2.070(5) Å, which are typical values for $Zn^{II}-N_{py}$ coordination distances.[29] The Cl(1)−Zn−Cl(2) bond angle [123.52(7)°] is larger than the N(1)−Zn−N(2A) bond angle [99.53(18)°], probably in order to minimize Cl···Cl interactions. The dihedral angle between the two pyridyl rings attached to Zn^{II} is 83.2°, which means that they are approximately perpendicular; 3,3′-bpp acts as an *exo*-bidentate ligand, where the pyridyl rings are slightly twisted with respect to the corresponding linking phenyl rings, with the dihedral angles between them being 24.7° and 26.5°, respectively. The two phenyl rings about the central bond have a drastic twisting, with the dihedral angle between them being 130.5°. The combination of these twistings allows 3,3′-bpp to link $ZnCl_2$ units into a dinuclear metallacycle. The Zn···Zn separation in the cycle is 14.015 Å, which is longer than in known zinc macrocycles.[29] Owing to the high distortion and flexibility of 3,3′-bpp, no enclathration of guest molecules is observed in **1**. There are no other noteworthy weak interactions between the adjacent macrocycles. Interestingly, every macrocycle has significant π−π interactions with its four closet neighbors. As shown in Figure 2, one phenyl ring of 3,3′-bpp and one pyridyl ring from the adjacent macrocycle are approximately parallel, with the dihedral angle between them being 24.7° and the distance between their centroids being 4.155 Å,[31] resulting in the formation of one-dimensional stacked macrocycles; the other phenyl ring of 3,3′-bpp and one phenyl ring from another adjacent macrocycle are completely parallel, with the distance between their centroids being 3.922 Å, further producing a layered network formed by stacked macrocycles.[32]

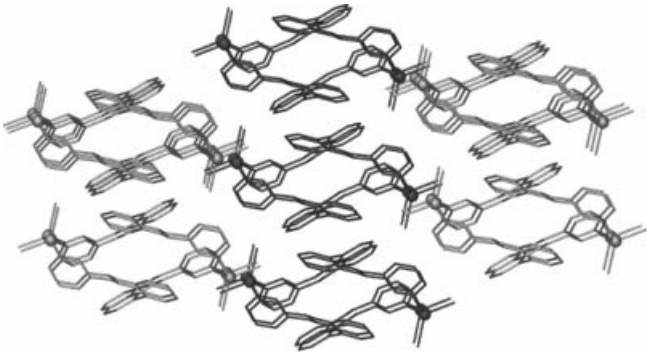

Figure 2. View of packing structure along *a* axis in **1** showing that there are no other interactions between adjacent macrocycles

$[Zn_2(3,3'\text{-bpp})_2Br_4]$ (2)

Compounds **1** and **2** are isomorphous, which suggests that the Br^- and Cl^- counteranions have no effect on the formation of the metallomacrocycle. As shown in Figure 3, Zn^{II} is coordinated by two nitrogen atoms from different 3,3′-bpp ligands and two terminal Br^- ligands in a distorted tetrahedral geometry. The Zn−N bond lengths and the N−Zn−N bond angle are 2.068(8)−2.085(9) Å and 98.6(3)°, respectively, similar to those in **1**. The dihedral angle of the two pyridyl rings coordinated to Zn^{II} is 81.0°. In the *exo*-bidentate 3,3′-bpp ligand, the dihedral angles between the two phenyl rings as well as between the phenyl rings and their corresponding linking pyridyl rings are 130.2, 28.5 and 26.1°, respectively. Thus, 3,3′-bpp connects $ZnBr_2$ units forming a dinuclear metallomacrocycle with a Zn···Zn separation of 14.113 Å. Similar to **1**, π−π interactions between every macrocycle and its four adjacent

 © 2004 Wiley-VCH Verlag GmbH & Co. KGaA, Weinheim

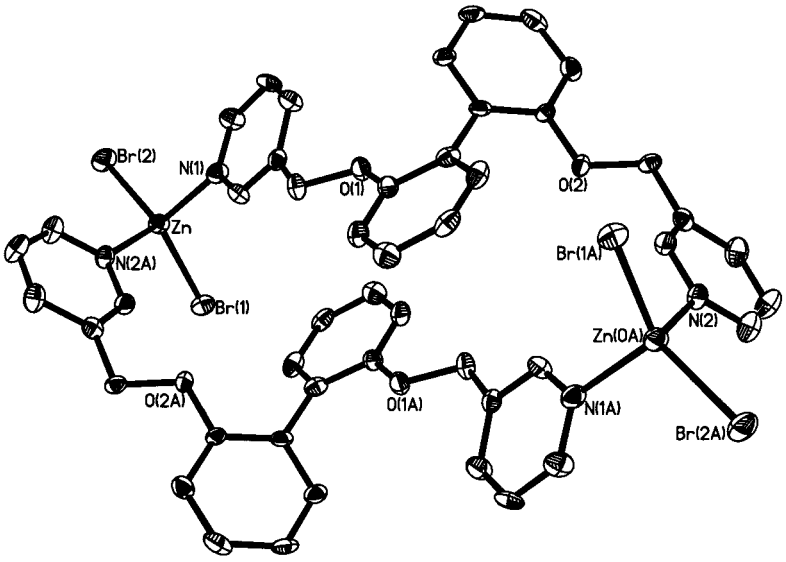

Figure 3. Molecular structure of complex **2** with the thermal ellipsoids at 30% probability level

macrocycles further stack it into a layered network structure.

$[Zn(4,4'\text{-bpp})Cl_2]_n$ (3)

The single-crystal X-ray structural analysis reveals that **3** is a one-dimensional zigzag chain formed through interconnection of $ZnCl_2$ units and 4,4′-bpp ligands. As shown in Figure 4, each Zn^{II} is coordinated by two nitrogen atoms from different 4,4′-bpp and two terminal Cl^- ligands in a distorted tetrahedral coordination environment. The Zn−N bond lengths are 2.041(5) and 2.057(4) Å, slightly shorter than those in **1**. However, the N(1)−Zn−N(2A) bond angle of 102.93(19)° is larger than that in **1**. All the 4,4′-bpp ligands behave in an *exo*-bidentate mode and lie on the same side of the polymer chain. The pyridyl rings are twisted with respcet to their corresponding linking phenyl rings, with the dihedral angles between them being 20.8 and 44.6°, respectively. The twisting angle of 76.2° between two phenyl rings about the central bond is smaller than those in **1** and **2**, which means that 4,4′-bpp connects the $ZnCl_2$ units into a one-dimensional polymeric chain instead of a macrocycle. The adjacent Zn···Zn separation bridged by 4,4′-bpp is 11.580 Å. It should be emphasized that there are significant π−π interactions between a pyridyl ring and the adjacent equivalent pyridyl rings from another chain (Figure 5); they are approximately parallel, with the dihedral angle between them being 12.9° and the distance between their centroids being 3.817 Å (Figure 6).[30] There are no other noteworthy weak interactions between the adjacent chains.

Figure 5. View of π−π interactions between the adjacent chains along the *c* axis in **3**

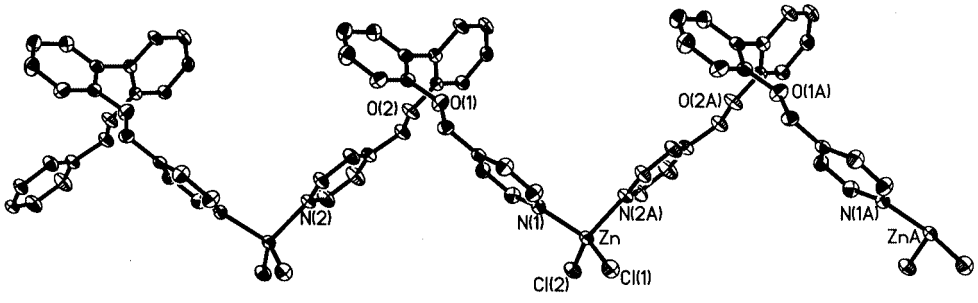

Figure 4. View of the one-dimensional polymeric chain in **3** with the thermal ellipsoids at 30% probability level

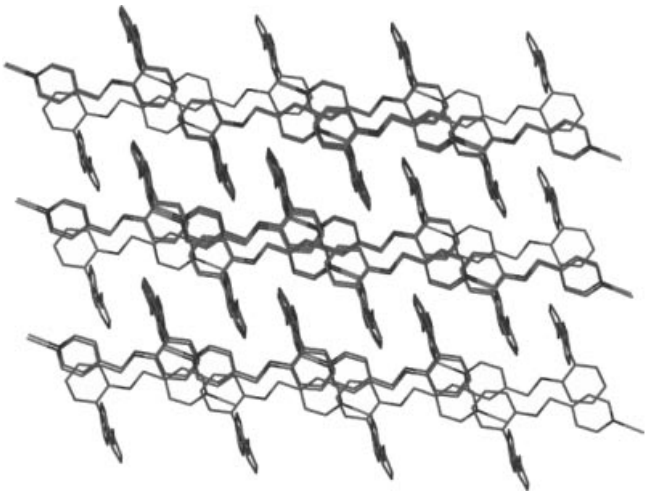

Figure 6. View of the packing structure along the *b* axis in complex **3**

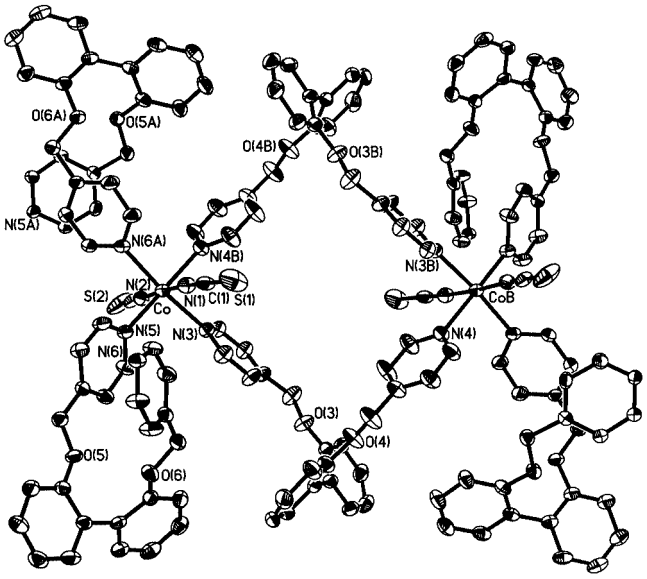

Figure 8. View of the folded rectangular box in **5** with the thermal ellipsoids at 30% probability level

$[Zn(4,4'\text{-bpp})Br_2]_n$ (4)

Compounds **3** and **4** are isomorphous. Zn^{II} is coordinated by two nitrogen atoms from different 4,4′-bpp and two terminal Br^- ligands in a distorted tetrahedral geometry. The Zn−N bond lengths and the N−Zn−N bond angles are 2.052(7)−2.069(7) Å and 101.5(1)°, respectively, similar to those in **3**. The Zn−Br bond lengths of 2.3512(15)−2.3560(13) Å and the Br(1)−Zn−Br(2) bond angle of 119.90(6)° are slightly smaller than their counterparts in **2**. An *exo*-bidentate 4,4′-bpp ligand bridges a pair of adjacent Zn^{II} centers on the same side forming a one-dimensional zigzag chain. The Zn···Zn separation bridged by 4,4′-bpp is 11.688 Å; π−π interaction between the pyridyl ring and an adjacent pyridyl ring from another chain stacks the polymeric chains into a network architecture (Figure 7).

$[Co(4,4'\text{-bpp})_2(SCN)_2]_n$ (5)

The single-crystal X-ray diffraction analysis reveals that **5** is a two-dimensional polymer consisting of folded rectangular boxes (Figure 8) and zigzag chains (Figure 9) bridged by Co^{II}. As shown in Figure 8, each Co^{II} has a compressed octahedral coordination environment with four pyridyl nitrogen atoms from different 4,4′-bpp situated in the equatorial plane and two *trans*-thiocyanato nitrogen atoms at the axial positions. The four pyridyl units associated with Co^{II} are arranged in a propeller fashion. The Co^{II} is approximately coplanar with the mean plane of four equatorial pyridyl nitrogen atoms, with a deviation of 0.0116 Å towards the axial donor atoms. The $Co-N_{py}$ bond lengths range from 2.162(5) to 2.239(5) Å [av. 2.201(5) Å], which are longer than the $Co-N_{NCS}$ bond lengths of 2.062(5) and 2.080(6) Å [av. 2.071(6) Å]. The SCN^- groups are almost linear, with N(1)−C(1)−S(1) and N(2)−C(2)−S(2) bond angles of 179.7(6) and 178.6(7)°, respectively. The connections between Co^{II} and SCN^- groups are slightly bent, with C(1)−N(1)−Co and C(2)−N(2)−Co bond angles of 170.1(6) and 174.7(5)°, respectively, suggesting that the two SCN^- ligands are not perpendicular to the equatorial plane. Interestingly, there are two independent 4,4′-bpp ligands in this complex, one bridges two Co^{II} centers forming a folded rectangular box of two planes.[24] The Co···Co separation within the box is 11.446 Å. This type of box is similar to that constructed by dipyridyl ligands with a 1,1′-bi-2-naphthol connector and $[Pt(dppp)(OSO_2CF_3)_2]$[24] [dppp = 1,3-bis(diphenylphosphanyl)propane] and very different from the common rectangular boxes derived from other *exo*-bidentate pyridyl-

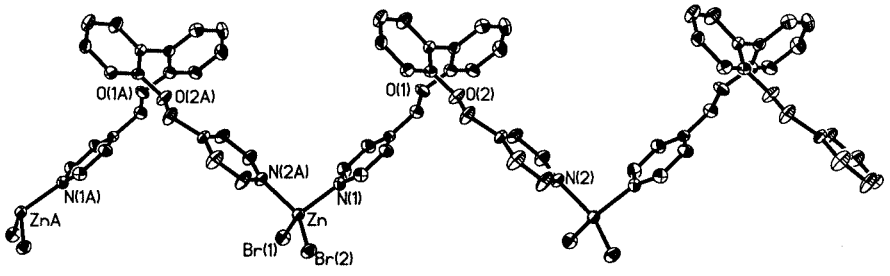

Figure 7. View of the one-dimensional polymeric chain in **4** with the thermal ellipsoids at 30% probability level

 © 2004 Wiley-VCH Verlag GmbH & Co. KGaA, Weinheim

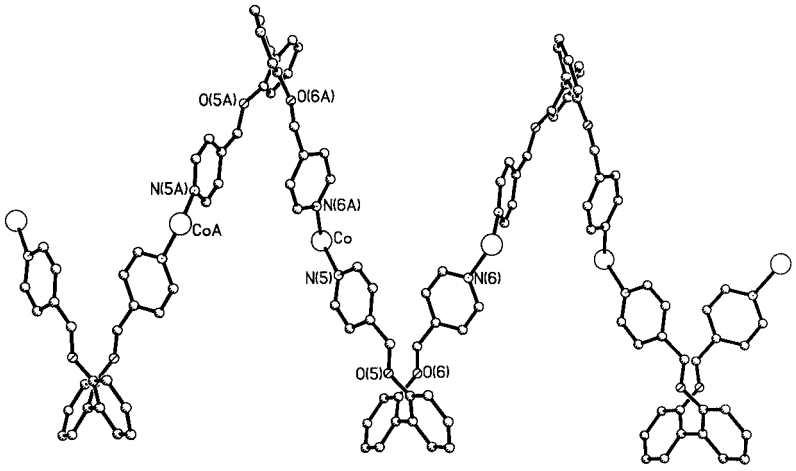

Figure 9. View of the zigzag chains in **5**

containing ligands.[31] In the 4,4′-bpp ligand the dihedral angle between the two phenyl rings is 65.6°. The dihedral angle of 50.8° between the two phenyl rings in the other independent 4,4′-bpp unit is smaller than that in the former and those in complexes **3** and **4**, which results in 4,4′-bpp linking two adjacent Co^{II} into a one-dimensional zigzag chain. Different from **3** and **4**, the 4,4′-bpp ligands lie on different sides of the zigzag chain. The closest Co···Co separation in the zigzag chain is 8.032 Å, which is much shorter than those in the zigzag chains of **3** and **4**. The most intriguing feature in **5** is that rectangular boxes and zigzag chains are fused into a two-dimensional polymer through $Co(NCS)_2$ units (Figure 10). To the best of our knowledge, this type of complex containing folded rectangular boxes and zigzag chains is unprecedented, which suggests that the distortion of the biphenyl connector has a great effect on the construction of novel structural motifs (Figure 11).

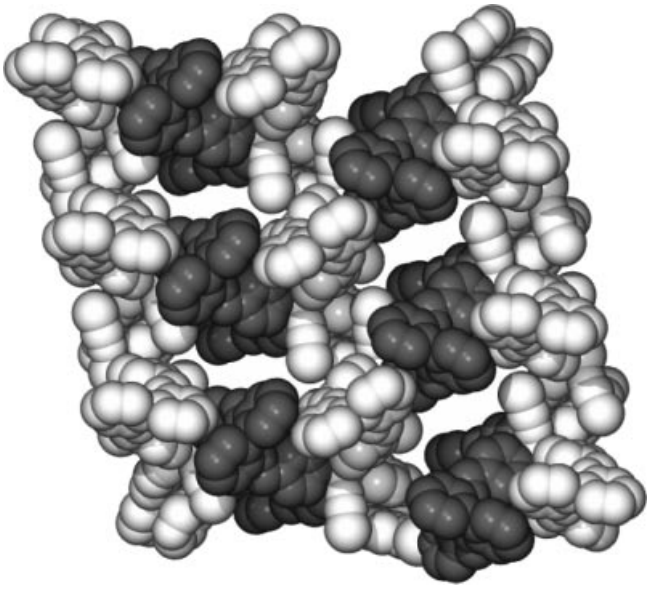

Figure 10. The two-dimensional structure formed by the folded rectangular boxes and zigzag chains in **5**

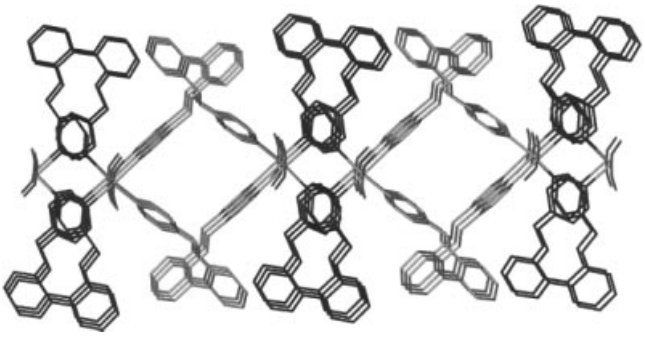

Figure 11. The packing structure along the *b* axis in **5** showing the linkage of the folded rectangular boxes and zigzag chains

$[\{Cd(4,4'\text{-bpp})_2(SCN)_2\}\cdot 2H_2O]_n$ (6)

Complex **6** is a polycatenated species[6] whose structure is made up of inclined interpenetrated two-dimensional layers. Each layer is composed of an alternating assembly of left-hand (*M*) and right-hand (*P*) cylindrical 2_1 helices along the *b* axis.[32] As shown in Figure 12, the coordination sphere of Cd^{II} is defined by four pyridyl nitrogen atoms from different 4,4′-bpp ligands situated in the equatorial plane and two *trans*-thiocyanato nitrogen atoms at the axial positions, resulting in a compressed octahedral coordination environment. The Cd^{II} is displaced 0.0240 Å out of the equatorial plane. The $Cd-N_{py}$ and $Cd-N_{SCN}$ bond lengths are in the range 2.379(5)−2.405(5) Å [av. 2.390(5) Å] and 2.308(7)−2.329(6) Å [av. 2.319(7) Å], respectively. The SCN^- groups are almost linear, with N(1)−C(1)−S(1) and N(2)−C(2)−S(2) bond angles of 177.9(9) and 174.0(8)°, respectively. The two SCN^- groups are not perpendicular to the equatorial plane and the C(1)−N(1)−Cd and C(2)−N(2)−Cd bond angles are 135.3(6) and 139.6(6)°,

 © 2004 Wiley-VCH Verlag GmbH & Co. KGaA, Weinheim

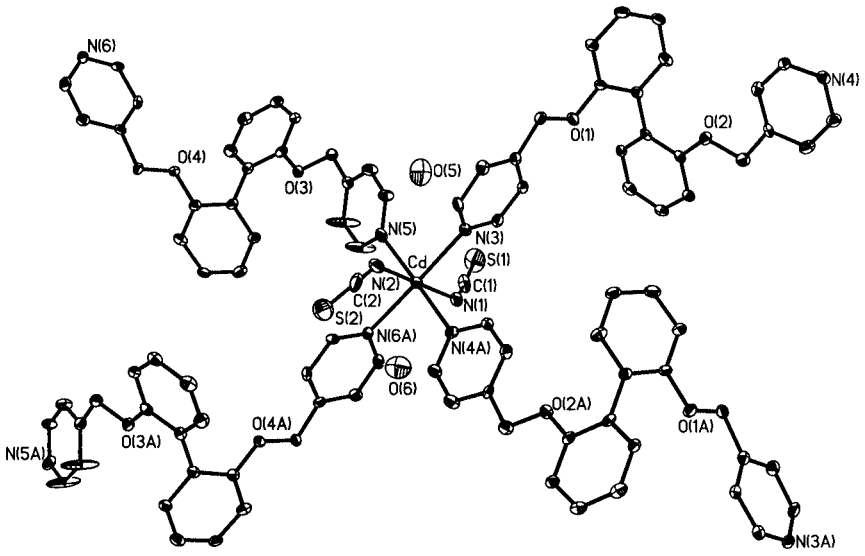

Figure 12. View of the coordination environment of Cd^{II} in **6** with the thermal ellipsoids at 30% probability level

respectively. These values are similar to those in complex **5**. It should be emphasized that there are two independent 4,4′-bpp ligands in this complex, one of which bridges six-coordinate Cd^{II} forming an (*M*) helical column (Figure 13). The repeating period in the helical column is 17.050 Å, which is slightly longer than the Cd···Cd distance bridged by 4,4′-bpp (16.590 Å). In the 4,4′-bpp ligand the dihedral angles between phenyl rings and their corresponding linking pyridyl rings are 23.3 and 6.0°, respectively. A drastic twisting is observed between two phenyl rings, with a dihedral angle of 116.9°, which is much larger than those in **3**−**5** and leads to the formation of the helical column. Interestingly, the other *cis* ligand coordinates to Cd^{II} and forms a (*P*) helical column (Figure 13). The distance of the helical pitch and Cd···Cd separation bridged by 4,4′-bpp are 17.050 and 16.668 Å, respectively. In the 4,4′-bpp ligand the dihedral angles between the two phenyl rings as well as between the phenyl rings and their corresponding linking pyridyl rings are 118.1, 32.9 and 10.9°, respectively, which are slightly different from the other 4,4′-bpp ligand These two types of cylindrical columns are alternatively connected, with the $Cd(SCN)_2$ units functioning as hinges, forming a unique two-dimensional layer structure (Figures 14 and 15). It should be emphasized that the longer helical pitch and the 4,4′-bpp ligands result in the formation of larger void cavities in the two-dimensional network, which greatly exceeds that required to accommodate the guest molecules in the reaction system. Thus, instead of forming an open, microporous structure, the potential voids are filled by mutually inclined interpenetration of identical two-dimensional frameworks (Figure 16). Uncoordinated water molecules act as guest molecules and further fill in its space.

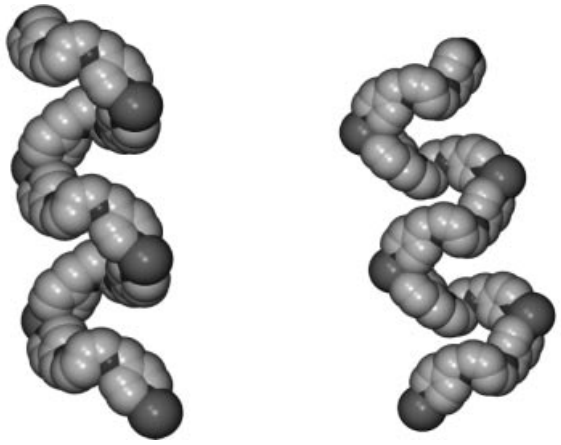

Figure 13. View of the left-hand and right-hand cylindrical 2_1 helices in **6** with uncoordinated water molecules omitted for clarity

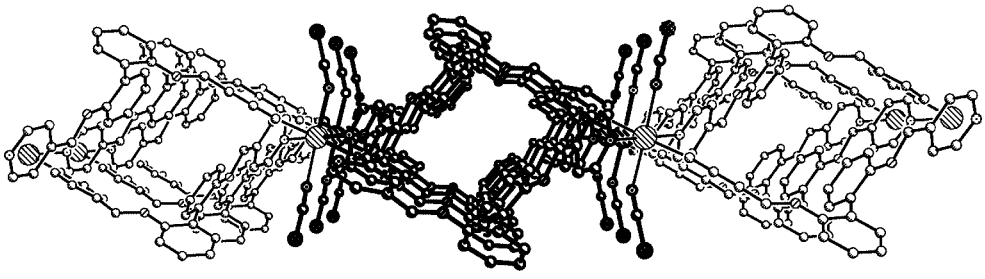

Figure 14. View of the two-dimensional layer along the *b* axis in **6** with uncoordinated water molecules omitted for clarity

 © 2004 Wiley-VCH Verlag GmbH & Co. KGaA, Weinheim

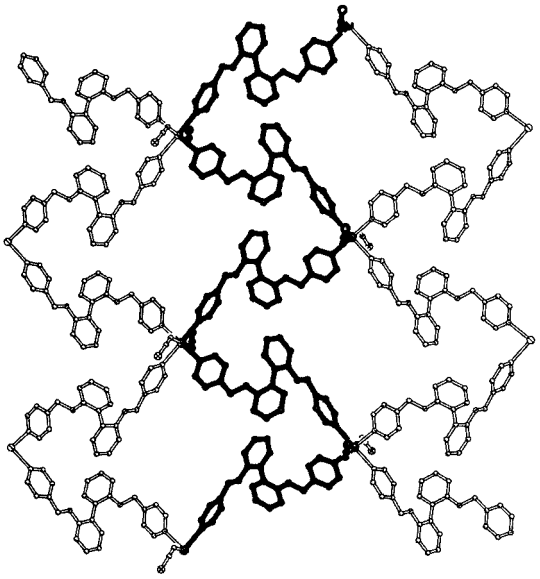

Figure 15. Packing structure along the *c* axis in **6** with uncoordinated water molecules omitted for clarity

Although there have been many helical coordination polymers reported, to the best our knowledge this type of helix-assembled polycatenated motif is unprecedented.

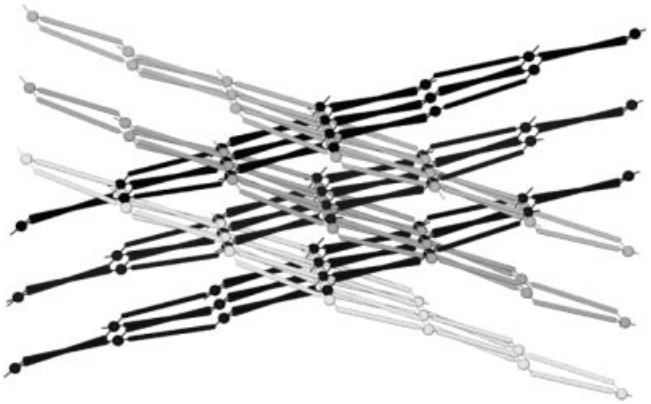

Figure 16. Packing structure of the inclined interpenetrating two-dimensional layers in **6** with partial atoms omitted for clarity

$[Cd(4,4'\text{-bpp})(dca)_2]_n$ (7)

Complex **7** consists of two-dimensional $Cd(dca)_2$ layers bridged by 4,4′-bpp ligands. As shown in Figure 17, Cd^{II} is coordinated by six nitrogen atoms in a distorted octahedral geometry, in which four nitrogen atoms from different dca^- ligands form the equatorial plane, and two pyridyl nitrogen atoms from different 4,4′-bpp occupy the apical positions. The $Cd-N_{dca}$ and $Cd-N_{py}$ bond lengths are in the range 2.317(6)−2.475(7) Å [av. 2.367(7) Å] and 2.321(6)−2.352(7) Å [av. 2.337(7) Å], respectively; dca^- has two distinctly different bridging modes: one adopts a usual end-to-end μ-1,5 bridging mode,[27] and the other acts as a rare μ-1,3 bridge through a terminal nitrile nitrogen atom and the middle nitrogen atom.[28] These two types of dca^- bridge Cd^{II} to form a neutral two-dimensional layer structure (Figure 18). The Cd···Cd separations bridged by μ-1,5- and μ-1,3-dca^- are 7.725 and 6.050 Å, respectively. The 4,4′-bpp ligand acts as an *exo*-bidentate ligand; the dihedral angle between two phenyl rings is 131.6°. However, the dihedral angles between the phenyl rings and their corresponding linking pyridyl rings are 10.1 and 19.1°, respectively. As a result, the 4,4′-bpp ligands are situated at two sides of the layers to saturate the six-coordinate Cd^{II} center and connect the Cd−dca layers into a three-dimensional network. It is note-

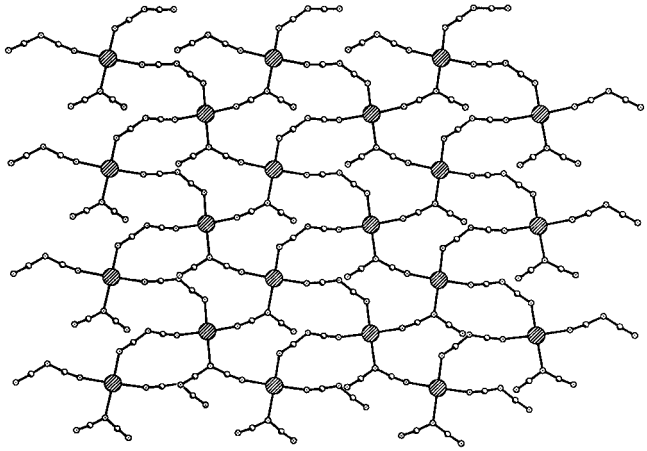

Figure 18. The two-dimensional layer formed by dca^- and Cd^{II} along the *c* axis in **7**

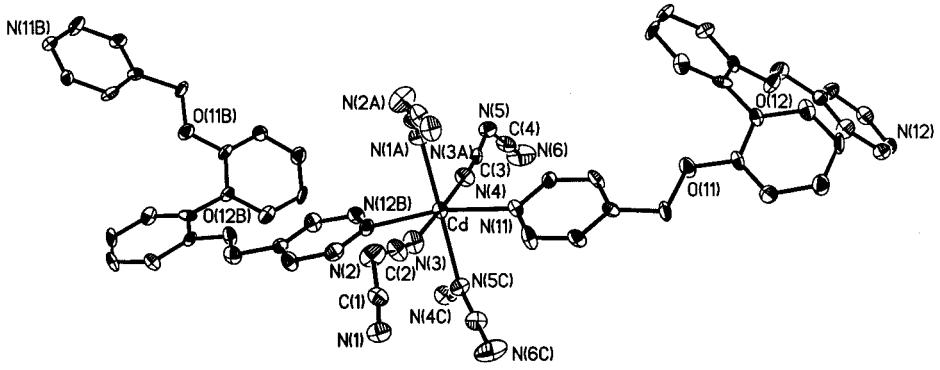

Figure 17. View of the coordination environment of Cd^{II} in **7** with the thermal ellipsoids at 30% probability level

 © 2004 Wiley-VCH Verlag GmbH & Co. KGaA, Weinheim

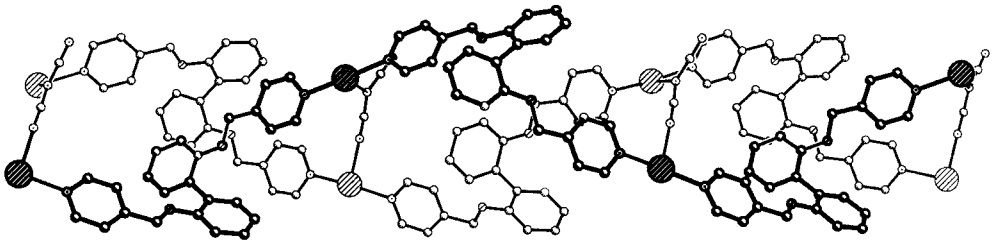

Figure 19. (*M*)- (light) and (*P*)-Cd-(4,4′-bpp) (dark) helical chains bridged by μ-1,3-dca in **7**

worthy that the 4,4′-bpp ligands bridge Cd^{II} to form (*M*) and (*P*) helical chains (Figure 19). Different from **6**, the adjacent (*M*) and (*P*) helical chains are connected by μ-1,3-dca ligands instead of metal centers. The distance of the helical pitch and Cd···Cd distance bridged by 4,4′-bpp are 29.629 and 15.697 Å, respectively. Hence, complex **7** can be regarded as the fusion of two-dimensional $Cd(dca)_2$ layers with (*M*)- and (*P*)-Cd-(4,4′-bpp) helical chains through Cd^{II} centers (Figure 20).

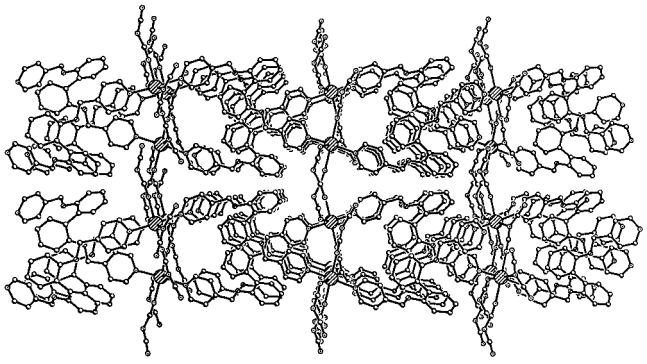

Figure 20. Packing structure along the *a* axis in **7** showing the linkage of the helical chains and the two-dimensional layer

It should be interesting and essential to compare the related structural data of 3,3′-bpp and 4,4′-bpp in complexes **1**−**7**. As suggested in Table 1, the twisting angles of the biphenyl connector about the central bond in 3,3′-bpp and 4,4′-bpp are responsible for the formation of the structural motifs. Owing to the steric hindrance from the relative orientation of the coordination sites in the pyridyl rings, 3,3′-bpp and 4,4′-bpp bridge $ZnCl_2$ or $ZnBr_2$ units generating metallomacrocycles and one-dimensional zigzag chains with 4,4′-bpp at the same sides, respectively. The distortion angles of the biphenyl connector in 3,3′-bpp (130.5° for **1** and 130.2° for **2**) are much larger than those in 4,4′-bpp (76.2° for **3** and 79.6° for **4**); however, the distortion angles of the biphenyl connector of 50.8 and 65.6° in 4,4′-bpp in **5**, which are smaller than those in the polymeric chains of **3** and **4**, lead to the formation of a one-dimensional zigzag chain with 4,4′-bpp at two sides and a folded rectangular box, respectively. When the distortion angles of the biphenyl connector in 4,4′-bpp increase to 116.9 and 118.1°, cylindrical 2_1 helical structures are generated. The largest distortion angle of the biphenyl connector in 4,4′-bpp (131.6°) results in a one-dimensional helical chain in complex **7**. Correspondingly, the dihedral angles between the phenyl rings and linking pyridyl rings are different in each type of structural motif. In the zigzag chain with 4,4′-bpp at two sides, the smallest twisting angle of the biphenyl connector in 4,4′-bpp (50.8°) results in the shortest distance between the metal centers bridged by 4,4′-bpp (8.032 Å) in **5**; the longest distance is found in the right-handed cylindrical 2_1 helix (16.668 Å) of complex **6**. It should be emphasized that the two phenyl rings in free 4,4′-bpp can rotate freely about the central bond, but the rotation is restricted in metal-organic complexes because of pyridyl-*N* coordination; consequently, this restricted rotation gives rise to two confor-

Table 1. Comparison of the structural data from 3,3′-bpp or 4,4′-bpp in **1**−**7**

Compound	Ligand	Dihedral angles [°]			Distance between metal centers bridged by ligand [Å]	Structure
		[a]	[b]	[c]		
1	3,3′-bpp	130.5	24.7 and 26.5	83.2	14.015	dimetallomacrocycle
2	3,3′-bpp	130.2	26.1 and 28.5	81.0	14.113	dimetallomacrocycle
3	4,4′-bpp	76.2	20.8 and 44.6	76.0	11.580	1D polymeric chain
4	4,4′-bpp	79.6	15.1 and 42.8	77.7	11.688	1D polymeric chain
5	4,4′-bpp	65.6	21.6 and 45.3	74.9	11.446	folded rectangular box
	4,4′-bpp	50.8	24.1 and 49.5	77.4	8.032	1D zigzag chain
6	4,4′-bpp	116.9	23.3 and 6.0	80.8	16.590	(*M*) cylindrical 2_1 helix
	4,4′-bpp	118.1	32.9 and 10.9	89.3	16.668	(*P*) cylindrical 2_1 helix
7	4,4′-bpp	131.6	10.1 and 19.1	18.6	15.697	1D helical chain

[a] Biphenyl connector in the ligand. [b] Between the phenyl ring and the corresponding linking pyridyl ring. [c] Between two pyridyl rings at the metal center.

 © 2004 Wiley-VCH Verlag GmbH & Co. KGaA, Weinheim

mations [(*M*) and (*P*)] in complexes **6** and **7**.[22] Therefore, the flexibility of ligands, the coordination propensity of metal ions and the secondary ligands play important roles in the formation of the final networks, meaning that the structural topologies of complexes **5**, **6**, and **7** are unusual.

Conclusions

Seven novel metal-organic complexes containing the flexible dipyridyl ligands 2,2′-bis(3-pyridylmethyleneoxy)-1,1′-biphenylene (3,3′-bpp) and 2,2′-bis(4-pyridylmethyleneoxy)-1,1′-biphenylene (4,4′-bpp) have been prepared and structurally characterized. In complexes **1**−**4**, *exo*-bidentate 3,3′-bpp and 4,4′-bpp ligands link ZnX_2 (X = Cl^- and Br^-) units into dinuclear metallomacrocycles and one-dimensional zigzag chains, respectively, in which the metal centers adopt a distorted tetrahedral geometry. This reveals that the relative orientation of the nitrogen donors in the pyridyl rings has a great influence on the construction of the supramolecular architectures. The metal centers in both **5** and **6** all have a compressed octahedral geometry, although $Co(SCN)_2$ and $Cd(SCN)_2$ hinges fuse one-dimensional zigzag chains and folded rectangular boxes as well as left-handed and right-handed cylindrical 2_1 helices into two distinctly different two-dimensional networks. The topological differences in complexes **3**−**6** are attributed to the different geometric requirement of the metal ions. The results of structural analyses of **3**−**6** containing 4,4′-bpp reveal that their structures mainly depend on the geometric requirement of the metal ions and are not influenced greatly by the counteranions, which only act as terminal ligands. The introduction of bridging dca^- counteranions into the reaction system produces a three-dimensional complex **7**, in which 4,4′-bpp functions as a bridge between the adjacent Cd−dca layers. Such differences in **1**−**7** are realized through the distortion of the biphenyl connector in 3,3′-bpp and 4,4′-bpp. In summary, this research shows that assembly of dipyridyl ligands with a biphenyl connector and metal ions can generate unique structural motifs, which cannot be obtained using normal rigid or flexible *exo*-bidentate organic ligands, such as 4,4′-bipy and related organic ligands. In this regard, we are currently using these results as probes for axial chiral ligands derived from 1,1′-bi-2-naphthol and extending our research to prepare chiral supramolecular species.

Experimental Section

General: 2,2′-Biphenol, 3-picolyl chloride hydrochloride and 4-picolyl chloride hydrochloride were purchased from Acros. All other chemicals are commercially available and were used as purchased without further purification. The NMR spectra were recorded with a Varian Inova-500 spectrophotometer at room temperature and the chemical shifts are quoted in δ (ppm) relative to the deuterated solvent used. The mass spectra were recorded in the Mass Spectrometry Laboratory of the Department of Applied Biology and Chemical Technology, The Hong Kong Polytechnic University with a Fisons VG platform. The IR spectra as KBr disks were recorded with a Magna 750 FT-IR spectrophotometer. C, H and N elemental analyses were determined with an Elementary Vario ELIII elemental analyzer.

Synthesis of 3,3′-bpp: A mixture of 2,2′-biphenol (1.86 g, 10 mmol), 3-picolyl chloride hydrochloride (3.61 g, 22 mmol) and NaOH (1.76 g, 44 mmol) in acetone (50 mL) was stirred at reflux under nitrogen for 3 d. After cooling to room temperature, the inorganic salt was removed by filtration and washed with acetone several times. The combined solutions were concentrated under reduced pressure and the red residue was dissolved in ethyl acetate and then washed twice with water and once with brine. The organic layer was dried with anhydrous Na_2SO_4 and filtered. After removal of the solvent under reduced pressure, the residue was purified by chromatography on silica gel to afford a colorless solid. Yield: 3.24 g (88% based on 2,2′-biphenol). ^{1}H NMR (500 MHz, $CDCl_3$): δ = 8.44 (d, J = 3.0 Hz, 2 H, H^2), 8.38 (s, 2 H, H^1), 7.40 (d, J = 7.5 Hz, 2 H, H^4), 7.30−7.34 (m, 2 H, H^3), 7.29 (d, J = 1.5 Hz, 2 H, H^9), 7.04−7.11 (m, 4 H, H^7, H^8), 7.00 (d, J = 8.5 Hz, 2 H, H^6), 4.96 (s, 4 H, H^5) ppm. ^{13}C NMR ($CDCl_3$, 125 MHz): δ = 155.6 (C^7), 148.7 (C^1), 148.0 (C^2), 134.4 (C^4), 132.7 (C^5), 131.4(C^{12}), 128.7(C^9, C^{11}), 123.1 (C^3), 121.2 (C^{10}), 112.9 (C^8), 67.9 (C^6) ppm. ES-MS: m/z = 368 [M^+ + 1]. HRMS: calcd for $C_{24}H_{20}N_2O_2$ [M^+ + 1]: m/z = 368.4342; found 368.4345.

Synthesis of 4,4′-bpp: The procedure was similar to the synthesis of 3,3′-bpp except that 4-picolyl chloride hydrochloride was used instead of 3-picolyl chloride hydrochloride. Yield: 2.75 g (75% based on 2,2′-biphenol). ^{1}H NMR (500 MHz, $CDCl_3$): δ = 8.37 (d, J = 6.0 Hz, 4 H, H^1), 7.27 (d, J = 7.5 Hz, 4 H, H^2), 7.04 (d, J = 7.0 Hz, 2 H, H^9), 6.97 (d, J = 5.5 Hz, 4 H, H^6 and H^8), 6.88 (d, J = 7.5 Hz, 2 H, H^7), 4.92 (s, 4 H, H^5) ppm. ^{13}C NMR ($CDCl_3$, 125 MHz): δ = 155.7 (C^5), 149.8 (C^1), 146.6 (C^3), 131.7 (C^7), 129.0 (C^{10}), 128.5 (C^9), 121.5 (C^8), 121.0 (C^2), 112.6 (C^6), 68.5 (C^4) ppm. ES-MS: m/z = 368 [M^+ + 1]. HRMS: calcd for $C_{24}H_{20}N_2O_2$ [M^+ + 1]: m/z = 368.4342; found 368.4349.

Synthesis of [Zn_2(3,3′-bpp)$_2Cl_4$] (1): A solution of $ZnCl_2$ (0.034 g, 0.25 mmol) in H_2O (10 mL) was slowly added to a stirring solution of 4,4′-bpp (0.092 g, 0.25 mmol) in MeOH (10 mL) to give a white precipitate. The reaction mixture was heated to 60 °C and DMF was added dropwise (about 1 mL) until the precipitate dissolved. The resulting solution was filtered and kept in air at room temperature for two weeks. Colorless crystals of **1** suitable for X-ray diffraction were obtained. Yield: 0.08 g (63%). $C_{24}H_{20}Cl_2N_2O_2Zn$ (504.69): calcd. C 57.11, H 3.96, N 5.55; found C 57.09, H 4.98, N 5.57. ^{1}H NMR (500 MHz, $CDCl_3$): δ = 8.44 (s, 4 H), 8.42 (s, 4 H), 7.58 (d, J = 7.5 Hz, 4 H), 7.33 (t, J = 7.5 Hz, 15 Hz, 4 H), 7.27−7.29 (m, 4 H), 7.23 (dd, J = 2.0, 7.5 Hz, 4 H), 7.16 (d, J = 8.0 Hz, 4 H), 7.02 (t, J = 7.0 Hz, 14 Hz, 4 H), 5.10 (s, 8 H) ppm. IR (KBr pellet): $\tilde{\nu}$ = 3121 cm^{-1} (vw), 3047 (w), 2913 (vw), 2858 (w), 1614 (m), 1593 (m), 1564 (w), 1504 (w), 1482 (s), 1456 (m), 1436 (s), 1431 (s), 1387 (m), 1335 (w), 1265 (s), 1234 (s), 1194 (m), 1163 (w), 1125 (s), 1057 (m), 1032 (s), 1002 (m), 933 (vw), 867 (w), 814 (w), 796 (m), 766 (s), 697 (m), 658 (m), 642 (w), 613 (vw), 540 (vw), 486 (vw), 453 (vw).

Synthesis of [Zn_2(3,3′-bpp)$_2Br_4$] (2): The procedure was similar to the synthesis of complex **1** except that $ZnBr_2$ (0.056 g, 0.25 mmol) was used instead of $ZnCl_2$. Yield: 0.10 g (67%). $C_{24}H_{20}Br_2N_2O_2Zn$ (593.61): calcd. C 48.56, H 3.37, N 4.72; found C 48.52, H 3.40, N 4.70. ^{1}H NMR (500 MHz, $CDCl_3$): δ = 8.44 (s, 4 H), 8.43 (s, 4 H), 7.58 (d, J = 7.0 Hz, 4 H), 7.33 (t, J = 8.5 Hz, 17 Hz, 4 H), 7.28−7.31 (m, 4 H), 7.23 (d, J = 6.0 Hz, 4 H), 7.16 (d, J = 7.0 Hz,

 © 2004 Wiley-VCH Verlag GmbH & Co. KGaA, Weinheim

4 H), 7.02 (t, J = 7.0 Hz, 14 Hz, 4 H), 5.10 (s, 8 H) ppm. IR (KBr pellet): $\tilde{\nu}$ = 3121 cm^{-1} (vw), 3045 (w), 2910 (w), 2858 (w), 1614 (m), 1595 (m), 1563 (vw), 1504 (w), 1483 (s), 1458 (m), 1437 (s), 1385 (m), 1335 (w), 1284 (w), 1263 (s), 1232 (s), 1194 (m), 1165 (w), 1124 (s), 1057 (m), 1034 (s), 1020 (m), 1001 (m), 933 (vw), 912 (vw), 866 (w), 793 (m), 764 (s), 698 (s), 658 (m), 615 (vw), 544 (vw), 486 (vw), 454 (vw).

Synthesis of $[Zn(4,4'\text{-bpp})Cl_2]_n$ (3): A solution of 4,4′-bpp (0.037 g, 0.1 mmol) in MeOH (5 mL) was carefully layered on top of a solution of $ZnCl_2$ (0.014 g, 0.1 mmol) in H_2O (5 mL). Diffusion between the two phases over a period of two weeks produced colorless crystals. Yield: 0.04 g (79%). $C_{24}H_{20}Cl_2N_2O_2Zn$ (504.69): calcd. C 57.11, H 3.96, N 5.55; found C 57.07, H 4.02, N 5.53. IR (KBr pellet): $\tilde{\nu}$ = 3121 cm^{-1} (vw), 3052 (w), 2916 (w), 2852 (w), 1624 (s), 1593(m), 1563 (w), 1504 (m), 1481 (m), 1450 (s), 1436 (s), 1390 (m), 1329 (vw), 1306 (m), 1265 (s), 1234 (s), 1163 (vw), 1121 (m), 1057 (m), 1032 (s), 1005 (w), 933 (vw), 866 (w), 814 (s), 786 (m), 752 (s), 642 (w), 613 (vw), 486 (w), 453 (vw).

Synthesis of $[Zn(4,4'\text{-bpp})Br_2]_n$ (4): The procedure was similar to the synthesis of complex **3** except that $ZnBr_2$ (0.023 g, 0.1 mmol) was used instead of $ZnCl_2$. Yield: 0.05 g (84%). $C_{24}H_{20}Br_2N_2O_2Zn$ (593.61): calcd. C 48.56, H 3.37, N 4.72; found C 48.51, H 3.39, N 4.68. IR (KBr pellet): $\tilde{\nu}$ = 3121 cm^{-1} (vw), 3062 (w), 2910 (w), 2856 (w), 1624 (s), 1593 (m), 1563 (w), 1504 (s), 1481 (s), 1440 (s), 1431 (s), 1387 (s), 1328 (w), 1284 (s), 1267 (s), 1234 (s), 1158 (w), 1121 (s), 1056 (s), 1030 (s), 1005 (m), 933 (vw), 912 (vw), 864 (w), 829 (w), 810 (s), 770 (s), 750 (s), 717 (w), 641 (m), 613 (vw), 544 (vw), 513 (vw), 486 (w), 454 (w).

Synthesis of $[Co(4,4'\text{-bpp})_2(SCN)_2]_n$ (5): The procedure was similar to the synthesis of complex **3** except that $Co(NO_3)_2{\cdot}6H_2O$ (0.029 g, 0.1 mmol) and NH_4SCN (0.015 g, 0.2 mmol) were used instead of $ZnCl_2$. Yield: 0.04 g (88% based on 4,4′-bpp). $C_{50}H_{40}CoN_6O_4S_2$ (911.93): calcd. C 65.85, H 4.39, N 9.21; found C 65.82, H 4.42, N 9.18. IR (KBr pellet): $\tilde{\nu}$ = 3423 cm^{-1} (w), 3064 (w), 2914 (w), 2854 (w), 2075 (vs), 1618 (s), 1595 (m), 1564 (w), 1504 (m), 1483 (m), 1441 (s), 1421 (s), 1385 (m), 1325 (w), 1271 (s), 1225 (s), 1163 (vw), 1113 (m), 1057 (m), 1016 (m), 939 (vw), 810 (m), 762 (s), 634 (w), 618 (vw), 494 (w).

Synthesis of $[\{Cd(4,4'\text{-bpp})_2(SCN)_2\}{\cdot}2H_2O]_n$ (6): The procedure was similar to the synthesis of complex **3** except that $Cd(NO_3)_2{\cdot}6H_2O$ (0.031 g, 0.1 mmol) and NH_4SCN (0.015 g, 0.2 mmol) were used instead of $ZnCl_2$. Yield: 0.04 g (80% based on 4,4′-bpp). $C_{50}H_{44}CdN_6O_6S_2$ (1001.4): calcd. C 59.96, H 4.39, N 8.39; found C 59.91, H 4.37, N 8.32%. IR (KBr pellet): $\tilde{\nu}$ = 3435 cm^{-1} (w), 3120 (w), 2914 (w), 2852 (w), 2033 (vs), 1615 (s), 1596 (m), 1562 (w), 1504 (w), 1479 (m), 1436 (s), 1423 (s), 1399 (m), 1324 (vw), 1269 (m), 1231 (s), 1161 (vw), 1126 (m), 1062 (m), 1013 (m), 939 (vw), 814 (m), 751 (m), 635 (w), 619 (vw), 486 (w).

Synthesis of $[Cd(4,4'\text{-bpp})(dca)_2]_n$ (7): The procedure was similar to the synthesis of complex **3** except that $Cd(NO_3)_2{\cdot}4H_2O$ (0.031 g, 0.1 mmol) and $Na(dca)_2$ (0.018 g, 0.2 mmol) were used instead of $ZnCl_2$. Yield: 0.05 g (82%). $C_{28}H_{20}CdN_8O_2$ (612.92): calcd. C 54.87, H 3.26, N 18.27; found C 54.85, H 3.29, N 18.25. IR (KBr pellet): $\tilde{\nu}$ = 3529 cm^{-1} (w), 3061 (w), 2916 (w), 2891 (w), 2845 (w), 2305 (s), 2258 (s), 2229 (vs), 2170 (vs), 1618 (m), 1597 (w), 1562 (w), 1504 (w), 1479 (m), 1425 (s), 1369 (m), 1327 (w), 1306 (m), 1263 (s), 1252 (s), 1227 (s), 1161 (vw), 1124 (m), 1061 (m), 1018 (m), 933 (w), 816 (s), 802 (m), 756 (s), 638 (w), 613 (vw), 510 (w), 490 (m), 467 (vw).

X-ray Crystallographic Study: Intensity data for complexes **1**−**7** were measured with a Siemens Smart CCD diffractometer with

Table 2. Selected bond lengths [Å] and angles [°] for **1**−**7**[a]

Complex **1**			
Zn−N(1)	2.061(4)	Zn−N(2A)	2.070(5)
Zn−Cl(1)	2.2245(17)	Zn−Cl(2)	2.2150(16)
N(1)−Zn−N(2A)	99.53(18)	N(1)−Zn−Cl(2)	108.83(14)
N(2A)−Zn−Cl(2)	105.96(14)	N(1)−Zn−Cl(1)	103.74(14)
N(2A)−Zn−Cl(1)	112.60(14)	Cl(2)−Zn−Cl(1)	123.52(7)
Complex **2**			
Zn−N(1)	2.068(8)	Zn−N(2A)	2.085(9)
Zn−Br(1)	2.3614(16)	Zn−Br(2)	2.3674(16)
N(1)−Zn−N(2A)	98.6(3)	N(1)−Zn−Br(1)	108.7(2)
N(2A)−Zn−Br(1)	106.9(2)	N(1)−Zn−Br(2)	105.1(2)
N(2A)−Zn−Br(2)	113.0(2)	Br(1)−Zn−Br(2)	121.92(6)
Complex **3**			
Zn−N(1)	2.041(5)	Zn−N(2A)	2.057(4)
Zn−Cl(1)	2.2155(17)	Zn−Cl(2)	2.2153(16)
N(1)−Zn−N(2A)	102.93(19)	N(1)−Zn−Cl(2)	108.90(14)
N(2A)−Zn−Cl(2)	108.58(14)	N(1)−Zn−Cl(1)	108.01(14)
N(2A)−Zn−Cl(1)	106.27(14)	Cl(2)−Zn−Cl(1)	120.71(7)
Complex **4**			
Zn−N(1)	2.052(7)	Zn−N(2A)	2.069(7)
Zn−Br(1)	2.3512(15)	Zn−Br(2)	2.3560(13)
N(1)−Zn−N(2A)	101.8(3)	N(1)−Zn−Br(1)	108.1(2)
N(2A)−Zn−Br(1)	107.9(2)	N(1)−Zn−Br(2)	109.5(2)
N(2A)−Zn−Br(2)	108.1(2)	Br(1)−Zn−Br(2)	119.90(6)
Complex **5**			
Co−N(1)	2.062(5)	Co−N(2)	2.080(6)
Co−N(5)	2.162(5)	Co−N(6A)	2.181(5)
Co−N(3)	2.222(5)	Co−N(4B)	2.239(5)
N(1)−Co−N(2)	176.6(2)	N(1)−Co−N(5)	87.1(2)
N(2)−Co−N(5)	92.15(19)	N(1)−Co−N(6A)	93.8(2)
N(2)−Co−N(6A)	89.53(19)	N(5)−Co−N(6A)	91.94(18)
N(1)−Co−N(3)	89.0(2)	N(2)−Co−N(3)	87.73(19)
N(5)−Co−N(3)	95.59(18)	N(6A)−Co−N(3)	172.08(18)
N(1)−Co−N(4B)	89.1(2)	N(2)−Co−N(4B)	91.78(19)
N(5)−Co−N(4B)	175.97(19)	N(6A)−Co−N(4B)	87.20(19)
N(3)−Co−N(4B)	85.45(19)	C(1)−N(1)−Co	170.1(6)
C(2)−N(2)−Co	174.7(5)	N(1)−C(1)−S(1)	179.7(6)
N(2)−C(2)−S(2)	178.6(7)		
Complex **6**			
Cd−N(1)	2.329(6)	Cd−N(2)	2.308(7)
Cd−N(3)	2.384(5)	Cd−N(4B)	2.405(5)
Cd−N(5)	2.393(5)	Cd−N(6A)	2.379(5)
N(2)−Cd−N(1)	178.2(2)	N(1)−Cd−N(6A)	90.6(2)
N(1)−Cd−N(3)	89.81(18)	N(1)−Cd−N(5)	88.5(2)
N(1)−Cd−N(4B)	93.37(18)	N(2)−Cd−N(3)	89.22(19)
N(2)−Cd−N(5)	93.0(2)	N(2)−Cd−N(6A)	90.4(2)
N(2)−Cd−N(4B)	85.14(19)	N(3)−Cd−N(5)	90.26(17)
N(3)−Cd−N(4B)	90.17(17)	N(5)−Cd−N(4B)	178.11(19)
N(6A)−Cd−N(4B)	91.37(17)	N(6A)−Cd−N(3)	178.39(17)
N(6A)−Cd−N(5)	88.19(17)	C(1)−N(1)−Cd	135.3(6)
C(2)−N(2)−Cd	139.6(6)	N(1)−C(1)−S(1)	177.9(9)
N(2)−C(2)−S(2)	174.0(8)		

 © 2004 Wiley-VCH Verlag GmbH & Co. KGaA, Weinheim

Table 2. *(continued)*

Complex **7**			
Cd−N(4)	2.318(8)	Cd−N(11)	2.322(9)
Cd−N(1A)	2.324(10)	Cd−N(3)	2.334(9)
Cd−N(12B)	2.359(9)	Cd−N(5C)	2.470(10)
N(4)−Cd−N(11)	93.2(3)	N(4)−Cd−N(1A)	90.3(3)
N(11)−Cd−N(1A)	92.9(4)	N(4)−Cd−N(3)	177.3(4)
N(11)−Cd−N(3)	86.2(3)	N(1A)−Cd−N(3)	87.0(3)
N(4)−Cd−N(12B)	92.1(3)	N(11)−Cd−N(12B)	169.0(3)
N(1A)−Cd−N(12B)	96.7(4)	N(3)−Cd−N(12B)	88.9(3)
N(4)−Cd−N(5C)	88.8(3)	N(11)−Cd−N(5C)	88.0(3)
N(1A)−Cd−N(5C)	178.7(3)	N(3)−Cd−N(5C)	93.8(3)
N(12B)−Cd−N(5C)	82.5(3)		

[a] Symmetry code: **1** (A): $-x + 2, -y, -z$; **2** (A): $-x + 1, -y + 1, -z$; **3** (A): $x + 1/2, y + 1/2, z$; **4** (A): $x + 1/2, y + 1/2, z$; **5** (A): $-x, y + 1/2, -z - 1/2$; **5** (B): $-x + 1, -y - 2, -z$; **6** (A): $-x + 2, -y, z + 1/2$; **6** (B): $-x + 1, -y + 1, z + 1/2$; **7** (A): $x + 1/2, -y + 1, z$; **7** (B): $-x + 1, -y, z - 1/2$; **7** (C): $x - 1/2, -y, z$.

graphite-monochromated Mo-K_α radiation (λ = 0.71073 Å) at room temperature. All empirical absorption corrections were applied with the SADABS program.[33] The structures were solved by direct methods[34] and refined on F^2 by full-matrix least squares using the SHELXL-97 program package.[35] The positions of H atoms were generated geometrically (C−H bond fixed at 0.96 Å), assigned isotropic thermal parameters, and allowed to ride on their parent carbon atoms before the final cycle of refinement. The selected bond lengths and angles for **1**−**7** are listed in Table 2. Crystal data and structure determination data for **1**−**7** are listed in Table 4. CCDC-232662 to -232668 (**1**−**7**, respectively) contain the supplementary crystallographic data for this paper. These data can be obtained free of charge at www.ccdc.cam.ac.uk/conts/retrieving.html [or from the Cambridge Crystallographic Data Centre, 12 Union Road, Cambridge CB2 1EZ, UK; Fax: (internat.) + 44-1223-336-033; E-mail: deposit@ccdc.cam.ac.uk].

Acknowledgments

This work was supported by grants from the National Nature Science Foundation of China (No. 20231020), the Nature Science Foundation of Fujian Province, and the Open Laboratory of Chirotechnology of the Hong Kong Polytechnic University (No. PolyU5306/01P).

[1] [1a] J. M. Lehn, *Supramolecular Chemistry: Concepts and Perspectives*, VCH, Weinheim, **1995**. [1b] J. W. Steed, J. L. Atwood, *Supramolecular Chemistry*, J. Wiley and Sons, New York, **2000**.
[2] [2a] S. A. Bourne, J. Lu, A. Mondal, B. Moulton, M. J. Zaworotko, *Angew. Chem. Int. Ed.* **2001**, *40*, 2111−2113. [2b] M. Munakata, L. P. Wu, T. Kuroda-Sowa, *Adv. Inorg. Chem.* **1999**, *46*, 173−303.
[3] [3a] M. Eddaoudi, D. B. Moler, H. Li, B. Chen, T. M. Reineke, M. O'Keeffe, O. M. Yaghi, *Acc. Chem. Res.* **2001**, *34*, 319−330. [3b] S. Leininger, B. Olenyuk, P. J. Stang, *Chem. Rev.* **2000**, *100*, 853−908.
[4] [4a] D. A. Beauchamp, S. J. Loeb, *Chem. Commun.* **2002**, 2484−2485. [4b] D. A. McMorran, P. J. Steel, *Chem. Commun.* **2002**, 2120−2121. [4c] M. Maekawa, H. Konaka, Y. Suenaga, T. Kuroda-Sowa, M. Munakata, *J. Chem. Soc., Dalton Trans.* **2000**, 4160−4166.
[5] [5a] O. R. Evan, W. B. Lin, *Acc. Chem. Res.* **2002**, *35*, 511−522 and references cited therein. [5b] C. Janiak, *Dalton Trans.* **2003**, 2781−2804.
[6] [6a] L. Carlucci, G. Ciani, D. M. Proserpio, *Cryst. Eng. Commun.* **2003**, *5*, 269−279. [6b] S. O. H. Gutschke, M. Molinier, A. K. Powell, R. E. P. Winpenny, P. T. Wood, *Chem. Commun.* **1996**, 823−824.
[7] [7a] S. Banfi, L. Carlucci, E. Caruso, G. Ciani, D. M. Proserpio, *J. Chem. Soc., Dalton Trans.* **2002**, 2714−2721. [7b] J. Keegan, P. E. Kruger, M. Nieuwenhuyzen, N. Martin, *Cryst. Growth Design* **2002**, *2*, 329−332.
[8] [8a] Y. Cui, S. J. Lee, W. Lin, *J. Am. Chem. Soc.* **2003**, *125*, 6014−6015. [8b] D. Braga, M. Polito, M. Bracaccini, D. D'Addario, E. Tagliavini, D. M. Proserpio, F. Grepioni, *Chem. Commun.* **2002**, 1081−1082. [8c] J. Schneider, M. Köckerling, R. Kopitzky, G. Henkel, *Eur. J. Inorg. Chem.* **2003**, 1727−1734.
[9] [9a] Y. B. Dong, J. Y. Cheng, R. Q. Huang, M. D. Smith, H. C. zur Loye, *Inorg. Chem.* **2003**, *42*, 5699−5706. [9b] M. L. Tong, S. L. Zheng, X. M. Chen, *Chem. Eur. J.* **2000**, *6*, 3729−3738.
[10] [10a] O. S. Jung, Y. J. Kim, Y. A. Lee, J. K. Park, H. K. Chae, *J. Am. Chem. Soc.* **2000**, *122*, 9921−9925. [10b] K. A. Hirsch, S. R. Wilson, J. S. Moore, *Inorg. Chem.* **1997**, *36*, 2960−2968.
[11] [11a] G. D. Munno, F. Cipriani, D. Armentano, M. Julve, J. A. Real, *New J. Chem.* **2001**, *25*, 1031−1036. [11b] R. W. Saalfrank, I. Bernt, M. M. Chowdhry, F. Hampel, G. B. M. Vaughan, *Chem. Eur. J.* **2001**, *7*, 2765−2769.
[12] [12a] O. S. Jung, S. H. Park, K. M. Kim, H. G. Jang, *Inorg. Chem.* **1998**, *37*, 5781−5785. [12b] T. L. Hennigar, D. C. MacQyarrie, P. Losier, R. D. Rogers, M. J. Zaworotko, *Angew. Chem. Int. Ed. Engl.* **1997**, *36*, 972−973.
[13] [13a] A. J. Blake, N. R. Champness, P. Hubberstey, W. S. Li, M. A. Withersby, M. Schröder, *Coord. Chem. Rev.* **1999**, *183*, 117−138. [13b] P. J. Hagrman, D. Hagrman, J. Zubieta, *Angew. Chem. Int. Ed.* **1999**, *38*, 2639−2684.
[14] [14a] S. Kitagawa, M. Kondo, *Bull. Chem. Soc. Jpn.* **1998**, *71*, 1799−1806. [14b] S. Belanger, J. T. Hupp, C. L. Stern, R. V. Slone, D. F. Watson, T. G. Carrell, *J. Am. Chem. Soc.* **1999**, *121*, 557−558.
[15] [15a] K. Biradha, M. Fujita, *J. Chem. Soc., Dalton Trans.* **2000**, 3805−3810. [15b] K. Biradha, Y. Hongo, M. Fujita, *Angew. Chem. Int. Ed.* **2000**, *39*, 3843−3845.
[16] [16a] X. H. Bu, W. Chen, S. L. Lu, R. H. Zhang, D. Z. Liao, W. M. Bu, M. Shionoya, F. Brisse, J. Ribas, *Angew. Chem. Int. Ed.* **2001**, *40*, 3201−3203. [16b] F. A. A. Paz, Y. Z. Khimyak, A. D. Bond, J. Rocha, J. Klinowski, *Eur. J. Inorg. Chem.* **2002**, 2823−2828. [16c] W. J. Belcher, C. A. Longstaff, M. R. Neckenig, J. W. Steed, *Chem. Commun.* **2002**, 1602−1603.
[17] [17a] P. L. Caradoc-Davies, D. H. Gregory, L. R. Hanton, J. M. Turnbull, *J. Chem. Soc., Dalton Trans.* **2002**, 1574−1580. [17b] D. M. L. Goodgame, D. A. Grachvogel, I. Hussain, A. J. P. White, D. J. Williams, *Inorg. Chem.* **1999**, *38*, 2057−2063 and references cited therein.
[18] M. C. Hong, Y. J. Zhao, W. P. Su, R. Cao, M. Fujita, Z. Y. Zhou, A. S. C. Chan, *J. Am. Chem. Soc.* **2000**, *122*, 4819−4820.
[19] M. C. Hong, Y. J. Zhao, W. P. Su, R. Cao, M. Fujita, Z. Y. Zhou, A. S. C. Chan, *Angew. Chem. Int. Ed.* **2000**, *39*, 2468−2470.
[20] R. H. Wang, M. C. Hong, W. P. Su, Y. C. Liang, R. Cao, Y. J. Zhao, J. B. Weng, *Bull. Chem. Soc. Jpn.* **2002**, *75*, 725−730.
[21] M. C. Hong, W. P. Su, R. Cao, M. Fujita, J. X. Lu, *Chem. Eur. J.* **2000**, *6*, 427−432.
[22] [22a] R. H. Wang, M. C. Hong, J. H. Luo, R. Cao, J. B. Weng, *Chem. Commun.* **2003**, 1018−1019. [22b] J.-M. Rueff, S. Pillet, N. Claiser, G. Bonaventure, M. Souhassou, P. Rabu, *Eur. J. Inorg. Chem.* **2002**, 895−900. [22c] H. Kumagai, K. Inoue, M. Kurmoo, *Bull. Chem. Soc. Jpn.* **2002**, *75*, 1283−1289.
[23] [23a] L. Pu, *Chem. Rev.* **1998**, *98*, 2405−2494. [23b] R. H. Wang, L. J. Xu, X. S. Li, Y. M. Li, Q. Shi, Z. Y. Zhou, M. C. Hong, A. S. C. Chan, *Eur. J. Inorg. Chem.* **2004**, 1595−1599.
[24] T. W. Kim, M. S. Lah, J. I. Hong, *Chem. Commun.* **2001**, 743−744.
[25] [25a] M. Kondo, M. Shimamura, S. Noro, S. Minakoshi, A. Asami, K. Seki, S. Kitagawa, *Chem. Mater.* **2000**, *12*, 1288−1299. [25b] X. M. Ouyang, B. L. Fei, T. Okamura, H. W. Bu, W. Y.

Sun, W. X. Tang, N. Ueyama, *Eur. J. Inorg. Chem.* **2003**, 618−627. [25c] C. Karunakaran, K. R. J. Thomas, A. Shunmugasundaram, R. Murugesan, *J. Mol. Struct.* **2000**, *523*, 213−221.

[26] [26a] H. P. Wu, C. Janiak, L. Uehlin, P. Klüfers, P. Mayer, *Chem. Commun.* **1998**, 2637−2638. [26b] M. Fettouhi, B. E. Ali, A. M. El-Ghanam, S. Golhen, L. Ouahab, N. Daro, J. P. Sutter, *Inorg. Chem.* **2002**, *41*, 3705−3712.

[27] [27a] S. R. Batten, K. S. Murray, *Coord. Chem. Rev.* **2003**, *246*, 103−130. [27b] P. Jensen, S. R. Batten, B. Moubaraki, K. S. Murray, *J. Chem. Soc., Dalton Trans.* **2002**, 3712−3722. [27c] S. Dalai, P. S. Mukherjee, E. Zangrando, N. R. Chaudhuri, *New J. Chem.* **2002**, *26*, 1185−1189. [27d] J. L. Manson, A. M. Arif, C. D. Incarvito, L. M. Liable-Sands, A. L. Rheingold, J. S. Miller, *J. Solid State Chem.* **1999**, *145*, 369−378.

[28] Z. M. Wang, B. W. Sun, J. Luo, S. Gao, C. S. Liao, C. H. Yan, Y. Li, *Inorg. Chim. Acta* **2002**, *332*, 127−134.

[29] [29a] C. Klcin, E. Graf, M. W. Hosseini, A. D. Cian, N. Kyritsakas, *Eur. J. Inorg. Chem.* **2003**, 1299−1302. [29b] L. Carlucci, G. Ciani, D. M. Proserpio, *J. Chem. Soc., Dalton Trans.* **1999**, 1799−1804. [29c] M. Sasa, T. Tanaka, X. H. Bu, M. Shiro, M. Shionoya, *J. Am. Chem. Soc.* **2001**, *123*, 10750−10751. [29d] R. Burth, H. Vahrenkamp, *Inorg. Chim. Acta* **1998**, *282*, 193−201.

[30] C. Janiak, *J. Chem. Soc., Dalton Trans.* **2000**, 3885−3896.

[31] [31a] M. Fujita, S. Nago, M. Iida, K. Ogata, K. Ogura, *J. Am. Chem. Soc.* **1993**, *115*, 1574−1575. [31b] K. Onitsuka, S. Yamamoto, S. Takahashi, *Angew. Chem. Int. Ed.* **1999**, *38*, 174−178. [31c] C. A. Hunter, L. D. Sarson, *Angew. Chem. Int. Ed. Engl.* **1994**, *33*, 2313−2317.

[32] [32a] M. Munakata, L. P. Wu, T. Kuroda-Sowa, *Adv. Inorg. Chem.* **1999**, *46*, 173−303. [32b] V. V. Ponomarova, V. V. Komarchuk, I. Boldog, A. N. Chernega, J. Sieler, K. V. Domasevitch, *Chem. Commun.* **2002**, 436−437. [32c] M. Kondo, M. Miyazawa, Y. Irie, R. Shinagawa, T. Horiba, A. Nakamura, T. Naito, K. Maeda, S. Utsuno, F. Uchida, *Chem. Commun.* **2002**, 2156−2157.

[33] G. M. Sheldrick, *SADABS, Program for Empirical Absorption Correction of Area Detector Data*, University of Göttingen, Göttingen, **1996**.

[34] G. M. Sheldrick, *SHELXS 97, Program for Crystal Structure Solution*, University of Göttingen, Göttingen, **1997**.

[35] G. M. Sheldrick, *SHELXS 97, Program for Crystal Structure Refinement*, University of Göttingen, Göttingen, **1997**.

Received March 3, 2004
Early View Article
Published Online July 14, 2004

 © 2004 Wiley-VCH Verlag GmbH & Co. KGaA, Weinheim

EurJIC
European Journal of Inorganic Chemistry

Issue 19/2004

Pages 3765–3958

Papers available ahead of print in Early View at www.interscience.wiley.com

Earliest available Table of Contents: Automatically, free of charge by e-mail through www.interscience.wiley.com/alerts

COVER PICTURE

The cover picture shows a flexible Pd metallocrown ether that has two SCS-pincer ligand moieties. A long bidentate ligand binds to the host in a bridging fashion to close the crown cavity, whereas a short one divides the cavity to give two small polyether rings. Details are discussed in the Short Communication by T. Nabeshima et al. on p. 3779 ff.

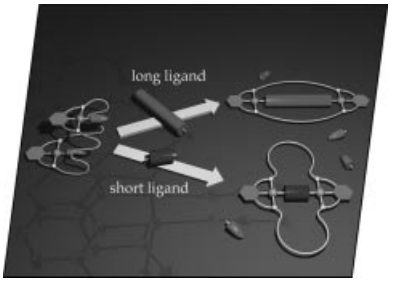

SHORT COMMUNICATION

Contents

3779 **T. Nabeshima,* D. Nishida, S. Akine, T. Saiki**

Synthesis, Structure and Complexation Ability of Novel Metalloreceptors Containing Two Pincer Complexes of Palladium(II)

Keywords: Host-guest systems / Pincer ligands / Palladium / Metalloreceptors / Crown ethers

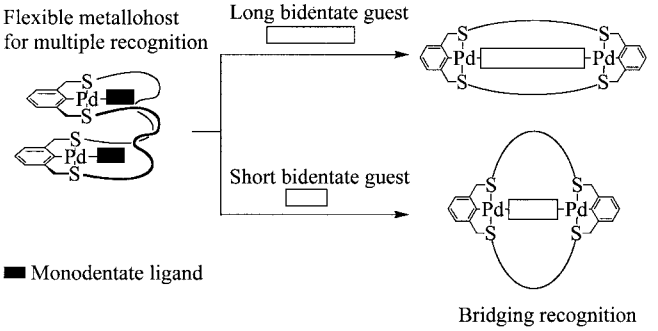

 © 2004 Wiley-VCH Verlag GmbH & Co. KGaA, Weinheim

FULL PAPERS

3783 **F. Thétiot, S. Triki,* J. S. Pala, J.-R. Galán-Mascarós, J. M. Martínez-Agudo, K. R. Dunbar**

Discrete Dinuclear Complexes and Two-Dimensional Architectures from Bridging Polynitrile and Bipyrimidine (bpym) Ligands: Syntheses, Structures and Magnetic Properties of $[M_2(bpym)(dcne)_4(H_2O)_2]$ (M = Mn^{II}, Co^{II}) and $[M_2(bpym)(dcne)_4(H_2O)_4]\cdot 2H_2O$ (M = Fe^{II}, Cu^{II}) ($dcne^- = [(CN)_2CC(O)OEt)]^-$)

Keywords: Bridging ligands / Coordination polymers / Magnetic properties / N ligands / Transition metals

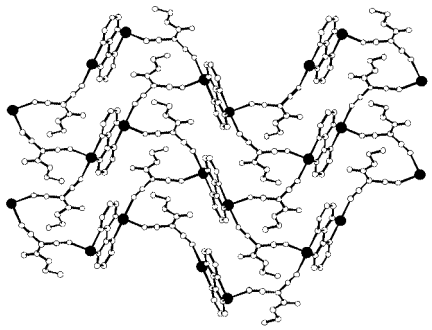

$[M_2(bpym)(dcne)_4(H_2O)_2]$ (M = Mn^{II}, Co^{II})

3792 **A. C. Stowe, S. Nellutla, N. S. Dalal,* U. Kortz***

Magnetic Properties of Lone-Pair-Containing, Sandwich-Type Polyoxoanions: A Detailed Study of the Heteroatomic Effect

Keywords: Copper / EPR spectroscopy / Magnetic properties / Polyoxometalates / Self assembly / Tungsten

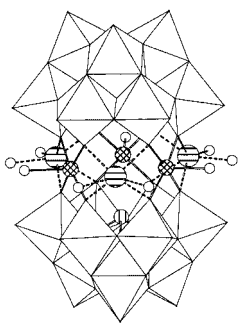

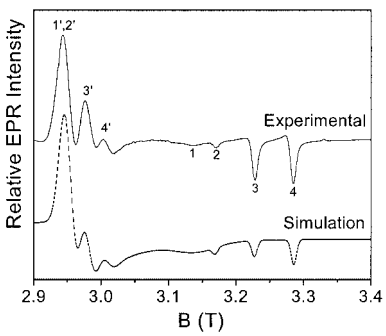

3798 **J. Van Droogenbroeck, K. Tersago, C. Van Alsenoy, S. M. Aucott, H. L. Milton, J. D. Woollins, F. Blockhuys***

Roesky's Ketone: Structure, Aromaticity and Reactivity

Keywords: Aromaticity / Density functional theory / Dithiadiazole / Reactivity / X-ray diffraction

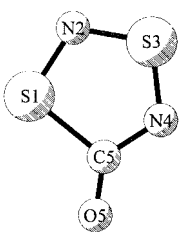

3806 **X. Sun, R. Li, D. Wang, J. Dou, P. Zhu, F. Lu, C. Ma, C.-F. Choi, D. Y. Y. Cheng, D. K. P. Ng, N. Kobayashi, J. Jiang***

Synthesis and Characterization of Mixed Phthalocyaninato and *meso*-Tetrakis(4-chlorophenyl)porphyrinato Triple-Decker Complexes − Revealing the Origin of Their Electronic Absorptions

Keywords: Phthalocyanines / Porphyrins / Rare earth metals / Sandwich complexes / Triple-decker complexes

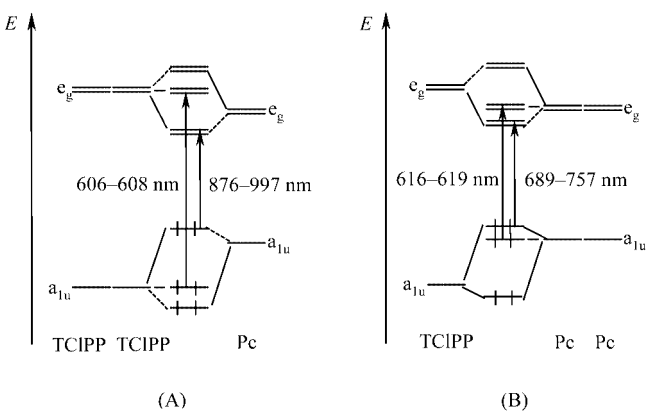

 © 2004 Wiley-VCH Verlag GmbH & Co. KGaA, Weinheim

3814 **A. Sebastián, P. Royo,* P. Gómez-Sal, C. Ramírez de Arellano**

Diastereoselective Insertion of Isocyanide into the Alkyl−Metal Bond of Methylbenz[*e*]indenyl *ansa*-Zirconocene Complexes

Keywords: Metallocenes / Zirconium / Insertion / Isocyanides / Polymerization

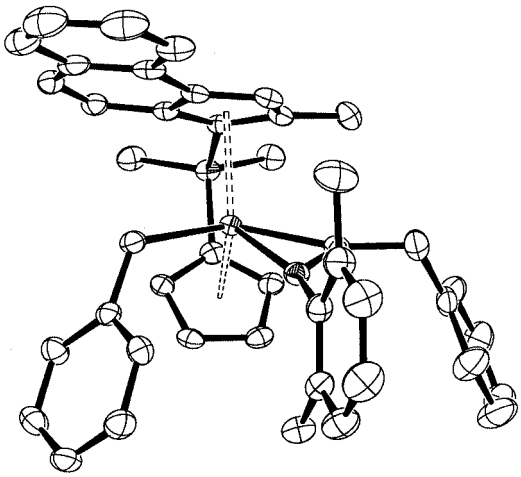

3822 **M. Alexiou, C. Dendrinou-Samara, C. P. Raptopoulou, A. Terzis, V. Tangoulis,* D. P. Kessissoglou***

A Cationic Tetranuclear $[Ni^{II}_4(MeOH)_2(pko)_6]^{2+}$ Cluster Showing Antiferro- and Ferromagnetic Features

Keywords: Cluster compounds / Magnetic properties / Oximato ligands / Nickel

3828 **A. Aissa, B. Badraoui, R. Thouvenot,* M. Debbabi***

Synthesis, X-ray Structural Analysis and Spectroscopic Investigations (IR and ^{31}P MAS NMR) of Mixed Barium/Strontium Fluoroapatites

Keywords: Barium / IR spectroscopy / NMR spectroscopy / Strontium / X-ray diffraction

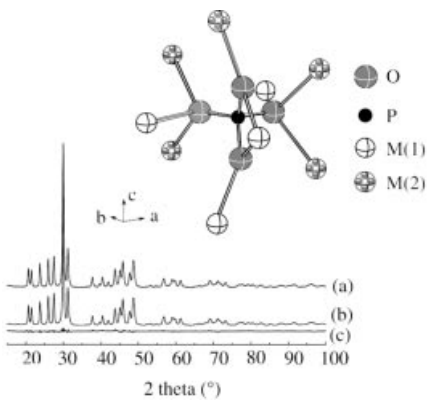

3837 **Y.-Q. Sun, J. Zhang,* J.-L. Chen, G.-Y. Yang**

Two Copper(II) Complexes Built from a Novel Redox-Active Bipyridinium Dimer Ligand and Oxalate Anions: Synthesis, Crystal Structure and Magnetic Properties

Keywords: Copper(II) / Bipyridium dimer / Oxalate / X-ray diffraction

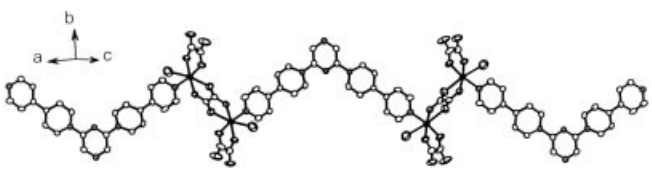

 © 2004 Wiley-VCH Verlag GmbH & Co. KGaA, Weinheim

3842 **A. Dimitrov,* I. Hartwich, P. Neubauer, M. Meisel**

2,4-*N*,*N*′-Bis(dialkylamido)-2,4-dithioxo-1,3,2λ^5,4λ^{5}dithiadiphosphetanes

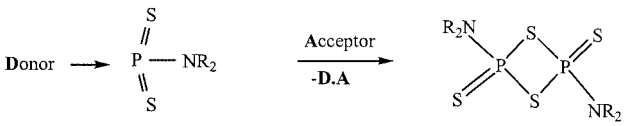

Keywords: Donor-acceptor systems / N-ligands / Fluorinated ligands / Sulfur / Phosphorus

3846 **S. Chakrabarti, S. K. Pati, M. A. Green, S. Natarajan***

Hydrothermal Synthesis, Structure and Magnetic Properties of a One-Dimensional Iron Arsenate, $^1_\infty[NH_3(CH_2)_2NH(CH_2)_2NH_3][Fe_2F_4(HAsO_4)_2]$

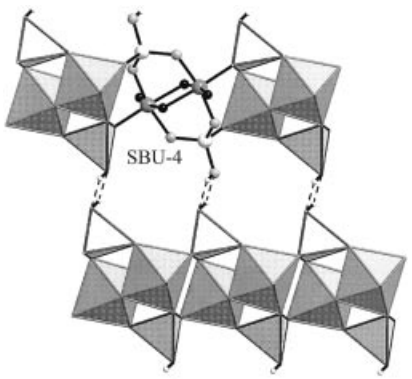

Keywords: Iron arsenate / Antiferromagnetism / Hydrothermal reactions / Iron / Magnetic properties

3852 **U. A. Böttger, B. O'Sullivan, B. Ziemer, H. Schumann, C. Mügge, H. Weißhoff***

Structure Comparison of Early and Late Lanthanide(III) Homodinuclear Macrocyclic Complexes with the Polyamine Polycarboxylic Ligand H_8OHEC

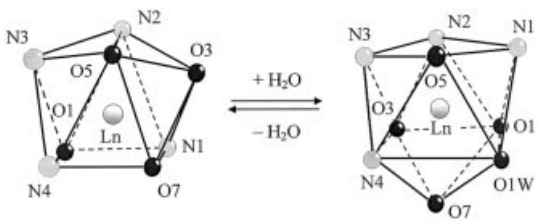

Keywords: Solid-state structures / Lanthanides / Macrocyclic ligands / Polyamine polycarboxylic acid / Solution thermodynamics

3865 **T. S. Cameron, A. Decken, E. G. Ilyin, G. B. Nikiforov, J. Passmore***

18-Crown-6 and Titanium Tetrafluoride − Preparation of the Ti^{IV} Fluoride Crown Ether Complexes $(TiF_4)_2$(18-Crown-6) and the Stabilization of *cis*-$TiF_4(H_2O)_2$ in [{*cis*-$TiF_4(H_2O)_2$}$_2$(18-Crown-6)]

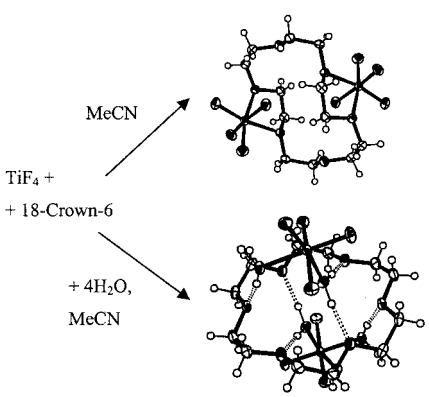

Keywords: Titanium(IV) / Fluorides / Crown ether / Macrocyclic ligands / Coordination modes / Host-guest systems

 © 2004 Wiley-VCH Verlag GmbH & Co. KGaA, Weinheim

3873 **C. Ruiz-Pérez,* P. Lorenzo-Luis, M. Hernández-Molina, M. M. Laz, F. S. Delgado, P. Gili, M. Julve**

1,2,4,5-Benzenetetracarboxylic Acid and 4,4′-Bipyridine as Ligands in Designing Low-Dimensional Coordination Polymers

Keywords: Hydrothermal / 1,2,4,5-Benzenetetracarboxylic acid / 4,4′-Bipyridine / Low-dimensional polymers / Manganese / Cobalt

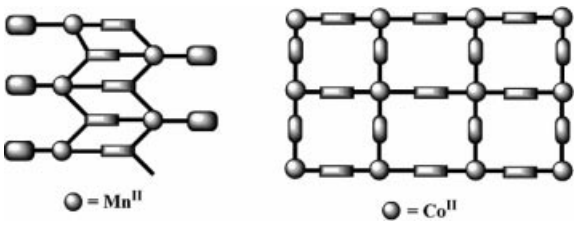

3880 **C. Mantel, C. Philouze, M.-N. Collomb,* C. Duboc***

Investigation of a Neat versus Magnetically Diluted Powdered Mononuclear Mn^{II} Complex by High-Field and High-Frequency EPR Spectroscopy

Keywords: Azide ligand / Electronic structure / EPR spectroscopy / Manganese / Magnetic dilution

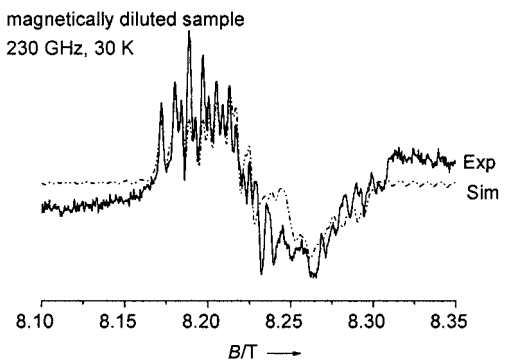

3887 **A. Caneschi, L. Sorace, U. Casellato, P. Tomasin,* P. A. Vigato**

d- or f-Mononuclear and Related Heterodinuclear Complexes With [1+1] Asymmetric Compartmental Macrocycles

Keywords: Heterometallic complexes / Macrocyclic ligands / Compartmental Schiff bases / Magnetic properties / EPR spectroscopy

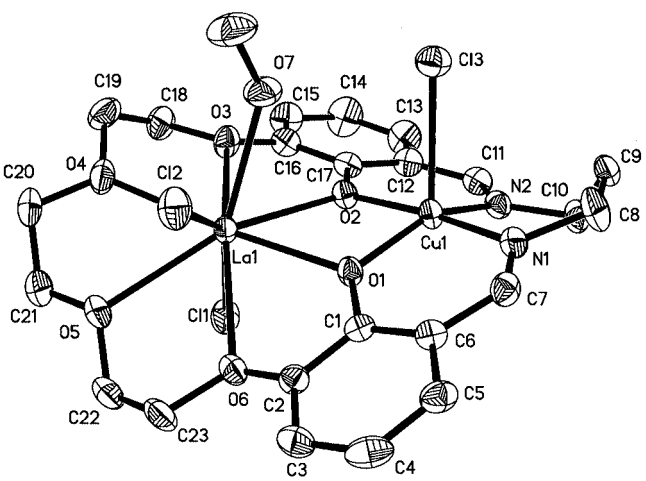

3901 **R. Della Pergola,* A. Fumagalli, F. Fabrizi de Biani, L. Garlaschelli, F. Laschi, M. C. Malatesta, M. Manassero,* E. Roda, M. Sansoni, P. Zanello**

Carbonyl-Nitrido Mixed-Metal Clusters: Synthesis, Reactivity, Electrochemical Behavior and Solid-State Structure of $[Co_5MoN(CO)_{14}]^{2-}$ and $[Co_5MoN(CO)_{14}AuPPh_3]^-$

Keywords: Cobalt / Molybdenum / Cluster compounds / Nitrides / Electrochemistry

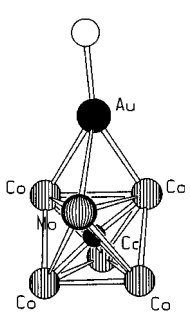

 © 2004 Wiley-VCH Verlag GmbH & Co. KGaA, Weinheim

3907 **L. Vieille-Petit, L. Karmazin-Brelot, G. Labat, G. Süss-Fink***

endo and *exo* Coordination of Indanol: Synthesis, Isolation and Structural Characterisation of $[H_3Ru_3(endo\text{-Indanol})(C_6Me_6)_2(O)]^+$ and $[H_3Ru_3(exo\text{-Indanol})(C_6Me_6)_2(O)]^+$ as Their Tetrafluoroborate Salts

Keywords: Arene ligands / Biphasic catalysis / Cluster compound / Hydrogenation / Ruthenium

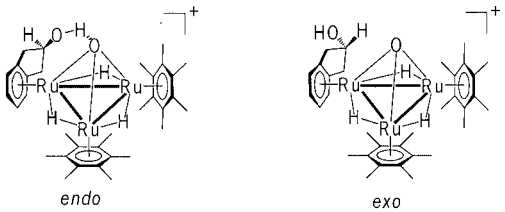

3913 **J. A. Fernandes, R. A. Sá Ferreira, M. Pillinger, L. D. Carlos,* I. S. Gonçalves, P. J. A. Ribeiro-Claro***

Spectroscopic Studies of Europium(III) and Gadolinium(III) Tris-β-diketonate Complexes with Diazabutadiene Ligands

Keywords: Ab initio calculations / Lanthanides / Luminescence / N ligands / Vibrational spectroscopy

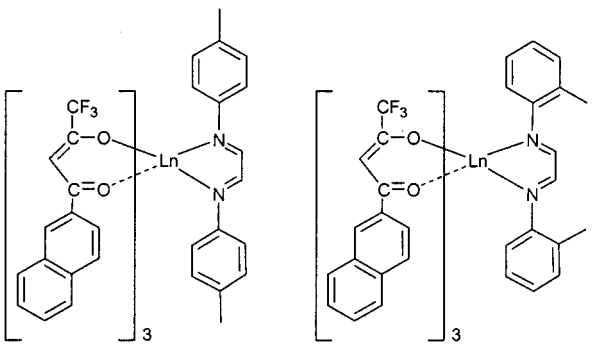

3920 **M. Iida,* M. Inoue, T. Tanase, T. Takeuchi, M. Sugibayashi, K. Ohta**

Formation of Thermotropic and Lyotropic Liquid Crystals of Bis(*N*-alkylethylenediamine)-silver(I) Nitrate

Keywords: Silver / N ligands / Liquid crystals / Microemulsions

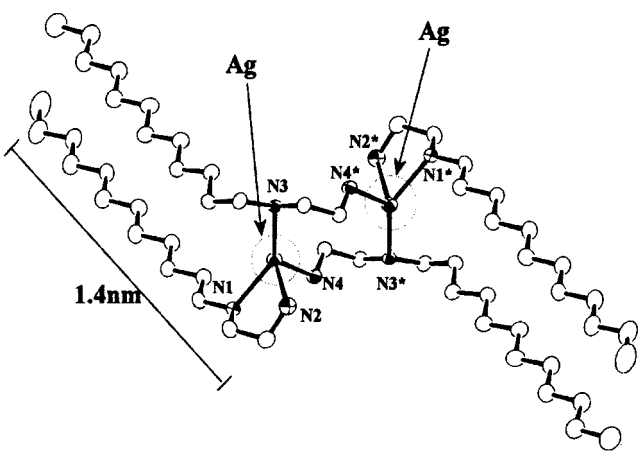

3930 **K. Mirosavljević, J. Sabolović, V. Noethig-Laslo***

Conformational Analysis of Bis(L-*N*,*N*-dimethylvalinato)copper(II) and Bis(L-*N*,*N*-dimethylleucinato)copper(II) in Different Solvents by EPR Spectroscopy and a Molecular Mechanics Study

Keywords: Complexes / Amino acids / N,O ligands / EPR spectroscopy / Force field

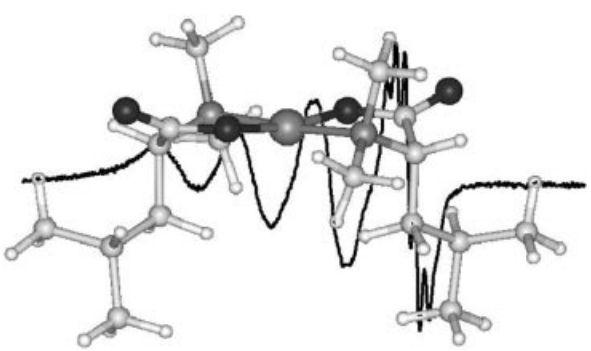

 © 2004 Wiley-VCH Verlag GmbH & Co. KGaA, Weinheim

3938 **D. Belli Dell'Amico,* F. Calderazzo, U. Englert, L. Labella, F. Marchetti, M. Specos**

New *N*,*N*-Diisopropylcarbamato Complexes of Ruthenium(II) as Catalytic Precursors for Olefin Hydrogenation

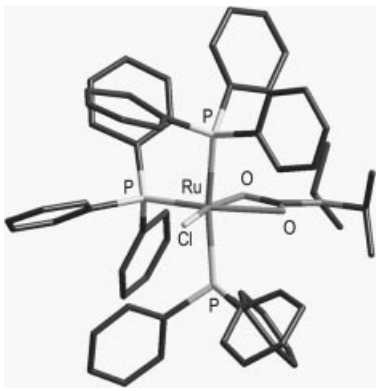

Keywords: *N*,*N*-Dialkylcarbamato complexes / Ruthenium / Hydrogenation

3946 **Y. Wei, H. Hou,* Y. Fan, Y. Zhu**

Transition Metal Ion Directed Self-Assembly of Polynuclear Coordination Complexes: Structural Characterization and Magnetic Properties

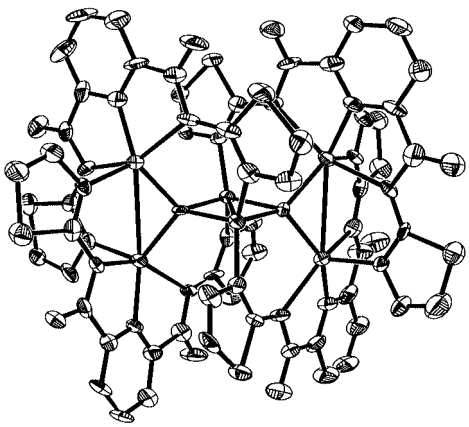

Keywords: Magnetic properties / Multidentate ligands / Organic-inorganic hybrid composites / Self-assembly / Transition metals

 © 2004 Wiley-VCH Verlag GmbH & Co. KGaA, Weinheim

Synthesis, Structure and Complexation Ability of Novel Metalloreceptors Containing Two Pincer Complexes of Palladium(II)

Tatsuya Nabeshima,*[a] Daisuke Nishida,[a] Shigehisa Akine,[a] and Toshiyuki Saiki[a]

Keywords: Host-guest systems / Pincer ligands / Palladium / Metalloreceptors / Crown ethers

Metalloreceptors **1a** and **1b** were synthesized by palladation of 42- and 54-membered crown ethers that have two SCS-pincer ligand moieties. The X-ray crystallographic analysis reveals that the metalloreceptor **1b** has a folded structure in which the two pincer-Pd moieties are stacked in a parallel manner. The metalloreceptor **1b** recognizes the aromatic bidentate guests 4,4′-bipyridine, pyrazine, and pyrimidine and binds to them in a bridging fashion to form the corresponding bimacrocyclic 1:1 complex.

(© Wiley-VCH Verlag GmbH & Co. KGaA, 69451 Weinheim, Germany, 2004)

Metalloreceptors have recently attracted much attention in supramolecular chemistry because the physical and chemical properties of the metal center can be applied in guest binding, sensing, and regulation of molecular functions.[1] In particular, the coordination of various ligands to metals is very useful for the formation of a stable supramolecular system.[2−6] Combination of the coordinate bonding and other intermolecular interactions provides a strong and selective recognition.

Complexes between Pd and pincer ligands are useful as they provide a nice coordination site for host-guest interaction.[7] For example, crown ethers containing a Pd center inside the ring and molecular recognition have been reported.[8−10] Cooperative binding of the Pd unit and the crown ether moiety to nucleobases such as cytosine and adenine was observed in this system.[11,12] However, a host molecule containing several pincer complexes as a binding site has not been synthesized although this type of host is very interesting as a multi-point receptor.

Here we report the synthesis, structure and molecular recognition ability of large macrocyclic hosts **1**, which contain two pincer complexes of Pd^{II}. The metallohosts are expected to bind bidentate guests of different sizes in the cavity because the framework of these hosts is flexible so as to cause induced-fit recognition (Scheme 1).

Metallohosts **1** containing the two Pd centers were prepared according to Scheme 2. Diols **2a**[13] and **2b**[14] were treated with *p*-toluenesulfonyl chloride to afford **3a** and **3b** in 80% and 63% yield, respectively. Reaction of dithiol **4**[15] with **3a, 3b** in the presence of K_2CO_3 afforded diols **5a, 5b**,

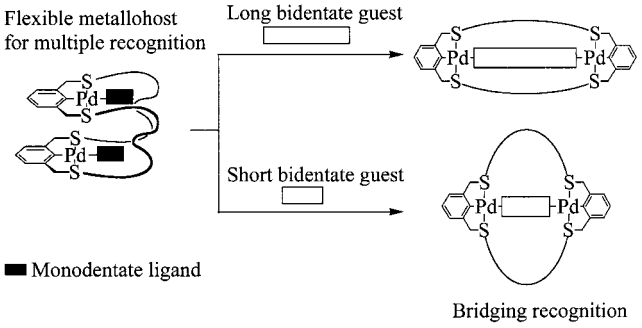

Scheme 1. Recognition of bidentate guests in a bridging fashion

and the following tosylation gave **6a, 6b**. The ditosylates **6a** and **6b** were then treated with **4** under high dilution conditions to give crown ethers **7a** and **7b** in 42% and 45% yield, respectively. Metallation of **7** with $[Pd(CH_3CN)_4](BF_4)_2$[16] yielded metallohosts **1a, 1b**.

All spectroscopic data are consistent with the formula of **1** (see Exp. Sect.). Palladation of **7** caused broadening of the ^1H NMR signals, probably due to the enhanced rigidity of the structure, which restricts the free rotation of the methylene group. On metallation, downfield shifts of the signals for the SCH_2CH_2 protons (e.g. $\delta = 2.60$ for **7b**, $\delta = 3.32$ for **1b**, Figure 1) and the benzyl protons is observed. This is elucidated by the decreased electron-density of these protons. ESI-MS for **1b** gave signals at $m/z = 614.1$ ($C_{52}H_{70}O_{12}S_4Pd_2$, $[\mathbf{1b}-2BF_4-2CH_3CN]^{2+}$) and $m/z = 1247.2$ ($C_{52}H_{70}FO_{12}S_4Pd_2$, $[\mathbf{1b}-2BF_4-2CH_3CN+F]^+$), (the F^- anion was obtained from decomposition of the BF_4^- anion during the ESI-MS measurements). In addition, the X-ray crystallographic analysis clarified the structure of **1b** (Figure 2). The two complex moieties exhibit square-planar geometry at Pd, with three donor atoms provided by the rigid SCS chelate. The Pd−S distances are in

[a] Department of Chemistry, University of Tsukuba, Tsukuba, Ibaraki 305-8571, Japan
Fax: (internat.) +81-29-853-6503
E-mail: nabesima@chem.tsukuba.ac.jp

Supporting information for this article is available on the WWW under http://www.eurjic.org or from the author.

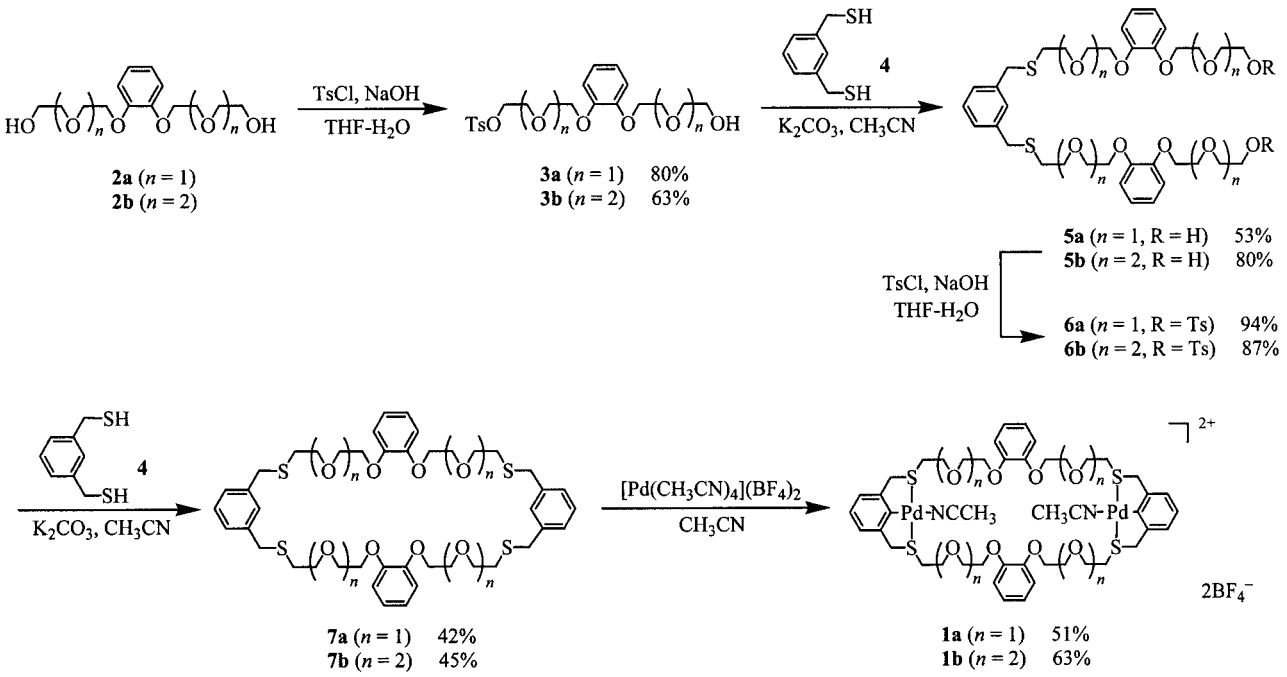

Scheme 2. Synthesis of metallohosts **1**

the range between 2.334 Å and 2.286 Å. The two aromatic rings, which bind the palladium atoms, are stacked. The distance between the mean planes of the benzene rings (3.4 Å) suggests the existence of π-π interactions. Furthermore, the palladium atoms are located in closely proximity of the sulfur atoms. The distance between Pd2−S2 (3.371 Å) is shorter than the sum of van der Waals radii for sulfur and palladium (3.43 Å). Two CH_3CN molecules coordinate to Pd, and the Pd1−N1 and Pd2−N2 distances are 2.105 Å and 2.092 Å, respectively.

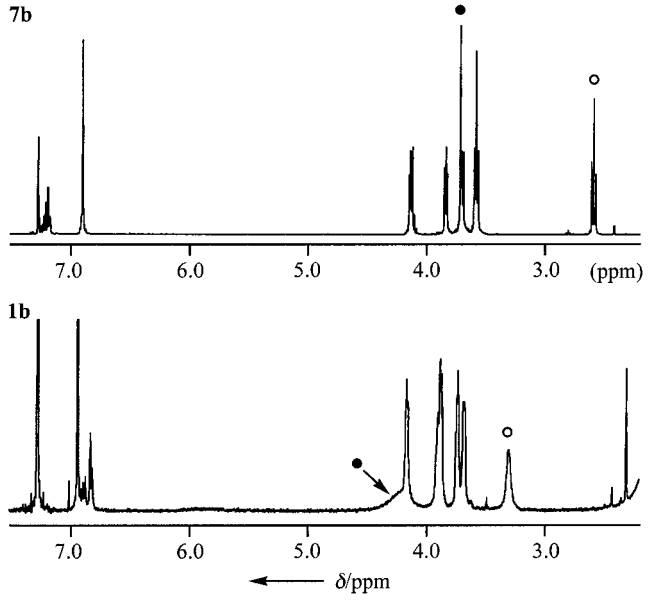

Figure 1. ^1H NMR spectral changes of **7b** upon palladation (400 MHz, $CDCl_3$); SCH_2CH_2O and benzyl protons are indicated with open and filled circles, respectively

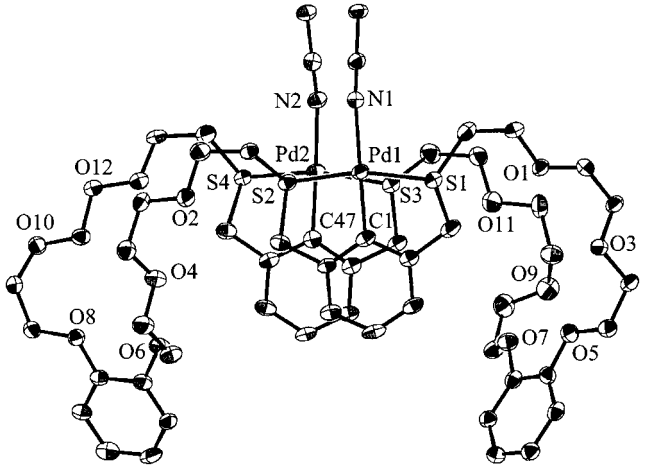

Figure 2. Crystal structure of **1b**; thermal ellipsoids are drawn at 30% probability level; the minor component of the disordered atoms, counter anions, and hydrogen atoms are omitted for clarity

The interaction between **1b** and 4,4′-bipyridine was evaluated by ^1H NMR spectroscopy (Figure 3). Signals of free **1b** disappear when 1.0 equiv. of 4,4′-bipyridine is added, and no change is observed in the presence of excess ligand. This result supports the 1:1 complexation between **1b** and 4,4′-bipyridine in a bridging fashion as illustrated in Scheme 1. ESI-MS also supports the 1:1 complexation. A mixture of **1b** and 4,4′-bipyridine gives a signal at m/z = 692.1 (calcd. for $C_{62}H_{78}N_2O_{12}S_4Pd_2$, $[\mathbf{1b}-2BF_4-2CH_3CN+4,4'\text{-bipyridine}]^{2+}$). In addition, the absorbance of **1b** at 304 nm increases until 1.0 equivalent of 4,4′-bipyridine is added (Figure 4). All the experiments described above indicate the 1:1 complexation between **1b** and 4,4′-

 © 2004 Wiley-VCH Verlag GmbH & Co. KGaA, Weinheim

bipyridine. Pyrazine and pyrimidine as bidentate ligands also give rise to 1:1 complexation, as seen by ^{1}H NMR spectroscopic experiments, although the distances involving the ligating nitrogen atoms of pyrazine and pyrimidine are much shorter than that of 4,4′-bipyridine.

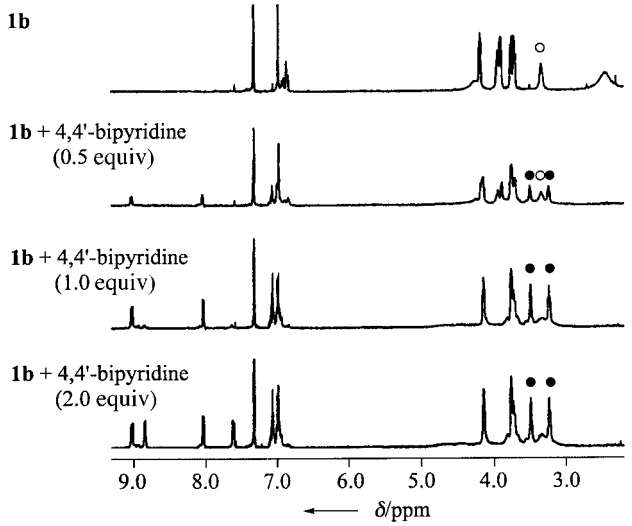

Figure 3. ^{1}H NMR spectral changes of **1b** upon addition of 4,4′-bipyridine (400 MHz, $CDCl_3$, [**1b**] = 2.0 mM); signals for free and complexed **1b** are indicated with open and filled circles, respectively

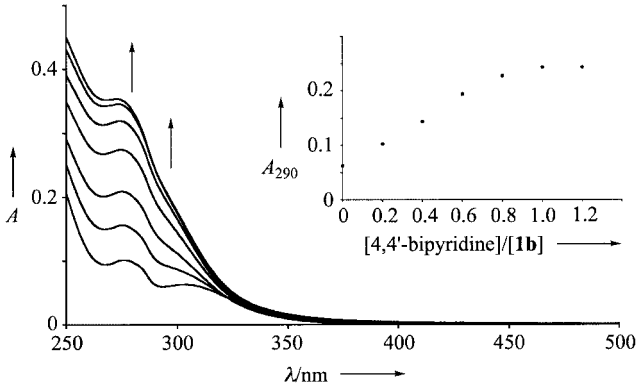

Figure 4. UV/Vis spectral changes of **1b** upon addition of 4,4′-bipyridine ($CHCl_3$, [**1b**] = 1.0×10^{-5} M)

Complexation of **1b** with these bidentate ligands should give two small cavities which are almost half as large as that of **1b** (Scheme 1). The change in cavity size is very interesting, because this strategy may be most useful to regulate recognition ability of artificial receptors.[17−19]

In conclusion, we have prepared metallohosts **1** bearing two Pd centers inside the cavity, and studied the structure and guest-binding ability of **1b** in detail by ^{1}H, ^{13}C NMR spectroscopy or X-ray crystallographic analysis. We are currently investigating this bridging strategy to control molecular recognition.

Experimental Section

Synthesis of 1a: A solution of $[Pd(CH_3CN)_4](BF_4)_2$ (302 mg, 0.680 mmol) in acetonitrile (10 mL) was added to a solution of crown ether **7a** (271 mg, 0.322 mmol) in acetonitrile (20 mL), and the mixture was stirred for 2 h at room temperature. The mixture was refluxed for 13 h, and then the solvent was evaporated. The residue was dissolved in dichloromethane (20 mL) and filtered. The filtrate was concentrated and dried in vacuo to afford **1a** (215 mg, 51%) as a yellow solid, which was further purified by recrystallization from acetonitrile to give pale yellow crystals. ^{1}H NMR (400 MHz, CD_3CN): δ = 3.30 (br. s, 8 H), 3.80 (t, J = 4.2 Hz, 8 H), 3.90 (br. t, 8 H), 4.12 (t, J = 4.2 Hz, 8 H), 4.29 (br. t, 8 H), 6.77 (d, J = 7.6 Hz, 4 H), 6.90−6.99 (m, 10 H) ppm. ^{13}C NMR (100 MHz, CD_3CN): δ = 40.00, 46.78 (br.), 69.20, 70.54 (×2, CH_2), 114.78, 122.39, 123.96, 126.65 (CH), 149.49, 151.65 (br.), 156 (br., C) ppm. ESI-MS: *m/z* found 1071.1 [**1a**−2BF_4−2CH_3CN+F]$^+$. $C_{48}H_{60}B_2F_8N_2O_8Pd_2S_4$: calcd. C 44.09, H 4.62, N 2.14; found C 43.78, H 4.57, N 2.28.

Synthesis of 1b: 1b was prepared from **7b** (319 mg, 0.315 mmol) and $[Pd(CH_3CN)_4](BF_4)_2$ (302 mg, 0.680 mmol) in 63% yield by a procedure similar to that for **1a**. **1b**: yellow oil. ^{1}H NMR (400 MHz, $CDCl_3$): δ = 3.32 (br. s, 8 H), 3.67−3.69 (m, 8 H), 3.73−3.75 (m, 8 H), 3.86−3.89 (m, 8 H), 3.90−3.92 (m, 8 H), 4.16 (t, J = 4.0 Hz, 8 H), 4.18 (br., 8 H), 6.79 (d, J = 7.0 Hz, 4 H), 6.85 (t, J = 7.0 Hz, 2 H), 6.92 (s, 8 H) ppm. ^{13}C NMR (100 MHz, CD_3CN): δ = 39.68, 46.35, 69.40, 70.50 (× 2), 71.29, 71.38 (CH_2), 115.09, 122.40, 124.01, 126.65 (CH), 149.62, 151.72, 156.59 (C) ppm. ESI-MS: *m/z* found 1247.2 [**1b**−2BF_4−2CH_3CN+F]$^+$. $C_{56}H_{76}B_2F_8N_2O_{12}Pd_2S_4$·$CHCl_3$: calcd. C 42.70, H 4.84, N 1.75; found C 42.30, H 5.06, N 2.08.

X-ray Crystallographic Analysis of 1b:[20] Pale yellow crystals (0.3 × 0.15 × 0.1 mm) were obtained after oily **1b** was allowed to stand at room temperature. $C_{56}H_{76}B_2F_8N_2O_{12}Pd_2S_4$, M = 1483.85. Intensity data were collected at 130 K on a Rigaku R-AXIS Rapid diffractometer with Mo-K_α radiation (λ = 0.71069 Å). Reflection data were corrected for Lorentz and polarization factors, and for absorption using the multi-scan method. Crystal system, triclinic, a = 13.2731(12) Å, b = 14.4368(16) Å, c = 18.1120(19) Å, α = 71.267(4)°, β = 71.424(3)°, γ = 86.580(3)°, V = 3112.0(6) Å^3, space group $P\bar{1}$, Z = 2, μ(Mo-K_α) = 0.797 mm^{-1}, $D_{calcd.}$ = 1.584 g/cm^3, $2\theta_{max}$ = 52°, collected reflections 25108, unique reflections 12053 (R_{int} = 0.0719). The structure was solved by Patterson methods (DIRDIF-99)[21] and refined by full-matrix least-squares on F^2 using SHELXL 97.[22] The non-hydrogen atoms were refined anisotropically except for the minor component of disordered sulfur atoms (S4 and S6). Hydrogen atoms were idealized by using the riding models. Occupancy factor involving the disordered sulfur atoms was refined to be 0.888(3) for S3 and S5, and 0.112(3) for S4 and S6. $R1$ = 0.0618 [$I > 2\sigma(I)$], $wR2$ = 0.1537 (all data), GOF (F^2) = 1.036 for 786 parameters.

Acknowledgments

This work was supported by Grants-in-Aid for Scientific Research from the Ministry of Education, Culture, Sports, Science, and Technology, Japan.

[1] J. -M. Lehn, *Supramolecular Chemistry, Concepts and Perspectives*, VCH: Weinheim, **1995**.
[2] T. Nabeshima, *Coord. Chem. Rev.* **1996**, *148*, 151−169.
[3] T. Nabeshima, S. Akine, T. Saiki, *Rev. Heteroat. Chem.* **2000**, *22*, 219−239.
[4] D. L. Caulder, K. N. Raymond, *J. Chem. Soc., Dalton Trans.* **1999**, 1185−1200.

 © 2004 Wiley-VCH Verlag GmbH & Co. KGaA, Weinheim

[5] M. Albrecht, *Chem. Rev.* **2001**, *101*, 3457−3497.
[6] T. Nabeshima, Y. Yoshihira, T. Saiki, S. Akine, E. Horn, *J. Am. Chem. Soc.* **2003**, *125*, 28−29.
[7] M. Albrecht, G. van Koten, *Angew. Chem. Int. Ed.* **2001**, *40*, 3750−3781.
[8] J. E. Kickham, S. J. Loeb, *J. Chem. Soc., Chem. Commun.* **1993**, 1848−1850.
[9] J. E. Kickham, S. J. Loeb, *Inorg. Chem.* **1994**, *33*, 4351−4359.
[10] J. E. Kickham, S. J. Loeb, *Inorg. Chem.* **1995**, *34*, 5656−5665.
[11] J. E. Kickham, S. J. Loeb, S. L. Murphy, *J. Am. Chem. Soc.* **1993**, *115*, 7031−7032.
[12] J. E. Kickham, S. J. Loeb, *Organometallics* **1995**, *14*, 3584−3587.
[13] S. Kopolow, T. E. Hogen Esch, J. Smid, *Macromolecules* **1973**, *6*, 133−142.
[14] S. Shinkai, K. Inuzuka, O. Miyazaki, O. Manabe, *J. Am. Chem. Soc.* **1985**, *107*, 3950−3955.
[15] T. Sato, K. Nishiyama, A. Morita, Y. Iitaka, *Bull. Chem. Soc. Jpn.* **1985**, *58*, 2366−2369.
[16] R. F. Schramm, B. B. Wayland, *J. Chem. Soc., Chem. Commun.* **1968**, 898−899.
[17] T. Nabeshima, H. Furusawa, Y. Yano, *Angew. Chem. Int. Ed. Engl.* **1994**, *33*, 1750−1751.
[18] T. Nabeshima, D. Nishida, *Tetrahedron Lett.* **2002**, *43*, 5719−5722.
[19] T. Nabeshima, D. Nishida, T. Saiki, *Tetrahedron* **2003**, *59*, 639−647.
[20] CCDC-241251 contains the supplementary crystallographic data for this paper. These data can be obtained free of charge at http://www.ccdc.cam.ac.uk/conts/retrieving.html [or from the Cambridge Crystallographic Data Centre, 12 Union Road, Cambridge CB2 1EZ, UK; Fax: (internat.) +44-1223-336-033; E-mail: deposit@ccdc.cam.ac.uk].
[21] P. T. Beurskens, G. Beurskens, R. de Gelder, S. Garcia-Granda, R. O. Gould, R. Israel, J. M. M. Smits, The DIRDIF-99 program system, Crystallography Laboratory, University of Nijmegen, The Netherlands, **1999**.
[22] G. M. Sheldrick, *SHELXL 97, Program for crystal structure refinement*, University of Göttingen, Germany, **1997**.

Received June 11, 2004

 © 2004 Wiley-VCH Verlag GmbH & Co. KGaA, Weinheim

Discrete Dinuclear Complexes and Two-Dimensional Architectures from Bridging Polynitrile and Bipyrimidine (bpym) Ligands: Syntheses, Structures and Magnetic Properties of $[M_2(bpym)(dcne)_4(H_2O)_2]$ ($M = Mn^{II}$, Co^{II}) and $[M_2(bpym)(dcne)_4(H_2O)_4]\cdot 2H_2O$ ($M = Fe^{II}$, Cu^{II}) ($dcne^- = [(CN)_2CC(O)OEt)]^-$)

Franck Thétiot,[a] Smail Triki,*[a] Jean Sala Pala,[a] José-Ramón Galán-Mascarós,[b,c] José M. Martínez-Agudo,[c] and Kim R. Dunbar[b]

Keywords: Bridging ligands / Coordination polymers / Magnetic properties / N ligands / Transition metals

One-pot reactions in aqueous solutions of the polynitrile anion dcne$^-$ {2,2-dicyano-1-ethoxyethenolate = $[(CN)_2CC(O)OEt)]^-$} with the M^{II} ions (M = Mn, Fe, Co, Cu) in the presence of bpym (2,2′-bipyrimidine) afford the first mixed dcne/bpym compounds $[M_2(bpym)(dcne)_4(H_2O)_2]$ (**1**: M = Mn; **2**: M = Co) and $[M_2(bpym)(dcne)_4(H_2O)_4]\cdot 2H_2O$ (**3**: M = Fe; **4**: M = Cu). The new compounds have been characterized by IR spectroscopy and X-ray crystallography. Compounds **1** and **2** are isostructural, with each metal ion being located in an MN_5O pseudo-octahedral environment with three N atoms coming from three dcne$^-$ ligands, two nitrogen atoms from bpym and one oxygen atom from a water molecule. The extended structures of **1** and **2** are best described as dcne-bridged zigzag chains of M^{II} ions running along the [100] direction; connections of these chains in the [010] direction, by the bis(chelating) bpym ligand, afford 2D structures. Compounds **3** and **4** are isostructural, and consist of discrete dinuclear units involving MN_4O_2 octahedrally coordinated M^{II} ions bridged by bis(bidentate) 2,2′-bipyrimidine and terminal dcne ligands. Magnetic measurements for the 2D compounds **1** and **2** exhibit maxima in the χ_m vs. *T* plots (at about 4.5 K for **1** and about 20 K for **2**) which are characteristic of weak antiferromagnetic exchange interactions between the high-spin metal centres. While the dinuclear iron complex **3** presents a similar behaviour (maximum in χ_m vs. *T* plot at 12 K), the antiferromagnetic exchange interactions are stronger in the copper complex **4**. Fits of magnetic data for compounds **1**, **3** and **4** with appropriate models led to *J* values of –0.6, –1.5 and –99.0 cm^{-1} respectively.

(© Wiley-VCH Verlag GmbH & Co. KGaA, 69451 Weinheim, Germany, 2004)

Introduction

Polynitrile molecules are interesting ligands for the preparation of a large variety of discrete and extended molecular structures due to the fact that their cyano groups are disposed in such a way that they cannot coordinate to the same metal cation and that association of the π electronic system of the CN groups with the π system of the central fragment induces electronic delocalization that facilitates transmission of electronic effects between the metal centers (Scheme 1).[1,2]

[a] UMR CNRS 6521, Laboratoire de Chimie, Electrochimie Moléculaires et Chimie Analytique, Université de Bretagne Occidentale,
B. P. 809, 29285 Brest cedex, France
Fax: (internat.) + 33-2-98017001
E-mail: triki@univ-brest.fr
[b] Department of Chemistry, Texas A&M University, College Station,
TX 77842-3012, USA
[c] Instituto de Ciencia Molecular, Universidad de Valencia,
Dr. Moliner 50, 46100 Burjasot, Spain

Reactions of dca$^-$,[3,4] tcm$^-$,[3,5] dcnm$^-$,[6] dcne$^-$,[7] tcnp$^-$,[8] tcpd^{2-} [9] and hcazpd$^-$ [10] with transition metal ions by us and others have led to the isolation of a variety of new compounds, many of which exhibit extended structures and interesting magnetic properties.

Taking into account the crucial role of the bridging ligands in the magnetic properties of such polynuclear or polymeric derivatives, we are interested in using polynitrile ligands in combination with other bridging ligands with the aim of generating new molecular architectures associated with new properties.[11] In this context, the 2,2′-bipyrimidine (bpym) ligand, which is known to transmit antiferromagnetic coupling between paramagnetic centers separated by more than 5.5 Å,[12] is a particularly interesting choice.[13–16] Recently reported results obtained for dca/bpym mixed-ligand complexes reveal that this combination affords a rich variation in molecular architectures. For example, $[M(dca)_2(bpym)(H_2O)]$ (M = Mn, Fe, Co) and $[Mn(dca)_2(bpym)]$ have 1D structures,[17,18]

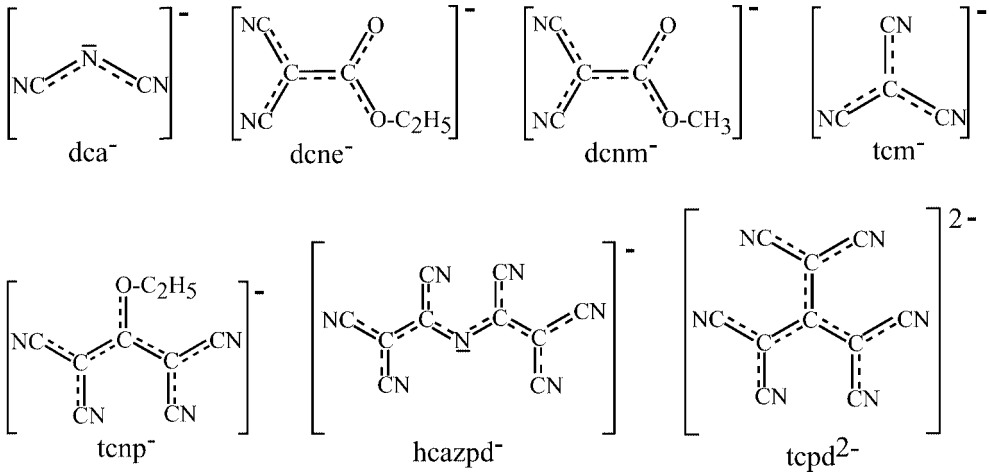

Scheme 1. Examples of polynitrile units with two to six CN groups

$[M_2(dca)_4(bpym)]\cdot H_2O$ (M = Fe, Co) and $[Fe_2(dca)_4(bpym)(H_2O)_2]$ 2D structures,[17,19] and $[M_2(dca)_4(bpym)]$ (M = Mn, Cu) 3D structures.[18,20]

Recently we described M^{II}–dcne binary derivatives of general formula $[M(dcne)_2(H_2O)_2]$ (M = Mn, Fe, Co, Ni, Zn) and $[Cu(dcne)_2(H_2O)]$ with the 2,2-dicyano-1-ethoxyethenolate ligand ($[(CN)_2CC(O)OEt]^-$ = $dcne^-$; Scheme 1). These compounds crystallize as one-dimensional structures with bridging polynitrile ligands.[7] Magnetic measurements indicated that very weak antiferromagnetic coupling occurs in these systems. In order to increase the dimensionality of the materials and therefore favour stronger magnetic coupling, we decided to introduce an auxiliary neutral bridging ligand in these binary systems. These efforts have resulted in the first examples of mixed M^{II}–dcne/bpym ternary compounds whose structures and properties are described herein.

Results and Discussion

Syntheses and IR Characterisation

One-pot reactions in aqueous solutions of the polynitrile anion $dcne^-$ {$[(CN)_2CC(O)OEt]^-$} with M^{II} ions (M = Mn, Fe, Co, Cu) in the presence of bpym (2,2′-bipyrimidine) afforded new mixed dcne/bpym compounds of formula $[M_2(bpym)(dcne)_4(H_2O)_2]$ (**1**: M = Mn; **2**: M = Co) and $[M_2(bpym)(dcne)_4(H_2O)_4]\cdot 2H_2O$ (**3**: M = Fe; **4**: M = Cu).

It is well known that IR spectroscopy can be used as a diagnostic tool for identifying the coordination modes of the 2,2′-bipyrimidine (bpym) ligand, which can act as a single chelate or as a bis(chelate) ligand.[13,16] The former is typically characterised by two intense, absorption features of nearly equal intensities at about 1580 and 1560 cm^{-1}, while the latter is indicated either by an asymmetric doublet or by a single, strong broad feature near 1580 cm^{-1}.[13,16] The single strong band observed near 1580 cm^{-1} in the spectra of **1**–**4** points to a bis(chelate) coordination mode of the bpym ligand.

For the dcne ligand, two absorption bands assigned to ν(CN) are observed in the range 2180–2240 cm^{-1}. The first mode is very similar to that observed for the uncoordinated $dcne^-$ moiety in K(dcne) (intense doublet centered at 2195 cm^{-1}), while the second feature is slightly shifted to higher wavenumbers.[7] These data are in good agreement with the presence of both coordinated and uncoordinated CN groups in compounds **1**–**4**, as confirmed by the X-ray structures.

For each compound, a broad feature indicative of the presence of water molecules [ν_s(OH) and ν_{as}(OH)] is observed (from 3279 cm^{-1} in **2** to 3472 cm^{-1} in **4**); this observation does not allow for the assignment of free versus coordinated H_2O.

Single-Crystal X-ray Studies of Compounds 1–4

The four compounds were characterised by X-ray crystallography. Selected bond lengths and bond angles are provided in Tables 1–3 and the molecular structures are displayed in Figures 1–4.

Structures of $[M_2(bpym)(dcne)_4(H_2O)_2]$ [M = Mn^{II} (1), Co^{II} (2)]

Compounds **1** and **2** are isostructural (see Exp. Sect). Their asymmetric unit consists of one M^{II} ion, two dcne anions and a water molecule, all on general positions, and one bpym molecule centered on the special position (0,0,0). Each metal ion resides in an MN_5O pseudo-octahedral environment with three nitrogen atoms (N3, N4 and N5) coming from three $dcne^-$ ligands, two nitrogen atoms (N1 and N2) from bpym and one oxygen atom (O5) from a water molecule (Figure 1). The metal-ion environment, which involves three $dcne^-$ ligands in a *fac* arrangement, is highly distorted due to the small bite angle of the bpym ligand [71.71(6)° for **1**, 76.44(6)° for **2**] (Table 1). It is noteworthy that the two M–N(bpym) bonds (average: 2.309 Å for **1**

 © 2004 Wiley-VCH Verlag GmbH & Co. KGaA, Weinheim

and 2.169 Å for **2**) are longer than the other four M−L bonds (average: 2.178 Å for **1** and 2.085 Å for **2**), the difference being more pronounced in **1** (ca. 0.13 Å) than in **2** (ca. 0.08 Å).

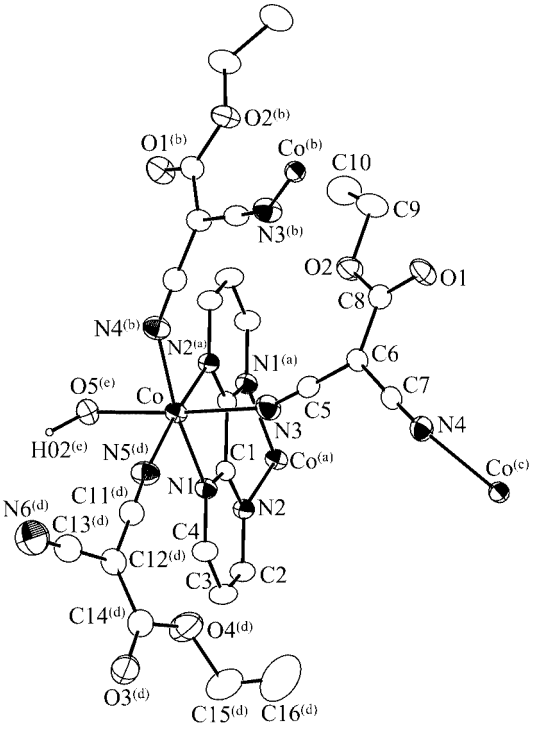

Figure 1. ORTEP view showing the metal environment and the atom labelling scheme in compound **1** (similar to compound **2**); codes of equivalent positions: (a): $-x, -y, -z$; (b): $1/2 + x, 1/2 - y, z$; (c): $-1/2 + x, 1/2 - y, z$; (d): $-1/2 + x, 1/2 - y, -1 + z$; (e): $1/2 - x, -1/2 + y, -z$

Table 1. Selected bond lengths [Å] and angles [°] for compounds **1** and **2**

	1	**2**
M−N1	2.292(2)	2.153(2)
M−N2	2.326(2)	2.185(2)
M−N3	2.208(2)	2.108(2)
M−N5	2.146(2)	2.063(2)
M−O5	2.152(2)	2.054(2)
M−N4	2.207(2)	2.117(2)
N1−M−N2	71.71(6)	76.44(6)
N1−M−N3	90.94(8)	90.02(8)
N1−M−N4	165.50(7)	170.02(7)
N1−M−N5	93.00(8)	94.13(7)
N1−M−O5	88.58(7)	90.90(7)
N2−M−N3	87.70(8)	90.03(8)
N2−M−N4	93.88(7)	94.16(7)
N2−M−N5	164.65(8)	170.26(7)
N2−M−O5	85.32(6)	86.26(7)
N3−M−N4	86.78(9)	86.60(8)
N3−M−N5	94.02(9)	92.44(8)
N3−M−O5	172.79(7)	175.86(7)
N4−M−N5	101.44(8)	95.39(8)
N4−M−O5	91.88(8)	91.83(7)
N5−M−O5	93.19(8)	91.52(7)

The two crystallographically equivalent dcne ligands exhibit μ_2-coordination modes while the other one is monodentate; the bpym ligand acts as a bis(bidentate) ligand. The extended structure resulting from these coordination modes is best described as dcne-bridged zigzag chains of M^{II} ions running along the [100] direction; connections of these chains, in the [010] direction, by the bis(chelating) bpym ligand afford the 2D structure shown in Figure 2. The metal−metal distances across the bpym bridges [6.1152(5) in **1** and 5.7853(4) Å in **2**] are close to those observed in other Mn^{II}−bpym (6.1−6.3 Å)[13] and Co^{II}−bpym (5.76−5.95 Å)[15] derivatives. The M···M distances across

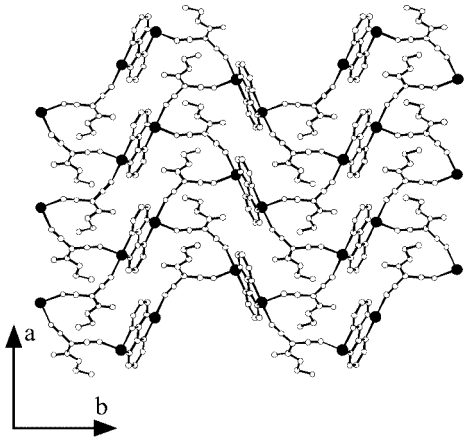

Figure 2. ORTEP view of compound **1** showing the two-dimensional structure (similar to compound **2**); the terminal dcne ligands have been omitted for the sake of clarity

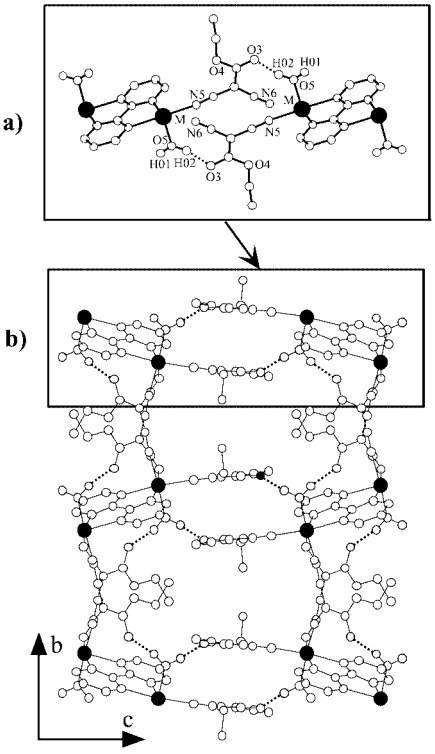

Figure 3. ORTEP view of compound **1** showing the hydrogen bonds between two adjacent sheets (similar to compound **2**)

 © 2004 Wiley-VCH Verlag GmbH & Co. KGaA, Weinheim

the span of the dcne bridges [8.1420(5) in **1** and 8.0867(4) Å in **2**] are longer than the analogous distances observed in the 1D binary compounds $[Co(dcne)_2(H_2O)_2]$ [7.4270(2) Å][7] and $[Mn(dcne)_2(H_2O)_2]$ [7.5906(3) Å].[21]

Careful examination of the inter-layer distances revealed the presence of hydrogen bonds between the terminal oxygen atom of the $dcne^-$ ligands (O3) and the oxygen atom of the water molecule (O5). These hydrogen bonds occur between adjacent sheets [O3···H02 1.731(2) Å and O3···H02−O5 157.6(1)° for **1**; 1.731(2) Å and 164.9(1)° for **2**] as shown in Figure 3, giving rise to overall 3D structures.

Structures of $[M_2(bpym)(dcne)_4(H_2O)_4]\cdot 2H_2O$ (M = Fe^{II}(3), Cu^{II} (4)]

Compounds **3** and **4** are isostructural (see Exp. Sect.). Their asymmetric unit consists of one M^{II} ion, two dcne anions and three water molecules, all on general positions, as well as one bpym molecule centered on the special position (0,1/2,1/2). Each metal ion resides in a *trans*-MN_4O_2 pseudo-octahedral geometry (Figure 4). The four nitrogen atoms are from bpym (N1 and N2) and from two independent *cis*-$dcne^-$ ligands (N3 and N5); the two oxygen atoms arise from water molecules (O5 and O6) in a *trans* arrangement.

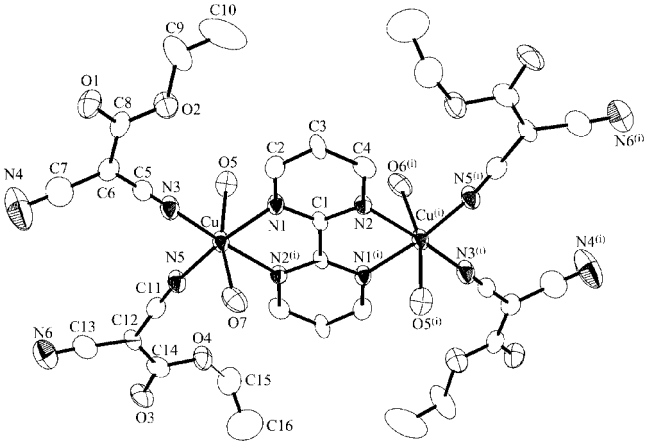

Figure 4. ORTEP view showing the metal environment and the atom labelling scheme in compound **3** (similar to compound **4**); code of equivalent position: (i): $-x$, $1-y$, $1-z$

As in the cases of **1** and **2**, the metal-ion environments are highly distorted due to the small bite angle of the bpym ligand [75.4(1)° for **3** and 80.8(2)° for **4**], but this distortion is more pronounced in compound **4** since the axial Cu−O bonds [2.338(3) and 2.494(3) Å] are much more longer than the four equatorial Cu−N ones (averaged $Cu-N_{bpym}$: 2.06 Å and averaged $Cu-N_{dcne}$: 1.96 Å; Table 2).

Table 2. Selected bond lengths [Å] and angles [°] for compounds **3** and **4**

	3	**4**
M−N1	2.212(4)	2.064(4)
M−N2	2.201(4)	2.045(4)
M−N3	2.121(4)	1.955(4)
M−N5	2.087(5)	1.965(5)
M−O5	2.117(4)	2.338(3)
M−O6	2.106(4)	2.494(3)
N1−M−N2	75.4(1)	80.8(2)
N1−M−N3	92.6(2)	92.0(2)
N1−M−N5	170.1(2)	172.7(1)
N1−M−O5	90.2(2)	87.2(1)
N1−M−O6	84.3(1)	80.0(1)
N2−M−N3	167.9(2)	171.7(2)
N2−M−N5	94.9(2)	92.3(2)
N2−M−O5	87.5(2)	89.3(1)
N2−M−O6	85.8(1)	84.6(1)
N3−M−N5	97.0(2)	94.6(2)
N3−M−O5	94.3(2)	94.5(2)
N3−M−O6	91.5(2)	90.2(1)
N5−M−O5	91.5(2)	95.2(2)
N5−M−O6	93.0(2)	97.1(1)
O5−M−O6	172.2(2)	166.5(1)

While the bpym ligand acts as a bis(bidentate) bridge as in **1** and **2**, all of the dcne ligands in this structure are monodentate, which results in the formation of discrete dinuclear units (Figure 4). The intradinuclear M···M distances through the bpym bridges [5.881(1) in **3** and 5.506(1) Å in **4**] are in the same range observed for other Fe^{II}−bpym (5.5−6.0 Å)[14] and Cu^{II}−bpym (5.3−5.7 Å)[16] derivatives. Careful examination of the inter-dinuclear distances clearly reveals an absence of hydrogen bonding.

Structure of the dcne Ligand

An examination of bond lengths and angles of the dcne ligand in **1**−**4** reveals that the metrical parameters of the dcne ligands are not significantly different in the series (Table 3). Apart from the terminal ethyl group, each dcne ligand is essentially planar within a maximum deviation of 0.1 Å (0.08, 0.10, 0.08 and 0.06 Å for **1**−**4**, respectively) from the corresponding mean plane. The two central carbon atoms of each dcne unit (C6−C8 and C12−C14) exhibit an sp^2 hybridization whereas the carbon atoms of the cyano groups are sp-hybridized, which permits a strong electronic delocalization as indicated by the C−C bonds with bond lengths from 1.390 to 1.436 Å in **1**−**4**. This delocalization is also evident from the rather short terminal C−O bond (range 1.223−1.248 Å), which deviates from a typical C−O single bond (1.50 Å), and by a C−OEt bond (range 1.334−1.350 Å) that also indicates some degree of multiple bonding. As previously reported for the binary system M^{II}−dcne,[7] the structural data in this work are in agreement with the electronic structure depicted in Scheme 2.

 © 2004 Wiley-VCH Verlag GmbH & Co. KGaA, Weinheim

Table 3. Selected bond lengths [Å] and angles [°] for the dcne ligands in compounds **1**−**4**

	1	**2**	**3**	**4**
O1−C8	1.223(3)	1.224(3)	1.227(6)	1.242(7)
O2−C8	1.340(3)	1.341(3)	1.334(7)	1.334(8)
N3−C5	1.147(4)	1.151(3)	1.147(7)	1.153(7)
N4−C7	1.149(3)	1.150(3)	1.154(9)	1.14(1)
C5−C6	1.397(4)	1.399(3)	1.395(7)	1.397(8)
C6−C7	1.403(3)	1.399(3)	1.402(9)	1.42(1)
C6−C8	1.435(3)	1.436(3)	1.428(7)	1.407(7)
O3−C14	1.226(3)	1.232(3)	1.248(6)	1.230(7)
O4−C14	1.350(3)	1.348(3)	1.343(7)	1.342(7)
N5−C11	1.143(3)	1.142(3)	1.160(7)	1.145(7)
N6−C13	1.135(4)	1.136(4)	1.130(8)	1.155(9)
C11−C12	1.390(3)	1.399(3)	1.392(7)	1.398(8)
C12−C13	1.414(4)	1.415(4)	1.420(8)	1.413(9)
C12−C14	1.419(4)	1.416(3)	1.415(8)	1.433(8)
C5−C6−C7	119.3(2)	120.0(2)	121.1(5)	118.6(5)
C5−C6−C8	122.1(2)	121.4(2)	121.2(5)	122.9(6)
C7−C6−C8	118.1(2)	118.0(2)	117.5(5)	118.4(5)
O1−C8−O2	123.8(2)	123.9(2)	123.0(5)	122.2(5)
O1−C8−C6	123.8(2)	123.4(2)	124.6(5)	124.5(6)
O2−C8−C6	112.3(2)	112.7(2)	112.5(4)	113.3(5)
C11−C12−C13	118.7(2)	118.7(2)	121.0(5)	120.4(5)
C11−C12−C14	121.2(2)	121.2(2)	119.5(5)	120.0(5)
C13−C12−C14	120.0(2)	120.2(2)	119.4(5)	119.5(5)
O3−C14−O4	121.8(3)	122.1(2)	120.8(5)	121.9(5)
O3−C14−C12	125.6(3)	125.1(2)	125.2(5)	124.8(6)
O4−C14−C12	112.6(2)	112.8(2)	113.9(4)	113.4(5)

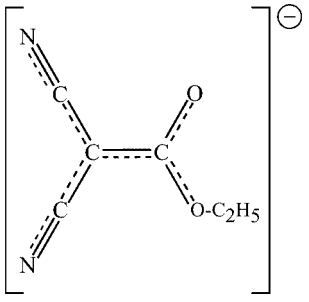

Scheme 2. Mean electronic structure of the dcne ligand

It is particularly noteworthy that the negative charge is not located on the terminal oxygen atom for the dcne ligand and therefore it is not surprising that this atom does not enter in the coordination sphere of the metal atom.

Magnetic Properties

The magnetic properties for compounds **1** (Figure 5), **2** (Figure 6), and **3** (Figure 7) are displayed as the thermal dependence of χ_m and the $\chi_m T$ product, where χ_m is the magnetic susceptibility per formula unit (2 mol of metal ions). These compounds exhibit similar behaviour in the temperature range 2−300 K. The room-temperature $\chi_m T$ values (8.4, 5.4 and 6.0 emu·K·mol^{-1} for **1**, **2** and **3**, respectively) are in good agreement with the expected values for two magnetically isolated high-spin ions [two Mn^{II} (S = 5/2), two Co^{II} (S = 3/2), and two Fe^{II} (S = 2) for **1**, **2** and **3**, respectively].[7,8,13−15] Upon cooling, the $\chi_m T$ products for **1** and **3** remain constant down to approximately 100 K, at which temperature the value decreases sharply and

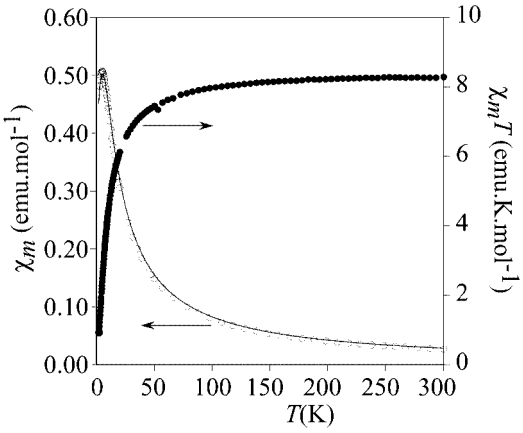

Figure 5. Thermal variations of the magnetic susceptibility in the form $\chi_m T$ (•••) and χ_m (ooo) for compound **1** (solid lines represent the best fit)

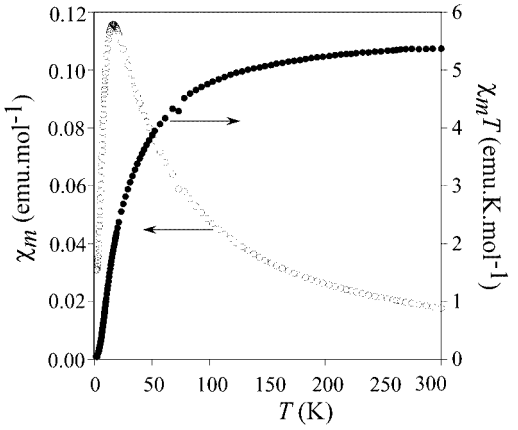

Figure 6. Thermal variations of the magnetic susceptibility in the form $\chi_m T$ (•••) and χ_m (ooo) for compound **2**

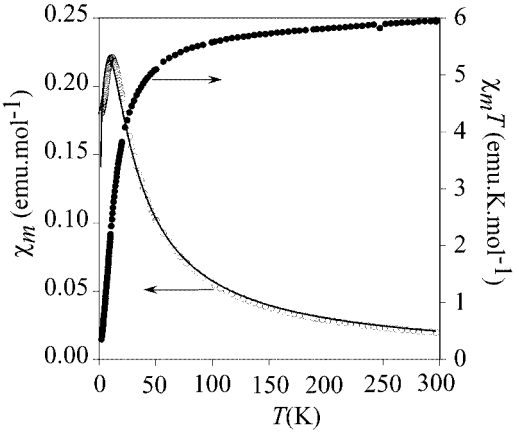

Figure 7. Thermal variations of the magnetic susceptibility in the form $\chi_m T$ (•••) and χ_m (ooo) for compound **3** (solid lines represent the best fit)

 © 2004 Wiley-VCH Verlag GmbH & Co. KGaA, Weinheim

reaches values of 0.92 and 0.36 emu·K·mol^{-1} at 2 K for **1** and **3**, respectively. For the Co derivative **2**, the decrease in the $\chi_m T$ product begins at higher temperatures due to the well-known orbital contribution for this ion,[22] and tends to a value close to zero at 2 K (Figure 6). These data are characteristic of antiferromagnetic exchange interactions between the metal ions and is corroborated by the presence of susceptibility maxima at 4.5, 20 and 12 K for **1**, **2** and **3**, respectively.

A perusal of magnetic data for various related compounds indicates that magnetic interactions through the dcne bridge are weaker ($-J_{dcne} \approx 0.04-0.40$ cm^{-1})[7,13−15] than those observed through a bis(bidentate) bpym ligand ($-J_{bpym} \approx 0.6-10$ cm^{-1} for M = Mn, Fe, Co).[7,13−15] This conclusion led us to fit the magnetic data with a model that only takes into account interactions through the bpym ligand. Thus, to treat the magnetic data we used the susceptibility expressions derived from the spin pairs (5/2-5/2, 3/2-3/2 and 2-2 for **1**−**3**, respectively) coupled through an isotropic exchange interaction J (the Hamiltonian is written as $H = -2JS_aS_b$).[22] This isotropic model cannot be used for the Co derivative **2**, however, due to the important zero-field splitting for this ion, as previously reported for $[Co_2(dca)_4(bpym)]\cdot H_2O$.[17] The analytical expressions are given in Equations (1) and (2) with $C = Ng^2\mu_B{}^2/(k_B)$, $x = J/(k_BT)$, and the parameters N, g, μ_B and k_B having their usual meanings.

$$\text{for } \mathbf{1}: \chi_m = 2(C/T)\{[e^{2x} + 5e^{6x} + 14e^{12x} + 30e^{20x} + 55e^{30x}]/[1 + 3e^{2x} + 5e^{6x} + 7e^{12x} + 9e^{20x} + 11e^{30x}]\} \quad (1)$$

$$\text{for } \mathbf{3}: \chi_m = 2(C/T)\{[e^{2x} + 5e^{6x} + 14e^{12x} + 30e^{20x}]/[1 + 3e^{2x} + 5e^{6x} + 7e^{12x} + 9e^{20x}]\} \quad (2)$$

For both compounds, a satisfactory agreement with the experimental data were observed over the entire temperature range (solid lines in Figures 5 and 7) with the sets of parameters displayed in Table 4. The J values are very similar to those reported for other dinuclear Mn^{II} (−0.4 to −0.6 cm^{-1})[13] and Fe^{II} (−1.5 to −2.1 cm^{-1})[14] derivatives with a bis(bidentate) bpym bridge.

For the Cu derivative **4**, the thermal variation of the magnetic susceptibility presents a broad susceptibility maximum at approximately 150 K (Figure 8) which is higher than the values observed for **1**−**3**, an indication of the presence of strong antiferromagnetic coupling between the two metal ions. The increase observed below 50 K is attributed to the presence of paramagnetic impurities. As for compounds **1** and **3**, the magnetic data were modelled using the susceptibility expression derived from the spin pair 1/2-1/2, by adding in this case a term to take into account a paramagnetic contribution. The analytical expression is given in Equation (3) where $\chi_D = 2(C/T)[1/(3 + e^{-2x})]$ and ρ represents the fraction of uncoupled impurities for which the molecular weight is the same as that of the investigated compound. The best fit, obtained with the values given in Table 4, is plotted as solid lines in Figure 8a.

$$\chi_m = (1 - \rho)\chi_D + (C/2T)\rho \quad (3)$$

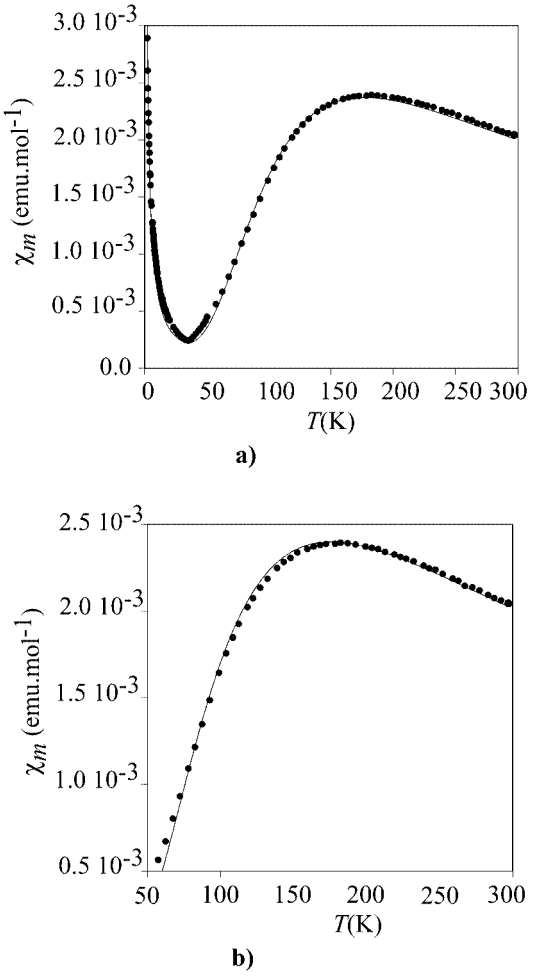

Figure 8. Thermal variations of the magnetic susceptibility for compound **4**, showing two fits of the magnetic data (solid lines): (a) using a model taking into account the paramagnetic impurities, and (b) using a simple model without paramagnetic impurities (see text)

Table 4. Magnetic parameters for compounds **1**, **3** and **4**.

Compound	S	J [cm^{-1}]	g	ρ
$[Mn_2(bpym)(dcne)_4(H_2O)_2]$ (**1**)	5/2	−0.6	2.00	
$[Fe_2(bpym)(dcne)_4(H_2O)_4]\cdot 2H_2O$ (**3**)	2	−1.5	2.05	
$[Cu_2(bpym)(dcne)_4(H_2O)_4]\cdot 2H_2O$ (**4**)	1/2	−99.0	2.12	0.008

In order to confirm the presence of the paramagnetic impurities, a second fit was carried out in the range 50−300 K using the same model but with no paramagnetic impurities ($\rho = 0$; $\chi_m = \chi_D$). The best agreement was obtained with $g = 2.12$ and $J = -98$ cm^{-1} (Figure 8b); these values are very similar to those obtained for the first fit (Table 4),

 © 2004 Wiley-VCH Verlag GmbH & Co. KGaA, Weinheim

which corroborates the hypothesis that the increase in χ_m below 50 K is due to paramagnetic impurities. Finally, it is worth pointing out that the magnetic coupling is much more stronger in the Cu derivative than in other compounds; such a difference has been reported previously in several other compounds with bpym bridges.[16]

Conclusion

This study, which reports a new series of transition-metal derivatives with two types of bridging ligands, confirms the ability of such mixed systems to generate a variety of molecular architectures. The combination of dcne with bpym as ligands afforded both 2D derivatives $[M_2(bpym)(dcne)_4(H_2O)_2]$ (**1**: M = Mn; **2**: M = Co) and discrete dinuclear compounds $[M_2(bpym)(dcne)_4(H_2O)_4]\cdot 2H_2O$ (**3**: M = Fe; **4**: M = Cu). Since compounds without the bpym ligand, such as $[M(dcne)_2(H_2O)_2]$ (M = Mn, Fe, Co, Ni, Zn) and $[Cu(dcne)_2(H_2O)]$, are known to exhibit 1D structures, it is obvious that the introduction of an additional bridging ligand induces significant structural modifications. In an effort to increase the dimensionality of these mixed polynitrile/co-ligand compounds, further work is in progress that involves a similar synthetic strategy with polynitrile anions that possess more than two nitrile substituents.

Experimental Section

Materials and Physical Measurements: All reagents were purchased from commercial sources and used as received (2,2′-bipyrimidine from Lancaster). The potassium 2,2-dicyano-1-ethoxyethenolate {K(dcne) = K[$(CN)_2CC(O)OEt$)]} was prepared according to a recently reported procedure.[7] Elemental analyses were obtained from the Service Central d'Analyses (Vernaison) and Service de Microanalyses de ICSN-CNRS (Gif-sur-Yvette). Infrared spectra were recorded in the range 4000−200 cm^{-1} as KBr pellets on a FT-IR NEXUS NICOLET Spectrometer. Magnetic studies were carried out on powder samples at 0.1 T after zero-field cooling, in the temperature range 2−300 K with an MPMS-XL SQUID magnetometer from Quantum Design housed in the Chemistry Department at Texas A&M University. The susceptibilities were corrected for the sample holder and the diamagnetic contributions of all atoms.

Syntheses: All syntheses were performed under aerobic conditions using the following procedure: 2,2′-Bipyrimidine (20 mg, 0.126 mmol) and K(dcne) (89 mg, 0.504 mmol) were successively added with continuous stirring to a hot aqueous solution of the hydrated metal(II) chloride (0.252 mmol). The resulting solution was filtered and then slowly concentrated to yield crystals which were removed by filtration and air-dried.

Compound 1: Yield 74% (79 mg). $C_{32}H_{30}Mn_2N_{12}O_{10}$ (852.54): calcd. C 45.08, H 3.55, N 19.72; found C 44.92, H 3.61, N 19.59. Colorless crystals. IR (KBr): $\tilde{\nu}$ = 3348 br. and 3290 br. ν(OH), 3114 s, 3082 w, 2996 w, 2980 w, 2229 m, 2219 s and 2194 s ν(CN), 1623 m, 1580 m, 1462 w, 1413 m, 1401 w, 1372 m, 1320 m, 1163 w, 1142 w, 1116 m, 1102 w, 760 w, 693 w, 673 w, 559 w, 550 w, 366 w.

Compound 2: Yield 69% (75 mg). $C_{32}H_{30}Co_2N_{12}O_{10}$ (860.53): calcd. C 44.66, H 3.51, N 19.53; found C 44.74; H 3.51; N 19.49. Orange crystals. IR (KBr): $\tilde{\nu}$ = 3347 br. and 3279 br. ν(OH), 3084 w, 2996 w, 2979 w, 2228 m and 2196 s ν(CN), 1622 s, 1584 m, 1462 w, 1418 m, 1402 w, 1372 m, 1321 m, 1163 w, 1113 m, 1012 w, 760 w, 693 w, 679 w, 547 w, 368 w.

Compound 3: Yield 64% (75 mg). $C_{32}H_{38}Fe_2N_{12}O_{14}$ (926.42): calcd. C 41.49, H 4.13, N 18.14; found C 41.22, H 4.22, N 17.99. Red

Table 5. Crystal data for compounds **1**−**4**

	1	**2**	**3**	**4**
Empirical formula	$C_{32}H_{30}Mn_2N_{12}O_{10}$	$C_{32}H_{30}Co_2N_{12}O_{10}$	$C_{32}H_{38}Fe_2N_{12}O_{14}$	$C_{32}H_{38}Cu_2N_{12}O_{14}$
Formul mass[a]	852.55	860.54	926.43	941.81
Space group	$P2_1/a$	$P2_1/a$	$P\bar{1}$	$P\bar{1}$
a [Å]	8.2320(2)	8.1772(2)	7.1857(4)	7.0670(3)
b [Å]	19.3486(5)	19.0699(5)	12.2737(6)	12.5536(5)
c [Å]	12.9429(3)	12.7165(4)	12.8907(7)	12.6724(5)
α [°]	90	90	102.2(1)	103.265(7)
β [°]	96.38(7)	96.9(1)	102.4(2)	102.941(6)
γ [°]	90	90	100.2(1)	102.612(7)
V (Å^3)	2048.7(4)	1968.6(6)	1055(2)	1022.4(2)
Z[a]	2	2	1	1
$D_{calcd.}$ [g·cm^{-3}]	1.38	1.45	1.46	1.53
μ [mm^{-1}]	0.654	0.906	0.759	1.117
F(000)	872	880	478	484
Refl. measured	6735	10157	6271	6122
2θ range [°]	5.0−50.70	5.0−60.10	5.0−51.0	5.0−52.02
Refl. unique/R_{int}	3623/0.026	5502/0.031	3675/0.051	3714/0.05
Refl. with [I > $n\sigma(I)$]	2459 (n = 3)	2904 (n = 3)	2141 (n = 2)	2150 (n = 2)
N_v	253	253	271	271
$R(F_o)$[b]/$R_w(F_o)$[c]	0.033/0.039	0.034/0.039	0.055/0.060	0.050/0.053
Goodness-of-fit[d]	1.146	1.300	1.229	1.053
$\Delta\rho_{max,/min}$ [e/Å^3]	+0.194/−0.329	+0.205/−0.388	+0.602/−0.450	+0.500/−0.492

[a] For compounds **1**−**4** the asymmetric unit contains half of the chemical formula. [b] $R = \Sigma||F_o| - |F_c||/|F_o|$. [c] $Rw = [\Sigma w(|F_o| - |F_c|)^2/w(F_o)^2]^{1/2}$. [d] G.O.F = $[(\Sigma w|F_o| - |F_c|)^2/(N_{obs} - N_{var})]^{1/2}$.

 © 2004 Wiley-VCH Verlag GmbH & Co. KGaA, Weinheim

crystals. IR (KBr): $\tilde{\nu}$ = 3349 br. ν(OH), 3090 w, 2994 w, 2980 w, 2214 m and 2187 s ν(CN), 1647 m, 1607 s, 1582 s, 1471 w, 1425 m, 1400 w, 1378 m, 1329 m, 1170 w, 1120 m, 1012 w, 755 w, 692 w, 667 w, 553 w, 365 w.

Compound 4: Yield 76% (90 mg). $C_{32}H_{38}Cu_2N_{12}O_{14}$ (941.82): calcd. C 40.81, H 4.07, N 17.85; found C 40.57, H 4.15, N 17.64. Brown crystals. IR (KBr): $\tilde{\nu}$ = 3472 br. ν(OH), 3082 w, 2990 w, 2971 w, 2209 s and 2181 s ν(CN), 1643 s, 1587 m, 1471 w, 1413 w, 1404 w, 1375 m, 1321 s, 1144 m, 1113 w, 1024 w, 754 w, 692 w, 685 w, 553 w, 364 w.

X-ray Structural Determinations: Data were collected at 288 K with a Nonius KappaCCD Diffractometer, equipped with an Oxford Cryosystem Cryostream cooler device and graphite-monochromated Mo-K_α radiation (λ = 0.71073 Å). The crystal structures were solved by direct methods and successive Fourier difference syntheses, and were refined on F^2 by weighted anisotropic full-matrix least-squares methods (Table 5).[23] The positions of all hydrogen atoms of the dcne ligands were calculated [d(C−H) = 0.95Å]; the thermal parameters were taken as $U_{iso} = 1.3U_{equ}$(C) and therefore included as isotropic fixed contributors to F_c in the four structures. The hydrogen atoms of the water molecules were not observed, except those of the coordinated water molecule O5 of compounds **1** and **2**, which were located by difference Fourier maps and refined isotropically. Scattering factors and corrections for anomalous dispersion were taken from the International Tables for X-ray Crystallography.[24] All calculations were performed with an Alphastation 255 4/233 computer. Selected bond lengths and angles are listed in Tables 1−3, pertinent crystal data in Table 5. CCDC-232956 to -232959 (**1**−**4**, respectively) contain the supplementary crystallographic data for this paper. These data can be obtained free of charge at www.ccdc.cam.ac.uk/conts/retrieving.html [or from the Cambridge Crystallographic Data Centre, 12 Union Road, Cambridge CB2 1EZ, UK; Fax: (internat. + 44-1223-336-033; E-mail: deposit@ccdc.cam.ac.uk].

Acknowledgments

F. T., S. T. and J. S. P. gratefully acknowledge the CNRS (Centre National de la Recherche Scientifique) and UMR CNRS 6521 for support of this work. F. T. thanks the Ministère de l'Education Nationale, de la Recherche et de la Technologie for a thesis grant. J.-R. G.-M. thanks the Ministerio de Educacion y Cultura for a Ramón y Cajal contract. K. R. D. gratefully acknowledges the National Science Foundation (CHE-9906583) for support.

[1] [1a] T. L. Cairns, R. A. Carboni, D. D. Coffman, V. A. Engelhardt, R. E. Heckert, E. L. Little, E. McGeer, B. C. McKusick, J. Middleton, R. M. Scribner, C. W. Theobald, H. E. Winberg, *J. Am. Chem. Soc.* **1958**, *80*, 2775−2778. [1b] W. J. Middleton, V. A. Engelhardt, *J. Am. Chem. Soc.* **1958**, *80*, 2788−2795. [1c] W. J. Middleton, E. L. Little, D. D. Coffman, V. A. Engelhardt, *J. Am. Chem. Soc.* **1958**, *80*, 2795−2806. [1d] T. L. Cairns, B. C. McKusick, *Angew. Chem.* **1961**, *73*, 520−525. [1e] O. W. Webster, W. Mahler, R. E. Benson, *J. Am. Chem. Soc.* **1962**, *84*, 3678−3684. [1f] L. R. Melby, R. J. Harder, W. R. Hertler, W. Mahler, R. E. Benson, W. E. Mochel, *J. Am. Chem. Soc.* **1962**, *84*, 3374−3387.

[2] [2a] K. R. Dunbar, *Angew. Chem.* **1996**, *108*, 1769−1771; *Angew. Chem. Int. Ed. Engl.* **1996**, *35*, 1659−1671. [2b] W. Kaim, M. Moscherosch, *Coord. Chem. Rev.* **1994**, *129*, 157−173. [2c] J. M. Manriquez, T. Y. Gordon, R. S. McLean, A. J. Epstein, J. S. Miller, *Science* **1991**, *252*, 1415−1417. [2d] R. Kato, H. Kobayashi, A. Kobayashi, *J. Am. Chem. Soc.* **1989**, *111*, 5224−5232. [2e] J. S. Miller, A. J. Epstein, W. M. Reiff, *Chem. Rev.* **1988**, *88*, 201−220.

[3] S. R. Batten, K. S. Murray, *Coord. Chem. Rev.* **2003**, *246*, 103−130, and references cited therein.

[4] [4a] M. R. Pederson, A. Y. Liu, T. Baruah, E. Z. Kurmaev, A. Moewes, S. Chiuzbaian, M. Neumann, C. R. Kmety, K. L. Stevenson, D. Ederer, *Phys. Rev. B* **2002**, *66*, 014446, 1−8. [4b] P. M. van der Werff, S. R. Batten, P. Jensen, B. Moubaraki, K. S. Murray, *Inorg. Chem.* **2001**, *40*, 1718−1722. [4c] P. M. van der Werff, S. R. Batten, P. Jensen, B. Moubaraki, K. S. Murray, E. H. K. Tan, *Polyhedron* **2001**, *20*, 1129−1138. [4d] P. Jensen, D. J. Price, S. R. Batten, B. Moubaraki, K. S. Murray, *Chem. Eur. J.* **2000**, *6*, 3186−3195. [4e] S. R. Batten, P. Jensen, B. Moubaraki, K. S. Murray, *Chem. Commun.* **2000**, 2331−2332. [4f] C. R. Kmety, Q.-Z. Huang, J. W. Lynn, R. W. Erwin, J. L. Manson, S. McCall, J. E. Crow, K. L. Stevenson, J. S. Miller, A. J. Epstein, *Phys. Rev. B* **2000**, *62*, 5576−5588. [4g] S. R. Batten, P. Jensen, C. J. Kepert, M. Kurmoo, B. Moubaraki, K. S. Murray, D. J. Price, *J. Chem. Soc., Dalton Trans.* **1999**, 2987−2997. [4h] P. Jensen, S. R. Batten, G. D. Fallon, B. Moubaraki, K. S. Murray, D. J. Price, *Chem. Commun.* **1999**, 177−178. [4i] S. R. Batten, P. Jensen, B. Moubaraki, K. S. Murray, R. Robson, *Chem. Commun.* **1998**, 439−440. [4j] M. Kurmoo, C. J. Kepert, *New J. Chem.* **1998**, *22*, 1515−1524. [4k] J. L. Manson, C. R. Kmety, Q. Z. Huang, J. W. Lynn, G. M. Bendele, S. Pagola, P. W. Stephens, L. M. Liable-Sands, A. L. Rheingold, A. J. Epstein, J. S. Miller, *Chem. Mater.* **1998**, *10*, 2552−2560.

[5] [5a] F. Thétiot, S. Triki, J. Sala Pala, S. Golhen, *Inorg. Chim. Acta* **2003**, *350*, 314−320. [5b] R. Feyerherm, A. Loose, J. L. Manson, *J. Phys.: Condens. Matter* **2003**, *15*, 663−673. [5c] J. L. Manson, E. Ressouche, J. S. Miller, *Inorg. Chem.* **2000**, *39*, 1135−1141. [5d] S. R. Batten, B. F. Hoskins, R. Robson, *Chem. Eur. J.* **2000**, *6*, 156−161. [5e] S. R. Batten, B. F. Hoskins, B. Moubaraki, K. S. Murray, R. Robson, *J. Chem. Soc., Dalton Trans.* **1999**, 2977−2986. [5f] H. Oshino, K. Iida, T. Kawamoto, T. Mori, *Inorg. Chem.* **1999**, *38*, 4229−4232. [5g] J. L. Manson, C. Campana, J. S. Miller, *Chem. Commun.* **1998**, 251−252. [5h] S. R. Batten, B. F. Hoskins, R. Robson, *New J. Chem.* **1998**, *22*, 173−175.

[6] C. Kremer, C. Melián, J. Torres, M. P. Juanicó, C. Lamas, H. Pezaroglo, E. Manta, H. Schumann, J. Pickardt, F. Girgsdies, O. N. Ventura, F. Lloret, *Inorg. Chim. Acta* **2001**, *314*, 83−90.

[7] F. Thétiot, S. Triki, J. Sala Pala, C. J. Gómez-García, *J. Chem. Soc., Dalton Trans.* **2002**, 1687−1693.

[8] F. Thétiot, S. Triki, J. Sala Pala, *Polyhedron* **2003**, *22*, 1837−1843.

[9] [9a] S. Triki, J. Sala Pala, M. Decoster, P. Molinié, L. Toupet, *Angew. Chem.* **1999**, *111*, 155−158; *Angew. Chem. Int. Ed.* **1999**, *38*, 113−115. [9b] S. Triki, J. Sala Pala, A. Riou, P. Molinié, *Synth. Met.* **1999**, *102*, 1472−1473.

[10] M. Decoster, J. E. Guerchais, Y. Le Mest, J. Sala Pala, S. Triki, L. Toupet, *Polyhedron* **1996**, *15*, 195−202.

[11] For mixed polynitrile/coligand transition-metal compounds, see for example: [11a] J. L. Manson, J. Gu, J. A. Schlueter, H. H. Wang, *Inorg. Chem.* **2003**, *42*, 3950−3955. [11b] C. M. Brown, J. L. Manson, *J. Am. Chem. Soc.* **2002**, *124*, 12600−12605. [11c] A. M. Kutasi, S. R. Batten, B. Moubaraki, K. S. Murray, *J. Chem. Soc., Dalton Trans.* **2002**, 819−821. [11d] A. M. Kutasi, S. R. Batten, A. H. Harris, B. Moubaraki, K. S. Murray, *Aust. J. Chem.* **2002**, *55*, 311−313. [11e] P. Jensen, S. R. Batten, B. Moubaraki, K. S. Murray, *J. Chem. Soc., Dalton Trans.* **2002**, 3712−3722. [11f] S. Martin, M. G. Barandika, J. M. Ezpeleta, R. Cortés, J. I. Ruiz de Larramendi, L. Lezama, T. Rojo, *J. Chem. Soc., Dalton Trans.* **2002**, 4275−4280. [11g] I. Riggio, G. A. van Albada, D. D. Ellis, A. L. Spek, J. Reedijk, *Inorg. Chim. Acta* **2001**, *313*, 120−124. [11h] P. Jensen, S. R. Batten, B. Moubaraki, K. S. Murray, *J. Solid State Chem.* **2001**, *159*, 352−361. [11i] J. L. Manson, Q.-Z. Huang, J. W. Lynn, H.-J. Koo, M.-H. Whangbo, R. Bateman, T. Otsuka, N. Wada, D. N. Argyriou,

J. S. Miller, *J. Am. Chem. Soc.* **2001**, *123*, 162−172. [11j] S. R. Batten, A. R. Harris, P. Jensen, K. S. Murray, A. Ziebell, *J. Chem. Soc., Dalton Trans.* **2000**, 3829−3835. [11k] P. Jensen, S. R. Batten, B. Moubaraki, K. S. Murray, *Chem. Commun.* **2000**, 793−794. [11l] B.-W. Sun, S. Gao, B.-Q. Ma, Z.-M. Wang, *New J. Chem.* **2000**, *24*, 953−954. [11m] J. L. Manson, C. D. Incarvito, A. L. Rheingold, J. S. Miller, *J. Chem. Soc., Dalton Trans.* **1998**, 3705−3706. [11n] S. R. Batten, B. F. Hoskins, R. Robson, *Inorg. Chem.* **1998**, *37*, 3432−3434.

[12] G. De Munno, M. Julve, *NATO ASI Ser. Ser. C* **1996**, *474*, 139−162 and references cited therein.

[13] For Mn−bpym complexes see for example: [13a] D. Armentano, G. De Munno, F. Guerra, J. Faus, F. Lloret, M. Julve, *Dalton Trans.* **2003**, *24*, 4626−4634. [13b] J. M. Herrera, D. Armentano, G. De Munno, F. Lloret, J. Faus, M. Julve, M. Verdaguer, *New J. Chem.* **2003**, *27*, 128−133. [13c] L. M. Toma, R. Lescouëzec, L. D. Toma, F. Lloret, M. Julve, J. Vaissermann, M. Andruh, *J. Chem. Soc., Dalton Trans.* **2002**, 3171−3176. [13d] S. Martin, M. G. Barandika, M. J. Ruiz de Larramendi, R. Cortès, M. Font-Bardia, L. Lezama, Z. E. Serna, X. Solans, T. Rojo, *Inorg. Chem.* **2001**, *40*, 3687−3692. [13e] G. De Munno, T. Poerio, M. Julve, F. Lloret, G. Viau, A. Caneschi, *J. Chem. Soc., Dalton Trans.* **1997**, 601−606. [13f] G. De Munno, G. Viau, M. Julve, F. Lloret, J. Faus, *Inorg. Chim. Acta* **1997**, *257*, 121−129. [13g] G. De Munno, M. Julve, G. Viau, F. Lloret, J. Faus, D. Viterbo, *Angew. Chem.* **1996**, *108*, 1931−1934; *Angew. Chem. Int. Ed. Engl.* **1996**, *35*, 1807−1810. [13h] R. Cortés, L. Lezama, J. L. Pizarro, M. I. Arriortua, T. Rojo, *Angew. Chem.* **1996**, *108*, 1934−1936; *Angew. Chem. Int. Ed. Engl.* **1996**, *35*, 1810−1812. [13i] G. De Munno, R. Ruiz, F. Lloret, J. Faus, R. Sessoli, M. Julve, *Inorg. Chem.* **1995**, *34*, 408−411.

[14] For Fe-bpym complexes see for example: [14a] D. Armentano, G. De Munno, F. Lloret, M. Julve, J. Curély, A. M. Babb, J. Y. Lu, *New J. Chem.* **2003**, *27*, 161−165. [14b] D. Armentano, G. De Munno, J. Faus, F. Lloret, M. Julve, *Inorg. Chem.* **2001**, *40*, 655−660. [14c] J. S. Sun, H. Zhao, X. Ouyang, R. Clérac, J. A. Smith, J. M. Clemente-Juan, C. Gomez-Garcia, E. Coronado, K. Dunbar, *Inorg. Chem.* **1999**, *38*, 5841−5855. [14d] G. De Munno, V. Walter, G. Viau, F. Lloret, J. Faus, M. Julve, *Inorg. Chem.* **1998**, *37*, 1458−1464. [14e] G. De Munno, T. Poerio, G. Viau, M. Julve, F. Lloret, *Angew. Chem. Int. Ed. Engl.* **1997**, *36*, 1459−1461. [14f] G. De Munno, M. Julve, J. A. Real, *Inorg. Chim. Acta* **1997**, *255*, 185−188. [14g] G. De Munno, T. Poerio, G. Viau, M. Julve, F. Lloret, Y. Journaux, E. Rivière, *Chem. Commun.* **1996**, 2587−2588. [14h] G. De Munno, M. Julve, J. A. Real, F. Lloret, R. Scopelliti, *Inorg. Chim. Acta* **1996**, *250*, 81−85. [14i] E. Andrès, G. De Munno, M. Julve, J. A. Real, F. Lloret, *J. Chem. Soc., Dalton Trans.* **1993**, 2169−2174. [14j] J. A. Real, J. Zarembovitch, O. Kahn, X. Solans, *Inorg. Chem.* **1987**, *26*, 2939−2943.

[15] For Co−bpym complexes see for example: [15a] G. De Munno, T. Poerio, M. Julve, F. Lloret, G. Viau, *New J. Chem.* **1998**, *22*, 299−305. [15b] G. De Munno, M. Julve, F. Lloret, J. Faus, A. Caneschi, *J. Chem. Soc., Dalton Trans.* **1994**, 1175−1183.

[16] For Cu−bpym complexes, see for example: [16a] Y. Rodriguez-Martin, J. Sanchiz, C. Ruiz-Pérez, F. Lloret, M. Julve, *Inorg. Chim. Acta* **2001**, *326*, 20−26. [16b] G. De Munno, T. Poerio, M. Julve, F. Lloret, J. Faus, A. Caneschi, *J. Chem. Soc., Dalton Trans.* **1998**, 1679−1685. [16c] G. De Munno, M. Julve, F. Lloret, J. Cano, A. Caneschi, *Inorg. Chem.* **1995**, *34*, 2048−2053. [16d] G. De Munno, M. Julve, F. Lloret, J. Faus, M. Verdaguer, A. Caneschi, *Inorg. Chem.* **1995**, *34*, 157−165. [16e] I. Castro, J. Sletten, L. K. Glaerum, J. Cano, F. Lloret, J. Faus, M. Julve, *J. Chem. Soc., Dalton Trans.* **1995**, 3207−3213. [16f] I. Castro, J. Sletten, L. K. Glaerum, F. Lloret, J. Faus, M. Julve, *J. Chem. Soc., Dalton Trans.* **1994**, 2777−2782. [16g] G. De Munno, J. A. Real, M. Julve, M. C. Munoz, *Inorg. Chim. Acta* **1993**, *211*, 227−233. [16h] G. De Munno, M. Julve, F. Nicolo, F. Lloret, J. Faus, R. Ruiz, E. Sinn, *Angew. Chem.* **1993**, *105*, 588−590; *Angew. Chem. Int. Ed. Engl.* **1993**, *32*, 613−615. [16i] G. De Munno, M. Julve, F. Lloret, J. Faus, R. Ruiz, E. Sinn, *Angew. Chem.* **1993**, *105*, 1122−1124; *Angew. Chem. Int. Ed. Engl.* **1993**, *32*, 1046−1048. [16j] G. De Munno, M. Julve, M. Verdaguer, G. Bruno, *Inorg. Chem.* **1993**, *32*, 2215−2220. [16k] M. Julve, M. Verdaguer, G. De Munno, J. A Real, G. Bruno, *Inorg. Chem.* **1993**, *32*, 795−802.

[17] S. R. Marshall, C. D. Incarvito, J. L. Manson, A. L. Rheingold, J. S. Miller, *Inorg. Chem.* **2000**, *39*, 1969−1973.

[18] [18a] S. Martin, M. G. Barandika, J. I. Ruiz de Larramandi, M. K. Urtiada, L. Lezama, M. I. Arriortua, T. Rojo, *Eur. J. Inorg. Chem.* **2001**, 2107−2113. [18b] S. Martin, M. G. Barandika, J. I. Ruiz de Larramandi, R. Cortés, M. Font-Bardia, L. Lezama, Z. E. Serna, X. Solans, T. Rojo, *Inorg. Chem.* **2001**, *40*, 3687−3692.

[19] S. Triki, F. Thétiot, J. R. Galán-Mascarós, J. Sala Pala, K. R. Dunbar, *New J. Chem.* **2001**, *25*, 954−958.

[20] B. Vangdal, J. Carranza, F. Lloret, M. Julve, J. Sletten, *J. Chem. Soc., Dalton Trans.* **2002**, 566−574.

[21] Structure of $[Mn(dcne)_2(H_2O)_2]$: S. Triki et al., unpublished results.

[22] O. Kahn, *Molecular Magnetism*, VCH Publishers, New York, **1993**.

[23] C. K. Fair, *MolEN, An Interactive Intelligent System for Crystal Structure Analysis*, User Manual, Enraf-Nonius, Delft, The Netherlands, **1985**.

[24] *International Tables for X-ray Crystallography*, Kynoch Press, Birmingham, U. K. **1975**, vol. 4.

Received March 12, 2004
Early View Article
Published Online July 27, 2004

 © 2004 Wiley-VCH Verlag GmbH & Co. KGaA, Weinheim

Magnetic Properties of Lone-Pair-Containing, Sandwich-Type Polyoxoanions: A Detailed Study of the Heteroatomic Effect

Ashley C. Stowe,[a] Saritha Nellutla,[a] Naresh S. Dalal,*[a] and Ulrich Kortz*[b]

Keywords: Copper / EPR spectroscopy / Magnetic properties / Polyoxometalates / Self assembly / Tungsten

Magnetic susceptibility and high-frequency EPR spectroscopy investigations were carried out on the isostructural family of tricopper(II)-substituted, sandwich-type polyoxotungstates $[Cu_3(H_2O)_3(\alpha\text{-}AsW_9O_{33})_2]^{12-}$ (**1**), $[Cu_3(H_2O)_3(\alpha\text{-}SbW_9O_{33})_2]^{12-}$ (**2**), $[Cu_3(H_2O)_3(\alpha\text{-}SeW_9O_{33})_2]^{10-}$ (**3**), and $[Cu_3(H_2O)_3(\alpha\text{-}TeW_9O_{33})_2]^{10-}$ (**4**) with the intention of examining the possible influence of the diamagnetic heteroatoms X (X = As^{III}, Sb^{III}, Se^{IV}, Te^{IV}) on the magnetic exchange properties of the three Cu^{2+} ions in the central belt. Magnetic susceptibility data indicate a single antiferromagnetic spin exchange constant J for the triangular Cu_3 belts in **1**–**4**. Variable-temperature, W-band (ca. 94 GHz) EPR spectra reveal that the Cu_3 units have $S_T = 1/2$ as the spin ground state with the excited state $S_T = 3/2$ located within a few cm^{-1}. We also determined the g matrix components for both the $S_T = 1/2$ and 3/2 states. The zero-field parameter D has been measured for the $S_T = 3/2$ state, and its sign is shown to be positive for **1**–**4**. From the analysis of the g matrix components for the molecular and the local Cu^{2+} site symmetry, the unpaired electrons are shown to occupy the $3d_{x^2-y^2}$ orbitals. The J values change from –1.36 to –1.04 cm^{-1} for **1** and **2**, and from –1.52 to –1.48 cm^{-1} for **3** and **4**, respectively. The g values follow a similar trend, but the D value for **4** implies a role of through-space as well as through-bond sources for the magnetic interactions in the Cu_3 belt. Our results suggest that the heteroatoms, containing lone pairs, allow the fine tuning of the magnetic parameters of **1**–**4**.

(© Wiley-VCH Verlag GmbH & Co. KGaA, 69451 Weinheim, Germany, 2004)

Introduction

Polyoxoanions constitute a rapidly growing class of molecular metal−oxygen clusters with an enormous diversity of structures.[1,2] These molecules also display a unique multitude of properties based on their highly alterable sizes, shapes, charge densities, and reversible redox potentials. As a consequence, possible applications span a wide range of domains including catalysis, electrocatalysis, medicine, materials science, photochemistry, analytical chemistry and magnetochemistry.[3−6]

The synthesis of new classes of compounds with ground states with high electronic spin, S, is a topic of high current interest in synthetic chemistry, fundamental theoretical understanding of quantum phenomenon and future nanotechnology.[7] Incorporation of multiple transition metal ions in lacunary polyoxoanion fragments can lead to species with various stoichiometries and structural features combined with interesting magnetic properties.[8] Thus, studies of well-characterized polyoxoanions containing exchange-coupled paramagnetic metal centers should add useful data to the literature on polyoxometalates. Polyoxoanions can be considered as intermediate in complexity between monomeric metal coordination complexes and high-spin multinuclear clusters that have received considerable attention.[9−12] Since in polyoxoanions the magnetic fragment is usually encapsulated by a diamagnetic tungsten−oxo cluster, they provide ideal structural supports for the study of the magnetic exchange interactions in clusters.[13,14]

Although an enormous number of polyoxoanions with different structures is known, there are relatively few isostructural polyoxoanion families that contain several, well-characterized members. Probably the best known examples are the tetrametal-substituted, sandwich-type polyoxotungstates of the Keggin type $\{[M_4(H_2O)_2(B\text{-}\alpha\text{-}XW_9O_{34})_2]$ (M = Mn^{2+}, Fe^{3+}, Co^{2+} etc.; X = P, As, Si, Ge)$\}$ and the Wells−Dawson analogues $\{[M_4(H_2O)_2(B\text{-}\alpha\text{-}X_2W_{15}O_{34})_2]$ (M = Mn^{2+}, Fe^{3+}, Co^{2+} etc.; X = P, As)$\}$.[8b,15] Over the last decade or so the magnetic properties of transition-metal-substituted polyanions have been investigated predominantly by Coronado et al.[16] In these studies the properties of derivatives containing different transition metals (e.g. Cu^{2+} vs. Mn^{2+}) were investigated. There is essentially no report on a systematic, comparative magnetic study of isostructural polyoxoanions involving the heteroatoms.

[a] Department of Chemistry and Biochemistry, Florida State University and National High Magnetic Field Laboratory and Center for Interdisciplinary Magnetic Resonance,
Tallahassee, FL 32306-4390, USA
Fax: (internat.) + 1-850-644-3398
E-mail: dalal@chemmail.chem.fsu.edu
[b] International University Bremen, School of Engineering and Science,
P. O. Box 750561, 28725 Bremen, Germany
Fax: (internat.) + 49-421-200-3229
E-mail: u.kortz@iu-bremen.de

 © 2004 Wiley-VCH Verlag GmbH & Co. KGaA, Weinheim **DOI: 10.1002/ejic.200400234**

The $(Cu^{2+})_3$ fragment represents the simplest example of a spin-frustrated system, provided (i) the exchange interaction is antiferromagnetic and (ii) the copper centers are symmetry-related through a C_3 axis. The compounds studied here belong to this class. Although many compounds containing a $(Cu^{2+})_3$ fragment have been reported, there is no system that allows one to fine-tune the magnetic interactions of the $(Cu^{2+})_3$ moiety.[17−25] Polyoxometalates appear to be an excellent candidate for such a study.

Recently Kortz et al. reported on the synthesis and structural characterization of the four copper(II)-substituted, lone-pair-containing polyoxotungstates $[Cu_3(H_2O)_3(\alpha\text{-}AsW_9O_{33})_2]^{12-}$ (**1**), $[Cu_3(H_2O)_3(\alpha\text{-}SbW_9O_{33})_2]^{12-}$ (**2**), $[Cu_3(H_2O)_3(\alpha\text{-}SeW_9O_{33})_2]^{10-}$ (**3**), and $[Cu_3(H_2O)_3(\alpha\text{-}TeW_9O_{33})_2]^{10-}$ (**4**).[26] The isostructural nature of polyanions **1**−**4** allows one to correlate the magnetic properties of these compounds with structural details.

We used high-frequency EPR spectroscopy and SQUID magnetometry to study the effects of heteroatomic substitution on the magnetic properties of **1**−**4** and we discovered an interesting trend.

Results and Discussion

For the study reported here we used $Na_{12}[Cu_3(H_2O)_3(\alpha\text{-}AsW_9O_{33})_2]\cdot 32H_2O$ (**Na-1**), $Na_{12}[Cu_3(H_2O)_3(\alpha\text{-}SbW_9O_{33})_2]\cdot 46H_2O$ (**Na-2**), $K_9Na[Cu_3(H_2O)_3(\alpha\text{-}SeW_9O_{33})_2]\cdot 16H_2O$ (**K-3**) and $K_9Na[Cu_3(H_2O)_3(\alpha\text{-}TeW_9O_{33})_2]\cdot 16H_2O$ (**K-4**) which were synthesized according to the published procedure.[26]

The copper(II)-substituted, lone-pair-containing polyoxotungstates $[Cu_3(H_2O)_3(\alpha\text{-}AsW_9O_{33})_2]^{12-}$ (**1**), $[Cu_3(H_2O)_3(\alpha\text{-}SbW_9O_{33})_2]^{12-}$ (**2**), $[Cu_3(H_2O)_3(\alpha\text{-}SeW_9O_{33})_2]^{10-}$ (**3**), and $[Cu_3(H_2O)_3(\alpha\text{-}TeW_9O_{33})_2]^{10-}$ (**4**) consist of two $(\alpha\text{-}XW_9O_{33})$ units joined by three equivalent Cu^{2+} ions (see Figure 1). All copper ions have one terminal water molecule resulting in a square-pyramidal coordination geometry. Therefore, these polyanions have idealized D_{3h} symmetry. The space in between the three transition metal ions is occupied by three sodium ions (X = As^{III}, Sb^{III}) or potassium ions (X = Se^{IV}, Te^{IV}) leading to a central belt of six metal atoms alternating in position.

The separations of the three copper ions and the two heteroatoms in polyanions **1**−**4** are summarized in Table 1.

Magnetic Susceptibility

Figure 2 shows a plot of $\chi_m T$ vs. T for compound **K-4**. This type of behavior indicates the presence of antiferromagnetic exchange interactions between the Cu^{2+} ions. The behavior of compounds **Na-1**, **Na-2** and **K-3** is very similar. The solid-state structures of polyanions **1**−**4** indicated that two of the three copper centers are crystallographically inequivalent, but nevertheless all three are oriented in a very regular triangular fashion.[26] Therefore, we used the equilateral triangle model in order to explain the observed magnetic properties of **Na-1**, **Na-2**, **K-3** and **K-4**. The Heisenberg spin exchange Hamiltonian corresponding to this model is given in Equation (1).[24,25,27] Here J is the spin exchange coupling constant, and $\hat{S}_i$ (i = 1, 2, 3) is the spin operator of the ith ion. The eigenvalues associated with the Hamiltonian in Equation (1) can be given as in

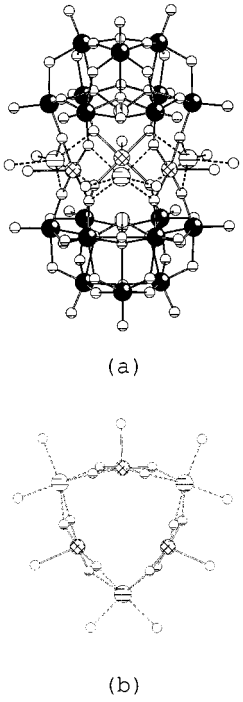

Figure 1. (a) Ball-and-stick diagram of $[Cu_3(H_2O)_3(\alpha\text{-}AsW_9O_{33})_2]^{12-}$ (**1**); this figure is also representative of $[Cu_3(H_2O)_3(\alpha\text{-}SbW_9O_{33})_2]^{12-}$ (**2**), $[Cu_3(H_2O)_3(\alpha\text{-}SeW_9O_{33})_2]^{10-}$ (**3**), and $[Cu_3(H_2O)_3(\alpha\text{-}TeW_9O_{33})_2]^{10-}$ (**4**); (b) representation of the central belt in **1**; Cu (cross-hatched), Na (horizontally hatched), As (vertically hatched), O (shaded), H_2O (unshaded)

Table 1. Cu···Cu and heteroatom (X···X) separations in polyanions **1**−**4**[26]

Polyanion	Cu···Cu [Å]	X···X [Å]
$[Cu_3(H_2O)_3(\alpha\text{-}AsW_9O_{33})_2]^{12-}$ (**1**)	4.69	5.34
$[Cu_3(H_2O)_3(\alpha\text{-}SbW_9O_{33})_2]^{12-}$ (**2**)	4.84	4.85
$[Cu_3(H_2O)_3(\alpha\text{-}SeW_9O_{33})_2]^{10-}$ (**3**)	4.84	5.38
$[Cu_3(H_2O)_3(\alpha\text{-}TeW_9O_{33})_2]^{10-}$ (**4**)	4.87	4.95

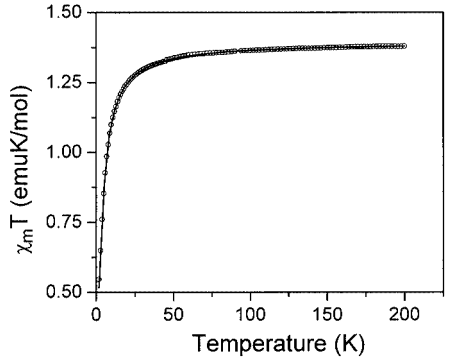

Figure 2. $\chi_m T$ vs. T plot of $K_9Na[Cu_3(H_2O)_3(\alpha\text{-}TeW_9O_{33})_2]\cdot 16H_2O$ (**K-4**) at H = 1000 G; the solid line represents the theoretical curve (see text)

 © 2004 Wiley-VCH Verlag GmbH & Co. KGaA, Weinheim

Equation (2),[24,25,27] where S_T is the total spin and S_i (i = 1, 2, 3) is the spin of each ion.

$$\hat{H} = -2J[\hat{S}_1\cdot\hat{S}_2 + \hat{S}_2\cdot\hat{S}_3 + \hat{S}_3\cdot\hat{S}_1] \quad (1)$$

$$E(S_T,S_1,S_2,S_3) = -J[S_T(S_T+1) - S_1(S_1+1) - S_2(S_2+1) - S_3(S_3+1)] \quad (2)$$

Since for each Cu^{2+} ion $S_1 = S_2 = S_3 = 1/2$, S_T can take values 1/2 ($\uparrow\uparrow\downarrow$), 1/2 ($\uparrow\downarrow\uparrow$) or 3/2 ($\uparrow\uparrow\uparrow$). The S_T = 1/2 state is thus doubly degenerate, with an energy of $-3J/2$, while the S_T = 3/2 state has an energy of $3J/2$. Substitution of these values into the standard Van Vleck equation[28] yields the expression for the molar magnetic susceptibility [Equation (3)]. Here N is the Avogadro number, g the Landé g factor, β the electronic Bohr magneton, k the Boltzmann constant and T the temperature in Kelvin.

$$\chi_m = \frac{Ng^2\beta^2}{4kT}\left[\frac{1+5\exp(3J/kT)}{1+\exp(3J/kT)}\right] \quad (3)$$

The experimental $\chi_m T$ data for **Na-1**, **Na-2**, **K-3** and **K-4** have been fitted to Equation (3) by treating g and J as adjustable parameters. The agreement between the theoretical curve and the measured data is quite satisfactory. The best least-squares fit parameters are given in Table 2. The negative sign of J indicates the presence of antiferromagnetic intra-trimer interactions and hence, the doubly degenerate S_T = 1/2 state is the ground spin state in all four compounds. The g values are consistent with the g_{iso} values obtained directly from the EPR measurements (vide infra).

As indicated above, two of the three copper centers in **1**−**4** are crystallographically inequivalent, which inevitably results in two different Cu···Cu separations. Although these differences are very small (< 0.04 Å), we also attempted to fit the experimental data to an isosceles triangle model [cf. Equation (4)],[28] where J_1 and J_2 represent the two kinds of exchange interactions. Due to the similar magnetic environment, however, we could not improve the fits by using the two spin exchange constants J_1 and J_2.

$$\chi_m = \frac{Ng^2\beta^2}{4kT}\left[\frac{1+10\exp(3J_1/kT)+\exp(2(J_1-J_2)/kT)}{1+2\exp(3J_1/kT)+\exp(2(J_1-J_2)/kT)}\right] \quad (4)$$

In all four polyanions **1**−**4**, the Cu $3d_{x^2-y^2}$ orbitals, which contain the unpaired electrons, are directed along the $Cu-O_{eq}$ vectors. Therefore, spin exchange coupling takes place by an indirect pathway involving two tungsten and three oxygen atoms of each XW_9O_{33} (X = As^{III}, Sb^{III}, Se^{IV}, Te^{IV}) fragment. Hence, we expected weak spin exchange interactions between the Cu^{2+} ions. The small magnitude of the observed J values (ca. 1 cm^{-1}) supports this model (see Table 2).

The coupling constants J for **Na-1**, **Na-2**, **K-3** and **K-4** are plotted as a function of the Cu···Cu separations in Figure 3. It can be seen that for **Na-1**/**Na-2** and **K-3**/**K-4** there is a decrease of J with increasing Cu···Cu separation. The average equatorial $Cu-O_{eq}$ distances in polyanions **1**−**4** are very similar [**1**, 1.921(6) Å; **2**, 1.937(6) Å; **3**, 1.918(9) Å; **4**, 1.927(9) Å], so that the differences in the Cu···Cu separations between **1**−**4** must be due to the different heteroatoms. The heteroatoms of **1** (As^{III}) and **2** (Sb^{III}) are from main group V, whereas the hetero groups of **3** (Se^{IV}) and **4** (Te^{IV}) are from main group VI.

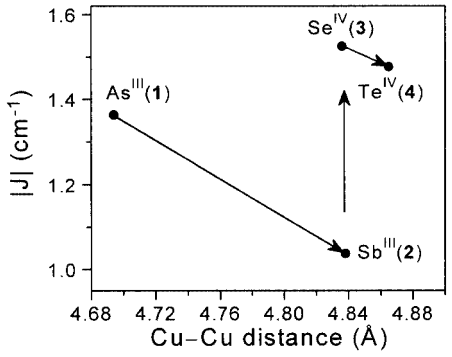

Figure 3. Dependence of the magnetic coupling constant J on the average Cu···Cu separations in $Na_{12}[Cu_3(H_2O)_3(\alpha\text{-}AsW_9O_{33})_2]\cdot 32H_2O$ (**Na-1**), $Na_{12}[Cu_3(H_2O)_3(\alpha\text{-}SbW_9O_{33})_2]\cdot 46H_2O$ (**Na-2**), $K_9Na[Cu_3(H_2O)_3(\alpha\text{-}SeW_9O_{33})_2]\cdot 16H_2O$ (**K-3**) and $K_9Na[Cu_3(H_2O)_3(\alpha\text{-}TeW_9O_{33})_2]\cdot 16H_2O$ (**K-4**)

When comparing **1** and **2**, it can be noted that both have the same charge, but the latter has the larger heteroatom. With the above in mind, the increase in the Cu···Cu separation in **2** compared to **1** must be due to an "equatorial expansion motion" of the former polyanion in the belt region. We believe that this is caused by lone pair···lone pair

Table 2. Magnetic parameters for polyanions **1**−**4** obtained from EPR and magnetic susceptibility measurements; the error in the g values is ± 0.005 and the error in J is ± 0.01

Polyanion	EPR							Susceptibility	
	S_T = 1/2			S_T = 3/2					
	$g_\parallel$	$g_\perp$	g_{iso}	$g_\parallel$	$g_\perp$	g_{iso}	D [cm^{-1}]	J [cm^{-1}]	g_{iso}
1 (X = As)[a]	2.117	2.254	2.208	2.060	2.243	2.182	0.0230	−1.36	2.209
2 (X = Sb)	2.128	2.257	2.219	2.061	2.231	2.175	0.0225	−1.04	2.223
3 (X = Se)	2.120	2.263	2.216	2.064	2.243	2.183	0.0219	−1.52	2.212
4 (X = Te)	2.127	2.288	2.234	2.065	2.239	2.181	0.0240	−1.48	2.226

[a] Ref.[8a]

 © 2004 Wiley-VCH Verlag GmbH & Co. KGaA, Weinheim

interaction of the two heteroatoms, which is more pronounced in **2** than in **1** due to the larger size of Sb^{III} compared to As^{III} (see Table 1). The same trend is observed for **3** and **4** and we suggest an analogous explanation.

When comparing the magnetic exchange coupling constants *J* of **1** and **3** it must be remembered that the charge of the polyanions differs by 2 units. This is due to the fact that the heteroatoms are As^{III} and Se^{IV}, respectively. In **1** and **3** the heteroatom separation is essentially equivalent (see Table 1), so that the differences in the average Cu···Cu separation must be due to charge effects. The Cu···Cu separation is larger in **3** than in **1** which indicates an "equatorial expansion motion" similar to above, but this time it must be caused by excess negative charge on the polyanion. However, the exchange coupling constant *J* is larger for **3** than for **1**, indicating that an increase of the negative charge on the polyanion leads to an increase of the magnetic coupling constant. The same trend is observed for **2** and **4** and we suggest an analogous explanation. Nevertheless it remains to be seen if this observation can be generalized.

The two straight lines in Figure 3 perfectly reflect the size differences of the 4p (As^{III}, Se^{IV}) vs. 5p (Sb^{III}, Te^{IV}) heteroatoms. The fact that the slope of both lines is very similar indicates that the same trend is valid for group V and group VI heteroatoms. We have also shown that magnetic exchange coupling constants can reflect structural details of heteropolyanions. We believe that the graph in Figure 3 can also be used to predict coupling constants of related polyanions that have not yet been synthesized, e.g. the Bi derivative of **1** and **2**. We expect that the hypothetical polyanion $[Cu_3(H_2O)_3(\alpha\text{-}BiW_9O_{33})_2]^{12-}$ has a coupling constant *J* which is smaller than 1 cm^{-1}.

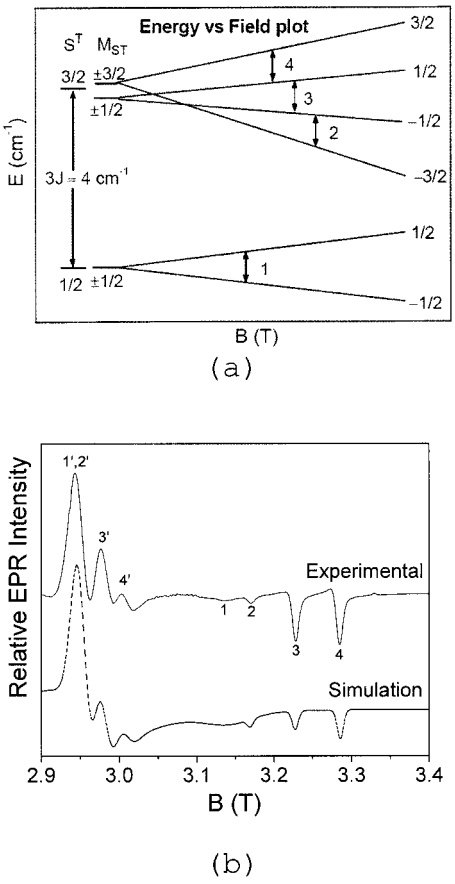

Figure 4. (a) Energy level diagram and the expected EPR transitions; (b) experimental and simulated W-band (ν = 93.494 GHz) powder EPR spectra of $K_9Na[Cu_3(H_2O)_3(\alpha\text{-}TeW_9O_{33})_2]\cdot 16H_2O$ (**K-4**) at 4 K

EPR Spectroscopy

Polycrystalline powder samples of **Na-1**, **Na-2**, **K-3** and **K-4** show similar EPR spectra with a quadruplet excited spin state at slightly higher energy than the S_T = 1/2 spin ground state (see Figure 4). The observed EPR spectra were analyzed using the spin Hamiltonian in Equation (5), where S_T is the total spin operator, *D* is the zero-field splitting parameter, and *g*, β, *B* have their usual meaning.

$$\hat{H} = \hat{S}_T \cdot D \cdot \hat{S}_T + \beta \cdot B \cdot g \cdot \hat{S}_T \quad (5)$$

The possible spin states correspond to a total spin of S_T = 3/2 or 1/2, which is expected for a frustrated triangle containing an unpaired electron et each vertex. Here we neglect the hyperfine structure due to the $^{63,65}Cu$ nuclei, since it is exchange-averaged. Also, we do not consider *J* here because its effect is not detected by standard EPR measurements, except through the detection of separate spectra from the ground and thermally accessible excited states. The small magnitude of exchange determined by magnetic susceptibility is not large enough to see intensity changes between different spin states.[25] Assuming axial symmetry, and the high-field limit ($g\beta B >> |D|$, as is the case here), the solution of Equation (5) is straightforward.[29] The line centers will be given by the *g* factor, and each line will be split into $2S_T$ components. For a system with axial symmetry, such as the $(Cu^{2+})_3$ moiety here, the fine structure splitting varies essentially as $D(3\cos^2\Theta - 1)$, where Θ is the angle between the applied field direction and the axis of symmetry. Thus, for an S_T = 3/2 spin state, the powder pattern in the limit $g\beta B >> |D|$ should consist of a triplet around the principal *g* components. The triplet separation around the *g* peak is 2*D* while the separation of perpendicular transitions around the $g_{\|}$ peak is 2|*D*|.

Figure 4 (a) shows the energy level diagram and the expected magnetic dipole ($\Delta M_{ST} = \pm 1$) transitions, labeled 1−4. Figure 4 (b) shows the 4 K experimental W-band EPR spectrum of the tellurium analog **K-4** with the best-fit simulation. The experimental spin Hamiltonian parameters used in this simulation and those obtained for compounds **Na-1**, **Na-2** and **K-3** are summarized in Table 2. Figure 5 shows the measured room-temperature and 4 K W-band EPR spectra for **K-4**. In the room-temperature spectrum, only the quadruplet fine structure transitions are observed for the quadruplet excited spin state. At 4 K, a fourth parallel peak centered at *g* = 2.117 was observed. The higher intensity of the lowest field line suggests that the perpendicular component of the S_T = 1/2 state is superimposed. This ob-

 © 2004 Wiley-VCH Verlag GmbH & Co. KGaA, Weinheim

servation lends credence to a lower energy spin state being present. The ground spin state for the $(Cu^{2+})_3$ triangle is therefore the doublet $S_T = 1/2$ state. Further analysis of the signal intensity with respect to temperature reveals the sign of the zero field splitting. At lowest temperature, only the lowest energy states are thermally populated. Hence, at 4 K, the fine structure line intensity shifts into the outermost parallel and perpendicular lines, indicating a positive sign for the D value. The $M_{ST} = \pm 1/2$ states are therefore of lower energy. Compounds **Na-1**, **Na-2**, **K-3** have analogous EPR spectra and show an $S_T = 1/2$ ground spin state; however, the magnetic parameters vary slightly. It should be noted that in all cases the quadruplet state transitions are still observed at 4 K because the spin exchange between states is small (ca. 4 cm^{-1}).

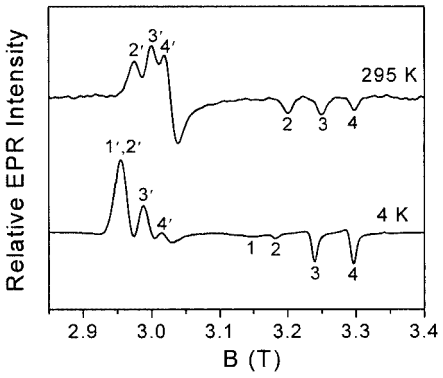

Figure 5. W-band (ν = 93.494 GHz) powder EPR spectra of $K_9Na[Cu_3(H_2O)_3(\alpha\text{-}TeW_9O_{33})_2]\cdot 16H_2O$ (**K-4**) at 295 K and 4 K as indicated; numbering corresponds to Figure 4 (a)

The geometrical arrangement of the CuO_5 groups in polyanions **1**−**4** is such that their perpendicular directions correspond to the C_3 axis of the heteropolyanion, while the parallel direction of each CuO_5 unit is perpendicular to the molecular C_3 axis. The square-pyramidal geometry of each CuO_5 unit has C_{4v} site symmetry. Since, the axial Cu−Ow distance in each unit is longer than the four equatorial Cu−O distances,[26] the $3d_{z^2}$ orbital is stabilized with respect to $3d_{x^2-y^2}$ such that the unpaired electron resides in the $3d_{x^2-y^2}$ orbital. Siedle et al. have shown that the observed EPR g matrix parameters can be transformed with respect to the g matrix of the individual copper centers.[30] If g(m) represents the g matrix of an individual CuO_5 unit, the relation between g(m) and the observed g values can be written as $g_{\|} = g_{\perp}(m)$ and $g_{\perp} = (1/2)[g_{\|}(m) + g_{\perp}(m)]$. Applying these relations to the polyanion **4**, for example, yields $g_{\|}(m)$ and $g_{\perp}(m)$ values as 2.449 and 2.127, respectively. With this geometrical framework $g_{\|}(m) > g_{\perp}(m) > g_e$, g_e being the free electron g value of 2.0023, proving that the $d_{x^2-y^2}$ orbital contains the unpaired electron.

Finally, an interesting observation from Table 2 is that for **4**, the D value magnitude does not fit the trend of the Cu···Cu distances. Normally, one would expect that the D value should fall off sensitively with the Cu···Cu separations. For **4**, however, while the Cu···Cu distance is the largest, the D value is also the largest. This breakdown in the D value vs. Cu···Cu distance relationship suggests a significant role for the through-bond interactions in **4**.

Conclusions

W-band EPR and SQUID measurements have enabled us to measure the influence of the charge and size properties of the lone pair containing heteroatoms on the central Cu^{2+} triangle embedded in a series of four isostructural polyoxometalates. The g_{iso} value calculated from EPR measurements for the ground spin state for compounds **Na-1**, **Na-2**, **K-3** and **K-4** varies from the best fit parameters determined by $\chi_m T$ vs. T plots. For **Na-1** and **K-3**, which have larger J values, the agreement between magnetic susceptibility and EPR spectroscopic results is within experimental error. For **Na-2** and **K-4**, a 3% difference was observed in the g values determined from the two techniques. We tentatively ascribe this difference to the fact that the susceptibility measurements extend over a wide temperature range.

In summary, we have performed the first systematic study of the magnetic properties of an isostructural family of polyoxoanions. Not surprisingly, magnetic susceptibility and EPR measurements have revealed that the magnetic exchange coupling constant J is a sensitive parameter that can reflect very small structural differences in the magnetic core (e.g. Cu···Cu separations) of polyanions. More importantly, we have also shown that these structural differences can be rationalized by size and charge effects of the heteroatoms. This means that magnetic measurements can be used as an indirect analytical tool, in order to investigate phenomena that originate in nonmagnetic regions of magnetic molecules.

Experimental Section

Synthesis: The polyoxoanions $Na_{12}[Cu_3(H_2O)_3(\alpha\text{-}AsW_9O_{33})_2]\cdot 32H_2O$ (**Na-1**), $Na_{12}[Cu_3(H_2O)_3(\alpha\text{-}SbW_9O_{33})_2]\cdot 46H_2O$ (**Na-2**), $K_9Na[Cu_3(H_2O)_3(\alpha\text{-}SeW_9O_{33})_2]\cdot 16H_2O$ (**K-3**) and $K_9Na[Cu_3(H_2O)_3(\alpha\text{-}TeW_9O_{33})_2]\cdot 16H_2O$ (**K-4**) were synthesized according to the published procedure.[26]

Magnetic Susceptibility Measurements: Magnetic susceptibility measurements on **Na-1**, **Na-2**, **K-3** and **K-4** were carried out using a Quantum Design MPMS-XL SQUID magnetometer. Data for polycrystalline samples were collected over 1.8−200 K at 1000 G, using approximately 70 mg of sample. The data were corrected for the sample holder, diamagnetism using Klemm constants,[31] and temperature-independent paramagnetism (TIP) contributions.

EPR Spectroscopy: Polycrystalline powder EPR spectra of **Na-1**, **Na-2**, **K-3** and **K-4** were recorded at W-band frequencies (ca. 94 GHz) at the high-field electron magnetic resonance facility at the National High Magnetic Field Laboratory in Tallahassee, as described elsewhere.[32,33] Temperature variation was measured from room temperature to 4 K. An Oxford Instruments Teslatron superconducting magnet, able to sweep between 0 and 17 T, was used to apply the Zeeman field. In all experiments the modulation

 © 2004 Wiley-VCH Verlag GmbH & Co. KGaA, Weinheim

amplitudes and microwave power were adjusted for optimal signal intensity and resolution. The Bruker XSophe EPR simulation program was used with the appropriate spin Hamiltonian to generate simulated EPR spectra. This program includes a Boltzmann term that considers thermal population of particular spin levels.

Acknowledgments

The work at NHMFL was supported in part by the NSF and the State of Florida. We wish to thank Dr. Johan van Tol for his helpful advice and discussions. U. K. thanks the International University Bremen for research support. Figure 1 was generated by Diamond Version 2.1e (© Crystal Impact GbR).

[1] M. T. Pope, *Heteropoly and Isopoly Oxometalates*, Springer, Berlin, **1983**.
[2] M. T. Pope, A. Müller, *Angew. Chem.* **1991**, *103*, 56−70; *Angew. Chem. Int. Ed. Engl.* **1991**, *30*, 34−48.
[3] *Polyoxometalates: from Platonic Solids to Anti Retroviral Activity* (Eds.: M. T. Pope, A. Müller), Kluwer, Dordrecht, **1994**.
[4] Special Thematic Issue on Polyoxometalates: *Chem. Rev.* **1998**, *98*, 1−389.
[5] *Polyoxometalate Chemistry: From Topology via Self-Assembly to Applications* (Eds.: M. T. Pope, A. Müller), Kluwer, Dordrecht, **2001**.
[6] *Polyoxometalate Chemistry for Nano-Composite Design* (Eds.: T. Yamase, M. T. Pope), Kluwer, Dordrecht, **2002**.
[7] [7a] For a recent review on the potential of high-spin systems for nanotechnology, see: J. Tejada, E. M. Chudnovsky, E. del Barco, J. M. Hernandez, *Nanotechnology* **2001**, *12*, 181−186. [7b] For their importance in fundamental research, see: D. Gatteschi, R. Sessoli, *Angew. Chem. Int. Ed.* **2003**, *42*, 268−297. [7c] For quantum computation, see: D. Loss, M. Leuenberger, *Nature (London)* **2000**, *410*, 789−793. [7d] For some general references, see: J. R. Friedman, M. P. Sarachik, J. Tejada, R. Ziolo, *Phys. Rev. Lett.* **1996**, *76*, 3830−3833; C. Sangregorio, T. Ohm, C. Paulsen, R. Sessoli, D. Gatteschi, *Phys. Rev. Lett.* **1997**, *78*, 4645−4648; A. L. Barra, D. Gatteschi, R. Sessoli, *Phys. Rev. B* **1997**, *56*, 8192−8198; J. A. A. J. Perenboom, J. S. Brooks, S. Hill, T. Hathaway, N. S. Dalal, *Phys. Rev. B* **1998**, *58*, 330−338; S. Hill, J. A. A. J. Perenboom, N. S. Dalal, T. Hathaway, T. Stalcup, J. S. Brooks, *Phys. Rev. Lett.* **1998**, *80*, 2453−2456; L. Bokacheva, A. D. Kent, M. A. Walters, *Phys. Rev. Lett.* **2000**, *85*, 4803−4806; E. M. Chudnovsky, D. A. Garanin, *Phys. Rev. B* **2002**, *65*, 094423−094431 and references cited therein for theoretical work.
[8] [8a] U. Kortz, S. Nellutla, A. C. Stowe, N. S. Dalal, J. van Tol, B. Bassil, *Inorg. Chem.* **2004**, *43*, 144−154. [8b] U. Kortz, S. Nellutla, A. C. Stowe, N. S. Dalal, U. Rauwald, W. Danquah, D. Ravot, *Inorg. Chem.* **2004**, *43*, 2308−2317, and references cited therein.
[9] R. Sessoli, D. Gatteschi, A. Caneschi, M. A. Novak, *Nature* **1993**, *365*, 141−143.
[10] O. Kahn, *Chem. Phys. Lett.* **1997**, *265*, 109−114.
[11] G. Aromí, S. M. J. Aubin, M. A. Bolcar, G. Christou, H. J. Eppley, K. Folting, D. N. Hendrickson, J. C. Huffman, R. C. Squire, H.- L. Tsai, S. Wang, M. W. Wemple, *Polyhedron* **1998**, *17*, 3005−3020.
[12] For detailed references, see: [12a] S. M. J. Aubin, Z. Sun, H. J. Eppley, E. M. Rumberger, E. A. Guzei, K. Folting, P. K. Gantzel, A. L. Rheingold, G. Christou, D. N. Hendrickson, *Inorg. Chem.* **2001**, *40*, 2127−2146. [12b] D. Gatteschi, R. Sessoli, *Angew. Chem.* **2003**, *115*, 278−309. [12c] G. Christou, D. Gatteschi, D. N. Hendrickson, R. Sessoli, *MRS Bull.* **2000**, *25*, 66−71.
[13] G. F. Kokoszka, F. Padula, A. S. Goldstein, E. L. Venturini, L. Azevedo, A. R. Siedle, *Inorg. Chem.* **1988**, *27*, 59−62.
[14] [14a] L. C. W. Baker, V. E. S. Baker, S. H. Wasfi, G. A. Candela, A. H. Kahn, *J. Am. Chem. Soc.* **1972**, *94*, 5499−5501. [14b] L. C. W. Baker, V. E. S. Baker, S. H. Wasfi, G. A. Candela, A. H. Kahn, *J. Chem. Phys.* **1972**, *56*, 4917−4923.
[15] Some recent references include: [15a] U. Kortz, S. Isber, M. H. Dickman, D. Ravot, *Inorg. Chem.* **2000**, *39*, 2915−2922. [15b] L.-H. Bi, R.-D. Huang, J. Peng, E.-B. Wang, Y.-H. Wang, C.-W. Hu, *J. Chem. Soc., Dalton Trans.* **2001**, 121−129. [15c] E. M. Limanski, M. Piepenbrink, E. Droste, K. Burgemeister, B. Krebs, *J. Cluster Sci.* **2002**, *13*, 369−379.
[16] [16a] C. J. Gómez-García, E. Coronado, J. J. Borrás-Almenar, *Inorg. Chem.* **1992**, *31*, 1667−1673. [16b] N. Casañ-Pastor, J. Bas-Serra, E. Coronado, G. Pourroy, L. C. W. Baker, *J. Am. Chem. Soc.* **1992**, *114*, 10380−10383. [16c] C. J. Gómez-García, E. Coronado, P. Gómez-Romero, N. Casañ-Pastor, *Inorg. Chem.* **1993**, *32*, 3378−3381. [16d] C. J. Gómez-García, J. J. Borrás-Almenar, E. Coronado, L. Ouahab, *Inorg. Chem.* **1994**, *33*, 4016−4022. [16e] J. M. Clemente-Juan, E. Coronado, J. R. Galán-Mascarós, C. J. Gómez-García, *Inorg. Chem.* **1999**, *38*, 55−63.
[17] E. Sinn, *Coord. Chem. Rev.* **1970**, *5*, 313−347.
[18] J. S. Griffith, *Struct. Bonding (Berlin)* **1972**, *10*, 87.
[19] B. S. Tsukerblat, V. M. Novotortsev, B. Y. Kuyavskaya, M. I. Belinsky, A. V. Ablov, A. N. Bazhan, V. T. Kalinnikov, *Sov. Phys. JETP Lett.* **1974**, *19*, 277−278.
[20] [20a] L. Banci, A. Bencini, D. Gatteschi, *Inorg. Chem.* **1983**, *22*, 2681−2683. [20b] L. Banci, A. Bencini, A. Dei, D. Gatteschi, *Inorg. Chem.* **1983**, *22*, 4018−4021.
[21] J. Padilla, D. Gatteschi, P. Chaudhuri, *Inorg. Chim. Acta* **1997**, *260*, 217−220.
[22] M. Azuma, T. Odaka, M. Takano, D. A. Vander Griend, K. R. Poeppelmeier, Y. Narumi, K. Kindo, Y. Mizuno, S. Maekawa, *Phys. Rev. B* **2000**, *62*, R3588−R3591.
[23] M. Kodera, Y. Tachi, T. Kita, H. Kobushi, Y. Sumi, K. Kano, M. Shiro, M. Koikawa, T. Tokii, M. Ohba, H. Okawa, *Inorg. Chem.* **2000**, *39*, 226−234.
[24] R. Clérac, F. A. Cotton, K. R. Dunbar, E. A. Hillard, M. A. Petrukhina, B. W. Smuckler, *C. R. Acad. Sci. Ser. IIc: Chim.* **2001**, *4*, 315−319.
[25] B. Cage, F. A. Cotton, N. S. Dalal, E. A. Hillard, B. Rakvin, C. M. Ramsey, *J. Am. Chem. Soc.* **2003**, *125*, 5270−5271; *C. R. Chim.* **2003**, *6*, 39−46.
[26] U. Kortz, N. K. Al-Kassem, M. G. Savelieff, N. A. Al Kadi, M. Sadakane, *Inorg. Chem.* **2001**, *40*, 4742−4749.
[27] K. Kambe, *J. Phys. Soc., Jpn.* **1950**, *5*, 48−51.
[28] O. Kahn, *Molecular Magnetism*, VCH, New York, **1993**.
[29] A. Abragam, B. Bleaney, *Electron Paramagnetic Resonance of Transition Ions*, Dover Publications, Inc., New York, **1970**.
[30] A. R. Siedle, F. Padula, J. Baranowski, C. Goldstein, M. DeAngelo, G. F. Kokoszka, L. Azevedo, E. L. Venturini, *J. Am. Chem. Soc.* **1983**, *105*, 7447−7448.
[31] S. G. Vulfson, *Molecular Magnetochemistry*, Gordon and Breach Science, The Netherlands, **1998**, p. 241.
[32] B. Cage, A. K. Hassan, L. Pardi, J. Krzystek, L.-C. Brunel, N. S. Dalal, *J. Magn. Reson.* **1997**, *124*, 495−498.
[33] A. K. Hassan, L. A. Pardi, J. Krzystek, A. Sienkiewicz, P. Goy, M. Rohrer, L.-C. Brunel, *J. Magn. Reson.* **2000**, *142*, 300−312.

Received March 23, 2004
Early View Article
Published Online July 29, 2004

 © 2004 Wiley-VCH Verlag GmbH & Co. KGaA, Weinheim

Roesky's Ketone: Structure, Aromaticity and Reactivity

Joris Van Droogenbroeck,[a] Karla Tersago,[a] Christian Van Alsenoy,[a] Stephen M. Aucott,[b] Heather L. Milton,[b] J. Derek Woollins,[b] and Frank Blockhuys*[a]

Keywords: Aromaticity / Density functional theory / Dithiadiazole / Reactivity / X-ray diffraction

The molecular and crystal structure of the title compound, 5-oxo-1,3,2,4-dithiadiazole or Roesky's ketone (**1**), is studied experimentally by re-determining the crystal structure and theoretically by calculations at the density functional level of theory using an extended basis set. A comprehensive set of properties, consisting of orbital topologies, atomic charges, atomic and molecular dipoles, aromaticity parameters and Fukui functions of the title compound and a number of its constitutional isomers was calculated in order to formulate a description of its structure, its aromaticity and reactivity.
(© Wiley-VCH Verlag GmbH & Co. KGaA, 69451 Weinheim, Germany, 2004)

Introduction

The discovery of the metallic properties of polymeric $(SN)_x$ in 1973,[1] and the finding that it becomes a superconductor at low temperatures two years later,[2] opened a new era in the research on conducting polymers. In $(SN)_x$ compounds the alternating sulfur and nitrogen atoms donate two π-electrons and one π-electron, respectively, which makes these compounds electron-rich and leads to a partial occupancy of the π*-orbital.[3,4] Such electron-rich compounds are known to be very reactive. One of the approaches to stabilize these interesting systems, and the one we adopted in this work, is to enclose chains of a limited length, for example an $(SN)_2$ unit, in a five- or six-membered ring, thus extending the π-delocalisation and stabilizing the heteroatomic fragment. The resulting new compounds have very different properties when compared with their hydrocarbon analogues. When, for example, naphthalene is compared with 1,3λ^{4}δ^2,2,4-benzodithiazine, its analogue containing an $(SN)_2$ unit, we see that upon changing the −C=C−C=C− fragment into an −N=S=N−S− one the number of double bonds is retained but, in addition, one lone pair from the singly bound sulfur atom is introduced into the π-system. This causes 1,3λ^{4}δ^2,2,4-benzodithiazine to become antiaromatic, while naphthalene itself is aromatic. These effects of electronic (de)localization, combined with the promising magnetic and electronic properties that result from the peculiar electronic structure, make these new compounds very interesting systems for further theoretical and experimental investigations.

Here we present an in-depth study of the structure, aromaticity and reactivity of one of these ring systems, in particular 5-oxo-1,3,2,4-dithiadiazole or Roesky's ketone, by combining the results from theoretical calculations and experimental techniques. A previous study on 1,3λ^{4}δ^2,2,4-benzodithiazine and its fluorinated derivatives[5,6] provided a unique way to gain a deeper understanding of the properties of the molecule and to find out the best suited theoretical level to describe these properties, by comparing calculated geometries with the results of a gas-phase electron diffraction (GED) experiment. To complement the work presented here the influence of the theoretical level and basis set on the structure of Roesky's ketone was recently performed.[7] The small number of atoms makes this molecule especially interesting in such a study as we were able to use very high-level theories and very extended basis sets. Roesky's ketone can thus act as a model system for more complicated $(SN)_2$ systems. We are currently performing a similar study on an organometallic $(SN)_2$ compound containing a cobalt atom.

Roesky's ketone was first synthesised by Roesky and Wehner[8] in 1975 and later by Neidlein and Leinberger.[9,10] In 1978, the crystal structure of the ketone was determined by Roesky et al.[11] by means of X-ray diffraction (XRD). In 1993 deLaat et al.[12] studied Roesky's ketone in the gas phase by infrared (IR) and photoelectron spectroscopy (PES), and by a limited theoretical study using semi-empirical and low-level ab initio methods. In this work Roesky's ketone is subjected to a low-temperature X-ray diffraction study, yielding data with a higher resolution than the existing set. This experimental structural study is complemented by the calculation of a theoretical gas-phase geometry which is compared with the XRD results. A further descrip-

[a] University of Antwerp, Department of Chemistry, Universiteitsplein 1, 2610 Wilrijk, Belgium
Fax: (internat.) + 32-3-820-2310
E-mail: frank.blockhuys@ua.ac.be
[b] University of St. Andrews, Department of Chemistry, St. Andrews KY16 9ST, United Kingdom
Supporting information for this article is available on the WWW under http://www.eurjic.org or from the author.

 © 2004 Wiley-VCH Verlag GmbH & Co. KGaA, Weinheim **DOI: 10.1002/ejic.200400361**

tion of the molecular properties of Roesky's ketone is given based on calculated atomic charges, molecular and atomic dipoles, deformation densities, bond orders, Nucleus-Independent Chemical Shift (NICS) values, Fukui functions and softnesses, to gain a complete insight into the structure, reactivity and aromaticity of the title compound. To tackle the issue of aromaticity three constitutional isomers of Roesky's ketone, given in Figure 1, were included in the study.

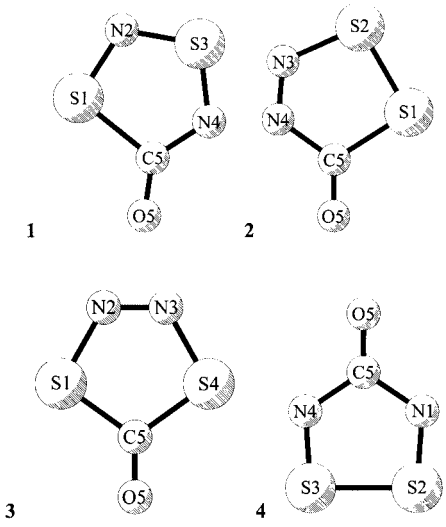

Figure 1. Molecular structure of Roesky's ketone (**1**) and its three constitutional isomers (see text for details); note that the numbering of the isomers is not systematic, but conforms to that of the parent compound for clarity

Results and Discussion

Experimental and Theoretical Geometry

The geometry of Roesky's ketone (**1**), which was synthesised as shown in Figure 2, was optimized at the DFT/B3LYP level of theory and the geometrical results are given in Table 1 together with the experimental solid-state geometry. The data show that the geometries of the two independent molecules in the unit cell are identical within the experimental errors; the torsion angles (not given in Table 1) are limited to 1.69(12)° and confirm the near-planar conformation of the compound in the solid state. This is in agreement with the planar conformation found in the calculations and suggests that the slight deformation in the crystal is due to packing effects. Keeping in mind that r_{XRD} are r_α-type distances which are compared to calculated (or r_e) distances, the agreement for the three N−S bonds is excellent for the longer one but less impressive for the two shorter ones, even though the relative bond lengths in the NSNS fragment are quite well reproduced. The difference between the calculated and the experimental bond length for the C−N and C−O bonds amounts to 0.02 Å; the calculation underestimates both. The only bond which is grossly overestimated by the DFT calculation is the C−S bond, with a difference of up to 0.11 Å compared to the experimental value. From a more systematic study of the influence of the level of theory, the functional used in DFT and the basis set on the calculated structure of Roesky's ketone, the results of which can be found elsewhere,[7] it is clear that B3LYP/6-311+G* leads to a high-quality structure in a relatively short computational time.

Table 1. Molecular geometry (r_e in Å and angles in °) calculated for 5-oxo-1,3,2,4-dithiadiazole (**1**) at the DFT/B3LYP/6-311+G* level of theory, and the experimental solid-state geometrical data (distances in Å and angles in °) for the two independent molecules in the asymmetric unit

	DFT	XRD	
S1−N2	1.6408	1.6395(14)	1.6425(15)
N2−S3	1.6083	1.5807(15)	1.5814(15)
S3−N4	1.5953	1.5763(15)	1.5750(16)
N4−C5	1.3650	1.386(2)	1.384(2)
C5−S1	1.9410	1.8305(17)	1.8293(16)
O5−C5	1.1939	1.211(2)	1.211(2)
S1−N2−S3	112.37	112.37(9)	112.04(8)
N2−S3−N4	106.78	106.13(7)	106.24(7)
S3−N4−C5	116.31	114.60(11)	114.74(11)
N4−C5−S1	107.86	109.73(11)	109.63(12)
C5−S1−N2	96.68	97.17(8)	97.32(8)
O5−C5−S1	120.82	123.79(13)	123.72(12)
O5−C5−N4	131.32	126.49(15)	126.65(15)

5-Oxo-1,3,2,4-dithiadiazole (**1**) is a five-membered-ring structure which is characterised by one longer (1.641 Å) and two shorter (av. 1.579 Å) S−N bonds, a regular-length C−N bond (1.385 Å), a longer C−S bond (1.830 Å) and a localised C=O double bond (1.211 Å). The internal angles of the ring are all centred around 110°, which is close to the ideal value of 108° for a regular pentagon, apart from the C5−S1−N2 angle, which severely distorts the structure, as can be seen in Figure 1. Figure 3 shows the crystal structure and packing of the title compound: the orthorhombic unit consists of 16 molecules (two in the asymmetric unit) packed in a parallel configuration, which are slightly distorted from the planar conformation.

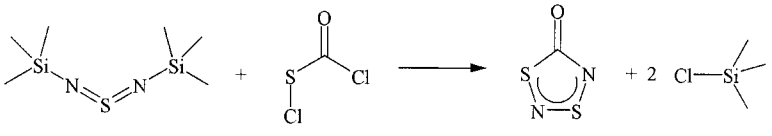

Figure 2. Synthetic pathway to 5-oxo-1,3,2,4-dithiadiazole (**1**)

 © 2004 Wiley-VCH Verlag GmbH & Co. KGaA, Weinheim

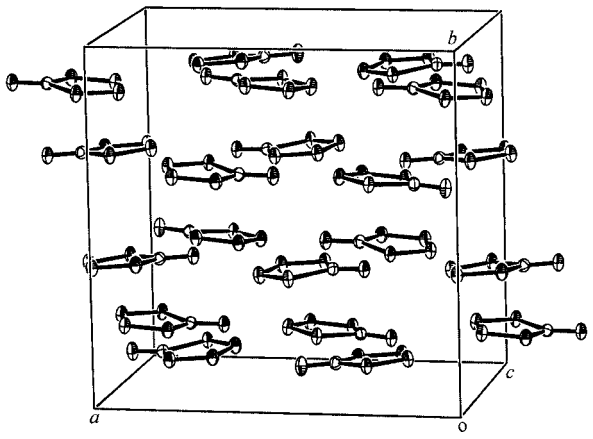

Figure 3. Crystal structure and packing of Roesky's ketone (**1**)

Frontier Orbitals and Geometries of the Anion and Cation

In Figure 4 the frontier orbitals are visualized using the program gOpenMol[13,14] for values of the contour surfaces of −0.035 and 0.035. Based on these pictures, the geometries of the anionic and cationic forms of Roesky's ketone can be rationalized. The geometries of the anion and the cation and the differences with the neutral molecule are given in Table 2. Based on the nodes of the HOMO, it is to be expected that the C5−S1, N4−C5 and N2−S3 bonds are longer in the cation than in the neutral molecule, as the HOMO has bonding character on these bonds: upon removing an electron from that orbital, the bonding will decrease, resulting in the lengthening of the bonds. This is indeed observed, as can be seen from Table 2: an increase in interatomic distance of up to 0.077 Å is found for the N2−S3 bond. The same reasoning can be applied for the three remaining bonds, which all become shorter. The removal of an electron from an orbital with anti-bonding character (the nodes in Figure 4a) will increase the bonding and shorten the bonds. Similar conclusions can be drawn for the anion, taking into account that here an extra electron is introduced into the LUMO. The bond lengths of the bonds where this orbital has anti-bonding character — all of them except N4−C5 — will increase, since the anti-bonding character is further increased. The bond length corresponding to the one bond in which there is bonding character (N4−C5) will decrease. All these trends can be found in the calculated geometry differences, given in Table 2.

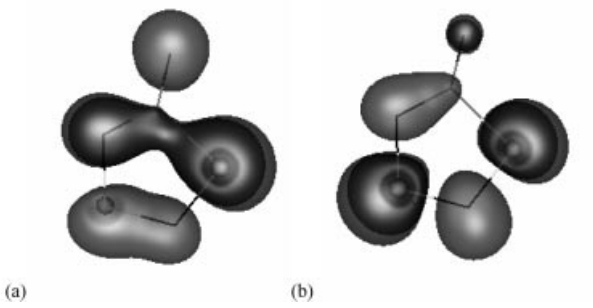

Figure 4. (a) HOMO and (b) LUMO of 5-oxo-1,3,2,4-dithiadiazole (**1**); see text for details

Table 2. Geometries of neutral 5-oxo-1,3,2,4-dithiadiazole (**1**), its cationic and anionic forms and the differences Δ (= $r_{ion} - r_{neutral}$); bond lengths are given in Å and angles in °

	Cation	Δ	Neutral	Anion	Δ
S1−N2	1.5797	−0.0611	1.6408	1.6834	0.0426
N2−S3	1.6852	0.0769	1.6083	1.7052	0.0969
S3−N4	1.5749	−0.0204	1.5953	1.6794	0.0841
N4−C5	1.3792	0.0142	1.3650	1.3156	−0.0494
C5−S1	2.0018	0.0608	1.9410	1.9618	0.0208
O5−C5	1.1808	−0.0131	1.1939	1.2236	0.0297
S1−N2−S3	115.02	2.65	112.37	109.38	−2.99
N2−S3−N4	104.50	−2.29	106.78	105.35	−1.44
S3−N4−C5	117.58	1.27	116.31	116.91	0.61
N4−C5−S1	107.37	−0.48	107.86	109.90	2.04
C5−S1−N2	95.53	−1.15	96.68	98.46	1.78
O5−C5−S1	121.39	0.57	120.82	117.25	−3.57
O5−C5−N4	131.23	−0.09	131.32	132.85	1.53

Charges and Dipoles

As the Hirshfeld partitioning of the electron density is an excellent way to attribute charges to atomic centers, stockholder charges, which are calculated according to this scheme, are known to be chemically very acceptable.[15−18] Stockholder charges were therefore calculated for the neutral 5-oxo-1,3,2,4-dithiadiazole (**1**) and for both its cation and anion; the obtained values are given in Table 3. Several features which are based on chemical knowledge, such as the dipole in the carbonyl group, the positive charges on the sulfur atoms and the negative charges on the nitrogen atoms, are reproduced well. The charges of the ionic forms of **1** will be used later in the reactivity discussion.

Table 3. Stockholder charges (in |e|) of neutral 5-oxo-1,3,2,4-dithiadiazole (**1**), its cationic and anionic forms and the differences Δ (= $q_{ion} - q_{neutral}$)

	Cation	Δ	Neutral	Anion	Δ
S1	0.435	0.291	0.144	−0.112	−0.257
N2	−0.056	0.100	−0.155	−0.281	−0.126
S3	0.520	0.203	0.318	−0.013	−0.330
N4	−0.042	0.143	−0.185	−0.280	−0.095
C5	0.196	0.068	0.128	0.065	−0.063
O5	−0.054	0.196	−0.250	−0.379	−0.129

The molecular dipole moment, μ, was calculated to be 3.104 D and its components are μ_x = −0.259 D and μ_y = −3.093 D, in the axis system given in Figure 5. The nth component of the molecular dipole, μ_n, with $n = x, y, z$, can be written as

 © 2004 Wiley-VCH Verlag GmbH & Co. KGaA, Weinheim

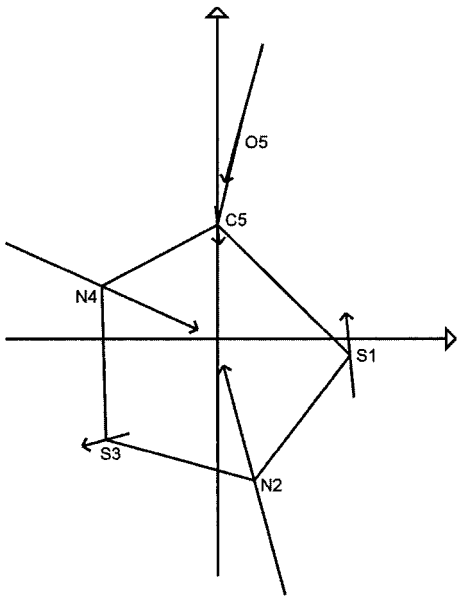

Figure 5. Atomic dipole moments in the Cartesian frame of the calculation; the size of the atomic dipole moment vector arrows has been increased by a factor of 100

$$\mu_n = \sum_A q_A R_{A,n} + \sum_A \mu_{A,n}$$

which is the sum of the contributions of charge transfer (first term, with q_A the stockholder charge and $R_{A,n}$ the coordinate of atom A) and of the intra-atomic charge polarization, calculated by the atomic dipole moment components $\mu_{A,n}$ (second term). Table 4 compiles these components for all six atoms in Roesky's ketone. It is clear that the contributions of the atomic dipoles, represented by the arrows in Figure 5, can be summed over the whole molecule to a net dipole with components of about 0.1 D in both the x and y directions. On the other hand, the charge-transfer contributions of the five ring atoms can be summed to a net zero charge transfer, indicating that the total charge transfer is determined solely by the value of the oxygen atom. Since the absolute values of the components of the total charge transfer outweigh those of the total atomic dipole, it can be said that the charge transfer of the oxygen atom indirectly determines the total molecular dipole moment. This is indeed found when the components of the charge transfer contribution of the oxygen atom (−0.336 and −2.819 in the x and y directions, respectively) are compared to the components of the total molecular dipole moment (−0.259 and −3.093 D in the x and y directions, respectively).

Table 4. Components, $\mu_{A,n}$, of the atomic dipole moment vectors, μ_A, and components, $q_A.R_{A,n}$, of the atomic charge transfers, in D, calculated for Roesky's ketone (**1**)

	$\mu_{A,x}$	$\mu_{A,y}$	$\mu_{A,z}$	$q_A.R_{A,x}$	$q_A.R_{A,y}$	$q_A.R_{A,z}$
S(1)	−0.020	0.224	0.000	0.963	−0.120	0.000
N(2)	−0.163	0.608	0.000	−0.287	1.096	0.000
S(3)	−0.125	−0.033	0.000	−1.782	−1.594	0.000
N(4)	0.508	−0.229	0.000	1.073	−0.488	0.000
C(5)	0.010	−0.102	0.000	0.000	0.730	0.000
O(5)	−0.102	−0.366	0.000	−0.336	−2.819	0.000
Sum	0.109	0.102	0.000	−0.369	−3.195	0.000

Aromaticity

Aromaticity remains a very complicated and debated issue in the whole of chemistry. Particularly in the field of computational chemistry, many researchers have tried to formulate unambiguous criteria for this elusive property during the past few decades; for a comprehensive work on aromaticity we refer to the book by Minkin, Glukhovstev and Simkin.[19] It is known that aromaticity involves the cyclic electron delocalisation coupled with an energetic stabilization, but the underlying physical nature of this aromatic stabilization is not known. An extensive set of criteria, which can be grouped into structural, energetic and magnetic criteria, can be found in literature, but it is believed that none of them alone can lead to an unambiguous definition of aromaticity. For this reason, an attempt is made in this work to combine a structural, an energetic and a magnetic criterion in order to ascertain whether the title compound is aromatic, anti-aromatic or nonaromatic.

In the first instance an attempt was made to qualitatively describe the influence on the aromaticity of the fragment closing the heterocyclic NSNS ring using structural and magnetic criteria. For a benzene ring as the closing fragment it was found in the gas-phase electron diffraction (GED) study[5] of 1,3λ²δ⁴,2,4-benzodithiadiazine that the heterocycle features one localized single S−N bond [1.697(5) Å] and two localized S=N double bonds [1.548(3) and 1.543(3) Å]; this trend was confirmed by a B3LYP/6-311+G* calculation yielding 1.717, 1.570 and 1.566 Å as the bond lengths, respectively. This geometrical data, together with a calculated NICS value of 14.99 ppm at the B3LYP/6-31+G* level,[6] indicates that the heterocyclic ring is anti-aromatic; a positive value indicates anti-aromaticity, a value approximating zero nonaromaticity and a negative value aromaticity. For 5-oxo-1,3,2,4-dithiadiazole (**1**), where the ring is closed by a carbonyl group, we find more intermediate bond lengths of 1.641, 1.608 and 1.595 Å, which suggest a higher degree of electron delocalisation and thus a higher degree of aromaticity. The NICS value of −11.13 ppm confirms the suggestion that the molecule is aromatic. Other structural criteria also express this electron delocalisation. Table 5 presents the calculated bond orders of Roesky's ketone (**1**), which can be conveniently combined with a graphical representation of the electron delocalisation in the form of a deformation electron density. For Roesky's ketone (**1**) the latter is plotted in Figure 6 through the molecular plane. It is clear from Figure 6 that the bond-order values can be correlated with the peak heights on the bonds in the deformation map: the three N−S bonds have similar bond orders (0.94, 1.23 and 0.98) and produce peaks of similar height in the density map, indicative of electron delocalisation. The C−N bond is somewhat stronger (1.33)

 © 2004 Wiley-VCH Verlag GmbH & Co. KGaA, Weinheim

Table 5. Selected geometrical data (r_e in Å and angles in °), bond orders (BO), total energies E (in H) and NICS values (in ppm) in the plane of the molecule [at the ring center, NICS(0)] and at 1 Å above the ring center [NICS(1)] of Roesky's ketone (**1**) and its constitutional isomers **2**−**4**

1		BO	**2**		BO	**3**		BO	**4**		BO
S1−N2	1.6408	0.94	S1−S2	2.0630	1.02	S1−N2	1.7423	0.67	N1−S2	1.5718	0.97
N2−S3	1.6083	1.23	S2−N3	1.7638	0.70	N2−N3	1.2376	2.07	S2−S3	2.1493	0.91
S3−N4	1.5953	0.98	N3−N4	1.2272	1.92	N3−S4	1.7423	0.67	S3−N4	1.5718	0.97
N4−C5	1.3650	1.33	N4−C5	1.4542	0.86	S4−C5	1.8121	0.87	N4−C5	1.4283	1.25
C5−S1	1.9410	0.74	C5−S1	1.8519	0.92	C5−S1	1.8121	0.87	C5−N1	1.4283	1.25
O5−C5	1.1939	1.94	O5−C5	1.1861	1.98	O5−C5	1.1939	2.08	O5−C5	1.1997	1.90
NICS(0)	−11.13		NICS(0)	−14.02		NICS(0)	−3.46		NICS(0)	−18.01	
NICS(1)	−7.73		NICS(1)	−9.54		NICS(1)	−4.17		NICS(1)	−11.88	
E	−1019.266		*E*	−1019.278		*E*	−1019.270		*E*	−1019.249	

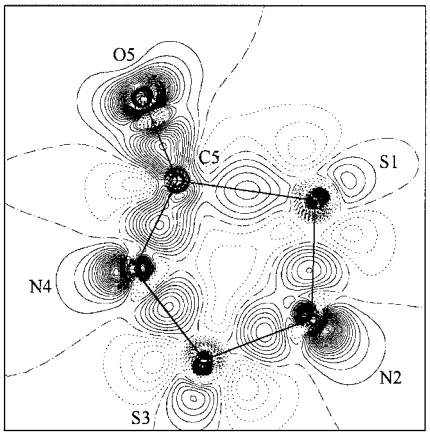

Figure 6. Deformation electron density of Roesky's ketone (**1**) in the molecular plane; full lines indicate positive electron density, dashed lines negative electron density and dashed-dotted lines zero electron density; isodensity lines were plotted every 0.05 e·Å^{-3}

and the C=O bond can be interpreted as a true double bond (1.94). The C−S bond (0.74), which is longer than expected, has indeed the lowest electron density between the two nuclei involved in the bond.

As the second part of this qualitative description, an energetic criterion was used as a measure of the (anti/non)aromatic character. For 1,3λ^{2}δ^4,2,4-benzodithiadiazine the UV/Vis absorption spectrum shows a maximum at 617 nm which is due to the heterocycle.[20] Our own measurements performed on Roesky's ketone produce a maximum absorption wavelength of 369 nm. The calculated value of the HOMO−LUMO gap, which is 342 nm at the B3LYP/6-311+G* level, is relatively close to the experimental one. It is known that the HOMO−LUMO separation may serve as an indicator of structural stability and reactivity; in the case of aromaticity, a larger HOMO−LUMO gap indicates a larger aromatic stabilisation (see ref.[19] and references cited therein). Based on this, the difference between the two λ_{max} values of the two compounds can serve to distinguish 5-oxo-1,3,2,4-dithiadiazine (aromatic) from 1,3λ^{2}δ^4,2,4-benzodithiadiazine (antiaromatic). The three criteria form a consistent set. As already mentioned in the introduction, the properties of compounds containing an NSNS fragment differ considerably from those of their hydrocarbon analogues. This can be illustrated here again by comparing Roesky's ketone (6 π-electrons), which is clearly aromatic, with its hydrocarbon analogue, the antiaromatic cyclopentadienone (4 π-electrons). These findings are in agreement with Hückel's $4n + 2$ π-electron rule.[21] In 1972 Banister[22] proposed that planar sulfur−nitrogen heterocycles are electron-rich compounds that show aromaticity, in agreement with Hückel's rule. He supported this contention with S_2N_2, S_4N_3 and S_5N_5 as examples. In our study we see that the aromaticity of our ring system, containing a carbonyl group besides the nitrogen and sulfur atoms, complies with Hückel's rule as well.

After this successful qualitative description of the aromaticity of the title compound, an attempt was made to obtain a quantitative insight into the combination of calculated bond orders, bond lengths and NICS values so that a description of the degree of aromaticity could be constructed. To do this, three constitutional isomers of 5-oxo-1,3,2,4-dithiadiazole (**1**), in which the sulfur and nitrogen atoms are permutated, were included in the calculations. The structures of the isomers 5-oxo-1,2,3,4-dithiadiazole (**2**), 5-oxo-1,4,2,3-dithiadiazole (**3**) and 5-oxo-2,3,1,4-dithiadiazole (**4**) are given in Figure 1. The molecular geometries, bond orders, total energies and NICS values of these three compounds are given in Table 5; the data for Roesky's ketone (**1**) is added for comparison. The NICS(0) values, calculated in the molecular plane, are negative for all isomers. It has been pointed out by Schleyer et al.[23] that there are some artifacts in NICS(0) values calculated in the plane of the molecule, due to the σ-framework of the molecule. In order to circumvent this, they proposed to calculate NICS(1) values at 1 Å above the ring center, since aromaticity rather involves the delocalization of the π-electrons. Based on the NICS(0) values, all molecules are aromatic. For **3** the NICS(0) and NICS(1) values are almost equal and considerably smaller than for the other isomers, suggesting that this isomer is nonaromatic. The bond orders and bond lengths of **3** indicate that all bonds are single, except the N=N and C=O bonds, which are localized double bonds. The localized nature of the latter bond is found in all isomers and we conclude that these π-electrons do not play any role in stabilizing the ring. The fact that all other bonds in **3** are single or localized double bonds is in

 © 2004 Wiley-VCH Verlag GmbH & Co. KGaA, Weinheim

accordance with the magnetic criterion NICS, and together they confirm that 5-oxo-1,4,2,3-dithiadiazole (**3**) is nonaromatic.

The other three isomers — **1**, **2** and **4** — all have larger negative values for NICS(0) and considerably negative values of NICS(1). These compounds must, therefore, all be aromatic, and the most aromatic of the series, according to this magnetic criterion, is 5-oxo-2,3,1,4-dithiadiazole (**4**). For this compound all bond orders have a value of about 1.00, which suggests there is maximum electron delocalization, i.e. a very narrow range of bond-order values of the bonds in the five-membered ring. This is in agreement with the two NICS values. The two remaining compounds, 5-oxo-1,3,2,4-dithiadiazole (**1**) and 5-oxo-1,2,3,4-dithiadiazole (**2**), could be classified as being of intermediate aromaticity, even though the structural and magnetic criteria put them in a different order.

We notice here that the overestimation of the C−S bond length at the B3LYP/6-311+G* level of theory has apparently no influence on the description of the electron delocalisation, whereas the excellent description of the relative bond lengths in the NSNS fragment by this method is obviously very important.

As a more general conclusion it can be stated that it is possible to qualitatively determine the (anti/non)aromatic nature of a system by combining structural, energetic and magnetic criteria. Some general quantitative trends can be found as well, even though a real numerical determination of the degree of aromaticity for Roesky's ketone (**1**) and its three studied isomers does not lead to an unambiguous order of aromaticity. Since these isomers cannot be interrelated by isodesmic reactions, no conclusion pertaining to their aromaticity can be drawn from the total energy values, which are also given in Table 5. The energy differences contain both different contributions due to the different kinds of bonds in the isomers and contributions due to the aromatic stabilization. Because these contributions cannot be separated, the total energies cannot be used as an aromaticity criterion.

Reactivity and Reactive Sites

We finally turn our attention to the local reactivity description by means of the condensed Fukui functions and local softnesses calculated for Roesky's ketone (**1**); these are given in Table 6. The stockholder charges, discussed above, will be used in this reactivity description as well. For all details on Fukui functions and local softnesses, and on the related global and local softness and hardness concept, we refer the reader to a recent review.[24] We mention here that a maximum value of the Fukui function, f^+, and local softness, s^+ (or f^- and s^-), indicates the most suitable place for nucleophilic (or electrophilic) attack by a soft species. As can be seen from Table 6, S3 has the largest s^+ value, and it also has the largest positive charge (Table 3). From these findings we know that S3 is the preferred site for a nucleophilic attack both by soft and hard reagents. The most likely site for an electrophilic attack is S1, but in view of its positive charge one does not expect a charge-controlled electrophilic attack to take place at this atom; rather, S1 is the favoured site for an orbital-controlled (based on the Fukui functions) electrophilic attack. The question of which site in Roesky's ketone (**1**) *is* favoured for a charge-controlled electrophilic attack can be answered in the following way.

The next highest value of f^- in Table 6 is found for S3 but, again, this site is disfavoured for a charge-controlled electrophilic attack due to its high positive atomic charge. Just below the value of S3 we find O5 and, even though it has a lower local softness value for electrophilic attack than both sulfur atoms, it has a pronounced negative charge and therefore is the most likely site for the charge-controlled attack by a hard electrophile. This has indeed been observed experimentally:[11] reactions between Roesky's ketone and electron-deficient hard Lewis acids like BF_3, $SbCl_5$ and $SnCl_4$ always yield adducts in which the metal atom is coordinated to the oxygen atom, the site predicted by assuming a charge-controlled regioselectivity.

Finally, we note that the local softness can also be seen as a measure of the ability of an atom to adapt its charge when electrons are added to or removed from a molecule. Upon inspection of the calculated stockholder charges of the cationic and anionic forms of Roesky's ketone (Table 3), we indeed find that the sulfur atoms — the softest atoms — are most suited as electron donor and as electron acceptor: upon oxidation or reduction of **1** the change of the atomic charge of both sulfur atoms is the largest in the molecule. More qualitatively, the softness of an atom can also be expressed by the diffuseness of the electron cloud surrounding it, and in this context we refer to the figure containing the deformation electron-density map (Figure 6): the lone pairs on the sulfur atoms — the softest atoms — are more diffuse than the ones on the harder nitrogen atoms.

Table 6. Fukui functions, f^+ and f^-, and local softnesses, s^+ and s^-, of the different atoms in Roesky's ketone (**1**)

	f^+	s^+	f^-	s^-
S(1)	0.256	0.864	0.280	0.945
N(2)	0.151	0.509	0.107	0.360
S(3)	0.320	1.082	0.212	0.715
N(4)	0.108	0.364	0.137	0.461
C(5)	0.056	0.191	0.064	0.216
O(5)	0.110	0.370	0.202	0.682

Conclusions

5-Oxo-1,3,2,4-dithiadiazole was synthesized and its structure re-determined experimentally by single-crystal X-ray diffraction. The experimental molecular geometry was compared to the B3LYP/6-311+G* geometry and a good agreement was found, except for the C−S bond, which is overestimated by the calculation. Further molecular and atomic properties were calculated at this level to obtain insight into the structure, aromaticity and reactivity of the title com-

 © 2004 Wiley-VCH Verlag GmbH & Co. KGaA, Weinheim

pound. A Hirshfeld partitioning of the electron density was used to calculate the atomic charges and dipoles, which led directly to the understanding of the origin of the molecular dipole. Based on frontier-orbital topologies, the geometries of the ionic forms of Roesky's ketone were explained. A consistent combination of structural, magnetic and energetic criteria confirmed that the compound is aromatic. An attempt to quantify the aromaticity, based on NICS values, bond lengths, bond orders and deformation densities, was made, and even though some general trends can be found, a real quantification was not possible for these compounds. Finally, a number of reactivity descriptors from conceptual DFT were calculated and the reactive sites within the molecule could be identified.

We note that, based on the finding that the π-system in the heterocycle of Roesky's ketone is delocalised over the entire ring, it would be incorrect to use the λ,δ-nomenclature, as this suggests localisation. The contrast between 1,3$\lambda^2\delta^4$,2,4-benzodithiadiazine (localised π-system and antiaromatic compound) and 5-oxo-1,3,2,4-dithiadiazole (**1**; delocalised π-system and aromatic compound) can now be conveniently made by omitting the λ,δ descriptors.

Experimental Section

Synthesis: 5-Oxo-1,3,2,4-dithiadiazole (**1**) was synthesised by a modification of a procedure reported by Neidlein and Gieren;[9] the reaction sequence is given in Figure 2. Unless otherwise stated, manipulations were performed under oxygen-free argon using standard Schlenk techniques and flame-dried Schlenk glassware. Hexane and chloroform were dried, purified and stored according to common procedures.[25] Chlorocarbonylsulfenyl chloride was purchased from Lancaster and used as received; bis(trimethylsilyl)-sulfur diimide was prepared according to a literature method.[26] The UV/Vis absorption spectrum was obtained from a solution in dry CH_2Cl_2 with a Hitachi U-2001 double-beam spectrometer. A solution of bis(trimethylsilyl)sulfur diimide (5.23 g, 5.97 mL, 25.33 mmol) in chloroform (30 mL) was added dropwise over a 40 min period to a stirred and cooled (0 °C) solution of chlorocarbonylsulfenyl chloride (3.32 g, 2.10 mL, 25.35 mmol) in chloroform (30 mL). Once the addition was complete, the stirred reaction mixture was slowly warmed to room temperature, then heated to 40 °C for 20 min and then allowed to cool to room temperature. Hexane (60 mL) was added and the mixture was filtered through a stainless steel cannula to remove any insoluble material. The volume of the filtrate was reduced in vacuo to approximately 50 mL and then stored at −14 °C overnight. The resulting yellow crystalline material was collected by suction filtration, washed with cooled (0 °C) hexane (10 mL) and then dried briefly in vacuo. The yield was 1.63 g (53%). UV/Vis (CH_2Cl_2): λ_{max} = 369 nm.

X-ray Structure Determination: Single crystals of 5-oxo-1,3,2,4-dithiadiazole (**1**) suitable for X-ray diffraction studies were obtained by slow sublimation of the bulk material at room temperature and pressure under argon over a two month period. Crystal structure data for the compound were collected at 125 K with a Bruker SMART CCD diffractometer equipped with an Oxford Instruments low-temperature attachment, using Mo-K_α radiation (λ = 0.71073 Å). The structure was solved by direct methods and refined by full-matrix least-squares methods on F^2. Refinements were performed using SHELXTL (Version 5.10, Bruker AXS, 1999). Crystal data for 5-oxo-1,3,2,4-dithiadiazole (**1**): CN_2OS_2, M = 120.15, orthorhombic, a = 13.029(3), b = 12.762(3), c = 9.145(2) Å, V = 1520.6(6) Å^3, T = 125(2) K, space group *Pbca*, Z = 16 with two nonequivalent molecules in the asymmetric unit, D_c = 2.099 g·cm^{-3}, μ(Mo-K_α) = 1.207 mm^{-1}, 1359 unique reflections (R_{int} = 0.0206) measured. Final R_1 [1097, $F \geq 2\sigma(F)$] = 0.0225, wR (all F^2) = 0.0580. CCDC-238171 contains the supplementary crystallographic data for this paper. These data can be obtained free of charge at www.ccdc.cam.ac.uk/conts/retrieving.html [or from the Cambridge Crystallographic Data Centre, 12 Union Road, Cambridge CB2 1EZ, UK; Fax: (internat.) + 44-1223-336-033; E-mail: deposit@ccdc.cam.ac.uk].

Calculations: All calculations were performed on isolated molecules using the BRABO[27] and Gaussian 98[28] suites of programs applying the Density Functional level of theory (DFT), using the Becke-type three-parameter hybrid functional,[29] B3LYP[30] and the 6-311+G*[31,32] basis set. Initially, the geometry of Roesky's ketone was calculated in C_1 symmetry, but the structure converted into a planar conformation. Consequently, the symmetry was raised to C_s, the geometry was re-calculated and a frequency calculation was performed to ascertain that the resulting structure was indeed an energy minimum. All subsequent calculations of molecular properties were performed at the B3LYP/6-311+G* geometry. Deformation densities were calculated by subtracting the pro-molecular density from the total molecular density. Stockholder charges were calculated as previously reported,[15] based on the Hirshfeld partitioning of the space.[33] Atomic dipole moments, μ_A, were calculated according to

$$\mu_{A,n} = -\int r_n \Delta\varrho_A(\vec{r}) \mathrm{d}\vec{r}$$

with $n = x, y, z$, $\vec{r}$ = the position vector of the atom and $\Delta\rho$ = the deformation density, as usually defined.[16] Nucleus-Independent Chemical Shifts (NICS)[34] were calculated at the B3LYP/6-311+G* level of theory, in the geometrical centre of the ring [NICS(0)] and at a distance of 1 Å perpendicularly above the ring centre [NICS(1)], using the Gauge Independent Atomic Orbitals (GIAO) method as implemented in Gaussian 98. Bond orders were calculated according to Mayer's definition.[35] The Fukui function[36] was calculated by the finite difference approach.[24] Geometries and molecular properties of the three constitutional isomers **2**−**4** and the anionic and cationic forms of Roesky's ketone (**1**) were calculated at the B3LYP/6-311+G* level. A procedure analogous to the one applied to the parent compound indicated that the constitutional isomers and the ionic forms also have C_s symmetry. Cartesian coordinates and energies of all compounds are given in the Supporting Information.

Acknowledgments

J. V. D. thanks the Flemish governmental institution IWT for a predoctoral grant. The authors are grateful to Prof. Frank De Proft of the University of Brussels (VUB) for his help with the interpretation and discussion of conceptual DFT.

[1] V. V. Walatka, M. M. Labes, J. H. Perlstein, *Phys. Rev. Lett.* **1973**, *31*, 1139−1142.
[2] R. L. Greene, G. B. Street, L. J. Suter, *Phys. Rev. Lett.* **1975**, *34*, 577−579.
[3] T. Chivers, *Chem. Rev.* **1985**, *85*, 341−365.
[4] T. Chivers, *Acc. Chem. Res.* **1984**, *17*, 166−171.

 © 2004 Wiley-VCH Verlag GmbH & Co. KGaA, Weinheim

[5] F. Blockhuys, S. L. Hinchley, A. Y. Marakov, Y. V. Gatilov, A. V. Zibarev, J. D. Woollins, D. W. H. Rankin, *Chem. Eur. J.* **2001**, *7*, 3592−3602.
[6] A. Y. Makarov, I. Y. Bagryanskaya, F. Blockhuys, C. Van Alsenoy, Y. V. Gatilov, V. V. Knyazev, A. M. Maksimov, T. V. Mikhalina, V. E. Platonov, M. M. Shakirov, A. V. Zibarev, *Eur. J. Inorg. Chem.* **2003**, 77−88.
[7] J. Van Droogenbroeck, K. Tersago, C. Van Alsenoy, F. Blockhuys, *Chem. Phys. Lett.*, submitted.
[8] H. W. Roesky, E. Wehner, *Angew. Chem. Int. Ed. Engl.* **1975**, *14*, 498−498.
[9] R. Neidlein, P. Leinberger, A. Gieren, B. Dederer, *Chem. Ber.* **1978**, *111*, 698−704.
[10] R. Neidlein, P. Leinberger, *Chem.-Ztg.* **1975**, *99*, 433−433.
[11] H. W. Roesky, E. Wehner, E. J. Zehnder, H. J. Deiseroth, A. Simon, *Chem. Ber.* **1978**, *111*, 1670−1676.
[12] R. H. Delaat, L. Durham, E. G. Livingstone, N. P. C. Westwood, *J. Phys. Chem.* **1993**, *97*, 11216−11220.
[13] D. L. Bergman, L. Laaksonen, A. Laaksonen, *J. Mol. Graphics* **1997**, *15*, 301−307.
[14] L. Laaksonen, *J. Mol. Graphics* **1992**, *10*, 33−34.
[15] B. Rousseau, A. Peeters, C. Van Alsenoy, *Chem. Phys. Lett.* **2000**, *324*, 189−194.
[16] F. De Proft, C. Van Alsenoy, A. Peeters, W. Langenaeker, P. Geerlings, *J. Comput. Chem.* **2002**, *23*, 1198−1209.
[17] F. De Proft, R. Vivas-Reyes, A. Peeters, C. Van Alsenoy, P. Geerlings, *J. Comput. Chem.* **2003**, *24*, 463−469.
[18] J. Olah, C. Van Alsenoy, A. B. Sannigrahi, *J. Phys. Chem. A* **2002**, *106*, 3885−3890.
[19] V. I. Minkin, M. N. Glukhovsev, B. Y. Simkin, *Aromaticity and Antiaromaticity*, John Wiley, New York, **1994**.
[20] A. W. Cordes, M. Hojo, H. Koenig, M. C. Noble, R. T. Oakley, W. T. Pennington, *Inorg. Chem.* **1986**, *25*, 1137−1145.
[21] E. Hückel, *Z. Phys.* **1931**, *70*, 204−286.
[22] A. J. Banister, *Nature (London), Phys. Sci.* **1972**, *237*, 92−93.
[23] P. V. Schleyer, M. Manoharan, Z. X. Wang, B. Kiran, H. J. Jiao, R. Puchta, N. Hommes, *Org. Lett.* **2001**, *3*, 2465−2468.
[24] P. Geerlings, F. De Proft, W. Langenaeker, *Chem. Rev.* **2003**, *103*, 1793−1873.
[25] D. D. Perrin, W. L. F. Armarego, *Purification of Laboratory Chemicals*, 3rd ed., Pergamon Press, Oxford, **1988**.
[26] C. P. Warrens, J. D. Woollins, *Inorg. Synth.* **1989**, *25*, 43−47.
[27] C. Van Alsenoy, A. Peeters, *J. Mol. Struct.* **1993**, *105*, 19−34.
[28] M. J. Frisch, G. W. Trucks, H. B. Schlegel, G. E. Scuseria, M. A. Robb, J. R. Cheeseman, V. G. Zakrzewski, J. J. A. Montgomery, R. E. Stratmann, J. C. Burant, S. Dapprich, J. M. Millam, A. D. Daniels, K. N. Kudin, M. C. Strain, O. Farkas, J. Tomasi, V. Barone, M. Cossi, R. Cammi, B. Mennucci, C. Pomelli, C. Adamo, S. Clifford, J. Ochterski, G. A. Petersson, P. Y. Ayala, Q. Cui, K. Morokuma, P. Salvador, J. J. Dannenberg, D. K. Malick, A. D. Rabuck, K. Raghavachari, J. B. Foresman, J. Cioslowski, J. V. Ortiz, A. G. Baboul, B. B. Stefanov, G. H. Liu, A. Liashenko, P. Piskorz, I. Komaromi, R. Gomperts, R. L. Martin, D. J. Fox, T. Keith, M. A. Al-Laham, C. Y. Peng, A. Nanayakkara, M. Challacombe, P. M. W. Gill, B. Johnson, W. Chen, M. W. Wong, J. L. Andres, C. Gonzalez, M. Head-Gordon, E. S. Replogle, J. A. Pople, *Gaussian 98*, Revision A.11, Gaussian Inc., Pittsburgh PA, **2001**.
[29] A. D. Becke, *J. Chem. Phys.* **1993**, *98*, 5648−5652.
[30] P. J. Stephens, F. J. Devlin, C. F. Chabalowski, M. J. Frisch, *J. Phys. Chem.* **1994**, *98*, 11623−11627.
[31] A. D. McLean, G. S. Chandler, *J. Chem. Phys.* **1980**, *72*, 5639−5648.
[32] R. Krishnan, J. S. Binkley, R. Seeger, J. A. Pople, *J. Chem. Phys.* **1980**, *72*, 650−654.
[33] F. L. Hirshfeld, *Theor. Chim. Acta* **1977**, *44*, 129−138.
[34] P. V. Schleyer, C. Maerker, A. Dransfeld, H. J. Jiao, N. Hommes, *J. Am. Chem. Soc.* **1996**, *118*, 6317−6318.
[35] I. Mayer, *Chem. Phys. Lett.* **1983**, *97*, 270−274.
[36] R. G. Parr, W. T. Yang, *J. Am. Chem. Soc.* **1984**, *106*, 4049−4050.

Received May 3, 2004
Early View Article
Published Online July 22, 2004

 © 2004 Wiley-VCH Verlag GmbH & Co. KGaA, Weinheim

Synthesis and Characterization of Mixed Phthalocyaninato and *meso*-Tetrakis(4-chlorophenyl)porphyrinato Triple-Decker Complexes – Revealing the Origin of Their Electronic Absorptions

Xuan Sun,[a] Renjie Li,[a] Daqi Wang,[b] Jianmin Dou,[b] Peihua Zhu,[a] Fanli Lu,[a] Changqin Ma,[a] Chi-Fung Choi,[c] Diana Y. Y. Cheng,[c] Dennis K. P. Ng,[c] Nagao Kobayashi,[d] and Jianzhuang Jiang*[a]

Keywords: Phthalocyanines / Porphyrins / Rare earth metals / Sandwich complexes / Triple-decker complexes

Two series of mixed phthalocyaninato and porphyrinato rare earth(III) triple-decker complexes $[M_2(Pc)(TClPP)_2]$ (**1a–10a**) and $[M_2(Pc)_2(TClPP)]$ (**1b–11b**) [M = Y, La–Er except Ce and Pm; Pc = phthalocyaninate; TClPP = tetrakis(4-chlorophenyl)-porphyrinate] have been prepared by treating the half-sandwich complexes [M(TClPP)(acac)] (acac = acetylacetonate), generated in situ from $[M(acac)_3]\cdot nH_2O$ and $H_2(TClPP)$, with $Li_2(Pc)$. All the triple-decker complexes have been characterized by a wide range of spectroscopic and electrochemical methods. The molecular structures of $[M_2(Pc)(TClPP)_2]$ (M = Y, Ho) have also been determined, and show a symmetrical disposition of ligands, with two outer domed TClPP and one inner Pc rings. A systematic investigation of the optical and electrochemical data of these complexes has revealed the nature of the HOMO and LUMO, as well as the origin of the electronic absorptions of these triple-decker complexes.
(© Wiley-VCH Verlag GmbH & Co. KGaA, 69451 Weinheim, Germany, 2004)

Introduction

Triple-decker rare-earth complexes with mixed phthalocyaninato and porphyrinato ligands have received considerable attention.[1] With two different classes of macrocyclic ligands, which can be arranged in different order in the complexes, this exotic class of compounds exhibits intriguing spectroscopic and electrochemical properties that cannot be found in non-sandwich counterparts. Owing to the high stability, the presence of multiple redox states, and the ability to store charge for a significant period of time, these triple-decker complexes are promising molecular-based materials for information-storage devices such as multistate counters and molecular capacitors.[2] Despite these important applications and other intrinsic interest in the structural and spectroscopic aspects, heteroleptic triple-deckers with these tetrapyrrole ligands remain rare and are confined to a number of lanthanides.[2–4] As part of our continuing interest in heteroleptic rare-earth complexes with tetrapyrrole ligands,[1,4] we describe herein a systematic study of two series of phthalocyaninato and porphyrinato triple-decker complexes, namely $[M_2(Pc)(TClPP)_2]$ (M = Y, La–Ho except Ce and Pm) and $[M_2(Pc)_2(TClPP)]$ (M = Y, La–Er except Ce and Pm), including their synthesis, spectroscopic and structural characterization, and electrochemical properties. A detailed examination of these properties has led to a better understanding of their electronic structure as well as the origin of the electronic transitions of these complexes.

Results and Discussion

Synthesis and Characterization

According to our previously described procedure,[4a,4b] treatment of [M(TClPP)(acac)] (M = Y, La–Er except Ce and Pm), generated in situ from $[M(acac)_3]\cdot nH_2O$ and $H_2(TClPP)$, with $Li_2(Pc)$ gave a mixture of the triple-deckers $[M_2(Pc)(TClPP)_2]$ and $[M_2(Pc)_2(TClPP)]$, which could be separated readily by column chromatography (Figure 1). The yields for both series of complexes {5–48% for $[M_2(Pc)(TClPP)_2]$ and 4–40% for $[M_2(Pc)_2(TClPP)]$} were higher for lanthanides with a moderate size, while both

[a] Department of Chemistry, Shandong University
Jinan 250100, China
Fax: (internat.) + 86-531-856-5211
E-mail: jzjiang@sdu.edu.cn
[b] Department of Chemistry, Liaocheng University
Liaocheng 252000, China
[c] Department of Chemistry, The Chinese University of Hong Kong
Shatin, N.T., Hong Kong, China
[d] Department of Chemistry, Graduate School of Science, Tohoku University
Sendai 980-8578, Japan
Supporting information for this article is available on the WWW under http://www.eurjic.org or from the author.

 © 2004 Wiley-VCH Verlag GmbH & Co. KGaA, Weinheim **DOI: 10.1002/ejic.200400289**

early and late lanthanide analogues gave a lower yield (Tables S1 and S2, and Figure S1 in the Supporting Information). Attempts to isolate the late lanthanide complexes $[M_2(Pc)(TClPP)_2]$ (M = Er−Lu) and $[M_2(Pc)_2(TClPP)]$ (M = Tm−Lu) were not successful. Apparently, mid-lanthanides have an appropriate size to optimize the separation of the three ligands so that they are close enough to maximize the stabilization due to π-π interactions yet the axial compression of the π-systems remains tolerable. This balance leads to a higher stability and therefore a higher yield of the complexes.

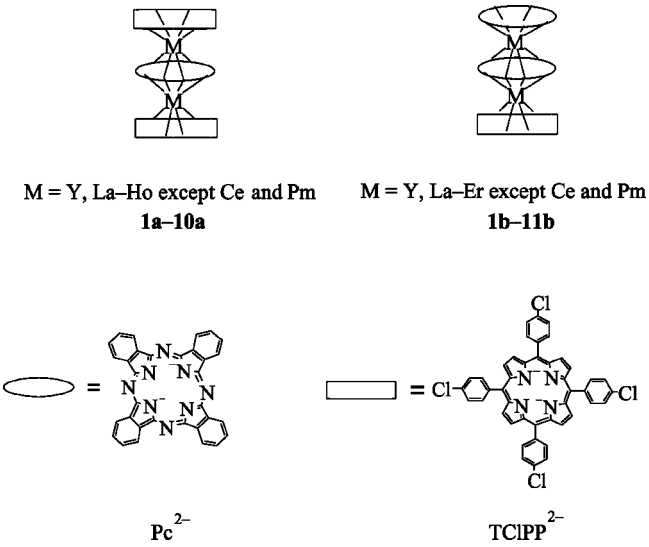

Figure 1. Schematic structures of the mixed-ring rare-earth triple-decker complexes with phthalocyaninato and *meso*-tetrakis(4-chlorophenyl)porphyrinato ligands

Except for a few early lanthanide triple-deckers, which are not very stable even in the solid state, all the triple-deckers gave satisfactory elemental analysis results (Tables S1 and S2). Intense molecular ion (or protonated molecular ion) peaks with expected isotopic patterns were also observed in the MALDI-TOF mass spectra for all these complexes. The mass spectroscopic data are also summarized in Tables S1 and S2, and a partial MALDI-TOF spectrum of $[Tb_2(Pc)(TClPP)_2]$ (**7a**) showing the isotopic distribution of the protonated molecular ion and the corresponding simulated spectrum is given in the Supporting Information (Figure S2) as an example.

Table 1 collects the ^1H NMR spectroscopic data of the triple-deckers $[M_2(Pc)(TClPP)_2]$ [M = Sm (**4a**), Y (**9a**)] and $[M_2(Pc)_2(TClPP)]$ [M = Sm (**4b**), Y (**9b**)] in $CDCl_3$. The spectral assignment could easily be made on the basis of the integration and multiplicity of the signals, and with reference to the previous results for the Eu analogues **5a** and **5b**,[4b] and the triple-deckers $[M_2(Pc)(TPyP)_2]$ [M = La, Eu; TPyP = *meso*-tetrakis(4-pyridyl)porphyrinate].[4f] Satisfactory NMR spectroscopic data, however, could not be obtained for the other triple-deckers due to the highly paramagnetic character of the metal centers.

Electronic Absorption Spectra

The electronic absorption spectra for both series of triple-decker complexes **1a**−**10a** and **1b**−**11b**, were measured in $CHCl_3$ and the data are compiled in Tables 2 and 3. Figures 2 and 3 display the spectra for $[M_2(Pc)(TClPP)_2]$ and $[M_2(Pc)_2(TClPP)]$ (M = Nd, Gd, Dy), respectively, as examples. For the first series of complexes, the Pc Soret band at 354−360 nm shifts slightly to the blue, while the Q-band absorptions at 485−494, 548−573, and 876−997 nm are all red-shifted due to the lanthanide contraction (Table 2). The TClPP Soret band at 418−420 nm and the remaining Q band at 606−608 nm remain relatively unshifted for the whole series of complexes.

Some of the absorption bands of **1b**−**11b** are also dependent on the size of the metal centers. As shown in Table 3, the TClPP Soret band at 411−418 nm and the longest-

Table 1. ^1H NMR spectroscopic data (δ) for the triple-deckers $[M_2(Pc)(TClPP)_2]$ (M = Sm, Y) and $[M_2(Pc)_2(TClPP)]$ (M = Sm, Y) in $CDCl_3$

Compound	Pc-H_α	Pc-H_β	TClPP-H_β	TClPP-H_{aryl}
$[Sm_2(Pc)(TClPP)_2]$ (**4a**)	8.10−8.18 (m, 8 H)	7.81−7.84 (m, 8 H)	6.67 (s, 16 H)	7.57 (dd, *J* = 1.8, 8.1 Hz, 8 H) 7.38 (dd, *J* = 1.8, 8.1 Hz, 8 H) 7.10 (dd, *J* = 1.8, 8.1 Hz, 8 H) 6.61 (dd, *J* = 1.8, 8.1 Hz, 8 H)
$[Y_2(Pc)(TClPP)_2]$ (**9a**)	9.46−9.49 (m, 8 H)	8.55−8.58 (m, 8 H)	7.29 (s, 16 H)	8.34 (dd, *J* = 2.1, 8.1 Hz, 8 H) 7.98 (dd, *J* = 2.1, 8.1 Hz, 8 H) 6.96 (dd, *J* = 2.1, 8.1 Hz, 8 H) 5.86 (dd, *J* = 2.1, 8.1 Hz, 8 H)
$[Sm_2(Pc)_2(TClPP)]$ (**4b**)	7.93−7.95 (m, 8 H) 7.83−7.86 (m, 8 H)	7.71−7.74 (m, 8 H) 7.65−7.68 (m, 8 H)	6.60 (s, 8 H)	7.90 (dd, *J* = 2.1, 8.1 Hz, 4 H) 7.88 (dd, *J* = 2.1, 8.1 Hz, 4 H) 7.13 (dd, *J* = 2.1, 8.1 Hz, 4 H) 6.78 (dd, *J* = 2.1, 8.1 Hz, 4 H)
$[Y_2(Pc)_2(TClPP)]$ (**9b**)	9.11−9.20 (m, 8 H) 8.48−8.59 (m, 8 H)	8.68−8.73 (m, 8 H) 8.05−8.12 (m, 8 H)	7.33 (s, 8 H)	8.48−8.59 (overlapped with one of the Pc-H_α multiplets) 8.02 (dd, *J* = 2.1, 8.1 Hz, 4 H) 6.98 (dd, *J* = 2.1, 8.1 Hz, 4 H) 5.98 (dd, *J* = 2.1, 8.1 Hz, 4 H)

 © 2004 Wiley-VCH Verlag GmbH & Co. KGaA, Weinheim

Table 2. Electronic absorption data for **1a**−**10a** in $CHCl_3$

Compound	λ_{max} [nm] (log ε)					
1a	360 (5.01)	420 (5.45)	485 (4.43)	551 (4.28)	608 (4.30)	876 (3.86)
2a	360 (4.99)	420 (5.38)	489 (4.39)	549 (4.15)	607 (4.29)	908 (3.83)
3a	358 (4.94)	420 (5.30)	489 (4.44)	548 (4.32)	607 (4.25)	919 (4.10)
4a	355 (4.96)	420 (5.27)	492 (4.49)	556 (4.40)	606 (4.29)	937 (3.96)
5a	354 (5.04)	419 (5.32)	492 (4.57)	559 (4.15)	605 (4.34)	950 (3.94)
6a	354 (5.05)	419 (5.36)	493 (4.55)	563 (4.05)	606 (4.24)	955 (4.04)
7a	354 (5.02)	419 (5.33)	494 (4.53)	565 (4.17)	606 (4.19)	973 (3.94)
8a	354 (5.10)	419 (5.38)	494 (4.64)	567 (4.20)	606 (4.30)	987 (3.89)
9a	354 (5.10)	418 (5.34)	494 (4.68)	566 (4.16)	607 (4.39)	995 (3.80)
10a	354 (5.09)	418 (5.33)	494 (4.68)	573 (4.18)	606 (4.40)	997 (3.77)

Table 3. Electronic absorption data for **1b**−**11b** in $CHCl_3$

Compound	λ_{max} [nm] (log ε)						
1b	342 (5.21)	418 (4.94)				616 (4.86)	689 (4.55)
2b	342 (5.14)	418 (5.08)	489 (4.43)		553 (4.36)	619 (4.75)	694 (4.61)
3b	342 (5.18)	417 (5.11)	489 (4.33)	524 (4.42)	556 (4.37)	617 (4.81)	705 (4.63)
4b	343 (5.20)	416 (5.03)	491 (4.32)	525 (4.47)	560 (4.37)	618 (4.87)	720 (4.61)
5b	342 (5.19)	414 (5.05)	491 (4.33)	521 (4.42)	557 (4.36)	617 (4.84)	723 (4.55)
6b	343 (5.22)	413 (5.03)	493 (4.32)	524 (4.40)	564 (4.37)	618 (4.84)	731 (4.50)
7b	343 (5.21)	413 (5.01)		523 (4.39)		618 (4.81)	737 (4.45)
8b	343 (5.19)	413 (4.98)		524 (4.37)		619 (4.76)	744 (4.39)
9b	343 (5.19)	412 (4.95)		523 (4.35)		618 (4.74)	747 (4.35)
10b	343 (5.17)	411 (4.94)		522 (4.34)		618 (4.71)	751 (4.31)
11b	343 (5.17)	412 (4.95)		521 (4.45)		617 (4.72)	757 (4.42)

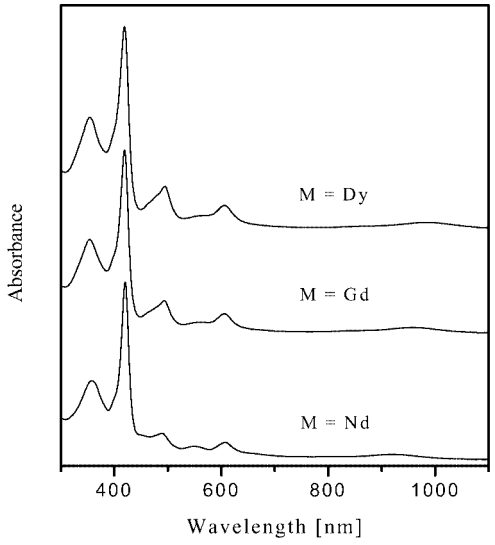

Figure 2. Electronic absorption spectra of $[M_2(Pc)(TClPP)_2]$ (M = Nd, Gd, Dy) in $CHCl_3$

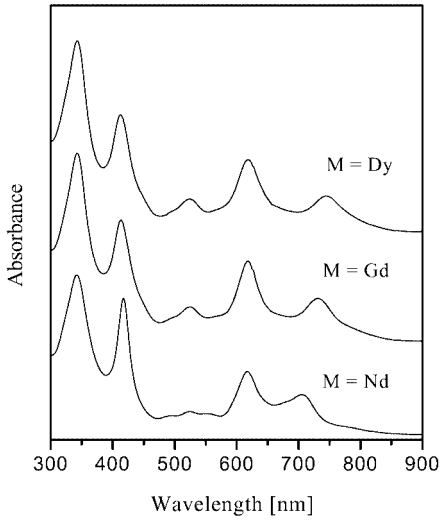

Figure 3. Electronic absorption spectra of $[M_2(Pc)_2(TClPP)]$ (M = Nd, Gd, Dy) in $CHCl_3$

wavelength Q-band at 689−757 nm are shifted to the blue and red, respectively, across the lanthanide series. For this series of complexes, the positions of the Pc Soret band (342−343 nm) and the other Q-bands in the visible region are not very sensitive to the metal centers.

In the mixed-ring triple-deckers $[M_2(Pc)(TClPP)_2]$ (**1a**−**10a**) and $[M_2(Pc)_2(TClPP)]$ (**1b**−**11b**), the close proximity of the three conjugated π-systems in a face-to-face configuration induces a splitting of the monomer (Pc and TClPP) molecular orbitals. As shown in Figure 4, the interactions of the doubly degenerate e_g LUMO of both ligands, the a_{1u} HOMO of Pc, and the a_{1u} second HOMO of TClPP result in the formation of three doubly degenerate lowest-unoccupied molecular orbitals (the bonding LUMO, second non-bonding LUMO, and third anti-bonding LUMO) and three non-degenerate highest-occupied molecular orbitals (the third bonding HOMO, second non-bonding

 © 2004 Wiley-VCH Verlag GmbH & Co. KGaA, Weinheim

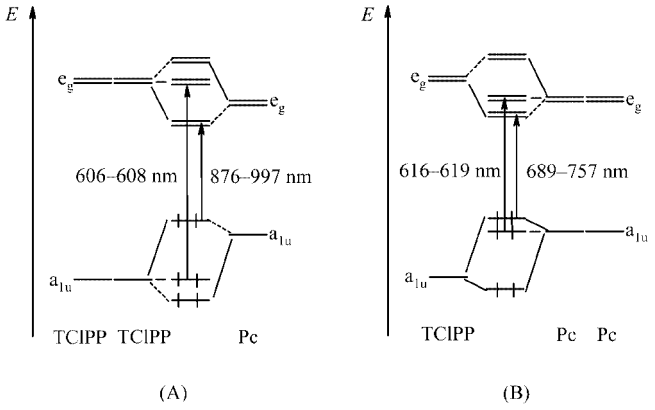

Figure 4. Partial molecular-orbital diagrams for $[M_2(Pc)(TClPP)_2]$ (A) and $[M_2(Pc)_2(TClPP)]$ (B)

HOMO, and first anti-bonding HOMO).[5] Due to the intrinsic difference in the electronic structure, the a_{1u} orbital of Pc is higher in energy than that of TClPP, while the e_g orbitals of Pc are lower than those of TClPP. Therefore, for both series of triple-deckers, the first anti-bonding HOMO and the first bonding LUMO are mainly from the phthalocyaninato ligand(s), whereas the third bonding HOMO and third anti-bonding LUMO have higher porphyrin character. The second non-bonding HOMO and non-bonding LUMO are pure TClPP and Pc orbitals, respectively, for $[M_2(Pc)(TClPP)_2]$ (**1a**−**10a**) and $[M_2(Pc)_2(TClPP)]$ (**1b**−**11b**). Along with the lanthanide contraction, the ring-to-ring interactions increase, resulting in an increase in the splitting between the first and second HOMOs as well as the second and third HOMOs of the triple-deckers. This simplified bonding picture can be used to interpret the electronic absorption data of these triple-decker complexes. For both series of complexes, the lowest-energy absorption band can be attributed to the electronic transition from the anti-bonding HOMO to the bonding LUMO, which is red-shifted across the lanthanide series (Tables 2 and 3). The second-lowest-energy absorption band can be ascribed to the transition from the second non-bonding HOMO to the second non-bonding LUMO, which remains essentially unchanged for the whole lanthanide series. Similarly, the Soret bands at 418−420 nm for $[M_2(Pc)(TClPP)_2]$ (**1a**−**10a**) and 342−345 nm for $[M_2(Pc)_2(TClPP)]$ (**1b**−**11b**) should also involve non-bonding orbitals with a pure TClPP or Pc character, respectively. It is worth noting that the dependence of the other Soret bands at 354−360 nm for $[M_2(Pc)(TClPP)_2]$ (**1a**−**10a**) and 412−418 nm for $[M_2(Pc)(TClPP)_2]$ (**1b**−**11b**) on the rare-earth ionic size clearly indicates the mixed phthalocyanine and porphyrin character of these transitions, suggesting the contributions from both porphyrin and phthalocyanine ligands to the molecular orbitals involved in these transitions.

IR Spectra

IR spectroscopy is a useful tool to reveal the nature of phthalocyaninato ligands in their rare-earth sandwich complexes. The IR characteristics of several series of double- and triple-decker phthalocyaninato and/or porphyrinato rare-earth compounds, namely $[M(Pc')_2]$, $[M(Pc')(Por)]$, $[M_2(Pc')(Por)_2]$, and $[M_2(Pc')_2(Por)]$ (Pc′ = general phthalocyaninate; Por = general porphyrinate) have been systematically studied.[6] An intense band at 1312−1323 cm^{-1} has been observed for neutral bis(phthalocyaninato) and mixed (phthalocyaninato)(porphyrinato) rare earth(III) double-decker complexes. This can be attributed to the $Pc^{\cdot-}$ IR marker band. On the other hand, a moderately strong band at ca. 1329 cm^{-1} has been observed for $[Ce^{IV}(Pc)_2]$ and $[M_2(Pc)_2\{Pc(OC_8H_{17})_8\}]$ $[Pc(OC_8H_{17})_8$ = 2,3,9,10,16,17,23,24-octaoctyloxyphthalocyaninate], which contain dianionic phthalocyanine rings. This band is therefore regarded as the characteristic IR band for Pc^{2-}.[6] For the present two series of complexes, the dianionic nature of the phthalocyaninato ligand(s) was unambiguously verified by the observation of the characteristic Pc^{2-} IR band at ca. 1330 cm^{-1}. As expected, the relative intensity of this band is higher for **1b**−**11b** than for **1a**−**10a** due to the higher Pc/TClPP ratio.

Structural Studies of $[M_2(Pc)(TClPP)_2]$ (M = Y, Ho)

The molecular structures of $[M_2(Pc)(TClPP)_2]$ [M = Y (**9a**), Ho (**10a**)] were determined by X-ray diffraction analysis. Both compounds are isostructural and crystallize in the same tetragonal system with a *P*4/*n* space group together with a disordered CH_2Cl_2 molecule. It is worth noting that structurally characterized mixed-ring triple-deckers remain rare so far, and to the best of our knowledge they are limited to [(TPP)Ce(Pc)Gd(OEP)] (TPP = *meso*-tetraphenylporphyrinate; OEP = octaethylporphyrinate),[7] $[Ce_2(Pc)_2(TOMePP)]$ [TOMePP = *meso*-tetrakis(4-methoxyphenyl)porphyrinate],[8] $[Ce_2\{Pc(OMe)_8\}(TPP)_2]$ [Pc-$(OMe)_8$ = 2,3,9,10,16,17,23,24-octamethoxyphthalocyaninate],[8] $[Nd_2(Pc)_2(TOMePP)]$,[9] and $[Nd_2(Nc)(OEP)_2]$ (Nc = naphthalocyaninate).[4d]

Figure 5 shows the molecular structure of $[Ho_2(Pc)(TClPP)_2]$ (**10a**) in two different perspective views. Each holmium center is octa-coordinated by the pyrrole and isoindole nitrogen atoms of an outer TClPP and the central Pc rings, respectively, confirming the arrangement of ligands as [(TClPP)Ho(Pc)Ho(TClPP)]. The two holmium centers, however, are not identical in terms of their coordination geometry and separation from the ligands. The Ho1 atom adopts a slightly distorted square-antiprismatic structure while the Ho2 atom exhibits a slightly distorted cubic geometry. The Pc ring is slightly domed toward the Ho2 atom. Both holmium centers lie closer to the TClPP ring due to its larger central cavity compared with the Pc ligand (1.131 vs. 2.004 Å for Ho1; 1.218 vs. 1.687 Å for Ho2), and are not equidistant from the TClPP and Pc ligands. These structural features are clearly different from those revealed in the triple-deckers $[Ce_2\{Pc(OMe)_8\}(TPP)_2]$[8] and $[Nd_2(Nc)(OEP)_2]$,[4d] which are centrosymmetric and have two identical metal environments. This could be attributed to the different crystal packing forces for these complexes.

 © 2004 Wiley-VCH Verlag GmbH & Co. KGaA, Weinheim

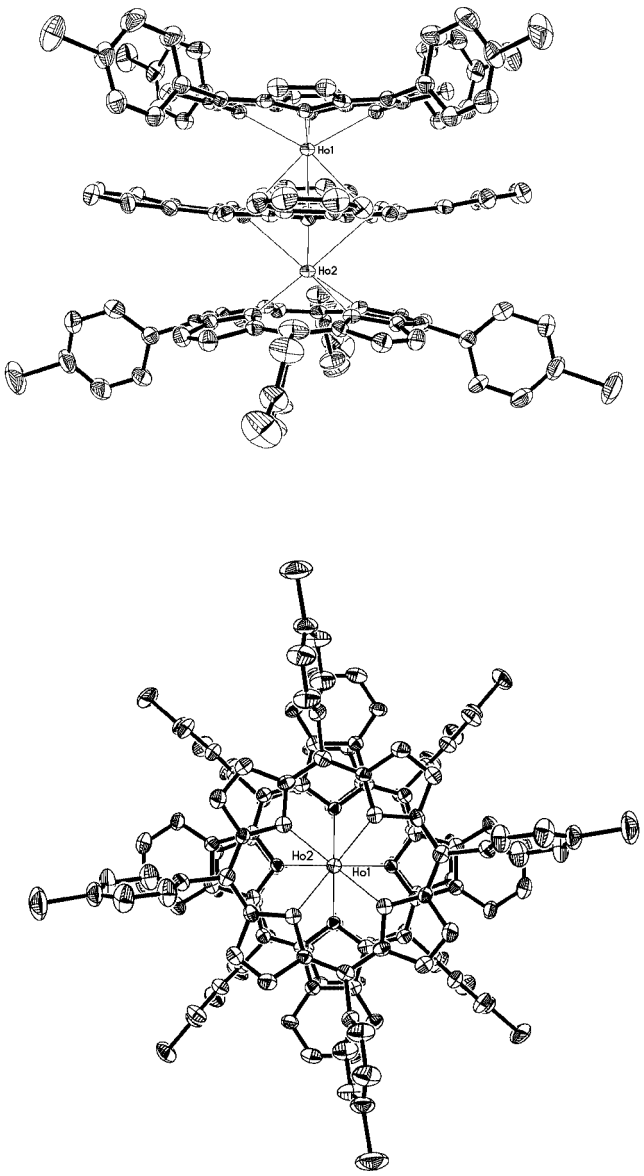

Figure 5. Molecular structure of $[Ho_2(Pc)(TClPP)_2]$ (**10a**) in two different perspective views; hydrogen atoms are omitted for clarity and the ellipsoids are drawn at the 30% probability level

Electrochemistry

The redox behavior of the mixed-ring triple-deckers **1a**−**10a** and **2b**−**11b** was studied by cyclic voltammetry (CV) and differential pulse voltammetry (DPV) in CH_2Cl_2. Within the electrochemical window of CH_2Cl_2, five quasi-reversible one-electron oxidations and up to four quasi-reversible one-electron reductions were revealed for **1a**−**10a**. An additional reduction couple was observed for most of the triple-deckers in the series $[M_2(Pc)_2(TClPP)]$ (**3b**−**9b** and **11b**). The half-wave potentials for these two series of complexes are summarized in Tables 4 and 5. All these redox processes can be attributed to the successive removal of electrons from, or addition of electrons to, the ligand-based orbitals, as the oxidation state of the central trivalent rare-earth metals does not change. Figure 6 displays the cyclic and differential pulse voltammograms of **3a** and Figure 7 shows the variation of the redox potentials of **1a**−**10a** with the rare-earth ionic radii. It can be seen that the half-wave potentials of the first (O^1) and second (O^2) oxidation processes for **1a**−**10a**, which involve the removal of electrons from the HOMO, decrease linearly as the size of the metal center decreases. In contrast, the potentials of the other oxidation processes, including O^3 and O^4, which involve the second HOMO, remain virtually unchanged at 1.37−1.43 and 1.60−1.65 V (except **1a**). These results indicate that along with the lanthanide contraction, the HOMO increases in energy while the energy level of the second-highest occupied orbital remains relatively unchanged. This directly reveals the anti- and non-bonding nature for the HOMO and second HOMO and indirectly suggests the bonding nature for the third HOMO. All the reduction processes (R^1, R^2, R^3, and R^4) also appear to be insensitive to the size of the rare earth metal centers, suggesting that the energy level of the first (as well as the second and the third) lowest unoccupied orbital remains relatively constant for the whole series. Therefore, the energy separation between the HOMO and the LUMO diminishes across the series, while that between the second-highest non-bonding occupied orbital and the second-lowest non-bonding unoccupied orbitals remains constant. The decrease in energy gap between the HOMO and LUMO is in agreement with the red-shift of the longest-wavelength near IR band at

Table 4. Half-wave redox potentials for **1a**−**10a** [V vs. SCE] in CH_2Cl_2 containing 0.1 M $[Bu_4N][ClO_4]$

	O^5	O^4	O^3	O^2	O^1	R^1	R^2	R^3	R^4	$\Delta E_{1/2}$ [a]
1a	+1.85[b]	+1.50	+1.31	+1.13	+0.85	−0.71	−1.25	−1.71[b]		1.56
2a	+1.84	+1.61	+1.38	+1.12	+0.80	−0.70	−1.20	−1.66	−1.88[b]	1.50
3a	+1.85[b]	+1.61	+1.37	+1.12	+0.78	−0.70	−1.21	−1.67[b]		1.48
4a	+1.85	+1.65	+1.41	+1.09	+0.73	−0.72	−1.23	−1.69	−1.89	1.45
5a	+1.86[b]	+1.62	+1.40	+1.08	+0.74	−0.72	−1.20	−1.64		1.46
6a	+1.84	+1.62	+1.40	+1.07	+0.72	−0.73	−1.24	−1.66	−1.87[b]	1.45
7a	+1.85[b]	+1.65	+1.42	+1.05	+0.67	−0.73[b]	−1.29	−1.67[b]	−1.96[b]	1.40
8a	+1.85[b]	+1.62	+1.40	+1.04	+0.66	−0.74	−1.22	−1.63	−1.84[b]	1.40
9a	+1.82	+1.63	+1.41	+1.03	+0.65	−0.74	−1.21	−1.65[b]	−1.90[b]	1.39
10a	+1.85[b]	+1.60	+1.43	+1.03	+0.64	−0.75	−1.22	−1.65[b]	−1.90[b]	1.39

[a] $\Delta E_{1/2}$ is the potential difference between the first oxidation and the first reduction processes. [b] Recorded by DPV.

 © 2004 Wiley-VCH Verlag GmbH & Co. KGaA, Weinheim

Table 5. Half-wave redox potentials for **1b**−**11b** [V vs. SCE] in CH_2Cl_2 containing 0.1 M $[Bu_4N][ClO_4]$

	O^5	O^4	O^3	O^2	O^1	R^1	R^2	R^3	R^4	R^5	$\Delta E_{1/2}$ [a]
2b	+1.98[b]	+1.58	+1.37	+1.03	+0.58	−0.62	−1.05[b]	−1.39[b]			1.20
3b	+1.95[b]	+1.60	+1.34	+1.00	+0.54	−0.66[b]	−1.12	−1.51	−1.72	−2.01	1.20
4b	+1.88	+1.63	+1.40	+0.97	+0.51	−0.64	−1.09	−1.51	−1.76[b]	−1.98[b]	1.15
5b	+2.00	+1.63	+1.42	+0.94	+0.47	−0.63	−1.11	−1.50	−1.57[b]	−1.92[b]	1.10
6b	+1.93	+1.61	+1.40	+0.93	+0.47	−0.64	−1.11	−1.48	−1.70[b]	−1.98[b]	1.11
7b	+1.93	+1.61	+1.41	+0.91	+0.44[b]	−0.65	−1.09[b]	−1.52	−1.76	−1.98[b]	1.09
8b	+1.93	+1.61	+1.42	+0.91	+0.44[b]	−0.64	−1.09	−1.48	−1.74	−1.97[b]	1.08
9b	+2.00[b]	+1.62	+1.41	+0.89	+0.43	−0.69	−1.07	−1.56	−1.69[b]	−1.95[b]	1.12
10b	+1.95	+1.61	+1.41	+0.89	+0.42	−0.65	−1.10	−1.54	−1.74[b]		1.07
11b	+1.94	+1.61	+1.41	+0.86	+0.39	−0.65	−1.08	−1.48	−1.73[b]	−1.97[b]	1.04

[a] $\Delta E_{1/2}$ is the potential difference between the first oxidation and the first reduction processes. [b] Recorded by DPV.

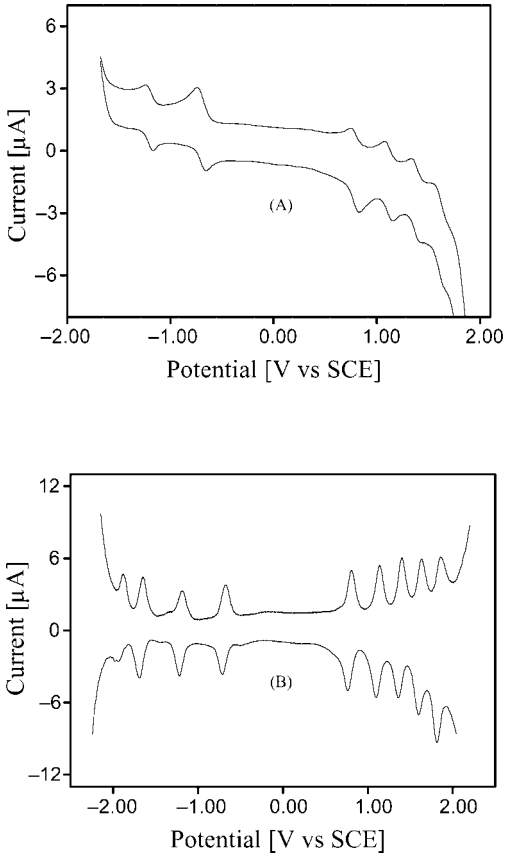

Figure 6. (A) Cyclic voltammogram and (B) differential pulse voltammogram of $[Nd_2(Pc)(TClPP)_2]$ (**3a**) in CH_2Cl_2 containing 0.1 M $[NBu_4][ClO_4]$ at a scan rate of 20 and 10 mV s^{-1}, respectively

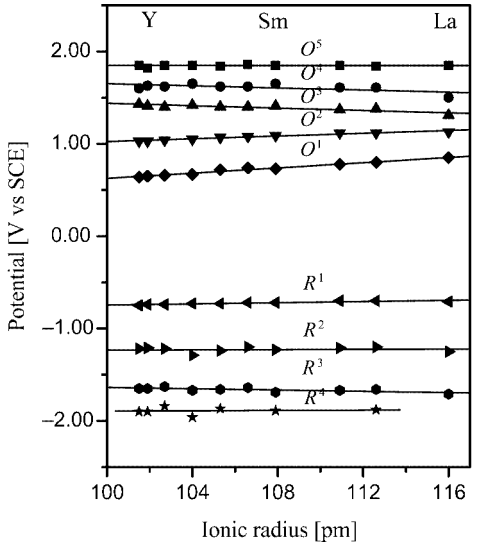

Figure 7. Plot of the half-wave potentials of the oxidation and reduction processes of $[M_2(Pc)(TClPP)_2]$ (**1a**−**10a**) as a function of the ionic radius of M^{III}

876−997 nm (Table 2). The main Q-band at 605−608 nm, which remains relatively unchanged for the whole series of complexes, can then be assigned to the electronic transition from the second-highest non-bonding occupied orbital to the second-lowest non-bonding unoccupied orbitals. The remaining weak Q-band at 551−573 nm is red-shifted as the size of the metal centers decreases (Table 2). This suggests that this absorption may arise from the electronic transition from the HOMO to the third-lowest unoccupied orbitals as the energy gap between these two sets of orbitals decreases across the series from La to Ho. Figure S3 (Supporting Information) compares the energy levels for the La (**1a**) and Ho (**10a**) triple-deckers.

The electrochemical behavior of $[M_2(Pc)_2(TClPP)]$ (**2b**−**11b**) is similar to that of $[M_2(Pc)(TClPP)_2]$ (**1a**−**10a**). Similar trends were observed for their redox potentials (Table 5) as a function of the ionic radius of the metal center. Thus, similar conclusions could be drawn about the frontier molecular orbitals and the corresponding electronic transitions for this series of complexes, except that the second-highest occupied orbitals and the second-lowest unoccupied orbitals are of pure Pc character instead of pure TClPP character in $[M_2(Pc)(TClPP)_2]$. By comparing the data in Tables 4 and 5, it can be seen that the $[M_2(Pc)_2(TClPP)]$ complexes undergo oxidation (O^1 and O^2) and reduction (R^1 and R^2) more readily than the corresponding $[M_2(Pc)(TClPP)_2]$ complexes.

As the first oxidation and the first reduction processes involve a one-electron transfer from the HOMO and to the LUMO of the molecule, respectively, the energy difference between these two redox processes, $\Delta E^\circ_{1/2}(O^1 - R^1)$, should reflect the energy required for the electronic transition from

 © 2004 Wiley-VCH Verlag GmbH & Co. KGaA, Weinheim

the HOMO to the LUMO. This should therefore correlate with the lowest-energy electronic transition. As shown in Tables 4 and 5, the HOMO−LUMO gap for $[M_2(Pc)(TClPP)_2]$ (**1a**−**10a**) (1.39−1.56 V) is larger than that for $[M_2(Pc)_2(TClPP)]$ (**2b**−**11b**) (1.04−1.20 V). However, the lowest-energy electronic absorption band of **1a**−**10a** appears at longer wavelength than that of **2b**−**11b** due to the different ligand composition and ring-ring interaction in the two series. According to the electrochemical and absorption data for both series of triple-deckers tabulated in Tables 2−5, the equations $\Delta E^{\circ}_{1/2}(O^1 - R^1) - h\nu = -0.14$ (±0.02) and $\Delta E^{\circ}_{1/2}(O^1 - R^1) - h\nu = -0.58$ (±0.02) eV could be established for the series **a** and **b**, respectively, instead of the equation $\Delta E^{\circ}_{1/2}(O^1 - R^1) - h\nu = 0.01$ eV established for monomeric metalloporphyrins containing a pure porphyrin ligand.[10]

Conclusions

Two series of mixed (phthalocyaninato)(porphyrinato) rare earth triple-decker complexes $[M_2(Pc)(TClPP)_2]$ and $[M_2(Pc)_2(TClPP)]$ have been prepared. All these compounds have been fully characterized with a wide range of spectroscopic and electrochemical techniques. The molecular structures of two triple-deckers $[M_2(Pc)(TClPP)_2]$ (M = Y, Ho) have also been determined. Systematic studies of the spectroscopic and electrochemical properties of both series of compounds reveal the nature of some frontier molecular orbitals and the electronic absorption bands of these complexes.

Experimental Section

General Remarks: Anhydrous TCB (Aldrich) was used as received. Details regarding the treatment of the other solvents, preparation of the starting materials, and the instrumentation have been described previously.[11]

General Procedure for the Preparation of $[M_2(Pc)(TClPP)_2]$ (1a−10a) and $[M_2(Pc)_2(TClPP)]$ (1b−11b): A mixture of $H_2(TClPP)$ (75 mg, 0.10 mmol) and $[M(acac)_3]\cdot nH_2O$ (ca. 150 mg, 0.30 mmol) in TCB (20 mL) was refluxed under a slow stream of nitrogen for 4 h. The resulting dark cherry-red solution was cooled to room temperature, then $Li_2(Pc)$ (80 mg, 0.15 mmol) was added. The mixture was refluxed for a further 6 h, then the solvent was removed under reduced pressure. The violet-blue residue was chromatographed on a silica gel column using $CHCl_3$/hexanes (1:1) as eluent to give an olive-green band, which contained mainly the triple-decker $[M_2(Pc)(TClPP)_2]$, and a small amount of the double-decker $[M(Pc)(TClPP)]$ and unchanged $H_2(TClPP)$. After collecting this band, the column was further eluted with $CHCl_3$ to give a mixture of the triple-decker $[M_2(Pc)_2(TClPP)]$ and the double-decker $[M(Pc)_2]$. The triple-decker products were further purified by chromatography, followed by recrystallization from $CHCl_3$ and MeOH to give dark green or dark blue microcrystals of $[M_2(Pc)(TClPP)_2]$ and $[M_2(Pc)_2(TClPP)]$, respectively.

X-ray Crystallographic Analysis of 9a and 10a: Crystals suitable for X-ray diffraction analysis were grown by layering MeOH onto a CH_2Cl_2 solution of the compounds. Crystal data and details of data collection and structure refinement are given in Table 6. Data were collected with a Bruker SMART CCD diffractometer with an Mo-K_α sealed tube (λ = 0.71073 Å) at 293 K, using the ω-scan mode with an increment of 0.3°. Preliminary unit-cell parameters were obtained from 45 frames. Final unit-cell parameters were obtained by global refinements of reflections obtained from integration of all the frame data. The collected frames were integrated using the preliminary cell-orientation matrix. SMART software was used for collecting frames of data, indexing reflections, and determination of lattice constants; SAINT-PLUS for integration of intensity of reflections and scaling;[12] SADABS for absorption correction;[13] and SHELXL for space group and structure determination, refinements, graphics, and structure reporting.[14] CCDC-208839 (**9a**) and -208840 (**10a**) contain the supplementary crystallographic data for this paper. These data can be obtained free of charge at www.ccdc.cam.ac.uk/conts/retrieving.html [or from the Cambridge Crystallographic Data Centre, 12 Union Road, Cambridge CB2 1EZ, UK; Fax: (internat.) + 44-1223-336033; E-mail: deposit@ccdc.cam.ac.uk].

Table 6. Crystallographic data for **9a** and **10a**

	9a·CH_2Cl_2	**10a**·CH_2Cl_2
Empirical formula	$C_{121}H_{66}Cl_{10}N_{16}Y_2$	$C_{121}H_{66}Cl_{10}Ho_2N_{16}$
Formula mass	2276.22	2428.26
Crystal size [mm]	0.35 × 0.18 × 0.12	0.40 × 0.25 × 0.12
Crystal system	tetragonal	tetragonal
Space group	*P*4/*n*	*P*4/*n*
a [Å]	23.546 (16)	23.437 (10)
b [Å]	23.546 (16)	23.437 (10)
c [Å]	12.556 (12)	12.580 (8)
V [Å]	6961 (9)	6910 (6)
Z	2	2
F (000)	2304	2416
ρ_{calcd} [Mg m^{-3}]	1.086	1.167
μ [mm^{-1}]	1.067	1.376
θ range [°]	2.52−25.00	2.75−25.00
Reflections collected	34772	34465
Independent reflections	6121 (R_{int} = 0.1411)	6081 (R_{int} = 0.0844)
Parameters	352	352
$R1$ [$I > 2\sigma(I)$]	0.0892	0.0633
$wR2$ [$I > 2\sigma(I)$]	0.2872	0.2182
Goodness of fit	1.014	1.010

Acknowledgments

Financial support from the National Natural Science Foundation of China (Grant No. 20171028, 20325105), the National Ministry of Science and Technology of China (Grant No. 2001CB6105-04), the National Ministry of Education of China, and Shandong University for J. J., and The Chinese University of Hong Kong for D. K. P. N. is gratefully acknowledged.

[1] [1a] D. K. P. Ng, J. Jiang, *Chem. Soc. Rev.* **1997**, *26*, 433. [1b] J. Jiang, K. Kasuga, D. P. Arnold, in *Supramolecular Photosensitive and Electroactive Materials* (Ed.: H. S. Nalwa), Academic Press, New York, **2001**, pp. 113−210. [1c] J. Jiang, W. Liu, D. P. Arnold, *J. Porphyrins Phthalocyanines* **2003**, *7*, 459.
[2] [2a] J. Li, D. Gryko, R. B. Dabke, J. R. Diers, D. F. Bocian, W.

 © 2004 Wiley-VCH Verlag GmbH & Co. KGaA, Weinheim

G. Kuhr, J. S. Lindsey, *J. Org. Chem.* **2000**, *65*, 7379. [2b] D. Gryko, J. Li, J. R. Diers, K. M. Roth, D. F. Bocian, W. G. Kuhr, J. S. Lindsey, *J. Mater. Chem.* **2001**, *11*, 1162. [2c] T. Gross, F. Chevalier, J. S. Lindsey, *Inorg. Chem.* **2001**, *40*, 4762. [2d] K.-H. Schweikart, V. L. Malinovskii, J. R. Diers, A. A. Yasseri, D. F. Bocian, W. G. Kuhr, J. S. Lindsey, *J. Mater. Chem.* **2002**, *12*, 808. [2e] K.-H. Schweikart, V. L. Malinovskii, A. A. Yasseri, J. Li, A. B. Lysenko, D. F. Bocian, J. S. Lindsey, *Inorg. Chem.* **2003**, *42*, 7431. [2f] Z. Liu, A. A. Yasseri, J. S. Lindsey, D. F. Bocian, *Science* **2003**, *302*, 1543. [2g] L. Wei, K. Padmaja, W. J. Youngblood, A. B. Lysenko, J. S. Lindsey, D. F. Bocian, *J. Org. Chem.* **2004**, *69*, 1461.

[3] [3a] M. Lachkar, A. De Cian, J. Fischer, R. Weiss, *Inorg. Chem.* **1986**, *25*, 2107. [3b] D. Chabach, M. Lachkar, A. De Cian, J. Fischer, R. Weiss, *New J. Chem.* **1992**, *16*, 431. [3c] T.-H. Tran-Thi, T. A. Mattioli, D. Chabach, A. De Cian, R. Weiss, *J. Phys. Chem.* **1994**, *98*, 8279. [3d] D. Chabach, A. De Cian, J. Fischer, R. Weiss, M. El Malouli Bibout, *Angew. Chem. Int. Ed. Engl.* **1996**, *35*, 898.

[4] [4a] J. Jiang, R. L. C. Lau, T. W. D. Chan, T. C. W. Mak, D. K. P. Ng, *Inorg. Chim. Acta* **1997**, *255*, 59. [4b] J. Jiang, W. Liu, W.-F. Law, D. K. P. Ng, *Inorg. Chim. Acta* **1998**, *268*, 49. [4c] D. P. Arnold, J. Jiang, *Chem. Lett.* **1999**, 483. [4d] J. Jiang, Y. Bian, F. Furuya, W. Liu, M. T. M. Choi, N. Kobayashi, H.-W. Li, Q. Yang, T. C. W. Mak, D. K. P. Ng, *Chem. Eur. J.* **2001**, *7*, 5059. [4e] N. Pan, J. Jiang, X. Cui, D. P. Arnold, *J. Porphyrins Phthalocyanines* **2002**, *6*, 347. [4f] X. Sun, X. Xui, D. P. Arnold, M. T. M. Choi, D. K. P. Ng, J. Jiang, *Eur. J. Inorg. Chem.* **2003**, 1555.

[5] [5a] M. J. Stillman, T. Nyokong, in *Phthalocyanines − Properties and Applications*, vol. 1 (Eds.: C. C. Leznoff, A. B. P. Lever), VCH, New York, **1989**, pp. 133−290. [5b]E. Orti, J. L. Bredas, *J. Chem. Phys.* **1990**, *92*, 1228. [5c] R. Rousseau, R. Aroca, M. L. Rodriguez-Mendez, *J. Mol. Struct.* **1995**, *356*, 49. [5d] N. Ishikawa, *J. Porphyrins Phthalocyanines* **2001**, *5*, 87.

[6] [6a] J. Jiang, D. P. Arnold, H. Yu, *Polyhedron* **1999**, *18*, 2129. [6b] F. Lu, M. Bao, C. Ma, X. Zhang, D. P. Arnold, J. Jiang, *Spectrochim. Acta A* **2003**, *59*, 3273. [6c] M. Bao, N. Pan, C. Ma, D. P. Arnold, J. Jiang, *Vib. Spectrosc.* **2003**, *32*, 175.

[7] D. Chabach, A. De Cian, J. Fischer, R. Weiss, M. El Malouli Bibout, *Angew. Chem. Int. Ed. Engl.* **1996**, *35*, 898.

[8] D. Chabach, M. Lachkar, A. De Cian, J. Fischer, R. Weiss, *New J. Chem.* **1992**, *16*, 431.

[9] M. Moussavi, A. De Cian, J. Fischer, R. Weiss, *Inorg. Chem.* **1986**, *25*, 2107.

[10] J.-H. Fuhrhop, K. M. Kadish, D. G. Davis, *J. Am. Chem. Soc.* **1973**, *95*, 5140.

[11] F. Lu, X. Sun, R. Li, D. Liang, P. Zhu, C.-F. Choi, D. K. P. Ng, T. Fukuda, N. Kobayashi, M. Bai, C. Ma, J. Jiang, *New J. Chem.*, accepted.

[12] *SMART* and *SAINT* for Windows NT Software Reference Manuals, Version 5.0, Bruker Analytical X-ray Systems, Madison, WI, **1997**.

[13] G. M. Sheldrick, *SADABS − A Software for Empirical Absorption Correction*, University of Göttingen, Germany, **1997**.

[14] *SHELXL*, Reference Manual, Version 5.1, Bruker Analytical X-ray Systems, Madison, WI, **1997**.

Received April 8, 2004
Early View Article
Published Online July 29, 2004

 © 2004 Wiley-VCH Verlag GmbH & Co. KGaA, Weinheim

Diastereoselective Insertion of Isocyanide into the Alkyl−Metal Bond of Methylbenz[*e*]indenyl *ansa*-Zirconocene Complexes

Alfredo Sebastián,[a] Pascual Royo,*[a] Pilar Gómez-Sal,[a] and Carmen Ramírez de Arellano[b]

Keywords: Metallocenes / Zirconium / Insertion / Isocyanides / Polymerization

Alkylation of *ansa*-zirconocene [Zr{(η^5-C_5H_5)$SiMe_2$-(MBI)}Cl_2] (MBI = η^5-2-Me–$C_{13}H_7$) with MgRCl gave the dimethyl complex [Zr{(η^5-C_5H_5)$SiMe_2$(MBI)}Me_2], but unresolvable mixtures containing mono-alkylated compounds were obtained when bulkier alkyls were used. However pure dialkyl complexes [Zr{(η^5-C_5H_5)$SiMe_2$(MBI)}R_2] (R = CH_2Ph, CH_2SiMe_3) were easily obtained using K(CH_2Ph) and Li(CH_2SiMe_3) as alkylating agents. Diastereoselective insertion into the MBI-unprotected Zr–R bond was observed when all of these dialkyl complexes were treated with 2,6-xylyl isocyanide to give the iminoacyl compounds [Zr{(η^5-C_5H_5)$SiMe_2$(MBI)}R{CR[η^2-*N*-(2,6-xylyl)]}] (R = Me, CH_2Ph, CH_2SiMe_3). All of the new complexes were characterized by NMR spectroscopy and the X-ray molecular structures of the dibenzyl and the imino-benzyl compounds were determined. The catalytic activity for ethene polymerization and ethene/1-hexene copolymerization of the dichloro zirconocenes [Zr{(η^5-C_5H_5)EMe_2(MBI)}Cl_2] (E = C, Si), activated with methylalumoxane (MAO), was measured.

(© Wiley-VCH Verlag GmbH & Co. KGaA, 69451 Weinheim, Germany, 2004)

Introduction

The rational design of different types of group 4 metallocenes to be used as olefin polymerization catalysts, after activation with methylalumoxane (MAO), has been the objective of a great number of scientific contributions.[1−5] Extensive studies have demonstrated the high degree of electronic and steric control provided by sterically demanding cyclopentadienyl ligands, making them powerful tools for producing convenient single-site catalysts for the known broad range of precisely functionalized, tacticity-controlled, branched and block polymers and copolymers.[6−8] The main targets of many of the studies have been the optimization of catalytic activity, stereospecificity and the modulation of the molecular weight of the resulting polymers.[9,10] It is well-known that the presence of condensed benzene rings in the indenyl ligands of metallocene-type complexes induces a remarkable increase in their catalytic activity, and the addition of a 2-methyl substituent in their Cp rings reduces the incidence of β-elimination processes, providing a significant increase in the molecular weight of the polymer. In this regard the 2-methylbenz[*e*]indenyl ligand (MBI) is an excellent choice for this purpose. The isolation of the first group 4 metallocenes containing this ligand has demonstrated high performance in ethylene and propylene polymerization[11,12] as well as in copolymerization processes using ethylene and octene[13] or ethylene/polar monomers such as 10-undecene-1-ol and allyl alcohol.[14,15]

Metal alkyl compounds are convenient models not only for olefin polymerization but also for other insertion and transmetallation reactions and as carbon−carbon bond formation precursors.[16−18] Insertion of unsaturated substrates into metal−alkyl bonds are basic reactions for which many synthetic, mechanistic and theoretical studies have been developed.[19] The migratory insertion of isocyanide has provided numerous iminoacyl complexes[20−24] and a solid knowledge of the steric and electronic effects of the ligands on the reactivity[25] and catalytic activity[9] of different systems.

We report herein the effect of the bulky MBI ligand on the stereoselectivity of the migratory insertion of 2,6-dimethylphenyl isocyanide into the metal−alkyl bonds of new dialkyl metallocenes prepared from the dichloro derivatives reported recently.[26] We also report the results found from our studies of catalytic activity of these dichloro-metallocenes in the homopolymerization of ethylene and copolymerization of ethylene/1-hexene.

Results and Discussion

The dichloro *ansa*-zirconocenes [Zr{(η^5-C_5H_5)EMe_2(η^5-2-Me−$C_{13}H_7$)}Me_2] (E = C: **1a**, E = Si: **1b**) containing the

[a] Departamento de Química Inorgánica, Universidad de Alcalá
Campus Universitario, 28871 Alcalá de Henares, Spain
Fax: (internat.) + 34-91-8854683
E-mail: pascual.royo@uah.es
[b] Departamento de Química Orgánica, Facultad de Farmacia, Universidad de Valencia
46100 Valencia, Spain

 © 2004 Wiley-VCH Verlag GmbH & Co. KGaA, Weinheim **DOI: 10.1002/ejic.200400333**

MBI ligand were isolated previously[26] by reaction in toluene of $ZrCl_4(THF)_2$ with the dilithium salts of the corresponding $-CMe_2-$ and $-SiMe_2$-bridged indenyl-cyclopentadienyl derivatives, as shown in Scheme 1.

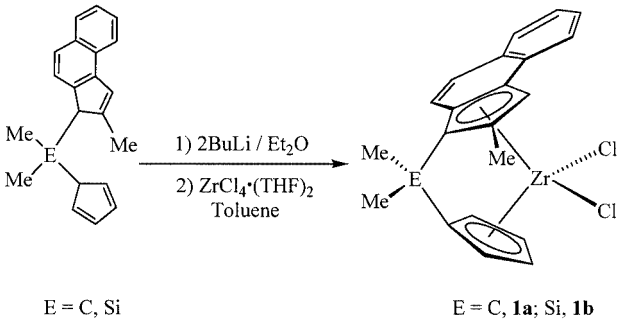

Scheme 1

The reaction of complex **1b** with 2 equiv. of MgClMe gave dimethyl zirconocene [Zr{(η^5-C_5H_5)$SiMe_2$(η^5-2-Me$-C_{13}H_7$)}Me_2] (**2**) in high yield. However this type of dialkyl compound is not so easily accessible when bulky substituents are located at the cyclopentadienyl β-carbon of rigid *ansa*-metallocenes. The steric demands of the benzene rings attached to the α and β positions of the η^5-cyclopentadienyl unit in the MBI ligand of complex **1b**, make dialkylation difficult when bulky alkyl groups are used. In fact alkylation of **1b** with two equiv. of $MgCl(CH_2Ph)$ gave low yields of the dibenzyl complex [Zr{(η^5-C_5H_5)$SiMe_2$(η^5-2-Me$-C_{13}H_7$)}$(CH_2Ph)_2$] (**3**) which was always contaminated by significant amounts of the monobenzyl compounds. However complex **3** could be isolated in high yield as the unique component when $K(CH_2Ph)$ was used as the alkylating agent. Similarly, $MgCl(CH_2SiMe_3)$ has been extensively used[27,28] to produce dialkyl derivatives of many metallocenes with free cyclopentadienyl ligands, whereas related *ansa*-metallocenes usually yield the corresponding monoalkyl compounds.[29] Consistently the dialkyl complex [Zr{(η^5-C_5H_5)$SiMe_2$(η^5-2-Me$-C_{13}H_7$)}$(CH_2SiMe_3)_2$] (**4**) could not be isolated using the Grignard reagent but was easily obtained in high yield with the lithium derivative $Li(CH_2SiMe_3)$. It is therefore evident that the steric hindrance due to the bulky MBI ligand may be overcome using more appropriate nucleophilic alkylating agents, as shown in Scheme 2. The air sensitive dialkyl compounds **2**–**4** are

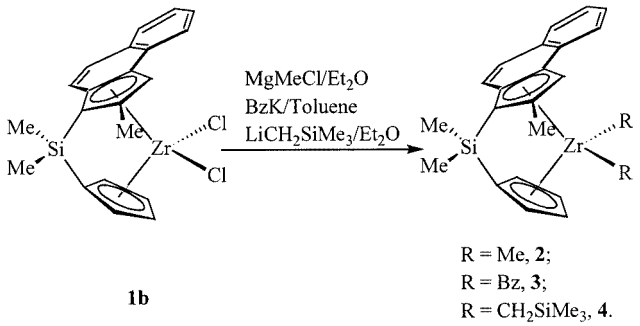

Scheme 2

stable in $CDCl_3$ under an inert atmosphere although they are transformed into the dichloro complex **1b** when heated at 110 °C in Teflon-valved NMR tubes.

The enantiotopic face of the MBI ligand makes these dialkyl compounds, **2**–**4,** asymmetric molecules with two nonequivalent alkyl groups. The ^{1}H NMR spectrum of **2** shows two singlets for the Zr-methyl groups, one shifted significantly highfield ($\delta = -1.29$) compared with the typical value ($\delta = 0.09$ ppm) observed for the other, which was in the range found for related methyl zirconocenes.[30] NOE experiments demonstrated that the highfield singlet is due to the methyl group located under the benzene ring attached to the indenyl moiety. Similar behavior was observed for the four doublets due to the two diastereotopic methylene protons of the benzyl (**3**) and methylsilyl (**4**) ligands. Two of the signals, corresponding to the alkyl group located under the ring-fused benzene, are shifted highfield ($\delta = 0.18$ ppm and 0.28 ppm for **3**; $\delta = -2.20$ ppm and -0.94 ppm for **4**) due to the anisotropic effect of the aromatic ring. However this anisotropic contribution was not observed in the ^{13}C and gHMQC NMR spectra (see Exp. Sect.). In addition, the ^{1}H NMR spectra of complexes **2**–**4** show the expected singlet for the MBI-methyl group, two singlets for Si–Me, four multiplets for the C_5H_4 ring and one singlet for the C_5H(MBI) ring proton. All of the remaining MBI nonequivalent protons give the set of signals corresponding to two AB and ABCD spin systems.

Slow cooling at −30 °C of a toluene solution of the dibenzyl complex **3** rendered appropriate crystals for X-ray diffraction studies. The X-ray structure of **3** is shown in Figure 1 with the atomic labeling scheme and selected bond lengths and angles are listed in Table 1.

The coordination geometry of the zirconium atom is the typical distorted tetrahedron formed by the two ring centro-

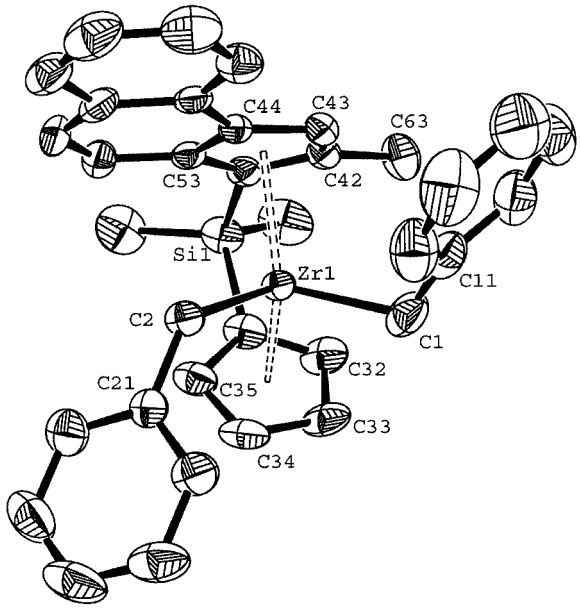

Figure 1. Ellipsoid plot of compound **3** (50% probability level); hydrogen atoms have been omitted for clarity

 © 2004 Wiley-VCH Verlag GmbH & Co. KGaA, Weinheim

Table 1. Selected interatomic distances (Å) and angles (°) for complex **3** (Cp is the centroid of C(31)−C(32)−C(33)−C(34)−C(35) ring; Cp_{MBI} is the centroid of C(41)−C(42)−C(43)−C(44)−C(45) ring)

Zr(1)−Cp	2.212	Zr(1)−C(33)	2.556(4)
Zr(1)-Cp_{MBI}	2.262	Zr(1)−C(34)	2.559(5)
Zr(1)−C(2)	2.308(4)	Zr(1)−C(35)	2.491(5)
Zr(1)−C(1)	2.315(6)	Zr(1)−C(41)	2.515(4)
C(1)−C(11)	1.478(8)	Zr(1)−C(42)	2.514(4)
C(2)−C(21)	1.481(6)	Zr(1)−C(43)	2.578(4)
Zr(1)−C(31)	2.491(5)	Zr(1)−C(44)	2.636(4)
Zr(1)−C(32)	2.487(5)	Zr(1)−C(53)	2.582(4)
C(2)−Zr(1)−C(1)	97.4(2)	C(11)−C(1)−Zr(1)	121.8(4)
Cp−Zr(1)−Cp_{MBI}	125.8	C(21)−C(2)−Zr(1)	125.5(3)

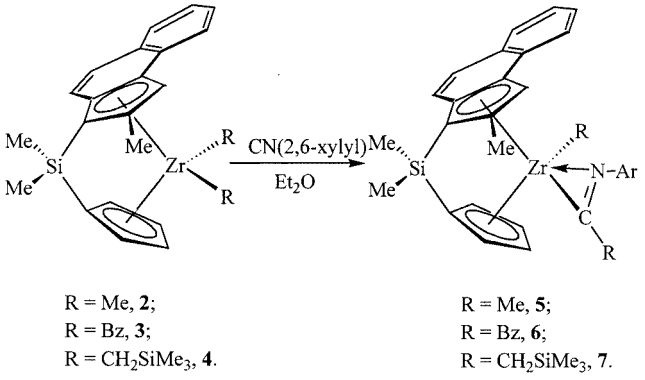

Scheme 3

ids and the carbon atoms of the benzyl ligands. The Cp(centroid)−Zr−Cp_{MBI}(centroid) [125.8°] and the C(2)−Zr(1)−C(1) [97.4(2)°] angles are similar to those observed for related *ansa*-MBI compounds and the Cp(centroid)−Zr distances [Cp 2.212Å and Cp_{MBI} 2.262Å] are in the range found in related indenyl zirconocenes.[12,26,31,32]

The most remarkable difference is the orientation of the two nonequivalent benzyl ligands. One is located above the plane (torsion angle Cp_{MBI}−Zr(1)−C(1)−C(11) 62.6°) while the other is located below (torsion angle Cp_{MBI}−Zr(1)−C(2)−C(21) 158.1°), with respect to the C(1)−Zr(1)−C(2) plane. The benzyl ligand eclipsed by the MBI system positions the methylene C(2) under the benzene ring condensed to the indenyl moiety with the phenyl ring oriented towards the other Cp system, whereas the benzyl ring located on the open side, far away from the MBI system, has its phenyl ring directed towards the moiety with the MBI system using the wide space. In spite of these different orientations both benzyl ligands show Zr−C distances [Zr−C(1) 2.315(6) Å and Zr−C(2) 2.308(4) Å] and Zr−C−C(Ph) angles [Zr−C(1)−C(11) 121.8(4)° and Zr−C(2)−C(21) 125.5(3)°] typical of σ-bonded benzyl groups without benzallylic interactions [Zr−C(11) 3.338 and Zr−C(21) 3.389 Å], and are similar to values found[31,33] for other benzyl zirconium compounds with bulky Cp systems.

Reaction of diethyl ether solutions of the dialkyl complexes **2**−**4** with 1 equiv. of 2,6-xylyl isocyanide at room temperature gave the corresponding iminoacyl compounds [Zr{(η^5-C_5H_5)$SiMe_2$(η^5-2-Me−$C_{13}H_7$)}R{CR[η^2-*N*-(2,6-xylyl)]}] (R = Me: **5**, CH_2Ph: **6**, CH_2SiMe_3: **7**) as shown in Scheme 3, which were isolated as solids and characterized by elemental analysis and NMR spectroscopy. When monitoring the reactions by ^1H NMR spectroscopy it was observed that insertion was easier for less bulky alkyl ligands following the order **5** < **6** < **7**. The η^2-coordination of the isocyanide ligand is consistent with the IR [(Nujol): $\tilde{\nu}_{C=N}$ = 1600, 1585 and 1590 cm^{-1}] and ^{13}C NMR spectroscopic data [δ = 245.4 (**4**), 244.5 (**5**), 245.4 (**6**)]. Further reactions with an additional 1 equiv. or an excess of isocyanide were not observed under any conditions, as was expected for these types of coordinately saturated 18e species.

These insertion reactions may lead to two diastereomers depending on which of the two nonequivalent alkyl groups migrate to the isocyanide ligand. The ^1H NMR spectra confirm that one unique diastereoisomer is obtained in all of these reactions, for which the signals due to the alkyl group located under the MBI system remain almost unmodified [δ = −1.20(s) (**5**), 0.27(d) and 0.56(d) (**6**), −1.86(d) and −2.97(d) (**7**)]. In contrast, signals due to the alkyl group located far from the MBI system are significantly shifted lowfield [δ = 2.36(s) (**5**), δ 3.60(d) and 3.68(d) (**6**), 2.45(d) and 2.63(d) (**7**)] as expected for the migrated C-bonded alkyl ligand. NOE experiments on the methyl derivative (**5**) demonstrate that the highfield shifted singlet corresponds to the methyl group located under the MBI system, which is affected by the anisotropic effect of the aromatic ring.

Similar behavior is also observed in the ^{13}C NMR spectra which show significant lowfield shifts for all the signals due to the migrated alkyl group bound to the iminoacylic carbon atom, appearing at δ = 22.2, 44.6 and 22.7 for **5**, **6** and **7**, respectively. All of the remaining ^1H and ^{13}C NMR signals show no significant changes.

The ^1H NMR spectrum of complex **7** represented in Figure 2 shows the typical pattern of signals observed for both dialkyl and iminoacyl complexes.

Therefore it is possible to conclude that the steric demands of the bulky MBI system have a significant effect on the high diastereoselectivity of all of these insertion reactions, although the electronic contribution demonstrated for related [MBI]-silyl-η^1-amido zirconium complexes (work still in progress),[34] for which electronic effects are significantly important, cannot be discarded. However the spectroscopic data do not distinguish between the *exo*-*N*-coordinated iminoacyl formed under kinetic control and the usually more favorable *endo*-*N*-coordinated iminoacyl isomer formed under thermodynamic control. The *endo*-configuration was confirmed for complex **6** by X-ray diffraction studies of its molecular structure.

Appropriate crystals of **6** were isolated by slow evaporation of a C_6D_6 solution. Figure 3 shows the X-ray molecular structure of **6** with the atomic labeling scheme. Selected bond lengths and angles are collected in Table 2.

The pseudotetrahedral coordination of the zirconium atom is defined by the Cp, the Cp_{MBI}, the benzyl methylene

 © 2004 Wiley-VCH Verlag GmbH & Co. KGaA, Weinheim

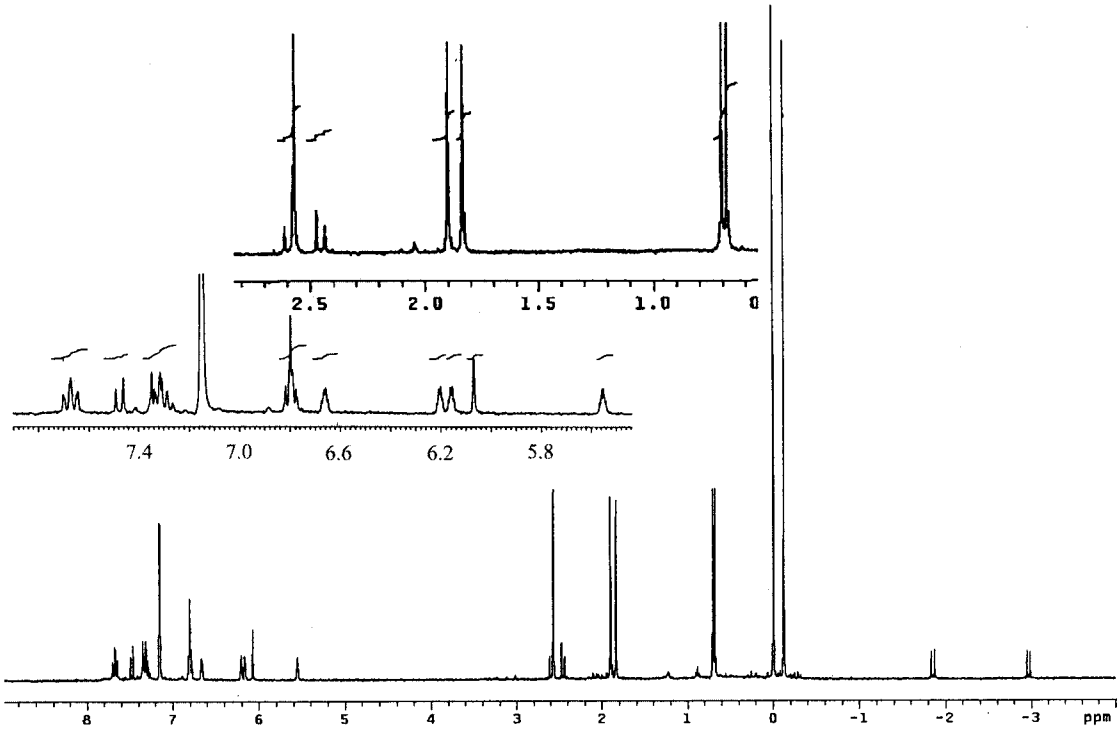

Figure 2. ^{1}H NMR for **7** in C_6D_6; the spectrum shows the normal pattern of signals for Zr(MBI−$SiMe_2$Cp)R_2 complexes

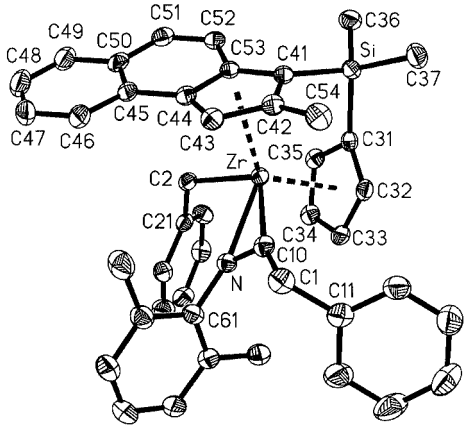

Figure 3. Ellipsoid plot of compound **6** (50% probability level); hydrogen atoms have been omitted for clarity

Table 2. Selected interatomic distances (Å) and angles (°) for complex **6**
Cp is the centroid of C(31)−C(32)−C(33)−C(34)−C(35) ring. Cp_{MBI} is the centroid of C(41)−C(42)−C(43)−C(44)−C(45) ring.

Zr−Cp_{MBI}	2.311	Zr−C(32)	2.547(2)
Zr−Cp	2.246	Zr−C(33)	2.605(2)
Zr−N	2.287(2)	Zr−C(34)	2.564(2)
Zr−C(10)	2.231(2)	Zr−C(35)	2.492(2)
Zr−C(2)	2.372(2)	Zr−C(41)	2.548(2)
C(1)−C(10)	1.513(3)	Zr−C(42)	2.530(2)
C(2)−C(21)	1.468(3)	Zr−C(43)	2.607(2)
N−C(10)	1.281(3)	Zr−C(44)	2.708(2)
Zr−C(31)	2.532(2)	Zr−C(53)	2.649(2)
Cp_{MBI}−Zr−Cp	124.3	C(21)−C(2)−Zr	123.24(13)
C(10)−Zr−N	32.92(6)	C(10)−N−Zr	71.12(12)
C(10)−Zr−C(2)	116.43(7)	C(61)−N−Zr	161.83(13)
N−Zr−C(2)	84.18(6)	N−C(10)−C(1)	124.31(19)
C(1)−C(10)−Zr	159.54(15)	N−C(10)−Zr	75.96(12)

carbon and the midpoint of the iminoacyl C−N bond. Both, the Cp−Zr and Cp_{MBI}−Zr lines are almost perpendicular to the corresponding C(31)−C(35) and C(41)−C(53) cyclopentadienyl main planes (87.3 and 85.0°, respectively). The Cp−Zr−Cp_{MBI} bond angle [124.3°] is closer than that observed for complex **3** indicating the larger bite of the cyclopentadienyl rings. The structure shows η^2-coordination of the iminoacyl ligand with the C−N bond almost perpendicular to the line going from the Zr atom to the C−N bond midpoint (87.4°). The iminoacylic-N adopts an *endo*-configuration, with a C(2)−Zr−C(10)−N torsion angle of 12.6(1)°, giving rise to a very open C(2)−Zr−C(10) angle [116.44(7)°]. The benzyl ligand is eclipsed by the MBI system, locating the methylene C(2) under the benzene ring condensed to the cyclopentadienyl moiety [C(2)−Zr−C(44)−C(45) torsion angle 16.4(2)°]. The phenyl group of the benzyl ligand [C(21)−C(26)] is *anti* to the MBI system with respect to the Zr−C(2) bond [C(21)−C(2)−Zr−Cp_{MBI} torsion angle 178.0°]. Thus, the benzyl group adopts a geometry similar to that observed for the eclipsed benzyl group in compound **3**.

The zirconium-carbon bond length [Zr−C(2) 2.372(2) Å] to the sp^3 methylene benzyl ligand is 0.06Å longer than that observed in complex **3** and longer than the distance to the sp^2 iminoacyl carbon atom[35] [Zr−C(10) 2.231(2) Å], which is in the range [2.164−2.363Å] observed for related iminoacyl zirconium compounds.[21,36] However the zirconium-nitrogen bond length [Zr−N 2.2872(16) Å] is

 © 2004 Wiley-VCH Verlag GmbH & Co. KGaA, Weinheim

slightly longer than those found in related zirconium iminoacyl compounds in the range 2.148−2.250Å.[37,38] The double bond character of the iminoacyl C(10)−N bond is confirmed by the 1.281(3) Å distance, which is longer than usual for related zirconium iminoacyl compounds and close to that known for organic C=N bonds [1.28Å].[35] All of these elongated bonds are consistent with the steric hindrance due to the bulky MBI ring and the benzyl and 2,6-xylyl substituents.

Both the iminoacyl N and the C(10) sp^2 atoms show a profoundly distorted trigonal planar disposition, although the sum of their angles is 360°. The distortion is mainly seen in the close C(10)−N−Zr [71.13(12)°] and N−C(10)−Zr [75.95(12)°] angles and together with the small angle at the zirconium center [C(10)−Zr−N 32.92(6)°] are a consequence of the η^2-coordination of the iminoacyl ligand.

The Zr−Cp distance [2.246Å] is shorter than the $Zr-Cp_{MBI}$ distance [2.311Å]. Consistently the distances from zirconium to the Cp ring carbon atoms [2.492(2)−2.605(2) Å] are slightly shorter than the corresponding distances to the MBI carbon atoms [2.530(2)−2.708(2) Å], the Zr−C(44) and Zr−C(53) bond lengths being unusually long [2.708(2) and 2.649(2) Å, respectively].

Olefin Polymerization Results

The dichlorozirconocenes **1a** and **1b**, activated with a large excess methylalumoxane (MAO), were used as catalyst precursors for the polymerization of ethylene and copolymerization of ethylene/1-hexene. All experiments were carried out at 70 °C in heptane for 15 min, under 4.0 bar of ethylene in a Büchi autoclave, with variable amounts of catalyst and a 10% toluene solution of MAO.

The reaction conditions, measured activities and properties of the resulting polymers are summarized in Table 3 and compared with data for $[ZrCp_2Cl_2]$ and $[Zr(SiMe_2Cp_2)Cl_2]$ used as references.

Both catalysts **1a** and **1b** polymerize ethylene to give linear polyethylene with high activities. Complex **1b** shows a catalytic activity four times higher than that observed for complex **1a** (entries 1, 6) leading to a polymer of much higher molecular weight, similar to that observed for $[ZrCp_2Cl_2]$, although their polydispersities are similar. Under similar conditions (entries 3, 9) complex **1b** is significantly more active than $[ZrCp_2Cl_2]$ and almost 10 times more active than $[Zr(SiMe_2Cp_2)Cl_2]$. Increasing Al/Zr ratios (entries 3, 4 and 5, 6) produce higher activities which were only slightly dependent on the catalyst concentration.

Both metallocenes show higher catalytic activities (entries 1, 2 and 4, 7, 8) in the presence of the comonomer 1-hexene as a consequence of the known "comonomer effect".[39] In all cases incorporation of 1-hexene to the polymer chain is rather high for both catalysts, and is significantly higher (6.69%) for the methylene-bridged complex **1a** with its more open bite compared to the silyl-bridged complex **1b**. The process was always accompanied by a very significant decrease in molecular weight due to the favored β elimination produced by the presence of terminal 1-hexene inserted units.

In most cases the polydispersity is close to the typical value expected for "single site" catalysts, although occasional values higher than 3.0 are observed.

Experimental Section

General Considerations: All manipulations were performed under argon using Schlenk and high-vacuum line techniques or a glove box model HE-63. The solvents were pre-dried over sodium wire prior to purification by distillation under argon using the appropriate drying/deoxygenated agent: toluene, hexane and pentane (sodium-potassium alloy) and diethyl ether, THF (sodium-benzophenone). After being collected, the dried solvent was stored under argon in an ampoule over potassium mirrors or 4 Å molecular sieves (THF). Deuterated solvents from Scharlau were dried, degassed and stored over molecular sieves. C, H and N microanalyses were performed on a Perkin−Elmer 240B and/or Heraeus CHN−O-Rapid microanalyzer. IR spectra were performed in nujol mulls on a Perkin−Elmer 883 spectrophotometer. NMR spectra, measured at 25 °C, were recorded on a Varian Unity FT-300 (^{1}H NMR at 300 MHz, ^{13}C NMR at 75 MHz) or FT-500 (^{1}H NMR at 500 MHz, ^{13}C NMR at 125 MHz) spectrometer and chemical shifts were referenced to the residual protons or carbons of the deuterated solvents. MgMeCl and (2,6-xylyl)isocyanide were purchased

Table 3. Ethylene polymerization and ethylene/1-hexene copolymerization with **1a** and **1b**/MAO

Polymerization	Entry	μmol Zr	Al/Zr	% $C_{6\ M}$ [a]	g PE	Activity[b]	Polymer % C_6[c]	*M*w[d]	*M*w/*M*n
1a	1	5.0	1500	−	10.7	$2.14\cdot10^6$	−	95100	3.8
	2	5.0	1500	39	21.9	$4.38\cdot10^6$	6.69	22600	1.8
1b	3	0.8	10000	−	14.47	$1.81\cdot10^7$	−	284600	−
	4	0.4	10000	−	4.33	$1.08\cdot10^7$	−	−	3.1
	5	0.8	5000	−	4.57	$5.71\cdot10^6$	−	−	−
	6	5.0	1500	−	13.83	$8.33\cdot10^6$	−	289800	3.1
	7	0.4	10000	24	4.44	$1.11\cdot10^7$	2.22	154000	2.3
	8	0.4	10000	39	8.1	$2.03\cdot10^7$	3.64	101800	1.9
A[e]	9	0.8	10000	−	8.42	$1.05\cdot10^7$	−	270000	2.0
B[e]	10	0.8	10000	−	0.9	$1.06\cdot10^6$	−	35000	2.2

[a] % mol of comonomer. [b] g PE/mol Zr·h·bar. [c] % molar in the polymer. Determined by ^{13}C NMR.[d] Mw measured by GPC.[e] **A** Cp_2ZrCl_2. **B** $(Me_2SiCp_2)ZrCl_2$.

 © 2004 Wiley-VCH Verlag GmbH & Co. KGaA, Weinheim

from Aldrich and used without further purification. [Zr{(η^5-2-$MeC_{13}H_8$)(η^5-C_5H_4)EMe_2}Cl_2] (E = C, Si)[26], Li(CH_2SiMe_3)[40] and K($CH_2C_6H_5$)[41] were prepared following the literature methods.

Preparation of [Zr{(η^5-2-$MeC_{13}H_7$)(η^5-C_5H_4)$SiMe_2$}Me_2] (2): A THF solution of ClMgMe (3.0 M, 0.5 mL, 1.52 mmol) was added to a stirred suspension of [Zr{(η^5-2-$MeC_{13}H_7$)(η^5-C_5H_4)$SiMe_2$}Cl_2] (**1b**) (0.35 g, 0.75 mmol) in diethyl ether (50 mL) at −78 °C. The mixture was allowed to warm to room temperature and stirred for a further 12 h. The solvent was removed under reduced pressure and the mixture was extracted into hexane. The supernatant solution was then filtered through celite from the $MgCl_2$ residue, concentrated (10 mL) and cooled to -35 °C to give **2** as a pale yellow powder. Yield 0.27 g, 84%. ^{1}H NMR (300 MHz, C_6D_6, 25 °C): δ = −1.29 (s, 3 H, ZrMe), 0.09 (s, 3 H, ZrMe), 0.41 (s, 3 H, SiMe), 0.53 (s, 3 H, SiMe), 1.95 (s, 3 H, CMe), 5.43 (m, 1 H, C_5H_4), 5.52 (m, 1 H, C_5H_4), 6.50 (m, 1 H, C_5H_4), 6.59 (m, 1 H, C_5H_4), 7.1−7.2 (m, 3 H, $C_{13}H_7$), 7.27 (m, 1 H, $C_{13}H_7$), 7.39 (m, 1 H, $C_{13}H_7$), 7.67 (m, 1 H, $C_{13}H_7$), 8.05 (m, 1 H, $C_{13}H_7$) ppm. ^{13}C{^{1}H} NMR (75 MHz, $CDCl_3$, 25 °C): δ = −1.2 (SiMe), −0.8 (SiMe), 18.0 (CMe), 31.0 (ZrMe), 35.5 (ZrMe), 86.2 (C_{ipso}, Si*C*), 100.2 (C_{ipso}, Si*C*), 110.2, 113.0, 113.6, 120.3, 120.6, 122.1, 123.7, 125.4, 125.9, 127.3, 128.9; (CH, C_5H_4, $C_{13}H_7$), 128.5, 129.2, 131.2, 131.5, 131.7; (C_{ipso}, C_5H_4, $C_{13}H_7$) ppm. $C_{23}H_{26}SiZr$ (421.76): calcd. C 65.60, H 6.21; found C 65.81, H 6.28.

Preparation of [Zr{(η^5-2-$MeC_{13}H_7$)(η^5-C_5H_4)$SiMe_2$}($CH_2C_6H_5$)$_2$] (3): Diethyl ether (50 mL) at −78 °C was added to a mixture of [Zr{(η^5-2-$MeC_{13}H_7$)(η^5-C_5H_4)$SiMe_2$}Cl_2] (**1b**) (0.4 g, 0.86 mmol) and K($CH_2C_6H_5$) (0.22 g, 1.72 mmol) and the resulting suspension was allowed to warm to room temperature and stirred for a further 12 h. The supernatant solution was then filtered through celite from the KCl residue, concentrated under reduced pressure (10 mL) and cooled to -35 °C to give **3** as an orange solid. Recrystallization from toluene/hexane gave **3** as a microcrystalline solid. Yield 0.38 g, 78%. ^{1}H NMR (300 MHz, C_6D_6, 25 °C): δ = −0.18 (d, 1 H, $ZrCH_2$, 11 Hz), 0.28 (d, 1 H, $ZrCH_2$, 11 Hz), 0.34 (s,3 H, SiMe), 0.46 (s, 3 H, SiMe), 1.75 (s, 3 H, CMe), 1.95 (d, 1 H, $ZrCH_2$, 11 Hz), 2.13 (d, 1 H, $ZrCH_2$, 11 Hz), 5.20 (m, 1 H, C_5H_4), 5.29 (m, 1 H, C_5H_4), 5.80 (m, 1 H, C_5H_4), 6.31 (m, 1 H, C_5H_4), 6.52 (m, 2 H, C_6H_5), 7.17−7.13 (m, 6 H, C_6H_5), 6.93 (s, 1 H, $C_{13}H_7$), 6.78 (m, 1 H, $C_{13}H_7$), 7.21(m, 1 H, $C_{13}H_7$), 7.22(m, 1 H, $C_{13}H_7$), 7.33(m, 2 H, C_6H_5), 7.41(m, 1 H, $C_{13}H_7$), 7.53(m, 1 H, $C_{13}H_7$), 7.89(m, 1 H, $C_{13}H_7$) ppm. ^{13}C{^{1}H} NMR (75 MHz, $CDCl_3$, 25 °C): δ = −0.7 (SiMe), −1.3 (SiMe), 17.2 (CMe), 61.4 (CH_2), 68.4 (CH_2), 85.7 (C_{ipso}, Si*C*), 100.7 (C_{ipso}, Si*C*), 111.6, 113.6, 116.1, 121.1, 121.3, 122.5, 124.0, 124.0, 124.3, 125.3, 125.3, 126.3, 126.4, 126.4, 126.6, 127.6, 128.5, 128.7, 128.7, 128.9, 129.3; (CH.), 125.0, 128.8, 130.3, 131.0, 132.3, 153.4, 154.6 (C_{ipso}) ppm. $C_{35}H_{34}SiZr$ (573.95): calcd. C 73.24, H 5.97; found C 73.02, H 5.76.

Preparation of [Zr{(η^5-2-$MeC_{13}H_7$)(η^5-C_5H_4)$SiMe_2$}(CH_2SiMe_3)$_2$] (4): In a procedure analogous to that described above for **3** a mixture of [Zr{(η^5-2-$MeC_{13}H_7$)(η^5-C_5H_4)$SiMe_2$}Cl_2] (**1b**) (0.35 g, 0.75 mmol) and Li(CH_2SiMe_3) (0.14 g, 1.52 mmol) were reacted in diethyl ether (50 mL) to yield a pale yellow powder characterized as **4**. Yield 0.29 g, 68%. ^{1}H NMR (300 MHz, C_6D_6, 25 °C): δ = −2.20 (d, 1 H, $ZrCH_2$, 11 Hz), −0.94 (d, 1 H, $ZrCH_2$, 11 Hz), −0.07 (d, 1 H, $ZrCH_2$, 11 Hz), −0.21 (s, 9 H, $SiMe_3$), 0.24 (s, 9 H, $SiMe_3$), 0.25 (d, 1 H, $ZrCH_2$, 11 Hz), 0.42 (s, 3 H, SiMe), 0.49 (s, 3 H, SiMe), 2.07 (s, 3 H, CMe), 5.58 (m, 1 H, C_5H_4), 5.66 (m, 1 H, C_5H_4), 6.68 (m, 1 H, C_5H_4), 6.79 (m, 1 H, C_5H_4), 7.15 (s, 1 H, $C_{13}H_7$), 7.17−7.4 (m, 5 H, $C_{13}H_7$), 7.60 (m, 1 H, $C_{13}H_7$), 8.07 (m, 1 H, $C_{13}H_7$) ppm. ^{13}C{^{1}H} NMR (75 MHz, $CDCl_3$, 25 °C): δ = −1.5 (SiMe), −0.5 (SiMe), 2.6 ($SiMe_3$), 3.5 ($SiMe_3$), 18.3 (CMe), 47.7 (CH_2), 49.4 (CH_2), 88.4 (C_{ipso}, Si*C*), 103.8 (C_{ipso}, Si*C*), 111.8, 112.6, 112.9, 116.6, 119.7, 123.1, 123.8, 125.9, 126.2, 127.5, 128.9; (CH.), 125.3, 126.7, 130.4, 130.8, 132.2 (C_{ipso}) ppm. $C_{29}H_{42}Si_3Zr$ (566.12): calcd. C 61.53, H 7.48; found C 61.38, H 7.34.

Preparation of [Zr{(η^5-2-$MeC_{13}H_7$)(η^5-C_5H_4)$SiMe_2$}{Me}{η^5-C(Me)N(2,6-xylyl)}] (5): Diethyl ether (50 mL) was added to a mixture of [Zr{(η^5-2-$MeC_{13}H_7$)(η^5-C_5H_4)$SiMe_2$}Me_2] (**2**) (0.4 g, 0.95 mmol) and CN(2,6-xylyl) (0.12 g, 0.95 mmol) and the resulting suspension was stirred for a further 5 h. The solvent was completely removed under vacuum and the product was washed with cool pentane (10 mL) to give a pale yellow powder characterized as **5**. Yield 0.49 g, 89%. IR (Nujol): $\tilde{\nu}$ = 1585 ($\nu_{C=N}$) cm^{-1}. ^{1}H NMR (300 MHz, C_6D_6, 25 °C): δ = −1.20 (s, 3 H, ZrMe), 0.67 (s, 3 H, SiMe), 0.71 (s, 3 H, SiMe), 1.65 (s, 3 H, CMe), 1.94 (s, 3 H, CMe), 1.97 (s, 3 H, CMe), 2.36 (3 H, ZrCMe), 5.18 (m, 1 H, C_5H_4), 5.72 (m, 1 H, C_5H_4), 5.91 (m, 1 H, C_6H_3), 5.94 (m, 1 H, C_5H_4), 5.99 (m, 1 H, C_5H_4), 6.80 (m, 2 H, C_6H_3), 6.82 (s, 1 H, $C_{13}H_7$), 7.21 (m, 2 H, $C_{13}H_7$), 7.30(m, 1 H, $C_{13}H_7$), 7.45(m, 1 H, $C_{13}H_7$), 7.68(m, 1 H, $C_{13}H_7$), 7.74 (m, 1 H, $C_{13}H_7$) ppm. ^{13}C{^{1}H} NMR (75 MHz, $CDCl_3$, 25 °C): δ = −0.9 (SiMe), −0.1 (SiMe), 19.2 (CMe), 19.4 (CMe), 19.6 (CMe), 22.2 (ZrCMe), 32.2 (ZrMe), 92.3 (C_{ipso}, Si*C*), 105.0(C_{ipso}, Si*C*), 106.2, 106.3, 106.4, 114.3, 118.6, 123.2, 123.7, 124.6, 125.0, 125.5, 126.2, 128.5, 128.9, 129.7 (*C*H, $C_{13}H_7$, C_6H_3), 119.8, 126.0, 127.8, 128.1, 129.4, 130.5, 132.6, 144.9; (C_{ipso}, $C_{13}H_7$, C_6H_3) 245.4 (*C*=N) ppm. $C_{34}H_{39}NSiZr$ (580.99): calcd. C 70.29, N 2.41, N 6.77; found C 70.41, N 2.52, H 6.82.

Preparation of [Zr{(η^5-2-$MeC_{13}H_7$)(η^5-C_5H_4)$SiMe_2$}{$CH_2C_6H_5$}{η^5-C($CH_2C_6H_5$)N(2,6-xylyl)}] (6): In a procedure analogous to that described above for **5** a mixture of [Zr{(η^5-2-$MeC_{13}H_7$)(η^5-C_5H_4)$SiMe_2$}($CH_2C_6H_5$)$_2$] (**3**) (0.5 g, 0.87 mmol) and CN(2,6-xylyl) (0.11 g, 0.87 mmol) were reacted in diethyl ether (50 mL) to yield an orange powder characterized as **6**. Recrystallization from toluene/hexane gave **6** as a microcrystalline solid. Yield 0.56 g, 91%. IR (Nujol): $\tilde{\nu}$ = 1600 ($\nu_{C=N}$) cm^{-1}. ^{1}H NMR (300 MHz, C_6D_6, 25 °C): δ = 0.27 (d, 1 H, $ZrCH_2$, 9 Hz), 0.56 (d, 1 H, $ZrCH_2$, 9 Hz), 0.54 (s, 3 H, SiMe), 0.67 (s, 9 H, $SiMe_3$), 1.32 (s, 3 H, CMe), 1.96 (s, 3 H, CMe), 2.29 (s, 3 H, CMe), 3.60 (d, 1 H, CCH_2, 9 Hz), 3.68 (d, 1 H, CCH_2, 9 Hz), 5.24 (m, 1 H, C_5H_4), 5.28 (m, 1 H, C_5H_4), 5.82 (m, 1 H, C_5H_4), 6.00 (m, 1 H, C_5H_4), 6.15 (m, 1 H, C_6H_n), 6.41 (m, 2 H, C_6H_n), 6.66 (m, 1 H, C_6H_n), 6.8−7.10 (m, 10 H, C_6H_n), 6.84 (s, 1 H, $C_{13}H_7$), 7.18 (m, 1 H, $C_{13}H_7$), 7.29 (m, 1 H, $C_{13}H_7$), 7.37 (m, 1 H, $C_{13}H_7$), 7.44 (m, 1 H, $C_{13}H_7$), 7.57 (m, 1 H, $C_{13}H_7$), 7.71 (m, 1 H, $C_{13}H_7$) ppm. ^{13}C{^{1}H} NMR (75 MHz, $CDCl_3$, 25 °C): δ = −0.4 (SiMe), −0.8 (SiMe), 19.5 (CMe), 19.7 (CMe), 20.6 (CMe), 44.6 (CCH_2), 47.0 ($ZrCH_2$), 94.9 (C_{ipso}, Si*C*), 106.3(C_{ipso}, Si*C*), 106.8, 108.9, 109.3, 118.4, 118.8, 119.4, 123.1, 124.0, 125.4, 125.5, 125.5, 125.8, 125.8, 125.9, 126.9, 127.2, 127.2, 128.3, 128.6, 128.7, 128.7, 129.0, 130.1, 130.1; ($C_{13}H_7$, C_6H_n), 122.9, 124.9, 125.7, 129.2, 129.3, 131.4, 136.2, 145.2, 155.9; (C_i, $C_{13}H_7$, C_6H_n), 244.5 (*C*=N; *n* = 3, 5) ppm. $C_{44}H_{43}NSiZr$ (705.13): calcd. C 74.95, N 1.99, H 6.15; found C 75.22, N 2.05, H 6.28.

Preparation of [Zr{(η^5-2-$MeC_{13}H_7$)(η^5-C_5H_4)$SiMe_2$}{CH_2SiMe_3}{η^5-C(CH_2SiMe_3)N(2,6-xylyl)}] (7): In a procedure analogous to that described above for **5** a mixture of [Zr{(η^5-2-$MeC_{13}H_7$)(η^5-C_5H_4)$SiMe_2$}(CH_2SiMe_3)$_2$] (**4**) (0.35 g, 0.62 mmol) and CN(2,6-xylyl) (0.08 g, 0.62 mmol) were reacted in diethyl ether (50 mL) to yield an orange powder characterized as **7**. Recrystallization from toluene/hexane gave **7** as a microcrystalline solid. Yield 0.37 g, 87%. IR (Nujol): $\tilde{\nu}$ = 1590 ($\nu_{C=N}$) cm^{-1}. ^{1}H NMR (300 MHz, C_6D_6, 25 °C): δ = −2.97 (d, 1 H, $ZrCH_2$, 12 Hz), −1.86 (d, 1 H, $ZrCH_2$, 12 Hz), −0.12 (s, 9 H, $SiMe_3$), −0.01 (s, 9 H, $SiMe_3$), 0.68 (s, 3 H,

 © 2004 Wiley-VCH Verlag GmbH & Co. KGaA, Weinheim

SiMe), 0.70 (s, 3 H, SiMe), 1.83 (s, 3 H, CMe), 1.90 (s, 3 H, CMe), 2.45 (d, 1 H, CCH_2, 12 Hz), 2.57 (s, 3 H, CMe), 2.63 (d, 1 H, CCH_2, 12 Hz), 5.55 (m, 1 H, C_6H_3), 6.07 (m, 1 H, C_5H_4), 6.19 (m, 1 H, C_5H_4), 6.21 (m, 1 H, C_5H_4), 6.66 (m, 1 H, C_5H_4), 6.79 (m, 3 H, $C_{13}H_7$), 7.29 (m, 3 H, $C_{13}H_7$, C_6H_3), 7.47 (m, 1 H, $C_{13}H_7$), 7.67 (m, 2 H, $C_{13}H_7$) ppm. $^{13}C\{^1H\}$ NMR (75 MHz, $CDCl_3$, 25 °C): δ = −0.43 (SiMe), −0.40 (SiMe), 0.9 ($SiMe_3$), 3.9 ($SiMe_3$), 19.6 (CMe), 20.4 (CMe), 20.6 (CMe), 22.7 (CCH_2), 32.3 ($ZrCH_2$), 96.5 (C_{ipso}, Si*C*), 106.2(C_{ipso}, Si*C*), 107.6, 107.7, 112.9, 115.6, 123.5, 124.2, 124.8, 125.3, 125.6, 127.8, 128.2, 128.5, 128.7, 128.8; ($C_{13}H_7$, C_6H_3), 124.6, 125.5, 129.6, 129.7, 130.6, 133.3, 134.8, 145.7; (C_i, $C_{13}H_7$, C_6H_3), 245.4 (*C*=N) ppm. $C_{38}H_{51}NSi_3Zr$ (697.30): calcd. C 65.45, N 2.01, H 7.37; found C 65.79, N 2.16, H 7.52.

X-ray Structure Determination for Complex 3: Orange crystals of compound **3** were obtained by cooling a concentrated toluene solution and a suitable sized crystal was mounted in a Lindemann tube and mounted on an Enraf−Nonius CAD 4 automatic four-circle diffractometer with graphite monochromated Mo-K_α radiation (λ = 0.71073Å). Crystallographic and experimental details are summarized in Table 4. Data were collected at room temperature. Intensities were corrected for Lorentz and polarization effects in the usual manner. No absorption or extinction corrections were made. The structure was solved by direct methods and refined by least-squares against F^2 (SHELXL 97).[42] All non-hydrogen atoms were refined anisotropically, and the hydrogen atoms were introduced from geometrical calculations and refined using a riding model with the exception of the hydrogens of the CH_2 groups which were found in the difference Fourier map. The hydrogen atoms of the disorder toluene molecule were not included.

X-ray Structure Determination for Complex 6: Data were recorded using Mo-K_α radiation (λ = 0.71073 Å), graphite monochromator and ω scans on a Nonius Kappa CCD diffractometer (see Table 4). The structure was refined anisotropically using the program SHELXL-97.[42] Hydrogen atoms were included using rigid methyl groups or a riding model.

CCDC-236220 (for **3**) and -236644 (for **6**) contains the supplementary crystallographic data for this paper. These data can be obtained free of charge at www.ccdc.cam.ac.uk/conts/retrieving.html [or from the Cambridge Crystallographic Data Centre, 12 Union Road, Cambridge CB2 1EZ, UK; Fax: (internat.) +44-1223-336-033; E-mail: deposit@ccdc.cam.ac.uk].

Polymerization Procedures

Ethylene Polymerizations: Polymerizations were carried out in a Büchi autoclave equipped with a heating bath, mechanical stirrer and connection to argon-vacuum lines. The reactor was evacuated, flushed several times with argon and then charged at 25 °C with 600 mL of freshly distilled heptane and variable amounts of a 10% toluene solution of MAO. The solution was saturated and pressurized with ethylene at 4.0 bar and the thermostat set at 70 °C. Polymerization was started by injection of variable volumes of a previously prepared toluene solution of the zirconocene catalyst. The reaction was stopped by addition of 5 mL of acidified methanol (HCl/methanol, 1:1). Polymers were recovered by filtration, washed with methanol and dried under vacuum at 80 °C for 1 day. The molecular weight of the resulting polyethylene was evaluated by GPC.

Ethylene/1-Hexene Polymerizations: The same procedure described above was followed for copolymerization experiments, the appropriate volume of 1-hexene being initially charged into the reactor together with the solvent. The resulting copolymer was characterized by ^{13}C NMR spectroscopy in $C_6D_3Cl_3$ to evaluate the ethylene/1-hexene ratio by reported methods.[43]

Table 4. Summary of X-ray data for compounds **3** and **6**

	3	**6**
Empirical formula	$C_{35}H_{35}SiZr\cdot 1/2C_7H_8$	$C_{44}H_{43}NSiZr$
Color	orange	pale yellow
Molecular mass	621.40	705.10
Crystal habit	block	prism
a (Å)	9.611(2)	17.2139(10)
b (Å)	18.532(4)	12.1819(9)
c (Å)	17.891(4)	16.4343(10)
β (°)	104.63(3)	93.884(9)
V (Å^3)	3083.3(12)	3438.3(4)
Z	4	4
T (K)	293(2)	150(2)
$D_{calcd.}$ (g·cm^{-3})	1.336	1.362
Crystal system	monoclinic	monoclinic
Space group	$P2_1/n$	$P2_1/c$
F(000)	1292	1472
Crystal size (mm)	0.35 × 0.30 × 0.25	0.28 × 0.26 × 0.10
μ (mm^{-1})	0.421	0.388
2θ (max.)	52.02	54.96
Total/indep. reflns.	6357/5986	26898/7873
Limiting indices (*h*, *k*, *l*)	−11/0, 0/22, −21/22	−22/22, −15/15, −21/21
Data/restraints/parameters	5986/0/370	7873/381/429
R_{int}	0.0746	0.0501
Goodness of fit F^2	1.083	1.026
R int. [all data]	*R*1 = 0.1000, *wR*2 = 0.1649	*R*1 = 0.0585, *wR*2 = 0.0817
Final *R* int [$I > 2\sigma(I)$]	*R*1 = 0.0567, *wR*2 = 0.1463	*R*1 = 0.0344, *wR*2 = 0.0742
Largest diff. peak and hole [e·Å^{-3}]	0.723 and −1.179	0.312 and −0.494

 © 2004 Wiley-VCH Verlag GmbH & Co. KGaA, Weinheim

Acknowledgments

Financial support of our work by MCyT (project MAT2001−1309) is gratefully acknowledged. We are grateful to Repsol-YPF for a fellowship (A. S.) and for the polymerization measurements.

[1] G. J. P. Britovsek, V. C. Gibson, D. F. Wass, *Angew. Chem. Int. Ed.* **1999**, *38*, 428−447.
[2] M. Bochmann, *J. Chem. Soc., Dalton Trans.* **1996**, 255−270.
[3] H. H. Brintzinger, D. Fischer, R. Mülhaupt, B. Rieger, R. M. Waymouth, *Angew. Chem. Int. Ed. Engl.* **1995**, *34*, 1143−1170.
[4] H. G. Alt, A. Koppl, *Chem. Rev.* **2000**, *100*, 1205−1221.
[5] C. Janiak, in *Metallocenes, vol. 2* (Eds.: A. Togni, R. L. Halterman), Wiley-VCH, Weinheim, **1998**, pp. 547−614.
[6] S. D. Ittel, L. K. Johnson, M. Brookhart, *Chem. Rev.* **2000**, *100*, 1169−1203.
[7] K. C. Jayaratne, L. R. Sita, *J. Am. Chem. Soc.* **2000**, *122*, 958−959.
[8] E. Y. Tshuva, I. Goldberg, M. Kol, *J. Am. Chem. Soc.* **2000**, *122*, 10706−10707.
[9] I. M. Lee, W. J. Gauthier, J. M. Ball, B. Iyengar, S. Collins, *Organometallics* **1992**, *11*, 2115−2122.
[10] W. Roll, H. H. Brintzinger, B. Rieger, R. Zolk, *Angew. Chem. Int. Ed. Engl.* **1990**, *29*, 279−280.
[11] W. Spaleck, F. Küber, A. Winter, J. Rohrmann, B. Bachmann, M. Antberg, V. Dolle, E. F. Paulus, *Organometallics* **1994**, *13*, 954−963.
[12] U. Stehling, J. Diebold, R. Kirsten, W. Roll, H. H. Brintzinger, S. Jungling, R. Mülhaupt, F. Langhauser, *Organometallics* **1994**, *13*, 964−970.
[13] G. X. Xu, E. Ruckenstein, *Macromolecules* **1998**, *31*, 4724−4729.
[14] J. Imuta, Y. Toda, T. Matsugi, H. Kaneko, S. Matsuo, S. Kojoh, N. Kashiwa, *Chem. Lett.* **2003**, *32*, 656−657.
[15] J. Imuta, N. Kashiwa, Y. Toda, *J. Am. Chem. Soc.* **2002**, *124*, 1176−1177.
[16] D. R. Swanson, C. J. Rousset, E. Negishi, T. Takahashi, T. Seki, M. Saburi, Y. Uchida, *J. Org. Chem.* **1989**, *54*, 3521−3523.
[17] S. L. Buchwald, R. B. Nielsen, *Chem. Rev.* **1988**, *88*, 1047−1058.
[18] H. Yasuda, A. Nakamura, *Angew. Chem. Int. Ed. Engl.* **1987**, *26*, 723−742.
[19] J. J. Alexander, *The Chemistry of the Metal-carbon Bond, vol. 2*, John Wiley & Sons, New York, **1985**.
[20] L. D. Durfee, I. P. Rothwell, *Chem. Rev.* **1988**, *88*, 1059−1079.
[21] A. M. Barriola, A. M. Cano, T. Cuenca, F. J. Fernández, P. Gómez-Sal, A. Manzanero, P. Royo, *J. Organomet. Chem.* **1997**, *542*, 247−253.
[22] E. L. Lyszak, J. P. O′Brien, D. A. Kort, S. K. Hendges, R. N. Redding, T. L. Bush, M. S. Hermen, K. B. Renkema, M. E. Silver, J. C. Huffman, *Organometallics* **1993**, *12*, 338−342.
[23] F. J. Berg, J. L. Petersen, *Organometallics* **1993**, *12*, 3890−3895.
[24] R. Fandos, A. Meetsma, J. H. Teuben, *Organometallics* **1991**, *10*, 2665−2671.
[25] M. Bühl, G. Hopp, W. vonPhilipsborn, S. Beck, M. H. Prosenc, U. Rief, H. H. Brintzinger, *Organometallics* **1996**, *15*, 778−785.
[26] A. Sebastián, P. Royo, P. Gómez-Sal, E. Herdtweck, *Inorg. Chim. Acta* **2003**, *350*, 511−519.
[27] M. F. Lappert, C. J. Pickett, P. I. Riley, P. I. W. Yarrow, *J. Chem. Soc., Dalton Trans.* **1981**, 805−813.
[28] M. F. Lappert, P. I. Riley, P. I. W. Yarrow, J. L. Atwood, W. E. Hunter, M. J. Zaworotko, *J. Chem. Soc., Dalton Trans.* **1981**, 814−821.
[29] A. Antiñolo, R. Fernández-Galán, B. Gallego, A. Otero, S. Prashar, A. M. Rodriguez, *Eur. J. Inorg. Chem.* **2003**, 2626−2632.
[30] R. Wolfgramm, C. Ramos, P. Royo, M. Lanfranchi, M. A. Pellingelli, A. Tiripicchio, *Inorg. Chim. Acta* **2003**, *347*, 114−122.
[31] H. R. H. Damrau, E. Royo, S. Obert, F. Schaper, A. Weeber, H. H. Brintzinger, *Organometallics* **2001**, *20*, 5258−5265.
[32] X. W. Zhang, Q. M. Zhu, I. A. Guzei, R. F. Jordan, *J. Am. Chem. Soc.* **2000**, *122*, 8093−8094.
[33] N. Schneider, F. Schaper, K. Schmidt, R. Kirsten, A. Geyer, H. H. Brintzinger, *Organometallics* **2000**, *19*, 3597−3604.
[34] A. Sebastián, P. Royo, O. Castaño, L. M. Frutos, C. Ramírez de Arellano, manuscript in preparation.
[35] F. H. Allen, O. Kennard, D. G. Watson, L. Brammer, A. G. Orpen, R. Taylor, *J. Chem. Soc., Perkin Trans. 2* **1987**, S1−S19.
[36] R. Fandos, M. Lanfranchi, A. Otero, M. A. Pellinghelli, M. J. Ruiz, P. Terreros, *Organometallics* **1996**, *15*, 4725−4730.
[37] U. Segerer, S. Blaurock, J. Sieler, E. Hey-Hawkins, *J. Organomet. Chem.* **2000**, *608*, 21−26.
[38] H. H. Karsch, K. A. Schreiber, M. Reisky, *Organometallics* **1998**, *17*, 5052−5060.
[39] R. Kravchenko, R. M. Waymouth, *Macromolecules* **1998**, *31*, 1−6.
[40] M. Wedler, F. Knosel, F. T. Edelmann, U. Behrens, *Chem. Ber./Recueil* **1992**, *125*, 1313−1318.
[41] M. Westerhausen, W. Schwarz, *Z. Naturforsch., Teil B* **1998**, *53*, 625−627.
[42] G. M. Sheldrick, *SHELXL-97*, University of Göttingen, Göttingen, Germany, **1998**.
[43] J. C. Randall, E. T. Hsieh, *ACS Symp Ser.* **1984**, *247*, 131−151.

Received April 26, 2004
Early View Article
Published Online August 12, 2004

 © 2004 Wiley-VCH Verlag GmbH & Co. KGaA, Weinheim

A Cationic Tetranuclear $[Ni^{II}_4(MeOH)_2(pko)_6]^{2+}$ Cluster Showing Antiferro- and Ferromagnetic Features

Maria Alexiou,[a] Catherine Dendrinou-Samara,[a] Catherine P. Raptopoulou,[b] Aris Terzis,[b] Vassilis Tangoulis,*[c] and Dimitris P. Kessissoglou*[a]

Keywords: Cluster compounds / Magnetic properties / Oximato ligands / Nickel

The majority of reported nickel tetranuclear clusters have a dicubane-like structural core. The compound presented here is the second example possessing an Ni_4O_2 core based on a chair or butterfly "out-of-face" topology. This compound also belongs to the family of compounds characterized as metallacrowns with an $[Ni–N–O–]_n$ linkage and is the only example with three Ni–O–N–Ni strands bridging the nickel atoms. The values obtained from the fitting procedure are $J_1 = 55.8$ cm^{-1}, $J_2 = -67.2$ cm^{-1}, $g = 2.2$, $\rho = 1.1\%$. These values suggest the presence of both ferromagnetic and antiferromagnetic interactions, while a small paramagnetic impurity is also present. This magnetic behaviour with antiferromagnetic internal coupling and ferromagnetic spin-alignment is the second example in the literature and the first in the metallacrown family.

(© Wiley-VCH Verlag GmbH & Co. KGaA, 69451 Weinheim, Germany, 2004)

Introduction

Our interest in polynuclear nickel[1–4] or manganese[5–10] complexes showing interesting structural and magnetic features has focused especially on metallacrowns, a molecular class that exhibits selective recognition of cations and anions. An attractive feature of metallacrowns is that they concentrate a large number of metal ions into a small area. These large concentrations of metal ions may lead to interesting magnetic behaviour.[1,10–12] The structural features of each metallacrown can lead to high magnetic moments per compound through ferromagnetic exchange or coupling to low-lying paramagnetic states. Previously reported metallacrowns[1–27] have been prepared using hydroxamic acids and/or ketone oximic acids as constructing ligands. Hpko is a bifunctional ligand that can bind metal atoms in either five- or six-membered chelate rings. The deprotonated di-2-pyridyl ketone oxime can act in two binding modes: (i) bichelate and (ii) monochelate. In (i) the ketone oxime oxygen atom (O_k) and one pyridine nitrogen atom (N) bind to one metal atom and the other pyridine nitrogen atom (N) plus the ketone oxime nitrogen atom (N_k) chelate an adjacent metal atom in a *syn-anti* arrangement (form A). In (ii) the ketone oxime nitrogen atom (N_k) and one pyridine nitrogen atom (N) are coordinated to one metal atom in a five-membered chelate ring in a *syn-syn* arrangement (form B_1) or the ketone oxime oxygen atom (O_k) and one pyridine nitrogen atom (N) are bound to one metal atom in a six-membered chelate ring in a *syn-anti* arrangement (form B_2). These juxtaposed five- and six-membered chelate rings form the basis of the metallacrown ring through the $[M-N-O-]_n$ linkage.

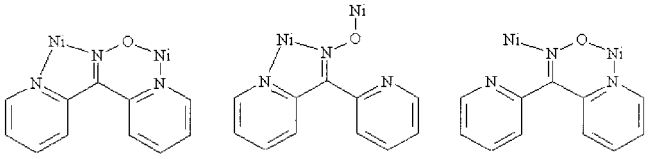

For tetranuclear nickel clusters the majority of the compounds reported have a dicubane-like structural core[28–41] with only one example possessing an Ni_4O_2 core based on a chair or butterfly "out-of-face" topology.[42] The compound presented here is the second example that may be characterized as having a chair topology and the only example showing a metallacrown $[M-N-O-]_n$ linkage with three Ni–O–N–Ni strands bridging the nickel atoms. This compound is also the first metallacrown showing antiferromagnetic internal coupling and ferromagnetic spin alignment.

Results and Discussion

The reaction of $Ni(ClO_4)_2$ with dipyridyl ketone oxime, $(2\text{-py})_2C{=}NOH$ (Hpko) in a 1:1 ratio in methanol in the

[a] Department of General and Inorganic Chemistry, Faculty of Chemistry, Aristotle University of Thessaloniki, 54124 Thessaloniki, Greece
[b] NCSR "Demokritos", Institute of Materials Science, 15310 Aghia Paraskevi Attikis, Greece
[c] Department of Materials Science, University of Patras, 26500 Patras, Greece

presence of NaOH gives red-brown crystals of the cluster $[Ni^{II}_4(CH_3OH)_2(pko)_6](OH)(ClO_4)\cdot 2CH_3OH\cdot 4H_2O$ (**1**) after slow evaporation of the solvent. The synthesis of cluster **1** was achieved by the reaction

$$4\ Ni(ClO_4)_2 + 6\ Hpko + 7\ NaOH \xrightarrow{Methanol} [Ni(II)_4(CH_3OH)_2(pko)_6](OH)(ClO_4) + 7\ NaClO_4 + 6\ H_2O$$

The compound crystallizes in the tetragonal space group *P4/n*. The asymmetric unit contains half of the tetranuclear cation, half a perchlorate and hydroxide counterion, two lattice water molecules and one methanol solvent molecule of crystallization. The tetranuclear $[Ni^{II}_4(pko)_6(CH_3OH)_2]^{2+}$ cation is centrosymmetric; the inversion center lies in the center of the Ni(2)−O(1)−Ni(2)−O(1) moiety. The whole structure can be characterized as having a "metallacrown chair" topology (Figure 1). Two nickel atoms with a distorted octahedral NO_5 coordination environment are bridged by two oxygen atoms from pko ligands to form the Ni_2O_2 core, in which the Ni(2)−O(1) or Ni(2)−O(1)# distances are found to be 2.086(8) Å and 2.101(8) Å, respectively, the Ni(2)···Ni(2)# and O(1)···O(1)# separations to be 3.059 Å and 2.861 Å, respectively, and the Ni(2)−O(1)−Ni(2)# and O(1)−Ni(2)−O(1)# angles to be 93.70° and 86.16°, respectively (Table 1). Each nickel atom of the Ni_2O_2 core is bound to two oximato oxygen atoms with Ni(2)−O(11) and Ni(2)−O(21) distances of 1.974(9) and 2.047(8) Å, respectively; the octahedron is completed by a methanol oxygen atom at a distance of 2.113(8) Å.

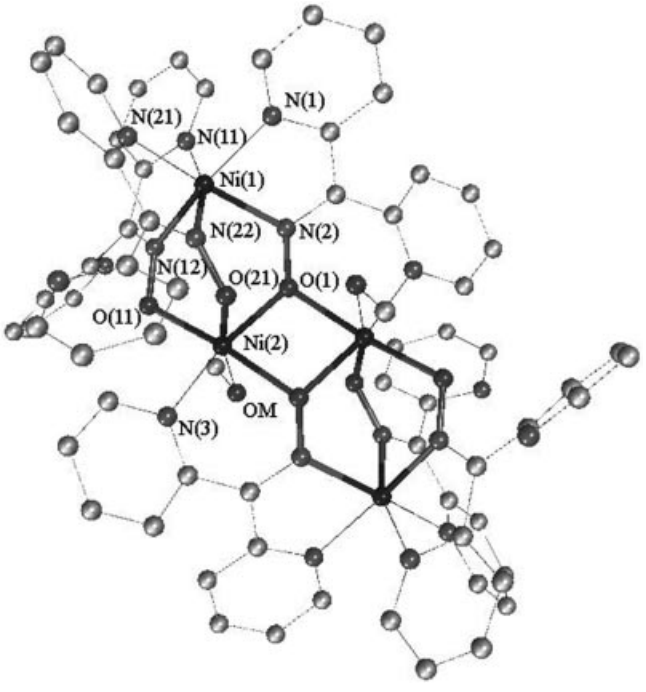

Figure 1. Crystal structure of the the $[Ni^{II}_4(pko)_6(CH_3OH)_2]^{2+}$ ion; the core and ring connectivity have been highlighted; perchlorate and hydroxy ions are not shown

Two pko oximato moieties bridge the core nickel atom with the "wing" nickel atom in a monochelate mode and a *syn-syn* arrangement(form B_1), while the third pko ligand bridges the "wing" nickel atom Ni(1) and the symmetrically equivalent Ni(2)# nickel atom through the oximato moity in bichelate mode and a *syn-anti* arrangement (form A). The two "wing" nickel atoms have a pure N_6 coordination environment with three nitrogen atoms coming from three oximato moieties [Ni(1)−$N_{oximato}$ (av.) = 2.036 Å] and three nitrogen atoms from three pko-pyridine groups [Ni(1)−$N_{pyridine}$ (av.) = 2.105 Å]. Four of the six pko ligands have the second pyridine nitrogen atom uncoordinated. The "wing" nickel atoms Ni(1) and Ni(1)# lie on opposite sides of the Ni_2O_2 parallelogram at 3.469 Å and 4.744 Å from the core nickel atoms Ni(2). The formation of the 12-membered metallacrown follows the pattern (Ni−N−O−Ni−O−N−Ni−N−O−Ni−O−N) and, in cooperation with the *syn-anti* mode of one pko-oximato ligand, allows the construction of the chair-like metallacrown shape.

Table 1. Selected bond lengths [Å] and angles [°] of **1**

Bond lengths			
Ni(1)−N(12)	2.025(10)	Ni(2)−O(11)	1.974(9)
Ni(1)−N(22)	2.040(11)	Ni(2)−N(3)#1	2.036(10)
Ni(1)−N(2)	2.043(10)	Ni(2)−O(21)	2.047(8)
Ni(1)−N(11)	2.100(10)	Ni(2)−O(1)	2.086(8)
Ni(1)−N(1)	2.107(11)	Ni(2)−O(1)#1	2.101(8)
Ni(1)−N(21)	2.108(11)	Ni(2)−OM1	2.113(8)
Ni(2)···Ni(2)#1	3.059	O(1)···O(1)#1	2.861
Ni(1)···Ni(2)	3.469		
Angles			
N(22)−Ni(1)−N(11)	163.3(4)	O(11)−Ni(2)−O(1)#1	174.7(3)
N(12)−Ni(1)−N(1)	164.7(4)	O(21)−Ni(2)−OM1	169.2(4)
N(2)−Ni(1)−N(21)	163.2(4)	N(3)#1−Ni(2)−O(1)	169.9(4)
N(2)−O(1)−Ni(2)#1	93.70(4)	O(1)−Ni(2)−O(1)#1	86.16(4)

Symmetry operation: #1: $-x, 1-y, 1-z$

Magnetic Study

The temperature dependence of the susceptibility data in the form of χ_M and $\chi_M T$ vs. T plots is shown in Figure 2.

The room-temperature value of $\chi_M T$ is 3.5 emu·mol^{-1}·K lower than the value expected for four uncorrelated $S = 1$ spins (4.0 emu·mol^{-1}·K for $g = 2.0$) showing that an overall antiferromagnetic behavior characterizes the magnetic interaction between the magnetic centers. As the temperature decreases the value of $\chi_M T$ also decreases until about 17 K, where its value is close to zero. After that temperature a plateau forms until 2 K, revealing that a paramagnetic impurity is present. This is shown better in the χ_M data, where a Curie tail appears below 7 K. Another important aspect of the χ_M data is the peak at about 67 K, which is evidence of different types of interaction in the cluster.

Magnetization measurements were carried out in the field range 0−12 T at 2 K in order to verify the ground state and possibly to observe a jump to an excited state (Figure 3). The reduced magnetization at 12 T is 0.0135 μ_B and this is

 © 2004 Wiley-VCH Verlag GmbH & Co. KGaA, Weinheim

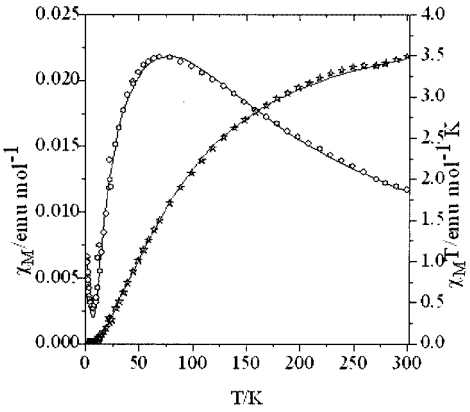

Figure 2. Temperature dependence of the susceptibility data in the form of χ_M (open circles) and $\chi_M T$ (open stars) vs. T plots in an applied field of 0.1 T; the solid lines represent the best fit according to Equation (1) (see text for details)

due to the paramagnetic impurity of the system; there is no population of the excited state with $S_{tot} > 0$ until 12 T.

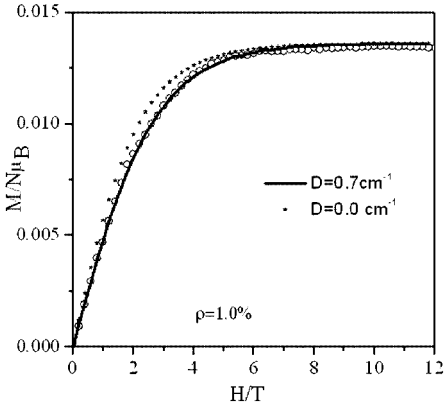

Figure 3. Magnetization data at 2 K and in the field range 0−12 T; the lines represent 1.0% of an $S = 1$ system with $D = 0$ cm^{-1} (dotted) and $D = 0.7$ cm^{-1} (solid)

The safe conclusions from the study of the magnetic experiments are: (a) there are both ferro- and antiferromagnetic interactions in the cluster, which lead to an overall antiferromagnetic behavior; (b) the ground state of the system is $S = 0$ with a small percentage of paramagnetic impurity of an $S = 1$ system.

In order to calculate the interactions between the magnetic ions the zero-field Hamiltonian according to Equation (1) was used, where the numbering of the spins and the exchange couplings are based on the magnetic model in Figure 4, according to crystallographic criteria.

$$H = J_1(S_1S_2 + S_3S_4) + J_2(S_2S_3) + J_3(S_1S_3 + S_2S_4) \quad (1)$$

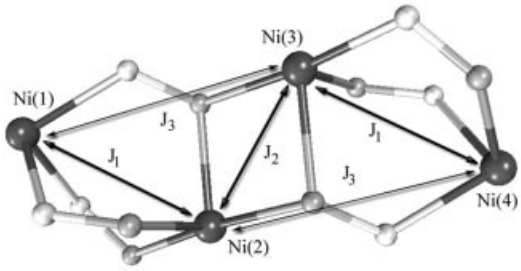

Figure 4. The magnetic model showing the interaction vectors; Ni(3) and Ni(4) are symmetry equivalents of Ni(2) and Ni(1), respectively

The fitting results are shown in Figure 2 in the form of solid lines and the values obtained are: $J_1 = 48.1$ cm^{-1}, $J_2 = -12.1$ cm^{-1}, $J_3 = 14.5$ cm^{-1}, $g = 2.2$, $\rho = 1.1\%$.

The interaction between the two central ions Ni(2) and Ni(3) is ferromagnetic, which is in accordance with the Ni−O−Ni angle (93.7°) and the small distance between the two ions (3.059 Å), while the interaction between Ni(1) and Ni(2) and Ni(3) and Ni(4) is antiferromagnetic due to the superexchange pathway [Ni(1)−N−O−Ni(2)] and the long distance between the magnetic ions (3.470 Å).

It is interesting to note that a third antiferromagnetic interaction exists between Ni(1) and Ni(3) and Ni(2) and Ni(4) despite the long distance between the Ni ions (4.743 Å). A ferromagnetic Ni−Ni interaction is observed when the Ni−O−Ni angle is close to orthogonal. Antiferromagnetic interactions have also been observed for Ni−O−Ni bridging angles larger than 99°. Following the lead of Christou et al.,[43] for comparison purposes the magnetic interactions (J) are represented in Figure 5 as a function of average Ni−O−Ni angles.

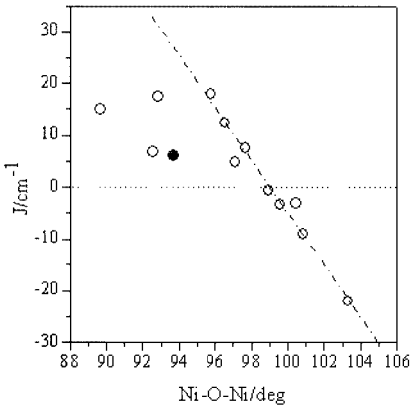

Figure 5. Exchange interaction (J) as a function of the Ni−O−Ni angle for different cores of the type Ni_4O_4 described in the literature (open circles)[36] and that reported in this contribution (solid circle)[44]

The energy scheme according to the previous parameters reveal that the ground state is $S = 0$, and that this is well separated from the first excited state ($S = 1$, $\Delta E = 36$ cm^{-1}; Figure 6).

 © 2004 Wiley-VCH Verlag GmbH & Co. KGaA, Weinheim

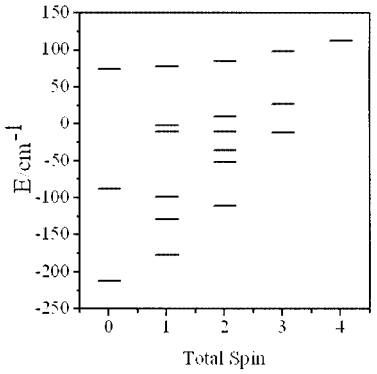

Figure 6. Energy scheme of the magnetic model according to fitting results (see text for details)

Concerning the magnetization data, a simulation procedure was carried out in order to obtain information about the paramagnetic impurity. Assuming that the ground state $S = 0$ is well isolated (which is true according to the susceptibility data) at 2 K the magnetization curve belongs to the paramagnetic impurity of an $S = 1$ system. The simple Brillouin function of a 0.008% $S = 1$ state is not completely superimposed on the data, which implies that the zero-field term may play an important role. By adding the zero-field term the best simulation was obtained for a D value of 0.7 cm^{-1}.

Conclusions

While tetranuclear nickel clusters have been reported, the compound presented here shows some very interesting features. It is the second example possessing an Ni_4O_2 core based on a "chair or butterfly out-of-face" topology. This compound also belongs to the family of compounds characterized as metallacrowns with an $[Ni-N-O-]_n$ linkage and is the only example with three strands Ni−O−N−Ni bridging the nickel atoms. The magnetic study shows the presence of both ferromagnetic and antiferromagnetic interactions. The magnetic behaviour with antiferromagnetic internal coupling and ferromagnetic spin alignment is the second example in the literature and the first in the metallacrown family.

Experimental Section

CAUTION: *Perchlorate compounds of metal ions are potentially explosive; only a small amount of material should be prepared and handled with caution!*

Materials: The chemicals for the synthesis of the compounds were used as purchased. DMF was distilled from calcium hydride (CaH_2) and CH_3OH from magnesium (Mg); they were both stored over molecular sieves (3 Å). Hpko and $Ni(ClO_4)_2·6H_2O$ were purchased from Aldrich Co. All chemicals and solvents were reagent grade.

Physical Measurements: Infrared spectra (200−4000 cm^{-1}) were recorded with a Perkin−Elmer FT-IR 1650 spectrometer with samples prepared as KBr pellets. UV/Vis spectra were recorded with a Shimadzu-160A dual-beam spectrophotometer. C, H and N elemental analysis was performed with a Perkin−Elmer 240B elemental analyser; Ni was determined by atomic absorption spectroscopy with a Perkin−Elmer 1100B spectrophotometer. Electrical-conductance measurements were carried out with a WTW model LF 530 conductivity outfit and a type-C cell, which had a cell constant of 0.996. This represents a mean value calibrated at 25 °C with potassium chloride. The temperature dependence of the magnetic susceptibility was measured on polycrystalline powder samples using a Cryogenics S600 SQUID Magnetometer with an applied field of 0.1−1.0 T in the temperature range 2−300 K. Data were corrected for sample-holder contribution and diamagnetism of the sample using standard procedures.

Synthesis of $[Ni^{II}_4(CH_3OH)_2(pko)_6](OH)(ClO_4)·2CH_3OH·4H_2O$ (1): Dipyridyl ketone oxime (1.19 g, 6 mmol) was added to a solution of sodium hydroxide (0.24 g, 6 mmol) in CH_3OH (20 mL). The resulting mixture was stirred for 1 h, generating a pale-yellow solution. $NiClO_4·6H_2O$ (1.46 g, 4 mmol) dissolved in CH_3OH (20 mL) was then added with stirring. The resulting red-brown solution was stirred for 1 h. Brown crystals suitable for X-ray diffraction studies were obtained by slow concentration. Yield 50%. $C_{70}H_{73}ClN_{18}Ni_4O_{19}$ (1740.8): calcd. C 48.3, H 4.2, N 14.5, Ni 13.4; found C 47.9, H 4.4, N 14.2, Ni 13.0. IR: $\tilde{\nu}$ = 1597 [vs, ν(C=N)], = 1462 [vs, ν(N=O)] cm^{-1}. UV/Vis (DMF): λ_{max} (ε [$dm^3·mol^{-1}·cm^{-1}$]) = 524 (722, sh) nm.

X-ray Crystal-Structure Determination: Slow crystallization of **1** from methanol yielded red prismatic crystals. A crystal with approximate dimensions 0.08 × 0.25 × 0.40 mm was mounted in a capillary. Diffraction measurements were made with a $P2_1$ Nicolet diffractometer upgraded by Crystal Logic using graphite-monochromated Cu radiation. Unit-cell dimensions were determined and refined by using the angular settings of 25 automatically centered reflections in the range $22° < 2\theta < 54°$. These data are given in Table 2. Intensity data were recorded using a θ-2θ scan to $2\theta(max) = 100°$ with a scan speed of 1.5°/min and scan range 2.4 plus a_1a_2 separation. Three standard reflections monitored every 97 reflections showed less than 3% variation and no decay. Lorentz, polarization and ψ-scan absorption corrections were applied using the Crystal Logic software. Symmetry-equivalent data were averaged with $R = 0.0703$ to give 4442 independent reflections from a total of 4725 collected. The structure was solved by direct methods using SHELXS-86 and refined by full-matrix least-squares techniques on F^2 with SHELXL-93 using 4442 reflections and refining 518 parameters.[45−47] The final values for $R1$, $wR2$ and GOF for observed data are given in Table 2, and for all data are 0.1724, 0.3409 and 1.057 respectively. The maximum and minimum residual peaks in the final difference map were 1.123 and −0.599 e/Å. The largest shift/esd in the final cycle was 0.017. CCDC-223110 contains the supplementary crystallographic data for this paper. These data can be obtained free of charge via www.ccdc.cam.ac.uk/conts/retrieving.html [or from the Cambridge Crystallographic Data Centre, 12 Union Road, Cambridge CB21EZ, UK; Fax: (internat.) + 44-1223-336-033; E-mail: deposit@ccdc.cam.ac.uk]. Structural remarks: The crystals were small and of poor quality (the peak scans showed small shoulders). For this reason we did not collect data above $2\theta = 100°$, and even for the data we did collect about 40% was unobserved. This problem is due especially to disordered perchlorate and hydroxy anions and solvent molecules. The quality of the $[Ni^{II}_4(pko)_6(CH_3OH)_2]^{2+}$ ion is very satis-

 © 2004 Wiley-VCH Verlag GmbH & Co. KGaA, Weinheim

factory, particularly for interpreting the magnetic data. All hydrogen atoms of the pko ligands were introduced at calculated positions as riding on bonded atoms. All non-hydrogen atoms were refined anisotropically. The perchlorate counterion was refined as follows: two independent chlorine atoms were found in the difference Fourier map, one located on a fourfold axis of symmetry, Cl(1), and the second on a fourfold inverse axis of symmetry, Cl(2). One of the oxygen atoms on Cl(1), O(31), is also located on the fourfold axis of symmetry, while the other three oxygen atoms, O(32), O(33), O(34), are on general positions and were refined with occupation factor 0.25 as disordered over the C_4 axis. Only one oxygen atom, O(41), was found near Cl(2), generating the perchlorate anion due to the fourfold inverse axis of symmetry. Atoms Cl1 and Cl2 were refined anisotropically, while all oxygen atoms were refined isotropically. The hydroxide counterion was refined as follows: two independent oxygen atoms were found in the difference Fourier map, both located on a fourfold axis of symmetry and were refined isotropically with occupation factors 0.25. The water and methanol solvent molecules were refined isotropically as follows: one of the water molecules, OW(1), was found disordered and it was refined over three positions with occupation factors of a total sum one. The second water molecule, OW(2), was also found disordered and it was refined over two positions with occupation factors of a total sum one. The methyl group of the methanol solvate was found disordered and it was refined over three positions with occupation factors of a total sum of one.

Table 2. Summary of crystal, intensity collection and refinement data of **1**

Empirical formula	$C_{70}H_{73}ClN_{18}Ni_4O_{19}$
Formula mass	1740.75
Temperature [K]	293
Radiation (Cu-K_a) [Å]	1.54180
Crystal system, space group	tetragonal, *P4/n*
a [Å]	22.798(2)
b [Å]	22.798(2)
c [Å]	16.633(2)
Volume [Å^3]	8645(2)
Z, calculated density [Mg/m^3]	4, 1.337
Absorption coefficient [mm^{-1}]	1.874
Crystal size [mm]	0.40 × 0.25 × 0.08
Reflections collected/unique	4725/4442 [R_{int} = 0.0703]
Data/restraints/parameters	4442/22/518
R_{int} [2528 refls. with $I > 2\sigma(I)$]	$R1$ = 0.1035, $wR2$ = 0.2600
R_{int} (all data)	$R1$ = 0.1724, $wR2$ = 0.3409

Acknowledgments

This work was supported by PENED 2001/1034. V. T. would like to thank Dr. Claudio Sangregorio and the Department of Chemistry of Florence, Italy for the magnetic measurements.

[1] C. Dendrinou-Samara, G. Psomas, L. Iordanidis, V. Tangoulis, D. P. Kessissoglou, *Chem. Eur. J.* **2001**, *7*, 5041−5051.
[2] C. Dendrinou-Samara, L. Alevizopoulou, L. Iordanidis, E. Samaras, D. P. Kessissoglou, *J. Inorg. Biochem.* **2002**, *89*, 89−96.
[3] M. Alexiou, C. Dendrinou-Samara, C. P. Raptopoulou, A. Terzis, D. P. Kessissoglou, *Inorg. Chem.* **2002**, *41*, 4732−4738.
[4] G. Psomas, C. Dendrinou-Samara, M. Alexiou, A. Tsohos, C. P. Raptopoulou, A. Terzis, D. P. Kessissoglou, *Inorg. Chem.* **1998**, *37*, 6556−6557.
[5] G. Psomas, A. J. Stemmler, C. Dendrinou-Samara, J. Bodwin, M. Schneider, M. Alexiou, J. Kampf, D. P. Kessissoglou, V. L. Pecoraro, *Inorg. Chem.* **2001**, *40*, 1562−1570.
[6] D. P. Kessissoglou, J. Bodwin, J. Kampf, C. Dendrinou-Samara, V. L. Pecoraro, *Inorg. Chim. Acta* **2002**, *331*, 73−80.
[7] D. P. Kessissoglou, J. Kampf, V. L. Pecoraro, *Polyhedron* **1994**, *13*, 1379−1391.
[8] M. Alexiou, C. Dendrinou-Samara, A. Karagianni, S. Biswas, C. M. Zaleski, J. Kampf, D. Yoder, J. E. Penner-Hahn, V. L. Pecoraro, D. P. Kessissoglou, *Inorg. Chem.* **2003**, *42*, 2185−2187.
[9] T. Afrati, C. Dendrinou-Samara, C. P. Raptopoulou, A. Terzis, V. Tangoulis, D. P. Kessissoglou, *Angew. Chem. Int. Ed.* **2002**, *41*, 2148−2150.
[10] C. Dendrinou-Samara, M. Alexiou, C. M. Zaleski, J. Kampf, D. Yoder, J. E. Penner-Hahn, M. L. Kirk, D. P. Kessissoglou, V. L. Pecoraro, *Angew. Chem. Int. Ed.* **2003**, *42*, 3763−3766.
[11] V. L. Pecoraro, A. J. Stemmler, B. R. Gibney, J. J. Bodwin, H. Wang, J. W. Kampf, A. Barwinski, *Prog. Inorg. Chem.* **1997**, *45*, 83.
[12] A. J. Stemmler, J. W. Kampf, M. L. Kirk, B. H. Atasi, V. L. Pecoraro, *Inorg. Chem.* **1999**, *38*, 2807−2817.
[13] B. R. Gibney, A. J. Stemmler, S. Pilotek, J. W. Kampf, V. L. Pecoraro, *Inorg. Chem.* **1993**, *32*, 6008−6015.
[14] A. J. Stemmler, J. W. Kampf, M. L. Kirk, V. L. Pecoraro, *J. Am. Chem. Soc.* **1995**, *117*, 6368−6369.
[15] A. J. Stemmler, A. Barwinski, M. J. Baldwin, V. Young, V. L. Pecoraro, *J. Am. Chem. Soc.* **1996**, *118*, 11962−11963.
[16] A. J. Stemmler, J. W. Kampf, V. L. Pecoraro, *Inorg. Chem.* **1995**, *34*, 2271−2272.
[17] M. S. Lah, B. R. Gibney, D. L. Tierney, J. E. Penner-Hahn, V. L. Pecoraro, *J. Am. Chem. Soc.* **1993**, *115*, 5857−5858.
[18] R. W. Saalfrank, I. Bernt, M. M. Chowdhry, F. Hampel, G. B. M. Vaughan, *Chem. Eur. J.* **2001**, *7*, 2765−2769.
[19] M. Eshel, A. Bino, I. Feiner, D. C. Johnston, M. Luban, L. L. Miller, *Inorg. Chem.* **2000**, *39*, 1376−1380.
[20] B. Kwak, H. Rhee, S. Park, M. S. Lah, *Inorg. Chem.* **1998**, *37*, 3599−3602.
[21] S.-X. Liu, S. Lin, B.-Z. Lin, C.-C. Lin, J.-O. Huang, *Angew. Chem. Int. Ed.* **2001**, *40*, 1084−1087.
[22] R. W. Saalfrank, R. Burak, S. Reihs, N. Löw, F. Hampel, H.-D. Stachel, J. Lentmaier, K. Peters, E.-M. Peters, H. G. von Schering, *Angew. Chem. Int. Ed. Engl.* **1995**, *34*, 993−995.
[23] R. W. Saalfrank, I. Bernt, E. Uller, F. Hampel, *Angew. Chem. Int. Ed. Engl.* **1997**, *36*, 2482.
[24] R. W. Saalfrank, N. Löw, S. Kareth, V. Seitz, F. Hampel, D. Stalke, M. Teichert, *Angew. Chem. Int. Ed.* **1998**, *37*, 172−175.
[25] R. W. Saalfrank, S. Trummer, U. Reiman, M. M. Chowdhry, F. Hampel, O. Waldmann, *Angew. Chem. Int. Ed.* **2000**, *39*, 3492−3494.
[26] H. Piotrowski, G. Hilt, A. Schulz, P. Mayer, K. Polborn, K. Severin, *Chem. Eur. J.* **2001**, *7*, 3196−3208.
[27] A. E. Pullen, J. Piotraschke, K. A. Abboud, J. R. Reynolds, *Inorg. Chem.* **1996**, *35*, 793−796.
[28] A. J. Edwards, B. F. Hoskins, E. H. Kachab, A. Markewiecz, K. S. Murray, R. Robson, *Inorg. Chem.* **1992**, *31*, 3585−3591.
[29] M. Bell, A. J. Edwards, B. F. Hoskins, E. H. Kachab, R. Robson, *J. Am. Chem. Soc.* **1989**, *111*, 3603−3610.
[30] K. Nanda, K. Venkatsubramanian, D. Majumdar, K. Nag, *Inorg. Chem.* **1994**, *33*, 1581−1582.
[31] S. Mohanta, K. K. Nanda, R. Werner, W. Haase, A. K. Mukherjee, S. K. Dutta, K. Nag, *Inorg. Chem.* **1997**, *36*, 4656−4664.
[32] M. A. Halcrow, G. Christou, *Chem. Rev.* **1994**, *94*, 2421−2481.
[33] E. Jabri, M. B. Carr, R. P. Hausinger, P. A. Karplus, *Science* **1995**, *268*, 998−1004.
[34] C. J. Matthews, K. Avery, Z. Xu, L. K. Thompson, L. Zhiao, D. O. Miller, K. Biradha, M. J. Zaworotko, C. Wilson, A. E. Goeta, J. A. K. Howard, *Inorg. Chem.* **1999**, *38*, 5266−5276.
[35] A. Escuer, R. Vicente, S. B. Kumar, F. A. Mautner, *J. Chem. Soc., Dalton Trans.* **1998**, 3473−3478.

 © 2004 Wiley-VCH Verlag GmbH & Co. KGaA, Weinheim

[36] J. M. Clemente-Juan, B. Chansou, B. Donnadieu, J.-P. Tuchagues, *Inorg. Chem.* **2000**, *39*, 5515−5519.

[37] J. M. Clemente-Juan, H. Andres, J. J. Borrás-Almenar, E. Coronado, H. U. Güdel, M. Aebersold, G. Kearly, H. Büttner, M. Zolliker, *J. Am. Chem. Soc.* **1999**, *121*, 10021−10027.

[38] C. J. Gómez-García, J. J. Borrás-Almenar, E. Coronado, L. Ouahab, *Inorg. Chem.* **1994**, *33*, 4016−4022.

[39] M. S. El Fallah, E. Rentschler, A. Caneschi, D. Gatteschi, *Inorg. Chim. Acta* **1996**, *247*, 231−235.

[40] Z. E. Serna, L. Lezama, M. K. Urtiaga, M. I. Arriortua, M. G. Barandika, R. Cortés, T. Rojo, *Angew. Chem.* **2000**, *112*, 352, *Angew. Chem. Int. Ed.* **2000**, *39*, 344−347.

[41] A. Escuer, M. Font-Bardía, S. J. Kumar, X. Solans, R. Vicente, *Polyhedron* **1999**, *18*, 909−914.

[42] V. V. Pavlishchuk, S. V. Kolotilov, A. W. Addison, M. J. Prushan, D. Schollmeyer, L. K. Thompson, E. A. Goreshnik, *Angew. Chem. Int. Ed.* **2001**, *40*, 4734−4737.

[43] M. A. Halcrow, J. S. Sun, J. C. Huffman, G. Christou, *Inorg. Chem.* **1995**, *34*, 4167.

[44] In order to compare our results (J-formalism, $H = J_{ij}\ S_iS_j$) with the other ones shown in Figure 5 ($-2J$-formalism, $H = -2J_{ij}\ S_iS_j$) we had to convert our value of $J_2 = -12.1\ cm^{-1}$ to $J_2' = 6.05\ cm^{-1}$.

[45] *International Tables for X-ray Crystallography*, Kynoch Press, Birmingham, **1974**, vol. IV.

[46] G. M. Sheldrick, *SHELXS 86: Structure Solving Program*, University of Göttingen, Germany, **1986**.

[47] G. M. Sheldrick, *SHELXL 93: Crystal Structure Refinement*, University of Göttingen, Germany, **1993**.

Received March 2, 2004
Early View Article
Published Online August 12, 2004

 © 2004 Wiley-VCH Verlag GmbH & Co. KGaA, Weinheim

Synthesis, X-ray Structural Analysis and Spectroscopic Investigations (IR and ^{31}P MAS NMR) of Mixed Barium/Strontium Fluoroapatites

Abdallah Aissa,[a] Béchir Badraoui,[a] René Thouvenot,*[b] and Mongi Debbabi*[a]

Keywords: Barium / IR spectroscopy / NMR spectroscopy / Strontium / X-ray diffraction

Continuous solid solutions of barium/strontium fluoroapatites $Ba_{(10-x)}Sr_x(PO_4)_6F_2$ ($Ba_{(10-x)}Sr_xFAp$; $0 \leq x \leq 10$) were obtained in an aqueous medium. They were investigated by Rietveld structure-refinement methods using powder X-ray diffraction patterns and by chemical analysis, IR spectroscopy and ^{31}P MAS NMR spectroscopy. Replacement of barium by strontium induces a regular decrease of the lattice constants *a* and *c* according to Vegard's law. The results of the powder-fitting structure refinements indicate a clear preference of strontium for the S(1) site of the apatitic structure. A high-wavenumber shift of the IR absorption bands characteristic of PO_4 internal modes is also observed, in agreement with the diminution of the ionic character of the M–O bonds. For increasing strontium content, a regular δ_{iso} increase is shown in the ^{31}P MAS NMR spectra, from $\delta = 0.91$ ppm for $Ba_{10}FAp$ to $\delta = 3.06$ ppm for $Sr_{10}FAp$. For all mixed Ba/Sr fluoroapatites, the low intensities of the spinning bands reflect the weak ^{31}P chemical-shift anisotropy, in agreement with the low distortion of the PO_4 tetrahedron, as shown by Rietveld refinement.
(© Wiley-VCH Verlag GmbH & Co. KGaA, 69451 Weinheim, Germany, 2004)

Introduction

Apatite is a general name for a large family of isomorphous compounds, with the structure belonging basically to the hexagonal space group $P6_3/m$.[1] The general chemical formula is $M_{10}(XO_4)_6Y_2$, where M corresponds to a divalent cation such as Ca^{2+}, Sr^{2+}, Ba^{2+}, Cd^{2+}, or Pb^{2+}, XO_4 is a trivalent anion, essentially PO_4^{3-}, VO_4^{3-} or AsO_4^{3-}, and Y a monovalent anion, like OH^-, F^-, Cl^-, Br^-.[2,3] Furthermore, M^{2+} may be partially replaced by mono- or trivalent cations (Na^+, K^+, Al^{3+}, ...) and XO_4^{3-} may be replaced by tetravalent anions like SiO_4^{4-} and divalent anions like CO_3^{2-} and SO_4^{2-}.

The natural fluoroapatite, $Ca_{10}(PO_4)_6F_2$, is considered as a good structural model for apatitic compounds.[1] The Ca^{2+} cations are located in two nonequivalent crystallographic sites (Figure 1). In each unit cell four Ca(1) atoms, located on the threefold axis, are coordinated by six oxygen atoms as nearest neighbors belonging to the PO_4 group. The site S(1), occupied by Ca(1) atoms, is 4f (symmetry C_3). The other six Ca(2) atoms in the unit cell are coordinated by six oxygen atoms from the PO_4 tetrahedra and by one F^- ion located on the sixfold axis. The site S(2), occupied by Ca(2), is 6h (symmetry C_s). This structure can accommodate a variety of substitutions which affect the physicochemical properties of the materials. In particular, ionic substitutions are involved in dental and bone pathologies, bioceramics for bone implants, pollution by phosphate fertilizers, ion-exchange ability for water treatment and radioactive-waste confinement, as well as in catalytic and luminescent properties.[4,5]

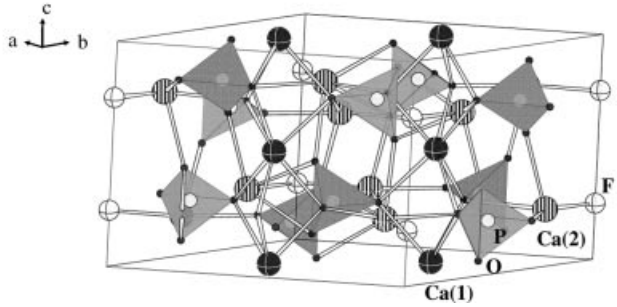

Figure 1. Perspective view of $Ca_{10}(PO_4)_6F_2$ structure

Fluoroapatites are known for the divalent metals Ca, Sr, Ba and Pb,[6–8] and dicationic systems of Sr-, Cd-, and Pb-substituted Ca fluoroapatites have been widely investigated.[9–11] For these systems the limit of miscibility may be correlated to the relative properties of the metals (polarisability, electronegativity and essentially cationic

[a] Laboratoire de Physico-chimie des Matériaux, Ecole Nationale d'Ingénieurs de Monastir,
5019 Monastir, Tunisia
Fax: (internat.) + 216-73-500-514
E-mail: mngdbb@enim.rnu.tn
[b] Laboratoire de Chimie Inorganique et Matériaux Moléculaires, UMR CNRS 7071,
Case courrier 42, Université Pierre et Marie Curie, 75252 Paris Cedex05, France
Fax: (internat.) + 33-1-44273841
E-mail: rth@ccr.jussieu.fr
Supporting information for this article is available on the WWW under http://www.eurjic.org or from the authors.

 © 2004 Wiley-VCH Verlag GmbH & Co. KGaA, Weinheim **DOI: 10.1002/ejic.200400224**

Table 1. Fractional atomic coordinates and equivalent thermal parameters, after Rietveld refinement, for the mixed Ba/Sr fluoroapatites (e.s.d. in parentheses)

$Ba_{(10-x)}Sr_xFAp$	Atom	x	y	z	B [Å^2]
Ba_{10} [a]	M(1)	0.3333	0.6667	0.0003(3)	0.4434
	M(2)	0.2391(2)	0.9806(1)	0.2500	0.4859
	P	0.3983(4)	0.3665(5)	0.2500	0.2044
	O(1)	0.341(2)	0.486(3)	0.2500	1.0306
	O(2)	0.576(1)	0.462(3)	0.2500	1.1393
	O(3)	0.339(3)	0.268(1)	0.087(1)	1.7448
	F	0.0000	0.0000	0.2981(7)	2.6703
$Ba_{9.01}Sr_{0.99}$ [b]	M(1)	0.3333	0.6667	0.0017(3)	0.4340
	M(2)	0.2382(1)	0.9800(2)	0.2500	0.4756
	P	0.4016(5)	0.3699(4)	0.2500	0.2001
	O(1)	0.346(2)	0.487(3)	0.2500	1.0086
	O(2)	0.573(3)	0.459(2)	0.2500	1.1148
	O(3)	0.341(2)	0.269(4)	0.089(1)	1.7079
	F	0.0000	0.0000	0.2562(5)	2.6127
$Ba_{6.92}Sr_{3.08}$ [c]	M(1)	0.3333	0.6667	−0.0017(6)	0.4075
	M(2)	0.2364(1)	0.9806(2)	0.2500	0.4471
	P	0.4085(8)	0.3758(6)	0.2500	0.1882
	O(1)	0.351(4)	0.491(3)	0.2500	0.9480
	O(2)	0.583(5)	0.455(2)	0.2500	1.0419
	O(3)	0.346(3)	0.271(2)	0.089(4)	1.6113
	F	0.0000	0.0000	0.2493(6)	2.4345
$Ba_{5.05}Sr_{4.95}$ [d]	M(1)	0.3333	0.6667	−0.0006(4)	0.3992
	M(2)	0.2363(2)	0.9803(1)	0.2500	0.4382
	P	0.4096(6)	0.3769(4)	0.2500	0.1844
	O(1)	0.352(1)	0.494(3)	0.2500	0.9290
	O(2)	0.584(1)	0.454(2)	0.2500	1.0198
	O(3)	0.345(3)	0.271(1)	0.089(1)	1.5802
	F	0.0000	0.0000	0.2521(2)	2.3811
$Ba_{2.92}Sr_{7.08}$ [e]	M(1)	0.3333	0.6667	−0.0025(6)	0.3909
	M(2)	0.2378(2)	0.9863(1)	0.2500	0.4293
	P	0.4038(5)	0.3711(6)	0.2500	0.1807
	O(1)	0.341(3)	0.487(2)	0.2500	0.9100
	O(2)	0.586(3)	0.465(4)	0.2500	0.9974
	O(3)	0.342(2)	0.275(5)	0.084(3)	1.5478
	F	0.0000	0.0000	0.2500	2.3267
$Ba_{1.03}Sr_{8.97}$ [f]	M(1)	0.3333	0.6667	−0.0009(2)	0.3705
	M(2)	0.2382(3)	−0.0162(2)	0.2500	0.4072
	P	0.4017(6)	0.3701(4)	0.2500	0.1714
	O(1)	0.337(1)	0.486(2)	0.2500	0.8629
	O(2)	0.582(1)	0.461(3)	0.2500	0.9433
	O(3)	0.345(2)	0.264(1)	0.079(3)	1.4720
	F	0.0000	0.0000	0.2487(5)	2.1975
Sr_{10} [g]	M(1)	0.3333	0.6667	−0.0008(4)	0.3636
	M(2)	0.2391(1)	0.9848(1)	0.2500	0.3996
	P	0.3980(5)	0.3663(3)	0.2500	0.1682
	O(1)	0.332(2)	0.482(2)	0.2500	0.8469
	O(2)	0.580(1)	0.462(1)	0.2500	0.9251
	O(3)	0.344(3)	0.262(2)	0.073(3)	1.4455
	F	0.0000	0.0000	0.2514(3)	2.1542

[a] a = 10.1611(2) Å, c = 7.7322(1) Å, R_p = 5.3, R_{Wp} = 6.9. The pattern R factor, R_p, is defined as $R_p = 100\{|Y_{oi} - Y_{ci}|/Y_{oi}\}$. The weighted pattern R factor, R_{Wp}, is defined as $R_{Wp} = 100\{W_i(Y_{oi} - Y_{ci})^2/W_i(Y_{oi})^2\}^{1/2}$. [b] a = 10.1074(3) Å, c = 7.6896(2) Å, R_p = 3.9, R_{Wp} = 5.4. [c] a = 10.0562(5) Å, c = 7.5939(5) Å, R_p = 5.6, R_{Wp} = 7.4. [d] a = 9.9288(5) Å, c = 7.4893(6) Å, R_p = 3.6, R_{Wp} = 4.7. [e] a = 9.8581(6) Å, c = 7.3590(4) Å, R_p = 6.5, R_{Wp} = 7.2. [f] a = 9.7636(3) Å, c = 7.3258(1) Å, R_p = 3.6, R_{Wp} = 4.9. [g] a = 9.7211(2) Å, c = 7.2869(1) Å, R_p = 5.1, R_{Wp} = 8.4.

size).[12,13] The lattice parameters of these mixed apatites decrease with increasing content of the smaller metal cation, and in the case of the Ca/Sr and Ca/Pb systems the results of powder pattern fitting refinement indicate a clear preference of Ca^{2+} for the site S(1) of the apatitic structure. On the contrary, for Ca/Cd fluoroapatites, the smaller Cd^{2+} cations prefer the S(2) site; this can be explained by a good affinity of cadmium to fluorine. To the best of our knowledge, no other mixed divalent-metal fluoroapatites have been reported.

In this paper we report the synthesis in aqueous medium and the chemical analysis of a continuous series of mixed strontium/barium fluoroapatites; the results of powder fitting structure refinement are discussed in relation with the spectroscopic data (IR and ^{31}P MAS NMR).

Results

X-ray Analysis

The results of X-ray diffraction pattern identification for all products $Ba_{(10-x)}Sr_x(PO_4)_6F_2$ (hereafter $Ba_{(10-x)}Sr_xFAp$; $0 \leq x \leq 10$) indicate that the samples are constituted of a single apatitic phase.

The structural analysis by Rietveld methods for seven samples gave the following formulae: $Ba_{10}FAp$, $Ba_{9.01}Sr_{0.99}FAp$, $Ba_{6.92}Sr_{3.08}FAp$, $Ba_{5.05}Sr_{4.95}FAp$, $Ba_{2.92}Sr_{7.08}FAp$, $Ba_{1.03}Sr_{8.97}FAap$ and $Sr_{10}FAp$. The results of the refined structural parameters for these samples are reported in Table 1. The stoichiometry of these samples is close to that of the synthesis and agrees very well with the chemical analysis (Table 2). Therefore, to simplify, from now onwards the samples will be named as $Ba_{(10-x)}Sr_xFAp$ where x corresponds to the stoichiometry of the synthesis.

The progressive replacement of barium by strontium leads to a slight decrease in the crystallographic parameters a and c; the variations are linear and obey Vegard's law[14] according to the following Equations.

$a = (10.173 - 0.045x)$ Å; $\sigma(a) = 4.5 \times 10^{-2}$ Å
$c = (7.726 - 0.045x)$ Å; $\sigma(c) = 2.3 \times 10^{-2}$ Å
$V = (691.4 - 9.6x)$ Å^3; $\sigma(V) = 0.7$ Å^3

As a typical comparison between the observed and calculated profiles the final plot for Ba_5Sr_5FAp is displayed in Figure 2.

The structural refinement shows that strontium occupies both the S(1) and S(2) sites of the apatitic structure. However, the occupancy in S(1) is always higher than expected from the statistical distribution, as shown in Figure 3 and in Table 3.

The bond lengths and angles for the two metal environments, obtained by DIAMOND,[15] and the distortion indexes of the phosphate tetrahedron calculated by Baur relations,[16] are reported in Table 4. The M−M, M−O, and M(2)−F distances decrease with increasing strontium content and the distortion indexes of the mixed phases are slightly larger than those of the limiting phases.

 © 2004 Wiley-VCH Verlag GmbH & Co. KGaA, Weinheim

Table 2. Strontium substitution (atom-%) in mixed Ba/SrFAp (e.s.d. in parentheses)

$Ba_{(10-x)}Sr_xFAp$	Sr(1)/[Sr(1) + Ba(1)]	Sr(1)/[Sr(1) + Sr(2)]	Sr(2)/[Sr(2) + Ba(2)]	Sr/(Sr + Ba)[a]	Sr/(Sr + Ba)[b]
$Ba_{9.01}Sr_{0.99}FAp$	21.9(2)	88.0(2)	1.9(1)	9.9(2)	9.2(5)
$Ba_{6.92}Sr_{3.08}$ FAp	67.22(2)	84.4(3)	8.3(3)	30.8(4)	31.2(2)
$Ba_{5.05}Sr_{4.95}FAp$	81.0(3)	65.3(5)	28.5(5)	49.5(1)	48.5(1)
$Ba_{2.92}Sr_{7.08}$ FAp	90.5(3)	51.1(3)	57.7(4)	70.8(2)	71.6(5)
$Ba_{1.03}Sr_{8.97}FAp$	97.7(1)	43.5(2)	84.4(5)	89.7(2)	91.8(1)

[a] Rietveld refinement. [b] Chemical analysis.

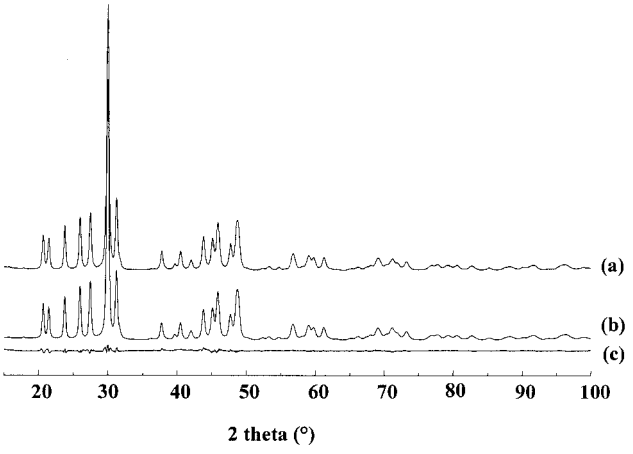

Figure 2. Comparison of the observed [curve (a)] and calculated [curve (b)] powder-diffraction patterns of Ba_5Sr_5FAp; curve (c) is the difference profile

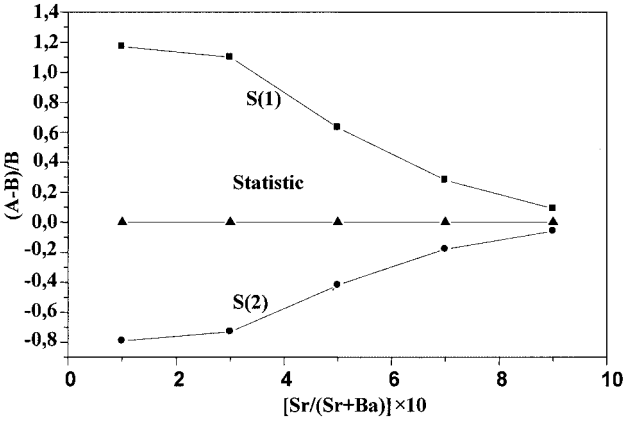

Figure 3. Distribution of strontium between the S(1) and S(2) crystallographic sites

Infrared Absorption Spectroscopy

The infrared spectra of the mixed fluoroapatites present the characteristic absorption bands (stretching and bending) of the PO_4^{3-} group and a band at about 300 cm^{-1} assigned to an M_3-F "ν_3-type stretching "of the 2[M_3-F] sublattice.[17] All IR data are displayed in Table 5 and two typical spectra are presented in the Supporting Information. The progressive replacement of the barium ions by strontium induces a regular shift of all the absorption bands towards greater wavenumbers (Figure 4). Furthermore there is a splitting of the ν_3-[M_3-F] band into two or three components; this effect is markedly pronounced for the intermediate phases, from Ba_6Sr_4FAp to Ba_1Sr_9FAp.

^{31}P Solid-State NMR Analysis

The ^{31}P MAS NMR spectra of the whole series of mixed Ba-SrFAp's are depicted in Figure 5 and the data are given in Table 6. For increasing Sr content, the isotropic signal (δ_{iso}) shows a regular shift towards high frequency between the two limiting phases $Ba_{10}FAp$ (δ_{iso} = 0.91 ppm) and $Sr_{10}FAp$ (δ_{iso} = 3.06 ppm; Figure 6). The low intensity of the spinning side bands (SSB) even at low spinning rate (2 kHz) indicates low chemical-shift anisotropy (CSA) of the phosphorus nucleus; this prevents the determination of the chemical shift tensor components by the classical analysis of the SSB intensity.[18]

As for the Sr/Pb hydroxyapatite system, only one isotropic signal is observed whatever the strontium content. However, for the mixed phases this signal appears complex and contains many components. Despite the weak amplitude of variation of δ_{iso}, numeric simulation allows the decomposition of the isotropic resonance into separate signals, corresponding to different phosphate environments (Figure 7). For the phases with low content of either Sr or Ba (x = 1, 8, 9), the decomposition allows the evaluation of

Table 3. Refinement occupancy compared with the statistic distribution for strontium in the two metal sites S(1) and S(2) of Ba/Sr fluoroapatites

$Ba_{10-x}Sr_xFAp$	Refinement distribution (A)		Statistic distribution (B)		(A − B/B)	
	S(1)	S(2)	S(1)	S(2)	S(1)	S(2)
Ba_9Sr_1FAp	0.87	0.12	0.40	0.59	+1.17	−0.79
Ba_7Sr_3FAp	2.59	0.49	1.23	1.85	+1.10	−0.73
Ba_5Sr_5FAp	3.23	1.72	1.98	2.97	+0.63	−0.42
Ba_3Sr_7FAp	3.62	3.46	2.83	4.25	+0.28	−0.18
Ba_1Sr_9FAp	3.90	5.07	3.59	5.38	+0.09	−0.06

 © 2004 Wiley-VCH Verlag GmbH & Co. KGaA, Weinheim

Table 4. Bond lengths, bond angles and PO_4 tetrahedron distortion indices in mixed Ba/Sr fluoroapatites (e.s.d. in parentheses)

	Ba_{10}FAp	Ba_9Sr_1FAp	Ba_7Sr_3FAp	Ba_5Sr_5FAp	Ba_3Sr_7FAp	Ba_1Sr_9FAp	Sr_{10}FAp
P−O(1)	1.57(4)	1.54(4)	1.54(3)	1.53(1)	1.55(2)	1.55(3)	1.54(1)
P−O(2)	1.55(5)	1.50(3)	1.49(6)	1.51(5)	1.52(3)	1.53(1)	1.53(2)
P−O(3)(*)	1.53(5)	1.52(4)	1.53(4)	1.52(3)	1.52(4)	1.53(5)	1.53(2)
P−O mean	1.55	1.52	1.52	1.52	1.53	1.53	1.53
O(1)−O(2)	2.51(5)	2.45(1)	2.53(5)	2.53(4)	2.41(6)	2.53(1)	2.51(2)
O(1)−O(3)(*)	2.53(2)	2.50(2)	2.49(3)	2.49(5)	2.53(7)	2.53(2)	2.52(8)
O(2)−O(3)(*)	2.55(1)	2.49(4)	2.46(2)	2.47(3)	2.49(3)	2.48(3)	2.49(1)
O(3)−O(3)	2.51(1)	2.46(6)	2.44(1)	2.41(1)	2.48(2)	2.49(6)	2.52(6)
O−O mean	2.53	2.48	2.48	2.47	2.49	2.51	2.51
O(1)−P−O(2)	107.1(2)	107.1(2)	111.2(4)	112.2(2)	112.(1)	110.6(5)	109.2(2)
O(1)−P−O(3)(*) (×2)	109.1(2)	109.4(4)	108.1(2)	109.3(2)	108.4(1)	110.4(5)	110.3(1)
O(2)−P−O(3)(*)	110.9(6)	111.2(1)	110.8(6)	109.5(1)	110.1(2)	108.3(4)	108.2(2)
O(3)−P−O(3)	109.5(7)	108.4(5)	106.8(2)	104.9(4)	107.0(3)	108.7(2)	110.6(3)
O−P−O mean	109.4	109.4	109.3	109.2	109.4	109.4	109.5
DI(P−O)	0.0084	0.007	0.010	0.006	0.007	0.003	0.0018
DI(O−P−O)	0.0047	0.007	0.010	0.011	0.012	0.008	0.0083
DI(O−O)	0.0096	0.010	0.015	0.013	0.013	0.009	0.0036
M(1)−O(1)(*) (×3)	2.69(2)	2.68(4)	2.59(2)	2.61(5)	2.55(3)	2.56(1)	2.56(2)
M(1)−O(2)(*)	2.73(3)	2.73(4)	2.67(5)	2.56(6)	2.59(1)	2.56(4)	2.57(6)
M(1)−O(3)(*)	3.13(3)	3.11(5)	3.08(5)	3.01(3)	2.99(2)	2.92(1)	2.91(3)
M(1)−O mean	2.85	2.84	2.78	2.72	2.71	2.68	2.68
M(2)−O(1)	2.91(1)	2.92(6)	2.93(1)	2.94(3)	2.82(5)	2.79(6)	2.75(2)
M(2)−O(2)	2.64(2)	2.65(2)	2.67(3)	2.66(3)	2.54(6)	2.55(4)	2.52(4)
M(2)−O(3) (*)	2.70(7)	2.71(2)	2.72(5)	2.65(5)	2.58(2)	2.54(2)	2.50 (3)
M(2)−O(3) (*)	2.86(2)	2.85(3)	2.85(6)	2.79(2)	2.78(4)	2.70(1)	2.68 (2)
M(2)−O mean	2.78	2.78	2.79	2.75	2.68	2.63	2.61
M(2)−F	2.53	2.51	2.47	2.45	2.41	2.41	2.40
M(2)−M(2)	4.39(1)	4.35(6)	4.30(2)	4.24(4)	4.18(1)	4.17(3)	4.16(2)
M(1)−M(2)	4.23(5)	4.20(1)	4.18(1)	4.14(2)	4.10(6)	4.08(6)	4.07(8)
M(1)−M(1)	3.87(2)	3.82(4)	3.77(2)	3.75(4)	3.67(5)	3.65(4)	3.63(5)

(*) Replicated by symmetry: $DI(PO)=\frac{(\sum_{i=1}^{4}|PO_i-PO_m|)}{4PO_m}$; $DI(OO)=\frac{(\sum_{i=1}^{6}|OO_i-OO_m|)}{6OO_m}$; $DI(OPO)=\frac{(\sum_{i=1}^{6}|OPO_i-OPO_m|)}{6OPO_m}$

Table 5. Infrared band positions [cm^{-1}] for mixed Ba/Sr fluoroapatites

Sample	ν_1	ν_2	ν_3	ν_4	ν_3 (M_3−F)
Ba_{10}FAp	934	444	1005, 1026, 1055	553, 573, 581	293
Ba_9Sr_1FAp	936	445	1007, 1034, 1059	554, 571, 582	295
Ba_7Sr_3FAp	939	448	1010, 1053, 1067	555, 573, 584	301
Ba_6Sr_4FAp	941	450	1013, 1055, 1071	556, 574, 586	301, 307
Ba_5Sr_5FAp	943	451	1015, 1057, 1073	557, 576, 588	301, 309
Ba_4Sr_6FAp	943	453	1016, 1061, 1074	558, 578, 588	297, 312
Ba_3Sr_7FAp	945	455	1018, 1063, 1076	559, 579, 589	301, 322
Ba_2Sr_8FAp	947	456	1019, 1065, 1077	559, 579, 590	304, 314, 322
Ba_1Sr_9FAp	948	457	1022, 1067, 1078	560, 581, 592	291, 314
Sr_{10}FAp	951	458	1026, 1069, 1080	561, 582, 594	322

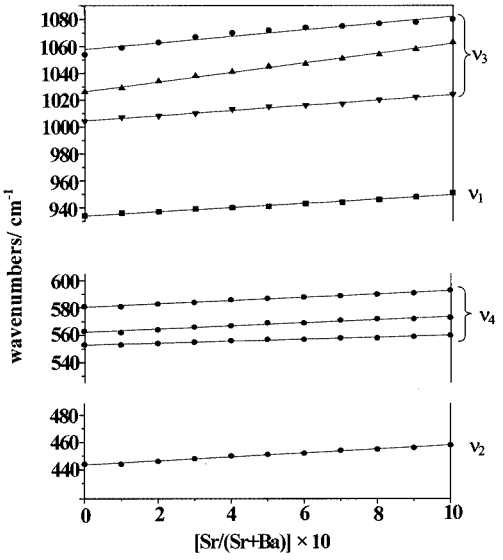

Figure 4. Evolution of the wavenumbers of the PO_4 IR absorption modes as a function of the strontium content

the respective populations of the phosphate sites (Table 7).

For all compositions, the static ^{31}P NMR spectra are quite symmetric, as can be seen in a typical plot (Figure 8); they exhibit a pseudo-Gaussian shape with full width at half maximum (fwhm) of about 14 ppm. The shape of the static spectrum is likely essentially determined by dipolar ^{31}P-^{19}F interactions.

Discussion

The results of this study indicate that the small difference between the cationic radius of Ba^{2+} (1.48 Å) and Sr^{2+} (1.32 Å)[19] allows the formation of a continuous solid solution of barium and strontium fluoroapatites. The replacement of barium in the apatitic structure by the smaller strontium cation induces, as expected, a linear decrease of the lattice

 © 2004 Wiley-VCH Verlag GmbH & Co. KGaA, Weinheim

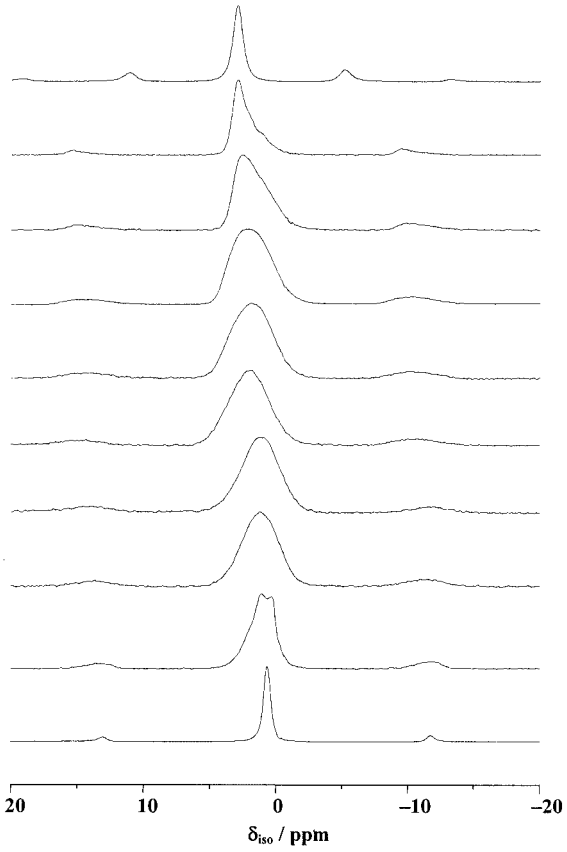

Figure 5. Part of the 162 MHz ^{31}P MAS spectra of the monocationic and mixed Ba/Sr fluoroapatites, showing only the isotropic signal and the spinning side bands; from bottom to top: $Ba_{10}FAp$ (spinning rate R_0 = 2 kHz, number of scans N_s = 1056), Ba_9Sr_1FAp (R_0 = 2 kHz, N_s = 104), Ba_7Sr_3FAp (R_0 = 2 kHz, N_s = 112), Ba_6Sr_4FAp (R_0 = 2 kHz, N_s = 80), Ba_5Sr_5FAp (R_0 = 2 kHz, N_s = 80), Ba_4Sr_6FAp (R_0 = 2 kHz, N_s = 88), Ba_3Sr_7FAp (R_0 = 2 kHz, N_s = 560), Ba_2Sr_8FAp (R_0 = 2 kHz, N_s = 64), Ba_1Sr_9FAp (R_0 = 2 kHz, N_s = 80), $Sr_{10}FAp$ (R_0 = 1.3 kHz, N_s = 272)

Table 6. ^{31}P solid-state NMR spectroscopic data for mixed Ba/Sr fluoroapatites

Samples	δ_{iso} [ppm]	$\Delta_{1/2}$ [ppm]	$\Delta_{1/2static}$ [ppm]
$Ba_{10}FAp$	0.91	0.65	13.5
Ba_9Sr_1FAp	1.2	1.85	14.82
Ba_7Sr_3FAp	1.73	3.18	14.49
Ba_6Sr_4FAp	2.01	3.30	13.81
Ba_5Sr_5FAp	2.2	3.47	13.54
Ba_4Sr_6FAp	2.44	3.61	14.04
Ba_3Sr_7FAp	2.61	3.52	14.75
Ba_2Sr_8FAp	2.83	3.07	14.08
Ba_1Sr_9FAp	2.87	1.90	13.74
$Sr_{10}FAp$	3.06	0.92	12.87

parameters. Despite the variation in the cell dimensions there are no dramatic distortions of the PO_4 tetrahedron (Table 4). The geometry of the phosphate anions remains regular (quasi T_d symmetry) with only small variations over the whole series.

Structural refinements by the Rietveld method show that the Sr^{2+} ions are distributed between the two crystallographic sites S(1) and S(2), with a strong preference for the smaller site S(1). This is particularly marked for low Sr concentrations (Figure 3). Moreover, as the metal−metal distances, determined for $Ba_{10}FAp$, differ markedly for the two types of metallic sites [Ba(1)−Ba(1) = 3.87 Å and Ba(2)−Ba(2) = 4.39 Å] the S(1) sites appear more suitable to accommodate small cations. Furthermore, in $Ba_{10}FAp$ the fluorine atom is shifted to the z position close to 0.3, whereas it is about 0.25 for all solid solutions. This displacement can be related to the sole presence of larger cations (Ba^{2+}) at the S(2) site and the weak affinity of the soft acid Ba^{2+} for the hard base F^-.

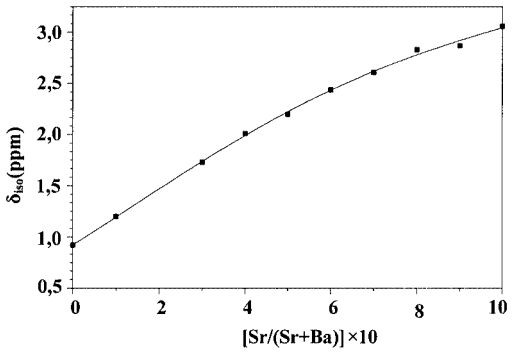

Figure 6. Variation of δ_{iso} as a function of Sr content

The infrared spectra of all mixed fluoroapatites are very similar, especially with respect to the phosphate bands. In particular, the splitting of the triply degenerate ν_3 and ν_4 bands and the intensity of the infrared-inactive bands (for T_d symmetry) ν_1 and ν_2 remain nearly constant over the whole series, in agreement with the minor geometrical perturbations of the PO_4 group (see above). Increasing the strontium content leads, however, to an increase of the frequencies of the PO_4 vibrational modes, and there is a quasi-linear variation of all wavenumbers with the strontium atomic ratio x (Figure 4). As noted by Fowler, who studied pure Ca and Sr hydroxyapatites, this might be due to increased anion−anion repulsions concomitant with decreased lattice dimensions,[17] and also by the higher covalency of the P−O bonds resulting from increased ionicity of the M−O bonds.[13]

According to Fowler,[17] the low-wavenumber bands around 300 cm^{-1} may be assigned to a "ν_3-type stretching" of the M_3−F unit. The multiplicity of these ν_3-[M_3−F] bands observed in the mixed phases can be explained by the various F^- environments — FBa_3, FBa_2Sr, $FBaSr_2$ and FSr_3 — and also by loss of the degeneracy of this E mode by symmetry lowering (D_{3h} to C_{2v}) through metal substitution. This splitting is observed only for the compositions between Ba_6Sr_4FAp and Ba_1Sr_9FAp, when the sites S(2) are significantly occupied by both cations according to the Rietveld refinements (15% Sr/85% Ba for Ba_6Sr_4FAp and 84% Sr/16% Ba in Ba_1Sr_9FAp). Outside this composition range, there is almost exclusively one symmetrical fluorine environment, either FBa_3 or FSr_3, which explains the single ν_3-[M_3−F] absorption band. Two relevant spectra, for

 © 2004 Wiley-VCH Verlag GmbH & Co. KGaA, Weinheim

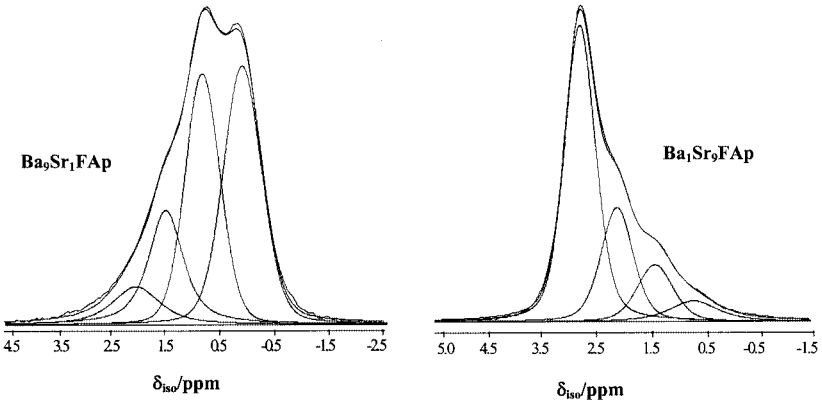

Figure 7. Linefit analysis of the isotropic signal for Ba_9Sr_1FAp and Ba_1Sr_9FAp

Table 7. Relative populations of the various phosphorus environments for Ba_9Sr_1, Ba_2Sr_8 and Ba_1Sr_9 fluoroapatites, from ^{31}P NMR MAS spectra line-fitting analysis

Phosphorus environment	Ba_9Sr_1FAp [a]	[b]	δ_{iso}	Ba_2Sr_8FAp [a]	[b]	δ_{iso}	Ba_1Sr_9FAp [a]	[b]	δ_{iso}
PBa_9	38.74	38	0.21	*	*		*	*	
PBa_8Sr_1	38.74	39	0.90	*	*		*	*	
PBa_7Sr_2	17.22	18	1.52	*	*		*	*	
PBa_6Sr_3	4.46	5	2.25	*	*		*	*	
PBa_5Sr_4	*	*		*	*		*	*	
PBa_4Sr_5	*	*		6.61	7.84	0.86	*	*	
PBa_3Sr_6	*	*		17.62	18.72	1.12	4.46	4	0.45
PBa_2Sr_7	*	*		30.20	29.72	1.98	17.22	18	1.46
PBa_1Sr_8	*	*		30.20	29.93	2.32	38.74	40	2.05
PSr_9	*	*		13.42	13.78	2.98	38.74	38	3.04

[a] Relative amount (%) from statistical formula. [b] Relative amount (%) from line-fitting analysis.

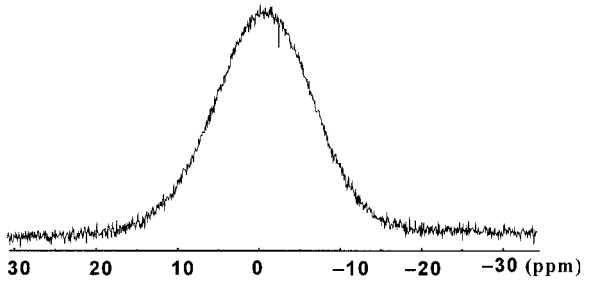

Figure 8. 162 MHz ^{31}P solid-state NMR static spectrum of Ba_5Sr_5FAp

Ba_4Sr_6FAp (38% Sr/Ba 62%) and Ba_5Sr_5FAp (28% Sr/Ba 72%), are given as Supporting Information.

Let us now consider the ^{31}P solid-state MAS NMR results. Solid-state MAS ^{31}P NMR spectra of phosphate compounds generally present a central resonance at δ_{iso} associated with a spinning side-band pattern, characteristic of the chemical shift anisotropy (CSA) of the phosphorus nucleus. In the present case the spectra of all fluoroapatites exhibit low-intensity spinning side-bands, even at moderate spinning rates (Figure 5). This corresponds to a very small CSA interaction, in agreement with the structural analysis, which shows a regular geometry of the phosphate anion for all species (see above).

The limiting phases Ba_{10}FAp and Sr_{10}FAp exhibit a single isotropic resonance, at δ = 0.91 and 3.06 ppm, respectively, in agreement with the equivalence of all phosphate groups in the apatitic structure. For the mixed Ba/Sr fluoroapatites there is a monotonic shift of the position of the isotropic resonance as a function of the strontium content (Figure 6). This regular deshielding of the P nucleus may be correlated to the regular contraction of the lattice parameters.[20]

The variation of δ_{iso} between Ba_{10}FAp and Sr_{10}FAp ($\Delta\delta$ = 2.15 ppm, ca. 350 Hz) is very weak compared to the linewidth of the isotropic signal of these phases (100 and 150 Hz, respectively). Therefore, contrary to what was observed in the Cd/Pb hydroxyapatites system,[21] the isotropic signals associated to different environments of phosphate ions are not resolved in the experimental spectra of the mixed phases. Actually, the ^{31}P resonances of the Ba/Sr fluoroapatites appear as relatively broad signals due to the distribution of the ^{31}P chemical shifts (Figure 5, Table 6). For the phases with low content of either metal — i.e. for x = 1, 8 and 9 — the isotropic resonance has an asymmetrical shape and may be easily decomposed into individual components by using the DOMFIT program.[18] For this analysis we considered that the ^{31}P chemical shift is primarily determined by the cationic environments of the phosphate groups.[22] In the apatitic structure, the phosphorus atoms display nine O−M contacts (Scheme 1). For the nine oxygen−metal contacts around each P atom, neglecting the incidence of the relative positions of Ba and Sr, one expects therefore 10 different P environments, noted $PBa_{(9-y)}Sr_y$ (y = 0, 1, ..., 9). Their relative proportions, which depend on the composition of the apatitic phase, are calculated according to

$$p[PBa_{(9-y)}Sr_y] = C_9^y (p_{Ba})^{(9-y)} (p_{Sr})^y$$

where

$$C_9^y = \frac{9!}{y!(9-y)!}$$

 © 2004 Wiley-VCH Verlag GmbH & Co. KGaA, Weinheim

is the binomial coefficient, and p_{Ba} and p_{Sr} are the atomic fractions of Ba and Sr, respectively (Supporting Information). Considering that P environments with less than about 5% abundance would not contribute to the ^{31}P isotropic signal, we can nicely simulate the spectra of Ba_9Sr_1FAp and Ba_1Sr_9FAp with four components (Figure 7). The decomposition of the isotropic signals for these phases give populations of the PO_4 environments close to the statistic weight obtained from their chemical composition (Table 7). From Figure 7, it appears that the linewidth of the individual $PBa_{(9-y)}Sr_y$ resonances increases as y increases (or decreases) towards 0.5. Moreover for "reverse" compositions, strontium-rich environments give broader resonances than their barium-rich analogues (compare Figure 7, right and left). Actually, according to Scheme 1, each $PBa_{(9-y)}Sr_y$ motif corresponds to various slightly different P environments, depending on the relative positions of Ba and Sr in the metallic sites. This may result in subtle variations in ^{31}P chemical shifts and finally in a broader signal than for the single environments PBa_9 and PSr_9. Of course, maximal broadening is expected for the PBa_5Sr_4 and PBa_4Sr_5 motifs. For small y values, corresponding to barium-rich samples, preferential location of strontium at S(1) leads to less-numerous $PBa_{(9-y)}Sr_y$ environments than for the reverse composition $PBa_ySr_{(9-y)}$.

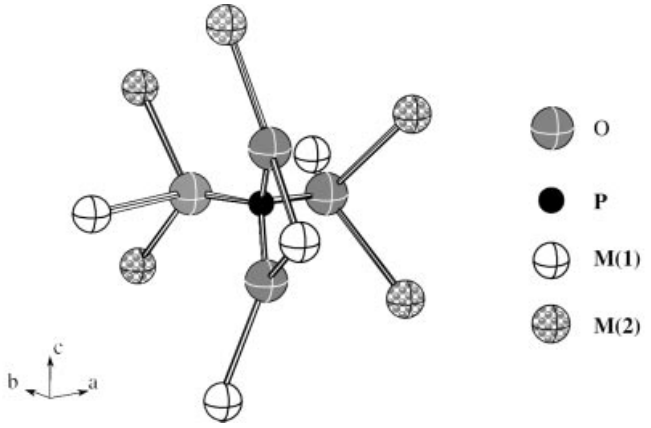

Scheme 1. The cationic environment of the phosphate group in apatitic structure

A more puzzling observation is that the individual lines of the various $PBa_{(9-y)}Sr_y$ motifs shifts more strongly through Ba/Sr substitution (up to 1 ppm, Table 7) than the experimentally observed isotropic signal (mean value of the shift about 0.2 ppm, Table 6 and Figure 6).

Moreover, whereas $\delta_{iso}(PSr_9)$ remains nearly constant (within the accuracy) in Ba_2Sr_8FAp (+2.98 ppm), Ba_1Sr_9FAp (+3.04 ppm) and $Sr_{10}FAp$ (+3.06 ppm), PBa_9 in Ba_9Sr_1FAp (+0.21 ppm, Table 7) is significantly shielded with respect to the same motif in the "pure" phase $Ba_{10}FAp$ (+0.91 ppm, Table 6). Even more surprisingly, PBa_3Sr_6 (in Ba_1Sr_9FAp) and PBa_4Sr_5 (in Ba_2Sr_8FAp) are shielded with respect to PBa_9 in $Ba_{10}FAp$. From all these observations it appears that the ^{31}P isotropic chemical shifts (and linewidths) of the $PBa_{(9-y)}Sr_y$ environments depend significantly on the composition of the apatitic phase; therefore the δ_{iso} values reported in Table 7 cannot be transferred for further simulations.

At variance with the hydroxyapatites,[23] the full width at half maximum ($\Delta\nu_{1/2}$) for the static signal does not change significantly throughout the whole series (14 ± 1 ppm, Table 6). As the P−F dipolar interaction is likely the dominant interaction, the quasi-invariance of $\Delta\nu_{1/2}$ for fluoroapatites shows that the P−F dipolar interaction does not vary when substituting Sr for Ba, in agreement with the P−F distances remaining always of the order of 3.7 Å. By contrast, for hydroxyapatites of space group $P6_3/m$ the statistical orientation of the OH^- ions gives different P−H distances and therefore different dipolar P−H interactions.

Conclusions

Barium strontium fluoroapatites form a continuous series of solid solutions. Structure refinements indicate a clear preference of strontium for the S(1) site of the apatitic structure. Despite the weak amplitude of variation of δ_{iso}, decomposition of the isotropic ^{31}P MAS-NMR resonance into separate signals, corresponding to different phosphate environments, was done for the phases with low content of either Sr or Ba.

Experimental Section

Synthesis: All chemicals, $Ba(CH_3CO_2)_2$, $Sr(NO_3)_2$, NH_4F, and $(NH_4)_2HPO_4$ were of reagent grade (Prolabo, 99% purity) and used without further purification. The mixed barium and strontium fluoroapatites $Ba_{(10-x)}Sr_xFAp$, with x ranging from 0 to 10, were obtained by a double decomposition method.[24,25] This method consists of the preparation in aqueous medium from a solution containing the two metallic cations (A) and a solution of phosphate and ammonium fluoride (B). Concentrations of the solutions in barium, strontium and phosphate ions correspond to the stoichiometry of the desired apatite. A mixture of barium acetate and strontium nitrate, with a total concentration of metal cations of 0.2 M (solution A, 250 mL) and 0.2 M ammonium dihydrogen phosphate solution (solution B, 150 mL) were prepared. Solution A was added dropwise to solution B, maintained at boiling temperature, under nitrogen. The pH of the slurry was maintained at approximately 11 by regular addition of small amounts of ammonia (d = 0.89; 28% aqueous solution). The resulting solid phase was kept in contact with the mother solution at boiling temperature for 1 h. The precipitate was then filtered, washed with hot distilled water, dried at 100 °C for 12 h and calcined at 500 °C for 4 h to improve its crystallinity. The compounds thus obtained were submitted to XRD, chemical analysis, IR spectroscopy and ^{31}P MAS NMR analyses.

Chemical Analyses and Instrumental Methods: Barium and strontium contents were determined with a Perkin−Elmer 3110 atomic absorption spectrophotometer. Phosphorus was determined colorimetrically as phosphovanadomolybdate, by measurement of its absorbance at 430 nm.[26] Fluorine content was determined by potent-

 © 2004 Wiley-VCH Verlag GmbH & Co. KGaA, Weinheim

iometry, using an ionometer equipped with a fluoride-specific electrode, at ambient temperature and a pH of about 6. The support electrolyte was a 1 M aqueous solution of sodium citrate. The crystallographic data were collected with a Philips PW1710 diffractometer equipped with a copper anode and a graphite monochromator. The investigated range was from 15 to 100° (2θ), with a step of 0.03° and a counting time of 15 s for each step. IR spectra were obtained from KBr pellets (1 mg sample and 300 mg KBr) with a Bio-Rad FTS 6000 IRFT spectrophotometer in the range 4000−200 cm^{-1}, with a spectral resolution of 4 cm^{-1}. The NMR experiments were performed on powdered samples at room temperature with a Bruker MSL400 spectrometer (9.4 T) operating at 162 MHz. A Doty probehead equipped with 4-mm (diameter) rotors was used for MAS spinning rates up to 6.5 kHz. The spinning rate was monitored by a Bruker pneumatic unit, allowing the control of bearing and drive-inlet air pressure. The spectral width was 45 kHz (280 ppm). The spectra were acquired using a simple one-pulse sequence with phase cycling (CYCLOPS sequence). Pulse duration was 1 μs, (15° flip angle) and the preacquisition and interpulse delays were 22 μs and 5 s, respectively. The 4 K free-induction decay was zero-filled to the size of 8 K and convoluted with an exponential function (exponential multiplication) using a 10-Hz line-broadening factor. The final digital resolution of the spectrum was 10 Hz (0.07 ppm). A better digital resolution, for more accurate determination of the isotropic chemical shifts (±0.05 ppm), was obtained after 16 K zero-filling and no window function. Chemical shifts are reported with respect to external 85% H_3PO_4 in the IUPAC convention, i.e. positive δ corresponds to a resonance at higher frequency (deshielding) than the reference.

Structural Analysis: Rietveld-method crystal-structure refinements from the powder diffraction data were carried out with the DBWS-9411 program.[27,28] The space group ($P6_3/m$) and the atomic positions of the $Ba_{10}(PO_4)_6F_2$ structure were used as starting data in the refinement. First of all, the scale factor and the background coefficients were refined. The peaks were fitted with a "pseudo-Voigt" function. The half-width of the diffraction peaks as a function of 2θ was evaluated by the Caglioti equation.[29] Successively, the pattern parameters (true 2θ zero, peak widths and their dependence on 2θ, asymmetry parameter, preferred orientation parameter) and the lattice parameters were allowed to vary. Finally, the structural parameters (occupancy factor, atomic coordinates) were refined. No constraint was imposed on the overall strontium content. The two sites S(1) and S(2) were imposed to be fully and complementarily occupied by barium and strontium. The occupancy factors of O and P were assumed as constant, in agreement with the apatite stoichiometry. The fractional atomic coordinates were refined starting from the atomic positions of the two metals. No attempt was made to differentiate the barium positions from strontium ones. Rietveld refinement was performed in several stages, the parameters obtained in each stage being deferred in the following. In the last refinement cycles, all 29 parameters were released. Then, the refined parameters were used as initial model for apatite with barium content immediately lower, and so on. The results of the refinement structural parameters (atomic positions, anisotropic thermal parameters, lattice parameters, reliability pattern factors R_p and weighted factors R_{Wp}) are reported in Table 1, while a comparison between the calculated and observed profiles of Ba_5Sr_5FAp is reported in Figure 2. Table 4 gives interatomic distances and distortion indices of phosphate tetrahedron. The strontium-ion distribution between the two sites and chemical analysis results are gathered in Table 2.

Equivalent thermal parameters

$$B_{eq} = \sum_i \sum_j \beta_{ij} (\vec{a}.\vec{b})$$

are calculated by the relation[30]

$$B_{eq} = 4(a^2\beta_{11} + b^2\beta_{22} + c^2\beta_{33} + ab\beta_{12}\cos(\gamma)/3$$

Further details of the crystal-structure investigation may be obtained from the Fachinformationszentrum Karlsruhe, 76344 Eggenstein-Leopoldshafen, Germany, on quoting the depository number CSD-414240.

Supporting Information (see footnote on the first page of this article): Table giving the relative (theoretical) proportions (%) of $PM_{(9-y)}M'_y$ environments as a function of x in the mixed apatites $M_{(10-x)}M'_x(PO_4)_6F_2$ [or $M_{(10-x)}M'_x(PO_4)_6(OH)_2$] (pale-blue background for proportions higher than 4%); Figure giving infrared spectra of Ba_5Sr_5FAp (top) and Ba_4Sr_6FAp (bottom).

Acknowledgments

We greatly acknowledge financial support from the Direction Générale de la Recherche Scientifique et Technique (Tunisie) and the Centre National de la Recherche Scientifique (France) in the frame of a bilateral join project. NMR measurements were performed at the NMR facility center (SIARE) of the Université Pierre et Marie Curie (Paris).

[1] M. I. Kay, R. A. Young, A. S. Posner, *Nature* **1964**, *204*, 1050−1052.
[2] D. McDonnel, *Apatite, Its Crystal Chemistry, Mineralogy, Utilization, and Geologic and Biologic Occurrences*, Springer, New York, N. Y., **1973**.
[3] G. Wright, G. Montel, *C. R. Acad. Sci., Paris* **1969**, *268C*, 2077−2080, *Chem. Abstr.* **1969**, *71*, 56134.
[4] P. Fourman, P. Royer, *Calcium et tissu osseux − Biologie et pathologie*, Flammarion, Paris, **1970**.
[5] T. Suzuki, Y. Hayakawa, *1st International Congress on Phosphorus Compounds*, Rabat, October 17−21, **1977**, p. 381.
[6] E. L. Belokoneva, E. A. Troneva, L. N. Dem′yanets, N. G. Duderov, N. V. Belov, *Kristallografiya* **1982**, *27*, 793−794; *Chem. Abstr.* **1982**, *97*, 118469.
[7] E. R. Kreidler, F. A. Hummel, *Am. Mineral.* **1970**, *55*, 170−184.
[8] M. Mathew, I. Mayer, B. Dickens, L. W. Schroeder, *J. Solid State Chem.* **1979**, *28*, 79−95.
[9] I. Khattech, M. Jemal, *Thermochim. Acta* **1997**, *298*, 23−30.
[10] A. Nounah, J. L. Lacout, *J. Solid State Chem.* **1993**, *107*, 444−451.
[11] I. Ntahomvukiye, I. Khattech, M. Jemal, *Ann. Chim. (Paris)* **1997**, *22*, 435−446; *Chem. Abstr.* **1998**, *128*, 42893.
[12] A. Hamad, B. Badraoui, M. Debbabi, *J. Soc. Chim. Tunisie* **2003**, *5*, 115−124.
[13] A. Aissa Hamad, B. Badraoui, M. Debbabi, *J. Soc. Alger. Chim.* **2003**, *13*, 131−140.
[14] L. Vegard, *Z. Phys.* **1922**, *9*, 395−410.
[15] K. Brandenburg, *DIAMOND*, Crystal Structure Information System, version 1.2, **1997**.
[16] W. H. Baur, *Acta Crystallogr., Sect. B* **1974**, *30*, 1195−1215.
[17] B. O. Fowler, *Inorg. Chem.* **1974**, *13*, 207−214.
[18] D. Massiot, F. Fayon, M. Capron, I. King, S. Le Calvé, B.

 © 2004 Wiley-VCH Verlag GmbH & Co. KGaA, Weinheim

Alonso, J.-O. Durand, B. Bujoli, Z. Gan, G. Hoatson, *Magn. Reson. Chem.* **2002**, *40*, 70−76.
[19] R. D. Shannon, *Acta Crystallogr., Sect. A* **1976**, *32*, 751−767.
[20] M. T. Weller, G. Wong, *J. Chem. Soc., Chem. Commun.* **1988**, 1103−1104.
[21] B. Badraoui, A. Bigi, M. Debbabi, M. Gazzano, N. Roveri, R. Thouvenot, *Eur. J. Inorg. Chem.* **2001**, 1261−1267.
[22] S. Aime, G. Digilio, R. Gobetto, A. Bigi, A. Ripamonti, N. Roveri, M. Gazzano, *Inorg. Chem.* **1996**, *35*, 149−154.
[23] B. Badraoui, A. Bigi, M. Debbabi, M. Gazzano, N. Roveri, R. Thouvenot, *Eur. J. Inorg. Chem.* **2002**, 1864−1870.
[24] A. Bigi, M. Gazzano, A. Ripamonti, E. Foresti, N. Roveri, *J. Chem. Soc., Dalton Trans.* **1986**, 241−244.
[25] A. Bigi, G. Falini, E. Foresti, M. Gazzano, A. Ripamonti, N. Roveri, *J. Inorg. Biochem.* **1993**, *49*, 69−78.
[26] K. P. Quinlan, M. A. De Sesa, *Anal. Chem.* **1955**, *27*, 1626−1629.
[27] H. M. Rietveld, *J. Appl. Crystallogr.* **1969**, *2*, 65−71.
[28] R. A. Young, A. Sakthivel, T. S. Moss, C. O. Paiva-Santos, *J. Appl. Crystallogr.* **1995**, *28*, 366−367.
[29] G. Caglioti, A. Paoletti, F. P. Ricci, *Nucl. Instrum.* **1958**, *3*, 223−228.
[30] M. Hata, K. Okada, S. Iwai, *Acta Crystallogr., Sect. B* **1978**, *34*, 3062−3064.

Received March 21, 2004
Early View Article
Published Online August 13, 2004

 © 2004 Wiley-VCH Verlag GmbH & Co. KGaA, Weinheim

Two Copper(II) Complexes Built from a Novel Redox-Active Bipyridinium Dimer Ligand and Oxalate Anions: Synthesis, Crystal Structure and Magnetic Properties

Yan-Qiong Sun,[a] Jie Zhang,*[a] Jing-Lin Chen,[a] and Guo-Yu Yang[a]

Keywords: Copper(II) / Bipyridium dimer / Oxalate / X-ray diffraction

The synthesis of a novel V-shaped redox-active bipyridinium dimer ligand, 2,6-bis(4′-pyridyl-1′-pyridiniumyl)pyrazine (**Bpypr**) dichloride and its copper complexes, (H_2**Bpypr**)[$Cu_2(C_2O_4)_4$] (**1**) and {[(**Bpypr**)$Cu_2(C_2O_4)_3$-$(H_2O)_2$]·$5H_2O$}$_n$ (**2**), are described. Single-crystal X-ray diffraction studies confirm that complex **1** contains one V-shaped H_2**Bpypr** cation and two essentially planar [$Cu(C_2O_4)_2$]$^{2-}$ anions, which participate in two hydrogen bonds through the two N–H moieties. Complex **2** has a 1D zigzag chain structure composed of [$Cu_2(C_2O_4)_3$]$^{2-}$ units bridged by V-shaped **Bpypr** cations. The magnetic study revealed the occurrence of a weak ferromagnetic interaction within the dinuclear copper unit of complex **2**.

(© Wiley-VCH Verlag GmbH & Co. KGaA, 69451 Weinheim, Germany, 2004)

Introduction

In recent years, the design and synthesis of metal-organic coordination polymers has attracted considerable attention in supramolecular chemistry and crystal engineering,[1−5] because these supramolecular assemblies have interesting structures as well as potentially useful properties such as magnetic, catalytic, and nonlinear optical activities or electrical conductivity, amongst others.[6−9] A developing strategy in this field is to build supramolecular arrays by use of polynuclear coordination complexes as the secondary architectural units, which introduces the appealing possibility of constructing porous materials[10,11] and molecular-scale wires.[12,13] In order to produce defined architectures and interesting functions in a controlled fashion, careful selection of the metal ions, peripheral ligands and modular bridging ligands is required.[14] At present, most of the systems studied are composed of molecular subunits, containing metal ions coordinated to appropriate ligands, and which are linked by extended bridging spacers such as alkanes, alkynes, or polycyclic aromatic groups. The geometry and photoelectrochemical properties of the assemblies are generally controlled by the presence of a polynuclear coordination complex.[15−17] Currently, not many bridging ligands with electrochemical and photochemical properties are available. Bipyridinium dimers, as derivatives of the viologens, exhibit photoelectrochemical activity and a change of spin multiplicity upon external stimulus.[18−20] Their terminal N-donor atoms and π-conjugated system can provide various coordination modes and structural motifs, which enable construction of versatile molecular assemblies and incorporation of optical, electronic and magnetic properties. In this paper, we report the design and synthesis of a novel V-shaped bipyridinium dimer bridging ligand (Scheme 1), 2,6-bis(4′-pyridyl-1′-pyridiniumyl)-pyrazine dichloride (**Bpypr**Cl_2), which exhibits two-step electrochemical reduction processes and photochemical activity. Two new copper complexes (H_2**Bpypr**)[$Cu_2(C_2O_4)_4$] (**1**) and {[(**Bpypr**)$Cu_2(C_2O_4)_3(H_2O)_2$]·$5H_2O$}$_n$ (**2**), possessing quite different architectures despite use of the same starting materials, were obtained by molecular self-assembly.

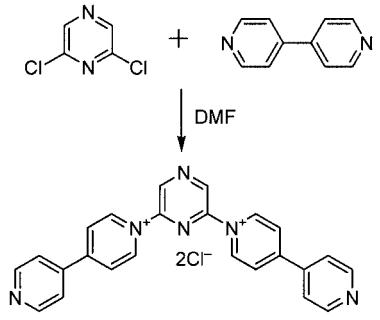

Scheme 1

[a] State Key Laboratory of Structural Chemistry, Fujian Institute of Research on the Structure of Matter, Chinese Academy of Sciences,
Fuzhou, Fujian 350002, China
Fax: (internat.) + 86-591-379-2871
E-mail: zhangjie@fjirsm.ac.cn

Supporting information for this article is available on the WWW under http://www.eurjic.org or from the author.

Results and Discussion

Redox and Photochemical Properties of the $BpyprCl_2$ Ligand

The electrochemical behavior of the **Bpypr**Cl_2 ligand was investigated by cyclic voltammetry in a 0.1 M acetonitrile solution of $(Bu_4N)PF_6$. The two-step quasi-reversible electron-transfer processes occurring at $E_{1/2} = -0.271$ V and -0.419 V vs. Ag^+/Ag, respectively, correspond to the first and second reduction of the **Bpypr**Cl_2 ligand. The photochemical activity of **Bpypr**Cl_2 was investigated spectrochemically in methanol solution. Under illumination with a 350-W xenon lamp, the absorption band of the ligand at 310 nm decreases in intensity and undergoes a slight blue-shift, while a new broad band appears between 400 to 600 nm, characteristic for the generation of photoinduced radicals.[21]

Structural Description

X-ray diffraction analysis reveals that complex **1** contains one V-shaped H_2**Bpypr** cation and two essentially planar $[Cu(C_2O_4)_2]^{2-}$ anions (Figure 1). Each cupric cation is coordinated by four oxygen atoms from two oxalate anions to give a square-planar geometry. The bond lengths of Cu−O range from 1.913(5) Å to 1.950(5) Å and the bond angles of O−Cu−O range from 85.3(2)° to 95.7(2)°. The H_2**Bpypr** ligand, with a two-fold axis passing through N(4) and N(3) atoms, is slightly twisted between the pyrazine ring and adjacent pyridyl rings, while the bipyridyl unit is close to planarity with a small dihedral angle of 7.82(25)°. Two $[Cu(C_2O_4)_2]^{2-}$ anions and one H_2**Bpypr** cation are involved in hydrogen-bonding interactions, having appropriate distances and orientation for N(1)−H(1)···O(7) [2.763(9) Å] and N(1)−H(1)···O(8) [3.012(9) Å], leading to the formation of a V-shaped dimer. These V-shaped dimers are cross-packed to yield an extended rhombic motif along the *a* axis, with $[Cu(C_2O_4)_2]^{2-}$ anions sitting in the center of the rhombus (Figure 2). No specific π−π stacking interactions are identifiable between N-heterocyclic rings.

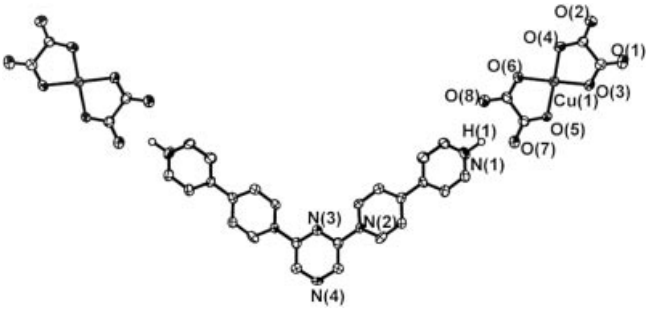

Figure 1. ORTEP drawing (50% probability level) with atom-numbering scheme of complex **1**, $(H_2Bpypr)[Cu_2(C_2O_4)_4]$, showing the local coordination environment of Cu^{II}; all hydrogen atoms are omitted for clarity with the exception of H(1) on the nitrogen atom

Complex **2** possesses a one-dimensional zigzag chain structure composed of $[Cu_2(C_2O_4)_3]^{2-}$ units bridged alternately by V-shaped **Bpypr** cations. As shown in Figure 3,

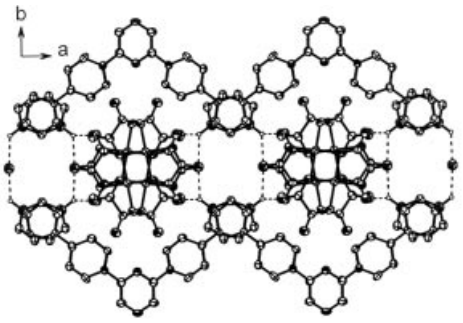

Figure 2. Packing structure for complex **1**, $(H_2$**Bpypr**$)[Cu_2(C_2O_4)_4]$, viewed along the *c* axis; all hydrogen atoms are omitted for clarity with the exception of H(1) on the nitrogen atom

the crystallographically independent copper ion has an elongated octahedral geometry with the equatorial plane defined by one nitrogen atom of the **Bpypr** ligand [Cu−N: 2.026 (5) Å] and three oxalate oxygen atoms [average Cu−O: 1.961(5) Å], with the axial sites occupied by one water molecule [Cu−O 2.618(7) Å] and one oxygen atom from a centrosymmetric bridging oxalate [Cu−O 2.334(6) Å]. The bridging oxalato ligand is almost planar, with an inversion center lying in the middle of the C−C bond. The C−O bond lengths are not equivalent [1.241(8) Å, 1.283(9) Å], and those involving axial coordination are shorter. The **Bpypr** ligand, with a two-fold axis passing through N(4) and N(3) atoms, shows a nonplanar configuration. The two adjacent pyridyl rings are twisted by 16.35(52)° with respect to each other, while the dihedral angle between the pyrazine ring and the neighboring pyridyl ring is 18.61(57)°.

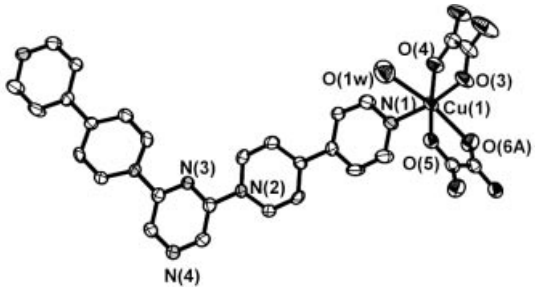

Figure 3. ORTEP drawing (50% probability level) with atom numbering scheme of complex **2**, $\{[($**Bpypr**$)Cu_2(C_2O_4)_3(H_2O)_2]\cdot 5H_2O\}_n$, showing the local coordination environment of Cu^{II}; the H atoms are omitted for clarity; atom labels having "A" refer to symmetry-generated atoms

The bridging oxalate ligand coordinates to a central-symmetry-related Cu^{II} ion in bis(bidentate) fashion to give the dinuclear $[Cu_2(C_2O_4)_3]^{2-}$ ions as a secondary building unit. The Cu−Cu′ distance across the oxalate ion is 5.581(2) Å, within the range observed in dinuclear Cu^{II} complexes containing oxalate bridges in an asymmetrical bis(bidentate) coordination between the two metal centers.[22,23] V-shaped **Bpypr** cations link the $[Cu_2(C_2O_4)_3]^{2-}$ dinuclear units to form polymeric chains running along the *c* axis of the unit cell (Figure 4). These chains are stacked on top of each other along [101] to yield a subunit motif consisting of

 © 2004 Wiley-VCH Verlag GmbH & Co. KGaA, Weinheim

alternate rhombic sheets with a plum-blossom-like configuration. The rhombic sheets are held together further by hydrogen bonds between the terminal oxygen atoms of the uncoordinated oxalate and water molecules [O···O = 2.627(24)−3.098(27) Å], resulting in a three-dimensional supramolecular network.

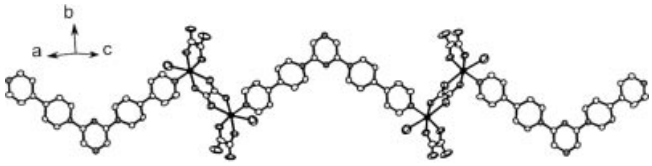

Figure 4. Zigzag chain of complex **2**, $\{[(\mathbf{Bpypr})Cu_2(C_2O_4)_3(H_2O)_2]\cdot 5H_2O\}_n$

Thermogravimetric Analysis

The thermal stabilities of the two complexes were determined by thermogravimetric analysis (TGA) under a flow of N_2. The TGA curve for **1** shows an initial weight loss of 65.23% from 40 °C to 455 °C which corresponds well to the loss of one H_2**Bpypr** cation and two oxalate anions per formula unit (calcd. 65.22%). Above 455 °C, the residual oxalate ion of complex **1** decomposes completely and the sample converts to cupric oxide above 800 °C. The TGA curve for **2** displays a three-step weight loss process. The initial weight loss of 10.31% between 50 and 120 °C corresponds to the loss of five uncoordinated water molecules per formula unit (calculated: 9.92%). The second weight loss of 50.14% is observed from 120 to 385 °C, and is attributed to the removal of two coordinated water molecules, one $\mathbf{Bpypr}^{2+}$ cation and one CO molecule (from incomplete decomposition of an oxalate anion) per formula unit (calculated: 50.07%). Above 385 °C, the residual oxalate ion of complex **2** starts to decompose and the sample converts to cupric oxide at 720 °C (residual CuO, calculated: 17.53%; found 17.38%).

Electron Spin Resonance Spectroscopy

X-band powder ESR spectra of complex **1** and **2** at room temperature show broad axial signals at $g_{\|} = 2.1527$, $g_{\perp} = 2.0792$ ($g_{av} = 2.1163$) for **1**, and $g_{\|} = 2.2816$, $g_{\perp} = 2.0747$ ($g_{av} = 2.1806$) for **2**, corresponding basically to a $d_{x^2-y^2}$ ground state for the Cu^{II} ion (inverted type with $g_{\|} > g_{\perp} > 2.0$). The g values are similar to those expected for the CuO_4 chromophores of **1** with a square-planar-type geometry around the copper ion, and for those $CuNO_3O_2'$ chromophores of **2** where the copper atom is in a very elongated octahedral environment.

Magnetic Behavior

The temperature dependence of the magnetic susceptibilities was measured in the temperature range 300 to 5 K in an applied field of 10 kOe. Figure 5 shows the magnetic behavior of complex **2** in the form of the $\chi_M T$ product (χ_M is the molar magnetic susceptibility per two Cu^{II} ions) versus temperature. At room temperature, $\chi_M T$ is 0.87 $cm^3\cdot K\cdot mol^{-1}$, in agreement with the expected spin-only value for two magnetically dilute Cu^{II} centers with $S = 1/2$ ($g = 2.15$). With decreasing temperature, the $\chi_M T$ value steadily increases attaining a value of 0.99 $cm^3\cdot K\cdot mol^{-1}$ at 5 K. This behavior suggests a weak ferromagnetic interaction between the Cu^{II} ions, which is further confirmed by a positive Weiss constant ($\theta = +1.16$ K). In order to evaluate the exchange interaction between neighbouring Cu^{II} atoms, the variable-temperature susceptibility data were analyzed using Equation (1) derived[24] from the Heisenberg isotropic spin Hamiltonian ($H = -JS_1\cdot S_2$), for two coupled $S = 1/2$ ions, given by the Bleaney−Bowers expression for a dinuclear Cu^{II} compound. The interaction between adjacent dinuclear units in the 1D chain was considered in molecular-field approximation; J is the intradimer coupling constant between Cu^{II} ions, zJ' is the interdimer magnetic exchange, treated in the molecular field approximation. A best fit, which affords the solid line in Figure 5, was obtained with values of $g = 2.15$, $J = 3.86\ cm^{-1}$, $zJ' = -0.28\ cm^{-1}$. The agreement factor R, defined as $\Sigma[(\chi_M)_{obsd.} - (\chi_M)_{calcd.}]^2/\Sigma(\chi_M)^2_{obsd.}$, is equal to 5.73×10^{-6}. The positive J value demonstrates a ferromagnetic coupling between the two Cu^{II} ions.

$$\chi_M = 2Ng^2\beta^2[kT - 2zJ'/(3 + \exp(-J/kT))]^{-1}[3 + \exp(-J/kT)]^{-1} \quad (1)$$

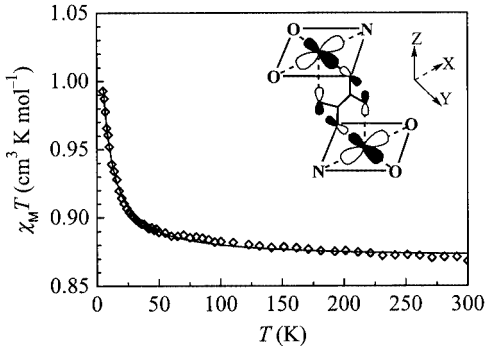

Figure 5. The temperature dependences of the product $\chi_M T$ (diamonds) for complex **2**, $\{[(\mathbf{Bpypr})Cu_2(C_2O_4)_3(H_2O)_2]\cdot 5H_2O\}_n$; the solid line corresponds to the best theoretical fit; the inset shows a model depicting the magnetic interaction in the oxalate-bridged Cu^{II} complex **2**

The complex **2** exhibits an elongated octahedral geometry, with the unpaired electron around each metal center described by a magnetic orbital of the $d_{x^2-y^2}$ type pointing toward the three oxalato oxygen atoms and one pyridyl nitrogen atom of the equatorial plane, which is perpendicular to the oxalate bridge. This situation corresponds to the coordination mode shown in the inset of Figure 5. Due to a poor overlap between the axial oxalato oxygen orbital and the metal $d_{x^2-y^2}$ orbital, a ferromagnetic coupling dominates the magnetic properties of the Cu dinuclear unit of complex **2**. The magnitude of the coupling observed is in the same range as several reported examples.[25,26]

 © 2004 Wiley-VCH Verlag GmbH & Co. KGaA, Weinheim

Conclusion

A novel V-shaped redox-active bipyridinium dimer ligand, 2,6-bis(4′-pyridyl-1′-pyridiniumyl)pyrazine (**Bpypr**) dichloride has been designed and synthesized. Two new copper complexes, $(H_2$**Bpypr**$)[Cu_2(C_2O_4)_4]$ (**1**) and $\{[($**Bpypr**$)Cu_2(C_2O_4)_3(H_2O)_2]\cdot 5H_2O\}_n$ (**2**), were obtained by assembling the **Bpypr**Cl_2 ligand with $(NH_4)_2Cu(C_2O_4)_2$. The 1-D zigzag chain of **2** is composed of $[Cu_2(C_2O_4)_3]^{2-}$ units bridged by V-shaped **Bpypr** cations in an alternating fashion. The variant assembly modes of **Bpypr** ligand with $(NH_4)_2Cu(C_2O_4)_2$ provide a great potential for construction of multifunctional organic-inorganic hybrid materials and for the observation of important structure-property relationships. More physical properties and further assemblies of the **Bpypr** ligand with other anionic donors is in progress.

Experimental Section

General Remarks: All chemicals were used as purchased without purification except those used for electrochemical measurements. The ^{1}H NMR spectrum was recorded with a Varian Unity 500 MHz spectrometer. IR spectra were measured as KBr pellets with a Bomem BM102 FT-IR in the range 400−4000 cm^{-1}. The elemental analyses were determined using a Vario EL III CHNOS elemental analyzer. Thermogravimetric data were collected with a Mettler Toledo TGA/SDTA 851^e analyzer under a stream of nitrogen at a heating rate of 5 °C/min. ESR spectra were recorded with a Bruker ER-420 spectrometer at the X-band frequency. Variable-temperature magnetic susceptibilities were measured from 300 K to 5 K with an applied field strength of 10 KOe using a Quantum Design MPMS-7 magnetometer. Diamagnetic corrections were estimated from Pascal's constants. Photochemistry of the samples in KBr pellets was investigated using a 350-W Xenon lamp. The cyclic voltammogram was obtained by use of a Perkin-Elmer potentiostat/galvanostat model 263A in 1 mM acetonitrile solution containing 0.1 M $(Bu_4N)PF_6$ as supporting electrolyte at a scan rate of 100 $mV\cdot s^{-1}$. Platinum and glassy graphite were used as working and counter electrodes, respectively. Potentials were referenced to Ag/AgCl.

Preparation of the BpyprCl$_2$ Ligand: A mixture of 4,4′-bipy(3.12 g, 20 mmol) and 2,6-dichloropyrazine (1.47 g, 10 mmol) was dissolved in 8 mL of DMF. After stirring at 120 °C under nitrogen for 4 h, the solution was concentrated to a small volume under reduced pressure. Then an excess of hot benzene was added and the precipitate was collected by filtration, washed with hot benzene and dried in vacuo to afford a pale yellow powder (1.62 g, 35.3%). ^{1}H NMR ($CDCl_3$, 500MHz): δ = 8.12 (d, 4 H), 8.85 (d, 4 H), 8.89 (d, 4 H), 9.88 (d, 4 H), 9.92 (s, 2 H) ppm. IR (KBr): $\tilde{\nu}$ = 3478 (s), 3413 (s), 3118 (w), 3033 (w), 1634 (vs), 1597 (m), 1557 (m), 1463 (w), 1438 (s), 1412 (s), 1347 (w), 1281 (m), 1263 (m), 1212 (m), 1161 (w), 1019 (m), 866 (m), 821 (s), 754 (m), 718 (m), 637 (w), 619 (w), 538 (w), 501 (m) cm^{-1}.

Synthesis of $(H_2$Bpypr$)[Cu_2(C_2O_4)_4]$ (1): A mixture of **Bpypr**Cl_2 (102.2 mg, 0.2 mmol) and $CuCl_2$ (34 mg, 0.2 mmol) was dissolved in water. The resulting solution was layered with an H_2O/DMSO (5:1, v/v) solution (20 mL) of $(NH_4)_2Cu(C_2O_4)_2$ (55.1 mg, 0.2 mmol) in a 1:1 ratio in a straight glass tube. Black-green prism crystals were obtained by slow interface diffusion after a few days. Yield 11%. IR (KBr): $\tilde{\nu}$ = 3556 (m), 3454 (m), 3114 (w), 3037 (w), 1707 (w), 1652 (vs), 1431 (s), 1415 (m), 1378 (s), 1278 (m), 1241 (m), 1201 (m), 1007 (m), 818 (m), 792 (m), 551 (w), 497 (m) cm^{-1}. $C_{32}H_{20}Cu_2N_6O_{16}$ (871.62): calcd. C 44.10, H 2.31, N 9.64; found C 43.76, H 1.86, N 9.54.

Synthesis of $\{[($Bpypr$)Cu_2(C_2O_4)_3(H_2O)_2]\cdot 5H_2O\}_n$ (2): A mixture of **Bpypr**Cl_2 (102.2 mg, 0.2 mmol) and $CuCl_2$ (34 mg, 0.2 mmol) was dissolved in water. The resulting solution was layered with an H_2O/DMSO (5:1, v/v) solution (20 mL) of $(NH_4)_2Cu(C_2O_4)_2$ (55.1 mg, 0.2 mmol) in a 1:1 ratio in a straight glass tube. Green needle crystals were obtained by slow interface diffusion after a few days. Yield 32%. IR (KBr): $\tilde{\nu}$ = 3416 (s), 3121 (w), 3038 (w), 1691 (vs),

Table 1. Crystallographic data for complexes **1** and **2**

	1	**2**
Empirical formula	$C_{32}H_{20}Cu_2N_6O_{16}$	$C_{30}H_{32}Cu_2N_6O_{19}$
Formula mass	871.62	907.70
Crystal system	monoclinic	monoclinic
Space group	*C*2/*c*	*C*2/*c*
T [K]	293	293
a [Å]	12.5637(5)	15.6288(6)
b [Å]	18.3206(8)	19.8960(1)
c [Å]	12.9832(3)	12.7179(5)
β [°]	116.49(1)	90.436(2)
V [Å^3]	2988.32(19)	3507.97(19)
Z	4	4
$D_{calcd.}$ [$g\cdot cm^{-3}$]	1.937	1.719
μ [mm^{-1}]	1.523	1.307
F(000)	1760	1856
Goodness-of-fit on F^2	1.069	1.099
Reflections collected/unique	4329/2466 [*R*(int) = 0.0505]	5279 / 3031 [*R*(int) = 0.0446]
Data/restraints/parameters	2466/0/258	3031 / 0 / 272
R_1/wR_2 [$I > 2\sigma(I)$]	0.0730/0.1453	0.0649/0.1597
R_1/wR_2 (all data)	0.1088/0.1660	0.1183/0.2091
Largest difference peak and hole	0.671 and −0.608 e·Å^{-3}	0.566 and −0.454 e·Å^{-3}

$R1 = \Sigma||F_o| - |F_c||/\Sigma|F_o|$. $wR2 = \{\Sigma[w(F_o^2 - F_c^2)^2]/\Sigma[w(Fo^2)^2]\}^{1/2}$ where $w = 1/[\sigma^2(F_o^2) + (AP)^2 + BP]$, with A = 0.0444 (**1**) and 0.1077 (**2**), B = 41.3993 (**1**) and 9.3117 (**2**), $P = (F_o^2 + 2F_c^2)/3$.

 © 2004 Wiley-VCH Verlag GmbH & Co. KGaA, Weinheim

Table 2. Selected bond lengths [Å] and angles [°] for **1** and **2**

Complex **1**			
Cu(1)−O(4)	1.913(5)	Cu(1)−O(5)	1.936(5)
Cu(1)−O(3)	1.934(5)	Cu(1)−O(6)	1.950(5)
O(4)−Cu(1)−O(3)	85.6(2)	O(3)−Cu(1)−O(5)	95.7(2)
O(4)−Cu(1)−O(6)	93.3(2)	O(5)−Cu(1)−O(6)	85.3(2)
O(4)−Cu(1)−O(5)	177.4(2)	O(3)−Cu(1)−O(6)	178.8(2)
Complex **2**			
Cu(1)−O(4)	1.959(5)	Cu(1)−N(1)	2.026(5)
Cu(1)−O(3)	1.958(5)	Cu(1)−O(6)#1	2.334(6)
Cu(1)−O(5)	1.965(5)	Cu(1)−O1W	2.618(7)
O(4)−Cu(1)−O(3)	83.6(2)	O(5)−Cu(1)−O(6)#1	77.11(19)
O(3)−Cu(1)−O(5)	89.4(2)	N(1)−Cu(1)−O(6)#1	94.7(2)
O(4)−Cu(1)−N(1)	94.5(2)	O(4)−Cu(1)−O(6)#1	103.1(2)
O(5)−Cu(1)−N(1)	86.7(2)	O(3)−Cu(1)−O(6)#1	94.8(2)

Symmetry transformations used to generate equivalent atoms: #1: $-x + 1/2, -y + 1/2, -z + 1$.

1636 (s), 1432 (s), 1413 (s), 1298 (m), 1289 (m), 1208 (m), 1011 (m), 822 (m), 798 (m), 717 (w), 555 (w), 499 (m) cm^{-1}. $C_{30}H_{32}Cu_2N_6O_{19}$ (907.70): calcd. C 39.70, H 3.55, N 9.26; found C 39.25, H 3.27, N 9.09.

X-ray Crystallography: Data sets for **1** and **2** were collected at room temperature using a Siemens SMART CCD diffractometer with graphite-monochromated Mo-K_α (λ = 0.71073 Å) radiation in the ω- and φ-scanning mode. An empirical absorption correction was applied using the SADABS program. The structures were solved by direct methods and refined by full-matrix least-squares on F^2 using the SHELXTL-97 program package.[27] All hydrogen atoms were generated geometrically (C−H = 0.93 Å) with the exception of the hydrogen atoms of all free water molecules and H(1) of **1**. H(1) of **1** was located in the difference Fourier map and its position and isotropic displacement parameters were refined. The crystallographic data for complexes **1** and **2** are listed in Table 1. Selected bond lengths and angles are shown in Table 2. CCDC-220468 (**1**) and -220467 (**2**) contain the supplementary crystallographic data for this paper. These data can be obtained free of charge at www.ccdc.cam.ac.uk/conts/retrieving.html [or from the Cambridge Crystallographic Data Centre, 12 Union Road, Cambridge CB2 1EZ, UK; Fax: (internat.) + 44-1223-336-033; E-mail: deposit@ccdc.cam.ac.uk].

Acknowledgments

The authors thank the National Natural Science Foundation of China (No. 20201010/50372069), the Ministry of Personnel of China, and the Natural Science Foundation of Fujian Province for financial support. The authors are also grateful to Prof. Zhong-Ning Chen for electrochemical measurements.

[1] H. J. Choi, M. P. Suh, *J. Am. Chem. Soc.* **1998**, *120*, 10622−10628.
[2] A. K. Cheetham, G. Férey, T. Loiseau, *Angew. Chem. Int. Ed.* **1999**, *38*, 3268−3292.
[3] D.-L. Long, A. J. Blake, N. R. Champness, M. Schröder, *Chem. Commun.* **2000**, 1369−1370.
[4] C. Janiak, *Dalton Trans.* **2003**, 2781−2804.
[5] S. L. James, *Chem. Soc. Rev.* **2003**, *32*, 276−288.
[6] E. Coronado, J. R. Galán-Mascarós, C. J. Gómez-García, V. Laukhin, *Nature* **2000**, *408*, 447−449.
[7] S. Karasawa, Y. Sano, T. Akita, N. Koga, T. Itoh, H. Iwamura, P. Rabu, M. Drillon, *J. Am. Chem. Soc.* **1998**, *120*, 10080−10087.
[8] O. M. Yaghi, H. Li, C. Davis, D. Richardson, T. L. Groy, *Acc. Chem. Res.* **1998**, *31*, 474−484.
[9] P. G. Lacroix, I. Malfant, S. Benard, P. Yu, E. Riviere, K. Nakatani, *Chem. Mater.* **2001**, *13*, 441−449.
[10] M. Eddaoudi, D. B. Moler, H. L. Li, T. M. Reineke, M. O′Keeffe, O. M. Yaghi, *Acc. Chem. Res.* **2001**, *34*, 319−330.
[11] H. K. Chae, J. Kim, O. D. Friedrichs, M. O′Keefe, O. M. Yaghi, *Angew. Chem. Int. Ed.* **2003**, *42*, 3907−3909.
[12] R. L. Carroll, C. B. Gorman, *Angew. Chem. Int. Ed.* **2002**, *41*, 4378−4400.
[13] J. L. Chen, L. Y. Zhang, Z. N. Chen, L. B. Gao, M. Abe, Y. Sasaki, *Inorg. Chem.* **2004**, *43*, 1481−1490.
[14] L. De Cola, P. Belser, *Coor. Chem. Rev.* **1998**, *177*, 301−346.
[15] C. H. Londergan, J. C. Salsman, S. Ronco, L. M. Dolkas, C. P. Kubiak, *J. Am. Chem. Soc.* **2002**, *124*, 6236−6237.
[16] Y. Hoshino, S. Higuchi, J. Fiedler, C.-Y. Su, A. Knodler, B. Schwederski, B. Sarkar, H. Hartmann, W. Kaim, *Angew. Chem. Int. Ed.* **2003**, *42*, 674−677.
[17] F. A. Cotton, J. P. Donahue, C. A. Murillo, *J. Am. Chem. Soc.* **2003**, *125*, 5436−5450.
[18] P. Rajakumar, K. Srinivasan, *Eur. J. Org. Chem.* **2003**, 1277−1284.
[19] T. Iyoda, M. M. Matsushita, T. Kawai, *Pure Appl. Chem.* **1999**, *71*, 2079−2084.
[20] J. Zhang, M. M. Matsushita, X. X. Kong, J. Abe, T. Iyoda, *J. Am. Chem. Soc.* **2001**, *123*, 12105−12106.
[21] M. M. Matsushita, M. Morikawa, T. Kawai, T. Iyoda, *Mol. Cryst. and Liq. Cryst.* **2000**, *343*, 87−96.
[22] M. Julve, M. Verdaguer, A. Gleizes, M. Philoche-Levisalles, O. Kahn, *Inorg. Chem.* **1984**, *23*, 3808−3818.
[23] Z. Smekal, Z. Travnicek, F. Loret, J. Marek, *Polyhedron* **1999**, *18*, 2787−2793.
[24] O. Kahn, *Molecular Magnetism*, VCH Publishers, New York, **1993**, p. 132.
[25] O. Costisor, M. Brezeanu, Y. Journaux, K. Mereiter, P. Weinberger, W. Linert, *Eur. J. Inorg. Chem.* **2001**, 2061−2066.
[26] Z. Smékal, Z. Trávníček, F. Lloret, J. Marek, *Polyhedron* **1999**, *18*, 2787−2793.
[27] G. M. Sheldrick, *SHELXL-97, Program for the Refinement of Crystal Structures*, University of Göttingen, Göttingen, Germany, **1997**.

Received March 23, 2004
Early View Article
Published Online August 3, 2004

 © 2004 Wiley-VCH Verlag GmbH & Co. KGaA, Weinheim

2,4-*N*,*N*′-Bis(dialkylamido)-2,4-dithioxo-1,3,2λ^5,4λ^5-dithiadiphosphetanes

Anton Dimitrov,*[a] Irmgard Hartwich,[a] Petra Neubauer,[a] and Manfred Meisel[a]

Keywords: Donor-acceptor systems / N-ligands / Fluorinated ligands / Sulfur / Phosphorus

Dialkylamide derivatives of the monometadithioxaphosphoric acid stabilised by pyridine as a donor, i.e. $[(C_5H_5N)PS_2NR_2]$, readily react with $AlCl_3$. The elimination of the donor and formation of the adduct $C_5H_5N{\cdot}AlCl_3$ liberates the unstable $\sigma^3\lambda^5$-phosphoranes (PS_2NR_2). The latter are stabilised by [2+2] "cycloaddition-dimerization" leading to the title compounds $[PS_2NR_2]_2$ in nearly quantitative yields. The synthesis and characterisation of two compounds possessing NR_2 substituents of very different basicities clearly demonstrate the generalisation of such a procedure as an easy way of accessing further derivatives in this class.

(© Wiley-VCH Verlag GmbH & Co. KGaA, 69451 Weinheim, Germany, 2004)

Introduction

Whereas studies of dithiadiphosphetane disulfides $(PS_2X)_2$ (X = alkyl, aryl, alkylthio, arylthio, and some "exotic substituents" such as ferrocenyl[1] or $[W(CO)_5]$[2]) have been well documented, with more than 20 published crystal structures[3], literature reports of the same class of substances with X = NR_2 remain rare, speculative or have been shown to be incorrect. During the reaction between P_4S_3 and $S[N(CH_3)_2]_2$, Fluck et al. observed the formation of the title compound $[PS_2NMe_2]_2$ (**1a**).[4] From numerous signals appearing in the ^{31}P NMR spectra of the reaction products, the authors assigned a singlet at δ = 23.9 ppm to compound **1a**. The decrease of its intensity in the mixture was concomitant with the formation of crystals. The remaining components of the reaction mixture were not characterised. After successful completion of the process, the isolated crystals showed practically no solubility in common organic solvents. By means of mass spectrometric, IR and Raman data the composition of the crystals was postulated as a mixture of the dimer **1a** and the trimer $[PS_2NMe_2]_3$. An X-ray investigation of a crystal from the heterogeneous solid mixture revealed the structure of **1a**, the only known crystal structure, up to now, of a bis(dialkylamido)dithiadiphosphetane. By attempting to reproduce the synthesis of Fluck et al.[4], we succeeded in the preparation of **1a** with a yield of about 7%. The ^{31}P NMR spectra taken from the product mixture revealed the inaccessibility of this synthesis: the main peaks were unknown and did not correspond to **1a**. Furthermore we were unable to confirm the reported[4] insolubility of **1a** in common organic solvents. Thus, **1a** prepared in nearly quantitative yield by our method [see Equation (2)] allows at least the convenient measuring of ^{31}P NMR spectra in toluene.

In 1994 Nizamov et al.[5] reported the reaction between P_4S_{10} and R_2NSR' as a high yield synthesis for the title compounds **1a** or $[PS_2NEt_2]_2$ **1b**, respectively.

$$P_4S_{10} + 4\ R_2NSR' \longrightarrow 2\ \text{(1a/1b)} + 2\ R'SSR' + 1/4\ S_8 \qquad (1)$$

1a R = Me, R' = Et, *i*Pr
1b R = Et, R' = Et, *i*Pr, *i*Bu

The authors' interpretation of the data obtained from Equation (1) is, however, clearly incorrect. All of the ^{31}P NMR spectra taken from the reaction products showed no signals in the chemical shift region which is typical for compounds having a dithiadiphosphetane ring (δ = 20−26 ppm, see below), but signals at much lower field (between δ = 90 and 120 ppm). Because the elemental analysis[5] of the reaction products supports the presence of compounds with a composition equal to **1a** and **1b**, the reported δ(^{31}P) values of the NMR spectra could only be explained if the reaction products are isomers of **1** with a P_2N_2 four membered ring such as 1,3-dialkyl-2,4-bis(alkylthio)-2,4-dithioxo-1,3-diaza-2λ^5,4λ^5-diphosphetidines[6] and/or some cyclic oligomers, $[R_2NPS_2]_n$ (n = 3,4). However, the various signals listed in reference 5 which result from the main products of the reaction between P_4S_{10} and alkylsulfendialkylamides (R_2NSR'), show that Equation (1) clearly results in a mixture of undefined (not identified) products with no measurable formation of **1**. Altogether, the data from the

[a] Institut für Chemie, Humboldt Universität zu Berlin,
Brook-Taylor-Straße 2, 12489 Berlin, Germany
Fax: (internat.) +49-(0)30-20937468
E-mail: anton.dimitrov@chemie.hu-berlin.de

 © 2004 Wiley-VCH Verlag GmbH & Co. KGaA, Weinheim **DOI: 10.1002/ejic.200400343**

literature reveal that at the present time, a suitable approach to the synthesis of **1** does not exist.

Results

During our investigations into the differences in the structures and reactivities of amides of the donor stabilised monometadithioxaphosphoric acid with various alkyl substituents, $(C_5H_5N)PS_2NR_2$ (**2**), we developed an easy synthesis for **1** by treating **2** with the Lewis acid $AlCl_3$.

R	**2** (^{31}P NMR Signal)
CH_3	**2a** (122.0 ppm)[7]
CH_2CH_3	**2b** (122.9 ppm)[8]
CH_2CF_3	**2c** (120.9 ppm)

$$2\,(C_5H_5N)PS_2NR_2 \;(\mathbf{2a–c}) + 2AlCl_3 \rightarrow 2\,C_5H_5N{\cdot}AlCl_3 + [PS_2NR_2]_2 \;(\mathbf{1a–c}) \quad (2)$$

1 (^{31}P NMR Signal)
1a (23.9 ppm)[4]
1b (21.8 ppm)[8]
1c (25.7 ppm)

The starting compounds **2** can be obtained very pure and in high yields by treating the pyridine stabilized σ^{4}λ^5-dithiochlorophosphorane, Py→PS_2Cl, with the corresponding *sec*-amines.[9] The single-crystal X-ray diffraction investigations of **2b**[10] and **2c**[11] (Figure 1) show the distorted tetrahedral surroundings of the P atoms in both compounds. By comparing the two structures, one can recognize that the lengthening of the P−N_{amide} bond in **2c**, caused as expected by the influence of the CF_3 groups, does not affect the P−N_{donor} and P=S distances at all.

Our high temperature ^{31}P NMR investigations confirm the formation of small amounts of **1b** by heating **2b**, an observation already noted by Meisel and Donath.[8] This observation has been explained by the liberation of σ^{3}λ^5-PS_2NEt_2 intermediates from **2b** at high temperatures as reactive species which undergo [2+2] cycloaddition reactions. This hypothesis[8] has been strongly supported by our results which make it seem very plausible. The reaction of **2** with the strong Lewis acid $AlCl_3$ which forms the adduct Py → $AlCl_3$ with the donor base pyridine, results exclusively in the formation of **1**, Equation (2).[13]

The molecular structures of **1b**[14] (Figure 2) and **1c**[15] show a completely planar P_2S_2 four member ring in each case, with a *trans* arrangement of the exocyclic ligands. The P centres are in distorted tetrahedral environments. The tetrahedra are joined along a common edge (built by the endocyclic S atoms) to the dimeric molecules **1**. The significant difference in the bond lengths between the two endocyclic S atoms and phosphorus within the dithiadiphosphetane ring reveals the tendency for a monomer formation in **1b** and **1c** but, surprisingly, not in **1a**. In Table 1 some selected bond angles and distances are given.

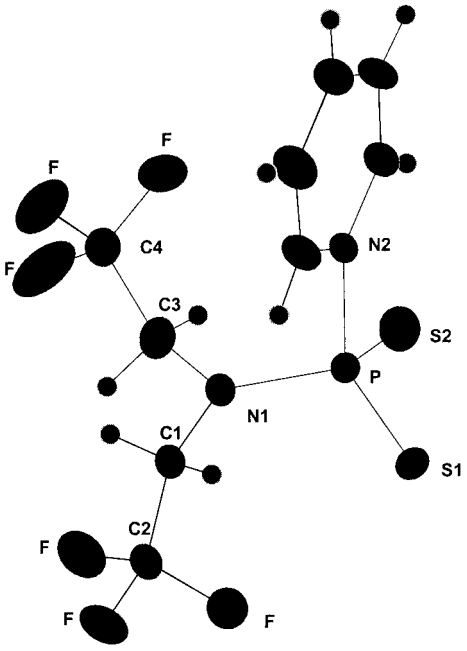

Figure 1. Structure of **2c** (DIAMOND[12], ellipsoids are shown at the 60% probability level) and selected bond lengths [pm] and angles (°) for **2c/2b**: P−S1 194.1(1)/194.9(2), P−S2 194.8(1)/195.2(1), P−N1 168.6(1)/164.0(1), P−N2 189.3(1)/189.8(2), N1−C1 146.2(2)/148.3(1), N1−C3 146.9(2)/148.0(1), C1−C2 151.6(2)/151.4(1), C3−C4 150.6(3)/152.2(1), S1−P−S2 122.81(3)/120.42(6), N1−P−N2 99.62(7)/101.82(5), N1−P−S1 111.65(5)/113.48(6), N1−P−S2 111.02(5)/112.58(8), N2−P−S1 103.14(5)/101.74(5), N2−P−S2 105.32(5)/103.65(5), C1−N1−C3 117.11(13)/115.56(7), C1−N1−P 121.84(11)/120.78(9), C3−N1−P 121.06(11)/123.60(4)

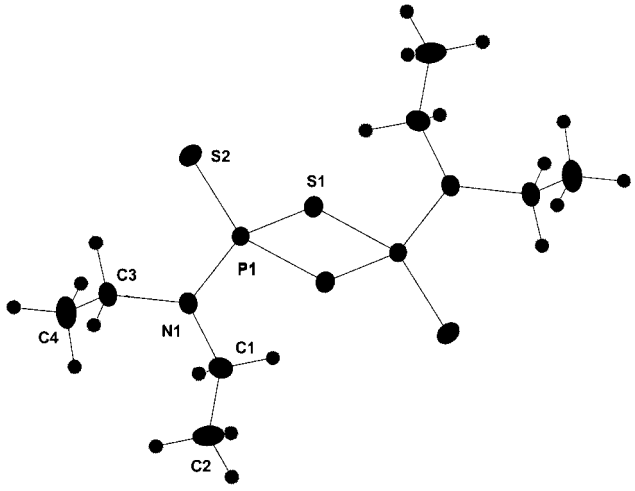

Figure 2. Structure of **1b** (DIAMOND,[12] ellipsoids are shown at the 60% probability level)

 © 2004 Wiley-VCH Verlag GmbH & Co. KGaA, Weinheim

Table 1. Selected bond lengths [pm] and angles (°) (* atoms generated by symmetry)

	P1−S1	P1−S1*	P1−S2	P1−N1	N1−C1	N1−C3	C1−C2	C3−C4
1a[4]	212.2(1)	212.2(1)	192.6(1)	163.3(3)	145.0(5)	145.1(6)		
1b	210.9(1)	215.2(1)	193.8(1)	163.8(2)	149.1((3)	147.4(3)	152.0(3)	151.6((3)
1c	209.7(1)	213.8(1)	190.8(1)	167.7(1)	146.8(2)	146.0(2)	151.5(2)	150.6(2)
	P1−S1−P1*	S1−P1−S1*	S2−P1−S1*	S1−P1−N1	S2−P1−N1	P1−N1−C1	P1−N1−C3	C1−N1−C3
1a[4]	86.86(3)	93.14(3)	115.57(4)	107.83(9)	114.66(9)	120.5(2)	124.0(2)	115.5(3)
1b	87.75(6)	92.25(6)	114.80(7)	110.00(8)	115.00(8)	119.7(2)	121.8(2)	116.9(2)
1c	86.44(2)	93.56(2)	115.35(2)	107.77(5)	114.12(0)	119.5(1)	122.0(1)	117.0(1)

Equation (2) which we have dealt with in this work leads, in its first step and under mild conditions, to the formation of reactive $\sigma^3\lambda^5$ phosphoranes. The subsequent [2+2] cycloaddition reaction immediately forms the stable dimeric title compounds **1**. At present we are investigating the viability of the analogous reactions of Py→$POSNR_2$ and Py→PO_2NR_2 with $AlCl_3$. By successfully applying these reactions it may be possible to access the corresponding dimeric compounds with P_2O_2 or P_2OS four membered rings.

Experimental Section

General Remarks: All experiments were performed under purified dry argon in a glove box and/or on a glass high-vacuum line. Py→PS_2Cl was prepared according to the literature procedure from P_4S_{10}, pyridine and $PSCl_3$ [16]. Toluene was heated to reflux over Na and freshly distilled prior to use. The NMR spectra were recorded with a 400 MHz Bruker spectrometer at the appropriate ^{31}P, ^{1}H, ^{13}C and ^{19}F frequencies using H_3PO_4, TMS and F11 as external standards, respectively.

Single-crystals suitable for X-ray analyses were isolated and prepared in a cold stream of nitrogen. Data collection was carried out with an IPDS diffractometer (Stoe & Cie) at 180 K using graphite-monochromated Mo-K_α radiation (71.073 pm) and a cryostream cooler (Oxford Cryosystems). The data set was collected in the φ-oscillation scan mode. The structures were solved[17] and refined[18] with SHELX 97 (see refs.[10−15]). CCDC-232449 (for **1b**), -232450 (for **1c**), -232451 (for **2b**) and -232448 (for **2c**) contain the supplementary crystallographic data for this paper. These data can be obtained free of charge at www.ccdc.cam.ac.uk/conts/retrieving.html [or from the Cambridge Crystallographic Data Centre, 12 Union Road, Cambridge CB2 1EZ, UK; Fax: +44-1223/336-033; E-mail: deposit@ccdc.cam.ac.uk].

Synthesis of 1: Compound **2** (5 mmol) was partially dissolved in toluene (15 mL) in a 50-mL Schlenk tube. To this suspension was added an equivalent amount of $AlCl_3$ (668 mg) dissolved in toluene (15 mL) and the reaction mixture became a clear solution. Within 1−2 hours the reaction was complete and the adduct $C_5H_5N{\cdot}AlCl_3$ separated as an oil and/or solid participate. The clear toluene phase was separated, its volume reduced to about 1/3 by evaporation of the solvent and stored overnight at −20 °C for crystallisation. The resultant crystals were separated, washed with toluene and dried in vacuo.

1b: Yield 80.5%, $C_8H_{20}N_2P_2S_2$ (334.45): calcd. C 28.73, H 6.03, N 8.38, P 18.52, S 38.34; found C 27.87, H 6.43, N 8.13, P. 18.92, S 38.29. NMR spectroscopic data ([D$_8$]toluene): ^{31}P NMR: δ = 21.8 ppm. ^{1}H NMR: δ = 0.92 (t, $^{3}J_{H,H}$ = 6.9 Hz, 6 H, CH_3), 3.42 (d/q, $^{3}J_{H,P}$ = 17.7, $^{3}J_{H,H}$ = 6.9 Hz, 4 H, CH_2) ppm. ^{13}C NMR: δ = 13.7 (s, CH_3), δ = 41.6 (s, CH_2) ppm.

1c: Yield 73.1%, $C_8H_8F_{12}N_2P_2S_4$ (550.33): calcd. N 5.09, P 11.26, S 22.3; found N 4.93, P 11.82, S 23.77. NMR spectroscopic data [D$_8$]toluene: ^{31}P NMR: δ = 25.7 ppm. ^{1}H NMR: δ = 3.93 (d/q, $^{3}J_{H,P}$ = 16.2, $^{3}J_{H,F}$ = 8.3 Hz, 4 H, CH_2) ppm. ^{13}C NMR: δ = 47.3 (q, $^{2}J_{C,F}$ = 33.5 Hz, CH_2), δ = 124.6 (q, $^{1}J_{C,F}$ = 282.1 Hz, CF_3) ppm. ^{19}F NMR: δ = −68.04 (t, $^{3}J_{F,H}$ = 8.3 Hz, CF_3) ppm.

Synthesis of 2: Py → PS_2Cl (10 mmol) was partially dissolved in toluene (25 mL) in a 75 mL Schlenk tube. To this suspension was added the corresponding *sec*-amine dissolved in toluene (10 mL). Two equivalents were used for **2b** and a single equivalent together with one equivalent of pyridine for **2c**. The reaction mixtures became clear solutions and after heating for 2 hours at 60 °C under an Argon atmosphere the reactions were complete. The precipitated amine hydrochlorides were filtered after cooling to room temperature and the clear filtrates stored overnight at −20 °C for crystallisation. The crystals were separated, washed with toluene and dried in vacuo.

2b: Yield 73.5%, $C_9H_{15}N_2PS_2$ (246.32): calcd. C 43.88, H 6.14, N 11.37, P 12.57, S 26.03; found C 43.20, H 6.14, N 10.93, P 12.85, S 26.07. NMR spectroscopic data (CD_3CN): ^{31}P NMR: δ = 123.3 ppm. ^{1}H NMR: δ = 0.95 (t, $^{3}J_{H,H}$ = 7.1 Hz, 6 H, CH_3), 3.50 (d/q, $^{3}J_{H,P}$ = 15.2, $^{3}J_{H,H}$ = 7.1 Hz, 4 H, CH_2), 7.81 (m, 2 H, β-CH), 8.25 (m, 1 H, γ-CH), 9.45 (m, 2 H, α-CH) ppm. ^{13}C NMR: δ = 14.2 (d, $^{3}J_{C,P}$ = 2.2 Hz, CH_3), 42.2 (d, $^{2}J_{C,P}$ = 3.6 Hz, CH_2), 126.9 (s, β-CH), 142.9(s, α-CH), 144.4 (s, γ-CH) ppm.

2c: Yield 69.1%, $C_9H_9F_6N_2PS_2$ (354.27): calcd. N 7.91, P 8.74, S 18.1; found N 7.51, P 9.26, S 18.46. NMR spectroscopic data (CD_3CN): ^{31}P NMR: δ = 120.9 ppm. ^{1}H NMR: δ = 4.47 (d/q, $^{3}J_{H,P}$ = 13.2, $^{3}J_{H,F}$ = 8.9 Hz, 4 H, CH_2), 7.9 (m, 2 H, β-CH), 8.4(m, 1 H, γ-CH), 8.7 (m, 2 H, α-CH) ppm. ^{13}C NMR: δ = 49.0 (q/d, $^{2}J_{C,F}$ = 32.7, $^{2}J_{C,P}$ = 5.0 Hz, CH_2), 125.8 (q/d, $^{1}J_{C,F}$ = 282, $^{3}J_{C,P}$ = 2.2 Hz, CF_3), 127.9 (s, β-CH), 143.1 (s, α-CH), 146.2 (s, γ-CH) ppm. ^{19}F-NMR: δ = −68.19 (t, $^{3}J_{F,H}$ = 8.9 Hz, CF_3) ppm.

[1] M. R. St. J. Foreman, A. M. Z. Slawin, J. D. Woollins, *J. Chem. Soc., Dalton Trans.* **1996**, 3653−3657.
[2] K. Merzweiler, H.-J. Kersten, *Z. Naturforsch., Teil B* **1993**, *48*, 541−543.
[3] See the deposited structures with the Cambridge Crystallographic Data Centre (CSD) and the corresponding literature by carrying out a CSD-search for the structural fragment S=(P_2S_2)=S.
[4] E. Fluck, G. Gonzalez, K. Peters, H. G. von Schnering, *Z. Anorg. Allg. Chem.* **1981**, *473*, 51−58.

 © 2004 Wiley-VCH Verlag GmbH & Co. KGaA, Weinheim

[5] I. S. Nizamov, L. A. Almetkina, V. A. Kuznetzov, E. S. Batyeva, *Phosphorus, Sulfur, Silicon* **1994**, *92*, 139−147.

[6] C. Donath, M. Meisel, K.-H. Jost, K. K. Palkina, S. I. Maksimova, N. T. Cibiskova, *Z. Naturforsch., Teil B* **1986**, *41*, 1201−1205.

[7] E. Fluck, P. J. Retuert, H. Binder, *Z. Anorg. Allg. Chem.* **1973**, *397*, 225−236.

[8] M. Meisel, Ch. Donath, *Phosphorus, Sulfur, Silicon* **1992**, *64*, 63−69.

[9] A. Rabis, *Dissertation*, **1999**, Humboldt University, Berlin.

[10] Crystal data for **2b**: Pale yellow colour, crystal size 0.54 × 0.42 × 0.32 mm, orthorhombic, space group *Pbca* (no. 61), a = 1729.6(12), b = 1735.8(23), c = 1665.5(15) pm, V = 5001(9) × 10^6 pm^3, Z = 8, $\rho_{calcd.}$ = 1.309 g·cm^{-3}, F(000) = 2080, μ(Mo-K_α) = 0.520 mm^{-1}; (h,k,l) = (± 17, 0 to +18, 0 to +12), θ = 2.06−21.77°, 4941 measured reflections (R_{int} = 0.0886), 272 parameters, R1 = 0.0693, 2214 reflections with $I > 2\sigma(I)$, wR2 = 0.1861 for 2625 unique reflections, ρ_{final}(max./min.) = 0.587/−1.065 × 10^{-6} e·pm^{-3}.

[11] Crystal data for **2c**: Colourless, crystal size 0.80 × 0.72 × 0.60 mm, monoclinic, space group P21/n (No. 14), a = 1102.2(3), b = 1095.0(3), c = 1180.0(3) pm, β = 97.94(3)°, V = 1410.6(7) × 10^6 pm^3, Z = 4, $\rho_{calcd.}$ = 1.668 g·cm^{-3}, F(000) = 712, μ(Mo-K_α) = 0.548 mm^{-1}; (h,k,l) = (±13, ±13, ±14), θ = 2.63−25.75°, 9303 measured reflections (R_{int} = 0.0265), 217 parameters, R1 = 0.0295, 2428 reflections with $I > 2\sigma(I)$, wR2 = 0.0757 for 2655 unique reflections, ρ_{final}(max./min.) = 0.524/−0.385 × 10^{-6} e·pm^{-3}.

[12] K. Brandenburg, M. Berndt, *Diamond* 2.1c, Crystal Impact GbR, Bonn, Germany, **1999**.

[13] All compounds of reaction (2) were fully characterised by elemental analyses and single-crystal X-ray diffraction studies. The crystal structures of **2a** and $C_5H_5N{\cdot}AlCl_3$ will be published in a separate paper.

[14] Crystal data for **1b**: Colourless, crystal size 0.68 × 0.60 × 0.24 mm, triclinic space group P-1 (no. 2), a = 658.0(2), b = 695.6(3), c = 891.9(5) pm, α = 86.17(6)°, β = 72.72(5)°, γ = 78.84(4)°, V = 382.4(3) × 10^6 pm^3, Z = 1, $\rho_{calcd.}$ = 1.452 g·cm^{-3}, F(000) = 176, μ(Mo-K_α) = 0.808 mm^{-1}; (h,k,l) = (±7, ±8, ±10), θ = 3.47−25.25°, 3789 measured reflections (R_{int} = 0.0919), 114 parameters, R1 = 0.0285, 1207 reflections with $I > 2\sigma(I)$, wR2 = 0.0762 for 1255 unique reflections, ρ_{final}(max./min.) = 0.374/−0.341 × 10^{-6} e·pm^{-3}.

[15] Crystal data for **1c**: Colourless, crystal size 0.52 × 0.40 × 0.28 mm, monoclinic space group P 21/c (no. 14), a = 1125.95(17), b = 580.54(5), c = 1432.6(2) pm, β = 99.572(17)°, V = 923.4(2) × 10^6 pm^3, Z = 2, $\rho_{calcd.}$ = 1.979 g·cm^{-3}, F(000) = 544, μ(Mo-K_α) = 0.802 mm^{-1}; (h,k,l) =(±13, ±6, ±17), θ = 2.88−25.23°, 5749 measured reflections (R_{int} = 0.0285), 143 parameter, R1 = 0.0227, 1526 reflections with $I > 2\sigma(I)$, wR2 = 0.0591 for 1645 unique reflections, ρ_{final}(max./min.) = 0.316/−0.270 × 10^{-6} e·pm^{-3}.

[16] M. Meisel, H. Grunze, *Z. Anorg. Allg. Chem.* **1968**, *360*, 277−283.

[17] G. M. Sheldrick, *Acta Crystallogr., Sect. A* **1990**, *46*, 467−473, for the program SHELXS-97.

[18] G. M. Sheldrick, SHELXL-97, *Program for Crystal Structure Refinement*, University of Göttingen, **1997**.

Received April 29, 2004
Early View Article
Published Online August 12, 2004

 © 2004 Wiley-VCH Verlag GmbH & Co. KGaA, Weinheim

Hydrothermal Synthesis, Structure and Magnetic Properties of a One-Dimensional Iron Arsenate, $^1_\infty[NH_3(CH_2)_2NH(CH_2)_2NH_3][Fe_2F_4(HAsO_4)_2]$

Sandip Chakrabarti,[a] Swapan K. Pati,[b] Mark A. Green,[c] and Srinivasan Natarajan*[a]

Keywords: Iron arsenate / Antiferromagnetism / Hydrothermal reactions / Iron / Magnetic properties

A novel one-dimensional iron arsenate, $^1_\infty[NH_3(CH_2)_2NH(CH_2)_2NH_3][Fe_2F_4(HAsO_4)_2]$, built up exclusively from SBU-4 units (two octahedral units sharing an edge and connected through two tetrahedra) with Fe^{3+} ions in the high-spin state has been synthesized by hydrothermal methods. Structure elucidation reveals that the compound is a two-leg ladder with very weak antiferromagnetic exchanges along the chains. The magnetic susceptibility data show activated behaviour at T = 14 K, suggesting a finite spin gap between the nonmagnetic ground state and the excited triplet state. We have estimated the exchange parameters theoretically based on the S = 5/2 Majumdar–Ghosh model with frustrations and dimerisations. Although the magnetic gap is quite small, this is the first example, to the best of our knowledge, where the rungs with two S = 5/2 spins form strong singlet dimers.

(© Wiley-VCH Verlag GmbH & Co. KGaA, 69451 Weinheim, Germany, 2004)

Introduction

In recent years, one-dimensional and quasi-one-dimensional systems have received considerable attention. Due to large quantum fluctuations, low-dimensional systems often show unusual properties such as a gap between a singlet ground state and a magnetic excited state; this leads to exponentially vanishing magnetic susceptibility at low temperature. Many low-dimensional systems have been realised experimentally, of which the Haldane gap spin-1 system is a good example.[1−3] Other examples include the spin-ladder systems in which a small number of chains interact with each other.[4,5] It has been observed that if each rung of the ladder contains an odd number of spin-1/2 sites, then the system effectively behaves like a spin-1/2 chain with a gapless low-energy spectrum. Such behaviour has been observed in $Sr_2Cu_3O_5$.[6] Conversely, ladders with an even number of spin-1/2 sites in the rung behave like an integer spin chain with a finite spin gap to the lowest excited spin state [for example, $SrCu_2O_3$,[7] $(VO)_2P_2O_7$,[8] $Cu_2(C_5H_{12}N_2)_2Cl_4$ [9]]. Another interesting observation in a quasi-one-dimensional spin system, $CuGeO_3$, is that it spontaneously dimerises below the spin-Peierls transition temperature leading to opening up of a spin gap.[10]

We have been interested in the intricate relationship between structure, dimensionality and magnetism. As part of a research program aiming to produce new compounds based on iron, a new iron arsenate, $^1_\infty[NH_3(CH_2)_2NH(CH_2)_2NH_3][Fe_2F_4(HAsO_4)_2]$ (**I**), possessing a one-dimensional structure was synthesized. Although the syntheses and structures of a large number of metal phosphates with open-framework structures have been reported in the literature,[11] research on metal arsenates is just beginning to emerge.[12−16] In many of the metal phosphates, the use of fluorine in the synthesis mixture appears to give rise to a variety of novel structures, especially in iron phosphates.[17] The concept of secondary building units has evolved to describe complex crystal structures based on tetrahedral connectivity.[18] During the last few years, this has been expanded to include nontetrahedral connectivity as well.[19] In the case of octahedral-tetrahedral structures, such as those present in iron phosphates and arsenates, the common structural features prompted Ferey to propose a set of secondary building units (SBUs) to describe and understand such structures.[20−22] The simplest of the SBUs is the one containing two octahedral and tetrahedral units (SBU-4), wherein the octahedral units share edges/corners and are connected through the tetrahedra. Compound **I**, described here, is the first one-dimensional structure built up exclusively from SBU-4 building units.

The two-leg ladder $^1_\infty[NH_3(CH_2)_2NH(CH_2)_2NH_3][Fe_2F_4(HAsO_4)_2]$ (**I**) consists of high-spin Fe^{3+} (S = 5/2) ions. Due to strong exchange interactions between the rung

[a] Framework Solids Laboratory, Chemistry and Physics of Materials Unit, Jawaharlal Nehru Centre for Advanced Scientific Research,
Jakkur P. O., Bangalore 560064, India
Fax: (internat.) + 91-80-2362-2766
E-mail: raj@jncasr.ac.in
[b] Theoretical Sciences Unit, Jawaharlal Nehru Centre for Advanced Scientific Research,
Jakkur P. O., Bangalore 560 064, India
[c] The Davy-Faraday Research Laboratory, The Royal Institution of Great Britain,
21 Albemarle Street, London, W2S 4BS, UK

 © 2004 Wiley-VCH Verlag GmbH & Co. KGaA, Weinheim DOI: 10.1002/ejic.200400127

spins, each rung can be considered as a singlet spin dimer. The magnetic susceptibility measurements show that the system has a spin gap of about 10 K. The theoretical fit to the experimental data suggests that the system is a weakly linked rung dimer. We have also measured magnetisation as a function of magnetic field at two different temperatures. At low field strength, both of the magnetisation curves follow unit-cell-polarised Brillouin functions (each unit cell contains two $S = 5/2$).

Results and Discussion

The asymmetric unit of **I** contains two crystallographically unique Fe and As atoms. Of these, Fe(1) and As(1), and Fe(2) and As(2) are connected together, giving rise to two independent one-dimensional ladders. Both the Fe atoms, Fe(1) and Fe(2), are octahedrally coordinated by three O and three F atoms with Fe−O/F bond lengths in the range 1.874(3)−2.064(3) Å (average 1.9852 Å). Each iron atom is linked to three arsenic atoms through three Fe−O−As bonds (average angle 127.5°), has two Fe−F−Fe bonds (average angle 101.43°) and possesses a terminal Fe−F bond. Each As atom also has three As−O−Fe bonds and one terminal As−O bond. The As atom is tetrahedrally coordinated by oxygen atoms with an average As−O distance of 1. 6832 Å and an O−As−O bond angle of 109.4°. The terminal As−O bonds, for both As(1) and As(2), are As−OH bonds; this agrees well with the proton position found next to the oxygen atoms in the difference Fourier map. The Brown−Altermatt formalism[23] for the bond length/bond valence relationship for Fe−O, Fe−F and As−O was used to calculate bond-order sums for the cations and anions (Table 3). The calculated bond-order sums for both cations and anions are in agreement with the formal oxidation states of +3, +5 and −2 for Fe, As and O atoms, respectively (Table 3).

The structure of **I** consists of FeO_3F_3 octahedral and $HAsO_4$ tetrahedral building units connected through their vertices. Thus, the connectivity between $Fe(1)O_3F_3$ and $As(1)O_3(OH)$, and $Fe(2)O_3F_3$ and $As(2)O_3(OH)$ gives rise to two distinctand independent one-dimensional structure units (Figure 1). The FeF_3O_3 octahedra are connected together through two Fe−F−Fe bridges forming edge-shared dimers. The $Fe_2F_4O_6$ dimers are linked through $AsO_3(OH)$ tetrahedra completing the basic building unit, which resembles the secondary building unit, SBU-4, enumerated by Ferey.[20−22] The SBU-4 units are joined together to give rise to the one-dimensional ladder structure (Figure 1). The charge-compensating doubly protonated diethylenetriamine (DETA) molecules are located between the ladders and interact through N−H···O and N−H···F hydrogen bonds. The view of the ladders and the arrangement of the SBU-4 units along the *c* axis are shown in Figure 2. The presence of terminal fluoride, along with OH groups, gives rise to a number of hydrogen-bond interactions involving the amine. Important hydrogen-bond interactions are listed in Table 1.

The presence of Fe_2F_2 dimers in **I**, and strong intrachain and weak interchain interactions between the SBU-4 units

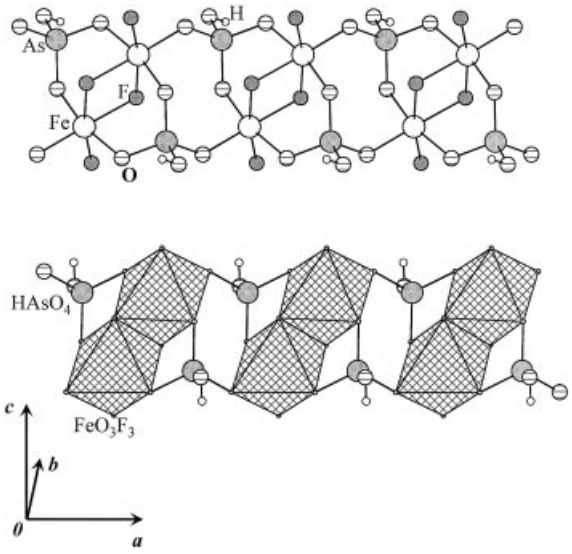

Figure 1. Structure of **I** showing the arrangement of the ladders; note that the SBU-4 units are connected through a four-membered ring; amine molecules are not shown for clarity

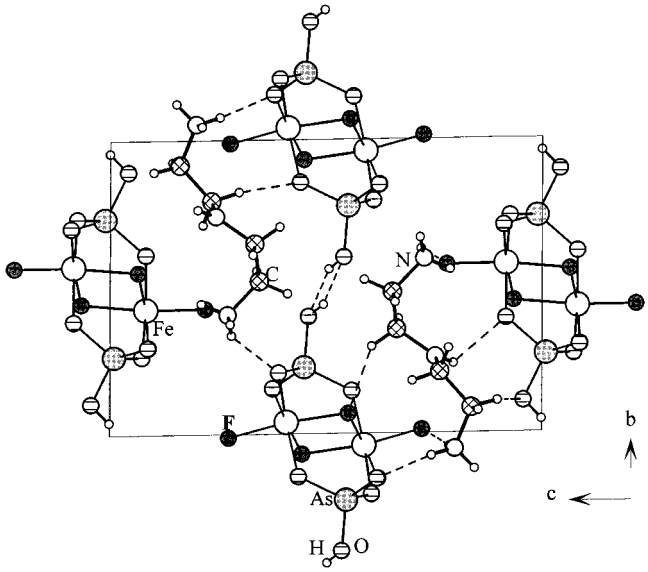

Figure 2. Structure of **I** viewed down the ladder axis; dotted lines represent possible hydrogen-bond interactions

prompted us to evaluate the magnetic properties of **I**. The magnetic characterization of **I** was carried out using a SQUID magnetometer in the temperature range 5−300 K. The temperature dependence of the magnetic susceptibility (χ) of **I** is shown in Figure 3. The special feature to be noticed is the activated behaviour at $T \approx 14$ K, below which the susceptibility (χ) drops exponentially to zero. This activated behaviour corresponds to a finite spin gap in the material. For low-dimensional spin-gap systems, considering the magnon excitations approximately, Troyer et al. have derived a general expression for χ: $\chi = (1/K_BT)z(K_BT)/[1 + 3z(K_BT)]$, with $z(K_BT) = 1/\pi \int \exp(-E_K/K_BT)dK$, where E_K is the nondegenerate triplet magnon dispersion.[24] For low temperature, the above expression can be approximated as

 © 2004 Wiley-VCH Verlag GmbH & Co. KGaA, Weinheim

Table 1. Important hydrogen-bond interactions in $^1_\infty[NH_3(CH_2)_2NH(CH_2)_2NH_3][Fe_2F_4(HAsO_4)_2]$ (**I**); symmetry operations used to generate equivalent atoms: #1: $1-x, y, 1+z$; #2: $2-x, 1-y, 3-z$; #3: $x, 1+y, 1+z$; #4: $x, 1+y, z$; #5: $1-x, 1-y, 3-z$

D−H···A	D−H [Å]	H···A [Å]	D···A [Å]	D−H···A [°]
N(1)−H(1)···O(6)	0.89	2.05	2.801(6)	141
N(1)−H(2)···F(11)#1	0.89	2.44	3.294(6)	161
N(2)−H(8)···O(1)#2	0.86	2.62	3.253(7)	144
N(3)−H(13)···O(3)#3	0.89	2.22	3.015(7)	148
N(3)−H(14)···O(8)#4	0.89	2.01	2.886(7)	170
N(3)−H(15)···F(10)#4	0.89	1.94	2.803(7)	162
O(7)−H(30)···O(7)[a]#2	0.82	1.78	2.524(6)	151
C(2)−H(7)···F(9)#4	0.97	2.25	3.092(7)	144
C(3)−H(10)···O(5)#2	0.97	2.29	3.238(8)	165
C(4)−H(11)···O(1)#5	0.97	2.43	3.327(8)	154

[a] Interchain interaction.

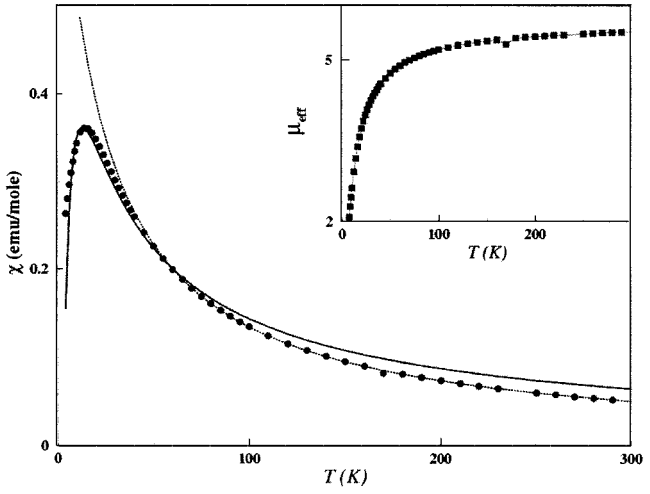

Figure 3. χ [emu/mol] vs. T plot at 100 Gauss; the solid line is the exponential fit at low temperature mentioned in the text; the dotted line is the Curie−Weiss law fit for χ at high temperature; the inset shows the effective magnetic moment μ_{eff} as a function of T

$\chi_{low\text{-}T} = A\cdot\exp(-\Delta/K_BT)/(K_BT)^{\zeta}$. This formulation can be applied for any half-integer spin with parabolic triplet magnon dispersion at low temperature.[25] Note that, at the dimer limit, $\Delta = 1$ and the exponent ζ becomes 1. However, for a gapped spin-1/2 extended lattice, it is shown that $\zeta = 1/2$. Clearly, this exponent relates the transition from a dimer limit to the extended system. By fitting the above form of $\chi_{low\text{-}T}$ with the experimental data, we find that the best fit is obtained with $A = 6$, $\Delta = 10.3$ K and $\zeta = 0.78$. The fit is shown as a solid line in Figure 3. At high temperature, the value of χ saturates to the paramagnetic value for two $S = 5/2$ spins. The high-temperature susceptibility, $\chi_{high\text{-}T}$, fits very well down to $T = 60$ K with a Curie−Weiss form $\chi_{cw} = C/(T-\Theta)$, with $C = 16.39$ and $\Theta = -22$ K (dotted line in Figure 3). The inset shows the effective magnetic moment μ_{eff} as a function of temperature. The room-temperature μ_{eff} per Fe is approximately equal to 5.5 μ_B, which steadily decreases to 1.45 μ_B at 5 K, indicating strong antiferromagnetic behaviour (see inset, Figure 3). This room-temperature value of μ_{eff} compares fairly well with the spin-only moment for high-spin Fe^{3+}.

The maximum and the subsequent decrease of χ with an increase in T correspond to short-range antiferromagnetic exchange interactions in the system. A careful investigation of the structure reveals that there are three different superexchange pathways as shown below in Scheme 1. All the superexchange angles between the corresponding pair of localised Fe^{3+} ions through the intervening atoms suggest that all three exchanges are antiferromagnetic, making the system highly frustrated. In addition, J_1 exchanges in the rung (Fe dimers) are through two fluorine atoms, while J_2 and J_3 are through $HAsO_4$ tetrahedral links. This clearly shows that the intradimer exchange interactions are much stronger than the interdimer exchanges. Although we specify two different exchanges between the rungs, they are similar in magnitude and are quite small relative to J_1.

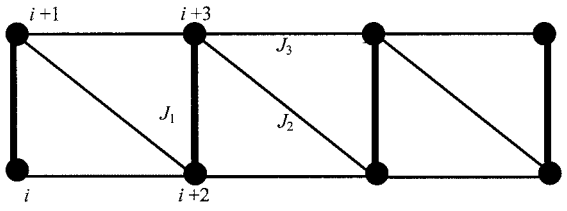

Scheme 1

If we neglect J_3, the system is a $S = 5/2$ J-alternating one-dimensional chain with exchange values J_1 and J_2 respectively. If $J_1 = J_2$, the system is an isotropic half-integer spin chain, which is gapless. Defining $\alpha = J_1/J_2$, for small J_2, the spin gap increases as $\alpha^{2/3}$ with increase in J_2. For a gap of $\Delta = 10.3$ K, J_2 would be more than 30 times smaller than J_1, which is quite small. For a proper estimation of the magnitudes of the three exchange constants (J_1, J_2 and J_3), we have chosen temperatures corresponding to two values of χ; one at the maximum and the other where χ saturates to its paramagnetic value. The Hamiltonian corresponding to this system can be written as $H = \Sigma_i\{[J + (-1)^{i-1}\delta]S_i\cdot S_{i+1} + J_3S_i\cdot S_{i+2}\}$, where $(J \pm \delta)$ corresponds to J_1 and J_2.[26] We solve this Majumdar−Ghosh Hamiltonian for a range of system sizes (two and three unit cells) with $S = 5/2$ spins and with exchange parameters J_1, J_2 and J_3. We find that the best fit to the experimental data is obtained with $J_2 = J_3 = 0.35J_1$. All three exchange interactions are antiferromagnetic and their magnitudes are also reasonable considering the distance between the corresponding spin centres.[27]

The dependence of magnetisation (M) as a function of magnetic field (B) at 5 and 15 K are shown in Figure 4. For both temperatures $M(B)$ increases rapidly with increasing B, indicating that the excited spin states are significantly populated. It is clear from the figure that at these temperatures there is no alignment of spins. For a comparison, we have computed Brillouin functions for two independent $S = 5/2$ spins in the unit cell and for a large unit cell with $S =$

 © 2004 Wiley-VCH Verlag GmbH & Co. KGaA, Weinheim

5. The $M = f(B)$ curve at $T = 15$ K is between the two Brillouin functions mentioned above. This proves that even at $T = 15$ K, the magnetic polarisation of the unit cell with two high-spin Fe^{3+} ions is not complete. Since the lowest excited spin state is a triplet with a gap of 10 K, the sharp initial rise in $M(B)$ for small B values corresponds to the Zeeman-coupling-assisted increase in population of the triplet state. With the fitted values of the exchange parameters ($J_2 = J_3 = 0.35J_1$), we have computed the magnetisation for the temperature values, $T = 5$, 15 and 30 K. For $T = 15$ and 30 K, they are plotted with the corresponding experimental $M = f(B)$ curves for comparison. In the inset of Figure 3, we have plotted all three theoretical $M = f(B)$ curves up to high magnetic field strengths. The $M = f(B)$ curve at $T = 5$ K closely follows Brillouin functions with one independent $S = 5$ unit-cell spin. Thus, at small T, the magnetisation corresponds to the magnetic polarisation of one unit cell (1 unit cell = 2 Fe^{3+} ions). We estimate theoretically that for the complete alignment of the spins on all the unit cells (complete polarisation) for this one-dimensional ladder would require magnetic field strengths of the order of 8 Tesla even at low temperatures (i.e. about 5 K).

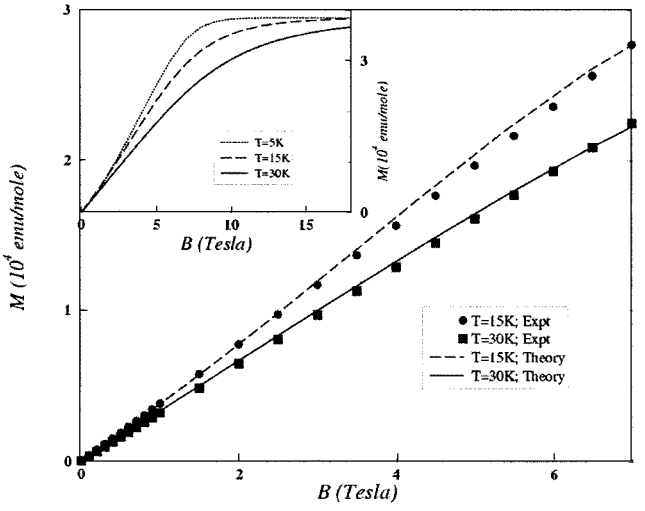

Figure 4. Magnetisation (M) as a function of magnetic field (B) at two different temperatures, $T = 5$ K (filled circles) and $T = 15$ K (filled squares); the dashed line and the solid line are the theoretical magnetisation plots for the corresponding T values; the inset shows the theoretical M vs. B curve for three different temperatures, $T = 5$ K (dotted line), $T = 15$ K (dashed line) and $T = 30$ K (solid line)

Conclusions

The synthesis, structure and magnetic characterization of a one-dimensional iron arsenate, $^1_\infty[NH_3(CH_2)_2NH(CH_2)_2NH_3][Fe_2F_4(HAsO_4)_2]$ (**I**), has been accomplished. The theoretical estimate of the exchange parameters based on the Majumdar−Ghosh model shows the presence of a frustrated solid with one strong and two weak short-range antiferromagnetic couplings. A two-dimensional layer structure built up exclusively from SBU-4 units has been reported recently by us,[28] and we have now stabilized SBU-4 in a one-dimensional structure. More importantly, the low-dimensional structures of the type investigated here provide an opportunity for the theoretical evaluations of the interplay between the coupling strength, the geometrical frustrations and the low-temperature phase transitions, as such materials are rarely isolated. We are vigorously pursuing further work in this direction.

Experimental Section

Compound **I** was synthesized hydrothermally in the presence of diethylenetriamine (DETA). In a typical synthesis iron acetylacetonate [Fe(acac)$_3$] (0.196 g) was dispersed in water (2 mL). To this, As_2O_5 (0.378 g) and HF (48%, 0.08 mL) were added while stirring continuously. Finally, DETA (0.25 mL) was added, and the mixture was homogenised at room temperature for 30 min. The reaction mixture with the composition Fe(acac)$_3$/As_2O_5/HF/DETA/H_2O (1:3:4:4:200) was transferred into a PTFE-lined stainless-steel pressure vessel (23 mL) and heated at 180 °C under autogenous pressure for 72 h. The initial pH of the reaction mixture was approximately equal to 5 and the pH after the reaction was approximately 4. The resulting product, a crop of fine pale-yellow rod-shaped crystals, was filtered, washed with water and dried at room temperature (yield 70% based on Fe). An EDAX analysis indicated that the ratio Fe/As was 1:1, and that fluorine was present. $C_4H_{17}As_2F_4Fe_2N_3O_8$ (572.75): calcd. C 8.4, H 3.0, N 6.3; found C.8.1, H 2.8, N 6.3. A potentiometric titration also confirmed the presence of fluorine (calcd. 13.27%; found 12.9%).[29]

A suitable single crystal was carefully selected under a polarising microscope and glued to a thin glass fibre. Crystal structure determination by X-ray diffraction was performed with a Siemens Smart-CCD diffractometer equipped with a normal focus, 2.4 kW sealed-tube X-ray source (Mo-K_α radiation, $\lambda = 0.71073$Å) op-

Table 2. Crystal data and structure refinement parameters for $^1_\infty[NH_3(CH_2)_2NH(CH_2)_2NH_3][Fe_2F_4(HAsO_4)_2]$ (**I**)

Empirical formula	$C_4H_{17}As_2F_4Fe_2N_3O_8$
Formula mass	572.75
Crystal size [mm]	0.06 × 0.16 × 0.16
Crystal system	triclinic
Space group	$P\bar{1}$ (No. 2)
a [Å]	5.5386(5)
b [Å]	9.5537(9)
c [Å]	13.6893(12)
α [°]	89.780(2)
β [°]	83.799(2)
γ [°]	76.230(2)
V [Å^3]	699.24(11)
Z	2
$D_{calcd.}$ [g·cm^{-3}]	2.720
μ [mm^{-1}]	6.865
Total data collected	2990
Unique data	1992
Observed data [$I > 2\sigma(I)$]	1726
R_{merg}	0.0476
R indexes [$I > 2\sigma(I)$]	$R_1 = 0.0319$[a]; $wR_2 = 0.0687$[b]
R indexes (all data)	$R_1 = 0.0409$[a]; $wR_2 = 0.0738$[b]

[a] $R_1 = \||F_o| - |F_c|\|/|F_o|$. [b] $wR_2 = \{[w(F_o^2 - F_c^2)^2]/[w(F_o^2)^2]\}^{1/2}$; $w = 1/[\sigma^2(F_o)^2 + (aP)^2 + bP]$, $P = [\max.(F_o^2,0) + 2(F_c)^2]/3$, where $a = 0.0164$ and $b = 2.9953$.

 © 2004 Wiley-VCH Verlag GmbH & Co. KGaA, Weinheim

Table 3. Selected bond lengths [Å] and angles [°] in $^1_\infty[NH_3(CH_2)_2NH(CH_2)_2NH_3][Fe_2F_4(HAsO_4)_2]$ (**I**); values in brackets are the bond valences; their sum SVB appears in bold type at the end of the list of the distances around every cation; symmetry transformations used to generate equivalent atoms: #1: $x-1, y, z$; #2: $-x, -y+1, -z+2$; #3: $x+1, y, z$; #4: $-x+3, -y, -z+3$

Bond		Bond	
As(1)−O(1)	1.669(4) [1.303]	Fe(1)−O(4)#2	1.992(4) [0.533]
As(1)−O(2)	1.678(4) [1.272]	Fe(1)−O(2)	1.999(4) [0.523]
As(1)−O(3)	1.687(4) [1.241]	Fe(1)−F(11)#2	2.024(3) [0.394]
As(1)−O(4)	1.685(4) [1.248]	Fe(1)−F(11)	2.054(3) [0.363]
Σ(As−O)	[5.065]	Σ(Fe−O/F)	[3.014]
As(2)−O(5)	1.679(4) [1.269]	Fe(2)−F(10)	1.913(3) [0.531]
As(2)−O(6)	1.693(4) [1.221]	Fe(2)−O(8)#3	1.941(4) [0.611]
As(2)−O(7)	1.665(4) [1.317]	Fe(2)−O(5)#4	1.978(4) [0.553]
As(2)−O(8)	1.710(4) [1.167]	Fe(2)−F(9)#4	1.982(3) [0.441]
Σ(As−O)	[4.974]	Fe(2)−O(6)	2.008(4) [0.510]
Fe(1)−F(12)	1.874(3) [0.590]	Fe(2)−F(9)	2.064(3) [0.353]
Fe(1)−O(3)#1	1.941(4) [0.611]	Σ(Fe−O/F)	[3.000]
Angle		**Angle**	
O(1)−As(1)−O(2)	110.9(2)	O(2)−Fe(1)−F(11)	83.43(15)
O(1)−As(1)−O(4)	104.77(19)	F(11)#2−Fe(1)−F(11)	78.52(14)
O(2)−As(1)−O(4)	113.64(19)	F(10)−Fe(2)−O(8)#3	92.25(15)
O(1)−As(1)−O(3)	108.5(2)	F(10)−Fe(2)−O(5)#4	90.68(15)
O(2)−As(1)−O(3)	108.97(19)	O(8)#3−Fe(2)−O(5)#4	98.22(17)
O(4)−As(1)−O(3)	109.89(18)	F(10)−Fe(2)−F(9)#4	168.03(14)
O(7)−As(2)−O(5)	110.4(2)	O(8)#3−Fe(2)−F(9)#4	99.71(14)
O(7)−As(2)−O(6)	111.6(2)	O(5)#4−Fe(2)−F(9)#4	87.18(14)
O(5)−As(2)−O(6)	111.06(19)	F(10)−Fe(2)−O(6)	90.65(15)
O(7)−As(2)−O(8)	104.7(2)	O(8)#3−Fe(2)−O(6)	93.82(16)
O(5)−As(2)−O(8)	110.79(18)	O(5)#4−Fe(2)−O(6)	167.82(16)
O(6)−As(2)−O(8)	108.07(18)	F(9)#4−Fe(2)−O(6)	89.02(14)
F(12)−Fe(1)−O(3)#1	90.58(16)	F(10)−Fe(2)−F(9)	89.46(13)
F(12)−Fe(1)−O(4)#2	90.10(15)	O(8)#3−Fe(2)−F(9)	176.36(15)
O(3)#1−Fe(1)−O(4)#2	98.63(16)	O(5)#4−Fe(2)−F(9)	84.96(14)
F(12)−Fe(1)−O(2)	92.72(16)	F(9)#4−Fe(2)−F(9)	78.62(13)
O(3)#1−Fe(1)−O(2)	92.40(16)	O(6)−Fe(2)−F(9)	82.95(14)
O(4)#2−Fe(1)−O(2)	168.59(16)	As(1)−O(2)−Fe(1)	126.4(2)
F(12)−Fe(1)−F(11)#2	171.96(14)	As(1)−O(3)−Fe(1)#3	132.6(2)
O(3)#1−Fe(1)−F(11)#2	97.35(14)	As(1)−O(4)−Fe(1)#2	124.2(2)
O(4)#2−Fe(1)−F(11)#2	87.46(14)	As(2)−O(5)−Fe(2)#4	124.3(2)
O(2)−Fe(1)−F(11)#2	88.24(15)	As(2)−O(6)−Fe(2)	125.3(2)
F(12)−Fe(1)−F(11)	93.66(14)	As(2)−O(8)−Fe(2)#1	132.1(2)
O(3)#1−Fe(1)−F(11)	174.18(15)	Fe(2)#4−F(9)-Fe(2)	101.38(13)
O(4)#2−Fe(1)−F(11)	85.36(14)	Fe(1)#2−F(11)-Fe(1)	101.48(13)

erating at 40 kV and 40 mA. An empirical absorption correction based on symmetry-equivalent reflections was applied with the SADABS program.[30] The structure was solved and refined using the SHELXTL-PLUS suite of programs.[31] All hydrogen atoms were located in the difference Fourier maps. For the final refinement the hydrogen atoms were placed geometrically and held in the riding mode. The final refinement included atomic positions for all atoms, anisotropic thermal parameters for all non-hydrogen atoms and isotropic thermal parameters for all hydrogen atoms. Full-matrix least-squares refinement against $|F^2|$ was carried out using the SHELXTL-PLUS[31] suite of programs. Details of the structure solution and final refinement for $^1_\infty[NH_3(CH_2)_2NH(CH_2)_2NH_3][Fe_2F_4(HAsO_4)_2]$ (**I**) are given in Table 2. CCDC-205336 contains the supplementary crystallographic data for this paper. These data can be obtained free of charge at www.ccdc.cam.ac.uk/conts/retrieving.html [or from the Cambridge Crystallographic Data Centre, 12 Union Road, Cambridge CB2 1EZ, UK; Fax: (internat.) + 44-1223-336-033; E-mail: deposit@ccdc.cam.ac.uk].

Acknowledgments

S. N. thanks the Council of Scientific and Industrial Research, (CSIR) Government of India and S. K. P. thanks the Department of Science and Technology (DST), Government of India for financial support.

[1] F. D. M. Haldane, *Phys. Rev. Lett.* **1983**, *50*, 1153−1156.
[2] W. L. J. Buyers, R. M. Morra, R. L. Armstrong, M. J. Hogan, P. Gerlach, K. Hirakawa, *Phys. Rev. Lett.* **1986**, *56*, 371−374.
[3] S. Ma, C. Broholm, D. H. Reich, B. J. Sternlieb, R. W. Erwin, *Phys. Rev. Lett.* **1992**, *69*, 3571−3574.
[4] D. J. Scalapino, *Nature* **1995**, *377*, 12−13.
[5] E. Dagotto, T. M. Rice, *Science* **1996**, *271*, 618−623.
[6] M. Azuma, Z. Hiroi, M. Takano, K. Ishida, Y. Kataoka, *Phys. Rev. Lett.* **1994**, *73*, 3463−3466.
[7] M. Azuma, Z. Hiroi, M. Takano, Y. Bando, Y. Takeda, *Nature* **1992**, *356*, 775−776.
[8] R. S. Eccleston, T. Barnes, J. Brody, J. W. Johnson, *Phys. Rev. Lett.* **1994**, *73*, 2626−2629.

 © 2004 Wiley-VCH Verlag GmbH & Co. KGaA, Weinheim

[9] G. Chaoussant, P. A. Crowell, L. P. Levy, O. Piovesana, A. Madouri, D. Mailly, *Phys. Rev. B* **1997**, *55*, 3046−3049.
[10] M. Hase, I. Terasaki, K. Uchinokura, *Phys. Rev. Lett.* **1993**, *70*, 3651−3654; M. Nishi, O. Fujita, J. Akimitsu, *Phys. Rev. B* **1994**, *50*, 6508−6510.
[11] A. K. Cheetham, G. Ferey, T. Loiseau, *Angew. Chem. Int. Ed.* **1999**, *38*, 3268−3292 and references therein.
[12] S. Ekambaram, S. Sevov, *Inorg. Chem.* **2000**, *39*, 2405−2410.
[13] P. Feng, T. Zhang, X. Bu, *J. Am. Chem. Soc.* **2001**, *123*, 8608−8609.
[14] A.-H. Liu, S.-L. Wang, *Inorg. Chem.* **1998**, *37*, 3415−3418.
[15] M.-Y. Lee, S.-L. Wang, *Chem. Mater.* **1999**, *11*, 3588−3594.
[16] S. Chakrabarti, S. Natarajan, *Angew. Chem. Int. Ed.* **2002**, *41*, 1224−1226.
[17] K.-H. Lii, Y.-F. Huang, V. Zima, C.-Y. Huang, H.-M. Lin, Y.-C. Jiang, F.-L. Liao, S.-L. Wang, *Chem. Mater.* **1998**, *10*, 2599−2609 and references therein.
[18] Ch. Baerlocher, L. B. McCusker, *Database of Zeolite Structures*: http://www.iza-structure.org/databases/
[19] M. Eddaoudi, D. B. Moler, H. L. Li, B. L. Chen, T. M. Reineke, M. O'Keeffe, O. M. Yaghi, *Acc. Chem. Res.* **2001**, *34*, 319−330.
[20] G. Ferey, *J. Fluorine Chem.* **1995**, *72*, 187−193 and references therein.
[21] M. Riou-Cavellec, D. Riou, G. Ferey, *Inorg. Chim. Acta* **1999**, *291*, 317−325.
[22] G. Ferey, *Chem. Mater.* **2001**, *13*, 3084−3098 and references therein.
[23] I. D. Brown, D. Altermatt, *Acta Crystallogr., Sect. B* **1985**, *41*, 244−247.
[24] M. Troyer, H. Tsunetsugu, D. Wurtz, *Phys. Rev. B* **1994**, *50*, 13515−13527.
[25] D. C. Johnston, R. K. Kremer, M. Troyer, X. Wang, A. Klümper, S. L. Bud'ko, A. F. Panchula, P. C. Canfield, *Phys. Rev. B* **2000**, *61*, 9558−9606.
[26] R. Chitra, S. K. Pati, H. R. Krishnamurthy, D. Sen, S. Ramasesha, *Phys. Rev. B* **1995**, *52*, 6581−6587.
[27] S. K. Pati, S. Ramasesha, D. Sen, *Magnetism: Molecules to Materials IV* (Eds. J. S. Miller, M. Drillon), Wiley-VCH, Weinheim, **2003**, p. 119.
[28] S. Chakrabarty, S. K. Pati, M. Green, S. Natarajan, *Eur. J. Inorg. Chem.* **2003**, 3820−3825.
[29] *Vogel's Textbook of Quantitative Chemical Analysis*, Vth ed., John Wiley & Sons Inc., New York, **1989**. p. 570.
[30] G. M. Sheldrick, *SADABS, Siemens Area Detector Absorption Correction Program*, University of Göttingen, Göttingen, Germany, **1994**.
[31] G. M. Sheldrick, *SHELXTL-PLUS, Program for Crystal Structure Solution and Refinement*, University of Göttingen, Göttingen, Germany, **1997**.

Received February 17, 2004
Early View Article
Published Online July 27, 2004

 © 2004 Wiley-VCH Verlag GmbH & Co. KGaA, Weinheim

Structure Comparison of Early and Late Lanthanide(III) Homodinuclear Macrocyclic Complexes with the Polyamine Polycarboxylic Ligand H_8OHEC

Ulrike A. Böttger,[a] Brendon O'Sullivan,[b] Burkhard Ziemer,[a] Herbert Schumann,[b] Clemens Mügge,[a] and Hardy Weißhoff*[a]

Keywords: Solid-state structures / Lanthanides / Macrocyclic ligands / Polyamine polycarboxylic acid / Solution thermodynamics

The solid-state structures of two new homodinuclear chelate complexes with the late lanthanide(III) ions Yb and Lu, $[Na_2(Yb_2OHEC)]\cdot 14.5H_2O$ (**1**), and $[Na_2(Lu_2OHEC)]\cdot 14.5H_2O$ (**2**) (H_8OHEC = 1,4,7,10,14,17,20,23-octaazacyclohexacosane- 1,4,7,10,14,17,20,23-octaacetic acid), have been determined by X-ray crystal structure analysis. Each lanthanide(III) ion is coordinated by eight donor atoms of the ligand and the geometry of the coordination polyhedron approaches a bicapped trigonal prism. These structures are compared with those of the homodinuclear chelate complexes with the same ligand and the mid to early lanthanide(III) ions Gd, Eu, La and also Y. A distinctive structural change occurs across the lanthanide series. The centrosymmetric mid to early lanthanide(III) complexes are all ninefold-coordinated in a capped square antiprismatic arrangement with a water molecule coordinated in a prismatic position. This structure is maintained in aqueous solution, together with an asymmetric minor isomer. The late lanthanide(III) OHEC complexes not only lack the inner-sphere water, but the change of coordination sphere also results in a loss of symmetry of the whole complex molecule. The observed change of coordination mode and number of the lanthanide ion may offer a geometric model for the isomerization process in eight- and ninefold-coordinated complex species that are isomers in a possible coordination equilibrium observed by NMR in aqueous solution. This model may also explain the intramolecular rearrangements necessary during water exchange in the inner coordination sphere of the complex $[(Gd_2OHEC)(H_2O)_2]^{2-}$ through a slow dissociative mechanism. Protonation constants of the H_8OHEC ligand and complex formation constants of this ligand with Gd^{III}, Ca^{II}, Cu^{II} and Zn^{II} have been determined by solution thermodynamic studies.
(© Wiley-VCH Verlag GmbH & Co. KGaA, 69451 Weinheim, Germany, 2004)

Introduction

H_8OHEC (1,4,7,10,14,17,20,23-octaazacyclohexacosane-1,4,7,10,14,17,20,23-octaacetic acid) is a macrocyclic polyaminocarboxylate with a 26-atom-membered ring formed from the eight amine and bridging ethylene or propylene groups. It was developed as a potential MRI contrast agent ligand, combining two aims: (i) to increase the rotational correlation time compared with conventional DOTA and DTPA, thereby enhancing the relaxivity, the measure of drug efficiency; (ii) to obtain previously unknown binuclear contrast agents with two closely sited gadolinium ions, and to study the intramolecular interaction of the two paramagnetic centres as well as their influence on the electronic relaxation. Previous studies focussed on the preparation[1] of this ligand and its properties as a chelator for lanthanides and small transition metals.[2] The crystal structures of the homodinuclear complexes of yttrium(III), gadolinium(III), europium(III), and lanthanum(III) with H_8OHEC have been discussed, as well as the solution structure and dynamics of its diamagnetic Y^{III} complex.[2,3] These complexes are almost isostructural in that they all crystallise in the monoclinic space group $P2_1/n$, and the conformation of the OHEC macrocycle as well as the coordination geometry around the metal ions is nearly the same. NMR studies on the yttrium complex revealed that the same centrosymmetric structure is maintained in aqueous solution as is found in the solid state. In addition, in aqueous solution the complexes are present in two isomeric forms.[3,4] The doubled NMR signal number of the second isomer obviously reveals an asymmetrical molecule, the geometry of which could not be deduced from the NMR spectroscopic data because of strongly overlapping signals with those of the main isomer.

Coordination polyhedra of the ninefold-coordinated complexes investigated by X-ray crystal structure analysis were interpreted with special regard to their metal-bound water molecule in the inner coordination sphere. A second inspection showed that these structures must be reconsidered. In this report they will be discussed anew together with the structures of two new homodinuclear OHEC com-

[a] Institut für Chemie, Humboldt Universität zu Berlin, Brook-Taylor-Str. 2, 12489 Berlin, Germany
Fax: (internat.) + 49-(0)30-2093-7561
E-mail: weiss@chemie.hu-berlin.de
[b] Institut für Chemie, Technische Universität Berlin, Strasse des 17. Juni 135, 10623 Berlin, Germany

 © 2004 Wiley-VCH Verlag GmbH & Co. KGaA, Weinheim **DOI: 10.1002/ejic.200400124**

plexes with the late lanthanides ytterbium(III) and lutetium(III).

The acidity constants of H_8OHEC and the thermodynamic stabilities of its complexes formed with Gd^{3+}, Ca^{2+}, Cu^{2+} and Zn^{2+} are reported here. These metals were chosen to examine the in vivo stability and selectivity of OHEC complexed gadolinium with respect to its possible application as a contrast agent for magnetic resonance imaging.

Results and Discussion

X-Ray Crystal Structures

Molecular Structures of 1 and 2

The crystals contain $[C_{34}H_{52}Ln_2N_8O_{16}]^{2-}$ anions, sodium cations, hydroxide ions, ethanol molecules and water of crystallization. Their compositions correspond to $[Na_2(Yb_2OHEC)]\cdot 14.5H_2O$, C_2H_5OH, 0.5NaOH (**1**) and $[Na_2(Lu_2OHEC)]\cdot 14.5\cdot H_2O$, C_2H_5OH, 0.5NaOH (**2**). The complexes are isostructural and crystallise in the triclinic space group $P\bar{1}$ (no. 2), which is centrosymmetric. There are the two molecules of the complex per unit cell, which are connected via sodium cations and are centrosymmetric with respect to each other. Crystals are built up from infinite one-dimensional chains of $[Ln_2(OHEC)]^{2-}$ units, arranged parallel to the *a* axis and linked by a network of $Na^+\cdots O$ contacts, involving the sodium cation, the carboxylate oxygen atoms and the water molecules associated with the cation. Thus, although **1** and **2** lack the inner-sphere water molecules, the complexes are wrapped in a water matrix. The shortest distances between bulk water molecules and metal ion centres are 430(14) ($O_{aqua(18)}-Yb_1$) / 453(8) pm ($O_{aqua(32)}-Yb_2$) for **1** and 432(5) ($O_{aqua(18)}-Lu_1$) / 451(10) pm ($O_{aqua(32)}-Lu_2$) for **2**. As the centre of symmetry lies outside the complex molecule, the two chemically identical halves of the complex molecules **1** and **2**, containing the Yb^{III} and Lu^{III} ions, respectively, can only be interconverted by a pseudo-C_2 symmetry operation. The complex molecule itself possesses no kind of symmetry.

Conformation of the Macrocycle in Lanthanide OHEC Complexes

The two lanthanide ions in **1** and **2** are completely encapsulated by the macrocyclic ligand (Figure 1). Each lanthanide ion is coordinated by the four nitrogen and four carboxylic oxygen atoms belonging to one-half of the overall hexadecadentate ligand.

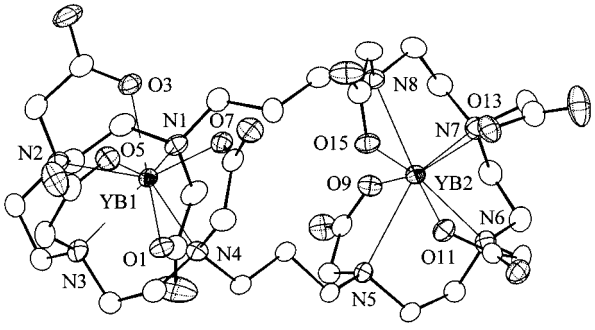

Figure 1. Solid-state conformation of $Na_2(Yb_2OHEC)$ (**1**)

Figure 2 shows the overall conformation of the OHEC macrocycle in the di-ytterbium complex **1**, together with the qualitative torsion angles. Measured torsion angles are listed in Table 1. In contrast to the light lanthanide(III) OHEC complexes, the rings of which adopt a centrosymmetric biangular conformation, {1313}, according to the terminology of Dale[5], the complexes with the smaller and heavier lanthanides ytterbium(III) and lutetium(III) form quadrangular ring conformations with four genuine corners, {7272}. This leads to essentially tighter folding of the ring around the central atoms, leaving no room for an inner-sphere water molecule. The fivefold repetition of *anti* torsion angles in the propylene chains allows for a maximal

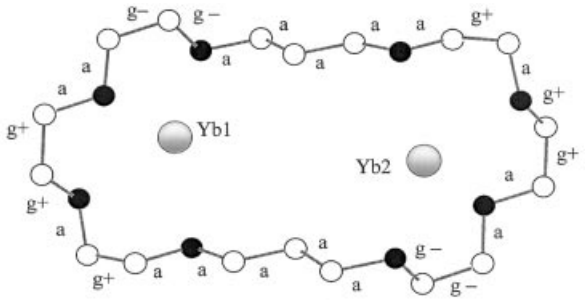

Figure 2. Conformation of the OHEC ligand in **1**, with corresponding qualitative torsion angles

Table 1. Measured torsion angles (°) of the OHEC macrocycle in the di-ytterbium complex **1**

Torsion angle				**1**	**2**
N1	C1	C2	N2	64.87(37)	65.76(46)
C1	C2	N2	C3	−170.81(27)	−171.33(34)
C2	N2	C3	C4	97.49(31)	96.84(39)
N2	C3	C4	N3	52.35(36)	52.43(45)
C3	C4	N3	C5	−171.13(26)	−171.17(34)
C4	N3	C5	C6	170.04(26)	169.43(34)
N3	C5	C6	N4	−63.45(34)	−63.41(44)
C5	C6	N4	C7	−88.08(31)	−89.09(39)
C6	N4	C7	C8	174.64(26)	174.44(33)
N4	C7	C8	C9	172.93(26)	173.01(32)
C7	C8	C9	N5	156.15(25)	157.11(329
C8	C9	N5	C10	170.64(25)	170.16(32)
C9	N5	C10	C11	−168.83(25)	−169.60(33)
N5	C10	C11	N6	66.07(33)	67.63(44)
C10	C11	N6	C12	170.86(26)	−168.59(34)
C11	N6	C12	C13	95.52(31)	93.3(4)
N6	C12	C13	N7	57.46(35)	57.85(45)
C12	C13	N7	C14	−171.74(27)	−173.27(34)
C13	N7	C14	C15	165.02(28)	167.14(34)
N7	C14	C15	N8	−65.33(36)	−67.30(43)
C14	C15	N8	C16	−87.45(33)	−85.48(40)
C15	N8	C16	C17	177.41(27)	175.73(35)
N8	C16	C17	C18	174.67(26)	174.50(34)
C16	C17	C18	N1	154.72(27)	155.49(35)
C17	C18	N1	C1	169.72(27)	170.87(34)
C18	N1	C1	C2	−167.96(27)	−168.67(35)

 © 2004 Wiley-VCH Verlag GmbH & Co. KGaA, Weinheim

separation of the two lanthanides, thereby minimizing electrostatic repulsion.

While the centrosymmetric conformation of the macrocyclic ring of the lighter lanthanide(III) OHEC complexes[3] as well as for the corresponding OHEC-amine ligand and its binuclear copper(II) complex $[Cu_2(OHEC\text{-}amine)](SO_4)_2$ [1] corresponds to the chair shape, for **1** and **2** the ring adopts the boat conformation with a typical pseudo-C_2 symmetry axis. In the OHEC complexes with the chair shape the central atoms as well as the inner-sphere water molecules lie alternately below and above a mean ring plane of the macrocycle, formed by the four propylene bridged nitrogen atoms.[1,3] No such mean plane is found for **1** and **2**. Here, the metal ions both sit on the same side, within the boat conformation of the macrocyclic ring. They are, in each case, sandwiched between nitrogen atoms and three carboxylate arms coordinating the metal from the upper side of the boat, while the forth carboxylate side arms fixed on N1 and N5 coordinate the metals from the lower side of the boat. The layout of the acetate arms depends on the inherent symmetries of these two types of rings. Whereas in the centrosymmetric conformations the pendent arms with up-up-up-down orientations are inverted for both molecule halves at the centre of symmetry, in the boat conformation the up-up-up-down orientations of the four pendant arms of each molecule half can be only interconverted by rotation around a pseudo-C_2 symmetry axis.

Coordination Geometry of the Late Lanthanide Ions

The two lanthanide ions in **1** and **2** are chelated by the hexadecadentate ligand H_8OHEC and adopt eight-coordinate geometry. The coordination sphere for each lanthanide ion consists of four amine nitrogens of the macrocycle and four carboxylic oxygens of the acetate side arms. The large OHEC-ring system is quite flexible but the accommodation of two lanthanide ions is a considerable steric demand. As all eight nitrogen donor atoms belong to one large macrocyclic system they experience a steric constraint. Moreover, as all faces of the polyhedra are built up by mixed donor atoms, by nitrogen atoms and carboxylate oxygens, significant deviations from the ideal geometry can be expected.

Using the criterion established by Haigh for distinguishing the types of structures in eightfold-coordinated complexes, based on a pattern of bond angles,[6] the 28 LML′ angles at the central atom the 16th, 17th and 18th lowest angles were compared. For Yb1 in **1** these are 91.99°, 97.22° and 118.60°, for Lu1 in **2** the corresponding values are 92.93°, 95.71° and 117.42°. The structure should be square antiprism (SAP) if the gap between the 16th and 17th lowest angles is more than 20°. This is not the case. As the gap between the 17th and 18th lowest LML′ angles is substantial the structure should be close to a bicapped trigonal prism (BCTP) (Figure 3). Compared with reclassified structures,[6] on the basis of Haigh's criterion the gap in **1** and **2** is large enough to assign the structure as distorted BCTP. The third possibility, a triangular dodecahedron, must be ruled out as the 16th, 17th and 18th LML′ angles are not close together.

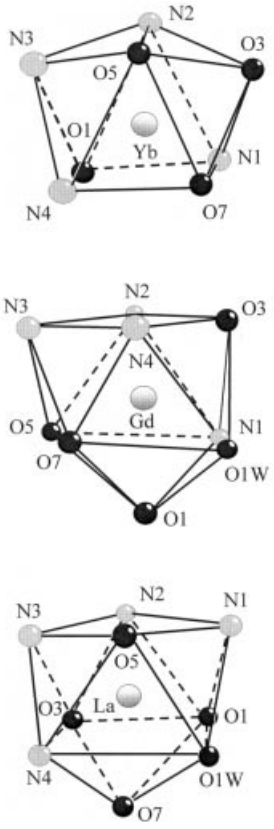

Figure 3. Coordination polyhedron about the ytterbium ion in **1** (top), gadolinium ion in **4** (middle) and lanthanum ion in **6** (bottom)

Comparison of the dihedral angles δ in the primary coordination sphere of the central atoms of **1** and **2**, which are sensitive to symmetry and shape, with those of an ideal D_{4d} (SAP) and C_{2v} (BCTP) geometry gives a more objective assessment of shape (Table 2).[7] The observed deviations from the ideal indicate the ligand's difficulty in satisfying the steric demands of the two central atoms. Of the two alternative polyhedra the polytopal shape of **1** and **2** is best described with the distorted BCTP geometry. For a SAP geometry the two square planes that should be nearly parallel to each other could not be found. Deviations from planarity of the second face are too large (Table 2).

The three different lengths of the prismatic heights of the coordination cage is also a measure of distortion from the ideal BCTP (Table 2). Therefore, the triangular faces of the polyhedra are far from being parallel.

For Yb1 in **1**, atoms N4, O7, O5 and O1, N1, N2 form the triangular faces and the capping positions are occupied by N3 and O3 (Figure 3). For Yb2 in **1** and the two Lu atoms in the isostructural complex **2** the same coordination geometry is found. The metal ions are close to the centre of the trigonal prism, slightly shifted toward the face capped with an acetate oxygen atom and shifted down toward the triangular face of the trigonal prism containing two oxygen donor atoms. The mean $Lu-O_{carboxylate}$ bond

 © 2004 Wiley-VCH Verlag GmbH & Co. KGaA, Weinheim

Table 2. Dihedral angles δ in eightfold coordination for lanthanide OHEC complexes. Estimated standard deviation of last reported digit in parentheses

Complex	δ in coordination cages	Angle (°)	Idealized angle (°)
1 (Yb1)	O1−N1−O7−N4	−0.09(10)	0.0 (BCTP); 0.0 (SAP)
	N3−O5−O3−N2	23.41(11)	21.8 (BCTP); 0.0 (SAP)
	N3−O1−N2−N1	28.18(15)	48.2 (BCTP); 52.4 (SAP)
	O1−N2−N1− O3	63.48(12)	48.2 (BCTP); 52.4 (SAP)
	N3−N4−O5−O7	44.36(12)	48.2 (BCTP); 52.4 (SAP)
	O3−O7−O5−N4	45.20 (11)	48.2 (BCTP); 52.4 (SAP)
1 (Yb2)	O15−N8−O9−N5	−0.07(13)	0.0 (BCTP); 0.0 (SAP)
	N7−N6−O11−O13	−26.62(11)	21.8 (BCTP); 0.0 (SAP)
	N7−O9−N6−N5	25.59(13)	48.2 (BCTP); 52.4 (SAP)
	O11−N5−N6− O9	64.46(11)	48.2 (BCTP); 52.4 (SAP)
	N7−O13−N8− O15	40.85(13)	48.2 (BCTP); 52.4 (SAP)
	O11−O15−O13−N8	44.21(12)	48.2 (BCTP); 52.4 (SAP)
1 (Yb1)	N3−O5−N2−O3	−151.39(14)	0 (SAP)
	N4−O1−O7−N1	−179.89(13)	0 (SAP)
1 (Yb2)	N5−O15−O9−N8	179.93(13)	0 (SAP)
	O11−N6−O13−N7	−145.42(14)	0 (SAP)
2 (Lu1)	O1−N1−O7−N4	−0.18(12)	0.0 (BCTP); 0.0 (SAP)
	N2−O3−O5−N3	22.68(13)	21.8 (BCTP); 0.0 (SAP)
	N3−O1−N2−N1	28.54(15)	48.2 (BCTP); 52.4 (SAP)
	O1−N2−N1− O3	63.52(13)	48.2 (BCTP); 52.4 (SAP)
	N3−N4−O5−O7	45.08(15)	48.2 (BCTP); 52.4 (SAP)
	O3−O7−O5−N4	43.54(14)	48.2 (BCTP); 52.4 (SAP)
2 (Lu2)	O15−N8− O9−N5	0.19(13)	0.0 (BCTP); 0.0 (SAP)
	N7−N6−O11−O13	−27.52(12)	21.8 (BCTP); 0.0 (SAP)
	N7−O9−N6−N5	25.01(16)	48.2 (BCTP); 52.4 (SAP)
	O11−N5−N6−O9	65.4(14)	48.2 (BCTP); 52.4 (SAP)
	N7−O13−N8−O15	43.03(16)	48.2 (BCTP); 52.4 (SAP)
	O11−O15−O13−N8	43.32(14)	48.2 (BCTP); 52.4 (SAP)
2 (Lu1)	N3−O5−N2−O3	−152.39(16)	0 (SAP)
	N4−O1−O7−N1	−179.77(15)	0 (SAP)
2 (Lu2)	N5−O15−O9−N8	179.76(16)	0 (SAP)
	O11−N6−O13−N7	−143.99(16)	0 (SAP)
Edge lengths of the prismatic heights in the BCTP polyhedron [pm]			
	N4−O1	O5−N2	O7−N1
1	299(17)	341(14)	367(13)
2	296(19)	341(16)	361(19)
	O15−N5	O13−N6	N8−O9
1	367(17)	322(18)	293(18)
2	366(18)	324(17)	295(19)

length in **2** is 224.3 pm, slightly shorter than in the ninefold-coordinated Na[LuDOTA(H_2O)] complex (227.9 pm).[8] Also, the mean Lu−N distance in **2** (254.9 pm) is shorter than in Na[LuDOTA(H_2O)] (261.4 pm). Consistent with the lanthanide contraction the mean distances in **1** are slightly longer than in **2** (mean Yb−$O_{carboxylate}$ 225.4 pm and mean Yb−N 256.3 pm). For the eight-coordinate K[Tm(DOTA)],[9] a complex with the lanthanide ion next to Yb^{3+} in the periodic table, the mean Tm−$O_{carboxylate}$ distance of 228 pm is, as expected, longer than in **1**, whereas the mean Tm−N distance of 252.9 pm is slightly shorter than in **1** and also than in **2**.

Table 3 lists the Ln−O and Ln−N distances of LnOHEC complexes, which reflect well the shrinkage of the ionic radii of the chelated lanthanide ions.

The differences between the maximum and minimum interatomic distances in **1** and **2** (Table 4) are too small to indicate distortions within the molecule caused by steric constraints.

Coordination Geometry of the Early to Mid Lanthanide Ions: Implications for the Inner-sphere Water Exchange and an Isomeric Coordination Equilibrium

Since Ln^{3+} aqua ions and other polyaminocarboxylate complexes have varying hydration numbers throughout the series, a varying coordination number may be expected in OHEC lanthanide complexes, depending upon the size of the Ln^{3+} cation.[10]

In the early to mid di-lanthanide complexes of the H_8OHEC ligand the central atoms are all ninefold-coordi-

 © 2004 Wiley-VCH Verlag GmbH & Co. KGaA, Weinheim

Table 3. Bond lengths in the metal coordination sphere

	(1)Yb	(2) Lu	(3)Y	(4)Gd	(5)Eu	(6)La
Ln(1)−O(1)	222.7(2)	221.8(3)	241.2(2)	246.5(3)	247.7(4)	252.9(5)
Ln(1)−O(3)	230.0(2)	229.1(3)	228.4(3)	234.9(3)	236.2(4)	246.4(5)
Ln(1)−O(5)	226.0(2)	224.9(3)	233.7(3)	235.9(3)	237.2(4)	246.4(5)
Ln(1)−O(7)	222.8(2)	221.4(3)	230.7(3)	234.7(3)	236.5(5)	252.9(5)
Average	225.4	224.3	233.5	238.0	239.4	249.6
Ln(1)−O(1W)	−	−	236.3(3)	240.6(3)	243.0(5)	252.6(6)
Ln(1)−N(1)	265.3(3)	264.8(3)	264.7(3)	262.3(4)	265.4(5)	275.3(6)
Ln(1)−N(2)	249.9(3)	248.0(3)	266.2(3)	269.3(3)	271.1(5)	277.6(6)
Ln(1)−N(3)	252.1(3)	250.1(4)	265.2(3)	270.0(3)	270.6(5)	277.6(6)
Ln(1)−N(4)	258.0(3)	256.9(3)	276.7(3)	276.7(4)	279.9(5)	275.4(6)
Average	256.3	254.9	268.2	269.6	271.8	276.5
Ln(1)−Ln(2)	658(8)	662(19)	665(3)	652(1)	652(2)	636(2)

nated.[2,3] Besides the eight donor atoms per metal ion provided by the ligand the ninth site in the metal coordination sphere is occupied by a water molecule. In most such polyamine polycarboxylate ligand complexes the oxygen atom of the inner-sphere water molecules occupies a special site in the coordination polyhedron: it takes a capping position both in the square antiprismatic structures in DOTA-like complexes[11,12] and in the trigonal prismatic structures of acyclic ligand complexes, e.g. as in $[Gd(BOPTA)(H_2O)]^{2-}$.[13]

Initial discussion regarding the structure of homodinuclear OHEC complexes $[Na_2(Y_2OHEC)(H_2O)_2]$ (**3**), $[Na_2(Gd_2OHEC)(H_2O)_2]$ (**4**), $[Na_2(Eu_2OHEC)(H_2O)_2]$ (**5**) and $[Cs_2(La_2OHEC)(H_2O)_2]$ (**6**) was led by the thought that the water molecule should occupy a capping position, as in the DOTA complexes, resulting in an irregular coordination polyhedron. After reinspecting the lanthanide environment in these complexes we found, in all cases, a distorted capped

Table 4. Selected structural parameters for lanthanide OHEC complexes

Complex (Ln)	C−N [pm]	C−C [pm]	$C-O_{carboxylate}$ [pm]	$C-O_{keto}$ [pm]
1 (Yb)	148.1−149.9(4)	150.0−153.6(4)	126.5−128.9(4)	123.1−124.9(5)
2 (Lu)	147.7−149.5(5)	150.0−153.4(5)	126.5−128.4(5)	121.7−124.4(5)
3 (Y)	147.9−150.8(5)	150.5−152.8(5)	124.9−128.4(5)	122.4−125.7(5)
4 (Gd)	146.8−149.9(5)	150.5−152.5(6)	125.8−128.9(5)	122.3−125.2(5)
5 (Eu)	146.9−150.1(9)	149.4−153.1(9)	123.1−125.4(8)	126.0−127.8(8)
6 (La)	146.3− 50.8(10)	150.0−154.4(10)	125.6−127.9(10)	122.2−125.0(9)

Table 5. Some face angles of the ninefold coordination polyhedra (OHEC complexes **3**−**6**)

Complex	Face 1	Face 2	Angle (°)	Idealized angle (polyhedron)
3	N1−N2−O5	N4−O7−O1W	27.4	0 (TTP)
	N3−N2−N4	O3−N2−N4	0.73	0 (CSAP)
	O5−O7−N1	O1−W−O7−N1	1.21	0 (CSAP)
	N2−N3−N4−O3	N1−O5−O7−O1W	4.5	0 (CSAP)
4	N1−N2−O5	N4−O7−O1W	27.6	0 (TTP)
	N3−N2−N4	O3−N2−N4	−0.83	0 (CSAP)
	O5−O7−N1	O1−W−O7−N1	1.03	0 (CSAP)
	N2−N3−N4−O3	N1−O5−O7−O1W	5.5	0 (CSAP)
	N7−O13−O15	N5−O11−O3W	17.8	0 (TTP)
	N6−N7−O11	N8−N7−O11	−178.74	0 (CSAP)
	N5−O13−O3W	O15−O13−O3W	−177.94	0 (CSAP)
	N6−N7−N8−O11	N5−O13−O15−O3W	6.2	0 (CSAP)
5	N1−N2−O5	N4−O7−O1W	27.8	0 (TTP)
	N3−N2−N4	O3−N2−N4	0.2	0 (CSAP)
	O5−O7−N1	O1−W−O7−N1	−1.18	0 (CSAP)
	N2−N3−N4−O3	N1−O5−O7−O1W	5.7	
	N7−O13−O15	N5−O11−O2W	16.9	
	N6−N7−O11	N8−N7−O11	−179.57	
	N5−O13−O2W	O15−O13−O2W	−177.63	
	N6−N7−N8−O11	N5−O13−O15−O2W	6.5	
6	N2−N3−N4−O3	N1−O5−O7−O1W	5.7	0 (CSAP)
	N2−O1−O3	N4−O5−O1W	13.7	0 (TTP)
	N3−N2−O5	N1−N2−O5	−5.5	0 (CSAP)
	O3−N4−O1	O1−W−O1−N4	2.38	0 (CSAP)
	N1−N2−N3−O5	N4−O1−O3−O1W	8.5	0 (CSAP)

 © 2004 Wiley-VCH Verlag GmbH & Co. KGaA, Weinheim

square antiprism (CSAP) as coordination polyhedron, as in DOTA-like complexes but, importantly, the inner-sphere water molecule occupies a prismatic position instead of a capping one (Figure 3). The positions of both square faces are occupied by mixed donor atoms of the ligand. For **3**, **4** and **5** the uncapped square is formed by three ring nitrogens (N2, N3 and N4) and O3, whereas the capped square face is formed by N1, two carboxylate oxygens, O5 and O7, and one inner-sphere water oxygen O1W. Considering the coordination geometry in **6** as a strongly distorted CSAP structure, the uncapped square is formed by N1, N2, N3 and O5. The capped square face is formed by N4, two carboxylate oxygens, O1 and O3, and one inner-sphere water oxygen O1W. For the gadolinium(III) complex **4** the polyhedron comes closest to the ideal CSAP structure. The uncapped square face deviates from planarity by less than 1°. Lanthanum(III) structure **6** shows the highest deviation (Figure 3). Table 5 summarises the most important angles characterising the coordination cage of the lanthanide ions in the four OHEC complexes.

The change of coordination number from nine for the early to mid lanthanides to eight for the late lanthanides in the same type of chelate complex as a result of the lanthanide contraction has been well investigated by NMR for lanthanide(III) DOTA complexes,[9,14] and has also been observed for other polyamine polycarboxylate ligands.[15,16] For lanthanide OHEC complexes, the change of complex geometry is accompanied by a loss of symmetry. This is clearly observable upon considering the CO−CH_2 connectivities in the HMBC spectra of the centrosymmetric Y_2OHEC (**3**, four cross peak pairs) and Lu_2OHEC without a centre of symmetry (**2**, eight cross peak pairs) (Figure 4).

For DOTA complexes, besides the two enantiomeric pairs of ninefold-coordinated stereoisomers, differing in the ligand conformation, a coordination change is superimposed.[14] The loss of the metal-bound water molecule leads to two further structures in which the metal ion is only eight-coordinate but where the coordination geometries are fundamentally maintained since the departing inner-sphere water occupies the capping position in a squared antiprism. This peculiar capping site provides a readily accessible intermediate to water exchange via a more dissociatively activated mechanism for the gadolinium(III) complexes,[17] which yields relatively rapid exchange rates, with $k_{ex}(298)$ in the range of 4.1×10^6 s^{-1} for DOTA[18] and 1.6×10^6 s^{-1} for DO3A−bz−NO_2 [19] for such compounds. As the square antiprism for DOTA-like complexes is unchanged during the exchange process for all investigated lanthanide(III) complexes, there is little difference in the energies between the nine- versus eight-coordinate complexes. Thus, despite the high rigidity of the inner-sphere structure in DOTA complexes the activation energy for the water exchange reaction is very small.[14]

NMR investigations of the di-yttrium complex **3** show that its geometry in aqueous solution is very similar to that in the solid state.[3,11] For each complex, two isomers undergoing conformational changes were proven. Interchange from the major to the minor isomer is accompanied by a loss of centrosymmetry. Figure 5 shows this by means of the Eu_2OHEC ^{1}H NMR spectrum. The same observations have been made for the lanthanide OHEC complexes with Ln^{III} = Eu, Gd, and Tb by means of NMR, UV/Vis, EPR and luminescence spectroscopy.[4] For the europium complex **5** and the gadolinium complex **4** the metal centres change their coordination number from 9 to 8 during isomerisation equilibrium, such as $[Ln_2(OHEC)_2(H_2O)_2]^{2-} \rightarrow [Ln_2(OHEC)]^{2-} + 2H_2O$. As the structures of these two isomers correspond to the two structure types of lanthanide OHEC complexes found in the solid state, the major isomer must have a centrosymmetric, nine-coordinate CSAP structure while the minor isomer has the distorted eight-coordinate BCTP structure without molecular symmetry. Therefore, the isomeric equilibrium not only involves changes of conformation but also of coordination. Figure 6 depicts the rearrangement of the complex molecule in an exchange equilibrium between the two isomers. In contrast to DOTA-like complexes, a water molecule that enters or leaves the metal coordination sphere in lanthanide OHEC complexes gives rise to a considerable reorganisation of the donor atoms and the ring conformation about the metal atom, as the inner-sphere water is less accessible at a prismatic position of the coordination polyhedron. Notably, this rearrangement does not require the release of ligand donor coordination bonds, while removal of the metal-bound water molecules, which are also stabilised by hydrogen bonds, can be considered as the first step in the isomerisation process.

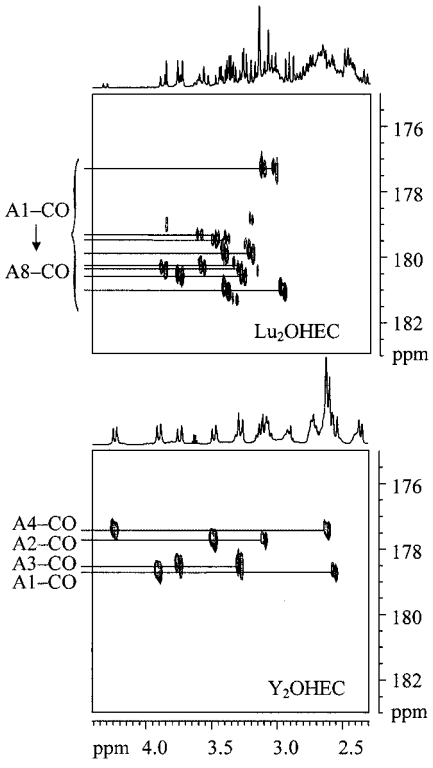

Figure 4. CO−CH_2 region of the HMBC spectra of Lu_2OHEC (**2**, top) and Y_2OHEC (**3**, bottom); there are twice as many NMR cross peaks for Lu_2OHEC than for the main isomer of Y_2OHEC, which can be correlated directly with the loss of symmetry

 © 2004 Wiley-VCH Verlag GmbH & Co. KGaA, Weinheim

During the structural change, only four of the eight donor atoms nearly keep their positions. The N1 atom, which carries the O1 atom, is probably moved by a conformational change of the macrocycle. Simple rotation of the acetate arms can accomplish all other changes of positions.

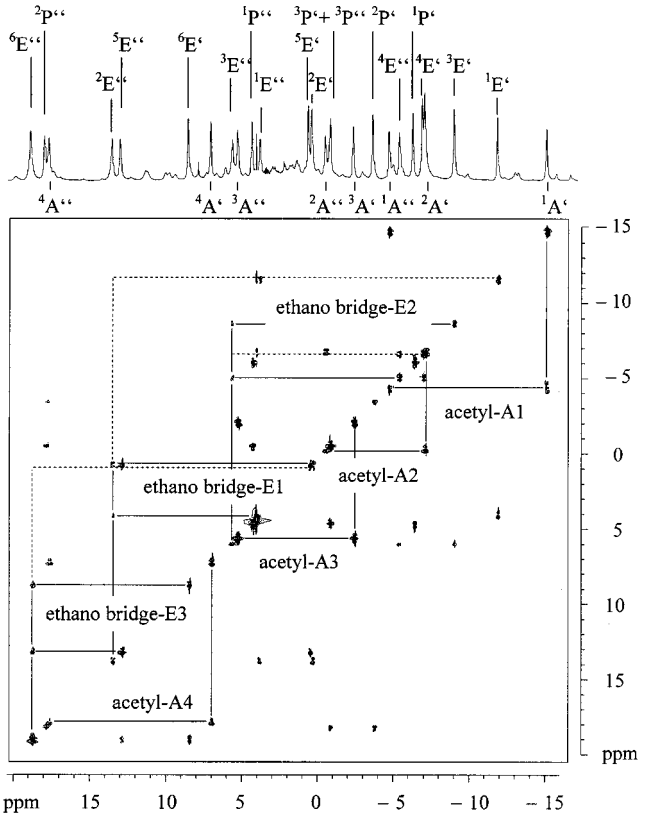

Figure 5. $^1H-^1H$ COSY spectrum of the binuclear Eu^{III} complex of OHEC at 600 MHz; assignment of the centrosymmetric, major isomer $Eu_2OHEC(H_2O)_2$ is shown; the protons can be classified into three ethylene groups (ethano bridge E1−E3, consisting of protons $^1E/^2E$, $^3E/^4E$ and $^5E/^6E$), four acetate arms A1−A4 and one propylene group; the symbols ′ and ″ refer to two geminal protons; assignment of the protons of the minor isomer, preformed using exchange spectroscopy (EXSY), is not shown for clarity

These ligand rearrangements, which take place simultaneously in both halves of the molecule, may account for the extremely slow isomerisation rate [$k_{is}(298) = 73.0\ s^{-1}$] and the very slow water exchange rate [$k_{ex}(298) = 0.40 \times 10^6\ s^{-1}$] in the $[Gd_2OHEC(H_2O)_2]^{2-}$ complex.[4] The rate constant is similar to that of DTPA-bis(amides).[18,20]

Interaction of this inner-sphere water with the gadolinium(III) ion and its exchange with bulk water is the basis for the action of MRI contrast agents of such compounds. However, the distances between the gadolinium atom and the water oxygen atom, and between the gadolinium atom and the acetate oxygen atom in most known polyamine polycarboxylate structures, show that the water ligand does not bind at an exceptionally different distance. Thus, the preferred capping position in DOTA-like complexes for the water molecule, as discussed above, results not from constraints imposed by the donor atoms but rather results from the favourable preorganisation of the ligand. The exchange process is fast on the proton NMR time scale, so that two isomers differing only in the water coordination number while retaining the same ligand conformation are indistinguishable.

Solution Thermodynamics

Potentiometry

Potentiometric titration data for the ligand OHEC may be represented conveniently by calculation of the average number of ligand-bound protons ($\tilde{n}_H$) for each point in the titrations, as in Figure 7. Equation (1) defines $\tilde{n}_H$ in terms of K_w, the ionisation constant of water, H_T and L_T, the total (analytical) concentrations of protons and the ligand, respectively, and $[H^+]$ the concentration of free protons. Notably, $\tilde{n}_H$ is calculated entirely from observable param-

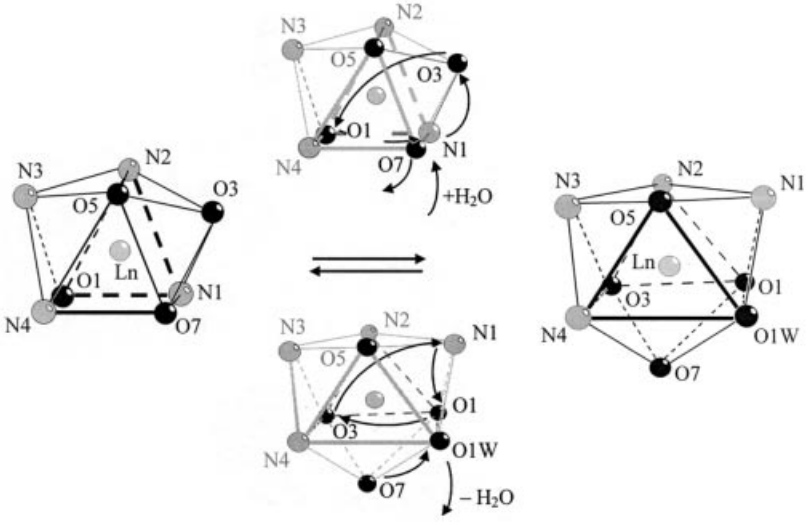

Figure 6. Coordination equilibrium for isomers of lanthanide(III) OHEC complexes

 © 2004 Wiley-VCH Verlag GmbH & Co. KGaA, Weinheim

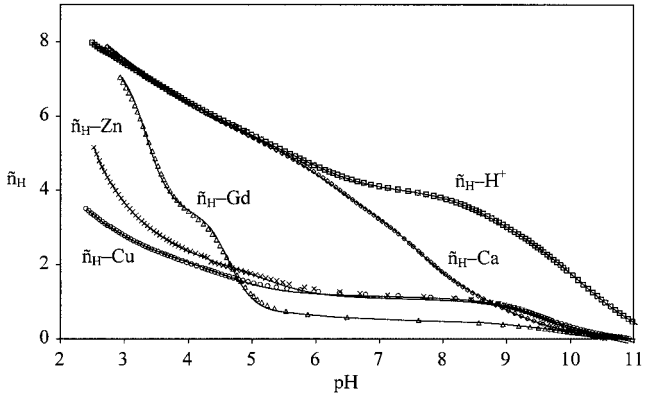

Figure 7. Average number of protons bound ($\tilde{n}_H$) to the ligand OHEC in the presence of the indicated metals, where H^+ indicates the absence of any coordinating metal ion; symbols give observed titration curves and lines the calculated fits to those curves; data were obtained using metal-to-ligand ratios for Cu of 1.9:1, Zn 1.95:1, Ca 1.86:1 and Gd 1.75:1

eters (observed pH and the analytical concentrations) and is, therefore, independent of the chemical model used to extract stability constants from the data. Thus, careful inspection of $\tilde{n}_H$ curves will reveal insights into the chemical equilibria present, and act as a guide in model selection. The solid lines in Figure 7 also give the $\tilde{n}_H$s as derived from the calculated pH. In this manner, the quality of fit between the observations and the refinements is presented.

$$\tilde{n}_H = \frac{H_T - [H^+] + K_W \cdot [H^+]^{-1}}{L_T} \quad (1)$$

All $\tilde{n}_H$ curves in Figure 7 approach zero above pH 11. In this highly basic region, OHEC forms only fully deprotonated species, either as the free ligand or as the various metal complexes. At lower, more acidic pHs, the $\tilde{n}_H-H^+$ curve climbs rapidly, indicating protonation of the ligand with up to eight protons by pH 2.5. In fact the $\tilde{n}_H-H^+$ curve shows no sign of reaching a plateau at this level and more than eight protonation constants might be calculated (OHEC contains up to 16 acid/base donor groups). This was indeed possible, giving protonation constants up to β_{019} (Table 6). The remaining protonation constants up to the 16th value are too acidic to allow measurement by conventional potentiometry.

The $\tilde{n}_H$ curve for Ca^{2+} coincides with that of $\tilde{n}_H-H^+$ below pH 6. Thus, for the conditions of the titration, no coordination with calcium is expected below pH 6, with relatively weak complexation at higher pHs. Indeed, the constants for calcium are the smallest of all metals in Table 6 and the distribution diagram of Figure 8 confirms the absence of calcium-binding below pH 6.

In contrast, OHEC is bound very strongly by Cu^{2+} and Zn^{2+}, affording $\tilde{n}_H$ curves well displaced from that for $\tilde{n}_H-H^+$, even at the strongly acidic pH of 2.5. In fact, the 3.5 protons that remain bound to OHEC at pH 2.5 in the presence of Cu^{2+} are barely enough to allow measurement of the stability constants by potentiometry. Interestingly, both Cu^{2+} and Zn^{2+} generate $\tilde{n}_H$ curves with wide plateaus between pH 6 and 9 at one bound proton, revealing a highly stable M_2LH species, while complete deprotonation of the two metal-centre complex is observed only above pH 9. These observations are reflected in the complexation constants of Table 6 and the lowermost species distribution diagram of Figure 8, which is calculated from those constants.

Finally, Gd^{3+} displays a coordination strength with OHEC that is between those of Ca^{2+} and Cu^{2+}. Below pH 3 the curve $\tilde{n}_H-Gd^{3+}$ rapidly approaches that for $\tilde{n}_H$-H^+, indicating acidic liberation of Gd^{3+} from the ligand. At higher pH, coordination proceeds rapidly and is complete by pH 5.5. The species distribution diagram of Figure 8 with the end species reflects this behaviour, Gd_2L dominating from pH 6 and higher.

Table 6. Protonation and metal complexation constants determined for the ligand OHEC, defined as in Equation (2); figures in parentheses give the standard deviation (σ) expressed in units of the least significant figure of each constant, calculated from the variation between repeat determinations; *n* is the number of determinations for each constant. Note that for the protonation constants the index m is always zero. Logarithms calculated with the decimal basis ($\log_{10}$)

Species	m	l	h	*H* (*m* = 0) log β_{0lh}	n	Gd log β_{mlh}	n	Ca log β_{mlh}	n	Cu log β_{mlh}	n	Zn log β_{mlh}	n
ML	1	1	0			18.32 (2)	6	7.7 (3)	6	18.7 (4)	4	17.4 (3)	4
MLH	1	1	1	10.7 (1)	8	28.53 (9)	5	17.9 (3)	8	28.9 (3)	6	27.7 (1)	6
MLH_2	1	1	2	20.88 (2)	8	37.84 (8)	7	27.4 (3)	12	38.5 (3)	6	37.0 (1)	6
MLH_3	1	1	3	30.36 (4)	8	43.82 (8)	9	35.0 (2)	13	45.6 (2)	6	44.5 (2)	6
MLH_4	1	1	4	38.94 (1)	8	47.8 (1)	10			50.3 (4)	6	49.6 (3)	5
MLH_5	1	1	5	45.14 (4)	8							53.1 (3)	5
MLH_6	1	1	6	50.22 (6)	8								
MLH_7	1	1	7	54.15 (7)	8								
MLH_8	1	1	8	57.21 (4)	8								
MLH_9	1	1	9	59.5 (3)	8								
M_2L	2	1	0			33.6 (1)	8	13.8 (4)	8	36.4 (4)	4	33.4 (3)	6
M_2LH	2	1	1					22.8 (3)	7	45.9 (1)	5	42.9 (2)	6
M_2LH_2	2	1	2							50.5 (2)	6	48.0 (2)	6
M_2LH_3	2	1	3							53.8 (3)	6	51.5 (2)	5

 © 2004 Wiley-VCH Verlag GmbH & Co. KGaA, Weinheim

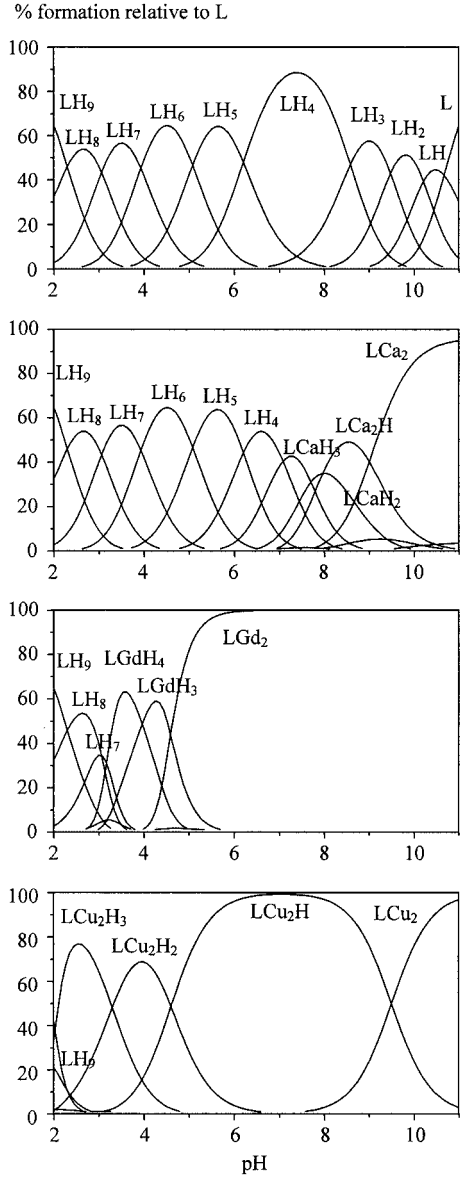

Figure 8. Species distribution diagrams for OHEC and indicated metals (top: calculated for the absence of a coordinating metal). All figures calculated for total concentrations of 5×10^{-4} M ligand and 1×10^{-3} M metal. "L" denotes the deprotonated ligand species OHEC

Comparison of OHEC with Similar Chelators

Macrocyclic OHECs are most easily compared with similar open-chain polyamine polycarboxylic acids by use of the parameter pM, the negative logarithm of the concentration of the free metal species formed at equilibrium for given total concentrations of metal, ligand and pH. Higher pMs indicate stronger complexation since the free metal concentration is depressed to a lower level. This parameter has the advantage that ligands of differing basicity, denticity and nucleacity may be compared directly, which is not the case when the absolute magnitude of stability constants is simply compared. pMs for OHEC and all the studied metals along with the values for the ligands DTPA, DOTA and EDTA are given in Table 7.[21−32] The relatively weak binding properties of OHEC are immediately apparent. Reading across the rows for each metal, OHEC gives rise to the smallest pM amongst all ligands. This is probably due to the binuclear nature of OHEC, such that the second metal centre is always more weakly bound than the first. Nonetheless, the binding strength of OHEC for Gd^{3+} remains very high and similar to that of the commercially applied contrast agents.

Table 7. pM for the ligands OHEC, DTPA, DOTA, and EDTA, calculated for a total metal concentration of 1×10^{-6} M and a total ligand concentration 1×10^{-5} M at pH 7.4; for OHEC the equilibrium constants determined in this work were used, for other ligands literature values were used[22−33]

pM	OHEC	DTPA	DOTA	EDTA
Gd	14.6	18.7	18.9	16.4
Ca	6.0	7.5	11.3	8.4
Cu	15.5	18.1	17.6	17.3
Zn	14.2	15.3	16.0	14.3

Also apparent from Table 7 is the improved selectivity of OHEC for Gd^{3+} over Ca^{2+} with respect to the selectivity of the commercially applied contrast agents DTPA and DOTA. Indeed, the pM for OHEC and Ca^{2+} is 6.0, indicating no complexation of the metal, i.e. all the Ca^{2+} exists as the free cation under the conditions of the calculation. In contrast, OHEC displays a poorer selectivity for Gd^{3+} over the transition metals Cu^{2+} and Zn^{2+}. The pM for OHEC and Zn^{2+} (14.2) approaches that for Gd^{3+} (14.6) while that for Cu^{2+} (15.5) even exceeds that of Gd^{3+}. Thus, the selectivity of OHEC for Gd^{3+} over these latter two transition metals most closely resembles that of EDTA, a ligand whose gadolinium complex gives rise to toxic impacts.[33] However, the in vivo concentration of Ca^{2+} within human blood serum (2.5−4 millimolar)[34] is much higher than the concentrations of Cu^{2+} and Zn^{2+} (1−10 micromolar and 10−50 micromolar, respectively).[34] The high selectivity of OHEC for Gd^{3+} over Ca^{2+} is therefore a positive result for the potential application of this ligand as a contrast agent for MRI.

The relatively weak binding of Ca^{2+} and Gd^{3+} by OHEC is consistent with the presence of propylene bridging groups in this ligand. These give rise to six-membered chelate rings and a significantly reduced "bite-size"[36] (2.5 Å in the idealised conformation) between the chelating nitrogen atoms of the amine. In the corresponding five-membered rings formed by ethylene-bridged amines this bite-size is 2.8 Å for the idealised conformation. The ligands of Table 7 to which OHEC is compared, all contain exclusively ethylene-bridged amines. As has been reviewed,[35] this decrease in bite-size for six-membered chelate rings has virtually no effect on the stability of complexes formed with Cu^{2+} and Zn^{2+} since these metals have relatively small ionic radii, 0.73 and 0.74 Å, respectively.[36] However, for the larger cations Ca^{2+} and Gd^{3+} (ionic radii of 1.12 and 1.053 Å, respectively)[36] the decrease in bite-size reduces complex

 © 2004 Wiley-VCH Verlag GmbH & Co. KGaA, Weinheim

stability since the six-membered chelate rings can no longer fully span the metal centres. With Gd^{3+}, however, the complex remains significantly stable since this trivalent cation has a higher charge density than Ca^{2+}. The identical trend in thermodynamic stabilities has been observed for complexes formed between the metals Cu^{2+}, Zn^{2+}, Ca^{2+}, and Gd^{3+} with DOTA and a pair of propylene-bridged derivative ligands.[22,37]

Conclusion

The polyaminocarboxylate macrocycle OHEC ligand developed here can bind two lanthanide ions in close proximity. Homodinuclear lanthanide complexes of OHEC show an interesting coordination equilibrium, depending on the ionic radii of the bound lanthanide ions. Whereas ninefold-coordinated CSAP solid-state structures are found for the mid to early lanthanide(III) ions (Gd, Eu, La) with larger radii, the late lanthanides (Lu, Yb) show eightfold coordination in BCTP structures. These two solid-state structures are the basis for the recently published extensive characterization of the isomerization equilibrium of Ln-OHEC complexes in solution and were used as starting structures for MD calculations.[4]

Ninefold-coordinated Ln-OHEC isomers have one water molecule per lanthanide ion in the inner coordination sphere; this is essential for the efficiency of Gd_2OHEC as a MRI contrast agent. The simultaneous presence of eightfold-coordinated metal centres in solution without water in the first coordination sphere results in a decrease of relaxivity according to the share in the isomerization equilibrium of about 25%.

Nevertheless, OHEC is a useful model ligand in investigating intramolecular electron-spin interactions caused by a short metal−metal distance between paramagnetic lanthanide ions, as shown for the Gd_2OHEC complex. EPR spectra of Gd^{III}- and mixed Gd^{III}/Y^{III} binuclear complexes clearly show that the two Gd^{III} centres interact intramolecularly, resulting in an enhancement of the electronic relaxation of the Gd^{III} electron spins.[38] Other candidates for the investigation of intramolecular electron-spin interactions include bimetallic azacryptates with $Ln^{III}-Ln^{III}$ distances of around 3.5 pm.[39]

The complex solution equilibria of the ligand OHEC have been studied successfully by potentiometry. Using just a single dependent variable, i.e. pH as a function of solution composition, the complete range of solution species and their thermodynamic stabilities could be determined. So much information was extracted from such a simple technique by taking considerable care in the analysis and interpretation of the data. The parameter $\tilde{n}_H$ provided an initial guide in developing a realistic speciation model. Chemical species were included in each metal/ligand/proton system on the basis of their effect upon Σ, the scaled sum of squares. Multiple titrations with suitable variations in concentration and in the metal to ligand ratio were performed for each system. Species that gave rise to highly variable stability constants between independent investigations were viewed as spurious and removed from the model. As a further precaution, titrations were collected for all systems from both forward (vs. KOH) and backward (vs. HCl) titrations. Thus, the equilibrium state was approached from both directions.

The thermodynamic studies revealed that the ligand OHEC is a relatively good chelator for Cu^{2+} and Zn^{2+} while the chelation of Gd^{3+}, and more dramatically Ca^{2+}, is weakened. These trends in complex stability are consistent with the introduction of propylene-bridged amines within the molecular structure of OHEC. The effective deselection of Ca^{2+} by OHEC is a positive result for the potential application of this ligand in a Gd^{3+}-based MRI contrast agent.

Experimental Section

Materials: All reagents used for the preparation of compounds were purchased from either Merck or Aldrich and used as received.

Synthesis: H_8OHEC was prepared by the published method.[1] The sodium salt of the complexes **1** and **2** was prepared by mixing Ln_2O_3, the ligand and NaOH in deionised water (50 mL). The resultant white suspension was heated at 80 °C for several days, until a clear solution was obtained. After cooling to room temperature, the reaction mixture was then filtered and centrifuged to remove undissolved solid material. The final solution was then evaporated to dryness to give a white solid.
Elemental analysis and FAB mass spectra confirmed the composition of the compounds. Elemental analysis: Perkin-Elmer 2400 Series CHNS/O Analyzer. MC: Double-focusing ZAB instrument, VG company (FAB).

X-ray Crystallographic Study: The molecular structures of the complexes **1** and **2** were determined by single-crystal X-ray diffraction. X-ray quality crystals were obtained from saturated aqueous solutions of the pure complexes by slow diffusion of ethanol into the solution of **1** and **2** or by dissolving the solid in a water−ethanol mixture that was kept at 4 °C for several weeks.
Single crystals of compounds **1** and **2** were measured on a STOE Stadi-4 four circle diffractometer at 180 K in a nitrogen atmosphere. Intensity data were corrected for Lorentz, polarisation and absorption (psi-scan technique).[40] Structures were solved by direct methods and refined by full-matrix least-squares against F^2 supported by STOE Xstep software.
Crystal data, data collection and refinement parameters of the structures **1** and **2** are listed in Table 8.
The thermal motion of all non-hydrogen atoms was treated anisotropically, that of hydrogen atoms isotropically and tied 1.2 times higher than the corresponding attached atom.
CCDC-230877 (for **1**) and -230876 (for **2**) contain the supplementary crystallographic data for this paper. These data can be obtained free of charge at www.ccdc.cam.ac.uk/conts/retrieving.html [or from the Cambridge Crystallographic Data Centre, 12 Union Road, Cambridge CB2 1EZ, UK; Fax: (internat.)+44-1223-336-033; E-mail: deposit@ccdc.cam.ac.uk].

NMR Spectroscopy: NMR spectra were recorded on a Bruker AMX 600 and an AVANCE 400 spectrometer equipped with a Silicon Graphics O2 workstation and a HP workstation x1100, respectively. All samples examined were dissolved in deuterated water,

 © 2004 Wiley-VCH Verlag GmbH & Co. KGaA, Weinheim

Table 8. Crystal data, details of data collection, and structure refinement for **1** and **2**

Compound	$[Na_2(Yb_2OHEC)]$ (**1**)	$[Na_2(Lu_2OHEC)]$ (**2**)
Crystal data		
Moiety formula	$[C_{34}H_{52}Yb_2N_8O_{16}]^{2-}$, 14,5$H_2O$, C_2H_5OH, 0.5NaOH	$[C_{34}H_{52}Lu_2N_8O_{16}]^{2-}$, 14,5$H_2O$, C_2H_5OH, 0.5NaOH
Space group	$P\bar{1}$ (no. 2)	$P\bar{1}$ (no. 2)
Crystal system	triclinic	triclinic
M_r [amu]	1540.19	1552.06
Crystal size (mm)	0.76 × 0.71 × 0.68	0.78 × 0.51 × 0.38
a [pm]	10.5840(14)	10.569(4)
b [pm]	15.436(2)	15.562(10)
c [pm]	19.1859(17)	19.143(14)
α (°)	110.330(11)	110.48(5)
β (°)	93.837(16)	93.71(5)
γ (°)	106.546(16)	106.67(4)
V [$pm^3 \times 10^6$]	2769.2(6)	2777(3)
$\rho_{calcd.}$ [gcm^{-3}]	1.847	1.856
F (000) [e]	1558	1570
μ(Mo-K_α) [mm^{-1}]	3.477	3.655
Z	2	2
Data collection	Stoe STADI-4	Stoe STADI-4
Radiation λ [pm]	Mo-K_α, 71.073	Mo-K_α, 71.073
T [K]	180	180
Reflections collected	14527	17771
Reflections unique, R_{int}	10298, 0.0328	10904, 0.0228
$2\Theta_{min/max}$ (°)	4.18/50.98	4.18/52.0
h/*k*/*l* ranges	−12,12/ −18,17/ −23,23	−13,13/ −19,18/ −23,23
Refinement	L. S. full-matrix on F^2	L. S. full-matrix on F^2
Data(n)/parameters(p)	10298/798	10904/805
R_1,[a] wR_2[b] [$I > 2\sigma(I)$]	0.0341, 0.0927	0.0264, 0.0642
R_1,wR_2, GoF[c] (all data)	0.0363, 0.0946, 1.109	0.0298, 0.0663, 1.062
$\Delta\rho_{max/min}$ [e $pm^{-3} \times 10^{-6}$]	1.97/−1.95	1.44/−0.91

[a] $R1 = \Sigma(|F_o| - |F_c|)/\Sigma|F_o|$. [b] $wR2 = \{\Sigma[w(F_o^2 - F_c^2)^2]/\Sigma[w(F_o^2)^2]\}^{1/2}$. [c] $GoF = \{[w(F_o^2 - F_c^2)^2]/(n - p)\}^{1/2}$.

which was also used as fixed internal reference. The signal due to residual HDO was suppressed by continuous low-power irradiation. To assign the spectra, 2D and 1D NOE difference experiments were carried out. 2D ^{1}H NMR experiments (H,H-COSY, TOCSY and EXSY) were recorded at 278 K with a sweep-width of δ = 12 ppm for non-paramagnetic compounds and δ = 60 ppm for Eu_2OHEC. Data matrices typically consisted of 4096 complex points in F2 for each of the 1024 F1 increments, the data being zero-filled to a 8192 × 2048 complex matrix before transformation. The EXSY spectrum was recorded using the conventional NOESY phase-sensitive pulse sequence ($90° - t_1 - 90° - \tau_m - 90° -$ acq) with a mixing time of 60 ms.

Solution Thermodynamics: Equilibrium constants were measured at 25 °C in aqueous solution with a supporting electrolyte of 0.1 M KCl. They are defined, Equation (2), as cumulative formation constants (β_{mlh}, where M, L and H refer to the free metal, ligand and proton species, respectively).

$$\beta_{mlh} = \frac{[M_m L_l H_h]}{[M]^m [L]^l [H]^h} \quad (2)$$

Determination of the solution equilibria formed by the ligand OHEC is a challenging problem. The ligand contains 16 donor atoms that simultaneously interact with solution protons and any coordinating metals present. The macrocyclic ring may incorporate up to two metal centres. Ultra-violet/visible spectroscopic measurements were not possible as the ligand is an aliphatic amino-carboxylate. Thus, classical potentiometry was applied.

Apparatus: Titrations were performed in a custom-built 100-mL cell and were held under a positive pressure of N_2 to eliminate ingress of CO_2. The cell was constructed of Pyrex glass with a water jacket for temperature control and a PVC lid with various openings for gas control and insertion of the electrode and burette tips. The glass-bulb pH electrode was obtained from Corning (General Purpose High Performance, catalogue no. 476146). An autoburette from Metrohm (model 716) was employed for titrant delivery and measurement of the electrode potential. The burette was controlled by a personal computer using the LABVIEW[41] programming environment, which allowed automated titration execution. An analytical grade balance (±0.05 mg) was used.

Electrode Calibration: The electrode was calibrated, using a published protocol, over the pH range 2.5 to 11.5 before each titration.[42] Data were analysed using the program GLEE.[43] The parameters E^0 (standard potential), *s* (slope of the electrode) and γ (correction factor of the base concentration) were refined while pK_w was fixed at 13.78.[44,45]

Reagents: All solutions were prepared from deionised (resistivity ≥ 18 MΩ) water. Dissolved CO_2 was removed by boiling and subsequent cooling under N_2. Acid and base solutions (≈0.1 M HCl and KOH) were prepared using Merck Titrisol ampoules and standardized to ±0.2% against potassium hydrogen phthalate (99.95% Aldrich) with phenolphthalein as a visual end-point indi-

 © 2004 Wiley-VCH Verlag GmbH & Co. KGaA, Weinheim

cator. Stock solutions of the various metals were prepared in 0.01 M HCl from high purity chloride salts ($GdCl_3$ 99.9% ChemPur, $CaCl_2$ 99% ChemPur, $CuCl_2$ 99.999% Alfa Aesar, $ZnCl_2$ 99.999% Alfa Aesar). These stock solutions were standardised by chelometric titration against a solution of EDTA ($Na_2EDTA{\cdot}2H_2O$ 99% Aldrich) which was in turn standardised by potentiometric titration against an HCl solution. For each metal ion, an appropriate buffer system and indicator dye was used in the chelometric standardisations: for Gd^{3+} Arsenazo III[46] in 0.05 M ammonium acetate, for Ca^{2+} and for Zn^{2+} Xylenol Orange[47] in 6×10^{-4} cetylpyridinium chloride and 0.05 M ammonium acetate adjusted to pH 9, and for Cu^{2+} Xylenol Orange[45] in 0.05 M ammonium acetate adjusted to pH 7. The particular batch of H_8OHEC used for the titrations was isolated as an hydrochloride salt and gave an analytical analysis: $C_{34}H_{60}N_8O_{16}{\cdot}3.5HCl{\cdot}4.5H_2O$ (1044.6): calcd. C 39.1, H 7.0, N 10.7, Cl 11.9; found C 38.7, H 6.5, N 10.4, Cl 12.3.

Titrations: Test solutions were assembled in the titration cell by combining an aliquot of the electrolyte solution (from an A-grade pipette) with a weighed portion of the ligand and, when appropriate, an aliquot of a metal stock solution. Care was taken to add the metal stock solution after dissolution of the ligand to avoid the possibility of metal ion hydrolysis. Concentrations in the range $2.4-9.2\times0^{-4}$ M H_8OHEC were used for protonation studies. Metal complexation experiments employed concentrations of $2.4-9.6\times10^{-4}$ M H_8OHEC and of $0.37-1.7\times10^{-3}$ M for the metal ion, with metal-to-ligand ratios ranging from 1:1 to 1.95:1. In titrations containing the weakly hydrolysed Ca^{2+} an excess of the metal above two equivalents was occasionally used, up to 2.2:1. The resulting solutions typically had an initial pH of ≈3 and were initially titrated to pH 11 with KOH, followed by back titration to pH 2.5 with HCl so that the equilibrium state was approached from both directions. Following addition of titrant the system was allowed to equilibrate for 90 s for ligand-only titrations, 180 s in the presence of a metal, after which time the electrode potential was measured. On obtaining 10 measurements with a standard deviation of ≤0.05 mV the electrode potential was considered stable, a pH measurement was recorded and the titration proceeded to the next point. Each titration contained approximately 120 points, collected between pH 2.5 and 11, each being a measurement of pH versus volume of titrant.

Data Treatment: Equilibrium constants were determined from the titration data by least-squares refinement using the computer program HYPERQUAD.[48] The data from each pair wise set of titrations, i.e. initial titration with KOH and back titration with HCl, were imported into the program along with values for the titrant concentration, initial volume and analytical concentrations of the reagents, as calculated from either the mass of ligand or volume of metal stock taken. The analytical concentration of protons was treated as a refinable parameter, always returning a value within 5% of the initial estimate. The "automatic" weighting scheme was selected with error estimates of 0.002 mL for the titre values and 0.002 pH. Following refinement of the equilibrium constants, the quality of fit was assessed with Σ, the scaled sum of squares, which has an expectation value of one for perfectly fit data. Obtained values ranged between 0.6 and 5.9 with an average of 2.4. Individual species were included into or rejected from the coordination model based on their effect upon Σ. Also, species that gave widely divergent equilibrium constants (standard deviation ≥ 0.5) between independent titrations were rejected. The resulting equilibrium constants, determined from a total of 53 titrations, are given in Table 6.

Acknowledgments

B. O'Sullivan gratefully acknowledges the support of the Alexander von Humboldt Foundation with the awarding of fellowship IV NEU/1070214 STP.

[1] H. Schumann, U. A. Böttger, K. Zietzke, H. Hemling, G. Kociok-Köhn, J. Pickardt, F.-E. Hahn, A. Zschunke, B. Schiefner, H. Gries, B. Radüchel, *Chem. Ber./Recueil* **1997**, *130*, 267−277.
[2] H. Schumann, U. A. Böttger, H. Weisshoff, B. Ziemer, A. Zschunke, *Eur. J. Inorg. Chem.* **1999**, 1735−1743.
[3] H. Schumann, U. A. Böttger, A. Zschunke, H. Weisshoff, B. Ziemer, *Mat. Sc. For.* **1999**, *128*, 315−317.
[4] G. M. Nicolle, Y. Fabrice, D. Imbert, U. A. Böttger, J.-C. Bünzli, A. E. Merbach, *Chem. Eur. J.* **2003**, *9*, 5453−5467.
[5] J. Dale, *Isr. J. Chem.* **1980**, *20*, 3−11.
[6] C. W. Haigh, *Polyhedron* **1995**, *14*, 2871−2878.
[7] E. L. Muetterties, L. J. Guggenberger, *J. Am. Chem. Soc.* **1974**, *96*, 1748−1756.
[8] S. Aime, A. Barge, M. Botta, M. Fasano, J. D. Ayala, G. Bombieri, *Inorg. Chim. Acta* **1996**, *26*, 423−429.
[9] F. Benetello, G. Bombieri, L. Calabi, S. Aime, M. Botta, *Inorg. Chem.* **2003**, *42*, 148−157.
[10] K. Micskei, L. Helm, E. Brücher, A. E. Merbach, *Inorg. Chem.* **1993**, *32*, 3844−3850.
[11] M.-R. Spirlet, J. Rebizant, J. F. Desreux, M.-F. Loncin, *Inorg. Chem.* **1984**, *23*, 359−363.
[12] J. A. Peters, E. Zitha-Bovens, D. M. Corsi, C. F. G. C. Geraldes, *The Chemistry of Contrast Agents in Medical Magnetic Resonance Imaging*, **2001**, p. 315−382.
[13] F. Uggeri, S. Aime, P. L. Anelli, M. Botta, M. Brochetta, C. DeHaen, G. Ermondi, M. Grandi, *Inorg. Chem.* **1995**, *34*, 633−642.
[14] S. Aime, M. Botta, M. Fasano, M. P. M. Marques, C. F. G. C. Geraldes, D. Pubanz, A. E. Merbach, *Inorg. Chem.* **1997**, *36*, 2059−2068.
[15] E. Bovens, M. A. Hoefnagel, E. Boers, H. Lammers, H. van Bekkum, J. A. Peters, *Inorg. Chem.* **1996**, *35*, 7679−7683.
[16] S. Aime, A. Barge, A. Borel, M. Botta, S. Chemerisov, A. E. Merbach, U. Müller, D. Pubanz, *Inorg. Chem.* **1997**, *36*, 5104−5112.
[17] É. Tóth, *The Chemistry of Contrast Agents in Medical Magnetic Resonance Imaging*, **2001**, p. 74−78.
[18] H. D. Powell, O. M. Ni Dhubhghaill, D. Pubanz, L. Helm, Y. Lebedev, W. Schlaepfer, A. E. Merbach, *J. Am. Chem. Soc.* **1996**, *118*, 9333−9346.
[19] E. Tóth, D. Pubanz, S. Vauthey, L. Helm, A. E. Merbach, *Chem. Eur. J.* **1996**, *2*, 1607−1615.
[20] E. Tóth, F. Connac, L. Helm, K. Adzamli, A. E. Merbach, *Eur. J. Inorg. Chem.* **1998**, 2017−2021.
[21] E. T. Clarke, A. E. Martell, *Inorg. Chim. Acta* **1991**, *190*, 27−36.
[22] E. W. Baumann, *J. Inorg. Nucl. Chem.* **1974**, *16*, 1827−1832.
[23] G. Anderegg, P. Nägeli, F. Müller, G. Schwarzenbach, *Helv. Chim. Acta* **1959**, *42*, 827−836.
[24] A. P. Brunetti, G. H. Nancollas, P. N. Smith, *J. Am. Chem. Soc.* **1969**, *91*, 4680−4683.
[25] J. D. Carr, D. G. Swartzfager, *J. Am. Chem. Soc.* **1975**, *97*, 315−321.
[26] S. Chaberek, A. E. Frost, M. A. Doran, N. J. Bicknell, *J. Inorg. Nucl. Chem.* **1959**, *11*, 184−196.
[27] R. Delgado, J. J. R. Fraústo Da Silva, *Talanta* **1982**, *29*, 815−822.
[28] E. J. Durham, D. P. Ryskiewich, *J. Am. Chem. Soc.* **1958**, *80*, 4812−4817.
[29] C. Gèze, C. Mouro, F. Hindré, M. Le Plouzennec, C. Moinet, R. Rolland, L. Alderighi, A. Vacca, G. Simmoneaux, *Bull. Soc. Chim. France* **1996**, *133*, 267−272.
[30] T. F. Gritmon, M. P. Goedken, G. R. Choppin, *J. Inorg. Nucl. Chem.* **1977**, *39*, 2021−2023.

 © 2004 Wiley-VCH Verlag GmbH & Co. KGaA, Weinheim

[31] K. Kumar, C. Allen Chang, L. C. Francesconi, D. D. Dischino, M. F. Malley, J. Z. Gougoutas, M. F. Tweedle, *Inorg. Chem.* **1994**, *33*, 3567−3575.
[32] R. A. Overvoll, W. Lund, *Anal. Chim. Acta* **1982**, *143*, 153−161.
[33] R. B. Lauffer, *Chem. Rev.* **1987**, *87*, 901−927.
[34] W. P. Cacheris, S. C. Quay, S. M. Rocklage, *Mag. Res. Imag.* **1990**, *8*, 467−481.
[35] R. D. Hancock, *J. Chem. Educ.* **1992**, *69*, 615−621.
[36] R. D. Shannon, *Acta Crystallogr., Sect. A* **1976**, *32*, 751−767.
[37] E. T. Clarke, A. E. Martell, *Inorg. Chim. Acta* **1991**, *190*, 37−46.
[38] G. M. Nicolle, L. Helm, A. E. Merbach, *Magn. Res. Chem.* **2003**, *41*, 794−799.
[39] F. Avecilla, C. Platas-Iglesias, R. Rodríguez-Cortiñas, G. Guillemot, J.-C. G. Bünzli, C. D. Brondino, C. F. G. C. Geraldes, A. de Blas, T. Rodríguez-Blas, *J. Chem. Soc., Dalton Trans.* **2002**, 4658−4665.
[40] N. Walker, D. Stuart, *Acta Crystallogr., Sect. A* **1983**, *39*, 158−166.
[41] *LABVIEW, 6.1*, National Instruments Corporation, http://www.ni.com/, 11500 N Mopac Expwy, Austin, TX 78759−3504.
[42] A. R. Johnson, B. O′Sullivan, K. N. Raymond, *Inorg. Chem.* **2000**, *39*, 2652−2660.
[43] P. Gans, B. O′Sullivan, *Talanta* **2000**, *51*, 33−37.
[44] H. S. Harned, B. B. Owen, *The Physical Chemistry of Electrolytic Solutions*, Reinhold Pub. Corp., New York, **1958**, p. 803.
[45] F. H. Sweeton, R. E. Mesmer, C. F. J. Baes, *J. Sol. Chem.* **1974**, *3*, 191−196.
[46] K. Ueno, T. Imamura, K. L. Cheng, *Handbook of Organic Analytical Reagents*, CRC Press, Boca Raton, FL, **1992**, p. 615.
[47] V. Svoboda, V. Chromý, *Talanta* **1965**, *12*, 431−436.
[48] P. Gans, A. Sabatini, A. Vacca, *Talanta* **1996**, *43*, 1739−1753.

Received February 15, 2004
Early View Article
Published Online August 12, 2004

 © 2004 Wiley-VCH Verlag GmbH & Co. KGaA, Weinheim

18-Crown-6 and Titanium Tetrafluoride − Preparation of the Ti^{IV} Fluoride Crown Ether Complexes $(TiF_4)_2$(18-Crown-6) and the Stabilization of *cis*-$TiF_4(H_2O)_2$ in [{*cis*-$TiF_4(H_2O)_2$}$_2$(18-Crown-6)]

T. Stanley Cameron,[a] Andreas Decken,[b] Evgeny G. Ilyin,[c] Grigori B. Nikiforov,[b] and Jack Passmore*[b]

Keywords: Titanium(IV) / Fluorides / Crown ether / Macrocyclic ligands / Coordination modes / Host-guest systems

Reaction of TiF_4 and 18-crown-6 in MeCN affords the molecular complex [(*cis*-$TiF_4)_2$(18-crown-6)] (**1**) only. Water and THF displace the 18-crown-6 in the tetrafluoro complex **1**, with the formation of *cis*-TiF_4L_2. The complex *cis*-$TiF_4(H_2O)_2$ and 18-crown-6 form [{*cis*-$TiF_4(H_2O)_2$}$_2$(18-crown-6)] (**2**), in which *cis*-$TiF_4(H_2O)_2$ and 18-crown-6 are connected by hydrogen bonding through the protons of coordinated H_2O in $TiF_4(H_2O)_2$ and the oxygen atoms of the crown ether. Complexes **1** and **2** were characterized by X-ray single crystal analysis, elemental analysis, IR, NMR and Mass spectroscopy. The relative basicities of the 18-crown-6 and the molecular donor ligands MeCN, THF, H_2O toward Ti^{IV} fluoride were established by NMR spectroscopic investigations of the substitution reactions. 18-crown-6 is slightly more basic than MeCN, similar to that of Et_2O, and less basic than THF and H_2O.
(© Wiley-VCH Verlag GmbH & Co. KGaA, 69451 Weinheim, Germany, 2004)

Introduction

Crown ethers are known as variable multidentate ligands that act as macrocycles and chelate ligands,[1] and form a variety of host guest complexes with the neutral molecules.[2] Interest in the crown ethers stems in part from its ability to stabilize metal cations,[1,2] cationic complexes, and aqua complexes of the transition metals.[1−3] Interaction of the transition metal chloride salt, for example $FeCl_3$, $CoCl_2$, $CuCl_2$, VCl_4, with the crown ether in the acetonitrile solution spontaneously yields cationic transition-metal complexes.[4] The group IV chlorides $TiCl_4$, $SnCl_4$,[5] and $TiCl_3$[3e] in the presence of moisture and 18-crown-6 give molecular donor-acceptor adducts with a rare bidentate bonding mode for the 18-crown-6 molecule. The crown ether pillared α-zirconium phosphonate phosphate $Zr_2(L)_{1.17}(PO_4)(HPO_4)_{0.83}F_2Cl_{0.17}(H_2O)_{1.69}$ (L = 1-aza-15-crown-5), according to the solid state NMR spectroscopy, contains the fluorine atom bonded to Zr, and was found to have selective ion exchange properties.[6] However, to the best of our knowledge, no structurally characterized group IV crown ether fluoride complexes are found in the literature.'

Titanium fluoride complexes have been attracting considerable attention for use in several fields including synthetic methodology, catalysis and theoretical studies. $TiHal_4$ (Hal = F, Cl) was used as a reference Lewis acid for the theoretical investigation of the nature of donor−acceptor bond in complexes of the type $TiHal_4L_2$ [L= $C(NH_2)_2$, NH_3, CO].[7] The complex $CpTiF_3$ is active in syndiospecific styrene polymerization in the presence of methylaluminoxane (MAO),[8] and $[TiF_2(NMe_2)_2]_4$ was found to have a relatively modest activity for the catalysis of olefin polymerizations in the presence of MAO.[9] An equimolar mixture of TiF_4 and (*S*)-(−/)-1,1′-bi-2-naphthol treated with 2 equiv. of allylsilane is an effective catalyst for enantioselective addition of allylsilanes to aldehydes.[10] In addition, titanium fluoride complexes have been extensively employed as complexing agents for LiF, NaF, MgF_2, CaF_2, Li_2O, ZnF_2, and preparation of hot-guest compounds, e. g. (Cp*$TiF_3)_4CaF_2$, [$(Cp^*TiF_3)_8(ZnF_2)_3$] etc., which are soluble in organic solvents.[11]

Our interest in the chemistry of titanium fluoride complexes is focused on the structure and reactivity of the complexes, and on the development of a simple high yield synthesis of the Ti^{IV} non-metallocene fluoride complexes. In this paper, we report the preparation, characterization and stability of the titanium(IV) fluoride complex with 18-

[a] Department of Chemistry, Dalhouse University, Halifax, NS B3H 4J3, Canada
[b] Chemistry Department, University of New Brunswick, E3B 6E2 Fredericton, N.B., Canada
Fax: (internat.) +1-506-453-48-21
E-mail: passmore@unb.ca
[c] N. S. Kurnakov Institute of General and Inorganic Chemistry of Russian Academy of Sciences
117907 Moscow GSP-1, Leninsky Prospect 31, Russia
E-mail: eilyin@igic.ras.ru
Supporting information for this article is available on the WWW under http://www.eurjic.org or from the author.

crown-6. In addition, 18-crown-6 was used to stabilize *cis*-$TiF_4(H_2O)_2$, which was found as an intermediate hydrolysis product of TiF_4.[12] The complex *cis*-$TiF_4(H_2O)_2$ was reported to be unstable to give $(H_3O)[TiF_4(OH)(H_2O)]$.[12]

Results and Discussion

Reaction of TiF_4 and Crown-6 in MeCN, Preparation of $[(TiF_4)_2(18\text{-Crown-6})]$ (1)

Interaction of 2 or 3 M TiF_4 and 1 M of 18-crown-6 in the MeCN led to the precipitation of crystalline $[(TiF_4)_2(18\text{-crown-6})]$ (**1**) with an isolated yield of approximately 50% (Scheme 1). Reaction of 1 M TiF_4 and 1 M 18-crown-6 in the same solvent led to the isolation of 18-crown-6 and complex **1**.

$$(2 \text{ or } 3)TiF_4 + [18\text{-Crown-6}] \xrightarrow{MeCN} [TiF_4]_2(18\text{-Crown-6}) \downarrow$$

Scheme 1

The structure of **1** consists of a discrete $[(TiF_4)(18\text{-crown-6})(TiF_4)]$ molecular complex (Figure 2),[13] with bidentate chelation by oxygen atoms of the crown ether to each titanium atom. The most related halogen containing complexes are $[PPh_4]_2[(VCl_4)_2(18\text{-crown-6})]$[3f] and $[TiCl_4(18\text{-crown-6})]$,[5] in which each metal atom is bidentately coordinated to oxygen atoms of 18-crown-6. Both M−O bond lengths in $[(VCl_4)_2(18\text{-crown-6})]$ [2.116(6) and 2.117(6) Å] and in $[TiCl_4(18\text{-crown-6})]$ [2.123(8) and 2.154(9) Å], and O−M−O angles 75.6(2)° and 75.5°, respectively, vary only slightly from those in **1** (Table 1). Complex **1** can also be compared with the binuclear anionic complex $[(TiF_4)(\mu\text{-}C_2O_4)(TiF_4)]^{2-}$,[14] in which each TiF_4 unit is coordinated to two oxygen atoms of the oxalato anion. The Ti−O bond lengths in **1** are similar to the corresponding bond lengths in the binuclear anion $[(TiF_4)(\mu\text{-}C_2O_4)(TiF_4)]^{2-}$.[14] The bidentate ligating mode of the crown ether is relatively rare and has been mostly observed for early transition metal chloride complexes of titanium and vanadium.[5,15]

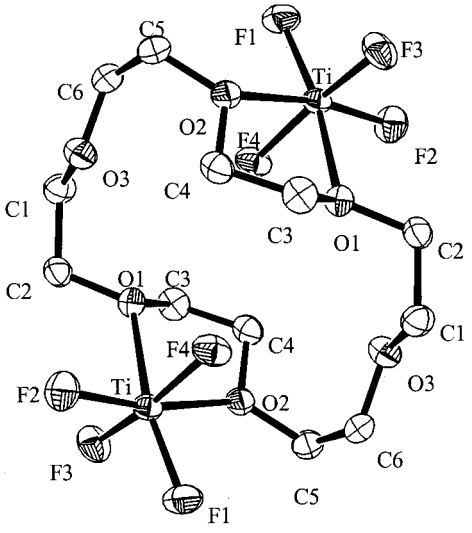

Figure 1. ORTEP drawing (50% thermal probability ellipsoids) of the crystal structure of $[(cis\text{-}TiF_4)_2(18\text{-crown-6})]$ (**1**) with atomic numbering scheme; hydrogen atoms are omitted for clarity

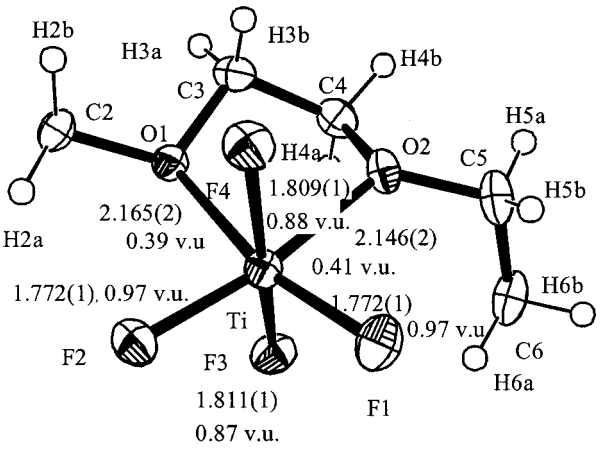

Figure 2. A portion of the $[(cis\text{-}TiF_4)_2(18\text{-crown-6})]$ (**1**) molecule showing the coordination sphere around titanium with the corresponding distances (Å) and bond valences (v.u.)[13]

Table 1. Selected bond lengths (Å) and angles (°) for **1** and **2**; symmetry transformations used to generate equivalent atoms in **1**: $1 - x + 1, -y + 1, -z + 2$; symmetry equivalent positions as x, y, z in **2**: $+x, +y, +z$; $1/2 - x, 1/2 + y, 1/2 - z$; $-x, -y, -z$; $1/2 + x, 1/2 - y, 1/2 + z$

Bond lengths (Å)		Angles (°)	
Complex **1**			
Ti−F(1)	1.772(2)	F(1)−Ti−F(2)	103.12(7)
Ti−F(2)	1.772(2)	F(1)−Ti−F(4)	94.61(6)
Ti−F(4)	1.809(2)	F(1)−Ti−O(1)	164.78(7)
Ti−F(3)	1.811(2)	F(1)−Ti−O(2)	88.95(6)
Ti−O(2)	2.146(2)	F(4)−Ti−F(3)	166.46(6)
Ti−O(1)	2.165(2)	O(2)−Ti−O(1)	75.86(6)
Complex **2**			
Ti−F(2)	1.831(3)	F(2)−Ti−F(3)	95.6(1)
Ti−F(3)	1.790(3)	F(2)−Ti−F(5)	93.4(1)
Ti−F(5)	1.808(3)	F(2)−Ti−O(4)	178.5(1)
Ti−F(6)	1.811(3)	F(2)−Ti−O(5)	92.7(1)
Ti−O(4)	2.087(3)	F(5)−Ti−F(6)	165.6(1)
Ti−O(5)	2.065(3)	O(4)−Ti−O(5)	86.0(1)

The Ti−F bonds of the *trans* F−Ti−O fragment of **1** are shorter than those of the ordinate F−Ti−F fragment due to the *trans* effect in octahedral Ti^{IV} complexes (Table 1). In previously reported *cis*-TiF_4L_2 (L=DMSO), Ph_3PO,[16,17] and $[(cis\text{-}TiF_4)(\mu\text{-}C_2O_4)(cis\text{-}TiF_4)]^{2-}$ [14] complexes, the *trans* effect was implied by the data, but the high Ti−F standard deviation and nonequivalence of all the Ti−F distances ruled out unambiguous interpretations. The Ti−F bond lengths for the F−Ti−F moiety in $[(TiF_4)(\mu\text{-}C_2O_4)(TiF_4)]^{2-}$ are 1.802(5) Å and 1.823(5) Å, and those for the F−Ti−O ordinate are 1.792(5) Å and 1.771(5) Å. In this work the standard deviation allows for the unambiguous observation of the *trans* effect in the titanium(IV) fluoride complex **1**. The average F−Ti−F angle of 96.0(1)°

 © 2004 Wiley-VCH Verlag GmbH & Co. KGaA, Weinheim

in **1** is substantially greater than the O−Ti−O angle of 75.9(1)°, reflecting the much greater Ti−F bond order (0.92 v.u. av.) than that of Ti−O (0.40 v.u. av.) and the presence of $p_\pi-d_\pi$ back bonding to titanium.[18]

Elemental analysis shows that complex **1** corresponds to $[TiF_4]_2$(18-crown-6). The crystals of **1** do not change appearance on storage in sealed ampoules at room temperature for several months, but decompose at 141 °C. The heaviest particle detected by EI-MS corresponds to the $[TiF_3(18\text{-crown-6})^+]$ cation. The $[(18\text{-crown-6})^+]$ and $[TiF_3^+]$ ions are also detected. Analysis of the isotope distribution from the EI-MS data also shows ions that are formed by the subtraction of $(CH_2)_2O$ and $O(CH_2)_2O$ from the 18-crown-6.

The observed bands due to Ti−F absorption of **1** [581(m), 648 (vs), 670 (vs) cm^{-1} (IR) and 582 (vs), 672 (vs) cm^{-1} (Raman)] are located in the 400−700 cm^{-1} region for Ti−F vibrations for known TiF_4L_2 complexes. For comparison, these absorptions are located at 560 (vs, br.) for *trans*-$TiF_4(bfq)_2$ (bfq = 5,6 benzoquinoline),[19a] 610 (vs) and 550 (s) for *cis*-$TiF_4(Me_2SO)_2$,[19b] 670 (vs, br.) and 585 (vs, br.) for *cis*-$TiF_4(DME)_2$ (DME = dimethoxyethane),[19b] and 634 (vs, br.) and 562 (s) for *cis*-$TiF_4(bipy)_2$ (bipy = 2,2′-bipyridyl).[19c]

The ^{19}F NMR spectrum of **1** in acetonitrile shows resonances assigned to $TiF_4(MeCN)_2$, $[Ti_2F_9]^-$, oligomeric complexes with bridging fluorine atoms, and *face*-$[TiF_3(MeCN)_3]^+$.[20,21] Two broad resonances at 230−232 and 156−159 ppm (−40 °C) are assigned to the titanium tetrafluoride crown ether complex [*cis*-TiF_4(18-crown-6)] (Supporting Information, Figure S1). Therefore, in the acetonitrile solution of **1**, a complex equilibrium is observed between oligomeric fluoride complexes with bridging fluorides, monomeric complexes of TiF_4 with acetonitrile and TiF_4 complexes with crown ether, since the donor properties of acetonitrile and 18-crown-6 toward TiF_4 are similar.

Resonances assigned to [TiF_4(18-crown-6)] as well as $[Ti_2F_9]^-$ are detected in the ^{19}F NMR spectrum of **1** in $CDCl_3$, which is a very poor donor toward Ti^{IV} fluorides. The corresponding cationic complex is not detected, possibly due to a rapid exchange process involving this complex.

Reaction of Complex 1 with THF and H_2O, Stabilization of *cis*-$TiF_4(H_2O)_2$ by Coordination with the Crown Ether

Complex **1** is very soluble in THF and insoluble in Et_2O. The NMR spectrum of **2** and excess THF in MeCN and $CDCl_3$ at room temperature and at low temperatures show resonances for *cis*-$TiF_4(THF)_2$,[22] as well as a single resonance for 18-crown-6. Therefore, THF displaces MeCN and 18-crown-6 in the titanium(IV) tetrafluoro complexes.

Complex **1** readily reacts with water. The ^{19}F NMR spectrum of **1** and 1−4 equivalents of water in MeCN shows resonances for $[Ti_2F_9]^-$,[21] four resonances for the intermediate oligomeric titanium fluoride complex (A) and *cis*-$TiF_4(H_2O)_2$. The relative concentration of the species in solution depends on the amount of added H_2O (Supporting Information, Figures S11 and S12).

Complex [{*cis*-$TiF_4(H_2O)_2$}$_2$(18-crown-6)] (**2**), formed from *cis*-$TiF_4(H_2O)_2$ and 18-crown-6, precipitates quantitatively as a white insoluble powder on reaction with 4 equivalents of H_2O in acetonitrile. Colorless crystals of **2** are formed from the acetonitrile solution and contain 2.2 mol of water per one mol of complex **1** at −24 °C.

The structure of **2** consists of $TiF_4(H_2O)_2$ and 18-crown-6 units connected through hydrogen bonding (Figure 3) between the protons H(14), H(15), and H(16) of the coordinated H_2O in $TiF_4(H_2O)_2$ and O1, O2, and O3 oxygen atoms of the crown ether. The H(14−16)···O(1−3) distances (Figure 4) in **2** are similar to the corresponding H···O distances in $TiCl_3(H_2O)$[18-crown-6][3e] (1.8 Å) and close to those observed in known hydrogen-bonded complexes

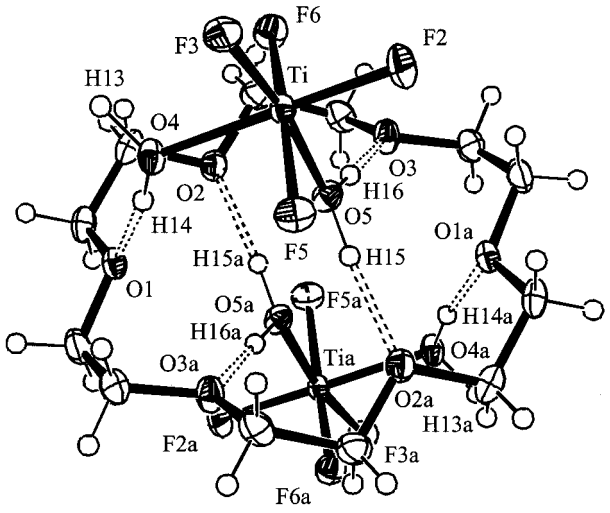

Figure 3. ORTEP drawing (50% thermal probability ellipsoids) of the crystal structure of [{*cis*-$TiF_4(H_2O)_2$}$_2$(18-crown-6)] (**2**) with atomic numbering scheme

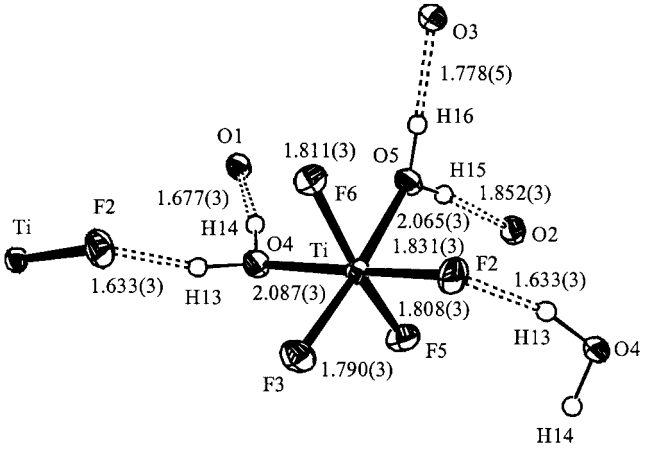

Figure 4. A portion of [{*cis*-$TiF_4(H_2O)_2$}$_2$(18-crown-6)] (**2**) showing the coordination sphere around titanium with the corresponding distances and hydrogen bonding between the protons H13−H16 of the coordinated H_2O and F2 of the neighboring $TiF_4(H_2O)_2$ unit and O1−O3 atoms of 18-crown-6

 © 2004 Wiley-VCH Verlag GmbH & Co. KGaA, Weinheim

(1.7−1.9 Å).[23] The $TiF_4(H_2O)_2$ units are joined together through H(13)···F(2) contacts 1.633(3) Å (Figure 4), which are similar to the H···F distances in related compounds, e.g. $CuF_2{\cdot}2H_2O$ (1.69 Å)[24] and $FeSiF_6{\cdot}6H_2O$ (1.86 Å).[24c]

Each titanium atom in the *cis*-$TiF_4(H_2O)_2$ moiety is connected to four fluorine atoms and two oxygen atoms to form a distorted octahedral environment around the titanium center (Figure 4). The Ti−F bond lengths are nonequivalent. The shortest bond is Ti−F(3) [1.790(3) Å, 0.92 v.u.] and involves the fluorine *trans* to H_2O. The two distances Ti−F(5) and Ti−F(6) in the *trans* F(5)−Ti−F(6) fragment of **2** [1.808(3) Å 0.88 v.u. and 1.811(3) Å 0.87 v.u.] are slightly greater than Ti−F(3) due to the *trans* effect in octahedral Ti^{IV} complexes. The hydrogen bonding between F(2) and H(13) leads to the longer Ti−F(2) bond [1.831(3) Å, 0.83 v.u.]. The titanium−oxygen bond length lies in the range for normal Ti−O distances [1.985(7)−2.160 (6) Å] in known complexes with the oxygen donor ligands.[14,16,17,25] The F−Ti−F, F−Ti−O and O−Ti−O angles (Table 1) around titanium are in agreement with VSEPR theory.[18]

Crystals of **2** change appearance in air due to reaction with H_2O. On storage in sealed ampoules at room temperature they are stable for several months, and decomposition occurs above 200 °C in sealed melting point tubes.

The EI-MS of the hydrolysis product shows $[M^+ - 2HF - C_6H_{12}O_3]$ {252 (2)} and $[M^+ - 2H_2F - C_6H_{12}O_3]$, as well as the cations $[TiF_2O^+]$ and $[TiF_3^+]$, which are formed by the decomposition of **2** during the EI-MS experiment. The strongest signals are for $[C_4H_8O_2^+]$, $[C_3H_6O^+]$, and $[C_2H_5O^+]$, which correspond to fragments of 18-crown-6.

Formation of OH···O hydrogen bonds in **2** is reflected by the strong, broad H_2O IR absorption band at 3350−3150 cm^{-1} (maximum at 3295 cm^{-1}). For comparison, the IR absorption bands for H_2O in $TiCl_3(H_2O){\cdot}$(18-crown-6) occurs at 3380 and 3328 cm^{-1}.[3e] Three TiF_4 absorption bands are observed at 667, 607, and 559 cm^{-1}. The skeletal stretches for 18-crown-6 (839, 900, 962 cm^{-1}) are shifted to higher frequencies relative to those of 18-crown-6 (827, 858, 943 cm^{-1})[26] due to interaction of the oxygen atoms of 18-crown-6 with the protons of the $TiF_4(H_2O)_2$ moieties.

The ^{19}F NMR spectra of **2** in MeCN at room temperature shows resonances assigned to $[Ti_2F_9]^-$, oligomeric titanium complex (A) and *cis*-$TiF_4(H_2O)_2$. Lowering the temperature leads to the disappearance of the resonances assigned to $[Ti_2F_9]^-$, and at −35 °C the ^{19}F NMR spectrum shows resonances for (A) and *cis*-$TiF_4(H_2O)_2$, which is consistent with a temperature-dependent equilibrium between the titanium fluoride complexes in solution.

Interaction between 18-crown-6 and *cis*-$TiF_4(H_2O)_2$ leads to a downfield shift of the proton resonance for 18-crown-6 detected at δ_H = 5.1 ppm [δ_H(18-crown-6) 4.3 ppm]. The proton resonance for the *cis*-$TiF_4(H_2O)_2$ moiety (δ_H = 7.4 ppm) detected at −35 °C also shifts 0.5 ppm downfield relative to that of *cis*-$TiF_4(H_2O)_2$ in MeCN, due to interaction of the protons of coordinated water with 18-crown-6 in solution.

An Estimation of the Basic Properties of 18-Crown-6 Toward Titanium Tetrafluoride

In order to establish the relative stability of the [TiF_4(18-crown-6)] complex, the relative basicity of the commonly used donors and 18-crown-6 was compared.

Previous authors have reported a linear relationship between Δδ (H NMR and F NMR spectroscopy) and ΔH^0 values for adduct formation between a series of bases and substituted phenols,[27] and a linear correlation between Δδ (F NMR spectroscopy) in [*cis*-TiF_4(L1)(L2)] (L1 = *N*,*N*-dimethylacetamide, L2 = *p*-substituted pyridine I-oxide) and the appropriate Hammett substituent parameters[28] and also the electronegativity of the substituent R in L1, L2−R_3PO.[29] A linear relationship was also observed between Δδ (F NMR spectroscopy) in $[TiF_5L]^-$ (L − neutral Lewis bases) and pK_α values.[30] This allows us the opportunity to estimate the donor properties of 18-crown-6 toward TiF_4 with the correlation between Δδ (F NMR) in *cis*-TiF_4L_2 and the donor properties of ligand L. We have observed a linear correlation between Δδ (F NMR) of F_A and F_x in *cis*-TiF_4L_2 (Table 2, Figure 5), and the relative basicities of the molecular ligands L (V.Gutmann, G. Olofsson).[31] From this dependence it was concluded that the basic properties of the crown ether (Table 2, Figure 5) are slightly greater than those of acetonitrile and similar to that of Et_2O.

Table 2. Chemical shifts for the *cis*-TiF_4L_2 complexes

Complex	Solvent	Temp. (K)	δ (CCl_3F) (ppm)	*J* (Hz)	Donor number L	Ref.
$TiF_4(MeCN)_2$	50%MeCN, 50%CH_2Cl_2	182 220	252.4; 169.9 253.3; 171.9	31.3	14.1(MeCN)[a]	[20,35]
$TiF_4(Et_2O)_2$	20%Et_2O, 80% MeCN	203	227.2; 163.2	−	19.2(Et_2O)[a]	[35]
		220	228.6; 164.0	−		
$TiF_4\{(MeO)_3PO\}_2$	MeCN	240	214.0; 149.4	41.3	23.0[a]	[20,35]
$TiF_4(THF)_2$	MeCN	240	214.8; 160.4		20.0[a]	this work
$TiF_4(H_2O)_2$	MeCN	240	215.8; 146.1		24.3[b]	this work
$TiF_4(Ph_3PO)_2$	MeCN	240	197.2; 142.4	41.3	27.0[c]	[20]
$TiF_4(Me_2SO)_2$	MeCN	240	188.4; 137.6	37.1	29.8[a]	[20]
$[TiF_6]^{2-}$	MeCN	240	79.8		53(±5)[c]	[20,36c]
[TiF_4(18-crown-6)]	MeCN	240	230−232; 156−159	−	20(±2)	this work
$TiF_4(H_2O)$(THF)	THF	240	219.5;212.2; 150.3	−		this work

[a] Ref.[31] [b] Ref.[32] [c] Ref.[36c]

 © 2004 Wiley-VCH Verlag GmbH & Co. KGaA, Weinheim

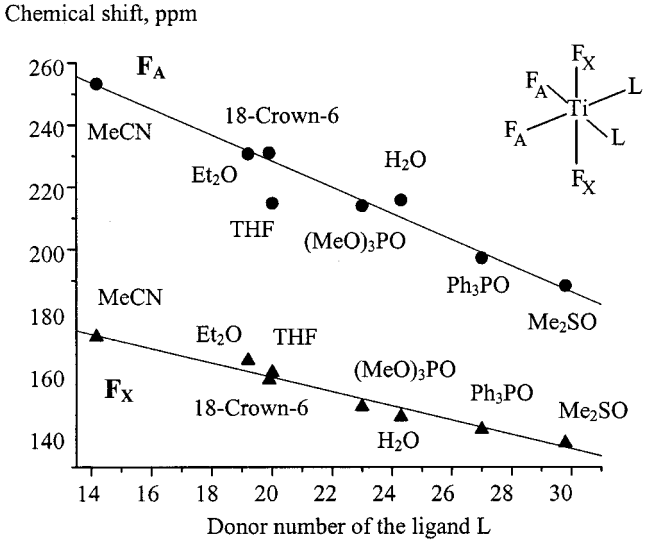

Figure 5. Relationship between the relative basicities of the ligands L (donor number) and chemical shifts of the ^{19}F resonances F_A and F_X in the *cis*-TiF_4L_2 complexes

The substitution reaction (Scheme 2) should proceed[32] if the donor strength of Base1 is greater than that of Base2. The displacement reactions involving TiF_4 and the above molecular donor ligands were studied[16,17,25,33–35] (this work, Supporting Information).

$$[TiF_4(\text{Base 1})] + (\text{Base 2}) \longrightarrow [TiF_4(\text{Base 2})] + (\text{Base 1})$$

Scheme 2

The 18-crown-6 displaces MeCN with the formation of complex **1** in acetonitrile, while THF and H_2O displace 18-crown-6 to give *cis*-TiF_4L_2 (L = THF, H_2O) in solution. Thus, 18-crown-6 is a stronger donor than MeCN, but weaker than THF and H_2O toward titanium tetrafluoride. The basicity of 18-crown-6 might be similar to that of Et_2O since the basic properties of the Et_2O are slightly weaker than those of THF and larger than that of MeCN. Our preliminary NMR spectroscopic study of TiF_4 in mixtures of MeCN and Et_2O show that the mixed complexes $[TiF_4(MeCN)_{2-x}(Et_2O)_x]$ and $[Ti_2F_9]^-$,oligomeric complexes with bridging fluoride atoms, are formed in solutions,[36] much like that in the solution of **1** in MeCN.

Finally, the order of the relative basicities of the ligands in the Ti^{IV} fluoride complexes was established to be MeCN $<$ Et_2O $\approx$ 18-crown-6 $<$ THF $<$ $(MeO)_3PO$ $<$ H_2O[37] $<$ Ph_3PO $<$ Me_2SO $<$ $[F]^-$.

Conclusions

Reaction of TiF_4 and 18-crown-6 in MeCN affords only one molecular complex [(*cis*-TiF_4)$_2$(18-crown-6)] (**1**). The crown ether 18-crown-6 bidentately coordinates through the oxygen atoms to titanium tetrafluoride in **1**, in a manner similar to that in the corresponding chloride complex [$TiCl_4$(18-crown-6)]. However, the stoichiometry of the fluoride and chloride complexes (2:1 and 1:1 respectively) differs from each other, and the complex [TiF_4(18-crown-6)] (1:1) was not isolated from the [TiF_4(18-crown-6)]/acetonitrile system.

Water and THF displaces 18-crown-6 in the tetrafluoro complex with the formation of *cis*-$TiF_4(L)_2$ (L= THF, H_2O) in solution. The complex *cis*-$TiF_4(H_2O)_2$ and 18-crown-6 form [{*cis*-$TiF_4(H_2O)_2$}$_2$(18-crown-6)] (**2**), in which *cis*-$TiF_4(H_2O)_2$ and 18-crown-6 are connected by hydrogen bonding through protons of coordinated H_2O in $TiF_4(H_2O)_2$ and oxygen atoms of the crown ether. Thus, reaction of TiF_4 and **2** with water yields the molecular adduct *cis*-$TiF_4(H_2O)_2$, which was observed in solution,[12] but has not hitherto been isolated and characterized.

The basic properties of 18-crown-6 toward TiF_4 were established from a linear correlation between $\Delta\delta$ (F NMR spectroscopy) of F_A and F_x in *cis*-TiF_4L_2 and the relative basicities of the molecular ligands L (V.Gutmann, G. Olofsson) as well as from the displacement reaction data involving complex **1**, MeCN, THF, and H_2O. The relative basicity of the ligands increase in the order MeCN $<$ Et_2O $\approx$ 18-crown-6 $<$ THF $<$ $(MeO)_3PO$ $<$ H_2O $<$ Ph_3PO $<$ Me_2SO $<$ $[F]^-$.

Thus the molecular donor ligands that have greater donor properties than Et_2O will displace 18-crown-6 in **1**, and THF, H_2O, Me_2SO, and other solvents cannot be used for the preparation and investigation of complex **1**.

Experimental Section

General Remarks: All operations were performed with standard Schlenk line techniques under a purified nitrogen atmosphere. Solid reagents and crystals were manipulated in a Vacuum Atmospheres Dri-Lab equipped with a Dri-Train (HE-493) and 1 kg of 3 Å molecular sieves contained in an internal circulating drying unit. Titanium tetrafluoride (99%, Across Organics) was purified by holding under 2.5 atm of F_2 for 4 days in the Monel metal vessel, 18-crown-6 (99.5%, Aldrich) was used as received, acetonitrile, THF, CH_2Cl_2, and $CDCl_3$ were dried over CaH_2 and degassed. NMR spectra were recorded with a Varian 400 NMR spectrometer. Proton shifts are reported in δ units downfield from Me_4Si, with the solvent as the reference signal. $CClF_3$ was used as a reference for the ^{19}F NMR spectra. NMR samples were prepared in 5 mm NMR tubes fitted with J. Young valves. Mass spectra were recorded on a KRATOS ms 50 TC mass spectrometer equipped with an EI source (30 eV), from samples sealed in dried glass m.p.t. tubes by the direct inlet method. FT-IR spectra were recorded on a Thermo Nicolet spectrometer (Nexus 470 FT-IR), and FT-Raman spectra were obtained from neat samples, sealed under a nitrogen atmosphere in glass capillaries, using an FT-IR spectrometer (Bruker IFS66)

 © 2004 Wiley-VCH Verlag GmbH & Co. KGaA, Weinheim

equipped with an FT-Raman accessory (Bruker FRA 106), incorporating a Nd-YAG laser (emission wavelength: 1064 nm; maximum laser power: 300 mW). Melting points were measured in sealed capillary tubes under nitrogen and are not corrected. Elemental analysis was carried out by Galbraith Laboratories, Inc.

Preparation of [$(TiF_4)_2$(18-Crown-6)] (1): Acetonitrile (30 mL) was condensed into the mixture of TiF_4 (0.8 g, 6.5 mmol) and 18-crown-6 (0.8 g, 3.0 mmol) at −79 °C, and the solution was warmed to 50 °C to dissolve the reagents. The obtained solution was filtered, concentrated to ca. 10−15 mL, and left at room temperature for 5 days. Colorless crystals were separated by filtration, washed three times with cold (−20 to −40 °C) CH_2Cl_2 (5 mL). Yield 0.8 g (50% based on 18-crown-6). M.p. 141−143 °C decomposition. $C_{12}H_{24}F_8O_6Ti_2$ (512.1): calcd. C 28.12, H 4.69, F 29.68; found C 28.00, H 4.55, F 29.20. EI-MS (30 eV, heating room temperature −170 °C): *m/z* = 368 (0.2) [TiF_3(18-crown-6)$^+$], 264 (5) [(18-crown-6)$^+$], 221 (8) [(18-crown-6)−$C_2H_4O^+$], 204 (1) [$TiF_2C_5O_3H_{10}^+$], 188 (3) [$TiF_2C_5H_{10}O_2^+$], 177 (50) [(18-crown-6)−$C_4H_8O_2^+$], 174 (12) [$TiF_2C_4H_8O_2^+$], 161 (3) [(18-crown-6)−$C_4H_8O_3^+$], 159 (3) [$TiF_2C_3H_5O_2^+$], 146 (4) [$TiF_2C_2H_4O_2^+$], 132 (65) [(18-crown-6)−$C_6H_{12}O_3^+$], 116 (35) [$TiF_2CH_2O^+$], 105 (90) [TiF_3^+], 88 (100) [$C_4H_8O_2^+$], calculated theoretical isotops distribution matched that experimentally observed for all peaks. ^{1}H NMR (400 MHz, $CDCl_3$, −60 °C, undissolved solid is present in the NMR ampoule): δ_H = 3.59 (br., 4 H, 7%), 3.64 (s, 4 H), 3.70 (s, 4 H), 3.73 (s, 4 H), sum of the relative intensities of the resonances 3.64, 3.70, 3.73 is 68%, 3.76 (s, 4 H, 2%), 3.80 (s, 4 H, 2%), 3.92 (br., 4 H, 7%), 4.36 (br., 4 H, 7%), 4.57 (br., 4 H, 7%) ppm. ^{19}F NMR (376.3 MHz, $CDCl_3$, −60 °C, undissolved solid is present in the NMR ampoule): δ_F = 260.1 (m, 6F, *face*-[TiF_3(μ-F)$_3$TiF_3]$^-$, 32%), 236.4 (br., [TiF_4(18-crown-6)], 26%), 149.7 (br., [TiF_4(18-crown-6)], 26%), −17.8 (br., 3F, *face*-[TiF$_3$(μ-*F*)$_3$TiF$_3$]$^-$, 16%), −51.3 (C−F), −69.1 (CDF_3), −73.8 (CDF_2Cl), −75.1 (CD*F*Cl$_2$) ppm. ^{19}F NMR (MeCN, room temperature): δ_F = 324 [*face*-TiF_3(MeCN)$_3$], 306 to −260 [{*face*-TiF_3(MeCN)$_x$(μ-F)$_{3-x}$}$_y$, *x* = 0−2], 263.5 (*face*-[TiF_3(μ-F)$_3$TiF_3]$^-$), 232 (br., [TiF_4(18-crown-6)]), 230.3 (br), 215 (br., *cis*-TiF_4-(MeCN)$_2$], 158 (br. [TiF_4(18-crown-6)]), 0 to −20 [{*face*-TiF$_3$(MeCN)$_x$(μ-*F*)$_{3-x}$}$_y$, *x* = 0−2], −20.7 (*face*-[TiF$_3$(μ-*F*)$_3$TiF$_3$]$^-$), (MeCN, −40 °C), 321 [*face*-TiF_3(MeCN)$_3$], 306−260 [{*face*-TiF_3(MeCN)$_x$(μ-F)$_{3-x}$}$_y$, *x* = 0−2], 264.5 (*face*-[TiF_3(μ-F)$_3$TiF_3]$^-$), 254 (m) 231 (br., [TiF_4(18-crown-6)]), 226.8 (br.), 228−202 (overlapped resonances of *cis*-TiF_4(MeCN)$_2$ and mixed monomeric complexes containing MeCN and 18-crown-6), 158 (br. [TiF_4(18-crown-6)]), 0 to −20 [{*face*-TiF$_3$(MeCN)$_x$(μ-*F*)$_{3-x}$}$_y$, *x* = 0−2], −21.6 (*face*-[TiF$_3$(μ-*F*)$_3$TiF$_3$]$^-$) ppm. IR (AgCl, Perflouroalkyl ether, Fluorolube mull): $\tilde{\nu}$ = 1363 (m), 1355 (m), 1305 (m), 1288 (w), 1276 (w), 1264 (m), 1247 (w), 1236 (m), 1142 (s), 1121 (w), 1107 (m), 1066 (s), 1040 (s), 1015 (m), 928 (s), 920 (s), 909 (s), 855 (s), 813 (w) 793 (m), 670 (vs, TiF_4), 648 (vs, TiF_4), 581 (m, TiF_4), 550 (w), 516 (m) cm^{-1}. Raman (solid): $\tilde{\nu}$ = 3026 (s), 3011 (s), 2965 (vs), 2932 (w), 2902 (m), 2874 (s), 2860 (m), 2826 (m), 2743 (w), 1473 (m), 1455 (s), 1425 (w), 1394 (w), 1378 (w), 1352(w), 1295 (m), 1268 (m), 1249 (m), 1236 (w), 1159 (w), 1139 (w), 1117 (w), 1098 (w), 1076 (w), 1060 (w), 1028 (w), 954 (w), 929 (m), 836 (m), 788 (m), 673 (vs, TiF_4), 589 (vs, TiF_4), 558 (w), 505 (w), 422 (w), 354 (w), 336 (w), 284 (m), 265 (m), 245 (m), 229 (w), 209 (w), 179 (w), 108 (w) cm^{-1}. Raman (160−4000 cm^{-1}) spectrum of the compound **1** is given in the Supporting Information (Figure S4).

Interaction of Complex 1 with H_2O: Complex **1** (0.1 g, 0.2 mmol) was loaded into a 5 mm NMR tube, and MeCN (0.7 mL) was added. Four aliquots of H_2O (4 × 0.003.510^{-3} mL) were added by means of a micro syringe. Addition of 3 or 4 equivalents of H_2O (0.6, 0.8 mmol of H_2O) to the solution of **1** leads to precipitation of the white product **2**. Finally, MeCN was removed by decantation, and the resulting solid dried under dynamic vacuum for 1 hour. Recovered 0.11 g of the solid **2**. Yield of **2** 95% (based on **1**). All NMR spectroscopic data are given in the Supporting Information. M.p. 205−207 °C decomposition. $C_{12}H_{32}O_{10}Ti_2F_8$ (584.2): calcd. Ti 16.43; found Ti 16.50. EI-MS (30 eV, heating room temperature −170 °C): *m/z* = 264 (1) [(18-crown-6)$^+$], 254 (2) [M^+ − 2HF − $C_6H_{12}O_3$], 252 (2) [M^+ − $2H_2F$ − $C_6H_{12}O_3$], 221 (1) [(18-crown-6)−$C_2H_4O^+$], 177 (6) [(18-crown-6)−$C_4H_8O_2^+$], 175 (2) [$TiF_2C_4H_9O_2^+$], 133 (10) [$TiFO_4H_2^+$], 117 (6) [$TiFO_3H_2^+$], 101 (20) [TiF_2O^+], 105 (15) [TiF_3^+], 88 (100) [$C_4H_8O_2^+$], 72 (30) [$C_4H_8O^+$], 58 (50) [$C_3H_6O^+$], 45 (100) [$C_2H_5O^+$], calculated theoretical isotope distribution matched that experimentally observed for all peaks. ^{1}H NMR (400 MHz, MeCN, room temperature): δ_H = 5.0 (br), 4.3 (18-crown-6) ppm. ^{1}H NMR (400 MHz, MeCN, −35 °C): δ_H = 7.5 (*H*$_2$O), 5.2 (br), 4.2 (18-crown-6) ppm. ^{19}F NMR (MeCN, room temperature): δ_F = 262.1 (m, 6F, *face*-[TiF_3(μ-F)$_3$TiF_3]$^-$, 10%), 233.0 (m, nF, 6%), 220.7 (m, 2nF, 12%), 214.5 (br., *cis*-TiF_4(H$_2$O)$_2$, 21%), 153.3 (br., *cis*-TiF_4(H$_2$O)$_2$, 21%), −11.7 (m, 2nF, 12%), −19.70 (m, 2nF, 12%), −21.6 (br., 3F, *face*-[TiF$_3$(μ-*F*)$_3$TiF$_3$]$^-$, 5%) ppm. ^{19}F NMR (MeCN, −35 °C): δ_F = 233.0 (m, nF, 7%), 220.7 (m, 2nF, 14%), 210.7 (*cis*-TiF_4(H$_2$O)$_2$, 24%), 148.3 (*cis*-TiF_4(H$_2$O)$_2$, 24%), −11.7 (m, 2nF, 14%), −19.70 (m, 2nF, 14%) ppm. IR (KBr, Perflouroalkyl ether, Fluorolube mull): $\tilde{\nu}$ = 3350−3150 [maximum 3295] (br., vs, H−O stretches), 2408 (w, H_2O), 1352 (s), 1298 (w), 1282 (m), 1269 (w) 1254 (m), 1244 (w), 1234 (w), 1197 (s), 1155 (m), 1124 (s), 1096 (vs), 962 (vs), 900 (s), 839 (s), 745 (m), 667 (s, TiF_4), 607 (s, TiF_4), 559 (s, TiF_4), 522 (m), 439 (w) cm^{-1}.

Reactions between TiF_4 and THF, and H_2O, leading to $TiF_4(THF)_2$ and $TiF_4(H_2O)_2$, respectively are described in the Supporting Information.

Crystal Growth and X-ray Crystallography: Crystals of **1** were grown by slow cooling of a saturated solution in acetonitrile from room temperature to +5 °C. Crystals of **2** were grown by slow diffusion of water vapor into a saturated solution of **1** at +5 °C. Single crystals were coated with Paratone-N oil, mounted using a glass fiber, and frozen in cold nitrogen and mounted on the goniometer. The structure of **1** was measured on a Bruker AXS P4/SMART 1000 diffractometer and that of **2** was measured on a Rigaku AFC5R diffractometer. The data of the major component of **1** and **2** were reduced (SAINT)[38] and corrected for absorption (SADABS).[39] The structures of **1** and **2** were solved by and expanded with Fourier techniques.[40] All non-hydrogen atoms were refined anisotropically. Hydrogen atoms were found in Fourier difference maps and refined isotropically. All calculations were performed with the SHELXTL[41a] (**1**) and teXsan[41] crystallographic software package of Molecular Structure Corporation (**2**). For the structure of **2**, neutral atom scattering factors were taken from Cromer and Waber.[42] Anomalous dispersion effects were included in $F_{calcd.}$;[43] the values for $\Delta f'$ and $\Delta f''$ were those of Creagh and McAuley.[44] The values for the mass attenuation coefficients are those of Creagh and Hubbell.[45]

CCDC-35610 and CCDC-235611 contain the supplementary crystallographic data for this paper. These data can be obtained free of charge at www.ccdc.cam.ac.uk/conts/retrieving.html [or from the Cambridge Crystallographic Data Centre, 12 Union Road, Cambridge CB2 1EZ, UK; Fax: (internat.) +44-1223-336-033; E-mail: deposit@ccdc.cam.ac.uk].

Table 3. Crystallographic data of the X-ray diffraction studies of **1** and **2**

	1	**2**
Empirical formula	$C_{12}H_{24}F_8O_6Ti_2$	$C_{12}H_{32}F_8O_{10}Ti_2$
M_r	512.11	584.16
Temperature (K)	198(1)	133(1)
Radiation used [λ (Å)]	Mo-K_α (0.71073)	Mo-K_α (0.71073)
Crystal description	Colorless, plate	colorless, block
Crystal size (mm)	0.075 × 0.1 × 0.25	0.22 × 0.20 × 0.42
Crystal system	Triclinic	Monoclinic
Space group	$P\bar{1}$	$P2_1/n$
a (Å)	7.3481(12)	8.975(4)
b (Å)	7.8660(13)	12.830(6)
c (Å)	8.9165(14)	11.024(4)
α (°)	111.851(2)	90
β (°)	96.136(2)	111.13(3)
γ (°)	95.348(2)	90
V (Å^3)	470.64(13)	1184.1(9)
Z	1	4
F (000)	260	600.00
$\rho_{calcd.}$ (g cm^{-3})	1.807	1.638
μ (mm^{-1})	0.952	0.780
Total reflections	2386	3832
Unique reflections	1548	3628
R(int)	0.0237	0.040
Scan range θ (°)	2.49 to 24.99	1.00 to 30.1
Completeness to θ_{max} (%)	93.5	100
Index ranges	$-8 \le h \le 7$	$0 \le h \le 12$
	$-8 \le k \le 9$	$0 \le k \le 18$
	$-10 \le l \le 10$	$-9 \le l \le 14$
Data/restrains/parameters	1548/0/175	3476/0/161
$R1$, $wR2$ [$I > 2\sigma(I)$][a]	0.0302, 0.0896	0.045, 0.1275
$R1$, $wR2$ (all data)[a]	0.0343, 0.0923	0.045, 0.1275
Refinement method	Full-matrix least-squares on F^2	Full-matrix least-squares on F
Goodness-of-fit on F^2	1.064	1.07
Max./min. el. dens. (e·Å^{-3})	0.451, −0.293	0.78, −0.76

[a] $wR2 = ([w(F_o^2 - F_c^2)2]/[F_o^4])1/2$, $R1 = ||F_o| - |F_c||/|F_o|$, Weight = $1/[\sigma^2(F_o^2) + (0{\cdot}0745P)^2]$, where $P = (\max [F_o^2] + 2F_c^2)/3$.

Acknowledgments

We would like to acknowledge NSERC (Canada) for support of this research.

[1] [1a] G. H. Robinson, *Coord. Chem. Rev.* **1992**, *112*, 227−245. [1b] N. B. Mikheev, A. N. Kamenskaya, *Coord. Chem. Rev.* **1991**, *109*, 1−59. [1c] Y. Liu, B.-H. Han, Y.-T. Chen, *Coord. Chem. Rev.* **2000**, *200−202*, 53−73. [1d] J. W. Steed, *Coord. Chem. Rev.* **2001**, *215*, 171−221. [1e] I. Ando, *Coord. Chem. Rev.* **2004**, *248*, 185−203. [1f] G. W. Gokel, W. M. Leevy, M. E. Weber, *Chem. Rev.* **2004**, in press.

[2] [2a] R. M. Izatt, J. J. Christensen, *Synthesis of Macrocycles: The Design of Selective Complexing Agents*; Wiley-Interscience, New York, **1987**, Vol. 3. [2b] F. Vogtle, E. Weber, *Host Guest Complex Chemistry Macrocycles*; Springer-Verlag:Berlin, **1985**. [2c] D. J. Cram, J. M. Cram, *Acc. Chem. Res.* **1978**, *11*, 8−14. [2d] T. J. Meade, D. H. Busch, *Progr. Inorg. Chem.* **1985**, *33*, 59−126. [2e] H. M. Colquhoun, J. F. Stoddart, D. J. Williams, *Angew. Chem. Int. Ed. Engl.* **1986**, *25*, 487−507; H. M. Colquhoun, J. F. Stoddart, D. J. Williams, *Angew. Chem.* **1986**, *98*, 483−493.

[3] [3a] U. Russo, G. Valle, G. J. Long, E. O. Schlemper, *Inorg. Chem.* **1987**, *26*, 665−670. [3b] A. Elbasyouny, H. J. Bruegge, K. Von Deuten, M. Dickel, A. Knochel, K. U. Koch, J. Kopf, D. Melzer, G. Rudolph, *J. Am. Chem. Soc.* **1983**, *105*, 6568−6577. [3c] D. Steinborn, O. Gravenhorst, H. Hartung, U. Baumeister, *Inorg. Chem.* **1997**, *36*, 2195−2199. [3d] J. Klimes, A. Knöchel, G. Rudolph, *Inorg. Nucl. Chem. Lett.* **1977**, *13*, 45−52. [3e] S. G. Bott, U. Kynast, J. Atwood, *J. Inclusion Phenomena* **1986**, *4*, 241−246. [3f] U. Kynast, S. G. Bott, J. L. Atwood, *J. Coord. Chem.* **1988**, *17*, 53−61.

[4] [4a] L. V. Ivakina, N. R. Strel'tsova, V. R. Bel'skii, P. A. Storozhenko, M. K. Bulichev, A. B. Tarasov, *Zhurnal Obshchei Khimii* **1987**, *57*, 1600−1605. [4b] W. Massa, T. Ernst, K. Dehnicke, *Z. Naturforsch., Teil B* **1990**, *45*, 563−566. [4c] D. Fenske, H. Goesmann, T. Ernst, K. Dehnicke, *Z. Naturforsch., Teil B* **1990**, *45*, 101−104. [4d] G. Frenzen, W. Massa, T. Ernst, K. Dehnicke, *Z. Naturforsch., Teil B* **1990**, *45*, 1393−1397. [4e] T. Ernst, Dissertation, University of Marburg, Germany **1990**.

[5] S. G. Bott, H. Prinz, A. Alvanipour, J. L. Atwood, *J. Coord. Chem.* **1987**, *16*, 303−309.

[6] [6a] B. Zhang, A. Clearfield, *J. Am. Chem. Soc.* **1997**, *119*, 2751−2752. [6b] Reports concerning the crown ether transition metal fluoride complexes are rare, copper(II) fluoride complex $[LCu_2(OH)_2BF_4]BF_4{\cdot}2H_2O$, L = l,l0-Bis(2,2′-bipyridyl-5-ylcarbonyl)-l,l0-diaza-4,7,13,16-tetraoxacyclooctadecane was reported in: C. F. Martens, A. P. H. J. Scheming, M. C. Feiters, J. Heck, G. Beurskens, P. T. Beurskens, E. Steinwender, R. J. M. Nolte, *Inorg. Chem.* **1993**, *32*, 3029−3033. [6c] [CpRu(benzo-15-crown-5)($NaPF_6$)]BPh_4 was reported in D. S. Glueck, A. R. Brough, P. Mountford, M. L. H. Green, *Inorg. Chem.* **1993**, *32*, 1893−1902. [6d] $[\{Li(Cp^*_2Ti_2F_7)\}_2(\mu_2\text{-}\eta1\text{:}\ \eta\ 1^-12\text{-crown-}4)]{\cdot}$(12-crown-4) contains 12-crown-4 coordinated to the $[Li]^+$: A. Pevec, F. Perdih, J. Košmrlj, B. Modec, H. W. Roesky, A. Demšar, *Dalton Transactions* **2003**, *3*, 420−425.

[7] A. Beste, O. Krämer, A. Gerhard, G. Frenking, *Eur. J. Inorg. Chem.* **1999**, 2037−2045.

[8] W. Kaminsky, S. Lenk, V. Scholz, H. W. Roesky, A. Herzog, *Macromolecules* **1997**, *30*, 7647−7650.

[9] D. A. Straus, M. Kamigaito, A. P. Cole, R. M. Waymouth, *Inorg. Chim. Acta* **2003**, *349*, 65−/68.

[10] D. R. Gauthier Jr., E. M. Carreira, *Angew. Chem. Int. Ed. Engl.* **1996**, *35*, 2363−2365.

[11] P. Yu, P. Müller, H. W. Roesky, M. Noltemeyer, A. Demsar, I. Usón, *Angew. Chem. Int. Ed.* **1999**, *38*, 3319−3321; *Angew. Chem.* **1999**, *111*, 3518−3520 and references therein.

[12] Yu. A. Buslaev, D. S. Dyer, R. O. Ragsdale, *Inorg. Chem.* **1967**, *6*, 2208−2212.

[13] [13a] I. D. Brown, *Structure and Bonding in Crystals* (Eds.: M. O'Keefe, A. Navrotsky), Academic Press, London, **1981**. [13b] I. D. Brown, D. Altermatt, *Acta Crystallogr., Sect. B* **1985**, *41*, 244−247. [13c] N. E. Brese, M. O'Keefe, *Acta Crystallogr., Sect. B* **1991**, *47*, 192−197. [13d] Values used: Ti(+4)−F(−1) R_o = 1.76, B = 0.37, Ti(+4)−O(−2) R_o = 1.815, B = 0.37.

[14] A. Penicaud, P. Batail, K. Bechgaard, J. Sala-Pala, *Synth. Met.* **1988**, *22*, 201−207.

[15] M. Plate, G. Frenzen, K. Dehnicke, *Z. Naturforsch., Teil B* **1993**, *48*, 149−155.

[16] E. G. Il'in, G. B. Nikiforov, G. G. Aleksandrov, V. S. Sergienko, Yu. A. Buslaev, *Doklady Chemistry* **1999**, *367*, 772−775.

[17] E. G. Il'in, G. G. Aleksandrov, G. B. Nikiforov, Yu. A. Buslaev, *Doklady Chemistry*, **2004**, to be published.

[18] R. G. Gillespie, I. Hargittai, *The VSEPR Model of Molecular Geometry*, Allyn and Bacon, a division of Simon and Schuster Inc., Boston, **1991**.

[19] [19a] S. A. A. Zaidi, T. A. Khan, B. S. Neelam, *J. Inorg. Nucl. Chem.* **1980**, *42*, 1525−1526. [19b] E. L. Muetterties, *J. Am. Chem. Soc.* **1960**, *82*, 1082−1087. [19c] R. G. H. Clark, W. Errington, *J. Chem. Soc. (A)* **1967**, 258−261.

[20] E. G. Il'in, G. B. Nikiforov, M. E. Ignatov, Yu. A. Buslaev, *Doklady Chemistry* **1999**, *369*, 770−777.

[21] ^{19}F chemical shift of $[Ti_2F_9]^-$ in SO_2: P. A. W. Dean, *Can. J. Chem.* **1973**, *51*, 4024−4030; ^{19}F chemical shift of $TiF_4(MeCN)_2$ at room temp. in MeCN: J. Pauli, W. Storek, L. Riesel, *Z. Chem.* **1988**. *H.6.*, B.226.

 © 2004 Wiley-VCH Verlag GmbH & Co. KGaA, Weinheim

[22] R. S Borden, R. N. Hammer, *Inorg. Chem.* **1970**, *9*, 2004−2009.
[23] [23a] W. C. Hamilton, J. A. Ibers, *Hydrogen Bonding in Solids*, Benjamin, New York, **1968**, 259−266. [23b] P. Schuster, *The Hydrogen Bond: Recent Developments in Theory and Experiments*, New York, American Elsevier Pub. Co., **1976**, *2*, 440−456. [23c]D. Steinborn, O. Gravenhorst, H. Hartung, U. Baumeister, *Inorg. Chem.* **1997**, *36*, 2195−2199. [23d] H. M. Colquhoun, G. Jones, J. M. Maud, J. F. Stoddart, D. J. Williams, *J. Chem. Soc. J. Chem. Soc., Dalton Trans.* **1984**, 63−66.
[24] [24a] S. C. Abrahams, E. Prince, *J. Chem. Phys.* **1962**, *36*, 50−55. [24b] S. C. Abrahams, *J. Chem. Phys.* **1962**, *36*, 56−61. [24c] W. C. Hamilton, *Acta Crystallogr.* **1962**, *15*, 353−354.
[25] E. G. Il'in, G. G. Aleksandrov, G. B. Nikiforov, Yu. A. Buslaev, *Doklady Chemistry* **2001**, *376*, 25−28.
[26] A. Elbasyouny, H. J. Briigge, K. von Deuten, M. Dickel, A. Knochel, K. U. Koch, J. Kopf, D. Melzer, G. Rudolph, *J. Am. Chem. Soc.* **1983**, *105*, 6568−6577.
[27] [27a] D. Gurka, R. W. Taft, *J. Am. Chem. Soc.* **1969**, *91*, 4794−4801. [27b] D. P. Eyman, R. S. Drago, *J. Am. Chem. Soc.* **1966**, *88*, 1617−1620.
[28] D. S. Dyer, R. O. Ragsdale, *Inorg. Chem.* **1967**, *6*, 8−11.
[29] M. E. Ignatov, E. G. Iliin, V. G. Iagodin, J. A. Buslaev, *Doklady Akademii Nauk SSSR* **1978**, *243*, 1179−1181.
[30] H. G. Lee, D. S. Dyer, R. O. Ragsdale, *J. Chem. Soc., Dalton Trans.* **1976**, 1325−1329.
[31] [31a] V. Gutmann, *Coordination Chemistry in Non-Aqueous Solutions*, Springer-Verlag, Berlin and New York, **1968**. [31b] V. Gutman, R. Schmid, *Coord. Chem. Rev.* **1973**, *12*, 263−293. [31c] *The Chemistry of Nonaqueous Solvents* (Ed.: J. J. Lagowsky),V. VA, Academic Press, New York. **1978**, pp. 63−119.
[32] [32a] G. Olofsson, *Acta Chem. Scand.* **1967**, *21*, 1887−1888. [32b] G. Olofsson, *Acta Chem. Scand.* **1968**, *22*, 1352−1353.
[33] A. F. Holleman, E. Wiberg, *Inorganic Chemistry*, Academic Press, Walter de Gruyter, Berlin and New York, **1995**, 358−371.
[34] According to the NMR study of the displacement reactions involving TiF_4 and molecular donor ligands Et_2O, THF, $(MeO)_3PO$, Ph_3PO, Me_2SO, $[F]^-$ displaces MeCN in the *cis*-$TiF_4(MeCN)_2$, while water displaces MeCN, Et_2O, THF, $(MeO)_3PO$ in the tetrafluorocomplex (this work and refs.[35,36]). The *cis*-$TiF_4(Ph_3PO)_2$ is stable in air toward moistire $[F]^-$ displaces all mentioned ligands with the formation of $[TiF_6]^{2-}$ (ref. 36).
[35] G. B. Nikiforov, S. G. Sakharov, E. G. Il′in, J. A. Buslaev, *Rus. J. Inorg. Chem.* **2001**, *46*, 1045−1054.
[36] [36a] E. G. Il'in, G. B. Nikiforov, J. A. Buslaev, *Doklady Chemistry* **2000**, *375*, 242−246. [36b] E. G. Il'in, G. B. Nikiforov, J. A. Buslaev, *Doklady Chemistry* **2001**, *376*, 8−15. [36c] G. B. Nikiforov, PhD Thesis, Institute of General and Inorganic Chemistry RAS, Moscow, Russia, **2001**.
[37] Titanium fluoride complexes in the Et_2O, mixtures of Et_2O and CH_2Cl_2: E. G. Il'in, G. B. Nikiforov, to be published.
[38] For water as a solvent DN = 33, greater than that of Me_2SO (ref. 31).
[39] *SAINT 6.02*, Bruker AXS, Inc., Madison, Wisconsin, USA, **1997−1999**.
[40] G. Sheldrick, *SADABS*, Bruker AXS, Inc., Madison,Wisconsin, USA, **1999**.
[41] [41a] G. Sheldrick, *SHELXTL 5.1*, Bruker AXS, Inc., Madison,-Wisconsin, USA, **1997**. [41b] P. T. Beurskens, G. Admiraal, G. Beurskens, W. P. Bosman, R. de Gelder, R. Israel, J. M. M. Smits, *The DIRDIF-94 program system*, Technical Report of the Crystallography Laboratory, University of Nijmegen, The Netherlands, **1994**.
[42] *teXsan for Windows version 1.06: Crystal Structure Analysis Package*, Molecular Structure Corporation, Texas, **1997−1999**.
[43] D. T. Cromer, J. T. Waber, *International Tables for X-ray Crystallography*, Vol. IV, Table 2.2 A, The Kynoch Press, Birmingham, England, **1974**.
[44] J. A. Ibers, W. C. Hamilton, *Acta Crystallogr.* **1964**, *17*, 781.
[45] D. C. Creagh & W. J. McAuley, *International Tables for Crystallography*, Vol C (Ed.: A. J. C. Wilson), Kluwer Academic Publishers, Boston, **1992**, Table 4.2.6.8, pp. 219−222.
[46] D. C. Creagh & J. H. Hubbell, *International Tables for Crystallography*, Vol C (Ed.: A. J. C. Wilson), Kluwer Academic Publishers, Boston, **1992**, Table 4.2.4.3, pp. 200−206.

Received April 15, 2004
Early View Article
Published Online August 3, 2004

 © 2004 Wiley-VCH Verlag GmbH & Co. KGaA, Weinheim

1,2,4,5-Benzenetetracarboxylic Acid and 4,4′-Bipyridine as Ligands in Designing Low-Dimensional Coordination Polymers

Catalina Ruiz-Pérez,*[a] Pablo Lorenzo-Luis,[b] María Hernández-Molina,[a] M. Milagros Laz,[c] Fernando S. Delgado,[a] Pedro Gili,[b] and Miguel Julve[d]

Keywords: Hydrothermal / 1,2,4,5-Benzenetetracarboxylic acid / 4,4′-Bipyridine / Low-dimensional polymers / Manganese / Cobalt

The combined use of 1,2,4,5-benzenetetracarboxylic acid (H_4bta) and 4,4′-bipyridine (bpy) as ligands with Mn^{II} and Co^{II} ions afforded two polymeric compounds with the formulae [Mn(Hbta)(Hbpy)(H_2O)$_2$] (**1**) and [H_2bpy][Co(bta)(bpy)(H_2O)$_2$] (**2**). **1** and **2** were prepared under hydrothermal conditions (145 °C, 3 h) and characterized by elemental analysis, IR spectroscopy, TG-DTA analysis and single-crystal X-ray diffraction methods. **1** exhibits a novel double chain structure growing along the *b* axis where the manganese atoms are linked by tris-monodentate $Hbta^{3-}$ ligands. The values of the manganese···manganese intrachain separations are 7.627(2) Å [Mn(1)···Mn(1c); c = –x + 1/2, y – 1/2, –z] and 9.274(4) Å [Mn(1)···Mn(1d); *d* = x, y + 1, –z]. Adjacent double chains in **1** are further linked through hydrogen bonds between the NH fragment of the $Hbpy^+$ cation and one of the carboxylate groups of the $Hbta^{3-}$ anion along the *a* axis, resulting in a sheetlike structure. **2** exhibits a rectangular grid arrangement of cobalt atoms bridged by bis-monodentate bta^{4-} and bpy ligands in the *bc* plane, the cobalt···cobalt separations across them being 6.228(2) and 10.074 (2) Å, respectively. The metal atoms in **1** and **2** are six-coordinate with two water molecules in *trans* positions (**1** and **2**), three (**1**)/two (**2**) carboxylate oxygen atoms and one (**1**)/two (**2**) pyridyl nitrogen atoms forming a distorted octahedral environment. The varying nature of the divalent metal ions [Mn **1** and Co **2**] along with the differing degrees of protonation of the tetracaboxylate [$Hbta^{3-}$ **1** and bta^{4-} **2**] and bipyridyl [$Hbpy^+$ **1** and bpy and H_2bpy^{2+} **2**] species account for the structural differences between **1** and **2**.

(© Wiley-VCH Verlag GmbH & Co. KGaA, 69451 Weinheim, Germany, 2004)

Introduction

The crystal engineering of supramolecular architectures or metal-organic coordination polymers is a growing field and it has attracted much attention in the past decades.[1−4] With the recent development of self-assembly supramolecular chemistry, it is possible to rationally design and synthesize supramolecular architectures or metal-organic coordination polymers based on covalent or supramolecular contacts (such as forces resulting from intermolecular non-bonded, non-covalent electrostatic forces (due to static and oscillating fixed charge interactions) and dispersion forces (due to induced transient charge interactions).[5−7] However, the assembly of molecular materials from organic ligands and metal ion building blocks to generate new supramolecular architectures is still a challenge.[8−10] Two main methods can be envisaged in order to construct open supramolecular architectures on the basis of the different interactions between the building blocks: one takes advantage of the covalent bonds and the other focuses on the supramolecular contacts.[11] The use of covalent bonds to link metal ions and organic molecules such as polycarboxylic acids or 4,4′-bipyridine (bpy), has resulted in a large number of porous frameworks with different dimensionalities and topologies.[12−15]

It is worth noting that the coordination ability of aromatic polycarboxylic acids towards transition metal complexes has received considerable attention due to the variety of the bridging modes of the carboxylate group with regards to the formation of extended frameworks.[16,17] The goal in the search for organic porous frameworks is not simply to mimic inorganic materials by using different

[a] Laboratorio de Rayos X y Materiales Moleculares, Dpto. de Física Fundamental II, Avda, Astrofísico Francisco Sánchez s/n. Facultad de Física, Universidad de La Laguna, 38204, Tenerife, Spain
E-mail: caruiz@ull.es
[b] Dpto. de Química Inorgánica (Facultad de Farmacia), Universidad de La Laguna, 38204, Tenerife, Spain
[c] Laboratorio de Rayos X y Materiales Moleculares, Dpto. de Edafología y Geología, Universidad de La Laguna, 38204, Tenerife, Spain
[d] Departament de Química Inorgànica/Instituto de Ciencia Molecular, Universitat de València, 46100 Burjassot, València, Spain
Supporting information for this article is available on the WWW under http://www.eurjic.org or from the author.

building blocks. Some of the properties of organic compounds, such as low stability and low Lewis acidity, are inherently different. In this sense, 1,2,4,5-benzenetetracarboxylic acid (hereafter noted H_4bta) possesses several interesting characteristics: (a) it has four carboxylic groups whose deprotonation (partial or total) and subsequent coordination to the metal ions affords interesting structures with tunable dimensionality; (b) it can act not only as a hydrogen bond acceptor but also as a hydrogen bond donor, depending upon the degree of deprotonation; (c) due to steric hindrance, some of the carboxylic groups may not lie in the plane of the phenyl ring upon complexation to the metal ions, and thus, they can connect metal ions in different directions. Hence, H_4bta is a good choice for the construction of polymeric structures, as proved by the large number of metal-organic structures obtained from the Cambridge Structural Database (CSD).[18] The versatility of the deprotonated forms of H_4bta as ligands is illustrated by Scheme 1.

Our research group is engaged in the design of extended arrays of metal ions with mixed ligands, and recently, we obtained a supramolecular loop-chain network of pillared layers via 4,4′-bipyridine.[19] Our first attempts, using H_4bta and bpy as ligands towards first row transition metal ions, afforded the new coordination polymers [Mn(Hbta)(Hbpy)$(H_2O)_2$] (**1**) and H_2bpy[Co(bta)(bpy)$(H_2O)_2$] (**2**) (see Scheme 2). To the best of our knowledge,[18] compound **1** exhibits an unprecedented connection mode for the H_4bta ligand (see Scheme 1). The preparation, structural characterization, spectroscopic and thermal investigations of complexes **1** and **2** are presented here.

Results and Discussion

Description of the Structures

[Mn(Hbta)(Hbpy)$(H_2O)_2$]$_n$ (1)

The structure of **1** is made up of neutral double zigzag chains of formula [Mn(Hbta)(Hbpy)$(H_2O)_2$] which run parallel to the *b* axis (Figure 1, a) with $Hbta^{3-}$ acting as a tris-monodentate bridging ligand. The resulting ribbon-like motifs are further linked via N−H···O hydrogen bonds involving the protonated pyridyl nitrogen of bpy [N(1)] and one of the carboxylate oxygen atoms [O(2b); b = $-x - 1/2, y - 1/2, z$] of the $Hbta^{3-}$ ligand (see Table 1) affording a sheet-like structure in the *ab* plane (Figure 1, b). The Mn(1) atom has a slightly distorted octahedral environment (MnO_5N) with two *trans* water molecules filling the axial positions (see Figure 2) The $Mn-O_{(carboxylate)}$ and $Mn-N_{(Hbpy^+)}$ bond lengths are in agreement with previous data of carboxylate- and bpy-containing manganese(II) complexes.[20] The $Hbta^{3-}$ anion is not planar since the dihedral angles between the COO groups and the aromatic ring of $Hbta^{3-}$ are 57.9(2) Å [O(1)−C(7)−O(2)], 64.5(2) Å [O(3)−C(8)−O(4)], 5.0(3) Å [O(5)−C(9)−O(6)] and 8.9(2) Å [O(7)−C(10)−O(8)]. The deprotonated carboxylate groups of each $Hbta^{3-}$ [O(1)−C(7)−O(2), O(3)−C(8)−O(4) and O(7)−C(10)−O(8)] are coordinated to three manganese atoms [Mn(1), Mn(1c) and Mn(1d) through O(7), O(1) and O(4), respectively; symmetry code: c = $-x + 1/2, y - 1/2, z$; d = $x, y + 1, -z$]. The values of the Mn···Mn separation through the $Hbta^{3-}$ ligand are 7.627(2) [Mn(1)···Mn(1c)] and 9.274(4) Å [Mn(1)···Mn(1d)]. The protonated carboxylic group remains uncoordinated but contributes to the stabilization of the structure through an extensive network of hydrogen bonds together with the water molecules and the free carboxylate oxygen atoms (see Table 1).

The pyridyl rings of the monoprotonated $Hbpy^+$ species are planar but the ligand as a whole is far from being planar [dihedral angle between the two pyridyl rings is 12.32(14)°]. $Hbpy^+$ acts as a terminal monodentate ligand being coordinated to the manganese atom through the nonprotonated N(2) pyridyl atom. The $Hbpy^+$ ligands are alternatively located right and left of each double chain (Figure 1, a) in such a way that the $Hbpy^+$ groups from two adjacent double chains are stacked along the *b* axis (Figure 1, b). The separation between the mean pyridyl planes of adjacent $Hbpy^+$ groups is 3.969(9) Å, a value that supports the occurrence of very weak π-π stacking interactions. Finally, weaker $C-H_{(Hbpy^+)}\cdots O_{(Hbta^{3-})}$ supramolecular interactions, the values of the C···O separations being less or equal than 3.22 Å (the sum of the van der Waals radii of the interacting atoms), are also observed.[18]

[H_2bpy]·[Co(bta)(bpy)$(H_2O)_2$]·(2)

The structure of this complex consists of a two-dimensional rectangular grid of *trans*-diaquacobalt(II) ions growing in the *ab* plane with bta^{4-} and bpy ligands acting as bis-monodentate bridges within each layer (Figure 3, a). These layers are connected to each other through hydrogen bonds between the protonated pyridyl nitrogen atoms of H_2bpy^{2+} [N(3)] and one of the uncoordinated carboxylate oxygen atoms [O(3)] (Figure 3, b and Table 1) to afford a three-dimensional network. In contrast to **1**, fully deprotonated bta^{4-} and both neutral bpy and diprotonated H_2bpy^{2+} are present in **2**. As in **1**, each Co^{II} ion has a somewhat distorted octahedral arrangement with two trans water molecules in the axial positions (Figure 4). The $Co-O_{(bta)}$ [2.077(2) Å] and $Co-N_{bpy}$ [2.169(3) Å] bond lengths are also in agreement with those reported for carboxylate- and bpy-containing cobalt(II) complexes.[21,22] The bta^{4-} ligand is not planar; the dihedral angles between the carboxylate groups and the mean plane of the phenyl ring are 56.75(10)° [C(1)−C(4)−O(1)−O(2)] and 33.94(9)° [C(5)−C(2)−O(3)−O(4)]. Each bta^{4-} group acts as a *trans* bis-monodentate ligand bridging two symmetry related Co^{II} ions thus affording a uniform chain of cobalt atoms along the (101) direction, the cobalt···cobalt separation across bridging H_2bta being 11.248(3) Å. These chains are cross-linked by bridging bis-monodentate bpy ligands along the *b* axis leading to a two dimensional quasi-square grid of cobalt atoms. The cobalt···cobalt separation through the

 © 2004 Wiley-VCH Verlag GmbH & Co. KGaA, Weinheim

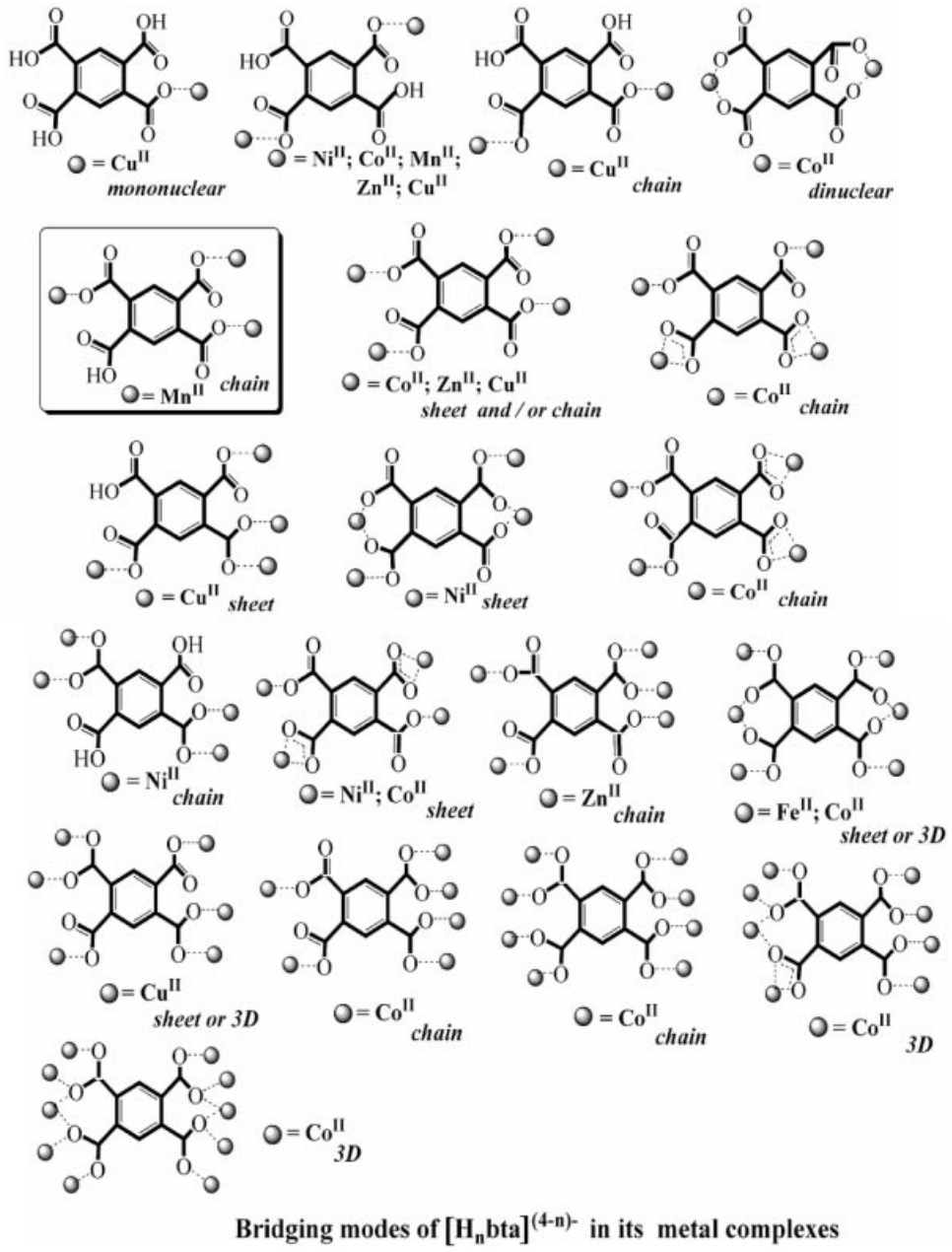

Scheme 1

bpy bridge is 11.476(2) Å. The pyridyl rings of bpy are practically planar within experimental error, but the ligand as a whole deviates significantly from planarity [the dihedral angle between the mean planes of the two pyridyl rings is 19.29(1)°]. Centrosymmetric H_2bpy^{2+} cations are placed between the layers and they link these layers into a three-dimensional network through hydrogen bonds of the type N−H···$O_{carboxylate}$, the shortest cobalt···cobalt interplanar separation being 8.977(3) Å. Additional hydrogen bonds involving coordinated water molecules and one carboxylate oxygen atom [2.728(4) Å for O(1w)···O(4c) (c = $-x, -y + 1, -z + 1$) contribute to the stabilization of this 3D network.

Infrared Spectra and TG-DTA Analysis

The infrared spectra of the two complexes are quite similar, with a broad band centered at ca. 3395−3370 which is due to the O−H stretching vibration of water molecules involved in extensive hydrogen bonding interactions.[23] Furthermore, they exhibit the $\nu_{as(OCO)}$ and $\nu_{s(OCO)}$ vibrations of the carboxylate groups which occur at 1690 and 1490 cm^{-1} for **1** and at 1680 and 1480 cm^{-1} for **2**, respectively. $\Delta\nu[\nu_{as(COO)} - \nu_{s(COO)}]$ is ca. 200 cm^{-1} for both complexes, a value which suggests the occurrence of monodentate coordination of the carboxylate groups.[24] This is also in agreement with the crystal structure (vide supra). Less

 © 2004 Wiley-VCH Verlag GmbH & Co. KGaA, Weinheim

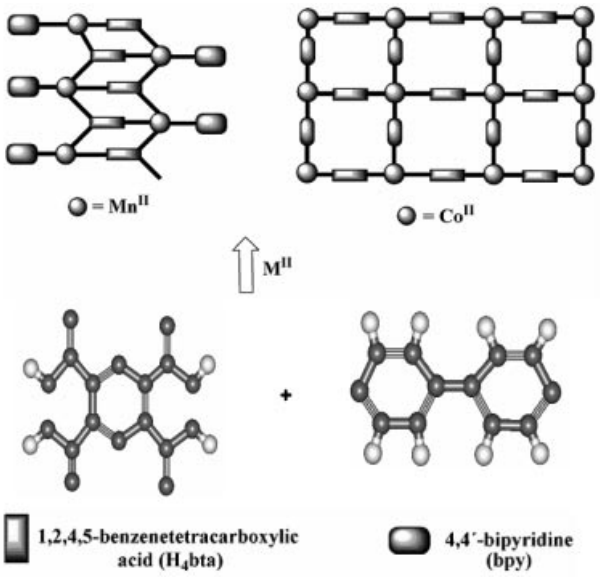

Scheme 2

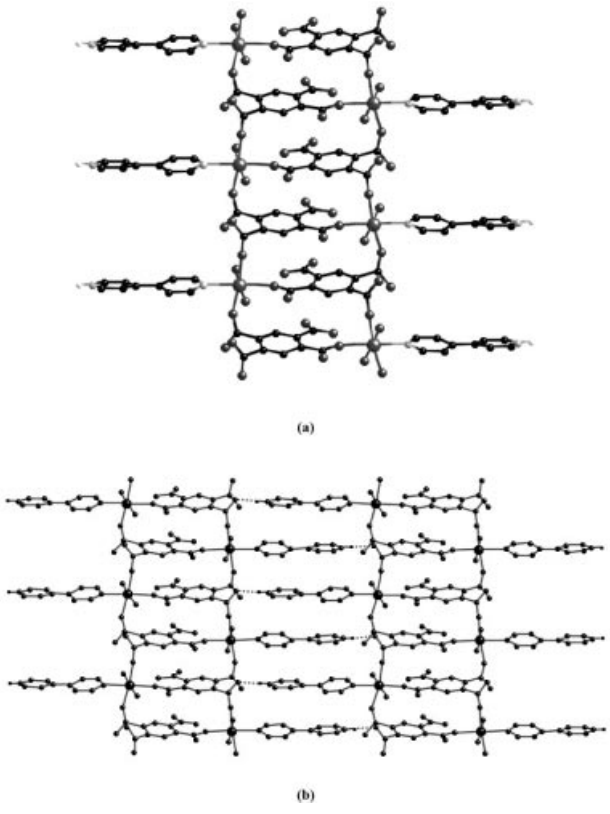

Figure 1. X-ray structure of $[Mn(Hbta)(Hbpy)(H_2O)_2]_n$ (**1**); (a) view along the *c*-axis illustrating the double-chain and (b) view of the layer structure formed through the N−H···O hydrogen bonds of adjacent double chains

significant absorptions occur at 3050 (stretching vibrations of aromatic C−H groups), 820−700 (out-of-plane C−H bending of phenyl and pyridyl rings) and 557 cm^{-1} ($\nu_{(M-N)}$ vibration).[25,26]

Table 1. Hydrogen bonds in **1** and **2**

D−H···A	D···A	H···A	<D−H···A
1[a][b][c]			
N(1)−H(1)···O(2b)	2.683(4)	1.834(2)	168.9(2)
O(1W)−H(12W)···O(3)	2.725(4)	1.834(2)	171.7(4)
O(1W)−H(11W)···O(3e)	2.831(4)	1.814(5)	167.4(5)
O(2W)−H(21W)···O(2a)	2.720(4)	1.848(6)	174.8(7)
O(2W)−H(22W)···O(8c)	2.708(4)	1.990(5)	165.6(5)
2[a][b][c]			
N(3)−H(3)···O(3ai)	2.596(4)	1.742(2)	171.3(2)
O(1W)−H(11W)···O(2bi)	2.649(3)	1.807(6)	154.7(5)
O(1W)−H(21W)···O(4ci)	2.728(3)	1.879(5)	168.8(5)

[a] Values of the interatomic distances and angles in Å and degrees, respectively. [b] D = donor and A = acceptor. [c] Symmetry code: a = x, $y-1$, z; b = $-x-1/2$, $y-1/2$, z; c = $-x+1/2$, $y-1/2$, z; e = $-x$, $y-1/2$, $-z+1/2$; ai = $-x+1/2$, $y-1/2$, z; bi = $-x$, y,$-z+1/2$; ci = $-x$, $-y+1$, $-z+1$.

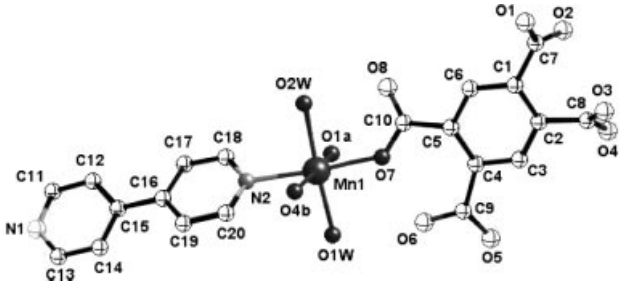

Figure 2. Coordination sphere of the manganese atom in $[Mn(Hbta)(Hbpy)(H_2O)_2]_n$ (**1**)

The $[Mn(Hbta)(Hbpy)(H_2O)_2]$ and H_2bpy $[Co(bta)(bpy)(H_2O)_2]$compounds show a similar thermal behavior. Two steps are observed in the TG-DTG/DTA curves of **1** and **2** (Figure S1, supplementary material): the first one, no thermal decomposition of the compounds occurs, confirming that the networks remain stable below ca. 174 °C; the second one, three overlapped weight loss peaks are observed {$[T_{strong\ peak}]_{DTG}$ ca. 230 °C; $[T_{little\ peak}]_{DTG}$ ca. 374 °C and $[T_{little\ peak}]_{DTG}$ ca. 455 °C}. This last process is followed by two strong endothermic peaks {$[T_{strong\ peaks}]_{DTA}$ ca. 190 and 233 °C for **1** and ca. 140 and 228 °C, for **2**} whose weight loss corresponds to the release of H_2O, H_4bta and bpy groups, in agreement with another similar complex $[H_2bpy][H_3bta]_2$, recently reported.[19]

Conclusion

Two polymeric complexes with chains or rectangular grids, $[Mn(Hbta)(Hbpy)(H_2O)_2]_n$ (**1**) and $[H_2bpy][Co(bta)(bpy)(H_2O)_2]$ (**2**), respectively, were constructed from 1,2,4,5-benzenetetracarboxylic acid (H_4bta) in the presence of an auxiliary ligand (4,4′-bipyridine) under hydrothermal conditions. The auxiliary ligand, play an important role in the synthesis of the complexes by engaging in coordination or acting as a template. The coordination modes of the H_4bta ligands in the two complexes are different, to the

 © 2004 Wiley-VCH Verlag GmbH & Co. KGaA, Weinheim

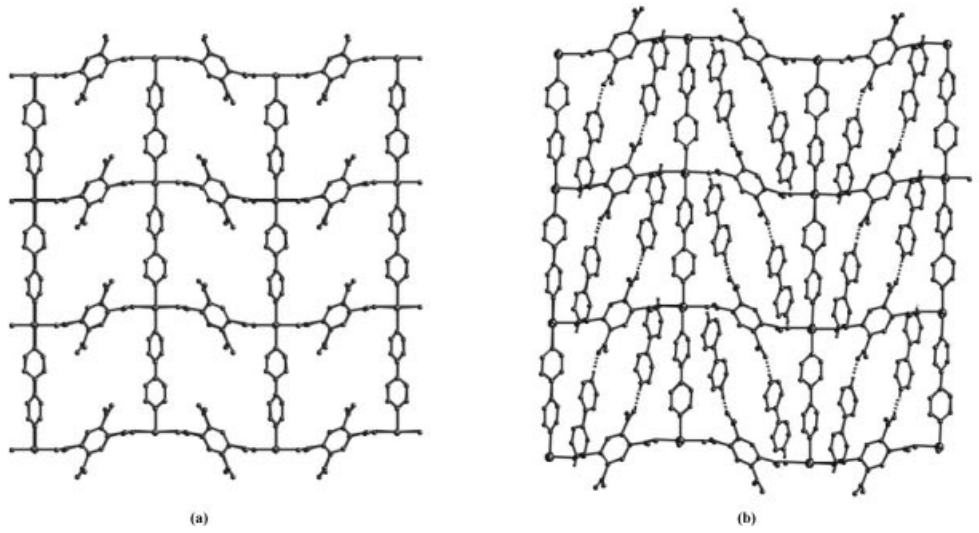

Figure 3. (a) Projection on the *ab*-plane of the two-dimensional layered architecture showing the quasi-square grids; (b) addition of the connecting $H_2bpy^{2\pm}$ illustrating the modus of growth of the 3D structure

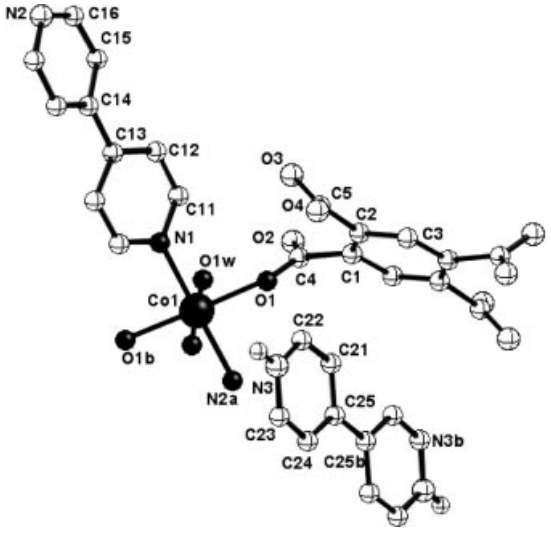

Figure 4. A perspective view of the locally expanded unit for **2**

best of our knowledge, where **1** exhibits an unprecedented connection mode. In both compounds, the introduction of mixed ligands provides the probability of generating multiple binding forces, such as coordination bonds, hydrogen bonding and other supramolecular interactions.

Experimental Section

General Remarks: Elemental analyses (C, N N) were carried out with an EA 1108 CHNS-0 automatic analyzer. FT-IR spectra were performed with a ThermoNicolet Avatar 360 FT-IR spectrometer on samples prepared as KBr pellets. Thermal analyses (TG-DTA) were done on a PerkinElmer Diamond TG-DTA system (SEGAI Service of the University of La Laguna) under a nitrogen atmosphere (flow rate: 80 $cm^3\ min^{-1}$) in the temperature range 290−550 °C. The samples [3.542 **1** and 1.351 mg **2**] were heated in an aluminium crucible (45 μL) at a rate of 10 °C min^{-1}. The TG curves were analyzed by mass loss as a function of temperature. The number of decomposition steps was identified by using the derivative thermogravimetric curve (DTG). The DTA curves were analyzed as differential thermal analysis [$\Delta T(\mu V)$].

$[Mn(Hbta)(Hbpy)(H_2O)_2]_n$ (1) and $[H_2bpy]\cdot[Co(bta)(bpy)(H_2O)_2]$ (2): The reagents and solvents were purchased from commercial sources (Aldrich) and used as received. These compounds were prepared similarly to $[H_2bpy][H_3bta]_2$.[19] Thus, for compound **1**, a sample of manganese acetate tetrahydrate (0.35 mmol) was dissolved in 5 mL of deionized water. 1,2,4,5-benzenetetracarboxylic acid H_4bta (0.39 mmol) was suspended in 5 mL of H_2O/NaOH (0.75 mmol) whilst stirring at ambient temperature for 10 min. A water solution of 4,4′-bipyridine bpy (0.75 mmol) was added dropwise to a 1,2,4,5-benzenetetracarboxylic acid solution. After that the clear solution, was mixed with the previously prepared manganese acetate whilst stirring. The mixture was then transferred to a

Table 2. Crystal data and structure refinement for **1** and **2**

	1	**2**
Empirical formula	$C_{20}H_{16}MnO_{10}N_2$	$C_{30}H_{24}CoO_{10}N_4$
Molecular mass	499.29	659.47
Crystal system	orthorhombic	monoclinic
Space group	*Pbca*	*C*2/*c*
a/Å	20.694(4)	15.255(3)
b/Å	7.627(2)	11.476(2)
c/Å	24.512(5)	15.972(3)
β/°		90.89(3)
V/Å^3	3868.8(15)	2795.8(9)
Z	4	4
$D_{calcd.}$/g cm^{-3}	1.714	1.538
μ/mm^{-1}	0.749	0.682
Independent reflections	5558	3993
Observed reflections [$I > 2\sigma(I)$]	3353	2642
Refined parameters	319	219
$R1\ (F2)$[a]	0.0744	0.0654
$wR2\ (F2)$[b]	0.1024	0.1047
S	1.118	1.095

[a] $R1 = \Sigma||F_o| - |F_c||/\Sigma|F_o|$. [b] $wR2 = [\Sigma w(|F_o|^2 - |F_c|^2)^2]/\Sigma w|F_o|^2]^{1/2}$.

 © 2004 Wiley-VCH Verlag GmbH & Co. KGaA, Weinheim

Table 3. Selected bond lengths (Å) and angles (°) for **1**; symmetry code: a = x, $y - 1$, z; b = $-x + 1/2$, $y - 1/2$, z

Mn(1)−O(1)	2.179(2)	Mn(1)−O(1w)	2.126(3)
Mn(1)−O(4a)	2.149(2)	Mn(1)−O(2w)	2.183(3)
Mn(1)−O(7b)	2.206(2)	Mn(1)−N(21)	2.276(3)
O(1)−Mn(1)−O(1W)	90.8(1)	O(4a)−Mn(1)−O(7b)	95.8(1)
O(1)−Mn(1)−O(2W)	85.5(1)	N(2)−Mn(1)−O(4a)	84.5(1)
O(1)−Mn(1)−N(2)	89.5(1)	N(2)−Mn(1)−O(7b)	177.1(1)
O(1)−Mn(1)−O(4a)	173.2(1)	O(1W)−Mn(1)−O(4a)	86.3(1)
O(1)−Mn(1)−O(7b)	90.2(1)	O(1W)−Mn(1)−O(7b)	90.0(1)
O(1W)−Mn(1)−O(2W)	175.3(1)	O(2W)−Mn(1)−O(4a)	95.9(1)
O(1W)−Mn(1)−N(2)	92.9(1)	O(2W)−Mn(1)−O(7b)	85.7(1)
O(2W)−Mn(1)−N(2)	91.4(1)		

Table 4. Selected bond lengths (Å) and angles (°) for **2**; symmetry code: a = $-x$, y, $-z$; b = $-x$, $y - 1$, z

Co(1)−O(1)	2.077(2)	Co(1)−N(1)	2.169(3)
Co(1)−O(1W)	2.114(2)		
O(1)−Co(1)−O(1a)	179.2(1)	O(1a)−Co(1)−O(1W)	89.5(1)
O(1)−Co(1)−O(1W)	90.5(1)	O(1W)−Co(1)−O(1Wa)	176.5(1)
O(1)−Co(1)−O(1Wa)	89.5(1)	O(1W)−Co(1)−N(1)	91.8(1)
O(1)−Co(1)−N(1)	89.6(1)	O(1W)−Co(1)−N(2b)	88.2(1)
O(1)−Co(1)−N(2b)	90.4(1)		

reaction vessel placed inside a preheated oven at 145° for 3 h. The compound **2**, was prepared similarly to the manganese compound from $Co(NO_3)_2{\cdot}6H_2O$ (0.36 mmol). After several days, crystals of **1** and **2** were manually harvested under the microscope and analyzed using single-crystal X-ray diffraction (see Table 2). (**1**) $C_{20}H_{16}MnN_2O_{10}$ (499.3): calcd. C 48.11, H 3.23, N 5.61; found C 48.21, H 3.45, N 5.76. (**2**) $C_{30}H_{24}CoN_4O_{10}$ (659.5): calcd. C 54.64, H 3.67, N 8.50; found C 53.82, H 3.58, N 8.05.

X-ray Crystallographic Study: Diffraction experiments for **1** and **2** were carried out with Mo-K_α radiation using a Nonius KappaCCD diffractometer at 273(1) K. A summary of the crystallography data and structure refinement is given in Table 2. Both structures were solved by direct methods and refined with the full-matrix least-squares technique on F^2 using the SHELXS-97[27] and SHELXL-97[28] programs. All non-hydrogen atoms were refined anisotropically. All hydrogen atoms bound to carbon were placed in calculated positions and refined isotropically. The hydrogen atoms of the water molecules and those of the carboxylic groups were found in a difference Fourier map and refined isotropically for compound **1**. The final full-matrix least-squares refinement was performed minimizing the function $\Sigma w(|F_o|^2 - |F|^2)$ with $w = 1/[\sigma^2(F_o)^2 + mP^2 + nP]$ and $P = (F_o^2 + 2F_c^2)/3$ with $m = 0.0197$ **1** and 0.0183 **2** and $n = 7.3045$ **1** and 12.1543 **2**. The values of the discrepancy indices $R1$ ($wR2$) for all data were 0.1437 (0.1186) for **1** and 0.1204 (0.1224) for **2**, whereas those listed in Table 2 correspond to the data with $I > 2\sigma(I)$. The final Fourier difference map showed maximum and minimum height peaks of 0.512 and −0.394 eÅ^{-3} for (**1**) and 0.523 and −0.515 eÅ^{-3} for (**2**). The final geometrical calculations and the graphical manipulations were carried out with PARST95[29] and PLATON[30] programs, respectively. Selected bond lengths (Å) and angles (°) for **1** and **2** are listed in Table 3 and Table 4, respectively. CCDC-231515 (for **1**) and -231516 (for **2**) contain the supplementary crystallographic data for this paper. These data can be obtained free of charge at www.ccdc.cam.ac.uk/conts/retrieving.html [or from the Cambridge Crystallographic Data Centre, 12 Union Road, Cambridge CB2 1EZ, UK; Fax: (internat.) +44-1223-336-033; E-mail: deposit@ccdc.cam.ac.uk].

Acknowledgments

This work was supported by the Ministerio Español de Ciencia y Tecnología (Project BQU2001−3794) and the Consejería de Educación, Cultura y Deportes del Gobierno Autónomo de Canarias (Project PI2002/175). F.S. Delgado thanks the Consejería de Educación, Cultura y Deportes del Gobierno Autónomo de Canarias for a predoctoral grant.

[1] P. Lightfoot, A. Snedden, *J. Chem. Soc., Dalton Trans.* **1999**, 3549.
[2] Y. B. Dong, M. D. Smith, R. C. Layland, H.-C. zur Loye, *J. Chem. Soc., Dalton Trans.* **2000**, 775.
[3] K. Biradha, K. V. Domasevitch, B. Moulton, C. Seward, M. J. Zaworotko, *Chem. Commun.* **1999**, 1327.
[4] H. Gudbjartson, K. Biradha, K. M. Poirier, M. J. Zaworotko, *J. Am. Chem. Soc.* **1999**, *117*, 2599.
[5] M. L. Tong, H. K. Lee, X. M. Chen, R. B. Huang, T. C. M. Mak, *J. Chem. Soc., Dalton Trans.* **1999**, 3657.
[6] L. R. MacGillivray, R. H. Groeneman, J. L. Atwood, *J. Am. Chem. Soc.* **1998**, *120*, 2676.
[7] C. H. Chang, K. C. Hwang, C. S. Liu, Y. Chi, A. J. Carty, L. Scoles, S. M. Peng, G. H. Lee, J. Reedijk, *Angew. Chem. Int. Ed.* **2001**, *40*, 4651.
[8] O. M. Yaghi, C. E. Davis, G. Li, H. L. Li, *J. Am. Chem. Soc.* **1997**, *119*, 2861.
[9] Y. Cui, H. L. Ngo, W. B. Lin, *Inorg. Chem.* **2002**, *41*, 1033.
[10] J. W. Ko, K. S. Min, M. P. Suh, *Inorg. Chem.* **2002**, *41*, 2151.
[11] V. G. Albano, M. C. Aragoni, M. Arca, C. Castellari, F. Demartin, F. A. Devillanova, F. Isaia, V. Lippolis, L. Loddo, G. Verani, *Chem. Commun.* **2002**, 1170.
[12] S. S. Y. Chui, S. M. F. Lo, J. P. H. Charmant, A. G. Orpen, I. D. Williams, *Science* **1999**, *283*, 1148.

 © 2004 Wiley-VCH Verlag GmbH & Co. KGaA, Weinheim

[13] R. Cao, D. F. Sun, Y. C. Liang, M. C. Hong, K. Tatsumi, Q. Shi, *Inorg. Chem.* **2002**, *41*, 2087.
[14] P. M. Foster, A. K. Cheetham, *Angew. Chem. Int. Ed.* **2002**, *41*, 457.
[15] M. Eddaoudi, D. B. Moler, H. L. Li, B. L. Chen, T. M. Reineke, M. O′Keeffe, O. M. Yaghi, *Acc. Chem. Res.* **2001**, *34*, 319.
[16] S. S.-Y. Chui, S. M.-F. Lo, J. P. H. Charmant, A. G. Orpen, I. D. Williams, *Science* **1999**, *283*, 1148.
[17] S. M.-F. Lo, S. S.-Y. Chui, L.-Y. Shek, Z.-Y. Lin, X. X. Zhang, G.-H. Wen, I. D. Williams, *J. Am. Chem. Soc.* **2000**, *122*, 6293.
[18] F. H. Allen, *Acta Crystallogr., Sect. B* **2002**, *58*, 380.
[19] C. Ruiz-Pérez, P. A. Lorenzo-Luis, M. Hernández-Molina, M. M. Laz, P. Gili, M. Julve, *Crystal Growth & Design* **2004**, *4*, 57.
[20] Y. Rodríguez-Martín, M. Hernández-Molina, J. Sanchiz, C. Ruiz-Pérez, F. Lloret, M. Julve, *Dalton Trans.* **2003**, 2359.
[21] F. S. Delgado, J. Sanchiz, C. Ruiz-Pérez, F. Lloret, M. Julve, *Cryst. Eng. Commun.* **2003**, *5*, 280.
[22] E. I. Stiefel, G. F. Brown, *Inorg. Chem.* **1972**, *11*, 434.
[23] E. Berti, F. Cecconi, C. A. Ghilardi, S. Midollini, A. Orlandini, E. Pitzalis, *Inorg. Chem. Commum.* **2002**, *5*, 1041.
[24] L. J. Zhang, J. Q. Xu, Z. Shi, W. Xu, T.-G. Wang, *Dalton Trans.* **2003**, 1148.
[25] G. B. Hix, K. D. M. Harris, *J. Mater. Chem.* **1998**, *8(3)*, 579.
[26] D. Cheng, M. A. Khan, R. P. Houser, *Inorg. Chim. Acta* **2003**, *351*, 2.
[27] G. M. Sheldrick, *SHELXS*, University of Göttingen, Germany, **1997**.
[28] G. M. Sheldrick, *SHELXL, Program for the Refinement of Crystal Structure*, University of Göttingen, Germany, **1997**.
[29] M. Nardelli, *PARST95* (An update to *PARST)* a system of *FORTRAN* routines for calculating molecular structure parameters from the results of crystal structure analyses, *J. Appl. Cryst.* **1995**, *28*, 659.
[30] A. L. Spek, *Acta Crystallogr., Sect. A* **1990**, *46*, 34.

Received March 18, 2004
Early View Article
Published Online July 29, 2004

 © 2004 Wiley-VCH Verlag GmbH & Co. KGaA, Weinheim

Investigation of a Neat versus Magnetically Diluted Powdered Mononuclear Mn^{II} Complex by High-Field and High-Frequency EPR Spectroscopy

Claire Mantel,[a,b] Christian Philouze,[c] Marie-Noëlle Collomb,*[b] and Carole Duboc*[a]

Keywords: Azide ligand / Electronic structure / EPR spectroscopy / Manganese / Magnetic dilution

The isolation, structural characterization and electronic properties of a new mononuclear, pentacoordinate Mn^{II} complex [Mn(*t*Buterpy)$(N_3)_2$] (**1**; *t*Buterpy = 4,4′,4′′-tri-*tert*-butyl-2,2′:6′,2′′-terpyridine) is reported. The X-ray structure of **1** reveals that the manganese ion lies in the center of a distorted trigonal bipyramid. The electronic properties of **1** were investigated by high-field and high-frequency EPR (HF-EPR) spectroscopy, allowing the determination of the spin-Hamiltonian parameters. HF-EPR spectra were recorded on a neat powder of **1** and also on **1** magnetically diluted in the corresponding zinc complex. From the neat powder HF-EPR spectra, the following *g* and zero-field-splitting terms, as well as the sign of *D*, were obtained: $D = -0.250(5)$ cm^{-1}, $E = 0.044(5)$ cm^{-1} and $g_x = g_y = g_z = 2.000(5)$. The magnetically diluted sample allows the determination of the hyperfine coupling constant *A* and confirms the values of the parameters determined with the neat powder: $|D| = 0.260(1)$ cm^{-1}, $E = 0.043(1)$ cm^{-1}, $g_x = g_y = 2.001(1)$ $g_z = 2.0005(5)$ and $A_{xx} = A_{yy} = A_{zz} = 77.5(5)$ G. A comparison between these two sets of spin-Hamiltonian parameters is discussed, as well as the correlation between the *D* parameter and the coordination number around the manganese ion for a coordination shell characterized by O and/or N atoms (i.e. Mn^{II}-containing proteins).

(© Wiley-VCH Verlag GmbH & Co. KGaA, 69451 Weinheim, Germany, 2004)

Introduction

Mononuclear Mn^{II} complexes are present in several metalloproteins implicated in various important biological processes. Examples include manganese superoxide dismutase, an antioxidant enzyme that catalyzes the dismutation of the superoxide radical,[1] concanavaline A, a saccharide-binding protein,[2] the fosfomycin resistance protein implicated in the resistance against the antibiotic fosfomycin,[3] and several others.[4] Since the manganese site is essential for their activity, a precise determination of the geometry and the coordination shell of the metallic ion is required to understand the reactivity of these proteins. One of the best techniques used to elucidate the electronic structure of a metallic center is EPR spectroscopy. In particular, X-band EPR spectroscopy (9.4 GHz) has been used to study several biological Mn^{II} sites.[1b−1d,2c,2d,3,4]

High-spin Mn^{II} ($3d^5$) is characterized by a fundamental electronic spin *S* of 5/2 and a nuclear spin *I* also of 5/2 (^{55}Mn, 100%). Its electronic properties are described by the spin-Hamiltonian of Equation (1).

$$H = \beta B \cdot g \cdot S + I \cdot A \cdot S + D[S_z^2 - 1/3S(S+1)] + E(S_x^2 - S_y^2) \quad (1)$$

The first two terms represent the electronic Zeeman and the electron nuclear hyperfine interactions, respectively, whereas the last two terms define the zero-field splitting (zfs) interaction, with *D* and *E* weighting the axial and rhombic parts.

A typical Mn^{II} EPR spectrum for mononuclear complexes with small zfs parameters, recorded under highly diluted conditions (in solution) and at high temperature, is characterized by a unique feature centered at $g \approx 2.0$ as a sextuplet. These six lines originate from the hyperfine splitting of the central transition $|5/2, -1/2> \rightarrow |5/2, +1/2>$, as shown in Figure 1. The shape of the sextuplet depends on the magnitude of the different spin-Hamiltonian terms. When the zfs terms increase, the X-band EPR spectrum becomes increasingly more complicated and almost impossible to interpret, with broad transitions between 0 and 0.5 mT. In this case, the way to simplify the Mn^{II} EPR spectra is to record them at higher microwave frequencies such as 35 GHz (Q-band EPR), 95 GHz or even up to 285 GHz

[a] Grenoble High Magnetic Field Laboratory, Laboratoire des Champs Magnétiques Intenses, CNRS UPR 5021, MPI
B. P. 166, 38042 Grenoble Cedex 9, France
Fax: (internat.) + 33-4-76855610
E-mail: duboc@grenoble.cnrs.fr
[b] Laboratoire d'Electrochimie Organique et de Photochimie Redox, Université Joseph Fourier, CNRS UMR 5630, Institut de Chimie Moléculaire de Grenoble (ICMG), FR CNRS 2607
B. P. 53, 38041 Grenoble cedex 9, France
Fax: (internat.) + 33-4-76514267
E-mail: Marie-Noelle.Collomb@ujf-grenoble.fr
[c] Laboratoire d'Etudes Dynamiques et Structurales de la Sélectivité, Université Joseph Fourier, CNRS UMR 5616, ICMG, FR CNRS 2607
B. P. 53, 38041 Grenoble cedex 9, France

 © 2004 Wiley-VCH Verlag GmbH & Co. KGaA, Weinheim **DOI: 10.1002/ejic.200400325**

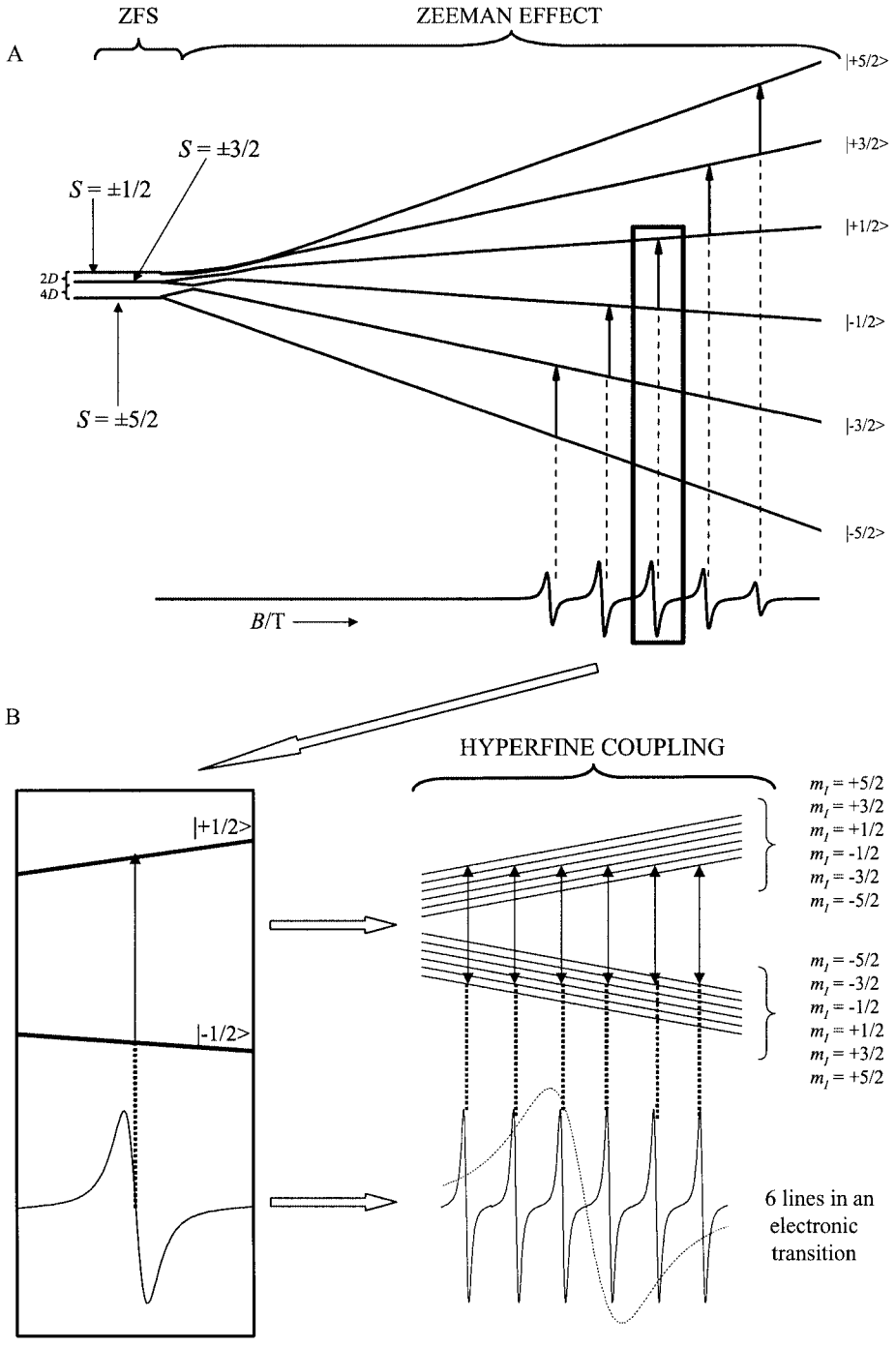

Figure 1. (A) Schematic representation of the energy level diagram of an $S = 5/2$ system undergoing axial zero field splitting (zfs) (negative D) and Zeeman effect with the field parallel to the z axis; (B) extended view of the $Ms = \pm 1/2$ energy levels showing the hyperfine levels for $I = 5/2$; arrows indicate the allowed transitions and the resulting spectra are given

(high-field EPR, HF-EPR). Indeed, HF-EPR spectroscopy (frequency 95 GHz) and derived techniques such as high-field ENDOR have proven to be useful tools.[1d,1e,2d,5] Under high-field conditions ($D << g\beta B$), EPR spectra recorded on an Mn^{II}-containing protein solution exhibit a simplified sextuplet from which the spin-Hamiltonian parameters can be extracted. However, when the magnitude of D is very large ($|D| > 0.2$ cm^{-1}), even at high field (285 GHz, $g = 2$ at 10.2 T), the central transition $|5/2, -1/2> \rightarrow |5/2, +1/2>$ appears as a signal characterized by more than six lines.[1d,1e] With such Mn^{II} systems, a multi-frequency HF-EPR study is necessary for a precise determination of the spin-Hamiltonian parameters.

Concerning the other transitions of the paramagnet $S = 5/2$ displayed in Figure 1, four others are expected along each magnetic axis. However, they are rarely observed and studied by X-band EPR spectroscopy, especially when the experiments are performed in solution.

 © 2004 Wiley-VCH Verlag GmbH & Co. KGaA, Weinheim

X- and Q-band EPR studies performed on powdered or crystalline samples of synthetic mononuclear Mn^{II} complexes have also been reported.[6] The analysis of the EPR spectra is feasible for systems with small *D* values due to the observation of some or all expected transitions. Nevertheless, Mn^{II} complexes are often characterized by relatively large axial zfs, and when *D* is larger than or similar to the energy provided by the EPR spectrometer, the spectra become more complicated and not interpretable. Furthermore, with neat powder samples the hyperfine interactions cannot be observed. In order to detect them, the manganese complexes need to be diluted into a diamagnetic host. In the few studies related to magnetic dilution,[7] the X- or Q-band EPR spectra show several transitions split by hyperfine interactions that can help with the determination of the spin-Hamiltonian parameters when *D* is relatively large.

Another way to obtain interpretable spectra of manganese(II) complexes with large *D* values is the use of HF-EPR spectroscopy. In this case, with neat powder samples more, or even all, transitions can be then observed than with X-band, allowing the precise determination of the spin-Hamiltonian parameters. To the best of our knowledge, only two HF-EPR studies, showing complete or quasi-complete EPR spectra of Mn^{II} complexes, have been reported so far.[8] The compounds were three series of synthetic mononuclear dihalo complexes with distorted octahedral[8a] or tetrahedral[8b] geometries. The HF-EPR experiments were carried out on neat powder samples at 94.5 and 250 GHz avoiding the observation of hyperfine splitting in the different electronic-spin transitions. The spin-Hamiltonian parameters were determined, although the sign of *D* was not extracted since the experiments were performed at room temperature.

In this paper, we report the synthesis, the crystallographic characterization and an HF-EPR study (190−285 GHz) of a new synthetic pentacoordinate inorganic complex: [Mn(*t*Buterpy)$(N_3)_2$] (**1**; *t*Buterpy = 4,4′,4′′-tri-*tert*-butyl-2,2′:6′,2′′-terpyridine). The EPR experiments were performed both on a neat powder of **1** and on the complex diluted into the corresponding zinc(II) complex, [Zn(Mn)(*t*Buterpy)$(N_3)_2$]. We chose this solid magnetic dilution rather than a dilution of **1** in a solvent in order to maintain the pentacoordination of **1**. This work allows us to compare the spin-Hamiltonian parameters obtained in both conditions (neat and magnetically diluted samples of **1**). We can thus discuss the validity of the approach developed for several Mn^{II} protein EPR studies in which only the sextuplet is used to determine the electronic structure of the Mn^{II} site.

Results

Description of the Crystal Structure of [Mn(*t*Buterpy)$(N_3)_2$] (1)

The crystal structure of complex **1** was determined by single-crystal X-ray crystallography and its structure is shown in Figure 2.[9] The principal crystallographic data are given in the Exp. Sect., while Table 1 summarizes selected bond lengths and angles.

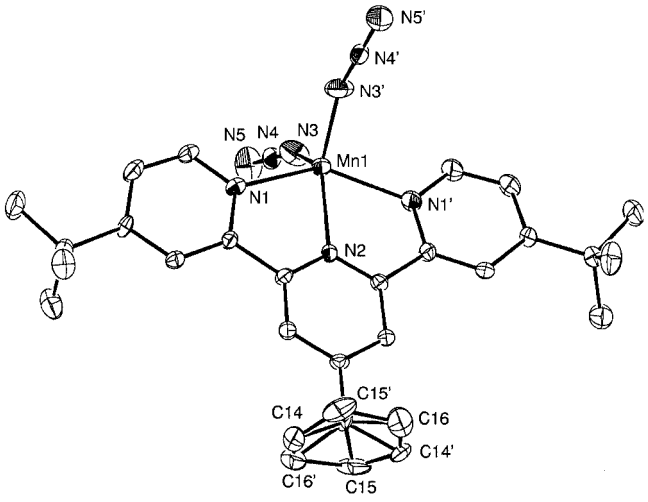

Figure 2. ORTEP view of [Mn(*t*Buterpy)$(N_3)_2$]; hydrogen atoms have been omitted for clarity

Table 1. Selected bond lengths [Å] and angles [°] for complex **1**

Mn−N(1)	2.249(5)	N(1)−Mn−N(1′)	144.1(2)
Mn−N(2)	2.206(5)	N(1)−Mn−N(3)	101.0(2)
Mn−N(3)	2.038(5)	N(1)−Mn−N(3′)	99.6(2)
N(1)−Mn−N(2)	72.0(1)	N(3)−Mn−N(3′)	108.8(3)
N(2)−Mn−N(3)	125.6(2)		

The manganese ion lies in the center of a distorted trigonal bipyramid. The equatorial plane is occupied by two nitrogen atoms of the two azide ligands [N(3) and N(3′)] and the central nitrogen atom [N(2)] of *t*Buterpy. The two distal *t*Buterpy nitrogen atoms [N(1) and N(1′)] are in the axial positions. The structure possesses a rotational C_2 symmetry axis passing through the Mn and N(2), atoms implying that the atoms N(3) and N(3′) are crystallographically equivalent, as are N(1) and N(1′). It can also be seen that the *tert*-butyl group of the central pyridine ring rotates around this C_2 axis. This implies that each carbon atom of the *tert*-butyl group [C(14), C(15) and C(16)] possesses two equivalent crystallographic sites whose occupancy ratio is 50%. The $Mn-N_{tButerpy}$ bond lengths and the angles N(1)−Mn−N(1′) and N(1)−Mn−N(2) are typical for mononuclear (terpy)Mn^{II} complexes.[10] The Mn−N(2) distance [2.206(5) Å] is shorter than the Mn−N(1) distance [2.249(5) Å].[10] The magnitude of the N(1)−Mn−N(1′) [144.1(2)°] is reduced from the theoretical value of 180° of an idealized trigonal bipyramid due to the rigidity of the *t*Buterpy ligand. The angles between the atoms in the equatorial positions are 125.6(2)° [N(2)−Mn−N(3){N(3′)}] and 108.8(3)° [N(3)−Mn−N(3′)]. These values are a measure of the distortion as a value of 120° is expected for an undistorted trigonal bipyramid. The $Mn-N_{azide}$ bonds [2.038(5)

 © 2004 Wiley-VCH Verlag GmbH & Co. KGaA, Weinheim

Å] in **1** are slightly shorter than those observed in $[Mn(phen)_2(N_3)(H_2O)]^+$ (2.151 Å) or $[Mn(phen)_2(N_3)_2]$ (av. 2.138 Å) (phen: 1,10-phenanthroline).[11]

HF-EPR Spectroscopy of a Neat Powder of [Mn(*t*Buterpy)-$(N_3)_2$]

The electronic properties of a neat powder sample of complex **1** were investigated by a multi-frequency EPR study between 190 and 285 GHz and over a temperature range of 5−30 K. Figure 3 shows experimental and simulated 285 GHz HF-EPR spectra recorded at 5 and 10 K. At this frequency, the spectra show transitions located between 9.0 and 11.2 T. Since high-field limit conditions are reached ($D << g\beta B$), all of the transitions are allowed, permitting an easy interpretation of the experimental data.

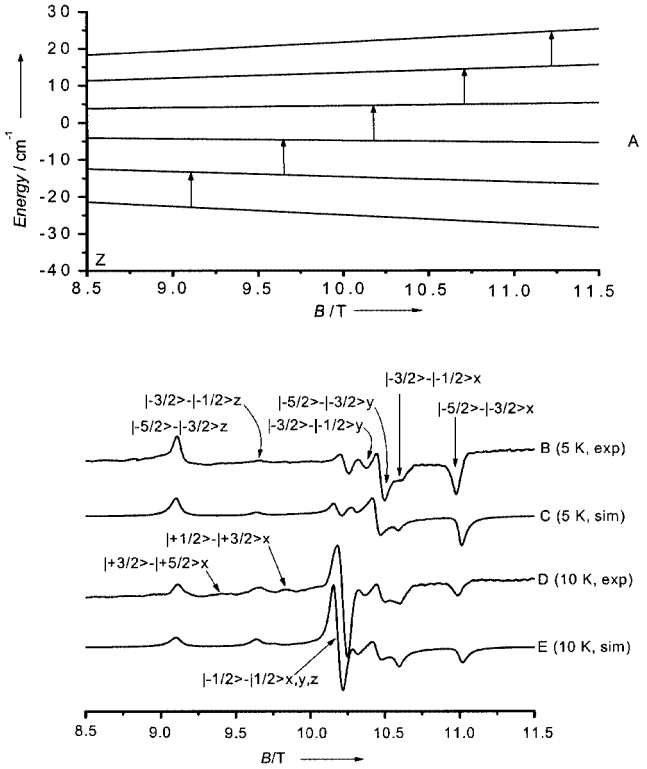

Figure 3. Plots of energy vs. field for the six levels arising from an $S = 5/2$ spin state using the parameters given below; the field is parallel to the molecular z axis (A); arrows indicate the observed resonances; experimental (B and D) and simulated (C and E) powder 285 GHz EPR spectra of **1**, recorded at 5 K (B and C) and 10 K (D and E); the parameters used for the simulation are: $D = -0.250(5)$ cm^{-1}, $E = 0.044(5)$ cm^{-1} and $g_x = g_y = g_z = 2.000(5)$

In the 5 K spectrum (Figure 3B), the furthest transition (9.11 T) from the center of the spectrum (close to $g = 2.00$ for Mn^{II};[12] 10.18 T at 285 GHz) is associated with the $|5/2,-5/2> \rightarrow |5/2,-3/2>$ transition along the z axis, since $D_{zz} > D_{xx}$ and D_{yy} (with $D_{zz} + D_{xx} + D_{yy} = 0$). This is in agreement with the fact that, at low temperature, only the first Zeeman levels (Ms) levels are populated ($|-5/2>$ and $|-3/2>$). From its field position, the sign and an estimate of the magnitude of D can be obtained. Since this transition is located in the low-field part of the spectrum at low temperature, we infer that the sign of D is negative. Its distance from the central field of the spectrum is $4D/g_z\beta$, implying a D value of 0.27 T or 0.25 cm^{-1} (with $g_z = 2.00$ as a first approximation). The intensity of the transition observed at 9.60 T increases from 5 to 10 K (Figure 3D), in agreement with the Boltzmann population of the Ms levels. Thus, it can be attributed to the $|5/2,-3/2> \rightarrow |5/2,-1/2>$ transition along z. Moreover, this transition is located at the expected field position of $+2D/g_z\beta$ from the $|5/2,-5/2> \rightarrow |5/2,-3/2>$ transition along z, confirming our analysis.

The other 5 K spectrum features are associated with x and y transitions. The 10.98 T and 10.59 T features are associated with the $|5/2,-5/2> \rightarrow |5/2,-3/2>$ and $|5/2,-3/2> \rightarrow |5/2,-1/2>$ transitions along the x axis, respectively. These assignments were confirmed thanks to the temperature effect on the intensity of the transitions. Indeed, the intensity of the first transition of the multiplet decreases on going from 5 to 10 K whereas the second feature increases. The E term can be extracted from the resonance-field difference of these two subsequent x transitions, which corresponds to $(3E - D)/g_x\beta$. This implies an E value of 0.038 cm^{-1}.

The transitions associated with the y axis for the $Ms = -5/2$ and $-3/2$ levels of **1** are observed at 10.47 T and 10.34 T, respectively, which yields a field difference of 0.13 T equal to $-(D + 3E)/g_y\beta$, giving an E value of 0.043 cm^{-1}. This value is similar to the previous one obtained from the x transitions.

Concerning the central feature located at $g = 2.0$ (10.18 T at 285 GHz), it corresponds to the contribution of the $|5/2,-1/2> \rightarrow |5/2,+1/2>$ transitions along the three magnetic axes. At 5 K, the major contribution comes from the y transition since the Ms level $|-1/2>$ is not populated in the x and z directions. On the contrary, at higher temperatures the $|5/2,-1/2> \rightarrow |5/2,+1/2>$ transitions along x, y and z contribute to the central feature. For this reason, this central transition is largely enhanced at 10 K compared to the other transitions.

The absence of observable splitting due to hyperfine interactions in the experimental spectra originates from the large line width of the spectral features. Different mechanisms can contribute to line broadening. In our case, the line width is not temperature-dependent, implying that the major contribution of the broadening comes from dipolar interactions between metallic centers.

As hyperfine interactions are not observable in the experimental data, the spin Hamiltonian of Equation (2) that describes our system under these conditions is simpler than in Equation (1).

$$H = \beta B \cdot g \cdot S + D[S_z^2 - 1/3S(S+1)] + E(S_x^2 - S_y^2) \quad (2)$$

The HF-EPR spectra were simulated using a full-matrix diagonalization procedure of the spin Hamiltonian [Equation (2)].[6a] The best simulation of the experimental spectra

 © 2004 Wiley-VCH Verlag GmbH & Co. KGaA, Weinheim

(Figure 3) was obtained using the following spin Hamiltonian parameters: $D = -0.250(5)$ cm^{-1}, $E = 0.044(5)$ cm^{-1} and $g_x = g_y = g_z = 2.000(5)$. These spin-Hamiltonian parameters also simulate successfully the HF-EPR spectra recorded at all temperatures and frequencies.

HF-EPR Spectroscopy of a Magnetically Diluted Powder of [Mn(tButerpy)(N$_3$)$_2$] in Zinc(II)

To experimentally observe the hyperfine interactions for determining the A term, one way is to minimize the line broadening by diluting the paramagnetic centers. A good way to magnetically dilute a paramagnetic center is to incorporate the sample in a diamagnetic host in order to decrease the dipolar interactions. We therefore diluted complex **1** in the corresponding zinc(II) complex at a concentration of approximately 5% by weight of manganese(II).

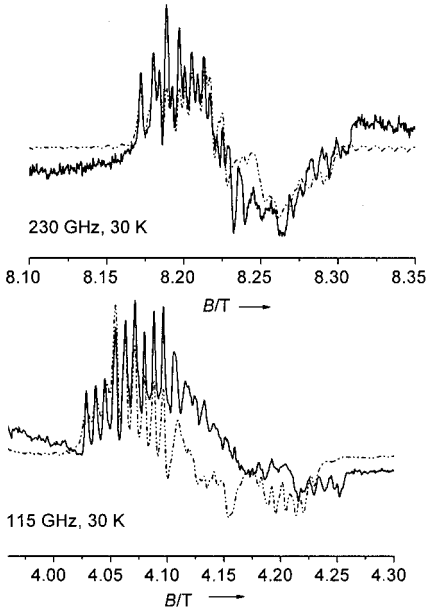

Figure 4. Experimental (bold line) and simulated (dashed line) EPR spectra recorded at 230 and 115 GHz of [Zn(Mn)(*t*Buterpy)(N$_3$)$_2$] at 30 K; the parameters used for the simulation are: $|D| = 0.260(1)$ cm^{-1}, $E = 0.043(1)$ cm^{-1}, $g_x = g_y = 2.001(1)$ $g_z = 2.0005(5)$ and $A_{xx} = A_{yy} = A_{zz} = 77.5$ (5) G

Figure 4 displays the 115 and 230 GHz experimental and simulated EPR spectra of [Zn(Mn)(*t*Buterpy)(N$_3$)$_2$]. As expected, this spectrum is characterized by a unique feature located at $g \approx 2.0$, split into multiple lines corresponding to the $|5/2,-1/2> \rightarrow |5/2,+1/2>$ transition along the three axes x, y and z. Since the two experimental spectra are centered at a g value of around 2.000, the Zeeman interaction is dominant above 4 T. As already observed by Un et al.,[1e] the total width of the spectra increases from 115 to 230 GHz (0.135 and 0.220 T, respectively) and the spectra appear better resolved at low field. Since the exact positions of all of these lines are dependent on the zfs terms (D and E) and g, simulations have been performed to extract the spin Hamiltonian parameters of these spectra.

A full-matrix diagonalization of Equation (1) was performed, and the best simulated spectra using $|D| = 0.260(1)$ cm^{-1}, $E = 0.043(1)$ cm^{-1}, $g_x = g_y = 2.001(1)$, $g_z = 2.0005(5)$ and $A_{xx} = A_{yy} = A_{zz} = 77.5$ (5) G are shown in Figure 4. The sign of D cannot be extracted from the multiplet.

Discussion and Conclusion

In this paper we have described the synthesis and the crystallographic characterization of a mononuclear Mn^{II} complex possessing two terminal azide ligands, [Mn(*t*Buterpy)(N$_3$)$_2$]. Such mononuclear complexes are not common since azide ions have mainly been used for their ability to bridge paramagnetic Mn^{II} centers into dimers, clusters, and polymers.[13] A large number of such compounds have been described in the literature including the dimer [Mn$_2^{II,II}$(μ-N$_3$)$_2$(terpy)$_2$](N$_3$)$_2$].[14]

We performed an HF-EPR study of **1** in order to determine the spin-Hamiltonian parameters of this complex. The experiments were performed in the solid state both on the neat compound and its magnetically diluted form. From the HF-EPR experiments carried out on the neat powder, we extracted the magnitude of g, D and E, as well as the sign of D. The unambiguous determination of the sign of D was possible by recording the spectra at low temperature. In previous HF-EPR studies on mononuclear Mn^{II} complexes, the sign of D was not determined since the experiments were performed at room temperature.[8] The experiments conducted under magnetically diluted conditions allow us to determine the A term and to confirm the value of the other spin-Hamiltonian parameters; the sign of D cannot

Table 2. Electronic characteristics and coordination number of Mn^{II} sites in enzymes

	D [10^{-4} cm^{-1}]	E [10^{-4} cm^{-1}]	A [Gauss]	Coord. number	Ref.
Mn^{2+}-FosA + substrate	2300	200	–	5	[3b]
Mn-SOD *R. capsulatus*	3588	146	86	5	[1e]
Mn-SOD *E. coli*	3548	305	85	5	[1e]
R. capsulatus + azide	720	193	81	6	[1e]
E. Coli + azide	462	91	82	6	[1e]
Mn^{2+}-FosA	600	60	–	6	[3b]
Mn^{2+} concanavaline A	216	23.7	92.5	6	[2d]
Mn^{2+} xylose isomerase	422–450	105.5–112.3	–	6	[4b]

 © 2004 Wiley-VCH Verlag GmbH & Co. KGaA, Weinheim

be extracted. Since both sets of parameters are essentially the same, a similar environment for each manganese ion can be postulated in both pure and diluted lattices.

In Table 2, we report the spin-Hamiltonian parameters of several mononuclear Mn^{II} complexes present in different metalloproteins. In all cases the spin-Hamiltonian parameters have been accurately determined from the EPR hyperfine split multiplet of the $|5/2,-1/2> \rightarrow |5/2,+1/2>$ transition using extended spectroscopic techniques such as Q-band EPR, HF-EPR or HF-ENDOR. The coordination number cannot be adequately correlated to A, although such a correlation has already been proposed.[4a,15] On the contrary, a good agreement is observed between the magnitude of D and the coordination number of the Mn^{II} ion. D is larger than 0.2 cm^{-1} for pentacoordinate complexes while it is smaller than 0.1 cm^{-1} for hexacoordinate ones. The D value found for **1** is in good agreement with a pentacoordinate complex. The large E/D value (0.176) reflects the distortions observed in the X-ray structure of complex **1**.

We found similar spin-Hamiltonian parameters to simulate both neat and magnetically diluted powder of **1**. This result shows that the analysis of the HF-EPR spectrum under diluted conditions is sufficient to allow an accurate determination of the electronic parameters of mononuclear Mn^{II} complexes. For the study of manganese sites present in metalloproteins, samples obviously correspond to diluted conditions where only the $|5/2,-1/2> \rightarrow |5/2,+1/2>$ transition can be observed. As shown in Table 2, where all spin-Hamiltonian parameters have been determined using Q-band or HF-EPR spectroscopy, the advantage of increasing the frequency is that the spectra are simpler than X-band spectra. Consistent with this view, our work confirms that HF-EPR spectroscopy permits the resolution of the electronic structure of mononuclear Mn^{II} complexes even for systems with a large D value, making it a promising tool for the study of Mn^{II} compounds, including metalloproteins.

Experimental Section

General: Reagents and solvents were purchased commercially and used as received. ***Caution:*** Both N_3^- and its complexes are potentially explosive; although we have encountered no such problems with complex **1**, it should still be handled with care; further, N_3^- releases explosive HN_3 on contact with acid solution!

Synthesis of [Mn(*t*Buterpy)$(N_3)_2$]: An ethanolic solution (10 mL) of *t*Buterpy (0.055 g, 0.136 mmol) was added, with stirring, to an aqueous solution (2 mL) of $MnCl_2$ (0.017 g, 0.136 mmol). An excess of solid NaN_3 was then added to the yellow solution. The solution was filtered to remove any impurities and the solvents were evaporated to dryness to give a yellow precipitate corresponding to complex **1**. Single crystals of [Mn^{II}(*t*Buterpy)$(N_3)_2$] were grown by slow diffusion of diethyl ether into a concentrated solution of **1** in a mixture of dichloromethane and acetonitrile (1:1). Yield: 0.032 g (22%). $C_{28}H_{38}MnN_9O_{0.5}$ (563): calcd. C 59.67, H 6.80, N 22.37; found C 60.42, H 6.70, N 22.40. IR (KBr): $\tilde{\nu}$ = 2959 (m) cm^{-1}, 2076 (vs), 1607 (s), 1549 (m), 1402 (m), 1364 (m), 1251 (m), 1013 (m), 845 (m).

Synthesis of [Zn(Mn)(*t*Buterpy)$(N_3)_2$]: $[Mn(O_2CCH_3)_2]\cdot 4H_2O$ (0.0032 g, 0.013 mmol) was added with stirring to a methanolic solution (5 mL) of $[Zn(O_2CCH_3)_2]\cdot 2H_2O$ (0.0551 g, 0.25 mmol). A solution of *t*Buterpy (0.1056 g, 0.263 mmol) in 100 mL of methanol was then added to this solution. Finally, an excess of solid NaN_3 was added. The solution was stirred for 1 h until formation of a white precipitate. The solution was filtered and the filtrate was concentrated to dryness to give a yellow precipitate of [Zn(Mn)(*t*Buterpy)$(N_3)_2$]. Yield: 0.045 g (31%).

Crystal-Structure Determination of [Mn(*t*Buterpy)$(N_3)_2$]: Diffraction data were collected with an Enraf-Nonius CAD4 diffractometer. The structures were solved by direct methods and refined using the TEXSAN software package (Single Crystal Structure Analysis Software, version 1.7, molecular structure corporation, 3200 Research Forest Drive, The Woodlands, TX 77381, USA, **1995**). Further details of the data collection and refinement are given in Table 3. CCDC-209520 (**1**) contains the supplementary crystallographic data for this paper. These data can be obtained free of charge at www.ccdc.cam.ac.uk/conts/retrieving.html [or from the Cambridge Crystallographic Data Centre, 12 Union Road, Cambridge CB2 1EZ, UK; Fax: (internat.) + 44-1223-336-033; E-mail: deposit@ccdc.cam.ac.uk].

Physical Measurements: IR spectra were obtained with a Perkin−Elmer Spectrum GX spectrophotometer, piloted by a Dell Optiplex GXa computer. Spectra were recorded with a solid sample at 1% in mass in a pellet of KBr. High-frequency and high-field EPR spectra were recorded with a home-made spectrometer.[16] Gunn diodes operating at 95 GHz and 115 GHz and equipped with a second-, third-, fourth-, and fifth-harmonic generator were used as the radiation source. The magnetic field was produced by a superconducting magnet (0−12 T). The HF-EPR experiments were performed on polycrystalline powder pellets of **1** in order to avoid magnetic orientation of crystals. Diluted samples of **1** were prepared by immobilizing the powder either in KBr or in *n*-icosane mull; identical HF-EPR spectra were obtained in both cases.

Table 3. Principal crystallographic data and parameters of complex **1**

Empirical formula	$C_{27}H_{35}MnN_9$
Formula mass	540.57
Crystal system	monoclinic
Space group	*C*2/*c*
Crystal dimensions [mm]	0.56 × 0.20 × 0.12
a [Å]	22.766(4)
b [Å]	11.718(4)
c [Å]	11.343(2)
β [°]	112.10
V [Å^3]	2804(1)
T [°C]	20
λ [Å]	0.7107
$\rho_{calcd.}$ [g·cm^{-3}]	1.281
Z	4
F(000)	1140
Abs coeff [cm^{-1}]	0.503
No. of reflections collected	10088
No. of independent reflections	3475
No. of observed reflections [$I > 2\sigma(I)$]	1634
No. of refined parameters	183
Largest peak/hole [e·Å^{-3}]	0.51/−0.37
R[a]	0.0628
R_w[b]	0.0902

[a] $R = \Sigma||F_o| - |F_c||/\Sigma|F_o|$. [b] $Rw = [(\Sigma w(|F_o| - |F_c|)^2/\Sigma w(F_o^2)]^{1/2}$.

 © 2004 Wiley-VCH Verlag GmbH & Co. KGaA, Weinheim

Acknowledgments

We thank Dr. H. Weihe from the Chemistry Department, University of Copenhagen, Denmark, for the simulation software.

[1] [1a] M. L. Ludwig, A.L. Metzger, K. A. Pattridge, W. C. Stallings, *J. Mol. Biol.* **1991**, *219*, 335−358. [1b] A. L. Schwartz, E. Yakilmaz, C. K. Vance, S. Varthyam, R. L. Koder, A.-F. Miller, *J. Inorg. Biochem.* **2000**, *80*, 247−256. [1c] M. M. Whittaker, J. W. Whittaker, *Biochemistry* **1997**, *36*, 8923−8931. [1d] S. Un, P. Dorlet, G. Voyard, L. C. Tabares, N. Cortez, *J. Am. Chem. Soc.* **2001**, *123*, 10123−10124. [1e] S. Un, L. C. Tabares, N. Cortez, B. Y. Hiraoka, F. Yamakura, *J. Am. Chem. Soc.* **2004**, *126*, 2720−2726.

[2] [2a] A. T. Deacon, T. Gleichmann, A. J. Kalb (Gilboa), J. Price, J. Raftery, G. Brabbrook, J. Yariv, J. R. Helliwell, *J. Chem. Soc., Faraday Trans.* **1997**, *93*, 4305−4312. [2b] Z. Zhang, M. Qian, Q. Huang, Y. Jia, Y. Tang, K. Wang, D. Cui, M. Li, *J. Prot. Chem.* **2001**, *20*, 423. [2c] E. Meirovitch, Z. Luz, A. J. Kalb, *J. Am. Chem. Soc.* **1974**, *96*, 7538−7542. [2d] R. Carmieli, P. Manikanda, A. J. Kalb (Gilboa), D. Goldfard, *J. Am. Chem. Soc.* **2001**, *123*, 8378−8386.

[3] [3a] B. A. Bernat, L. T. Laughlin, R. N. Armstrong, *Biochemistry* **1999**, *38*, 7462−7469. [3b] S. K. Smoukov, J. Telser, B. A. Bernat, C. L. Rife, R. N. Armstrong, B. M. Hoffman, *J. Am. Chem. Soc.* **2002**, *124*, 2318−2326.

[4] [4a] A. K. Whiting, Y. R. Bolt, M. P. Hendrich, L. P. Wackett, L. Que Jr., *Biochemistry* **1996**, *35*, 160−170. [4b] R. Bogumil, R. Kappl, J. Hüttermann, H. Witzel, *Biochemistry* **1997**, *36*, 2345−2352. [4c] L. Requena, S. Bornemann, *Biochem. J.* **1999**, *343*, 185−190.

[5] [5a] C. Buy, G. Girault, J.-L. Zimmermann, *Biochemistry* **1996**, *35*, 9880−9891. [5b] H. Käss, F. MacMillan, B. Ludwig, T. Prisner, *J. Phys. Chem. B* **2000**, *104*, 5362−5371.

[6] [6a] C. J. H. Jacobsen, E. Pedersen, J. Villardsen, H. Weihe, *Inorg. Chem.* **1993**, *32*, 1216−1221. [6b] C. Bucher, E. Duval, J.-M. Barbe, J.-N. Verpeaux, C. Amatore, R. Guilard, L. Le Pape, J.-M. Latour, S. Dahaoui, C. Lecomte, *Inorg. Chem.* **2001**, *40*, 5722−5726. [6c] L. R. Gahan, V. A Grillo, T. W. Hambley, G. R. Hanson, C. J. Hawkins, E. M. Proudfoot, B. Moubaraki, K. S. Murray, D. Wang, *Inorg. Chem.* **1996**, *35*, 1039−1044. [6d] E. Meirovitch, Z. Luz, J. Kalb, *J. Am. Chem. Soc.* **1974**, *96*, 7538−7542. [6e] R. D. Dowsing, J. F. Gibson, *J. Chem. Phys.* **1969**, *50*, 294. [6f] F. E. Mabbs, D. Collison, *Electron Paramagnetic Resonance of Transition Metal Compounds*, Elsevier, Amsterdam, **1992**, vol. 16; and references cited therein.

[7] [7a] R. D. Dowsing, J. F. Gibson, D. M. L. Goodgame, M. Goodgame, P. J. Hayward, *J. Chem. Soc. A* **1969**, 1242−1248. [7b] R. B. Birdy, M. Goodgame, *Inorg. Chim. Acta* **1981**, *50*, 183−187. [7c] G. M. Woltermann, J. R. Wasson, *Inorg. Chem.* **1973**, *12*, 2366−2370. [7d] R. A. Palmer, M. C. L. Yang, J. C. Hempel, *Inorg. Chem.* **1978**, *17*, 1200−1203. [7e] D. Vivien, J. F. Gibson, *J. Chem. Soc., Faraday Trans. 2* **1975**, 1640−1653. [7f] C. A. Kosky, J.-P. Gayda, J. F. Gibson, S. F. Jones, D. J. Williams, *Inorg. Chem.* **1982**, *21*, 3173−3179.

[8] [8a] W. B. Lynch, R.S. Boorse, J. H. Freed, *J. Am. Chem. Soc.* **1993**, *115*, 10909−10915. [8b] R. M. Wood, D. M. Stucker, L. M. Jones, W. B. Lynch, S. K. Misra, J. H. Freed, *Inorg. Chem.* **1999**, *38*, 5384−5388.

[9] Due to the disorder of the *tert*-butyl group and the thickness of the needle-type crystals, we were only able to obtain a structure with a reasonable resolution.

[10] L. S. Erre, G. Micera, E. Garribba, A. Cs. Bényei, *New. J. Chem.* **2000**, *24*, 725−728.

[11] P.-Y. Bu, L. Z. Zhang, L.-C. Li, Y. Dai, P. Cheng, S.-P. Yan, Z.-H. Jiang, D.-Z. Liao, *J. Coord. Chem.* **2002**, *55*, 1263.

[12] A. Abragam, B. Bleaney, in *Electron Paramagnetic Resonance of Transition Ions*, Clarendon Press, Oxford, **1970**.

[13] J. Ribas, A. Escuer, M. Monfort, R. Vicente, R. Cortés, L. Lezama, T. Rojo, *Coord. Chem. Rev.* **1999**, 193−195; J. Ribas, A. Escuer, M. Monfort, R. Vicente, R. Cortés, L. Lezama, T. Rojo, *Coord. Chem. Rev.* **1999**, 1027−1068.

[14] [14a] R. Cortés, J. L. Pizarro, L. Lezama, M. I. Arriortua, T. Rojo, *Inorg. Chem.* **1994**, *33*, 2697−2700. [14b] Z.-H. Zhang, X.-H. Bu, Z.-H. Ma, W.-M. Bu, Y. Tang, Q.-H. Zhao, *Polyhedron* **2000**, *19*, 1559.

[15] J. W. Whittaker, M. M. Whittaker, *J. Am. Chem. Soc.* **1991**, *113*, 5528−5540.

[16] [16a] A.-L. Barra, L.-C. Brunel, J. B. Robert, *Chem. Phys. Lett.* **1990**, *165*, 107. [16b] F. Muller, M. A. Hopkins, N. Coron, M. Grynberg, L.-C. Brunel, G. Martinez, *Rev. Sci. Instrum.* **1989**, *60*, 3681−3684.

Received April 23, 2004
Early View Article
Published Online July 22, 2004

 © 2004 Wiley-VCH Verlag GmbH & Co. KGaA, Weinheim

d- or f-Mononuclear and Related Heterodinuclear Complexes With [1+1] Asymmetric Compartmental Macrocycles

Andrea Caneschi,[a] Lorenzo Sorace,[a] Umberto Casellato,[b] Patrizia Tomasin,*[b] and Pietro Alessandro Vigato[b]

Keywords: Heterometallic complexes / Macrocyclic ligands / Compartmental Schiff bases / Magnetic properties / EPR spectroscopy

d- or f-mononuclear and d,f-heterodinuclear complexes with the [1+1] asymmetric compartmental macrocycles H_2L_A, H_2L_B, H_2L_C or H_2L_D, derived from the condensation of 1,2-diaminoethane or 1,3-diaminopropane with 3,3′-(3-oxapentane-1,5-diyldioxy)bis(2-hydroxybenzaldehyde) or 3,3′-(3,6-dioxaoctane-1,8-diyldioxy)bis(2-hydroxybenzaldehyde), have been synthesized and characterized, including by single-crystal X-ray structural determinations. The influence of coordinating size and the number of donor atoms of the two adjacent chambers on the preparation of stable d,f-heterodinuclear complexes has also been tested. The X-ray structure of the isostructural complexes $[MLn(L)(Cl)_3(CH_3OH)]$ (MLn = LaCu, LaZn, TbCu) shows the metal(II) ion residing in the N_2O_2 site in a square-pyramidal coordination, the fifth apical position being filled by a chloride ion, while each lanthanide(III) ion is located in the O_2O_4 site and reaches nona-coordination by linking six oxygen atoms of the macrocyclic ligand, two chloride ions and the oxygen atom of a methanol molecule. Magnetic susceptibility data, complemented by EPR spectroscopy, of the heterodinuclear complexes, studied over the range 2–300 K, show a ferromagnetic coupling for the CuGd complex, whereas, when comparing CeCu and TbCu derivatives with the corresponding Zn derivatives, no appreciable interaction could be detected for the former and a ferromagnetic interaction seems to dominate in the latter.

(© Wiley-VCH Verlag GmbH & Co. KGaA, 69451 Weinheim, Germany, 2004)

Introduction

A wide range of compartmental ligands, containing adjacent similar or dissimilar coordination sites, has been designed and used in the preparation of mono- and polynuclear complexes and in studying the peculiar properties arising from the close proximity of the metal ions.[1−9]

These ligands, acyclic or cyclic, often originate from the condensation of appropriately designed formyl and amine precursors. While the acyclic ligands are always asymmetric, the cyclic ligands can be symmetric or asymmetric. X-ray structural determinations or, when lacking suitable crystals, mass spectrometry reveals conveniently their molecular complexity.[10−16] Suitable infrared and NMR investigations have added the information necessary to identify exhaustively their nature.

Asymmetric compartmental ligands have received particular attention in the last decade as they can give rise to specific molecular recognition at the two adjacent, different compartments.[17−19] Thus, they can recognize two different metal ions; the resulting heterodinuclear complexes generally show considerably different chemical and physical behaviours from those derived from the sum of the related properties of the single metal ions surrounded by the same coordination moiety.

In addition, when homodinuclear complexes are formed, the two metal ions can be varied by appropriate reactions, i.e. the selective oxidation or reduction of one metal ion, the further ligand coordination to one metal ion with the consequent variation of the coordination polyhedron, etc. These reactions, however, are difficult to fine-tune and often do not occur. Further possibilities include the migration of one metal ion from one site to the other to afford positional isomers, the substitution of one metal ion by transmetallation (inducing a consequent migration from one site to the other), and modification of the coordination environment about one metal ion through its oxidation or reduction. These molecular movements can be reversed by changing the reaction conditions or the external stimulus. Such systems are potential molecular machines, and several molecular or nanomolecular sensors or devices based on these processes have been successfully proposed.[20−22]

We have investigated recently the coordinating properties of [1+1] asymmetric cyclic Schiff bases derived from the condensation of 3,3′-(3-oxapentane-1,5-diyldioxy)bis(2-hydroxybenzaldehyde) or 3,3′-(3,6-dioxaoctane-1,8-diyl-

[a] Department of Chemistry and INSTM Research Unit, University of Florence,
Via della Lastruccia 3, 50019 Sesto Fiorentino (Fi), Italy
[b] Istituto di Chimica Inorganica e delle Superfici,
Area della Ricerca, C.so Stati Uniti 4, 35127 Padova, Italy
Fax: (internat.) + 39-049-8702911
E-mail: patrizia.tomasin@icis.cnr.it

dioxy)bis(2-hydroxybenzaldehyde) with a series of polyamines. These ligands contain an N_2O_2 or N_3O_2 Schiff base chamber and an adjacent O_2O_3 or O_2O_4 crown-ether-like chamber. They are particularly suitable for testing the chemical preference of different metal ions in coordinating one of the two adjacent coordination sites. Notably, d- or 4f-metal ions, when treated with these ligands, occupy the Schiff base or the crown-ether-like chamber, respectively, according to their "soft" or "hard" character.[23−25]

Conversely, in the presence of s-metal ions strongly coordinated in the crown-ether-like chamber, an incoming lanthanide ion is forced into the Schiff base moiety, affording well-defined heterodinuclear complexes without positional isomers, as ascertained for the complexes $[LnNa(L)(Cl)_2(CH_3OH)]$.[23] This chemical behaviour has been used successfully to design and use these systems as suitable shift reagents for the qualitative and quantitative recognition of the sodium ion. The ^{23}Na NMR resonance of the sodium cation is markedly shifted from that of the free ion by the paramagnetic Ln^{III} centre, making the heterodinuclear Ln−Na complexes very promising candidates for the development of highly effective shift reagents for metal cations of biological importance.[26−28]

Given the remarkable tendency of Schiff bases to coordinate the d-metal ions, combined with the high preference of the "hard" lanthanide(III) ions for the crown-ether site, we aimed to obtain positional pure heterodinuclear d,f complexes and studied the physicochemical properties arising from this aggregation. The two coordination chambers were progressively enlarged to find the most appropriate donor set configuration (coordination moiety) for pure, stable heterodinuclear d,f complexes.

Accordingly, the four macrocycles H_2L_A, H_2L_B,H_2Lc and H_2L_D were employed for the synthesis and physicochemical characterisation of a series of d- or f-mononuclear and d,f-heterodinuclear complexes. In particular, the X-ray single-crystal structures of some of these d,f complexes with H_2L_D and their magnetic properties were investigated in detail.

The paper aims to verify whether the reaction pathway of Scheme 1 can be followed, the difficulty encountered with the different synthetic methodologies, the best fit of the coordination chambers for the different metal ions and the physicochemical properties resulting from the close proximity of a d- and 4f-metal ion, particularly their magnetic behaviour.

Results and Discussion

Preparation of the Ligands and Related Complexes

The [1+1] asymmetric cyclic compartmental Schiff bases H_2L_A, H_2L_B, H_2L_C and H_2L_D were prepared by self-condensation of diformyl precursors 3,3′-(3-oxapentane-1,5-diyldioxy)bis(2-hydroxybenzaldehyde) or 3,3′-(3,3-dioxaoctane-1,8-diyldioxy)bis(2-hydroxybenzaldehyde)[23−25,29,31] with an equimolar amount of the appropriate diamine (1,2-diaminoethane or 1,3-diaminopropane). For the larger macrocycles H_2L_C and H_2L_D high-dilution conditions (methanol/diethyl ether, 1:200) are necessary; when high-dilution conditions are not employed, the [1+1] cyclic Schiff bases are variously contaminated by [2+2] or higher homologues.

These Schiff bases are yellow solids, stable in air, soluble in $CHCl_3$ and CH_3OH, and slightly soluble in C_2H_5OH. A

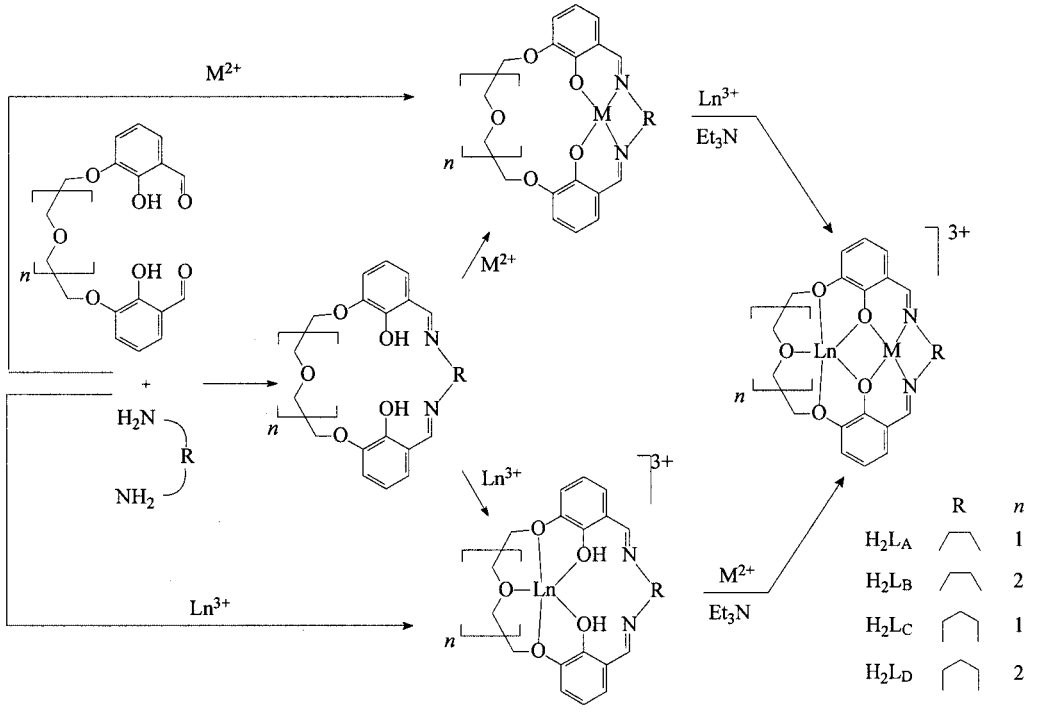

Scheme 1

 © 2004 Wiley-VCH Verlag GmbH & Co. KGaA, Weinheim

strong IR band at 1635−1627 cm^{-1} due to $\nu_{C=N}$, and the absence of bands attributable to $\nu_{C=O}$ or ν_{NH2}, show that condensation occurs. ^1H NMR spectroscopy provided further evidence of condensation reactions. In particular the peaks at δ = 9.94 ppm, due to the formyl protons (CH=O), disappear and new peaks at δ = 8.30−8.19 ppm, due to the iminic protons CH=N, are clearly detectable. The other peaks, due to aliphatic or the aromatic protons, also vary because of the condensation reaction.

The [1+1] cyclic nature of $H_2L_A\cdots H_2L_D$ was inferred by FAB and ESI mass spectrometry, which clearly show two peaks at the appropriate *m*/*z* value, characteristic of the protonated $[MH]^+$ and the cationized $[MNa]^+$.

The macrocyclic Schiff bases H_2L_A, H_2L_B, H_2L_C and H_2L_D contain two adjacent coordination sites, one N_2O_2 and one O_3O_2 or O_4O_2, that are sufficiently different to give rise to two different, well-defined complexation reactions with a d- or 4f-metal ion. The N_2O_2 Schiff base site is filled exclusively by the d-metal ion while the 4f-metal ions, owing to their "harder" character, invariably coordinate the crown-like O_2O_3 or O_2O_4 chamber. The small Schiff base cavity is unsuitable for 4f-metal ion encapsulation; conversely, the "crown-ether" character of the other chamber does not favour the coordination of d-metal ions. The result is the formation of pure positional mononuclear isomers.

The appropriate diformyl derivative, 3,3′-(3,6-dioxaoctane-1,8-diyldioxy)bis(2-hydroxybenzaldehyde) or 3,3′-(3-oxapentane-1,5-diyldioxy)bis(2-hydroxybenzaldehyde), reacts in methanol in a 1:1 molar ratio with 1,2-diaminoethane or 1,3-diaminopropane in the presence of the desired transition metal(II) chloride or acetate (Cu^{2+}, Ni^{2+}, Zn^{2+}) or lanthanide(III) chloride hydrate to form the corresponding mononuclear complexes $M(L)\cdot nH_2O$ or $[Ln(H_2L)(H_2O)_4](Cl)_3$. The crude product was recrystallised from an alcoholic solution and then characterized by the usual methods.

In particular, when copper(II) salts were used, the complexes $[Cu(L)]\cdot H_2O$ were obtained, as confirmed by ESI mass spectra, which exhibits the parent peak $[Cu(L)]^+$ at the appropriate *m*/*z* value. With the other metal ions M(L), M(HL)(X) or $M(H_2L)(X)_2$ (X = Cl^- or CH_3COO) are obtained, depending on the experimental conditions. In strong basic media the complexes $M(L)\cdot nH_2O$ are obtained. These data are in line with a parallel potentiometric study showing that the different complexes $[M(H_2L)]^{2+}$, $[M(HL)]^+$ and [M(L)] are the predominant species in particular pH ranges.[32] These investigations also prove that the coordination of a metal ion (i.e. Cu^{2+}) strongly stabilises the Schiff bases over a large pH range (2−12) and prevents their easy hydrolysis. Interestingly, this result affords the possible use of these systems in solutions usually forbidden to the Schiff bases.

Although the preformed Schiff base can give rise to the same d- or f-mononuclear complexes, when treated with the appropriate metal salt the above template procedure has to be preferred owing to the tedious and time-consuming procedure for obtaining the [1+1] macrocycle with acceptable purity. Moreover, template procedures increase considerably the yield of the complexes.

The formation of the mononuclear complexes $[Ln(H_2L)(H_2O)_n](Cl)_3$ was inferred by IR spectra, where the $\nu_{C=N}$ band was observed in the range 1637−1653 cm^{-1} depending on the macrocycle and the lanthanide ion. NMR spectra in CD_3OD were useful only for diamagnetic or weakly paramagnetic compounds, showing the HC=N signal at δ = 8.87−8.74 ppm for the lanthanum complexes and at δ = 12.47−10.56 ppm for the cerium ones.

Proton migration from the phenol to the iminic group upon complexation, which has been seen in other similar compounds,[33] was not seen in these complexes − the experimental conditions (the use of methanol as deuterated solvent) probably prevented this observation. Furthermore, X-ray structures of H_2L_B and $[La(H_2L_B)(H_2O)_4](Cl)_3$ show the lanthanum(III) ion residing in the O_3O_2 chamber, in a monocapped square-antiprismatic coordination environment, but does not allow us to define whether the protons are linked to the phenolic oxygen atom or to iminic C=N groups.[31] The same structure was found for other lanthanide(III) complexes with H_2L_B.

The three pathways summarized in Scheme 1 {reaction of $M(L)\cdot nH_2O$ with $LnCl_3\cdot nH_2O$, reactions of $[Ln(H_2L)(H_2O)_n](Cl)_3$ with metal(II) chloride, one-pot reaction} give rise to the same complexes although at times with a different solvent content. However, it was verified that the complexes $[Ln(H_2L)(H_2O)_4](Cl)_3$ are the most convenient "ligand" precursors and thus all the complexes were prepared by using the second procedure. The other two procedures were successfully tested to verify their feasibility. The one-pot reaction, in particular, clearly shows that these ligands have the correct coordination moiety for simultaneous recognition of a d- and a 4f-metal ion.

However, notably, the stability, especially in solution, of the heterodinuclear complexes $[LnM(L)(Cl)_3(CH_3OH)]$ varies considerably when changing the coordination shape of the two chambers. Thus, because the complexes $[LnM(L_A)(Cl)_3(CH_3OH)]$, though formed, are not stable enough in solution and attempts to crystallise them failed, we enlarged progressively the two bites. Again, with H_2L_B and H_2L_C, the resulting heterodinuclear complexes are unstable in solution and tend to eliminate partially one of the two metal ions. With the correct coordination shape, i.e. with ligand H_2L_D, enlarging the aliphatic chain from CH_2CH_2 to $CH_2CH_2CH_2$ in the N_2O_2 chamber and changing the crown-ether chain from O_2O_3 to O_2O_4 with the addition of a $-CH_2CH_2O-$ group, the resulting complexes are very stable in solution and readily crystallised.

Heterodinuclear complexes have been synthesised by treating $Ln(H_2L)Cl_3\cdot nH_2O$ in alcoholic solution with MCl_2 (M = Cu, Ni, Zn) in the presence of Et_3N. The solution was heated slightly during stirring: a precipitate usually formed after 20−30 min. The powder, collected by filtration and washed with $MeOH/Et_2O$, was then dissolved in an alcoholic solvent. Slow diffusion of diethyl ether into the resulting alcoholic solution produced crystals of $MLn(L_D)Cl_3\cdot nCH_3OH\cdot mEtOH$ (Ln = La, Ce, Gd, Tb; *n* =

 © 2004 Wiley-VCH Verlag GmbH & Co. KGaA, Weinheim

0−1; m = 0−2). The IR spectra of $MLn(L)Cl_3$ show a strong band ($\nu_{C=N}$) in the range 1618−1638 cm^{-1} (NiLn) or 1625−1647 cm^{-1} (CuLn) with a general lowering, more or less evident, compared to the $Ln(H_2L)Cl_3$ compounds owing to the coordination of the transition metal(II) ion into the Schiff base site. ^1H NMR spectroscopy was useful only for characterizing diamagnetic and some paramagnetic compounds. Interestingly, the coordination of M^{2+} provokes a large shift of the C=N band (for LnNi at δ = 19.38−19.45 ppm, for CeCu at δ = 53.61 ppm), confirming coordination in the Schiff base site. In these heterodinuclear complexes the Ni^{II} ion is in a high-spin state; therefore, the analogous Zn^{II} compounds were chosen as diamagnetic references in the magnetic studies reported below. SEM-EDS analysis were very useful in confirming the homogeneity of the complexes and the presence of the two metal ions in the correct ratio (Ln/M/Cl = 1:1:3).

In conclusion, the ligand H_2L_D is designed correctly for the formation of stable heterodinuclear LnM complexes. Thus, while mononuclear complexes can be obtained with all the macrocycles, the formation of heterodinuclear complexes, and especially their stability in solution, strongly depends on the experimental conditions and, above all, on the size of the donor chambers. By obtaining pure, stable heterodinuclear complexes we have clearly shown the need for appropriate molecular design of the coordinating systems.

Crystal Structures of the Heterodinuclear Complexes

Crystals of La−Cu, La−Zn and Tb−Cu complexes $[LnM(L_D)(Cl)_3(CH_3OH)]$ were obtained by slow diffusion of diethyl ether in methanolic solutions. All three complexes are monoclinic (space group $P2_1/n$) and isostructural, with four molecules in the unit cell (see Exp. Sect.). Figures 1 and 2 show ORTEP representations of the crystal structure and the coordination surroundings of the only La−Cu complex.

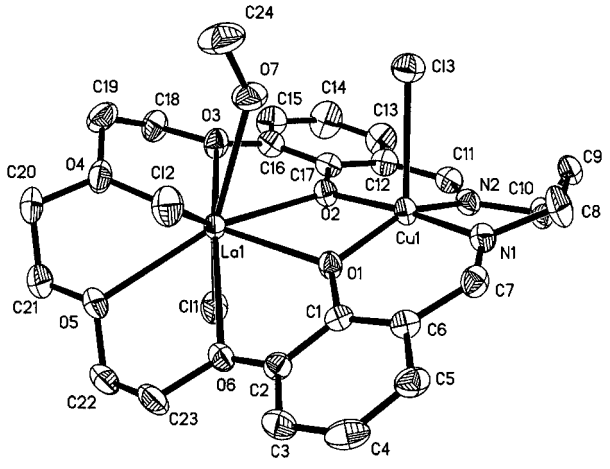

Figure 1. ORTEP diagram of the La−Cu complex showing the atom-labelling scheme; thermal ellipsoids are drawn at the 50% probability level; La−Zn and Tb−Cu complexes present an identical drawing

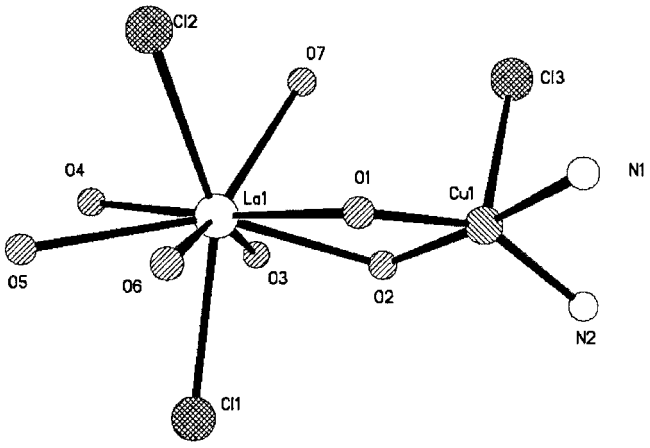

Figure 2. ORTEP diagram of the La−Cu coordination core showing the atom-labelling scheme

The macrocyclic ligand presents two coordination compartments: an N_2O_2 chamber and an O_2O_4 crown-like one. Each lanthanide metal ion is located in the O_2O_4 site and reaches the coordination number of nine by bonding six oxygen atoms of the ligand, two chlorine ions and the oxygen atom of one methanol molecule. O(3), O(4) O(5) and O(6) are etheric, whereas O(1) and O(2) are phenolic. The transition metal ions, copper and zinc, occupy the N_2O_2 chamber, the phenolic O(1) and O(2) atoms work as bridges between the coordinated metal ions.

The dimension change of the coordinated metal ions has little influence on the coordination geometry in the three complexes. Tb^{3+} (0.923Å) is smaller than La^{3+} (1.016 Å) and Cu^{2+} (0.72 Å) is smaller than Zn^{2+} (0.74 Å). Of the five possible coordination polyhedra with nine vertices, the tricapped trigonal prism and the capped square antiprism are the most stable and common in the lanthanide complexes. In our complexes, probably owing to the different nature of the coordinated oxygen atoms [etheric, phenolic and alcoholic, from O(1) to O(7)] and the presence of two chlorine ions, none of the above polyhedra can represent well the geometry around the lanthanide atoms. The best would be an hexagonal bipyramid where the base is formed by the two phenolic oxygen atoms and the four etheric oxygen atoms. One vertex is a chlorine ion, Cl(1), the other is the mid-point between the second chlorine ion, Cl(2), and the oxygen atom of the coordinated methanol molecule. The mean plane formed by the six oxygen atoms, O(1) to O(6), presents deviations in the range ±0.480 Å [the largest are +0.482 Å, for O(1), and −0.440 Å for O(4)] in both the lanthanum complexes, while the deviations are within ±0.580 Å (involving the same oxygen atoms) in the terbium complex. The lanthanide ions, in all complexes, are displaced by about 0.32 Å from the mean plane toward the Cl(2) and O(7) atoms (because of the larger hindrance of these two atoms) in relation to the only chlorine atom [Cl(1)] present in the opposite side, which forces the macrocyclic ligand to assume an umbrella-like shape. There are considerable differences in coordination bond angles on

 © 2004 Wiley-VCH Verlag GmbH & Co. KGaA, Weinheim

Table 1. Metal−oxygen and metal−chlorine bonds [Å] and selected bond angles [°] in the coordination sphere of lanthanides

Donor atom	Central lanthanide ion (Ln)		
	La−Cu complex La	La−Zn complex La	Tb−Cu complex Tb
O(1)	2.460(4)	2.479(4)	2.370(8)
O(2)	2.521(4)	2.474(4)	2.447(8)
O(3)	2.710(4)	2.743(5)	2.655(8)
O(4)	2.571(5)	2.588(5)	2.480(9)
O(5)	2.662(4)	2.670(5)	2.589(10)
O(6)	2.686(4)	2.679(5)	2.650(9)
O(7)	2.566(5)	2.618(6)	2.417(11)
Cl(1)	2.804(2)	2.797(2)	2.671(4)
Cl(2)	2.818(2)	2.823(2)	2.700(3)
O(1)−Ln−O(2)	60.1(1)	61.7(1)	61.0(3)
O(1)−Ln−O(6)	60.8(1)	60.8(1)	62.2(3)
O(2)−Ln−O(3)	59.6(1)	59.1(1)	60.7(3)
O(3)−Ln−O(4)	60.6(1)	59.9(2)	61.1(3)
O(4)−Ln−O(5)	61.2(2)	60.9(2)	62.7(4)
O(5)−Ln−O(6)	60.9(1)	61.0(2)	60.4(3)
Cl(2)−Ln−O(7)	73.9(1)	73.3(1)	75.4(2)
Cl(1)−Ln−O(1)	99.3(1)	101.1(1)	101.3(2)
Cl(1)−Ln−O(2)	79.1(1)	80.1(1)	78.7(2)
Cl(1)−Ln−O(3)	74.2(1)	74.6(1)	73.3(3)
Cl(1)−Ln−O(4)	86.5(1)	85.6(2)	92.4(3)
Cl(1)−Ln−O(5)	76.0(1)	75.8(1)	74.8(3)
Cl(1)−Ln−O(6)	81.5(1)	82.3(1)	80.3(2)
Cl(1)−Ln−O(7)	138.8(1)	138.7(2)	138.5(1)
Cl(1)−Ln−Cl(2)	146.92(6)	147.22(7)	145.7(1)

changing the lanthanide ion or the transition metal ion in the complexes. Coordination bond lengths are affected by the ionic radii, which decrease on going from the lanthanum to the terbium ion and increase from the copper to the zinc ion (Tables 1 and 2).

The butterfly shape adopted by the cyclic ligand around the central ions has two phenyl rings as wings; they form a dihedral angle of between 37.3 and 38.9° in the three complexes.

The dihedral angles defined by M−O(1)−O(2) and Ln−O(1)−O(2) planes are similar in the La−Cu and Tb−Cu complexes [16.5(2) and 15.4(2)°, respectively] but is 22.9(2)° in the La−Zn complex. In the complexes, copper is more effectively replaced with zinc than lanthanum is with terbium. The polyhedron around the transition-metal ions, present in the coordination site N_2O_2, is well depicted as a square pyramid, where the base is formed by the two phenolic bridging oxygen atoms and by the two iminic nitrogen atoms, and the apex is occupied by the third chlorine ion, Cl(3). The transition-metal ion is displaced from the mean N_2O_2 plane by about 0.247 Å (mean) in the two copper-containing complexes and by 0.533 Å in the zinc complex.

The torsion angles of the ligands (O−C−C−O) and (N−C−C−C−N) are very similar (Table 3). No remarkable hydrogen-bond networks are present.

X-ray powder diffractograms of five dinuclear complexes, $CeCu(L_D)Cl_3{\cdot}CH_3OH$, $GdCu(L_D)Cl_3{\cdot}CH_3OH$, $CeZn(L_D)Cl_3{\cdot}CH_3OH$, $GdZn(L_D)Cl_3{\cdot}3H_2O$ and $TbZn(L_D)Cl_3{\cdot}EtOH$, have been compared with that obtained by calculation from single crystal diffraction data of the La−Cu complex. We conclude that Ce−Cu, Ce−Zn, Gd−Cu and La−Cu complexes are all isostructural.

Conversely, the diffractograms of Tb−Zn and Gd−Zn complexes differ from each other and from the La−Cu one. In any case, the results obtained through other physicochemical characterization techniques strongly suggest that the coordination environment of the metal ion is closely related to that observed in LaCu and isostructural compounds. This assumption, of particular importance in the following discussion on magnetic properties, is sound as the use of a compartmental ligand constrains the mutual positions of metal and bonding atoms to a fixed geometry. In this framework, the different powder diffractometric patterns observed should be ascribed more to differences in crystal packing and cell settings than to differences in coordination geometries.

Magnetic and ESR Data

The magnetic properties of coupled lanthanide ions have been the focus of intense research.[34] The main problem when dealing with these systems is the combination of the effects of the first-order angular momentum of the ground state of the lanthanide ions − with the exception of Gd^{III}− and of the crystal-field splitting, which is usually of the order of kT at room temperature. This implies that the thermal dependence of the populations of the Stark sublevels

 © 2004 Wiley-VCH Verlag GmbH & Co. KGaA, Weinheim

Table 2. M−N, M−O and M−Cl bonds [Å] and selected bond angles [°] in the coordination sphere of the transition metal atoms

Donor atom	La−Cu complex Cu	La−Zn complex Zn	Tb−Cu complex Cu
O(1)	1.968(4)	2.056(4)	1.957(8)
O(2)	1.952(4)	2.065(4)	1.929(8)
N(1)	1.970(5)	2.067(6)	1.959(10)
N(2)	1.978(5)	2.058(6)	1.977(9)
Cl(3)	2.694(2)	2.347(2)	2.687(5)
Ln···M contacts	3.630(1)	3.675(1)	3.554(1)

	Dihedral angles LaCu	LaZn	TbCu
$M_4O(1)-O(2)/Ln_4O(1)-O(2)$	16.5(2)°	22.9(2)°	15.4(2)°

Central transition metal ion (M)	Cu	Zn	Cu
O(1)−M−O(2)	79.1(2)	76.1(2)	78.0(3)
O(1)−M−N(1)	92.2(2)	89.2(2)	92.6(4)
O(2)−M−N(2)	92.8(2)	88.3(2)	92.7(4)
N(1)−M−N(2)	95.5(2)	94.2(3)	96.0(4)
Cl(3)−M−O(1)	115.0(1)	120.7(1)	113.8(3)
Cl(3)−M−O(2)	86.3(1)	92.7(1)	86.9(3)
Cl(3)−M−N(1)	96.4(2)	104.6(2)	96.4(4)
Cl(3)−M−N(2)	92.4(1)	102.3(2)	92.3(4)

Table 3. Representative torsion angles [°] for the three complexes

Involved atoms	Complexes La−Cu	La−Zn	Tb−Cu
O(3)−C(18)−C(19)−O(4)	−53	−53	−51
C(19)−O(4)−C(20)−C(21)	145	145	136
O(4)−C(20)−C(21)−O(5)	55	54	49
C(20)−C(21)−O(5)−C(22)	175	176	172
O(5)−C(22)−C(23)−O(6)	−57	−57	−53
C(7)−N(1)−C(8)−C(9)	170	168	169
N(1)−C(8)−C(9)−C(10)	−46	−52	−45
C(8)−C(9)−C(10)−N(2)	82	85	82
C(9)−C(10)−N(2)−C(11)	122	126	123

has to be taken into account implicitly and an important anisotropy of the magnetic susceptibility is usually observed, preventing the use of a spin-only Hamiltonian for isotropic exchange to analyse the data. Consequently, the overwhelming majority of magnetic studies on Ln−M complexes concerns Gd^{III}-containing systems, for which the usual isotropic Heisenberg spin Hamiltonian can be employed and the interpretation of the data is straightforward.[35−40]

As a first step we determined the magnetic properties of the LaCu complex: its EPR spectrum clearly shows the features of an elongated tetragonal coordination of Cu^{II} with two broad transitions yielding $g_\perp = 2.078$ and $g_\parallel = 2.241$ (Figure 3). This is in the range usually observed for N_2O_2Cl coordination around the copper ion.[41] These results are confirmed by susceptibility measurements, which follow the Curie−Weiss law over the whole investigated temperature range (inset of Figure 3). Best-fit results to $1/\chi = (T + \theta)/C$, yielded $C = 0.422$ cm^3·K·mol^{-1} (cf. a theoretical value of 0.427 cm^3·K·mol^{-1} results from EPR) and a θ of 0.185 K, which indicates the existence of only weak antiferromagnetic intermolecular interactions.

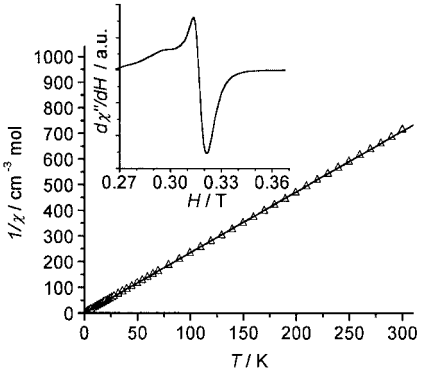

Figure 3. Curie−Weiss plot for the LaCu derivative between 2 and 300 K with the best-fit line (see text for details); inset: X-band EPR spectrum of the same complex ($g = 2.00$ is lying at $H = 0.33$ T)

The low-temperature X-band EPR spectrum of the GdZn derivative (Figure 4) exhibits fine structure due to zero-field splitting of the $S = 7/2$ state. The spectrum was satisfactorily simulated[42] by assuming a simple second-order spin Hamiltonian [$H = \beta\mathbf{B}\cdot\mathbf{g}\cdot\mathbf{S} + D\mathbf{S}_z^2 + E(\mathbf{S}_x^2-\mathbf{S}_y^2)$]

 © 2004 Wiley-VCH Verlag GmbH & Co. KGaA, Weinheim

for $S = 7/2$. The best simulation was obtained using $g = 1.995 \pm .005$, $D = 0.058 \pm .002$ cm^{-1}, $E = 0.0125 \pm .001$ cm^{-1}.

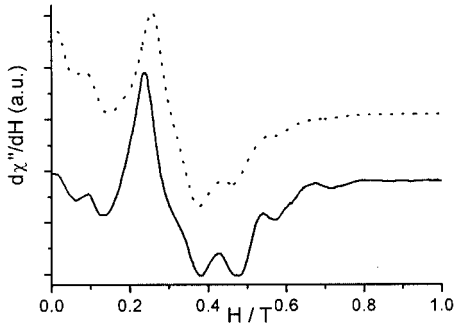

Figure 4. X-band EPR spectrum obtained for the GdZn derivative (continuous line) at 4 K, and best simulation (dotted line) obtained with parameters reported in the text; $g = 2.00$ lies at $H = 0.3300$ T

Independent determination of single-ion Cu^{II} and Gd^{III} properties was used successively to reduce the number of parameters used to fit the χT curve of GdCu (Figure 5). The χT room-temperature value obtained for this complex, 8.38 cm^3·K·mol^{-1}, is a little higher than the expected theoretical value for the two isolated $S = 1/2$ and $S = 7/2$ spins (assuming $g = 1.995$ for Gd^{III} and summing the values observed for LaCu gives 8.26 cm^3·K·mol^{-1}). On decreasing temperature, χT increases monotonically, indicating an intramolecular ferromagnetic coupling between Cu^{II} and Gd^{III} that is widely accounted for in similar systems.[35−38] The GdCu curve was then simulated by using the Hamiltonian $\mathbf{H} = J\,\mathbf{S}_{Gd}\cdot\mathbf{S}_{Cu}$ [43]

$$\chi = \frac{N\beta^2}{3kT}\cdot\frac{g_{S=4}{}^2 84 + g_{S=3}{}^2 180\exp\left(-\frac{4J}{kT}\right)}{7 + 9\exp\left(-\frac{4J}{kT}\right)}$$

where $g_{S=3} = 9/8g_{Gd} - 1/8g_{Cu}$ and $g_{S=4} = 7/8g_{Gd} + 1/8g_{Cu}$, and both g_{Cu} and g_{Gd} have been fixed to the value determined by EPR spectra of LaCu and GdZn, respectively.

Given the very small single-ion contribution to the zero-field splitting of Gd^{III} and the fairly large distance between magnetic centres of neighbouring molecules, which implies very weak intermolecular interactions, no correction[44] for these two phenomena was taken into account. The best-fit curve was obtained for $J = -2.49 \pm 0.05$ cm^{-1}, [$R^2 = \Sigma(\chi T_{calcd.} - \chi T_{obsd.})^2/\Sigma(\chi T_{obsd.})^2 = 0.9994$] meaning that the ground state $S = 4$ is separated in energy from the state $S = 3$ by about 10 cm^{-1}.

For the remaining lanthanides the situation is, as already noted, more difficult. However, some studies on the magnetic properties of anisotropic rare-earth ions coupled to either transition-metal ions or organic radicals have been reported recently.[45−50] In all these studies, the crystal-field effects on the magnetic properties of the lanthanides were determined separately by measuring a series of isomorphous complexes containing a diamagnetic counterpart (e.g. Zn^{II} or square-planar Ni^{II} in place of Cu^{II}). In the latter systems, deviation of the magnetic susceptibility compared to the Curie law is entirely due to the varying thermal population of the Ln^{III} Stark components, and this effect is assumed to be the same in systems with another paramagnetic species. In this framework, the variation with temperature of the curve obtained by subtracting the susceptibility of the complex containing the diamagnetic counterpart (e.g. LnZn) compared to that of the system with coupled centres (in our case, LnCu) ($\Delta\chi T_{LnM} = \chi T_{LnM} - \chi T_{LnZn}$) will only be due to exchange coupling interaction between the two paramagnetic centres. In detail, a positive variation of $\Delta\chi T_{LnM}$ on lowering T indicates a ferromagnetic coupling and a negative one an antiferromagnetic coupling. The same method can be applied to magnetisation measurements whenever a confirmation or a discrimination of the obtained results is needed.[47] Given the observed isostructurality of LaCu, CeCu, CeZn and TbCu, and the assumption of a closely related coordination environment for TbZn (see above), we applied this qualitative method to the family here described. Differences in crystal packing and intermolecular distances that, based on diffractometric powder pattern, might exist for TbZn are not important at this level of approximation as intermolecular interaction will not be considered.

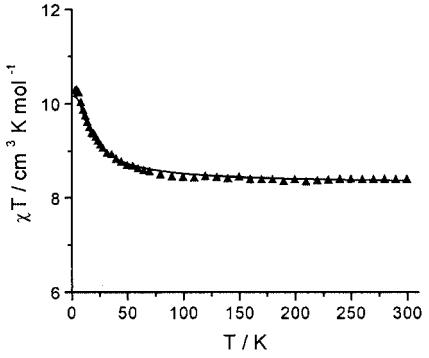

Figure 5. χT vs. T experimental curve measured between 2 and 300 K for GdCu (filled triangles), and the best-fit curve (continuous line) obtained with parameters reported in the text

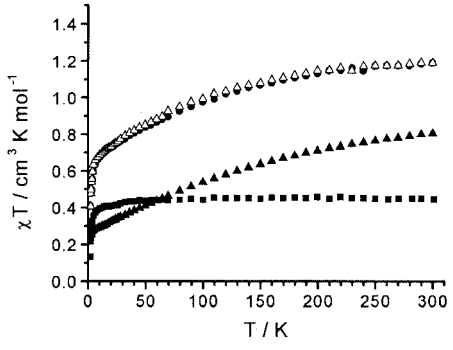

Figure 6. χT vs. T experimental curves measured between 2 and 300 K for CeCu (filled circles) and CeZn (filled triangles) and LaCu (filled squares) and the summed curve for LaCu + CeZn (open triangles)

 © 2004 Wiley-VCH Verlag GmbH & Co. KGaA, Weinheim

The room-temperature value observed for the CeZn derivative, 0.80 $cm^3 \cdot K \cdot mol^{-1}$, agrees with that expected on the basis of spin-only behaviour,[51] the slow decrease observed on lowering the temperature being due to the progressive depopulation of $^2F_{5/2}$ excited Stark components (Figure 6).

Comparison of the curve resulting from the sum of LaCu and CeZn with that of CeCu clearly shows that no appreciable interaction can be observed, as the two curves are almost perfectly superimposable over the entire temperature range. Comparison of M vs. H curves measured at 2.5 K (Figure 7) might suggest the existence of a weak antiferromagnetic interaction.

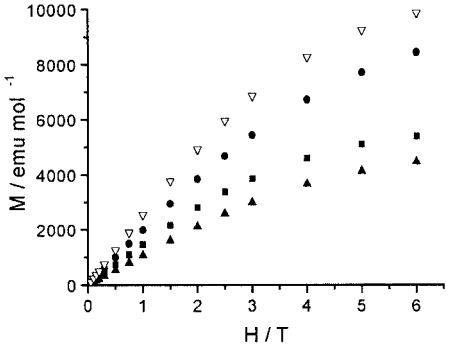

Figure 7. Comparison of the M vs. H curves at 2.5 K for CeCu (filled circles), CeZn (filled triangles), and LaCu (filled squares) with the sum (open inverted triangles) of the two latter curves

Indeed, the CeCu curve lies below the sum of LaCu and CeZn. However, in the absence of anisotropic magnetic data, diamagnetic substitution methods should not be pushed too far, and some caution should be exercised in deriving fine details.[52] In particular, some low-temperature discrepancies might well be due to small differences in crystal-field effects or intermolecular interactions and not to exchange coupling between 3d- and 4f-metal ions.

The observed χT values for the TbZn derivative at room temperature, 11.25 $cm^3 \cdot K \cdot mol^{-1}$, agrees with what is expected for this $^7F_6$ ion: on lowering the temperature the progressive depopulation of excited sublevels leads to the decrease of χT (Figure 8).

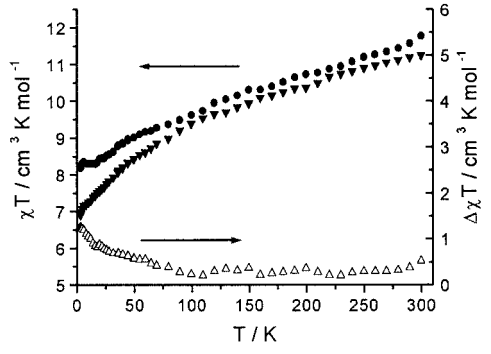

Figure 8. χT vs. T experimental curves measured between 2 and 300 K for TbCu (filled circles) and TbZn (filled inverted triangles) and their difference $\Delta\chi T$ (open triangles)

At 5 K a prominent EPR signal observed in zero field indicates that the two lowest sublevels are separated by $\Delta E = 0.3$ cm^{-1} (inset Figure 9). The results shown in Figure 8 for comparison of the χT curves of TbCu and TbZn clearly suggest a ferromagnetic coupling. Indeed, on lowering the temperature, $\Delta\chi T_{TbCu}$ increases from 0.415 $cm^3 \cdot K \cdot mol^{-1}$ at room temperature (in agreement with that observed for the LaCu derivative) to 1.25 $cm^3 \cdot K \cdot mol^{-1}$.

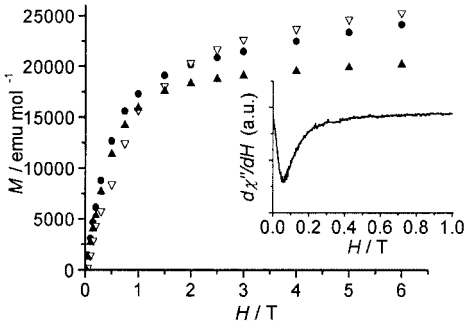

Figure 9. M vs. H curves at 2.5 K for TbCu (filled circles) and TbZn (filled triangles) compared with the sum of the latter and the experimental curve of LaCu (open inverted triangles); inset: low-temperature X-band EPR spectrum observed for the TbZn derivative

Ferromagnetic behaviour is confirmed by analysis of the M vs. H curves measured at 2.5 K (Figure 9). At low field the sum of LaCu and TbZn is lower than TbCu; however, for fields higher than 2 T the picture is reversed, which might suggest that the situation is not as simple as could be anticipated from the analysis of χT curves.

Conclusion

A series of LnM heterodinuclear complexes $[LnM(L)(Cl)_3(CH_3OH)]$ has been prepared, starting from the corresponding mononuclear complexes. It was confirmed that the transition-metal ion coordinates into the N_2O_2 Schiff base chamber while the lanthanide(III) ion prefers the O_2O_3 or O_2O_4 crown-like chamber. The two compartments of the asymmetric macrocyclic ligands have been progressively enlarged to find the best coordination moiety for heterodinuclear complexation. The larger macrocycle H_2L_D, derived from the condensation of 1,3-diaminopropane and 3,3′-(3,6-dioxaoctane-1,8-diyldioxy)bis(2-hydroxybenzoldehyde), has the most appropriate shape for forming stable heterodinuclear species. Furthermore, the large difference between two adjacent chambers assures the formation of only one species of heterodinuclear complexes, avoiding transmetallation, scrambling, migration reactions, etc. The ascertained stabilisation of the Schiff bases in consequence of the metal ion coordination opens up interesting possibilities in using these systems in solutions usually not allowed to Schiff bases.

The formation of isomerically pure, stable heterodinuclear complexes $[LnM(L_D)(Cl)_3\ (CH_3OH)]$ reported here

 © 2004 Wiley-VCH Verlag GmbH & Co. KGaA, Weinheim

clearly shows the need for prior appropriate molecular design of the coordinating systems.

The prepared complexes are isostructural, with the exception of TbZn and GdZn complexes. These crystallographic differences may be ascribed more to different solvent content than to different coordination shapes about the two metal ions. Further work is in progress to clarify the origin of the crystallographic discrepancies.

As expected, we observed a ferromagnetic coupling for the GdCu complex, and the availability of a series of isomorphous LnM complexes allowed an empirical determination of the coupling interaction for two anisotropic LnCu derivatives. While no meaningful interaction was detected for the CeCu derivative, a clear sign of ferromagnetic coupling was observed for TbCu. In the absence of a simple model to explain the sign and magnitude of exchange coupling between a rare earth and an unpaired spin, we can only compare our data with the available literature results. In this respect, the observed ferromagnetic coupling for TbCu agrees with what has been found for all reported TbM couples (see ref.[49] and references cited therein), whereas a clear antiferromagnetic interaction has been reported for a different Schiff base containing CeCu complex.[45] Here, even subtle chemical and structural changes produced an observed variation of exchange coupling interaction with the Ce^{III} ion. This result points out again the need for a large wealth of data to build up a reliable magnetostrucutral correlation for complexes containing exchange-coupled lanthanide ions, in analogy to what has been done for 3d-metal ions.

Finally, functionalising these systems at the periphery of the coordination moiety with suitable hydrophilic or hydrophobic groups will increase their solubility in aqueous or non-aqueous solvents, and/or will favour their interaction and anchorage on suitable surfaces to obtain ferri- or ferromagnetic molecular nanosystems and devices. Preliminary results are very encouraging.

Experimental Section

General: All solvents, reagents and metal salts were purchased from Aldrich or Fluka and used without further purification. Dimethyl sulfoxide was purified by distillation.[53] The diformyl precursors 3,3′-(3-oxapentane-1,5-diyldioxy)bis(2-hydroxybenzaldehyde) and 3,3′-(3,6-dioxaoctane-1,8-diyldioxy)bis(2-hydroxybenzaldehyde) were prepared according to the literature.[29]

Physicochemical Characterization: Elemental analyses (C,H,N) were carried out using a Fison 1108 analyzer. IR spectra were recorded as KBr pellets with a Mattson 500 FT-IR spectrometer. ^1H and ^{13}C NMR spectra of the ligands and related complexes were performed with a Bruker AMX300 spectrometer, equipped with a 5-mm BB multinuclear probe, operating at 300.13 MHz for ^1H and 75.43 MHz for ^{13}C. 2D NOESY, 2D COSY and HMQC experiments for the ligands and complexes were performed with a Bruker AMX300 spectrometer. All the samples examined were dissolved in deuterated methanol or chloroform, which were used also as internal references. The morphology, homogeneity, and the metal/chlorine ratio of the complexes were investigated by using a Philips XL40 model scanning electron microscope equipped with an EDAXDX PRIME X-ray energy dispersive spectrometer. The solvent content (H_2O or MeOH) was evaluated by thermal analysis curves using Netzsch STA 429 thermoanalytical equipment; tests were performed under nitrogen (flux rate 250 mL/min, heating rate 5 °C min^{-1}) and in air under the same conditions. Neutral alumina (Carlo Erba, Milano, Italy) was used as reference material. ESI-MS data were recorded using a Finnigan LCQ mass spectrometer and methanolic solutions of the samples (10^{-3} M).[57] Mass spectrometric measurements were also performed using a ZAB2F instrument (Micromass, Manchester, UK) operating under FAB conditions. Nitrobenzyl alcohol solutions of the compounds were bombarded by 8 keV Xe atoms.[57] Magnetic susceptibilities of polycrystalline powders of LaCu, CeCu, CeZn, GdCu, GdZn, TbCu and TbZn were measured between 2 and 300 K with applied magnetic fields of 0.1 and 1 Tesla using a Cryogenic S600 SQUID magnetometer. To avoid the preferential orientation of polycrystalline powders, which might eventually result in a much higher apparent magnetic moment of the complexes, the powders were pressed in pellets. Data were corrected for the magnetism of the sample holder, which was determined separately in the same temperature range and field, and the underlying diamagnetism of each sample was estimated from Pascal's constants. Magnetisation measurements were performed on the same samples at 2.5 K with a field up to 6.0 T. Polycrystalline EPR powder spectra of the same complexes were recorded at the X-band (9.24 GHz) with a Varian E9 spectrometer equipped with a ^4He continuous-flow cryostat. Powders were blocked in wax to avoid preferential orientation of the crystallites.

Synthesis of Macrocycles and Complexes

H_2L_A: H_2L_A was prepared according to the literature.[31]

$Ln(H_2L_A)Cl_3{\cdot}nH_2O$ (Ln = La, Ce, Gd, Tb, Lu; n = 2−5): $LnCl_3{\cdot}6H_2O$ (2 mmol) in MeOH (5 mL) and, subsequently, ethylenediamine (120 mg, 2 mmol) in methanol (5 mL) were added to a pale yellow solution of 3,3′-(3-oxapentane-1,5-diyldioxy)bis(2-hydroxybenzaldehyde) (692 mg, 2 mmol) in methanol (50 mL). The obtained yellow solution was heated under reflux for 2.5 h and then reduced in volume. The addition of Et_2O (50 mL) to the resulting solution gave rise to a yellow precipitate that was filtered off, washed with MeOH/Et_2O (1:4), and dried in vacuo. 75% average yield.

$La(H_2L_A)Cl_3{\cdot}2H_2O$: 1004 mg, 77% yield. $C_{20}H_{22}Cl_3LaN_2O_5{\cdot}2H_2O$ (651.68): calcd. C 36.86, H 4.02, N 4.30; found C 36.14, H 3.82, N 4.27. IR: $\tilde{\nu}$ = 1648 cm^{-1} ($\nu_{C=N}$, s). ^1H NMR (300 MHz, CD_3OD, 25 °C): δ = 4.36 (m, 4 H, CH_2O), 4.39 (s, 4 H, CNCH_2), 4.45 (m, 4 H, CH_2O−Ar), 6.68 (t, 2 H, Ar−*H*), 7.15 (d, 2 H, Ar−*H*), 7.23 (d, 2 H, Ar−*H*), 8.78 (s, 2 H, *H*C=N). SEM-EDS: La/Cl = 1:3.

$Ce(H_2L_A)Cl_3{\cdot}1H_2O$: 990 mg, 78% yield. $C_{20}H_{22}CeCl_3N_2O_5{\cdot}H_2O$ (634.88): calcd. C 37.84, H 3.81, N 4.41; found C 37.62, H 3.68, N 4.54. IR: $\tilde{\nu}$ = 1649 cm^{-1} ($\nu_{C=N}$, s). ^1H NMR (300 MHz, CD_3OD, 25 °C): δ = −13.19 (d, 4 H, CH_2O), −1.19 (s, 4 H, CNCH_2), 4.20 (d, 4 H, CH_2O−Ar), 12.12 (t, 2 H, Ar−*H*), 12.47 (s, 2 H, *H*C=N), 13.05 (d, 2 H, Ar−*H*), 14.50 (d, 2 H, Ar−*H*). SEM-EDS: Ce/Cl = 1:3.

$Gd(H_2L_A)Cl_3{\cdot}2H_2O$: 994 mg, 74% yield. $C_{20}H_{22}Cl_3GdN_2O_5{\cdot}2H_2O$ (670.02): calcd. C 35.85, H 3.91, N 4.18; found C 35.16, H 4.49, N 4.63. IR: $\tilde{\nu}$ = 1637 cm^{-1} ($\nu_{C=N}$, s). SEM-EDS: Gd/Cl = 1:3.

$Tb(H_2L_A)Cl_3{\cdot}2H_2O$: 994 mg, 74% yield. $C_{20}H_{22}Cl_3N_2O_5Tb{\cdot}2H_2O$ (671.70): calcd. C 35.76, H 3.90, N 4.17; found C 35.26, H 3.72, N 4.12. IR: $\tilde{\nu}$ = 1637 cm^{-1} ($\nu_{C=N}$, s). SEM-EDS: Tb/Cl = 1:3.

 © 2004 Wiley-VCH Verlag GmbH & Co. KGaA, Weinheim

Lu(H_2L_A)Cl_3·5H_2O: 1068 mg, 72% yield. $C_{20}H_{22}Cl_3LuN_2O_5$·5H_2O (741.78): calcd. C 32.38, H 4.35, N 3.78; found C 31.57, H 3.93, N 4.46. IR: $\tilde{\nu}$ = 1647cm^{-1} ($\nu_{C=N}$, s). SEM-EDS: Lu/Cl = 1:3.

Yb(H_2L_A)Cl_3·2H_2O: $YbCl_3$·6H_2O (765 mg, 2 mmol) in EtOH (20 mL) was added to a solution of H_2L_A (741 mg, 2 mmol) in chloroform (50 mL). The resulting solution was heated under reflux for 2.5 h and then reduced in volume. Addition of Et_2O (50 mL) to this solution afforded a yellow precipitate that was filtered off, washed with MeOH/Et_2O (1:4), and dried in vacuo. 878 mg, 64% yield. $C_{20}H_{22}N_2O_5YbCl_3$·2H_2O (685.81): calcd. C 35.03, H 3.82, N 4.08; found C 35.16, H 4.49, N 4.63. IR: $\tilde{\nu}$ = 1637 cm^{-1} ($\nu_{C=N}$, s). SEM-EDS: Yb/Cl = 1:3.

NiLn(L_A)Cl_3·*n*H_2O (Ln = La, Ce, Gd, Tb, Yb, Lu; *n* = 0−5): $NiCl_2$·6H_2O (237.7 mg, 1 mmol) in MeOH (5 mL) was added to a yellow solution of Ln(H_2L_A)Cl_3·*n*H_2O (1 mmol) in methanol (50 mL). After 10 min, triethylamine (202 mg, 2 mmol) was added dropwise and the resulting yellow-red solution was heated under reflux for 2.5 h. After evaporation of the solvent to dryness, the residue was treated with $CHCl_3$ (25 mL) and stirred. The orange powder obtained was filtered off, washed with Et_2O and dried in vacuo. 60% average yield.

LaNi(L_A)Cl_3·2H_2O: 452 mg, 64% yield. $C_{20}H_{20}Cl_3LaN_2NiO_5$·2$H_2O$ (708.38): calcd. C 33.07, H 3.61, N 3.86; found (%) C 33.38, H 4.46, N 3.28. IR: $\tilde{\nu}$ = 1619 cm^{-1} ($\nu_{C=N}$, s). ^{1}H NMR (300 MHz, CD_3OD, 25 °C): δ = 4.01 (s, 4 H, CH_2O), 4.77 (s, 4 H, CH_2O−Ar), 5.64 (br. s, 4 H, CNCH_2), 6.87 (t, 2 H, Ar−*H*), 7.35 (d, 2 H, Ar−*H*), 7.65 (d, 2 H, Ar−*H*), 19.38 (br. s, 2 H, *H*C=N). SEM-EDS: Ni/La/Cl = 1:1:3.

CeNi(L_A)(OH)Cl_2·H_2O: 417 mg, 62% yield. $C_{20}H_{20}CeCl_2N_2NiO_5$-(OH)·$H_2O$ (673.12): calcd. C 35.66, H 2.99, N 4.16; found C 35.33, H 3.42, N 4.22. IR: $\tilde{\nu}$ = 1618 cm^{-1} ($\nu_{C=N}$, s). ^{1}H NMR (300 MHz, CD_3OD, 25 °C): δ = −5.44 (br. s, 4 H, CH_2O), −0.24 (br. s, 4 H, CH_2O−Ar), 5.57 (d, 2 H, Ar−*H*), 6.62 (t, 2 H, Ar−*H*), 8.34 (s, 4 H, CNCH_2), 8.57 (d, 2 H, Ar−*H*), 19.45 (br. s, 2 H, *H*C=N). SEM-EDS: Ni/Ce/Cl = 1:1:2.

GdNi(L_A)Cl_3·2H_2O: 425 mg, 59% yield. $C_{20}H_{20}Cl_3GdN_2NiO_5$·2$H_2O$ (726.72): calcd. C 33.06, H 3.33, N 3.85; found C 33.69, H 4.27, N 4.46. IR: $\tilde{\nu}$ = 1634 cm^{-1} ($\nu_{C=N}$, s). SEM-EDS: Ni/Gd/Cl = 1:1:3.

TbNi(L_A)Cl_3·H_2O: 428 mg, 60% yield. $C_{20}H_{20}Cl_3N_2NiO_5Tb$·$H_2O$ (710.38): calcd. C 33.82, H 3.12, N 3.94; found (%) C 33.65, H 3.02, N 3.95. IR: $\tilde{\nu}$ = 1619 cm^{-1} ($\nu_{C=N}$, s). SEM-EDS: Ni/Tb/Cl = 1:1:3.

YbNi(L_A)$(OH)_2$Cl·5H_2O: 448 mg, 59% yield. $C_{20}H_{22}ClN_2NiO_5$-Yb$(OH)_2$·5H_2O (759.64): calcd. C 31.62, H 4.25, N 3.69; found C 30.84, H 3.70, N 4.55. IR: $\tilde{\nu}$ = 1634 cm^{-1} ($\nu_{C=N}$, s). SEM-EDS: Ni/Yb/Cl = 1:1:3.

LuNi(L_A)Cl_3·5H_2O: 460 mg, 58% yield. $C_{20}H_{20}Cl_3LuN_2NiO_5$·5$H_2O$ (798.48): calcd. C 30.09, H 3.79, N 3.51; found C 29.10, H 3.91, N 4.38 IR: $\tilde{\nu}$ = 1628 cm^{-1} ($\nu_{C=N}$, s). SEM-EDS: Ni/Lu/Cl = 1:1:3.

CuLn (L_A)Cl_3·*n*H_2O (Ln = La, Ce, Gd, Tb, Yb, Lu; *n* = 0−5): $CuCl_2$·2H_2O (170.48 mg, 1 mmol) in MeOH (5 mL) was added to a yellow solution of Ln(H_2L_A)Cl_3·*n*H_2O (1 mmol) in methanol (50 mL). After 10 min, triethylamine (202 mg, 2 mmol) was added dropwise and the resulting yellow-red solution was heated under reflux for 2.5 h. After evaporation of the solvent to dryness, the residue was treated with $CHCl_3$ (25 mL) and stirring continued. The green powder obtained was filtered off, washed with Et_2O and dried in vacuo. ca. 60% average yield.

LaCu(L_A)Cl_3·H_2O: 430 mg, 62% yield. $C_{20}H_{20}Cl_3CuN_2O_5La$·$H_2O$ (695.20): calcd. C 34.55, H 3.19, N 4.03; found C 33.73, H 3.29, N 3.42. IR: $\tilde{\nu}$ = 1645 cm^{-1} ($\nu_{C=N}$, s). SEM-EDS: Cu/La/Cl = 1:1:3.

CeCu(L_A)Cl_3·4H_2O: 484 mg, 64% yield. $C_{20}H_{20}CeCl_3CuN_2O_5$·4$H_2O$ (750.45): calcd. C 32.01, H 3.76, N 3.73; found C 31.42, H 4.12, N 3.84. IR: $\tilde{\nu}$ = 1647 cm^{-1} ($\nu_{C=N}$, s). ^{1}H NMR (300 MHz, CD_3OD, 25 °C): δ = −7.79 (s, 4 H, CH_2O−Ar), −5.44 (s, 4 H, CH_2O), −0.88 (s, 4 H, CNCH_2), 7.82 (t, 2 H, Ar−*H*), 9.49 (d, 2 H, Ar−*H*), 22.63 (d, 2 H, Ar−*H*), 53.61 (s, 2 H, *H*C=N). SEM-EDS: Cu/Ce/Cl = 1:1:3.

GdCu(L_A)Cl_3·4H_2O: 470 mg, 61% yield. $C_{20}H_{20}Cl_3CuGdN_2$-O_5·4H_2O (767.58): calcd. C 29.91, H 3.51, N 3.49; found C 29.11, H 3.98, N 4.08. IR: $\tilde{\nu}$ = 1638 cm^{-1} ($\nu_{C=N}$, s). SEM-EDS: Cu/Gd/Cl = 1:1:3.

TbCu(L_A)(OH)Cl_2·3H_2O: 442 mg, 60% yield. $C_{20}H_{20}Cl_2CuN_2O_5$-Tb(OH)·3H_2O (732.79): calcd. C 32.78, H 3.71, N 3.82; found C 32.39, H 3.10, N 3.79. IR: $\tilde{\nu}$ = 1626 cm^{-1} ($\nu_{C=N}$, s). SEM-EDS: Cu/Tb/Cl = 1:1:2.

YbCu(L_A)(OH)Cl_2·6H_2O: 456 mg, 57% yield. $C_{20}H_{20}Cl_2CuN_2O_5$-Yb(OH)·6H_2O (800.94): calcd. C 29.99, H 4.15, N 3.50; found C 29.54, H 3.40, N 4.44. IR: $\tilde{\nu}$ = 1640 cm^{-1} ($\nu_{C=N}$, s). SEM-EDS: Cu/Yb/Cl = 1:1:2.

LuCu(L_A)Cl_3·H_2O: 402 mg, 55% yield. $C_{20}H_{20}Cl_3CuLuN_2O_5$·$H_2O$ (731.26): calcd. C 32.85, H 3.03, N 3.83; found C 32.43, H 3.41, N 4.50 IR: $\tilde{\nu}$ = 1636 cm^{-1} ($\nu_{C=N}$, s). SEM-EDS: Cu/Lu/Cl = 1:1:3.

ZnLn(L_A)Cl_3·*n*H_2O (Ln = La, Ce, Tb; *n* = 0−5): $ZnCl_2$ (136.28 mg, 1 mmol) in MeOH (5 mL) was added to a yellow solution of Ln(H_2L_A)Cl_3·*n*H_2O (1 mmol) in methanol (50 mL). After 10 min, triethylamine (202 mg, 2 mmol) was added dropwise and the resulting yellow-red solution was heated under reflux for 2.5 h. After evaporation of the solvent to dryness, the resultant residue was treated with $CHCl_3$ (25 mL) and stirred. The pale yellow powder obtained was filtered off, washed with Et_2O and dried in vacuo. 60% average yield.

LaZn(L_A)Cl_3: 408 mg, 60% yield. $C_{20}H_{20}Cl_3LaN_2O_5Zn$ (679.01): calcd. C 35.38, H 2.97, N 4.13; found C 35.97, H 3.10, N 4.11. IR: $\tilde{\nu}$ = 1644 cm^{-1} ($\nu_{C=N}$, s). ^{1}H NMR (300 MHz, CD_3OD, 25 °C): δ = 3.57 (dd, 2 H, CH_2O), 3.88 (t, 2 H, CH_2O), 3.97 and 4.10 (dd, 4 H, CNCH_2), 4.31 (dd, 2 H, CH_2O), 4.88 (t, 2 H, CH_2O), 6.73 (t, 2 H, Ar−*H*), 7.18 (d, 2 H, Ar−*H*), 7.20 (d, 2 H, Ar−*H*), 8.62 (s, 2 H, *H*C=N). SEM-EDS: Zn/La/Cl = 1:1:3.

CeZn(L_A)Cl_3: 415 mg, 61% yield. $C_{20}H_{20}CeCl_3N_2O_5Zn$ (680.22): calcd. C 35.32, H 2.96, N 4.12; found C 36.08, H 3.33, N 4.17. IR data: $\tilde{\nu}$ = 1644 cm^{-1} ($\nu_{C=N}$, s). ^{1}H NMR (300 MHz, CD_3OD, 25 °C): δ = −9.88 (br. s, 2 H, CH_2O−Ar), −7.59(d, 2 H, CH_2O−Ar), −5.20 (s, 2 H, CH_2O), −3.33 (br. s, 2 H, CH_2O), 2.23 (d, 2 H, Ar−*H*), 5.48 (t, 2 H, Ar−*H*), 8.44 (s, 2 H, Ar−*H*), 8.80 (d, 2 H, CNCH_2), 9.82 (d, 2 H, CNCH_2), 12.82 (s, 2 H, *H*C=N). SEM-EDS: Zn/Ce/Cl = 1:1:3.

TbZn(L_A)Cl_3·H_2O: 422 mg, 59% yield. $C_{20}H_{20}Cl_3N_2O_5TbZn$·$H_2O$ (717.04): calcd. C 33.50, H 3.09, N 3.91; found C 33.13, H 3.34, N 3.85. IR: $\tilde{\nu}$ = 1641 cm^{-1} ($\nu_{C=N}$, s). SEM-EDS: Zn/Tb/Cl = 1:1:3.

H_2L_B: H_2L_B was prepared according to the literature.[31]

Ln(H_2L_B)Cl_3·*n*H_2O (Ln = La, Ce, Tb; *n* = 0−3): $LnCl_3$·6H_2O (2 mmol) in MeOH (5 mL) and, subsequently, ethylenediamine (120 mg, 2 mmol) in methanol (5 mL) were added to a pale yellow solution of 3,3′-(3,6-dioxaoctane-1,8-diyldioxy)bis(2-hydroxybenz-

 © 2004 Wiley-VCH Verlag GmbH & Co. KGaA, Weinheim

aldehyde) (780.8 mg, 2 mmol) in methanol (50 mL). The obtained yellow solution was heated under reflux for 2.5 h and the resultant yellow precipitate was filtered off, washed with MeOH/Et_2O (1:4), and dried in vacuo. It was then recrystallised from MeOH/EtOH. 65% average yield.

$La(H_2L_B)Cl_3{\cdot}4H_2O$: 975 mg, 67% yield. $C_{22}H_{26}Cl_3LaN_2O_6{\cdot}4H_2O$ (731.76): calcd. C 36.11, H 4.68, N 3.83; found C 36.20, H 4.70, N 3.78 IR: $\tilde{\nu}$ = 1644 cm^{-1} ($\nu_{C=N}$, s). ^1H NMR (300 MHz, CD_3OD, 25 °C): δ = 4.21 (4 + 4 H, CH_2O + $CNCH_2$), 4.38 (t, 4 H, CH_2O), 4.55 (t, 4 H, CH_2O-Ar), 6.76 (t, 2 H, Ar−*H*), 7.23 (dd, 2 H, Ar−*H*), 7.37 (dd, 2 H, Ar−*H*), 8.87 (s, 2 H, *H*C=N). SEM-EDS: La/Cl = 1:3.

$Ce(H_2L_B)Cl_3$: 857 mg, 65% yield. $C_{22}H_{26}CeCl_3N_2O_6$ (660.91): calcd. C 39.98, H 3.97, N 4.24; found C 39.05, H 3.73, N 4.93. IR: $\tilde{\nu}$ = 1645 cm^{-1} ($\nu_{C=N}$, s). ^1H NMR (300 MHz, CD_3OD, 25 °C): δ = 0.14 (s, 4 H, CH_2O), 2.71 (s, 4 H, CH_2O), 4.50 (d, 2 H, Ar−*H*), 5.95 (t, 2 H, Ar−*H*), 6.24 (s, 4 H, $CNCH_2$), 7.63 (d, 2 H, Ar−*H*), 7.67 (s, 4 H, CH_2O), 10.56 (s, 2 H, *H*C=N). SEM-EDS: Ce/Cl = 1:3.

$Tb(H_2L_B)Cl_3{\cdot}3H_2O$: 931 mg, 63% yield. $C_{22}H_{26}Cl_3N_2O_6Tb{\cdot}3H_2O$ (733.76): calcd. C 36.01, H 4.40, N 3.82; found C 35.97, H 4.22, N 4.24. IR: $\tilde{\nu}$ = 1647 cm^{-1} ($\nu_{C=N}$, s). SEM-EDS: Tb/Cl = 1:3.

$NiLa(L_B)Cl_3{\cdot}nH_2O$ and $CuLa(L_B)Cl_3{\cdot}nH_2O$: These compounds were prepared according to the literature.[31]

H_2L_C: A methanolic solution (3 mL) of 1,3-diaminopropane (74 mg, 1 mmol) was diluted with diethyl ether (400 mL). A $CHCl_3$ solution (5 mL) of 3,3′-(3-oxapentane-1,5-diyldioxy)bis(2-hydroxybenzaldehyde) (346 mg, 1 mmol) was then added dropwise at room temperature. The resultant yellow precipitate was stirred for 20 min, then filtered off, washed well with a diethyl ether/light petroleum solution and dried in vacuo. 211 mg, 55% yield. $C_{21}H_{24}N_2O_5$ (384.41): calcd. C 65.62, H 6.29, N 7.29; found C 66.52, H 6.41, N 7.41. IR: $\tilde{\nu}$ = 1631 cm^{-1} ($\nu_{C=N}$, s). ^1H NMR (300 MHz, $CDCl_3$, 25 °C): δ = 2.04 (quint, 2 H, $CNCH_2CH_2$), 3.66 (t, 4 H, $CNCH_2$), 3.96 (t, 4 H, CH_2O), 4.21 (t, 4 H, CH_2O-Ar), 6.73 (t, 2 H, Ar−*H*), 6.84 (dd, 2 H, Ar−*H*), 6.94 (dd, 2 H, Ar−*H*), 8.30 (s, 2 H, *H*C=N), 13.82 (br. s, OH) ppm. MS: 385 $[M + H]^+$.

$La(H_2L_C)Cl_3{\cdot}4H_2O$: $LaCl_3{\cdot}6H_2O$ (743 mg, 2 mmol) in MeOH (5 mL) and, subsequently, 1,3-propanediamine (148 mg, 2 mmol) in methanol (5 mL) were added to a pale yellow solution of 3,3′-(3-oxapentane-1,5-diyldioxy)bis(2-hydroxybenzaldehyde) (692 mg, 2 mmol) in methanol (50 mL). The resultant yellow solution was heated under reflux for 2.5 h and then reduced in volume. The obtained yellow precipitate was filtered off, washed with MeOH/Et_2O (1:4), and dried in vacuo. 1010 mg, 72% yield. It was then recrystallised from MeOH and slow diffusion of Et_2O. $C_{21}H_{24}Cl_3LaN_2O_5{\cdot}4H_2O$ (701.74): calcd. C 35.94, H 4.60, N 3.99; found C 35.34, H 4.41, N 4.85. IR: $\tilde{\nu}$ = 1651 cm^{-1} ($\nu_{C=N}$, s). ^1H NMR (300 MHz, CD_3OD, 25 °C): δ = 2.55 (quint, 2 H, $CNCH_2CH_2$), 4.08 (t, 4 H, $CNCH_2$), 4.44 (dd, 8 H, CH_2O), 6.62 (t, 2 H, Ar−*H*), 7.00 (dd, 2 H, Ar−*H*), 7.21 (dd, 2 H, Ar−*H*), 8.74 (s, 2 H, *H*C=N). SEM-EDS: La/Cl = 1:3.

$LaNi(L_C)Cl_3$: Triethylamine (202 mg, 2 mmol) and $NiCl_2{\cdot}6H_2O$ (237.7 mg, 1 mmol), dissolved in EtOH (2 mL), were added to a yellow solution of $La(H_2L_C)Cl_3{\cdot}4H_2O$ (702 mg, 1 mmol) in ethanol (20 mL) that was slightly heated (30 °C). After stirring for 10 min, a green precipitate formed. The suspension was stirred for further 20 min and then cooled to room temperature. The resultant green powder was collected by filtration, washed with Et_2O and dried in vacuo. 357 mg, 52% yield. $C_{21}H_{22}Cl_3LaN_2NiO_5$ (686.38): calcd. C 36.75, H 3.23, N 4.08; found C 36.05, H 3.53, N 3.80 IR: $\tilde{\nu}$ = 1627 cm^{-1} ($\nu_{C=N}$, s). SEM-EDS: Ni/La/Cl = 1:1:3.

H_2L_D: A methanolic solution (3 mL) of 1,3-diaminopropane (74 mg, 1 mmol) was diluted with diethyl ether (400 mL). A $CHCl_3$ solution (5 mL) of 3,3′-(3,6-dioxaoctane-1,8-diyldioxy)bis(2-hydroxybenzaldehyde) (392 mg, 1 mmol) was then added dropwise at room temperature. The resultant yellow precipitate was stirred for 20 min, then filtered off, washed well with a diethyl ether/light petroleum solution and dried in vacuo. 300 mg, 70% yield. $C_{23}H_{28}N_2O_6$ (428.46): calcd. C 64.48, H 6.59, N 6.54; found C 64.02, H 6.42, N 6.45. IR: $\tilde{\nu}$ = 1635−1627 cm^{-1} ($\nu_{C=N}$, s). ^1H NMR (300 MHz, $CDCl_3$, 25 °C): δ = 2.03 (quint., 2 H, $CNCH_2CH_2$), 3.65 (t, 4 H, $CNCH_2$), 3.73 (s, 4 H, CH_2O), 3.88 (t, 4 H, CH_2O), 4.18 (t, 4 H, CH_2O-Ar), 6.72 (t, 2 H, Ar−*H*), 6.83 (dd, 2 H, Ar−*H*), 6.93 (dd, 2 H, Ar−*H*), 8.29 (s, 2 H, *H*C=N), 13.83 (br. s, OH) ppm. MS: 429 $[M + H]^+$.

$Ln(H_2L_D)Cl_3{\cdot}nH_2O$ (Ln = La, Ce, Gd, Tb; n = 0−7): $LnCl_3{\cdot}nH_2O$ (2 mmol) in MeOH (5 mL) and, subsequently, 1,3-diaminopropane (148 mg, 2 mmol) in methanol (5 mL) were added to a pale yellow solution of 3,3′-(3,6-dioxaoctane-1,8-diyldioxy)bis(2-hydroxybenzaldehyde) (780.8 mg, 2 mmol) in methanol (50 mL). This yellow solution was then heated under reflux for 2.5 h and subsequently reduced to dryness.

$La(H_2L_D)Cl_3$: The obtained yellow residue was recrystallised from MeOH/EtOH, filtered off and dried in vacuo. 997 mg, 74% yield. $C_{23}H_{28}Cl_3LaN_2O_6$ (673.73): calcd. C 41.00, H 4.19, N 4.16; found (%) C 40.60, H 4.43, N 3.79. IR: $\tilde{\nu}$ = 1648 cm^{-1} ($\nu_{C=N}$, s). ^1H NMR (300 MHz, CD_3OD, 25 °C): δ = 2.43 (quint, 2 H, $CNCH_2CH_2$), 4.01 (t, 4 H, $CNCH_2$), 4.21 (s, 4 H, CH_2O), 4.37 (t, 4 H, CH_2O), 4.54 (t, 4 H, CH_2O-Ar), 6.73 (t, 2 H, Ar−*H*), 7.18 (dd, 2 H, Ar−*H*), 7.33 (dd, 2 H, Ar−*H*), 8.79 (s, 2 H, *H*C=N). SEM-EDS: La/Cl = 1:3.

$Ce(H_2L_D)Cl_3$: The yellow residue was recrystallised from MeOH/*i*PrOH, filtered off, washed with Et_2O and dried in vacuo. 931 mg, 69% yield. $C_{23}H_{28}CeCl_3N_2O_6$ (674.94): calcd. C 40.93, H 4.18, N 4.15; found C 41.61, H 4.64, N 4.31. IR: $\tilde{\nu}$ = 1639 cm^{-1} ($\nu_{C=N}$, s). ^1H NMR (300 MHz, CD_3OD, 25 °C): δ = 0.56 (s, 4 H, CH_2O), 2.36 (t, 4 H, CH_2O), 3.63 (m, 2 H, $CNCH_2CH_2$), 5.24 (d, 2 H, Ar−*H*), 5.53 (t, 4 H, $CNCH_2$), 6.35 (t, 2 H, Ar−*H*), 7.41 (t, 4 H, CH_2O), 7.94 (d, 2 H, Ar−*H*), 10.57 (s, 2 H, *H*C=N). SEM-EDS: Ce/Cl = 1:3.

$Gd(H_2L_D)Cl_3{\cdot}2H_2O$: The yellow residue was recrystallised from EtOH/*i*PrOH, filtered off, washed with Et_2O and dried in vacuo. 1077 mg, 74% yield. $C_{23}H_{28}Cl_3GdN_2O_6{\cdot}2H_2O$ (728.10): calcd. C 37.94, H 4.43, N 3.85; found C 38.42, H 5.13, N 3.81. IR: $\tilde{\nu}$ = 1653 cm^{-1} ($\nu_{C=N}$, s). SEM-EDS: Gd/Cl = 1:3.

$Tb(H_2L_D)Cl_3{\cdot}7H_2O$: The yellow residue was treated with MeOH/Et_2O and dried in vacuo. 1181 mg, 72% yield. $C_{23}H_{28}Cl_3N_2O_6Tb{\cdot}7H_2O$ (819.84): calcd. C 33.70, H 5.16, N 3.42; found C 33.39, H 4.65, N 3.86. IR: $\tilde{\nu}$ = 1637 cm^{-1} ($\nu_{C=N}$, s). SEM-EDS: Tb/Cl = 1:3.

$NiLn(L_D)Cl_3{\cdot}nH_2O{\cdot}m$EtOH (Ln = La, Ce, Gd, Tb, n = 0−2, m = 0−2): Triethylamine (202 mg, 2 mmol) and $NiCl_2{\cdot}6H_2O$ (237.7 mg, 1 mmol), dissolved in MeOH (2 mL), were added to a yellow solution of $Ln(H_2L_D)Cl_3{\cdot}nH_2O$ (1 mmol) in MeOH/EtOH (for La) or MeOH/*i*PrOH (for Ce,Gd,Tb) (20 mL) that was slightly heated (30 °C). After stirring for 10 min, a pale green precipitate formed. The

 © 2004 Wiley-VCH Verlag GmbH & Co. KGaA, Weinheim

suspension was then stirred for a further 20 min and subsequently cooled to room temperature. The resultant pale green powder was collected by filtration, washed with Et_2O and dried in vacuo. Slow diffusion of Et_2O into an EtOH/MeOH solution of the compound produced green crystals. 62% average yield.

$LaNi(L_D)Cl_3$: 464 mg, 63% yield. $C_{23}H_{26}Cl_3LaN_2NiO_6$ (730.42): calcd. C 37.82, H 3.59, N 3.84; found C 37.75, H 4.11, N 3.40 IR: $\tilde{\nu}$ = 1636 cm^{-1} ($\nu_{C=N}$, s). SEM-EDS: Ni/La/Cl = 1:1:3.

$CeNi(L_D)Cl_3$: 461 mg, 63% yield. $C_{23}H_{26}CeCl_3N_2NiO_6$ (731.63): calcd. C 37.76, H 3.58, N 3.83; found C 37.57, H 4.28, N 3.72. IR: $\tilde{\nu}$ = 1634 cm^{-1} ($\nu_{C=N}$, s). SEM-EDS: Ni/Ce/Cl = 1:1:3.

$GdNi(L_B)Cl_3{\cdot}2H_2O{\cdot}EtOH$: 516 mg, 62% yield. $C_{23}H_{26}Cl_3GdN_2NiO_6{\cdot}2H_2O{\cdot}EtOH$ (830.86): calcd. C 36.14, H 4.37, N 3.37; found C 36.50, H 5.08, N 3.45. IR: $\tilde{\nu}$ = 1638 cm^{-1} ($\nu_{C=N}$, s). SEM-EDS: Ni/Gd/Cl = 1:1:3.

$TbNi(L_B)Cl_3{\cdot}2EtOH$: 504 mg, 60% yield. $C_{23}H_{26}Cl_3N_2NiO_6Tb{\cdot}2EtOH$ (842.57): calcd. C 38.49, H 4.55, N 3.32; found C 38.13, H 4.89, N 3.41. IR: $\tilde{\nu}$ = 1628 cm^{-1} ($\nu_{C=N}$, s). SEM-EDS: Ni/Tb/Cl = 1:1:3.

$CuLn(L_D)Cl_3{\cdot}CH_3OH$ (Ln = La, Ce, Gd, Tb): Triethylamine (202 mg, 2 mmol) and $CuCl_2{\cdot}2H_2O$ (170.5 mg, 1 mmol), dissolved in MeOH (2 mL), were added to a yellow solution of $Ln(H_2L_D)Cl_3{\cdot}nH_2O$ (1 mmol) in methanol (for La) or MeOH/EtOH (for Ce,Gd, Tb) (20 mL) that was slightly heated (30 °C). After stirring for 10 min, a green precipitate formed; the suspension was stirred for further 20 min and then cooled to room temperature. The resultant green powder was collected by filtration, washed with Et_2O and dried in vacuo. Slow diffusion of Et_2O into an EtOH/MeOH solution of the compound produced green crystals. 63% average yield.

$LaCu(L_D)Cl_3{\cdot}CH_3OH$: 492 mg, 64% yield. $C_{23}H_{26}Cl_3CuLaN_2O_6{\cdot}CH_3OH$ (767.30): calcd. C 37.57, H 3.94, N 3.60; found C 38.49, H 3.77, N 3.60. IR: $\tilde{\nu}$ = 1625 cm^{-1} ($\nu_{C=N}$, s). SEM-EDS: Cu/La/Cl = 1:1:3.

$CeCu(L_D)Cl_3{\cdot}CH_3OH$: 480 mg, 62% yield. $C_{23}H_{26}CeCl_3CuN_2O_6{\cdot}CH_3OH$ (768.51): calcd. C 37.51, H 3.93, N 3.65; found C 37.84, H 4.02, N 3.87. IR: $\tilde{\nu}$ = 1627 cm^{-1} ($\nu_{C=N}$, s). SEM-EDS: Cu/Ce/Cl = 1:1:3.

$GdCu(L_D)Cl_3{\cdot}CH_3OH$: 495 mg, 63% yield. $C_{23}H_{26}Cl_3CuGdN_2O_6{\cdot}CH_3OH$ (785.64): calcd. C 36.69, H 3.85, N 3.57; found C 37.40, H 3.53, N 3.45. IR: $\tilde{\nu}$ = 1627 cm^{-1} ($\nu_{C=N}$, s). SEM-EDS: Cu/Gd/Cl = 1:1:3.

$TbCu(L_D)Cl_3{\cdot}CH_3OH$: 494 mg, 63% yield. $C_{23}H_{26}N_2O_6TbCuCl_3{\cdot}CH_3OH$ (787.31): calcd. C 36.61, H 3.84, N 3.56; found C 36.82, H 3.94, N 3.74. IR: $\tilde{\nu}$ = 1627 cm^{-1} ($\nu_{C=N}$, s). SEM-EDS: Cu/Tb/Cl = 1:1:3.

$ZnLn(L_D)Cl_3{\cdot}nH_2O{\cdot}mROH$ (Ln = La, Ce, Gd, Tb; n = 0−3; m = 0−1; R = CH_3, CH_3CH_2): Triethylamine (202 mg, 2 mmol) and $ZnCl_2$ (136.28 mg, 1 mmol), dissolved in MeOH (2 mL), were added to a yellow solution of $Ln(H_2L_D)Cl_3{\cdot}nH_2O$ (1 mmol) in methanol or MeOH/EtOH (for La, Gd) (20 mL) that was slightly heated (30 °C). After stirring for 10 min, a pale yellow precipitate formed. The suspension was then stirred for further 20 min and subsequently cooled to room temperature. The obtained pale yellow powder was collected by filtration, washed with Et_2O and dried in vacuo. Slow diffusion of Et_2O into an EtOH/MeOH solution of the compound produced pale yellow crystals. 55% average yield.

$LaZn(L_D)Cl_3{\cdot}CH_3OH$: 439 mg, 57% yield. $C_{23}H_{26}Cl_3LaN_2O_6Zn{\cdot}CH_3OH$ (769.12): calcd. C 37.48, H 3.93, N 3.64; found C 36.86, H 3.49, N 3.53. IR: $\tilde{\nu}$ = 1631 cm^{-1} ($\nu_{C=N}$, s). ^1H NMR (300 MHz, CD_3OD, 25 °C): δ = 2.19 (quint, 2 H, $CNCH_2CH_2$), 4.00 (t, 4 H, $CNCH_2$), 4.20 (s, 4 H, CH_2O), 4.37 (t, 4 H, CH_2O), 4.56 (t, 4 H, CH_2O−Ar), 6.85 (t, 2 H, Ar−*H*), 7.13 (dd, 2 H, Ar−*H*), 7.28 (dd, 2 H, Ar−*H*), 8.41 (s, 2 H, *H*C=N). SEM-EDS: Zn/La/Cl = 1:1:3.

$CeZn(L_D)Cl_3{\cdot}CH_3OH$: 412 mg, 53% yield. $C_{23}H_{26}CeCl_3N_2O_6Zn{\cdot}CH_3OH$ (770.33): calcd. C 37.42, H 3.93, N 3.64; found C 37.42, H 3.68, N 3.66. IR: $\tilde{\nu}$ = 1630 cm^{-1} ($\nu_{C=N}$, s). ^1H NMR (300 MHz, CD_3OD, 25 °C): δ = 0.80 (br. s, 4 H, CH_2O), 1.81 (br. s, 4 H, CH_2O), 2.97 (m, 2 H, $CNCH_2CH_2$), 4.59 (m, 4 H, $CNCH_2$), 5.81 (br. s, 2 H, Ar−*H*), 6.60 (t, 2 H, Ar−*H*), 7.26 (br. s, 4 H, CH_2O), 7.63 (d, 2 H, Ar−*H*), 9.28 (s, 2 H, *H*C=N). SEM-EDS: Zn/Ce/Cl = 1:1:3.

Table 4. Crystal and intensity data for La−Cu, La−Zn and Tb−Cu complexes

Coordinated metals	La−Cu	La−Zn	Tb−Cu
Empirical formula	$C_{24}H_{30}Cl_3CuLaN_2O_7$	$C_{24}H_{30}Cl_3LaN_2O_7Zn$	$C_{24}H_{30}Cl_3CuN_2O_7Tb$
Formula mass	764.30	769.13	787.31
Crystal system	monoclinic	monoclinic	monoclinic
Space group	$P2_1/n$ (No. 14)	$P2_1/n$ (No. 14)	$P2_1/n$ (No. 14)
a [Å]	11.041(2)	11.186(2)	10.967(2)
b [Å]	14.034(3)	14.076(3)	13.851(3)
c [Å]	18.590(4)	18.558(4)	18.625(4)
β [°]	102.74(3)	103.35 (3)	102.68(3)
Cell volume [$Å^3$]	2809(1)	2843(1)	2760(1)
Z	4	4	4
Calcd. density [g/cm^3]	1.814	1.797	1.895
Absorption μ [mm^{-1}] (Mo-K_α)	2.588	2.653	3.648
Range of relative transmission factors [%][a]	91−100	88−100	81−100
θ limits [°]	6.9−56	6.2−56	6.3−56
Data collected/unique	6215/6028	6156/5981	3789/3636
Data observed	5958 [$F \geq 3.5\sigma(F)$]	5878 [$F \geq 3.5\sigma(F)$]	3557 [$F \geq 3.5\sigma(F)$]
No. of parameters (observed per parameter)	320 (18.6)	320 (18.4)	320 (11.1)
R [$\Sigma(\|F_o\| - \|F_c\|)/\Sigma\|F_o\|$]	0.051	0.063	0.067
R_w [$\Sigma w(\|\|F_o\| - \|F_c\|\|)^2/\Sigma w(F_o)^2]^{1/2}$	0.130	0.14	0.15
Highest map residual [$e^-/Å^3$]	1.67	1.22	1.18

[a] Corrections: Lorentz polarization and absorption (empirical, ψ scan).

 © 2004 Wiley-VCH Verlag GmbH & Co. KGaA, Weinheim

$GdZn(L_D)Cl_3 \cdot 3H_2O$: 445 mg, 55% yield. $C_{23}H_{26}Cl_3GdN_2O_6Zn \cdot 3H_2O$ (809.46): calcd. C 34.13, H 3.98, N 3.46; found C 33.43, H 3.90, N 3.53. IR: $\tilde{\nu}$ = 1631 cm^{-1} ($\nu_{C=N}$, s). SEM-EDS: Zn/Gd/Cl = 1:1:3.

$TbZn(L_D)Cl_3 \cdot EtOH$: 439 mg, 55% yield. $C_{23}H_{26}Cl_3N_2O_6TbZn \cdot CH_3CH_2OH$ (803.16): calcd. C 37.39, H 4.02, N 3.49; found C 36.82, H 3.80, N 3.51. IR: $\tilde{\nu}$ = 1632 cm^{-1} ($\nu_{C=N}$, s). SEM-EDS: Zn/Tb/Cl = 1:1:3.

X-ray Crystallography: Diffraction data were collected at room temperature with a Philips PW1100 automatic four-circle diffractometer (FEBO System) using graphite-monochromated Mo-K_α radiation and the ω-2θ scan mode. Lattice parameters were obtained from least-squares refinement of the setting angles of 25 reflections with $10° \leq 2\theta \leq 24°$. Table 4 summarises the crystallographic data and structure refinement. No sign of crystal deterioration was revealed by monitoring three standard reflections after every 200 measurements. Structures were solved by standard Patterson methods and subsequently completed by a combination of least-squares techniques and Fourier syntheses with the SHELX program.[54] All benzene rings were refined as rigid bodies, hydrogen atoms were included in idealised positions with fixed C−H distances (0.97Å) and isotropic temperature factors fixed to 1.2 times U(eq) of the respective carbon atom. Selected bond lengths and angles pertinent to the coordination spheres are given in Tables 1 and 2 and representative torsion angles in Table 3. Additional crystallographic data, atomic coordinates, anisotropic thermal parameters, and full listings of bond lengths and angles are provided as supplementary material. CCDC-244706, -244707 and -244708 contain the supplementary crystallographic data for this paper. These data can be obtained free of charge at www.ccdc.cam.ac.uk/conts/retrieving.html [or from the Cambridge Crystallographic Data Centre, 12 Union Road, Cambridge CB2 1EZ, UK; Fax: (internat.) + 44-1223-336-033; E-mail: deposit@ccdc.cam.ac.uk]. Final geometrical calculations and drawings were carried out with the PARST program[55] and the XP utility of the Siemens package,[56] respectively, running on a DIGITAL ALPHA-AXP 300 computer. X-ray powder diffraction measurements were carried out with a Philips X'Pert diffractometer (40 kV, 35 mA) using graphite-monochromated Cu-K_α radiation in the range $5° < 2\theta < 80°$. The simulated powder diffraction pattern was obtained by means of the SHELXTL program (Bruker ASX, 1998) using the single-crystal diffraction data of the La−Cu complex.

Acknowledgments

We thank Mr. A. Aguiari, Mr. E. Bullita and Mrs. A. Moresco for their technical assistance. We also thank MIUR project FIRB-RBNE019H9 K for financial support. A. C. and L. S. thank FIRB RBNE01YLKN and CNR, Italy.

[1] P. A. Vigato, S. Tamburini, *Coord. Chem. Rev.*, in press.
[2] [2a] N. F. Curtis, *Coord. Chem. Rev.* **1968**, *3*, 3. [2b] D. H. Busch, *Science* **1971**, *171*, 241. [2c] S. M. Nelson, *Pure Appl. Chem.* **1980**, *52*, 2461.
[3] V. Alexander, *Chem. Rev.* **1995**, *95*, 273.
[4] [4a] D. E. Fenton, H. Okawa, *Chem. Ber./Recueil* **1997**, *130*, 433. [4b] S. R. Collinson, D. E. Fenton, *Coord. Chem. Rev.* **1996**, *148*, 19. [4c] D. E. Fenton, *Pure Appl. Chem.* **1986**, *58*, 1437.
[5] [5a] L. F. Lindoy, *The Chemistry of Macrocyclic Ligand Complexes*, Cambridge University, Cambridge, U. K., **1989**. [5b] L. F. Lindoy, *Pure Appl. Chem.* **1989**, *61*, 1575. [5c] L. F. Lindoy *Synthesis of Macrocycle: The Design of Selective Complexing Agents* (Eds: R. M. Izatt, J. J. Christensen), Wiley, New York, **1987**, p. 53.
[6] P. Guerriero, S. Tamburini, P. A. Vigato, *Coord. Chem. Rev.* **1995**, *139*, 17.
[7] O. Kahn, *Advances in Inorganic Chemistry* (Ed.: A. G. Sykes), Academic Press, S. Diego (USA), **1995**, vol. 43, p. 179.
[8] K. S. Murray, *Advances in Inorganic Chemistry* (Ed.: A. G. Sykes), Academic Press, S. Diego (USA), **1995**, vol. 43, p. 261.
[9] [9a] *Crown Compounds: Toward Future Applications* (Ed.: S. R. Coper), VCH Publishers Inc., New York, **1992**. [9b] *Coordination Chemistry of Macrocyclic Compounds* (Ed.: G. A. Melson), Plenium Press, New York, **1979**. [9c] A. Martell, J. Penitka, D. Kong, *Coord. Chem. Rev.* **2001**, *55*, 216−217.
[10] P. A. Vigato, P. Guerriero, S. Tamburini, R. Seraglia, P. Traldi, *Org. Mass Spectrom.* **1990**, *25*, 420.
[11] P. Guerriero, S. Tamburini, P. A. Vigato, R. Seraglia, P. Traldi, *Org. Mass Spectrom.* **1992**, *27*, 231.
[12] P. Guerriero, S. Tamburini, P. A. Vigato, S. Catinella, P. Traldi, *Rapid Commun. Mass Spectrom.* **1992**, *6*, 741.
[13] S. Catinella, P. Traldi, P. Guerriero, S. Tamburini, P. A. Vigato, *Rapid Commun. Mass Spectrom.* **1994**, *8*, 111.
[14] M. Coppola, S. Catinella, P. Traldi, P. Guerriero, S. Tamburini, P. A. Vigato, *Org. Mass Spectrom.* **1994**, *29*, 566.
[15] P. Tomasin, S. Tamburini, P. A. Vigato, M. D'Alpaos, P. Traldi, *Rapid Commun. Mass Spectrom.* **1997**, *11*, 494.
[16] M. D'Alpaos, S. Tamburini, P. Tomasin, P. A. Vigato, P. Traldi, *Rapid Commun. Mass Spectrom.* **1997**, *11*, 1909.
[17] P. A. Vigato, S. Tamburini, D. E. Fenton, *Coord. Chem. Rev.* **1990**, *106*, 25.
[18] D. E. Fenton, P. A. Vigato, *Chem. Soc. Rev.* **1988**, *17*, 89.
[19] H. Okawa, H. Furutachi, D. E. Fenton, *Coord. Chem. Rev.* **1998**, *174*, 51.
[20] V. Amendola, C. Brusoni, L. Fabbrizzi, C. Mangano, H. Miller, P. Pallavicini, A. Pernotti, A. Taglietti, *J. Chem. Soc., Dalton Trans.* **2001**, 3528.
[21] [21a] V. Amendola, L. Fabbrizzi, L. Granelli, C. Maggi, C. Mangano, P. Pallavicini, M. Zema, *Inorg. Chem.* **2001**, *40*, 3579. [21b] V. Amendola, L. Fabbrizzi, P. Pallavicini, E. Sartirana, A. Taglietti, *Inorg. Chem.* **2003**, *42*, 1632.
[22] L. Fabbrizzi, F. Foti, P. Pallavicini, S. Patroni, A. Taglietti, *Atti del VI Congresso Nazionale di Chimica Supramolecolare*, Urbino, **2003**, P62, p. 201.
[23] M. Botta, U. Casellato, C. Scalco, S. Tamburini, P. Tomasin, P. A. Vigato, S. Aime, *Chem. Eur. J.* **2002**, *8*, 3917.
[24] N. Brianese, U. Casellato, S. Tamburini, P. Tomasin, P. A. Vigato, *Inorg. Chem. Commun.* **1999**, *2*, 149.
[25] U. Casellato, S. Tamburini, P. Tomasin, P. A. Vigato, S. Aime, A. Barge, M. Botta, *Chem. Commun.* **2000**, 145.
[26] A. D. Sherry, C. F. G. C. Geraldes in *Lanthanide Probes in Life, Chemical and Earth Sciences* (Eds.: J.-C. G. Bunzli, G. R. Choppin), Elsevier, Amsterdam, **1989**, chapter 4.
[27] [27a] R. B. Hutchinson, J. I. Shapiro, *Concepts Magn. Reson.* **1991**, *3*, 215. [27b] C. S. Springer, Jr., in *NMR Techniques in the Study of Cardiovascular Structure and Function* (Eds.: M. Osbakken, J. Haselgrove), Futura Publishing, New York, **1988**, chapter 4.
[28] A. Barge, M. Botta, S. Tamburini, P. A. Vigato, *VI Congresso Nazionale di Chimica Supramolecolare*, Urbino, September 7−10, **2003**, P64, p.205.
[29] C. J. Van Staveren, J. Van Erden, F. C. J. M. Van Veggel, S. Harkema, D. Reinhoudt, *J. Am. Chem. Soc.* **1988**, *110*, 4994.
[30] [30a] F. C. J. M. Van Veggel, M. Bos, S. Harkema, W. Verboom, D. N. Reinhoudt, *Angew. Chem. Int. Ed. Engl.* **1989**, *28*, 749. [30b] F. C. J. M. Van Veggel, M. Bos, S. Harkema, H. Van Bovenkamp, W. Verboom, J. Reedijk, D. N. Reinhoudt, *J. Org. Chem.* **1991**, *56*, 22.
[31] N. Brianese, U. Casellato, S. Tamburini, P. Tomasin, P. A. Vigato, *Inorg. Chim. Acta* **1999**, *293*, 178.
[32] P. Di Bernardo, P. Zanonato, personal communication.
[33] [33a] J.-P. Costes, F. Dahan, F. Nicodeme, *Inorg. Chem.* **2003**, *42*, 6556. [33b] W. Xie, M. J. Heeg, P. G. Wang, *Inorg. Chem.* **1999**, *38*, 2541. [33c] K. Binnemans, Y. G. Galyametdinov, R.

 © 2004 Wiley-VCH Verlag GmbH & Co. KGaA, Weinheim

Van Deun, D. W. Bruce, S. R. Collinson, A. P. Polishchuk, I. Bikchantaev, W. Haase, A. V. Prosvirin, L. Tinchurina, I. Litvinov, A. Gubajdullin, A. Rakhmatullin, K. Uytterhoeven, L. Van Meervelt, *J. Am. Chem. Soc.* **2000**, *122*, 4335.
[34] C. Benelli, D. Gatteschi, *Chem. Rev.* **2002**, *102*, 2369 and references cited therein.
[35] A. Bencini, A. Benelli, A. Caneschi, R. L. Carlin, A. Dei, D. Gatteschi, *J. Am. Chem. Soc.* **1985**, *107*, 8128.
[36] M. Andruh, I. Ramade, E. Codjovi, O. Guillou, O. Kahn, J. C. Trombe, *J. Am. Chem. Soc.* **1993**, *115*, 1822.
[37] J. P. Costes, F. Dahan, A. Dupuis, J. P. Laurent, *Inorg. Chem.* **1996**, *35*, 2400.
[38] J.-P. Sutter, M. L. Kahn, S. Golhen, L. Ouahab, O. Kahn, *Chem. Eur. J.* **1998**, *4*, 571.
[39] J. P. Costes, F. Dahan, A. Dupuis, J. P. Laurent, *Inorg. Chem.* **2000**, *39*, 169.
[40] Y. Kobayashi, S. Ueki, T. Ishida, T. Nogami, *Chem. Phys. Lett.* **2003**, *378*, 337.
[41] A. Bencini., D. Gatteschi in *Transition Metal Chemistry* (Eds.: B. N. Figgis, G. Melson) Marcel Dekker, New York, **1982**, vol. 8, p. 1.
[42] C. J. H. Jacobsen, E. Pedersen, J. Villadsen, H. Weihe, *Inorg. Chem.* **1993**, *32*, 1216.
[43] O. Kahn, *Molecular Magnetism*, VCH, New York, **1993**.
[44] C. J. O'Connor, *Prog. Inorg. Chem.* **1982**, *29*, 103.
[45] J. P. Costes, F. Dahan, A. Dupuis, J. P. Laurent, *Chem. Eur. J.* **1998**, *4*, 1616.
[46] M. L. Kahn, C. Mathoniere, O. Kahn, *Inorg. Chem.* **1999**, *38*, 3692.
[47] M. L. Kahn, J. P. Sutter, S. Golhen, P. Guionneau, L. Ouahab, O. Kahn, D. Chasseau, *J. Am. Chem. Soc.* **2000**, *122*, 3413.
[48] J. P. Sutter, M. L. Kahn, O. Kahn, *Adv. Mater.* **1999**, *11*, 863.
[49] A. Figuerola, C. Diaz, J. Ribas, V. Tangoulis, J. Granell, F. Lloret, J. Mahia, M. Maestro, *Inorg. Chem.* **2003**, *42*, 641.
[50] A. Caneschi, A. Dei, D. Gatteschi, S. Poussereau, L. Sorace, *Dalton Trans.*, submitted for publication.
[51] R. D. L. Carlin, *Magnetochemistry*, Springer Verlag, Berlin, **1986**.
[52] A. Caneschi, A. Dei, D. Gatteschi, C. A. Massa, L. A. Pardi, S. Poussereau, L. Sorace, *Chem. Phys. Lett.* **2003**, *371*, 694.
[53] D. D. Perrin, W. L. Armarego, D. R. Perrin, *Purification of Laboratory Chemicals*, 2nd ed., Pergamon Press, Oxford, **1982**, p. 229.
[54] G. M. Sheldrick, C. Kruger, R. Goddard (Eds.), *SHELX-86, Crystallographic Computing 3*, Oxford University Press, London, **1985**, p. 175; G. M. Sheldrick, *SHELXL-93, Program for Crystal Structure Refinement*, University of Göttingen, Germany, **1993**.
[55] M. Nardelli, *J. Appl. Crystallogr.* **1995**, *28*, 659.
[56] G. M. Sheldrick, *SHELXTL-PLUS*, version 4.2, Siemens Analytical X-ray Instruments Inc., Madison, WI, **1991**.
[57] [57a] P. P. Morgan, J. M. Beynon, R. M. Bateman, B. M. Green, *Int. J. Mass Spectrom. Ion Phys.* **1978**, *28*, 171. [57b] M. Barber, R. S. Bordoli, R. D. Sedgwick, A. M. Taylor, *Chem. Commun.* **1981**, *7*, 1716.

Received February 17, 2004
Early View Article
Published Online August 3, 2004

 © 2004 Wiley-VCH Verlag GmbH & Co. KGaA, Weinheim

Carbonyl-Nitrido Mixed-Metal Clusters: Synthesis, Reactivity, Electrochemical Behavior and Solid-State Structure of $[Co_5MoN(CO)_{14}]^{2-}$ and $[Co_5MoN(CO)_{14}AuPPh_3]^-$

Roberto Della Pergola,*[a] Alessandro Fumagalli,[b] Fabrizia Fabrizi de Biani,[c] Luigi Garlaschelli,[d] Franco Laschi,[c] Maria Carlotta Malatesta,[d] Mario Manassero,*[e] Elena Roda,[d] Mirella Sansoni,[e] and Piero Zanello[c]

Keywords: Cobalt / Molybdenum / Cluster compounds / Nitrides / Electrochemistry

The dianionic cluster $[Co_5MoN(CO)_{14}]^{2-}$ (**1**) was synthesized from $[Co_6N(CO)_{15}]^-$ and $[Mo_2(CO)_{10}]^{2-}$ in refluxing acetonitrile. The solid-state structure of the $[Ph_4P]^+$ salt was determined. It consists of an octahedral metal cage, enclosing a six-coordinate nitrido ligand. Typical bond lengths are: Co–N 1.88 Å, Mo–N 2.03 Å, Co–Co 2.61 Å and Co–Mo 2.84 Å, showing that there is very little, if any, preferential interaction of the interstitial atom with that of molybdenum. The cluster reacts with $Au(PPh_3)Cl$ in THF at room temperature forming the derivative $[Co_5MoN(CO)_{14}\{AuPPh_3\}]^-$ (**2**). The gold atom caps an $MoCo_2$ face of the octahedron, with short Au–Co (2.68 Å) and long Au–Mo (3.16 Å) bonds, showing that both metal atoms are necessary for coordination, but Au^I binds better with the cobalt atoms. Electrochemical studies have pointed out that cluster **1** has good redox capabilities in that it is able to support reversibly the progressive addition of three electrons. EPR measurements on the corresponding trianion confirm the lack of preferential interaction between the Mo site and the interstitial nitride atom.

(© Wiley-VCH Verlag GmbH & Co. KGaA, 69451 Weinheim, Germany, 2004)

Introduction

Recently, we described the synthesis and the chemical characterization of octahedral mixed-metal clusters of iron and a metal of group 6 (Mo or W), containing an interstitial nitride. Even if the yields were only just acceptable, they were obtained selectively, using different complexes with ligands of a different nature (CO, Cp, MeCN).[1] As an extension of this type of chemistry, we moved to the synthesis of Co−Mo nitrides. The choice of these two elements was based on the industrial relevance of Mo and Co in hydrodesulfurization (HDS) and hydrodenitrogenation (HDN) reactions.[2] Molecular organometallic complexes have many applications in this field, since they contribute to clarifying the mechanism of the hydrogenation of thio and aza compounds.[3] In this context, clusters are especially of value, since they can homogeneously catalyze the hydrogenation of heterocycles[4] or model the interaction between N- and S-donors with multimetallic sites.[5] Even more important, sulfido Co−Mo clusters can stoichiometrically desulfurize thio compounds by a mechanism that is believed to closely mimic heterogeneous HDS.[6] Additionally, dimetallic sulfides can be prepared from a molecular precursor, either by supporting heterometallic Co−Mo clusters,[7] or by co-impregnation of homometallic carbonyl complexes.[8]

We started these investigations hoping that clusters containing Co, Mo and N could help us to understand the mutual relationships between the three elements. The first results of our efforts is the reproducible synthesis of a new cluster, $[Co_5MoN(CO)_{14}]^{2-}$, which could be fully characterized through a combination of chemical, spectroscopic, electrochemical and X-ray analyses. The yields of the anion are moderate, but its preparation is much simpler than those reported for other Co−Mo nitride complexes,[9] mak-

[a] Dipartimento di Scienze dell'Ambiente e del Territorio, Università di Milano-Bicocca,
Bicocca-piazza della Scienza 1, 20126 Milano, Italy
E-mail: roberto.dellapergola@unimib.it
[b] Dipartimento di Biologia Strutturale e Funzionale, Università degli Studi dell'Insubria,
Via J. H. Dunant 3, 21100 Varese, Italy
[c] Dipartimento di Chimica dell'Università di Siena,
Via A. Moro, 53100 Siena, Italy
[d] Dipartimento di Chimica Inorganica, Metallorganica ed Analitica, Università di Milano,
Via G. Venezian 21, 20133 Milano, Italy
[e] Dipartimento di Chimica Strutturale e Stereochimica Inorganica, Università di Milano,
Via G. Venezian 21, 20133 Milano, Italy
E-mail: m.manassero@csmtbo.mi.cnr.it.
Supporting information for this article is available on the WWW under http://www.eurjic.org or from the author.

ing the cluster available on a decigram scale for further investigations.

Results

Synthesis and Reactivity

With the aim of synthesizing a nitrido Co−Mo cluster, we tried the same synthetic approach as was successfully used for the Fe−Mo analogs,[1] i.e. the condensation of a cobalt nitride, having a small negative charge, with a highly reduced carbonyl anion of molybdenum. Thus, the new product $[Co_5MoN(CO)_{14}]^{2-}$ (**1**) was obtained by reaction of $[Co_6N(CO)_{15}]^-$ (K^+ salt) and $[Mo_2(CO)_{10}]^{2-}$ (NEt_4^+ salt) in refluxing acetonitrile. IR monitoring shows that the reaction proceeds smoothly, the only by-products detectable in solution being the mononuclear carbonyl complexes $[Co(CO)_4]^-$ and $[Mo(CO)_6]$.[10] However, a fairly large amount of decomposition product is formed, which can easily be eliminated by filtration. Dianion **1** can be purified by metathesis with $[Ph_4P]^+$ in MeOH, which induces precipitation. We tested other less reducing complexes of molybdenum, such as $[Mo(CO)_3(NCEt)_3]$ or $[HMo_2(CO)_{10}]^-$, but the resulting yields were even lower. Thus, the formation of **1** can be formally represented by the reaction

$$[Co_6N(CO)_{15}]^- + [Mo_2(CO)_{10}]^{2-} \rightarrow [Co_5MoN(CO)_{14}]^{2-} + [Mo(CO)_6] + [Co(CO)_4]^- + CO$$

The reactivity of **1** with several potential sources of S- or N-ligands (such as quinoline, $NOBF_4$, Ph_2S_2) was examined. In order to perform ligand substitution, we attempted both the direct carbonyl displacement and "oxidative substitution",[11] analogous with what has been used for other dianionic octahedral clusters.[12] Unfortunately, no stable derivatives were ever obtained. Attempts to add hydride ligands to **1** by protonation resulted in the formation of $[Co_6N(CO)_{15}]^-$, in keeping with a weak interaction between the nitrogen and the molybdenum atom. All these disappointing results led us to further investigate the redox capability of **1**, thus prompting electrochemical investigations (see later). By contrast, the reaction between **1** and $Au(PPh_3)Cl$ in THF at room temperature is fast and clean, quantitatively yielding $[Co_5MoN(CO)_{14}\{AuPPh_3\}]^-$ within a few minutes. The isolation of this adduct demonstrated that the poor reactivity of the dianion **1** cannot be attributed to the absence of nucleophilic character, nor steric crowding of its carbonyl ligands. Due to its composition of early-, late- and post-transition elements, the trimetallic $[Co_5MoN(CO)_{14}\{AuPPh_3\}]^-$ can be well classified among the "very-mixed"-metal carbonyl clusters.[13]

The Solid-State Structures

The crystal structure of cluster **1** was determined on the $[Ph_4P]_2$**1** salt, and the geometry of the anion is shown in Figure 1.[14] Average values of bond lengths are collected in Table 1, and compared with the corresponding parameters determined in **2**. The individual values are reported in Table S4 of the Supporting Information. The six metal atoms define an octahedron, centered by an interstitial nitride. As normally observed in Co clusters, the four unbridged edges are definitely longer than the bridged ones.[15] Examining the metal−metal and the metal−nitrogen bond lengths of other nitrido Co−Mo complexes,[9] Dahl discovered that Mo−N interactions are shorter than expected, and concluded that the Mo−N bond order was higher than the Co−N bond order. The same arguments were also used for nitrido Fe−Mo clusters,[1] with a strong interaction between the electron-deficient molybdenum atoms and the nitride (a well-known strong π-donor).[16] In the present case the uncertainty of the metallic radius of the cobalt atoms is high, since the Co−Co bond lengths are scattered by the

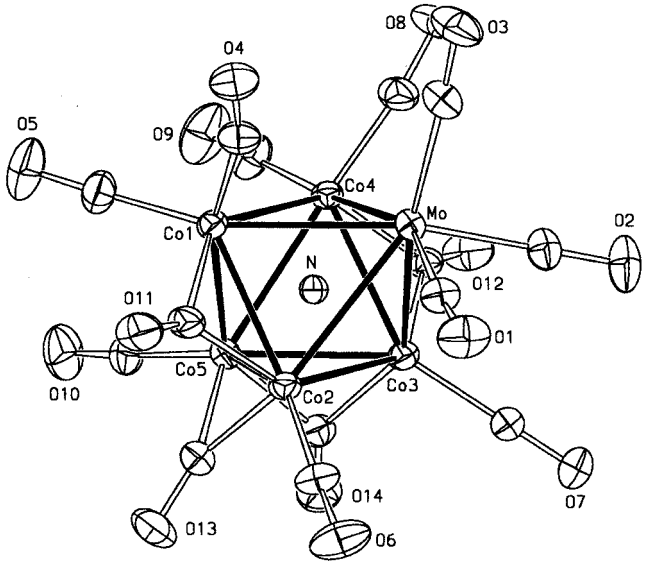

Figure 1. The solid-state structure of $[Co_5MoN(CO)_{14}]^{2-}$; carbon atoms are labeled using the oxygen atom to which they are attached

Table 1. Average interatomic distances [Å] in the clusters **1** and **2** (t = terminal, br = bridging); numbers in parentheses are esds on unique values, ± numbers are rmsds on average bond lengths

	1	**2**
Co−Mo	2.84 ± 0.04	2.85 ± 0.05
Co−Co (unbridged)	2.72 ± 0.01	2.65 ± 0.04
Co−Co (bridged)	2.50 ± 0.07	2.531 ± 0.004
Au−Mo	−	3.159(1)
Au−Co	−	2.68 ± 0.07
Au−P	−	2.312(1)
Mo−N	2.025(1)	2.061(1)
Co−N	1.88 ± 0.01	1.88 ± 0.01
Mo−CO_t	1.96 ± 0.03	2.00 ± 0.01
Co-CO_t	1.76 ± 0.01	1.77± 0.02
Co-CO_{br}	1.94	1.96
C_t−O_t	1.15	1.15
C_{br}−O_{br}	1.16	1.17

 © 2004 Wiley-VCH Verlag GmbH & Co. KGaA, Weinheim

presence of bridged and unbridged bonds (the root mean square deviations are listed in Table 1). The average values in **1** are 2.61 ± 0.12 Å for the Co−Co distances and 2.84 ± 0.04 Å for the Mo−Co bonds. Therefore the metallic radius of the Co atom can be estimated as being 0.23 ± 0.12 Å smaller than that of Mo. On the other hand, the average Co−N bond is only 0.15 ± 0.01 Å shorter than the Mo−N distance. The discrepancy between the two values (0.08 Å) is obviously smaller than the root mean square deviations and statistically uninformative. Nevertheless, with this difference being similar to that of other related clusters,[9] one would be tempted to presume that in **1** a small displacement of the nitride towards the Mo atom occurs.

The idealized symmetry of the whole anion is C_s, with the mirror plane passing through Mo, N and the midpoint of the Co2−Co3 edge. The cluster is surrounded by ten terminal and four edge-bridging carbonyl groups, distributed in such a way that all metal atoms are connected to three ligands. The Mo and Co atoms differ in the bonding mode of the ligands, due to their different valence electrons: Mo is connected to terminal ligands only, Co1 and Co4 to two terminal and one bridging group, Co2 and Co3 to one terminal and two bridging CO groups. With respect to this, it is remarkable that the dimetallic cluster **1** displays the same arrangement of bridging ligands found in $[Co_6N(CO)_{13}]^-$, with four μ-CO groups "spanning a sequence of four bonds".[15] As a matter of fact the octahedral clusters of Rh and Co that contain an interstitial atoms and thirteen ligands, all adopt a different stereochemistry of the carbonyls.[15,17]

The solid-state structure of cluster **2** was determined on the $[Ph_4P]$**2** salt. The anion is shown in Figure 2, selected structural parameters are listed in Table S4 of the Supporting Information.

Also in this case, six metal atoms define an octahedron, centered by the interstitial nitride. The gold atom is situated on the triangular face composed of Mo, Co1 and Co4. The Co and Mo atoms bind differently to the gold atom. As in **1**, the Mo−N, Mo−CO and Mo−Co distances are longer by about 0.2 Å than the corresponding cobalt bonds, whereas the difference between Mo−Au and Co−Au is almost 0.5 Å. The different abilities of the two metals to coordinate gold can probably be explained by their electronic configuration: the Mo atom, already depleted of electron density, is less prone to adding the electrophilic fragment than the Co atom. The addition of the Au−PPh_3 moiety brings about little change to the average structural parameters, but several distortions on the individual values, which can be related to electronic rather than to steric factors. As a matter of fact, the Co1−Co4 edge becomes abnormally long (2.810 Å), suggesting some reduction in its electron density. To compensate, N−Co1 and N−Co4 bonds are shortened, whereas Mo−N is lengthened, in contrast to the expected effect between the N(−3) donor and the Au(+1) acceptor. Also in **2**, no convincing conclusions can be drawn on the strength of Co−N and Mo−N interactions, since the difference in metallic radii, estimated from

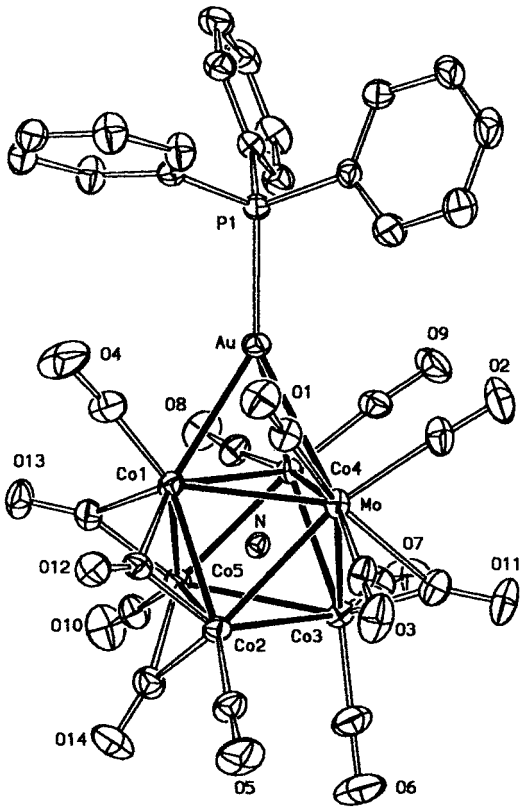

Figure 2. The solid-state structure of $[Co_5MoN(CO)_{14}\{AuPPh_3\}]^-$; carbon atoms are labeled using the oxygen atom to which they are attached

metal−metal and metal−nitrogen bond lengths, is even smaller than in **1** (0.07 ± 0.10 Å).

A very small lengthening of the M−CO (comparable, however, with uncertainties) might be indicative of reduced back-donation. The architecture of the bridging ligands is modified in **2**, and a "true" μ-CO group, spanning a Co−Mo edge, is formed. The other three bridging carbonyl groups are located on the edges of the Co1, Co2, Co5 cluster face, which has the shortest Co−Co bonds. Thus, the shortening effect of the bridging ligands can also be observed in **2**.

Electrochemistry and Joint EPR Measurements

Figure 3 illustrates the cyclic voltammetric behavior of $[Co_5MoN(CO)_{14}]^{2-}$ in MeCN solution.

Three sequential reductions with features of chemical reversibility are clearly detected together with an irreversible process interposed between the second and the third step. Taking into account that this latter process occurs at the same potential than that of an authentic sample of $[Ph_4P]Br$, we assign it to the countercation of the cluster dianion.

Controlled potential coulometry corresponding to the first reduction (E_w = −1.5 V) consumed one electron per molecule. In order to confirm the long-term chemical reversibility of such a process, cyclic voltammetry was performed on the exhaustively reduced solution, affording pro-

 © 2004 Wiley-VCH Verlag GmbH & Co. KGaA, Weinheim

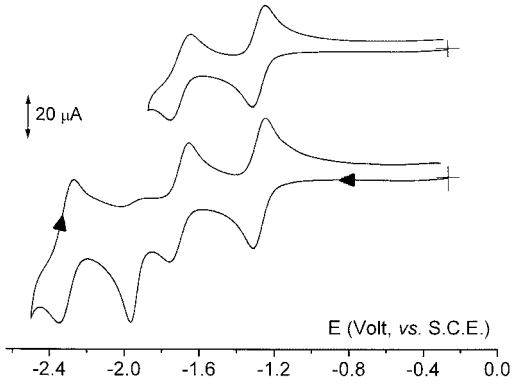

Figure 3. Cyclic voltammetric responses recorded at a gold electrode in an MeCN solution of $[Ph_4P]_2[Co_5MoN(CO)_{14}]$ (1.7×10^{-3} mol·dm^{-3}); $[Bu_4N][PF_6]$ (0.2 mol·dm^{-3}); scan rate 0.2 V s^{-1}

files quite complementary to the original ones. On this basis we assign the series of chemically reversible reduction steps to the four-membered sequence $[Co_5MoN(CO)_{14}]^{2-/3-/4-/5-}$.

Analysis of the $[Co_5MoN(CO)_{14}]^{2-/3-}$ process with scan rates increasing from 0.02 to 1.00 Vs^{-1} not only agrees with the chemical reversibility of the process (i_{pa}/i_{pc} constantly equal to unity), but also reveals its electrochemical reversibility (ΔE_p constantly equal to 59 mV), thus suggesting that no significant geometrical reorganization accompanies the electron addition.[18]

The formal electrode potentials of the processes discussed above are compiled in Table 2. Finally, we point out that $[Co_5MoN(CO)_{14}]^{2-}$ also exhibits an irreversible multielectron oxidation ($E_p = +0.13$ V).

In view of the chemical stability of the trianion $[Co_5MoN(CO)_{14}]^{3-}$, EPR investigations have been carried out on the complex after its electrogeneration at −20 °C. Figure 4 shows the X-band EPR spectrum of the MeCN solution of the trianion recorded under glassy conditions ($T = 100$ K).

Table 2. Formal electrode potentials [V, vs. SCE] and peak-to-peak separations [mV] for the redox processes exhibited by $[Co_5MoN(CO)_{14}]^{2-}$ in MeCN solution

$E°'_{(2-/3-)}$	ΔE_p[a]	$E°'_{(3-/4-)}$	ΔE_p[a]	$E°'_{(4-/5-)}$	ΔE_p[a]	E_p[a] [b]
−1.28	59	−1.70	85	−2.31	65	−1.97

[a] Measured at 0.2 V s^{-1}. [b] Process centered on $[PPh_4]^+$, see text.

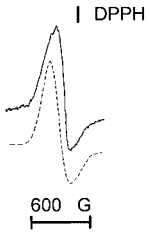

Figure 4. X-band EPR spectra of the frozen solution of $[Co_5MoN(CO)_{14}]^{3-}$; $T = 100$ K; MeCN solution; solid line: first derivative experimental spectrum; dashed line: simulated spectrum

The lineshape analysis is suitably carried out assuming an $S = 1/2$ axial electron spin hamiltonian with poor resolution of the overall anisotropic signal, which is constituted by two absorptions overlapped in the intermediate field.[19] The computed[20] g_i anisotropic parameters display a noticeable metal character ($g_\perp > g_\parallel > g_{electron} = 2.0023$):

$g_\parallel = 1.985(8)$, $g_\perp = 2.160(8)$; $<g> = 1/3(g_\parallel + 2g_\perp) = 2.102(8)$

$\Delta H_\parallel = 110(5)$ G; $\Delta H_\perp = 95(5)$ G

Neither Co (^{59}Co: $I = 7/2$; natural abundance = 100%) nor Mo (^{97}Mo, ^{99}Mo: $I = 5/2$; natural abundance = 15.8 and 9.6%, respectively) hyperfine (hpf) or superhyperfine (shpf) splittings are detected, as a consequence of the noticeable anisotropic line widths largely overlapping the underlying metal magnetic couplings, if any, i.e.

$\Delta H_\parallel = 110(5)$ G $\geq a_i(^{59}Co, ^{97,99}Mo, ^{14}N)$;

$\Delta H_\perp = 95(5)$ G $\geq a_i(^{59}Co, ^{97,99}Mo, ^{14}N)$

The actual paramagnetic features indicate the complete delocalization of the $S = 1/2$ unpaired spin density onto the octahedral metal frame without any evidence for significant individual metal interaction. The fact that the interstitial nitride nucleus (^{14}N: $I = 1$; natural abundance = 99.6%) does not exhibit resolved anisotropic splittings, confirms this.

Raising the temperature of the glassy-fluid transition phase ($T = 227.5$ K) results in the axial signal disappearing and the paramagnetic solution becoming EPR-mute. Rapidly refreezing the fluid solution only partially recovers the original anisotropic signal, indicating chemical lability of the electrogenerated trianion in fluid solution under a non-inert gas.

Conclusions

The synthesis of the new cluster $[Co_5MoN(CO)_{14}]^{2-}$ was pursued hoping that substitution or addition of nitrogen or sulfur donors would highlight the cooperativity of the two metals in the coordination of the ligands and the cleavage of C−N and C−S bonds.[3] Even if it does not react directly with these types of ligands, the formation of $[Co_5MoN(CO)_{14}\{AuPPh_3\}]^-$ shows that more ligands can be added to its metal cage, and that both metallic elements are important for activation and coordination of electrophiles. Moreover, in contrast with what has been found in related dimetallic compounds,[9] the solid-state structure of both clusters allows us to exclude a preference of the nitride for the Co or Mo atom. The redox reactivity of the anion was studied by electrochemical and ESR experiments, that may suggest an alternative way to achieve substitution, through Electron Chain Transfer Catalysis (ECTC).[21] Therefore, we feel that the isolation of this dimetallic cluster can be relevant for material sciences, since it can be used as a molecular precursor to provide dimetallic nitrides, which

 © 2004 Wiley-VCH Verlag GmbH & Co. KGaA, Weinheim

are active catalysts for the HDN reactions and for ammonia synthesis.[22] Additionally, after the discovery of an interstitial μ_6-N atom in the Fe−Mo cofactor of nitrogenase,[23] carbonyl-nitrido clusters will also play an important role in the field of bioinorganic chemistry and N_2 activation, either as starting materials for synthetic studies,[24] or as reliable references for spectroscopy.[25]

Experimental Section

General: All solvents were purified and dried by conventional methods and stored under nitrogen. All reactions were carried out under oxygen-free nitrogen using the Schlenk-tube technique.[26] $K[Co_6N(CO)_{15}]$,[27] $[Et_4N]_2[Mo_2(CO)_{10}]$,[28] were prepared by literature methods. Infrared spectra in solution were recorded with a Nicolet Avatar FT-IR spectrophotometer, using calcium fluoride cells previously purged with N_2. Elemental analyses were carried out by the staff of the Laboratorio di Analisi of the Dipartimento di Chimica Inorganica, Metallorganica e Analitica. The materials and apparatus for the electrochemistry and joint-EPR measurements have been described elsewhere.[29] All of the potential values were referenced to the saturated calomel electrode (SCE). Under the present experimental conditions, the one-electron oxidation of ferrocene occurs at +0.38 V.

Synthesis of $[Co_5MoN(CO)_{14}]^{2-}$ from $[Co_6N(CO)_{15}]^-$ and $[Mo_2(CO)_{10}]^{2-}$: $K[Co_6N(CO)_{15}]$ (1.21 g; 1.47 mmol) and $[Et_4N]_2[Mo_2(CO)_{10}]$ (0.58 g; 0.79 mmol) were dissolved in MeCN (70 mL) and refluxed, while monitoring by IR spectroscopy. After about 7 h, the starting materials were completely consumed, the solution was cooled to room temperature and filtered to eliminate the insoluble material. The solvent was removed in vacuo and the residue was dissolved with methanol. Addition of $[Ph_4P]Br$ caused precipitation of microcrystalline $[Ph_4P]_2$**1**, which was filtered off, washed with 2-propanol and dried. It was then dissolved in the minimum amount of THF, and the solution layered with 2-propanol. Crystals of the salt $[Ph_4P]_2$**1** were obtained in 20% yield. IR (THF; cm^{-1}): ν(CO) = 2019 w, 1960 vs, 1832 m (see Figure S5 of the Supporting Information). $C_{62}H_{40}Co_5MoNO_{14}P_2$ (1475.5): calcd. C 50.47, H 2.73, N 0.95; found C 50.24, H 2.15, N 0.85.

Synthesis of $[Co_5MoN(CO)_{14}\{AuPPh_3\}]^-$: $[Ph_4P]_2[Co_5MoN(CO)_{14}]$ (0.10 g; 0.064 mmol) and $Au(PPh_3)Cl$ (0.03 g; 0.062 mmol) were dissolved in THF (10 mL) and stirred at room temperature. After 15 min, the reaction was completed, the solvent was then removed in vacuo, and the solid was repeatedly washed with 2-propanol. It was then dissolved in a minimum amount of THF, and the solution was layered with 2-propanol. Yield 44 mg of $[Ph_4P]$**2** (43%). IR (THF; cm^{-1}): ν(CO) = 2038 m, 1986 vs, 1861 m, 1838 w in THF (see Figure S5 of the Supporting Information). $C_{56}H_{35}AuCo_5MoNO_{14}P_2$ (1595.4): calcd. C 42.16, H 2.21, N 0.88; found C 42.08, H 1.86, N 0.85. ^{31}P NMR (CD_2Cl_2): δ = 23.9 ppm ($[Ph_4P]^+$), 60.26 ppm ($AuPPh_3$).

X-ray Data Collections and Structure Determinations: Crystal data are summarized in Table 3; for further experimental details see Supporting Information and ref.[14] The diffraction experiments were carried out with a Bruker SMART CCD area-detector diffractometer at 223 K. The collected frames were processed with the software SAINT,[30] and an empirical absorption correction was applied (SADABS)[31] to the collected reflections. The calculations were performed using the Personal Structure Determination Package[32] and the physical constants tabulated therein.[33] The structures were solved by direct methods (SHELXS)[34] and refined by full-matrix least squares using all reflections and minimizing the function $\Sigma w(F_o^2 - kF_c^2)^2$ (refinement on F^2). Anisotropic thermal factors were refined for all the non-hydrogen atoms. The hydrogen atoms were placed in their ideal positions (C−H = 0.97 Å), with the thermal parameter B = 1.10 times that of the carbon atom to which they are attached, and not refined. For noncentrosymmetric $[Ph_4P]_2$**1** full refinement of the correct structure model led to R_2 = 0.064 and R_{2w} = 0.090, full refinement of the inverted structure led to R_2 = 0.065 and R_{2w} = 0.092. In the final Fourier maps the maximum residuals were 1.87(15) e·Å^{-3} at 0.78 Å from Co(3) and 0.92(18) e·Å^{-3} at 0.89 Å from Au for $[Ph_4P]_2$**1** and $[Ph_4P]$**2**, respectively.

Supporting Information: See footnote on the first page of this article.

Acknowledgments

This work was financially supported by MIUR (cofin 2003 and FAR) and by Facoltà di Farmacia, Università di Milano.

Table 3. Crystallographic data and collection parameters for compounds $[Ph_4P]_2$**1** and $[Ph_4P]$**2**

	$[Ph_4P]_2$**1**	$[Ph_4P]$**2**
Empirical formula	$C_{62}H_{40}Co_5MoNO_{14}P_2$	$C_{56}H_{35}AuCo_5MoNO_{14}P_2$
Formula mass	1475.56	1595.42
Crystal system	monoclinic	monoclinic
Space group	*Pc*	$P2_1/c$
a [Å]	12.574(1)	11.828(1)
b [Å]	13.242(1)	13.936(2)
c [Å]	18.936(2)	35.084(4)
β [°]	107.09(1)	94.89(1)
V [Å^3]	3013.7(5)	5762(1)
Z	2	4
T [K]	223	223
μ(Mo-K_α) [cm^{-1}]	16.6	42.6
Reciprocal space explored	full sphere	full sphere
No. of reflections (total; independent)	50289, 18147	73246, 14505
R_{int}	0.033	0.038
Final R_2 and R_{2w} indices (F^2, all reflections)	0.064, 0.090	0.046, 0.056
Conventional R_1 index $I > 2\sigma(I)$	0.038	0.027

 © 2004 Wiley-VCH Verlag GmbH & Co. KGaA, Weinheim

[1] R. Della Pergola, M. Branchini, A. Fumagalli, L. Garlaschelli, M. Manassero, M. Sansoni, *Eur. J. Inorg. Chem.* **2000**, 1759−1765.
[2] T. Kabe, A. Ishihara, W. Qian, *Hydrodesulfurization and hydrodenitrogenation*, Wiley-VCH, Weinheim, **2000**.
[3] [3a] R. J. Angelici, *Acc. Chem. Res.* **1988**, *21*, 387−394. [3b] C. Bianchini, A. Meli, *Acc. Chem. Res.* **1998**, *31*, 109−116. [3c] R. A. Sánchez-Delgado, *Organometallic Modeling of the Hydrodesulfurization and Hydrodenitrogenation Reactions*, Kluwer, Dordrecht, **2002**.
[4] S.-I. Murahashi, Y. Imada, Y. Hirai, *Tetrahedron Lett.* **1987**, *28*, 77−80.
[5] [5a] A. Eisenstadt, C. M. Giandomenico, M. F. Frederick, R. M. Laine, *Organometallics* **1985**, *4*, 2033−2039. [5b] M. Brorson, J. D. King, K. Kiriakidou, F. Prestopino, E. Nordlander, in *Metal Cluster in Chemistry* (Eds.: P. Braunstein, L. A. Oro, P. R. Raithby), Wiley-VCH, Weinheim, **1999**, vol. 2, p. 741−777. [5c] J. A. Cabeza, J. M. Fernández-Colinas, S. García-Granda, A. Llamares, F. López-Ortíz, V. Riera, J. F. Van der Maelen, *Organometallics* **1994**, *13*, 426−428.
[6] M. D. Curtis, S. H. Drucker, *J. Am. Chem. Soc.* **1997**, *119*, 1027−1036.
[7] M. D. Curtis, J. E. Penner-Hahn, J. Schwank, O. Baralt, D. J. McCabe, L. Thompson, G. Waldo, *Polyhedron* **1988**, *7*, 2411−2420.
[8] Y. Okamoto, T. Kubota, *Cat. Surv. Jpn.* **2001**, *5*, 3−16.
[9] C. P. Gibson, L. W. Dahl, *Organometallics* **1988**, *7*, 543−552.
[10] The main IR band of **1** and that of $Mo(CO)_6$ overlap to a large extent.
[11] K. Lee, J. R. Shapley, *Organometallics* **1998**, *17*, 4368−4373.
[12] [12a] R. Della Pergola, L. Garlaschelli, M. Manassero, N. Masciocchi, *J. Organomet. Chem.* **1995**, *488*, 199−204. [12b] R. Della Pergola, A. Ceriotti, A. Cinquantini, F. Fabrizi de Biani, L. Garlaschelli, M. Manassero, R. Piacentini, M. Sansoni, P. Zanello, *Organometallics* **1998**, *17*, 802−806.
[13] S. M. Waterman, N. T. Lucas, M. G. Humphrey, *Adv. Organomet. Chem.* **2001**, *46*, 47−143.
[14] CCDC-230660 (for $[Ph_4P]_2$**1**) and -230661 (for $[Ph_4P]$**2**) contain the supplementary crystallographic data for this paper. These data can be obtained free of charge at www.ccdc.cam.ac.uk/conts/retrieving.html [or from the Cambridge Crystallographic Data Centre, 12 Union Road, Cambridge CB2 1EZ, UK; Fax: (internat.) + 44-1223-336-033; E-mail: deposit@ccdc.cam.ac.uk].
[15] G. Ciani, S. Martinengo, *J. Organomet. Chem.* **1986**, *306*, C49−C52.
[16] N. N. Greenwood, A. Earnshaw, *Chemistry of the Elements*, Pergamon Press, Oxford, **1989**, p 480.
[17] V. G. Albano, D. Braga, F. Grepioni, R. Della Pergola, L. Garlaschelli, a. Fumagalli, *J. Chem. Soc., Dalton Trans.* **1989**, 879−883.
[18] P. Zanello, *Inorganic Electrochemistry. Theory, Practice and Application*, Royal Society of Chemistry, **2003**.
[19] F. E. Mabbs, D. Collison, *Electron Paramagnetic Resonance of d Transition Metal Compounds*, Vol. 6 of the series *Studies in Inorganic Chemistry*, Elsevier, New York, **1992**.
[20] P. Lozos, B. M. Hofmann, C. G. Franz, *Quantum Chemistry Program Exchange*, Indiana University, **1974**, *295*, 20.
[21] D. Astruc, *Angew. Chem. Int. Ed. Engl.* **1988**, *27*, 643.
[22] [22a] S. Ramanathan, C. C. Yu, S. T. Oyama, *J. Catal.* **1998**, *173*, 10−16. [22b] P. Clark, B. Dhandapani, S. T. Oyama, *Appl. Catal. A: General* **1999**, *184*, L175−L180. [22c] V. Schwartz, S. T. Oyama, *J. Mol. Catal., A: Chem.* **2000**, *163*, 269−282.
[23] O. Einsle, F. A. Tezcan, S. L. A. Andrade, B. Schmid, M. Yoshida, J. B. Howard, D. C. Rees, *Science* **2002**, *297*, 1696−1700.
[24] S. C. Lee, R. H. Holm, *Chem. Rev.* **2004**, *104*, 1135−1157.
[25] B. M. Leu, M. Z. Zgierski, G. R. A. Wyllie, W. R. Scheidt, W. Sturhahn, E. E. Alp, S. M. Durbin, J. Sage, *J. Am. Chem. Soc.* **2004**, *126*, 4211−4227.
[26] D. F. Shriver, M. A. Dredzon, *The Manipulation of air-sensitive compounds*, 2nd ed., Wiley, New York, **1986**.
[27] S. Martinengo, G. Ciani, A. Sironi, B. T. Heaton, J. Mason, *J. Am. Chem. Soc.* **1979**, *101*, 7095−7097.
[28] J. K. Ruff, W. J. Schlientz, *Inorg. Synth.* **1974**, *15*, 88−90.
[29] G. Ciani, A. Sironi, S. Martinengo, L. Garlaschelli, R. Della Pergola, P. Zanello, F. Laschi, N. Masciocchi, *Inorg. Chem.* **2001**, *40*, 3905−3911.
[30] *SAINT Reference manual*, Siemens Energy and Automation, Madison, WI, **1994−1996**.
[31] G. M. Sheldrick, *SADABS, Empirical Absorption Correction Program*, University of Göttingen, **1997**.
[32] B. A. Frenz, *Comput. Phys.* **1988**, *2*, 42.
[33] *Crystallographic Computing 5*, Oxford University Press, Oxford, U. K., **1991**, chapter 11, p. 126.
[34] G. M. Sheldrick, *SHELXS 86, Program for the solution of crystal structures*, University of Göttingen, Germany, **1985**.

Received February 10, 2004
Early View Article
Published Online July 22, 2004

 © 2004 Wiley-VCH Verlag GmbH & Co. KGaA, Weinheim

endo and *exo* Coordination of Indanol: Synthesis, Isolation and Structural Characterisation of $[H_3Ru_3(endo\text{-Indanol})(C_6Me_6)_2(O)]^+$ and $[H_3Ru_3(exo\text{-Indanol})(C_6Me_6)_2(O)]^+$ as Their Tetrafluoroborate Salts

Ludovic Vieille-Petit,[a] Lydia Karmazin-Brelot,[a] Gaël Labat,[a] and Georg Süss-Fink*[a]

Keywords: Arene ligands / Biphasic catalysis / Cluster compound / Hydrogenation / Ruthenium

The reaction of 2,3,4,7-tetrahydro-1*H*-inden-2-ol with ruthenium chloride hydrate in refluxing ethanol yields the chloro-bridged dinuclear complex $[RuCl_2(indanol)]_2$ (**1**). The mononuclear complex $[Ru(indanol)(H_2O)_3]^{2+}$ (**2**), formed in situ from **1** in aqueous solution, reacts with the dinuclear complex $[H_3Ru_2(C_6Me_6)_2]^+$ to give a trinuclear arene-ruthenium cluster as a mixture of two isomers, the cations $[H_3Ru_3(endo\text{-indanol})(C_6Me_6)_2(O)]^+$ (**3a**) and $[H_3Ru_3(exo\text{-indanol})(C_6Me_6)_2(O)]^+$ (**3b**), in a 1:1 ratio. The hydroxy function of the indanol ligand is oriented towards the μ_3-oxo cap of **3a**, whereas the OH group is bent away from the metal skeleton of **3b**. These two isomers, which can easily be separated by silica-gel chromatography, were isolated and characterised as their tetrafluoroborate salts. The single-crystal X-ray structure analysis of $[\mathbf{3a}][BF_4]$ shows a strong intramolecular hydrogen bond between the μ_3-oxo ligand and the hydroxyl function, which even persists in acetone solution, as demonstrated by NMR spectroscopy. On the other hand, the hydroxy function of **3b** was found to be free in the solid state as well as in solution, as shown by an X-ray crystal structure analysis and by NMR spectroscopy. The catalytic activities of the water-soluble trinuclear cations **3a** and **3b** for the hydrogenation of benzene to give cyclohexane under biphasic conditions are considerably different, the *exo* isomer **3b** being more active than the *endo* isomer **3a**.

(© Wiley-VCH Verlag GmbH & Co. KGaA, 69451 Weinheim, Germany, 2004)

Introduction

We reported recently that the cluster cation $[H_3Ru_3(C_6H_6)(C_6Me_6)_2(O)]^+$, used as its water-soluble tetrafluoroborate salt, efficiently catalyses the hydrogenation of benzene to cyclohexane under biphasic conditions.[1] From experimental and molecular modelling studies we concluded that the substrate molecule is incorporated into the hydrophobic pocket spanned by the three arene ligands, suggesting that the catalytic reaction occurs within this host-guest complex without prior coordination of the substrate (''supramolecular cluster catalysis'').[2] Furthermore, we were able to isolate the catalyst-substrate host-guest complexes postulated for two hydroxyalkyl derivatives as their tetrafluoroborate or hexafluorophosphate salts $[C_6H_6{\subset}H_3Ru_3\{C_6H_5(CH_2)_2OH\}(C_6Me_6)_2(O)][PF_6]$ and $[C_6H_6{\subset}H_3Ru_3\{C_6H_5(CH_2)_3OH\}(C_6Me_6)_2(O)][BF_4]$.[3] However, on the basis of the data obtained so far,[4] we cannot exclude catalysis by ''soluble'' metallic species (nanoclusters or colloids), and we are presently engaged in a collaborative effort to refute or support this alternative hypothesis.[5a] In this context, we also tried to design new trinuclear arene-ruthenium cluster cations with functional substituents at one η^6-moiety which could give rise to more stable catalysts which may be particularly active or selective.

Herein we report the synthesis and characterisation of a new chloro-bridged arene-ruthenium dimer, $[RuCl_2(indanol)]_2$ (**1**), which is used to synthesise a trinuclear cluster cation containing indanol as one of the three arene ligands: $[H_3Ru_3(indanol)(C_6Me_6)_2(O)]^+$ (**3**). Surprisingly, **3** was obtained as a mixture of two isomers, **3a** and **3b**, which were easily separated by silica-gel chromatography. Single-crystal X-ray structure analyses of $[\mathbf{3a}][BF_4]$ and $[\mathbf{3b}][BF_4]$ have been performed to establish unambiguously the molecular structures of these two isomers. The different catalytic activities of **3a** and **3b** in the hydrogenation of benzene to cyclohexane under biphasic conditions are also discussed. This is the first time that indanol has been used as a ligand in ruthenium chemistry and that both the *endo* and the *exo* isomers of the corresponding complexes have been characterised by single-crystal X-ray crystallography.

Results and Discussion

The reaction of 2,3,4,7-tetrahydro-1*H*-inden-2-ol, accessible from the Birch reduction of commercially available 2-indanol,[6] with ruthenium(III) chloride hydrate, in refluxing ethanol, gives the chloro-bridged dimer $[RuCl_2(indanol)]_2$ (**1**), which is obtained quantitatively as an orange powder

[a] Institut de Chimie, Université de Neuchâtel, Case postale 2, 2007 Neuchâtel, Switzerland
E-mail address: georg.suess-fink@unine.ch

(Scheme 1). Compound **1** is expected to exist as a mixture of three possible isomers, since the OH groups of the two indanol ligands may be folded outwards (*exo*) or inwards (*endo*). Unfortunately, as **1** is insoluble in all solvents except water and dimethyl sulfoxide, in which **1** decomposes to give mononuclear species, we cannot tell whether or not the orange powder of **1** contains only one or all three possible isomers *exo*,*exo*-**1**, *exo*,*endo*-**1** and *endo*,*endo*-**1**. The molecular formula $[RuCl_2(indanol)]_2$ for **1** has been confirmed by electrospray-mass spectroscopy and micro-analysis.

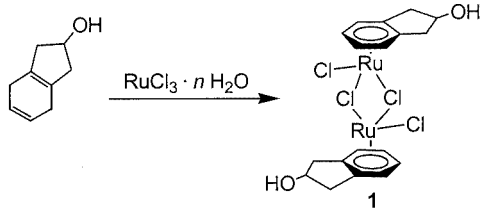

Scheme 1

In aqueous solution, the dimer **1** seems to form the mononuclear complex $[Ru(indanol)(H_2O)_3]^{2+}$ (**2**), an analogue of the known cation $[Ru(C_6H_6)(H_2O)_3]^{2+}$.[7] In order to characterise this intermediate by NMR spectroscopy, we prepared the deuterated analogue $[Ru(indanol)(D_2O)_3]^{2+}$ (**2′**) by cleavage of **1** with two equivalents of Ag_2SO_4 in deuterated water. The ^1H NMR spectrum of the solution obtained after elimination of the AgCl precipitate shows the expected two sets of well-defined signals which can be assigned to the two isomers $[Ru(endo\text{-indanol})(D_2O)_3]^{2+}$ (**2a′**) and $[Ru(exo\text{-indanol})(D_2O)_3]^{2+}$ (**2b′**) in a 10:7 ratio (Scheme 2).

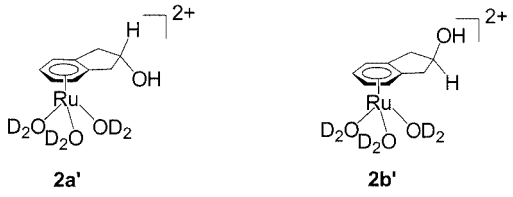

Scheme 2

In aqueous solution, the mononuclear intermediate **2** (a mixture of isomers **2a** and **2b**) reacts with the dinuclear complex $[H_3Ru_2(C_6Me_6)_2]^+$ [8] to give a trinuclear arene-ruthenium cluster as a mixture of two isomers, the cations $[H_3Ru_3(endo\text{-indanol})(C_6Me_6)_2(O)]^+$ (**3a**) and $[H_3Ru_3(exo\text{-indanol})(C_6Me_6)_2(O)]^+$ (**3b**), in a 1:1 ratio. The oxo cap in the clusters **3a** and **3b** seems to arise from one of the H_2O ligands in the precursors **2a** and **2b**. The hydroxy function of the indanol ligand is oriented towards the μ_3-oxo cap of **3a**, whereas it is bent away from the metal skeleton of **3b** (Scheme 3). Compounds **3a** and **3b** are easily separated as their tetrafluroborate salts by preparative thin-layer silica-gel chromatography.

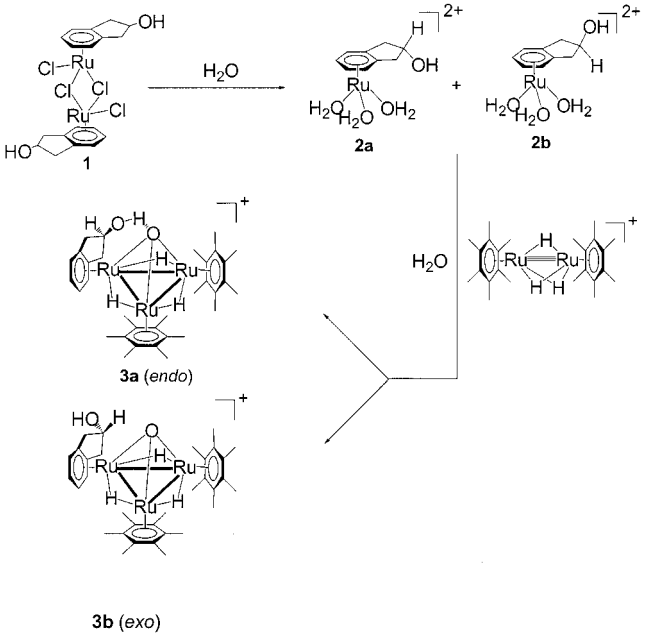

Scheme 3

Like the known analogues $[H_3Ru_3(\eta^6\text{-arene})(\eta^6\text{-arene}')_2(O)]^+$,[1,3,9] compounds **3a** and **3b** also give rise to two hydride signals each in the ^1H NMR spectra, a triplet centred at $\delta = -19.92$ ppm for **3a** and $\delta = -20.07$ ppm for **3b** and a doublet centred at $\delta = -19.30$ ppm for **3a** and $\delta = -19.41$ ppm for **3b**, integrating for one and two protons, respectively. The isolated compounds [**3a**][BF_4] and [**3b**][BF_4] were analysed by single-crystal X-ray crystallography. The molecular structures of [**3a**]$^+$ and [**3b**]$^+$ are shown in Figure 1.

While [**3b**][BF_4] crystallises in a monoclinic space group with one cation and one anion in the asymmetric unit, in the case of **3a** (triclinic space group) the asymmetric unit comprises two independent cations and two anions, two dichloromethane molecules, and half a molecule of dichloromethane disordered with half a water molecule. Only one molecule of **3a** is shown in Figure 1 as the other one is identical.

In both **3a** and **3b** the metal core consists of three ruthenium atoms, the three Ru−Ru distances being in accordance with a metal−metal single bond. The three ruthenium atoms are capped by a μ_3-oxo ligand which is almost symmetrically coordinated. Selected bond lengths and angles are listed in Table 1 and 2 for **3a** and **3b**, respectively. The indanol ligand adopts an envelope conformation in which the five-membered ring is folded towards the ruthenium atom. The *endo* conformation of the indanol ligand in **3a** allows a strong intramolecular hydrogen bond between the hydroxyl substituent and the μ_3-oxo cap, the distances between the oxygen atoms and the hydroxide protons being 1.90 Å for molecule 1 and 1.84 Å for molecule 2. The triruthenium framework of the *exo* conformation in **3b** shows intermolecular hydrogen bonds between the indanol ligand and the tetrafluoroborate ion, the distances between the hy-

 © 2004 Wiley-VCH Verlag GmbH & Co. KGaA, Weinheim

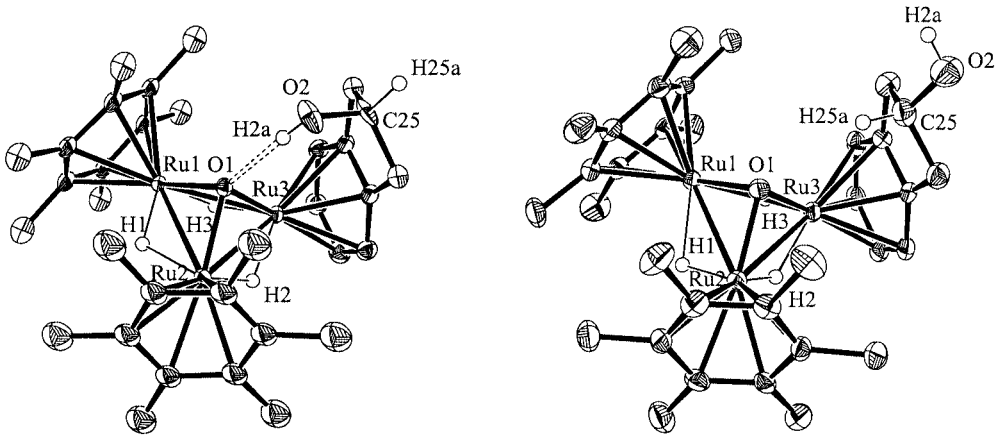

Figure 1. ORTEP views of $[\mathbf{3a}]^+$ (left) and $[\mathbf{3b}]^+$ (right) with displacement ellipsoids at the 50% probability level; hydrogen atoms, except for the hydroxide proton, the three hydrido ligands and the α-hydrogen atom of the indanol moiety, are omitted for clarity

Table 1. Selected bond lengths (Å) and angles (°) in $[\mathbf{3a}][BF_4]\cdot 1.25CH_2Cl_2\cdot 0.25H_2O$

Interatomic distances		Bond angles	
Ru(1)−Ru(2)	2.7892(7)	Ru(1)−Ru(2)−Ru(3)	59.053(17)
Ru(2)−Ru(3)	2.7565(7)	Ru(1)−Ru(3)−Ru(2)	61.069(18)
Ru(1)−Ru(3)	2.7332(6)	Ru(2)−Ru(1)−Ru(3)	59.878(17)
Ru(4)−Ru(5)	2.7978(6)	Ru(4)−Ru(5)−Ru(6)	59.338(17)
Ru(5)−Ru(6)	2.7627(7)	Ru(4)−Ru(6)−Ru(5)	60.965(18)
Ru(4)−Ru(6)	2.7525(7)	Ru(5)−Ru(4)−Ru(6)	59.697(18)
Ru(1)−O(1)	2.014(4)	Ru(1)−O(1)−Ru(2)	87.70(14)
Ru(2)−O(1)	2.012(4)	Ru(1)−O(1)−Ru(3)	85.43(14)
Ru(3)−O(1)	2.015(4)	Ru(2)−O(1)−Ru(3)	86.41(14)
Ru(4)−O(3)	2.009(4)	Ru(4)−O(3)−Ru(5)	88.45(15)
Ru(5)−O(3)	2.003(4)	Ru(4)−O(3)−Ru(6)	86.35(13)
Ru(6)−O(3)	2.014(4)	Ru(5)−O(3)−Ru(6)	86.90(15)
Ru(1)−H(1)	1.4313	H(1)−Ru(1)−H(3)	92.8
Ru(2)−H(1)	1.9805	H(1)−Ru(2)−H(2)	86.5
Ru(2)−H(2)	1.8025	H(2)−Ru(3)−H(3)	85.9
Ru(3)−H(2)	1.6113	H(4)−Ru(4)−H(6)	81.4
Ru(1)−H(3)	1.6563	H(4)−Ru(5)−H(5)	79.2
Ru(3)−H(3)	1.6218	H(5)−Ru(6)−H(6)	83.9
Ru(4)−H(4)	1.8259		
Ru(5)−H(4)	1.5825		
Ru(5)−H(5)	1.6071		
Ru(6)−H(5)	1.8146		
Ru(4)−H(6)	1.4543		
Ru(6)−H(6)	1.9076		

Table 2. Selected bond lengths (Å) and angles (°) in $[\mathbf{3b}][BF_4]$

Interatomic distances		Bond angles	
Ru(1)−Ru(2)	2.7717(9)	Ru(1)−Ru(2)−Ru(3)	59.59(2)
Ru(2)−Ru(3)	2.7437(9)	Ru(1)−Ru(3)−Ru(2)	60.72(2)
Ru(1)−Ru(3)	2.7405(8)	Ru(2)−Ru(1)−Ru(3)	59.70(2)
Ru(1)−O(1)	1.994(5)	Ru(1)−O(1)−Ru(2)	88.4(2)
Ru(2)−O(1)	1.980(5)	Ru(1)−O(1)−Ru(3)	86.7(2)
Ru(3)−O(1)	1.997(5)	Ru(2)−O(1)−Ru(3)	87.2(2)
Ru(1)−H(1)	1.8944	H(1)−Ru(1)−H(3)	89.9
Ru(2)−H(1)	1.5997	H(1)−Ru(2)−H(2)	90.6
Ru(2)−H(2)	1.2305	H(2)−Ru(3)−H(3)	95.4
Ru(3)−H(2)	1.7800		
Ru(1)−H(3)	2.0056		
Ru(3)−H(3)	1.3846		

droxide proton and two of the fluorine atoms being 2.44 Å and 2.25 Å.

The strong intramolecular hydrogen bond found in the solid state for **3a** seems to persist also in acetone solution. The ^1H NMR spectrum of **3a** in $[D_6]$acetone shows a well-defined doublet centred at $\delta = 6.77$ ppm, attributed to the proton of the OH group coupled to the α-proton of the indanol ligand, the coupling constant being 13 Hz. On the other hand, the ^1H NMR spectrum of **3b** in $[D_6]$acetone shows a badly defined doublet centred at $\delta = 4.44$ ppm for the OH group, the coupling constant being 4.48 Hz (see Figure 2).

The water-soluble cations **3a** and **3b** are indeed found to be catalytically active for the hydrogenation of benzene to cyclohexane under biphasic conditions; they show a catalytic activity of 67 and 125 h^{-1} (average TOF), respectively, for a catalyst/substrate ratio of 1:1000, at 110 °C under 60 bar of H_2 during three hours. The catalytic activity of **3a** and **3b** is not as high as that of the benzene analogue $[H_3Ru_3(C_6H_6)(C_6Me_6)_2(O)]^+$, which under the same conditions has an average catalytic turnover frequency of 296 h^{-1}.[4]

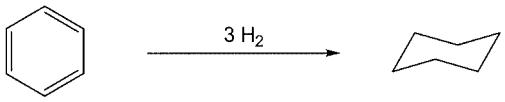

After a catalytic run the cationic clusters **3a** or **3b** can be recovered unchanged from the aqueous phase in 90 to 95% yield. As a small quantity of black solid (presumably metallic ruthenium) is formed during the catalytic run, it is certainly possible, if not probable,[5a,5b] that the catalytic reaction involves highly dispersed metallic species ("nanoclusters") formed by partial degradation of the catalyst precursor under hydrogen pressure. The difference in the catalytic activity of **3a** and **3b** could be due to the different stability of these clusters with respect to the formation of nanopart-

 © 2004 Wiley-VCH Verlag GmbH & Co. KGaA, Weinheim

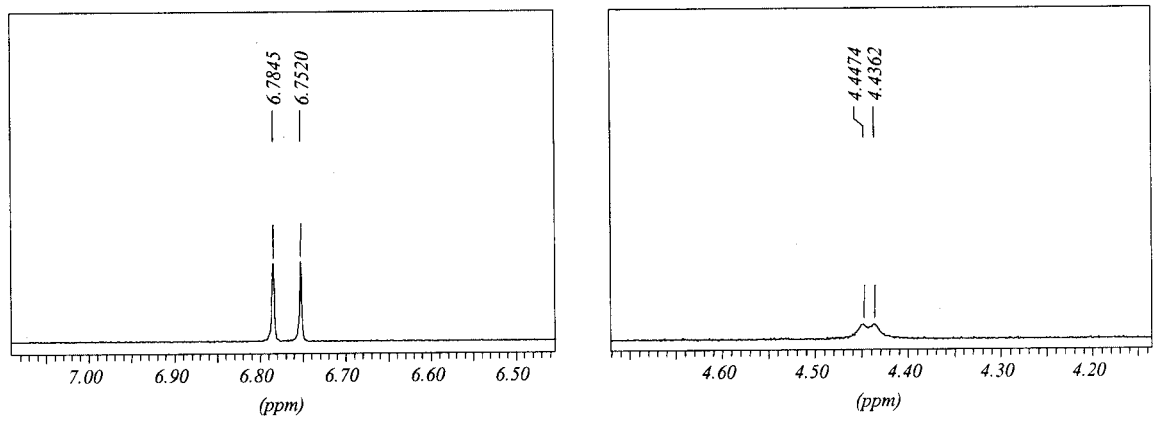

Figure 2. ^{1}H NMR spectra (O*H* signals) of **3a** (left) and **3b** (right) in [D$_6$]acetone (400 MHz)

icles under the catalytic conditions. Further work is underway in order to answer this question unequivocally.[5a]

Conclusion

Indanol, C_9H_9OH, has been used as a ligand in ruthenium chemistry for the first time. The new dimeric complex $[RuCl_2(indanol)]_2$ (**1**) serves as a dinuclear building block for the assembly of the isomeric trinuclear cluster cations $[H_3Ru_3(endo\text{-indanol})(C_6Me_6)_2(O)]^+$ (**3a**) and $[H_3Ru_3(exo\text{-indanol})(C_6Me_6)_2(O)]^+$ (**3b**), isolated as their tetrafluoroborate salts. For the first time, both *endo* and *exo* isomers of a ruthenium indanol complex have been characterised by X-ray crystallography.

Experimental Section

General Remarks: All manipulations were carried out under an inert argon atmosphere using standard Schlenk techniques. Doubly distilled water was degassed and saturated with argon prior to use. Organic solvents used for chromatography were distilled under argon prior to use. Silica-gel G used for preparative thin-layer (20 × 20 cm) chromatography was purchased from Macherey−Nagel GmbH. Deuterated NMR solvents were purchased from Cambridge Isotope Laboratories, Inc. NMR spectra were recorded using a Bruker 400 MHz spectrometer and treated using the 1D WIN NMR spectroscopy software. The mass spectra were recorded at the University of Fribourg by Prof. Titus Jenny. Microanalyses were carried out by the Mikroelementaranalytisches Laboratorium, ETH Zürich (Switzerland). 2,3,4,7-Tetrahydro-1*H*-inden-2-ol was prepared by sodium reduction of 2-indanol in liquid ammonia.[6] The starting dinuclear dichloro complex $[RuCl_2(C_6Me_6)]_2$ was synthesised according to published methods.[10]

$[RuCl_2(indanol)]_2$ (1): 2,3,4,7-Tetrahydro-1*H*-inden-2-ol (6 g, 44.4 mmol) was added to a solution of ruthenium trichloride hydrate (1.70 g, 6.5 mmol) in absolute degassed ethanol (100 mL) and the mixture was refluxed overnight. After cooling to room temperature, the resulting orange precipitate was filtered, washed with diethyl ether, and dried under vacuum to give pure $[RuCl_2(indanol)]_2$ as an orange powder. Yield: 1.90 g (95%). $C_{18}H_{20}Cl_4O_2Ru_2$ (612.30): calcd. C 35.31, H 3.29; found C 35.22, H 3.44. MS (ESI positive mode, methanol): m/z = 576.8 $[M - Cl]^+$.

$[Ru(endo\text{-indanol})(D_2O)_3]^{2+}$ (2a′) and $[Ru(exo\text{-indanol})(D_2O)_3]^{2+}$ (2b′): In a 250 mL brown-glass Schlenk tube, compound **1** (150 mg, 0.245 mmol) was mixed with a solution of Ag_2SO_4 (153 mg, 0.490 mmol) in 5 mL of D_2O. The suspension was stirred at room temperature until the orange solid had completely dissolved to give a yellow solution of **2a′** and **2b′**. The white precipitate of AgCl formed was removed from the aqueous solution by filtration through filter pulp and the resulting clear solution was directly analysed by NMR spectroscopy. ^{1}H NMR spectroscopic data for the mixture of **2a′** and **2b′** (400 MHz, D_2O, 25 °C): δ = 2.53 [dd, ^2J = 16.38, ^3J = 7.30 Hz, 2 H, (C*H*)$_2$CHOH], 2.81 [d, ^2J = 17.79 Hz, 2 H, (C*H*)$_2$CHOH], 2.98 [dd, ^2J = 17.79, ^3J = 5.50 Hz, 2 H, (C*H*)$_2$CHOH], 3.17 [dd, ^2J = 16.38, ^3J = 7.17 Hz, 2 H, (C*H*)$_2$CHOH], 4.83 [m, 1 H, (CH)$_2$C*H*OH], 4.89 [m, 1 H, (CH)$_2$C*H*OH], 5.83 to 6.00 (m, 8 H, H_{arom}) ppm.

$[H_3Ru_3(endo\text{-indanol})(C_6Me_6)_2(O)][BF_4]$ (cation 3a) and $[H_3Ru_3(exo\text{-indanol})(C_6Me_6)_2(O)\ [BF_4]$ (cation 3b): In a 250 mL brown-glass Schlenk tube, $[RuCl_2(C_6Me_6)]_2$ (300 mg, 0.449 mmol) was mixed with a solution of Ag_2SO_4 (282 mg, 0.904 mmol) in 30 mL of water. The suspension was stirred at room temperature until the orange solid had completely dissolved to give a yellow solution of $[Ru(C_6Me_6)(H_2O)_3]^{2+}$ (ca. one hour). The white precipitate of AgCl formed was removed from the aqueous solution by filtration through filter pulp. The resulting clear yellow filtrate was cooled in an ice bath for 30 minutes. In a separate 50 mL Schlenk tube, $NaBH_4$ (75 mg, 1.974 mmol) was dissolved in 15 mL of water at room temperature. After stirring for five minutes, the $NaBH_4$ solution was transferred very slowly through a cannula into the cooled $[Ru(C_6Me_6)(H_2O)_3][SO_4]$ solution. The colour of the solution changed to black, due to the formation of $[H_3Ru_2(C_6Me_6)_2]^+$. The resulting solution was immediately filtered trough filter pulp under argon to remove insoluble black particles. Solid $[RuCl_2(indanol)]_2$ (260 mg, 0.425 mmol) was added to the dark clear solution containing $[H_3Ru_2(C_6Me_6)_2]^+$. The mixture was stirred at room temperature until the orange solid had completely dissolved. The solution was then transferred under argon into a 300 mL closed Schlenk pressure-tube and stirred under argon pressure (two atmospheres) at 60 °C for 4 d. During this time the colour of the solution changed from black to red. After cooling to room temperature, the red solution containing **3a** and **3b** was filtered through filter pulp. A large excess (200 mg) of solid $NaBF_4$ was then added

 © 2004 Wiley-VCH Verlag GmbH & Co. KGaA, Weinheim

to the filtrate in order to precipitate the mixture of [**3a**][BF_4] and [**3b**][BF_4]. After stirring for one hour at room temperature, the red precipitate was centrifuged at 1500 rpm for 10 min and the aqueous solution was then removed from the centrifuge tube with a glass pipette. The red solid was dissolved in CH_2Cl_2 and again filtered through filter pulp, in order to eliminate unreacted $NaBF_4$. The solution was then concentrated to 15 mL in vacuo. The resulting concentrate was subjected to preparative thin-layer chromatography on silica-gel using CH_2Cl_2/acetone (2:1) as eluent. The pure compounds were extracted with acetone from the first ([**3a**][BF_4]) and the second ([**3b**][BF_4]) red bands. Evaporation of acetone under vacuum gave 62 mg of [**3a**][BF_4] and 65 mg of [**3b**][BF_4] as red powders (total yield: 32%). Crystals suitable for X-ray diffraction analyses were grown by slow diffusion of hexane into a CH_2Cl_2 solution of [**3a**][BF_4] or an acetone solution of [**3b**][BF_4]. $C_{33}H_{49}BF_4O_2Ru_3$ ([**3a**][BF_4]) (867.76): calcd. C 45.68, H 5.69; found C 45.42, H 5.81. $C_{33}H_{49}B_1F_4O_2Ru_3$ ([**3b**][BF_4]) (867.76): calcd. C 45.68, H 5.69; found C 45.44, H 5.87.

Spectroscopic Data for 3a: ^{1}H NMR (400 MHz, [D_6]acetone, 25 °C): $\delta = -19.92$ (t, $^2J = 3.83$ Hz, 1 H, hydride), −19.30 (d, $^2J = 3.83$ Hz, 2 H, hydride), 2.34 [s, 36 H, $C_6(CH_3)_6$], 2.43 [d, $^2J = 16.73$ Hz, 2 H, $(CH)_2$CHOH], 3.02 [dd, $^2J = 16.73$, $^3J = 5.54$ Hz, 2 H, $(CH)_2$CHOH], 4.52 [m, 1 H, $(CH)_2CH$OH], 5.69 [dd, $^3J = 3.83$, $^4J = 2.13$ Hz, 2 H, H_{arom}], 5.96 [dd, $^3J = 3.83$, $^4J = 2.13$ Hz, 2 H, H_{arom}], 6.77 [d, $^3J = 13.00$ Hz, 1 H, $(CH)_2$CHOH] ppm. $^{13}C\{^1H\}$ NMR (100 MHz, CD_2Cl_2, 25 °C): $\delta = 18.2$ [$C_6(CH_3)_6$], 40.8 [$(CH)_2$CHOH], 70.8 [$(CH)_2CH$OH], 78.0, 82.8, 95.3, 101.8 (C_{arom}) ppm. MS (ESI positive mode, acetone): $m/z = 782.1$ [M + H]$^+$.

Spectroscopic Data for 3b: ^{1}H NMR (400 MHz, [D_6]acetone, 25 °C): $\delta = -20.07$ (t, $^2J = 4.05$ Hz, 1 H, hydride), −19.41 (d, $^2J = 4.05$ Hz, 2 H, hydride), 2.32 [s, 36 H, $C_6(CH_3)_6$], 2.69 [dd, $^2J = 14.92$, $^3J = 7.88$ Hz, 2 H, $(CH)_2$CHOH)], 2.87 [dd, $^2J = 14.92$, $^3J = 6.82$ Hz, 2 H, $(CH)_2$CHOH], 4.44 [d, $^3J = 4.48$ Hz, 1 H, $(CH)_2CHOH$)], 4.84 [m, 1 H, $(CH)_2CH$OH], 5.53 [dd, $^3J = 3.83$, $^4J = 2.23$ Hz, 2 H, H_{arom}], 5.84 (dd, $^3J = 3.83$, $^4J = 2.23$ Hz, 2 H, H_{arom}] ppm. $^{13}C\{^1H\}$ NMR (100 MHz, CD_2Cl_2, 25 °C): $\delta = 18.1$ [$C_6(CH_3)_6$], 39.8 [$(CH)_2$CHOH], 72.1 [$(CH)_2CH$OH], 79.3, 81.3, 95.1, 101.0 (C_{arom}) ppm. MS (ESI positive mode, acetone): $m/z = 782.1$ [M + H]$^+$.

Catalytic Runs: In a typical experiment, a solution of [**3a**][BF_4] or [**3b**][BF_4] (10 mg) in 10 mL of water was placed in a 100 mL stainless-steel autoclave equipped with a glass-lined vessel, and the benzene substrate was added in a 1:1000 catalyst/substrate ratio. After purging four times with hydrogen, the autoclave was pressurised with hydrogen (60 bar), heated to 110 °C in an oil bath for 15 minutes, and the mixture stirred vigorously. After 3 h the autoclave was cooled in an ice-bath and the pressure released. The two-phase system was separated by decanting. The aqueous phase containing the catalyst was discarded and the organic phase containing cyclohexane and benzene was analysed by NMR spectroscopy and GC.

X-ray Crystallographic Study

[3a][BF_4]·1.25CH_2Cl_2·0.25H_2O: A red crystal of [**3a**][BF_4]·1.25CH_2Cl_2·0.25H_2O was mounted on a Stoe Imaging Plate Diffractometer System (Stoe & Cie, 1995) equipped with a one-circle φ goniometer and a graphite-monochromator. Data collection was

Table 3. Crystallographic data for the structures of {[**3a**][BF_4]}$_2$·2.5 CH_2Cl_2·0.5H_2O and [**3b**][BF_4]

	{[**3a**][BF_4]}$_2$·2.5 CH_2Cl_2·0.5H_2O	[**3b**][BF_4]
Empirical formula	$C_{34.25}H_{52}O_{2.25}Ru_3BF_4Cl_{2.50}$	$C_{33}H_{49}O_2Ru_3BF_4$
Molecular mass	978.40	867.74
Crystal colour and shape	red block	orange needle
Crystal size	0.300 × 0.200 × 0.100	0.400 × 0.183 × 0.050
Crystal system	triclinic	monoclinic
Space group	$P\bar{1}$	$P2_1/n$
a (Å)	15.4090(11)	8.6447(6)
b (Å)	16.5547(12)	17.7673(7)
c (Å)	18.0306(13)	21.0089(14)
α (°)	116.023 (8)	90.00
β (°)	111.549(8)	97.543(5)
γ (°)	90.509(9)	90.00
V (Å^3)	3763.9(5)	3198.9(3)
Z	4	4
D_{calc} (g·cm^{-3})	1.727	1.802
μ (Mo-K_α) (mm^{-1})	1.416	1.451
Temperature (K)	153(2)	153(2)
F(000)	1964	1744
Scan range (°)	$2.28 < \theta < 25.90$	$1.95 < \theta < 29.55$
Cell refinement parameters reflections	8000	29717
Reflections measured	28873	46056
Independent reflections	13696	8868
Reflections observed [$I > 2\sigma(I)$]	10385	6505
R_{int}	0.0463	0.1220
Final R_{int} [$I > 2\sigma(I)$]	$R_1 = 0.0442$, $wR_2 = 0.1249$[a]	$R_1 = 0.0726$, $wR_2 = 0.1635$[a]
R_{int} (all data)	$R_1 = 0.0619$, $wR_2 = 0.1392$[a]	$R_1 = 0.1013$, $wR_2 = 0.1717$[a]
Goodness-of-fit	1.009	1.181
Residual density: max./min. $\Delta\rho$ (e·Å^{-3})	1.898, −1.526	1.997, −0.983

[a] Structure was refined on F_o^2: $wR_2 = \{\Sigma[w(F_o^2 - F_c^2)^2]/\Sigma w(F_o^2)^2\}^{1/2}$, where $w^{-1} = [\Sigma(F_o^2) + (aP)^2 + bP]$ and $P = [\max(F_o^2, 0) + 2F_c^2]/3$.

 © 2004 Wiley-VCH Verlag GmbH & Co. KGaA, Weinheim

performed at −120 °C using Mo-K_α radiation (λ = 0.71073 Å). 193 Exposures (3 min per exposure) were obtained at an image plate distance of 70 mm with $0 < \varphi < 193°$ and with the crystal oscillating through 1° in θ. The resolution was D_{min} − D_{max} 12.45−0.81 Å.

The structure was solved by direct methods using the program SHELXS-97[11] and refined by full-matrix least-squares on F^2 with SHELXL-97.[12] The six hydrido ligands (H1, H2, H3, H4, H5 and H6) and the two hydrogen atoms (H5a and H5b) of the water molecule were derived from difference Fourier maps and refined with the Ru−H and O−H distances constrained to the theoretical value; the remaining hydrogen atoms were included in calculated positions and treated as riding atoms using the SHELXL-97 default parameters. All non-hydrogen atoms were refined anisotropically, except for one dichloromethane molecule which is shared with a water molecule. One BF_4 counteranion is disordered. An empirical absorption correction was applied using DIFABS (PLATON99,[13] $T_{min.}$ = 0.348, $T_{max.}$ = 0.768).

[3b][BF$_4$]: An orange crystal of [**3b**][BF_4] was mounted on a Stoe Mark II-Imaging Plate Diffractometer System (Stoe & Cie, 2002) equipped with a graphite monochromator. Data collection was performed at −120 °C using Mo-K_α radiation (λ = 0.71073 Å). 265 Exposures (3 min per exposure) were obtained at an image plate distance of 100 mm, 180 frames with $\varphi = 0°$ and $0 < \omega < 180°$, and 85 frames with $\varphi = 90°$ and $0 < \omega < 85°$, with the crystal oscillating through 1° in ω. The resolution was D_{min} − D_{max} 17.78−0.72 Å.

The structure was solved by direct methods using the program SHELXS-97[11] and refined by full-matrix least-squares on F^2 with SHELXL-97.[12] The three hydrido ligands H1, H2 and H3 were derived from difference Fourier maps and refined with the Ru−H distance constrained to the theoretical value; the remaining hydrogen atoms were included in calculated positions and treated as riding atoms using the SHELXL-97 default parameters. All non-hydrogen atoms were refined anisotropically. An empirical absorption correction was applied using DIFABS (PLATON99,[13] $T_{min.}$ = 0.139, $T_{max.}$ = 0.611). All of the tested crystals were twinned; the structure was solved and refined on data collected from one domain of such a crystal.

Crystallographic details are given in Table 3 and significant bond lengths and bond angles are listed in Table 1 (**3a**) and Table 2 (**3b**). The figures were drawn with ORTEP.[14]

CCDC-235554 (for [**3a**][BF_4]·1.25CH_2Cl_2·0.25H_2O) and -235555 (for [**3b**][BF_4]) contain the supplementary crystallographic data for this paper. These data can be obtained free of charge at www.ccdc.cam.ac.uk/conts/retrieving.html [or from the Cambridge Crystallographic Data Centre, 12 Union Road, Cambridge CB2 1EZ, UK; Fax: +44-1223-336-033; E-mail: deposit@ccdc.cam.ac.uk].

Acknowledgments

The authors are grateful to the Fonds National Suisse de la Recherche Scientifique for financial support. A generous loan of ruthenium chloride hydrate from the Johnson Matthey Technology Centre is gratefully acknowledged. We thank Dr. Antonia Neels and Prof. Helen Stoeckli-Evans for helpful discussions.

[1] M. Faure, M. Jahncke, A. Neels, H. Stoeckli-Evans, G. Süss-Fink, *Polyhedron* **1999**, *18*, 2679.
[2] G. Süss-Fink, M. Faure, T. R. Ward, *Angew. Chem.* **2002**, *114*, 105; *Angew. Chem. Int. Ed.* **2002**, *41*, 99.
[3] L. Vieille-Petit, B. Therrien, G. Süss-Fink, T. R. Ward, *J. Organomet. Chem.* **2003**, *684*, 117.
[4] G. Süss-Fink, B. Therrien, L. Vieille-Petit, M. Tschan, V. B. Romakh, T. R. Ward, M. Dadras, G. Laurenczy, *J. Organomet. Chem.* **2004**, *689*, 1362.
[5] [5a] In order to check the possibility of nanocluster catalysis, we started a collaboration with Professor Richard G. Finke (Colorado State University) for a detailed kinetic study of this reaction under biphasic conditions. The results will be published in due course. [5b]A review of the "Is It Homogeneous or Heterogeneous Catalysis?" question is available: J. A. Widegren, R. G. Finke, *J. Mol. Catal. A: Chemical* **2003**, *198*, 317.
[6] [6a] M. E. Kuehne, B. F. Lambert, *Org. Synth.* **1973**, *5*, 400. [6b] L. Vieille-Petit, B. Therrien, G. Süss-Fink, *Polyhedron* **2004**, *23*, 687.
[7] M. Stebler-Röthlisberger, W. Hummel, P. A. Pittet, H.-B. Bürgi, A. Ludi, A. E. Merbach, *Inorg. Chem.* **1988**, *27*, 1358.
[8] [8a] M. A. Bennett, J. P. Ennett, K. I. Gell, *J. Organomet. Chem.* **1982**, *233*, C17. [8b] M. A. Bennett, J. P. Ennett, *Inorg. Chim. Acta* **1992**, *198−200*, 583. [8c] M. Jahncke, G. Meister, G. Rheinwald, H. Stoeckli-Evans, G. Süss-Fink, *Organometallics* **1997**, *16*, 1137.
[9] [9a] L. Vieille-Petit, S. Unternährer, B. Therrien, G. Süss-Fink, *Inorg. Chim. Acta* **2003**, *355*, 335. [9b] L. Vieille-Petit, B. Therrien, G. Süss-Fink, *Inorg. Chim. Acta* in press. [9c] L. Vieille-Petit, B. Therrien, G. Süss-Fink, *Inorg. Chim. Acta* **2003**, *355*, 394.
[10] M. A. Bennett, T.-N. Huang, T. W. Matheson, A. K. Smith, *Inorg. Synth.* **1982**, *21*, 74.
[11] G. M. Sheldrick, *Acta Crystallogr., Sect. A* **1990**, *46*, 467.
[12] G. M. Sheldrick, *SHELXL-97, Program for crystal structure refinement*, University of Göttingen, Germany (**1997**).
[13] A. L. Spek, *Acta Crystallogr., Sect. A* **1990**, *46*, C34.
[14] L. J. Farrugia, *J. Appl. Cryst.* **1997**, *30*, 565.

Received April 4, 2004
Early View Article
Published Online August 12, 2004

 © 2004 Wiley-VCH Verlag GmbH & Co. KGaA, Weinheim

Spectroscopic Studies of Europium(III) and Gadolinium(III) Tris-β-diketonate Complexes with Diazabutadiene Ligands

José A. Fernandes,[a] Rute A. Sá Ferreira,[b] Martyn Pillinger,[a] Luís D. Carlos,*[b] Isabel S. Gonçalves,[a] and Paulo J. A. Ribeiro-Claro*[a]

Keywords: Ab initio calculations / Lanthanides / Luminescence / N ligands / Vibrational spectroscopy

Adducts of the type $Ln(NTA)_3$·L [Ln = Eu, Gd; NTA = 1-(2-naphthoyl)-3,3,3-trifluoroacetonate; L = 1,4-diaza-1,3-butadiene RN=CHCH=NR (R = *p*-tolyl, *o*-tolyl)] were prepared by treatment of $Ln(NTA)_3·2H_2O$ with one equivalent of the chelating N–N ligand. The mixed ligand complexes were characterised by elemental analysis, thermogravimetric analysis, IR and Raman spectroscopy, and photoluminescence (PL) spectroscopy. Ab initio calculations were carried out in order to predict coordination geometries and also to interpret the vibrational spectra. For the europium(III) compounds, new Raman-active bands at approximately 440 and 479 cm^{-1} are tentatively assigned to $(\nu Eu–N)_{sym}$ and $(\nu Eu–N)_{as}$ modes, respectively. A second band at 1185 cm^{-1} is associated with the symmetric stretching of the N–C(ring) and C–C (DAB) bonds, and is shifted about 20 cm^{-1} to a higher wavenumber relative to the corresponding band for the free ligand. The room-temperature PL spectra of the two Eu complexes are composed of the typical Eu^{3+} red emission, assigned to transitions between the first excited state ($^5D_0$) and the ground multiplet ($^7F_{0–4}$). Based on the room-temperature emission spectra and lifetime measurements, the quantum efficiencies of the $^5D_0$ Eu^{3+} excited state were estimated and found to be quite low (e.g. 2–3%). The low efficiencies are attributed to the presence of thermally activated nonradiative channels involving ligand-to-metal charge-transfer (LMCT) states. Indeed, a low-lying LMCT band was detected for the Eu complex containing the ligand *p*-tolyl-DAB by comparison of the room-temperature diffuse reflectance spectrum for this complex with that of the corresponding Gd analogue.

(© Wiley-VCH Verlag GmbH & Co. KGaA, 69451 Weinheim, Germany, 2004)

Introduction

Over the past 40 years there has been considerable interest in the luminescence and lasing ability of certain diketonates of lanthanides, particularly europium(III) and terbium(III).[1–4] Two classes of complexes may be distinguished depending on whether the ratio of diketonate ion to metal ion in the product is 3:1 (tris complex) or 4:1 (tetrakis complex).[5,6] The tris-β-diketonates are usually coordinatively unsaturated and, therefore, form adducts with a variety of Lewis base ligands, to give seven-, eight- or even nine-coordinate complexes.[7–19] Some of us recently reported on the luminescence features and the absolute quantum yield of europium(III) tris[1-(2-naphthoyl)-3,3,3-trifluoroacetonate] complexes, $Eu(NTA)_3·2L$ (NTA = 1-(2-naphthoyl)-3,3,3-trifluoroacetonate, L = H_2O and DMSO).[19] The experimental quantum yield measured for $Eu(NTA)_3·2DMSO$ (0.75) is one of the highest so far reported for solid-state europium complexes. Replacement of the solvent molecules in these complexes by organic ligands is one way to further modify the luminescence properties of the parent tris complex. The complex with 2,2′-bipyridine (bipy) has already been reported.[9] In the present work, $Eu(NTA)_3$ complexes containing 1,4-diaza-1,3-butadienes (DAB) of the type RN=CR′CR′=NR (R = *p*-tolyl, *o*-tolyl; R′ = H) have been prepared and characterised. For comparison, the corresponding Gd^{III} complexes have also been prepared. To the best of our knowledge, very few studies have been carried out on diazabutadiene compounds of rare earths,[20–22] especially with regard to their photophysical properties. This is surprising since, as α-diimine ligands, DAB ligands have electronic and structural similarities to the more extensively studied heteroaromatic chelating agents bipy and 1,10-phenanthroline.[23] Added flexibility arises from the presence of the substituents R and R′, perhaps allowing luminescence behaviour to be tuned by variation of steric and electronic effects.

Results and Discussion

Synthesis and Thermogravimetric Analysis

The mononuclear complexes $Ln(NTA)_3$·*p*-tolyl−DAB [Ln = Eu (**1**), Gd (**3**)] and $Ln(NTA)_3$·*o*-tolyl−DAB [Ln =

[a] Department of Chemistry, CICECO, University of Aveiro, 3810-193 Aveiro, Portugal
Fax: (internat.) + 351-234-370084
E-mail: pclaro@dq.ua.pt
[b] Department of Physics, CICECO, University of Aveiro, 3810-193 Aveiro, Portugal

Eu (**2**), Gd (**4**)] were prepared in reasonable yields by the treatment of solutions of $Ln(NTA)_3{\cdot}2H_2O$ in chloroform with one equivalent of the respective diazabutadiene ligand.

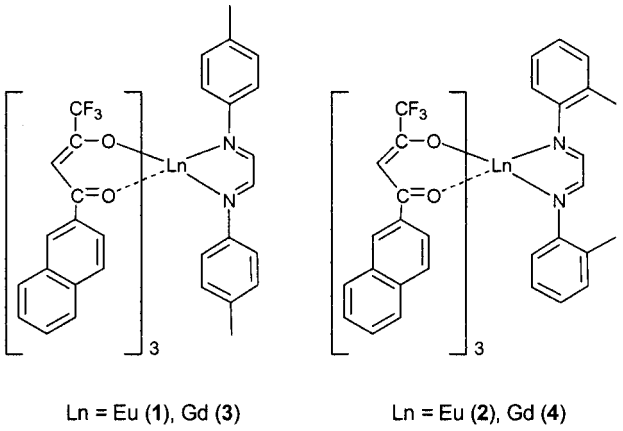

Figure 1 shows the TGA results for *o*-tolyl−DAB, $Eu(NTA)_3{\cdot}2H_2O$ and $Eu(NTA)_3{\cdot}$*o*-tolyl−DAB (**2**). Similar traces were obtained for the compounds *p*-tolyl−DAB, $Gd(NTA)_3{\cdot}2H_2O$ and $Ln(NTA)_3{\cdot}$L (**1**,**3**,**4**), respectively. The compounds *o*-tolyl−DAB and *p*-tolyl−DAB sublime in the temperature range 100−230 °C. The precursors $Ln(NTA)_3{\cdot}2H_2O$ undergo a mass loss up to 100 °C, which corresponds to the removal of coordinated water. Further decomposition takes place in two steps; the first of these occurs between 100 and 350 °C (54% mass loss for Eu, 63% for Gd), and the second between 350 and 600 °C (21% mass loss for Eu, 19% for Gd). Finally, a small mass loss of 2% occurs between 600 and 700 °C for both compounds, leaving a residual mass of 17.7% for Eu and 13.8% for Gd. The TGA curves of the adducts **1**−**4** are very similar to each other and to the reagents $Ln(NTA)_3{\cdot}2H_2O$, and all steps for these six compounds take place at the same temperatures. There is no step characteristic of "free" ligand, indicating that the ligands are coordinated to the metal centres. The first mass loss (3.0% for **1**) corresponds to the removal of water content. Following this, the mass loss for the step between 100 and 350 °C is smaller than that observed for the reagents (47.2% for compound **1**). Conversely, the step between 350 and 600 °C corresponds to a larger amount (34.3% for compound **1**). Finally, the TGA shows a mass loss of about 2% between 575 and 720 °C, leaving a residual mass of about 16% for compounds **1** and **2**, and 14% for compounds **3** and **4**.

Ab Initio Calculations and Vibrational Spectra

Figure 2 shows the calculated coordination geometry of DAB in **1** (NTA ligands are shown in wireframe). The complexed tolyl−DAB adopts a propeller-like configuration; the phenyl rings are rotated 33° and 42° from the N=C−C=N plane, in opposite directions. In the free ligand, the lowest energy form presents a similar rotation angle (approximately 37°), but to the same side of the N=C−C=N plane (therefore, the phenyl rings are co-planar). Similar results were obtained for the simulation of *o*-tolyl−DAB

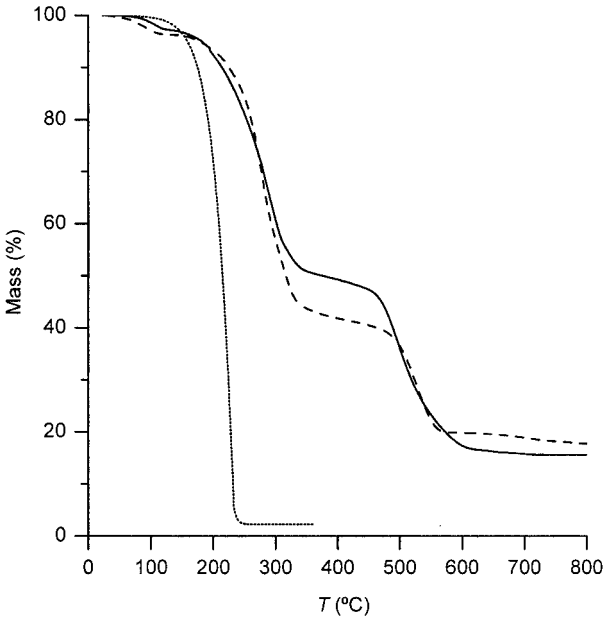

Figure 1. TGA of $Eu(NTA)_3{\cdot}$*o*-tolyl−DAB (**2**) (−), *o*-tolyl−DAB (···) and $Eu(NTA)_3{\cdot}2H_2O$ (− − −)

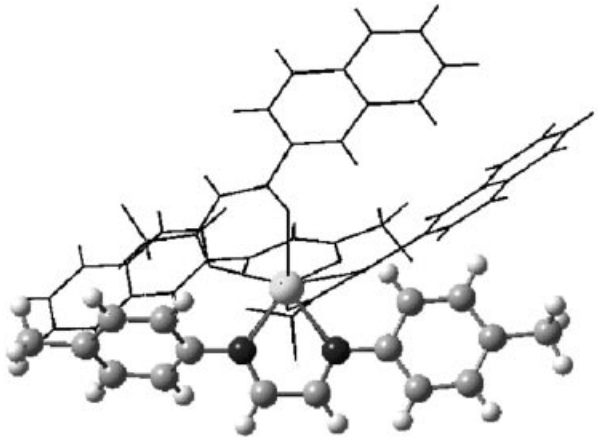

Figure 2. Lowest energy structure calculated for the model $Eu[O(CH)_3O]_3{\cdot}$*p*-tolyl−DAB; the $(NTA)_3$ framework was obtained from the X-ray single crystal structure for $Eu(NTA)_3{\cdot}$phenanthroline[24]

(**2**), with the exception of the twist angles of the phenyl ring, which are about 10° larger than those for **1** due to the presence of the *ortho* methyl groups. Calculated Eu−N distances are about 233 pm, and the N−Eu−N angle is 72° in both **1** and **2**. The Eu−N bond lengths are shorter than those calculated at the same level for the 2,2′-bipyrimidine and 1,10-phenanthroline derivatives,[24] suggesting a stronger Eu−N interaction in the case of the present ligands. As a result, the calculated frequencies for the Eu−N stretching modes are higher than those usually reported. In fact, ab initio calculations predict the νEu−N stretching modes at about 460 cm^{-1} (after scaling), with a moderately strong Raman intensity and weak IR intensity.

An important geometrical change upon complexation is revealed in the bond lengths of the diazabutadiene fragment. From the free DAB ligand to complex **1**, the

 © 2004 Wiley-VCH Verlag GmbH & Co. KGaA, Weinheim

$C_{(ring)}-N$, C=N and C−C bond lengths are reduced by approximately 2.2, 1.8 and 3.3 pm, respectively. From the free ligand to complex **2**, the corresponding values are 1.7, 1.8 and 2.9 pm, respectively. The effect is residual in the aromatic C−C bonds (< 1 pm) and is absent in the $C-CH_3$ bonds. This contraction affects the vibrational modes involving the diazabutadiene fragment, which are predicted to be generally shifted to higher wavenumbers upon complexation. The effect is particularly evident in the mode combining the symmetric stretching of the $N-C_{(ring)}$ and C−C (DAB) bonds, with a strong Raman intensity, for which a shift of 20 cm^{-1} is predicted. The calculated scaled values are 1164 cm^{-1} for the free DAB ligands and 1184 cm^{-1} for the complex model. These predictions find experimental support from the vibrational spectra, as discussed below.

The vibrational spectra of **1** and **2** are well-described by the sum of the spectra of their reagents, with some additional details ascribed to the complexation process. Figure 3 shows two relevant regions in the Raman spectra of compound **1** [trace (c)], the reagents $Eu(NTA)_3{\cdot}2H_2O$ [trace (b)] and *p*-tolyl−DAB [trace (a)].

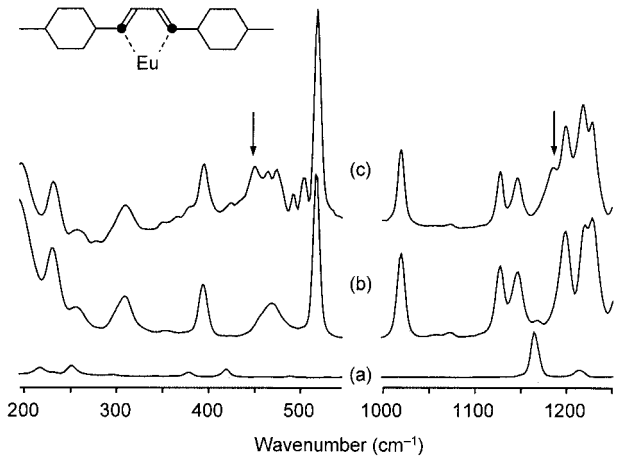

Figure 3. Raman spectra of (a) *p*-tolyl−DAB, (b) $Eu(NTA)_3{\cdot}2H_2O$ and (c) $Eu(NTA)_3$·*p*-tolyl−DAB (**1**); the arrows point to the bands assigned to the *ν*Eu−N modes (about 460 cm^{-1}) and symmetric stretching of the N−C(ring) and C−C (DAB) bonds (1185 cm^{-1})

The vibrational modes involving the Eu−N bonds were searched for in the low wavenumber region. The two bands observed at approximately 440 and 479 cm^{-1} are not present in the spectra of the reagents and fit the intensity and wavenumber predicted from ab initio calculations. In this way, they have been tentatively assigned to $(\nu Eu-N)_{sym}$ and $(\nu Eu-N)_{as}$, respectively. Identical bands are observed at 449 cm^{-1} and 473 cm^{-1} in the Raman spectrum of **2**, supporting this assignment. Analysis of the IR spectrum in this region was inconclusive, due to band overlap.

The effect of complexation can also be observed in the higher wavenumber region of Figure 3. The bands corresponding to the symmetric stretching of the $N-C_{(ring)}$ and C−C (DAB) bonds are easily identified in the spectra of the free ligands and products due to their strong Raman intensity. As can be seen, the strong band at 1165 cm^{-1} for the pure DAB ligand [trace (a)] moves to about 1185 cm^{-1} in **1** [trace (c)]. The ca. 20 cm^{-1} upwards shift upon complexation is in agreement with the contraction of the C−C and N−C bonds from the free ligand to the complexes.

Photoluminescence Studies

Figure 4 shows the room-temperature PL spectra of compounds **1** and **2** obtained under the excitation wavelength that maximises the emission intensity. Both spectra are composed of the typical Eu^{3+} red emission, assigned to transitions between the first excited state ($^5D_0$) and the ground multiplet ($^7F_{0-4}$). It is possible to identify 3 and 5 Stark components for the $^5D_0 \rightarrow {}^7F_{1-2}$ transitions, which indicates that the Eu^{3+} ions are located in a low site symmetry group, without an inversion centre according to the higher intensity of the $^5D_0 \rightarrow {}^7F_2$ transition. Changes in the excitation wavelength did not produce significant alterations either in the number of emission components or in their energy. The presence of only one component for the $^5D_0 \rightarrow {}^7F_0$ transition suggests only one Eu^{3+} local environment. However, the high value found for the full width at half maximum (fwhm) in both compounds(26 cm^{-1}) indicates a large distribution of local coordination sites,[25] probably induced by the amorphous nature of the compounds. The similarity between the two spectra is also apparent in the energy and fwhm of the $^5D_0 \rightarrow {}^7F_{0-2}$ transitions. This fact, in particular the comparable energies for the $^5D_0 \rightarrow {}^7F_0$ transition, indicates that the Eu^{3+} first coordination sphere might be very similar for the two compounds. This is based on the knowledge that the energy of this transition is usually related to the so-called *nephelauxetic* effect induced by the ion′s first neighbours.[26] Such conclusions are also supported by the PL spectra measured at 14 K. Apart from small changes in the relative intensity of the $^5D_0 \rightarrow {}^7F_2$ transition Stark components, the energy, fwhm and number of emission components of the intra-$4f^6$ transitions are essentially the same as observed at room

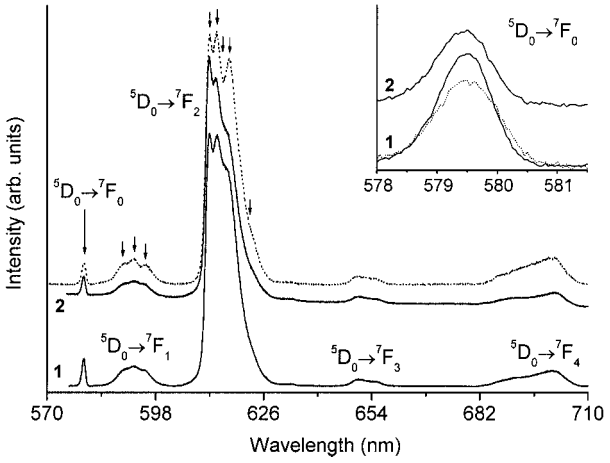

Figure 4. Room-temperature PL spectra of compounds **1** and **2** excited at 345 nm; The dotted line corresponds to the PL spectrum of **1** detected at 14 K and excited at 365 nm

 © 2004 Wiley-VCH Verlag GmbH & Co. KGaA, Weinheim

temperature. However, the integrated intensity of the emission arising from the $^5D_0$ level strongly depends on the selected temperature, presenting the behaviour shown in Figure 5 for **1**. For both compounds, no emission from the ligands could be detected, suggesting an effective interaction between them and the Eu^{3+} ions.

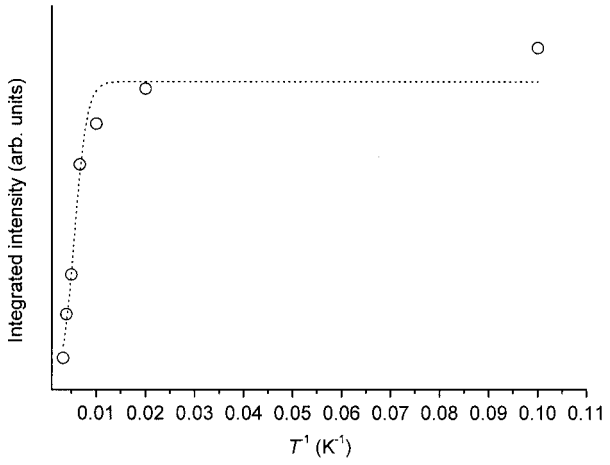

Figure 5. Temperature-dependence (14−300 K) of the Eu^{3+} $^5D_0$ emission for compound **1** (open circles); the dotted line is the best fit to the data using Equation (4)

The excitation spectra (PLE), monitored around the most intense line of the cation (Figure 6), enable us to draw the same conclusion. The spectra exhibit a large broad band between 280 and 420 nm, with a maximum at around 345 nm, and no lines associated with the direct excitation of the intra-$4f^6$ levels are detected. This strongly suggests an efficient sensitization process between the ligands and the metal ion. Lowering the temperature to 14 K induces a red-shift to 365 nm, and a low-intensity line associated with the excitation of the $^5D_2$ level is observed, as shown in Figure 6 for **1**. This large band may originate from the ligand levels involving the NTA and diimine components, since the PLE spectrum acquired for $Eu(NTA)_3{\cdot}2H_2O$ under identical experimental conditions is different from those plotted in Figure 6.[19]

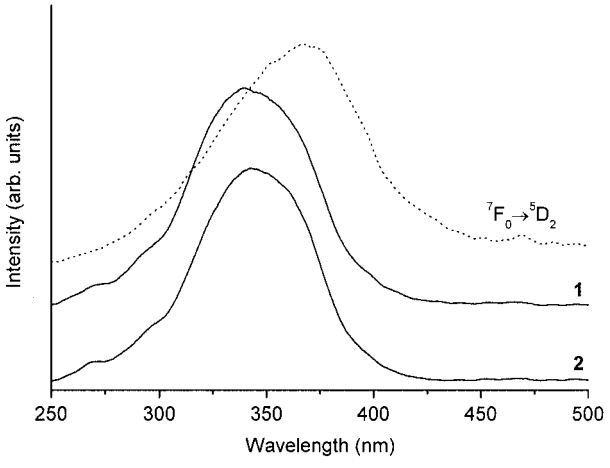

Figure 6. room-temperature PLE spectra of compounds **1** and **2** monitored around 612 nm; the dotted line is the PLE spectrum of **1** detected at 14 K

The $^5D_0$ lifetime, τ, was measured around the most intense PL line (not shown). For both compounds the data are well described by a single exponential function, revealing lifetime values of 0.038 ± 0.001 and 0.030 ± 0.001 ms for compounds **1** and **2**, respectively. These values are smaller than the lifetime value previously found for the precursor complex.[19]

Based on the room-temperature emission spectra and on the lifetime measurements we can estimate the efficiency, q, of the $^5D_0$ Eu^{3+} excited state, considering that only nonradiative and radiative processes are essentially involved in the depopulation of the $^5D_0$ state,[3,19,27,28] where k_r and k_{nr} are the radiative and nonradiative transition probabilities, respectively, ($k_{exp} = 1/\tau_{exp} = k_r + k_{nr}$).

$$q = \frac{k_r}{k_r + k_{nr}} \tag{1}$$

The emission intensity, I, taken as the integrated intensity, S, of the emission curves, for the $^5D_0 \rightarrow {}^7F_{0-4}$ transitions, is expressed by Equation (2): where i and j represent the initial ($^5D_0$) and final ($^7F_{0-6}$) levels, respectively, $\hbar w_{i\rightarrow j}$ is the transition energy, $A_{i\rightarrow j}$ corresponds to Einstein's coefficient of spontaneous emission and N_i is the population of the $^5D_0$ emitting level.[3,19,27,28]

$$I_{i\rightarrow j} = \hbar w_{i\rightarrow j} A_{i\rightarrow j} N_i \equiv S_{i\rightarrow j} \tag{2}$$

The radiative contribution may be calculated from the relative intensities of the $^5D_0 \rightarrow {}^7F_{0-6}$ transitions. Since the $^5D_0 \rightarrow {}^7F_1$ transition can be considered as a reference due to its dipolar magnetic nature, k_r can be calculated according to Equation (3), where $A_{0\rightarrow 1}$ is the Einstein's coefficient of spontaneous emission between the $^5D_0$ and the $^7F_1$ Stark levels.

$$k_r = A_{0\rightarrow 1} \frac{\hbar\omega_{0\rightarrow 1}}{S_{0\rightarrow 1}} \sum_{J=0}^{6} \frac{S_{0-J}}{\hbar\omega_{0-J}} \tag{3}$$

The $^5D_0 \rightarrow {}^7F_{5,6}$ transitions were not measured experimentally and so the branching ratio for these transitions, which is usually very small, can be neglected. Therefore, we can ignore their influence in the depopulation of the $^5D_0$ excited state. The $^5D_0 \rightarrow {}^7F_1$ transition does not depend on the local ligand field seen by Eu^{3+} ions and, thus, may be used as a reference for the whole spectrum; in vacuo $A(^5D_0 \rightarrow {}^7F_1) = 14.65\ s^{-1}$.[28] The values found for q, k_r and k_{nr} for compounds **1** and **2** are gathered in Table 1. An average index of refraction equal to 1.5 was considered for both compounds leading to an approximate $A(^5D_0 \rightarrow {}^7F_1)$ value of $50\ s^{-1}$.[29]

 © 2004 Wiley-VCH Verlag GmbH & Co. KGaA, Weinheim

Table 1. Experimental $^5D_0$ lifetimes (τ) and decay rates (k_{exp}), calculated radiative (k_r) and nonradiative (k_{nr}) $^5D_0$ decay rates and quantum efficiency (q) for compounds **1** and **2**

	τ (ms)	k_{exp} (ms^{-1})	k_r (ms^{-1})	k_{nr} (ms^{-1})	q (%)
1	0.038 ± 0.001	26.32	0.82	25.50	3.1
2	0.030 ± 0.001	33.33	0.72	32.61	2.2

Compound **1** has the highest q value, induced by higher k_r (12%) and lower k_{nr} (22%) values. However, both compounds present lower values for the $^5D_0$ quantum efficiency compared with that found for the precursor complex $Eu(NTA)_3{\cdot}2H_2O$ (q = 29%)[19] that may be induced by the higher k_{nr} contribution found in **1** and **2**. In fact, the temperature-dependence of the Eu^{3+} emission-integrated intensity, I_{int} (Figure 5), suggests a thermally activated nonradiative mechanism. Such nonradiative de-excitation is well-described by the following expression:

$$I_{int} = \frac{1}{1 + A\exp(-E_a/K_BT)} \quad (4)$$

where A is related to the ratio between the nonradiative (at $T = 0$) and radiative rates, K_B is the Boltzmann constant and E_a is the energy of activation of the de-excitation channel with respect to the energy of the $^5D_0$ level. The energy activation obtained is 550 ± 136 cm^{-1}, which places the nonradiative level in a position resonant with the Eu^{3+} emitting level.

In Eu^{3+} complexes such thermally activated nonradiative channels may involve ligand-to-metal charge-transfer (LMCT) states, formed by the orbital overlap of the ligand and Eu^{3+} energy levels.[30−32] Quenching of the Eu^{3+} PL by low-lying thermally activated LMCT transitions is a well-known phenomenon in molecular solids and complexes in solution.[31−34] These states are usually difficult to detect by absorption and emission spectroscopy, and indeed their unequivocal assignment and detection have only been performed for a few lanthanide compounds.[3,31−34] Due to the difficulties in detecting LMCT states, they are usually claimed to exist in order to explain low PL quantum yields and/or the strong dependence of the emission intensity with temperature. The comparison of Eu^{3+} and Gd^{3+} reflectance spectra is a useful tool to perceive and ascribe the LMCT transitions, since the energetic difference between the Gd^{3+} first excited state and the fundamental levels is too high to allow the detection of a charge-transfer state in the UV/Vis range. Therefore, in the Gd^{3+} spectrum we expect to measure only the contributions that are not related with the LMCT processes.

Figure 7 shows the room-temperature diffuse reflectance spectra of compounds **1** and **3**. The arithmetic difference between the two curves is also represented, showing the presence of a low-lying LMCT band (centred at about 17800 cm^{-1}). As far as we know, this is one of the clearest examples where the arithmetic difference between the diffuse reflectance spectra of isostructural Eu^{3+} and Gd^{3+} compounds allows the explicit identification of ligand-to-metal charge transfer states by direct means. Unfortunately, and in agreement with the mentioned difficulties, these states cannot be identified so visibly in the reflectance spectra of compounds **2** and **4**.

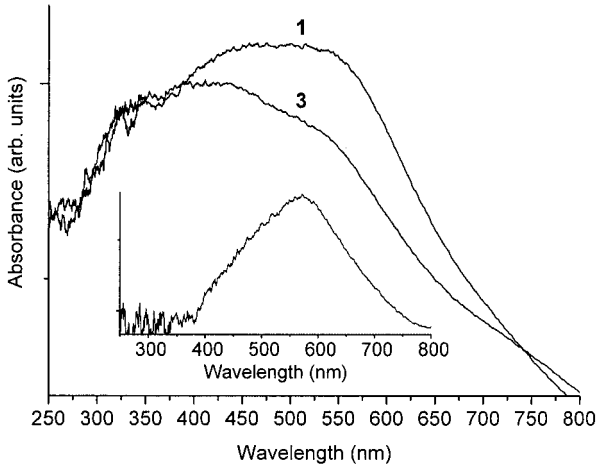

Figure 7. room-temperature diffuse reflectance spectra of compounds **1** and **3**; the arithmetic difference between the two curves is also represented

The charge-transfer band observed in the reflectance spectrum of compound **1** (Figure 7) does not appear at all as an excitation band (see the PLE spectra of Figure 6), indicating that the LMCT band in these compounds is predominantly a quenching channel. This is exactly the conclusion arrived at previously from the temperature-dependence of the Eu^{3+} emission integrated intensity of compound **1** (Figure 5). Actually, the energy of the thermally activated nonradiative level derived from Equation (4), 550 ± 136 cm^{-1} above the $^5D_0$ level (about 17256.3 cm^{-1}, Figure 4), is in excellent agreement with the maximum of the LMCT band discerned from the arithmetic difference between the reflectance spectra of **1** and **3** (approximately 17800 cm^{-1}, Figure 7). Therefore, the low $^5D_0$ quantum efficiency observed for compounds **1** and **2** can be reliably assigned to a nonradiative decay through the LMCT state of Eu^{3+}, which is at rather low energies in these diimine compounds. This is in agreement with previously reported experimental results that indicate that the $^5D_0$ quantum efficiency decreases as the energy of the LMCT states decreases.[31,32] Moreover, recent theoretical results on energy transfer mechanisms between these LMCT states and the ligand and Eu^{3+} levels demonstrate that the quantum yield of the complex (and thus the $^5D_0$ quantum efficiency) decreases drastically as the LMCT barycentre becomes resonant with the $^5D_0$ level.[35]

 © 2004 Wiley-VCH Verlag GmbH & Co. KGaA, Weinheim

Concluding Remarks

New europium and gadolinium tris-β-diketonate complexes have been prepared, containing diazabutadiene (DAB) ligands coordinated to the metal centres. Accordingly, the complexes with the general formula $Ln(NTA)_3{\cdot}nL$ (Ln = Eu, Gd) are now known with L = H_2O, DMSO, 2,2′-bipyridine, 1,10-phenanthroline and DAB. Binuclear complexes of the type $[Ln(NTA)_3]_2{\cdot}$bpym (bpym = 2,2′-bipyrimidine) have also been reported. The motivation for the preparation of these derivatives stems from the fact that the experimental quantum yield measured for $Eu(NTA)_3{\cdot}2DMSO$ (0.75) is one of the highest so far reported for solid-state europium complexes. It has been found that the $^5D_0$ quantum efficiencies for these complexes vary considerably depending on the nature of L, decreasing in the order L = DMSO (62%), phen (40%), bpym (39%), H_2O (29%) and DAB (2−3%). The low $^5D_0$ quantum efficiencies for the diazabutadiene adducts can be reliably assigned to a nonradiative decay through the LMCT state of Eu^{3+}, which is at rather low energies in these diimine compounds. The use of photoluminescence spectroscopy, together with vibrational spectroscopy and ab initio calculations, therefore allows us to build up quite a detailed picture about the nature of the metal−ligand interactions in these tris-β-diketonate complexes.

Experimental Section

Materials and Methods: $Eu(NTA)_3{\cdot}2H_2O$,[36] $Gd(NTA)_3{\cdot}2H_2O$,[36] *p*-tolyl−DAB,[37] and *o*-tolyl−DAB[37] were prepared by literature methods.

Microanalyses were performed at the Instituto de Tecnologia Química e Biológica (ITQB), Lisbon. Thermogravimetric analyses (TGA) were performed using a Mettler TA3000 system at a heating rate of 5 K min^{-1} under a static atmosphere of air. IR spectra were obtained as KBr pellets with a FTIR Mattson-7000 infrared spectrophotometer. Raman spectra were recorded with a Bruker RFS100/S FT instrument (Nd:YAG laser, 1064 nm excitation, InGaAs detector). The photoluminescence spectra (PL) were recorded on a Jobin Yvon-Spex spectrometer (HR, 460) coupled to a R928 Hamamatsu photomultiplier (14−300 K). A 300 W Xe arc lamp coupled to a Jobin Yvon-Spex (TRIAX 180) monochromator was used as the excitation source. All the spectra were corrected for the response of the detector. The lifetime measurements were carried out at room temperature (r.t.) on a modular double grating excitation spectrofluorimeter with a TRIAX 320 emission monochromator (Fluorolog-3, Jobin Yvon-Spex) in front face mode coupled to a R928 Hamamatsu photomultiplier.

Preparation of Complexes: A solution of the diimine (0.102 g, 0.432 mmol) in $CHCl_3$ (5 mL) was added to a solution of $Ln(NTA)_3{\cdot}2H_2O$ (0.432 mmol) in $CHCl_3$ (15 mL). The reaction mixture was stirred for 3 h at room temperature. The solvent was then removed, and the resultant brown solid was washed with hexane and dried in vacuo.

$Eu(NTA)_3{\cdot}$*p*-tolyl−DAB (1): Yield: 0.455 g (89%). $C_{58}H_{40}EuF_9N_2O_6$ (1183.9): calcd. C 58.84, H 3.41, N 2.37; found C 58.89, H 3.46, N 2.37. IR (KBr, selected): $\tilde{\nu}_{max.}$ = 3065 (w), 2961 (w), 2927 (w), 1614 (s), 1593 (m), 1570 (m), 1531 (m), 1510 (m), 1460 (m), 1384 (w), 1353 (w), 1298 (s), 1251 (m), 1198 (m), 1135 (m), 1074 (w), 959 (w), 865 (w), 792 (m), 749 (w), 684 (m), 568 (w), 472 (w) cm^{-1}. Raman: 3058 (m), 1629 (s), 1596 (m), 1468 (s), 1432 (w), 1386 (s), 1298 (m), 1228 (w), 1199 (w), 1019 (w), 771 (m), 517 (m) cm^{-1}.

$Eu(NTA)_3{\cdot}$*o*-tolyl−DAB (2): Yield: 0.441 g (82%). $C_{58}H_{40}EuF_9N_2O_6$ (1183.9): calcd. C 58.84, H 3.41, N 2.37; found C 58.78, H 3.33, N 2.28. IR (KBr, selected): $\tilde{\nu}_{max.}$ = 3060 (w), 2959 (w), 2924 (w), 1613 (vs), 1593 (s), 1570 (s), 1532 (s), 1509 (s), 1460 (m), 1384 (w), 1353 (w), 1298 (vs), 1251 (m), 1198 (s), 1136 (s), 1074 (w), 958 (w), 864 (w), 793 (m), 749 (m), 684 (m), 569 (w), 519 (w), 472 (w) cm^{-1}. Raman: 3056 (m), 1628 (s), 1596 (m), 1532 (m), 1468 (s), 1432 (w), 1386 (s), 1297 (m), 1228 (w), 1198 (w), 1019 (w), 771 (m), 517 (m) cm^{-1}.

$Gd(NTA)_3{\cdot}$*p*-tolyl−DAB (3): Yield: 0.255 g (46%). $C_{58}H_{40}F_9GdN_2O_6$ (1189.2): calcd. C 58.58, H 3.39, N 2.36; found C 58.43, H 3.21, N 2.29. IR (KBr, selected): $\tilde{\nu}_{max.}$ = 3058 (w), 2960 (w), 2958 (w), 1615 (s), 1570 (m), 1532 (m), 1510 (m), 1384 (vs), 1299 (m), 1198 (m), 1135 (m), 959 (w), 792 (m), 684 (m), 570 (w), 471(w) cm^{-1}. Raman: 3057 (m), 1629 (s), 1596 (m), 1468 (s), 1432 (w), 1386 (s), 1299 (m), 1228 (w), 1198 (w), 1019 (w), 770 (m), 517 (m) cm^{-1}.

$Gd(NTA)_3{\cdot}$*o*-tolyl−DAB (4): Yield: 0.168 g (39%). $C_{58}H_{40}F_9GdN_2O_6$ (1189.2): calcd. C 58.58, H 3.39, N 2.36; found C 58.75, H 3.33, N 2.38. IR (KBr, selected): $\tilde{\nu}_{max.}$ = 3058 (w), 2960 (w), 2926 (w), 1614 (vs), 1594 (s), 1570 (s), 1531 (s), 1509 (s), 1460 (m), 1384 (m), 1353 (m), 1298 (s), 1251 (m), 1187 (s), 1135 (s), 1074 (w), 958 (w), 865 (w), 792 (m), 748 (m), 684 (m), 568 (w), 472 (w) cm^{-1}. Raman: 3057 (m), 1628 (s), 1596 (m), 1532 (m), 1467 (s), 1432 (w), 1386 (s), 1297 (m), 1227 (w), 1197 (w), 1019 (w), 770 (m), 517 (m) cm^{-1}.

Ab Initio Calculations: Ab initio calculations were performed using the G03w program package,[38] running on a personal computer. The fully optimised geometry, the harmonic vibrational frequencies, and the infrared and Raman intensities were obtained at the B3LYP level, using the Effective Core Potentials (ECP) of Pacios and Christiansen[39] and *f* function (zeta = 0.591) for the Eu atom, and the Stevens/Basch/Krauss[40,41] ECP minimal basis set (CEP-4G option of G03) for the remaining atoms. Due to the large size of the systems, the NTA ligands were replaced by the coordination fragment $[O(CH)_3O]^-$. This model consistently yields Eu−O and Eu−N bond lengths shorter than the reported X-ray values for the phenanthroline,[24] bipyridine,[24] and diaquo[42] analogues, by 16% and 7%, respectively. The calculated wavenumbers were scaled by a factor of 0.90 before comparison with the experimental values.

Acknowledgments

The authors are grateful to FCT, POCTI and FEDER for financial support (Project POCTI/CTM/46780/2002). J. F. thanks the University of Aveiro and the FCT for research grants.

[1] L. C. Thompson, in *Handbook on the Physics and Chemistry of Rare Earths* (Eds.: K. A. Gscheidner, Jr. and L. Eyring), North-Holland, Amsterdam, **1979**, vol. 3, chapter 25.
[2] W. DeW. Horrocks, M. Albin, *Prog. Inorg. Chem.* **1984**, *31*, 1.
[3] G. F. de Sá, O. L. Malta, C. de Mello Donegá, A. M. Simas, R. L. Longo, P. A. Santa-Cruz, E. F. da Silva, *Coord. Chem. Rev.* **2000**, *196*, 165.
[4] K. C. Joshi, V. N. Pathak, *Coord. Chem. Rev.* **1977**, *22*, 37.
[5] L. R. Melby, N. J. Rose, E. Abramson, J. C. Caris, *J. Am. Chem. Soc.* **1964**, *86*, 5117.

 © 2004 Wiley-VCH Verlag GmbH & Co. KGaA, Weinheim

[6] H. Bauer, J. Blanc, D. L. Ross, *J. Am. Chem. Soc.* **1964**, *86*, 5125.
[7] A. K. Trikha, L. B. Zinner, K. Zinner, P. C. Isolani, *Polyhedron* **1996**, *15*, 1651.
[8] H. J. Batista, A. V. M. de Andrade, R. L. Longo, A. M. Simas, G. F. de Sá, N. K. Ito, L. C. Thompson, *Inorg. Chem.* **1998**, *37*, 3542.
[9] L. C. Thompson, F. W. Atchison, V. G. Young, *J. Alloys Compd.* **1998**, *275−277*, 765.
[10] K. Iftikhar, M. Sayeed, N. Ahmed, *Inorg. Chem.* **1982**, *21*, 80.
[11] D. F. Moser, L. C. Thompson, V. G. Young Jr., *J. Alloys Compd.* **2000**, *303−304*, 121.
[12] O. L. Malta, M. A. Couto dos Santos, L. C. Thompson, N. K. Ito, *J. Lumin.* **1996**, *69*, 77.
[13] V. Tsaryuk, J. Legendziewicz, L. Puntus, V. Zolin, J. Sokolnicki, *J. Alloys Compd.* **2000**, *300−301*, 464.
[14] R. C. Holz, L. C. Thompson, *Inorg. Chem.* **1993**, *32*, 5251.
[15] L. C. Thompson, S. Berry, *J. Alloys Compd.* **2001**, *323−324*, 177.
[16] R. C. Holz, L. C. Thompson, *Inorg. Chem.* **1988**, *27*, 4640.
[17] O. L. Malta, H. F. Brito, J. F. S. Menezes, F. R. Gonçalves e Silva, C. de Mello Donegá, S. Alves Jr., *Chem. Phys. Lett.* **1998**, *282*, 233.
[18] O. L. Malta, H. F. Brito, J. F. S. Menezes, F. R. Gonçalves e Silva, S. Alves Jr., F. S. Farias Jr., A. V. M. de Andrade, *J. Lumin.* **1997**, *75*, 255.
[19] L. D. Carlos, C. de Mello Donegá, R. Q. Albuquerque, S. Alves Jr., J. F. S. Menezes, O. L. Malta, *Mol. Phys.* **2003**, *101*, 1037.
[20] G. van Koten, K. Vrieze, *Adv. Organomet. Chem.* **1982**, *21*, 151.
[21] F. G. N. Cloke, H. C. Delemos, A. A. Sameh, *J. Chem. Soc., Chem. Commun.* **1986**, 1344.
[22] F. G. N. Cloke, *Chem. Soc. Rev.* **1993**, *22*, 17.
[23] M. N. Bochkarev, A. A. Trifonov, F. G. N. Cloke, C. I. Dalby, P. T. Matsunaga, R. A. Andersen, H. Schumann, J. Loebel, H. Hemling, *J. Organomet. Chem.* **1995**, *486*, 177.
[24] J. A. Fernandes, R. A. Sá Ferreira, M. Pillinger, L. D. Carlos, J. Jepsen, A. Hazell, P. Ribeiro-Claro, I. S. Gonçalves, *J. Lumin.,* in press.
[25] J.-C. G. Bünzli, in *Lanthanide Probes in Life, Chemical, and Earth Sciences* (Eds.: J.-C. G. Bünzli, G. R. Choppin), Elsevier, Amsterdam, **1989**, p. 219.
[26] [26a] L. D. Carlos, R. A. Sá Ferreira, V. de Zea Bermudez, C. Molina, L. A. Bueno, S. J. L. Ribeiro, *Phys. Rev. B* **1999**, *60*, 10042. [26b] O. L. Malta, H. J. Batista, L. D. Carlos, *Chem. Phys.* **2002**, *282*, 21.
[27] [27a] O. L. Malta, M. A. Couto dos Santos, L. C. Thompson, N. K. Ito, *J. Lumin.* **1996**, *69*, 77. [27b] O. L. Malta, H. F. Brito, J. F. S. Menezes, F. R. Gonçalves e Silva, S. Alves Jr., F. S. Farias Jr., A. V. M. de Andrade, *J. Lumin.* **1997**, *75*, 255.
[28] M. H. V. Werts, R. T. F. Jukes, J. W. Verhoeven, *Phys. Chem. Chem. Phys.* **2002**, *4*, 1542.
[29] M. F. Hazenkamp, G. Blasse, *Chem. Mater.* **1990**, *2*, 105.
[30] C. W. Struck, W. H. Fonger, *Understanding Luminescence Spectra and Efficiency Using Wp and Related Functions*, Springer-Verlag, Berlin, **1978**.
[31] C. de Mello Donegá, S. J. L. Ribeiro, R. R. Gonçalves, G. Blasse, *J. Phys. Chem. Solids* **1996**, *11*, 1727.
[32] G. Blasse, N. Sabbatini, *Mater. Chem. Phys.* **1987**, *16*, 237.
[33] J.-C. G. Bünzli, P. Froidevaux, J. M. Harrowfield, *Inorg. Chem.* **1993**, *32*, 3306.
[34] R. Longo, F. R. Gonçalves e Silva, O. L. Malta, *Chem. Phys. Lett.* **2000**, *328*, 67.
[35] O. L. Malta, personal communication.
[36] R. G. Charles, A. Perrotto, *J. Inorg. Nucl. Chem.* **1964**, *26*, 373.
[37] R. Colton, I. B. Tomkins, *Aust. J. Chem.* **1965**, *18*, 447.
[38] M. J. Frisch, G. W. Trucks, H. B. Schlegel, G. E. Scuseria, M. A. Robb, J. R. Cheeseman, V. G. Zakrzewski, J. A. Montgomery, R. E. Stratmann, J. C. Burant, S. Dapprich, J. M. Millam, A. D. Daniels, K. N. Kudin, M. C. Strain, O. Farkas, J. Tomasi, V. Barone, M. Cossi, R. Cammi, B. Mennucci, C. Pomelli, C. Adamo, S. Clifford, J. Ochterski, G. A. Petersson, P. Y. Ayala, Q. Cui, K. Morokuma, D. K. Malick, A. D. Rabuck, K. Raghavachari, J. B. Foresman, J. Cioslowski, J. V. Ortiz, B. B. Stefanov, G. Liu, A. Liashenko, P. Piskorz, I. Komaromi, R. Gomperts, R. L. Martin, D. J. Fox, T. Keith, M. A. Al-Laham, C. Y. Peng, A. Nanayakkara, C. Gonzalez, M. Challacombe, P. M. W. Gill, B. G. Johnson, W. Chen, M. W. Wong, J. L. Andres, M. Head-Gordon, E. S. Replogle, J. A. Pople, GAUSSIAN 98 (Revision A.1), Gaussian, Inc., Pittsburgh, PA, **1998**.
[39] L. F. Pacios, P. A. Christiansen, *J. Chem. Phys.* **1985**, *82*, 2664.
[40] W. Stevens, H. Basch, J. Krauss, *J. Chem. Phys.* **1984**, *81*, 6026.
[41] W. J. Stevens, M. Krauss, H. Basch, P. G. Jasien, *Can. J. Chem.* **1992**, *70*, 612.
[42] L. VanMeervelt, A. Froyen, W. D'Olieslager, C. WalrandGorller, I. Drisque, G. S. D. King, S. Maes, A. T. H. Lenstra, *Bull. Soc. Chim. Bel.* **1996**, *105*, 377.

Received March 9, 2004
Early View Article
Published Online July 29, 2004

 © 2004 Wiley-VCH Verlag GmbH & Co. KGaA, Weinheim

Formation of Thermotropic and Lyotropic Liquid Crystals of Bis(*N*-alkylethylenediamine)silver(I) Nitrate

Masayasu Iida,*[a] Michiko Inoue,[a] Tomoaki Tanase,[a] Takae Takeuchi,[a] Makiko Sugibayashi,[b] and Kazuchika Ohta[b]

Keywords: Silver / N ligands / Liquid crystals / Microemulsions

We have synthesized bis(*N*-hexylethylenediamine)silver(I) nitrate ([Ag(hex-en)$_2$]NO_3), bis(*N*-octylethylenediamine)silver(I) nitrate ([Ag(oct-en)$_2$]NO_3), and bis(*N*-dodecylethylenediamine)silver(I) nitrate ([Ag(dod-en)$_2$]NO_3) and investigated the aggregation behavior of [Ag(dod-en)$_2$]NO_3 and [Ag(oct-en)$_2$]NO_3 in the liquid state. An X-ray crystallographic analysis revealed that [Ag(dod-en)$_2$]NO_3 has a dinuclear structure in the crystalline state — the molecular composition unit is [Ag_2(dod-en)$_4$](NO_3)$_2$, where the two dod-en ligands bridge two silver ions that are coordinated by four nitrogen atoms. The dinuclear complex is appreciably dissociated into a mononuclear complex in solution. It was found that [Ag(oct-en)$_2$]NO_3 and [Ag(dod-en)$_2$]NO_3 form thermotropic liquid crystals in the temperature ranges 48–67 °C and 59–96 °C, respectively, and a lyotropic liquid crystal was also observed for [Ag(dod-en)$_2$]NO_3 in *n*-heptane at around room temperature in the presence of a small amount of water. The structures of the thermotropic and lyotropic liquid crystals of [Ag(dod-en)$_2$]NO_3 were identified as a typical smectic A (S_A) type and a nematic one, respectively.
(© Wiley-VCH Verlag GmbH & Co. KGaA, 69451 Weinheim, Germany, 2004)

Introduction

The field of metallomesogens has developed rapidly in recent years.[1−5] Despite this, however, the lyotropic behavior of thermotropic metallomesogens has rarely been studied.[3−5] Furthermore, although metallosurfactants have characteristic structures and unique properties that are not seen in conventional surfactants, detailed and systematic studies on their aggregation behavior in solutions have not been carried out even for simple types of surfactants.[6−11]

Bis(*N*-alkylethylenediamine)metal complex surfactants form a variety of aggregates, since they have a delicate hydrophile-lipophile balance, and their double-chained molecular shape is favorable for the formation of highly ordered aggregates.[8−11] They easily form aggregates with appropriate amounts of encapsulating water in organic solvents of low dielectric constant, such as benzene and chloroform. One (M. Iida) of the present authors and coworkers has systematically investigated the physical properties and structural characterizations of highly aggregated systems such as bis(*N*-alkylethylenediamine)zinc(II), with various anions, dichlorobis(*N*-octylethylenediamine)cadmium(II), and bis(*N*-octylethylenediamine)palladium(II) chloride complexes in water/benzene or water/chloroform systems.[10,11] In a series of these studies, we have revealed the change in the geometry of the hydrocarbon chains of *N*-octylethylenediamine ligands in the zinc(II) complex from *transoid* to *cisoid* upon transfer from the crystalline state to the water/benzene interface in a microemulsion using Atomic Face Microscope (AFM) and Transmission Electron Microscope (TEM) methodologies.[10,11b,11c] Furthermore, the same group has synthesized and isolated bis(*N*-hexadecylethylenediamine)silver(I) nitrate ([Ag(hexd-en)$_2$]NO_3).[12] This complex is highly soluble in neat *n*-heptane and can be reduced in contact with an aqueous sodium borohydride solution to form silver(0) nanoparticles. An assembly of the silver ions of [Ag(hexd-en)$_2$]NO_3 in the *n*-heptane solution is advantageous to control the formation of silver(0) nanoparticles by changing the concentrations of the solutions, although the aggregation behavior has not been studied. A detailed characterization of this complex has also not been performed, although we have confirmed its formula and purity by elemental analysis and by ^{13}C NMR spectra. This complex is appreciably hydrophobic and we observed that it hardly incorporates water in *n*-hexane and therefore aggregation does not occur to a large extent.

For mesophases of silver(I) complexes, silver alkoxystilbazole complexes, including dinuclear complexes, have been extensively prepared, and the formation of both lyotropic and thermotropic liquid crystals has been studied.[4,5b] Con-

[a] Department of Chemistry, Nara Women's University, Kitauoya-nishi-machi, Nara 630-8506, Japan
[b] Department of Functional Polymer Science, Shinshu University, Ueda 386-8567, Japan
Supporting information for this article is available on the WWW under http://www.eurjic.org or from the author.

 © 2004 Wiley-VCH Verlag GmbH & Co. KGaA, Weinheim **DOI: 10.1002/ejic.200400167**

cerning (amine)silver(I) complexes, the formation of thermotropic liquid crystal of $[Ag(n\text{-}C_nH_{2n+1}NH_2)_2]NO_3$ has been reported.[13] This complex shows a lamellar phase consisting of U-shaped (double-chained) molecules. For the *N*-alkyl-substituted (ethylenediamine)silver complexes, however, a detailed molecular structure and the molecular assembly in the liquid state have not been reported.

In the present study we have synthesized and investigated the molecular aggregation behavior of $[Ag(dod\text{-}en)_2]NO_3$ in comparison with $[Ag(hex\text{-}en)_2]NO_3$ and $[Ag(oct\text{-}en)_2]NO_3$ (the three complexes are represented by $[Ag(alkyl\text{-}en)_2]NO_3$ and found that the structure of $[Ag(dod\text{-}en)_2]NO_3$ is dinuclear from the X-ray crystallographic analysis and that a thermotropic liquid crystal is formed below 100 °C. We furthermore found that $[Ag(dod\text{-}en)_2]NO_3$ forms a lyotropic liquid crystal in *n*-heptane by incorporating small amounts of water. We performed the characterization of the lyotropic liquid crystals and the studies on the aggregation behavior of the complexes in water/organic mixed solvents. The aggregation behavior of the silver complexes in water/organic mixed solvent systems was mainly studied by measurement of the self-diffusion of the silver complexes.

Results and Discussion

X-ray Crystallographic Analysis

An ORTEP drawing of the complex is given in Figure 1; selected crystal data are given in the Exp. Sect. Four *N*-dodecylethylenediamine ligands coordinate to the two silver ions in the crystalline state; the coordination geometry around each silver ion is tetrahedral. The nitrate ions are arranged between the silver ions only as counterions. The diamine complexes previously reported tend to form ethylenediamine-bridged polymeric structures such as $[Ag(en)^+]_\infty$ and $[Ag(tn)^+]_\infty$ (tn = 1,3-propanediamine); in these systems, the coordination number of the silver ions is two.[14a,14c] In the present complex, on the other hand, polymerization does not occur and the dod-en ligands bridge two silver ions. The substitution of the diamine protons by alkyl chains in the silver complex obviously has a blocking effect on the polymerization. A related dinuclear silver complex, $[Ag_2H_2(en)_3]^{4+}$, has previously been identified by X-ray crystallographic analysis.[14b] In that case, the ethylenediamine bridges are cleaved by protonation to form a dinuclear complex where only one ethylenediamine ligand bridges two silver ions; the coordination number of the silver ion is two.

Although the present result reveals the structure in the crystalline state to be dinuclear, this complex should be appreciably dissociated into a mononuclear one in organic solvents, as will be described below, and thus we express the three silver complexes by the rational formula $[Ag(dod\text{-}en)_2]NO_3$ from here on.

Formation of Thermotropic Liquid Crystals

The formation of thermotropic liquid crystals was established by Differential Scanning Calorimetry (DSC) and polarizing microscopic observations for the neat complexes as follows. $[Ag(dod\text{-}en)_2]NO_3$ is crystalline below 59 °C and forms a mesophase over the temperature range 59−96 °C. Large and small endothermic peaks were observed in the DSC curves for the respective transitions. The transition data are listed in Table 1. This mesophase gave an oily streak texture accompanied by spontaneous homeotropic alignment, as shown in Figure 2; the oily streak means that the phase should be a smectic A one. Thus, X-ray diffraction measurement was carried out at 75 °C. The profile is

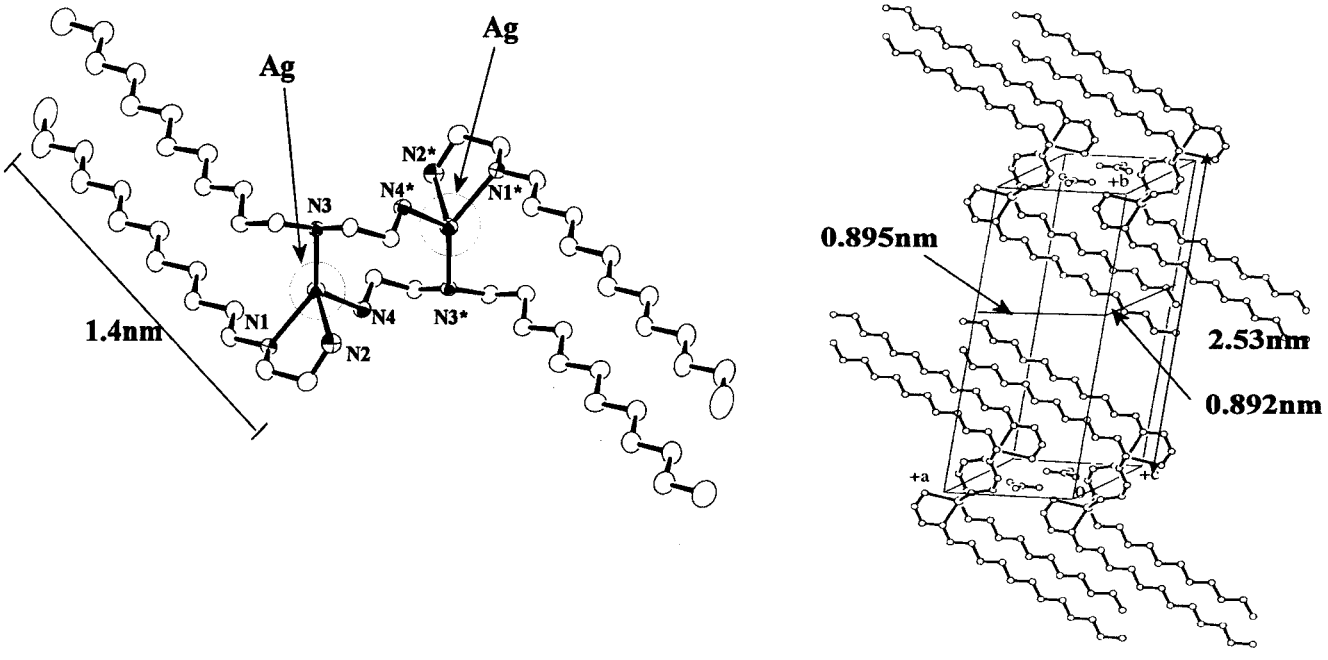

Figure 1. ORTEP diagram and atom-numbering system of $[Ag(dod\text{-}en)_2]No_3$

 © 2004 Wiley-VCH Verlag GmbH & Co. KGaA, Weinheim

described in Figure 3 and the peak data are summarized in Table 2. As can be seen in this table, it shows a series of periodic reflections characteristic of a lamellar structure. Therefore, this mesophase could be characterized as a smectic A phase, as illustrated in Figure 4. According to the X-ray crystallographic analysis (Figure 1), twice the alkyl chain length is around 2.8 nm (1.4 nm × 2), which is close to the lamellar layer length (3.1 nm). As shown in Figure 4, if the contribution of the headgroup to the layer length is significant, the alkyl chain is possibly shortened in the mesophase.

Table 1. Thermal data for the phase transitions in the complexes $[Ag(dod\text{-}en)_2]NO_3$ and $[Ag(oct\text{-}en)_2]NO_3$[a]

	K ⇄ LC	LC ⇄ IL
$[Ag(dod\text{-}en)_2]NO_3$	$T = 59$; $\Delta H = 148$	$T = 96$; $\Delta H = 3.6$
$[Ag(oct\text{-}en)_2]NO_3$	$T = 48$; $\Delta H = 98$	$T = 67$; $\Delta H = 3.2$

[a] Temperatures are given in °C and ΔH values in $kJ \cdot mol^{-1}$; K = crystal, LC = liquid crystal, IL = isotropic liquid.

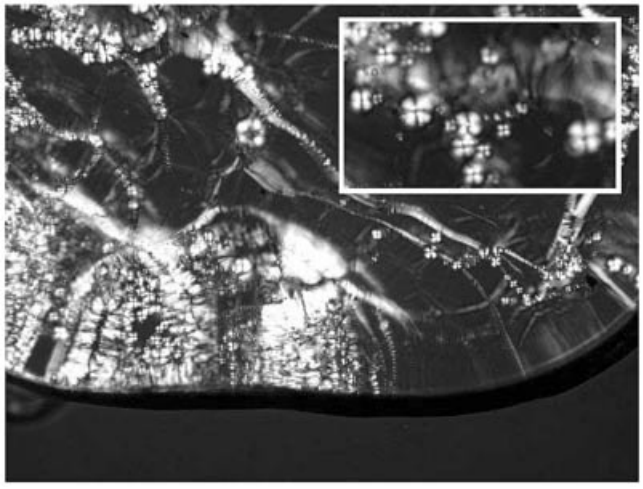

Figure 2. Optical textures observed for the neat $[Ag(dod\text{-}en)_2]NO_3$ complex at 75 °C

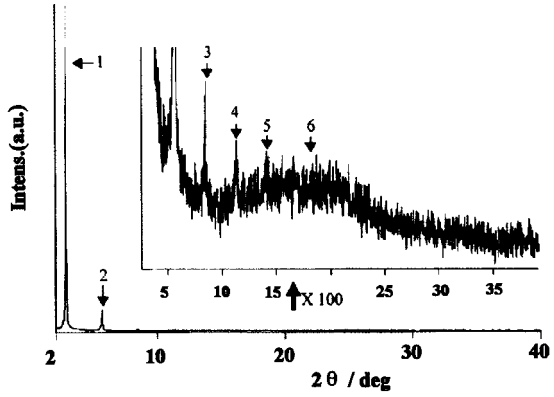

Figure 3. X-ray diffraction profile of the neat $[Ag(dod\text{-}en)_2]NO_3$ complex at 75 °C

$[Ag(oct\text{-}en)_2]NO_3$ also forms thermotropic liquid crystals but the formation is weaker than that for $[Ag(dod\text{-}en)_2]NO_3$. The thermal data are listed in Table 1; no liquid-crystalline phase was detected for $[Ag(hex\text{-}en)_2]NO_3$.

Table 2. X-ray data for the $[Ag(dod\text{-}en)_2]NO_3$ thermotropic liquid crystal at 75 °C

Peak no.	Spacings [Å]		Miller indices (*hkl*)	Lattice constant [Å]
	Observed	Calculated		
1	31.1	31.3	(001)	
2	15.7	15.6	(002)	
3	10.4	10.4	(003)	S_A; $c = 31.3$
4	7.81	7.82	(004)	
5	6.27	6.25	(005)	
6	ca. 4.7	–	[a]	

[a] Halo of molten alkyl chains.

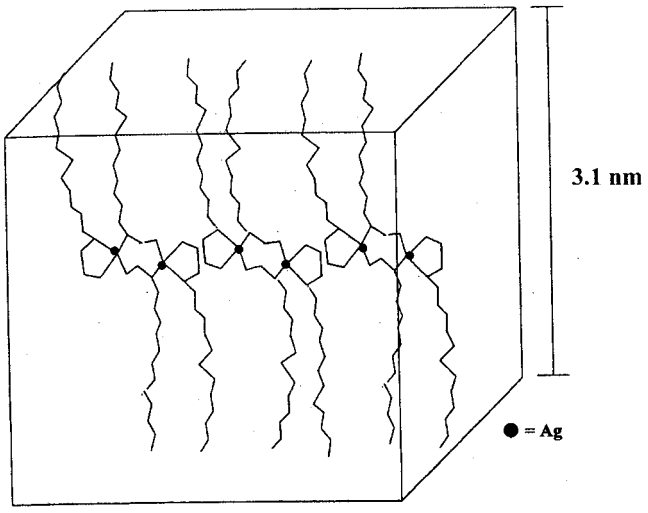

Figure 4. Schematic representation of the smectic A phase for the $[Ag(dod\text{-}en)_2]NO_3$ complex

Solubility of $[Ag(alkyl\text{-}en)_2]NO_3$ in Organic Solvents and Formation of a Lyotropic Liquid Crystal of $[Ag(dod\text{-}en)_2]NO_3$ in Water/*n*-Heptane

$[Ag(dod\text{-}en)_2]NO_3$ is soluble in only a few solvents. At 25 °C this complex is soluble [> 10% (wt/v)] in dichloromethane, and sparingly soluble [a few % (wt/v)] in methanol and ethanol. The $[Ag(oct\text{-}en)_2]NO_3$ complex, on the other hand, is readily soluble in DMF, acetone, benzene, and 1,4-dioxane, and sparingly soluble in dichloromethane, ethyl acetate, diethyl ether, and chloroform. This complex is not stable in methanol and ethanol. The most hydrophilic complex, $[Ag(hex\text{-}en)_2]NO_3$, is readily soluble in many solvents, such as water, DMF, methanol, ethanol, acetone, dichloromethane, ethyl acetate, and 1,4-dioxane. As this complex seems to have similar properties to common surfactants, a detailed study of its aggregation behavior has not been performed.

It is noteworthy that the solubility of $[Ag(dod\text{-}en)_2]NO_3$ in *n*-heptane and 1,4-dioxane and that of $[Ag(oct\text{-}en)_2]NO_3$ in *n*-heptane are largely enhanced by the presence of small amounts of water. Such a solubility phenomenon does not

 © 2004 Wiley-VCH Verlag GmbH & Co. KGaA, Weinheim

occur for $[Ag(hex\text{-}en)_2]NO_3$. This solubility enhancement suggests the formation of aggregates of the metal complexes surrounding a water "pool", where the hydrophilic sites of the silver complex ions would be collected. Figure 5 shows three-component phase diagrams of the $[Ag(dod\text{-}en)_2]NO_3$ and $[Ag(oct\text{-}en)_2]NO_3$ systems for the formation of transparent and homogeneous solutions in water/1,4-dioxane and water/*n*-heptane mixed solvent systems. It is interesting to compare the preferable interaction between the silver complexes and solvents with those of our previous studies for $[ZnCl_2(oct\text{-}en)_2]$, $[CdCl_2(oct\text{-}en)_2]$, and $[Pd(oct\text{-}en)_2]Cl_2$.[11,15] The zinc complex of a weak electrolyte and the palladium complex of a strong electrolyte are extensively dissolved in water/benzene and water/chloroform mixed solvents, respectively, to form large aggregates (microemulsions). The higher affinity of the $[Ag(dod\text{-}en)_2]NO_3$ and $[Ag(oct\text{-}en)_2]NO_3$ complexes for *n*-heptane than for more polar solvents such as benzene and chloroform indicates their higher hydrophobicity compared to $[ZnCl_2(oct\text{-}en)_2]$ and $[CdCl_2(oct\text{-}en)_2]$ despite their being strong electrolytes. The $[Ag(hexd\text{-}en)_2]NO_3$ complex previously reported is soluble in neat *n*-heptane without water[12] and does not incorporate even small amounts of water in *n*-heptane. The result of the $[Ag(dod\text{-}en)_2]NO_3$/water/*n*-heptane system (Figure 5b) shows that the transparent and homogeneous phase is especially large in the $[Ag(dod\text{-}en)_2]NO_3$ complex; this feature reflects the moderate hydrophile/lipophile balance of this complex. The dinuclear complex is almost completely changed to the mononuclear complex in solution, as will be described below. This structural change may also cause the unique solubility phenomena.

We also found a very narrow phase region of lyotropic liquid crystals in the $[Ag(dod\text{-}en)_2]NO_3$/water/*n*-heptane system (Figure 5b). The structural characterization and studies of the physical properties are discussed below.

Vapor-Pressure Depression, Electric Conductivity, and Mass Spectrometric Studies for the $[Ag(dod\text{-}en)_2]NO_3$ Complex in Some Organic Solvents

We measured the physical properties of solutions to determine the aggregation behavior of the $[Ag(dod\text{-}en)_2]NO_3$ complex. The apparent molecular weight (MW_{app}) of the complex was estimated from the vapor-pressure depression Δp [which is proportional to ΔT of Equation (2) in the Exp. Sect.] of the solutions (methanol, dichloromethane, and *n*-hexane systems) as a function of the silver complex concentrations (m; $g \cdot kg^{-1}$). As a first approximation, we estimated the MW_{app} values by assuming that the silver complex is a nonelectrolyte. The ΔT vs. m plots are slightly curved for dichloromethane and methanol solutions. The MW_{app}/MW ratios (R_{MW}) obtained for $[Ag(dod\text{-}en)_2]NO_3$ (626.72) were 1.5−2.5 in dichloromethane {$[Ag(dod\text{-}en)_2]NO_3$ =

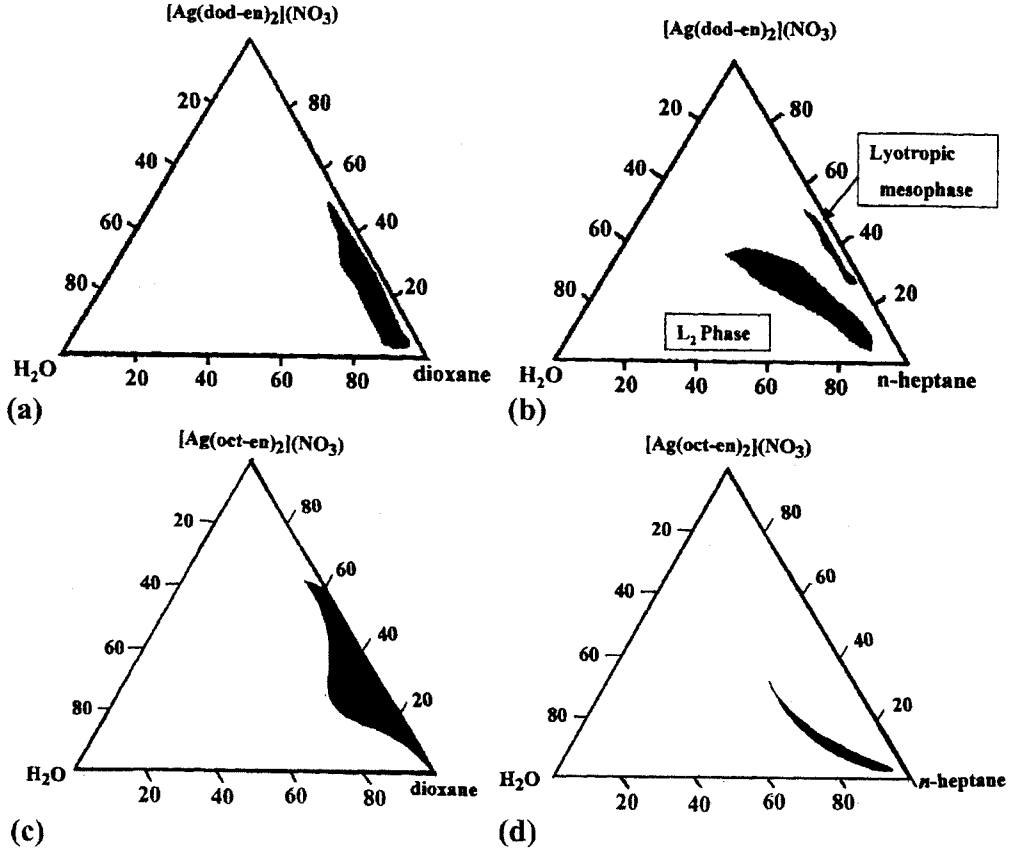

Figure 5. (a) Partial mass (wt.-%) ternary phase diagrams for the transparent and homogeneous solutions in the $[Ag(dod\text{-}en)_2]NO_3$/1,4-dioxane/water system at 30 °C; (b) partial mass (wt.-%) ternary phase diagrams for the homogeneous solutions in the $[Ag(dod\text{-}en)_2]NO_3$/*n*-heptane/water system at 30 °C; L_2 is water in oil phase

 © 2004 Wiley-VCH Verlag GmbH & Co. KGaA, Weinheim

0.19−1.29 mol·kg^{-1}}, 0.8−1.1 in methanol {[Ag(dod-en)$_2$]NO_3 = 0.04−0.51 mol kg^{-1}}, and 15.5 in *n*-heptane {[Ag(dod-en)$_2$]NO_3 = 0.97−1.32 mol kg^{-1}}, where a small amount of water is present and the phase is a lyotropic liquid crystal. The obtained R_{MW} values are < 2 under some conditions. This is due to two factors, one of which is the dissociation of the salt into the silver complex ion and the nitrate ion and the other is the dissociation of the dinuclear complex into the mononuclear one. Concerning the former factor, we measured electric conductivities of the [Ag(dod-en)$_2$]NO_3 methanol solutions in the concentration range 0.01−0.12 mol·dm^{-3}. At lower concentrations, the molar electric conductivities depend on the concentration and almost obey the Onsager equation assuming a 1:1 electrolyte (Supporting Information; Figure S1a). As the dependence of the electric conductivity on the concentration is larger than that of the self-diffusion, we estimated the limiting molar conductivity of the silver complex ion in order to obtain a more accurate value by use of the self-diffusion coefficient of the silver complex ion according to the Nernst equation.[16] [The limiting molar conductivity (Λ^0) of the silver complex thus obtained was 8.7 × 10^{-3} S·m^2·mol^{-1} by using λ_0 = 6.1 × 10^{-3} S·m^2·mol^{-1} for the nitrate ion in methanol at 25 °C; this Λ^0 value is reasonable as an extrapolated value.] This result indicates that at lower concentrations in methanol this complex would be completely dissociated into [Ag(dod-en)$_2$]$^+$ and NO_3^-. At higher concentrations, where the vapor-pressure depression was measured, the Onsager plot is largely curved and the ionic interactions become stronger and more complicated. The R_{MW} value of 0.8−1.0 obtained from the VPO measurement in this concentration range means that the interaction between [Ag(dod-en)$_2$]$^+$ and NO_3^- is stronger than that at lower concentrations. In methanol, the electric conductivities (κ) are around 0.1−0.5 S·m^{-1} at 0.01−0.2 mol·dm^{-3}, whereas in dichloromethane they are around 0.1−0.2 S·m^{-1} at 0.12−0.90 mol·dm^{-3} (Supporting Information; Figure S1b). The significantly smaller electric conductivities in dichloromethane mean that the dissociation of the silver complex into the monomer or into the ions occurs to a lesser extent in dichloromethane than in methanol. This trend is consistent with the result of the vapor-pressure depression.

In order to determine the nature of the species in solution, we also measured nano-ESI mass spectra of the silver dod-en complexes in methanol and in dichloromethane. A typical spectrum is shown in Figure 6. The percentages of the peak areas of [Ag$_2$(dod-en)$_4$]NO_3^+ (*m*/*z* = 1188.82, $^{12}C_{56}{}^{1}H_{128}{}^{107}Ag_2{}^{14}N_9{}^{16}O_3$)/[Ag$_2$(dod-en)$_3$]$NO_3^+$ (*m*/*z* = 960.57, $^{12}C_{42}{}^{1}H_{96}{}^{107}Ag_2{}^{14}N_7{}^{16}O_3$)/[Ag(dod-en)$_2$]$^+$ (*m*/*z* = 563.42, $^{12}C_{28}{}^{1}H_{64}{}^{107}Ag^{14}N_4$) were as follows: 2.4%/4.6%/93% for a 0.048 mol·dm^{-3} methanol solution, 7.2%/7.2%/85.6% for a 0.064 mol·dm^{-3} dichloromethane solution, and 10.2%/15.6%/74.2% for a 0.16 mol·dm^{-3} dichloromethane solution. Although the percentages obtained do not necessarily reflect the distribution of each species in solution due to complicated ionization processes, this result does not conflict with the view that the dinuclear complex found in the crystalline state would be appreciably dissociated into the mononuclear complex even at moderate concentrations in organic solvents. A similar formation of mixed mononuclear and dinuclear ethylenediamine (en) complexes of silver such as Ag(en)$^+$, Ag$_2$(en)$^{2+}$, Ag(en)$_2^+$, and Ag$_2$(en)$_2^{2+}$ has been previously reported in water.[17] For the en complex, a

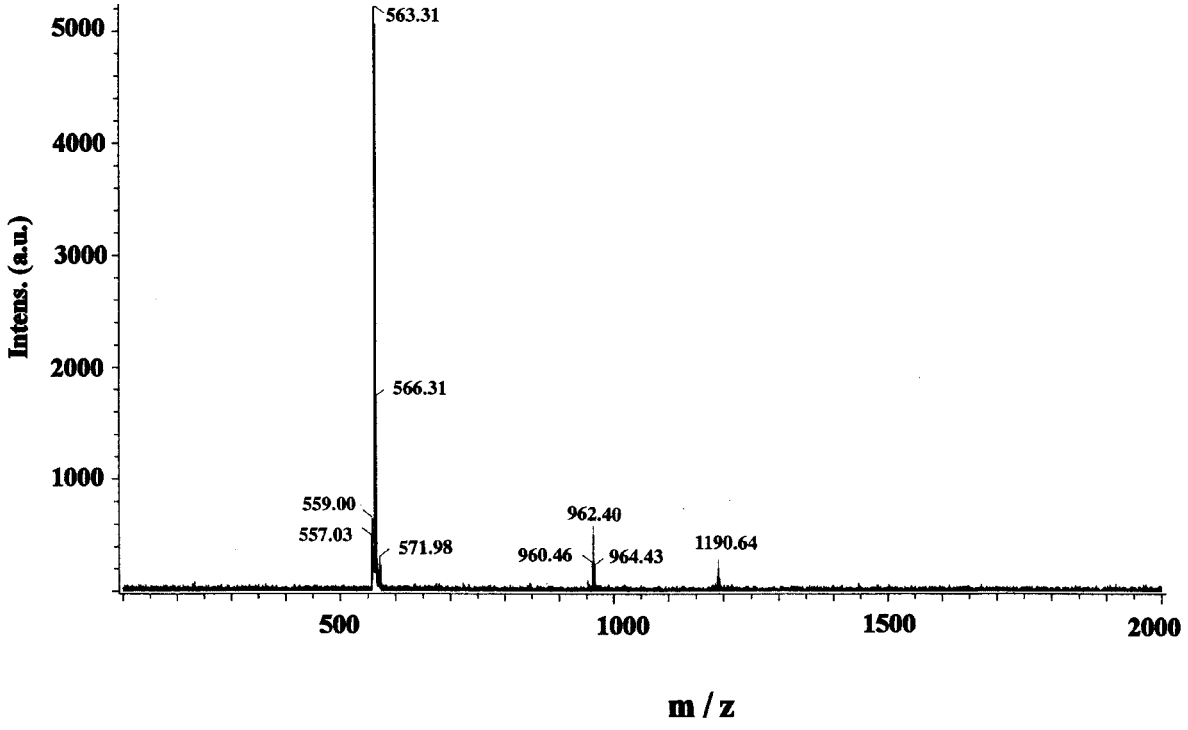

Figure 6. Nano-ESI-TOF mass spectrum of 0.16 M [Ag$_x$(dod-en)$_y$](NO$_3$)$_z$ complexes in dichloromethane

 © 2004 Wiley-VCH Verlag GmbH & Co. KGaA, Weinheim

polynuclear structure in the solid state decomposes into the dinuclear and mononuclear complexes in water.

Observation of the Lyotropic Liquid Crystal by Micrograph for the [Ag(dod-en)$_2$]NO$_3$/Water/n-Heptane System

Figure 7 shows a photomicrograph of the lyotropic mesophase in [Ag(dod-en)$_2$]NO$_3$/water/*n*-heptane mixtures at room temperature. It gave a schlieren texture containing both two and four brushes, which is characteristic of a nematic phase.[18] Hence, this lyotropic mesophase can be identified as a nematic phase. As the molecular structure of this dinuclear and double-chained complex is favorable to form thermotropic liquid crystals at temperatures higher than room temperature, this molecule furthermore loses order in one dimension in the water-containing *n*-heptane to form a nematic lyotropic liquid crystal. The presence of small amounts of water plays an important role in the stabilization of the liquid-crystalline structure by assembling the headgroup of the silver complex and by organizing the supramolecules. This difference in the superstructure of this complex between the neat state and the solution state can be attributed to a loss of molecular orderings in the assemblies by the presence of *n*-heptane. It is notable that the dinuclear complex in the crystalline state would be significantly dissociated into a monomer in organic solvents as described above. The presence of small amounts of water will promote this dissociation. Thus, the lyotropic liquid crystal may be mainly composed of a mononuclear double-chained [Ag(dod-en)$_2$]NO$_3$ complex. As the dissociation of the nitrate ions from the silver salt in the water/*n*-heptane system may be slight because of a large excess of *n*-heptane over water in the lyotropic liquid crystalline phase, the R_{MW} value (15.5) obtained from the vapor-pressure depression in the water/*n*-heptane system will be close to the aggregation number of [Ag(dod-en)$_2$]NO$_3$ ion-pairs.

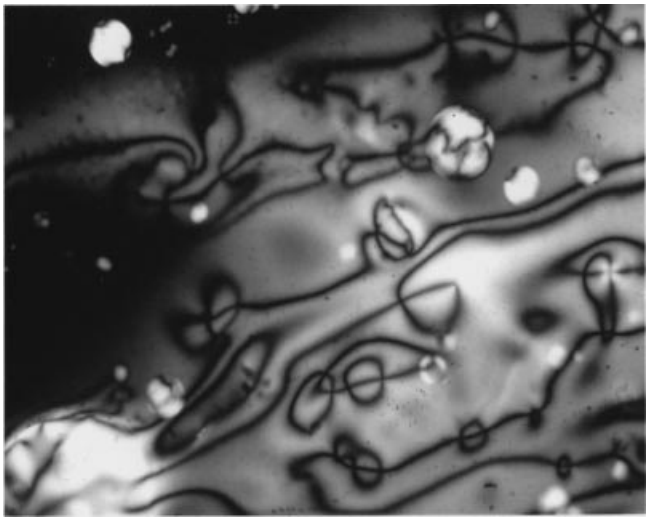

Figure 7. Optical texture observed for the lyotropic liquid crystal of the [Ag(dod-en)$_2$]NO$_3$/water/*n*-heptane system

^{2}H NMR Spectra and Small-Angle X-ray Scattering (SAXS) for the Lyotropic Mesophase

The lyotropic liquid crystal forms in very narrow composition and temperature ranges, and the small amounts of water play an important role in forming the mesophase. In order to monitor the formation of lyotropic mesophases containing water from a microscopic viewpoint, we expected the ^{2}H NMR spectra to provide useful information. As the water content in the present lyotropic mesophase is small (W_0 = [water]/[silver complex] < 2), most water molecules can be regarded as water of hydration. Thus, we can directly monitor the nature of the aggregates in the ne-

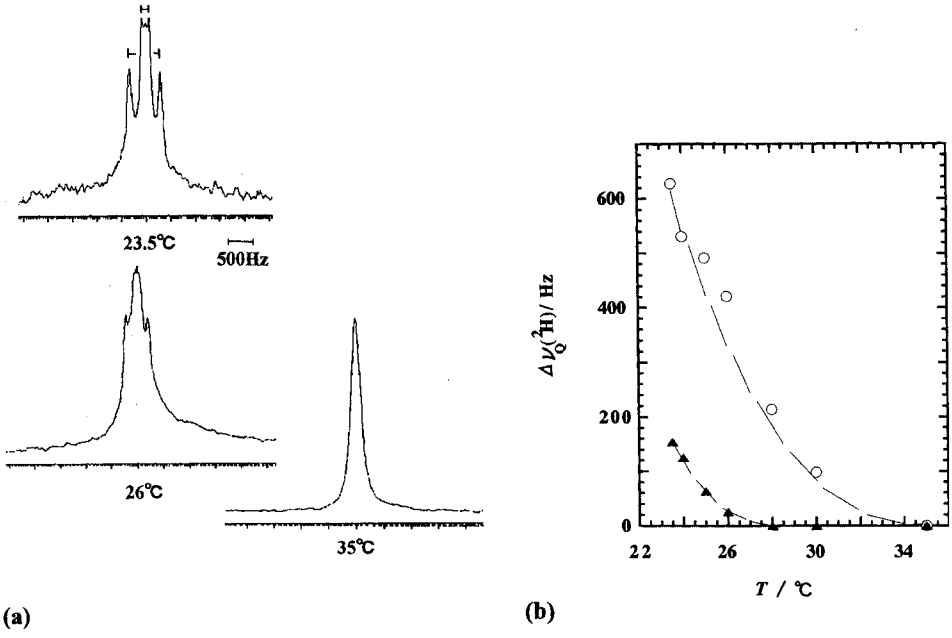

Figure 8. (a) ^{2}H NMR spectra of the trace water in the [Ag(dod-en)$_2$]NO$_3$/water/*n*-heptane system as a function of temperature (W_0 = 1.7 and m = 1.2 mol kg^{-1}); (b) change in the ^2H_2O quadrupole splitting for the two kinds of liquid crystalline peaks

 © 2004 Wiley-VCH Verlag GmbH & Co. KGaA, Weinheim

matic lyotropic mesophase by ^{2}H NMR spectroscopy. Figure 8a shows the ^{2}H NMR spectra of trace water in the $[Ag(dod\text{-}en)_2]NO_3$/water/*n*-heptane system as a function of temperature. The ^{2}H NMR quadrupole splittings of the liquid-crystalline spectra as a function of temperature are shown in Figure 8b. The absolute values of the quadrupole splittings are consistent with a nematic phase.[19] This figure indicates the presence of two kinds of hydration modes. As the exchange of the hydration water between the two states is slow enough on the NMR timescale, the two kinds of water would reflect those of molecular assemblies.

We observed one SAXS peak at $2\theta = 1.4°$ ($d = 6.3$ nm, which is nearly twice the bilayer thickness of 3.1 nm) in the same lyotropic mesophase as used for the ^{2}H NMR spectra; no clear peak was observed in the SAXS spectrum for the isotropic microemulsions (L_2 phase in Figure 5b). Therefore, it is possible that the smaller ^{2}H NMR splitting arises from hydration of the domains close to the isotropic microemulsions.

The narrow temperature and concentration ranges of the nematic lyotropic mesophase mean that the mesophase could form because of the delicate balance of the hydrophilicity/lipophilicity of the silver complex and the selective hydration in *n*-heptane solution.

Self-Diffusion Studies for the Aggregation of $[Ag(dod\text{-}en)_2]NO_3$ in Solution

The self-diffusion coefficients of the solvent and solute were calculated to monitor the extent of aggregation, especially in mixed-component systems. We thus measured the diffusion coefficients of the $[Ag(dod\text{-}en)_2]NO_3$ complex and the solvents in water/*n*-heptane and dichloromethane in comparison with those in methanol where aggregation hardly occurs.

Figure 9 shows the results for water and the silver complex as a function of the silver complex concentrations. In the water/*n*-heptane system, the solute concentration is expressed for the neat *n*-heptane solvent (neglecting small amounts of water). In Figure 9a, the diffusion coefficients in methanol could be obtained only in a very narrow concentration range due to solubility limitations; those at low concentration are regarded as those of the monomer.

The diffusion coefficients obtained can be interpreted on the basis of the Stokes−Einstein equation at infinite dilution according to Equation (1), where R is the Stokes radius for the monomer, k the Boltzmann constant, T the absolute temperature, and η_0 the viscosity of the solvent.

$$R = kT/6\pi\eta_0 D_0 \quad (1)$$

We can estimate the Stokes radius for the silver complex in dilute methanol solution or in dichloromethane by an extrapolation of the diffusion coefficients to an infinite dilution in Figure 9a; we obtain a D_0 value in methanol of 6.8×10^{-10} m^2·s^{-1} and in dichloromethane of 8.4×10^{-10} m^2·s^{-1}. By using an η_0 value for methanol of 0.542 mPa s[20] and a value for dichloromethane of 0.41 mPa·s at 25 °C[20] the R values are 0.67 nm and 0.71 nm, respectively. The larger size in dichloromethane is consistent with the results of the vapor-pressure depression and mass spectrometric measurements. The significant decrease in the diffusion coefficients at higher concentrations indicates the extensive aggregation.[21]

As deuterated *n*-heptane is unobtainable, we measured the diffusion coefficients of the silver complex in water/*n*-heptane solutions indirectly as will be described in the Exp. Sect. The measurements of diffusion coefficients in the *n*-heptane/water system were performed in both the water in oil (w/o) microemulsion phase (larger W_0 regions) and the lyotropic liquid-crystalline phase (smaller W_0 regions) (Figure 9b). We can furthermore estimate the Stokes radius for the metal complex in *n*-heptane ($D_0 = 8.7 \times 10^{-11}$ m^2·s^{-1})

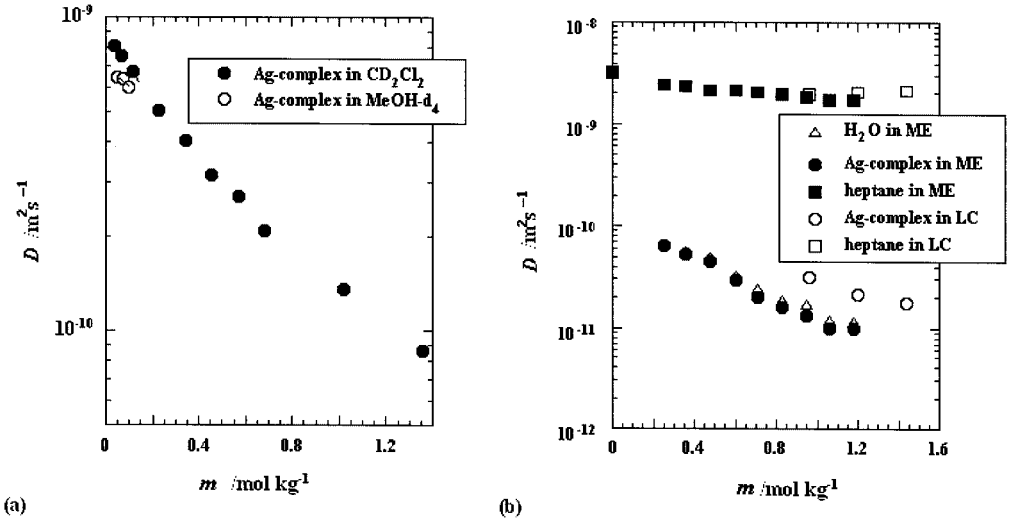

Figure 9. (a) Diffusion coefficients for the $[Ag(dod\text{-}en)_2]NO_3$ complex in $[D_4]$MeOH and $[D_2]$dichloromethane as a function of the mononuclear silver complex concentration; (b) diffusion coefficients for water, *n*-heptane, and the complex in the $[Ag(dod\text{-}en)_2](NO_3)_2$/*n*-heptane/water system [in the microemulsion (ME) and liquid crystal (LC) systems] as a function of the mononuclear silver complex concentrations ($W_0 = 30$ in the ME system and $W_0 = 1.7$ in the LC system)

 © 2004 Wiley-VCH Verlag GmbH & Co. KGaA, Weinheim

by neglecting small amounts of water. (η_0 = 0.397 mPa·s for *n*-heptane) The obtained value of 6.4 nm is appreciably larger than those in methanol and dichloromethane. This result clearly indicates that the silver complex is readily dissolved in *n*-heptane only when large aggregates are formed by incorporation of water.

We can see the other two characteristic features in Figure 9b. Firstly, the diffusion coefficient of water is appreciably smaller than that of *n*-heptane and is slightly larger than that of the silver complex. Secondly, the diffusion coefficients of the silver complex in the liquid-crystalline region are significantly larger and those of solvent *n*-heptane are also slightly larger than those in the microemulsion systems. The first feature in the water diffusion means that water tends to move together with the silver complex and is motionally restricted to a large extent. This indicates the formation of reversed micelles or W/O microemulsions. The second feature is consistent with a nematic liquid crystal characterized by a polarizing microscope, since the viscosity of the nematic lyotropic liquid crystal will be lower than that of the isotropic phase of the same surfactant concentration. The water content is appreciably smaller in the lyotropic liquid crystal than in the W/O microemulsion state in spite of the slightly larger concentration of the silver complex in the former state. This difference of the silver complex concentration will tend to make the diffusion coefficient in the liquid crystal phase smaller than that in the W/O microemulsion system. However, the result obtained is opposite to this prediction, which may reflect the lower viscosity of the nematic-type liquid crystal. Although *n*-heptane seems to be an unfavorable solvent to form lyotropic liquid crystals due to a lower molecular rigidity and a lower polarity, the rigid structure of the present complex and the small amounts of incorporated water may play important roles in forming the anisotropic superstructure.

In order to see the water effect on the aggregation, we furthermore measured the diffusion coefficients of the silver complexes depending on the water content in the 1,4-dioxane and *n*-heptane systems. Figure 10a shows that in the 1,4-dioxane/water system the diffusion coefficients of $[Ag(hex\text{-}en)_2]^+$, $[Ag(oct\text{-}en)_2]^+$, and $[Ag(dod\text{-}en)_2]^+$ slightly increase with increasing water content. In this figure, the silver complex concentration is expressed for the neat 1,4-dioxane solvent. The diffusion coefficients increase probably due to the dilution of the solution with an addition of water. The dod-en complex is dissolved in 1,4-dioxane in the presence of water and the effect of water on the aggregation of $[Ag(dod\text{-}en)_2]^+$ is only slight, contrary to the dilution effect. This result means that water assists the dissolution of this complex in 1,4-dioxane by the formation of aggregates.

This effect of water on the diffusion appears more clearly in the *n*-heptane system, as shown in Figure 10b, where it is characteristic that addition of water decreases the diffusion coefficients of the $[Ag(dod\text{-}en)_2]^+$ complex and of both solvents. In this system, water clusters move together with the silver complex aggregates and assist the aggregation of the silver complex. As the diffusion of *n*-heptane is also decreased by addition of water, water will assist the aggregation of the silver complex to form a W/O microemulsion more than in the 1,4-dioxane system. The effect of the aggregation on the diffusion would be larger than the opposite effect on aggregation due to dilution with an increase in the water content, and thus the diffusion is decreased by addition of water.

In conclusion, we have synthesized and characterized new amphiphilic alkylethylenediamine dinuclear silver complexes. Although the ligand is regarded as a simple and common type, a unique rigid structure of the tetrakis(dodecyl)-substituted complex gives rise to a formation of therm-

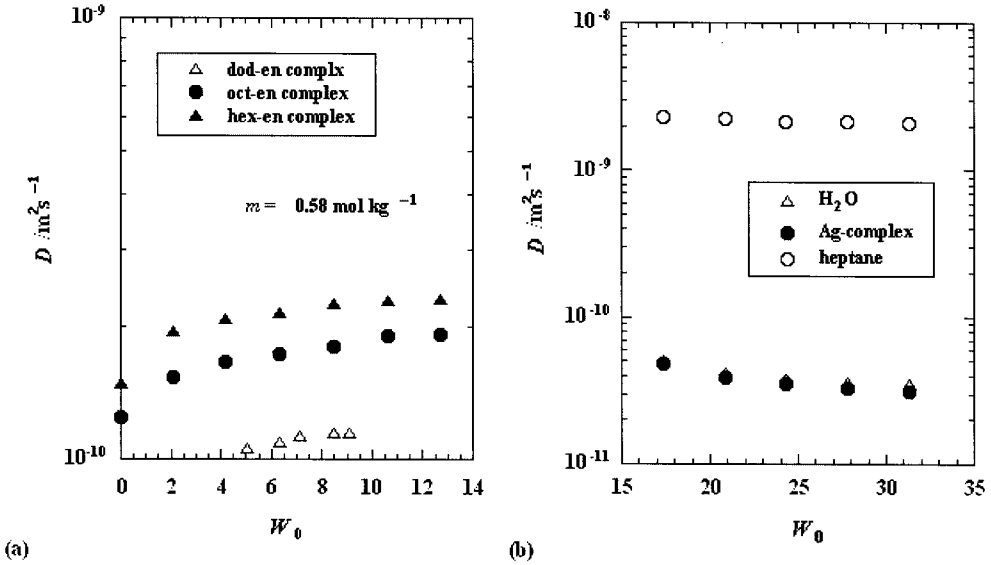

Figure 10. (a) Diffusion coefficients of $[Ag(hex\text{-}en)_2]^+$, $[Ag(oct\text{-}en)_2]^+$, and $[Ag(dod\text{-}en)_2]^+$ in water-containing $[D_8]$1,4-dioxane systems as a function of the water content; (b) diffusion coefficients of $[Ag(dod\text{-}en)_2]^+$ and the solvents in the water-containing *n*-heptane system as a function of the water content

 © 2004 Wiley-VCH Verlag GmbH & Co. KGaA, Weinheim

otropic liquid crystals. Small amounts of water play an important role in concentrating the silver headgroup in the nanosized water pools and thereby aligning the assemblies of the silver complex for the superstructure.

Experimental Section

Materials: *N*-Hexylethylenediamine, *N*-octylethylenediamine, and *N*-dodecylethylenediamine were prepared according to reported procedures.[11a,11b] The silver complexes were synthesized according to a similar procedure as described for the *N*-hexadecylethylenediamine complex but the crystallization from the reaction mixtures was performed by the addition of cyclohexane to a methanol solution. The molecular formula and purity were determined by elemental analyses and ^{13}C NMR spectroscopy. The yields after recrystallization were about 80%. $[Ag(hex\text{-}en)_2]NO_3$: $C_{16}H_{40}AgN_5O_3$ (458.41): calcd. C 41.92, H 8.80, N 15.28; found C 41.69, H 8.80, N 15.17. $[Ag(oct\text{-}en)_2]NO_3$: $C_{20}H_{48}AgN_5O_3$ (514.50): calcd. C 46.69, H 9.40, N 13.61; found C 46.64, H 9.31, N 13.47. $[Ag(dod\text{-}en)_2]NO_3$: $C_{28}H_{64}AgN_5O_3$ (626.7): calcd. C 53.66, H 10.29, N 11.17; found C 53.92, H 10.15, N 11.20. Chloroform, dichloromethane, methanol, and 1,4-dioxane were guaranteed grades supplied by Wako Pure Chemical Industries. Chloroform was purified as previously reported.[11d] Dichloromethane was dried with calcium chloride and then distilled; the water content was $< 1 \times 10^{-3}$ %. Methanol and 1,4-dioxane were distilled once before use. Water was distilled twice. The deuterated solvents (D_2O, $[D_4]$MeOH, $[D_2]$dichloromethane, and $[D_8]$1,4-dioxane) were supplied by Merck Co.

Single-Crystal X-ray Diffraction Analysis for $[Ag(dod\text{-}en)_2]NO_3$: A colorless plate ($0.30 \times 0.25 \times 0.05$ mm) was fixed on the top of a glass fiber with Paraton N oil, and 3854 reflections ($6° < 2\theta < 52°$) were measured with a Rigaku/MSC Mercury CCD diffractometer with graphite-monochromated Mo-K_α radiation at −70 °C. An absorption correction by a spherical multiscan method was applied ($\mu = 6.1$ cm^{-1}). The structure was solved by direct methods using the program SIR92[22] and was refined with full-matrix least-squares techniques to $R = 0.061$ and $R_w = 0.066$ for 4517 independent reflections with $I > 2\sigma(I)$. All non-hydrogen atoms were refined anisotropically and the hydrogen atoms, located in ideal positions, were not refined. All calculations were performed with a Silicon Graphics O2 Station with the teXsan program system.[23] The crystal data and experimental details are summarized in Table 3. CCDC-244806 contains the supplementary crystallographic data for this paper. These data can be obtained free of charge at www.ccdc.cam.ac.uk/conts/retrieving.html [or from the Cambridge Crystallographic Data Centre, 12 Union Road, Cambridge CB2 1EZ, UK; Fax: (internat.) + 44-1223-336-033; E-mail: deposit@ccdc.cam.ac.uk].

Observations of the Structures of the Liquid Crystals: Thermotropic and lyotropic mesomorphisms were established using the samples exhibiting satisfactory elemental analysis data of C, H and N. For the thermotropic mesomorphism, the phase-transition phenomenon was observed using a polarizing microscope (Olympus BH2), equipped with a heating plate controlled by a thermo-regulator (Mettler FP80 hot stage, Mettler FP82 central processor), and measured by a differential scanning calorimeter (Shimadzu DSC-50). The X-ray diffraction measurement for the thermotropic liquid crystal was performed with Cu-K_α radiation (Rigaku RAD) equipped with a hand-made heating plate[24] controlled by a thermo-regulator. For the lyotropic system, the mesophase at room temperature was characterized by the polarizing microscope, ^2H_2O NMR spectroscopy, and small-angle X-ray scattering ($0.5° < 2\theta < 5°$) with Cu-K_α radiation (Rigaku RAD), where a plastic cell of 3 mm thickness with mica windows was used and the intensity distribution was measured with a position-sensitive proportional counter (PSPC).

Table 1. Crystallographic and experimental data for $[Ag(dod\text{-}en)_2]NO_3$

Empirical formula	$C_{56}H_{128}Ag_2N_{10}O_6$
Formula mass	1253.43
Crystal system	triclinic
Crystal size [mm]	$0.30 \times 0.25 \times 0.05$
Space group	$P\bar{1}$ (no. 2)
a [Å]	8.9479(2)
b [Å]	25.318(3)
c [Å]	8.9207(2)
α [°]	80.33(2)
β [°]	118.51(2)
γ [°]	95.64(2)
V [Å^3]	1750.2(4)
Z	1
T [°C]	70
D_{calcd} [g cm^{-3}]	1.189
Abs coeff [cm^{-1}]	6.06
Diffractometer	Rigaku/MSC Mercury CCD
ω oscillation range [°]	70.0−100.0
Exposure rate [s/°]	120
Data images	1440
2θ range [°]	$6 < 2\theta < 52$
No. of unique data	6135
No. of obsd. data	4517 [$I > 2\sigma(I)$]
No. of variables	335
Data/parameters	13.48
R[a]	0.061
R_w[a]	0.066
GOF[b]	1.50

[a] $R = \Sigma||F_o| - |F_c||/\Sigma|F_o|$; $Rw = [\Sigma w(|F_o| - |F_c|)^2/\Sigma w|F_o|^2]^{1/2}$ [$w = 1/\sigma^2(F_o)$]. [b] GOF $= [\Sigma w(|F_o| - |F_c|)^2/[N_o - N_p]^{1/2}$ (N_o = number of data, N_p = number of variables).

NMR Measurements: The aggregation behavior in solution was monitored by NMR spectroscopy. The ^2H NMR spectra were obtained with a JEOL JNM EX-270 FT NMR spectrometer operating at 41.5 MHz for 20% enriched ^2H_2O, small amounts of which are contained in the lyotropic liquid crystalline system. The self-diffusion coefficients were measured by the NMR PFG (Pulsed Field Gradient) technique.[25] The measurements were performed with a JEOL FX-90 spectrometer operating at 90 MHz for ^1H. The spectrometer was equipped with an apparatus that produced a field gradient in the range 0.3−1.0 T/m. For water, the change in the intensity of the ^1HDO signal was monitored. For the surfactant, the intensity of the methylene ^1H signals of the alkyl chains was monitored. In the *n*-heptane (deuterated reagent was not supplied) system, the ^1H peaks of the silver complex were completely covered by those of the solvent. However, the attenuation of the spin-echo amplitude after the Fourier transformation of the solvent peaks decayed much more rapidly with a change in the duration (δ) of the applied gradient pulses ($0.2 < \delta < 5$ ms) than that of the silver complex. Thus, we could obtain the diffusion coefficients of the silver complexes even in the *n*-heptane system. The accuracy of the measured diffusion coefficients is estimated to be better than ±5%, although that for the silver complex in the *n*-heptane system is somewhat worse.

 © 2004 Wiley-VCH Verlag GmbH & Co. KGaA, Weinheim

Other Measurements: The vapor-pressure depressions for the solutions of methanol, dichloromethane, and *n*-heptane containing small amounts of water[26] were measured with a Knauer Vapor Pressure Osmometer (VPO) at 45 °C. The magnitude of the depression is proportional to the difference in temperatures (ΔT) between a solvent-wetted thermistor and a solution-wetted one. If the dissociation of the counterion is negligible, Equation (2) can be applied, where k is a constant depending on the solvent and the apparatus used, M_1 the apparent molecular weight of the solute, and m' the solute concentration in g·kg^{-1}.

$$\Delta T = km'/M_1 \quad (2)$$

The k value was determined from benzil solutions. The electric conductivities of the methanol and dichloromethane solutions were measured using an admittance linear bridge (FUSO 362A) operated at 1 kHz. The mass spectra of the silver dod-en complexes in methanol and dichloromethane were measured with a Jeol JMS-T100 (AccuTOF) ESI-TOF mass spectrometer.

[1] [1a] T. Sierra, *Metallomesogens* (Ed.: J. L. Serrano), VCH, Weinheim, **1996**, chapter 2. [1b] A. M. Giroud-Godquin, *Metal-Containing Liquid Crystals* (Eds.: D. Demus, J. Goodby, G. W. Gray, H. -W. Spiess, V. Vill), Wiley-VCH, Weinheim, **1998**, vol. 2B, chapter 14. [1c] D. W. Bruce, *Inorganic Materials* (Eds.: D. W. Bruce, D. O'Hare), Wiley, Chichester, **1996**, chapter 8.

[2] [2a] K. Binnemans, L. Jongen, C. G. Walrand, W. D'Olieslager, D. Hinz, G. Meyer, *Eur. J. Inorg. Chem.* **2000**, 1429. [2b] K. Binnemans, C. G-Walrand, *Chem. Rev.* **2002**, *102*, 2303.

[3] B. Donnio, *Curr. Opin. Colloid Interf. Sci.* **2002**, *7*, 371.

[4] D. W. Bruce, *Acc. Chem. Res.* **2000**, *33*, 831.

[5] See, for example: [5a] D. W. Bruce, D. A. Dunmur, P. M. Maitlis, J. M. Watkins, G. J. T. Tiddy, *J. Mater. Chem.* **1993**, *3*, 911. [5b] A. I. Smirnova, D. W. Bruce, *Chem. Commun.* **2002**, 176. [5c] T. Terech, C. Chachaty, J. Gaillard, A. M. Giroud-Godquin, *J. Phys.* **1987**, *48*, 663. [5d] M. Ibn-Elhaj, D. Guillon, A. Skoulios, A. M. Giroud-Godquin, J. C. Marchon, *J. Phys. II* **1992**, *2*, 2197. [5e] K. Ohta, M. Moriya, M. Ikejima, H. Hasebe, N. Kobayashi, I. Yamamoto, *Bull. Chem. Soc. Jpn.* **1997**, *70*, 1199. [5f] K. Praefcke, J. D. Holbrey, N. Usolt'seva,, *Mol. Cryst. Liq. Cryst.* **1996**, *288*, 189. [5g] K. Praefcke, B. Bilgin, N. Usolt'seva, B. Heinrich, D. J. Guillon, *J. Mater. Chem.* **1995**, *5*, 2257. [5h] N. Usolt'seva, K. Praefcke, B. Bilgin, D. Singer, B. Gündoan, *Liq. Cryst.* **1994**, *16*, 601. [5i] K. Praefcke, J. D. Holbrey, N. Usolt'seva, D. Blunk, *Mol. Cryst. Liq. Cryst.* **1997**, *292*, 123.

[6] [6a] J. Bowers, M. Danks, D. W. Bruce, R. K. Heenan, *Langmuir* **2003**, *19*, 292. [6b] J. Bowers, M. Danks, D. W. Bruce, J. R. P. Webster, *Langmuir* **2003**, *19*, 299.

[7] [7a] S. S. Zhu, T. M. Swager, *Adv. Mater.* **1995**, *7*, 280. [7b] P. C. Griffiths, I. A. Fallis, D. J. Willock, A. Paul, C. L. Barrie, P. M. Griffiths, G. M. Williams, S. M. King, R. K. Heenan, R. Görgl, *Chem. Eur. J.* **2004**, *10*, 2022.

[8] D. A. Jaeger, V. B. Reddy, N. Arulsamy, D. S. Bohle, D. W. Grainger, B. Berggren, *Langmuir* **1997**, *13*, 533.

[9] X. Lu, Z. Zhang, Y. Liang, *J. Chem. Soc., Chem. Commun.* **1994**, 2731; *Langmuir* **1996**, *12*, 5501; *Langmuir*, **1996**, *12*, 5501.

[10] Y. Ikeda, T. Imae, J.-C. Hao, M. Iida, T. Kitano, N. Hisamatsu, *Langmuir* **2000**, *16*, 7618.

[11] [11a] M. Iida, A. Yonezawa, J. Tanaka, *Chem. Lett.* **1997**, 663. [11b] M. Iida, T. Tanase, N. Asaoka, A. Nakanishi, *Chem. Lett.* **1998**, 1275. [11c] M. Iida, H. Er, N. Hisamatsu, T. Tanase, *Chem. Lett.* **2000**, 518. [11d] M. Iida, K. Asayama, S. Ohkawa, *Bull. Chem. Soc. Jpn.* **2002**, *75*, 521.

[12] A. Manna, T. Imae, M. Iida, N. Hisamatsu, *Langmuir* **2001**, *17*, 6000.

[13] [13a] A. M. Levelut, *Mol. Cryst. Liq. Cryst.* **1992**, *215*, 31. [13b] A. C. Albéniz, J. Barberá, P. Espinet, M. C. Lequerisa, A. M. Levelut, F. J. López-Marcos, J. L. Serrano, *Eur. J. Inorg. Chem.* **2000**, 133.

[14] [14a] E. Bang, *Acta Chem. Scand., Ser. A* **1978**, *32*, 555. [14b] U. Timper, G. Heller, *Z. Naturforsch., Teil B* **1994**, *49*, 215. [14c] E. Bang, *Acta Chem. Scand., Ser. A* **1996**, *50*, 952.

[15] H. Er, M. Iida, N. Asaoka, T. Imae, *Colloids Surf. A* **2003**, *221*, 119.

[16] The diffusion coefficient at an infinite dilution can be correlated with the molar conductivity. According to the Nernst equation, the diffusion coefficient (D_{0j}) for a univalent ion j is simply correlated with its molar conductivity (λ_{0j}) at an infinite dilution: $D_{0j} = 2.68 \times 10^{-7}\ \lambda_{0j}$ at 25 °C. From this equation we estimated the λ_{0j} value to be 2.6×10^{-3} S·m^2·mol^{-1} for the silver ion.

[17] G. Schwarzenbach, H. Ackermann, B. Maissen, G. Anderegg, *Helv. Chim. Acta* **1952**, *35*, 2337.

[18] G. W. Gray, J. W. G. Goodby, *Smectic Liquid Crystals*, Leonard Hill, Glasgow and London, **1984**, p. 58.

[19] B. J. Forrest, L. W. Reeves, *Chem. Rev.* **1981**, *81*, 1.

[20] A. Weissberger, *Organic Solvents*, 4th ed., Wiley, New York, **1986**. The value for dichloromethane is obtained by an interpolation to 25 °C.

[21] T. Erdey-Grûz, *Transport Phenomena in Aqueous Solutions*, Adam Hilger, London, **1974**, p. 151, 228.

[22] A. Altomare, M. C. Burla, M. Camalli, M. Cascarano, C. Giacovazzo, A. Guagliardi, G. Polidori, *J. Appl. Crystallogr.* **1994**, *27*, 435.

[23] teXcan, Crystal Structure Analysis Package, Molecular Structure Corp., **1999**.

[24] H. Ema, Masters thesis, Shinshu University, Ueda, Japan, **1988**, chaper 7; H. Hasebe, Masters thesis, Shinshu University, Ueda, Japan, **1991**, chapter 5.

[25] P. Stilbs, *Progr. Nucl. Magn. Reson. Spectrosc.* **1986**, *19*, 1.

[26] The result of the vapor-pressure depression may not be significantly affected by the presence of small amounts of water in organic solvent, and therefore the result in the water/*n*-heptane system is almost certain; see: [26a] J. M. Corkill, J. F. Goodman, T. Walker, *Trans. Faraday Soc.* **1965**, *61*, 589. [26b] A. Kitahara, *J. Phys. Chem.* **1965**, *69*, 2788.

Received February 28, 2004
Early View Article
Published Online August 12, 2004

 © 2004 Wiley-VCH Verlag GmbH & Co. KGaA, Weinheim

Conformational Analysis of Bis(L-*N*,*N*-dimethylvalinato)copper(II) and Bis(L-*N*,*N*-dimethylleucinato)copper(II) in Different Solvents by EPR Spectroscopy and a Molecular Mechanics Study

Krunoslav Mirosavljević,[a] Jasmina Sabolović,[b] and Vesna Noethig-Laslo*[a]

Keywords: Complexes / Amino acids / N,O ligands / EPR spectroscopy / Force field

An EPR study on the Brownian motion of bis(L-*N*,*N*-dimethylvalinato)copper(II), Cu(L-Me_2Val)$_2$ and bis(L-*N*,*N*-dimethylleucinato)copper(II), Cu(L-Me_2Leu)$_2$, dissolved in different solvents (CD_3OD, CH_3CH_2OH, $CDCl_3$) as a function of temperature is presented. The theoretical fits of the EPR spectra revealed different EPR behaviour for the two copper(II) complexes in hydrogen bond making solvents. In order to examine whether the different behaviour could be explained on conformational (steric) grounds, a conformational analysis of the copper(II) complexes with L-*N*,*N*-dimethylated amino acids was performed with a molecular mechanics force field. The ability of the most stable conformations to bind a water molecule in the copper(II) first coordination sphere was also examined using the force field.
(© Wiley-VCH Verlag GmbH & Co. KGaA, 69451 Weinheim, Germany, 2004)

Introduction

Copper(II) complexes with amino acids and small peptides have been intensively studied in relation to their biological importance and possible pharmacological activity (here we refer only to few).[1−7] These compounds are also regarded as good model systems for copper binding sites in copper-containing enzymes and other proteins (e.g. prions).[8−10] Most of the biologically important interactions are achieved by the side-chains of the amino acids in proteins. These interactions may have a significant role in the oxidation state changes of the copper ion in copper-containing metalloproteins.[11]

Amino acid side-chain interactions such as those of the van der Waals type may also be important in the low molecular-weight copper(II) complexes with amino acids. Sigel and co-workers[12,13] studied amino acid side-chain interactions in the copper(II) complexes by glass electrode potentiometry. They pointed out that intramolecular van der Waals interactions formed by the two amino acid side-chains in the bis(chelated) copper(II) complexes could be formed only when 2N/2O donor amino acid atoms were arranged in a *trans* position in the equatorial plane of the copper(II) coordination sphere. Only the *trans*-CuN_2O_2 configuration was confirmed in a number of copper(II) complexes with L-*N*,*N*-dialkylated amino acids (other than glycine) dissolved in organic solvents by EPR spectroscopy[14,15] as well as by X-ray structural methods.[16−19] However, the *trans*-isomer of bis(glycinato)copper(II) was found to be more stable that the *cis*-isomer in the solid and gaseous phases, with a very quick isomerization reaction form *cis* to *trans* in the gas phase at ambient temperature.[20]

The effect of water molecules dissolved in organic solvents on the electronic states of copper(II) complexes with L-*N*,*N*-dialkylated amino acids was studied.[15] It was suggested that if the amino acid side chains were long enough to form aliphatic intramolecular van der Waals contacts, then the presence of water in the organic solvent might induce the conformation change of the complex.

Thus, the effects of the water binding to the fifth (apical) position in the copper(II) coordination sphere on the length of the *N*-alkyl substituents in bis(chelates) with *N*,*N*-dialkyl amino acids were studied.[21,22] It was found that the water molecule bound to the copper(II) coordination sphere in the *N*,*N*-dialkylated alaninato complex could be easily released from the copper(II) but only when the *N*-alkyl chain was longer than methyl, whereas the apical water molecule was essential for the stability of the copper(II) complex with L-*N*,*N*-dimethylalanine.[21,22] However, EPR spectroscopic measurements of the copper(II) complexes of L-*N*,*N*-dimethylvaline or L-*N*,*N*-dimethylisoleucine revealed considerable influence of the water molecules dissolved in organic solvents on the resultant EPR spectra[15] and suggested that in these complexes, dissolved in organic solvents, the apically bound water molecule could be easily released from the copper(II) coordination sphere. Thus, considerable influence of the aliphatic amino acid residues on binding or release of

[a] Rudjer Bošković Institute, Department of Physical Chemistry, Bijenička cesta 54, 10002 Zagreb, Croatia
Fax: (internat.) +385-1-4680-245
E-mail: laslo@rudjer.irb.hr
[b] Institute for Medical Research and Occupational Health, Ksaverska cesta 2, P. O. Box 291, 10001 Zagreb, Croatia
Fax: (internat.) +385-1-4673-303
E-mail: jasmina.sabolovic@imi.hr

 © 2004 Wiley-VCH Verlag GmbH & Co. KGaA, Weinheim **DOI: 10.1002/ejic.200300781**

the water molecule from the copper(II) coordination sphere could be envisaged.[22,23] Namely, a change in the conformation of the isoleucine side-chains in bis(L-*N,N*-dimethylisoleucinato)copper(II), i.e. Cu(L-Me_2Ile)$_2$, dissolved in deuterated methanol associated with the water molecule released from the copper(II) coordination sphere was suggested from the first study on the temperature dependence of the Brownian motion of the copper(II) amino acid complexes using EPR spectroscopy recorded at different frequencies.[22]

EPR spectroscopy is a powerful technique for the study of the electronic structures of the copper(II) complexes in order to gain information about the solute-solvent interactions as a function of the solvent, temperature and pH.[24,25] Interpretation of the results is sometimes difficult because of the lack of structural data. On the other hand, a recently proposed molecular mechanics (MM) force field (FFW) developed for modelling of anhydrous and hydrated copper(II) amino acid complexes[26] offers a unique possibility to gain qualitative insight into the arrangements that a chosen number of water molecules may adopt around the studied complexes. A combination of EPR spectroscopy and molecular mechanics calculations has become a valuable tool for identifying the preferred structure between different conformers.[27,28]

As a continuation of our previous investigations, we herein present an EPR study of the temperature dependence of the Brownian motion of bis(L-*N,N*-dimethylvalinato)copper(II), Cu(L-Me_2Val)$_2$, and bis(L-*N,N*-dimethylleucinato)-copper(II), Cu(L-Me_2Leu)$_2$, dissolved in CD_3OD, CH_3CH_2OH and $CDCl_3$. These bis(L-dimethylamino acidato)copper(II) complexes have the two N-atoms in the copper(II) coordination sphere in the *trans*-position,[16−19] thus a similar temperature dependence of the ligand field parameters may be envisaged. The conformational analysis of these compounds was performed with the MM force field FFW[26,29] in order to find the most stable conformations. The ability of the most stable conformations to bind a water molecule in the copper(II) first coordination sphere (i.e. apical water) was examined. The combined EPR and MM studies are aimed at establishing whether different EPR behaviour of the copper(II) complexes examined in this work may be due to the aliphatic amino acid side-chain interactions, i.e. conformational (steric) in nature.

Results and Discussion

A) EPR Analysis

The EPR spectra and the rotational correlation time, τ_θ, of the complexes calculated from the spectra of Cu(L-Me_2-Leu)$_2$ dissolved in CD_3OD and in $CDCl_3$, respectively, are compared in Figure 1. The spectra of the complex dissolved in one particular solvent could be fitted well with the same spectral parameters (Table 1) characteristic for that solvent in the whole temperature interval examined (i.e. 277−317 K in CD_3OD and 274−304 K in $CDCl_3$). The spectra of the complex dissolved in $CDCl_3$ (c and d) exhibit five well resolved superhyperfine lines due to the two nitrogen atoms in the copper(II) coordination sphere in the *trans*-position.[30,31] The resolved superhyperfine lines in the spectra also depend on the rotational correlation time, τ_θ.[24,32] A negligible influence of the anisotropic components ($a_{N\parallel}$ and $a_{N\perp}$) of the superhyperfine coupling tensor can be determined from spectrum c.[33,34] Well resolved superhyperfine lines suggest that the copper and nitrogen atoms are positioned in the equatorial plane of the copper(II) coordination sphere. The spectra of the complex dissolved in CD_3OD which are characterised by different EPR parameters (Table 1), albeit with the similar τ_θ values[24,32] as in $CDCl_3$, show five much broader superhyperfine lines in the whole temperature range studied. This is due to a displacement of the nitrogen atoms from of the copper(II) equatorial plane most probably by the apical water molecule in the complex.[15,35] A larger hyperfine splitting constant a_o, concomitant with decreased g_o values (Table 1) was determined from the spectra c and d (Figure 1) in $CDCl_3$. A comparison of this with the values determined from the spectra a and b in CD_3OD suggests more covalent character for the Cu−ligand bonds of the complex in $CDCl_3$.[35] This is in accordance with the finding that small deviations from the square-planar coordination shifts the hyperfine splitting constant to smaller values (see Table 1).[36]

Figure 2 shows the EPR spectra of Cu(L-Me_2Val)$_2$ dissolved in $CDCl_3$ (a and b), CD_3OD (c and d) and CH_3CH_2OH (e and f) recorded at two temperatures and their corresponding theoretical fits. In $CDCl_3$ the spectra were fitted well with the same parameters (Table 1) in the whole temperature range studied. As in the case of the leuc-

Table 1. EPR parameters of the copper(II) complexes

	g_0	$g_\parallel$	$g_\perp$	a_0/mT	$A_\parallel$/mT	$A_\perp$/mT
Cu(L-Me_2Leu)$_2$						
CD_3OD (277−317 K)	2.133 ± 0.001	2.244 ± 0.001	2.078 ± 0.001	7.8 ± 0.1	17.8 ± 0.1	2.8 ± 0.1
$CDCl_3$ (274−304 K)	2.115 ± 0.001	2.243 ± 0.001	2.051 ± 0.001	9.4 ± 0.1	17.8 ± 0.2	5.2 ± 0.2
Cu(L-Me_2Val)$_2$						
CD_3OD (276−296 K)	2.129 ± 0.001	2.245 ± 0.001	2.071 ± 0.001	8.2 ± 0.2	18.5 ± 0.1	3.1 ± 0.2
CD_3OD (296−316 K)	2.127 ± 0.001	2.245 ± 0.001	2.068 ± 0.001	8.4 ± 0.1	18.5 ± 0.1	3.4 ± 0.2
C_2H_5OH (284−308 K)	2.128 ± 0.001	2.244 ± 0.001	2.070 ± 0.001	8.4 ± 0.1	18.4 ± 0.1	3.4 ± 0.1
C_2H_5OH (308−328 K)	2.125 ± 0.001	2.244 ± 0.001	2.067 ± 0.001	8.6 ± 0.1	18.4 ± 0.1	3.7 ± 0.1
$CDCl_3$ (264−304 K)	2.116 ± 0.001	2.250 ± 0.001	2.050 ± 0.001	9.5 ± 0.1	17.9 ± 0.1	5.3 ± 0.1

 © 2004 Wiley-VCH Verlag GmbH & Co. KGaA, Weinheim

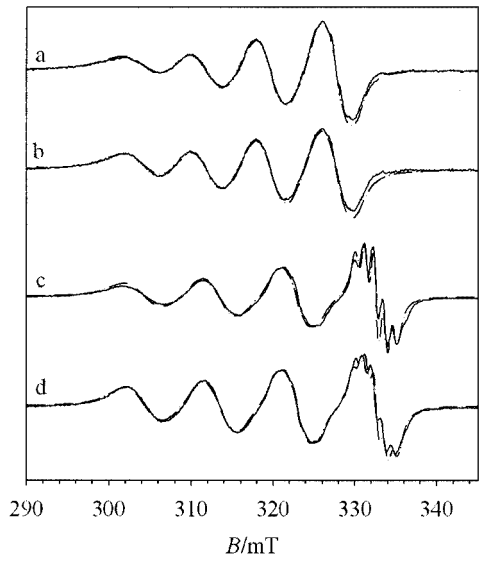

Figure 1. EPR spectra of Cu(L-Me_2Leu)$_2$ dissolved in CD_3OD taken at: (a) 294 K ($\tau_\theta = 9.1\cdot10^{-11}$ s), (b) 317 K ($\tau_\theta = 7.0\cdot10^{-11}$ s) and in $CDCl_3$ at (c) 274 K ($\tau_\theta = 8.6\cdot10^{-11}$ s), (d) 304 K ($\tau_\theta = 8.0\cdot10^{-11}$ s); full lines represent experimental spectra and dotted lines show the theoretical fit obtained with the EPR parameters a_o, g_o, $A_\parallel$ and $g_\parallel$ displayed in Table 1

inato complex, the spectra are characterised by well resolved superhyperfine structures due to the two nitrogen atoms in the copper(II) equatorial plane.

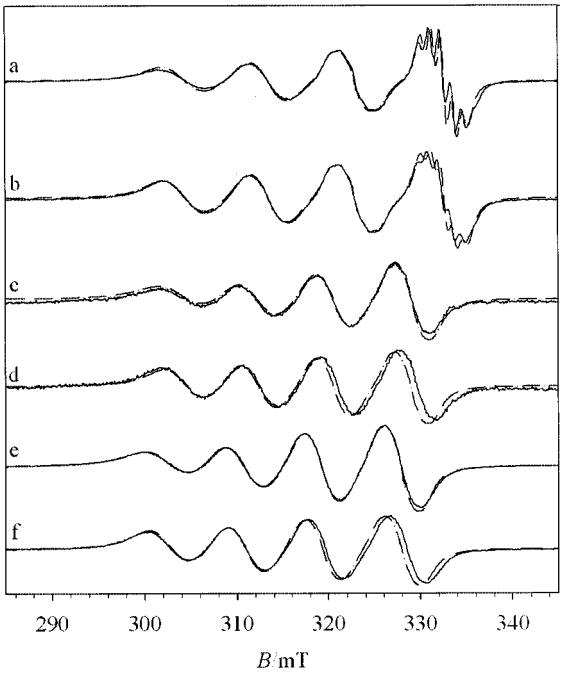

Figure 2. EPR spectra of Cu(L-Me_2Val)$_2$ dissolved in $CDCl_3$ at (a) 274 K ($\tau_\theta = 6.6\cdot10^{-11}$ s), (b) 304 K ($\tau_\theta = 5.4\cdot10^{-11}$ s); in CD_3OD at (c) 292 K ($\tau_\theta = 6.9\cdot10^{-11}$ s), (d) 316 K ($\tau_\theta = 4.3\cdot10^{-11}$ s); in CH_3CH_2OH at (e) 292 K ($\tau_\theta = 7.1\cdot10^{-11}$ s) and (f) 320 K ($\tau_\theta = 4.0\cdot10^{-11}$ s); full lines represent experimental spectra and dotted lines represent the theoretical fit with the EPR parameters of the lower-temperature ranges given in Table 1

However, in addition to the blurred superhyperfine structure of the spectra c−f (Figure 2), the theoretical fit of the spectra with the EPR parameters for the valine complex dissolved in CD_3OD and CH_3CH_2OH (i.e. in the hydrogen-bond making solvents) was satisfactory only in the lower temperature interval (see Table 1), assuming one type, the aqua complex, for the first copper(II) coordination sphere. In order to fit the experimental spectra d and f well (Figure 2), an increased a_o and a decreased g_o value, as determined from the experimental spectra were taken into account. This suggested an increase of the covalent character of the Cu−ligands bonds[36] of the complex represented by the experimental spectra d and f.

The reorientation correlation times, τ_θ, of the complexes which describe their Brownian motion in solution (see Methods) were calculated from the fitted spectra. Figure 3 shows a comparison of τ_θ calculated from the fit of the spectra of Cu(L-Me_2Leu)$_2$ and Cu(L-Me_2Val)$_2$ dissolved in CD_3OD.

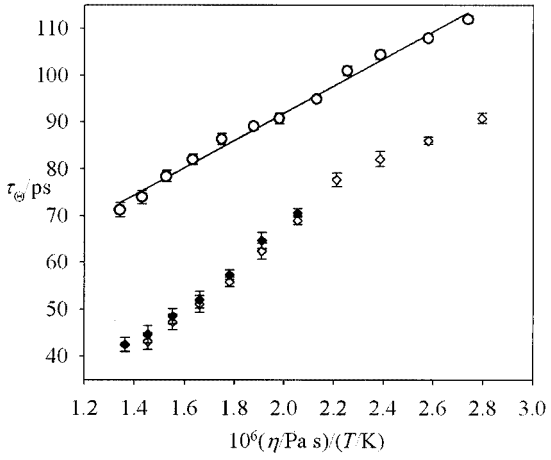

Figure 3. The reorientation correlation times, τ_θ, calculated from the fit of the spectra of Cu(L-Me_2Leu)$_2$ (white circles) and Cu(L-Me_2Val)$_2$ (white squares − fitted with the parameters required for the good fit of the spectra at the lower temperatures; black squares − fitted with parameters required for the good fit of the spectra at higher temperatures (see Table 1) dissolved in CD_3OD as a function of η/T

The linear dependence of τ_θ on η/T obtained with the parameters (Table 1) of the fitted spectra of Cu(L-Me_2Leu)$_2$ suggests an unchanged effective volume of the complex over the whole temperature range studied and indicates the presence of one conformation of the complex in the whole temperature interval examined. On the other hand, τ_θ calculated from the fit of the spectra of Cu(L-Me_2Val)$_2$ dissolved in CD_3OD, exhibited no linear dependence on η/T. An increase of a_o concomitant with a decrease of g_o which was determined from the spectra above 296 K (Table 1) is reflected in the function $\tau_\theta = f(\eta/T)$ as a deviation from linearity. Above 296 K increased a_o values (Table 1) suggest a higher covalent character of the Cu−ligand bonds whereas the nonlinearity of the function $\tau_\theta = f(\eta/T)$ suggests a changed solvated volume of the complex, indicating a conformation change.

 © 2004 Wiley-VCH Verlag GmbH & Co. KGaA, Weinheim

When the two complexes were dissolved in $CDCl_3$ (Figure 4), a linear function of τ_θ against η/T was obtained and the spectra were fitted well with a single value for a_o and a single value for g_o (Table 1) in the whole range of temperatures examined. It can be seen that the values of τ_θ, calculated from the spectra of the complexes, as well as the slopes of the straight lines, $\tau_\theta = f[V_{eff}(\eta/T)]$, ($V_{eff}$ denotes the effective volume of the solvated complexes), are different. This result suggests that the motion of Cu(L-Me_2Leu)$_2$ is slower than that of Cu(L-Me_2Val)$_2$.

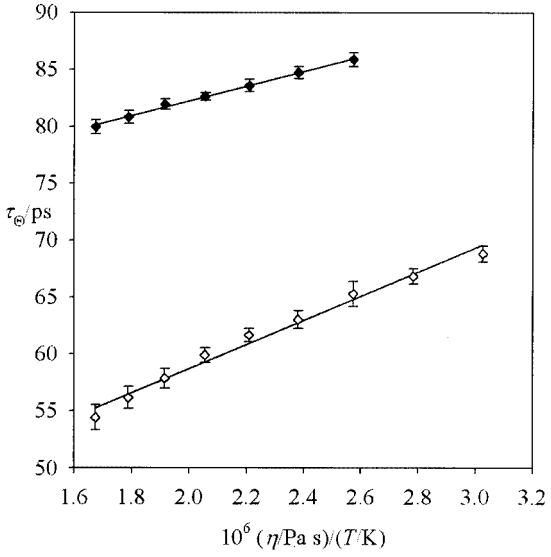

Figure 4. τ_θ calculated from the fit of the spectra of Cu(L-Me_2Val)$_2$ (white squares) and Cu(L-Me_2Leu)$_2$ (black squares) dissolved in $CDCl_3$ as a function of η/T using the parameters shown in Table 1

Cu(L-Me_2Val)$_2$ dissolved in CH_3CH_2OH exhibited a linear dependence of τ_θ on η/T (Figure 5), although an increase of a_o and a decrease of g_o were determined above 308 K. The linear dependence of τ_θ on η/T indicates that the solvated volume of the complex did not change above 308 K, although there was a change in the copper(II) electronic state resulting from an increase in the covalent character of the copper−ligand bonds.

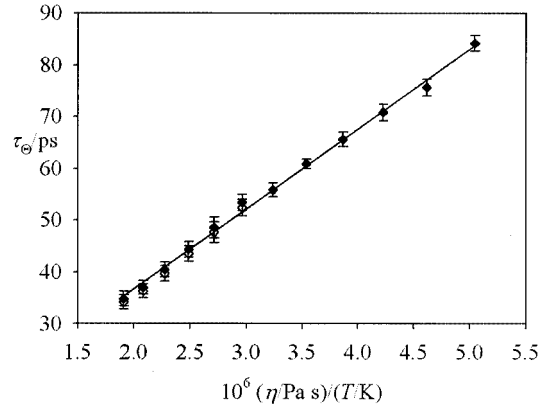

Figure 5. τ_θ calculated from the fit of the spectra of Cu(L-Me_2Val)$_2$ dissolved in CH_3CH_2OH as a function of η/T (black squares fit with g_o = 2.128, a_o = 8.4 mT; white squares fit with g_o = 2.125, a_o = 8.6 mT)

B) Conformational Analysis

The conformational analysis of Cu(L-Me_2Val)$_2$ and Cu(L-Me_2Leu)$_2$ were performed with the MM force field FFW[26,29] developed for anhydrous and hydrated copper(II) amino acid complexes.

From stereochemical considerations it can be proposed that each chelate ring of Cu(L-Me_2Val)$_2$ can have 6 conformations (3 conformers with the valine side-chains in the axial position and 3 conformers with them in the equatorial position with respect to the chelate ring planes) and that each chelate ring of Cu(L-Me_2Leu)$_2$ can have 18 conformations (9 conformers with the C^β-axial and 9 conformers with the C^β-equatorial positions). The results of in vacuo strain energy minimisations for the two systems, Cu(L-Me_2Val)$_2$ and Cu(L-Me_2Leu)$_2$, are listed in Table 2. Figure 6 shows their most stable conformations.

The conformational analysis was extended to the conformers interacting with water molecules (Table 2) in order to study the influence of amino acid side-chains on water binding in the first copper(II) coordination sphere. Due to the low number of water molecules dissolved in the studied organic solvents we limited the number of water molecules surrounding the copper complexes to 4. The initial atomic positions used for water oxygens and water hydrogens were the same for all the studied conformers.

The calculated equilibrium structures suggest that four water molecules may occur around the copper(II) amino acid complexes (Figures 7 and 8). It may be expected that FFW overestimates the distance between Cu and the axial water oxygen (denoted as O_w in Figures 7 and 8) by an average of 0.2 Å.[26] We suggest that every axially placed O_w at a distance longer than 3 Å cannot be considered as an apically bound water molecule.[37] The apically bound water molecule can be defined as the one that may influence the electronic structure of the copper(II), i.e. cause changes in the EPR spectral parameters.

The a6−a6 minimum of Cu(L-Me_2Val)$_2$ (Figure 6, Table 2) corresponds to the conformation of the anhydrous complex determined by the X-ray diffraction experiment.[16] The a6−e2 axial-equatorial minimum in the same compound (Figure 7) corresponds to the experimental crystalline conformation of the corresponding aqua-copper(II) complex.[18] The crystal structure of Cu(L-Me_2Leu)$_2$ has not yet been determined.

The conformers having the lowest strain conformational energies for the anhydrous complexes (Figure 6) also remained the most stable when four water molecules were present in the systems (Table 2). They have C^β in their axial positions as may be seen in Figures 6−8. Among the conformers with the same C^β-axial conformations in both chelate rings, only one conformer of Cu(L-Me_2Val)$_2$ (a5−a5, Table 2) can bind the apical water molecule in the first copper(II) coordination sphere when surrounded with more than two water molecules. In all other axial-axial conformers presented in Table 2, the methyl groups on the nitrogen atoms, as well as the close van der Waals contacts between two valine side-chains, prevent the apical water molecule

 © 2004 Wiley-VCH Verlag GmbH & Co. KGaA, Weinheim

Table 2. Minimum strain energies for the conformers having two chelate rings in the same conformations for anhydrous complexes and for complexes surrounded with four water molecules

Conformer	φ_1 [a]	φ_2	φ_3	φ_4	Strain energy[b]	Strain energy
		$Cu(L\text{-}Me_2Val)_2$				$Cu(L\text{-}Me_2Val)_2{\cdot}4H_2O$
				C^β-equatorial		
e1−e1	152.4	−143.7	167.6		14.92	20.55
e2−e2	147.4	−159.8	89.3		20.33	14.14
e3−e3	155.9	−153.1	−56.4		55.26	50.40
e1a−e1a	126.0	−152.7	176.1		22.39	29.34
				C^β-axial		
a4−a4	−158.6	−82.8	50.2		36.35	36.77
a5−a5	−154.7	−78.6	−91.2		10.03	7.53
a6−a6	−151.6	−89.7	−173.5		0.00	0.00
		$Cu(L\text{-}Me_2Leu)_2$				$Cu(L\text{-}Me_2Leu)_2{\cdot}4H_2O$
				C^β-equatorial		
e1−e1	134.6	−144.4	−72.3	175.4	33.91	34.67
e1a−e1a	146.1	−165.5	−95.6	166.6	38.41	38.38
e2−e2	130.4	−139.2	−90.9	−35.3	92.27	92.19
e3−e3	155.5	−154.1	88.6	84.4	42.79	41.81
e4−e4	154.9	−150.0	−177.3	158.1	19.75	19.43
e5−e5	154.6	−149.2	−178.4	−74.9	32.27	34.62
e6−e6	138.3	−162.2	−174.2	68.5	11.61	15.14
				C^β-axial		
a7−a7	−155.2	−76.9	−94.2	−73.7	25.94	26.28
a8−a8	−146.6	−108.7	96.2	62.5	84.20	86.21
a9−a9	−151.6	−95.4	68.2	−157.9	26.25	29.22
a10−a10	−152.2	−79.8	−178.7	−77.3	6.91	12.91
a11−a11	−151.9	−80.2	177.8	49.8	16.05	15.88
a12−a12	−151.6	−80.1	172.6	−174.8	0.00	0.00

[a] Torsion angles φ*1*, φ*2* and φ*3* correspond to O−Cu−N−C_{methyl}, $C^\alpha-C^\beta-N-$Cu and $C^\gamma-C^\beta-C^\alpha$-N (see Figure 6). Torsion angle φ*4* corresponds to the angle $C^\delta-C^\gamma-C^\beta-C^\alpha$ for $Cu(L\text{-}Me_2Leu)_2$ (see Figure 6). Torsion angles are in degrees. [b] Strain energies are in kcal mol^{-1}. Zero point energies: −4844.11 kcal mol^{-1} for $Cu(L\text{-}Me_2Val)_2$; −5337.15 kcal mol^{-1} for $Cu(L\text{-}Me_2Val)_2{\cdot}4H_2O$; −5628.95 kcal mol^{-1} for $Cu(L\text{-}Me_2Leu)_2$ and −6124.77 kcal mol^{-1} for $Cu(L\text{-}Me_2Leu)_2{\cdot}4H_2O$.

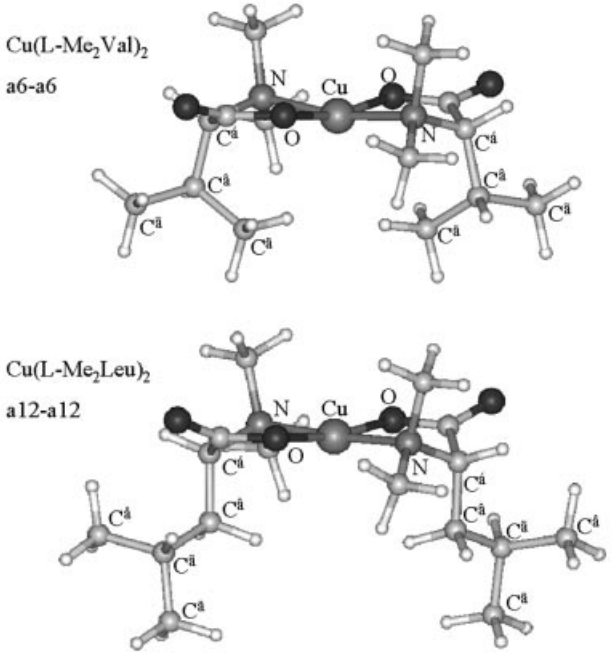

Figure 6. The most stable conformations of the two copper(II) complexes with L-*N*,*N*-dimethylated amino acids calculated with the FFW force field

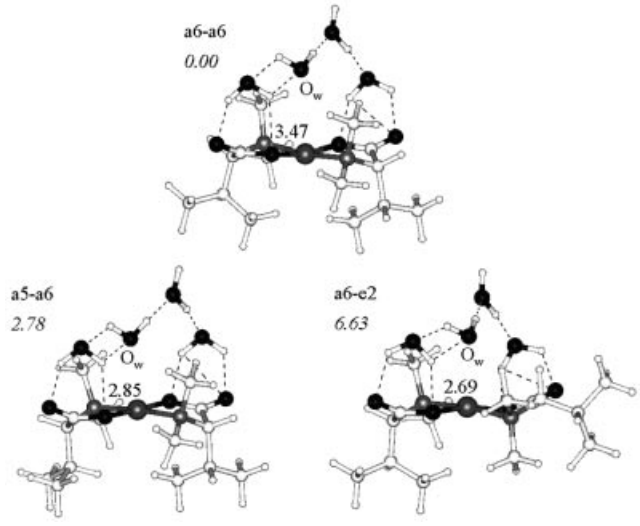

Figure 7. Three minima of $Cu(L\text{-}Me_2Val)_2{\cdot}4H_2O$ with the lowest conformation energy; the values in italics are energy values expressed in kcal mol^{-1}; the values in Å are copper(II) to O_w distances

from approaching Cu^{II} (e.g. see a6−a6 in Figure 7). However, the conformers with C^β-equatorial in both chelate rings and in the mixed axial-equatorial positions do not

 © 2004 Wiley-VCH Verlag GmbH & Co. KGaA, Weinheim

hinder the water molecule from closely approaching the copper(II) (Figure 7).

On the other hand, almost all the minima of Cu(L-Me_2-Leu)$_2$, including the most stable conformer a12-a12, can apically bind a water molecule to the axial position in the copper(II) coordination sphere when surrounded with more than two water molecules (Figure 8).

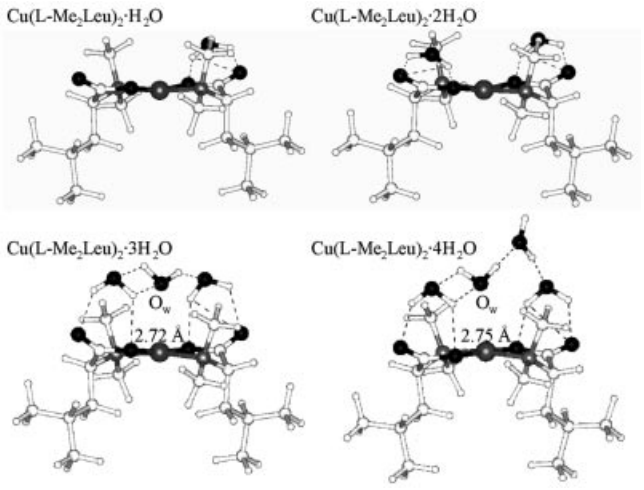

Figure 8. The a12−a12 conformer of Cu(L-Me_2Leu)$_2$ interacting with up to four water molecules; the values in Å are copper(II) to O_w distances.

According to the results obtained with the FFW force field, the interactions with four water molecules increase the energy differences between the most stable conformer and other conformations of Cu(L-Me_2Leu)$_2$, resulting in the a12−a12 as well as the11−a11 minima being even more stable than in the anhydrous system (Table 2). However, when four water molecules are present in Cu(L-Me_2Val)$_2$, the energy difference between the lowest energy minimum a6−a6 and the first above it becomes lower (Table 2 and Figure 7). These changes in the strain energy distributions among the conformers of the two theoretically examined systems, i.e. between the anhydrous system and the system containing four water molecules (Table 2), may suggest an even smaller energy difference between the hydrated conformers and the a6−a6 conformer of Cu(L-Me_2Val)$_2$ in more complicated system such as in real hydrogen-bond making solutions. With increased molecular vibrations at higher temperatures, the system may attain enough energy for the transformation from an equatorial-equatorial or an axial-equatorial to the axial-axial conformer, followed by the release of the water molecule from the copper(II) first coordination sphere. Such a conformer a12−a12 (the most stable for the two studied systems presented in Table 2, Figures 6 and 8) can easily accept and release the water molecule to and from the copper(II) coordination polyhedron.

Conclusions

The results of the EPR analysis of the temperature dependence of the Brownian motion point to different behaviour for Cu(L-Me_2Leu)$_2$ and Cu(L-Me_2Val)$_2$ dissolved in the hydrogen-bond making solvents CD_3OD and CH_3CH_2OH. This cannot be due to different temperature dependencies of the ligand field in the two complexes because both complexes have the same copper(II) coordination sphere.

For Cu(L-Me_2Leu)$_2$, a satisfactory match between the experimental and theoretical fits of the spectra with the EPR parameters characteristic for the chosen solution (Figure 1, Table 1) and the linear function $\tau_\theta = f(\eta/T)$ were obtained, suggesting an unchanged effective volume of the complex, i.e. an unchanged conformation of the side-chains.

For Cu(L-Me_2Val)$_2$, the unchanged effective volume was determined only from the spectra of the complex dissolved in $CDCl_3$. The non-linear dependence of τ_θ on (η/T) for Cu(L-Me_2Val)$_2$ in CD_3OD combined with changed a_o and g_o values above 296 K in CD_3OD, suggests a change in the effective volume of Cu(L-Me_2Val)$_2$ and consequently a different conformation. Different EPR parameters a_o and g_o observed for Cu(L-Me_2Val)$_2$ (Table 1) in the hydrogen-bond making solvents above a solvent dependent temperature reflect changes in the bonding and/or solvation of the complex. A decrease in g_o with a concomitant increase in a_o in the EPR spectra suggests more covalent character of the metal−ligand bonds in the equatorial plane of this complex. The isotropic hyperfine splitting constant a_o and the superhyperfine coupling constant a_N are highly sensitive to the geometric distortions. The changes in a_o and a_N determined from the spectra of Cu(L-Me_2Val)$_2$ on going from $CDCl_3$ to CH_3CH_2OH indicate pronounced flexibility of the copper(II) coordination polyhedron in this complex. This is in accordance with the findings[38] that with intramolecular and/or intermolecular strain the distortion of the copper(II) polyhedron from planarity was more energetically favourable than the changes in the valinato chelate rings' conformations. Thus, the non-linear dependence of τ_θ on (η/T) for Cu(L-Me_2Val)$_2$ in CD_3OD combined with a change in a_o suggests not only a change in the effective volume of Cu(L-Me_2Val)$_2$ above 296 K and consequently a different conformation, but also a differently distorted copper(II) coordination polyhedron.

The results of the theoretical conformational analysis offer an explanation for the differing EPR behaviour of Cu(L-Me_2Val)$_2$ and Cu(L-Me_2Leu)$_2$. The different behaviour may come from the lack of a bulky CH_3 group at C^β in Cu(L-Me_2Leu)$_2$ (Figure 6) compared with in Cu(L-Me_2Val)$_2$. The lack of the CH_3 group consequently allows the possibility of closer intramolecular contacts between aliphatic leucine side-chains in the two chelate rings upon water binding to the first copper(II) coordination sphere (Figure 8). That is, the most stable conformer of Cu(L-Me_2Val)$_2$ (a6−a6 in Figure 7) cannot accept a water molecule in the copper(II) first coordination sphere because of intramolecular steric effects. For Cu(L-Me_2Val)$_2$, we may conclude that the fifth copper(II) coordination site can be occupied only for some con-

 © 2004 Wiley-VCH Verlag GmbH & Co. KGaA, Weinheim

formations and that the conformational changes (most probably triggered by solute-solvent interactions) can open and close the copper(II) accessibility to the water molecule. Conversely, Cu(L-Me_2Leu)$_2$ can bind and release the apical water molecule without the need for the conformational changes.

Experimental Section

Methods

A) EPR Spectroscopy: The EPR spectra of bis(amino acidato)copper(II) complexes are characterized by four resonances arising from the hyperfine coupling between an electron spin (S = 1/2) of the copper(II) (configuration $3d^9$) and the nuclear spin of the copper (I_{Cu} = 3/2), determined by the hyperfine coupling tensor $\hat{A}$ and the g-tensor related to the spin-orbit coupling. In solution, the average of the diagonal tensor values g_o and a_o is observed. Further splitting of the hyperfine lines may reveal the coupling of the copper electron spin with the nuclear spin of two nitrogens (I_N = 1) bonded to the copper(II)[30,31] resulting in the superhyperfine structures of the spectra (see Figure 1).

In this study we simulated the experimental EPR spectra of the complexes with the WIN-EPR Simfonia software (BRUKER) and the fast motion approximation. τ_θ was calculated from the linewidth (ΔB/mT) of the spectra which is dependent on the nuclear magnetic moment m_{Cu}:

$$\Delta B(m_{Cu}) = a + bm_{Cu} + cm_{Cu}^2$$

where a, b, c, are parameters for the lineshape fit.

The calculations of the reorientation correlation time, τ_θ, describing McConnell's tumbling mechanism[39] were performed following the procedure given elsewhere.[21]

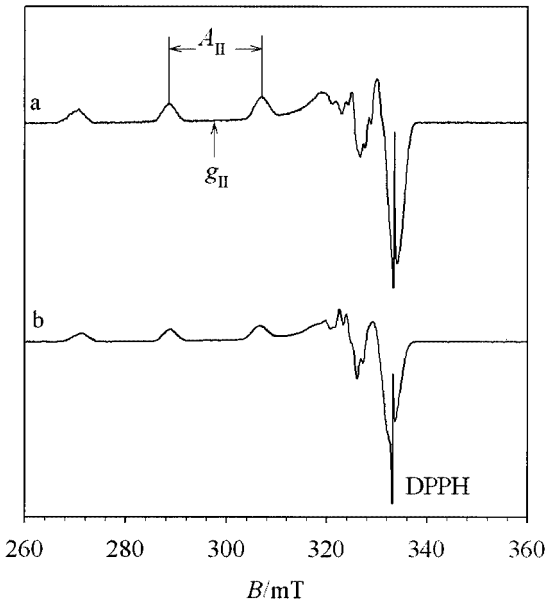

Figure 9. EPR spectra of (a) Cu(L-Me_2Val)$_2$ and (b) Cu(L-Me_2Leu)$_2$, dissolved in CD_3OD and recorded at 105 K (see Table 1)

The reorientation correlation time, τ_θ, of the complex describes the Brownian motion in solution and may be expressed as $\tau_\theta = (1/k)\, V_{eff}\, (\eta/T)\, \kappa$, where V_{eff} is the effective volume of the complex, η/T the viscosity over temperature, k is the Boltzmann constant and κ is the anisotropic interaction parameter, the second rank tensor related to EPR spectral parameters.[40] If the complex retains one conformation in the examined temperature interval, τ_θ will be a linear function of η/T with the coefficient of linearity proportional to the effective volume of the dissolved complex.[22]

The parameters $A_\parallel$ and $g_\parallel$ required for the calculation of τ_θ were determined from the EPR spectra of the glassy state recorded at 105 K (Figure 9). The spectra indicate only one type of the copper(II) complex in solution with axial symmetry ($g_\parallel > g_\perp$) of the ligand field with the $d_{x^2-y^2}$ ground state.

EPR spectra were measured using a Varian E-109 spectrometer (X-band) equipped with a BRUKER variable temperature control unit. The g-factor was measured relative to diphenyl-picryl-hydrazil (DPPH) as an external marker (g_{DPPH} = 2.0036 ± 0.0003). The temperature dependence of the viscosity η of the solvents was determined from published tables.[41]

B) Molecular Mechanics Calculations: The strain energy minimisations were performed with the CFF program for conformational analysis[42–44] with the FFW force field[26,29] suited for modelling anhydrous and hydrated copper(II) amino acid complexes with both a *trans*- and a *cis*-CuN_2O_2 coordination polyhedron. A detailed description of the potential energy functions used, the FFW's development as well as a discussion on the efficacy of the force field in simulation and prediction of experimental crystal and molecular structures and quantum-chemically calculated vacuum structures of a series of anhydrous and hydrated copper(II) amino acid complexes can be found in our earlier paper.[26] FFW correctly predicted the most stable conformations of the copper(II) amino acid complexes in vacuo and reproduced well the hydrogen-bonding pattern between water molecules and amino acid atoms.[26] It also simulates the result obtained from quantum chemical calculations for aqua-copper(II) glycinato systems[26,45] in which the formation of hydrogen bonds between water molecules and amino and carboxylato groups competes with axial Cu···OH_2 interactions.

Materials:

The ligands L-*N*,*N*-dimethylvaline and L-*N*,*N*-dimethylleucine were prepared using a modified method of Bowman and Stroud[46] (i.e. by methylation of the amino acids through condensation with formaldehyde, followed by a catalytic hydrogenation in an ethanol/water solution at room temperature). The corresponding copper(II) complexes were prepared according to the modified procedure of Nash and Schaefer[47] (i.e. by means of the reaction of copper(II) acetate monohydrate with the sodium salt of the ligand in dichloroethane solution to obtain Cu(L-Me_2Val)$_2$, and in dry dichloromethane to obtain Cu(L-Me_2Leu)$_2$). The C, N and Cu elemental analyses confirmed the compositions of the ligands and complexes.

Concentrations of approximately 0.1 mmol dm^{-3} of the copper(II) complexes (in CH_2CH_3OH, $CDCl_3$, CD_3OD) were used. Organic solvents were dried over Type 4 Linde Na–Al-silicate molecular sieves with a pore radius of 4 Å (SERVA, Heidelberg, Germany).

Acknowledgments

We would like to thank Dr. N. Paulic for the synthesis of the L-*N*,*N*-methylated amino acids and the copper(II) complexes. Financial support from the Ministry of Science and Technology of the Republic of Croatia, Grants 0022017 and 0098040, is acknowledged.

 © 2004 Wiley-VCH Verlag GmbH & Co. KGaA, Weinheim

[1] B. Bóka, A. Myani, I. Sóvágó, N. Hadjiliadis, *J. Inorg. Biochem.* **2004**, *98*, 113−122.
[2] Z. Arkosi, T. Szabó-Plánka, A. Rockenbauer, N. V. Nagy, L. Lázár, F. Fülöp, *Inorg. Chem.* **2003**, *16*, 4842−4848.
[3] M. D. Apostolova, P. R. Bontchev, B. B. Ivanova, W. R. Russell, D. R. Mehandjiev, J. H. Beattie, C. K. Nachev, *J. Inorg. Biochem.* **2003**, *95*, 321−333.
[4] G. Facchin, M. H. Torre, E. Kremer, O. E. Piro, E. E. Castellano, E. J. Baran, *J. Inorg. Biochem.* **2002**, *89*, 174−180.
[5] T. Szabó-Plánka, N. Nagy, A. Rockenbauer, L. Korecz, *Polyhedron* **2000**, *19*, 2049−2057.
[6] R. Pogni, M. C. Baratto, E. Busi, R. Basosi, *J. Inorg. Biochem.* **1999**, *73*, 153−165.
[7] G. Branica, N. Paulić, B. Grgas, D. Omanović, *Chem. Spec. Bioavail.* **1999**, *11*, 125−134.
[8] D. R. Brown, V. Guantieri, G. Grasso, G. Impellizzeri, G. Pappalardo, E. Rizzarelli, *J. Inorg. Biochem.* **2004**, *98*, 133−143.
[9] M. J. Pushie, A. Rauk, *J. Biol. Inorg. Chem.* **2003**, *8*, 53−65.
[10] M. Orfei, M. C. Alcaro, G. Marcon, M. Chelli, M. Ginanneschi, H. Kozlowski, J. Brasun, L. Messori, *J. Inorg. Biochem.* **2003**, *97*, 299−307.
[11] P. Comba, *Coord. Chem. Rev.* **2000**, *200−202*, 217−245.
[12] G. Liang, R. Tribolet, H. Sigel, *Inorg. Chem. Acta* **1989**, *27*, 273−280.
[13] H. Sigel, *Pure Appl. Chem.* **1989**, *61*, 923−932.
[14] V. Noethig-Laslo, N. Paulić, *J. Chem. Soc., Dalton Trans.* **1992**, 2045−2047.
[15] V. Noethig-Laslo, N. Paulić, *Z. Anorg. Allg. Chem.* **1995**, *62*, 84−88.
[16] B. Kaitner, N. Paulić, N. Raos, V. Simeon, *J. Coord. Chem.* **1987**, *15*, 373−381.
[17] B. Kaitner, N. Paulić, N. Raos, *J. Coord. Chem.* **1991**, *22*, 269−279.
[18] B. Kaitner, G. Pavlović, N. Paulić, N. Raos, *J. Coord. Chem.* **1995**, *36*, 327−338.
[19] B. Kamenar, M. Penavić, A. Škorić, N. Paulić, N. Raos, V. Simeon, *J. Coord. Chem.* **1988**, *17*, 85−94.
[20] C. S. Tautermann, J. Sabolović, A. F. Voegele, K. R. Liedl, *J. Phys. Chem. B* **2004**, *198*, 2098−2102.
[21] V. Noethig-Laslo, N. Paulić, *Polyhedron* **1999**, *18*, 1609−1614.
[22] V. Noethig-Laslo, N. Paulić, R. Pogni, R. Bassosi, *Polyhedron* **2002**, *21*, 1643−1649.
[23] J. Sabolović, V. Noethig-Laslo, *Cellul. Mol. Biol. Lett.* **2002**, *7*, 151−153.
[24] R. Basosi, W. A. Antholine, J. S. Hyde, *Biological Magn. Res.* **1993**, *13*, 103−150.
[25] R. Pogni, G. della Lunga, R. Basosi, *J. Am. Chem. Soc.* **1993**, *115*, 1546−1550.
[26] J. Sabolović, C. S. Tautermann, T. Loerting, K. R. Liedl, *Inorg. Chem.* **2003**, *42*, 2268−2279.
[27] C. Conato, A. Contino, G. Maccaone, A. Magri, M. Remelli, G. Tabbi, *Thermochim. Acta* **2000**, *362*, 13−23.
[28] B. A. Goodman, C. G. Palivan, H. Palivan, S. Tomas, *Appl. Magn, Reson.* **2003**, *25*, 13−28.
[29] B. Kaitner, N. Paulić, G. Pavlović, J. Sabolović, *Polyhedron* **1999**, *18*, 2301−2311.
[30] B. A. Goodman, D. B. McPhail, H. K. J. Powell, *J. Chem. Soc., Dalton Trans.* **1981**, 822−827.
[31] B. A. Goodman, D. B. McPhail, *J. Chem. Soc., Dalton Trans.* **1985**, 1717−1719.
[32] M. Pasenkiewicz-Gierula, W. Froncisz, R. Basosi, W. E. Antholine, J. S. Hyde, *Inorg. Chem.* **1987**, *26*, 801−805.
[33] A. Rockenbauer, *J. Magn. Res.* **1979**, *35*, 429−438.
[34] T. Szabo-Planka, A. Rockenbauer, L. Korecz, D. Nagy, *Polyhedron* **2000**, *19*, 1123−1131.
[35] D. B. McPhail, B. A. Goodman, *J. Chem. Soc., Faraday Trans.* **1987**, 3683−3692.
[36] J. Peisach, W. E. Blumberg, *Arch. Biochem. Biophys.* **1974**, *165*, 691−708.
[37] P. Comba, P. Jursic, Y. D. Lampeka, A. Peters, A. I. Prikhod′ko, H. Pritzkow, *Inorg. Chim. Acta* **2001**, *324*, 99−107.
[38] J. Sabolović, K. R. Liedl, *Inorg. Chem.* **1999**, *38*, 2764−2774.
[39] H. M. McConnell, *J. Chem. Phys.* **1956**, *25*, 709−711.
[40] F. G. Hering, J. M. Park, *J. Magn. Res.* **1979**, *36*, 311−323.
[41] *CRC Handbook of Chemistry and Physics*, 58th edition, CRC PRESS, **1977−1978**.
[42] S. R. Niketić, K. Rasmussen, *The Consistent Force Field: A Documentation; Lectures Notes in Chemistry*; Springer-Verlag: Berlin Heidelberg New York, **1977**, vol. 3.
[43] K. Rasmussen, *Potential Energy Functions in Conformational Analysis; Lectures Notes in Chemistry*; Springer-Verlag: Berlin, Heidelberg, New York, **1985**, Vol. 37.
[44] K. Rasmussen, S. B. Engelsen, J. Fabricius, B. Rasmussen in the *Recent Experimental and Computational Advances in Molecular Spectroscopy* (Ed.: R. Fausto), NATO ASI Series C: Mathematical and Physical Sciences; Kluwer Academic Publishers: Dordrecht, The Netherlands, **1993**, vol. 406, pp. 381−419.
[45] T. J. M. de Bruin, T. M. Marcelis, H. Zuilhof, E. J. R. Sudhölter, *Phys. Chem. Chem. Phys.* **1999**, *1*, 4157−4163.
[46] R. E. Bowman, H. H. Stroud, *J. Chem. Soc.* **1950**, 1342−1349.
[47] C. P. Nash, W. P. Schaefer, *J. Am. Chem. Soc.* **1969**, *91*, 1319−1324.

Received October 24, 2003
Early View Article
Published Online August 12, 2004

 © 2004 Wiley-VCH Verlag GmbH & Co. KGaA, Weinheim

New *N*,*N*-Diisopropylcarbamato Complexes of Ruthenium(II) as Catalytic Precursors for Olefin Hydrogenation

Daniela Belli Dell'Amico,*[a] Fausto Calderazzo,[a] Ulli Englert,[b] Luca Labella,[a] Fabio Marchetti,[a] and Monica Specos[a]

Keywords: *N*,*N*-Dialkylcarbamato complexes / Ruthenium / Hydrogenation

During the synthesis of $[Ru(O_2CN\mathit{i}Pr_2)_2(PPh_3)_2]$ (**1**), the $[RuCl_2(PPh_3)_3]/NH\mathit{i}Pr_2/CO_2$ system produces the intermediates $[NH_2\mathit{i}Pr_2][Ru_2Cl_2(\mu\text{-}Cl)_3(PPh_3)_4]$ (**2**) and $[RuCl(O_2CN\mathit{i}Pr_2)(PPh_3)_3]$ (**3**) which have been isolated and fully characterised. Compound **2** contains the dinuclear anionic triply chloride-bridged ruthenium(II) species. Compound **3** is mononuclear, the octahedral ruthenium centre being coordinated to the bidentate carbamato ligand. The reactions of compounds **1** and **3** with dihydrogen have been studied at room temperature and atmospheric pressure with respect to their catalytic hydrogenation of 1-octene.

(© Wiley-VCH Verlag GmbH & Co. KGaA, 69451 Weinheim, Germany, 2004)

Introduction

Olefin hydrogenation using ruthenium(II) complexes has been studied extensively.[1] Some precursors containing carboxylato ligands have been shown to be catalytically active under homogeneous conditions.[2] *N*,*N*-Dialkylcarbamato complexes of ruthenium(II) with tertiary phosphanes as ancillary ligands have been prepared in our laboratories[3] and elsewhere.[4] The *N*,*N*-dialkylcarbamato group, R_2NCO_2, is geometrically similar to the carboxylato ligand and is a good leaving group, prompt CO_2 evolution being observed in the presence of proton-active substances.[5] Moreover, this ligand may undergo a change of hapticity from bidentate to monodentate, thus allowing coordination of a further ligand. This observation has been established for the reaction of **1** with CO, the two bidentate carbamato groups being sequentially converted into monodentate groups by addition of carbon monoxide yielding $[Ru(O_2CN\mathit{i}Pr_2)_2(CO)(PPh_3)_2]$ and $[Ru(O_2CN\mathit{i}Pr_2)_2(CO)_2(PPh_3)_2]$.[3a] This is reminiscent of earlier data on the hexacoordinate ruthenium(II) cation $[Ru(O_2CNMe_2)(PMe_2Ph)_4]^+$ which is converted into $[Ru(CO)(O_2CNMe_2)(PMe_2Ph)_4]^+$. Both were isolated as their hexafluorophosphate derivatives.[4a,4b] Such coordination flexibility is an important prerequisite for catalysis.

In relation to the use of carboxylato and carbamato derivatives of ruthenium(II) in catalysis, $[Ru(O_2CMe)_2(PPh_3)_2]$ was reported to assist olefin hydrogenation in the presence of strong protic acids such as CF_3SO_3H,[2a] with $[Ru(PPh_3)_n]^{2+}$ being postulated as the catalytically active species. Moreover, it is worth noting that in the ruthenium-catalysed conversion of $CO_2/HNMe_2/H_2$ to $HCONMe_2$ at 125 °C, the intermediacy of a (carbamato)ruthenium complex was excluded on the basis of deuteration studies.[6a] The possible role played by the *N*,*N*-dialkylcarbamato group in this process urged us to study the behaviour of this ligand in ruthenium-promoted catalytic hydrogenation. This paper reports some new data regarding the reaction of $[RuCl_2(PPh_3)_3]$, a pentacoordinate mononuclear ruthenium complex,[6b] with the $NH\mathit{i}Pr_2/CO_2$ system leading to new derivatives of ruthenium(II). Moreover, results are presented on the reaction of the (carbamato)ruthenium(II) complexes with dihydrogen, some of them acting as catalyst precursors for olefin hydrogenation.

Results and Discussion

Synthesis and Characterisation of the Ruthenium Complexes

The reaction of $[RuCl_2(PPh_3)_3]$ with $NH\mathit{i}Pr_2$ and CO_2 to afford **1** is rather slow, the conversion of 4 g of the precursor requiring several days at room temperature in the presence of a large excess of the amine [Equation (1)].[3a]

$$[RuCl_2(PPh_3)_3] + 4\ NH\mathit{i}Pr_2 + 2\ CO_2 \longrightarrow \underset{\mathbf{1}}{[Ru(O_2CN\mathit{i}Pr_2)_2(PPh_3)_2]} + 2\ [NH_2\mathit{i}Pr_2]Cl + PPh_3 \quad (1)$$

[a] Dipartimento di Chimica e Chimica Industriale, Università di Pisa,
Via Risorgimento 35, 56126 Pisa, Italy
Fax: (internat.) + 39-050-2219-246
E-mail: belli@dcci.unipi.it
[b] Institut für Anorganische Chemie der RWTH,
Professor-Pirlet-Strasse 1, 52074 Aachen, Germany

 © 2004 Wiley-VCH Verlag GmbH & Co. KGaA, Weinheim DOI: 10.1002/ejic.200400014

A more appropriate synthesis of **1** has now been found (vide infra) and this required further work on the reactivity of $[RuCl_2(PPh_3)_3]$. In spite of its low solubility in toluene, $[RuCl_2(PPh_3)_3]$ rapidly dissolves in the presence of $NHiPr_2$ and CO_2. We have now found that two intermediates, **2** and **3**, can be intercepted, presumably formed according to Equation (2).

$$3\,[RuCl_2(PPh_3)_3] + 2\,NHiPr_2 + CO_2 \longrightarrow \underset{\mathbf{2}}{[NH_2iPr_2][Ru_2Cl_5(PPh_3)_4]} + \underset{\mathbf{3}}{[RuCl(O_2CNiPr_2)(PPh_3)_3]} + 2\,PPh_3 \quad (2)$$

It is reasonable to assume that the relatively slow substitution of one chloro ligand by the carbamate anion $[O_2CNiPr_2]^-$, formed in situ from carbon dioxide and the amine, yields **3** and $[NH_2iPr_2]Cl$, the latter being promptly sequestered by the unchanged starting material to afford **2**. The formation of **2** in a 69% yield has been established independently by treating $[RuCl_2(PPh_3)_3]$ with $[NH_2iPr_2]Cl$ in toluene in a molar ratio of 2 [Equation (3)].

$$2\,[RuCl_2(PPh_3)_3] + [NH_2iPr_2]Cl \longrightarrow \underset{\mathbf{2}}{[NH_2iPr_2][Ru_2Cl_5(PPh_3)_4]} + 2\,PPh_3 \quad (3)$$

The successful replacement of the phosphane ligand by chloride in this reaction can be easily understood since the starting compound $[RuCl_2(PPh_3)_3]$, which is mononuclear with a pentacoordinate ruthenium atom, is converted into the anionic dinuclear product containing a hexacoordinate ruthenium atom (vide infra).

The salt-like product **2** has been found to be a convenient starting material for the synthesis of **1**. Since it contains two phosphane ligands per ruthenium atom, the poorly soluble phosphane is not released and **1** is obtained pure, in a satisfactory yield of about 55%, without contamination by **3** [Equation (4)].

$$\underset{\mathbf{2}}{[H_2NiPr_2][Ru_2Cl_5(PPh_3)_4]} + 8\,NHiPr_2 + 4\,CO_2 \longrightarrow 2\,\underset{\mathbf{1}}{[Ru(O_2CNiPr_2)_2(PPh_3)_2]} + 5\,[NH_2iPr_2]Cl \quad (4)$$

The ^{31}P NMR spectrum of **2** in C_6D_6 shows a singlet at $\delta = 46.8$ ppm. This suggests a symmetrical arrangement of the ligands which was subsequently confirmed by X-ray diffraction methods.

The anion contains two hexacoordinate ruthenium centres bridged by three chloro ligands, the coordination of each ruthenium atom being completed by two phosphane ligands and one terminal chloro ligand (Figure 1). In addition, hydrogen interactions are present between the cation and the terminal chloro ligands of the anion, the N(1)···Cl(4) and N(1)···Cl(5) distances being 3.29 and 3.23 Å, respectively. Similar interactions have already been reported in $[Et_2NH_2][Ru_2Cl_2(\mu\text{-}Cl)_3(DPB)_2]$ [DPB = 1,2-bis(diphenylphosphanyl)benzene],[7a] $[tBu_2MePH][Ru_2Cl_2(\mu\text{-}Cl)_3(CO)_2(PtBu_2Me)_2]$[7b] and in $[Et_2NH_2][Ru_2Cl_2(\mu\text{-}Cl)_3\{(R)\text{-}p\text{-MeO-BINAP})\}_2]$ [*p*-MeO-BINAP = 2,2′-bis(diphenylphosphanyl)-1,1′-binaphthyl].[8a] The formation of ion pairs is presumably responsible for the high solubility of these species in aromatic solvents. Crystal packing is created by the ion pairs where the two partners are tightly linked, the shortest distance separating the centroids of neighbouring pairs being 11.8 Å.

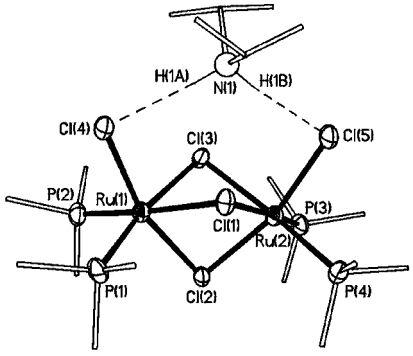

Figure 1. View of the molecular structure of the ion pair $[iPr_2NH_2][Ru_2Cl_2(\mu\text{-}Cl)_3(PPh_3)_4]$ (**2**) with thermal ellipsoids at the 30% probability level; the phenyl groups of triphenylphosphane and the isopropyl hydrogen atoms have been omitted for clarity

Table 1. Bond lengths [Å] and angles [°] around the Ru atoms in **2**

Ru(1)−Cl(1)	2.466(7)	Ru(2)−Cl(1)	2.437(6)
Ru(1)−Cl(2)	2.439(6)	Ru(2)−Cl(2)	2.411(6)
Ru(1)−Cl(3)	2.478(6)	Ru(2)−Cl(3)	2.487(6)
Ru(1)−Cl(4)	2.404(6)	Ru(2)−Cl(5)	2.414(7)
Ru(1)−P(1)	2.288(7)	Ru(2)−P(3)	2.311(7)
Ru(1)−P(2)	2.308(8)	Ru(2)−P(4)	2.302(7)
N(1)···Cl(4)	3.29(2)	N(1)···Cl(5)	3.23(2)
P(1)−Ru(1)−P(2)	98.9(3)	P(3)−Ru(2)−Cl(5)	95.5(2)
P(1)−Ru(1)−Cl(4)	93.2(3)	P(4)−Ru(2)−Cl(2)	100.1(2)
P(2)−Ru(1)−Cl(4)	92.8(2)	P(3)−Ru(2)−Cl(2)	93.4(2)
P(1)−Ru(1)−Cl(2)	98.3(3)	Cl(5)−Ru(2)−Cl(2)	163.8(2)
P(2)−Ru(1)−Cl(2)	98.4(2)	P(4)−Ru(2)−Cl(1)	89.6(2)
Cl(4)−Ru(1)−Cl(2)	162.5(2)	P(3)−Ru(2)−Cl(1)	169.0(3)
P(1)−Ru(1)−Cl(1)	90.3(2)	Cl(5)−Ru(2)−Cl(1)	89.4(2)
P(2)−Ru(1)−Cl(1)	170.7(3)	Cl(2)−Ru(2)−Cl(1)	79.7(2)
Cl(4)−Ru(1)−Cl(1)	88.2(2)	P(4)−Ru(2)−Cl(3)	167.5(2)
Cl(2)−Ru(1)−Cl(1)	78.6(2)	P(3)−Ru(2)−Cl(3)	92.2(2)
P(1)−Ru(1)−Cl(3)	167.5(2)	Cl(5)−Ru(2)−Cl(3)	88.9(2)
P(2)−Ru(1)−Cl(3)	93.2(2)	Cl(2)−Ru(2)−Cl(3)	77.2(2)
Cl(4)−Ru(1)−Cl(3)	89.1(2)	Cl(1)−Ru(2)−Cl(3)	78.0(2)
Cl(2)−Ru(1)−Cl(3)	76.9(2)	Ru(2)−Cl(1)−Ru(1)	86.8(2)
Cl(1)−Ru(1)−Cl(3)	77.6(2)	Ru(2)−Cl(2)−Ru(1)	88.0(2)
P(4)−Ru(2)−P(3)	100.1(3)	Ru(1)−Cl(3)−Ru(2)	85.5(2)
P(4)−Ru(2)−Cl(5)	91.6(3)		

As can be seen in Table 1, the coordination environment around the ruthenium centre is pseudo-octahedral. The Ru(1)···Ru(2) distance is 3.370 Å, a value beyond the maximum generally accepted for a bonding interaction. A significant difference is found between the ruthenium−chlorine distances *trans* to the phosphane ligands (mean value 2.467 Å) and those *trans* to the terminal chloro ligands (mean value 2.425 Å).

 © 2004 Wiley-VCH Verlag GmbH & Co. KGaA, Weinheim

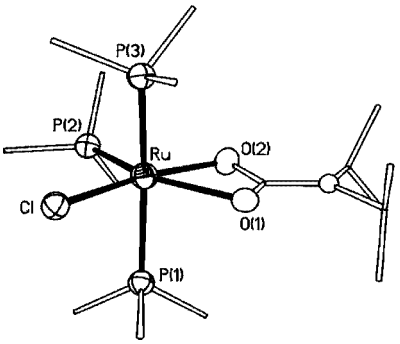

Figure 2. View of the molecular structure of [RuCl(O_2CN*i*Pr_2)(PPh_3)$_3$] (**3**) with thermal ellipsoids at the 30% probability level; the phenyl groups of the triphenylphosphane and isopropyl hydrogen atoms have been omitted for clarity

The presence of two face-bridged octahedra with three bridging chloro ligands is common in ruthenium chemistry. On the other hand, a few examples exist in the literature of *anionic* species containing tertiary phosphanes as ligands, namely those mentioned above as well as [Et_2NH_2][Ru_2Cl_2(μ-Cl)$_3$(dppb)$_2$] [dppb = 1,4-bis(diphenylphosphanyl)butane].[8b] A rational synthesis of this class of anionic species was reported for [H_2NR_2][(Ru_2Cl_2(μ-Cl)$_3$(dppb)$_2$][8b] involving the addition of [R_2NH_2]Cl to the pentacoordinate [$RuCl_2$(dppb)(PPh_3)]. Closely connected are the results by Caulton and co-workers[7b] on the reaction of $RuX_2(CO)L_2$ with M^IX (M^I = alkali metal; X = halide) which affords $M^I[Ru_2X_5(CO)_2L_2]$. Reactions which involve elimination of a ligand L from the metal coordination sphere, followed by dimerization of the metal-containing fragments through bridging halo ligands, can be explained by the need torelieve steric congestion and to obtain the 18-electron configuration in the triply bridged anion.

To obtain pure **3**, it is necessary to use an excess of the amine (amine/Ru molar ratio ca. 4) in a relatively dilute toluene solution [Equation (5)]. In fact, with a *i*Pr_2NH/[$RuCl_2$(PPh_3)$_3$] molar ratio of 2, the reaction according to Equation (2) still operates and a mixture of **2** and **3** was found even after long reaction times together with unchanged starting material. It is important to note that contamination of **3** with **1** does not occur since complete removal of the chloro ligands from the ruthenium atom requires a large excess of the amine [Equation (1)]. The reaction of **3** towards the amine/(carbon dioxide) system is slow [Equation (6)].

$$[RuCl_2(PPh_3)_3] + 2\ NHiPr_2 + CO_2 \rightleftharpoons \underset{\mathbf{3}}{[RuCl(O_2CNiPr_2)(PPh_3)_3]} + [NHiPr_2]Cl \quad (5)$$

$$\underset{\mathbf{3}}{[RuCl(O_2CNiPr_2)(PPh_3)_3]} + 2\ NHiPr_2 + CO_2 \longrightarrow \underset{\mathbf{1}}{[Ru(O_2CNiPr_2)_2(PPh_3)_2]} + [NHiPr_2]Cl + PPh_3 \quad (6)$$

Moreover, the formation of **1** would be accompanied by PPh_3 elimination which is clearly counteracted by the presence of free triphenylphosphane. Thus, when good yields of pure **3** are required, addition of some free triphenylphosphane to the reaction mixture totally prevents the formation of **1**. A similar situation has already been encountered with [RuCl(O_2CNR_2)(η^6-cymene)] (R = Et, *i*Pr) which does not yield [Ru(O_2CNR_2)$_2$(η^6-cymene)] even under severe conditions of temperature and pressure and with elevated amine/Ru molar ratios.[3c]

The ruthenium complex **3**, recrystallized from a toluene/heptane mixture, has been studied by single-crystal X-ray diffraction (Figure 2, Table 2). The compound has a mononuclear structure with the metal centre in a distorted octahedral geometry. The coordination sites are occupied by a chloro ligand, an asymmetric bidentate carbamato ligand and three phosphane ligands in *mer* positions.

Table 2. Bond lengths [Å] and angles [°] around the Ru atom in **3**

Ru−Cl	2.415(6)	Ru−P(3)	2.419(7)
Ru−P(1)	2.375(7)	Ru−O(1)	2.27(2)
Ru−P(2)	2.271(6)	Ru−O(2)	2.12(2)
O(2)−Ru−P(2)	91.2(5)	O(1)−Ru−Cl	106.5(4)
O(1)−Ru−O(2)	60.0(6)	P(1)−Ru−Cl	81.8(2)
P(2)−Ru−O(1)	151.1(4)	O(2)−Ru−P(3)	98.9(5)
O(2)−Ru−P(1)	94.9(5)	P(2)−Ru−P(3)	98.2(2)
P(2)−Ru−P(1)	98.8(2)	O(1)−Ru−P(3)	89.5(5)
O(1)−Ru−P(1)	82.4(5)	P(1)−Ru−P(3)	157.9(2)
O(2)−Ru−Cl	166.5(5)	Cl−Ru−P(3)	80.9(2)
P(2)−Ru−Cl	102.2(2)		

Major distortions from ideal octahedral geometry are due to the small O(1)−Ru−O(2) angle of 60.0° and the P(1)−Ru−P(3) bond angle, involving the two *trans*-phosphane ligands, of 157.9°. The Ru−O(1) bond of 2.27 Å is longer than Ru−O(2) (2.12 Å), possibly due to O(1) being *trans* to P(2). The Ru−P(2) bond is significantly shorter than the other two distances, as found elsewhere for other *mer* complexes.[9a,9b] The easy displacement of one of the weakly bonded phosphane ligands leading to [*cis*-Ru(O_2CN*i*Pr_2)$_2$(PPh_3)$_2$] can therefore be easily understood.

Compound **3** was subjected to conventional spectroscopic investigations. The presence of bidentate carbamato ligands was confirmed by the absence of IR bands above 1600 cm^{-1}.[5b] The ^{31}P NMR solution spectrum of **3** at −40 °C shows the presence of free PPh_3 with a signal at δ = −4.2 ppm and two doublets at δ = 27.7 and 51.0 ppm (J = 68 Hz) as well as a triplet at δ = 46.5 ppm coupled with the doublet at δ = 50.1 ppm (J = 66 Hz). For comparison, [RuCl(O_2CMe)(PPh_3)$_3$][9c] shows signals at δ = 31.0 (t) and 50.5 (d) ppm. At room temperature the signals of **3** are broad. These results may be explained by assuming that equilibrium [Equation (7)] occurs in solution, the dinuclear species being responsible for the additional signals.

$$2\ \underset{\mathbf{3}}{[RuCl(O_2CNiPr_2)(PPh_3)_3]} \rightleftharpoons [Ru_2(\mu\text{-}Cl)_2(O_2CNiPr_2)_2(PPh_3)_4] + 2\ PPh_3 \quad (7)$$

 © 2004 Wiley-VCH Verlag GmbH & Co. KGaA, Weinheim

Similar to other examples in the literature,[10] the equilibrium is suppressed by addition of an excess of phosphane. In the dinuclear compound, each ruthenium atom is assumed to be hexacoordinate with two bridging chloro ligands, two phosphane ligands and a terminal bidentate carbamato ligand, the ruthenium(II) centre again reaching the 18-electron configuration.[10a] The rather simple NMR spectra of $[RuCl(O_2CMe)(PPh_3)_3]$[9c] suggest the absence of ligand dissociation.

Reactivity of the Ruthenium Complexes with Dihydrogen

Olefin complexation is believed to be the primary process in a catalytic hydrogenation cycle and a few olefin complexes of ruthenium(II) have been isolated and crystallographically characterised.[11–15] $RuHCl(PPh_3)_3$[16] was reported to be unreactive towards 1-hexene, 1-heptene and 2-octene, whereas an alkyl derivative was detected (NMR) with ethylene at 35 atm. We have observed that the carbamato complexes **1** and **3** do not react with 1-octene, although it was conceivable that they could add the olefin by converting the carbamato ligand from a bidentate to a monodentate ligating mode.

Compound **3** is converted by dihydrogen at room temperature and atmospheric pressure in toluene solution into both the soluble $[Ru(H)_2(H_2)(PPh_3)_3]$ and the poorly soluble violet $[RuHCl(PPh_3)_3]$. These compounds have been identified on the basis of their spectroscopic data and by comparison with data in the literature.[16,17] The intermediate $[RuH(O_2CN\mathit{i}Pr_2)(PPh_3)_3]$ (**4**) was also detected by ^{31}P NMR spectroscopy in solution (vide infra). These results are consistent with the reactions shown in Equations (8) and (9). On the other hand, direct hydrogenation of **3** may lead to $[RuH(Cl)(PPh_3)_3]$ [Equation (10)]. We have also established that when **3** is hydrogenated in the presence of an excess of $NH\mathit{i}Pr_2$, only the soluble $[Ru(H)_2(H_2)(PPh_3)_3]$ is formed, together with $[NH_2\mathit{i}Pr_2]Cl$. HCl elimination from $[RuH(Cl)(PPh_3)_3]$ is favoured under these conditions. It is interesting to note that $[Ru(H)_2(H_2)(PPh_3)_3]$[17,18] is prepared by the action of relatively strong reducing agents such as $NaBH_4$ or AlR_3 on $[RuCl_2(PPh_3)_3]$.[19a,19b] Our synthesis operates under mild conditions in aromatic hydrocarbons.

$$\underset{\mathbf{3}}{[RuCl(O_2CN\mathit{i}Pr_2)(PPh_3)_3]} + H_2 \longrightarrow \underset{\mathbf{4}}{[RuH(O_2CN\mathit{i}Pr_2)(PPh_3)_3]} + HCl \quad (8)$$

$$\underset{\mathbf{4}}{[RuH(O_2CN\mathit{i}Pr_2)(PPh_3)_3]} + 2\,H_2 \rightleftharpoons [Ru(H)_2(H_2)(PPh_3)_3] + CO_2 + NH\mathit{i}Pr_2 \quad (9)$$

$$\underset{\mathbf{3}}{[RuCl(O_2CN\mathit{i}Pr_2)(PPh_3)_3]} + H_2 \longrightarrow [RuH(Cl)(PPh_3)_3] + CO_2 + NH\mathit{i}Pr_2 \quad (10)$$

The carbamato derivative **1** does not react with dihydrogen at room temperature and atmospheric pressure. By gradually increasing the temperature, a reaction was found to occur at about 80 °C, accompanied by some decomposition, presumably due to the low thermal stability of the intermediate $[Ru(H)_2(H_2)_2(PPh_3)_2]$.[17a,17b] The experiment at 80 °C was therefore repeated in the presence of 1 equiv. of triphenylphosphane. Under these conditions, $[Ru(H)_2(H_2)(PPh_3)_3]$ was detected as the sole final ruthenium-containing compound [Equation (11)].

$$[Ru(O_2CN\mathit{i}Pr_2)_2(PPh_3)_2] + 3\,H_2 + PPh_3 \longrightarrow [Ru(H)_2(H_2)(PPh_3)_3] + 2\,CO_2 + 2\,NH\mathit{i}Pr_2 \quad (11)$$

Upon monitoring the reaction by ^{31}P NMR spectroscopy, signals attributable to the intermediate formation of $[RuH(O_2CN\mathit{i}Pr_2)(PPh_3)_3]$ [Equation (12)] were detected, namely a triplet at $\delta = 76.8$ ppm coupled with a doublet at $\delta = 41.7$ ppm ($J = 68$ Hz). These signals can be attributed to three phosphane ligands in a *mer* configuration if a comparison is made with [*mer*-$RuH(O_2CMe)(PPh_3)_3$], the latter showing resonances at $\delta = 77.6$ (t) and 43.8 (d) ppm.[10b]

$$\underset{\mathbf{1}}{[Ru(O_2CN\mathit{i}Pr_2)_2(PPh_3)_2]} + H_2 + PPh_3 \longrightarrow [RuH(O_2CN\mathit{i}Pr_2)(PPh_3)_3] + CO_2 + NH\mathit{i}Pr_2 \quad (12)$$

The ^1H NMR spectrum of $[RuH(O_2CN\mathit{i}Pr_2)(PPh_3)_3]$ shows a quadruplet at $\delta = -17.6$ ppm, equivalent to an overlapping doublet of triplets which would be expected for the coupling with the three phosphorus atoms. This is analogous with the quadruplet at $\delta = -19.8$ ppm exhibited by $[RuH(O_2CMe)(PPh_3)_3]$.[1d] A possible structure for $[RuH(O_2CN\mathit{i}Pr_2)(PPh_3)_3]$, similar to that of **3** with three *mer*-phosphane ligands, is consistent with the observed spectrum (Figure 2).

The reaction according to Equation (9) is reversible: in toluene, $[Ru(H)_2(H_2)(PPh_3)_3]$ rapidly reverts to $[RuH(O_2CN\mathit{i}Pr_2)(PPh_3)_3]$ in the presence of $\mathit{i}Pr_2NH/CO_2$ (amine/ruthenium molar ratio ca. 8) which is the only species present in solution after 1 h. By adding a large excess of amine, $[Ru(O_2CN\mathit{i}Pr_2)_2(PPh_3)_2]$ was obtained after one week.

Catalysis

All ruthenium derivatives reported in this paper have been tested as potential catalysts for the hydrogenation of 1-octene in toluene at room temperature, with activity being shown by **1** and **3**.

Once it was established that **1** does not react at room temperature and atmospheric pressure either with 1-octene or with H_2, hydrogenation of 1-octene was observed using $10^{-2}/10^{-3}$ M solutions of **1**, as evidenced by both gas chromatography, ^1H NMR spectroscopy and gas-volumetric measurements. Immediately after the catalyst precursor comes into contact with the reaction mixture, olefin hydrogenation occurs with no induction time being observed. The initial rate was found to correspond to approximately 300 mmol·L^{-1} h^{-1}, the olefin/ruthenium molar ratio being 28 and the initial olefin concentration being 2.6×10^{-1} M. After normalization with respect to the concentration of both the catalyst precursor and the olefin and to the H_2

 © 2004 Wiley-VCH Verlag GmbH & Co. KGaA, Weinheim

partial pressure, the initial reaction rate (r_i), was calculated to be 163 mol·L^{-1} h^{-1}. No other ruthenium complexes other than the starting material were detected in solution by NMR spectroscopy after hydrogenation. More than 90% of **1** remained unchanged.[19c] It is reasonable to assume that in the course of the process, vacant sites for olefin or hydrogen coordination are made available on **1** by a haptic-ity change of the carbamato ligand from bidentate to monodentate.

Hydrogenation of 1-octene was also studied in the presence of **3** as a catalytic precursor. After about 6 h in toluene at room temperature, complete hydrogenation was established as indicated by gas chromatography and ruthenium was recovered as $[RuHCl(PPh_3)_3]$. No $[RuH_2(H_2)(PPh_3)_3]$ was present in the solution and gas-volumetric measurements showed that 89% of the olefin was hydrogenated in about 3 h.

In contrast to the earlier report on the use of the anionic complex $[Ru_2Cl_2(\mu\text{-}Cl)_3\{(R)\text{-}p\text{-MeO-BINAP})\}_2]^-$ [8a] in the asymmetric hydrogenation of olefins, $[iPr_2NH_2][Ru_2Cl_5(PPh_3)_4]$ was found to be inactive for the hydrogenation of 1-octene, the latter being slowly converted into (*E*)-4-octene. Similarly, in an attempted hydrogenation of 1-octene, the carbonyl complex $[Ru(CO)(O_2CNiPr_2)_2(PPh_3)_2]$ gave only a slow olefin isomerization.

Conclusions

In the reaction of $[RuCl_2(PPh_3)_3]$ with iPr_2NH and CO_2, optimum conditions have been identified for the preparation of the new species **3**. Moreover, a new convenient synthesis of **1** was carried out using **2** as a precursor.

The hydrogenation of some (carbamato)ruthenium(II) complexes was found to depend on the nature of the ligands. Compound **3** promptly reacts at room temperature, producing a mixture of $[RuHCl(PPh_3)_3]$ and $[RuH_2(H_2)(PPh_3)_3]$. When the reaction was carried out in the presence of an HCl scavenger, for instance iPr_2NH, only $[RuH_2(H_2)(PPh_3)_3]$ was detected as the final ruthenium-containing product through the intermediate $[RuH(O_2CNiPr_2)(PPh_3)_3]$.

No reaction with dihydrogen was observed for **1** at room temperature with $[RuH_2(H_2)(PPh_3)_3]$ being formed at 80 °C in the presence of PPh_3. Both **1** and **3** promote the hydrogenation of 1-octene at room temperature and atmospheric pressure, the highest activity being exhibited by the former which was largely recovered unchanged after catalysis in toluene. No other complexes were detected in solution by ^{31}P NMR spectroscopy. This suggests that catalysis does not require complete cleavage of the $Ru-O_2CNiPr_2$ bond. The flexibility of the carbamato ligand changing its coordination mode from η^2 to η^1 and allowing easy access to the metal atom may explain the results. Consistent with this interpretation both $[Ru(O_2CNiPr_2)_2CO(PPh_3)_2]$ and $[Ru(O_2CNiPr_2)_2(CO)_2(PPh_3)_2]$, which contain monodentate carbamato groups and strongly bonded ancillary ligands, are inactive towards olefin hydrogenation under comparable conditions. The importance of the carbamato ligand in the dihydrogen activation is apparent from the observation that the chloride-bridged anion of ruthenium(II) in the $[iPr_2NH_2][Ru_2Cl_5(PPh_3)_4]$ derivative was found to be inactive. As a result of recent mechanistic studies on ruthenium-catalysed hydrogenations,[20a–20c] the hydrogenation experiments reported in this paper will be extended to other unsaturated substrates.

Experimental Section

General: All procedures were carried out in standard Schlenk tubes. Solvents were freshly distilled from conventional drying agents under nitrogen and all manipulations were carried out under nitrogen, unless otherwise specified. The compounds $[RuCl_2(PPh_3)_3]$,[21] $[Ru(CO)(O_2CNiPr_2)_2(PPh_3)_2]$,[3a] and $[Ru(CO)_2(O_2CNiPr_2)_2(PPh_3)_2]$[3a] were prepared according to the literature. Commercial (Aldrich) triphenylphosphane, 1-octene and diisopropylamine were purified by conventional methods. Elemental analyses (C, H, N) were performed by the Laboratorio di Microanalisi della Facoltà di Farmacia, Università di Pisa, with a Carlo Erba model 1106 elemental analyser. IR spectra were recorded with a Perkin-Elmer FT-IR model 1725X spectrophotometer. Nuclear magnetic resonance spectra were recorded using a Varian Gemini 200BB instrument, the data being expressed in ppm relative to TMS for ^1H and ^{13}C and to 85% H_3PO_4 in D_2O for ^{31}P.

Synthesis of $[RuCl(O_2CNiPr_2)(PPh_3)_3]$ (3): To a solution of diisopropylamine (2.6 mL, 18.4 mmol) in toluene (300 mL), saturated with carbon dioxide, $[RuCl_2(PPh_3)_3]$ (4.35 g, 4.54 mmol) was quickly added together with PPh_3 (3.63 g, 13.8 mmol). After stirring under carbon dioxide for 4 d, $[iPr_2NH_2]Cl$ was removed by filtration. The ^{31}P NMR spectroscopic measurements on the filtrate gave the following results: δ = −4.2 ppm, 27.7 ppm (br. s), 46.5 (t, J = 66.0 Hz), 50.1 (d, J = 66.0 Hz), 51.0 (br., s) ppm. After removing the volatiles in vacuo, the resultant residue was dissolved in toluene (25 mL). By addition of heptane (75 mL), the title compound was recovered by filtration and then dried in vacuo at room temperature for 3 h (3.48 g, 71.8% yield). $C_{68}H_{75}ClNO_2P_3Ru$ (1167.8): calcd. C 69.9, H 6.5, N 1.2; found C 70.5, H 5.5, N 0.8. ^{31}P NMR (C_6D_6): δ = 27.7 (br. s), 46.5 (br. t, J = 68 Hz), 50.1 (br. d, J = 68 Hz), 51.0 (br. s) ppm. ^1H NMR (C_6D_6): δ = 0.9 (d, J = 68 Hz, C*H*$_3$ *i*Pr), 1.2 (d, C*H*$_3$ *i*Pr), 1.3 (d, C*H*$_3$ *i*Pr), 3.7 (m, C*H* *i*Pr), 4.4 (m, C*H* *i*Pr), 6.7 (m, 27 H, *m*,*p*-C*H*), 7.7 (m, 18 H, *o*-C*H*) ppm. ^{13}C NMR (C_6D_6): δ = 21.7 (s, *C*H$_3$ *i*Pr), 21.8 (s, *C*H$_3$ *i*Pr), 44.4 (s, *C*H *i*Pr), 44.5 (s, *C*H *i*Pr), 44.6 (s, *C*H *i*Pr), 163.5 (s) and 164.0 (s) (*C*O$_2$) ppm. Addition of triphenylphosphane caused the signals at δ = 27.7 and 51.0 ppm to decrease leading to a better resolution of the signals at δ = 50.1 (d) and 46.5 (t) ppm.

Synthesis of $[NH_2iPr_2][Ru_2Cl_5(PPh_3)_4]$ (2): A suspension of $[RuCl_2(PPh_3)_3]$ (0.44 g, 0.46 mmol) in toluene (25 mL) was treated with $[iPr_2NH_2]Cl$ (0.03 g, 0.22 mmol) under argon. The resultant dark-red solution showed a single ^{31}P NMR peak at δ = 46.9 ppm. After filtration and evaporation of the solvent to a small volume, the title crystalline compound was precipitated by addition of heptane (20 mL), filtered and dried in vacuo (0.23 g, 69% yield). $C_{78}H_{76}Cl_5NP_4Ru_2$ (1530.8): calcd. C 61.2, H 5.0, N 0.9; found C 59.6, H 5.2, N 0.6. ^{31}P NMR (C_6D_6): δ = 46.8 (s) ppm. ^1H NMR (C_6D_6): δ = 1.2 (dd, J = 6.0 Hz, 12 H, C*H*$_3$ *i*Pr), 3.5 (m, 2 H, C*H* *i*Pr), 6.8 (m, 36 H, *m*,*p*-C*H*), 7.6 (m, 24 H, *o*-C*H*), 8.2 (br. s, 2 H, N*H*) ppm. IR (nujol, KBr): $\tilde{\nu}$ = 3049 (m), 1586 (w),1482 (m), 1434 (s), 1311 (w) cm^{-1}.

 © 2004 Wiley-VCH Verlag GmbH & Co. KGaA, Weinheim

Synthesis of $[Ru(O_2CN{i}Pr_2)_2(PPh_3)_2]$ (1) from $[NH_2{i}Pr_2][Ru_2Cl_5(PPh_3)_4]$ (2): Under carbon dioxide, iPr_2NH (25 mL) was added to a toluene solution of **2** prepared from $[RuCl_2(PPh_3)_3]$ (3.61 g, 3.76 mmol) and iPr_2NH_2Cl (0.25 g, 1.82 mmol). After stirring at ambient temperature for 4 d, the ammonium salt was removed by filtration and the filtrate was concentrated to dryness in vacuo. The resultant residue was suspended in heptane and the product was recovered by filtration and subsequent drying in vacuo (1.96 g, 57% yield). ^{31}P NMR (C_6D_6): δ = 66.2 (s) ppm. ^1H NMR (C_6D_6): δ = 1.1 (d, CH_3, *i*Pr), 3.6 (sept, CH, *i*Pr), range 6.6−7.5 (aromatic, m, CH) ppm.[3a]

Reaction of $[RuCl(O_2CN{i}Pr_2)(PPh_3)_3]$ (3) with H_2: A solution of **3** (1.21 g, 1.13 mmol) in toluene (100 mL) was placed under hydrogen. After 4 h, a violet precipitate was observed and a ^{31}P NMR spectrum of the liquid phase showed signals at δ = 58.5 $[RuH_2(H_2)(PPh_3)_3]$[17a] and 76.9 (t) and 41.7 (d) $\{[RuH(O_2CN{i}Pr_2)(PPh_3)_3]\}$ ppm. The latter signals disappeared with time such that after 1 d only the signal at δ = 58.5 was present. The violet solid was filtered and dried in vacuo (0.52 g, 49.6% yield). ^{31}P NMR ($C_2D_2Cl_4$): δ = 59.0 (br. s) ppm. ^1H NMR ($C_2D_2Cl_4$): δ = −18.4 (q, *J* = 26.0 Hz), 1.4 (br. s, CH_3), 3.4 (m, CH *i*Pr), 6.9 (m, *m*,*p*-CH), 7.7 (m, *o*-CH), 9.0 (br. s, NH) ppm. IR (Nujol, KBr, range 2200−1900 cm^{-1}): $\tilde{\nu}$ = 2030 cm^{-1}. To a solution of $[RuCl(O_2CN{i}Pr_2)(PPh_3)_3]$ (0.73 g, 0.68 mmol) in toluene (50 mL), iPr_2NH (0.4 mL, 2.86 mmol) was added and the mixture was stirred under dihydrogen for 4 h. The ^{31}P NMR spectrum of the liquid phase showed peaks due to $[RuH(O_2CN{i}Pr_2)(PPh_3)_3]$. After 24 h of stirring, the ^{31}P NMR of the liquid phase showed only a signal at δ = 58.5 $\{[RuH_2(H_2)(PPh_3)_3]\}$ ppm.[17a]

Treatment of $[Ru(O_2CN{i}Pr_2)_2(PPh_3)_2]$ with H_2. Reversible Formation of $[RuH_2(H_2)(PPh_3)_3]$: A solution of $[Ru(O_2CN{i}Pr_2)_2(PPh_3)_2]$ (0.38 g, 0.42 mmol) in toluene (50 mL) was stirred under hydrogen at room temperature for 3 h. No change was indicated by ^{31}P NMR spectroscopy even after treatment at 30 and 60 °C. Treatment at 80 °C for 4 h led to a mixture with a complex ^{31}P NMR spectrum containing a resonance at δ = 58.5 $\{[RuH_2(H_2)(PPh_3)_3]\}$ ppm. Longer treatment led to extensive decomposition. In an experiment where 1 equiv. of PPh_3 had been added, a solution of $[Ru(O_2CN{i}Pr_2)_2(PPh_3)_2]$ (0.32 g, 0.35 mmol) and PPh_3 (0.10 g, 0.38 mmol) in C_6D_6 (4 mL) was treated with hydrogen at atmospheric pressure. As in the previous experiment, no NMR spectroscopic changes were noted at room temperature, 40 or 60 °C, whereas a reaction did occur at 80 °C. After 12 h at 80 °C under hydrogen, the solution showed the following ^{31}P NMR resonances: δ = 76.8 (t, *J* = 68 Hz) and 41.7 (d, *J* = 68 Hz) $\{[RuH(O_2CN{i}Pr_2)(PPh_3)_3]\}$, 58.5 $\{$s, $[RuH_2(H_2)(PPh_3)_3]\}$ ppm. ^1H NMR: δ = −17.6 (q, *J* = 26.0 Hz), −7.1 (br. s), 0.75 (d, CH_3), 0.9 (d, CH_3 of free amine), 1.05 (d, CH_3 of the carbamato group), 2.7 (m, C*H* of free amine), 3.1 and 4.1 (m, C*H*), range 6.6−7.8 (aromatic C*H*), 9.0 (s, amine N*H*) ppm. ^{13}C NMR: δ = 164.6 (br. s), 45.4 (amine *C*H), 44.0 (*C*H of the carbamato group), 23.7 (amine *C*H_3), 21.8 (*C*H_3 of the carbamato group) ppm. After an additional 12 h at 80 °C, the solution turned yellow and only the resonance at δ = 58.5 $\{[RuH_2(H_2)(PPh_3)_3]\}$ ppm was observed. To this solution was added iPr_2NH (0.2 mL, 1.42 mmol) under carbon dioxide. After 1 h, the solution turned red and had the following spectroscopic features. ^{31}P NMR: δ = 76.8 (t, *J* = 68 Hz), 41.7 (d, *J* = 68 Hz) and 58.5 ppm. ^1H NMR: δ = −17.6 (q, *J* = 26 Hz), −7.1 (br. s), 0.75 (d, CH_3 of the carbamato groups), 0.9 (d, amine CH_3), 1.05 (d, CH_3 of the carbamato groups), 2.7 (m, amine C*H*), 3.1 and 4.1 (m, C*H* of the carbamato groups), range 6.6−7.8 (aromatic C*H*), 9.0 (s, amine N*H*) ppm. After 12 h, the ^{31}P NMR showed signals at δ = 76.8 (t) and 41.6 (d) $\{[RuH(O_2CN{i}Pr_2)(PPh_3)_3]\}$ ppm. By addition of an excess (5 mL) of iPr_2NH, a signal at δ = 66.4 $\{$s, $[Ru(O_2CN{i}Pr_2)_2(PPh_3)_2]\}$ ppm[3a] was present in the ^{31}P NMR spectrum after 1 week.

Reaction of $[Ru(CO)_2(O_2CN{i}Pr_2)_2(PPh_3)_2]$ with H_2: A solution of $[Ru(CO)_2(O_2CN{i}Pr_2)_2(PPh_3)_2]$ (0.19 g, 0.19 mmol) in toluene (10 mL) was placed under hydrogen and heated at 50 °C for 1 d. ^{31}P NMR spectra of the solution showed the progressive decrease of the signal of the starting material (δ = 29.9 ppm), the presence of an intermediate signal at δ = 43.5 ppm and the increase of the final signal at δ = 57.8 ppm attributable to $[RuH_2(CO)_2(PPh_3)_2]$.[2g,22] Once the reaction was complete, the pale-yellow $[RuH_2(CO)_2(PPh_3)_2]$ precipitated upon cooling to room temperature (30 mg, 22.4% yield). ^{31}P NMR (C_6D_6): δ = 57.7(s) ppm. ^1H NMR (C_6D_6): δ = −6.35 (t, *J* = 25 Hz), range 6.9−7.8 (aromatic C*H*) ppm. IR (Nujol): $\tilde{\nu}$ = 2010, 1974 (CO stretching), 1880 and 1815 (Ru−H stretching) cm^{-1}.

Treatment of $[{i}Pr_2NH_2][Ru_2Cl_5(PPh_3)_4]$ (2) with 1-Octene and with 1-Octene/H_2: To a C_6D_6 (3 mL) solution of **2** (0.37 g, 0.24 mmol) was added 1-octene (0.1 mL, 0.64 mmol). The solution was monitored by ^{31}P NMR spectroscopy with no change being noted. After introducing hydrogen, ^1H NMR signals due to (*E*)-4-octene [δ = 5.4 (m), 1.9 (m), 1.5 (m), 0.85 (t) ppm] were noted in addition to those of 1-octene.

Hydrogenation of 1-Octene in the Presence of $[Ru(O_2CN{i}Pr_2)_2(PPh_3)_2]$ (1) or $[RuCl(O_2CN{i}Pr_2)(PPh_3)_3]$ (3): The olefin (1-octene, 1.46 mmol) in C_6D_6 (4 mL) was stirred under H_2 at room temperature in the presence of **1** (0.15 mmol). After 12 h, the ^1H NMR spectrum of the reaction mixture showed the absence of the signals of 1-octene, the latter being completely converted into octane (gas chromatography, ATWAX capillary column). A hydrogenation experiment was carried out directly in an NMR tube: 1-octene (1.02 mmol) and **1** (86 mg, 9.44 × 10^{-2} mmol) were dissolved in C_6D_6 (0.7 mL) under N_2 with aqueous 85% H_3PO_4 contained in a flame-sealed capillary being used as a reference. The ^{31}P NMR spectrum showed signals at δ = 0 ppm due to phosphoric acid and at δ = 66.2 ppm due to **1** with an intensity ratio of 7.3. The content of the tube was then exposed to H_2 (*p* = 760 Torr) for 3 d. A new ^{31}P NMR spectrum showed signals at δ = 0 and 66.2 ppm with a ratio of 7.7, corresponding to more than 90% of the original complex **1** being unconverted. No other resonances were observed, while the ^1H NMR spectrum showed that complete hydrogenation to octane had occurred. A solution of **3** (0.14 g, 0.13 mmol) and 1-octene (0.2 mL, 1.27 mmol) in toluene (50 mL) was stirred for a few hours with no change in the ^{31}P NMR spectrum being noted. The solution was then placed under H_2 and stirred for 6 h. A violet solid was formed. A gas chromatogram of the liquid phase with an ATWAX capillary column showed a single peak due to octane. The violet solid spectroscopically identified as $[RuHCl(PPh_3)_3]$ was filtered and dried (50 mg, 41.2% yield). ^{31}P NMR ($C_2D_2Cl_4$): δ = 59.0 (br. s) ppm. ^1H NMR ($C_2D_2Cl_4$): δ = −18.4 (q, $J_{H,P}$ = 26 Hz), range 6.9−7.8 (m) ppm. The hydrogenation of 1-octene was monitored by gas volumetry, using both **1** and **3** as catalytic precursors. In a typical experiment, the solution of the olefin in toluene (20 mL) was prepared and a fragile flame-sealed ampoule containing the ruthenium complex was introduced. After thermostatting the system under H_2 (p_{H2} = 740 Torr), the ampoule was broken by magnetic stirring and the hydrogen absorption with time was noted, no induction being observed. The hydrogenation of 1-octene (0.8 mL, 5.1 mmol) in the presence of **1** (0.16 g, 0.18 mmol) at 20.6 °C in toluene (20 mL) gave a dihydrogen absorption corresponding to a conversion of about 70% in 165 min, the initial rate being 300 mmol·L^{-1} h^{-1} ([Ru] = 9.0 × 10^{-3} M).

 © 2004 Wiley-VCH Verlag GmbH & Co. KGaA, Weinheim

The hydrogenation of 1-octene (0.3 mL, 1.91 mmol) in the presence of **3** (0.21 g, 0.20 mmol) at 21.2 °C in toluene (20 mL) was similarly monitored, the absorption of dihydrogen corresponding to 88.8% of the theoretical amount in 165 min. The initial rate was 153 mmol·L^{-1} h^{-1}, the ruthenium concentration being 1.0×10^{-2} M.

X-ray Crystallographic Studies: The crystallographic measurements on both samples were carried out on four-circle diffractometers. Cu-K_α radiation ($\lambda = 1.54184$ Å) was used for **3** due to the length of the *b* parameter, whereas Mo-K_α radiation ($\lambda = 0.71073$ Å) was used for **2**. All data were collected in the ω-2θ scan mode and three standard reflections were monitored every 97 measurements in order to check for crystal decay and equipment stability. For both samples, particularly for **3**, weak diffractions which rapidly dropped below the observation threshold were measured at increasing 2θ angles. Data reduction was performed using the DARX2000 and SDP program packages.[23,24] Crystals of **2**, prepared as described before, are red-brown blocks. An approximately tetrahedral splinter cut from one of them, with the edge about 0.30 mm long, was sealed in a glass capillary under N_2 and the unit cell parameters listed in Table 3 were derived from the setting angles of 35 strong reflections. A set of 6633 reflections were collected between $\theta = 1.8$ and 22.5° which were corrected for Lorentz and polarization effects and for absorption using the Ψ-scan method. After merging the equivalent reflections $\{R_{int} = [\Sigma|F_o^2 - F_o^2(\text{mean})|/\Sigma(F_o^2)] = 0.0483\}$, 4553 unique reflections satisfying the condition $I > 2\sigma(I)$ were obtained. The systematic absences indicated the $P2_1/c$ space group. After location of all the heavy atoms of the $[Ru_2Cl_5(PPh_3)_4]^-$ anion and of the $[i\text{Pr}_2\text{NH}_2]^+$ cation and the introduction of the hydrogen atoms in calculated positions, several large peaks were found in the difference Fourier map in the cavities between the ion pairs. These peaks were attributed to a disordered lattice solvent (heptane), but a reliable model for this substance was not found. This contributed to the relatively high reliability factors of the refinement which was carried out with anisotropic thermal factors for the Ru, Cl and P atoms only. The final reliability factors are listed in Table 3. Calculations were carried out using the SHELX-97 program.[25] Crystals of **3** are red prisms. A crystal of dimensions 0.20 × 0.25 × 0.38 mm, sealed in a glass capillary under N_2, exhibited the cell parameters listed in Table 3. Due to the poor diffraction properties of the crystal, only 3157 independent intensities having $I > 2\sigma(I)$ were collected in the range $3.69° \le \theta \le 70.0°$. They were corrected for Lorentz and polarization effects and for absorption using the Ψ-scan method. The structure was solved in the $P2_1/n$ space group by direct methods and refined by least-squares methods based on *F* (SHELXTL).[26] As in the structure of **2**, several peaks present in the difference Fourier map were attributed to a disordered lattice solvent (heptane) molecule. The last refinement cycle was carried out using anisotropic thermal factors for Ru, Cl and P atoms only. The final reliability factors are listed in Table 3. Final atomic parameters, thermal factors and the details of the structural determinations have been deposited in the form of a CIF file with the Cambridge Crystallographic Data Centre. CCDC-228267 (for **2**) and -228268 (for **3**) contain the supplementary crystallographic data for this paper. These data can be obtained free of charge at www.ccdc.cam.ac.uk/conts/retrieving.html [or from the Cambridge Crystallographic Data Centre, 12 Union Road, Cambridge CB2 1EZ, UK; Fax: (internat.) + 44-1223-336-033; E-mail: deposit@ccdc.cam.ac.uk].

Table 3. Crystal data and structural refinements for **2** and **3**

	2·heptane	**3**·heptane
Empirical formula	$C_{85}H_{92}Cl_5NP_4Ru_2$	$C_{68}H_{75}ClNO_2P_3Ru$
Formula mass	1630.87	1167.72
Wavelength [Å]	0.71069	1.54184
Crystal system	monoclinic	monoclinic
Space group	$P2_1/c$ (No. 14)	$P2_1/n$ (No. 14)
a [Å]	19.922(5)	10.583(2)
b [Å]	15.385(2)	46.516(9)
c [Å]	27.423(4)	12.990(3)
β [°]	91.15(2)	104.29(3)
V [Å^3]	8403(3)	6197(2)
Z	4	4
$D_{calcd.}$ [Mg·m^{-3}]	1.289	1.252
μ [mm^{-1}]	0.636	3.507
No. observed [$I > 2\sigma(I)$]	4553	3157
No. parameters	296	367
R, *wR*	0.1226, 0.3116	0.1061, 0.2769
Goodness of fit on F^2	1.607	0.994

Acknowledgments

The authors wish to thank the Ministero dell' Istruzione Universitaria e della Ricerca (MIUR), Programmi di Rilevante Interesse Nazionale 2002-3 and the Consiglio Nazionale delle Ricerche, Progetto CNR/MIUR "Sviluppo di microcelle a combustibile" for financial support.

[1] [1a] *Comprehensive Coordination Chemistry*, vol. 4 (Eds.: G. Wilkinson, R. D. Gillard, J. A. McCleverty), Pergamon Press, Oxford, **1988**.[1b] *Comprehensive Coordination Chemistry II*, vol. 4 (Eds.: J. A. McCleverty, T. J. Meyer), Elsevier Ltd., Oxford, **2004**. [1c] *Comprehensive Organometallic Chemistry II*, vol. 7 (Eds.: E. W. Abel, F. G. A. Stone, G. Wilkinson), Pergamon Press, Oxford, **1995**. [1d] D. Rose, J. D. Gilbert, R. P. Richardson, G. Wilkinson, *J. Chem. Soc.* **1969**, 2610−2615, and references cited therein.

[2] [2a] R. W. Mitchell, A. Spencer, G. Wilkinson, *J. Chem. Soc., Dalton Trans.* **1973**, 846−854. [2b] S. D. Robinson, M. F. Uttley, *J. Chem. Soc., Dalton Trans.* **1973**, 1912−1920. [2c] A. Dobson, S. D. Robinson, M. F. Uttley, *J. Chem. Soc., Dalton Trans.* **1975**, 370−377. [2d] C. J. Creswell, A. Dobson, D. S. Moore, S. D. Robinson, *Inorg. Chem.* **1979**, *18*, 2055−2059. [2e] M. Rotem, Z. Stein, Y. Shvo, *J. Organomet. Chem.* **1990**, *387*, 95−101. [2f] T. Arligule, B. Chaudret, G. Chung, F. Dahan, *Organometallics* **1991**, *10*, 2973−2977. [2g] P. Frediani, C. Faggi, A. Salvini, M. Bianchi, F. Piacenti, *Inorg. Chim. Acta* **1998**, *272*, 141−149. [2h] G. Sbrana, G. Braca, E. Giannetti, *J. Chem. Soc., Dalton Trans.* **1976**, 1847−1852.

[3] [3a] D. Belli Dell'Amico, F. Calderazzo, L. Labella, F. Marchetti, *J. Organomet. Chem.* **2000**, *596*, 144−151. [3b] D. Belli Dell' Amico, F. Calderazzo, A. Grazzini, L. Labella, F. Marchetti, *Inorg. Chim. Acta* **2002**, *334*, 411−418. [3c] D. Belli Dell'Amico, F. Calderazzo, L. Labella, F. Marchetti, E. Sbrana, *J. Organomet. Chem.* **2002**, *651*, 52−59.

[4] [4a] T. V. Ashworth, M. Nolte, E. Singleton, *J. Organomet. Chem.* **1976**, *121*, C57−C60. [4b] T. V. Ashworth, M. J. Nolte, E. Singleton, *S. Afr. J. Chem.* **1978**, *31*, 149−152. [4c] T. Tsuda, M. Shiro, *Organometallics* **1999**, *18*, 2741−2743.

[5] [5a] A. Belforte, D. Belli Dell′Amico, F. Calderazzo, U. Giurlani, L. Labella, *Gazz. Chim. Ital.* **1993**, *123*, 119−127. [5b] D. Belli Dell'Amico, F. Calderazzo, L. Labella, F. Marchetti, G. Pampaloni, *Chem. Rev.* **2003**, *103*, 3857−3897.

[6] [6a] P. Haynes, L. H. Slaugh, J. F. Kohnle, *Tetrahedron Lett.* **1970**, 365−368. [6b] S. J. La Placa, J. A. Ibers, *Inorg. Chem.* **1965**, *4*, 778−783.

[7] [7a] K. Mashima, T. Nakamura, Y. Matsuo, K. Tani, *J. Organomet. Chem.* **2000**, *607*, 51−56. [7b] D. Huang, K. Folting, K. G. Caulton, *Inorg. Chem.* **1996**, *35*, 7035−7040.

 © 2004 Wiley-VCH Verlag GmbH & Co. KGaA, Weinheim

[8] [8a] T. Ohta, Y. Tonomura, K. Nozaki, H. Takaya, K. Mashima, *Organometallics* **1996**, *15*, 1521−1523. [8b] K. S. MacFarlane, I. S. Thorburn, P. W. Cyr, D. E. K.-Y. Chau, S. J. Rettig, B. R. James, *Inorg. Chim. Acta* **1998**, *270*, 130−144.
[9] [9a] A. C. Skapski, P. G. H. Troughton, *J. Chem. Soc., Chem. Commun.* **1968**, 1230−1231. [9b] A. C. Skapski, F. A. Stephens, *J. Chem. Soc., Dalton Trans.* **1974**, 390−395. [9c] V. V. Mainz, R. A. Andersen, *Organometallics* **1984**, *3*, 675−678.
[10] [10a] P. W. Armit, A. S. F. Boyd, T. A. Stephenson, *J. Chem. Soc., Dalton Trans.* **1975**, 1663−1672. [10b] P. R. Hoffman, K. G. Caulton, *J. Am. Chem. Soc.* **1975**, *97*, 4221−4228.
[11] J. Halpern, J. F. Harrod, B. R. James, *J. Am. Chem. Soc.* **1966**, *88*, 5150−5155.
[12] [12a] S. Komiya, A. Yamamoto, S. Ikeda, *J. Organomet. Chem.* **1972**, *42*, C65−C66. [12b] S. Komiya, A. Yamamoto, *Bull. Chem. Soc. Jpn.* **1976**, *49*, 2553−2559.
[13] T. V. Ashworth, E. Singleton, *J. Organomet. Chem.* **1976**, *117*, C113−C115.
[14] G. G. A. Balavoine, T. Boyer, *Organometallics* **1992**, *11*, 456−459.
[15] B. de Klerk-Engels, J. G. P. Delis, K. Vrieze, K. Goubitz, J. Fraanje, *Organometallics* **1994**, *13*, 3269−3278.
[16] P. S. Hallman, B. R. McGarvey, G. Wilkinson, *J. Chem. Soc. A* **1968**, 3143−3150.
[17] [17a] D. E. Linn, J. Halpern, *J. Am. Chem. Soc.* **1987**, *109*, 2969−2974. [17b] L. S. Van Der Sluys, G. J. Kubas, K. G. Caulton, *Organometallics* **1991**, *10*, 1033−1038. [17c] E. Hoel, M. F. Hawthorne, *Inorg. Synth.* **1974**, *15*, 31−34. [17d] W. H. Knoth, *J. Am. Chem. Soc.* **1972**, *94*, 104−109.
[18] [18a] T. V. Ashworth, E. Singleton, *J. Chem. Soc., Chem. Commun.* **1976**, 705−706. [18b] R. H. Crabtree, D. G. Hamilton, *J. Am. Chem. Soc.* **1986**, *108*, 3124−3125. [18c] R. H. Crabtree, D. G. Hamilton, *J. Am. Chem. Soc.* **1988**, *110*, 4126−4133.
[19] [19a] R. O. Harris, N. K. Hota, L. Sadavoy, M. C. Yuen, *J. Organomet. Chem.* **1973**, *54*, 259−264. [19b] T. Ito, S. Kitazume, A. Yamamoto, S. Ikeda, *J. Am. Chem. Soc.* **1970**, *92*, 3011−3016. [19c] Under the best conditions, the molar quantity of $OPPh_3$ contained in the catalytic runs did not exceed 1% (by ^{31}P NMR spectroscopy).
[20] [20a] K. Abdur-Rashid, A. J. Lough, R. H. Morris, *Organometallics* **2000**, *19*, 2655−2657. [20b] C. P. Casey, S. W. Singer, D. R. Powell, R. K. Hayashi, M. Kavana, *J. Am. Chem. Soc.* **2001**, *123*, 1090−1100. [20c] K. Abdur−Rashid, S. E. Clapham, A. Hadzovic, J. N. Harvey, A. J. Lough, R. H. Morris, *J. Am. Chem. Soc.* **2002**, *124*, 15104−15118.
[21] P. S. Hallman, T. A. Stephenson, G. Wilkinson, *Inorg. Synth.* **1970**, *12*, 237−240.
[22] F. L′Eplattenier, F. Calderazzo, *Inorg. Chem.* **1968**, *7*, 1290−1293.
[23] A. Pifferi, L. Barba, *DARX2000 V1.0.3*, CNR-IC, Montelibretti, Roma, Italy, **2000**.
[24] *ENRAF-Nonius SDP V5.0*, Delft, The Netherlands, **1989**.
[25] G. M. Sheldrick, *SHELX-97, Programs for Crystal Structure Analysis* (Release 97-2), University of Göttingen, Germany, **1998**.
[26] G. M. Sheldrick, *SHELXTL-Plus, Rel. 5.03*, Bruker AXS, Madison, Wisconsin, USA, **1995**.

Received January 9, 2004
Early View Article
Published Online July 27, 2004

 © 2004 Wiley-VCH Verlag GmbH & Co. KGaA, Weinheim

Transition Metal Ion Directed Self-Assembly of Polynuclear Coordination Complexes: Structural Characterization and Magnetic Properties

Yongli Wei,[a] Hongwei Hou,*[a] Yaoting Fan,[a] and Yu Zhu[a]

Keywords: Magnetic properties / Multidentate ligands / Organic-inorganic hybrid composites / Self-assembly / Transition metals

The reactions of different transition metals with the multidentate ligand *N*,*N*′-bis(1,3,4-thiadiazol-2-yl)-2,6-pyridinedicarboxamide (btapca) afford six new polynuclear complexes: the hexanuclear complexes [{$Zn_6(O)_2(btapca)_4$}·3DMF·2H_2O] (**1**) and [{$Zn_6(O)_2(btapca)_4$}·DMF·MeOH·H_2O] (**2**); the pentanuclear complexes [{$Zn_5(OH)_2(btapca)_4$}·4DMF·H_2O] (**3**), [{$Co_5(OH)_2(btapca)_4$}·4DMF·MeOH·H_2O] (**4**) and [{$Ni_5(OH)_2(btapca)_4$}·4DMF·MeOH] (**5**); and the trinuclear complex [{$Fe_3(OH)(btapca)_3$}·2DMF·2MeOH] (**6**). The dominant characteristic of these polynuclear complexes is that there are μ_3- or μ_4-oxygen atoms in the metal polyhedrons. The hexanuclear complexes **1** and **2** show similar octahedral features based on zinc centers. The five metal centers in complexes **3**, **4** and **5** arrange into two triangles with one common vertex. As for complex **6**, three iron(II)/iron(III) atoms form a plane with a μ_3-OH^- in the center. We also report the magnetic properties of complexes **4**, **5** and **6**. Complex **4** exhibits intramolecular antiferromagnetic exchange, while the analogous complex **5** is dominated by very strong intramolecular ferromagnetic coupling. The trinuclear complex [{$Fe_3(OH)(btapca)_3$}·2DMF·2MeOH] (**6**) shows comparable weak antiferromagnetic coupling.
(© Wiley-VCH Verlag GmbH & Co. KGaA, 69451 Weinheim, Germany, 2004)

Introduction

"Self-assembly", defined by Whitesides as "the spontaneous assembly of molecules into structured, stable, noncovalently joined aggregates",[1] was borrowed from biology and since then has been widely used in modern coordination chemistry.[2] In traditional studies of supramolecular self-assembly, hydrogen bonds are most frequently employed, as they are in all biological systems.[3] In recent years, strong metal−ligand interactions in supramolecular architectures aroused great interest. Consequently, the self-assembly of organic ligands and inorganic metal ions became one of the most efficient and widely utilized approaches to the construction of organic/inorganic coordination superarchitectures,[4] which have intriguing properties induced by direct or indirect M−M interactions or a consequence of the positioning and identity of the coordination pockets within the ligand and the ability of metal ion to read these sites in terms of its own coordination algorithms.[5] Thus, such architectures exhibit potential applications in catalysis, electrical conductivity, molecular-based magnets, and host-guest chemistry,[6] and can be exploitated for the design of new materials with desirable properties and the manufacturing of devices and molecular machinery.[7−9]

Thus far, various sophisticated supramolecules have been constructed by self-assembly, such as squares, helices, metallacoronates, cages, capsules, tubes, cylinders, and many high-dimensional structures.[3a,10−17] Amongst these diverse architectures, polynuclear metal clusters have attracted much attention.[18−20] For the preparation of such architectures, well-designed organic ligands with the appropriate choice of donors and bridging groups have become the focus of a great deal of research work. It is well-known that polypyridyl groups have been very useful as programmed components in self-assembly processes,[21] and many polypyridyl ligands have been proved to be very useful in the construction of polynuclear complexes. For example, the alkoxy-diazine ligands have produced a series of high-nuclearity complexes;[5] the pendent-arm ligand 1,4,7-tris-(acetophenoneoxime)-1,4,7-triazacyclononane has resulted in the formation of Cu^{II}, $Co^{II,III}$, Ni_4^{II}, and $Mn_3^{II,III}$ complexes;[22] the bis-chelating ligand 1,2-bis(2,2′-bipyridine-6-yl)ethane has afforded a number of Mn complexes.[18] In most cases, combining with the chelating ligands, oxide bridges are always dominant in these polynuclear species, and they enhance the superexchange between paramagnetic metal ions. Chemists have also paid a great deal of attention to magnetic properties in addition to the versatile structures,[23] and have found that such complexes exhibit unusual supramolecular magnetic properties.[18,22,24−30]

In recent years, our group has been engaged in the study of functional coordination complexes, including polymers[31−34] and polynuclear complexes.[35,36] The design

[a] Department of Chemistry, Zhengzhou University, Henan 450052, P. R. China
Fax: (internat.) + 86-371-776-1744
E-mail: houhongw@zzu.edu.cn

 © 2004 Wiley-VCH Verlag GmbH & Co. KGaA, Weinheim DOI: 10.1002/ejic.200400110

of ideal multifunctional ligands is one of our main themes. In this context, we prepared the ligand *N*,*N*′-bis(1,3,4-thiadiazol-2-yl)-2,6-pyridinedicarboxamide (btapca) and explored its coordination properties. We found that it can produce different polynuclear complexes when reacted with different metal ions: the hexanuclear complexes $[\{Zn_6(O)_2(btapca)_4\}\cdot 3DMF\cdot 2H_2O]$ (**1**) and $[\{Zn_6(O)_2(btapca)_4\}\cdot DMF\cdot MeOH\cdot H_2O]$ (**2**); the pentanuclear complexes $[\{Zn_5(OH)_2(btapca)_4\}\cdot 4DMF\cdot H_2O]$ (**3**), $[\{Co_5(OH)_2(btapca)_4\}\cdot 4DMF\cdot MeOH\cdot H_2O]$ (**4**) and $[\{Ni_5(OH)_2(btapca)_4\}\cdot 4DMF\cdot MeOH]$ (**5**); and the trinuclear complex $[\{Fe_3(OH)(btapca)_3\}\cdot 2DMF\cdot 2MeOH]$ (**6**). The magnetic properties of complexes **4**, **5**, and **6** are also reported here. The occurrence of indirect metal−metal interactions and metal-oxygen-metal bridging functions leads to dominant magnetic superexchange interactions.

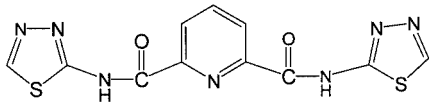

btapca

Results and Discussion

Synthesis

Complexes **1**−**6** were synthesized by the reaction of *N*,*N*′-bis(1,3,4-thiadiazol-2-yl)-2,6-pyridinedicarboxamide (btapca) with different metal salts MX_2 (M = Zn^{II}, Co^{II}, Ni^{II}, Fe^{II}; X = NO_3, OAc, Cl, I) in methanol and DMF solution.

The reaction of $Zn(NO_3)_2\cdot 6H_2O$ with btapca in methanol and DMF (1:1) yielded the hexanuclear complex $[\{Zn_6(O)_2(btapca)_4\}\cdot 3DMF\cdot 2H_2O]$ (**1**). Replacement of $Zn(NO_3)_2\cdot 6H_2O$ with $Zn(OAc)_2\cdot 2H_2O$ in the above reaction led to the related hexanuclear complex $[\{Zn_6(O)_2(btapca)_4\}\cdot DMF\cdot MeOH\cdot H_2O]$ (**2**), which crystallized in a different crystal system and space group to those of complex **1**. In contrast to complexes **1** and **2**, we found that the reaction of ZnI_2 with btapca in a mixture of THF and DMF (1:1) did not afford the hexanuclear complex, but gave the pentanuclear complex $[\{Zn_5(OH)_2(btapca)_4\}\cdot 4DMF\cdot H_2O]$ (**3**) instead, which exhibits a "bow-tie" backbone. Interestingly, we also obtained pentanuclear complexes $[\{Co_5(OH)_2(btapca)_4\}\cdot 4DMF\cdot MeOH\cdot H_2O]$ (**4**) and $[\{Ni_5(OH)_2(btapca)_4\}\cdot 4DMF\cdot MeOH]$ (**5**) in the presence of $CoCl_2\cdot 6H_2O$ and $Ni(NO_3)_2\cdot 6H_2O$, respectively, their structures are similar to that of complex **3**. The reaction of $FeCl_2\cdot 4H_2O$ with btapca led to the trinuclear complex $[\{Fe_3(OH)(btapca)_3\}\cdot 2DMF\cdot 2MeOH]$ (**6**), which has a planar unit completely different from the structures of the other five complexes.

The following chart illustrates the syntheses and structural relationships based on the above discussions.

Crystal Structure of $[\{Zn_6(O)_2(btapca)_4\}\cdot 3DMF\cdot 2H_2O]$ (1)

The crystal structure of complex **1** is illustrated in Figure 1. In the structure, there are six Zn^{II} ions bound by four ligands in the available coordination polyhedron. These six zinc atoms show two different kinds of coordination environments. The inner Zn(3) and Zn(4) atoms are coordinated in a roughly tetrahedral fashion, with two N atoms from different btapca ligands, and O(9) and O(10). The Zn(3)−N(O) bond lengths lie in a fairly narrow range [1.979(9)−2.022(14) Å], and the N−Zn(3)−O angles vary from 109.5° to 117.2°. The corresponding bond lengths and angles around Zn(4) are identical to those of Zn(3), in the range 1.964(9)−2.00(2) Å and 107.7(5)−115.8(5)°, respectively. The Zn(3)···Zn(4) distance is 2.802(2) Å, suggesting that there is a strong interaction between Zn(3) and Zn(4). Such short Zn···Zn distances are unusual in polynuclear zinc complexes.[37−43]

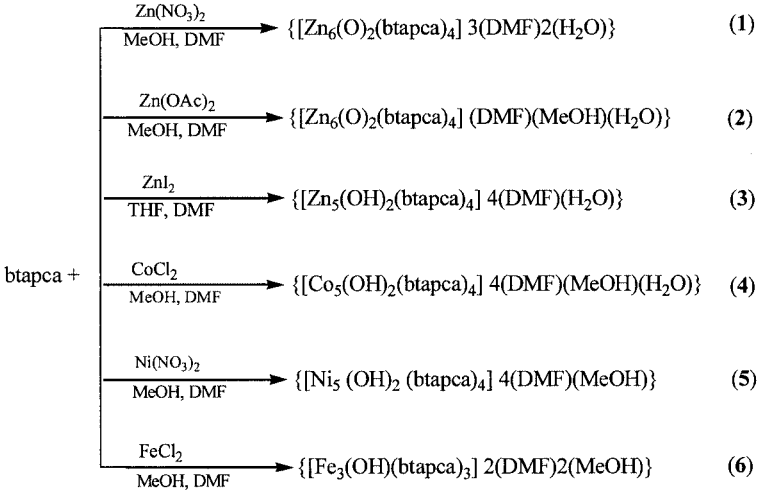

 © 2004 Wiley-VCH Verlag GmbH & Co. KGaA, Weinheim

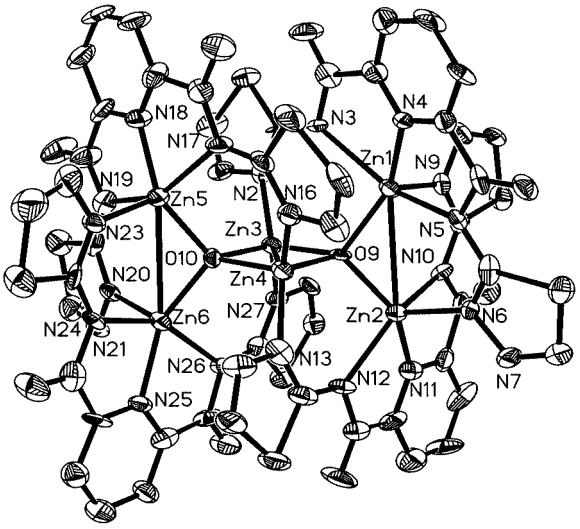

Figure 1. The hexanuclear backbone of $[\{Zn_6(O)_2(btapca)_4\}\cdot 3DMF\cdot 2H_2O]$ (**1**)

The other four zinc atoms Zn(1), Zn(2), Zn(5) and Zn(6) are connected to Zn(3) and Zn(4) through the O(9) and O(10) atoms. All these four Zn atoms are five coordinate and exhibit an approximately tetragonal pyramidal coordination geometry. In the polyhedron of Zn(5), N(17), N(18), N(19), O(10) lie in the basal plane, with a best least-squares deviation of 0.1274 Å, and N(23) occupies the apex. Zn(6) is identical to Zn(5). The slightly longer Zn(1)···Zn(2) [3.129(3) Å] and Zn(5)···Zn(6) [3.144(3) Å] distances suggest weaker interactions between the Zn atoms than Zn(3)···Zn(4), but still show a close Zn···Zn contact compared to those in the literature (falling in the range 3.0−4.4 Å).[37−43]

Considering the six zinc atoms as the symmetry core, the motif can be described as a rough octahedron. There is a pseudo-fourfold axis along Zn(3) and Zn(4). The basal plane is made up of Zn(1), Zn(2), Zn(5) and Zn(6), with a deviation of 0.0540 Å, and the four edges are 3.129, 3.144, 4.995 and 5.161 Å, respectively. Zn(3) and Zn(4) occupy the two apical sites.

The skeleton of **1** can also be described as edge-shared double tetrahedrons. Two isolated oxygen atoms are located in the center of each tetrahedron, and Zn(3)···Zn(4) is the common edge. In the outside of the Zn_6O_2 core, four ligands coil in a tetra-helical style.

The asymmetric unit contains two formula units; all the asymmetric units pack in a three-dimensional fashion based on hydrogen bonding. Along the crystallographic *a* direction, every $[Zn_6(O)_2(btapca)_4]$ unit is linked through O(2)···S(7) and O(2)···H−C(7). O(3)···H−C(33) hydrogen bonds form in the *b* direction, and O(8)···H−C(28) and O(1)···H−C(17) bonds in the *c* direction. All these contacts are weak van der Waals interactions, whose distances are in the range 2.375−3.140 Å. Although these interactions are comparatively weak, they may play a role in the stabilization of the crystal structure. The solvent DMF and H_2O molecules do not influence the structure of $[Zn_6(O)_2(btapca)_4]$, and are dispersed in the spaces of the structure.

Crystal Structure of $[\{Zn_6(O)_2(btapca)_4\}\cdot DMF\cdot MeOH\cdot H_2O]$ (2)

Complex **2** has a different space group from complex **1**, but its crystal structure is similar to that of **1** except for the solvent molecules. The two Zn−N distances are in the ranges 2.020(6)−2.284(6) Å and 1.972(6)−1.996(6) Å, and the Zn−O distances are in the range 1.939(5)−1.989(5) Å, slightly shorter than the corresponding distances in **1**. The shortest Zn···Zn distance is 2.8103 Å, and the longest 3.1456 Å. The asymmetric units also pack in a three-dimensional fashion through hydrogen bonding [O(4)···H(47), O(13)···H(11), O(2)···H(7) and S(6)···H(5)]. The lengths of these hydrogen bonds range from 2.470 to 2.934 Å.

The crystal structures of hexanuclear complexes **1** and **2** are very novel, although various Zn-containing polynuclear complexes have been reported previously. For example, in the hexanuclear zinc(II) cage $[Zn_6Cl_4(3,5\text{-}Me_2PzH)_8(PhPO_3)_4]$ (Me_2PzH = 3,5-dimethylpyrazole), the six zinc centers are arranged in a chair-like conformation.[38] The tetranuclear complex $[Zn_2L(\mu_{1,1}\text{-}HCO_2)(\mu_{1,3}\text{-}HCO_2)]_2(ClO_4)_2$ {L = 2,6-bis[*N*-2-(2′-pyridylethyl)formimidoyl]-4-methylphenol}[37] consists of two identical dinuclear $[Zn_2L(\mu_{1,1}\text{-}HCO_2)(\mu_{1,3}\text{-}HCO_2)]^+$ subunits which connect to each other through an interaction between the dangling oxygen of the formate and the zinc atom of the other subunit. The structure of the trinuclear compound $[Zn_3Cl(3,5\text{-}Me_2Pz)_4(t\text{BuPO}_3)_2]$[38] contains a planar trizinc assembly containing two bicapping $\mu_3[t\text{BuPO}_3]^{2-}$ ligands and terminal pyrazole and chloride ligands. The trinuclear complex $[Zn_3L(NH_3)_3(H_2O)_3]Cl\cdot H_2O$[44] [L = tris(2-hydroxybenzylidene)triaminoguanidine] adopts a propeller-like conformation. The six zinc centers in complexes **1** and **2** arrange in a completely different way, with a roughly octahedral conformation.

Crystal Structure of $[\{Zn_5(OH)_2(btapca)_4\}\cdot 4DMF\cdot H_2O]$ (3)

The pentanuclear backbone is based on a $Zn_5(\mu_3\text{-}OH)_2$ "bow-tie" cluster in which two triangles share one vertex [Zn(2)]. The three edges of each triangle are 3.413, 3.269, 3.269 Å, respectively, making it close to isosceles. The structural unit is illustrated in Figure 2. There is a 4(1)/*n* symmetry axis running through the central Zn(2) atom, and each asymmetric unit contains two formula units.

Zn(1) is six-coordinate by N(3), N(4), N(5), O(3), N(2), N(7) from three ligands. N(3), N(4), N(5) and O(3) comprise the equatorial plane, with a deviation of 0.0622 Å, and N(2) and N(7) occupy the two axial positions. Zn(2) is also in an octahedral coordination environment, with four N atoms in the equatorial plane and two O atoms at the axis. The Zn(2)−O distances fall in the range 1.940(11)−2.041(8) Å. O(3) is located in the mean plane of Zn(1)−Zn(1A)−Zn(2) with a best least-squares deviation of 0.1751 Å. The Zn−O−Zn angles fall in a fairly narrow range [110.4(4)−119.2(6)°]. The Zn−O and Zn−N bond

 © 2004 Wiley-VCH Verlag GmbH & Co. KGaA, Weinheim

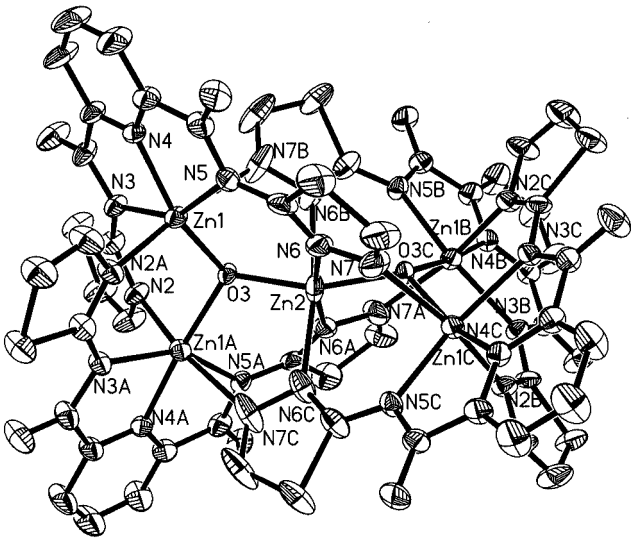

Figure 2. The pentanuclear unit of $[\{Zn_5(OH)_2(btapca)_4\}\cdot 4DMF\cdot H_2O)$ (**3**)

lengths are similar to those reported in the literature,[9,39,40,45–47] which are in the range 1.92–2.42 Å.

Complex **3** has a cage-like skeleton taking into account the hydrogen bonds. The solvent DMF and H_2O molecules are located in the cages and do not take part in the hydrogen bonding. The hydrogen bonds are formed between O(2)···H(1) and O(1)···H(11) with distances of 2.561 and 2.557 Å, respectively; the O(2)···S(1) distance is 3.180 Å, which indicates a weak van der Waals interaction.

Crystal Structure of $[Co_5(OH)_2(btapca)_4]\cdot 4DMF\cdot MeOH\cdot H_2O]$ (4)

The molecular structure of complex **4** is depicted in Figure 3. The pentanuclear backbone is similar to **3**: a 4(1)/*n* symmetry axis runs through the central Co(2) atom and each asymmetric unit contains two formula units. Each triangle has a μ_3-OH at its center and is held together by four peripheral ligands in a manner similar to the polymer $[\{Co_5(OH)_2\{1,2,4,5\text{-}(O_2C)_4C_6H_2\}_2(H_2O)_4\}\cdot xH_2O\}_n$.[48] Five cobalt centers share four ligands. Co(1) is coordinated by three ligands and two oxygens, while Co(2) is bound to four ligands and two oxygens. The two Co_3 triangles, joined through a Co(2) vertex, are almost isosceles, with edges of 3.346, 3.359, 3.359 Å, respectively. The dihedral angle of the two triangles is 90.0°. The longer distances Co(1B)···Co(1A) and Co(1B)···Co(1) are 6.288 Å. Consequently, a virtual S_2 axis through Co(2) atom can be postulated from the Co_5 core. In the tetranuclear $[Co_4O_4(O_2CR)_2(bpy)_4]^{3+}$ (bpy = 2,2′-bipyridine) salts,[49] the Co···Co distances are in the range 2.874(1)–2.641(1) Å; such short Co···Co distances are the result of short bridges formed only by oxygen atoms. On the contrary, the Co···Co distances in the trinuclear cation $[L_2Co_2^{III}Co^{II}]^{2+}$ [H_3L = 1,4,7-tris(acetophenoneoxime)-1,4,7-triazacyclononane][22] are much longer [3.402(2) and 6.805(4) Å, respectively]. Generally, the reported Co···Co distances range from 2.4 Å to 3.5 Å.[50–53] The Co···Co distances in **4** (about 3.3 Å) are in this range.

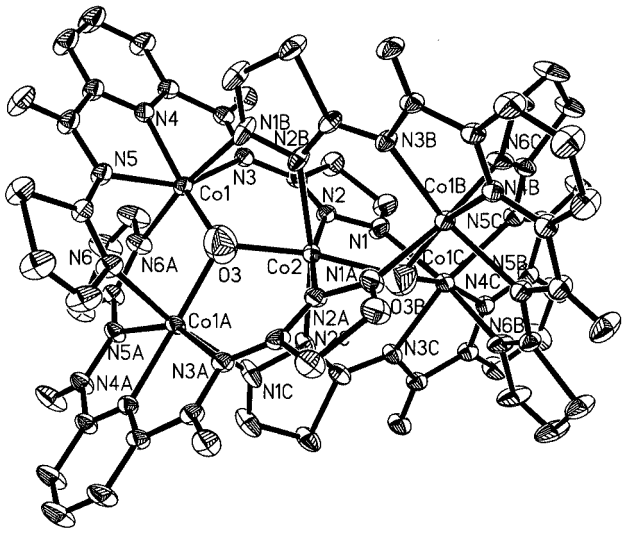

Figure 3. The pentanuclear unit of $[\{Co_5(OH)_2(btapca)_4\}\cdot 4DMF\cdot MeOH\cdot H_2O)$ (**4**) in which two triangles share one common vertex based on cobalt centers

Complex **4** can also be described as four Co(btapca) fragments joined to the Co(2) atom through oxygen bridges. The central Co(2) is bonded by N(2), N(2A), N(2B) and N(2C) from different ligands and two μ_3-O(3) atoms. The four nitrogen atoms from the equatorial plane and the two oxygen atoms occupy the axial positions. The O(3)–Co(2)–O(3B) bond angle of 158.0(3)° is far from the octahedral value of 180°. The Co(2)–O(3) distance [2.021(7) Å] is significantly shorter than the Co–O distance [2.082(3) Å] in the cation $[L_2Co_2^{III}Co^{II}]^{2+}$.[22] This phenomenon is expected for an axially compressed Jahn–Teller ion: "The high-spin Co^{II} ($t_{2g}^5e_g^2$) complexes are susceptible to Jahn–Teller distortions although the structural effect would be expected to be considerably less pronounced, since the degeneracy occurs in the t_{2g} d-orbital set rather than in the e_g set".[22] The antiferromagnetic effect of complex **4** further confirms the high-spin d^7 electronic configuration of the Co centers.

Each Co(1) atom is also in a distorted octahedral environment surrounded by N(3), N(4), N(5), N(6), N(1) and O(3). The Co(1B) atom is located in the mean plane of N(3B)–N(4B)–N(5B)–O(3B) with a deviation of 0.0912 Å. Along the axial direction, the two apical positions are occupied by N(1A) and N(6C), which come from another two ligands. The Co(1)–N(O) distances are in the range 1.998(10)–2.262(5) Å, and are in agreement with the high-spin description of the Co^{II} centers.

All the structural units are loosely packed in line along the *a* axis, and there are only weak O(1)···S(2) (3.228 Å) interactions between every two units. Solvent molecules occupy the space between the units.

 © 2004 Wiley-VCH Verlag GmbH & Co. KGaA, Weinheim

Crystal Structure of [{$Ni_5(OH)_2(btapca)_4$}·4DMF·MeOH] (5)

As in the cases of **3** and **4**, the structure of **5** also consists of a pentanuclear [$Ni_5(OH)_2(btapca)_4$], a 4(1)/*n* symmetry axis runs through the central Ni(2) atom, and each asymmetric unit contains two formula units. The structural unit is illustrated in Figure 4. Five Ni^{II} ions are bridged by 24 nitrogen atoms, with four ligands coiling round the [$Ni_5(OH)_2$] core. The distance between two adjacent Ni(1) atoms is 3.444 Å, and the Ni(1)···Ni(2) distances are 3.287 Å. In this point it is similar to **3**, in which the distances between two adjacent Zn(1) atoms are about 3.4 Å, while the Zn(1)···Zn(2) distances are much shorter (about 3.2 Å). The $Ni(1)-N_{(amide)}$ distances fall in the range 2.129(7)−2.151(7) Å, and the $Ni(2)-N_{(thiazole)}$ distances are slightly longer [2.276(7) Å]; the $Ni-N_{(py)}$ distance [1.966(7) Å] is much shorter.

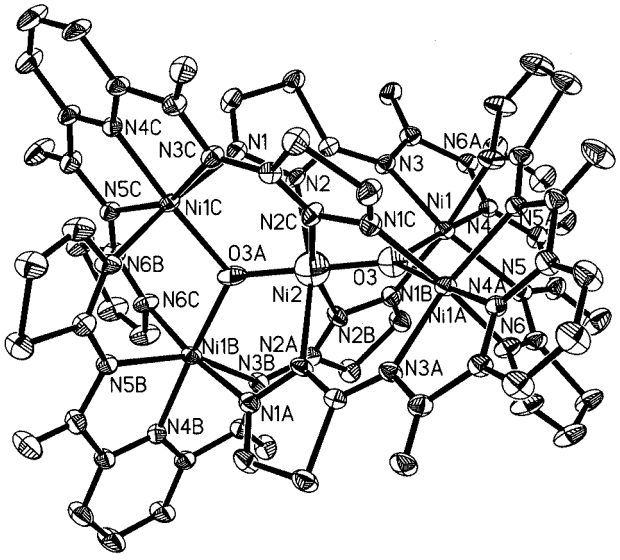

Figure 4. The pentanuclear structure of [{$Ni_5(OH)_2(btapca)_4$}·4DMF·MeOH) (**5**), showing similar feature to those of complex **3** and **4**; the μ_3-OH has been located exactly

The structure of **5** is loosely packed in three dimensions. O(1)···S(2) (3.236 Å) and S(1)···H(7) (2.941 Å) hydrogen bonds are found to connect the whole structure. Channels can be easily seen along the direction perpendicular to the *ac* plane, and the solvent molecules are found in these channels.

Although the skeleton of **5** is similar to those of **3** and **4**, there is a major difference between them. In **3** or **4**, the μ_3-OH is disordered in the center of the M_3 core whereas in **5**, μ_3-OH can be located exactly, with a $Ni(1)-O_{(\mu3)}$ distance of 2.041(6) Å and a $Ni(2)-O_{(\mu3)}$ distance of 1.703(10) Å. The short length of the $Ni(1)-O_{(\mu3)}-Ni(2)$ bridge (about 3.74 Å) leads to active superexchange between the metal ions, as shown by their magnetic-exchange phenomena.

There are many Ni-based complexes with nuclearities ranging from two to eight. The octanuclear ring [$Ni_8(DPKOH\text{-}2H)_4(H_2O)_8](BF_4)_8\cdot 16H_2O$[54] {DPKOH-2H = 1,2-bis[di(pyridin-2-yl)methyleneamino]oxalodiimidic acid}, for example, has a square grouping of six-coordinate Ni^{II} centers arranged in the external ligand pockets. Tetranuclear Ni^{II} complexes are also common,[22,28,29,55−57] for example the [2 × 2] square tetranuclear grid [$Ni_4(POAP\text{-}H)_4(H_2O)_4](NO_3)_4\cdot 8H_2O$ (POAP = alkoxydiazine ligand),[55] the dimer of dimers complex [$Ni_4(ICIMP)_2(Ph_2Ac)_2(urea)(H_2O)][ClO_4]_2$ [56] [ICIMP = 2-{*N*-isopropyl-*N*-[(1-methylimidazolyl)methyl]aminomethyl}-6-{*N*-carboxylmethyl)-*N*-[(1-methylimidazolyl)methyl]aminomethyl}-4-methylphenol], the cation [{$(L^2)Ni_2(\mu\text{-}pydz)(N_3)_2\}_2]^{2+}$ {L^2 = *N*,*N*′-bis[(2-thio-3-aminomethyl-5-*tert*-butylbenzyl)-propane-1,3-diamine]},[57] which contains a rectangular array of four Ni^{II} ions, tetrameric [$Ni_4L_3(H_2O)][ClO_4]_2\cdot 2H_2O$ [H_2L = bis(3-propionyloxy)-1,5-diazacyclooctane],[29] which has a planar triangular Ni_4 topology, the dicubane-like tetramer [Ni(dpk·OH)$(N_3)]_4\cdot 2H_2O$ [dpk = di(2-pyridyl) ketone],[28] and the planar trigonal-shaped tetranuclear Ni^{II} species $[Ni_4(HL)_3]^{2+}$[22] [HL = 1,4,7-tris(acetophenone-oxime)1,4,7-triazacyclononane]. There are also several reported dinuclear nickel(II) complexes,[58−60] while only a limited number of pentanuclear Ni^{II} complexes have been reported, such as the five-membered ring [$Ni_5(bptz)_5(CH_3CN)_{10}][SbF_6]_{10}$ [bptz = 3,6-bis(2-pyridyl)1,2,4,5-tetrazine].[61] As for the pentanuclear Ni^{II} species **5**, its conformation is completely different. The pentanuclear backbone is based on a $Ni_5(\mu_3\text{-}OH)_2$ "bow-tie" cluster, in which two triangles have a common vertex. Comparing complex **5** with these reported Ni^{II} complexes, we found that all of them have O atoms as bridges and similar Ni···Ni distances and Ni−O−Ni angles.

Crystal Structure of [{$Fe_3(OH)(btapca)_3$]·2DMF·2MeOH] (6)

The molecular structure of complex **6** (Figure 5) is based on an isosceles triangular Fe_3 fragment with a bridging μ_3-OH at the center of the triangle. A C_2 symmetry axis through Fe(2) and the central O(4) atom can be found. Three ligands join three iron atoms through nitrogen atoms from the thiadiazole ring; the bridging μ_3-OH reinforces the trianglar framework. The Fe(1)−Fe(1A), Fe(1)−Fe(2) and Fe(1A)−Fe(2) distances are 3.261, 3.227 and 3.227 Å, respectively, within the range of 2.93−3.65 Å reported in the literature.[26,62] A μ_3-O(4) atom bridges three iron atoms [Fe(1), Fe(1A) and Fe(2)] with Fe−O distances of 1.878(3), 1.878(3) and 1.853(7) Å, respectively. The distance of 1.853(7) Å is typical for $Fe^{3+}-O^{2-}$ bonds in trinuclear (carboxylato)(μ_3-oxo) complexes.[63] A comparison of the μ_3-O−Fe distances in complex **6** with corresponding distances in [$Fe_3O(O_2CC(CH_3)_3]_6(C_5H_5N)_3$] ($\mu_3$-O−$Fe^{3+}$ 1.85, at 295 K),[64] favors the assumption that the oxidation state of the Fe(2) atom is +3. The valence of the other two Fe atoms remains to be +2.

 © 2004 Wiley-VCH Verlag GmbH & Co. KGaA, Weinheim

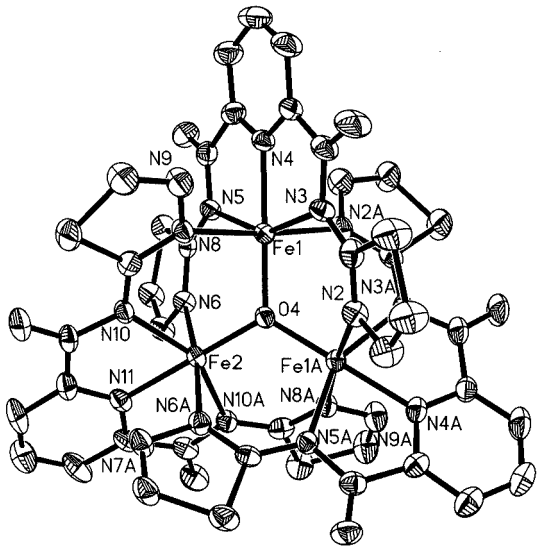

Figure 5. The triangle plane of [{$Fe_3(OH)(btapca)_3$}·2DMF·2MeOH) (**6**), consisting of mixed-valence Fe^{II} and Fe^{III} ions connected together through a μ_3-OH group

Both the Fe^{II} and Fe^{III} ions in **6** have a distorted octahedral geometry with a μ_3-oxygen and five nitrogen atoms. Each Fe center is coordinated simultaneously by three ligands. For example, in the coordination environment of Fe(1), the N(3), N(4) and N(5) donors come from one ligand, N(2A) from the other, and N(8) from the third. μ_3-O(4) and $N(4)_{(py)}$ are at the *trans* positions for all three Fe centers. The four equatorial coordination sites are occupied by N(3), N(4), N(5) and O(4), which are essentially coplanar, with a deviation of 0.0015 Å. Fe(1) is almost in the center of the coordination plane, which deviates from the mean plane by only 0.0019 Å. N(2A) and N(8) from the other two ligands bond to the Fe(1) axial positions to complete the octahedral geometry. The Fe−N distances fall in the range 2.085(9)−2.229(6) Å, which is the typical range for these systems. Three ligands overlap each other like a Chinese knot. Three iron atoms support the triangle knot through a μ_3-oxygen atom. Thus, a closer Fe···Fe contact is found in complex **6**, which benefits the magnetic exchange between the iron centers.

The structure of **6** packs in a large cage-like fashion, in which all the [$Fe_3(OH)(btapca)_3$] units are linked through hydrogen bonding [O(1)···H(11): 2.468 Å; O(3)···H(1): 2.535 Å]. DMF and MeOH solvent molecules occupy the large cages, and the DMF molecules form further hydrogen bonds with [$Fe_3(OH)(btapca)_3$] units [O(5)···H(6): 2.526 Å].

Magnetic Study

The magnetic characterization of **4**−**6** was carried out by measurement of the thermal variation of the paramagnetic susceptibilities χ_p under a magnetic field of 500 G. Because Zn^{II} has no unpaired electrons, complexes **1**−**3** are expected to be diamagnetic.

The magnetic properties of **4** were investigated as described in Figure 6. The χ_pT product exhibits a regular decrease from 3.36 $cm^3·K·mol^{-1}$ at 241 K to 0.97 $cm^3·K·mol^{-1}$ at 5 K, indicating a dominant antiferromagnetic interaction and the spin-orbit coupling of the octahedral Co^{II} centers. Because of this, the μ_{eff} value (5.15 μ_B) of **4** at room temperature is larger than the spin-only value of high-spin cobalt(II) (3.87 μ_B; $\mu_{so} = [4S(S + 1)]^{1/2}$; $S = 3/2$). From 241 to 261 K, χ_pT gradually decreases from 3.36 to 3.24 $cm^3·K·mol^{-1}$, which is an anomaly. This may be due to a transition, possibly associated with the freezing of solvent molecules in the structure and some structural modification. From 261 to 299 K, χ_pT gradually increases from 3.24 to 3.32 $cm^3·K·mol^{-1}$. The close agreement between the experimental and expected μ_{eff} values when the spin momentum and orbital momentum exist independently [5.20 μ_B; $\mu_{1s} = [L(L + 1) + 4S(S + 1)]^{1/2}$; $L = 3$,

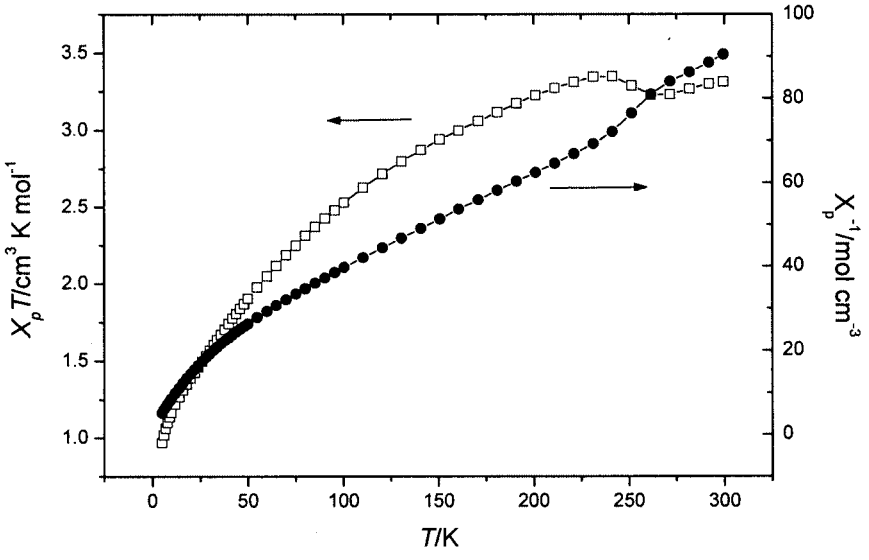

Figure 6. Thermal evolution of χ_pT and χ_p^{-1} of [{$Co_5(OH)_2(btapca)_4$}·4(DMF·MeOH·H_2O) **4**. (χ_p is the paramagnetic susceptibility of **4**)

 © 2004 Wiley-VCH Verlag GmbH & Co. KGaA, Weinheim

$S = 3/2$] suggests that there is a contribution of the orbital angular momentum typical for the $^4T_{1g}$ ground state.

The inverse susceptibility varies linearly with temperatures in the experimental regime (85 K $\leq T \leq$ 242 K) and is well fitted in this region by using the Curie−Weiss law, giving $C = 3.71$ cm^3·K·mol^{-1} and $\theta = -37$ K, which further prove the antiferromagnetic exchange. At lower and higher temperatures, χ_p^{-1} shows a characteristic curvature.

In complex **4** there are three kinds of magnetic exchange pathways, namely a Co^{II}-Co^{II} interaction via the μ_3-OH bridge, a magnetic coupling between Co^{II} and Co^{II} through the $N_{(thiazole)}-N_{(thiazole)}$ pathway (5.89 Å), and a Co^{II}-Co^{II} interaction via the $N_{(amide)}-C-N_{(thiazole)}$ bridge (7.077 Å). In consideration of the structural framework, the spin-bearing centers would like to couple antiferromagnetically in triangular or tetrahedral arrays.[65,66] When the unpaired electrons are aligned at 120° and 109° in the triangular and tetrahedral units, respectively, the overall spin vector is equal to zero, as is required for antiferromagnetic coupling.[65] In the spin Co_3O core the Co−O−Co bond angles are about 113°, in accordance with antiferromagnetic behaviour.

The magnetic properties of **5** were studied in the range 5−302 K and the results are given in Figure 7 in the form of χ_pT vs. T and χ_p^{-1} vs. T plots. The variation of χ_p^{-1} is well described by the Curie−Weiss law from 302 to 5 K. The value $C_m = 5.07$ cm^3·K·mol^{-1} and Weiss temperature $\theta = +2$ K are characteristic of a ferromagnetic superexchange. The magnitude of χ_pT increases continuously with decreasing temperature from 5.11 cm^3·K·mol^{-1} (five Ni atoms) at room temp., with a small peak of 5.46 cm^3·K·mol^{-1} at 50 K. From 50 to 44 K, the value of χ_pT decreases slightly from 5.46 to 5.43 cm^3·K·mol^{-1}. After further cooling, the curve rapidly increases to 6.25 cm^3·K·mol^{-1} at 6 K, and then χ_pT begins to decrease. The small peak at around 50 K may be due to molecular oxygen. These results are indicative of the occurrence of ferromagnetic coupling between the metallic centers. The effective magnetic moment at room temperature is 6.4 μ_B, which agrees very well with the spin-only value for five Ni atoms (6.32 μ_B).

In spite of their structural similarity, complex **5** exhibits quite different magnetic behaviour from **4**. We attributed this to the different exchange centers. The metallic centers have superexchange through different pathways, including the btapca ligands and a μ_3-O. Regularly, if the Ni−O−Ni angle is 120°, the complex will exhibit an antiferromagnetic behavior.[67] For face-sharing dioctahedral nickel complexes, Ni−X−Ni bridging angles of (90 ± 14°) are an indication of a ferromagnetic interaction.[29,57,68] The Ni−O−Ni angles in structure **5** are 115.1(5)° and 122.5(2)°, but we can still see a ferromagnetic interaction from the experimental data. Thus, the magnetic exchange through the btapca ligands could dominate even though the pathway through the μ_3-O is much shorter. The low efficiency of these exchange pathways explains the weak ferromagnetic behavior observed for **5**, although the magnetic exchange centers are relatively close to each other. Moreover, the distortions of octahedral geometry around the Ni ion [Ni−N distances ranging from 1.966(7) to 2.276(7) Å with Ni−O lengths of 2.041(6) and 1.704(10) Å] account for the slight weakening of the observed ferromagnetic coupling. Consequently, differences in the bond lengths around Ni ions are directly related to the overlap between the d_{x2-y2} orbital and thus affect the magnitude of the ferromagnetic coupling.

The magnetic behavior of complex **6** is shown in Figure 8 in the form of a χ_pT vs. T plot. χ_pT decreases continuously from 3.14 cm^3·K·mol^{-1} at 302 K to 0.67 cm^3·K·mol^{-1} at 4 K. This behavior is consistent with an antiferromagnetic interaction between the exchange centers. The magnetic susceptibility, plotted as χ_p^{-1} vs. T in Figure 8, follows the Curie−Weiss expression $\chi_p = C/(T - \theta)$ between 110 K and 300 K, with a Curie constant of 3.30 cm^3·K·mol^{-1} and a

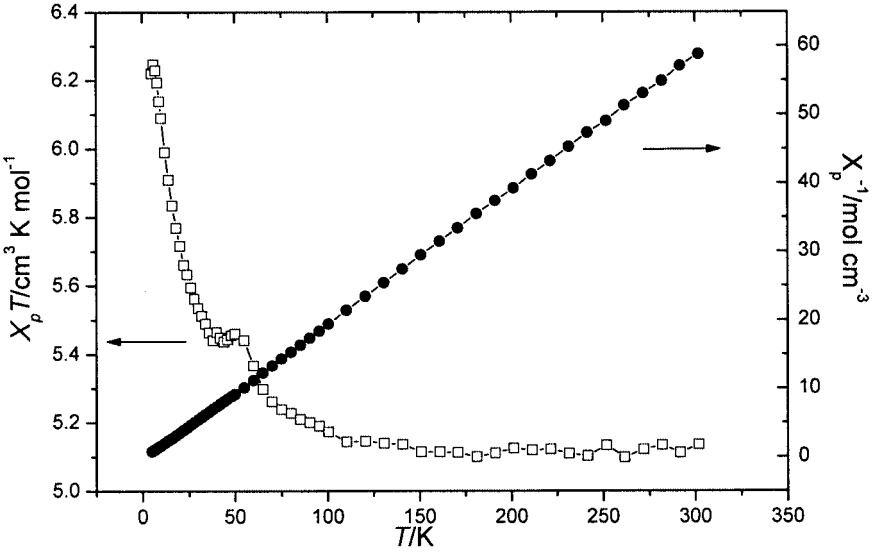

Figure 7. Thermal evolution of χ_pT and χ_p^{-1} of [{$Ni_5(OH)_2(btapca)_4$}·4DMF·MeOH) (**5**); χ_p is the paramagnetic susceptibility of **5**

 © 2004 Wiley-VCH Verlag GmbH & Co. KGaA, Weinheim

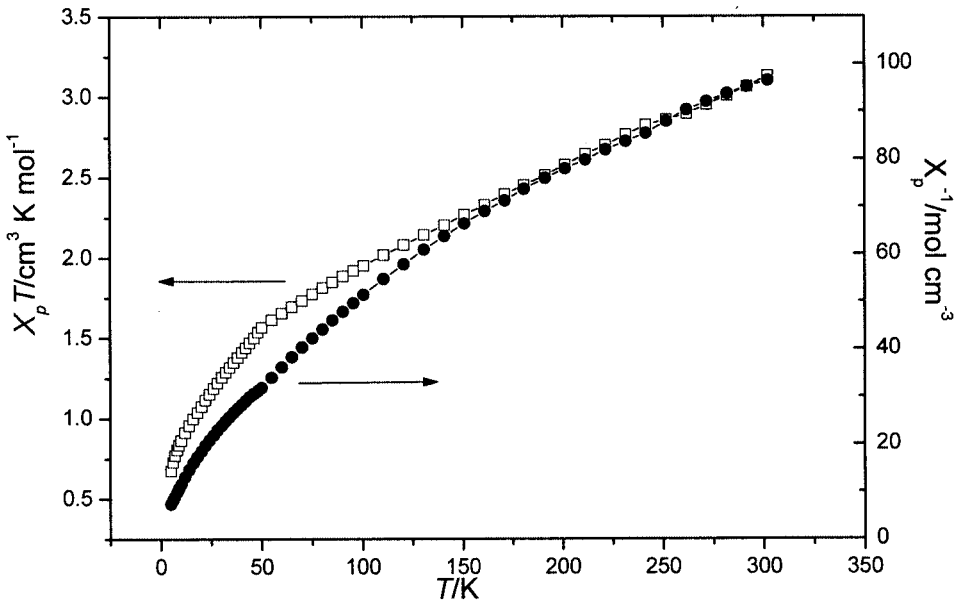

Figure 8. Plots of $\chi_p T$ and χ_p^{-1} vs. T for [{Fe_3(OH)(btapca)$_3$}·2DMF·2MeOH) (**6**); χ_p is the paramagnetic susceptibility of **6**

Curie−Weiss temperature, θ, of −49 K. Below 110 K, the data do not strictly obey the Curie−Weiss law. The effective paramagnetic moment, μ_{eff}, is 5.0 μ_B, indicating a high-spin state for both Fe^{II} (S = 2) and Fe^{III} (S = 5/2) centers. The negative sign for θ suggests an overall antiferromagnetic coupling between the mixed-valence Fe^{II}-Fe^{III} centers.

The magnetic interactions between Fe ions in **6** are achieved mainly through the μ_3-O atom. Although the presence of N−C−N bridges provides an additional exchange pathway (Fe-*N*-C-*N*-Fe about 7.04 Å), they can be neglected due to the shorter Fe−O−Fe bridges (Fe−O−Fe about 3.73 Å). The Fe···Fe distances (about 3.2 Å) differ by only 0.04 Å, and the average Fe−O−Fe angle is 120°. The restricted Fe−O−Fe angle in the iron-$O_{\mu 3}$ plane structures allows magneto-structural correlations. The typical obtuse angle of 120° induces an antiferromagnetic interaction.

The Mössbauer spectrum of complex **6** is similar to that observed for another trimeric, mixed-valent, oxo-centered complex,[69] although it is remarkably different from other trimeric, mixed-valence, oxo-centered complexes.[70,71] The doublets in the Mössbauer spectrum of **6** at room temperature are far from the ratio of 2:1, with isomer shifts and quadrupole splittings of δ_I = 0.27 mm·s^{-1}, ΔE_{QI} = 1.75 mm·s^{-1} and δ_{II} = 0.72 mm·s^{-1}, ΔE_{QII} = 2.63 mm·s^{-1} (Figure 9). This denotes some degree of delocalization (valence detrapping) of the extra electron over the three Fe sites. At room temperature only one doublet is usually found for trimeric, mixed-valent, oxo-centered transition metal complexes due to full delocalization of the "excess" electron over the three iron sites ("valence-detrapped state").[69,70] Complex **6** exhibits a partially valence-delocalized (partially valence-detrapped) state which is similar to the case of a reported Fe^{II}/Fe^{III} complex.[69]

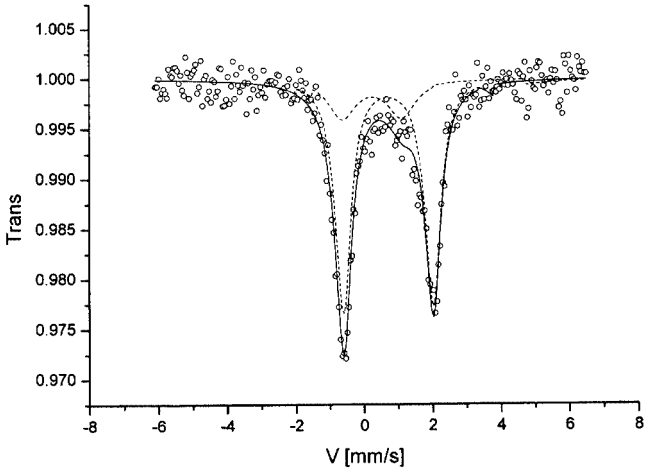

Figure 9. The Mössbauer spectrum of complex [{Fe_3(OH)(btapca)$_3$}·2DMF·2MeOH) (**6**) at room temperature

Conclusion

We have succeeded in obtaining a series of polynuclear complexes constructed from polydentate ligands and different transition-metal salts. The number of metal atoms in these polynuclear complexes ranges from 3 to 6. A μ_3-O atom is a dominant feature in the formation of all these structures. The magnetic behavior of complex **5** shows a ferromagnetic interaction between the Ni^{II} ions, while complexes **4** and **6** both exhibit typical antiferromagnetic exchange between the metal centers.

 © 2004 Wiley-VCH Verlag GmbH & Co. KGaA, Weinheim

Experimental Section

General Techniques: 2-Amino-1,3,4-thiadiazole (TBA) was prepared according to a published method.[72] All the other starting chemicals and solvent were commercially available with analytical purity and were used without further purification. A PE 240C Elemental Analyzer was used to perform the elemental analysis. Infrared spectra were measured on a Bruker Tensor 27 infrared spectrophotometer. Fast atom bombardment (FAB) mass spectra were obtained on a Bruker Esquire 3000 mass spectrometer. NMR spectra were obtained using a Bruker DPX-400 spectrometer.

Preparation of *N*,*N*′-Bis(1,3,4-thiadiazol-2-yl)-2,6-pyridinedicarboxamide (btapca): 2,6-Pyridinedicarboxylic acid (1.67 g, 10 mmol) was dissolved in 20 mL of $SOCl_2$. The mixture was refluxed until the white powder dissolved completely. The residual $SOCl_2$ was then removed under reduced pressure. The resulting 2,6-pyridinedicarbonyl dichloride was dissolved in 10 mL of anhydrous pyridine. This pyridine solution of 2-aminodithiazole (2.02 g, 20 mmol) was added dropwise to the 2,6-pyridinedicarbonyl dichloride whilst stirring in an ice bath. Stirring for 4 h resulted in the formation of a white precipitate, which was filtered under reduced pressure and washed with water and methanol. Yield: 2.25 g (70%). $C_{11}H_7N_7O_2S_2$ (333.01): calcd. C 39.64, H 2.12, N 29.41; found C 39.84, H 2.27, N 28.11. ^{1}H NMR (400 MHz, DMSO): δ = 8.39 (q, H), 8.50 (d, 2 H), 9.36 (s, 2 H), 13.73 (d, 2 H) ppm. Positive-ion, ESI-MS: m/z = 333.9 [btapca + H^-].

Synthesis of [{$Zn_6(O)_2$(btapca)$_4$}·3DMF·2H_2O] (1): A DMF solution (5 mL) of btapca (0.1 mmol, 0.0333 g) was added to a methanol solution (5 mL) of $Zn(NO_3)_2$·6H_2O (0.2 mmol, 0.0595 g). The mixture solution was then evaporated to 30% of the original volume at room temperature. Colorless crystals were collected after two weeks with a yield of 30%. IR (KBr pellets): $\tilde{\nu}$ = 3082, 1625, 1667, 1293 cm^{-1}. $C_{53}H_{45}N_{31}O_{15}S_8Zn_6$ (2004.9): calcd. C 31.72, H 2.24, N 21.65; found C 31.51, H 2.31, N 21.22.

Synthesis of [{$Zn_6(O)_2$(btapca)$_4$}·DMF·MeOH·H_2O] (2): A DMF solution (5 mL) of btapca (0.1 mmol, 0.0333 g) was added to a methanol solution (5 mL) of $Zn(OAc)_2$·2H_2O (0.2 mmol, 0.0439 g). The mixture was allowed to stand in air at room temperature for a week resulting in colorless crystals suitable for X-ray diffraction. Yield: 46%. IR (KBr pellets): $\tilde{\nu}$ = 3450, 1626, 1467, 1427, 1376, 1070, 959, 885, 529 cm^{-1}. $C_{48}H_{33}N_{29}O_{13}S_8Zn_6$ (1872.7): calcd. C 30.76, H 1.76, N 21.68; found C 30.95, H 1.58, N 22.01.

Synthesis of [{$Zn_5(OH)_2$(btapca)$_4$}·4DMF·H_2O] (3): A DMF solution (5 mL) of btapca (0.1 mmol, 0.0333 g) was added to a THF solution (5 mL) of ZnI_2 (0.2 mmol, 0.0638 g). A light-yellow solution was obtained after filtration, and this was placed under air. Colorless polyhedral crystals appeared after two weeks. Yield: 25%. IR (KBr pellets): $\tilde{\nu}$ = 3445, 3095, 1639, 1538, 1466, 1444, 1377, 1075, 959, 889 cm^{-1}. $C_{56}H_{52}N_{32}O_{15}S_8Zn_5$ (1996.6): calcd. C 33.66, H 2.60, N 22.44; found C 33.36, H 2.83, N 22.37.

Synthesis of [{$Co_5(OH)_2$(btapca)$_4$}·4DMF·MeOH·H_2O] (4): A DMF solution (5 mL) of btapca (0.1 mmol, 0.0333 g) was added dropwise to a methanol solution (5 mL) of $CoCl_2$·6H_2O (0.2 mmol, 0.0476 g). The resulting red solution produced dark-red crystals suitable for X-ray analysis after four days. Yield: 52%. IR (KBr

Table 1. Crystal data and structure refinement for complexes **1**−**6**

	1	**2**	**3**	**4**	**5**	**6**
Empirical formula	$C_{53}H_{45}N_{31}O_{15}S_8Zn_6$	$C_{48}H_{33}N_{29}O_{13}S_8Zn_6$	$C_{56}H_{52}N_{32}O_{15}S_8Zn_5$	$C_{57}H_{52}Co_5N_{32}O_{17}S_8$	$C_{57}H_{54}N_{32}Ni_5O_{15}S_8$	$C_{41}H_{38}Fe_3N_{23}O_{11}S_6$
Molecular mass	2004.90	1872.73	1996.63	2008.44	1977.35	1388.85
Temperature	291(2) K	291(2) K	291(2) K	291(2) K	293(2) K	291(2) K
Wavelength	0.71073 Å	0.71073 Å	0.71073 Å	0.71073 Å	0.71073 Å	0.71073 Å
Crystal system	triclinic	monoclinic	tetragonal	tetragonal	tetragonal	monoclinic
Space group	$P\bar{1}$	$P2_1/n$	$P4_2/n$	$P4_2/n$	$P4_2/n$	$C2/c$
Unit cell dimensions	a = 14.634(3) Å	a = 13.112(3) Å	a = 14.821(2) Å	a = 14.805(2) Å	a = 14.792(2) Å	a = 15.981(3) Å
	b = 20.794(4) Å	b = 37.227(7) Å	b = 14.821(2) Å	b = 14.805(2) Å	b = 14.792(2) Å	b = 20.199(4) Å
	c = 12.904(3) Å	c = 14.510(3) Å	c = 18.462(4) Å	c = 18.421(4) Å	c = 18.108(4) Å	c = 19.513(4) Å
	α = 99.14(3)°	α = 90°	α = 90°	α = 90°	α = 90°	α = 90°
	β = 96.24(3)°	β = 108.56(3)°	β = 90°	β = 90°	β = 90°	β = 102.47(3)°
	γ = 71.48(3)°	γ = 90°	γ = 90°	γ = 90°	γ = 90°	γ = 90°
Volume	3668.8(13) Å^3	6714(2) Å^3	4055.5(11) Å^3	4037.7(11) Å^3	3962.0(11) Å^3	6150(2) Å^3
Z	2	4	2	2	2	4
Calculated density	1.815 Mg/m^3	1.853 Mg/m^3	1.635 Mg/m^3	1.652 Mg/m^3	1.657 Mg/m^3	1.501 Mg/m^3
Absorption coefficient	2.243 mm^{-1}	2.441 mm^{-1}	1.743 mm^{-1}	1.296 mm^{-1}	1.459 mm^{-1}	0.973 mm^{-1}
F(000)	2016	3744	2020	2034	2016	2832
Index ranges	$0 \le h \le 17$	$-15 \le h \le 14$	$-17 \le h \le 17$	$0 \le h \le 17$	$-17 \le h \le 17$	$-18 \le h \le 14$
	$-21 \le k \le 24$	$-44 \le k \le 43$	$0 \le k \le 17$	$-17 \le k \le 17$	$0 \le k \le 17$	$14 \le k \le 24$
	$-15 \le l \le 15$	$0 \le l \le 17$	$-21 \le l \le 21$	$-21 \le l \le 21$	$-21 \le l \le 20$	$-22 \le l \le 22$
Reflections collected/unique	8194/8194 [R(int) = 0.0000]	15422/9468 [R(int) = 0.0631]	9960/3331 [R(int) = 0.0478]	10257/3115 [R(int) = 0.0463]	10847/3304 [R(int) = 0.0442]	7745/4499 [R(int) = 0.0436]
Refinement method	full-matrix least-squares on F^2	full-matrix least-squares on F^2	full-matrix least-squares on F^2	full-matrix least-squares on F^2	full-matrix least-squares on F^2	full-matrix least-squares on F^2
Data/restraints/parameters	8194/6/934	9468/0/938	3331/5/241	3115/2/272	3304/4/241	4499/0/347
Final R(int) [$I > 2\sigma(I)$]	$R1$ = 0.0773	$R1$ = 0.0556	$R1$ = 0.0768	$R1$ = 0.0580	$R1$ = 0.0832	$R1$ = 0.0737
	$wR2$ = 0.1739	$wR2$ = 0.1003	$wR2$ = 0.1947	$wR2$ = 0.1594	$wR2$ = 0.2615	$wR2$ = 0.2000
Largest diff. peak and hole	1.306 and −0.684 e·Å^{-3}	1.158 and −0.811 e·Å^{-3}	0.979 and −0.438 e·Å^{-3}	0.698 and −0.926 e·Å^{-3}	1.470 and −3.822 e·Å^{-3}	0.810 and −0.570 e·Å^{-3}

 © 2004 Wiley-VCH Verlag GmbH & Co. KGaA, Weinheim

pellets): $\tilde{\nu}$ = 3435, 3069, 1709, 1667, 1612, 1437, 1366, 1077, 954, 888 cm^{-1}. $C_{57}H_{52}Co_5N_{32}O_{17}S_8$ (2008.4): calcd. C 34.06, H 2.59, N 22.31; found C 35.22, H 2.27, N 22.65.

Synthesis of [{$Ni_5(OH)_2(btapca)_4$}·4DMF·MeOH] (5): $Ni(NO_3)_2·6H_2O$ (0.1 mmol, 0.0291 g) was dissolved in 5 mL methanol, and a DMF solution (5 mL) of btapca (0.1 mmol, 0.0333 g) was added dropwise to the above solution. The resulting solution was kept at room temperature. Brown crystals suitable for X-ray diffraction were obtained. Yield: 33%. IR (KBr pellets): $\tilde{\nu}$ = 3442, 3075, 1637, 1598, 1465, 1360, 1074, 959, 889 cm^{-1}. $C_{57}H_{54}N_{32}Ni_5O_{15}S_8$ (1977.4): calcd. C 34.59, H 2.73, N 22.66; found C 34.89, H 2.57, N 22.74.

Synthesis of [{$Fe_3(OH)(btapca)_3$}·2DMF·2MeOH] (6). Solutions of btapca (0.1 mmol, 0.0333 g) in DMF and $FeCl_2·4H_2O$ (0.2 mmol, 0.0398 g) in methanol were mixed. Dark-red microcrystals were obtained at room temperature. Yield: 62%. IR (KBr pellets): $\tilde{\nu}$ = 3452, 3079, 1636, 1422, 1358, 1283, 1158, 1043, 959, 888 cm^{-1}.

Table 2. Selected bond lengths (Å) and angles (°) for complexes **1**–**3**

Complex **1**

Zn(1)–O(9)	1.947(9)	Zn(3)–Zn(4)	2.802(2)
Zn(2)–O(9)	1.940(9)	Zn(5)–Zn(6)	3.145(3)
Zn(3)–O(10)	1.979(9)	O(10)–Zn(3)–O(9)	89.5(4)
Zn(3)–O(9)	1.982(9)	O(9)–Zn(4)–O(10)	89.9(4)
Zn(4)–O(9)	1.965(9)	Zn(2)–O(9)–Zn(1)	107.2(4)
Zn(4)–O(10)	1.981(9)	Zn(2)–O(9)–Zn(4)	114.6(5)
Zn(5)–O(10)	1.925(9)	Zn(1)–O(9)–Zn(4)	114.1(4)
Zn(6)–O(10)	1.955(10)	Zn(2)–O(9)–Zn(3)	116.5(4)
Zn(1)–N(9)	2.014(12)	Zn(1)–O(9)–Zn(3)	113.6(5)
Zn(1)–N(3)	2.337(12)	Zn(4)–O(9)–Zn(3)	90.5(4)
Zn(2)–N(6)	2.020(12)	Zn(5)–O(10)–Zn(6)	108.3(4)
Zn(2)–N(12)	2.277(13)	Zn(5)–O(10)–Zn(3)	116.8(5)
Zn(3)–N(27)	1.992(12)	Zn(6)–O(10)–Zn(3)	111.7(4)
Zn(4)–N(13)	1.995(15)	Zn(5)–O(10)–Zn(4)	113.5(4)
Zn(5)–N(19)	2.218(13)	Zn(6)–O(10)–Zn(4)	115.9(5)
Zn(6)–N(24)	2.255(11)	Zn(3)–O(10)–Zn(4)	90.1(4)
Zn(1)–Zn(2)	3.130(3)		

Complex **2**

Zn(1)–O(10)	1.939(5)	Zn(1)–Zn(2)	3.1457(14)
Zn(1)–N(2)	2.021(7)	Zn(3)–Zn(4)	2.8103(13)
Zn(2)–O(10)	1.943(5)	Zn(5)–Zn(6)	3.0927(14)
Zn(2)–N(5)	2.234(6)	Zn(5)–O(9)–Zn(6)	105.7(2)
Zn(3)–O(9)	1.968(5)	Zn(5)–O(9)–Zn(3)	115.0(2)
Zn(3)–N(27)	1.971(6)	Zn(6)–O(9)–Zn(3)	114.9(2)
Zn(3)–O(10)	1.974(5)	Zn(5)–O(9)–Zn(4)	114.7(2)
Zn(3)–N(13)	1.988(6)	Zn(6)–O(9)–Zn(4)	115.8(2)
Zn(4)–O(9)	1.980(5)	Zn(3)–O(9)–Zn(4)	90.8(2)
Zn(4)–O(10)	1.989(5)	Zn(1)–O(10)–Zn(2)	108.2(2)
Zn(4)–N(6)	1.987(6)	Zn(1)–O(10)–Zn(3)	113.6(2)
Zn(4)–N(16)	1.996(6)	Zn(2)–O(10)–Zn(3)	116.2(2)
Zn(5)–O(9)	1.940(5)	Zn(1)–O(10)–Zn(4)	114.2(2)
Zn(5)–N(26)	2.260(6)	Zn(2)–O(10)–Zn(4)	113.7(2)
Zn(6)–O(9)	1.941(5)	Zn(3)–O(10)–Zn(4)	90.3(2)
Zn(6)–N(17)	2.284(6)		

Complex **3**[a]

Zn(1)–O(3)	1.940(11)	O(3)–Zn(1)–N(4)	154.7(4)
Zn(1)–N(4)	2.029(6)	O(3)–Zn(1)–O(3)#1	27.2(5)
Zn(1)–O(3)#1	2.041(12)	N(4)–Zn(1)–O(3)#1	174.2(3)
Zn(1)–N(2)#1	2.128(7)	O(3)–Zn(1)–N(2)#1	107.0(4)
Zn(1)–N(5)	2.167(6)	N(4)–Zn(1)–N(2)#1	96.5(3)
Zn(1)–N(3)	2.215(6)	O(3)#1–Zn(1)–N(2)#1	84.2(3)
Zn(1)–N(7)#2	2.451(9)	O(3)–Zn(1)–N(5)	109.8(3)
Zn(2)–O(3)#3	2.018(8)	N(4)–Zn(1)–N(5)	76.8(3)
Zn(2)–O(3)#1	2.018(8)	O(3)#3–Zn(2)–O(3)#1	161.0(4)
Zn(2)–O(3)#2	2.018(8)	O(3)#3–Zn(2)–O(3)#2	27.0(5)
Zn(2)–O(3)	2.018(8)	O(3)#1–Zn(2)–O(3)#2	161.0(4)
Zn(2)–N(6)	2.293(8)	O(3)#3–Zn(2)–O(3)	161.0(4)
Zn(2)–N(6)#3	2.293(8)	O(3)#1–Zn(2)–O(3)	27.0(5)
Zn(2)–N(6)#2	2.293(8)	O(3)#3–Zn(2)–N(6)	74.5(4)
Zn(2)–N(6)#1	2.293(8)	O(3)#1–Zn(2)–N(6)	86.9(4)
Zn(1)–O(3)–Zn(2)	119.2(6)	Zn(1)–O(3)–Zn(1)#1	110.4(4)
Zn(2)–O(3)–Zn(1)#1	114.5(5)		

[a] Symmetry transformations used to generate equivalent atoms: #1 $-x + 3/2$, $-y + 3/2$, z; #2 y, $-x + 3/2$, $-z + 1/2$; #3 $-y + 3/2$, x, $-z + 1/2$.

Table 3. Selected bond lengths (Å) and angles (°) for complexes **4**–**6**

Complex **4**[a]

Co(1)–O(3)#1	1.998(10)	O(3)#1–Co(1)–O(3)	31.5(4)
Co(1)–O(3)	2.016(9)	O(3)#1–Co(1)–N(4)	169.0(2)
Co(1)–N(4)	2.020(4)	O(3)–Co(1)–N(4)	159.3(3)
Co(1)–N(3)	2.160(4)	O(3)#1–Co(1)–N(3)	94.8(2)
Co(1)–N(5)	2.168(4)	O(3)–Co(1)–N(3)	113.2(2)
Co(1)–N(6)#1	2.197(5)	O(3)–Co(2)–O(3)#3	158.0(3)
Co(1)–N(1)#2	2.262(5)	O(3)–Co(2)–O(3)#2	158.0(3)
Co(2)–O(3)	2.021(7)	O(3)#3–Co(2)–O(3)#2	31.2(4)
Co(2)–O(3)#3	2.021(7)	O(3)–Co(2)–O(3)#1	31.2(4)
Co(2)–O(3)#2	2.021(7)	O(3)#3–Co(2)–O(3)#1	158.0(3)
Co(2)–O(3)#1	2.021(7)	O(3)#2–Co(2)–O(3)#1	158.0(3)
Co(2)–N(2)	2.238(4)	O(3)–Co(2)–N(2)	105.9(2)
Co(2)–N(2)#1	2.238(4)	O(3)#3–Co(2)–N(2)	73.3(3)
Co(2)–N(2)#3	2.238(4)	O(3)#2–Co(2)–N(2)	96.0(3)
Co(2)–N(2)#2	2.238(4)	O(3)#1–Co(2)–N(2)	84.7(2)

Complex **5**[b]

Ni(1)–N(4)	1.966(7)	Ni(2)–N(2)#3	2.276(7)
Ni(1)–O(3)	2.041(6)	Ni(2)–N(2)#1	2.276(7)
Ni(1)–N(5)	2.129(7)	Ni(2)–N(2)	2.276(7)
Ni(1)–N(3)	2.131(7)	O(3)#2–Ni(2)–O(3)	180.000(1)
Ni(1)–N(6)#1	2.140(7)	O(3)#2–Ni(2)–N(2)#2	97.23(17)
Ni(1)–N(1)#2	2.151(7)	O(3)–Ni(2)–N(2)#2	82.77(17)
Ni(2)–O(3)#2	1.704(10)	O(3)#2–Ni(2)–N(2)#3	97.23(17)
Ni(2)–O(3)	1.704(10)	O(3)–Ni(2)–N(2)#3	82.77(17)
Ni(2)–N(2)#2	2.276(7)	N(2)#2–Ni(2)–N(2)#3	165.5(3)
N(4)–Ni(1)–O(3)	175.0(2)	N(4)–Ni(1)–N(6)#1	93.3(3)
N(4)–Ni(1)–N(5)	78.5(3)	O(3)–Ni(1)–N(6)#1	91.7(2)
O(3)–Ni(1)–N(5)	100.8(3)	N(5)–Ni(1)–N(6)#1	93.6(3)
N(4)–Ni(1)–N(1)#2	92.5(3)	N(5)–Ni(1)–N(1)#2	91.1(3)
O(3)–Ni(1)–N(1)#2	82.5(2)	N(3)–Ni(1)–N(1)#2	86.6(3)

Complex **6**[c]

Fe(1)–O(4)	1.878(3)	Fe(2)–O(4)–Fe(1)#1	119.76(18)
Fe(1)–N(4)	2.085(6)	Fe(2)–O(4)–Fe(1)	119.76(18)
Fe(1)–N(5)	2.132(6)	Fe(1)#1–O(4)–Fe(1)	120.5(4)
Fe(1)–N(3)	2.141(6)	O(4)–Fe(1)–N(4)	179.6(2)
Fe(1)–N(8)	2.226(6)	O(4)–Fe(1)–N(5)	104.1(2)
Fe(1)–N(2)#1	2.229(6)	N(4)–Fe(1)–N(5)	76.0(2)
Fe(2)–O(4)	1.853(7)	O(4)–Fe(1)–N(2)#1	91.8(2)
Fe(2)–N(11)	2.085(9)	N(4)–Fe(1)–N(2)#1	88.5(2)
Fe(2)–N(10)	2.131(6)	N(5)–Fe(1)–N(2)#1	90.3(2)
Fe(2)–N(10)#1	2.131(6)	N(3)–Fe(1)–N(2)#1	89.0(3)
Fe(2)–N(6)	2.209(5)	O(4)–Fe(2)–N(10)	104.31(18)
Fe(2)–N(6)#1	2.209(5)	N(11)–Fe(2)–N(10)	75.69(18)
O(4)–Fe(1)#1	1.878(3)	O(4)–Fe(2)–N(10)#1	104.31(18)
O(4)–Fe(2)–N(11)	180.000(1)		

[a] Symmetry transformations used to generate equivalent atoms: #1 $-x + 5/2$, $-y + 5/2$, z; #2 y, $-x + 5/2$, $-z - 1/2$; #3 $-y + 5/2$, x, $-z - 1/2$; #4 y, $-x + 5/2$, $-z + 1/2$. [b] Symmetry transformations used to generate equivalent atoms: #1 $-x + 3/2$, $-y + 3/2$, z; #2 y, $-x + 3/2$, $-z + 1/2$; #3 $-y + 3/2$, x, $-z + 1/2$; #4 $-y + 3/2$, x, $-z + 3/2$; #5 y, $-x + 3/2$, $-z + 3/2$. [c] Symmetry transformations used to generate equivalent atoms: #1 $-x$, y, $-z + 1/2$; #2 $-x + 1/2$, $-y + 3/2$, $-z$.

 © 2004 Wiley-VCH Verlag GmbH & Co. KGaA, Weinheim

$C_{41}H_{38}Fe_3N_{23}O_{11}S_6$ (1388.9): calcd. C 35.42, H 2.74, N 23.18; found C 35.12, H 2.80, N 23.52.

Magnetic Studies: Temperature-dependent magnetic-susceptibility measurements on powdered solid samples were carried out on a SQUID magnetometer (MPMS Quantum Design) over the temperature range 5−300 K. The magnetic field applied was 500 G. The observed susceptibility data were corrected for underlying diamagnetism by using Pascal's constants.[73]

Mössbauer Measurement: Mössbauer spectra were obtained in transmission mode using a ^{57}Co source in a Rh matrix. 64.8 mg of the samples was used and the spectra were measured on an Austin S-600 Mössbauer spectrometer. The spectra were recorded at room temperature at a speed of 6 mm/s. The source was kept at room temperature. The hyperfine field parameters were obtained by fitting the raw data with Lorentz-shaped lines using the program "Mössbauer spectra for Fitting" by Prof. Z. X. Xu (Material Physics and Chemistry Department, University of Science and Technology Beijing). The hyperfine field data are referenced against α-Fe.

X-ray Crystallographic Study: The diffraction intensities of prismatic crystals of complexes **1**, **2**, **3**, **4**, **5** and **6** were collected with graphite-monochromated Mo-K_α radiation (λ = 0.71073 Å) using a Rigaku R-AXIS-IV diffractometer at 291(2) K to a maximum 2θ value of 50°. The unit-cell parameters were determined from the reflections collected on oscillation frames and were then refined. The data were corrected for Lorentz and polarization effects. The structures were solved by direct methods with SHELXS-97[74] and subsequent Fourier-difference synthesis and refined by the full-matrix least-squares method on F^2 with SHELXL-97.[75] All non-hydrogen atoms, except atoms in disordered parts, were refined anisotropically; hydrogen atoms were placed at calculated positions and refined as riding atoms with isotropic displacement parameters. Crystal data and structure refinement details for the seven compounds are given in Table 1. Selected bond lengths and angles of complexes **1**−**6** are listed in Table 2 and 3.
CCDC-212348 (for **1**), -212349 (for **2**), -212351 (for **3**), -212350 (for **4**), -212352 (for **5**) and -212354 (for **6**) contain the supplementary crystallographic data for this paper. These data can be obtained free of charge at www.ccdc.cam.ac.uk/conts/retrieving.html [or from the Cambridge Crystallographic Data Centre, 12 Union Road, Cambridge CB2 1EZ, UK; Fax: +44-1223-336033; E-mail: deposit@ccdc.cam.ac.uk].

Acknowledgments

This work was supported by the National Natural Science Foundation of China (Nos. 20001006 and 20371042), the Excellent Young Teachers Program In Higher Education Institute and Henan Province.

[1] G. M. Whitesides, J. P. Mathias, C. T. Seto, *Science* **1991**, *254*, 1312−1319.
[2] G. F. Swiegers, T. J. Malefetse, *Chem. Rev.* **2000**, *100*, 3483−3537.
[3] [3a] S. S. Sun, A. J. Lee, *J. Am. Chem. Soc.* **2000**, *122*, 8956−8967. [3b] D. S. Lawrence, T. Jiang, M. Levett, *Chem. Rev.* **1995**, *95*, 2229−2260.
[4] Y. B. Dong, M. D. Smith, H. C. Z. Loye, *Angew. Chem. Int. Ed.* **2000**, *39*, 4271−4273.
[5] L. K. Thompson, L. Zhao, Z. Xu, D. O. Miller, W. M. Reiff, *Inorg. Chem.* **2003**, *42*, 128−139.
[6] E. Colacio, M. Ghazi, H. Stoeckli-Evans, F. Lloret, J. M. Moreno, C. Pérez, *Inorg. Chem.* **2001**, *40*, 4876−4883.
[7] *Monographs in Supramolecular Chemistry* (Ed.: J. F. Stoddart), Royal Society of Chemistry, Cambridge, UK, **1989, 1991, 1994−1996**; vols. 1−6.
[8] D. B. Amabilino, J. F. Stoddart, *Chem. Rev.* **1995**, *95*, 2725−2828.
[9] D. B. Amabilino, M. Asakawa, P. R. Ashton, R. Ballardini, V. Balzani, M. Belohradský, A. Credi, M. Higuchi, F. M. Raymo, T. Shimizu, J. F. Stoddart, M. Venturi, K. Yase, *New J. Chem.* **1998**, *22*, 959−972.
[10] S. Leininger, B. Olenyuk, P. J. Stang, *Chem. Rev.* **2000**, *100*, 853−908.
[11] [11a] K. S. Jeong, Y. L. Cho, J. U. Song, H. Y. Chang, M. G. Choi, *J. Am. Chem. Soc.* **1998**, *120*, 10982−10983. [11b] F. A. Cotton, L. M. Daniels, C. Lin, C. A. Murillo, *Chem. Commun.* **1999**, 841−842. [11c] S. M. Woessner, J. B. Helms, J. F. Houlis, B. P. Sullivan, *Inorg. Chem.* **1999**, *38*, 4380−4381. [11d] S. S. Sun, A. S. Silva, I. M. Brinn, A. J. Lees, *Inorg. Chem.* **2000**, *39*, 1344−1345.
[12] [12a] R. V. Slone, K. D. Benksrein, S. Bélanger, J. T. Hupp, I. A. Guzei, A. L. Rheingold, *Coord. Chem. Rev.* **1998**, *171*, 221−243. [12b] S. Bélanger, J. T. Hupp, C. L. Stern, R. V. Slone, D. F. Watson, T. G. Carrell, *J. Am. Chem. Soc.* **1999**, *121*, 557−563. [12c] S. Bélanger, J. T. Hupp, *Angew. Chem. Int. Ed.* **1999**, *38*, 2222−2224.
[13] [13a] Y. Zhang, S. Wang, G. D. Enright, S. R. Breeze, *J. Am. Chem. Soc.* **1998**, *120*, 9398−9399. [13b] K. Onitsuka, S. Yamamoto, S. Takahashi, *Angew. Chem. Int. Ed.* **1999**, *38*, 174−176.
[14] Y. L. Cho, H. Uh, S. Y. Chang, H. Y. Chang, M. G. Choi, I. Shin, K. S. Jeong, *J. Am. Chem. Soc.* **2001**, *123*, 1258−1259.
[15] [15a] M. Fujita, *Chem. Soc. Rev.* **1998**, *27*, 417−425. [15b] D. L. Caulder, K. N. Raymond, *Acc. Chem. Res.* **1999**, *32*, 975−982.
[16] [16a] R. D. Schnebeck, E. Freisinger, F. Glahé, B. Lippert, *J. Am. Chem. Soc.* **2000**, *122*, 1381−1390. [16b] F. Würthner, A. Sautter, *Chem. Commun.* **2000**, 445−446. [16c] A. J. Blake, N. R. Champness, A. N. Khlobystov, S. Parsons, M. Schröder, *Angew. Chem. Int. Ed.* **2000**, *39*, 2317−2320. [16d] K. D. Benkstein, J. T. Hupp, C. L. Stern, *Angew. Chem. Int. Ed.* **2000**, *39*, 2891−2893.
[17] [17a] N. Takeda, K. Umemoto, K. Yamaguchi, M. Fujita, *Nature* **1999**, *398*, 794−796. [17b] B. Olenuyuk, J. A. Whiteford, A. Fechtenkötter, P. J. Stang, *Nature* **1999**, *398*, 796−799. [17c] A. Ikeda, M. Yoshimura, H. Udzu, C. Fukuhara, S. Shinkai, *J. Am. Chem. Soc.* **1999**, *121*, 4296−4297. [17d] N. P. Tatjana, M. Scherer, K. N. Raymond, *Angew. Chem. Int. Ed.* **2000**, *39*, 1239−1242. [17e] M. Yoshizawa, T. Kusukawa, M. Fujita, K. Yamaguchi, *J. Am. Chem. Soc.* **2000**, *122*, 6311−6312.
[18] E. C. Sãnudo, V. A. Grillo, M. J. Knapp, J. C. Bollinger, J. C. Huffman, D. N. Hendrickson, G. Christou, *Inorg. Chem.* **2002**, *41*, 2441−2450.
[19] [19a] M. Soler, P. Artus, K. Folting, J. C. Huffman, D. N. Hendrickson, G. Christou, *Inorg. Chem.* **2001**, *40*, 4902−4912. [19b] R. Sessoli, H.-L. Tsai, A. R. Schake, S. Wang, J. B. Vincent, K. Folting, D. Gatteschi, G. Christou, D. N. Hendrickson, *J. Am. Chem. Soc.* **1993**, *115*, 1804−1816. [19c] S. Wang, K. Folting, W. E. Streib, E. A. Schmitt, J. K. McCusker, D. N. Hendrickson, G. Christou, *Angew. Chem. Int. Ed. Engl.* **1991**, *30*, 305−306. [19d] J. K. McCusker, J. B. Vincent, E. A. Schmitt, M. L. Mino, K. Shin, D. K. Coggin, P. M. Hagen, J. C. Huffman, G. Christou, D. N. Hendrickson, *J. Am. Chem. Soc.* **1991**, *113*, 3012−3021.
[20] [20a] A. Bino, M. Ardon, D. Lee, B. Spingler, S. J. Lippard, *J. Am. Chem. Soc.* **2002**, *124*, 4578−4579. [20b] E. Y. Tshuva, D. Lee, W. Bu, S. J. Lippard, *J. Am. Chem. Soc.* **2002**, *124*, 2416−2417. [20c] S. C. Burdette, S. J. Lippard, *Coord. Chem. Rev.* **2001**, *216−217*, 333−361. [20d] S. C. Burdette, S. J. Lippard, *PNAS Perspect.* **2003**, *100*, 3605−3610. [20e] D. Lee, S. J. Lippard, *J. Am. Chem. Soc.* **2001**, *123*, 4611−4612.
[21] A. Kamiyama, T. Noguchi, T. Kajiwara, T. Ito, *Inorg. Chem.* **2002**, *41*, 507−512.
[22] V. Pavlishchuk, F. Birkelbach, T. Weyhermüller, K. Wieghardt, P. Chaudhuri, *Inorg. Chem.* **2002**, *41*, 4405−4416.

 © 2004 Wiley-VCH Verlag GmbH & Co. KGaA, Weinheim

[23] L. K. Thompson, *Coord. Chem. Rev.* **2002**, *233−234*, 193−206.
[24] T. L. Borgne, E. Rivière, J. Marrot, P. Thuéry, J. J. Girerd, M. Ephritikhine, *Chem. Eur. J.* **2002**, *8*, 774−783.
[25] J. M. Clemente-Juan, C. Mackiewicz, M. Verelst, F. Dahan, A. Bousseksou, Y. Sanakis, J. P. Tuchagues, *Inorg. Chem.* **2002**, *41*, 1478−1491.
[26] K. S. Gavrilenko, A. Vértes, G. Vanko, L. F. Kiss, A. W. Addison, T. Weyhermüller, V. V. Pavlishchuk, *Eur. J. Inorg. Chem.* **2002**, 3347−3355.
[27] P. E. Kruger, B. Moubaraki, G. D. Fallon, K. S. Murray, *J. Chem. Soc., Dalton Trans.* **2000**, 713−718.
[28] Z. E. Serna, M. G. Barandika, R. Cortés, M. K. Urtiaga, G. E. Barberis, T. Rojo, *J. Chem. Soc., Dalton Trans.* **2000**, 29−34.
[29] M. Du, X. H. Bu, Y. M. Guo, L. Zhang, D. Z. Liao, J. Ribas, *Chem. Commun.* **2002**, 1478−1479.
[30] M. J. Hossain, M. Yamasaki, M. Mikuriya, A. Kuribayashi, H. Sakiyama, *Inorg. Chem.* **2002**, *41*, 4058−4062.
[31] X. R. Meng, Y. L. Song, H. W. Hou, Y. T. Fan, G. Li, Y. Zhu, *Inorg. Chem.* **2003**, *42*, 1306−1315.
[32] H. W. Hou, X. R. Meng, Y. L. Song, Y. T. Fan, Y. Zhu, H. J. Lu, C. X. Du, W. H. Shao, *Inorg. Chem.* **2003**, *42*, 4068−4075.
[33] H. W. Hou, Y. L. Song, H. Xu, Y. L. Wei, Y. T. Fan, Y. Zhu, L. K. Li, C. X. Du, *Macromolecules* **2003**, *36*, 999−1008.
[34] H. W. Hou, Y. L. Wei, Y. L. Song, Y. Zhu, L. K. Li, Y. T. Fan, *J. Mater. Chem.* **2002**, *12*, 838−843.
[35] H. W. Hou, G. Li, L. K. Li, Y. Zhu, X. R. Meng, Y. T. Fan, *Inorg. Chem.* **2003**, *42*, 428−435.
[36] G. Li, Y. L. Song, H. W. Hou, L. K. Li, Y. T. Fan, Y. Zhu, X. R. Meng, L. W. Mi, *Inorg. Chem.* **2003**, *42*, 913−920.
[37] B. H. Ye, X. Y. Li, L. D. Williams, X. M. Chen, *Inorg. Chem.* **2002**, *41*, 6426−6431.
[38] V. Chandrasekhar, S. Kingsley, B. Rhatigan, M. K. Lam, A. L. Rheingold, *Inorg. Chem.* **2002**, *41*, 1030−1032.
[39] W. N. Lipscomb, N. Sträter, *Chem. Rev.* **1996**, *96*, 2375−2434.
[40] D. E. Wilcox, *Chem. Rev.* **1996**, *96*, 2435−2458.
[41] N. Sträter, W. N. Lipscomb, T. Klabunde, B. Krebs, *Angew. Chem. Int. Ed. Engl.* **1996**, *35*, 2024−2055.
[42] X. M. Chen, Y. X. Tong, T. C. W. Mak, *Inorg. Chem.* **1994**, *33*, 4586−4588.
[43] P. Chaudhuri, C. Stckheim, K. Wieghardt, W. Deck, R. Gregorzik, H. Vahrenkamp, B. Nuber, J. Weiss, *Inorg. Chem.* **1992**, *331*, 1451−1457.
[44] I. S. Müller, R. Robson, *Angew. Chem. Int. Ed.* **2000**, *39*, 4357−4359.
[45] M. Dey, C. P. Rao, P. Saarenketon, K. Rissanen, E. Kolehmainen, *Eur. J. Inorg. Chem.* **2002**, 2207−2215.
[46] D. Walther, T. Döhler, N. Theyssen, H. Görls, *Eur. J. Inorg. Chem.* **2001**, 2049−2060.
[47] O. P. Anderson, A. L. Cour, A. Dodd, A. D. Garrett, M. Wicholas, *Inorg. Chem.* **2003**, *42*, 122−127.
[48] S. O. H. Gutschke, D. J. Price, A. K. Powell, P. T. Wood, *Eur. J. Inorg. Chem.* **2001**, 2739−2741.
[49] D. Katerina, D. B. Angelica, E. C. Thomas, R. L. Arnold, C. George, *Chem. Commun.* **2001**, 1284−1285.
[50] X. Fan, R. Cao, M. Hong, W. Su, D. Sun, *J. Chem. Soc., Dalton Trans.* **2001**, 2961−2962.
[51] T. A. Chesnokova, E. V. Zhezlova, K. A. Kornev, Y. V. Fedotova, L. N. Mushtina, G. A. Domrachev, *J. Organomet. Chem.* **2002**, *642*, 20−31.
[52] K. Yamamoto, S. Nakazawa, A. Matsufuji, T. Taguchi, *J. Chem. Soc., Dalton Trans.* **2001**, 251−258.
[53] V. Schwartz, R. Prins, X. Wang, W. M. H. Sachtler, *J. Phys. Chem. B* **2002**, *106*, 7210−7217.
[54] Z. Q. Xu, L. K. Thompson, V. A. Milway, L. Zhao, T. Kelly, D. O. Miller, *Inorg. Chem.* **2003**, *42*, 2950−2959.
[55] L. K. Thompson, C. J. Matthews, L. Zhao, Z. Xu, D. O. Miller, C. Wilson, M. A. Leech, J. A. K. Howard, S. L. Heath, A. G. Whitteker, R. E. P. Winpenny, *J. Solid State Chem.* **2001**, *159*, 308−320.
[56] H. Carlsson, M. Haukka, E. Nordlander, *Inorg. Chem.* **2002**, *41*, 4981−4983.
[57] B. Kersting, G. Steinfeld, D. Siebert, *Chem. Eur. J.* **2001**, *7*, 4253−4258.
[58] A. Escuer, M. Font-Bardía, E. Peñalba, N. Sanz, X. Solans, R. Vicente, *J. Chem. Soc., Dalton Trans.* **1999**, 3115−3119.
[59] A. Escuer, C. J. Harding, Y. Dussart, J. Nelson, V. McKee, R. Vicente, *J. Chem. Soc., Dalton Trans.* **1999**, 223−227.
[60] I. Castro, M. L. Calatayud, J. Sletten, F. Lloret, M. Julve, *J. Chem. Soc., Dalton Trans.* **1997**, 811−817.
[61] C. S. Campos-Fernández, R. Clérac, J. M. Koomen, D. H. Russell, K. R. Dunbar, *J. Am. Chem. Soc.* **2001**, *123*, 773−774.
[62] D. B. D. Amico, D. Boschi, F. Calderazzo, S. Ianelli, L. Labella, F. Marchetti, G. Pelizzi, E. G. F. Quadrelli, *Inorg. Chim. Acta* **2000**, *300−302*, 882−891.
[63] S. G. Shova, I. G. Kadelnik, M. Gdanec, Yu. A. Simonove, T. K. Zhovmir, V. M. Meriacre, G. Filotti, K. I. Turte, *Zh. Strukt. Khim.* **1998**, *39*, 917−933.
[64] C. Wilson, B. B. Iversen, J. Overgaard, F. K. Larsen, G. Wu, S. P. Palii, G. A. Timco, N. V. Gerbeleu, *J. Am. Chem. Soc.* **2000**, *122*, 11370−11379.
[65] S. R. Marshall, A. L. Rheingold, L. N. Dawe, W. W. Shum, C. Kitamura, J. S. Miller, *Inorg. Chem.* **2002**, *41*, 3599−3601.
[66] J. E. Greedan, *J. Mater. Chem.* **2001**, *11*, 37−53.
[67] B. N. Figgis, E. S. Kucharski, M. Vrtis, *J. Am. Chem. Soc.* **1993**, *115*, 176−181.
[68] K. K. Nanda, L. K. Thompson, J. N. Bridson, K. Nag, *J. Chem. Soc., Chem. Commun.* **1994**, 1337−1338 and references cited therein.
[69] V. Coropceanu, V. Schünemann, C. Ober, M. Gerdan, A. X. Trautwein, J. Köhler, R. W. Saalfrank, *Inorg. Chim. Acta* **2000**, *300−302*, 875−881.
[70] R. D. Cannon, R. P. White, *Prog. Inorg. Chem.* **1988**, *36*, 195−298, and references cited therein.
[71] C. C. Wu, H. G. Jang, A. L. Rheingold, P. Gütlich, D. N. Hendrickson, *Inorg. Chem.* **1996**, *35*, 4137−4147.
[72] R. Q. Huang, H. L. Wang, J. Zhou, *Synthesis of Organic Intermediates*, Chemistry Engineering Publisher, Peking, **1996**, p.134.
[73] R. L. Carlin, *Magnetochemistry*, Springer, Berlin, Heidelberg, New York, Tokyo, **1986**.
[74] G. M. Sheldrick, *Acta Crystallogr., Sect. A* **1990**, *46*, 467−473.
[75] G. M. Sheldrick, *SHELXL-97, Program for the Refinement of Crystal Structures*, University of Göttingen, **1997**.

Received February 11, 2004
Early View Article
Published Online July 22, 2004

 © 2004 Wiley-VCH Verlag GmbH & Co. KGaA, Weinheim

EurJIC
European Journal of Inorganic Chemistry

Issue 20/2004

Pages 3959–4146

Papers available ahead of print in Early View at www.interscience.wiley.com

Earliest available Table of Contents:
Automatically, free of charge by e-mail through
www.interscience.wiley.com/alerts

COVER PICTURE

The cover picture shows the low-temperature ^{31}P NMR signals and simplified 3D representations of *exo* and *endo* isomers of an (η^3-1,3-diphenylallyl)palladium(II) complex in which the metal center is coordinated by a chiral xanthene-derived diphospholane ligand. Such complexes are intermediates in palladium-catalyzed allylic substitution, and their structures determined by 2D NMR spectroscopy allow for the interpretation of the enantioselectivities of the catalytic process in terms of preferential rotation of the allyl group. Key methyl groups of the chiral ligand that govern this rotation are represented by yellow spheres in the background. Details on these complexes and others and on asymmetric catalysis can be found in the article by J. A. Osborn, L. Barloy et al. on p. 3987ff. The authors are indebted to Bernard Lafleuriel (CURRI-Visu) for his help concerning the artwork of the cover picture.

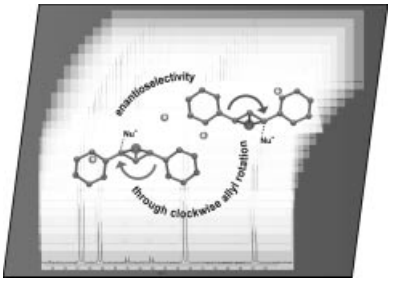

MICROREVIEW

Contents

3971 **R. Blasius, C. Moucheron, A. Kirsch-De Mesmaeker***

Photoadducts of Metallic Compounds with Nucleic Acids – Role Played by the Photoelectron Transfer Process and by the TAP and HAT Ligands in the Ru^{II} Complexes

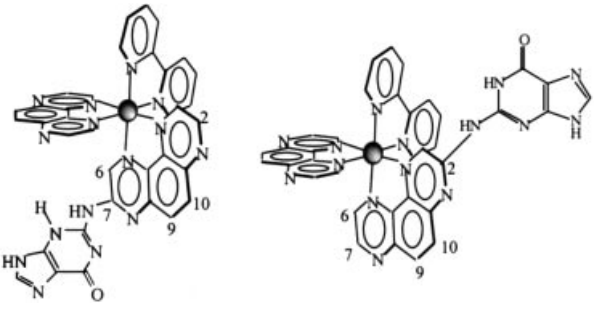

Keywords: Photoadducts / Electron transfer / Ruthenium(II) complexes / GMP / DNA

 © 2004 Wiley-VCH Verlag GmbH & Co. KGaA, Weinheim

SHORT COMMUNICATIONS

3981 **A. Lavalette, G. A. Lawrance, N. W. Alcock,* M. J. Hannon***

Channel Structures in a Simple Inorganic Salt − An Open Framework Formed through Structural Integration of Distinct Sodium Acetate and Sodium Perchlorate Domains

Keywords: Channel structures / Microporous materials / Crystal engineering / Zeolite analogues

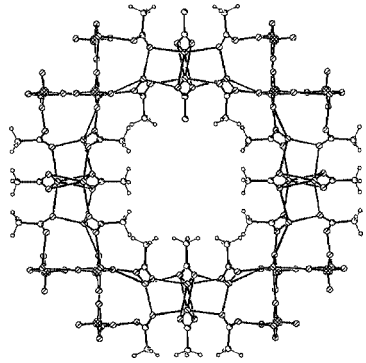

3984 **D. Martineau, P. Gros,* M. Beley,* Y. Fort**

New Ruthenium Complexes with 4-(1*H*-Pyrrol-1-yl)-Substituted Polypyridine Ligands − Electrochemical and Spectroscopic Properties

Keywords: Nitrogen heterocycles / Ruthenium / N donor ligands

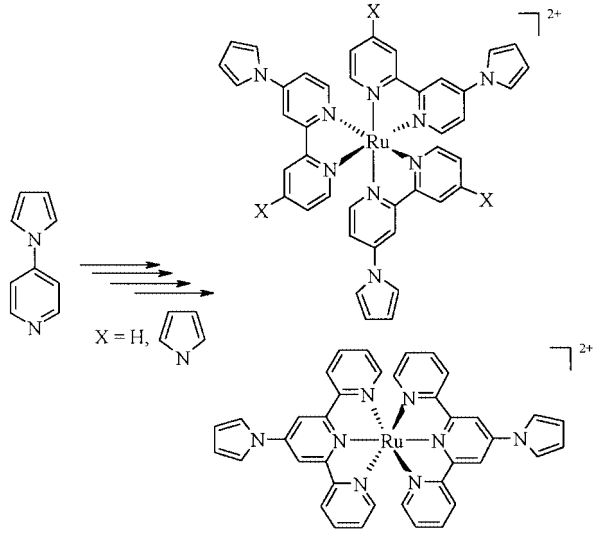

FULL PAPERS

3987 **G. Malaisé, S. Ramdeehul, J. A. Osborn,* L. Barloy,* N. Kyritsakas, R. Graff**

Palladium Complexes with Chiral Diphospholane Ligands: Comparative Catalytic Properties and Analysis of (η^3-Allyl)palladium Species

Keywords: Palladium / Allyl ligands / Reaction intermediates / Asymmetric catalysis / Enantioselectivity

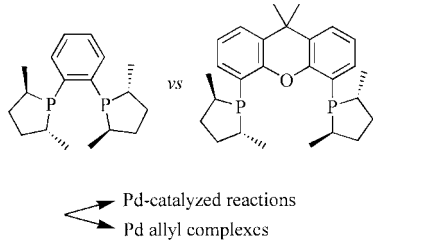

4002 **D. Shamir,* I. Zilbermann, E. Maimon, D. Meyerstein**

Oxidation of CH_3NH_2 and $(CH_3)_2NH$ by $Ni^{III}(cyclam)(H_2O)_2^{3+}$ in Aqueous Solutions

Keywords: Pendant primary amines / Amines / Cyclam / Nickel / Electrocatalysts

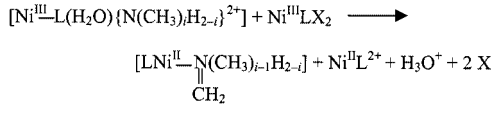

4006 **O. S. Oleneva, A. V. Olenev, E. V. Dikarev, A. V. Shevelkov***

From Discrete to Extended Guests: A Novel Supramolecular $[Hg_6As_4](AgCl_3)_2$ Assembly Featuring One-Dimensional $(AgCl_3)^{2-}$ Anions

Keywords: Arsenic / Host–guest systems / Mercury / Silver / Supramolecular chemistry

4011 **G. E. Herberich,* U. Englert, A. Fischer, D. Wiebelhaus**

Anion Binding of 1,1′-Bis(dialkylboryl)cobaltocenium Complexes – Structures of $[Co\{C_5H_4(BMe_2)\}_2]PF_6$, $Co[C_5H_4(BMe_2)][C_5H_4(BMe_2Cl)]$, $Co[C_5H_4(BiPr_2)]_2(\mu\text{-}F)$ and $NMe_4[Co\{C_5H_4(BiPr_2F)\}_2]$

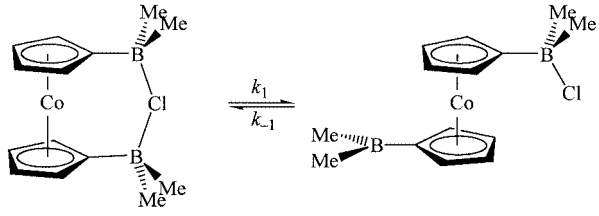

Keywords: Anion binding / Borates / Boron / Cobalt / Sandwich complexes

4021 **D. B. Werz, R. Gleiter,* F. Rominger**

Mono(alkyne)cobalt Complexes and Electron-Rich Alkynes – The Formation of an Alkyne-Bridged Dinuclear Cobalt Complex by a One-Pot Procedure

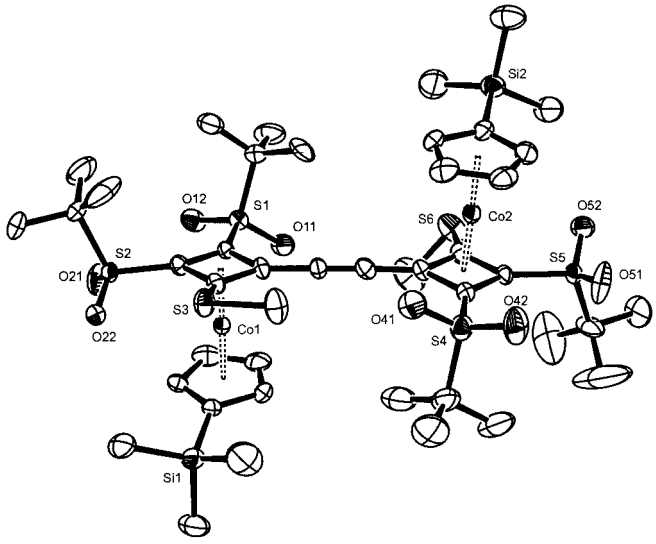

Keywords: Alkynes / Chalcogens / Cobalt / Cyclobutadiene complexes

4028 **S. Zhang, C. Tu, X. Wang, Z. Yang, J. Zhang, L. Lin, J. Ding, Z. Guo***

Novel Cytotoxic Copper(II) Complexes of 8-Aminoquinoline Derivatives: Crystal Structure and Different Reactivity towards Glutathione

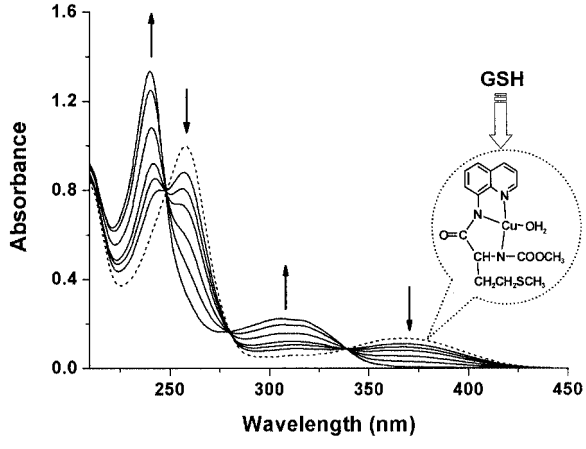

Keywords: Antitumor agents / Bioinorganic chemistry / Copper / N ligands

 © 2004 Wiley-VCH Verlag GmbH & Co. KGaA, Weinheim

4036 **I. A. Koval, M. Huisman, A. F. Stassen, P. Gamez, O. Roubeau, C. Belle,* J.-L. Pierre, E. Saint-Aman, M. Lüken, B. Krebs, M. Lutz, A. L. Spek, J. Reedijk***

Dinuclear Cu^{II} Complexes with a New Phenol-Based Ligand Bearing Pyridine and Thiophene Substituents: Synthesis, Characterization and Interaction with Catechol Substrates

Keywords: Copper / Dinuclear complexes / Catechol oxidase / Magnetochemistry / Electrochemistry

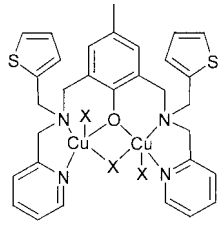

X = Cl or Br

4046 **H. Zhu, J. Chai, A. Stasch, H. W. Roesky,* T. Blunck, D. Vidovic, J. Magull, H.-G. Schmidt, M. Noltemeyer**

Reactions of the Aluminum(I) Monomer LAl [L = HC{(CMe)(NAr)}$_2$; Ar = 2,6-*i*Pr$_2$C$_6$H$_3$] with Imidazol-2-ylidene and Diphenyldiazomethane. A Hydrogen Transfer from the L Ligand to the Central Aluminum Atom and Formation of the Diiminylaluminum Compound LAl(N=CPh$_2$)$_2$

Keywords: Aluminum / Carbenes / Diazo compounds / Hydrogen transfer / N ligands

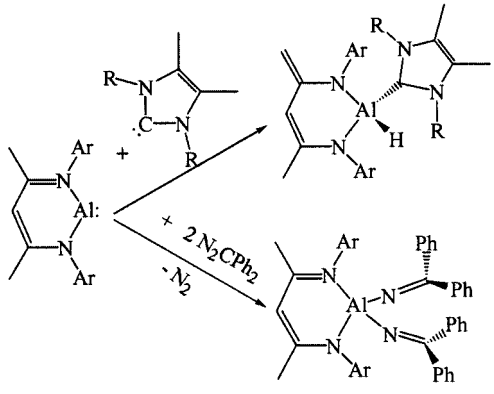

Ar = 2,6-*i*Pr$_2$C$_6$H$_3$; R = Me, or *i*Pr

4052 **A. Stasch, S. Singh, H. W. Roesky,* M. Noltemeyer, H.-G. Schmidt**

Adducts of Aluminum and Gallium Trichloride with a *N*-Heterocyclic Carbene and an Adduct of Aluminum Trichloride with a Thione

Keywords: Adducts / Aluminum / Carbenes / Gallium / Lewis acids

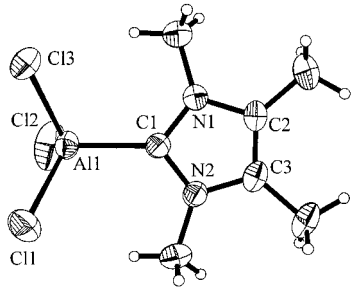

4056 **A. Stasch, S. S. Kumar, V. Jancik, H. W. Roesky,* J. Magull, M. Noltemeyer**

Methyl Substitution of Aluminum−Hydride Bonds in a Carbaalane and an Aluminum Imide

Keywords: Aluminum / Cluster Compounds / Hydrides

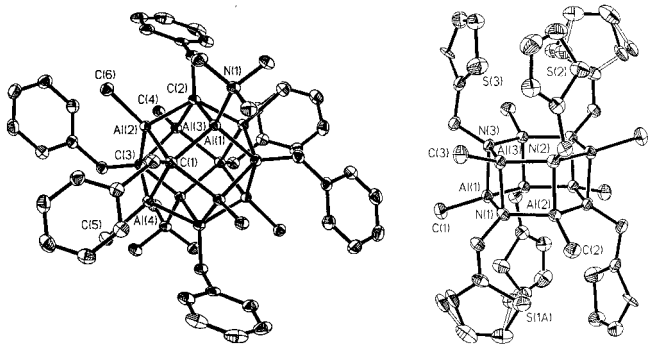

 © 2004 Wiley-VCH Verlag GmbH & Co. KGaA, Weinheim

4061 **J. Aguilar, A. Bencini,* E. Berni, A. Bianchi,* E. García-España,* L. Gil, A. Mendoza, L. Ruiz-Ramírez, C. Soriano**

Dinuclear Zn^{II} Complexes of Polydentate Polyamines as Minimalist Models of Hydrolytic Reactions

Keywords: Enzyme models / Hydrolysis / Macrocycles / N ligands / NMR spectroscopy / Zinc

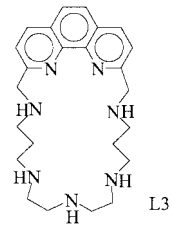

4072 **Y. Zhao, J.-J. Zhu,* J.-M. Hong, N. Bian, H.-Y. Chen**

Microwave-Induced Polyol-Process Synthesis of Copper and Copper Oxide Nanocrystals with Controllable Morphology

Keywords: Copper / Copper oxides / Microwaves / Nanostructures / UV / Vis spectroscopy

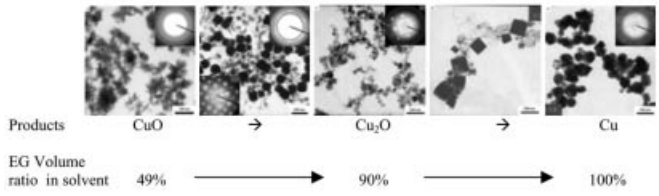

4081 **J. Pasán, J. Sanchiz, C. Ruiz-Pérez,* F. Lloret, M. Julve**

Phenylmalonate-Containing Copper(II) Complexes: Synthesis, Crystal Structure and Magnetic Properties

Keywords: Copper / Magnetic properties / N ligands / O ligands

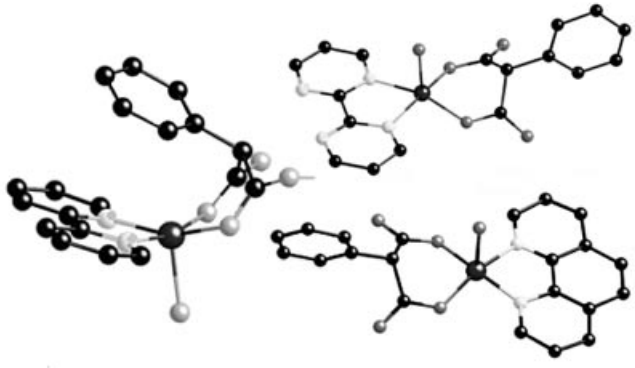

4091 **D. V. Gribkov, F. Hampel, K. C. Hultzsch***

Synthesis and Characterization of Alkyllanthanum Biphenolate Complexes as Catalysts for Hydroamination/Cyclization and Hydrosilylation

Keywords: Asymmetric catalysis / Hydroamination / Hydrosilylation / Lanthanum / O ligands

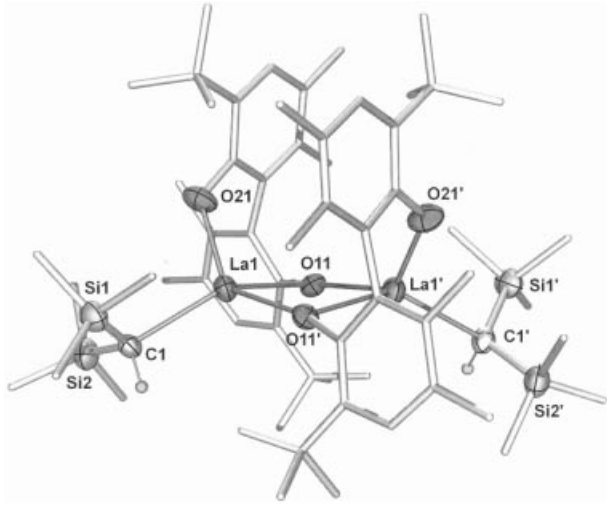

 © 2004 Wiley-VCH Verlag GmbH & Co. KGaA, Weinheim

4102 **N. Hao, E. Shen,* Y.-G. Li, E.-B. Wang,* C.-W. Hu, L. Xu**

Novel Cadmium(II) Adipate Coordination Polymers with Structural Transformation via Oxalate Ligand: Syntheses, Structures and Fluorescence Properties

Keywords: Cadmium / Coordination polymers / Fluorescence / Hydrothermal synthesis / Interpenetration

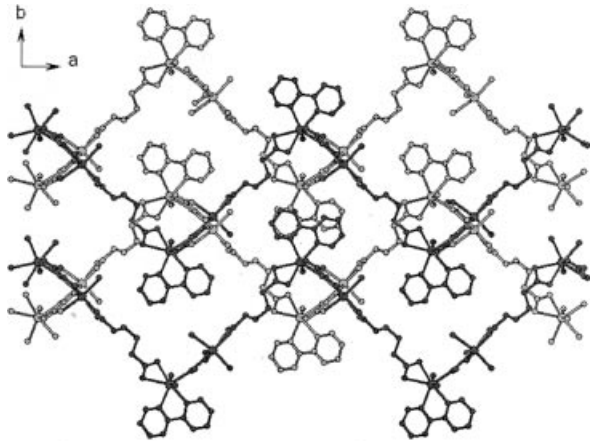

4108 **E. Robé, J.-C. Daran, S. Vincendeau, R. Poli***

A New Synthetic Method and Solution Equilibria for the Chlorotitanate(IV) Anions − Evidence for the Existence of a New Species: $[Ti_2Cl_{11}]^{3-}$

Keywords: Anions / Electrochemistry / Infrared spectroscopy / Titanium

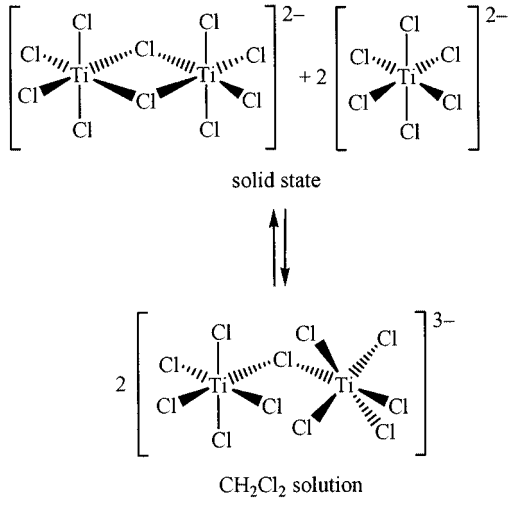

4115 **T. G. Roy,* S. K. S. Hazari, B. K. Dey, H. A. Miah, C. Bader, D. Rehder***

Copper(II) and Nickel(II) Complexes of *N*,*N*-Bis(2-hydroxyethyl)octamethyl-1,4,8,11-tetraazacyclotetradecane

Keywords: Antimicrobial activity / Copper / Macrocyclic ligands / N ligands / Nickel

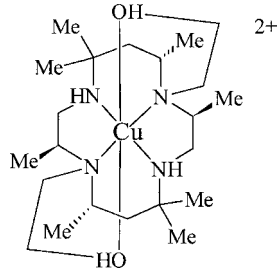

4124 **V. Nahum, B. Fischer***

Boranophosphate Salts as an Excellent Mimic of Phosphate Salts: Preparation, Characterization, and Properties

Keywords: Bioisosters / Boranophosphates / NMR spectroscopy / Phosphate mimics

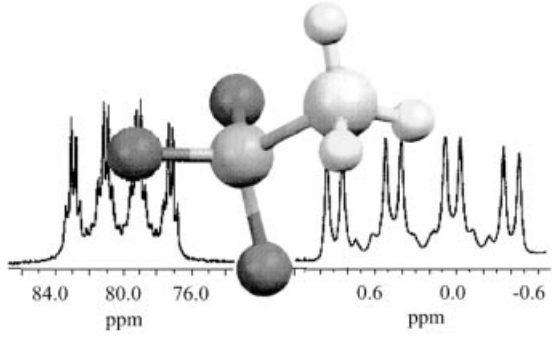

 © 2004 Wiley-VCH Verlag GmbH & Co. KGaA, Weinheim

4132 **I.-M. Mbomekalle, B. Keita, Y. W. Lu, L. Nadjo,* R. Contant, N. Belai, M. T. Pope**

Synthesis and Electrochemistry of the Monolacunary Dawson-Type Tungstoarsenate $[H_4AsW_{17}O_{61}]^{11-}$ and Some First-Row Transition-Metal Ion Derivatives

Keywords: Polyoxometalates / Dawson dissymmetrical polyoxometalates / Arsenic / Tungsten / Electrochemistry / Electrocatalysis

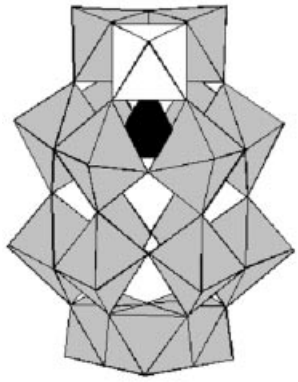

4140 **K. Jitsukawa,* H. Takahashi, R. Hyuga, H. Arii, H. Masuda***

Sequence-Specific Oxidative Degradation of Tripeptides by a Cobalt(III) Complex Containing a Terpyridine Ligand

Keywords: Cleavage reactions / Cobalt / N ligands / Oxidation / Peptides

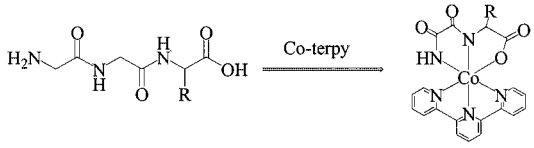

CORRECTION

4146 **P. González-Duarte,* A. Lledós, R. Mas-Ballesté**

Extending The Reaction Landscape of the {Pt(μ-S)$_2$Pt} Core: From Metal Centers to Non-Metallic Electrophiles

Keywords: Platinum / Sulfur / Metalloligand / Nucleophile / Building block

 © 2004 Wiley-VCH Verlag GmbH & Co. KGaA, Weinheim

Photoadducts of Metallic Compounds with Nucleic Acids − Role Played by the Photoelectron Transfer Process and by the TAP and HAT Ligands in the Ru^{II} Complexes

Romain Blasius,[a][‡] Cécile Moucheron,[a] and Andrée Kirsch-De Mesmaeker*[a]

Keywords: Photoadducts / Electron transfer / Ruthenium(II) complexes / GMP / DNA

The properties that are characteristic of TAP (1,4,5,8-tetraazaphenanthrene) and HAT (1,4,5,8,9,12-hexaazatriphenylene) Ru^{II} complexes under illumination are highlighted and compared with those of other metallic complexes. In particular, the photo-oxidizing power of their ^{3}MLCT states leads to a quenching of luminescence accompanied by a photoreaction when they are in presence of nucleic acids. The proton-coupled photoinduced electron transfer with the guanine nucleobases produces metallic adducts on DNA guanine units. The mechanism of formation, structure, and possible applications of these photoadducts are discussed and compared with other DNA metallic adducts currently in the literature.
(© Wiley-VCH Verlag GmbH & Co. KGaA, 69451 Weinheim, Germany, 2004)

Introduction

During the last 15 years, transition-metal complexes have been extensively studied in the presence of nucleic acids. The interest focused on these complexes stems mainly from their photophysical and photochemical properties, which can be easily tuned by the type of ligands and nature of the metallic centre. The platinum complexes such as *cis*-$[PtCl_2(NH_3)_2]$, known as cisplatin, and its derivatives are well-known examples of metallic compounds that have been widely applied in anticancer chemotherapy.[1−4] They have turned testicular cancer into a curable disease. The activity of these platinum complexes against a variety of cancers is

[a] Université Libre de Bruxelles, Chimie Organique et Photochimie, CP 160/08,
50 avenue F. D. Roosevelt, 1050 Brussels, Belgium
Fax: (internat.) + 32-2-650-3018
E-mail: akirsch@ulb.ac.be
[‡] Present address: Laboratoire de Biologie Moléculaire et Cellulaire du Cancer, Hôpital Kirchberg,
9 rue Edward Steichen, 2540 Luxembourg, Luxembourg

Romain Blasius was born in 1976 in Luxembourg. In 1995 he moved to the Université Libre de Bruxelles (Brussels, Belgium), where he received his BSc degree in chemistry in 1999. He then went on to complete his Ph.D. studies under the supervision of A. Kirsch and C. Moucheron in the area of photochemistry and photophysics of transition metal complexes with DNA and received his Ph.D. in 2003. He subsequently moved to the Laboratoire de Biologie Moléculaire et Cellulaire du Cancer in Luxembourg, where he is currently carrying out his research on the resistance of cancer cells towards chemotherapeutic drugs and the inhibition of this resistance through the use of natural compounds.

Cécile Moucheron was born in 1966 in Leuven. She received her doctoral degree in 1992 at the Université Libre de Bruxelles (ULB, Belgium) in the area of aromatic synthesis and coordination chemistry. She worked with Dr. J.-P. Sauvage on semicatenanes and copper(I) complexes at the Université Louis Pasteur in Strasbourg. She then joined the laboratory of photochemistry at the ULB. In 1994, she spent several months at the Université Joseph Fourier in Grenoble (UJF, France) where she contributed to research on new intercalating derivatives with Prof. J. Lhomme and Dr. M. Demeunynck. She continued her career as assistant professor at the ULB. From 2003, she was elected as Professor in the Department of Chemistry at the ULB. Her research includes the synthesis of polyazaaromatic complexes and their study with DNA or as antenna systems.

Andrée Kirsch-De Mesmaeker received her doctoral degree in 1972 at the Université Libre de Bruxelles (ULB, Belgium) in the area of photochemistry and electrochemistry. She subsequently moved to Germany at the Max Planck Institut für Strahlenchemie in Mülheim a.d. Ruhr to carry out post-doctoral research with Professor Schulte-Frohlinde and Dr von Sonntag on γ and pulsed radiolysis of sugar (1972−1974). She then moved to the University of North Carolina at Chapel Hill (USA) (1974−1975) where she contributed to research on dyes photochemistry with Dr. G. Wyman. Back at the ULB as FNRS researcher (Fonds National pour la Recherche Scientifique, Belgium), she performed research in photoelectrochemistry and has obtained an award from the Belgian Academy of Sciences. She continued her career as Director of Research at the FNRS and spent a sabbatical year at Columbia University in New York in 1989. From 1999 she was elected as full Professor in the Department of Chemistry at the ULB. Her current research includes photochemistry and photophysics of transition metal complexes with DNA.

MICROREVIEWS: This feature introduces the readers to the authors' research through a concise overview of the selected topic. Reference to important work from others in the field is included.

attributed to their reactivity with nucleic acids, mainly by substitution of their chloride ligands by water and ultimately by two adjacent guanines of DNA,[5,6] which results in covalent binding of the metallic species to the genetic material. However, treatment by these drugs leads to important toxic side effects. Therefore, there is still an urgent need for other metallic compounds that would be active mainly at the level of the genetic material and that could exhibit an equal or higher activity against other types of cancer but with a lower toxicity.

The use of a photoreactive metallic drug would be rather advantageous because the action of the drug could be triggered at a chosen time and at selected sites by using optical fibers. There is thus a motivation to develop metallic compounds that are photoreactive towards DNA. The illumination of metallic complexes that interact with DNA generally leads to cleavage (direct cleavage and a cleavage that is revealed by treatment with piperidine) or to the formation of photoadducts with a covalent bond between the metallic compound and a DNA base. These metallic photoadducts could play an important role in chemotherapy in the future, a role similar to that played by the Pt compounds. Some of them have indeed been shown to inhibit DNA replication or synthesis so that they may be regarded as potential antitumor drugs.[7]

In this review, we describe different mechanisms for the formation of metallic photoadducts with DNA and polynucleotides. The particular role played by the Ru^{II} complexes formed with the ligands TAP and HAT (TAP = 1,4,5,8-tetraazaphenanthrene, HAT = 1,4,5,8,9,12-hexaazatriphenylene, Figure 1) is highlighted. The Ru^{II} complexes can be used also as photoprobes of DNA structures or topologies, and for this particular aspect, the reader should refer to already published reviews.[8−14]

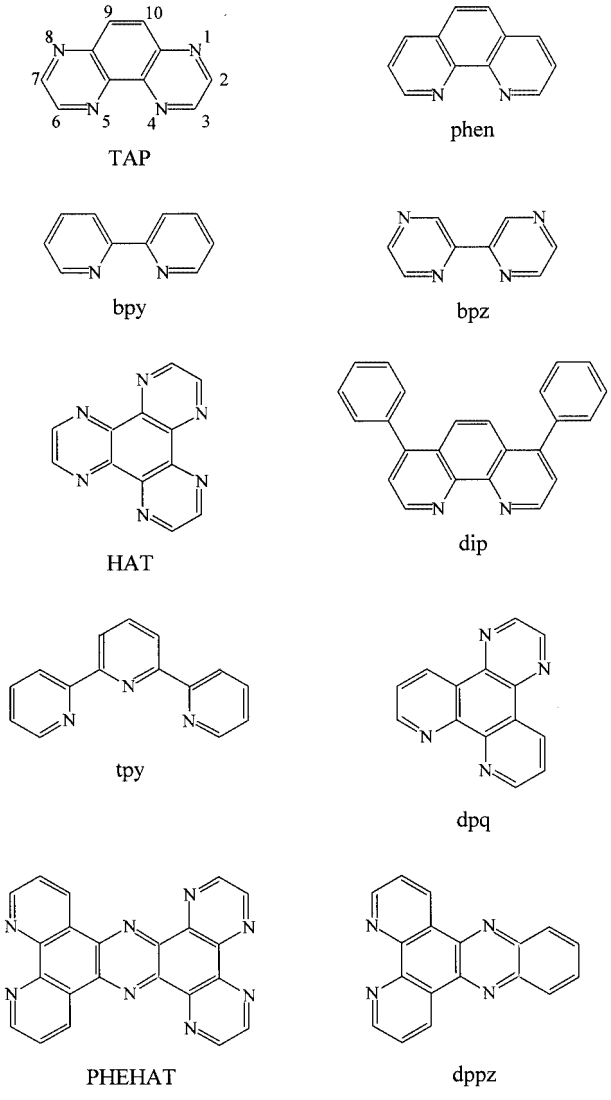

Figure 1. Structure of the different ligands

Different Types of Metallic Photoadducts with DNA

1. With Rhodium, Chromium, and Ruthenium Complexes. Photoadducts Formed by Ligand Substitution

Morrison's team has shown that irradiation of *cis*-dichlorobis(1,10-phenanthroline)rhodium(III) chloride (Figure 2) in the presence of 2′-deoxyguanosine (Figure 2) under aerobic conditions gives rise to the formation of a photoproduct in which the metal is bound to the N1 site of the deoxyguanosine (Figure 3, A); another photoproduct in which Rh^{III} is bound to the guanine either through the oxygen atom at C6 or the amino group at C2[15,16] is also formed. The illumination of the same starting complex, un-

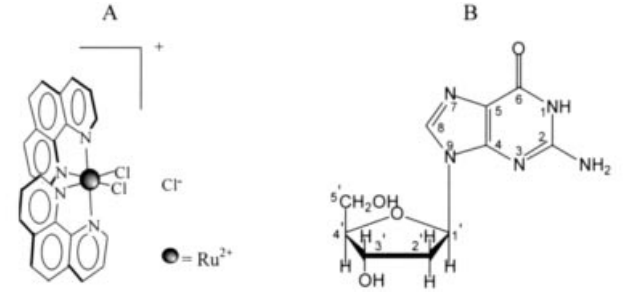

Figure 2. Structure of *cis*-dichlorobis(1,10-phenanthroline)-rhodium(III) (A) and 2′-deoxyguanosine (B)

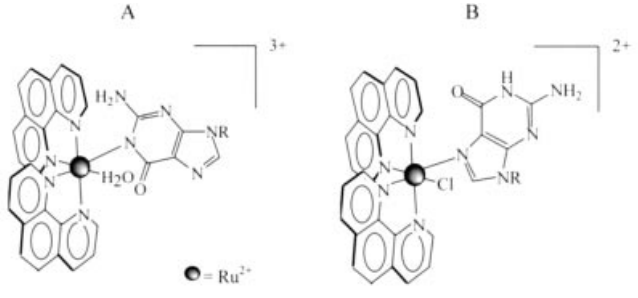

Figure 3. Proposed structure for the rhodium-guanine adducts; A: N1 bound adduct,[15] with 2′-deoxyguanosine, aerobic conditions; B: N7-bound adduct[17] with 2′-deoxyguanosine, anaerobic conditions; R represents the sugar group of dG

 © 2004 Wiley-VCH Verlag GmbH & Co. KGaA, Weinheim

der aerobic conditions, in the presence of calf thymus DNA leads to the identical photoadduct (linked through the N1 position of the guanine) that was isolated after enzymatic digestion of the nucleic acid.[15]

Under anaerobic conditions, illumination of the Rh^{III} complex in the presence of 2′-deoxyguanosine also forms a photoadduct, but in this case, the metal centre is linked to the N7 atom of the guanine moiety (Figure 3B).[17] Furthermore, this photoreaction (in the absence of oxygen) proceeds with a quantum efficiency greater than 1, which has been explained by a chain reaction initiated by a photoinduced electron transfer.[17] However, the irradiation of *cis*-dichlorobis(1,10-phenanthroline)Rh^{III} chloride in the presence of calf thymus DNA under anaerobic conditions leads to the same photoadduct as that detected in the presence of oxygen.[18]

The key step of the mechanism for the formation of these photoadducts is an electron transfer from the guanine base to the excited-state metal complex (step 2).[15,16]

$$cis\text{-}[Rh^{III}(phen)_2Cl_2]^+ \xrightarrow{h\nu} cis\text{-}[Rh^{III}(phen)_2Cl_2]^{+*} \quad (1)$$

$$cis\text{-}[Rh^{III}(phen)_2Cl_2]^{+*} + dG \longrightarrow cis\text{-}[Rh^{II}(phen)_2Cl_2] + dG^{\bullet+} \quad (2)$$

A chain reaction begins with the loss of one Cl^- ligand from the Rh^{II} complex (step 3). In the absence of oxygen, a subsequent reaction with the most nucleophilic site of dG leads to an N7−guanine adduct on the Rh complex (step 4). Another electron transfer (in the dark) between the Rh^{II} adduct and the starting dichloro complex completes the first turnover of this chain reaction and leads to the formation of the final Rh^{III} photoadduct under anaerobic conditions (step 5). Finally, the chain reaction is terminated by a back electron-transfer from the Rh^{II} intermediate species to $dG^{\cdot+}$ (step 6).

Under aerobic conditions, however, oxygen can kill the chain propagation by oxidising the *cis*-$[Rh^{II}(phen)_2Cl]^+$ species formed during step 3, with the simultaneous addition of a water molecule and production of a chloroaquo complex and a superoxide anion (step 4a).

The formation of this chloroaquo compound and its reaction with $dG^{\cdot}$ (obtained by chemical oxidation−deprotonation of the guanosine) finally leads to the adduct.[16] Different sites have been proposed for the radical position on the guanine; the localisation on N1 explains the structure of the *cis*-$[Rh^{III}(phen)_2(N1-dG)(OH_2)]^{3+}$ adduct formed under aerobic conditions. Coupling with the radical at either the oxygen atom at C6 or the amino group at C2 has been postulated to explain the unidentified adduct.

In conclusion, the preferential binding of *cis*-$[Rh^{III}(phen)_2Cl_2]^+$ to guanine moieties rather than other nucleobases is due to the initiation step of the chain reaction, i.e. a primary electron transfer from a base to the excited complex. This process occurs, of course, preferentially with a guanine because it is the nucleobase with the lowest reduction potential for the cation radical.

Interestingly, thanks to this Rh photoreactivity, irradiation of *cis*-dichlorobis(1,10-phenanthroline)rhodium(III) chloride in the presence of packaging RNA (which forms a hexameric complex to gear the DNA translocation process) leads to some crosslinking of this RNA.[18,19]

It has also been reported that [*cis*-$Cr(phen)_2Cl_2$] upon excitation with visible light in the presence of DNA leads to the covalent attachment of the metal.[20] This Cr complex also undergoes aquation, which originates from both thermal and photochemical pathways. The photochemical pathway stems again from an electron transfer from dG to the excited state metal complex, with the exchange of one or two Cl^- ligands.[20]

The photoreactivity of complexes such as $[Ru(tpy)(X)Cl]^+$ {tpy = 2,2′:6′,2′′-terpyridine; X = bipyridine (bpy), 1,10-phenanthroline (phen) and dipyrido[3,2-*a*:2′,3′-*c*]phenazine (dppz)},[21] has also been investigated in the frame of the search for novel photoreagents that are reactive towards DNA. When these Ru complexes are photolysed, the Cl^- ligand is easily substituted by a H_2O molecule, which leads to the aquaruthenium complex. This latter complex, like the Rh species, is reactive towards the DNA bases and forms a coordination bond with a heterocyclic nitrogen atom[22] of a nucleobase. The covalent binding of such aqua Ru complexes to DNA has been demonstrated by ultrafiltration, extensive dialysis and ethanol precipitation.[23,24] However, the reaction between $[Ru(tpy)(X)(H_2O)]^{2+}$ and double-stranded DNA proceeds with a rather poor yield ($[Ru]_{bound}$/[DNA-nucleotide] is approximately 0.02) because of the important steric hindrance due to the presence of the polypyridyl (X) ligands and the incoming reactive DNA base.[22]

2. The Ru^{II} Complexes Containing TAP and HAT Ligands

2a. Formation of Photoadduct by Substitution

In 1994 Lecomte et al. showed that $[Ru(TAP)_3]^{2+}$ can form photoadducts with AMP (adenosine 5′-monophosphate) by photosubstitution of one TAP ligand.[25] This

$$cis\text{-}[Rh^{II}(phen)_2Cl_2] \longrightarrow cis\text{-}[Rh^{II}(phen)_2Cl]^+ + Cl^- \quad (3)$$

$$cis\text{-}[Rh^{II}(phen)_2Cl]^+ + dG \longrightarrow cis\text{-}[Rh^{II}(phen)_2(N7\text{–}dG)Cl]^+ \quad (4)$$

$$cis\text{-}[Rh^{II}(phen)_2(N7\text{–}dG)Cl]^+ + cis[Rh^{III}(phen)_2Cl_2]^+ \longrightarrow cis[Rh^{III}(phen)_2(N7\text{–}dG)Cl]^{2+} + cis[Rh^{II}(phen)_2Cl_2] \quad (5)$$

$$cis\text{-}[Rh^{II}(phen)_2(N7\text{–}dG)Cl]^+ + dG^{\bullet+} \longrightarrow cis\text{-}[Rh^{III}(phen)_2(N7\text{–}dG)Cl]^{2+} + dG \quad (6)$$

$$cis\text{-}[Rh^{II}(phen)_2Cl]^+ + O_2 \xrightarrow{H_2O} cis\text{-}[Rh^{III}(phen)_2Cl(OH_2)]^{2+} + O_2^{\bullet-} \quad (4a)$$

 © 2004 Wiley-VCH Verlag GmbH & Co. KGaA, Weinheim

photoreactivity is thus similar to that discussed above in which the initial chelation sphere around the Ru^{II} centre is transformed. The origin of this photoreactivity can easily be explained. It has been demonstrated (see later) that the ^{3}MLCT (metal to ligand charge-transfer) state of this complex is efficiently thermally activated to a ^{3}MC (metal-centred) state, which produces a rather high quantum yield of photodechelation (loss of a ligand under illumination).[26] Therefore, $[Ru(TAP)_3]^{2+}$ exhibits, under illumination, a higher probability of substitution of one of its TAP ligands by a DNA base than complexes with lower photodechelation quantum yields. The photoreactivity of this complex in the presence of AMP has been studied by UV/Vis absorbance and laser flash photolysis,[25] and it indicates the formation of $[Ru(TAP)_2(AMP)(X)]^{n+}$ (X = H_2O, Cl^-), which absorbs in the 500 nm region. It is important to note that such photosubstitution reactions are not observed with GMP as mononucleotide (see further for the explanation).

In conclusion, in the photoadducts described up to now in which a metal−nitrogen bond is formed, the chelation sphere around the metal centre is destroyed relative to that in the starting complex. This ligand substitution can be triggered either by a photoelectron transfer, as is the case for the Rh complexes, or by crossing from the ^{3}MLCT state to the ^{3}MC state at room temperature, as observed with $[Ru(TAP)_3]^{2+}$ in the presence of AMP.

2b. Formation of a New Type of Photoadduct

Quite different photoadducts were seen for the first time when analyses of the illuminated solution of $[Ru(TAP)_3]^{2+}$ in the presence of ^{32}P-labeled oligonucleotides were performed by denaturing polyacrylamide gel electrophoresis (PAGE). These PAGE experiments exhibit the unexpected appearance of bands of lower mobility than the starting 5′-^{32}P-labeled single-stranded oligomer,[27,28] whereas $[Ru(phen)_3]^{2+}$ or $[Ru(bpy)_3]^{2+}$ lead to photoinduced strand breaks by a mechanism involving singlet oxygen.[29,30] The slower bands were attributed to covalent photoadducts of $[Ru(TAP)_3]^{2+}$ with the oligonucleotide. Interestingly, such low mobility bands have also been observed with $[Ru(TAP)_2(bpy)]^{2+}$, but not with $[Ru(bpy)_2(TAP)]^{2+}$.[27] Further evidence for photoadduct formation was obtained by dialysis experiments coupled with detection by UV/visible spectroscopy.[28] The absorption spectrum indicates that the photoproduct cannot originate from dechelation/substitution, as discussed in Section 2a of this article, because no increasing absorption is detected around 500 nm, but a strong hypsochromic shift with a hyperchromic effect appears in the 350−400 nm region. The same spectral changes appear after illumination of $[Ru(TAP)_3]^{2+}$ in the presence of GMP, and are thus different from those described above in the presence of AMP.

Further evidence for the formation of a new type of photoadduct is furnished by electrospray mass spectrometry (ESMS).[31,32] Strong peaks corresponding to $[M - 2H - 2PF_6^-]^{2+}$ and $[M - 2H - PF_6^-]^+$, where M = [Ru(TAP)$_3$(PF$_6$)$_2$ + guanine or + guanosine monophosphate], are typical of the mass of the purified adduct as the PF_6^- salt, isolated after illumination of $[Ru(TAP)_3]^{2+}$ in the presence of GMP or $[Ru(TAP)_2(bpy)]^{2+}$ and DNA after hydrolysis of the DNA.[32] Thus, the results show that in the photoadduct, the chelation sphere has remained intact and a covalent bond between one of the ligands of the Ru complex and guanine is formed with the simultaneous loss of two hydrogen atoms.

In 1997, Vicendo et al. showed by ICP (inductively coupled plasma) and absorption spectroscopy that $[Ru(bpz)_3]^{2+}$ (bpz = 2,2′-bipyrazine) also forms photoadducts with calf thymus DNA[33] and dGMP. Spectroscopic changes similar to those described with the TAP complexes, appear after illumination of $[Ru(bpz)_3]^{2+}$ in the presence of DNA or dGMP. Subsequently, the same research team confirmed the occurrence of a photoadduct by gel electrophoresis experiments performed on illuminated $[Ru(bpz)_3]^{2+}$ with single- and double-stranded oligonucleotides.[34]

Quite recently, photoadduct formation has also been detected by visible illumination of $[Ru(HAT)_2(phen)]^{2+}$ in the presence of GMP, calf thymus DNA and synthetic oligonucleotides.[35] ESMS analyses of the isolated photoproduct with GMP confirms the addition of one GMP to the Ru complex, without loss of the polyazaaromatic ligands. Furthermore, photoadduct formation with $[Ru(HAT)_2(phen)]^{2+}$ appears only with guanine-containing synthetic oligonucleotides,[35] as shown by gel electrophoresis experiments.

In conclusion, TAP, HAT, and bpz Ru^{II} complexes containing at least two such ligands form photoadducts with GMP or G-containing polynucleotides that are quite different from those formed with Pt, Rh or other Ru complexes.

Mechanism for Formation of the New Photoadducts

In order to provide evidence for the primary processes responsible for the formation of the photoadducts, photophysical and redox properties of these particular complexes have to be considered. Figure 4 represents the classical photophysical scheme proposed for most Ru^{II} complexes with three bidentate ligands such as $[Ru(bpy)_3]^{2+}$.[36,37] Illumination of such polyazaaromatic complexes leads to the population of a ^{1}MLCT state, which deactivates rapidly

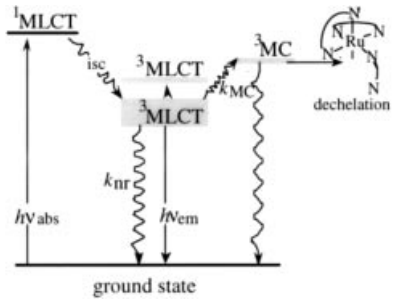

Figure 4. Photophysical scheme for $[Ru(bpy)_3]^{2+}$

 © 2004 Wiley-VCH Verlag GmbH & Co. KGaA, Weinheim

(less than 1 ps) by intersystem crossing to a ^{3}MLCT state with a quantum yield of unity.[38] This ^{3}MLCT state can deactivate radiatively (k_r), giving rise to the emission of the complex, or nonradiatively (k_{nr}). A conversion into a higher ^{3}MC state can also take place by thermal activation from the ^{3}MLCT. The ^{3}MC state can either deactivate nonradiatively or lead to dechelation (the loss of one polyazaaromatic ligand). This process is important for $[Ru(TAP)_3]^{2+}$ and is responsible for the formation of the first type of photoadduct with AMP, as discussed in section 2a.

The emission and the excited state lifetime associated with the ^{3}MLCT state strongly depends on the environment. Generally, the interaction of such compounds with polynucleotides leads to an increase in the luminescence intensity and lifetime. This effect is attributed to the protection of the metallic complex by the DNA hydrophobic environment (protection from water and oxygen quenching). However, the behaviour of TAP or HAT complexes that contain at least two or three TAP (or HAT) ligands (thus with $[Ru(bpy)_n(TAP/HAT)_{3-n}]^{2+}$ when $n = 0$ or 1) is different. Instead of a luminescence enhancement, a luminescence quenching appears in the presence of CT-DNA and poly(dG-dC)$_2$[27,39,40] (see also Figure 5 for $[Ru(HAT)_2(phen)]^{2+}$). The emission is thus quenched by G-C containing polynucleotides. As described below this quenching is due to a photoelectron transfer. In Table 1 we have presented the results on the effect of increasing polynucleotide concentrations on the luminescence of different Ru^{II} complexes.

An emission quenching for the same complexes also appears in the presence of mononucleotides. Large quenching rate constants of luminescence (of the order of 10^9 M^{-1}·s^{-1}) by GMP are characteristic of complexes containing two or three TAP (or HAT) ligands, whereas the other complexes exhibit extremely weak or no quenching at all by GMP.

Actually, the ruthenium(II) complexes containing at least two π-deficient ligands (TAP or HAT) with low-lying unoccupied molecular orbitals centred on the ligand are strongly oxidising in their ^{3}MLCT state.[41] Therefore, this excited

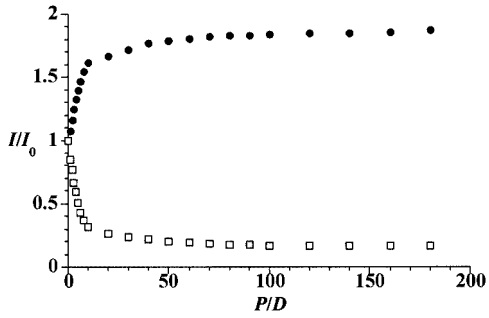

Figure 5. Effect of the polynucleotide/dye (P/D, D = ruthenium complex) ratio on the emission intensity of $[Ru(HAT)_2(phen)]^{2+}$; [Ru] = 5.2×10^{-5} M in 10 mm TRIS buffer; the excitation has been performed at 410 nm; I = emission intensity in the presence of the polynucleotide; I_0 = emission intensity in the absence of the polynucleotide; solid circles: effect of [poly(dA-dT)]$_2$. open squares: effect of DNA

species can abstract one electron from a guanine unit of DNA or GMP. The oxidising power can be estimated from the reduction potentials of the ground state and the energy of the emission maximum ($\Delta E_{\lambda_{max}}$) (Table 2):

$$E_{red}^* \approx E_{red} + \Delta E_{\lambda_{max}}$$

Taking into account the oxidation potential of GMP (E_{ox} = +0.92 V vs. SCE[11] or +1.35 V vs. SCE[42]) it is concluded that depending on the value, the excited complexes may or may not be able to oxidise GMP.

The plot of the logarithms of the quenching rate constants (k_q in water) as a function of the reduction potential of the excited state of different TAP and HAT complexes in MeCN (Figure 6) gives a curve typical of quenching by electron transfer; one where a plateau value is reached, and which corresponds to the diffusion rate constant. Actually, it has been demonstrated for some complexes that the electron transfer is coupled to a proton transfer in water,[43] as evidenced from a decrease in k_q from H_2O to D_2O. This

Table 1. Effect of increasing concentrations of various polynucleotides on the emission intensity of different ruthenium(II) complexes; ↑: increase of the luminescence; ↓: quenching of luminescence

Complex	CT-DNA	[poly(dG-dC)]$_2$	[poly(dA-dT)]$_2$	Reference
$[Ru(HAT)_3]^{2+}$	↓	–	↓	[39][40]
$[Ru(TAP)_3]^{2+}$	↓	↓	↑	[27][44]
$[Ru(HAT)_2(TAP)]^{2+}$	↓	–	↓	[39]
$[Ru(TAP)_2(HAT)]^{2+}$	↓	↓	↑	[39]
$[Ru(HAT)_2(phen)]^{2+}$	↓	–	↑	[35]
$[Ru(TAP)_2(phen)]^{2+}$	↓	↓	↑	[55]
$[Ru(HAT)(TAP)(bpy)]^{2+}$	↓	–	↑	[39]
$[Ru(HAT)_2(bpy)]^{2+}$	↓	–	↑	[40][56]
$[Ru(TAP)_2(bpy)]^{2+}$	↓	–	↑	[27]
$[Ru(bpy)_2(HAT)]^{2+}$	↑	–	↑	[40][56]
$[Ru(bpy)_2(TAP)]^{2+}$	↑	–	↑	[27][39]
$[Ru(phen)_2(PHEHAT)]^{2+}$	↑	–	↑	[57]
$[Ru(TAP)_2(dppz)]^{2+}$	↓	–	↑	[43]
$[Ru(phen)_2(dppz)]^{2+}$	↑	–	↑	[57]

 © 2004 Wiley-VCH Verlag GmbH & Co. KGaA, Weinheim

Table 2. Oxidation (E_{ox}) and reduction (E_{red}) potentials of a series of complexes and the corresponding oxidation (E_{ox}*) and reduction (E_{red}*) potentials in the excited state (the data are expressed in V vs. SCE)

Complex	E_{ox}	E_{red}	E_{ox}*	E_{red}*	Reference
$[Ru(HAT)_3]^{2+}$	+ 2.07	− 0.62	− 0.01	+ 1.46	[41]
$[Ru(HAT)_2(TAP)]^{2+}$	+ 2.03	− 0.64	− 0.04	+ 1.43	[41]
$[Ru(TAP)_2(HAT)]^{2+}$	+ 2.02	− 0.68	− 0.02	+ 1.36	[41]
$[Ru(TAP)_3]^{2+}$	+ 1.94	− 0.75	− 0.12	+ 1.32	[26]
$[Ru(HAT)_2(phen)]^{2+}$	+ 1.86	− 0.66	− 0.03	+ 1.23	[40]
$[Ru(HAT)_2(bpy)]^{2+}$	+ 1.79	− 0.76	− 0.08	+ 1.12	[41]
$[Ru(HAT)(TAP)(bpy)]^{2+}$	+ 1.78	− 0.75	− 0.08	+ 1.11	[41]
$[Ru(TAP)_2(dppz)]^{2+}$	+ 1.77	− 0.80	− 0.18	+ 1.15	[43]
$[Ru(TAP)_2(phen)]^{2+}$	+ 1.73	− 0.83	− 0.16	+ 1.06	[40]
$[Ru(TAP)_2(bpy)]^{2+}$	+ 1.70	− 0.83	− 0.19	+ 1.06	[40]
$[Ru(bpy)_2(HAT)]^{2+}$	+ 1.56	− 0.84	− 0.11	+ 0.83	[41]
$[Ru(bpy)_2(TAP)]^{2+}$	+ 1.51	− 0.88	− 0.23	+ 0.86	[26]
$[Ru(phen)_2(PHEHAT)]^{2+}$	+ 1.35	− 0.84	− 0.52	+ 1.03	[57]
$[Ru(phen)_2(dppz)]^{2+}$	+ 1.30	− 1.00	− 0.76	+ 0.97	[57]
$[Ru(bpy)_3]^{2+}$	+ 1.28	− 1.35	− 0.73	+ 0.66	[26]

proton coupling could explain the appearance of quenching by electron transfer, even with an oxidation potential value for GMP as positive as +1.35 V/SCE.

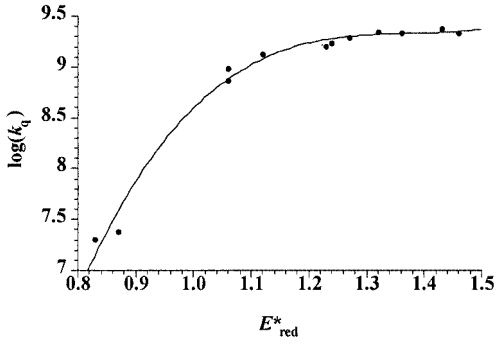

Figure 6. Plot of $\log(k_q)$ in water as a function of the estimated reduction potentials of the excited complexes (E^*_{red}) in MeCN; k_q = luminescence quenching rate constant

The electron transfer generates an oxidised $GMP^{\cdot+}$ species and a reduced complex $[Ru(L_2)(L^{\cdot-})]^+$ (the percentage of protonated reduced species depends on the pH). If instead of GMP, AMP is present, the excited ^{3}MLCT state cannot be quenched reductively, therefore its thermal crossing to the ^{3}MC state is possible and is accompanied by the loss of a TAP ligand and by a possible substitution by AMP (see section 2a).

The presence of an electron-transfer process with guanine units was demonstrated by laser flash photolysis experiments. The monoreduced complex and monooxidized GMP could be detected after the laser pulse.[40,44]

$$[Ru(L)_3]^{2+*} + GMP \rightarrow [Ru(L)_2(L^{\cdot-})]^+ + GMP^{\cdot+}$$
$$[Ru(L)_2(L^{\cdot-})]^+ + GMP^{\cdot+} \rightarrow [Ru(L)_3]^{2+} + GMP$$

The differential transient absorption measured at about 500−550 nm, characteristic of the absorption of the monoreduced complex, disappears according to a bimolecular, equimolecular process in the absence of oxygen, which indicates the presence of a back electron-transfer process in a few hundred μs. In the presence of oxygen, the decay of the transient at the same wavelength becomes pseudo-monomolecular and takes place in a few ten μs, due to the reoxidation of the reduced complex by oxygen. The remaining absorption still present after this decay corresponds to the absorption of the deprotonated radical cation of $GMP^{\cdot+}$. By flash photolysis experiments with DNA, a transient absorption at the same wavelength could also be observed; however, the amplitude of the decay is too small to perform a kinetic analysis of the signal, which indicates that the back electron-transfer is faster with DNA than with GMP. Moreover, the signal does not decay to zero but to a permanent absorption corresponding to that of the photoadduct.

In conclusion, the results with the mononucleotides and polynucleotides highlight a correlation between the reduction potential of the excited complex (thus the oxidation power of the excited state), the proton-coupled photoinduced electron transfer from guanine units, and the formation of photoadducts. Thus, the latter could result from the reaction of the intermediate radicals produced by the electron transfer. Determination of the structure of the photoadduct is a key element, which allows the confirmation of this conclusion.

Structure of the New Photoadducts

The determination of the structure of the photoadducts formed between the TAP and HAT complexes and GMP was performed mainly by NMR spectroscopy, first with the system $[Ru(TAP)_3]^{2+}$ and GMP.[31] From the integration of the different peaks in the NMR spectra, two protons are missing relative to the spectrum of one equivalent of $[Ru(TAP)_3]^{2+}$ and one equivalent of GMP. This indicates that the photoadduct, as concluded from the ESMS data, contains the starting complex plus one GMP, minus two H. One of the missing hydrogen atoms corresponds to that on position 2 of the TAP ligand (see Figure 1 for the numbering), which indicates the formation of a covalent bond between the position 2 of TAP and a guanine moiety. This is in agreement with the chemical shift of proton 3 of TAP, which is induced by this addition.[31] The other hydrogen atom missing belongs to the exocyclic amine (position 2 on GMP); the signal for the remaining amine proton is shifted downfield by δ = 5 ppm relative to that for the exocyclic amine protons of the free guanine. Thus, the covalent bond with the TAP ligand is formed with the exocyclic N atom of the guanine.[31] The structure of this photoadduct, as deduced from the NMR-COSY spectrum and the above arguments, is depicted in Figure 7.

 © 2004 Wiley-VCH Verlag GmbH & Co. KGaA, Weinheim

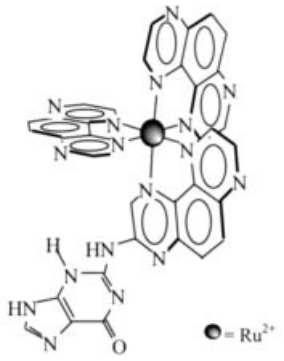

Figure 7. Structure of the photoadduct formed after illumination of $[Ru(TAP)_3]^{2+}$ in the presence of GMP; the structure shown corresponds to the photoadduct after acid hydrolysis to remove the sugar-phosphate moiety

The structure of the photoadduct formed between $[Ru(TAP)_2(bpy)]^{2+}$ and CT-DNA has also been studied. In that case, CT-DNA was hydrolysed or digested by enzymes after illumination.[32] The NMR spectrum obtained corresponds to a mixture of two products, i.e. two geometrical isomers (Figure 8), the covalent bond forms with the exocyclic-N of the guanine residue.[32] This was confirmed by mass spectrometry data that showed a fragmentation product corresponding to $[Ru(TAP\text{-}NH_2)(TAP)(bpy)]^{2+}$.

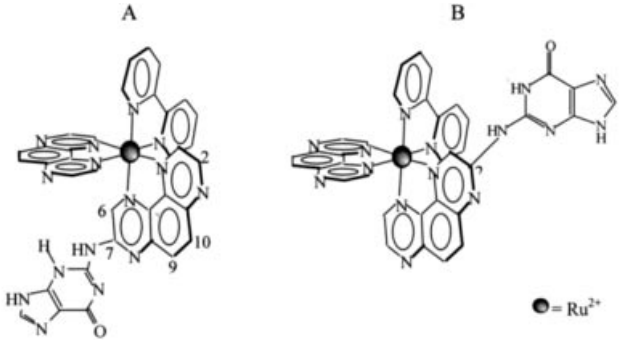

Figure 8. Structure of the two geometrical isomers for the photoadducts formed after illumination of $[Ru(TAP)_2(bpy)]^{2+}$ in the presence of CT-DNA; the structures have been obtained after enzymatic digestion and acidic treatment of CT-DNA

More recently, the structure of the photoadducts between a HAT-containing complex, i.e. $[Ru(HAT)_2(phen)]^{2+}$ and GMP, was examined.[35] In this case, two geometrical isomers were also detected from the NMR spectroscopic data, as with $[Ru(TAP)_2(bpy)]^{2+}$. However, a difference appears at the level of the protons of the guanine moiety, which suggests that the covalent bond with the HAT ligand is formed, in this case, with the O6 atom of the guanine unit. The difference in the structures of the photoadducts with the HAT and TAP complexes (i.e. addition at the O6 or at the exocyclic-N of the guanine unit) cannot be explained. With $[Ru(HAT)_2(phen)]^{2+}$ illuminated in the presence of GMP, in addition to the two geometrical isomers mentioned above, two supplementary photoadducts were detected by ESMS analyses :(i) a photoproduct containing a supplementary oxygen atom, which could correspond, for example, to the addition of an 8-oxoguanosine monophosphate to the complex; and (ii) a photoproduct not involving a 1:1 stoichiometry, i.e. a biadduct corresponding to the addition of two guanosine monophosphate moieties to one ruthenium(II) complex.[35] The structure of these species has not yet been determined.

On the other hand, the origin of the structures of the photoadducts with one GMP can be explained on the basis of the proton-coupled photoinduced electron transfer,[40,44] i.e.:

$$[Ru(TAP/HAT)_2phen]^{2+}* + GMP \rightarrow \{[Ru(TAP/HAT)(phen)(TAPH^{\cdot}/HATH^{\cdot}]^{+},(GMP-H)^{\cdot}\}$$

The proton transferred to the $TAP^{\cdot -}$ or $HAT^{\cdot -}$ moiety can stem from the GMP radical cation. Indeed the radical cation of guanine has a pK_a of 3.9, $GMP^{\cdot +}$ [45–47] thus deprotonates at pH 7 to give a guanine radical. Monoreduced $[Ru(TAP)_3]^{2+}$ has a pK_a of 7.6, which means that it should be protonated after electron transfer.[44] Similar pK_a values can be expected for complexes like $[Ru(TAP)_2(bpy)]^{2+}$ and $[Ru(HAT)_2(phen)]^{2+}$. In conclusion, the coupling of the two radical species resulting from the proton-coupled electron transfer, followed by rearomatisation, could explain the formation of the isolated photoadducts (reactions 7 and 8).

The formation of photoadducts with nucleic acids should obviously be preceded by the interaction of the two partners. The question which may be raised is whether the geometry of interaction of the complexes with the polynucleotides would play an important role in photoadduct formation.

Actually, it has been shown that $[Ru(TAP)_3]^{2+}$ and $[Ru(TAP)_2(bpy)]^{2+}$ [27,48] bind to the surface DNA grooves and interact with a rather low affinity (10^3-10^4 M^{-1}). In contrast, $[Ru(HAT)_2(phen)]^{2+}$, as probed by monitoring of the spectroscopic changes of the complex while interacting with DNA and by DNA viscosity measurements, intercalates one of its HAT ligands between the stacking of bases, and its affinity for the polynucleotides reaches $3.8 \cdot 10^5$ M^{-1}.[35] We may thus conclude that both geometries of interaction, adsorption or intercalation, produce photoadducts since they are detected in both cases.

Applications

One major disadvantage of metallic complexes that react in the dark with DNA, like cisplatin, or that photoreact

$$\{[Ru(TAP)(phen)(TAPH^{\bullet})]^{2+},GMP(-H)^{\bullet}\} \longrightarrow [Ru(TAP)(phen)(TAPH\text{-}GMP(-H))]^{2+} \quad (7)$$

$$[Ru(TAP)(phen)(TAPH\text{-}GMP(-H))]^{2+} \xrightarrow{-2H} [Ru(TAP)(phen)(TAP(-H)\text{-}GMP(-H))]^{2+} \quad (8)$$

 © 2004 Wiley-VCH Verlag GmbH & Co. KGaA, Weinheim

with DNA, like the TAP and HAT complexes, is their non-specificity of (photo)reaction. Indeed, they do not interact with a specific targeted gene, thus a specific base sequence. This represents a drawback if the expression of this sequence has to be inhibited by using the Ru complex as DNA photoreagent. The antigene or antisense strategies are well-known to provide means to inhibit such genes. Unfortunately, after hybridization with the synthetic oligonucleotide, the system formed (double helix for the antisense and triple helix for the antigene strategy) is recognised by the enzymes and destroyed. Many efforts have been focused on different possible ways of increasing the stability of the pairing of the synthetic oligonucleotide with the targeted sequence. In this context, the use of synthetic oligonucleotides derivatised by photoreactive Ru^{II} complexes could be promising as one can take advantage of the formation of the photoadduct on the nucleobases. This strategy has been developed with complexes that show the two types of photoadducts (without and with destruction of the chelation sphere), thus (i) with the TAP complexes and (ii) with the precursors of aqua complexes. (i) A photoreactive TAP complex is chemically anchored to an oligonucleotide with a sequence complementary to the sequence of the targeted gene. After hybridization of the Ru^{II}-labeled sequence to the target sequence, and after illumination of the attached complex, the formation of the photoadduct can be "directed" towards a specific guanine unit of the target strand. Such a photoreaction should result in the photocrosslinking of the two strands and could inhibit the expression of the specific gene. The existence of such photocrosslinkings was demonstrated by gel electrophoresis with $[Ru(TAP)_2(dip)]^{2+}$ (dip = 4,7-diphenylphenanthroline) tethered on different probe sequences (Figure 9).[49−53] Moreover, it was shown that enzymes such as DNA polymerase and exonuclease III are blocked at the level of the photocrosslinking.[54] Thus, a 17-*mer* Ru^{II}-labeled oligodesoxyribonucleotide was hybridised to its complementary sequence located on the 5′-side of a 40-*mer* matrix. After illumination, the elongation of a 13-*mer* DNA primer hybridised to the 3′-end of the same matrix stopped at a position corresponding to the formation of the photoadduct with an efficiency of 100%.

(ii) On the other hand, oligonucleotide conjugates bearing a Ru^{II} complex such as $[Ru(tpy)(dppz)(CH_3CN)]^{2+}$ (tpy = 2,2′:6′,2″-terpyridine)[22] have also been tested. This complex, chemically attached to a probe sequence, can lead to successful crosslinkings with the complementary sequence. Actually, the attached $[Ru(tpy)(dppz)(CH_3CN)]^{2+}$ is simply transformed under illumination into the corresponding aqua complex $[Ru(tpy)(dppz)(H_2O)]^{2+}$ which reacts (dark reaction) with a base unit of the complementary strand.

It should be stressed at this stage that the use of the above complexes in the frame of the antisense strategy would be limited to treatments of specific cancer cells in dermatology or hematopoietic cells that can be illuminated outside the patient. Indeed the visible light (in contrast to IR wavelengths) does not penetrate deeply in tissues, which would prevent an efficient treatment. However, it should be noted

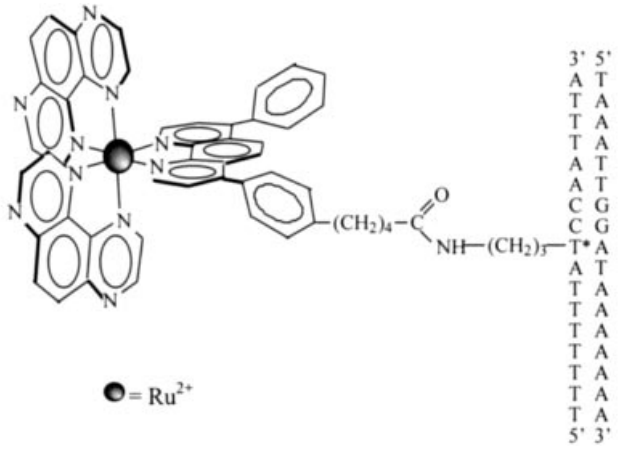

Figure 9. $[Ru(TAP)_2(dip)]^{2+}$-labeled oligonucleotide in the presence of its complementary sequence

that the recognition of a target nucleotidic sequence by an oligonucleotide probe derivatized with a photoreactive complex, followed by photocrosslinking between the two strands as described above, could also be applied in biotechnology without problems with the visible illumination in this case.

Conclusions

In this review, we tried to highlight the properties brought about by π-deficient TAP or HAT ligands in the resulting Ru^{II} complexes. Thus the complexes with at least 2 of these ligands induce a photoinduced electron-transfer with the guanine bases of DNA, a process that generates an adduct between the two partners. In this photoadduct, the complex and the guanine species are attached by a covalent bond without destruction of the chelation sphere.

One could speculate on the important role which could be played in the future by these complexes. For example, as outlined above, the Ru derivatised oligonucleotides could be applied in biotechnology or for treatments of specific cancers in the frame of the antigene or antisense strategy, whose effect could be triggered by light. The important problem which remains to be solved is the penetration and transport of the photoreactive agent into the cell. Research, with this aim, is presently being carried out.

Acknowledgments

R. B. thanks the Luxembourg Ministry of Education and Vocational Training for a Ph.D. research grant. The COST D14 and Action Lions Vaincre le Cancer are also acknowledged. The authors are grateful to the ARC program (02/07−286) and the LEA (Laboratoire Européen Associé, Belgian FNRS-French CNRS) for financial support.

[1] K. T. Douglas, *Chem. & Ind.* **1984**, 738−742.
[2] S. E. Sherman, S. J. Lippard, *Chem. Rev.* **1987**, *87*, 1153−1181.
[3] W. I. Sundquist, S. J. Lippard, *Coord. Chem. Rev.* **1990**, *100*, 293−322.

 © 2004 Wiley-VCH Verlag GmbH & Co. KGaA, Weinheim

[4] Y. Mikata, Q. He, S. J. Lippard, *Biochemistry* **2001**, *40*, 7533−7541.
[5] J. Reedijk, *Chem. Commun.* **1996**, 801−806.
[6] T. W. Hambley, *J. Chem. Soc., Dalton Trans.* **2001**, *19*, 2711−2718.
[7] M. Pauly, I. Kayser, M. Schmitz, M. Dicato, A. Del Guerzo, I. Kolber, C. Moucheron, A. Kirsch-De Mesmaeker, *Chem. Commun.* **2002**, 1086−1087.
[8] C. Moucheron, A. Kirsch-De Mesmaeker, J. M. Kelly, in *Structure and Bonding*, vol. 92 Springer Verlag, Berlin, **1998**.
[9] A. Kirsch-De Mesmaeker, C. Moucheron, N. Boutonnet, *J. Phys. Org. Chem.* **1998**, *11*, 566−576.
[10] A. Kirsch-De Mesmaeker, J.-P. Lecomte, J. M. Kelly, *Topics in Current Chemistry* **1996**, *177*, 25−76.
[11] C. Moucheron, A. Kirsch-De Mesmaeker, J. M. Kelly, *J. Photochem. Photobiol. B: Biol.* **1997**, *40*, 91−106.
[12] I. Ortmans, C. Moucheron, A. Kirsch-De Mesmaeker, *Coord. Chem. Rev.* **1998**, *168*, 233−271.
[13] K. E. Erkkila, D. T. Odom, J. K. Barton, *Chem. Rev.* **1999**, *99*, 2777−2795.
[14] B. Nordén, P. Lincoln, B. Akerman, E. Tuite, in *Metal Ions in Biological Systems*, vol. 33 (*Probing of Nucleic Acids by Metal Ion Complexes of Small Molecules*) (Eds.: A. Sigel, H. Sigel), Marcel Dekker, Inc., New York, Basel, Hong Kong, **1996**.
[15] R. E. Mahnken, M. A. Billadeau, E. P. Nikonowicz, H. Morrison, *J. Am. Chem. Soc.* **1992**, *114*, 9253−9265.
[16] M. A. Billadeau, K. V. Wood, H. Morrison, *Inorg. Chem.* **1994**, *33*, 5780−5784.
[17] H. L. Harmon, H. Morrison, *Inorg. Chem.* **1995**, *34*, 4937−4938.
[18] H. Morrison, H. Harmon, *Photochem. Photobiol.* **2000**, *72*, 731−738.
[19] T. Mohammad, C. Chen, P. Guo, H. Morrison, *Bioorg. Med. Chem. Lett.* **1999**, *9*, 1703−1708.
[20] M. A. Billadeau, H. Morrison, *J. Inorg. Biochem.* **1995**, *57*, 249−270.
[21] N. C. Pramanik, K. Pramanik, P. Ghosh, S. Bhattacharya, *Polyhedron* **1998**, *17*, 1525−1534.
[22] D. Ossipov, S. Gohil, J. Chattopadhyaya, *J. Am. Chem. Soc.* **2002**, *124*, 13416−13433.
[23] N. Grover, N. Gupta, H. H. Thorp, *J. Am. Chem. Soc.* **1992**, *114*, 3390−3393.
[24] N. Grover, T. W. Welch, T. A. Fairley, M. Cory, H. H. Thorp, *Inorg. Chem.* **1994**, *33*, 3544−3548.
[25] J.-P. Lecomte, A. Kirsch-De Mesmaeker, J. M. Kelly, *Bull. Soc. Chim. Belg.* **1994**, *5−6*, 193−200.
[26] A. Masschelein, L. Jacquet, A. Kirsch-De Mesmaeker, J. Nasielski, *Inorg. Chem.* **1990**, *29*, 855−860.
[27] J. M. Kelly, M. M. Feeney, A. B. Tossi, J.-P. Lecomte, A. Kirsch-De Mesmaeker, *Anti-Cancer Drug Des.* **1990**, *5*, 69−75.
[28] M. M. Feeney, J. M. Kelly, A. B. Tossi, A. Kirsch-De Mesmaeker, J.-P. Lecomte, *J. Photochem. Photobiol. B: Biol.* **1994**, *23*, 69−78.
[29] J. M. Kelly, A. B. Tossi, D. J. McConnell, C. OhUigin, *Nucleic Acids Res.* **1885**, *13*, 6017.
[30] M. B. Fleisher, K. C. Waterman, N. J. Turro, J. K. Barton, *Inorg. Chem.* **1986**, *25*, 3549−3551.
[31] L. Jacquet, J. M. Kelly, A. Kirsch-De Mesmaeker, *J. Chem. Soc., Chem. Commun.* **1995**, 913−914.
[32] L. Jacquet, R. J. H. Davies, A. Kirsch-De Mesmaeker, J. M. Kelly, *J. Am. Chem. Soc.* **1997**, *119*, 11763−11768.
[33] P. Vicendo, S. Mouysset, N. Paillous, *Photochem. Photobiol.* **1997**, *65*, 647−655.
[34] E. Gicquel, N. Paillous, P. Vicendo, *Photochem. Photobiol.* **2000**, *72*, 583−589.
[35] R. Blasius, H. Nierengarten, J.-F. Constant, E. Defrancq, P. Dumy, M. Luhmer, C. Moucheron, A. Kirsch-De Mesmaeker, *Chem. Eur. J.,* submitted.
[36] T. J. Meyer, *Pure Appl. Chem.* **1986**, *58*, 1193−1206.
[37] A. Juris, V. Balzani, F. Barigelletti, S. Campagna, P. Belser, A. von Zelewsky, *Coord. Chem. Rev.* **1988**, *84*, 85−277.
[38] J. N. Demas, D. G. Taylor, *Inorg. Chem.* **1979**, *18*, 3177−3179.
[39] A. Kirsch-De Mesmaeker, G. Orellana, J. K. Barton, N. J. Turro, *Photochem. Photobiol.* **1990**, *52*, 461−472.
[40] J.-P. Lecomte, A. Kirsch-De Mesmaeker, M. M. Feeney, J. M. Kelly, *Inorg. Chem.* **1995**, *34*, 6481−6491.
[41] L. Jacquet, A. Kirsch-De Mesmaeker, *J. Chem. Soc., Faraday Trans.* **1992**, *88*, 2471−2480.
[42] S. Steenken, S. V. Jovanovic, *J. Am. Chem. Soc.* **1997**, *119*, 617−618.
[43] I. Ortmans, B. Elias, J. M. Kelly, C. Moucheron, A. Kirsch-De Mesmaeker, *Dalton Trans.* **2004**, 668−676.
[44] J.-P. Lecomte, A. Kirsch-De Mesmaeker, J. M. Kelly, A. B. Tossi, H. Görner, *Photochem. Photobiol.* **1992**, *55*, 681−689.
[45] J. Reynisson, S. Steenken, *Phys. Chem. Chem. Phys.* **2002**, *4*, 527−532.
[46] J. Reynisson, S. Steenken, *Phys. Chem. Chem. Phys.* **2002**, *4*, 5346−5352.
[47] S. C. Weatherly, I. V. Yang, H. H. Thorp, *J. Am. Chem. Soc.* **2001**, *123*, 1236−1237.
[48] J.-P. Lecomte, A. Kirsch-De Mesmaeker, M. Demeunynck, J. Lhomme, *J. Chem. Soc., Faraday Trans.* **1993**, *89*, 3261−3269.
[49] O. Lentzen, J.-F. Constant, E. Defrancq, M. Prévost, S. Schumm, C. Moucheron, P. Dumy, A. Kirsch-De Mesmaeker, *ChemBioChem* **2003**, *4*, 195−202.
[50] S. Schumm, M. Prévost, D. Garcia-Fresnadillo, O. Lentzen, C. Moucheron, A. Kirsch-De Mesmaeker, *J. Phys. Chem. B* **2002**, *106*, 2763−2768.
[51] D. Garcia-Fresnadillo, N. Boutonnet, S. Schumm, C. Moucheron, A. Kirsch-De Mesmaeker, E. Defrancq, J.-F. Constant, J. Lhomme, *Biophysical Journal* **2002**, *82*, 978−987.
[52] I. Ortmans, S. Content, N. Boutonnet, A. Kirsch-De Mesmaeker, W. Bannwarth, J.-F. Constant, E. Defrancq, J. Lhomme, *Chem. Eur. J.* **1999**, *5*, 2712−2721.
[53] J.-F. Constant, E. Defrancq, J. Lhomme, N. Boutonnet, S. Content, I. Ortmans, A. Kirsch-De Mesmaeker, *Nucleosides & Nucleotides* **1999**, *18*, 1319−1320.
[54] O. Lentzen, E. Defrancq, J.-F. Constant, S. Schumm, D. Garcia-Fresnadillo, C. Moucheron, P. Dumy, A. Kirsch-De Mesmaeker, *J. Biol. Inorg. Chem.* **2003**, *9*, 100−108.
[55] A. Del Guerzo, A. Kirsch-De Mesmaeker, *Inorg. Chem.* **2002**, *41*, 938−945.
[56] F. de Buyl, A. Kirsch-De Mesmaeker, A. B. Tossi, J. M. Kelly, *J. Photochem. Photobiol. A: Chem.* **1991**, *60*, 27−45.
[57] C. Moucheron, A. Kirsch-De Mesmaeker, S. Choua, *Inorg. Chem.* **1997**, *36*, 584−592.

Received June 9, 2004

 © 2004 Wiley-VCH Verlag GmbH & Co. KGaA, Weinheim

Channel Structures in a Simple Inorganic Salt − An Open Framework Formed through Structural Integration of Distinct Sodium Acetate and Sodium Perchlorate Domains

Arnaud Lavalette,[a] Geoffrey A. Lawrance,[b] Nathaniel W. Alcock,*[a] and Michael J. Hannon*[a]

Keywords: Channel structures / Microporous materials / Crystal engineering / Zeolite analogues

The novel mixed salt of sodium acetate and perchlorate reported herein, $Na_4(OAc)_3(ClO_4)$, has a distinctive lattice structure formed from sodium acetate planes linked together by sodium perchlorate cylinders. In total contrast to the component salts, the structure contains channels parallel to the *c* axis. The integration of the two molecular-level structural motifs of the two component salts thus leads to a supramolecular/macromolecular-level structure which is very different from those of the components. A template mechanism is implicated in the formation.
(© Wiley-VCH Verlag GmbH & Co. KGaA, 69451 Weinheim, Germany, 2004)

Introduction

The design of new porous materials is a field of much current activity driven by the plethora of applications based around zeolite chemistry.[1] Much of the work has focused on crystal engineering approaches based on organic ligands or metallo-organic coordination frameworks in which supramolecular assembly principles are extended to polymeric solid-state materials.[2] However, relatively simple inorganic salts can also be used to create porous materials - the encapsulation of fullerene molecules inside the pores of a silver nitrate framework is a particularly striking example.[3] We have fortuitously prepared a remarkable mixed inorganic salt of sodium acetate and perchlorate, which has a distinctive lattice structure containing porelike channels (that hold a small amount of disordered solvent), and we report this finding herein.

Results

The mixed salt $Na_4(OAc)_3(ClO_4)\cdot 0.25(MeOH)$ was obtained serendipitously in the course of our studies on aggregation of supramolecular units into larger polymeric solid-state arrays[4] during the attempted preparation of the Ag complex of a chiral bispyridylimine ligand.[5] A methanolic solution of 5-hydroxypyridine-2-carboxaldehyde and (*S*)-(−)-1,1′-binaphthalene-2,2′-diamine was heated at reflux and then treated with silver acetate. Following further heating, the solution was treated with excess sodium perchlorate. Crystals were observed 4 days after addition of diethyl ether. It appears that the presence of the organic ligand or its constituents are significant in this preparation (possibly by a templating/nucleating mechanism) as extensive attempts to prepare the material from mixtures of sodium acetate and perchlorate were unsuccessful, generally leading to the formation of either hydrated sodium acetate or sodium perchlorate. The crystal structure determination indicates that Ag is absent from the crystals.

A search of the Cambridge Crystallographic Database[6] indicates that the complex is the only known simple, mixed acetate-perchlorate salt. The crystal structure determination reveals a remarkable supramolecular structure in a large high-symmetry cell, and channels run through the structure parallel to the *c* axis (Figure 1). These channels are lined with inward-pointing methyl groups. The channel diameters are about 8 Å (H···H) and contain a small amount of highly disordered solvent.

The presence of the channels is particularly striking since the structures of neither of the individual component salts contain cavities: Structures of two polymorphs of anhydrous sodium acetate have been reported.[7] Both forms contain two-dimensional layers in which a sodium carboxylate framework is lined on each side by the acetate methyl groups. In each form, the sodium ions are six-coordinate and bound to one bidentate acetate and four unidentate acetate groups with Na−O distances in the range

[a] Centre for Supramolecular and Macromolecular Chemistry, Department of Chemistry, University of Warwick, Gibbet Hill Road, Coventry, CV4 7AL, UK
Fax: (internat.) + 44-24-7652-4112
E-mail: n.w.alcock@warwick.ac.uk
m.j.hannon@warwick.ac.uk
[b] Discipline of Chemistry, School of Environmental and Life Sciences, The University of Newcastle, Callaghan, N.S.W. 2308, Australia
Supporting information for this article is available on the WWW under http://www.eurjic.org or from the author.

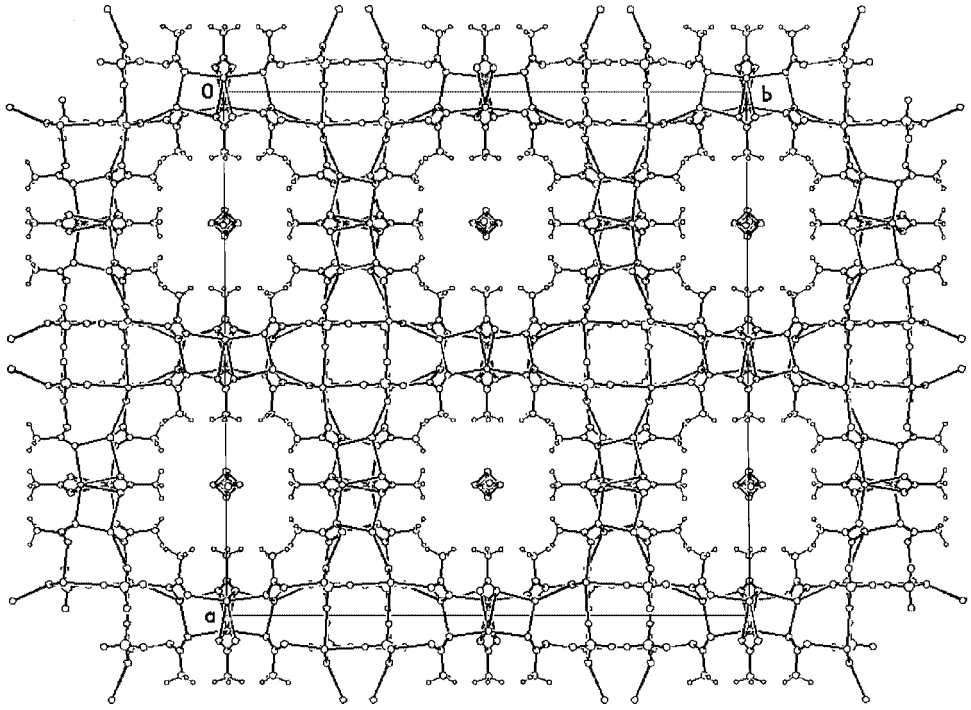

Figure 1. The $Na_4(OAc)_3(ClO_4).0.25(MeOH)$ structure viewed down the *c* axis, showing the channels through the structure

2.34−2.67 Å. Sodium perchlorate has orthorhombic symmetry and contains eight-coordinate sodium cations bound to two bidentate and four unidentate perchlorate ions with Na−O distances in the range 2.38−2.71 Å.[8] Above 581 K it undergoes a phase change and adopts a cubic structure (as NaCl) with rotating perchlorate anions.[9]

Inspection of the structure of the present mixed acetate-perchlorate salt reveals that the structure is made up of discrete domains of sodium acetate linked by domains of sodium perchlorate: the four sides of the channels are formed from planes containing six-coordinate sodium ions surrounded by acetate ions. The sodium atoms have two environments within these planes: one sodium atom [Na(1)] is bound to one bidentate acetate and four unidentate acetate groups (Na−O 2.36−2.56 Å), while the other [Na(3)] binds one bidentate and three unidentate acetate groups and its coordination sphere is completed by a unidentate perchlorate group (Na−O 2.34−2.80 Å) that links the planes to the sodium perchlorate domains. The structure of the planes is very similar to the two-dimensional layers in polymorph (I) of sodium acetate, but is approximately 8.5 Å in width (corresponding to three sodium atoms and three acetate groups) in one direction (rather than infinite).

These sodium acetate planes are held together by cylindrical sodium perchlorate domains that form the corners of the square channels and are very similar to the cubic phase of sodium perchlorate (without the perchlorate orientational disorder associated with that phase). The sodium [Na(2)] in this domain is bound to four perchlorate and two unidentate acetate groups to give an apparent coordination number of 6 (Na−O 2.39−2.50 Å). However two of the perchlorate groups form additional long contacts (Na−O 2.98 Å) and, if regarded as bidentate, increase the coordination number to eight. The different coordination spheres of the three types of sodium(I) centres in the structure are illustrated in Figure 2, and figures illustrating the structural similarities between the discrete domains and the corresponding bulk materials (sodium acetate and sodium perchlorate) are included in the Supporting Information.

The perchlorate domains act as four-way connectors linking linear sodium acetate planes into the grid-like framework. It is significant that this can be achieved without major distortions to the known structural motifs of the individual salts. While the molecular-level structures are retained, their integration gives rise to a very different (cavity containing) supramolecular-level structure from the components. Although open-frame network structures have been prepared by combining ligands and metals,[2] and ligands and salts,[1] this appears to be the first example in which discrete salt domains are linked by other discrete salt domains to give rise to such structures.

Although a serendipitous finding, the structure herein represents a remarkable example of a porous network assembled from very simple inorganic components. Guest-framework interactions have previously been identified as key factors in the creation of porous materials from simple inorganic salts. For example, silver···fullerene interactions appear significant in the formation of the remarkable fullerene-encapsulated silver nitrate network mentioned above.[3] However, no such interactions seem to be at work herein (indeed the solvent is disordered, consistent with a lack of specific interactions, and the channels only partially occupied). Nevertheless, the inability to recreate the network simply by mixing the individual components implicates

 © 2004 Wiley-VCH Verlag GmbH & Co. KGaA, Weinheim

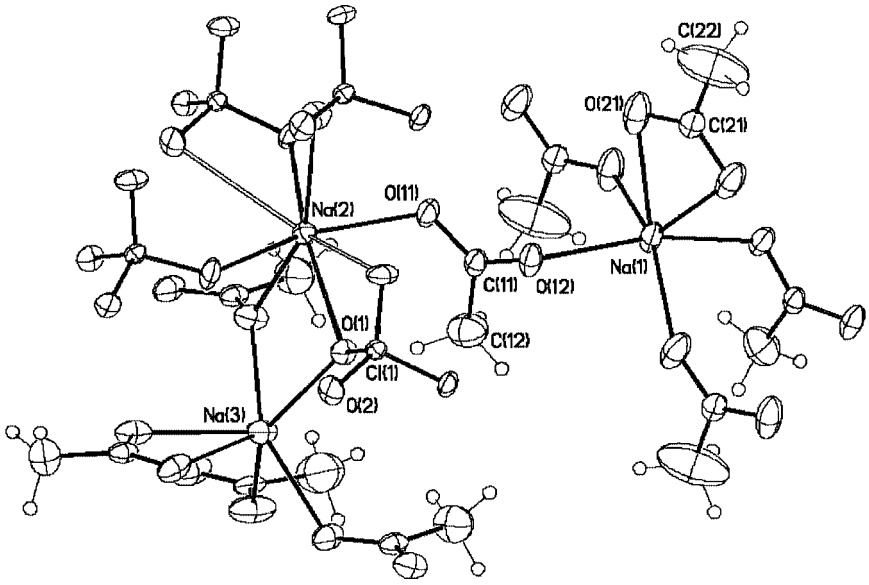

Figure 2. View of the complex, showing the full environment of each sodium ion; displacement ellipsoids are drawn at the 50% probability level

some form of templated nucleation in its formation. Indeed the size of cavity is defined by the length of the sodium acetate domains, which the template nucleation might affect or determine. Organic ligands and metal complexes have been used to direct formation of open-framework structures;[10] however, the template is usually included in the resulting structure. We can also suggest a relationship between the formation of this unusual structure and the nucleation of simple inorganic salts to afford complex and differing structures, which is a common theme in biological systems, particularly with regard to biomineralisation of calcium phosphate and carbonate salts, and which has also been exploited in chemical systems.[11]

CCDC-230080 contains the supplementary crystallographic data for this paper. These data can be obtained free of charge at www.ccdc.cam.ac.uk/conts/retrieving.html [or from the Cambridge Crystallographic Data Centre, 12, Union Road, Cambridge CB2 1EZ, UK; Fax: (internat.) +44-1223-336-033; E-mail: deposit@ccdc.cam.ac.uk].

Supporting Information (see also the footnote on the first page of this article): Figures illustrating the structural similarity between the discrete domains and the corresponding bulk materials (sodium acetate and sodium perchlorate), synthetic and crystallographic experimental details.

Acknowledgments

This work was supported by an EU Marie Curie Fellowship (A. L.; MCFI-2000-01003). M.J.H. is the Royal Society of Chemistry Sir Edward Frankland Fellow 2004−2005. We thank EPSRC and Siemens Analytical Instruments for grants in support of the diffractometer.

[1] See for example: *Comprehensive Supramolecular Chemistry, Vol 7* (Eds.: J. L. Atwood, J. E. D. Davies, J.-M. Lehn, D. D. MacNicol, F. Vögtle); Vol. Eds.: G. Alberti, T. Bein; Pergamon: Oxford, **1996**; M. E. Davis, *Nature* **2002**, *417*, 813−821; F. Schuth, W. Schmidt, *Adv. Mater.* **2002**, *14*, 629; G. Férey, *Chem. Mater.* **2001**, *13*, 3084−3098.

[2] G.R. Desiraju, *Crystal Engineering: The Design of Organic Solids*; Elsevier, Amsterdam, **1989**; A. Gavezzotti, *Curr. Opin. Solid State Mater. Sci.* **1996**, *1*, 501−505; G. R. Desiraju, *Curr. Opin. Solid State Mater. Sci.,* **1997**, *2*, 451−454; I. Manners, *Angew. Chem., Int. Ed. Engl.* **1996**, *35*, 1603−0621; O. M. Yaghi, H. Li, C. Davis, D. Richardson, T. L. Groy, *Acc. Chem. Res.* **1998**, *31*, 474−484; S. R. Batten,R. Robson, *Angew. Chem., Int. Ed. Engl.* **1998**, *37*, 1460−1494; R. Robson, in: *Comprehensive Supramolecular Chemistry, Vol 6* (Eds.: J. L. Atwood, J. E. D. Davies, J.-M. Lehn, D. D. MacNicol, F. Vögtle, Pergamon, Oxford, **1996**; M. J. Zaworotko, *Angew. Chem., Int. Ed. Engl.* **2000**, *39*, 3052−3054; N. R. Champness, M. Schröder, *Curr. Opin. Solid State Mater. Sci.* **1998**, *3*, 419−24; T. J. Prior, M. J. Rosseinsky, *Inorg. Chem.* **2003**, *42*, 1564−1575; P. A. Prassad, S. Neeraj, S. Natarajan, C. N. R. Rao, *Chem. Commun.* **2000**, 1251−1252; S. L. James, *Chem. Soc. Rev.* **2003**, *32*, 276−288.

[3] M. M. Olmstead, K. Maitra, A. L. Balch, *Angew. Chem. Int. Ed.* **1999**, *38*, 231−233.

[4] A. Lavalette, F. Tuna, J. Hamblin, A. Jackson, G. Clarkson, N. W. Alcock, M. J. Hannon, *Chem. Commun.* **2003**, 2666−2667.

[5] J. Hamblin, L. J. Childs, N. W. Alcock, M. J. Hannon, *J. Chem. Soc., Dalton Trans.* **2002**, 164−169.

[6] F. H. Allen, *Acta Crystallogr., Sect. B* **2002**, *58*, 380−388.

[7] L.-Y. Hsu, C. E. Nordman, *Acta Crystallogr., Sect. C* **1983**, *39*, 690−694.

[8] R. Wartchow, H. J. Berthold, *Z. Kristallogr.* **1978**, *147*, 307.

[9] J. Liu, C.-G. Duan, W.N. Mei, R. W. Smith, J. R. Hardy, *J. Solid State Chem.* **2002**, *163*, 294−299 and refs. therein.

[10] Z.-E. Lin, J. Zhang, S. T. Zheng, G.-Y. Yang, *Eur. J. Inorg. Chem.* **2004**, 953−955; J. A. Rodgers, W. T. A. Harrison, *Chem. Commun.* **2000**, 2385−2386 and refs. therein.

[11] See for example: S. Mann, *Angew. Chem. Int. Ed.* **2000**, *39*, 3393−3406 and refs. therein.

Received May 4, 2004

 © 2004 Wiley-VCH Verlag GmbH & Co. KGaA, Weinheim

New Ruthenium Complexes with 4-(1*H*-Pyrrol-1-yl)-Substituted Polypyridine Ligands − Electrochemical and Spectroscopic Properties

David Martineau,[b] Philippe Gros,*[a] Marc Beley,*[b] and Yves Fort[a]

Keywords: Nitrogen heterocycles / Ruthenium / N donor ligands

Three new pyrrole-containing ligands and their ruthenium complexes have been prepared. The pyrrole ring bound by nitrogen to pyridine was found to significantly modify photophysical and electrochemical properties compared to parent bi- and terpyridines.

(© Wiley-VCH Verlag GmbH & Co. KGaA, 69451 Weinheim, Germany, 2004)

Introduction

The design of new ruthenium(II) complexes that are able to harvest light and turn it into electricity has been the focus of many research works for the development of organic solar cells or luminescence sensors.[1] The nature of the ligands around the metal has been found to play a crucial role during the energy conversion process. Particularly, modification of the classically used bpy and tpy ligands with electron-donor substituents have been found to dramatically improve the absorption in the visible region, which is necessary for sunlight collection. Studies dealing with the effect of several substituents on bipyridines (bpy) in the $Ru(bpy)_3^{2+}$ series revealed that the highest values for $\lambda_{max.}$ were obtained with dimethylamino groups.[2] Moreover, the introduction of a 2-thienyl moieties at the 4′-position in terpyridine (tpy) also led to efficient visible light absorption.[3] From these data, the binding of a nitrogen-containing electron-rich ring such as pyrrole could be expected to tune the photophysical and electrochemical properties of the corresponding complexes. Herein, we report on the preparation of the new homoleptic ruthenium complexes **4a**, **5a** and **7a** from 4-(1*H*-pyrrol-1-yl)pyridine-containing ligands and on the study of their photophysical and electronic properties.

[a] Synthèse Organométallique et Réactivité, UMR 7565, Faculté des Sciences, Université Henri Poincaré,
Nancy I, Boulevard des Aiguillettes, BP239, 54506 Vandoeuvre-Les-Nancy, France
Fax: (internat.) +33-3-83684785
E-mail: Philippe.Gros@sor.uhp-nancy.fr
[b] LIMBP, UFR SciFA, LIMBP-IPEM 1,
Boulevard Arago, Metz Technopole, 57078 Metz, France
Fax: (internat.) +33-3-87315301
E-mail: beley@sciences.univ-metz.fr

Results and Discussion

Synthesis

We first synthesized the C-2 chlorinated precursors **2** and **3** needed for further organometallic couplings (Scheme 1). The electron-releasing effect of the pyrrole moiety was exploited to selectively direct lithiation at the position alpha to the pyridine nitrogen atom,[4] thus allowing for introduction of the halogens in high yield. An efficient iterative lithiation of compound **2** afforded the expected 2,6-dichloro derivatives **3** (Scheme 1).

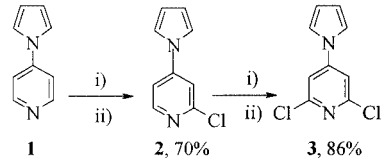

1 **2**, 70% **3**, 86%

Scheme 1. Preparation of **2** and **3**: i) BuLi/$Me_2N(CH_2)_2OLi$ (3 equiv.), toluene, −78 °C, 1 h; ii) C_2Cl_6 (3.5 equiv.), toluene, −78 °C to room temperature

The symmetrical ligand **4** was then prepared efficiently by nickel-catalysed homocoupling of **2**, while **5** and **7** were obtained by Stille cross-coupling of 2-(tributylstannyl)pyridine with **2** and **6**, respectively (Scheme 2).[5] Attempts to obtain **7** by a one-pot coupling remained limited to the formation of compound **6**, and the two-step procedure was preferred for the formation of **7** in an acceptable 50% yield after crystallization in ether.

We then turned our focus to the preparation of the corresponding homoleptic ruthenium complexes **4a**, **5a** and **7a** (Scheme 3). In our first attempts, stoichiometric proportions of the ligands classically reacted overnight with $RuCl_3(H_2O)_x$ in refluxing DMF. Unfortunately, incomplete incorporation of the ligands was observed leading only to complex mixtures. This is assumed to be a result of the pyr-

 © 2004 Wiley-VCH Verlag GmbH & Co. KGaA, Weinheim DOI: 10.1002/ejic.200400385

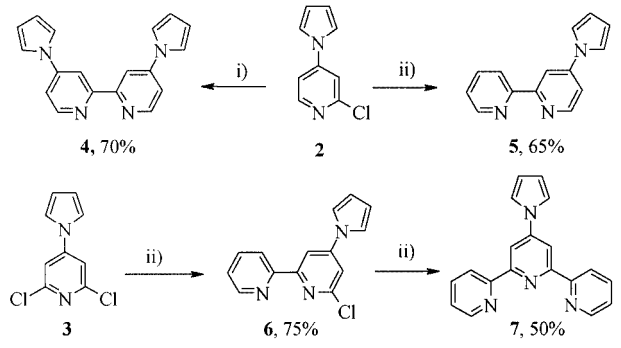

Scheme 2. Preparation of ligands **4**−**7**: i) $NiCl_2$ (1.1 equiv.), PPh_3 (4.4 equiv.), Zn (1.1 equiv.), degassed DMF, 50 °C, 1.5 h, ii) 2-(tributylstannyl)pyridine (1.1 equiv.), $[PdCl_2(PPh_3)_2]$ (5 mol %), PPh_3 (10 mol %), degassed xylene, reflux, 24 h

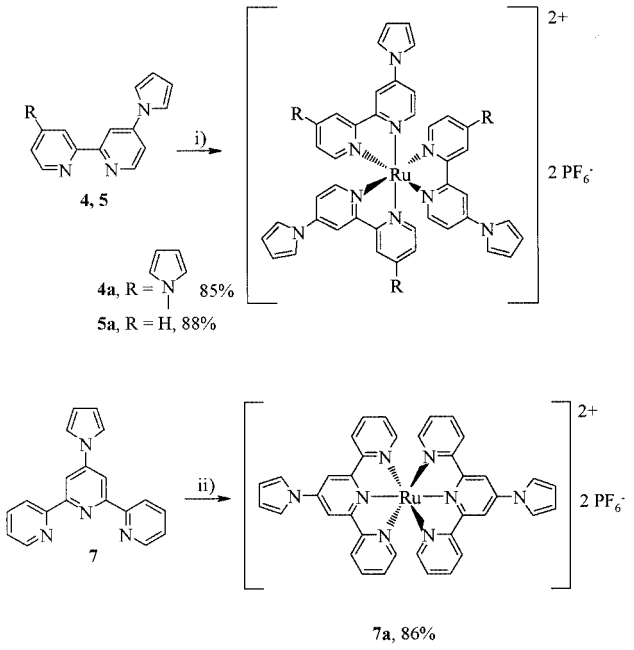

Scheme 3. Preparation of ruthenium complexes: i) $RuCl_3(H_2O)_x$ (0.33 equiv.), *N*-ethylmorpholine (2 drops), ethylene glycol, microwave irradiation, 200 °C, 5 min, ii) $RuCl_3(H_2O)_x$ (0.5 equiv.), *N*-ethylmorpholine (2 drops), ethylene glycol, microwave irradiation, 200 °C, 5 min

role-induced lower π-accepting power of the ligands. Indeed, the corresponding unsubstituted bpys and tpy are known to react smoothly under the same conditions leading to $[Rubpy_3]^{2+}$ and $[Rutpy_2]^{3+}$ complexes, respectively.[5] Complexation under microwave irradiation was then attempted (see Exp. Sect.). We were pleased to observe the formation of the target complexes **4a**, **5a** and **7a** in high yields after 3 min at 200 °C in ethylene glycol (Scheme 3).

Properties

Electrochemical and photophysical data of **4a**, **5a** and **7a** are reported in Table 1 and are compared with those of the corresponding parent complexes.

All complexes display a reversible Ru^{II} to Ru^{III} oxidation wave. No ligand reduction waves are detected for **7a**. This may be attributed to the formation of a nonconducting layer by adsorption at the electrode surface.[3b] An irreversible oxidation wave of the pyrrole moiety is distinctively observed only with complex **7a** at 0.8V, while overlap with the Ru^{III}/Ru^{II} oxidation wave is observed for **4a** and **5a**. The oxidation of pyrrole-containing complexes is observed at a less positive voltage than those of $[Rubpy_3]^{2+}$ and $[Rutpy_2]^{3+}$.

Comparison of the values obtained for **4a** and **5a** show that the introduction of a second pyrrole unit on the bpy ligand has a much lower effect than the introduction of the first unit. All these results indicate a significant destabilisation of the metal d orbital due to the electron-donor effect induced by the pyrrole substituent bound by the nitrogen atom to the pyridine ring. This property is also clearly evidenced by electronic transition spectra in acetonitrile. Indeed, all the MLCT absorptions in the visible region are red-shifted. Values for $\lambda_{max.}$ from 465 to 490 nm are observed; the larger effect is observed for complex **4a** bearing ligands with two pyrrole units. Electron-donor groups like pyrrol-1-yl destabilise the HOMO (π t_{2g}) metal orbital more than the LUMO (π^*) ligand orbital.[8] Consequently, both absorption and emission maxima of **4a**, **5a** and **7a** are shifted to longer wavelengths than those of $[Ru(bpy)_3]^{2+}$and $[Ru(terpy)_2]^{2+}$. For the same reasons the oxidation processes on **4a**, **5a** and **7a** occur with greater ease than those on their parent complexes. A consequence of the electron-donor effect is a $^3MLCT \rightarrow {}^3MC$ energy gap decrease,[9] and thus, the following order is obtained for quantum yields $\Phi_{\mathbf{5a}} < \Phi_{\mathbf{4a}} < \Phi_{[Ru(bpy)_3]^{2+}}$.

However, for **4a** and **5a** the reduction potentials are shifted to higher values than for $[Rubpy_3]^{2+}$. The corresponding stabilization of the LUMO (π^*) ligand orbital

Table 1. Electrochemical and photophysical data for ruthenium complexes

Complex[a]	$E_{1/2,ox}$ (V)[b] R^{III}/Ru^{II} (ΔEp/mV)	Ligand processes (V)	λ_{abs} (nm)	$\varepsilon \times 10^{-3}$ (M^{-1} cm^{-1})	λ_{em} (nm)[c]	φem (%)
$Ru(bpy)_3(PF_6)_2$	1.27 (90)[d]	−1.31 (rev.)/−1.50 (rev.)/−1.77 (rev.)	451[d]	14.0[d]	615[e]	0.059[f]
4a	1.12(90)	−1.20 (rev.)/−1.32 (rev.)/−1.52 (rev.)	480	22.2	630	0.044
5a	1.16 (90)	−1.21 (rev.)/−1.37 (rev.)/−1.60 (rev.)	465	8.6	650	0.022
$[Ru(tpy)_2]$ $(PF_6)_2$ [g]	1.30 (100)	−1.24 (rev.)/−1.49 (rev.)	474	10.4	629	$<5 \times 10^{-6}$
7a	1.18 (100)	n.d.	490	38.5	n.d.	n.d.

[a] All measurements performed in degassed acetonitrile solutions at 298 K. [b] First potential standardised with Fc as internal standard and converted into SCE scale by adding 0.38 V [$E_{1/2}$ (Fc^+/Fc)]. Recorded at 100mV/s with $LiCLO_4$ as supporting electrolyte. [c] DO < 0.1. [d] See ref.[6]. [e] See ref.[7]. [f] See ref.[8]. [g] See ref.[9].

 © 2004 Wiley-VCH Verlag GmbH & Co. KGaA, Weinheim

does not correspond to an electron-donor effect. A possible explanation may be based on the fact that the observed electronic transitions involve the HOMO and the SLUMO (second lowest unoccupied MO) centred on the pyridine ring, whereas the electrochemical reduction processes involve the LUMO localised on the remote *N*-pyrrolyl group. Such an anomalous electrochemical and/or spectroscopic behaviour has been observed in the case of $[Ru(taphen)_3]^{2+}$(taphen = dipyrido[3,2-*c*:2′,3′-*e*]pyridazine).[10] On the taphen ligand, the LUMO is strongly localised on the −N=N− bridge between the two pyridine rings.

Also of high interest is the dramatic increase in the ε values induced by incorporation of the pyrrole units on the ligands in complexes **4a** and **7a**, while a surprising decrease is observed with **5a**. In the latter case, dissymmetry of ligand **5** allows for the formation of the *fac*- and *mer*-isomers of complex **5a**.[11] The expected strongly different dipole moments of the two isomers may be responsible for the decrease in the ε value. The incorporation of a second pyrrole on the bpy ligand induces a huge increase from 8600 in **5a** to 22200 $M^{-1}cm^{-1}$ in **4a**. For **7a**, the value (38400 $M^{-1}cm^{-1}$) is similar to that obtained with the complex $[Ru(tsite)_2]^{2+}$ (tsite = 4,4′,4′′-triphenyl-2,2′,2′′-terpyridine), which displays one of the highest known ε values (38400 $M^{-1}cm^{-1}$) in terpy complex series.[12]

Conclusion

In summary, we have prepared new homoleptic ruthenium complexes from bpy and tpy pyrrole-containing ligands. The electron-donor effect of the pyrrole moiety was clearly demonstrated by the lower Ru^{II}/Ru^{III} oxidation potential and by the significant red-shifted MLCT absorption and emission maxima relative to those of the unsubstituted ligands. The use of bpy ligands bearing two pyrrole units leads to a high ε value. These new complexes are promising for developing novel solar harvesting devices. Work is now in progress to investigate the electropolymerisation of the pyrrole moiety for preparation of new photosensitising materials.

Experimental Section

General Procedure for Preparation of Complexes 4a, 5a and 7a: The ligand **4** or **5** (0.19 mmol) or **7** (35.9 mg, 0.12 mmol) and $RuCl_3(H_2O)_x$ (15.7 mg, 0.06 mmol) were dissolved in ethylene glycol (5 mL) and *N*-ethylmorpholine (2 drops) was added. The reaction mixture was then placed into a synthesis microwave oven and irradiated at 200 °C (300 W) for 3 min. After cooling down to room temperature, a saturated aqueous solution of KPF_6 (25 mL) was poured into the glazing orange mixture. The resulting orange precipitate was filtered and washed with diethyl ether and toluene to remove uncomplexed ligands. The filter cake was then dissolved in a minimum amount of acetonitrile and poured into deionised water. After filtration and drying, complexes were obtained in almost quantitative yields. The complexes were characterized by ^1H NMR (CD_3CN) and mass spectrometry. Spectral data for complexes: **4a:** ^1H NMR (200 MHz, CD_3CN): δ = 8.51−8.74 (m, 6 H), 7.69−8.0 (m, 6 H), 7.53−7.65 (m, 12 H), 7.40−7.54 (m, 6 H), 6.30−6.73 (m, 12 H) ppm. MS (ESI): *m*/*z* = 1105.3 $[M - PF_6]^+$, 961.4 $[M - 2PF_6]^+$, 480.2 $[M - 2PF_6]^{2+}$. UV/Vis (CH_3CN): $\lambda_{max.}$ ($\varepsilon_{max.}$, $L \cdot mol^{-1} \cdot cm^{-1}$) = 480 nm (22200). **5a:** ^1H NMR (200 MHz, CD_3CN): δ = 8.58−8.82 (m, 3 H), 8.39−8.57 (m, 3 H), 7.98−8.22 (m, 3 H), 7.61−7.96 (m, 6 H), 7.25−7.60 (m, 12 H), 6.25−6.72 (m, 6 H) ppm. MS (ESI): *m*/*z* = 910.2 $[M - PF_6]^+$, 764.2 $[M - 2PF_6]^+$, 382.6 $[M - 2PF_6]^{2+}$. UV/Vis (CH_3CN): $\lambda_{max.}$ ($\varepsilon_{max.}$, $L \cdot mol^{-1} \cdot cm^{-1}$) = 465 nm (8600). **7a:** ^1H NMR (200 MHz, CD_3CN): δ = 8.79−8.97 (m, 4 H), 8.59−8.73 (m, 4 H), 7.92−8.09 (m, 4 H), 7.83−7.92 (m, 4 H), 7.44−7.54 (m, 4 H), 7.15−7.34 (m, 4 H), 6.58−6.78 (m, 4 H) ppm. MS (ESI): *m*/*z* = 985.3 $[M^+]$, 843.2 $[M - PF_6]^+$, 697.2 $[M - 2PF_6]^+$, 349.1 $[M - 2PF_6]^{2+}$. UV/Vis (CH_3CN): $\lambda_{max.}$ ($\varepsilon_{max.}$, $L \cdot mol^{-1} \cdot cm^{-1}$) = 490 nm (38500).

[1] [1a] A. Juris, V. Balzani, F. Barigelletti, S. Campagna, P. Belser, A. von Zelewsky, *Coord. Chem. Rev.* **1988**, *84*, 85. [1b] B. O'Regan, M. Grätzel, *Nature* **1991**, *353*, 737. [1c] A. Hagfeldt, M. Grätzel, *Chem. Rev.* **1995**, *95*, 49. [1d] R. Argazzi, A. Bignozzi, G. M. Hasselmann, G. J. Meyer, *Inorg. Chem.* **1998**, *27*, 4533. [1e] X. Schulze, J. Serin, A. Adronov, J. M. J. Fréchet, *Chem. Commun.* **2001**, 1160. [1f] M. I. J. Polson, N. J. Taylor, G. S. Hanan, *Chem. Commun.* **2002**, 1356. [1g] E. Figgemeier, V. Aranyos, E. C. Constable, R. W. Handel, C. E. Housecroft, C. Risinger, A. Hagfeldt, E. Mukhtar, *Inorg. Chem. Commmun.* **2004**, *7*, 117.

[2] M. J. Cook, A. P. Lewis, G. S. McAulife, V. Skarda, A. J. Thomson, *J. Chem. Soc., Perkin Trans. 2* **1984**, 1293.

[3] [3a] J. Hjelm, E. C. Constable, E. Figgemeier, A. Hagfeldt, R. Handel, C. E. Housecroft, E. Mukhtar, E. Chofield, *Chem. Commun.* **2002**, 284. [3b] E. R. Schofield, Ph. D. Dissertation, University of Basel, Switzerland, **1999**.

[4] [4a] Ph. Gros, Y. Fort, *Eur. J. Org. Chem.* **2002**, 3375. [4b] D. Cuperly, Ph. Gros, Y. Fort, *J. Org. Chem.* **2002**, *67*, 238.

[5] Detailed studies on selective lithiation of **1** and coupling reactions will be published in due course.

[6] B. P. Sullivan, J. A. Baumann, T. J. Meyer, D. J. Salmon, H. Lehmann, A. Ludi, *J. Am. Chem. Soc.* **1977**, *99*, 7368.

[7] E. C. Constable, C. E. Housecroft, E. R. Schofield, S. Encinas, N. Armaroli, F. Barigelletti, L. Flamigni, E. Figgenmeier, J. G. Vos, *Chem. Commun.* **1999**, 869.

[8] K. Nakamaru, *Bull. Chem. Soc. Jpn.* **1982**, *55*, 1639.

[9] M. Maestri, N. Armaroli, V. Balzani, E. W. Constable, A. M. W. Cargill Thomson, *Inorg. Chem.* **1995**, *34*, 2759.

[10] F. Barigelletti, A. Juris, V. Balzani, P. Belser, A. von Zelewsky, *Inorg. Chem.* **1987**, *26*, 4115

[11] The ^1H NMR spectrum of **5a** did not allow to distinguish between the *fac*- and *mer* isomer.

[12] M. L. Stone, G. A. Crosby, *Chem. Phys. Lett.* **1981**, *79*, 169.

Received May 11, 2004
Early View Article
Published Online September 2, 2004

 © 2004 Wiley-VCH Verlag GmbH & Co. KGaA, Weinheim

Palladium Complexes with Chiral Diphospholane Ligands: Comparative Catalytic Properties and Analysis of (η^3-Allyl)palladium Species

Grégory Malaisé,[a] Shailesh Ramdeehul,[a] John A. Osborn,*[a][†] Laurent Barloy,*[a] Nathalie Kyritsakas,[b] and Roland Graff[c]

Dedicated to the memory of Jean-Marc Kern

Keywords: Palladium / Allyl ligands / Reaction intermediates / Asymmetric catalysis / Enantioselectivity

The chiral diphospholane ligands Duphos (**1**) and Duxantphos (**2**), which can be differentiated by their bite angle, were applied to palladium-catalysed asymmetric reactions, essentially allylic alkylations with symmetrically (**3a**–**d**) or unsymmetrically (**5a**,**b**) substituted allylic acetates as substrates. The most interesting results were found with the first series of substrates in which **2** was more reactive and/or selective than **1**. The model complexes of the catalytic intermediates [Pd{(*S*,*S*)-**1**}(η^3-cyclohexenyl)](BF_4) (**10**) and *exo*-[Pd{(*R*,*R*)-**2**}(η^3-cyclohexenyl)](SbF_6) (**11**) could be characterised by X-ray crystallography. ^{1}H and ^{31}P NMR spectroscopic analyses of [Pd{(*R*,*R*)-**2**}(η^3-diphenylallyl)](SbF_6) (**12**) and [Pd{(*R*,*R*)-**2**}(η^3-allyl)](SbF_6) (**13**) revealed the presence of exchanging isomers in solution. Structural data provided by these techniques combined with the preferential rotation model led to a satisfactory interpretation of the catalytic allylic alkylation results. It appears that the bite angle plays a crucial role in the positioning of the proximal methyl groups, which determines the distribution of allyl isomeric intermediates and the balance between clockwise and anticlockwise rotations in the enantioselective step.

(© Wiley-VCH Verlag GmbH & Co. KGaA, 69451 Weinheim, Germany, 2004)

Introduction

Asymmetric palladium-catalysed reactions have attracted enormous interest over the past years, especially for allylic substitutions[1,2a] or the Heck reaction.[2b] Allylic alkylation is of considerable use in organic synthesis and proceeds smoothly under mild conditions. A large amount of work has been devoted to the design and synthesis of chiral ligands, with the aim of increasing the enantioselectivity of the catalysts. Very good asymmetric inductions have been achieved, most of them with the benchmark substrate 1-acetoxy-1,3-diphenylprop-2-ene, but also with sterically less demanding substrates such as 1-acetoxycyclohex-2-ene.[1,2a] Structural analyses of allyl palladium intermediates have been helpful in understanding the intimate steric and/or electronic grounds for enantioselectivity.[1a−1c,2a,3]

The catalytic properties of two chiral xanthene-derived ligands for use in allylic alkylations have been previously reported in the laboratory.[4] These ligands combine the advantages of having chiral phospholane donor groups, which have met with great success in catalysis,[5] and a wide bite angle. The advantages of large bite angle ligands in homogeneous catalysis are well known[6] and, furthermore, an increase of the P−Pd−P angle imposed by the ligand is likely to improve the control of allylic alkylation enantioselectivity through enhancement of the depth of the chiral pocket.[1b]

The purpose of this paper is to report a systematic comparison between one of these ligands, 4,5-bis[(2*R*,5*R*)-2,5-dimethylphospholanyl)]-9,9-dimethylxanthene, hereafter abbreviated (*R*,*R*)-Duxantphos [(*R*,*R*)-**2**], with the homologous bidentate, narrow bite angle ligand (*R*,*R*)-Duphos[5] [(*R*,*R*)-**1**] or its enantiomer (*S*,*S*)-**1**. This comparison relates to their application in palladium-catalysed asymmetric reactions and to the three-dimensional structural properties of their respective allyl palladium(II) complexes in order to rationalise their catalytic behaviour.

[a] Laboratoire de Chimie des Métaux de Transition et de Catalyse, UMR 7513 CNRS, Institut Le Bel, Université Louis Pasteur, 4 rue Blaise Pascal, 67070 Strasbourg Cedex, France
Fax: (internat.) + 33-3-90241329
E-mail: barloy@chimie.u-strasbg.fr
[b] Service commun des Rayons X, Faculté de Chimie, Institut Le Bel, Université Louis Pasteur, 4 rue Blaise Pascal, 67070 Strasbourg Cedex, France
[c] Service commun de RMN, Faculté de Chimie, Université Louis Pasteur, 1 rue Blaise Pascal, 67008 Strasbourg Cedex, France
[†] Deceased; please address further correspondence to L. Barloy

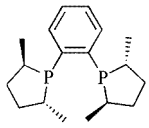

(*R*,*R*)-Duphos
(*R*,*R*)-**1**

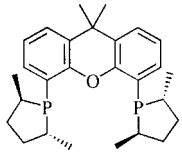

(*R*,*R*)-Duxantphos
(*R*,*R*)-**2**

Results

Homogeneous Catalysis

The ligands Duphos (**1**) and Duxantphos (**2**) were first tested in palladium-catalysed allylic alkylation with the racemic allylic acetates **3**−**6** as substrates, the standard dimethyl malonate anion as the nucleophile and $[Pd(C_3H_5)Cl]_2$ as the palladium source. The results are shown in Table 1. All tests were run using ligands with the (*R*,*R*) configuration, except one (Entry 11). The nucleophile was generated from dimethyl malonate either using sodium hydride, or in situ with *N*,*O*-bis(trimethylsilyl)acetamide (BSA) and a catalytic amount of sodium acetate.

These results show interesting differences between **1** and **2** with regard to reactivity and selectivity. In general, the Pd catalyst is less reactive with ligand **1** than with ligand **2**. BSA does not appear to be an appropriate base for **1** (Entries 6, 9, 11), leading at best to low yields (0−30%). Quantitative yields are obtained only with NaH. On the contrary, the catalytic alkylation reactions are complete with ligand **2** whatever the base, solvent or temperature. Furthermore, with the cyclic substrates 1-acetoxycyclohex-2-ene (**3c**) or 1-acetoxycyclopent-2-ene (**3d**), the reactions are finished within very short time ranges (5−10 min, see Entries 10, 12−14).

With 1-acetoxy-1,3-diphenylprop-2-ene (**3a**) as substrate, both ligands give rise to high *ee* values which is also the case for a host of chiral ligands reported in the literature.[1] Under the same conditions, ligand **1** leads to a 97% *ee* in 4 h, whereas ligand **2** affords a faster reaction (1 h) but with a lower enantioselectivity (85% *ee*) (Entries 1 and 2). Although the configurations of **1** and **2** are the same [viz (*R*,*R*)], the configurations of the major enantiomer of product **4a** are the opposite. The *ee* value found for **1** is practically identical to that reported by Pregosin et al. (98%) for the same reaction run with (*R*,*R*)-**1** but with conditions slightly different from ours (BSA/CH_2Cl_2).[7] With ligand **2**, the *ee* could be increased to up to 97% by modifying the base and solvent and to a higher extent by lowering the temperature (Entries 3 and 4).

The difference between both diphospholane ligands with regards to enantio-differentiation is far more striking with the sterically less demanding substrates **3b**−**d**, with a marked superiority of **2** over **1**. Low enantiomeric excesses were observed using ligand **1** (5−10%, Entries 5, 8, 11). In contrast, ligand **2** affords high *ee* values with 2-acetoxypent-3-ene (**3b**) and 1-acetoxycyclohex-2-ene (**3c**) (75%, Entry 7 and 83%, Entry 10, respectively). The performance of ligand (*R*,*R*)-**2** in terms of enantioselectivity is similar to that previously reported under somewhat different reaction conditions.[4] The asymmetric induction is, however, less efficient (50−54% *ee*) when one switches to the cyclopentenyl substrate **3d** (Entries 12−14) but **2** still remains superior to **1**. Incidentally, the configurations of the major enantiomers of **4c** and **4d** are the same (*S*) with ligand **2**.

Table 1. Palladium-catalysed asymmetric allylic alkylations of racemic allylic acetates **3a**−**d** with dimethyl malonate using diphospholane ligands **1** and **2**

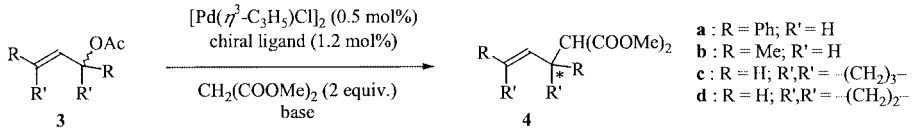

3 **4**

Entry	Substrate	Ligand	Base	Solvent	Temperature	Time[a]	*ee* [%][b]
1	**3a**	(*R*,*R*)-**1**	NaH	THF	room temp.	4 h	97 (*S*)
2	**3a**	(*R*,*R*)-**2**	NaH	THF	room temp.	1 h	85 (*R*)
3	**3a**	(*R*,*R*)-**2**	BSA/KOAc	CH_2Cl_2	room temp.	1 h	89 (*R*)
4	**3a**	(*R*,*R*)-**2**	BSA/KOAc	CH_2Cl_2	0 °C	3 h	97 (*R*)
5	**3b**	(*R*,*R*)-**1**	NaH	THF	room temp.	4 h	9 (*R*)
6	**3b**	(*R*,*R*)-**1**	BSA/KOAc	CH_2Cl_2	room temp.	24 h	—[c]
7	**3b**	(*R*,*R*)-**2**	BSA/KOAc	CH_2Cl_2	room temp.	3.5 h	75 (*S*)
8	**3c**	(*R*,*R*)-**1**	NaH	THF	room temp.	3 h	5 (*S*)
9	**3c**	(*R*,*R*)-**1**	BSA/KOAc	CH_2Cl_2	room temp.	24 h	—[d]
10	**3c**	(*R*,*R*)-**2**	NaH	THF	0 °C	10 min	83 (*S*)
11	**3d**	(*S*,*S*)-**1**	BSA/KOAc	CH_2Cl_2	room temp.	24 h	10 (*R*)[e]
12	**3d**	(*R*,*R*)-**2**	BSA/KOAc	CH_2Cl_2	room temp.	10 min	50 (*S*)
13	**3d**	(*R*,*R*)-**2**	BSA/KOAc	THF	room temp.	5 min	52 (*S*)
14	**3d**	(*R*,*R*)-**2**	NaH	THF	0 °C	7 min	54 (*S*)

[a] The yields determined by GC (using dodecane as internal standard) were quantitative unless otherwise stated. [b] See Exp. Sect. The absolute configuration is given in parentheses. [c] No reaction. [d] 1% yield. [e] 30% yield.

 © 2004 Wiley-VCH Verlag GmbH & Co. KGaA, Weinheim

Table 2. Palladium-catalysed asymmetric allylic alkylations of racemic allylic acetates **5a**−**b** with dimethyl malonate using diphospholane ligands **1** and **2**

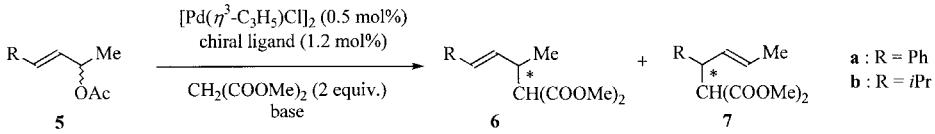

5 6 7

Entry	Substrate	Ligand	Base	Solvent	Time[a]	Yield (*ee*) [%] **6**	Yield (*ee*) [%] **7**
1	**5a**	(*S*,*S*)-**1**	BSA/KOAc	CH_2Cl_2	24 h	96 (12)[b]	4 (80)
2	**5a**	(*R*,*R*)-**2**	BSA/KOAc	CH_2Cl_2	24 h	95 (3)[c]	1 (60)
3	**5a**	(*R*,*R*)-**2**	BSA/KOAc	THF	2 h	98 (16)[b]	2 (55)
4	**5a**	(*R*,*R*)-**2**	NaH	THF	5 min	98 (3)[b]	2 (15)
5	**5b**	(*S*,*S*)-**1**	NaH	THF	24 h	3 (nd)[d]	0
6	**5b**	(*R*,*R*)-**2**	NaH	THF	1 h	90 (0)	0
7	**5b**	(*R*,*R*)-**2**	BSA/KOAc	THF	24 h	0	0
8	**5b**	(*R*,*R*)-**2**	BSA/KOAc	CH_2Cl_2	24 h	20 (0)	0

[a] See Exp. Sect.The reactions were performed at room temperature and the yields determined by GC using dodecane as internal standard. [b] (*S*) configuration. [c] (*R*) configuration. [d] nd = not determined.

We were also interested in the regiochemical and stereochemical outcome of the alkylation by dimethylmalonate of unsymmetrically substituted allylic acetates, viz 2-acetoxy-4-phenylbut-3-ene (**5a**) and 3-acetoxy-2-methylhex-4-ene (**5b**), catalysed by palladium associated with the diphospholane ligands (Table 2). With substrate **5a** the conversion is always complete, but the reaction time strongly depends on the reaction conditions from 5 min (Entry 4) to 24 h (Entry 2). The nucleophile attacks overwhelmingly on the Me side of the allyl intermediate to yield **6a** as the major product, whatever the ligand. This is a general trend with this substrate,[8−10] due to delocalization of the C=C bond with the phenyl substituent. The *ee* values of **6a** are poor (3−16%), whereas they are far better for the minor regioisomer **7a** (up to 80%). This situation mirrors the predictions and experimental results reported by Norrby, Åkermark, Helquist et al. for the same substrate.[9] The differences between both ligands **1** and **2** are rather minor. Under the same conditions (BSA/CH_2Cl_2), Duphos (**1**) performs slightly better than Duxantphos (**2**) in terms of enantioselectivity (Entries 1 and 2), but the *ee* of **6a** can be improved to 16% with **2** using THF as the solvent (Entry 3). Substrate **5b** appears less reactive and it is necessary to use NaH as a base to achieve a good conversion (90%) with ligand **2**. Under the same conditions, ligand **1** is almost inactive (3% conversion in 24 h, Entry 5). Only one regioisomeric product, **6b**, was formed and no asymmetric induction was observed. Under our conditions, the allyl palladium intermediates derived from (*R*)-**5a**,**b** do not interconvert with those derived from (*S*)-**5a**,**b**. A powerful memory effect can therefore be expected which results in poor global *ee* values,[11] taking into account that allylic alkylation proceeds with overall retention of configuration and that the regioisomers **6a**,**b** are the overwhelmingly major catalysis products.[2a]

The good performance of ligand (*R*,*R*)-**2** with small substrates (vide supra) prompted us to carry out the alkylation of the simple allyl acetate (2 equiv.) with the prochiral nucleophile (1 equiv.) derived from 2-methyl-1-tetralone (Scheme 1).[12] However, the selectivity was disappointing. According to some of the experimental procedures of Trost and Schroeder,[13] we used LDA as a base either in THF or DME. Both experiments quantitatively afforded the allylation product, in 5 min and 1 h, respectively, but with a low enantioselectivity (12%). Replacement of LDA with the BSA/KOAc system only led to a 2% conversion in 24 h.

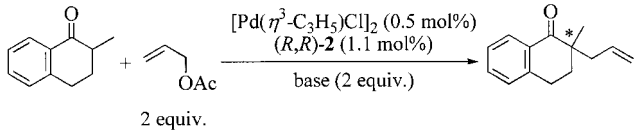

Scheme 1. Palladium-catalysed asymmetric allylic alkylation of allyl acetate with 2-methyl-1-tetralone

Finally, we tested the diphospholane ligands in another Pd-catalysed process, the benchmark asymmetric Heck reaction between phenyl triflate and 2,3-dihydrofuran (Scheme 2).[14] Ligand (*R*,*R*)-**2** associated with $Pd(OAc)_2$ as a palladium source led to very low yields and *ee* values [**8**: 5% yield, 12% *ee* (*S*); **9**: 5% yield, 2% *ee* (*R*)], whereas no reaction was observed under the same conditions with ligand (*R*,*R*)-**1**. With **2**, the Heck reaction with $Pd(DBA)_2$ instead of $Pd(OAc)_2$ gave racemic products in low yields (**8**: 3%; **9**: 8%).

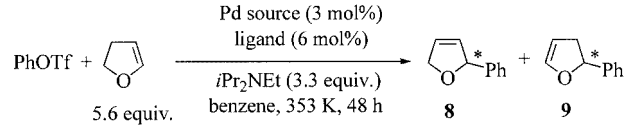

Scheme 2. Palladium-catalysed asymmetric Heck reaction

 © 2004 Wiley-VCH Verlag GmbH & Co. KGaA, Weinheim

Allylpalladium Complexes

In order to clarify how each of the chiral diphospholane ligands affects the stereochemical outcome of the catalytic reactions, we attempted to elucidate the three-dimensional structures of some cationic allyl palladium catalytic intermediates through solid-state (crystallography) and/or solution (NMR) studies. For this purpose, a series of cationic (η^3-allyl)palladium complexes (**10**−**13**) was synthesised in acceptable to very good yields (55−93%) according to a classical procedure. Abstraction of Cl^- from the chloride-bridged dimer $[Pd(\eta^3\text{-}C_6H_9)Cl]_2$ with $AgBF_4$ or $AgSbF_6$, followed by addition of (*S*,*S*)-**1** or (*R*,*R*)-**2** afforded the cyclohexenyl complexes **10** and **11**. Complexes **12** and **13** were obtained in a similar way from (*R*,*R*)-**2**, starting from $[Pd(\eta^3\text{-}Ph_2C_3H_3)Cl]_2$ or $[Pd(\eta^3\text{-}C_3H_5)Cl]_2$. The synthesis, NMR analysis, and X-ray structure of the related compound [Pd{(*R*,*R*)-Duphos}(η^3-1,3-diphenylallyl)](CF_3SO_3) have been reported by Drago and Pregosin.[7]

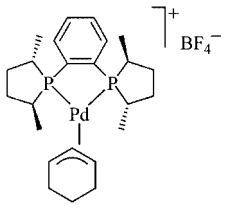

10

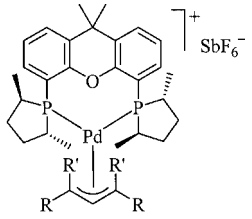

11 : R = H; R',R' = –$(CH_2)_3$–
12 : R = Ph; R' = H
13 : R = R' = H

Crystallographic Studies

Single-crystals of **10** and **11** suitable for X-ray diffraction analyses were obtained from slow liquid-phase diffusion of *n*-heptane and vapour-phase diffusion of pentane, respectively, into a dichloromethane solution of the complex. The X-ray crystallographic structures are depicted in Figures 1

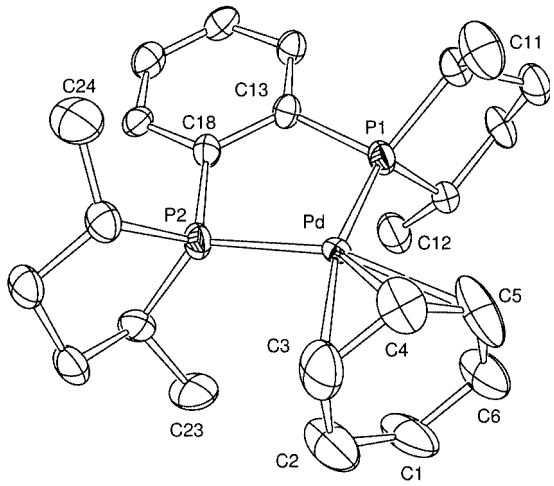

Figure 1. ORTEP drawing of [Pd{(*S*,*S*)-Duphos}(C_6H_9)](BF_4) (**10**) showing 30% probability thermal ellipsoids and the atom-numbering scheme; hydrogen atoms and the BF_4^- anion have been omitted for clarity

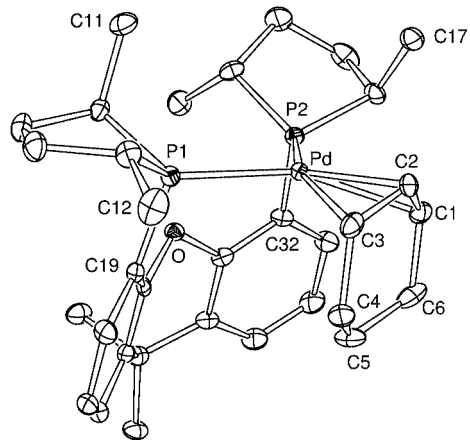

Figure 2. ORTEP drawing of [Pd{(*R*,*R*)-Duxantphos}(C_6H_9)](SbF_6) (**11**) showing 30% probability thermal ellipsoids and the atom-numbering scheme; hydrogen atoms and the SbF_6^- anion have been omitted for clarity

and 2 and selected bond lengths and angles are given in Tables 3 and 4. Complexes **10** and **11** crystallise as monocationic, pseudo-square-planar complexes with noncoordinating anions. Each metallic centre is coordinated by the three allylic carbon atoms and the two phosphorus atoms of the bidentate diphospholane **1** or **2**. Crystallographic disorder is present in the structure of **10**: the palladium atom occupies two positions (Pd and Pd′, 50% occupancy ratio each). Pd is bound to C3, C4, and C5, whereas Pd′, which is located slightly below, is bound to C6, C1, and C2. This

Table 3. Selected bond lengths [Å] and angles [°] in [Pd{(*S*,*S*)-Duphos}(C_6H_9)](BF_4) (**10**)

Pd−P1	2.278(3)	Pd−C3	2.39(2)
Pd−P2	2.323(3)	Pd−C4	2.23(1)
C3−C4	1.43(2)	Pd−C5	2.41(3)
C4−C5	1.44(3)		
P1−Pd−P2	86.40(9)	C3−Pd−C5	61.8(6)
P1−Pd−C3	167.0(4)	P2−Pd−C5	162.8(5)
P1−Pd−C5	105.5(5)	P2−Pd−C3	105.5(5)
Pd−P1−C7	117.5(3)	Pd−P2−C18	106.4(3)
Pd−P1−C10	121.6(3)	Pd−P2−C19	129.6(3)
Pd−P1−C13	107.5(3)	Pd−P2−C22	109.4(3)
C3−C4−C5	118(1)		

Table 4. Selected bond lengths [Å] and angles [°] for [Pd{(*R*,*R*)-Duxantphos}(C_6H_9)](SbF_6) (**11**)

Pd−P1	2.321(1)	Pd−C1	2.247(5)
Pd−P2	2.335(1)	Pd−C2	2.136(4)
C1−C2	1.377(8)	Pd−C3	2.206(5)
C2−C3	1.403(8)		
P1−Pd−P2	105.02(4)	C1−Pd−C3	64.9(2)
P1−Pd−C1	156.4(1)	P2−Pd−C3	156.9(1)
P1−Pd−C3	96.7(1)	P2−Pd−C1	92.0(1)
Pd−P1−C7	122.0(2)	Pd−P2−C13	116.3(2)
Pd−P1−C10	124.2(2)	Pd−P2−C16	125.7(2)
Pd−P1−C19	106.7(2)	Pd−P2−C32	107.7(2)
C1−C2−C3	118.6(5)		

 © 2004 Wiley-VCH Verlag GmbH & Co. KGaA, Weinheim

disorder results in large thermal ellipsoids for the 6 cyclohexenyl carbon atoms. For the sake of clarity, only Pd is shown in Figure 1.

The overall structure of **11** is very close to the reported structure of [Pd{(*R*,*R*)-Duthixantphospholane}(cyclohexenyl)]$^+$.[4a] The conformational characteristics of the Duxantphos ligand in complex **11** are similar to those of achiral xanthene-based ligands coordinated to palladium.[15,16] The main difference between **10** and **11** lies in the fact that in **10** the aromatic backbone of the ligand is approximately in the coordination plane and keeps a pseudo-C_2 symmetry axis, whereas in **11** the xanthene scaffold is almost perpendicular to the coordination plane. Indeed, the P1−Pd−P2 plane subtends an angle of only 14.8(1)° with the best-fit plane defined by the six aromatic Duphos carbons in **10**, while in **11** both xanthene aromatic rings (also defined by best-fit six-carbons planes) are bent by 77.08(4) and 75.67(4)° with regard to the P1−Pd−P2 plane. In **11**, the tricycle is folded along an O···CMe_2 axis, the oxygenated six-membered ring being in a boat conformation, and the angle between the mean aromatic planes reaches 45.32(4)°. Another marked difference is the angle between the mean phospholane planes (defined by their five atoms) and the P1−Pd−P2 plane: 70.6(1) and 78.3(1)° in **10** compared with only 13.41(4) and 34.52(4)° in **11**.

The loss of symmetry of the Duxantphos ligand upon coordination to the palladium centre induces *exo*/*endo* isomerism in the complex. The *exo* species can be defined as the conformer where the xanthene backbone is located on the same side of the coordination plane as the cyclohexenyl or, in a more general way, where the central allylic proton is on the opposite side with regard to the backbone.[4a] It is indeed the observed conformer for **11** as well as for [Pd{(*R*,*R*)-duthixantphospholane}(cyclohexenyl)]$^+$.

In both structures, the Pd−P bond lengths (2.278−2.335 Å) are within the expected range for complexes with phospholanes coordinated to palladium.[4a,7,17] As expected, the bite angle P1−Pd−P2 is much larger in **11** [105.02(4)°] than in **10** [86.40(9)°]. Because of the strong *trans* influence of the phospholanes, the palladium−terminal allylic carbon bonds (**10**: 2.39−2.41 Å; **11**: 2.206−2.247 Å) are longer than in other reported Pd−η^3-cyclohexenyl complexes.[17] In addition, they appear much longer in **10** than in **11** which is probably linked to the crystallographic disorder observed in **10** (vide supra). For the same reason, the cyclohexenyl carbons look, artificially, nearly coplanar in **10**, whereas in **11** the cyclohexenyl is in a chair conformation.

The ''twist angle'' τ defined by Helmchen et al.[18] is useful here for describing the inclination of the allyl in a front view. It corresponds to the dihedral angles P1−P2−C3−C5 in **10** and P1−P2−C1−C3 in **11** and reaches the values of −7.0(6)° and −8.7(2)°, respectively, which are very close. In other words, in a front view of the molecule where the allyl is positioned in the foreground, the allyl appears rotated slightly clockwise so that steric interactions between it and the proximal phospholane methyls (**10**: C11 and C23; **11**: C12 and C17) are minimised. It is worth noting that within the five-membered phospholane cycles, the proximal methyls of **10** are both *syn* with regard to the coordinating electron pair of the phosphorus atom, whereas in **11** C17 is *syn* but C12 is *anti*.

In **10** the mean phospholane planes are nearly parallel to the mean cyclohexenyl plane [5.7(2) and 9.0(1)°] and therefore the shortest spatial distance between a terminal allylic carbon and a chiral carbon of a phospholane is 4.015(20) Å (C3···C22). In contrast, the phospholanes of **11** make an angle of 72.94(5) and 89.57(6)° with the cyclohexenyl and the C3···C10 and C1···C13 distances are shorter at 3.878(7) and 3.548(7) Å, respectively. This observation mirrors exactly what Kamer et al. noted about palladium allyl complexes coordinated either by 1,2-bis(diphenylphosphanyl)-ethane or xantphos.[15] The consequence is a stronger protrusion of the proximal methyls into the cyclohexenyl ligand. Their distances from the cyclohexenyl mean plane are 2.031(2) Å (C12) and 1.962(2) Å (C17) in **11**, compared with 2.657(6) Å (C11) and 3.428(6) Å (C23) in **10**. In connection with the steric repulsion between C12 and the allyl of **11**, the P1−Pd−C3 angle is slightly but significantly larger than P2−Pd−C1 [96.7(1)° vs. 92.0(1)°] and Pd−P1−C10 is also larger than Pd−P2−C13 [124.2(2)° vs. 116.3(2)°].

NMR Investigations

We have also compared the NMR spectroscopic data of complexes **10** and **11** in solution. Like its crystallographic features, the NMR characteristics of **11** are closely akin to those of *exo*-[Pd{(*R*,*R*)-Duthixantphospholane}(cyclohexenyl)]$^+$. Upon coordination of the C_2-symmetric ligands **1** and **2** to the Pd centre, the loss of the symmetry axis is revealed by the $^{31}P\{^1H\}$, ^1H, and $^{13}C\{^1H\}$ NMR spectra. Many signals are duplicated, e.g. the phosphorus resonances which appear as an AB system, or the four ^1H NMR signals of the methyl groups borne by the phospholanes which are doublets of doublets. The $J_{P,P}$ values measured from the $^{31}P\{^1H\}$ spectra are slightly larger in **11** than in **10** (41 Hz vs. 36 Hz) which may be the consequence of an increased P−Pd−P angle.

The chemical shifts of the phosphorus nuclei are higher in the Duphos complex **10** (δ = 68.2 and 71.9 ppm) than in the Duxantphos complex **11** (δ = 33.7 and 35.5 ppm). This deshielding could be expected in view of the ring contribution (Δ_R) parameter[19] which reaches a high value for a five-membered metallacycle. The chemical shift difference between the terminal allylic ^{13}C signals is a useful tool to account for asymmetry in the allyl bonding.[7] Here, we observed that this difference is only Δδ = 5.2 ppm in **10**, but reaches Δδ = 12.0 ppm in **11**.

The case of complex [Pd{(*R*,*R*)-**2**}(η^3-1,3-diphenylallyl)](SbF_6) (**12**) appears to be more complicated. In spite of numerous efforts, we did not manage to grow single crystals for X-ray analysis. Its room-temperature $^{31}P\{^1H\}$ and ^1H NMR spectra exhibit broad signals which sharpen when the

 © 2004 Wiley-VCH Verlag GmbH & Co. KGaA, Weinheim

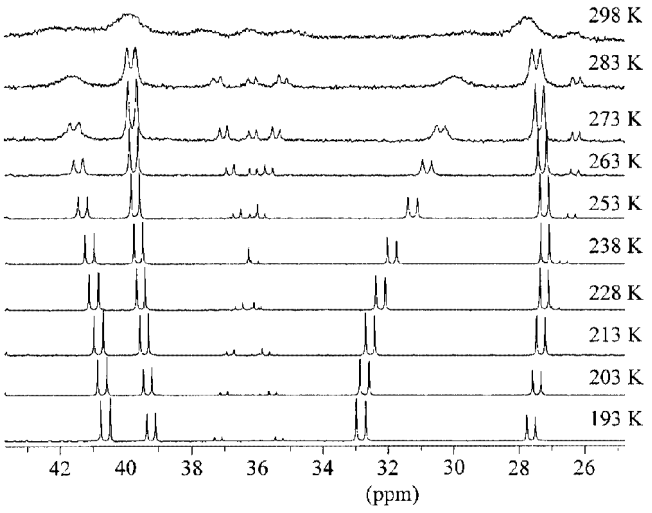

Figure 3. 202.5 MHz $^{31}P\{^1H\}$ NMR spectra of [Pd{(*R*,*R*)-Duxantphos}($Ph_2C_3H_3$)](SbF_6) (**12**) in CD_2Cl_2 in the range 193−298 K

temperature is decreased (Figure 3). Below 273 K, the ^{31}P NMR spectra exhibit eight narrow doublets between δ = 26 and 42 ppm with 45 Hz < $J_{P,P}$< 57 Hz, values which are all close to those found for complex **11**. Measurement of the P−P coupling constants associated with a $^{31}P\{^1H\}$ COSY spectrum recorded at 193 K allowed us to identify them as four AB systems, corresponding to two major (**12a**,**b**) and two minor (**12c**,**d**) isomeric species where a Pd atom is chelated by the diphospholane. If we assume that we can rely on the integration of the $^{31}P\{^1H\}$ NMR signals, their relative ratios are 35:25:4:1 at 193 K. **12a** and **12b** are predominant whatever the temperature. Coalescence of the ^{31}P and ^1H signals of the four isomers upon warming to room temperature indicates that they undergo fast exchange processes.

2D-^1H NMR spectroscopy has proved to be a very useful tool for the investigation of the 3D structures of allyl Pd complexes.[3] Indeed, although many signals of the 1D-^1H NMR spectrum of **12** recorded at 193 K overlap, 2D-NMR analysis combined with phosphorus-decoupled proton NMR spectroscopy allowed us to assign most of the signals of both major isomers and identify them as *exo*,*syn*,*syn* (**12a**) and *endo*,*syn*,*syn* (**12b**) (Scheme 3). In each isomer, all the ^1H signals of the diphospholane ligand (except the methylene signals) could be assigned with the help of 2D-^1H COSY and ROESY spectra, each proton being connected to another by scalar coupling and/or by spatial proximity (NOE effect). The aromatic protons located in the *ortho* position with regard to the phospholane substituents are characterised by a $^3J_{H,P}$ value of ca. 7 Hz. We can unambiguously identify the signals of the key proximal phospholane methyl groups that point in the foreground towards the allyl moiety. In the 2D-^1H ROESY spectrum, the left-side proximal methyl group displays a strong NOE with the adjacent *ortho*-xanthene proton (e.g. at δ = 7.35 ppm in the *exo* isomer), whereas the other *ortho* proton (e.g. *exo*: δ = 6.76 ppm) shows an NOE with the methylidyne group that

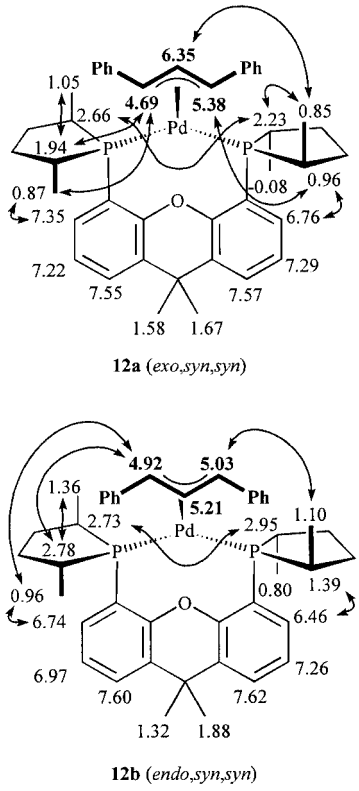

Scheme 3. Representation of relevant NOE contacts in **12a** and **12b** from ^1H ROESY; for the sake of clarity, NOEs associated with scalar couplings are not shown

is geminal with the right-side proximal methyl group. In the background, NOEs are observed between both phospholane distal methylidyne groups (e.g. *exo*: δ = 2.23 and 2.66 ppm) which is an indication that the xanthene backbone is folded as in the X-ray structure of **11**.

Six allyl signals are spread over a rather large range, i.e. δ = 4.69−6.35 ppm. The *syn*,*syn* geometry of the allyl ligand was established in both isomers from NOE cross-peaks between the lateral allyl signals (δ = 4.69−5.38 and 4.92−5.03 ppm; see Scheme 4). This is also suggested by the large values of the coupling constants between the central and lateral allylic protons (10−14 Hz), although this fact alone would not be definite proof.[3a] We note, however, that within each allyl ligand, both values of $^3J_{H,H}$ are not equal which suggests that the allyl group undergoes deformations.

The assignment of the allyl configuration (*exo* or *endo*) is essentially based on the interligand NOEs that the lateral-right and central allylic protons cause or do not cause with the right-side proximal phospholane methyl group and its *gem*-methylidyne group (Scheme 3). The *endo* structure of isomer **12b** is supported by the very intense NOE cross-peak of the allyl proton signal at δ = 5.03 ppm with the methyl signal at δ = 1.10 ppm (Figure 4). In the *exo* isomer **12a**, the lateral allyl proton (δ = 5.38 ppm) shows a close NOE contact with the proximal methylidyne group (δ = 0.96 ppm) but not with the methyl group (δ = 0.85 ppm). In addition, an NOE signal between the *exo* central allyl signal at δ = 6.35 ppm and the proximal methyl signal at

 © 2004 Wiley-VCH Verlag GmbH & Co. KGaA, Weinheim

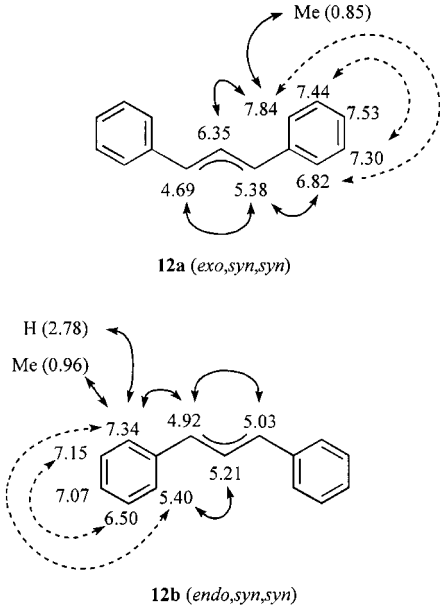

Scheme 4. Representation of relevant NOE contacts (plain arrows) and chemical exchanges (broken arrows) within the allyl ligand in **12a** and **12b** from ROESY experiments; for the sake of clarity, NOEs associated with scalar couplings are not shown

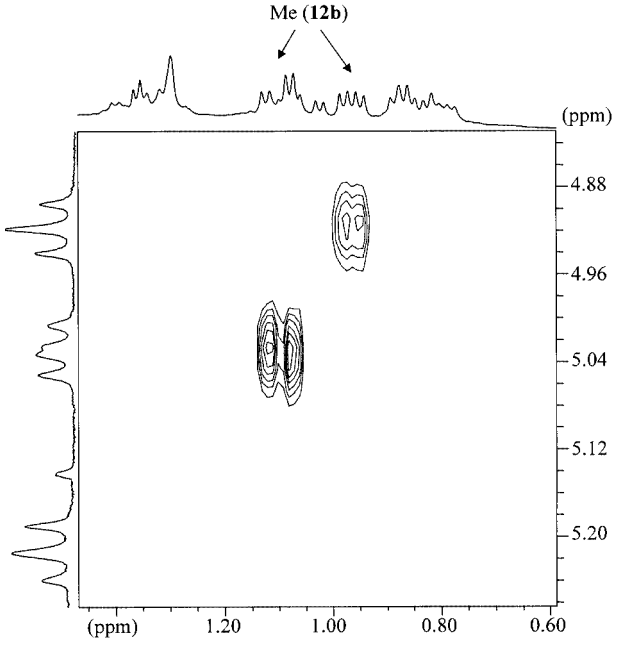

Figure 4. Section of the ^{1}H ROESY spectrum of **12** recorded in CD_2Cl_2 at 193 K; a section of the aliphatic region is represented horizontally and the three allylic proton signals of **12b** vertically

δ = 0.85 ppm can be observed. However, **12a** and **12b** cannot be differentiated by the left-side lateral allylic proton (**12a**: δ = 4.69 ppm; **12b**: δ = 4.92 ppm) because they both display NOEs with the proximal, left-side methyl group and methylidyne group.

The low frequency shift of some of the protons is consistent with their positioning in the anisotropy cone of the aromatic rings. The *exo* central allylic proton resonates in the normal range (δ = 6.35 ppm). In comparison, the chemical shift of the central proton of [Pd(Duphos)(1,3-diphenylallyl)]$^+$ is δ = 6.84 ppm, although the signal of the homologous proton of the *endo* isomer that lies in the anisotropy cone of both xanthene aromatic cycles is shifted upfield by more than 1 ppm (δ = 5.21 ppm). Conversely, the signals of several protons belonging to the diphospholane ligand are shifted upfield, such as (1) on the right side of the *exo* isomer, the *ortho*-xanthene proton (δ = 6.76 ppm), the proximal methylidyne group (δ = 0.96 ppm) and even the distal methyl group (δ = −0.08 ppm) as well as (2) on the *endo* isomer, both *ortho*-xanthene protons (δ = 6.46 and 6.74 ppm) and the proximal methylidyne group on the right (δ = 1.39 ppm). These shifts are probably related to the anisotropy cone of the phenyl substituents of the allyl moiety.

In each isomer, only the ^{1}H signals of one phenyl substituent can be identified, i.e. the right-side phenyl group in the *exo* form and the left-side one in the *endo* form (Scheme 4). For each of them, five distinct resonances can be observed. This means that their rotation is frozen at 193 K because of the steric effect of the proximal methyl groups. However, positive exchange (EXSY) cross-peaks related to this rotation, between the *ortho* and *meta* protons of each phenyl group, can be found in the ^{1}H ROESY spectrum. The protons oriented downwards resonate at low frequencies (e.g. the *endo*,*ortho* proton signal at δ = 5.40 ppm) because of their location in the anisotropy cone of the xanthene backbone (vide supra).

The ^{1}H NMR signals of both minor isomers **12c** and **12d** could hardly be detected in the spectra because of overlapping of the signals of the major isomers **12a** and **12b**. However, in view of related (1,3-diphenylallyl)palladium complexes,[3] it seems highly probable that they are *syn*,*anti* isomers (vide infra). Such *syn*,*anti* (1,3-diphenylallyl)palladium complexes are generally less stable than *syn*,*syn* isomers because of unfavorable $Ph_{anti}-H_{anti}$ steric interactions.

From the integration of the respective ^{1}H NMR signals of **12a** and **12b** in CD_2Cl_2, we observed that the [**12a**]/[**12b**] ratio in solution increased with the temperature and that a plot of ln$K$ (K = [**12a**]/[**12b**]) vs. 1/T is a straight line (Figure 5). This allowed us to estimate the thermodynamic data of the equilibrium, viz. $\Delta H° \approx 4$ kJ·mol^{-1} and $\Delta S° \approx 18$ J·mol^{-1}·K^{-1}. Upon warming form 193 to 298 K, the intensity of the AB system at δ ≈ 28 and 39 ppm in the ^{31}P NMR spectrum increased, whereas that of the AB pattern at δ ≈ 31−33 and 40−42 ppm decreased (Figure 3). We can, therefore, assign the first couple of signals to **12a** and the second to **12b**, by comparison with the variable-temperature ^{1}H NMR spectroscopic data.

The broadening of the ^{1}H and ^{31}P{^{1}H} NMR signals of **12** upon increasing the temperature from 193 K to room temperature is characteristic of fluxional processes. We tried to record a high-temperature (323 K) ^{31}P{^{1}H} NMR spectrum of **12** in CD_3NO_2 but unfortunately it decomposed upon heating before any narrowing of the signals could be observed. We envisioned that the equilibria between the isomers of **12** could be visualised by low-temperature 2D

 © 2004 Wiley-VCH Verlag GmbH & Co. KGaA, Weinheim

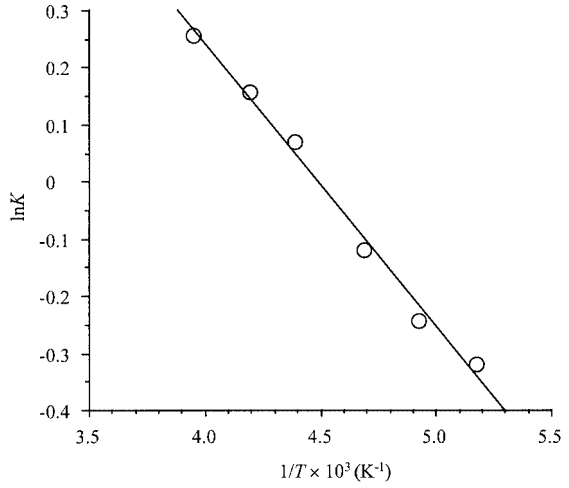

Figure 5. ln K vs. $1/T$ curve (K = [**12a**]/[**12b**] in CD_2Cl_2)

exchange NMR spectroscopy. No exchange cross-peaks involving allylic protons were found in the ^1H ROESY spectrum, probably because the exchange rates are too low at 193 K. However, we could observe two cross-peaks which reveal very selective chemical exchanges of phosphorus nuclei in a $^{31}P\{^1H\}$ ROESY spectrum recorded at 263 K (Figure 6). This can be interpreted as the consequence of a conformational equilibrium between the major isomers **12a**

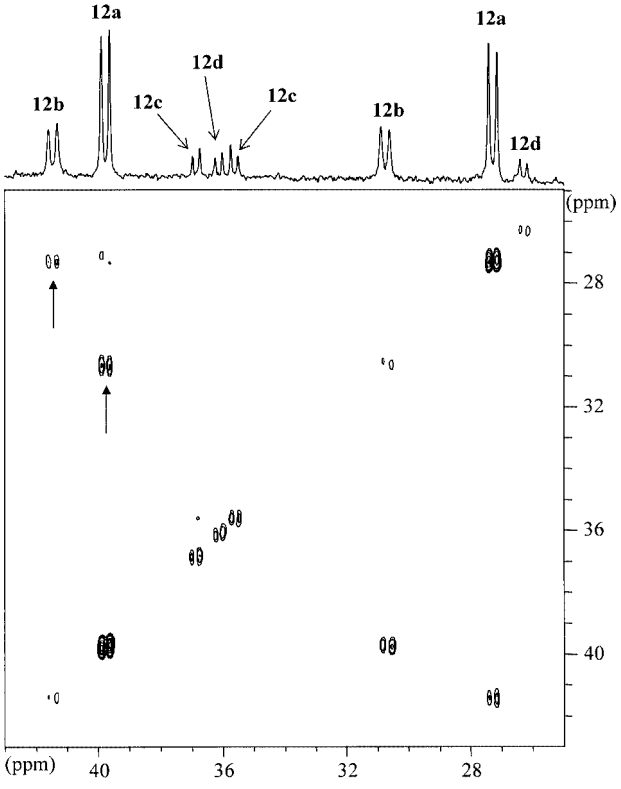

Figure 6. ^{31}P ROESY spectrum of **12** recorded in CD_2Cl_2 at 263 K; exchange cross-peaks between **12a** and **12b** are designated by arrows

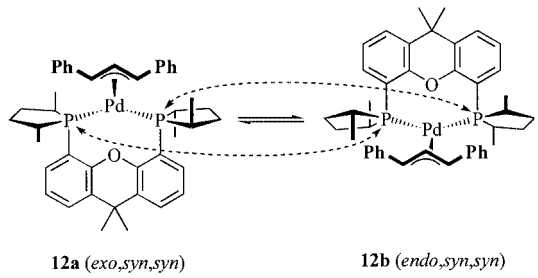

Scheme 5. Hypothetical conformational equilibrium between **12a** and **12b** accounting for the phosphorus nuclei exchanges (broken arrows) observed by ^{31}P ROESY

and **12b** (Scheme 5), where the xanthene backbone moves upwards rotating around the P···P axis (flip−flop). Very similar NMR observations of a Pd(diphosphane)(η^3-allyl) complex have been reported.[20] No exchange cross-peaks were found in the ^{31}P ROESY spectrum between the signals of the major *syn*,*syn* and the minor hypothetically *syn*,*anti* isomers, which means that $\eta^3-\eta^1-\eta^3$ isomerization is too slow to be observed at 263 K. It is plausible that this process, which involves Pd−C bond breaking, is slower than a conformational equilibrium.

A $^{13}C\{^1H\}$ NMR spectrum of **12** was recorded at 263 K in CD_3NO_2, a solvent in which the complex is reasonably soluble (a spectrum recorded in CD_2Cl_2 resulted in a poor signal-to-noise ratio). Although the spectrum is complicated because many species are present in solution, we assigned the most intense signals to **12a** which is by far the predominant species at this temperature. One of the terminal allylic carbon atoms has olefin-like character[3b] with a high-frequency chemical shift of δ = 100.2 ppm. As in the cyclohexenyl series, the $\Delta\delta_{C\ terminal\ allyl}$ value is much larger with Duxantphos (δ = 22.4 ppm) than with Duphos (δ = 10.3 ppm[7]). Indeed, δ = 22.4 ppm is particularly high for a (1,3-diphenylallyl)Pd complex chelated by two donor atoms of the same type.[3b] The terminal allyl carbon signals of **12a** are doublets (as in the cyclohexenyl analogue **11**) and the coupling constants with their respectively *trans*-positioned phosphorus atom are quite different (δ = 77.8 ppm, 30 Hz vs. δ = 100.2 ppm, 20 Hz). All these observations are consistent with an allyl deformation or tilt which was suggested by the values of the H-H coupling constants within the allyl (vide supra).

Like **12**, complex [Pd(*R*,*R*)-**2**](η^3-allyl)](SbF$_6$) (**13**) could not be analysed by X-ray crystallography. Instead, a detailed NMR spectroscopic analysis was carried out. Its low-temperature $^{31}P\{^1H\}$ NMR spectrum revealed the presence of *exo* and *endo* isomers in very different proportions, i.e. with a ratio > 10 (Figure 7). At 183 K, the major compound was characterised by an AB system at δ = 33.2 and 34.3 ppm ($J_{P,P}$ = 40 Hz), whereas only one doublet of the minor species was visible at δ = 31.3 ppm ($J_{P,P}$ = 40 Hz). Upon heating, we observed a coalescence of the signals which led to a single averaged AB system at room temperature. The coalescence temperature can be roughly estimated as 223 K. This suggests that the energy barrier of the fluxional process is lower for **13** than for **12**. A straightfor-

 © 2004 Wiley-VCH Verlag GmbH & Co. KGaA, Weinheim

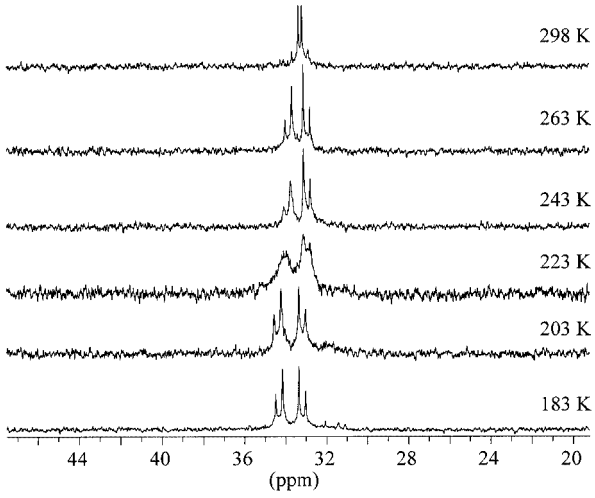

Figure 7. 121.5 MHz $^{31}P\{^1H\}$ NMR spectra of [Pd{(*R*,*R*)-Duxantphos}(C_3H_5)](SbF$_6$) (**13**) in CD_2Cl_2 in the range 183−298 K

ward explanation based on the steric effect of the bulky 1,3-diphenylallyl moiety can be proposed.

It is highly probable that the major species at low temperature is also largely predominant at room temperature, i.e. above the coalescence temperature. Therefore, the diagnostic cross-peaks observed in the ^1H ROESY NMR spectrum recorded at room temperature must be characteristic of that major isomer. Most of the protons of Duxantphos in **13** could be identified with the help of that spectrum, in connection with key Me···H$_{ar}$ and CH···H$_{ar}$ NOE cross-peaks. Several indications tend to show that it corresponds to the *exo* isomer shown in Scheme 6. In an *endo* isomer, a strong NOE interaction between H$_{anti}$ (δ = 2.55 ppm) and the phospholane methyl group (δ = 1.33 ppm) on the right side would be expected, which is not the case. Furthermore, by comparison with reported [Pd(trialkylphosphane)$_2$(allyl)]$^+$ complexes,[21] the chemical shifts of the *anti* protons are rather low, possibly because they are located in the anisotropy cone of the backbone aromatic rings in the *exo* conformation. Unfortunately, this assignment is not unambiguous, since each allylic *syn* proton displays NOEs with a methyl group and a methylidyne group, whereas the allylic *anti* or central protons show no significant NOE with any of the Duxantphos protons.

We found two distinct chemical exchange (positive) cross-peaks in the ROESY spectrum between both *ortho*-xanthene protons and also between two methyl groups (Scheme 6). Other exchange cross-peaks involving Duxantphos protons could not be distinguished because the chemical shifts of the exchanging nuclei were too close. Besides, the four terminal allyl protons all exchange with each other. All these exchange cross-peaks can be interpreted as the result of a flip−flop of the diphospholane ligand similar to that shown in Scheme 5 (leading to the minor isomer), followed by an isomerization back to the major species through a classical $\eta^3-\eta^1-\eta^3$ allyl rearrangement mechanism.[1b]

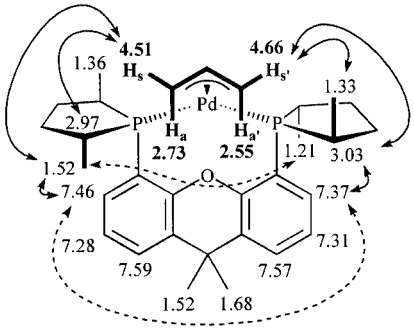

Scheme 6. Representation of relevant NOE contacts (plain arrows) and chemical exchanges (broken arrows) in **13** from ^1H ROESY; for the sake of clarity, NOEs associated with scalar couplings are not shown

Discussion

The purpose of this discussion is to try to establish a link between the structural information provided by the analysis of allyl palladium complexes and some of our most valuable results of palladium-catalysed allylic alkylations with diphospholane ligands, i.e. with substrates **3a** and **3c**.

As a result of the bite angle of the diphospholane, the conformation of the scaffold generates *exo*/*endo* isomerism in the Duxantphos complexes **11**−**13** and both forms are in equilibrium. In contrast, Duphos maintains a pseudo-C_2 symmetry when it is coordinated to the metal atom and there is no such isomerism. We have represented, in Scheme 7, some simplified front views of the allyl palladium complexes, in analogy with previously reported representations.[4] This allows us to visualise the interactions of the proximal methyl groups of the (*R*,*R*)-diphospholane ligands with the allyl moiety. The proximal methyl groups [(a) = down; (b) = up] have dramatically different positions depending on the ligand: with (*R*,*R*)-Duphos, (a) is on the right and (b) on the left, whereas the reverse is true with (*R*,*R*)-Duxantphos. However, this picture does not account for the distances between the methyl groups and the allyl plane which are shorter with Duxantphos than with Duphos (vide supra).

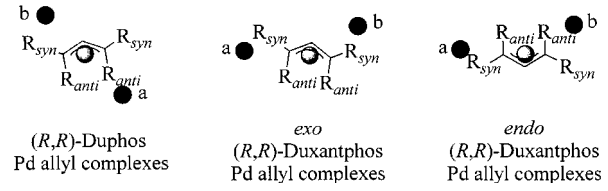

Scheme 7. Front-view representation of [Pd(diphospholane)(allyl)]$^+$ complexes; black circles = proximal methyl groups; gray circle = palladium centre

The example of the cyclohexenyl complex **11** {or of [Pd{(*R*,*R*)-Duthixantphospholane}(cyclohexenyl)]$^+$ [4a]} indicates that a methyl group (b) cannot accommodate an

 © 2004 Wiley-VCH Verlag GmbH & Co. KGaA, Weinheim

anti substituent on the right in the *endo* isomer. Therefore, an *endo* isomer of **11** could not be detected. On the other hand, when the allyl group is *syn*,*syn*-substituted with large phenyl groups (complex **12**), the *exo* and *endo* forms coexist in comparable proportions. Both undergo some internal steric congestion, as illustrated by the restricted rotation of some phenyl groups because of the proximity of phospholane methyl groups (Scheme 4, vide supra). *syn*,*anti* 1,3-Diphenylallyl complexes are normally destabilised by $H_{anti}-Ph_{anti}$ steric repulsion but can be present in significant quantity with a large, intrusive ancillary ligand.[22] Indeed, minor isomers of **12**, which are very probably *syn*,*anti*, coexist with the major *syn*,*syn* isomers, whereas [Pd(Duphos)(η^3-1,3-diphenylallyl)]$^+$ is exclusively *syn*,*syn*,[7] in connection with the fact that Duphos is less intrusive than Duxantphos. When Ph is replaced by a smaller Me on the Duxantphos complex, the *syn*,*anti* species become predominant.[4b] In brief, it appears that the proportion of each stereoisomer of a given allyl complex, whether it is related to *exo*/*endo* or to *syn*/*anti* isomerism, is the result of a subtle balance between various steric effects.

A general trend in our catalytic results in the field of allylic alkylation is a higher reactivity of ligand **2** compared with ligand **1**. Here, the reaction rate increases with the bite angle. Such an effect has already been reported in Pd-catalysed allylic alkylations, but it is not always the rule.[15,23] It can be interpreted as the consequence of a greater stability of the Pd^0-alkene complex which results from the nucleophilic attack on a $Pd^{II}-$allyl species, assuming that it is the rate-limiting step of the catalytic cycle.[24a] The origin of this stabilisation can be interpreted as the result of a decrease of the HOMO energy level, as suggested by Walsh diagrams.[6a]

With substrates that generate a symmetrically substituted η^3-allyl ligand (viz. substrates **3a**−**d**), the enantioselectivity of the catalytic process arises from the regioselectivity of the nucleophilic attack where the $Pd^{II}-\eta^3$-allyl complex is converted into a $Pd^0-\eta^2$-alkene complex. An interpretation of the origin of the enantioselectivity is provided by the concept of preferential rotation of the allyl group,[4,9] also referred to as torquoselectivity.[25] This interpretation is based on the hypothesis of a medium to late transition state[24] in which unhindered, thermodynamically more stable Pd^0-olefin products would be favoured. In the present case, enantiodiscrimination is governed by steric interactions between the proximal methyl groups and the coordinated alkene product (Schemes 7 and 8).

An explanation that accounts for the catalytic superiority of **2** over **1** with **3c** as the substrate is given in Scheme 8. In Scheme 8A, the methyl group (a) of (*R*,*R*)-Duphos is located low and far from the allylic carbon atoms and interacts very little with the cyclohexenyl moiety. Therefore, no major steric clash is expected whether the allyl group rotates clockwise or anticlockwise. This correlates well with the poor enantioselectivity of the reaction (5% *ee*). On the contrary, the situation with (*R*,*R*)-Duxantphos is the same as with (*R*,*R*)-Duthixantphos.[4] That is, an anticlockwise rotation is unfavourable because of the steric strain between

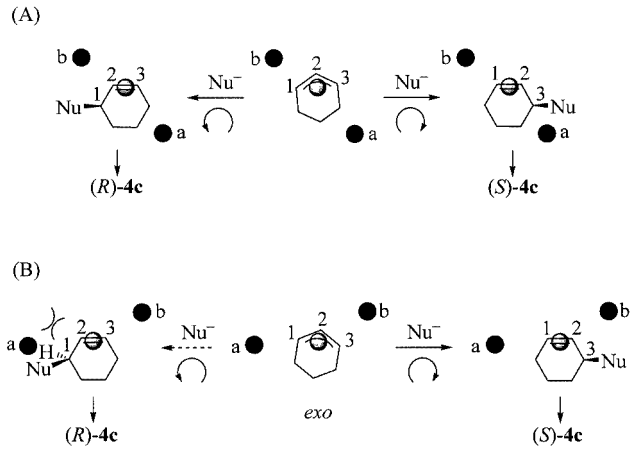

Scheme 8. Interpretation of the selectivity of the nucleophilic attack of the Pd−cyclohexenyl intermediate with (A) (*R*,*R*)-**1** or (B) (*R*,*R*)-**2** as ligands; Nu = $CH(COOMe)_2$

C1−H and the methyl group (a) in the Pd^0-olefin species, whereas no such strain hinders a clockwise rotation of the allyl group (Scheme 8B). Indeed, compound (*S*)-**4** is formed with a high *ee* (83%) in the catalytic process run with ligand (*R*,*R*)-**2**.

It has been reported that in palladium-catalysed asymmetric allylic alkylation, a twist of the allyl group (observed by X-ray crystallography) toward a product-like state might influence the regioselectivity of the nucleophilic attack.[16,24c] However, in complex [Pd{(*R*,*R*)-Duphos}(cyclohexenyl)]$^+$ which is the mirror image of **10**, the allyl group is twisted anticlockwise according to the crystal structure of **10**. Nevertheless, a clockwise rotation is slightly favoured. Hence, this is another argument against an early transition state with these ligands.

With the encumbered substrate **3a**, chirality transfer was very efficient in the catalytic reaction. The configurations of **4a** were found to be opposite with both diphospholane ligands, obviously because the positions of the proximal methyl groups (a) and (b), which undergo repulsive interaction with the phenyl substituents, are inverse (Scheme 9). If the nucleophile attacks the C3 atom of [Pd{(*R*,*R*)-Duphos}(cyclohexenyl)]$^+$, a very severe steric clash occurs between barrier (b) and the left-side phenyl group and, to a lesser extent, between barrier (a) and the right-side phenyl group (Scheme 9A). Nucleophilic attack at C1 accompanied with anticlockwise rotation of the allyl group does not experience a high energy barrier related to steric strain. This is in agreement with the formation of (*S*)-**4a** with 97% *ee*.

Things are more complicated with Duxantphos, with 4 diastereomers of the 1,3-diphenylallyl complex **12** being detected by $^{31}P\{^1H\}$ NMR spectroscopy (Scheme 9B). It is reasonable to suppose that the minor isomers **12c** and **12d** are the two *syn*,*anti* species shown in Scheme 9 (among four possible isomers), where no major steric clash exists between the proximal methyl groups and the phenyl substituents. *cis*-**4a** was not detected in the catalysed reaction. This implies that anticlockwise rotation upon nucleophilic attack

 © 2004 Wiley-VCH Verlag GmbH & Co. KGaA, Weinheim

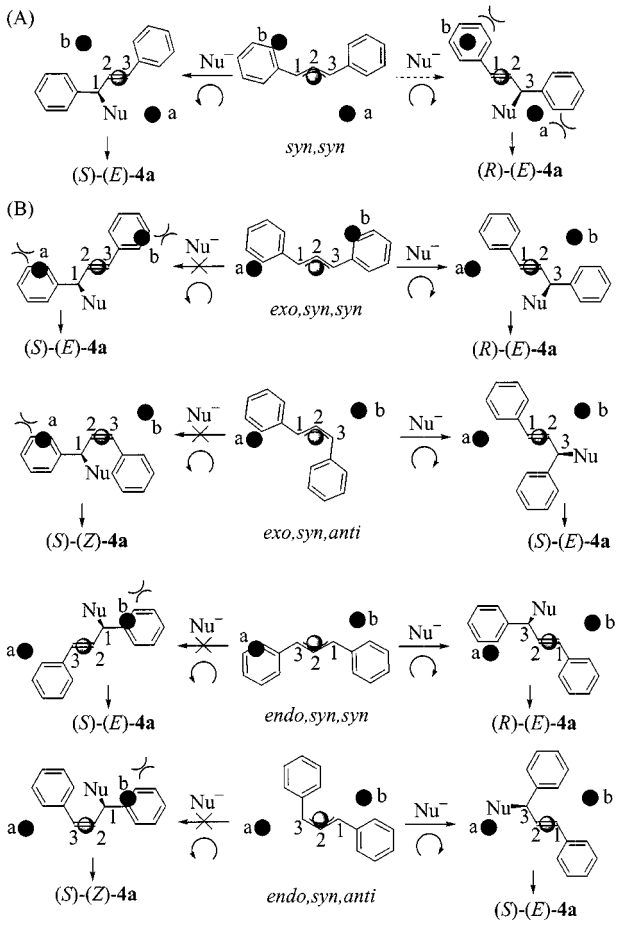

Scheme 9. Interpretation of the selectivity of the nucleophilic attack of the Pd−1,3-diphenylallyl intermediate with (A) (*R*,*R*)-**1** or (B) (*R*,*R*)-**2** as ligands; Nu = $CH(COOMe)_2$

of the *syn*,*anti* allyl complexes is forbidden because of steric repulsion of one of the phenyl groups with the methyl group (a) (*exo*) or (b) (*endo*). This raises the question as to why a sterically hindered movement of the allyl group is forbidden and not just slowed down. We propose two arguments to explain this: (1) from the comparison with the Duxantphos cyclohexenyl complex, it appears that the *syn* substituent is a bulky phenyl group and not a proton and (2), as stated above, the proximal methyl groups of Duxantphos are much closer to the allyl plane than those of Duphos. Since the environment of C1 is the same in the *exo*,*syn*,*syn* and the *exo*,*syn*,*anti* species represented in Scheme 9, an anticlockwise rotation of the *exo*,*syn*,*syn* allyl group must also be forbidden. The same reasoning is valid for the *endo* species.

Hence, only clockwise rotations occur in the four isomers of **12**, in analogy with the interpretation reported for the 1,3-dimethylallyl system.[4b] Both major *syn*,*syn* isomers lead to the (*R*) alkylated product, whereas the minor *syn*,*anti* species lead to the (*S*) product. Our interpretation based on the hypothesis of Curtin−Hammett conditions[24a] is in agreement with the high measured *ee* values (85−89%) of (*R*)-**4a**. In comparison with the case of Duphos, the presence of *syn*,*anti* catalytic intermediates is detrimental to the enantioselectivity. We are, however, aware that the interpretation proposed here is qualitative since we know nothing of the relative nucleophilic attack rate on each diastereomer of **12**. In particular, it looks probable that this rate is superior for **12a** than for **12b**: in the latter, a clockwise rotation may be somewhat hindered by the methyl group (a).

Conclusion

In this paper we have compared the catalytic and structural properties of the two chiral diphospholane ligands coordinated to Pd, viz. **1** and **2** which differ in their bite angle. Palladium-catalysed allylic alkylation tests have confirmed the success of xanthene-based diphospholane with the "symmetrical" allylic substrates **3a**−**d**[4] but this success was found to be somewhat limited. Attempts to use other kinds of substrates or nucleophiles, for example, led to modest selectivities at best. However, a strong positive bite angle effect was found in allylic alkylation with small, sterically unhindered substrates such as **3b**−**d**, where Duxantphos was much superior to Duphos in terms of reactivity and especially enantioselectivity.

Investigations of the 3D structures of the allyl complexes **10**−**13** were carried out by NMR spectroscopy and, whenever possible, by X-ray crystallography. Overall, these analyses have provided accurate indications about the structural differences between Duphos and Duxantphos. The increase in the bite angle induces a loss of C_2 symmetry of the ligand upon coordination and renders its proximal methyl groups more intrusive towards the allyl group. These differences have major consequences on the nature and distribution of the Pd−allyl intermediates and, furthermore, on the intimate mechanism of catalytic selectivity which is based on steric factors. We applied the preferential rotation concept which proved to be a very suitable model to account for the catalytic results. With (*R*,*R*)-Duxantphos, we found that a clockwise rotation in the nucleophilic attack step is the preferred, and sometimes the exclusive motion of the allyl group. (*R*,*R*)-Duphos, on the other hand, leads to anticlockwise rotation but only if the allyl group carries bulky phenyl substituents. In conclusion, the comparison of Duphos (**1**) with Duxantphos (**2**) emphasises the advantages of large bite angle ligands.

Experimental Section

General Procedures: All experiments were carried out under nitrogen or argon using a vacuum line or Vacuum Atmospheres glovebox equipped with a Dri-Train HE-493 inert gas purifier. Pentane, benzene, diethyl ether, and THF were distilled from sodium and benzophenone whereas acetonitrile and dichloromethane were distilled over calcium hydride under nitrogen immediately before use. Column chromatography was carried out on Merck silica gel 60, 70−230 mesh ASTM and thin layer chromatography on Macherey−Nagel 0.25 mm Polygram® Sil G/UV_{254} precoated silica gel plates. Commercial reagents were used as received: Strem: (*R*,*R*)- and (*S*,*S*)-Duphos, $AgBF_4$; Aldrich: dimethyl malonate,

 © 2004 Wiley-VCH Verlag GmbH & Co. KGaA, Weinheim

N,*O*-bis(trimethylsilyl)acetamide (BSA), potassium acetate, (*rac*)-2-methyl-1-tetralone, allyl acetate, 2,3-dihydrofuran, phenyl triflate, *N*,*N*-diisopropylethylamine, europium tris[3-(heptafluoropropylhydroxymethylene)-(+)-camphorate] [Eu(hfc)$_3$], $AgSbF_6$; Prolabo: *n*-heptane. NaH (60% in mineral oil; Fluka) was washed three times with pentane, dried in vacuo, and stored in the glovebox. (*R*,*R*)-Duxantphos was prepared according to ref.[4] The compounds listed hereafter were synthesised according to reported procedures: (*rac*)-(*E*)-1-acetoxy-1,3-diphenylprop-2-ene (**3a**),[26] (*rac*)-(*E*)-2-acetoxypent-3-ene (**3b**),[27] (*rac*)-1-acetoxycyclohex-2-ene (**3c**),[28] (*rac*)-1-acetoxycyclopent-2-ene (**3d**),[29] (*rac*)-(*E*)-2-acetoxy-4-phenylbut-3-ene (**5a**),[8] (*rac*)-(*E*)-3-acetoxy-2-methylhex-4-ene (**5b**),[30] bis[(η^3-allyl)chloropalladium],[31] bis[(η^3-cyclohexenyl)chloropalladium],[32] bis[(η^3-1,3-diphenylallyl)chloropalladium].[24f] NMR spectra were recorded at room temperature (unless otherwise indicated) with Bruker spectrometers. ^1H NMR spectra were recorded at 300.16 MHz (AC-300 instrument) or 500.13 MHz (ARX-500) and referenced to $SiMe_4$. The assignments and measurements of coupling constants were supported by irradiations. $^1H\{^{31}P\}$, ^1H COSY, and/or $^{31}P\{^1H\}$ COSY spectra were recorded with the ARX-500 instrument. $^{13}C\{^1H\}$ NMR spectra (broadband-decoupled) were recorded at 75.48 MHz (AC-300), 100.62 MHz (AM-400), or 125.76 MHz (ARX-500) and referenced to $SiMe_4$. The assignments were supported by DEPT-135°. $^{31}P\{^1H\}$ spectra (broadband-decoupled) were recorded at 121.51 MHz (AC-300) or 202.46 MHz (ARX-500) and referenced to 85% aqueous H_3PO_4. The phase-sensitive 2D ROESY spectra[33] were recorded with the ARX-500 spectrometer using mixing times of 0.25 s (^1H) or 0.1 s ($^{31}P\{^1H\}$). FAB MS spectra were carried out at the corresponding facilities at the Fédération de Recherche de Chimie, Université Louis Pasteur, Strasbourg and elemental analyses by the Service Central d'Analyses, CNRS, Vernaison. Optical rotations were checked with a Perkin−Elmer Otopol III polarimeter (λ = 589 nm). GC analyses were performed with a Hewlett Packard 5890 series II apparatus equipped with a 30 m × 0.25 mm SGE 25QC2 capillary column (for conversion measurements) or with a 30 m × 0.25 mm Restek Rt-βDEXse capillary column (for enantiomeric excess determinations). HPLC analyses were carried out with a Hewlett Packard series 1100 apparatus equipped with 250 mm × 4.6 mm Daicel Chiralcel® AD or OD analytical columns.

General Procedure for Palladium-Catalysed Allylic Alkylation with Dimethyl Malonate: A mixture of the diphospholane ligand (12 μmol) and [Pd(η^3-C_3H_5)Cl]$_2$ (1.8 mg, 5 μmol) in the appropriate solvent (CH_2Cl_2 or THF, 2 mL) was stirred at room temperature for 20 min. When BSA was used as a base, a suspension of KOAc (1 mg, 10 μmol) in the solvent (1 mL) was added to the catalyst solution, followed by a mixture of dimethyl malonate (264 mg, 2 mmol) and BSA (407 mg, 2 mmol) in the solvent (4 mL) and a solution of the substrate (1 mmol) in the solvent (1 mL). When NaH was used as a base, a solution of dimethyl sodiomalonate was prepared by allowing a solution of dimethyl malonate (264 mg, 2 mmol) in THF (1 mL) to react with a suspension of NaH (48 mg, 2 mmol) in THF (4 mL). A solution of the substrate (1 mmol) in THF (1 mL) was added to the catalyst solution, followed by the nucleophile solution. In both cases, the conversion was periodically monitored by GC. When the reaction was complete, water (25 mL) was added, and the organic phase was extracted with Et_2O (3 × 30 mL). The extract was dried with $MgSO_4$ and the solvent was removed under reduced pressure. The crude product was purified by column chromatography on silica gel with pentane/Et_2O (4:1, v/v). By comparison with literature data, the alkylation products were identified and, if necessary, their absolute stereochemistry was determined by polarimetry: dimethyl (*E*)-(1,3-diphenylprop-2-en-1-yl)malonate (**4a**),[34] dimethyl (*E*)-(pent-3-en-2-yl)malonate (**4b**),[35] dimethyl (cyclohex-2-en-1-yl)malonate (**4c**) and dimethyl (cyclopent-2-en-1-yl)malonate (**4d**),[36] dimethyl (*E*)-(4-phenylbut-3-en-2-yl)malonate (**6a**) and dimethyl (*E*)-(1-phenylbut-2-en-1-yl)malonate (**7a**),[8,9] dimethyl (*E*)-(5-methylhex-3-en-2-yl)malonate (**6b**) and dimethyl (*E*)-(2-methylhex-4-en-3-yl)malonate (**7b**).[35] The *ee* values were measured with the following methods: **4a**, chiral HPLC (Chiralcel AD, 1 mL·min^{-1}; eluent *n*-hexane/*i*PrOH, 95:5, v/v); **4b** and **4c**, chiral GC; **4d**, **6a**, **7a**, **6b**, and **7b**, ^1H NMR in $CDCl_3$ using Eu(hfc)$_3$ as a chiral shift reagent.

General Procedure for Palladium-Catalysed Allylic Alkylation with 2-Methyl-1-Tetralone: The procedure was adapted from ref.[13] To a solution or suspension of base (1.85 mmol) in THF (2 mL) was added 2-methyl-1-tetralone (150 mg, 0.94 mmol). A mixture of ligand **2** (4.4 mg, 10 μmol) and [Pd(η^3-C_3H_5)Cl]$_2$ (1.8 mg, 5 μmol) in THF (1 mL) was stirred at room temperature for 20 min. To the catalyst solution was added allyl acetate (187 mg, 1.87 mmol), followed by the nucleophile solution. The conversion was periodically monitored by GC. When the reaction was complete, the mixture was added to a 0.2 M aqueous HCl solution (25 mL) and extracted with Et_2O (3 × 30 mL). The extract was treated with saturated $NaHCO_3$ (aq.) and dried with $MgSO_4$. The solvent was removed under reduced pressure and the crude 2-allyl-2-methyl-1-tetralone purified by column chromatography on silica gel with pentane/EtOAc (v/v, 9:1; R_f = 0.52). The *ee* of the product was determined by chiral HPLC (Chiralcel OD, 0.7 mL·min^{-1}; eluent *n*-hexane/*i*PrOH, 99.9:0.1, v/v) and its absolute stereochemistry was assigned by comparison with ref.[13]

General Procedure for the Heck Reaction: The procedure was adapted from ref.[14] A mixture of diphospholane ligand (24 μmol) and the Pd source (12 μmol) in benzene (2 mL) was stirred at room temperature for 20 min. To the catalyst solution were successively added a solution of PhOTf (89 mg, 0.394 mmol) in benzene (1 mL), N*i*Pr$_2$Et (168 mg, 1.30 mmol), 2,3-dihydrofuran (155 mg, 2.21 mmol) and additional benzene (2 mL). The mixture was heated to reflux for 48 h. The solvent was removed under reduced pressure and the crude products were purified by column chromatography on silica gel with pentane/EtOAc (9:1, v/v). The absolute stereochemistry of the product was determined by comparing the sign of its optical rotation with data from ref.[14] The *ee* values were measured by chiral GC.

[Pd{(*S*,*S*)-Duphos}(η^3-cyclohexenyl)](BF$_4$) (10): To a solution of [Pd(η^3-C_6H_9)Cl]$_2$ (35 mg, 0.078 mmol) in acetonitrile (4 mL) was added dropwise in the dark at room temperature a solution of $AgBF_4$ (35 mg, 0.180 mmol) in acetonitrile (3 mL). After 10 min of stirring, the suspension was filtered through Celite and a suspension of (*S*,*S*)-Duphos (48 mg, 0,157 mmol) in acetonitrile (1 mL) was added to the colourless filtrate. A pale orange solution was obtained after 30 min of stirring. The solvent was evaporated in vacuo to afford a brown powder which was washed with diethyl ether. The product was recrystallized from dichloromethane/pentane as colourless crystals. Yield: 50 mg (55%). $^{31}P\{^1H\}$ NMR (CD_2Cl_2, 121 MHz): δ = 68.2 (d, $^2J_{P,P}$ = 36 Hz, 1 P), 71.9 (d, $^2J_{P,P}$ = 36 Hz, 1 P) ppm. ^1H NMR (CD_3CN, 300 MHz): δ 0.62 (dd, $^3J_{H,H}$ = 7.0, $^3J_{H,P}$ = 15.6 Hz, 3 H, CH_3), 0.85 (dd, $^3J_{H,H}$ = 7.0, $^3J_{H,P}$ = 15.6 Hz, 3 H, CH_3), 1.12 (dd, $^3J_{H,H}$ = 7.0, $^3J_{H,P}$ = 20.8 Hz, 3 H, CH_3), 1.35 (dd, $^3J_{H,H}$ = 7.1, $^3J_{H,P}$ = 20.5 Hz, 3 H, CH_3), 1.60−3.20 (m, 18 H, CH + CH_2), 5.33 (t, $^3J_{H,H}$ = 7.1 Hz, 1 H, H^2), 5.90 (m, 2 H, H^1 + H^3), 7.60−7.90 (m, 4 H, H_{ar}) ppm. $^{13}C\{^1H\}$ NMR (CD_2Cl_2, 75 MHz): δ = 14.8 (s, 2 CH_3), 18.4 (d, $^2J_{C,P}$ = 12 Hz, CH_3), 18.7 (d, $^2J_{C,P}$ = 12 Hz, CH_3), 20.4 (s, CH_2), 28.1 (d, $^2J_{C,P}$ = 5 Hz, CH_2), 29.4 (d, $^2J_{C,P}$ = 5 Hz, CH_2), 36.2 (d,

 © 2004 Wiley-VCH Verlag GmbH & Co. KGaA, Weinheim

$^2J_{C,P}$ = 5 Hz, CH_2), 36.5 (d, $^2J_{C,P}$ = 5 Hz, CH_2), 37.2 (s, CH_2), 37.5 (s, CH_2), 38.6 (d, $^1J_{C,P}$ = 24 Hz, CH), 40.7 (d, $^1J_{C,P}$ = 22 Hz, CH), 41.0 (d, $^1J_{C,P}$ = 26 Hz, CH), 41.3 (d, $^1J_{C,P}$ = 24 Hz, CH), 81.9 (dd, $^2J_{C,P}$ = 29, $^2J_{C,P}$ = 3 Hz, $C_{allyl\ terminal}$), 87.1 (dd, $^2J_{C,P}$ = 29, $^2J_{C,P}$ = 3 Hz, $C_{allyl\ terminal}$), 113.8 (t, $^2J_{C,P}$ = 7 Hz, $C_{allyl\ central}$), 132.6 (s, 2 CH_{ar}), 134.1 (d, $^2J_{C,P}$ = 12 Hz, CH_{ar}), 134.3 (d, $^2J_{C,P}$ = 12 Hz, CH_{ar}), 141.2 (m, 2 C_{ar}) ppm. MS (FAB^+, NBA matrix): *m*/*z* (%) = 493.0 (100) $[M - BF_4]^+$, 412.9 (37) $[M + 1 - BF_4 - C_6H_9]^+$. $C_{24}H_{37}BF_4P_2Pd$ (580.71): calcd. C 49.64, H 6.42, P 10.67; found C 49.59, H 6.34, P 10.80.

[Pd{(*R*,*R*)-Duxantphos}(η³-cyclohexenyl)](SbF₆) (11): To a solution of $[Pd(\eta^3\text{-}C_6H_9)Cl]_2$ (20 mg, 0.045 mmol) in THF (2 mL) was added dropwise in the dark at room temperature a solution of $AgSbF_6$ (32 mg, 0.093 mmol) in THF (2 mL). After 15 min of stirring, the suspension was filtered through Celite and a solution of (*R*,*R*)-Duxantphos (42 mg, 0.096 mmol) in THF (2 mL) was added to the colourless filtrate. A yellow solution was obtained after 30 min of stirring and the solvent was evaporated in vacuo to afford a yellow powder which was washed with pentane. The product was recrystallized from dichloromethane/diethyl ether. Yield: 72 mg (93%). $^{31}P\{^1H\}$ NMR (CD_2Cl_2, 121 MHz): δ = 33.7 (d, $^2J_{P,P}$ = 41 Hz, 1 P), 35.5 (d, $^2J_{P,P}$ = 41 Hz, 1 P) ppm. ^1H NMR (CD_2Cl_2, 300 MHz): δ = 0.06 (m, 1 H, CH_2), 0.24 (m, 1 H, CH_2), 0.46 (m, 1 H, CH_2), 0.60−0.80 (m, 2 H, CH_2), 1.13 (dd, $^3J_{H,H}$ = 7.3, $^3J_{H,P}$ = 14.7 Hz, 3 H, $CH_{3\ phospholane}$), 1.25 (dd, $^3J_{H,H}$ = 7.6, $^3J_{H,P}$ = 20.5 Hz, 3 H, $CH_{3\ phospholane}$), 1.32 (dd, $^3J_{H,H}$ = 7.6, $^3J_{H,P}$ = 19.3 Hz, 3 H, $CH_{3\ phospholane}$), 1.20−1.75 (m, 3 H, CH_2), 1.41 (s, 3 H, $CH_{3\ xanthene}$), 1.79 (s, 3 H, $CH_{3\ xanthene}$), 1.80 (dd, $^3J_{H,H}$ = 7.3, $^3J_{H,P}$ = 14.2 Hz, 3 H, $CH_{3\ phospholane}$), 2.07−2.40 (m, 5 H, CH_2), 2.63 (m, 1 H, CH_2), 2.80−3.00 (m, 3 H, CH), 3.09 (m, 1 H, CH), 5.20 (t, $^3J_{H,H}$ = 7.1 Hz, 1 H, H^2), 5.60−5.75 (m, 2 H, H^1 + H^3), 7.13−7.30 (m, 2 H, H_{ar}), 7.36 (m, 1 H, H_{ar}), 7.50−7.62 (m, 3 H, H_{ar}) ppm. $^{13}C\{^1H\}$ NMR (CD_3CN, 75 MHz): δ = 14.5 (s, $CH_{3\ phospholane}$), 17.5 (d, $^2J_{C,P}$ = 5 Hz, $CH_{3\ phospholane}$), 19.4 (d, $^2J_{C,P}$ = 9 Hz, $CH_{3\ phospholane}$), 20.0 (s, CH_2), 20.2 (d, $^2J_{C,P}$ = 14 Hz, $CH_{3\ phospholane}$), 24.2 (s, $CH_{3\ xanthene}$), 26.9 (d, $^2J_{C,P}$ = 5 Hz, CH_2), 27.2 (d, $^2J_{C,P}$ = 5 Hz, CH_2), 32.1 (s, CH_2), 32.4 (s, $CH_{3\ xanthene}$), 32.6 (s, CH_2), 32.9 (d, $^1J_{C,P}$ = 22 Hz, CH), 33.6 (s, CH_2), 33.9 (d, $^1J_{C,P}$ = 20 Hz, CH), 34.0 (d, $^1J_{C,P}$ = 14 Hz, CH), 34.7 (s, CH_2), 36.8 [s, $C(CH_3)_2$], 37.0 (d, $^1J_{C,P}$ = 27 Hz, CH), 81.3 (d, $^2J_{C,P}$ = 28 Hz, $C_{allyl\ terminal}$), 93.3 (d, $^2J_{C,P}$ = 25 Hz, $C_{allyl\ terminal}$), 109.1 (t, $^2J_{C,P}$ = 5 Hz, $C_{allyl\ central}$), 119.2 (d, $^2J_{C,P}$ = 27 Hz, C_{ar}), 120.1 (d, $^2J_{C,P}$ = 23 Hz, C_{ar}), 125.4 (d, $^3J_{C,P}$ = 4 Hz, CH_{ar}), 126.2 (d, $^3J_{C,P}$ = 4 Hz, CH_{ar}), 128.3 (s, CH_{ar}), 128.8 (s, 2 CH_{ar}), 130.9 (s, CH_{ar}), 134.4 (s, C_{ar}), 135.2 (s, C_{ar}), 153.4 (d, $^1J_{C,P}$ = 7 Hz, C_{ar}), 153.8 (d, $^1J_{C,P}$ = 7 Hz, C_{ar}) ppm. MS (FAB^+, NBA matrix): *m*/*z* (%) = 625.2 (68) $[M - SbF_6]^+$, 545.1 (100) $[M + 1 - SbF_6 - C_6H_9]^+$.

[Pd{(*R*,*R*)-Duxantphos}(η³-1,3-diphenylallyl)](SbF₆) (12): To a suspension of $[Pd(\eta^3\text{-}Ph_2C_3H_3)Cl]_2$ (30 mg, 0.045 mmol) in CH_2Cl_2 (3 mL) was added dropwise in the dark at room temperature a solution of $AgSbF_6$ (31 mg, 0.090 mmol) in CH_2Cl_2 (2 mL). After 20 min of stirring, the suspension was filtered through Celite and a solution of (*R*,*R*)-Duxantphos (40 mg, 0.091 mmol) in CH_2Cl_2 (2 mL) was added to the red filtrate. An orange-brown solution was obtained after 20 min of stirring. The product precipitated upon slow addition of pentane. It was then separated from the yellow supernatant, washed with diethyl ether, and dried. Yield: 70 mg (80%). HRMS (FAB^+, NBA matrix): *m*/*z* calcd. for $C_{42}H_{49}OP_2{}^{105}Pd$ 736.23094; found 736.23067.

***syn*,*syn*,*exo*-12a:** $^{31}P\{^1H\}$ NMR (CD_2Cl_2, 202.5 MHz, 193 K): δ = 27.6 (d, $^2J_{P,P}$ = 52 Hz, 1 P), 39.2 (d, $^2J_{P,P}$ = 52 Hz, 1 P) ppm. ^1H NMR (CD_2Cl_2, 500 MHz, 193 K), selected data (see also Scheme 3): δ = −0.08 (dd, $^3J_{H,H}$ = 7.0, $^3J_{H,P}$ = 14.9 Hz, 3 H, $CH_{3\ phospholane}$), 0.85 (dd, $^3J_{H,H}$ = 7.4, $^3J_{H,P}$ = 22.2 Hz, 3 H, $CH_{3\ phospholane}$), 0.87 (dd, $^3J_{H,H}$ = 7.1, $^3J_{H,P}$ = 14.0 Hz, 3 H, $CH_{3\ phospholane}$), 1.05 (dd, $^3J_{H,H}$ = 7.4, $^3J_{H,P}$ = 22.2 Hz, 3 H, $CH_{3\ phospholane}$), 1.58 (s, 3 H, $CH_{3\ xanthene}$), 1.65 (s, 3 H, $CH_{3\ xanthene}$), 4.69 (t, $^3J_{H,H}$ = $^3J_{H,P}$ = 10.8 Hz, 1 H, H_{allyl}), 5.38 (dd, $^3J_{H,H}$ = 13.7, $^3J_{H,P}$ = 9.4 Hz, 1 H, H_{allyl}), 6.35 (ddd, $^3J_{H,H}$ = 14.0, $^3J_{H,H}$ = 10.0, $^3J_{H,P}$ = 2.2 Hz, 1 H, H_{allyl}) ppm. $^{13}C\{^1H\}$ NMR (CD_3NO_2, 125 MHz, 263 K), selected data: δ = 14.6 (s, $CH_{3\ phospholane}$), 15.2 (s, 2 $CH_{3\ phospholane}$), 17.8 (s, $CH_{3\ phospholane}$), 21.3 (d, $^1J_{C,P}$ = 14 Hz, CH), 22.5 (d, $^1J_{C,P}$ = 13 Hz, CH), 25.0 (s, $CH_{3\ xanthene}$), 29.2 (s, $CH_{3\ xanthene}$), 33.2 (s, CH_2), 34.9 (s, CH_2), 35.1 (s, CH_2), 36.3 (s, CH_2), 36.7 (d, $^1J_{C,P}$ = 20 Hz, CH), 38.2 (d, $^1J_{C,P}$ = 19 Hz, CH), 38.6 [s, $C(CH_3)_2$], 77.8 (d, $^2J_{C,P}$ = 30 Hz, $C_{allyl\ terminal}$), 100.2 (d, $^2J_{C,P}$ = 20 Hz, $C_{allyl\ terminal}$), 110.4 (s, $C_{allyl\ central}$) ppm.

***syn*,*syn*,*endo*-12b:** $^{31}P\{^1H\}$ NMR (CD_2Cl_2, 202.5 MHz, 193 K): δ = 32.8 (d, $^2J_{P,P}$ = 57 Hz, 1 P), 40.6 (d, $^2J_{P,P}$ = 57 Hz, 1 P) ppm. ^1H NMR (CD_2Cl_2, 500 MHz, 193 K), selected data (see also Scheme 3): δ = 0.80 (dd, $^3J_{H,H}$ = 7.2, $^3J_{H,P}$ = 14.5 Hz, 3 H, $CH_{3\ phospholane}$), 0.96 (dd, $^3J_{H,H}$ = 7.4, $^3J_{H,P}$ = 15.1 Hz, 3 H, $CH_{3\ phospholane}$), 1.10 (dd, $^3J_{H,H}$ = 7.6, $^3J_{H,P}$ = 22.4 Hz, 3 H, $CH_{3\ phospholane}$), 1.32 (s, 3 H, $CH_{3\ xanthene}$), 1.36 (dd, $^3J_{H,H}$ = 7.3, $^3J_{H,P}$ = 18.8 Hz, 3 H, $CH_{3\ phospholane}$), 1.88 (s, 3 H, $CH_{3\ xanthene}$), 4.92 (t, $^3J_{H,H}$ = $^3J_{H,P}$ = 11.1 Hz, 1 H, H_{allyl}), 5.03 (dd, $^3J_{H,H}$ = 13.0, $^3J_{H,P}$ = 9.2 Hz, 1 H, H_{allyl}), 5.21 (t, $^3J_{H,H}$ = 12.5 Hz, 1 H, H_{allyl}) ppm.

Minor Isomer 12c: $^{31}P\{^1H\}$ NMR (CD_2Cl_2, 202.5 MHz, 193 K): δ = 35.3 (d, $^2J_{P,P}$ = 45 Hz, 1 P), 37.2 (d, $^2J_{P,P}$ = 45 Hz, 1 P) ppm.

Minor Isomer 12d: $^{31}P\{^1H\}$ NMR (CD_2Cl_2, 202.5 MHz, 193 K): δ = 28.3 (d, $^2J_{P,P}$ = 46 Hz, 1 P), 36.0 (d, $^2J_{P,P}$ = 46 Hz, 1 P) ppm.

[Pd{(*R*,*R*)-Duxantphos}(η³-allyl)](SbF₆) (13): To a solution of $[Pd(\eta^3\text{-}C_3H_5)Cl]_2$ (35 mg, 0.096 mmol) in CH_2Cl_2 (4 mL) was added dropwise in the dark at room temperature a solution of $AgSbF_6$ (63 mg, 0.183 mmol) in CH_2Cl_2 (1 mL). After 10 min of stirring, the suspension was filtered through Celite and a solution of (*R*,*R*)-Duxantphos (80 mg, 0.182 mmol) in CH_2Cl_2 (2 mL) was added to the yellow filtrate. A brown solution was obtained after 10 min of stirring. The volume was reduced in vacuo and the product was precipitated by slow addition of pentane and collected on a frit as a brown powder. Yield: 115 mg (77%). $^{31}P\{^1H\}$ NMR (CD_2Cl_2, 121 MHz) : δ = 33.1 (d, $^2J_{P,P}$ = 38 Hz, 1 P), 33.5 (d, $^2J_{P,P}$ = 38 Hz, 1 P) ppm. ^1H NMR (CD_2Cl_2, 500 MHz), selected data (see also Scheme 6): δ = 1.21 (dd, $^3J_{H,H}$ = 7.3, $^3J_{H,P}$ = 14.6 Hz, 3 H, $CH_{3\ phospholane}$), 1.33 (dd, $^3J_{H,H}$ = 7.5, $^3J_{H,P}$ = 20.2 Hz, 3 H, $CH_{3\ phospholane}$), 1.36 (dd, $^3J_{H,H}$ = 7.5, $^3J_{H,P}$ = 19.5 Hz, 3 H, $CH_{3\ phospholane}$), 1.52 (dd, $^3J_{H,H}$ = 7.2, $^3J_{H,P}$ = 14.5 Hz, 3 H, $CH_{3\ phospholane}$), 1.52 (s, 3 H, $CH_{3\ xanthene}$), 1.68 (s, 3 H, $CH_{3\ xanthene}$), 1.60−2.10 (m, 4 H, CH_2), 2.20−2.40 (m, 3 H, CH_2), 2.51 (m, 1 H, CH_2), 2.55 (dd, $^3J_{H,H}$ = 13.6, $^3J_{H,P}$ = 8.8 Hz, 1 H, H_{anti}), 2.73 (dd, $^3J_{H,H}$ = 13.1, $^3J_{H,P}$ = 9.6 Hz, 1 H, H_{anti}), 2.85−3.10 (m, 4 H, CH), 4.51 (dddd, $^3J_{H,H}$ = 7.4, $^4J_{H,H}$ = 2.3, $^3J_{H,P}$ = 2.2, 0.6 Hz, 1 H, H_{syn}), 4.66 (dddd, $^3J_{H,H}$ = 7.2, $^4J_{H,H}$ = 2.5, $^3J_{H,P}$ = 2.9, 0.6 Hz, 1 H, H_{syn}), 5.18 (tt, $^3J_{H,H}$ = 13.3, $^3J_{H,H}$ = 7.3 Hz, 1 H, $H_{central}$), 7.28 (td, $^3J_{H,H}$ = 7.7, $^4J_{H,P}$ = 1.5 Hz, 1 H, H_{ar}), 7.31 (td, $^3J_{H,H}$ = 7.6, $^4J_{H,P}$ = 1.5 Hz, 1 H, H_{ar}), 7.37 (ddd, $^3J_{H,H}$ = 7.7, $^4J_{H,H}$ = 1.4, $^3J_{H,P}$ = 6.3 Hz, 1 H, H_{ar}), 7.46 (ddd, $^3J_{H,H}$ = 7.7, $^4J_{H,H}$ = 1.2, $^3J_{H,P}$ = 7.6 Hz, 1 H, H_{ar}), 7.57 (ddd, $^3J_{H,H}$ = 7.7, $^4J_{H,H}$ = 1.3, $^5J_{H,P}$ = 0.8 Hz, 1 H, H_{ar}), 7.59 (ddd, $^3J_{H,H}$ = 7.8, $^4J_{H,H}$ = 1.4, $^5J_{H,P}$ = 0.7 Hz, 1 H, H_{ar}) ppm. $^{13}C\{^1H\}$ NMR (CD_2Cl_2, 100 MHz): δ = 14.9 (d, $^2J_{C,P}$ = 2 Hz, $CH_{3\ phospholane}$), 15.9 (d, $^2J_{C,P}$ = 4 Hz, $CH_{3\ phospholane}$), 19.3

 © 2004 Wiley-VCH Verlag GmbH & Co. KGaA, Weinheim

Table 5. Crystal and refinement data for compounds **10** and **11**

	10	**11**
Empirical formula	$C_{24}H_{37}P_2Pd{\cdot}BF_4$	$C_{33}H_{45}OP_2Pd{\cdot}SbF_6$
Formula mass	580.72	861.81
Colour	colourless	colourless
Crystal system	monoclinic	orthorhombic
a [Å]	8.2100(2)	12.041(1)
b [Å]	18.6150(7)	12.425(2)
c [Å]	8.5920(3)	22.917(4)
β [°]	97.553(2)	90
V [Å^3]	1301.7(1)	3428(1)
Z	2	4
$D_{calcd.}$ [g cm^{-3}]	1.48	1.67
*F*000	596	1728
Wavelength [Å]	0.71073	0.71073
μ [mm^{-1}]	0.874	1.459
Space group	P 1 2_1 1	P 2_1 2_1 2_1
Diffractometer	KappaCCD	MACH3 Nonius
Cryst dimens [mm]	0.15 × 0.12 × 0.12	0.40 × 0.25 × 0.20
Temperature [K]	173	173
Radiation	Mo-K_α graphite-monochromated	Mo-K_α graphite-monochromated
Scan mode	φ scans	θ/2θ
hkl limits	−10/10, −26/26, −12/12	0/15, −15/0, 0/28
θ limits [°]	2.5/30.56	2.5/26.29
No. of data measured	19463	3917
No. of data with $I > 3\sigma(I)$	2887	3318
Weighting scheme	$4F_o^2/[\sigma^2(F_o^2) + 0.0004\ F_o^4] + 1.0$	$4F_o^2/[\sigma^2(F_o^2) + 0.0016\ F_o^4]$
No. of variables	297	397
R	0.067	0.025
R_w	0.088	0.031
Flack parameter	0.0(1)	−0.02(3)
Largest peak in final difference [e·Å^{-3}]	0.738	0.567
GOF	1.612	1.096

(d, $^2J_{C,P}$ = 9 Hz, $CH_{3\ phospholane}$), 19.9 (d, $J_{C,P}$ = 10 Hz, $CH_{3\ phospholane}$), 25.9 (s, $CH_{3\ xanthene}$), 29.4 (s, $CH_{3\ xanthene}$), 32.0 (s, CH_2), 32.4 (s, CH_2), 32.7 (s, CH_2), 33.3 (s, CH_2), 33.4 (dd, $^1J_{C,P}$ = 23, $^3J_{C,P}$ = 2 Hz, CH), 33.7 (dd, $^1J_{C,P}$ = 17, $^3J_{C,P}$ = 2 Hz, CH), 34.0 (dd, $^1J_{C,P}$ = 19, $^3J_{C,P}$ = 3 Hz, CH), 35.3 (dd, $^1J_{C,P}$ = 22, $^3J_{C,P}$ = 3 Hz, CH), 36.1 [s, $C(CH_3)_2$], 66.8 (dd, $^2J_{C,P}$ = 26, $^2J_{C,P}$ = 3 Hz, $CH_{allyl\ terminal}$), 72.6 (dd, $^2J_{C,P}$ = 25, $^2J_{C,P}$ = 3 Hz, $CH_{allyl\ terminal}$), 118.2 (dd, $^2J_{C,P}$ = 27, $^4J_{C,P}$ = 2 Hz, C_{ar}), 118.5 (dd, $^2J_{C,P}$ = 24, $^4J_{C,P}$ = 2 Hz, C_{ar}), 118.7 (t, $^2J_{C,P}$ = 5 Hz, $CH_{allyl\ central}$), 124.8 (d, $^2J_{C,P}$ = 6 Hz, CH_{ar}), 125.3 (d, $^2J_{C,P}$ = 5 Hz, CH_{ar}), 127.3 (s, CH_{ar}), 127.6 (d, $^3J_{C,P}$ = 2 Hz, CH_{ar}), 127.9 (d, $^3J_{C,P}$ = 2 Hz, CH_{ar}), 128.6 (s, CH_{ar}), 134.1 (d, $^3J_{C,P}$ = 3 Hz, C_{ar}), 134.4 (d, $^3J_{C,P}$ = 3 Hz, C_{ar}), 153.2 (d, $^1J_{C,P}$ = 6 Hz, C_{ar}), 153.4 (d, $^1J_{C,P}$ = 6 Hz, C_{ar}) ppm. HRMS (FAB$^+$, NBA matrix): *m*/*z* calcd. for $C_{30}H_{41}OP_2{}^{105}Pd$ 584.1683; found 584.1689.

X-ray Crystallographic Studies: Details of data collection parameters and refinement results are listed in Table 5. The structures were solved by direct methods. Hydrogen atoms were introduced as fixed contributors in calculated positions [C−H = 0.95 Å, *B*(H) = 1.3 B_{equiv}]. Final difference maps revealed no significant maxima. All calculations were performed using the Nonius OpenMoleN package.[37] Neutral atom scattering factor coefficients and anomalous dispersion coefficients were taken from a standard source.[38] CCDC-236309 (**10**) and -236310 (**11**) contain the supplementary crystallographic data for this paper. These data can be obtained free of charge at www.ccdc.cam.ac.uk/conts/retrieving.html [or from the Cambridge Crystallography Data Centre, 12 Union Road, Cambridge CB2 1EZ, UK [Fax: + 44-1223/336-033; E-mail: deposit@ccdc.cam.ac.uk].

Acknowledgments

We thank Denis Sinou for helpful discussions and Rafael Aguado and Peter Dierkes for a gift of ligand **2**. Financial support from the Centre National de la Recherche Scientifique is gratefully acknowledged.

[1] Reviews and selected papers: [1a] C. G. Frost, J. Howarth, J. M. J. Williams, *Tetrahedron: Asymmetry* **1992**, *3*, 1089−1122. [1b] B. M. Trost, D. L. Van Vranken, *Chem. Rev.* **1996**, *96*, 395−422. [1c] G. Helmchen, *J. Organomet. Chem.* **1999**, *576*, 203−214. [1d] K. H. Ahn, C.-W. Cho, J. Park, S. Lee, *Tetrahedron: Asymmetry* **1997**, *8*, 1179−1185. [1e] A. Saitoh, M. Misawa, T. Morimoto, *Tetrahedron: Asymmetry* **1999**, *10*, 1025−1028. [1f] W. Zhang, T. Shimanuki, T. Kida, Y. Nakatsuji, I. Ikeda, *J. Org. Chem.* **1999**, *64*, 6247−6251. [1g] D. A. Evans, K. R. Campos, J. D. Tedrow, F. E. Michael, M. R. Gagné, *J. Am. Chem. Soc.* **2000**, *122*, 7905−7920. [1h] K. Ito, R. Kashiwagi, S. Hayashi, T. Uchida, T. Katsuki, *Synlett* **2001**, 284−286. [1i] S. J. Greenfield, A. Agarkov, S. R. Gilbertson, *Org. Lett.* **2003**, *5*, 3069−3072.

[2] [2a] A. Pfaltz, M. Lautens, in: *Comprehensive Asymmetric Catalysis* (Eds.: E. Jacobsen, A. Pfaltz, H. Yamamoto), Springer, Berlin, **1999**, vol. II, chapter 24, pp. 833−884. [2b] M. Shibasaki, E. M. Vogl, in: *Comprehensive Asymmetric Catalysis* (Eds.: E. Jacobsen, A. Pfaltz, H. Yamamoto), Springer, Berlin, **1999**, vol. I, chapter 14, pp. 457−487.

[3] [3a] P. S. Pregosin, G. Trabesinger, *J. Chem. Soc., Dalton Trans.* **1998**, 727−734. [3b] P. S. Pregosin, R. Salzmann, *Coord. Chem. Rev.* **1996**, *155*, 35−68.

 © 2004 Wiley-VCH Verlag GmbH & Co. KGaA, Weinheim

[4] [4a] P. Dierkes, S. Ramdeehul, L. Barloy, A. De Cian, J. Fischer, P. C. J. Kamer, P. W. N. M. van Leeuwen, J. A. Osborn, *Angew. Chem. Int. Ed.* **1998**, *37*, 3116−3118. [4b] S. Ramdeehul, P. Dierkes, R. Aguado, P. C. J. Kamer, P. W. N. M. van Leeuwen, J. A. Osborn, *Angew. Chem. Int. Ed.* **1998**, *37*, 3118−3121.
[5] M. J. Burk, *Acc. Chem. Res.* **2000**, *33*, 363−372.
[6] [6a] P. Dierkes, P. W. N. M. van Leeuwen, *J. Chem. Soc., Dalton Trans.* **1999**, 1519−1529. [6b] P. W. N. M. van Leeuwen, P. C. J. Kamer, J. N. H. Reek, P. Dierkes, *Chem. Rev.* **2000**, *100*, 2741−2769. [6c] Z. Freixa, P. W. N. M. van Leeuwen, *Dalton Trans.* **2003**, 1890−1901.
[7] D. Drago, P. S. Pregosin, *J. Chem. Soc., Dalton Trans.* **2000**, 3191−3196.
[8] T. Hayashi, A. Yamamoto, T. Hagihara, *J. Org. Chem.* **1986**, *51*, 723−727.
[9] E. Peña-Cabrera, P.-O. Norrby, M. Sjögren, A. Vitagliano, V. De Felice, J. Oslob, S. Ishii, D. O′Neill, B. Åkermark, P. Helquist, *J. Am. Chem. Soc.* **1996**, *118*, 4299−4313.
[10] K. Selvakumar, M. Valentini, M. Wörle, P. S. Pregosin, A. Albinati, *Organometallics* **1999**, *18*, 1207−1215.
[11] [11a] I. J. S. Fairlamb, G. C. Lloyd−Jones, Š. Vyskočil, P. Kočovský, *Chem. Eur. J.* **2002**, *8*, 4343−4353. [11b] L. Gouriou, G. C. Lloyd−Jones, Š. Vyskočil, P. Kočovský, *J. Organomet. Chem.* **2003**, *687*, 525−537.
[12] J. C. Fiaud, A. Hibon de Gournay, M. Larchevêque, H. B. Kagan, *J. Organomet. Chem.* **1978**, *154*, 175−185.
[13] B. M. Trost, G. M. Schroeder, *J. Am. Chem. Soc.* **1999**, *121*, 6759−6760.
[14] F. Ozawa, A. Kubo, Y. Matsumoto, T. Hayashi, E. Nishioka, K. Yanagi, K. Moriguchi, *Organometallics* **1993**, *12*, 4188−4196.
[15] M. Kranenburg, P. C. J. Kamer, P. W. N. M. van Leeuwen, *Eur. J. Inorg. Chem.* **1998**, 25−27.
[16] R. J. van Haaren, K. Goubitz, J. Fraanje, G. P. F. van Strijdonck, H. Oevering, B. Coussens, J. N. H. Reek, P. C. J. Kamer, P. W. N. M. van Leeuwen, *Inorg. Chem.* **2001**, *40*, 3363−3372.
[17] A. C. Albéniz, P. Espinet, B. Martín-Ruiz, *Chem. Eur. J.* **2001**, *7*, 2481−2489.
[18] M. Kollmar, B. Goldfuss, M. Reggelin, F. Rominger, G. Helmchen, *Chem. Eur. J.* **2001**, *7*, 4913−4927.
[19] P. E. Garrou, *Chem. Rev.* **1981**, *81*, 229−266.
[20] I. J. S. Fairlamb, G. C. Lloyd-Jones, *Chem. Commun.* **2000**, 2447−2448.
[21] [21a] R. S. Paonessa, A. L. Prignano, W. C. Trogler, *Organometallics* **1985**, *4*, 647−657. [21b] F. Ozawa, T.-i. Son, S. Ebina, K. Osakada, A. Yamamoto, *Organometallics* **1992**, *11*, 171−176.
[22] P. Barbaro, P. S. Pregosin, R. Salzmann, A. Albinati, R. W. Kunz, *Organometallics* **1995**, *14*, 5160−5170.
[23] R. J. van Haaren, H. Oevering, B. B. Coussens, G. P. F. van Strijdonck, J. N. H. Reek, P. C. J. Kamer, P. W. N. M. van Leeuwen, *Eur. J. Inorg. Chem.* **1999**, 1237−1241.
[24] The question of an early or late transition state for this step has been a matter of debate: [24a] P. B. Mackenzie, J. Wheland, B. Bosnich, *J. Am. Chem. Soc.* **1985**, *107*, 2046−2054. [24b] J. Sprinz, M. Kiefer, G. Helmchen, M. Reggelin, G. Huttner, O. Walter, L. Zsolnai, *Tetrahedron Lett.* **1994**, *35*, 1523−1526. [24c] A. Togni, U. Burckhardt, V. Gramlich, P. S. Pregosin, R. Salzmann, *J. Am. Chem. Soc.* **1996**, *118*, 1031−1037. [24d] B. M. Trost, L. Weber, P. E. Strege, T. J. Fullerton, T. J. Dietsche, *J. Am. Chem. Soc.* **1978**, *100*, 3416−3426. [24e] J. M. Brown, D. I. Hulmes, P. J. Guiry, *Tetrahedron* **1994**, *50*, 4493−4506. [24f] P. von Matt, G. C. Lloyd-Jones, A. B. E. Minidis, A. Pfaltz, L. Macko, M. Neuburger, M. Zehnder, H. Rüegger, P. S. Pregosin, *Helv. Chim. Acta* **1995**, *78*, 265−284. [24g] P. E. Blöchl, A. Togni, *Organometallics* **1996**, *15*, 4125−4132. [24h] H. Steinhagen, M. Reggelin, G. Helmchen, *Angew. Chem. Int. Ed. Engl.* **1997**, *36*, 2108−2110. [24i] H. Hagelin, B. Åkermark, P.-O. Norrby, *Chem. Eur. J.* **1999**, *5*, 902−909.
[25] G. C. Lloyd-Jones, S. C. Stephen, M. Murray, C. P. Butts, Š. Vyskočil, P. Kočovský, *Chem. Eur. J.* **2000**, *6*, 4348−4357.
[26] P. R. Auburn, P. B. Mackenzie, B. Bosnich, *J. Am. Chem. Soc.* **1985**, *107*, 2033−2046.
[27] J. C. McKew, M. J. Kurth, *J. Org. Chem.* **1993**, *58*, 4589−4595.
[28] A. Heumann, B. Åkermark, S. Hansson, T. Rein, *Org. Synth. Coll. Vol.* **1993**, *8*, 137−140.
[29] [29a] W. H. Bunnelle, T. A. Isbell, *J. Org. Chem.* **1992**, *57*, 729−740. [29b] B. M. Trost, M. G. Organ, G. A. O'Doherty, *J. Am. Chem. Soc.* **1995**, *117*, 9662−9670.
[30] I. Fleming, D. Higgins, N. J. Lawrence, A. P. Thomas, *J. Chem. Soc., Perkin Trans. 1* **1992**, 3331−3349.
[31] F. R. Hartley, S. R. Jones, *J. Organomet. Chem.* **1974**, *66*, 465−473.
[32] B. M. Trost, P. E. Strege, L. Weber, T. J. Fullerton, T. J. Dietsche, *J. Am. Chem. Soc.* **1978**, *100*, 3407−3415.
[33] D. G. Davis, A. Bax, *J. Mag. Res.* **1985**, *64*, 533.
[34] P. von Matt, A. Pfaltz, *Angew. Chem. Int. Ed. Engl.* **1993**, *32*, 566−568.
[35] P. A. Evans, J. D. Nelson, *J. Am. Chem. Soc.* **1998**, *120*, 5581−5582.
[36] P. Sennhenn, B. Gabler, G. Helmchen, *Tetrahedron Lett.* **1994**, *35*, 8595−8598.
[37] *OpenMoleN, Interactive Structure Solution*, Nonius B. V., Delft, The Netherlands, **1997**.
[38] D. T. Cromer, J. T. Waber, *International Tables for X-ray Crystallography*, The Kynoch Press, Birmingham, **1974**, vol. IV, [38a] Table 2.2b, [38b] Table 2.3.1.

Received April 19, 2004
Early View Article
Published Online September 10, 2004

 © 2004 Wiley-VCH Verlag GmbH & Co. KGaA, Weinheim

Oxidation of CH_3NH_2 and $(CH_3)_2NH$ by $Ni^{III}(cyclam)(H_2O)_2^{3+}$ in Aqueous Solutions

Dror Shamir,*[a] Israel Zilbermann,[a,b] Eric Maimon,[a,b] and Dan Meyerstein[a,c]

Keywords: Pendant primary amines / Amines / Cyclam / Nickel / Electrocatalysts

Ni^{II}(1,4,8,11-tetraazacyclotetradecane)$^{2+}$, $Ni^{II}L^{2+}$, is a good electrocatalyst for the oxidation of CH_3NH_2 and $(CH_3)_2NH$ but not of $(CH_3)_3N$. The oxidation kinetics of the amines by $Ni^{III}L(H_2O)_2^{3+}$ indicate that the amines are good axial ligands to the tervalent nickel complex. The complexes $Ni^{III}L[N(CH_3)_iH_{3-i}](H_2O)^{3+}$ are stronger oxidants than the complexes $Ni^{III}L[N(CH_3)_iH_{3-i}]_2^{3+}$. The oxidation is base-catalyzed and obeys a second-order rate law in $Ni^{III}LX_2$. It is proposed that the key step is Ni^{III}–$L(H_2O)[N(CH_3)_iH_{2-i}]^{2+}$ + Ni^{II}-$^{I}LX_2$ → LNi^{II}–$N(=CH_2)(CH_3)_{i-1}H_{2-i}$ + $Ni^{II}L^{2+}$ + H_3O^+ + 2 X. Naturally, $N(CH_3)_3$ is not oxidized by this mechanism. Of special interest is the observation that the axial ligands CH_3NH_2 and $(CH_3)_2NH$ are oxidized by the central cation, while the cyclam ligand, which has four secondary amine groups bound to the nickel(III) ion, and axially bound pendant primary amine groups, which are covalently linked to the macrocyclic ligand, are relatively stable. This difference in the behavior of axially bound amine groups is attributed to the free rotation of the axially bound $N(CH_3)_iH_{3-i}$ ligands that is required for the oxidation to proceed.
(© Wiley-VCH Verlag GmbH & Co. KGaA, 69451 Weinheim, Germany, 2004)

Introduction

$Ni^{III}L^i(H_2O)_2^{3+}$ complexes, where L^i is a neutral tetraazamacrocyclic ligand, are stabilized by axial coordination of a variety of anions.[1−3] The $Ni^{III}L^i$ complexes are also stabilized by pendant amine substituents of the macrocyclic ligands, which are capable of binding axially to the central nickel cation.[4−7] Therefore, it seemed reasonable to try and stabilize $Ni^{III}L^i(H_2O)_2^{3+}$ complexes by axial coordination of amines. As the ligating groups of L^i are four secondary amines and as the pendant substitutes studied were primary amines,[4−7] it seemed reasonable to assume that axially bound amines will not be oxidized by the central Ni^{III} cation. Surprisingly, it was observed that $Ni^{II}L^{2+}$, where L = 1,4,8,11-teraazacyclotetradecane, is an electrocatalyst for the oxidation of CH_3NH_2 and $(CH_3)_2NH$. The mechanism of the oxidation of the amines was studied and the plausible reasons for the different oxidation resistance of free axial and pendant amines are discussed.

[a] Chemistry Department, Ben-Gurion University of the Negev, Beer-Sheva, Israel
[b] Nuclear Research Centre Negev, Beer-Sheva, Israel
[c] Biological Chemistry Department, College of Judea and Samaria, Ariel, Israel
Supporting information for this article is available on the WWW under http://www.eurjic.org or from the author.

Results and Discussion

Electrochemistry

Cyclic voltammograms of NiL^{2+} in the presence of methylamine and dimethylamine (Figures 1 and 2) clearly demonstrate that the nickel complex is an electrocatalyst for the oxidation of these amines. On the other hand, the voltammogram in the presence of trimethylamine (Figure 3) reveals that this amine is not electrocatalytically oxidized in the presence this complex. From the small shift of the wave in the presence of $N(CH_3)_3$, the pH, and the pK_a of $HN(CH_3)_3^+$ (pK_a = 9.8) one can calculate, with the use of the Nernst equation, that the binding constant of $N(CH_3)_3$ to $Ni^{III}L(H_2O)_2^{2+}$ is smaller than 4.0×10^5 M^{-1}.

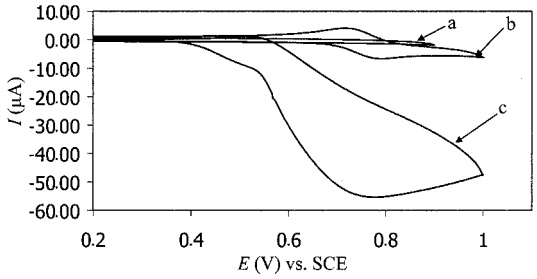

Figure 1. Voltammogram of NiL^{2+} in the presence of methylamine; solution composition: pH = 7.0; 0.1 M ($NaClO_4$); a: $NH_3CH_3^+$ 0.02 M; b: NiL^{2+} 0.0001 M; c: $NH_3CH_3^+$ 0.02 M, NiL^{2+} 0.0001 M; scan rate 50 mV/s

 © 2004 Wiley-VCH Verlag GmbH & Co. KGaA, Weinheim **DOI: 10.1002/ejic.200400033**

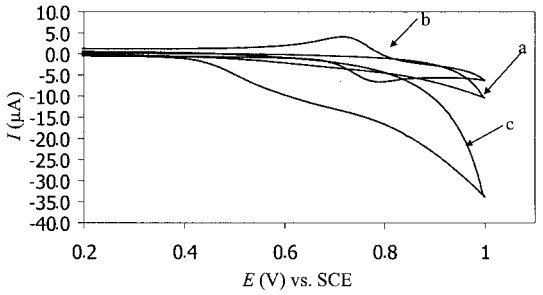

Figure 2. Voltammogram of NiL^{2+} in the presence of dimethylamine; solution composition: pH = 7.0; 0.1 M ($NaClO_4$); a: $NH_2(CH_3)_2^+$ 0.02 M; b: NiL^{2+} 0.0001 M; c: $NH_2(CH_3)_2^+$ 0.02 M, NiL^{2+} 0.0001 M; scan rate 50 mV/s

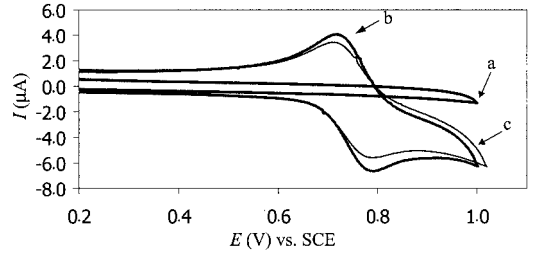

Figure 3. Voltammogram of NiL^{2+} in the presence of trimethylamine; solution composition: pH = 7.0; 0.1 M ($NaClO_4$); a: $NH(CH_3)_3^+$ 0.02 M; b: NiL^{2+} 0.0001 M; c: $NH(CH_3)_3^+$ 0.02 M, NiL^{2+} 0.0001 M; scan rate 50 mV/s

Kinetic Studies

When solutions containing 0.0001 M $Ni^{III}L(SO_4)_2^-$ are mixed with excess $NH_3CH_3^+$ or $NH_2(CH_3)_2^+$ at a constant ionic strength of 0.1 M ($NaClO_4$), fast disappearance of the spectrum due to the complex $Ni^{III}LX_2$ is observed, see for example Figure 4. The kinetics of this process fit a second-order rate law with respect to $[Ni^{III}LX_2]$.

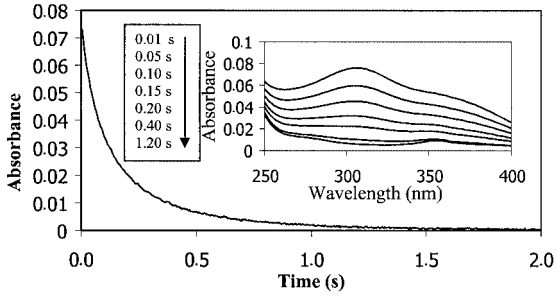

Figure 4. Oxidation of $NH_3CH_3^+$ by $Ni^{III}L(SO_4)_2^-$ at pH = 7.0; solution composition: $NH_3CH^+_3$ 0.01 M; $Ni^{III}L(SO_4)_2^-$ 0.0001 M; BIS TRIS buffer 0.0001 M; measured at 306 nm; inset: time-dependent spectra of the solution

Surprisingly, when the concentration of the amines is changed at constant pH, the rates of the processes decrease somewhat with an increase in the concentration of the amines (Table 1). These results clearly indicate that the equilibria according to Equations (1)−(3) exist in solution and that $Ni^{III}L[N(CH_3)_iH_{3-i}]_2^{3+}$ is more stable than $Ni^{III}L(H_2O)[N(CH_3)_iH_{3-i}]^{3+}$.

Table 1. Observed rates for the oxidation of amines by $Ni^{III}L(SO_4)_2^-$; solution composition: $NiL(SO_4)_2^-$ 0.0001 M; BIS TRIS buffer 0.0001 M; pH = 7.0

$2k$ [$M^{-1}s^{-1}$] for $NH_2(CH_3)_2^+$	$2k$ [$M^{-1}s^{-1}$] for $NH_3CH_3^+$	$NH_3CH_3^+$/ $NH_2(CH_3)_2^+$ [M]
5550 ± 50	49.0 ± 0.3	1.60×10^{-2}
5750 ± 50	63.5 ± 0.3	1.25×10^{-2}
5850 ± 40	72.5 ± 0.4	1.00×10^{-2}
5950 ± 40	85.0 ± 0.4	5.00×10^{-3}
6250 ± 50	88.0 ± 0.5	2.50×10^{-3}
6350 ± 50	92.0 ± 0.8	1.60×10^{-3}
6400 ± 50	97.0 ± 0.8	1.25×10^{-3}

$$Ni^{III}L_{aq} + N(CH_3)_iH_{3-i} \rightleftarrows Ni^{III}L(H_2O)N(CH_3)_iH_{3-i}^{3+} \ (i = 1 \text{or } 2) \quad (1)$$

$$Ni^{III}L(H_2O)N(CH_3)_iH_{3-i}^{3+} + N(CH_3)_iH_{3-i} \rightleftarrows Ni^{III}L[N(CH_3)_iH_{3-i}]_2^{3+} + H_2O \quad (2)$$

$$N(CH_3)_iH_{3-i} + H_3O^+ \rightleftarrows N(CH_3)_iH_{4-i}^+ \quad (3)$$

The maximum rate is observed at the lowest amine concentration studied, $[N(CH_3)_iH_{4-i}]^+ = 1.25 \times 10^{-3}$ M at pH = 7.0. This result indicates that already at this concentration at least one amine is bound to the nickel complex. From this value, assuming that at least 90% of the nickel(III) complexes have at least one bound amine at this pH, one calculates:

$$K_{1app} = \frac{[Ni^{III}L(H_2O)\{N(CH_3)_iH_{3-i}\}^{3+}]}{[Ni^{III}L(H_2O)_2^{3+}]\,[N(CH_3)_iH_{4-i}^+]} \geq 10 / 1.25\times10^{-3} = 8\times10^3\ M^{-1}$$

As the pK_a values of $N(CH_3)H_3^+$ and $N(CH_3)_2H_2^+$ are 10.64 and 10.72, respectively, one calculates from the results that (Supporting Information; see footnote on the first page of this article):

$$K_1 = \frac{[Ni^{III}L(H_2O)N(CH_3)H_2^{3+}]}{[Ni^{III}L(H_2O)_2^{3+}][N(CH_3)H_2]} \geq 3.4\times10^7\ M^{-1}$$

$$K_1 = \frac{[Ni^{III}L(H_2O)N(CH_3)H_2^{3+}]}{[Ni^{III}L(H_2O)_2^{3+}][N(CH_3)_2H]} \geq 4.1\times10^7\ M^{-1}$$

The estimation of the stability constant for the binding of the second amine molecule is considerably more difficult:

$$K_2 = \frac{[Ni^{III}L\{N(CH_3)_iH_{3-i}\}_2^{3+}]}{[Ni^{III}L(H_2O)\{N(CH_3)_iH_{3-i}\}^{3+}][N(CH_3)_iH_{3-i}]}$$

 © 2004 Wiley-VCH Verlag GmbH & Co. KGaA, Weinheim

For this calculation one has to make one of two assumptions:

a) The rate of decomposition of $Ni^{III}L[N(CH_3)_iH_{3-i}]_2^{3+}$ is negligible relative to that of $Ni^{III}L(H_2O)[N(CH_3)_iH_{3-i}]^{3+}$. With this assumption, a lower limit for K_2 can be calculated.

b) The observed rate of decomposition at the highest concentration of $N(CH_3)_iH_{4-i}^{+}$ used is the rate of decomposition of $Ni^{III}L[N(CH_3)_iH_{3-i}]_2^{3+}$. With this assumption, an upper limit for K_2 is calculated.

Thus, $4.8 \times 10^5 < K_2 < 9.6 \times 10^6$ M^{-1} and $4.0 \times 10^5 < K_2 < 8.9 \times 10^6$ M^{-1} for $N(CH_3)H_2$ and $N(CH_3)_2H$, respectively, are obtained.

The pH effect on the rates of oxidation of CH_3NH_2 and $(CH_3)_2NH$ by $Ni^{III}L(SO_4)_2^{-}$ was studied. The results (Figure 5) indicate that the rate depends linearly on $[OH^-]$ over the entire pH range studied. This result is in agreement with the expectation that the axially bound amine has a pK_a, i.e.

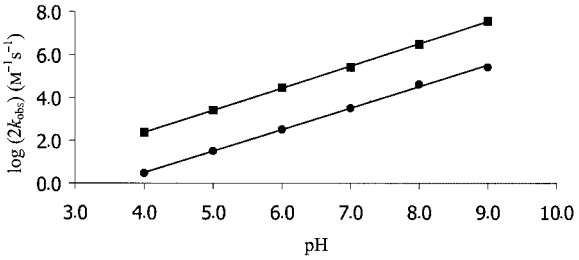

Figure 5. Dependence of the observed rate of oxidation of $NH_3CH_3^+$ (circles) and $NH_2(CH_3)_2^+$ (squares) on pH; solution composition: $NH_3CH_3^+/NH_2(CH_3)_2^+$ 0.01 M; $Ni^{III}L(SO_4)_2^-$ 0.0001 M; BIS TRIS buffer 0.0001 M (pH range 5.8−7.2); TRIS BASE buffer 0.0001 M (pH range 8.0−9.0); TRIS ACID buffer 0.0001 M (pH range 4.0−5.0)

Thus, the kinetic results agree with the following mechanism for the oxidation of CH_3NH_2 and $(CH_3)_2NH$ by $Ni^{III}L(H_2O)_2^{3+}$; As the concentration of SO_4^{2-} in solution is 2×10^{-4} M, the complex loses the sulfate ligands when dissolved:[9]

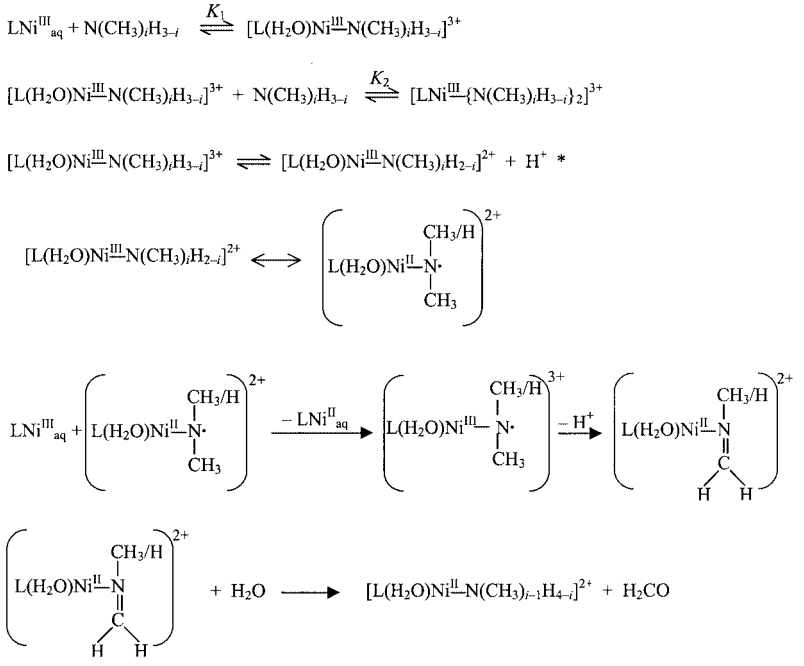

* For simplicity only this possibility is drawn; however, clearly analogous reactions for $[LNi^{III}(N(CH_3)_iH_{3-i})_2]^{3+} \rightleftharpoons [L\{N(CH_3)_iH_{3-i}\}Ni^{III}N(CH_3)_iH_{2-i}]^{2+} + H^+$ have to be considered.

that one of its protons is lost and that the alkaline form $N(CH_3)_iH_{2-i}^{2+}$ is the one that is oxidized:

$$LNi^{III}-N(CH_3)_iH_{3-i}^{3+} + OH^- \rightleftarrows LNi^{III}-N(CH_3)_iH_{2-i}^{2+} + H_2O$$

The results indicate that the pK_a s of the bound amines are ≥ 10. The latter finding is in agreement with the suggestion that the secondary amines of the macrocyclic ligands in the Ni^{III} complexes have pK_a values > 10.[8]

This mechanism is in agreement with the suggested mechanism for the oxidation of the macrocyclic ligand by the central Ni^{III} ion, which occurs considerably slower.[8]

As the $N(CH_3)_iH_{3-i}$ ligands stabilize the central Ni^{III} ion by lowering the oxidation potential of the complex, $LNi^{III}-[N(CH_3)_iH_{3-i2}]$ decomposes slower than $L(H_2O)Ni^{III}N(CH_3)_iH_{3-i}$.

The proposed mechanism predicts that H_2CO will be one of the products of the reaction. Indeed, analysis indicates that the yield of H_2CO is 42 ± 4% of the $Ni^{III}L(SO_4)_2^-$

 © 2004 Wiley-VCH Verlag GmbH & Co. KGaA, Weinheim

used; this is in good agreement with the proposed mechanism.

Concluding Remarks

The results point out two relatively unexpected conclusions:

1. The binding constant of $N(CH_3)_3$ to $Ni^{III}L(H_2O)_2^{3+}$ is smaller by over two orders of magnitude than that of CH_3NH_2 and $(CH_3)_2NH$. This result is in agreement with previous results that show that tertiary amines are poor ligands to high-valent transition metal cations due to their hydrophobic nature.[10−12]

2. The free axial ligands $(CH_3)NH_2$ and $(CH_3)_2NH$ are oxidized faster by many orders of magnitude than axial pendant primary amines, which are bound as substituents to the macrocyclic ligand. The source of this difference seems to be that the transformation of

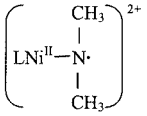

into

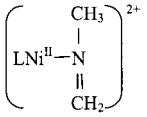

through oxidation requires a relatively free rotation around the $N-CH_3$ bond. This rotation is hindered around the C−N bonds of the macrocyclic ligand and around the C−N bonds in complexes with the general structure:

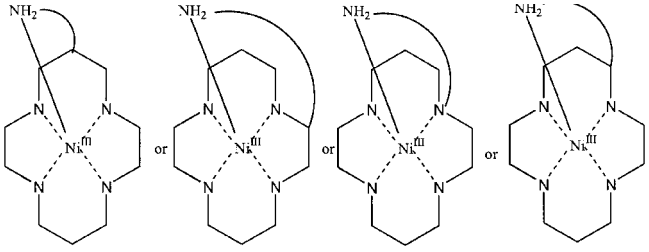

A similar interpretation was given previously to explain the different stabilities of the *rac* and *meso* diastereoisomers of Ni^{III}(5,7,7,12,14,14-hexamethyl-1,4,8,11-tetraazacyclotetradecane)$^{3+}$.[8]

Experimental Section

Materials: The ligand L = 1,4,8,11-tetraazacyclotetradecane and the complex $Ni^{II}L(ClO_4)_2$ were synthesized by a previously reported method.[13] All other chemicals used were of analytical grade, and were used without further purification. All solutions were prepared with heat-distilled water, which was further purified by passing through a Millipore Milli-Q water purification system, to a final resistance >10 $^{m}\Omega$.

Preparation of $Ni^{III}L(SO_4)_2$: The tervalent complex was prepared by oxidation of $Ni^{II}L^{2+}$ by $Na_2S_2O_8$ at pH = 3.0. The complex thus prepared is relatively stable in aqueous solutions, $t_{1/2}$ = several hours.[9] The yield was determined spectrophotometrically by measuring the absorption at λ = 306 nm (ε = 9600 $M^{-1}cm^{-1}$).[9]

Electrochemical Procedures: Cyclic voltammetric studies were carried out using an EG&G Princeton Applied Research potentiostat/galvanostat, model 263 A, operated by a Research Electrochemistry software EG&G PARC, with a three-electrode assembly consisting of a glassy carbon working electrode (A = 0.07 cm^2), a platinum counter electrode, and a saturated calomel electrode as the reference electrode.

Kinetic Studies: Slow reactions were monitored spectrophotometrically with an HP 8452-A diode array spectrophotometer, in an anaerobic UV/Vis quartz cell. Fast reactions were studied with a stopped-flow Applied Photo Physics, Model SX 18-MV apparatus.

H_2CO Analysis: Formaldehyde was determined by a colorimetric method[14] from its yellow complex with acetyl acetone (diacetyldihydrolutidine) measuring the absorption at 412 nm.

Acknowledgments

This study was supported in part by a grant from the Budgeting and Planning Committee of The Council of Higher Education and the Israel Atomic Energy Commission. D. M. wishes to express his thanks to Mrs. Irene Evens for her ongoing interest and support.

[1] I. Zilbermann, A. Meshulam, H. Cohen, D. Meyerstein, *Inorg. Chim. Acta* **1993**, *206*, 127.
[2] A. G. Lappin, A. McAuley, *Adv. Inorg. Chem.* **1988**, *32*, 241.
[3] E. Zeigerson, I. Bar, J. Bernstein, L. J. Kirschenbaum, D. Meyerstein, *Inorg. Chem.* **1982**, *21*, 73.
[4] B. Korybut-Daszkiewicz, J. Taraszewska, B. Kamienski, *Eur. J. of Inorg. Chem.* **2001**, 645.
[5] E. Kimura, M. Haruta, T. Koike, M. Shionoya, K. Takenouchi, Y. Iitaka, *Inorg. Chem.* **1993**, *32*, 2779.
[6] P. S. Pallavicini, A. Perotti, A. Poggi, B. Seghi, L. Fabbrizzi, *J. Am. Chem. Soc.* **1987**, *109*, 5139.
[7] J. Taraszewska, G. Roslonek, B. Korybut-Daszkiewicz, *J. Electroanal. Chem.* **1991**, *297*, 245.
[8] E. Zeigerson, G. Ginzburg, J. Y. Becker, L. J. Kirschenbaum, H. Cohen, D. Meyerstein, *Inorg. Chem.* **1981**, *20*, 3988.
[9] E. Zeigerson, G. Ginzburg, L. J. Kirschenbaum, D. Meyerstein, *J. Electroanal. Chem.* **1981**, *127*, 113.
[10] D. Meyerstein, *Coord. Chem. Rev.* **1999**, *186*, 141.
[11] G. Golub, H. Cohen, P. Paoletti, A. Bencini, L. Messori, I. Bertini, D. Meyerstein, *J. Am. Chem. Soc.* **1995**, *117*, 8353.
[12] T. Clark, M. Hennemann, R. van Eldik, D. Meyerstein, *Inorg. Chem.* **2002**, *41*, 2927.
[13] E. J. B. D. T. Pierce, *Inorg. Chem.* **1997**, *36*, 2950.
[14] T. Nash, *Nature* **1952**, *170*, 976.

Received January 15, 2004
Early View Article
Published Online August 13, 2004

 © 2004 Wiley-VCH Verlag GmbH & Co. KGaA, Weinheim

From Discrete to Extended Guests: A Novel Supramolecular $[Hg_6As_4](AgCl_3)_2$ Assembly Featuring One-Dimensional $(AgCl_3)^{2-}$ Anions

Olga S. Oleneva,[a] Andrei V. Olenev,[a] Evgeny V. Dikarev,[b] and Andrei V. Shevelkov*[a]

Keywords: Arsenic / Host–guest systems / Mercury / Silver / Supramolecular chemistry

A novel supramolecular assembly $[Hg_6As_4](AgCl_3)_2$ has been prepared and its structure determined. It crystallizes in the monoclinic system, space group $I2/a$ (no. 15), with the unit-cell dimensions a = 14.690(1), b = 9.1851(7), c = 20.285(1) Å, β = 93.17(1)°, and Z = 4. The crystal structure comprises a three-dimensional cationic host framework, $[Hg_6As_4]^{4+}$, built of mercury and arsenic atoms and one-dimensional $^1_\infty(AgCl_3)^{2-}$ guest anions built of corner-sharing $[AgCl_4]$ tetrahedra. The title compound is the first example of a perfectly ordered supramolecular architecture having an infinite chain anion as a guest moiety embedded into a mercury–pnicogen cationic framework.
(© Wiley-VCH Verlag GmbH & Co. KGaA, 69451 Weinheim, Germany, 2004)

Introduction

The formation of supramolecular assemblies is usually controlled by the size, shape, and, where appropriate, charge of guest species that template the host framework.[1] The use of rigid guests enables prediction and successful realization of the desired host-framework topology. Supramolecular architectures form spontaneously through a self-assembly process; the resulting structures typically exhibit perfect ordering of the guests within the cavities of the framework. Such an ordering is achieved due to a reasonably large number of weak host–guest interactions.[2] The process of self-assembly is hard to follow and control in the case of high-temperature ampoule synthesis,[3] therefore only knowledge of typical host frameworks and guest units that can form in a given system can be used for predicting new architectures. Such knowledge is frequently based merely on trends in oxidation states, coordination numbers, and bond lengths.[4]

A broad family of supramolecular assemblies based on the mercury–pnicogen cationic frameworks has been reported in the past decade.[2,5] In these frameworks, mercury atoms possess linear coordination while pnicogen atoms have a tetrahedral environment. There are many possible arrangements of mercury and pnicogen atoms, leading to different topologies of the cationic framework guided by the size, shape, and charge of the guest anions. The guests that take their "assigned" positions within the cavities of the framework have been represented so far by discrete anions only. Octahedral,[5] tetrahedral,[6] pyramidal,[7] and triangular[2] anions have been successfully embedded into closed cavities of host frameworks of complementary topology. We therefore tried to find out if infinite anions could be accommodated by a mercury–pnicogen cationic matrix. Group 11 elements seemed to be a logical choice for such work since they frequently form infinite anions through condensation of different building units.[8] In particular, the $AgX_n^{(n-1)-}$ anions are well known[9,10] to form chains of condensed tetrahedra in the presence of different inorganic and organic cations.

In this article, we report the first supramolecular architecture in which a one-dimensional (1D) anionic chain, instead of a discrete anion, serves as a guest unit in an $[Hg_6As_4](AgCl_3)_2$ supramolecular assembly.

Results and Discussion

$[Hg_6As_4](AgCl_3)_2$ was prepared by a stoichiometric ampoule synthesis at elevated temperatures (see Exp. Sect. for details) as a bright-red, polycrystalline solid that is stable in moist air. It crystallizes in the monoclinic space group $I2/a$. The crystal structure comprises a three-dimensional (3D) host framework built of mercury and arsenic atoms and one-dimensional (1D) guest anions built of corner-sharing $[AgCl_4]$ tetrahedra (Figure 1).

There are six crystallographic positions occupied by mercury atoms (Table 1), each having linear coordination by two arsenic atoms. The Hg–As distances (Table 2) are similar to those reported in the literature.[5–7,11] The As–Hg–As angles (Table 3) deviate significantly from 180° only for the Hg(1) and Hg(2) atoms, each experiencing an influence of two distant chlorine atoms. The corresponding

[a] Inorganic Synthesis Laboratory, Department of Chemistry, Moscow State University,
Leninskie Gory 1/3, Moscow 119992, Russia
E-mail: shev@inorg.chem.msu.ru
[b] Department of Chemistry, University of Albany,
Albany 12222, NY, USA

 © 2004 Wiley-VCH Verlag GmbH & Co. KGaA, Weinheim **DOI: 10.1002/ejic.200400205**

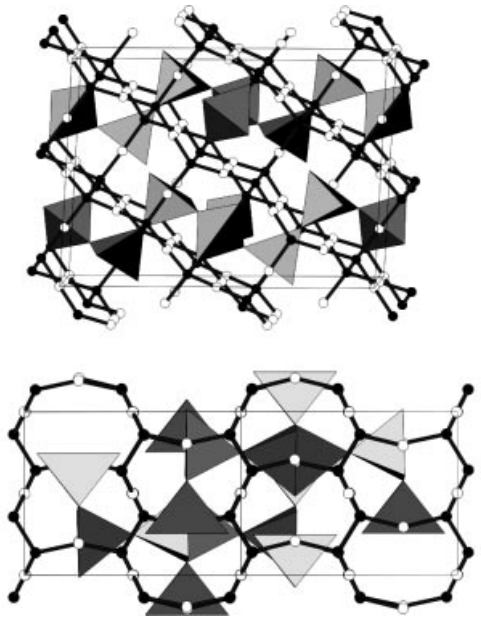

Figure 1. Crystal structure of $[Hg_6As_4](AgCl_3)_2$: (top) view almost along the *c* axis; (bottom) projection onto the (101) plane; the mercury and arsenic atoms composing the cationic framework are shown as open and filled spheres, respectively; $[AgCl_4]$ anions are represented by tetrahedra

Table 1. Atomic positions for $[Hg_6As_4](AgCl_3)_2$

Atom	Position	*x/a*	*y/b*	*z/c*	U_{eq} [Å^2][a]
Hg(1)	8f	0.0814(1)	0.2071(1)	0.3324(1)	0.0103(1)
Hg(2)	4e	1/4	0.8067(1)	0	0.0103(1)
Hg(3)	4b	0	0	1/2	0.0093(1)
Hg(4)	4a	0	0	0	0.0093(1)
Hg(5)	8f	0.1663(1)	0.0000(1)	0.1686(1)	0.0094(1)
Hg(6)	8f	0.3338(1)	0.0009(1)	0.3343(1)	0.0095(1)
As(1)	8f	0.2157(1)	0.1416(1)	0.2687(1)	0.0039(2)
As(2)	8f	0.1173(1)	0.86334(9)	0.0671(1)	0.0044(2)
As(3)	8f	0.9508(1)	0.1420(1)	0.3999(1)	0.0039(2)
Ag(1)	8f	0.1036(1)	0.7197(1)	0.3320(1)	0.0383(2)
Ag(2)	4e	1/4	0.3427(2)	0	0.0493(4)
Cl(1)	8f	0.9950(2)	0.3881(3)	0.2370(1)	0.0200(5)
Cl(2)	8f	0.1722(1)	0.5760(3)	0.9240(1)	0.0145(5)
Cl(3)	8f	0.1379(2)	0.4823(3)	0.3873(1)	0.0191(5)
Cl(4)	4c	1/4	3/4	1/4	0.0156(7)
Cl(5)	8f	0.1211(2)	0.2545(2)	0.0633(1)	0.0210(5)

[a] U_{eq} is defined as one third of the trace of the orthogonalized U_{ij} *tensor.*

Hg···Cl interactions (2.80−2.87 Å) are much longer than typical Hg−Cl covalent bonds of 2.27−2.29 Å,[12] but do not exceed the Hg···Cl host−guest separations of 3.07−3.34 Å observed in other supramolecular architectures of general formula $[Hg_6Pn_4](MCl_6)Cl$ (Pn = P or As; M = Ti, Mo, or In).[13]

All three crystallographically independent arsenic atoms display similar tetrahedral coordination. They each form one As−As bond and three Hg−As bonds. The As−As bond length (Table 2) is typical for a single bond,[14] which leads to the assignment of a −2 oxidation state to the arsenic atoms. Linear coordination of the mercury atoms with

Table 2. Selected interatomic distances [Å] for $[Hg_6As_4](AgCl_3)_2$

As(1)−As(1)	2.375(1)
As(1)−Hg(1)	2.4909(9)
As(1)−Hg(5)	2.4855(9)
As(1)−Hg(6)	2.4892(9)
As(2)−As(3)	2.379(1)
As(2)−Hg(2)	2.4928(9)
As(2)−Hg(4)	2.4775(9)
As(2)−Hg(5)	2.4843(9)
As(3)−As(2)	2.379(1)
As(3)−Hg(1)	2.4907(9)
As(3)−Hg(3)	2.4875(9)
As(3)−Hg(6)	2.4881(9)
Hg(1)···Cl(1)	2.802(2)
Hg(1)···Cl(3)	2.867(2)
Hg(2)···Cl(2)	2.825(2) × 2
Ag(1)−Cl(3)	2.491(3)
Ag(1)−Cl(1)	2.494(3)
Ag(1)−Cl(2)	2.795(3)
Ag(1)−Cl(4)	2.804(1)
Ag(2)−Cl(5)	2.481(3) × 2
Ag(2)−Cl(2)	2.843(3) × 2

Table 3. Selected bond angles [°] for $[Hg_6As_4](AgCl_3)_2$

As(3)−Hg(1)−As(1)	152.06(4)	Hg(5)−As(2)−Hg(2)	111.03(3)
As(2)−Hg(2)−As(2)	155.88(4)	As(2)−As(3)−Hg(3)	109.00(4)
As(3)−Hg(3)−As(3)	180.0	As(2)−As(3)−Hg(6)	108.22(4)
As(2)−Hg(4)−As(2)	180.0	Hg(3)−As(3)−Hg(6)	108.70(3)
As(2)−Hg(5)−As(1)	178.75(3)	As(2)−As(3)−Hg(1)	107.38(4)
As(3)−Hg(6)−As(1)	179.41(3)	Hg(3)−As(3)−Hg(1)	112.13(3)
As(1)−As(1)−Hg(5)	106.72(5)	Hg(6)−As(3)−Hg(1)	111.31(3)
As(1)−As(1)−Hg(6)	108.11(5)	Cl(3)−Ag(1)−Cl(1)	153.11(10)
Hg(5)−As(1)−Hg(6)	109.19(3)	Cl(3)−Ag(1)−Cl(2)1	103.31(7)
As(1)−As(1)−Hg(1)	108.99(5)	Cl(1)−Ag(1)−Cl(2)	97.75(9)
Hg(5)−As(1)−Hg(1)	110.24(3)	Cl(3)−Ag(1)−Cl(4)	102.21(6)
Hg(6)−As(1)−Hg(1)	113.36(3)	Cl(1)−Ag(1)−Cl(4)	92.70(6)
As(3)−As(2)−Hg(4)	107.29(4)	Cl(2)−Ag(1)−Cl(4)	93.98(6)
As(3)−As(2)−Hg(5)	107.77(4)	Cl(5)−Ag(2)−Cl(5)	141.88(13)
Hg(4)−As(2)−Hg(5)	111.10(3)	Cl(5)−Ag(2)−Cl(2)	105.12(7) × 2
As(3)−As(2)−Hg(2)	109.21(4)	Cl(5)−Ag(2)−Cl(2)	103.38(7) × 2
Hg(4)−As(2)−Hg(2)	110.32(3)	Cl(2)−Ag(2)−Cl(2)	82.16(10)

no Hg−Hg bonds present points to a +2 oxidation state of mercury. Consequently, the host framework carries a +4 charge per formula unit that can be formulated as $[Hg_6As_4]^{4+}$. The formula of the cationic framework is the same as in the series of supramolecular complexes with general formula $[Hg_6As_4](MX_6)Y$ (M = Ti, Mo, Cr, Fe, In, Sb, Hg; Y = Cl, Br, I, Hg).[5] However, the frameworks of the latter assemblies have a different topology (Figure 2). They possess two types of symmetric cavities capable of trapping guests of two different sizes. The guests carry a total charge of −4 to compensate for the positive charge of the framework. In the case where M is a trivalent metal, this compensation is achieved by a combination of two guest anions, $M^{III}X_6^{3-}$ and Y^-, occupying the larger and smaller cavities, respectively. If M is a divalent metal, the octahedral $M^{II}X_6^{4-}$ anions do not require additional charge-compensating guests, whereas the smaller cavities either trap zerovalent mercury or remain empty. In the title compound, all the cavities are almost of the same size and less symmetric.

 © 2004 Wiley-VCH Verlag GmbH & Co. KGaA, Weinheim

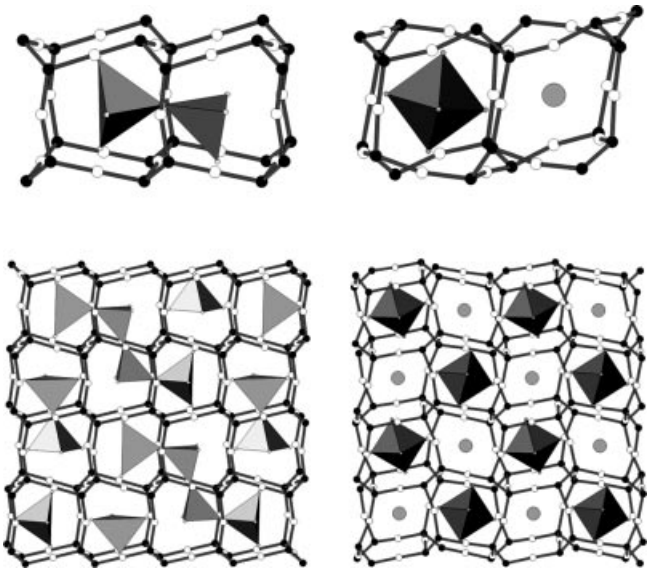

Figure 2. Topology of the $[Hg_6As_4]$ framework in the title compound (left) and in the $[Hg_6Pn_4](MX_6)Y$ complexes (right): two adjacent cages (top) and a 4×4 grid (bottom); mercury: open circles; pnicogen: filled circles; guest units are shown in polyhedral presentation save for the monoatomic guest shown as large gray circles

The difference in the framework topology reflects their different hierarchical origin. The title compound framework originates from a 4-connected As net having a lonsdaleite[15] topology in which three of four edges are expanded[16] by mercury atoms. On the other hand, the framework in the $[Hg_6As_4](MX_6)Y$ compounds originates from the γ-Si[17] topology. As a consequence, while the compositions of the frameworks are the same, their topologies are different.

The guest part of the structure is the 1D anionic chain composed of $AgCl_4$ tetrahedra sharing the corners (Figure 3). Two types of tetrahedra compose each chain; however, the environment of the Ag(1) and Ag(2) atoms centering the tetrahedra appears to be very similar. Each silver atom is surrounded by four chloride ions so that there are two short (2.48−2.49 Å) and two long (2.80−2.84 Å) Ag−Cl interactions involving terminal and bridging chlorine atoms, respectively. The Ag−Cl bond lengths fall in the range of 2.37−2.92 Å reported in the literature[9,18] for similar anions. The tetrahedral coordination of a silver atom by chloride ions is very common; moreover, there are examples of corner-sharing $[AgCl_4]$ tetrahedra in Cs_2AgCl_3 and Rb_2AgCl_3, for instance,[9] although the resulting chains are straight rather than spiral as in the title compound. The oxidation states for the silver and chlorine atoms apparently are +1 and −1, respectively, giving the formulation of the anionic chain as $^1_\infty(AgCl_3)^{2-}$. Hence, the notation of the supramolecular assembly as $[Hg_6As_4](AgCl_3)_2$ indicates the host−guest charge balance.

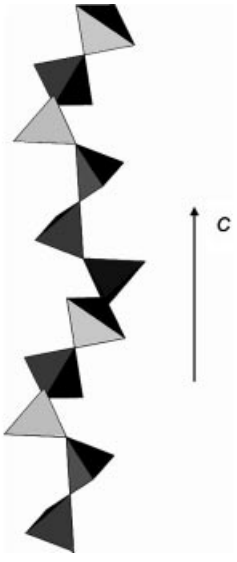

Figure 3. View of the 6-step $(AgCl_3)^{2-}$ anionic chain

The conformation of the 1D $(AgCl_3)^{2-}$ anion is best described as a 6-step spiral chain of tetrahedra,[19] reflecting the repeat unit (Figure 3). The chains are chiral; both enantiomers are present in the centrosymmetric structure. At this stage we cannot explain the observed conformation of the anionic chains. It is clear, though, that there are several factors that control the geometry and conformation of the guest unit. Firstly, a high negative charge of a single $AgCl_4^{3-}$ anion favors condensation of tetrahedra in a vertex-sharing fashion. Secondly, three of five independent chlorine atoms [Cl(1), Cl(2), and Cl(3)] have rather distant contacts with the mercury atoms of the host framework, ensuring that the host and guest units assemble into an ordered supramolecular architecture through weak host−guest interactions. The dimensions of the $[AgCl_4]$ tetrahedra and their fitting into the cavities of the framework should also be taken into account.

In general, this research confirms that it is possible to accommodate infinite anions within a host cationic framework. The title compound is the first example of a supramolecular architecture having a chiral tetrahedral chain as a guest moiety embedded into a mercury−pnicogen framework. The lack of structural data does not allow us to explain the observed features or to predict similar architectures. Nevertheless, the principal direction of a search for new compounds having infinite anions embedded into a mercury−pnicogen framework is clear. It is based on the propensity of the Group 11 elements to form condensed polyhedral anions of flexible geometry, with variable coordination and oxidation number of the central atom. A search for new compounds of this type is currently underway.

Experimental Section

Synthesis: A stoichiometric mixture of mercury(I) chloride, gray arsenic, and silver powder (all > 99.99% purity, total weight 0.5 g) was sealed in a silica tube, annealed at 680 K for 6 d, and then furnace-cooled. A comparison of the diffraction pattern [STADI-P (Stoe), Cu-$K_{\alpha 1}$ radiation] of the red, air-stable product with the theoretical one calculated on the basis of the data obtained during the crystal structure refinement revealed that the product was a desired new phase. However, the profile analysis of the diffractogram enabled us to suggest that only slight admixtures of mercury(II)

 © 2004 Wiley-VCH Verlag GmbH & Co. KGaA, Weinheim

chloride and silver chloride were present. For a single-crystal preparation, a mixture of Hg_2Cl_2, As, and Ag taken in a 3:4:2 molar ratio was annealed in a silica tube at 680 K for 5 d. Red crystals were found in the furnace-cooled product.

Crystal Structure Determination: A red crystal with approximate dimensions 0.09 mm × 0.04 mm × 0.03 mm was selected from the reaction product for X-ray crystallographic analysis. The X-ray intensity data were recorded at 173(2) K (Bruker KRYO-FLEX) with a Bruker SMART APEX CCD-based X-ray diffractometer system equipped with graphite-monochromated Mo-K_α radiation (λ = 0.71073 Å) operated at 1800 W. The detector was placed at a distance of 6.140 cm from the crystal. The data collection covered approximately a hemisphere of the reciprocal space. A total of 1850 frames were collected with a scan width of 0.3° in ω and an exposure time of 20 s/frame. The frames were integrated with the Bruker SAINT software package[20] using a narrow-frame integration algorithm. The integration of the data using a monoclinic unit-cell yielded a total of 11582 reflections to a maximum 2θ angle of 56.45° (0.75 Å resolution), of which 3204 were independent (R_{int} = 0.0389). The final cell constants are based upon the refinement of the *XYZ*-centroids of 4394 reflections above $20\sigma(I)$. Analysis of the duplicate reflections showed negligible decay during data collection. Data were corrected for absorption effects using the empirical method (SADABS),[21] the ratio of minimum/maximum apparent transmission was 0.3865. The structure was solved and refined by a full-matrix least-squares procedure on $|F^2|$ in the *I*2/*a* space group using the Bruker SHELXTL (Version 6.12) software package.[22] The positions of six mercury and three arsenic atoms were found in direct-method *E* maps. The remaining atoms were located from a combination of least-squares refinement and difference Fourier synthesis. The isotropic refinement of the obtained model led to $R1$ = 0.078 with the slightly enlarged thermal displacement parameters of both silver atoms. However, refinement of the occupancies of these atoms proved full occupation for the corresponding positions. Attempts to refine the structure with split positions of the silver atoms did not lead to satisfactory results. Final anisotropic refinement led to the composition $[Hg_6As_4](AgCl_3)_2$, that is in excellent agreement with synthesis data, and to the atomic and structural parameters listed in Tables 1 and 4, respectively. Further details of the crystal structure determination may be obtained from the Fachinformationzentrum Karlsruhe, 76344 Eggenstein-Leopoldshafen, Germany, on quoting the depository number CSD-413821.

Table 4. Data collection and structure refinement parameters for $[Hg_6As_4](AgCl_3)_2$

Empirical formula	$Ag_2As_4Cl_6Hg_6$
T [K]	173(2)
Space group	*I*2/*a*
a [Å]	14.690(1)
b [Å]	9.1851(7)
c [Å]	20.285(1)
β [°]	93.170(1)
V [Å^3]	2732.8(4)
Z	6
Density (calcd.) [Mg/m^3]	7.042
μ [1/mm]	60.523
λ [Å]	0.71073
Data collection range [°]	$2.01 < \theta < 28.23$
Reflections collected	11582
Independent reflections	3204 (R_{int} = 0.0389)
Parameters refined	129
Transmission factors	
Extinction coefficient	
$R1$,[a] $wR2$[b] [$I > 4\sigma(I)$]	0.0387, 0.1023
$R1$, $wR2$ (all data)	0.0509, 0.1100
Largest difference peak/hole [e/Å^3]	3.801/−5.111
Quality-of-fit[c]	1.026

[a] $R1 = \Sigma||F_o| - |F_c||/\Sigma|F_o|$. [b] $wR2 = \{\Sigma[w(F_o^2 - F_c^2)^2]/\Sigma[w(F_o^2)^2]\}^{1/2}$. [c] Quality-of-fit = $\{\Sigma[w(F_o^2 - F_c^2)^2]/(N_{obs} - N_{params})\}^{1/2}$, based on all data.

Acknowledgments

This work was supported by the U. S. Civilian Research & Development Foundation for the Independent States of the Former Soviet Union (award No. 12735), the Russian Foundation for Basic Research (grant No. 04-03-32351a), and the European Commission 5th Framework Program (contract HPRN-CT-2002-00193). E. V. D. is grateful to the National Science Foundation for funding the CCD diffractometer (CHE-0130985) at the University of Albany. A. V. S. thanks the Russian Science Support Foundation for a research award.

[1] [1a] J.-M. Lehn, *Supramolecular Chemistry*, VCH, Weinheim, **1995**. [1b] A. Müller, H. Reuter, S. Dillinger, *Angew. Chem.* **1995**, *107*, 2505−2539; *Angew. Chem. Int. Ed. Engl.* **1995**, *34*, 2328−2361.

[2] A. V. Olenev, A. I. Baranov, O. S. Oleneva, I. I. Vorontsov, M. Y. Antipin, A. V. Shevelkov, *Eur. J. Inorg. Chem.* **2003**, 1053−1057.

[3] G. Férey, *J. Solid State Chem.* **2000**, *152*, 37−48.

[4] [4a] C. Gieck, F. Rocker, V. Ksenofontov, Ph. Gütlich, W. Tremel, *Angew. Chem.* **2001**, *113*, 946−948; *Angew. Chem. Int. Ed.* **2001**, *40*, 908−911. [4b] M. Eddaoudi, J. Kim, M. O'Keefe, O. M. Yaghi, *J. Am. Chem. Soc.* **2002**, *124*, 376−377. [4c] R. Vaidhyanathan, S. Natarajan, C. N. R. Rao, *Eur. J. Inorg. Chem.* **2003**, 1675−1680.

[5] A. V. Olenev, O. S. Oleneva, M. Lindsjö, L. A. Kloo, A. V. Shevelkov, *Chem. Eur. J.* **2003**, 3201−3208, and references cited therein.

[6] A. V. Olenev, A. V. Shevelkov, *Angew. Chem.* **2001**, *113*, 2415−2416; *Angew. Chem. Int. Ed.* **2001**, *40*, 2353−2354.

[7] A. V. Olenev, A. I. Baranov, A. V. Shevelkov, B. A. Popovkin, *Eur. J. Inorg. Chem.* **2002**, 547−553.

[8] A. F. Wells, *Structural Inorganic Chemistry*, 5th ed., Clarendon Press, Oxford, **1986**, chapter 25.

[9] [9a] C. Brink, *Acta Crystallogr.* **1949**, *2*, 158−163. [9b] C. Hasselgren, S. Jagner, *Acta Crystallogr., Sect. C* **1999**, *55*, 1208−1210.

[10] [10a] C. Brink, H. A. Stenfert-Kröse, *Acta Crystallogr.* **1952**, *5*, 433−436. [10b] M. M. Thackeray, J. Cötzer, *Acta Crystallogr., Sect. B* **1976**, *32*, 1619−1620. [10c] G. Helgesson, M. Josefsson, S. Janger, *Acta Crystallogr., Sect. C* **1988**, *44*, 1729. [10d] R. Böse, D. Bläser, W. Hüben, *Z. Kristallogr.* **1990**, *191*, 135−136. [10e] M. Hoyer, H. Hartl, *Z. Anorg. Allg. Chem.* **1996**, *622*, 308−312. [10f] B. Ahrens, S. Friedrichs, R. Herbst-Irmer, P. G. Jones, *Eur. J. Inorg. Chem.* **2000**, 2017−2029.

[11] [11a] A. Rebbah, J. Yazbeck, A. Leclaire, A. Deschanvres, *Acta Crystallogr., Sect. B* **1980**, *36*, 771−773. [11b] A. V. Shevelkov, E. V. Dikarev, B. A. Popovkin, *J. Solid State Chem.* **1994**, *113*, 116−119.

[12] V. Subramanian, K. Seff, *Acta Crystallogr., Sect. B* **1980**, *36*, 2132−2135.

[13] [13a] J. Beck, U. Neisel, *Z. Anorg. Allg. Chem.* **2000**, *626*, 1620−1626. [13b] A. V. Olenev, A. V. Shevelkov, *J. Solid State Chem.* **2001**, *160*, 88−92. [13c] A. V. Olenev, A. I. Baranov, M.

 © 2004 Wiley-VCH Verlag GmbH & Co. KGaA, Weinheim

M. Shatruk, A. S. Tyablikov, A. V. Shevelkov, *Izv. Akad. Nauk, Ser. Khim.* **2002**, *51*, 414−418; *Russ. Chem. Bull.* **2002**, *51*, 444−448.
[14] H. G. von Schnering, *Angew. Chem.* **1981**, *93*, 44−62; *Angew. Chem. Int. Ed. Engl.* **1981**, *20*, 33−51.
[15] [15a] F. P. Bundy, J. S. Kasper, *J. Chem. Phys.* **1967**, *46*, 3437−3446. [15b] P. D. Ownby, X. Yang, J. Liu, *J. Am. Ceram. Soc.* **1992**, *75*, 1876−1883.
[16] M. O'Keefe, M. Eddaoudi, H. Li, T. Reineke, O. M. Yaghi, *J. Solid State Chem.* **2000**, *152*, 3−20.
[17] J. S. Kasper, S. M. Richards, *Acta Crystallogr.* **1964**, *17*, 752−755.
[18] [18a] N. Elliott, L. Pauling, *J. Am. Chem. Soc.* **1938**, *60*, 1846−1851. [18b] L. Schröder, H. L. Keller, *Z. Anorg. Allg. Chem.* **1988**, *562*, 123−130. [18c] G. Meyer, F. Stenzel, *Z. Anorg. Allg. Chem.* **1993**, *619*, 652−660.
[19] F. Liebau, *Structural Chemistry of Silicates*, Springer-Verlag, Berlin, **1985**, pp. 101−104.
[20] *SAINT, Software for the CCD Detector System*, version 6.02, Bruker Analytical X-ray Systems, Madison, WI, **2000**.
[21] *SADABS, Program for absorption correction based on the methods of Robert Blessing*: R. H. Blessing, *Acta Crystallogr., Sect. A* **1995**, *51*, 33.
[22] *SHELXTL*, version 6.12, Bruker Analytical X-ray Systems, Madison, WI, **2001**.

Received March 13, 2004
Early View Article
Published Online August 13, 2004

 © 2004 Wiley-VCH Verlag GmbH & Co. KGaA, Weinheim

Anion Binding of 1,1′-Bis(dialkylboryl)cobaltocenium Complexes − Structures of $[Co\{C_5H_4(BMe_2)\}_2]PF_6$, $Co[C_5H_4(BMe_2)][C_5H_4(BMe_2Cl)]$, $Co[C_5H_4(BiPr_2)]_2(\mu\text{-}F)$ and $NMe_4[Co\{C_5H_4(BiPr_2F)\}_2]$[‡]

Gerhard E. Herberich,*[a] Ulli Englert,[a] Andreas Fischer,[a][‡‡] and Dag Wiebelhaus[a][‡‡‡]

Keywords: Anion binding / Borates / Boron / Cobalt / Sandwich complexes

The cobaltocenium salts $[Co\{C_5H_4(BiPr_2)\}_2]PF_6$ [(**1a**)PF_6] and $[Co\{C_5H_4(BMe_2)\}_2]PF_6$ [(**1b**)PF_6] are strong Lewis acids. With pyridine (**1a**)PF_6 forms a mono-adduct **2** and a di-adduct **3** which show NMR spectra in the low-temperature regime of pyridine exchange. With chloride from PPh_4Cl the adduct formed is dynamic; quite remarkably, the formation of an anionic di-adduct is also observed. The mono-adducts (**1a**)X (X = F, Cl, Br, I, OH, and NH_2) and (**1b**)X (X = F, Cl, and OH) as well as the di-adduct salts $NMe_4[(\mathbf{1a})F_2]$ (**5**) and $K[(\mathbf{1a})(OH)_2]$ (**6**) are made by treating the salts (**1a**,**b**)PF_6 in CH_2Cl_2 or $MeNO_2$ with salts PPh_4X, NMe_4F, or powders of $NaNH_2$ or KOH in the appropriate ratios. X-ray single-crystal structures of the salt $[Co\{C_5H_4(BMe)_2\}_2]PF_6$ [(**1b**)PF_6], the semi-quaternized mono-adduct $Co[C_5H_4(BMe_2)][C_5H_4(BMe_2Cl)]$ (**4bd**) [B–Cl = 1.969(2) Å], the inverse chelate $Co[C_5H_4(BiPr_2)]_2(\mu\text{-}F)$ (**4ac**) with the very rare feature of fluorine bridging two boron centers [C_2 symmetric; B–F = 1.641(4) Å, B–F–B′ = 148.4(3)°], and the doubly quaternized di-adduct $NMe_4[Co\{C_5H_4(BiPr_2F)\}_2]$ (**5**) [exactly centrosymmetric; B–F = 1.477(4) Å] are given. Solution structures of the 1:1 products greatly depend on the nature of the anion, displaying i) exclusively ionic structures for (**1a**)PF_6 and (**1b**)PF_6, ii) semi-quaternized structures for the heavier halides (**1a**)Br (**4ae**) and (**1a**)I (**4af**) with some noticeable ionic dissociation, iii) semi-quaternized structures in equilibrium with minor amounts of inverse chelate isomers for (**1a**)F (**4ac**), (**1b**)Cl (**4bd**), and very likely for (**1a**)Cl (**4ad**), and iv) stable inverse chelate structures for $Co[C_5H_4(BiPr_2)]_2(\mu\text{-}NH_2)$ (**4aa**) (static in variable temperature NMR spectra, with diastereotopic Me groups), $Co[C_5H_4(BR_2)]_2(\mu\text{-}OH)$ [**4ab**: R = *i*Pr; **4bb**: R = Me; dynamic; for **4ab** T_c = 95 ± 5 °C, $\Delta G^{\neq}_{368}$ = 75(1) kJ·mol^{-1} for interchange of the diastereotopic Me groups], and $Co[C_5H_4(BMe_2)]_2(\mu\text{-}F)$ (**4bc**). The stability of the inverse chelates decreases in the order amide (**4aa**) > hydroxides (**4ab** and **4bb**) > fluorides (**4ac** and **4bc**) > chlorides (**4ad** and **4bd**), and also in the order BMe_2 > $BiPr_2$ (specifically **4bc** > **4ac**, and **4bd** > **4ad**). Variable temperature NMR spectra of solutions of **4bd** (CD_2Cl_2, 173–243 K) show that i) the ring-opening of the chelated chloride ($\Delta G^{\neq}_{368} \approx 45$ kJ·mol^{-1}) is energetically easier than for the chelated hydroxide **4ab**, ii) the predominance of the semi-quaternized isomer over the inverse chelate ($\Delta_R H$ = 2.5 ± 1.1 kJ·mol^{-1}, $\Delta_R S$ = 37.6 ± 5.4 kJ·mol^{-1}·K^{-1}) in the equilibrium is entropic in nature, and iii) the semi-quaternized isomer still undergoes fast chloride-exchange in the low-temperature regime of this equilibrium, proving the existence of an independent, intermolecular chloride-exchange mechanism.

(© Wiley-VCH Verlag GmbH & Co. KGaA, 69451 Weinheim, Germany, 2004)

Introduction

Anion recognition is one of the central themes of supramolecular chemistry,[3] and has been the subject of numerous reviews.[4] The binding of an anionic guest species to a host molecule may be caused mainly by one of three effects: electrostatic attraction by cationic centers, formation of polar bonds with Lewis-acidic centers, and formation of hydrogen bonds; these effects often act in combination.

The earliest example was the discovery in 1966, by Shriver and Biallas, that the 1,2-diborylethane $F_2BCH_2CH_2BF_2$ reacts with the trityl ether Ph_3COMe to give ether cleavage and formation of an inverse chelate $Ph_3C[(CH_2BF_2)_2(\mu\text{-}OMe)]$[5] with the anion being bonded simultaneously by two Lewis acid centers. Katz subsequently introduced 1,8-diborylnaphthalenes, which differ from the above-mentioned diborylethane in that they have their boron centers sterically fixed and thus are more close to the idea of a molecular pincer species.[6] This preorganization[7] of the chelating ligand ensures more efficient anion chelation since the reaction entropy is less unfavorable than in the case of the conformationally flexible 1,2-bis(difluoro-

[‡] Bis(boryl)metallocenes, 3; Part 2: Ref.[1] This work also forms part of a dissertation.[2]

[a] Institut für Anorganische Chemie, Technische Hochschule Aachen
52056 Aachen, Germany
Fax: +49-241-809-2288
E-mail: gerhard.herberich@ac.rwth-aachen.de
[‡‡] Current address: Grünenthal GmbH
Postfach 50 04 44, 52099 Aachen, Germany
[‡‡‡] Current address: BASF AG, Competence Center Global Purchasing, GR/S
Benckieserplatz 1 − BZM1, 67056 Ludwigshafen, Germany

boryl)ethane. Conformationally rigid chelate ligands have also been made by other groups[8] and have recently been used for the construction of highly electrophilic anion pincers.[9]

In this paper we treat anion binding by cationic two-boron host species, the two 1,1′-bis(dialkylboryl)cobaltocenium cations **1a**$^+$ and **1b**$^+$, in the form of their hexafluorophosphate salts. These cationic anion pincers possess a skeletal flexibility similar to that of a diborylethane, but in contrast to the older two-boron examples, they are cationic and exert an electrostatic field effect which adds stability to their anion complexes.

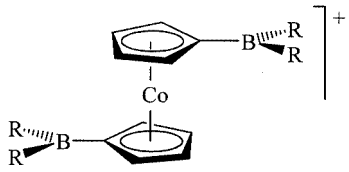

1a$^+$: R = *i*Pr; **1b**$^+$: R = Me

Cations of type **1** give rise to strong cation-anion interactions, and four structural types are encountered: type **A** with purely ionic interactions, a semi-quaternized type **B** with a zwitterionic situation, type **C** with an inverse chelate structure, and finally the doubly quaternized type **D**. In our preliminary communication of this topic we have already described one example each of types **A**−**C** [the compounds (**1a**)PF_6, (**1a**)Cl, and (**1a**)(OH), respectively],[10] while an example of type **D** structures will be given below for the first time.

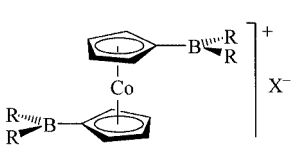

A

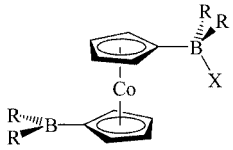

B

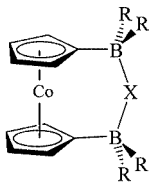

C

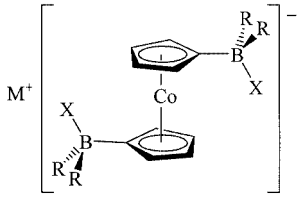

D

Before becoming more specific we note a detail of great analytical value. The pincer cation **1a** with the diisopropylboryl substituents will have diastereotopic methyl groups in the structures of type **C** and **D** and for one of the ligands of type **B**, provided these structures are not dynamic. In all other cases the methyl groups are equivalent. This feature will provide us with insights which remain hidden in case of the dimethylboryl analogue **1b**$^+$.

Results and Discussion

Synthesis of the Anion Binding Cobaltocenium Ions

The diisopropylboryl compound (**1a**)PF_6 can be made in a straightforward two-step synthesis.[10] First, the cobaltocene **1a** is prepared from Li[C_5H_4(B*i*Pr$_2$)][11]/$CoBr_2$(DME). Subsequent oxidation with [$FeCp_2$]PF_6 [12] in dichloromethane affords the desired compound, which was characterized structurally as an ionic compound without specific cation-anion interactions.

The dimethylboryl analogue (**1b**)PF_6 could potentially be made by an analogous sequence. For practical reasons it seemed more convenient to synthesize it by a different route. First we prepared the cobaltocene Co[C_5H_4-{B(NEt_2)$_2$}]$_2$ and, by quantitative oxidation with C_2Cl_6, the corresponding chloride [Co{C_5H_4[B(NEt_2)$_2$]}$_2$]Cl.[1] Subsequent treatment with BCl_3 and then with Al_2Me_6 afforded the salt (**1b**)$AlCl_4$, and, by anion metathesis, (**1b**)PF_6.[1]

First Observations

In a first series of NMR-tube experiments a solution of (**1a**)PF_6 in CD_2Cl_2 was treated with varying amounts of pyridine. Formation of a mono-adduct **2** and of a di-adduct **3** was observed, quite as expected. If the ratio of the reactants py/**1a**$^+$ is chosen close to 1:1 or to 2:1 the respective adducts can be isolated by crystallization at −30 °C; they were not characterized in detail.

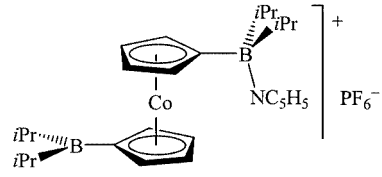

2

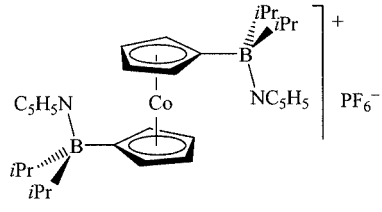

3

Several observations are of interest. First, the reaction mixtures are close to the slow-exchange regime, and all species involved can be observed separately in the ^1H, ^{13}C, and ^{11}B NMR spectra. However, the hyperfine structure of the ring protons is blurred and the two different rings of **2** cannot be distinguished in the $^1H\{^1H\}$ NOE difference

 © 2004 Wiley-VCH Verlag GmbH & Co. KGaA, Weinheim

spectrum, indicating a slow exchange of the pyridine. The adduct-formation equilibria are far on the right side as no free pyridine is seen at py/**1a**$^+$ ratios below two. Also, the adduct formation to give **3** is less strong than the formation of **2** as no di-adduct **3** is seen at py/**1a**$^+$ ratios lower than one. These observations are remarkable since the pyridine adducts of the known uncharged complexes $M(CO)_2\{C_5H_4(BMe_2)\}$ (M = Co, Rh) show fast exchange with excess pyridine.[13] Hence the cation **1a**$^+$ is a comparatively stronger Lewis acid, even in the second stage.

In a second experiment we titrated (**1a**)PF_6 with PPh_4Cl in dichloromethane solution and monitored the ensuing reaction by ^{11}B NMR spectroscopy (Figure 1). Only one ^{11}B NMR signal is seen over the entire range of the titration, indicating a fast-exchange regime for the interaction of cation **1a**$^+$ and Cl^-.

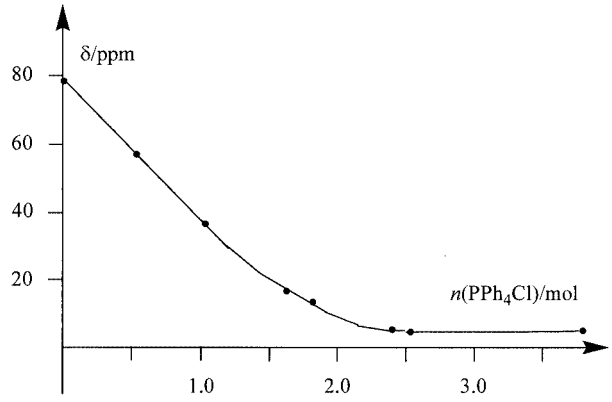

Figure 1. Boron chemical shifts during titration of (**1a**)PF_6 with PPh_4Cl in CD_2Cl_2

The chemical shift at the beginning of the titration (δ = 79 ppm) is that of **1a**$^+$ and conforms to the expected value for dialkylarylboranes, while the final chemical shift (δ = 5 ppm) indicates the presence of a fully quaternized species, the anionic species $[(\mathbf{1a})Cl_2]^-$.[14] The first addition of Cl^- to **1a**$^+$ is energetically rather favorable since we observe a straight line for the chemical-shift values up to a ratio of $Cl^-/\mathbf{1a}^+ \leq 1$. The product (**1a**)Cl is dynamic and shows a chemical shift (δ = 37 ppm) which can be understood as the mean of the chemical shifts for one trigonal and one tetrahedral boron center. Hence, the product (**1a**)Cl possesses the same semi-quaternized structure in solution that has also been found in the crystal.[10] The second addition of Cl^- is less favorable energetically, as indicated by the curvature of the line, and an excess of Cl^- (almost 2.5 mol) is needed to complete the formation of $PPh_4[(\mathbf{1a})Cl_2]$, the doubly quaternized end-product. Below we shall discuss the nature of the observed chloride-exchange process for (**1a**)Cl and also give a more thorough comment on its solution structure.

Synthetic Methods I: Uncharged Complexes

Complexes of types **B** and **C** were made by essentially the same general method. We treated the salts (**1a**,**b**)PF_6 in CH_2Cl_2, or occasionally in nitromethane, with a second salt such as NMe_4F, PPh_4Cl, PPh_4Br, and PPh_4I in a 1:1 ratio. The large organic cations ensured a sufficient solubility. If such salts were not readily available, inorganic salts such as KOH and $NaNH_2$ had to be used in powdered form, and long reaction times were required. After completion of the reaction the polar solvent was removed. The product was then extracted with toluene and isolated from that solvent. When crystals were desired the material was recrystallized from CH_2Cl_2/toluene. Yields were mostly very good, but no reactions were achieved with NMe_2^-, OMe^-, and OPh^-, and attempted addition of hydride induced decomposition. In some cases oxidation of the cobaltocene **1a** could be used as an alternative method, and (**1a**)Cl (**4ad**) and (**1a**)(OH) (**4ab**) were made in this way (Scheme 1).[10]

$$[Co\{C_5H_4(BR_2)\}_2]PF_6 \xrightarrow[-ZPF_6]{+ZX} Co[C_5H_4(BR_2)]_2 * X$$

(**1a**,**b**)PF_6 — **4**

Z = NMe_4, PPh_4

4, R = *i*Pr	**aa**	**ab**	**ac**	**ad**	**ae**	**af**
R = Me		**bb**	**bc**	**bd**		
X	NH_2	OH	F	Cl	Br	I

Scheme 1

Synthetic Methods II: Doubly Quaternized Complexes

The salt $PPh_4[(\mathbf{1a})Cl_2]$ that was observed in the titration experiment was not stable enough to be isolated. However, with the more Lewis basic anions F^- and OH^- salts with doubly quaternized anionic complexes could be isolated. When (**1a**)PF_6 in CH_2Cl_2 was treated with NMe_4F in a 1:2 ratio, the ammonium fluoride dissolved despite its low solubility in that solvent (Scheme 2). Since the resulting robust product $NMe_4[(\mathbf{1a})F_2]$ (**5**) readily dissolves in toluene it can be isolated by the same general technique described above. It was crystallized by slowly concentrating its solution in toluene or by recrystallization from CH_2Cl_2/Et_2O. The analogous treatment of (**1a**)PF_6 in CH_2Cl_2 with an excess of finely ground KOH afforded the potassium salt $K[(\mathbf{1a})(OH)_2]$ (**6**), which can be crystallized from toluene/hexane. Treatment of the hydroxide **4ab** with KOH also produces complex **6**. The conceivable alternative of a deprotonation is not observed.

$$[Co\{C_5H_4(BiPr_2)\}_2]PF_6 \xrightarrow[-ZPF_6]{+2\,ZX} Z[Co\{C_5H_4(BiPr_2X)\}_2]$$

(**1a**)PF_6 — **5**: Z = NMe_4, X = F; **6**: Z = K, X = OH

Scheme 2

Crystal Structures of (1b)PF_6, 4bd, 4ac, and 5

We present four crystal structures which exemplify the four archetypal cation-anion interactions (**A**−**D**) mentioned

 © 2004 Wiley-VCH Verlag GmbH & Co. KGaA, Weinheim

above. Compound (**1b**)PF_6 is ionic with essentially purely electrostatic interaction between the anion and **1b**$^+$ (type **A**; Figure 2). The chloride **4bd** displays a semi-quaternized structure (type **B**; Figure 3). For **4ac** an inverse chelate type is observed (type **C**; Figure 4), and **5** finally has a doubly quaternized structure (type **D**; Figure 5).

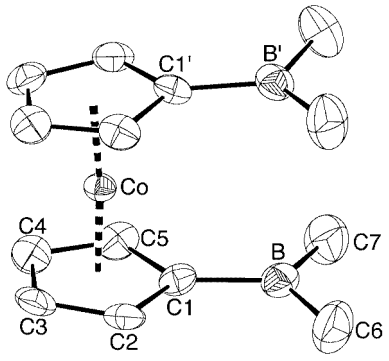

Figure 2. Structure of the cation of (**1b**)PF_6 (PLATON plot[15] at the 50% probability level); selected bond lengths (Å): Co−C 2.032 (av.) [range 2.021(3)−2.055(4)], C1−B 1.566(6), C6−B 1.554(6), C7−B 1.542(7)

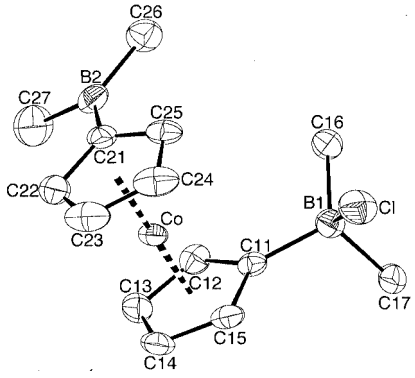

Figure 3. Structure of the chloride **4bd** (PLATON plot[15] at the 50% probability level); selected bond lengths (Å): Co−C(Cp1) 2.034 (av.) [with one long bond Co−C11 2.074(2)], B1−Cl 1.968(2), C11−B1 1.614(3), C16−B1 1.628(3), C17−B1 1.654(3), Co−C(Cp2) 2.038 (av.) [range 2.027(2)−2.044(2)], C21−B2 1.567(3), C26−B2 1.551(3), C27−B2 1.563(3)

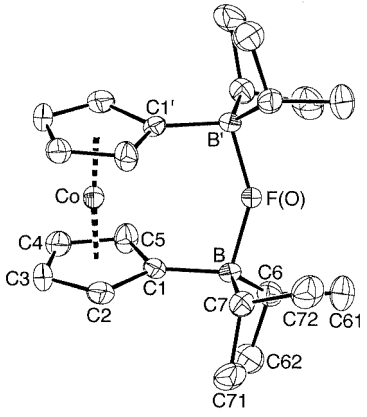

Figure 4. Structure of the inverse chelate **4ac** (PLATON plot[15] at the 50% probability level); selected bond lengths (Å) and angles (°): Co− C 2.023 (av.) [range 2.012(3) − 2.033(3)], B−F 1.641(4), C1−B 1.629(4), C6−B 1.606(5), C7−B 1.620(5), F(O)−H 0.9390(19); B−F−B′ 148.4(3), B−F(O)−H 105.80(13)

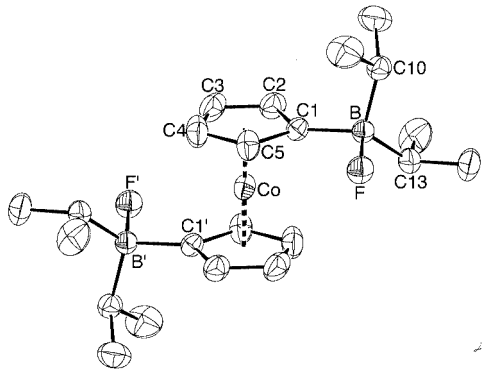

Figure 5. Structure of the anion of **5** (PLATON plot[15] at the 30% probability level); selected bond lengths (Å): Co−C1 2.095(3), Co−C2 2.022(4), Co−C3 2.007(4), Co−C4 2.018(4), Co−C5 2.031(3), B−F 1.478(3), C1−B 1.627(4), C10−B 1.634(4), C13−B 1.626(4)

All structures contain a cobaltocenium moiety with the usual metal−ring distance for formal cobalt(III) (close to 1.63 Å), regardless of its actual overall charge. The salt (**1b**)PF_6 displays crystallographic mirror symmetry and hence an exactly eclipsed conformation. The resulting transannular repulsion is reflected in a ring tilt of 6.3(2)°; all other structures contain parallel planar ring systems. The torsion angle (B−cog-cog′−B′)[16] varies from exactly 0° for (**1b**)PF_6 through 26° for **4ac** and 83° for **4bd** to exactly 180° for **5**. This last compound displays crystallographic centrosymmetry which places the two negative charge centers of the anion $[Co\{C_5H_4(BiPr_2F)\}_2]^-$ at maximum distance. In all other cases the ring-ring torsional mode should be very soft, and the torsional angle observed should largely be determined by lattice forces.

Next we consider the distance B···B′. This distance is 3.543(7) Å in the structure of (**1b**)PF_6, and would be 3.270 Å for the same cation with parallel eclipsed rings. In the inverse chelate $Co[C_5H_4(BF_2)]_2(\mu\text{-}OH)$ it amounts to only 2.752(4) Å,[1] demonstrating a variation of the B···B′ distance of up to 0.8 Å for eclipsed conformations. Ring-ring rotation adds further variability to the pincer bite of the cations **1a**,**b**$^+$.

Of general interest are the boron−anion distances as they should be related qualitatively to the strength of the cation−anion interaction. Bond lengths for chlorine fixed to a quaternized boron center vary within a wide range of 1.76 to 1.92 Å.[17] The average value is about 1.83 Å[18] and distances at the higher end of the given range are considered as weak.[17a] We should, however, remember in this context that the sizeable electrostatic contribution to the bonding interaction varies roughly with 1/*r* and thus is only weakly affected by small bond-length variations. The B−Cl distance for the *B*-methyl compound **4bd** is even longer, with a value of 1.969(2) Å. The same distance in the *B*-*i*Pr compound **4ad** [1.982(3) Å] is marginally longer;[10] a marked steric influence of the isopropyl groups is not seen here.

The reported B−F bond lengths (for bonds with terminal fluorine) lie in a comparatively narrow range from 1.36 to 1.43 Å for quaternized boron centers.[19] All of these dis-

 © 2004 Wiley-VCH Verlag GmbH & Co. KGaA, Weinheim

tances are from compounds with more than one fluorine atom directly attached to boron. Substitution of fluorine with an alkyl substituent leads to less-positive boron centers and, consequently, to longer distances for the remaining B−F bonds. Thus, for BF_4^- an average of 1.37 Å has been found,[18] whereas for $MeBF_3^-$ a value of 1.424 Å has been reported.[19e] Therefore the observed value of 1.477(4) Å for **5** seems to conform to expectations for a fluorotriorganoborate.

Before discussing the B−F distance in **4ac**, we have to consider the identity of the material isolated as **4ac**. In our previous work an attempted synthesis of $Co[C_5H_4(BF_2)]_2(\mu\text{-}F)$ resulted in the isolation of $Co[C_5H_4(BF_2)]_2(\mu\text{-}OH)$,[1] thus indicating a strong preference for OH^- binding of the corresponding pincer cation. In the present case, the ^1H NMR spectra showed the presence of small admixtures of the hydroxo compound **4ab** which increased when the material was manipulated, for instance in a recrystallization procedure. The structural data for **4ac** are very similar to those reported for **4ab**,[10] showing the same space group (*Pccn* no. 56), the same crystallographic C_2 symmetry of the inverse chelate, and rather similar atomic coordinates, bond lengths, and angles. These observations suggested that the two compounds might cocrystallize; hence the structure was refined assuming cocrystallization of **4ac** and **4ab**. The refinement converged for a **4ac/4ab** ratio of 79(3)/21(3). Thus, a high predominance of the fluoride **4ac** in the crystal picked for the structure determination can be considered as certain.

The structure of the inverse chelate **4ac** is highly unusual in that it displays a fluorine bridging two boron centers. A search in the Cambridge Structural Database (CSD)[20,21] resulted in only two hits, a structure with the heptafluorodiborate ion $B_2F_7^-$ [B−F = 1.50(1) and 1.51(1) Å with B−F−B = 128.1(7)°],[22] and the structure of 9-fluoro-9-borabicyclo[3.3.1]nonane, which displays an unsymmetrical self-association with a long bond between a tetracoordinate boron center and a bridging fluorine [B−F = 1.652(5) Å].[23] For the inverse chelate **4ac** the B−F bond length [1.641(4) Å] is, not surprisingly, longer than in $B_2F_7^-$ and similar to that of the comparable bond of 9-fluoro-9-borabicyclo[3.3.1]nonane**.** The bond angle around the bridging fluorine of 148.4(3)° seems remarkably large; a shift of the fluorine atom toward the cobalt center decreases the transannular repulsion of the two B*i*Pr$_2$ groups (for evidence of this repulsion see below) and increases the electrostatic attraction between the negative fluorine and the positive metallocenium region of **4ac**.

Structure in Solution I

Boron chemical shifts give first indications as to which structures exist in solution. Figure 6 gives an overview over the chemical-shift values observed. Three regions may be distinguished. At the high (left) end of the scale the salts (**1a**,**b**)PF_6 mark the position of the "naked" trigonal boron (δ = 78 ppm). At the low end are the inverse chelate molecules (δ = 1.4 to −8.5 ppm) with exclusively tetrahedral boron centers which, in fact, display their signal in the same region as the doubly quaternized salts **5** and **6**. In the central region the chlorides **4ad** and **4bd** mark the region of the semi-quaternized molecules (δ = 37 ppm) with a mean chemical shift for one trigonal (δ = 78 ppm) and one tetrahedral boron (roughly δ = 0 ppm). The higher chemical-shift values for the bromide **4ae** and even more so for the iodide **4af** indicate that there is more tricoordinate boron than tetracoordinate boron, in other words, that there is a dissociation equilibrium (Scheme 3). Finally, while the fluoride **4bc** fits the overall picture, the sterically more crowded diisopropylboryl analogue **4ac** shows an anomalously high chemical shift which will be discussed further below.

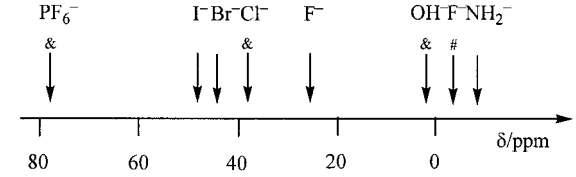

Figure 6. Boron chemical shifts of the combinations (**1a**)PF_6/X^-; &: the related combination (**1b**)PF_6/X^- shows the same chemical shift; #: the signal for (**1b**)PF_6/F^- appears at higher field

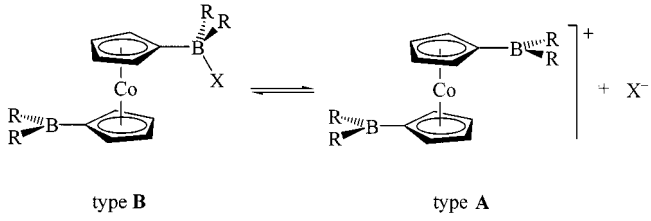

R = *i*Pr, Me; X = Cl−, Br−, I−

Scheme 3

Structure in Solution II: Inverse Chelates

The inverse chelate complexes **4aa**, **4ab**, and **4ac** possess two types of diastereotopic methyl groups (within their B*i*Pr$_2$ groups) which should give rise to two doublets in the ^1H NMR spectra. In the case of the rather stable hydroxide **4ab**[10] these two doublets are seen at ambient temperature. However, when a solution of **4ab** in $C_2D_2Cl_4$ is warmed up, line-broadening sets in at 60 °C. Despite the onset of decomposition fast measurements give a coalescence temperature, T_c, of 95 ± 5 °C which corresponds to a barrier $\Delta G^{\neq}_{368}$ of 75(1) kJ·mol^{-1}. The underlying dynamic process must imply ring-opening of the chelate and rotation of a diisopropylboryl group. In the case of the robust amide **4aa** the doublets are sharp even at 115 °C. Thus the chelate structure of the amide is more stable than that of the hydroxide. On the other hand, the fluoride **4ac** is already dynamic at ambient temperature, showing only one doublet. These observations show that the stability of the inverse

 © 2004 Wiley-VCH Verlag GmbH & Co. KGaA, Weinheim

chelate forms increases in the order fluoride **4ac** < hydroxide **4ab** < amide **4aa**.

The anomalously high chemical shift for **4ac** mentioned above indicates a fast equilibrium between the semi-quaternized form **4ac-B** and the chelate form **4ac-C** (Scheme 4). We may take the shift of the methyl compound **4bc** (δ = −2.5 ppm) as representative of the chelate form **4ac-C**, and estimate a 65% contribution of the open form **4ac-B** to the equilibrium mixture (NMR tube, ambient temperature). Furthermore, the comparison of **4ac** and **4bc** proves that the sterically more demanding isopropyl groups effect a marked destabilization of the chelate structure **C**.

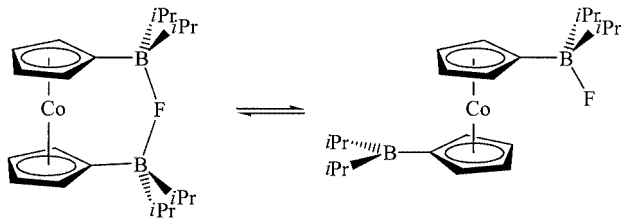

4ac-C **4ac-B**

Scheme 4

Structure in Solution III: The Chlorides 4ad and 4bd

A more direct observation of the equilibrium between semi-quaternized form **B** and chelate form **C** (cf. Scheme 4) seemed desirable. Variable temperature NMR spectra (173−243 K) of the chloride **4bd** in CD_2Cl_2 solutions revealed that this chloride may also form a chelate isomer (Scheme 5). The exchange reaction is slow below 200 K, and the chelate isomer contributes 5−7% to the equilibrium mixture. Note in this context that a chloride bridging two boron centers has previously been observed in the structurally characterized compound $(Ph_3PNPPh_3)[1,8\text{-}C_{10}H_6(BCl_2)_2(\mu\text{-}Cl)]$ derived from the rigid pincer molecule 1,8-bis(dichloroboryl)naphthalene.[6c]

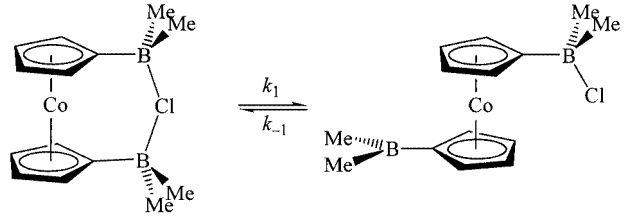

4bc-C **4bc-B**

Scheme 5

The equilibrium is close to thermoneutral ($\Delta_R H$ = 2.5 ± 1.1 kJ·mol^{-1}), showing that the bond strength for the bridging B−Cl bond is about half that of the terminal B−Cl bond. Ring-opening of the chelate **4bd-C** is endotropic ($\Delta_R S$ = 37.6 ± 5.4 kJ·mol^{-1}·K^{-1}), and the equilibrium is entropy driven in the accessible temperature range. The sign of the reaction enthalpy suggests, though with only moderate significance, that the major isomer **4bd-B** does not represent the ground-state isomer.

Line-shape analysis (^{1}H and ^{13}C NMR, 193−243 K) with the help of the program D NMR-SIM[24] provided rate constants, and from these activation parameters.[25] The estimated free enthalpy of activation for the ring-opening of **4bd-C** is estimated to be about 45 kJ·mol^{-1}, much less than in the case of the hydroxide **4ab** discussed above, as expected.

The low-temperature NMR spectra hold another surprise: the major isomer **4bd-B**, quite unexpectedly, shows only a single ligand pattern of effective C_{2v} symmetry. Since we do see separate spectra for the two isomers, the *intra*molecular chloride exchange implied in Scheme 5 is frozen out at 200 K. What is still possible is an *inter*molecular chloride-exchange mechanism with the chloride migrating from the boron in one open molecule **4bd-B** to the next one. Several detailed mechanisms are conceivable; for instance, a dissociation with formation of $\mathbf{1b}^+$ and free Cl^- analogous to Scheme 3 and subsequent chloride transfer between **4bd-B** and the trace cation $\mathbf{1b}^+$ is a likely possibility.

In the case of the chloride **4ad** variable temprature NMR spectra revealed line-broadening in an intermediate temperature range (as for **4bd**), but no chelate isomer **4ad-C** could be detected in the low-temperature regime (< 200 K). This seemingly puzzling situation can now easily be understood. From what we have seen in the fluoride cases we should expect that the contribution of the chelate form **4ad-C** is smaller than for the methyl compound **4bd**. Experimentally it is obviously below the level of detection (< 2%), but the line-broadening still observed is again evidence of a dynamic process, most likely analogous to that of Scheme 5.

Concluding Remarks

The chelating properties of pincer molecules may be influenced (inter alia) by preorganization of the coordinating centers and by field effects. The pincer cations $\mathbf{1a,b}^+$ allow ring-ring rotation, and thus have little preorganization, but they possess a positive charge which favors anion binding. Three features are particularly noteworthy: formation of Lewis base adducts in the slow-exchange regime (with pyridine), formation of anionic di-adducts with anions (with F^-, OH^-, and in solution with Cl^-), and formation of inverse chelates with monoatomic anions, surprisingly including F^-. In summary, our observations strongly underline the favorable effect of the positive charge on the anion binding properties of pincer cations such as $\mathbf{1a,b}^+$.

Experimental Section

General Remarks: Reactions were carried out under an atmosphere of dinitrogen by means of conventional Schlenk techniques. Hexane was distilled from potassium, THF from sodium benzophenone ketyl, dichloromethane from calcium hydride and nitromethane was condensed after passing through a column of acti-

 © 2004 Wiley-VCH Verlag GmbH & Co. KGaA, Weinheim

vated alumina. Silica and alumina were heated under vacuum at 300 °C and kept under dinitrogen.

KOH was prepared from KH and water in THF. $NaNH_2$ was bought as a suspension in xylene, washed with hexane and dried under vacuum to yield a grey powder. NMe_4F was bought from Acros; all other reagents were from Aldrich and were used without purification.

NMR spectra were recorded on a Varian Unity 500 spectrometer (^{1}H: 500 MHz; ^{13}C: 125.7 MHz), a Varian VXR 300 (^{1}H: 300 MHz; ^{13}C: 75.4 MHz), Bruker WM-250 FT (^{1}H: 250 MHz; ^{13}C: 62.9 MHz) or a Rototec/Piccinotti Mini-FID (^{11}B: 29 MHz) and calibrated using referenced solvent signals. Mass spectra were recorded on a Finningan MAT-95 spectrometer. Elemental analyses were determined by the Analytische Laboratorien Malissa and Reuter, Lindlar, Germany.

Pyridine Adducts 2 and 3: A solution of (**1a**)PF_6 in CD_2Cl_2 was treated with defined successive portions of pyridine (from 0.7 to 2.2 equivalents). After each addition NMR spectra were recorded.
2: ^{1}H NMR (500 MHz, CD_2Cl_2): δ = 0.52 and 0.63 (d, $^3J \approx$ 6.8 Hz, 2 × 6 H, 2 Me′ each), 1.15 (d, ^3J = 7.3 Hz, 4 Me), 1.23 (sept, ^3J = 7.3 Hz, 2 BCH′), 1.99 (sept, ^3J = 7.3 Hz, 2 BCH), 5.20 (br. s, 2-/5-H′), 5.51 (br. s, 3-/4-H′), 5.84 (br. s, 2-/5-H), 5.95 (br. s, 3-/4-H), 7.91 (m, 2 H_m), 8.25 (m, H_p), 8.76 (m, 2 H_o) ppm. ^{11}B{^{1}H} NMR (160 MHz, CD_2Cl_2): δ = 78.7, 2.0 ppm. ^{13}C{^{1}H} NMR (126 MHz, CD_2Cl_2): δ = 18.5 (br., BCH′), 18.66 (Me), 18.94 and 19.99 (Me′), 23.26 (br., BCH), 82.08 (C-2′,5′), 87.13 (C-3′,4′), 89.91 (C-2,5), 90.27 (C-3,4) ppm; pyridine: δ = 126.58 (C-3,5), 141.92 (C-4), 145.86 (C-2,6) ppm.
3: ^{1}H NMR (500 MHz, CD_2Cl_2): δ = 0.58 and 0.65 (br. d, $^3J \approx$ 7.0 Hz, 2 × 12 H, 4 Me each), 1.26 (sept, 4 BCH), 5.18 (m, 2 2-/5-H), 5.60 (m, $N = {}^3J_{2,3} + {}^4J_{2,4}$ = 3.7 Hz, 2-/3-/4-H), 7.83 (m, 4 H_m), 8.22 (m, 2 H_p), 8.82 (m, 4 H_o) ppm. ^{11}B{^{1}H} NMR (160 MHz, CD_2Cl_2): δ = 2.3 ppm. ^{13}C{^{1}H} NMR (126 MHz, CD_2Cl_2): δ = 18.7 (br., BCH), 19.17 and 20.18 (Me), 83.76 (C-3,4), 86.70 (C-2,5) ppm; pyridine: δ = 126.28 (C-3,5), 141.70 (C-4), 146.02 (C-2,6) ppm.

Co[C_5H_4(B*i*Pr$_2$)]$_2$(μ-F) (4ac): Solid NMe_4F (206.5 mg, 2.22 mmol) was added with stirring to a solution of (**1a**)PF_6 (1.17 g, 2.22 mmol) in CD_2Cl_2 (20 mL) at room temperature. After 30 minutes all volatiles were removed under vacuum. The yellow powdery residue was transferred to a frit and extracted with toluene until the filtrate remained colorless. The combined solutions were freed from solvent to give the product **4ac** (428.3 mg, 49%) as a yellow microcrystalline solid, m.p. 127 °C (dec.); the product always contained an admixture of the hydroxy compound **4ab**. $C_{22}H_{36}B_2CoF$ (400.1) calcd. C 66.05, H 9.07; found C 66.35, H 9.32. SIMS (K/T): positive ions *m*/*z* (%) = 381 (100) [M^+ − F], 357 (31) [M^+ − *i*Pr]; negative ions *m*/*z* (%) = 400 (100) [M^-], 357 (17) [M^- − *i*Pr], 137 (23) [C_5H_4B*i*PrF$^-$], 65 (35) [Cp^-]. ^{1}H NMR (500 MHz, CD_2Cl_2): δ = 0.92 (d, ^3J = 7.3 Hz, 8 Me), 1.15 (sept, ^3J = 7.3 Hz, 4 BCH), 5.40 (m, 2 C_5H_4) ppm. ^{11}B{^{1}H} NMR (160 MHz, CD_2Cl_2): δ = 26.4 ppm. ^{13}C{^{1}H} NMR (126 MHz, CD_2Cl_2): δ = 20.50 (Me), 21.6 (br., BCH), 83.68 (C-3,4), 87.92 (C-2,5) ppm. ^{19}F NMR (470 MHz, C_6D_6): δ = −158 ($\nu_{1/2}$ = 207 Hz).

Co[C_5H_4(BMe$_2$)]$_2$(μ-F) (4bc): A preparation as described for (**1a**)F from NMe_4F (58.2 mg, 0.410 mmol) and (**1b**)PF_6 (171.0 mg, 0.413 mmol) gave **4bc** (113.0 mg, 96%) as a yellow powder which could be recrystallized from toluene/CD_2Cl_2. SIMS (DTE/DTT/Sul): positive ions *m*/*z* (%) = 269 (100) [M^+ − F], 229 (64) [CoCp{C_5H_4(BMe$_2$)}$^+$]. ^{1}H NMR (250 MHz, CD_2Cl_2): δ = −0.10 (s, 4 Me), 5.19 (m, 2 2-/5-H), 5.25 (m, N = 3.7 Hz, 2 3-/4-H) ppm. ^{11}B{^{1}H} NMR (29 MHz, CD_2Cl_2): δ = −2.5 ppm. ^{13}C{^{1}H} NMR (63 MHz, CD_2Cl_2): δ = 11.5 (br., Me), 82.79 (C-3,4), 87.45 (C-2,5) ppm.

Co[C_5H_4(B*i*Pr$_2$)][C_5H_4(B*i*Pr$_2$Cl)] (4ad): Solutions of (**1a**)PF_6 (281.7 mg, 0.536 mmol) and PPh_4Cl (206.5 mg, 0.551 mmol) in CD_2Cl_2 (5 mL each) were combined with stirring. After 10 minutes the solvent was removed under vacuum. The residue was suspended in toluene and transferred to a frit with a layer of silica. After filtration the solid was extracted with more toluene until the filtrate remained colorless. The combined solutions were concentrated to a volume of less than 5 mL and left for crystallization at −30 °C to give **4ad** (163.9 mg, 73%) as yellow crystals. $C_{22}H_{36}B_2CoCl$ (416.5) calcd. C 63.44, H 8.71; found C 63.30, H 8.52. ^{1}H NMR (250 MHz, $CDCl_3$): δ = 0.96 (d, ^3J = 7.3 Hz, 8 Me), 1.43 (sept, ^3J = 7.3 Hz, 4 BCH), 5.52 (m, 2 2-/5-H), 5.54 (m, 2 3-/4-H) ppm. ^{11}B{^{1}H} NMR (160 MHz, CD_2Cl_2): δ = 36.9 ppm. ^{13}C{^{1}H} NMR (63 MHz, $CDCl_3$): δ = 20.02 (Me), 22.0 (br., BCH), 85.12 (C-3,4), 88.24 (C-2,5) ppm.

Co[C_5H_4(BMe$_2$)][C_5H_4(BMe$_2$Cl)] (4bd): A preparation as described for (**1a**)Cl from (**1b**)$AlCl_4$ [1] (437.4 mg, 1.00 mmol) and PPh_4Cl (368.3 mg, 0.98 mmol) gave **4bd** (299.0 mg, 100%) as a yellow powder which was crystallized from Et_2O/CD_2Cl_2 at −30 °C; m.p. 96 °C (dec.). [The use of (**1b**)$AlCl_4$ instead of (**1b**)PF_6 is more convenient here since (**1b**)PF_6 was made from (**1b**)$AlCl_4$ by anion metathesis.] $C_{14}H_{20}B_2ClCo$ (304.3) calcd. C 55.26, H 6.62; found C 54.68, H 6.84. SIMS (DTE/DTT/Sul): positive ions *m*/*z* (%) = 269 (100) [M^+ − Cl], 229 (16) [CoCp{C_5H_4(BMe$_2$)}$^+$]. ^{1}H NMR (500 MHz, CD_2Cl_2, room temp.): δ = 0.54 (s, 4 Me), 5.48 (m, 2 2-/5-H), 5.51 (m, N = 3.7 Hz, 2 3-/4-H) ppm; the assignment for the ring protons is based on ^{1}H{^{1}H}NOE difference spectra. ^{11}B{^{1}H} NMR (160 MHz, CD_2Cl_2, room temp.): δ = 36.8 ppm. ^{13}C{^{1}H} NMR (126 MHz, CD_2Cl_2, room temp.): δ = 13.0 (br., Me), 85.69 (C-3,4), 87.94 (C-2,5) ppm; the assignment for the ring-carbon nuclei is based on heteronuclear correlation spectra or (^{1}H, ^{13}C) HMQC spectra.

Variable Temperature NMR Spectra of 4bd in CD_2Cl_2: ^{1}H and ^{13}C{^{1}H} NMR spectra of **4bd** in CD_2Cl_2 show decoalescence and the presence of two species at low temperatures (Scheme 5). Both species display effective C_{2v} symmetry, but their constitutions could be assigned by means of systematic comparisons of the chemical shifts observed for various species **4**; note especially the large difference of chemical shifts for the B-Me groups [δ = 0.60 ppm for **4bd-B** and δ = −0.15 ppmfor **4bd-C**]. The semi-quaternized isomer **4bd-B** is the major isomer and the chelate form **4bd-C** the minor isomer over the entire temperature range. The relative concentrations measured and the deduced thermodynamic parameters are collected in Table 1. Rate constants for the ring-opening reaction were obtained from line-shape analyses for the spectra of the minor isomer. The ^{1}H signals of the B-Me groups and the ^{13}C{^{1}H} signals of the carbon atoms C-2,5 and C-3,4 were suitable; the remaining signals were not used because the coupling constants of the ring

Table 1. Equilibrium data for **4bd** (see Scheme 5)

T (K)	K	$\Delta_R G$ (kJ·mol^{-1})
173	15.1	−3.90
183	16.5	−4.27
193	17.7	−4.61
203	19.8	−5.03
$\Delta_R H$ = (2.6 ± 1.1) kJ·mol^{-1}		
$\Delta_R S$ = (37.6 ± 5.4) J·K^{-1}·mol^{-1}		

 © 2004 Wiley-VCH Verlag GmbH & Co. KGaA, Weinheim

protons are not easily accessible with the necessary precision and because the carbon atoms attached to boron are quadrupole-broadened. Rate constants for the ring-closure reaction were calculated using the equation $k_{-1} = K/k$. The resulting activation parameters in terms of the Eyring equation are collected in Table 2.

Table 2. Kinetic data and activation parameters for **4bd**

T (K)	K	k_1 (s^{-1})	K_{-1} (s^{-1})
193	17.7	15	0.85
203	19.8	70	3.54
213	21.2	250	11.79
243	25.4	2600	102.36
For the ring opening:		$\Delta H^{\neq}_1 = (38.0 \pm 3.0)$ kJ·mol^{-1}	
		$\Delta S^{\neq}_1 = (-18 \pm 13)$ J·K^{-1}·mol^{-1}	
For the ring closure:		$\Delta H^{\neq}_{-1} = (35.2 \pm 3.0)$ kJ·mol^{-1}	
		$\Delta S^{\neq}_{-1} = (-56 \pm 13)$ J·K^{-1}·mol^{-1}	

Data for 4bd-B: C_s symmetry, 94.7% at −90 °C. ^{1}H NMR (500 MHz, CD_2Cl_2, −90 °C): δ = 0.60 (s, 4 Me), 5.56 (s, 2 C_5H_4) ppm. $^{13}C\{^1H\}$ NMR (126 MHz, CD_2Cl_2, −90 °C): δ = 12.9 (br., Me), 86.28 (C-3,4), 87.77 (C-2,5) ppm.
Data for 4bd-C: C_{2v} symmetry, 5.3% at −90 °C. ^{1}H NMR (500 MHz, CD_2Cl_2, −90 °C): δ = −0.15 (s, 4 Me), 5.26 (s, 2 C_5H_4) ppm. $^{13}C\{^1H\}$ NMR (126 MHz, CD_2Cl_2, −90 °C): δ = 10.6 (br., Me), 83.20 (C-3,4), 86.99 (C-2,5) ppm.

Co[C_5H_4(B*i*Pr$_2$)][C_5H_4(B*i*Pr$_2$Br)] (4ae) and Co[C_5H_4(B*i*Pr$_2$)][C_5H_4(B*i*Pr$_2$I)] (4af): These compounds were prepared as described for **4ac** and **4ad** with PPh_4Br and PPh_4I, respectively. $^{11}B\{^1H\}$ NMR (160 MHz, CD_2Cl_2): δ = 43.8 for **4ae** and δ = 48.5 ppm for **4af**.

Co[C_5H_4(B*i*Pr$_2$)]$_2$(μ-OH) (4ab): Freshly powdered KOH (25.6 mg, 0.46 mmol) was added to (**1a**)PF_6 (253.1 mg, 0.48 mmol) in CH_2Cl_2 (15 mL). The suspension was then stirred for 1 d. Workup as described for **4ac** gave **4ab** (124.3 mg, 69%) as a brownish yellow solid. ^{1}H NMR (500 MHz, CD_2Cl_2): δ = 0.86 (s, 4 Me + 4 BCH), 1.01 (br. d, ^3J = 5.8 Hz, 4 Me), 2.37 (s, OH), 5.19 (m, 2 2-/5-H), 5.24 (m, 2 3-/4-H) ppm. $^{11}B\{^1H\}$ NMR (160 MHz, CD_2Cl_2): δ = 1.4 ppm. $^{13}C\{^1H\}$ NMR (126 MHz, CD_2Cl_2): δ = 21.48 and 22.28 (Me), 22.1 (br., BCH), 82.81 (C-3,4), 88.04 (C-2,5) ppm.

Co[C_5H_4(BMe$_2$)]$_2$(μ-OH) (4bb): Preparation from powdered KOH (27.3 mg, 0.49 mmol) and (**1b**)PF_6 (212.0 mg, 0.51 mmol) in nitromethane instead of CH_2Cl_2 gave **4bb** (128.6 mg, 92%) as an orange microcrystalline solid; m.p. 125 °C. $C_{14}H_{21}B_2CoO$ (285.9) calcd. C 58.82, H 7.40; found C 58.82, H 7.41. SIMS (DTE/DTT/Sul): positive ions m/z (%) = 269 (100) [M^+ − OH]. ^{1}H NMR (500 MHz, CD_2Cl_2): δ = −0.12 (s, 4 Me), 1.95 (s, OH), 5.17 (m, $N \approx$ 3.8 Hz, 2 2-/5-H), 5.24 (m, 2 3-/4-H) ppm. $^{11}B\{^1H\}$ NMR (160 MHz, CD_2Cl_2): δ = −1.9 ppm. $^{13}C\{^1H\}$ NMR (126 MHz, CD_2Cl_2): δ = 10.8 (br., Me), 82.71 (C-3,4), 87.30 (C-2,5) ppm.

Co[C_5H_4(B*i*Pr$_2$)]$_2$(μ-NH$_2$) (4aa): A solution of (**1a**)PF_6 (641.4 mg, 1.22 mmol) in CH_2Cl_2 (20 mL) was added to solid sodium amide (254.8 mg, 6.53 mmol). The resulting suspension was stirred for 7 d. The solvent was then removed under vacuum. The residue was suspended in toluene and filtered through silica. Removal of the solvent left **4aa** (434.0 mg, 90%) as a brown-orange solid which was recrystallized from toluene at −30 °C; m.p. 152 °C. $C_{22}H_{38}B_2CoN$ (397.1) calcd. C 66.54, H 9.65, N 3.53. SIMS (K/T): positive ions m/z (%) = 396 (2) [M^+ − H], 354 (100) [M^+ − *i*Pr], 228 (19) [M^+ − *i*Pr − $2C_3H_6$]; negative ions m/z (%) = 397 (100) [M^-], 354 (22) [M^- − *i*Pr], 161 (6) [C_5H_4B*i*Pr$_2^-$]. ^{1}H NMR (250 MHz, CD_2Cl_2): δ = 0.86 (overlapping, 4 BCH), 0.88 (d, J = 5.5 Hz, 4 Me), 0.96 (d, J = 6.2 Hz, 4 Me), 2.19 (br. s, NH_2), 5.15 (m, 2 2-/5-H), 5.17 (m, 2 3-/4-H) ppm; coupling constants in C_6D_6 solution: N = 3.7 Hz for C_5H_4 part and $^3J \approx$ 7.2 Hz for *i*Pr groups. $^{11}B\{^1H\}$ NMR (160 MHz, C_6D_6): δ = −8.5 ppm. $^{13}C\{^1H\}$ NMR (63 MHz, CD_2Cl_2): δ = 22.20 and 22.97 (Me), 82.23 (C-3,4), 87.59 (C-2,5) ppm.

NMe$_4$[Co{C_5H_4(B*i*Pr$_2$F)}$_2$] (5): A solution of (**1a**)PF_6 (456.6 mg, 0.868 mmol) in CH_2Cl_2 (10 mL) was added to solid NMe_4F (172.4 mg, 1.851 mmol). After stirring for 3 h all volatiles were removed under vacuum. The residue was suspended in toluene and filtered through a frit. The remaining solid was intensively washed with more toluene. The combined filtrates were liberated from solvent to give **5** (380 mg, 89%) as orange microcrystals; m.p. 160 °C (dec.). $C_{26}H_{48}B_2CoF_2N$ (493.2) calcd. C 63.31, H 9.81, N 2.84; found C 63.44, H 10.01, N 2.91. SIMS (K/T): positive ions m/z (%) = 74 (100) [NMe_4^+]; negative ions m/z (%) = 419 (100) [M^- − NMe_4], 400 (10) [419 − F], 376 (23) [419 − C_3H_7], 333 (7) [Co(C_5H_4B*i*PrF)$_2^-$]. ^{1}H NMR (500 MHz, CD_2Cl_2): δ = 0.62 (sept, 4 BCH), 0.71 and 0.75 (d, ^3J = 7.0 Hz, 4 Me each), 3.36 (s, NMe_4), 5.05 (m, 2 2-/5-H), 5.16 (br. m, N = 3.7 Hz, 2 3-/4-H) ppm. $^{11}B\{^1H\}$ NMR (160 MHz, CD_2Cl_2): δ = 3.4 (d, $^1J_{F,B}$ = 61 Hz) ppm. $^{13}C\{^1H\}$ NMR (126 MHz, CD_2Cl_2): δ = 21.14 and 21.21 (d, $^3J_{F,C}$ = 5.5 Hz, Me), 21.6 (br., BCH), 56.41 (t, $^1J_{N,C}$ = 3.8 Hz, NMe_4), 80.70 (C-3,4), 85.29 (d, $^3J_{F,C}$ = 5.5 Hz, C-2,5) ppm. ^{19}F NMR (470 MHz, C_6D_6): δ = −194 ($\nu_{1/2}$ = 153 Hz) ppm.

K[Co{C_5H_4(B*i*Pr$_2$OH)}$_2$] (6): Freshly powdered KOH (24.5 mg, 0.44 mmol) was added to a solution of **4ab** (135.2 mg, 0.34 mmol) in THF (10 mL). After stirring the suspension for 24 h it was filtered through silica. The volatiles were removed from the orange filtrate under vacuum. The resulting brown oil was dissolved in toluene (3 mL) and diluted with hexane (10 mL). After standing for several days at room temperature brownish yellow needles of **6** (67.7 mg, 44%) had formed; m.p. > 210 °C. $C_{22}H_{38}B_2CoKO_2$ (454.2) calcd. C 58.18, H 8.43; found C 58.04, H 8.53. SIMS (K/T): negative ions m/z (%) = 471 (100) [M + OH^-]; positive ions m/z (%) = 303 (100) [K^+ + [18]-crown-6]. ^{1}H NMR (500 MHz, [D_8]THF): δ = 0.07 (br. s, 2 OH), 0.54 (sept, 4 BCH), 0.69 and 0.73 and (d, ^3J = 7.1 Hz, 4 Me each), 5.09 (m, 2 × 2-/5-H), 5.11 (m, 2 × 3-/4-H) ppm. $^{11}B\{^1H\}$ NMR (160 MHz, [D_8]THF): δ = −3.1 ppm. $^{13}C\{^1H\}$ NMR (126 MHz, [D_8]THF): δ = 21.40 and 21. 76 (Me), 22.7 (br., BCH), 80.19 (C-3,4), 86.10 (C-2,5) ppm.

X-ray Crystal Structure Determinations: Geometry and intensity data were collected with ENRAF-Nonius CAD4 diffractometers (Mo-K_α radiation with graphite monochromators). Crystal data, data-collection parameters, and convergence results for the compounds (**1b**)PF_6, **4bd**, **4ac**, and **5** are listed in Table 3. The structures of (**1b**)PF_6, **4bd**, and **5** were solved by direct methods[26a] and subsequent Fourier difference syntheses, whereas the coordinates of the corresponding hydroxo compound **4ab** provided the structure model for **4ac**. In the full-matrix least-squares refinements on intensities[26b] non-hydrogen atoms were assigned anisotropic displacement parameters and hydrogen atoms were included with standard geometry. The refinement of **4ac** deserves a comment: This compound is isomorphous with the hydroxide **4ab** with similar, but significantly different, lattice parameters. Refinement of the chelated anion site with the scattering factor for *F* results in clearly superior reliability factors than a model for chelated hydroxide. The best results were obtained when a mixed occupancy of the anion site was refined; convergence was reached for an approximate F:O ratio of 4:1, in good agreement with spectroscopic evidence. CCDC-232238 for (**1b**)PF_6, -232239 for **4bd**, -232240 for **4ac**, and -232241 for **5** contain the supplementary crystallographic data of

 © 2004 Wiley-VCH Verlag GmbH & Co. KGaA, Weinheim

Table 3. Crystal data, data collection parameters, and convergence results for (**1b**)PF_6, **4bd**, **4ac** and **5**

	(**1b**)PF_6	**4bd**	**4ac**	**5**
Empirical formula	$C_{14}H_{20}B_2CoF_6P$	$C_{14}H_{20}B_2ClCo$	$C_{22}H_{36.2}B_2CoF_{0.8}O_{0.2}$	$C_{26}H_{48}B_2CoF_2N$
Molecular mass	413.82	304.30	399.66	493.20
Crystal system	monoclinic	triclinic	orthorhombic	monoclinic
Space group	$P2_1/m$ (11)	$P\bar{1}$ (2)	$Pccn$ (56)	$C2/c$ (15)
Radiation (λ, Å)	Mo-K_α (0.71073)	Mo-K_α (0.71073)	Mo-K_α (0.71073)	Mo-K_α (0.71073)
a (Å)	8.040(2)	8.153(3)	7.8665(9)	15.2028(12)
b (Å)	12.574(3)	9.390(2)	14.3884(18)	7.7185(4)
c (Å)	8.612(2)	10.373(3)	18.710(2)	25.2446(11)
α (°)		94.01(2)		
β (°)	100.95(2)	92.37(2)		102.574(5)
γ (°)		113.490(18)		
V (Å^3)	854.8(4)	724.4(4)	2117.7(4)	2891.2(3)
Z	2	2	4	4
$d_{calcd.}$ (g/cm^3)	1.608	1.395	1.254	1.133
F(000)	420	316	856	1064
μ (mm^{-1})	1.150	1.346	0.821	4.845
Absorption correction	numerical	numerical	none	empirical
Max./min. transmission	0.877/0.758	0.721/0.640		0.530/0.377
θ range (°)	3−28	3−26	2−28	6−74
Temperature (K)	203	203	203	293
Scan mode	ω	ω−2θ	ω−2θ	ω−2θ
Crystal size (mm)	0.45 × 0.24 × 0.12	0.70 × 0.40 × 0.26	0.2 × 0.2 × 0.2	0.25 × 0.15 × 0.15
Reflections collected	5136	3086	5300	4925
Reflections unique	1841	2837	2559	2898
Refls. observed $I > 2\sigma(I)$	1443	2615	1130	1488
Variables	138	328	120	177
R_1[a] observed (all data)	0.0519 (0.0730)	0.0275 (0.0315)	0.0620 (0.1696)	0.0471 (0.1483)
wR_2[b] observed (all data)	0.1406 (0.1494)	0.0746 (0.0761)	0.0860 (0.0975)	0.1066 (0.1215)
GOF[c]	1.077	1.059	0.958	0.925
Max. resd. density (e/Å^3)	0.962	0.357	0.659	0.190

[a] $R_1 = \|F_o| - |F_c\|/|F_o|$. [b] $wR_2 = [w(F_o^2 - F_c^2)^2/w(F_o^2)^2]^{1/2}$, where $w = 1/[\sigma^2(F_o^2) + (aP)^2]$ and $P = [\max(F_o^2,0) + 2F_c^2]/3$. [c] GOF = $[w(F_o^2 - F_c^2)^2/(n - p)]^{1/2}$.

this paper. These data can be obtained free of charge at www.ccdc.cam.ac.uk/conts/retrieving/html or from the Cambridge Crystallographic Data Centre, 12 Union Road, Cambridge CB2 1EZ, UK [Fax: (internat.) + 44-1223-336-033; E-mail: deposit@ccdc.cam.ac.uk].

Acknowledgments

This work was generously supported by the Deutsche Forschungsgemeinschaft and the Fonds der Chemischen Industrie.

[1] G. E. Herberich, U. Englert, A. Fischer, D. Wiebelhaus, *Organometallics* **1998**, *17*, 4769−4775.
[2] D. Wiebelhaus, Dissertation, Technische Hochschule Aachen, Aachen, Germany, **1998**.
[3] [3a] J.-M. Lehn, *Supramolecular Chemistry*, VCH, Weinheim, **1995**. [3b] F. Vögtle, *Supramolecular Chemistry*, John Wiley & Sons, Chichester, England, **1993**. [3c] *Molecular Recognition* (Ed.: S. H. Gellman), Thematic issue of *Chem. Rev.* (July/August), **1997**.
[4] [4a] C. Suksai, T. Tuntulani, *Chem. Soc. Rev.* **2003**, *32*, 192−202. [4b] P. D. Beer, P. A. Gale, *Angew. Chem.* **2001**, *113*, 502−532; *Angew. Chem. Int. Ed.* **2001**, *40*, 486−516. [4c] F. P. Schmidtchen, M. Berger, *Chem. Rev.* **1997**, *97*, 1609−1646. [4d] *The Supramolecular Chemistry of Anions* (Eds.: A. Bianchi, K. Bowman-James, E. Garcia-España), Wiley-VCH, Weinheim, **1997**.
[5] [5a] M. J. Biallas, D. F. Shriver, *J. Am. Chem. Soc.* **1966**, *88*, 375−376. [5b] D. F. Shriver, M. J. Biallas, *J. Am. Chem. Soc.* **1967**, *89*, 1078−1081. [5c] M. J. Biallas, *J. Am. Chem. Soc.* **1969**, *91*, 7290−7292.
[6] [6a] H. E. Katz, *J. Am. Chem. Soc.* **1985**, *107*, 1420−1421. [6b] H. E. Katz, *J. Org. Chem.* **1985**, *50*, 5027−5032. [6c] H. E. Katz, *Organometallics* **1987**, *6*, 1134−1136.
[7] D. H. Busch, *Chem. Rev.* **1993**, *93*, 847−860.
[8] [8a] D. J. Saturnino, M. Yamauchi, W. R. Clayton, R. W. Nelson, S. G. Shore, *J. Am. Chem. Soc.* **1975**, *97*, 6063−6070. [8b] R. Köster, G. Seidel, *Chem. Ber.* **1992**, *125*, 627−636. [8c] R. Köster, G. Seidel, K. Wagner, B. Wrackmeyer, *Chem. Ber.* **1993**, *126*, 305−317.
[9] V. C. Williams, G. J. Irvine, W. E. Piers, Z. Li, S. Collins, W. Clegg, M. R. J. Elsegood, T. B. Marder, *Organometallics* **2000**, *19*, 1619−1621.
[10] G. E. Herberich, A. Fischer, D. Wiebelhaus, *Organometallics* **1996**, *15*, 3106−3108.
[11] G. E. Herberich, A. Fischer, *Organometallics* **1996**, *15*, 58−67.
[12] [12a] N. G. Connelly, W. E. Geiger, *Chem. Rev.* **1996**, *96*, 877−910. [12b] A. N. Nesmeyanov, R. B. Materikova, I. R. Lyatifov, T. K. Kurbanov, N. S. Kochetkova, *J. Organomet. Chem.* **1978**, *145*, 241−243.
[13] J. F. Klang, D. B. Collum, *Organometallics* **1988**, *7*, 1532−1537.
[14] For reference data see: [14a] H. Nöth, B. Wrackmeyer, in *NMR Basic Principles and Progress* (Eds.: P. Diehl, E. Fluck, R. Kosfeld), Springer Verlag, Berlin, **1978**, vol. 14. [14b]B. Wrackmeyer, *Annu. Rep. NMR Spectrosc.* **1988**, *20*, 61−203. [14c] A. R. Siedle, *Annu. Rep. NMR Spectrosc.* **1988**, *20*, 205−314.

 © 2004 Wiley-VCH Verlag GmbH & Co. KGaA, Weinheim

[15] A. L. Spek, *Acta Crystallogr., Sect. A* **1990**, *46*, C34.
[16] The acronym *cog* denotes the center of gravity of the C5 ring.
[17] [17a] C. K. Narula, H. Nöth, *Inorg. Chem.* **1985**, *24*, 2532−2539. [17b] T. Wagner, U. Eigendorf, G. E. Herberich, U. Englert, *Struct. Chem.* **1994**, *5*, 233−237.
[18] F. H. Allen, O. Kennard, D. G. Watson, L. Brammer, A. G. Orpen, R. Tylor, *J. Chem. Soc., Perkin Trans. 2* **1987**, S1−S19.
[19] [19a] T. D. Coyle, F. G. A. Stone, in *Progress in Boron Chemistry* (Eds.: H. Steinberg, A. L. McCoskey), Pergamon Press, Oxford, **1964**, vol. 1, 83−166. [19b]D. Mootz, M. Steffen, *Z. Anorg. Allg. Chem.* **1981**, *483*, 171−1180. [19c] D. J. Brauer, H. Bürger, G. Pawelke, *Inorg. Chem.* **1977**, *16*, 2305−2314. [19d] D. J. Brauer, H. Bürger, G. Pawelke, *J. Organomet. Chem.* **1980**, *192*, 305−317. [19e] D. J. Brauer, H. Bürger, G. Pawelke, *J. Organomet. Chem.* **1982**, *238*, 267−279. [19f] M. J. R. Clark, H. Lynton, *Can. J. Chem.* **1970**, *48*, 405−409.
[20] F. H. Allen, *Acta Crystallogr., Sect. B* **2002**, *58*, 380−388.
[21] *X-Blackboard*, Version 2.3.8; number of records searched, April 2003: 272066 (no disorder, coordinates available, error-free, $R < 0.1$).
[22] P. Braunstein, L. Douce, J. Fischer, N. C. Craig, G. Goetz-Grandmont, D. Matt, *Inorg. Chim. Acta* **1992**, *194*, 151−156.
[23] R. Köster, W. Schüßler, R. Boese, *Chem. Ber.* **1990**, *123*, 1945−1952.
[24] R. Fuhler, T. Lenzen, G. Hägele, *Comp. Chem.* **1995**, *19*, 277−282.
[25] J. Sandström, *Dynamic NMR Spectroscopy*, Academic Press, London, England, **1982**.
[26] [26a] G. M. Sheldrick, *SHELXS-97: Program for Structure Solution*; University of Göttingen, Göttingen, Germany, **1997**. [26b] G. M. Sheldrick, *SHELXL-97: Program for Structure Refinement*; University of Göttingen, Göttingen, Germany, **1997**.

Received April 2, 2004
Early View Article
Published Online August 12, 2004

 © 2004 Wiley-VCH Verlag GmbH & Co. KGaA, Weinheim

Mono(alkyne)cobalt Complexes and Electron-Rich Alkynes − The Formation of an Alkyne-Bridged Dinuclear Cobalt Complex by a One-Pot Procedure

Daniel B. Werz,[a] Rolf Gleiter,*[a] and Frank Rominger[a]

Keywords: Alkynes / Chalcogens / Cobalt / Cyclobutadiene complexes

[η^2-Bis(*tert*-butylsulfonyl)acetylene](carbonyl)(η^5-trimethylsilylcyclopentadienyl)cobalt (**2c**) proved to be reactive towards bis(telluro)- and bis(seleno)-substituted alkynes **3** and **4**, respectively, to yield *push-pull*-substituted CpCo-stabilized cyclobutadiene complexes. By utilizing the unsymmetrical diyne **6** and the symmetrical bis(thio)-substituted triyne **7** it was shown that only the most electron-rich triple bond was attacked by the electrophilic compound **2c**. In the case of **7** a dinuclear CpCo-stabilized cyclobutadiene complex **14** bridged by one acetylene moiety was obtained. All the reactions could be carried out at room temperature under rather mild conditions. X-ray investigations of **8**, **12**, **14a**, and **15** show almost equal C–C bond lengths in the cyclobutadiene moieties.
(© Wiley-VCH Verlag GmbH & Co. KGaA, 69451 Weinheim, Germany, 2004)

Introduction

Nearly 50 years ago dicarbonyl(η^5-cyclopentadienyl)cobalt [$CpCo(CO)_2$] was synthesized for the first time.[1,2] Since that time this compound has proved to be a very convenient and efficient reagent for the di- and trimerization of alkynes.[3] Several useful and theoretically attractive molecules like cyclobutadienes,[4] cyclopentadienones,[5,6] and benzene derivatives[7] have been synthesized by this reagent. As one possible mechanism, the subsequent replacement of the CO units by acetylene fragments was proposed yielding first a monoacetylene, then a diacetylene complex that is converted by a metal-mediated cycloaddition process into a 16-electron metallacycle.[7,8] The latter species has the ability to react with a further acetylene fragment or to form the cyclobutadiene[4] by a reductive elimination process. To obtain more insight into the mechanism, several intermediates were isolated and characterized crystallographically. Krebs and Jessel succeeded in the isolation of a mono(alkyne)cobalt complex **1** by using the highly strained 3,3,6,6-tetramethyl-1-thiacycloheptyne.[9] Our group was able to synthesize a variety of mono(alkyne)cobalt complexes[10] **2a**−**f** with the very electron-deficient compound bis(*tert*-butylsulfonylacetylene) (BTSA).[11]

In the course of our in-depth study of electron-rich alkynes[12−14] and their reactions with electrophilic metal fragments, we elucidated the reaction of our mono(alkyne)-cobalt complexes **2a**−**f** with several electron-rich alkynes under mild conditions.[15] Until now we have treated only thio- or carbon-substituted symmetrical acetylene fragments with the mono(alkyne) cobalt complexes.[15] The more electron-rich thio-substituted acetylenes reacted faster and with greater ease than the carbon-substituted compounds, for which heating was needed to initiate the reaction.[15] Therefore, we raised the question whether other elements such as selenium or tellurium are also able to act in the same way as sulfur. Furthermore, we are interested in the reaction of polyacetylene systems in which the mono(alkyne) complex has the choice to discriminate between acetylene units with slightly different electron densities, or even to react twice with the polyalkyne molecule. As model compounds we chose bis(methylseleno)acetylene (**3**),[16] bis(methyltelluro)acetylene (**4**),[17] bis(methylthio)butadiyne (**5**),[14b] (methylthio)(trimethylsilyl)butadiyne (**6**),[14b] and bis(methylthio)hexatriyne (**7**).[14b]

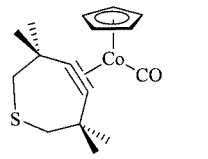

1

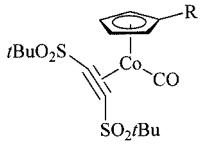

2a–2f
(R = H, CH_3, $SiMe_3$, CO_2Me, Ac, Et_4Me)

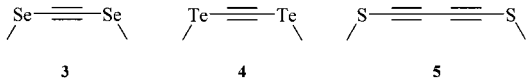

3 **4** **5**

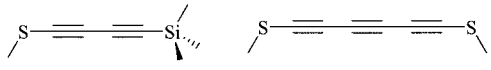

6 **7**

[a] Organisch-Chemisches Institut der Universität Heidelberg, Im Neuenheimer Feld 270, 69120 Heidelberg, Germany
Fax: (internat.) + 49-6221-544205
E-mail: rolf.gleiter@urz.uni-heidelberg.de

Results and Discussion

To ensure reasonable solubilities of the products, we chose **2c** because the $Si(CH_3)_3$ substituent at the Cp ring enhances the solubility in toluene.[10] The reaction between the mono(alkyne)cobalt complex **2c** and alkynes **3**−**7** were carried out in toluene at room temperature and in the dark since the electron-rich alkynes are light-sensitive. The two monoacetylenic substrates **3** and **4** afforded the selenium- and tellurium-substituted cyclobutadiene complexes **8** and **9**, respectively, in 54−63% yield (Scheme 1). Due to the high-lying HOMO of **3** and **4**, the activation energy of this reaction is low.

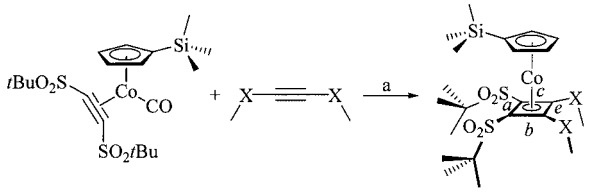

2c **3** (X = Se), **4** (X = Te) **8** (X = Se) 54%, **9** (X = Te) 63%

a) toluene, r.t.

Scheme 1

The reaction of **2c** with the two butadiynes **5** and **6** yielded cyclobutadiene complexes **10** and **12**, respectively. Even by using a high excess of mono(alkyne)cobalt complex, a second attack to the still unchanged triple bond did not take place. Complex **12** was obtained as the only product in the reaction of **2c** with **6**. The subtle differences in the electron density between the two triple bonds in **6** should therefore be important in determining the regioselectivity of the electrophilic attack by the mono(alkyne) complex. Furthermore, in the reaction of **2c** with **5**, a decomposition process of the mono(alkyne)cobalt species took place: the highly electron-deficient BTSA reacted in a Diels−Alder reaction with the CpH(TMS) moiety to afford the norbornadiene derivative **11** in 40% yield.

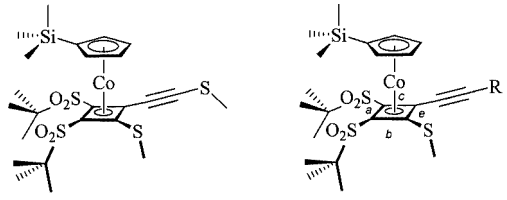

10 **12** (R = $SiMe_3$), **15** (R = H)

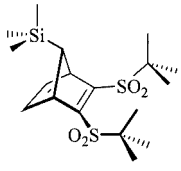

11

We ascribe the observation that the second triple bond in **5** did not react to steric repulsion between the two adjacent cobalt fragments. Thus, the reaction of the electron-rich hexatriyne **7** with excess **2c** was now even more interesting. The analysis of the reaction products showed that only the terminal triple bonds with the higher electron density (relative to the central one) were attacked. Two compounds resulted, the mono- and the disubstituted products **13** and **14**.

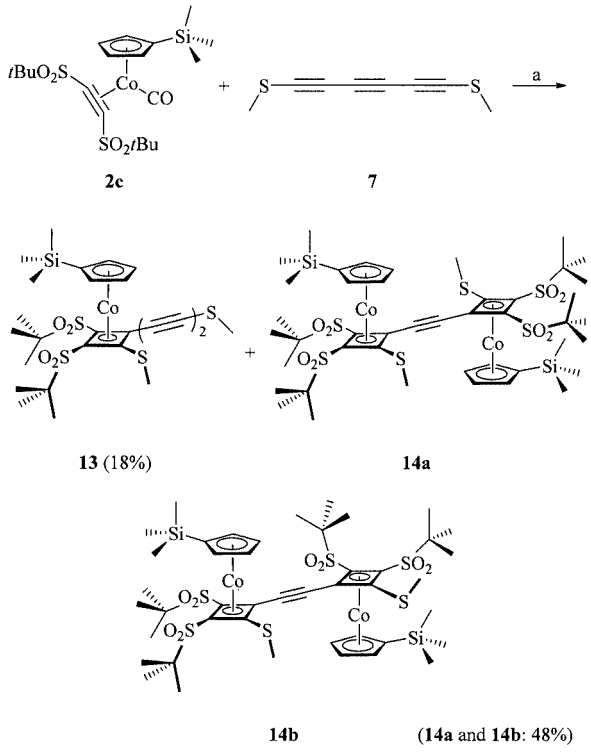

2c **7**

13 (18%) **14a**

14b (**14a** and **14b**: 48%)

a) toluene, r.t.

Scheme 2

For the dinuclear compound, three stereoisomers **14a** and **14b** are possible. NMR spectroscopic investigations revealed their ratio to be approximately 1:1. Separation by column chromatography proved to be unsuccessful, and therefore recrystallization experiments were carried out instead. From a mixture of dichloromethane and diethyl ether the C_i-symmetrical stereoisomer **14a** was obtained as a pure compound.

This reaction reveals an interesting alternative route to bridged dinuclear cyclobutadiene complexes;[18] this is important especially because the introduction of only one acetylene fragment between two metal-stabilized cyclobutadiene fragments is still a difficult goal to reach. The usual method by Bunz et al. is a multi-step sequence starting with the lithiation of metal-capped cyclobutadiene complexes to afford, after treatment with iodine, the corresponding iodides. According to this, with a Stille-type reaction, coupling with the acetylene fragment takes place.[18,19] Even tri- and tetranuclear complexes have been achieved in combination with Glaser-type reactions in this manner.[18,19] Efforts to synthesize dinuclear complexes with bridging butadiyne moieties by a deprotection reaction of **12** (yielding **15**) and

 © 2004 Wiley-VCH Verlag GmbH & Co. KGaA, Weinheim

a subsequent Glaser coupling of the deprotected cobalt complex **15** failed. We ascribe this behavior to the divalent sulfur atom in the starting material that may hinder the catalytic activity of the copper species.

All the cyclobutadiene complexes were yellow to red in color, and were remarkably stable as they are inert towards moisture and air. The characteristic features of the ^{13}C NMR spectra are the chemical shifts of the cyclobutadiene ring atoms that show values between $\delta = 75$ and 85 ppm. Only in the case of the tellurium-substituted cyclobutadiene complex **9** do we encounter signals at $\delta = 53.6$ ppm for the carbon atoms adjacent to the tellurium atoms. Such a "heavy-atom effect" that influences this relatively low-frequency resonance has been reported before.[14a,20]

Four cyclobutadiene complexes **8**, **12**, **14a**, and **15** yielded single crystals which could be investigated by X-ray crystal-

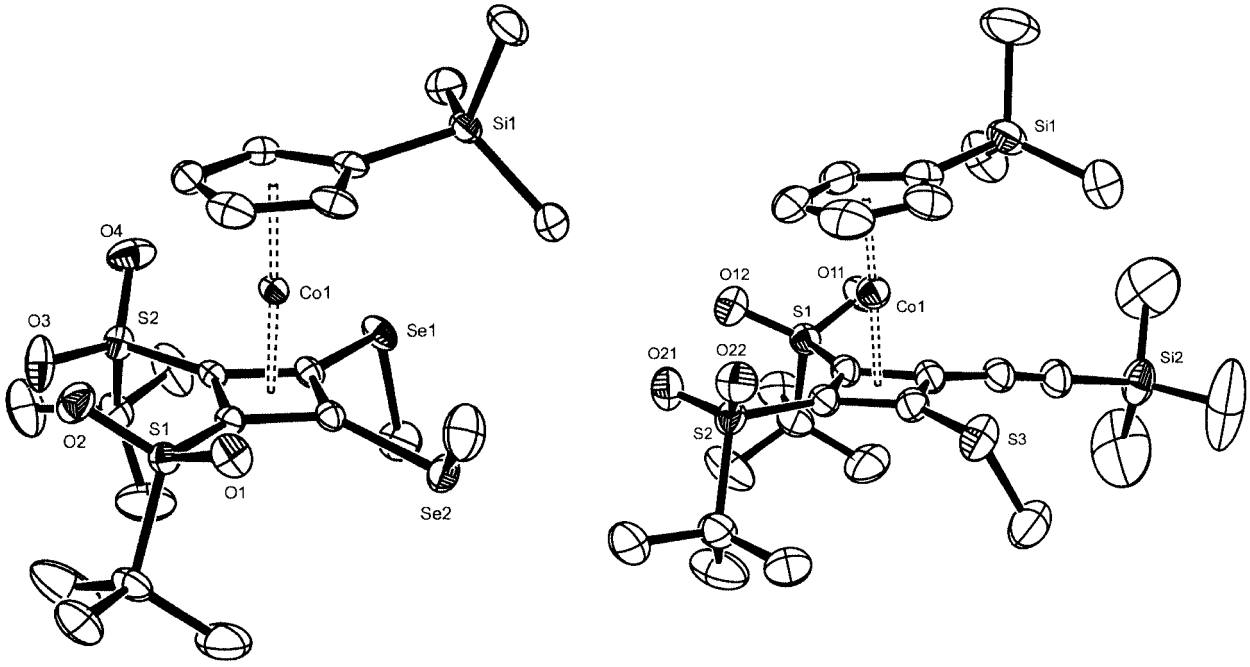

Figure 1. ORTEP plots (50% ellipsoid probability) of the molecular structures of **8** (left) and **12** (right)

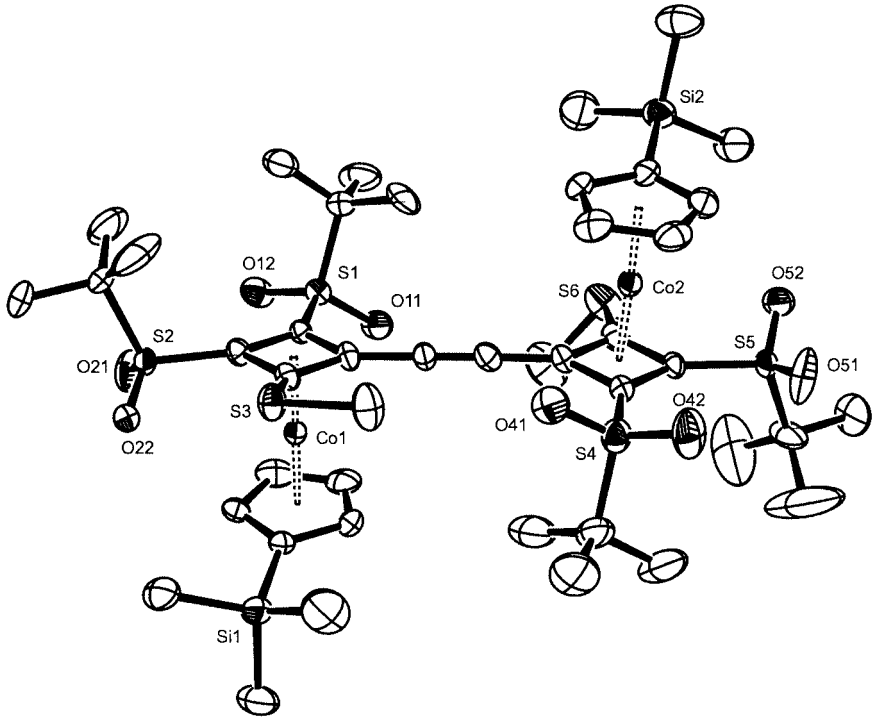

Figure 2. ORTEP plot (50% ellipsoid probability) of the molecular structure of **14a**

 © 2004 Wiley-VCH Verlag GmbH & Co. KGaA, Weinheim

Table 1. Selected distances [pm] and interplanar angles φ [°] of **8**, **12**, **14a**, and **15**; for the definition see Scheme 1

Compound	*d*(Co−Cp)	*d*(Co−Cbd)	φ(Cp−Cbd)	*a*	*b*	*c*	*e*
8	167.5	168.1	4.8	149.1	147.9	147.4	146.2
12[a]	166.7	168.3	6.1	148.6	146.5	147.3	146.1
	166.0	167.2	5.5	148.3	148.2	147.1	145.7
14a	166.1	167.3	5.0	150.0	144.3	146.6	147.5
	167.1	167.8	8.1	148.2	146.0	146.6	144.3
15[b]	165.9	167.0	4.5	148.6	146.3	146.9	144.7

[a] Two independent molecules exist in the asymmetric unit. [b] Disorder between the SMe and the C_2H moieties, the values should be considered imprecise.

lography. As examples, we show the molecular structures of the mononuclear complexes **8** and **12** in Figure 1 and the dinuclear cobalt complex **14a** in Figure 2.

All the conformations in the solid state are highly influenced by the rather bulky *tert*-butylsulfonyl groups. In all cases they point away from the metal center, and to avoid steric interactions with the rather voluminous $Si(CH_3)_3$ substituent at the Cp ring, the latter points in the opposite direction. This behavior allows an almost parallel orientation of the Cp and the Cbd rings. In Table 1, we have compared the interplanar angles of the π-systems as well as the most relevant distances.

The mean distance between the cobalt atom and the four-membered cycle is slightly larger than the distance between the cobalt atom and the five-membered cycle. An examination of the CpCo-stabilized cyclobutadiene systems shows only weak variations. Due to steric repulsions, the longest bond is found to be between the two adjacent *tert*-butylsulfonyl groups (*a*). Any indication of bond alternation in the four-membered ring was not found as can be seen in Table 1. Relative to the unsubstituted $CpCo(C_4H_4)$[21] ($a = b = c = e = 144$ pm), the cyclobutadiene moiety in our systems is slightly enlarged due to the repulsion described above.

Conclusions

We have shown that the CO group in mono(alkyne)cobalt complexes can be replaced by seleno- and telluro-substituted alkynes to yield seleno- and telluro-substituted cyclobutadiene complexes. An important parameter that affects this substitution reaction under mild conditions is the HOMO energy of the alkyne and not the type of heteroatom attached to it. Furthermore, our studies reveal that mono(alkyne)cobalt complexes are able to differentiate between triple bonds with slightly different electron densities in a polyalkyne system, where the attack always takes place at the most electron-rich triple bond. In the case of a hexatriyne system, the attack of two mono(alkyne)cobalt complexes affords a dinuclear complex bridged by one triple bond. Our X-ray investigations reveal that the various substitution patterns do not strongly influence the C−C bond lengths within the metal-capped π-system.

Experimental Section

General Methods: Moisture- and oxygen-sensitive reactions were conducted in oven-dried glassware under argon using dried solvents. Materials used for column chromatography: Neutral alumina (Merck), Celite (Fluka). Elemental analyses were carried out by the Mikroanalytisches Laboratorium der Universität Heidelberg. All melting points are uncorrected. ^{1}H NMR and ^{13}C NMR spectra were recorded with a Bruker WH 300 (^{1}H at 300 MHz and ^{13}C at 75.47 MHz) and Bruker Avance 500 (^{1}H at 500 MHz and ^{13}C at 125.77 MHz) using the solvent as internal standard. IR spectra were recorded with a Bruker Vector 22 FT-IR. UV light absorption data were recorded with a Hewlett Packard 8452A spectrometer. High resolution mass spectra were recorded using a JEOL JMS-700. The starting materials **3**−**7** were prepared according to literature methods.[10][14b,16,17]

General Procedure for the Preparation of the Cyclobutadiene Complexes from Mono(alkyne)cobalt Complex 2c and Electron-Rich Alkynes: To a solution of the mono(alkyne)cobalt complex **2c** in toluene (50 mL) was added the corresponding electron-rich polyalkyne in one portion. To avoid any light, the reaction flask was wrapped with aluminum foil. The reaction mixture was stirred at room temperature for 7−14 d. After completion of the reaction (shown by thin-layer chromatography), the solvent was removed by rotary evaporation, and the crude product was purified by column chromatography.

[η^4-1,2-Bis(*tert*-butylsulfonyl)-3,4-bis(methylseleno)cyclobutadiene](η^5-trimethylsilylcyclopentadienyl)cobalt(I) (8): Starting materials: $CpSiMe_3Co(CO)(BTSA)$ (**2c**) (100 mg, 0.20 mmol) and 2,5-diselenahex-3-yne (**3**) (47 mg, 0.20 mmol). Column chromatography with light petroleum/diethyl ether (2:1) as eluent afforded 73 mg (54%) of **8** as a yellow solid. M.p. 135 °C. ^{1}H NMR (300 MHz, $CDCl_3$): δ = 0.32 (s, 9 H, CH_3), 1.45 (s, 18 H, CH_3), 2.31 (s, 6 H, CH_3), 5.20 (ps, 2 H, CpH), 5.74 (ps, 2 H, CpH) ppm. ^{13}C NMR (75 MHz, $CDCl_3$): δ = −0.2 (CH_3), 10.5 (CH_3), 24.8 (CH_3), 61.6 (C), 77.0 (C), 78.1 (C), 88.5 (CH), 89.5 (CH), 94.1 (C) ppm. UV/Vis (CH_2Cl_2): λ_{max} (log ε) = 248 (4.17), 288 (4.00), 322 (3.96), 372 (3.37) nm. IR (KBr) $\tilde{\nu}$ = 2930, 1628, 1458 cm^{-1}. HRMS (FAB+): calcd. for $C_{22}H_{37}CoO_4S_2{}^{80}Se_2Si$ 675.9565 [M$^+$]; found 675.9593. $C_{22}H_{37}CoO_4S_2Se_2Si$ (675.9): calcd. C 39.17, H 5.53; found C 39.35, H 5.59.

[η^4-1,2-Bis(*tert*-butylsulfonyl)-3,4-bis(methyltelluro)-cyclobutadiene](η^5-trimethylsilylcyclopentadienyl)cobalt(I) (9): Starting materials: $CpSiMe_3Co(CO)(BTSA)$ (**2c**) (60 mg, 0.12 mmol) and 2,5-ditellurahex-3-yne (**4**) (38 mg, 0.12 mmol). Column chromatography with light petroleum/diethyl ether (2:1) as eluent afforded 58 mg (63%) of **9** as an orange solid. M.p. 18 °C.

 © 2004 Wiley-VCH Verlag GmbH & Co. KGaA, Weinheim

^{1}H NMR (500 MHz, $CDCl_3$): δ = 0.32 (s, 9 H, CH_3), 1.40 (s, 18 H, CH_3), 2.10 (s, 6 H, CH_3), 5.07 (ps, 2 H, CpH), 5.64 (ps, 2 H, CpH) ppm. ^{13}C NMR (125 MHz, $CDCl_3$): δ = −12.9 (CH_3), 0.3 (CH_3), 25.1 (CH_3), 53.6 (C), 61.5 (C), 82.7 (C), 88.5 (CH), 89.9 (CH), 94.5 (C) ppm. UV/Vis (CH_2Cl_2): λ_{max} (log ε) = 262 (4.14), 290 (4.02), 324 (3.69), 356 (3.41), 584 (3.21) nm. IR (KBr): $\tilde{\nu}$ = 2929, 1628, 1459 cm^{-1}. HRMS (FAB+): calcd. for $C_{22}H_{37}CoO_4S_2Si^{128}Te_2$ 771.9324 [M$^+$]; found 771.9326. $C_{22}H_{37}CoO_4S_2SiTe_2$ (771.9): calcd. C 34.23, H 4.83; found C 34.69, H 4.91.

[η^4-1,2-Bis(*tert*-butylsulfonyl)-3-(methylthio)-4-(methylthioethynyl)-cyclobutadiene](η^5-trimethylsilylcyclopentadienyl)cobalt(I) (10) and the Norbornadiene Derivative 11: Starting materials: $CpSiMe_3Co(CO)(BTSA)$ (**2c**) (100 mg, 0.20 mmol) and 2,7-dithiaocta-3,5-diyne (**5**) (14 mg, 0.10 mmol). Column chromatography with hexane/diethyl ether (1:1) as eluent afforded 30 mg (49%) of **10** as a yellow highly viscous oil and 32 mg (40%) of **11** as a colorless solid.

10: ^{1}H NMR (500 MHz, $CDCl_3$): δ = 0.33 (s, 9 H, CH_3), 1.42 (s, 18 H, CH_3), 2.40 (s, 3 H, CH_3), 2.46 (s, 3 H, CH_3), 5.16 (ps, 1 H, CpH), 5.39 (ps, 1 H, CpH), 5.70 (ps, 1 H, CpH), 5.80 (ps, 1 H, CpH) ppm. ^{13}C NMR (125 MHz, $CDCl_3$): δ = −0.5 (CH_3), 18.4 (CH_3), 18.7 (CH_3), 24.5 (CH_3), 24.7 (CH_3), 61.3 (C), 61.8 (C), 76.3 (C), 76.5 (C), 77.4 (C), 85.2 (C), 85.4 (C), 87.9 (CH), 88.4 (CH), 89.3 (CH), 90.2 (C), 90.9 (CH), 92.8 (C) ppm. UV/Vis (CH_2Cl_2): λ_{max} (log ε) = 262 (4.47), 324 (4.20), 358 (3.68), 364 (3.82), 404 (3.73) nm. IR (film): $\tilde{\nu}$ = 2930, 2145, 1475, 1432, 1315 cm^{-1}. HRMS (FAB+): calcd. for $C_{24}H_{37}CoO_4S_4Si$ 604.0676 [M$^+$]; found 604.0693.

11: M.p. 173 °C. ^{1}H NMR (300 MHz, $CDCl_3$): δ = −0.1 (s, 9 H, CH_3), 1.41 (s, 18 H, CH_3), 2.58 (s, 1 H, CH), 4.20 (s, 2 H, CH), 6.97 (s, 2 H, CH) ppm. ^{13}C NMR (75 MHz, $CDCl_3$): δ = −0.8 (CH_3), 24.1 (CH_3), 61.9 (CH), 62.4 (CH), 84.5 (CH), 142.5 (CH), 166.3 (C) ppm. UV/Vis (CH_2Cl_2), λ_{max} (log ε) = 262 (3.47) nm. IR (KBr) $\tilde{\nu}$ = 2954, 1629, 1476, 1317 cm^{-1}. HRMS (FAB+): calcd. for $C_{18}H_{32}O_4S_2Si$ 405.1589 [M$^+$]; found 405.1558. $C_{18}H_{32}O_4S_2Si$ (405.2): calcd. C 53.43, H 7.97, S 15.85; found C 53.44, H 8.04, S 15.94.

[η^4−1,2-Bis(*tert*-butylsulfonyl)-3-(methylthio)-4-(trimethylsilylethynyl)cyclobutadiene](η^5-trimethylsilylcyclopentadienyl)cobalt(I) (12): Starting materials: $CpSiMe_3Co(CO)(BTSA)$ (**2c**) (80 mg, 0.16 mmol) and (methylthio)(trimethylsilyl)butadiyne (**6**) (33 mg, 0.20 mmol). Column chromatography with hexane/diethyl ether (2:1) as eluent afforded 46 mg (45%) of **12** as a yellow solid. ^{1}H NMR (500 MHz, $CDCl_3$): δ = 0.17 (s, 9 H, CH_3), 0.33 (s, 9 H, CH_3), 1.41 (s, 9 H, CH_3), 1.42 (s, 9 H, CH_3), 2.47 (s, 3 H, CH_3), 5.13 (ps, 1 H, CpH), 5.39 (ps, 1 H, CpH), 5.70 (ps, 1 H, CpH), 5.82 (ps, 1 H, CpH) ppm. ^{13}C NMR (125 MHz, $CDCl_3$): δ = −0.5 (CH_3), −0.4 (CH_3), 17.7 (CH_3), 24.4 (CH_3), 24.8 (CH_3), 61.2 (C), 62.0 (C), 62.8 (C), 76.2 (C), 76.9 (C), 85.5 (C), 88.0 (CH), 88.5 (CH), 89.5 (CH), 90.9 (CH), 93.1 (C) ppm. UV/Vis (CH_2Cl_2): λ_{max} (log ε) = 262 (4.22), 322 (4.01), 370 (3.44) nm. IR (KBr) $\tilde{\nu}$ = 2958, 2145, 1631, 1426, 1312, 1249 cm^{-1}. HRMS (FAB+): calcd. for $C_{26}H_{34}CoO_4S_3Si_2$ 630.1194 [M$^+$]; found 630.1152.

[η^4-1,2-Bis(*tert*-butylsulfonyl)-3-(methylthio)-4-(methylthiobutadiynyl)cyclobutadiene](η^5-trimethylsilylcyclopentadienyl)cobalt(I) (13) and the Dinuclear Cyclobutadiene Cobalt(I) Complex 14: Starting materials: $CpSiMe_3Co(CO)(BTSA)$ (**2c**) (155 mg, 0.32 mmol) and 2,9-dithiadeca-3,5,7-triyne (**7**) (24 mg, 0.14 mmol). Column chromatography with *n*-hexane/diethyl ether (1:1) as eluent afforded 16 mg (18%) of **13** as an orange oil and 76 mg (48%) of a mixture of **14a** and **14b** as an orange solid.

13: ^{1}H NMR (500 MHz, $CDCl_3$: δ = 0.33 (s, 9 H, CH_3), 1.42 (s, 18 H, CH_3), 2.45 (s, 3 H, CH_3), 2.47 (s, 3 H, CH_3), 5.18 (ps, 1 H, CpH), 5.42 (ps, 1 H, CpH), 5.70 (ps, 1 H, CpH), 5.81 (ps, 1 H, CpH) ppm. ^{13}C NMR (125 MHz, $CDCl_3$): δ = −1.0 (CH_3), 18.4 (CH_3), 19.0 (CH_3), 24.2 (CH_3), 24.4 (CH_3), 61.3 (C), 61.6 (C), 62.5 (C), 72.9 (C), 77.4 (C), 77.4 (C), 78.3 (C), 79.0 (C), 82.0 (C), 86.7 (C), 87.7 (CH), 88.8 (CH), 89.0 (CH), 90.8 (CH), 93.3 (C) ppm. UV/Vis (CH_2Cl_2): λ_{max} (log ε) = 236 (4.58), 252 (4.59), 270 (4.49), 324 (4.11), 378 (3.73) nm. IR (KBr) $\tilde{\nu}$ = 2967, 2931, 2174, 2097, 1628, 1458, 1314, 1250 cm^{-1}. HRMS (FAB+): calcd. for $C_{26}H_{38}CoO_4S_4Si$ 629.0755 [M$^+$ + H]; found 629.0751.

14a: ^{1}H NMR (500 MHz, $CDCl_3$): δ = 0.33 (s, 18 H, CH_3), 1.46 (ps, 36 H, CH_3), 2.47 (s, 6 H, CH_3), 5.21 (ps, 2 H, CpH), 5.33 (ps, 2 H, CpH), 5.71 (ps, 4 H, CpH) ppm. ^{13}C NMR (125 MHz, $CDCl_3$): δ = −0.3 (CH_3), 19.1 (CH_3), 24.7 (CH_3), 24.9 (CH_3), 61.5 (C), 61.5 (C), 63.5 (C), 76.0 (C), 78.4 (C), 84.3 (C), 88.3 (CH), 88.8 (C), 88.8 (CH), 89.9 (CH), 90.0 (CH), 94.6 (C) ppm. UV/Vis (CH_2Cl_2): λ_{max} (log ε) = 264 (4.48), 318 (4.34), 404 (3.85) nm. IR (KBr) $\tilde{\nu}$ = 2969, 1631, 1461, 1313, 1249 cm^{-1}. HRMS (FAB+): calcd. for $C_{44}H_{69}Co_2O_6S_6Si_2$ 1091.1520 [M$^+$ + H]; found 1091.1492.

[η^4-1,2-Bis(*tert*-butylsulfonyl)-3-(methylthio)-4-(ethynyl)cyclobutadiene](η^5-trimethylsilylcyclopentadienyl)cobalt(I) (15): Starting materials: **12** (59 mg, 0.09 mmol) and a solution of sodium hydroxide (0.3 mL, 0.30 mmol of 1.0 N) in methanol (30 mL). The mixture was stirred for 3 h and extracted with diethyl ether. Column chromatography with hexane → hexane/diethyl ether (1:1) as eluent afforded 31 mg (59%) of **15** as a yellow solid. M.p. 130 °C (dec.). ^{1}H NMR (500 MHz, $CDCl_3$): δ = 0.33 (s, 9 H, CH_3), 1.43 (s, 9 H, CH_3), 1.43 (s, 9 H, CH_3), 2.47 (s, 3 H, CH_3), 3.39 (s, 1 H, CH), 5.20 (ps, 1 H, CpH), 5.35 (ps, 1 H, CpH), 5.74 (ps, 1 H, CpH), 5.83 (ps, 1 H, CpH) ppm. ^{13}C NMR (75 MHz, $CDCl_3$): δ = −0.5 (CH_3), −18.4 (CH_3), 24.5 (CH_3), 24.7 (CH_3), 61.4 (C), 61.7 (C), 63.1 (C), 76.6 (C), 77.0 (C), 77.6 (C), 85.1 (C), 85.8 (CH), 88.3 (CH), 88.7 (CH), 89.2 (CH), 90.9 (CH), 93.7 (C) ppm. UV/Vis (CH_2Cl_2): λ_{max} (log ε) = 258 (4.48), 282 (4.27), 320 (4.31), 376 (3.55) nm. IR (KBr): $\tilde{\nu}$ = 2969, 1628, 1461, 1416, 1312, 1249, 1164 cm^{-1}. HRMS (FAB+): calcd. for $C_{23}H_{35}CoO_4S_3Si$ 558.0735 [M$^+$]; found 558.759. $C_{23}H_{35}CoO_4S_3Si$ (558.1): calcd. C 49.44, H 6.31, S, 17.22; found C 49.10, H 6.32, S 16.80.

X-ray Diffraction Analyses: The reflections were collected at 200(2) K with a Bruker Smart CCD diffractometer (Mo-K_α radiation, graphite monochromator). Intensities were corrected for Lorentz and polarization effects, an empirical absorption correction was applied using SADABS[22] based on the Laue symmetry of the reciprocal space. The structures were solved by direct methods. The structural parameters of the non-hydrogen atoms were refined anisotropically according to a full-matrix least-squares technique (F^2). The hydrogen atoms were calculated according to stereochemical aspects. In the case of **12**, two independent molecules were found in the asymmetric unit. In **15**, the ethynyl moiety and the methylthio unit were disordered (2:1). Structure solution and refinement were carried out with the SHELXTL (5.10) software package.[22] ORTEP drawings were obtained using the ORTEP-3 for Windows program by L. Farrugia.[23] Table 2 contains the crystallographic information and details of the refinement procedure. CCDC-225694 to -225698 contain the supplementary crystallographic data for this paper. These data can be obtained free of charge at www.ccdc.cam.ac.uk/conts/retrieving.html [or from the Cambridge Crystallographic Data Centre, 12 Union Road, Cambridge CB2 1EZ, UK; Fax: (internat.) + 44-1223-336-033; E-mail: data_request@ccdc.cam.ac.uk].

 © 2004 Wiley-VCH Verlag GmbH & Co. KGaA, Weinheim

Table 2. Crystallographic data and details of the refinement procedure for **8**, **11**, **12**, **14a**, and **15**

	8	**11**	**12**	**14a**	**15**
Empirical formula	$C_{22}H_{37}CoO_4S_2Se_2Si$	$C_{18}H_{32}O_4S_2Si$	$C_{26}H_{43}CoO_4S_3Si_2$	$C_{44}H_{68}Co_2O_8S_6Si_2$	$C_{23}H_{35}CoO_4S_3Si$
Formula mass [g/mol]	674.60	404.66	630.92	1091.43	558.74
Crystal size [mm]	0.40 × 0.20 × 0.09	0.40 × 0.32 × 0.06	0.32 × 0.30 × 0.30	0.32 × 0.20 × 0.16	0.36 × 0.05 × 0.03
Crystal color	yellow	colorless	yellow	red	yellow
Crystal shape	polyhedron	polyhedron	polyhedron	polyhedron	needle
Crystal system	monoclinic	monoclinic	monoclinic	monoclinic	monoclinic
Space group	*Cc*	$P2_1/n$	$P2_1/c$	*Cc*	$P2_1/c$
a [Å]	10.5834(1)	10.1921(1)	29.0406(2)	23.4650(1)	14.8676(2)
b [Å]	16.2163(2)	12.1916(1)	19.3468(1)	20.0117(3)	10.1951(2)
c [Å]	16.3188(2)	17.4848(2)	11.6699(2)	12.2655(2)	13.1370(2)
β [°]	98.579(1)	98.633(1)	92.854(1)	112.077(1)	94.627(1)
V [Å^3]	2769.35(5)	2148.50(4)	6548.52(13)	5337.27(12)	2740.19(7)
$D_{calcd.}$ [g/cm^3]	1.618	1.251	1.280	1.358	1.354
Z	4	4	8	4	4
h_{min}/h_{max}	−13/13	−13/13	−37/37	−30/30	−18/18
k_{min}/k_{max}	−20/20	−15/15	−25/25	−25/25	−12/12
l_{min}/l_{max}	−20/21	−22/22	−15/15	−15/15	−22/21
μ [mm^{-1}]	3.47	0.32	0.82	0.95	0.92
$T_{max.}/T_{min.}$	1.00/0.77	1.00/0.93	0.82/0.71	0.89/0.71	0.97/0.73
Refl. collected	12188	21643	67395	27315	23966
Refl. unique	6144	4907	15014	12125	5210
Refl. observed	5605	3882	9708	9548	3184
Parameter	300	235	675	580	307
R(*F*)	0.022	0.035	0.047	0.043	0.065
$R_w(F^2)$	0.048	0.083	0.110	0.101	0.151
S (Gof) on F^2	0.83	1.04	1.02	1.01	1.03
$(\Delta\rho)_{max}$ [e·Å^{-3}]	0.25	0.39	0.96	1.38	0.74
$(\Delta\rho)_{min}$ [e·Å^{-3}]	−0.33	−0.30	−0.42	−0.44	−0.63

Acknowledgments

We are grateful to the Deutsche Forschungsgemeinschaft (SFB 623), the Fonds der Chemischen Industrie, and BASF Aktiengesellschaft, Ludwigshafen, for financial support. D. B. W. thanks M. Basler for preparative assistance and the Studienstiftung des deutschen Volkes for a graduate fellowship. We thank Prof. W. Siebert for helpful discussions.

[1] T. S. Piper, F. A. Cotton, J. Wilkinson, *Inorg. Nucl. Chem.* **1955**, *1*, 165−174.
[2] E. O. Fischer, R. Jira, *Z. Naturforsch., Teil B* **1955**, *10*, 355.
[3] [3a] R. D. W. Kemmit, D. R. Russell in *Comprehensive Organometallic Chemistry*, vol.5 (Eds.: F. G. A. Stone, E. W. Abel), Pergamon Press, New York, **1982**. [3b] J. P. Collman, L. S. Hegedus, J. R. Norton, R. G. Finke, *Principles and Applications of Organotransition Metal Chemistry*, University Science Books, Mill Valley, CA, **1987**.
[4] Reviews: [4a] A. Efraty, *Chem. Rev.* **1977**, *77*, 691−744. [4b] R. Gleiter, *Angew. Chem.* **1992**, *104*, 29−46; *Angew. Chem. Int. Ed. Engl.* **1992**, *31*, 27−44.
[5] Reviews: [5a] W. I. Hübel in *Organic Synthesis via Metal Carbonyls*, Wiley, New York, **1968**, vol. 1, p. 273. [5b] P. Pino, G. Braca in *Organic Synthesis via Metal Carbonyls*, vol. 2 (Eds.: I. Wender, P. Pino), Wiley, New York, **1977**, p. 419.
[6] N. Schore, *Chem. Rev.* **1988**, *88*, 1081−1119.
[7] Reviews: [7a] K. P. C. Vollhardt, *Angew. Chem.* **1984**, *96*, 525−541, *Angew. Chem. Int. Ed. Engl.* **1984**, *23*, 539−555. [7b] H. Bönnemann, W. Brijoux, R. Brinkmann, W. Meurers, R. Mynott, W. von Philipsborn, T. Egolf, *J. Organomet. Chem.* **1984**, *272*, 231−249.
[8] [8a] M. D. Rausch, G. F. Westover, E. Mintz, G. M. Reisner, I. Bernal, A. Clearfield, J. M. Troup, *Inorg. Chem.* **1979**, *18*, 2605−2615. [8b] J. H. Hardesty, J. B. Koerner, T. A. Albright, G.-Y. Lee, *J. Am. Chem. Soc.* **1999**, *121*, 6055−6067.
[9] [9a] B. Jessel, Dissertation, Universität Hamburg, **1984**. [9b] A. Krebs, J. Wilke, *Top. Curr. Chem.* **1983**, *109*, 189−233.
[10] C. Benisch, J. Chávez, R. Gleiter, B. Nuber, H. Irngartinger, T. Oeser, H. Pritzkow, F. Rominger, *Eur. J. Inorg. Chem.* **1998**, 629−632.
[11] [11a] A. Riera, F. Cabré, A. Moyano, M. A. Pericàs, J. Santamaria, *Tetrahedron Lett.* **1990**, *31*, 2169−2172. [11b] A. Riera, M. Marti, A. Moyano, M. A. Pericàs, J. Santamaria, *Tetrahedron Lett.* **1990**, *31*, 2173−2176.
[12] [12a] C. Benisch, S. Bethke, R. Gleiter, T. Oeser, H. Pritzkow, F. Rominger, *Eur. J. Org. Chem.* **2000**, 2479−2488. [12b] D. B. Werz, R. Gleiter, F. Rominger, *J. Org. Chem.* **2002**, *67*, 4290−4297.
[13] [13a] R. Gleiter, D. B. Werz, B. J. Rausch, *Chem. Eur. J.* **2003**, *9*, 2676−2683. [13b] D. B. Werz, R. Gleiter, F. Rominger, *J. Am. Chem. Soc.* **2002**, *124*, 10638−10639.
[14] [14a] D. B. Werz, R. Gleiter, F. Rominger, *Organometallics* **2003**, *22*, 843−849. [14b] D. B. Werz, R. Gleiter, *J. Org. Chem.* **2003**, *68*, 9400−9405.
[15] [15a] C. Benisch, R. Gleiter, T. H. Staeb, B. Nuber, T. Oeser, H. Pritzkow, F. Rominger, *J. Organomet. Chem.* **2002**, *641*, 102−112. [15b] C. Benisch, D. B. Werz, R. Gleiter, F. Rominger, T. Oeser, *Eur. J. Inorg. Chem.* **2002**, 1099−1112.
[16] L. Brandsma, *Preparative Acetylene Chemistry*, 2nd ed., Elsevier, Amsterdam, **1988**.
[17] R. W. Gedridge Jr., L. Brandsma, R. A. Nissan, H. D. Verkruijsse, S. Harder, R. L. P. de Jong, C. J. O'Connor, *Organometallics* **1992**, *11*, 418−422.
[18] [18a] J. E. C. Wiegelmann, U. H. F. Bunz, *Organometallics* **1993**, *12*, 3792−3794. [18b] U. H. F. Bunz, J. E. C. Wiegelmann-Kreiter, *Chem. Ber.* **1996**, *129*, 785−797.
[19] [19a] U. H. F. Bunz, V. Enkelmann, *Angew. Chem.* **1993**, *105*, 1712−1714; *Angew. Chem. Int. Ed. Engl.* **1993**, *32*, 1653−1655. [19b] M. Altmann, V. Enkelmann, U. H. F. Bunz, *Chem. Ber.* **1996**, *129*, 269−273.

 © 2004 Wiley-VCH Verlag GmbH & Co. KGaA, Weinheim

[20] M. Kaupp, O. L. Malkina, V. G. Malkin, P. Pyykkö, *Chem. Eur. J.* **1998**, *4*, 118−126.
[21] P. E. Riley, R. E. Davies, *J. Organomet. Chem.* **1976**, *113*, 157−166.
[22] G. M. Sheldrick, Bruker Analytical X-ray Division, Madison, WI, **1997**.
[23] ORTEP-3 for Windows: A Version of ORTEP-III with a Graphical User Interface (GUI): L. J. Farrugia, *J. Appl. Crystallogr.* **1997**, *30*, 565.

Received April 28, 2004
Early View Article
Published Online August 17, 2004

 © 2004 Wiley-VCH Verlag GmbH & Co. KGaA, Weinheim

Novel Cytotoxic Copper(II) Complexes of 8-Aminoquinoline Derivatives: Crystal Structure and Different Reactivity towards Glutathione

Shouchun Zhang,[a] Chao Tu,[a] Xiongyong Wang,[a] Zhen Yang,[a] Junyong Zhang,[a] Liping Lin,[b] Jian Ding,[b] and Zijian Guo*[a]

Keywords: Antitumor agents / Bioinorganic chemistry / Copper / N ligands

Two novel Cu^{II} complexes [Cu(CMQA)(H_2O)] (**1**) (CMQA = *N*-carboxymethyl-L-methionine-*N*′-8-quinolylamide) and [Cu(MQA)(OAc)] (**2**) (MQA = L-methionine-*N*′-8-quinolylamide, OAc = CH_3COO^-) have been synthesized and structurally characterized. Complex **1** crystallizes in the orthorhombic system with space group $P2_12_12_1$ [a = 5.556(1) Å, b = 15.002(3) Å, c = 20.886(4) Å] while complex **2** crystallizes in the monoclinic system with space group $C2$ [a = 28.463(6) Å, b = 5.264(1) Å, c = 13.345(3) Å, β = 109.142(3)°]. In both complexes the Cu^{II} center is coordinated by three N atoms of the ligand and one O atom of H_2O (**1**) or OAc (**2**). The in vitro cytotoxicity of both complexes and their corresponding ligands have been tested against the murine leukemia P-388 and lung adenocarcinoma A-549 cell lines. Complex **2** shows a potent activity against both cell lines with an inhibitory rate of 100% for the murine leukemia P-388 cell line and 93.4% for the lung adenocarcinoma A-549 cell line at a concentration of 10^{-6} mol·L^{-1}, while complex **1** shows only a marginal activity against the same cell lines. The reactivity of the two complexes towards γ-glutathione (GSH) has been investigated and is discussed in association with their different cytotoxicity.
(© Wiley-VCH Verlag GmbH & Co. KGaA, 69451 Weinheim, Germany, 2004)

Introduction

The application of metal complexes in medicine has become increasingly prevalent since the clinical success of cisplatin for treatment of several human malignant tumors decades ago.[1−4] Copper has a long history of medical use, and its potential antitumor properties have attracted attention recently because it is thought to be less toxic than nonessential metals such as platinum.[5] For example, Cu^{II} complexes of thiosemicarbazone are a family of the most promising non-platinum compounds with antitumor potential.[6−8] Some tertiary Cu^{II}-amino acid-phenanthroline complexes (Casiopeinas) exhibit high antitumor activity towards a variety of tumor cell lines.[9,10] More recently, some Cu^{II} complexes with macrocyclic ligands[11,12] or nitrogen-containing heterocyclic ligands[13,14] have also been reported to show potent antitumor activities.

As a part of our interest in the design of quinoline-based metallo-antitumor complexes,[15−17] we describe here the crystal structure and in vitro cytotoxicity of two novel copper complexes [Cu(CMQA)(H_2O)] (**1**) and [Cu(MQA)(OAc)] (**2**; Scheme 1). The interactions of complexes **1** and **2** with γ-glutathione (GSH) have been studied and the implications for their cytotoxicity are discussed.

[a] State Key Laboratory of Coordination Chemistry, Coordination Chemistry Institute, Nanjing University, Nanjing 210093, P. R. China
Fax: +86-25-8331-4502
E-mail: zguo@nju.edu.cn
[b] Division of Anti-tumor Pharmacology, State Key Laboratory for New Drug Research, Shanghai Institute of Materia Medica, Shanghai Institute of Biological Science, Shanghai 200031, P. R. China
Supporting information for this article is available on the WWW under http://www.eurjoc.irg or from the author.

Results and Discussion

Synthesis

The reaction of $Cu(OAc)_2·H_2O$ with ligands **L** and **L**′ resulted in two related complexes **1** and **2** (Scheme 1). In the reaction of **L** with $Cu(OAc)_2·H_2O$, the $OC(CH_3)_3$ group of **L** is replaced by OCH_3 from the solvent methanol. This ester-exchange reaction has been reported previously in similar reactions.[17] During Cu^{II} coordination all the amide groups of the ligands are deprotonated, giving rise to a stable delocalized electronic system.[18,19] Complex **1** dissolves readily in CH_3OH, DMSO, and DMF but barely in H_2O, while complex **2** can dissolve fairly well both in organic solvents such as CH_3OH, DMSO, DMF and in water.

Structures

The crystal data, data collection, structural solution and refinement parameters for ligand **L** and complexes **1** and **2** are summarized in the Exp. Sect; selected bond lengths and angles are listed in Table 1. The crystal structure of ligand **L** is shown in Figure 1. All the bond lengths and bond

 © 2004 Wiley-VCH Verlag GmbH & Co. KGaA, Weinheim DOI: 10.1002/ejic.200400357

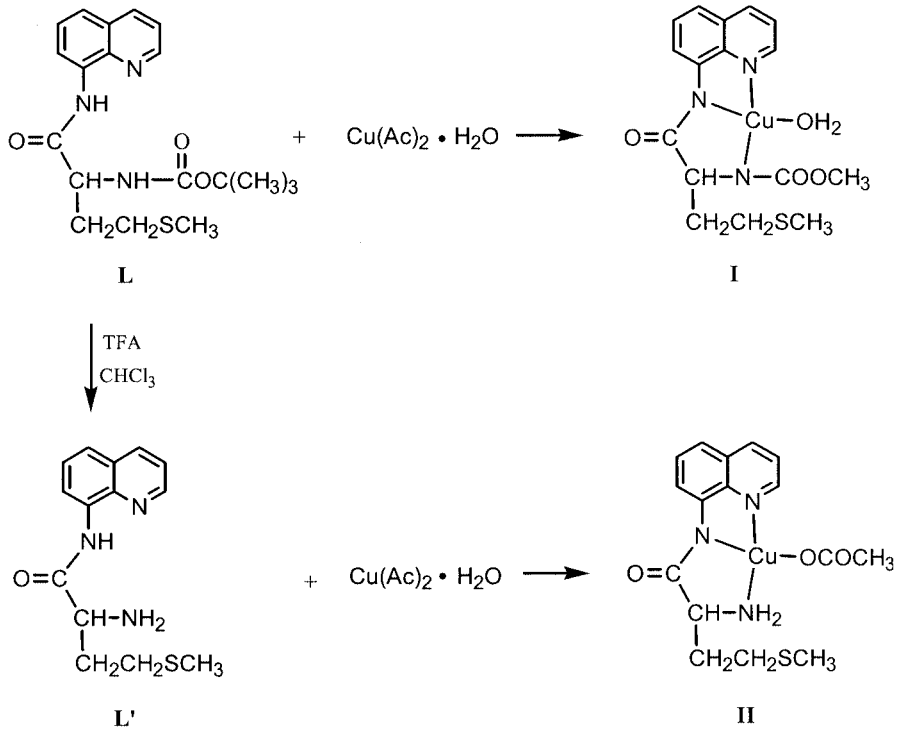

Scheme 1

angles of **L** are within the normal ranges. The N(2)−C(8) and N(2)−C(10) bond lengths are similar to those of similar ligands.[20,21] The crystal packing of ligand **L** is shown in Figure S1. The distance between the two adjacent quinoline planes is 3.390 Å, suggesting the presence of strong intermolecular p-π stacking interactions between the adjacent molecules. Intermolecular hydrogen bonds between the hydrogen atom on N(1) and the O(2) atom of a neighboring molecule are observed. The D···A separation is 2.968 Å for N(1)···O(2) (symmetry code: $x + 1$, y, z) and the D−H···A angle is about 156.72° for N(1)−H(1A)···O(2). The crystal structures of complexes **1** and **2** are shown in Figure 2 and 3, respectively. In both complexes the ligand acts as a tridentate chelator coordinated to Cu^{II} through the quinolyl N(3) and amide N(1) and N(2) atoms. The fourth coordination position of Cu^{II} is occupied by either a water molecule through O(1W) in complex **1** or an acetate through O(2) in complex **2**. In general, the $Cu-N_{amido}$ and $Cu-N_{quinolyl}$ bond lengths and the bond angles in **1** and **2** are similar to those of related complexes.[17] The bond angles show that the geometry around Cu^{II} is slightly distorted from the regular square-planar geometry in both complexes. For example, the N(1)−Cu(1)−N(3) and N(2)−Cu(1)−O(1W or 2) angles are contracted from the ideal value of 180° for a regular square-planar structure. Such distortion is often observed in Cu^{II} complexes of tridentate chelating agents.[22−24] It is notable that the CuN_3O [Cu(1), N(1), N(2), N(3), O(1W) (for **1**) or O(2) (for **2**)] plane is nearly co-planar with the quinoline ring in both complexes (see Figure S2 and Figure S3 in the Supporting Information for this article; see also the footnote on the first page of this article), and the mean deviation from the large best plane is 0.004 Å for **1** and 0.026 Å for **2**. There are strong intermolecular π-π stacking interactions between the adjacent molecules in both complexes, and the distance between the adjacent planes is 3.506 Å for **1** and 3.574 Å for **2**. There is an intramolecular hydrogen bond (Table S1) in the crystal structure of complex **1**; the D···A separation is 2.545 Å for O(1W)···O(2). The D−H···A angle is about 151° for O(1W)−H(1WA)···O(2). This intramolecular hydrogen bond may be responsible for the poor solubility of complex **1** in water. Intermolecular hydrogen bonds are observed in complex **2** between the hydrogen atoms of the solvent water molecule and N(1) and O(3). No intramolecular hydrogen bond is observed in **2**.

Cytotoxic Activity

The in vitro cytotoxicity of ligands **L** and **L′** and their copper complexes **1** and **2** was evaluated against the murine leukemia P-388 and lung adenocarcinoma A-549 cell lines with cisplatin as a positive control. The cytotoxicity profiles are shown in Figure 4. The results indicate that the inhibitory rates of complexes **1** and **2** are significantly higher than those of ligands **L** and **L′**, which are inactive to the tested cell lines. This observation is in accordance with the general phenomenon that copper complexes demonstrate enhanced biological activity than their parent ligands.[25,26] Complex **2** is far more active than complex **1** against both cell lines under the same conditions, with the latter being active only at concentrations as high as 10^{-4} mol·L^{-1}. At a concentration of 10^{-6} mol·L^{-1}, complex **2** still retains a high in-

 © 2004 Wiley-VCH Verlag GmbH & Co. KGaA, Weinheim

Table 1. Selected bond lengths (Å) and angles (°) of ligand **L** and complexes **1** and **2**

Ligand **L**					
N(2)−C(10)	1.356(4)	N(2)−C(8)	1.400(4)	N(3)−C(11)	1.447(4)
C(10)−C(11)	1.531(4)	C(11)−C(12)	1.534(4)	O(1)−C(10)	1.208(4)
C(10)−N(2)−C(8)	128.0(3)	O(1)−C(10)−N(2)	124.8(3)	N(3)−C(11)−C(10)	113.4(2)
N(2)−C(8)−C(9)	115.0(3)	N(2)−C(10)−C(11)	114.5(3)	N(3)−C(9)−C(8)	117.7(3)
Complex **1**					
Cu(1)−N(1)	1.939(7)	Cu(1)−N(2)	1.906(6)	Cu(1)−N(3)	1.986(7)
Cu(1)−O(1 W)	1.949(5)	N(3)−C(1)	1.328(10)	N(3)−C(9)	1.372(10)
N(2)−C(10)	1.334(9)	N(2)−C(8)	1.386(10)	C(8)−C(9)	1.443(10)
N(1)−C(11)	1.481(9)	N(1)−C(15)	1.308(10)	O(1)−C(10)	1.232(9)
N(1)−Cu(1)−N(3)	167.5(2)	N(1)−Cu(1)−O(1W)	97.0(2)	N(2)−Cu(1)−O(1W)	178.4(3)
N(2)−Cu(1)−N(3)	83.1(3)	N(2)−Cu(1)−N(1)	84.4(3)	C(11)−N(1)−Cu(1)	113.3(5)
C(10)−N(2)−Cu(1)	117.9(5)	C(8)−N(2)−Cu(1)	115.3(5)	C(1)−N(3)−Cu(1)	129.9(6)
C(9)−N(3)−Cu(1)	112.7(5)	O(1W)−Cu(1)−N(3)	95.4(2)	C(15)−N(1)−Cu(1)	125.4(5)
Complex **2**					
Cu(1)−N(1)	2.017(8)	Cu(1)−N(2)	1.887(8)	Cu(1)−N(3)	1.993(8)
Cu(1)−O(2)	1.923(8)	N(3)−C(1)	1.313(14)	N(3)−C(9)	1.357(15)
N(2)−C(10)	1.350(12)	N(2)−C(8)	1.400(13)	C(8)−C(9)	1.456(15)
N(1)−C(11)	1.502(13)	O(1)−C(10)	1.202(14)	O(2)−C(15)	1.225(15)
N(1)−Cu(1)−N(3)	167.7(4)	N(1)−Cu(1)−O(2)	101.0(3)	N(2)−Cu(1)−O(2)	173.7(4)
N(2)−Cu(1)−N(3)	83.3(4)	N(2)−Cu(1)−N(1)	84.4(3)	C(11)−N(1)−Cu(1)	107.4(6)
C(10)−N(2)−Cu(1)	117.4(7)	C(8)−N(2)−Cu(1)	116.7(7)	C(1)−N(3)−Cu(1)	128.8(8)
C(9)−N(3)−Cu(1)	111.9(7)	O(2)−Cu(1)−N(3)	91.4(4)	C(15)−O(2)−Cu(1)	133.8(8)

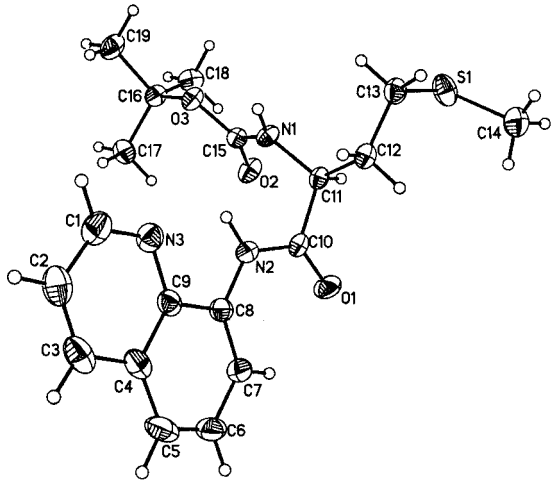

Figure 1. Crystal structure of ligand **L** (ORTEP drawing)

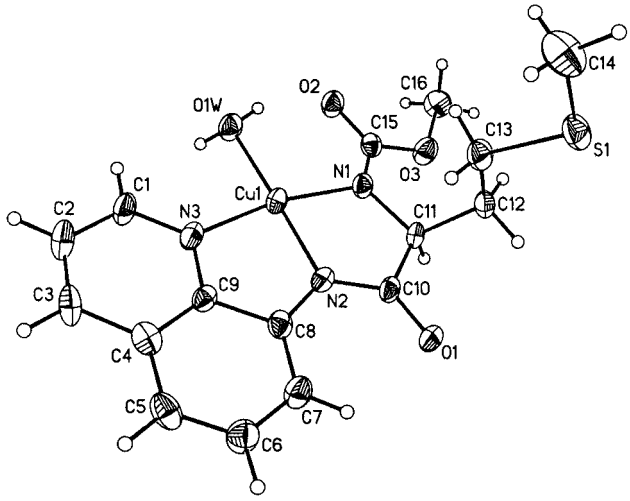

Figure 2. Crystal structure of complex **1** (ORTEP drawing)

hibitory rate against both the murine leukemia P-388 cell line (100%) and lung adenocarcinoma A-549 cell line (93.4%), and is about two to three times more potent than cisplatin. In fact, the activity of complex **2** is more potent than cisplatin at most experimental concentrations.

Interactions with DNA and GSH

It is commonly believed that DNA is the main cellular target of metal-based antitumor agents.[27] DNA-binding studies were therefore carried out to reveal the potential biological target for complexes **1** and **2**. To our surprise, the CD data (Figure S3, Supporting Information) do not show significant changes upon addition of the complexes to calf thymus DNA. The UV data (Figure S4, Supporting Information) also suggest that these complexes do not bind to DNA under the experimental conditions studied. This result suggests that another biological target may exist for complexes **1** and **2**.

As one of the most widely distributed intracellular reductants, GSH also plays an important role in metal detoxification.[28−31] Recently, a quantitative study has shown that GSH is a crucial contributor to protect against Cu cytotoxicity and it may function both in concert with, or

 © 2004 Wiley-VCH Verlag GmbH & Co. KGaA, Weinheim

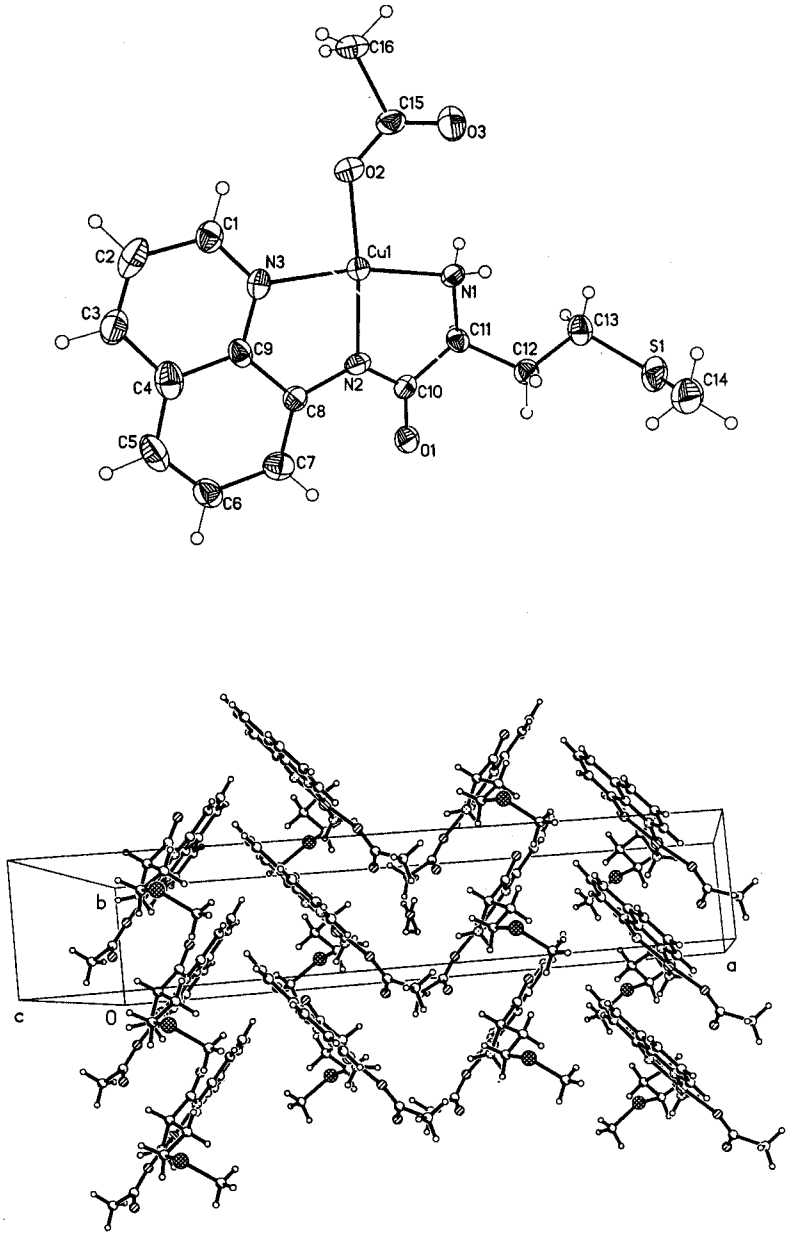

Figure 3. Crystal structure (ORTEP drawing) (top) and structure packed along the *b* axis (bottom) of complex **2**

independently of, metallothionein.[32] We thus studied the interaction of complexes **1** and **2** with GSH. As shown in Figure 5, the absorbances of complex **1** at 259 and 365 nm decrease gradually while the absorbances at about 241 and 302 nm increase upon the addition of GSH. When the concentration of GSH was increased to 3.33×10^{-5} mol·L^{-1}, equivalent to that of complex **1**, the absorption bands at 259 and 365 nm disappeared completely. In contrast to complex **1**, no new absorption bands and only inconspicuous absorption changes were observed in the UV spectra upon addition of GSH to a solution of **2**. Interestingly, this result is closely correlated with the cytotoxicity of these complexes. The GSH-reactive complex **1** is biologically inactive against tumor cells, while GSH-inactive complex **2** is biologically active. This relationship between reactivity and cytotoxicity may result from the Cu detoxification by intracellular GSH. Upon entering tumor cells, complex **1** would react with intracellular GSH and thus prevent it from reaching its desired target and exhibiting cytotoxicity. Complex **2** does not react with GSH, therefore its cytotoxicity in tumor cells is retained. It is therefore tempting to suggest that GSH could be used as a probe to select cytotoxic copper(II) complexes, although many more complexes need to be tested.

The electrochemical behavior of complexes **1** and **2** was also studied to explain the different reactivity of both complexes toward GSH (Figure S5). Complex **2** undergoes a reduction process at about −900 mV, which is far more negative than that of complex **1** (about −600 mV). The difference in activation energies ($\Delta G^{\ddagger}$) of both complexes re-

 © 2004 Wiley-VCH Verlag GmbH & Co. KGaA, Weinheim

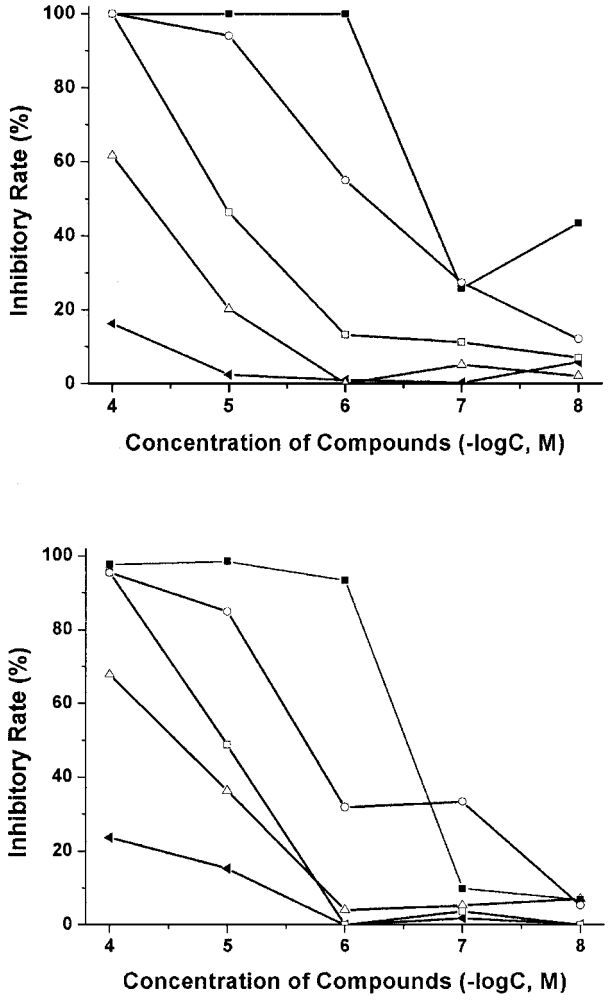

Figure 4. Cytotoxic activity of compounds against murine leukemia P-388 cell line (top) and lung adenocarcinoma A-549 cell line (bottom) (solid triangle: ligand **L**; hollow triangle: ligand **L′**; hollow square: complex **1**; solid square: complex **2**; hollow circle: cisplatin)

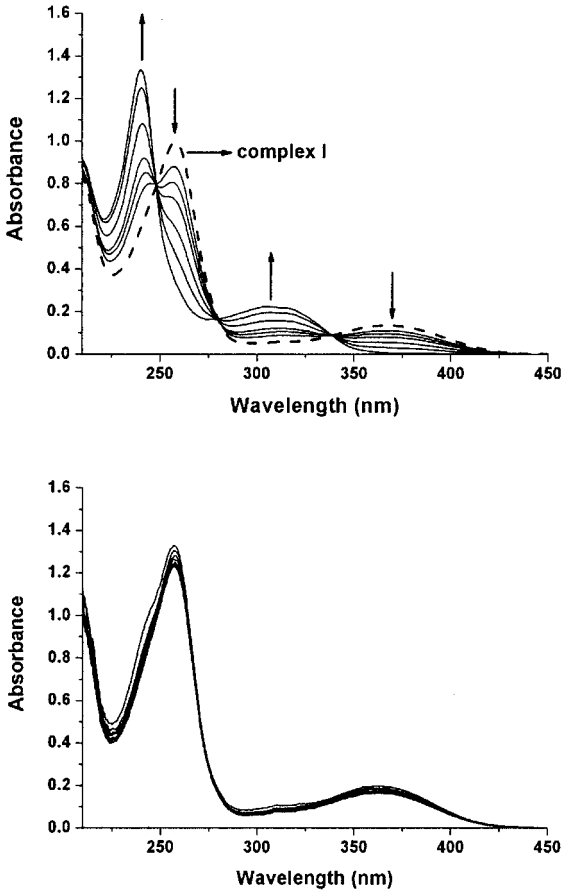

Figure 5. UV absorption spectra of complexes **1** (top) and **2** (bottom) in methanol with increasing concentration of GSH. [**1**] = [**2**] = 3.33×10^{-5} mol·L^{-1}; [GSH] = 0, 0.55×10^{-5}, 0.83×10^{-5}, 1.11×10^{-5}, 1.67×10^{-5}, 2.22×10^{-5}, 3.33×10^{-5} mol·L^{-1}; the time span between two successive spectra was 10 min

duced on the surface of the electrode was about 29 kJ·mol^{-1}, indicating that a higher activation energy is needed to drive the charge-transfer process for complex **2** than for **1**, which is consistent with their different reactivity toward GSH. Additionally, the poor cytotoxicity of complex **1** may also result from its low solubility. The adequate solubility of complex **2** in both organic solvents and water facilitates its transport and absorption in cells, and makes it easier to reach the target.

Conclusion

Although complex **1** and **2** have similar distorted square-planar configurations, their cytotoxicity and reactivity toward GSH are very different. The in vitro cytotoxicity of complex **2** against murine leukemia P-388 and lung adenocarcinoma A-549 cell lines is more potent than cisplatin at most experimental concentrations, whereas complex **1** only shows a marginal cytotoxicity against the same cells. Complex **1** is reactive toward GSH while complex **2** is inert. This fact implies that GSH may be used as a useful probe to predict the cytotoxicity of copper complexes.

Experimental Section

General Remarks: Solvents such as methanol, tetrahydrofuran, acetone, anhydrous diethyl ether, chloroform, *N*,*N*-dimethylformamide (DMF) and common reagents such as $Cu(OAc)_2 \cdot H_2O$, triethylamine and trifluoroacetic acid (TFA) were all of analytical grade and used as received. 8-Aminoquinoline and di-*tert*-butyl dicarbonate were purchased from Acros Organics. L-Methionine, the disodium salt of calf thymus DNA (CT DNA) and the reduced γ-glutathione were purchased from Sigma. The infrared spectra were recorded on a Bruker VECTOR22 spectrometer as KBr pellets (4000−500 cm^{-1}), and elemental analysis was performed on a Perkin−Elmer 240C analytical instrument. Electrochemical measurements were made at 20 °C on an EG&G PAR Model 273 potentiostat. A three-electrode setup comprising a platinum working electrode, platinum wire auxiliary electrode, and an Ag/AgCl reference electrode was used for voltammetric work. Tetrabutylammonium perchlorate (TBAP) was used as the supporting electrolyte in DMF.

 © 2004 Wiley-VCH Verlag GmbH & Co. KGaA, Weinheim

N-(*tert*-Butoxycarbonyl)-L-methionine-*N*′-8-quinolylamide (**L**) and its deprotected counterpart L-methionine-*N*′-8-quinolylamide (**L**′) were synthesized following a procedure described previously.[17] Colorless single crystals of **L** suitable for X-ray diffraction were obtained by slow evaporation of an acetone solution.

Complex 1: This complex was prepared by mixing a methanol solution of $Cu(OAc)_2 \cdot H_2O$ (0.5 mmol, 6 mL) and **L** (6 mL) in a 1:1 molar ratio. The resulting solution was refluxed for about 2 h, and then cooled to room temperature. Brownish-red single crystals suitable for X-ray diffraction were obtained by slow evaporation of the solvent. Yield 164 mg (80%). $C_{16}H_{19}CuN_3O_4S$ (412.94): calcd. C 45.2, H 4.27, N 10.5; found C 45.5, H 4.33, N 10.4. IR (KBr): $\tilde{\nu}$ = 3446.8 (m), 3207.9 (m), 1600.7 (s), 1567.6 (s), 1498.3 (m), 1468.1 (m), 1417.4 (m), 1347.3 (s), 1072.9 (w), 1013.4 (w), 829.9 (m), 752.1 (w) cm^{-1}.

Complex 2: This complex was synthesized following the same procedure as for complex **1** except the starting ligand was replaced by **L**′. Dark-purple single crystals suitable for X-ray diffraction were obtained by slow evaporation of the solvent. Yield 166 mg (82%). $C_{16}H_{20}CuN_3O_{3.50}S$ (405.95): calcd. C 47.4, H 4.79, N 10.6; found C 47.0, H 4.76, N 10.5. IR (KBr): $\tilde{\nu}$ = 3472.1 (m), 1685.1 (s), 1594.0 (s), 1571.8 (s), 1501.8 (m), 1467.4 (m), 1412.5 (s), 1206.3 (s), 1140.0 (m), 830.9 (m), 788.6 (w), 725.5 (w) cm^{-1}.

X-ray Crystallographic Study: The main crystallographic data for ligand **L** and complexes **1** and **2** are summarized in Table 2. The crystals of ligand **L** and complex **1** were determined on a Siemens P4 four-circle diffractometer at 293 K. An empirical absorption correction was made (ψ-scan). The structure was solved by Patterson methods and completed by iterative cycles of least-squares refinement and ΔF syntheses. H-atoms were located in their calculated positions and treated as riding on the atoms to which they are attached. All non-hydrogen atoms were refined anisotropically. All calculations were carried out with the SHELXTL program.[33] The crystal of complex **2** was determined on a Siemens SMART CCD diffractometer at 293 K. The program SAINT[34] was used for data reduction and an empirical absorption correction was carried out using the SADABS program.[35] The structure was solved by Patterson methods that revealed the position of all non-hydrogen atoms and refined using the full-matrix least-squares method on F^2_{obs} with the SHELXTL software package.[33] All non-hydrogen atoms were placed in calculated positions. Atomic scattering factors and anomalous dispersion corrections were taken from ref.[36] CCDC-223042 (for **L**), -223043 (for **1**) and -223044 (for **2**) contain the supplementary crystallographic data for this paper. These data can be obtained free of charge at www.ccdc.cam.ac.uk/conts/retrieving.html [or from the Cambridge Crystallographic Data Centre, 12 Union Road, Cambridge CB2 1EZ, UK; Fax: +44-1223-336-033; E-mail: deposit@ccdc.cam.ac.uk].

Cytotoxicity Assays: The cytotoxicity assays of **L** and **L**′ and their Cu^{II} complexes **1** and **2** were performed as follows. Tumor cell lines were grown in RPMI-1640 medium supplemented with 10% (v/v) heat-inactivated fetal bovine serum, 2 mM glutamine, 100 U/mL penicillin, and 100 μg/mL streptomycin (GIBCO, Grand Island, NY) in a highly humidified atmosphere of 95% air with 5% CO_2 at 310 K.

The growth inhibitory effect on the murine leukemia P-388 cell line was measured by the microculture tetrazolium [3-(4,5-dimethylthiazol-2-yl)-2,5-diphenyltetrazolium bromide, MTT] assay.[37] Briefly, cells in 100 μL of culture medium were plated in each well of 96-

Table 2. Crystal data and structure refinement for ligand **L**, complexes **1** and **2**

	Ligand **L**	Complex **1**	Complex **2**
Empirical formula	$C_{19}H_{25}N_3O_3S$	$C_{16}H_{19}CuN_3O_4S$	$C_{16}H_{20}CuN_3O_{3.50}S$
Molecular mass	375.48	412.94	405.95
T (K)	293(2)	293(2)	293(2)
Crystal size (mm)	0.25×0.20×0.15	0.35×0.25×0.18	0.30×0.25×0.15
Crystal habit, color	block, colorless	prism, brownish-red	prism, dark purple
Crystal system	orthorhombic	orthorhombic	monoclinic
Space group	$P2_12_12_1$	$P2_12_12_1$	$C2$
a (Å)	5.157(1)	5.556(1)	28.463(6)
b (Å)	19.052(4)	15.002(3)	5.264(1)
c (Å)	19.593(4)	20.886(4)	13.345(3)
β (°)			109.142(3)
V (Å^3)	1925.0(7)	1740.9(6)	1888.8(7)
Z	4	4	4
Calculated density (mg·m^{-3})	1.296	1.576	1.428
Absorption coefficient (mm^{-1})	0.192	1.401	1.288
F(000)	800	852	840
θ range for data collection (°)	1.49 to 25.00	1.67 to 24.96	1.82 to 27.98
Limiting indices	$0 \le h \le 6$ $0 \le k \le 22$ $-23 \le l \le 23$	$0 \le h \le 6$ $0 \le k \le 17$ $0 \le l \le 24$	$-29 \le h \le 37$ $-6 \le k \le 6$ $-17 \le l \le 17$
Reflections collected/unique	3867/3367 (R_{int} = 0.0388)	1801/1801 (R_{int} = 0.0025)	5608/3827 (R_{int} = 0.0513)
Absorption corrections	empirical	empirical	empirical
Data/restraints/parameters	3367/0/236	1801/0/226	3827/8/223
Goodness-of-fit on F^2	1.066	1.023	1.046
Final R_{int} [$I > 2\sigma(I)$][a]	$R1$ = 0.0386, $wR2$ = 0.1181	$R1$ = 0.0375 $wR2$ = 0.0933	$R1$ = 0.1064, $wR2$ = 0.2824
R_{int} (all data)[a]	$R1$ = 0.0614, $wR2$ = 0.1604	$R1$ = 0.0653, $wR2$ = 0.1432	$R1$ = 0.1225, $wR2$ = 0.2941
Largest diff. peak, hole (e·A^{-3})	0.210, −0.210	0.337, −0.374	2.052, −0.624

[a] $R1 = \Sigma||F_o| - |F_c||/\Sigma|F_o|$; $wR2 = [\Sigma w(F_o^2 - F_c^2)^2/\Sigma w(F_o^2)^2]^{1/2}$.

 © 2004 Wiley-VCH Verlag GmbH & Co. KGaA, Weinheim

well plates (Falcon, Calif.). The cells were treated in triplicate with grade concentrations of the ligands, copper complexes and the reference drug cisplatin at 310 K for 48 h. A 20 μL aliquot of MTT solution (5 mg/mL) was added directly to all the appropriate wells. The culture was then incubated for 4 h. Then 100 μL of "triplex solution" (10% SDS/5% isobutanol/12 mM HCl) was added. After incubating the plates at 310 K overnight, they were measured by the absorbance at 570 nm using a multiwell spectrophotometer (VERSA Max, Molecular Devices, USA).

For the lung adenocarcinoma A-549 cell line, the growth inhibition was analyzed by the sulforhodamine B (SRB) assay.[38] Briefly, adherent cells in 100 μL of medium were seeded in 96-well plates and allowed to attach for 24 h before drug addition. The cell densities were selected based on preliminary tests to maintain control cells in an exponential phase of growth during the period of the experiment and to obtain a linear relationship between the optical density (OD) and the number of viable cells. Each cell line was exposed to grade concentrations of the compounds at desired final concentrations for 72 h and each concentration was tested in triplicate wells. After exposure, cells were fixed by gentle addition of 100 μL of cold (277 K) 10% trichloroacetic acid to each well, followed by incubation at 277 K for 1 h. The plates were washed with deionized water five times and allowed to dry in air. The cells were stained by addition of 100 μL of SRB solution [0.4% SRB (w/v) in 1% acetic acid (v/v)] to the wells for 15 min. The plates were then quickly washed five times with 1% acetic acid to remove any unbound dye and allowed to dry in air. Bound dye was solubilized with 10 mmol·mL^{-1} Tris (pH 10.5) prior to reading the plates. The OD value was read at a wavelength of 515 nm. Media and DMSO control wells, in which compounds were absent, were included in all the experiments. The growth inhibitory rate of treated cells was calculated by $(OD_{control} - OD_{test})/OD_{control} \times 100\%$.

Spectral Studies of Interactions with DNA and GSH: The concentration of DNA was determined by measuring the UV absorption at 260 nm and taking the molar absorption coefficient (ε_{260}) of CT-DNA as 6600 L·mol^{-1}·cm^{-1}.[39] Circular dichroism (CD) spectra were recorded on a Jasco J-810 spectropolarimeter. Each sample solution was scanned in the range 225−300 nm. A CD spectrum was generated which represented the mean of three scans from which the solvent background had been subtracted. The UV/Vis spectra of complexes **1** and **2** on addition of CT DNA were obtained on a UV-3100 spectrometer at a molar ratio (DNA/copper) of 0.0, 0.2, 0.4, 0.6. The UV/Vis spectroscopic titrations were carried out at room temperature by adding increasing amounts of GSH (0, 0.55×10^{-5}, 0.83×10^{-5}, 1.11×10^{-5}, 1.67×10^{-5}, 2.22×10^{-5}, 3.33×10^{-5} mol·L^{-1}) to a solution of complexes **1** or **2** at a fixed concentration (3.33×10^{-5} mol·L^{-1}) contained in a quartz cell. The time span between two successive spectra was 10 min.

Acknowledgments

We thank the financial support from the National Natural Science Foundation of China (No.s 20231010 and 20228102) and the Ministry of Education for Specialized Research Fund for the Doctoral Program of Higher Education (No. 20010284029).

[1] K. H. Thompson, C. Orvig, *Science* **2003**, *300*, 936−939.
[2] E. Wong, C. M. Giandomenico, *Chem. Rev.* **1999**, *99*, 2451−2466.
[3] M. J. Clarke, F. C. Zhu, D. R. Frasca, *Chem. Rev.* **1999**, *99*, 2511−2534.
[4] Z. J. Guo, P. J. Sadler, *Adv. Inorg. Chem.* **2000**, *49*, 183−306.
[5] G. J. Brewer, *Curr. Opin. Chem. Biol.* **2003**, *7*, 207−212.
[6] G. J. van Giessen, J. A. Crim, D. H. Petering, H. G. Petering, *J. Natl. Cancer Inst.* **1973**, *51*, 139−146.
[7] J. Easmon, G. Pürstinger, G. Heinisch, T. Roth, H. H. Fiebig, W. Holzer, W. Jäger, M. Jenny, J. Hofmann, *J. Med. Chem.* **2001**, *44*, 2164−2171.
[8] M. B. Ferrari, F. Bisceglie, G. Pelosi, P. Tarasconi, R. Albertini, P. P. Dall'Aglio, S. Pinelli, A. Bergamo, G. Sava, *J. Inorg. Biochem.* **2004**, *98*, 301−312.
[9] A. De Vizcaya-Ruiz, A. Rivero-Muller, L. Ruiz-Ramirez, G. E. N. Kass, L. R. Kelland, R. M. Orr, M. Dobrota, *Toxicol. in Vitro* **2000**, *14*, 1−5.
[10] I. Gracia-Mora, L. Ruiz-Ramírez, C. Gómez-Ruiz, M. Tinoco-Méndez, A. Márquez-Quiñones, L. R. de Lira, A. Marín-Hernández, L. Macías-Rosales, M. E. Bravo-Gómez, *Met.-Based Drugs* **2001**, *8*, 19−28.
[11] D. Y. Kong, C. Qin, L. H. Meng, Y. Y. Xie, *Bioorg. Med. Chem. Lett.* **1999**, *9*, 1087−1092.
[12] I. Dovinová, H. Paulíková, P. Rauko, L. Hunáková, E. Hanušovská, E. Tibenská, *Toxicol. in Vitro* **2002**, *16*, 491−498.
[13] D. Y. Kong, A. E. Martell, R. J. Motekaitis, *Inorg. Chem.* **2001**, *86*, 298.
[14] J. A. Broomhead, G. Camm, M. Sterns, L. Webster, *Inorg. Chim. Acta* **1998**, *271*, 151−159.
[15] J. Y. Zhang, X. Y. Wang, C. Tu, J. Lin, J. Ding, L. P. Lin, Z. M. Wang, C. He, C. H. Yan, X. Z. You, Z. J. Guo, *J. Med. Chem.* **2003**, *46*, 3502−3507.
[16] T. Yang, C. Tu, J. Y. Zhang, L. P. Lin, X. M. Zhang, Q. Lin, J. Ding, Q. Xu, Z. J. Guo, *Dalton Trans.* **2003**, *17*, 3419−3424.
[17] J. Y. Zhang, X. K. Ke, C. Tu, J. Lin, J. Ding, L. P. Lin, H. K. Fun, X. Z. You, Z. J. Guo, *BioMetals* **2003**, *16*, 485−496.
[18] R. L. Chapman, F. S. Stephens, R. S. Vagg, *Inorg. Chim. Acta* **1980**, *43*, 29−33.
[19] J. M. Rowland, M. L. Thornton, M. M. Olmstead, P. K. Mascharak, *Inorg. Chem.* **2001**, *40*, 1069−1073.
[20] J. Y. Zhang, Q. Liu, Y. Xu, Y. Zhang, X. Z. You, Z. J. Guo, *Acta Crystallogr., Sect. C* **2001**, *57*, 109−110.
[21] Y. Shao, C. Tu, J. Y. Zhang, Z. J. Guo, *Acta Crystallogr., Sect E* **2003**, *59*, 527−529.
[22] D. X. West, H. Gebremedhin, R. J. Butcher, J. P. Jasinski, A. E. Liberta, *Polyhedron* **1993**, *12*, 2489−2497.
[23] M. Akbar Ali, K. K. Dey, M. Nazimuddin, R. J. Butcher, F. E. Smith, J. P. Jasinski, J. M. Jasinski, *Polyhedron* **1996**, *15*, 3331−3339.
[24] M. Akbar Ali, A. H. Mirza, R. J. Butcher, *Polyhedron* **2001**, *20*, 1037−1043.
[25] A. Mohindru, J. M. Fisher, M. Rabinovitz, *Nature (London)* **1983**, *303*, 64−65.
[26] E. W. Ainscough, A. M. Brodie, W. A. Denny, G. J. Finlay, J. D. Ranford, *J. Inorg. Biochem.* **1998**, *70*, 175−185.
[27] E. R. Jamieson, S. J. Lippard, *Chem. Rev.* **1999**, *99*, 2467−2498.
[28] P. A. Andrews, M. P. Murphy, S. B. Howell, *Cancer Chemother. Pharmacol.* **1987**, *19*, 149−154.
[29] Y. T. Kang, M. D. Enger, *Toxicology* **1988**, *48*, 93−101.
[30] T. Ochi, F. Otsuka, K. Takahashi, M. Ohswa, *Chem.-Biol. Interact.* **1988**, *65*, 1−14.
[31] D. E. Conner, A. H. Ringwood, *Aquat. Toxicol.* **2000**, *50*, 341−349.
[32] J. F. Jiang, C. M. S. Croix, N. Sussman, Q. Zhao, B. R. Pitt, V. E. Kagan, *Chem. Res. Toxicol.* **2002**, *15*, 1080−1087.
[33] G. M. Sheldrick, *SHELXTL v5, Reference Manual*, Siemens Analytical X-ray Systems, Madison, WI. **1996**.

 © 2004 Wiley-VCH Verlag GmbH & Co. KGaA, Weinheim

[34] G. M. Sheldrick, *SAINT v4, Software Reference Manual*, Siemens Analytical X-ray Systems, Madison, WI. **1996**.
[35] G. M. Sheldrick, *SADABS, Program for Empirical Absorption Correction of Area Detector Data*, University of Göttingen, Germany. **1996**.
[36] A. J. Wilson, *International Table for X-ray Crystallography*, Kluwer Academic Publishers, Dordrechet. **1992**, vol. C, Tables 6.1.1.4 (p.500) and 4.2.6.8 (p. 219), respectively.
[37] M. C. Alley, D. A. Scudiero, A. Monks, M. L. Hursay, M. J. Czerwinski, D. Fine, B. J. Abbott, J. G. Mayo, R. H. Shoemaker, M. R. Boyd, *Cancer Res.* **1988**, *48*, 589−601.
[38] P. Skehan, R. Storeng, D. Scudiero, A. Monks, J. McMahon, D. Vistica, J. T. Warren, H. Bokesch, S. Kenney, M. R. Boyd, *J. Natl. Cancer Inst.* **1990**, *82*, 1107−1112.
[39] M. E. Reichmann, S. A. Rice, C. A. Thomas, P. Doty, *J. Am. Chem. Soc.* **1954**, *76*, 3047−3053.

Received May 1, 2004
Early View Article
Published Online August 12, 2004

 © 2004 Wiley-VCH Verlag GmbH & Co. KGaA, Weinheim

Dinuclear Cu^{II} Complexes with a New Phenol-Based Ligand Bearing Pyridine and Thiophene Substituents: Synthesis, Characterization and Interaction with Catechol Substrates

Iryna A. Koval,[a] Mieke Huisman,[a] Arno F. Stassen,[a] Patrick Gamez,[a] Olivier Roubeau,[b] Catherine Belle,*[c] Jean-Louis Pierre,[c] Eric Saint-Aman,[d] Matthias Lüken,[e] Bernt Krebs,[e] Martin Lutz,[f] Anthony L. Spek,[f] and Jan Reedijk*[a]

Keywords: Copper / Dinuclear complexes / Catechol oxidase / Magnetochemistry / Electrochemistry

The reaction of the phenol-based ligand 4-methyl-2,6-bis{[(2-methylpyridyl)(2-methylthiophenyl)amino]methyl}phenol-(Hpy2th2s), containing pyridine and thiophene substituents, with copper(II) chloride and bromide yields two new dinuclear complexes with the composition $[Cu_2(py2th2s)X_3]$, where X = Cl or Br. In both complexes, the copper(II) ions are pentacoordinate and bridged by the deprotonated phenolate anion and by one halogen anion. Both complexes exhibit geometric asymmetry, as the coordination environment around one of the two copper ions is square-pyramidal, whereas the geometry around the other can be best described as a distorted trigonal bipyramid. The complexes were characterized by means of X-ray single-crystal diffraction, ligand field and EPR spectroscopy, mass spectrometry, and electrochemically. Magnetic susceptibility measurements indicate an antiferromagnetic coupling between the two metal centers ($2J \approx -200$ cm^{-1}). The interaction of the complexes with model substrates 3,5-di-*tert*-butylcatechol and tetrachlorocatechol is reported.

(© Wiley-VCH Verlag GmbH & Co. KGaA, 69451 Weinheim, Germany, 2004)

Introduction

The copper-containing proteins with a type-3 active site, e.g. hemocyanin, tyrosinase and catechol oxidase, have the ability to reversibly bind and activate dioxygen at ambient conditions.[1] For this reason, modeling of the active site of these proteins has attracted significant scientific interest during the last few decades.[2−8] Hemocyanin functions as a dioxygen-carrier protein in some mollusks and arthropods, whereas tyrosinase and catechol oxidase utilize dioxygen to perform selective oxidation of various organic substrates. Tyrosinase catalyzes the hydroxylation of tyrosine to dopa [3-(3,4-dihydroxyphenyl)alanine] (cresolase activity) and its subsequent oxidation to dopaquinone (catecholase activity), the initial steps in melanin biosynthesis. Catechol oxidase lacks the cresolase activity of tyrosinase and only catalyzes the aerial oxidation of *o*-diphenols to the corresponding *o*-diquinones.

The crystal structure of catechol oxidase has been determined in 1998 by Krebs and co-workers.[9] Its active site is characterized by a dinuclear copper center, in which each copper ion is surrounded by nitrogen donor atoms of three histidine residues from a protein backbone. A catalytic cycle for catechol oxidase activity has been proposed from a combination of biochemical, spectroscopic, and structural data[10] and by comparison with the tyrosinase-related cycle.[1] It begins with the interaction of the catechol substrate with the met form of the enzyme, which contains two copper(II) ions singly bridged by a hydroxo group, resulting in the formation of a stoichiometric amount of the quinone.

Dinucleating phenol-based compartmental ligands have been previously successfully applied to model the type-3 active site.[6,7,11,12] Recent studies on the copper complexes of H-BPMP ligand, published by some of us,[7] allowed to propose a new catalytic mechanism, emphasizing the role of the μ-hydroxo bridge between the two metal centers. It includes the monodentate coordination of the substrate to one of the metal centers with the concomitant cleavage of the OH bridge, and the subsequent proton transfer from

[a] Leiden Institute of Chemistry, Leiden University,
P. O. Box 9502, 2300 RA Leiden, The Netherlands
Fax: (internat.) + 31-71-527-42-61
E-mail: reedijk@chem.leidenuniv.nl
[b] Centre de Recherche Paul Pascal − CNRS UPR 8641,
115 avenue du Dr. A. Schweitzer, 33600 Pessac, France
[c] LEDSS, Chimie Biomimétique, UMR CNRS 5616, Université J. Fourier,
B. P. 53, 38041 Grenoble Cedex, France
E-mail: Catherine.Belle@ujf-grenoble.fr
[d] Laboratoire d'Electrochimie Organique et de Photochimie Redox, UMR CNRS 5630, Université J. Fourier,
B. P. 53, 38041 Grenoble Cedex, France
[e] Institut für Anorganische und Analytische Chemie der Westfälischen Wilhelms-Universität Münster,
Wilhelm-Klemm-Strasse 8, 48149 Münster, Germany
[f] Bijvoet Center for Biomolecular Research, Crystal and Structural Chemistry, Utrecht University,
Padualaan 8, 3584 CH Utrecht, Netherlands

the second OH group of the catechol substrate to the hydroxy group bound to the second copper center.[7] The release of a water molecule results in a bridging coordination of the catecholate, which undergoes an oxidation to quinone. In order to further demonstrate the importance of a μ-hydroxo bridge on the catalytic cycle, we report the synthesis of two dinuclear copper(II) chloride and bromide complexes with the new phenol-based ligand 4-methyl-2,6-bis[[(2-methylpyridyl)(2-methylthiophenyl)amino]methyl}phenol (abbreviated as Hpy2th2s), their structural, spectroscopic, magnetic and electrochemical properties, and their interaction with the model substrates 3,5-di-*tert*-butylcatechol (3,5-DTBC) and tetrachlorocatechol (TCC). In these complexes, the two metal ions are doubly bridged by the oxygen atom of the phenolate group and a halogen anion. It can be expected that the substitution of the μ-hydroxo group by a halogen anion should hamper the cleavage of the bridge and the subsequent proton transfer, thereby preventing the coordination of the catecholate in the bridging bidentate fashion, and thus hampering the catalytic cycle.

Results and Discussion

Synthesis

An interesting structural feature encountered in the active site of catechol oxidase from sweet potatoes (*Ipomoea batatas*)[9] and in active sites of some hemocyanins[13,14] is an unusual thioether bond between a carbon atom of one of the histidine ligands and the sulfur atom of a nearby cysteine residue from the protein backbone. There is also sequence homology evidence for this type of bridge in tyrosinase from *Neurospora crassa*.[15] Such a moiety was also encountered in the mononuclear copper enzyme galactose oxidase, in which it was proposed to stabilize the tyrosine radical generated during catalysis. However, the absence of this bridge in hemocyanins of arthropods and in human tyrosinase does not support the hypothesis about its direct involvement in the electron transfer process.[9]

Although a very large number of synthetic models of the type-3 active site appeared in the literature in the past few decades, relatively little attention has been paid to this thioether bond. In an attempt to mimic this quite unusual structural feature we prepared a new dinucleating phenol-based ligand Hpy2th2s with two pendant arms, containing pyridine and thiophene residues. The synthesis of this ligand is depicted in Figure 1.

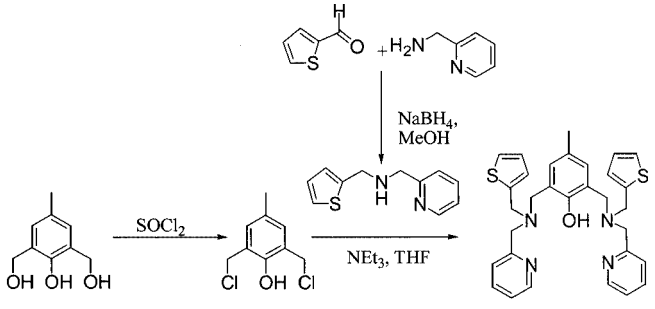

Figure 1. Reaction scheme of the synthesis of the ligand Hpy2th2s

The starting compound for the ligand synthesis, (2-picolyl)(2-thiophenyl)amine, was prepared by reaction of the commercially available 2-formylthiophene and (pyridin-2-ylmethyl)amine, followed by the reduction of the in situ generated imine by $NaBH_4$. Another starting compound 2,6-bis(chloromethyl)-4-methylphenol was prepared as described previously.[16] The reaction of 2,6-bis(chloromethyl)-4-methylphenol with a stoichiometric amount of (2-picolyl)(2-thiophenyl)amine in the presence of excess NEt_3 resulted in the formation of the ligand, which was isolated as a transparent light yellow oil. The reaction of Hpy2th2s with copper(II) chloride and bromide led to the formation of two new dinuclear copper complexes, which were isolated as dark brown and dark purple crystals, respectively.

Characterization of the Complexes

Crystal Structure Descriptions

[Cu_2(py2th2s)Cl_3]·CH_3OH (1)

Rectangular reddish-brown crystals of complex **1** were obtained by diethyl ether diffusion into a methanol solution containing stoichiometric amounts of copper(II) chloride and the ligand. A Platon[17] projection of the crystal structure of the complex is shown in Figure 2. Selected bond lengths and angles are presented in Table 1. The complex crystallizes as methanol solvate in space group $P2_1/n$ with four formula units present per unit cell. The dinuclear core is composed of two copper(II) ions, bridged on the one side by the endogenous cresolato bridge and on the other side by the chloride anion. The Cu···Cu separation in the complex is 3.185(1) Å. Both copper(II) ions are pentacoordinate with an identical N_2OCl_2 donor sets. However, the complex possesses geometrical asymmetry, as the coordination geometry around Cu1 is almost a regular square pyramid (τ = 0.10),[18] whereas the coordination environment around the Cu2 ion can be best described as a heavily distorted trigonal bipyramid (τ = 0.63).[18] The basal plane of the square pyramid around the Cu1 ion is made up of the nitrogen atom N1 of the tertiary amine group, the N2 atom of the pyridine ring, the oxygen atom O1 of the cresolate moiety, and the bridging chloride atom Cl1, whereas another chloride anion Cl2 occupies the apical position. In the case of the Cu2 ion, the nitrogen atom N3 of the tertiary amine group, the bridging chloride anion Cl1, and the chloride anion Cl3 form the equatorial plane of the trigonal bipyramid. The axial positions are occupied by the nitrogen atom N4 of the pyridine ring and the oxygen atom O1 of the cresolate group. The thiophene rings of the ligand remain noncoordinated; the Cu···S separations are > 5 Å. One of the thiophene rings shows disorder; the sulfur atom is refined on two independent positions, with occupancy factors of 78% (S1) and 22% (S1a). One noncoordinated disordered

 © 2004 Wiley-VCH Verlag GmbH & Co. KGaA, Weinheim

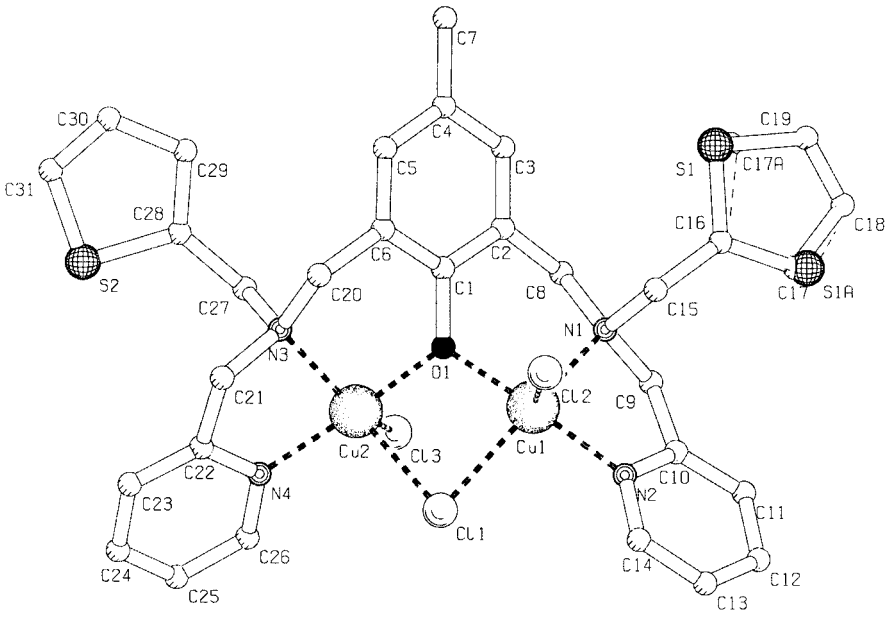

Figure 2. Platon[17] projection of the crystal structure $[Cu_2(py2th2s)Cl_3]\cdot CH_3OH$; hydrogen atoms and noncoordinated solvent molecule are omitted for clarity

Table 1. Selected bond lengths and bond angles of the complex $[Cu_2(py2th2s)Cl_3]\cdot CH_3OH$ (**1**)

Bond lengths [Å]			
Cu1−O1	1.9209(19)	Cu2−O1	1.911(2)
Cu1−N2	1.975(2)	Cu2−N4	1.972(2)
Cu1−N1	2.103(2)	Cu2−N3	2.083(2)
Cu1−Cl1	2.3922(8)	Cu2−Cl1	2.4717(9)
Cu1−Cl2	2.3931(10)	Cu2−Cl3	2.3636(10)
Cu1−Cu2	3.185(1)		
Bond angles [°]			
O1−Cu1−N2	159.33(9)	O1−Cu2−N4	168.80(9)
O1Cu1−N1	90.47(8)	O1−Cu2−N3	90.59(8)
N2−Cu1−N1	81.53(9)	N4−Cu2−N3	82.01(9)
O1−Cu1−Cl1	82.70(6)	O1−Cu2−Cl1	80.76(6)
N2−Cu1−Cl1	95.90(7)	N4−Cu2−Cl1	97.76(7)
N1−Cu1−Cl1	153.25(6)	N3−Cu2−Cl1	131.18(6)
O1−Cu1−Cl2	100.79(7)	O1−Cu2−Cl3	94.77(7)
N2−Cu1−Cl2	99.74(7)	N4−Cu2−Cl3	96.43(7)
N1−Cu1−Cl2	106.18(6)	N3−Cu2−Cl3	130.53(6)
Cl1−Cu1−Cl2	100.50(3)	Cl1−Cu2−Cl3	98.17(4)

methanol molecule is present per formula unit, which is hydrogen-bonded to the chloride anion Cl3.

[Cu₂(py2th2s)Br₃] (2)

Very dark purple needles of complex **2** were obtained by slow concentration of an acetonitrile solution containing stoichiometric amounts of copper(II) bromide and the ligand. A Platon[17] projection of the crystal structure is shown in Figure 3. Selected bond lengths and angles are presented in Table 2. The complex crystallizes in space group $P\bar{1}$. The asymmetric unit consists of two independent formula units. As in the case of the chloride complex **1**, two copper(II) ions are doubly bridged by the oxygen atom of the cresolate moiety and the halogen anion. The Cu···Cu distances are 3.2710(10) and 3.2394(10) Å, respectively. The copper ions are pentacoordinate, with N_2OBr_2 donor sets. One of the two independent formula units (Cu11, Cu12) possesses geometrical asymmetry. The geometry around the Cu11 ion is a slightly distorted square pyramid (τ = 0.17),[18] whereas the geometry around the Cu12 ion is a very distorted trigonal bipyramid (τ = 0.58).[18] The nitrogen atom N11 of the tertiary amine group, the nitrogen atom N12 of the pyridine ring, the bridging oxygen atom O11, and the bridging bromide anion Br11 form the basal plane of the square pyramid around the Cu11 ion, whereas the monocoordinated bromide anion Br12 occupies the axial position. The equatorial plane of the trigonal bipyramid around the Cu12 ion is formed by the nitrogen atom N13 of the tertiary amine group and the bromide atoms Br11 and Br13. The axial positions of the bipyramid are occupied by the bridging oxygen atom of the cresolate group and the nitrogen atom N14 of the pyridine ring. One of the noncoordinated thiophene rings is rotationally disordered. Thus, the first orientation has an occupancy factor of 85%, while the 180° rotated orientation has an occupancy factor of 15%.

In the second independent formula unit, both copper(II) ions (Cu21 and Cu22) have significantly distorted square-pyramidal surroundings (τ = 0.26 for the Cu21 ion and 0.45 for the Cu22 ion)[18]. The basal plane around the Cu21 ion is made up of, as in the case of the Cu11 ion, the two nitrogen atoms N21 and N22, the oxygen atom O21 of the cresolate group, and the bridging halogen atom Br21, whereas the bromide anion Br22 occupies the apical position. For the Cu22 ion, the nitrogen atom N23 of the ter-

 © 2004 Wiley-VCH Verlag GmbH & Co. KGaA, Weinheim

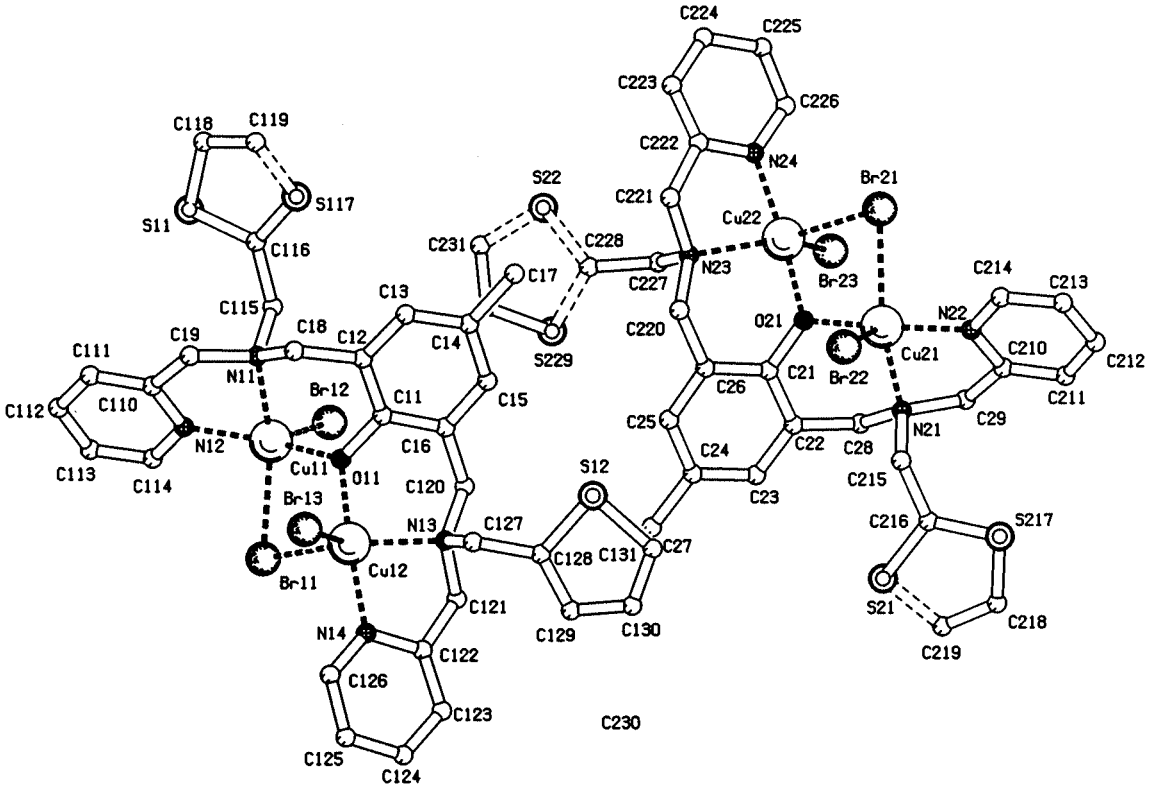

Figure 3. Platon[17] projection of the two independent formula units of $[Cu_2(py2th2s)Br_3]$; hydrogen atoms are omitted for clarity; three of the thiophene rings are rotationally disordered

tiary amine group, the nitrogen atom N24, the bridging oxygen atom O21, and the bridging bromide anion Br21 form the basal plane of the square pyramid, and its apical position is occupied by the Br23 atom. Thus, two square pyramids share one side through the atoms O21 and Br21, with their apical positions *trans*-located to each other. Both thiophene rings of the ligand remain noncoordinated (Cu···S separations are > 5 Å) and exhibit rotational disorder. Thus, the thiophene ring at S21 was refined on two orientations with occupancies of 0.72 and 0.28, respectively, and the thiophene ring at S22 with occupancies of 0.55 and 0.45, respectively.

Physical Methods

Ligand Field Spectroscopy

The ligand field spectra of both complexes, recorded in the solid state (diffuse reflectance), exhibit almost identical features. Both spectra are characterized by the presence of the charge-transfer band from the phenolate moiety to the copper ions[11] around 500 nm (483 nm for complex **1** and 521 nm for complex **2**) and the d-d transition band of the copper(II) ions. The latter band, observed at 774 nm for the chloride complex and at 806 nm for the bromide complex, is asymmetric in both cases, with a shoulder observed at higher wavelengths. As shown previously, such spectroscopic behavior (high-energy absorption band in the visible region with a low-energy shoulder) is typical for square-pyramidal copper(II) complexes.[19] In acetonitrile solution, the charge-transfer band is observed at 472 nm for complex **1** (ε = 1851 $M^{-1}\cdot cm^{-1}$) and at 500 nm for complex **2** (ε = 1812 $M^{-1}\cdot cm^{-1}$). The d-d band is located at 771 nm (ε = 464 $M^{-1}\cdot cm^{-1}$) for complex **1** and 791 nm (ε = 534 $M^{-1}\cdot cm^{-1}$) for complex **2**. A small shift of the d-d bands upon dissolution of the complexes in acetonitrile may suggest the coordination of the solvent to the metal centers. However, the partial dissociation of the complexes due to the exchange of the halide anions with acetonitrile molecules can also not be excluded.

EPR and Magnetic Susceptibility Studies

Both complexes **1** and **2** are EPR-silent in the solid state and in a frozen acetonitrile solution at 100 K, suggesting an antiferromagnetic coupling between the copper ions. Such a behavior is confirmed by the temperature dependence of the molar magnetic susceptibility χ_M depicted in Figure 4, which is typical for complexes of antiferromagnetically coupled copper(II) dimers. Indeed the χ_M vs. T curves present a broad maximum centered around 160 and 190 K for **1** and **2**, respectively, while the values of χ_M at high temperatures (2.10×10^{-3} and 1.85×10^{-3} $cm^3\cdot mol^{-1}$ at 300 K, respectively) are slightly lower than expected for two uncoupled copper(II) ions (2.5×10^{-3} $cm^3\cdot mol^{-1}$ for g = 2). Below 40 K, a Curie tail ascribed to paramagnetic impurity is observed, which is usual in such copper(II) complexes. These experimental data were reproduced correctly using

 © 2004 Wiley-VCH Verlag GmbH & Co. KGaA, Weinheim

Table 2. Selected bond lengths and bond angles of the complex $[Cu_2(py2th2s)Br_3]$ (**2**)

Bond lengths [Å]			
Cu11−O11	1.925(3)	Cu12−O11	1.931(4)
Cu11−N12	1.977(4)	Cu12−N14	1.986(5)
Cu11−N11	2.099(4)	Cu12−N13	2.096(4)
Cu11−Br11	2.5620(9)	Cu12−Br11	2.5226(8)
Cu11−Br12	2.5314(8)	Cu12−Br13	2.4870(9)
Cu21−O21	1.931(3)	Cu22−O21	1.918(4)
Cu21−N22	1.968(4)	Cu22−N24	1.981(5)
Cu21−N21	2.112(4)	Cu22−N23	2.113(4)
Cu21−Br21	2.5535(10)	Cu22−Br21	2.5666(9)
Cu21−Br22	2.5166(9)	Cu22−Br23	2.4953(9)
Cu11−Cu12	3.2710(10)	Cu21−Cu22	3.2394(10)
Bond angles [°]			
O11−Cu11−N12	159.37(17)	O11−Cu12−N14	165.93(17)
O11−Cu11−N11	91.14(16)	O11−Cu12−N13	91.70(17)
N11−Cu11−N12	81.55(17)	N13−Cu12−N14	81.61(19)
Br11−Cu11−O11	81.00(11)	Br11−Cu12−O11	81.95(10)
Br11−Cu11−N12	95.53(13)	Br11−Cu12−N14	93.07(13)
Br11−Cu11−N11	149.47(13)	Br11−Cu12−N13	130.96(12)
Br12−Cu11−O11	97.77(11)	Br13−Cu12−O11	96.52(11)
Br12−Cu11−N12	102.84(12)	Br13−Cu12−N14	97.54(13)
Br12−Cu11−N11	108.72(13)	Br13−Cu12−N13	119.60(12)
Br11−Cu11−Br12	101.58(3)	Br11−Cu12−Br13	109.44(3)
O21−Cu21−N22	162.14(18)	O21−Cu22−N24	164.78(18)
O21−Cu21−N21	91.15(16)	O21−Cu22−N23	90.99(17)
N21−Cu21−N22	81.54(17)	N23−Cu22−N24	81.71(19)
Br21−Cu21−O21	83.16(12)	Br21−Cu22−O21	83.04(11)
Br21−Cu21−N22	93.90(14)	Br21−Cu22−N24	93.39(15)
Br21−Cu21−N21	146.37(13)	Br21−Cu22−N23	137.81(12)
Br22−Cu21−O21	99.57(12)	Br23−Cu22−O21	95.20(11)
Br22−Cu21−N22	98.26(13)	Br23−Cu22−N24	99.98(14)
Br22−Cu21−N21	110.29(13)	Br23−Cu22−N23	122.65(12)
Br21−Cu21−Br22	103.34(3)	Br21−Cu22−Br23	99.51(3)
Cu11−O11−Cu12	116.04(18)	Cu21−O21−Cu22	114.63(19)
Cu11−Br11−Cu12	80.08(3)	Cu21−Br21−Cu22	78.50(3)

the modified Bleaney−Bowers equation [Equation (1)], where χ_M is the magnetic susceptibility per dimer. In this equation, $2J$ corresponds to the singlet-triplet energy gap, ρ to the fraction of paramagnetic impurity, and TIP to a term to account for temperature-independent paramagnetism, while N_A, β, k_B, and g have their usual meaning. The paramagnetic impurity was assumed to be a mononuclear copper(II) species and g was fixed to 2. The best-fit parameters were then obtained as $2J = -177(2)$ cm^{-1}, ρ = 1.8(1)% and TIP = 2.9(1) × 10^{-4} cm^3·mol^{-1} for complex **1**, and $2J = -219(1)$ cm^{-1}, ρ = 0.6(1)% and TIP = 2.0(1) × 10^{-4} cm^3·mol^{-1} for complex **2**.

$$\chi_M = (1-\rho)\frac{2N_A\beta^2g^2}{k_BT}\left[3+\exp(-2J/k_BT)\right]^{-1} + 2\rho\left(\frac{N_A\beta^2}{k_BT}\right) + TIP \quad (1)$$

These medium antiferromagnetic couplings should be correlated to a significant overlap between the two magnetic orbitals of the two copper(II) ions in complexes **1** and **2**, through both the halide and phenolate bridges. The short

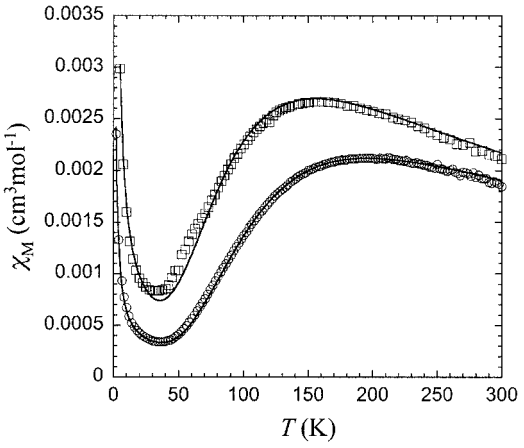

Figure 4. χ_M vs. T curve for complexes **1** (squares) and **2** (circles); see text for further details

Cu−O bonds and the large Cu−O−Cu angles of the phenolate bridge in **1** and **2**, relative to the long Cu−X bonds, point at a dominant coupling through the phenolate bridge. The coordination sphere around one of the two copper ions is intermediate between a square pyramid and a trigonal bipyramid, while the other has a square-pyramidal environment. In the former case, the unpaired electron of copper(II) occupies either the d_{z^2} or the $d_{x^2-y^2}$ orbital, which would both point along the Cu−O(phenolate) bond. Short Cu−O bonds and large Cu−O−Cu angles in square-pyramidal phenolate-bridged Cu dimers result in a strong overlap of $d_{x^2-y^2}$ orbitals and thus produce strong to very strong antiferromagnetic couplings.[20] On the other hand, if one of the copper ions in such dimers has a trigonal-bipyramidal environment, weaker overlap is expected, and even weak ferromagnetic coupling has been observed.[21,22] Therefore, the smaller singlet-triplet energy gap in **1** can be related to a smaller Cu−O−Cu angle in **1** (ca. 112°) relative to **2** (on average over the two dimeric units about 115.3°), but also to a more distorted trigonal-bipyramidal coordination sphere in **2** (τ = 0.58, Cu12) than in **1** (τ = 0.63, Cu2). Most likely, the difference in the singlet-triplet energy gap results from both structural differences.

Electrochemistry

The electrochemical behavior of both complexes was investigated by cyclic voltammetry (CV) and rotating disk electrode voltammetry (RDE) in acetonitrile solution, with tetra-*n*-butylammonium perchlorate (TBAP) as supporting electrolyte (0.1 M). The potentials were referred to an Ag/10 mM $AgNO_3$ + CH_3CN +0.1 M TBAP reference electrode.

When scanning towards the negative region of potentials, the CV curve for both complexes **1** and **2** is characterized by three successive electrochemical signals (Figures 5 and 6). The first signal for **1**, at $E_{pc} = -0.52$ V, is irreversible, and re-oxidation of the reduced species is seen on the reverse scan at +0.23 V (Figure 5, curve a), while that for **2** appears to be weakly reversible at $E_{1/2} = -0.34$ V (ΔE_p =

 © 2004 Wiley-VCH Verlag GmbH & Co. KGaA, Weinheim

0.12 V, Figure 6, curve a). Coulometric titrations give n = 1 for the exchanged electron per complex, allowing to attribute this electrochemical process to the complexed $Cu_2^{II,II}/Cu_2^{II,I}$ redox couple. The UV/Vis spectra of the one-electron reduced complexes exhibit one very broad band around 680 nm. The lack of reversibility of the first electrochemical reduction of **1** and **2** suggests a change in the coordination sphere around the metal center upon reduction, likely a partial dissociation of the exogenous halide ligand and a change in the geometry of the coordination sphere. Additional electrochemical measurements performed at −40 °C showed that the course of these coupled chemical reactions is not prevented at low temperature. The second electrochemical signal, weakly reversible at $E_{1/2}$ = −0.78 V for **1** and at $E_{1/2}$ = −0.72 V for **2**, also corresponds to a one-electron process, leading to the complexed $Cu_2^{II,I}/Cu_2^{I,I}$ redox couple. Finally, the third electrochemical signal at E_{pc} = −1.45 V for **1** and −1.04 V for **2** corresponds to a two-electron process, suggesting the reduction of Cu^{I} ions to the Cu^0 state and the deposition of metallic copper on the electrode surface. Accordingly, an additional sharp anodic peak is observed on the reverse scan, which is caused by the redissolution of metallic copper.

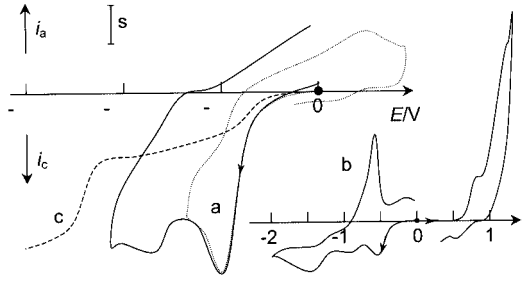

Figure 5. Electrochemical curves recorded in a 0.67 mM solution of **1** in CH_3CN + TBAP 0.1 M on a Pt disc [diameter = 5 (a, b) or 3 (c) mm]; curves a, b: CV curves, ν = 0.1 $V{\cdot}s^{-1}$; curve c: RDE curve, N = 600 rpm; V vs. $Ag/AgNO_3$ mM + CH_3CN + TBAP 0.1 M; scale s = 20 μA (curve a), 120 μA (curve b) or 10 μA (curve c)

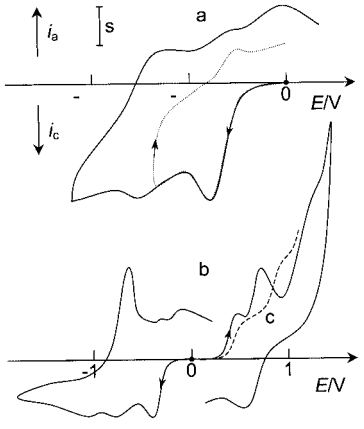

Figure 6. Electrochemical curves recorded in a 0.67 mM solution of **2** in CH_3CN + TBAP 0.1 M on a Pt disc [diameter = 5 (a, b) or 3 (c) mm]; curves a, b: CV curves, ν = 0.1 $V{\cdot}s^{-1}$; curve c: RDE curve, N = 600 rpm; V vs. $Ag/AgNO_3$ mM + CH_3CN + TBAP 0.1 M; scale s = 20 μA (curve a), 40 μA (curve b, c)

The anodic behavior of complexes **1** and **2** differs. The anodic part of the CV curve for **1** (Figure 5, b) is characterized by two electrochemical signals, whereas three signals are observed on the CV curve for **2** (Figure 6, b). For **1**, the first signal at $E_{1/2}$ = 0.64 V (ΔE_p = 0.26 V) corresponds to a one-electron quasi-reversible oxidation of **1**. The electron transfer is likely to be centered on the phenolate bridge, as previously shown for other phenolate-bridged dinuclear copper(II) complexes.[11,23] This process is followed by the oxidation of the chloride anions, which is seen as a shoulder at the negative foot of the over-oxidation wave of the complex (free chloride anions are reversibly oxidized at 0.72 V under our experimental conditions). The CV curve recorded in a solution of **2** shows an additional fully irreversible one-electron process at E_{pa} = 0.47 V. This is assumed to be due to the one-electron oxidation of bromide anions; free bromide anions are irreversibly oxidized at E_{pa} = 0.39 V under our experimental conditions. The one-electron phenolate-based oxidation of complex **2**, similarly to **1**, is observed as a quasi-reversible pair of peaks at $E_{1/2}$ = 0.76 V (ΔE_p = 0.18 V), and is followed at higher potentials by the over-oxidation of the complex.

These results have been confirmed by rotating disk electrode (RDE) voltammetric experiments (Figures 5 and 6). The RDE curves display one anodic wave at $E_{1/2}$ = 0.84 V for **1** and two successive well-behaved anodic waves at $E_{1/2}$ = 0.42 V and 0.82 V (Figure 6, curve c) for **2**. For both complexes, three successive cathodic waves are seen. For **1** and **2**, the first one at $E_{1/2}$ = −0.42 V and −0.40 V, respectively, is followed by a second ill-behaved wave at $E_{1/2}$ = −0.78 V and −0.80 V, respectively. The third cathodic wave corresponding to the deposition of metallic copper onto the electrode surface is observed at $E_{1/2}$ = −1.22 V and −1.20 V, respectively.

Conductivity Measurements

The conductivity measurements of the complexes **1** and **2** were performed on 0.5 mM solutions of the complexes in acetonitrile. The calculated values for equivalent conductivities of both compounds are roughly the same and are equal to 52 $cm^2{\cdot}mol^{-1}{\cdot}\Omega^{-1}$ for complex **1** and 55 $cm^2{\cdot}mol^{-1}{\cdot}\Omega^{-1}$ for complex **2**. Previously, the conductivity range for complexes corresponding to the 1:1-type electrolytes was suggested to lie between 120 and 160 $cm^2{\cdot}mol^{-1}{\cdot}\Omega^{-1}$ if acetonitrile was utilized as a solvent.[24] Although values as low as 90 $cm^2{\cdot}mol^{-1}{\cdot}\Omega^{-1}$ were also reported in some cases, the observed conductivities of both complexes **1** and **2** are still too low for them to be considered as 1:1 electrolytes. As shown previously,[25] such small conductivity values in acetonitrile are often found for nonelectrolytes, due to coordinating and solvating properties of this solvent. Some authors[25] argue that they may indicate a partial exchange of counter anions with the solvent molecules. Small changes in the positions of UV/Vis/NIR d-d bands of the complexes upon their dissolution in acetonitrile, observed in our case, appear to sustain this assumption.

 © 2004 Wiley-VCH Verlag GmbH & Co. KGaA, Weinheim

Interaction of the Complexes with the Model Substrates

Catecholase Activity Measurements

To evaluate the ability of the complexes to behave as functional models of catechol oxidase, they were tested as catalysts in the oxidation of 3,5-di-*tert*-butylcatechol (3,5-DTBC), a widely used model substrate, to the respective quinone. Both complexes exhibit only negligible catecholase activity (TON $<$ 1 after 30 min), making a detailed kinetic analysis dispensable. These results are as expected, confirming that the substitution of the μ-hydroxo bridge by a halogen anion precludes catecholase activity. However, these results do not provide information on whether or not the binding of the substrate to the metal centers takes place *at all*. Reim et al. have previously shown that, in the case of essentially inactive complexes, no interaction between the dimetal core and the substrate occurred.[6] To evaluate whether or not the first step of the catalytic cycle, e.g. the binding of catechol to the metal centers, takes place, we studied the interaction of the complexes with tetrachlorocatechol (TCC). The latter catechol has a very high oxidation potential due to its electron-withdrawing substituents and is not oxidized by copper complexes.

TCC Binding Studies

The titration of 5×10^{-4} M solutions of the complexes in acetonitrile with TCC was monitored by means of UV/Vis and EPR spectroscopy. The changes observed in the UV/Vis spectra of complex **1** upon addition of TCC (up to 4 equiv.) are depicted in Figure 7. Quite significant changes in the spectrum of the original complex indicate the interaction between the substrate and the metal centers. The presence of two isosbestic points at 570 nm and 724 nm shows the presence of only two absorbing species in solution. The Cu^{II} d-d transition band shifts gradually from 789 nm to 718 nm, whereas its absorbance decreases to about 50% of its initial value. Also, the extinction coefficient of the LMCT band decreases from 1851 to about 1600 $M^{-1}\cdot cm^{-1}$ (Figure 7).

Whereas the chloride complex obviously reacts with TCC, no changes were observed in the UV/Vis spectrum upon addition of TCC to the bromide complex. Taking into account the great structural similarity between the two complexes, it seems reasonable to us to suggest that the difference in their behavior is caused by the different halogen anions coordinated to the copper ions. The Cu−Cl bond has a more ionic character than the Cu−Br bond, which facilitates the substitution of (at least one of) the chloride anions by catechol, whereas no exchange of Br anions by TCC occurs.

Titration of complex **1** with TCC, monitored by X-band EPR spectroscopy, revealed that no evolution of the EPR signal is observed upon addition of TCC. This indicates that the two copper ions are strongly antiferromagnetically coupled, suggesting that they probably remain doubly bridged by the phenolate group and the chloride anion. Although a few structures of copper(II) complexes with bridging catecholate were previously described,[8,26] no magnetic properties of these compounds have been reported. However, we believe that the cleavage of the halide bridge would lead to a decrease in strength of the magnetic coupling, similarly to the behavior seen in previously reported μ-hydroxo complexes with phenol-based ligands[7] after the cleavage of the hydroxo bridge. Thus, the reaction of TCC with the chloride complex probably results in the substitution of at least one of the apical chloride anions.

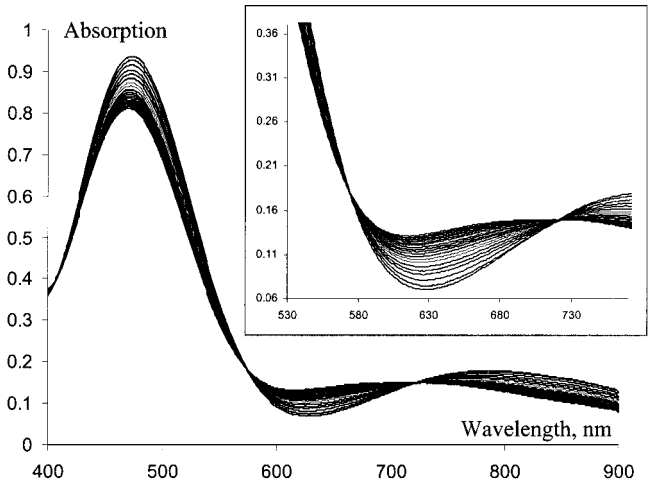

Figure 7. UV/Vis titration of complex **1** (0.5 mM solution in acetonitrile) with TCC (from 0 to 4 equiv.); the inset shows the enlargement of the spectroscopic curves in the range 530−780 nm

In order to further confirm this hypothesis, the conductivity of complex **1** in acetonitrile solution before and after addition of TCC was studied. The equivalent conductivity of TCC itself is negligible.

The values of the equivalent conductance observed after addition of 1−4 equiv. of TCC to 0.5 mM solution of complex **1** are listed in Table 3. As can be seen, a substantial increase is observed after 1 equiv. of TCC has been added. Further addition of TCC leads to a slight increase in conductivity, until a final value of 118 $cm^2\cdot mol^{-1}\cdot\Omega^{-1}$ is reached. This value fits perfectly in a range suggested for the 1:1 electrolytes in acetonitrile.[24] The interaction of **1** with TCC leads to the release of one chloride anion in solution; complete release is reached in the presence of an excess of TCC as shown by the slight increase in the conductivity above 1 mol-equiv. added. The reversible nature of this process is further confirmed by UV/Vis titration experiments

Table 3. Calculated values of equivalent conductivity upon treating 0.5 mM solution of **1** in acetonitrile with TCC

Number of equiv. of TCC	Equivalent conductivity [$cm^2\cdot mol^{-1}\cdot\Omega^{-1}$]
0	52
1	100
2	110
3	117
4	118

 © 2004 Wiley-VCH Verlag GmbH & Co. KGaA, Weinheim

that showed that the maximal perturbation in the UV/Vis spectra was reached in the presence of at least 3 equiv. of TCC (Figures 7 and 8).

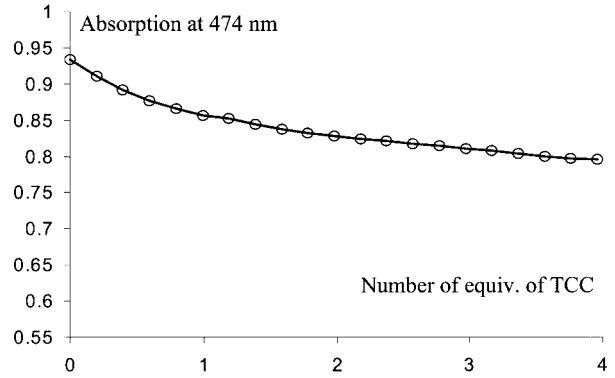

Figure 8. Decrease in the LMCT band (474 nm) upon titration of the solution of **1** (0.5 mM) in acetonitrile with TCC

Not surprisingly, additions of TCC to the bromide complex do not lead to an increase in conductivity, in complete agreement with the hypothesis that substitution of Br^- anions by TCC is not possible.

General Discussion

Previously, many attempts to establish a correlation between the structural parameters of the complexes and their catalytic activity in the oxidation of catechols were described in the literature. Three most important criteria influencing the catalytic properties of the complexes can now be distinguished: (i) the distance between the metal centers,[11,27,28] (ii) the nature of the bridging group between the metal ions,[29,30] (iii) the electronic properties of the complexes.[23] Some other factors, e.g. the imposed strain in the complex due to the rigidity of either the ligand and/or the bridging group, may also play a role.[6] Results published by Reim et al.[6] indicate that complexes with strained structures show catalytic activity, whereas complexes present in relaxed and energetically favored conformations are essentially inactive towards catechol oxidation. In the chloride and bromide complexes **1** and **2**, the metal−metal distance and the redox potentials of the metal ions are similar to the values previously determined for catalytically active complexes;[6,11,29] thus, the absence of catalytic activity is not likely to be due to these two factors. Also, the coordination spheres around the copper ions in both complexes exhibit quite a large distortion from a regular square-pyramidal geometry, resulting in relatively strained structures. Thus, the main reason for the absence of catalytic activity lies in the nature of the bridging groups between the two copper ions in the complexes. As discussed above, the crucial steps of the mechanism that was proposed earlier[7] is the cleavage of the OH bridge between the two metal ions and the subsequent proton transfer from the catechol substrate to the hydroxy anion, leading to the release of one water molecule. We have shown that the reaction of catechol with the complexes **1** and **2** does not result in a cleavage of the bridge, although binding of the substrate to the chloride complex undoubtedly takes place. These results thus emphasize the influence of the bridging group between the copper centers on the catecholase activity of the complexes and underline the importance of the exogenous hydroxo bridge for the catalytic mechanism. This hydroxo ligand appears to be the key factor to achieve the complete deprotonation of catechol, leading to a bridging catecholate prior to the electron transfer. Upon substitution of the hydroxo bridge with the halogen anion, no proton transfer can occur, precluding the binding of catecholate in a bidentate bridging fashion, and thus the subsequent catalytic cycle.

Conclusion

The synthesis of a new phenol-based ligand Hpy2th2s bearing thiophene- and pyridine-containing pendant arms was successfully accomplished. Two dinuclear copper(II) complexes with this ligand were isolated and characterized by means of single-crystal X-ray analysis, UV/Vis and EPR spectroscopy, magnetochemistry and electrochemistry. Both complexes were found to be essentially inactive in the catalytic oxidation of 3,5-di-*tert*-butylcatechol to the respective quinone. The presence of chloride and bromide anions as bridging ligands between the two metal centers precludes the deprotonation of catechol and its binding in a bidentate bridging fashion to the copper ions, and thus from further oxidation. Studies to establish a better structure-activity relationship for dinuclear copper(II) complexes as structural models of catechol oxidase are currently in progress.

Experimental Section

General Remarks: All starting materials were commercially available and used as purchased. 2,6-Bis(chloromethyl)-4-methylphenol was prepared as described previously.[16] The NMR spectra were recorded with a JEOL FX-200 (200 MHz) FT NMR spectrometer. The ligand field spectra of the solids (300−2000 cm^{-1}, diffuse reflectance) were taken with a Perkin−Elmer 330 spectrophotometer equipped with a data station. The ligand field spectra in solution were recorded with a Varian Cary 50 Scan UV/Vis spectrophotometer. Electrospray mass spectra (ESI-MS) in acetonitrile solutions were recorded with a Thermo Finnigan AQA apparatus. X-band electron paramagnetic resonance (EPR) measurements were performed at 77 K in the solid state with a Jeol RE2x electron spin resonance spectrometer, using DPPH (g = 2.0036) as a standard, and at 100 K as acetonitrile frozen solutions with a Bruker ESP 300E spectrometer operating at 9.4 GHz (X-band). The conductivity measurements were performed with a Philips PW9526 digital conductivity meter and PW 9552/60 measuring cell with 0.5 mM solutions of the complexes in acetonitrile. The electrochemical behavior of the complexes was investigated in a 0.1 M solution of tetra-*n*-butylammonium perchlorate (TBAP) in acetonitrile using an EGG 273 potentiostat coupled with a Kipp&Zonen *x*-*y* recorder. The experiments were performed at room temperature or at −40 °C in a three-compartment cell. Potentials are referred to

 © 2004 Wiley-VCH Verlag GmbH & Co. KGaA, Weinheim

an Ag/10 mM $AgNO_3$ + CH_3CN +0.1 M TBAP reference electrode. The working electrode was a platinum disk with a 5 mm diameter for the cyclic voltammetry (CV, 0.1 V/s) experiments or 3 mm diameter for the rotating disk electrode (RDE, 600 rpm) voltammetry experiments. The working electrode was polished with 1 μm diamond paste prior to each recording. Bulk magnetizations of polycrystalline samples were performed on the crystals of complexes **1** (11.11 mg) and **2** (16.88 mg) in the temperature range 5−400 K with a Quantum Design MPMS-5S SQUID magnetometer in a 1 kG applied field. The data were corrected for the experimentally determined contribution of the sample holder. Corrections for the diamagnetic responses of the complexes, as estimated from Pascal's constants, were applied.[31]

Catecholase Activity Study: The catecholase activity of the complexes was evaluated by reaction with 3,5-di-*tert*-butylcatechol at 25 °C. The absorption at 400 nm, characteristic of the formed quinone, was measured as a function of time. The experiments were performed under 1 atm of dioxygen; 3 mL of $2.5 \cdot 10^{-4}$ M solution of complex in acetonitrile was placed in 1-cm path-length cell, and 75 μL of a 1 M solution of the substrate in the same solvent was added. After thorough shaking, the changes in UV/Vis spectra were recorded over 30 min. The titration of the complexes with tetrachlorocatechol (TCC) was carried out by adding 3 μL aliquots of 0.1 M solution of TCC (corresponding to 0.198 equiv. of TCC/1 equiv. of the complex) to 3 mL of 5×10^{-4} M solution of complex in acetonitrile.

(2-Picolyl)(2-thiophenyl)amine: A solution of (pyridin-2-ylmethyl)-amine (2.00 g, 18.5 mmol) was added dropwise, while stirring, to a solution of 2-formylthiophene (2.08 g, 18.5 mmol) in MeOH. The resulting solution was stirred at room temperature overnight. Afterwards, $NaBH_4$ (2.1 g, 56 mmol, 3 equiv. per 1 CH=N) was added slowly, and the resulting solution was heated at 50 °C for 3 h. After concentration, the obtained oil was redissolved in a mixture of dichloromethane and water. The organic and aqueous layers were separated, and the water layer was washed twice with a small amount of dichloromethane. After combining and drying of the dichloromethane layers with Na_2SO_4 and concentration, the pure product was obtained as a light yellow oil. The product is light-sensitive and should preferably be stored in darkness at low temperatures. Yield: 3.59 g (95%). ^{1}H NMR ($CDCl_3$): δ = 2.28 (s, 1 H, NH), 3.95 (s, 2 H, NHCH_2th), 4.03 (s, 2 H, NHCH_2py), 6.93 (d, 1 H, 3′th), 6.96 (s, 1 H, 4′th), 7.20 (d, 1 H, 5′th), 7.15 (t, 1 H, 5′py), 7.30 (d, 1 H, 3′py), 7.62 (t, 1 H, 4′py), 8.55 (d, 1 H, 6′py) ppm.

4-Methyl-2,6-bis{[(2-methylpyridyl)(2-methylthiophenyl)amino]-methyl}phenol (Hpy2th2s): A solution of (2-picolyl)(2-thiophenyl)-amine (0.7 g, 3.4 mmol) and Et_3N (0.7 g, 7 mmol) in THF was added dropwise, while stirring, to a solution of 2,6-bis(chloromethyl)-4-methylphenol (0.35 g, 1.7 mmol) in THF. After refluxing for 2 h, the solution was cooled to room temperature. Filtration of the triethylammonium salt and subsequent evaporation of the solvent resulted in an oil, which was dissolved in acidified water and washed with dichloromethane. The water layer was made alkaline by adding a concentrated aqueous solution of NH_3, and the resulting suspension was extracted three times with dichloromethane. The combined organic layers were dried with Na_2SO_4 and the solvents evaporated under reduced pressure. The resulting oil was found to be the pure product. Yield: 0.77 g (84%). ^{1}H NMR ($CDCl_3$): δ = 2.28 (s, 3 H, CH_3), 3.82 (s, 4 H, NCH_2th), 3.85 (s, 4 H, phCH_2N), 3.89 (s, 4 H, NCH_2py), 6.95 (m, 4 H, 3′th + 4′th), 7.04 (s, 2 H, 3′ph + 5′ph), 7.15 (t, 2 H, 5′th), 7.24 (d, 2 H, 3′py), 7.53 (d, 2 H, 5′th), 7.66 (t, 2 H, 4′py), 8.56 (d, 2 H, 6′py), 10.40 (1 H, OH) ppm. ESI-MS: m/z = 541 [M + H$^+$].

[Cu_2(py2th2s)(μ-Cl)Cl_2]·CH_3OH (1): Hpy2th2s (0.15 g, 0.28 mmol) and copper chloride (0.10 g, 0.54 mmol) were dissolved in methanol (10 mL). Addition of diethyl ether (20 mL) resulted in the precipitation of the complex as a dark brown powder. Yield: 102 mg (46%). Single crystals of the complex were obtained by slow diffusion of diethyl ether into a 0.01 M solution of the complex. [Cu_2(symth2py2)Cl_3]·CH_3OH. $C_{32}H_{36}Cl_3Cu_2N_4O_2S_2$ (806.2): calcd. C 47.73, H 4.38, N 6.96, S 7.96; found C 45.73, H 4.14, N 7.25, S 7.91. ESI-MS: m/z = 737 [Cu_2(py2th2s)Cl_2]$^+$.

[Cu_2(py2th2s)(μ-Br)Br_2] (2): Hpy2th2s (0.15 g, 0.28 mmol) and copper bromide (0.12 g, 0.54 mmol) were dissolved in of methanol (10 mL). After addition of diethyl ether to the resulting solution, the complex precipitated as a dark purple crystalline powder. Yield: 155 mg (64%). Crystals suitable for X-ray diffraction were obtained by slow diffusion of diethyl ether into a 0.01 M solution of the complex in acetonitrile. $C_{31}H_{31}Br_3Cu_2N_4OS_2$ (906.5): calcd. C 40.95, H 3.76, N 5.97, S 6.83; found C 39.76, H 3.42, N 6.07, S 6.50. ESI-MS: m/z = 827 [Cu_2(py2th2s)Br_2]$^+$.

X-ray Structures

Compound 1: A single crystal of [Cu_2(py2th2s)(μ-Cl)Cl_2]·CH_3OH (**1**) was mounted at 150 K on a ᵇruker AXS SMART 6000 diffractometer, equipped with Cu-K_α radiation (λ = 1.54184 Å). $C_{32}H_{35}Cl_3Cu_2N_4O_2S_2$, M = 802.17, rectangular reddish-brown plate, 0.23 × 0.21 × 0.05 mm, a = 7.984(2) Å, b = 34.589(7) Å, c = 12.554(3) Å, β = 94.31(3)°, Z = 4, V = 3457(2) Å^3, $\rho_{calcd.}$ = 1.541 g·cm^{-3}, μ = 5.068 mm^{-1}, absorption correction with SADABS,[32] monoclinic, space group $P2_1/n$ (no. 14), 19864 reflections collected, 6317 independent reflections (R_{int} = 0.0386). The structure was solved by direct methods and refined using the SHELX program package.[33,34] All hydrogen atoms were placed on idealized positions riding on their carrier atoms with isotropic displacement parameters. The final cycle of full-matrix least-squares refinement, including 438 parameters, converted into $R1$ = 0.0352 ($R1$ = 0.0430 all data) and $wR2$ = 0.1009 ($wR2$ = 0.1038 all data) with a maximum (minimum) residual electron density of 0.535 (−0.466) e·Å^{-3}.

Compound 2: $C_{31}H_{31}Br_3Cu_2N_4OS_2$ + solvent, M = 906.53, red needle, 0.60 × 0.06 × 0.03 mm, triclinic, $P\bar{1}$ (no. 2), a = 8.4207(2) Å, b = 17.9812(4) Å, c = 24.2238(6) Å, α = 71.2709(9), β = 81.2708(7), γ = 80.6146(11)°, V = 3407.66(14) Å^3, Z = 4, $\rho_{calcd.}$ = 1.767 g·cm^{-3}, 43713 measured reflections, 12061 unique reflections (R_{int} = 0.0734), 8080 observed reflections [$I > 2\sigma(I)$], 775 refined parameters, no restraints; R (obsd. refl.): $R1$ = 0.0461, $wR2$ = 0.1121; R (all data): $R1$ = 0.0776, $wR2$ = 0.1286; S = 1.085; residual electron density between −1.08 and 1.17 e·Å^{-3}. Intensities were measured with a Nonius KappaCCD diffractometer with rotating anode (Mo-K_α, λ = 0.71073 Å) at a temperature of 150 K. An absorption correction based on multiple measured reflections was applied (μ = 4.920 mm^{-1}, 0.59−0.86 transmission). The structure was solved with direct methods with the program SHELXS-97,[35] and refined with the program SHELXL-97[34] against F^2 of all reflections up to a resolution of $(\sin/\lambda)_{max.}$ = 0.60 Å^{-1}. Non-hydrogen atoms were refined freely with anisotropic displacement parameters. Hydrogen atoms were refined as rigid groups. Three of the thiophene rings were rotationally disordered and refined with occupancies of 0.85:0.15, 0.72:0.28, and 0.55:0.45, respectively. The crystal structure contains large voids (150.9 Å^3/unit cell) filled with disordered solvent molecules. Their contribution to the structure factors was secured by back-Fourier transformation (program

 © 2004 Wiley-VCH Verlag GmbH & Co. KGaA, Weinheim

PLATON,[17] CALC SQUEEZE; 22 e^-/unit cell). The drawings, structure calculations, and checking for higher symmetry was performed with the program PLATON.[17]

CCDC-230014 (**1**) and -230015 (**2**) contain the supplementary crystallographic data for this paper. These data can be obtained free of charge at www.ccdc.cam.ac.uk/conts/retrieving.html [or from the Cambridge Crystallographic Data Centre, 12 Union Road, Cambridge CB2 1EZ, UK; Fax: + 44-1223-336-033; E-mail: deposit@ccdc.cam.ac.uk].

Acknowledgments

Support from the NRSC Catalysis (a Research School Combination of HRSMC and NIOK) is kindly acknowledged. Also support and sponsorship from COST Action D21/003/2001 is kindly acknowledged. This project was financially supported by the Dutch Economy, Ecology, Technology (EET) program, a joint program of the Ministry of Economic Affairs, the Ministry of Education, Culture and Science, and the Ministry of Housing, Spatial Planning and the Environment. This work was supported in part (M. L., A. L. S.) by The Netherlands Foundation for Chemical Sciences (CW) with financial aid from the Netherlands Organization for Scientific Research (NWO).

[1] E. I. Solomon, U. M. Sundaram, T. E. Machonkin, *Chem. Rev.* **1996**, *96*, 2563−2605.
[2] T. Plenge, R. Dillinger, L. Santagostini, L. Casella, F. Tuczek, *Z. Anorg. Allg. Chem.* **2003**, *629*, 2258−2265.
[3] L. Santagostini, M. Gullotti, R. Pagliarin, E. Monzani, L. Casella, *Chem. Commun.* **2003**, *17*, 2186−2187.
[4] K. D. Karlin, J. C. Hayes, Y. Gultneh, R. W. Cruse, J. W. McKown, J. P. Hutchinson, J. Zubieta, *J. Am. Chem. Soc.* **1984**, *106*, 2121−2128.
[5] K. D. Karlin, T. Zoltan, A. Farooq, M. S. Haka, P. Ghosh, R. W. Cruse, Y. Gultneh, J. C. Hayes, P. J. Toscano, J. Zubieta, *Inorg. Chem.* **1992**, *31*, 1436−1451.
[6] J. Reim, B. Krebs, *J. Chem. Soc., Dalton Trans.* **1997**, 3793−3804.
[7] S. Torelli, C. Belle, S. Hamman, J. L. Pierre, E. Saint-Aman, *Inorg. Chem.* **2002**, *41*, 3983−3989.
[8] H. Börzel, P. Comba, H. Pritzkow, *Chem. Commun.* **2001**, 97−98.
[9] T. Klabunde, C. Eicken, J. C. Sacchettini, B. Krebs, *Nat. Struct. Biol.* **1998**, *5*, 1084−1090.
[10] C. Eicken, B. Krebs, J. C. Sacchettini, *Curr. Opin. Struct. Biol.* **1999**, *9*, 677−683.
[11] S. Torelli, C. Belle, I. Gautier-Luneau, J. L. Pierre, E. Saint-Aman, J. M. Latour, L. Le Pape, D. Luneau, *Inorg. Chem.* **2000**, *39*, 3526−3536.
[12] M. Thirumavalavan, P. Akilan, M. Kandaswamy, Kandaswamy Chinnakali, G. Senthil Kumar, H. K. Fun, *Inorg. Chem.* **2003**, *42*, 3308−3317.
[13] M. E. Cuff, K. I. Miller, K. E. van Holde, W. A. Hendrickson, *J. Mol. Biol.* **1998**, *278*, 855−870.
[14] C. Gielens, N. de Geest, X. Q. Xin, B. Devreese, J. van Beeumen, G. Preaux, *Eur. J. Biochem.* **1997**, *248*, 879−888.
[15] K. Lerch, *J. Biol. Chem.* **1982**, *257*, 6414−6419.
[16] A. S. Borovik, V. Papaefthymiou, L. F. Taylor, O. P. Anderson, L. Que, *J. Am. Chem. Soc.* **1989**, *111*, 6183−6195.
[17] A. L. Spek, *J. Appl. Crystallogr.* **2003**, *36*, 7−13.
[18] A. W. Addison, T. N. Rao, J. Reedijk, J. van Rijn, G. C. Verschoor, *J. Chem. Soc., Dalton Trans.* **1984**, 1349−1356.
[19] U. Rajendran, R. Viswanathan, M. Palaniandavas, N. Laskiminaraya, *J. Chem. Soc., Dalton Trans.* **1994**, 1219−1226.
[20] E. Ruiz, P. Alemany, S. Alvarez, J. Cano, *J. Am. Chem. Soc.* **1997**, *119*, 1297−1303.
[21] K. Bertoncello, G. D. Fallon, J. H. Hodgkin, K. S. Murray, *Inorg. Chem.* **1988**, *27*, 4750−4758.
[22] T. N. Sorrel, C. J. O′Connor, O. P. Anderson, J. H. Reibenspies, *J. Am. Chem. Soc.* **1985**, *107*, 4199−4206.
[23] C. Belle, C. Beguin, I. Gautier-Luneau, S. Hamman, C. Philouze, J. L. Pierre, F. Thomas, S. Torelli, E. Saint-Aman, M. Bonin, *Inorg. Chem.* **2002**, *41*, 479−491.
[24] W. J. Geary, *Coord. Chem. Rev.* **1971**, *7*, 81−122.
[25] R. A. Walton, *Quart. Rev.* **1965**, *19*, 126−143.
[26] K. D. Karlin, Y. Gultneh, T. Nicholson, J. Zubieta, *Inorg. Chem.* **1985**, *24*, 3725−3727.
[27] C. Fernandes, A. Neves, A. J. Bortoluzzi, A. S. Mangrich, E. Rentschler, B. Szpoganicz, E. Schwingel, *Inorg. Chim. Acta* **2001**, *320*, 12−21.
[28] C.-H. Kao, H.-H. Wei, Y.-H. Liu, G.-H. Lee, Y. Wang, C.-J. Lee, *J. Inorg. Biochem.* **2001**, *84*, 171−178.
[29] A. Neves, L. M. Rossi, A. J. Bortoluzzi, B. Szpoganicz, C. Wiezbicki, E. Schwingel, W. Haase, S. Ostrovsky, *Inorg. Chem.* **2002**, *41*, 1788−1794.
[30] J. Mukherjee, R. Mukherjee, *Inorg. Chim. Acta* **2002**, *337*, 429−438.
[31] I. M. Kolthoff, P. J. Elving, *Treatise on Analytical Chemistry*, Interscience Encyclopedia, Inc., New York, **1963**, vol. 4.
[32] *SAINT Plus V 6.02*, Bruker AXS, Inc., Madison, WI, **1999**.
[33] G. M. Sheldrick, *SHELXTL PLUS*, University of Göttingen, Germany, **1990**.
[34] G. M. Sheldrick, *SHELXL-97, Program for the refinement of crystal structures*, University of Göttingen, Germany, **1997**.
[35] G. M. Sheldrick, *SHELXS-97, Program for crystal structure solution*, University of Göttingen, Germany, **1997**.

Received February 4, 2004
Early View Article
Published Online August 17, 2004

 © 2004 Wiley-VCH Verlag GmbH & Co. KGaA, Weinheim

Reactions of the Aluminum(I) Monomer LAl [L = HC{(CMe)(NAr)}$_2$; Ar = 2,6-*i*Pr$_2$C$_6$H$_3$] with Imidazol-2-ylidene and Diphenyldiazomethane. A Hydrogen Transfer from the L Ligand to the Central Aluminum Atom and Formation of the Diiminylaluminum Compound LAl(N=CPh$_2$)$_2$

Hongping Zhu,[a] Jianfang Chai,[a] Andreas Stasch,[a] Herbert W. Roesky,*[a] Torsten Blunck,[a] Denis Vidovic,[a] Jörg Magull,[a] Hans-Georg Schmidt,[a] and Mathias Noltemeyer[a]

Dedicated to Professor Axel Zeeck on the occasion of his 65th birthday

Keywords: Aluminum / Carbenes / Diazo compounds / Hydrogen transfer / N ligands

The solid-state reaction of LAl and imidazol-2-ylidene at elevated temperature (120 °C) yielded the aluminum monohydride *N*-heterocyclic carbene adduct [{HC[C(CH$_2$)NAr](CMeNAr)}AlH-{CN(R)C$_2$Me$_2$N(R)}] [R = *i*Pr (**1**), Me (**2**)]. Compounds **1** and **2** have been characterized by spectroscopic (IR, and ^{1}H and ^{13}C NMR), mass spectrometric, and elemental analyses, and **1** was further characterized by X-ray structural analysis. These experimental data indicate that the Al–H bond is formed by hydrogen migration from one of the methyl groups of the β-diketiminato ligand backbone. The reaction of LAl with two equivalents of diphenyldiazomethane afforded the diiminylaluminum compound LAl(N=CPh$_2$)$_2$ (**3**), while an excess of diphenyldiazomethane resulted in the formation of Ph$_2$C=N–N=CPh$_2$. This suggests that Ph$_2$C=N–N=CPh$_2$ is initially generated and then reacts further by oxidative addition to yield **3**. The X-ray structural analysis reveals that compound **3** contains the shortest Al–N$_{iminyl}$ bond among those with a four-coordinate aluminum center.

(© Wiley-VCH Verlag GmbH & Co. KGaA, 69451 Weinheim, Germany, 2004)

Introduction

Monovalent group-13 species are of considerable interest not only for their syntheses, structures, and theoretical investigations,[1] but also for their reactivity.[2] In the last decade, a variety of new reactions has been intensively explored for generating tetrameric aluminum(I) compounds.[3] The compound (Cp*Al)$_4$ has been reported to have a remarkable tendency to dissociate in solution and give a monomeric fragment in the gas phase.[4] Reactions involving such species have also been investigated to some extent and a number of novel compounds have been isolated and structurally characterized.[5] Recently, we have prepared the first monomeric aluminum(I) complex LAl [L = HC{(CMe)(NAr)}$_2$, Ar = 2,6-*i*Pr$_2$C$_6$H$_3$], which is stable at room temperature.[6] Ab initio calculations show that this monomer possesses a nonbonded electron pair at the central two-coordinate Al atom and is isoelectronic with a singlet carbene. Subsequent reaction of LAl with organic azides at low temperature or with P$_4$ at room temperature indicates its reactivity, leading to the formation of a five-membered AlN$_4$ heterocycle [LAl{(NSiMe$_3$)$_2$N$_2$}], a monomeric aluminum imide [LAl(*N*-2,6-trip$_2$C$_6$H$_3$)] (trip = 2,4,6-*i*Pr$_3$C$_6$H$_2$), and a sandwich compound [(LAl)$_2$P$_4$] containing a P$_4^{4-}$ unit.[7] These results are markedly different from those in which (Cp*Al)$_4$ is used in related reactions. Obviously, the steric and electronic stabilization of the bulky β-diketiminato ligand enables its monomeric nature and therefore its unique chemical behavior, and allows further investigation of its reactivity.

Imidazol-2-ylidene is a stable neutral *N*-heterocyclic carbene which has been prepared in recent years.[8] Diphenyldiazomethane can be used as an effective precursor for the generation of transient :CPh$_2$.[9] The reaction of imidazol-2-ylidene with monovalent group-13 compounds has only been reported for InBr; a disproportionation reaction is observed.[10] More recently, a handful of reactions involving treatment of imidazol-2-ylidene with trivalent group-13 species have been investigated; the *N*-heterocyclic carbene functions as a Lewis base.[11] The corresponding reactions of diphenyldiazomethane with monovalent group-13 species have not been described so far. We now report on the reaction of LAl with imdazol-2-ylidene and diphenyldiazome-

[a] Institut für Anorganische Chemie der Universität Göttingen, Tammannstrasse 4, 37077 Göttingen, Germany
Fax: +49-551-39-3373
E-mail: hroesky@gwdg.de

 © 2004 Wiley-VCH Verlag GmbH & Co. KGaA, Weinheim **DOI: 10.1002/ejic.200400159**

thane. The formation of the aluminum monohydride *N*-heterocyclic carbene adduct of composition [{HC[C(CH_2)NAr](CMeNAr)}AlH{CN(R)C_2Me_2N(R)}] [R = *i*Pr (**1**), Me (**2**)] indicates a hydrogen transfer from the L ligand to the aluminum center. The formation of a diiminylaluminum compound [LAl(N=CPh_2)$_2$] (**3**) might proceed through the initial generation of Ph_2C=N−N=CPh_2 followed by its oxidative addition to LAl.

Results and Discussion

Reaction of LAl with Imdazol-2-ylidenes

The initial reaction of LAl with 1,3-diisopropyl-4,5-dimethylimidazol-2-ylidene was conducted in toluene in the temperature range from 25 to 80 °C. However, due to the low solubility of the *N*-heterocyclic carbene, this reaction was not successful. Therefore both starting materials were mixed in the solid state at 120 °C for 5 h. A softening of 1,3-diisopropyl-4,5-dimethylimidazol-2-ylidene and a subsequent color change of LAl from red black to light yellow were observed. Extraction of the product with hot toluene and keeping the eluate at room temperature afforded crystalline [{HC[C(CH_2)NAr](CMeNAr)}AlH{CN(*i*Pr)C_2Me_2N(*i*Pr)}] (**1**, Scheme 1).

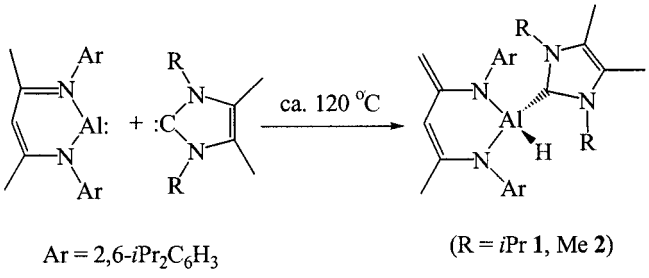

Scheme 1

Compound **1** is colorless and soluble in hot toluene and benzene while sparingly soluble in *n*-hexane and pentane. It was characterized by spectroscopic and elemental analyses. The mass spectrum exhibits the molecular ion of **1** {*m*/*z* (%) = 624 (5) [M^+], 609 (40) [M^+ − Me], 581 (100) [M^+ − *i*Pr]}. The ^{1}H and ^{13}C NMR spectra recorded in C_6D_6 are consistent with a pseudo-tetrahedral geometry and C_s symmetry about aluminum, giving rise to six isopropyl C*H* resonances and twelve diastereotopically split isopropyl CH_3 resonances due to the chiral environment of the Al center. The proton resonance of the β-CH_3 group on the L ligand backbone (δ = 1.72 ppm) integrates for three protons, while two other singlets are observed downfield (δ = 3.98 and 3.30 ppm) and integrate for one proton each. The former corresponds to the normal terminal CH_3−C group, and the latter is assigned to the terminal CH_2=C group which gives rise to two nonequivalent protons due to the restricted rotation about the C=C double bond. One broad proton resonance centered at δ = 4.80 ppm is characteristic for aluminum hydrides.[12] The IR spectrum exhibits a single band at 1809 cm^{-1} for Al−H absorption.[13]

Complex **1** was also characterized by X-ray structural analysis. The molecular structure of **1** is shown in Figure 1. Due to the poor quality of the crystal data the bond lengths and angles for **1** will not be discussed in detail. The quality of the crystals gave no improvement in the refinement of the structure even after recrystallization from several different solvents. Nonetheless, the structural solution of **1** offers important structural information which is in agreement with its spectral analysis. Compound **1** is monomeric and the central Al atom adopts a distorted tetrahedral geometry. The Al−N bond lengths [1.844(3) and 1.853(2) Å] appear to be shorter than other Al−$N_{\beta\text{-diketiminato}}$ bonds [1.875(4)−1.957(2) Å],[5,14] and are closer to those found in diamidoaluminum monohydride [{ArN(CH_2)$_3$NAr}-AlH(NMe_3)] [1.820(1) and 1.828(1) Å].[13c] In the ligand backbone, the terminal C−C bond lengths [C(4)−C(5): 1.507(4) Å; C(1)−C(2): 1.363(4) Å] are indicative of a single and double bond, respectively, as are the others within the backbone [C(2)−C(3): 1.458(4) Å; C(3)−C(4): 1.351(4) Å]. The adjacent N−C bond lengths [1.411(3) and 1.413(3) Å] are intermediate between N−C double and single bonds.

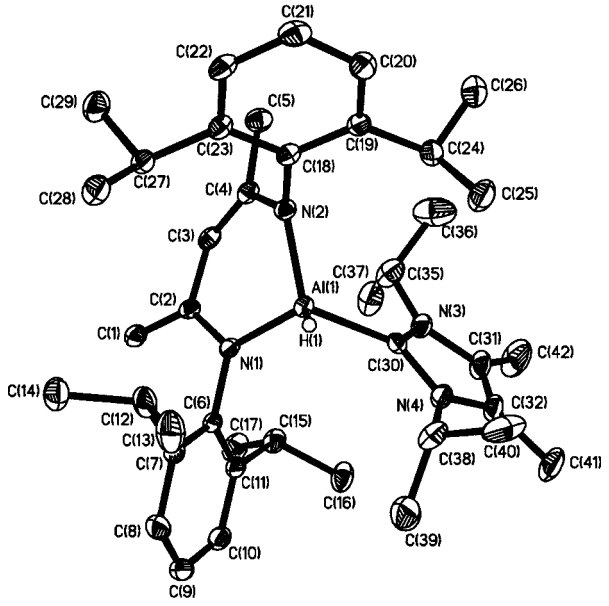

Figure 1. Molecular structure of **1**; H atoms are omitted for clarity except for the Al−H hydrogen atom

Obviously, the Al−H hydrogen comes from one of the terminal methyl groups of the L ligand, although whether this hydrogen transfer occurs via a proton, a hydrogen radical, or a hydride is not clear.

The reaction of LAl with less bulky *N*-substituted 1,3,4,5-tetramethylimidazol-2-ylidene was also performed in a similar manner (method A) to the preparation of **1** in order to investigate the effect of the steric bulk on the reaction product. As a result, [{HC[C(CH_2)NAr](CMeNAr)}AlH-{CN(Me)C_2Me_2N(Me)}] (**2**) was obtained in a relatively low yield. All the spectroscopic data (IR, EI mass, and ^{1}H and ^{13}C NMR) confirm a structure analogous to that of **1**.

 © 2004 Wiley-VCH Verlag GmbH & Co. KGaA, Weinheim

Reaction of LAl with N_2CPh_2

In the majority of organic and organometallic reactions diphenyldiazomethane is used as a precursor for the generation of transient :CPh_2 carbene.[9] Therefore, it was selected as another electron-rich species for the reaction with LAl. However, treatment of LAl with two equivalents of N_2CPh_2 under heating unexpectedly afforded [LAl(N=CPh_2)$_2$] (**3**; Scheme 2), the first example of a diiminylaluminum compound. When LAl was treated with an excess of N_2CPh_2 under the same conditions Ph_2C=N−N=CPh_2 was isolated.[15] Therefore, we assumed that the formation of **3** proceeds by the initial generation of Ph_2C=N−N=CPh_2 followed by its oxidative addition to LAl. In order to test this assumption a toluene solution of LAl was heated under reflux with one equivalent of Ph_2C=N−N=CPh_2 and complex **3** was formed, as expected, in an almost quantitative yield.[16]

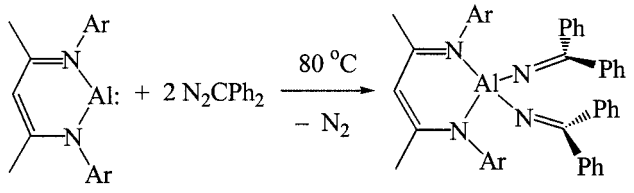

Scheme 2

Complex **3** is an orange-yellow crystalline solid that is thermally stable, as indicated by its high melting point (344−346 °C). The most intense ion in the EI mass spectrum appears at m/z = 624 [M^+ − $NCPh_2$]; the peak at m/z = 805 (20%) is assigned to the molecular ion [M^+].

X-ray quality single crystals of **3** had formed from a 1:1 solvent mixture (*n*-hexane, diethyl ether) at 4 °C after two days. The structural analysis unambiguously ascertains the composition of **3**. The molecular structure is shown in Figure 2 and selected bond lengths and angles are listed in Table 1. The central Al atom is bound to two β-diketiminato nitrogen atoms and two iminyl nitrogen atoms. The AlN_4 core exhibits a distorted tetrahedral geometry with *trans*-N−Al−N angles ranging from 97.23(18)° to 117.6(2)°. The Al−$N_{\beta\text{-diketiminato}}$ bond lengths [1.899(4) and 1.901(4) Å] are in the expected range [1.875(4)−1.957(2) Å].[5,14] However, the Al−N_{iminyl} distances [1.774(4) and 1.785(4) Å] are the shortest yet found in four-coordinate Al−N complexes.[17] Comparable Al−N bond lengths have only been observed in three-coordinate [trip$_2$Al{N(H)dipp}] [1.784(3) Å],[18a] [MeAl(Ndipp)]$_3$ [1.782(4) Å][18b] and Al[N(SiMe$_3$)$_2$]$_3$ [1.78(2) Å].[18c] Surprisingly, the N−C distances of the iminyl group [1.249(6) and 1.269(6) Å] are shorter than that of a C=N bond.[19] The short Al−N_{iminyl} bond can be considered to be highly ionic, and the shortening of the N=C bond may be due to a charge delocalization over the phenyl groups. The Al(1)−N(4)−C(50) [163.4(5)°] and Al(1)−N(3)−C(30)

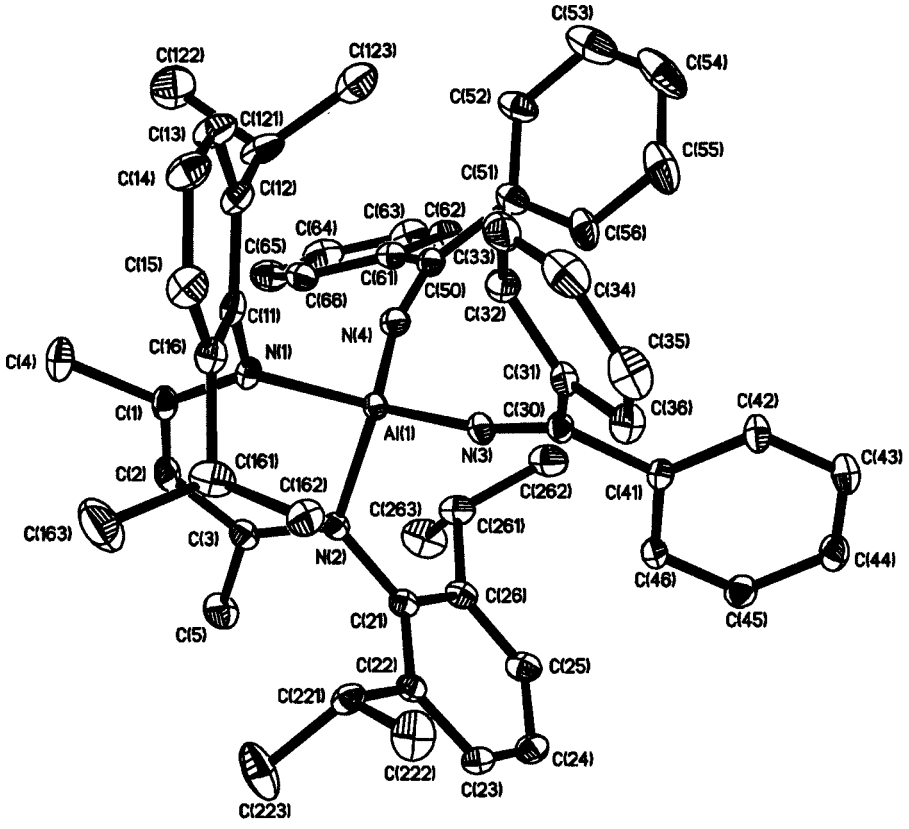

Figure 2. Molecular structure of **3**; H atoms are omitted for clarity

 © 2004 Wiley-VCH Verlag GmbH & Co. KGaA, Weinheim

[169.4(4)°] angles show a less-bent arrangement of the Al−N=C group. The observation of two sets of resonances for the iminyl phenyl rings in the ^{1}H and ^{13}C NMR spectra suggests a restricted rotation of the phenyl rings around the N=C bond. This was confirmed by a high-temperature proton NMR spectral analysis (40, 60, and 80 °C), where two corresponding sets of resonances are always observed.

Table 1. Selected bond lengths (Å) and angles (deg) for compound **3**

Al(1)−N(1)	1.901(4)	Al(1)−N(2)	1.899(4)
Al(1)−N(3)	1.774(4)	Al(1)−N(4)	1.785(4)
N(3)−C(30)	1.249(6)	N(4)−C(50)	1.269(6)
N(1)−Al(1)−N(2)	97.23(18)	N(3)−Al(1)−N(4)	116.1(2)
N(1)−Al(1)−N(3)	117.6(2)	N(1)−Al(1)−N(4)	107.4(2)
N(2)−Al(1)−N(3)	109.5(2)	N(2)−Al(1)−N(4)	106.9(2)
C(30)−N(3)−Al(1)	169.4(4)	C(50)−N(4)−Al(1)	163.4(5)

Conclusions

In summary, we have reacted the aluminum(I) monomer LAl with imidazol-2-ylidene and diphenyldiazomethane and obtained the new compounds [{HC[C(CH$_2$)NAr]-(CMeNAr)}AlH{CN(R)C$_2$Me$_2$N(R)}] [R = *i*Pr (**1**), Me (**2**)] and [LAl(N=CPh$_2$)$_2$] (**3**). This further shows the unique reaction behavior of LAl, and exhibits its properties as a carbene analog. Inspired by these results, we are now exploring the reaction of LAl with metal carbonyl complexes to compare the electronic equivalence of LAl with CO.

Experimental Section

All manipulations were carried out under a purified nitrogen atmosphere using Schlenk techniques. The solvents were dried by standard methods. Chemicals were purchased from Aldrich or Fluka and used as received. LAl,[6] [CN(R)C$_2$Me$_2$N(R)] (R = Me, *i*Pr),[8] and N$_2$CPh$_2$ [9a] were prepared as described in the literature.

Elemental analyses were performed by the Analytisches Labor des Instituts für Anorganische Chemie der Universität Göttingen. ^{1}H (300.13 MHz), ^{13}C (125.76 MHz) and ^{27}Al NMR (65.17 MHz) spectra were recorded on a Bruker AM 200 or a Bruker AM 250 spectrometer and IR spectra on a Bio-Rad Digilab FTS-7 spectrometer. EI mass spectra were measured on a Finnigan MAT 8230 or a Varian MAT CH5 instrument. Melting points were measured in sealed glass tubes and are not corrected.

Synthesis of [{HC[C(CH$_2$)NAr](CMeNAr)}AlH{CN(*i*Pr)C$_2$Me$_2$-N(*i*Pr)}] (1). Method A: A suspension of LAlI$_2$ (2.08 g, 3.0 mmol) and finely divided potassium (0.25 g, 6.3 mmol) in toluene (50 mL) was stirred vigorously for 3 d at room temperature until all the potassium had disappeared. After filtration the dark-red filtrate was slowly dried in vacuo and some red microcrystals of LAl were observed to deposit on the walls of the flask. [CN(*i*Pr)C$_2$Me$_2$N-(*i*Pr)] (0.36 g, 2 mmol) was added to the resulting solid. The mixture was heated slowly to about 120 °C and kept for 5 h. After cooling to room temperature, the yellow product was extracted with hot toluene (30 mL) and the extract was kept at room temperature for 24 h to afford X-ray quality colorless block crystals, which were collected by filtration (0.42 g). The mother liquor was concentrated (ca. 5 mL) and kept at 4 °C for 24 h to give another crop of colorless crystals (0.25 g). Total yield of **1**: 0.67 g {47%, based on [CN(*i*Pr)C$_2$Me$_2$N(*i*Pr)]}. M.p. 298−300 °C (>250 °C decomp.). ^{1}H NMR (C$_6$D$_6$, 300 K): δ = 0.38, 0.50, 0.76, 0.82, 1.19, 1.32, 1.46, 1.50, 1.53, 1.55, 1.57, 1.59 [d, 12 × 3 H, CH*Me*$_2$ and N(CH*Me*$_2$)], 1.38, 1.62 (s, 2 × 3 H, C$_2$*Me*$_2$), 1.72 (s, 3 H, β-C*H*$_3$), 3.30, 3.98 (s, 2 × 1 H, β-C*H*$_2$), 3.28, 3.62, 4.18, 4.26 (sept, 4 × 1 H, *CH*Me$_2$), 4.80 (br., 1 H, Al-*H*), 5.60 (s, 1 H, γ-C*H*), 5.44, 5.62 [sept, 2 × 1 H, N(*CH*Me$_2$)], 7.10−7.38 (m, 6 H, *Ar*) ppm. ^{13}C NMR (C$_6$D$_6$, 300 K): δ = 9.9, 10.0 (C$_2$*Me*$_2$), 20.7, 21.1, 21.4, 22.0, 23.3, 23.7, 23.8, 24.4, 24.5, 24.7, 25.6, 25.7, 26.4, 27.1, 27.7, 28.4, 28.9 [N(CH*Me*$_2$), *CH*Me$_2$, CH*Me*$_2$ and β-*C*H$_3$], 50.9, 53.0 [N(*CH*Me$_2$)], 80.8 (β-*C*H$_2$), 106.6 (γ-*C*), 123.0, 124.5, 124.7, 124.9, 125.6, 126.6, 127.8, 128.5, 129.3, 143.4, 144.7, 145.6, 146.1, 147.2, 148.4, 149.0 (*Ar*, *C*N and *C*$_2$Me$_2$), 154.5 (Al-*C*) ppm. ^{27}Al NMR ([D$_8$]toluene, 300 K): no resonances were observed. IR (Nujol): ν_{Al-H} = 1809 cm^{-1} (m), $\nu_{C=C}$ = 1619 (m). MS (EI): *m*/*z* (%) = 624 (5) [M$^+$], 609 (40) [M$^+$ − Me], 581 (100) [M$^+$ − *i*Pr]. C$_{40}$H$_{61}$AlN$_4$ (624.94): calcd. C 76.87, H 9.84, N 8.97; found C 77.07, H 9.55, N 8.86.

Method B: A suspension of LAlI$_2$ (2.08 g, 3.0 mmol), [CN(*i*Pr)C$_2$Me$_2$N(*i*Pr)] (0.54 g, 3 mmol) and finely divided potassium (0.25 g, 6.3 mmol) in toluene (50 mL) was stirred vigorously for 3 d at room temperature until all the potassium had disappeared. After filtration the orange filtrate was concentrated (ca. 20 mL) and *n*-hexane (20 mL) was added. The solution was kept at 4 °C for one week to afford colorless block crystals (0.72 g). The mother liquor was further concentrated (ca. 5 mL) and kept at 4 °C for 2 d to give another crop of colorless crystals (0.32 g). Total yield of **1**·toluene: 1.04 g (48%). The IR, ^{1}H and ^{13}C NMR spectroscopic data are essentially the same as those of **1** except for one extra molecule of toluene.

Synthesis of [{HC[C(CH$_2$)NAr](CMeNAr)}AlH{CN(Me)C$_2$-Me$_2$N(Me)}] (2): Compound **2** was prepared in a similar manner (method A) as **1**. LAlI$_2$ (2.08 g, 3.0 mmol), finely divided potassium (0.25 g, 6.3 mmol) and [CN(Me)C$_2$Me$_2$N(Me)] (0.24 g, 2.0 mmol) were used. The extract (10 mL) was added to *n*-hexane (10 mL) and kept at −26 °C for 48 h to afford colorless crystals of **2** {yield: 0.42 g, 25%, based on [CN(Me)C$_2$Me$_2$N(Me)]}. M.p. 252−253 °C. ^{1}H NMR ([D$_8$]toluene, 300 K): δ = 1.45, 1.47 (s, 2 × 3 H, C$_2$*Me*$_2$), 0.29, 0.30, 1.16, 1.46, 1.58, 1.60, 1.61, 1.62 (d, 8 × 3 H, CH*Me*$_2$), 1.69 (s, 3 H, β-C*H*$_3$), 3.70, 3.75 (s, 2 × 3 H, N(*Me*)), 3.10, 3.85 (s, 2 × 1 H, β-C*H*$_2$), 3.21, 3.25, 4.15, 4.21 (sept, 4 × 1 H, C*H*Me$_2$), 4.80 (br., 1 H, Al-*H*), 5.39 (s, 1 H, γ-C*H*), 7.04−7.38 (m, 6 H, *Ar*) ppm. ^{13}C NMR ([D$_8$]toluene, 300 K): δ = 7.9, 8.0 (C$_2$*Me*$_2$), 23.6, 24.0, 24.2, 24.3, 24.8, 24.9, 25.4, 25.8, 26.0, 26.4, 26.5, 27.1, 27.8, 28.7, 29.0 [N(*Me*), *C*HMe$_2$, CH*Me*$_2$ and β-*C*H$_3$), 80.1 (β-*C*H$_2$), 102.3 (γ-*C*), 122.9, 123.7, 124.2, 124.6, 124.9, 125.1, 125.3, 127.7, 128.0, 143.2, 143.8, 145.4, 146.3, 147.4, 148.2, 149.0 (*Ar*, *C*N and *C*$_2$Me$_2$), 155.2 (Al-*C*) ppm. MS (EI): *m*/*z* (%) = 568 (15) [M$^+$], 553 (100) [M$^+$ − Me]. IR (Nujol): ν_{Al-H} = 1810 cm^{-1} (m), $\nu_{C=C}$ = 1616 (m). C$_{36}$H$_{53}$AlN$_4$ (568.83): calcd. C 76.01, H 9.29, N 9.85; found C 76.50, H 9.60, N 9.40.

Synthesis of LAl(NCPh$_2$)$_2$ (3): A solution of N$_2$CPh$_2$ (0.37 g, 1.90 mmol) in toluene (15 mL) was added to a solution of LAl (0.42 g, 0.94 mmol) in toluene (25 mL) at room temperature. The mixture was slowly heated to 60 °C and kept for 12 h; a yellow solution developed. All volatiles were then removed in vacuo and the residue was washed with *n*-hexane (5 mL) to afford an orange-yellow crystalline solid of **3** (0.36 g, 48%). M.p. 344−346 °C. ^{1}H NMR (C$_6$D$_6$, 300 K): δ = 0.82, 1.02 (d, 8 × 3 H, CH*Me*$_2$), 1.64 (s, 2 × 3 H, β-C*H*$_3$), 3.21 (sept, 4 × 1 H, C*H*Me$_2$), 5.28 (s, 1 H, γ-C*H*), 6.92−7.00 (m, 2 × 5 H, *Ph*), 7.00−7.08 (m, 2 × 5 H, *Ph*),

 © 2004 Wiley-VCH Verlag GmbH & Co. KGaA, Weinheim

7.18−7.32 (m, 6 H, *Ar*) ppm. ^{13}C NMR (C_6D_6, 300 K): δ = 23.8, 24.4, 24.9, 28.5 (*C*HMe$_2$, CH*Me*$_2$, β-*C*H$_3$), 98.8 (γ-*C*), 124.5, 126.9, 127.6, 127.6, 127.9, 128.1, 128.3, 128.3, 129.4, 142.4, 143.1, 144.7 (*Ar*, *Ph*), 166.9 (N*C*Ph$_2$), 171.0 (*C*N) ppm. MS (EI): *m*/*z* (%) = 805 (20) [M$^+$], 790 (30) [M$^+$ − Me], 624 (100) [M$^+$ − NCPh$_2$]. IR (Nujol): $\nu_{C=C}$ = 1667 cm^{-1} (w), $\nu_{C=N}$ = 1624, 1554 (w). $C_{55}H_{61}AlN_4$ (805.10): calcd. C 82.05, H 7.64, N 6.96; found C 82.11, H 7.74, N 7.05. X-ray quality crystals were obtained by recrystallization from a 1:1 *n*-hexane/diethyl ether solution at 4 °C for one week.

X-ray Structure Determination and Refinement: The crystallographic data for compound **1** were collected on a Stoe IPDS II-array detector system and for **3** on a Stoe−Siemens−Huber four-circle-diffractometer coupled to a Siemens CCD area-detector. In both cases graphite-monochromated Mo-K_α radiation (λ = 0.71073 Å) was used. Both structures were solved by direct methods (SHELXS-96) and refined against F^2 using SHELXL-97.[20,21] All non-hydrogen atoms were located by difference Fourier synthesis and refined anisotropically, and hydrogen atoms were included using the riding model with U_{iso} tied to the U_{iso} of the parent atoms, except for the Al−H hydrogen atom, which was located by difference Fourier synthesis and refined isotropically. A summary of cell parameters, data collection, and structure solution and refinement is given in Table 2.

CCDC-231677 (for **1**) and -231678 (for **3**) contain the supplementary crystallographic data for this paper. These data can be obtained free of charge at www.ccdc.cam.ac.uk/conts/retrieving.html [or from the Cambridge Crystallographic Data Centre, 12, Union Road, Cambridge CB2 1EZ, UK; fax: +44-1223-336-033; E-mail: deposit@ccdc.cam.ac.uk].

Table 2. Crystallographic data for compounds **1** and **3**

	1	**3**
Empirical formula	$C_{40}H_{61}AlN_4$	$C_{55}H_{61}AlN_4$
Formula mass	624.91	805.06
Temp. (K)	133(2)	203(2)
Crystal system	monoclinic	orthorhombic
Space group	$P2_1/c$	$P2(1)2(1)2(1)$
a (Å)	10.161(2)	12.285(2)
b (Å)	17.380(4)	12.981(2)
c (Å)	22.274(5)	30.001(6)
α (°)		
β (°)	101.89(3)	
γ (°)		
V (Å^3)	3849.1(13)	4784.4(16)
Z	4	4
ρ_c (Mg/m^3)	1.078	1.118
μ (mm^{-1})	0.084	0.082
F(000)	1386	1728
θ range (°)	1.87−24.71	3.55−25.01
Index ranges	$-11 \le h \le 11$	$0 \le h \le 14$
	$-20 \le k \le 20$	$-1 \le k \le 15$
	$-26 \le l \le 24$	$-35 \le l \le 35$
No. of reflections collected	33356	4675
No. of independent reflns. (R_{int})	6560 (0.1511)	4658 (0.0188)
No. of data/restraints/parameters	6560/0/424	4658/0/555
GoF/F^2	0.911	1.096
*R*1,[a] *wR*2[b] [$I > 2\sigma(I)$]	0.0541, 0.0974	0.0614, 0.1530
*R*1,[a] *wR*2[b] (all data)	0.1198, 0.1096	0.0848, 0.1740
largest difference peak/hole (e·Å^{-3})	0.313/−0.271	0.271/−0.282

[a] $R = \Sigma||F_o| - |F_c||/\Sigma|F_o|$. [b] $wR2 = [\Sigma w(F_o^2 - F_c^2)^2/\Sigma w(F_o^2)]^{1/2}$.

Acknowledgments

This work was supported by the Deutsche Forschungsgemeinschaft, the Fonds der Chemischen Industrie and the Göttinger Akademie der Wissenschaften.

[1] [1a] P. P. Power, *J. Chem. Soc., Dalton Trans.* **1998**, 2939−2951. [1b] P. P. Power, *Chem. Rev.* **1999**, *99*, 3463−3503.
[2] [2a] W. Uhl, *Rev. Inorg. Chem.* **1998**, *18*, 239−282, and references cited therein. [2b] M. N. S. Rao, H. W. Roesky, G. Anantharaman, *J. Organomet. Chem.* **2002**, *646*, 4−14, and references cited therein.
[3] [3a] C. Dohmeier, C. Robl, M. Tacke, H. Schnöckel, *Angew. Chem.* **1991**, *103*, 594−595; *Angew. Chem. Int. Ed. Engl.* **1991**, *30*, 564−565. [3b] E. P. Schram, N. Sudha, *Inorg. Chim. Acta* **1991**, *183*, 213−216. [3c] S. Schulz, H. W. Roesky, H. J. Koch, G. M. Sheldrick, D. Stalke, A. Kuhn, *Angew. Chem.* **1993**, *105*, 1828−1830; *Angew. Chem. Int. Ed. Engl.* **1993**, *32*, 1729−1731. [3d] C. Schnitter, H. W. Roesky, C. Röpken, R. Herbst-Irmer, H.-G. Schmidt, M. Noltemeyer, *Angew. Chem.* **1998**, *110*, 2059−2062; *Angew. Chem. Int. Ed.* **1998**, *37*, 1952−1955. [3e] M. Schormann, K. S. Klimek, H. Hatop, S. P. Varkey, H. W. Roesky, C. Lehmann, C. Röpken, R. Herbst-Irmer, M. Noltemeyer, *J. Solid State Chem.* **2001**, *162*, 225−236. [3f] M. Schiefer, N. D. Reddy, H. W. Roesky, D. Vidovic, *Organometallics* **2003**, *22*, 3637−3638.
[4] [4a] J. Gauss, U. Schneider, R. Ahlrichs, C. Dohmeier, H. Schnöckel, *J. Am. Chem. Soc.* **1993**, *115*, 2402−2408. [4b] A. Haaland, K.-G. Martinsen, S. A. Shlykov, H. V. Volden, C. Dohmeier, H. Schnöckel, *Organometallics* **1995**, *14*, 3116−3119.
[5] [5a] C. Dohmeier, H. Schnöckel, C. Robl, U. Schneider, R. Ahlrichs, *Angew. Chem.* **1994**, *106*, 225−227; *Angew. Chem. Int. Ed. Engl.* **1994**, *33*, 199−201. [5b] S. Schulz, L. Häming, R. Herbst-Irmer, H. W. Roesky, G. M. Sheldrick, *Angew. Chem.* **1994**, *106*, 1052−1054; *Angew. Chem. Int. Ed. Engl.* **1994**, *33*, 969−971. [5c] C. Dohmeier, H. Krautscheid, H. Schnöckel, *Angew. Chem.* **1994**, *106*, 2570−2571; *Angew. Chem. Int. Ed. Engl.* **1994**, *33*, 2482−2483. [5d] S. Schulz, T. Schoop, H. W. Roesky, L. Häming, A. Steiner, R. Herbst-Irmer, *Angew. Chem.* **1995**, *107*, 1015−1016; *Angew. Chem. Int. Ed. Engl.* **1995**, *34*, 919−920. [5e] S. Schulz, A. Voigt, H. W. Roesky, L. Häming, R. Herbst-Irmer, *Organometallics* **1996**, *15*, 5252−5263.
[6] C. Cui, H. W. Roesky, M. Noltemeyer, H.-G. Schmidt, H. Hao, F. Cimpoesu, *Angew. Chem.* **2000**, *112*, 4444−4446; *Angew. Chem. Int. Ed.* **2001**, *39*, 4274−4276.
[7] [7a] C. Cui, H. W. Roesky, H. Hao, H.-G. Schmidt, M. Noltemeyer, *Angew. Chem.* **2000**, *112*, 4705−4707; *Angew. Chem. Int. Ed.* **2000**, *39*, 4531−4533. [7b] N. J. Hardman, C. Cui, H. W. Roesky, W. H. Fink, P. P. Power, *Angew. Chem.* **2001**, *113*, 2230−2232; *Angew. Chem. Int. Ed.* **2001**, *40*, 2172−2174. [7c] Y. Peng, H. Fan, H. Zhu, H. W. Roesky, J. Magull, *Angew. Chem.* **2004**, *116*, 3525−3527; *Angew. Chem. Int. Ed.* **2004**, *43*, 3443−3445.
[8] N. Kuhn, T. Kratz, *Synthesis* **1993**, 561−562.
[9] [9a] H. Staudinger, E. Anthes, F. Pfenninger, *Ber. Dtsch. Chem. Ges.* **1916**, *49*, 1928−1941. [9b] K. Ziegler, H.-G. Gellert, H. Lehmkuhl, W. Pfohl, K. Zosel, *Justus Liebigs Ann. Chem.* **1960**, *629*, 1−13. [9c] W. A. Herrmann, J. L. Hubbard, I. Bernal, J. D. Korp, B. L. Haymore, G. L. Hillhouse, *Inorg. Chem.* **1984**, *23*, 2978−2983.
[10] R. J. Baker, R. D. Farley, C. Jones, M. Kloth, D. M. Murphy, *Chem. Commun.* **2002**, 1196−1197.
[11] [11a] A. J. Arduengo III, H. V. R. Dias, J. C. Calabrese, F. Davidson, *J. Am. Chem. Soc.* **1992**, *114*, 9724−9725. [11b] X.-X. Li, J. Su, G. H. Robinson, *Chem. Commun.* **1996**, 2683−2684. [11c] C. J. Carmalt, A. H. Cowley, *Adv. Inorg. Chem.* **2000**, *50*, 1−61, and references cited therein. [11d] R. J. Baker, A. J. Davies, C. Jones, M. Kloth, *J. Organomet. Chem.* **2002**, *656*, 203−210. [11e]

 © 2004 Wiley-VCH Verlag GmbH & Co. KGaA, Weinheim

J. D. Gorden, C. L. B. Macdonald, A. H. Cowley, *J. Organomet. Chem.* **2002**, *643−644*, 487−489.
[12] C. Cui, H. W. Roesky, M. Noltemeyer, H.-G. Schmidt, *Inorg. Chem.* **2000**, *29*, 3678−3689.
[13] [13a] A. H. Cowley, H. S. Isom, A. Decken, *Organometallics* **1995**, *14*, 2589−2592. [13b] C. Klein, H. Nöth, M. Tacke, M. Thomann, *Angew. Chem.* **1993**, *105*, 923−926; *Angew. Chem. Int. Ed. Engl.* **1993**, *32*, 886−889. [13c] H. Zhu, J. Chai, H. W. Roesky, M. Noltemeyer, H.-G. Schmidt, D. Vidovic, J. Magull, *Eur. J. Inorg. Chem.* **2003**, *17*, 3113−3119.
[14] C. Cui, S. Köpke, R. Herbst-Irmer, H. W. Roesky, M. Noltemeyer, H.-G. Schmidt, B. Wrackmeyer, *J. Am. Chem. Soc.* **2001**, *123*, 9091−9098.
[15] The azine $Ph_2C{=}N{-}N{=}CPh_2$ was obtained as colorless crystals with a melting point of 174 °C. Its spectroscopic data (EI mass, IR, ^1H and ^{13}C NMR) and elemental analysis confirmed the composition. It is well-known that many salts and complexes of Cu^I and Cu^{II} are used as catalysts for the decomposition of diphenyldiazomethane. The reaction of LAl and diphenyldiazomethane to give $Ph_2C{=}N{-}N{=}CPh_2$ may indicate that the LAl plays a catalytic role. [15a] W. Kirmse, *Carbene Chemistry* 2nd edition, Academic Press, New York, **1971**, 85−128, and references cited therein. [15b] D. Bethell, K. L. Handoo, S. A. Fairhurst, L. H. Sutcliffe, *J. Chem. Soc., Chem. Commun.* **1977**, 326−328.
[16] A mixture of equivalent amounts of LAl and $Ph_2C{=}N{-}N{=}CPh_2$ in toluene (20 mL) was allowed slowly to heat to reflux and kept for 3 h. After cooling to room temperature, the solution was dried in vacuo and the residue was washed with *n*-hexane (5 mL) to give an orange-yellow crystalline solid in almost quantitative (yield, > 90%). The melting point and the spectroscopic data (EI mass and IR) are essentially the same as those of **3**.
[17] P. J. Brothers, P. P. Power, *Adv. Organomet. Chem.* **1996**, *39*, 1−69.
[18] [18a] K. M. Waggoner, H. Hope, P. P. Power, *Angew. Chem.* **1988**, *100*, 1765−1766; *Angew. Chem. Int. Ed. Engl.* **1988**, *27*, 1699−1700. [18b] K. M. Waggoner, P. P. Power, *J. Am. Chem. Soc.* **1991**, *113*, 3385−3393. [18c] G. M. Sheldrick, W. S. Sheldrick, *J. Chem. Soc. A* **1969**, 2279−2293.
[19] For the structural model $X_{1,2}{-}C{=}N{-}Y$, the range of C=N double-bond lengths is 1.279−1.302 Å. [19a] F. H. Allen, P. Kennard, D. G. Waston, L. Brammer, A. G. Orpen, R. Taylor, *J. Chem. Soc., Perkin Trans. 2* **1987**, S1−S19.
[20] G. M. Sheldrick, SHELXS-90, Program for Structure Solution, *Acta Crystallogr., Sect. A* **1990**, *46*, 467−473.
[21] G. M. Sheldrick, SHELXL-97, *Program for Crystal Structure Refinement*, University of Göttingen, Germany, **1997**.

Received February 25, 2004

 © 2004 Wiley-VCH Verlag GmbH & Co. KGaA, Weinheim

Adducts of Aluminum and Gallium Trichloride with a *N*-Heterocyclic Carbene and an Adduct of Aluminum Trichloride with a Thione

Andreas Stasch,[a] Sanjay Singh,[a] Herbert W. Roesky,*[a] Mathias Noltemeyer,[a] and Hans-Georg Schmidt[a]

Keywords: Adducts / Aluminum / Carbenes / Gallium / Lewis acids

The reactions of $AlCl_3$ and $GaCl_3$ with 1,3,4,5-tetramethylimidazole-2-ylidene in toluene at room temperature affords the 1:1 adducts **5** and **6**, respectively. The use of a bulky *N*-heterocyclic carbene (NHC) in toluene/THF and $AlCl_3$ results in the formation of an imidazolium salt **7** with the tetrachloroaluminate anion. A 1:1 adduct **8** of 1,3,4,5-tetramethylimidazole-2(3*H*)-thione with $AlCl_3$ is obtained in toluene. The crystal structures of **5**·0.5C_7H_8, **7**·THF and **8** were determined.

(© Wiley-VCH Verlag GmbH & Co. KGaA, 69451 Weinheim, Germany, 2004)

Introduction

The use of *N*-heterocyclic carbenes (NHC)[1,2] as good σ-donor molecules to stabilize trivalent group 13 compounds was established with the isolation of the first alane adduct of an imidazol-2-ylidene **1**.[3] The stability of these complexes is demonstrated by the melting point of **1** (246−247 °C). Compound **1** melts without decomposition, whereas AlH_3·NMe_3 decomposes above 100 °C.[4] The properties of the corresponding gallium and indium compounds allow their isolation and characterization.[5,6] However, adducts of a NHC with aluminum or gallium halides have not been reported. The reaction of a bidentate NHC ligand with $AlCl_3$ in diethyl ether resulted in an imidazolium salt in moderate yield and in by-products, although moisture was excluded from the reaction mixture.[7] Only adducts of a phosphanylsilylcarbene with MCl_3 (M = Al **2**, Ga **3**, In **4**) were reported and the X-ray single-crystal structure of **3** was determined.[8] From reactions of a NHC with InX_3 (X = Cl, Br) under different conditions, carbene adducts with a composition of 1:1 and 1:2 ratios as well as imidazolium salts of carbene-stabilized indates were obtained and structurally characterized.[9]

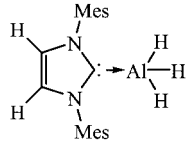

1

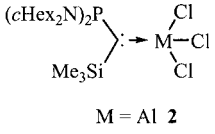

M = Al **2**
= Ga **3**
= In **4**

[a] Institut für Anorganische Chemie der Georg-August-Universität Göttingen,
Tammannstr. 4, 37077 Göttingen, Germany
E-mail: hroesky@gwdg.de

Results and Discussion

$AlCl_3$ was treated with one equivalent of 1,3,4,5-tetramethylimidazole-2-ylidene[10] in toluene at room temperature; $AlCl_3$ dissolved after 30 minutes. The mixture was filtered and concentrated. Colorless plates of **5** were obtained in 56% yield at low temperature. The ^{1}H NMR spectrum of **5** shows two singlets (δ = 1.15 and δ = 3.23 ppm) for the protons of the methyl groups of the carbene ligand. They are shifted upfield relative to the free carbene 1,3,4,5-tetramethylimidazole-2-ylidene (δ = 1.59 and δ = 3.35 ppm). No resonances for an imidazolium salt were detected. A weak and broad ^{13}C NMR resonance (δ = 154 ppm) can be assigned to the carbene carbon atom. The ^{27}Al NMR spectrum shows a resonance at δ = 103 ppm, which is typical for four-coordinate aluminum and in the region of the resonances for hydride derivatives. EI mass spectrometry presents a molecular ion peak at *m*/*z* = 256 in the correct isotopic pattern and free 1,3,4,5-tetramethylimidazole-2-ylidene as the base peak. Compound **5** crystallizes with half a molecule of toluene in the triclinic space group $P\bar{1}$. It exhibits the expected assembly (see Figure 1), and selected bond lengths and angles are given in Table 1. The Al−C distance in **5** is 2.009(5) Å, which is shorter than the corresponding bond length in the adduct of 1,3,4,5-tetra-

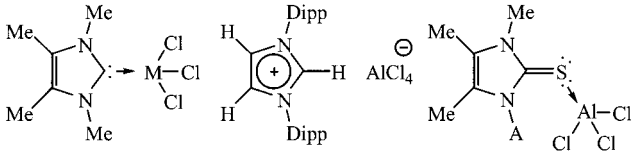

M = Al **5**
= Ga **6**

7

8

 © 2004 Wiley-VCH Verlag GmbH & Co. KGaA, Weinheim **DOI: 10.1002/ejic.200400247**

methylimidazole-2-ylidene with $Al(C{\equiv}CtBu)_3$ [2.051(2) Å].[11]

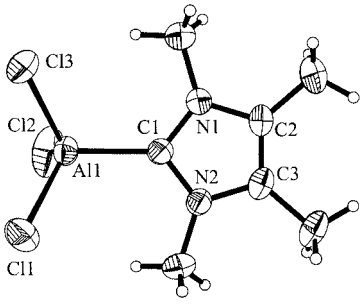

Figure 1. Crystal structure of **5**·0.5C_7H_8; toluene omitted for clarity

Table 1. Selected bond lengths (Å) and angles (°) of **5**·0.5C_7H_8

Al1−C1	2.009(5)	Al1−Cl1	2.134(4)
Al1−Cl2	2.121(5)	Al1−Cl3	2.131(3)
N1−C1	1.352(5)	N1−C2	1.392(5)
N2−C1	1.353(5)	N2−C3	1.387(5)
C2−C3	1.343(6)		
C1−Al1−Cl1	111.1(2)	Cl2−Al1−Cl1	110.43(17)
N2−C1−N1	104.8(3)	C3−C2−N1	106.9(4)

The gallium analogue of **5** could be prepared and crystallized by a comparable method in 62% yield. Due to the dimeric nature of $GaCl_3$ and its good solubility in hydrocarbon solvents, in contrast to polymeric $AlCl_3$ in the solid state, $GaCl_3$ was cooled with liquid nitrogen while a solution of 1,3,4,5-tetramethylimidazole-2-ylidene in toluene was added, and the mixture was slowly warmed to room temperature. No single crystals were obtained for **6** but the ^{1}H NMR spectrum shows a ratio of ca.1:0.70 ratio of **6** and toluene. The $GaCl_3$ adduct **6** is less soluble than **5**. The resonances for the methyl groups (δ = 1.05 and 3.19 ppm) are in the region of the resonances for **5**. A resonance for the carbene carbon atom was not observed in the ^{13}C NMR spectrum, as seen before for comparable compounds.[7,9] The EI mass spectrum shows the molecular ion peak M^+ at *m*/*z* = 300 with the expected isotopic pattern as well as $M^+ - Cl$ at *m*/*z* = 265. A gallium triiodide adduct of a NHC was very recently prepared in our group from the corresponding hydride and was structurally characterized.[12] The computed M−C distance for the adduct of MCl_3 (M = Al, Ga) with diaminocarbene are 2.060 Å for Al and 2.079 Å for Ga.[13] These bond lengths are nearly identical. We also found a very similar bond length for the carbene adduct of $Ga(C{\equiv}CtBu)_3$ with 1,3,4,5-tetramethylimidazole-2-ylidene [2.057(3) Å][14] and the corresponding aluminum compound [2.051(2) Å, see above]. The Ga−C bond length in **3** is 1.978(10) Å.

The reaction of a bulky imidazolylidene with $AlCl_3$ in THF/toluene afforded the imidazolium salt **7**·THF in moderate yield (Figure 2). The very poorly soluble compound **7**·THF was characterized by an X-ray single-crystal structure determination. Selected bond lengths and angles are summarized in Table 2. Only the cationic species for the corresponding imidazolium salt could be detected in the FAB mass spectrum at (*m*/*z* = 389), and no peak for the tetrachloroaluminate anion was observed. However, the EI-mass spectrum of the salt shows the ions for the corresponding $AlCl_3$ carbene adduct with one chlorine less (*m*/*z* = 484) and with only one chlorine (*m*/*z* = 451) in the expected isotopic pattern. It is known that $AlCl_3$ dissociates in THF[15,16] and other donor solvents[17,18] to form donor-stabilized salts of the type $[AlCl_2(Do)_x][AlCl_4]$. Moreover, we assume that the hydrogen atoms in the backbone (here on C2 and C3) of the imidazolylidene are responsible for the protonation and the formation of the imidazolium salt.

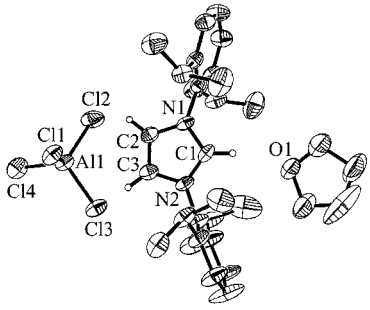

Figure 2. Crystal structure of **7**·THF; only hydrogen atoms on the imidazolium ring are shown

Table 2. Selected bond lengths (Å) and angles (°) of **7**·THF

Al1−Cl2	2.129(2)	Al1−Cl3	2.140(2)
C1−N1	1.334(6)	C1−N2	1.322(7)
N1−C2	1.379(7)	N2−C3	1.391(6)
Cl1−Al1−Cl2	109.34(10)	N2−C1−N1	108.6(4)

In a comparable route, 1,3,4,5-tetramethylimidazole-2(3*H*)-thione, which is a common starting material for the preparation of 1,3,4,5-tetramethylimidazole-2-ylidene by reduction with potassium in THF,[10] reacts with $AlCl_3$ in toluene to afford adduct **8** (Figure 3). The latter compound is less soluble than **5**. The ^{1}H NMR resonances of the ligand exhibit singlets at δ = 1.27 and δ = 3.12 ppm. Only the free thione was detected by EI mass spectrometry. Compound **8** crystallizes in the orthorhombic space group *Pbca*. Selected bond lengths and angles are given in Table 3. The Al−S bond length is 2.2661(13) Å. The C=S bond length

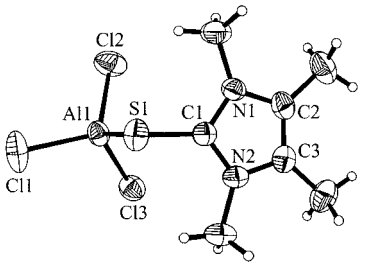

Figure 3. Crystal structure of **8**

 © 2004 Wiley-VCH Verlag GmbH & Co. KGaA, Weinheim

in the free thione [1.690(2) Å][19] is elongated upon coordination with $AlCl_3$ in **8** [1.739(3) Å] by nearly 0.05 Å. The $AlCl_3$ moiety is coordinated to one lone pair of the sulfur atom to give a C1−S1−Al1 angle of 98.79(9)°. The adduct **8** is a model compound for the activation of a carbonyl function by a Lewis acid.

Table 3. Selected bond lengths (Å) and angles (°) of **8**

Al1−Cl1	2.1242(12)	Al1−Cl2	2.1300(13)
Al1−Cl3	2.1318(12)	Al1−S1	2.2661(13)
S1−C1	1.739(3)	C1−N1	1.347(4)
C1−N2	1.338(4)	N1−C2	1.399(4)
N2−C3	1.391(4)	C2−C3	1.351(4)
Cl1−Al1−Cl2	113.48(6)	Cl3−Al1−S1	110.09(5)
C1−S1−Al1	98.79(9)	N1−C1−S1	125.7(2)
C3−C2−N1	106.9(2)	N2−C1−N1	107.4(2)

The N1−C1−N2 angle in the imidazole ring of **5** [104.8(3)°] lies between the corresponding angles of the free carbene 1,3,4,5-tetramethylimidazole-2-ylidene [101.3(2)° from X-ray, and 101.9(1)° and 102.0(1)° from neutron diffraction experiments on the perdeuterated compound][20] and that of an imidazolium salt [e.g. 108.6(4)° in **7**·THF]. These findings are in agreement with those of previously reported compounds.[1,2] For comparison, the N1−C1−N2 angle in **8** is 107.4(2)°.

In summary, we have prepared the first NHC adducts of an aluminum and a gallium trihalide, and report the first X-ray crystal structure of an aluminum halide carbene adduct. Moreover, an imidazolium tetrachloroaluminate and a thione adduct of $AlCl_3$ were also synthesized and structurally characterized.

Experimental Section

All manipulations were performed under a dry and oxygen-free atmosphere (N_2 or Ar) using Schlenk line and glove box techniques. Melting points are not corrected. X-ray single-crystal structure analyses were performed on a Stoe−Siemens four circle (**5**·0.5C_7H_8 and **8**) or a Stoe IPDS2 (**7**·THF) diffractometer with Mo-K_α radiation (λ = 0.71073 Å). The structures were solved by direct methods and refined with full-matrix least-squares on F^2 using SHELX-97.[21] Crystallographic data are summarized in Table 4. CCDC-234360 (**5**·0.5C_7H_8), -234361 (**7**·THF) and -234362 (**8**) contain the supplementary crystallographic data for this paper. These data can be obtained free of charge at www.ccdc.cam.ac.uk/conts/retrieving.html [or from the Cambridge Crystallographic Data Centre, 12 Union Road, Cambridge CB2 1EZ, UK; Fax: (internat.) +44-1223-336-033; E-mail: deposit@ccdc.cam.ac.uk].

Preparation of 5: Toluene (30 mL) was added at room temperature to a mixture of $AlCl_3$ (0.64 g, 4.80 mmol, 1.12 equiv.) and 1,3,4,5-tetramethylimidazole-2-ylidene[10] (0.55 g, 4.27 mmol, 1.0 equiv.). The mixture was stirred for 30 min, and the $AlCl_3$ dissolved. The mixture was filtered and concentrated in vacuo to 15 mL. A brown

Table 4. Crystallographic data

	5·0.5C_7H_8	**7**·THF	**8**
Formula	$C_{10.50}H_{16}AlCl_3N_2$	$C_{31}H_{45}AlCl_4N_2O$	$C_7H_{12}AlCl_3N_2S$
M	303.58	630.47	289.58
T	200(2) K	133(2) K	200(2) K
Crystal system	triclinic	triclinic	orthorhombic
Space group	$P\bar{1}$	$P\bar{1}$	$Pbca$
a (Å)	8.583(10)	9.937(3)	13.022(3)
b (Å)	8.903(10)	12.702(7)	13.368(4)
c (Å)	10.73(3)	14.265(5)	15.025(5)
α (°)	85.3(2)	82.85(3)	90
β (°)	79.20(6)	82.25(3)	90
γ (°)	68.57(7)	78.66(4)	90
V (nm^3)	0.75(1)	1.7404(12)	2.6155(12)
Z	2	2	8
$\delta_{calcd.}$ (Mg m^{-3})	1.344	1.203	1.471
μ (mm^{-1})	0.649	0.390	0.894
F(000)	314	668	1184
Crystal size (mm)	1.00 × 0.70 × 0.60	0.30 × 0.30 × 0.20	1.00 × 0.80 × 0.20
θ (°)	3.71−24.95	2.08−24.63	3.69−25.06
Index range	$-9 \le h \le 10$, $-10 \le k \le 10$, $-5 \le l \le 12$	$-11 \le h \le 11$, $-14 \le k \le 14$, $-16 \le l \le 16$	$-3 \le h \le 15$, $-15 \le k \le 15$, $-17 \le l \le 17$
Reflexes, collected/unique	3031/2600	32460/5821	3030/2295
R_{int}	0.0351	0.0948	0.0700
Completeness to θ (%)	99.0	99.0	99.5
Data/Restraints/Parameter	2600/265/170	5821/0/360	2295/0/132
Goodness-of-fit on F^2	1.103	1.010	1.049
R values [$I > 2\sigma(I)$]	$R_1 = 0.0726$, $wR_2 = 0.2270$	$R_1 = 0.0801$, $wR_2 = 0.1821$	$R_1 = 0.0540$, $wR_2 = 0.1348$
R values (all data)	$R_1 = 0.0757$, $wR_2 = 0.2314$	$R_1 = 0.1094$, $wR_2 = 0.1985$	$R_1 = 0.0584$, $wR_2 = 0.1411$
Largest diff. peak and hole [max and min] (e· Å^{-3})	1.483, −0.778	0.872, −0.408	0.737, −0.550

 © 2004 Wiley-VCH Verlag GmbH & Co. KGaA, Weinheim

oily by-product was also formed and could be separated off during filtration. The solution was stored for two weeks at −25 °C to give colorless crystals of **5**. Colorless plates of **5**·0.5C_7H_8 suitable for X-ray single-crystal structure analysis were obtained from a concentrated solution in toluene at 4 °C. The crystals were dried in vacuo. Yield 0.62 g (2.41 mmol, 56%). M.p. 130 °C. ^{1}H NMR (500 MHz, C_6D_6): δ = 1.15 (s, 6 H, NCH_3), 3.23 (s, 6 H, CCH_3) ppm. ^{13}C NMR (126 MHz, C_6D_6): δ = 7.9 [C(4,5)*C*H$_3$], 34.0 (N*C*H$_3$), 125.6 [*C*(4,5)], 154 (very broad, carbene-*C*) ppm. ^{27}Al NMR (78.2 MHz, C_6D_6): δ = 103 ppm. MS (EI): *m*/*z* = 256 [M^+, 3], 221 (M^+ − Cl, 13), 124 ($C_7H_{12}N_2$, 100). IR (Nujol, KBr plates): $\tilde{\nu}$ = 1643, 1580, 1207, 1100, 1031, 487 cm^{-1}. $C_7H_{12}AlCl_3N_2$·$C_{3.5}H_4$ (257.52): calcd. C 32.65, H 4.70, N 10.88; found C 33.11, H 4.65, N 10.67.

Preparation of 6: A solution of 1,3,4,5-tetramethylimidazole-2-ylidene (0.40 g, 3.23 mmol, 1.0 equiv.) in toluene (18 mL) was slowly added to cooled (−196 °C) $GaCl_3$ (0.57 g, 3.24 mmol, ca. 1.0 equiv.). The mixture was slowly warmed to room temperature while stirring, and stirring was continued for an additional 30 min at this temperature. The mixture was concentrated to about 12 mL, filtered, and stored at −25 °C to afford a colorless crystalline material of **6**·0.70C_7H_8. Small amounts of a brown oily by-product formed during the reaction could be separated during filtration. Yield 0.73 g (2.00 mmol, 62%) of **6**·0.70C_7H_8. M.p. approximately 110 °C. ^{1}H NMR (300 MHz, C_6D_6) [toluene resonances are not given]: δ = 1.05 (s, 6 H, NCH_3), 3.19 (s, 6 H, CCH_3) ppm. ^{13}C NMR (126 MHz, C_6D_6): δ = 7.6 [C(4,5)*C*H$_3$], 33.8 (N*C*H$_3$), 125.6 [*C*(4,5)] ppm. MS (EI): *m*/*z* = 300 [M^+, 1], 265 (M^+ − Cl, 25), 124 ($C_7H_{12}N_2$, 100). IR (Nujol, KBr plates): $\tilde{\nu}$ = 1645, 1261, 1093, 1031, 848, 800, 570, 370 cm^{-1}. $C_7H_{12}Cl_3GaN_2$·$C_{4.9}H_{5.6}$ (364.77): calcd. C 39.18, H 4.68, N 7.68; found C 38.98, H 4.65, N 7.50.

Preparation of 7: Toluene (50 mL) and THF (50 mL) were added to a mixture of $AlCl_3$ (0.56 g, 4.20 mmol, 1.1 equiv.) and 1,3-bis(2,6-diisopropylphenyl)imidazole-2-ylidene (1.47 g, 3.80 mmol, 1.0 equiv.). The mixture was stirred for 1 h and subsequently filtered. Yellow crystals of **7**·THF were obtained at 2 °C. Yield 0.98 g (1.56 mmol, 41%). M.p. 260 °C: ^{1}H NMR (300 MHz, CD_3OD) [THF resonances are not given]: δ = 1.22 [d, *J* = 6.9 Hz, 12 H, CH(CH_3)$_2$], 1.34 [d, *J* = 6.9 Hz, 12 H, CH(CH_3)$_2$], 2.45 [sept, *J* = 6.9 Hz, 4 H, C*H*(CH$_3$)$_2$], 7.50 (d, *J* = 7.6 Hz, 4 H, *m*-ArH), 7.67 (t, *J* = 7.6 Hz, 2 H, *p*-ArH), 8.27 (d, *J* = 2.5 Hz, 2 H, C*H*), 9.97 (t, *J* = 2.5 Hz, 1 H, N_2CH) ppm. ^{13}C NMR (126 MHz, CD_3OD): δ = 23.9, 24.7, 30.4, 126.0, 127.6, 131.5, 133.4, 141.1, 146.5 ppm. MS (EI): *m*/*z* = 484 [$AlCl_2C_3N_2H(Dipp)_2^+$, 15], 451 [$AlClC_3N_2H(Dipp)_2^+$, 2], 389 [$C_3N_2H_3(Dipp)_2^+$, 100]. MS (FAB) cations: *m*/*z* = 389 [$C_3N_2H_3(Dipp)_2^+$, 100]. IR (Nujol, KBr plates): $\tilde{\nu}$ = 1643, 1600, 1540, 1331, 1206, 1062, 953, 804, 756, 683, 616, 491 cm^{-1}. $C_{27}H_{37}AlCl_4N_2$·C_4H_8O (630.49): calcd. C 59.05, H 7.19, N 4.44; found C 58.55, H 7.03, N 4.68.

Preparation of 8: Toluene (25 mL) was added to a mixture of $AlCl_3$ (0.50 g, 3.75 mmol, 1.0 equiv.) and 1,3,4,5-tetramethylimidazole-2(3*H*)-thione[10] (0.585 g, 3.75 mmol, 1.0 equiv.), stirred for 15 h at room temperature, 30 min at 50 °C, and finally filtered at this temperature. Storing the solution at 4 °C afforded crystals of **8**. Yield 0.63 g (2.18 mmol, 58%). M.p. approximately 165 °C (decomposed; in general decomposition at temperatures above about 100 °C). ^{1}H NMR (300 MHz, C_6D_6): δ = 1.27 (s, 6 H, NCH_3), 3.12 (s, 6 H, CCH_3) ppm. ^{13}C NMR (126 MHz, C_6D_6): δ = 8.4, 31.5, 120.1, 161.6 ppm. MS (EI): *m*/*z* = 156 [{MeCCN(Me)}$_2$C=S, 100]. IR (Nujol, KBr plates): $\tilde{\nu}$ = 1639, 1262, 1100, 1020, 801, 612 cm^{-1}. $C_7H_{12}AlCl_3N_2S$ (289.59): calcd. C 29.03, H 4.18, N 9.67; found C 28.70, H 4.22, N 9.44.

Acknowledgments

This work was supported by the Deutsche Forschungsgemeinschaft and the Göttinger Akademie der Wissenschaften.

[1] Stable Carbenes: D. Bourissou, O. Guerret, F. P. Gabbaï, G. Bertrand, *Chem. Rev.* **2000**, *100*, 39−91.
[2] Main Group Complexes: C. J. Carmalt, A. H. Cowley, *Adv. Inorg. Chem.* **2000**, *50*, 1−32.
[3] A. J. Arduengo III, H. V. Rasika Dias, J. C. Calabrese, F. Davidson, *J. Am. Chem. Soc.* **1992**, *114*, 9724−9725.
[4] C. L. Raston, *J. Organomet. Chem.* **1994**, *475*, 15−24.
[5] C. D. Abernethy, M. L. Cole, C. Jones, *Organometallics* **2000**, *19*, 4852−4857.
[6] M. D. Francis, D. E. Hibbs, M. B. Hursthouse, C. Jones, N. A. Smithies, *J. Chem. Soc., Dalton Trans.* **1998**, 3249−3254.
[7] R. J. Baker, M. L. Cole, C. Jones, M. F. Mahon, *J. Chem. Soc., Dalton Trans.* **2002**, 1992−1996.
[8] A. H. Cowley, F. P. Gabbaï, C. J. Carrano, L. M. Mokry, M. R. Bond, G. Bertrand, *Angew. Chem.* **1994**, *106*, 584−586; *Angew. Chem. Int. Ed. Engl.* **1994**, *33*, 578−580.
[9] S. J. Black, D. E. Hibbs, M. B. Hursthouse, C. Jones, K. M. A. Malik, N. A. Smithies, *J. Chem. Soc., Dalton Trans.* **1997**, 4313−4319.
[10] N. Kuhn, T. Kratz, *Synthesis* **1993**, 561−562.
[11] M. Schiefer, N. D. Reddy, H.-J. Ahn, A. Stasch, H. W. Roesky, A. C. Schlicker, H.-G. Schmidt, M. Noltemeyer, *Inorg. Chem.* **2003**, *42*, 4970−4976.
[12] H.-J. Ahn, H. W. Roesky, M. Noltemeyer, H.-G. Schmidt, unpublished results.
[13] A. Beste, O. Krämer, A. Gerhard, G. Frenking, *Eur. J. Inorg. Chem.* **1999**, 2037−2045.
[14] A. Stasch, H. W. Roesky, A. C. Schlicker, unpublished results.
[15] J. Derouault, M. T. Forel, *Inorg. Chem.* **1977**, *16*, 3207−3113.
[16] J. Derouault, P. Granger, M. T. Forel, *Inorg. Chem.* **1977**, *16*, 3214−3118.
[17] P. Pullmann, K. Hensen, J. W. Bats, *Z. Naturforsch., Teil B* **1982**, *37*, 1312−1315.
[18] M. Dalibart, J. Derouault, P. Granger, *Inorg. Chem.* **1982**, *21*, 2241−2246.
[19] N. Kuhn, J. Fahl, R. Fawzi, M. Steinmann, *Z. Krist. New Cryst. Struct.* **1998**, *213*, 434.
[20] A. J. Arduengo III, H. V. R. Dias, D. A. Dixon, R. L. Harlow, W. T. Klooster, T. F. Koetzle, *J. Am. Chem. Soc.* **1994**, *116*, 6812−6822.
[21] G. M. Sheldrick, *SHELXL-97, Program for Crystal Structure Refinement*, University of Göttingen, Germany, **1997**.

Received March 29, 2004
Early View Article
Published Online August 3, 2004

 © 2004 Wiley-VCH Verlag GmbH & Co. KGaA, Weinheim

Methyl Substitution of Aluminum−Hydride Bonds in a Carbaalane and an Aluminum Imide

Andreas Stasch,[a] S. Shravan Kumar,[a] Vojtech Jancik,[a] Herbert W. Roesky,*[a] Jörg Magull,[a] and Mathias Noltemeyer[a]

Keywords: Aluminum / Cluster Compounds / Hydrides

The methylated compounds $[(AlMe)_6(AlNMe_3)_2(CCH_2Ph)_6]$ (**4**), $[(AlMe)_6(AlNMe_3)_2(CCH_2CH_2SiMe_3)_6]$ (**5**) and $[(AlMe)_6(NCH_2C_4H_3S)_6]$ (**6**) were synthesized in good yields from the corresponding hydride derivatives by treatment with $AlMe_3$ in toluene. The X-ray single crystal structures of **4**·xC_7H_8, **4**·4C_7H_8 and **6** were determined. In **4**·xC_7H_8 the solvent molecules are arranged in infinite channels along the *c* axis.
(© Wiley-VCH Verlag GmbH & Co. KGaA, 69451 Weinheim, Germany, 2004)

The chemistry of carbaalanes and aluminum imide (or iminoalane) cage compounds is growing rapidly. After the synthesis of the cluster cores their derivatisation is an attractive goal for synthetic chemists. The aluminum−hydride bonds in the hydroalumination products can be converted into other functionalities. Recently, we have used various reagents to substitute the hydrides in the carbaalane $[(AlH)_6(AlNMe_3)_2(CCH_2R)_6]$ (R = Ph **1**, CH_2SiMe_3 **2**) and in the aluminum imide $[(AlH)_6(NCH_2C_4H_3S)_6]$ (**3**) to yield halogen and alkynyl derivatives.[1−6] Herein we report further attempts to substitute the hydrides by methyl groups.

Initial investigations were carried out with protic reagents such as alcohols and secondary amines. The reaction of **1** with six equivalents of isopropanol results in the formation of impure compounds and decomposition of the cluster. The reaction of **1** with six equivalents of R_2NH (R = Et, $SiMe_3$) in toluene gave no gas evolution either at room temperature or upon heating the mixture to its boiling point; crystals of **1** were recovered from the reaction mixture. Similar reactions were undertaken with **3**. Again, reactions with alcohols led to decomposition of the cage and amines did not properly react with the hydrides. A partial substitution of **1**, however, was achieved with a protic reagent: ethynylferrocene reacted at elevated temperatures leading to the formation of terminal alkynyl-substituted products.[3]

Bis(trimethylsilyl) ether $[(Me_3Si)_2O]$ reacts with neat iBu_2AlH under reflux conditions to form $(Me_3SiOAliBu_2)_2$, while $AlH_3{\cdot}NMe_3$ does not react under these conditions.[7] However, we found no reaction or significant solubility of **1** in neat boiling $(Me_3Si)_2O$ (b.p. 101 °C). $AlH_3{\cdot}NMe_3$ forms the soluble aluminum sulfide compounds $[(Me_3NAl)_4S_6]$ and $[(Me_3NAl)_2(Me_3NAlH)_2S_5]$ upon reaction with $(Me_3Si)_2S$ in hot toluene.[8] Treatment of **1** with an excess (ca. 18 equiv.) of $(Me_3Si)_2S$ in boiling toluene for one day, and subsequent workup, afforded crystals of the starting material in moderate yield. Moreover, $(Me_3Si)_2$ did not react with **1** under similar conditions and crystals of **1** were again recovered. No reaction of $(Me_3Si)_2$ with iBu_2AlH has been reported.[9]

When a suspension of **1** in toluene is treated with an excess of $AlMe_3$ at room temperature the solubility improves, and after several hours of stirring the precipitate that forms is converted into fine, colorless, needle- or rod-shaped crystals. Filtering off these crystals and storing the solution at 4 °C afforded additional crystals of the same shape. The X-ray single crystal structure analysis showed these to be the expected compound $[(AlMe)_6(AlNMe_3)_2(CCH_2Ph)_6]$ (**4**) with toluene. Crystals of $[(AlMe)_6(AlNMe_3)_2(CCH_2Ph)_6]{\cdot}4C_7H_8$ (**4**) 4C_7H_8) were obtained at −25 °C from the supernatant solution. The reaction of **2** with $AlMe_3$ for four hours afforded $[(AlMe)_6(AlNMe_3)_2(CCH_2CH_2SiMe_3)_6]$ (**5**) in good purity after removal of all volatiles at 50 °C in vacuo (Scheme 1).

In the same manner, the hexameric aluminum imide $[(AlH)_6(NCH_2C_4H_3S)_6]$ **3** was treated with $AlMe_3$ in toluene at room temperature to yield the methylated species $[(AlMe)_6(NCH_2C_4H_3S)_6]$ (**6**). The reaction of **3** with diethylzinc in THF/toluene at room temperature gave $[(AlEt)_6(NCH_2C_4H_3S)_6]$ (**7**), where the hydrides have been substituted by ethyl groups; no coordination of diethylzinc to the thiophenyl groups was found. The substitution of the hydridic hydrogens of hexameric aluminum imides, prepared from aluminum hydrides and primary amines, was first reported in the 1970s. Partially and fully alkylated

[a] Institut für Anorganische Chemie der Georg-August-Universität Göttingen,
Tammannstrasse 4, 37077 Göttingen, Germany
Fax: + 49-551-393-373
E-mail: hroesky@gwdg.de

 © 2004 Wiley-VCH Verlag GmbH & Co. KGaA, Weinheim **DOI: 10.1002/ejic.200400347**

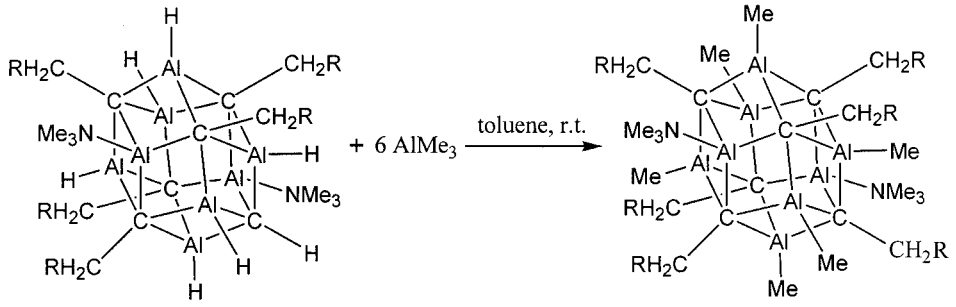

1 R = Ph
2 R = CH_2SiMe_3

4 R = Ph
5 R = CH_2SiMe_3

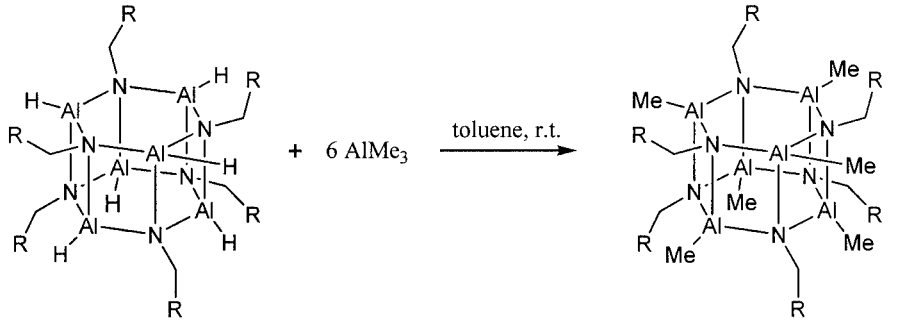

3 R = C_4H_3S

6 R = C_4H_3S

Scheme 1

species were isolated from reactions with AlR_3 (R = Me, Et) giving rise to **6** and **7**, which were not structurally characterized.[10] Only substitution and no degradation of the cage or cluster structures is observed upon treatment with AlR_3 (R = Me, Et) in these reactions. Methyl-substituted aluminum imides prepared from primary amines and $AlMe_3$ at elevated temperatures often show different degrees of oligomerization depending on the size of the organic groups.[11] A prominent example is the planar alumazene.[12]

The first crystals of compound **4** with toluene crystallize in the trigonal space group $R\bar{3}$. The solvent molecules (toluene) are disordered and are located in channels along the *c* axis that are only partially occupied and could not be successfully refined. The packing of **4** is shown in Figure 1. The width of the channels is about 12.2 Å (calculated from the centers of the atoms), which is approximately the size of **4**. A similar packing was found in the crystal structure of an iron compound with seven hexane molecules within the channel.[13] Compound **4**·$4C_7H_8$ crystallizes at −25 °C in the monoclinic space group *C*2/*c* with one half of a molecule and two molecules of toluene in the asymmetric unit (Figure 2 and Table 1). Compound **6** crystallizes in the triclinic space group $P\bar{1}$ with half a molecule in the asymmetric unit (Figure 3 and Table 2). One thiophenyl group is distorted and two positions of the thiophene ring were refined for S(1). The basic structure of the new compounds is

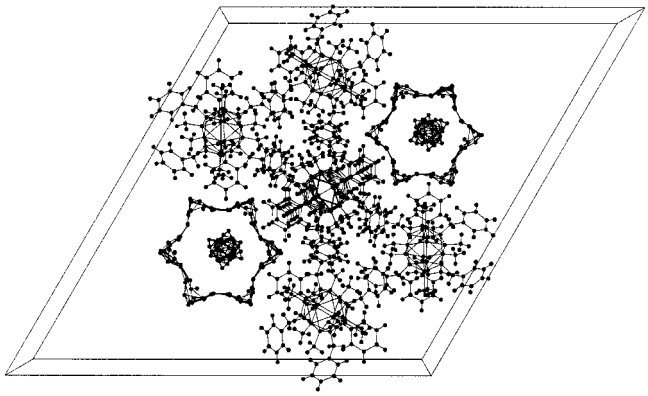

Figure 1. Packing diagram of **4**·xC_7H_8; perspective view along the *c* axis; the disordered solvent molecules are pictured as simple dots; the centers of the channels are located on the C_3 axes

nearly identical to their starting materials. The Al−C bond lengths for the methyl groups range from 1.973(2) Å to 1.976(2) Å in **4**·$4C_7H_8$ and 1.937(4) Å to 1.978(5) Å in **6**. For comparison, the Al−C bond lengths in the cluster **4** are longer [from 2.036(2) Å to 2.118(2) Å] than the single bonds of the methyl groups to aluminum.

Compound **4** is only poorly soluble and no NMR spectra of sufficient quality could be recorded. The EI mass spectrum only shows C−H fragments. The methyl groups of **5** appear as a singlet in the ^1H NMR spectrum (δ = 0.2 ppm).

 © 2004 Wiley-VCH Verlag GmbH & Co. KGaA, Weinheim

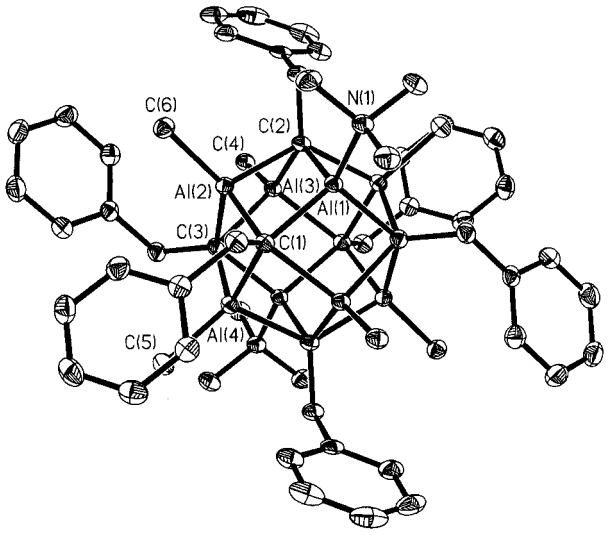

Figure 2. Molecular structure of **4**·4C_7H_8; hydrogen atoms and solvent molecules are omitted for clarity

Table 1. Selected bond lengths (Å) and angles (°) for **4**·4C_7H_8

Al(1)−N(1)	2.008(1)	Al(2)−C(6)	1.973(2)
Al(1)−C(2)	2.036(2)	Al(2)−C(2)	2.117(2)
Al(1)−Al(32)	2.585(1)	Al(3)−Al(2)	2.667(1)
C(6)−Al(2)−C(3)	129.4(1)	C(6)−Al(2)−C(1)	113.5(1)
C(6)−Al(2)−C(2)	112.4(1)	C(4)−Al(3)−C(2)	130.8(1)
C(4)−Al(3)−C(3)	112.4(1)	C(4)−Al(3)−C(3)	112.0(1)

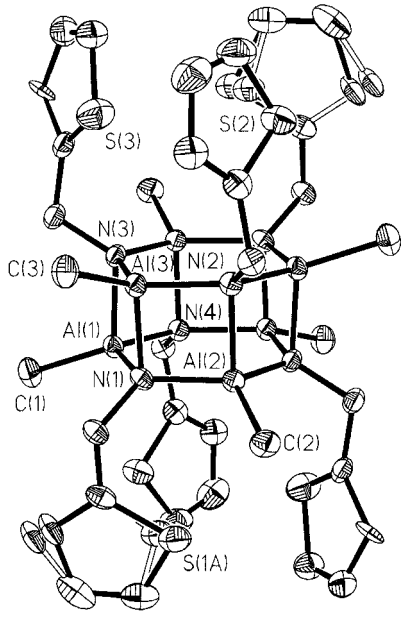

Figure 3. Molecular structure of **6**; hydrogen atoms are omitted for clarity

The cluster carbon atoms resonate at δ = 20.3 ppm in the ^{13}C NMR spectrum and a broad singlet (δ = 155.4 ppm) is observed in the ^{27}Al NMR spectrum of **5**. In general, the NMR resonances of **5** are shifted downfield compared to the starting material **2** and its halogen derivatives, except for the cluster carbon atoms in the ^{13}C NMR spectrum.

Table 2. Selected bond lengths (Å) and angles (°) for **6**

Al(1)−N(1)	1.886(4)	Al(1)−N(3)	1.986(3)
Al(1)−C(1)	1.978(5)	Al(2)−N(1)	1.877(3)
Al(2)−N(2)	1.982(3)	Al(2)−C(2)	1.937(4)
Al(3)−N(3)	1.879(3)	Al(3)−N(1)	1.986(3)
Al(3)−C(3)	1.94(1)		
N(4)−Al(1)−N(1)	113.8(2)	N(1)−Al(1)−N(3)	91.3(2)
N(1)−Al(1)−C(1)	119.3(2)	N(1)−Al(1)−C(1)	119.6(2)

The EI mass spectrum provides a molecular ion peak at m/z = 1102.6 for **5**. The singlet resonance for the protons of the methyl groups in the ^1H NMR spectrum of **6** is at δ = −0.52 ppm and is not shifted as far downfield as that for **5**. The NMR resonances are in agreement with the observed composition. The EI mass spectrum provides no molecular ion peak for **6**, although an ion corresponding to [$M^+ - CH_4$] was observed at m/z = 903.

In conclusion, the cluster cores of both the carbaalane and aluminum imide containing reactive Al−H bonds can be effectively replaced by methyl groups upon reaction with $AlMe_3$.

Experimental Section

General Remarks: All manipulations were performed under a dry and oxygen-free atmosphere (N_2 or Ar) using Schlenk-line and glove-box techniques. The samples for spectral measurements were prepared in a dry box. Solvents were purified according to conventional procedures and were freshly distilled prior to use. NMR spectra were recorded on a Bruker AM 200 instrument, and the chemical shifts are reported with reference to TMS. IR spectra were recorded on a Bio-Rad Digilab FTS7 spectrometer. Melting points were obtained on a HWS−SG 3000 apparatus and are uncorrected. CHN analyses were performed at the Analytical Laboratory of the Institute of Inorganic Chemistry at Göttingen, Germany.

Synthesis of [(AlMe)$_6$(AlNMe$_3$)$_2$(CCH$_2$Ph)$_6$] (4): $AlMe_3$ (1.90 mL of a 2.0 M solution in toluene, 3.80 mmol, 20 equiv.) was added to a fine suspension of **1** (0.18 g, 0.188 mmol, 1.0 equiv.) in toluene (20 mL). The mixture was stirred for 15 h during which time the solid turned into fine crystals. After filtration, additional needle- or rod-shaped crystals with of **4**·xC_7H_8 were obtained at 4 °C. Storing the supernatant solution at −25 °C gave crystals of **4**·4C_7H_8. The crystals were dried in vacuo. Yield 0.17 g (0.16 mmol, 87%). M.p.: ca. 240 °C (decomposition). IR (Nujol, KBr plates): $\tilde{\nu}$ = 1653, 1262, 1100, 971, 810, 750, 574 cm^{-1}. $C_{60}H_{78}Al_8N_2$ (1043.13): calcd. C 69.08, H 7.54, N 2.69; found 67.83, H 7.58, N 2.85.

Synthesis of [(AlMe)$_6$(AlNMe$_3$)$_2$(CCH$_2$CH$_2$SiMe$_3$)$_6$] (5): $AlMe_3$ (1.00 mL of a 2.0 M solution in toluene, 2.00 mmol, 15.6 equiv.) was added to a solution of **2** (0.13 g, 0.128 mmol, 1.0 equiv.) in toluene (5 mL). The solution was stirred for 4 h, all volatiles were removed in vacuo and the crude product was dried at 50 °C in vacuo giving **5** in a quantitative yield possibly admixed with a little Me_2AlH. M.p.: 210 °C (color change), 246 °C (full decomposition). ^1H NMR (300 MHz, C_6D_6): δ = 0.10 [s, 54 H, Si(CH_3)$_3$], 0.2 (br. s, 18 H, AlCH_3), 1.00 (ddd, J = 9.0, 4.1, 4.1 Hz, 12 H, Me_3SiCH_2), 2.16 (ddd, J = 9.0, 4.1, 4.1 Hz, 12 H, CCH_2), 2.17 [s, 18 H, N(CH_3)$_3$] ppm. ^{13}C NMR (126 MHz, C_6D_6): δ = −4.1 (broad, AlCH_3), −1.63 [Si(CH_3)$_3$], 20.3 (cluster-*C*), 25.9 (Me_3SiCH_2), 27.9

 © 2004 Wiley-VCH Verlag GmbH & Co. KGaA, Weinheim

(CH_2C), 46.9 [N(CH_3)$_3$] ppm. ^{27}Al NMR (78.2 MHz, C_6D_6): δ = 155.4 (s, very broad) ppm. ^{29}Si NMR (99.4 MHz, CD): δ = −0.82 ppm. MS (EI): *m*/*z* (%) = 1102.6 (3) [M^+], 1043.5 (48) [M^+ − NMe], 998.5 (71) [M^+ − NMe − NHMe], 984.5 (100) [M^+ − 2NMe]. IR (Nujol, KBr plates): $\tilde{\nu}$ = 1318, 1258, 1182, 1022, 862, 828, 763, 723, 672, 593, 485 cm^{-1}. $C_{48}H_{114}Al_8N_2Si_6$ (1103.80): calcd. C 52.23, H 10.41, N 2.54; found C 51.98, H 10.34, N 2.61.

Synthesis of [(AlMe)$_6$(NCH$_2$C$_4$H$_3$S)$_6$] (6): $AlMe_3$ (2.7 mL of a 2.0 M solution in heptane, 5.40 mmol, 9.0 equiv.) was added dropwise to a solution of **3** (0.50 g, 0.60 mmol, 1.0 equiv.) in toluene (20 mL). The resultant mixture was stirred overnight at room temperature and filtered. The filtrate was reduced to 20 mL in vacuo and stored at 0 °C for several days to obtain colorless crystals of **6** (0.40 g, 0.435 mmol, 73%). M.p.: 246 °C (decomposition). ^{1}H NMR (200 MHz, $CDCl_3$, 25 °C, TMS): δ = −0.52 (s, 18 H, AlCH_3), 4.28 (s, 12 H, NCH_2), 6.70, 6.80, 7.20 (m, 18 H, C_4H_3S) ppm. ^{13}C NMR (125 MHz, $CDCl_3$, 25 °C, TMS): δ = −7.2 (Al−CH_3), 43.5 (NCH_2), 123.7, 124.9, 127.5, 148.3 (C_4H_3S) ppm. IR (nujol, NaCl plates): $\tilde{\nu}$= 1340 (m), 1254 (m), 1210 (s), 1167 (w), 1059 (w), 1014 (s), 980 (s), 965 (s), 943 (s), 848 (s), 747 (s), 734 (s), 683 (s) cm^{-1}. EI-MS: *m*/*z* (%) = 903 (100) [M^+ − CH_4], 835 (8) [$C_{30}H_{36}Al_6N_6S_6^+$], 113 (52) [$CH_2C_4H_3SNH_2^+$], 97 (72) [$CH_2C_4H_3S^+$]. $C_{36}H_{48}Al_6N_6S_6$ (919.04): calcd. C 47.05, H 5.26, N 9.14; found C 46.53, H 4.89, N 8.96.

X-ray Structure Determination of 4·4C$_7$H$_8$, 4·*x*C$_7$H$_8$ and 6: A suitable crystal of each compound was mounted on a glass fiber and coated with paraffin oil. Diffraction data for **4**·4C_7H_8 were collected on SMART instrument, and for **4**·*x*C_7H_8 and **6** the data were collected on a STOE IPDS2 diffractometer. The structures were solved by direct methods and refined with full-matrix least-squares on F^2 using SHELX-97.[14,15] All non-hydrogen atoms were refined anisotropically. Neutral-atom scattering factors (including anomalous scattering) were taken from the International Tables for X-ray Crystallography.[16] Hydrogen atoms were included at geometrically calculated positions and refined using a riding model. The restraints in **4**·4C_7H_8 are due to the distortions of the toluene molecules and in **6** the quality of the data is not as good as expected due to the breakdown of the low-temperature equipment and disorder in one of the thiophenyl groups. The crystallographic data is summarized in Table 3.

CCDC-237048 (for **4**·*x*C_7H_8), -237049 (for **4**·4C_7H_8) and -237050 (for **6**) contain the supplementary crystallographic data for this paper. These data can be obtained free of charge at www.ccdc.cam.ac.uk/conts/retrieving.html [or from the Cambridge Crystallographic Data Centre, 12 Union Road, Cambridge CB2 1EZ, UK [Fax: +44-1223-336-033; E-mail: deposit@ccdc.cam.ac.uk].

Acknowledgments

Financial support by the Deutsche Forschungsgemeinschaft and the Göttinger Akademie der Wissenschaften is gratefully acknowledged.

[1] A. Stasch, M. Ferbinteanu, J. Prust, W. Zheng, F. Cimpoesu, H. W. Roesky, J. Magull, H.-G. Schmidt, M. Noltemeyer, *J. Am. Chem. Soc.* **2002**, *124*, 5441−5448.
[2] A. Stasch, H. W. Roesky, D. Vidovic, J. Magull, H.-G. Schmidt, M. Noltemeyer, *Inorg. Chem.* **2004** *43*, 3625−3630.

Table 3. Crystal data and refinement details. Compound **4**·xC_7H_8 was refined without the solvent molecules

Compound	**4**·*x*C_7H_8	**4**·4C_7H_8	**6**
Empirical formula	$C_{60}H_{78}Al_8N_2$	$C_{88}H_{110}Al_8N_2$	$C_{36}H_{48}Al_6N_6S_6$
Molecular mass	1043.08	1411.62	919.04
T	133(2) K	100(2) K	133(2) K
Wavelength	0.71073 Å	1.54178 Å	0.71073 Å
Crystal system	trigonal	monoclinic	triclinic
Space group	$R\bar{3}$	*C*2/*c*	$P\bar{1}$
Unit cell dimensions	*a* = 40.445(6) Å	*a* = 25.468(5) Å	*a* = 10.347(9) Å
	b = 40.445(6) Å	*b* = 15.899(3) Å	*b* = 10.284(9) Å
	c = 11.670(2) Å	*c* = 23.256(5) Å	*c* = 10.955(9) Å
	α = 90°	*α* = 90°	*α* = 99.537(7)°
	β = 90°	*β* = 122.69(3)°	*β* = 100.632(7)°
	γ = 120°	*γ* = 90°	*γ* = 101.027(7)°
V	16530(10) Å^3	7925(3) Å^3	1099.99(16) Å^3
Z	9	4	1
D_{calcd}	0.943 Mg/m^3	1.183 Mg/m^3	1.387 Mg/m^3
μ	0.142 mm^{-1}	1.317 mm^{-1}	0.466 mm^{-1}
F(000)	5004	3024	480
Crystal size	0.30 × 0.20 × 0.10 mm^3	0.10 × 0.10 × 0.05 mm^3	0.20 × 0.20 × 0.10 mm^3
θ	1.74 to 24.76°	3.46 to 59.06°	1.93 to 25.08°
Index range	−47 ≤ *h* ≤ 47	−27 ≤ *h* ≤ 28	−12 ≤ *h* ≤ 11
	−47 ≤ *k* ≤ 45	−17 ≤ *k* ≤ 17	−11 ≤ *k* ≤ 12
	−13 ≤ *l* ≤ 13	−25 ≤ *l* ≤ 25	−12 ≤ *l* ≤ 12
Reflexes collected/unique	57395/6280	17157/5549	6421/3579
Completeness to θ	99.7%	96.9%	91.5%
R_{int}	0.2439	0.0246	0.0431
Data/restraints/parameters	6280/0/357	5549/92/484	3579/0/254
Goodness-of-fit on F^2	1.035	1.051	1.046
R values [$I > 2\sigma(I)$]	R_1 = 0.0873, wR_2 = 0.1747	R_1 = 0.0281, wR_2 = 0.0746	R_1 = 0.0589, wR_2 = 0.1574
R values (all data)	R_1 = 0.1501, wR_2 = 0.2267	R_1 = 0.0310, wR_2 = 0.0766	R_1 = 0.0745, wR_2 = 0.1693
Largest diff. peak and hole (max and min)	0.704 and −0.485 e·Å^{-3}	0.232 and −0.190 e·Å^{-3}	0.883 and −0.738 e·Å^{-3}

 © 2004 Wiley-VCH Verlag GmbH & Co. KGaA, Weinheim

[3] S. S. Kumar, J. Rong, S. Singh, H. W. Roesky, D. Vidovic, J. Magull, D. Neculai, V. Chandrasekhar, M. Baldus, *Organometallics* **2004**, *23*, 3496−3500.
[4] N. D. Reddy, H. W. Roesky, M. Noltemeyer, H.-G. Schmidt, *Inorg. Chem.* **2002**, *41*, 2374−2378.
[5] S. S. Kumar, N. D. Reddy, H. W. Roesky, D. Vidovic, J. Magull, R. F. Winter, *Organometallics* **2003**, *22*, 3348−3350.
[6] N. D. Reddy, S. S. Kumar, H. W. Roesky, D. Vidovic, J. Magull, M. Noltemeyer, H.-G. Schmidt, *Eur. J. Inorg. Chem.* **2003**, 442−448.
[7] C. Rennekamp, H. Wessel, H. W. Roesky, P. Müller, H.-G. Schmidt, M. Noltemeyer, I. Uson, A. R. Barron, *Inorg. Chem.* **1999**, *38*, 5235−5240.
[8] R. J. Wehmschulte, P. P. Power, *J. Am. Chem. Soc.* **1997**, *119*, 9566−9567.
[9] C. Rennekamp, *Dissertation*, University of Göttingen, **1999**.
[10] S. Cucinella, T. Salvatori, C. Busetto, M. Cesari, *J. Organomet. Chem.* **1976**, *121*, 137−147.
[11] K. M. Waggoner, P. P. Power, *J. Am. Chem. Soc.* **1991**, *113*, 3385−3393.
[12] K. M. Waggoner, H. Hope, P. P. Power, *Angew. Chem.* **1988**, *100*, 1765−1766; *Angew. Chem. Int. Ed. Engl.* **1988**, *27*, 1699−1700.
[13] Rhombohedral space group $R\bar{3}$: S. Doherty, M. R. J. Elsegood, W. Clegg, D. Mampe, *Organometallics* **1997**, *16*, 1186−1192.
[14] G. M. Sheldrick, *Acta Crystallgr., Sect. A* **1990**, *46*, 467−473.
[15] G. M. Sheldrick, SHELXL-97, *Program for Crystal Structure Refinement*, University of Göttingen, Germany, **1997**.
[16] *International Tables for X-ray Crystallography*, Kynoch Press, Birmingham, England, **1969**; Vol. IV, p. 55, 99, 149.

Received April 29, 2004
Early View Article
Published Online August 13, 2004

 © 2004 Wiley-VCH Verlag GmbH & Co. KGaA, Weinheim

Dinuclear Zn^{II} Complexes of Polydentate Polyamines as Minimalist Models of Hydrolytic Reactions

Juan Aguilar,[a] Andrea Bencini,*[b] Emanuela Berni,[b] Antonio Bianchi,*[b] Enrique García-España,*[a] Laura Gil,[a] Angel Mendoza,[c] Lena Ruiz-Ramírez,[c] and Conxa Soriano[a]

Keywords: Enzyme models / Hydrolysis / Macrocycles / N ligands / NMR spectroscopy / Zinc

The synthesis of the novel macrocycle 2,6,9,12,16-pentaaza-[17](2,9)(1,10)phenanthrolinophane (L3) is reported. Speciation studies on the systems Zn^{II}–L3 and Zn^{II}–L2 (L2 = 2,6,10,13,17,21-hexaaza[22]metacyclophane) performed in aqueous solution show the formation of mono- and dinuclear Zn^{II} complexes. In the two systems, the dinuclear complexes readily hydroxylate, with the hydroxo species being the main ones in solution at relatively low pH values. This feature makes these complexes promising hydrolytic agents for carboxy and phosphate esters. The hydrolytic ability of the L1–L3 dinuclear complexes toward the carboxy and phosphate ester bond was tested by addition of *p*-nitrophenyl acetate (NA) and bis(*p*-nitrophenyl)phosphate (BNP). While in the case of NA the cleavage takes place through a simple bimolecular mechanism and the hydrolysis rate depends on the nucleophilicity of the Zn^{II}–OH functions, in the case of BNP the hydrolytic mechanism involves substrate interaction with the metal ions and nucleophilic attack of a Zn^{II}-bound hydroxide ion at the phosphorus atom. The L3 complex gives rise to the highest hydrolysis rate constant {$k = 62 \times 10^{-5}$ $M^{-1}\cdot s^{-1}$ vs. $k = 8 \times 10^{-5}$ and 4×10^{-5} $M^{-1}\cdot s^{-1}$ for $[Zn_2L2(OH)_2]^{2+}$ and $[Zn_2L1(OH)_2]^{2+}$, respectively}. This may be related to a stronger interaction with the substrate due to the synergetic role in BNP binding played by the phenanthroline unit, which can give π-stacking and hydrophobic interactions with the aromatic units of the substrate, and by the two Zn^{II} ions, which can act cooperatively in BNP coordination.

(© Wiley-VCH Verlag GmbH & Co. KGaA, 69451 Weinheim, Germany, 2004)

Introduction

A model compound of a metalloprotein can be defined as a structurally simpler metal complex, without the protein ligand, that is able to reproduce key features of its active center and/or its spectroscopic properties and/or its biochemical function. In this respect, throughout the last few years a great deal of experimental work has been addressed to the development of Zn^{II} complexes with unsaturated coordination spheres able to mimic features of the active site of Zn^{II} hydrolases.[1–23] Many of these enzymes use two Zn^{II} centers for the activation of the substrate and very often the nucleophile is a hydroxy group generated from deprotonation of a coordinated water molecule.[22,23] The right compromise between the thermodynamic stability of the complex and its rapid dynamic reorganization following the mechanism of the reaction, the hydrophilic/hydrophobic balance of the environment, the possibility of formation of hydrogen bonds with the substrate, and the presence of noncoordinated basic groups that can assist the process are other factors that influence the catalytic activity.

Macrocyclic structures are very appealing for the construction of these mimics because they intrinsically provide a certain organization of their reactive functions. In this context many aza or oxaaza macrocycles have been shown to yield interesting performances as models for the cleavage of carboxy or phosphate esters. One representative example was provided by the binucleating oxaaza ligand 1,4,7,16,19,22-hexaaza-10,13,25,28-tetraoxacyclotriacontane ([30]aneN_6O_4), which contains two triamine moieties separated by two dioxa chains.[24]

Here we report on the catalytic ability towards carboxy- and phosphate-ester cleavage of three compounds of different structure. L1 is an open-chain hexaamine consisting of a symmetrical array of four propylenic chains and one central ethylenic chain connecting the set of nitrogen atoms,[25] L2 presents a classical 1:1 cyclophane structure in which the

[a] Departamento de Química Inorgánica, CMOL, Universidad de Valencia,
C/ Dr. Moliner 46100, Burjassot (Valencia), Spain
E-mail: enrique.garcia-es@uv.es
[b] Università di Firenze, Polo Scientifico, Dipartimento di Chimica,
Via della Lastruccia 3, 50019 Sesto Fiorentino, Firenze, Italy
[c] Departamento de Química Inorgánica, Facultad de Química, Universidad Nacional Autónoma de México, UNAM
Av. Universidad 3000, Ciudad Universitaria, México D.F., 04510, Mexico

Supporting information for this article is available on the WWW under http://www.eurjic.org or from the author.

hexamine L1 has been linked through methylene groups to a *meta*-benzene spacer,[26] and L3 is a novel phenanthrolinophane ligand consisting of the pentaamine 4,7,10-triazatridecane-1,13-diamine linked through methylene groups to the 2- and 9-positions of a 1,10-phenanthroline moiety (Scheme 1). We present the synthesis of L3 and we discuss the Zn^{II} coordination capabilities of the three ligands L1, L2 and L3 as well as their potentialities as hydrolytic mimics.

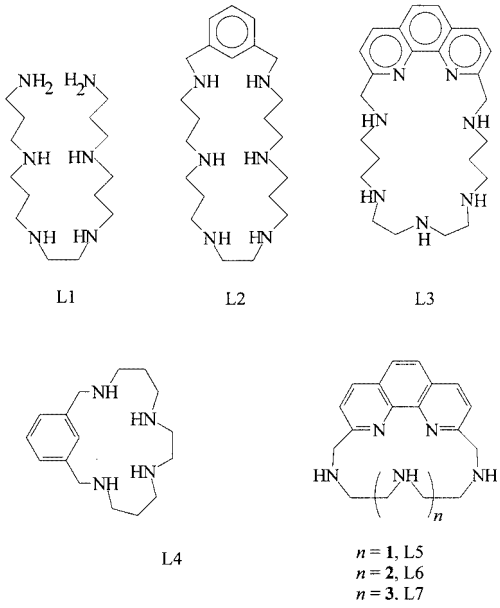

Scheme 1

Results and Discussion

Synthesis of L3

The synthesis of L3 was achieved according to a route different to that reported for the preparation of related cyclophanes[27] and similar phenanthrolinophanes.[28] The procedure consists of a condensation reaction of the partly tosylated amine 4,7,10-tris(*p*-tolylsulfonyl)-4,7,10-triaazatridecane-1,13-diamine (**1**) with 1,10-phenanthroline-2,9-dicarboxaldehyde (**2**), which yields the tosylated imine **3**. Compound **3** is then reduced with $NaBH_4$ to give the partly tosylated macrocycle (**4**; Scheme 2). The reductive cleavage of the amine to give L3 was performed with HBr/AcOH in PhOH. L3 was handled as its hexahydrobromide salt. The overall yield of the reaction was about 40%.

Speciation Studies

Table 1 gathers the stability constants for the formation of Zn^{II} complexes of L1, L2 and L3. Formation of both mono- and dinuclear complexes was detected in all three systems. L1 and L2 form protonated mononuclear complexes with protonation degrees varying between 2 and 0 and between 2 and −1, respectively. The speciation studies

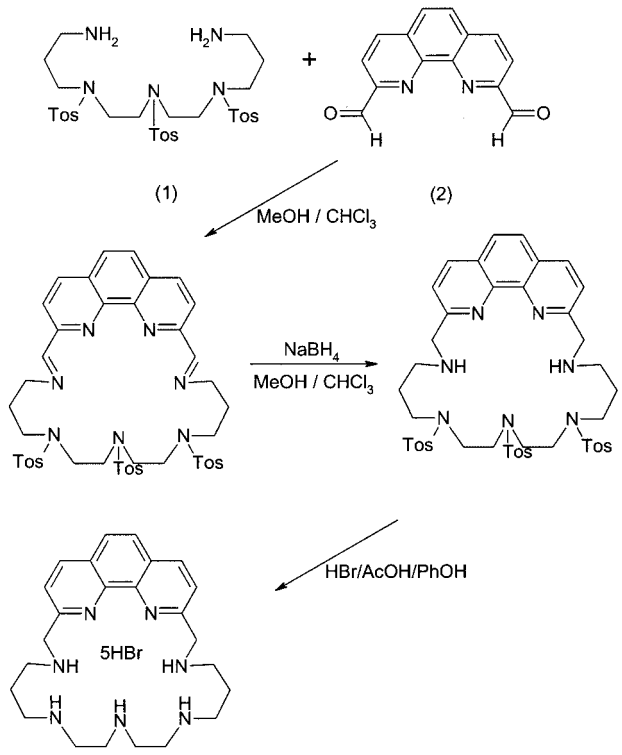

Scheme 2

for the Zn^{II}−L3 system show the formation of mononuclear complexes with stoichiometries $[ZnH_xL]^{(2+x)}$ with x ranging from 4 to 0. With respect to the dinuclear complexes, while in the systems Zn^{II}−L1 and Zn^{II}−L2 only hydroxylated species are detected, in the system Zn^{II}−L3 formation of a neutral and of a monoprotonated dinuclear complex is also observed.

In a previous report,[25] some of us analysed the coordination capabilities towards Zn^{II} of the open-chain ligand L1. Taking into account the values of the stability constants, the NMR spectra of the complex and the comparison with related polyamines and the other metal ions of the second part of the first transition series, a coordination number of four was confidently established for its mononuclear Zn^{II} complexes. A similar analysis can be performed for the system Zn^{II}−L2. First of all, a direct comparison with L1 shows that the formation constant of $[ZnL2]^{2+}$ is even a little bit lower than that of $[ZnL1]^{2+}$ (Table 1). The formation constant of $[ZnL2]^{2+}$ is, on the other hand, similar to those of open-chain tetraamines like 3,6-diazaoctane-1,8-diamine (trien) ($\log K_{ZnL/Zn\cdot L} = 12.0$) with all ethylenic chains, 4,7-diazadecane-1,10-diamine (2,2,2-tet, $\log K_{ZnL/Zn\cdot L} = 11.25$) with a symmetrical disposition of two propylenic and one ethylenic chain or 4,8-diazadecane-1,11-diamine (3,2,3-tet, $\log K_{ZnL/Zn\cdot L} = 10.46$) with all ethylenic chains and larger than those obtained for open-chain triamines like 3-azapentane-1,5-diamine (2,2-tri, $\log K_{ZnL/Zn\cdot L} = 8.8$).[29] If we compare tetraazacycloalkanes like 1,4,8,11-tetraazacyclotetredecane (cyclam, $\log K_{ZnL/Zn\cdot L} = 15.5$) or 1,4,7,10-tetraazacyclododecane (cyclen, $\log K_{ZnL/Zn\cdot L} = 16.2$), then the formation constant of $[ZnL]^{2+}$ is clearly

 © 2004 Wiley-VCH Verlag GmbH & Co. KGaA, Weinheim

Table 1. Logarithms of the stability constants for the formation of Zn^{2+} complexes of ligands L1, L2 and L3 determined at 298.1 K in 0.15 M ionic strength

Reaction	L1[a][b]	L2[b]	L3[c]
$Zn^{2+} + L + 4H^+ \rightarrow ZnH_4L^{6+}$			36.44(3)
$Zn^{2+} + L + 3H^+ \rightarrow ZnH_3L^{5+}$			32.48(2)
$Zn^{2+} + L + 2H^+ \rightarrow ZnH_2L^{4+}$	28.25(1)	26.31(2)	26.37(2)
$Zn^{2+} + L + H^+ \rightarrow ZnHL^{3+}$	20.09(1)	18.65(2)	19.41(2)
$Zn^{2+} + L \rightarrow ZnL^{2+}$	10.53(2)	10.19(3)	10.96(2)
$Zn^{2+} + L + H_2O \rightarrow ZnL(OH)^+ + H^+$		0.39(3)	
$Zn^{2+} + L + H_2O \rightarrow ZnL(OH)_2 + 2H^+$		−10.18(5)	
$2Zn^{2+} + L + H^+ \rightarrow Zn_2HL^{5+}$			22.54(7)
$2Zn^{2+} + L \rightarrow Zn_2L^{4+}$			16.26(3)
$2Zn^{2+} + L + H_2O \rightarrow Zn_2L(OH)^{3+} + H^+$	7.55(3)	5.80(4)	8.48(4)
$2Zn^{2+} + L + 2H_2O \rightarrow Zn_2L(OH)_2^{2+} + 2H^+$	−1.98(8)	−2.63(3)	−1.35(5)
$ZnH_3L^{5+} + H^+ \rightarrow ZnH_4L^{6+}$			4.0[d]
$ZnH_2L^{4+} + H^+ \rightarrow ZnH_3L^{5+}$			6.1
$ZnHL^{3+} + H^+ \rightarrow ZnH_2L^{4+}$	8.2	7.7	7.0
$ZnL^{2+} + H^+ \rightarrow ZnHL^{3+}$	9.6	8.6	8.5
$Zn_2L^{4+} + H^+ \rightarrow Zn_2HL^{5+}$			6.3
$Zn_2L^{4+} + OH^- \rightarrow Zn_2L(OH)^{3+}$			6.0
$Zn_2L^{4+} + H_2O \rightarrow Zn_2L(OH)^{3+} + H^+$			−7.8
$Zn_2L(OH)^{3+} + OH^- \rightarrow Zn_2L(OH)_2^{2+}$	4.2	5.3	3.9
$Zn_2L(OH)^{3+} + H_2O \rightarrow Zn_2L(OH)_2^{2+} + H^+$	−9.5	−8.4	−9.8

[a] Taken from ref.[25] [b] 0.15 M $NaClO_4$. [c] 0.15 M NaCl. [d] Just one decimal figure is included in the calculated stepwise constants.

lower as a result of the important macrocyclic effect that is operative in these small-sized saturated azamacrocycles. A comparison with the triazamacrocycles 1,4,7-triazacyclononane ([9]aneN_3, log $K_{ZnL/Zn\cdot L}$ = 11.6) and 1,5,10-triazacyclododecane ([12]aneN_3, log $K_{ZnL/Zn\cdot L}$ = 8.6) shows an intermediate constant for $[ZnL2]^{2+}$ between the macrocycle with all ethylenic chains and that with only propylenic chains. A last comparison of relevance refers to tetraazametacyclophanes like 2,6,9,13-tetraaza[14]metacyclophane (L4; Scheme 1) for which the number of coordinated nitrogen atoms was deduced to be three (log $K_{ZnL/Zn\cdot L}$ = 8.73).[30] Therefore, all these data suggest that in the Zn^{II}−L1 mononuclear complexes the metal ion is coordinated by four nitrogen donors of the macrocycle. The two high, stepwise protonation constants obtained for $[ZnL2]^{2+}$ also give support to the tetracoordination of the metal ion. The nitrogen atoms undergoing protonation would be noncoordinated ones and this is the reason for such high values of their protonation constants.

The analysis of the stability constants for the interaction of Zn^{II} with the phenanthrolinophane L3 leads to similar conclusions. Firstly, the value for the formation constant of $[ZnL3]^{2+}$ (Table 1) is of the same order of magnitude as found for the other polyamines studied in the present work (L1 and L2); this could indicate that, as has been just discussed, four is the most likely coordination number. However, in this case the presence of the strong π-acceptor phenanthroline spacer can produce some modification in the analysis. Therefore, it is interesting to compare L3 with similar phenanthrolinophanes reported previously.[31] Indeed the $[ZnL]^{2+}$ complex of the phenanthrolinophane receptor 2,5,8-triaza[9](2,9)(1,10)phenanthrolinophane (L5; Scheme 1) displays a stability constant of 16.15, which is much higher than those reported here for the analogous complexes of L1−L3. In spite of this, the crystal structure of its complex cation $[ZnL(H_2O)]^{2+}$ revealed that Zn^{II} is coordinated only by the phenanthroline donors, by the central nitrogen atom of the polyamine bridge and by a water molecule, with a tetrahedral disposition of the donor atoms. This again points out the difficulties of deriving coordination numbers just from free-energy terms. Nevertheless, one has to consider that such an enhancement of the stability of Zn^{II} complexes by ligands favoring tetrahedral arrangements is quite usual as can be seen from the relevant data for the tripodal tetraamine tris(2-aminoethyl)amine, which has a higher stability constant than any other open-chain tetraamine.[29]

However, the larger 2,5,8,11-tetraaza[12](2,9)(1,10)phenanthrolinophane (L6 in Scheme 1) and 2,5,8,11,13-pentaaza[14](2,9)(1,10)phenanthrolinophane (L7) have lower constants — log $K_{ZnL/Zn\cdot L}$ = 14.29 and 12.38, respectively.[31] In the case of L3, the stability constant obtained follows this tendency, being even lower (Table 1). Additionally, the number of protonated species found is very large. All this can be interpreted on the grounds of an increasing strained coordination geometry imposed by the macrocyclic conformation and to a low coordination number that should involve either three or at most four nitrogen donors, including those of the spacer.

The most relevant aspect with respect to the dinuclear complexes is the ready hydroxylation observed for the three systems at relatively low pH values (see Figure 1). In the case of L1 and L2, $[Zn_2L]^{4+}$ species are not even detected in solution due to the marked tendency of the dinuclear Zn^{II} complexes to form hydroxylated complexes. In the case of L3, a pK_a value of 7.8 for deprotonation of a Zn^{II}-coordinated water molecule of $[Zn_2L3]^{4+}$ was found. Similar low pK_a values are generally observed in the case of a bridging

 © 2004 Wiley-VCH Verlag GmbH & Co. KGaA, Weinheim

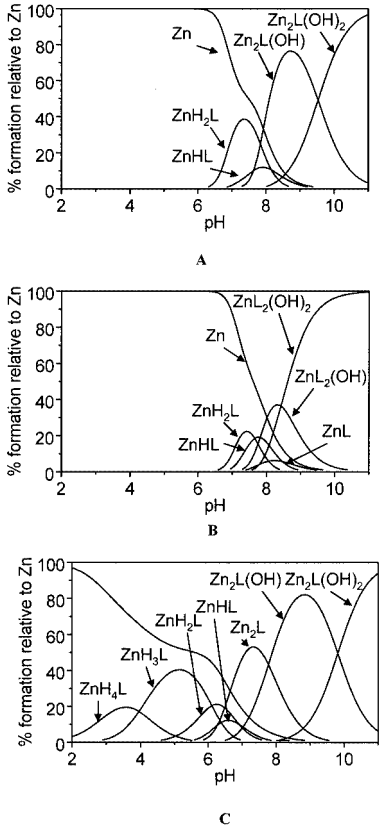

Figure 1. Distribution diagrams for the systems $Zn^{II}-L1$, $Zn^{II}-L2$ and $Zn^{II}-L3$ for molar ratios $Zn^{II}/L = 2:1$ ($[Zn^{II}] = 2 \times 10^{-3}$ M)

disposition of hydroxide between two metal ions[24,32,33] or in the case of mononuclear complexes containing a water molecule placed as a fourth ligand of a Zn^{II} moiety coordinated by three nitrogen donors.[4,30] Therefore, the coordinatively unsaturated first coordination spheres of these dinuclear complexes provide nucleophilic OH^- functions, which could play a key role in the hydrolytic process (vide infra).

Kinetics of p-Nitrophenyl Acetate (NA) Hydrolysis

NA hydrolysis was monitored by UV/Vis spectroscopy by monitoring the appearance of the *p*-nitrophenolate anion at 403 nm (298.1 K, $I = 0.15$ M $NaClO_4$). All ligands form dinuclear complexes in aqueous solution. In the case of L3 the formation of the dinuclear $[Zn_2L3]^{4+}$ complex takes place at a pH > 6, with almost simultaneous deprotonation of a coordinated water molecule to give the monohydroxo species $[Zn_2L3(OH)]^{3+}$. The rather low pK_a (7.8 log units) suggests a bridging coordination of the hydroxide ion between the two metal centers, as is often found in dizinc complexes with macrocyclic ligands, where the two metal atoms are kept at a short distance by the cyclic framework, thus favoring the assembly of $Zn_2(\mu\text{-OH})$ units.[24,32,33] The formation of a dihydroxo $[Zn_2L3(OH)_2]^{2+}$ complex is observed at alkaline pH values, with $pK_{a2} = 9.8$ (298 K). This pK_a value is higher than those usually found for bridging hydroxide ions and is generally related to the formation of a single-metal-bound hydroxide function.[24,32,33] L1 and L2 display a somewhat different behavior, since the formation of the $[Zn_2L]^{4+}$ complex is not observed and only the dinuclear hydroxylated species $[Zn_2L(OH)]^{3+}$ and $[Zn_2L(OH)_2]^{2+}$ are present in neutral and alkaline aqueous solutions, respectively. For all the three ligands, both the dinuclear complexes $[Zn_2L(OH)]^{3+}$ and $[Zn_2L(OH)_2]^{2+}$ promote NA hydrolysis; second-order kinetics is monitored at different pH values. As shown in Figure 2 for the dinuclear L1 complexes, plots of the k_{NA} values as a function of the percentages of $[Zn_2L1(OH)]^{3+}$ (Figure 2a) and $[Zn_2L1(OH)_2]^{2+}$ (Figure 2b) give rise to straight lines. Similar plots were also obtained for the dinuclear complexes with L2 and L3. For all the dinuclear complexes under investigation, no effect is observed at pH < 7.5, where such species are absent in solutions. Finally, experiments carried out on solutions containing ligands L1, L2 or L3 and Zn^{II} in a 1:1 molar ratio in the pH range 7−9 (under these conditions mononuclear complexes are largely prevalent in solution) do not show significant increases of the hydrolysis rate, indicating that the mononuclear Zn^{II} complexes are not active in this hydrolytic process.

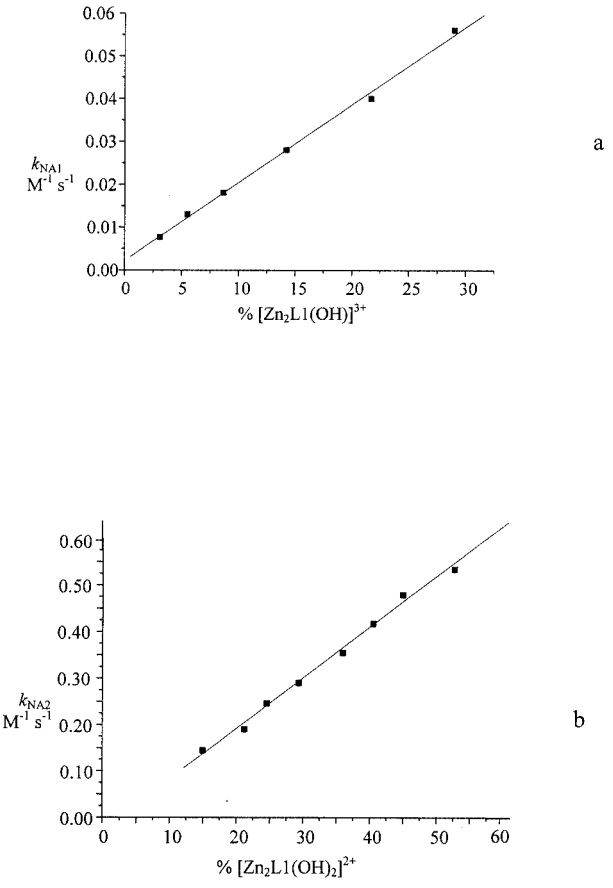

Figure 2. Second-order rate constants for NA hydrolysis (k_{NA}) as a function of the percentage of $[Zn_2L1(OH)]^{3+}$ (a) and as a function of the percentage of $[Zn_2L1(OH)_2]^{2+}$ (b)

 © 2004 Wiley-VCH Verlag GmbH & Co. KGaA, Weinheim

Only the mono- and dihydroxo complexes $[Zn_2L(OH)]^{3+}$ and $[Zn_2L(OH)_2]^{2+}$ are the kinetically active species, meaning that the $Zn^{II}-OH$ function is indeed nucleophilic. Furthermore, Figure 2 clearly shows that the dihydroxo complex $[Zn_2L1(OH)_2]^{2+}$ is much more active in NA hydrolysis than the monohydroxo complex $[Zn_2L1(OH)]^{3+}$. Similarly, the dinuclear dihydroxo complexes with L2 and L3 show a higher activity in promoting NA cleavage than the monohydroxo ones.

The $[Zn_2L(OH)]^{3+}$ and $[Zn_2L(OH)_2]^{2+}$ complexes (L = L1, L2 or L3) are formed in at most 70% yield in the pH ranges used in the kinetic measurements. Therefore, in order to quantify the different activity in NA hydrolysis of the present complexes, second-order rate constants k'_{NA} have been determined from the maximum k_{NA} values by using the equation:

$$v = k_{NA}[\text{total } Zn^{II}\text{complex}][NA] = k'_{NA}[Zn_2L(OH)_x^{4-x}][NA];\ x = 1 \text{ or } 2$$

The k'_{NA} values for the present complexes are listed in Table 2, together with the rate constants found for Kimura's mononuclear Zn^{II} complexes **1** and **2** (Scheme 3).[34]

Table 2. Second-order rate constants k'_{NA} [M^{-1} s^{-1}] for hydrolysis of *p*-nitrophenyl acetate

Nucleophile	k'_{NA} [M^{-1} s^{-1}]	pK_a
$[Zn_2L1(OH)]^{3+}$	0.18 ± 0.01	–
$[Zn_2L1(OH)_2]^{2+}$	1.1 ± 0.05	9.5
$[Zn_2L2(OH)]^{3+}$	0.06 ± 0.003	–
$[Zn_2L2(OH)_2]^{2+}$	0.80 ± 0.4	8.4
$[Zn_2L3(OH)]^{3+}$	0.069 ± 0.04	7.8
$[Zn_2L3(OH)_2]^{2+}$	2.2 ± 0.05	9.8
1	0.041[a]	7.2
2	0.11[a]	7.9

[a] From ref.[34]; I = 0.15 M $NaClO_4$.

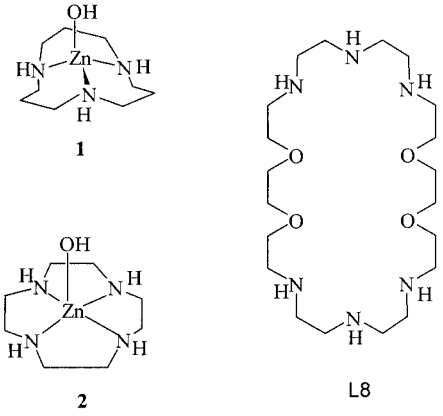

Scheme 3

Table 2 clearly shows that the monohydroxo $[Zn_2L(OH)]^{3+}$ complexes exhibit a remarkably lower rate constant than the corresponding dihydroxo $[Zn_2L(OH)_2]^{2+}$ complexes. The much lower hydrolytic properties of the $[Zn_2L(OH)]^{3+}$ species can be ascribed to the bridging coordination of the hydroxide ion, as is often found in dizinc complexes with hexa- and heptaamine ligands.[22,24,32] In fact, the simultaneous binding to two electrophilic metal centers reduces the nucleophilicity of the generated hydroxide ion. The k'_{NA} of $[Zn_2L(OH)]^{3+}$ is, however, similar to those found for the monohydroxo complexes **1** and **2**.

Addition of a second hydroxide anion to a Zn^{II} ion may lead to detachment of the bridging OH ion from one of the metal atoms or to a weakening of the Zn(μ-OH) bond, giving a more "open" conformation of the complex, which can leave catalytic sites accessible on the two Zn^{II} ions. As a matter of fact, the dihydroxo complexes $[Zn_2L(OH)_2]^{2+}$ give much higher rate constants in NA hydrolysis than the monohydroxo complexes **1** and **2**, indicating an enhanced nucleophilicity of the $Zn-OH$ functions in $[Zn_2L(OH)_2]^{2+}$. Actually, a bridging hydroxide ion in $[Zn_2L(OH)]^{3+}$ reduces the positive charge on the metal ions. This determines the rather high pK_{a2} values found for deprotonation of a Zn^{II}-bound water molecule to give the $[Zn_2L(OH)_2]^{2+}$ complexes and increases the nucleophilic character of the resulting $Zn-OH$ functions.

Comparing the different abilities of these species in NA cleavage, Table 2 shows that the k'_{NA} values increase in the sequence L2 < L1 < L3. The mechanism generally accepted for NA hydrolysis involves a simple nucleophilic attack of the metal-bound hydroxide ion to the carbonyl group of the ester and release of *p*-nitrophenolate.[8,35] The two Zn^{II} ions do not play any cooperative role in substrate activation and a simple bimolecular mechanism is predominant. For this reason, for a series of analogous complexes, such as **1** and **2**, the ability of $Zn-OH$ functions in NA hydrolysis increases with their pK_a values. From this point of view, the increasing pK_{a2} value observed on passing from L2 to L1 would explain the higher k'_{NA} value found for $[Zn_2L1(OH)_2]^{2+}$ with respect to $[Zn_2L2(OH)_2]^{2+}$. On the other hand the $[Zn_2L3(OH)_2]^{2+}$ complex displays a pK_{a2} value similar to that of the corresponding L1 complex {pK_{a2} = 9.8 and 9.5 for $[Zn_2L3(OH)_2]^{2+}$ and $[Zn_2L1(OH)_2]^{2+}$, respectively}, but, at the same time, is twice as active in NA hydrolysis {k'_{NA} = 2.2 and 1.1 $M^{-1}{\cdot}s^{-1}$ for $[Zn_2L3(OH)_2]^{2+}$ and $[Zn_2L1(OH)_2]^{2+}$, respectively}. A tentative explanation for this behavior could reside in the presence of a large heteroaromatic unit — phenanthroline — in the L3 cyclic framework. It is known, in fact, that phenanthroline-containing receptors can give host–guest adducts with substrates containing aromatic moieties, stabilized by strong π-stacking and hydrophobic interactions between the two aromatic units.[2,36–38] In the present case, these interactions between phenanthroline and the aromatic moiety of NA would stabilise the transient state of the nucleophilic attack, leading to the observed higher hydrolytic ability of the L3 complex. At the same time phenanthroline is poorly solvated in water. Therefore, the presence of this unit within the cyclic framework can provide a rather hydrophobic environment for the $Zn-OH$ function, enhancing its nucleophilic activity.

 © 2004 Wiley-VCH Verlag GmbH & Co. KGaA, Weinheim

The high activity of the present complexes in NA hydrolysis prompted us to study their hydrolytic ability toward the phosphate ester bond, by using bis(*p*-nitrophenyl)phosphate (BNP) as substrate. It is known, in fact, that BNP hydrolysis in the presence of Zn^{II} complexes generally takes place through an "associative" mechanism,[33−35] in which substrate binding and activation by the metal center is followed by a nucleophilic attack at the phosphorus atom. Hydrophobic and π-stacking interactions would lead, in principle, to a stronger association between BNP and the Zn^{II} complex with L3, and, therefore, to an increased substrate activation of the hydrolytic process

BNP Binding by the Zn^{II} Complexes with L1−L3

Binding of BNP to the Zn^{II} complexes with ligands L1−L3 was monitored by means of ^{31}P NMR spectra recorded on MeOD/CD_3CN (50:50, v/v) solutions containing BNP (1×10^{-2} M) and the complexes in different molar ratios. Solutions containing BNP and increasing amounts of the dinuclear complexes display a progressive upfield shift of the BNP signals (Figure 3). In the case of the dizinc complexes with L3 (Figure 3c), the plot of $\Delta\delta$ (where $\Delta\delta$ is the difference between the chemical shift of BNP in the presence and in absence of the complex) as a function of the $[Zn_2L3](ClO_4)_4{\cdot}2H_2O$/[BNP] molar ratio ($R$) gives a straight line for $R < 0.8$. Then, the slope changes almost suddenly to give a straight line parallel to the x axis for $R > 1.2$ (at this point $\Delta\delta = 2.8$ ppm). This behavior indicates the formation of a stable 1:1 complex between the dizinc complex and BNP. A similar plot is obtained with the dizinc complex with L2; the slope change, however, is less sudden than in the case of the L3 complex and a lower $\Delta\delta$ value ($\delta = 1.9$ ppm) is reached for $R > 1.5$ (Figure 3b). Finally, in the presence of the dizinc complex with L1 a very smooth curve is observed up to $R = 5$ ($\Delta\delta = 0.55$ ppm), where precipitation of a 1:1 complex between the dizinc complex and BNP takes place. {A solid compound of stoichiometry $[Zn_2L1](BNP)(ClO_4)_3{\cdot}2H_2O$ was isolated and characterized by elemental analysis. $C_{26}H_{48}Cl_3N_8O_{20}PZn_2$ (1060.82): calcd. C 29.54, H 4.58, N 10.61, P 2.93; found C 28.99, H 4.50, N 10.25, P 2.73.} These data are in agreement with the formation of 1:1 complexes with BNP, whose stability increases in the order $[Zn_2L1]^{4+} < [Zn_2L2]^{4+} < [Zn_2L3]^{4+}$. Furthermore, the rather large shift for the signal of the phosphate ester bound to the L2 and L3 dinuclear complexes would suggest interaction of BNP with both Zn^{II} ions through a bridging coordination of the phosphate anion. From this point of view, it is of interest to note that no shift of the BNP signal is observed in the presence of the mononuclear Zn^{II} complexes with ligands L1−L3. Most likely, in the mononuclear complexes the Zn^{II} ion is almost coordinately saturated by the ligand donors and no free binding site is available at the metal for BNP coordination.

The ^{31}P NMR spectra recorded in D_2O solution display minor shifts of the BNP signal, even in the presence of a large excess of the dinuclear complexes ($\delta = 0.5$ and 0.3 ppm in the case of L3 and L2, respectively, and $\delta \approx$ 0.1 ppm for L1), probably due to a much lower percentage of coordinated BNP in this more solvating medium. In the case of L2 and L3, ^{31}P NMR titrations at pD = 10 (see Supporting Information), carried out by adding increasing amounts of $[Zn_2L3](ClO_4)_4{\cdot}2H_2O$ or $[Zn_2L2](ClO_4)_4{\cdot}4H_2O$ to a BNP solution lead to calculate a log K value of 2.5 ± 0.2 and 1.7 ± 0.1 for the addition of BNP to the dinuclear

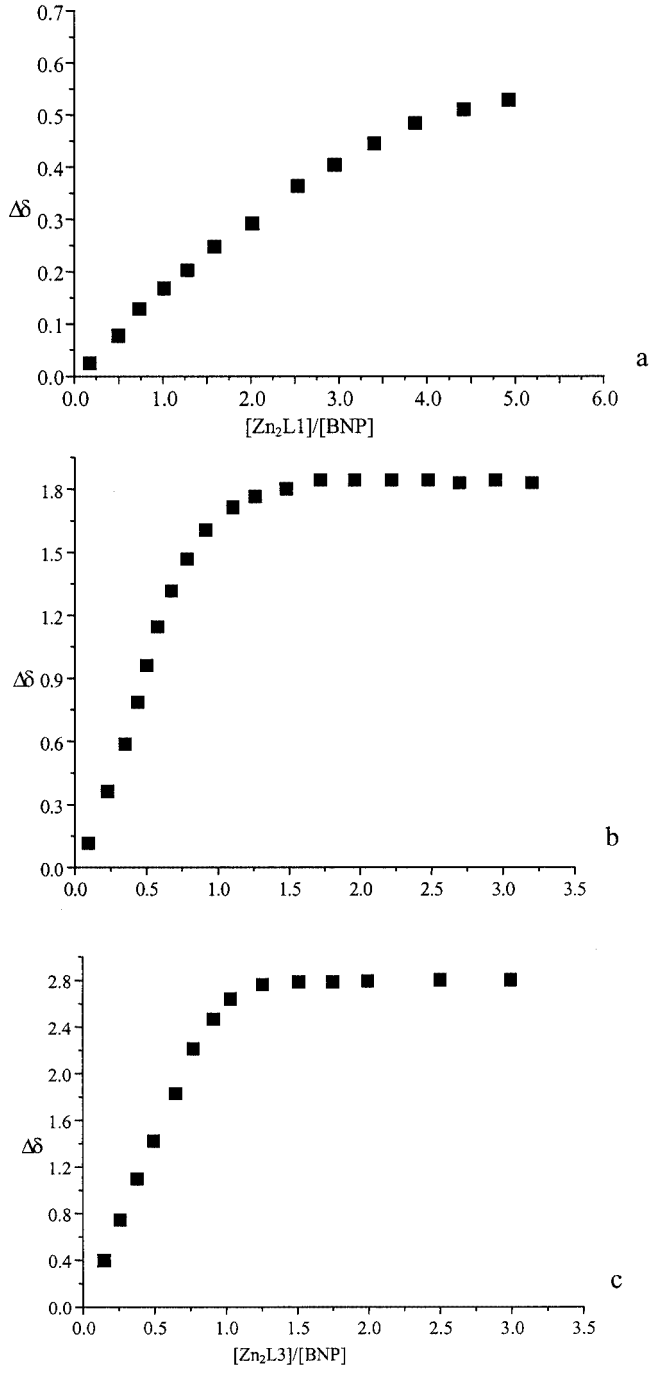

Figure 3. Plot of the ^{31}P NMR chemical shifts of BNP ($\Delta\delta = \delta_{BNP} - \delta_{OBS}$, where δ_{BNP} = chemical shift of the unbound BNP ester and δ_{OBS} = observed chemical shift in the presence of the dinuclear complexes with L1−L3) as a function of the [$[Zn_2L1](ClO_4)_4{\cdot}2H_2O$]/[BNP] (a), [$[Zn_2L2](ClO_4)_4{\cdot}4H_2O$]/[BNP] (b) and [$[Zn_2L3](ClO_4)_4{\cdot}2H_2O$]/[BNP] molar ratios (MeOD/CD_3CN solution, 298 K, [dizinc complex] = 1×10^{-2} M)

 © 2004 Wiley-VCH Verlag GmbH & Co. KGaA, Weinheim

Zn^{II} complex with L3 and L2, respectively. In the case of the dizinc complex with L1, the observed shift of the ^{31}P NMR signal is too low to confidently determine the addition constant of BNP to the complex.

To obtain further information on the interaction mode of the BNP anion with our dizinc complexes, we also recorded ^{1}H NMR spectra of solutions containing BNP and increasing amounts of dinuclear Zn^{II} complexes with L1−L3. Although the ^{1}H NMR spectra of the ligands in their Zn^{II} complexes are rather fluxional and do not allow a correct determination of the ^{1}H chemical shifts, the resonances of the aromatic protons of BNP [two doublets at δ = 7.98 (H1; for atom labelling see Figure 4) and δ = 7.13 ppm (H2) in the absence of the Zn^{II} complexes] are generally easily recognizable. The ^{1}H NMR signals of BNP are almost unaffected by the presence, even in large excess, of the dizinc complexes with ligand L1 and L2. On the contrary, addition of the dizinc complex with L3 to a BNP solution gives rise to a significant upfield shift of both the BNP signals (Figure 4). As in the case of the ^{31}P NMR spectra, the plot of the $\Delta\delta$ values as a function of the [dinuclear L3 complex]/[BNP] molar ratio (R) gives a straight line for $R < 0.8$; subsequently, the slope changes to give a straight line parallel to the x axis for $R > 1.2$ (at this point $\Delta\delta$ = 0.42 and 0.37 ppm for the protons H1 and H2, respectively). The upfield shifts observed for the BNP signals are indicative of a π-stacking interaction between the aromatic rings of the ester and the large phenanthroline unit. This interaction seems to be absent in the case of the zinc complexes with L2, which contains a smaller aromatic unit.

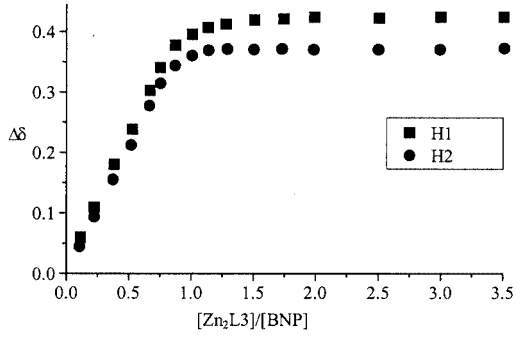

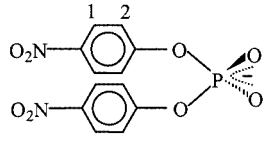

Figure 4. Plot of the ^{1}H NMR chemical shifts of BNP ($\Delta\delta = \delta_{BNP} - \delta_{OBS}$, where δ_{BNP} = chemical shift of the unbound BNP ester and δ_{OBS} = observed chemical shift in the presence of the dinuclear complexes with L1−L3) as a function of the $[[Zn_2L3](ClO_4)_4{\cdot}2H_2O]$/[BNP] molar ratios (MeOD/CD_3CN solution, 298 K, $[[Zn_2L3](ClO_4)_4{\cdot}2H_2O] = 1 \times 10^{-2}$ M)

Both the ^{31}P and ^{1}H NMR experiments account for a higher overall interaction between the phosphate ester and the dizinc complex with L3, probably due to the synergetic effect in BNP binding exerted by the two metal centers, which can act cooperatively in substrate coordination, and by the phenanthroline moiety, which can interact with BNP by π-stacking.

To shed further light on the role played by substrate interaction and activation by the present metal complexes, we decided to carry out a comparative kinetic study on the ability of the L1−L3 complexes to hydrolyze BNP.

BNP Hydrolysis Promoted by the Zn^{II} Complexes with L1−L3

A kinetic analysis of BNP cleavage shows that only the dinuclear complexes with L1−L3 promote BNP hydrolysis, while the mononuclear complexes are totally unable to hydrolyze this ester. Figure 5 shows the second-order rate constants for BNP cleavage (k_{BNP}) in the presence of the ligand L3 and increasing amounts of Zn^{II} at pH = 10. No hydrolytic effect is observed with molar ratios $R < 1$ for Zn^{II}/L3, when only mononuclear complexes are formed in aqueous solutions; for $1 < R < 2$, the k_{BNP} values increase almost linearly with R, due to the formation of increasing amounts of the dinuclear complex. The maximum k_{BNP} value is obtained when $R = 2$, where only the dinuclear complex is present in solution at pH = 10. Addition of further Zn^{II} ($R > 2$) does not change the hydrolysis rate.

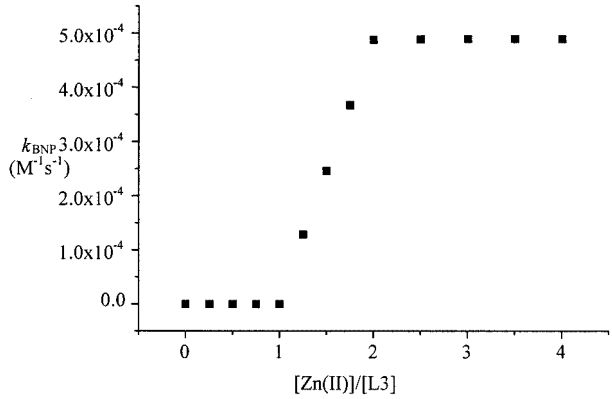

Figure 5. Second-order rate constants for BNP cleavage (k_{BNP}) as a function of the $[Zn^{II}]$/[L3] molar ratio at pH = 10 (CHES buffer)

For all the three ligands, only the dihydroxo complexes $[Zn_2L(OH)_2]^{2+}$ promote BNP hydrolysis in aqueous solution, to give mono(*p*-nitrophenyl phosphate) (MNP) and *p*-nitrophenolate, while the monohydroxo species $[Zn_2L(OH)]^{3+}$ do not promote this process (Figure 5), in agreement with the very much lower activity in NA hydrolysis found for this species. Plots of the second-order rate constants k_{BNP} for the L1, L2 and L3 dizinc complexes as a function of pH fit the distribution curves of the $[Zn_2L1(OH)_2]^{2+}$, $[Zn_2L2(OH)_2]^{2+}$, and $[Zn_2L3(OH)_2]^{2+}$ species (Figure 6), pointing out that these dihydroxo complexes are the kinetically active species. As in the case of NA hydrolysis, second-order rate constants k'_{BNP} can be

 © 2004 Wiley-VCH Verlag GmbH & Co. KGaA, Weinheim

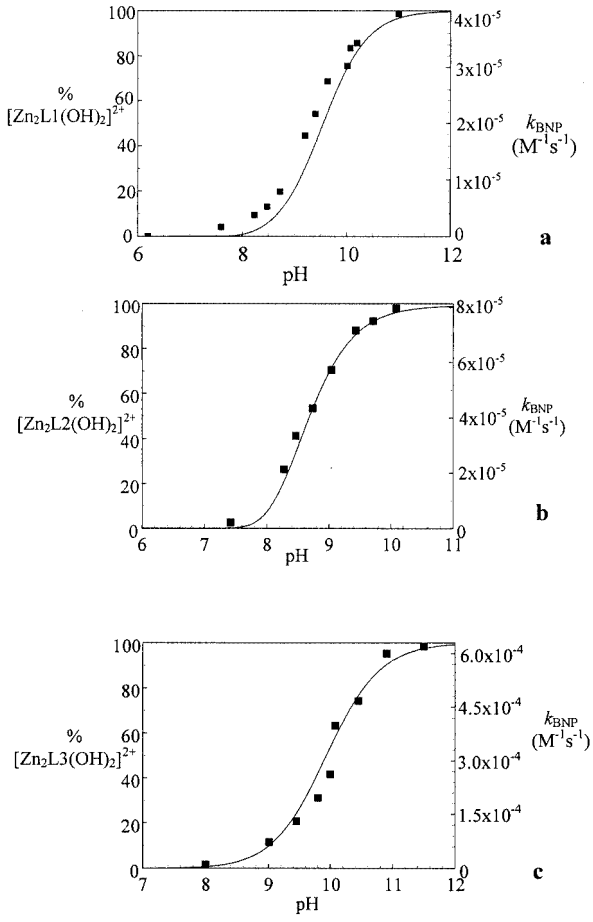

Figure 6. Plots of the distribution curves of $[Zn_2L1(OH)_2]^{2+}$ (a), $[Zn_2L2(OH)_2]^{2+}$ (b) and $[Zn_2L3(OH)_2]^{2+}$ (c) (solid line, right *y* axes) and k_{BNP} values (squares, left *y* axes) as a function of pH

calculated from the maximum k_{BNP} value by using the expression:

$$v = k_{BNP}[\text{total } Zn^{II}\text{complex}][BNP] = k'_{BNP}[Zn_2L(OH)_2{}^{2+}][BNP]$$

Table 3. Second-order rate constants *k'BNP* [M^{-1} s^{-1}] for hydrolysis of bis(4-nitrophenyl)phosphate

Nucleophile	$k'_{BNP}\cdot10^5$ [M^{-1} s^{-1}]	pK_a
$[Zn_2L1(OH)_2]^{2+}$	4.0 ± 0.2	9.5
$[Zn_2L2(OH)_2]^{2+}$	8.0 ± 0.4	8.4
$[Zn_2L3(OH)_2]^{2+}$	62 ± 3	9.8
1	8.5[a]	7.2
2	2.1[a]	7.9
$[Zn_2L8(OH)_2]^{2+}$	11.0[b]	9.1

[a] From ref.[40]; I = 0.15 M $NaClO_4$. [b] From ref.[24]; I = 0.1 M NaCl.

Table 3 reports the k'_{BNP} values for the $[Zn_2L(OH)_2]^{2+}$ complexes, in comparison with the corresponding pK_{a2} values. The k'_{BNP} values reported for the mononuclear complexes **1** and **2**[34] and for the dinuclear complex with L8[24] (Scheme 3) are also reported for comparison. Considering L1 and L2, the activity of their complexes in BNP hydrolysis decreases from L2 to L1, i.e., the hydrolytic properties decrease as the pK_a of the complexes increases, which is the opposite behavior to that found in NA cleavage. Thus, in BNP cleavage the hydrolytic properties of these complexes are not only determined by the nucleophilicity of the Zn−OH functions. This behavior has been already observed in both mono- and dinuclear Zn^{II} complexes and can be explained in terms of an "associative" mechanism,[24,32−34] in which the substrate approaches the $[Zn_2L(OH)_2]^{2+}$ complexes and the oxygen atoms of BNP associate with the electrophilic Zn^{II} ions, probably through a bridging coordination. A zinc-bound hydroxide ion then nucleophilically attacks the substrate (Figure 7). Lower pK_a values generally imply a better ability in substrate binding. The L2 complex, which contains the less nucleophilic Zn^{II}−OH functions, would give a stronger interaction with BNP during the hydrolytic process, leading to enhanced substrate activation and to higher rate acceleration. This is in agreement with the ^{31}P NMR results, which point out a higher interaction of BNP with the dinuclear L2 complex.

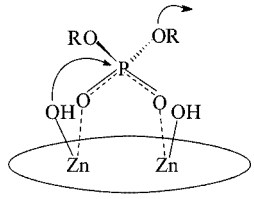

Figure 7. Proposed mechanism for BNP hydrolysis promoted by the dinuclear Zn^{II} complex with L2 and L3

Actually, the hydrolytic activity of the dinuclear complex with L2 is similar to that found for the mononuclear complex **1** and somewhat lower than that of the dinuclear Zn^{II} complex with [30]aneN_6O_4 (L8 in Scheme 3). The L2 complex, however, shows a better ability in BNP hydrolysis than the mononuclear complex **2**. However, experiments performed on solutions containing ligand L2 and Zn^{II} in 1:1 molar ratio in the alkaline pH region (pH = 7−10) showed that the mononuclear complex with L2 is completely unable to promote BNP hydrolysis. This suggests a cooperative effect of the two metal ions in BNP hydrolysis through a bridging coordination of the substrate to the two Zn^{II} ions, as actually confirmed by the marked upfield shift observed for the ^{31}P NMR signal of BNP upon coordination to the L2 complex.

The most interesting finding in Table 2, however, is the remarkably high k_{BNP} value found for $[Zn_2L3(OH)_2]^{2+}$, which is almost eight times more active than the corresponding L2 complex. A tentative explanation for this effect could reside in the stronger interaction of the L3 complex with BNP suggested by the ^1H and ^{31}P NMR results. Although precipitation of a solid complex {a compound of stoichiometry $[Zn_2L3](BNP)_2(ClO_4)_2$ precipitates at pH = 10 with a molar ratio of BNP/dizinc complex > 5; $C_{48}H_{56}Cl_2N_{11}O_{24}P_2Zn_2$ (1434.67): calcd. C 40.22, H 3.93, N 10.74, P 4.32; found C 40.76, H 4.08, N 10.55, P 4.5} at high molar ratios between BNP and the L3 dizinc complex prevents a Michaelis−Menten analysis of this hydrolytic

 © 2004 Wiley-VCH Verlag GmbH & Co. KGaA, Weinheim

process, the simultaneous bridging coordination of the phosphate ester to the two metal centers and π-stacking and/or hydrophobic interactions between phenanthroline and the *p*-nitrophenylene groups of BNP could reinforce the interaction between the dizinc complex and the substrate.

Conclusions

Ligands L1−L3 present similar binding features toward Zn^{II}, giving rise to both mono- and dinuclear complexes in aqueous solutions. The dizinc complexes are characterized by a marked tendency to form hydroxo species; the relatively low number of nitrogen donors, in fact, cannot fulfil the coordination sphere of two metal ions and, therefore, facile deprotonation of Zn^{II}-bound water molecules occurs on going from from neutral to alkaline pH values. This feature parallels the behavior of Zn^{II}-based hydrolytic enzymes, where Zn−OH functions behave as nucleophilic agents in the overall catalytic process.

Despite the similar coordination properties of L1−L3, their dizinc complexes display remarkably different hydrolytic ability. While the dinuclear Zn^{II} complexes with L1 and L2 show a hydrolytic activity toward NA and BNP similar to that reported for other Zn^{II} complexes developed as functional models for hydrolytic metalloenzymes, the dinuclear Zn^{II} complexes with L3, which contain a large and hydrophobic heteroaromatic moiety, give remarkably higher rate enhancements; among synthetic dizinc complexes, the L3 complex is one of the most active in both NA and BNP hydrolysis. The synergetic role in BNP binding of phenanthroline, which can give π-stacking and hydrophobic interactions with the aromatic rings of the substrate, and of the two metal ions, which act cooperatively in substrate coordination, probably gives a higher BNP activation.

Experimental Section

General Procedures: Ligands L1 and L2 were prepared as described elsewhere and handled as their hydrochloride salts.[25,26] UV/Vis spectra were recorded with a Shimadzu UV-2101PC spectrophotometer.

NMR Measurements: The ^1H and ^{13}C NMR spectra were recorded with Varian UNITY 300 and UNITY 400 spectrometers, operating at 299.95 and 399.95 MHz for ^1H and at 75.43 and 100.58 MHz for ^{13}C. The spectra were obtained at room temperature in D_2O or $CDCl_3$ solutions. For the ^{13}C NMR spectra dioxane was used as a reference standard (δ = 67.4 ppm) and for the ^1H NMR spectra the solvent signal. Adjustments to the desired pH were made by adding drops of DCl or NaOD solutions. The pH was calculated from the measured pD values using the correlation pH = pD − 0.4.[39] In the ^{31}P and ^1H NMR titrations, increasing amounts of 1 × 10^{-2} M solutions in MeOD/CD_3CN (50:50, v/v) or in D_2O at pH = 10 of the preformed Zn^{II} complexes with L1−L3 (see below) were added to a 5 × 10^{-3} M solution of BNP. The addition constants of BNP to dizinc complexes with L2 and L3 were calculated by means of the HYP NMR program.[40] TMS or DSS were used as internal standard.

2,6,9,12,16-Pentaaza[17](2,9)(1,10)phenanthrolinophane Pentahydrobromide (L3·5HBr): 4,7,10-Tris(*p*-tolylsulfonyl)-4,7,10-triaazatridecane-1,13-diamine (2.5 g, 3.68 mmol)[41] and 1,10-phenanthroline-2,9-dicarboxaldehyde (0.88 g, 3.73 mmol) were stirred overnight in a mixture of $CHCl_3$ and MeOH (1:5; 300 mL) to give the imine. Sodium borohydride (0.57 g, 15.2 mmol) was added and the mixture was stirred at room temperature for 24 h. The solvent was then removed at reduced pressure. The resulting residue was treated with water (50 mL) and extracted with dichloromethane (2 × 45 mL). Then, it was dried with Na_2SO_4 and the solvent removed by rotary evaporation. The tosyl groups of tritosylated L3 (3 g, 3.39 mmol) were removed by reductive cleavage with a 33% HBr/AcOH mixture (120 mL) and phenol (15 g, 160 mmol) heating at 90 °C for 18 h and then cooling to obtain a white solid. The resulting solid was filtered off and washed several times with CH_2Cl_2 and EtOH. The macrocycle was obtained as its hydrobromide salt (1.2 g, yield 44%). ^1H NMR (D_2O): δ = 1.95−2.03 (m, 4 H), 2.99 (t, J = 8 Hz, 4 H), 3.12 (t, J = 8 Hz, 4 H), 3.31−3.39 (m, 8 H), 4.6 (s, 4 H), 7.63 (d, J = 8 Hz, 2 H), 7.75 (s, 2 H), 8.34 (d, 2 H) ppm. ^{13}C NMR (D_2O): δ = 22.9, 43.3, 43.7, 45.1, 45.5, 51.9, 123.7, 127.5, 129.4, 139.9, 150.9 ppm. $C_{24}H_{40}N_7$·5HBr (831.19): calcd. C 34.89, H 4.88, N 11.88; found C 35.0, H 4.9, N 12.0.

Synthesis of the Dinuclear Zn^{II} Complexes with L1−L3: The Zn^{II} complexes $[Zn_2L1](ClO_4)_4$·$2H_2O$, $[Zn_2L2](ClO_4)_4$·$4H_2O$ and $[Zn_2L3](ClO_4)_4$·$2H_2O$ were obtained by slow evaporation of the solvent from butanol solutions containing ligands L1−L3 and $Zn(ClO)_4$·$6H_2O$ in a 1:2 molar ratio and characterized by means of elemental analysis. $[Zn_2L1](ClO_4)_4$·$2H_2O$: $C_{14}H_{40}Cl_4N_6O_{18}Zn_2$ (853.19): calcd. C 19.71, H 4.73, Cl 16.62, N 9.85; found C 19.99, H 4.78, Cl 16.3, N 10.01. $[Zn_2L2](ClO_4)_4$·$4H_2O$: $C_{22}H_{50}Cl_4N_6O_{20}Zn_2$ (991.26): calcd. C 26.66, H 5.08, Cl 14.31, N 8.48; found C 26.75, H 5.12, Cl 14.2, N 8.57. $[Zn_2L3](ClO_4)_4$·$2H_2O$: $C_{24}H_{39}Cl_4N_7O_{18}Zn_2$ (986.20): calcd. C 29.23, H 3.39, Cl 14.38, N 9.94; found C 29.79, H 3.51, Cl 14.2, N 10.05.

emf Measurements: The potentiometric titrations were carried out at 298.1 ± 0.1 K using 0.15 M $NaClO_4$ as supporting electrolyte. The experimental procedure (burette, potentiometer, cell, stirrer, microcomputer, etc.) has been fully described elsewhere.[42] The acquisition of the emf data was performed with the computer program PASAT.[43] The reference electrode was an Ag/AgCl electrode in saturated KCl solution. The glass electrode was calibrated as a hydrogen-ion-concentration probe by titration of previously standardized amounts of HCl with CO_2-free NaOH solutions and determining the equivalent point by Gran's method,[44] which gives the standard potential, $E^{0\prime}$, and the ionic product of water [pK_w = 13.73(1)]. The computer program HYPERQUAD was used to calculate the protonation and stability constants.[45] The protonation constants of L1 and L2 were taken from refs.[25,26], respectively. Protonation constants of L3 determined in 0.15 M NaCl at 298.1 K are as follows: log $K_{HL/H\cdot L}$ = 10.0(1), log $K_{H2L/HL\cdot H}$ = 9.15(1), log $K_{H3L/H2L\cdot H}$ = 7.81(1), log $K_{H4L/H3L\cdot H}$= 6.42(1), log $K_{H5L/H4L\cdot H}$ = 2.97(2). The pH range investigated was 2.5−10.5 and the concentration of the Zn^{II} ions and that of the ligands ranged from 1 × 10^{-3} to 5 × 10^{-3} M with Zn^{II}/L molar ratios varying between 2:1 and 1:2. The different titration curves for each system (at least two) were treated either as a single set or as separate curves without significant variations in the values of the stability constants. Finally, the sets of data were merged and treated simultaneously to give the final stability constants.

Kinetics of *p*-Nitrophenyl Acetate (NA) and Bis(*p*-nitrophenyl)phosphate (BNP) Hydrolysis: The hydrolysis rate of 4-nitrophenyl acetate in the presence of the dizinc complexes of L1, L2 and L3 was

 © 2004 Wiley-VCH Verlag GmbH & Co. KGaA, Weinheim

measured by an initial-slope method monitoring the increase in the 403-nm absorption of the released 4-nitrophenolate ion at 298.1 ± 0.1 K by using the procedure reported previously.[24] The ionic strength was adjusted to 0.15 M with $NaClO_4$. The reaction solution was maintained at 298.1 ± 0.1 K. MOPS (pH = 7.0−7.8), TAPS (pH = 7.8−8.9), CHES (pH = 8.9−9.7) and CAPSO (pH = 9.1−10.2) buffers were used (50 mM). In a typical experiment, after 4-nitrophenyl acetate and the dizinc complexes $[Zn_2L1](ClO_4)_4{\cdot}2H_2O$, $[Zn_2L2](ClO_4)_4{\cdot}4H_2O$ and $[Zn_2L3](ClO_4)_4{\cdot}2H_2O$ (0.1−1.0 mM) in 10% CH_3CN solutions at appropriate pH (the reference experiment does not contain the Zn^{II} complex) were mixed, the UV absorption decay was recorded immediately and was monitored generally until 2% decay of 4-nitrophenyl acetate. For all three ligands, two species — $[Zn_2LOH]^{3+}$ and $[Zn_2L(OH)_2]^{2+}$ — promote NA hydrolysis; in the case of L1, measurements in the pH range 7.5−8.2, where the $[Zn_2L1(OH)_2]^{2+}$ complex is absent from the solution, allowed us to determine second-order k_{NA1} rate constants for promoted hydrolysis by the monohydroxo species $[Zn_2L1OH]^{3+}$ and to extrapolate the k_{NA2} values for this species in the pH range 8.7−10.0, where both species are present in solution. Measurements in the pH range 8.7−10.0 allowed us to determine k_{OBS} values. The second-order rate constants k_{NA2} for the dihydroxo complex $[Zn_2L1(OH)_2]^{2+}$ are calculated by subtracting from the k_{OBS} value at a given pH the k_{NA1} value at the same pH. An analogous procedure was used for the L2 and L3 complexes. Errors in k_{NA} values were generally 5%. The hydrolysis rate of BNP to give mono(*p*-nitrophenyl)phosphate (MNP) and *p*-nitrophenolate (the hydrolysis products were identified by means of ^1H and ^{31}P NMR spectroscopy) in the presence of the dizinc complexes with L1−L3 was measured by an initial-slope method monitoring the increase in the 403 nm absorption of the *p*-nitrophenolate at 308.1 ± 0.1 K using a similar procedure to that reported for NA. The ionic strength was adjusted to 0.1 with NMe_4NO_3. The reaction solution was maintained at 308.1 ± 0.1 K. MOPS (pH = 6.5−7.8), TAPS (pH = 7.8−8.9), CHES (pH = 8.9−10.1) and CAPS (pH = 10.1−11.4) buffers were used (50 mM). Freshly prepared stock solutions of the zinc complexes and of BNP (1−10 mM) where used in the measurements. In a typical experiment, immediately after BNP and the zinc complexes were mixed in aqueous solutions at the appropriate pH value (the reference experiment does not contain the Zn^{II} complex), the UV absorption spectrum was recorded and monitored generally until 2% decay of BNP (for each second-order rate constant determination at least five experiments were monitored until 20−30%). For all systems, only the dihydroxo complexes $[Zn_2L(OH)_2]^{2+}$ (L = L1−L3) promote BNP hydrolysis. A plot of the hydrolysis rate vs. BNP concentration (0.1−1.0 mM) at a given pH value gave a straight line, and then we determined the slope/[zinc complex] ratio as the second-order rate constants k_{BNP} [M^{-1} s^{-1}]. Errors in k_{BNPP} values were about 5%.

Acknowledgments

Financial support by the DGCYT Generalitat Valenciana Project CTIDIB/2002/244 (Spain) Project no. BQU2003-09215-CO3-01, and Italian Ministero dell'Istruzione, dell'Università e della Ricerca (COFIN 2002) is gratefully acknowledged.

[1] [1a] E. Kimura, *Prog. Inorg. Chem.* **1994**, *41*, 443−441. [1b] E. Kimura, T. Koike, *Adv. Inorg. Chem.* **1997**, *44*, 229. [1c] E. Kimura, H. Hashimoto, T. Koike, *J. Am. Chem. Soc.* **1996**, *118*, 10963−10970.

[2] T. Darbre, C. Dubs, E. Rusanov, H. Stoeckli-Evans, *Eur. J. Inorg. Chem.* **2002**, 3284−3291.

[3] H. Aït-Haddou, J. Sunoaka, S. L. Wiskur, J. F. Folmer-Andersen, E. V. Anslyn, *Angew. Chem. Int. Ed.* **2002**, *41*, 4014−4016.

[4] B. Altava, M. I. Burguete, S. V. Luis, J. F. Miravet, E. García-España, V. Marcelino, C. Soriano, *Tetrahedron* **1997**, *53*, 4751−4761.

[5] [5a] P. Molenveld, J. F. J. Engbersen, D. N. Reinhoudt, *Eur. J. Org. Chem.* **1999**, 3269−3275. [5b] P. Molenveld, J. F. J. Engbersen, *Chem. Soc. Rev.* **2000**, *29*, 75−86.

[6] J. Blasko, T. C. Bruice, *Acc. Chem. Res.* **1999**, *32*, 475−484 and references therein.

[7] E. L. Hegg, J. N. Burstyn, *Coord. Chem. Rev.* **1998**, *173*, 133−165 and references therein. R. Krämer, *Coord. Chem. Rev.* **1999**, *182*, 243 and references therein.

[8] [8a] M. Yashiro, A. Ishikubo, M. Komiyama, *J. Chem. Soc., Chem. Commun.* **1995**, 1793−1794. [8b] M. Yashiro, A. Ishikubo, M. Komiyama, *Chem. Commun.* **1997**, 83−84. [8c] S. Matsuda, M. Yashiro, A. Kuzuya, A. Ishikubo, M. Komiyama, *Angew. Chem. Int. Ed. Eng.* **1998**, *37*, 3284−3286.

[9] P. Rossi, F. Felluga, P. Tecilla, F. Formaggio, M. Crisma, C. Toniolo, P. Scrimin, *Biopolymers* **2000**, *55*, 496−501. C. Sissi, P. Rossi, F. Felluga, F. Formaggio, M Palumbo, P. Tecilla, C. Toniolo, P. Scrimin, *J. Am. Chem. Soc.* **2001**, *123*, 3169−3170.

[10] D. Lee, P.-L. Hung, B. Sp bingler, S. J. Lippard, *Inorg. Chem.* **2002**, *41*, 521−531 and references therein. D. Kong, A. E. Martell, J. Reibenspies, *Inorg. Chim. Acta* **2002**, *333*, 7−14.

[11] W. H. Chapman Jr., R. Breslow, *J. Am. Chem. Soc.* **1995**, *117*, 5462−5469.

[12] S. Kondo, K. Shinbo, T. Yamaguchi, K. Yoshida, Y. Yano, *J. Chem. Soc., Perkin Trans. 2* **2001**, 128−131.

[13] F. Nihan, M. S. Akkaya, E. U. Akkaya, *J. Mol. Catal. A: Chem.* **2001**, *165*, 291−294.

[14] S. Kawahara, T. Uchimaru, *Eur. J. Inorg. Chem.* **2001**, 2437−2442.

[15] D. E. Fenton, H. Okawa, *Chem. Ber./Recueil* **1997**, *130*, 433−442.

[16] S.-A. Li, D.-X. Yang, D.-F. Li, J. Huang, W.-X. Tang, *New J. Chem.* **2002**, *26*, 1831−1837.

[17] C. Vichard, T. A. Kaden, *Inorg. Chim. Acta* **2002**, *337*, 173−180.

[18] K. Yamada, Y. Takahashi, H. Yamamura, S. Araki, K. Saito, M. Kawai, *Chem. Commun.* **2000**, 1315−1316.

[19] O. Iranzo, A. Y. Kovalevski, J. R. Morrow, J. P. Richard, *J. Am. Chem. Soc.* **2003**, *125*, 1988−1993.

[20] K. Worm, F. Chu, K. Matsumoto, M. D. Best, V. Linch, E. V. Anslyn, *Chem. Eur. J.* **2003**, *3*, 741−747.

[21] S. R. Korupoju, N. Mangayarkarasi, P. S. Zacharias, J. Mizuthani, H. Nishihara, *Inorg. Chem.* **2002**, *41*, 4099−4101.

[22] [22a] B. M. Trost, V. S. C. Yeh, *Angew. Chem. Int. Ed.* **2002**, *41*, 861−863. [22b] H. I. Park, L.-J. Ming, *Angew. Chem. Int. Ed.* **1999**, *38*, 2914−2916.

[23] For recent reviews, see: [23a] W. N. Lipscomb, N. Sträter, *Chem. Rev.* **1996**, *96*, 2375−2433. [23b] D. E. Wilcox, *Chem. Rev.* **1996**, *96*, 2435−2458. [23c] N. Sträter, W. N. Lipscomb, T. Klabunde, B. Krebs, *Angew. Chem. Int. Ed. Engl.* **1996**, *35*, 2024−2055. [23d] H.-J. Schneider, A. Yatsimirsky, in *Metal Ions in Biological Systems* (Eds.: H. Sigel, A. Sigel), Marcel Dekker, New York, **2003**, vol. 40, p. 369−462.

[24] C. Bazzicalupi, A. Bencini, A. Bianchi, V. Fusi, C. Giorgi, P. Paoletti, B. Valtancoli, D. Zanchi, *Inorg. Chem.* **1997**, *36*, 2784−2790.

[25] J. A. Aguilar, A. Bianchi, E. García-España, S. V. Luis, J. M. Llinares, J. A. Ramírez, C. Soriano, *J. Chem. Soc., Dalton Trans.* **1994**, 637−644.

[26] [26a] J. A. Aguilar, E. García-España, J. A. Guerrero, S. V. Luis, J. M. Llinares, J. F. Miravet, J. A. Ramírez, C. Soriano, *J. Chem. Soc., Chem. Commun.* **1995**, 2237−2239. [26b] J. A. Aguilar, E. García-España, J. Guerrero, S. V. Luis, J. M. Llinares, J. A. Ramírez, C. Soriano, *Inorg. Chim. Acta* **1996**, *246*, 287−294.

 © 2004 Wiley-VCH Verlag GmbH & Co. KGaA, Weinheim

[27] A. Bencini, M. I. Burguete, E. García-España, S. V. Luis, J. F. Miravet, C. Soriano, *J. Org. Chem.* **1993**, *58*, 4749−4753.
[28] C. Bazzicalupi, A. Bencini, V. Fusi, C. Giorgi, P. Paoletti, B. Valtancoli, *J. Chem. Soc., Dalton Trans.* **1999**, 393−399.
[29] R. M. Smith, A. E. Martell, *NIST Stability Constants Database*, version 4, National Institute of Standards and Technology, Washington, DC**, 1997**.
[30] [30a] E. García-España, S. V. Luis, *Supramol. Chem.* **1996**, *6*, 257−266. [30b] S. Andrés, B. Escuder, A. Doménech, E. García-España, S. V. Luis, V. Marcelino, J. M. Llinares, J. A. Ramírez, C. Soriano, *J. Phys. Org. Chem.* **2001**, *14*, 495−500.
[31] [31a] C. Bazzicalupi, A. Bencini, A. Bianchi, C. Giorgi, V. Fusi, B. Valtancoli, M. A. Bernardo, F. Pina, *Inorg. Chem.* **1999**, *38*, 3806−3813. [31b] A. Bencini, M. A. Bernardo, A. Bianchi, V. Fusi, C. Giorgi, F. Pina and B Valtancoli, *Eur. J. Inorg. Chem.* **1999**, 1911−1918.
[32] C. Bazzicalupi, A. Bencini, A. Bianchi, V. Fusi, P. Paoletti, G. Piccardi, B. Valtancoli, *Inorg. Chem.* **1995**, *34*, 5622−5631.
[33] A. Bencini, E. Berni, A. Bianchi, V. Fedi, C. Giorgi, P. Paoletti, B. Valtancoli B, *Inorg. Chem.* **1999**, *38*, 4115−4122.
[34] T. Koike, E. Kimura, *J. Am. Chem. Soc.* **1991**, *113*, 8935−8941.
[35] E. Kimura, *Tetrahedron* **1992**, *30*, 6175−6217.
[36] [36a] C. Bazzicalupi, A. Beconcini, A. Bencini, C. Giorgi, V. Fusi, A. Masotti, B. Valtancoli, *J. Chem. Soc., Perkin Trans. 2* **1999**, 1675−1682. [36b] C. Bazzicalupi, A. Bencini, E. Berni, A. Bianchi, P. Fornasari, C. Giorgi, C. Marinelli, B. Valtancoli, *Dalton Trans.* **2003**, 2564−2572. [36c] C. Bazzicalupi, A. Bencini, E. Berni, A. Bianchi, P. Fornasari, C. Giorgi, B. Valtancoli, *Eur. J. Inorg. Chem.* **2003**, 1974−1983.
[37] M. Bastian, H. Sigel, *Inorg. Chem.* **1997**, *36*, 1619−1624 and references therein.
[38] G. Liang, R. Tribolet, H. Sigel, *Inorg. Chem.* **1988**, *27*, 2877−2887.
[39] A. K. Convington, M. Paabo, R. A. Robinson, R. G. Bates, *Anal. Chem.* **1968**, *40*, 700−708.
[40] C. Frassineti, S. Gelli, P. Gans, A. Sabatini, M. S. Moruzzi, A. Vacca, *Anal. Biochem.* **1995**, *231*, 374−382.
[41] [41a] J. A. Aguilar, P. Díaz, F. Escartí, E. García-España, L. Gil, C. Soriano, B. Verdejo, *Inorg. Chim. Acta* **2002**, *339*, 307−316. [41b] H. Gampp, D. Haspra, M. Maeder, A. D. Zuberbuehler, *Inorg. Chem.* **1984**, *23*, 3724−3730.
[42] E. García-España, M.-J. Ballester, F. Lloret, J.-M. Moratal, J. Faus, A. Bianchi, *J. Chem. Soc., Dalton Trans.* **1988**, 101−104.
[43] M. Fontanelli, M. Micheloni, *Proceedings of the I Spanish-Italian Congress on Thermodynamics of Metal Complexes*, Diputación de Castellón, Castellón, Spain, **1990**. Program for the automatic control of the microburette and the acquisition of the electromotive force readings.
[44] [44a] G. Gran, *Analyst (London)* **1952**, *77*, 661−671. [44b] F. J. Rossotti, H. Rossotti, *J. Chem. Educ.* **1965**, *42*, 375−378.
[45] P. Gans, A. Sabatini, A. Vacca, *Talanta* **1996**, *43*, 1739−1753.

Received February 27, 2004
Early View Article
Published Online August 12, 2004

 © 2004 Wiley-VCH Verlag GmbH & Co. KGaA, Weinheim

Microwave-Induced Polyol-Process Synthesis of Copper and Copper Oxide Nanocrystals with Controllable Morphology

Yu Zhao,[a] Jun-Jie Zhu,*[a] Jian-Min Hong,[a] Ningsheng Bian,[a] and Hong-Yuan Chen[a]

Keywords: Copper / Copper oxides / Microwaves / Nanostructures / UV / Vis spectroscopy

Different morphologies of copper and copper oxide nanocrystallites, including radially arrayed whiskers, cubic particles and sphere particles, have been successfully synthesized by a microwave-induced method under ambient conditions. In aqueous solution containing different ethylene glycol concentrations, copper acetate hydrate produces different reduction products. The as-prepared copper and copper oxide crystallites were characterized by various techniques, including X-ray powder diffraction, transmission electron microscopy, selected-area electron diffraction and UV/Vis absorption spectroscopy. It was found that microwave irradiation plays a critical role in the formation of the products; temperature was also found to be important in the reaction. The irradiation time and copper acetate concentration also affect the morphology of the products. The possible formation mechanism is also discussed.
((c) Wiley-VCH Verlag GmbH & Co. KGaA, 69451 Weinheim, Germany, 2004)

Introduction

Nanometer-sized metals, semiconductors, and oxides are of great interest because they can have physical and chemical properties that are not characteristic of the atoms or of their bulk counterparts. The large surface area to volume ratio can contribute to some of the unique properties of nanoparticles.[1−5] Among them, Cu, Cu_2O and CuO are industrially important materials that are widely used in fields such as magnetic storage media, solar energy transformation, electronics, sensors, catalysis, batteries, resonance imaging and so forth.[6−12] In the past, some successful attempts have been made to synthesize nanoparticles of copper and copper oxides, such as sonochemical methods,[13−15] microwave irradiation,[16] photochemical methods,[17−20] hydrothermal and solvothermal methods,[21,22] electrochemical methods,[23−31] sol-gel methods,[32−35] solid-state reactions,[36] chemical reduction and decomposition route[37−42] and so on.

Microwaves are a portion of the electromagnetic spectrum with frequencies in the range of 300 MHz to 300 GHz. The corresponding wavelengths of these frequencies are 1 m to 1 mm. The most commonly used frequency is 2.45 GHz. The degree of interaction of microwaves with a dielectric medium is related to the material′s dielectric constant and dielectric loss.[43] When microwaves penetrate and propagate through a dielectric solution or suspension, the internal electric fields generated within the affected volume induce translation motions of free or bound charges such as electrons or ions and rotate charged complexes such as dipoles.[43] The resistance of these induced motions due to inertial, elastic, and frictional force, which are frequency dependent, causes losses and attenuates the electric field. Compared to ultrasonic irradiation, there is no similar bubble formation during microwave heating, although superheating occurs in localized spots. The main advantages of microwave-assisted reactions over conventional methods in synthesis are: (a) the kinetics of the reaction are increased by one to two orders of magnitude, (b) novel phases are formed, (c) the initial heating is rapid, which can lead to energy savings, and (d) selective formation of one phase over another often occurs.[44−46] One possible hypothesis for these microwave-induced effects is the generation of localized high temperatures at the reaction sites to enhance reaction rates in an analogous manner to that of ultrasonic waves,[47] where both high temperatures and pressures have been reported during reactions. The enhanced kinetics of crystallization can lead to energy savings of up to 90%.[48]

The polyol method is a low-temperature process that is environmentally benign because the reactions are carried out under closed-system conditions. It was first introduced to produce metal submicron-sized powders.[49−51] In this method, a suitable solid metal salt is suspended in a liquid polyol. The suspension is stirred and heated to a certain temperature; the reduction of the starting compound yields fine metal powders. The polyol itself acts not only as a solvent in the process but also as a stabilizer, limiting particle growth and prohibiting agglomeration.[52−54] Recently, this method has also been extended to the preparation of metal oxides[55−57] and metal chalcogenides.[58−60] Tarascon and co-workers have demonstrated that in these reactions the

[a] State Key Laboratory of Coordination Chemistry, Department of Chemistry, Nanjing University, Nanjing, 210093, P. R. China
Supporting information for this article is available on the WWW under http://www.eurjic.org or from the author.

 © 2004 Wiley-VCH Verlag GmbH & Co. KGaA, Weinheim DOI: 10.1002/ejic.200400258

temperature is a dominant factor in affecting the reactivity. Three factors are influenced by the temperature: (1) the reduction potential of ethylene glycol, (2) the rupture and creation of chemical bonds, and (3) diffusion.[61] All these factors make microwave-heating techniques favorable for the fabrication of metal and metal oxides by using ethylene glycol as a solvent. The ethylene glycol is an excellent susceptor for the microwave radiation because of its high permanent dipole. The metallic particles produced as intermediates in the polyol reaction are also good for this purpose.

In this paper, we present a novel microwave-induced polyol route to synthesize different morphologies of Cu, Cu_2O and CuO nanoparticles. Ethylene glycol (EG) aqueous solutions with different concentration were used in order to control the reaction temperature during the microwave heating. Cu, Cu_2O or CuO were formed in the different conditions. The effect on the morphology of the nanoparticles was also investigated. It was found to be a fast, convenient, mild, energy efficient and environmentally friendly route to produce nanoparticles of Cu, Cu_2O and CuO.

Results and Discussion

In order to study the nature and morphology of the products, various techniques such as X-ray diffraction (XRD), transmission electron microscopy (TEM), selected-area electron diffraction (SAED) and UV/Vis absorption spectroscopy were employed.

The results of the powder XRD analysis are shown in Figure 1 (see a−e). The diffraction peaks correspond to the reflection of: (a) CuO (CCID file no. 801916 monoclinic), (b) CuO mixed with Cu_2O, (c) Cu_2O (CCID file no. 782076 cubic), (d) Cu_2O mixed with Cu, and (e) Cu (CCID file no. 040836 cubic). In all the reactions, highly crystalline products were obtained. The positions of the peaks are in good agreement with literature values.

TEM images of the products are presented in Figure 2 (see a−e), where the different morphologies that be achieved simply by changing the water/EG ratio of the solvent can be clearly observed. Figure 2 (a) depicts the morphology of CuO, which shows radially arrayed whiskers. In this image, a single whisker is calculated to be about 80 nm in length and less than 10 nm in diameter; the SAED pattern of the products is shown in the inset. Figure 2 (b) shows a mixture of whiskers and cubic particles. Two different phases can be observed clearly in this picture. According to the SEAD images, and compared with the other SEAD patterns shown in Figure 2 (see a and c), it can be concluded that the whiskers are CuO of monoclinic phase [SAED pattern inset top right in Figure 2 (b)], and the cubes are Cu_2O in the cubic phase (SAED pattern inset bottom left). Cu_2O particles are observed as shown in Figure 2 (c); they are around 50 nm cubic nanoparticles. The SAED pattern of a single crystal of one of these particles is shown in the inset. Figure 2 (d) depicts Cu mixed with Cu_2O particles; the products are not clearly separated. We conclude it to be mixture only by the XRD pattern in Figure 1. Figure 2 (e) depicts Cu particles, the size of which ranges from 100−120 nm. The SEAD pattern of these copper particles is inset.

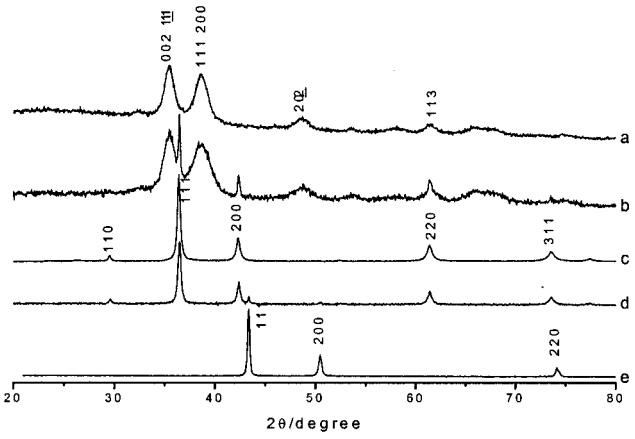

Figure 1. XRD patterns of: (a) CuO; (b) CuO mixed with Cu_2O; (c) Cu_2O; (d) Cu_2O mixed with Cu; (e) Cu

In order to elucidate the mechanism of temperature control in the EG aqueous solution, we first supposed that the ethylene glycol and water mixture is an ideal binary system, which therefore behaves according to Raoults Law

$$y_A = x_A \cdot P^*_A / P$$

with y_A = mol fraction of substance A in the vapor phase equilibrium with the solution, X_A = mol fraction of substance A in the solution; P^*_A = equilibrium vapor pressure of substance A; P = vapor pressure of the whole system.

We calculated the theoretical boiling point of the system at different water volume ratios; the results are depicted in Figure 3. In our microwave dielectric heating process, the system temperature elevates rapidly. The reaction temperatures measured fit well with the theoretical values. As a result, an accurate and average temperature can be controlled in our microwave dielectric heating system.

As far as we know, when the solvent is pure ethylene glycol copper acetate is only partly dissolved and no chemical reaction occurs at 108 °C; when the solvent is water, copper acetate is completely soluble. On the contrary, in the EG aqueous solution, when the reaction temperature varies between 90 and 108 °C, CuO can be produced. We propose the process of producing CuO as follows: first, copper acetate hydrate dissolves in the solution; then EG esterifies with OAc^- to produce ethylene glycol monoacetate and OH^-; finally OH^- and Cu^{2+} ion combine in solution and then dehydrate to form CuO. The reaction can be schematized as follows:

$$CH_3COO^- + HOCH_2CH_2OH \xrightarrow{\Delta} CH_3COOCH_2CH_2OH + OH^- \quad (1)$$

$$Cu^{2+} + 2\,OH^- \xrightarrow{\Delta} CuO\,(s) + H_2O \quad (2)$$

 © 2004 Wiley-VCH Verlag GmbH & Co. KGaA, Weinheim

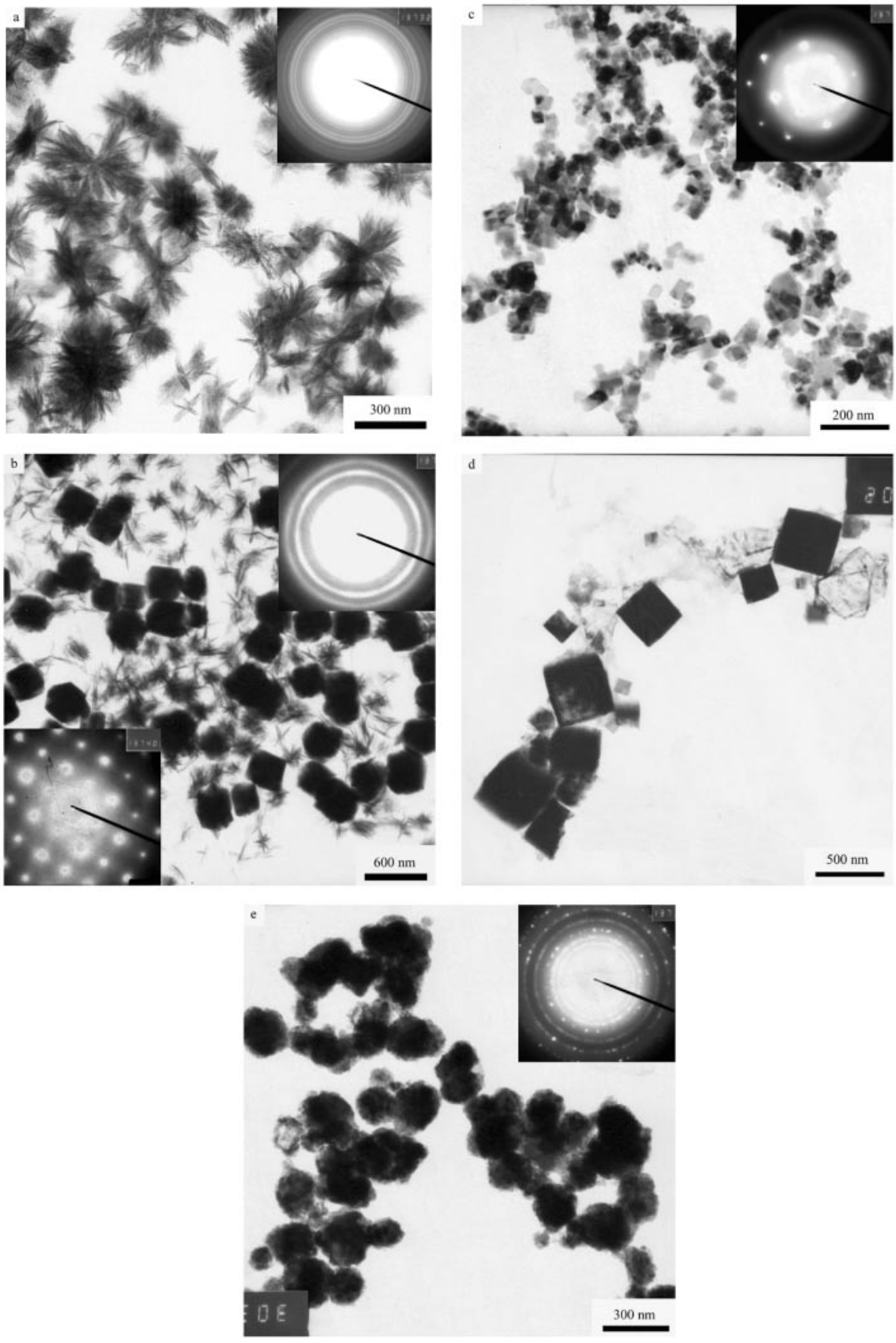

Figure 2. The TEM images of as-prepared: (a) CuO (inset: SEAD of CuO); (b) CuO mixed with Cu_2O (inset bottom left: SAED of the whiskers; top right: SAED of a single cube); (c) Cu_2O (inset: SEAD pattern of Cu_2O) (d) Cu_2O mixed with Cu; (e) Cu (inset: SAED pattern of Cu particles)

 © 2004 Wiley-VCH Verlag GmbH & Co. KGaA, Weinheim

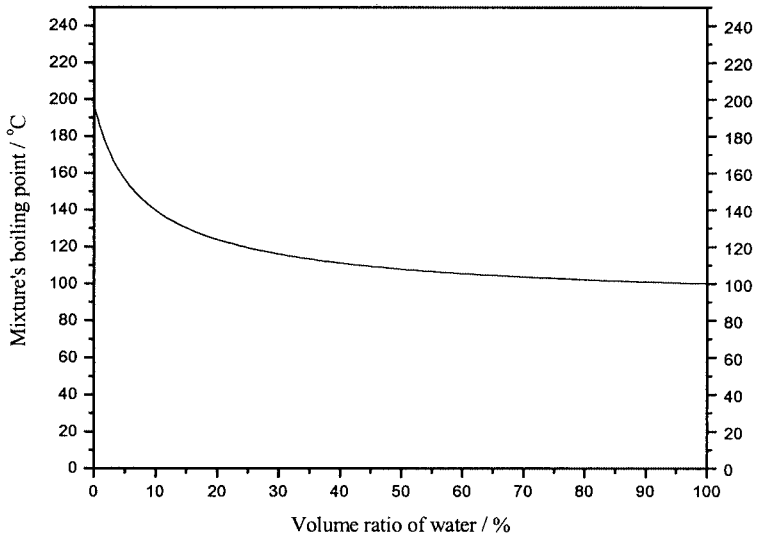

Figure 3. Theoretical boiling points with different EG volume ratios in the EG aqueous system

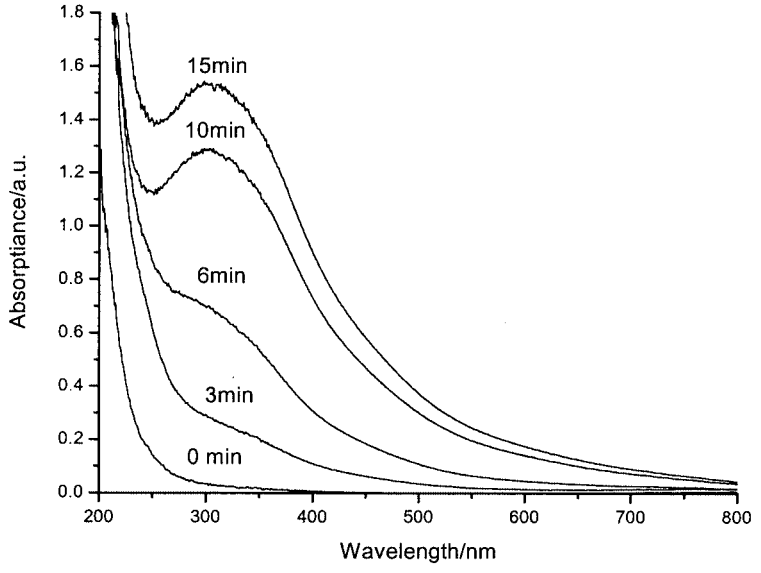

Figure 4. The UV/Vis absorption spectra of a suspension of copper acetate (0.03 g/40 mL) suspended in 49% EG aqueous solution after different microwave irradiation times; the numbers on the spectra indicate the time of irradiation; path length = 1 cm

To prove the reaction mechanism, we removed the water from the solvent for GC-MS detection after removing the precipitate by centrifugation. The results show that ethylene glycol monoacetate is the only reaction product remaining in solution.

To demonstrate the formation process of CuO nanocrystals, we recorded UV/Vis absorption spectra at different reaction times (Figure 4). There is no absorption present at the beginning of the reaction (0 min). As the reaction proceeds, however, an absorption shoulder appears at around 310 nm. After 15 minutes irradiation, the suspension becomes dark-brown, and a broad absorption peak centered at 310 nm can be observed. There is no obvious shift of the absorption peak with time. This means that the crystal size changes very little during the whole precipitation process. As an ionic reaction, reaction 2 is comparatively fast, so the formation of CuO nanocrystals is determined by reaction 1. In this process, the single whiskers prepared from different copper acetate concentration have the same size.

Figure 5 (see a−d) shows the change in morphology of as-prepared CuO as a function of time. The growth of CuO-whisker arrays can be described by three steps. First, crystal seeds of CuO are formed. These seeds then grown into whiskers, and, in the end, the CuO whiskers assemble into radially arrayed whiskers.

The concentration of copper acetate also plays a dramatic role in determining the morphology (Figure 6). In the case of a single whisker of the CuO nanocrystals, the crystal size is almost the same for all copper acetate concentration, but the morphology varies: the higher the concentration is, the denser the radial arrays will be. As we can see, when the

 © 2004 Wiley-VCH Verlag GmbH & Co. KGaA, Weinheim

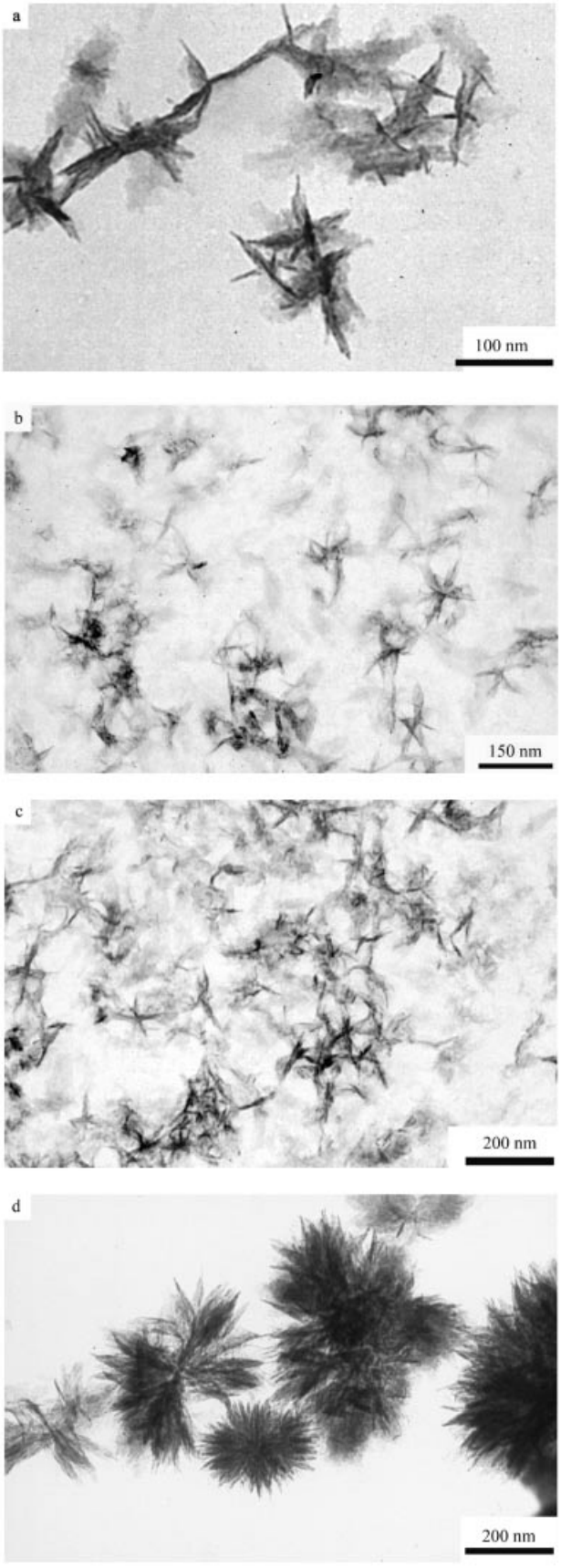

Figure 5. TEM images of CuO as a function of reaction time: a) 3 min; b) 6 min; c) 10 min; d) 15 min (0.03 g/40 mL copper acetate in 49% EG aqueous solution)

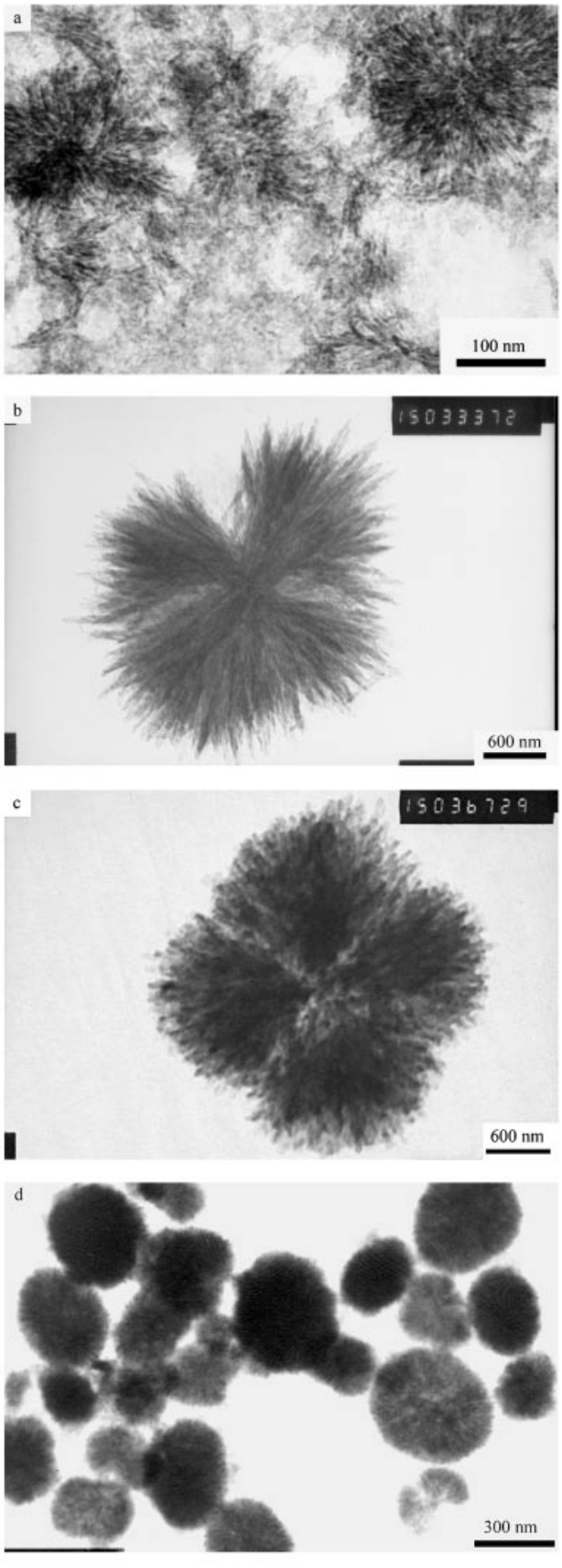

Figure 6. TEM images of CuO at various copper acetate concentrations: a) 0.03 g; b) 0.30 g; c) 0.70 g; d) 1.00 g (in 40 mL 49% EG aqueous solution)

 © 2004 Wiley-VCH Verlag GmbH & Co. KGaA, Weinheim

copper acetate concentration increases to 0.70 g/40 mL, the CuO radical arrays are so dense that they look like a sphere (see d in Figure 6). Interestingly we also found that the growth of the radial whisker arrays is directed mainly along the axes of a tetrahedron.

Cu and Cu_2O nanocrystals can also be prepared by this method; they follow a reduction mechanism. At 197 °C, the reduction product is Cu. Fievet et al.[2] have proposed that the metal particles are formed by nucleation and growth from the solution. According to this mechanism, we have proposed a formation process for the Cu nanoparticles: first, under dielectric heating, copper acetate hydrate dissolves completely in ethylene glycol, and then the intermediate solid phase between the starting material and the final metal powder is formed; during the second stage of the reaction the re-dissolution of the intermediate solid phase takes place. The reduction action of ethylene glycol is due to diacetyl, which is formed by a duplicative oxidation of acetaldehyde previously produced by dehydration of ethylene glycol.

The reaction can be schematized as follows:

$$2\ CH_2OH\text{-}CH_2OH \xrightarrow{-H_2O} 2\ CH_3CHO$$

Intermediate phase

$$\longrightarrow CH_3\text{-}CO\text{-}CO\text{-}CH_3 + H_2O + 2\ Cu$$

UV/Vis spectra were taken as a function of time (Figure 7). After six minutes irradiation, an absorption shoulder appears at around 490 nm, which indicates an intermediate phase. The phase will be shown to be Cu_2O later. After nine minutes, colloidal copper has formed with an absorption peak at 580 nm. This absorption can be attributed to the plasma resonance absorption of the copper particles. As the reaction progresses, the copper colloid aggregates and precipitates. As a result, after 15 minutes the absorption peak at 580 nm has almost disappeared.

Figure 8 (a−d) depict the change in morphology of copper as a function of time. After six minutes, Cu_2O cubic particles of about 300 nm have formed. This Cu_2O is continuously being reduced to give dispersedCu particles with a dispersed particle size of about 15 nm in diameter (c in Figure 8). However, after reaction for 15 minutes, the Cu aggregates into particles of about 60 nm.

Cu_2O is obtained at 140 °C. UV/Vis absorption spectra were recorded after different reaction times to investigate the reaction (Figure 9). Only after 12 minutes did the absorption shoulder at around 460 nm appear. This peak can be attributed to Cu_2O, and corresponds well with the absorption band of the intermediate phase in the preparation of Cu nanoparticles.

The growth of Cu_2O nanoparticles was also investigated (Figure 10). As can be seen from the morphology of Cu_2O after different reaction times, the Cu_2O is formed as cubes of about 40 nm (Figure 10, a). As the reaction proceeds the particles grow further. It is interesting that hexagons [Figure 10 (d)] and truncated cubes [Figure 10 (e)] are also found in the reaction products; they can be regarded as intermediate morphologies en route to cubic particles. An SEAD pattern was also measured. As calculated, the inserted SEAD pattern of a truncated cube in Figure 10 (d) shows the (001) face and the hexagon in Figure 10 (e) shows the (111) face; they are both Cu_2O of primitive cubic phase. As the reaction time is prolonged to 30 minutes, we can get cubic Cu_2O as large as 500 nm. It is therefore possible to control the size of the Cu_2O crystals.

Conclusion

Using a novel microwave-induced polyol process, we have successfully synthesized copper, cuprites and copper(II) oxides systematically. The EG aqueous solution was heated by microwave irradiation, easy and precise control on the temperature was realized. By varying the conditions we

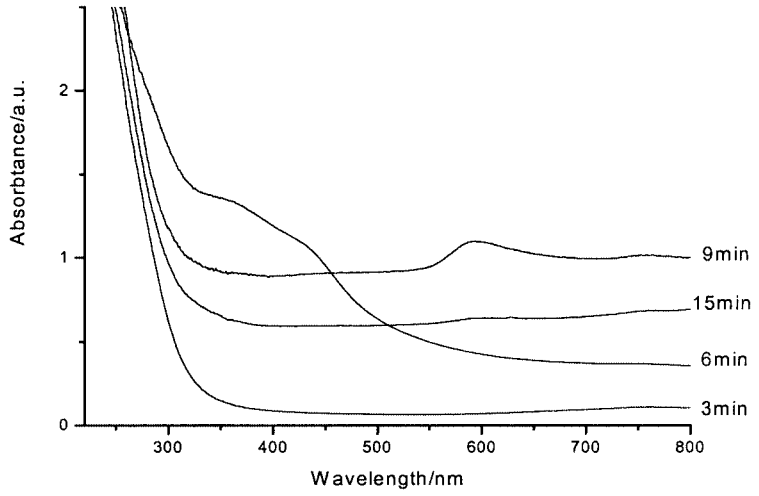

Figure 7. The UV/Vis absorption spectra of a suspension of copper acetate (0.03 g/40 mL) in pure EG solution as a function of irradiation time; the numbers on the spectra indicate the time of irradiation; path length = 1 cm

 © 2004 Wiley-VCH Verlag GmbH & Co. KGaA, Weinheim

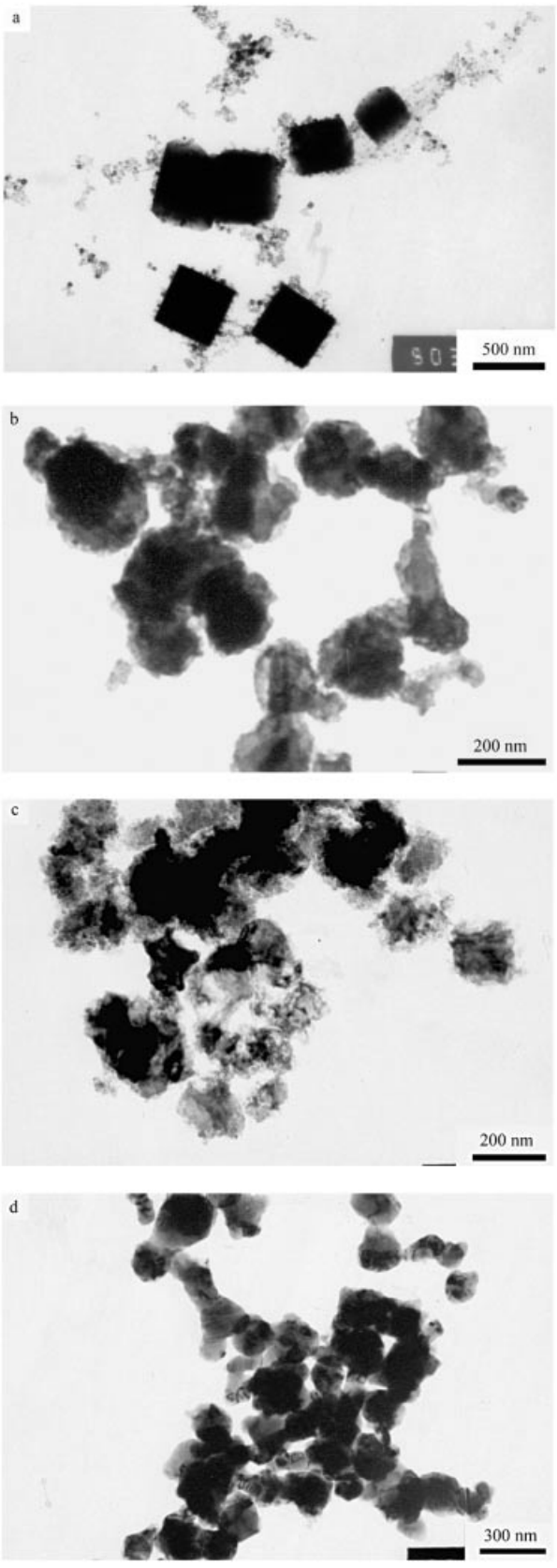

Figure 8. The TEM images in the formation of Cu as a function of reaction time: a) 6 min; b) 8 min; c) 9 min; d) 15 min (0.03 g/40 mL copper acetate in pure EG solution)

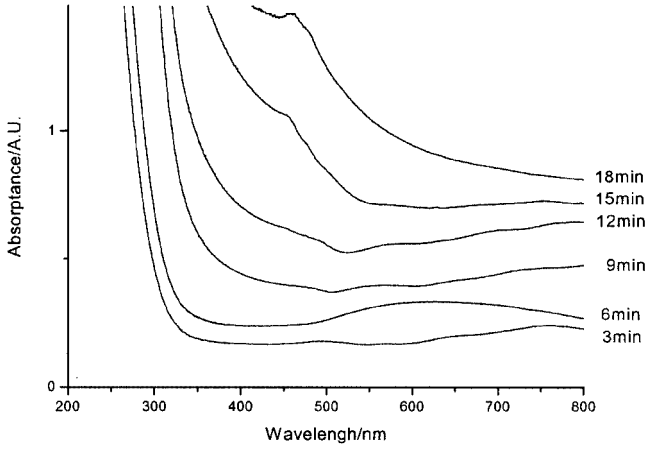

Figure 9. The UV/Vis absorption spectra of a suspension of copper acetate (0.03 g/40 mL) in 90% EG aqueous solution after different irradiation times; the numbers on the spectra indicate the irradiation time; path length = 1 cm

were able to prepare products with different morphology and particle sizes. A formation mechanism of the as-prepared products was proposed and the effects on the morphology and size were investigated. This kind of method is advantageous as it is a one-step reaction that occurs at relatively mild temperatures and gives well-dispersed products. Its extension to the preparation of other materials is currently being investigated.

Experimental Section

General: All the experiments were performed in a modified National frequency-convertible microwave oven (NN-S570MFS). A reflux system was connected to the microwave oven. X-ray powder diffraction (XRD) measurements were performed on a Philips X′pert X-ray diffractometer at a scanning step of 0.03°, continue time 10 seconds, in the 2q range from 20° to 80°, with graphite monochromated Cu-K_a radiation (l = 0.15418 nm) and a nickel filter. Transmission electron microscopy (TEM) images and selected-area electron diffraction (SAED) images were recorded on a JEOL-JEM 200CX transmission electron microscope, at an accelerating voltage of 200 kV. The samples used for TEM observations were prepared by dispersing some products in ethanol followed by ultrasonic vibration for 30 min, then placing a drop of the dispersion onto a copper grid coated with a layer of amorphous carbon. A Shimazu UV-2401PC photospectrometer was used to record the UV/Vis absorption spectra of the as-prepared samples dispersed in water.

Synthesis of Copper and Copper Oxides: In a typical procedure, the appropriate amount of $Cu(OAc)_2 \cdot H_2O$ was added into an 80 mL round-bottomed flask, and then 40 mL of EG aqueous solution was added into the same flask. The mixture was placed into the microwave reflux system and the reaction was carried out under ambient conditions for 15 minutes at a power of 365 W. The detailed reaction conditions in various EG aqueous solutions are listed in Table 1. The reactants dissolved in the EG aqueous solution after irradiating for 3 min. As the reaction progressed a large amount of precipitate formed (dark-brown for CuO, reddish yellow for Cu_2O, and red for Cu). After the reaction, the suspension was

 © 2004 Wiley-VCH Verlag GmbH & Co. KGaA, Weinheim

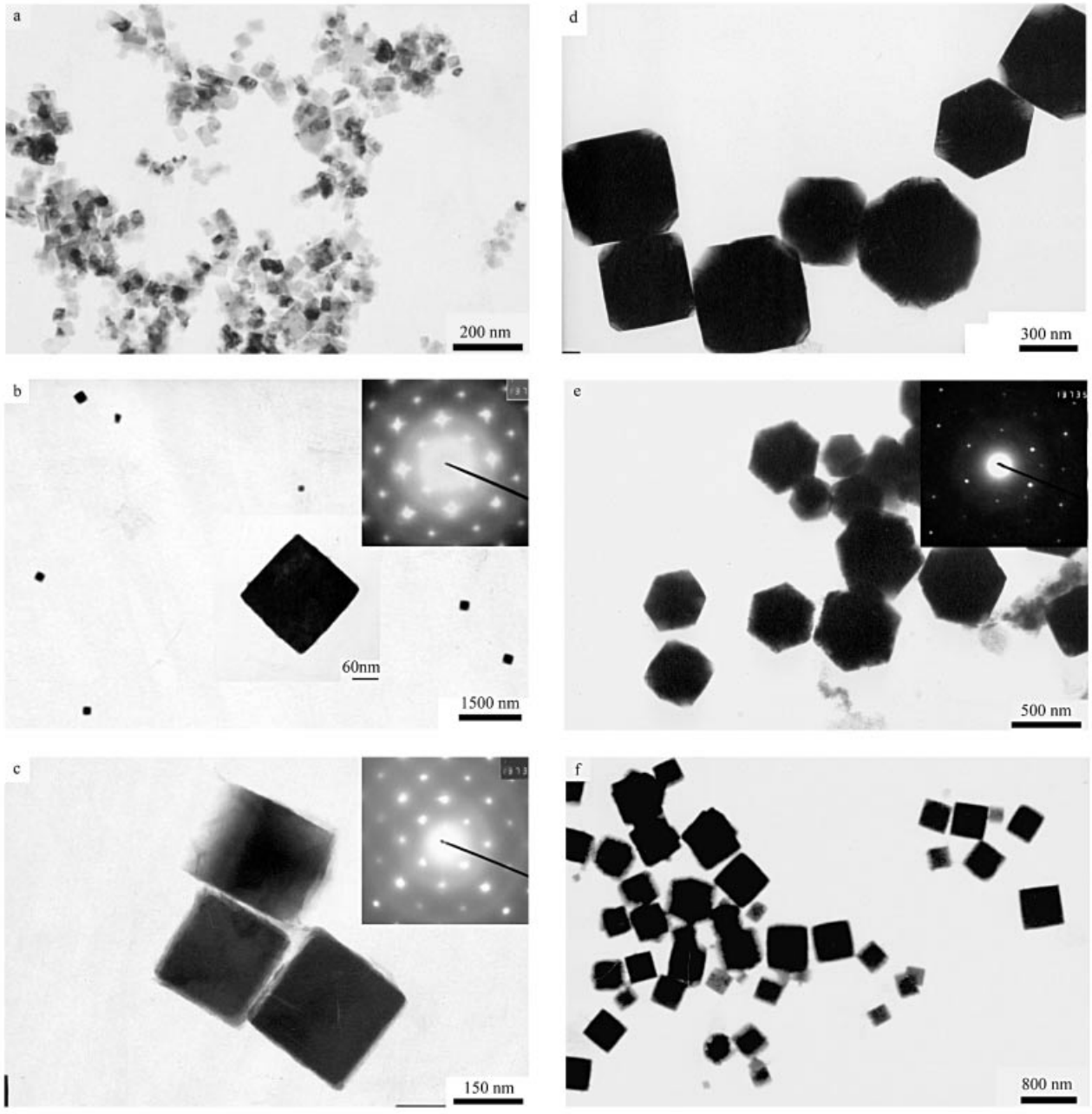

Figure 10. The TEM images of Cu_2O as a function of reaction time: a) 3 min; b) 6 min; c) 9 min; d) and e) 15 min; f) 30 min (0.03 g/40 mL copper acetate in 90% EG aqueous solution)

Table 1. The reaction conditions in various EG aqueous solutions and products via Microwave dielectric heating

Condition	EG volume ratio (%)	Water volume ratio (%)	Reaction temp. (°C)	Precipitate
o	0	100	100	–
a	49	51	108	CuO
b	75	25	119	CuO and Cu_2O
c	90	10	140	Cu_2O
d	95	5	156	Cu_2O and Cu
e	100	0	197	Cu

cooled to room temperature and the precipitate was centrifuged, washed with distilled water, absolute ethanol and acetone in sequence and dried in vacuo at room temperature. The final products were collected for characterizations. The products of the different reactions are also listed in Table 1.

Acknowledgments

This work was supported by the National Natural Science Foundation of China (No.20325516, 90206037) and the Research Foundation for the Doctoral Program of the Ministry of Education of China (Grant No. 20020284022). The authors also thank Prof. Xinhua Xia and Mr. Zhengwei Shi for allowing us to use their facilities.

[1] M. D. Morse, *Chem. Rev.* **1986**, *86*, 1049−1109.
[2] W. P. Halperin, *Rev. Mod. Phys.* **1986**, *58*, 533−603.
[3] A. Henglein, *Chem. Rev.* **1989**, *89*, 1861−1873.

 © 2004 Wiley-VCH Verlag GmbH & Co. KGaA, Weinheim

[4] G. D. Stucky, J. E. MacDougall, *Science* **1990**, *247*, 669−678.
[5] V. V. Kresin, *Phys. Rep.* **1992**, *220*, 1−52.
[6] A. Inoue, B. L. Shen, *J. Mater. Res.* **2003**, *18*, 2799−2806.
[7] S. Krongelb, L. T. Romankiw, J. A. Tornello, *IBM J. Res. Dev.* **1998**, *42*, 575−585.
[8] T. Mitsuyu, O. Yamakazi, K. Ohji, K. Wasa, *Ferroelectrics* **1982**, *42*, 233−240.
[9] M. M. Viitanen, W. P. A. Jansen, R. G. van Welzenis, H. H. Brongersma, D. S. Brands, E. K. Poels, A. Bliek, *J. Phys. Chem. B* **1999**, *103*, 6025−6029.
[10] U. Bjoerksten, J. Moser, M. Graetze, *Chem. Mater.* **1994**, *6*, 858−863.
[11] J. Tamaki, K. Shimanoe, Y. Yamada, Y. Yamamoto, N. Miura, N. Yamazoe, *Sens. Actuat. B* **1998**, *49*, 121−125.
[12] Y. Jiang, S. Decker, C. Mohs, K. J. Klabunde, *J. Catal.* **1998**, *180*, 24−35.
[13] R. V. Kumar, Y. Mastai, Y. Diamant, A. Gedanken, *Chem. Mater.* **2000**, *12*, 2301−2305.
[14] R. V. Kumar, Y. Mastai, Y. Diamant, A. Gedanken, *J. Mater. Chem.* **2001**, *11*, 1209−1213.
[15] N. A. Dhas, C. P. Raj, A. Gedanken, *Chem. Mater.* **1998**, *10*, 1446−1452.
[16] H. Wang, J. Z. Xu, J. J. Zhu, H. Y. Chen, *J. Cryst. Growth* **2002**, *244*, 88−94.
[17] G. G. Condorelli, L. L. Costanzo, I. L. Fragala, S. Giuffrida, G. Ventimiglia, *J. Mater. Chem.* **2003**, *13*, 2409−2411.
[18] S. Kapoor, T. Mukherjee, *Chem. Phys. Lett.* **2003**, *370*, 83−87.
[19] A. V. Loginov, V. V. Gorbunova, T. B. Boitsova, *J. Nanopart. Res.* **2002**, *4*, 193−205.
[20] T. B. Boitsova, A. V. Loginov, V. V. Gorbunova, *Russ. J. Appl. Chem.* **1997**, *70*, 1507−1512.
[21] Z. Liu, Y. Yang, J. Liang, Z. Hu, S. Li, S. Peng, Y. J. Qian, *J. Phys. Chem. B* **2003**, *107*, 12658−12661.
[22] S. J. Chen, X. T. Chen, Z. L. Xue, L. H. Li, X. Z. You, *J. Cryst. Growth* **2002**, *246*, 169−175.
[23] M. G. Shumsky, J. A. Switzer, *Chem. Mater.* **1999**, *11*, 2289−2291.
[24] J. K. Barton, A. A. Vertegel, E. W. Bohannan, J. A. Switzer, *Chem. Mater.* **2001**, *13*, 952−959.
[25] L. Huang, H. Wang, Z. Wang, A. Mitra, D. Zhao, Y. Yan, *Chem. Mater.* **2002**, *14*, 876−880.
[26] S. Kenane, L. Piraux, *J. Mater. Res.* **2002**, *17*, 401−406.
[27] M. E. T. Molares, V. Buschmann, D. Dobrev, R. Neumann, R. Scholz, I. U. Schuchert, J. Vetter, *Adv. Mater.* **2001**, *13*, 62−65.
[28] I. Enculescu, Z. Siwy, D. Dobrev, C. Trautmann, M. E. T. Molares, R. Neumann, K. Hjort, L. Westerberg, R. Spohr, *Appl. Phys. A, Mater. Sci. Process.* **2003**, *77*, 751−755.
[29] Y. Konishi, M. Motoyama, H. Matsushima, Y. Fukunaka, R. Ishii, Y. Ito, *J. Electroanal. Chem.* **2003**, *559*, 149−153.
[30] T. Gao, G. W. Meng, Y. W. Wang, S. H. Sun, L. Zhang, *J. Phys.: Condens. Matter* **2002**, *14*, 355−363.
[31] D. K. Sarkar, X. J. Zhou, A. Tannous, M. Louie, K. T. Leung, *Solid State Commun.* **2003**, *125*, 365−368.
[32] C. L. Kitchens, M. C. McLeod, C. B. Roberts, *J. Phys. Chem. B* **2003**, *107*, 11331−11338.
[33] L. Armelao, D. Barreca, M. Bertapelle, G. Bottaro, C. Sada, E. Tondello, *Thin Solid Films* **2003**, *442*, 48−52.
[34] J. C. S. Wu, I. H. Tseng, W. C. Chang, *J. Nanopart. Res.* **2001**, *3*, 113−118.
[35] M. Epifani, G. T. De, A. Licciulli, L. Vasanelli, *J. Mater. Chem.* **2001**, *11*, 3326−3332.
[36] W. H. Wang, Y. J. Zhan, G. H. Wang, *Chem. Commun.* **2001**, 727−728.
[37] M. Yang, J. J. Zhu, *J. Cryst. Growth* **2003**, *256*, 134−138.
[38] W. Wang, Z. Liu, Y. Liu, C. Xu, C. Zheng, G. Wang, *Appl. Phys. A, Mater. Sci. Process.* **2003**, *76*, 417−420.
[39] C. K. Xu, Y. K. Liu, G. D. Xu, G. H. Wang, *Mater. Res. Bull.* **2002**, *37*, 2365−2372.
[40] W. Z. Wang, G. H. Wang, X. S. Wang, Y. J. Zhan, Y. K. Liu, C. L. Zheng, *Adv. Mater.* **2002**, *14*, 67−69.
[41] L. F. Gou, C. J. Murphy, *Nano. Lett.* **2003**, *3*, 231−234.
[42] M. H. Cao, C. W. Hu, Y. H. Wang, Y. H. Guo, C. X. Guo, E. B. Wang, *Chem. Commun.* **2003**, 1884−1885.
[43] W. H. Sutton, *Am. Ceram. Soc. Bull.* **1989**, *68*, 376.
[44] H. Katsuki, S. Komarneni, *J. Am. Ceram. Soc.* **2001**, *84*, 2313−2317.
[45] S. Komarneni, R. Roy, Q. H. Li, *Mater. Res. Bull.* **1992**, *27*, 1393−1405.
[46] S. Komarneni, *Ionics* **1995**, *21*, 95.
[47] K. S. Suslick, *Science* **1990**, *247*, 1439−1445.
[48] Brochure on AultraCLAVE by Milestone, Microwave Laboratory Systems (Monroe, CT).
[49] M. Figlarz, F. Fievet, J. P. Lagier, Europe patent no. 0113281; USA no. 4539041; Japan: application no. 24303783, **1985**.
[50] F. Fievet, J. P. Lagier, B. Bin, *Solid State Ionics* **1989**, *32*, 198−205.
[51] C. Feldmann, *Adv. Funct. Mater.* **2003**, *13*, 101−107.
[52] Y. G. Sun, Y. N. Xia, *Adv. Mater.* **2002**, *14*, 833−837.
[53] S. Komarneni, D. Li, B. Newalkar, H. Katsuki, A. S. Bhalla, *Langmuir* **2002**, *18*, 5959−5962.
[54] C. Feldmann, H. O. Jungk, *Angew. Chem. Int. Ed.* **2001**, *40*, 359−362.
[55] O. Palchik, J. J. Zhu, A. Gedanken, *J. Mater. Chem.* **2000**, *10*, 1251−1254.
[56] T. Yamamoto, Y. Wada, H. B. Yin, T. Sakata, H. Mori, S. Yanagida, *Chem. Lett.* **2002**, *10*, 964−965.
[57] F. Kooli, V. Rives, W. Jones, *Chem. Mater.* **1997**, *9*, 2231−2235.
[58] R. Harpeness, O. Palchik, A. Gedanken, V. Palchik, S. Amiel, M. A. Slifkin, A. M. Weiss, *Chem. Mater.* **2002**, *14*, 2094−2102.
[59] H. Grisaru, O. Palchik, A. Gedanken, M. A. Slifkin, A. M. Weiss, V. Palchik, *Inorg. Chem.* **2003**, *42*, 7148−7155.
[60] H. Grisaru, O. Palchik, A. Gedanken, V. Palchik, M. A. Slifkin, A. M. Weiss, Y. R. Hacohen, *Inorg. Chem.* **2001**, *40*, 4814−4815.
[61] F. Bonet, C. Guery, D. Guyromard, R. Herrera Urbina, K. Tekaia-Elhsissen, J. M. Tarascon, *Int. J. Inorg. Mater.* **1999**, *1*, 47−51.

Received March 30, 2004
Early View Article
Published Online August 26, 2004

 © 2004 Wiley-VCH Verlag GmbH & Co. KGaA, Weinheim

Phenylmalonate-Containing Copper(II) Complexes: Synthesis, Crystal Structure and Magnetic Properties

Jorge Pasán,[a] Joaquín Sanchiz,[b] Catalina Ruiz-Pérez,*[a] Francesc Lloret,[c] and Miguel Julve[c]

Keywords: Copper / Magnetic properties / N ligands / O ligands

Three new copper(II) complexes of formula [Cu(2,2′-bpy)(Phmal)(H_2O)]·2H_2O (**1**), [{Cu(2,2′-bpym)(Phmal)}]$_n$ (**2**) and [{Cu(phen)(Phmal)}]$_n$·3$n$$H_2O$ (**3**) (Phmal = phenylmalonate; 2,2′-bpy = 2,2′-bipyridine; 2,2′-bpym = 2,2′-bipyrimidine; phen = 1,10-phenanthroline) have been prepared and their structures determined by X-ray diffraction techniques. Complex **1** is mononuclear whereas **2** and **3** are uniform chain compounds. The copper atoms in **1**–**3** are distorted square-pyramidal: two nitrogen atoms from the bidentate nitrogen heterocycle and two carboxylate oxygen atoms from the phenylmalonate ligand build the equatorial plane; the axial position is filled either by a water molecule (**1**) or a carboxylate oxygen atom from another phenylmalonate group (**2** and **3**). The values of the intrachain copper–copper separation through the phenylmalonate-carboxylate bridge in the *anti-syn* conformation are 4.6853(7) (**2**) and 5.014(3) Å (**3**). The phenyl ring of the Phmal ligand in **1** produces an unusual intramolecular π–π stacking interaction with the Cu^{II}–(aromatic 2,2′-bpy) chelate ring. Intrachain edge-to-face phenyl–pyridyl and offset phen–phen-type interactions occur in **2** and **3**, respectively. Magnetic susceptibility measurements of **2** and **3** in the temperature range 1.9–290 K show the occurrence of weak intrachain ferromagnetic interactions between the copper(II) ions through the phenylmalonate-carboxylate bridge [J = +0.10(1) (**2**) and +0.31(1) cm^{-1} (**3**)]. These values are compared with those reported for malonate-containing copper(II) complexes with the same exchange pathway through the *anti-syn* carboxylate bridge.
(© Wiley-VCH Verlag GmbH & Co. KGaA, 69451 Weinheim, Germany, 2004)

Introduction

The design of synthetic pathways to obtain systems with desired properties continues to be a challenge for inorganic chemists. In this context, a great interest has been devoted to the development of rational synthetic routes to novel polynuclear compounds of tuneable dimensionality which may have applications as molecule-based magnetic materials.[1−3] Many recent reports have focused on the synthesis and magneto-structural characterization of polymeric transition metal compounds using malonate (dianion of propanedioic acid, H_2mal) as both blocking and bridging ligand.[4−10] In the framework of our research with malonate-containing metal complexes[8−13] we have been able to prepare a large number of compounds with different structures and properties whose dimensionality goes from zero in the mononuclear species [Cu(mal)(2,2′-bpym)][14] (2,2′-bpym = 2,2′-bipyrimidine) to three in the compound [Cu(mal)(pyz)]$_n$ (pyz = pyrazine).[15] The variety of the coordination modes of the malonate ligand in these compounds has been reviewed very recently.[9] From a magnetic point of view, the parameters governing the nature and magnitude of the magnetic interactions between copper(II) ions are the conformation of the bridge (*anti-anti*, *anti-syn*, *syn-syn*), the environment of the metal atom,[16,17] and the relative orientation of the malonate-carboxylate bridge with respect to the metal environment (equatorial-equatorial, equatorial-apical and apical-apical with relatively strong, weak and negligible interactions, respectively), in addition to the Cu−O(carboxylate) distances.[10]

More recently, we have started a systematic study on copper(II) complexation by substituted malonate ligands such as phenylmalonate (dianion of phenylmalonic acid, H_2Phmal). One of the aims of this study is to analyze the influence that factors such as the withdrawing effect, the rigidity and the possibility of specific attractive interactions between phenyl rings can exert on the structure and magnetic coupling of phenylmalonate-containing copper(II) complexes.[17] In a previous work, we have observed that

[a] Laboratorio de Rayos X y Materiales Moleculares, Departamento de Física Fundamental II, Universidad de La Laguna,
Av. Astrofísico Francisco Sánchez s/n, 38206 La Laguna (Tenerife), Spain
E-mail: caruiz@ull.es
[b] Laboratorio de Rayos X y Materiales Moleculares, Departamento de Química Inorgánica, Universidad de La Laguna,
Av. Astrofísico Francisco Sánchez s/n, 38204 La Laguna (Tenerife), Spain
[c] Departament de Química Inorgànica/Instituto de Ciencia Molecular, Facultat de Química, Universitat de València,
Av. Dr. Moliner 50, 46100 Burjassot (Valencia), Spain

the complex $[\{Cu(H_2O)_3\}\{Cu(Phmal)_2\}]_n$ has a layered structure induced by the phenyl groups and intralayer ferromagnetic couplings through phenylmalonate-carboxylate and -oxo bridges. Here we show how the structure and magnetic properties of this layered system are modified by the presence of coligands such as 2,2′-bipyridine (2,2′-bpy), 2,2′-bipyrimidine (2,2′-bpym) and 1,10-phenanthroline (phen). These are all aromatic nitrogen heterocycles that, in addition to their good coordinating ability (metal−ligand bonds), can interact with the phenyl ring of the Phmal group (supramolecular interactions), making this system very appropriate to illustrate the effects of both types of interactions.

We report herein the synthesis, crystallographic analysis and magnetic study of the copper(II) complexes of formula $[Cu(2,2'\text{-bpy})(Phmal)(H_2O)]\cdot 2H_2O$ (**1**), $[\{Cu(2,2'\text{-bpym})(Phmal)\}]_n$ (**2**) and $[\{Cu(phen)(Phmal)\}]_n\cdot 3nH_2O$ (**3**). Complex **1** is a magnetically isolated mononuclear species whereas **2** and **3** are uniform chains with intrachain ferromagnetic interactions.

Results and Discussion

Synthesis of the Complexes

Complexes **1**−**3** were prepared by reaction of stoichiometric amounts copper(II) phenylmalonate with the appropriate heterocyclic N-donor in a methanol water mixture. X-ray quality crystals of the mononuclear complex **1** and the chain compounds **2** and **3** were grown from concentrated solutions by slow solvent evaporation.

Description of the Crystal Structures

[Cu(2,2′-bpy)(Phmal)(H$_2$O)]·2H$_2$O (1)

The structure of **1** consists of neutral [Cu(Phmal)(2,2′-bpy)(H$_2$O)] mononuclear entities (Figure 1a) and crystallization water molecules. The molecular units are linked by hydrogen bonding involving the uncoordinated phenylmalonate oxygen atoms and the crystallization water molecules, with O···O distances ranging from 2.667(3) to 2.972(4) Å (see Table 1). A surprising two-dimensional (6,3) net results (Figure 2) which contributes to the stabilization of the whole structure. Adjacent layers are linked by weak offset π−π-stacking interactions between pyridyl rings. The shortest offset angle between pyridyl rings is 28.5° while the shortest centroid−centroid contact is 3.966(4) Å, values which are slightly larger than the average values in π−π interactions with pyridine-like groups previously reported.[18]

The molecular structure of **1** is remarkably similar to that of the recently reported[19,20] complexes $[Cu(Bzmal)(phen)(H_2O)]\cdot 3H_2O$ and $[Cu(Bzmal)(2,2'\text{-bpy})(H_2O)]\cdot 2H_2O$ (Bzmal = 2-benzylmalonate) compounds. The phenyl rings of Bzmal and Phmal are located over the N−C−C−N−Cu chelate ring in the three complexes and metalloaromaticity was pointed out to be the factor responsible for this structural feature.[19] A search in the Cambridge Structural Database has shown the existence of several compounds which present the same conformation (listed in Table 2). The value of the dihedral angle between the mean planes in complex **1** is larger (25.5°) than in the other compounds (1.2−14.5°) due to geometrical constraints that preclude the parallel arrangement of the phenyl group above the chelate ring. All the structures found in the search contain a ligand with the nitrogen atoms inside the aromatic rings (i.e. always 2,2′-bpy or phen but never *N*,*N*′-ethylenediamine). According to Janiak,[18] phenyl rings do not like to stack above each other but to adopt an offset (parallel displaced) arrangement, thus leading to C−H···π-type interactions. Therefore, we suggest that this is responsible for the situation of the phenyl group above the chelate ring (i.e. displaced from the stacked position over the pyridyl groups). We can compare this structure with that of the reported mononuclear complex $[Cu(2,2'\text{-bpy})(mal)(H_2O)]\cdot H_2O$,[30] where the monomeric units are distributed in bilayers in the *bc* plane through hydrogen bonds involving the malonate-carboxylate groups and the coordinated and uncoordinated water molecules. The hydrophobic interactions in **1** form layers of different hydrophilic character with the aromatic rings in one and the phenylmalonate oxygen atoms and water molecules in the other one. A remarkable difference between both compounds is the position of the methylene group: it is directed toward the coordinated water molecule in the malonate compound whereas the metalloaromaticity in the case of **1** causes the methylene C−H bond to point towards the opposite side of the coordinated water molecule.

Each copper atom in **1** exhibits a somewhat distorted square-pyramidal environment, with a τ value[31] of 0.14. The copper atom is bound to two 2,2′-bpy nitrogen atoms [2.001(2) and 1.998(2) Å for Cu(1)−N(1) and Cu(1)−N(2), respectively] and to two carboxylate oxygen atoms from the Phmal ligand [1.954(2) and 1.933(2) Å for Cu(1)−O(2) and Cu(1)−O(4)] in the basal plane, and to a water molecule in the apical position [2.143(2) Å for Cu(1)−O(1w)]. The 2,2′-bpy and Phmal groups in **1** adopt a bidentate coordination mode, the values of the angles subtended at the copper atom by them being 80.53(8)° and 90.09(7)°, respectively. The 2,2′-bpy ligand is practically planar [the value of the dihedral angle between the mean pyridyl planes is 1.1(1)°] and its bond lengths and angles are in agreement with those reported for free 2,2′-bpy.[32] The Phmal group exhibits the boat conformation as in $[\{Cu(H_2O)_3\}\{Cu(Phmal)_2\}]_n$.[17] However, the Phmal group in this last compound simultaneously exhibits bidentate (through two oxygen atoms of the two carboxylate groups) and bis(monodentate) (through two *trans* carboxylate oxygen atoms from two Phmal ligands) coordination modes, leading to a layered structure. The $[Cu(Phmal)_2]^{2-}$ units in this compound tend also to align their aromatic rings in the same direction, preventing the occupation of one of the axial positions of the copper(II) coordination sphere, while the other apical site is filled by another $[Cu(Phmal)_2]^{2-}$ unit. This also occurs in **1** where the aromatic ring practically fills one of the axial

 © 2004 Wiley-VCH Verlag GmbH & Co. KGaA, Weinheim

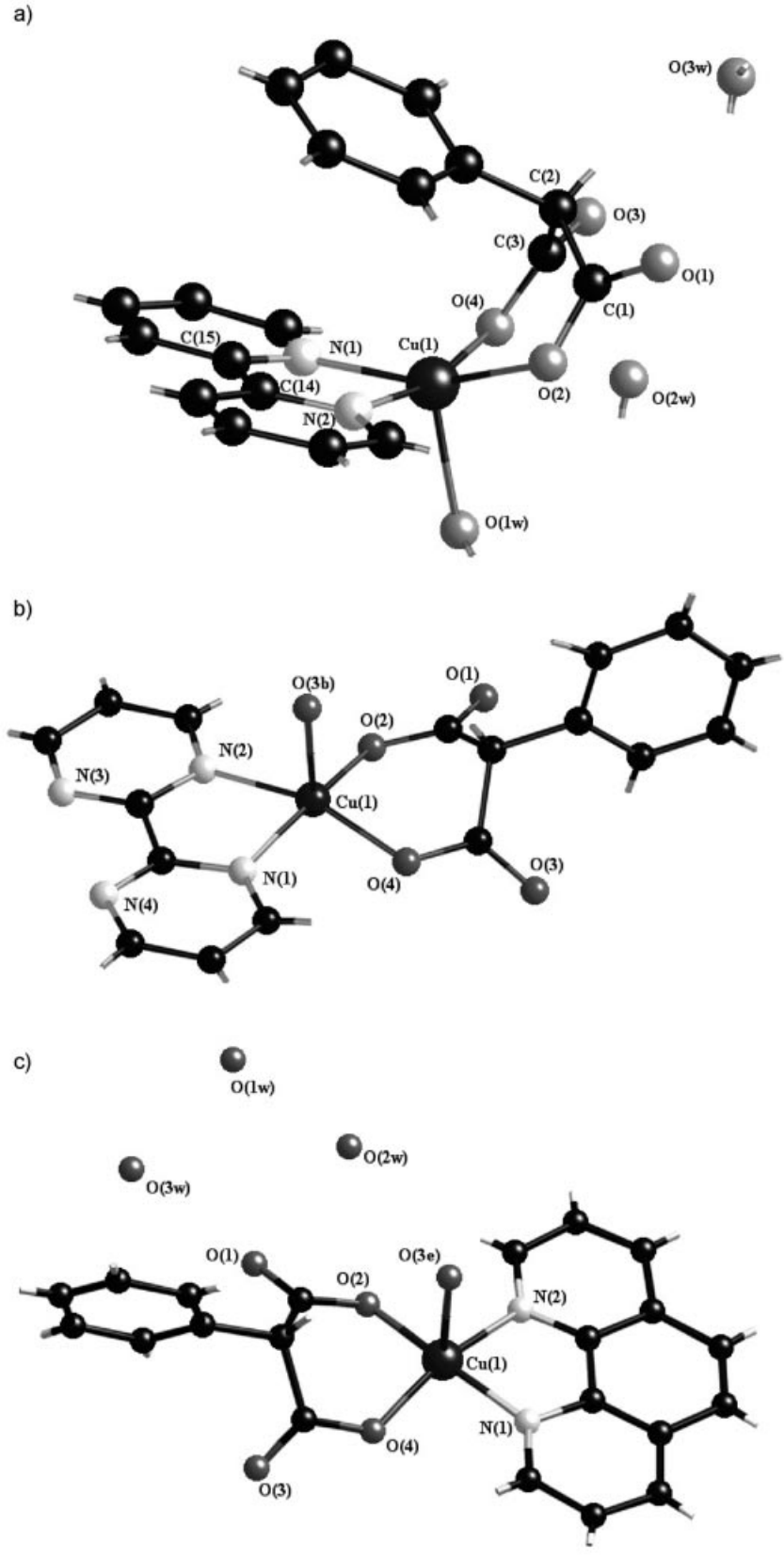

Figure 1. Asymmetric unit of [Cu(2,2′-bpy)(Phmal)(H_2O)]·2H_2O (**1**) (a) and molecular fragments of [{Cu(2,2′-bpym)(Phmal)}]$_n$ (**2**) (b) and [{Cu(phen)(Phmal)}]$_n$·3$n$$H_2O$ (**3**) (c) with the numbering scheme

 © 2004 Wiley-VCH Verlag GmbH & Co. KGaA, Weinheim

Table 1. Hydrogen bonds in complex **1**

D−H···A[a]	D···A	∠D−H···A[b]	Symmetry operator[c]
O(1w)−H(1wa)···O(2w)	2.667(3)	170(4)	$x, y - 1, z + 1$
O(1w)−H(1wb)···O(3)	2.735(3)	172(4)	$x + 1/2, -y, -z + 5/2$
O(2w)−H(2wa)···O(1)	2.881(4)	172(6)	$x, y + 1/2, -z + 3/2$
O(2w)−H(2wb)···O(3w)	2.763(4)	171(4)	$x + 1, y, z$
O(3w)−H(3wa)···O(3)	2.972(4)	167(5)	$x - 1/2, -y + 1/2, z - 1$
O(3w)−H(3wb)···O(1)	2.815(3)	158(5)	$x - 1/2, -y + 1, -z + 3/2$

[a] Values of the distances and angles in Å and °, respectively. [b] D = donor and A = acceptor. [c] Symmetry operation concerning the acceptor atom.

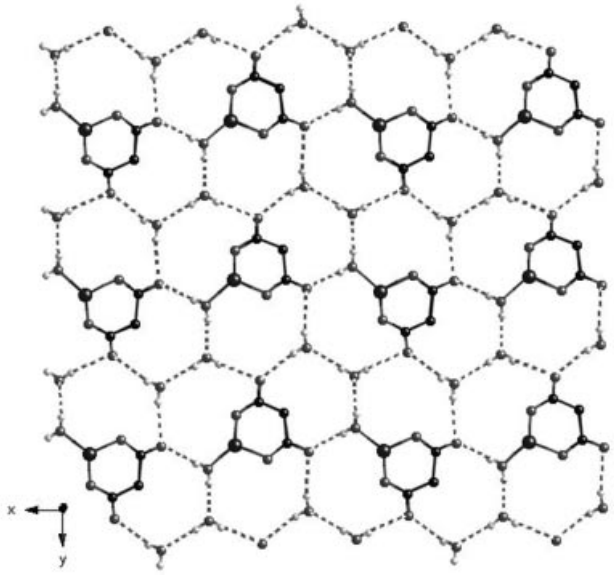

Figure 2. (6,3) pattern formed by hydrogen bonding involving the coordinated and crystallization water molecules and the malonate oxygen atoms; such a regular net contributes to the stabilization of the structure; the 2,2′-bpy ligands have been omitted for clarity

positions of the copper coordination sphere and the other one is occupied by a water molecule. The shortest intermolecular copper−copper separation in **1** is 7.6494(5) Å [Cu(1)−Cu(1a); (a) = $-x + 2, -y, -z + 2$].

[{Cu(2,2′-bpym)(Phmal)}]$_n$ (2)

The structure of **2** consists of chains of [Cu(2,2′-bpym)(Phmal)] units that are linked through one phenylmalonate-carboxylate group in an *anti-syn* conformation (Figure 1b). These chains run parallel to the *a* axis and interact between themselves by means of π−π- and C−H···π-type interactions (Figure 3). There are two hydrophobic cavities where 2,2′-bpym molecules and the phenyl rings from the Phmal groups are constrained. The 2,2′-bpym groups are involved in π−π interactions, with the shortest centroid−centroid contact being 3.798(6) Å and the shortest parallel displacement angle between pyrimidyl rings being 25.7°, values which are similar to the average ones observed in π−π interactions with pyridine-like groups.[18] Weak C−H···π interactions are also present between the phenyl rings and 2,2′-bpym groups inside the chains and between phenyl groups of different chains, with the shortest H···centroid distance being 2.86(4) Å, and C−H···centroid

Table 2. Stacking parameters of some compounds found in the Cambridge Structural Database with the same conformation as complex **1**

Compound	Stacking parameters[a]			Ref.
	$d(c_1-c_2)$ [Å]/α [°]	$d[\perp c_1-P(2)]$ [Å]/β [°]	$d[\perp c_2-P(1)]$ [Å]/γ [°]	
[Cu(L1)(L2)]SbF_6·CH_2Cl_2 [b]	3.58/1.2	3.49/13.1	3.49/13.2	[21]
[Cu(L3)(L4)(L5)]	3.49/7.2	3.45/14.3	3.38/8.2	[22]
[Cu(L3)(L4)]$(NO_3)_2$·$3H_2O$	3.50/10.2	3.43/18.5	3.32/11.4	
catena-[Cu(L4)(L6)]ClO_4·H_2O	3.44/6.46	3.37/8.0	3.41/12.1	[23]
[Cu(L7)(L8)H_2O]BF_4·$3H_2O$	3.39/10.1	3.38/14.2	3.29/4.3	[24]
[Cu(L9)(L8)H_2O]Cl·H_2O	3.53/14.5	3.32/15.8	3.39/19.7	[25]
[Cu(L10)(L4)H_2O]·$3H_2O$	3.49/2.1	3.39/15.5	3.36 /13.9	[19]
[Cu(L10)(L8)H_2O]·$2H_2O$	3.51/8.2	3.37/10.7	3.45/16.4	[20]
[Cu(L11)(L8)H_2O]NO_3·MeOH·H_2O	3.48/5.2	3.41/15.7	3.35/11.3	[26]
[Cu(L9)(L4)H_2O]ClO_4·$1.5H_2O$	3.38/8.8, 3.38/5.4	3.31/16.6, 3.32/12.0	3.24/11.8, 3.30/10.3	[27]
[Cu(L12)(L4)Cl]·$3H_2O$	3.45/6.7	3.41/5.6	3.44/9.2	[27]
[Cu(L12)(L8)H_2O]ClO_4	3.37/7.4	3.35/13.2	3.28/5.8	[28]
[Cu(L9)(L13)H_2O]ClO_4·H_2O	3.42/3.7	3.29/17.1	3.27/16.1	[29]
1	3.683/25.5	3.152/31.5	3.562/14.7	this work

[a] P(1) = plane 1; P(2) = plane 2; c_1 = centroid of P(1); c_2 = centroid of P(2); α = angle between mean planes; β = angle between the normal of P(1) and P(2); γ = angle between the normal of P(2) and P(1). [b] L1 = (*S*,*S*)-2,6-bis(4-phenyl-2-oxazolin-2-yl)pyridine; L2 = benzyloxyacetaldehyde; L3 = L-4,5-dihydroxyphenylalanine; L4 = 1,10-phenanthroline; L5 = *n*-propanol; L6 = L-tryptophanate; L7 = D,L-2,5-dihydroxytyrosine; L8 = 2,2′-bipyridine; L9 = L-tyrosinate; L10 = 2-benzylmalonate; L11 = L-3-iodotyrosinate; L12 = L-phenylalanine; L13 = 1,4,8,9-tetraazatriphenylene.

 © 2004 Wiley-VCH Verlag GmbH & Co. KGaA, Weinheim

groups being almost collinear. The building units of the chain are rotated 90° through the normal axis of the planar 2,2′-bpym group in a twist fashion (i.e. odd units in the same position and even units rotated by 90°; Figure 3).

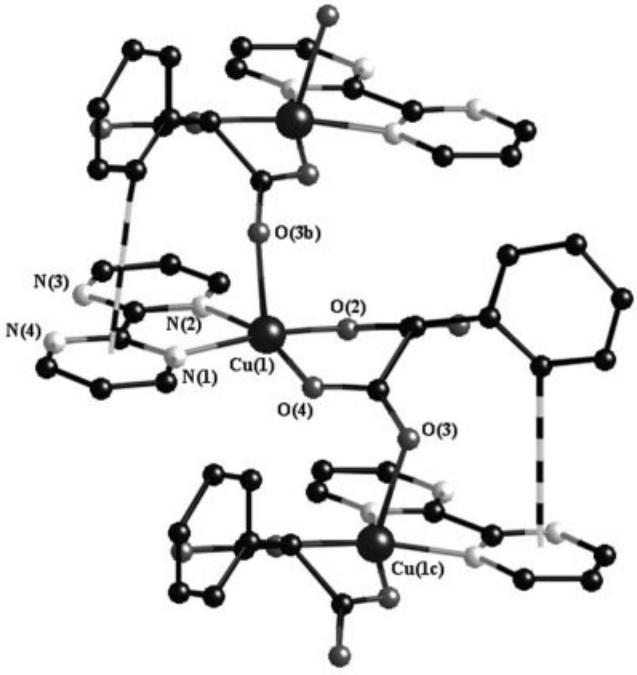

Figure 3. Fragment of the uniform chain of compound **2** showing the rotation of the units by 90° and the intrachain C−H···π interaction (dashed line)

Each copper(II) atom has a slightly distorted square-pyramidal surrounding, the τ value[31] being 0.08. Two nitrogen atoms of the 2,2′-bpym ligand [N(1) and N(2)] and two carboxylate oxygen atoms from the Phmal ligand [O(2) and O(4)] build the basal plane, whereas the symmetry-related carboxylate oxygen atom [O(3b); (b) = $-1/2 + x$, $1/2 - y$, z] occupies the apical position. The equatorial bond lengths vary in the range 1.900(3)−2.003(3) Å and the apical bond length is 2.262(3) Å. The 2,2′-bpym ligand is quasi planar [the dihedral angle between the pyrimidyl rings being 3.5(1)°] and it acts as a bidentate ligand through two [N(1) and N(2)] of its four nitrogen atoms. This coordination mode has previously been observed in several mono- and polynuclear 2,2′-bpym-containing copper(II) complexes.[14,33,34] The outer N(3) and N(4) 2,2′-bpym nitrogen atoms remain free, the N(3)···N(4) bite distance being somewhat longer [2.811(6) Å] than the N(1)···N(2) one [2.584(5) Å] due to the bidentate coordination of the 2,2′-bpym to the copper atom through N(1) and N(2). The inter-ring carbon−carbon bond length of 2,2′-bpym in **2** [1.480(6) Å for C(13)−C(14)] is close to that found in the free ligand in the solid state [1.497(1) and 1.502(4) Å].[35] As in **1**, the Phmal ligand adopts a boat conformation; the phenyl ring in **2** is placed perpendicular to the boat skeleton of the malonate in order to establish the weak intrachain C−H(phenyl)···π (pyrimidyl) interactions mentioned above. Finally, a comparison between the structure of **2** and that of the related mononuclear complex [Cu(2,2′-bpym)(mal)(H$_2$O)]·6H$_2$O[14] shows once more the structural influence of the hydrophobic phenyl ring of the Phmal ligand. The complexation reaction between the preformed [Cu(2,2′-bpym)]$^{2+}$ species and the dicarboxylate mal and Phmal ligands affords neutral hydrated mononuclear (mal) and anhydrous chain (Phmal, **2**) compounds. The structure of the former exhibits extensive hydrogen bonds involving coordinated and uncoordinated water molecules, whereas carboxylate-bridging and supramolecular C−H···π-type interactions counterbalance the lack of hydrogen bonds in the latter.

The shortest intrachain copper−copper separation in **2** is 4.6853(7) Å [Cu(1)···Cu(1c); (c) = $1/2 + x$, $1/2 - y$, z], a value which is much shorter than the shortest interchain metal−metal distance [7.3634(8) Å for Cu(1)···Cu(1d); (d) = $-x$, $1 - y$, $1 - z$].

[{Cu(phen)(Phmal)}]$_n$·3nH$_2$O (3)

The structure of complex **3** consists of chains of [Cu(phen)(Phmal)] units linked through *anti-syn* carboxylate bridges and crystallization water molecules (Figure 1c). The chains run parallel to the *a* axis and they are linked by pairs along the [011] direction through hydrogen bonds involving the water molecules and noncoordinated carboxylate oxygen atoms [the values of the O···O distance range from 2.338(13) to 3.084(5) Å; Figure 4]. Intrachain offset π−π interactions between phen ligands occur, the shortest centroid−centroid distance being 3.907(4) Å and parallel displacement angle being 28.6°, in agreement with previously reported values.[18]

Each copper(II) atom presents a slightly distorted square-pyramidal environment, with a τ value[31] of 0.10. Two carboxylate oxygen atoms from the Phmal ligand [O(2) and O(4)] and the two nitrogen atoms of phen [N(1) and N(2)] form the equatorial plane, whereas a symmetry-related carboxylate oxygen atom [O(3e); (e) = $x + 1$, y, z] occupies the apical position. The equatorial bond lengths vary in the range 1.913(2)−2.026(3) Å and the apical bond amounts to 2.314(3) Å. The angle subtended by the planar bidentate phen ligand at the copper atom is 81.86(11)°. The bond lengths and angles of the phen ligand in **3** agree well with those reported for the free molecule.[36] The conformation and coordination mode of the Phmal ligand in **3** are identical to those in **2**. However, π−π stacking between phen ligands occurs in **3** instead of the C−H(phenyl)···π(N-heterocycle)-type interaction which occurs in **2**. Moreover, the [Cu(phen)(Phmal)] chain units in **3** are not rotated by 90°, in contrast to what it is observed in **2**; this modification of the crystal packing in **3** is due most likely to the crystallization water molecules which are present in the structure of the latter compound. A comparison between the structure of **3** and that of the mononuclear complex [Cu(phen)(mal)(H$_2$O)]·1.5H$_2$O[37] reveals that weak π−π stacking interactions between phen ligands are present in both compounds. However, the mononuclear units are grouped by pairs in the malonato-containing complex, whereas a uniform chain is formed in **3**.

 © 2004 Wiley-VCH Verlag GmbH & Co. KGaA, Weinheim

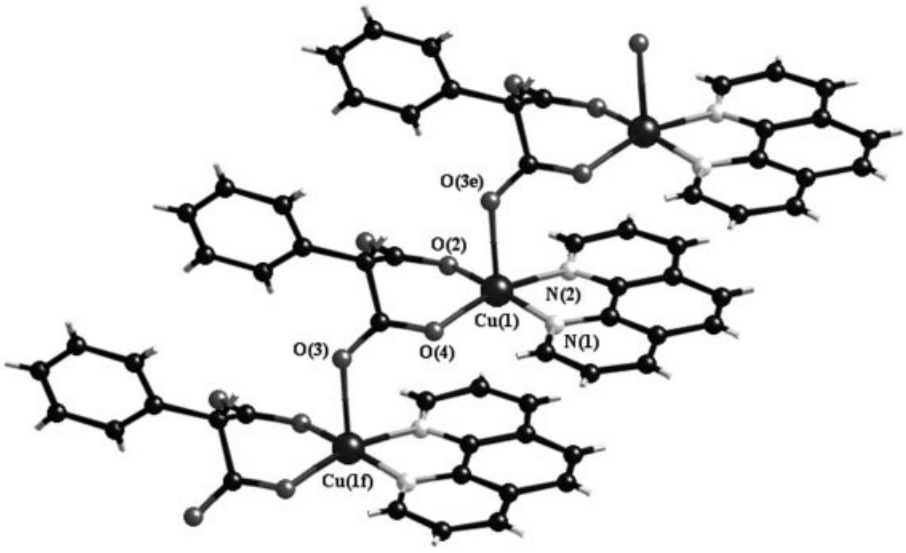

Figure 4. View of the uniform chain of compound **3** showing the phenylmalonate-carboxylate bridge in axial-equatorial *anti-syn* conformation

The shortest intrachain copper−copper separation is 5.014(3) Å [Cu(1)−Cu(1f); (f) = −1 + *x*, *y*, *z*], a value which is much shorter than the shortest interchain metal−metal distance [7.5872(16) Å for Cu(1)−Cu(1g); (g) = −1/2 + *x*, 1/2 − *y*, −1/2 + *z*].

Magnetic Properties

The $\chi_M T$ product of compound **1** obeys the Curie law in the 5−300 K temperature range. Its value is 0.365 $cm^3mol^{-1}K$, as expected for a magnetically isolated spin doublet of a copper(II) ion. This is in agreement with its mononuclear nature.

The magnetic properties of compounds **2** and **3** in the form of $\chi_M T$ vs. *T* plots [χ_M being the molar susceptibility per copper(II) ion] are shown in Figure 5; $\chi_M T$ at room temperature is 0.41 $cm^3mol^{-1}K$ for both compounds, a value which is as expected for a magnetically isolated spin doublet. Upon cooling, $\chi_M T$ remains almost constant for compound **2** down to 10 K and then smoothly increases at lower temperatures to reach a value of 0.44 $cm^3mol^{-1}K$ at 1.9 K; $\chi_M T$ remains constant upon cooling down to 25 K for compound **3** and then it increases at lower temperatures reaching a value of 0.50 $cm^3mol^{-1}K$ at 2.0 K. These features are indicative of an overall weak ferromagnetic coupling between the copper(II) ions in both compounds. Given that the structures of **2** and **3** consist of uniform chains, where the copper(II) ions are bridged by the phenylmalonate-carboxylate group, we analyzed their magnetic properties through the numerical expression proposed by Baker and Rushbrooke[38] for a ferromagnetic uniform copper(II) chain [Equation (1)]:

$$\chi_M = (N\beta^2 g^2/4kT)(A/B)^{2/3} \quad (1)$$

where

$$A = 1.0 + 5.7979916y + 16.902653y^2 + 29.376885y^3 + 29.832959y^4 + 14.036918y^5 \quad (2)$$

$$B = 1.0 + 2.7979916y + 7.0086780y^2 + 8.6538644y^3 + 4.5743114y^4 \quad (3)$$

and $y = J/2kT$, the spin Hamiltonian, *H*, being defined as $\Sigma_i -J\, S_i\, S_{i+1}$; *J* is the intrachain magnetic-coupling parameter and *N*, *g*, and β have their usual meanings.

The best fit obtained using a nonlinear regression analysis leads to $J = +0.10(1)$ cm^{-1}, $g = 2.091(1)$ and $R = 2.6 \times 10^{-5}$ for compound **2** and $J = +0.31(1)$ cm^{-1}, $g = 2.092(1)$ and $R = 2.1 \times 10^{-6}$ for compound **3** (*R* is the agreement factor defined as $\Sigma_i[(\chi_M T)_{obsd.}(i) - (\chi_M T)_{calcd.}(i)]^2/\Sigma[(\chi_M T)_{obsd.}(i)]^2$. The calculated curves match very well the experimental data in the whole temperature range, as seen in Figure 5. The fact that the magnetization data of **3** at 2.0 K (see inset of Figure 5) are clearly above the Brillouin function for a magnetically isolated spin doublet (this is also observed for the corresponding plot in **2**) confirms the ferromagnetic nature of the intrachain magnetic coupling.

The weak ferromagnetic interactions in **2** and **3** can be understood in a simple manner by analysing the exchange pathway which is involved and the relative arrangement of the magnetic orbitals. The unpaired electron of the copper(II) ion in **2** and **3** (square-pyramidal environment) lies in the equatorial plane [N(1)N(2)O(2)O(4)] and it is defined by a $d_{x^2-y^2}$-type magnetic orbital [the *x* and *y* axes corre-

 © 2004 Wiley-VCH Verlag GmbH & Co. KGaA, Weinheim

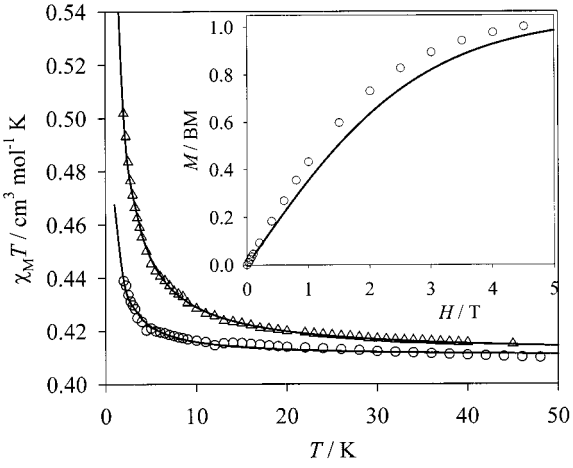

Figure 5. Experimental temperature dependence of the $\chi_M T$ product of **2** (circles) and **3** (triangles) at $T < 50$ K; (—) curves calculated from Equation (1); the inset shows the magnetization versus H plot for **3** at 2.0 K, experimental data (circles), (—) Brillouin function for a magnetically isolated spin doublet with $g = 2.09$

sponding roughly to the equatorial bonds to the copper atom]. The O(4)C(3)O(3) carboxylate bridge provides the intrachain exchange pathway in **2** and **3**: it links one equatorial position from Cu(1) [O(4)] with the axial one [O(3)] at Cu(1c) (**2**) and Cu(1f) (**3**) (see Scheme 1) adopting the *anti-syn* bridging mode. This exchange pathway produces a very poor overlap between the magnetic orbitals due to the weak spin density in the apical site.[39] Thus, the antiferromagnetic contribution, which is proportional to the square of the overlap between the magnetic orbitals, is minimized and the resulting magnetic coupling is most likely ferromagnetic, as observed.[40]

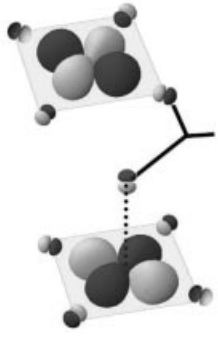

Scheme 1

Previous examples of carboxylate-(*anti-syn*-)bridged copper(II) complexes with an axial-equatorial exchange pathway exhibit ferromagnetic couplings with values of J ranging from +0.05 to +1.9 cm^{-1} (see Table 3).[8,10,16,41–43] The intensity of the magnetic coupling is affected by the Cu–O(axial) distance and the distortion of the metal environment — the longer the distance and the greater the distortion, the weaker the coupling is. The values of J for **2** and **3** fall in this range, but they are smaller than those with similar structural parameters [distortion and Cu–O(axial) distance]. The low value observed for the coupling constant for **2** [$J = +0.10(1)$ cm^{-1}] could be due to the greater value of the angle between the apical-oxygen-to-copper vector and the normal to the equatorial mean plane of the copper atom (7° in **2** and only 3.6° in **3**). In general, this shift influences the effectiveness of the bridge in the transmission of the magnetic coupling because it modifies the overlap between the magnetic orbitals.

Another interesting point looking at the results listed in Table 3 concerns compounds **3** and [{Cu(mal)(Im)}]$_n$. Although the structural parameters of **3** are similar to those of [{Cu(mal)(Im)}]$_n$, the value of the ferromagnetic coupling for **3** is somewhat smaller. Most likely, the carboxylate group of the phenylmalonate is less effective in the transmission of the magnetic coupling than the carboxylate group of the malonate ligand. The magnetic coupling is essentially an electronic effect and the phenylene ring of the phenylmalonate exerts an electron-withdrawing effect that delocalizes some electron density of the copper(II) towards the aromatic ring, decreasing the electronic delocalization towards the carboxylate bridge. The decrease of the electron delocalization towards the bridge would decrease the size of the magnetic coupling. This could be one of the factors to account for the weaker magnetic interaction between the copper(II) ions in **3** (and also in **2**) through the phenylmalonate-carboxylate bridge with respect to the malonate-carboxylate one.

Conclusions

Three new compounds have been prepared in which the phenylmalonate ligand acts either as blocking (**1**) or as bridging ligand (**2** and **3**). Weak interactions (hydrogen bonding and π–π stacking) govern the structure of the compounds leading to molecular (**1**) and one-dimensional (**2** and **3**) structures. A comparison with the related malonato-containing complexes reveals that the influence of the phenyl group in the Phmal compounds is decisive: [Cu(2,2′-bpy)(mal)(H_2O)]·H_2O presents different conformation and crystal packing of the mononuclear units from those in compound **1**; compounds **2** and **3** are uniform chains whereas the malonato-containing copper(II) complexes of 2,2′-bpym and phen are mononuclear compounds. The nature of the magnetic coupling between copper(II) ions through the phenylmalonate-carboxylate bridge (ferromagnetic) is the same as that through the malonate-carboxylate, but its magnitude is somewhat smaller, probably due to the electron-withdrawing effect which is exerted by the phenyl ring. In the near future, magneto-structural studies on phenylmalonate-containing copper(II) complexes will be pursued to check this observation and to gain further insights into the structural possibilities they provide.

Experimental Section

General: Phenylmalonic acid (H_2Phmal), copper(II) acetate hydrate ([Cu($CH_3COO)_2$·H_2O]), 2,2′-bipyridine (2,2′-bpy), 2,2′-bipyrim-

 © 2004 Wiley-VCH Verlag GmbH & Co. KGaA, Weinheim

Table 3. Selected magneto-structural data for some (malonate-/phenylmalonate-)carboxylate-bridged copper(II) complexes

Compound[a]	Carboxylate pathway	Cu−(O)ap	τ[31] Cu1/Cu2	J [cm^{-1}][b]	Ref.
$[Cu(H_2O)_4][Cu(mal)_2(H_2O)_2]$	equatorial-apical	2.383	oct[c]/0.05	+1.8	[8]
$[Cu(H_2O)_4]_2[Cu(mal)_2(H_2O)]^{2+}$	equatorial-apical	2.381	oct[c]/0.12	+1.2	[8]
$[\{Cu(H_2O)_3\}\{Cu(mal)_2(H_2O)\}]_n$	equatorial-apical	2.185	0.24/0.28	+1.9	[8]
$[Cu(Im)_2(mal)]_n$	equatorial-apical	2.394	0.02/0.02	+1.6	[16]
$[Cu(2\text{-}MeIm)_2(mal)]_n$	equatorial-apical	2.270	0.18/0.18	+0.4	[16]
$\{(H_2bpe)[Cu(mal)_2]\}_n \cdot 4nH_2O$	equatorial-apical	2.611	oct[c]/oct[c]	+0.049	[41]
2	equatorial-apical	2.262	0.08/0.08	+0.10	this work
3	equatorial-apical	2.314	0.10/0.10	+0.31	this work

[a] Abbreviations: Im = imidazole; 2-MeIm = 2-methylimidazole; bpe = 1,2-bis(4-pyridyl)ethylene. [b] Values of the coupling constant (J). [c] Octahedral.

idine (2,2′-bpym), 1,10-phenanthroline (phen) and methanol were purchased from Aldrich and used as received. Elemental analyses (C, H and N) were performed with an EA 1108 CHNS-O microanalytical analyzer. IR spectra (450−4000 cm^{-1}) were recorded with a Bruker IF S55 spectrophotometer with the sample prepared as KBr pellets. Magnetic susceptibility measurements on polycrystalline samples of compounds **1**−**3** were carried out in the temperature range 1.9−290 K with a Quantum Design SQUID magnetometer. Diamagnetic corrections of the constituent atoms were estimated from Pascal's constants[44] as -228×10^{-6}, -189×10^{-6} and -251×10^{-6} cm^3·mol^{-1} for compounds **1**, **2** and **3**, respectively. Experimental susceptibilities were also corrected for the temperature-independent paramagnetism (60×10^{-6} cm^3·mol^{-1} per Cu^{II}) and the magnetization of the sample holder.

Synthesis: The general procedure to prepare compounds **1**−**3** starts with the preparation of an aqueous solution (15 mL) of copper(II) phenylmalonate (1 mmol) which was prepared by adding phenylmalonic acid (0.180 g, 1 mmol) to a warm methanolic solution (20 mL) of copper(II) acetate (1 mmol, 0.200 g) under continuous stirring. The resulting pale-blue solution was concentrated to dryness in a rotary evaporator. The green solid obtained was washed thoroughly with acetone to remove the acetic acid and then the green product was dissolved in water (15 mL).

$[Cu(2,2'\text{-bpy})(Phmal)(H_2O)]\cdot 2H_2O$ (1): 2,2′-Bipyridine (0.156 g, 1 mmol) was dissolved in methanol/water (50:50, 10 mL) and then an aqueous solution (15 mL) of copper(II) phenylmalonate was added whilst stirring. The solution was allowed to concentrate in a fumehood at room temperature. Prismatic blue single crystals of **1** had grown after a few days. Yield: 0.34 g (75% based on copper). $C_{19}H_{20}CuN_2O_7$ (451.55): calcd. C 50.49, H 4.43, N 6.20; found C 50.41, H 4.40, N 6.05. IR (KBr): ν(C−H, =C−H): 3090, 3062, 2950, 2923; ν(C=C, COO): 1637, 1605, 1590, 1577, 1445, 1409 cm^{-1}.

$[\{Cu(2,2'\text{-bpym})(Phmal)\}]_n$ (2): Compound **2** was prepared similarly to **1** but using a solution of 2,2′-bpyrimidine (0.158 g, 1 mmol) instead of 2,2′-bipyridine. Prismatic greenish-blue single crystals of **2** were grown after a few days. Yield: 0.24 g (60% based on copper).

Table 4. Crystallographic data for complexes **1**−**3**

	1	**2**	**3**
Empirical formula	$C_{19}H_{20}CuN_2O_7$	$C_{17}H_{12}CuN_4O_4$	$C_{21}H_{20}CuN_2O_7$
Formula mass	451.91	399.85	475.88
Crystal system	orthorhombic	orthorhombic	monoclinic
Space group	*Pcab*	*Pcab*	$P2_1/n$
a [Å]	14.6113(5)	8.9331(3)	5.014(3)
b [Å])	16.1928(4)	11.7577(3)	26.403(3)
c [Å]	16.5067(5)	29.8171(4)	14.685(3)
β [°]	90	90	94.75
V [Å^3]	3905.5(2)	3131.77(14)	1937.3(12)
Z	8	8	4
μ(Mo-K_α) [cm^{-1}]	11.63	14.28	11.76
T [K]	293(2)	293(2)	293(2)
$\rho_{calcd.}$ [gcm^{-3}]	1.537	1.696	1.611
λ [A]	0.71073	0.71073	0.71073
Index ranges	$-18 \le h \le 20$	$-12 \le h \le 9$	$-7 \le h \le 5$
	$-22 \le k \le 22$	$-16 \le k \le 16$	$-32 \le k \le 37$
	$-23 \le l \le 13$	$-41 \le l \le 41$	$-13 \le l \le 20$
Independent reflections (R_{int})	5537 (0.060)	4545 (0.132)	5284 (0.051)
Observed reflections [$I > 2\sigma(I)$]	3552	2985	2872
Parameters	343	283	336
Goodness-of-fit	1.043	1.138	1.012
R [$I > 2\sigma(I)$]	0.0429	0.0742	0.0591
R_w [$I > 2\sigma(I)$]	0.0837	0.1462	0.1098
R (all data)	0.0866	0.1217	0.1376
R_w (all data)	0.1004	0.1615	0.1302

 © 2004 Wiley-VCH Verlag GmbH & Co. KGaA, Weinheim

$C_{17}H_{12}CuN_4O_4$ (399.55): calcd. C 51.05, H 3.00, N 14.02; found C 51.20, H 3.14, N 14.10. IR (KBr): ν(C−H, =C−H): 3057, 3027, 2925; ν(C=C, COO): 1646, 1606, 1578, 1557, 1420, 1403 cm^{-1}.

[{Cu(phen)(Phmal)}]$_n$·3nH$_2$O (3): Compound **3** was prepared similarly to **1** but using a solution of 1,10-phenanthroline (0.180 g, 1 mmol) instead of 2,2′-bipyridine. Prismatic blue single crystals of **3** separated from the mother liquor on standing at room temperature after a week. Yield: 0.38 g (80% based on copper). $C_{21}H_{20}CuN_2O_7$ (475.55): calcd. C 52.99, H 4.21, N 5.89; found C 52.79, H 4.32, N 5.80. IR (KBr): ν(C−H, =C−H): 3060, 3030, 2923, 2850; ν(C=C, COO): 1628, 1615, 1595, 1576, 1425, 1405 cm^{-1}.

X-ray Crystallographic Study: Single crystals of **1**−**3** were used for data collection with a Nonius KappaCCD diffractometer. The data collection was carried out at 293 K using graphite-monochromated Mo-K_α radiation (λ = 0.71073 Å). A summary of the crystallographic data and structure refinement is given in Table 4 and selected interatomic distances and angles are listed in Table 5. The structures were solved by direct methods and refined with a full-matrix least-squares technique on F^2 using the SHELXL-97[45] program included in the WINGX[46] software package. All non-hydrogen atoms were refined anisotropically. All hydrogen atoms of structures **1**−**3** were located from difference maps and refined with isotropic temperature factors, except those of the water molecules of complex **3**. The final geometrical calculations and graphical manipulations were carried out with PARST97[47] and CRYSTALMAKER[48] programs. CCDC-235074 (**1**), -235075 (**2**) and -235076 (**3**) contain the supplementary crystallographic data for this paper. These data can be obtained free of charge at www.ccdc.cam.ac.uk/conts/retrieving.html [or from the Cambridge Crystallographic Data Centre, 12 Union Road, Cambridge CB2 1EZ, UK; Fax: (internat.) + 44-1223-336-033; E-mail: deposit@ccdc.cam.ac.uk].

Table 5. Selected bond lengths [Å] and bond angles [°] for compounds **1**−**3**[a]

1			
Cu(1)−O(2)	1.954(2)	Cu(1)−N(2)	1.998(2)
Cu(1)−O(4)	1.933(2)	Cu(1)−O(1w)	2.143(2)
Cu(1)−N(1)	2.001(2)		
O(2)−Cu(1)−O(4)	90.09(7)	O(4)−Cu(1)−N(2)	166.47(8)
O(2)−Cu(1)−N(1)	158.23(8)	O(4)−Cu(1)−O(1w)	97.46(9)
O(2)−Cu(1)−N(2)	92.89(8)	N(1)−Cu(1)−N(2)	80.53(8)
O(2)−Cu(1)−O(1w)	96.85(9)	N(1)−Cu(1)−O(1w)	104.38(9)
O(4)−Cu(1)−N(1)	91.89(8)	N(2)−Cu(1)−O(1w)	95.29(9)
2			
Cu(1)−O(2)	1.922(3)	Cu(1)−N(2)	1.996(3)
Cu(1)−O(4)	1.900(3)	Cu(1)−O(3b)	2.262(3)
Cu(1)−N(1)	2.003(3)		
O(2)−Cu(1)−O(4)	92.93(11)	O(4)−Cu(1)−N(2)	162.02(14)
O(2)−Cu(1)−N(1)	166.90(14)	O(4)−Cu(1)−O(3b)	100.05(12)
O(2)−Cu(1)−N(2)	93.31(13)	N(1)−Cu(1)−N(2)	80.53(13)
O(2)−Cu(1)−O(3b)	106.32(12)	N(1)−Cu(1)−O(3b)	85.78(12)
O(4)−Cu(1)−N(1)	89.79(12)	N(2)−Cu(1)−O(3b)	94.33(12)
3			
Cu(1)−O(2)	1.913(2)	Cu(1)−N(2)	2.026(3)
Cu(1)−O(4)	1.934(2)	Cu(1)−O(3e)	2.314(2)
Cu(1)−N(1)	1.992(3)		
O(2)−Cu(1)−O(4)	92.80(9)	O(4)−Cu(1)−N(2)	162.66(10)
O(2)−Cu(1)−N(1)	168.52(11)	O(4)−Cu(1)−O(3e)	101.46(9)
O(2)−Cu(1)−N(2)	90.63(10)	N(1)−Cu(1)−N(2)	81.86(11)
O(2)−Cu(1)−O(3e)	92.74(10)	N(1)−Cu(1)−O(3e)	96.59(10)
O(4)−Cu(1)−N(1)	91.90(10)	N(2)−Cu(1)−O(3e)	95.35(10)

[a] Estimated standard deviations in the last significant digits are given in parentheses. Symmetry codes: (b) −1/2 + x, 1/2 − y, z; (e) x + 1, y, z.

Acknowledgments

This work was supported by the Ministerio Español de Ciencia y Tecnología (project BQU2001-3794) and the Gobierno Autónomo de Canarias (project PI2002/175). J. P. acknowledges the Ministerio Español de Educación, Cultura y Deporte for a predoctoral fellowship (ref. AP2001-3322).

[1] D. Gatteschi, O. Kahn, J. S. Miller, F. Palacio, *Magnetic Molecular Materials*, Kluwer Academic Publishers, Dordrecht, The Netherlands, **1991**.
[2] *Polyhedron* **2001**, *20* (11−14) entire issue.
[3] *Polyhedron* **2003**, *22* (14−17) entire issue.
[4] D. Chattopadhyay, S. K. Chattopadhyay, P. R. Lowe, C. H. Schwalke, S. K. Mazumber, A. Rana, S. Ghosh, *J. Chem. Soc., Dalton Trans.* **1993**, 913.
[5] I. Gil de Muro, F. A. Mautner, M. Insausti, L. Lezama, M. I. Arriortua, T. Rojo, *Inorg. Chem.* **1998**, *37*, 3243.
[6] C. Ruiz-Pérez, J. Sanchiz, M. Hernández-Molina, F. Lloret, M. Julve, *Inorg. Chim. Acta* **2000**, *298*, 202.
[7] C. Ruiz-Pérez, M. Hernández-Molina, P. Lorenzo-Luis, F. Lloret, J. Cano, M. Julve, *Inorg. Chem.* **2000**, *39*, 3845.
[8] C. Ruiz-Perez, J. Sanchiz, M. H. Molina, F. Lloret, M. Julve, *Inorg. Chem.* **2000**, *39*, 1363.
[9] Y. Rodríguez-Martín, M. Hernández-Molina, F. S. Delgado, J. Pasán, C. Ruiz-Pérez, J. Sanchiz, F. Lloret, M. Julve, *CrystEngComm* **2002**, *4*, 522.
[10] J. Pasán, F. S. Delgado, Y. Rodríguez-Martín, M. Hernández-Molina, C. Ruiz-Pérez, J. Sanchiz, F. Lloret, M. Julve, *Polyhedron* **2003**, *22*, 2143.
[11] Y. Rodríguez-Martín, M. Hernández-Molina, J. Sanchiz, C. Ruiz-Pérez, F. Lloret, M. Julve, *Dalton Trans.* **2003**, 2359.
[12] C. Ruiz-Pérez, M. Hernández-Molina, J. Sanchiz, T. López, F. Lloret, M. Julve, *Inorg. Chim. Acta* **2000**, *298*, 245.
[13] C. Ruiz-Pérez, Y. Rodríguez-Martín, M. Hernández-Molina, F. S. Delgado, J. Pasan, J. Sanchiz, F. Lloret, M. Julve, *Polyhedron* **2003**, *22*, 2111.
[14] Y. Rodríguez-Martín, J. Sanchiz, C. Ruiz-Pérez, F. Lloret, M. Julve, *Inorg. Chim. Acta* **2001**, *326*, 20.
[15] Y. Rodríguez-Martín, M. Hernández-Molina, F. S. Delgado, J. Pasan, C. Ruiz-Pérez, J. Sanchiz, F. Lloret, M. Julve, *CrystEngComm* **2002**, *4*, 440.
[16] J. Sanchiz, Y. Rodríguez-Martín, C. Ruiz-Pérez, A. Mederos, F. Lloret, M. Julve, *New J. Chem.* **2002**, *26*, 1624−1628.
[17] J. Pasán, J. Sanchiz, C. Ruiz-Pérez, F. Lloret, M. Julve, *New J. Chem.* **2003**, *27*, 1557.
[18] C. Janiak, *J. Chem. Soc., Dalton Trans.* **2000**, 3885.
[19] A. Castiñeiras, A. G. Sicilia-Zafra, J. M. González-Pérez, D. Choquecillo-Lazarte, J. Niclós-Gutiérrez, *Inorg. Chem.* **2003**, *41*, 6956.
[20] W. Guan, J. Y. Sun, X. D. Zhang, Q. T. Liu, *Chem. Res. Chin. Univ.* **1998**, *19*, 5.
[21] D. A. Evans, M. C. Kozlowski, J. A. Murry, C. S. Burgey, K. R. Campos, B. T. Connell, R. T. Staples, *J. Am. Chem. Soc.* **1999**, *121*, 669.
[22] S. Suzuki, K. Yamaguchi, N. Nakamura, Y. Tagawa, H. Kuma, T. Kawamoto, *Inorg. Chim. Acta* **1998**, *283*, 260.

 © 2004 Wiley-VCH Verlag GmbH & Co. KGaA, Weinheim

[23] H. Masuda, O. Matsumoto, A. Odani, O. Yamauchi, *J. Chem. Soc. Jpn.* **1988**, 783.
[24] N. Nakamura, T. Kohzuma, H. Kuma, S. Suzuki, *J. Am. Chem. Soc.* **1992**, *114*, 6550.
[25] X. Solans, L. Ruiz-Ramírez, A. Martinez, L. Gasque, R. Moreno-Esparza, *Acta Crystallgr., Sect. C* **1992**, *48*, 1785.
[26] F. Zhang, T. Yajima, H. Masuda, A. Odani, O. Yamauchi, *Inorg. Chem.* **1997**, *36*, 5777.
[27] T. Sugimori, H. Masuda, N. Ohata, K. Koiwai, A. Odani, O. Yamauchi, *Inorg. Chem.* **1997**, *36*, 576.
[28] P. S. Subramanian, E. Suresh, P. Dastidar, S. Waghmode, D. Srinivas, *Inorg. Chem.* **2001**, *40*, 4291.
[29] X.-Y. Le, M.-L. Tong, Y.-L. Fu, L.-N. Ji, *Acta Chim. Sinica* **2002**, *60*, 367.
[30] E. Suresh, M. M. Bhadbhade, *Acta Crystallogr., Sect. C* **1997**, *53*, 193.
[31] A. W. Addison, T. N. Rao, J. Reedijk, J. van Rijn, G. C. Verschoor, *J. Chem. Soc., Dalton Trans.* **1984**, 1349.
[32] L. L. Merrit, E. D. Schroeder, *Acta Crystallogr.* **1956**, *9*, 801.
[33] [33a] G. de Munno, G. Bruno, M. Julve, M. Romeo, *Acta Crystallogr., Sect. C* **1990**, *46*, 1828. [33b] L. W. Morgan, W. T. Pennington, J. D. Petersen, R. R. Ruminski, D. W. Bennet, J. S. Rommel, *Acta Crystallogr., Sect. C* **1992**, *48*, 163. [33c] G. De Munno, M. Julve, M. Verdaguer, G. Bruno, *Inorg. Chem.* **1993**, *32*, 561. [33d] G. De Munno, M. Julve, F. Nicolò, F. Lloret, J. Faus, R. Ruiz, E. Sinn, *Angew. Chem. Int. Ed. Engl.* **1993**, *32*, 613. [33e] I. Castro, J. Sletten, L. K. Glaerum, F. Lloret, J. Faus, M. Julve, *J. Chem. Soc., Dalton Trans.* **1994**, 2777. [33f] I. Castro, J. Sletten, L. K. Glaerum, J. Cano, F. Lloret, J. Faus, M. Julve, *J. Chem. Soc., Dalton Trans.* **1995**, 3207. [33g] S. Decurtins, H. W. Schmalle, P. Schneuwly, L. M. Zheng, *Acta Crystallogr., Sect. C* **1996**, *52*, 561.
[34] [34a] I. Castro, M. Julve, G. De Munno, G. Bruno, J. A. Real, F. Lloret, J. Faus, *J. Chem. Soc., Dalton Trans.* **1992**, 1739. [34b] M. Julve, M. Verdaguer, G. De Munno, J. A. Real, G. Bruno, *Inorg. Chem.* **1993**, *32*, 795. [34c] J. A. Real, G. De Munno, R. Chiappetta, M. Julve, F. Lloret, Y. Journaux, J. C. Colin, G. Blondin, *Angew. Chem. Int. Ed. Engl.* **1994**, *33*, 1184. [34d] G. De Munno, M. Julve, F. Lloret, J. Faus, M. Verdaguer, A. Caneschi, *Inorg. Chem.* **1995**, *34*, 157. [34e] G. De Munno, M. Julve, F. Lloret, J. Cano, A. Caneschi, *Inorg. Chem.* **1995**, *34*, 2048. [34f] G. De Munno, M. G. Lombardi, P. Paoli, F. Lloret, M. Julve, *Inorg. Chim. Acta* **1998**, *282*, 252.
[35] L. Fernholt, C. Rømming, S. Samdal, *Acta Chem. Scand., Ser. A* **1981**, *35*, 707.
[36] S. Nishigaki, H. Yoshioka, K. Nakatsu, *Acta Crystallogr., Sect. B* **1978**, *34*, 875.
[37] [37a] W.-L. Kwik, K.-P. Ang, H. S.-O. Chan, V. Chebolu, S. A. Koch, *J. Chem. Soc., Dalton Trans.* **1986**, 2519. [37b] E. Borghi, *Gazz. Chim. Ital.* **1987**, *117*, 557.
[38] G. A. Baker, G. S. Rushbrooke, H. E. Gilbert, *Phys. Rev.* **1964**, *135*, A1272.
[39] A. Rodríguez-Fortea, P. Alemany, S. Álvarez, E. Ruiz, *Chem. Eur. J.* **2001**, *7*, 627.
[40] O. Kahn, *Molecular Magnetism*, VCH, New York, **1993**.
[41] F. S. Delgado, J. Sanchiz, C. Ruiz-Pérez, F. Lloret, M. Julve, *Inorg. Chem.* **2003**, *42*, 5938−5948.
[42] Y. Rodríguez-Martín, C. Ruiz-Pérez, J. Sanchiz, F. Lloret, M. Julve, *Inorg. Chim. Acta* **2001**, *318*, 159−165.
[43] E. Colacio, J. M. Domínguez-Vera, M. Ghazi, R. Krekäs, M. Klinga, J. M. Moreno, *Eur. J. Inorg. Chem.* **1999**, 441.
[44] A. Earnshaw, *Introduction to Magnetochemistry*, Academic Press, London, **1968**.
[45] G. M. Sheldrick, *SHELXL-97, SHELXS-97, Program for Crystal Structure Refinement*, Universität Göttingen, Germany, **1998**.
[46] L. J. Farrugia, *J. Appl. Crystallogr.* **1999**, *32*, 837.
[47] PARST95: M. Nardelli, *J. Appl. Crystallogr.* **1995**, *28*, 659.
[48] CrystalMaker 4.2.1, CrystalMaker Software, P. O. Box 183, Bicester, Oxfordshire, OX26 3TA, UK.

Received March 31, 2004
Early View Article
Published Online August 17, 2004

 © 2004 Wiley-VCH Verlag GmbH & Co. KGaA, Weinheim

Synthesis and Characterization of Alkyllanthanum Biphenolate Complexes as Catalysts for Hydroamination/Cyclization and Hydrosilylation

Denis V. Gribkov,[a] Frank Hampel,[a] and Kai C. Hultzsch*[a]

Keywords: Asymmetric catalysis / Hydroamination / Hydrosilylation / Lanthanum / O ligands

The homochiral, dimeric biphenolate alkyllanthanum complex [La{(*R*)-Biphen}{CH(SiMe$_3$)$_2$}]$_2$ can be prepared by facile alkane elimination starting from [La{CH(SiMe$_3$)$_2$}$_3$] and enantiopure (*R*)-3,3′-di-*tert*-butyl-5,5′,6,6′-tetramethyl-1,1′-biphenyl-2,2′-diol [H$_2${(*R*)-Biphen}]. Single-crystal X-ray diffraction revealed that the two La{(*R*)-Biphen}{CH(SiMe$_3$)$_2$} fragments are connected through bridging phenolate groups of the biphenolate ligands. The two different phenolate groups undergo an intramolecular exchange process in solution leading to their equivalence on the NMR timescale. The biphenolate alkyl complex shows high catalytic activity for hydroamination/cyclization of aminoalkenes, similar to previously known lanthanocene catalysts, but only low enantioselectivity. Addition of THF to [La{(*R*)-Biphen}{CH(SiMe$_3$)$_2$}]$_2$ leads to a monomeric tris-THF adduct [La{(*R*)-Biphen}{CH(SiMe$_3$)$_2$}(THF)$_3$] with higher catalytic activity than the THF-free homochiral dimer in the cyclization of 2,2-dimethylpent-4-enylamine, suggesting that the dimeric structure of the catalyst system prevails under catalytic conditions in the absence of THF. Addition of HN(SiHMe$_2$)$_2$ to [La{(*R*)-Biphen}{CH(SiMe$_3$)$_2$}(THF)$_3$] results in the formation of [La{(*R*)-Biphen}{N(SiHMe$_2$)$_2$}(THF)$_3$] which is in equilibrium with its homochiral dimer [La{(*R*)-Biphen}{N(SiHMe$_2$)$_2$}(THF)]$_2$ at elevated temperatures. The biphenolate alkyl complexes exhibit good catalytic activity and diastereoselectivity in the hydrosilylation of styrene. Hydrosilylation of 1-hexene and norbornene also proceeds with high diastereoselectivity but rather low activity.
(© Wiley-VCH Verlag GmbH & Co. KGaA, 69451 Weinheim, Germany, 2004)

Introduction

The chemistry of organometallic rare-earth-metal compounds has advanced significantly over the last two decades and many catalytic applications of these species in polymer chemistry[1,2] and organic synthesis,[3] notably hydroamination,[4−25] hydrophosphination,[26,27] hydrosilylation,[28−47] and hydroboration,[48,49,50] have been investigated. Most catalytic studies have relied on catalyst systems based on organometallic rare-earth-metal complexes containing at least one cyclopentadienyl-type ligand.[51] The chemistry of non-metallocene complexes[52−54] is much less developed and only a limited number of catalytic investigations have been reported.[45,55−69] One significant disadvantage of cyclopentadienyl-based chiral rare-earth-metal catalysts is their facile epimerisation in the presence of donor molecules, such as ethers and amines.[15,70−73] Cyclopentadienyl-free catalyst systems could solve this problem by providing a configurationally stable catalytic site and we[60,65] and others[59,62−64] have reported significant progress over the last year.

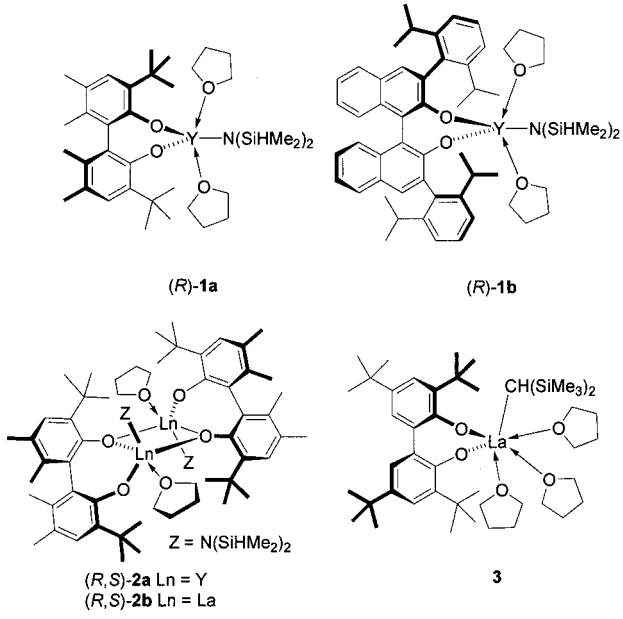

(*R*)-**1a** (*R*)-**1b**

(*R*,*S*)-**2a** Ln = Y
(*R*,*S*)-**2b** Ln = La

3

Recently we reported the synthesis of monomeric biphenolate and binaphtholate rare-earth-metal amido complexes of the type [Ln{diolate}{N(SiHMe$_2$)$_2$}(THF)$_2$] (**1**) as well as their application in enantioselective hydroamination/cyclization reactions.[60] Based on the high thermal stability of the complexes and the small decrease of enantioselectiv-

[a] Institut für Organische Chemie, Friedrich-Alexander Universität Erlangen-Nürnberg,
Henkestr. 42, 91054 Erlangen, Germany
Fax: + 49-9131-852-6865
E-mail: hultzsch@chemie.uni-erlangen.de

ity with increasing temperature, these complexes are assumed to be configurationally stable under catalytic conditions, even at temperatures as high as 100 °C. Although these catalysts can be prepared quite conveniently by a simple amine-elimination reaction, they require relatively high reaction temperatures (≥ 50 °C) in order to achieve reasonable turnover frequencies.[74] Additionally, we found that complexes derived from the sterically less-hindered racemic 3,3′-di-*tert*-butyl-5,5′,6,6′-tetramethyl-1,1′-biphenyl-2,2′-diol [H_2(Biphen)][75][76] readily dimerize to give a phenolate-bridged heterochiral dimer. A presumably homochiral dimeric amidolanthanum species could be observed in situ upon heating heterochiral (*R*,*S*)-[La(Biphen){N(SiHMe$_2$)$_2$}(THF)]$_2$ [(*R*,*S*)-**2b**],[60] but all attempts to obtain the former in pure form starting from enantiopure Biphen ligand have failed to date.

We therefore became interested in understanding the source of the low catalytic activity of complexes [Ln{diolate}{N(SiHMe$_2$)$_2$}(THF)$_2$] (**1**). Possible reasons could be inhibition by THF coordination, sluggish initiation caused by the low basicity of the bis(dimethylsilyl)-amido ligand or the electronic properties of our chiral chelating diolate ligand system.

Schaverien reported the synthesis of biphenolate and binaphtholate alkyllanthanum complexes in 1992,[77] but little is known about their reactivity or catalytic activity. Although the structure of the monomeric tris-THF adduct [La{1,1′-(2-OC$_6$H$_2$*t*Bu$_2$-3,5)$_2$}{CH(SiMe$_3$)$_2$}(THF)$_3$] (**3**) was elucidated by single-crystal X-ray diffraction analysis, the structure of its base-free precursor, formulated as the monomeric species [La{1,1′-(2-OC$_6$H$_2$*t*Bu$_2$-3,5)$_2$}{CH(SiMe$_3$)$_2$}], remained unknown.

Herein we report the synthesis, characterization and catalytic activity of related biphenolate alkyllanthanum complexes derived from (*R*)-Biphen. As it turned out, the initial base-free lanthanum complex of this chiral biphenolate ligand exists as a homochiral dimer.[78]

Results and Discussion

Reaction of (*R*)-H_2(Biphen)[76] with the trialkyllanthanum complex [La{CH(SiMe$_3$)$_2$}$_3$][79] at −10 °C in toluene solution resulted in the smooth formation of a single species **4** of the general formula "La{(*R*)-Biphen}{CH(SiMe$_3$)$_2$}" (Scheme 1). Although the reaction seems to proceed relatively cleanly according to NMR spectroscopy, we could only obtain 35% of the product in isolated yield due to its high solubility in pentane. The ^{1}H NMR spectrum at room temperature exhibits only one broad set of signals for the biphenolate ligand, suggesting that both phenolate rings are equivalent at this temperature, as well as two signals for the diastereotopic trimethylsilyl groups (Figure 1). The lanthanum-bound methyne carbon atom resonates in the ^{13}C NMR spectrum at δ = 55.0 ppm ($^1J_{C,H}$ = 101 Hz). The signals of the biphenolate ligand decoalesce into two separate sets of signals for the two phenolate rings upon cooling to 0 °C. Similar temperature-dependent spectroscopic features of the biphenolate ligand have been observed in the heterochiral dimer (*R*,*S*)-[La(Biphen){N(SiHMe$_2$)$_2$}(THF)]$_2$ [(*R*,*S*)-**2b**].[60] The equivalence of both phenolate rings in (*R*,*S*)-**2b** on the NMR timescale at 25 °C is caused by an intramolecular exchange process of terminal and bridging phenolate groups. An analogous intramolecular exchange process of terminal and bridging phenolate groups seems to be operational for (*R*,*R*)-**4** (Scheme 2). The homochiral dimeric structure of (*R*,*R*)-**4** was also confirmed by X-ray crystallographic analysis (vide infra). It seems likely that the related complex [La{1,1′-(2-OC$_6$H$_2$*t*Bu$_2$-3,5)$_2$}{CH(SiMe$_3$)$_2$}] pre-

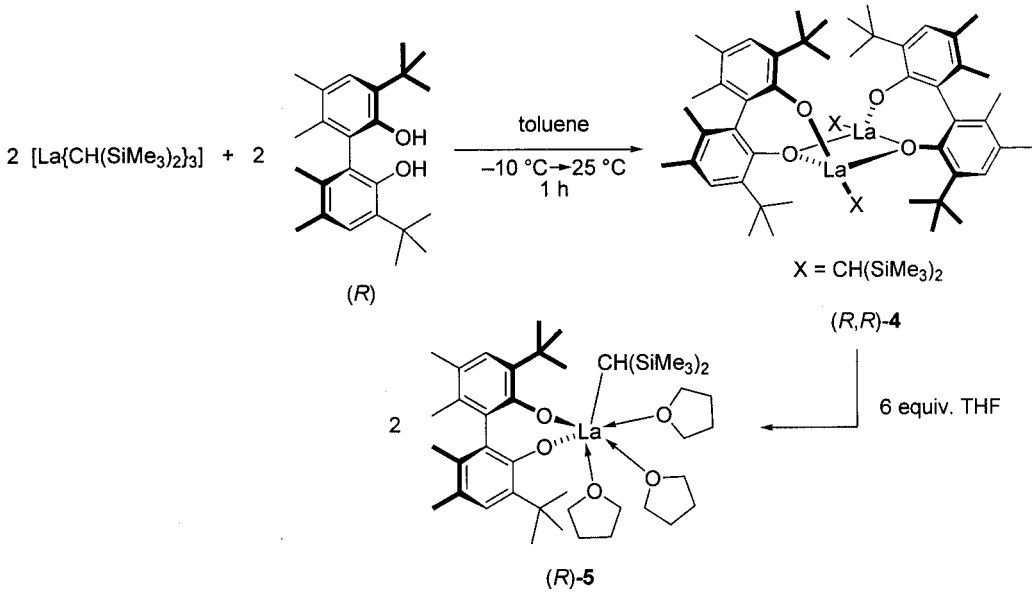

Scheme 1

pared by Schaverien[77] from [La{CH(SiMe$_3$)$_2$}$_3$] and 3,3′,5,5′-tetra-*tert*-butylbiphenyl-2,2′-diol is also dimeric. The signal of the lanthanum-bound methyne proton of this species appears at $\delta = -1.46$ ppm in the ^{1}H NMR spectrum and the lanthanum-bound carbon atom is found at $\delta =$ 59.4 ppm ($^1J_{C,H} = 95$ Hz).[77] Based on the differences in the NMR spectra of [La{1,1′-(2-OC$_6$H$_2$*t*Bu$_2$-3,5)$_2$}{CH(SiMe$_3$)$_2$}] and (*R*,*R*)-**4** one can rule out a homochiral dimeric structure. A heterochiral[78] dimeric structure is more likely and should be thermodynamically more stable due to the absence of unfavorable steric interactions.

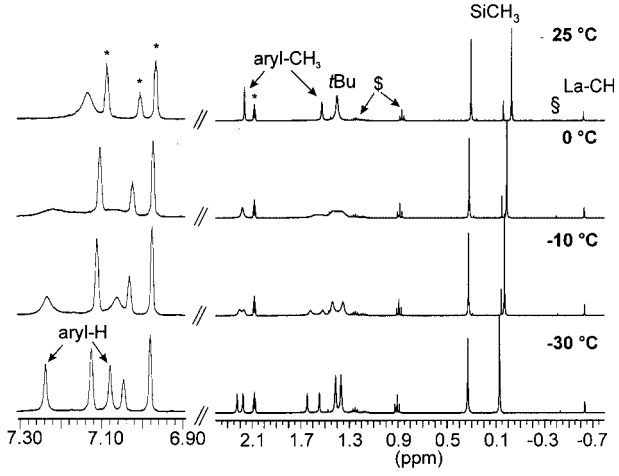

Figure 1. Variable temperature ^{1}H NMR spectra of (*R*,*R*)-**4** in [D$_8$]toluene (*) showing the aliphatic (right) and aromatic region (left, threefold expanded) [$ = *n*-pentane, § = CH$_2$(SiCH$_3$)$_2$]

Addition of six equivalents of THF to (*R*,*R*)-**4** led to the formation of a monomeric species (*R*)-**5** (Scheme 1), which is analogous to the crystallographically characterized biphenolate lanthanum complex **3**.[77] Formation of (*R*)-**5** from (*R*,*R*)-**4** does not proceed instantaneously, but within 30 min. The signal of the lanthanum-bound methyne proton is shifted to higher field at $\delta = -1.64$ ppm in the ^{1}H NMR spectrum and the methyne carbon atom resonates in the ^{13}C NMR spectrum at $\delta = 51.5$ ppm with a $^1J_{C,H}$ value of 97.6 Hz. Addition of three equivalents of THF yields a mixture of (*R*,*R*)-**4**, (*R*)-**5** and a new species at $\delta = -1.12$ ppm, which we believe to be a dimeric mono-THF adduct [La{(*R*)-Biphen}{CH(SiMe$_3$)$_2$}(THF)]$_2$ in a 1:1.2:1.2 ratio (based on the integration of the lanthanum-bound methyne proton signals in the ^{1}H NMR spectrum). Unfortunately, isolation of (*R*)-**5** on a preparative scale was hampered by its high solubility in pentane at −78 °C as well as partial loss of THF under reduced pressure, giving a mixture of the tris-THF adduct (*R*)-**5**, the mono-THF adduct and the THF-free starting material (*R*,*R*)-**4**. Furthermore, (*R*)-**5** could only be obtained when THF was added to complex (*R*,*R*)-**4**, whereas reaction of [La{CH(SiMe$_3$)$_2$}$_3$] with (*R*)-H$_2$(Biphen) in the presence of THF (5 equiv.) in [D$_6$]benzene solution resulted in the slow formation of several products. Complex (*R*)-**5** accounted for only 15% of this mixture after 70% consumption of [La{CH(SiMe$_3$)$_2$}$_3$]. Reactions of (*R*)-H$_2$(Biphen) with [Y{CH(SiMe$_3$)$_2$}$_3$] performed in the presence or absence of THF were unsuccessful as well, producing a mixture of products which did not contain an yttrium−carbon bond.

Interestingly, attempts to synthesize the racemic analogue of (*R*,*R*)-**4** from [La{CH(SiMe$_3$)$_2$}$_3$] and racemic H$_2$(Biphen) yielded only a mixture of complexes. This contrasts our previous observation in the preparation of biphenolate amido complexes using the tris(amido) complex [La{N(SiHMe$_2$)$_2$}$_3$(THF)$_2$] as starting material, which gave isolable products only when racemic H$_2$(Biphen) was used.[60] Attempts to synthesize an enantiopure biphenolate lanthanum amido complex resulted in the formation of a mixture of at least three products. In the present study the reactivity seems to be opposite. Using the trialkyllanthanum complex [La{CH(SiMe$_3$)$_2$}$_3$] we were able to prepare the homochiral dimer (*R*,*R*)-**4**, while the synthesis of a racemic complex failed. The formation of biphenolate rare-earth-metal complexes by amine or alkane elimination is very sensitive to the reactivity and steric hindrance of the rare-earth-metal precursor. The desired biphenolate rare-earth-metal alkyl or amido complexes are obtained as kinetic products.

The X-ray diffraction analysis of (*R*,*R*)-**4** (orthorhombic, space group $P2_12_12$) reveals a C_2-symmetric homochiral dimeric structure (Figure 2). It shows a similar binding motif for the biphenolate ligand as was observed in the heterochiral dimer (*R*,*S*)-**2b** and the thiobinaphtholate complex [Sm{1,1′-S(2-OC$_{10}$H$_4$*t*Bu$_2$-3,6}(OC$_6$H$_3$*t*Bu$_2$-2,6)]$_2$.[80] Selected bond lengths and angles of (*R*,*R*)-**4** and (*R*,*S*)-**2b** are summarized in Table 1 for a better comparison.

The two biphenolate metal moieties are connected by two bridging phenolate units and the tetrahedral geometry

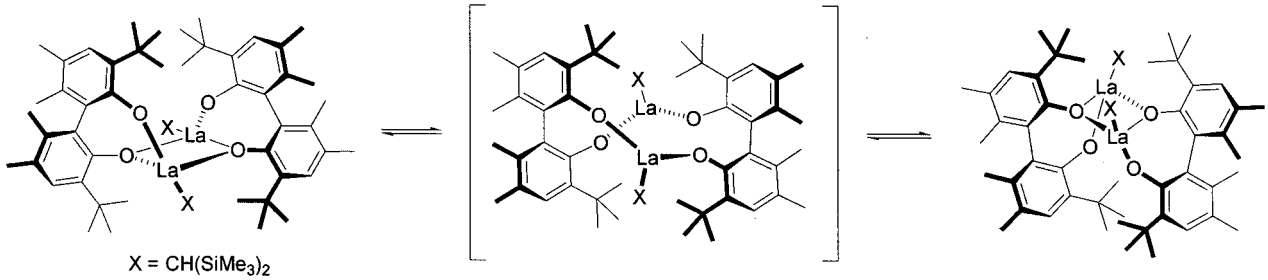

Scheme 2

 © 2004 Wiley-VCH Verlag GmbH & Co. KGaA, Weinheim

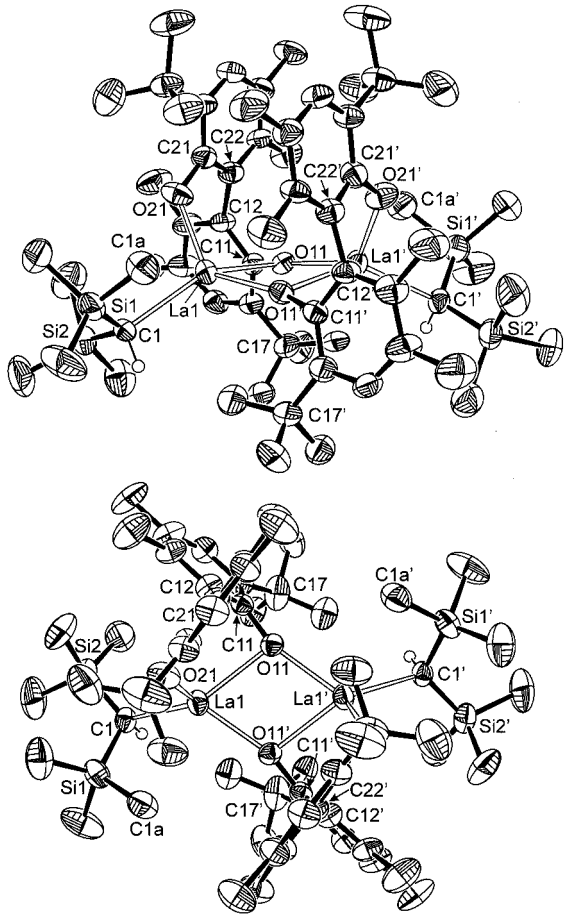

Figure 2. ORTEP diagram of the molecular structure of (*R*,*R*)-**4** (top) and alternative view from the top (bottom); thermal ellipsoids are drawn at the 50% probability level; hydrogen atoms, except for those on C1 and C1′, as well as one position of the disordered *tert*-butyl group on C17 have been omitted for the sake of clarity

around lanthanum is significantly distorted. Both terminal phenolate groups have a *syn* relationship relative to the La_2O_2 core, with their aromatic rings being stacked parallel to each other in order to avoid destabilizing steric interactions of the *tert*-butyl groups.

The La_2O_2 core displays an even more distorted geometry than was observed in (*R*,*S*)-**2b**[60] (Table 1). The lanthanum−oxygen bond to the bridging phenolate oxygen atom of the same biphenolate metal moiety (La1−O11) is 0.14 Å longer than the corresponding bond to the bridging phenolate oxygen atom of the other biphenolate metal moiety (La1−O11′). The terminal lanthanum−oxygen bond La1−O21 is 0.34 Å (for La1−O11) and 0.20 Å (for La1−O11′) shorter than the bond to the bridging phenolates [typical range La−OAr(term.) = 2.17−2.32 Å; La−OAr(bridg.) = 2.32−2.43 Å].[60] The dihedral angle between the two phenol rings [−97.0(7)° for (*R*,*R*)-**4**] is about 9° larger than in (*R*,*S*)-**2b** [87.8(4)°][60] and 24° larger than in [La{1,1′-(2-$OC_6H_2tBu_2$-3,5)$_2$}{$CH(SiMe_3)_2$}$(THF)_3$] (**3**) [72.9(1.9)°],[77] due to its lower coordination number. The O11−La1−O21 bite angle of the biphenolate ligand for (*R*,*R*)-**4** [95.86(12)°] is larger than the values of 88.83(7)° for (*R*,*S*)-**2b**[60] and 88.1(3)° for [La{1,1′-(2-$OC_6H_2tBu_2$-3,5)$_2$}{$CH(SiMe_3)_2$}$(THF)_3$].[77] The La···La separation [3.8750(5) Å] is the shortest observed for complexes with an La_2O_2 core (usual range for La: 3.96−4.02 Å),[60][81−84] in accordance with the observations mentioned earlier.

Table 1. Comparison of selected bond lengths (Å), atomic distances (Å) and angles (°) for (*R*,*R*)-**4** (E = C1) and (*R*,*S*)-**2b**[60] (E = N1)

	(*R*,*R*)-**4** E = C1	(*R*,*S*)-**2b**[60] E = N1
La1−O21	2.169(4)	2.234(2)
La1−O11	2.506(3)	2.503(2)
La1−O11′	2.364(3)	2.407(2)
La1−E	2.543(5)	2.416(3)
La1··· La1′	3.8750(5)	3.9954(3)
La1···C11	2.899(5)	2.911(3)
La1···C1A	3.088(7)	−
La1···Si1	3.3685(16)	3.5240(11)
La1···Si2	3.8643(18)	3.3703(10)
O11−La1−O21	95.86(12)	88.83(7)
O11−La1−O11′	73.24(11)	71.10(8)
O21−La1−O11′	124.07(13)	108.79(8)
E−La1−O11	137.47(16)	123.41(9)
E−La1−O11′	119.42(15)	142.14(9)
E−La1−O21	105.51(17)	106.41(9)
La1−O11−La1′	105.39(11)	108.90(8)
La1−O11−C11	91.9(3)	92.81(16)
La1−O21−C21	125.0(4)	132.5(2)
La1−E−Si1	99.2(2)	116.17(14)
La1−E−Si2	124.0(3)	109.56(14)
Si1−E−Si2	118.4(3)	133.94(17)
C11−C12−C22−C21	−97.0(7)	87.8(4)

The lanthanum−carbon bond [2.543(5) Å] in (*R*,*R*)-**4** is similar in length to that in [La(Cp*){$CH(SiMe_3)_2$}$_2$] [2.537(5) and 2.588(4) Å],[85] but significantly shorter than in [La{1,1′-(2-$OC_6H_2tBu_2$-3,5)$_2$}{$CH(SiMe_3)_2$}$(THF)_3$] (**3**) [2.676(13) Å][77] and [La(Cp*){$CH(SiMe_3)_2$}$_2$(THF)] [2.651(8) and 2.627(10) Å].[85] The alkyl ligand avoids unfavorable steric interactions with the bridging phenolate groups by increasing C1−La1−O11 [137.47(16)°] and C1−La1−O11′ [119.42(15)°], while C1−La1−O21 [105.51(17)°] is slightly decreased from an ideal tetrahedral geometry around lanthanum. The geometry of the alkyl ligand displays a β-SiC monoagostic interaction [La−C−Si = 99.2(2)°, 124.0(3)°; La···C = 3.088(7) Å] resembling those found in previously characterized coordinatively unsaturated bis(trimethylsilyl)methyl rare-earth-metal complexes[86][87] such as [La(Cp*){$CH(SiMe_3)_2$}$_2$] [La−C−Si = 99.6(3)°, 126.4(4)° and 98.8(3)°, 129.6(3)°; La···C = 2.978(6), 2.988(6) Å],[85] [La(Cp*)-{$CH(SiMe_3)_2$}$_2$(THF)] [La−C−Si = 102.9(4)°, 134.8(6)° and 103.6(4)°, 131.1(5)°; La···C = 3.241(19), 3.265(14) Å].[85] One silicon−carbon bond is distorted towards the metal center with La1···Si1 [3.3685(16) Å] and La1···C1A [3.088(7) Å] being within the sum of the van der Waals radii. Note that the coordinatively saturated monomeric biphenolate complex **3** [La−C−Si = 116.5(7)° and 118.7(6)°][77] does not display such an agostic interaction.

Reaction of (*R*,*R*)-**4** with tetramethyldisilazane in the presence of six equivalents of THF results in the formation

 © 2004 Wiley-VCH Verlag GmbH & Co. KGaA, Weinheim

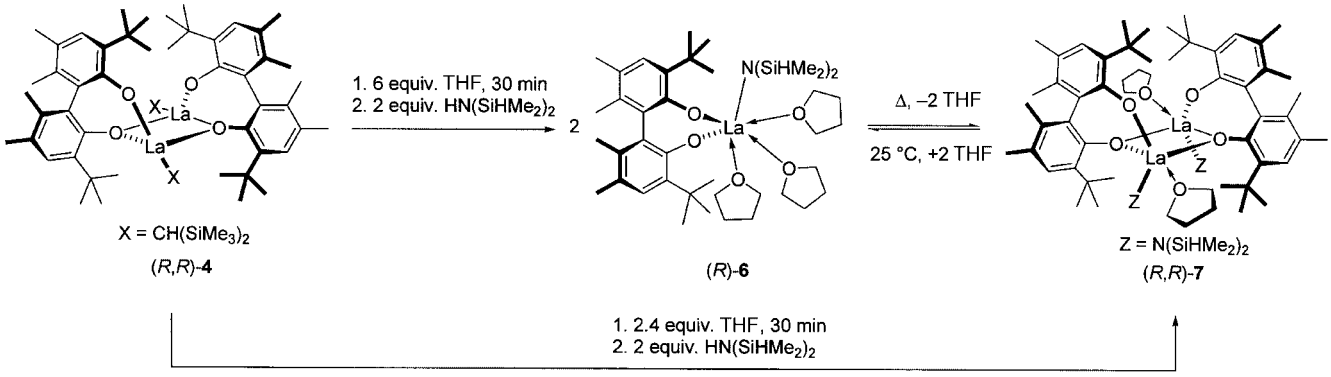

Scheme 3

of [La{(*R*)-Biphen}{N(SiHMe$_2$)$_2$}(THF)$_3$] [(*R*)-**6**] as the major product (Scheme 3), which is not available from the reaction of (*R*)-H$_2$(Biphen) with [La{N(SiHMe$_2$)$_2$}$_3$-(THF)$_2$]. The ^{1}H NMR spectrum of (*R*)-**6** has similar features to the previously characterized (*R*)-**1a**,[60] showing two doublets for the methyl groups on silicon at δ = 0.24 and 0.28 ppm ($^3J_{H,H}$ = 2.9, 3.0 Hz) and a septet for SiH at δ = 5.00 ppm in (*R*)-**6** compared to δ = 0.32 and 0.38 ppm ($^3J_{H,H}$ = 3.0 Hz) and δ = 5.12 ppm in (*R*)-**1a**. In addition to the signals of (*R*)-**6**, small quantities of a second species can be observed to appear over the course of 2 h in the ^{1}H NMR spectrum. The equilibrium is shifted towards this second species upon heating, which we believe to be the homochiral dimer [La{(*R*)-Biphen}{N(SiHMe$_2$)$_2$}(THF)]$_2$ [(*R*,*R*)-**7**]. The equilibrium between (*R*)-**6** and (*R*,*R*)-**7** is shifted from 3:1 at 25 °C to 1:1.5 at 60 °C and 1:3.2 at 80 °C (Figure 3). Formation of (*R*,*R*)-**7** is reversible and the initial 3:1 ratio of (*R*)-**6** to (*R*,*R*)-**7** is regenerated upon cooling back to 25 °C (however, equilibration generally requires 1−2 h at room temperature). (*R*,*R*)-**7** has identical spectroscopic data to the species that is formed upon heating (*R*,*S*)-**2b** in [D$_8$]toluene.[60] Reaction of (*R*,*R*)-**4** with tetramethyldisilazane in the presence of only 2.4 equivalents of THF gives (*R*,*R*)-**7** as the major product.

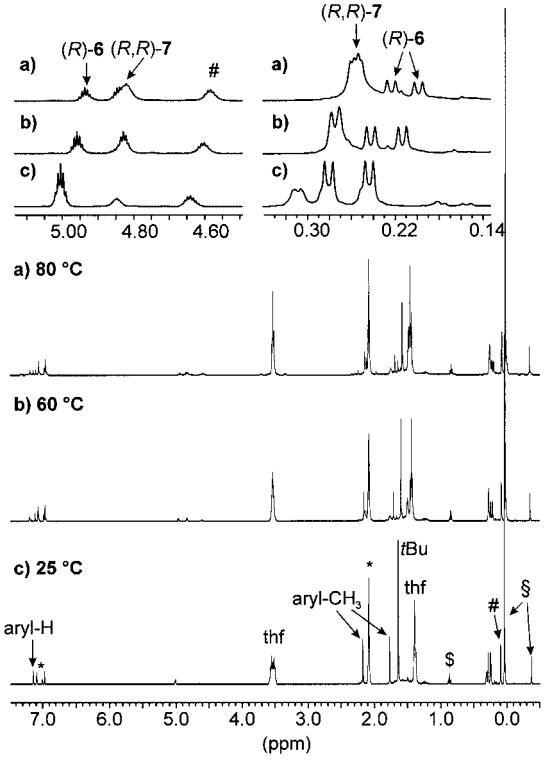

Figure 3. ^{1}H NMR spectrum of the equilibrium between (*R*)-**6** and (*R*,*R*)-**7** in [D$_8$]toluene at: a) 80 °C, b) 60 °C and c) 25 °C [# = HN(SiHMe$_2$)$_2$, § = CH$_2$(SiMe$_3$)$_2$, $ = pentane]

Catalytic Evaluation

Complexes (*R*,*R*)-**4** and (*R*)-**5** were evaluated for their catalytic activity in hydroamination/cyclization and hydrosilylation reactions (Table 2 and 3 respectively). The most notable feature of alkyl complexes (*R*,*R*)-**4** and (*R*)-**5** in comparison to bis(dimethylsilylamido) complexes **1** and **2** is their significantly higher catalytic activity for the hydroamination/cyclization of aminoalkenes. Especially noteworthy seems to be the almost twofold increase in catalytic activity of complex (*R*)-**5** compared to the dimer (*R*,*R*)-**4** in the cyclization of 2,2-dimethylpent-4-enylamine (**8**; Table 2, entries 1 and 2). This strongly suggests that (*R*,*R*)-**4** remains dimeric under the catalytic conditions, which is in accordance with our earlier finding that (*R*,*S*)-**2a** has a lower catalytic activity than **1a**. However, (*R*,*R*)-**4** and (*R*)-**5** show similar rates in the cyclization of the sterically less bulky pent-4-enylamine **10** (Table 2, entry 3 and 4).

The turnover frequency of 61 h^{-1} for complex (*R*)-**5** in the cyclization of substrate **8** is of the same magnitude as that of other highly active lanthanocene catalysts, such as [Cp*$_2$LaCH(SiMe$_3$)$_2$] (95 h^{-1} at 25 °C),[13] and twice as active as the lanthanum bisoxazoline complex [{(4*R*,5*S*)-Ph$_2$Box}La{N(SiMe$_3$)$_2$}$_2$] (25 h^{-1} at 23 °C).[25] Unfortunately, both lanthanum catalysts (*R*,*R*)-**4** and (*R*)-**5** achieve significantly lower enantioselectivities than the yttrium biphenolate complex (*R*)-**1a**[60] — pyrrolidines **9** and **11** are produced in essentially racemic form. The larger atomic radius (0.900 Å for Y vs. 1.032 Å for La)[88] concomitant with the low steric hindrance presented by the *tert*-butyl substituents of the biphenolate ligand results in a low level of stereodifferentiation.

 © 2004 Wiley-VCH Verlag GmbH & Co. KGaA, Weinheim

Table 2. Catalytic hydroamination/cyclization reactions

Entry	Substrate	Product	Cat.[a]	*T* [°C]	Time[b] [h]	Conv. [%]	TOF [h^{-1}]	*ee* Product;[c] dr
1	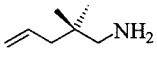	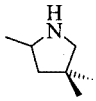	(*R*,*R*)-**4**	25	1.5	95	35	8
2	**8**	**9**	(*R*)-**5**	25	1	98	61	8
3	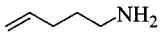		(*R*,*R*)-**4**	60	19	> 99	5	2
4	**10**	**11**	(*R*)-**5**	60	25	98	5.3	0
5	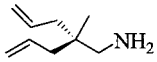	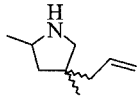	(*R*,*R*)-**4**	29	0.4	> 99	≥ 120	5 / 18; 1.15:1
6	**12**	**13**	(*R*)-**5**	25	0.15	> 99	≥ 330	1 / 28 ; 1.4:1
7	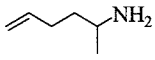	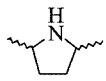	(*R*,*R*)-**4**	25	49	93	1.7[d]	nd; 9:1 (*trans*:*cis*)
8	**14**	**15**	(*R*)-**5**	60	5	95	23[d]	nd; 5.3:1 (*trans*:*cis*)
9	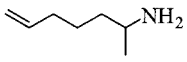	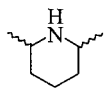	(*R*,*R*)-**4**	80	38	> 96	3.5[d]	nd; 1:3.7 (*trans*:*cis*)
10	**16**	**17**	(*R*)-**5**	80	42	87	3.8[d]	nd; 1:4 (*trans*:*cis*)

[a] Reaction conditions: 2 mol % cat., C_6D_6, Ar atm. [b] Reaction time. [c] Determined by ^{19}F NMR spectroscopy of the Mosher amides. [d] The reactions are not zero order in substrate concentration. TOF is based on the initial rate. nd = not determined.

Table 3. Catalytic hydrosilylation of olefins with $PhSiH_3$ [93]

Entry	Substrate	Product	Cat.[a]	Time[b] [h]	Conv. [%]	dr[c]
1		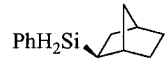	(*R*,*R*)-**4**[d]	22	79	> 30:1
	18	**19**				
2	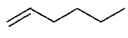	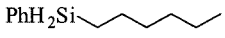	(*R*,*R*)-**4**[d]	22	87	38:1
3	**20**	**21**	(*R*)-**5**	66.5	81	52:1
4	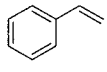	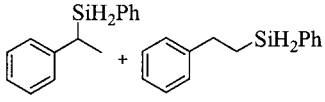	(*R*,*R*)-**4**	2	95	17:1
5	**22**	**23a** + **23b**	(*R*)-**5**	6.7	82	18:1

[a] Reaction conditions: 2 mol % cat., C_6D_6, 1 equiv. $PhSiH_3$, 60 °C, Ar atm. [b] Reaction time. [c] Determined by ^1H NMR spectroscopy. [d] 4 mol % cat.

The amino diolefin **12** cyclizes very rapidly to diastereomeric 4-allyl-2,4-dimethylpyrrolidine (**13**) with a similarly low diastereoselectivity [1.15:1 for (*R*,*R*)-**4** and 1.4:1 for (*R*)-**5**] as observed for (*R*)-**1b**.[60] Interestingly, whereas (*R*)-**1b** gave both diastereomers in almost identical enantiomeric ratios,[60] (*R*,*R*)-**4** and (*R*)-**5** deliver the minor diastereomer with higher enantioselectivity than the almost racemic major diastereomer.

 © 2004 Wiley-VCH Verlag GmbH & Co. KGaA, Weinheim

Cyclization of 1-methylpent-4-enylamine (**14**) in the presence of (*R*,*R*)-**4** at 25 °C gives 2,5-dimethylpyrrolidine (**15**) with a good diastereoselectivity of 9:1 (*trans*:*cis*). The monomeric catalyst (*R*)-**5** produces **15** with a somewhat lower diastereoselectivity of 5.3:1, albeit at 60 °C. Cyclization of 1-methylhex-5-enylamine (**16**), on the other hand, yields preferentially *cis*-2,5-dimethylpiperidine (*cis*-**17**) in a roughly 1:4 ratio (*trans:cis*) using either (*R*,*R*)-**4** or (*R*)-**5**, which is similar to the diastereoselectivity observed with a catalyst system prepared from [Y{N(SiMe$_3$)$_2$}$_3$] and *N*,*N*′-diarylethane-1,2-diamines.[58] Formation of the six-membered ring requires heating to 80 °C for both biphenolate lanthanum catalysts. Preferred formation of *trans*-2,5-dimethylpyrrolidine can be rationalized by a minimization of the 1,3-diaxial interaction in the seven-membered cyclization transition state.[23] Similar considerations explain the preferred formation of *cis*-2,5-dimethylpiperidine via an eight-membered transition state.[22]

Cyclization of 2,2-dimethylpent-4-enylamine (**8**) using (*R*,*R*)-**4** or (*R*)-**5** as catalysts proceeds with a zero-order rate dependence on substrate concentration (Figure 4). This result is in accordance with the generally accepted mechanism of lanthanocene-catalyzed hydroamination reactions, in which olefin insertion into the rare-earth-metal amido bond is the rate-determining step.[13] However, this result contrasts our previous finding that ring-closing of **8** using bis(dimethylsilyl)amido complexes **1** and **2** proceeds with a first- [(*R*)-**1b** and **2**] or second-order rate dependence [(*R*)-**1a**] on substrate concentration.[60]

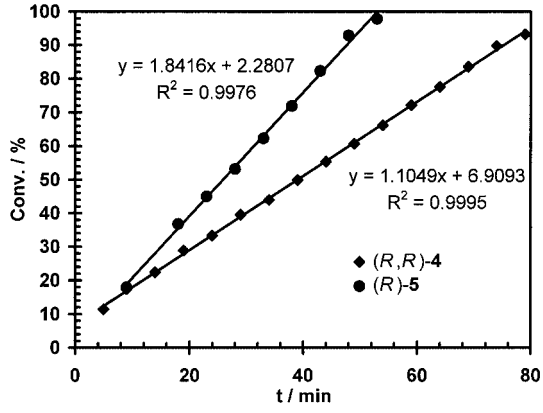

Figure 4. Hydroamination/cyclization of **8** (0.63 M) with 1 mol % (*R*,*R*)-**4** (= 2 mol % La) and 2 mol % (*R*)-**5** at 25 °C in C_6D_6

(*R*,*R*)-[La(Biphen){N(SiHMe$_2$)$_2$}(THF)] [(*R*,*R*)-**7**], prepared in situ by reaction of (*R*,*R*)-**4** with HN(SiHMe$_2$)$_2$ and one equivalent of THF, shows a significantly reduced catalytic activity in the ring-closing of substrate **8**, with an initial rate of 0.36 h^{-1} at 60 °C. Similar to the amidoyttrium biphenolate complex (*R*)-**1a**, ring-closing of **8** with (*R*,*R*)-**7** proceeds with a second-order rate dependence (**1a**) on substrate concentration. The ^{1}H NMR spectra of the catalytic reaction show free tetramethyldisilazane as well as unchanged catalyst, indicating that only 36% of the catalyst is activated. The unchanged catalyst most likely exists as a monomeric species of the general type [La{(*R*)-Biphen}{N(SiHMe$_2$)$_2$}(THF)(L)$_n$] (L = substrate **8** or pyrrolidine **9**; n = 1 or 2) based on the well-separated doublets for the amido silicon methyl groups at δ = 0.30 and 0.35 ppm ($^3J_{H,H}$ = 2.9 Hz) in the ^{1}H NMR spectrum, which is typical for the monomeric biphenolate complexes (*R*)-**1a** and (*R*)-**6**. Therefore, the low catalytic activity of bis(dimethylsilyl)amido complexes **1**, **2** and (*R*)-**6** in comparison to alkyl catalysts (*R*,*R*)-**4** and (*R*)-**5** has to be attributed mainly to the low basicity of the bis(dimethylsilyl)amido ligand resulting in incomplete protonolysis of the amido ligand by the aminoalkene substrate [Scheme 4, X = N(SiHMe$_2$)$_2$, K_{eq} < 1]. Protonolysis of the biphenolate alkyl complexes, on the other hand, is instantaneous and quantitative [Scheme 4, X = CH(SiMe$_3$)$_2$, K_{eq} >> 1]. Complexes with the bis(trimethylsilyl)amido ligand generally give similar catalytic activity to that of alkyl complexes.[13][89] Tetramethyldisilazane (pK_a = 22.8)[90] is more acidic than hexamethyldisilazane (pK_a = 25.8).[91] Obviously, this slight difference in basicity between the two amido ligands renders the bis(dimethylsilyl)amido ligand an unsuitable leaving group for the catalyst precursor.[92] Coordinated THF in the bis(dimethylsilyl)amido complexes cannot contribute significantly to the low catalytic activity, because rare-earth-metal-based hydroamination catalysts generally show only a small decrease in rate in the presence of THF.[13,65,66]

Both complexes (*R*,*R*)-**4** and (*R*)-**5** are also active in the hydrosilylation of various olefinic substrates (Table 3).[93] However, catalytic activity for the monomeric tris-THF adduct (*R*)-**5** is generally lower than for the THF-free dimer (*R*,*R*)-**4**.

Hydrosilylation of styrene proceeds with good activity to give the Markovnikov product with high selectivity. Plausible reasons for the preferred formation of this isomer can be derived from the electronically preferred secondary insertion of styrene into the metal−hydride bond of the catalytically active rare-earth-metal hydrido species.[33,94] In contrast to previously investigated lanthanocene[33] and diamidobiphenyl[45] catalyst systems, the catalytic activities of complexes (*R*,*R*)-**4** and (*R*)-**5** in the hydrosilylation of 1-hexene or norbornene are significantly lower than for styrene, and higher catalyst loadings are required to complete the reaction. The stereoselectivity substrates is very high for these, giving exclusively 1,2-addition for 1-hexene and the *exo* adduct for norbornene.

The reason for the low catalytic activity in the hydrosilylation of 1-hexene and norbornene is not completely clear at present. NMR spectroscopic investigation could not reveal an identifiable species during the catalysis, for example a lanthanum hydride species. Schaverien noted that replacing a six-electron π-donor cyclopentadienyl ligand in a lanthanocene complex by a four-electron donating aryloxide ligand results in reduced activity in the polymerization of α-olefins due to the formation of deactivated μ-hydrido and μ-alkyl species.[95] Insertion of linear terminal olefins proceeded exclusively in a 1,2-fashion and no μ-isoalkyls were observed. Similarly, the highly electrophilic biphenolate lanthanum complexes can be expected to form stable μ-hydrido

 © 2004 Wiley-VCH Verlag GmbH & Co. KGaA, Weinheim

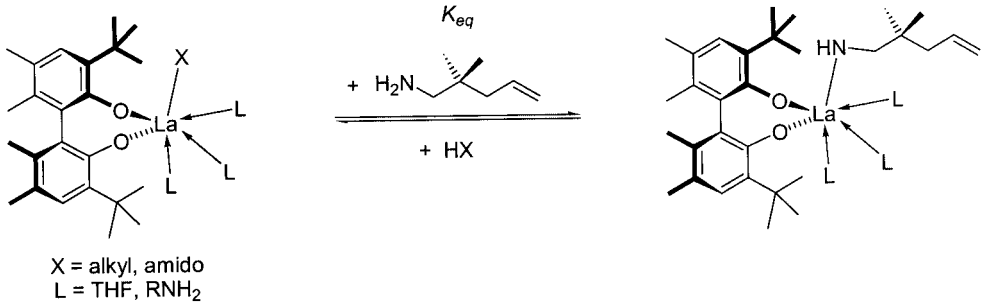

Scheme 4

and μ-alkyl species[96] with reduced reactivity towards olefin insertion or phenylsilane σ-bond metathesis (Scheme 5a). Whereas insertion of 1-hexene into a terminal lanthanum hydride species is expected to give an appreciable amount of branched product[33,39] due to the sterically undemanding features of the biphenolate ligand, insertion into a bridging μ-hydrido would explain the high regioselectivity observed in the hydrosilylation of 1-hexene. The secondary insertion product formed in the reaction of the lanthanum hydride species with styrene on the other hand should adopt an η^3-benzylic coordination mode[94] rather than a bridging μ-benzyl arrangement. The terminal η^3-benzyl group should be significantly more reactive towards phenylsilane than a μ-alkyl species.

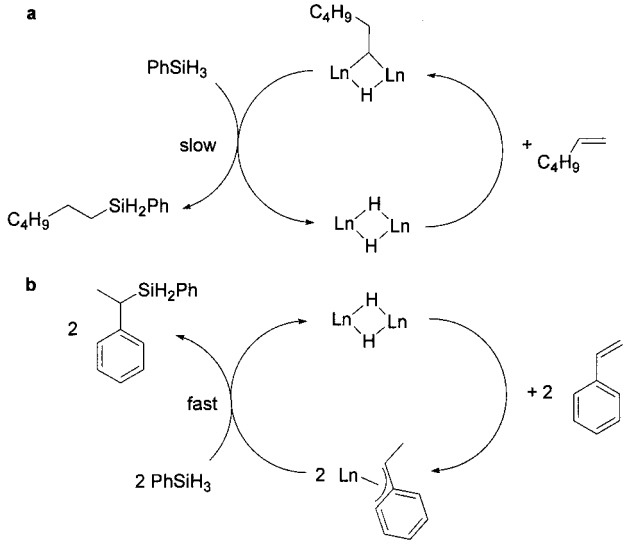

Scheme 5

Conclusion

We have presented here the facile synthesis of chiral biphenolate alkyllanthanum complexes. These complexes show good catalytic activity for the hydroamination/cyclization of aminoalkenes, which is of comparable magnitude to well established lanthanocene catalysts. The catalytic activity is significantly higher than previously prepared biphenolate bis(dimethylsilyl)amido complexes. This can be attributed to a sluggish catalyst initiation in the case of the amido complexes caused by the low basicity of the bis(dimethylsilyl)amido ligand. Despite their high catalytic activity, practical use of the biphenolate alkyl complexes for asymmetric hydroamination is limited by the low enantiomeric excess in the product heterocycles, because the *tert*-butyl groups of the biphenolate ligand have an insufficient stereodifferentiating effect. However, catalysts with larger substituents should be more enantioselective, as shown by yttrium complexes bearing tris(aryl) substituted binaphtholate ligands,[65] while retaining the high catalytic activity. Although the biphenolate lanthanum complexes show good regioselectivity in the hydrosilylation of olefins, they are less attractive catalysts than lanthanocene complexes due to their lower catalytic activity.

Experimental Section

General Remarks: All operations were performed under an inert atmosphere of nitrogen or argon using standard Schlenk-line or glovebox techniques. After drying over KOH, THF was distilled from sodium benzophenone ketyl. Hexanes, pentane and toluene were purified by distillation from sodium/triglyme benzophenone ketyl. [Ln{$CH(SiMe_3)_2$}$_3$] (Ln = Y, La),[79] (*R*)-H_2(Biphen)[76] and substrates **8**,[97] **10**,[13] **12**,[60] **14**[98][99] and **16**[58] were synthesized as described in the literature. Olefins for hydrosilylation reactions were distilled from sodium and stored over molecular sieves. The substrates were dried by distillation from CaH_2 and stored over molecular sieves. (*R*)-(+)-α-Methoxy-α-trifluoromethylphenylacetic acid (RCA, Freiburg, Germany) was transformed into its acid chloride by reaction with oxalyl chloride/DMF in hexanes.[100] Mosher amides were prepared and analyzed by ^{19}F NMR spectroscopy as described earlier.[60] All other chemicals were commercially available and used as received. ^1H, ^{13}C and ^{19}F NMR spectra were recorded on a Bruker Avance 300 (300.1, 75.5 and 282.4 MHz for ^1H, ^{13}C, and ^{19}F, respectively) or Avance 400 (400.1 and 100.6 MHz for ^1H and ^{13}C, respectively) spectrometer. Spectra were referenced internally using the residual solvent resonances (^1H, ^{13}C) or referenced externally to $CFCl_3$ (^{19}F; δ = 0 ppm). Elemental analyses were performed by the Microanalytical Laboratory of this department. Although metal complexes were combusted with V_2O_5 as burning aid, analyses often gave low carbon content repeatedly, presumably due to carbide formation.

(*R*,*R*)-[La(Biphen){$CH(SiMe_3)_2$}]$_2$ [(*R*,*R*)-4]: A solution of (*R*)-H_2(Biphen) (156 mg, 0.44 mmol) in toluene (1 mL) was added to a solution of [La{$CH(SiMe_3)_2$}$_3$] (280 mg, 0.454 mmol) in toluene (1 mL) over 10 min at −10 °C with a syringe. The mixture was stirred at room temperature for 1 h and the solvent was evaporated

 © 2004 Wiley-VCH Verlag GmbH & Co. KGaA, Weinheim

in vacuo. The remaining yellow residue was dried in vacuo. Pentane (2 mL) was added to the residue and the mixture was heated to 50 °C and left in a fridge overnight. The solvent was decanted at −30 °C, acetone bath) from a slightly yellow crystalline precipitate, and the precipitate was washed with pentane (0.5 mL) and dried in vacuo. Yield 110 mg (35%). The crystals contain one equiv. of pentane per molecule of the dimer. ^{1}H NMR (400.1 MHz, [D$_8$]toluene, 25 °C): δ = 7.13 (br. s, 4 H, Biphen), 2.16 (br. s, 12 H, aryl-CH$_3$), 1.53 (br. s, 12 H, aryl-CH$_3$), 1.40 (br. s, 36 H, C(CH$_3$)$_3$], 0.30 [s, 18 H, Si(CH$_3$)$_3$], −0.03 [s, 18 H, Si(CH$_3$)$_3$], −0.62 (s, 2 H, LaCH). ^{1}H NMR (400.1 MHz, [D$_8$]toluene, −30 °C): δ = 7.24 (s, 2 H, Biphen), 7.08 (s, 2 H, Biphen), 2.22 (s, 6 H, aryl-CH$_3$), 2.18 (s, 6 H, aryl-CH$_3$), 1.65 (s, 6 H, aryl-CH$_3$), 1.55 (s, 6 H, aryl-CH$_3$), 1.41 [s, 18 H, C(CH$_3$)$_3$], 1.37 [s, 18 H, C(CH$_3$)$_3$], 0.33 [s, 18 H, Si(CH$_3$)$_3$], 0.07 [s, 18 H, Si(CH$_3$)$_3$], −0.63 (s, 2 H, LaCH) ppm. ^{13}C{^{1}H} NMR (100.6 MHz, [D$_8$]toluene, −30 °C): δ = 156.1, 150.3, 137.8, 137.3, 137.2, 137.0, 135.0, 133.4, 131.2, 130.1, 128.5, 126.6, (aryl), 55.0 (LaCH), 35.0 [*C*(CH$_3$)$_3$], 32.2, 30.7 [C(*C*H$_3$)$_3$], 20.0, 17.5 (aryl-CH$_3$), 4.8, 4.5 [Si(CH$_3$)$_3$] ppm. C$_{62}$H$_{102}$La$_2$O$_4$Si$_4$·(C$_5$H$_{12}$) (1373.8): calcd. C 58.58, H 8.36; found C 57.73, H 8.10.

(*R*)-[La(Biphen){CH(SiMe$_3$)$_2$}(THF)$_3$] [(*R*)-5]: THF (7.2 μL, 89 μmol, 3 equiv. per lanthanum) was added to a solution of (*R*,*R*)-**4** (20 mg, 14.6 μmol) in [D$_6$]benzene (0.5 mL). Removal of the solvent in vacuo led to partial loss of THF, therefore the catalyst was always prepared in situ directly prior to use. ^{1}H NMR (400.1 MHz, [D$_6$]benzene): δ = 7.17 (s, 2 H, Biphen), 3.55 (br. m, 12 H, THF), 2.15 (s, 6 H, aryl-CH$_3$), 1.74 (s, 6 H, aryl-CH$_3$), 1.63 [s, 18 H, C(CH$_3$)$_3$], 1.30 (br. m, 12 H, THF), 0.35 (s, 9 H, SiMe$_3$), 0.33 (s, 9 H, SiMe$_3$), −1.64 [s, 1 H, *CH*(SiMe$_3$)$_2$] ppm. ^{13}C{^{1}H} NMR (100.6 MHz, [D$_6$]benzene): δ = 156.3, 138.3, 136.4, 130.7, 128.9, 124.4 (aryl), 68.9 (THF), 51.5 (LaCH), 35.2 [*C*(CH$_3$)$_3$], 30.7 [C(*C*H$_3$)$_3$], 25.4 (THF), 20.4 (aryl-CH$_3$), 16.2 (aryl-CH$_3$), 5.1 (SiMe$_3$), 5.0 (SiMe$_3$) ppm.

(*R*)-[La(Biphen){N(SiHMe$_2$)$_2$}(THF)$_3$] [(*R*)-6]: THF (6.3 μL, 78 μmol, 3.5 equiv. per lanthanum) was added to a solution of (*R*,*R*)-**4** (15 mg, 10.9 μmol) in [D$_8$]toluene (0.5 mL). The solution was kept at 25 °C for 30 min and then tetramethyldisilazane (4.0 μL, 23 μmol) was added. Removal of the solvent in vacuo led to partial loss of THF. ^{1}H NMR (400.1 MHz, [D$_8$]toluene, 25 °C): δ = 7.14 (s, 2 H, Biphen), 5.00 (sept, $^3J_{H,H}$ = 3.0 Hz, 2 H, SiH), 3.55 (m, THF), 3.50 (br. m, THF), 2.17 (s, 6 H, aryl-CH$_3$), 1.77 (s, 6 H, aryl-CH$_3$), 1.64 [s, 18 H, C(CH$_3$)$_3$], 1.38 (m, THF), 0.28 [d, $^3J_{H,H}$ = 3.0 Hz, 6 H, SiH(C*H*$_3$)$_2$], 0.24 [d, $^3J_{H,H}$ = 2.9 Hz, 6 H, SiH(C*H*$_3$)$_2$] ppm. ^{13}C{^{1}H} NMR (100.6 MHz, [D$_8$]toluene, 25 °C): δ = 156.6, 139.1, 136.3, 131.4, 128.4, 123.9 (aryl), 68.6 (THF), 35.3 [*C*(CH$_3$)$_3$], 30.6 [C(*C*H$_3$)$_3$], 25.6 (THF), 16.2 (aryl-CH$_3$), 3.0 [SiH(CH$_3$)$_2$], 2.9 [SiH(CH$_3$)$_2$] ppm.

(*R*,*R*)-[La(Biphen){N(SiHMe$_2$)$_2$}(THF)]$_2$ [(*R*,*R*)-7]: THF (1.4 μL, 17.3 μmol, 1.2 equiv. per lanthanum) was added to a solution of (*R*,*R*)-**4** (10 mg, 7.3 μmol) in [D$_6$]benzene (0.5 mL). The solution was kept at 25 °C for 30 min and then tetramethyldisilazane (3.1 μL, 17.8 μmol) was added. The ^{1}H and ^{13}C NMR spectra show broad signals for the biphenolate ligand at room temperature. ^{1}H NMR (400.1 MHz, [D$_6$]benzene, 60 °C): δ = 7.23 (s, 2 H, Biphen), 4.90 (br. sept, 2 H, SiH), 3.58 (br. m, THF), 3.50 (br. m, THF), 2.15 (br. s, 6 H, aryl-CH$_3$), 1.80 (br. s, 6 H, aryl-CH$_3$), 1.54 [br. s, 18 H, C(CH$_3$)$_3$], 1.33 (m, THF), 0.32 [m, 12 H, SiH(C*H*$_3$)$_2$] ppm. ^{13}C{^{1}H} NMR (100.6 MHz, [D$_6$]benzene, 60 °C): δ = 138.4, 137.3, 136.2, 129.6, 128.6, 124.7 (aryl), 69.3 (THF), 35.3 [*C*(CH$_3$)$_3$], 34.9 [*C*(CH$_3$)$_3$], 30.7 [C(*C*H$_3$)$_3$], 30.5 [C(*C*H$_3$)$_3$], 25.3 (THF), 20.0, 16.3 (aryl-CH$_3$), 3.2 [SiH(CH$_3$)$_2$], 3.1 [SiH(CH$_3$)$_2$] ppm.

X-ray Crystallographic Study: Clear, colourless crystals of (*R*,*R*)-**4** suitable for X-ray diffraction analysis were obtained by cooling a concentrated pentane solution to −30 °C. Data were collected on a Nonius KappaCCD area detector. Crystal data: C$_{62}$H$_{102}$La$_2$O$_4$Si$_4$·C$_5$H$_{12}$, M_r = 1373.78, crystal size 0.10 × 0.10 × 0.10 mm, orthorhombic, space group $P2_12_12$ (No. 18), a = 16.3814(7) Å, b = 17.5277(5) Å, c = 12.9592(6) Å, V = 3721.0(3) Å^3, Z = 2, $\rho_{calcd.}$ = 1.225 g cm^{-3}, F(000) = 1434, Mo-K_α radiation (λ = 0.71073 Å), T = 173(2) K, μ = 1.237 mm^{-1}, 8519 independent reflections measured, GOF = 0.945, R [$I > 2\sigma(I)$] = 0.0473, wR_2 (all data) = 0. 1084, absolute structure parameter = −0.04(2), largest e-max, e-min = 0.555 and −0.767 e·Å^{-3}. Cell parameters for (*R*,*R*)-**4** were obtained from 10 frames using a 10° scan and refined with 4689 reflections. Lorentz, polarization, and empirical absorption corrections were applied.[101,102] The space group was determined from systematic absences and subsequent least-squares refinement. The structures were solved by direct methods. The parameters were refined with all data by full-matrix least-squares on F^2 using SHELXL-97.[103] Hydrogen atoms were fixed in idealized positions using a riding model. Non-hydrogen atoms were refined anisotropically. The methyl groups attached to C17 are disordered and were refined with two independent orientations (position occupation of 48.52% and 51.48%, respectively). Scattering factors and $\Delta f'$ and $\Delta f''$ values were taken from the literature.[104] Graphical representations were prepared with ORTEP-III for Windows.[105] CCDC-235041 contains the supplementary crystallographic data for this paper. These data can be obtained free of charge at www.ccdc.cam.ac.uk/conts/retrieving.html [or from the Cambridge Crystallographic Data Centre, 12 Union Road, Cambridge CB2 1EZ, UK; Fax: +44-1223-336-033; E-mail: deposit@ccdc.cam.ac.uk].

General Procedure for NMR-Scale Catalytic Hydroamination/Cyclization Reactions: In a glovebox, a screw-cap NMR tube was charged with 10 μmol of the catalyst, C$_6$D$_6$ (0.5 mL) and the substrate (0.33 mmol) in that order. The NMR tube was then placed in a pre-heated oil bath and conversion followed by ^{1}H NMR spectroscopy (for acquisition parameters see below). Final conversion was determined by ^{1}H NMR spectroscopy (disappearance of olefinic signals) and by GC analysis. Diastereomeric ratios of pyrrolidines **13** and **15** as well as piperidine **17** were determined by vacuum-transfer of all volatiles and subsequent ^{1}H NMR spectroscopic analysis of characteristic signals.

General Procedure for Kinetic Catalytic Hydroamination/Cyclization Reactions: In a glovebox, a screw-cap NMR tube was charged with 10 μmol of the catalyst, C$_6$D$_6$ (0.5 mL) and the substrate (0.33 mmol) in that order. The NMR tube was then placed in the thermostatted probe (± 0.5 °C) of the Bruker Avance 400 spectrometer. The conversion was monitored by ^{1}H NMR spectroscopy by following the disappearance of the olefinic signals of the substrate relative to the internal standard CH$_2$(SiMe$_3$)$_2$. NMR spectra were taken at 5 min time intervals using the *multizg* script from the Bruker XWin NMR software package. In order to ensure accurate integration, a 10 s delay between 30° pulses was utilized (number of scans = 4, acquisition time = 4 s). Substrate and catalyst concentration was verified by comparison of the integrals of characteristic signals [olefinic signals for substrates; Si(CH$_3$) signal of CH$_2$(SiMe$_3$)$_2$]. The linear part of the data (minimum two half-lives) was fit by least-squares analysis and the turnover frequency (TOF) was determined from the slope a. TOF = a × [subst]$_0$/[cat]

General Procedure for NMR-Scale Catalytic Hydrosilylation Reactions: In the glovebox, a screw-cap NMR tube was charged with (*R*,*R*)-**4** (5.0 mg, 3.6 μmol), C$_6$D$_6$ (0.5 mL), the olefin (0.30 mmol) and phenylsilane (33 mg, 0.30 mmol) in that order. The NMR tube

 © 2004 Wiley-VCH Verlag GmbH & Co. KGaA, Weinheim

was then placed in a pre-heated oil bath and conversion followed by ^{1}H NMR spectroscopy. Final conversion was determined by ^{1}H NMR spectroscopy (disappearance of olefinic signals). Diastereomeric ratios were determined by ^{1}H NMR spectroscopic analysis of characteristic signals in comparison to literature spectroscopic data.[30,33]

Acknowledgments

Generous financial support by the Deutsche Forschungsgemeinschaft (DFG) and the Fonds der Chemischen Industrie is gratefully acknowledged. K. C. H. is a DFG Emmy Noether fellow (2001−2005) and thanks Professor John A. Gladysz for generous support.

[1] H. Yasuda, *Top. Organomet. Chem.* **1999**, *2*, 255−283.
[2] Z. Hou, Y. Wakatsuki, *Coord. Chem. Rev.* **2002**, *231*, 1−22.
[3] G. A. Molander, J. A. C. Romero, *Chem. Rev.* **2002**, *102*, 2161−2185.
[4] R. Taube, in *Applied Homogeneous Catalysis*, vol. 1 (B. Cornils, W. A. Herrmann, Eds.), Wiley-VCH: Weinheim, **1996**, pp. 507−520. For other general reviews on this topic see refs.[5−12]
[5] T. E. Müller, M. Beller, *Chem. Rev.* **1998**, *98*, 675−703.
[6] M. Nobis, B. Drießen-Hölscher, *Angew. Chem.* **2001**, *113*, 4105−4108; *Angew. Chem. Int. Ed.* **2001**, *40*, 3983−3985.
[7] J. J. Brunet, D. Neibecker, in *Catalytic Heterofunctionalization from Hydroamination to Hydrozirconation* (A. Togni, H. Grützmacher, Eds.), Wiley-VCH: Weinheim, **2001**, pp. 91−141.
[8] J. Seayad, A. Tillack, C. G. Hartung, M. Beller, *Adv. Synth. Catal.* **2002**, *344*, 795−813.
[9] M. Beller, C. Breindl, M. Eichberger, C. G. Hartung, J. Seayad, O. R. Thiel, A. Tillack, H. Trauthwein, *Synlett* **2002**, 1579−1594.
[10] F. Pohlki, S. Doye, *Chem. Soc. Rev.* **2003**, *32*, 104−114.
[11] I. Bytschkov, S. Doye, *Eur. J. Org. Chem.* **2003**, 935−946.
[12] P. W. Roesky, T. E. Müller, *Angew. Chem.* **2003**, *115*, 2812−2814; *Angew. Chem. Int. Ed.* **2003**, *42*, 2708−2710.
[13] M. R. Gagné, C. L. Stern, T. J. Marks, *J. Am. Chem. Soc.* **1992**, *114*, 275−294.
[14] M. A. Giardello, V. P. Conticello, L. Brard, M. Gagné, T. J. Marks, *J. Am. Chem. Soc.* **1994**, *116*, 10241−10254.
[15] M. R. Douglass, M. Ogasawara, S. Hong, M. V. Metz, T. J. Marks, *Organometallics* **2002**, *21*, 283−292.
[16] Y. Li, T. J. Marks, *J. Am. Chem. Soc.* **1996**, *118*, 9295−9306.
[17] Y. Li, T. J. Marks, *J. Am. Chem. Soc.* **1998**, *120*, 1757−1771.
[18] V. M. Arredondo, F. E. McDonald, T. J. Marks, *J. Am. Chem. Soc.* **1998**, *120*, 4871−4872.
[19] A. T. Gilbert, B. L. Davis, T. J. Emge, R. D. Broene, *Organometallics* **1999**, *18*, 2125−2132.
[20] V. M. Arredondo, S. Tian, F. E. McDonald, T. J. Marks, *J. Am. Chem. Soc.* **1999**, *121*, 3633−3639.
[21] G. A. Molander, E. D. Dowdy, *J. Org. Chem.* **1999**, *64*, 6515−6517.
[22] G. A. Molander, E. D. Dowdy, S. K. Pack, *J. Org. Chem.* **2001**, *66*, 4344−4347.
[23] J.-S. Ryu, T. J. Marks, F. E. McDonald, *Org. Lett.* **2001**, *3*, 3091−3094.
[24] J.-S. Ryu, G. Y. Li, T. J. Marks, *J. Am. Chem. Soc.* **2003**, *125*, 12584−12605.
[25] S. Hong, A. M. Kawaoka, T. J. Marks, *J. Am. Chem. Soc.* **2003**, *125*, 15878−15892.
[26] M. R. Douglass, C. L. Stern, T. J. Marks, *J. Am. Chem. Soc.* **2001**, *123*, 10221−10238.
[27] A. M. Kawaoka, M. R. Douglass, T. J. Marks, *Organometallics* **2003**, *22*, 4630−4632.
[28] G. A. Molander, E. C. Dowdy, *Top. Organomet. Chem.* **1999**, *2*, 119−154.
[29] T. Sakakura, H.-J. Lautenschlager, M. Tanaka, *J. Chem. Soc., Chem. Commun.* **1991**, 40−41.
[30] G. A. Molander, M. Julius, *J. Org. Chem.* **1992**, *57*, 6347−6351.
[31] S.-Y. Onozawa, T. Sakakura, M. Tanaka, *Tedrahedron Lett.* **1994**, *35*, 8177−8180.
[32] G. A. Molander, P. J. Nichols, *J. Am. Chem. Soc.* **1995**, *117*, 4415−4416.
[33] P.-F. Fu, L. Brard, Y. Li, T. J. Marks, *J. Am. Chem. Soc.* **1995**, *117*, 7157−7168.
[34] G. A. Molander, W. H. Retsch, *Organometallics* **1995**, *14*, 4570−4575.
[35] G. A. Molander, P. J. Nichols, *J. Org. Chem.* **1996**, *61*, 6040−6043.
[36] G. A. Molander, J. Winterfeld, *J. Organomet. Chem.* **1996**, *524*, 275−279.
[37] G. A. Molander, W. H. Retsch, *J. Am. Chem. Soc.* **1997**, *119*, 8817−8825.
[38] H. Schumann, M. R. Keitsch, J. Winterfeld, S. Mühle, G. A. Molander, *J. Organomet. Chem.* **1998**, *559*, 181−190.
[39] G. A. Molander, E. C. Dowdy, B. C. Noll, *Organometallics* **1998**, *17*, 3754−3758.
[40] G. A. Molander, E. C. Dowdy, *J. Org. Chem.* **1998**, *63*, 3386−3396.
[41] H. Schumann, M. R. Keitsch, J. Demtschuk, G. A. Molander, *J. Organomet. Chem.* **1999**, *582*, 70−82.
[42] G. A. Molander, C. P. Corrette, *J. Org. Chem.* **1999**, *64*, 9697−9703.
[43] G. A. Molander, M. H. Schmitt, *J. Org. Chem.* **2000**, *65*, 3767−3770.
[44] A. R. Muci, J. E. Bercaw, *Tedrahedron Lett.* **2000**, *41*, 7609−7612.
[45] T. I. Gountchev, T. D. Tilley, *Organometallics* **1999**, *18*, 5661−5667.
[46] A. A. Trifonov, T. P. Spaniol, J. Okuda, *Organometallics* **2001**, *20*, 4869−4874.
[47] Y. Horino, T. Livinghouse, *Organometallics* **2004**, *23*, 12−14.
[48] K. N. Harrison, T. J. Marks, *J. Am. Chem. Soc.* **1992**, *114*, 9220−9221.
[49] E. A. Bijpost, R. Duchateau, J. H. Teuben, *J. Mol. Catal. A* **1995**, *95*, 121−128.
[50] G. A. Molander, D. Pfeiffer, *Org. Lett.* **2001**, *3*, 361−363.
[51] H. Schumann, J. A. Meese-Marktscheffel, L. Esser, *Chem. Rev.* **1995**, *95*, 865−986.
[52] F. T. Edelmann, *Angew. Chem.* **1995**, *107*, 2647−2669; *Angew. Chem. Int. Ed. Engl.* **1995**, *34*, 2466−2488.
[53] F. T. Edelmann, D. M. M. Freckmann, H. Schumann, *Chem. Rev.* **2002**, *102*, 1851−1896.
[54] W. E. Piers, D. J. H. Emslie, *Coord. Chem. Rev.* **2002**, *233−234*, 131−155.
[55] M. R. Bürgstein, H. Berberich, P. W. Roesky, *Organometallics* **1998**, *17*, 1452−1454.
[56] Y. K. Kim, T. Livinghouse, J. E. Bercaw, *Tedrahedron Lett.* **2001**, *42*, 2933−2935.
[57] M. R. Bürgstein, H. Berberich, P. W. Roesky, *Chem. Eur. J.* **2001**, *7*, 3078−3085.
[58] Y. K. Kim, T. Livinghouse, *Angew. Chem.* **2002**, *114*, 3797−3799; *Angew. Chem. Int. Ed.* **2002**, *41*, 3645−3647.
[59] P. N. O′Shaughnessy, P. D. Knight, C. Morton, K. M. Gillespie, P. Scott, *Chem. Commun.* **2003**, 1770−1771.
[60] D. V. Gribkov, K. C. Hultzsch, F. Hampel, *Chem. Eur. J.* **2003**, *9*, 4796−4810.
[61] Y. K. Kim, T. Livinghouse, Y. Horino, *J. Am. Chem. Soc.* **2003**, *125*, 9560−9561.
[62] P. N. O′Shaughnessy, P. Scott, *Tedrahedron: Asymmetry* **2003**, *14*, 1979−1983.
[63] S. Hong, S. Tian, M. V. Metz, T. J. Marks, *J. Am. Chem. Soc.* **2003**, *125*, 14768−14783.
[64] J. Collin, J.-D. Daran, E. Schulz, A. Trifonov, *Chem. Commun.* **2003**, 3048−3049.

 © 2004 Wiley-VCH Verlag GmbH & Co. KGaA, Weinheim

[65] D. V. Gribkov, K. C. Hultzsch, *Chem. Commun.* **2004**, 730−731.
[66] K. C. Hultzsch, F. Hampel, T. Wagner, *Organometallics* **2004**, *23*, 2601−2612.
[67] However, the chemistry of inorganic rare-earth-metal Lewis-acid catalysts for organic synthesis is well developed, see: M. Shibasaki, N. Yoshikawa, *Chem. Rev.* **2002**, *102*, 2187−2210 and refs.[68,69].
[68] S. Kobayashi, M. Sugiura, H. Kitagawa, W. W.-L. Lam, *Chem. Rev.* **2002**, *102*, 2227−2302.
[69] K. Mikami, M. Terada, H. Matsuzawa, *Angew. Chem.* **2002**, *114*, 3704−3722; *Angew. Chem. Int. Ed.* **2002**, *41*, 3554−3571.
[70] M. A. Giardello, V. P. Conticello, L. Brard, M. Sabat, A. L. Rheingold, C. L. Stern, T. J. Marks, *J. Am. Chem. Soc.* **1994**, *116*, 10212−10240.
[71] K. C. Hultzsch, T. P. Spaniol, J. Okuda, *Organometallics* **1997**, *16*, 4845−4856.
[72] J. C. Yoder, M. W. Day, J. E. Bercaw, *Organometallics* **1998**, *17*, 4946−4958.
[73] J. Eppinger, PhD Dissertation, Technische Universität, München, **1999**.
[74] For related 3,3′-bis[tris(aryl)silyl]-substituted binaphtholate arylyttrium complexes, displaying improved catalytic activity and enantioselectivity compared to the amido complexes reported in ref.[60], see ref.[65]
[75] H_2(Biphen) is commercially available from Strem Chemicals, Inc. in enantiopure form. This ligand has been successfully employed in asymmetric ring-closing metathesis reactions, see: R. R. Schrock, A. H. Hoveyda, *Angew. Chem.* **2003**, *115*, 4740−4782; *Angew. Chem. Int. Ed.* **2003**, *42*, 4592−4633.
[76] J. B. Alexander, R. R. Schrock, W. M. Davis, K. C. Hultzsch, A. H. Hoveyda, J. H. Houser, *Organometallics* **2000**, *19*, 3700−3715.
[77] C. J. Schaverien, N. Meijboom, A. G. Orpen, *J. Chem. Soc., Chem. Commun.* **1992**, 124−126.
[78] One should note that in contrast to the Biphen ligand system employed in our study, Schaverien's biphenolate complexes can only be synthesized in racemic form. The 3,3′,5,5′-tetra-*tert*-butyl-1,1′-biphenyl-2,2′-diol ligand cannot form atropisomers due to lack of sterically congesting substituents in the 6- and 6′-positions.
[79] P. B. Hitchcock, M. F. Lappert, R. G. Smith, R. A. Bartlett, P. P. Power, *J. Chem. Soc., Chem. Commun.* **1988**, 1007−1008.
[80] P. L. Arnold, L. S. Natrajan, J. J. Hall, S. J. Bird, C. Wilson, *J. Organomet. Chem.* **2002**, *647*, 205−215.
[81] R. Anwander, *Top. Curr. Chem.* **1996**, *179*, 149−245.
[82] C. Runschke, G. Meyer, *Z. Anorg. Allg. Chem.* **1997**, *623*, 1493.
[83] W. J Evans, R. E. Golden, J. W. Ziller, *Inorg. Chem.* **1991**, *30*, 4963−4968.
[84] L.-W. Yang, S. Liu; E. Wong, S. J. Rettig, C. Orvig, *Inorg. Chem.* **1995**, *34*, 2154−2178.
[85] H. van der Heijden, C. J. Schaverien, A. G. Orpen, *Organometallics* **1989**, *8*, 255−258.
[86] C. J. Schaverien, *Adv. Organomet. Chem.* **1994**, *36*, 283−362.
[87] W. T. Klooster, L. Brammer, C. J. Schaverien, P. H. M. Budzelaar, *J. Am. Chem. Soc.* **1999**, *121*, 1381−1382.
[88] R. D. Shannon, *Acta Crystallogr., Sect. A* **1976**, *32*, 751−767.
[89] In fact, bis(trimethylsilyl)methyl- and bis(trimethylsilyl)amido-lanthanum binaphtholate complexes show identical catalytic activity: D. V. Gribkov, K. C. Hultzsch, unpublished results.
[90] J. Eppinger, M. Spiegler, W. Hieringer, W. A. Herrmann, R. Anwander, *J. Am. Chem. Soc.* **2000**, *122*, 3080−3096.
[91] R. R. Fraser, T. S. Mansour, S. Savard, *J. Org. Chem.* **1985**, *50*, 3232−3234.
[92] For similar discussions see refs.[62,66]
[93] Because of the inferior enantioselectivities observed in the hydroamination reactions using catalysts (*R*,*R*)-**4** and (*R*)-**5**, the enantiomeric excess of silanes **19** and **23a** was not determined.
[94] K. C. Hultzsch, P. Voth, K. Beckerle, T. P. Spaniol, J. Okuda, *Organometallics* **2000**, *19*, 228−243.
[95] C. J. Schaverien, *Organometallics* **1994**, *13*, 69.
[96] The formation of higher aggregated species such as trimers or tetramers seems to be conceivable, as we believe that it is very likely that the dimeric μ-phenolate cage of (*R*,*R*)-**4** remains intact during the catalytic cycle.
[97] Y. Tamaru, M. Hojo, H. Higashimura, Z.-I. Yoshida, *J. Am. Chem. Soc.* **1988**, *110*, 3994−4002.
[98] H. O. House, L. F. Lee, *J. Org. Chem.* **1976**, *41*, 863−869.
[99] K. Harding, S. R. Burks, *J. Org. Chem.* **1981**, *46*, 3920−3922.
[100] P. M. Smith, E. J. Thomas, *J. Chem. Soc., Perkin Trans. 1* **1998**, 3541−3556.
[101] "Collect" data collection software, Nonius B. V., **1998**.
[102] "Scalepack" data processing software: Z. Otwinowski, W. Minor, *Methods in Enzymology* **1997**, *276*, (Macromolecular Crystallography, Part A), 307.
[103] G. M. Sheldrick, *SHELX-97, Program for the refinement of crystal structures*, University of Göttingen, **1997**.
[104] D. T. Cromer, J. T. Waber, in *International Tables for X-ray Crystallography* (Eds.: J. A. Ibers, W. C. Hamilton), Kynoch, Birmingham, England, **1974**.
[105] L. J. Farrugia, *Ortep-3 for Windows, J. Appl. Crystallogr.* **1997**, *30*, 565.

Received April 1, 2004
Early View Article
Published Online August 17, 2004

 © 2004 Wiley-VCH Verlag GmbH & Co. KGaA, Weinheim

Novel Cadmium(II) Adipate Coordination Polymers with Structural Transformation via Oxalate Ligand: Syntheses, Structures and Fluorescence Properties

Na Hao,[a] Enhong Shen,*[a] Yang-Guang Li,[a] En-Bo Wang,*[a] Chang-Wen Hu,[a] and Lin Xu[a]

Keywords: Cadmium / Coordination polymers / Fluorescence / Hydrothermal synthesis / Interpenetration

Two novel cadmium adipate coordination polymers $[Cd\{O_2C(CH_2)_4CO_2\}\{1,10\text{-phen}\}]_n$ (**1**) and $[Cd_2(C_2O_4)\{O_2C(CH_2)_4CO_2(OH_2)_2\}\{2,2'\text{-bipy}\}]\cdot H_2O$ (**2**) [adipic acid = $HO_2C(CH_2)_4CO_2H$] have been hydrothermally synthesized and characterized by elemental analyses, IR spectroscopy, thermogravimetric analysis and single-crystal X-ray diffraction. Crystallographic data for **1**: monoclinic, *C*2/*c*, *a* = 16.186(3) Å, *b* = 15.487(3) Å, *c* = 14.052(3) Å, *β* = 112.73(3)°, *Z* = 8. Crystal data for **2**: monoclinic, *Cc*, *a* = 23.448(5) Å, *b* = 11.826(2) Å, *c* = 8.3163(17) Å, *β* = 99.08(3)°, *Z* = 4. The structural analysis reveals that **1** forms a novel one-dimensional chain in which the binuclear Cd centers are linked by adipate anions. Compound **2** is the first example in which both a 2,2′-bipy ligand and an oxalate group are found in the {M/adipate} system. Compound **2** possesses one-dimensional sine- or cosine-type chains, which are alternately connected together by the oxalate group to form a three-dimensional framework. The structural determination reveals that the introduction of the oxalate ligand causes the dimensional transformation of the compounds. Compounds **1** and **2** show strong fluorescent properties at room temperature.

(© Wiley-VCH Verlag GmbH & Co. KGaA, 69451 Weinheim, Germany, 2004)

Introduction

Research on metal-templated coordination polymers with different dimensions is of current interest in the field of supramolecular chemistry and crystal engineering, not only because of their intriguing structural motifs but also because of their potential applications due to their unique electro-conductive, nonlinear optical and magnetic properties.[1−6] In this respect, the selection of inorganic and organic building blocks possessing specific features to fulfil special needs of transition metals, such as versatile binding modes and coordination abilities to form hydrogen bonding, is the key to the construction of a desired framework.[7,8] It is noteworthy that dicarboxylates such as malonate, fumarate and 1,4-benzenedicarboxylate have been widely used in constructing novel different dimensional metal-organic hybrid compounds.[9] In contrast, the dicarboxylate ligand adipate has rarely been used. There are at least three intriguing structural features of the adipate ligand. In the first place, it contains two bridging moieties, which leads to a variety of connection modes with transitional metal centers and provides abundant structural motifs. In the second place, it can act both as a hydrogen-bond donor and acceptor. And finally, it contains six carbon atoms that may construct high dimensional and pore structures. Although several interesting compounds containing adipate have been reported by Jung, Ribas, Bakalbassis and their co-workers,[10] the introduction of chelating ligands containing N- or O-donors, such as 2,2′-bipy, 1,10-phen and oxalate anion ($C_2O_4^{2-}$), to the {M/adipate} system has not been explored hitherto. A chelating N-containing ligand usually inhibits the expansion of polymeric frameworks due to the "passivation" of the metal sites by the N donors of the organic groups, which may decrease the dimensionality of these metal-organic hybrid compounds.[11,12] However, the O-containing ligand $C_2O_4^{2-}$ has more geometrical coordination modes to provide both rigidity and preferred coordination specificity for metal centers,[7] thus making it easier to form 1-D chains and thereby allow the formation of higher-dimensional frameworks. Taking into account these factors, we became motivated to design and synthesize novel metal-organic coordination polymers containing adipate and one or more kind of organic ligands containing N- or O-donors under hydrothermal conditions.

In this paper, we report two novel cadmium-containing coordination polymers $[Cd\{O_2C(CH_2)_4CO_2\}\{1,10\text{-phen}\}]_n$ (**1**) and $[Cd_2(C_2O_4)\{O_2C(CH_2)_4CO_2(OH_2)_2\}\{2,2'\text{-bipy}\}]\cdot H_2O$ (**2**). Compounds **1** and **2** possess different dimensionality due to the introduction of the oxalate ligand. Compound **1**

[a] Institute of Polyoxometalate Chemistry, Department of Chemistry, Northeast Normal University, Changchun, 130024, P. R. China
Fax: +86-431-568-4009
E-mail: wangenbo@public.cc.jl.cn

Supporting information for this article is available on the WWW under http://www.eurjic.org or from the author.

 © 2004 Wiley-VCH Verlag GmbH & Co. KGaA, Weinheim **DOI: 10.1002/ejic.200400291**

exhibits an interesting 1-D chain in which the binuclear Cd centers are linked by adipate anions. Compound **2** not only has 1-D sine- or cosine-type chains, but also exhibits a novel three-dimensional framework in which the sine- and cosine-type curves are connected alternately by oxalate anions along the *c* axis. Furthermore, both compounds show intense fluorescence at room temperature.

Results and Discussion

The hydrothermal reaction of a solution of $Cd(NO_3)_2{\cdot}4H_2O$, adipic acid, 1,10-phenanthroline (1,10-phen), NaOH and H_2O gives rise to **1** as colorless crystals. Single crystal X-ray diffraction analysis reveals that **1** is a 1-D chain-like polymer with one crystallographically unique Cd center in the asymmetric unit (see Figure S1 in the Supporting Information). The Cd(1) site coordinates to two nitrogen atoms of one 1,10-phen group and five carboxyl oxygen atoms of different adipate ligands. The average Cd−N bond length is 2.346 Å and the Cd−$O_{(carboxyl)}$ bond lengths are in the range 2.289(2)−2.587(3) Å. The N(O)−Cd−O(N) bond angles range from 80.65(9)° to 153.85(10)° (see Table S2 in the Supporting Information). Thus, the Cd center displays a distorted pentagonal bipyramidal geometry to form one $[CdO_5N_2]$ unit. Two such $[CdO_5N_2]$ units are connected together by μ_3-O atoms in an edge-sharing mode to form dinuclear Cd centers. In addition, two carboxylate groups of the adipate ligand exhibit two kinds of coordination modes with Cd centers (see a in Scheme 1) — one carboxylate group acts as a bis-chelating ligand to bridge one Cd center, while the other exhibits an unusual bidentate bridging mode to link two Cd centers. Thus, one adipate ligand is connected to three different Cd centers, which has not been observed previously. To the best of our knowledge, this is the first example for adipate anions in which the carboxylates exhibit a bis-chelating and bidentate bridging mode toward metal centers. On the basis of this connection mode, all dinuclear Cd centers are linked by four bridging adipate ligands to form a 1-D chain along the *a* axis (see Figure 1). In contrast to the reported compounds in the {M/adipate} (M = transition metal ions) system, compound **1** is the first dinuclear compound connected by mixed adipate and 1,10-phen ligands. In the packing arrangement of **1**, the adjacent 1-D chains are parallel to each other and construct a 2-D framework through π-π interactions between the aromatic groups of the 1,10-phen ligands.[13a] The narrowest interplanar distance of the aromatic units is about 3.41 Å. Adjacent 2-D frameworks are further connected together to form a 3-D network by hydrogen-bonding interactions. The π-π interactions and the hydrogen bonds enhance the stability of the compound.

Valence-sum calculations give a value of 1.92 for the Cd atom, indicating that the Cd center is in the +2 oxidation state. Atoms O(1)−O(4) have bond-valence sums of 1.66,

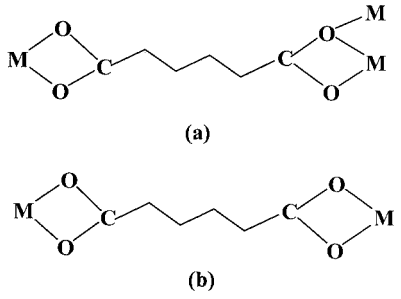

Scheme 1. Coordination modes of the adipate ligand in compounds **1** (a) and **2** (b)

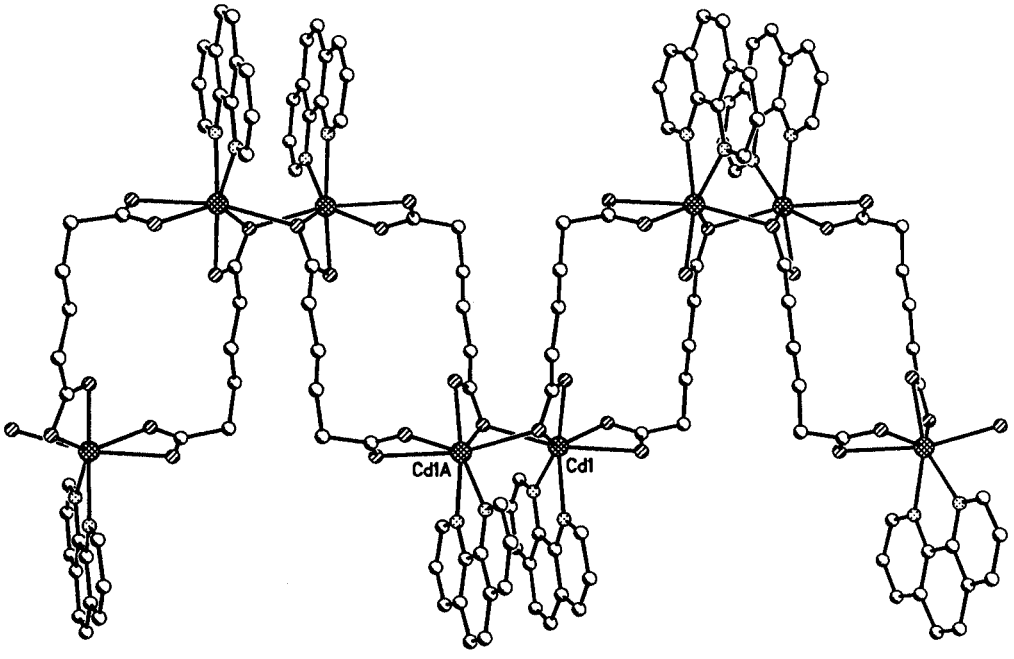

Figure 1. The 1-D chain of compound **1** viewed along the *b* axis

 © 2004 Wiley-VCH Verlag GmbH & Co. KGaA, Weinheim

1.79, 1.85, and 1.62, respectively, suggesting that all carboxyl groups are deprotonated.[13b] These results are consistent with the charge-balance considerations and alkaline synthetic conditions of compound **1**.

The hydrothermal reaction of a solution of $Cd(NO_3)_2{\cdot}4H_2O$, adipic acid, 2,2′-bipy, $H_2C_2O_4$, NaOH and H_2O gives rise to **2** as colorless crystals. X-ray crystallographic analysis reveals that compound **2** forms an interesting 3-D network. There are two crystallographically unique Cd centers in the asymmetric unit (see Figure S2). The Cd(1) center is coordinated by two oxygen atoms [Cd(1)−O(3) 2.438(6) Å, Cd(1)−O(4) 2.302(6) Å] of one carboxylate group, four oxygen atoms of two different oxalate anions, including one μ_3-oxygen atom [Cd(1)−O(6) 2.630(6) Å], and one oxygen atom of a water molecule [Cd(1)−$O_{(water)}$ 2.267(6) Å]. The O−Cd(1)−O bond angles range from 52.66(17)° to 166.6(2)°. The Cd(2) center is bonded to two nitrogen atoms of one 2,2′-bipy ring with an average Cd(2)−N bond length of 2.347(6) Å, two oxygen atoms [Cd(2)−O(1) 2.467(6) Å, Cd(2)−O(2) 2.320(6) Å] of one carboxylate group, and two oxygen atoms of one oxalate anion [Cd(2)−O(5) 2.406(5) Å, Cd(2)−O(6) 2.353(5) Å]. The O−Cd(2)−O bond angles range from 54.1(2)° to 156.29(19)°, and the O(N)−Cd(2)−N(O) bond angles range from 81.1(2)° to 166.9(2)° (shown in Table S3). Therefore, both Cd centers display a distorted pentagonal bipyramidal geometry. The [CdO_7] unit and [CdO_5N_2] unit are linked by $C_2O_4^{2-}$ anions to form a pseudo-binuclear Cd center through the μ_3-O(6) atom. The Cd(1)···Cd(2) distance bridged by one μ_3-O(6) atom is 4.881 Å. As opposed to compound **1**, the two carboxyl groups of the adipate ligand in compound **2** exhibit another kind of coordination mode with the Cd atoms, as shown in Scheme 1b — all the carboxyl groups adopt a bis-chelating mode to connect the two Cd atoms. These pseudo-binuclear Cd centers are connected to each other by adipate anions to form a 1-D wave-like chain along the *c* axis, just like a sine- or cosine-type curve (see Figure 2). Furthermore, the $C_2O_4^{2-}$ anions also display two interesting kinds of connection mode with the Cd centers, as shown in Scheme 2. One carboxylate group binds in a bis-chelating mode to bridge one Cd center, while the two oxygen atoms from two different carboxyl groups exhibit an unusual bidentate bridging mode to link with another Cd center. Thus, one $C_2O_4^{2-}$ anion is connected with three Cd centers, as shown in Figure 3. To the best of our knowledge, this is the first example containing $C_2O_4^{2-}$ anions in which the oxalate group binds in both a bis-chelating and a bridging mode toward the metal centers. Based on the connection mode of $C_2O_4^{2-}$ anions, the sine-type and cosine-type chains are connected alternately by $C_2O_4^{2-}$ anions, forming a novel 3-D framework (see Figure 4). It is noteworthy that this 3-D network contains approximately square channels constructed by the adipate and oxalate ligands and the Cd centers, where the 2,2′-bipy ligands reside.

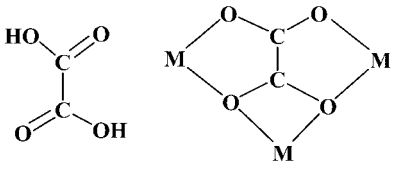

Scheme 4. Coordination modes of the oxalate ligand in compound **2**

Compound **2** is the first example in which both 2,2′-bipy and oxalate ligands are introduced into the {M/adipate} system. Furthermore, the introduction of the oxalate ligand leads to the dimensional transformation of the metal adipate coordination polymers.

Valence-sum calculations give values of 2.17 and 1.98 for the Cd(1) and Cd(2) atoms, respectively, indicating that each Cd center is in the +2 oxidation state. The coordinated oxygen atoms Ow(1) and Ow(2) have bond-valence sums of 0.27 and 0.37, respectively, suggesting that Ow is a coordinated water molecule. Atoms O(1)−O(8) have bond valence sums of 1.69, 1.77, 1.78, 1.83, 1.73, 1.71, 1.76 and 1.76, respectively, showing that all the carboxyl groups have been deprotonated.[13b] These results are consistent with charge-balance considerations and the alkaline synthetic conditions of compound **2**.

The IR spectrum of compound **1** shows characteristic bands of carboxyl groups at 1560 cm^{-1} for the antisymmetric stretching and at 1447 and 1409 cm^{-1} for symmetric

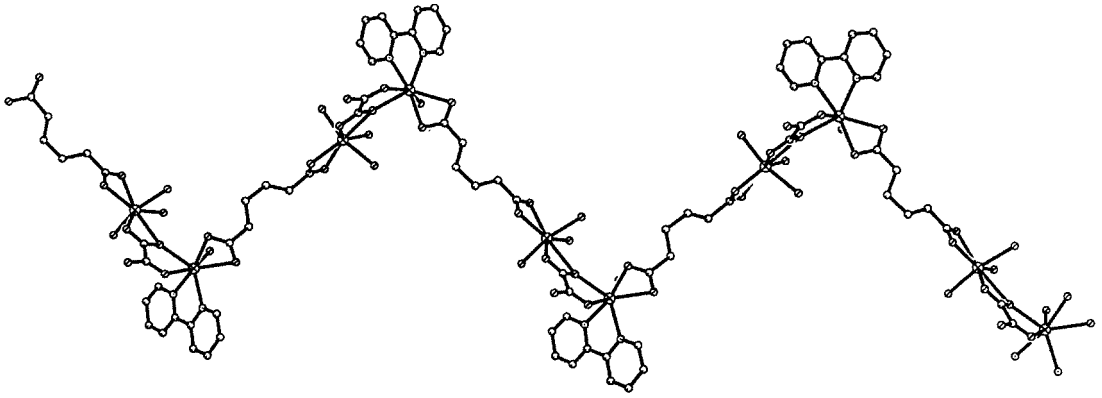

Figure 2. The 1-D chain of compound **2** viewed along the *c* axis

 © 2004 Wiley-VCH Verlag GmbH & Co. KGaA, Weinheim

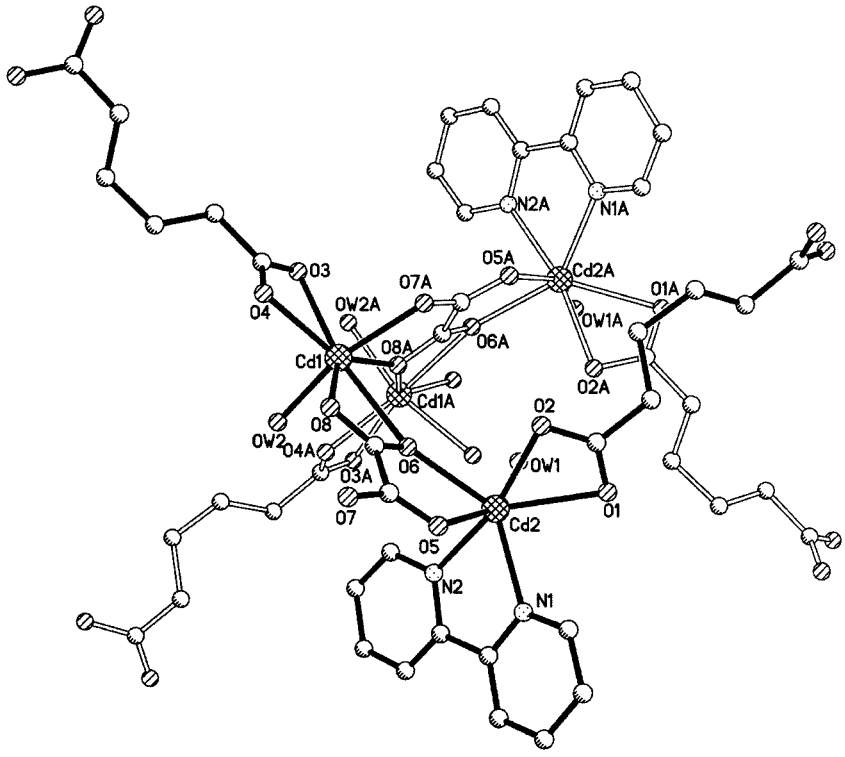

Figure 3. Perspective view of the connection mode of sine- and cosine-type chains connected to each other by oxalate in compound **2**

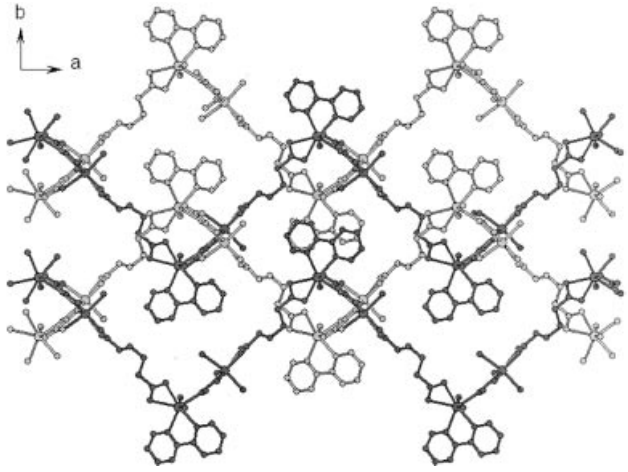

Figure 4. The 3-D framework of compound **2** along the *c* axis

stretching (see Figure S3a). The separations ($\Delta\nu$) between $\nu_{asym}(CO_2)$ and $\nu_{sym}(CO_2)$ indicate the presence of both chelating (113 cm^{-1}) and monodentate (151 cm^{-1}) coordination modes in compound **1**. The IR spectrum of compound **2** exhibits characteristic bands of carboxyl groups at 1630 cm^{-1} and 1603 cm^{-1} for the antisymmetric stretching and at 1437 cm^{-1} for symmetric stretching (see Figure S3b). The separations ($\Delta\nu$) between the $\nu_{asym}(CO_2)$ and $\nu_{sym}(CO_2)$ bands show that the carboxylate groups bind in a bis-chelating fashion to the metal centers.[14]

In the TGA curve of compound **1** (see Figure S4a), there is only one weight loss of 70.50% in the range 320−540 °C, corresponding to the release of 1,10-phen and adipate ligands (calcd. 70.60%). The remaining weight of 29.50% corresponds to the percentage (29.40%) of Cd and O components, indicating that the final product is CdO. The TGA curve of compound **2** exhibits three weight-loss stages. The first weight loss is 3.09% (calcd. 2.70%) in the range of 133−185 °C, corresponding to the release of water molecules of crystallization. The second weight loss is 18.27% (calcd. 18.59%) in the range 265−360 °C, corresponding to the release of coordinated water and oxalate ligand. The last weight loss is 40.48% (calcd. 40.22%) in the temperature range 375−565 °C, corresponding to the release of 2,2′-bipy and adipate ligands. The residue is CdO. The whole weight loss (61.84%) is in good agreement with the calculated value (61.51%; see Figure S4b).

Photoluminescence Properties

The emission spectra of compounds **1** and **2** in the solid state at room temperature are depicted in Figure 5, with intense emissions at 443 nm (see a in Figure 5, λ_{ex} = 383 nm) for **1** and 422 nm (see b in Figure 5, λ_{ex} = 346 nm) for **2**. The difference between the two emission bands may be due to the different coordination environments of the Cd atom in these compounds. According to the literature,[15] the emissions at 443 nm and 422 nm can be assigned to ligand-to-metal charge-transfer (LMCT) bands. These observations indicate that compounds **1** and **2** may be excellent candidates for photoluminescent materials.

 © 2004 Wiley-VCH Verlag GmbH & Co. KGaA, Weinheim

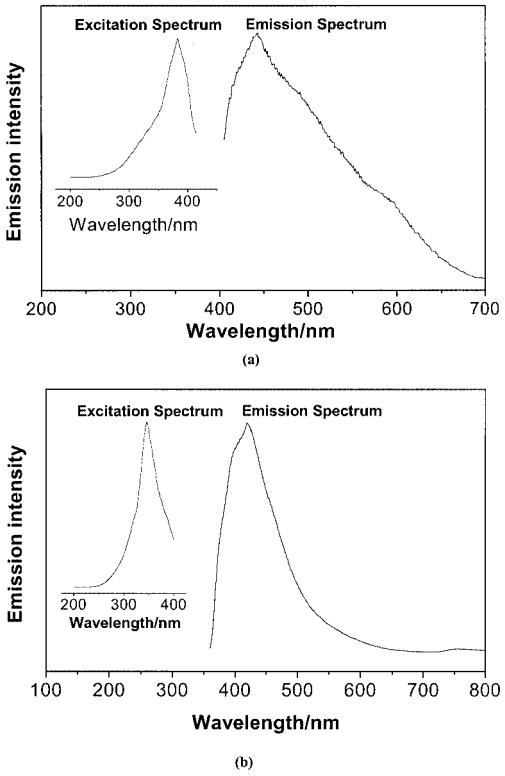

Figure 5. Solid-state emission spectra of the complexes at room temperature: (a) **1**, (b) **2**

Conclusion

We have successfully combined the merits of Cd metal and adipate with other organic ligands and synthesized two novel coordination polymers — $[Cd\{O_2C(CH_2)_4CO_2\}\{1,10\text{-phen}\}]_n$ (**1**) and $[Cd_2(C_2O_4)\{O_2C(CH_2)_4CO_2(OH_2)_2\}\{2,2'\text{-bipy}\}]\cdot H_2O$ (**2**) — with different dimensionalities and different coordination architectures. Comparing the structures of **1** and **2**, it has been found that the different coordination modes of the ligand may have a significant effect on the formation and dimension of the resulting structures. The successful preparation of compounds **1** and **2** provides a valuable approach for the construction of many other coordination polymers with different dimensional structures by the introduction of another kind of organic ligand. Furthermore, the strong fluorescent properties of compounds **1** and **2** make them excellent candidates for potential photoactive materials.

Experimental Section

General Methods: All chemicals were commercially purchased and used without further purification. Elemental analyses (C, H and N) were performed with a Perkin-Elmer 2400 CHN Elemental Analyzer; Cd was determined with a PLASMA-SPEC(I) ICP atomic emission spectrometer. IR spectra were recorded in the range 400−4000 cm^{-1} with an Alpha Centaurt FT/IR Spectrophotometer using KBr pellets. TG analyses were performed with a Perkin-Elmer TGA7 instrument in flowing N_2 with a heating rate of 10 °C·min^{-1}. Excitation and emission spectra were obtained with a Spex FL-2T2 spectrofluorometer equipped with a 450-W-xenon lamp as the excitation source.

Synthesis of 1: Compound **1** was synthesized from a reaction mixture containing $Cd(NO_3)_2\cdot 4H_2O$ (0.15 g, 0.5 mmol), adipic acid (0.073 g, 0.5 mmol), 1,10-phen (0.018 g, 0.1 mmol), NaOH (0.04 g, 1.0 mmol) and H_2O (6 mL, 333 mmol) in an 18-mL Teflon-lined autoclave under autogenous pressure at 160 °C for four days, followed by slow cooling (10 °C/h) to room temperature. The product was washed with distilled water and air-dried. The product was of high quality in the form of colorless crystals. Yield: 0.112 g (75% based on Cd). Elemental analyses. $C_{18}H_{16}CdN_2O_4$: calcd. C 49.5, H 3.7, N 6.4, Cd 25.7; found C 49.6, H 3.5, N 6.5, Cd 25.9. Selected FT-IR data (KBr pellet): $\tilde{\nu}$ = 3427 (s), 3053 (w), 2991 (m), 1560 (s), 1516 (w), 1418 (s), 1409 (s), 1355 (w), 1316 (m), 1103 (s), 1053 (s), 858 (s), 787 (m), 753 (m), 730 (s), 638 (m), 601 (w), 470 (s), 420 (w) cm^{-1}.

Synthesis of 2: Compound **2** was synthesized from a reaction mixture containing $Cd(NO_3)_2\cdot 4H_2O$ (0.15 g, 0.5 mmol), adipic acid (0.073 g, 0.5 mmol), 2,2′-bipy (0.023 g, 0.15 mmol), $H_2C_2O_4$ (0.009 g, 0.1 mmol), NaOH (0.04 g, 1.0 mmol) and H_2O (6 mL, 333 mmol) in na 18-mL Teflon-lined autoclave under autogenous pressure at 160 °C for four days, followed by slow cooling (10 °C/h) to room temperature. The product was washed with distilled water and air-dried. The product was of high quality in the form of colorless crystals. Yield: 0.108 g (72% based on Cd). $C_{18}H_{22}Cd_2N_2O_{11}$: calcd. C 32.4, H 3.3, N 4.2, Cd 33.7; found C 32.5, H 3.2, N 4.4, Cd 33.9. Selected FT-IR data (KBr pellet): $\tilde{\nu}$ = 3382 (s), 3269 (w), 2876 (w), 1639 (m), 1603 (m), 1550 (s), 1460 (w), 1437 (s), 1361 (w), 1309 (s), 1214 (m), 1176 (w), 1155 (m), 1073 (w), 1060 (w), 1018 (s), 971 (w), 910 (w), 804 (s), 765 (s), 737 (m), 651 (m), 627 (w), 583 (w), 493 (m), 449 (w) cm^{-1}.

X-ray Crystallography: Single crystals of compounds **1** and **2** with dimensions 0.532 × 0.485 × 0.396 mm and 0.467 × 0.413 × 0.345 mm, respectively, were glued onto a glass fiber. Data were collected on a Rigaku R-AXIS RAPID IP diffractometer with Mo-K_α graphite-monochromated radiation (λ = 0.71073 Å) at 293 K in the range $1.89 < \theta < 27.48°$ and $1.76 < \theta < 27.44°$, respectively. An empirical absorption correction was applied. The structures were solved by direct methods and refined by the full-matrix least-squares method on F^2 using the SHELXL crystallographic software package.[16] Anisotropic thermal parameters were used to refine all non-hydrogen atoms. Hydrogen atoms were located from difference Fourier maps. The space group of the compound **2** was selected to be *Cc*. Although *Cc* and *C*2/*c* possess the same extinction rules, it can be presumed that the structure of compound **2** is noncentrosymmetric based on the lower CFOM value and the mean value of $<E^2-1>$ 0.651, which is lower than 0.736. Furthermore, as the value of $<E^2-1>$ is very low, the structure may be twinned. Thus, during the structural absolute refinement, a twin refinement was used. The final structural Flack parameter (k = 0.00), suggesting the absolute configuration of compound **2**, was confirmed. Selection of the *C*2/*c* space group to solve the structure did not give the correct structural model.

Crystal Data for 1: $C_{18}H_{16}CdN_2O_4$, M_r = 436.73, monoclinic, *C*2/*c*, a = 16.186(3) Å, b = 15.487(3) Å, c = 14.052(3) Å, $\alpha = \gamma = 90°$, β = 112.73(3)°, U = 3248.7(11) $Å^3$, Z = 8, D_c = 1.786 g·cm^{-3}, μ = 1.371 mm^{-1}, $F(000)$ = 1744, $R1$ = 0.0305, $wR2$ = 0.0685 and

 © 2004 Wiley-VCH Verlag GmbH & Co. KGaA, Weinheim

S = 0.999 for 3728 reflections with $I > 2\sigma(I)$ and 226 parameters ($R1$ = 0.0464, $wR2$ = 0.0864 for all 7266 data).

Crystal Data for 2: $C_{18}H_{22}Cd_2N_2O_{11}$, M_r = 667.18, monoclinic, Cc, a = 23.448(5) Å, b = 11.826(2) Å, c = 8.3163(17) Å, β = 99.08(3)°, U = 2277.3(8) Å^3, Z = 4, D_c = 1.928 g·cm^{-3}, μ = 1.928 mm^{-1}, $F(000)$ = 1312, $R1$ = 0.0323, $wR2$ = 0.0884 and S = 0.996 for 4775 reflection with $I > 2\sigma(I)$ and 293 parameters ($R1$ = 0.0384, $wR2$ = 0.0971 for all 4778 data).

CCDC-220446 (for **1**) and -223954 (for **2**) contain the supplementary crystallographic data for this paper. These data can be obtained free of charge at www.ccdc.cam.ac.uk/conts/retrieving.html [or from the Cambridge Crystallographic Data Centre, 12, Union Road, Cambridge CB2 1EZ, UK; Fax: +44-1223-336-033; E-mail: deposit@ccdc.cam.ac.uk].

Supporting Information: Crystal data and structure refinement, bond lengths and angles, the perspective view of the Cd^{II} coordination environments, the IR spectra, the TGA curves for compounds **1** and **2** (Tables S1−3, Figures S1−S4; see also the footnote on the first page of this article).

Acknowledgments

This work was financially supported by the National Natural Science Foundation of China (20171010).

[1] [1a] P. J. Stang, B. Olenyuk, *Acc. Chem. Res.* **1997**, *30*, 502−518. [1b] S. Leininger, B. Olenyuk, P. J. Stang, *Chem. Rev.* **2000**, *100*, 853−908. [1c] G. F. Swiegers, T. J. Malefetse, *Chem. Rev.* **2000**, *100*, 3483−3538. [1d] C. T. Chen, K. S. Suslick, *Coord. Chem. Rev.* **1993**, *128*, 293−322.

[2] [2a] P. J. Hagrman, D. Hagrman, J. Zubieta, *Angew. Chem. Int. Ed.* **1999**, *38*, 2638−2684. [2b] D. Hagrman, R. P. Hammond, R. Haushalter, J. Zubieta, *Chem. Mater.* **1998**, *10*, 2091−2100.

[3] [3a] X.-M. Zhang, M.-L. Tong, X.-M. Chen, *Angew. Chem. Int. Ed.* **2002**, *41*, 1029−1031. [3b] G.-F. Liu, B.-H. Ye, Y.-H. Ling, X.-M. Chen, *Chem. Commun.* **2002**, 1442−1443. [3c] X.-H. Bu, W. Chen, S.-L. Lu, R.-H. Zhang, D.-Z. Liao, W.-M. Bu, M. Shionoya, F. Brisse, J. Ribas, *Angew. Chem. Int. Ed.* **2001**, *40*, 3201−3203. [3d] X.-H. Bu, W. Chen, W.-F. Hou, M. Du, R.-H. Zhang, F. Brisse, *Inorg. Chem.* **2002**, *41*, 3477−3482.

[4] [4a] W.-B. Lin, O. R. Evans, R.-G. Xiong, Z. Y. Wang, *J. Am. Chem. Soc.* **1998**, *120*, 13272−13273. [4b] Y. Cui, O. R. Evans, H. L. Ngo, P. S. White, W.-B. Lin, *Angew. Chem. Int. Ed.* **2002**, *41*, 1159−1162. [4c] Y. Cui, H. L. Ngo, W.-B. Lin, *Inorg. Chem.* **2002**, *41*, 1033−1035.

[5] [5a] N. Takeda, K. Umemoto, K. Yamaguchi, M. Fujita, *Nature* **1999**, *398*, 794−796. [5b] A. Caneschi, D. Gatteschi, N. Lalioti, C. Angregorio, R. Sessoli, G. Venturi, A. Vindigni, A. Rettori, M. G. Pini, M. A. Navak, *Angew. Chem. Int. Ed.* **2001**, *40*, 1760−1763. [5c] Y.-Q. Tian, C.-X. Cai, Y. Ji, X.-Z. You, S.-M. Peng, G. H. Lee, *Angew. Chem. Int. Ed.* **2002**, *41*, 1384−1386.

[6] [6a] Y.-H. Wang, L.-Y. Feng, Y.-G. Li, C.-W. Hu, E.-B. Wang, N.-H. Hu, H.-Q. Jia, *Inorg. Chem.* **2002**, *41*, 6351−6357. [6b] M. Yuan, Y.-G. Li, E.-B. Wang, Y. Lu, C.-W. Hu, N.-H. Hu, H.-Q. Jia, *J. Chem. Soc., Dalton Trans.* **2002**, 2916−2920. [6c] Y.-G. Li, N. Hao, E.-B. Wang, M. Yuan, C.-W. Hu, N.-H. Hu, H.-Q. Jia, *Inorg. Chem.* **2003**, *42*, 2729−2735. [6d] Y.-G. Li, N. Hao, Y. Lu, E.-B. Wang, Z.-H. Kang, C.-W. Hu, *Inorg. Chem.* **2003**, *42*, 3119−3124. [6e] Y.-G. Li, N. Hao, E.-B. Wang, Y. Lu, C.-W. Hu, *Eur. J. Inorg. Chem.* **2003**, 2567−2571.

[7] J.-K. Lu, M.-A. Lawandy, J. Li, *Inorg. Chem.* **1999**, *38*, 2695−2704.

[8] [8a] C.-D. Wu, C.-Z. Lu, W.-B. Yang, S.-F. Lu, H.-H. Zhuang, J.-S. Huang, *Eur. J. Inorg. Chem.* **2002**, *41*, 797−800. [8b] R. Cao, D.-F. Sun, Y.-C. Liang, M.-C. Hong, K. Tatsumi, Q. Shi, *Inorg. Chem.* **2002**, *41*, 2087−2094.

[9] [9a] S. Konar, P. S. Mukherjee, E. Zangrando, F. Lloret, N. Ray Chaudhuri, *Angew. Chem. Int. Ed.* **2002**, *41*, 1561−1563. [9b] P. S. Mukherjee, S. Dalai, G. Mostafa, E. Zangrando, T.-H. Lu, G. Rogez, T. Mallah, N. Ray Chaudhuri, *Chem. Commun.* **2001**, 1346−1347. [9c] P. S. Mukherjee, S. Konar, E. Zangrando, C. Diaz, J. Ribas, N. Ray Chaudhuri, *J. Chem. Soc., Dalton Trans.* **2002**, 3471−3476.

[10] [10a] Y. Kim, D.-Y. Jung, *Inorg. Chem.* **2000**, *39*, 1470−1475. [10b] Y. Kim, E. Lee, D.-Y. Jung, *Chem. Mater.* **2001**, *13*, 2684−2690. [10c] E. G. Bakalbassis, M. K. A. Michailides, J. Mrozinski, C. Raptopoulou, S. Skoulika, A. Terzis, D. Tsaousis, *J. Chem. Soc., Dalton Trans.* **2001**, *6*, 850−857. [10d] P. S. Mukherjee, S. Konar, E. Zangrando, T. Mallah, J. Ribas, N. Ray Chaudhuri, *Inorg. Chem.* **2003**, *42*, 2695−2703.

[11] [11a] Y. Lu, E.-B. Wang, M. Yuan, G.-Y. Luan, Y.-G. Li, *J. Chem. Soc., Dalton Trans.* **2002**, 3029−3031. [11b] Y.-G. Li, E.-B. Wang, H. Zhang, G.-L. Luan, C.-W. Hu, *J. Solid State Chem.* **2002**, *163*, 10−16. [11c] X.-L. Wang, C. Qin, E.-B. Wang, Y.-G. Li, C.-W. Hu, L. Xu, *Chem. Commun.* **2004**, 378−379.

[12] [12a] P. J. Hagrman, J. Zubieta, *Inorg. Chem.* **2000**, *39*, 3252−3260. [12b] P. J. Zapf, R. C. Haushalter, J. Zubieta, *Chem. Mater.* **1997**, *9*, 2019−2024.

[13] [13a] C. Janiak, *J. Chem. Soc., Dalton Trans.* **2000**, 3885−3896. [13b] I. D. Brown, D. Altermatt, *Acta Crystallogr., Sect. B* **1985**, *41*, 244−247.

[14] K. Nakamoto, *Infrared Spectra and Raman Spectra of Inorganic and Coordination Compounds*, John Wiley & Sons, New York, **1986**.

[15] [15a] V. W. W. Yam, K. K. W. Lo, *Chem. Soc. Rev.* **1999**, *28*, 323−334. [15b] J. Tao, J.-X. Shi, M.-L. Tong, X.-X. Zhang, X.-M. Chen, *Inorg. Chem.* **2001**, *40*, 6328−6330. [15c] L.-C. Dai, X.-T. Wu, Z.-Y. Fu, C.-P. Cui, S.-M. Wu, W.-X. Du, L.-M. Wu, H.-H. Zhang, Q.-Q. Sun, *Inorg. Chem.* **2002**, *41*, 1391−1396. [15d] W. Chen, J.-Y. Wang, C. Chen, Q. Yue, H.-M. Yuan, J.-X. Chen, S.-N. Wang, *Inorg. Chem.* **2003**, *42*, 944−946.

[16] [16a] G. M. Sheldrick, *SHELXS 97, Program for Crystal Structure Refinement*, University of Göttingen, Germany, **1997**. [16b] G. M. Sheldrick, *SHELXL 97, Program for Crystal Structure Solution*, University of Göttingen, Germany, **1997**.

Received April 8, 2004
Early View Article
Published Online August 12, 2004

 © 2004 Wiley-VCH Verlag GmbH & Co. KGaA, Weinheim

A New Synthetic Method and Solution Equilibria for the Chlorotitanate(IV) Anions − Evidence for the Existence of a New Species: $[Ti_2Cl_{11}]^{3-}$

Emmanuel Robé,[a] Jean-Claude Daran,[b] Sandrine Vincendeau,[b] and Rinaldo Poli*[a]

Keywords: Anions / Electrochemistry / Infrared spectroscopy / Titanium

$TiCl_3$ is oxidized by $SOCl_2$ in the presence of the appropriate amount of $[NEt_3Bz]Cl$ or $[PPN]Cl$ [Bz = benzyl; PPN = bis(triphenylphosphanyl)iminium] to afford the corresponding salts of $[Ti_2Cl_9]^-$, $[Ti_2Cl_{10}]^{2-}$ or $[TiCl_6]^{2-}$. The results of cyclic voltammetric and solution IR studies in the Ti–Cl stretching region are interpreted in terms of a rapid chloride-redistribution equilibrium between $[Ti_2Cl_{10}]^{2-}$ on one side and a mixture of $[Ti_2Cl_9]^-$ and a previously unreported $[Ti_2Cl_{11}]^{3-}$ species on the other side. In the solid state, however, a compound with the $[PPN]_3[Ti_2Cl_{11}]$ stoichiometry exists as a mixture of $[PPN]_2[Ti_2Cl_{10}]$ and $[PPN]_2[TiCl_6]$. The PPN salt of $[Ti_2Cl_9]^-$ has been structurally characterized by X-ray diffractometry.

(© Wiley-VCH Verlag GmbH & Co. KGaA, 69451 Weinheim, Germany, 2004)

Introduction

Homoleptic chlorometallates are a wide class of fundamentally important coordination compounds. They are in general easily accessible by addition of the required amount of halide ions to the neutral metal halide. For Ti^{IV}, four different anionic complexes are known, the enneachlorodititanate $[Ti_2Cl_9]^-$, the decachlorodititanate $[Ti_2Cl_{10}]^{2-}$, the pentachlorotitanate $[TiCl_5]^-$, and the hexachlorotitanate $[TiCl_6]^{2-}$, formally related to $TiCl_4$ by the addition of one half, one, or two Cl^- ions per titanium, respectively (Scheme 1).[1] The choice between mononuclear or dinuclear pentachlorotitanate seems to be controlled by the size of the counterion.[2] Since $TiCl_3$ is used extensively as a precursor of Ziegler−Natta polymerization catalysts,[3−8] its coordination chemistry has been widely explored. However, the only reported chlorotitanate(III) anions are apparently the edge-sharing bioctahedral $[Ti_2Cl_9]^{3-}$ and the mononuclear octahedral $[TiCl_6]^{3-}$.[9−11] Furthermore, these ions are prepared at high temperatures in the solid state (no solvent),[12,13] and therefore little information is available on their properties in solution.

In an attempt to gain access to soluble versions of these anionic complexes and perhaps to prepare the as-yet unknown[14] decachlorodititanate(III) tetraanion $[Ti_2Cl_{10}]^{4-}$, we have investigated the interaction between $TiCl_3$ and chloride salts in solution. Given the hydrolytic sensitivity of Ti^{III}, our approach consists of the use of $SOCl_2$ as solvent, since this is a well-known medium for ensuring anhydrous conditions for transition metal chlorides.[15] The results of this interaction, yielding metal oxidation, are reported here. Furthermore, we present new information on the solution behavior of the $[Ti_2Cl_{10}]^{2-}$ ion and spectroscopic and electrochemical evidence for the existence of a previously unreported $[Ti_2Cl_{11}]^{3-}$ ion in solution.

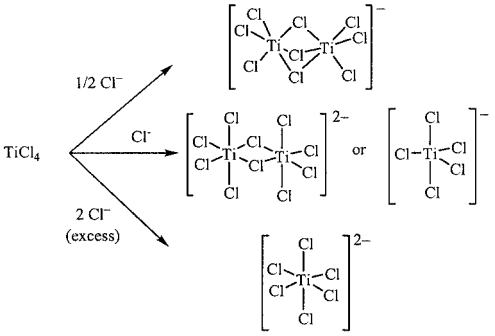

Scheme 1

Results and Discussion

Syntheses

The addition of one equivalent of chloride, either as the triethylbenzylammonium (Et_3BzN) or the bis(triphenylphosphanyl)iminium (PPN) salt, to $TiCl_3$ in $SOCl_2$ results in a smooth reaction at room temperature accompanied by a sharp color change from dark purple to yellow. The color is

[a] Laboratoire de Synthèse et d'Electrosynthèse Organométalliques (LSEO UMR 5632), Université de Bourgogne, Faculté de Sciences "Gabriel",
6 boulevard Gabriel, 21000 Dijon, France
Fax: (internat.) +33-5-61553003
E-mail: poli@lcc-toulouse.fr
[b] Laboratoire de Chimie de Coordination (LCC UPR 8241), 205 Route de Narbonne, 31077 Toulouse Cedex, France

indicative of chloro complexes of Ti^{IV}. Indeed, the selective product of the reactions are the decachlorodititanate(IV) salts [Equation (1)]. The products were obtained in a pure state and in good yields. They are moderately soluble in dichloromethane, the PPN salt being more soluble than the ammonium salt. The dinuclear nature of these salts is demonstrated by their IR properties (vide infra).

$$2\ TiCl_3 + 2\ [Cat]Cl + 2\ \{Cl\} \xrightarrow{SOCl_2} [Cat]_2[Ti_2Cl_{10}] \quad (1)$$

(Cat = NEt_3Bz, PPN)

By changing the stoichiometry to one or four equivalents of chloride salt per two of $TiCl_3$, the ennachlorodititanate(IV) $[Ti_2Cl_9]^-$, and the hexachlorotitanate(IV) $[TiCl_6]^{2-}$ were obtained in good yields [Equation (2) and Equation (3), respectively]. We have also obtained a product with the stoichiometry $[PPN]_3[Ti_2Cl_{11}]$ by using a 3:2 PPNCl/$TiCl_3$ ratio. The solid state and solution nature of these products will be discussed in the next section. The necessary chlorine atoms for the stoichiometries of Equation (1), Equation (2) and Equation (3) are undoubtedly provided by the thionyl chloride solvent, which must therefore be reduced. The oxidizing properties of thionyl chloride relative to low-valent metal halides do not appear to have been extensively explored. A metal oxidation process has been witnessed for the dehydration of $SnCl_2{\cdot}2H_2O$ (leading to $SnCl_4$ while elemental sulfur was found amongst the reduction products), whereas the dehydration of $TlCl_3{\cdot}xH_2O$, which is affected by a spontaneous reduction to TlCl when the salt is thermally dehydrated, leads to pure $TlCl_3$ when using $SOCl_2$.[15] Another potentially reducing metal chloride is $CrCl_2$, although the dehydration of the corresponding hydrate with $SOCl_2$ has apparently never been described[16] (whereas it *is* known with $COCl_2$).[15] Unlike the above-mentioned dehydration of $SnCl_2$, we have not witnessed the formation of any elemental sulfur. It is known that $SOCl_2$ decomposes at high temperatures to yield Cl_2, SO_2 and S_2Cl_2,[17,18] but, remarkably, the Ti oxidation process that we report here occurs smoothly at room temperature. We have not explored the nature of the reduced sulfur products in this reaction further.

$$2\ TiCl_3 + [PPN]Cl + 2\ \{Cl\} \xrightarrow{SOCl_2} [PPN][Ti_2Cl_9] \quad (2)$$

$$TiCl_3 + 2\ [PPN]Cl + \{Cl\} \xrightarrow{SOCl_2} [PPN]_2[TiCl_6] \quad (3)$$

Electrochemical and Spectroscopic Characterization

Still with the goal in mind of exploring the solution chemistry of the chlorotitanate(III) complexes, we have carried out electrochemical investigations of the chlorotitanate(IV) anions. Previous electrochemical investigations on Ti^{IV} chloride systems appear to be limited to $TiCl_4$ in $AlCl_3$/chloride melts.[19,20] Basic melts (Cl/Al > 4) exhibit only a reversible reduction that has been attributed to the $[TiCl_6]^{2-}$ ion,[19] whereas Lewis-acidic melts show less reversible features that are attributed to less chloride-rich anions, whose nature depends on the melt composition.[20] It is reasonable to expect that the reduction process to Ti^{III} correlates with the effective charge at the metal center, a greater electron density leading to a more difficult reduction process. Therefore, one could reasonably expect a trend of reduction potentials in the order $[TiCl_6]^{2-} < [Ti_2Cl_{10}]^{2-} < [Ti_2Cl_9]^-$.

A cyclic voltammetric analysis of $[Ti_2Cl_{10}]^{2-}$ in CH_2Cl_2 shows that the Ti^{IV} center undergoes the expected reduction process, which is irreversible. This irreversibility is probably linked to loss of chloride ions upon reduction, induced by the accumulation of too much negative charge and by the possible rearrangement to a triply bridged, face-sharing bioctahedral $[Ti_2Cl_9]^{2-}$ species. Such a mixed-valence complex is apparently not yet known. The surprising observation, however, is the complexity of the reduction wave (see Figure 1), which shows at least two distinct processes, the main one having a cathodic peak potential, $E_{p,c}$, of −1.03 V, with a broad shoulder between about −0.8 and −0.6 V.

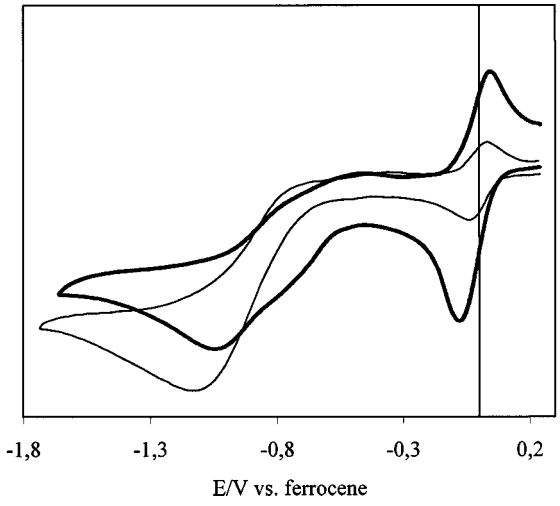

Figure 1. Cyclic voltammograms of solutions of $[NBzEt_3]_2[Ti_2Cl_{10}]$ alone (thicker line) and with two equiv. of $[NBzEt_3]Cl$ (thinner line); both solutions also contain the internal ferrocene standard (reversible wave at $E_{1/2} = 0$); solvent: CH_2Cl_2

The possibility that the complexity of this voltammetric response could result from sample impurities was soon excluded by the reproducibility when measuring several samples obtained from different syntheses. The key to understanding this complexity comes from the voltammetric measurement after the addition of excess chloride ions, which should quantitatively convert the electroactive species to the $[TiCl_6]^{2-}$ ion (see Scheme 1), according to the literature. The single irreversible reduction wave at $E_{p,c} = -1.13$ V that is obtained under these conditions (see Figure 1) may therefore be attributed to the reduction of this ion. Note that this wave is irreversible, whereas full reversibility is observed in an $AlCl_3$/chloride melt.[19] This obser-

 © 2004 Wiley-VCH Verlag GmbH & Co. KGaA, Weinheim

vation agrees fully with the likely instability of a reduced $[TiCl_6]^{3-}$ ion towards chloride-ion loss. This wave occurs at a very similar potential as the main wave of the $[Ti_2Cl_{10}]^{2-}$ solution in the absence of free chloride ions. The second species is reduced at a less negative potential, therefore it must contain a higher effective positive charge on the metal center (lower Cl/Ti ratio). A logical hypothesis is to assign this wave to the $[Ti_2Cl_9]^-$ ion. Indeed, the cyclic voltammogram for a solution prepared from the isolated $[Ti_2Cl_9]^-$ salt shows an irreversible wave with $E_{p,c} = -0.76$ V, corresponding closely to the shoulder of the $[Ti_2Cl_{10}]^{2-}$ solution in the absence of free chloride ions. Therefore, we conclude that a chloride-dissociation equilibrium exists in solution starting from the dianionic decachloro species, according to Equation (4). The chloride ions that are freed up in solution can then break the bridge bonds of the decachloro species to yield a more chloride-rich species. It would seem reasonable to assume that this species is the mononuclear dianion $[TiCl_6]^{2-}$. However, the results obtained from a parallel IR investigation tell a different story.

$$[Ti_2Cl_{10}]^{2-} \rightleftharpoons [Ti_2Cl_9]^- + Cl^- \quad (4)$$

An independent investigation of the solution equilibria is complicated by the absence of available spectroscopic probes such as spin-1/2 nuclei for an NMR investigation or unpaired electrons for an EPR investigation. The use of ^{47}Ti and ^{49}Ti NMR spectroscopy is unsatisfactory for compounds where the Ti center has lower than cubic symmetry.[20,21] A suitable solution is provided by infrared spectroscopy in the low wavenumber region, which is sensitive to the Ti−Cl stretching vibrations. Infrared studies of chlorotitanate ions have been published previously, but these have mostly been confined to solid samples[2,22−24] as the solubility of most available salts (e.g. with K^+, Rb^+, Cs^+, $Et_2NH_2^+$, and Et_4N^+)[23] is too low. The PPN salts reported here are sufficiently soluble in dichloromethane to yield reasonable intensities ($A > 1$ for some bands in 0.5 mm pathlength polyethylene cells, see Figure 2). It should be noted that the PPN^+ ion does not interfere in the investigated region, since it shows only a very weak band at 464 cm^{-1}.

First, we shall comment on the dichotomy between $[Ti_2Cl_{10}]^{2-}$ and its mononuclear version, the pentachlorotitanate(IV) anion $[TiCl_5]^-$,[2,22,25−27] and then on the species with a different Cl/Ti ratio. Previous studies have shown that, in the solid state, the pentachlorotitanate(IV) salts feature a dichloro-bridged bioctahedral geometry for the anion in the presence of small cations, whereas salts of larger cations are mononuclear.[2] The PCl_4^+ salt has been shown to undergo a temperature-dependent monomer-dimer equilibrium.[22] The solid-state spectrum of the mononuclear salt is characterized by a very strong band at 348 cm^{-1}, which is absent from the solution spectrum of $[PPN]_2[Ti_2Cl_{10}]$. On the other hand, the solid-state spectra of dinuclear anions are characterized by a very strong band at around 380 cm^{-1} (385 cm^{-1} for the NEt_4 salt and 377 cm^{-1} for the PCl_4 salt).[2] A band in this region is indeed observed in the solution spectrum of $[PPN]_2[Ti_2Cl_{10}]$ (maximum at 370 cm^{-1}). The solid-state spectrum of $[PPN]_2[Ti_2Cl_{10}]$ (see a in Figure 3), is characterized by a strong band at around 365 cm^{-1}, in-between those previously reported for the mono- and dinuclear ions, but quite close to the major band that is observed in solution. The overall shape of the two spectra, in dichloromethane solution and in the solid state, is very similar. We conclude that the compound structure is most certainly dinuclear both in solution and in the solid state. Thus, the rule stating that the pentachlorotitanate(IV) is mononuclear with large cations does not appear to have general validity, since PPN^+ is perhaps the largest cation with which this anion has ever been crystallized.

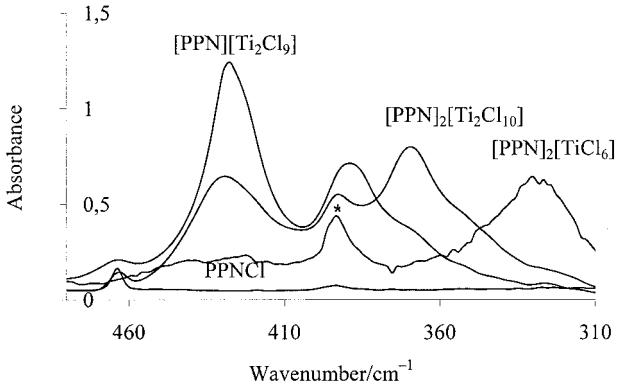

Figure 2. Infrared spectra of various chlorotitanate(IV) PPN salts in CH_2Cl_2 solution (Ti concentration = 2×10^{-2} M); the starred peak corresponds to an oxo impurity (see text)

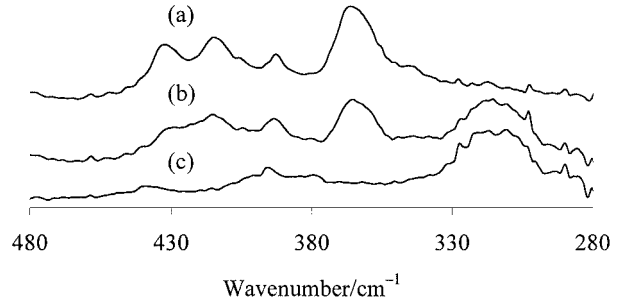

Figure 3. Solid state (nujol mull) infrared spectra of: (a) $[PPN]_2[Ti_2Cl_{10}]$, (b) $[PPN]_3[Ti_2Cl_{11}]$, and (c) $[PPN]_2[TiCl_6]$

The spectra of the $[Ti_2Cl_9]^-$ and $[TiCl_6]^{2-}$ salts, also shown in Figure 2, are quite different from that of the $[Ti_2Cl_{10}]^{2-}$ ion, demonstrating the suitability of IR spectroscopy in this spectral region for the analysis of the species present in solution. Complex $[Ti_2Cl_9]^-$ has a very strong band centered at 428 cm^{-1} and a strong band at 390 cm^{-1}. The shoulder on the right-hand side of the latter band may be due to minor amounts of the $[Ti_2Cl_{10}]^{2-}$ salt. Complex $[TiCl_6]^{2-}$, on the other hand, is characterized by a strong and broad band centered at 327 cm^{-1}. This corresponds to the frequency reported in the literature for the IR-active stretching vibration (ν_3, T_{1u}) of this ion (ca. 330 cm^{-1} depending on the counterion).[23,24,28] It is worth noting the

 © 2004 Wiley-VCH Verlag GmbH & Co. KGaA, Weinheim

weak band observed at 392 cm^{-1}. Only two IR-active bands (the ν_3 stretching and the ν_4 bending, both of T_{1u} type) are expected for the O_h $[TiCl_6]^{2-}$ ion. According to the literature, these are located around 330 cm^{-1} and 183 cm^{-1}, respectively. Therefore, the weak band at 392 cm^{-1} cannot belong to this ion. We believe that this band is due to oxo impurities deriving from a small amount of hydrolysis, given the extreme moisture sensitivity of the $Ti^{IV}-Cl$ bonds. In support of this hypothesis, we have observed that the relative intensity of this band changes as a function of the care with which the solutions are handled and increases when undried dichloromethane is used as solvent, but we have been unable to completely eliminate it. The reported spectrum was recorded in carefully dried solvent and all glassware and transfer syringes were silylated by rinsing with a 10% v/v chloroform solution of Me_3SiCl. It is possible that some hydrolysis occurred during the isolation procedure (washings and transfer into the storage ampoules), as suggested by the observation of the same weak band in the IR spectrum of the solid sample (see c in Figure 3). Following this consideration, the band observed at about 390 cm^{-1} for the $[Ti_2Cl_{10}]^{2-}$ solution may also be due to a product of partial hydrolysis.

The spectrum of the $[TiCl_6]^{2-}$ salt was also reproduced (except for the variable relative intensity of the 392 cm^{-1} band as outlined above) upon addition of ≥ 2 equivalents of PPNCl to the solution of $[Ti_2Cl_{10}]^{2-}$. The addition of just one equivalent of PPNCl to the same solution, on the other hand, shows the complete disappearance of the bands of $[Ti_2Cl_{10}]^{2-}$ and the appearance of a very strong band centered at 355 cm^{-1} (Figure 4). It should be noted that the band of $[TiCl_6]^{2-}$ is also absent from this spectrum. This suggests the formation of a complex having the stoichiometry $[Ti_2Cl_{11}]^{3-}$. Addition of PPNCl to this solution generated again the spectrum of $[TiCl_6]^{2-}$.

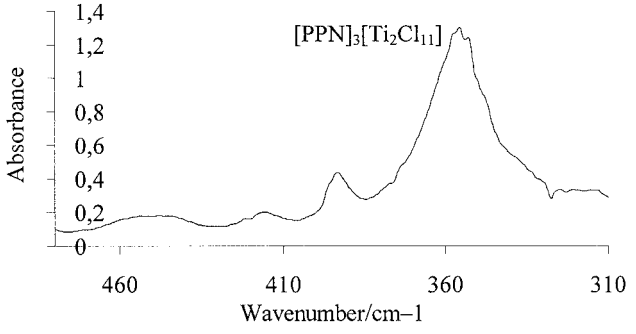

Figure 4. Infrared spectrum of a CH_2Cl_2 solution of $[PPN]_3[Ti_2Cl_{11}]$ (Ti concentration = 2×10^{-2} M)

The $[Ti_2Cl_{11}]^{3-}$ anion does not appear to have been reported in the literature. Its structure most likely corresponds to a corner-sharing bioctahedron [Equation (5)]. On the basis of VSEPR theory, the geometry around the bridging Cl atom should be bent and the IR spectrum can be predicted to be quite similar to that of mononuclear octahedral $[TiCl_6]^{2-}$ if vibrational coupling across the Cl bridge is weak. Thus, the slight shift to higher frequency on going from $[TiCl_6]^{2-}$ to $[Ti_2Cl_{11}]^{3-}$ (327 to 355 cm^{-1}) suggests a force-constant increase upon reduction of the metal effective charge. Although the weak band at 392 cm^{-1} is identical to that observed for the $[TiCl_6]^{2-}$ solution, and is therefore attributable to minor amounts of a hydrolytic product, its attribution to a genuine normal mode of the $[Ti_2Cl_{11}]^{3-}$ cannot be excluded. Once again, this spectrum was found to depend highly on the rigor with which the solution was prepared, and the band at 392 cm^{-1} could never be completely eliminated. The reported spectrum was obtained from a solution prepared in silylated glassware and in carefully dried dichloromethane, from a solid sample that was obtained by direct synthesis in $SOCl_2$, according to the stoichiometry of Equation (6).

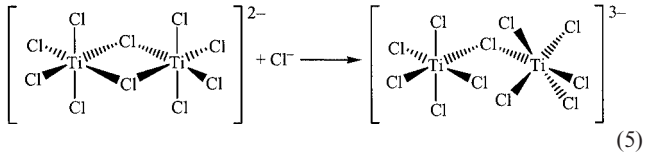

(5)

$$2\ TiCl_3 + 3\ [PPN]Cl + 2\ \{Cl\} \xrightarrow{SOCl_2} [PPN]_3[Ti_2Cl_{11}] \quad (6)$$

An additional interesting feature is shown by the IR spectrum of the $[PPN]_3[Ti_2Cl_{11}]$ compound in the solid state (see b in Figure 3). This is quite clearly the superposition of the spectra of the $[PPN]_2[Ti_2Cl_{10}]$ and $[PPN]_2[TiCl_6]$ salts that are shown in the same figure, whereas the band observed for the same compound in solution is absent. This observation demonstrates that the species $[Ti_2Cl_{11}]^{3-}$ exists only in solution, and the crystallization process forces a ligand redistribution to yield $[Ti_2Cl_{10}]^{2-}$ and $[TiCl_6]^{2-}$. In other words, the ligand-redistribution equilibrium shown in Equation (7) lies on the left in dichloromethane solution and on the right in the solid state for PPN salts.

$$2\ [Ti_2Cl_{11}]^{3-} \rightleftharpoons [Ti_2Cl_{10}]^{2-} + 2\ [TiCl_6]^{2-} \quad (7)$$

As a final relevant observation, note that the solution spectrum of the $[Ti_2Cl_{10}]^{2-}$ salt (Figure 2) does not show a significant absorption at 355 cm^{-1}, thus excluding the presence of large amounts of $[Ti_2Cl_{11}]^{3-}$ at equilibrium. A shoulder on the low-frequency side of the 368 cm^{-1} band signals the possible presence of minor amounts of $[Ti_2Cl_{11}]^{3-}$, which could be related to an imprecise stoichiometry during the synthesis, or to a chloride-redistribution equilibrium as shown in Equation (8). In the latter case, the equilibrium must necessarily be shifted almost completely towards the $[Ti_2Cl_{10}]^{2-}$ ion.

$$2\ [Ti_2Cl_{10}]^{2-} \rightleftharpoons [Ti_2Cl_9]^{-} + [Ti_2Cl_{11}]^{3-} \quad (8)$$

In the light of the IR study, we can now re-interpret the result of the cyclic voltammetric experiment on the $[Ti_2Cl_{10}]^{2-}$ salt by assigning the wave at -1.03 V to the

 © 2004 Wiley-VCH Verlag GmbH & Co. KGaA, Weinheim

reduction of the $[Ti_2Cl_{11}]^{3-}$ complex and the shoulder at about −0.7 V to the reduction of $[Ti_2Cl_9]^-$. The cyclic voltammetric results seem to indicate the presence of large amounts of the $[Ti_2Cl_9]^-$ + $[Ti_2Cl_{11}]^{3-}$ species, i.e. the equilibrium of Equation 8 seems shifted extensively toward the right-hand side. This, however, contrasts with the IR results (see above). There is in fact no contradiction between these two results because of the dynamic nature of the electrochemical experiment. Since the equilibration process described in Equation (8) may be quite fast, and since the $[Ti_2Cl_9]^-$ complex is reduced at a less-negative potential, its consumption by the reduction process shifts the equilibrium to the right-hand side at the expense of the $[Ti_2Cl_{10}]^{2-}$ ion in the electrode diffusion layer.

Structural Characterization of [PPN][Ti_2Cl_9]

Single crystals of the PPN salt of the $[Ti_2Cl_9]^-$ species were grown from dichloromethane/pentane solution and were investigated by X-ray diffraction. The structure confirms the expected face-sharing bioctahedral geometry (see Figure 5). The bond lengths and angles within the anion are given in the Exp. Sect. The Ti−Cl bond lengths involving the bridging chlorine atoms are longer [2.4775(8) Å to 2.5098(8) Å] than the terminal ones [2.1955(8) Å to 2.2216(8) Å] as reported for related compounds containing the $[Ti_2Cl_9]^-$ anion.[1,29−33]

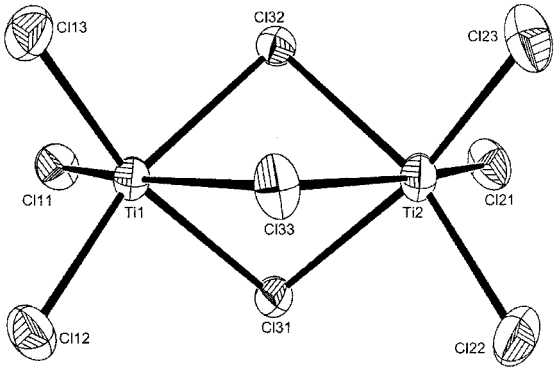

Figure 5. An ORTEP view of the anion of compound $[PPN]_2[Ti_2Cl_9]$; ellipsoids are drawn at the 50% probability level

Conclusions

The two main novelties of this new study of the well-developed coordination chemistry of chlorititanate(IV) complexes are: (*i*) the oxidation of $TiCl_3$ by thionyl chloride in the presence of chloride salts, and (*ii*) the complex chloride dissociation and redistribution equilibria that are established by these anions, with the unambiguous identification in solution of the previously unknown, yet simple, $[Ti_2Cl_{11}]^{3-}$ species. The combined IR and electrochemical study has shown that: (*i*) complex $[Ti_2Cl_{10}]^{2-}$ is dinuclear in dichloromethane solution and in the solid state as a PPN^+ salt; (ii) this ion is stable in dichloromethane but a chloride-redistribution equilibrium to yield a mixture of $[Ti_2Cl_9]^-$ and the novel $[Ti_2Cl_{11}]^{3-}$ complex is induced by the more facile electrochemical reduction of the former species; (*iii*) $[PPN]_3[Ti_2Cl_{11}]$ is not a stable species in the solid state and redistributes to a mixture of $[PPN]_2[Ti_2Cl_{10}]$ and $[PPN]_2[TiCl_6]$ upon crystallization.

Experimental Section

General Procedures. All manipulations were carried out under an atmosphere of dry and oxygen-free argon with standard Schlenk techniques. CH_2Cl_2 was purified by reflux and distillation over P_4O_{10} under argon. Pentane was purified by reflux over sodium benzophenone ketyl and distilled under argon. Cyclic voltammograms were recorded with an EG&G 362 potentiostat connected to a Macintosh computer through MacLab hardware/software. The electrochemical cell was fitted with an Ag-AgCl reference electrode, a platinum disk working electrode and a platinum wire counter-electrode. $[Bu_4N]PF_6$ (ca. 0.1 M) was used as supporting electrolyte in CH_2Cl_2. All potentials are reported relative to the ferrocene standard, which was added to each solution and measured at the end of the experiments. The infrared spectra were recorded on a Bruker Vector 22 instrument equipped with a Globar (MIR) source. The solution spectra in the far IR (480−300 cm^{-1}) region were obtained from CH_2Cl_2 solutions in polyethylene cells (0.5 mm path length). The elemental analyses were carried out by the analytical services of LSEO and LCC with Fisons EA 1108 and Perkin−Elmer 2400 instruments, respectively. Titanium(III) chloride (Aldrich), triethylbenzylammonium chloride (Aldrich) and bis(triphenylphosphanyl)iminium (PPN) chloride (Aldrich) were used as received.

Synthesis of [$NEt_3Bz]_2[Ti_2Cl_{10}$]: A Schlenk tube was charged with $TiCl_3$ (0.114 g, 0.74 mmol) and $[NEt_3Bz]Cl$ (0.174 g, 0.76 mmol). Thionyl chloride (20 mL) was added by syringe under magnetic stirring and the apparatus was connected to an oil bubbler. ***Warning****: The reaction between $SOCl_2$ and water (potentially present as a contaminant in the starting salts) produces toxic SO_2 and HCl, therefore the reaction must be carried out under a well-ventilated fume hood.* The dark-purple suspension transformed gradually into a yellow solution. After four hours of stirring at room temperature, pentane (50 mL) was added, causing the precipitation of the product as a yellow powder. After filtration, the solid was washed with pentane and dried under vacuum for three hours. Yield: 0.276 g (45%). $C_{26}H_{44}Cl_{10}N_2Ti_2$: calcd. C 37.4, H 5.3, N 3.4; found C 37.8, H 5.1, N 3.3.

Synthesis of [PPN]$_2$[Ti_2Cl_{10}]: Following an identical procedure as described above for $[NEt_3Bz]_2[Ti_2Cl_{10}]$, 0.834 g (88%) of $[PPN]_2[Ti_2Cl_{10}]$ was obtained starting from $TiCl_3$ (0.192 g, 1.24 mmol) and PPNCl (0.715 g, 1.25 mmol). $C_{72}H_{60}Cl_{10}N_2P_4Ti_2$: calcd. C 56.6, H 4.0, N 1.8; found C 56.0, H 3.7, N 1.8.

Synthesis of [PPN][Ti_2Cl_9]: A Schlenk tube was charged with $TiCl_3$ (0.565 g, 3.67 mmol) and PPNCl (1.050 g, 1.83 mmol). Thionyl chloride (30 mL) was added by syringe under magnetic stirring and the apparatus was connected to an oil bubbler. ***Warning****: the reaction between $SOCl_2$ and water (potentially present as a contaminant in the starting salts) produces toxic SO_2 and HCl, therefore the reaction must be carried out under a well ventilated fume hood.* The dark-purple suspension transformed gradually into a yellow solution. After cooling to room temperature, it was concentrated until approximately 10 mL and pentane (60 mL) was added, causing the precipitation of the product as a yellow powder. After filtration, the solid was washed with pentane and dried under vacuum. Yield:

 © 2004 Wiley-VCH Verlag GmbH & Co. KGaA, Weinheim

1.574 g (87%). $C_{36}H_{30}Cl_9NP_2Ti_2$: calcd. C 45.3, H 3.2; found C 44.3, H 2.8.

Synthesis of $[PPN]_2[TiCl_6]$: Following an identical procedure as described above for $[PPN][Ti_2Cl_9]$, 0.822 g (96%) of $[PPN]_2[TiCl_6]$ was obtained starting from $TiCl_3$ (0.099 g, 0.64 mmol) and PPNCl (0.740 g, 1.29 mmol). $C_{72}H_{60}Cl_{10}N_2P_4Ti_2$: calcd. C 64.6, H 4.5, N 2.1; found C 63.8, H 4.1, N 2.0. The solid state and solution IR characterization is presented in the Results and Discussion section.

Synthesis of a Product with Stoichiometry $[PPN]_3[Ti_2Cl_{11}]$: Following an identical procedure as described above for $[PPN][Ti_2Cl_9]$, $TiCl_3$ (0.112 g, 0.73 mmol) and PPNCl (0.628 g, 1.09 mmol) yielded 0.712 g (93%) of a solid product corresponding to the $[PPN]_3[Ti_2Cl_{11}]$ stoichiometry. $C_{108}H_{90}Cl_{11}N_3P_6Ti_2$: calcd. C 61.7, H 4.3, N 2.0; found C 60.6, H 3.8, N 1.9. The solid state and solution IR characterization is presented in the Results and Discussion section.

X-ray Structural Determinations for Compound $[PPN][Ti_2Cl_9]$: A single crystal was mounted under inert perfluoropolyether at the tip of a glass fiber and cooled in the cryostream of the Oxford-Diffraction XCALIBUR CCD diffractometer. Data were collected using monochromatic Mo-K_α radiation (λ = 0.71073). The structures was solved by direct methods (SIR97)[34] and refined by least-squares procedures on F^2 using SHELXL-97.[35] All H-atoms attached to carbon were introduced in calculation in idealised positions [d(CH) = 0.96 Å] and treated as riding models. The drawing of the molecules (Figure 1) was realised with the help of ORTEP32.[36] Crystal data and refinement parameters are shown in Table 1 and selected bond lengths and angles are listed in Table 2. CCDC-233004 contains the supplementary crystallographic data for this paper. These data can be obtained free of charge at www.ccdc.cam.ac.uk/conts/retrieving.html [or from the Cambridge Crystallographic Data Centre, 12 Union Road, Cambridge CB2 1EZ, UK; Fax: +44-1223-336-033; E-mail: deposit@ccdc.cam.ac.uk].

Table 1 Crystal data and structure refinement for $[PPN][Ti_2Cl_9]$

Empirical formula	$C_{36}H_{30}Cl_9NP_2Ti_2$
Molecular mass	953.40
Temperature	293(2) K
Wavelength	0.71073 Å
Crystal system	triclinic
Space group	$P\bar{1}$
Unit cell dimensions	a = 9.9904(10) Å
	b = 12.0458(12) Å
	c = 17.4335(14) Å
	α = 86.057(8)°
	β = 82.379(8)°
	γ = 83.861(8)°
Volume	2064.4(3) Å^3
Z	2
Density (calculated)	1.534 Mg/m^3
Absorption coefficient	1.075 mm^{-1}
F(000)	960
Crystal size	0.16 × 0.09 × 0.04 mm^3
Theta range for data collection	2.95 to 26.37°
Index ranges	$-12 \le h \le 9$
	$-15 \le k \le 15$
	$-21 \le l \le 21$
Reflections collected	16046
Independent reflections	8414 [R(int) = 0.0421]
Completeness to theta = 26.37°	99.7%
Absorption correction	analytical
Max. and min. transmission	0.92334 and 0.78155
Refinement method	full-matrix least-squares on F^2
Data/restraints/parameters	8414/0/451
Goodness-of-fit on F^2	0.795
Final R(int) [$I > 2\sigma(I)$]	$R1$ = 0.0348, $wR2$ = 0.0496
R(int) (all data)	$R1$ = 0.0706, $wR2$ = 0.0554
Largest diff. peak and hole	0.349 and −0.428 e·Å^{-3}

Table 2. Bond lengths (Å) and angles (°) for $[PPN][Ti_2Cl_9]$

Ti(1)−Ti(2)	3.3922(7)		
Ti(1)−Cl(11)	2.2216(8)	Ti(2)−Cl(21)	2.2124(9)
Ti(1)−Cl(12)	2.1955(8)	Ti(2)−Cl(22)	2.2175(9)
Ti(1)−Cl(13)	2.2046(9)	Ti(2)−Cl(23)	2.2031(9)
Ti(1)−Cl(31)	2.4620(8)	Ti(2)−Cl(31)	2.4937(8)
Ti(1)−Cl(32)	2.5098(8)	Ti(2)−Cl(32)	2.4785(8)
Ti(1)−Cl(33)	2.4775(8)	Ti(2)−Cl(33)	2.4496(8)
Cl(12)−Ti(1)−Cl(11)	98.02(3)	Cl(21)−Ti(2)−Cl(22)	97.49(4)
Cl(13)−Ti(1)−Cl(11)	97.12(3)	Cl(23)−Ti(2)−Cl(21)	96.84(3)
Cl(12)−Ti(1)−Cl(13)	99.71(3)	Cl(23)−Ti(2)−Cl(22)	98.94(4)
Cl(11)−Ti(1)−Cl(31)	91.45(3)	Cl(21)−Ti(2)−Cl(31)	91.30(3)
Cl(11)−Ti(1)−Cl(32)	90.86(3)	Cl(21)−Ti(2)−Cl(32)	89.43(3)
Cl(11)−Ti(1)−Cl(33)	166.67(3)	Cl(21)−Ti(2)−Cl(33)	166.33(3)
Cl(12)−Ti(1)−Cl(31)	91.01(3)	Cl(22)−Ti(2)−Cl(31)	89.23(3)
Cl(12)−Ti(1)−Cl(32)	165.52(3)	Cl(22)−Ti(2)−Cl(32)	165.02(3)
Cl(12)−Ti(1)−Cl(33)	91.65(3)	Cl(22)−Ti(2)−Cl(33)	92.14(3)
Cl(13)−Ti(1)−Cl(31)	165.17(3)	Cl(23)−Ti(2)−Cl(31)	167.58(3)
Cl(13)−Ti(1)−Cl(32)	90.45(3)	Cl(23)−Ti(2)−Cl(32)	93.37(3)
Cl(13)−Ti(1)−Cl(33)	90.21(3)	Cl(23)−Ti(2)−Cl(33)	91.19(3)
Cl(31)−Ti(1)−Cl(32)	77.29(3)	Cl(32)−Ti(2)−Cl(31)	77.29(3)
Cl(31)−Ti(1)−Cl(33)	79.18(3)	Cl(33)−Ti(2)−Cl(31)	79.11(3)
Cl(33)−Ti(1)−Cl(32)	77.92(3)	Cl(33)−Ti(2)−Cl(32)	79.04(3)

Acknowledgments

We are grateful to the French Ministry of Research, to the Centre National de la Recherche Scientifique, and to Polimeri Europa for support of this work, and to Mr. Sébastien Maria for technical assistance.

[1] T. J. Kistenmacher, G. D. Stucky, *Inorg. Chem.* **1971**, *10*, 122−132.
[2] C. Creaser, J. Creighton, *J. Chem. Soc., Dalton Trans.* **1975**, 1402−1405.
[3] G. Natta, *Angew. Chem.* **1956**, *68*, 393.
[4] G. Natta, P. Corradini, G. Allegra, *J. Polymer Sci.* **1961**, *51*, 399.
[5] E. G. M. Tornqvist, J. T. Richardson, Z. W. Wilchinsky, R. W. Looney, *J. Catal.* **1967**, *8*, 189−196.
[6] Z. W. Wilchinsky, R. W. Looney, E. G. M. Tornqvist, *J. Catal.* **1973**, *28*, 351−367.
[7] H. Sinn, W. Kaminsky, *Adv. Organomet. Chem.* **1980**, *18*, 99−149.
[8] P. Pino, R. Mulhaupt, *Angew. Chem. Int. Ed. Engl.* **1980**, *19*, 857−875.
[9] C. G. Barraclough, A. K. Gregson, *J. Chem. Soc., Faraday Trans. 2* **1972**, *68*, 177−180.
[10] O. Kahn, *Proc. Int. Conf. Coord. Chem. 16th* **1974**, 2.28a, 23 pp.
[11] A. Ceulemans, G. A. Heylen, L. F. Chibotaru, T. L. Maes, K. Pierloot, C. Ribbing, L. G. Vanquickenborne, *Inorg. Chim. Acta* **1996**, *251*, 15−27.
[12] P. C. Crouch, G. W. A. Fowles, R. A. Walton, *J. Chem. Soc. A* **1969**, 972−976.
[13] B. Briat, O. Kahn, I. Morgensternbadarau, J. C. Rivoal, *Inorg. Chem.* **1981**, *20*, 4193−4200.

 © 2004 Wiley-VCH Verlag GmbH & Co. KGaA, Weinheim

[14] D. Armstrong, P. Perkins, J. Stewart, *Rev. Roum. Chim.* **1974**, *19*, 1695−1707.
[15] H. Hecht, *Z. Anorg. Chem.* **1947**, *254*, 37−51.
[16] R. Colton, J. H. Canterford, *Halides of the First Row Transition Metals*, Wiley-Interscience, London, **1969**.
[17] H. Heumann, P. Köchlin, *Ber.* **1883**, *16*, 1625.
[18] H. Stavdinger, W. Kreis, *Helv. Chim. Acta* **1924**, *8*, 71.
[19] H. Linga, Z. Stojek, R. A. Osteryoung, *J. Am. Chem. Soc.* **1981**, *103*, 3754−3760.
[20] R. T. Carlin, R. A. Osteryoung, J. S. Wilkes, J. Rovang, *Inorg. Chem.* **1990**, *29*, 3003−3009.
[21] N. Hao, B. Sayer, G. Denes, D. Bickley, C. Detellier, M. Mcglinchey, *J. Magn. Reson.* **1982**, *50*, 50−63.
[22] A. F. Demiray, W. Brockner, B. N. Cyvin, S. J. Cyvin, *Z. Naturforsch., Teil A* **1979**, *34*, 362−368.
[23] R. Clark, L. Maresca, R. Puddephat, *Inorg. Chem.* **1968**, *7*, 1603.
[24] W. Van Bronswyk, R. Clark, L. Maresca, *Inorg. Chem.* **1969**, *8*, 1395.
[25] O. Poleshchuk, J. Latosinska, B. Nogaj, *J. Mol. Struct.* **1996**, *380*, 277−282.
[26] C. Ding, Y. Yu, R. Jensen, W. Balfour, C. Qian, *Chem. Phys. Lett.* **2000**, *331*, 163−169.
[27] A. Shiga, H. Kawamurakuribayashi, T. Sasaki, *J. Mol. Catal.* **1994**, *87*, 243−261.
[28] D. M. Adams, J. Chatt, J. M. Davidson, J. Gerratt, *J. Chem. Soc.* **1963**, 2189−2194.
[29] E. Solari, C. Floriani, A. Chiesi-Villa, C. Guastini, *J. Chem. Soc., Chem. Commun.* **1989**, 1747−1749.
[30] E. Solari, C. Floriani, K. Schenk, A. Chiesi-Villa, C. Rizzoli, M. Rosi, A. Sgamellotti, *Inorg. Chem.* **1994**, *33*, 2018−2028.
[31] S. Castro, W. Streib, J. Huffman, G. Christou, *Chem. Commun.* **1996**, 2177−2178.
[32] R. Bettenhausen, W. Milius, W. Schnick, *Chem. Eur. J.* **1997**, *3*, 1337−1341.
[33] Q. Feng, S. Luo, M. Olmstead, T. Rauchfuss, P. Stafford, *Chem. Mater.* **1997**, *9*, 641−643.
[34] A. Altomare, M. Burla, M. Camalli, G. Cascarano, C. Giacovazzo, A. Guagliardi, A. Moliterni, G. Polidori, R. Spagna, *J. Appl. Cryst.* **1999**, *32*, 115−119.
[35] G. M. Sheldrick, *SHELXL-97. Program for Crystal Structure refinement*, University of Göttingen, Göttingen, Germany, **1997**.
[36] L. J. Farrugia, *J. Appl. Crystallogr.* **1997**, *32*, 565.

Received April 10, 2004
Early View Article
Published Online August 17, 2004

 © 2004 Wiley-VCH Verlag GmbH & Co. KGaA, Weinheim

Copper(II) and Nickel(II) Complexes of *N*,*N*-Bis(2-hydroxyethyl)octamethyl-1,4,8,11-tetraazacyclotetradecane

Tapashi G. Roy,*[a] Saroj K. S. Hazari,[a] Benu K. Dey,[a] Hazarat A. Miah,[a] Cerstin Bader,[b] and Dieter Rehder*[b]

Keywords: Antimicrobial activity / Copper / Macrocyclic ligands / N ligands / Nickel

Reaction of ethylene oxide with the 1,4,8,11-tetraazacyclotetradecanes Me_8[14]ane L_B (diaxial-diequatorial with respect to the methyl substituents at the secondary ring carbons) and L_C (axial-triequatorial) yielded the N4,N11-disubstituted 2-hydroxyethyl (Y) derivatives L_{BY} (diaxial-diequatorial) and L_{AY} (all-equatorial). These new ligands interact with $Cu(ClO_4)_2$ to produce octahedral blue-violet $[CuL_{BY}][ClO_4]_2$ and deep-blue $[CuL_{AY}][ClO_4]_2$, with the hydroxyl groups of the $-CH_2-CH_2-OH$ arms in axial positions. Reaction of L_{BY} with nickel(II) acetate and subsequent addition of $Li(ClO_4)$ yielded square-planar yellow $[NiL_{BY}][ClO_4]_2$. Characterisation has been carried out on the basis of analytical, spectroscopic, conductometric and magneto-chemical data. The structures of L_{BY} and $[CuL_{AY}][ClO_4]_2$ have been confirmed by X-ray diffraction analyses. The antifungal and antibacterial activities of these compounds have been studied against some phytopathogenic fungi and bacteria.

(© Wiley-VCH Verlag GmbH & Co. KGaA, 69451 Weinheim, Germany, 2004)

Introduction

Biogenic macrocyclic tetraaza ligands employed in metal-ion complexation such as in heme proteins, chlorophyll, vitamin B_{12}, or the factor F_{430} of methyl-coenzyme-M reductase in methanogenesis are structurally complex systems which, generally and perhaps simplistically, may be considered rigid planar cyclic structures carrying pendent functional groups acting as functional components at the coordination sites.[1,2] The design and synthesis of macrocyclic systems carrying such functional groups, mimicking the properties of their natural counterparts, is thus a multifarious problem.

In order to synthesise the requisite type of super-structured macrocycles, the obvious approach is to first prepare the more basic macrocyclic ligand, and then attach suitable pendent hydrocarbon chains to the periphery. Thus, a number of macrocycles carrying N-substituents have been prepared by alkylation reactions,[3] starting from the basic isomeric octamethyltetraazacyclotetradecanes Me_8[14]anes L_A, L_B and L_C, where the indexes A, B and C denote the differing stereochemistries with respect to the methyl substituents attached to the chiral carbons of the [14]ane in its chair conformation. Thus, A represents all-equatorial, B diaxial-diequatorial and C axial-triequatorial orientations.[4,5] To approach the biogenic ligands, attempts have been made to attach pendent functional groups to the N donors and consequently to influence the ligating ability of the original N-donor ligands. Thus, in the reactions of L_B with acrylonitrile, two of the NH protons have been substituted by $-CH_2CH_2CN$.[6] This bis(2-cyanoethyl) derivative of L_B has been designated L_{BX}, and the dimethyl derivatives of L_B and L_C, prepared by methylation with methyl iodide,[7] have been denoted L_{BZ} and L_{CZ}. The structures of L_{BX} [6] and L_{BZ} [7] have been confirmed by X-ray crystallography. In the present contribution, we report on the synthesis and coordination behaviour towards Cu^{II} and Ni^{II} of the reaction products obtained by reacting L_B and L_C with ethylene oxide, yielding the bis(2-hydroxyethyl)-substituted ligands L_{BY} and L_{AY} where, in the case of the formation of L_{AY}, a conformational change took place.

[a] Department of Chemistry, University of Chittagong, Chittagong 4331, Bangladesh
[b] Universität Hamburg, Institut für Anorganische und Angewandte Chemie, 20146 Hamburg, Germany

Results and Discussion

Ligands L_{BY} and L_{AY}

Passage of ethylene oxide through aqueous suspensions of L_B and L_C, and subsequent extraction with chloroform, evaporation of the $CHCl_3$ extracts and re-crystallisation from $CH_3OH/CHCl_3$ (L_{BY}) or CH_3OH/Et_2O (L_{AY}) yielded the ligands in the form of white products (Scheme 1). The melting points of L_{BY} (175 °C) and L_{AY} (160 °C) clearly differ from those of the parent ligands L_B (122 °C) and L_C (85 °C). Formation of the bis- rather than the tetrakis(2-hydroxyethyl) derivatives observed in case of the analogous cyclam-type macrocycles[8] can be attributed to steric effects

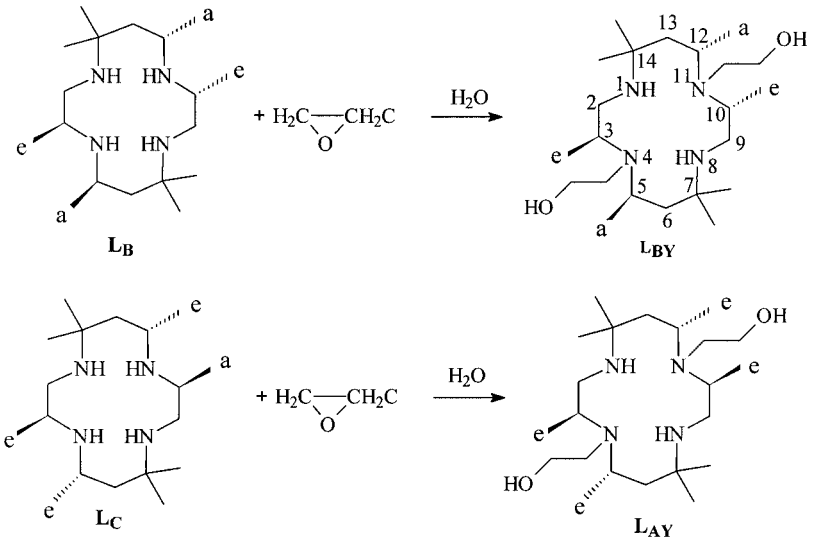

Scheme 1

created by the eight peripheral methyl groups. The fragmentation patterns obtained from the mass spectra of L_{BY} and L_{AY} (vide infra) clearly indicate that substitution of N−H protons by $-CH_2CH_2-OH$ groups has taken place at N4 and N11 only. This substitution was confirmed by the X-ray structure of L_{BY} and the copper(II) complex of L_{AY}. X-ray and ^1H NMR analyses (vide infra) of L_{BY} and L_{AY} reveal that the diaxial-diequatorial arrangement for L_{BY} is retained, while the configuration has changed to all-equatorial in the case of L_{AY}.

The infrared spectra (Table 1) show the ν_{N-H}, ν_{C-H}, ν_{C-C} and ν_{CH_3} stretching bands in the expected region. A band at 3740 cm^{-1} for L_{BY}, and 3500 cm^{-1} for L_{AY}, indicates the presence of the OH group in these compounds, as do the ν_{C-OH} bands at 1260 and 1060 cm^{-1}; the primary alcoholic hydroxyl group usually shows strong ν_{CO} stretching bands at 1350 to 1260, and 1050 cm^{-1}.

Table 1. Selected IR data (cm^{-1})

	ν_{N-H}	ν_{C-H}	ν_{CH_3}	ν_{C-C}	ν_{M-N}	ν_{ClO_4}	ν_{OH}
L_{BY}	3110	2990	1360	1160	–	–	3740
L_{AY}	3250	2970	1380	1135	–	–	3500
$[NiL_{BY}][ClO_4]_2$	3100	2985	1390	1180	540	1110, 625	3720
$[CuL_{BY}][ClO_4]_2$	3200	2990	1390	1175	570	1140, 625	3500
$[CuL_{AY}][ClO_4]_2$	3190	2995	1380	1175	525	1100, 620	3400

The mass spectrum of L_{BY} exhibits the molecular-ion peak at m/z = 400, while that of L_{AY} is at m/z = 403, corresponding to $[M + 3]^+$. Both the isomeric ligands show more or less the same fragmentation pattern, although the intensities of the peaks differ. The basic peaks are at m/z = 199 for L_{BY} and 171 for L_{AY}. This difference may reflect the stereochemical differences. The prominent fragmentations are presented in Schemes 2−5. The basic peak at m/z = 199 for L_{BY} comes about by the concomitant cleavage of the C2−C3 and C9−C10 bonds (α-cleavage),[4,9,10] followed by the loss of one H atom (path A in Scheme 2). The second intense peak at m/z = 201 also arises from this cleavage with capture of an H atom (path B). The molecular ion can also undergo fragmentation by C−N bond rupture of one of the N-pendent groups with elimination of vinyl alcohol, followed by hydrogen rearrangement and elimination of an H_2O molecule from the other 2-hydroxyethyl group, providing an ion at m/z = 340 (Scheme 3).

Additionally, the molecular ion can successively lose two methyl radicals from the more crowded α-carbons C7 and C14 to form ions at m/z = 370, from which removal of vinyl alcohol by C−N bond rupture in one of the N-pendent groups, followed by rearrangement of H atoms and finally

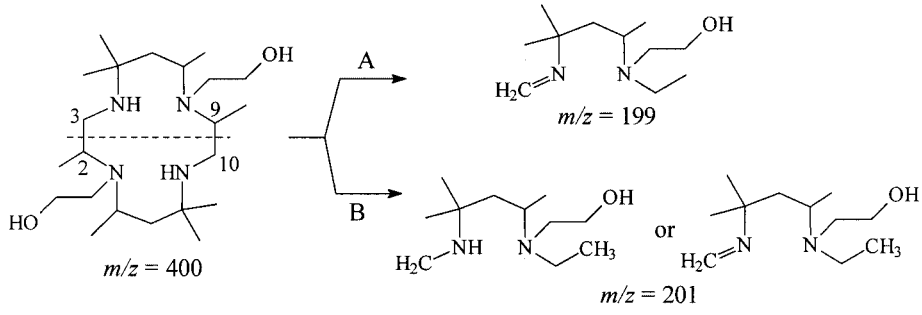

Scheme 2

 © 2004 Wiley-VCH Verlag GmbH & Co. KGaA, Weinheim

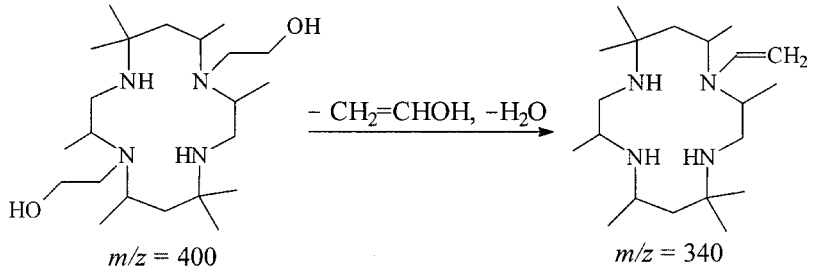

Scheme 3

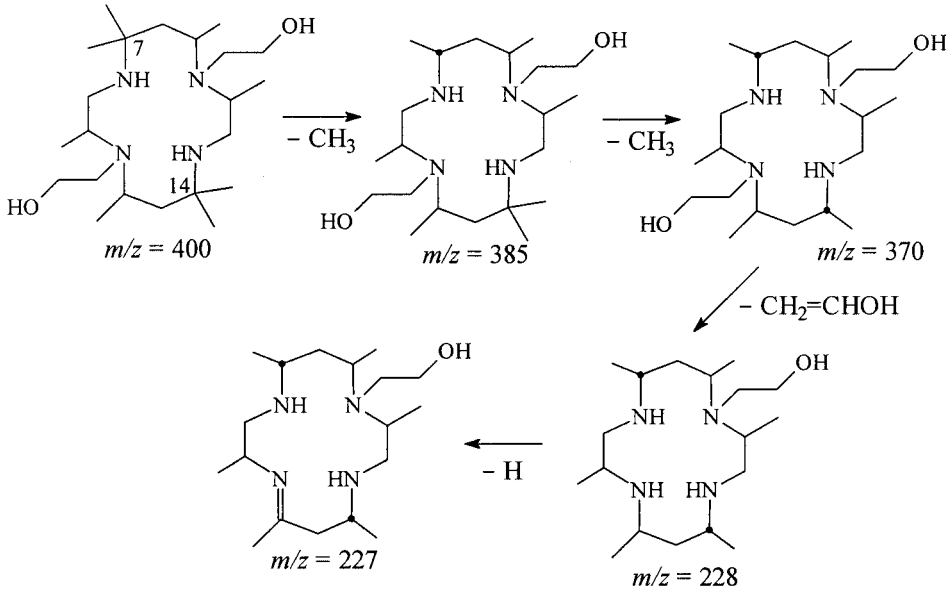

Scheme 4

elimination of H_2, results in an ion at m/z = 227 (Scheme 4).

Alternatively, the basic peak at m/z = 171 for L_{AY} (Scheme 5) may arise from the m/z = 201 fragment by C3−N4 bond rupture with elimination of ethylene, followed by rearrangement and successive removal of H_2. The resulting fragment at m/z = 171 can further lose a hydrogen molecule to provide the peak at m/z = 169. This fragment, on removal of hydrogen cyanide, yields an ion at m/z = 142 which, by C15−N4 bond cleavage and elimination of vinyl alcohol, can produce the ion at m/z = 98.

The ^{1}H NMR spectrum of ligand L_{BY} (Table 2) shows two singlets at δ = 1.108 and 1.147 ppm corresponding to six protons each that can be assigned to the geminal bis(methyl) groups. In addition, there are two doublets at δ = 0.982 and 0.879 ppm, each corresponding to six protons. This requires that C3,C10 and C5,C12 should be in pairwise equivalent configurations. The upfield doublet can be

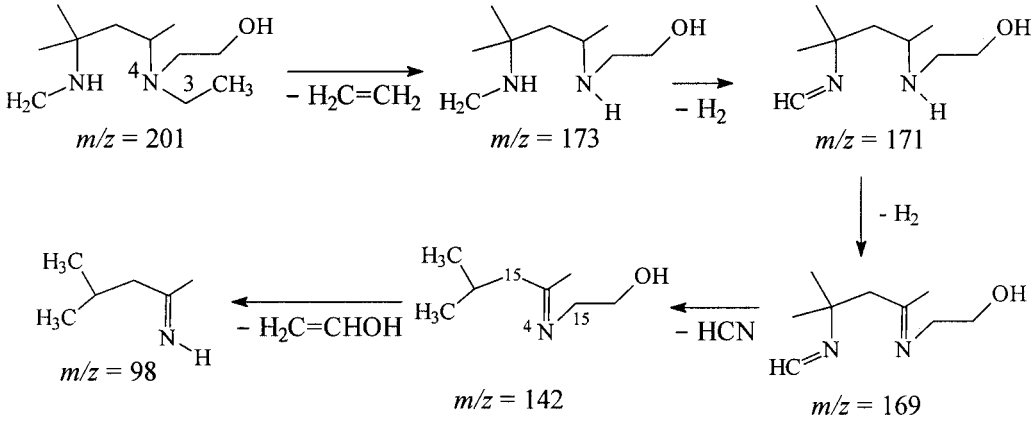

Scheme 5

 © 2004 Wiley-VCH Verlag GmbH & Co. KGaA, Weinheim

Table 2. ^{1}H NMR spectroscopic data of the ligands[a]

Ligands	Geminal dimethyl	Methyl on chiral carbon atoms	CH_2, CH and NH	OH
L_{BY}	1.108 s (*e*, 6 H) 1.147 s (*a*, 6 H)	0.982 d (*a*, 6 H) 0.879 d (*e*, 6 H)	2.047 m 2.353 m 3.168 m 3.408 m	not resolved
L_{AY}	1.082 s (*e*, 6 H) 1.369 s (*a*, 6 H)	1.145 d (*e*, 6 H) 1.199 d (*e*, 6 H)	2.20−2.45 m 3.10−3.35 m	2.897 br

[a] s = singlet, d = doublet, *a* = axial, *e* = equatorial, br = broad, m = multiplet.

assigned to the equatorial and the downfield doublet to the axial methyls. Thus, a diaxial-diequatorial arrangement has been assigned to L_{BY}, in analogy to its parent ligand L_B, an assignment which is confirmed by its X-ray structure. The presence of a hydroxyl group in L_{BY}, confirmed by IR spectroscopy, is not reflected by any clear singlet for OH protons in the ^{1}H NMR spectroscopy. This may be due to rapid intermolecular chemical exchange of the hydroxyl protons. The α- and β-methylene, methine and NH protons appear as poorly resolved multiplets at δ = 2.047, 2.353, 3.168 and 3.408 ppm, respectively.

The geminal bis(methyl) groups of L_{AY} are represented by two singlets at δ = 1.082 (equatorial) and 1.369 ppm (axial). Two doublets at δ = 1.145 and 1.199 ppm, each representing six protons, correspond to the methyl groups C3, C5, C10 and C12 in the equatorial positions. This all-equatorial arrangement was also confirmed by the X-ray structure of $[CuL_{AY}][ClO_4]_2$ (see below). A sharp singlet at δ = 2.897 ppm in the ^{1}H NMR spectrum of ligand L_{AY} can be assigned to the OH protons. The signals due to methylene, methine and N−H protons overlap and could not be resolved clearly.

Representations of the molecular structure of L_{BY}, including the numbering scheme, and the unit cell are shown in Figure 1, the caption of which also contains selected bonding parameters. The molecules are pairwise related to each other by an inversion centre. The cyclic [14]ane skeleton is in the chair conformation, with the methyl groups on the secondary ring carbons (C5, C9, C16, C20) alternately in the axial and the equatorial positions. The angles between the normals of the mean planes constituting the two chairs are as follows (cf. also Figure 1, bottom): molecule 1: C5,C11,C2A,N1A,C4A,C11A,C3,N1,C4 (plane 1)/C5,N2,C9,C11 = 92.6°; (plane 1)/C5A,N2A,C9A,C11A =

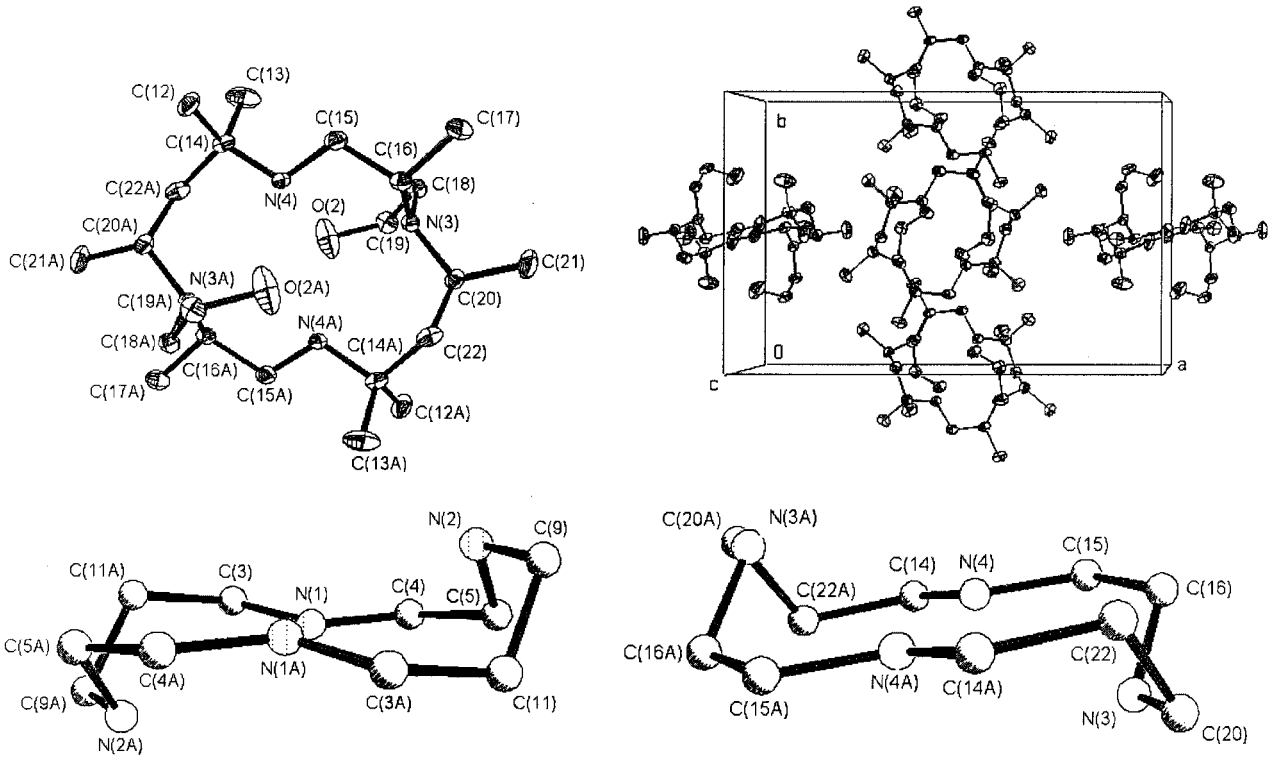

Figure 1. ORTEP presentation of the molecular structure (top left), cell drawing (top right) and the [14]ane skeletons (bottom) of L_{BY}; selected bond lengths (Å) and angles (°): N1−C4 1.464(2), N1−C3 1.484(2), N2−C5 1.4709(19), N2−C9 1.473(2), N2−C7 1.4591(19), C7−C8 1.528(2), C8−O1 1.409(2); C3−N1−C4 115.60(12), C5−N2−C9 117.87(12), C7−N2−C9 113.06(12), C7−N2−C5 115.66(12), N2−C7−C8 111.74(12), C7−C8−O1 112.88(13)

 © 2004 Wiley-VCH Verlag GmbH & Co. KGaA, Weinheim

72.3°; molecule 2: C16,C22,C14A,N4A,C15A,C16A,-C22A,C14,N4,C15 (plane 2)/C16,N3,C20,C22 = 87.7°; (plane 2)/C16A,N3A,C20A,C22A = 106.6°. The pendent ethanol substituents on N2 and N3 are oriented axially, with the OH groups bent towards the cavity spanned by the four nitrogens. Only one of the OH groups, O1, is involved in an intramolecular hydrogen bonding interaction [*d*(OH···N2) = 2.839Å].

Complexes $[Ni(L_{BY})][ClO_4]_2$ and $[CuL][ClO_4]_2$ (L = L_{BY} or L_{AY})

The reaction of nickel(II) acetate tetrahydrate with L_{BY} and subsequent addition of lithium perchlorate in methanolic solution yielded yellow, square-planar $[Ni(L_{BY})][ClO_4]_2$. The formulation is assigned on the basis of analytical data, conductance and magneto-chemical measurements, and IR- and UV-spectral analyses. The IR spectrum (Table 1) of the complex shows a ν_{N-H} band at around 3200 cm^{-1}, and the perchlorate bands around 1100 cm^{-1} and 620 cm^{-1}. A band at 3720 cm^{-1} demonstrates the presence of the pendent OH group. The molar conductivity value of 173 $\Omega^{-1}\cdot cm^2\cdot mol^{-1}$ (Table 3) in acetonitrile correspond to a 1:2 electrolyte — the two ClO_4^- anions are outside the coordination sphere. Similar results were found in aqueous solution (Table 3). The magneto-chemical measurement of $[Ni(L_{BY})][ClO_4]_2$ is in good agreement with square-planar diamagnetic nickel(II). The stereochemical assignment was based on ^1H NMR spectroscopy.

The electronic absorption spectrum of $[Ni(L_{BY})][ClO_4]_2$ displays a *d*-*d* band at 474 nm, which can be assigned to the $^1A_1g \rightarrow {}^1B_1g$ transition. The results of our complexes fit well with those for Ni^{II} complexes of other saturated aza macrocycles.[11] The relatively high ε_{max} value of 82 $dm^3\cdot mol^{-1}\cdot cm^{-1}$ indicates that the axial positions are free. Octahedral Ni^{II} complexes have low extinction coefficients in the range of 20−30 $dm^3\cdot mol^{-1}\cdot cm^{-1}$. The pendent hydroxy groups of L_{BY} in principle do have coordinating properties. The experimental evidence — the yellow colour, the comparatively high ε for the transition in the visible, and the lack of a shift of the IR band corresponding to OH —, however, shows that this group does not coordinate in the present case. The absorption band at 237 nm in the UV region is assigned to a charge-transfer transition. This band does not provide any information related to the geometry of these complexes. On complexation, the "up" and "down" positions of methyls on chiral carbons in the ligand are retained — no configurational change in the ligand system is to be expected as L_{BY} coordinates.[11,12] The proposed structure of $[Ni(L_{BY})][ClO_4]_2$ is shown in Scheme 6.

Interaction of copper(II) perchlorate hexahydrate with the ligands L_{BY} or L_{AY} in methanolic solution yields the blue-violet to deep-blue complexes $[CuL][ClO_4]_2$. The infrared spectra (Table 1) show ν_{N-H} bands around 3200 cm^{-1} and the perchlorate bands at 1100 and 620 cm^{-1}, as well as the ν_{C-H}, ν_{C-C}, ν_{CH_3} and ν_{Cu-N} bands in the expected positions. For $[CuL][ClO_4]_2$, a strong band at 3500 (L = L_{BY}) and a broad band at 3400 cm^{-1} (L = L_{AY}) are found, corresponding to OH. The low-frequency shift of these bands with respect to the free ligands indicates coordination of OH to the copper(II) ion, forming octahedral complexes, a coordination mode which was confirmed by the X-ray structure analysis of $[Cu(L_{AY})][ClO_4]_2$.

The molar conductivity of 168−170 in aqueous solution and 148−165 $\Omega^{-1}\cdot cm^2\cdot mol^{-1}$ in acetonitrile corresponds to 1:2 electrolytes — an ionic situation. The colour change (from blue-violet and deep-blue to pink) as these complexes are dissolved in water indicates the formation of new complexes in water. The most obvious explanation is the replacement of the hydroxy ligands by water — the formation of diaqua complexes $[CuL(H_2O)_2]^{2+}$ — as in the Cu^{II} complexes with the parent ligands L_B and L_C.[13] On the other hand, solutions of $[Cu(L_{BY})][ClO_4]_2$ and $[Cu(L_{AY})][ClO_4]_2$ in chloroform do not show any conductance, suggesting that the ClO_4^- ions have entered into the coordination sphere to form octahedral bis(perchlorato) complexes $[CuL(ClO_4)_2]$.

The complexes $[CuL][ClO_4]_2$ show broad *d*-*d* bands at 507−564 nm in acetonitrile, as do other Cu^{II} complexes with tetraza macrocycles.[14,15] Bands around 300 nm can be attributed to copper-ligand charge-transfer transitions. The magnetic moments of 1.68−1.83 μ_B are in good agreement with "normal" copper(II) complexes having one unpaired electron. As the ^1H NMR spectra could not be measured for these paramagnetic complexes, the exact stereochemistry (i.e. axial and equatorial positions of methyls on chiral carbons) could not be determined by NMR spectroscopy. As in the case of the nickel complex (vide supra), and based on the structural determination of the Cu^{II} complex with

Table 3. Selected physico-chemical properties of the complexes[a]

	$[Ni(L_{BY})][ClO_4]_2$	$[Cu(L_{BY})][ClO_4]_2$	$[Cu(L_{AY})][ClO_4]_2$
Solid state	pale yellow	blue-violet	deep blue
μ_{eff} (μ_B)	diamagnetic	1.83	1.68
In MeCN	yellow	pink-violet	blue
λ_{max} (nm) (ε)	474 (82)	507 (194), 303	564 (200), 301
Λ ($\Omega^{-1}\cdot cm^2\cdot mol^{-1}$)	173	165	148
In H_2O	yellow	pink	pink
Λ ($\Omega^{-1}\cdot cm^2\cdot mol^{-1}$)	165	170	168
In $CHCl_3$	−	blue-violet	deep blue
Λ ($\Omega^{-1}\cdot cm^2\cdot mol^{-1}$)	−	none	none

[a] μ = Magnetic moment at 298 K, λ = wavelength in the UV/Vis spectrum, ε = extinction coefficient, Λ = conductivity.

 © 2004 Wiley-VCH Verlag GmbH & Co. KGaA, Weinheim

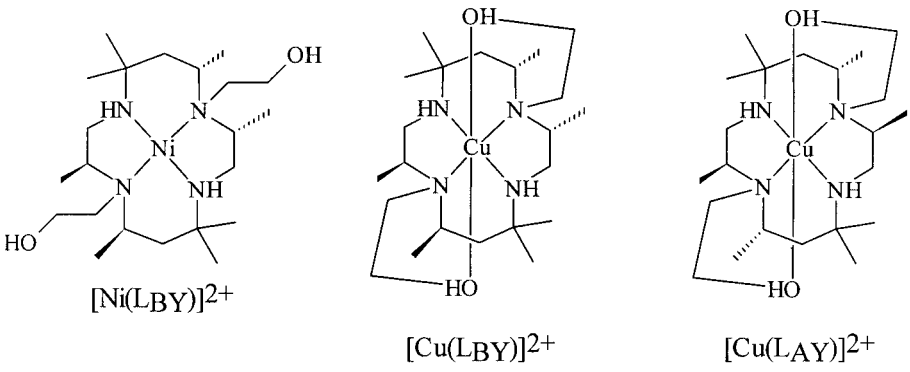

Scheme 6

L_{AY}, configurational changes on complexation are not expected. For structural formulae of the two copper complexes see Scheme 6.

An ORTEP drawing of the molecular structure of the cation $[Cu(L_{AY})]^{2+}$ is represented in Figure 2, showing the distorted octahedral coordination geometry for the copper ion. For selected bonding parameters see the caption to Figure 2. Cu lies on a crystallographic inversion centre. The two ring carbons C6 and C7, and the methyl group C9 (attached to C6), are disordered over two equally populated positions. Together with the four nitrogen donors, the copper ion forms an ideal plane. The deviations of the ring carbons from this plane are as follows (in Å): C3 −0.648, C4 −0.029, C6 −0.47, C6# −1.045, C7 −1.517, C7# −0.606, C8 −0.921. The OH functions are above and below this plane. The O1−Cu−O1A axis is not exactly perpendicular to this plane, but inclined towards the axis N1−Cu−N1A by 13.7°, and towards the axis N2−Cu−N2A by 4.3° (average angle between the normal of the plane and the O1−Cu−O1A axis: 95.6°). The Cu−O distances [2.432(3) Å] are rather long, indicating relatively weak coordination and thus the above-mentioned possibility of the replacement of the two axial positions by water or perchlorate. These OH functions are additionally hydrogen-bonded to the axially oriented perchlorate anions [$d(ClO_4^-\cdots OH)$ = 2.797 and 3.206 Å]. The angles at the carbons of the 2-hydroxyethyl arm of coordinated L_{AY} deviate somewhat from those of the free ligand L_{BY} (116.5° at C1 vs. 111.5°; 108.6° at C2 vs. 113.6°). The angles at N1 are 111.5° (C1−N1−C3) and 121.7° (C1−N1−C6), as compared to 115.6° and 113.1° of the corresponding angles in free L_{BY} — coordination of the hydroxyethyl arms to Cu^{II} can only be achieved by moving the arms towards the coordination centre.

Antimicrobial Activity Studies

Since only a few recent reports exist on the antifungal activities of macrocycles and their complexes,[13,15] it ap-

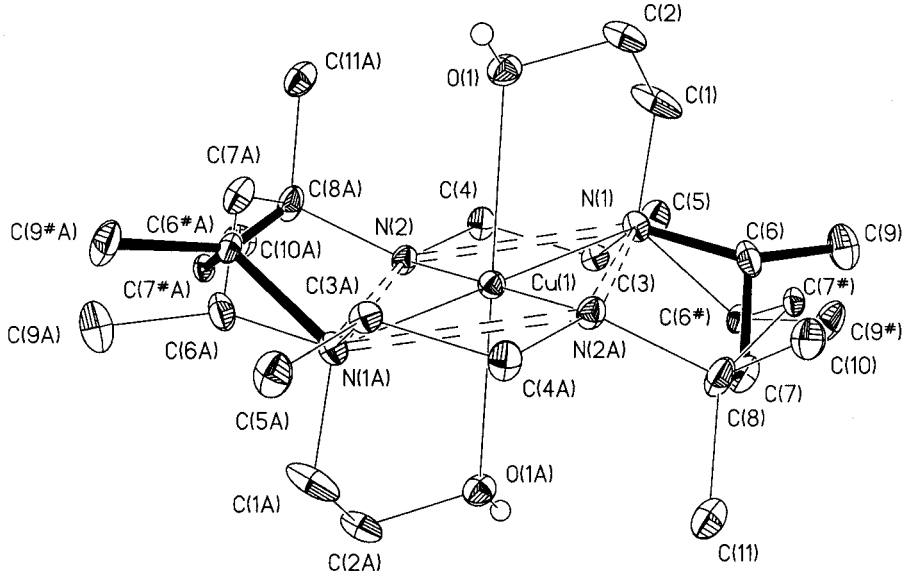

Figure 2. ORTEP plot (30% probability level), including disorder information, of $[Cu(L_{AY})]^{2+}$; "A" refers to symmetry related atoms, # and bold bonds to disordered regions; the plane spanned by the four nitrogen donors is emphasized by dashed lines; selected bond lengths (Å) and angles (°): Cu−N1 2.157(3), Cu−N2 1.992(3), Cu−O1 2.432(3), O1−C2 1.419(6); N1−Cu−N2 85.96(12), N1−Cu−N2A 94.04(12), N1−C1−C2 116.4(4), C2−O1−Cu 106.7(2) N1−Cu−O1 76.30(11), N1A−Cu−O1 103.70(11), N2−Cu−O1 94.46(12), N2A−Cu−O1 85.54(12)

 © 2004 Wiley-VCH Verlag GmbH & Co. KGaA, Weinheim

Table 4. In vitro antifungal activities of ligands and their metal complexes

	Inhibition of mycelial growth (%)				
	Macrophomina phaseolina	*Alternaria alternata*	*Fusarium equiseti*	*Colletotrichum corcolei*	*Botrgodiplodia theobromal*
L_{BY}	52.00	36.00	38.68	39.69	47.58
L_{AY}	40.40	37.00	36.87	39.42	32.98
$[CuL_{BY}][ClO_4]_2$	32.00	21.22	27.00	2.58	31.36
$[CuL_{AY}][ClO_4]_2$	51.00	36.50	22.60	35.00	22.08
$[NiL_{AY}][ClO_4]_2$	13.00	0.00	0.00	3.50	31.00

peared interesting to see whether the compounds involved in the present study exhibit any such activity. We therefore investigated the antifungal potential of the ligands L_{BY} and L_{AY}, and their Cu^{II} and Ni^{II} complexes against five selective phytopathogenic fungi — (i) *Macrophomina phaseolina*, (ii) *Alternaria alternata*, (iii) *Fusarium equiseti*, (iv) *Colletotrichum corcolei*, and (v) *Botrgodiplodia theobromal*. It is evident from the results (Table 4) that the macrocycles and their complexes under investigation show some antifungal behaviour, which is more pronounced against *M. phaseolina* than against the other four organisms. The activity decreases upon coordination of the ligands to Cu^{II} and Ni^{II} in most cases, with the nickel complex showing the lowest activity. It has been noted that the N-substituted ligands (such as L_{BY}) exhibit a higher rate of inhibition on mycelial growth than their parent ligands (such as L_B).[13] The antifungal potential of the coordinated *N*-substituted ligands thus compares to that of the parent ligands; it also compares to the activities of copper[13] and nickel complexes[16] of the parent L_B and L_C.

Antibacterial activities of the macrocycles and their complexes have not been studied so far. Here, we report on the antibacterial activities against *Salmonella typhi*, *Shigella dysenteriae*, *Escherichia coli* and *Bacillus cerelus.* The results are contained in Table 5, which shows that the ligands do not exhibit any antibacterial activity, although some activity is noted for the complexes. Hence, unlike their behaviour towards fungi, some of the complexes exhibit higher antibacterial activities than their corresponding ligands. For a clear understanding, however, of the differentiation in function towards microorganisms, additional systematic studies will be necessary.

Table 5. Antibacterial activities of ligands and their metal complexes[a]

	Salmonella typhi	*Shigella dysenteriae*	*Escherichia coli*	*Bacillus cerelus*
L_{BY}	0	0	0	0
L_{AY}	0	0	0	0
$[CuL_{BY}][ClO_4]_2$	8	7	0	0
$[CuL_{AY}][ClO_4]_2$	12	14	3	0
$[NiL_{AY}][ClO_4]_2$	6	11	10	21

[a] Diameter of zone of inhibition in mm after 24 hours (see Exp. Sect. for details).

Conclusion

Two new tetraaza macrocyclic ligands belonging to the Me_8[14]ane family, and carrying pendent 2-hydroxyethyl substituents (Y) on two of the nitrogen functions, have been obtained by reacting the basic tetraaza ligands L_B and L_C with ethylene oxide. In the case of diaxial-diequatorial (with respect to the four methyl groups attached to chiral carbons) L_B as the starting product, the diaxial-diequatorial ligand L_{BY} is formed. When the reaction is carried out with axial-triequatorial L_C, a configurational change to all-equatorial L_{AY} was observed. With Ni^{II}, L_{BY} yields a square-planar complex $[Ni(L_{BY})]^{2+}$, where the hydroxyethyl functions are coordinatively inert towards Ni^{II}. With Cu^{II}, however, the octahedral complexes $[Cu(L)]^{2+}$ (L = L_{BY} and L_{AY}) are formed, in which the OH functions weakly coordinate in the axial positions [Cu−O = 2.432(3) Å]. The counterion in the Ni and Cu complexes is ClO_4^-; the ionic nature has been confirmed by conductivity measurements in acetonitrile. In water, $[Cu(L)]^{2+}$ converts to $[Cu(L)(H_2O)_2]^{2+}$, whereas in chloroform the axial positions are occupied by perchlorate — the neutral complex $[Cu(L)(ClO_4)_2]$ is formed. Contrasting the ligands, the complexes show some anti-bacterial activity, while the anti-fungal activity of the complexes is generally lower than that of the ligands.

Experimental Section

Materials and Equipment: All chemicals were of analytical reagent grade and used without further purification. Synthesis of the parent ligand 3,10-*C*-*meso*-Me_8[14]diene dihydroperchlorate, reduction of this diene with $NaBH_4$ and separation into the three isomers of Me_8[14]ane (L_A, L_B and L_C) was carried out according to literature procedures.[4,17]

Caution*: *Perchlorates can be explosive in the presence of organic materials.

Microanalyses (C,H,N) were carried out by the combustion method at the Analytical Section of the Chemistry Department, University of Hamburg. For nickel and copper, standard titrimetric methods have been employed.

Infrared spectra were taken as KBr pellets in the range 4000−400 cm^{-1} on a Perkin−Elmer 883 infrared spectrophotometer. Electronic absorption spectra were recorded on a Schimadzu UV/Visible spectrophotometer. The mass spectral measurement of the li-

 © 2004 Wiley-VCH Verlag GmbH & Co. KGaA, Weinheim

gands was carried out with the help of a Varian MAT 311A (70 eV, EI) instrument. ^{1}H and ^{13}C NMR spectra were recorded on a 200 MHz Varian Gemini instrument. Conductance measurements of the metal complexes were done in water, acetonitrile and chloroform solutions, using a HANNA instrument equipped with a HI 8820N conductivity cell. Magnetic measurements were carried out at room temperature with a Gouy balance, calibrated against $Hg[Co(NCS)_4]$; susceptibilities were corrected for diamagnetic increments.

Ligand Syntheses: Ligands were synthesised by modified literature procedures for analogous, N-pendent ligands.[8]

***trans*-4,11-Bis(2-hydroxyethyl)-3,5,7,7,10,12,14,14-octamethyl-1,4,8,11-tetraazacyclotetradecane (L_{BY}):** L_B (0.312 g, 1.0 mmol) was suspended in 25 mL of distilled water and the temperature was maintained at 16 ± 2 °C. The mixture was stirred while a gentle stream of ethylene oxide was passed through the suspension for 5 h. The reaction mixture became milky and then oily. Undissolved compounds were removed by filtration and the clear filtrate was extracted with 200 mL (four 50 mL portions) of chloroform. On evaporation of the chloroform extract, a sticky material was obtained, which was washed three times with 2 mL portions of methanol to give L_{BY} as a crude, white solid. This was re-crystallised from 10 mL of a 1:2 chloroform/methanol mixture and dried in vacuo over silica gel to yield pure L_{BY}. Melting point: 175 °C. Yield 0.202 g (50%). $C_{22}H_{48}N_4O_2$ (400.65): calcd. C 65.95, H 12.08, N 13.98; found C 65.86, H 11.95, N 13.88.

***trans*-4,11-Bis(2-hydroxyethyl)-3,5,7,7,10,12,14,14-octamethyl-1,4,8,11-tetraazacyclotetradecane (L_{AY}):** L_{AY} was prepared analogously to L_{BY} from L_C (0.312 g, 1.0 mmol) and ethylene oxide at a temperature of 10 ± 2 °C. Evaporation of the chloroform left behind a pasty substance, which was dissolved in 10 mL of methanol and filtered. The filtrate, on evaporation, yielded white, solid L_{AY}, which was re-crystallised three times from 10 mL portions of diethyl ether and dried under vacuum over silica gel. Melting point: 160 °C. Yield 0.22 g (50%). $C_{22}H_{48}N_4O_2$ (400.65): calcd. C 65.95, H 12.08, N 13.98; found C 65.79, H 11.91, N 14.06.

$[NiL_{BY}][ClO_4]_2$: L_{BY} (0.400 g, 1.0 mmol) and nickel(II) acetate (0.256 g, 1.05 mmol) tetrahydrate were dissolved separately in 50 mL of cold, dry methanol. The ligand solution was added dropwise to the boiling nickel(II) acetate solution with stirring. The reaction mixture was heated on a steam bath for one hour, and the volume reduced to 20 mL. An orange colour developed. After adding 0.5 g of lithium perchlorate trihydrate, the solution was heated for another 10 min and allowed to stand for about 2 h. The yellow product $[NiL_{BY}][ClO_4]_2$ was filtered off, washed with methanol and diethyl ether, and dried in vacuo. Yield 0.165 g (25%). $C_{22}H_{48}Cl_2N_4NiO_{10}$ (658.24): calcd. C 40.14, H 7.35, N 8.51, Ni 8.92; found C 39.88, H 7.30, N 8.48, Ni 8.88.

$[CuL_{BY}][ClO_4]_2$: L_{BY} (0.40 g, 1.0 mmol) and copper(II)perchlorate hexahydrate (0.371 g, 1.0 mmol) were dissolved separately in 25 mL of dry, hot methanol and mixed while hot. A pink colour appeared. The volume was reduced to 20 mL by heating the mixture on a water bath. On cooling, pink $[CuL_{BY}][ClO_4]_2$ crystallised out, which was separated by filtration, washed with methanol and re-crystallised from 10 mL of acetonitrile/methanol (1:2). The product was dried in a vacuum desiccator over silica gel. Yield 0.221 g (33%). $C_{22}H_{48}Cl_2CuN_4O_{10}$ (663.09): calcd. C 39.85, H 7.30, N 8.45, Cu 9.58; found C 39.80, H 7.32, N 8.36, Cu 9.49.

$[CuL_{AY}][ClO_4]_2$: L_{AY} (0.40 g, 1.0 mmol) and copper(II)perchlorate hexahydrate (0.371 g, 1.0 mmol) were dissolved separately in 20 mL of dry, hot methanol. The solutions were mixed while hot. The deep-blue reaction mixture was heated on a water bath to reduce the volume to 10 mL. On cooling, a blue solid precipitated out, which was separated by filtration and re-crystallised from 10 mL of acetonitrile/methanol (1:1), and dried in vacuo over silica gel. Yield 0.331 g (50%). $C_{22}H_{48}Cl_2CuN_4O_{10}$ (663.09): calcd. C 39.85, H 7.30, N 8.45, Cu 9.58; found C 39.79, H 7.24, N 8.43, Cu 9.48.

Table 6. Structure and refinement data for L_{BY} and $[Cu(L_{AY})][ClO_4]_2$

	L_{BY}	$[Cu(L_{AY})][ClO_4]_2$
Empirical formula	$C_{22}H_{48}N_4O_2$	$C_{22}H_{48}Cl_2CuN_4O_{10}$
Molecular mass (g·mol^{-1})	400.64	663.08
Temperature (K)	153(2)	293(2)
Crystal system	monoclinic	orthorhombic
Space group	$P2_1/c$	*Pbca*
a (Å)	18.9914(9)	12.0059(10)
b (Å)	12.2427(6)	14.2108(12)
c (Å)	10.2633(5)	17.4931(14)
β (°)	96.3670(10)	
Cell volume (Å^3)	2371.6(2)	2984.6(4)
Z	4	4
Calculated density (g·cm^{-3})	1.122	1.476
Absorption coefficient (mm^{-1})	0.072	0.968
F(000)	896	1404
Crystal size (mm)	0.9 × 0.7 × 0.2	0.3 × 0.3 × 0.2
θ range for data collection (°)	1.08 to 25.00	2.33 to 25.06
Index ranges	$-22 \le h \le 22$, $-14 \le k \le 14$, $-12 \le l \le 12$	$-14 \le h \le 14$, $-16 \le k \le 16$, $-20 \le l \le 20$
Reflections collected	43378	23697
Independent reflections	4171 [*R*(int) = 0.0536]	3422 [*R*(int) = 0.0423]
Completeness to theta = 32.56°	99.9%	99.7%
Goodness-of-fit on F^2	1.082	1.040
Final R_{int} [$I > 2\sigma(I_0)$]	*R*1 = 0.0494, *wR*2 = 0.1277	*R*1 = 0.0693, *wR*2 = 0.1988
R_{int} (all data)	*R*1 = 0.0540, *wR*2 = 0.1316	*R*1 = 0.0929, *wR*2 = 0.2142
Largest diff. peak and hole (e·Å^{-3})	0.391 and −0.536	0.622 and −1.769

 © 2004 Wiley-VCH Verlag GmbH & Co. KGaA, Weinheim

Crystals of $[CuL_{AY}][ClO_4]_2$ suitable for the X-ray diffraction study were prepared by slow evaporation of acetonitrile-methanol solution of the complex.

X-ray Crystallographic Determination: X-ray structure analyses were performed with Mo-K_α irradiation (λ = 0.71073 Å, graphite monochromator), on a Smart Apex CCD diffractometer. The hydrogen atoms of the hydroxy groups of L_{BY} and $[Cu(L_{AY})][ClO_4]_2$ and the NH groups of $[Cu(L_{AY})][ClO_4]_2$ were found; other H atoms were calculated at their idealized positions and included in the last cycles of refinement. Absorption corrections were carried out automatically by Mult Scan. Crystal data and details of the data collection and refinement are collated in Table 6.
CCDC-235762 (for L_{BY}) and -235880 (for $[Cu(L_{AY})][ClO_4]_2$) contain the supplementary crystallographic data of this paper. These data can be obtained free of charge at www.ccdc.cam.ac.uk/conts/retrieving/html or from the Cambridge Crystallographic Data Centre, 12 Union Road, Cambridge CB2 1EZ, UK (Fax: +44-1223-336-033; E-mail: deposit@ccdc.cam.ac.uk).

Antimicrobial Activity: The in vitro antifungal activities of the compounds against selected phytopathogenic fungi were assessed by the poisoned food technique. Potato Dextros Agar (PDA) was used as a growth medium. DMF was used as the solvent to prepare solutions of the compounds. The solutions were then mixed with the sterilized PDA so as to maintain concentrations of the compounds of 0.01%. 20 mL portions of this mixture were poured into petri dishes. After the medium had solidified, a 5 mm mycelial disc of the fungus was placed in the centre of each assay plate, including a control. Linear growth of the fungus (in mm) was noted after five days of incubation at 25 ± 2 °C.
The antibacterial activities of the test materials were measured by the disc diffusion method. Paper discs of 6 mm diameter, and petri dishes (70 mm in diameter) were used throughout. Pour plates were prepared from sterilized molten NA (Nutrient Agar) at 45 °C. After solidification of the pour plates, suspensions of the test organisms were spread uniformly over the pour plate with a sterilised glass rod. After soaking the paper discs with the test chemicals (1% in $CHCl_3$ solutions), they were placed in the centre of the inoculated pour plate. A control plate was maintained in each case with $CHCl_3$. The plates were kept for 4 h at low temperature (4 °C) in order to allow the test chemicals to diffuse from the paper disc to the surrounding medium. The plates were then incubated at 35 ± 2 °C for growth of the test organisms, and checked at 24-hour intervals. The antibacterial activity was expressed in terms of the diameter (in mm) of the zone of inhibition. Each experiment was repeated three times.

Acknowledgments

The authors thank the University Grants Commission of Bangladesh for a fellowship to H. A. M. and the Ministry of Science and Technology, Government of People's Republic of Bangladesh, for a grant to T. G. R. and for providing a fellowship to H. A. M., and the German Academic Exchange Service (DAAD) for granting a stipend to T. G. R. Further, we wish to thank Prof. Dr. N. Anwar, Department of Microbiology, University of Chittagong, for his support of the antifungal and antibacterial studies.

[1] D. G. Pillsbury, D. H. Bush, *J. Am. Chem. Soc.* **1976**, *98*, 7836.
[2] W. P. Schammel, K. S. B. Mertes, G. G. Christoph, D. H. Bush, *J. Am. Chem. Soc.* **1979**, *101*, 1622.
[3] [3a] R. W. Hay, R. Bembi, *Inorg. Chim. Acta* **1982**, *65*, L227. [3b] C. M. Madeyski, J. P. Micheal, R. D. Hancock, *Inorg. Chem.* **1984**, *23*, 1487. [3c] K. P. Wainwright, *J. Chem. Soc., Dalton Trans.* **1983**, 1149. [3d] P. Clarke, S. F. Lincoln, K. P. Wainwright, *Inorg. Chem.* **1991**, *30*, 134.
[4] T. G. Roy, R. Bembi, *J. Bangladesh Chem. Soc.* **2002**, *15*, 23; *Chem. Abstr.* **2003**, *139*, 230266.
[5] R. Bembi, S. M. Sondhi, A. K. Singh, R. Singh, T. G. Roy, A. K. Jhanji, J. W. Lown, R. G. Ball, *Bull. Chem. Soc. Jpn.* **1989**, *62*, 3701.
[6] T. G. Roy, S. K. S. Hazari, B. K. Dey, H. A. Miah, E. R. T. Tiekink, *Acta Crystallogr.* **2001**, *E57*, 524.
[7] H. A. Miah, PhD Thesis, Department of Chemistry, Chittagong University, Bangladesh, **2003**.
[8] R. W. Hay, D. M. S. Clark, *Inorg. Chim. Acta* **1984**, *83*, L23.
[9] R. M. Silverstein, *Mass Spectrometry*, John Wiley & Sons, New York, **1967**, 2nd ed., pp. 4−63.
[10] H. Budzikiewicz, C. Dierassi, D. H. Williams, *Interpretation of Mass Spectra of Organic Compounds*, Holden-Day Inc., San Francisco, **1964**, pp. 63−110.
[11] T. G. Roy, R. Bembi, S. K. S. Hazari, B. K. Dey, T. K. Acharjee, E. Horn, E. R. T. Tiekink, *J. Coord. Chem.* **2002**, *55*, 853.
[12] R. Bembi, M. G. B. Drew, R. Singh, T. G. Roy, *Inorg. Chem.* **1991**, *30*, 1403.
[13] S. K. S. Hazari, T. G. Roy, B. K. Dey, S. C. Das, E. R. T. Tiekink, *Metal-Based Drugs* **1997**, *4*, 255.
[14] R. Bembi, R. Singh, T. G. Roy, A. K. Jhanji, *J. Coord. Chem.* **1985**, *14*, 119.
[15] T. G. Roy, S. K. S. Hazari, B. K. Dey, S. Chakraborty, E. R. T. Tiekink, *Metal-Based Drugs* **1997**, *6*, 345.
[16] T. K. Acharjee, M. Sc. Thesis, Department of Chemistry, Chittagong University, **2000**.
[17] N. F. Curtis, D. A. Swann, T. N. Waters, I. E. Maxwell, *J. Am. Chem. Soc.* **1969**, *91*, 4588.

Received April 13, 2004
Early View Article
Published Online August 12, 2004

 © 2004 Wiley-VCH Verlag GmbH & Co. KGaA, Weinheim

Boranophosphate Salts as an Excellent Mimic of Phosphate Salts: Preparation, Characterization, and Properties

Victoria Nahum[a] and Bilha Fischer*[a]

Keywords: Bioisosters / Boranophosphates / NMR spectroscopy / Phosphate mimics

We report on the preparation of boranophosphate salts, BPi (**2**), and the exploration of their properties with a view to developing a new mimic of the parent phosphate. BPi salts were easily prepared in excellent yield in a one-pot two-step reaction from tris(trimethylsilyl) phosphite, and were characterized by X-ray crystallography and IR, ^{1}H and ^{31}P NMR spectroscopy. We evaluated the acid/base character of BPi by determining its acidity constants. Likewise, we evaluated the stability of BPi at various pH values, and calculated the decomposition-rate constants at highly acidic pH. We also monitored the H-bonded clustering of BPi in organic solvents, including MeOH. Finally, we explored the chemical behavior of BPi with respect to various organic and inorganic reagents. BPi is stable under the following conditions: both basic and acidic pH (pH $>$ 2), in the presence of amines, and in the presence of Mg^{2+} ions. However, a P–B bond cleavage is observed upon the reaction of BPi with carbodiimides or upon catalytic hydrogenation. The reducing nature of the BH_3 moiety is drastically decreased in BPi. Likewise, the nucleophilicity of BPi's oxygen atom is lower than in phosphate, Pi, salts. Based on its water solubility, acid-base character, and H-bonding properties, BPi appears as a perfect mimic of Pi and is an attractive alternative to the known phosphate isosters.
(© Wiley-VCH Verlag GmbH & Co. KGaA, 69451 Weinheim, Germany, 2004)

Introduction

Phosphates and phosphate-containing molecules play a major role in numerous biological systems.[1] However, the unwanted lability of the ester P−O bond has promoted the search for suitable bioisosters — phosphate analogues — which retain the biological activity but possess diminished lability. The search for bioisosters was initiated by the need to produce phosphate probes for various studies, such as probing the stereochemical requirements of enzymes.[2] In addition, phosphate bioisosters have been developed for improving the pharmacological effects of nucleotide-based drugs, for example anti-sense agents.[3]

A widely used isoster of phosphate is phosphorothioate and its analogues, proposed in the pioneering work of Eckstein et al.[4] In these analogues, the nonbridging oxygen atom is replaced by a sulfur atom. Other chemical modifications of the phosphate moiety include the substitution of the labile phosphate ester oxygen atom by a carbon or nitrogen atom, to give phosphonates and phosphoramidate analogues, respectively.[5]

During the last decade, pioneering studies by Spielvogel and Ramsay-Shaw have proposed boranophosphate anaclogues **1** as bioisosters of natural nucleotides[6] and as important tools for biochemists.[7]

This emerging field of novel nucleotide bioisosters has expanded significantly and has provided many important applications of the boranophosphate analogues. For instance, nonterminal *P*-boronated nucleotides, existing as a pair of diastereoisomers, have been used as stereochemical probes to elucidate enzymatic catalysis.[8] Oligodeoxyribonucleotides bearing boranophosphate linkages have been used for polymerase chain reaction (PCR) sequencing and DNA diagnostics,[9] and boranophosphate nucleotides have been found to be highly potent and stable P2Y-receptor agonists.[10] Oligonucleotides bearing boranophosphate linkages have also been considered as potentially useful anti-sense agents.[11] These analogues were also tested for the treatment of cancer as carriers of ^{10}B isotope in boron neutron-capture therapy.[12]

As mentioned above, the field of boranophosphates covers, in-depth, related nucleotide/oligonucleotide analogues. However, to the best of our knowledge, no attention has been given to the unique and chemically interesting inorganic boranophosphate **2** (BPi). Although the related dimethyl boranophosphate potassium salt **3** has been described by Imamoto et al.[13] and by Wada and Saigo,[14] the preparation of inorganic boranophosphate **2** has not been reported.

We present here the preparation, characterization, and unique chemical properties of inorganic boranophosphate. In addition, we demonstrate that BPi is an excellent mimic of phosphate.

[a] Department of Chemistry, Gonda-Goldschmied Medical Research Center, Bar-Ilan University,
Ramat-Gan 52900, Israel
Fax: (internat.) + 972-3-535-1250
E-mail: bfischer@mail.biu.ac.il

 © 2004 Wiley-VCH Verlag GmbH & Co. KGaA, Weinheim **DOI: 10.1002/ejic.200400142**

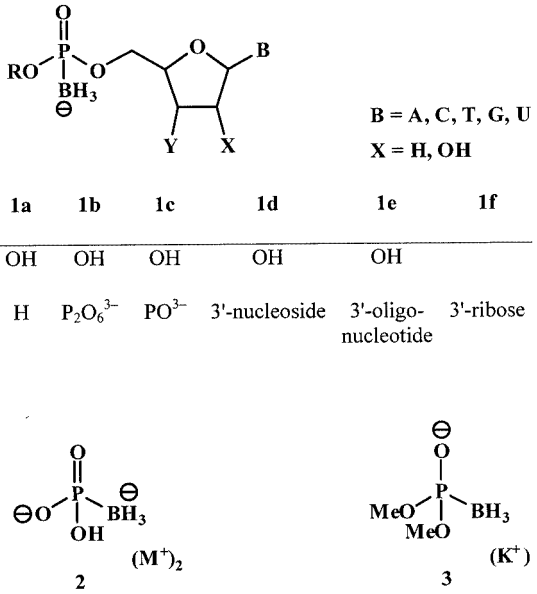

Results and Discussion

Synthesis

For the preparation of boranophosphate, we first attempted the treatment of chlorobis(diisopropylamino)phosphane (**4**) with BH_3·SMe_2 complex,[15] followed by acidic hydrolysis (pH = 3 or 1; Scheme 1A). This attempt resulted in a mixture of several phosphorus species. Alternatively, dibenzyl H-phosphonate **6** was treated with bis(silyl)acetamide, followed by boranation of intermediate **7** with BH_3·SMe_2, and hydrolysis of **8** with concentrated ammonium hydroxide. In this way, dibenzyl boranophosphate **9** was obtained in 71% overall yield (Scheme 1B). However, attempts to remove the benzyl groups by either catalytic hydrogenation or acidic hydrolysis (pH = 1.3) resulted in the cleavage of the P−B bond, leading to phosphorus acid instead of BPi.

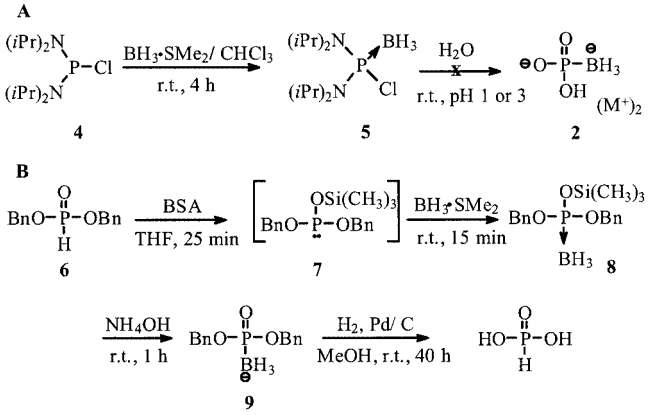

Scheme 1

Eventually, we were able to obtain BPi in an excellent overall yield in a two-step, one-pot reaction starting from tris(trimethylsilyl) phosphite[16] (**10**; Scheme 2). Phosphite **10** was treated with BH_3·SMe_2 in dry acetonitrile under an inert gas for 15 min. Subsequently, intermediate **11** was treated with 2 M methanolic ammonia for 1 h to give the BPi **2a** as a white solid in 93% yield. No further purification was conducted, since volatile silyl derivatives and the unreacted BH_3·SMe_2 were removed by evaporation. Alternatively, intermediate **11** was treated with $NH_4OH_{(aq)}$ solution (pH = 10), Bu_3N in MeOH, or 0.5 M triethylammonium hydrogencarbonate buffer (pH = 7.5) and freeze-dried or concentrated to provide **2a**, **2b**, or **2c**, respectively.

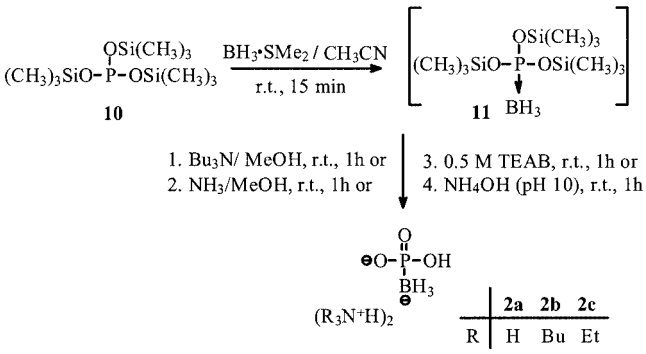

Scheme 2

Product **2a** is highly water-soluble, whereas **2b** dissolves only in organic solvents such as MeOH, CH_3CN, DMF, and $CHCl_3$. Product **2c** is highly soluble both in water and in organic solvents.

Characterization

NMR Spectroscopy

Compound **2a** in water was characterized by ^{31}P NMR spectroscopy. It shows a signal at $\delta \approx 80$ ppm (Figure 1). The boranophosphate ^{31}P NMR spectrum shows a typical pattern including two overlapping signals: the larger signal is due to coupling of P to the ^{11}B isotope, and the smaller signal is due to coupling with the ^{10}B isotope. The relative height of the smaller peak to the larger one is 0.14 (Figure 1A).[17] BPi's hydrogen-coupled ^{31}P NMR spectrum shows further splitting of the lines into a quadruplet (Figure 1B). The ^1H NMR spectrum shows a typical doublet of quadruples pattern, at $\delta \approx 0.2$ ppm, due to coupling of H to both ^{11}B and ^{31}P (Figure 1C). This pattern overlaps a more complex pattern due to coupling of H to both ^{10}B and ^{31}P.

The chemical shift of BPi is pH-dependent. For instance, at pH = 4.87 and 13.20, the phosphorus atom of BPi resonates at δ = 84 and 63 ppm, respectively. Likewise, the P−B coupling constant is also pH-dependent, and is reduced as the pH decreases (e.g. 147 and 183 Hz for pH = 4.87 and 13.2, respectively). The pH-dependent BPi spectrum indicates structural changes of BPi, which are due to

 © 2004 Wiley-VCH Verlag GmbH & Co. KGaA, Weinheim

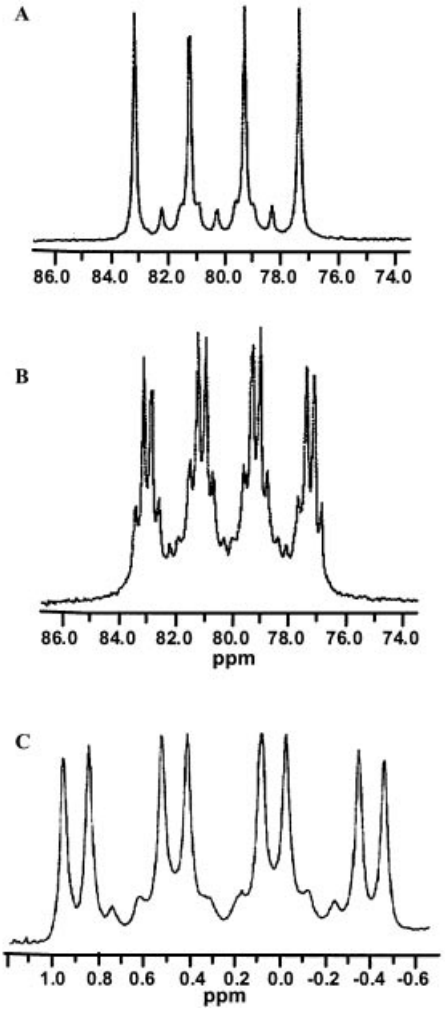

Figure 1. NMR spectra of BPi: A) ^{1}H-decoupled ^{31}P NMR spectrum in D_2O at 81 MHz; B) ^{1}H-coupled ^{31}P NMR spectrum in D_2O at 81 MHz; C) ^{1}H NMR spectrum in D_2O at 200 MHz

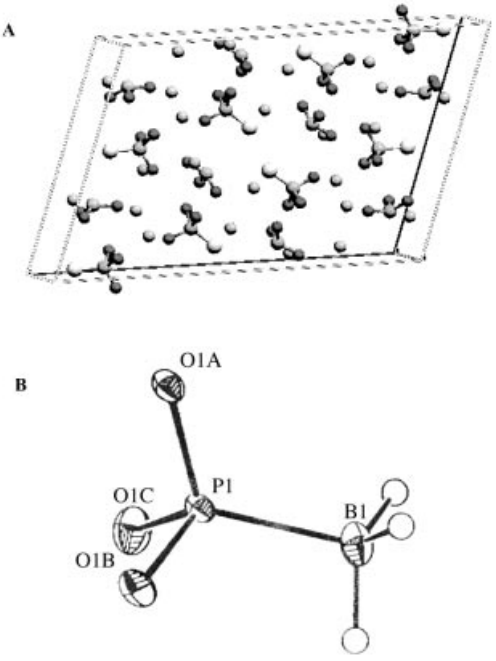

Figure 2. X-ray crystal structure of BPi: A) unit cell includes eight BPi molecules, eight H-phosphonate molecules, and 24 ammonium ions; hydrogen atoms are omitted to clarify the BPi geometry; B) ORTEP drawing of BPi; crystal data of **2a**: monoclinic, $P2_1/c$; a = 23.616(5) Å, b = 6.3470(13) Å, c = 15.325(3) Å; V = 2172.9(8) Å^3; Z = 12; $D_{calcd.}$ = 1.623 g/cm^3; $F(000)$ = 1104; 3094 reflections collected, R = 0.1015, Rw = 0.2345, GOF = 1.286; selected bond lengths [Å] and angles [°]: P(1)−O(1A) 1.524(7), P(1)−O(1B) 1.617(7), P(1)−O(1C) 1.583(7), P(1)−B(1) 1.891(11); O(1A)−P(1)−O(1C) 104.0(4), O(1A)−P(1)−O(1B) 105.3(4), O(1C)−P(1)−O(1B) 104.4(4), O(1A)−P(1)−B(1) 118.2(5), O(1C)−P(1)−B(1) 113.0(5), O(1B)−P(1)−B(1) 110.7(5)

the reduction of O−P−O angles upon protonation of the molecule.

X-ray Crystallography

To obtain structural information on BPi, compound **2a** was crystallized from an aqueous solution (pH = 7). In addition to compound **2a**, the crystal contained phosphorus acid (H-phosphonate) in a 1:1 ratio. This unexpected ratio does not reflect the molar ratio in the original BPi solution, in which phosphorus acid was less than 5%.

The unit cell contains eight BPi ions, eight H-phosphonate ions, and 24 ammonium ions (Figure 2A). Apparently, for each BPi anion, one ammonium counterion is observed, whereas two ammonium counterions are observed around each H-phosphonate group.

For BPi, the average P−B bond length is 1.892 Å, whereas for the three P−O bonds, the average lengths are 1.585, 1.605 Å, and 1.524 Å, respectively (Figure 2B). A deviation from tetrahedral angles was observed with values of 111−118° for B−P−O, and 104−105° for the O−P−O angles.

Comparison with X-ray crystal data obtained for the related dimethyl boranophosphate salt (**3**)[13] indicated similar values for the B−P (1.895 Å) and O−P (1.490, 1.597 and 1.612 Å) bond lengths. For dimethyl boranophosphate, one potassium ion was found near one of the oxygen atoms at a distance of 2.66 Å. Based on a comparison of the bond lengths of dimethyl boranophosphate salt with BPi, we assume that the BPi bears two H atoms, which were not found in the crystallographic data.

The shortest P−O bond (1.524 Å) indicates a partial double-bond character, and is in accordance with values found in the structures of phosphate diesters (1.47−1.51 Å) and monoesters (1.49−1.53 Å). This P−O bond is significantly longer than the bond observed in phosphate triesters (1.38−1.44 Å).[18]

IR Spectroscopy

The IR spectra of **2a** or **2b** in KBr pellet indicated characteristic bands for P−B and B−H in addition to bands associated with P−OH and P=O. Specifically, three absorptions at 2350, 2381, 2407 cm^{-1} (s) correspond to B−H stretches, and the absorption at 654 cm^{-1} (m) is the

 © 2004 Wiley-VCH Verlag GmbH & Co. KGaA, Weinheim

P−B stretch.[19] Typical absorptions were observed for P−OH and P=O stretches at 900−1080 cm^{-1} and at 1140−1250 cm^{-1}, respectively.

For an evaluation of the effects of the solvents on the H-bonds between BPi ions, IR spectra of BPi **2a** in aqueous and methanolic solutions (see below "H-bonding of BPi") were measured in a germanium cell and compared to the corresponding spectrum of a neat sample of BPi (Figure 3B). Comparison of those spectra indicated only minor differences. For instance, a shift of about 10 cm^{-1} to lower frequencies was observed for the P=O stretch of BPi, either in the neat sample or in MeOH, relative to BPi in aqueous solution. This shift is probably due to H-bonding-based clustering in the neat sample and MeOH. The typical fine-structure for the P=O stretch in a neat sample of BPi, in the range of 1144−1178 cm^{-1}, which is possibly also due to H-bonded clusters, is lost in water. The corresponding spectrum in MeOH appears as an average of the neat sample and aqueous solution spectra, probably indicating the presence of both BPi clusters and solvent H-bonded species.

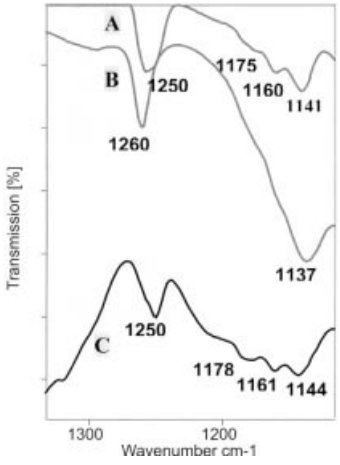

Figure 3. IR spectra of BPi **2c** (germanium cell; 1300−1100 cm^{-1}; cutoff: 680 cm^{-1}): A) methanolic solution; B) aqueous solution; C) neat sample

Chemical Properties

Acid/Base Properties

The acid/base character of BPi was studied by ^{31}P NMR-monitored pH-titration. The chemical shift of compound **2a** was plotted against the pH (Figure 4). For the pH range 4.8−13.2, two inflection points were observed. The second derivatives of the fitted function provided two pK_a values — 7.12 and 12.54 — with R^2 values of 0.999 and 0.997, respectively. These values are similar to the corresponding values of the second and third protonation equilibria of phosphoric acid (7.21 and 12.67), and they are higher than those for phosphorus acid (1.8 and 6.2).

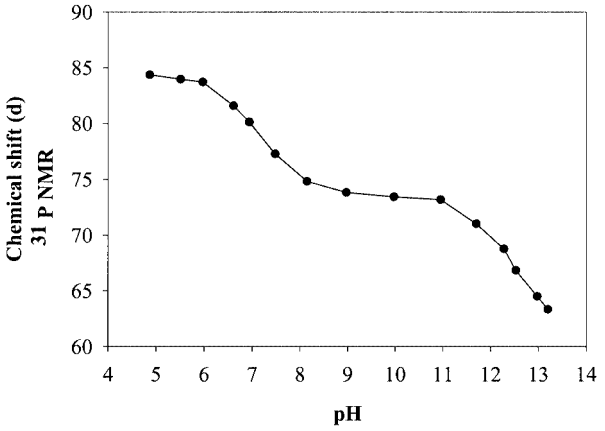

Figure 4. Determination of pK_a values of BPi; plot of BPi's ^{31}P NMR chemical shift in H_2O as a function of the pH; two inflection points are observed in the pH range 4.87−13.20

Stability of BPi

BPi is stable in neutral and basic solutions. For instance, after 48 h at room temperature at pH = 13.7, no degradation of BPi was observed by ^{31}P NMR spectroscopy. BPi is also relatively stable in acidic solution at pH values > 2. At pH = 2, BPi slowly degrades to phosphorus acid at a rate of 7×10^{-7} s^{-1}, $R^2 = 1.00$ ($t_{1/2}$ = 275 h), as monitored by ^{31}P NMR spectroscopy.

Under highly acidic conditions (pH < 2), the evolution of H_2 is clearly observed, the P−B bond is cleaved, and boric acid is formed together with phosphorus acid (Scheme 3).[20] Phosphorus acid was observed in the ^{31}P NMR spectrum as a doublet at δ = 3.5 ppm (J = 633 Hz). The borane reacts with water to liberate hydrogen gas and boric acid.

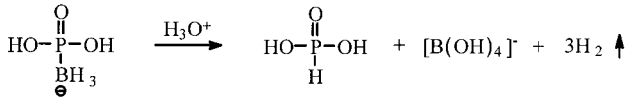

Scheme 3

The stability of inorganic boranophosphate, resulting from neutral hydrolysis of thymidine 5′-boranomonophosphate at 50 °C, has been reported earlier.[20]

H-Bonding of BPi

Solutions of **2b** or **2c** in organic solvents ($CHCl_3$, CH_3CN, DMF, and even MeOH), show unexpected ^{31}P NMR spectra. Product **2b** in MeOH apparently consists of three different but pattern-related signals. The signals with chemical shifts of δ = 80.0 (A), 86.2 (B), and 90.8 (C) ppm, each have an identical BPi-typical pattern (Figure 5).

Several minutes after the dissolution of **2b** in MeOH, signals A, B, and C are observed in the ^{31}P NMR spectrum, with A and B as the major peaks (C constitutes ca. 5% of the mixture). The composition of the initial mixture is time-dependent due to the interconversion of the species. When monitoring this process with 0.14 M **2b** in CD_3OD (ε = 33)

 © 2004 Wiley-VCH Verlag GmbH & Co. KGaA, Weinheim

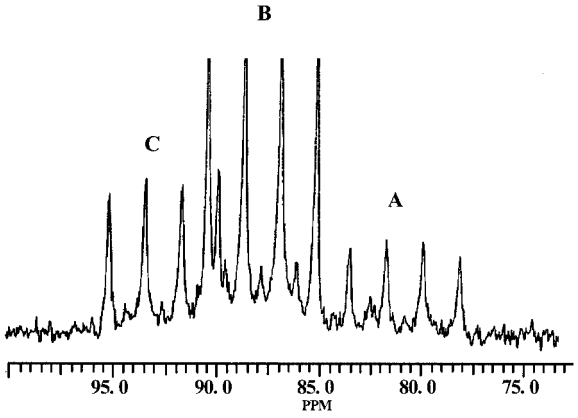

Figure 5. ^{31}P NMR spectrum of BPi **2b** in methanolic solution

at room temperature for 160 h, we noted the conversion of A and B to C, with a final C/B ratio of 4.4:1 (A disappeared completely). The ^{1}H-coupled ^{31}P NMR spectrum indicated H-split quadruplet signals for B and C — no D/H exchange occurred.

A spectrum similar to the one shown in Figure 5, and time-dependent interconversion of the species, was also observed for **2b** in DMF, CH_3CN, and $CHCl_3$.

The possibility that the additional BPi-like species are the corresponding mono- or dimethyl esters, due to a reaction of **2b** with MeOH, was ruled out because their ^{13}C and ^{1}H NMR spectra in $CDCl_3$ are devoid of a methyl ester signal.

The three signals seen in the ^{31}P NMR spectrum of **2c** in organic solvents converged into one, probably A (δ = 79.8 ppm) after solvent evaporation and dissolution in D_2O. The possibility that signals B and C are due to boranophosphate anhydrides, resulting from **2c** in the NMR sample, is unlikely as the formation of the related phosphoric acid anhydrides requires drastic conditions (up to 250 °C at very low pH, or the presence of a condensation agent).[21] Obviously, these conditions do not exist in the NMR samples of BPi.

The possibility of B and C being anhydrides formed during the preparation of BPi, was also ruled out as the ^{31}P NMR spectrum of **2c**, which exhibits several signals in organic solvents, shows only one signal when measured in water. In contrast, the hydrolysis of condensed phosphates is known to be quite slow (i.e. several weeks at 60 °C, pH = 5).[22]

Phosphoric acid and its derivatives form strongly H-bonded clusters including cyclic dimers, trimers, and chains.[23,24] Dimerization occurs in the solid state,[25] in highly concentrated phosphoric acid,[24,26] in freons,[23b] or in aprotic organic solvents.[27,28] Therefore, it is likely that the new BPi-like signals are indicative of clustering of BPi in organic solvents, and even in a highly polar and H-bonding solvent such as MeOH. These clusters are not large (< 30 Å) based on light-scattering measurements.

To assess the possibility of observing different H-bond-clustered species on the NMR timescale, we measured the ^{31}P NMR spectrum of the parent phosphate bis(tributylammonium) salt in benzene, where clustering is known to occur.[28] Indeed, three signals were clearly observed at δ = 3.63, 3.23, and 2.93 ppm, demonstrating that different H-bonded phosphate clusters can be detected by ^{31}P NMR spectroscopy. These three phosphate signals, seen in benzene, converged into one in acetonitrile and MeOH, indicating the collapse of the Pi clusters in polar/protic solvents.

Based on our observations of the pH-dependent chemical shift of BPi, and on the determination of BPi's acidity constants (Figure 4), we propose the following assignment of signals A, B, and C. Signal A corresponds to the monomeric BPi, whose chemical shift at $\delta \approx 80$ ppm indicates that half the BPi monomer population bears two protons, and the other half bears one proton (Figure 4). Signal B, at δ = 86 ppm, corresponds to a BPi moiety that has one BPi H-bonded neighbor. Namely, signal B could result both from BPi dimers and higher clusters (Scheme 4). In these cases, each BPi is associated with an additional proton (Bu_3NH^+ ions neutralize the negative charges). Therefore, the chemical shift of the BPi dimer shifts downfield (δ = 86 ppm, as at pH = 4.7). As indicated by signal C, BPi also forms clusters, corresponding to a BPi moiety that has two H-bonded BPi neighbors (Scheme 4). A BPi moiety in the middle of a cluster is associated with three protons, resulting in an additional downfield shift to δ = 91 ppm, corresponding to that of BPi at pH = 2.

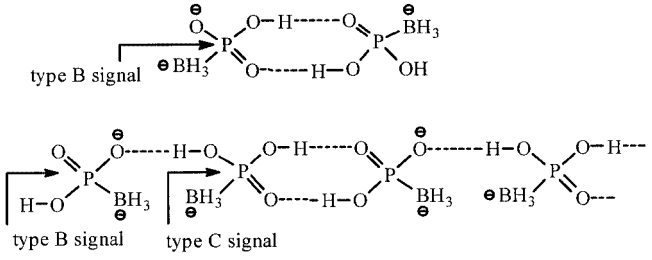

Scheme 4

Small H-bonded clusters (i.e. dimers and trimers) are formed almost instantaneously. This is probably the stage of nucleation. Once a critical nucleus is formed, a slow process of high-order clustering occurs. At this stage the concentration of A in solution is drastically reduced. This H-bonding-based clustering mechanism is also supported by the observation that, upon evaporation of the organic solvent from the species mixture and dissolution in water, only A is detected.

The fact that BPi forms clusters even in MeOH, whereas Pi forms clusters only in benzene, implies that BH_3 may play a role in the pre-organization of the BPi clusters. The lipophilic BH_3 moieties possibly form the core of the cluster due to hydrophobic interactions (in MeOH). This core is then further stabilized by P−O$^-$···HO−P hydrogen bonds.

Reactions of BPi with Selected Reagents

The reactivity of BPi towards various organic and inorganic reagents was explored as part of the characterization

 © 2004 Wiley-VCH Verlag GmbH & Co. KGaA, Weinheim

of the chemical nature of BPi. These reagents include aqueous acid solution, nitrile, amide, carbodiimide, pyridine and imidazole, tosyl chloride, phosphorus oxychloride, H_2, and Zn^{2+} and Mg^{2+} ions.

Although BH_3, in complexes with a variety of sulfur/amine/oxygen compounds, is an efficient reducing agent, its reducing nature is drastically altered in BPi. For instance, while hydride transfer from "BH_3" to water occurs readily, the BH_3 moiety in BPi transfers hydride only in a highly acidic solution (pH $<$ 2). Likewise, while BH_3·THF complex readily reduces nitriles and amides to the corresponding amines,[29] the borane moiety in BPi does not reduce acetonitrile and dimethyl formamide, as evidenced by the complete stability of BPi in these solutions.

A carbodiimide reagent is used for the condensation of phosphate derivatives to provide the corresponding phosphoric anhydride. The reaction of **2a** with an excess of 1-(3-dimethylaminopropyl)-3-ethylcarbodiimide (EDC) was explored in water (pH = 6.5) at 37 °C for 4 h. The addition of EDC to BPi resulted in excessive loss of this compound due to complete P−B bond cleavage of **2a** to yield phosphorus acid (72% of **2a** was degraded after 4 h, based on the ^{31}P NMR spectrum). This finding is in contrast to diethyl phosphite (cyano- or methoxycarbonyl)borane analogues, which are stable to dicyclohexylcarbodiimide (DCC).[30]

The P−B bond was also found to be sensitive to catalytic hydrogenation. Thus, when compound **9** was subjected to hydrogenation (in the presence of Pd/C), the P−B bond was also reduced, yielding phosphorus acid.

The reactivity of BPi with imidazole and pyridine was also studied. Specifically, a solution of BPi with 2 or 10 equiv. of imidazole in CD_3OD remained unchanged for 96 h, based on the ^{31}P NMR spectra. Likewise, only a negligible cleavage of the P−B bond was observed after 113 h for a solution of BPi in pyridine. BPi is apparently more stable to imidazole and pyridine than the related analogue tetramethyl boranopyrophosphate.[31] The reaction of 5′-DMT-2′-deoxythymidine with tetramethyl boranopyrophosphate in the presence of *N*-methylimidazole was reported to proceed with the partial removal of the borane group. Likewise, when pyridine was used as a solvent, partial removal of the borane group was observed.[31]

The presence of divalent metal ions such as Zn^{2+} and Mg^{2+} in DMF and water for 48 h and 4 h, respectively, left BPi unchanged.

Whereas dimethyl boranophosphate monopotassium salt (**3**) plays the role of an efficient nucleophile,[13] the related BPi is a poor nucleophile. Thus, when BPi was treated with tosyl chloride or mesyl chloride (with or without amine) in acetonitrile for 24 h, even at 60 °C, no reaction occurred. Likewise, the reaction of BPi with phosphorus oxychloride and its derivatives [P(O)Cl_2R] yielded no product. The reason for BPi's reduced nucleophilicity, as compared to **3**, might be due to the "carboxylate-like" nature of BPi, as compared to the "alkoxide-like" nature of dimethyl boranophosphate.

Conclusions

The quest for phosphate bioisosters over the last several decades has included the synthesis of phosphonates, α-halo phosphonates,[32,33] phosphorothioates,[4] and boranophosphate analogues.[6,34,35] Despite the extensive study of boranophosphate nucleoside analogues, the exploration of the parent inorganic boranophosphate has not been reported. The various potential applications of a phosphate isoster, together with the limitations of the currently available isosters, justify the continued search for the perfect inorganic phosphate mimic. Therefore, the unique and chemically interesting inorganic boranophosphate **2** has been investigated here as a mimic of phosphate with respect to properties such as water solubility, geometry, acid/base character, H-bonding, and chemical reactivity. The great similarity of BPi to the inorganic phosphate, Pi, is demonstrated here by the BPi's high water solubility, and geometry that is in accordance with that of the parent compound, except for the long P−B bond (1.892 Å) and B−P−O angles that are slightly larger than tetrahedral angles. Furthermore, the acid/base character of BPi is essentially not altered in comparison to Pi. This finding is in contrast to the corresponding phosphorothioate isoster, where there is a reduction of about two log units in the acidity relative to Pi.[36] Likewise, pK_{a2} values of α-mono- and -difluorophosphonate isosters are one and two log units, respectively, lower than the pK_{a2} value of phosphoric acid.[33]

Indications for H-bond-based clustering of BPi in organic solvents, including polar and protic solvents, were obtained from the IR and ^{31}P NMR spectra.

BPi is stable under both highly basic and acidic conditions (at pH $>$ 2). In addition, BPi is stable in the presence of imidazole, pyridine, and Mg^{2+} ions. However, the P−B bond cleavage is observed upon the reaction of BPi with carbodiimides. A loss of BPi's borane moiety also occurs at pH values $<$ 2.

A drastic alteration in the chemical nature of BPi as compared to Pi and BH_3 complexes is observed. While Pi is a nucleophile,[37] BPi is a poor nucleophile. Likewise, the reducing nature of the BH_3 group in BPi is drastically lower than in other BH_3 complexes.

Based on the geometry, water solubility, acid/base character, and H-bonding properties, BPi appears to be a perfect mimic of Pi, and an attractive alternative to the thiophosphate and α-halophosphonate isosters.

Experimental Section

General: All air- and moisture-sensitive reactions were performed in flame-dried, nitrogen-flushed flasks sealed with rubber septa; the reagents were introduced with a syringe. The progress of the reactions was monitored by TLC on precoated Merck silica-gel plates (60 K-254). Column chromatography was performed with Merck silica gel 60 (230−400 mesh). Compounds were characterized by NMR spectroscopy using Bruker DPX-300, DMX-600, or AC-200 spectrometers. NMR spectra were recorded with a Bruker AC-200 spectrometer with a ^{31}P NMR probe (isotope frequency of

 © 2004 Wiley-VCH Verlag GmbH & Co. KGaA, Weinheim

81 MHz) using 85% H_3PO_4 as an external reference. IR spectra of BPi in KBr pellets were recorded with a Nicolet Impact 400D spectrometer using the OMNIC program. IR spectra of BPi in solution were measured using a Bruker Vector 22 equipped with a liquid-nitrogen-cooled MCT detector. For the ATR measurements, a Harrick variable-angle ATR accessory was used. For one spectrum, 100 scans were co-added at a resolution of 4 cm^{-1}. The clean ATR germanium crystal (Harrick Scientific Corporation) was measured for the background spectra (cutoff 680 cm^{-1}). Crystallographic data were collected with a Nonius KappaCCD diffractometer at 120 K with scans of 1° collected at a speed of 1°/20 s; the merging *R*-factor on the data was 0.046 with 36867 reflections collected and 2979 unique. BPi crystals were obtained as colorless needles. Further details of the crystal structure investigation may be obtained from the Fachinformationzentrum Karlsruhe, 76344 Eggenstein-Leopoldshafen, Germany, on quoting the depository number CSD-413735. Melting points were measured using a Fisher-Johns melting-point apparatus. Apparent pH values were measured with a Hanna Instruments pH-meter (HI 8521), equipped with an Orion micro-combination pH electrode (9802). Compounds **2** are all inorganic boranophosphate salts having different ammonium counterions (ammonium in **2a**, tributylammonium in **2b**, triethylammonium in **2c**, and tetrabutylammonium in **2d**, see Experimental for **2a** below). The preparation of salts **2a**−**2c** for elemental analysis involved a freeze-drying process. Unfortunately, it was impossible to obtain reliable elemental analyses for salts **2a**−**2c** due to loss of some of the amine during this freeze-drying process (as observed in their ^1H NMR spectra). Therefore, we chose the tetrabutylammonium salt **2d** for performing a representative elemental analysis, since in this case there is no partial loss of the amine during freeze-drying.

Boranophosphate 2a: $BH_3{\cdot}SMe_2$ complex in THF (2 M, 1.35 mL, 2.7 mmol) was added to a solution of tris(trimethylsilyl) phosphite (600 μL, 1.795 mmol) in dry CH_3CN (5 mL) under N_2 at 0 °C. The resulting solution was kept at room temperature for 15 min. Dry MeOH (15 mL) and 2 M NH_3 in EtOH (1.8 mL, 3.6 mmol) were added and the mixture was stirred at room temperature for 1 h. The solvent was then removed under reduced pressure, and the product was obtained as a white solid in 93% yield (202 mg, 1.556 mmol), m.p. > 240 °C. ^1H NMR (D_2O, 200 MHz): δ = 0.27 (d of 1:1:1:1 quadruplet, $J_{P,H}$ = 22, $J_{B,H}$ = 87 Hz, 3 H) ppm. ^{31}P NMR (D_2O, 81 MHz): δ = 80.38 (1:1:1:1 quadruplet, J = 156 Hz; 1:1:1:1:1:1:1 septuplet, J = 52 Hz) ppm. IR (KBr): $\tilde{\nu}$ = 2412, 2378, 2352, 1181, 1149, 1077−903, 654 cm^{-1}. Compound **2a** was converted into the corresponding tetraethylammonium salt as follows: **2a** was passed through a Sephadex-CM C-25 − tetraethylammonium-form column (prepared from the corresponding sodium-form resin upon loading with excess Et_4NCl) and the column was washed with about 20 volumes of deionized water. The solution was freeze-dried to yield tetraethylammonium BPi (**2d**) as a white solid. Based on the pH value of the **2d** solution, the ^{31}P NMR spectrum, and correlation with the plot of BPi ^{31}P NMR shifts vs. pH (Figure 4), the expected empirical formula is $BH_3O_3PH_{1.5}(Et_4N)_{1.5}$ (289.3): calcd. H 11.9, P 10.7; found H 11.3, P 9.5.

Boranophosphate 2b: The tributylammonium salt of boranophosphate was prepared as described above for **2a**. However, Bu_3N (0.85 mL, 3.57 mmol) was added instead of NH_3/EtOH. The product was obtained as a white solid in 93% yield (645 mg, 1.385 mmol), m.p. 83−84 °C. IR (KBr): $\tilde{\nu}$: 2407, 2381, 2350, 1184, 1150, 1100−850, 655 cm^{-1}.

Determination of the pK_a Values of Boranophosphate 2a: The pK_a values of **2a** were evaluated by ^{31}P NMR spectroscopy at room temperature. Solutions of **2a** (0.15−0.18 M) at different pH values were prepared by adding dilute sodium hydroxide or hydrochloric acid solutions. The ^{31}P NMR chemical shift was monitored as a function of the pH. A five-parameter sigmoid function was fitted to the data using Sigma Plot 2000 (SPSS, Inc.): $\delta = \delta_0 + a/[1 + e^{-\{(pH-pH^\circ)/b\}}]^c$. The inflection point, which is determined by the second derivative of the fitted sigmoid function, is the pK_a value.

Determination of the Decomposition Rate of BPi 2a at pH = 2: The stability of **2a** in acidic solution was evaluated by ^{31}P NMR spectroscopy at room temperature, monitoring the formation of the deboranation product (phosphorus acid). A 0.16 M solution of **2a** at pH = 2 was prepared by adding dilute hydrochloric acid to a solution of inorganic boranophosphate (NH_4^+ salt) in H_2O and 10% D_2O. The percentage of decomposition of **2a** is based on integrations of PBi and phosphorus-acid signals (δ = 90.93 and 3.3 ppm, respectively). The decomposition rate was determined by measuring changes in the integration of the respective NMR signals within 96 h.

Acknowledgments

The authors would like to thank the Marcus Center for Medicinal Chemistry, and the German Bundesministerium fuer Bildung und Forschung (BMBF) and the Israeli Ministry of Science, Culture and Sport (MOS) for financial support (grant number 1812). In addition, the authors gratefully acknowledge Dr. D. T. Major for the calculation of the IR spectrum of BPi, Prof. S. Specher and I. Mastai for a helpful discussion, and Prof. C. Sukenik and Dr. T. Bayer for their help with IR measurements in a Ge cell.

[1] [1a] F. H. Westheimer, *Science* **1987**, 1173−1178. [1b] F. H. Westheimer, *Phosphorus Chemistry − Developments in American Science* (Eds.: E. N. Walsh, E. J. Griffith, R. W. Parry, L. D. Quin), ACS Symposium Series 486ACS, Washington DC, **1992**.
[2] [2a] P. J. Roumaniuk, F. Eckstein, *J. Biol. Chem.* **1981**, *256*, 7322−7328. [2b] B. A. Conolly, F. Eckstein, *Biochemistry* **1982**, *21*, 6158−6167.
[3] [3a] S. Agrawal, *Biochim. Biophys. Acta* **1999**, *1489*, 53−67. [3b] C. A. Stein, *Chem. Biol.* **1996**, *3*, 319−323.
[4] [4a] S. R. Nahorski, V. B. L. Potter, *Trends Pharamacol. Sci.* **1989**, *10*, 139−144. [4b] F. Eckstein, *Ann. Rev. Biochem.* **1985**, *54*, 367−402. [4c] F. Eckstein, *Angew. Chem. Int. Ed. Engl.* **1983**, *22*, 423−439. [4d] F. Eckstein, *Antisense Nucleic Acid Drug Dev.* **2000**, *10*, 117−121.
[5] R. Engel, *Chem. Rev.* **1977**, *77*, 349−367.
[6] [6a] A. Sood, B. R. Shaw, B. F. Spielvogel, *J. Am. Chem. Soc.* **1990**, *112*, 9000−9001. [6b] B. R. Shaw, D. Sergueev, K. He, K. Porter, J. S. Summers, Z. Sergueeva, V. Rait, *Methods Enzymol.* **2000**, *313*, 226−257.
[7] [7a] V. Rait, D. S. Sergueev, J. S. Summers, K. He, F. Huang, B. Krzyzanowska, B. R. Shaw, *Nucleosides Nucleotides* **1999**, *18*, 1379−1380. [7b] J. Zhang, T. Terhorst, M. D. Matteucci, *Tetrahedron Lett.* **1997**, *38*, 4957−4960. [7c] K. W. Porter, D. J. Briley, B. R. Shaw, *Nucleic Acids Res.* **1997**, *25*, 1611−1617.
[8] Z. A. Sergueeva, D. S. Sergueev, A. A. Ribeiro, J. S. Summers, B. R. Shaw, *Helv. Chim. Acta* **2000**, *83*, 1377−1391, and references cited therein.
[9] [9a] K. He, K. W. Porter, A. Hasan, J. D. Briley, B. R. Shaw, *Nucleic Acids Res.* **1999**, *27*, 1788−1794. [9b] K. W. Porter, J. D. Briley, B. R. Shaw, *Nucleic Acids Res.* **1997**, *25*, 1611−1617.
[10] V. Nahum, G. Zündorf, S. A. Levesque, R. Beaudoin, G. Reiser, B. Fischer, *J. Med. Chem.* **2002**, *45*, 5384−5396.
[11] J. S. Summers, B. R. Shaw, *Curr. Med. Chem.* **2001**, *8*, 1147−1155.
[12] B. F. Spielvogel, A. Sood, B. R. Shaw, I. H. Hall, R. G. Fairch-

 © 2004 Wiley-VCH Verlag GmbH & Co. KGaA, Weinheim

ild, B. H. Laster, C. Gordon, *Prog. Neutron Capture Ther. Cancer* **1992**, 211−213.
[13] T. Imamoto, E. Nagato, Y. Wada, H. Masuda, A. Yamaguchi, T. Uchimaru, *J. Am. Chem. Soc.* **1997**, *119*, 9925−9926.
[14] T. Wada, M. Shimizu, N. Oka, K. Saigo, *Tetrahedron Lett.* **2002**, *43*, 4137−4140.
[15] A. Longeau, P. Knochel, *Tetrahedron Lett.* **1996**, *37*, 6099−6102.
[16] A. Sood, C. K. Sood, I. H. Hall, B. F. Spielvogel, *Tetrahedron* **1991**, *47*, 6915−6930.
[17] R. K. Harris, *Nuclear Magnetic Resonace Spectroscopy: A Physicochemical View*, Longman Scientific and Technical, Somerset, NJ, **1986**.
[18] D. E. C. Corbridge, *The Structural Chemistry of Phosphorous*, Elsevier, Amsterdam, **1974**.
[19] [19a] D. E. C. Corbridge, *Phosphorous: An Outline of its Chemistry, Biochemistry and Technology*; *Studies in Inorganic Chemistry*, Elsevier, Amsterdam, **1995**, vol. 20, pp 1141−2. [19b] We also based our IR assignment on quantum mechanical calculations as follows. The boranophosphate anion was optimized using the B3LYP functional in conjunction with the 6-31+6(d) basis set. Frequency calculation was performed to obtain the IR spectrum and the harmonic vibrational frequencies were scaled by a factor of 0.9614. The calculations employed the Gaussian 98 program: M. J. Frisch, G. W. Trucks, H. B. Schlegel, G. E. Scuseria, M. A. Robb, J. R. Cheeseman, V. G. Zakrzewski, J. A. Montgomery, R. E. Stratmann, J. C. Burant, S. Dapprich, J. M. Millam, A. D. Daniels, K. N. Kudin, M. C. Strain, O. Farkas, J. Tomasi, V. Barone, M. Cossi, R. Cammi, B. Mennucci, C. Pomelli, C. Adamo, S. Clifford, J. Ochterski, G. A. Petersson, P. Y. Ayala, Q. Cui, K. Morokuma, D. K. Malick, A. D. Rabuck, K. Raghavachari, J. B. Foresman, J. Cioslowski, J. V. Ortiz, B. B. Stefanov, G. Liu, A. Liashenko, P. Piskorz, I. Komaromi, R. Gomperts, R. L. Martin, D. J. Fox, T. Keith, M. A. Al-Laham, C. Y. Peng, A. Nanayakkara, C. Gonzalez, M. Challacombe, P. M. W. Gill, B. G. Johnson, W. Chen, M. W. Wong, J. L. Andres, M. Head-Gordon, E. S. Replogle, J. A. Pople, *Gaussian 98* (Revision A.7), Gaussian, Inc., Pittsburgh, PA, **1998**.
[20] H. Li, C. Hardin, B. R. Shaw, *J. Am. Chem. Soc.* **1996**, *118*, 6606−6614.
[21] Ref.[18], p. 180, 214, 261.
[22] Ref.[18], p. 213.
[23] [23a] A. Onoda, T.-A. Okamura, Y. Hitoshi, N. Ueyama, *Mol. Cryst. Liq. Cryst.* **2002**, *379*, 401−406. [23b] C. Detering, P. M. Tolstoi, N. S. Golubev, G. S. Denisov, H. H. Limbach, *Dok. Akad. Nauk* **2001**, *379*, 353−356; *Chem. Abstr.* **2002**, *136*, 20119.
[24] Y. Kameda, K. Sugawara, T. Hosaka, T. Usuki, O. Uemura, *Bull. Chem. Soc. Jpn.* **2000**, *73*, 1105−1112.
[25] E. Gebert, A. H. Reis Jr., S. W. Peterson, L. I. Katzin, G. W. Mason, D. F. Peppard, *J. Inorg. Nucl. Chem.* **1981**, *43*, 1451−1464.
[26] D. L. Wertz, G. A. Cook, *J. Solution Chem.* **1985**, *14*, 41−8.
[27] M. Hojo, H. Hasegawa, Z. Chen, *Bull. Chem. Soc. Jpn.* **1996**, *69*, 2215−2220.
[28] [28a] D. F. Peppard, J. R. Ferraro, G. W. Mason, *J. Inorg. Nucl. Chem.* **1958**, *7*, 231−244. [28b] D. F. Peppard, J. R. Ferraro, G. W. Mason, *J. Inorg. Nucl. Chem.* **1957**, *4*, 371−372. [28c] Ref.[18a], pp. 1049−1064.
[29] H. C. Brown, *Borane in Organic Chemistry*, Cornell University Press, Ithaca, **1972**, pp. 230−235.
[30] K. Vyakaranam, G. Rana, B. F. Spielvogel, J. A. Maguire, N. S. Hosmane, *Nucleosides, Nucleotides Nucleic Acids* **2002**, *21*, 581−598.
[31] T. Wada, M. Shimizu, N. Oka, K. Saigo, *Tetrahedron Lett.* **2002**, *43*, 4137−4140.
[32] G. M. Blackburn, *Chem. Ind.* **1981**, 134. G. M. Blackburn, D. A. England, F. Kolkman, *J. Chem. Soc., Chem. Commun.* **1981**, 930−932.
[33] G. M. Blackburn, D. Brown, S. J. Martin, M. J. Parratt, *J. Chem. Soc., Perkin Trans. 1* **1987**, 181−186.
[34] J. S. Summers, D. Roe, P. D. Boyle, M. Colvin, B. R. Shaw, *Inorg. Chem.* **1998**, *37*, 4158−4159.
[35] B. R. Shaw, J. Madison, A. Sood, B. F. Spielvogel, *Methods Mol. Biol. (Totowa, NJ, U. S.)*, **1993**, *20, 225−243.*
[36] [36a] E. K. Jaffe, M. Cohn, *Biochemistry* **1978**, *17*, 652−657. [36b] J. A. Gerlt, M. A. Reynolds, P. C. Demou, G. L. Kenyon, *J. Am. Chem. Soc.* **1983**, *105*, 6469−6474.
[37] [37a] S. Saxena, *Ind. J. Chem. Sect. A* **2002**, *41A*, 718−722; *Chem. Abstr.* **2002**, *137*, 140554. [37b] O. A. El Seoud, M.-F. Ruasse, W. A. Rodrigues, *J. Chem. Soc., Perkin Trans. 2* **2002**, 1053−1058. [37c] P. M. Cullis, G. A. Fawcett, M. J. Harger, M. Lee, *J. Am. Chem. Soc.* **2001**, *123*, 4147−54. [37d] H. Bundgaard, J. Hansen, *Int. J. Pharm.* **1981**, *9*, 273−283.

Received February 19, 2004
Early View Article
Published Online August 12, 2004

 © 2004 Wiley-VCH Verlag GmbH & Co. KGaA, Weinheim

Synthesis and Electrochemistry of the Monolacunary Dawson-Type Tungstoarsenate $[H_4AsW_{17}O_{61}]^{11-}$ and Some First-Row Transition-Metal Ion Derivatives

Israel-Martyr Mbomekalle,[a] Bineta Keita,[a] Yu Wei Lu,[a] Louis Nadjo,*[a] Roland Contant,[b] Nebebech Belai,[c] and Michael T. Pope[c]

Keywords: Polyoxometalates / Dawson dissymmetrical polyoxometalates / Arsenic / Tungsten / Electrochemistry / Electrocatalysis

The novel family of the Dawson-type tungstomonoarsenate $[H_4AsW_{18}O_{62}]^{7-}$ has been extended by preparing for the first time its monolacunary species and its first-row transition-metal ion substituted derivatives. All compounds were characterized by elemental analysis, IR and UV/Vis spectroscopy and representative examples by ^{183}W NMR spectroscopy. Several lines of experimental evidence converge to indicate that the substitution occurs in the α_2 position. The lacunary species, unlike its phosphorus analogue, was sufficiently stable for a few voltammetric runs. Therefore, the cyclic voltammetric properties of substituted compounds were studied as a function of pH and systematically compared with those of the lacunary precursor rather than with those of their analogues derived from the symmetrical species $[As_2W_{18}O_{62}]^{6-}$. The electrocatalytic properties of all compounds were illustrated by the reduction of nitrite by reduced $[H_4AsW_{18}O_{62}]^{7-}$ and of nitrate by reduced α_2-$[(H_2O)Cu(H_4AsW_{17}O_{61})]^{9-}$.

(© Wiley-VCH Verlag GmbH & Co. KGaA, 69451 Weinheim, Germany, 2004)

Introduction

Polyoxometalates (POMs) are early transition metal−oxygen anionic clusters. They simultaneously exhibit many properties that make them attractive for applications in catalysis, separations, imaging, materials science and medicine.[1−8] The scope for varying the atomic compositions of these complexes is virtually enormous and new structures continue to be discovered. Even though complete rationalisation of the construction of these structures is lacking at present, very many of them might be recognised as being derived, at least partly, from lacunary Keggin and Dawson fragments. Recently, we have been interested in the possibility of obtaining Dawson structures with two different central heteroatoms. We were stimulated by the pioneering work[9] of one of the present authors who reported the synthesis of the novel Dawson-type tungstophosphate $[H_4PW_{18}O_{62}]^{7-}$ and its lacunary and zinc-substituted derivatives $[H_4PW_{17}O_{61}]^{11-}$ and $[Zn(H_2O)(H_4PW_{17}O_{61})]^{9-}$. In these species, the two anionic halves are of the A-type with only one of them containing a central heteroatom in the +v oxidation state. Soon afterwards, our group confirmed the feasibility of this synthesis for the As^V-containing analogue,[10] also obtaining the corresponding trilacunary species and achieving the synthesis of two sandwich-type derivatives, $[Zn_4(H_2O)_2(H_4AsW_{15}O_{56})_2]^{18-}$ and $[Cu_4(H_2O)_2(H_4AsW_{15}O_{56})_2]^{18-}$. With a systematic study of the relevant parameters, we have also established[11] the best experimental conditions for the synthesis of $[H_4AsW_{18}O_{62}]^{7-}$ and demonstrated that these conditions are essentially different from those necessary to obtain the well-known symmetric species $[As_2W_{18}O_{62}]^{6-}$. The same kind of rationalisation was achieved in the comparable syntheses of $[P_2W_{18}O_{62}]^{6-}$ and $[H_4PW_{18}O_{62}]^{7-}$.[12,13] Recently, we have extended the work on this new family of dissymmetric Dawson-type heteropolyanions to the first-row transition-metal ion substituted derivatives of $[H_4PW_{18}O_{62}]^{7-}$.[13]

Herein, we report the synthesis, characterization and electrochemistry of the hitherto unknown monolacunary species of $[H_4AsW_{18}O_{62}]^{7-}$ and its first-row transition-metal ion substituted derivatives. Their electrochemistry reveals differences from the corresponding symmetric heteropolyanions and with the phosphorus analogues. In addition, an evaluation of their electrocatalytic properties for the reduction of nitrate and nitrite is provided.

[a] Laboratoire de Chimie Physique, UMR 8000, CNRS, Electrochimie et Photoélectrochimie, Université Paris-Sud, Bâtiment 420, 91405 Orsay Cedex, France
Fax: (internat.) + 33-1-69154328
E-mail: nadjo@lcp.u-psud.fr
[b] Laboratoire de Chimie Inorganique et des Matériaux Moléculaires, UMR 7071, CNRS, Université Paris VI, 4, place Jussieu, 75252 Paris Cedex 05, France
[c] Department of Chemistry, Georgetown University, Box 571227, Washington, DC 20057, USA

Supporting information for this article is available on the WWW under http://www.eurjic.org or from the author.

 © 2004 Wiley-VCH Verlag GmbH & Co. KGaA, Weinheim **DOI: 10.1002/ejic.200400186**

Results and Discussion

Prolonged heating of the reaction mixture during the synthesis of $[H_4AsW_{18}O_{62}]^{7-}$ results in the formation of the pure so-called α-isomer.[11] All the POMs in the present study are primarily derived from α-$[H_4AsW_{18}O_{62}]^{7-}$ (AsW_{18}) and their formulae will be written as $MAsW_{17}$, with omission of oxygen atoms and overall charges when no confusion is likely to arise; M represents the substituent metal cation. In close analogy with the case of α-$[H_4PW_{18}O_{62}]^{7-}$, the results of electrochemistry and IR spectroscopy demonstrate that the mild alkaline degradation of AsW_{18} results in the removal of a W atom from the "cap" in the half of this molecule containing the single As atom, thus creating the first vacancy in one of the so-called α_2 positions. Scheme 1 illustrates the α-structure proposed for α-$[H_4AsW_{18}O_{62}]^{7-}$ and one of its monosubstituted derivatives, α_2-$[M(H_2O)H_4AsW_{17}O_{61}]^{9-}$, where M represents a divalent transition metal ion and the water molecule is omitted.

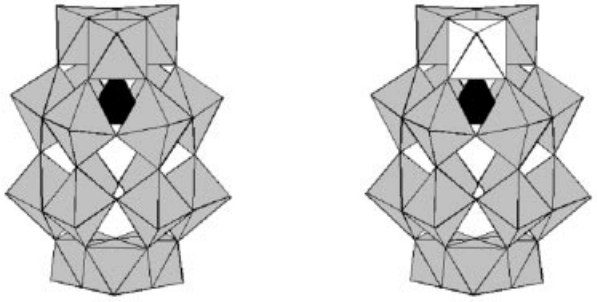

Scheme 1. Schematic representations of the Dawson-type tungstomonoarsenate and a monosubstituted tungstomonoarsenate

Synthesis

The synthesis and purification of $[H_4AsW_{18}O_{62}]^{7-}$ has been described previously in detail.[11] As will be described in the Exp. Sect., the monolacunary derivative was obtained under mild conditions, provided the addition of $KHCO_3$ was sufficient to maintain the pH around 8 during the process. Two slightly different experimental conditions were applied for the synthesis of metal cation substituted derivatives, depending on the terminal ligand on the substituent metal atom in the final product. As is usual with Keggin- and Dawson-type POMs, the sixth coordination site on the metal atom in the 1:1 complexes may be occupied by a variety of ligands.[1,13] We were interested in two kinds of ligands: on one hand, in the substitution by $V^{5+/4+}$ or $Mo^{6+/5+}$, the terminal oxo group can be considered to reconstitute the structure of a saturated POM; on the other hand, for all other metal cations of interest in this work, the sixth position is occupied by a water molecule.

UV/Vis and IR Spectroscopic Characterisation

As expected, no specific fingerprint signals were found in the UV/Vis spectra in the series in order to distinguish one compound from the next. However, recording these spectra over a period of at least 24 h was helpful in assessing the stability of the complexes as a function of pH. This delay was selected as a compromise between the time needed for electrochemical characterisation of the complexes and that for eventual long-lasting or preparative-scale catalytic or electrocatalytic processes. The precursor lacunary H_4AsW_{17} was found to be sufficiently stable for a few cyclic voltammetric runs to be performed, a remarkable difference from its phosphorus analogue for which no stability domain could be found. The so-called "saturated" substituted compounds, $MAsW_{17}$ (M = Mo or V), show stabilities close to that of the unsubstituted compound, with complete stability observed from pH = 0.3 to 4. Table 1 shows complementary details as well as the stability domains for all the other substituted derivatives. Black indicates the domain in which a particular derivative is stable; dark grey corresponds to a decomposition less than or equal to 20% and light grey indicates a decomposition of between 20 and 70%. It is worth pointing out the complete identity of this behaviour with that of the corresponding phosphorus analogues, except for the difference in stability of their respective monolacunary derivatives.[12] The only exception concerns the Cu derivatives. $CuAsW_{17}$ is stable from pH = 0.3 to 5 and $CuPW_{17}$ is only stable from pH = 2 to 5.

The locations of the main IR bands are summarized in the Supporting Information and show a comparison between As_2W_{18} and AsW_{18} (Table SI1). Substitution into the vacancy of the lacunary species AsW_{17} can be expected to restore the symmetry present in AsW_{18}, at least as far as IR spectra are concerned. Then, only a relative weakening of the bond force constants would be mainly expected as a result of substitution. Table SI1 confirms this general trend, even though the observed variations are modest. Despite this, the IR spectra support the conclusion that no important structural changes appear from one compound to the next.

^{183}W NMR Spectroscopy

Table 2 shows the ^{183}W NMR chemical shifts for the Zn- and Ni-monosubstituted derivatives of the Dawson-type tungstomonophosphate and tungstomonoarsenate. The chemical shifts for the corresponding tungstodiphosphates were obtained from the pioneering work of Jorris and coworkers[14] and are shown for comparison. The chemical shifts measured in this work compare well with those of the corresponding MP_2W_{17}. In full agreement with expectations, all tungsten centres can be observed for the Zn-substituted anions, as shown in the Supporting Information (Figure SI1). Peak integrations confirm this observation (Table 2). The signals of all tungsten atoms, except two pairs, are seen for the Ni-substituted anions. It is likely that the two lines observed at low field are from the two remaining belt tungsten atoms in the XW_9 half of the anion. The Fe- and Cu-substituted derivatives were too paramagnetic to give useful results.

 © 2004 Wiley-VCH Verlag GmbH & Co. KGaA, Weinheim

Table 1. Stability, monitored by UV/Vis spectroscopy as a function of pH over 24 h for α-As_2W_{18}, α-AsW_{18} and the α_2-$AsW_{17}M$ derivatives of the latter complex

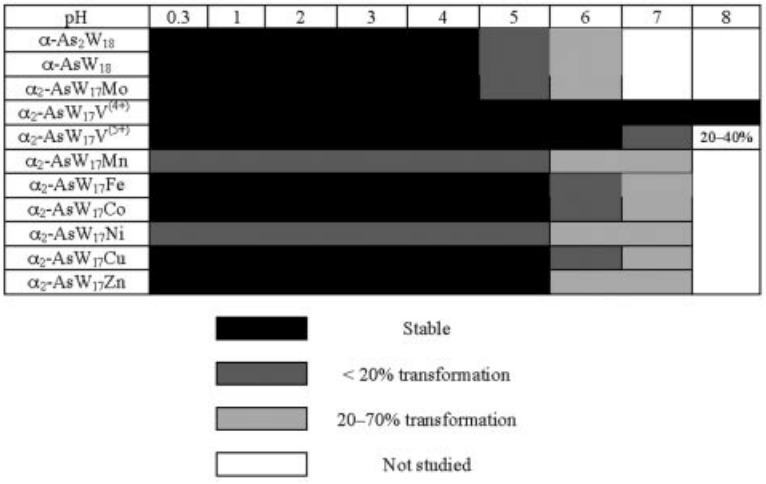

Table 2. Comparison of ^{183}W NMR chemical shifts of MXW_{17} where M = Zn or Ni and X = As or P with transition-metal monosubstituted Wells-Dawson heteropolytungstates from ref.[14]

Compound	^{183}W NMR chemical shifts	Ref.
α_2-$[(D_2O)Zn^{2+}P_2W_{17}O_{61}]^{8-}$	−84.4 (2 W), −138.7 (2 W), −180 (1 W), −186.7 (2 W), -208.6 (2 W), −214.8 (6 W), −242.7 (2 W)	[14]
α_1-$[(D_2O)Zn^{2+}P_2W_{17}O_{61}]^{8-}$	−99.4, −117.4, −123.0, −146.1, −151.9, −157.7, −167.6, −174.2, −175.7, −177.3, −193.3, −200.1, −203.7, −210.3, −214.1, −214.6, −225.5 (each 1 W)	[14]
$[Zn(H_4PW_{17}O_{61})]^{9-}$	−98 (2 W), −135 (2 W), −147 (2 W), −176 (2 W), −195 (2 W), −200 (2 W), −205 (2 W), −208 (2 W), −222 (1 W)	this work
$[Zn(H_4AsW_{17}O_{61})]^{9-}$	−85 (2 W), −137 (2 W), −166 (2 W), −169 (2 W), −175 (2 W), −191 (4 W), −201 (2 W), −228 (1 W)	this work
α_2-$[(D_2O)Ni^{2+}P_2W_{17}O_{61}]^{8-}$	+468.3 (2 W), +338.7 (2 W), −142 and −146 (4 W), −200 and −202 (3 W), −230.5 (2 W)	[14]
$[Ni(H_4PW_{17}O_{61})]^{9-}$	+468 (2 W), +386 (2 W), −140 (2 W), −164 (2 W), −167 (2 W), −187 (2 W), −245 (1 W)	this work
$[Ni(H_4AsW_{17}O_{61})]^{9-}$	+613 (2 W), +349 (2 W), −140 (2 W), −153 (2 W), −160 (2 W), −175 (2 W), −246 (1 W)	this work

A comparison of the results in Table 2 strongly suggests that the substitution site is the α_2 position, in complete analogy with the phosphorus systems.[12]

Electrochemistry

We have previously shown by cyclic voltammetry, the difference in basicity between the several first reduction species of As_2W_{18} and AsW_{18}.[10] Typically, in a pH = 0.3 sulfate medium, the part of the pattern of As_2W_{18} of interest here consists of two one-electron waves followed by two two-electron waves. These waves correspond to reversible diffusion-controlled processes. In contrast, in the same medium, AsW_{18} exhibits three two-electron chemically reversible diffusion-controlled waves. As a cross-check, the first wave was also shown by controlled potential coulometry to feature a two-electron process. Furthermore, we found that this first wave split into two one-electron waves at pH = 4 while the pattern for As_2W_{18} did not change. This behaviour can be understood in terms of the higher basicity of the first several reduced species of AsW_{18} over those of As_2W_{18}. The complete analogy between this and the comparable behaviour of PW_{18} and P_2W_{18} must be stressed.[12] The electrochemistry of monosubstituted derivatives of AsW_{18} can be discussed straightforwardly in comparison with the corresponding As_2W_{18}-derived analogues. Owing to the marginal variations in the behaviour of the corresponding compounds from one series to the next, the main outcome of such a study turned out to be the confirmation that α_2-substituted derivatives were indeed formed in the $MAsW_{17}$ series.

In contrast to the lacunary species PW_{17}, its analogue AsW_{17} is sufficiently stable to allow a few voltammetric runs in the pH = 3 and pH = 5 media used. This observation opens up the way for comparison between the electrochemical behaviour of $MAsW_{17}$ derivatives with that of their precursor lacunary compound. Such a comparison is appropriate because those substituted derivatives bearing a terminal water molecule as the sixth ligand on the substituent metal cation are expected to behave much like the lacunary precursor, at least as far as the electrochemistry of the POM framework is concerned.[15−18] In addition, the differences brought about by the presence of As instead of P in MXW_{17} (X = P or As) were selected as a basis for further interesting comparisons. In short, two issues were

 © 2004 Wiley-VCH Verlag GmbH & Co. KGaA, Weinheim

found pertinent for this electrochemical study: (i) the redox behaviour of the electroactive substituent cations within the POM framework and (ii) the influence of the nature of the substituent cation and of the central heteroatom on the reduction of the W^{VI} centre.

Redox Behaviour of the Electroactive Substituent Transition Metal Ions within $MAsW_{17}$

The reduction or oxidation peak potentials for reducible or oxidizable cations within the substituted POMs are listed in Table 3. In general, most of the peak potentials are pH-dependent, indicating proton intervention in the overall redox mechanism. The other trends observed for the phosphorus analogues are also seen here. Reduction of the Cu^{2+} centre is merged with the first tungsten reduction, precluding any accurate determination of its peak potential location. Oxidation of the Mn^{2+} centre is observed, but at a highly positive potential. Oxidation of the Co^{2+} centre is difficult to achieve.

Table 3. Potential locations of the cations which may be reduced or oxidized within α_2-$AsW_{17}M$ in a pH = 3.00 and a pH = 5.00 medium; E_{pc} = cathodic peak potential; E_{pa} = anodic peak potential; scan rate: 10 $mV{\cdot}s^{-1}$; working electrode: glassy carbon; reference electrode: SCE

Reducible cations	$-E_{pc}$ [V]	
	pH = 3	pH = 5
Fe^{3+} in $AsW_{17}Fe$	0.150	0.230
Cu^{2+} in $AsW_{17}Cu$	–	0.348
Mo^{6+} in $AsW_{17}Mo$	−0.096	−0.082
Oxidizable cations	E_{pa} [V]	
	pH = 3	pH = 5
V^{4+} in $AsW_{17}V^{IV}$	0.456	0.378
Mn^{2+} in $AsW_{17}Mn$	1.060	0.892
Co^{2+} in $AsW_{17}Co$	–	1.406

Influence of the Central Heteroatom on the First Tungsten Reduction Wave within $XW_{17}M$ (X = P or As)

Figure 1 (A and B) illustrate two typical examples of the limiting behaviour observed at pH = 3. For the Mn^{2+}-substituted derivatives, the peak potential for the first tungsten reduction wave is hardly displaced in Figure 1A, irrespective of whether the central heteroatom is As or P. In contrast, for the Cu^{2+} complexes, Figure 1B shows a 154 mV positive shift for the first tungsten reduction peak potential in the As compound compared with the P derivative. It must be pointed out that a combined Cu and W first wave was observed at pH = 3 for both P and As derivatives. In both cases, controlled potential coulometry beyond the peak potential of this composite wave consumes four electrons per molecule for complete reduction at pH = 3. Electrolysis conducted at the half-wave potential and combined with spectroelectrochemistry or simple inspection of the solution colour indicates that the two-electron reduction of the Cu^{2+} centre is completed before that of the W^{6+} centres begins. The first tungsten reduction peak potentials at pH = 3 are shown in Table 4 for all the substituted derivatives along with the value for H_4AsW_{17}. It appears from these data that the difference $\Delta E_p = E_p$(lacunary) − E_p(substituted), available only for As compounds, depends on the nature of the substituent. At pH = 3, the largest effect was obtained for $AsW_{17}Mo$ in which the first tungsten wave was driven 144 mV in the positive potential direction compared with the same wave in the lacunary precursor. All other differences are modest and range between +14 mV to −62 mV. The value of ΔE_p for the V^{4+} complex is remarkable and is comparable with those found for substituted derivatives bearing a terminal water molecule and not with a compound such as $AsW_{17}Mo$ bearing a terminal oxo group. Analogous trends were also obtained previously in the study of the α_1- and α_2-$P_2W_{17}M$ series.[16−18]

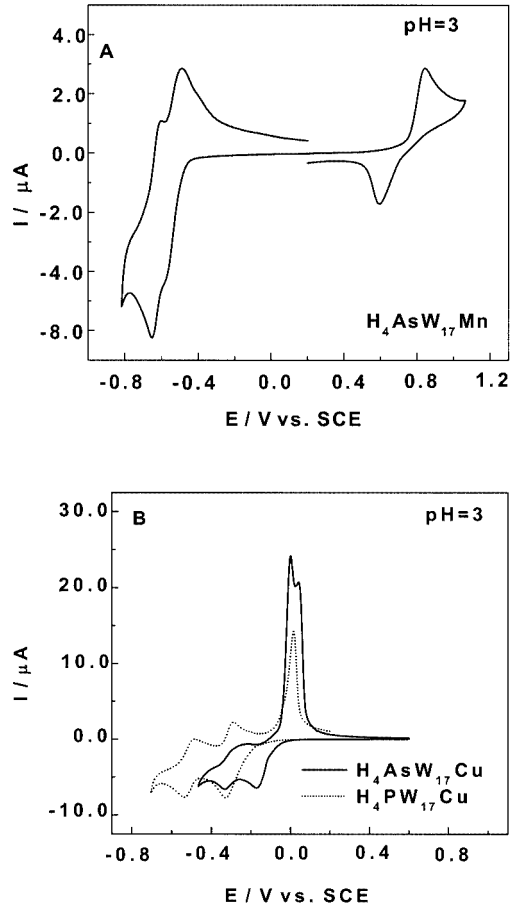

Figure 1. Cyclic voltammograms recorded on 5×10^{-4} M solutions of the relevant polyoxometalate in a pH = 3 medium (0.2 M Na_2SO_4 + H_2SO_4); scan rate: 10 $mV{\cdot}s^{-1}$; working electrode: glassy carbon; reference electrode: SCE; A: α-$[H_4Mn(H_2O)AsW_{17}O_{61}]^{9-}$; B: α-$[H_4Cu(H_2O)AsW_{17}O_{61}]^{9-}$ (solid line) and α-$[H_4Cu(H_2O)PW_{17}O_{61}]^{9-}$ (dotted line)

The influence of the nature of the central heteroatom X within $XW_{17}M$ (X = P or As) leads to modest peak potential shifts ranging between −30 mV and +30 mV, except in the case of the Cu^{2+}-substituted derivatives. In fact, the pK_a

 © 2004 Wiley-VCH Verlag GmbH & Co. KGaA, Weinheim

Table 4. Potential locations of the first tungsten wave for $AsW_{17}M$ derivatives and their differences with the corresponding wave of the precursor lacunary species in a pH = 3 medium; scan rate: 10 mVs^{-1}; working electrode: glassy carbon; reference electrode: SCE; E_{pc}: cathodic peak potential; $\Delta E_{pc} = (E_{pc\ lacunary} - E_{pc\ substituted})$

Substituent	$-E_{pc}$ [mV]	ΔE_{pc} [mV]
Lacunary	372	0
V^{4+}	400	28
Mn^{2+}	358	−14
Fe^{3+}	434	62
Co^{2+}	432	60
Ni^{2+}	420	48
Zn^{2+}	388	16
Mo^{6+}	280	−144

values for the substituted complexes and for their reduction species might be different, thus rendering complicated any study of the nature of the central heteroatom and of the pH effect.

Electrocatalytic Reductions of Nitrite and Nitrate

The behaviour of AsW_{18} and its substituted derivatives $AsW_{17}M$ towards the electrocatalytic reductions of nitrite and nitrate were tested in the pH-stable ranges of these POMs. In the potential region explored, no direct reduction of nitrite or nitrate on the glassy carbon electrode surface could be observed.[19,20] It was also deemed interesting to look, in particular, for cases in which a catalytic current could be observed on the first wave or the first several waves of each POM, in such potential regions. Under these conditions, the processes occur in solution and, usually, no permanent modification of the electrode surface by the POM was obtained.[21] Conclusions from our previous work[10,12,20] were confirmed here and indicate that only Cu- and Ni-substituted derivatives catalyse the reduction of nitrate, while most derivatives catalyse the reduction of nitrite. Typically, Figure 2 (A and B) illustrates selected representative examples of electrocatalytic reductions of nitrite by AsW_{18} or by $AsW_{17}Cu$, respectively. At pH = 2 and in the absence of nitrite, the first two waves of AsW_{18} are closely spaced (Figure 2, A). Upon addition of even modest amounts of nitrite, a large cathodic current enhancement was observed (Figure 2, B). This cathodic current was slightly composite and no longer had any associated anodic counterpart. Increasing the concentration of nitrite through adjustment of the excess parameter γ ($\gamma = C_{NO_2^-}/C_{POM}$) still enhanced the cathodic current. Thus, efficient catalysis of nitrite reduction[22] was achieved during the reduction of AsW_{18}. This current increase can be expressed more quantitatively through the catalytic efficiency CAT defined as $CAT = 100 \times [I_{(POM + NO_2^-)} - I^d_{(POM)}]/I^d_{(POM)}$ where $I_{(POM + NO_2^-)}$ represents the reduction peak current of the POM in the presence of nitrite and $I^d_{(POM)}$ the reduction peak current for the POM alone.

In the experiment described in Figure 2, CAT was found to vary from 634% to 1185% for $\gamma = 10$ and $\gamma = 30$, respectively. While electrocatalysis by AsW_{18} is triggered by reduced W centres, a more complex pathway must be considered in the case of $AsW_{17}Cu$. Figure 2, C shows at pH = 3 the first combined Cu/W cathodic wave for this POM with the characteristic stripping oxidation pattern on potential reversal. Superimposed on this is the cyclic voltammogram obtained in the presence of nitrite. The main obser-

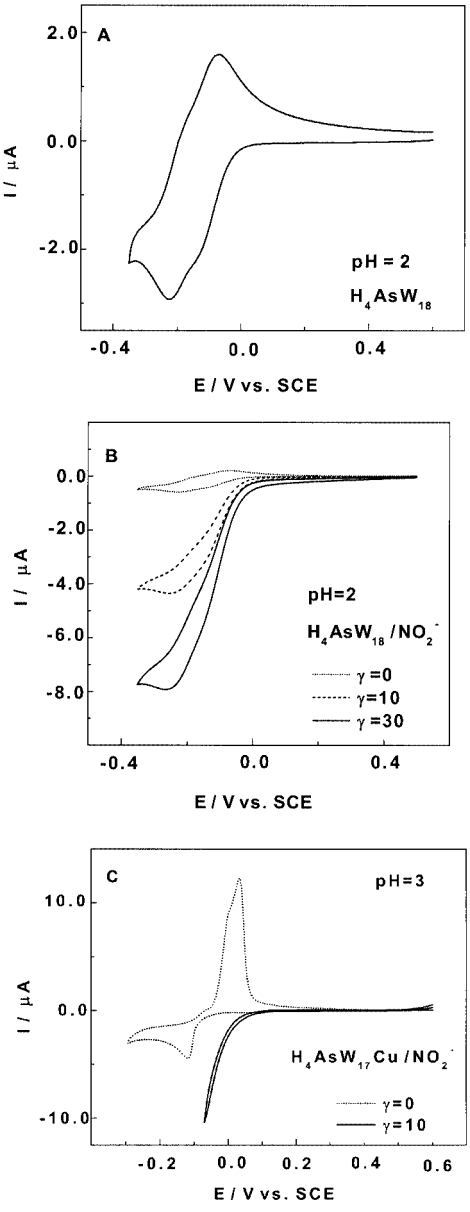

Figure 2. Cyclic voltammograms recorded on 5×10^{-4} M solutions of the relevant polyoxometalate; scan rate: 2 $mV \cdot s^{-1}$; working electrode: glassy carbon; reference electrode: SCE; for the definition of the excess parameter γ, see text; A: first two waves of α-$[H_4AsW_{18}O_{62}]^{7-}$ alone in a pH = 2 medium (0.2 M Na_2SO_4 + H_2SO_4); B: same conditions as in A with the addition of increasing amounts of nitrite; C: α-$[H_4Cu(H_2O)AsW_{17}O_{61}]^{9-}$ in the absence and presence of nitrite in a pH = 3 medium (0.2 M Na_2SO_4 + H_2SO_4)

 © 2004 Wiley-VCH Verlag GmbH & Co. KGaA, Weinheim

vations can be summarized as follows: (i) copper deposition can be obtained upon scanning the first combined Cu/W cathodic wave; (ii) nitrite electrocatalytic reduction begins in a potential region in which the reduction current of $AsW_{17}Cu$ is very weak; (iii) the electrocatalytic reduction of nitrite is very fast, so that no copper deposition could be detected in the potential range explored, at least as far as cyclic voltammetry is concerned.

The electrocatalytic reduction of nitrate by reduced $AsW_{17}Cu$ adds a new example to the few described in our previous work.[10,12,20] Figure 3 summarises the observations at pH = 3 and 5. Figure 3, A (obtained at pH = 3) shows that the nitrate electrocatalytic reduction is effective and is enhanced with increasing γ values. A comparison of Figures 2 and 3, A requires, at the very least, the following two remarks: (i) the electrocatalytic reduction of nitrite begins at a potential substantially less negative than that for the nitrate; (ii) a much larger excess parameter value is needed to observe a clear catalytic effect in the case of nitrate compared with that of nitrite. Figure 3, B indicates that the electrocatalytic reduction of nitrate remains effective at pH = 5. It is worth noting that two cathodic steps

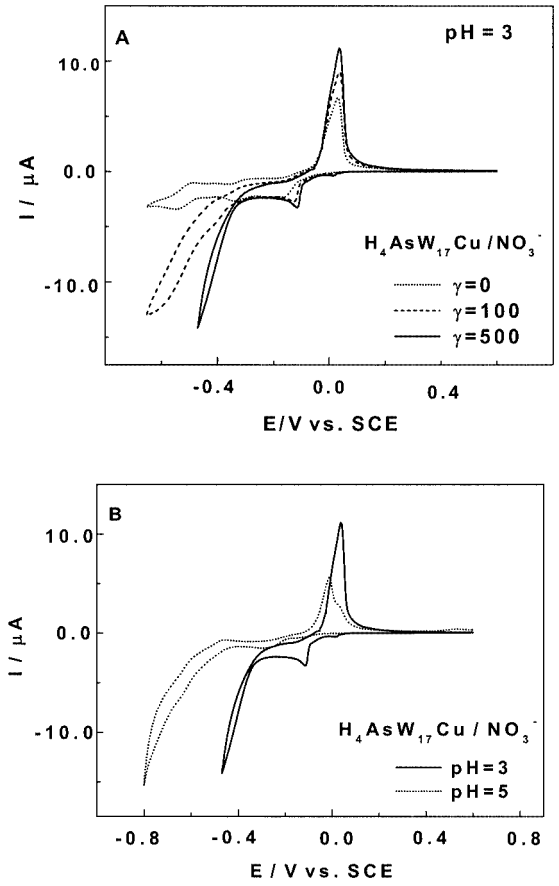

Figure 3. Cyclic voltammograms recorded on 5×10^{-4} M solutions of α-$[H_4Cu(H_2O)AsW_{17}O_{61}]^{9-}$ in the absence and presence of nitrate; scan rate: 2 mV·s^{-1}; working electrode: glassy carbon; reference electrode: SCE; for the definition of the excess parameter γ, see text; A: in a pH = 3 medium (0.2 M Na_2SO_4 + H_2SO_4), with increasing amounts of nitrate; B: comparison of the cyclic voltammograms run in the presence of nitrate in a pH = 3 medium and in a pH = 5 medium, respectively (0.4 M CH_3COONa + CH_3COOH)

were observed for copper reduction processes in this medium. The potential shift for nitrate reduction also falls in the range of 100 mV per pH unit. Finally, we found qualitatively that the central heteroatom X in $XW_{17}Cu$ (X = P or As) has little influence on the electrocatalytic reduction of nitrate.

Conclusions

The present work expands our earlier results which were previously limited to the synthesis and comparison of the electrochemical behaviour of AsW_{18} and its symmetrical analogue As_2W_{18}. The monolacunary species AsW_{17} was synthesized for the first time and served as a precursor to introduce first-row transition-metal ions in the framework of the novel Dawson-type tungstomonoarsenate. Several lines of experimental evidence converge to indicate that the substitution occurs in the α_2 position. The short-term stability of AsW_{17} in solution contrasts with the instability of its phosphorus analogue. This situation allows a comparison between the electrochemical behaviour of this lacunary POM and the transition-metal ion substituted systems. Most of the latter complexes were expected to behave like the lacunary precursor, at least with respect to the redox properties of the W framework. The results confirm this expectation. The efficiency of $AsW_{17}Cu$ towards the electrocatalytic reduction of nitrate is a new example in addition to the few previously published.

Experimental Section

Preparations: All chemicals were of reagent grade and were used as received. The isolated yields of the final pure products ranged constantly from 60 to 95% in all the preparations. α-$K_7[H_4AsW_{18}O_{62}]\cdot 18H_2O$ was synthesized as described previously.[11]

α-$K_{11}[H_4AsW_{17}O_{61}]\cdot 18H_2O$ (H_4AsW_{17}): A sample of α-$K_7[H_4AsW_{18}O_{62}]\cdot 18H_2O$ (8 g, 1.6 mmol) was dissolved in Millipore water (20 mL) with stirring. To the clear solution, was added $KHCO_3$ (17 mL of a 1 M solution) and a white precipitate gradually formed. Stirring was continued for roughly 1 h. The solid was then left to settle and was filtered, washed twice with ethyl alcohol, twice with diethyl ether and was air-dried by suction through a flask with an aspirator (yield 7.5 g, 95%). $K_{11}[H_4AsW_{17}O_{61}]\cdot 18H_2O$ (4934.5): calcd. As 1.52, K 8.72, W 63.34, H_2O 6.57; found As 1.59, K 8.91, W 62.81, H_2O 6.31.

α-$K_9[H_4Zn(H_2O)AsW_{17}O_{61}]\cdot 20H_2O$ ($AsW_{17}Zn$): A sample of $Zn(NO_3)_2\cdot 6H_2O$ (0.30 g, ca. 1 mmol) was dissolved in Millipore water (45 mL) and α-$K_{11}[H_4AsW_{17}O_{61}]\cdot 18H_2O$ (4 g, 0.82 mmol) was added in small portions while heating the mixture on a water bath (ca. 60 °C). After 30 min, the cloudy mixture was filtered hot and the clear filtrate left in a beaker. Large white crystals appeared upon cooling. This material was filtered, washed with ethyl alcohol and left to dry in the open air (yield 2.8 g, 70%). Recrystallization was performed with a minimum amount of Millipore water. $K_9[H_4Zn(H_2O)AsW_{17}O_{61}]\cdot 20H_2O$ (4975.7): calcd. As 1.51, K 7.10, W 63.07, Zn 1.32; found As 1.42, K 6.97, W 65.2, Zn 1.66.

 © 2004 Wiley-VCH Verlag GmbH & Co. KGaA, Weinheim

α-$K_9[H_4Cu(H_2O)AsW_{17}O_{61}]\cdot 18H_2O$ ($AsW_{17}Cu$): A sample of $Cu(NO_3)_2\cdot 3H_2O$ (0.25 g, ca. 1 mmol) was dissolved in Millipore water (45 mL) and α-$K_{11}[H_4AsW_{17}O_{61}]\cdot 18H_2O$ (4 g, 0.82 mmol) was added in small portions while heating the mixture on a water bath (ca. 60 °C). After 30 min, the cloudy greenish mixture was filtered hot and the green clear filtrate left in a beaker. Large green crystals appeared upon cooling. This material was filtered, washed with ethyl alcohol and left to dry in the open air. Recrystallization was performed from a minimum amount of Millipore water (yield 2.6 g, 65%). $K_9[H_4Cu(H_2O)AsW_{17}O_{61}]\cdot 18H_2O$ (4937.8): calcd. As 1.52, Cu 1.29, K 7.13, W 63.30; found As 1.60, Cu 1.27, K 7.26, W 62.81.

α-$K_9[H_4Ni(H_2O)AsW_{17}O_{61}]\cdot 21H_2O$ ($AsW_{17}Ni$): A sample of $Ni(NO_3)_2\cdot 6H_2O$ (0.30 g, ca. 1 mmol) was dissolved in Millipore water (45 mL) and α-$K_{11}[H_4AsW_{17}O_{61}]\cdot 18H_2O$ (4 g, 0.82 mmol) was added in small portions while heating the mixture on a water bath (ca. 60 °C). After 30 min, the green clear mixture was filtered hot and the green clear filtrate left in a beaker. A pale green yellow crystalline material appeared upon cooling. This material was filtered, washed with ethyl alcohol and left to dry in the open air. Recrystallization was performed from a minimum amount of Millipore water (yield 3.8 g, 95%). $K_9[H_4Ni(H_2O)AsW_{17}O_{61}]\cdot 21H_2O$ (4987): calcd. As 1.50, K 7.06, Ni 1.18, W 62.67; found As 1.32, K 7.03, Ni 1.24, W 63.16.

α-$K_9[H_4Co(H_2O)AsW_{17}O_{61}]\cdot 18H_2O$ ($AsW_{17}Co$): A sample of $Co(NO_3)_2\cdot 6H_2O$ (0.30 g, ca. 1 mmol) was dissolved in Millipore water (45 mL) and $K_{11}[H_4AsW_{17}O_{61}]\cdot 18H_2O$ (4 g, 0.82 mmol) was added in small portions while heating the mixture on a water bath (ca. 60 °C). After 30 min, the dark red cloudy mixture was filtered hot and the clear dark red filtrate left in a beaker. A clear sand-coloured crystalline material appeared upon cooling. This material was filtered, washed with ethyl alcohol and left to dry in the open air. Recrystallization was performed from a minimum quantity of Millipore water (yield 3.8 g, 95%). $K_9[H_4Co(H_2O)AsW_{17}O_{61}]\cdot 18H_2O$ (4933.2): calcd. As 1.52,Co 1.19, K 7.13, W 63.36; found As 1.46, Co 1.15, K 7.06, W 63.52.

α-$K_8[H_4Fe(H_2O)AsW_{17}O_{61}]\cdot 19H_2O$ ($AsW_{17}Fe$): A sample of $Fe(NO_3)_3\cdot 9H_2O$ (0.40 g, ca. 1 mmol) was dissolved in Millipore water (45 mL) and α-$K_{11}[H_4AsW_{17}O_{61}]\cdot 18H_2O$ (4 g, 0.82 mmol) was added in small portions while heating the mixture on a water bath (ca. 60 °C). After 30 min, the pale yellow suspension was filtered hot and the yellow clear filtrate transferred to a beaker. Upon treatment of this filtrate with KCl (10 g), a pale yellow crystalline material appeared. This material was filtered, washed with ethyl alcohol and left to dry in the open air. Recrystallization was performed from a minimum quantity of Millipore water (yield 2.4 g, 60%). $K_8[H_4Fe(H_2O)AsW_{17}O_{61}]\cdot 19H_2O$ (4909): calcd. As 1.53, Fe 1.14, K 6.37, W 63.67; found As 1.43, Fe 1.26, K 6.94, W 62.74.

α-$K_9[H_4Mn(H_2O)AsW_{17}O_{61}]\cdot 19H_2O$ ($AsW_{17}Mn$): A sample of $Mn(NO_3)_2\cdot 4H_2O$ (0.25 g, ca. 1 mmol) was dissolved in Millipore water (45 mL) and α-$K_{11}[H_4AsW_{17}O_{61}]\cdot 18H_2O$ (4 g, 0.82 mmol) was added in small portions while heating the mixture on a water bath (ca. 60 °C). After 30 min, the dark beige suspension was filtered hot and the dark beige clear filtrate left in a beaker. Large chestnut-coloured crystals appeared upon cooling. This material was filtered, washed with ethyl alcohol and left to dry in the open air. Recrystallization was performed from a minimum amount of Millipore water (yield 3.6 g, 90%). $K_9[H_4Mn(H_2O)AsW_{17}O_{61}]\cdot 19H_2O$ (4947.2): calcd. As 1.51, K 7.11, Mn 1.11, W 63.18; found As 1.47, K 7.23, Mn 1.24, W 62.40.

α-$K_9[H_4As^{IV}W_{17}O_{62}]\cdot 18H_2O$ ($AsW_{17}V^{IV}$): A sample of $VOSO_4\cdot 5H_2O$ (0.42 g, 1.7 mmol) was dissolved in Millipore water (90 mL) and acidified with 4 M HCl (8.5 mL). α-$K_{11}[H_4AsW_{17}O_{61}]\cdot 18H_2O$ (8 g, 1.64 mmol) was then added in small portions with stirring. The black solution was stirred for roughly 30 min and then filtered and treated with KCl (10 g). The grey black precipitate that resulted was filtered, washed with ethyl alcohol and dried in the open air. This material was recrystallized from a minimum of acidified water (HCl solution pH < 1) (yield 5.6 g, 70%). $K_9[H_4As^{IV}W_{17}O_{62}]\cdot 18H_2O$ (4923.2): calcd. As 1.52, K 7.15, V 1.03, W 63.48; found As 1.55, K 8.14, V 0.99, W 64.7.

α-$K_8[H_4As^{V}W_{17}O_{62}]\cdot 18H_2O$ ($AsW_{17}V^{V}$): A sample of $NaVO_3$ (0.21 g, 1.7 mmol) was dissolved in Millipore water (90 mL) and acidified with 4 M HCl (8.5 mL). α-$K_{11}[H_4AsW_{17}O_{61}]\cdot 18H_2O$ (8 g, 1.64 mmol) was then added in small portions with stirring. The yellow solution was stirred for roughly 30 min, filtered, then treated with KCl (10 g). The yellow precipitate that resulted was filtered, washed with ethyl alcohol and dried in the open air. This material was recrystallized from a minimum of acidified water (HCl solution pH < 1) (yield 4.8 g, 60%). $K_8[H_4P^{(5+)}W_{17}O_{62}]\cdot 18H_2O$ (4884.1): calcd. As 1.53, K 6.40, V 1.04, W 63.99; found As 1.61, K 6.27, V 1.00, W 63.2.

α-$K_7[H_4AsMoW_{17}O_{62}]\cdot 18H_2O$ ($AsW_{17}Mo$): A sample of $Na_2MoO_4\cdot 2H_2O$ (0.40 g, 1.7 mmol) was dissolved in Millipore water (90 mL) and acidified with 4 M HCl (8.5 mL). α-$K_{11}[H_4AsW_{17}O_{61}]\cdot 18H_2O$ (8 g, 1.64 mmol) was then added in small portions whilst stirring. The clear yellow solution was stirred for roughly 30 min, then filtered and treated with KCl (10 g). The fine yellow precipitate that resulted was filtered, washed with ethyl alcohol and dried in the open air. This material was recrystallized from a minimum of acidified water (HCl solution pH < 1) (yield 4.4 g, 55%). $K_7[H_4AsMoW_{17}O_{62}]\cdot 18H_2O$ (4890): calcd., As 1.53, K 5.60, Mo 1.96, W 63.92; found As 1.49, K 5.33, Mo 1.61, W 65.27.

General Methods and Materials: Pure water was used throughout. It was obtained by passing through a RiOs 8 unit followed by a Millipore-Q Academic purification set. All reagents were of high-purity grade and were used as purchased without further purification. Elemental analyses were performed by Kanti Labs Ltd, Mississauga, Canada. The IR spectra were recorded in KBr pellets with a Perkin-Elmer Spectrum One FT-IR spectrophotometer. The UV/Vis spectra were recorded with a Perkin-Elmer Lambda 19 spectrophotometer on 2.5×10^{-5} M solutions of the relevant polyanion. Matched 1.000-cm optical path quartz curvets were used. The compositions of the various media were as follows: for pH = 0.33: 0.5 M H_2SO_4; for pH = 1−3: 0.2 M Na_2SO_4 + H_2SO_4; for pH = 4 and 5: 0.4 M CH_3COONa + CH_3COOH; for pH = 6 and 7: 0.4 M NaH_2PO_4 + NaOH.

Electrochemical Experiments: The media used for UV/Vis spectroscopy were also used for electrochemistry except that the polyanion concentration was 5×10^{-4} M. All cyclic voltammograms were recorded at a scan rate of 10 $mV\cdot s^{-1}$ unless otherwise stated. The solutions were deoxygenated thoroughly for at least 30 min with pure argon and kept under a positive pressure of this gas during the experiments. The source, mounting and polishing of the glassy carbon (GC, Tokai, Japan) electrodes has been described.[23] The glassy carbon samples had a diameter of 3 mm. The electrochemical apparatus was an EG & G 273 A driven by a PC with the M270 software. Potentials are quoted relative to the saturated calomel electrode (SCE). The counter electrode was a platinum gauze of large surface area. All experiments were performed at room temperature.

 © 2004 Wiley-VCH Verlag GmbH & Co. KGaA, Weinheim

Acknowledgments

This work was supported by the CNRS (UMR, 8000 and UMR 7071), the Universities Paris XI, Paris VI and Georgetown University. We also thank Benoît Faure for assistance with several electrochemistry experiments.

[1] M. T. Pope *Heteropoly and Isopoly Oxometalates*, Springer-Verlag, Berlin, **1983**.
[2] M. T. Pope; A. Müller, *Angew. Chem. Int. Ed. Engl.* **1991**, *30*, 34−48.
[3] *Polyoxometalates: From Platonic Solids to Anti-Retroviral Activity* (Eds.: M. T. Pope, A. Müller), Kluwer, Dordrecht, The Netherlands, **1994**.
[4] Topical issue on polyoxometalates: C. L. Hill, *Chem. Rev.* **1998**, *98*, 1−389.
[5] *Polyoxometalate Chemistry: From Topology via Self-Assembly to Applications* (Eds.: M. T. Pope, A. Müller), Kluwer, Dordrecht, The Netherlands, **2001**.
[6] *Polyoxometalate Chemistry for Nano-Composite Design* (Eds.: T. Yamase, M. T. Pope), Nanostructure Science and Technology, Kluwer Academic/Plenum Publishing, New York, **2002**.
[7] M. T. Pope, *Polyoxo Anions: Synthesis and Structure* in *Comprehensive Coordination Chemistry II*, vol. 4 (Ed.: A. G. Wedd), Elsevier Science, New York **2004**, p. 635−678.
[8] C. L. Hill, *Polyoxometalates: Reactivity* in *Comprehensive Coordination Chemistry II*, vol. 4 (Ed.: A. G. Wedd), Elsevier Science, New York **2004**, p. 679−759.
[9] R. Contant, S. Piro-Sellem, J. Canny, R. Thouvenot, *C. R. Acad. Sci., Ser. IIc:Chim.* **2000**, *3*, 157−161.
[10] B. Keita, I. M. Mbomekalle, L. Nadjo, R. Contant, *Electrochem. Commun.* **2001**, *3*, 267−273.
[11] I. M. Mbomekalle, B. Keita, L. Nadjo, R. Contant, N. Belai, M. T. Pope, *Inorg. Chim. Acta* **2003**, *342*, 219−228.
[12] I. M. Mbomekalle, B. Keita, L. Lu, L. Nadjo, R. Contant, N. Belai, M. T. Pope, *Eur. J. Inorg. Chem.* **2004**, 276−285.
[13] R. Contant, M. Abbessi, J. Canny, A. Belhouari, B. Keita, L. Nadjo, *Inorg. Chem.* **1997**, *36*, 4961−4967.
[14] T. L. Jorris, M. Kozik, N. Casan-Pastor, P. J. Domaille, R.G. Finke, W. K. Miller, L. C. W. Baker, *J. Am. Chem. Soc.* **1987**, *109*, 7402−7408.
[15] B. Keita, A. Belhouari, L. Nadjo, R. Contant, *J. Electroanal. Chem.* **1998**, *442*, 49−57.
[16] B. Keita, Y. W. Lu, L. Nadjo, R. Contant, M. Abbessi, J. Canny, M. Richet, *J. Electroanal. Chem.* **1999**, *477*, 146−157.
[17] B. Keita, F. Girard, L. Nadjo, R. Contant, J. Canny, M. Richet, *J. Electroanal. Chem.* **1999**, *478*, 76−82.
[18] R. Contant, M. Abbessi, J. Canny, M. Richet, B. Keita, A. Belhouari, L. Nadjo, *Eur. J. Inorg. Chem.* **2000**, 567−574.
[19] A. Belhouari, B. Keita, L. Nadjo, R. Contant, *New J. Chem.* **1998**, 83−86.
[20] B. Keita, E. Abdeljalil, L. Nadjo, R. Contant, R. Belghiche, *Electrochem. Commun.* **2001**, *3*, 56−62.
[21] B. Keita, L. Nadjo, *Mater. Chem. Phys.* **1989**, *22*, 77−103.
[22] At pH = 1, the actual active species should be HNO_2 and/or NO. In fact, the following sequence is known: $HNO_2 \rightarrow H^+ + NO_2^-$ $pK_a = 3.3$ at 18 °C and HNO_2 disproportionates in fairly acidic solution: $3\ HNO_2 \rightarrow HNO_3 + 2\ NO + H_2O$. The rate of this reaction is known to be low.
[23] B. Keita, F. Girard, L. Nadjo, R. Contant, R. Belghiche, M. Abbessi, *J. Electroanal. Chem.* **2001**, *508*, 70−80.

Received March 8, 2004
Early View Article
Published Online August 12, 2004

 © 2004 Wiley-VCH Verlag GmbH & Co. KGaA, Weinheim

Sequence-Specific Oxidative Degradation of Tripeptides by a Cobalt(III) Complex Containing a Terpyridine Ligand

Koichiro Jitsukawa,*[a] Hiroshi Takahashi,[a] Ryoji Hyuga,[a] Hidekazu Arii,[a] and Hideki Masuda*[a]

Keywords: Cleavage reactions / Cobalt / N ligands / Oxidation / Peptides

A sequence-specific oxidative degradation of an oligopeptide consisting of aliphatic amino acids was performed with a ternary cobalt(III) complex. Under aerobic conditions the reaction of [Co(CO_3)(OH)(terpy)] and an equimolar amount of tripeptide at 40 °C at pH 8.5 gave two fraction bands (**a** and **b**) with water and then two bands (**c** and **d**) with NaCl solution, respectively, after column separation. In the case of gly-gly-leu (ggl, **1**), [Co(gg′l)(terpy)] [**1a**, gg′l = glycyl(2-oxoglycyl)leucine], [Co(g′l)(terpy)] [**1b**, g′l = *N*-(2-oxoglycyl)leucine], [Co(ggl)(terpy)]$^{+}$ (**1c**), and [Co(terpy)$_2$]$^{3+}$ (**1d**) were obtained. The crystal structure of **1c**, which was the main product, revealed that the starting ggl ligand was cleaved to give a bis-amide compound, g′l, which might be generated by loss of N-terminal glycine and carbonylation of the α-carbon of the N-2 glycine residue. Although the source of the oxygen of the newly generated carbonyl group is not clear, gg′l is supposed to be an intermediate for g′l on the basis of time-dependent HPLC analyses. NMR investigation of other tripeptides [βala-gly-leu (**2**), gly-gly-phe (**3**), and gly-gly-ala (**4**)] containing a bulky C-terminal aliphatic side chain indicated the formation of the corresponding oxidation complexes. On the other hand, peptides containing a C-terminal glycine residue [gly-gly-gly (**5**) and phe-gly-gly (**6**)] or an N-2 β-alanine residue [gly-βala-leu (**7**)] did not give such a transformation product. The crystal structure of [Co(fgg)-(terpy)] (**6c**) revealed that the tripeptide is coordinated to cobalt with a tridentate N-terminal *N*-*N*-*N* geometry. Such sequence specificity demonstrated in the reaction of the aliphatic tripeptide complexes is interpreted by the interligand interaction between the side chain of the C-terminal amino acid residue and terpy.

(© Wiley-VCH Verlag GmbH & Co. KGaA, 69451 Weinheim, Germany, 2004)

Introduction

In oxidative transformation of proteins, which plays a major role in many oxidation processes within cells, the radicals generated damage both the peptide backbone and the side chains.[1] In C−N bond dissociation during the peptide degradation, active oxygen species, such as HO$^{\cdot}$, and HOO$^{\cdot}$, attack at the α-position of the amino-acid residues to generate a carbon-centered radical.[2,3] Once formed, this reacts further with molecular oxygen to form peroxy radicals, which expel superoxide species to give carbocations, and are then hydrolyzed to give the corresponding alcohols or are deprotonated to give the corresponding imines.[4,5] Some iron edta complexes attached to cysteine residue of proteins site-specifically cleaved the peptide backbone, in which the iron-hydroperoxo species directly attacked the amide carbonyl moiety.[6] Recently, we have reported selective α-hydroxylation of the C-terminal amino-acid residue of a dipeptide (DP) mediated by a ternary cobalt complex with the 2,2′:6′,2′′-terpyridine (terpy) ligand under aerobic conditions, which is a model reaction for the peptidylglycine α-hydroxylating monooxygenase (PHM) reaction.[7] The terpy ligand is known to accelerate the oxidative transformation of another ligand coordinated *trans* to it,[8] and a ternary complex with the terpy ligand could therefore cause the oxidative degradation of a peptide compound. Herein, we describe a sequence-specific oxidative degradation of tripeptides (TPs), such as GGL (**1**), BGL (**2**), and GGF (**3**), whose reactivities are compared with the cases of GGA (**4**),

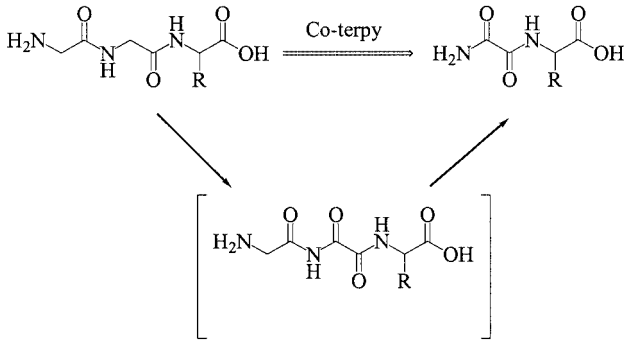

Scheme 1. Oxidative cleavage of tripeptides

[a] Nagoya Institute of Technology,
Gokiso-cho, Showa-ku Nagoya 466-8555, Japan
Fax: +81-52-7355240
E-mail: jitsukawa.koichiro@nitech.ac.jp
jitkk@ach.nitech.ac.jp

 © 2004 Wiley-VCH Verlag GmbH & Co. KGaA, Weinheim **DOI: 10.1002/ejic.200400261**

GGG (**5**), FGG (**6**), and GBL (**7**) (Scheme 1 and 2). Upon the formation of the ternary cobalt(III) complexes, some tripeptides containing bulky aliphatic amino acids at the C-terminus are cleaved to give unprecedented dipeptide derivatives on account of the assistance of the terpy ligand.

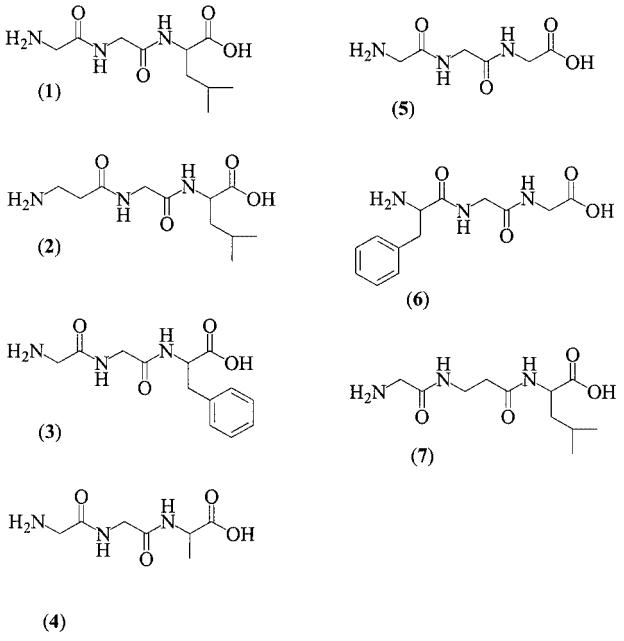

Scheme 2. Tripeptides employed: gly-gly-leu (GGL; **1**), βala-gly-leu (BGL; **2**), gly-gly-phe (GGF; **3**), gly-gly-ala (GGA; **4**), gly-gly-gly (GGG; **5**), phe-gly-gly (FGG; **6**), gly-βala-leu (GBL; **7**)

Results and Discussion

Characterization of the Ternary Complexes

The reaction of the cobalt carbonyl complex and an equimolar amount of tripeptides **1**−**7** was carried out at pH 8.5 and 40 °C in an aqueous solution for 10 h under aerobic conditions. After passing the reaction mixture through a cation-exchange column, four fractional bands containing cobalt(III) complexes (**a**−**d**) were obtained (see Exp. Sect.). In order to clarify the structure of the cobalt(III) complexes isolated from the column separation a ^{1}H NMR spectroscopic investigation was carried out. Transformation of the TP ligand was observed in the ternary complexes prepared from **1**−**3** (Table 1). Complex **1a** shows α-proton peaks of N-1 (N-terminal) at δ = 2.60 and 2.90 ppm, and that of the C-terminal (N-3) leucine at δ = 5.07 ppm, but no peaks corresponding to those of the N-2 (central) residue. Neither the α-proton peaks corresponding to N-1 nor N-2 glycine residues were detected in the spectrum of complex **1b**, while that of N-3 was detected at δ = 5.07 ppm. In complex **1c**, all α-proton peaks of GGL were detected. The spectroscopic and column behavior of the cobalt complexes prepared from BGL (**2**) and GGF (**3**) was similar to that of GGL (**1**), indicating that transformation of the glycine moieties takes place in the peptide backbone of **1a**, **1b**, **2a**, **2b**, **3a**, and **3b**.

Fortunately, a single crystal of **1b** suitable for X-ray analysis was obtained from the column eluent by allowing it to stand at room temperature. The crystal structure of **1b** (Figure 1)[11] reveals an unprecedented formation of the bisamide compound *N*-(2-oxoglycyl)leucine (G′L), as expected from the NMR spectroscopic data. The crystal data are summarized in the Exp. Sect. In order to determine the species substituted at the α-position of the N-2 residue in G′L, a positive-ion ESI mass spectrum of **1b** was measured. The obtained prominent peaks at *m*/*z* = 492.2 and 514.2 corresponding to the $[\{Co(g'l)(terpy)\} + H]^+$ and $[\{Co(g'l)(terpy)\} + Na]^+$ ions, respectively, indicate that the newly substituted atom is oxygen, although the oxygen source is not yet clear. Formation of a [Co(g′l)(terpy)] complex is also supported by the elemental analysis. Moreover, the relatively short bond length [1.22(2) Å] between the α-carbon [C(16)] and the newly generated atom [O(1)] and the sp^2 character around C(16) [O(1)−C(16)−N(4) = 128(1)° and O(1)−C(16)−C(17) = 119(1)°] in the crystal structure of **1b** indicate the formation of a C=O group at the α-position of the N-2 residue. The cleavage of the amide bond between the N-1 and N-2 residues in the GGL ligand took place in **1b**, but the α-protons of N-1 and N-3 moieties still remain in **1a** and **1c**.

In the case of GGA (**4**), complete column separation of **4a** and **4b** was not accomplished, although their ^{1}H NMR spectra indicated formation of the corresponding cleavage product. Due to the smaller size of the C-terminal side chain in **4** in comparison with the those in **1**−**3**, it is hard to separate complexes **4a** and **4b**. In the cases of some tripeptide ligands, for example GGG (**5**), FGG (**6**), and GBL (**7**), which have either an N-terminal glycine or N-2 β-alanine moiety, the main product was the $[Co(tp)(terpy)]^+$ complex (**5c**, **6c**, or **7c**), accompanied by a small amount of $[Co(terpy)_2]^{3+}$ (**d**).[9] Transformation compounds corresponding to **a** or **b** were not obtained. The ^{1}H NMR spectral patterns of the N1-, N2- and N3-α-proton moieties in **5c**, **6c**, and **7c** are very similar to that of **1c**. On the basis of the spectral analogy among the complexes **1c**−**7c**, the coordination mode of the tripeptide to cobalt is an N-terminal *N*-*N*-*N* form (N-1 terminal amine nitrogen, N-2 amide nitrogen, N-3 amide nitrogen), which agrees well with the empirical rule.[10,11] The tridentate coordination of FGG in **6c** is indicated by the upfield shift of the α-protons of the C-terminal glycine moiety (δ = 2.52 and 2.62 ppm) in comparison with the tetradentate coordination of FGG in $[Co(NH_3)_2(fgg)]$, where the corresponding protons are observed at δ = 4.00 ppm.[12] A complex-formation shift was not observed in the C-terminal α-position of **1c**−**7c**. The single-crystal structure of **6c**, shown in Figure 2, reveals that the cobalt ion is coordinated by two tridentate ligands, terpy and FGG, in which the coordination mode of the FGG to cobalt is an N-terminal *N*-*N*-*N* geometry, as expected from the NMR spectroscopic data. Moreover, the benzene ring of the N-terminal amino-acid side chain is very close to the terpy ring, with a distance of about 3.45 Å (the closest interatomic carbon-carbon distance).

 © 2004 Wiley-VCH Verlag GmbH & Co. KGaA, Weinheim

Table 1. NMR spectroscopic data for the ternary complexes

Tripeptide	Column Band	N-terminal α-H	N-terminal β-H	N-2 (center) α-H	N-2 (center) β-H	C-terminal α-H	C-terminal β-H
ggl	**a**	2.60 (d)	–	not detected		5.07 (q)	2.12 (m)
(**1**)		2.90 (d)					2.38 (m)
	b	not detected		not detected		5.07 (q)	2.10 (m)
							2.40 (m)
	c	3.42 (s)	–	5.28 (s)	–	4.00 (q)	1.34 (m)
bgl	**a**	2.30 (m)	1.75 (m)	2.13 (d)	–	4.95 (m)	2.08 (m)
(**2**)			1.85 (m)				
	b	not detected		not detected		5.01 (q)	2.00 (m)
							2.51 (m)
	c	hard to identify					
ggf	**a**	2.31 (d)	–	not detected		5.17 (m)	3.63 (dd)
(**3**)		2.97 (d)					4.43 (dd)
	b	not detected		not detected		5.22 (m)	3.67 (dd)
							4.45 (dd)
	c	3.30 (dd)	–	4.57 (dd)		2.31 (dd)	2.59 (dd)
		3.38 (dd)		4.69 (dd)			2.95 (dd)
gga	**a** + **b**	mixture of complexes (hard to identify)					
(**4**)	**c**	3.50 (dd)	–	4.75 (d)	–	2.50 (b)	0.41 (d)
				4.81 (d)			
ggg	**a**	not isolated					
(**5**)	**b**	not isolated					
	c	3.49 (s)	–	4.68 (s)	–	2.85 (s)	–
fgg	**a**	not isolated					
(**6**)	**b**	not isolated					
	c	3.84 (t)	2.78 (dd)	4.52 (d)	–	2.52 (d)	
			3.39 (dd)	4.72 (d)		2.62 (d)	
gbl	**a**	not isolated					
(**7**)	**b**	not isolated					
	c	3.23 (d)	–	2.65 (t), 4.16 (t)		3.53 (m)	1.17 (m)

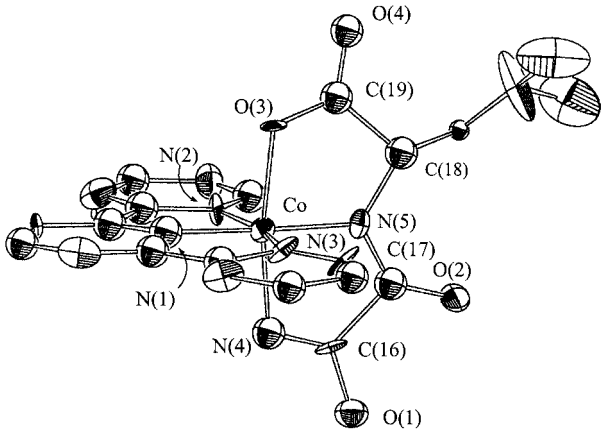

Figure 1. Molecular structure of the transformation compound [Co(g′l)(terpy)] (**1b**); hydrogen atoms are omitted for clarity; selected bond lengths (Å) and angles (°): Co−N(1) 1.87(1), Co−N(2) 1.99(1), Co−N(3) 1.93(1), Co−O(3) 1.92(1), Co−N(4) 1.91(1), Co−N(5) 1.88(2); O(3)−Co−N(4) 168.7(5), O(3)−Co−N(5) 84.0(6), N(1)−Co−N(5) 178.6(6), N(2)−Co−N(3) 162.0(7)

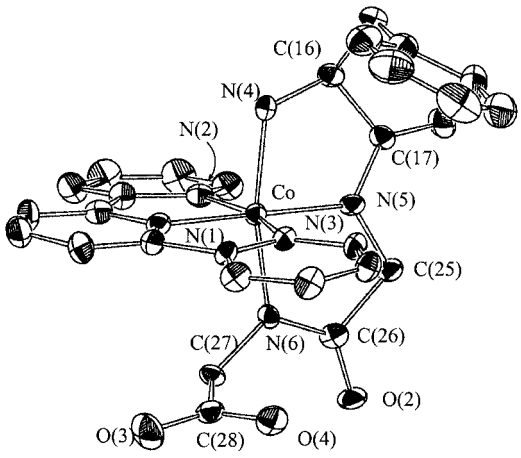

Figure 2. Molecular structure of the tripeptide compound, [Co(fgg)(terpy)] (**6c**); hydrogen atoms are omitted for clarity; selected bond lengths (Å) and angles (°): Co−N(1) 1.850(8), Co−N(2) 1.974(8), Co−N(3) 1.934(9), Co−N(4) 1.961(9), Co−N(5) 1.887(8), Co−N(6) 1.942(9); N(4)−Co−N(6) 166.5(3), N(4)−Co−N(5) 83.5(4), N(1)−Co−N(5) 180.0(4), N(2)−Co−N(3) 164.9(3)

Oxidative Degradation Pathway of the Peptide Bond

In this reaction, **1c** is considered as the starting compound for **1a** and **1b**, because the yield of **1c** decreases after a long reaction time. HPLC analysis of the reaction mixture also revealed that it is the primary product of the complex formation with Co-terpy and GGL. Similar time-dependent product distributions found by HPLC were observed in the reaction with BGL (**2**) and GGF (**3**). The reaction pathway from **1c** to **1b** is obviously different from the cobalt(III)-promoted hydrolysis, which generally gives both amine and carboxylic compounds.[11,13,14] The G′L ligand in **1b** is gen-

 © 2004 Wiley-VCH Verlag GmbH & Co. KGaA, Weinheim

erated by the loss of N-terminal glycine and oxygenation of the α-position of the N-2 glycine residue of the starting GGL. The structure of complex **1a**, a plausible intermediate for **1b**, is suggested by the positive ion ESI mass spectrum: The prominent peaks at m/z = 549.2 and 571.0 indicate the formation of a tripeptide complex containing glycyl(2-oxoglycyl)leucine (GG′L), which is consistent with the NMR spectroscopic data (no signal of N-2 protons in Table 1). Such an unprecedented cleavage reaction takes place only in tripeptides (**1**−**4**) with an alkyl side-chain at the C-terminal amino-acid residue, and not in the C-terminal glycine (**5** and **6**) and N-2 β-alanyl compounds (**7**). These results indicate that the oxidative degradation of the tripeptide ligand mediated by the ternary cobalt(III) terpy complex occurs sequence-specifically.

Although the detailed mechanism for this cleavage reaction is not yet clear, the downfield shift of the α-protons of the N-2 glycine moiety in **1c** relative to the metal-free GGL (δ = 4.01 and 4.03 ppm), might be essential for the reaction. Since the GGL ligand in **1c** strongly coordinates to the metal center in an N-terminal N-N-N manner, a nucleophile in aqueous solution (e. g. hydroxide ion) prefers to attack an electro-deficient state at the N-2 moiety. The α-proton of the glycine moiety is known to be easily abstracted to give a glycyl radical, whose stability is explained by the captodative effect.[15] In the oxidative transformation of the dipeptide ligand previously reported, the downfield shift of the α-proton attached to the N-2 residue of the dipeptide is important for the abstraction of the proton.[7] The radical intermediate generated at this position is attacked by dioxygen to give a peroxy radical, which decomposes by the Haber−Weiss mechanism to give the α-carbonyl compound **1a** because the transition metal-terpy system acts as a redox center for the electron-transfer reaction (Scheme 3).[8] Such an oxidative transformation of a methylene moiety adjacent to an amide group has also been reported in the case of iron(III) and cobalt(III) complexes with an *N*-(picolyl)picolinamide ligand under aerobic alkaline conditions, although the reaction mechanism is also unclear.[16] In aqueous conditions the amide complex **1a** might be hydrolyzed to give **1b**. Under anaerobic conditions, however, the transformation product **1b** was not detected in the HPLC analysis.

The terpy ligand is known to demonstrate very attractive features in electron-transfer, photochemical, and related reactions[8] and activate the *trans*-positioned ligand through the central metal,[17,18] which is attributed to the vacant low-lying π* orbitals that attract electron density from the metal.[19] Moreover, the assistance of terpy for hydrolysis of diribonucleoside monophosphate diesters has been demonstrated with a manganese(II) complex.[20] The interligand interaction caused by terpy is also known to regulate the α-hydroxylation of dipeptides.[7] From these results, we consider that the terpy ligand in this ternary cobalt(III) complex plays an important role in the oxidative transformation of the tripeptide. For sequence specificity, the interligand interaction between the C-terminal side chain and terpy in **1c** is important to abstract the α-proton or to stabilize the radical intermediate that gives **1a** under aerobic conditions. In the ternary complex **1c**, the CH-π interaction between the peptide and terpy ligands, as shown from the upfield shifts

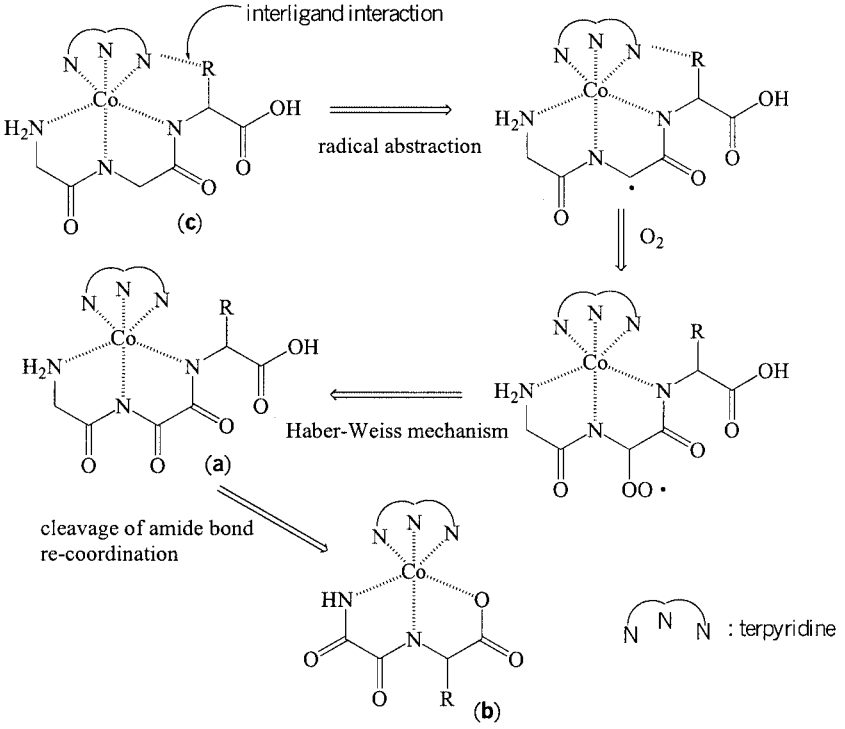

Scheme 3. Plausible oxidation pathway of the cleavage reaction

 © 2004 Wiley-VCH Verlag GmbH & Co. KGaA, Weinheim

of γ-H (δ = 0.82 ppm) and the δ-H's (δ = 0.23 and 0.58 ppm) of the leucine moiety, seems to fix the C-terminal side chain of GGL on the terpy ring. On the other hand, in the ternary complexes **5c** or **6c**, where the C-terminal residues are glycine, such upfield shifts are not observed. Consequently, the corresponding oxidative-degradation compounds were not generated in the cases of **5** and **6**. It is clear that the interligand interaction caused by the bulkiness of the C-terminal side-chain controls the sequence specificity of this reaction. The reason why the cleavage reaction does not take place in GBL (**7**), which contains a C-terminal bulky side-chain might be explained by the difficulty of abstraction of the protons attached on the N-2 β-alanine residue.

Conclusion

A new type of oxidative transformation of peptide compounds is carried out nonenzymatically in the presence of transition metal complexes containing a terpy ligand. The sequence-specific cleavage of peptides consisting of C-terminal aliphatic amino acids occurs because of the interligand interactions. Previously, the regioselective hydrolysis of peptides containing histidine or methionine residues has been reported with palladium(II) complexes,[21] in which coordination of the functional group of the peptide side chain to the palladium center was the key step for generating the selectivity. As compared with the previous reactions, our finding that the bulkiness of the aliphatic side chain — a nonfunctional group of the amino-acid residue — controls the specificity is the first report of the oxidative degradation of a peptide due to intramolecular noncovalent interactions with a ternary cobalt(III) complex.

Experimental Section

General: Reagents used for synthesis were of the highest grade available and were employed without further purification. The starting cobalt(III) complex, [Co(CO_3)(OH)(terpy)], was prepared according to the reported method.[22] All solvents for spectroscopic measurements were purified by distillation before use. Electronic absorption spectra were recorded on a JASCO UVIDEC-660 spectrometer. ^{1}H NMR spectra were measured on a Varian VXR-300S or JEOL Lambda-500 spectrometer with TMS as an internal standard. Crystal-structure analyses were performed with an Enraf−Nonius CAD4-EXPRESS four-circle diffractometer. Single crystals of the complexes suitable for the X-ray diffraction measurement were mounted on a glass capillary. The diffraction data were collected with graphite-monochromated Mo-K_α radiation with the ω-2θ scan technique at room temperature. Crystal data and experimental details are listed in Table 2, in which weighted refinement values (Rw) are obtained as follows: $Rw = [\Sigma w(F_o^2 - F_c^2)^2/\Sigma w(F_o^2)^2]^{1/2}$. At the appropriate time of the reaction with GGL, the yields of [Co(gg′l)(terpy)] (**1a**), [Co(g′l)(terpy)] (**1b**), and [Co(ggl)(terpy)] (**1c**) were determined by HPLC analysis (column, ODS CrestPak C18s. eluent, MeOH/water gradient method (5:95 → 35:65). UV-detector, wavelength = 513 nm). The ratio of these complexes varied during the reaction.

Complexation and Characterization of Ternary Cobalt(III) Complexes: Under aerobic conditions, the reaction of [Co(CO_3)(OH)(terpy)] (0.37 g, 2 mmol) and an equimolar amount of tripeptide [GGL (**1**), BGL (**2**), GGF (**3**), GGA (**4**), GGG (**5**), FGG (**6**), or GBL (**7**)] was carried out at pH 8.5 and 40 °C in an aqueous solution (50 mL). After 10 h, separation of the reaction mixture on a SP Sephadex C-25 column gave three separation patterns. In the cases of **1**−**3** as the first group separation pattern, two fraction bands (**a** and **b**) containing a neutral complex were eluted with water, one (**c**) containing a positively charged complex was eluted with 0.1 M NaCl solution, and one (**d**) was eluted with 0.2 M solution. In the case of **4** as the second group, one fraction band (**a** + **b**) was eluted with water, in which obvious separation of **4a** and **4b**

Table 2. Crystal data for the complexes **1b** and **6c**

Complex	{[Co(g′l)(terpy)]}$_2$·3.5H_2O (**1b**)	[Co(fgg)(terpy)]·2H_2O (**6c**)
Formula	$Co_2C_{46}H_{51}N_{10}O_{11.5}$	$CoC_{28}H_{29}N_6O_6$
Fw	1045.84	604.51
Crystal system	triclinic	triclinic
Space group	*P*1	*P*1
a (Å)	11.336(6)	8.884(1)
b (Å)	14.668(6)	11.694(2)
c (Å)	8.304(4)	7.594(2)
α (°)	96.50(3)	96.75(2)
β (°)	100.06(4)	105.75(2)
γ (°)	96.92(4)	72.55(1)
V (Å^3)	1336(1)	723.8(3)
Z	1	1
$\rho_{calcd.}$ (g cm^{-3})	1.299	1.387
μ (cm^{-1})	6.85	6.44
R_1 [a]	0.083	0.067
*R*w[b]	0.275	0.190
λ. Å	0.71070	0.71070
No. of reflections used [$I > 2\sigma(I)$]	3805	2500
No. of variables	631	371

[a] $R_1 = \Sigma||F_o| - |F_c||/\Sigma|F_o|$. [b] $Rw = [\Sigma w(F_o^2 - F_c^2)^2/\Sigma w(F_o^2)^2]^{1/2}$; $w = 4F_o^2/\sigma^2(F_o)^2$.

 © 2004 Wiley-VCH Verlag GmbH & Co. KGaA, Weinheim

from the column was not accomplished, and two bands, containing (**4c**) and (**4d**), were eluted with 0.1 M NaCl, and 0.2 M NaCl solution, respectively. In the case of the reaction with **5**−**7**, no fractional band corresponding to **a** or **b** was eluted with water; one band (**c**) was eluted with 0.1 M NaCl solution and another (**d**) with 0.2 M NaCl solution. These column patterns for the fractional bands are typical for the sequence of tripeptides employed here. In all cases, the complex contained in the last band (**d**) was identified as $[Co(terpy)_2]^{3+}$.[9] In the case of GGL (**1**), the amounts of **1b** increased with increasing reaction time. The structure of **1b** was confirmed by elemental analysis as well as by X-ray single crystal and ^1H NMR analysis. Elemental analysis of **1b**: $[Co(g'l)(terpy)]\cdot 4H_2O$; $C_{23}H_{30}CoN_5O_8$ (563.45): calcd. C 49.03, H 5.37, N 12.43; found C 49.23, H 5.30, N 12.13.

After 24 h, the isolated yield of **1b** was over 70% based on the starting cobalt complex, while the total yields of **1a** and **1c** were under 10%. Reverse-phase HPLC analyses of the reaction mixture indicated that the primary product of the complex formation with Co-terpy and GGL at the initial stage of the reaction was **1c**, which was oxidized to **1a** under aerobic conditions. Under anaerobic conditions, however, **1a** was not detected in the HPLC analyses. Similar time-dependent product distributions were observed in the reaction with BGL (**2**) and GGF (**3**). In the case of GGG (**5**), FGG (**6**), and GBL (**7**), the positively charged complexes, **5c** (75%), **6c** (65%), and **7c** (60%), eluted with 0.1 M NaCl solution, were the main products, respectively; neutral products, corresponding to **5a**, **5b**, **6a**, **6b**, **7a**, and **7b**, were not detected even after 24 h. NMR measurement of all complexes isolated from the eluting solution was carried out in D_2O solution. These data are listed in Table 1. The X-ray analyses of the single crystals of **1b** and **6c** were performed according to the previous methods.[7] Crystal data are summarised in Table 2. During the crystallization of **6c** at room temperature, the positively charged complex eluted from the column changed to a neutral one (presumably, carbonate ions generated from carbon dioxide in the atmosphere might act as a reagent for charge neutralization), presumably because a neutral compound crystallizes more easily than a positive one.

Acknowledgments

This research was supported in part by a Grant-in-Aid for Scientific Research from the Ministry of Education, Science, Sports and Culture.

[1] C. L. Hawkins, M. J. Davies, *Biochem. Biophys. Acta* **2001**, *1504*, 196−219.
[2] W. M. Garrison, *Chem. Rev.* **1987**, *87*, 381−398.
[3] E. R. Stadtman, *Methods. Enzymol.* **1995**, *258*, 379−393.
[4] M. Jonsson, H.-B. Kaartz, *J. Chem. Soc., Perkin Trans. 2* **1997**, 2673−2676.
[5] R. T. Dean, S. Fu, R. Stocker, M. J. Davies, *Biochem. J.* **1997**, *324*, 1−18.
[6] [6a] T. M. Rana, C. F. Meares, *J. Am. Chem. Soc.* **1990**, *112*, 2457−2458. [6b] T. M. Rana, C. F. Meares, *Proc. Natl. Acad. Sci. USA* **1991**, *88*, 10578−10582.
[7] K. Jitsukawa, T. Irisa, H. Einaga, H. Masuda, *Chem. Lett.* **2001**, 30−31.
[8] E. C. Constable, *Tetrahedron* **1992**, *48*, 10013−10059, and references cited therein.
[9] H. Elsbernd, J. K. Beattie, *J. Inorg. Nucl. Chem.* **1972**, *34*, 771−774.
[10] J. K. Moran, C. F. Mears, *Dictionary of Inorganic Compounds*, Chapman and Hall, London, **1992**, p. 3075.
[11] P. A. Sutton, D. A. Buckingham, *Acc. Chem. Res.* **1987**, *20*, 357−364.
[12] E. J. Evans, J. E. Grice, C. J. Hawkins, M. R. Heard, *Inorg. Chem.* **1980**, *19*, 3496−3502.
[13] D. A. Buckingham, C. E. Davis, D. M. Foster, A. M. Sargeson, *J. Am. Chem. Soc.* **1970**, *92*, 5571−5579.
[14] J. Chin, *Acc. Chem. Res.* **1991**, *24*, 145−152.
[15] F. Himo, P. E. M. Siegbahn, *Chem. Rev.* **2003**, *103*, 2412−2456.
[16] J. M. Rowland, M. M. Olmstead, P. K. Mascharak, *Inorg. Chem.* **2002**, *41*, 2754−2760.
[17] K. Jitsukawa, T. Hata, T. Yamamoto, H. Masuda, H. Einaga, *Chem. Lett.* **1994**, 1169−1172.
[18] M. Bakir, P. S. White, A. Dovletoglou, T. J. Meyer, *Inorg. Chem.* **1991**, *30*, 2835−2836.
[19] [19a] F. Barigelletti, L. Flamigni, V. Balzani, J.-P. Collin, J.-P. Sauvage, A. Sour, E. C. Constable, A. M. W. C. Thompson, *J. Am. Chem. Soc.* **1994**, *116*, 7692−7699. [19b] B. J. Coe, D. W. Thompson, C. T. Culbertson, J. R. Schoonover, T. J. Meyer, *Inorg. Chem.* **1995**, *34*, 3385−3395.
[20] M. Yashiro, M. Higuchi, M. Komiyama, Y. Ishii, *Bull. Chem. Soc. Jpn.* **2003**, *76*, 1813−1817.
[21] [21a] T. J. Parac, G. M. Ullmann, N. M. Kostic, *J. Am. Chem. Soc.* **1999**, *121*, 3127−3135. [21b] N. M. Milovic, N. M. Kostic, *J. Am. Chem. Soc.* **2002**, *124*, 4759−4769.
[22] E. S. Kucharski, B. W. Skelton, A. H. White, *Aust. J. Chem.* **1978**, *31*, 47−51.

Received March 31, 2004
Early View Article
Published Online August 12, 2004

 © 2004 Wiley-VCH Verlag GmbH & Co. KGaA, Weinheim

Extending The Reaction Landscape of the {Pt(μ-S)$_2$Pt} Core: From Metal Centers to Non-Metallic Electrophiles

Pilar González-Duarte,*[a] Agustí Lledós,[a] and Rubén Mas-Ballesté[a]

Keywords: Platinum / Sulfur / Metalloligand / Nucleophile / Building block

Figure 4 on p. 3595 of the original article[1] was inadvertently reproduced incorrectly. The correct figure is given below.

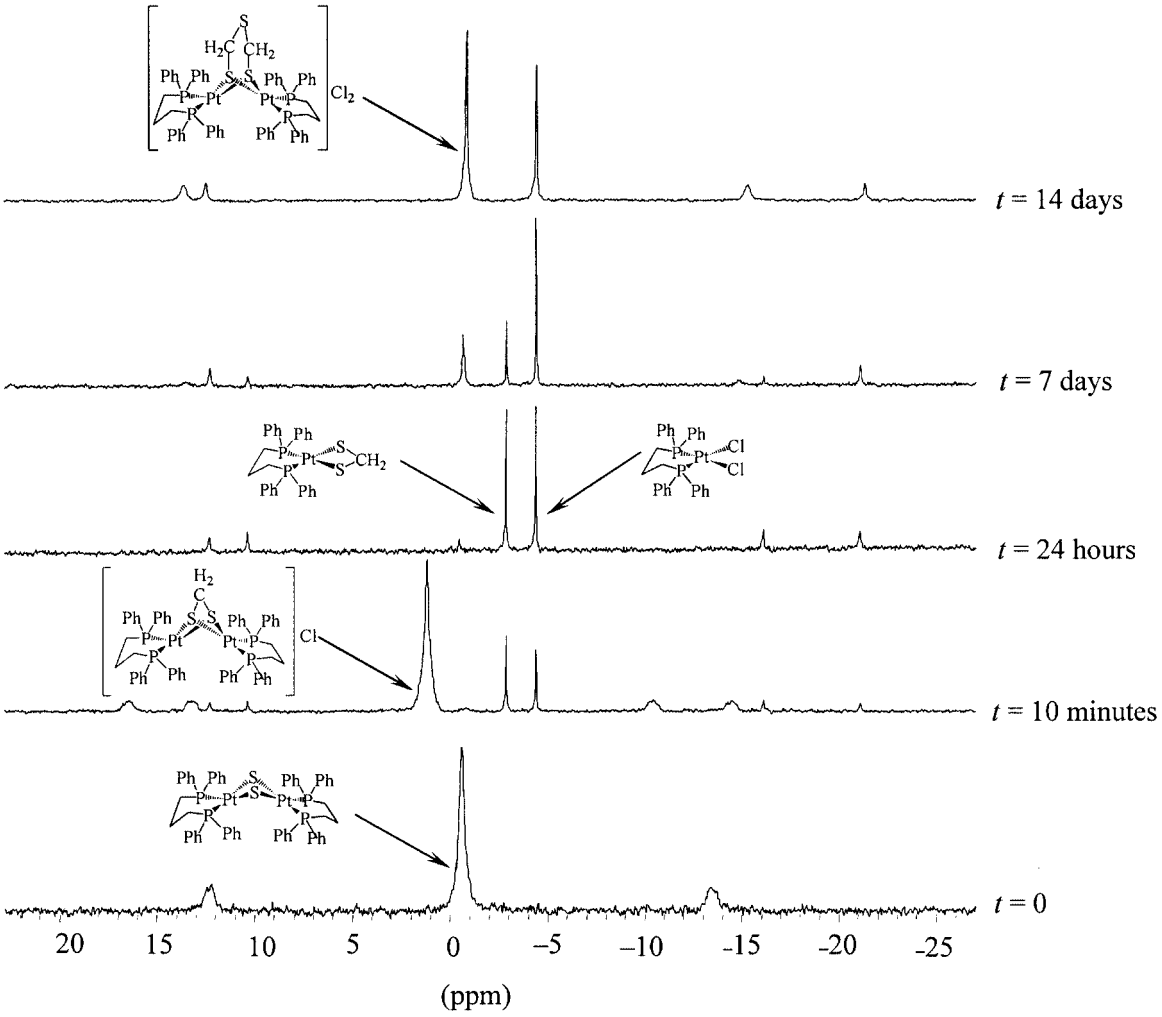

Figure 4. Progression of [Pt$_2$(dppp)$_2$(μ-S)$_2$] in CH_2Cl_2 as a function of time monitored by $^{31}P\{^1H\}$ NMR spectroscopy

[1] P. González-Duarte, A. Lledós, R. Mas-Ballesté, *Eur. J. Inorg. Chem.* **2004**, 3585−3599 (DOI: 10.1002/ejic.200400422).

Received September 13, 2004
The Editors

[a] Departament de Química, Universitat Autònoma de Barcelona, 08193 Bellaterra, Barcelona, Spain
Fax (internat.): +34-935-813-101
E-mail: Pilar.Gonzalez.Duarte@uab.es

 © 2004 Wiley-VCH Verlag GmbH & Co. KGaA, Weinheim **DOI: 10.1002/ejic.200400762**

EurJIC
European Journal of Inorganic Chemistry

Issue 21/2004

Pages 4147–4338

Papers available ahead of print in Early View at www.interscience.wiley.com

Earliest available Table of Contents:
Automatically, free of charge by e-mail through
www.interscience.wiley.com/alerts

COVER PICTURE

The cover picture shows the structure of the Fe^{III}-selective chelating agent ICL670 (R = COOH). ICL670 has a high potential for the oral treatment of iron overload, a condition that originates from regular blood transfusions, as are necessary in the treatment of β-Thalassaemia. However, a possible problem arising from this treatment is the production of $OH^{\cdot}$ radicals, which can be catalysed by redox-cycling of labile Fe^{II}/Fe^{III} species. For a conclusive consideration of potential oxidative stress, a careful elucidation of the stability and redox properties of the various Fe^{II}/Fe^{III} species, which are present at physiological conditions, has been performed. Details are discussed in the article by K. Hegetschweiler et al. on p. 4177 ff..

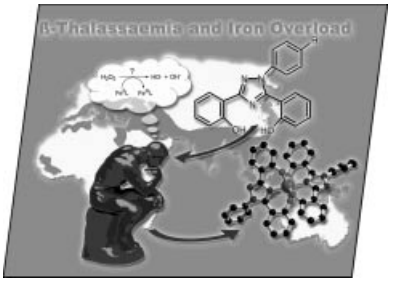

MICROREVIEW

Contents

4161 **C. Gemel, T. Steinke, M. Cokoja, A. Kempter, R. A. Fischer***

Transition Metal Chemistry of Low Valent Group 13 Organyls

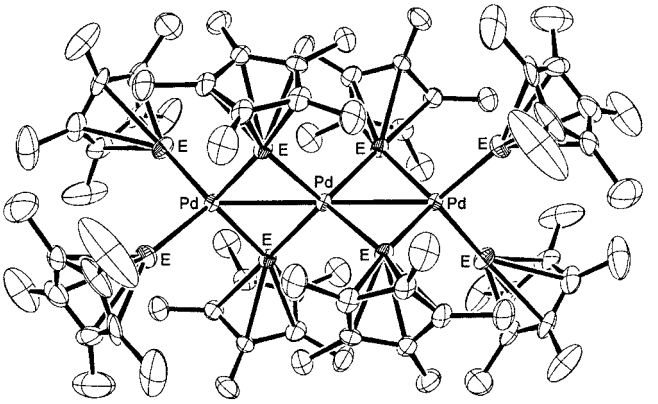

Keywords: Group 13 elements / Transition metals / Main group elements / Carbene homologues

 © 2004 Wiley-VCH Verlag GmbH & Co. KGaA, Weinheim

FULL PAPERS

4177 **S. Steinhauser, U. Heinz, M. Bartholomä, T. Weyhermüller, H. Nick, K. Hegetschweiler***

Complex Formation of ICL670 and Related Ligands with Fe^{III} and Fe^{II}

Keywords: Iron / Ligand design / Chelates / N,O ligands / Redox chemistry

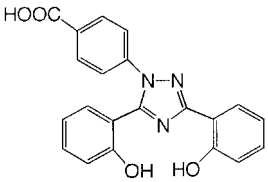

ICL670

4193 **J. I. van der Vlugt, J. M. J. Paulusse, E. J. Zijp, J. A. Tijmensen, A. M. Mills, A. L. Spek, C. Claver, D. Vogt***

Coordination Chemistry and Asymmetric Catalysis with a Chiral Diphosphonite

Keywords: Diphosphonite compounds / Asymmetric hydrogenation / Palladium / Rhodium / Asymmetric hydroformulation / Enantioselectivity

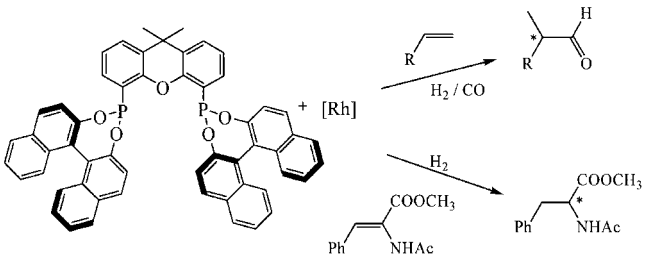

4202 **S. Konar, S. C. Manna, E. Zangrando, T. Mallah, J. Ribas,* N. Ray Chaudhuri***

Structural and Magnetic Properties of Two Carboxylato-Bridged Manganese(II) Complexes with N-Donor Coligands

Keywords: Manganese(II) / Dicarboxylates / N-donor ligands / Crystal structure / Magnetic study

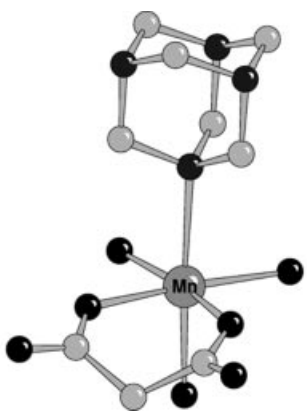

Mn + malonato + htm = 3D

Mn + *m*-phth + bpp = 1D

4209 **S. Mukherjee, T. Weyhermüller, E. Bill, P. Chaudhuri***

Tetranuclear Copper(II) and Nickel(II) Complexes Incorporating a New Imidazole-Containing Ligand

Keywords: Imidazolate bridging / Copper / Nickel / Magnetic properties

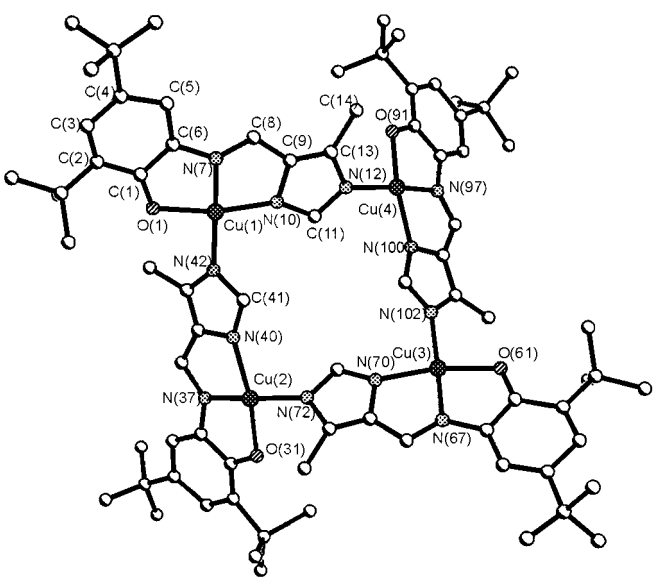

 © 2004 Wiley-VCH Verlag GmbH & Co. KGaA, Weinheim

4216 **H. Houjou,* N. Schneider, Y. Nagawa, M. Kanesato, R. Ruppert, K. Hiratani**

NMR Observations of Interligand Interference in the Molecular Motion of Double-Stranded Dinuclear Helicates

Keywords: DNA / Helical structures / NMR spectroscopy / Palladium / Schiff-base ligands

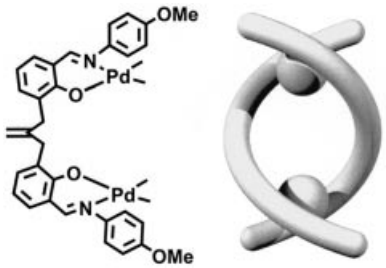

4223 **A. Goswami, H. Pritzkow, F. Rominger, W. Siebert***

Synthesis, Structures and Reactivity of Mono- and Diborylacetylenes

Keywords: Alkynes / Boranes / Cobalt / Cyclooligomerization

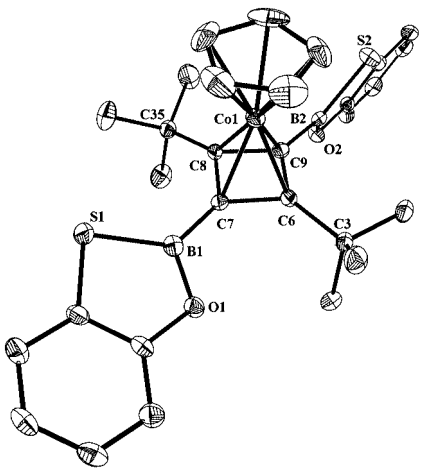

4232 **N. Biricik, Z. Fei, R. Scopelliti, P. J. Dyson***

Isolation of an Intermediate during the Decomposition of a Tetragold-Phosphane Complex

Keywords: N,P Ligands / Diphosphanylamines / Gold complexes

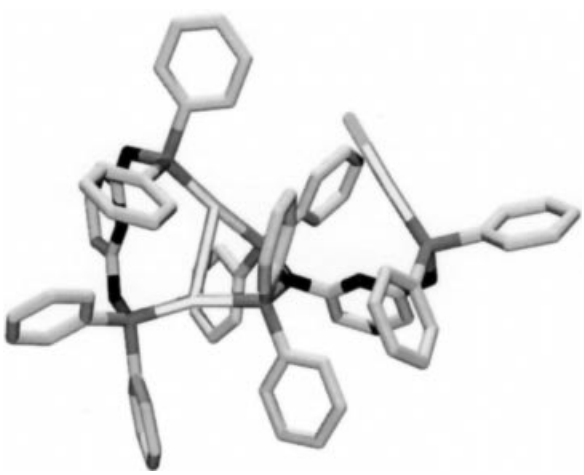

4237 **J. D. Crane,* D. J. Moreton, E. Rogerson**

Nonbridging and Monodentate Carboxylate Coordination of Calcium(2+) Through the Use of Intramolecular Hydrogen Bonding in a New Sterically Hindered Carboxylate Ligand

Keywords: Calcium / Hydrogen bonds / Carboxylate ligands / Sterically hindered ligands

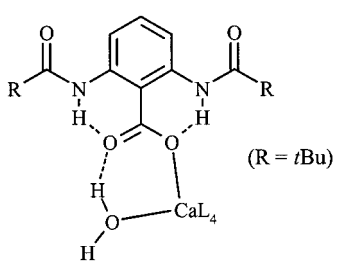

 © 2004 Wiley-VCH Verlag GmbH & Co. KGaA, Weinheim

4242 **V. Pawlowski, H. Kunkely, C. Lennartz,* K. Böhn, A. Vogler***

Synthesis, Structure, Optical Properties and Theoretical Studies of $Pt(P-P)(CN)_2$ with P−P = 1,2-Bis(diphenylphosphanyl)benzene and 2,2′-Bis(diphenylphosphanyl)-1,1′-binaphthyl − Luminescence from Metal-to-Ligand Charge Transfer and Intraligand States

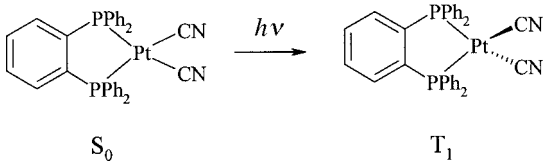

Keywords: Electronic spectra / Luminescence / Platinum complexes / Phosphane complexes / Quantumchemical calculations

4247 **J.-X. Chen, Q.-F. Xu, Y. Xu, Y. Zhang, Z.-N. Chen, J.-P. Lang***

Solid-State Reactions of AgAc with $TabHPF_6$ at Room Temperature − Isolation and Structural Characterisation of an Unusual Octadecanuclear Silver Thiolate Cluster $[Ag_9(Tab)_8(MeCN)_8]_2(PF_6)_{18}\cdot 4MeCN$ [Tab = 4-(trimethylammonio)benzenethiolate]

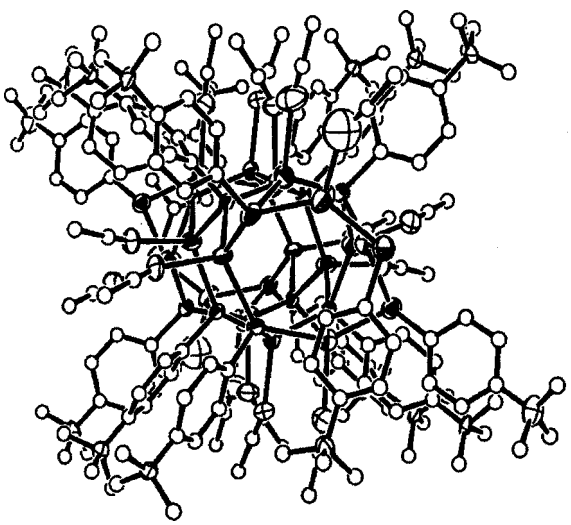

Keywords: Solid-state reactions / Thiolates / Silver / Clusters

4253 **T.-T. Luo, Y.-H. Liu, H.-L. Tsai, C.-C. Su, C.-H. Ueng,* K.-L. Lu***

A Novel Hybrid Supramolecular Network Assembled from Perfect π−π Stacking of an Anionic Inorganic Layer and a Cationic Hydronium-Ion-Mediated Organic Layer

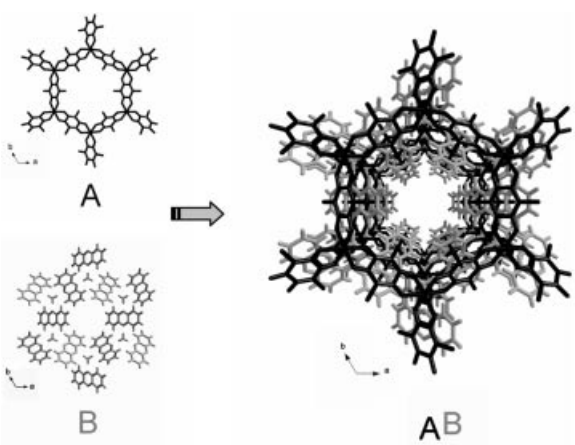

Keywords: Coordination polymers / Hydrogen bonds / Self-assembly / Stacking interactions

 © 2004 Wiley-VCH Verlag GmbH & Co. KGaA, Weinheim

4259 **K. Hassler,* R. Hummeltenberg, G. Tekautz**

The (Chloromethyl)dihalosilanes X_2HSiCH_2Cl (X = F, Cl, Br, I): Synthesis, Multinuclear NMR Spectroscopy and Rotational Isomerism Examined by Raman Spectroscopy

Keywords: Infrared spectroscopy / NMR spectroscopy / Raman spectroscopy / Silanes / Synthesis

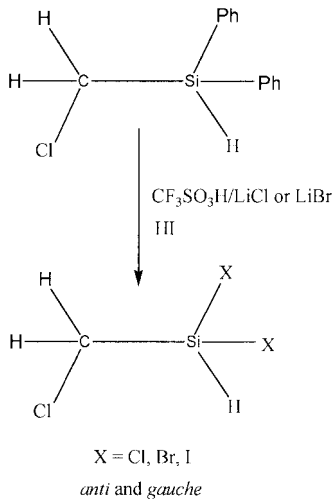

X = Cl, Br, I
anti and *gauche*

4266 **R. Dreos,* G. Nardin, L. Randaccio,* P. Siega, S. Scagliola, G. Tauzher**

The Effect of the Steric Bulk of the Ligand on the Geometry of the Species Self-Assembled from Co^{III} Bis(dioximates) and Boronic Acids

Keywords: Boronic acid / Cobalt / Dioximes / Self-assembly / Solid-state structures

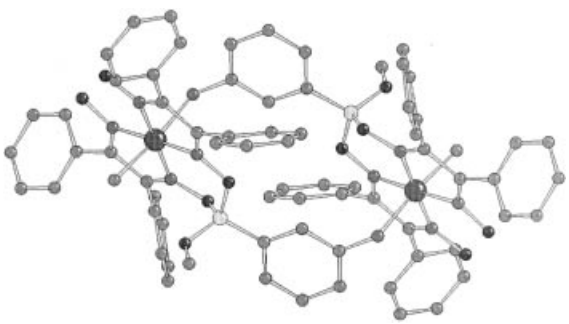

4272 **A. Murso, D. Stalke***

The C_α-Deprotonated Iminophosphorane $Ph_2P(CH_2Py)(NSiMe_3)$ as an *N*,*N*-Chelating Ligand for Iron and Zinc

Keywords: Chelates / Hypervalent compounds / Iminophosphoranes / Iron / N ligands

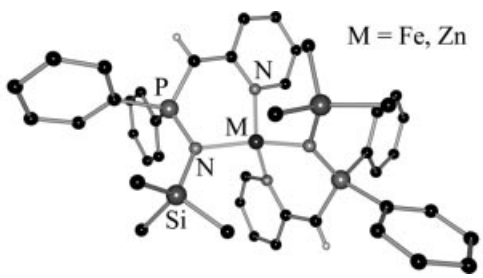

4278 **J. A. Brito, M. Gómez,* G. Muller, H. Teruel,* J.-C. Clinet, E. Duñach, M. A. Maestro**

Structural Studies of Mono- and Dimetallic Mo^{VI} Complexes − A New Mechanistic Contribution in Catalytic Olefin Epoxidation Provided by Oxazoline Ligands

Keywords: Molybdenum / Chiral oxazolines / Selective epoxidation / Oxo peroxo complexes / Catalysis

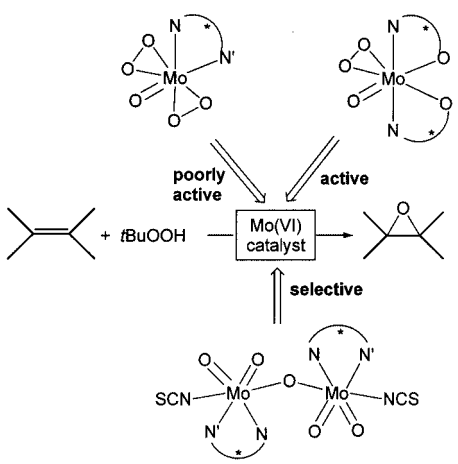

 © 2004 Wiley-VCH Verlag GmbH & Co. KGaA, Weinheim

4286 A. Newport, C. J. Carmalt, I. P. Parkin,* S. A. O'Neill

Formation of VN from VCl_4 and $NH(SiMe_3)_2$ by APCVD − a Potential Solar Control Coating

Keywords: Chemical vapour deposition / Nitrides / Solar control coatings

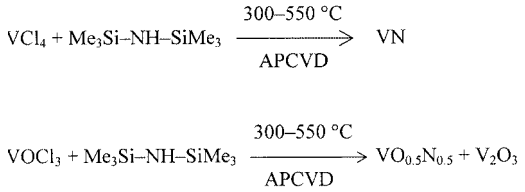

4291 D. Sellmann, R. Prakash,* F. W. Heinemann

Reactivity of a Thiolate-Bridged Dinuclear Ruthenium Complex with Nitrogenous Molecules: Spectroscopic Identification of a Labile Dinitrogen Complex

Keywords: N ligands / Nitrogenases / Nitrogen fixation / Ruthenium / S ligands

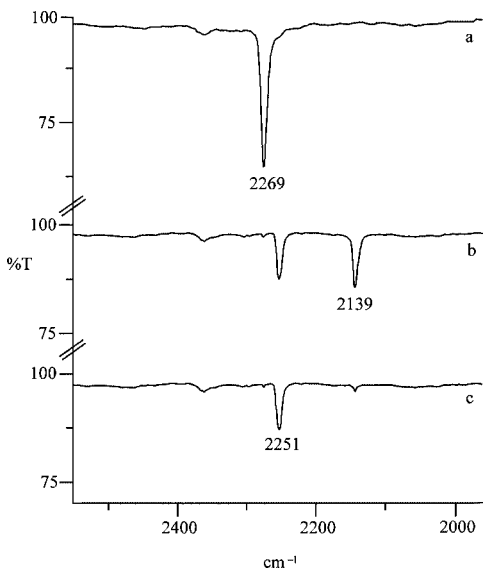

4300 A. Friedrich, U. Radius*

A Calix[4]arene Monoalkyl Ether as a Model of a Tris(phenolate) Ligand with a Hemilabile Anisole Moiety: Syntheses, Molecular Structures and Bonding of Calix[4]arene Ether Supported Titanium Complexes and Their Catalytic Activity in Epoxidation Reactions

Keywords: Calixarenes / Density functional calculations / Epoxidation / Supported catalysts / Titanium

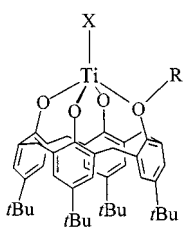

4317 G.-P. Yong, Z. Y. Wang,* Y. Cui

Synthesis, Structural Characterization and Properties of Copper(II) and Zinc(II) Coordination Polymers with a New Bridging Chelating Ligand

Keywords: Coordination polymers / Copper / N,O ligands / Zinc

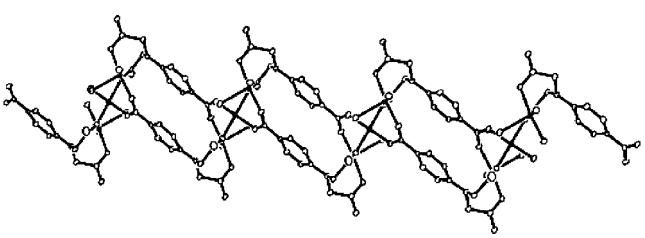

 © 2004 Wiley-VCH Verlag GmbH & Co. KGaA, Weinheim

4324 **C. D. Antoniadis, S. K. Hadjikakou,* N. Hadjiliadis,* M. Kubicki, I. S. Butler**

Synthesis, X-ray Characterisation and Studies of the New Ionic Complex [Bis(pyridin-2-yl) disulfide] Triiodide, Obtained by Oxidation of 2-Mercaptopyridine with I_2 − Implications in the Mechanism of Action of Antithyroid Drugs

Keywords: Bioinorganic chemistry / Iodine complexes / Polyiodides / S ligands / Crystal structures

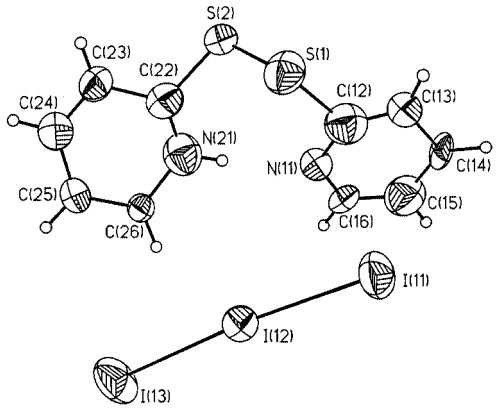

4330 **K. Müller-Buschbaum,* C. C. Quitmann**

Homoleptic Rare-Earth Carbazolates and the Trends of Their $E_{Ln}^{II/III}$ Redox Potentials: Mixed-Valent Samarium in $^1_\infty[Sm_2(Cbz)_5](CbzH)$ (CbzH = carbazole) and Trivalent Thulium, Neodymium and Gadolinium in $[Ln_2(Cbz)_6]$

Keywords: Solvent-free synthesis / Lanthanides / Carbazolates / N ligands

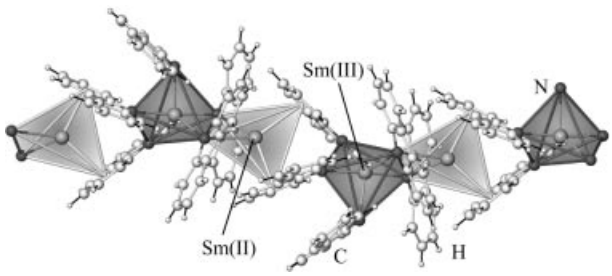

 © 2004 Wiley-VCH Verlag GmbH & Co. KGaA, Weinheim

Transition Metal Chemistry of Low Valent Group 13 Organyls

Christian Gemel,[a] Tobias Steinke,[a] Mirza Cokoja,[a] Andreas Kempter,[a] and Roland A. Fischer*[a]

Keywords: Group 13 elements / Transition metals / Main group elements / Carbene homologues

The coordination of low-valent group 13 organyls E^IR [E = Al, Ga, In; R = Cp*, $C(SiMe_3)_3$] to transition metals has attracted increasing interest over the past decade. Complexes and cluster compounds of these new ligands with a number of transition metals have been isolated and characterised. The E^IR moiety is formally isolobal with CO and PR_3 (R = alkyl, Cp*) or carbenes (R = chelating group) with varying σ-donor and π-acceptor properties depending on the organic group R as well as the group 13 metal E. In this review, different ways of forming M–E bonds such as substitution reactions of labile ligands or insertion of E^IR into transition metal halide bonds are described. Furthermore, the reactivity of homoleptic complexes $M_a(E^IR)_b$ is discussed, outlining the use of these new complex types in bond activation reactions.
(© Wiley-VCH Verlag GmbH & Co. KGaA, 69451 Weinheim, Germany, 2004)

1. Introduction

Since the pioneering discovery by H. Schnöckel in 1989 that the low valent group 13 metals Al^I and Ga^I can be stabilised by coordination of Cp*[1−3] and the subsequent development of convenient synthetic procedures for AlCp*[4,5] and GaCp*[6,7] by H. Roesky and P. Jutzi, much work has been devoted to the coordination of these compounds to transition metal centres.[8,9]

The E^IR fragment is isolobal with CO and PR_3, i.e. it exhibits σ-donation as well as π-accepting properties. The extent of σ-donation and π-acceptance is, of course, dependent on the nature of the metals, but also to a large extent

[a] Anorganische Chemie II, Organometallics and Materials Chemistry, Ruhr Universität Bochum,
Universitätsstrasse 150, 44780 Bochum, Germany
Fax: (internat.) + 49-(0)234-321-4174
E-mail: roland.fischer@ruhr-uni-bochum.de

Roland A. Fischer (far right), born in 1961 in Rosenheim, Germany, studied chemistry at the Technische Universität München (1981−1986). In 1989 he received his doctorate for his work on alkyne complexes of rhenium under the guidance of W. A. Herrmann. After a postdoctoral fellowship at the University of California at Los Angeles with H. D. Kaesz (1989−1990), he returned to the Technische Universität München and completed his habilitation in 1995 on the coordination chemistry of aluminium, gallium and indium at transition metals and on the use of these complexes as MOCVD sources for intermetallic phases. From 1996 to 1997 he was Professor of Inorganic Chemistry at the Ruprecht-Karls-University Heidelberg and in 1998 he moved to the Ruhr-Universität Bochum. His research interests deal with various aspects of organometallic and materials chemistry with some emphasis on precursor chemistry for MOCVD. His scientific work has been honoured among others with the Heinz-Meier-Leibnitz award from the Bundesministerium für Bildung und Forschung (Federal Ministry for Education and Science) (1993), a Karl-Winnacker scholarship (1995) and the award of the Alfried-Krupp-von-Bohlen-und-Halbach Foundation (1996).

Christian Gemel (centre) was born in 1971 in Vienna, Austria. From 1990−1996 he studied Chemistry at the Technical University of Vienna, receiving his Doctorate in 1997 for his work on organoruthenium chemistry in the group of Karl Kirchner. After postdoctoral visits to Kenneth G. Caulton, Indiana University (1998) and Klaus Richard Poerschke, MPI Mülheim (2000−2001), he joined the group of Prof. Roland Fischer in 2002. He became a permanent research staff member in 2004.

Tobias Steinke (far left), born in 1974 in Bochum, Germany trained as a teacher of chemistry from 1995−2000. In 2001 he started to work on his PhD under the guidance of Prof. Fischer on the coordination chemistry of ECp to transition metals. His doctoral work has been awarded with the Wolfgang-Seel-Preis.*

Mirza Cokoja (centre left) was born in 1979, Oberhausen, Germany and studied chemistry at the Ruhr University Bochum from 1998−2003. He received his Diploma in 2003 for his work on the insertion reactions of ECp into Ru−Cl Bonds.*

Andreas Kempter (centre right) was born in 1978, Sigmaringen, Germany and studied chemistry at the Ruhr University Bochum from 1999−2004. He received his Diploma in 2004 for his work on the coordination chemistry of sterically encumbered low valent group 13 metals.

MICROREVIEWS: This feature introduces the readers to the author's research through a concise overview of the selected topic. Reference to important work from others in the field is included.

on the organic group R. For R = Cp*, for example, the vacant p-orbitals of the group 13 metal are partially populated by the π-donor orbitals of the Cp* groups thus diminishing the π-acceptor properties of the ligand. In fact, the contribution of the σ-donation has been calculated to be very large, resulting in the highest contribution of the bond energy being the electrostatic attraction between the partially positive group 13 metal and the partially negative transition metal, following the order Al > Ga > In.[10]

In contrast to the chemistry of transition metal borylene complexes which has been recently reviewed by H. Braunschweig,[11–13] the free ligands E^IR are stable and isolable. This facilitates access to their transition metal complexes since classic organometallic synthetic approaches can be applied. Substitution of labile ligands by E^IR is the most general route of forming transition metal-group 13 element bonds. Homoleptic as well as heteroleptic complexes $[M_a(E^IR)_bL_c]$ are accessible from a wide range of transition metal complexes such as carbonyl, olefin or phosphane complexes. The ease of oxidation of E^IR provides less common synthetic pathways. Thus, E^IR can act as in situ reducing agents towards higher oxidation state transition metal complexes $[L_nMX_n]$, giving either insertion products if the oxidised group 13 metal remains coordinated to the transition metal centre or low oxidation state complexes $[M_a(E^IR)_b]$ by cleavage of X_2ER.

In this review we wish to highlight recent developments in this particular field from a mainly synthetic point of view. Fundamental bonding and general structural issues have been intensively discussed in the literature previously.[10,14–17] However, interest in E^IR has somewhat diminished during the last few years most likely because the chemistry of these new species has been considered to be quite unexciting. In contrast, our recent results which focus particularly on the transition metal chemistry of AlCp*, GaCp* and InCp* have revealed the unexpected potential of these compounds in classic organometallic and cluster chemistry. Herein we hope to convince the reader that these "exotic" ligands and related compounds hold much promise for the future.

2. Carbonyl Complexes $M_a(CO)_b(ER)_c$

Since the first isolation of E^IR, investigations of their properties as ligand towards transition metals have mostly involved metal carbonyl fragments. In particular, the reaction of E^IR with homoleptic transition metal carbonyls has been studied in detail. Hence, the complexes $[Mn_2(CO)_8\{\mu^2\text{-}[InC(SiMe_3)_3]\}_2]$,[18] $[Co_2(CO)_6(\mu^2\text{-}ECp^*)_2]$ (**1a**: E = Al,[19] **1b**: Ga[6]) or $[Ni_4(\mu^2\text{-}GaCp^*)_4(CO)_6]$[6] were obtained by treatment of the homoleptic metal carbonyl clusters with E^IR. The compounds $[Cr(CO)_5(ECp^*)]$ (E = Al,[20] Ga,[6] In[21]), $[(GaCp^*)_2Mo(CO)_4]$,[22] $[Fe_2(CO)_6\{\mu^2\text{-}In[C(SiMe_3)_3]\}_2]$ (**2**)[23] and $[Fe(CO)_4(GaCp^*)]$ (**3a**)[6] were obtained by substitution of chelating olefin ligands such as cyclooctene, norbornadiene, cyclooctatetraene and cycloheptatriene, respectively. Some carbonyl complexes, such as $[Fe(CO)_4(AlCp^*)]$ (**3b**),[24] are also available by salt metathesis from carbonylmetallates and $E^{III}RX_2$.[25–27]

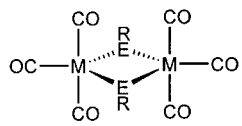

1a (M = Co, ER = AlCp*)
1b (M = Co, ER = GaCp*)
2 (M = Fe, ER = $InC(SiMe_3)_3$)

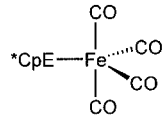

3a (E = Ga)
3b (E = Al)

A recent example of ligand substitution on metal carbonyl fragments is the reaction of [*fac*-$(RCN)_3M(CO)_3$] (R = Me, M = Mo; R = Et, M = W) with GaCp* giving the monomeric compounds [*fac*-$(GaCp^*)_3M(CO)_3$] (**4a**: M = Mo, **4b**: W).[28] It was shown that compound **4a** can act as a building block for the synthesis of dinuclear complexes affording $[Mo_2(CO)_6\{\mu^2\text{-}(GaCp^*)\}_3]$ (**5**) upon reaction with [*fac*-$(MeCN)_3Mo(CO)_3$] (Scheme 1).

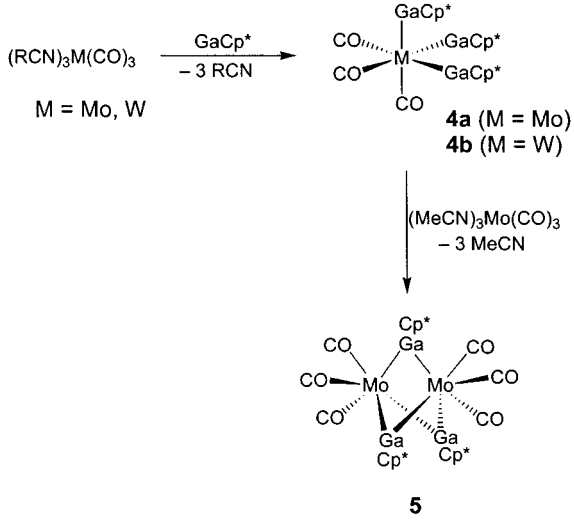

Scheme 1. Synthesis of $[Mo_2(CO)_6\{\mu^2\text{-}(GaCp^*)\}_3]$ (**5**)

In contrast to the well explored substitution reactions of ECp*, the addition to coordinatively unsaturated centres is only known for the in situ formed $[(dcpe)_2Pt]$ complex [dcpe = bis(dicyclohexylphosphanyl)ethane] leading to $[(dcpe)_2Pt(E^IR)_2]$.[29,30] The unsaturated 14 VE fragment $[(dcpe)_2Pt]$ is thermally formed from $[(dcpe)_2PtH(neopentyl)]$ and trapped in the presence of E^IR ligands (Scheme 2).

An unsaturated carbonyl system which has been studied in more detail is the reaction of GaCp* with the multiple bonded dimeric complexes $[CpM(CO)_2]_2$ (M = Mo, W). Reaction with GaCp* yields the addition products $[Cp(CO)_2M(\mu\text{-}GaCp^*)]_2$ (**6a**: M = Mo, **6b**: M = W) (Scheme 3).[28]

An unusual feature of **6a** and **6b** is the η^1-coordination mode of the Cp* moieties bound to the bridging Ga atoms, presumably a consequence of the steric overcrowding in the

 © 2004 Wiley-VCH Verlag GmbH & Co. KGaA, Weinheim

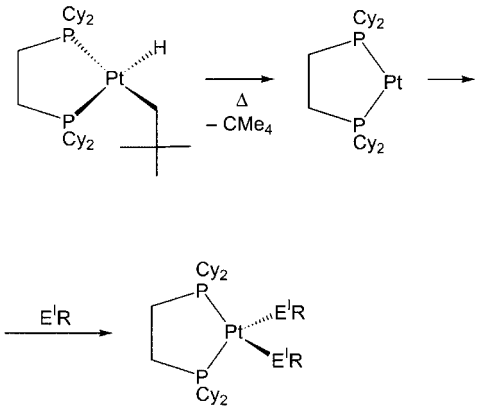

Scheme 2. Trapping of the unsaturated fragment $[(dcpe)_2Pt]$ with E^IR

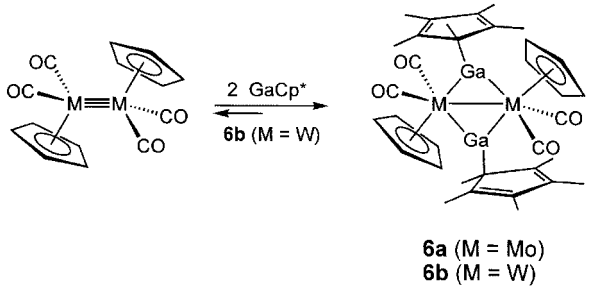

Scheme 3. Synthesis of $[Cp(CO)_2M(\mu\text{-}GaCp^*)]_2$ (**6a**: M = Mo, **6b**: M = W)

molecules. The GaCp* coordination in the tungsten complex is surprisingly weak and shows a temperature dependent association/dissociation equilibrium.

3. Homoleptic Complexes of the Type $[M_a(ECp^*)_b]$ (M = Ni, Pd, Pt)

3.1 Monomeric Complexes $[M(ECp^*)_4]$

The COD ligands in $[Pt(COD)_2]$ and $[Ni(COD)_2]$ (COD = 1,5-cyclooctadiene) can be readily replaced by ECp* or $E[C(SiMe_3)_3]$ yielding monomeric complexes of the type $[M(E^IR)_4]$ (M = Pt, Ni; R = Cp*; Figure 1).[22,31,32] Analogous Pd compounds can be obtained by treatment of $[Pd(tmeda)(CH_3)_2]$ with ECp*. In contrast to the reaction of $[Pd(tmeda)(CH_3)_2]$ (tmeda = *N*,*N*,*N*′,*N*′-tetramethylethylenediamine) with PR_3 giving $Pd(PR_3)_n$ which usually proceeds via a ligand-assisted reductive elimination of ethane, the reaction with ECp* includes a methyl group migration and reduction of the palladium centre by ECp*.[33]

All complexes $[M(E^IR)_4]$ are kinetically inert, indicating the high bond energy of the ECp* to transition metal linkage. Substitution reactions with PR_3 or CO do not take place and a coalescence of $[M(E^IR)_4]$ and the free E^IR is not observed in the NMR spectra. Also, the synthesis of heteroleptic complexes $[M(ECp^*)_n(E'Cp^*)_m]$ ($n + m = 4$) is not possible by ligand substitution. Interestingly, in the series $[M(ECp^*)_4]$ (M = Ni, Pd, Pt and E = Al, Ga, In), only $[Pt(InCp^*)_4]$ seems to be thermally unstable, decomposing at temperatures above −30 °C. This indicates weaker σ-donor properties of InCp* compared with $InC(SiMe_3)_3$, AlCp* or GaCp*.

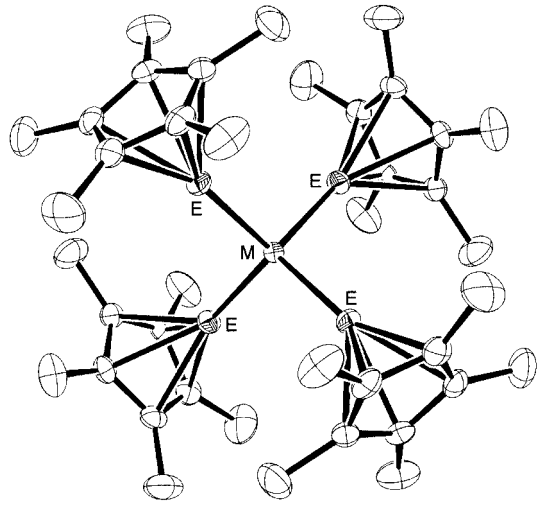

Figure 1. Monomeric Clusters $[M(ECp^*)_4]$

3.2 Cluster Complexes $[M_2(ECp^*)_5]$ and $[M_3(ECp^*)_8]$

Compared with the above examples, neutral homoleptic cluster compounds of the type $[M_a(ECp^*)_b]$ (M = Pd, Pt; $b > a > 1$) represent quite a novel and more promising field in the coordination chemistry of E^IR (E = Al, Ga, In). Recent studies concerning the synthesis of cluster compounds have been focused on the coordination of E^IR to transition metal carbonyl fragments $[(CO)_nM_a]$. Constitution and structural characteristics of new GaCp*-substituted Ni_4 [6] and Rh_6 carbonyl clusters[34] or $[\{(CpNi)(\mu_2\text{-}AlCp^*)\}_2]$[35] are directly related to classical transition metal carbonyl cluster structures. In contrast, the novel homoleptic series $[M_a(ECp^*)_b]$ has no direct structural analogue in classical carbonyl or phosphane cluster chemistry, although recently the coordination chemistry of PR_3 has been extended to include a bridging mode.[36] These complexes exhibiting bridging and terminal E^IR ligands are still rare in comparison with other M−E complexes. In principle, access to $[M_a(ECp^*)_b]$ proceeds via two different reaction pathways: (i) by building block synthesis and (ii) via direct methods. In both cases, E^IR reacts with a transition metal complex bearing labile ligands (e.g. olefins) with full substitution of the ligands, the nature of the products being determined mainly by kinetic factors.

3.2.1 Building Block Synthesis of Homoleptic Clusters $[MPt(GaCp^*)_5]$

The monomeric compounds $[M(GaCp^*)_4]$ (**7a**: M = Pt, **7b**: M = Pd; Figure 1) can serve as building blocks for the synthesis of the dinuclear cluster complexes $[MPt(GaCp^*)_5]$ (**8a**: M = Pt, **8b**: M = Pd) with terminal and bridging GaCp* ligands (Scheme 4). The reaction of $[Pt(COD)_2]$

 © 2004 Wiley-VCH Verlag GmbH & Co. KGaA, Weinheim

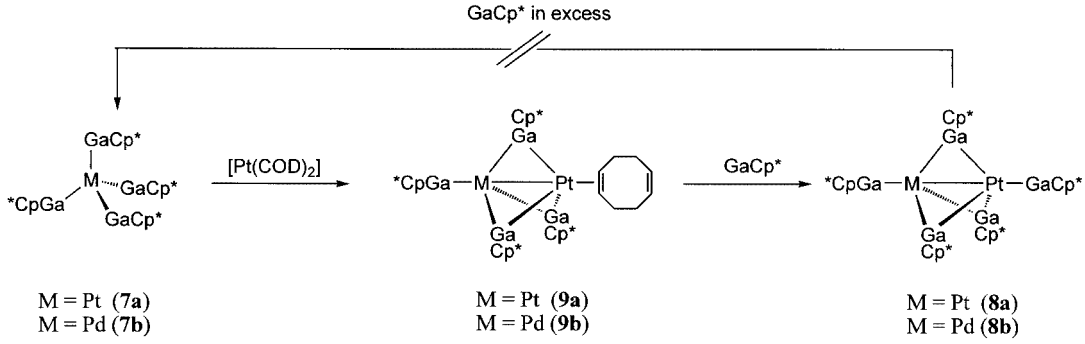

Scheme 4. Building block synthesis of clusters $M_a(ECp^*)_b$

with an equimolar amount of $[M(GaCp^*)_4]$ and subsequent addition of GaCp* yields $[Pt_2(GaCp^*)_2(\mu^2\text{-}GaCp^*)_3]$ (**8a**) and the analogous "trimetallic" heterodinuclear compound $[PtPd(GaCp^*)_2(\mu^2\text{-}GaCp^*)_3]$ (**8b**).

It has been shown that the $[M(GaCp^*)_4]$ species form reactive yet isolable dinuclear associates with $[Pt(COD)_2]$. Based on variable temperature NMR spectroscopic data these intermediates were identified as $[Pt_2(GaCp^*)(\mu^2\text{-}GaCp^*)_3(\eta^2\text{-}COD)]$ (**9a**) and $[PtPd(GaCp^*)(\mu^2\text{-}GaCp^*)_3(\eta^2\text{-}COD)]$ (**9b**).[33]

3.2.2 Direct Synthesis of Homoleptic Clusters $[M_a(ECp^*)_b]$

The reaction of ECp* with transition metal complexes having olefin ligands generally leads to a full substitution of the olefins by ECp*. However, in most cases the ratio of the reactants does not directly determine the composition of the products. Instead, the formation of mono-, di- or trinuclear products is influenced by kinetic factors, i.e. by the reaction temperature, the nature of the transition metal-olefin complex or simply the solubilities of the starting materials and products.

The first direct synthesis of a homoleptic cluster complex was reported in 2000 (Scheme 5). $[Pt_2(GaCp^*)_2(\mu^2\text{-}GaCp^*)_3]$ (**8a**) is quantitatively formed from the reaction of $[Pt(C_2H_4)_3]$ with an excess of GaCp* and could be isolated in analytically pure form in high yields.[37]

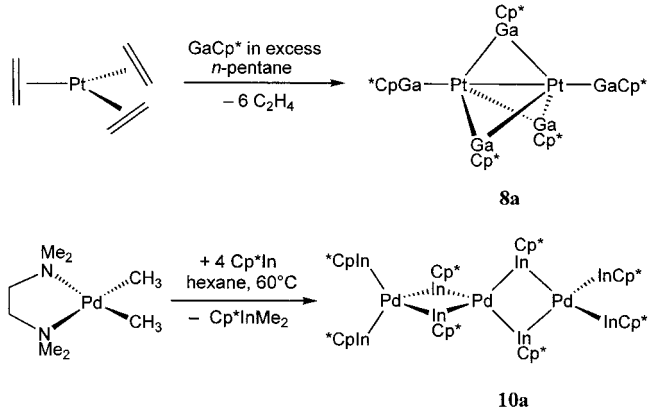

Scheme 5. Synthesis of $[Pt_2(GaCp^*)_2(\mu^2\text{-}GaCp^*)_3]$ (**8a**) and $[Pd_3(InCp^*)_4(\mu^2\text{-}InCp^*)_4]$ (**10a**)

The monomeric complex $[Pt(GaCp^*)_4]$ (**7a**) which is quantitatively formed in the reaction of $[Pt(COD)_2]$ with GaCp* was not observed in this reaction. It was shown

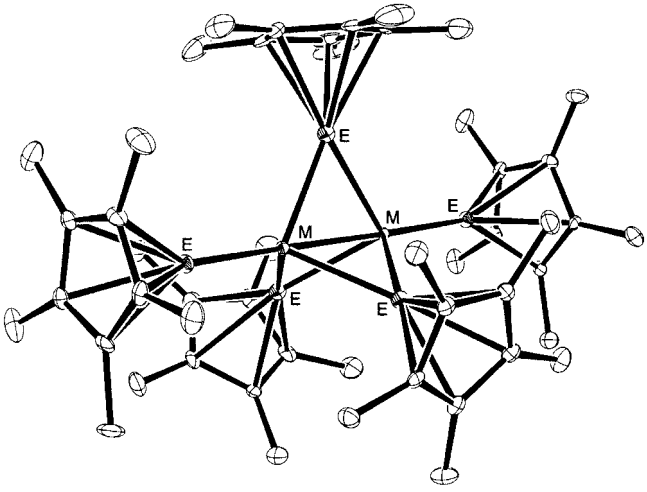

Figure 2. Dimeric clusters $[M_2(ECp^*)_5]$

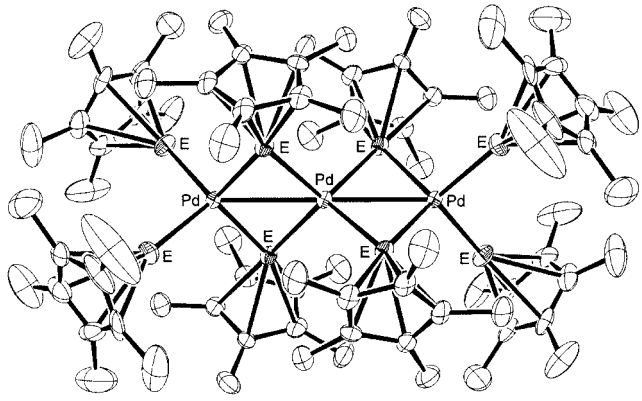

Figure 3. Trimeric clusters $[Pd_3(ECp^*)_8]$

 © 2004 Wiley-VCH Verlag GmbH & Co. KGaA, Weinheim

later that $[Pt_2(GaCp^*)_2(\mu^2\text{-}GaCp^*)_3]$ (**8a**) is also kinetically stable in the presence of free GaCp* and does not react to give $[Pt(GaCp^*)_4]$ (**7a**).[33]

When $[(tmeda)Pd(CH_3)_2]$ is treated with an excess of InCp*, the trinuclear complex $[Pd_3(InCp^*)_4(\mu^2\text{-}InCp^*)_4]$ (**10a**) is quantitatively formed. Complex **10a** is also kinetically inert and does not react to give mononuclear $[Pd(InCp^*)_4]$ in the presence of InCp*.[38]

A good illustrative example of the subtle kinetic control of cluster formation is the reaction of $[Pd_2(dvds)_3]$ with GaCp* (dvds = 1,3 divinyl-1,1,3,3-tetramethyldisiloxane). Depending on the reaction conditions, two different homoleptic clusters are formed. At −30 °C in hexane the reaction yields the dinuclear compound $[Pd_2(GaCp^*)_2(\mu^2\text{-}GaCp^*)_3]$ (**8c**) in quantitative yields. Only trace amounts (< 3%) of the monomeric compound $[Pd(GaCp^*)_4]$ (**7b**) are observed. The reaction in toluene at room temperature yields the trinuclear complex $[Pd_3(GaCp^*)_4(\mu^2\text{-}GaCp^*)_4]$ (**10b**) in high yield, while the dimeric species **8c** is formed in only very small amounts (< 2%) under these conditions (Scheme 6).

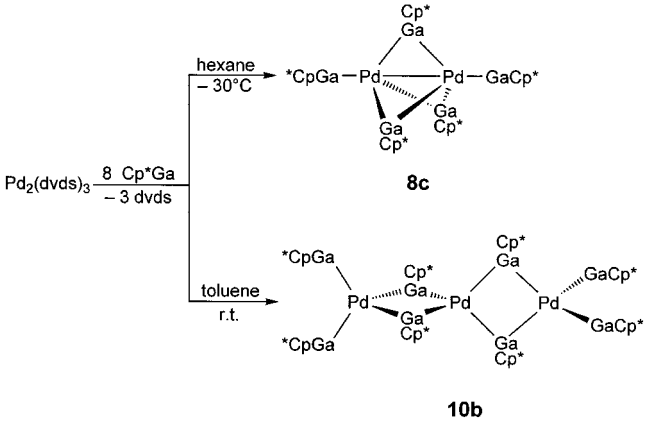

Scheme 6. Synthesis of $[Pd_2(GaCp^*)_2(\mu^2\text{-}GaCp^*)_3]$ (**8c**) and $[Pd_3(GaCp^*)_4(\mu^2\text{-}GaCp^*)_4]$ (**10b**)

3.2.3 Reactivity of Homoleptic Cluster Complexes $[M_a(ECp^*)_b]$ (M = Pd, Pt)

While the syntheses and structural chemistry of M−E complexes and their use as precursors to new materials have attracted widespread interest, remarkably little is still known about their general chemical reactivity. The coordinate M−E bond in such complexes is relatively polar and strong when E = Al, Ga[16] and the steric demand of the E^IR ligands is rather large.[22] Thus, neither dissociative nor associative reactions are very likely to occur at the central metal. Hence, the organometallic chemistry of such compounds would appear to be rather unfruitful. Indeed, the electronically and sterically saturated monomeric complexes $[M(ECp^*)_4]$ turn out to be completely kinetically inert.[39] In sharp contrast, however, the related unsaturated cluster complexes $[M_a(ER)_b]$ ($b > a > 1$) react with a selection of ligands (Cp*Al, CO, phosphanes, isocyanides) to give new di- and trinuclear substitution products (Scheme 7).[40]

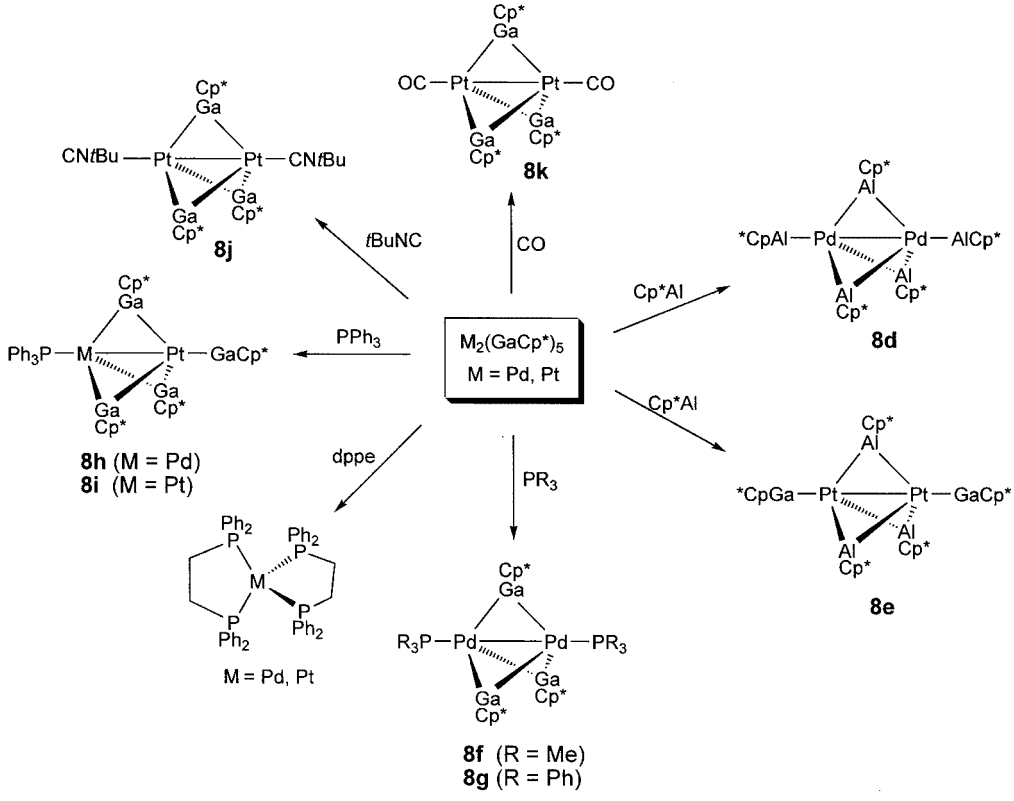

Scheme 7. Reactivity of $[M_2(GaCp^*)_2(\mu^2\text{-}GaCp^*)_3]$

 © 2004 Wiley-VCH Verlag GmbH & Co. KGaA, Weinheim

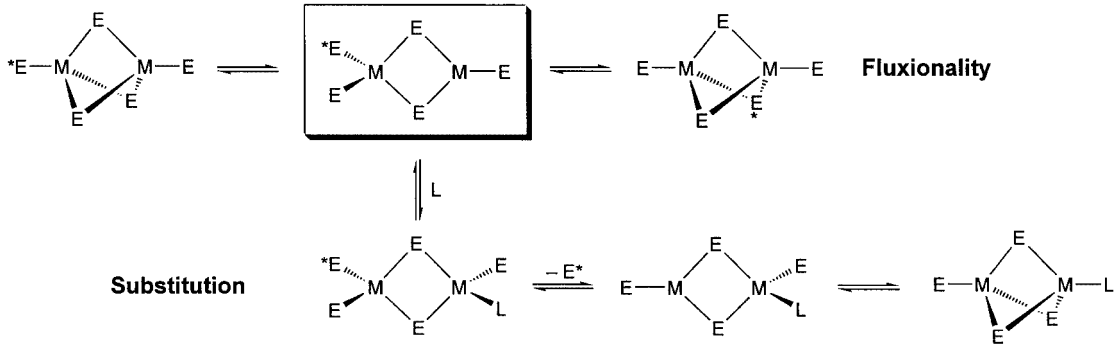

On the basis of quantum chemical calculations by Frenking, the substitution of GaCp* or InCp* by AlCp* in homoleptic complexes is a thermodynamically favourable reaction.[16] Indeed, treatment of $[M_2(GaCp^*)_2(\mu^2\text{-}GaCp^*)_3]$ with AlCp* quantitatively yields the "trimetallic" compound $[Pt_2(GaCp^*)_2(\mu^2\text{-}AlCp^*)_3]$ (**8e**) or the fully substituted dinuclear complex $[Pd_2(AlCp^*)_2(\mu^2\text{-}AlCp^*)_3]$ (**8d**).

The reaction of $[M_2(GaCp^*)_2(\mu^2\text{-}GaCp^*)_3]$ with PPh_3 quantitatively yields the mono- or disubstituted complexes $[MPt(GaCp^*)(PPh_3)(\mu^2\text{-}GaCp^*)_3]$ (**8h**: M = Pd, **8i**: M = Pt) and $[Pd_2(PPh_3)_2(\mu^2\text{-}GaCp^*)_3]$ (**8g**). Whereas the substitution reactions at Pd centres giving **8f** and **8g** readily occur at room temperature, the substitution of GaCp* by PPh_3 in the related Pt_2Ga_5 complex **8a** requires both a longer reaction time and a higher temperature (90 °C). In the case of the "trimetallic" compound **8b**, the substitution can only be observed at the Pd centre, leaving the Pt-GaCp* bond unchanged. This is in good agreement with the fluxionality of $[M_2(E^IR)_5]$ in solution (vide infra). Whereas ligands attached to a palladium centre usually show fast exchange between the terminal and bridging positions, such processes are slower on platinum centres. A dissociative mechanism of the bridging ligands forming unsaturated metal centres as intermediates is assumed for the substitution reactions as well as for the fluxional processes of $[M_2(E^IR)_5]$.

Generally, heteroleptic monomeric complexes of the type $[M(GaCp^*)_{4-x}(L)_x]$ ($x = 1-4$) are not accessible via substitution reactions. However, when the chelating diphosphane ligand dppe [dppe = bis(diphenylphosphanylethane)] is added to $[M_2(GaCp^*)_2(\mu^2\text{-}GaCp^*)_3]$, all Cp*Ga units are substituted and the monomeric complexes $[M(dppe)_2]$ (M = Pd, Pt) are formed quantitatively. The reaction of $[Pt_2(GaCp^*)_2(\mu^2\text{-}GaCp^*)_3]$ (**8a**) with the strong π-acceptors CN*t*Bu or CO gives the disubstitution products $[Pt_2(CNtBu)_2(\mu^2\text{-}GaCp^*)_3]$ (**8j**) and $[Pt_2(CO)_2(\mu^2\text{-}GaCp^*)_3]$ (**8k**), respectively, with the GaCp* ligands preferring the bridging positions.

In contrast to the substitution reactions of $[M_2(GaCp^*)_2(\mu^2\text{-}GaCp^*)_3]$ complexes, where the cluster core is always retained, the reaction of the trinuclear compound $[Pd_3(InCp^*)_8]$ (**10a**) with PPh_3 or dppe leads to a rearrangement of the linear Pd_3 core to give the triangular Pd_3 clusters $[Pd_3(InCp^*)_3(PPh_3)_3]$ (**10c**) and $[Pd_3(InCp^*)_3(dppe)_2]$ (**10d**) (Scheme 8).

In both complexes two InCp* units cap both faces of a Pd triangle resulting in a trigonal bipyramidal geometry.

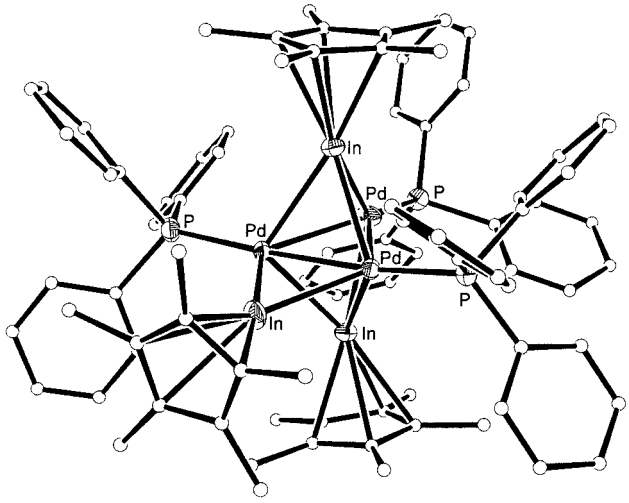

Figure 4. Triangular cluster **10c**

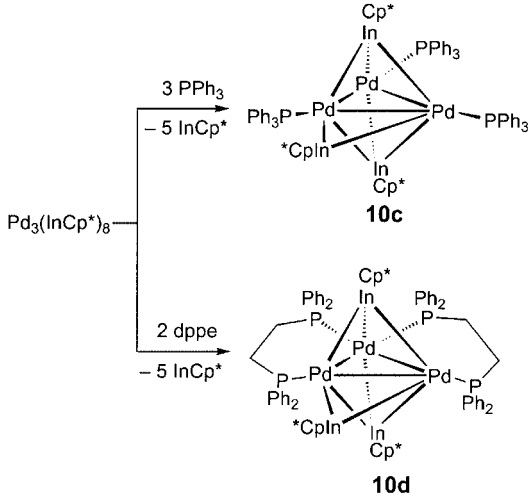

Scheme 8. Synthesis of $[Pd_3(InCp^*)_3(PPh_3)_3]$ (**10c**) and $[Pd_3(InCp^*)_3(dppe)_2]$ (**10d**)

The third InCp* ligand is found in a μ^2-coordination mode parallel to the Pd_3 plane. Additionally, each Pd centre is coordinated by one or two terminal phosphane ligands.

3.2.4 Solution Structures and NMR Spectroscopy

Whereas $[Pt_2(GaCp^*)_2(\mu^2\text{-}GaCp^*)_3]$ (**8a**) exhibits a static NMR spectrum at room temperature, i.e. two well dis-

 © 2004 Wiley-VCH Verlag GmbH & Co. KGaA, Weinheim

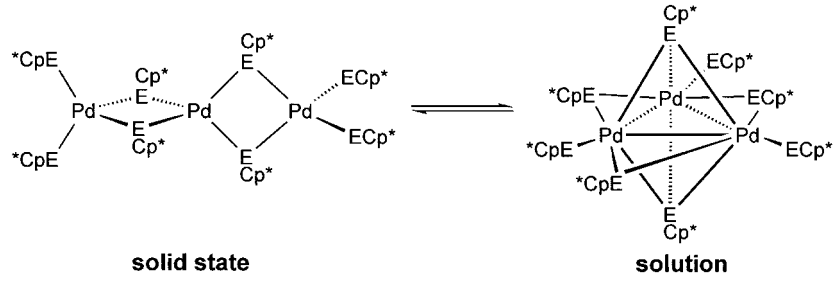

tinguishable signal sets (singlets) for the bridging and the terminal GaCp* ligands, the corresponding palladium cluster $[Pd_2(GaCp^*)_2(\mu^2\text{-}GaCp^*)_3]$ (**8c**) is dynamic in solution and gives rise to only one Cp* signal set. The ^1H NMR spectrum of $[PtPd(GaCp^*)_2(\mu^2\text{-}GaCp^*)_3]$ (**8b**) at room temperature shows two resonances with an integral ratio of 1:4. Clearly the fluxional process involves only the Pd centre of the dimeric structure, leaving the terminal Pt bound GaCp* unchanged. With regards to the dependence on the group 13 metal, it was found that the fluxional process in $[Pd_2(AlCp^*)_2(\mu^2\text{-}AlCp^*)_3]$ (**8d**) is slower than in $[Pd_2(GaCp^*)_2(\mu^2\text{-}GaCp^*)_3]$ (**8c**). These results are in very good agreement with the calculated bond energies in $[M\{E(CH_3)\}_4]$ (M = Ni, Pd, Pt; E = B − Tl) by Frenking.[16] For the transition metal the order Ni ≈ Pt > Pd can be observed, while for the group 13 elements the trend is B > Al > Ga ≈ In > Tl.

The ^1H NMR spectrum of $[Pd_3(GaCp^*)_4(\mu^2\text{-}GaCp^*)_4]$ (**10b**) at room temperature exhibits two resonances with an integral ratio of 1:3, whereas $[Pd_3(InCp^*)_4(\mu^2\text{-}InCp^*)_4]$ (**10a**) shows this signal splitting only at −80 °C. The reason for the unusual ratio of 1:3 is still uncertain and is not in agreement with the solid-state structure. A dissociation of the trinuclear component into two $[Pd(ECp^*)_3]$ fragments and one $[Pd(ECp^*)_2]$ (E = Ga, In) unit cannot be excluded. However, the addition of an excess of InCp* does not yield the saturated mononuclear species $[Pd(InCp^*)_4]$. The reactivity of these cluster complexes with phosphanes (PPh_3 or dppe) suggests that the nuclearity is sustained in solution (vide supra). Thus a triangular structure of **10a** and **10b** similar to the triangular phosphane clusters **10c** and **10d** in solution has been suggested. The structure bears two axial and six equatorial ligands. The equatorial ligands (terminal as well as bridging) are presumed to be fluxional in solution, giving a coalesced signal corresponding to six ligands.

3.3 Bond Activation Reactions by $M(ECp^*)_n$

The donor acceptor bond in $[L_nM\leftarrow ECp^*]$ has been calculated to be rather polar in the case of E = Al and Ga. The electron density of the transition metal centre on coordination should therefore increase considerably.[10,16,17,24,31,41] This is an intrinsically interesting feature especially from the point of view of classical bond activation reactions being relevant in organometallic chemistry (H_2, C−H, Si−H, B−H, etc.). Whereas CO, phosphanes or NHCs (nitrogen heterocyclic carbenes) are widely used as supporting and directing ligands for reactivity and selectivity in organometallic chemistry, almost nothing is known about the corresponding potential of E^IR ligands.

The reaction of $[Ni(COD)_2]$ with four equivalents of AlCp* in benzene does not yield the expected complex $[Ni(AlCp^*)_4]$ (**7c**) but instead gives $[NiH(AlCp^*)_3(AlCp^*Ph)]$ (**11**) in almost quantitative yields (Scheme 9).[39]

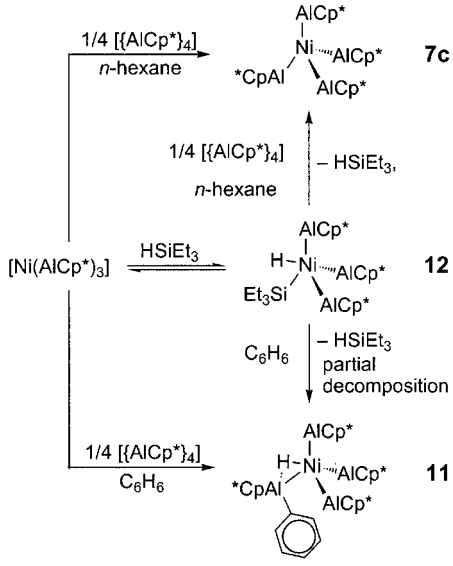

Scheme 9. Synthesis of **7c**, **11** and **12**

As shown by NMR spectroscopy, the C_6H_6 in **11** is not exchanged by C_6D_6, showing the kinetic inertness of complex **11**. It is assumed that the activation of benzene, which does not occur in the case of $[Ni(CO)_n]$, $[Ni(PR_3)_n]$ or other d^{10} Ni complexes, takes place on a reactive, low-coordinate fragment $[Ni(AlCp^*)_n]$ ($n < 4$) giving an intermediate of the type $[(AlCp^*)_nNi(H)(C_6H_5)]$. The reactive fragment $[Ni(AlCp^*)_n]$ is not formed from $[Ni(AlCp^*)_4]$ (**7c**) by a dissociative process but, rather, is an intermediate in the course of the formation of kinetically inert **7c** and is apparently trapped in the presence of suitable reaction partners prior to the formation of **11**. The subsequent migration of the phenyl group to an AlCp* ligand, accompanied by oxidation of the aluminium and formation of a strong Al−C bond, as well as the coordination of a fourth equivalent of AlCp* contribute to the driving force of the whole activation reaction.

 © 2004 Wiley-VCH Verlag GmbH & Co. KGaA, Weinheim

Similarly, in the presence of $HSiEt_3$ (Scheme 9), the formation of the hydrosilyl complex $[Ni(AlCp^*)_3(H)(SiEt_3)]$ (**12**) can be observed. In contrast to **11**, the hydride may be found in a terminal and not in a bridging position, showing the electron deficient nature of the Al^{III} centre in **11**. Compound **12** selectively reacts with C_6H_6 giving **11** via cleavage of $HSiEt_3$, indicating that $[Ni(AlCp^*)_3]$ is the probable relevant intermediate for the C−H activation of benzene.

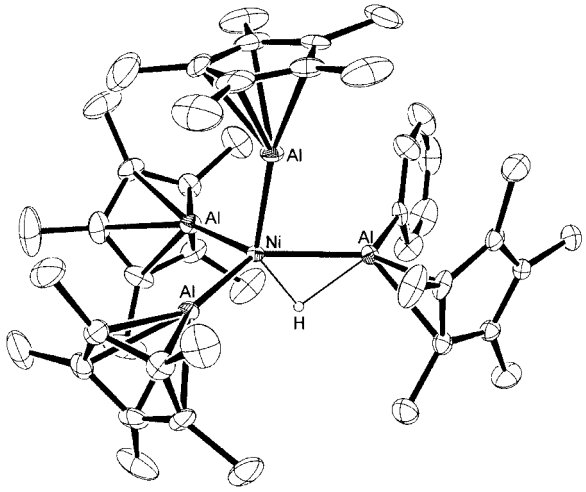

Figure 5. $[NiH(AlCp^*)_3(AlCp^*Ph)]$ (**11**)

Another example of C−H bond activation was found in the reaction of $[(\eta^6\text{-}C_6H_5CH_3)Fe(\eta^4\text{-}C_4H_8)]$ with AlCp* giving a product with the empirical formula $[Fe(AlCp^*)_5]$ (**13**).[42] The solid-state structure of **13** indeed exhibits a central iron atom in a distorted trigonal bipyramidal coordination environment. However, two C−H bonds of two Cp* ring methyl groups are attached to adjacent AlCp* ligands, giving an unusual $Cp^*Al-CH_2(C_5Me_4)Al-CH_2(C_5Me_4)Al$ chelating system (Figure 6). The hydrides occupy a bridging position between the Fe and Al centres. It is noteworthy that the Fe^0 source is inert in the presence of Cp*Ga or Cp*In, accentuating again the role of Cp*Al as a suitable ligand for bond activation reactions.

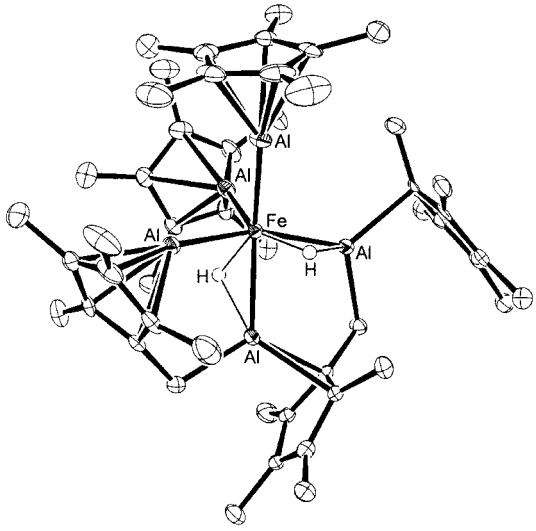

Figure 6. $[Fe(AlCp^*)_5]$ (**13**)

However, bond activations are not only restricted to Cp*Al, as shown by the reaction of $[Cp^*Rh(CH_3)_2L]$ (L = dimethyl sulfoxide, pyridine) with GaCp* (Scheme 10). In the first step of this reaction sequence, the ligand L is substituted by GaCp* giving $[Cp^*Rh(GaCp^*)(CH_3)_2]$ (**14**). This is isostructural with the starting complex. Complex **14** is thermally unstable and slowly reacts further in solution at room temperature to give the zwitterionic rhodium species $[Cp^*Rh\{(\eta^5\text{-}C_5Me_4)Ga(CH_3)_3\}]$ (**15**).[43]

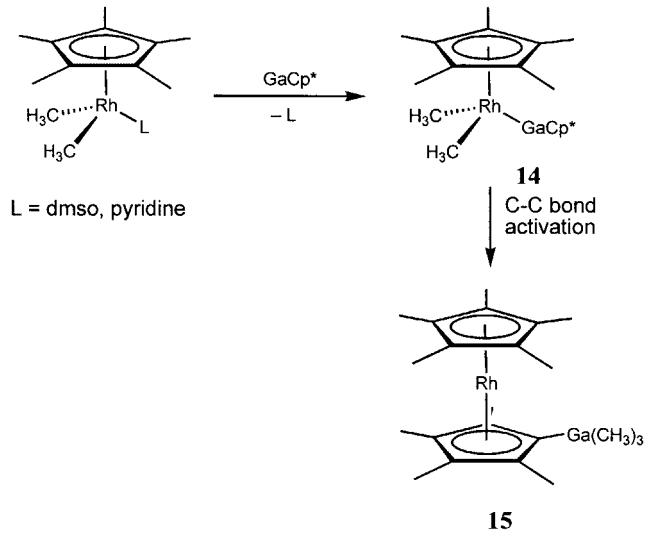

Scheme 10. Reaction of $[Cp^*Rh(CH_3)_2L]$ (L = dmso, pyridine) with GaCp*

The mechanism of this reaction sequence is still uncertain. However, the driving force presumably includes the migration of the methyl groups to ECp* (E = Al, Ga) accompanied by oxidation of the group 13 metal centre and the formation of a strong E−C bond. This is a rather general point in the reactions of M−C bonds with ECp* and is very similar to the classical alkyl migration to transition metal bonded electrophilic π-ligands such as CO and olefins.

4. Insertion Reactions of ECp* into Metal−Halide and Metal−Metal Bonds

Insertion reactions of E^IX (X = halide) have been known for a long time and date back to the studies of Graham, Chatt and Hsieh more than 30 years ago. In particular, the insertion of InX (X = Cl, Br) has been the focus of much research. In the 1960s, Graham et al. reported insertions of InBr into the metal−metal bonds of $[Co_2(CO)_8]$ and $[Mn_2(CO)_{10}]$ which they assumed to give $[(\mu^2\text{-}Br)_2\text{-}In\{Co(CO)_4\}_2]_2$ and $[BrInMn(CO)_5]_2$, respectively.[44−47] Later, Chatt et al. studied the insertion of InCl into the Pt−Cl bond of [*trans*-$Pt(Cl)(SiPh_3)\{PMe_2(Ph)\}_2$] and

 © 2004 Wiley-VCH Verlag GmbH & Co. KGaA, Weinheim

claimed that the product was [*trans*-Pt($InCl_2$)($SiPh_3$)-(PMe_2Ph)$_2$].[48] A. T. T. Hsieh reported a number products from the insertion of InX into metal-metal and metal-halide bonds of carbonyl and carbonyl free complexes of tungsten, molybdenum, manganese, iron, mercury and the metals of the cobalt triad.[49−52] Hsieh also investigated the behaviour of InCl towards Ph_3PAuCl, suggesting the formation of $Ph_3PAuInCl_2$.[53] Due to the insolubility of the products, however, the structural proposals were solely based on infrared spectroscopy, elemental analyses and comparisons of the melting points.

The actual complexity of these reactions was first shown by H. Schmidbaur[54] who isolated gold/indium clusters from a reaction analogous to that of Hsieh.[53] Treatment of (PPh_3)AuCl with InCl in THF yielded the In^{II} dimer [$In_2Cl_4(THF)_4$], whereas addition of a chelating ligand such as dppe led to the cluster [(dppe)$_2Au_3In_3Cl_6(THF)_6$]. A slight change in the stoichiometry gave the ionic cluster [(dppe)$_2$Au]$^+$[(dppe)$_2Au_3In_3Br_7(THF)$]$^-$.[55] The reaction of InBr with [CpNi(Br)(PR_3)] (R = Me, Ph) typically yields ionic [CpNi(PR_3)$_2$]$^+$[$InBr_4$]$^-$ "*ate*" complexes,[56,57] while only special conditions such as the presence of strong Lewis-bases (e.g. Ph_3P=O, quinuclidine) suppress this reaction so that Ni−In bonded compounds can be isolated.

These examples clearly show that insertion reactions of E^IX are extremely sensitive to the reaction conditions and that many possible reaction pathways have to be considered. The access to E^IR species with enhanced solubility and their ability to stabilise intermediates stimulated a re-examination of these classic insertion reactions. Jutzi reported on the insertion of GaCp* into the Fe−Cl bonds of $FeCl_2$ giving [Cp*Fe(GaCp*)$_2$($GaCl_2$·thf)] (**16**) and revealing the potential of E^IR as reducing and Cp*-transfer reagents together with the capacity to behave as stabilising "spectators" (Scheme 11).[58]

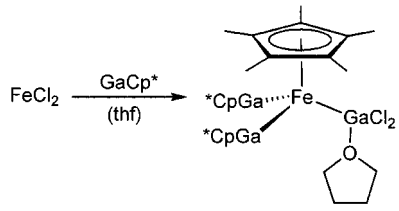

16

Scheme 11. Reaction of $FeCl_2$ with GaCp*

4.2 Rhodium- and Ruthenium−ECp* Coordination Compounds and Clusters

In general, depending on stoichiometry as well as reaction conditions, a variety of insertion products may be formed from the reactions of ECp* (E = Ga, In) and the isolobal d^6 complexes [{Cp*$RhCl_2$}$_2$][59,60] or [{(*p*-cymene)$RuCl_2$}$_2$][61] (Scheme 12 and 13). The reaction of [{RhCp*Cl_2}$_2$] with six equivalents of E^IR in toluene

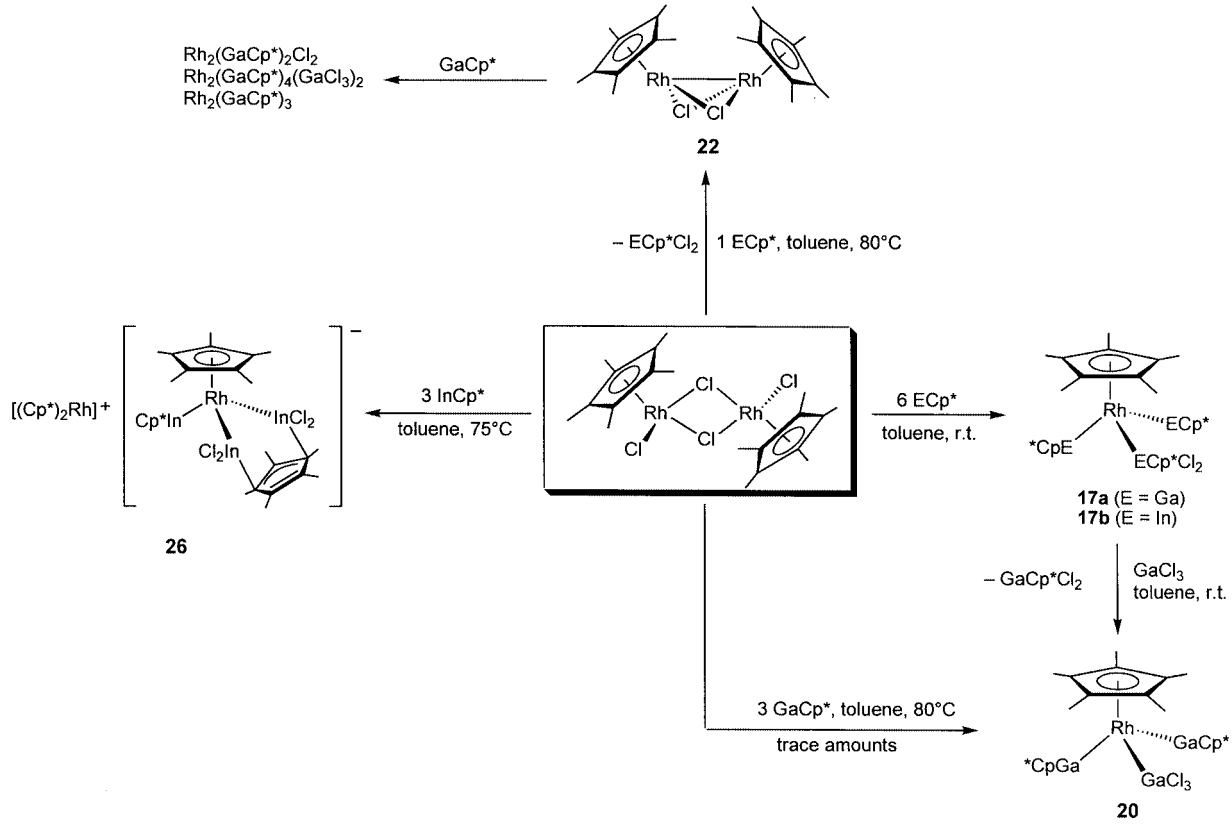

Scheme 12. Reactions of ECp* with [{Cp*$RhCl_2$}$_2$]

 © 2004 Wiley-VCH Verlag GmbH & Co. KGaA, Weinheim

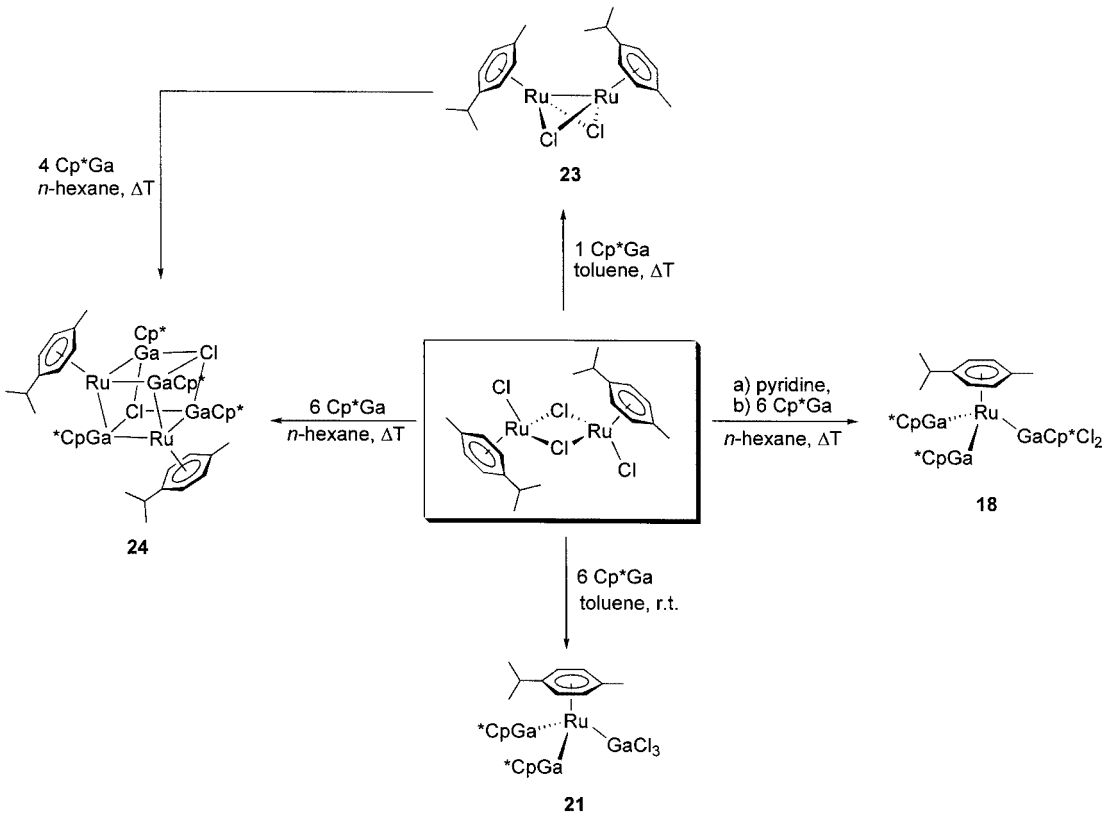

Scheme 13. Reactions of GaCp* with $[\{(p\text{-cymene})RuCl_2\}_2]$

at room temperature leads to simple, monomeric insertion products $[RhCp^*(ECp^*)_3Cl_2]$ (**17a**: E = Ga**, 17b**: E = In). The analogous ruthenium complex $[(p\text{-cymene})Ru(GaCp^*)_3Cl_2]$ (**18**) can be obtained from the reaction of GaCp* with $[\{(p\text{-cymene})RuCl_2\}_2]$ only by prior treatment of the dimeric starting complex with pyridine. The formation of the intermediate monomer $[(p\text{-cymene})RuCl_2(pyridine)]$ is followed by insertion of GaCp* into the Ru−Cl bonds and substitution of pyridine by GaCp*. If dmso is used instead of pyridine, the substitution can be suppressed yielding $[(p\text{-cymene})Ru(GaCp^*)_2(Cl)_2(DMSO)]$ (**19**). However, in contrast to the isolobal Rh complex, only GaCp* gave defined reaction products, whereas InCp* yielded intractable product mixtures under all conditions tested.

The compound $[Cp^*Rh(GaCp^*)_3Cl_2]$ (**17a**) reacts readily in the presence of Lewis acids. When **17a** is treated with one equivalent of $GaCl_3$ in toluene, the Lewis acid-base adduct $[Cp^*Rh(GaCp^*)_2(GaCl_3)]$ (**20**) is immediately formed. Complex **20** is also formed as a side product in the thermal decomposition of complex **17a**, showing the lability of the Cp*−Ga bond. In the case of the Ru(*p*-cymene) fragment, the corresponding complex $[(p\text{-cymene})Ru(GaCp^*)_2(GaCl_3)]$ (**21**) can be isolated in the stoichiometrically quantitative yield of 67% ("quantitative" is based on the amount of chlorine in the starting material) if $[\{(p\text{-cymene})RuCl_2\}_2]$ is treated directly with GaCp* in the absence of pyridine. Clearly the dimeric structure starting material is retained in some of the reaction intermediates, facilitating the Cp*−Cl exchange between two Ga centres.

Changing the stoichiometric ratio of the reactants or the reaction conditions leads to new structural types for the insertion products. The reaction of $[\{RhCp^*Cl_2\}_2]$ with only one equivalent of ECp* gives the Rh^{II} dimer $[\{RhCp^*Cl\}_2]$ (**22**) which is also accessible from the reaction of the precursor with Na/Hg[62,63] or elemental gallium.[64] The analogous Ru^I-Ru^I complex $[\{(p\text{-cymene})RuCl\}_2]$ (**23**), which has not been reported in literature before, can be obtained by treatment of $[\{(p\text{-cymene})RuCl_2\}_2]$ with one equivalent of GaCp* in toluene. Several attempts to use classic reducing agents (Li, K, C_8K, sodium naphthalide) for this reduction failed, resulting only in the uncontrolled formation of Ru metal.

Further reaction of **23** with four equivalents of GaCp* gives the dimeric cage compound **24** in very good yields. The cube-like cage core consists of two Ru(*p*-cymene), four GaCp* ligands and two μ^3-bridging chlorine atoms. Complex **24** can also be prepared by direct treatment of GaCp* with $[\{(p\text{-cymene})RuCl_2\}_2]$, albeit in very low yields.

Several products can be obtained from the reaction of $[\{Cp^*RhCl\}_2]$ with ECp*. However, the molecular structures of these products are not clear yet. The homoleptic cluster complex $[(RhCp^*)_2(GaCp^*)_3]$ (**25**) could be isolated as a thermal decomposition product of one of these insertion products.

 © 2004 Wiley-VCH Verlag GmbH & Co. KGaA, Weinheim

The reaction of $[\{Cp^*RhCl_2\}_2]$ with only three equivalents of InCp* (instead of six as in the synthesis of **17b**) leads to the salt $[Cp^*_2Rh][Cp^*Rh(InCp^*)\{In_2Cl_4(\mu^2\text{-}Cp^*)\}]$ (**26**). The molecular structure of the anionic part exhibits a distorted tetrahedral $RhIn_3$ core. The striking feature of the anion is the Cp* ring bridging two indium centres. The C_5 ring takes an almost parallel arrangement to the Cl−In−Cl planes with deviations smaller than 10°. Complex **26** is the first example of an intramolecular bridging Cp* ring. The only structural analogies are the solid-state structures of Et_2GaCp and $EtGaCp_2$, consisting of linear polymers with intermolecular bridging C_5H_5 ligands.[65]

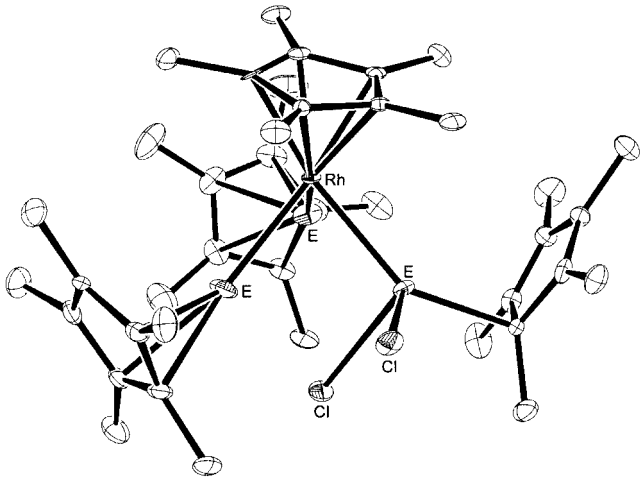

Figure 7. $[Cp^*Rh(ECp^*)_3Cl_2]$ (**17a**: E = Ga, **17b**: E = In)

4.2.1 Solution Structures and NMR Spectroscopy

The monomeric insertion products **17a** and **17b** as well as **18** can be regarded as acid-base adducts between Cp* ECl_2 and the basic d^8 transition metal centres in $[Cp^*Rh(ECp^*)_2]$ and $[(p\text{-cymene})Ru(ECp^*)_2]$, respectively. However, the NMR spectroscopic data are not consistent with simple acid-base adducts. Instead, in all these complexes the three ECp* ligands are equivalent on the NMR time scale down to −80 °C. Clearly a fast exchange of the chlorides between all group 13 atoms takes place, resulting in three coalesced ECp* ligands. A similar fluxional process was observed in the acid-base adducts of GaCp* and $GaCp^*X_2$ (X = Cl, Br). In this case, coalescence of the Cp* rings at −80 °C in $[D_8]$toluene was observed.[66] DFT calculations on the systems R_3E-ER and their isomers R_2E-ER_2 revealed that the difference in energy between these two forms is strongly dependent on both the groups R as well as the group 13 metal E. The adducts Cl_3B-GaH and Cl_3B-InH for example, exhibit bridging chlorines in the energetic minimum.[67]

Additionally, in solution, a fast Cp* exchange of the InCp* units in the anionic part of complex **26** can be assumed. The NMR spectra show three signal sets for the Cp* groups in a ratio of 2:2:1. Also, complex **26** does not show any decoalescence even at −80 °C.

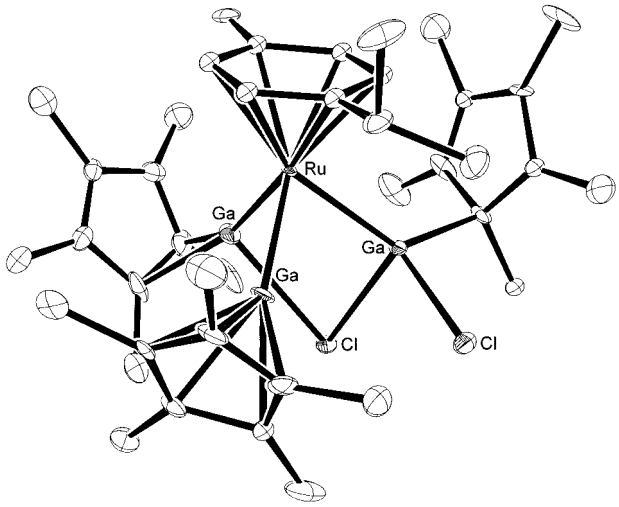

Figure 8. $[(p\text{-cymene})Ru(GaCp^*)_3Cl_2]$ (**18**)

4.2.2 Solid State Structures

The molecular structures of $[RhCp^*(ECp^*)_3Cl_2]$ (**17a**, **17b**) and $[(p\text{-cymene})Ru(GaCp^*)_3Cl_2]$ (**18**) exhibit cage-like motifs with E−Cl−E bridges. Generally, only one of the chlorine atoms is found in a bridging position, while the second chlorine is terminally coordinated. The strong difference in hapticity of the Cp* rings is a common feature of these structures. The Cp* ring on the ECl_2 unit is σ-bonded, while the Cp* group in the ECp* ligand showing no chloride interactions is clearly η^5-bonded. The bridging chloride atom exhibits some ground state *cis* effect on the coordination of the Cp* on the ECl unit which shows a "nonclassical" hapticity best described as η^3 or η^2. The free p-electron pairs at the Cl atoms effectively compete with the π-density at the Cp* for the empty p-orbitals on the group 13 metal centre. Therefore, the fluxional process in solution is reflected in the solid-state structures which can be re-

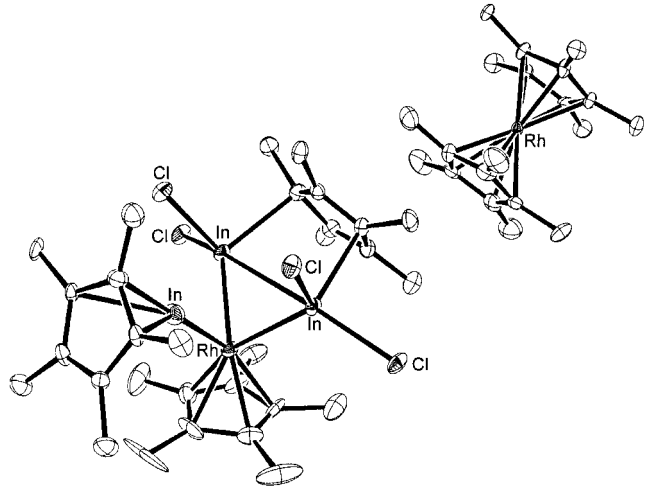

Figure 9. $[Cp^*_2Rh][Cp^*Rh(InCp^*)\{In_2Cl_4(\mu^2\text{-}Cp^*\}]$ (**26**)

 © 2004 Wiley-VCH Verlag GmbH & Co. KGaA, Weinheim

garded as trapped "intermediates" of a chlorine exchange between two ECp* centres.

In contrast, the $GaCl_3$ complexes $[Cp^*Rh(GaCp^*)_2(GaCl_3)]$ (**20**) and [(*p*-cymene)$Ru(GaCp^*)_2(GaCl_3)$] (**21**) are simple acid-base adducts without Ga−Cl−GaCp* interactions. Consequently, all Cp* units in both complexes are η^5-bonded to the Gallium centres.

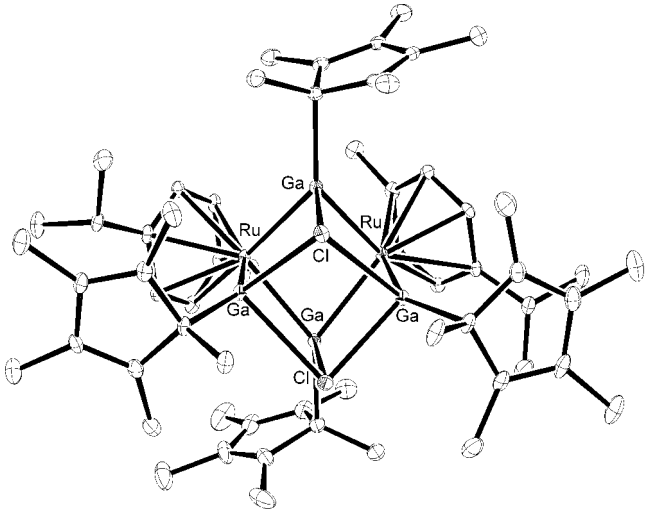

Figure 10. [Ru(*p*-cymene)$(GaCp^*)_2Cl]_2$ (**24**)

4.3 Reaction of ECp* with other Ruthenium Complexes

In contrast to [{(*p*-cymene)$RuCl_2\}_2$], [{$Cp^*RuCl\}_4$] reacts both with GaCp* and InCp* to give the monomeric "piano-stool" complexes $[Cp^*Ru(ECp^*)_3Cl]$ [E = Ga (**27a**), In (**27b**)] (Scheme 14).

In solution, all three ECp* ligands of **27a** and **27b** are equivalent on the NMR time scale down to −80 °C, due to a fast exchange of the chlorides between the three group 13 metals. In the solid state the chloride is either terminally coordinated to gallium (**27a**) or bridging two indium atoms (**27b**). As in complexes **17a**, **17b** and **18**, the influence of the chlorine coordination on the hapticity of adjacent Cp* ligands can be observed.

The reaction of ECp* with $[Cp^*RuCl]_4$ can be described as redox-neutral. The neutral *p*-cymene ligand is a stronger π-acceptor in comparison with the anionic Cp* ligand and thus has a more polarised bond to ruthenium. This situation leads to an increased electron density on all metal centres. Indeed, the chloride of compound **27a** can be easily removed by treatment with $NaBPh_4$, giving the cationic complex $[Cp^*Ru(GaCp^*)_3]^+[BPh_4]^-$ (**27c**). In contrast, **17a**, **17b** or **18** do not show any reaction with $NaBPh_4$. Notably, the cation **27c** can also be obtained by treatment of $[\{RuCp^*Cl_2\}_2]$ with GaCp*, thus having $[Cp^*GaCl_3]^-$ as the counterion instead of $[BPh_4]^-$.

The reaction of GaCp* with $[(Ph_3P)_3RuCl_2]$ leads to a complete substitution of the PPh_3 ligands and insertion of GaCp* into the ruthenium-halide bonds (Scheme 15). The product is the octahedral homoleptic complex $[Ru(GaCp^*)_6Cl_2]$ (**28**) which exhibits fluxional chloride ligands and coalescence of all GaCp* moieties.

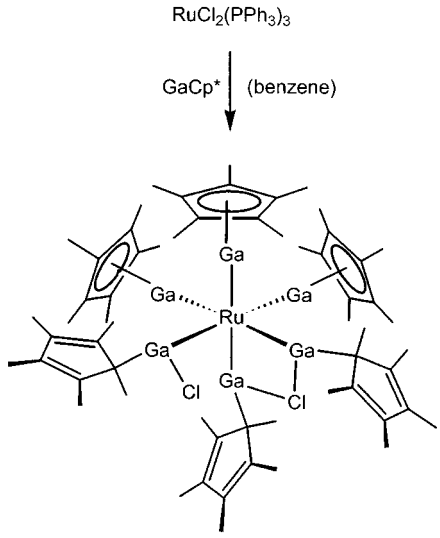

28

Scheme 15. Reaction of GaCp* with $[(Ph_3P)_3RuCl_2]$

5. Coordination Chemistry of Sterically Bulky Ligands

While the coordination chemistry of ECp* is a well explored field, sterically encumbered low-valent group 13 ligands such as E^ITrip {E = Al, Ga, In; Trip = Bis[2,5-(2,4,6-*i*$Pr_3C_6H_3$)phenyl]},[14,15,68−73] E^ITp [E = Al, Ga, In; Tp = Tris(pyrazoyl)hydroborato][74−82] or E^I(DDP) (E = Al, Ga; DDP = 2-Diisopropylphenylamino-4-diisopropylphenylimino-2-pentene[83−88] have been little used as li-

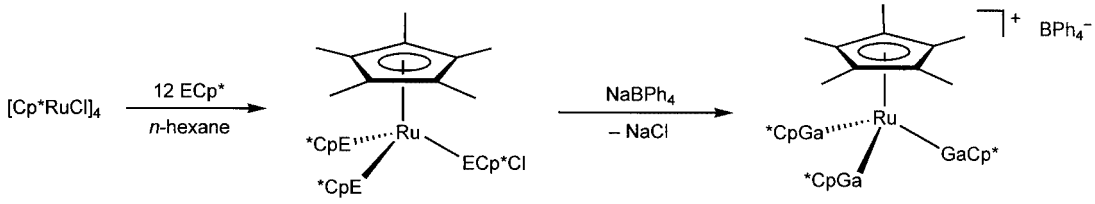

27a (E = Ga)
27b (E = In)

27c

Scheme 14. Synthesis of $[Cp^*Ru(E^ICp^*)_3Cl]$

 © 2004 Wiley-VCH Verlag GmbH & Co. KGaA, Weinheim

gands in transition metal chemistry. The iron carbonyl complexes $[(CO)_4Fe-E^IR]$ (E = Ga; R = DDP, Trip, Tp; E = In, R = Tp)[14,89–91] and the tungsten complex $[(CO)_5W-In^ITp]$[91] are the only such complexes reported so far. The difference in the steric demand as well as in the electronic properties of these ligands compared with ECp* points to a different coordination chemistry. As an example for this class of bulky ligands, the coordination chemistry of Ga(DDP) has recently been studied in more detail.[92]

The reactions of ML_n (M = Ni, Pd, Pt; L = olefin) with GaCp* lead to a full substitution of the olefinic ligands and give homoleptic monomeric, di- or trimeric clusters in all cases (vide supra). However, according to Scheme 16, the reaction of $[Pd_2(dvds)_3]$ with Ga(DDP) does not lead to complete substitution but, rather, gives the monosubstituted complex [{(DDP)Ga}Pd(dvds)] (**29a**). Similarly, the reaction of $[Pt(COD)_2]$ with Ga(DDP) leads to the disubstituted complex $[(1,3\text{-}COD)Pt\{Ga(DDP)\}_2]$ (**29b**). Clearly, complete substitution of the olefins is prevented by the high steric demand of Ga(DDP).

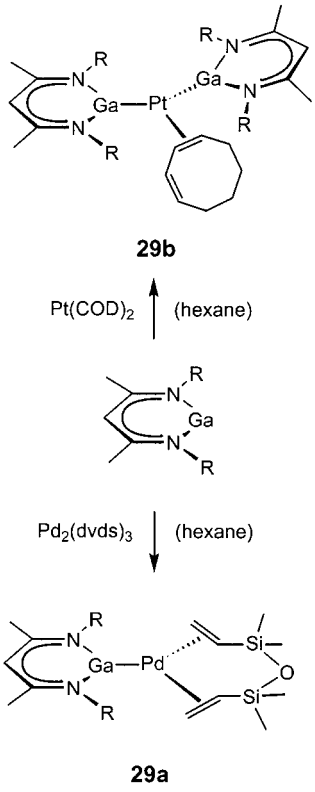

Scheme 16. Reactions of Ga(DDP) with $[Pd_2(dvds)_3]$ and $[Pt(COD)_2]$

In contrast to $[M(ECp^*)_4]$ complexes, which are kinetically inert, the electronically unsaturated complexes **29a** and **29b** are substitutionally labile and form dimeric, Ga(DDP) bridged complexes on reaction with CO.

Ga(DDP) shows similar reducing abilities to GaCp*. However, the steric demand of the organic group as well as the reduced Lewis acidity of the gallium centre somehow

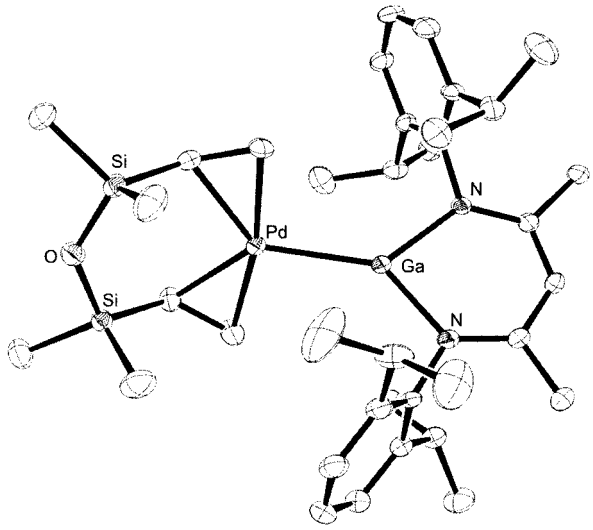

Figure 11. [{(DDP)Ga}Pd(dvds)] (**29a**)

limits the kinetic access to halide transfer reactions. A reaction mixture of $[\{Cp^*RhCl_2\}_2]$ and Ga(DDP) shows oxidised gallium species but the highly reactive Rh^I-products are not stable under these conditions and nonspecific decomposition is observed.

A representative example of the difference between Ga(DDP) and GaCp* is their reactivity towards $[(Ph_3P)_3RuCl_2]$. Whereas GaCp* causes complete substitution of the Ph_3P ligands and the insertion of GaCp* into the ruthenium-halide bonds with the conservation of the oxidation state of Ru^{II} (vide supra), Ga(DDP) leads to a selective reduction of Ru^{II} to Ru^0. A free Ga^{III}-species was detected by ^1H NMR spectroscopy which, in contrast to Cp^*GaCl_2, is not acidic and does not stabilise the Ru^0 centre. Instead, the highly reactive Ru^0 is stabilised by orthometallation of one of the phenyl-rings by reoxidation of the ruthenium centre (Scheme 17). Similar orthometallation reactions are known to take place in the reactions of $[(PPh_3)_3RuCl_2]$ with other reducing agents such as potassium naphthalide.[93,94]

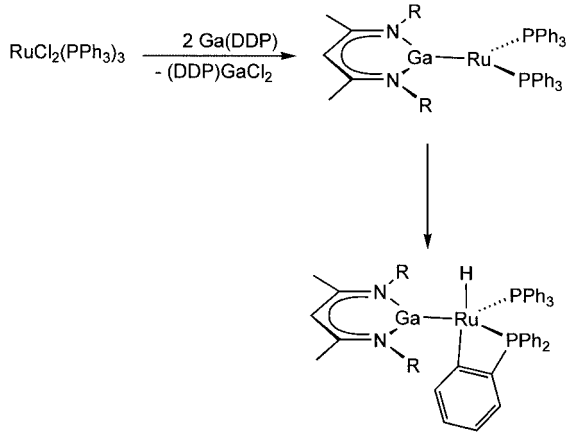

Scheme 17. Reaction of $[(PPh_3)_3RuCl_2]$ with Ga(DDP)

 © 2004 Wiley-VCH Verlag GmbH & Co. KGaA, Weinheim

In contrast, reactions of Ga(DDP) with transition metal halides in the oxidation state +I do not give Ga(DDP)Cl_2 but, rather, lead to insertion of Ga(DDP) into the transition metal halide bond.

The Rh^I-compound [$(Ph_3P)_3RhCl$] reacts with Ga(DDP) to give the monomeric complex [$(PPh_3)_2RhCl${Ga(DDP)}] (**30**) (Figure 12). However, the chloride can be found in a bridging position between the gallium and the rhodium centre. This is the first example of a halide-bridged transition-metal group 13 metal complex reported so far. Interestingly, the Lewis acidic properties of coordinated Ga(DDP) are not sufficiently strong to cause a complete migration of the chlorine atom.

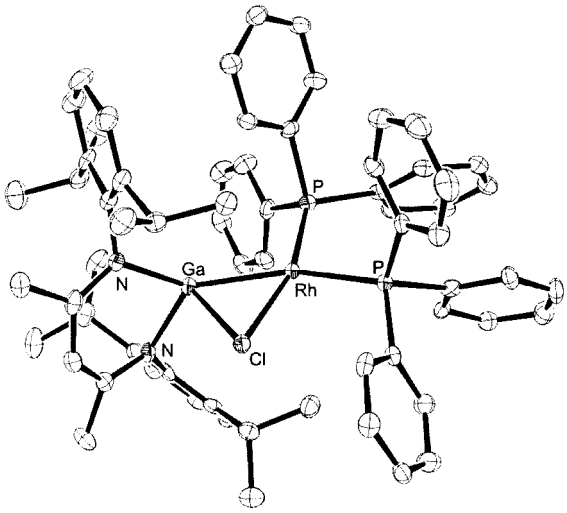

Figure 12. [$(PPh_3)_2RhCl${Ga(DDP)}] (**30**)

Whereas the reaction of [$(PPh_3)AuCl$] with GaCp* leads to unselective decomposition, the reaction with Ga(DDP) yields the complexes [$(Ph_3P)Au${Ga(DDP)}Cl] (**31a**) and [{(DDP)Ga}Au{Ga(DDP)}Cl] (**31b**) (Scheme 18). In these compounds, an insertion of a Ga(DDP) into a gold−halide bond with full migration of the chloride is observed.

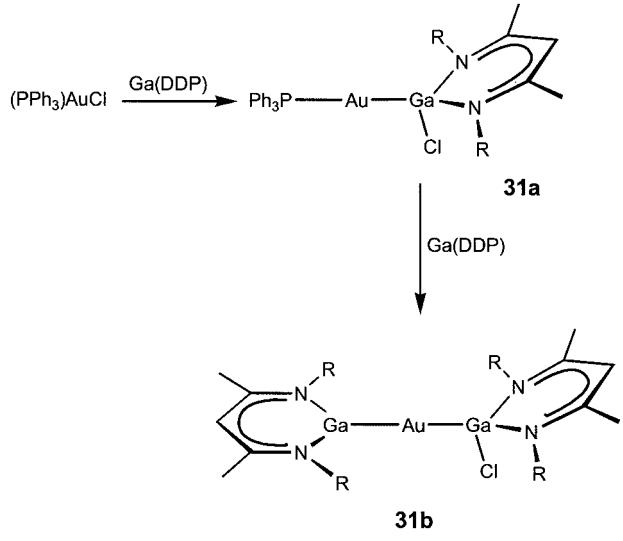

Scheme 18. Reaction of [$(PPh_3)AuCl$] with Ga(DDP)

6. Summary and Outlook

Since their discovery, the low valent group 13 organyls GaCp* and AlCp* have attracted much attention as ligands towards transition metals. They are formally isolobal with CO, phosphanes and NHCs but in contrast, their bonds to transition metals have been calculated to be very polar, the strongest contribution being the coulombic attraction between the metals. Early research concentrated on transition metal carbonyl fragments in order to elucidate the general properties of this new class of ligand. However, recent research is focussing on more reactive transition metal fragments, without competing strong π-acceptor ligands such as CO. The strong polarity of the metal−metal bond is quite interesting in the context of organometallic chemistry. In particular, for bond activation reactions the high increase in electron density of transition metal centres by E^IR is potentially useful or, qualitatively speaking, it should facilitate oxidative addition reactions. In particular, the reactivity of the unsaturated fragments [$M(E^IR)_n$] is not understood and will necessitate further research. In addition, the chemistry of sterically demanding ligands E^IR with R = DDP, Tp^R or similar substituents holds much promise for the discovery of novel and unusual reactions. Based on the above examples we speculate that these exotic "metallic" ligands E^IR may well be very useful in a classical sense as ancillary ligands in organometallic chemistry. However, it should be mentioned here that the title compounds [$M_a(ECp^*)_b$] may also be regarded as the basic building blocks of Schnöckels elaborate cluster [$Al_{38}(AlCp^*)_{12}$][95] showing that ECp*, in general, seems to be a suitable stabilising ligand for large metal clusters. The use of [$M_a(E^IR)_b$] as building blocks for the synthesis of larger transition metal ECp* clusters as well as molecular precursors for intermetallic M/E nanoparticles seems worthy of exploration.

[1] C. Dohmeier, C. Robl, M. Tacke, H. Schnöckel, *Angew. Chem.* **1991**, *103*, 594−595; *Angew. Chem. Int. Ed. Engl.* **1991**, *30*, 564−565.
[2] D. Loos, H. Schnöckel, *J. Organomet. Chem.* **1993**, *463*, 37−40.
[3] C. Dohmeier, D. Loos, H. Schnöckel, *Angew. Chem.* **1996**, *108*, 141−161; *Angew. Chem. Int. Ed. Engl.* **1996**, *35*, 129−149.
[4] M. Schormann, K. S. Klimek, H. Hatop, S. P. Varkey, H. W. Roesky, C. Lehmann, C. Röpken, R. Herbst-Irmer, M. Noltemeyer, *J. Solid State Chem.* **2001**, *162*, 225−236.
[5] S. Schulz, H. W. Roesky, H. J. Koch, G. M. Sheldrick, D. Stalke, A. Kuhn, *Angew. Chem.* **1993**, *105*, 1828−1830; *Angew. Chem. Int. Ed. Engl.* **1993**, *32*, 1729−1731.
[6] P. Jutzi, B. Neumann, G. Reumann, H.-G. Stammler, *Organometallics* **1998**, *17*, 1305−1314.
[7] P. Jutzi, L. O. Schebaum, *J. Organomet. Chem.* **2002**, *654*, 176−179.
[8] R. Murugavel, V. Chandrasekhar, *Angew. Chem.* **1999**, *111*, 1289−1293; *Angew. Chem. Int. Ed.* **1999**, *38*, 1211−1215.
[9] R. A. Fischer, J. Weiss, *Angew. Chem.* **1999**, *111*, 3002−3022; *Angew. Chem. Int. Ed.* **1999**, *38*, 2830−2850.

 © 2004 Wiley-VCH Verlag GmbH & Co. KGaA, Weinheim

[10] J. Uddin, C. Boehme, G. Frenking, *J. Am. Chem. Soc.* **2000**, *19*, 571−582.
[11] H. Braunschweig, M. Colling, *Coord. Chem. Rev.* **2001**, *223*, 1−51.
[12] H. Braunschweig, M. Colling, *Eur. J. Inorg. Chem.* **2003**, 393−403.
[13] H. Braunschweig, *Angew. Chem.* **1998**, *110*, 1882−1898; *Angew. Chem. Int. Ed.* **1998**, *37*, 1786−1801.
[14] J. Su, X.-W. Li, R. C. Crittendon, C. F. Campana, G. H. Robinson, *Organometallics* **1997**, *16*, 4511−4513.
[15] X.-W. Li, W. T. Pennington, G. H. Robinson, *J. Am. Chem. Soc.* **1995**, *117*, 7578−7579.
[16] J. Uddin, G. Frenking, *J. Am. Chem. Soc.* **2001**, *123*, 1683−1693.
[17] C. Boehme, G. Frenking, *Chem. Eur. J.* **1999**, *5*, 2184−2190.
[18] W. Uhl, S. U. Keimling, W. Hiller, M. Neumayer, *Chem. Ber.* **1995**, *128*, 1137−1139.
[19] C. Üffing, A. Ecker, R. Köppe, H. Schnöckel, *Organometallics* **1998**, *17*, 2373−2375.
[20] Q. Yu, A. Purath, A. Donchev, H. Schnöckel, *J. Organomet. Chem.* **1999**, *584*, 94−97.
[21] P. Jutzi, B. Neumann, G. Reumann, L. O. Schebaum, H.-G. Stammler, *Organometallics* **1999**, *18*, 2550−2552.
[22] P. Jutzi, B. Neumann, L. O. Schebaum, A. Stammler, H.-G. Stammler, *Organometallics* **1999**, *18*, 4462−4464.
[23] W. Uhl, M. Pohlmann, *Organometallics* **1997**, *16*, 2478−2480.
[24] J. Weiss, D. Stetzkamp, B. Nuber, R. A. Fischer, C. Boehme, G. Frenking, *Angew. Chem.* **1997**, *109*, 95−97; *Angew. Chem. Int. Ed. Engl.* **1997**, *36*, 70−72.
[25] G. Linti, W. Köstler, *Chem. Eur. J.* **1998**, *4*, 942−949.
[26] E. Leiner, M. Scheer, *J. Organomet. Chem.* **2002**, *646*, 247−254.
[27] E. Leiner, O. Hampe, M. Scheer, *Eur. J. Inorg. Chem.* **2002**, 584−590.
[28] M. Cokoja, C. Gemel, T. Steinke, T. Welzl, M. Winter, R. A. Fischer, *J. Organomet. Chem.* **2003**, 277−286.
[29] D. Weiss, T. Steinke, M. Winter, R. A. Fischer, N. Fröhlich, J. Uddin, G. Frenking, *Organometallics* **2000**, *19*, 4583−4588.
[30] D. Weiss, M. Winter, K. Merz, A. Knüfer, R. A. Fischer, N. Fröhlich, G. Frenking, *Polyhedron* **2002**, *21*, 535−542.
[31] W. Uhl, M. Benter, S. Melle, W. Saak, G. Frenking, J. Uddin, *Organometallics* **1999**, *18*, 3778−3780.
[32] W. Uhl, M. Pohlmann, R. Wartchow, *Angew. Chem.* **1998**, *110*, 1007−1009; *Angew. Chem. Int. Ed.* **1998**, *37*, 961−963.
[33] C. Gemel, T. Steinke, D. Weiss, M. Cokoja, M. Winter, R. A. Fischer, *Organometallics* **2003**, *22*, 2705−2710.
[34] E. V. Grachova, P. Jutzi, B. Neumann, L. O. Schebaum, H.-G. Stammler, S. P. Tunik, *Dalton Trans.* **2002**, 302−304.
[35] C. Dohmeier, H. Krautscheid, H. Schnöckel, *Angew. Chem.* **1994**, *106*, 2570−2571; *Angew. Chem. Int. Ed. Engl.* **1995**, *33*, 2482−2483.
[36] T. Pechmann, C. T. Brandt, H. Werner, *Angew. Chem.* **2000**, *112*, 4069−4072; *Angew. Chem. Int. Ed.* **2000**, *39*, 3909−3911.
[37] D. Weiss, M. Winter, R. A. Fischer, C. Yu, K. Wichmann, G. Frenking, *Chem. Commun.* **2000**, 2495−2496.
[38] T. Steinke, C. Gemel, M. Winter, R. A. Fischer, *Angew. Chem.* **2002**, *114*, 4955−4957; *Angew. Chem. Int. Ed.* **2002**, *41*, 4761−4763.
[39] T. Steinke, C. Gemel, M. Cokoja, M. Winter, R. A. Fischer, *Angew. Chem.* **2004**, *116*, 2349−2352; *Angew. Chem. Int. Ed.* **2004**, *43*, 2299−2302.
[40] T. Steinke, C. Gemel, R. A. Fischer, *Chem. Eur. J.* **2004**, submitted for publication.
[41] W. Uhl, S. Melle, G. Frenking, M. Hartmann, *Inorg. Chem.* **2001**, *40*, 750−755.
[42] T. Steinke, *Dissertation*, Ruhr-Universität, Bochum, **2004**.
[43] T. Cadenbach, C. Gemel, R. Schmid, S. Block, R. A. Fischer, *Dalton Trans.*, in press.
[44] D. J. Patmore, W. A. G. Graham, *J. Chem. Soc., Chem. Commun.* **1965**, 1.
[45] D. J. Patmore, W. A. G. Graham, *Inorg. Chem.* **1966**, *5*, 1405−1407.
[46] D. J. Patmore, W. A. G. Graham, *Inorg. Chem.* **1966**, *5*, 1586−1590.
[47] J. Hoyano, D. J. Patmore, W. A. G. Graham, *Inorg. Chem. Nucl. Lett.* **1968**, *4*, 201−203.
[48] J. Chatt, C. Eaborn, P. N. Kapoor, *J. Organomet. Chem.* **1970**, *23*, 109−115.
[49] A. T. T. Hsieh, M. J. Mays, *Inorg. Chem. Nucl. Lett.* **1971**, *7*, 223−225.
[50] A. T. T. Hsieh, M. J. Mays, *J. Chem. Soc., Dalton Trans.* **1972**, 516−521.
[51] A. T. T. Hsieh, M. J. Mays, *J. Organomet. Chem.* **1972**, *37*, 9−14.
[52] A. T. T. Hsieh, *Inorg. Chim. Acta* **1975**, *14*, 87−104.
[53] A. T. T. Hsieh, PhD thesis, Cambridge, **1971**.
[54] F. P. Gabbai, A. Schier, J. Riede, H. Schmidbaur, *Inorg. Chem.* **1995**, *34*, 3855−3856.
[55] F. P. Gabbai, S.-C. Chung, A. Schier, S. Krüger, N. Rösch, H. Schmidbaur, *Inorg. Chem.* **1997**, *36*, 5699−5705.
[56] J. Weiss, T. Priermeier, R. A. Fischer, *Inorg. Chem.* **1996**, *35*, 71−75.
[57] J. Weiss, A. Frank, E. Herdtweck, S. Nlate, M. Mattner, R. A. Fischer, *Chem. Ber.* **1996**, *129*.
[58] P. Jutzi, B. Neumann, L. O. Schebaum, A. Stammler, H.-G. Stammler, *Organometallics* **2000**, *19*, 1445−1447.
[59] T. Steinke, C. Gemel, M. Cokoja, R. A. Fischer, *Dalton Trans.* **2004**, in press.
[60] T. Steinke, C. Gemel, M. Cokoja, M. Winter, R. A. Fischer, *Chem. Commun.* **2003**, 1066−1067.
[61] M. Cokoja, C. Gemel, T. Steinke, F. Schröder, R. A. Fischer, *Dalton Trans.* **2004**, in press.
[62] P. R. Sharp, D. W. Hoard, C. L. Barnes, *J. Am. Chem. Soc.* **1990**, *112*, 2024.
[63] D. W. Hoard, P. R. Sharp, *Inorg. Chem.* **1993**, *32*, 612.
[64] M. Scheer, M. Kaupp, A. V. Virovets, S. N. Konchenko, *Angew. Chem.* **2003**, *115*, 5237−5240; *Angew. Chem. Int. Ed.* **2003**, *42*, 5083−5086.
[65] O. T. Beachley, D. B. Rosenblum, M. R. Churchill, C. H. Lake, L. M. Krajkowski, *Organometallics* **1995**, *14*, 4402−4408.
[66] P. Jutzi, B. Neumann, G. Reumann, L. O. Schebaum, H.-G. Stammler, *Organometallics* **2001**, *20*, 2854−2858.
[67] A. Y. Timoshkin, G. Frenking, *J. Am. Chem. Soc.* **2002**, *124*, 7240−7248.
[68] S. T. Haubrich, P. P. Power, *J. Am. Chem. Soc.* **1998**, *120*, 2202−2203.
[69] M. Niemeyer, P. P. Power, *Angew. Chem.* **1998**, *110*, 1291−1294; *Angew. Chem. Int. Ed.* **1998**, *37*, 1277−1279.
[70] J. Su, X.-W. Li, C. Crittendon, G. H. Robinson, *J. Am. Chem. Soc.* **1997**, *119*, 5471−5472.
[71] N. Takagi, M. W. Schmidt, S. Nagase, *Organometallics* **2001**, *20*, 1646−1651.
[72] B. Twamley, P. P. Power, *Angew. Chem.* **2000**, *112*, 3643−3646; *Angew. Chem. Int. Ed.* **2000**, *39*, 3500−3503.
[73] T. Yamaguchi, K. Ueno, H. Ogino, *Organometallics* **2001**, *20*, 501−507.
[74] M. C. Kuchta, J. B. Bonanno, G. Parkin, *J. Am. Chem. Soc.* **1996**, *118*, 10914−10915.
[75] M. C. Kuchta, H. V. R. Dias, S. G. Bott, G. Parkin, *Inorg. Chem.* **1996**, *35*, 943−948.
[76] M. Kuchta, J. B. Bonanno, G. Parkin, *J. Am. Chem. Soc.* **1996**, *1996*, 10914−10915.
[77] M. Kuchta, H. V. R. Dias, S. G. Bott, G. Parkin, *Inorg. Chem.* **1996**, *1996*, 943−948.
[78] H. V. R. Dias, L. Huai, W. Jin, S. G. Bott, *Inorg. Chem.* **1995**, *34*, 1973−1974.
[79] H. V. R. Dias, W. Jin, *Inorg. Chem.* **1996**, *35*, 267−268.
[80] H. V. R. Dias, W. Jin, *Inorg. Chem.* **2000**, *39*, 815−819.
[81] A. Frazer, B. Piggott, M. B. Hursthouse, M. Mazid, *J. Am. Chem. Soc.* **1994**, *116*, 4127−4128.
[82] D. L. Rege, D. G. Garza, *Organometallics* **1998**, *17*, 3624−3626.

 © 2004 Wiley-VCH Verlag GmbH & Co. KGaA, Weinheim

[83] N. J. Hardman, B. E. Eichler, P. P. Power, *Chem. Commun.* **2000**, 1991−1992.
[84] N. Hardman, P. P. Power, J. Gordon, C. L. B. Macdonald, A. H. Cowley, *Chem. Commun.* **2001**, 1866.
[85] N. Hardman, P. P. Power, *Inorg. Synth.* **2001**, *40*, 2474−2475.
[86] N. Hardman, P. J. Ragogna, K. N. Robertson, T. S. Cameron, *Chem. Commun.* **2002**, 382−383.
[87] N. J. Hardman, R. J. Wright, A. D. Phillips, P. P. Power, *J. Am. Chem. Soc.* **2003**, *125*, 2667−2679.
[88] M. Stender, B. E. Eichler, N. Hardman, P. P. Power, *Inorg. Chem.* **2001**, *2001*, 2794−2799.
[89] N. Hardman, R. J. Wright, A. D. Philips, P. P. Power, *J. Am. Chem. Soc.* **2003**, *125*, 2667−2679.
[90] D. L. Reger, D. G. Garza, A. L. Rheingold, G. P. A. Yap, *Organometallics* **1998**, *17*, 3624−3626.
[91] D. L. Reger, S. S. Mason, A. L. Rheingold, B. S. Haggerty, F. P. Arnold, *Organometallics* **1994**, *13*, 5049−5053.
[92] [92a] A. Kempter, C. Gemel, R. A. Fischer, **2004**, paper to be submitted for publication.[92b] A. Kempter, *Diploma Thesis*, Ruhr-Universität, Bochum, **2004**.
[93] G. P. Pez, R. A. Grey, J. Corsi, *J. Am. Chem. Soc.* **1981**, *1981*, 7528−7535.
[94] W. A. Fordyce, R. Wilcyzynski, J. Halpern, *J. Organom. Chem.* **1985**, *1985*, 115−125.
[95] J. Vollet, J. R. Hartig, H. Schnöckel, *Angew. Chem.* **2004**, *116*, 3248−3252; *Angew. Chem. Int. Ed.* **2004**, *43*, 3186−3189.

Received June 30, 2004

 © 2004 Wiley-VCH Verlag GmbH & Co. KGaA, Weinheim

Complex Formation of ICL670 and Related Ligands with Fe^{III} and Fe^{II}

Stefan Steinhauser,[a] Uwe Heinz,[a] Mark Bartholomä,[a] Thomas Weyhermüller,[b] Hanspeter Nick,[c] and Kaspar Hegetschweiler*[a]

Keywords: Iron / Ligand design / Chelates / N,O ligands / Redox chemistry

Complex formation of 4-[3,5-bis(2-hydroxyphenyl)-1,2,4-triazol-1-yl]benzoic acid (ICL670, H_3L^x), 4-[3,5-bis(2-hydroxyphenyl)-1,2,4-triazol-1-yl]benzosulfonic acid (H_3L^y), and 3,5-bis(2-hydroxyphenyl)-1-phenyl-1,2,4-triazole (H_2L^z) with Fe^{3+} and Fe^{2+} was investigated in H_2O and in H_2O/DMSO mixtures by potentiometry, spectrophotometry and cyclic voltammetry. ICL670 has previously been considered as a promising drug for an oral treatment of iron overload. In this paper, the stability and redox properties of the various Fe^{II} and Fe^{III} complexes were elucidated with a particular focus on their potential involvement in the generation of oxidative stress. The overall stability constants of $[Fe^{III}(L^x)]$ and $[Fe^{III}(L^x)_2]^{3-}$ (25 °C, 0.1 M KCl in H_2O) are log β_1 = 22.0 and log β_2 = 36.9, respectively. The affinity of these ligands for Fe^{2+} is remarkably poor. In particular, the 1:2 complexes $[Fe^{II}(L^x)_2]^{4-}$ and $[Fe^{II}(L^y)_2]^{4-}$ were found to be less stable. As a consequence, the redox chemistry of the $[Fe^{III}(L^x)]/[Fe^{II}(L^x)]^-$ and the $[Fe^{III}(L^x)_2]^{3-}/[Fe^{II}(L^x)_2]^{4-}$ couples differs significantly. $[Fe^{III}(L^x)_2]^{3-}$ is a very weak oxidizing agent ($E_{1/2}$ is approximately –0.6 V versus NHE) and reduction of $[Fe^{III}(L^x)_2]^{3-}$ is not anticipated under physiological conditions. The reduction potential of the $[Fe^{III}(L^x)]/[Fe^{II}(L^x)]^-$ couple is considerably less negative and was estimated to be +0.1 V (versus NHE). The possible roles of the various Fe complexes as catalysts for the Fenton reaction in biological media are discussed. The crystal structures of H_3L^x, $Na[Fe(L^z)_2]\cdot 4EtOH$, $Na[Al(L^z)_2]\cdot 4EtOH$, and $[Cu(L^z)(pyridine)]_2$ were investigated by single-crystal X-ray diffraction, and the possible influence of the particular steric requirements of these ligands on the stability of the metal complexes has been analyzed.
(© Wiley-VCH Verlag GmbH & Co. KGaA, 69451 Weinheim, Germany, 2004)

1. Introduction

Iron, an essential bioelement, is toxic when present in excess.[1] Iron overload is a particularly grave condition, because the human body lacks a physiological mechanism for actively excreting iron. There are a variety of different causes for the excessive loading of iron in a person; an important one is regular blood transfusions, necessary in the treatment of hematological defects such as β-Thalassaemia. Consequently, transfusion therapy must be combined with the administration of an iron-binding agent, transforming excess body iron into a chelated, excretable form. Presently, the microbial siderophore desferrioxamine (desferal, DFO) is used for this purpose (Scheme 1). This ligand, however, has some drawbacks. DFO is orally inactive and has a rather short plasma half-life. The need for new orally active iron chelators has been recognized for more than 30 years.[2] Deferiprone (L1), a hydroxy-pyridinone, can be taken orally; however, its application does suffer from some side effects.[3] The compound 4-[3,5-bis(2-hydroxyphenyl)-1,2,4-triazol-1-yl]benzoic acid (ICL670, deferasirox) is also an orally active iron chelator.[4] In previous animal studies, it proved to be more effective than parenteral DFO,[5] ICL670 is presently in Phase III of clinical trials.

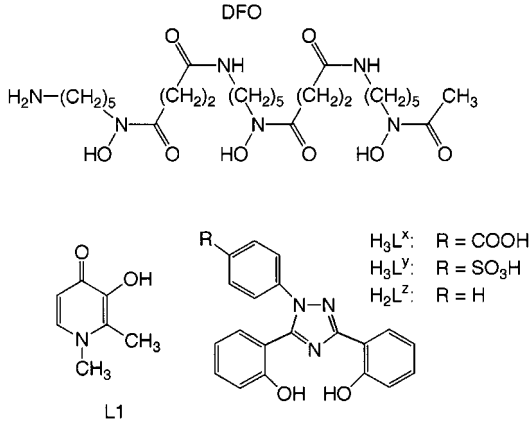

Scheme 1

A potential problem associated with iron chelation is the generation of oxidative stress.[6] Reactive oxygen species (ROS), and in particular the $OH^{\cdot}$ radical, have a consider-

[a] Anorganische Chemie, Universität des Saarlandes, Postfach 15 11 50, 66041 Saarbrücken, Germany
Fax: +49-681-302-2663
E-mail: hegetschweiler@mx.uni-saarland.de
[b] Max-Planck-Institut für Bioanorganische Chemie, Postfach 10 13 65, 45413 Mülheim an der Ruhr, Germany
[c] Novartis Institutes for BioMedical Research, WKL-136.P.72, Klybeckstrasse 141, 4002 Basel, Switzerland
Supporting information for this article is available on the WWW under http://www.eurjic.org or from the author.

able potential to damage a variety of cellular components.[7] There has been – and still is – a debate on the precise mechanism of oxidative stress.[8–11] It has been proposed that $OH^{\cdot}$ is generated by an Fe-catalyzed process; Fe^{III} is reduced by $O_2^{\cdot-}$ to Fe^{II}, which in turn reduces H_2O_2 to $OH^{\cdot}$ and OH^-.[7] It has also been argued that the level of O_2 in the cell would be much higher than that of H_2O_2, and that the initial step of oxidative stress could be assigned to the reaction of Fe^{II} with O_2 rather than H_2O_2.[12] Moreover, the reduction of Fe^{III} to Fe^{II} is not necessarily mediated by $O_2^{\cdot-}$, but could occur through the use of abundant biological reducing agents such as ascorbate and thiols.[7]

Although the precise mechanism of oxidative stress is not completely understood, it is generally accepted that iron can catalyze the production of ROS in terms of redox cycling, when it is available in a labile, redox-active form.[6–9,13–15] It is noteworthy that either a very high or a very low redox potential of an iron complex prevents oxidative stress. Ligands such as desferrioxamine or 1,10-phenanthroline, having either a high preference for the ferric or the ferrous form, appear to be inactive in terms of oxygen toxicity, whereas aminopolycarboxylates such as NTA^{3-}, $EDTA^{4-}$ or $DTPA^{5-}$ efficiently catalyze the production of single and double strand breaks of DNA and of modified nucleobases.[14] The reduction potential of possible $Fe^{III}L_n$/$Fe^{II}L_m$ species is thus a crucial parameter when developing new iron chelators for therapeutic use (Figure 1).[16]

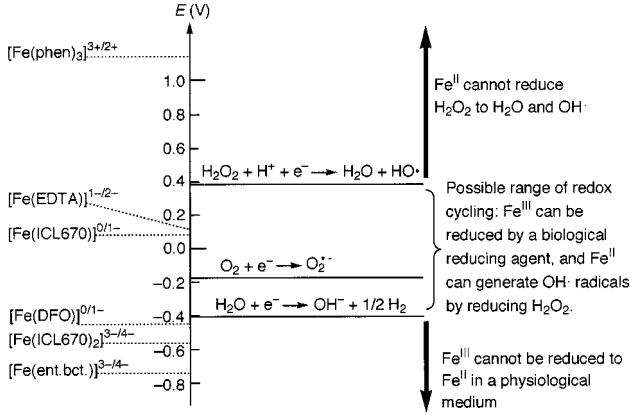

Figure 1. The possibility for redox cycling induced by different Fe^{III}/Fe^{II} complexes in biological media according to ref.[16]; the redox potentials are listed for pH 7, they were taken from refs.[16,18] and from this work (Fe–ICL670); the $O_2/O_2^{\cdot-}$ potential of −0.16 V refers to equal concentrations of dissolved O_2 and $O_2^{\cdot-}$, and not to the standard state (1 M $O_2^{\cdot-}$, 1 atm O_2); DFO = desferrioxamine, ent.bct = enterobactine, phen = 1,10-phenanthroline

In the present investigation, we address the problem of the possible redox activity of Fe–ICL670 complexes. For this purpose, we have studied the various species that form in solution, using a variety of physicochemical methods. Some preliminary results have already been published.[17] Herein, we present a comprehensive report on the complex formation of ICL670 (H_3L^x) and the related ligands H_3L^y and H_2L^z (Scheme 1) with Fe^{II} and Fe^{III}.[19–21]

2. Results

2.1. Solid-State Structures

2.1.1. Free Ligands

The unsubstituted derivative H_2L^z was first described by Ryabukhin.[21] We recently reported its crystal structure and documented the importance of the O–H···N hydrogen-bonding interactions between the phenolic hydroxy groups and N1 or N3 of the triazole ring.[22] Both O–H groups of H_2L^z are involved in intramolecular hydrogen bonds forming six-membered ring structures. O–H···N hydrogen bonding was also observed in the carboxylic acid derivative H_3L^x (ICL670), but in this ligand, only one of the hydroxy groups formed an intramolecular hydrogen bond (Figure 2). The other O–H···N bond was intermolecular, leading to infinite zigzag chains parallel to the crystallographic *z*-axis. These chains, which are further stabilized by some stacking interactions, are interconnected by the well-known pairing of the carboxylic acid moieties. The resulting two-dimensional sheets are oriented parallel to the *y*-*z* plane. Only one of the phenolic rings is roughly coplanar with the central triazole ring (the torsional angle is 2.3 °), while the other

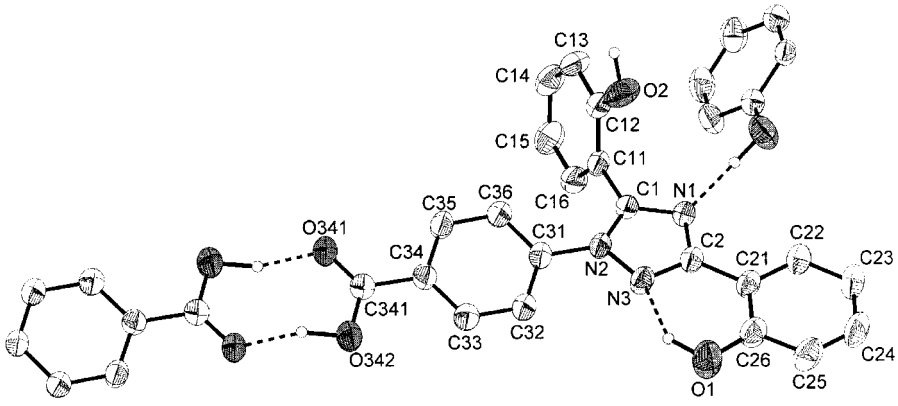

Figure 2. Molecular structure of H_3L^x (ICL670); the benzoic acid moiety and one phenol moiety of two neighboring H_3L^x molecules are also shown in order to illustrate the various types of intra- and intermolecular hydrogen bonding; atomic displacement ellipsoids are drawn at the 30% probability level; H(–O) hydrogen atoms are shown as spheres of arbitrary size; H(–C) hydrogen atoms are omitted for clarity. Bond lengths and angles are as expected

 © 2004 Wiley-VCH Verlag GmbH & Co. KGaA, Weinheim

phenolic ring with a torsional angle of 77.7° stands almost perpendicular to the triazole moiety. The benzoic acid moiety is tilted slightly out of the triazole plane by an angle of 13.9°.

2.1.2. Metal Complexes

There have been several unsuccessful attempts to crystallize metal complexes with H_3L^x and H_3L^y. However, complex formation with H_2L^z yielded, a variety of crystalline materials. Single crystals of $Na[Fe(L^z)_2]\cdot 4EtOH$ were found to be very fragile and disintegrated rapidly in air (loss of EtOH). Moreover, the crystal structure of this complex proved to be severely disordered. Refinement of a data set collected at room temperature resulted in rather poor agreement factors.[23] This disorder could partially be resolved in a low-temperature experiment (100 K). Two superimposed conformers in a 2:1 ratio were located (Figure 3), and some constraints had to be used to model the C−C distances in the peripheral phenyl ring realistically. The $[Fe(L^z)_2]^-$ anion was located on a crystallographic C_2 axis. This resulted in additional disorder of the sodium counterion, which was found in proximity of this axis (the disorder remained when the data was refined in the lower-symmetry space group *C*/*c*). The structure of $Na[Al(L^z)_2]\cdot 4EtOH$ is isotypic, showing the same type of disorder as observed for the Fe complex.[24]

$[Fe(L^z)_2]^-$ adopts the expected bis-structure with a meridional coordination mode of the two L^z entities, a distorted octahedral coordination environment, and Fe−O distances at the short end of the range expected for high-spin Fe^{III}.[25] The Fe−N distance of 2.092(5) Å is also remarkably short. It is worth noting that the ligand in this complex is once again not planar. The torsional angles between the phenolate rings and the central triazole unit are 14.1° and 23.5° (for the isostructural $[Al(L^z)_2]^-$, the corresponding values are 14.0° and 19.6°).[24] The sodium counterion is associated with one phenoxo group of each ligand. Four EtOH moieties complete the roughly octahedral NaO_6 coordination environment.

The combination of solutions of $CuBr_2$, H_2L^z, and a base resulted in the precipitation of $Cu(L^z)$. A polymeric chain structure has been proposed by Ryabukhin for this compound.[21] The green solid redissolved in boiling pyridine, and addition of MeOH and water resulted in the deposition of green crystals with the composition $[Cu(L^z)(pyridine)]_2$ (Figure 4). The dimeric complex is centrosymmetric; the two Cu^{II} cations have a slightly distorted square-pyramidal coordination geometry. The basal plane is defined by the O−N−O donor set of L^z and the pyridine *N* donor *trans* to the triazole nitrogen atom. Two $[Cu(L^z)(pyridine)]$ units are paired by mutual bridging through a coordinated phenoxo group. This phenoxo bridge represents the apex of the CuN_2O_3 pyramid. The Cu−O bond lengths fall in expected ranges.[26] However, it is interesting to note that the two Cu−N lengths (1.935 and 2.052 Å) differ significantly, the distance to the pyridine donor being longer. The bridging interaction of the phenoxo group is asymmetric with a long Cu−O distance to the donor in apical position. The two phenoxo moieties are again twisted with torsional angles of 19.2° and 24.0°. The structure is stabilized by some stacking interactions between the triazole and the pyridine moieties. As expected, the dimeric complex shows antiferromagnetic coupling between the two Cu^{II} centers with an $S = 0$ ground state.

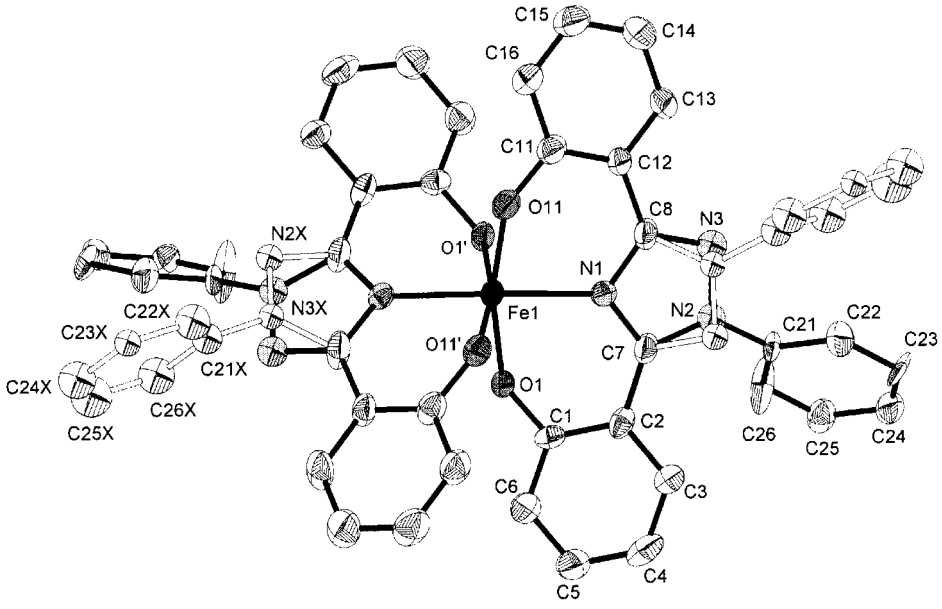

Figure 3. Molecular structure of the $[Fe(L^z)_2]^-$ anion, showing the major and minor components of the disordered structure; the atomic displacement ellipsoids are drawn at the 30% probability level; hydrogen atoms are omitted for clarity; selected bond lengths [Å] and angles (°): Fe1−O11 1.958(4), Fe1−O1 2.002(4), Fe1−N1 2.092(5), O11−Fe1−O11′ 92.4(3), O11−Fe1−O1 166.5(2), O11−Fe1−O1′ 90.6(2), O1−Fe1−O1′ 89.7(2), O11−Fe1−N1 84.1(2), O11−Fe1−N1′ 101.0(2), O1−Fe1−N1 82.4(2), O1−Fe1−N1′ 92.5(2), N1−Fe1−N1 172.7(3)

 © 2004 Wiley-VCH Verlag GmbH & Co. KGaA, Weinheim

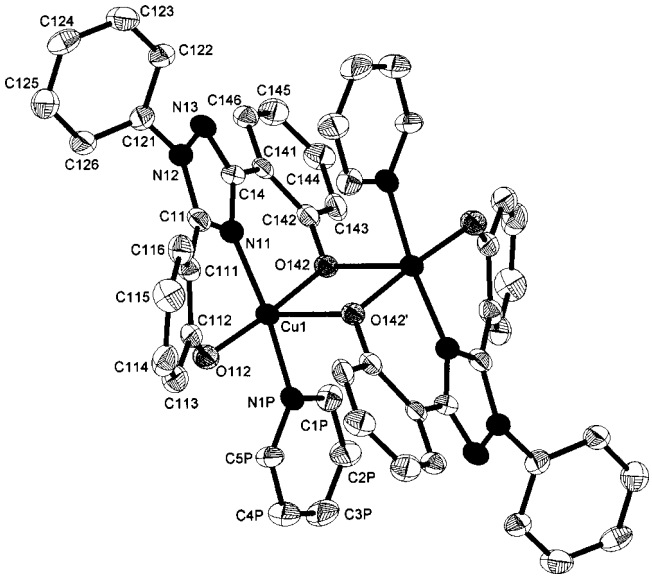

Figure 4. Molecular structure of the dinuclear $[Cu(L^z)(pyridine)]_2$ complex; the atomic displacement ellipsoids are drawn at the 30% probability level; hydrogen atoms are omitted for clarity; selected bond lengths [Å] and angles (°): Cu1−O112 1.922(6), Cu1−N11 1.935(6), Cu1−O142 1.946(5), Cu1−N1P 2.052(6), Cu1−O142′ 2.360(5), O112−Cu1−N11 89.6(2), O112−Cu1−O142 176.2(2), N11−Cu1−O142 86.8(2), O112−Cu1−O142′ 96.9(2), N11−Cu1−O142′ 96.5(2), O142−Cu1−O142′ 84.8(2), O112−Cu1−N1P 92.7(3), N11−Cu1−N1P 166.3(3), O142−Cu1−N1P 90.4(3), N1P−Cu1−O142′ 96.7(2)

2.2. pK_a Values of the Free Ligands

The pK_as were measured by potentiometric and spectrophotometric titrations (25 °C, 0.1 M KCl/KNO_3). In their fully protonated forms all three derivatives show rather low solubility in H_2O. Therefore, some of the deprotonation studies were performed in H_2O/DMSO solutions with $0.06 \leq x_{DMSO} \leq 0.20$ (x_{DMSO} is the mol fraction of DMSO). The dependence of the pK_as on x_{DMSO} was found to be roughly linear (Figure 5), and some of the missing values for pure H_2O could be estimated by extrapolation: $pK_{a,i}(x > 0) = pK_{a,i}(x = 0) + a \times x$, with $4.7 < a < 7.4$. Inspection of these data (Table 1) showed no significant differences for $pK_{a,2}$ and $pK_{a,3}$ between the three ligands H_3L^x, H_3L^y and H_2L^z. Moreover, the influence of the inert electrolyte (KCl or KNO_3) appears to be negligible, and the interpolation procedure yielded reliable estimates for the pK_as in H_2O, with an accuracy of about ±0.1. For an appropriate interpretation of these data, it is important to note that the ionic product (apparent $K_w = Q_c = [H^+] \times [OH^-]$) in the H_2O/DMSO system is considerably smaller than in pure H_2O.[27] As a consequence, the pH scale for $x_{DMSO} = 0.2$ is extended to a range of 0−15.6, and neutral solutions have a pH value of about 7.8.

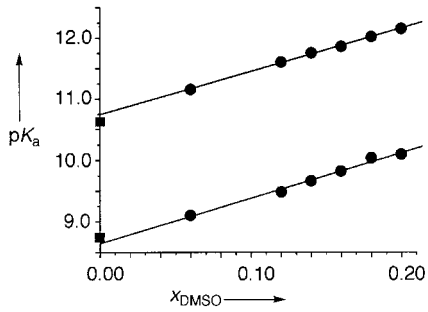

Figure 5. The dependence of the $pK_{a,2}$ and $pK_{a,3}$ of H_3L^y on x_{DMSO}; circles indicate values with $x_{DMSO} \geq 0.06$, squares refer the experimental values in pure water; the fitted line illustrates the reliability of the extrapolation procedure ($x_{DMSO} \rightarrow 0$) with an accuracy of the $x_{DMSO} = 0$ values of about ±0.1

The observed pK_a values can be grouped in three categories:

(a) $pK_a < 2$. Such low values could not be determined by conventional potentiometric methods and were therefore measured spectrophotometrically. All the investigated ligands showed significant spectral changes in the range $0 < pH < 2$. A ^1H NMR spectroscopic study of H_3L^x showed considerable shifts for the hydrogen atoms of the two phenol rings, whereas the resonances for the C_6H_4−COO hydrogen atoms (which appeared as a characteristic AA′XX′ spin system) remained virtually constant. Obviously, these changes must be attributed to protonation of a triazole nitrogen atom (for the unsubstituted 1,2,4-triazole, a pK_a of 2.19 is reported in the literature).[28] According to the ^1H

Table 1. pK_a values (25 °C, 0.1 M KCl or KNO_3) of H_3L^x, H_3L^y, and H_2L^z in H_2O and in H_2O/DMSO solutions with a mol fraction $x_{DMSO} = 0.2$; uncertainties (3σ) are given in parentheses

	H_3L^x (ICL670)		H_3L^y			H_2L^z	
	$x_{DMSO} = 0.20$						
$pK_{a,1}$[a]	4.61(2)[b] [c]	4.61(4)[d] [e]	<2				
$pK_{a,2}$[a]	10.12(2)[b][c]	10.00(3)[d][e]	10.10(4)[d][e]			10.12(1)[c][d]	10.0(1)[d][e]
$pK_{a,3}$[a]	12.08(2)[b][c]	12.12(4)[d][e]	12.15(2)[d][e]			12.21(3)[c][d]	12.2(1)[d][e]
	H_2O only						
$pK_{a,1}$[a]	−[f]	3.7(1)[d][g]	<2[c][d]	1.1(1)[d][e]			
$pK_{a,2}$[a]	8.80(1)[d][h]	9.0(1)[d][g]	8.74(1)[c][d]	8.76(3)[d][e]	8.6[d][g]	−[f]	
$pK_{a,3}$[a]	10.61(1)[d][h]	10.6(1)[d][g]	10.63(1)[c][d]	10.67(3)[d][e]	10.7[d][g]	−[f]	

[a] $pK_{a,i} = -\log K_{a,i}$, $K_{a,i} = [H_{3-i}L] \times [H] \times [H_{4-i}L]^{-1}$. [b] 0.1 M KNO_3. [c] pH titration of H_mL with KOH. [d] 0.1 M KCl. [e] Spectrophotometric titration. [f] Insufficient solubility. [g] Extrapolated for $x_{DMSO} \rightarrow 0$. [h] pH titration of $L^{x\,3-}$ with HCl.

 © 2004 Wiley-VCH Verlag GmbH & Co. KGaA, Weinheim

NMR spectroscopic characteristics, protonation of the nitrogen atom is also observed for the sulfonic acid derivative H_3L^y. Consequently, H_3L^y must be present predominantly in a zwitterionic form in strongly acidic aqueous media (Scheme S1, Supporting Information).

(b) $3 < pK_a < 5$ was only observed for H_3L^x and corresponds to the deprotonation of the carboxylic acid group.

(c) $pK_a > 8$. These values are characteristic of the deprotonation of the phenolic OH groups. Although the two OH groups are structurally inequivalent, it appears highly probable that they are deprotonated simultaneously, and that the observed pK_as represent averages of the individual (microscopic) acidity constants.[29]

2.3. Complex Formation with Fe^{III}

The formation of Fe^{III} complexes with H_3L^x, H_3L^y and H_2L^z was also studied in H_2O/DMSO by potentiometric and spectrophotometric methods. The overall stability constants, which are defined according to: $mFe^{3+} + nL^{u-} + qH^+ \rightleftarrows Fe_mL_nH_q^{3m-un+q}$, $\beta_{mnq} = [Fe_mL_nH_q^{3m-un+q}] \times [Fe^{3+}]^{-m} \times [L^{u-}]^{-n} \times [H^+]^{-q}$, ($L^x$, L^y: $u = 3$, L^z: $u = 2$), are summarized in Table 2.

In acidic solution (pH <3.5), formation of a 1:1 complex was verified by Job′s plots and was further confirmed by spectrophotometric batch titrations for all three ligands (Figures S5−S7, Supporting Information). Below pH 4, ICL670 forms a protonated complex $[Fe(HL^x)]^+$ (indicated as 111 in Scheme 2). This species could be deprotonated to $[Fe(L^x)]$ (110). We propose that the additional proton is bonded to the peripheral carboxylate group of the ligand. This assignment is consistent with the observation that a corresponding 111 species does not form with the sulfonic acid H_3L^y and the phenyl derivative H_2L^z. Clearly, the peripheral sulfonate group of H_3L^y is not sufficiently basic

Table 2. Overall formation constants (log β_{mnq}) of Fe^{III} complexes with H_3L^x, H_3L^y, and H_2L^z (25 °C, 0.1 M KCl or KNO_3) in H_2O or in H_2O/DMSO solutions with a mol fraction $x_{DMSO} = 0.20$; uncertainties (3σ) are given in parentheses

log β_{mnq}[a]	H_3L^x (ICL670)	H_3L^y	H_2L^z
mnq	$x_{DMSO} = 0.20$		
111	27.5(1)[b][c]		
110	23.33(3)[d][e], 23.5(1)[b][c]	22.50(1)[b][c]	22.85(1)[b][c]
122	48.7(1)[d][e]		
121	44.36(1)[d][e], 44.5(1)[b][c]	43.05(6)[b][c]	not determined[f]
120	38.56(2)[d][e], 38.6(1)[b][c]	37.46(9)[b][c]	not determined[f]
	H_2O only		
111	24.3[b][g]		
110	22.0[b][g]	21.30(4)[b][c], 21.2[b][g]	not determined[f]
122	43.4[b][g][h]		
121	41.2[b][g]	40.89(3)[b][e], 40.79(4)[b][c], 40.9[b][g]	not determined[f]
120	36.9[b][g]	35.95(5)[b][e], 36.06(4)[b][c], 35.8[b][g]	not determined[f]

[a] $\beta_{mnq} = [Fe_mL_nH_q] \times [Fe]^{-m} \times [L]^{-n} \times [H]^{-q}$. [b] 0.1 M KCl. [c] Spectrophotometric titration. [d] 0.1 M KNO_3. [e] Potentiometric titration. [f] Insufficient solubility. [g] Extrapolated for $x_{DMSO} \rightarrow 0$. [h] This species does not appear in the equilibrium in pure H_2O to a significant extent.

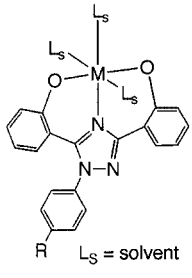

110: R = COO^-, SO_3^-, H
111: R = COOH

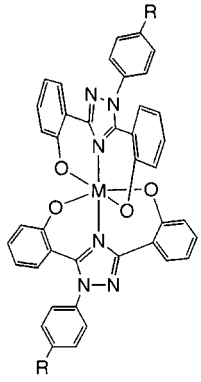

120: R = COO^-, SO_3^-, H

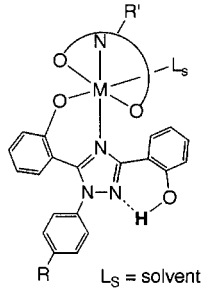

121: R = R' = COO^-, SO_3^-, H
122: R = COO^-, R' = COOH

Scheme 2

 © 2004 Wiley-VCH Verlag GmbH & Co. KGaA, Weinheim

to allow protonation in aqueous solution. Moreover, $[Fe(HL^x)]^+$ and $[Fe(L^x)]$ have very similar optical spectra (Figure 6b). Since the observed bands in the Vis spectra are mainly charge-transfer transitions, protonation of the peripheral carboxylate group does not modify the chromophore of this complex to a significant extent.

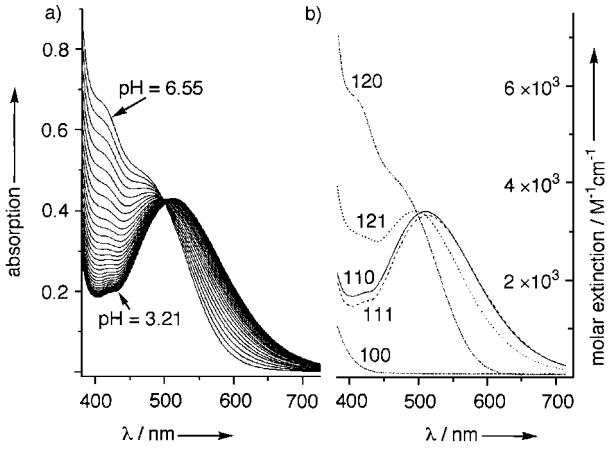

Figure 6. Determination of the formation constants log β_{mnq} of $[Fe_m(L^x)_nH_q]^{3m-3n+q}$; a) the sample spectra of the spectrophotometric titration with total [Fe]:total [L^x] = 1:3 in the range 3.2 < pH < 6.6 (x_{DMSO} = 0.2); b) calculated spectra of the individual $[Fe_m(L^x)_nH_q]^{3m-3n+q}$ species indicated as *mnq*; the spectra of Fe^{3+} (= 100) and of $[Fe(HL^x)]^+$ (= 111) were measured separately and were imported without refinement

At higher pH, complex formation with H_3L^x and H_3L^y was explored by continuous titrations (Figure 6). An additional ligand is bound to the metal center above pH 4, and a series of 1:2 complexes are formed. Experiments with H_2L^z could not be evaluated due to precipitation. Formation of a reddish-violet solid was always observed, even if a very low concentration of total Fe (10^{-4} M) and a large excess of ligand (total L^z: total Fe > 4) was used. The precipitation began after addition of about 1.2 equivalents of base, and the precipitate redissolved completely above pH 6. Obviously, a bis complex of zero charge is formed with a tentative composition $[Fe(L^z)(HL^z)]$ (indicated as 121 in Scheme 2). Formation of a similar 121 intermediate was also established for the sulfonic acid H_3L^y by potentiometric and spectrophotometric methods. However, due to the anionic nature of $[Fe(L^y)(HL^y)]^{2-}$, an insoluble solid did not form. The 121 complex deprotonated around pH 5−6 to form $[Fe(L^y)_2]^{3-}$ (= 120), which was then present as the sole species up to pH 12. The carboxylic acid H_3L^x behaved similarly, although an additional doubly protonated bis complex $[Fe(HL^x)_2]^-$ (= 122) was detected as a minor species in the region 4 < pH < 5.

For the mono complex, the reaction $[Fe(L^x)] + H^+ \rightarrow [Fe(HL^x)]^+$ was attributed to a simple protonation of the peripheral carboxylate group (vide supra). However, for the bis complexes, a different type of reaction must be considered, since $[Fe(L^y)_2]^{3-}$ and $[Fe(L^z)_2]^-$ have no peripheral sites available for protonation around pH 5 (Figure 7). Conclusive evidence for the nature of this complex is obtained from an analysis of the Vis spectroscopic data, which established that the spectra of $[Fe(L^x)(HL^x)]^{2-}$ (121) and $[Fe(L^x)_2]^{3-}$ (120) are distinctly different (Figure 6b). The situation is similar for $[Fe(L^y)(HL^y)]^{2-}$ and $[Fe(L^y)_2]^{3-}$ (see Figure S8, Supporting Information). Obviously, the two complexes must have different coordination spheres, and we therefore propose a bidentate coordination mode for one of the ligands in the 121 complex with the triazole nitrogen and one of the phenolic oxygen donors as the only coordinating atoms (Scheme 2). The second phenolic oxygen donor is protonated and probably hydrogen bonded to the free triazole nitrogen atom (as observed for the free ligands, see Figure 2). Further evidence for this particular structure is provided by FAB^+ MS (measured in EtOH). The spectrum shows the formation of the species $[Fe(L^z)_2(EtOH)]^+$ with rather high intensity. The binding of one (and only one) EtOH molecule can be nicely explained, if the complex is formulated as $[Fe(L^z)(HL^z)OEt]^+$, with a bidentate HL ligand and the sixth position in the coordination sphere occupied by an OEt^- moiety.

The spectra of the monoprotonated $[Fe(L^x)(HL^x)]^{2-}$ and the doubly protonated $[Fe(HL^x)_2]^-$ do not differ to any significant extent, and we therefore assign the reaction of $[Fe(L^x)(HL^x)]^{2-}$ with H^+ to a simple protonation of one of the peripheral carboxylate groups. The similarity of the two spectra, together with a rather low abundance of these species, prevents the determination of the formation constant β_{122} of $[Fe(HL^x)_2]^-$ by spectrophotometric methods. The value for log β_{122} could only be established by potentiometric titrations. In agreement with this assignment, the doubly protonated $[Fe(HL^y)_2]^-$ and $[Fe(HL^z)_2]^+$ species were not observed.

A comparison of the various log β values (Table 2) shows the following trends:

(a) *Dependence on DMSO concentration.* The sulfonic acid derivative has significantly enhanced solubility, and the entire range $0 \le x_{DMSO} \le 0.2$ could thus be investigated. A steady increase of log β was generally noted for an increase in the mol fraction of DMSO. The difference $\Delta\log\beta = \log\beta_{x(DMSO)=0.2} - \log\beta_{x(DMSO)=0}$ is 1.2 for $[Fe(L^y)]$, and 1.5 for $[Fe(L^y)_2]^{3-}$. Complex formation of H_3L^x with Fe^{3+} was performed in solutions with a mol fraction x_{DMSO} of 0.22, 0.20 and 0.18. The extrapolation $x_{DMSO} \rightarrow 0$ yielded $\Delta\log\beta_{110}$ = 1.3 and $\Delta\log\beta_{120}$ = 1.6. The similar behavior of the two ligands H_3L^x and H_3L^y and the linear dependence of log β on x as observed for H_3L^y justify application of the extrapolation procedure as described above for the pK_a values (Figure 5). As a result, we note that $Fe^{III}-L^x$ complexes with a peripheral COOH group are much stronger acids in H_2O than in H_2O/DMSO mixtures. Corresponding pK_a values derived from the overall formation constants (Table 2) are 2.3/2.2 (H_2O) and 4.2/4.3 (x_{DMSO} = 0.2) for $[Fe(HL^x)]^+$/$[Fe(HL^x)_2]^-$. We attribute this effect to the different solvation properties of the two media. Consequently, such protonated species appear in a substantial amount in the H_2O/DMSO mixture (Figure 7a), whereas in pure H_2O, their formation is of minor relevance or not significant at all (Figure 7b).

 © 2004 Wiley-VCH Verlag GmbH & Co. KGaA, Weinheim

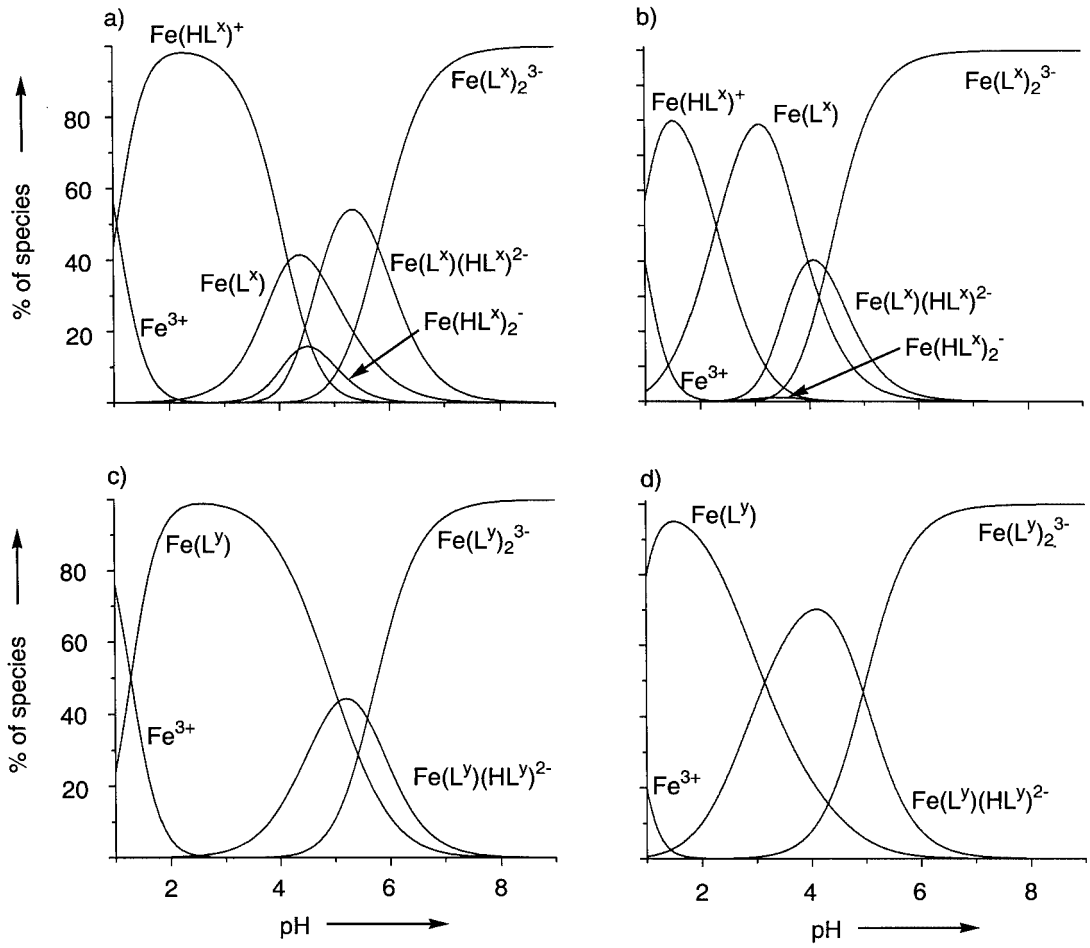

Figure 7. Species distribution plots for equilibrated solutions of $Fe^{III}-H_3L$ systems; a) H_3L^x, $x_{DMSO} = 0.2$; b) H_3L^x, $x_{DMSO} = 0.0$; c) H_3L^y, $x_{DMSO} = 0.2$; d) H_3L^y, $x_{DMSO} = 0.0$; total Fe and total ligand concentrations are 1.0 mM, and 2.0 mM, respectively; only metal-containing species are shown (total Fe = 100%); the equilibrium constants listed in Tables 1 and 2 were used for the calculations

(b) *Comparison of the different ligands.* The stability of [FeL] with $x_{DMSO} = 0.2$ decreases in the order $H_3L^x > H_2L^z > H_3L^y$. However, the differences are relatively minor. In general, the iron binding properties of H_3L^x and H_3L^y are indeed closely related: the pFe values[30] for H_3L^x and H_3L^y (total [L] = 10 μM, total Fe = 1 μM, pH = 7.4, H_2O, $I = 0.1$ M) are 21.5 and 20.6, respectively.

2.4. Complex Formation with Fe^{II}

The formation of Fe^{II} complexes with H_3L^y was again studied in H_2O/DMSO mixtures ($x_{DMSO} = 0.20$). However, a quantitative determination of the formation constants proved extremely difficult, because the ferrous complexes reacted as strong reducing agents and were readily oxidized to the corresponding Fe^{III} species. This oxidation process could easily be observed by the intense red or purple color of the Fe^{III} complexes (the Fe^{II} complexes are virtually colorless). It was thus of utmost importance to remove any traces of oxygen from the sample solutions. A series of potentiometric titrations was performed under Ar to determine the corresponding formation constants. However, it was not possible to suppress the oxidatively induced side reactions completely. In particular, the 1:2 complex $[Fe^{II}(L^y)_2]^{4-}$ was found to be a strong enough reducing agent to be oxidized even in the complete absence of oxygen. Corresponding CV measurements (see section 2.5.2) confirmed that $[Fe^{II}L_2]^{4-}$ is able to reduce H_2O (formation of H_2) in neutral solution. It was therefore not possible to determine any formation constant for the ferrous 1:2 complex with this method. The potentiometric measurements could, however, be used to investigate the formation of the 1:1 complex $[Fe^{II}(L^y)]^-$, according to the reaction $Fe^{2+} + H_3L^y \rightleftarrows [Fe(L^y)]^- + 3\ H^+$. The overall formation constant β_{110} (referring to the reaction $Fe^{2+} + L^{3-} \rightleftarrows [FeL]^-$) was determined in H_2O/DMSO ($x_{DMSO} = 0.2$) to be $\log \beta_{110} = 11.5(2)$. As expected, this number is substantially lower than the corresponding value for Fe^{3+} (22.5, see Table 2).

2.5. Redox Properties of the $Fe^{II}/Fe^{III}-H_3L$ System

2.5.1. Redox Chemistry in Acidic Solutions

Below pH 3, the 1:1 complexes $[Fe(HL^x)]^+$ and $[Fe(L^y)]$ are predominantly formed, even when the ligand is present in excess (Figure 7). The redox characteristics of these two complexes have been investigated thoroughly by means of cyclic voltammetry. The two complexes behave rather similarly, and we will focus here on the behavior of $[Fe(HL^x)]^+$ (Figure 8) and present the results for $[Fe(L^y)]$ in an abbrevi-

 © 2004 Wiley-VCH Verlag GmbH & Co. KGaA, Weinheim

ated manner. A Pt working electrode was used exclusively in acidic solution, and all experiments were performed in a H_2O/DMSO medium ($x_{DMSO} = 0.2$) to avoid precipitation of the insoluble H_3L. The use of DMSO as a particularly useful solvent in electrochemistry is well-established.[31]

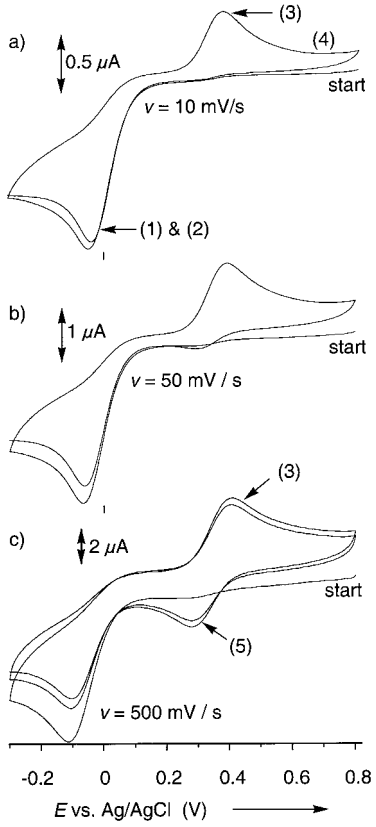

Figure 8. Cyclic voltammograms of $[Fe(HL^x)]^+$ (pH = 2.9, total [Fe] = 2.5 mM, total [L^x] = 5 mM, $x_{DMSO} = 0.2$ using a Pt working electrode at scan rates as indicated

Reduction of $[Fe(HL^x)]^+$ resulted in the formation of the corresponding Fe^{II} complex according to the reaction:

$$[Fe^{III}(HL^x)]^+ + e^- \rightarrow [Fe^{II}(HL^x)] \quad (1)$$

However, the ferrous complex is not stable and decomposes immediately and completely according to the reaction:

$$[Fe^{II}(HL^x)] + 2\,H^+ \rightarrow Fe^{2+} + H_3L^x \quad (2)$$

The electron uptake and complex decomposition described by the above reactions [Equation (1) and Equation (2)] was indicated by a characteristic irreversible peak in the range +100 mV to −150 mV (versus Ag/AgCl). As indicated by Equation (2), the decomposition is strongly pH dependent. The peak shifted to less positive values at higher pH with a slope of 109 mV/pH ([Fe(L^y)]: 129 mV/pH), indicating a transfer of two protons per electron (Figure S13, Supporting Information). The cathodic peak current was found to be linearly dependent on the square root of the scan rate, as expected for a diffusion controlled reaction (Figure S12, Supporting Information). The peak potential of the reduction slightly shifted to less positive values with increasing scan rate, and this is consistent with an irreversible process. As a result of the complete decomposition of the complex, the reverse scans showed a half wave indicative of the reoxidation of the free Fe^{2+} to Fe^{3+} at about 400 mV (versus Ag/AgCl) according to:

$$Fe^{2+} \rightarrow Fe^{3+} + e^- \quad (3)$$

This assignment is further supported by a characteristic time dependence, which was observed in subsequent scans. If a sufficiently slow scan rate was used (< 50 mV/s), enough time was available for the re-formation of the ferric complex after reoxidation of Fe^{2+} to Fe^{3+}, according to:

$$Fe^{3+} + H_3L^x \rightarrow [Fe^{III}(HL^x)]^+ + 2\,H^+ \quad (4)$$

Consequently, the second scan was identical to the first scan. Further scans did not result in any change in the behavior. However, if a higher scan rate of about 50−500 mV/s was applied, $[Fe^{III}(HL^x)]^+$ was only partially recovered [Equation (4)], and in the following scan, the solution still contained some free Fe^{3+}, which was reduced to Fe^{2+}:

$$Fe^{3+} + e^- \rightarrow Fe^{2+} \quad (5)$$

The above reaction [Equation (5)] resulted in the appearance of a new reduction wave at around 300 mV (versus Ag/AgCl), and as a consequence, two reduction waves [see Equation (1) and Equation (5)] were now observable. The ratio of their intensity varied characteristically with scan rate. Increasing scan rates resulted in an increase in the suppression of Equation (4), and therefore in an increase in the amount of free Fe^{3+} and a decrease in the amount of $[Fe^{III}(HL^x)]^+$. Consequently, the intensity of the peak at 300 mV increased with increasing scan rate, whereas that of the peak at around −100 mV (its counterpart) diminished. At a scan rate higher than 500 mV/s, the amount of complex formed after the first cycle was less than 50%, and the quasi-reversible pattern for the free Fe^{2+}/Fe^{3+} couple [Equation (3) and Equation (5)] was observed. This time-dependence was found to be in good agreement with the kinetics of $[Fe(HL^x)]^+$ formation, which was established previously by stopped flow experiments.[17]

If the pH was lowered to ≤2, the acidity of this medium was high enough to lead to the partial decomposition of $[Fe^{III}(HL^x)]^+$ (Figure 7):

$$[Fe^{III}(HL^x)]^+ + 2\,H^+ \rightarrow Fe^{3+} + H_3L^x \quad (6)$$

 © 2004 Wiley-VCH Verlag GmbH & Co. KGaA, Weinheim

Consequently, two reduction waves were observed already in the first scan, and it was not possible to suppress the peak at 300 mV by sufficiently slow scan rates.

2.5.2. Redox Chemistry in Neutral and Alkaline Solutions

Above pH 6, 1:2 complexes are predominantly formed, and the relevant reduction reaction is thus:

$$[Fe^{III}(L)_2]^{3-} + e^- \rightarrow [Fe^{II}(L)_2]^{4-} \quad (7)$$

However, CV experiments with an Au, Pt or glassy carbon working electrode did not show any redox activity for $[Fe^{III}(L)_2]^{3-}$. Obviously, $[Fe^{II}(L)_2]^{4-}$ is a stronger reducing agent than H_2 (see section 2.4), and the failure to observe any redox activity is due to the production of hydrogen prior to the reduction of the complex. An Hg (hanging drop) electrode was thus used to circumvent the problem of hydrogen formation, and the quasi-reversible reduction of $[Fe^{III}(L)_2]^{3-}$ [Equation (7)] could then be detected above pH 12 (Figure 9). The peak separations ΔE_P were 93 mV and 102 mV, and the reduction potentials for the $[Fe^{III/II}(L)_2]^{3-/4-}$ couple were −0.92 V and −0.89 V for H_3L^x and H_3L^y, respectively (x_{DMSO} = 0.2, vs. Ag/AgCl). As expected, this value does not depend on pH (Figure S14). Plots of the cathodic peak current vs. the square root of scan rate established a purely diffusion-controlled process (Figure S12). At pH <12, the two waves of to this redox process were still visible; however, additional peaks were observed in the reverse scan at more positive values (Figure S15). We attribute these characteristics to a partial dissociation of the ferrous complex [Equation (8)]:

$$[Fe^{II}L_2]^{4-} + nH^+ \rightarrow [Fe^{II}L]^- + H_nL^{n-3} \quad (8)$$

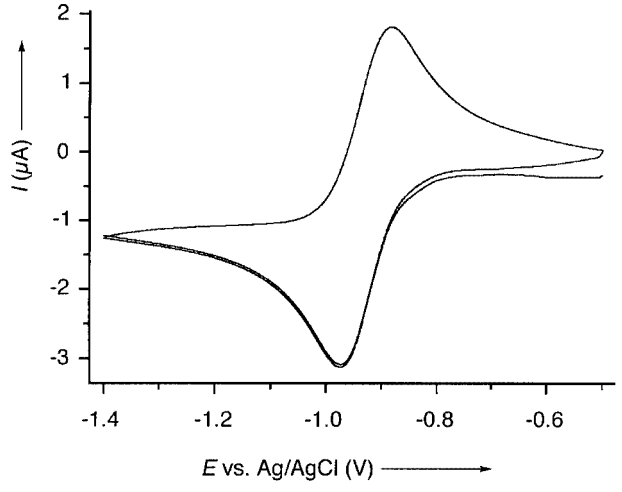

Figure 9. Cyclic voltammogram of $[Fe(L^x)_2]^{3-}$ (pH = 12.7, total [Fe] = 2.5 mM, total [L^x] = 5 mM, x_{DMSO} = 0.2 at a Hg (hanging drop) working electrode with a scan rate of 50 mV/s

For ICL670 (H_3L^x), the reduction of $[Fe^{III}(L)_2]^{3-}$ [Equation (7)] was also investigated in H_2O, and a very similar behavior was noted. The observed reduction potential was determined as −0.58 V (versus NHE). Excess ligand was used as buffer in our aqueous experiments, to stabilize the pH in the range 11−12 (the free ligand is electrochemically inactive). Moreover, the excess ligand also inevitably served to suppress the decomposition of $[Fe^{II}L_2]^{4-}$ [Equation (8)].

3. Discussion

3.1. Structure and Selectivity

It has been suggested that the application of ICL670 in the therapy of iron overload could be problematic due to the lack of sufficient selectivity.[2] In particular, the presence of an sp^2 nitrogen atom would generate a donor set with a significant tendency to bind divalent biometal cations such as Zn^{2+}. Although the affinity of high-spin Fe^{III} for six negative oxygen donors generally appears to be overestimated,[32] it is true that an increasing number of nitrogen donors would enhance the stability of metal complexes with late divalent transition metal cations (Ni^{2+}, Cu^{2+}, Zn^{2+}), because an sp^2 nitrogen donor is somewhat softer than a negative oxygen donor.[33,34] However, the metal selectivity of a complexing agent cannot be explained simply in terms of the hardness of the donor set. Additional steric factors of the ligand must also be considered,[33] and it appears that in discussing the metal-ion selectivity of ICL670, these steric aspects have not received the necessary attention in some of the previous reports.

With regard to the particular steric properties of ICL670, it is important to recognize that an entirely planar L−M unit with an O−M−O angle of 180° (Scheme 3a) would imply an M−O bond length of 1.60 Å and an M−N bond length of 1.90 Å. Only very small cations are capable of forming such a short M−O bond. It has been shown by Hancock that ligands forming six-membered chelate rings have a distinct preference for small metal centers, whereas five-membered chelate rings are more suited for larger cations.[35] Clearly, with its rigid structure and its constraint of two six-membered chelate rings, ICL670 will have a strong preference to bind small metal cations. As a consequence, *all* complexes of ICL670 with di- and trivalent transition-metal cations must be regarded as strained, and this strain increases significantly with increasing ionic size. This result is of importance with regard to selectivity of this ligand in biological systems. It is noteworthy that most of the competing biometal cations such as Zn^{2+} are larger than Fe^{3+}, and binding of these elements to ICL670 is thus clearly discriminated on the basis of steric considerations. The bond strain in such complexes can be absorbed to a large extent by angle deformation, and the M−O distance can be widened by out-of-plane twisting of the two phenyl rings (Scheme 3b). As already noted in the results section (2.1.2), this type of twist has generally been observed in the crystal structures of such metal complexes, and the corresponding twist angle increases, as expected, with increasing ionic ra-

 © 2004 Wiley-VCH Verlag GmbH & Co. KGaA, Weinheim

dius. However, the rotation of the two phenoxo rings inevitably results in a compression of the M−N bond. Corresponding M−N distances observed in the crystal structures are indeed rather short. Again, the compression is partially compensated by deformation of the *cis*−O−M−N and *trans*−O−M−O angles (Scheme 3c).

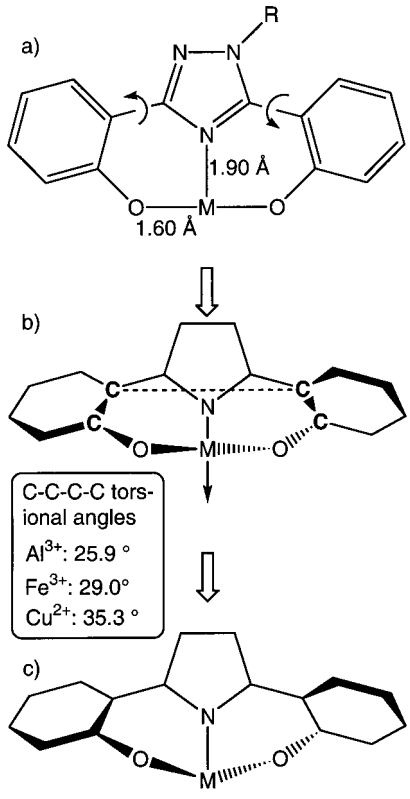

Scheme 3

The favored binding of small metal cations is nicely illustrated by the stability constants of $[M(L^x)]$ complexes with Mg^{2+} (log K = 7.6) and Ca^{2+} (log K = 5.5).[17] These values should be compared with values for other ligands that have a mixed *O*,*N* donor set such as NTA^{3-} (log K_{MgNTA} = 5.5, log K_{CaNTA} = 6.3) or EDTA (log K_{MgEDTA} = 8.8, log K_{CaEDTA} = 10.7).[36] The two aminopolycarboxylate ligands exclusively form five-membered chelate rings, and as a consequence, the complexes with the larger cation (Ca^{2+}) are more stable. For ICL670, the reverse trend is observed, and the complexes with the smaller Mg^{2+} are about two orders of magnitude more stable. Consequently, replacement of the ferric iron by the larger Zn^{2+} ion, according to $[Fe(L^x)_2]^{3-} + Zn^{2+} \rightleftarrows [Zn(L^x)_2]^{4-} + Fe^{3+}$, is strongly disfavored. The equilibrium constant for this reaction is 7.9×10^{-22}.[17] The significant stress, even in the ferric complex, also explains the rather unexpected formation of the protonated species $[Fe(L)(HL)]^{2-}$ (L = L^x, L^y) or [Fe(L)(HL)] (L = L^z) that was observed for all three ligands. Obviously, the transformation to a bidentate coordination mode arises because of the release of strain induced by the detachment of one of the coordinated phenoxo groups. Such a detachment of a basic donor atom by protonation is well-established for strained chelate rings.[37]

In the bis complexes of ICL670, the discussion of structure-stability correlations requires the analysis of additional interligand interactions. For this purpose, it is necessary to briefly discuss the different stereoisomers that are possible for such an ML_2 complex. In the simple ML unit, the twist of the two phenyl rings can either occur in a clockwise or counter-clockwise manner relative to the central triazole unit (Scheme 4a). By analogy with the usual nomenclature, the O···O line will be used in this work to refer to the two forms as the λ or δ enantiomer, and the combination in a bis complex would give either a λδ or a δδ (or λλ) form (Scheme 4b). The two forms adopt considerably different geometries. In the λδ isomer, the two ligands are oriented perpendicularly, whereas the δδ isomer has a rather flat shape with an almost parallel orientation of the four phenyl rings that allow for some π-stacking to occur. Due to the nonequivalence of the two noncoordinating nitrogen atoms, the symmetry of the λδ isomer is C_1. For the δδ isomer, the addition of a substituent to one of the nitrogen atoms results either in a *cisoid* or *transoid* structure. Both of these have C_2 symmetry. $[Fe^{III}(L^z)_2]^-$ and $[Al^{III}(L^z)_2]^-$ − as observed in the crystalline compounds − correspond to the C_2 isomer with the transoid configuration being predominant (Figure 3). Inspection of the different structures reveals that for all possible isomers, *repulsive* interligand interactions are relatively minor. The exclusive formation of the λλ/δδ form in the Fe^{III} and Al^{III} complexes may be attributed to the possible stabilization by intramolecular π-stacking and also to the better accessibility of the Na^+ counterion for its bonding to two phenoxo oxygen atoms (indicated by arrows in Scheme 4b).

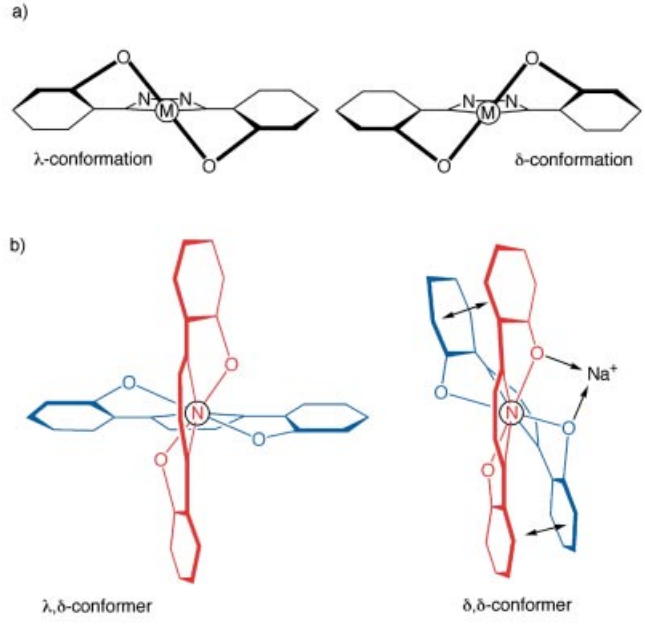

Scheme 4. a) The two enantiomeric ML conformations; b) the possible ML_2 forms (λ,δ and δ,δ)

 © 2004 Wiley-VCH Verlag GmbH & Co. KGaA, Weinheim

3.2. Species Distribution and Redox Properties of the Fe^{III}−ICL670 System

As outlined in the introduction, the abundance and redox potential of every single component must be considered when discussing the problem of possible redox cycling. As a tridentate ligand, ICL670 can form ML and ML_2 complexes, and both species must be regarded as possible redox catalysts. A conventional species distribution diagram for the ICL670−Fe^{3+} system is shown in Figure 7 (see a and b). However, in this type of representation, the amount of total Fe in solution is arbitrary. In contrast, Figure 10 illustrates a situation in which the different ferric complexes are in equilibrium with solid FeOOH. The concentration of free Fe^{3+} is then mediated by the solubility product of this solid phase, and the total amount of dissolved Fe is a direct measure of the efficacy of a ligand for Fe^{III} chelation at a given pH.[38] This type of representation more closely reflects the condition in an iron-overloaded patient. Figure 10 shows the amount of dissolved Fe for total ligand concentrations of 100 μM, 1 μM, and 10 nM (the corresponding value in the serum of an iron-overloaded patient during oral treatment with ICL670 falls in the range 10 μM−100 μM).[4] As expected, ICL670 displays optimum activity in neutral and slightly alkaline solutions ($6 < pH < 10$).[38] High concentrations of H^+ or OH^- favor either competitive protonation of the ligand or render the solid hydroxide very insoluble. At physiological conditions, more than 80% of the ligand is still loaded with Fe^{III} as $[FeL_2]^{3-}$ even at low total L concentrations such as 1 μM, and the fraction of the 1:1 complex is less than 3%, even if the level of total L is 10 nM. The protonated 1:2 complex is not of importance at physiological conditions as well.

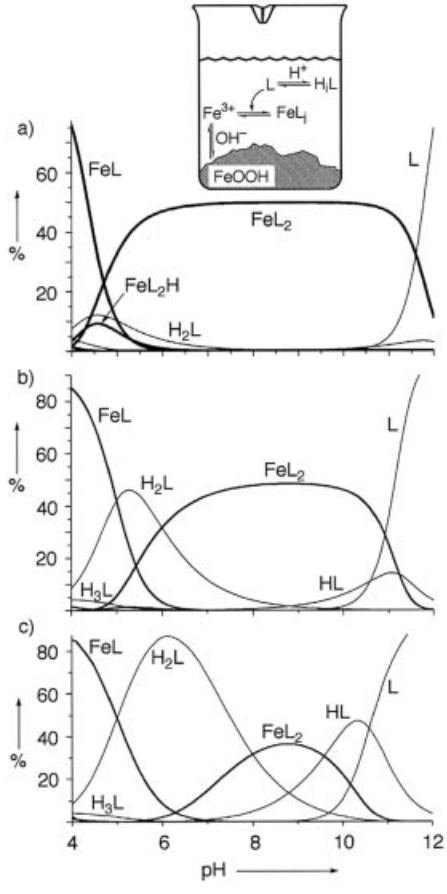

Figure 10. Sequestering ability of ICL670 in H_2O (0.1 M KCl, 25 °C) as a function of pH; the equilibrium concentration of the various species is shown as a fraction of total L concentration (= L_{tot}) with (a) L_{tot} = 100 μM, (b) L_{tot} = 1 μM, and (c) L_{tot} = 10 nM; the solubility product K_{S0}(FeOOH) = 10^{-39} M^4 corresponds to the solubility of ferrihydrite, (ref.[1]); the curves for iron-containing species are in bold

The stability of ferrous $[Fe^{II}(L^y)]^-$ (log β_{110} = 11.5) can be compared with the corresponding value log β_{110} = 13.3 reported for $[Zn(L^x)]^-$.[17] The ratio of these values corresponds closely to the expectations from a linear free energy relation $\Delta G^{Zn}/\Delta G^{Fe}$ = constant.[33] For a variety of ligands having similar, mixed *N*,*O* donor sets and a related charge or denticity, the ratio log $\beta_{110}([Zn^{II}L])$/log $\beta_{110}([Fe^{II}L])$ is 1.1−1.2 (Table 3). The corresponding ratio of 1.16 for log $\beta([Zn^{II}(L^x)]^-)$/log $\beta([Fe^{II}(L^y)]^-)$ corroborates the potentiometric results of the present investigation.[39] The value for β_{120} for the ferrous complex could not be determined directly due to instantaneous oxidation of $[FeL_2]^{4-}$. An analogous free energy relation as described for log β_{110} gave log β_{120} = 14.8 (x_{DMSO} = 0.2, see Table 3). With the use of an appropriate correction for $x_{DMSO} \rightarrow 0.0$ (Table 2), we estimate log β_{120} = 13.5 for pure water. This value is in good agreement with log β_{120} = 14.0 calculated from the reduction potential and from log β_{120} = 36.9 for $[Fe^{III}L_2]^{3-}$ (Scheme 5).

Table 3. Linear free energy relation for Zn^{2+} and Fe^{2+} complex formation

	Zn^{2+}		Fe^{2+}		log β (Zn^{2+})/log β (Fe^{2+})	
	log β_{110}	log β_{120}	log β_{110}	log β_{120}	log β_{110}	log β_{120}
$dipic^{2-}$[a]	6.35[b]	11.88[b]	5.71[b]	10.36[b]	1.11	1.15
nta^{3-} [a]	10.45[c]	14.24[c]	8.90[c]	11.98[c]	1.17	1.19
ida^{2-} [a]	6.58[d]	11.8[d]	5.45[d]	9.82[d]	1.21	1.20
L^{3-}	13.3[e]	16.0[f]	11.5[g]	14.0[h]	1.16	1.17

[a] Abbreviation of ligands: nitrilotriacetic acid (H_3nta), iminodiacetic acid (H_2ida), dipicolinic acid (H_2dipic). [b] From ref.[36], 20 °C, *I* = 0.1 M. [c] From reference [36], 25 °C, *I* = 0.1 M. [d] From ref.[36], 25 °C, *I* = 1.0 M. [e] From ref.[17], L = L^x, x_{DMSO} = 0.20, 25 °C, *I* = 0.1 M. [f] Ref.[17] listed the value log β_2 = 17.5 for L = L^x, x_{DMSO} = 0.20. This value was adjusted for pure H_2O (x_{DMSO} = 0) by adding an increment of −1.5 (see Table 2). [g] This work, L = L^y, x_{DMSO} = 0.20, 25 °C, I = 0.1 M.[h] L = L^x, estimated for H_2O (25 °C, I = 0.1 M) from the reduction potential $E_{1/2}(FeL_2)$ = −0.58 V and log β_{120} (Fe^{3+}) = 36.9 (see Scheme 5 and Table 2).

The low stability of $[Fe^{II}L_2]^{4-}$ (L = L^x, L^y) is an important result from this investigation. This complex is not only a very strong reducing agent, but also dissociates very easily to give the 1:1 complex. The individual association constant for the second ligand has a value of log $K_2 \approx 4$, and the pH-dependent constant according to Equation (8), *n* = 2, $K = [Fe^{II}L^-] \times [H_2L^-] \times [Fe^{II}L_2{}^{4-}]^{-1} \times [H^+]^{-2}$, is log *K* = −15.4. At pH 7, this equilibrium is clearly shifted to the right, and $[Fe^{II}L_2]^{4-}$ is only stable at a relatively high ligand concentration and high pH. The very low stability of

 © 2004 Wiley-VCH Verlag GmbH & Co. KGaA, Weinheim

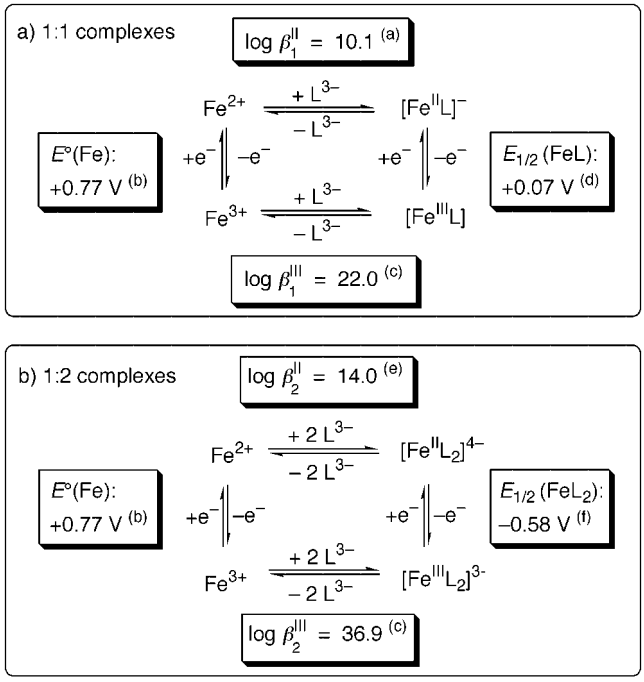

Scheme 5. Synopsis of complex stability and redox chemistry for iron complexes of H_3L^x in H_2O (0.1 M KCl, 25 °C); (a) this work (section 2.4), corrected for pure H_2O; (b) from ref.[18b]; (c) this work (see Table 2); (d) calculated as $E_{1/2}(FeL) = E^0(Fe) - 0.059V \times (\log \beta_1^{III} - \log \beta_1^{II})$; (e) calculated as $\log \beta_2^{II} = \log \beta_2^{III} - [E^0(Fe) - E_{1/2}(FeL_2)]/0.059V$; (f) this work (section 2.5.2)

the ferrous bis complex is attributed (a) to an unfavorable electrostatic repulsion between the two trianionic ligand entities, and (b) to the distinct selectivity of this ligand for small metal ions. As already discussed in section 3.1, *all* complexes of ICL670 with di- and trivalent transition metal cations must be regarded as significantly strained, and this strain increases with increasing ionic size. The addition of one electron to the ferric complex results in an increase in the effective ionic radius from 0.645 Å (high-spin Fe^{III}) to 0.780 Å (high-spin Fe^{II}).[40]

In addition to the complete dissociation of one ligand from $[Fe^{II}L_2]^{4-}$, the formation of a species with a partially coordinated and partially protonated ligand (e.g. $[Fe^{II}(L^x)(HL^x)]^{3-}$) must be taken into account. Moreover, it should be noted that $[Fe^{II}L]^-$ is susceptible to the binding of another ligating agent A^{m-} which may be present in the medium. Formation of such a ternary complex $[Fe^{II}(L^x)(A)]^{(1+m)-}$ appears to be particularly likely if this ligating agent could stabilize the ferrous form. The simple, pH-independent reduction potential [Equation (7)] must therefore be determined at a sufficiently high pH.[41] It is noteworthy that a cyclic voltammogram of the bis complex recorded at pH 12.6 showed a quasi-reversible electron transfer, whereas at lower pH, additional peaks were observed for the anodic wave at more positive potentials (Figure S15). This observation is a clear indication that additional species (protonation products of $[Fe^{II}L_2]^{4-}$ or ternary mixed ferrous complexes) are formed. However, at the present stage, it is not possible to derive any conclusive information about the nature of such species.

The formation of polynuclear species is another possibility for the stabilization of the 1:1 complex at the ferrous stage.[2] As already noted by Ryabukhin, the reaction of H_2L^z with divalent transition metal cations resulted in the precipitation of insoluble polymers.[21] A bis-bidentate coordination mode (binding of a first metal cation to N1 and O2, and a second cation to N3 and O1, see Figure 2) was proposed for the resulting $\{M(L^z)\}_n$ structure. In turn, each metal center would be chelated by two ligand entities. For H_3L^x, the corresponding oligomers $[\{Fe^{II}(L^x)\}_n]^{n-}$ would carry a negative charge at physiological pH, and they could therefore stay in solution. However, the smooth reaction of $Cu(L^z)$ with pyridine (Figure 4) demonstrates that such aggregates depolymerize readily in the presence of an additional coordinating agent.

With regard to the role of Fe^{III}−ICL670 complexes as possible catalysts for redox cycling, one can clearly state that the bis complex [Equation (7)] is redox inactive in any physiological medium. If partial dissociation and formation of the ternary $[Fe^{II}(L^x)(A)]^{(1+m)-}$ species at the ferrous stage is considered, then the result is unchanged, as long as the ligating agent A^{m-} further stabilizes the ferric form. This is indeed the case for many biological low-molecular-weight ligands such as citrate or ATP.

Although the reduction potential of $[Fe^{III}L]$ cannot be measured directly due to immediate decomposition of the complex after reduction in acidic solution (2.5.1), it can be calculated from the corresponding formation constants β_{110} for $[Fe^{II}L]^-$ and $[Fe^{III}L]$. The estimated $E_{1/2}$ for the 1:1 complex is +0.07 V (versus NHE), a value which is in good agreement with the irreversible cathodic wave (Figure 8) observed in acidic media in the range from +100 mV to −150 mV (versus Ag/AgCl). Clearly, $[Fe^{II}L]^-$ is a significantly weaker reducing agent than $[Fe^{II}L_2]^{4-}$. The redox potential of the 1:1 complex falls in a similar range to that of the $Fe^{III/II}$−EDTA couple (Figure 1).

4. Conclusions

A survey of the various formation constants and corresponding redox potentials of the Fe^{II} and Fe^{III} complexes with ICL670 (H_3L^x) in H_2O is summarized in Scheme 5. The other ligands (H_3L^y and H_2L^z) behave very similarly. Our study confirmed that these ligands are highly selective for Fe^{III}, and that the affinity for Fe^{II} is, in general, low. However, there is a distinct difference between the 1:1 and 1:2 complexes. $[Fe^{II}(L^x)]^-$ is sufficiently stable to be formed at moderate ligand concentrations around pH 6, whereas $[Fe^{II}(L^x)_2]^{4-}$ is generally not stable in aqueous solution. In view of a possible role in redox catalysis, reduction of $[Fe^{III}(L^x)_2]^{3-}$ is not possible in a physiological medium, and the 1:2 complex is thus redox inactive. On the other hand, the 1:1 complex $[Fe^{II}(L^x)]^-$ must be regarded as a somewhat milder reducing agent, and its formation from the ferric species could well be anticipated in the presence of a bio-

 © 2004 Wiley-VCH Verlag GmbH & Co. KGaA, Weinheim

logical electron donor. In particular, reduction by $O_2^{\cdot-}$ could occur (Figure 1), and reoxidation by H_2O_2 would also be possible. However, the formation of $[Fe^{III}(L^x)]$ is only relevant in acidic solutions. At pH 7−8, a ligand redistribution reaction, followed by precipitation of solid iron hydroxide according to: $2[Fe^{III}(L^x)] + 3OH^- \rightarrow FeOOH(s) + [Fe(L^x)_2]^{3-} + H_2O$, would be favored (Figure 10). Therefore, it appears rather unlikely that any possible enhancement of oxidative stress (Fenton chemistry etc.) needs to be considered under physiological conditions. This is clearly different at lower pH values, where $[Fe^{III}(L^x)_2]^{3-}$ will partially dissociate to $[Fe^{III}(L^x)]$, and this species can be reduced to $[Fe^{II}(L^x)]^-$. As a matter of fact, the partial dissociation of Fe^{III} complexes in slightly acidic solutions appears to be a general problem for di- and tridentate iron chelators such as L1 or ICL670.[42] This is, of course, different for ligands with a higher denticity such as DFO, where an "all-or-nothing" coordination mode prevents possible formation of partially coordinated, "dangerous" species.

Experimental Section

Materials, Instrumentation and Analyses: The chemicals used for the synthetic work were commercially available products of reagent grade quality and were used as obtained. H_2O was distilled twice (quartz apparatus). DMSO was from Fluka (puriss., p.a.). MeOH and EtOH (reagent grade) were purified by distillation prior to use. For the potentiometric and spectrophotometric titrations, metal salts of highest available quality (>99.95%) were used. $FeCl_3$ (anhydrous) was from Fluka, $(NH_4)_2Fe(SO_4)_2{\cdot}6H_2O$ (>99.997%) from Aldrich. ^1H and $^{13}C\{^1H\}$ NMR spectra were measured in [D$_6$]DMSO (28 °C) with a Bruker DRX 500 spectrometer (resonance frequencies: 500.13 MHz for ^1H and 125.9 MHz for ^{13}C). Chemical shifts (in ppm) are given relative to tetramethylsilane as an internal standard (= 0 ppm). EI^+-MS were measured on a Varian MAT 311 spectrometer (Dr. Graf, Universität des Saarlandes), and FAB^+-MS were recorded on a VG ZAB-VSEQ spectrometer (Dr. W. Amrein, R. Häfliger, ETH Zürich). Samples for FAB were dissolved in EtOH with 3-nitrobenzyl alcohol as a matrix. C,H,N analyses were performed by H. Feuerhake (Universität des Saarlandes).

2-(2-Hydroxyphenyl)-benzo-4*H*-[1,3]-oxazin-4-one:[43] Salicylic acid (24.9 g, 0.18 mol), salicylamide (20.6 g, 0.15 mol) and pyridine (1.5 mL) were refluxed in xylene (30 mL). Thionyl chloride (23.7 mL, 0.33 mol) was added with vigorous stirring over a period of 4 h. An intense evolution of SO_2 and HCl was noted. At the end of the addition, the product started to crystallize. Stirring was continued for an additional 30 min, and the xylene was removed by distillation at reduced pressure. The resulting solid residue was suspended in EtOH (60 mL) and acetic acid (1.5 mL). The mixture was heated gently and then allowed to cool to 20 °C. The precipitate was filtered and recrystallized from 2-methoxyethanol (70 mL). Yield: yellow needles (19.78 g, 82.7 mmol, 55%). The product decomposed slowly when exposed to moisture, forming bis(salicyl)-imide. $C_{14}H_9NO_3$ (239.2): calcd. C 70.29, H 3.79, N 5.85; found C 70.80, H 3.88, N 5.70. ^1H NMR ([D$_6$]DMSO): δ = 7.09 (m, 2 H), 7.62 (m; 2 H), 7.78 (d, 1 H), 7.94 (t, 1 H), 8.07 (d, 1 H), 8.20 (d, 1 H), 8.78 (OH) ppm. ^{13}C NMR ([D$_6$]DMSO): δ = 111.4, 117.4, 117.8, 117.9, 119.5, 126.7, 127.2, 129.0, 136.0, 136.7, 153.8, 161.8, 163.4, 164.8 ppm. UV/Vis (H_2O, 25 °C): λ_{max} = 371, 323 nm.

4-[3,5-Bis(2-hydroxyphenyl)-1,2,4-triazol-1-yl]benzoic Acid (H_3L^x):[19] 4-Hydrazino-benzoic acid (1.75 g, 11.5 mmol) and NEt_3 (1.16 g, 11.5 mmol) were dissolved in boiling EtOH (80 mL). To the clear solution was added 2-(2-Hydroxyphenyl)-4*H*-3,1-benzoxazin-4-one (2.50 g, 10.45 mmol), and the reaction mixture was refluxed for an additional 2 h. The solution was then allowed to cool to room temperature, and H_2O was added until some perturbation (i.e. a first sign of precipitation) was observed. The mixture was concentrated to a total volume of 50% under reduced pressure and aqueous 6 M HCl (40 mL) was added. The resulting solid was filtered and dried for 24 h in vacuo (3.11 g, 8.34 mmol, 80%). $C_{21}H_{15}N_3O_4$ (373.37): calcd. C 67.56, H 4.05, N 11.25; found C 67.76, H 3.85, N 11.14. ^1H NMR ([D$_6$]DMSO): δ = 6.90 (d, 1 H), 7.00−7.04 (m, 3 H), 7.37 (m, 2 H), 7.55 (d, 1 H), 7.58 (d, 2 H), 8.02 (d, 2 H), 8.08 (d, 1 H) 10.05 (s, OH), 10.81 (s, OH), 13.20 (broad, OH) ppm. ^{13}C NMR ([D$_6$]DMSO): δ = 113.6, 114.4, 116.2 (CH), 117.0 (CH), 119.4 (CH), 119.6 (CH), 123.2 (2 CH), 126.7 (CH), 130.2 (2 CH), 130.5, 131.0 (CH), 131.4 (CH), 132.5, 141.2 (CH), 152.0, 155.2, 156.4, 159.9, 166.4 ppm. UV/Vis (H_2O/DMSO, x_{DMSO} = 0.2, pH <2, 25 °C): λ_{max} (ε) = 284 nm (1.5×10^4), 296 (sh). FAB^+-MS: *m*/*z* = 374 (100%, $[H_4L^x]^+$). Single crystals of H_3L^x were grown by slow evaporation of a MeOH solution at room temperature. The solid was allowed to stand exposed to the air to form the monohydrate $H_3L^x{\cdot}H_2O$. $C_{21}H_{17}N_3O_5$ (391.39): calcd. C 64.45 H 4.38, N 10.74; found C 64.11, H 4.60, N 10.44.

4-[3,5-Bis(2-hydroxyphenyl)-1,2,4-triazol-1-yl]benzosulfonic Acid (H_3L^y):[20] 4-Hydrazino-benzosulfonic acid (2.4 g, 12.75 mmol) was suspended in EtOH (300 mL). The solid was dissolved by the addition of one equivalent of NEt_3 (1.29 g, 12.75 mmol). The solution was refluxed, and 2-(2-hydroxyphenyl)-4*H*-3,1-benzoxazin-4-one (3.00 g, 12.5 mmol) was added. Heating was continued for an additional 20 h. The clear solution was then allowed to cool to room temperature, and 6 M aqueous HCl (60 mL) was added. The resulting acidic solution was evaporated under reduced pressure until a white solid started to precipitate. A further portion of 6 M aqueous HCl (60 mL) was added. The solid was then separated by filtration and washed with a small portion of cold H_2O, and dried in vacuo over P_4O_{10} for 24 h (4.37 g, 10.67 mmol, 85%). $C_{20}H_{15}N_3O_5S$ (409.42): calcd. C 58.67, H 3.69, N 10.26; found C 58.99, H 3.90, N 9.88. ^1H NMR ([D$_6$]DMSO): δ = 6.91 (d, 1 H), 6.95−7.01 (m, 2 H), 7.05 (d, 1 H), 7.36−7.40 (m, 2 H), 7.46 (d, 2 H), 7.51 (d, 1 H), 7.72 (d, 2 H), 8.02 (d, 1 H) ppm. ^{13}C NMR (DEPT90, [D$_6$]DMSO): δ = 113.3, 113.4, 116.4 (CH), 117.1 (CH), 119.5 (CH), 119.8 (CH), 123.4 (2 CH), 126.7 (2 CH), 127.4 (CH), 131.2 (CH), 131.9 (CH), 132.9 (CH), 137.7, 148.1, 151.6, 155.5, 156.4, 158.4 ppm. UV/Vis (H_2O; pH <2; 25 °C): λ_{max} (ε) = 255 (1.4×10^4); 295 nm (1.2×10^4). FAB^+-MS: *m*/*z* = 410 (100) $[H_4L^y]^+$. The solid was allowed to stand exposed to the air, which resulted in the formation of the monohydrate $H_3L^y{\cdot}H_2O$. $C_{20}H_{17}N_3O_6S$ (427.44): calcd. C 56.20, H 4.01, N 9.83; found C 56.02, H 4.24, N 9.61.

3,5-Bis(2-hydroxyphenyl)-1-phenyl-1,2,4-triazole (H_2L^z):[43] Phenylhydrazine hydrochloride (1.45 g, 10.03 mmol) was dissolved in boiling EtOH (80 mL). 2-(2-hydroxyphenyl)-4*H*-3,1-benzoxazin-4-one (2.0 g, 8.36 mmol) was added, and the resulting clear yellow solution was heated under reflux for an additional 2 h. The yellow color disappeared, and the colorless solution was allowed to cool to room temperature. Addition of aqueous 1 M HCl (40 mL) resulted in precipitation of a white solid, which was filtered off and dried for 12 h in vacuo. Recrystallization from hot MeOH yielded a crystalline material that was suitable for single-crystal X-ray analysis. Yield: (1.72 g, 5.23 mmol, 62.5%). $C_{20}H_{15}N_3O_2$ (329.36): calcd. C 72.94, H 4.59, N 12.76; found C 72.61, H 4.36, N 12.64.

 © 2004 Wiley-VCH Verlag GmbH & Co. KGaA, Weinheim

^{1}H NMR ([D$_6$]DMSO): δ = 6.89 (d, 1 H), 6.94 (t, 1 H), 6.98−7.04 (m, 2 H), 7.37 (t, 2 H), 7.42−7.48 (m, 6 H), 7.85 (d, 1 H), 9.88 (s, OH), 10.71 (s, OH) ppm. ^{13}C NMR ([D$_6$]DMSO): δ = 113.7, 114.5, 116.0, 116.9, 119.1, 119.4, 123.6 (2 CH), 126.5, 128.5, 129.0 (2 CH), 130.8, 131.1, 132.1, 137.7, 151.6, 155.3, 156.2, 159.4 ppm. UV/Vis (H$_2$O/DMSO, x_{DMSO} = 0.2; pH <7; 25 °C): λ_{max} (ε) = 255 (1.5 × 10^4); 300 nm (1.2 × 10^4). MS-EI$^+$: m/z = 329.4 (100) [H$_2$L^z]$^+$.

Na[Fe(L^z)$_2$]·2H$_2$O·C$_2$H$_5$OH: FeCl$_3$ (324 mg, 2 mmol) dissolved in abs. EtOH (15 mL) was added to a solution of H$_2$L^z (660 mg, 2 mmol) in ethanol (15 mL). The resulting solution turned deep purple, indicating the formation of the 1:1 complex [Fe(L^z)]$^+$. In a separate reaction, solid Na was added to abs. EtOH to saturation.This NaOEt solution (1 mL) was then layered with the Fe^{III}−L^x solution (0.5 mL). After some hours, the deposition of deep red crystals was observed at the boundary of the two phases. It is important that the crystals remained in this intermediate medium and do not sink into the NaOEt solution. They were subsequently removed and immediately cooled to 100 K for the X-ray diffraction study. The single crystal analysis established the composition as Na[Fe(L^z)$_2$]·4C$_2$H$_5$OH. However, the crystal disintegrated rapidly and the compound that formed had the composition Na[Fe(L^z)]·2H$_2$O·C$_2$H$_5$OH. C$_{42}$H$_{36}$FeN$_6$NaO$_7$ (815.63): calcd. C 61.85, H 4.45, N 10.30; found C 62.49, H 4.15, N 10.02. FAB$^+$-MS: m/z = 709.5−714.5 (20%, superposition of [Fe(L^z)$_2$]$^+$, [Fe(L^z)(HL^z)]$^+$, [Fe(HL^z)$_2$]$^+$), 731.5−736.5 (100%, superposition of [NaFe(L^z)$_2$]$^+$ and [NaFe(L^z)(HL^z)]$^+$), 754.5−758.5 (79%, [Fe(L^z)$_2$(EtOH)]$^+$).

Na[Al(L^z)$_2$]·H$_2$O·C$_2$H$_5$OH: The procedure reported for the preparation of the corresponding Fe^{III} complex was used. Single crystals of composition Na[Al(L^z)$_2$]·4C$_2$H$_5$OH were obtained. They disintegrated rapidly to form Na[Al(L^z)$_2$]·H$_2$O·C$_2$H$_5$OH. C$_{42}$H$_{34}$AlN$_6$NaO$_6$ (768.75): calcd. C 65.62, H 4.46, N 10.93; found C 65.73, H 4.20, N 10.56.

Cu(L^z):[21] CuBr$_2$ (223 mg, 1 mmol) was added to a solution of H$_2$L^z (329 mg, 1 mmol) in EtOH (10 mL). The mixture was stirred until a green solid precipitated. The precipitation was completed by adding a concentrated solution of NaOMe in MeOH. Yield 290 mg (742 μmol, 74%). C$_{20}$H$_{13}$CuN$_3$O$_2$ (390.89): calcd. C 61.46, H 3.35, N 10.75; found C 61.96, H 3.35, N 10.73.

[Cu(L^z)(pyridine)]$_2$: The procedure, reported by Uhlemann and coworkers[44] for the preparation of a Cu^{II} complex with a related tridentate [O,N,O]-ligand, was used with some minor modifications: Solid Cu(L^z) (290 mg, 742 μmol) was dissolved in boiling pyridine (20 mL). This solution (2 mL) was mixed with MeOH (1 mL). H$_2$O (100 μL) was then layered on the resulting green solution. Dark green crystals of [Cu(L^z)(pyridine)]$_2$ suitable for single-crystal X-ray analysis grew within 24 h at 4 °C.

Potentiometric Measurements: All titrations were carried out at an ionic strength of 0.1 M (KCl or KNO$_3$) using a Metrohm 665 piston burette, a Metrohm 6.0222.100 glass electrode with an incorporated Ag/AgCl reference (aqueous), and a Metrohm 713 pH/mV meter. The pH meter and the piston burette were controlled by a PC.[45] The samples (50 mL) were placed in a double-jacketed beaker, and the temperature was maintained at 25.0 ± 0.1 °C using a Lauda ecoline103 thermostat. KOH (0.10 M, Merck Titrisol) having the same H$_2$O/DMSO molar ratio as the corresponding sample solution was used as titrant. The H$_2$O/DMSO samples were prepared using published values of the partial molar volumes of the two components (the H$_2$O/DMSO mixtures show a significant deviation from ideal behavior).[46] Titrations of the Fe^{II} complexes were performed under Ar, which was scrubbed with an alkaline solution of pyrogallol to remove traces of O$_2$. The other titrations were performed under N$_2$, which was passed through a 0.1 M aqueous KCl solution. The apparent ionization constant of the different H$_2$O/DMSO media was determined by multiple acid−base titrations. The pK_as of the ligands were measured using solid, analytically pure samples of H$_3$L^x, H$_3$L^y, and H$_2$L^z. The formation constants of the ferric complexes were determined using stock solutions of the ligands (0.01 M), which were standardized by acid−base titrations, and stock solutions of Fe^{III}, which were standardized photometrically as tris-phenanthroline-Fe^{II}.[47] Additional acid (HCl or HNO$_3$) was added to the Fe^{III} stock solutions to prevent partial hydrolysis prior to the titration. Complex formation with Fe^{III} was found to be sluggish, and additional back titrations were performed to ensure complete equilibration. A measuring time of 800−920 s per point proved necessary to avoid a significant hysteresis. Total ligand and total Fe concentrations ranged from 5×10^{-4} to 2×10^{-3} M.[48]

Spectrophotometric Titrations: The titration cell used for potentiometry was equipped with an immersion probe (HELLMA), which was connected to a diode array spectrophotometer (J&M, TIDAS-UV/NIR/100−1). A PC was used to trigger the recording of a spectrum just prior to the addition of each new aliquot of titrant.[45] For the pK_a determination of H$_3$L^x, H$_3$L^y, and H$_2$L^z, the total ligand concentration was about 10^{-5}−10^{-4} M, and absorption data in the range 250 < λ < 400 nm were collected. For the formation constants of the Fe^{III} complexes, total [Fe] was in the range 9.1×10^{-5}−3.5×10^{-4} M, and total [L] in the range 9.1×10^{-5}−9.7×10^{-4} M. The p$K_{a,1}$ of H$_3$L^y and the formation constants of [Fe(HL^x)]$^+$, [Fe(L^y)], and [Fe(L^z)]$^+$ were determined by a batch method with 10−40 individually sealed 10-mL samples in the range 1 < pH < 2 (25.0 °C) allowing an equilibration time of 24 h.[48]

Calculations of Equilibrium Constants: The computer programs HYPERQUAD[49] and SPECFIT[50] were used to evaluate the potentiometric and spectrophotometric data, respectively. All equilibrium constants were calculated as concentration constants, and pH was defined as −log [H$^+$]. For pure aqueous solutions, a pK_w of 13.78 was used.[36] In H$_2$O/DMSO solutions, the apparent ionization constant Q_c = [H$^+$]×[OH$^-$] depended linearly on x_{DMSO} in the range 0.1 ≤ x_{DMSO} ≤ 0.2 with pQ_c = 14.65 (x_{DMSO} = 0.10) and pQ_c = 15.59 (x_{DMSO} = 0.20). These values are in good agreement with those reported in the literature.[27] A graphical representation of pQ_c versus x_{DMSO} is shown in the supporting information (Figure S2). The pK_w (or pQ_c) and the total concentrations of the reactants were always treated as fixed values. Additionally, the protonation constants of the ligands were fixed when refining formation constants of metal-containing species. Because Fe(NH$_4$)$_2$(SO$_4$)$_2$·6H$_2$O was used as a Fe^{II} source, the pK_a of NH$_4^+$ was determined to be 8.90 (x_{DMSO} = 0.2). However, the formation of [Fe^{II}(L^y)]$^-$, which was investigated in the range of 5.9 < pH < 6.9, did not interfere with the deprotonation of NH$_4^+$. For the evaluation of the spectrophotometric titrations, the spectrum of free Fe^{3+} was measured separately for each H$_2$O/DMSO ratio, and was then imported and treated as fixed during refinement. Only absorption data with λ >400 nm were used for the evaluation of metal complex formation, and the free ligands and their protonation products could therefore be considered as colorless (see Figures S3 and S4).

Electrochemistry: Cyclic voltammograms were recorded in H$_2$O or H$_2$O/DMSO (x_{DMSO} = 0.2) using 0.1 M KCl as supporting electrolyte at ambient temperature (23 ± 3 °C). A BAS C2 cell equipped with a BAS 100B/W 2 potentiostat, a Pt counter electrode, and an

 © 2004 Wiley-VCH Verlag GmbH & Co. KGaA, Weinheim

Table 4. Crystallographic data for ICL670 (H_3L^x), $Na[Fe(L^z)_2]\cdot 4EtOH$, and $[Cu(L^z)(pyridine)]_2$

	ICL670	$Na[Fe(L^z)_2]\cdot 4EtOH$	$[Cu(L^z)(pyridine)]_2$
Empirical formula	$C_{21}H_{15}N_3O_4$	$C_{48}H_{50}FeN_6NaO_8$	$C_{50}H_{36}Cu_2N_8O_4$
Molecular weight	373.36	917.78	939.95
Crystal system	monoclinic	monoclinic	monoclinic
Space group	$P2_1/c$ (No. 14)	$C2/c$ (No. 15)	$P2_1/c$ (No. 14)
a [Å]	8.900(2)	23.933(4)	10.944(2)
b [Å]	26.946(5)	8.7399(12)	10.476(2)
c [Å]	7.558(2)	24.166(4)	18.419(4)
β [°]	94.77(3)	107.84(3)	100.05(3)
V [Å^3]	1806.3(7	4811.8(13)	2079.3(7)
Z	4	4	2
T [K]	215(2)	100(2)	293(2)
$D_{calcd.}$ [g cm^{-3}]	1.373	1.267	1.501
μ [mm^{-1}]	0.097	0.380	1.082
Crystal size [mm]	0.3 × 0.2 × 0.2	0.35 × 0.18 × 0.18	0.08 × 0.05 × 0.02
θ_{min}, θ_{max}	2.42, 24.13	1.79, 24.00	2.25, 23.99
Trans (min., max)	−	0.5567, 0.9625	−
Data set	−10/10; −30/30; −8/8	−28/24; −10/9; −27/26	−11/11; −11/11; −20/21
Total/Unique data	11218, 2810	9450, 3738	12786, 3077
Parameter/Restraints	313/0	269/9	289/0
R_1, wR_2, [$I > 2\sigma(I)$]	0.0468, 0.1033	0.0870, 0.2352	0.0599, 0.1143
R_1, wR_2, (all data)	0.0755, 0.1133	0.1456, 0.2832	0.1595, 0.1450
Max. peak/hole [e/ Å^3]	0.227/−0.218	1.240/−0.550	0.375/−0.442

Ag/AgCl reference electrode was used. The total iron concentration was 2.5 mM. Measurements at pH <4 ($E > -200$ mV vs. Ag/AgCl) were performed using a Pt working electrode. For the high pH samples (pH >6, $E < -400$ mV vs. Ag/AgCl) a hanging Hg drop working electrode was used.

Crystal Structure Determination:[51] X-ray diffraction data of H_3L^x (215 K), $Na[Fe(L^z)_2]\cdot 4EtOH$ (293 K),[23] and $[Cu(L^z)(pyridine)]_2$ (293 K) were collected on a STOE IPDS diffractometer. Data collection of $Na[Al(L^z)_2]\cdot 4EtOH$ was performed on a Siemens SMART CCD diffractometer at 293(2) K. Additionally, a data set of the Fe complex was collected at 100(2) K on the SMART CCD diffractometer. Graphite monochromated Mo-K_α radiation (λ = 0.71073 Å) was used for all structures. Crystallographic data for H_3L^x, the Fe complex at 100 K, and the Cu complex are summarized in Table 4. The Al complex proved to be isotypic with the Fe complex; however, the reflections were rather weak, and the data could not be refined satisfactorily.[24] All data sets were corrected for Lorentz and polarization effects, and an absorption correction was applied to the data of the Fe complex collected at 100 K. Minimal and maximal transmission factors were 0.5567 and 0.9625. All structures were solved by direct methods (SHELXS-97) and refined by full-matrix least-squares calculations on F^2 (SHELXL-97).[52] Anisotropic displacement parameters were refined for all non-hydrogen atoms of H_3L^x and $[Cu(L^z)(pyridine)]_2$. In the low-temperature structure of the Fe complex, the $[Fe(L^z)_2]^-$ anion was modeled as a superposition of two orientations, having the Fe center, the phenoxo rings, and the C−N−C moieties of the triazole rings in common. For the two outer nitrogen atoms (N2 and N3) and the peripheral phenyl ring, a major (66%) and a minor (34%) component were located. Non-hydrogen atoms of the nondisordered part and of the major component (except N2 and N3) of the anion, as well as the Na position and the C and O positions of a nondisordered EtOH molecule were refined with anisotropic displacement parameters. All C and N atoms of the minor component, N2 and N3 of the major component, and the C and O position of a second, disordered EtOH molecule were refined isotropically. The hydroxy hydrogen atom H(80) of the nondisordered EtOH was located and refined isotropically with $U_{iso} = 1.3 \times U_{eq}$ of the oxygen atom. All other H atom positions of the two metal complexes were calculated (riding model). Isotropic displacement parameters were used with $U_{iso} = 1.5 \times U_{eq}$(C) for methyl groups and $U_{iso} = 1.2 \times U_{eq}$(C) for all other hydrogen atoms. The H atom positions of H_3L^x could all be located. They were successfully refined with variable isotropic displacement parameters.

Acknowledgments

X-ray diffraction data for H_3L^x (ICL670), $Na[Fe(L^z)_2]\cdot 4EtOH$ (293 K) and $[Cu(L^z)(pyridine)]_2$ were recorded by Dr. Volker Huch (Saarbrücken). The structure of $[Cu(L^z)(pyridine)]_2$ was solved and refined by Dr. Jürgen Sander (Saarbrücken). Some of the CV measurements were performed by Michael Krämer (Saarbrücken). We thank Prof. G. Schwitzgebel (Saarbrücken, retired) for helpful discussions in interpreting the CV measurements, and Dr. Peter Osvath (Melbourne) for valuable advice.

[1] R. Crichton, *Inorganic Biochemistry of Iron Metabolism − From Molecular Mechanisms to Clinical Consequences*, 2nd Edition, John Wiley, Chichester, **2001**.
[2] [2a] Z. D. Liu, R. C. Hider, *Coord. Chem. Rev.* **2002**, *232*, 151. [2b] Z. D. Liu, R. C. Hider, *Med. Res. Rev.* **2002**, *22*, 26.
[3] R. C. Hider, Z. D. Liu, *Curr. Med. Chem.* **2003**, *10*, 1051.
[4] E. Nisbet-Brown, N. F. Olivieri, P. J. Giardina, R. W. Grady, E. J. Neufeld, R. Sechaud, A. J. Krebs-Brown, J. R. Anderson, D. Alberti, K. C. Sizer, D. G. Nathan, *Lancet* **2003**, *361*, 1597.
[5] [5a] C. Hershko, A. M. Konijn, H. P. Nick, W. Breuer, Z. I. Cabantchik, G. Link, *Blood* **2001**, *97*, 1115. [5b] H. Nick, P. Acklin, R. Lattmann, P. Buehlmayer, S. Hauffe, J. Schupp, D. Alberti, *Curr. Med. Chem.* **2003**, *10*, 1065.
[6] R. S. Britton, K. L. Leicester, B. R. Bacon, *Int. J. Hematol.* **2002**, *76*, 219.
[7] S. I. Liochev, *Met. Ions Biol. Syst.* **1999**, *36*, 1.
[8] M. J. Burkitt, *Prog. React. Kinet. Mech.* **2003**, *28*, 75.
[9] H. B. Dunford, *Coord. Chem. Rev.* **2002**, *233−234*, 311.
[10] [10a] W. H. Koppenol, *Redox Rep.* **2001**, *6*, 229. [10b] S. I. Liochev, I. Fridovich, *Redox Rep.* **2002**, *7*, 55.

 © 2004 Wiley-VCH Verlag GmbH & Co. KGaA, Weinheim

[11] W. H. Koppenol, *Redox Rep.* **2001**, *6*, 339.
[12] S. Y. Qian, G. R. Buettner, *Free Radic. Biol. Med.* **1999**, *26*, 1447.
[13] S. J. Stohs, D. Bagchi, *Free Radic. Biol. Med.* **1995**, *18*, 321.
[14] [14a] S. Toyokuni, *Free Radic. Biol. Med.* **1996**, *20*, 553. [14b] R. Meneghini, *Free Radic. Biol. Med.* **1997**, *23*, 783.
[15] B. P. Esposito, W. Breuer, P. Sirankapracha, P. Pootrakul, C. Hershko, Z. I. Cabantchik, *Blood* **2003**, *102*, 2670.
[16] M. Fontecave, J. L. Pierre, *Bull. Soc. Chim. Fr.* **1993**, *130*, 77.
[17] U. Heinz, K. Hegetschweiler, P. Acklin, B. Faller, R. Lattmann, H. P. Schnebli, *Angew. Chem.* **1999**, *111*, 2733; *Angew. Chem. Int. Ed.* **1999**, *38*, 2568.
[18] [18a] A.-F. Miller, *Compr. Coord. Chem. II* **2004**, *8*, 479. [18b] D. R. Lide (Ed.), *CRC Handbook of Chemistry and Physics 83rd Edition 2002−2003*, CRC-Press, Washington D. C. **2002**.
[19] R. Lattmann, P. Acklin (Novartis Pharma AG), PCT Int. Appl. WO 9749395 A1 **1997** [*Chem. Abstr.* **1998**, *128*, 114953e].
[20] F. Bachmann, J. Dannacher, G. Schlingloff, M. Hazenkamp, G. Haensler, K. Hegetschweiler, U. Heinz, (Ciba Specialty AG), PCT Int. Appl. WO 2003053986 A1 **2003** [*Chem. Abstr.* **2003** 139, 87009].
[21] Y. I. Ryabukhin, N. V. Shibaeva, A. S. Kuzharov, V. G. Korobkova, A. V. Khokhlov, A. D. Garnovskii, *Koord. Khim.* **1987**, *13*, 869; English Translation: *Soviet J. Coord. Chem.* **1987**, *13*, 493.
[22] U. Heinz, J. Sander, K. Hegetschweiler, *Z. Kristallogr. New Cryst. Struct.* **2001**, *216*, 113.
[23] Crystal data: $C_{48}H_{50}FeN_6NaO_8$, a = 24.138(5), b = 8.855(2), c = 24.597(5), β = 107.77(3), V = 5006.6(18), Z = 4, T = 293(2) K, space group $C2/c$, reflections: 15286 collected, 3741 unique, 2689 observed with $I > 2\sigma(I)$. R_1(observed data) = 0.1224, wR_2(all data) = 0.3476.
[24] Crystal data: $C_{48}H_{50}AlN_6NaO_8$, a = 23.922(9), b = 8.712(3), c = 24.168(10), β = 107.26(3), V = 4810.0(32), Z = 4, T = 293(2) K, space group $C2/c$, reflections: 7299 collected, 2578 unique, 1232 observed with $I > 2\sigma(I)$. R_1(observed data) = 0.1402, wR_2(all data) = 0.4545.
[25] [25a] Z. Travnicek, Z. Sindelar, J. Marek, *Z. Kristallogr. New Cryst. Struct.* **1997**, *212*, 125. [25b] I. Vencato, A. Neves, B. R. Vincent, C. Erasmus-Buhr, W. Haase, *Acta Crystallogr., Sect. C* **1994**, *50*, 386. [25c] B. S. Snyder, G. S. Patterson, A. J. Abrahamson, R. H. Holm, *J. Am. Chem. Soc.* **1989**, *111*, 5214. [25d] T. Weyhermüller, T. K. Paine, E. Bothe, E. Bill, P. Chaudhuri, *Inorg. Chim. Acta* **2002**, *337*, 344. [25e] H. Aneetha, K. Panneerselvam, T.-F. Liao, T.-H. Lu, C.-S. Chung, *J. Chem. Soc., Dalton Trans.* **1999**, 2689.
[26] [26a] M. T. Garland, J. Y. Le Marouille, E. Spodine, *Acta Crystallogr., Sect. C* **1985**, *41*, 855. [26b] P. Lemoine, D. Nguyen-Huy, B. Viossat, J.-M. Leger, A. Tomas, *Acta Crystallogr., Sect. C* **1999**, *55*, 2068. [26c] R. M. Buchanan, C. Wilson-Blumenberg, C. Trapp, S. K. Larsen, D. L. Greene, C. G. Pierpont, *Inorg. Chem.* **1986**, *25*, 3070. [26d] N. Matsumoto, M. Mimura, Y. Sunatsuki, S. Eguchi, Y. Mizuguchi, H. Miyasaka, T. Nakashima, *Bull. Chem. Soc., Jpn.* **1997**, *70*, 2461. [26e] Y. Sunatsuki, M. Nakamura, N. Matsumoto, F. Kai, *Bull. Chem. Soc., Jpn.* **1997**, *70*, 1851. [26f] C. A. Otter, S. M. Couchman, J. C. Jeffery, K. L. V. Mann, E. Psillakis, M. D. Ward, *Inorg. Chim. Acta* **1998**, *278*, 178. [26g] Y. Sunatsuki, T. Matsuo, M. Nakamura, F. Kai, N. Matsumoto, J.-P. Tuchagues, *Bull. Chem. Soc., Jpn.* **1998**, *71*, 2611. [26h] A. Bavoso, L. Menabue, M. Saladini, M. Sola, *Inorg. Chim. Acta* **1996**, *244*, 207. [26i] P. Lemoine, A. Mazurier, I. Billy, D. Nguyen-Huy, B. Viossat, *Z. Kristallogr. New Cryst. Struct.* **2000**, *215*, 523.
[27] [27a] E. M. Woolley, L. G. Hepler, *Anal. Chem.* **1972**, *44*, 1520. [27b] P. Fiordiponti, F. Rallo, F. Rodante, *Z. Phys. Chem.* **1974**, *88*, 149.
[28] T. Eicher, S. Hauptmann, *The Chemistry of Heterocycles*, 2nd edn, WILEY-VCH, Weinheim, **2003**.
[29] A. E. Martell, R. D. Hancock, *Determination and Use of Stability Constants*, 2nd Edition, VCH Publishers, New York, **1992**.
[30] W. R. Harris, K. N. Raymond, F. L. Weitl, *J. Am. Chem. Soc.* **1981**, *103*, 2667.
[31] [31a] J. N. Butler, *J. Electroanal. Chem.* **1967**, *14*, 89. [31b] D. T. Sawyer, J. L. Roberts, Jr., *Experimental Electrochemistry for Chemists*, John Wiley, **1974**, New York.
[32] [32a] K. Hegetschweiler, M. Ghisletta, L. Hausherr-Primo, T. Kradolfer, H. W. Schmalle, V. Gramlich, *Inorg. Chem.* **1995**, *34*, 1950. [32b] K. Hegetschweiler, M. Weber, V. Huch, M. Veith, H. W. Schmalle, A. Linden, R. J. Geue, P. Osvath, A. M. Sargeson, A. C. Willis, W. Angst, *Inorg. Chem.* **1997**, *36*, 4121.
[33] A. E. Martell, R. D. Hancock, *Metal Complexes in Aqueous Solutions*, Plenum Press, New York, **1996**.
[34] R. G. Pearson, *Chemical Hardness*, WILEY-VCH, New York, **1997**.
[35] [35a] R. D. Hancock, *Prog. Inorg. Chem.* **1989**, *37*, 187. [35b] R. D. Hancock, *Acc. Chem. Res.* **1990**, *23*, 253.
[36] R. M. Smith, A. E. Martell, R. J. Motekaitis, *Critically Selected Stability Constants of Metal Complexes*, NIST Standard Reference Database 46; Version 7.0; Gaithersburg, MD, USA **2003**.
[37] P. Paoletti, R. Walser, A. Vacca, G. Schwarzenbach, *Helv. Chim. Acta* **1971**, *54*, 243.
[38] K. Hegetschweiler, *Chem. Soc. Rev.* **1999**, *28*, 239.
[39] The minor differences between the two ligands L^x and L^y can be ignored for these rather general considerations.
[40] R. D. Shannon, *Acta Crystallogr., Sect. A* **1976**, *32*, 751.
[41] It can be assumed that a hypothetical protonated complex $[Fe^{II}(L^x)(HL^x)]^{3-}$ would in any case be more acidic than the free ligand HL^{2-}.
[42] A. El-Jammal, D. M. Templeton, *Inorg. Chim. Acta* **1996**, *245*, 199.
[43] Yu. I. Ryabukhin, L. N. Faleeva, V. G. Korobkova, *Chem. Heter. Com.* (Engl. Trans.) **1983**, *19*, 332.
[44] E. Ludwig, U. Schilde, E. Uhlemann, H. Hartl, I. Brüdgam, *Z. Anorg. Allg. Chem.* **1996**, *622*, 701.
[45] *Messlabor, a computer program for the control of potentiometric and spectrophotometric titrations*, Scientec GmbH, Saarbrücken, **2002**.
[46] J. T. W. Lai, F. W. Lau, D. Robb, P. Westh, G. Nielsen, C. Trandum, A. Hvidt, Y. Koga, *J. Solution Chem.* **1995**, *24*, 89.
[47] A. I. Vogel, *A Textbook of Quantitative Inorganic Analysis*, 5th edn, Longmans, London, **1987**.
[48] Further details of the titration experiments (Tables S1−S13 and Figures S3, S4, S6−S8) are provided as Supporting Information.
[49] P. Gans, A. Sabatini, A. Vacca, *Talanta* **1996**, *43*, 1739.
[50] [50a] R. A. Binstead, B. Jung, A. D. Zuberbühler, SPECFIT/32 Version 3.0, Spectrum Software Associates, Marlborough, MA 01752, USA, **2000**. [50b] H. Gampp, M. Maeder, C. J. Meyer, A. D. Zuberbühler, *Talanta* **1985**, *32*, 95.
[51] Crystallographic data (excluding structure factors) for $Na[Fe(L^z)_2]\cdot 4EtOH$ (293 K), $[Cu(L^z)(pyridine)]_2$, H_3L^x (ICL670), $Na[Fe(L^z)_2]\cdot 4EtOH$ (100 K), and $Na[Al(L^z)_2]\cdot 4EtOH$ (293 K) have been deposited with the Cambridge Crystallographic Data Center as supplementary publication nos. CCDC 237449−237453. Copies of the data can be obtained free of charge on application to CCDC, 12 Union Road, Cambridge CB2 1EZ, UK [Fax (internat.): +44-1223-336033; E-mail: deposit@ccdc.cam.ac.uk].
[52] [52a] G. M. Sheldrick, *SHELXS-97 Program for Crystal Structure Solution*, Göttingen, **1990**. [52b] G. M. Sheldrick, *SHELXL-97 Program for Crystal Structure Refinement*, Göttingen, **1997**.

Received May 4, 2004
Early View Article
Published Online September 13, 2004

 © 2004 Wiley-VCH Verlag GmbH & Co. KGaA, Weinheim

Coordination Chemistry and Asymmetric Catalysis with a Chiral Diphosphonite

Jarl Ivar van der Vlugt,[a] Jos M. J. Paulusse,[a] Eric J. Zijp,[a] Jason A. Tijmensen,[a] Allison M. Mills,[b] Anthony L. Spek,[b] Carmen Claver,[c] and Dieter Vogt*[a]

Keywords: Diphosphonite compounds / Asymmetric hydrogenation / Palladium / Rhodium / Asymmetric hydroformulation / Enantioselectivity

The improved synthesis of the chiral diphosphonite, XantBino (**1**), based on a xanthene backbone and bearing chiral binaphthyl groups on both P-atoms is described together with its Pd^{II} and Rh^{I} complexes. The ^{31}P NMR spectra of both complexes point out that the two phosphorus atoms are chemically inequivalent. The complex *cis*-[$PdCl_2$(**1**)] (**2**) is structurally characterized by NMR spectroscopy and X-ray crystallography. The molecular structure reveals an unusually small bite angle for this member of the xantphos family of only 100°. The rhodium-catalyzed asymmetric hydroformylation of styrene and vinyl acetate as well as the asymmetric hydrogenation of methyl (Z)-2-acetamidocinnamate, applying this chiral diphosphonite **1**, are described. Low enantiomeric excesses are obtained in the asymmetric hydroformylation, while use of the catalyst precursor [Rh(cod)(**1**)]BF_4 (**3**) results in a promising enantiomeric excess in the Rh-catalyzed asymmetric hydrogenation.

(© Wiley-VCH Verlag GmbH & Co. KGaA, 69451 Weinheim, Germany, 2004)

Introduction

The rhodium-catalyzed asymmetric hydroformylation of vinylarenes, with styrene as a model substrate, using rhodium-based catalysts, is a typical benchmark reaction for the comparison of new catalyst systems.[1] A number of ligand classes have been applied in this reaction, aiming at a thorough understanding of both the kinetics and the origin of enantioselectivity, for example, diphosphanes,[2] phosphane-phosphites,[3] diphosphites,[4] aminophosphane-phosphinites,[5] aminophosphanes,[6] and other bifunctional systems.[7] However, only few catalytic systems show satisfactory enantioselectivity for the desired branched aldehyde, with BINAPHOS ($\mathbf{L_1}$) as the current benchmark ligand in many respects (Figure 1). Phosphonites have been largely overlooked in homogeneous catalysis to date. Recently, some reports have appeared on diphosphonites in asymmetric hydrogenation[8] as well as in hydroboration,[9] making use of several backbones. Next to this, monophosphonites have attracted some attention, especially for the asymmetric hydrogenation of enamides,[8c] the copper-catalyzed addition of diethylzinc to enones,[10] and the hydroformylation of octenes.[11] Little precedent exists on the application of (chiral) diphosphonites in the transition metal catalyzed hydroformylation of alkenes or vinyl arenes. Dahlenburg and coworkers reported on chiral dialkyl-derived diphosphonites $\mathbf{L_2}$, their platinum complexes, and the Pt/Sn-catalyzed hydroformylation of styrene, but only very low enantioselectivities were obtained.[12] The groups of Schmutzler and Börner published a joint study on calix[4]arene-based achiral diphosphonites $\mathbf{L_2}$ in the Rh-catalyzed hydroformylation of terminal alkenes. The regioselectivities remained well below 2, indicating only monodentate behavior of these ligands systems.[13]

We have previously reported on the use of chiral xanthene-based diphosphonites in the asymmetric hydrocyanation of vinyl arenes that showed good enantioselectivities of up to 63% for 4-isobutylstyrene.[14] We recently published on the synthesis and use of sterically constrained achiral diphosphonites $\mathbf{L_4}$ in the rhodium-catalyzed hydroformylation of alkenes and showed that these systems are well-suited for the conversion of 2-butene into *n*-pentanal.[15] Together with our studies on the coordination chemistry of these xanthene-derived diphosphonites towards various transition metals,[16] this prompted us to explore the potential of chiral diphosphonite **1** in various asymmetric catalytic reactions. In this paper we report on the improved synthesis of compound **1**, its coordination with palladium and

[a] Schuit Institute of Catalysis, Laboratory of Homogeneous Catalysis, Eindhoven University of Technology,
P. O. Box 513, 5600 MB Eindhoven, The Netherlands
[b] Laboratory for Crystal and Structural Chemistry, Department of Chemistry, Utrecht University,
Padualaan 8, 3584 CH Utrecht, The Netherlands
[c] Departament de Química Física i Inorgànica, Universitat Rovira i Virgili,
Pl. Imperial Tàrraco 1, 43005 Tarragona, Spain
Fax: (internat.) + 31-40-2455054
E-mail: d.vogt@tue.nl

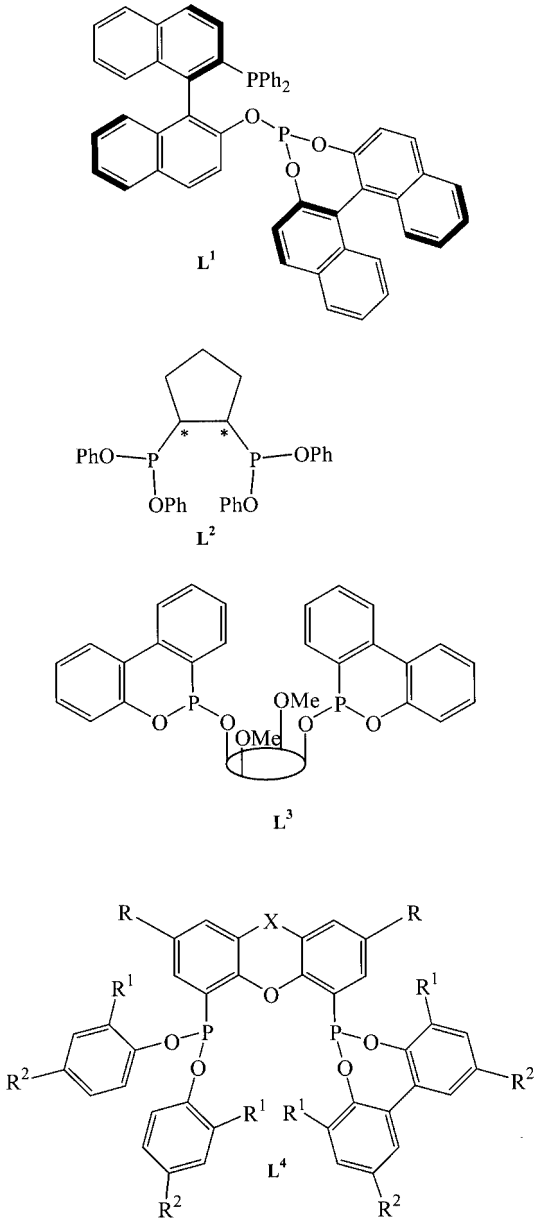

Figure 1. Representation of several reported literature ligand systems: $\mathbf{L_1}$) Nozaki's BINAPHOS; $\mathbf{L_2}$) cyclopentane-based diphosphonites by Dahlenburg; $\mathbf{L_3}$) calix[4]arene-derived diphosphonite of Schmutzler and Börner (the ellipsoid represents a *p-tert*-butylcalix[4]arene unit); $\mathbf{L_4}$) our own sterically constrained achiral diphosphonites

rhodium, and the use of this ligand in the rhodium-catalyzed asymmetric hydroformylation of styrene and vinyl acetate and in the asymmetric hydrogenation of methyl (*Z*)-2-acetamidocinnamate (Figure 2).

Results and Discussion

Synthesis of Diphosphonite 1 and Its Dichloropalladium Complex 2

Diphosphonite **1** was prepared in a straightforward manner, using a two-step procedure, as illustrated in Scheme 1. The [bis(diethylamino)]diphosphonite was derived from the commercial starting material 9,9-dimethylxanthene in mod-

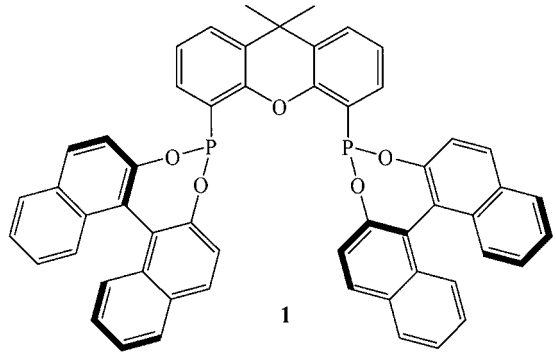

Figure 2. Chiral xanthene-based diphosphonite used in this study

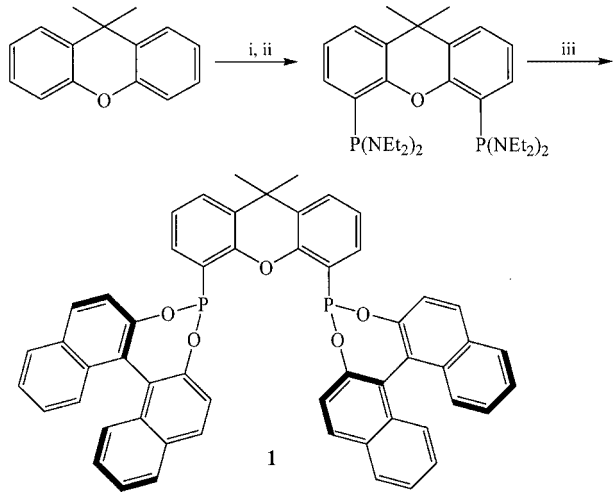

Scheme 1. Synthetic route to compound **1**: i) *n*BuLi, TMEDA, Et_2O, −40 °C, 16 h; ii) $ClP(NEt_2)_2$, pentane, −60 °C, 16 h.; iii) 2,2′-dihydroxy-1,1′-binaphthyl (2 equiv.), toluene, tetrazole, ΔT, 1 day

erate to good yield.[14] Subsequently, the chiral binaphthyl groups were introduced to obtain the desired chiral diphosphonite. This reaction is catalyzed by tetrazole as protonation agent, which is a slight but important modification of the literature procedure. Addition of tetrazole shortened the reaction time considerably, analogous to the synthesis of sterically constrained diphosphonites previously reported by our group.[15] The pure compound was obtained by layering a solution of the crude product in dichloromethane with acetonitrile. This was omitted in the earlier methodology. In general, the second step led to an unwanted side-product (<10%), most likely the monophosphonite, which justified the crystallization step. The ^{31}P NMR spectrum of the pure compound showed a singlet at $\delta = 178.0$ ppm, which seems remarkably low-field, even for a phosphonite moiety. This value reflects the fact that both electronic factors as well as conformational constraints strongly affect the chemical shift of the ^{31}P nucleus.

We were interested in the detailed coordination behavior of XantBino (**1**) towards palladium and rhodium. Previously, only the bischelate $Ni(\mathbf{1})_2$ was described.[14] From the reaction of $PdCl_2(cod)$ with ligand (*R*,*R*)-**1** at room temperature, a yellow compound was obtained, for which the ^{31}P NMR spectrum shows two doublets at $\delta = 143.1$ ppm

 © 2004 Wiley-VCH Verlag GmbH & Co. KGaA, Weinheim

and 137.4 ppm. The observed coupling constant $J_{P\text{-}P}$ is 46.5 Hz, apparently indicating that the phosphorus atoms are chemically inequivalent. This is attributed to the chiral, bulky binaphthyl units. From the ^{1}H NMR spectrum, it appears that the methyl groups in the backbone are also inequivalent, indicating that the aromatic skeleton of the xanthene is bent.[14,17]

Single crystals suitable for X-ray analysis were grown by layering a dichloromethane solution of complex **2** with acetonitrile. The molecular structure of *cis*-[$PdCl_2$(**1**)] is presented in Figure 3, together with selected bond lengths and angles. It is evident that ligand **1** acts as a bidentate ligand, coordinating in a *cis*-fashion to the palladium atom.

The coordination around the central palladium atom is distorted square-planar, with a P^1-Pd-P^2 angle of 99.99(3)°, while the $Cl^1-Pd-Cl^2$ angle is 90.15(4)°. There are few examples on palladium diphosphonite complexes known in literature. However, the bond lengths for Pd−P [$Pd-P^1$ is 2.2449(9) Å and $Pd-P^2$ is 2.2532(9) Å] and Pd−Cl [$Pd-Cl^1$ is 2.3412(10) Å and $Pd-Cl^2$ is 2.3442(9) Å] are normal, in agreement with those found by Agbossou[18] and Schmutzler.[19] Compared with crystal structures of Pd complexes known for xanthene diphosphane ligands, the bite angle of 100° for ligand **1** is unusually small. For instance, we previously reported on *trans*-coordinated diphosphonites[16] and both van Leeuwen et al.[20] and Buchwald et al.[21] reported on *trans*-Pd(Xantphos) complexes. Only in the case of Pd^0 complexes or with cationic palladium species has *cis*-coordination of Xantphos been observed by X-ray crystallography.[20,22] In complex **2**, the angles $Pd-P^1-C^{41}$ and $Pd-P^2-C^{54}$ were 109.87(11)° and 108.57(12)°, respectively (Figure 4). The dihedral angle between the metal plane $Cl^1-Pd-Cl^2$ and the ligand plane $P^1-P^2-C^{41}$ is 115.7°, indicating that the palladium is actually positioned outside the plane defined by the backbone and the phosphorus atoms, as illustrated in This is quite unusual for *cis*-Pd-diphosphorus complexes. A similar structural disposition of the metal atom, together with a small ligand bite angle, was found for an unexpected *ortho*-

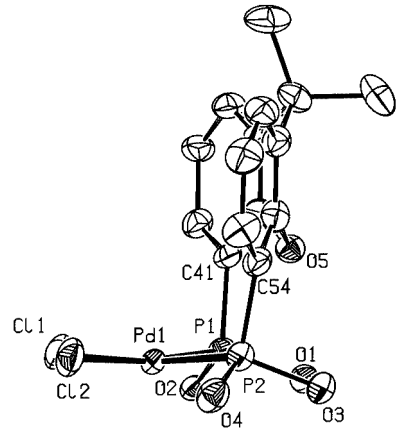

Figure 4. Illustration of the geometry around the square-planar palladium atom in complex **2**, showing the dihedral angle between the metal plane and the ligand plane

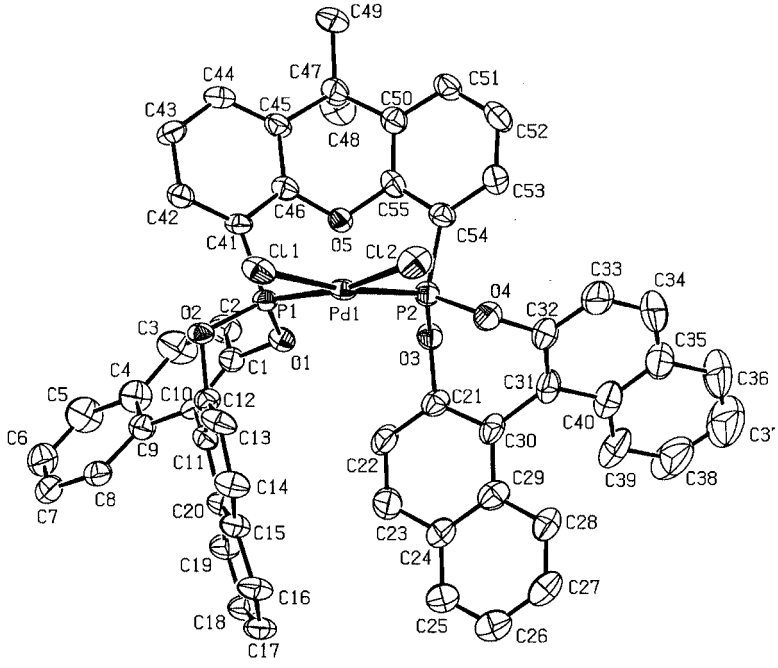

Figure 3. ORTEP representation of complex **2**, *cis*-[$PdCl_2$(**1**)]; displacement ellipsoids are drawn at the 50% probability level; all hydrogen atoms and solvent molecules are omitted for clarity; $Pd-P^1$ 2.2449(9); $Pd-P^2$ 2.2532(9); $Pd-Cl^1$ 2.3412(10); $Pd-Cl^2$ 2.3442(9); P^1-O^1 1.613(2); P^1-O^2 1.601(2); P^2-O^3 1.800(3); P^2-O^4 1.604(3); P^1-C^{41} 1.800(3); P^2-C^{54} 1.815(3); O^5-C^{46} 1.380(4); O^5-C^{55} 1.388(4); $Pd-O^5$ 3.284(2); P^1-P^2 3.4455(12); $Cl^1-Pd-Cl^2$ 90.15(4); P^1-Pd-P^2 99.99(3); Cl^1-Pd-P^1 82.70(3); Cl^1-Pd-P^2 172.15(3); Cl^2-Pd-P^1 170.01(3); Cl^2-Pd-P^2 86.23(3); $O^1-P^1-O^2$ 102.46(12); $O^3-P^2-O^4$ 103.07(13); $Pd-P^1-O^1$ 116.50(9); $Pd-P^1-O^2$ 117.78(9); $Pd-P^2-O^3$ 123.91(9); $Pd-P^2-O^4$ 110.02(10); $Pd-P^1-C^{41}$ 109.87(11); $Pd-P^2-C^{54}$ 108.57(12); $C^{46}-O^5-C^{56}$ 112.6(3); $C^{45}-C^{47}-C^{50}$ 106.8(3); $O^1-P^1-C^{41}$ 106.07(13); $O^2-P^1-C^{41}$ 102.70(13); $O^3-P^2-C^{54}$ 102.50(14); $O^4-P^2-C^{54}$ 107.67(15)

 © 2004 Wiley-VCH Verlag GmbH & Co. KGaA, Weinheim

metallated Pd-diphosphonite species described previously by our group.[16]

The structure of complex **2** also bears close resemblance to the molecular structures for the related platinum complex of ligand **1**, which will be communicated elsewhere,[23] as well as for *cis*-[$PtCl_2$(Xantphos)].[24] This indicates that such dispositioning of the metal atom is highly favored in the crystal packing regardless of the metal atom involved. This phenomenon must therefore be based on steric crowding induced by the binaphthyl units. The dihedral angle of the two aromatic rings in the xanthene backbone is found to be 107.8°. The distance between the two phosphorus atoms is 3.4455(12) Å, while the distance between the palladium atom and the oxygen atom in the backbone is 3.284(2) Å, which is too long to expect any interaction.[25]

When ligand (*R*,*R*)-**1** was reacted with Rh(cod)(acac), the ^{31}P NMR spectrum reveals two doublets of doublets, ascribed to the cationic complex **3**, [Rh(cod)(**1**)]BF_4. The average signals appear at δ = 169.7 ppm and at δ = 161.4 ppm, with coupling constants $^1J_{Rh\text{-}P}$ of 218 Hz and $^2J_{P,P}$ of 24 Hz. Although no further characterization was performed on this compound, the existence of this ABX pattern implies that the two phosphorus atoms are chemically inequivalent in the rhodium complex, as in the palladium case. The Rh−P coupling constant is similar to values reported by Börner,[13] Puddephatt,[26] and Shum,[27] although the latter report dealt with a Rh(acac)-diphosphonite derivative, with a $^1J_{Rh\text{-}P}$ of 266 Hz.

Asymmetric Hydroformylation

In order to evaluate the catalytic properties of enantiomerically pure (*R*,*R*)-**1**, it was applied in the rhodium-catalyzed asymmetric hydroformylation of styrene (Scheme 2). To the best of our knowledge, no reports have appeared on the use of chiral diphosphonite ligands in rhodium-catalyzed asymmetric hydroformylation. As a rhodium precursor, Rh(acac)$(CO)_2$ was used. Before addition of the substrate, the catalytic system was activated for 1 h with 20 bar syngas at the reaction temperature to generate the catalytic resting state.

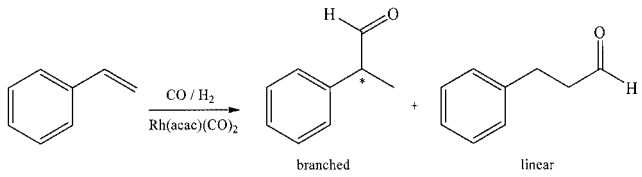

Scheme 2. General reaction scheme for the Rh-catalyzed hydroformylation of styrene

Several hydroformylation experiments were performed at different synthesis gas pressures (10 and 20 bar) and at different temperatures (40−100 °C). The amount of hydrogenation was usually less than 1% and no other side products were formed. The results obtained are summarized in Table 1. At 40 °C, a pressure of 20 bar instead of 10 bar led to an increase in the reaction rate of approximately 33%. The enantiomeric excess was found to be lower (entry 2 vs. 1). The selectivity for the branched aldehyde remained constant within experimental error. Turnover frequencies were determined at conversion levels of around 20−40% from the linear increase of conversion in time. Several samples were taken throughout the reaction without pressure loss.

The effect of pressure on the reaction rate is more significant at temperatures of 60 °C and higher. In all cases, the initial activity (TOF) is lower at higher pressures. Also, the enantioselectivity is lower at higher pressure. The regioselectivity shows a reverse trend, viz. a positive effect of pressure on the regioselectivity to branched product and a negative influence of the reaction temperature. This is more pronounced at a pressure of 10 bar, as the regioselectivity is only 56% at 100 °C and increases to 81% at 20 bar. In all cases, the enantiomeric excess (*ee*) is poor, with a maximum of 33% at 100 °C.

No attempts were made to modify the ligand system in order to obtain higher enantioselectivity. Goertz et al. already showed that for the asymmetric hydrocyanation, the introduction of bulky substituents in the 3,3′-positions of the binaphthyl units can lead to higher ee's.[14] Buisman et al. observed a similar effect in the asymmetric hydrofor-

Table 1. Rh-catalyzed asymmetric hydroformylation of styrene applying (*R*,*R*)-XantBino (**1**)

Entry[a]	*T* [°C]	*p* [bar]	Time [h]	Conversion [%][b]	Sel.$_{branched}$ [%][b]	*ee* [%][c]	TOF [h^{-1}][d]
1[e]	40	10	48	63	91	17 (*R*)	12
2[e]	40	20	72	90	92	13 (*R*)	17
3	60	10	5	54	85	22 (*R*)	260
4	60	20	8	93	87	16 (*R*)	140
5	80	10	3	99	80	27 (*R*)	880
6	80	20	3	100	85	20 (*R*)	720
7	100	10	2	94	56	33 (*R*)	n.d.
8	100	20	2	96	81	24 (*R*)	n.d.

[a] Reaction conditions: 1.55 mL styrene (13.5 mmol); 3.45 mL toluene; [Rh(acac)$(CO)_2$] = 0.9 mM, L:Rh = 1.2:1; styrene:Rh = 1000:1. [b] Determined by GC analysis. [c] Enantiomeric excess, determined by chiral GC analysis. [d] Turnover frequency determined at 20−40% conversion; defined as (mol substrate converted)·(mol rhodium)$^{-1}$·h^{-1}. [e] Preformation time 15 hours.

 © 2004 Wiley-VCH Verlag GmbH & Co. KGaA, Weinheim

mylation of styrene but with diphosphites derived from less rigid backbones.[4e] Furthermore, steric crowding around these positions led to a significant decrease in enantioselectivity.

As with thermodynamic control of the stereoselection, the *ee* decreases when the temperature is increased, and experiments are usually conducted at low temperature.[28–30] There are nonetheless some studies on the rhodium-catalyzed hydroformylation of styrene in which the enantioselectivity increased with increasing temperature.[31–34] Hanson et al. studied the Pt/Sn-catalyzed asymmetric hydroformylation with diamino-substituted versions of the known ligands CHIRAPHOS and BDPP. A linear decrease in the *ee* with temperature was observed using the CHIRAPHOS derivative, while with the BDPP ligand the sign of enantioselection changed with temperature. The (*S*)-enantiomer was formed in excess at low temperature, while the (*R*)-enantiomer was the major product at 60 °C and above. Furthermore, the enantioselectivity of the (*R*)-enantiomer increased with reaction temperature, contradictory to the "normal' behavior seen with CHIRAPHOS. This phenomenon, already discussed by Scharf in a review on dramatic temperature effects on selectivities in catalysis,[35] was explained by the existence of competing pathways of diastereomeric intermediates of a single chelate conformation of the catalyst system, hence indicating kinetic control.

For the catalytic system with ligand **1** we also observed a positive dependency of the enantiomeric excess on the reaction temperature, as illustrated in Figure 5. The highest *ee* of 33% is found at 100 °C and 10 bar. The *ee* is lower at higher pressure (for example, entries 3 and 4 vs. 5 and 6 in Table 1). A discussion on the proposed mechanism for this particular system is discussed hereafter (vide infra).

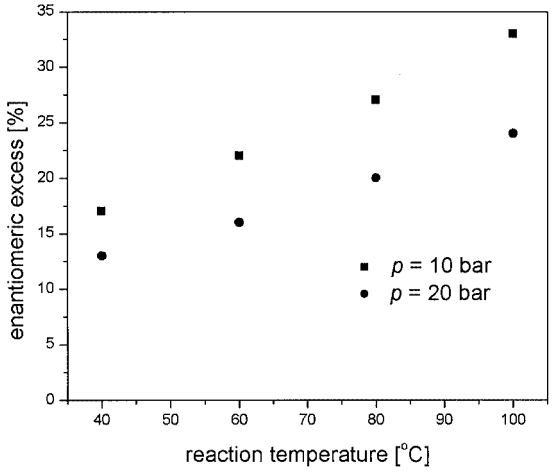

Figure 5. Plot of the positive relationship between the *ee* and the reaction temperature, at two pressures

It is known that the results obtained in the rhodium-catalyzed asymmetric hydroformylation of vinyl acetate can be drastically different when applying the same catalytic system.[36] We were therefore interested to see how our Rh/(**1**) system would perform in this specific reaction (Scheme 3). The substrate vinyl acetate differs from styrene in two important aspects, viz. a) vinyl acetate cannot form η^3 complexes and b) the carbonyl oxygen can participate in bonding to the metal.

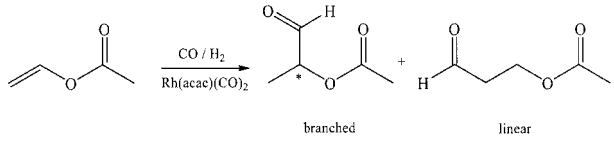

Scheme 3. General reaction scheme for the Rh-catalyzed hydroformylation of vinyl acetate

In all catalytic runs the catalyst was preformed for 1 hour at 60 °C and 10 bar. Reaction at 60 °C and 20 bar of H_2 led to an enantiomeric excess of 51%, which is significantly higher than for styrene. The regioselectivity was extremely high with an b/l ratio exceeding 90. The reaction of vinyl acetate showed the normal temperature dependence; the *ee* dropped to 33% at a reaction temperature of 80 °C. This supports the hypothesis that the η^3-benzyl intermediate might induce kinetic control of the *ee* with styrene as a substrate, leading to an unusual temperature effect. Since this intermediate species is absent in the case of vinyl acetate, no such dependence was found for this substrate.

Asymmetric Hydrogenation

As a third test reaction, diphosphonite **1** was applied in the Rh-catalyzed asymmetric hydrogenation of methyl (*Z*)-2-acetamidocinnamate (**I**) (Scheme 4).[37]

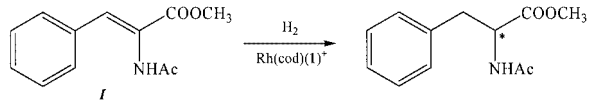

Scheme 4. General reaction scheme for the Rh-catalyzed hydrogenation of methyl (*Z*)-2-acetamidocinnamate

The catalysis was carried out at ambient temperature, with a substrate to rhodium ratio (S/Rh) of 100:1. Before addition of the substrate, a concentrated solution of [Rh(cod)(**1**)]BF_4, complex **3**, in methanol was stirred for 3 hours under 1.2 bar of H_2 in order to preform the catalyst. During catalysis a static H_2 pressure (1.2 or 5 bar) was applied. The reaction rate was constant up to 80% conversion for the reaction that applied 1.2 bar of H_2, indicating that the catalyst system remains stable and active. Also the *ee* remained constant at 54% over the full conversion range. Substrate depletion leads to the expected drop in reaction rate at even higher conversion. Under these nonoptimized conditions, the rates were low (about 40 h^{-1}) relative to rates reported by Reetz[8a] and Claver[8b] for the hydrogenation of different substrates that applied diphosphonites. For the paracyclophane-based diphosphonite system employed by Zanotti-Gerosa,[8c] TON's of up to 2000 h^{-1} were reported.

 © 2004 Wiley-VCH Verlag GmbH & Co. KGaA, Weinheim

The enantioselectivity of 54% with the present [Rh(cod)(**1**)]BF_4 system **3** is promising, but still moderate compared with the diphosphonite systems mentioned before (vide supra). The (*S*)-enantiomer is formed in excess with the catalyst containing (*R*,*R*)-(**1**). Similar catalytic results were obtained when applying a pressure of 5 bar H_2. After 2 hours, the conversion reached 94%, with an *ee* of 47%. The higher activity is expected since the concentration of hydrogen is evidently increased.

Temperature Dependence in Asymmetric Hydroformylation of Styrene

In the case of transition metal catalyzed functionalization of vinyl arenes, participation of η^3-benzyl intermediates (Scheme 5) have been discussed.[38−41] Depending on the ligand influence and on the temperature, pre-equilibria can exist that involve coordination of the substrate, σ-alkyl and η^3-benzyl intermediates. Obviously chirality is already induced during substrate binding but the direction could be influenced by a reversible insertion step. With (our) π-acceptor ligands the η^3-benzyl species could be favored, especially at low temperature giving rise to thermodynamic control over the enantioselection. At higher temperature, the σ-alkyl species could become more important, possibly resulting in a kinetically controlled process. This is in line with the pressure dependence of the *ee* and of the b/l ratio observed (vide supra) as higher CO pressure will slow down pre-equilibria and enhance product formation from intermediates once they are formed. Definitely, this effect is very interesting, and shedding more light on the underlying processes will give new insight into the stereoselection mechanism of the asymmetric hydroformylation. Unfortunately, the available data do not allow any conclusions yet. Detailed studies on this phenomenon are presently underway.

Conclusions

The synthesis of diphosphonite ligand **1** (XantBino) has been improved. The coordination chemistry of this ligand was explored for palladium and rhodium. The molecular structure for *cis*-[$PdCl_2$(**1**)], complex **2**, has been described, revealing an out-of-plane positioning of the metal atom at a dihedral angle of 115°. The bite angle of 100° of the diphosphonite ligand is unusually small for a xanthene-derived phosphorus ligand. The first application of a chiral diphosphonite in the rhodium-catalyzed asymmetric hydroformylation of styrene is reported, leading to high activities with turnover frequencies of up to 1420 h^{-1}. The maximum enantioselectivity obtained was low; however an interesting increase was observed at higher temperature. In the asymmetric hydrogenation of methyl (*Z*)-2-acetamidocinnamate, low activities were found, yet the enantioselectivity was promising, with an enantiomeric excess of 54%, which is encouraging, given the nonoptimized structure and conditions.

Experimental Section

General: Chemicals were purchased from Aldrich, Acros and Merck, and used as received. Synthesis gas (CO/H_2, 1:1) was purchased from Carburos Metalicos. All preparations were carried out under argon using standard Schlenk techniques. Solvents were distilled from sodium/benzophenone (THF, ether, toluene, hexane and ethanol) or calcium hydride (CH_2Cl_2 and $CDCl_3$) prior to use. All glassware was dried by heating under vacuum. The NMR spectra were recorded on a Varian Mercury 400 spectrometer (^1H, $^{13}C\{^1H\}$, $^{31}P\{^1H\}$). Chemical shifts are given in ppm referenced to solvent (^1H, $^{13}C\{^1H\}$) or an 85% aqueous solution of H_3PO_4 ($^{31}P\{^1H\}$). GC spectra were recorded on a Hewlett−Packard 5890A Chromatograph equipped with a Ultra-2 column (styrene) or a Shimadzu 17A with a PONA column (vinyl acetate and hydro-

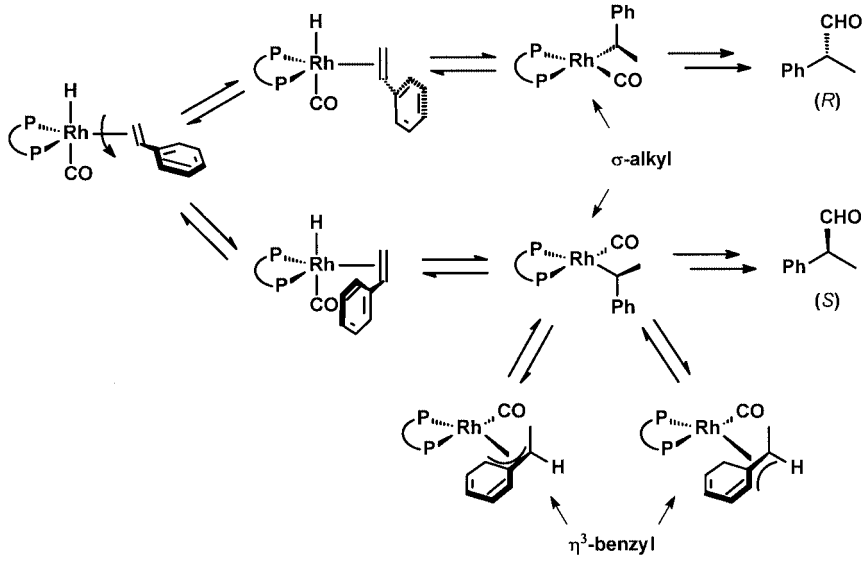

Scheme 5. Proposed stereoselection mechanism in the rhodium-catalyzed asymmetric hydroformylation of styrene (and other vinyl arenes)

 © 2004 Wiley-VCH Verlag GmbH & Co. KGaA, Weinheim

genation). Enantiomeric excesses were determined on a Hewlett−Packard 5890A with a Cyclodex β-I/P column (styrene) a GC Vega 6000 equipped with a Cyclodex β-I/P column (vinyl acetate) or a Shimadzu 2010 equipped with a Chirasil-L-Val column (hydrogenation). $PdCl_2(cod)$,[42] $[Rh(cod)Cl]_2$,[43] and [Rh(cod)(acac)][44] were prepared according to literature procedures.

4,5-Bis[bis(diethylamino)phosphonito]-9,9-dimethylxanthene:[14] 9,9-dimethylxanthene (2.85 g, 13.56 mmol) and *N,N,N′,N′*-tetramethylethylenediamine (TMEDA) (3.32 g, 28.48 mmol) were dissolved in diethyl ether (50 mL). The solution was cooled to −40 °C. *n*-Butyllithium (11.4 mL, 2.5 M in hexane) was added to the mixture dropwise. The solution was allowed to warm up to room temperature and stirred overnight. $ClP(NEt_2)_2$ (6.0 g, 18.99 mmol) was dissolved in diethyl ether (40 mL) and added to the reaction mixture at −80 °C. The solution was allowed to warm up to room temperature and stirred overnight. The solvent was removed by evaporation, and the resulting solid was dissolved in pentane (40 mL) and filtered to remove solids. Excess TMEDA was removed by azeotropic evaporation with toluene (3 × 20 mL). Pentane (10 mL) was added to the solid, and the mixture was stored overnight at −25 °C. The crystals that had formed were separated from the solution by filtration. The crystals were dried in vacuo, yielding a pure dark yellow solid. Yield (4.64 g, 61.3%). ^1H NMR ($CDCl_3$): δ = 7.38 (m, 4 H), 7.02 (d, 2 H), 3.05 (m, 16 H, NCH_2), 1.60 (6 H, CCH_3), 1.00 (m, 24 H, NCH_3) ppm. $^{31}P\{^1H\}$ NMR ($CDCl_3$): δ = 91.5 (s) ppm.

(*R*,*R*)-4,5-Bis(dinaphtho[*d*,*f*][1,3,2]dioxaphosphepin-4-yl)-9,9-dimethylxanthene (1): This is a modification of a literature procedure.[14] 4,5-Bis[bis(diethylamino)phosphonito]-9,9-dimethylxanthene (2.00 g, 3.58 mmol) and (*R*)-(+)-2,2′-dihydroxy-1,1′-binaphthyl (2.05 g, 7.16 mmol) were dissolved in toluene (50 mL). A catalytic quantity of tetrazole (about 10 mg, 0.14 mmol) was added as a protonation agent. The solution was heated to 90 °C for 16 hours. Diethylamine formed during the reaction was removed twice under vacuum. After reaction, the solvent was removed in vacuo, and the remaining crude product was dissolved in CH_2Cl_2 (5 mL) and layered with acetonitrile (20 mL). The precipitated product was isolated by filtration and washed with acetonitrile (10 mL). After drying, a yellow powder was obtained as a pure product (0.70 g, 31%). The other enantiomer can be obtained by the same procedure. ^1H NMR ($CDCl_3$): δ = 7.94 (d, ^1J = 8.8 Hz, 2 H, binolH), 7.90 (d, ^1J = 8.0 Hz, 2 H, binolH), 7.84 (d, ^1J = 8.0 Hz, 2 H, binolH), 7.63 (d, ^1J = 8.8 Hz, 2 H, binolH), 7.58 (d, ^1J = 8.8 Hz, 2 H, binolH), 7.55 (dd, ^1J = 8.0, ^2J = 0.8 Hz, 2 H, binolH), 7.42 (t, ^1J = 8.8 Hz, 6 H, ArH), 7.32 (d, ^1J = 8.4 Hz, 2 H, binolH), 7.28 (dquin, 4 H, ^1J = 8.0, ^2J = 1.2 Hz, binolH) 7.18 (d, ^1J = 8.8 Hz, 2 H, binolH), 6.92 (d, ^1J = 8.8 Hz, 2 H, binolH), 6.90 (d, ^1J = 7.2 Hz, 4 H, binolH), 1.79 [s, 6 H, $C(CH_3)_2$] ppm. ^{13}C NMR ($CDCl_3$): δ = 152.6, 149.9, 149.1, 133.0, 132.5, 131.5, 130.9, 130.4, 129.9, 129.0 (d, $J_{P,C}$ = 16.8 Hz), 128.5, 128.2 (d, $J_{P,C}$ = 6.8 Hz), 126.9 (d, $J_{P,C}$ = 3.8 Hz), 125.8 (d, $J_{P,C}$ = 19.0 Hz), 124.6 (d, $J_{P,C}$ = 20.6 Hz), 123.3, 121.9 (d, $J_{P,C}$ = 5.3 Hz), 34.1 [$C(CH_3)_2$], 31.9 [$C(CH_3)_2$] ppm. $^{31}P\{^1H\}$ NMR ($CDCl_3$): δ = 178.0 (s) ppm. $C_{55}H_{36}O_5P_2$ (838.82 g mol^{-1}): calcd. C 78.75, H 4.33; found C 78.52, H 4.18%.

***cis*-[$PdCl_2$((*S*,*S*)-1)] (complex 2):** $PdCl_2(cod)$ (13.2 mg, 46.2 μmol) and (*S*,*S*)-**1** (38.7 mg, 46.2 μmol) were dissolved in CH_2Cl_2 (5 mL) and stirred for 1 hour at room temperature. The solvent was removed in vacuo to leave a light-yellow solid. Yellow block-shaped crystals of complex **2** were grown by slow diffusion of acetonitrile into a dichloromethane solution. ^1H NMR ($CDCl_3$): δ = 8.37 (d, ^1J = 8.8 Hz, 1 H), 8.20 (d, ^1J = 8.8 Hz, 1 H), 8.16 (d, ^1J = 8.8 Hz, 1 H), 8.08 (d, ^1J = 8.8 Hz, 1 H), 8.03 (t, ^1J = 8.8 Hz, 1 H), 8.00 (d, ^1J = 8.8 Hz, 1 H), 7.95 (dd, ^1J = 8.0, ^2J = 4.8 Hz, 2 H), 7.89 (d, ^1J = 8.8 Hz, 1 H), 7.81 (m, 2 H), 7.70 (m, 3 H), 7.65 (dt, ^1J = 8.4, ^2J = 1.2 Hz, 1 H), 7.58 (t, ^1J = 8.8 Hz, 1 H), 7.56 (t, ^1J = 8.0 Hz, 2 H), 7.51 (dd, ^1J = 7.2, ^2J = 1.2 Hz, 1 H), 7.46 (m, 1 H), 7.46 (t, ^1J = 8.0 Hz, 1 H), 7.34 (m, 2 H), 7.23 (m, 2 H), 7.21 (t, ^1J = 6.8 Hz, 1 H), 7.13 (m, 1 H), 7.09 (dd, ^1J = 6.4, ^2J = 2.0 Hz, 1 H), 6.90 (d, ^1J = 8.8 Hz, 1 H), 6.09 (d, ^1J = 9.6 Hz, 1 H), 1.96 (s, 3 H, CCH_3), 1.67 (s, 3 H, CCH_3) ppm. $^{31}P\{^1H\}$ NMR ($CDCl_3$): δ = 143.1 (d, $J_{P,P}$ = 46.5 Hz), 137.4 ($J_{P,P}$ = 46.5 Hz) ppm. $C_{55}H_{36}Cl_2O_5P_2Pd$ (1016.14 g mol^{-1}): calcd. C 65.01, H 3.57; found C 65.34, H 3.63%.

[Rh(cod)((*R*,*R*)-1)]BF_4 (complex 3): This is a modification of a generic literature procedure.[45] [Rh(cod)(acac)] (0.047 g, 0.15 mmol) was dissolved in THF (2 mL). HBF_4 (54% solution in diethyl ether) (0.053 g, 0.60 mmol) was added. During addition, the solution colored darker. (*R*,*R*)-**1** (0.126 g, 0.15 mmol) was dissolved in THF (2 mL) and added to the solution, yielding an orange suspension. Diethyl ether (approximately 20 mL) was added, and the mixture was stirred vigorously for 5 minutes. The yellow precipitate formed was isolated and washed with diethyl ether (10 mL). Volatiles were removed in vacuo to leave a yellow/orange solid. Yield 68% (0.14 g, 0.10 mmol). $^{31}P\{^1H\}$ NMR ($CDCl_3$): δ = 169.3 (dd, J_{Rh-P} = 219, J_{P-P} = 24 Hz), 161.1 (dd, J_{Rh-P} = 216, J_{P-P} = 24 Hz.) ppm.

Hydroformylation of Styrene: Reactions were performed using a stainless steel autoclave (75 mL) equipped with an inner glass beaker. Styrene was filtered through neutral alumina before use. Generally, $Rh(acac)(CO)_2$ (3.5 mg, 13.5 μmol) and **1** (1.2 equiv.) were both dissolved in toluene (5 mL), and the combined solution was brought into the preheated autoclave, which was then pressurized to 20 bar of synthesis gas. After the appropriate preformation time, the autoclave was depressurized, and the substrate solution, containing styrene (1.55 mL, 13.5 mmol) in toluene (3.45 mL) was added, and 20 bar of synthesis gas was applied. During catalysis, samples were withdrawn without pressure loss for GC analysis. After reaction, the autoclave was cooled and depressurized, and the reaction mixture taken out. Oxidation of the aldehydes to the carboxylic acids was done directly afterwards, to prevent racemization and to allow for analysis by chiral GC.

Hydroformylation of Vinyl Acetate: Reactions were performed using a stainless steel autoclave (75 mL) equipped with an inner glass beaker. Generally, $Rh(acac)(CO)_2$ (3.0 mg, 11.6 μmol) and **1** (2 equiv.) were both dissolved in benzene (10 mL), and the combined solution was charged into the autoclave, which was then pressurized to 20 bar of synthesis gas and heated to reaction temperature. After preformation, vinyl acetate (1.5 mL, 16.3 mmol) in benzene (5 mL) was added. After reaction, the reaction mixture was quantitatively withdrawn, and a weighed amount of ethyl propionate (0.5 mL, 4.4 mmol) was added. After a quantitative distillation, an aliquot was withdrawn for GC analysis (both for conversion and enantiomeric excess).

Hydrogenation of Methyl (*Z*)-2-Acetamidocinnamate (I): Reactions were carried out in a stainless steel autoclave (75 mL). **3** (11.4 mg, 0.01 mmol) was dissolved in methanol (1 mL), and the solution was activated under 1 bar of H_2 for 2 hours. Methyl (*Z*)-2-acetamidocinnamate (0.22 g, 1.00 mmol) was dissolved in methanol (9 mL), and the substrate solution was charged into the catalyst solution, and the appropriate H_2 pressure was applied. During reaction, samples were withdrawn for GC analysis.

Crystal Structure Determination of 2: Intensity data were collected using graphite-monochromated Mo-K_α radiation, on a Nonius KappaCCD diffractometer. A correction for absorption was con-

 © 2004 Wiley-VCH Verlag GmbH & Co. KGaA, Weinheim

sidered unnecessary. The structure was solved by automated direct methods using SHELXS-97,[46] and refined on F^2 using SHELXL-97.[47] The absolute configuration of **2** was established by anomalous dispersion effects to be (*S*,*S*)-[$PdCl_2$(**1**)], Flack parameter 0.013(19). The crystal structure contains voids (1406.0 Å^3/unit cell) filled with disordered solvent molecules (dichloromethane/acetonitrile). Their contribution to the structure factors was ascertained using PLATON/SQUEEZE (499 e/unit cell). All non-hydrogen atoms were refined with anisotropic displacement parameters. All hydrogen atoms were constrained to idealized geometries and allowed to ride on their carrier atoms with an isotropic displacement parameter related to the equivalent displacement parameter of their carrier atoms. Structure validation and molecular graphics preparation were performed with the PLATON package.[48] CCDC-231720 contains the supplementary crystallographic data for this paper. These data can be obtained free of charge at www.ccdc.cam.ac.uk/conts/retrieving.html (or from the CCDC, 12 Union Road, Cambridge CB2 1EZ, UK; Fax: +44-1223-336033; E-mail: deposit@ccdc.cam.ac.uk).

Table 2. Selected crystallographic data for complex **2**, *cis*-[$PdCl_2$(**1**)]; $R_{int} = \Sigma[|F_o^2 - F_o^2\,(\text{mean})|] / \Sigma[F_o^2]$; $wR(F^2) = \{\Sigma[w(F_o^2 - F_c^2)^2] / \Sigma[w(F_o^2)^2]\}^{1/2}$; $R(F) = \Sigma(||F_o| - |F_c||) / \Sigma|F_o|$

	2
Formula	$C_{55}H_{36}Cl_2O_5P_2Pd$ + solvent
M (g mol^{-1})	1016.08[a]
Crystal size (mm)	0.06 × 0.12 × 0.30
Crystal system	orthorhombic
Space group	$P2_12_12_1$ (no. 19)
a (Å)	11.3183(1)
b (Å)	17.4368(1)
c (Å)	27.4181(3)
V (Å^3)	5411.10(8)
Z	4
$d_{calcd.}$ (g cm^{-3})	1.247[a]
μ(Mo-K_α) (mm^{-1})	0.544[a]
T (K)	150
Total reflections	59674
Unique reflections (R_{int})	12279 (0.064)
R_F	0.0411
wR_2 (F^2) (all data)	0.0975
F(000)	2064[a]

[a] Without disordered solvent.

Acknowledgments

This research was supported by The National Research School Combination on Catalysis (NRSC-C), Avantium Technologies (E. J. Z.) and in part by the Netherland's Organisation for Scientific Research (CW-NWO) (A. M. M. and A. L. S.). OMG is thanked for a generous gift of precious metals. The Erasmus Program of the European Union is acknowledged for a travel grant (J. P.). Scientific discussions with Dr. Rafael Sablong are highly valued.

[1] [1a] B. Breit, *Acc. Chem. Res.* **2003**, *36*, 264−275. [1b] B. Breit, W. Seiche, *Synthesis* **2001**, 1−36; C. Claver, P. W. N. M. van Leeuwen, in *Rhodium Catalyzed Hydroformylation* (P. W. N. M. van Leeuwen, C. Claver, Eds.), Kluwer, Amsterdam, **2000**, 107. [1d] F. Agbossou, J.-F. Carpentier, A. Mortreux, *Chem. Rev.* **1995**, 2485−2506. [1e] S. Gladiali, J. C. Bayon, C. Claver, *Tetrahedron: Asymmetry* **1995**, *6*, 1453−1474.

[2] [2a] A. Aghmiz, A. Orejón, M. Diéguez, M. D. Miquel-Serrano, C. Claver, A. M. Masdeu-Bultó, D. Sinou, G. Laurenczy, *J. Mol. Cat. A.: Chem.* **2003**, *195*, 113−124. [2b] C. Hegedus, J. Madarasz, H. Gulyas, A. Szollosy, J. Bakos, *Tetrahedron: Asymmetry* **2001**, *12*, 2867−2873. [2c] C. Bianchini, P. Barbaro, G. Scapacci, *J. Organomet. Chem.* **2001**, *621*, 26−33. [2d] U. Nettekoven, P. C. J. Kamer, M. Widhalm, P. W. N. M. van Leeuwen, *Organometallics* **2000**, *19*, 4596−4607. [2e] S. Lu, X. Li, A. Wang, *Catal. Today* **2000**, *63*, 531−536.

[3] [3a] F. Shibahara, K. Nozaki, T. Hiyama, *J. Am. Chem. Soc.* **2003**, *125*, 8555−8560. [3b] K. Nozaki, T. Matsuo, F. Shibahara, T. Hiyama, *Organometallics* **2003**, *22*, 594−600. [3c] O. Pamies, G. Net, A. Ruiz, C. Claver, *Tetrahedron: Asymmetry* **2002**, *12*, 3441−3445. [3d] V. Beghetto, A. Scrivanti, U. Matteoli, *Catal. Commun.* **2001**, *2*, 139−143. [3e] N. Sakai, S. Mano, K. Nozaki, H. Takaya, *J. Am. Chem. Soc.* **1993**, *115*, 7033−7034.

[4] [4a] M. Dieguez, O. Pamies, A. Ruiz, C. Claver, *New J. Chem.* **2002**, *26*, 827−833. [4b] Z. Freixa, C. J. Bayon, *J. Chem. Soc., Dalton Trans.* **2001**, 2067−2068. [4c] P. Uriz, E. Fernandez, N. Ruiz, C. Claver, *Inorg. Chem. Commun.* **2000**, *3*, 515−519. [4d] Y. Jiang, S. Xue, Z. Li, J. Deng, A. Mi, A. S. C. Chan, *Tetrahedron: Asymmetry* **1998**, *9*, 3185−3189. [4e] G. J. H. Buisman, L. A. van der Veen, A. Klootwijk, W. G. J. de Lange, P. C. J. Kamer, P. W. N. M. van Leeuwen, D. Vogt, *Organometallics* **1997**, *16*, 2929−2939. [4f] J. E. Babin, G. T. Whiteker (to Union Carbide) WO 93/03939 [*Chem. Abstr.* **1993**, *119*, 159872 h].

[5] [5a] F. Agbossou-Niedercorn, I. Suisse, *Coord. Chem. Rev.* **2003**, *242*, 145−158. [5b] R. Ewalds, E. B. Eggeling, A. C. Hewat, P. C. J. Kamer, P. W. N. M. van Leeuwen, D. Vogt, *Chem. Eur. J.* **2000**, *6*, 1496−1504.

[6] [6a] For a recent review see: J. Ansell, M. Wills, *Chem. Soc. Rev.* **2002**, *31*, 259−268. [6b] E. J. Zijp, J. I. van der Vlugt, M. Fioroni, D. M. Tooke, A. L. Spek, C. Müller, D. Vogt, unpublished work.

[7] [7a] M. T. Reetz, M. Pastó, *Tetrahedron Lett.* **2000**, *41*, 3315−3317. [7b] M. Laly, R. Broussier, B. Gautheron, *Tetrahedron Lett.* **2000**, *41*, 1183−1185.

[8] [8a] M. T. Reetz, A. Gosberg, R. Goddard, S.-H. Kyung, *Chem. Commun.* **1998**, 2077−2078. [8b] C. Claver, E. Fernandez, A. Gillon, K. Heslop, D. J. Hyett, A. Martorell, A. G. Orpen, P. G. Pringle, *Chem. Commun.* **2000**, 961−962. [8c] A. Zanotti-Gerosa, C. Malan, D. Herzberg, *Org. Lett.* **2001**, *3*, 3687−3690.

[9] M. T. Reetz, D. Moulin, A. Gosberg, *Org. Lett.* **2001**, *3*, 4083−4085.

[10] A. Martorell, R. Naasz, B. L. Feringa, P. G. Pringle, *Tetrahedron: Asymmetry* **2001**, *12*, 2497−2499.

[11] [11a] D. Selent, K. D. Wiese, D. Röttger, A. Börner, *Angew. Chem. Int. Ed.* **2000**, *39*, 1639−1641. [11b] D. Selent, W. Baumann, R. Kempe, A. Spannenberg, D. Röttger, K. D. Wiese, A. Börner, *Organometallics* **2003**, *22*, 4265−4271.

[12] [12a] L. Dahlenburg, *Eur. J. Inorg. Chem.* **2003**, 2733−2747. [12b] L. Dahlenburg, S. Mertel, *J. Organomet. Chem.* **2001**, *630*, 221−224. [12c] L. Dahlenburg, C. Becker, J. Höck, S. Mertel, *J. Organomet. Chem.* **1998**, *564*, 155−166.

[13] C. Kunze, D. Selent, I. Neda, M. Freytag, P. G. Jones, R. Schmutzler, W. Baumann, A. Börner, *Z. Anorg. Allg. Chem.* **2002**, *628*, 779−787.

[14] W. Goertz, P. C. J. Kamer, P. W. N. M. van Leeuwen, D. Vogt, *Chem. Eur. J.* **2001**, *7*, 1614−1618.

[15] [15a] W. Ahlers, D. Wiebelhaus, R. Paciello, M. Bartsch, R. Baumann, D. Vogt, A. C. Hewat (to BASF AG) WO 02/22261, **2002** [*Chem. Abstr.* **2002**, *136*, 249380]. [15b] J. I. van der Vlugt, A. C. Hewat, S. Neto, R. Sablong, A. M. Mills, M. Lutz, A. L. Spek, C. Müller, D. Vogt, *Adv. Synth. Catal.* **2004**, *346*, 993−1003. [15c] J. I. van der Vlugt, R. Sablong, P. C. M. M. Magusin, A. M. Mills, A. L. Spek, D. Vogt, *Organometallics* **2004**, *23*, 3177−3183.

[16] J. I. van der Vlugt, R. Sablong, A. M. Mills, H. Kooijman, A. L. Spek, A. Meetsma, D. Vogt, *Dalton Trans.* **2003**, 4690−4699.

 © 2004 Wiley-VCH Verlag GmbH & Co. KGaA, Weinheim

[17] W. Goertz, W. Keim, D. Vogt, U. Engler, M. D. K. Boele, L. A. van der Veen, P. C. J. Kamer, P. W. N. M. van Leeuwen, *J. Chem. Soc., Dalton Trans.* **1997**, 2981−2988.
[18] S. Agbossou, M. C. Bonnet, F. Dahan, I. Tkatchenko, *Acta Crystallogr., Sect. C* **1989**, *45*, 1149−1152.
[19] A. Karaçar, M. Freytag, P. G. Jones, R. Bartsch, R. Schmutzler, *Z. Anorg. Allg. Chem.* **2001**, *627*, 1571−1581.
[20] M. A. Zuideveld, B. H. G. Swennenhuis, M. D. K. Boele, Y. Guari, G. P. F. van Strijdonck, J. N. H. Reek, P. C. J. Kamer, K. Goubitz, J. Fraanje, M. Lutz, A. L. Spek, P. W. N. M. van Leeuwen, *J. Chem. Soc., Dalton Trans.* **2002**, 2308−2317.
[21] J. Yin, S. L. Buchwald, *J. Am. Chem. Soc.* **2002**, *124*, 6043−6048.
[22] M. Kranenburg, J. G. P. Delis, P. C. J. Kamer, P. W. N. M. van Leeuwen, K. Vrieze, N. Veldman, A. L. Spek, K. Goubitz, J. Fraanje, *J. Chem. Soc., Dalton Trans.* **1997**, 1839−1849. [22b] R. J. van Haaren, K. Goubitz, J. Fraanje, G. P. F. van Strijdonck, H. Oevering, B. Coussens, J. N. H. Reek, P. C. J. Kamer, P. W. N. M. van Leeuwen, *Inorg. Chem.* **2001**, *40*, 3363−3372.
[23] R. van Duren, J. H. J. Huibers, J. I. van der Vlugt, A. M. Mills, A. L. Spek, D. Vogt, unpublished results.
[24] R. van Duren, J. I. van der Vlugt, J. Meeuwissen, H. Kooijman, A. L. Spek, D. Vogt, unpublished work.
[25] Typical Pd−O distances observed are within the range 2.02−2.14 Å, see: [25a] P. L. Alsters, J. Boersma, W. J. J. Smeets, A. L. Spek, G. van Koten, *Organometallics* **1993**, *12*, 1639−1647. [25b] P. L. Alsters, J. Boersma, H. Kooijman, A. Sicherer-Roetman, A. L. Spek, G. van Koten, *Organometallics* **1992**, *11*, 4124−4135.
[26] R. Kumar, R. J. Puddephatt, F. R. Fronczek, *Inorg. Chem.* **1990**, *29*, 4850−4851.
[27] S. P. Shum, S. D. Pastor, G. Rihs, *Inorg. Chem.* **2002**, *41*, 127−131.
[28] S. Cserépi-Szücs, J. Bakos, *Chem. Commun.* **1997**, 635−636.
[29] G. J. H. Buisman, M. E. Martin, E. J. Vos, A. Klootwijk, P. C. J. Kamer, P. W. N. M. van Leeuwen, *Tetrahedron: Asymmetry* **1995**, *6*, 719−738.
[30] M. Diéguez, M. M. Pereira, A. M. Masdeu-Bultó, C. Claver, J. C. Bayón, *J. Mol. Cat. A: Chem.* **1999**, *75*, 111−122. See also ref. 4c.
[31] C. J. A. Daley, S. H. Bergens, *J. Am. Chem. Soc.* **2002**, *124*, 3680−3691.
[32] P. Haelg, G. Consiglio, P. Pino, *J. Organomet. Chem.* **1985**, *296*, 281−290.
[33] [33a] L. Kollár, J. Bakos, I. Tóth, B. Heil, *J. Organomet. Chem.* **1988**, *350*, 277−284. [33b] L. Kollár, J. P. Sándor, G. Szalontai, *J. Mol. Cat. A: Chem.* **1991**, *67*, 191−198. [33c] L. Kollár, T. Kégl, J. Bakos, *J. Organomet. Chem.* **1993**, *453*, 155−158.
[34] I. Tóth, I. Guo, B. E. Hanson, *Organometallics* **1993**, *12*, 848−852.
[35] H. Buschmann, H. Scharf, N. Hoffmann, P. Esser, *Angew. Chem. Int. Ed. Engl.* **1991**, *30*, 477−515.
[36] S. W. Breeden, D. J. Cole-Hamilton, D. F. Foster, G. J. Schwarz, M. Wills, *Angew. Chem. Int. Ed.* **2000**, *39*, 4106−4108.
[37] [37a] W. S. Knowles, M. J. Sabacky, B. D. Vineyard, D. J. Weinkauff, *J. Am. Chem. Soc.* **1975**, *97*, 2567−2568. [37b] W. S. Knowles, M. J. Sabacky, *J. Chem. Soc., Chem. Commun.* **1968**, 1445−1446.
[38] Modified from: A. van Rooij, E. N. Orij, P. C. J. Kamer, P. W. N. M. van Leeuwen, *Organometallics* **1995**, *14*, 34−43.
[39] With Ni: [39a] T. J. Anderson, D. A. Vicic, *Organometallics* **2004**, *23*, 623−625. [39b] A. L. Casalnuovo, T. V. RajanBabu, T. A. Ayers, T. H. Warren, *J. Am. Chem. Soc.* **1994**, *116*, 9869−9882.
[40] With rhodium: [40a] F. W. Kwok, D. J. Wink, *Organometallics* **1993**, *12*, 1954−1959 and references cited therein. [40b] C. Botteghi, S. Paganelli, *J. Organomet. Chem.* **1991**, *417*, C41−C45; H.-O. Stühler, *Angew. Chem.* **1980**, *92*, 475−476.
[41] With Pt: L. E. Crascall, S. A. Litster, A. D. Redhouse, J. L. Spencer, *J. Organomet. Chem.* **1990**, *394*, C35−C38. With Pd, see: [41a] F. Bergamin, F. Morandini, A. Turco, *Gazz. Chim. Ital.* **1990**, *120*, 57−59. [41b] F. Bergamin, F. Morandini, A. Turco, *Gazz. Chim. Ital.* **1990**, *120*, 705−709. [41c] Y. Becker, J. K. Stille, *J. Am. Chem. Soc.* **1978**, *100*, 845−850. [41d] J. S. Roberts, K. J. Klabunde, *J. Am. Chem. Soc.* **1977**, *99*, 2509−2515.
[42] D. R. Drew, J. R. Doyle, *Inorg. Synth.* **1972**, *13*, 52.
[43] J. Chatt, L. M. Venanzi, *J. Chem. Soc.* **1957**, 4735−4741.
[44] R. Cramer, *J. Am. Chem. Soc.* **1964**, *60*, 217−222.
[45] J. M. Brown, P. A. Chaloner, A. G. Kent, B. A. Murrer, P. N. Nicholson, D. Parker, P. J. Sidebottom, *J. Organomet. Chem.* **1981**, *216*, 263−276.
[46] G. M. Sheldrick, *SHELXS-97*; University of Göttingen, Germany, **1997**.
[47] G. M. Sheldrick, *SHELXL-97*; University of Göttingen, Germany, **1997**.
[48] A. L. Spek, *PLATON*, A Multi-purpose Crystallographic Tool; Utrecht University, The Netherlands, **2003**.

Received February 18, 2004
Early View Article
Published Online September 7, 2004

 © 2004 Wiley-VCH Verlag GmbH & Co. KGaA, Weinheim

Structural and Magnetic Properties of Two Carboxylato-Bridged Manganese(II) Complexes with N-Donor Coligands

Sanjit Konar,[a] Subal Chandra Manna,[a] Ennio Zangrando,[b] Talal Mallah,[c] Joan Ribas,*[d] and Nirmalendu Ray Chaudhuri*[a]

Keywords: Manganese(II) / Dicarboxylates / N-donor ligands / Crystal structure / Magnetic study

Two polymeric Mn^{II} complexes, $[(m\text{-phth})(Mn)(bpp)_2]\cdot 0.5H_2O$ (**1**) and $[(mal)_2(Mn)_2(H_2O)_2(hmt)]$ (**2**) [mal = malonate; hmt = hexamethylenetetramine; bpp = 1,3-bis(4-pyridyl)propane; *m*-phth = 1,3-benzenedicarboxylate] have been synthesized. Complex **1** consists of 1D chains (with monocoordinated bpp) that are held together to form a 2D extended network of hydrogen bonding between lattice water molecules and uncoordinated bpp donors. Variable-temperature magnetic susceptibility data of the complex have been fitted applying the formula used for dinuclear complexes of Mn^{II} ions, considering interdimer interactions (J'). The following parameters were obtained from the best fit: $J = -0.88 \pm 0.02$ cm^{-1}, $J' = -0.1$ cm^{-1} and $g = 1.99 \pm 0.01$. The agreement factor $R = \Sigma(\chi_m T_{obsd.} - \chi_m T_{calcd.})^2/\Sigma(\chi_m T_{calcd.})^2$ is 1.1×10^{-5}. Complex **2** is a 3D polymeric network where *syn/anti*-bridging malonate ligands and Mn^{II} centers are assembled in the form of $[Mn(H_2O)(mal)]_n$ layers, which are further connected by hexamethylenetetramine. The magnetic data have been fitted considering the complex as a pseudo-two-dimensional sheet of Mn^{II} cations and malonate anions since the coupling through the hexamethylenetetramine ligand is almost zero. We have followed two approaches for fitting the data, (a) through the expansion series of Line's equation for the $S = 5/2$ antiferromagnetic quadratic layer and (b) by using the equation based on an infinite 2D square lattice composed of isotropically coupled classical spin $S = 5/2$. Both approaches result in excellent theoretical fits and similar J values of –0.24 cm^{-1} and –0.21 cm^{-1} for the Line's and Curély equations, respectively.

(© Wiley-VCH Verlag GmbH & Co. KGaA, 69451 Weinheim, Germany, 2004)

Introduction

Carboxylates are interesting ligands because of their wide variety of coordination modes which make them an attractive choice for the synthesis of polynuclear metal complexes, from discrete dimer to 1D, 2D, or 3D networks.[1] Metal-organic frameworks built up by transition metal cations and dicarboxylate anions are of interest from a variety of viewpoints, including magnetic materials,[2] open-framework structures with micropores for ion exchange or catalysis[3] and also compounds that are biologically relevant.[4] Therefore, a considerable number of transition metal compounds using dicarboxylates have been reported during the last decade.[1–8] In our own investigations we also prepared and characterized several coordination polymers of transition metals containing dicarboxylate groups in combination with multidentate N-donor coligands such as 4,4′-bipyridine, pyrazine, 1,2-bis(4-pyridyl)ethane etc.[5–8] In continuation of our interest in this research field, we have synthesized two new polynuclear Mn^{II}–dicarboxylate complexes. Complex **1**, $[(m\text{-phth})Mn(bpp)_2]\cdot 0.5H_2O$ [bpp = 1,3-bis(4-pyridyl)propane; *m*-phth = 1,3-benzenedicarboxylate], is a 1D chain comprising a rigid dicarboxylate and a flexible N-donor coligand, whereas complex **2**, $[(mal)_2(Mn)_2(H_2O)_2(hmt)]$ [mal = malonate; hmt = hexamethylenetetramine] is a 3D coordination polymer derived from a flexible dicarboxylate and a rigid N-donor coligand. Both complexes show weak antiferromagnetic interactions between the metal centers. Magnetic data have been fitted using different theoretical approaches.

[a] Department of Inorganic Chemistry, Indian Association for the Cultivation of Science,
Kolkata 700032, India
E-mail: icnrc@mahendra.iacs.res.in
[b] Dipartimento di Scienze Chimiche, University of Trieste,
34127 Trieste, Italy
[c] Laboratoire de Chimie Inorganique, UMR CNRS 8613, Universit de Paris-Sud,
91405 Orsay, France
[d] Departament de Química Inorgànica, Universitat de Barcelona,
Diagonal 647, 08028 Barcelona, Spain
E-mail: joan.ribas@qi.ub.es

Supporting information for this article is available on the WWW under http://www.eurjic.org or from the author.

 © 2004 Wiley-VCH Verlag GmbH & Co. KGaA, Weinheim **DOI: 10.1002/ejic.200400148**

Results and Discussion

Synthesis of the Complexes

The complexes have been synthesized adopting procedures which are schematically given below:

$$MnCl_2 \cdot 4H_2O + 2\ bpp + Na_2(m\text{-phth}) \xrightarrow[\text{water/methanol (2:1)}]{\text{refluxing (1h)}} [(m\text{-phth})Mn(bpp)_2] \cdot 0.5H_2O\ (\mathbf{1}) + 2\ NaCl + 3.5\ H_2O$$

$$2\ MnCl \cdot 4H_2O + hmt + 2\ Na_2(mal) \xrightarrow[\text{water/methanol (2:1)}]{\text{stirring (1h)}} [(mal)_2Mn_2(H_2O)_2(hmt)](\mathbf{2}) + 4\ NaCl + 6\ H_2O$$

Description of the Structures

Complex 1

The structure of **1** consists of 1D polymeric chains (see Figures 1 and 2), built up by distorted octahedral Mn^{II} centers with dicarboxylate anions and *trans*-situated monocoordinated 1,3-bis(4-pyridyl)propane. One of the carboxylate groups of *m*-phthalate acts as a chelating ligand while the other, in a distorted *syn-syn* conformation, as bismonodentate) towards two crystallographically related metal centers, yielding a ribbon running parallel to the *b* axis. The polymer displays centro-symmetric 8- and 16-membered rings with metal−metal separations of 4.397 and 7.276 Å, respectively (Figure 1). The benzene ring forms a dihedral angle of 25.6(1)° with the former carboxylate but is almost coplanar with the other [angle of 8.7(1)°], resulting in a rather undulated chain. Thus the hexacoordinate Mn center possesses an N_2O_4 environment by virtue of four carboxylate oxygen atoms, and two bpp nitrogen donors. In the equatorial plane, the Mn−O(3) and Mn−O(4) distances of 2.113(2) and 2.114(2) Å, respectively, are in the range of those observed in Mn(*m*-phth) structures containing 2,2′-bipy[9] or 1,10-phen[10] ligands. On the other hand, the Mn−O distances generated by the chelating carboxylate are somewhat longer [2.262(2) and 2.288(2) Å] and appear comparable in length with the axial Mn−N bonds [Mn−N(1) = 2.313(3), Mn−N(2) = 2.285(3) Å, Table 1]. The two crystallographically independent flexible bpp ligands assume *gauche*/*anti* and *gauche*/*gauche* conformations, with the torsion angles along the propane chain being 64.3(5), 171.6(4)° and 71.7(11), 67.8(11)°, respectively. A disordered lattice water molecule connects the uncoordinated bpp nitrogen atoms of adjacent chains (N−O distances of ca. 3.0 Å) through hydrogen bonds, promoting the dimensionality of the compound. However, based on the

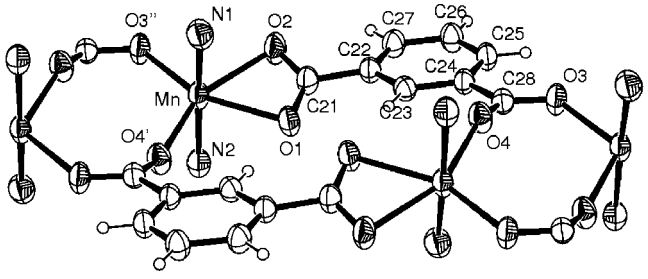

Figure 1. ID polymeric structure of **1** developed along axis *b*, showing the metal coordination environment (ellipsoid probability 40%); O4′ at: 1 − *x*, 1 − *y*, 1 − *z*; O3″ at: *x*, 1 − *y*, *z*

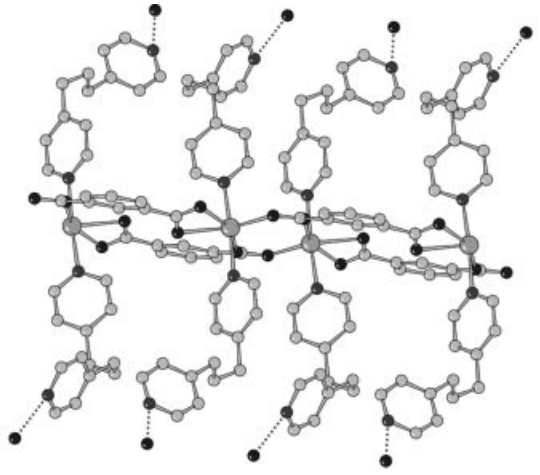

Figure 2. Polymeric chain of **1** showing bpp ligands hydrogen-bonded (dotted lines) to lattice water molecules through uncoordinated nitrogen atoms

Table 1. Selected bond lengths [Å] and angles [°] for complexes **1** and **2**

Complex **1**

Distances [Å]			
Mn−O(3″)	2.113(2)	Mn−O(2)	2.288(2)
Mn−O(4′)	2.114(2)	Mn−N(1)	2.313(3)
Mn−O(1)	2.262(2)	Mn−N(2)	2.262(2)
Angles [°]			
O(3″)−Mn−O(4′)	112.58(8)	O(1)−Mn−N(1)	88.1(1)
O(3″)−Mn−O(1)	151.56(8)	O(1)−Mn−N(2)	88.41(9)
O(3″)−Mn−O(2)	94.17(8)	O(2)−Mn−N(1)	89.5(1)
O(3″)−Mn−N(1)	97.4(1)	O(2)−Mn−N(2)	94.15(9)
O(3″)−Mn−N(2)	88.76(9)	N(1)−Mn−N(2)	172.64(9)
O(4′)−Mn−O(1)	95.38(8)	C(21)−O(1)−Mn	90.36(16)
O(4′)−Mn−O(2)	153.22(8)	C(21)−O(2)−Mn	89.33(17)
O(4′)−Mn−N(1)	88.5(1)	C(28″)−O(3″)−Mn	125.40(19)
O(4′)−Mn−N(2)	85.41(9)	C(28′)−O(4′)−Mn	152.1(2)
O(1)−Mn−O(2)	57.85(7)		

Symmetry codes: ′: 1 − *x*, 1 − *y*, 1 − *z*; ″: *x*, 1 − *y*, *z*

Complex **2**

Distances [Å]			
Mn−O(1)	2.154(2)	Mn−O(1w)	2.235(3)
Mn−O(2)	2.163(2)	Mn−N(1)	2.342(3)
Angles [°]			
O(1)−Mn−O(1′)	83.0(1)	O(2)−Mn−O(1w)	89.46(7)
O(1)−Mn−O(2)	86.43(8)	O(2)−Mn−N(1)	84.66(6)
O(1)−Mn−O(2′)	169.40(7)	O(1w)−Mn−N(1)	170.4(1)
O(1)−Mn−O(1w)	91.51(8)	C(1)−O(1)−Mn	129.8(1)
O(1)−Mn−N(1)	95.66(8)	C(1)−O(2″)−Mn″	130.8(2)
O(2)−Mn−O(2′)	104.1(1)		

Symmetry codes: ′: *x*, −*y*, *z*; ″: 1/2 − *x*, 1/2 − *y*, 1/2 + *z*; ‴: −*x*, −*y*, *z*

 © 2004 Wiley-VCH Verlag GmbH & Co. KGaA, Weinheim

peak height in the difference Fourier map, an occupancy factor of 0.5 was assigned to this water oxygen atom.

Complex 2

The X-ray structural determination of **2** evidences covalently bonded $[Mn(H_2O)(mal)]_n$ layers connected by hmt ligands to form a 3D polymer. The malonate anion, in its frequently found coordination mode[11−13] acts as a chelating and a bis(monodentate) ligand towards three metal ions. A selection of bond lengths and angles is reported in Table 1, and the structure with the atomic labeling scheme is shown in Figure 3. The octahedral coordination geometry of the metal atom consists of four planar equatorial carboxylate oxygen atoms [Mn−O(1) = 2.154(2) and Mn−O(2) = 2.163(2) Å], while the axial positions are occupied by an axial water molecule and an hmt nitrogen atom with significantly longer bond lengths [Mn−O(1w) = 2.235(3), Mn−N(1) 2.342(3) Å; Table 1]. These distances are similar to those found in the analogous $[Mn_2(mal)_2(4,4'\text{-bipy})(H_2O)_2]_n$,[11] with the exception of a slightly longer Mn−N(hmt) bond in the present case. In the square grids (4,4) of side dimension 5.517 Å, the coordinated water molecule forms two intralayer hydrogen bonds (2.719 Å) with the oxygen atoms of the anion chelating neighboring metal atoms (Figure 4). It is worth noting some features emerging from the 3D structure of the present compound and of the derivative containing the 4,4′-bipy ligands.[11] Figures 5, 6 and 7 show similar $[Mn(H_2O)(mal)]_n$ undulated layers with a zig-zag arrangement of the equatorial coordination planes. However, in the presently reported compound **2**, the sheets are separated by 8.029 Å and stack on top of each other with reference to a symmetry plane. The adamantoid hmt ligands connect the metal ions at 6.29 Å with angular Mn−N(hmt)−Mn links that outline a herringbone arrangement. A view of the packing along axis *c* indicates channels formed by the mal(Mn) layers and hmt ligands, the filled space being 74.8% (Figure 6). On the other hand, in $[Mn_2(mal)_2(4,4'\text{-bipy})(H_2O)_2]_n$, the distance between the mean planes through the sheets is slightly larger, 9.386 Å, but the rod-like 4,4′-bipy spacers cause sliding between the connected layers (Figure 7).

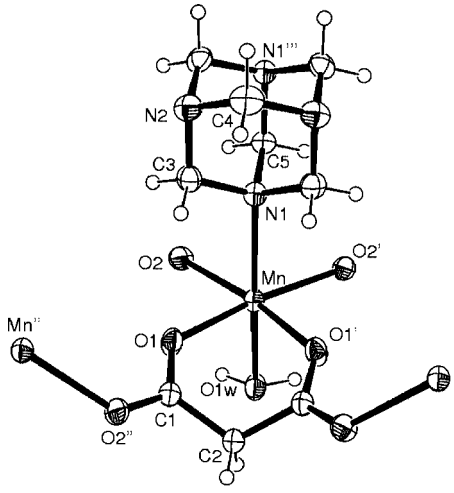

Figure 3. Structural fragment showing the Mn^{II} coordination sphere of **2** (ellipsoid probability at 40%); the hmt base is centered about an *mm2* crystallographic site (the twofold axis passing through C4−C5)

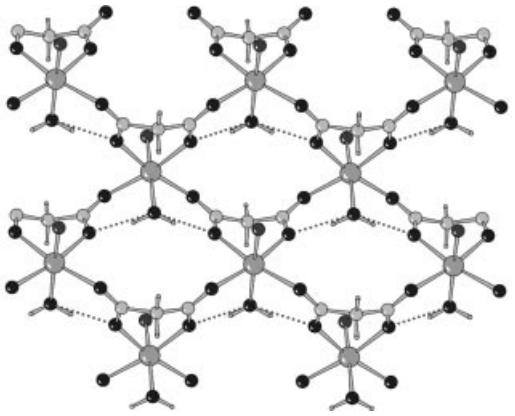

Figure 4. The $[Mn(H_2O)(malonate)]_n$ layer of complex **2** in the *bc* plane with hydrogen bonds (indicated by dotted lines) formed by the water molecules (for hmt only N donors are indicated)

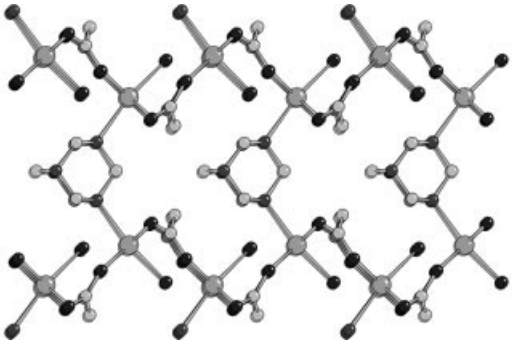

Figure 5. Crystal packing in **2** along axis *b* with staircase-like arrangement of $[Mn(H_2O)(mal)]_n$ layers

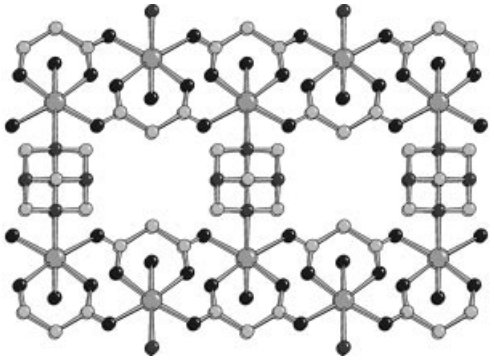

Figure 6. View of crystal packing in **2** along axis *c*, evidencing voids between hmt ligands

Magnetic Properties

Complex 1

The temperature dependence of χ_M (inset) and $\chi_M T$ (χ_M being the magnetic susceptibility for two Mn^{II} ions) for complex **1** is shown in Figure 8. The χ_M value (0.028

 © 2004 Wiley-VCH Verlag GmbH & Co. KGaA, Weinheim

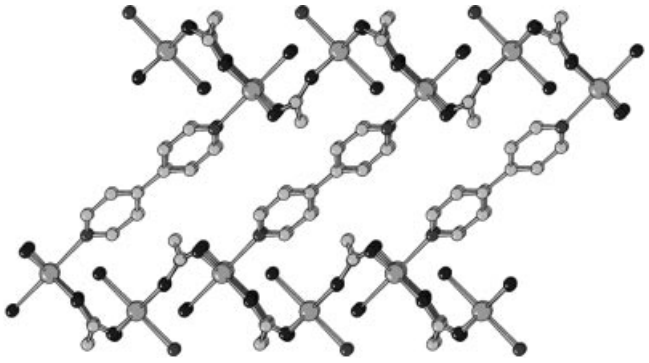

Figure 7. Crystal packing of $[Mn_2(mal)_2(4,4'\text{-bipy})(H_2O)_2]_n$ with layers connected by 4,4′-bipy ligands

cm^3mol^{-1} at 300 K) increases on decreasing the temperature. From room temp. to 100 K there is a smooth increase and from 100 K to 2 K the increase is more pronounced with a maximum at 4 K (χ_M = 0.717 cm^3mol^{-1}). Finally from 4 K to 2 K there is a slight decrease to 0.68 cm^3mol^{-1} at 2 K. χ_MT at 300 K is 8.42 $cm^3mol^{-1}K$, a value which is as expected for two "isolated" Mn^{II} ions. χ_MT is almost invariable up to 100 K and then gradually decreases while cooling to reach 1.36 $cm^3mol^{-1}K$ at 2 K. The shape of these curves is characteristic of the occurrence of weak antiferromagnetic interactions between the Mn^{II} centers.

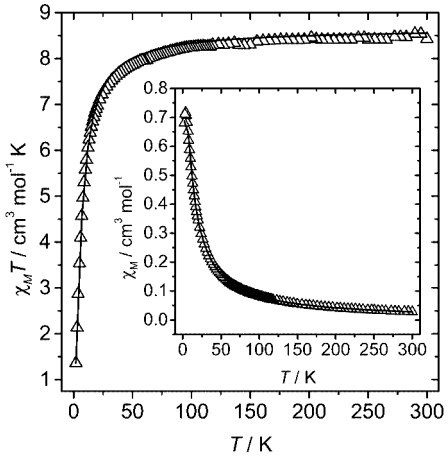

Figure 8. Temperature dependence (300−2 K) of χ_M (inset) and χ_MT (χ_M being the magnetic susceptibility for two Mn^{II} ions) for complex **1**; the solid line represents the best theoretical fit (see text for details)

The structure is one-dimensional, but from a magnetic point of view it can be considered as a dinuclear entity in which two Mn^{II} ions are linked by two distorted *syn-syn*-carboxylate bridges. These entities are linked together by an *m*-phthalate unit [monodentate to one Mn^{II} ion and chelated to the other], through a skeleton of five carbon atoms at distance of 7.276 Å. Thus, the only magnetic pathway is through Mn−O(4)−C(28)−O(3)−Mn in *syn-syn* conformation, which creates weak antiferromagnetic coupling (see below),[1b,14] although weak ferromagnetic coupling has also been reported in some cases.[2e]

Taking into account the pseudo-dinuclearity of **1**, the susceptibility data have been fitted applying the formula for a dinuclear complex of Mn^{II} (S = 5/2),[14] and the initial results were improved by adding a possible J' (intermolecular coupling) using the mean-field approach. The employed Hamiltonian was $H = -JS_1S_2 + g\beta S_zH - zJ'<S_z>S_z$.[1b] The best fit is given by the following parameters: $J = -0.88 \pm 0.02$ cm^{-1}, $J' = -0.1$ cm^{-1} and $g = 1.99 \pm 0.01$. The factor $R = \Sigma(\chi_mT_{obsd.} - \chi_mT_{calcd.})^2/\Sigma(\chi_mT_{calcd.})^2$ is 1.1×10^{-5} corroborating an excellent agreement between experiment and theory.

Complex 2

The temperature dependence of χ_M (inset) and χ_MT (χ_M being the magnetic susceptibility for one Mn^{II} ion) for complex **2** is shown in Figure 9. The χ_M value is 0.0144 cm^3mol^{-1} at 295 K. On decreasing the temperature the value of χ_M increases; from room temperature to 100 K there is a smooth increase and from 100 K to 2 K the increase is more pronounced (χ_M = 0.54 cm^3mol^{-1} at 2 K). In this case there is no maximum in the χ_M curve, as observed in complex **1**; only a tendency to a maximum is shown close to 2 K. χ_MT at 300 K is 4.24 $cm^3mol^{-1}K$, a value which is as expected for an "isolated" Mn^{II} ion. χ_MT is almost invariable up to 100 K (4.10 $cm^3mol^{-1}K$) and gradually decreases while cooling to reach 1.08 $cm^3mol^{-1}K$ at 2 K. The shape of these curves is characteristic of the occurrence of weak antiferromagnetic interactions between the Mn^{II} centers.

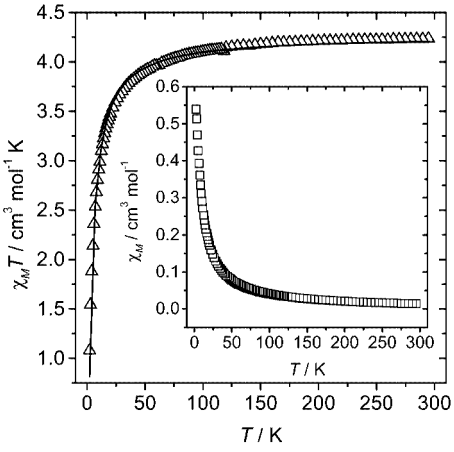

Figure 9. Temperature dependence (300−2 K) of χ_M (inset) and χ_MT (χ_M being the magnetic susceptibility for one Mn^{II} ion) for complex **2**; solid line represents their best theoretical fit (see text for details)

Taking into account that the structure is a three-dimensional network, it is impossible to fit the susceptibility data in order to find an appropriate J value. But, the structure can be considered as two-dimensional sub-lattices, consisting of Mn^{II} ions and malonate bridging ligands (Figure 4), which are linked to each other by hmt ligands. The Mn−N(1) distance [2.342(3) Å] is the longest in the distorted octahedral environment of Mn^{II}, which serves to simplify the calculations. The Mn−O(1) and Mn−O(2) distances [malonate bridge Mn−O(2)−C(1)−O(1)−Mn in *syn-anti* conformation] are shorter [2.154(2) and 2.163(2) Å, respectively]. Thus, owing to these differences in Mn−O/N

 © 2004 Wiley-VCH Verlag GmbH & Co. KGaA, Weinheim

distances and the large Mn−Mn separation (8.029Å), we can assume that the magnetic coupling through hmt will be almost negligible. Thus, with the pseudo two-dimensional character of **2**, the susceptibility data have been fitted according to two approaches:

a) By the expansion series[15] of Line's equation for an $S = 5/2$ antiferromagnetic quadratic layer, based on the exchange Hamiltonian $H = -\Sigma_{nn} JS_iS_j$, where Σ_{nn} runs over all pairs of nearest-neighbor spins i and j [Equation (1)], where $\theta = kT/|J|S(S+1)$, $C_1 = 4$, $C_2 = 1.448$, $C_3 = 0.228$, $C_4 = 0.262$, $C_5 = 0.119$, $C_6 = 0.017$ and N, g and β have their usual meanings.

$$Ng^2\beta^2/\chi|J| = 3\theta + (\Sigma C_n/\theta^{n-1}) \quad (1)$$

The best fit is obtained with $J = -0.24 \pm 0.03$ cm^{-1} and $g = 1.99 \pm 0.01$. The factor $R = \Sigma(\chi_m T_{obsd.} - \chi_m T_{calcd.})^2/\Sigma(\chi_m T_{calcd.})^2$ is 1.57×10^{-4}, which actually corresponds to an excellent experiment-theory agreement.

b) By means of the analytical expression derived by Curély for an infinite 2D square lattice composed of classical spins ($S = 5/2$), isotropically coupled, and based on the exchange Hamiltonian $H = -\Sigma_{nn} JS_iS_j$, where S_{nn} runs over all pairs of nearest-neighbor spins i and j (Heisenberg couplings)[16] [Equation (2)], where N is the Avogadro number, β the Bohr magneton, k the Boltzmann constant, and u is the well-known Langevin function defined as $u = L[JS(S+1)/kT] = \coth[JS(S+1)/kT] - kT/JS(S+1)$.

$$\chi = [Ng^2\beta^2 S(S+1)(1+u)^2]/[3kT(1-u)^2] \quad (2)$$

The best fit leads to $J = -0.21 \pm 0.01$ cm^{-1}; $g = 1.99 \pm 0.01$. The factor $R = \Sigma(\chi_m T_{obsd.} - \chi_m T_{calcd.})^2/\Sigma(\chi_m T_{calcd.})^2$ is 1.46×10^{-4}, which gives excellent agreement between experimental and theory.

The J values obtained by Line's or Curély expressions are very close: -0.24 cm^{-1} and -0.21 cm^{-1}, respectively. Taking into account that the Curély formula is more accurate and is valid up to 0 K (the Line's formula is only valid up to the maximum of χ_M, approximately), the value of -0.21 cm^{-1} seems to be the most precise for **2**.

Conclusion

As indicated in recent papers on manganese carboxylate, the most common feature for carboxylate bridges is the *syn-syn* mode.[17] The *syn-anti* bridge appears to be rather uncommon for Mn^{II} complexes, and only in a few cases have the magnetic properties been reported to date.[11,17,18] Corbella et al. have recently demonstrated that magnetic interactions through a *syn-anti*-carboxylate bridge in manganese complexes should be very sensitive to small structural changes: Mn−O distances, the O_{anti}−Mn−O_{syn} angle, the planarity of the bridge, etc.[19] A complete Table of this kind of complexes, including the magnetic data, has recently been gathered by Durot et al.[17] In general, *syn-anti* bridges induce very small antiferromagnetic J values because of the mismatch in the orientation of magnetic orbitals. All reported exchange coupling constants are reported to be between 0 cm^{-1} (no coupling) and -2 cm^{-1}.

Thus, although both complexes **1** and **2** have the same kind of bridging ligand; carboxylate in a distorted *syn-syn* conformation for **1** and a *syn-anti* conformation for **2**, the more antiferromagnetic J value in **1** can be ascribed to the smaller Mn−O distances (2.113 and 2.114 Å) in comparison with those found in **2** (2.154 and 2.164 Å). Moreover, in complex **2**, the simultaneous presence of hmt, as the bridging ligand that is further away, allows us to attribute the weak antiferromagnetic coupling only to the carboxylate bridging group. A contribution from the hmt ligand (if any) should be partial and very small.

Experimental Section

Materials: High-purity 1,3-bis(4-pyridyl)propane (bpp) and hexamethylenetetramine (hmt, also known as urotropine) were purchased from Aldrich Chemical Company Inc. and E. Merck (India) Ltd., respectively, and used as received. All the other chemicals were of A.R. grade.

Physical Measurements: Elemental analyses (carbon, hydrogen and nitrogen) were performed using a Perkin−Elmer elemental analyzer. IR spectra (4000−600 cm^{-1}) were taken in KBr pellets using a Jasco FT-IR (model 300E). The magnetic measurements were carried out on polycrystalline samples with a Quantum Design MPMS SQUID magnetometer (applied field 0.1 T) working in the temperature range 300−2 K. Diamagnetic corrections were estimated from Pascal's tables.[1b]

X-ray Structure Determination: Diffraction data of both structures were collected at room temperature with a Nonius DIP-1030H system equipped with a graphite monochromator and Mo-K_α radiation ($\lambda = 0.71073$ Å). A total of 30 frames were collected, each with an exposure time of 20 min with a rotation angle of 6° about φ, the detector being at 90 mm from the crystal. Cell refinement, indexing and scaling for both the data sets were carried out using Mosflm[20] and Scala.[20] The structures were solved by Patterson and Fourier analyses[21] and refined by the full-matrix least-squares method based on F^2 with all observed reflections.[21] Hydrogen atoms were located in idealized geometries. All the calculations were performed by means of the WinGX System, Ver. 1.64.05.[22] The crystal data and structure refinements are given in Table 2. CCDC-231735 (**1**) and -231736 (**2**) contain the supplementary crystallographic data for this paper. These data can be obtained free of charge at www.ccdc.cam.ac.uk/conts/retrieving.html [or from the Cambridge Crystallographic Data Centre, 12 Union Road, Cambridge CB2 1EZ, UK; Fax: (internat.) + 44-1223-336-033; E-mail: deposit@ccdc.cam.ac.uk].

Synthesis of [(*m*-phth)Mn(bpp)$_2$]·0.5H$_2$O (1): An aqueous solution (5 mL) of bpp = 1,3-bis(4-pyridyl)propane (2 mmol, 0.369 g) was added dropwise to an aqueous solution (5 mL) of $MnCl_2 \cdot 4H_2O$ (1 mmol, 0.197 g) with constant stirring for 5 min until the mixture became turbid. To this resulting mixture an aqueous solution (5 mL) of disodium *m*-phthalate (1 mmol, 0.210 g) was added dropwise yielding a transparent solution. The reaction mixture was refluxed for 1 h and filtered, the filtrate was kept in a $CaCl_2$ desiccator. After a few days, colorless crystals suitable for X-ray analysis

 © 2004 Wiley-VCH Verlag GmbH & Co. KGaA, Weinheim

Table 2. Crystal data and refinement details of complexes **1** and **2**

	1	**2**
Empirical formula	$C_{34}H_{33}MnN_4O_{4.50}$	$C_{12}H_{20}Mn_2N_4O_{10}$
Formula mass	624.58	490.20
T [K]	293(2)	293(2)
Crystal system	triclinic	orthorhombic
Space group	$P\bar{1}$	$Imm2$
a [Å]	9.444(2)	16.058(3)
b [Å]	10.226(3)	7.704(2)
c [Å]	16.511(3)	7.098(3)
α [°]	85.09(2)	90.00
β [°]	77.16(1)	90.00
γ [°]	80.08(1)	90.00
V [Å^3]	1529.6(6)	878.1(5)
Z	2	2
$D_{calcd.}$ [g cm^{-3}]	1.356	1.854
μ(Mo-K_α) [mm^{-1}]	0.478	1.502
F(000)	652	500
Reflections collected	10176	1522
Unique reflections/R(int)	6145 /0.0449	1443 /0.0433
Reflections observed [$I > 2\sigma(I)$]	4332	1400
No. parameters refined	403	79
$R1$	0.0514	0.0349
$wR2$	0.1338	0.0880
GoF	1.040	1.121
Residuals [e·Å^{-3}]	0.458, −0.456	0.466, −0.325

were obtained. Yield 0.437 g (70%). $C_{34}H_{33}MnN_4O_{4.5}$ (624.58): calcd. C 65.38, H 5.29, N 8.97; found C 65.65, H 5.22, N 8.91. IR: $\tilde{\nu}$ = 3429 (w, v br.), 3071 (w), 2925 (w), 1610 (vs), 1570 (s), 1543 (s), 1447 (m), 1390 (vs), 1222 (w), 1023 (w), 752 (m) 716 (w), 512 (vw) cm^{-1}.

Synthesis of [(mal)$_2$(Mn)$_2$(H$_2$O)$_2$(hmt)] (2): An aqueous solution (5 mL) of hmt (0.5 mmol, 0.070 g) was added dropwise, with constant stirring, to a methanolic solution (5 mL) of $MnCl_2{\cdot}4H_2O$ (1 mmol, 0.197 g). An aqueous solution (5 mL) of disodium malonate (1 mmol, 0.148 g) was added to this solution yielding a colorless compound. The single crystals suitable for X-ray analysis were obtained by allowing a methanolic solution (10 mL) of $MnCl_2{\cdot}4H_2O$ to diffuse into an aqueous layer of disodium malonate and hmt (1:1 mixture) (10 mL) in a tube. The colorless crystals were found at the junction of the two solutions after three weeks. Yield 0.147 g (60%). $C_{12}H_{20}Mn_2N_4O_{10}$ (490.20): calcd. C 29.38, H 4.08, N 11.42; found C 29.65, H 3.97, N 11.61. IR: $\tilde{\nu}$ = 3436−3239 (s, v br.), 2980 (w), 1572 (vs), 1445 (m), 1357 (s), 1225 (m), 1025 (w), 992 (s), 691 (m), 577 (w) cm^{-1}.

Supporting Information: A figure showing the 2D sheet of complex **1** (formed by hydrogen bonding between the lattice water and uncoordinated bpp nitrogen atoms of the adjacent chains) and a table containing the H bond parameters [Å, °] for **1** and **2** have also been deposited.

Acknowledgments

N. R. C. thanks the Council of Scientific and Industrial Research, New Delhi and J. R. thanks the Spanish Government (BQU2003/0791) for financial support.

[1] [1a] C. Oldham, *Comprehensive Coordination Chemistry* (Eds.: G. Wilkinson, R. D. Gillard, J. A. McCleverty), Pergamon Press, Oxford, U. K. **1987**, vol. 2, p. 435. [1b] O. Kahn, *Molecular Magnetism*; VCH, New York, **1993**. [1c] M. Eddaoudi, J. Kim, N. Rosi, D. Vodak, J. Wachter, M. O'Keeffe, O. M. Yaghi, *Science* **2002**, *295*, 469. [1d] M. D. Hollingsworth, *Science* **2002**, *295*, 2410. [1e] K. O. Kongshaug, H. Fjellvag, *Solid State Sci.* **2002**, *4*, 443. [1f] Y. Kim, D.-Y. Jung, *Inorg. Chem.* **2000**, *39*, 1470. [1g] R. Kuhlman, G. L. Schimek, J. W. Kolis, *Inorg. Chem.* **1999**, *38*, 194. [1h] S. S.-Y. Chui, S. M.-F. Lo, J. P. H. Charmant, A. G. Orpen, I. D. Williams, *Science* **1999**, *283*, 1148. [1i] D. M. L. Goodgame, D. A. Grachvogel, I. Hussain, A. J. P. White, D. J. Williams, *Inorg. Chem.* **1999**, *38*, 2057. [1j] Z. Y. Zhang, C. Brouca-Cabarrecq, C. Hemmert, F. Dahan, J. P. Tuchagues, *J. Chem. Soc., Dalton Trans.* **1995**, 1453. [1k] O. Horner, E. Anxolabe'he're-Mallart, M.-F. Charlot, L. Tchertanov, I.-J. Guilhem, T. A. Mattioli, A. Boussac, J. Girerd, *Inorg. Chem.* **1999**, *38*, 1222. [1l] N. Matsumoto, Y. Sunatsuki, H. Miyasaka, Y. Hashimoto, D. Luneau, J. P. Tuchagues, *Angew. Chem. Int. Ed.* **1999**, *38*, 171. [1m] M. W. Wemple, H.-L. Tsai, S. Wang, J. P. Claude, W. E. Streib, J. C. Huffman, D. N. Hendrickson, G. Christou, *Inorg. Chem.* **1996**, *35*, 6437. [1n] J. Cano, G. De Munno, J. L. Sanz, R. Ruiz, J. Faus, F. Lloret, M. Julve, A. Caneschi, *J. Chem. Soc., Dalton Trans.* **1997**, 1915. [1o] D. Dakternieks, A. Duthie, D. R. Smyth, C. P. D. Stapleton, E. R. T. Tiekink, *Organometallics* **2003**, *22*, 4599. [1p] W. Chen, J.-Y. Wang, C. Chen, Q. Yue, H.-M. Yuan, J.-S. Chen, S.-N. Wang, *Inorg. Chem.* **2003**, *42*, 944. [1q] H. Chun, D. Kim, D. N. Dybtsev, K. Kim, *Angew. Chem. Int. Ed.* **2004**, *43*, 971. [1r] X.-H. Bu, M.-L. Tong, H.-C. Chang, S. Kitagawa, S. R. Batten, *Angew. Chem. Int. Ed.* **2003**, *43*, 192.

[2] [2a] H.-L. Sun, B.-Q. Ma, S. Gao, G. Su, *Chem. Commun.* **2001**, 2586. [2b] F. Lloret, M. Julve, J. Cano, G. De Munno, *Mol. Cryst. Liq. Cryst.* **1999**, *334*, 569. [2c] J. L. Manson, A. M. Arif, J. S. Miller, *Chem. Commun.* **1999**, 1479. [2d] S. Noro, S. Kitagawa, M. Yamashita, T. Wada, *Chem. Commun.* **2002**, 222. [2e] Q.-D. Liu, J.-R. Li, S. Gao, B.-Q. Ma, H.-Z. Kou, L. Ouyang, R.-L. Huang, X.-X. Zhang, K.-B. Yu, *Eur. J. Inorg. Chem.* **2003**, *4*, 731. [2f] S. T. Xiang, F. X. Dao, X. T. Wen, S. Jie, *Polyhedron* **1997**, *16*, 689.

[3] [3a] T. M. Reineke, M. Eddaoudi, M. O. O'Keeffe, O. M. Yaghi, *Angew. Chem. Int. Ed.* **1999**, *38*, 2590. [3b] M. J. Zaworotko, *Angew. Chem. Int. Ed.* **2000**, *39*, 3052. [3c] S. R. Batten, B. F.

 © 2004 Wiley-VCH Verlag GmbH & Co. KGaA, Weinheim

Hoskins, R. Robson, *Chem. Eur. J.* **2000**, *6*, 156. [3d] M. Eddaoudi, H. Li, O. M. Yaghi, *J. Am. Chem. Soc.* **2000**, *122*, 1391.

[4] [4a] G. Christou, *Acc. Chem. Res.* **1989**, *22*, 328. [4b] K. Wieghardt, *Angew. Chem. Int. Ed. Engl.* **1989**, *28*, 1153. [4c] G. B. Conyers, G. Wu, M. J. Bessman, A. S. Mildvan, *Biochemistry* **2000**, *39*, 2347. [4d] M. C. J. Wilce, C. S. Bond, N. E. Dixon, H. C. Freeman, J. M. Guss, P. E. Lilley, J. A. Wilce, *Proc. Nat. Acad. Sci. U. S. A.* **1998**, *95*, 3472.

[5] [5a] P. S. Mukherjee, S. Dalai, G. Mostafa, E. Zangrando, T.-H. Lu, G. Rogez, T. Mallah, N. Ray Chaudhuri, *Chem. Commun.* **2001**, 1346. [5b] P. S. Mukherjee, T. K. Maji, G. Mostafa, J. Ribas, M. S. El Fallah, N. Ray Chaudhuri, *Inorg. Chem.* **2001**, *40*, 928. [5c] S. Dalai, P. S. Mukherjee, E. Zangrando, F. Lloret, N. Ray Chaudhuri, *J. Chem. Soc., Dalton Trans.* **2002**, 822. [5d] S. Sain, T. K. Maji, G. Mostafa, T.-H. Lu, N. Ray Chaudhuri, *New. J. Chem.* **2003**, *27*, 185.

[6] [6a] S. Konar, P. S. Mukherjee, E. Zangrando, F. Lloret, N. Ray Chaudhuri, *Angew. Chem. Int. Ed.* **2002**, *41*, 1561. [6b] S. Konar, M. Corbella, E. Zangrando, J. Ribas, N. Ray Chaudhuri, *Chem. Commun.* **2003**, 1424.

[7] [7a] S. Konar, E. Zangrando, M. G. B. Drew, J. Ribas, N. Ray Chaudhuri, *Dalton Trans.* **2004**, 260.

[8] S. Konar, P. S. Mukherjee, J. Ribas, M. G. B. Drew, N. Ray Chaudhuri, *Inorg. Chem.* **2003**, *42*, 2545.

[9] [9a] X. S. Tan, D. F. Xiang, W. X. Tang, K. B. Yu, *Polyhedron* **1997**, *16*, 1411. [9b] M. Hu, D. Xu, D. Cheng, *J. Coord. Chem.* **2002**, *55*, 11. [9c] M. Devereux, M. McCann, V. Leon, M. Geraghty, V. McKee, J. Wikaira, *Met.-Based Drugs* **2000**, *7*, 275.

[10] [10a] J. Nie, L. Liu, Y. Luo, D. Xu, *J. Coord. Chem.* **2001**, *53*, 365. [10b] X. S. Tan, J. Sun, D. F. Xiang, W. X. Tang, *Inorg. Chim. Acta* **1997**, *255*, 157.

[11] T. K. Maji, S. Sain, G. Mostafa, T.-H. Lu, J. Ribas, M. Monfort, N. Ray Chaudhuri, *Inorg. Chem.* **2003**, *42*, 709 and references cited therein.

[12] P. Lightfoot, A. Snedden, *J. Chem. Soc., Dalton Trans.* **1999**, 3549.

[13] T. Lis, J. Matuszewski, *Acta Crystallogr., Sect. B* **1979**, *35*, 2212.

[14] W. E. Hatfield, *The Theory and Applications of Molecular Paramagnetism* (Eds.: E. A. Boudreaux, L. N. Mulay), John Wiley and Sons, Inc., New York, **1976**, chapter 6.

[15] [15a] M. E. Lines, *J. Phys. Chem. Solids* **1970**, *31*, 101. [15b] A. Escuer, R. Vicente, M. A. S. Goher, F. A. Mautner, *J. Chem. Soc., Dalton Trans.* **1997**, 4431.

[16] [16a] J. Curély, *Europhys. Lett.* **1995**, *32*, 529. [16b] J. Curély, *Physica B* **1998**, *245*, 263. [16c] J. Curély, *Physica B* **1998**, *254*, 277. [16d] J. Curély, J. Rouch, *Physica B* **1998**, *254*, 298.

[17] S. Durot, C. Policar, G. Pelosi, F. Bisceglie, T. Mallah, J.-P. Mahy, *Inorg. Chem.* **2003**, *42*, 8072.

[18] [18a] C. Policar, F. Lambert, M. Cesario, I. Morgenstern-Badarau, *Eur. J. Inorg. Chem.* **1999**, 2201 and references cited therein. [18b] V. Tangoulis, G. Psomas, C. Dendrinou-Samara, C. P. Raptopolou, A. Terzis, D. P. Kessissoglou, *Inorg. Chem.* **1996**, *35*, 7655. [18c] X. M. Chen, Y. X. Tong, Z. T. Xu, T. C. W. Mak, *J. Chem. Soc., Dalton Trans.* **1995**, 4001. [18d] H. Oshio, E. Ino, I. Mogi, T. Ito, *Inorg. Chem.* **1993**, *32*, 5697. [18e] H. Adams, N. A. Bailey, N. Debaecker, D. E. Fenton, W. Kanda, J.-M. Latour, H. Okawa, H. Sakiyama, *Angew. Chem. Int. Ed. Eng.* **1995**, *34*, 2535. [18f] H. Iikura, T. Nagata, *Inorg. Chem.* **1998**, *37*, 4702.

[19] G. Fernández, M. Corbella, J. Mahía, M. A. Maestro, *Eur. J. Inorg. Chem.* **2002**, 2502.

[20] Collaborative Computational Project, Number 4, *Acta Crystallogr. Sect. D* **1994**, *50*, 760.

[21] G. M. Sheldrick, *SHELX97, Programs for Crystal Structure Analysis* (Release 97−2), University of Göttingen, Germany, **1998**.

[22] L. J. Farrugia, *J. Appl. Crystallogr.* **1999**, *32*, 837.

Received February 21, 2004
Early View Article
Published Online August 26, 2004

 © 2004 Wiley-VCH Verlag GmbH & Co. KGaA, Weinheim

Tetranuclear Copper(II) and Nickel(II) Complexes Incorporating a New Imidazole-Containing Ligand

Soumen Mukherjee,[a] Thomas Weyhermüller,[a] Eckhard Bill,[a] and Phalguni Chaudhuri*[a]

Keywords: Tetranuclear complexes / Imidazolate bridging / Copper / Nickel / Magnetic properties

The ligating properties of a new tridentate imidazole- and phenol-containing ligand H_3L towards nickel(II) and copper(II) ions have been studied. The ligand generates, in the presence of air and base, iminosemiquinone radical anions, which are not stable in the presence of the metal ions. The amine bond >C–NH– of the parent ligand becomes oxidized to >C=N– bonds upon coordination with Ni^{II} or Cu^{II}. The imidazole N atom becomes deprotonated and the resulting imidazolate group acts as a bridging ligand to generate tetranuclear complexes $[Cu^{II}{}_4L'_4]$ and $[Ni^{II}{}_4L'_4]$, where $[L']^{2-}$ is the dianionic new Schiff base formed after oxidation of the parent ligand. The square-planar tetranickel(II) complex is diamagnetic, as expected, whereas the four copper centres bridged by imidazolate anions in the complex $[Cu^{II}{}_4L'_4]$ are antiferromagnetically exchange coupled (J = –49 cm^{-1}), which has been supported by the EPR measurements. A simple magnetostructural correlation for the imidazolate-bridged copper(II) complexes is yet to emerge.
(© Wiley-VCH Verlag GmbH & Co. KGaA, 69451 Weinheim, Germany, 2004)

Introduction

Imidazole (ImH) occurs in proteins as part of the side chain of the amino acid histidine and constitutes all or part of the binding sites of various transition metal ions such as Ni^{2+}, Cu^{2+} or Zn^{2+} in a large number of metalloproteins.[1–4] Particularly, copper–imidazole interactions are widely known in biological systems. As for example, the conjugate base imidazolate ion (Im^-) is present as a bridging ligand between copper(II) and zinc(II) in superoxide dismutase,[5] which catalyses the disproportionation of the harmful superoxide radical anion.

In order to understand the unusual spectroscopic properties and the catalytic mechanisms of copper proteins, the development of relatively simple synthetic models of the active sites of copper proteins is of considerable interest. Since imidazole is present in many natural enzymes and proteins, we have been interested for some time in low molecular weight copper complexes with imidazole[6,7] and imidazolate-containing ligands which may serve as structural as well as spectroscopic models for the active site of copper proteins. As a continuation of this program, we report here a new tridentate ligand, 2,4-di-*tert*-butyl-6-[(5-methyl-3*H*-imidazol-4-ylmethyl)amino]phenol (H_3L) and its copper(II) and nickel(II) complexes.

This new ligand affords tetranuclear complexes, $[L'_4Ni^{II}_4]$ (**1**) and $[L'_4Cu^{II}_4(THF)_4]$ (**2**), where $[L']^{2-}$ is the dianionic Schiff-base form of the parent ligand H_3L after oxidation.

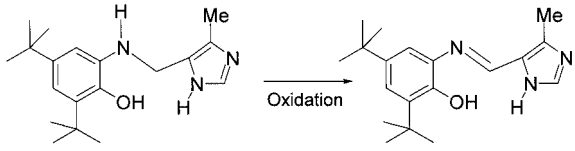

H_3L H_2L'

Complexes **1** and **2** have been characterised not only structurally but also by magnetic susceptibility measurements and EPR spectroscopy, in order to identify the exchange coupling for this tetracopper(II) complex **2** and hopefully to add a new brick to the construction of the correlation between structure and exchange coupling in imidazolate-bridged copper(II) complexes.

Results and Discussion

The ligand H_3L has been prepared in a two-step process involving first a Schiff-base condensation of 6-amino-2,4-di-*tert*-butylphenol with the appropriate 5-methyl-3*H*-imidazole-4-carbaldehyde and the subsequent reduction of the Schiff base by $NaBH_4$ in methanol. The ligand H_3L precipitates as a white solid in an aqueous medium. The ligand was fully characterised by ^1H, ^{13}C NMR, and IR spectroscopy, mass spectrometry and microanalysis together with its melting point determination (see Exp. Sect.). The IR bands due to ν(OH), ν(NH), ν(C–H of *tert*-butyl), ν(C=N), ν(C=C) and ν(C–O) are readily identified for the free H_3L which occur as strong peaks at ca. 3500, 3299, 2959, 1615, 1591 and 1233 cm^{-1}, respectively, and serve as a useful indication for complex formation. There is a distinct

[a] Max Planck Institute for Bioinorganic Chemistry, Stiftstraße 34–36, 45470 Mülheim an der Ruhr, E-mail: chaudh@mpi-muelheim.mpg.de

bathochromic shift typical for coordination of the deprotonated ligand to transition metal centres. The EI mass spectrometric molecular peak at m/z = 315 for H_3L is consistent with the elemental analysis.

A methanolic solution of the ligand, made basic by a few drops of triethylamine, is susceptible to aerial oxidation and forms a radical, presumably an iminosemiquinone, as evidenced by the EPR spectrum (Figure 1) at ambient temperature. A simulation of the spectrum yields the hyperfine coupling constants for the nitrogen atom and three protons to be a_N = 4.74 G, $a_{H(1)}$ = 9.30 G and $a_{H(2)}$ = 3.59 G. The simulated g value of 2.0049 clearly shows that the ligand is "noninnocent" and forms radicals in air. This ligand radical is not stable in the presence of a metal centre, which is shown by the X-ray crystal structures of **1** and **2**, confirming the ligand to be present in an iminophenolate form after complexation. The imine >C=N− character of the coordinated ligand $[L']^{2-}$ is also exhibited in the solid-state IR spectra for **1** and **2**; a sharp strong band appears at 1600 cm^{-1} for **1** and 1595cm^{-1} for **2**.

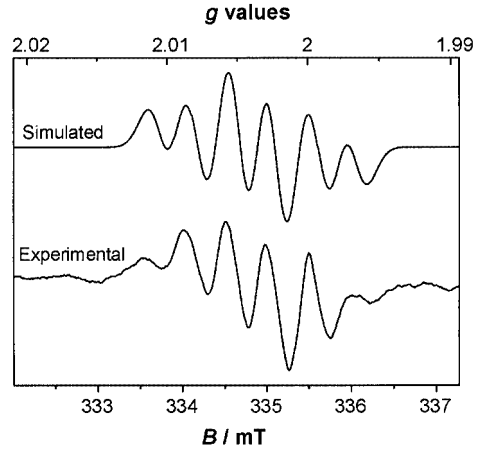

Figure 1. EPR spectrum of the ligand H_3L at room temperature in the presence of triethylamine in methanol

Mass spectrometry in the ESI positive mode (in CH_2Cl_2) is not very helpful in identifying the nuclearity of the nickel(II) complex **1**. The peak at m/z (%) = 683.4 (100) corresponds to the mononuclear species NiL'_2. But for **2**, the Cu^{II} complex, peaks at m/z = 374, 748, 1124 and 1496 with respective isotope distribution clearly show the tetranuclear nature of the copper complex.

Complex **1**, a tetrameric square-planar nickel(II) complex, is diamagnetic as expected, as is evidenced from the magnetic susceptibility as well as the ^1H NMR spectrum. In the ^1H NMR spectrum, the ratio of protons *tert*-butyl/*tert*-butyl/methyl/imine/aromatic/imidazole is 9:9:3:1:2:1, which is to be expected from the oxidized deprotonated ligand (see Exp. Sect.).

Molecular Structure of $[L'_4Ni_4]\cdot 9CH_2Cl_2$ (1)

From a dichloromethane/methanol (1:1) solvent mixture orange red X-ray quality crystals of **1** were obtained and they were subjected to diffractometric studies. The molecule consists of a neutral tetranuclear nickel complex along with 9 CH_2Cl_2 solvent molecules. The neutral molecule with its atom-labelling scheme is shown in Figure 2. Selected bond lengths and angles are listed in Table 1. Each of the nickel centres is in a distorted square-planar geometry with N_2O coordination from the deprotonated ligand and the fourth donor atom being the nitrogen atom of the imidazolate ring originating from the adjacent NiN_2O unit. Worth noting is the short C(8)−N(7) distance of 1.297(11) Å with a >C=N− character indicating oxidation of the >CH_2−NH− bond of the ancillary ligand H_3L. The average Ni−O (phenol), Ni−N (imine), Ni−N (imidazole) and Ni−N (adjacent imidazole) bond lengths of 1.856, 1.850, 1.891 and 1.850 Å, respectively, are similar to those in other square-planar Ni^{II} complexes.[8] The four nickel centres are arranged in the form of a "butterfly" with the Ni(1)−Ni(1A)−Ni(1B) and Ni(1C)−Ni(1A)−Ni(1B) planes forming the "wings" of the butterfly (see b in Figure 2).[9] The dihedral angle between these two planes is 107.7°. All the adjacent Ni···Ni distances are equal with a value of 5.851 Å.

Molecular Structure of $[L'_4Cu_4(THF)_4]$ (2)

Although the analytical data unambiguously show the presence of a CuL′ core as the smallest unit in **2**, the magnetic susceptibility data exhibit a strong temperature dependence with effective moments as 1.52 μ_B at 290 K and 0.09 μB at 2 K, refuting the mononuclear formulation. Hence, an X-ray analysis was undertaken to remove the doubts regarding connectivity. Unfortunately, crystals of **2** obtained from a THF/methanol mixture diffract X-rays very weakly.[10] In spite of the high R factor and large standard deviations due to the severity of the disorder and weakness of the data collected from a poorly diffracting small crystal, the crystal structure analysis of **2** confirmed its tetranuclear nature. Because of its unacceptable quality, we are unable to publish the crystal data in detail. It is not clear how many THF molecules are present in the unit cell. The structure consists of distinct $[L'_4Cu_4(THF)_4]$ molecules (Figure 3).

Selected interatomic distances and angles are given in Table 2. As observed in **1**, oxidation of the ligand occurs at the same position [C(8)−N(7) = 1.31 Å]. The structure consists of a distorted square-pyramidal tetranuclear neutral molecule with the Cu centres forming a "butterfly structure" (Figure 3). A THF molecule occupies the fifth position of the coordination site in each copper centre. The dihedral angle between the plane defined by connecting Cu(1)−Cu(2)−Cu(4) and Cu(3)−Cu(2)−Cu(4) is 150.1°. The average Cu−O (phenol), Cu−N (imine), Cu−N (imidazolate) and Cu−N (imidazolate of adjacent ligand) bond lengths are 1.942 Å, 1.942 Å, 1.992 Å and 1.948 Å, respectively, which are similar to other square-planar/pyramidal Cu^{II} complexes.[6,7,11] It is observed that the Cu(1)−N(10) bond is more elongated than it is for the other coordinating atoms. This tendency is the same for the other copper centres and is due to a Jahn−Teller effect which is present for d^9 systems thus making **2** less symmetric than **1**, a d^8

 © 2004 Wiley-VCH Verlag GmbH & Co. KGaA, Weinheim

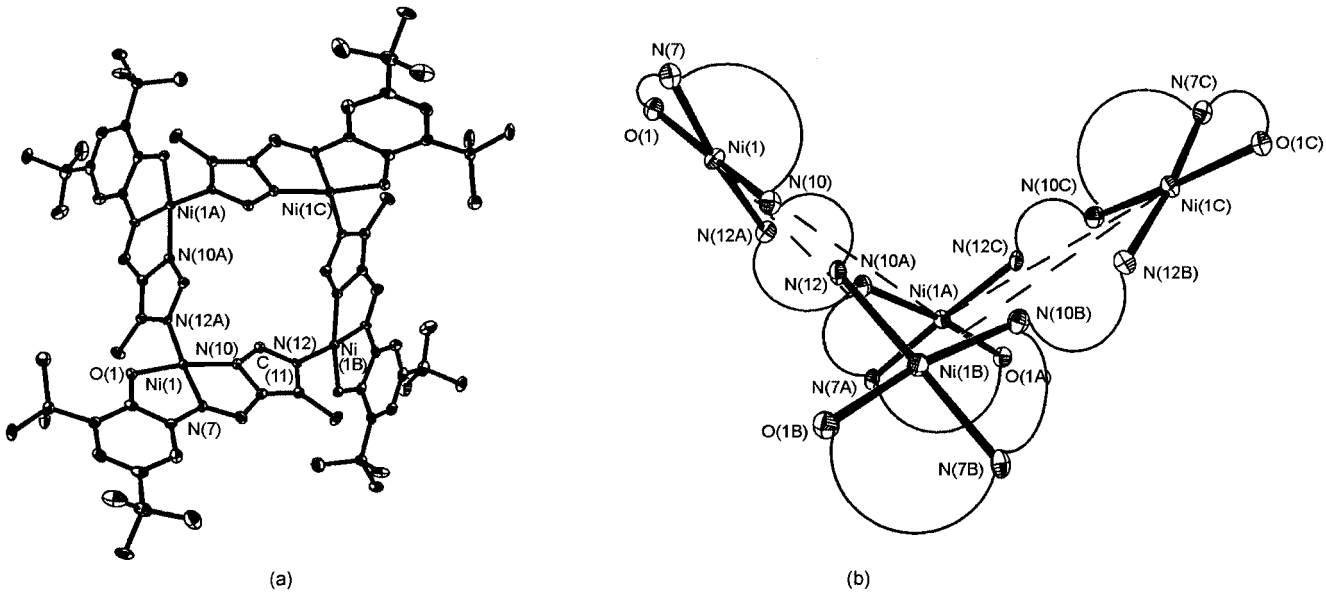

Figure 2.(a) ORTEP diagram of $[Ni_4L'_4]$ **1**; (b) view of **1** highlighting the butterfly nature of the four nickel centres; the ligand is denoted only by the donor atoms joined by the curved lines

Table 1. Selected bond lengths [Å] and angles [°] for **1**

Ni(1)−N(7)	1.850(7)	C(4)−C(5)	1.405(12)
Ni(1)−N(12A)	1.891(6)	C(5)−C(6)	1.405(11)
Ni(1)−N(10)	1.885(7)	C(1)−C(6)	1.407(12)
Ni(1)−O(1)	1.856(5)	C(9)−N(10)	1.381(10)
C(1)−O(1)	1.355(9)	N(12)−C(11)	1.332(11)
C(6)−N(7)	1.391(10)	C(13)−N(12)	1.362(10)
N(7)−C(8)	1.297(11)	C(11)−N(10)	1.297(11)
C(1)−C(2)	1.396(11)	C(8)−C(9)	1.447(11)
C(2)−C(3)	1.411(12)	C(9)−C(13)	1.370(11)
C(3)−C(4)	1.368(13)	C(13)−C(14)	1.489(11)
Ni(1A)−Ni(1)−Ni(1B)	77.8		
O(1)−Ni(1)−N(7)	86.5(3)	N(12A)−Ni(1)−N(10)	94.1(3)
N(7)−Ni(1)−N(10)	84.0(3)	N(12A)−Ni(1)−O(1)	95.6(3)
N(7)−Ni(1)−N(12A)	174.6(3)	N(10)−Ni(1)−O(1)	170.2(3)
C(1)−O(1)−Ni(1)	111.8(5)	Ni(1)−N(10)−C(9)	112.4(5)
C(8)−N(7)−C(6)	129.8(7)	C(11)−N(12A)−Ni(1)	123.8(5)
Ni(1)−N(10)−C(11)	142.8(6)	C(13)−N(12A)−Ni(1)	130.5(5)
C(8)−N(7)−Ni(1)	117.3(6)	C(6)−N(7)−Ni(1)	112.8(5)
Ni(1)···Ni(1A)	5.851		
Ni(1A)···Ni(1B)	7.351		

system; Cu(1) is displaced by 0.11 Å from the mean basal plane of the three nitrogen atoms [N(7), N(10), N(42)] and one oxygen atom [O(1)]. The dihedral angles between the plane N(42)O(1)N(7)N(10) containing the Cu(1) ion and the planes N(42)C(43)C(39)N(40)C(41) and N(10)-C(9)C(13)N(12)C(11) describing the two imidazolate bridging groups are 47.2° and 82.2°, respectively. It is interesting to note that the angle between the Cu(1)−N_{im}(42) and Cu(2)−N_{im}(40) vectors is 142.2° and that between the Cu(1)−N_{im}(10) and Cu(4)−N_{im}(12) vectors is 132.6°. The angle between the planes defined by Cu(1)O(1)N(7)N-(10)N(42) and Cu(2)O(31)N(37)N(40)N(72) is 139.1°.

Magnetochemistry and EPR Studies with 2

The magnetic susceptibility data for a polycrystalline sample of **2** was measured from 2 to 290 K in an applied magnetic field of 1 T to characterise the nature and magnitude of the exchange interaction propagated by the bridging ligands. The Heisenberg spin Hamiltonian used was in the form $\hat{H} = -2J \sum_{ij} \vec{S}_i \cdot \vec{S}_j$ for an isotropic exchange coupling. The experimental magnetic data were simulated using a least-squares fitting computer program[12] with a full-matrix diagonalisation of exchange coupling, Zeeman splitting,

 © 2004 Wiley-VCH Verlag GmbH & Co. KGaA, Weinheim

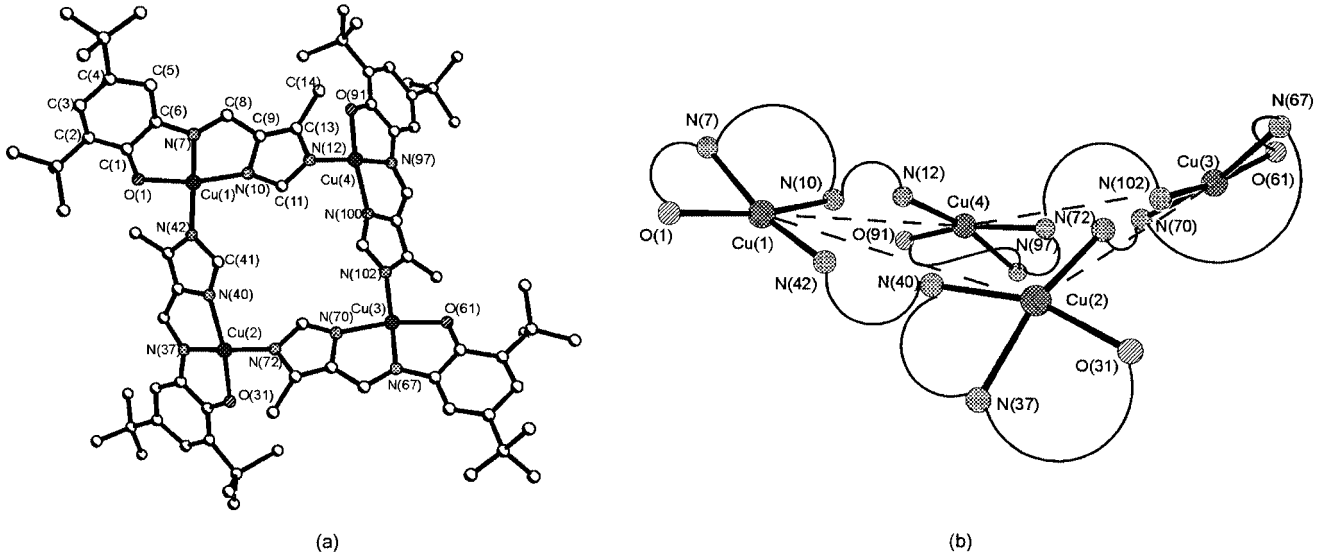

Figure 3.(a) Molecular structure of $[Cu_4L'_4]$ **2**; (b) view of **2** highlighting the butterfly dispositions of the copper centres

Table 2. Selected bond lengths [Å] and angles [°] for **2**

Cu(1)−N(7)	1.913(17)	Cu(2)−N(37)	1.964(16)
Cu(1)−N(42)	1.925(17)	Cu(2)−N(72)	1.957(16)
Cu(1)−N(10)	1.952(16)	Cu(2)−N(40)	2.020(16)
Cu(1)−O(1)	1.955(12)	Cu(2)−O(31)	1.965(13)
C(1)−O(1)	1.316(25)	C(9)−N(10)	1.462
C(6)−N(7)	1.420	N(12)−C(11)	1.347
N(7)−C(8)	1.310	C(13)−N(12)	1.408
C(1)−C(2)	1.422	C(11)−N(10)	1.381
C(2)−C(3)	1.399	C(8)−C(9)	1.461
C(3)−C(4)	1.365	C(9)−C(13)	1.341
C(4)−C(5)	1.399	C(13)−C(14)	1.525
C(5)−C(6)	1.409		
C(1)−C(6)	1.377		
Cu(1)−Cu(2)−Cu(3)	89.8	Cu(3)−Cu(4)−Cu(1)	89.8
Cu(2)−Cu(3)−Cu(4)	86.3	Cu(4)−Cu(1)−Cu(2)	85.9
O(1)−Cu(1)−N(7)	82.6	O(31)−Cu(2)−N(37)	81.6
N(7)−Cu(1)−N(10)	83.4	N(37)−Cu(2)−N(40)	81.7
N(7)−Cu(1)−N(42)	164.7	N(37)−Cu(2)−N(72)	163.2
N(42)−Cu(1)−N(10)	99.5	N(72)−Cu(2)−O(31)	93.8
N(42)−Cu(1)−O(1)	94.2	N(72)−Cu(2)−N(40)	100.9
N(10)−Cu(1)−O(1)	166.0	N(40)−Cu(2)−N(31)	162.7
Cu(1)−N(10)−C(11)	146.14(16)	Cu(2)−N(40)−C(41)	142.8(17)
Cu(1)−N(42)−C(41)	123.59(16)	Cu(4)−N(12)−C(11)	123.89(16)
Cu(1)···Cu(2)	6.054	Cu(3)···Cu(4)	6.034
Cu(1)···Cu(4)	6.044	Cu(1)···Cu(3)	8.524
Cu(2)···Cu(3)	6.019	Cu(2)···Cu(4)	8.245

and axial single-ion zero-field interactions $D\vec{S}_z^{\,2}$, if necessary. The susceptibility data were corrected for diamagnetism (Pascal corrections), temperature-independent paramagnetism (TIP) and the presence of paramagnetic monomer impurities (P) in the following way: $\chi_{calcd.} = (1 - P)\chi + \chi_{TIP} + P\chi_{mono}$.

The nature of the μ_{eff} vs. T plot for **2** (Figure 4) shows a behaviour typical for antiferromagnetic spin coupling. The effective moment μ_{eff} decreases monotonically with the decrease in temperature; the values of μ_{eff} are 3.051 μ_B at 290 K and 0.180 μ_B at 2 K. The magnetic data reveal an energetically well-isolated ground state of total spin $S_t = 0$, discernible from the decline of effective moments at temperatures below 100 K. The residual moment of 0.180 μ_B at 2 K is attributed to a monomeric ($S = 1/2$) impurity (2.0%). Monomeric species were also detected in weak abundance in the EPR spectra, as will be mentioned later. The susceptibility data could be simulated considering exchange coupling between adjacent Cu^{II} pairs with local spins ($S = 1/2$), as shown in the inset in Figure 4. The multiplets $|S_A S_B S_t>$ are labelled by the "pair spins", S_A ($\vec{S}_A = \vec{S}_1 + \vec{S}_3$) and S_B ($\vec{S}_B = \vec{S}_2 + \vec{S}_4$). The ground state is a singlet $|S_A S_B S_t> = |110>$ and the first excited state at energy $2J$ is a triplet $|111>$ (Figure 4). The states $|011>$, $|000>$ and $|101>$ are degenerate at energy $4J$ and the highest state at energy $6J$ is a quintuplet $|112>$. In zero field the multiplets remain degenerate in energy with pure magnetic quantum numbers,

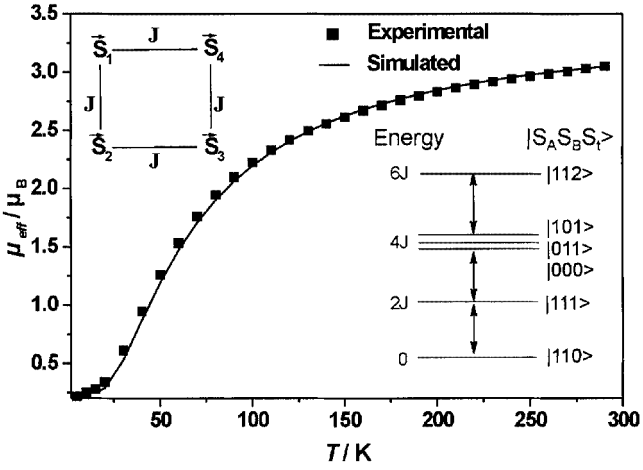

Figure 4. Plot of μ_{eff} vs. T for **2**; the solid line represents the simulated curve; insets: model used to simulate the spin coupling in **2** and corresponding spin states resulting from the spin Hamiltonian used (see text)

 © 2004 Wiley-VCH Verlag GmbH & Co. KGaA, Weinheim

according to their multiplicity. Projections of local spins S_i on the total spin S_t ($\vec{S}_t = \vec{S}_A + \vec{S}_B$)[13] reveal identical g_t values for all multiplets $S_t \neq 0$. The simulation of the experimental susceptibility data for the tetramer yielded an exchange coupling constant $J = -49$ cm^{-1}, $g = 2.022$, a paramagnetic impurity (P: $S = {}^1/_2$) of 2% and a temperature-independent paramagnetism (TIP) of 240×10^{-3} emu.

X-band EPR spectra for **2** in the solid state from 11.7 K to 62.1 K are dominated by a strong almost isotropic signal at $g = 2.08$ which shows the usual Curie behaviour, $I \sim 1/T$, for the given temperature range. Therefore, the strong derivative signal at $g \approx 2$ is attributed to the monomeric paramagnetic impurity (2%) present in the solid-state susceptibility measurements. In addition to the prominent line there are a number of weak signals in the measured field range extending from 50 to 600 mT. Their appearance is typical of integer spin manifolds arising for the exchange-coupled Cu^{II} tetramer, because competing Zeeman and zero-field splitting are expected due to dipolar coupling and anisotropic exchange. As a consequence, the resonances are widely spread over a large field range and the derivative signals appear to be weak (not the intensity). On increasing the temperature, changes in the relative intensities of these features are observed between 150 and 260 mT and between 380 and 600 mT (Figure 5), which is typical of integer spin signals from excited spin multiplets.

In order to elucidate the correlation between the EPR spectra and the spin multiplets of the coupled system, the change of intensity (I) of the derivative peak at 480 mT was scanned over the entire temperature (T) range. As the population of the excited state in the first order is dependent on the Boltzmann function of resonating levels, the product intensity·temperature, $I \cdot T$, was plotted versus temperature (Figure 5b). The fading below 10 K and the strong rise at elevated temperatures prove that the signals arise from excited states and that the ground state is diamagnetic and EPR-silent, in accordance with the susceptibility findings. For quantitative analysis, the experimental data were compared with the theoretical Boltzmann functions derived from the spin-coupling model (Figure 4). It is to be noted that values up to 40 K were taken as line broadening, which occurs above this temperature. The best agreement was obtained for $I_{111}T$, describing the thermal population of the first excited triplet state $|111>$, $I_{111}\ T \approx [\exp(2J/kT)]/Z$, where $Z = 1 + 3\exp(2J/kT) + 7\exp(6J/kT) + 5\exp(12J/kT)$. The solid line is a fit with $J = -42$ cm^{-1}, which is close to the exchange coupling constant of $J = -49$ cm^{-1} evaluated from the susceptibility measurements. Therefore, particular non-Kramers resonance at $B = 480$ mT, and probably the whole complex EPR spectrum in the field range 380−600 mT appears to arise from the first excited triplet state $|111>$ of the tetramer.

In an imidazolate-bridged system, there can be two pathways used to explain the magnetic interaction, viz. the σ- and the π-exchange pathways. Generally, it is agreed that the π orbitals are not involved in the coupling.[7,14] It has been stated that, since the magnetic orbitals are σ-antibonding for square-planar and square-pyramidal complexes, the relevant exchange pathway through the imidazolate bridge is of the σ-type. The imidazolate orbitals responsible for this sort of interaction are essentially parallel to the N−N′ (or C−C) direction.[7,11c]

Several studies have already been reported,[7,11c] in which structural data have been used to find correlations between structure and exchange coupling in imidazolate-bridged copper(II) complexes. Comparison of the numerical data shows that a simple magnetostructural correlation for imidazolate-bridged Cu complexes does not exist. However, as the values of J are independent of θ, the angle between the copper and imidazole coordination planes, a π-exchange pathway can be discarded. It has been concluded from EHMO calculations[11c] that the extent of anti-ferromagnetic coupling will increase when the N−N and other Cu−N bonds are parallel to the imidazolate carbon−carbon bond, thus favoring a σ-exchange pathway. Although the coupling constant for **2** is strong compared with the other complexes, the values of J cannot be strictly attributed to the values of α, the angle between the Cu−N and N−N vectors. This indicates that σ-superexchange cannot be the only mechanism for the exchange coupling for

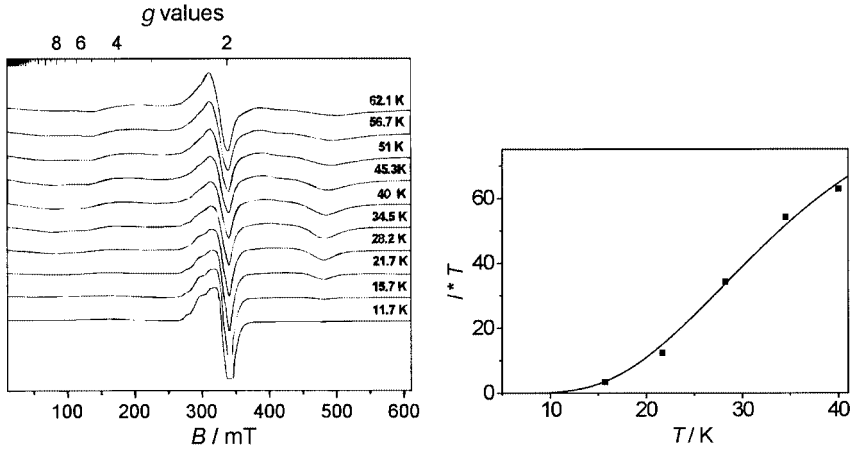

Figure 5. (a) EPR spectra of a powdered sample of **2** recorded as a function of temperature; (b) temperature dependence of the temperature-weighted intensity ($I \cdot T$) of the EPR subspectra; the solid line is the calculated Boltzmann function $I_{111} \cdot T$ with $J = -42$ cm^{-1}

 © 2004 Wiley-VCH Verlag GmbH & Co. KGaA, Weinheim

this compound. The presence of ligand−ligand interactions may also play a part in this type of exchange coupling. Recently, a theoretical DFT study[15] on the magneto-structural correlation in imidazolate-bridged dicopper(II) complexes showed that the exchange coupling constant *J* mainly depends on the Cu−*N*−C(Im) bond angle and is insensitive to the variation of the Cu−N(Im) distance and the dihedral angle between the bridged imidazolate ring and copper coordination planes.

Concluding Remarks

The ligating properties of a new tridentate ligand, 2,4-di-*tert*-butyl-6-[(5-methyl-3*H*-imidazol-4-ylmethyl)amino]-phenol containing an imidazole N-donor atom together with a phenol O-donor and amine N-donors towards the nickel(II) and copper(II) centers are described. The imidazole N atom becomes deprotonated and the resulting imidazolate group serves as a bridging ligand to generate tetranuclear complexes of the said metal centres. Although the ligand generates the iminosemiquinone monoanion radical very easily in the presence of a base and air, as evidenced by EPR spectroscopy, the radical form could not be stabilized in the presence of the metal centres. The C−NH bonds from the parent ligand have been oxidized to C=N bonds upon coordination with the Ni^{II} or Cu^{II} centres. The realization that the present phenol as well as imidazole-containing ligand can generate polynuclear complexes highlights the prospect of designing a generic ligand system, which should form polynuclear species with other metal centres.

The imidazolate-bridged copper(II) complexes are, as expected, antiferromagnetically exchange-coupled yielding diamagnetic ground states. No simple magneto-structural correlation has yet emerged for these imidazolate-bridged complexes. The synthesis of more of these imidazolate-bridged copper(II) complexes would therefore be warranted in order to resolve this complex problem of magnetostructural correlation.

Experimental Section

Materials and Physical Measurements: Commercial grade chemicals were used for synthetic purposes, and solvents were distilled and dried before use. Fourier transform IR spectroscopy on KBr pellets was performed with a Perkin−Elmer 2000 FT-IR instrument. Mass spectra were recorded either in the EI or the ESI (in CH_2Cl_2) modes with a Finnigan MAT95 or 8200 spectrometer. Magnetic susceptibilities of the polycrystalline samples were recorded with a SQUID magnetometer (MPMS, Quantum Design) in the 2−290 K temperature range with an applied field of 1 T. Diamagnetic contributions were estimated for each compound by the use of Pascal's constants. ^1H and ^{13}C NMR spectra were recorded using a Bruker ARX 250, or DRX 400 spectrometer. The spectra are referenced to TMS, using the ^{13}C or residual ^1H signals of the deuterated solvents as internal standards. X-band EPR spectra were recorded with a Bruker ESP 300E spectrometer equipped with a helium flow cryostat (Oxford Instruments ESR 910), an NMR field probe (Bruker 035M) and a microwave frequency counter HP 5352B.

X-ray Crystallographic Data Collection and Refinement of the Structures: A single crystal of **1** was coated with perfluoropolyether, picked up with glass fibres, and mounted on a Nonius Kappa-CCD diffractometer equipped with a cryogenic nitrogen cold stream operating at 100(2) K. Graphite-monochromated Mo-K_α radiation (λ = 0.71073 Å) was used. Intensity data were corrected for Lorentz and polarisation effects. The intensity data set of **1** was corrected for absorption with the program SADABS[16] The Siemens SHELXTL software package[17] was used for solution, refinement, and artwork of the structure, and neutral atom scattering factors of the program were used. All structures were solved and refined by direct methods and difference Fourier techniques. Non-hydrogen atoms were refined anisotropically, and hydrogen atoms were placed at calculated positions and refined as riding atoms with isotropic displacement parameters. Details of data collection and structure refinements are summarized in Table 3. CCDC-236872 contains the supplementary crystallographic data for this paper. These data can be obtained free of charge at www.ccdc.cam.ac.uk/conts/retrieving.html [or from the Cambridge Crystallographic Data Centre, 12 Union Road, Cambridge CB2 1EZ, UK; Fax: + 44-1223-336-033; E-mail: deposit@ccdc.cam.ac.uk].

Table 3. Crystal data and structure refinement for **1**, $[Ni_4L'_4]\cdot 9CH_2Cl_2$

	1
Empirical formula	$C_{76}H_{100}N_{12}Ni_4O_4\cdot 9CH_2Cl_2$
Formula mass	2244.85
Temperature [K]	100(2)
Wavelength [Å]	0.71073
Crystal system	tetragonal
Space group	$P\bar{4}2_1/c$ (No. 114)
Unit cell dimensions [Å]	a = 20.74(3)
	c = 12.1538(10)
Volume [Å^3]; Z	5227.9(12); 2
Density (calcd.) [Mg/m^3]	1.426
Absorp. coeff. [mm^{-1}]	1.220
F(000)	2324
θ range for data collection [°]	1.94−25.00
Index ranges	$-31 \le h \le 32$
	$-10 \le k \le 31$
	$-18 \le l \le 17$
Reflections collected	39793
Independent reflections	4608
Absorption correction	SADABS
Data/restraints/parameters	4591/16/289
Goodness-of-fit on F^2	1.048
Final R int [$I > 2\sigma(I)$]	$R1$ = 0.0786, $wR2$ = 0.2180
R int (all data)	$R1$ = 0.0982, $wR2$ = 0.2366

Ligand Synthesis

2,4-Di-*tert*-butyl-6-[(5-methyl-3*H*-imidazol-4-ylmethyl)amino]-phenol (H_3L): 2-Amino-4,6-di-*tert*-butylphenol (2.2 g, 10 mmol) and 5-methyl-3*H*-imidazole-4-carbaldehyde (1.1 g, 10 mmol) were added to deaerated methanol (50 mL) and the resulting solution was refluxed under argon for 2 h. The red solution was cooled and $NaBH_4$ was added portionwise until the solution turned a faint yellow. The precipitation of a white solid was initiated by dropwise addition of water. The white solid was collected by filtration and dried under vacuum. Yield: 2.8 g (89%). M.p. 186 °C. $C_{19}H_{29}N_3O$ (315.5): calcd. C 72.34, H 9.27, N 12.84; found C 71.0, H 9.2, N

 © 2004 Wiley-VCH Verlag GmbH & Co. KGaA, Weinheim

12.8. ^{1}H NMR ([D$_6$]DMSO): δ = 1.21 (s, 9 H), 1.31 (s, 9 H), 2.15 (s, 3 H), 4.02 (s, 2 H), 6.5 (t, 2 H), 7.4 (s, 1 H) ppm. ^{13}C NMR ([D$_6$]DMSO): δ = 30.0 (s), 34.1 (s), 34.5 (s), 48.6 (s), 107.5 (s), 111.1 (s), 133.2 (s), 136.3 (s), 140.3 (s), 141.9 (s) ppm. IR (KBr): $\tilde{\nu}$ = 3299 s, 2959 s, 1615 s, 1591 s, 1233 s cm^{-1}. EI-MS: *m*/*z* = 315 [M$^+$].

Complex 1 [Ni$_4$L′$_4$]: The ligand H_3L (1 mmol, 0.315 g) was dissolved in 25 mL of deaerated methanol. Solid $Ni(ClO_4)_2 \cdot 6H_2O$ (1 mmol, 0.365 g) along with NEt_3 (0.15 mL) were added to the ligand solution. The resulting orange-red solution was refluxed under argon for 1 h and then stirred in air for 0.5 h, whereupon a microcrystalline orange-red solid precipitated. The solid was filtered, dried in air. Yield: 0.21 g (58%). $C_{76}H_{100}N_{12}Ni_4O_4$ (1480.5): calcd. C 61.66, H 6.81, N 11.35, Ni 1586; found C 58.8, H 5.8, N 10.7, Ni 15.5. IR (KBr): $\tilde{\nu}$ = 2952, 1600, 1474, 1399, 1253, 1130, 861 cm^{-1}. X-ray quality crystals for **1** $[Ni_4L_4] \cdot 9CH_2Cl_2$ were obtained from a mixture of dichloromethane/methanol (1:1).

Complex 2 [Cu$_4$L′$_4$]: The ligand H_3L was dissolved in 15 mL of methanol. Solid $Cu(CH_3COO)_2 \cdot 4H_2O$ (0.5 mmol, 0.10 g) was added to the ligand solution, and the whole solution was made basic by adding NEt_3 (0.15 mL). The resulting light orange-red solution was refluxed for 1 h and then cooled to room temperature, whereupon a red-orange microcrystalline solid precipitated. The microcrystalline solid separated by filtration was recrystallised from a tetrahydrofuran/methanol solvent mixture. Yield: 0.120 g (64%). $C_{76}H_{100}Cu_4N_{12}O_4$ (1499.9): calcd. C 60.86, H 6.72, Cu 16.95, N 11.21; found C 59.8, H 6.6, Cu 17.3, N 11.1. IR (KBr): $\tilde{\nu}$ = 2951, 1595, 1470, 1398, 1257, 1126, 857, 647 cm^{-1}.

Acknowledgments

Financial support from the DFG (Priority Program Ch111/2-2) is gratefully acknowledged. Thanks go to Mrs. H. Schucht and Mr. A. Göbels for skilful technical assistance.

[1] T. E. Creighton, in *Proteins, Structures and Molecular Properties* (Ed.: W. H. Freeman), New York, **1984**.
[2] H. C. Freeman, in *Inorganic Biochemistry* (Ed.: G. L. Eichhorn), Elsevier, New York **1973**, chapter 4.
[3] R. J. Sundberg, R. B. Martin, *Chem. Rev.* **1974**, *74*, 471.
[4] "Bioinorganic Chemistry − State of the Art", *J. Chem. Educ.* **1985**, *62*, 917−1001.
[5] J. S. Richardson, K. A. Thomas, B. H. Rubin, D. C. Richardson, *Proc. Natl. Acad. Sci. U. S. A.* **1975**, *72*, 1349.
[6] P. Chaudhuri, I. Karpenstein, M. Winter, C. Butzlaff, E. Bill, A. X. Trautwein, U. Flörke, H.-J. Haupt, *J. Chem. Soc., Chem. Commun.* **1992**, 321.
[7] P. Chaudhuri, I. Karpenstein, M. Winter, M. Lengen, C. Butzlaff, E. Bill, A. X. Trautwein, U. Flörke, H.-J. Haupt, *Inorg. Chem.* **1993**, *32*, 888 and references cited therein.
[8] For example: D. J. White, N. Laing, H. Miller, S. Parsons, S. Coles, P. A. Tasker, *Chem. Commun.* **1999**, 2077.
[9] V. V. Pavlishchuk, S. V. Kolotilov, A. W. Addison, M. J. Prushan, D. Schollmeyer, L. K. Thomspon, E. A. Goreshnik, *Angew. Chem. Int. Ed.* **2001**, *40*, 4734.
[10] $[C_{76}H_{100}N_{12}Cu_4\ (C_4H_8O)_4] \cdot x$THF, monoclinic, space group $P2_1/c$, a = 24.916(5) Å, b = 17.296(4) Å, c = 33.004(7) Å, β = 91.72°, V = 14216 Å^3, Z = 4, T = 100(2) K, final R = 0.151 for 10569 independent reflections.
[11] Selected references: [11a] G. Ivarsson, B. K. S. Lundberg, N. Ingri, *Acta Chem. Scand.* **1972**, *26*, 3005. [11b] Kolks, S. J. Lippard, J. V. Waszczak, H. R. Lilienthal, *J. Am. Chem. Soc.* **1982**, *104*, 717. [11c] A. Bencini, C. Benelli, D. Gatteschi, C. Zanchini, *Inorg. Chem.* **1986**, *25*, 398. [11d] C. A. Salata, M. T. Youinou, C. J. Burrows, *Inorg. Chem.* **1991**, *30*, 3454. [11e] H. Nie, S. M. J. Aubin, M. S. Mashuta, R. A. Porter, J. F. Richardson, D. N. Hendrickson, R. M. Buchanan, *Inorg. Chem.* **1996**, *35*, 3325. [11f] G. Tabbi, W. L. Driessen, J. Reedijk, R. P. Bonomo, N. Veldman, A. J. Spek, *Inorg. Chem.* **1997**, *36*, 1168. [11g] N. Matsumoto, Y. Motoda, T. Matsuo, T. Nakashima, N. Re, F. Dahan, J.-P. Tuchagues, *Inorg. Chem.* **1999**, *38*, 1165. [11h] E. Colacio, M. Ghazi, R. Kivekäs, M. Klinga, F. Lloret, J. M. Moreno, *Inorg. Chem.* **2000**, *39*, 2770.
[12] V. Staemmler, F. Birkelbach, C. Krebs, unpublished, Bochum, Germany, **1997**.
[13] A. Bencini, D. Gatteschi, *Electron Paramagnetic Resonance of Exchange Coupled Systems*, Springer-Verlag, Berlin **1990**.
[14] [14a] D. N. Hendrickson, M. S. Haddad, *Inorg. Chem.* **1978**, *17*, 2622. [14b] M. S. Haddad, E. N. Duester, D. N. Hendrickson, *Inorg. Chem.* **1979**, *18*, 141. [14c] C. Benelli, R. K. Bunting, D. Gatteschi, C. Zanchini, *Inorg. Chem.* **1984**, *23*, 3074.
[15] Y.-M. Sun, C.-B. Liu, X.-J. Lin, S. W. Bi, *New J. Chem.* **2004**, *28*, 270.
[16] G. M. Sheldrick, University of Göttingen, Germany, **1994**.
[17] G. M. Sheldrick, *SHELXL-97, Program for refinement of crystal structures and program for solution of crystal structures*, University of Göttingen, Germany, **1997**.

Received April 29, 2004
Early View Article
Published Online September 2, 2004

 © 2004 Wiley-VCH Verlag GmbH & Co. KGaA, Weinheim

NMR Observations of Interligand Interference in the Molecular Motion of Double-Stranded Dinuclear Helicates

Hirohiko Houjou,*[a][‡] Nathanaëlle Schneider,[b] Yoshinobu Nagawa,[a] Masatoshi Kanesato,[a] Romain Ruppert,[b] and Kazuhisa Hiratani[c]

Keywords: DNA / Helical structures / NMR spectroscopy / Palladium / Schiff-base ligands

Double-stranded dinuclear complexes with either twisted or parallel arrangements were obtained by reaction between Schiff-base ligands and Pd^{II} ions. Linear ligands mainly afforded twisted arrangements, while macrocyclic ligands forced the complex to adopt parallel arrangements. In these dinuclear complexes, one isomer could not be converted into the other even upon prolonged heating. The NMR spectra showed that the chemical shifts of the diastereotopic protons can be used as an indicator to distinguish between the arrangements. The NOE cross-peak characteristics of the complexes with twisted arrangements are interpreted with reference to the crystal structure of a Cu^{II} complex as an isostructural model of the Pd^{II} complex. Variable-temperature measurements revealed the rotational interference between the ligands of the counterpart strands, the first time that this has been observed for helically arranged complexes.
(© Wiley-VCH Verlag GmbH & Co. KGaA, 69451 Weinheim, Germany, 2004)

Introduction

The spontaneous assembly of coordination compounds is an important tool for the construction of such fascinating architectures as a nanoscale molecule with well-defined polyhedral shape, or an infinite coordination polymer with a regularly arranged cavity.[1−4] Amongst the various three-dimensional structures, the helix is an attractive one to investigate. Many studies on helically arranged complexes have so far served as the foundation of molecular design, synthetic strategy, thermodynamics, kinetics, stereochemistry, and molecular architectonics in metallo-supramolecular chemistry.[5−7] Recently, helical complexes have been studied not only as a subject in basic chemistry, but also as a useful building block for functional materials.[8−12]

There have been many attempts to prepare double- or triple-stranded helical complexes by using metal-directed self-assembly.[13−22] For the efficient construction of helical structures the design of the linker connecting the chelating units is quite important, because a ligand could afford either a homochiral complex (helicate) with twisted arrangement or a heterochiral complex (*meso*-helicate, mesocate, or side-by-side complex) with parallel arrangement depending on the linker's shape and symmetry (Figure 1).[13] Since the potential advantages of the helical structures originate in their chirality, much attention has been paid to the thermodynamics of the complexes. It is known, for example, that in some cases the helical and nonhelical forms are in equilibrium in solution, resulting in the racemization of the compound.[23−25] This kind of dynamic interconversion is an inevitable result of entropy-driven molecular aggregation.

Another possible process to construct the helical structures is enthalpy-driven molecular aggregation, which

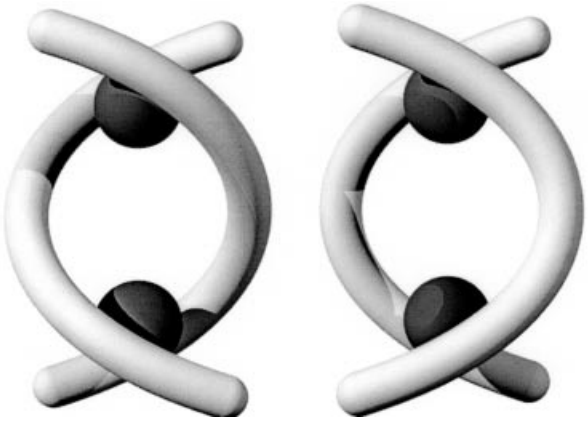

Figure 1. Model drawings of double-stranded dinuclear complexes with twisted (left) and parallel (right) arrangements

[a] Nanoarchitectonics Research Center, National Institute of Advanced Industrial Science and Technology (AIST), 1-1-1 Higashi, Tsukuba, Ibaraki 305-8562, Japan
[b] Faculté de Chimie, Université Louis Pasteur, 1 rue Blaise Pascal, 67008 Strasbourg Cedex, France
[c] Department of Applied Chemistry, Utsunomiya University, 7-2-1 Youtou, Utsunomiya 321-8585, Japan
[‡] Current address: Institute of Industrial Science, University of Tokyo, 4-6-1 Meguro-ku Tokyo 153-8505, Japan, E-mail: houjou@iis.u-tokyo.ac.jp

 © 2004 Wiley-VCH Verlag GmbH & Co. KGaA, Weinheim **DOI: 10.1002/ejic.200400407**

would afford thermally stable products. However, this method has an intrinsic difficulty in controlling the products because the reaction is largely kinetically controlled. Thus, a desirable ligand should maintain a conformation suitable for the formation of a helix during the complexation. We have investigated a variety of Schiff bases containing a 2-methylenepropane-1,3-diyl (isobutenylene) chain as a linker, as a promising ligand that would fulfill this requirement.[26] We have succeeded in synthesizing dinuclear complexes of Ti^{IV}, Y^{III}, Ni^{II}, and Cu^{II}.[27–29] Among these complexes, we found that Ni^{II} and Cu^{II} species have a helical arrangement in which the coordination site adopts a square-planar geometry.[29] This finding suggested a possible access to an isostructural complex of Pd^{II}. Such complexes with diamagnetic properties could be studied by NMR techniques, leading to the understanding of their formation mechanisms as well as their structure in solution and thermodynamic behavior. In this article we describe the synthesis and characterization of Pd^{II} complexes of our Schiff-base ligands. We will highlight the difference in NMR features between the complexes with twisted and parallel arrangements. Those NMR results are successfully interpreted based on a comparative study of the crystal structures between the Pd^{II} and Cu^{II} complexes. In particular, interligand interference in molecular motion is observed for the first time for the complexes with a twisted arrangement.

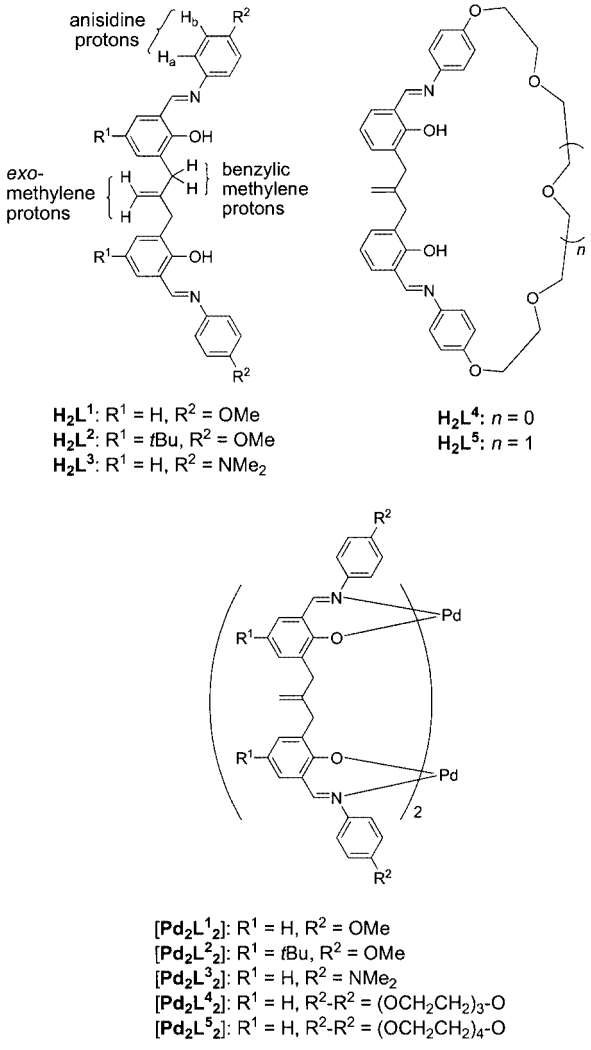

Figure 2. Chemical structures of the ligands and complexes; some specific protons referred to in the text are denoted

Results and Discussion

Characterization of the Helical and Nonhelical Complexes

The reaction of the Schiff-base ligands (H_2L^1 to H_2L^3; see Figure 2) and palladium(II) acetate afforded yellowish orange solids. The major products show ESI-MS peaks corresponding to a 2:2 assembly of ligand and palladium ion. Based on the results of our previous studies,[29] the products were expected to be the double-stranded dinuclear palladium complexes $[Pd_2L^1_2]$, $[Pd_2L^2_2]$ and $[Pd_2L^3_2]$, as shown in Figure 2. Their NMR spectra and elemental analyses were also in agreement with the proposed structure.

The ^1H NMR spectrum of $[Pd_2L^1_2]$ shows a split pair of doublets at δ = 1.87 ppm (^2J = 14.2 Hz) and 2.34 ppm (^2J = 14.2 Hz), which were assigned to the benzylic methylene protons (Figure 2) of the isobutenylene linker. This AB-type geminal coupling suggests a constraint of molecular motion which makes the two protons diastereotopic. These benzylic protons and the *exo*-methylene protons (δ = 4.75 ppm) exhibit NOE cross-peaks, among which one peak (between δ = 1.87 and 4.75 ppm) is significantly stronger than the other one (between δ = 2.34 and 4.75 ppm). These biased cross-peaks suggested a difference in distance ($d_{H\cdots H}$) between the benzylic proton and the *exo*-methylene proton. In view of the possible rotamers of the isobutenylene group,[26c,26d,30] one benzylic proton should be located in the in-plane region ($d_{H\cdots H} \approx 2.3$ Å) with respect to the π-plane of the ethylene group, while the other should be located in the out-of-plane region ($d_{H\cdots H} \approx 3.3$ Å). Therefore, we assigned the signal at δ = 1.87 ppm to the in-plane proton, and the signal at δ = 2.34 ppm to the out-of-plane proton. The NMR spectra of $[Pd_2L^2_2]$ and $[Pd_2L^3_2]$ also show similar features. The chemical shifts of the in-plane and out-of-plane protons are summarized in Table 1.

The ^1H NMR spectrum of the crude precipitate obtained after the reaction between Pd^{II} and ligand L^1 indicates the presence of a by-product that gives a split pair of doublets at δ = 2.02 and 2.20 ppm in the region of the benzylic methylene protons (Table 1). After purification, we were able to obtain a by-product-rich sample and a major product-rich sample, for which the ratio of the two components did not change even after the sample was heated at 80 °C for several hours. This indicates that these components are kinetically controlled products, which are not thermally interconvertible. The mass spectra recorded before and after the purification show no significant change, suggesting that the major product and the by-product have the same molecular weight. This observation led to the assumption that the major and minor components are two isomers with twisted and parallel arrangements (see Figure 1).

 © 2004 Wiley-VCH Verlag GmbH & Co. KGaA, Weinheim

Table 1. The chemical shift[a] (in ppm) of the benzylic methylene protons, and the presumed arrangement of the complexes

Compound	In-plane proton	Out-of-plane proton	$\Delta\delta$	Arrangement
$[Pd_2L^1{}_2]$	1.87 (14.2)	2.34 (14.2)	0.47	twisted
$[Pd_2L^1{}_2]$ (by-product)	2.02 (14)	2.20 (14)	0.18	parallel
$[Pd_2L^2{}_2]$	1.88 (14.1)	2.49 (14.1)	0.61	twisted
$[Pd_2L^3{}_2]$	1.84 (14.5)	2.40 (14.4)	0.56	twisted
$[Pd_2L^4{}_2]$	2.38 (14.1)	2.53 (14.5)	0.15	parallel
$[Pd_2L^5{}_2]$	2.32 (14.5)	2.59 (14.4)	0.27	parallel

[a] Every peak appears as a doublet. The coupling constants (^2J in Hz) are given in parentheses.

To clarify the difference between the two isomers — the twisted and parallel forms — we prepared similar dinuclear palladium complexes with the ligands H_2L^4 and H_2L^5 (Figure 2) that would not allow the helical arrangement owing to their macrocyclic structure. Figure 3 shows the crystal structure of $[Pd_2L^5{}_2]$. As expected, the ligand adopts a parallel arrangement around the two palladium atoms, to which two nitrogen atoms and two oxygen atoms are bound in a slightly distorted square-planar geometry with *trans* coordination. If only electronic factors are taken into account, the coordination geometry around the palladium(II) ion is expected to be *cis* for N−O chelating ligands.[31−33] In the present case, however, since the nitrogen atom is substituted by an aromatic group, the geometry around the palladium ion is defined by steric factors. Although the crystallographic symmetry of $[Pd_2L^5{}_2]$ is C_i, the NMR spectra show a C_{2h}-like behavior of the molecule, probably due to thermal fluctuations.

The ^{1}H NMR spectra of $[Pd_2L^4{}_2]$ and $[Pd_2L^5{}_2]$ show a split pair of doublets, which are again assigned to the benzylic protons (Table 1). The pattern of these signals is similar to that observed for $[Pd_2L^1{}_2]$ to $[Pd_2L^3{}_2]$, except that the resonances are significantly shifted downfield. Table 1 also lists the difference ($\Delta\delta$) of chemical shift between the out-of-plane and in-plane protons. It should be noticed that the $\Delta\delta$ values (0.15 and 0.27 ppm) measured for complexes $[Pd_2L^4{}_2]$ and $[Pd_2L^5{}_2]$, respectively, are much lower than those found for complexes $[Pd_2L^1{}_2]$ to $[Pd_2L^3{}_2]$ (0.47−0.61 ppm), and are very close to the $\Delta\delta$ value (0.18 ppm) measured for the by-product formed along with $[Pd_2L^1{}_2]$. These distinctive $\Delta\delta$ values may arise from differences in the chemical environment of the benzylic methylene groups in the twisted arrangement and in the parallel one. In other words, the $\Delta\delta$ value can be an indicator of the arrangement of the complexes. Based on the above results, we presume that $[Pd_2L^1{}_2]$ to $[Pd_2L^3{}_2]$ have a twisted arrangement, while $[Pd_2L^4{}_2]$, $[Pd_2L^5{}_2]$, and the by-product of $[Pd_2L^1{}_2]$ have a parallel arrangement (Table 1).

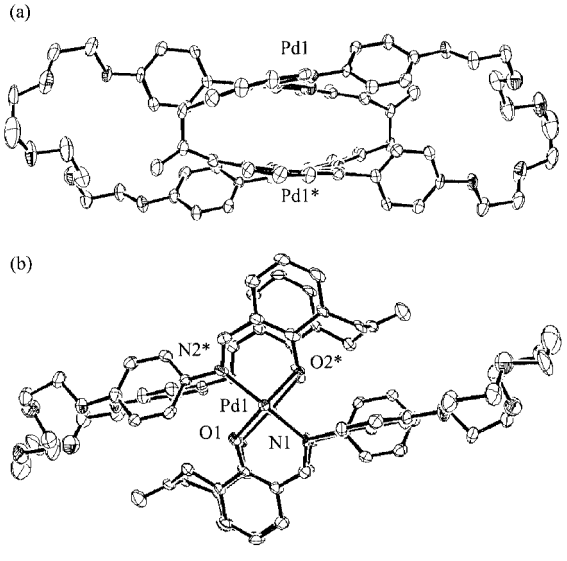

Figure 3. Crystal structure of $[Pd_2L^5{}_2]$: (a) view from the direction perpendicular to the Pd1···Pd1* line (pseudo-C_2 axis); (b) view nearly along the pseudo-C_2 axis; selected interatomic distances [Å] and bond angles [°]: O1−Pd1 1.995, O2*−Pd1 1.977, N1−Pd1 2.024, N2*−Pd1 2.042, Pd1−Pd1* 4.151; O1−Pd1−O2* 172.0, N1−Pd1−N2* 172.2; the hydrogen atoms have been omitted for clarity

NMR Features in Helical Complexes

An analysis of the crystal structures would provide helpful information to interpret the NMR spectra. Although the crystal structures of $[Pd_2L^1{}_2]$ to $[Pd_2L^4{}_2]$ have not been obtained, a comparison of the crystal structures between palladium and copper complexes confirms the assumption that these complexes have very similar structures. As shown in Figure 4, the crystal structure of $[Cu_2L^5{}_2]$ is highly reminiscent of that described above for $[Pd_2L^5{}_2]$ (see Figure 3). As expected, as copper is a first-row transition metal and palladium a second-row one, the main differences are found in the M−O and M−N distances; the other main interatomic distances in the two complexes are very close. For example, the distance between the two *exo*-methylene carbon atoms of $[Pd_2L^5{}_2]$ is 12.768 Å, while that of $[Cu_2L^5{}_2]$ is 12.685 Å, a difference of only 0.7%. Figure 5 shows the crystal structure of $[Cu_2L^2{}_2]$, which demonstrates the helical arrangement of the ligands around the two copper atoms.[12] In spite of the difference in arrangement, the geometry around each coordination site of $[Cu_2L^2{}_2]$ is quite similar to that of $[Cu_2L^5{}_2]$. From all these observations, it is reasonable to assume that the structure of $[Pd_2L^2{}_2]$ is also similar to that of $[Cu_2L^2{}_2]$.

The NOESY spectra of $[Pd_2L^1{}_2]$ to $[Pd_2L^3{}_2]$ show the characteristic cross-peaks that would be expected from a twisted arrangement. For $[Pd_2L^2{}_2]$, for example, we observed correlation peaks between the *tert*-butyl protons and the methoxy protons of the anisidine unit, and between the benzylic protons out of the plane of the ethylene group and

 © 2004 Wiley-VCH Verlag GmbH & Co. KGaA, Weinheim

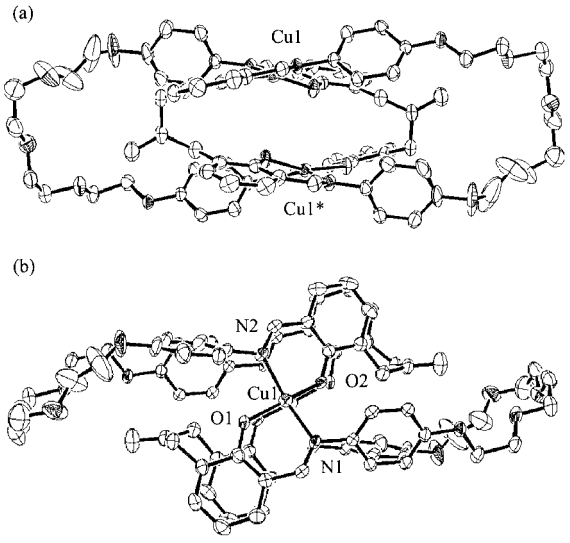

Figure 4. Crystal structure of $[Cu_2L^5_2]$: (a) view from the direction perpendicular to the Cu1···Cu1* line (pseudo-C_2 axis); (b) view nearly along the pseudo-C_2 axis; selected interatomic distances [Å] and bond angles [°]: O1−Cu1 1.881, O2−Cu1 1.892, N1−Cu1 2.002, N2−Cu1 1.999, Cu1−Cu1* 4.113; O1−Cu1−O2* 161.0, N1−Cu1−N2 158.6; the hydrogen atoms and the solvent of crystallization ($CHCl_3$) have been omitted for clarity

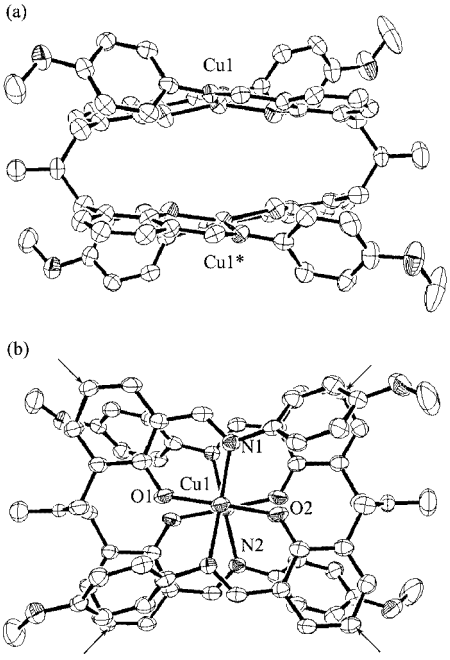

Figure 5. Crystal structure of $[Cu_2L^2_2]$: (a) view from the direction perpendicular to the Cu1···Cu1* line (pseudo-C_2 axis); (b) view nearly along the pseudo-C_2 axis; selected interatomic distances [Å] and bond angles [°]: O1−Cu1 1.880, O2−Cu1 1.864, N1−Cu1 1.984, N2−Cu1 1.991, Cu1−Cu1* 3.887; O1−Cu1−O2 159.2, N1−Cu1−N2 161.2; the hydrogen atoms and the solvent of crystallization (CH_2Cl_2) have been omitted for clarity; the *tert*-butyl groups have also been omitted for clarity, but the four carbon atoms to which they are attached are indicated by arrows in (b)

the aromatic protons (H_a and H_b, see Figure 2) of the anisidine unit. For a better understanding of these NOESY results, we analyzed the crystal structure of $[Cu_2L^2_2]$ as a model of $[Pd_2L^2_2]$. Figure 6 shows a partial structure of $[Cu_2L^2_2]$ in which the hydrogen atoms of interest are noted. The distances between the protons accurately account for the cross-peaks. First, the protons of the *tert*-butyl groups of the ligand are close to the methoxy group protons of the anisidine units of its counterpart (dashed lines A in Figure 6). This type of contact occurs only when the complex adopts a twisted arrangement. Secondly, the out-of-plane protons of the ligand are in close proximity to the anisidine units of its counterpart (dashed lines B and C in Figure 6). In addition, Figure 6 clearly shows the arrangement of the in-plane and out-of-plane benzylic protons (dashed lines D in Figure 6), which could cause the biased NOE cross-peak signals with the *exo*-methylene proton. Similarly, we were able to explain the NOE cross-peaks of the complexes with parallel arrangements — $[Pd_2L^4_2]$ and $[Pd_2L^5_2]$ — on the basis of the crystal structure of $[Pd_2L^5_2]$ (Figure 3).

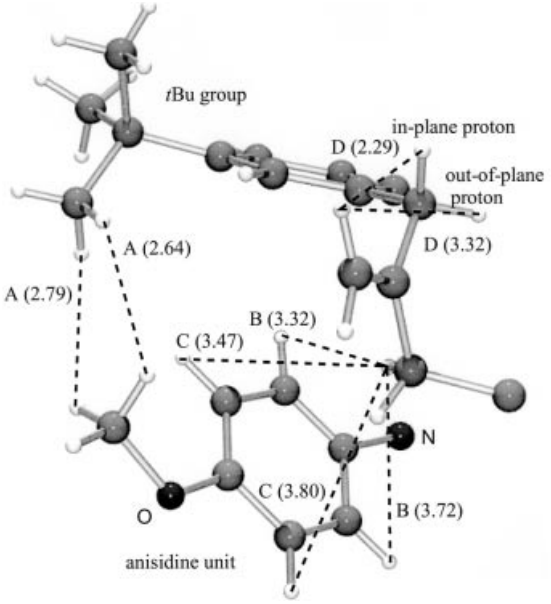

Figure 6. The crystal structure of $[Cu_2L^2_2]$ as a model of $[Pd_2L^2_2]$; notations A−D indicate a pair of protons in close proximity and their distance (in parentheses [Å])

Variable-temperature NMR measurements revealed a critical difference between the complexes with twisted and parallel arrangements. For $[Pd_2L^2_2]$, the H_a and H_b signals (anisidine protons denoted in Figure 2) appear as two doublets at $\delta = 6.56$ and 6.29 ppm, respectively, at 323 K, indicating that the anisidine ring freely rotates within the NMR timescale. At 213 K, as indicated by dashed lines in Figure 7, the H_a signal splits into two doublets at $\delta = 7.13$ and $\delta = 6.02$ ppm, while the H_b signal splits into two doublets at $\delta = 6.67$ and 5.81 ppm. The coalescence temperature is close to 253 K for both H_a and H_b. This spectral change suggests that the four protons become chemically inequivalent due to interference in the rotation of the anisidine moieties. Based on the temperature dependence of the line

 © 2004 Wiley-VCH Verlag GmbH & Co. KGaA, Weinheim

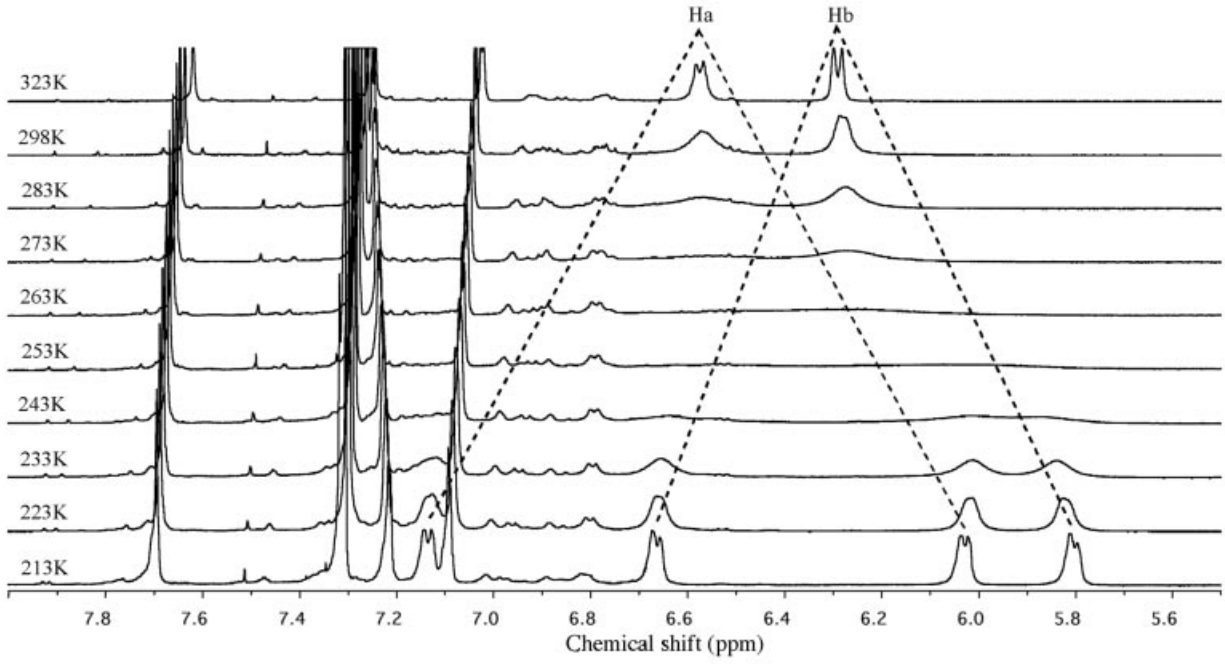

Figure 7. The temperature dependence of the ^{1}H NMR signals of the anisidine protons H_a and H_b

shape, the rotational barrier was estimated to be 47.8 kJ/mol. A similar temperature dependence was observed for $[Pd_2L^1_2]$, but with a lower coalescence temperature (243 K) and lower rotational barrier (45.4 kJ/mol). The difference in the barrier is attributable to the *tert*-butyl group on the phenolate, implying that the phenolate moiety acts as a hindrance to the rotating anisidine moiety. An influence due to contact with the benzylic methylene group is ruled out because a similar contact is also observed in the parallel complexes, which do not show interference in the anisidine rotation. To explain these phenomena, we need to assume a close contact between the anisidine moiety of one ligand and the phenolate moiety of the other, as shown in Figure 6, since the approach of these two moieties would be impossible in a single ligand molecule. Consequently, such an interligand steric hindrance is a phenomenon exclusively observed for the complexes with a twisted arrangement. On the other hand, the corresponding ^{1}H NMR signals of the complex with a parallel arrangement show little dependence on temperature. For example, the signals of H_a and H_b of $[Pd_2L^5_2]$ are observed as two doublets at δ = 7.20 and 6.87 ppm at 298 K, and they show only a slight shift to δ = 7.09 and 6.79 ppm, respectively, at 213 K.

Remarks on the Formation Mechanism

As described above, several characteristic NMR features enable us to distinguish the arrangement of the dinuclear Pd^{II} complexes. With the ligand H_2L^1, we obtained two isomers, namely the twisted form as a major product and the parallel form as a by-product. These isomers could not be interconverted, even after prolonged heating, demonstrating their thermodynamic stability. Similarly, for the other two linear ligands (H_2L^2 and H_2L^3), the major product of the reaction is the twisted isomer. By contrast, when the ligands have mechanical constraints due to their macrocyclic structures (H_2L^4 and H_2L^5), the parallel forms are the major reaction products. These results suggest that the acyclic ligands prefer a conformation that can induce a twisted arrangement in the dinuclear complexes. At this point it is worth mentioning the nature of the linker unit connecting the two chelating units in terms of symmetry. Albrecht et al. have introduced the "even-odd principle", which accounts for the relation between the arrangement and the ligand used to actively control the formation of helicates and *meso*-helicates.[34] Namely, an alkyl chain with an even number of methylene units has C_2 symmetry, which favors a helicate, whereas an alkyl chain with an odd number of methylene units has C_{2v} symmetry, which favors a *meso*-helicate. As for the present system, the isobutenylene chain can adopt several stable conformers with various symmetry such as skew-skew (C_2 symmetry), *syn-syn* (C_{2v} symmetry) and skew-skew′ (C_s symmetry). As already remarked in the previous paper, the isobutenylene chains have the skew-skew form in the helical Ni^{II} and Cu^{II} complexes. Since the helical Pd^{II} complexes are suggested to be isostructural to them, the chains should also adopt the skew-skew form. As for the nonhelical complexes, Figure 3 shows that the isobutenylene chains of $[Pd_2L^5_2]$ adopt the skew-skew′ form. According to an ab initio study (MP2/6-311**G//HF/6-311G** level of theory) of model compounds, the skew-skew form is more stable than the skew-skew′ form by 8.28 kJ/mol.[30] Although the calculated energy difference is rather small, it is suggested that the thermodynamic preference for the skew-skew conformation contributes to the efficient formation of the helical complexes to some extent.

 © 2004 Wiley-VCH Verlag GmbH & Co. KGaA, Weinheim

Consequently, the present system is a good example of enthalpy-driven molecular aggregation during which the ligand component effectively controls the arrangement of the products.

Conclusion

We have described the synthesis and structure of several dinuclear palladium(II) complexes of double-stranded Schiff-base ligands with either twisted or parallel arrangements. In the present system the complexation is enthalpy driven, and the product is largely kinetically controlled. Due to this formation mechanism, the twisted and parallel isomers are thermodynamically inconvertible in solution, such that we can observe the characteristic NMR features of a given complex with a definite arrangement. To the best of our knowledge, this is the first work that clearly exhibits the interligand interactions exclusively brought into helically arranged complexes.

Experimental Section

Measurements: NMR measurements were performed using a Bruker AVANCE500 (500 MHz for ^{1}H nuclei) spectrometer. The temperature was set at 298 K unless otherwise noted. The samples were dissolved in $CDCl_3$, and TMS was used as an internal standard. The chemical shifts of ^{1}H and ^{13}C nuclei were assigned by using NOESY, ROESY, COSY, and DQF-COSY techniques. Variable-temperature measurements were performed for dynamic NMR spectroscopic analysis. Calculations for complete line-shape analyses were carried out with an IBM R-32 computer using the computer program g NMR version 4.1.[35] Theoretical spectra were calculated to obtain an optimum fit with the observed spectra by varying the exchange-rate constants. The activation parameters were obtained using the Eyring equation.[36]

For X-ray diffraction of a single crystal, the data were collected with a Rigaku RAXIS-RAPID Imaging Plate diffractometer, λ(Mo-K_α) = 0.7107 Å radiation. The structure was solved by direct methods and expanded using Fourier techniques. The nonhydrogen atoms' coordinates were refined anisotropically. Hydrogen atoms' coordinates were calculated. The final cycle of full-matrix least-squares refinement was based on the observed reflections with $I > 1.5\sigma(I)$ and variable parameters. The refinement converged with the unweighted and weighted agreement factors, R_1 and R_w. All the calculations were performed with RIGAKU Corporation's Crystal-Structure software package.[37] ORTEP drawings were created with ellipsoids of 50% probability by using the ORTEP-3 software package.[38]

Synthesis of the Pd^{II} Complexes: The Schiff-base ligands H_2L^1 to H_2L^5 (Figure 2) were prepared from the corresponding bis(hydroxybenzaldehyde) and aniline derivative according to reported methods.[26] For example, a stoichiometric amount (L^1/Pd = 1:1) of palladium(II) acetate and a few drops of methanol and acetonitrile were added to a solution of H_2L^1 (507 mg, 1.0 mmol) in chloroform (10 mL). The solution was stirred at 25 °C for several days. After confirming the disappearance of the starting material by TLC, a large quantity of methanol was added to precipitate a yellowish orange solid. Similarly, ligands H_2L^2 to H_2L^5 were allowed to react with the palladium salt. Since we found it difficult to elute the products from a silica gel column, we attempted the purification by reprecipitation from a diethyl ether/chloroform system.

[Pd$_2$L$^1_2$]: Yield: 61 mg (10%). ^{1}H NMR: δ = 1.87 (d, J = 14.2 Hz, 4 H, Ar−CH_2−), 2.34 (d, J = 14.2 Hz, 4 H, Ar−CH_2−), 3.64 (s, 12 H, −OCH_3), 4.73 [s, 4 H, −C(=CH_2)−], 6.31 (d, J = 8.0 Hz, 8 H, ArH−OCH$_3$), 6.60 (dd, J = 7.4 Hz, 7.3 Hz, 4 H, ArH−OPd), 6.61 (d, J = 7.4 Hz, 8 H, ArH−OCH$_3$), 7.09 (d, J = 7.3 Hz, 4 H, ArH−OPd), 7.11 (d, J = 7.6 Hz, 4 H, ArH−OPd), 7.61 (s, 4 H, −CH=N−) ppm. ^{13}C NMR (213 K): δ = 32.8, 55.7, 111.6, 113.1, 114.0, 114.4, 118.7, 124.7, 125.0, 131.8, 132.8, 134.3, 142.7, 149.9, 156.9, 162.6, 162.9 ppm. ESI(+) MS: m/z = 1245.5 (calcd. for [M + Na$^+$] 1245.0). IR (KBr): $\nu_{C=N}$ = 1609 cm^{-1}. $C_{64}H_{56}N_4O_8Pd_2$ (1221.97): calcd. C 62.90, H 4.62, N 4.58; found C 63.03, H 4.71, N 4.51.

[Pd$_2$L$^2_2$]: Yield: 72 mg (10%). ^{1}H NMR: δ = 1.30 [s, 36 H, −C(CH_3)$_3$], 1.88 (d, J = 14.1 Hz, 4 H, Ar−CH_2−), 2.49 (d, J = 14.1 Hz, 4 H, Ar−CH_2−), 3.61 (s, 12 H, −OCH_3), 4.78 [s, 4 H, −C(=CH_2)−], 6.29 (m, 8 H, ArH−OCH$_3$), 6.57 (m, 8 H, ArH−OCH$_3$), 7.03 (d, J = 2.7 Hz, 4 H, ArH−OPd), 7.25 (d, J = 2.0 Hz, 4 H, ArH−OPd), 7.64 (s, 4 H, −CH=N−) ppm. ^{13}C NMR (213 K): δ = 31.5, 32.9, 33.6, 55.6, 111.3, 112.6, 114.4, 117.7, 125.0, 125.2, 128.0, 130.9, 132.2, 135.8, 143.3, 151.0, 156.6, 161.3, 163.1 ppm. ESI(+) MS: m/z = 1469.6 (calcd. for [M + Na$^+$] 1269.4). IR (KBr): $\nu_{C=N}$ = 1613 cm^{-1}. $C_{80}H_{88}N_4O_8Pd_2(H_2O)_3$ (1500.43): calcd. C 64.03, H 6.31, N 3.73; found C 64.17, H 6.23, N 3.64.

[Pd$_2$L$^3_2$]: Yield: 427 mg (67%). ^{1}H NMR: δ = 1.84 (d, J = 14.5 Hz, 4 H, Ar−CH_2−), 2.40 (d, J = 14.4 Hz, 4 H, Ar−CH_2−), 2.78 [s, 24 H, −N(CH_3)$_2$], 4.68 [s, 4 H, −C(=CH_2)−], 6.16 [d, J = 8.0 Hz, 8 H, ArH−N(CH$_3$)$_2$], 6.56 (dd, J = 7.5 Hz, 7.5 Hz, 4 H, ArH−OPd), 6.57 [d, J = 7.6 Hz, 8 H, ArH−N(CH$_3$)$_2$], 7.05 (d, J = 6.6 Hz, 4 H, ArH−OPd), 7.07 (d, J = 7.9 Hz, 4 H, ArH−OPd), 7.62 (s, 4 H, −CH=N−) ppm. ^{13}C NMR (298 K): δ = 33.2, 41.2, 112.2, 112.8, 114.1, 119.3, 124.8, 132.1, 132.5, 133.9, 140.8, 149.1, 151.3, 162.5, 163.7 ppm. ESI(+) MS: m/z = 1297.2 (calcd. for [M + Na$^+$] 1297.1). IR (KBr): $\nu_{C=N}$ = 1611 cm^{-1}. $C_{68}H_{68}N_8O_4Pd_2(H_2O)_{0.5}$ (1283.15): calcd. C 63.65, H 5.42, N 8.73; found C 63.72, H 5.30, N 8.49.

[Pd$_2$L$^4_2$]: Yield: 293 mg (42%). ^{1}H NMR: δ = 2.38 (d, J = 14.1 Hz, 4 H, Ar−CH_2−), 2.53 (d, J = 14.5 Hz, 4 H, Ar−CH_2−), 3.79 (s, 8 H, −OCH_2CH_2O−), 3.89 (m, 8 H, Ar−OCH$_2$CH_2O−), 4.26 (m, 8 H, Ar−OCH_2CH$_2$O−), 4.76 [s, 4 H, −C(=CH_2)−], 6.02 (dd, J = 7.3 Hz, 7.5 Hz, 4 H, ArH−OPd), 6.58 (d, J = 7.5 Hz, 4 H, ArH−OPd), 6.64 (d, J = 8.0 Hz, 4 H, ArH−OPd), 6.93 (d, J = 8.6 Hz, 8 H, ArH−OCH$_2$−), 7.14 (d, J = 8.6 Hz, 4 H, ArH−OCH$_2$−), 7.46 (s, 4 H, −CH=N−) ppm. The ^{13}C NMR spectrum was not measured due to low solubility. ESI(+) MS: m/z = 1417.2 (calcd. for [M + Na$^+$] 1417.1). IR (KBr): $\nu_{C=N}$ = 1610 cm^{-1}. $C_{72}H_{68}N_4O_{12}Pd_2$ (1394.14): calcd. C 62.03, H 4.92, N 4.02; found C 61.81, H 5.07, N 4.13.

[Pd$_2$L$^5_2$]: Yield: 348 mg (47%). ^{1}H NMR: δ = 2.32 (d, J = 14.5 Hz, 4 H, Ar−CH_2−), 2.59 (d, J = 14.4 Hz, 4 H, Ar−CH_2−), 3.81 (m, 16 H, −OCH_2CH_2O−), 3.93 (m, 8 H, Ar−OCH$_2$CH_2O−), 4.18 (m, 8 H, Ar−OCH_2CH$_2$O−), 4.75 [s, 4 H, −C(=CH_2)−], 6.02 (dd, J = 7.3 Hz, 7.3 Hz, 4 H, ArH−OPd), 6.59 (d, J = 6.7 Hz, 4 H, ArH−OPd), 6.61 (d, J = 7.8 Hz, 4 H, ArH−OPd), 6.87 (d, J = 8.7 Hz, 8 H, ArH−OCH$_2$−), 7.20 (d, J = 8.7 Hz, 4 H, ArH−OCH$_2$−), 7.47 (s, 4 H, −CH=N−) ppm. ^{13}C NMR (213 K): δ = 35.0, 66.5, 67.9, 69.7, 69.2, 112.7, 112.7, 113.0, 116.7, 125.2, 129.2, 130.7, 132.7, 142.2, 147.5, 155.5, 160.9, 161.6 ppm. ESI(+) MS: m/z = 1505.4 (calcd. for [M + Na$^+$] 1505.2). IR (KBr):

 © 2004 Wiley-VCH Verlag GmbH & Co. KGaA, Weinheim

$\nu_{C=N}$ = 1609 cm^{-1}. $C_{76}H_{76}N_4O_{14}Pd_2(H_2O)_3$ (1536.30): calcd. C 59.41, H 5.38, N 3.65; found C 58.99, H 4.98, N 3.40. A single crystal suitable for X-ray analysis was obtained by recrystallization from chloroform/diethyl ether. Crystal data: $C_{38}H_{38}N_2O_7Pd$ (741.12); crystal system: monoclinic; space group: *C*2/*c* (no. 15); Z = 8 in a cell of dimensions a = 21.259(8), b = 19.594(6), c = 17.239(6) Å, β = 111.15(3)°, V = 6697.2(4) $Å^3$, $D_{calcd.}$ = 1.470 g/cm^3, μ = 6.11 cm^{-1}, 30806 measured and 7612 unique reflections ($2\theta_{max}$ = 55.0°, R_{int} = 0.128); R_1 = 0.045, R_w = 0.082.

Synthesis of $[Cu_2L^5_2]$: A methanol solution (25 mL) of copper(II) acetate monohydrate (20 mg, 0.1 mmol) was added to a solution of H_2L^5 (64 mg, 0.1 mmol) in chloroform (25 mL). The solution was left at 25 °C without stirring for several hours. The resultant precipitate was collected by filtration. Yield: 64 mg (92%). ESI(+) MS: *m*/*z* = 1419.3 (calcd. for [M + Na^+] 1419.5). IR (KBr): $\nu_{C=N}$ = 1611 cm^{-1}. $C_{76}H_{76}Cu_2N_4O_{14}(CHCl_3)_2$ (1635.25): calcd. C 57.36, H 4.81, N 3.43; found C 57.97, H 4.38, N 3.31. A single crystal as precipitated was used for the X-ray analysis. Crystal data: $C_{38}H_{38}CuN_2O_7(CHCl_3)_2$ (937.03); crystal system: triclinic; space group: $P\bar{1}$ (no. 2); Z = 2 in a cell of dimensions a = 11.968(1), b = 12.0109(9), c = 17.706(2) Å, α = 74.666(5)°, β = 70.671(4)°, γ = 60.561(4)°, V = 2075.6(3) $Å^3$, $D_{calcd.}$ = 1.499 g/cm^3; μ = 9.63 cm^{-1}, 19156 measured and 8909 unique reflections ($2\theta_{max}$ = 54.8°, R_{int} = 0.040); R_1 = 0.084, R_w = 0.211.

Acknowledgments

Predoctoral fellowships for N. S. by the Région Alsace and the Chemistry Department of the Université Louis Pasteur are acknowledged.

[1] M. Fujita, K. Umemoto, M. Yoshizawa, N. Fujita, T. Kusukawa, K. Biradha, *Chem. Commun.* **2001**, 509−518.
[2] B. J. Holliday, C. A. Mirkin, *Angew. Chem. Int. Ed.* **2001**, *40*, 2022−2043.
[3] O. M. Yaghi, M. O'Keeffe, N. W. Ocking, H. K. Chae, M. Eddaoudi, J. Kim, *Nature* **2003**, *423*, 705−714.
[4] S. Kitagawa, M. Kondo, *Bull. Chem. Soc. Jpn.* **1998**, *71*, 1739−1753.
[5] J.-M. Lehn, *Supramolecular Chemistry: Concepts and Perspectives*, VCH, Weinheim, **1995**.
[6] E. C. Constable, *Metals and Ligand Reactivity*, VCH, Weinheim, **1996**.
[7] *Transition Metals in Supramolecular Chemistry* (Ed.: J.-P. Sauvage), John Wiley & Sons, Chichester, **1999**.
[8] R. Ziessel, *Coord. Chem. Rev.* **2001**, *216−217*, 195−223.
[9] L. Brunsveld, E. W. Meijer, R. B. Prince, J. S. Moore, *J. Am. Chem. Soc.* **2001**, *123*, 7978−7984.
[10] H.-C. Zhang, W.-S. Huang, L. Pu, *J. Org. Chem.* **2001**, *66*, 481−487.
[11] A. Lavalette, J. Hamblin, A. Marsh, D. M. Haddleton, M. J. Hannon, *Chem. Commun.* **2002**, 3040−3041.
[12] H. Houjou, Y. Shimizu, N. Koshizaki, M. Kanesato, *Adv. Mater.* **2003**, *15*, 1458−1461.
[13] M. Albrecht, *Chem. Rev.* **2001**, *101*, 3457−3479.
[14] E. C. Constable, M. J. Hannon, D. A. Tocher, *Angew. Chem. Int. Ed. Engl.* **1992**, *31*, 230−232.
[15] S. Ruettimann, C. Piguet, G. Brenardinelli, B. Bocquet, A. F. Williams, *J. Am. Chem. Soc.* **1992**, *114*, 4230−4237.
[16] D. E. Fenton, R. W. Matthews, M. McPartlin, B. P. Murphy, I. J. Scowen, P. A. Tasker, *J. Chem. Soc., Chem. Commun.* **1994**, 1391−1392.
[17] [17a] J. Hamblin, A. Jackson, N. W. Alcock, M. J. Hannon, *J. Chem. Soc., Dalton Trans.* **2002**, 1635−1641. [17b] J. Hamblin, L. J. Childs, N. W. Alcock, M. J. Hannon, *J. Chem. Soc., Dalton Trans.* **2002**, 164−169. [17c] M. J. Hannon, S. Bunce, A. J. Clarke, N. W. Alcock, *Angew. Chem. Int. Ed.* **1999**, *38*, 1277−1278.
[18] [18a] M. Elhabiri, R. Scopelliti, J.-C. G. Bünzli, C. Piguet, *J. Am. Chem. Soc.* **1999**, *121*, 10747−10762. [18b] J.-C. G. Bünzli, C. Piguet, *Chem. Rev.* **2002**, *102*, 1897−1928.
[19] [19a] C. O. Dietrich-Buchecker, J.-P. Sauvage, A. De Cian, J. Fischer, *J. Chem. Soc., Chem. Commun.* **1994**, 2231−2232. [19b] G. Rapenne, B. T. Patterson, J. -P. Sauvage, F. R. Keene, *Chem. Commun.* **1999**, 1853−1854.
[20] B. Hasenknopf, J.-M. Lehn, N. Boumediene, A. Dupont−Gervais, A. Van Dorsselaer, B. Kneisel, D. Fenske, *J. Am. Chem. Soc.* **1997**, *119*, 10956.
[21] [21a] P. L. Jones, K. J. Byrom, J. C. Jeffery, J. A. McCleverty, M. D. Ward, *Chem. Commun.* **1997**, 1361−1362. [21b] M. D. Ward, J. A. McCleverty, J. C. Jeffery, *Coord. Chem. Rev.* **2002**, *222*, 251−272.
[22] [22a] M. Albrecht, R. Fröhlich, *J. Am. Chem. Soc.* **1997**, *119*, 1656−1661. [22b] M. Albrecht, *Chem. Soc. Rev.* **1998**, *27*, 281−287. [22c] M. Albrecht, O. Blau, R. Fröhlich, *Proc. Natl. Acad. Sci. USA* **2002**, *99*, 4867−4872.
[23] [23a] P. Comba, A. Fath, T. W. Hambley, A. Vielfort, *J. Chem. Soc., Dalton Trans.* **1997**, 1691−1695. [23b] P. Comba, A. Kuener and A Peters, *J. Chem. Soc., Dalton Trans.* **1999**, 509−516.
[24] J. Xu, T. N. Parac, K. Raymond, *Angew. Chem. Int. Ed.* **1999**, *38*, 2878−2882.
[25] M. Elhabiri, J. Hamacek, J.-C. G. Bünzli, A.-M. Albrecht-Gary, *Eur. J. Inorg. Chem.* **2004**, 51−62.
[26] [26a] H. Houjou, S.-K. Lee, Y. Hishikawa, Y. Nagawa, K. Hiratani, *Chem. Commun.* **2000**, 2197−2198. [26b] H. Houjou, Y. Nagawa, K. Hiratani, *Tetrahedron Lett.* **2001**, *42*, 3861−3863. [26c] H. Houjou, S. Tsuzuki, Y. Nagawa, K. Hiratani, *Bull. Chem. Soc. Jpn.* **2002**, *75*, 831−839. [26d] H. Houjou, S. Tsuzuki, Y. Nagawa, M. Kanesato, K. Hiratani, *Bull. Chem. Soc. Jpn.* **2003**, *76*, 2405−2411.
[27] M. L. N. Rao, H. Houjou, K. Hiratani, *Chem. Commun.* **2002**, 420−421.
[28] M. Kanesato, H. Houjou, Y. Nagawa, K. Hiratani, *Inorg. Chem. Commun.* **2002**, *5*, 984−988.
[29] H. Houjou, A. Iwasaki, T. Ogihara, M. Kanesato, S. Akabori, K. Hiratani, *New J. Chem.* **2003**, *27*, 886−889.
[30] S. Tsuzuki, H. Houjou, Y. Nagawa, K. Hiratani, *J. Chem. Soc., Perkin Trans. 2* **2000**, 2448−2452.
[31] R. H. Holm, M. J. O'Connor, *Prog. Inorg. Chem.* **1971**, *14*, 241−401.
[32] A. W. Maverick, F. R. Fronczek, D. P. Martone, J. R. Bradbury, *J. Coord. Chem.* **1989**, *20*, 149−161.
[33] S. Richeter, C. Jeandon, J.-P. Gisselbrecht, R. Graff, R. Ruppert, H. J. Callot, *Inorg. Chem.* **2004**, *43*, 251−263.
[34] M. Albrecht, *Chem. Eur. J.* **2000**, *6*, 3485−3489.
[35] P. H. M. Budzelaar, *Simulation of One-Dimensional NMR Spectra*, Cherwell Scientific Limited, Oxford, **1999**.
[36] M. Oki, *Application of Dynamic NMR Spectroscopy to Organic Chemistry, Methods in Stereochemical Analysis*, vol. 4, VCH, Orlando, **1985**.
[37] *CrystalStructure*, version 3.10, Rigaku Coorporation and Rigaku/MSC, Tokyo, Japan, **2002**.
[38] ORTEP-3 for Windows: L. J. Farrugia, *J. Appl. Crystallogr.* **1997**, *30*, 565.

Received May 16, 2004
Early View Article
Published Online September 7, 2004

 © 2004 Wiley-VCH Verlag GmbH & Co. KGaA, Weinheim

Synthesis, Structures and Reactivity of Mono- and Diborylacetylenes

Avijit Goswami,[a] Hans Pritzkow,[a] Frank Rominger,[b] and Walter Siebert*[a]

Dedicated to Professor Margot Becke on the occasion of her 90th birthday

Keywords: Alkynes / Boranes / Cobalt / Cyclooligomerization

The reaction of [bis(diisopropylamino)boryl]acetylene with 2 equiv. of HCl and 1 equiv. of dithiocatechol or 2-hydroxythiophenol yields the corresponding monoborylacetylenes **1** and **2**, respectively. Diborylacetylenes **3** and **4** are obtained from the reactions of bis(trimethylstannyl)acetylene with 2 equiv. of bromoboranes. Treatment of chlorobis(diisopropylamino)-borane with LiC≡C–EMe$_3$ (E = C, Si) leads to the corresponding element-substituted [bis(diisopropylamino)boryl]-acetylenes **5a**,**b**. The syntheses of monoborylacetylenes **6a**,**b**–**8a**,**b** are achieved by the reaction of **5a**,**b** with 2 equiv. of HCl and 1 equiv. of catechol, dithiocatechol or 2-hydroxythiophenol, respectively. Stoichiometric amounts of [CpCo(CO)$_2$] react with **1**–**4** in refluxing toluene to give the corresponding (η^4-cyclobutadiene)cobalt complexes **9**–**12**. Analogous isomeric mixtures of (η^4-cyclobutadiene)cobalt complexes **13a/13a′**–**15a/15a′** are obtained from 1-*tert*-butyl-2-borylacetylenes **6a**–**8a** and [CpCo(C$_2$H$_4$)$_2$], whereas isomeric mixtures of (η^4-cyclohexatriene)(η^5-cyclopentadienyl)-cobalt complexes **13b/13b′**–**15b/15b′** are formed with 1-boryl-2-silylacetylenes **6b**–**8b** under similar conditions. Hydrolysis of **13a**–**15a** yields the (η^4-1,3-di-*tert*-butylcyclobutadiene)cobalt complex **16**. Catalytic trimerizations of mono- (**1**, **2**) and diborylacetylenes (**3**, **4**) with Co$_2$(CO)$_8$ lead to isomeric mixtures of triboryl- (**17/17′**, **18/18′**) and hexaborylbenzene derivatives (**19**, **20**), respectively. The new compounds are characterized by NMR spectroscopy and mass spectrometry as well as by X-ray structure analyses for **1b**, **5b**, **6b**, **14a**, **15a** and **16**.
(© Wiley-VCH Verlag GmbH & Co. KGaA, 69451 Weinheim, Germany, 2004)

Introduction

Over the past three decades, cobalt-mediated cyclooligomerization reactions of acetylenes have been recognized as a powerful tool for the synthesis of various compounds.[1] In general, catalytic cyclotrimerizations of less bulky substituted acetylenes with [CpCoL$_2$] (L = CO, C$_2$H$_4$) lead to benzene derivatives,[2] whereas CpCo complexes of cyclobutadiene[3] and/or cyclopentadienone[4] (with benzene derivatives as side products) are obtained with stoichiometric amounts of [CpCoL$_2$] complexes.

Recently, we have reported the synthesis of oxygen- and sulfur-substituted monoborylacetylenes.[5] Surprisingly, it was found that oxygen-substituted borylacetylenes formed only benzene derivatives in catalytic as well as stoichiometric reactions with [CpCoL$_2$]. On the other hand, with sulfur-substituted borylacetylenes only (η^4-cyclobutadiene)cobalt complexes were achieved. This unique heteroatom effect in borylacetylenes encouraged us to perform further studies. The monoborylacetylenes **1** and **2** and the diborylacetylenes **3** and **4** were synthesized and found to follow the same reaction trend to undergo dimerization with [CpCoL$_2$] to furnish (η^4-cyclobutadiene)cobalt complexes **9**−**12**. This indicated that the aryl groups have less electronic or steric influences on the reactivity of previously reported 1-aryl-2-borylacetylenes.[5]

In order to shed further light on the influence of bulky substituents on the borylacetylenes, we have prepared 1-boryl-2-*tert*-butylacetylenes and 1-boryl-2-silylacetylenes **6**−**8**, in which two oxygen atoms (in **6**), two sulfur atoms (in **7**) and one oxygen and one sulfur atom (in **8**) are bound to the boron atom. It is expected that the bulky substituents have different steric and electronic effects on the reactivity of the acetylenes **6**−**8**. In this paper, we report on the syntheses, structures and reactivity of the above-mentioned acetylenes **1**−**4** and **6**−**8**.

Results and Discussion

Synthesis and Properties of Mono- and Diborylacetylenes

The preparation of sulfur-substituted borylacetylenes was achieved by treatment of [bis(diisopropylamino)boryl]-acetylene with 2 equiv. of HCl and 1 equiv. of dithiocatechol or 2-hydroxythiophenol in THF, to give the mono-

[a] Anorganisch-Chemisches Institut der Universität,
Im Neuenheimer Feld 270, 69120 Heidelberg, Germany
Fax: + 49-6221-54-5609
E-mail: walter.siebert@urz.uni-heidelberg.de
[b] Organisch-Chemisches Institut der Universität,
Im Neuenheimer Feld 270, 69120 Heidelberg, Germany
Fax: + 49-6221-54-5244
E-mail: rominger@phindigo.oci.uni-heidelberg.de

borylacetylenes **1a**,**b** and **2**, respectively, in moderate yields (Scheme 1). The colorless solids were characterized by ^{1}H, ^{11}B and ^{13}C NMR spectroscopy, and by mass spectrometry.

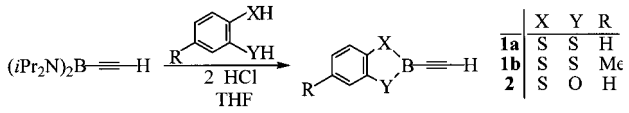

	X	Y	R
1a	S	S	H
1b	S	S	Me
2	S	O	H

Scheme 1

In the ^{11}B NMR spectrum the signals at δ = 47 (**1a**), 48 (**1b**) and 38 (**2**) ppm indicate trigonal-planar boryl groups, which was confirmed by the solid-state structure of **1b** (Figure 1). The ^{1}H NMR spectra of **1a**,**b** and **2** exhibit a characteristic singlet for the acetylenic proton at δ = 3.71 (**1a**), 3.70 (**1b**) and 3.17 (**2**) ppm. In the ^{13}C NMR spectrum the signals for B−C_{sp} are not observed; the signals for H−C_{sp} (δ = 90−100 ppm) are shifted to lower field compared to those of alkylacetylenes (δ = 70−80 ppm).

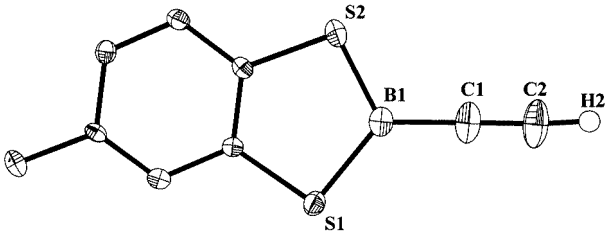

Figure 1. Molecular structure of **1b** in the solid state; selected bond lengths [Å] and bond angles [°]: B1−S1 1.849(3), B1−S2 1.728(3), B1−C1 1.521(2), C1−C2 1.188(3); C2−C1−B1 178.3(2), C1−C2−H2 175.9(2), C1−B1−S2 117.9(2), C1−B1−S1 128.4(2), S2−B1−S1 113.5(1)

Diborylacetylenes **3** and **4** were prepared by the reaction of bis(trimethylstannyl)acetylene with 2 equiv. of bromoboranes (Scheme 2). The colorless, air-sensitive solids formed are well soluble in chloroform and toluene, but less so in hexane and pentane. The ^{11}B NMR spectra show broad signals at δ = 47 (**3**) and 37 (**4**) ppm.

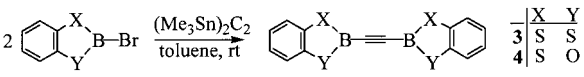

	X	Y
3	S	S
4	S	O

Scheme 2

The synthesis of the [bis(diisopropylamino)boryl]acetylenes **5a**,**b** was performed according to a literature procedure[6] by treating chlorobis(diisopropylamino)borane with LiC≡C−EMe_3 (E = C, Si). The products were isolated in almost quantitative yields (Scheme 3).

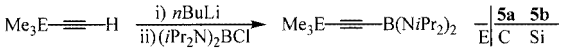

E	5a	5b
	C	Si

Scheme 3

The light-yellow acetylenes **5a**,**b** were characterized by ^{1}H, ^{11}B and ^{13}C NMR spectroscopy, and by mass spectrometry. The X-ray structure analysis of **5b** (Figure 2) reveals an almost linear B−C≡C−Si moiety; the C≡C distance (1.21 Å) is slightly longer than in other R−C≡C−R compounds (1.18 Å).[7]

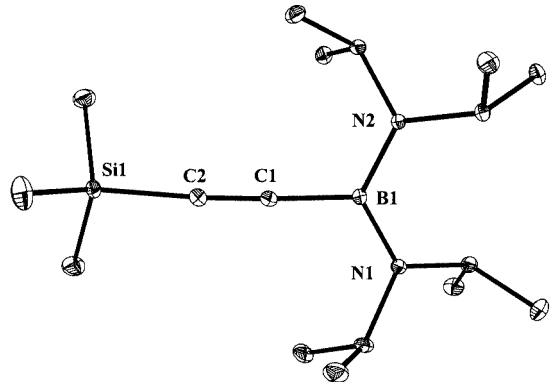

Figure 2. Molecular structure of **5b** in the solid state; hydrogen atoms are omitted for clarity; selected bond lengths [Å] and bond angles [°]: B1−C1 1.564(1), C1−C2 1.214(1), Si1−C2 1.830(1), N1−B1 1.428(1), N2−B1 1.439(1); C2−C1−B1 177.3(1), C1−C2−Si1 174.54(9), N1−B1−N2 124.40(8), N2−B1−C1 117.46(8), N1−B1−C1 118.13(8)

The synthesis of compounds **6**−**8** was achieved by the reaction of the [(diisopropylamino)boryl]acetylenes **5a**,**b** with 2 equiv. of HCl and 1 equiv. of catechol, dithiocatechol or 2-hydroxythiophenol, respectively, in THF (Scheme 4). Compounds **7a** and **7b** are colorless solids, whereas **6a**,**b**[8] and **8a**,**b** are pale-yellow liquids, which are readily soluble in common organic solvents.

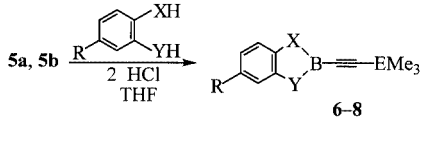

	X	Y	E	R
6a	O	O	C	H
6b	O	O	Si	H
7a	S	S	C	Me
7b	S	S	Si	Me
8a	S	O	C	H
8b	S	O	Si	H

Scheme 4

The ^{11}B NMR spectra exhibit broad signals at δ = 24 (**6a**), 23 (**6b**), 48 (**7a**), 47 (**7b**), 38 (**8a**) and 37 (**8b**) ppm. In the ^{1}H NMR spectra of **6b**−**8b** and **6a**−**8a** singlets appear at δ = 0.2−0.3 ppm ($SiMe_3$) and 1.2−1.3 ppm (CMe_3). Single crystals of **6b** were obtained at −20 °C. The molecular structure of **6b** (Figure 3) indicates an almost linear B−C≡C−Si moiety with a slightly elongated C≡C bond. The boron atom is trigonal coordinated and the heterocycle is almost planar.

 © 2004 Wiley-VCH Verlag GmbH & Co. KGaA, Weinheim

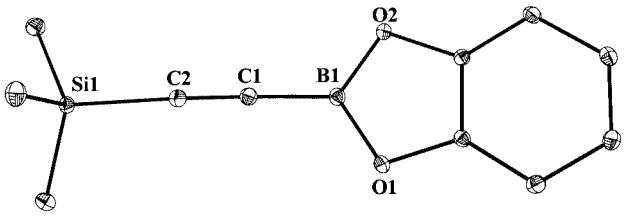

Figure 3. Molecular structure of **6b** in the solid state; hydrogen atoms are omitted for clarity; selected bond lengths [Å] and bond angles [°]: Si1−C2 1.853(1), B1−C1 1.524(2), C1−C2 1.209(2), O1−B1 1.386(1), O2−B1 1.387(1); C2−C1−B1 172.8(1), C1−C2−Si1 175.3(1), O1−B1−O2 112.13(9), O1−B1−C1 122.7(1), O2−B1−C1 125.0(1)

(η^4-Cyclobutadiene)cobalt Complexes 9−12

CpCo-mediated cyclodimerization has proved particularly efficient for tolerating the presence of varied functionalities on the alkyne.[9] As a result, the $[CpCoL_2]$ (L = CO, PR_3, olefin) complex family has been utilized for intensive studies, culminating in the isolation of numerous (η^4-cyclobutadiene)cobalt complexes. In refluxing toluene the mono- (**1a**, **2**) and diborylacetylenes (**3**, **4**) formed the (η^4-cyclobutadiene)cobalt complexes **9**−**12** in the presence of stoichiometric amounts of $[CpCo(CO)_2]$ (Scheme 5). Purification of complexes **9**−**12** was performed by repeated washing with hexane and toluene. The red-brown solids of **9**−**12** are partially soluble in chloroform; in methanol a fast reaction leads to the formation of $B(OMe)_3$.

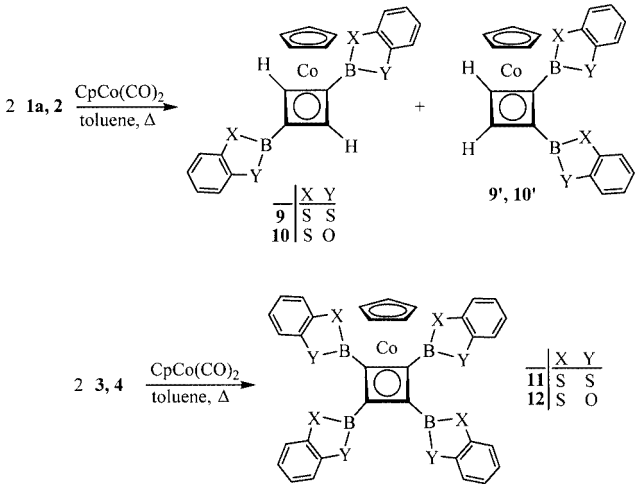

Scheme 5

Complexes **9**−**12** were characterized by ^1H, ^{11}B and ^{13}C NMR spectroscopy, and by mass spectrometry. The ^{11}B NMR spectra show broad signals at δ = 60 (**9**), 48 (**10**), 63 (**11**) and 50 (**12**) ppm. The ^1H NMR spectra of **9**−**12** exhibit multiplets in the region δ = 6.6−8.2 ppm for thr aromatic protons in addition to the Cp resonances (δ = 4.7−5.4 ppm). The *cis* isomers **9′**, **10′** could not be identified by NMR spectroscopy; however, analysis of the fragmentation patterns in the mass spectra in terms of the degradation of the cyclobutadiene ring clearly indicates the presence of trace amounts of *cis* isomers in the isomeric mixtures. It is worth mentioning that no benzene derivative was formed in the catalytic cyclotrimerization (thermal or photochemical) reactions of $[CpCo(CO)_2]$ with the borylacetylenes **1**−**4**.

Reactions of $[CpCo(C_2H_4)_2]$ with 6a−8a

The reaction of borylacetylenes **6a**−**8a** with stoichiometric amounts of $[CpCo(CO)_2]$ in refluxing toluene led only to 50−60% conversion of the starting acetylenes to an isomeric mixture of (η^4-cyclobutadiene)cobalt complexes **13a/13a′**, **14a/14a′** and **15a/15a′**, respectively. Using the more reactive complex $[CpCo(C_2H_4)_2]$[10] resulted in complete conversion of the borylacetylenes to the CpCo complexes **13a/13a′**−**15a/15a′** (Scheme 6).

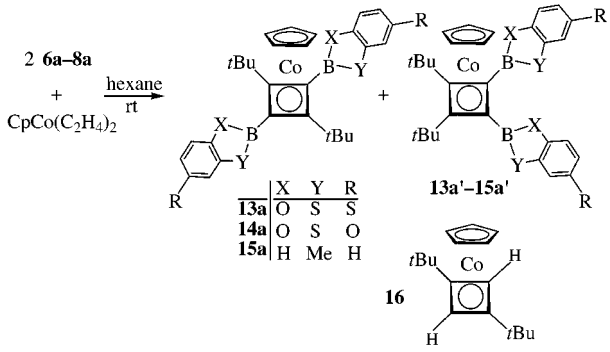

Scheme 6

Attempts to separate the isomeric mixtures of the cobalt complexes **13a/13a′**−**15a/15a′** by column chromatography led to the known complex $[CpCo(\eta^4\text{-}C_4tBu_2H_2)]$ (**16**).[11] Compounds **13a/13a′**−**15a/15a′** and **16** are soluble in common organic solvents and were characterized by ^1H, ^{11}B and ^{13}C NMR spectroscopy, mass spectrometry as well as by X-ray analyses for **14a**, **15a** and **16**. The ^{11}B NMR spectra show broad signals at δ = 36 (**13a/13a′**), 63 (**14a/14a′**) and 50 (**15a/15a′**) ppm. The ^1H NMR spectra of **13a**−**15a** exhibit singlets in the region δ = 4.8−5.2 ppm for H_{Cp} in addition to the *tert*-butyl group resonances (δ = 1.2−1.4 ppm). The molecular-ion peaks of **13a**−**15a** were detected with the expected isotopic pattern by mass spectrometry. The presence of very small amounts of *cis* isomers (**13a′**, **14a′** and **15a′**) in the isomeric mixtures was confirmed by analyzing the major peaks in the mass spectra (analogous to **9′**, **10′**).

Complexes **14a** and **15a** were characterized by performing a single-crystal X-ray diffraction analysis (Figures 4 and 5), which revealed that the *tert*-butyl and boryl groups are in *trans* positions. Neither of the boron heterocycles of **14a** lies in the cyclobutadiene plane, whereas one of the boron heterocycles of **15a** is coplanar with the cyclobutadiene ring.

 © 2004 Wiley-VCH Verlag GmbH & Co. KGaA, Weinheim

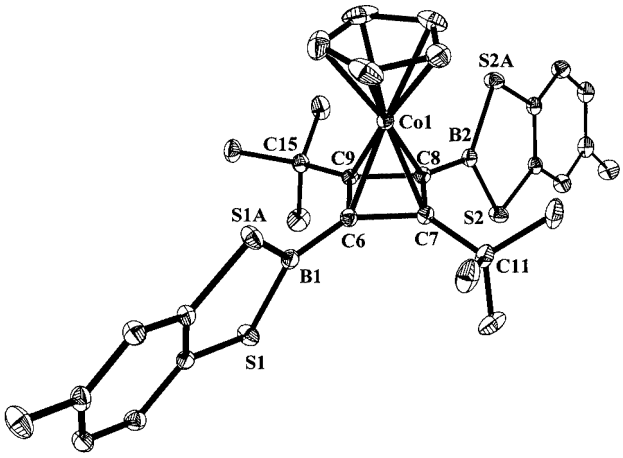

Figure 4. Molecular structure of **14a** in the solid state; hydrogen atoms are omitted for clarity; selected bond lengths [A] and bond angles [°]: C6−C9 1.467(3), C6−C7 1.475(3), C7−C8 1.468(3), C8−C9 1.467(3), B1−S1 1.803(3), B2−S2 1.795(3); C9−C6−C7 88.6(2), C6−C7−C8 91.1(2), C9−C8−C7 88.8(2), C6−C9−C8 91.5(2)

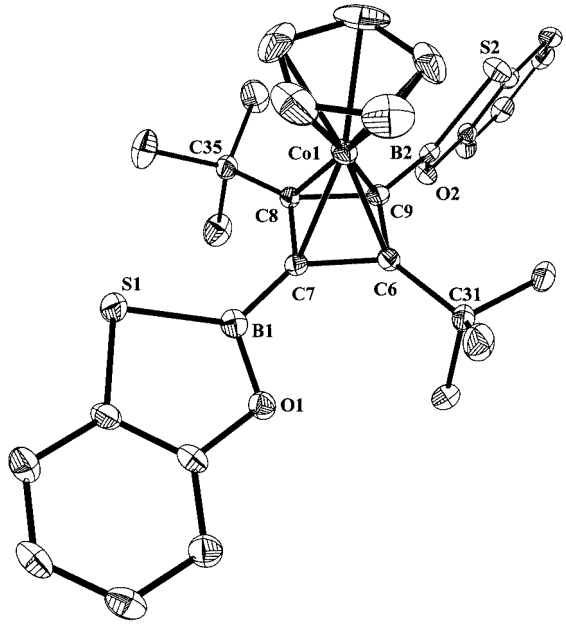

Figure 5. Molecular structure of **15a** in the solid state; hydrogen atoms are omitted for clarity; selected bond lengths [A] and bond angles [°]: C6−C9 1.459(4), C6−C7 1.477(4), C7−C8 1.482(4), C8−C9 1.467(4), B1−O1 1.379(4), B2−O2 1.376(4), B1−S1 1.824(4), B2−S2 1.814(4); C9−C6−C7 91.3(2), C6−C7−C8 88.3(2), C9−C8−C7 90.8(2), C6−C9−C8 89.6(2)

A solid-state structure analysis of **16** was carried out on a single crystal. This complex crystallizes with two independent molecules in the asymmetric unit with very similar distances and angles; only one structure is shown in Figure 6 and the average values are listed in the caption.

[CpCo(η⁴-cyclohexatriene)] Complexes 13b/13b′−15b/15b′

Reaction of **6b−8b** with $[CpCo(C_2H_4)_2]$[12] led to the [CpCo(η⁴-cyclohexatriene)] complexes **13b/13b′−15b/15b′**

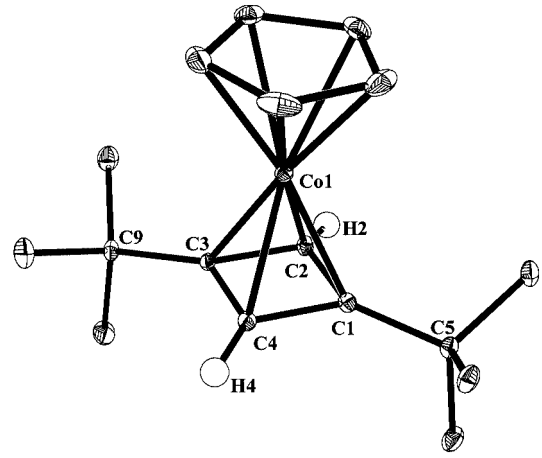

Figure 6. Molecular structure of **16** in the solid state; hydrogen atoms are omitted for clarity; selected bond lengths [A] and bond angles [°]: C1−C2 1.449(3), C1−C4 1.455(3), C2−C3 1.455(3), C3−C4 1.461(3); C2−C1−C4 89.8(2), C1−C2−C3 90.7(2), C2−C3−C4 89.3(2), C1−C4−C3 90.2(2)

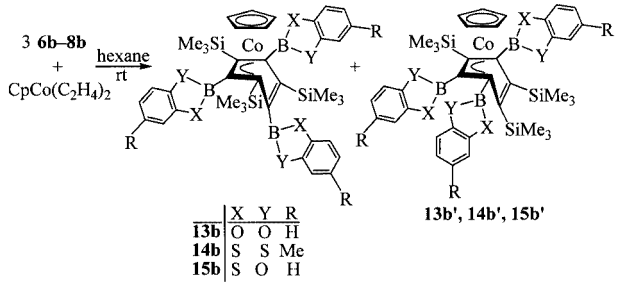

Scheme 7

in moderate yields (Scheme 7). They were purified by column chromatography on Florosil and isolated as reddish-brown oils, which were characterized by ^1H, ^{11}B, ^{13}C and ^{29}Si NMR spectroscopy, and by mass spectrometry.

The ^{11}B NMR spectra show broad signals at $\delta = 32$ (**13b/13b′**), 60 (**14b/14b′**) and 49 (**15b/15b′**) ppm and the ^1H NMR spectra exhibit multiplets in the aromatic region of $\delta = 6.3-7.5$ ppm in addition to the Cp resonances ($\delta = 4.9-5.3$ ppm). The EI-MS data confirm the identity of complexes **13b−15b** by the appearance of the molecular-ion peaks with the correct isotopic pattern.

[$Co_2(CO)_8$]-Catalyzed Cyclotrimerization of 1−4

In refluxing toluene the mono- and diborylacetylenes **1−4** form the corresponding benzene derivatives **17−20** in the presence of a catalytic amount of $Co_2(CO)_8$ (Scheme 8).[13] The air-stable colorless solids **17−20** are not soluble in common organic solvents, although triborylbenzene derivatives **17** and **18** are partially soluble in chloroform. In general, for unsymmetrical acetylenes one can expect to achieve mixtures of both 1,3,5 and 1,2,4 isomers in variable ratios. Due to their low solubility, the mixtures of isomers **17/17′** and **18/18′** could not be separated by column chromatography.[14] Purification of the compounds was accomplished by repeated washing with hexane and toluene. Compounds **17** and **18** were characterized by ^1H, ^{11}B and

 © 2004 Wiley-VCH Verlag GmbH & Co. KGaA, Weinheim

^{13}C NMR spectroscopy, and by mass spectrometry. In the ^{13}C NMR spectra of **17** and **18** the signals for the central benzene rings are not observed. Therefore, one cannot rule out the possibility that the isomers **17**/**17′** and **18**/**18′** are present. The hexaborylbenzene derivatives **19** and **20** were identified by mass spectrometry by the appearance of molecular-ion peaks with the correct isotopic pattern. Owing to their very low solubility, NMR measurements were not possible for **19** and **20**.

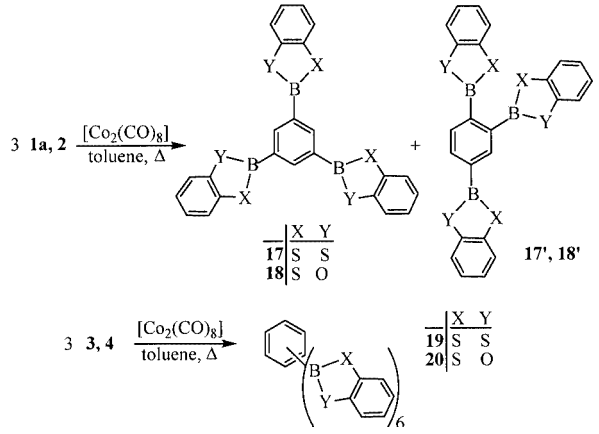

Scheme 8

Under similar reaction conditions no triborylbenzene derivative was found from the reactions with 1-alkyl-2-borylacetylenes **6**−**8**.

Conclusions

The reaction of borylacetylenes with catalytic as well as stoichiometric amounts of $[CpCo(CO)_2]$, $[CpCo(C_2H_4)_2]$ and $[Co_2(CO)_8]$ have been studied. Benzene derivatives are not formed by [2+2+2] catalytic cyclotrimerization reactions of $[CpCoL_2]$ (L = CO, C_2H_4) with borylacetylenes **1**−**4** and **6**−**8**. The (η^4-cyclobutadiene)cobalt complexes **9**−**12** are, however, formed by the reaction of mono- (**1**, **2**) and diborylacetylenes (**3**, **4**) with stoichiometric amounts of $[CpCo(CO)_2]$. Analogous (η^4-cyclobutadiene)cobalt complexes **13a**−**15a** have been prepared by the reaction of the corresponding *tert*-butylborylacetylenes **6a**−**8a** in the presence of $[CpCo(C_2H_4)_2]$. The interaction of a sulfur atom with the cobalt atom in the coordinatively unsaturated cobaltacyclopentadiene derivative probably does not allow the approach of a third acetylene molecule to the cobalt center; therefore formation of benzene derivatives does not occur by [2+2+2] catalytic cycloaddition reactions of the monoboryl acetylenes **1**−**4**, **7a** and **8a**. As similar oxygen−cobalt interactions are not known, steric bulkiness may be the reason for obtaining only (η^4-cyclobutadiene)cobalt complexes from the reaction of **6a** with $[CpCo(C_2H_4)_2]$. In **7a** and **8a**, the presence of the bulky *tert*-butyl group obviously hinders the formation of benzene derivatives.

Surprisingly, such types of cyclobutadienylcobalt complexes are not found in the reactions of 1-boryl-2-silylacetylenes **6b**−**8b** under similar reaction conditions. On the other hand, treatment of **6b**−**8b** with $[CpCo(C_2H_4)_2]$ at ambient temperature led to the novel (η^4-cyclohexatriene)(η^5-cyclopentadienyl)cobalt complexes **13b**−**15b**. Reaction of mono- and diborylalkynes (**1**−**4**) with catalytic amounts of $[Co_2(CO)_8]$ gives rise to triboryl- (**17**/**17′** and **18**/**18′**) and hexaborylbenzene derivatives (**19** and **20**), respectively.

Experimental Section

General: All reactions were performed under nitrogen using standard Schlenk techniques. Solvents were dried with the appropriate drying agents and distilled under nitrogen. Glassware was dried with a heat gun under high vacuum. Column chromatography: Florosil® (Fluka), 100−200 mesh. ^1H, ^{11}B and ^{13}C NMR: Bruker AC 200 spectrometer; ^1H and ^{13}C spectra were referenced to $Si(CH_3)_4$; ^{11}B spectra to $F_3B{\cdot}OEt_2$. Mass spectra were obtained with Finnigan MAT 8230 plus spectrometers using the EI technique. Melting points (uncorrected) were obtained with a Büchi apparatus, using capillaries which were filled under nitrogen and sealed. (iPr$_2$N)$_2$BCl[15] and [bis(diisopropylamino)boryl]acetylene[16] were prepared according to literature procedures. Bromo(dithiocatechol)-borane and bromo-1,3,2-benzooxathiaborole, not previously reported in the literature, were prepared by the reactions of dithiocatechol and 2-hydroxythiophenol with excess of BBr_3. Catechol, dithiocatechol, 4-methyldithiocatechol, 2-mercaptophenol and bis(trimethylstannyl)acetylene were purchased from Aldrich.

(1,3,2-Benzodithiaborol-2-yl)acetylene (1a), (5-Methyl-1,3,2-benzodithiaborol-2-yl)acetylene (1b) and (1,3,2-Benzooxathiaborol-2-yl)-acetylene (2): $HCl{\cdot}OEt_2$ (2 M; 10.5 mL, 21 mmol) was added to a stirred solution of [bis(diisopropylamino)boryl]acetylene (2.40 g, 10.1 mmol) in 50 mL of THF at −78 °C within 15 min. Stirring was continued at room temp. for 2 h. Then, 10.1 mmol of the corresponding aromatic diol (**1a**: 1.43 g of dithiocatechol; **1b**: 1.57 g of 4-methyldithiophenol; **2**: 1.27 g of 2-hydroxythiophenol; in 15 mL of THF) was added to the white suspension and the reaction mixture was stirred overnight at room temp. After filtration, the solution was concentrated almost to dryness, and a crystalline solid was obtained.

1a: Yield: 0.98 g (55%), m.p. 62 °C (dec.). ^1H NMR (200.1 MHz, $CDCl_3$): δ = 3.71 (s, 1 H, C≡CH), 7.20, 7.80 (m, 4 H, C_6H_4) ppm. ^{11}B NMR (64.2 MHz, $CDCl_3$): δ = 47 ppm. ^{13}C NMR (50.3 MHz, $CDCl_3$): δ = 94.10 (C≡*C*H), 126.0, 126.8, 140.8 (C_6H_4) ppm; C_{sp}−B signal not observed. MS (70 eV, EI): *m*/*z* (%) = 176 (20) [M^+]. MS (70 eV, HR-EI): *m*/*z* (%) = 175.9915 (13) [M^+; $^{12}C_8{}^1H_5{}^{32}S_2{}^{11}B$: 175.9926]; Δmmu = −1.1.

1b: Yield: 0.97 g (51%), m.p. 71 °C. ^1H NMR (200.1 MHz, $CDCl_3$): δ = 2.43 (s, 3 H, CH_3), 3.70 (s, 1 H, C≡CH), 7.20, 7.62 (m, 3 H, C_6H_3) ppm. ^{11}B NMR (64.2 MHz, $CDCl_3$): δ = 48 ppm. ^{13}C NMR (50.3 MHz, $CDCl_3$): δ = 21.06 (CH_3), 96.24 (C≡*C*H), 126.2, 126.9, 127.3, 136.2, 137.6, 140.9 (C_6H_3) ppm; C_{sp}−B not observed.

2: Yield: 0.79 g (49%), m.p. 56 °C. ^1H NMR (200.1 MHz, $CDCl_3$): δ = 3.17 (s, 1 H, C≡CH), 7.1−7.7 (m, 4 H, C_6H_4) ppm. ^{11}B NMR (64.2 MHz, $CDCl_3$): δ = 38 ppm. ^{13}C NMR (50.3 MHz, $CDCl_3$): δ = 97.23 (C≡*C*H), 115.1, 120.9, 124.1, 126.4, 127.8, 156.5 (C_6H_4) ppm; C_{sp}−B signal not observed. MS (70 eV, EI): *m*/*z* (%) = 160 (10) [M^+].

 © 2004 Wiley-VCH Verlag GmbH & Co. KGaA, Weinheim

[Bis(1,3,2-benzodithiaborol-2-yl)]acetylene (3) and [Bis(1,3,2-benzooxathiaborol-2-yl)]acetylene (4): The bromoborane (2.62 g of $C_6H_4S_2BBr$; 2.43 g of C_6H_4OSBBr; 11.4 mmol; in 10 mL of toluene) was added to a solution of $(Me_3Sn)_2C_2$ (2.0 g, 5.7 mmol) in toluene (50 mL) at −78 °C. The reaction mixture was allowed to warm to room temp. and stirred overnight. After removal of the solvent under vacuum, the brown-red residue was sublimed to yield colorless, air-sensitive crystals.

3: Yield: 1.18 g (64%), m.p. 132 °C. ^{1}H NMR (200.1 MHz, $CDCl_3$): δ = 7.37, 7.85 (m, 8 H, C_6H_4) ppm. ^{11}B NMR (64.2 MHz, $CDCl_3$): δ = 47 ppm. ^{13}C NMR (50.3 MHz, $CDCl_3$): δ = 93.14 (BC), 126.0, 126.7, 140.8 (C_6H_4) ppm. MS (70 eV, EI): *m*/*z* (%) = 326 (100) [M^+]. MS (70 eV, HR-EI): *m*/*z* (%) = 325.9699 (100) [M^+; $^{12}C_{14}{}^1H_8{}^{32}S_4{}^{11}B_2$: 325.9694]; Δmmu = 0.5.

4: Yield: 1.0 g (60%), m.p. 102 °C (dec.). ^{1}H NMR (200.1 MHz, $CDCl_3$): δ = 7.3−7.6 (m, 8 H, C_6H_4) ppm. ^{11}B NMR (64.2 MHz, $CDCl_3$): δ = 37 ppm. ^{13}C NMR (50.3 MHz, $CDCl_3$): δ = 115.1, 124.2, 125.5, 126.6, 127.9, 156.5 (C_6H_4) ppm; C_{sp}−B signal not observed. MS (70 eV, EI): *m*/*z* (%) = 294 (100) [M^+]. MS (70 eV, HR-EI): *m*/*z* (%) = 294.0164 (3.6) [M^+; $^{12}C_{14}{}^1H_8{}^{16}O_2{}^{32}S_2{}^{11}B_2$: 294.0152]; Δmmu = 1.2.

1-[Bis(diisopropylamino)boryl]-2-(*tert*-butyl)acetylene (5a) and 1-[Bis(diisopropylamino)boryl]-2-(trimethylsilyl)acetylene (5b): *n*BuLi (2.5 M in hexane; 5.8 mL, 14.6 mmol) was added slowly at −78 °C to a solution of alkylacetylene [**5a**: 1.2 g of (*tert*-butyl)acetylene; **5b**: 1.44 g of (trimethylsilyl)acetylene; 14.6 mmol; in 40 mL of hexane]. The reaction mixture was allowed to warm to room temp. and stirred for 2 h. A solution of chlorobis(diisopropylamino)borane (3.6 g, 14.6 mmol) in 10 mL of hexane was added and the mixture stirred at room temp. overnight. The solid was separated, the solvent removed under vacuum, and a light-yellow liquid was distilled.

5a: Yield: 3.5 g (82%), b.p. 48 °C/0.01 mbar. ^{1}H NMR (200.1 MHz, $CDCl_3$): δ = 1.21 [d, $^3J_{H,H}$ = 7.1 Hz, 24 H, $CH(CH_3)_2$], 1.23 [s, 9 H, $C(CH_3)_3$], 3.37 [sept, 4 H, $^3J_{H,H}$ = 7.1 Hz, $CH(CH_3)_2$] ppm. ^{11}B NMR (64.2 MHz, $CDCl_3$): δ = 26 ppm. ^{13}C NMR (50.3 MHz, $CDCl_3$): δ = 24.00 [$CH(CH_3)_2$], 30.36 [$C(CH_3)_3$], 30.79 [$C(CH_3)_3$], 46.38 [$CH(CH_3)_2$], 90.89 (C_{sp}-C_{ipso}) ppm; C_{sp}-B signal not observed. MS (70 eV, EI): *m*/*z* (%) = 292 (25) [M^+], 277 (100) [M^+ − Me], 249 (95) [M^+ − *i*Pr]. MS (70 eV, HR-EI): *m*/*z* (%) = 292.3038 (30) [M^+; $^{12}C_{18}{}^1H_{37}{}^{14}N_2{}^{11}B$: 292.3049]; Δmmu = −1.1.

5b: Yield: 3.2 g (71%), b.p. 51 °C/0.03 mbar. ^{1}H NMR (200.1 MHz, $CDCl_3$): δ = 0.13 (s, 9 H, $SiMe_3$), 1.21 [d, $^3J_{H,H}$ = 7.2 Hz, 24 H, $CH(CH_3)_2$], 3.36 [sept, $^3J_{H,H}$ = 7.1 Hz, 4 H, $CH(CH_3)_2$] ppm. ^{11}B NMR (64.2 MHz, $CDCl_3$): δ = 25 ppm. ^{13}C NMR (50.3 MHz, $CDCl_3$): δ = −0.19 ppm($SiMe_3$), 24.30 [$CH(CH_3)_2$], 46.87 [$CH(CH_3)_2$], 112.7 (C_{sp}-C_{ipso}) ppm; C_{sp}−B signal not observed. ^{29}Si NMR (39.8 MHz, $CDCl_3$): δ = −4.7 ppm. MS (70 eV, EI): *m*/*z* (%) = 308 (10) [M^+], 293 (100) [M^+ − Me], 265 (90) [M^+ − *i*Pr].

1-(1,3,2-Benzodioxaborol-2-yl)-2-(*tert*-butyl)acetylene (6a), 1-(*tert*-Butyl)-2-(5-methyl-1,3,2-benzodithiaborol-2-yl)acetylene (7a) and 1-(1,3,2-Benzooxathiaborol-2-yl)-2-(*tert*-butyl)acetylene (8a): $HCl{\cdot}OEt_2$ (2 M; 15.5 mL, 31 mmol) was added to a stirred solution of 1-bis(diisopropylamino)boryl-2-*tert*-butylacetylene (**5a**; 4.08 g, 14.0 mmol; in 40 mL of THF) at −78 °C within 15 min. Stirring was continued for 1 h and then 14.0 mmol of the corresponding aromatic diol (**6a**: 1.54 g of catechol; **7a**: 2.18 g of 4-methyldithiocatechol; **8a**: 1.76 g of 2-hydroxythiophenol; dissolved in 15 mL of THF) was added at room temp. The reaction mixture was stirred overnight. After filtration, the solvent was removed to yield **6a** and **8a** as colorless liquids and **7a** as a solid.

6a:[8] Yield: 1.8 g (64%), b.p. 49 °C/0.1 mbar. ^{1}H NMR (200.1 MHz, $CDCl_3$): δ = 1.33 [s, 9 H, $C(CH_3)_3$], 7.05, 7.18 (m, 4 H, C_6H_4) ppm. ^{11}B NMR (64.2 MHz, $CDCl_3$): δ = 24 ppm. ^{13}C NMR (50.3 MHz, $CDCl_3$): δ = 30.31 [$C(CH_3)_3$], 32.19 [$C(CH_3)_3$], 86.90 (C_{sp}-C_{ipso}), 112.2, 122.4, 148.2 (C_6H_4) ppm; C_{sp}−B signal not observed.

7a: Yield: 1.9 g (57%), m.p. 51 °C. ^{1}H NMR (200.1 MHz, $CDCl_3$): δ = 1.33 [s, 9 H, $C(CH_3)_3$], 2.34 (s, 3 H, CH_3), 6.86, 7.61 (m, 3 H, C_6H_3) ppm. ^{11}B NMR (64.2 MHz, $CDCl_3$): δ = 48 ppm. ^{13}C NMR (50.3 MHz, $CDCl_3$): δ = 30.86 [$C(CH_3)_3$], 31.58 [$C(CH_3)_3$], 125.9, 126.7, 126.9, 135.6, 137.5, 140.9 (C_6H_3) ppm; C_{sp}−B signal not observed. MS (70 eV, EI): *m*/*z* (%) = 246 (100) [M^+], 231 (90) [M^+ − Me]. MS (70 eV, HR-EI): *m*/*z* (%) = 246.0700 (100) [M^+; $^{12}C_{13}{}^1H_{15}{}^{32}S_2{}^{11}B$: 246.0708]; Δmmu = −0.8.

8a: Yield: 1.84 g (61%), b.p. 53 °C/0.1 mbar. ^{1}H NMR (200.1 MHz, $CDCl_3$): δ = 1.34 [s, 9 H, $C(CH_3)_3$], 7.1−7.6 (m, 4 H, C_6H_4) ppm. ^{11}B NMR (64.2 MHz, $CDCl_3$): δ = 38 ppm. ^{13}C NMR (50.3 MHz, $CDCl_3$): δ = 30.40 [$C(CH_3)_3$], 30.88 [$C(CH_3)_3$], 114.6, 123.7, 125.3, 126.1, 126.9, 156.5 (C_6H_4) ppm; C_{sp}−B signal not observed. MS (70 eV, EI): *m*/*z* (%) = 216 (100) [M^+]. MS (70 eV, HR-EI): *m*/*z* (%) = 216.0788 (92) [M^+; $^{12}C_{12}{}^1H_{13}{}^{16}O^{32}S^{11}B$: 216.0781]; Δmmu = 0.7.

1-(1,3,2-Benzodioxaborol-2-yl)-2-(trimethylsilyl)acetylene (6b), 1-(5-Methyl-1,3,2-benzodithiaborol-2-yl)-2-(trimethylsilyl)acetylene (7b) and 1-(1,3,2-Benzooxathiaborol-2-yl)-2-(trimethylsilyl)acetylene (8b): $HCl{\cdot}OEt_2$ (2 M; 16 mL, 32 mmol) was added to a stirred solution of 1-[bis(diisopropylamino)boryl]-2-(trimethylsilyl)acetylene (**5b**; 4.62 g, 15.0 mmol; in 40 mL of THF) at −78 °C within 15 min. Stirring was continued for 1 h and then 15.0 mmol of the corresponding aromatic diol (**6b**: 1.65 g of catechol; **7b**: 2.34 g of 4-methyldithiocatechol; **8b**: 1.89 g of 2-hydroxythiophenol; dissolved in 15 mL of THF) was added at room temp. The reaction mixture was stirred overnight. After filtration, the solvent was removed to yield colorless liquids **6b** and **8b**, and solid **7b**.

6b: Yield: 2.16 g (67%), b.p. 63 °C/0.1 mbar. ^{1}H NMR (200.1 MHz, $CDCl_3$): δ = 0.25 (s, 9 H, $SiMe_3$), 7.11, 7.19 (m, 4 H, C_6H_4) ppm. ^{11}B NMR (64.2 MHz, $CDCl_3$): δ = 23 ppm. ^{13}C NMR (50.3 MHz, $CDCl_3$): δ = −0.28 ($SiMe_3$), 113.0, 123.5, 147.9 (C_6H_4) ppm; C_{sp}−B signal not observed. ^{29}Si NMR (39.7 MHz, $CDCl_3$): δ = −15.7 ppm. MS (70 eV, EI): *m*/*z* (%) = 216 (35) [M^+], 201 (100) [M^+ − Me]. MS (70 eV, HR-EI): *m*/*z* (%) = 216.0799 (39) [M^+; $^{12}C_{11}{}^1H_{13}{}^{16}O_2{}^{28}Si^{11}B$: 216.0778]; Δmmu = 2.1.

7b: Yield: 2.88 g (73%), m.p. 67 °C. ^{1}H NMR (200.1 MHz, $CDCl_3$): δ = 0.23 (s, 9 H, $SiMe_3$), 2.36 (s, 3 H, CH_3), 7.12, 7.67 (m, 3 H, C_6H_3) ppm. ^{11}B NMR (64.2 MHz, $CDCl_3$): δ = 47 ppm. ^{13}C NMR (50.3 MHz, $CDCl_3$): δ = −0.46 ppm($SiMe_3$), 21.04 (CH_3), 126.1, 126.8, 127.1, 131.6, 135.9, 140.7 (C_6H_3) ppm; C_{sp}−B signal not observed. ^{29}Si NMR (39.7 MHz, $CDCl_3$): δ = −16.9 ppm. MS (70 eV, EI): *m*/*z* (%) = 262 (50) [M^+], 247 (100) [M^+ − Me]. MS (70 eV, HR-EI): *m*/*z* (%) = 262.0476 (54) [M^+; $^{12}C_{12}{}^1H_{15}{}^{32}S_2{}^{28}Si^{11}B$: 262.0477]; Δmmu = −0.1.

8b: Yield: 2.31 g (66%), b.p. 70 °C/0.1 mbar. ^{1}H NMR (200.1 MHz, $CDCl_3$): δ = 0.26 (s, 9 H, $SiMe_3$), 7.1−7.6 (m, 4 H, C_6H_4) ppm. ^{11}B NMR (64.2 MHz, $CDCl_3$): δ = 37 ppm. ^{13}C NMR (50.3 MHz, $CDCl_3$): δ = −0.53 ppm($SiMe_3$), 114.8, 123.9, 125.4, 126.3, 126.7, 156.4 (C_6H_4) ppm; C_{sp}−B signal not observed. ^{29}Si NMR (39.7 MHz, $CDCl_3$): δ = −16.4 ppm. MS (70 eV, EI): *m*/*z* (%) =

 © 2004 Wiley-VCH Verlag GmbH & Co. KGaA, Weinheim

232 (60) [M^+], 217 (100) [M^+ − Me]. MS (70 eV, HR-EI): *m/z* (%) = 232.0557 (31) [M^+; $^{12}C_{11}{}^{1}H_{13}{}^{16}O^{32}S^{28}Si^{11}B$: 232.0550]; Δmmu = 0.7.

[η⁴-Bis(4-methyldithiocatecholborol-2-yl)cyclobutadiene](η⁵-cyclopentadienyl)cobalt(I) (9/9′), [η⁴-Bis(1,3,2-benzooxathiaborol-2-yl)cyclobutadiene](η⁵-cyclopentadienyl)cobalt(I) (10/10′), (η⁵-Cyclopentadienyl)[η⁴-tetrakis(dithiocatecholborol-2-yl)cyclobutadiene]cobalt(I) (11) and (η⁵-Cyclopentadienyl)[η⁴-tetrakis(1,3,2-benzooxathiaborol-2-yl)cyclobutadiene]cobalt(I) (12): Borylalkyne (**1b**: 1.52 g; **2**: 1.28 g; **3**: 2.60 g; **4**: 2.32 g; 8 mmol) was added at room temp. to a solution of dicarbonyl(η⁵-cyclopentadienyl)cobalt (0.72 g, 4 mmol) in 30 mL of toluene. The reaction mixture was heated under reflux for 4 d. After cooling, the precipitate was collected by filtration, washed several times with hexane and dried in vacuo.

9/9′: Yield: 0.98 g (51%), brown solid, m.p. 170−174 °C. ^{1}H NMR (200.1 MHz, $CDCl_3$): δ = 3.44 (s, 2 H, CH), 4.75 (s, 5 H, H_{Cp}), 6.56, 7.07, 8.24 (m, 8 H, H_{aryl}) ppm. ^{11}B NMR (64.2 MHz, $CDCl_3$): δ = 60 (br.) ppm. ^{13}C NMR (50.3 MHz, $CDCl_3$): δ = 80.98 (C_{Cp}), 83.54 (C_{4ring}), 126.1, 126.8, 140.9 (dithiocatechol) ppm. MS (70 eV, EI): *m/z* (%) = 476 (100) [M^+], 300 (75) [$M^+ - C_6H_4S_2BC_2H$], 150 (3) [$M^+ - C_6H_4S_2BC{\equiv}CBS_2C_6H_4$]. MS (70 eV, HR-EI): *m/z* (%) = 475.9581 (100) [M^+; $^{12}C_{21}{}^{1}H_{15}{}^{32}S_4{}^{11}B_2{}^{59}Co$: 475.9574]; Δmmu = 0.7.

10/10′: Yield: 0.80 g (45%), red-brown solid, m.p. 160−163 °C. ^{1}H NMR (200.1 MHz, $CDCl_3$): δ = 3.75 (s, 2 H, CH), 5.45 (s, 5 H, H_{Cp}), 6.90, 7.18, 7.88 (m, 8 H, H_{aryl}) ppm. ^{11}B NMR (64.2 MHz, $CDCl_3$): δ = 50 (br.) ppm. ^{13}C NMR (50.3 MHz, $CDCl_3$): δ = 81.34 (C_{Cp}), 83.97 (C_{4ring}), 115.1, 120.9, 124.2, 125.8, 126.7, 156.5 (2-hydroxythiophenol) ppm. MS (70 eV, EI): *m/z* (%) = 444 (100) [M^+], 284 (80) [$M^+ - C_6H_4OSBC_2H$], 150 (5) [$M^+ - C_6H_4OSBC{\equiv}CBOSC_6H_4$], 124 [CpCo]. MS (70 eV, HR-EI): *m/z* (%) = 444.0042 (100) [M^+; $^{12}C_{21}{}^{1}H_{15}{}^{16}O_2{}^{32}S_2{}^{11}B_2{}^{59}Co$: 444.0031]; Δmmu = 1.1.

11: Yield: 1.48 g (47%), red solid, m.p. 232 °C. ^{1}H NMR (200.1 MHz, $CDCl_3$): δ = 4.87 (s, 5 H, H_{Cp}), 7.32, 7.79, 8.09 (m, 16 H, H_{aryl}) ppm. ^{11}B NMR (64.2 MHz, $CDCl_3$): δ = 63 (br.) ppm. ^{13}C NMR (50.3 MHz, $CDCl_3$): δ = 79.90 (C_{Cp}), 84.38 (C_{4ring}), 125.4, 126.4, 141.4 (dithiocatechol) ppm. MS (70 eV, EI): *m/z* (%) = 776 (50) [M^+], 450 (70) [$M^+ - C_6H_4S_2BC{\equiv}CBS_2C_6H_4$]. MS (70 eV, HR-EI): *m/z* (%) = 775.9119 (80) [M^+; $^{12}C_{33}{}^{1}H_{21}{}^{32}S_8{}^{11}B_4{}^{59}Co$: 775.9113]; Δmmu = 0.6.

12: Yield: 1.30 g (45%), brown solid, m.p. 213 °C (dec.). ^{1}H NMR (200.1 MHz, $CDCl_3$): δ = 5.37 (s, 5 H, H_{Cp}), 7.2−7.6 (m, 16 H, H_{aryl}) ppm. ^{11}B NMR (64.2 MHz, $CDCl_3$): δ = 50 (br.) ppm. ^{13}C NMR (50.3 MHz, $CDCl_3$): δ = 83.47 (C_{Cp}), 86.07 (C_{4ring}), 115.1, 121.0, 124.2, 125.5, 126.6, 127.9, 156.5 (2-hydroxythiophenol) ppm. MS (70 eV, EI): *m/z* (%) = 712 (50) [M^+], 418 (100) [$M^+ - C_6H_4OSBC{\equiv}CBOSC_6H_4$]. MS (70 eV, HR-EI): *m/z* (%) = 712.0046 (100) [M^+; $^{12}C_{33}{}^{1}H_{21}{}^{16}O_4{}^{32}S_4{}^{11}B_4{}^{59}Co$: 712.0026]; Δmmu = 2.0.

[η⁴-Bis(*tert*-butyl)bis(catecholborol-2-yl)cyclobutadiene](η⁵-cyclopentadienyl)cobalt(I) (13a/13a′), [η⁴-Bis(*tert*-butyl)bis(4-methyldithiocatecholborol-2-yl)cyclobutadiene](η⁵-cyclopentadienyl)cobalt(I) (14a/14a′) and [η⁴-Bis(1,3,2-benzooxathiaborol-2-yl)bis(*tert*-butyl)cyclobutadiene](η⁵-cyclopentadienyl)cobalt(I) (15a/15a′): Borylacetylene (**6a**: 0.80 g; **7a**: 0.98 g; **8a**: 0.86 g; 4 mmol) was added at −20 °C to a solution of (η⁵-cyclopentadienyl)bis(ethene)cobalt (0.36 g, 2 mmol) in 40 mL of hexane. The reaction mixture was stirred at room temp. for 2 d. After filtration, the solvent was evaporated almost to dryness. The resulting orange-yellow solid was crystallized from toluene.

13a/13a′: Yield: 0.73 g (70%), orange-yellow solid, m.p. 145−150 °C. ^{1}H NMR (200.1 MHz, $CDCl_3$): δ = 1.36 [s, 18 H, $C(CH_3)_3$], 5.02 (s, 5 H, H_{Cp}), 7.09, 7.23 (m, 8 H, H_{aryl}) ppm. ^{11}B NMR (64.2 MHz, $CDCl_3$): δ = 36 (br.) ppm. ^{13}C NMR (50.3 MHz, $CDCl_3$): δ = 30.83 [$C(CH_3)_3$], 32.20 [$C(CH_3)_3$], 80.15 (C_{Cp}), 101.8 (C_{4ring}), 112.2, 122.3, 148.5 (catechol) ppm. MS (70 eV, EI): *m/z* (%) = 524 (100) [M^+], 509 (90) [M^+ − Me], 467 (10) [M^+ − *t*Bu], 387 (35) [$M^+ - t$BuC≡C*t*Bu + 1], 324 (38) [$M^+ - H_4C_6O_2BC{=}Ct$Bu], 124 (75) [CpCo]. MS (70 eV, HR-EI): *m/z* (%) = 524.1727 (100) [M^+; $^{12}C_{29}{}^{1}H_{31}{}^{16}O_4{}^{11}B_2{}^{59}Co$: 524.1740]; Δmmu = −1.3.

14a/14a′: Yield: 0.80 g (65%), orange-yellow solid, m.p. 162−165 °C. ^{1}H NMR (200.1 MHz, $CDCl_3$): δ = 1.16 [s, 18 H, $C(CH_3)_3$], 2.43 (s, 6 H, CH_3), 5.18 (s, 5 H, H_{Cp}), 7.14, 7.65 (m, 6 H, H_{aryl}) ppm. ^{11}B NMR (64.2 MHz, $CDCl_3$): δ = 63 (br.) ppm. ^{13}C NMR (50.3 MHz, $CDCl_3$): δ = 21.49 (CH_3), 31.41 [$C(CH_3)_3$], 32.25 [$C(CH_3)_3$], 79.95 (C_{4ring}), 80.66 (C_{Cp}), 125.3, 125.8, 126.3, 126.6, 129.0, 131.6 (4-methyldithiocatechol) ppm. MS (70 eV, EI): *m/z* (%) = 616 (10) [M^+], 370 (9) [$M^+ - H_3CH_3C_6S_2BC{\equiv}Ct$Bu], 124 (85) [CpCo]. MS (70 eV, HR-EI): *m/z* (%) = 616.1163 (100) [M^+; $^{12}C_{31}{}^{1}H_{35}{}^{32}S_4{}^{11}B_2{}^{59}Co$: 616.1139]; Δmmu = 2.4.

15a/15a′: Yield: 0.72 g (64%), orange-yellow solid, m.p. 154−159 °C. ^{1}H NMR (200.1 MHz, $CDCl_3$): δ = 1.20 [s, 18 H, $C(CH_3)_3$], 5.07 (s, 5 H, H_{Cp}), 7.02−7.55 (m, 8 H, H_{aryl}) ppm. ^{13}C NMR (50.3 MHz, $CDCl_3$): δ = 31.58 [$C(CH_3)_3$], 32.63 [$C(CH_3)_3$], 80.67 (C_{Cp}), 85.20 (C_{4ring}) 114.3, 123.2, 124.9, 125.6, 128.3, 156.8 (2-hydroxythiophenol) ppm. ^{11}B NMR (64.2 MHz, $CDCl_3$): δ = 50 (br.) ppm. MS (70 eV, EI): *m/z* (%) = 556 (70) [M^+], 541 (15) [M^+ − Me], 499 (10) [M^+ − *t*Bu], 419 (10) [$M^+ - t$BuC≡C*t*Bu + 1], 340 (38) [$M^+ - H_4C_6OSBC{\equiv}Ct$Bu], 124 (100) [CpCo]. MS (70 eV, HR-EI): *m/z* (%) = 556.1312 (100) [M^+; $^{12}C_{29}{}^{1}H_{31}{}^{16}O_2{}^{32}S_2{}^{11}B_2{}^{59}Co$: 556.1284]; Δmmu = 2.8.

(η⁵-Cyclopentadienyl)[η⁴-tris(catecholborol-2-yl)tris(trimethylsilyl)cyclohexatriene]cobalt(I) (13b/13b′), (η⁵-Cyclopentadienyl)[η⁴-tris(4-methyldithiocatecholborol-2-yl)tris(trimethylsilyl)cyclohexatriene]cobalt(I) (14b/14b′) and (η⁵-Cyclopentadienyl)[η⁴-tris(1,3,2-benzooxathiaborol-2-yl)tris(trimethylsilyl)cyclohexatriene]cobalt(I) (15b/15b′): 1-Boryl-2-silylacetylene (**6b**: 1.29 g; **7b**: 1.48 g; **8b**: 1.39 g; 6 mmol) was added at room temp. to a solution of (η⁵-cyclopentadienyl)bis(ethene)cobalt (0.36 g, 2 mmol) in 40 mL of hexane. The reaction mixture was stirred at room temp. for 3 d. The solution was concentrated and a brown-red residue was obtained. Purification by column chromatography (Florosil/hexane) with hexane/toluene (2:1) afforded an air-sensitive red oil.

13b/13b′: Yield: 0.65 g (42%). ^{1}H NMR (200.1 MHz, C_6D_6): δ = 0.18, 0.20 (s, 27 H, $SiMe_3$), 5.05 (s, 5 H, H_{Cp}), 6.35, 6.75, 6.82 (m, 12 H, H_{aryl}) ppm. ^{11}B NMR (64.2 MHz, C_6D_6): δ = 33 (br.) ppm. ^{13}C NMR (50.3 MHz, C_6D_6): δ = −0.51, −0.04, 0.40, 0.56 ($SiMe_3$), 82.61 (C_{Cp}), 112.0, 122.1, 148.7 (catechol), 122.0, 122.5, 146.4, 149.9 (central C_{6ring}) ppm. ^{29}Si NMR (39.7 MHz, C_6D_6): δ = −21.8, −18.1, −0.7, 20.3 ppm. MS (70 eV, EI): *m/z* (%) = 772 (100) [M^+], 699 (7) [M^+ − Me]. MS (70 eV, HR-EI): *m/z* (%) = 772.2056 (100) [M^+; $^{12}C_{38}{}^{1}H_{44}{}^{16}O_6{}^{28}Si_3{}^{11}B_3{}^{59}Co$: 772.2057]; Δmmu = −0.1.

14b/14b′: Yield: 0.73 g (40%). ^{1}H NMR (200.1 MHz, $CDCl_3$): δ = 0.20 (s, 27 H, $SiMe_3$), 2.28 (s, 9 H, CH_3), 5.45 (s, 5 H, H_{Cp}), 7.01−7.90 (m, 12 H, H_{aryl}) ppm. ^{11}B NMR (64.2 MHz, $CDCl_3$): δ = 60 (br.) ppm. ^{13}C NMR (50.3 MHz, $CDCl_3$): δ = 0.29 ($SiMe_3$), 20.98 (CH_3), 79.76 (C_{Cp}), 124.5, 126.6, 130.1, 132.8, 140.2 (4-

 © 2004 Wiley-VCH Verlag GmbH & Co. KGaA, Weinheim

methyldithiocatechol), 126.4 (central C_{6ring}) ppm. ^{29}Si NMR (39.7 MHz, $CDCl_3$): $\delta = -21.9$ ppm. MS (70 eV, EI): *m/z* (%) = 910 (25) [M^+], 895 (10) [$M^+ - Me$], 837 (10) [$M^+ - SiMe_3$], 745 (20) [$M^+ - H_3CC_6H_3S_2B$]. MS (70 eV, HR-EI): *m/z* (%) = 910.1175 (100) [M^+; $^{12}C_{41}{}^1H_{50}{}^{32}S_6{}^{28}Si_3{}^{11}B_3{}^{59}Co$: 910.1155]; Δmmu = 2.0.

15b/15b′: Yield: 0.62 g (38%). ^{1}H NMR (200.1 MHz, $CDCl_3$): δ = 0.21 (s, 27 H, $SiMe_3$), 4.96 (s, 5 H, H_{Cp}), 6.20−6.99 (m, 12 H, H_{aryl}) ppm. ^{11}B NMR (64.2 MHz, $CDCl_3$): δ = 49 (br.) ppm. ^{13}C NMR (50.3 MHz, $CDCl_3$): $\delta = -0.34$ ($SiMe_3$), 81.24 (C_{Cp}), 115.0, 124.1, 125.6, 126.5, 126.8, 156.6 (2-hydroxythiophenol), 132.2 (central C_{6ring}) ppm. ^{29}Si NMR (39.7 MHz, $CDCl_3$): $\delta = -20.2$ ppm. MS (70 eV, EI): *m/z* (%) = 820 (100) [M^+]. MS (70 eV, HR-EI): *m/z* (%) = 820.1392 (30) [M^+; $^{12}C_{38}{}^1H_{44}{}^{16}O_3{}^{32}S_3{}^{28}Si_3{}^{11}B_3{}^{59}Co$: 820.1371]; Δmmu = 2.1.

[η^4-Bis(*tert*-butyl)cyclobutadiene](η^5-cyclopentadienyl)cobalt(I) (16): In attempts to purify **13a**, **14a** or **15a** by column chromatography on Florosil, the crude products were eluted with hexane; only hydrolysis to **16** was observed. Yellow solid, m.p. 68 °C. ^{1}H NMR (200.1 MHz, $CDCl_3$): δ = 1.03 [s, 18 H, $C(CH_3)_3$], 3.56 (s, 2 H, CH), 4.82 (s, 5 H, H_{Cp}) ppm. ^{13}C NMR (50.3 MHz, $CDCl_3$): δ = 29.65 [$C(CH_3)_3$], 29.81 [$C(CH_3)_3$], 78.81 (CCp), 50.88, 90.36 (C_{4ring}) ppm. MS (70 eV, EI): *m/z* (%) = 288 (100) [M^+], 273 (80) [$M^+ - Me$], 124 (10) [CpCo]. MS (70 eV, HR-EI): *m/z* (%) = 288.1283 (100) [M^+; $^{12}C_{17}{}^1H_{25}{}^{59}Co$: 288.1289]; Δmmu = −0.6.

Tris(1,3,2-benzodithiaborol-2-yl)benzene (17/17′), Tris(1,3,2-benzooxathiaborol-2-yl)benzene (18/18′), Hexakis(1,3,2-benzodithiaborol-2-yl)benzene (19) and Hexakis(1,3,2-benzooxathiaborol-2-yl)benzene (20): Borylalkyne (**1a**: 0.52 g; **2**: 0.48 g; **3**: 0.98 g; **4**: 0.88 g; 3 mmol) and octacarbonyldicobalt (0.05 g, 0.15 mmol, 5 mol-%) were heated under reflux in 20 mL of toluene for 4 d. The solid was separated, washed several times with small amounts of solvents (**17/17′** and **18/18′**: hexane and toluene; **19** and **20**: toluene and CH_2Cl_2) and dried in vacuo.

17/17′: Yield: 0.40 g (77%), colorless solid, m.p. 192−194 °C. ^{1}H NMR (200.1 MHz, $CDCl_3$): δ = 7.34, 7.89, 8.42 (m, 15 H, H_{aryl}) ppm. ^{11}B NMR (64.2 MHz, $CDCl_3$): δ = 61 (br.) ppm. ^{13}C NMR (50.3 MHz, $CDCl_3$): δ = 126.8, 131.1, 140.1 (dithiocatechol) ppm; owing to low solubility,the signals of the central benzene ring carbon atoms were not observed. MS (70 eV, EI): *m/z* (%) = 528 (100) [M^+]. MS (70 eV, HR-EI): *m/z* (%) = 527.9781 (100) [M^+; $^{12}C_{24}{}^1H_{15}{}^{32}S_6{}^{11}B_3$: 527.9777]; Δmmu = 0.4.

18/18′: Yield: 0.30 g (62%), colorless solid, m.p. 176−179 °C. ^{1}H NMR (200.1 MHz, $CDCl_3$): δ = 6.9−8.7 (m, 15 H, H_{aryl}) ppm. ^{11}B NMR (64.2 MHz, $CDCl_3$): δ = 51 (br.) ppm. ^{13}C NMR (50.3 MHz, $CDCl_3$): δ = 111.8, 115.1, 121.1, 130.5, 135.5, 156.2 (2-hydroxythiophenol) ppm; the signals of the central benzene ring carbon atoms were not found. MS (70 eV, EI): *m/z* (%) = 480 (100) [M^+]. MS (70 eV, HR-EI): *m/z* (%) = 480.0489 (100) [M^+; $^{12}C_{24}{}^1H_{15}{}^{16}O_3{}^{32}S_3{}^{11}B_3$: 480.0462]; Δmmu = 2.7.

19: Yield: 0.70 g (71%), colorless solid, m.p. > 300 °C. MS (70 eV, EI): *m/z* (%) = 978 (100) [M^+]. MS (70 eV, HR-EI): *m/z* (%) = 977.9128 (20) [M^+; $^{12}C_{42}{}^1H_{24}{}^{32}S_{12}{}^{11}B_6$: 977.9085]; Δmmu = 4.3.

20: 0.69 g (78%), colorless solid, m.p. > 300 °C. MS (70 eV, EI): *m/z* (%) = 882 (100) [M^+]. MS (70 eV, HR-EI): *m/z* (%) = 882.0461 (100) [M^+; $^{12}C_{42}{}^1H_{24}{}^{16}O_6{}^{32}S_6{}^{11}B_6$: 882.0455]; Δmmu = 0.6.

X-ray Crystal-Structure Determinations of 1b, 5b, 6b, 14a, 15a and 16: Crystal data and details of the structure determinations are listed in Table 1. Reflections covering a whole sphere in the reciprocal space were collected with a Bruker-AXS SMART 1000 diffractometer (Mo-K_α radiation, λ = 0.71073 Å, graphite mono-

Table 1. Crystal data and structure refinement for **1b**, **5b**, **6b**, **14a**, **15a** and **16**

	1b	**5b**	**6b**	**14a**	**15a**	**16**
Empirical formula	$C_{15}H_{23}BClNS_2$	$C_{17}H_{37}BN_2Si$	$C_{11}H_{13}BO_2Si$	$C_{31}H_{35}B_2CoS_4$	$C_{29}H_{31}B_2CoO_2S_2$	$C_{17}H_{25}Co$
Formula mass	327.72	308.39	216.11	616.38	556.21	288.30
Crystal system	monoclinic	orthorhombic	monoclinic	triclinic	orthorhombic	orthorhombic
Space group	$P2_1/c$	*Pbca*	$P2_1/c$	$P\bar{1}$	*Pbcn*	$Pna2_1$
a [Å]	16.2143(9)	18.6824(9)	18.282(2)	9.2159(1)	20.2951(4)	35.667(2)
b [Å]	7.5937(4)	11.8851(6)	5.4417(6)	9.2834(1)	8.9817(2)	5.9534(3)
c [Å]	15.5136(9)	19.0239(10)	11.7267(13)	18.0504(3)	30.1865(3)	14.3418(6)
α [°]	90	90	90	89.922(1)	90	90
β [°]	106.953(1)	90	95.612(2)	84.980(1)	90	90
γ [°]	90	90	90	88.738(1)	90	90
V [Å^3]	1827.1(2)	4224.1(4)	1161.1(2)	1538.0(3)	5502.5(2)	3045.4(2)
Z	4	8	4	2	8	8
$D_{calcd.}$ [g·cm^{-3}]	1.191	0.970	1.236	1.33	1.343	1.258
μ [mm^{-1}]	0.428	0.109	0.178	0.85	0.80	1.109
F(000)	696	1376	456	644	2320	1232
Crystal size [mm]	0.40 × 0.32 × 0.16	0.57 × 0.20 × 0.14	0.50 × 0.50 × 0.30	0.40 × 0.08 × 0.08	0.16 × 0.14 × 0.06	0.35 × 0.18 × 0.10
θ_{max} [°]	32.06	32.04	32.03	27.5	22.3	32.03
Index ranges	−24/22, 0/11, 0/23	0/27, 0/17, 0/28	−26/26, 0/ 7, 0/17	−11/11, −12/12, −23/23	−21/21, −9/9, −32/32	0/53, 0/8, −21/16
Reflections collected	32418	48978	19854	16166	34030	27277
Reflections independent (R_{int})	6329 (0.0341)	7305 (0.0449)	3961 (0.0399)	6996 (0.0363)	3477 (0.0740)	9051(0.0426)
Parameters	335	338	188	362	331	524
Goodness-of-fit on F^2	1.069	1.041	1.058	1.03	1.02	1.051
*R*1 [$I > 2\sigma(I)$]	0.0376	0.0417	0.0361	0.0360	0.0345	0.0392
*wR*2 (all reflections)	0.1042	0.1128	0.0994	0.0852	0.0814	0.0899
T [K]	103(2)	103(2)	103(2)	200(2)	200(2)	103(2)
Residual electron density [e/Å^3]	0.37/−0.24	0.48/−0.19	0.48/−0.23	0.36/−0.29	0.21/−0.28	0.67/−0.64

 © 2004 Wiley-VCH Verlag GmbH & Co. KGaA, Weinheim

chromator, ω-scan). Empirical absorption corrections were applied. The structures were solved by direct methods (SHELXS-86)[17] and refined by least-squares methods based on F^2 with all measured reflections (SHELXL-97).[18] All non-hydrogen atoms were refined anisotropically. In **1b** the dithiocatechol is disordered and the cell contains one diisopropylamino hydrochloride. CCDC-238364 (**1b**), -238365 (**5b**), -238366 (**6b**), -238367 (**15a**), -238368 (**16**) and -238369 (**14a**) contain the supplementary crystallographic data for this paper. These data can be obtained free of charge at www.ccdc.cam.ac.uk/conts/retrieving.html [or from the Cambridge Crystallographic Data Centre, 12 Union Road, Cambridge CB2 1EZ, UK; Fax: + 44-1223-336-033; E-mail: deposit@ccdc.cam.ac.uk].

Acknowledgments

This work was supported by the SFB 623 and the Fonds der Chemischen Industrie. We wish to thank Prof. R. Gleiter for fruitful discussions.

[1] [1a] H. Pelissier, J. Rodriguez, K. C. P. Vollhardt, *Chem. Eur. J.* **1999**, *5*, 3549−3561. [1b] S. Ito, H. Inabe, T. Okujima, N. Morita, M. Watanabe, N. Harada, K. Imafuku, *J. Org. Chem.* **2001**, *66*, 7090−7101. [1c] A. H. M. Elwahy, K. Hafner, *Tetrahedron Lett.* **2000**, *41*, 2859−2862.

[2] [2a] K. P. C. Vollhardt, *Angew. Chem.* **1984**, *96*, 525−542; *Angew. Chem. Int. Ed. Engl.* **1984**, *23*, 539−644. [2b] H. Bönnemann, W. Brijoux, R. Brinkmann, W. Meurers, R. Mynott, W. von Phillipsborn, T. Egolf, *J. Organomet. Chem.* **1984**, *272*, 231−249.

[3] [3a] A. Efraty, *Chem. Rev.* **1977**, *77*, 691−744. [3b] R. Gleiter, *Angew. Chem.* **1992**, *104*, 29−46; *Angew. Chem. Int. Ed. Engl.* **1992**, *31*, 27−44. [3c] A. Nakamura, N. Hagihara, *Bull. Chem. Soc. Jpn.* **1961**, *34*, 452−453. [3d] M. D. Rausch, R. A. Genetti, *J. Am. Chem. Soc.* **1967**, *89*, 5502−5503. [3e] J. L. Boston, D. W. A. Sharp, G. Wilkinson, *J. Chem. Soc.* **1962**, 3488−3494.

[4] N. Schore, *Chem. Rev.* **1988**, *88*, 1081−1119.

[5] A. Goswami, C. J. Maier, H. Pritzkow, W. Siebert, *Eur. J. Inorg. Chem.* **2004**, 2635−2645.

[6] J. Haberecht, A. Krummland, F. Breher, B. Gebhardt, H. Rüegger, R. Nesper, H. Grützmacher, *Dalton Trans.* **2003**, 2126−2132.

[7] F. H. Allen, O. Kennard, D. G. Watson, L. Brammer, A. G. Orpen, R. Taylor, *J. Chem. Soc., Perkin Trans. 2* **1987**, S1−S19.

[8] H. Yao, M. Sabat, R. N. Grimes, *Organometallics* **2003**, *22*, 2581−2593.

[9] J. P. Collman, L. S. Hegedus, J. R. Norton, R. G. Finke, *Principles and Applications of Organometransition Metal Chemistry*, University Science Book, Mill Valley, **1987**.

[10] J. K. Cammack, S. Jalisatgi, A. J. Matzger, A. Negron, K. P. C. Vollhardt, *J. Org. Chem.* **1996**, *61*, 4798−4800.

[11] H. Borwieck, O. Walter, E. Dinjus, J. Rebizant, *J. Organomet. Chem.* **1998**, *570*, 121−127.

[12] [12a] U. Koelle, B. Fuss, M. V. Rajasekharan, B. L. Ramakrishna, J. H. Ammeter, M. C. Böhm, *J. Am. Chem. Soc.* **1984**, *106*, 4152−4160. [12b] U. Koelle, B. Fuss, *Chem. Ber.* **1986**, 116−128. [12c] D. W. Macomber, A. G. Verma, *Organometallics* **1988**, *7*, 1241−1253.

[13] [13a] M. E. Arnett, J. M. Bollinger, *J. Am. Chem. Soc.* **1964**, *86*, 4729−4731. [13b] C. Ester, A. Maderna, H. Pritzkow, W. Siebert, *Eur. J. Inorg. Chem.* **2000**, 1177−1184.

[14] Y. Gu, H. Pritzkow, W. Siebert, *Eur. J. Inorg. Chem.* **2001**, 373−379.

[15] P. Y. Chavant, M. Vaultier, *J. Organomet. Chem.* **1993**, *455*, 37−46.

[16] H. Schulz, G. Gabbert, H. Pritzkow, W. Siebert, *Chem. Ber.* **1993**, *126*, 1593.

[17] G. M. Sheldrick, *SHELXS-86*, Univ. Göttingen, **1986**.

[18] G. M. Sheldrick, *SHELXL-97*, Univ. Göttingen, **1997**.

Received May 21, 2004
Early View Article
Published Online September 10, 2004

 © 2004 Wiley-VCH Verlag GmbH & Co. KGaA, Weinheim

Isolation of an Intermediate during the Decomposition of a Tetragold-Phosphane Complex

Nermin Biricik,[a] Zhaofu Fei,[a] Rosario Scopelliti,[a] and Paul J. Dyson*[a]

Keywords: N,P Ligands / Diphosphanylamines / Gold complexes

Reaction of the diphosphanylamine 2,6-{$(Ph_2P)_2N$}$_2C_5H_3N$ with four equivalents of Au(tht)Cl (tht = tetrahydrothiophene) affords the tetragold complex 2,6-{$(ClAuPh_2P)_2N$}$_2C_5H_3N$ in high yield. Decomposition of the tetragold compound results in the formation of the digold complex 2,6-{$(ClAuPh_2P)HN$}$_2C_5H_3N$ and colloidal gold. A trigold intermediate, which contains a Au–Au interaction [2.9886(5) Å] has been isolated, and while ultimately unstable, it is thought to be partially stabilised by virtue of the aurophilic nature of gold.
(© Wiley-VCH Verlag GmbH & Co. KGaA, 69451 Weinheim, Germany, 2004)

Introduction

Gold(I)-phosphane complexes and clusters have been extensively studied over the years.[1] Apart from fundamental interest in these types of compounds, they exhibit a number of interesting properties which gives rise to a wide range of different applications. Gold(I) complexes display anticancer activity and are employed in clinics for the treatment of rheumatoid arthritis.[2] In addition, they exhibit interesting photophysical[3] and catalytic properties.[4] From the plethora of studies involving gold(I) complexes, interactions between linearly coordinated gold(I) centres have been found to be extremely common, leading to self-assembled suprastructures through Au−Au intermolecular contacts.[5] In many cases these suprastructures exhibit strong photo-luminescence.[6] The term used to describe the affinity of gold to form Au−Au interactions is "aurophilicity",[7] which was introduced in 1989, and theoretical studies have since placed the effect on a solid foundation.[8]

Many different phosphane ligands have been used to form complexes with gold, in particular heterodentate phosphanes, which tend to afford multi-nuclear complexes containing Au−Au interactions.[9] Such interactions have been shown to persist in solution.[10] Aurophilicity is especially favoured where several phosphorus centres are in close proximity, enabling intramolecular auration, for example, in calix[3]arene and calix[4]arene based phosphane systems.[11] Complexes with diphosphanylamine ligands are also known.[12] Diphosphanylamines comprise a P−N−P backbone and some of their gold(I) complexes are light/moisture sensitive,[13] presumably due to the instability of both the P−N and Au−P bonds, resulting in the formation of colloidal gold particles. Formation of gold colloids, typically denoted by the precipitation of a purple/black powder, is frequently observed in gold(I) chemistry, however, the intermediate species formed during the decomposition process and decomposition mechanism remain essentially unknown. In this paper we describe the synthesis of a tetragold-diphosphanylamine complex and its decomposition to a digold species in which an intermediate trigold compound is isolated and characterised, providing insight into the decomposition mechanism.

[a] Institut des Sciences et Ingénierie Chimiques, Ecole Polytechnique Fédérale de Lausanne, EPFL-BCH,
1015 Lausanne, Switzerland
E-mail: paul.dyson@epfl.ch

Results and Discussion

The diphosphanylamine ligand 2,6-{$(Ph_2P)_2N$}$_2C_5H_3N$ (**L_1**) has previously been shown to undergo a remarkable reaction with H^+ to form the iminobiphosphane 2,6-$(Ph_2P-Ph_2P=N)_2C_5H_3NH^+$.[14] Since H^+ and certain gold fragments are isolobal[15] we thought that it would be interesting to explore the reactivity of **L_1** towards gold. Thus, under an inert atmosphere, **L_1** was treated with four equivalents of Au(tht)Cl (tht = tetrahydrothiophene) in dichloromethane at room temperature yielding 2,6-{$(ClAuPh_2P)_2N$}$_2C_5H_3N$ (**1**) as the only product (Scheme 1). The ^{31}P NMR spectrum of the reaction solution exhibits a sharp singlet at $\delta = 84.0$ ppm indicating that all of the phosphorus atoms are equivalent. In addition, the electrospray ionisation mass spectrum of **1** in dichloromethane exhibits a parent peak at $m/z = 1775$ which corresponds to the protonated intact parent ion $[M + H]^+$. After removal of the solvent under reduced pressure **1** was obtained as a white powder.

Compound **1** is stable in the solid state, but decomposes slowly in solution on exposure to air/moisture. The decomposition reaction can be monitored by ^{31}P NMR spectroscopy. The ^{31}P NMR spectrum in dichloromethane exhi-

 © 2004 Wiley-VCH Verlag GmbH & Co. KGaA, Weinheim **DOI: 10.1002/ejic.200400439**

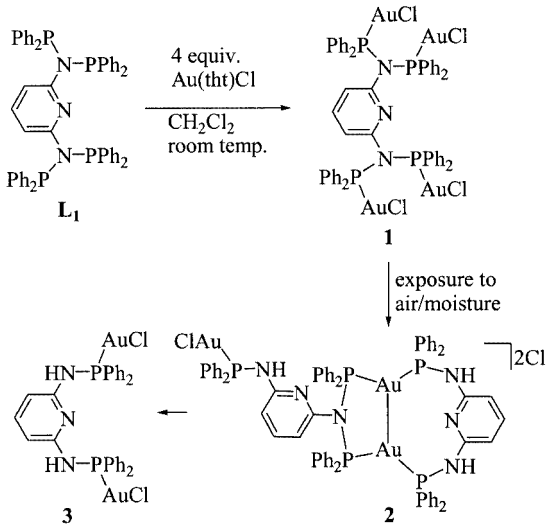

Scheme 1. Degradation of **1** and its decomposition to **3** via **2**, following exposure to air/light

bits, in the first instance, the signal at δ = 84.0 ppm corresponding to **1**, which decreases in intensity until it has completely disappeared after six hours. In its place three broad signals at 97.0, 68.9, 52.2 ppm (for which the P−P coupling could not be resolved) together with signals at δ = 35.6 ppm and −20.6 ppm ($J_{P\text{-}P}$ = 229.0 Hz) which are readily attributed to $Ph_2P(O)PPh_2$,[16] are observed. Simultaneously, the reaction mixture turns from colourless to purple, a characteristic colloid colouration, due to the formation of elemental gold. The three unidentified signals correspond to a new complex **2**, which by virtue of being a salt, precipitates from solution, on addition of diethyl ether. After filtration and removal of the solvent, the solid was washed with diethyl ether and obtained in its pure form and recrystallised from chloroform to afford crystals suitable for analysis by X-ray diffraction. The structure of the dication in **2** is shown in Figure 1 and key bond parameters are listed in the caption. Crystal data and details of the structure determination are listed in Table 1 and further details are given in the Experimental Section.

Compound **2** contains three gold centres and two different ligands, 2-{$(Ph_2P)_2N$}-6-{$(Ph_2P)HN$}-C_5H_3N (**L_2**) and 2,6-{$(Ph_2P)HN$}$_2C_5H_3N$ (**L_3**) (see Figure 2), both derived from the diphosphanylamine ligand **L_1** by substitution of one and two Ph_2P units by a proton, respectively. The Au−P and Au−Cl distances in **2** are similar to those observed in structurally related compounds;[17] whereas the Au−Au distance is 2.9886(5) Å, which is somewhat longer than those usually found in complexes containing Au−Au bonds within an "A"-frame structure involving a five-membered ring.[18] However, this distance is not long when compared to those observed in complexes where the gold centres are not orientated in such close proximity. The Au(1)−P(1) [2.301(2) Å], Au(1)−P(3) [2.312(2) Å], Au(2)−P(2) [2.303(2) Å] and Au(2)−P(4) [2.299(2) Å] distances are all similar, being slightly longer than the Au(3)−P(5) [2.219(3) Å] distance which involves the P−Au−Cl system. While the P(5)−Au(3)−Cl(1) fragment is nearly linear with an angle of 177.33(9)°, the P(1)−Au(1)−P(3) and P(2)−Au(2)−P(4) units form angles

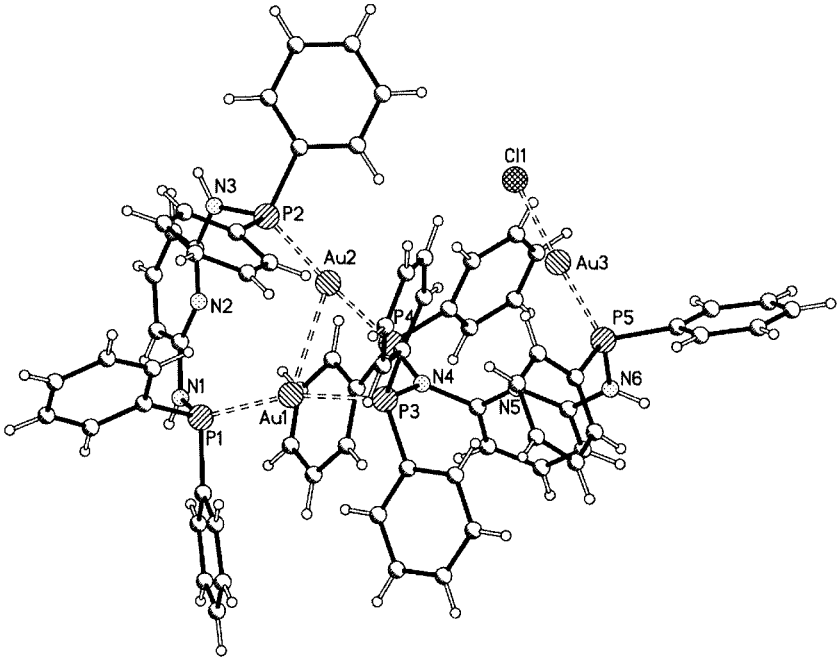

Figure 1. Molecular structure of **2** in the solid state (ball-and-stick representation showing just the cation with a partial labelling scheme, the Cl anions and all the solvent molecules have been omitted for clarity); key bond lengths (Å) and angles (°) include: Au(1)−P(1) 2.301(2), Au(1)−P(3) 2.312(2), Au(1)−Au(2) 2.9886(5), Au(2)−P(4) 2.299(2), Au(2)−P(2) 2.303(2), Au(3)−P(5) 2.219(3), Au(3)−Cl(1) 2.305(3), P(1)−N(1) 1.670(7), P(2)−N(3) 1.673(8), P(3)−N(4) 1.694(7), P(4)−N(4) 1.702(8), P(5)−N(6) 1.676(8), P(1)−Au(1)−P(3) 163.94(8), P(1)−Au(1)−Au(2) 112.58(6), P(3)−Au(1)−Au(2) 80.68(6), P(4)−Au(2)−P(2) 174.23(8), P(4)−Au(2)−Au(1) 78.00(6), P(2)−Au(2)−Au(1) 107.24(6), P(5)−Au(3)−Cl(1) 177.33(9)

 © 2004 Wiley-VCH Verlag GmbH & Co. KGaA, Weinheim

Table 1. Crystal data and details of the structure determination for **2** and **3**

	2	**3**
Empirical formula	$C_{78}H_{67}Au_3Cl_{27}N_6P_5$	$C_{30.5}H_{28}Au_2Cl_5N_3P_2$
Molecular mass	2791.28	1069.68
Crystal system	triclinic	triclinic
Space group	$P\bar{1}$	$P\bar{1}$
a (Å)	15.8163(11)	10.0883(7)
b (Å)	16.2804(8)	12.4008(9)
c (Å)	22.6502(12)	15.1675(10)
a (°)	83.714(4)	112.597(7)
b (°)	73.581(5)	95.294(5)
g (°)	65.340(6)	99.932(6)
V (Å^3)	5084.1(5)	1699.1(2)
Z	2	2
$D_{calcd.}$ (g cm^{-3})	1.823	2.091
F(*000*)	2696	1010
m (mm^{-1})	5.150	9.138
Temp. (K)	140(2)	140(2)
Wavelength (Å)	0.71073	0.71073
Measured reflections	29979	9959
Unique reflections	15710	5244
Unique reflections with $I > 2\sigma(I)$	12810	4698
Data/parameters	15710/1075	5244/388
$R^{[a]}$ [$I > 2\sigma(I)$]	0.0563	0.0280
$wR2^{[a]}$ (all data)	0.1602	0.0745
GoF	1.051	1.070

[a] $R = \Sigma||F_o| - |F_c||/\Sigma|F_o|$, $wR2 = \{\Sigma[w(F_o^2 - F_c^2)^2]/\Sigma[w(F_o^2)^2]\}^{1/2}$. [b] GoF = $\{\Sigma[w(F_o^2 - F_c^2)^2]/(n - p)\}^{1/2}$ where *n* is the number of data and *p* is the number of parameters refined.

to **2** steadily disappear, with the concomitant formation of a new singlet resonance at δ = 55.1 ppm. The peak at δ = 55.1 ppm has been assigned to **3**, which has been isolated in its pure form following the decomposition of **2** in dichloromethane on a preparative scale. In addition, **3** can be prepared directly from the reaction of Au(tht)Cl with 2,6-{$(Ph_2P)HN\}_2C_5H_3N$ (see below). The other components from the reaction, as denoted by ^{31}P NMR spectroscopy, have been tentatively assigned as $Ph_2P(O)PPh_2$ (see above), with lesser amounts of $Ph_2P(O)OH$ and Ph_2POH, as represented by signals of low relative intensity at δ = 35.5 and 24.0 ppm. A dark purple precipitate is observed which presumably corresponds to gold colloid. The structure of **3** has been established in the solid-state by single-crystal X-ray diffraction on crystals grown from a dichloromethane/diethyl ether solution at room temperature. The molecular structure of **3** is shown in Figure 3 and key bond parameters are listed in the caption.

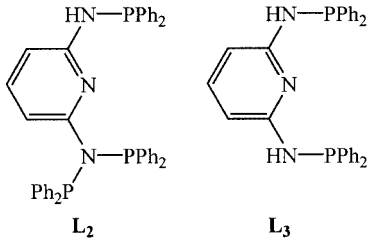

Figure 2. Ligands $\mathbf{L_2}$ and $\mathbf{L_3}$

of 163.94(8) and 174.23(8)°, respectively. The deviation from linearity is presumably due to the bulky ligands surrounding the Au−Au unit, which also results in the relatively long Au−Au contact.

Compound **2** is stable in the solid-state, but decomposes in solution on exposure to air/light. The decomposition reaction of complex **2** in dichloromethane was followed in situ by ^{31}P NMR spectroscopy. The peaks corresponding

Compound **3** is based on a $\mathbf{L_3}$-type ligand in which a Au−Cl fragment coordinates to each phosphorus(III) centre. The parameters in **3** are largely in accordance with the structurally similar compounds.[12,13] The Au(1)−P(1) [2.2377(14) Å] and Au(2)−P(2) [2.2359(15) Å] bond lengths are similar and somewhat longer than the related Au(3)−P(5) bond of 2.219(3) Å in **2**. The P(1)−Au(1)−Cl(1) and P(2)−Au(2)−Cl(2) units are essen-

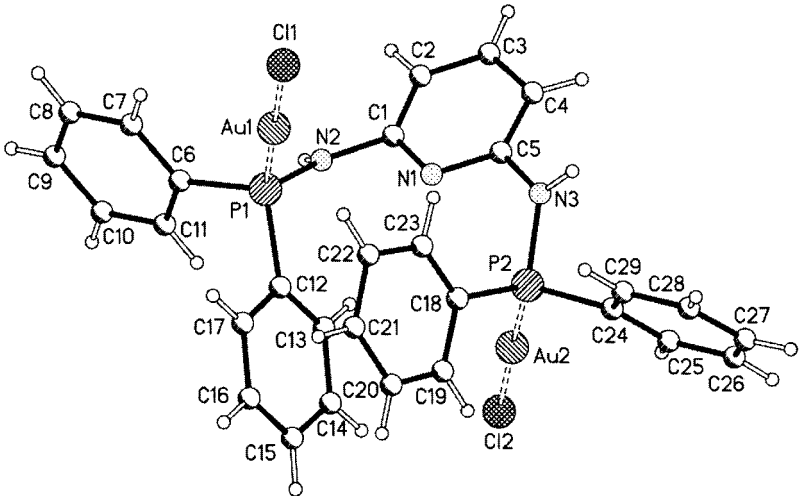

Figure 3. Molecular structure of **3** in the solid-state (ball-and-stick representation showing the labelling scheme, the solvent molecules have been omitted); key bond lengths (Å) and angles (°) include: Au(1)−P(1) 2.2377(14), Au(1)−Cl(1) 2.3229(13), Au(2)−P(2) 2.2359(15), Au(2)−Cl(2) 2.3063(14), P(1)−N(2) 1.698(5), P(2)−N(3) 1.710(5), P(1)−Au(1)−Cl(1) 179.59(5), P(2)−Au(2)−Cl(2) 178.69(6)

 © 2004 Wiley-VCH Verlag GmbH & Co. KGaA, Weinheim

tially linear with bond angles of 179.59(5) and 178.69(6)°, respectively.

The decomposition process **1** → **2** → **3** is worth some further comment since **2** cannot be prepared by a rational route. Complex **2** contains two different aminophosphane ligands, $\mathbf{L_2}$ and 2,6-{$(Ph_2P)HN$}$_2C_5H_3N$ ($\mathbf{L_3}$) which are derived from $\mathbf{L_1}$ by substitution of one and two Ph_2P units by a proton, respectively. Ligand $\mathbf{L_3}$ has been reported before,[19] and attempts to prepare $\mathbf{L_2}$ using a rational route, viz. reaction of one equivalent of 2,6-diaminopyridine with three equivalents of Ph_2PCl, are only partially successful. The main product from this reaction is $\mathbf{L_1}$ based on ^{31}P NMR spectroscopy and electrospray ionisation mass spectrometry. The formation of $\mathbf{L_2}$ was identified in the reaction mixture by electrospray ionisation mass spectrometry which contained peaks corresponding to $\mathbf{L_1}$ and $\mathbf{L_2}$, the peak at m/z = 662 corresponds to $[\mathbf{L_2}+H]^+$, but it has, as yet, not been possible to isolate $\mathbf{L_2}$ from the mixture, although attempts are ongoing.

Reaction of $\mathbf{L_3}$ with Au(tht)Cl in a 1:2 molar ratio gave complex **3** in quantitative yield, however, all attempts to prepare **2** from different combinations of $\mathbf{L_1}$ and $\mathbf{L_3}$ and Au(tht)Cl were unsuccessful. The reason that **2** is isolated at all is probably due to the lower solubility of **2** relative to **1** and **3** since it is a salt which facilitates precipitation from the reaction solution. However, this property alone does not fully explain the stability of **2** and we propose that the aurophilicity of gold, resulting in the Au−Au interaction, further stabilises the intermediate and facilitates its isolation. This property frequently results in structural diversity in gold(I) complexes.[20] However, we believe that compound **2** is especially pleasing as all researchers preparing novel gold complexes are frequently frustrated by decomposition to (or formation of) gold colloids, and in our system, we were fortunate enough to isolate a decomposition intermediate.

Experimental Section

The ligands 2,6-{$(Ph_2P)_2N$}$_2C_5H_3N$ ($\mathbf{L_1}$)[21] and 2,6-{$(Ph_2P)HN$}$_2C_5H_3N$ ($\mathbf{L_3}$)[19] and the complex Au(tht)Cl (tht = tetrahydrothiophene)[22] were prepared according to literature methods. Solvents were dried using appropriate reagents and distilled prior to use. NMR spectra were recorded in $CDCl_3$ at 20 °C with a Bruker DMX 200 instrument using $SiMe_4$ as the external standard for the ^1H NMR spectroscopy and 85% H_3PO_4 for the ^{31}P NMR spectroscopy. ESI-MS spectra were recorded on a ThermoFinnigan LCQ↗ Deca XP Plus quadrupole ion trap instrument using a literature method.[23] Samples were infused directly into the source at 5 μL min^{-1} using a syringe pump. The spray voltage was set at 5 kV and the capillary temperature at 50 °C. The MS detector was tuned automatically on the base peak, which optimised the remaining parameters. Elemental analyses was carried out at the Institute of Molecular and Biological Chemistry at the EPFL.

Synthesis of 1: Au(tht)Cl (256 mg, 0.80 mmol) was added to a solution of 2,6-{$(Ph_2P)_2N$}$_2C_5H_3N$ (170 mg, 0.20 mmol) in dichloromethane (10 mL) at 0 °C. The reaction mixture was allowed to warm to room temperature and stirred for 15 minutes. The solvent was removed under vacuum and the resulting white solid was washed with diethyl ether (2 × 2 mL) to give the product **1** as a white powder. Yield: 330 mg, 94%. ^1H NMR: δ = 6.5−8.20 (m, aromatic H) ppm. ^{31}P NMR: δ = 84.0 (s) ppm. ESI-MS$^+$ m/z: 1775 $[M + H]^+$. $C_{53}H_{43}Au_4Cl_4N_3P_4$ (1775.52): H 2.44, C 35.85, N 2.37; found H 2.47, C 35.89, N 2.34.

Synthesis of 2: A solution of **1** (300 mg, 0.17 mmol) in dichloromethane (10 mL) was stirred in air for 6 h at room temperature, after which time the ^{31}P NMR spectra showed the absence of the starting material **1**. The solvent was removed under reduced pressure and the remaining solid was washed with diethyl ether (3 × 10 mL) to give **2** as a white powder. Colourless crystals were obtained by slow evaporation of a solution in $CDCl_3$ at room temperature. Yield: 105 mg, 22%. M.p. 147 °C. ^1H NMR: δ = 6.5−8.20 (m, aromatic H); 6.30 (broad signal, NH) ppm. ^{31}P NMR: δ = 97.0 (broad signal), 68.9 (broad signal), 52.2 (broad signal) ppm. ESI-MS$^+$ m/z: 1765 [cation]$^+$. $C_{70}H_{59}Au_3Cl_3N_6P_5$ (1836.40): H 3.24, C 45.78, N 4.58; found H 3.31, C 45.89, N 4.60.

Synthesis of 3. Method A: A solution of **2** (190 mg, 0.10 mmol) in dichloromethane (10 mL) was stirred in air in for 24 hours at room temperature. The solvent was removed under reduced pressure and the remaining solid was washed with diethyl ether (3 × 10 mL). Colourless crystals were obtained by slow evaporation of a solution in dichloromethane at room temperature in two days. Yield: 40 mg, 41%.

Method B: Au(tht)Cl (64 mg, 0.20 mmol) was added to a solution of $\mathbf{L_3}$ (47 mg, 0.10 mmol) in dichloromethane (10 mL) at 0 °C. The reaction mixture was allowed to warm to room temperature and stirred for 30 minutes. The solvent was removed under vacuum and the resulting white solid was washed with diethyl ether (2 × 2 mL) to give the product **3** as a white powder. Yield: 90 mg, 95%. M.p. 163 °C (decmp.). ^1H NMR: δ = 6.5−8.20 (m, aromatic H); 6.50 (br., NH) ppm. ^{31}P NMR: δ = 55.1 (s) ppm. ESI-MS$^+$ m/z: 942 $[M + H]^+$. $C_{29}H_{25}Au_2Cl_2N_3P_2$ (942.32): H 2.67, C 36.96, N 4.46; found H 2.71, C 37.04, N 4.39.

X-ray Sructure Determination: Details about the crystals and their structure refinement are listed in Table 1, whereas relevant geometrical parameters, including bond lengths and angles are included in the figure captions. Data collections for both compounds were performed at 140 K on a 4-circle goniometer having kappa geometry and equipped with an Oxford Diffraction KM4 Sapphire CCD. Data reduction was carried out with CrysAlis RED, release 1.7.0.[24] Absorption corrections[25] have been applied to both data sets. Structure solution and refinement as well as molecular graphics and geometrical calculations were performed for both structures with the SHELXTL software package, release 5.1.[26] The structures were refined using the full-matrix least-squares on F^2 with all of the non-H atoms defined anisotropically. H atoms were placed in calculated positions using the "riding model".

CCDC-242559 (for **2**) and -242560 (for **3**) contain the supplementary crystallographic data for this paper. These data can be obtained free of charge at www.ccdc.cam.ac.uk/conts/retrieving.html [or from the Cambridge Crystallographic Data Centre, 12 Union Road, Cambridge CB2 1EZ, UK; Fax: +44-1223-336-033; E-mail: deposit@ccdc.cam.ac.uk].

Acknowledgments

We thank the Swiss National Science Foundation and the EPFL for financial support.

 © 2004 Wiley-VCH Verlag GmbH & Co. KGaA, Weinheim

[1] For an excellent overview covering all aspects of gold chemistry see, *Gold: Progress in Chemistry, Biochemistry and Technology* (Ed.: H. Schmidbaur), John Wiley & Sons, Chichester, **1999**.
[2] [2a] M. C. Gimeno, A. Laguna, *Chem. Rev.* **1997**, *97*, 511. [2b] C. F. Shaw III, *Chem. Rev.* **1999**, *99*, 2589.
[3] V. W. W. Yam, K. K.-W. Lo, K. M.-C. Wong, *J. Organomet. Chem.* **1999**, *578*, 3.
[4] [4a] D. Thompson, *Gold Bull.* **1999**, *32*, 12. [4b] J. H. Teles, S. Brode, M. Chabanas, *Angew. Chem. Int. Ed.* **1998**, *37*, 1415. [4c] E. Mizushima, K. Sato, T. Hayashi, M. Tanaka, *Angew. Chem. Int. Ed.* **2002**, *41*, 4563.
[5] For some recent examples see: [5a] C. Hollatz, A. Schier, H. Schmidbaur, *J. Am. Chem. Soc.* **1997**, *119*, 8115. [5b] J. D. E. T. Wilton-Ely, A. Schier, N. W. Mitzel, S. Nogai, H. Schmidbaur, *J. Organomet. Chem.* **2002**, *643*, 313. [5c] W. J. Hunks, M. C. Jennings, R. J. Puddephatt, *Inorg. Chem.* **2002**, *41*, 4590.
[6] [6a] C.-M. Che, H.-L. Kwong, V. W.-W. Yam, K.-C. Cho, *J. Chem. Soc., Chem. Commun.* **1989**, 885. [6b] C. King, J. C. Wang, M. N. I. Khan, J. P. Fackler Jr., *Inorg. Chem.* **1989**, *28*, 2145. [6c] V. W.-W. Yam, E. C.-C. Chen, Z.-Y. Zhao, *Angew. Chem. Int. Ed.* **2000**, *39*, 1683. [6d] C. D. Delfs, H. J. Kitto, R. Stranger, G. F. Swiegers, S. B. Wild, A. C. Willis, G. J. Wilson, *Inorg. Chem.* **2003**, *42*, 4469.
[7] [7a] P. G. Jones, *Gold Bull.* **1981**, *14*, 102. [7b] S. S. Pathaneni, G. R. Desiraju, *J. Chem. Soc., Dalton Trans.* **1993**, 319.
[8] H. Schmidbaur, *Gold Bull.* **2000**, *33*, 3.
[9] [9a] H. Schmidbaur, C. Paschalidis, O. Steigelmann, G. Müller, *Chem. Ber.* **1989**, *122*, 1851. [9b] D. S. Eggleston, J. V. McArdle, G. E. Zuber, *J. Chem. Soc., Dalton Trans.* **1987**, 677. [9c] P. Sakhaii, I. Neda, M. Freytag, H. Thönnessen, P. G. Jones, R. Schmutzler, *Z. Anorg. Allg. Chem.* **2000**, *626*, 1246.
[10] J. Zank, A. Schier, H. Schmidbaur, *J. Chem. Soc., Dalton Trans.* **1998**, 323.
[11] [11a] C. B. Dieleman, D. Matt, I. Neda, R. Schmutzler, A. Harriman, R. Yaftian, *Chem. Commun.* **1999**, 1911. [11b] C. B. Dieleman, D. Matt, I. Neda, R. Schmutzler, H. Thönnessen, P. G. Jones, A. Harriman, *J. Chem. Soc., Dalton Trans.* **1998**, 2115.
[12] [12a] V. W.-W. Yam, C.-L. Chan, K.-K. Cheung, *J. Chem. Soc., Dalton Trans.* **1996**, 4019. [12b] P. Lange, A. Schier, H. Schmidbaur, *Z. Naturforsch., Teil B* **1997**, *52*, 769. [12c] J. S. Field, J. Grieve, R. J. Haines, N. May, M. M. Zulu, *Polyhedron* **1998**, *17*, 3021. [12d] A. M. Z. Slawin, M. B. Smith, J. D. Woollins, *J. Chem. Soc., Dalton Trans.* **1998**, 1537. [12e] I. Neda, A. Fischer, T. Kaukorat, P. G. Jones, R. Schmutzler, *Chem. Ber.* **1994**, *127*, 1579.
[13] [13a] M. M. Taqui Khan, E. Rama Rao, *Polyhedron* **1987**, *6*, 1727. [13b] A. Bauer, W. Mitzel, A. Schier, D. W. H. Rankin, H. Schmidbaur, *Chem. Ber./Recueil* **1997**, *130* 323. [13c] D. Walther, T. Döhler, K. Heubach, O. Klobes, B. Schweder, H. Görls, *Z. Anorg. Allg. Chem.* **1999**, *625*, 923.
[14] Z. Fei, N. Biricik, D. Zhao, R. Scopelliti, P. J. Dyson, *Inorg. Chem.* **2004**, *43*, 2228.
[15] D. G. Evans, D. M. P. Mingos, *J. Organomet. Chem.* **1982**, *232*, 171.
[16] S. Berger, S. Braun, H.-O. Kalinowski, *NMR-Spektroskopie von Nichtmetallen*, vol. 3, ^{31}P *NMR-Spektroskopie,* Georg Thieme Verlag, Stuttgart, New York, **1993**.
[17] [17a] R. Uson, A. Laguna, M. Laguna, M. N. Fraile, P. G. Jones, G. M. Sheldrick, *J. Chem. Soc., Dalton Trans.* **1986**, 291. [17b] A. M. Z. Slawin, M. B. Smith, J. D. Woollins, *Polyhedron* **1999**, *18*, 1135. [17c] P. A. Bella, O. Crespo, E. J. Fernández, A. Fischer, P. G. Jones, A. Laguna, J. M. López-de-Luzuriagaa, M. Mongea, *J. Chem. Soc., Dalton Trans.* **1999**, 4009. [17d] Q. Zhang, G. Hua, P. Bhattacharyya, A. M. Z. Slawin, J. D. Woollins, *Dalton Trans.* **2003**, 3250.
[18] [18a] P. Schwerdtfeger, H. L. Hermann, H. Schmidbaur, *Inorg. Chem.* **2003**, *42*, 1334. [18b] M. D. Irwin, H. E. Abdou, A. A. Mohamed, J. P. Fackler Jr., *Chem. Commun.* **2003**, 2882.
[19] [19a] W. Schirmer, U. Floerke, H. J. Haupt, *Z. Anorg. Allg. Chem.* **1987**, *545*, 83. [19b] W. Schirmer, U. Floerke, H. J. Haupt, *Z. Anorg. Allg. Chem.* **1989**, *574*, 239.
[20] [20a] J. P. Fackler Jr., *Inorg. Chem.* **2002**, *41*, 6959. [20b] J. D. E. T. Wilton-Ely, A. Schier, N. W. Mitzel, H. Schmidbaur, *J. Chem. Soc., Dalton Trans.* **2001**, 1058. [20c] J. D. E. T. Wilton-Ely, A. Schier, H. Schmidbaur, *Organometallics* **2001**, *20*, 1895.
[21] N. Biricik, Z. Fei, R. Scopelliti, P. J. Dyson, *Helv. Chim. Acta* **2003**, *86*, 3281.
[22] R. Uson, A. Laguna, M. Laguna, *Inorg. Synth.* **1989**, *26*, 85.
[23] P. J. Dyson, J. S. McIndoe, *Inorg. Chim. Acta* **2003**, *354*, 68.
[24] Oxford Diffraction Ltd., Abingdon, Oxfordshire, UK, **2003**.
[25] DELABS, N. Walker, D. Stuart, *Acta Crystallogr., Sect. A* **1983**, *39*, 158.
[26] G. M. Sheldrick, University of Göttingen, Germany, **1997**; Bruker AXS, Inc., Madison, Wisconsin, 53719, USA, **1997**.

Received May 26, 2004
Early View Article
Published Online September 7, 2004

 © 2004 Wiley-VCH Verlag GmbH & Co. KGaA, Weinheim

Nonbridging and Monodentate Carboxylate Coordination of Calcium(2+) Through the Use of Intramolecular Hydrogen Bonding in a New Sterically Hindered Carboxylate Ligand

Jonathan D. Crane,*[a] David J. Moreton,[b] and Eleanor Rogerson[a]

Keywords: Calcium / Hydrogen bonds / Carboxylate ligands / Sterically hindered ligands

The sterically hindered carboxylate ligand 2,6-bis(2,2-dimethylpropionylamino)benzoic acid (**HL**) has been prepared. The two intramolecular hydrogen bonds in **HL** are exploited to restrict the corresponding carboxylate anion ($\mathbf{L}^-$) to nonbridging coordination and to preorganise its sterically bulky substituents proximal to the first and second coordination sphere of the bound metal ion. The crystal structures of the ligand anion as the ammonium salt $[NH_4][\mathbf{L}]$ and the distorted octahedral calcium complex $Ca\mathbf{L}_2(H_2O)_2$, in which $\mathbf{L}^-$ binds to the calcium(2+) ion in a monodentate, nonbridging mode, are described.

(© Wiley-VCH Verlag GmbH & Co. KGaA, 69451 Weinheim, Germany, 2004)

Introduction

Sterically hindered ligands are commonly used to control the coordination environment of metal ions, and hence their properties, through favouring lower coordination numbers and/or by preventing the unwanted formation of polynuclear species that often arise through ligand bridging.[1] This approach is particularly challenging for carboxylate ligands, nevertheless over recent years the application of this strategy has proven to be effective for the synthesis of some low molecular weight model compounds for transition metal ion sites in proteins, in which the role of the protein in providing a preorganised arrangement of carboxylate ligands at a metal ion binding site has been to some extent reproduced by the use of steric hindrance.[2] With sterically hindered carboxylate ligands the challenge is not primarily to limit coordination numbers, but rather to inhibit the strong natural tendency of the carboxylate group to bridge between two or more metal ions which results in the undesired formation of polymeric or highly polynuclear species. This is particularly problematic for the coordination chemistry of calcium(2+) which has an ionic radius of 0.99 Å, substantially larger than divalent transition metal ions [e.g., high-spin iron(2+), 0.78 Å], and as a consequence the triply bridging motif **I** and related structures are commonplace for simple carboxylate ligands.[3] In contrast, monodentate, nonbridging carboxylates are common ligands for calcium(2+) in proteins,[4] and although there are several examples of such calcium(2+) coordination for small molecules in the Cambridge Crystallographic Database,[5] these are all apparently serendipitous, arising unpredictably from the use of polydentate ligands and/or fortuitous packing arrangements.[6]

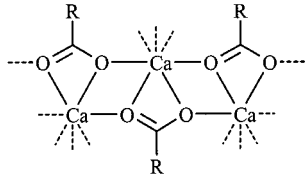

I

We wished to design a sterically hindered carboxylate ligand that specifically excludes the possibility of laterally bridging coordination to calcium(2+) or other metal ions. The sterically hindered 2,6-dialkyl- or 2,6-diarylbenzoic acid derivatives currently used for transition metal studies were not considered appropriate as the carboxylate group is free to rotate out of the plane of the aromatic ring and thus bridging is still allowed to occur.[2] The chosen design strategy was to use two intramolecular hydrogen bonds from adjacent amide groups to constrain the carboxylate group to be coplanar with the aromatic ring and therefore prevent lateral bridging to metal ions, whilst preorganising two sterically bulky groups proximal to the first and second coordination spheres of any bound metal ion. We herein report the synthesis of the *tert*-butyl-substituted ligand **HL**, the structure of its anion (as the ammonium salt) and its complexation with calcium(2+). Moreover, the straightforward synthesis of **HL** should allow the facile preparation of derivatives with a wide variety of R substituents, thus

[a] Department of Chemistry, University of Hull
Cottingham Road, Kingston-upon-Hull, HU6 7RX,UK
E-mail: j.d.crane@hull.ac.uk
[b] Lubrizol International Laboratories
Belper, Derby, DE56 1QN, UK

providing the opportunity for further control over the first and second coordination spheres of any metal ion and greater scope for the design of metallobiosite model complexes where restriction of the carboxylate coordination mode is required.

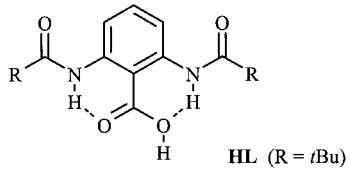

Results and Discussion

The carboxylic acid **HL** was readily prepared in 41% yield by the oxidation of the aromatic methyl group of diamide **1**[7] with potassium permanganate in aqueous pyridine at reflux (Scheme 1).[12] The two intramolecular hydrogen bonds in **HL** would be expected to stabilise the corresponding carboxylate anion, but less so than for 2,6-dihydroxybenzoic acid (vide supra).[13] In nonprotogenic solvents (e.g., chloroform) the carboxylic acid **HL** was found readily to eliminate water over several hours to form the benzoxazine **2**. ^{1}H and ^{13}C NMR spectroscopy showed that in chloroform an equilibrium (1:2) mixture of **HL/2** (and water) was formed after approximately 24 h. Pure **2** could be obtained in quantitative yield by the deliberate dehydration of a toluene solution of **HL** with excess acetic anhydride. Under mildly basic conditions in the presence of water both **HL** and **2** were found to rapidly reform the carboxylate anion $\mathbf{L}^{-}$.

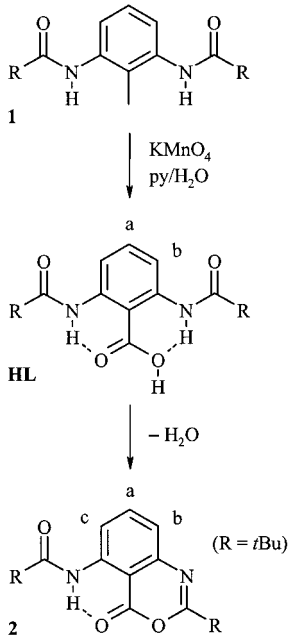

Scheme 1

The structure of the carboxylate anion $\mathbf{L}^{-}$ is revealed by the single-crystal X-ray structure determination of the ammonium salt **3** (Figure 1). As expected, there are intramolecular hydrogen bonds between the two amide N−H groups and the carboxylate oxygen atoms. The X-ray diffraction data were of sufficient quality for the amide N−H hydrogen atoms to be located in the difference Fourier map and freely refined; the N−H bond lengths of 0.90(3) Å indicate that there is no significant lengthening of the N−H bonds compared with the expected value of 0.85−0.90 Å, as determined by X-ray diffraction.[5] In addition, the N(1)···O(1) and N(2)···O(2) distances of 2.564(3) and 2.571(3) Å are relatively long, and the N(1)−H(1)···O(1) and N(2)−H(2)···O(2) angles of 142(2) and 147(3)° are significantly more acute than the usual range of 160−180° for strong hydrogen bonds. Furthermore, the carboxylate and two amide groups are slightly twisted out of the plane of the central aromatic ring with torsional angles between the respective pairs of least-squares planes of 21.3(1), 10.6(1) and 18.7(1)°. All these structural parameters suggest that these hydrogen bonds are weaker than in the near-planar 2,6-dihydroxybenzoate anion (Table 1),[13] and indicate that **HL** should be a weaker acid than 2,6-dihydroxybenzoic acid. However, the most important effect of these hydrogen bonds is that they successfully preorganise the planar, *trans*-primary-amide groups and therefore position the bulky *tert*-butyl groups to restrict coordination to the carboxylate group. In the lattice of **3** the packing of the carboxylate anions leaves cavities that are each occupied by a pair of ammonium counterions, with an inter-ammonium cation (N···N) distance of 3.675(3) Å, which, although short, is typical for ammonium carboxylate structures.[14] This electrostatically unfavourable arrangement is compensated for by the formation of hydrogen bonds to all four of the ammonium N−H bonds, thus the two ammonium ions are imprisoned in a cage of eight appropriately positioned hydrogen bond acceptor oxygen atoms (Figure 2, Table 2).

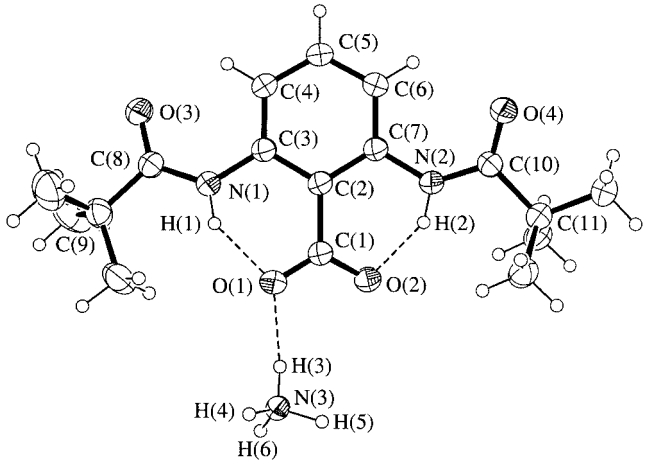

Figure 1. ORTEP[18] view of the molecular structure of **3** with thermal ellipsoids shown at 40%; hydrogen bonds are denoted by dashed lines; selected bond lengths [Å]: C(8)−N(1) 1.344(3), C(8)−O(3) 1.228(3), C(10)−N(2) 1.342(3), C(10)−O(4) 1.222(3)

 © 2004 Wiley-VCH Verlag GmbH & Co. KGaA, Weinheim

Table 1. Structural parameters related to the intramolecular hydrogen bonding of the carboxylate group in **3** and **4**

Compound	$\{ArCO_2^-\}$[a]	**3**	**4**
Hydrogen-bonding geometry	(X = O)	(X = N)	(X = N)
X(1)−H(1), X(2)−H(2) [Å]	0.81(2), 0.83(2)	0.90(3), 0.90(4)	0.88(3), 0.90(3)
H(1)···O(1), H(2)···O(2) [Å]	1.78(2), 1.77(2)	1.79(3), 1.77(4)	1.93(3), 1.88(3)
X(1)···O(1), X(2)···O(2) [Å]	2.511(2), 2.542(2)	2.564(3), 2.571(3)	2.683(2), 2.622(2)
X(1)−H(1)···O(1), X(2)−H(2)···O(2) [°]	149(2), 153(2)	142(3), 147(3)	142(2), 138(2)
O(5)−H(3) [Å]	−	−	0.88(3)
H(3)···O(2) [Å]	−	−	1.82(3)
O(5)···O(2) [Å]	−	−	2.671(2)
O(5)−H(3)···O(2) [°]	−	−	162(3)
Carboxylate group geometry			
C(1)−O(1), C(2)−O(2) [Å]	1.283(2), 1.260(2)	1.235(3), 1.248(3)	1.270(2), 1.255(2)
C(1)−C(2) [Å]	1.481(2)	1.519(3)	1.519(2)
Ar−CO_2^- torsional angle [°]	1.4(1)	21.3(1)	33.6(1)

[a] 2,6-Dihydroxybenzoate anion, ref.[13]

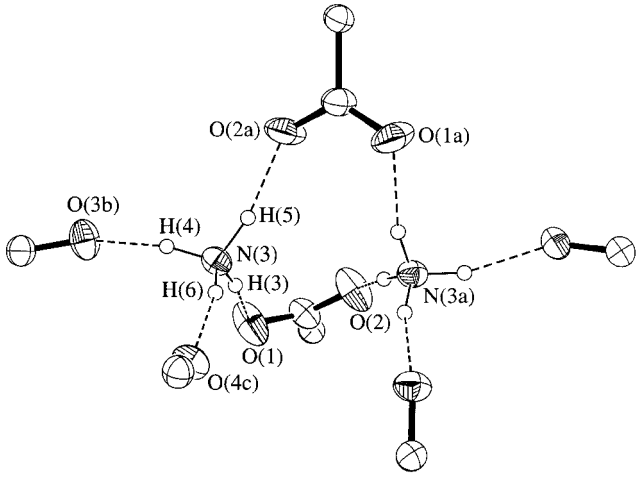

Figure 2. ORTEP[18] view of the ammonium cation hydrogen-bonding environment in **3** with thermal ellipsoids shown at 40%; hydrogen bonds are denoted by dashed lines; the majority of the ligand structures have been omitted for clarity; symmetry transformations: a: 2 − *x*, 1 − *y*, *z*; b: 3/2 − *x*, 1/2 + *y*, *z*; c: *x*, 1/2 + *y*, 1/2 + *z*

Table 2. Hydrogen-bonding geometry of the ammonium cation in **3**

D−H···A[a]	D−H	H···A	D···A	∠D−H···A
N(3)−H(3)···O(1)	0.90(3)	1.83(3)	2.713(3)	166(3)
N(3)−H(4)···O(3b)	0.99(3)	1.79(3)	2.750(3)	160(2)
N(3)−H(5)···O(2a)	1.00(3)	1.77(3)	2.749(3)	168(3)
N(3)−H(6)···O(4c)	0.95(3)	1.85(3)	2.776(3)	166(3)

[a] Symmetry transformations: a: 2 − *x*, 1 − *y*, *z*; b: 3/2 − *x*, 1/2 + *y*, *z*; c: *x*, 1/2 + *y*, 1/2 + *z*.

The structure of **4** (Figure 3) shows that the carboxylate ligand is bound to the calcium ion in the desired monodentate and nonbridging manner, and that the calcium ion is restricted to six coordination and a distorted octahedral geometry. Indeed, the "average" coordination environment for calcium(2+) in proteins is octahedral, and moreover with a mixture of carboxylate, peptide carbonyl and water ligands,[4] coincidently very similar to the specific structure described here. The average Ca−O bond length is 2.359 Å, only slightly longer than the value of 2.337 Å found for the comparable, unhindered octahedral complex $Ca(acac)_2(H_2O)_2$.[15] The Ca−O(1) distance is the longest in the calcium coordination sphere in **4**, 2.3830(11) Å, presumably due to the steric congestion of the carboxylate group, and the carboxylate is clearly monodentate with a very long Ca(1)···O(2) distance of 3.7205(12) Å. It is particularly noteworthy that this coordination mode is preferred over a more symmetrical bidentate coordination, or the formation of simple second coordination sphere $[Ca(H_2O)_n]^{2+}$ hydrogen-bonded salts of the ligand anion. One possible reason for the stability of **4** is that the long Ca−O(1) bond is supported by a strong hydrogen bond between the adjacent water ligand and the nonbound carboxylate oxygen atom

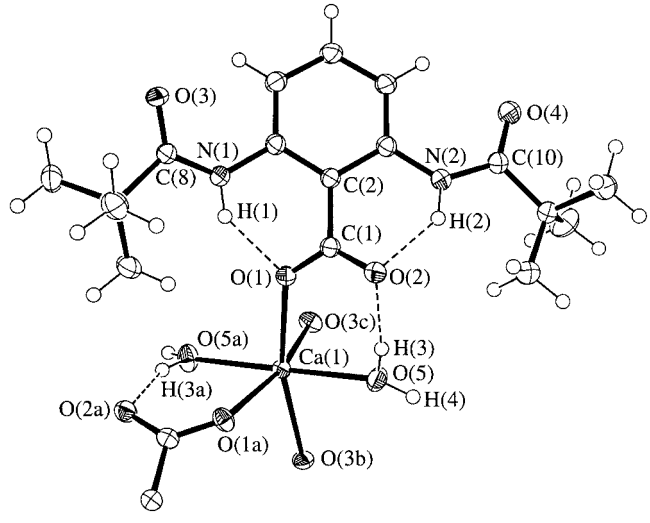

Figure 3. ORTEP[18] view of the structure of **4** with thermal ellipsoids shown at 50%; hydrogen bonds are denoted by dashed lines; for clarity only one ligand is shown in its entirety; selected bond lengths [Å] and angles [°]: Ca(1)−O(1) 2.3830(11), Ca(1)−O(5) 2.3378(11), Ca(1)−O(3b) 2.3560(11), C(8)−N(1) 1.349(2), C(8)−O(3) 1.241(2), C(10)−N(2) 1.362(2), C(10)−O(4) 1.232(2); O(1)−Ca(1)−O(5) 80.45(4), O(1)−Ca(1)−O(1a) 93.16(6), O(1)−Ca(1)−O(3b) 164.67(4), O(3b)−Ca(1)−O(3c) 90.37(6), O(3b)−Ca(1)−O(5) 84.29(4), O(5)−Ca(1)−O(5b) 177.44(7); symmetry transformations: a: 3 − *x*, *y*, 3/2 − *z*; b: 1/2 + *x*, 1/2 + *y*, *z*; c: 5/2 − *x*, 1/2 + *y*, 3/2 − *z*

 © 2004 Wiley-VCH Verlag GmbH & Co. KGaA, Weinheim

O(2) (Table 1); thus the carboxylate group is effectively acting as a bidentate ligand to a $Ca-OH_2$ group. Indeed, several similar structural motifs have been described over recent years in the transition metal chemistry of sterically hindered carboxylate ligands,[2] and in calcium(2+) coordination chemistry.[16] The coordination sphere of the calcium ion is completed by one amide carbonyl group from each of two equivalent neighbouring molecules, and the Ca(1)−O(3a) bond length of 2.3560(11) Å and Ca(1)−O(3a)−C(8a) angle of 169.98(11)° are typical of a predominantly electrostatic interaction with the metal ion. This interaction also results in a slight perturbation of the amide group with a longer C(8)=O(3) distance of 1.241(2) Å and shorter C(8)−N(1) distance of 1.349(2) Å compared to 1.232(2) and 1.362(2) Å, respectively for the other, non-coordinated amide group. Similar to as described above for **3**, the carboxylate and two amide groups in **4** are twisted out of the plane of the central aromatic ring. The torsional angles between the respective pairs of least-squares planes of 33.6(1), 25.0(1) and 10.1(1)° show that the ligand in **4** has larger distortions from planarity than in **3**, particularly with regard to the carboxylate group. For **3** and **4** these variations in torsional angles probably primarily arise from different packing effects and bonding requirements of the ammonium and calcium(2+) ions, respectively.

In conclusion, the sterically hindered ligand **HL** designed for nonbridging coordination to metal ions has been successfully prepared and its desired mode of coordination structurally characterised for a mononuclear calcium(2+) complex. The coordination chemistry of **HL** and related ligands with transition metal and lanthanide ions is currently under investigation.[17]

Experimental Section

General: *N*-[3-(2,2-Dimethylpropionylamino)-2-methylphenyl]-2,2-dimethylpropionamide (**1**) was prepared from 2,6-diaminotoluene and trimethylacetyl chloride by a literature method.[7] Elemental analyses were obtained with a Fisons EA1108 CHNS analyser. IR spectra were recorded as KBr disks with a Perkin−Elmer Paragon-100 FT-IR spectrophotometer. NMR spectra were recorded using a Jeol JNM-LA400 spectrometer at room temperature (20 °C) and are reported relative to tetramethylsilane. Mass spectra were recorded with a Finnigan 1200 (EI) mass spectrometer.

2,6-Bis(2,2-dimethylpropionylamino)benzoic Acid (HL): Potassium permanganate (4.75 g, 30 mmol) and diamide **1** (4.35 g, 15 mmol) in pyridine/water (1:1, 150 mL) was heated at reflux with constant stirring for 2 h, or until the purple colour of the permanganate had disappeared. The reaction mixture was allowed to cool to room temperature, water (250 mL) added, then the solution filtered to remove the dark brown precipitate of hydrated manganese dioxide. The pale yellow filtrate was concentrated to near dryness under reduced pressure and water (150 mL) added. The insoluble residue of unchanged **1** was filtered off, concentrated hydrochloric acid (20 mL) added to the filtrate and the precipitate of **HL** extracted into dichloromethane (3 × 40 mL). The dichloromethane extracts were combined, dried ($MgSO_4$), filtered, and the solvents evaporated to dryness under reduced pressure. Yield: 2.55 g (53%). The product was sufficiently pure for subsequent use, but an analytically pure sample could not be obtained by recrystallisation due to the facile conversion of **HL** to ***N*-(2-*tert*-butyl-4-oxo-4*H*-benzo-[*d*][1,3]oxazin-5-yl)-2,2-dimethylpropionamide (2)**. ^{1}H NMR (400 MHz, $CDCl_3$): δ = 1.32 (s, 18 H, CH_3), 7.20 (br. s, 1 H, CO_2H), 7.49 (t, ^3J = 8.3 Hz, 1 H, H^a), 8.26 (d, ^3J = 8.3 Hz, 2 H, H^b), 10.44 (s, 2 H, NH) ppm. ^{13}C NMR (100.6 MHz, $CDCl_3$): δ = 27.6, 40.3, 106.8, 117.1, 134.3, 140.9, 169.6, 177.5 ppm. IR (KBr): ṽ = 3407 (m), 2970 (m), 2874 (w), 1694 (s), 1636 (m), 1610 (m), 1582 (s), 1514 (s), 1464 (s), 1368 (m), 1294 (m), 1222 (s), 1163 (m), 1125 (w), 812 (m), 785 (m), 752 (m), 701 (w), 420 cm^{-1} (w). MS (EI): *m*/*z* (%) = 320 (14) [M^+], 302 (26) [$M^+ - H_2O$].

***N*-(2-*tert*-Butyl-4-oxo-4*H*-benzo[*d*][1,3]oxazin-5-yl)-2,2-dimethylpropionamide (2):** In nonaqueous solutions (e.g., chloroform) **HL** was found to eliminate water over a period of a few hours to give an equilibrium mixture of **HL**, the benzoxazine **2** and water. The deliberate dehydration of **HL** with excess acetic anhydride in toluene gave a near quantitative yield of pure **2**. A sample for analysis was recrystallised from petroleum ether (boiling range 60−80 °C) as colourless needles. $C_{17}H_{22}N_2O_3$ (302.37): calcd. C 67.53, H 7.33, N 9.26; found C 67.49, H 7.46, N 9.25. ^{1}H NMR (400 MHz, $CDCl_3$): δ = 1.37 (s, 9 H, CH_3), 1.40 (s, 9 H, CH_3), 7.26 (d, ^3J = 8.2 Hz, 1 H, H^b), 7.75 (t, ^3J = 8.2 Hz, 1 H, H^a), 8.79 (d, ^3J = 8.2 Hz, 1 H, H^c), 11.39 (s, 1 H, NH) ppm. ^{13}C NMR (100.6 MHz, $CDCl_3$): δ = 27.5, 27.6, 37.8, 40.6, 103.9, 118.2, 120.8, 137.9, 141.6, 147.1, 162.5, 167.2, 178.5 ppm. IR (KBr): ṽ = 3298 (w), 2968 (m), 1716 (m), 1698 (s), 1645 (m), 1610 (m), 1580 (s), 1542 (m), 1475 (m), 1291 (m), 1182 (m), 1157 (s), 1049 (m), 914 (w), 817 (s), 715 (m), 690 (m), 556 cm^{-1} (w). MS (EI): *m*/*z* (%) = 302 (31) [M^+], 245 (100) [$M^+ - C_4H_9$].

Ammonium 2,6-Bis(2,2-dimethylpropionylamino)benzoate, [NH$_4$]L (3): Carboxylic acid **HL** (0.96 g, 3 mmol) and potassium hydroxide (0.16 g, 2.9 mmol) were dissolved in methanol/water (1:1, 40 mL). Concentrated aqueous ammonia (20 mL) was added, the solution filtered and allowed to concentrate slowly. Large, colourless, X-ray quality crystals of **3** were obtained after 2−3 d. Yield: 0.56 g (55%). $C_{17}H_{27}N_3O_4$ (337.42): calcd. C 60.51, H 8.07, N 12.45; found C 60.35, H 8.32, N 12.32. ^{1}H NMR (400 MHz, [D$_6$]DMSO): δ = 1.20 (s, 18 H, CH_3), 7.14 (t, ^3J = 8.2 Hz, 1 H, H^a), 7.24 (br. s, 4 H, NH_4^+), 8.21 (d, ^3J = 8.2 Hz, 2 H, H^b), 14.04 (br. s, 2 H, NH) ppm. ^{13}C NMR (100.6 MHz, [D$_6$]DMSO): δ = 27.5, 111.5, 113.1, 129.1, 141.6, 171.3, 176.3 (the *t*Bu peak at ca. 40 ppm is masked by the solvent peak). IR (KBr): ṽ = 3080 (m), 2970 (m), 2155 (w), 1943 (w), 1654 (m), 1611 (m), 1580 (s), 1473 (s), 1433 (s), 1362 (s), 1252 (m), 916 (w), 839 (m), 785 (m), 709 (w), 548 (w), 421 cm^{-1} (w).

Calcium Bis[2,6-bis(2,2-dimethylpropionylamino)benzoate] Dihydrate, CaL$_2$(H$_2$O)$_2$ (4): Carboxylic acid **HL** (0.96 g, 3 mmol) and potassium hydroxide (0.16 g, 2.9 mmol) were dissolved in water (45 mL). A solution of calcium acetate monohydrate (0.24 g, 1.5 mmol) in water (5 mL) was added and the resulting solution was filtered. Large, colourless, X-ray quality crystals of **4** were obtained after 3−4 d. Yield: 0.68 g (63%). $C_{34}H_{50}CaN_4O_{10}$ (714.87): calcd. C 57.13, H 7.05, N 7.84; found C 56.97, H 7.01, N 7.66. ^{1}H NMR (400 MHz, [D$_6$]DMSO): δ = 1.21 (s, 18 H, CH_3), 3.35 (br. s, 2 H, H_2O), 7.16 (t, ^3J = 8.3 Hz, 1 H, H^a), 8.22 (d, ^3J = 8.3 Hz, 1 H, H^b), 13.85 (br. s, 2 H, NH) ppm. ^{13}C NMR (100.6 MHz, [D$_6$]DMSO): δ = 27.5, 111.0, 113.2, 129.4, 141.7, 172.2, 176.3 (the *t*Bu peak at ca. 40 ppm is masked by the solvent peak). IR (KBr): ṽ = 3398 (m), 3133 (m), 2967 (m), 1652 (m), 1626 (m), 1591 (m), 1480 (s), 1441 (m), 1360 (s), 1306 (m), 1252 (m), 1172 (m), 991 (w), 917 (w), 831 (m), 783 (m), 747 (m), 640 (w), 549 (w), 416 cm^{-1} (w).

Crystal Structure Determinations: Data were collected at 150(2) K employing a wavelength of 0.71073 Å (Mo-K_α) with a Stoe IPDS

 © 2004 Wiley-VCH Verlag GmbH & Co. KGaA, Weinheim

Table 3. Crystal data and structure refinement for **3** and **4**

Compound	**3**	**4**
Empirical formula	$C_{17}H_{27}N_3O_4$	$C_{34}H_{50}CaN_4O_{10}$
M_r [g mol^{-1}]	337.42	714.86
Crystal system	orthorhombic	orthorhombic
Space group	*Aba*2	$C222_1$
a [Å]	20.6625(17)	12.6255(6)
b [Å]	11.3308(10)	13.7423(8)
c [Å]	17.0301(12)	21.4274(11)
V [Å^3]	3987.1(6)	3717.7(3)
Z, $D_{calcd.}$ [g cm^{-3}]	8, 1.124	4, 1.277
μ(Mo-K_α) [mm^{-1}]	0.080	0.228
F(000)	1456	1528
Crystal dimensions [mm]	0.40 × 0.35 × 0.20	0.60 × 0.50 × 0.40
$\theta_{min}/\theta_{max}$ [°]	1.97/29.74	2.90/34.85
h, k, l ranges	−28/24, −15/15, −23/21	−20/20, −21/21, −33/34
Collected/unique reflections	14100/2928	28175/8040
Restraints, parameters	1, 242	0, 241
T_{min}/T_{max}	−	0.8410/0.9402
R_{int}	0.0842	0.0500
Goodness-of-fit on F^2	0.924	1.116
R indices [$I > 2\sigma(I)$]	$R_1 = 0.0480$, $wR_2 = 0.1137$	$R_1 = 0.0555$, $wR_2 = 0.1469$
R indices (all data)	$R_1 = 0.0617$, $wR_2 = 0.1214$	$R_1 = 0.0586$, $wR_2 = 0.1516$
Flack parameter	−	0.00(3)
Largest difference peak/hole [e·Å^{-3}]	0.232/−0.220	0.602/−0.552

II image plate diffractometer. Space groups were determined by an examination of the systematic absences in the data, and their correct identification was confirmed by the successful solution and refinement of the structures. Solutions were provided by direct methods using SHELXS-97 and refined by full-matrix least squares on F^2 using SHELXL-97.[8] Numerical absorption corrections were applied to **4** using X-RED/X-SHAPE.[9] All non-hydrogen atoms were refined anisotropically. All hydrogen atoms were placed in calculated positions with U_{iso} set at 1.2 times the U_{eq} of the parent atom, and methyl groups were allowed to rotate about their X−C bonds; the positions of all N−H and O−H groups were freely refined. The analysis of the structures was carried out with PLATON[10] and WinGX.[11] Details are given in Table 3. Supplementary data for **3** and **4** are available free of charge from the Cambridge Crystallographic Data Centre (CCDC), 12 Union Road, Cambridge, CB2 1EZ, UK [Fax: + 44-1223-336-033; E-mail: deposit@ccdc.cam.ac.uk], quoting the deposition numbers CCDC-239602 and -239601, respectively.

Acknowledgments

We acknowledge Lubrizol and the University of Hull for support.

[1] [1a] B. Twamley, S. T. Haubrich, P. P. Power, *Adv. Organomet. Chem.* **1999**, *44*, 1−65. [1b] C. C. Cummins, *Prog. Inorg. Chem.* **1998**, *47*, 685−836.
[2] [2a] J. R. Hagadorn, T. I. Zahn, L. Que, Jr., W. B. Tolman, *J. Chem. Soc., Dalton Trans.* **2003**, 1790−1794. [2b] D. Lee, S. J. Lippard, *Inorg. Chem.* **2002**, *41*, 2704−2719. [2c] D. Lee, P. L. Hung, B. Spingler, S. J. Lippard, *Inorg. Chem.* **2002**, *41*, 521−531. [2d] D. Lee, S. J. Lippard, *Inorg. Chim. Acta* **2002**, *341*, 1−11. [2e] D. Lee, L. Sorace, A. Caneschi, S. J. Lippard, *Inorg. Chem.* **2001**, *40*, 6774−6781.
[3] [3a] R. Murugavel, V. V. Karambelkar, G. Anantharaman, M. G. Walawalkar, *Inorg. Chem.* **2000**, *39*, 1381−1390. [3b] A. Karipides, C. White, K. Peiffer, *Acta Crystallogr., Sect. C* **1992**, *48*, 1015−1018. [3c] R. Helems, L. B. Cole, E. M. Holt, *Inorg. Chim. Acta* **1988**, *152*, 9−16. [3d] A. Karipides, C. Miller, *J. Am. Chem. Soc.* **1984**, *106*, 1494−1495.
[4] E. Pidcock, G. R. Moore, *J. Biol. Inorg. Chem.* **2001**, *6*, 479−489.
[5] D. A. Fletcher, R. F. McMeeking, D. Parkin, *J. Chem. Inf. Comput. Sci.* **1996**, *36*, 746−749.
[6] A. Kaufman Katz, J. P. Glusker, S. A. Beebe, C. W. Bock, *J. Am. Chem. Soc.* **1996**, *118*, 5752−5763.
[7] B. D. Andrews, I. D. Rae, *Aust. J. Chem.* **1971**, *24*, 413−422.
[8] [8a] G. M. Sheldrick, *SHELXS-97 Program for the Solution of Crystal Structures*; Universität Göttingen, **1997**. [8b] G. M. Sheldrick, *SHELXL-97 Program for the Refinement of Crystal Structures*; Universität Göttingen, **1997**.
[9] Stoe & Cie, *X-RED and X-SHAPE*, Stoe & Cie GmbH, Darmstadt, **2001**.
[10] A. L. Spek, *PLATON A Multipurpose Crystallographic Tool*, Utrecht University, **2000**.
[11] L. J. Farrugia, *J. Appl. Crystallogr.* **1999**, *32*, 837−838.
[12] M. V. Sargent, *J. Chem. Soc., Perkin Trans. 1* **1982**, 1095−1098.
[13] F. Cariati, L. Erre, G. Micera, A. Panzanelli, G. Ciani, A. Sironi, *Inorg. Chim. Acta* **1983**, *80*, 57−65.
[14] [14a] H. Hosomi, Y. Ito, S. Ohba, *Acta Crystallogr., Sect. C* **1998**, *54*, 142−145. [14b] H. A. Barnes, J. C. Barnes, *Acta Crystallogr., Sect. C* **1996**, *52*, 731−736. [14c] H. Herbertsson, B. Hedman, *Acta Crystallogr., Sect. B* **1982**, *38*, 320−322. [14d] E. J. Gabe, J. P. Glusker, J. A. Minkin, A. L. Patterson, *Acta Crystallogr.* **1967**, *22*, 366−375.
[15] J. J. Sahbari, M. M. Olmstead, *Acta Crystallogr., Sect. C* **1983**, *39*, 208−211.
[16] [16a] L. R. Nassimbeni, H. Su, *J. Chem. Soc., Dalton Trans.* **2000**, 349−352. [16b] A. M. Bahl, S. Krishnaswamy, N. G. Massand, D. J. Burkey, T. P. Hanusa, *Inorg. Chem.* **1997**, *36*, 5413−5415. [16c] M. B. Inoue, P. Oram, M. Inoue, Q. Fernando, *Inorg. Chim. Acta* **1996**, *246*, 401−412. [16d] S. R. Breeze, S. Wang, *Inorg. Chem.* **1994**, *33*, 5113−5121.
[17] J. D. Crane, D. J. Moreton, E. Rogerson, unpublished results.
[18] L. J. Farrugia, *J. Appl. Crystallogr.* **1997**, *30*, 565.

Received May 26, 2004
Early View Article
Published Online September 7, 2004

 © 2004 Wiley-VCH Verlag GmbH & Co. KGaA, Weinheim

Synthesis, Structure, Optical Properties and Theoretical Studies of $Pt(P-P)(CN)_2$ with P−P = 1,2-Bis(diphenylphosphanyl)benzene and 2,2′-Bis(diphenylphosphanyl)-1,1′-binaphthyl − Luminescence from Metal-to-Ligand Charge Transfer and Intraligand States

Valeri Pawlowski,[a] Horst Kunkely,[a] Christian Lennartz,*[b] Karlheinz Böhn,[b] and Arnd Vogler*[a]

Keywords: Electronic spectra / Luminescence / Platinum complexes / Phosphane complexes / Quantumchemical calculations

The complexes $Pt^{II}(P–P)(CN)_2$ with P–P = 1,2-bis(diphenylphosphanyl)benzene (dppb) and 2,2′-bis(diphenylphosphanyl)-1,1′-binaphthyl (binap) were synthesised and characterised by elemental analysis, ESI MS and electronic spectroscopy. The structure of $Pt(dppb)(CN)_2$ was resolved by single-crystal X-ray diffraction. This compound consists of mononuclear Pt^{II} complexes with an almost planar PtP_2C_2 coordination. While both complexes are not luminescent in solution, they show an emission in the solid state under ambient conditions. It is suggested that the luminescence of $Pt(dppb)(CN)_2$ originates from a (Pt^{II}→dppb) metal-to-ligand charge transfer (MLCT) triplet with some dppb intraligand (IL) contribution. This assignment is confirmed by calculations which provide further insight into the excited state properties of the complex. In solution the phosphorescence is absent because the MLCT/IL state is deactivated to a non-emissive ligand field (LF) triplet, which is located at rather low energies owing to its distortion towards a tetrahedral structure. In the solid state this distortion is hindered. In the case of solid $Pt(binap)(CN)_2$, the phosphorescence is apparently of the IL type as the ππ* triplet of the binaphthyl chromophore occurs at low energies. Again, in solution the phosphorescence is absent owing to the interference by a distorted LF state.
(© Wiley-VCH Verlag GmbH & Co. KGaA, 69451 Weinheim, Germany, 2004)

1. Introduction

A variety of square-planar Pt^{II} complexes has been shown to be luminescent under ambient conditions.[1−3] Diverse potential applications have stimulated interest in these compounds.[3] Generally, mononuclear Pt^{II} complexes emit from their lowest-energy triplet, which may be of the metal-to-ligand charge transfer (MLCT), ligand-to-ligand charge transfer (LLCT) or intraligand (IL) type. Pt^{II} complexes with low-energy ligand field (LF) triplets are not emissive at room temperature. The complex $Pt(1,2\text{-diimine})(CN)_2$ with 1,2-diimine = 4,7-diphenyl-1,10-phenanthroline is a typical example of a Pt^{II} complex which emits from an IL triplet.[4] This room temperature phosphorescence is facilitated by the low energy of the ππ* diimine IL states as well as by the strong LF strength of the cyanide ligands which push interfering LF states to rather high energies.[4] The number of emissive Pt^{II} complexes may be increased considerably if the diimines of $Pt(1,2\text{-diimine})(CN)_2$ are replaced by other strong-field ligands with low-energy excited states. Promising candidates are bidentate phosphanes that carry aromatic chromophores. We explored this possibility and selected the complex $Pt^{II}(P-P)(CN)_2$ with P−P = 1,2-bis(diphenylphosphanyl)benzene (dppb) and 2,2′-bis(diphenylphosphanyl)-1,1′-binaphthyl (binap) for the present study (Scheme 1).

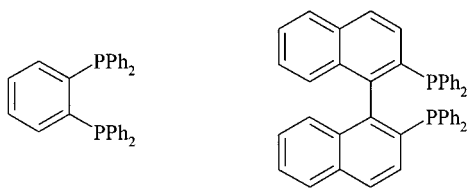

dppb binap

Scheme 1

The aromatic chromophores of these ligands were expected to serve as luminophores[5] of both complexes. In this context it should be mentioned that a few Pt^{II} phosphane complexes have been reported to display luminescence. However, these emissions do not originate from IL states. In some cases the phosphanes are only spectator

[a] Institut für Anorganische Chemie, Universität Regensburg, 93040 Regensburg, Germany
E-mail: arnd.vogler@chemie.uni-regensburg.de, christian.lennartz@basf-ag.de
[b] BASF AG, Computational Chemistry and Biology, GVC/C-A30, 67057 Ludwigshafen, Germany

ligands and are not directly involved in emission.[6−8] In other cases the luminescence is associated with metal−metal interactions in binuclear Pt^{II} complexes.[9,10] Our target compounds $Pt(P-P)(CN)_2$ were expected to be accessible by simple synthetic procedures.

2. Results and Discussion

Experimental Results

The complexes $Pt(dppb)(CN)_2$ and $Pt(binap)(CN)_2$ were obtained as white or slightly yellow solids by the reaction of $Pt(CN)_2$ with dppb and binap, respectively. The composition was confirmed by elemental analysis and mass spectroscopy. The positive ion electrospray mass spectrum (+ESI MS) of $[Pt(dppb)(CN)_2]$ in CH_3CN (+ 1% CH_3COOH) consists of peaks at m/z = 693, 694, 695, 696 and 697. The complex has apparently added one proton at the cyanide ligands. In addition, peaks at 1358, 1359, 1360, 1361, 1362, 1363 and 1364 indicate the presence of the dimer $Pt_2(dppb)_2(CN)_4$ which has lost one cyanide ligand. The +ESI MS spectrum of the binap complex shows an analogous pattern. The complex $Pt(binap)(CN)_2$ in its monoprotonated form displays peaks at 869, 870, 871, 872 and 873, while peaks of the cation $[Pt_2(binap)_2(CN)_4]^+$ appear at 1710, 1711, 1712, 1713, 1714, 1715, 1716 and 1717. In all cases there is a good agreement between the calculated and observed isotopic peak pattern.

The electronic spectrum of dppb in CH_3CN/CH_2Cl_2 (1:1) exhibits an absorption at λ_{max} = 276 nm (ε = 17 920 M^{-1} cm^{-1}). At room temperature, solutions of dppb are not emissive, but in ethanol glasses at 77 K a strong phosphorescence appears at λ_{max} = 502 nm. The absorption spectrum of $Pt(dppb)(CN)_2$ in CH_3CN (Figure 1) shows bands at λ_{max} = 295 (1420), 267 (12 940) and 225 nm (sh, 51 570). Solutions of the complex do not emit. However, at room temperature the solid compound shows a slightly structured luminescence (Figure 1) at λ_{max} = 502 nm with shoulders at approximately 480 and 540 nm. The absorption spectrum of $Pt(binap)(CN)_2$ in CH_3CN (Figure 2) contains bands at λ_{max} = 343 (3500) and shoulders at about 314 (5100), 290 (8500), 262 (33 500) and 220 nm (86 000). Again, in solution the complex does not emit, but the solid compound exhibits a luminescence at λ_{max} = 513 nm with distinct structural features at 470, 550, 600 and 640 nm (Figure 2).

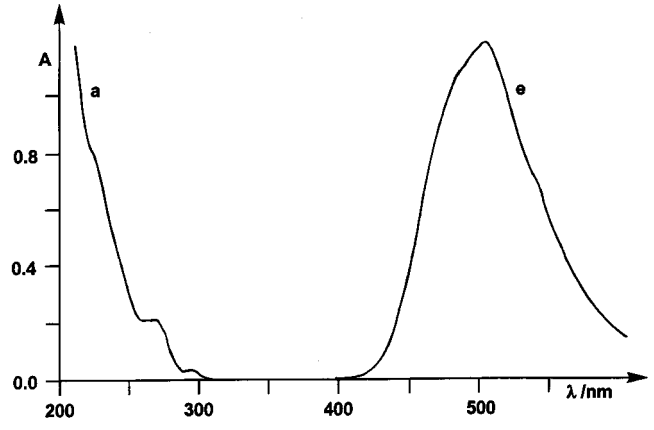

Figure 1. Electronic absorption (a) and emission (e) spectrum of $Pt(dppb)(CN)_2$ at room temperature; absorption: 1.54×10^{-5} M in CH_3CN, 1-cm cell; emission: solid, λ_{exc} = 300 nm, intensity in arbitrary units

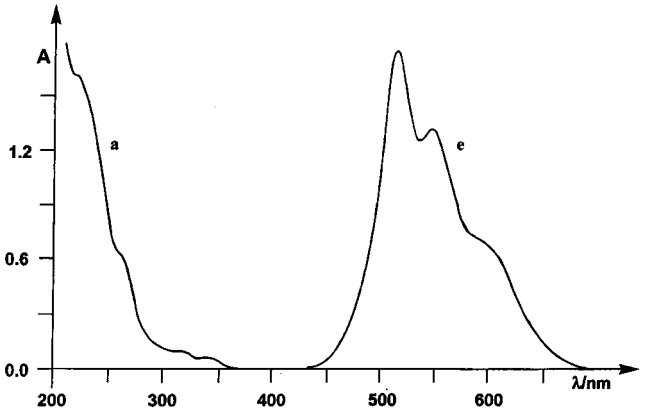

Figure 2. Electronic absorption (a) and emission (e) spectrum of $Pt(binap)(CN)_2$ at room temperature; absorption: 2.06×10^{-5} M in CH_3CN, 1-cm cell; emission: solid, λ_{exc} = 350 nm, intensity in arbitrary units

Interpretation

Complexes with the general composition $Pt^{II}(P-P)(CN)_2$ may be monomeric or dimeric[9,10] (Scheme 2).

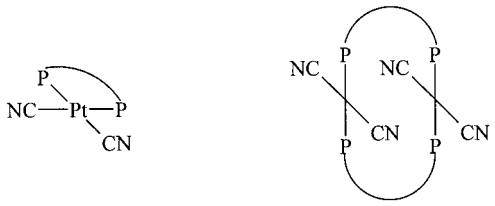

Scheme 2

In the dimers the cyanide ligands occupy *trans* positions and both square-planar Pt^{II} complex moieties are connected by bridging phosphanes. With regard to the complexes $Pt(dppb)(CN)_2$ and $Pt(binap)(CN)_2$, our analytical data do not provide an unambiguous distinction. The MS spectra indicate the presence of monomers as well as dimers. However, the dimers $Pt_2(P-P)_2(CN)_4$ with P−P = bis(diphenylphosphanyl)methane, bis(dimethylphosphanyl)methane and bis(dicyclohexyl-phosphanyl)methane show an intense absorption ($\varepsilon > 10^4$) around 330 nm, which is associated with the Pt−Pt interaction.[9,10] These absorptions do not appear in the spectra of $Pt(dppb)(CN)_2$ and $Pt(binap)(CN)_2$. Accordingly, the latter complexes are either monomeric at least in solution, or dimeric but with large Pt−Pt distances that prevent any efficient metal−metal interaction.

For $Pt(dppb)(CN)_2$, the monomeric structure was confirmed by single-crystal X-ray diffraction (Figure 3). The complex is essentially planar with P−Pt−P and C−Pt−C bond angles of 86.6° and 89.3°, respectively. The average

 © 2004 Wiley-VCH Verlag GmbH & Co. KGaA, Weinheim

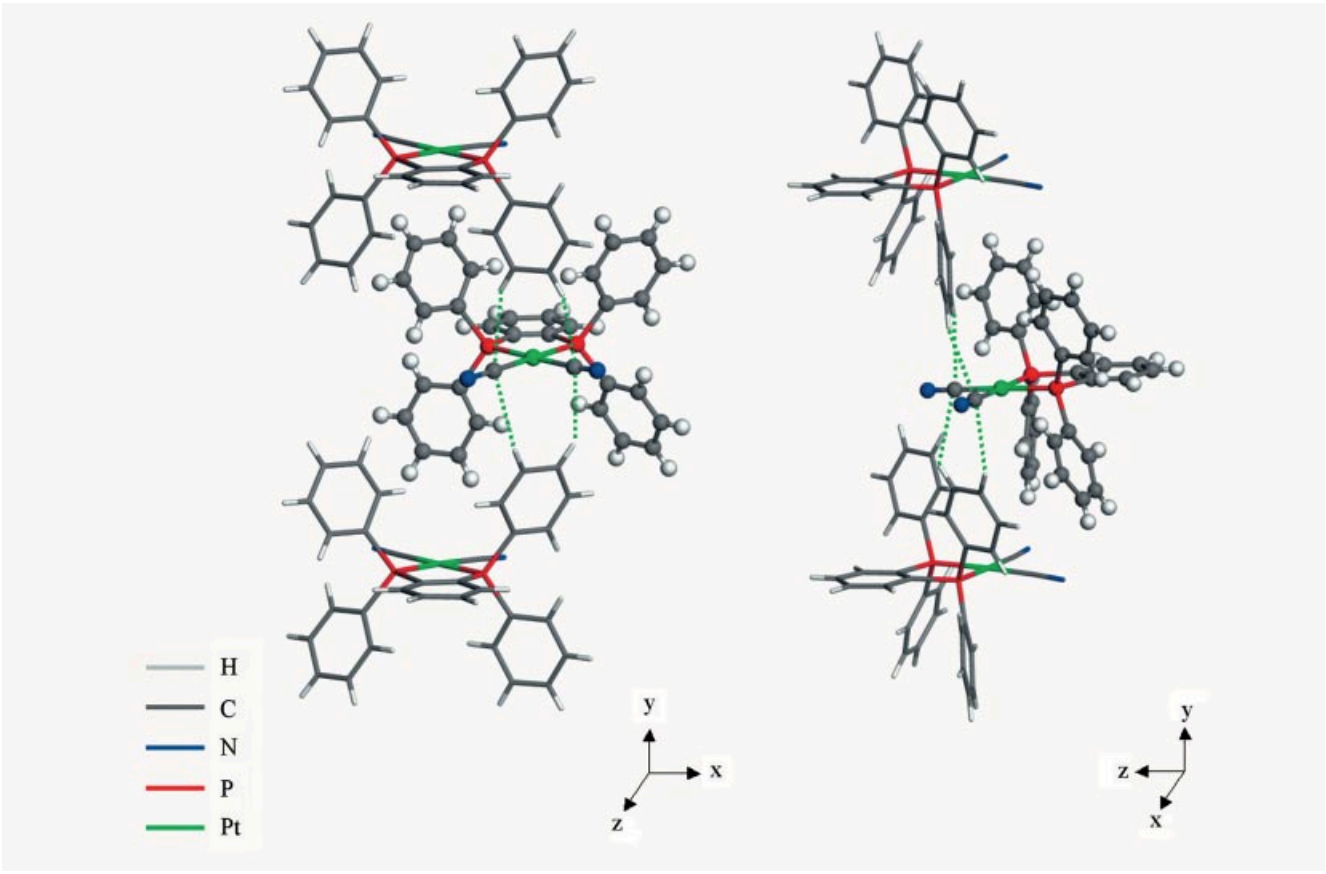

Figure 3. Crystal structure of monomeric Pt(dppb)$(CN)_2$: visualisation of the steric interactions between the Pt$(CN)_2$ fragment and two phenyl groups from neighbouring molecules

metal−ligand bond lengths are 2.26 Å for Pt−P and 1.98 Å for Pt−C. Cyanide is coordinated in a linear fashion.

The lowest-energy excited state of Pt(dppb)$(CN)_2$ seems to be of the IL type since the complex and the free ligand show this phosphorescence at the same wavelength (λ_{max} = 502 nm). However, the lowest-energy transitions of simple aromatic phosphanes are associated with the promotion of an electron from the lone pair (l) at the phosphorus atom to the π* orbitals of the aromatic substituents.[11] Upon coordination the lone pair is stabilised by σ-bonding. As a consequence, the l→π* transition of the phosphane becomes a σ→π* IL transition that should be shifted to higher energies.[11] This concept does not seem to apply to dppb and Pt(dppb)$(CN)_2$. Fortunately, theory provides a satisfactory explanation. According to density functional calculations, the emitting state of the complex is a MLCT state that contains a σ→π* IL contribution. The HOMO is essentially metal-based but also includes the Pt−P bonds, while the LUMO is largely restricted to the aromatic substituents (Figure 4).

To get further insight into the electronic structure and geometry of the excited state of the Pt(dppb)$(CN)_2$ molecule, additional density functional calculations were performed. Optimising the geometries of the singlet-ground state (S_0) and the first triplet state (T_1) results in a quadratic-planar coordination geometry with respect to Pt^{II} for

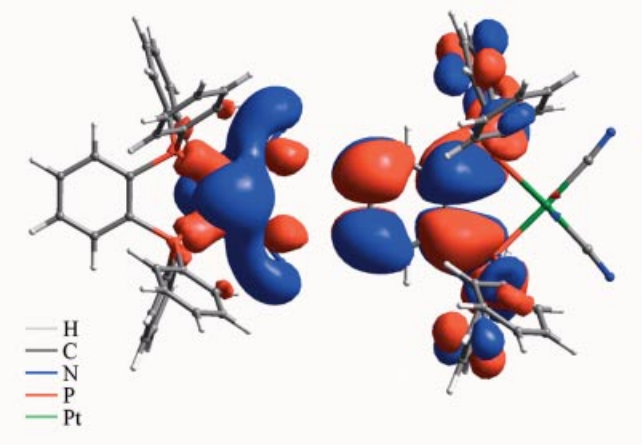

Figure 4. Frontier orbitals of the electronic transition at planar geometry: HOMO (left) and LUMO (right)

the ground state, while the geometry is heavily distorted in the triplet state yielding a deformed tetrahedral geometry as indicated in Scheme 3.

The angle between the cyanocarbons and Pt amounts to 160°, thus resembling more a linear coordination geometry regarding platinum and the two cyano groups than a true tetrahedron. Due to this distortion, the calculated energy gap between the triplet state and the ground state is reduced

 © 2004 Wiley-VCH Verlag GmbH & Co. KGaA, Weinheim

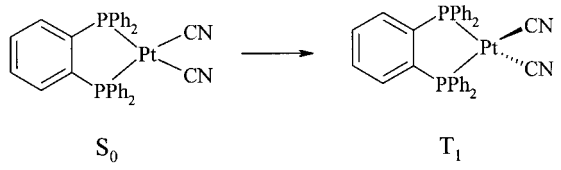

Scheme 3

to 0.1 eV at the triplet geometry. Therefore energetic relaxation of the triplet state should be dominated by nonradiative vibrational relaxation, thereby explaining the nonemissive behaviour of the molecule in solution.

To understand the origin of this distortion an orbital correlation diagram was derived from the density functional calculations. A schematic version is shown in Figure 5. Starting on the left the excitation process promotes one electron from the HOMO to the LUMO and generates the S_1-state. The character of this transition is best described as MLCT, which can be seen in Figure 4, where the frontier orbitals are shown. If the geometry of the S_1-state is now slightly distorted in a tetrahedral way due to corresponding normal modes, then orbital 28a′′ will be substantially stabilised, while orbital 30a' will be destabilised, in such a way that these two orbitals now become the frontier orbitals and a net stabilisation energy for the whole system is gained. Spin-orbit coupling yields the final triplet state. The reason for this orbital behaviour can be seen from the schematic orbital pictures. While an antibonding interaction in orbital 28a′′ vanishes during the rotation, an antibonding character is introduced into orbital 30a′ resulting in a completely different frontier orbital structure for the triplet state. As can be seen from orbitals 22a′′ and 38a′, the electronic transition to the ground state is now basically of a d-d (LF) type.

The crystal structure of $Pt(dppb)(CN)_2$ (Figure 3) shows that, in contrast to the isolated molecule, the triplet distortion is hindered by intermolecular steric interactions between the $Pt(CN)_2$ fragment and two phenyl groups from neighbouring molecules. These groups are oriented perpendicular to the plane spanned by Pt and the two CN groups.

For the complex $Pt(binap)(CN)_2$, the situation could be different as the binaphthyl substituent is characterised by an extended π-electron system. Accordingly, the lowest-energy transition of binap may not be of the l→π* type but rather a ππ* transition of the binaphthyl moiety. This assumption is supported by a comparison of the absorption and emission spectra of $Pt(binap)(CN)_2$ and $Au_2Cl_2(binap)$.[12] For the latter complex it is quite clear that the lowest-energy transitions are of the binap IL type as gold(I) complexes do not have available metal-centred or MLCT excited states at low energies.[13] Indeed, the long-wavelength region of the absorption spectrum of $Pt(binap)(CN)_2$ between 270 and 400 nm (Figure 2) is very similar to that of $Au_2Cl_2(binap)$. Moreover, the emission spectra of both complexes are also rather similar and resemble the phosphorescence of the free binap ligand which, however, is only observed at low temperatures.[14] The IL assignment for the phosphorescence of $Pt(binap)(CN)_2$ is also supported by the fact that the emission shows a pronounced structure which is typical for the phosphorescence from IL states.[1,15] The phosphorescence of $Pt(binap)(CN)_2$ appears only in the solid state and is absent in solution. Again, it is suggested that a rigid structure of the solid compound prevents a distortion towards a tetrahedral structure of a low-energy LF state that does not emit in solution.

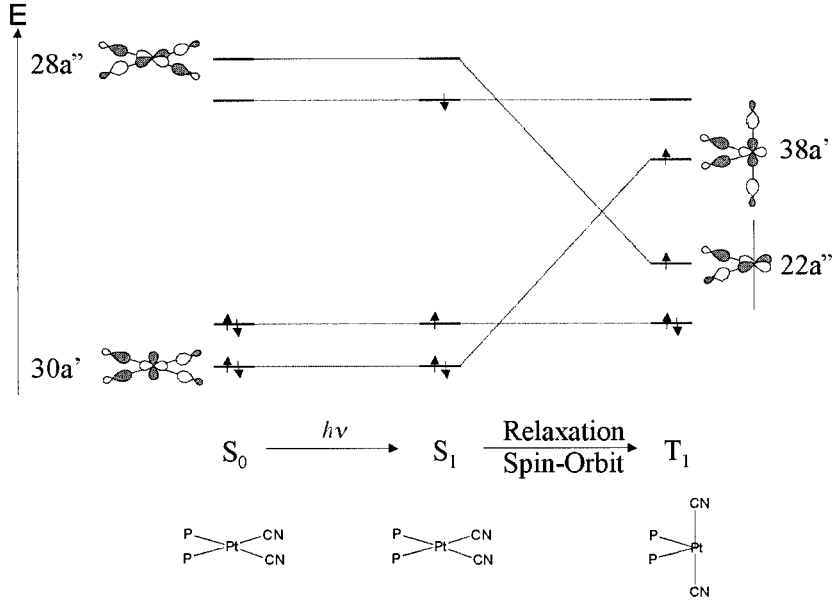

Figure 5. Schematic view of the orbital correlation diagram; only the orbitals responsible for the geometric rearrangement are shown

 © 2004 Wiley-VCH Verlag GmbH & Co. KGaA, Weinheim

In summary, solid compounds of the type $Pt(P-P)(CN)_2$ with bidentate phosphane ligands such as dppb and binap, which carry aromatic chromophores, are triplet emitters under ambient conditions. This phosphorescence originates from MLCT and/or IL states.

Experimental Section

Materials: All solvents used for spectroscopic measurements were of spectrograde quality. $Pt(CN)_2$, dppb and binap were commercially available (Aldrich and Strem) and used without further purification. The complexes $Pt(P-P)(CN)_2$ were obtained by the following procedures.

[Pt(dppb)(CN)$_2$]: A mixture of $Pt(CN)_2$ (0.76 g, 3 mmol) and dppb (1.38 g, 3 mmol) in dimethylformamide (70 mL) was refluxed for 6 h. A white powder slowly precipitated. It was collected by filtration, washed with diethyl ether and dried over silica gel under reduced pressure. The resulting white material was purified by recrystallisation from dichloroethane/ether yielding 0.92 g (43%). $C_{32}H_{24}N_2P_2Pt$ (693.58): calcd. C 55.42, H 3.49, N 4.04; found C 55.06, H 3.60, N 3.94.

[Pt(binap)(CN)$_2$] × H$_2$O: A mixture of $Pt(CN)_2$ (0.25 g, 1 mmol) and binap (0.63 g, 1 mmol) in dimethylformamide (40 mL) was refluxed for 20 h. After filtration, ether was added to the solution. A slightly yellow powder precipitated. It was collected by filtration, washed with diethyl ether and dried over silica gel under reduced pressure. The resulting slightly yellow material was recrystallised from dichloromethane/ether yielding 0.58 g (65%). $C_{46}H_{34}N_2OP_2Pt$ (887.82): calcd. C 62.23, H 3.86, N 3.16; found C 62.68, H 3.90, N 3.07.

X-ray Crystallographic Data for [Pt(dppb)(CN)$_2$]: $C_{32}H_{24}N_2P_2Pt$, M = 693.6; T = 203(2) K; monoclinic, $P2_1/n$ (no. 14); a = 10.031(2) Å, b = 14.885(7) Å, c = 18.812(5) Å, β = 98.138 (5); V = 2781(2) Å^3; Z = 4; Data from 2817 reflections, 2626 unique [R(int.) = 0.047], were collected with a Siemens P4 diffractometer by use of Cu-K_α radiation. The structure was refined by full-matrix least-squares refinement with the SHELXL-97 programmes. All non-H atoms were refined anisotropically, hydrogen atoms were included in riding mode with U_{iso}(H) = 1.2 U_{eq}(C) to give $R1$ = 0.051, $wR2$ = 0.137 [$I > 2\sigma(I)$] and $R1$ = 0.067, $wR2$ = 0.146 (all data).
CCDC-226785 contains the supplementary crystallographic data for this paper. These data can be obtained free of charge at www.ccdc.cam.ac.uk/conts/retrieving.html [or from the Cambridge Crystallographic Data Centre, 12 Union Road, Cambridge CB2 IEZ, UK: Fax: +44-1223-336-033; E-mail: deposit@ccdc.cam.ac.uk].

Instrumentation: Absorption spectra were measured with a Shimadzu 2100 spectrophotometer. Emission spectra were recorded on a Hitachi 850 spectrofluorometer equipped with a Hamamatsu 928 photomultiplier for measurements up to 900 nm. The mass spectra were obtained using a TSQ 7000 Finnigan Thermoquest mass spectrometer.

Calculations: Geometries and energies were calculated with the use of density functional theory involving the BP86 functional,[16] in combination with a split-valence basis set with polarisation functions on all heavy atoms [SV(P)].[17] For platinum, an effective core potential with relativistic corrections (ecp-60-mwb: derived from a multielectron fit to the quasi-relativistic Wood−Boring total valence energies) was employed.[18] The corresponding valence part was of SVP quality.[19,20] Triplet states were optimised with the unrestricted KS approach. Resolution of identity techniques[19] was used throughout. All calculations were carried out with the TURBOMOLE software package.[21]
The orbital correlation diagram is based on the assumption that the relevant excitations are sufficiently described by one-electron transitions between orbitals. We performed additional TD-DFT calculations using the same functional and basis set as described above to check for the single excitation character of the corresponding transitions. The weight of the leading configuration amounts to more then 80% for all relevant singlet excitations. This is also true in the case of the lowest triplet excitation based on the same singlet ground state orbitals for nondistorted geometries. For the distorted triplet geometry the UKS orbitals closely resemble the corresponding RKS orbitals. Therefore the one-electron interpretation is justified.

Acknowledgments

Financial support of the Regensburg group by BASF is gratefully acknowledged.

[1] A. Vogler, H. Kunkely, *Top. Curr. Chem.* **2001**, *213*, 143.
[2] J. M. Bevilacqua, R. Eisenberg, *Inorg. Chem.* **1994**, *33*, 2913.
[3] J. Brooks, Y. Babayan, S. Lamansky, P. I. Djurovich, I. Tsyba, R. Bau, M. E. Thompson, *Inorg. Chem.* **2002**, *41*, 3055, and references cited therein.
[4] H. Kunkely, A. Vogler, *J. Am. Chem. Soc.* **1990**, *112*, 5625.
[5] A. Vogler, H. Kunkely, *Coord. Chem. Rev.* **2002**, *230*, 243.
[6] V. W.-W. Yam, P. K.-Y. Yeung, K.-K. Cheung, *J. Chem. Soc., Dalton Trans.* **1994**, 2587.
[7] J. M. Bevilacqua, J. A. Zuleta, R. Eisenberg, *Inorg. Chem.* **1994**, *33*, 258.
[8] J. DePriest, G. Y. Zheng, N. Goswami, D. M. Eichhorn, C. Woods, D. P. Rillema, *Inorg. Chem.* **2000**, *39*, 1955.
[9] C.-M. Che, V. W.-W. Yam, W.-T. Wong, T.-F. Lai, *Inorg. Chem.* **1989**, *28*, 2908.
[10] B.-H. Xia, C.-M. Che, D. L. Phillips, K.-H. Leung, K.-K. Cheung, *Inorg. Chem.* **2002**, *41*, 3866.
[11] C. Kutal, *Coord. Chem. Rev.* **1990**, *99*, 213.
[12] V. Pawlowski, H. Kunkely, A. Vogler, *Inorg. Chim. Acta* **2004**, *357*, 1309.
[13] A. Vogler, H. Kunkely, *Coord. Chem. Rev.* **2001**, *219−221*, 489.
[14] H. Kunkely, A. Vogler, *Inorg. Chem. Commun.* **1999**, *2*, 533.
[15] H. Kunkely, A. Vogler, *Chem. Phys. Lett.* **2000**, *319*, 486.
[16] J. P. Perdew, *Phys. Rev. B* **1986**, *33*, 8822; A. D. Becke, *Phys. Rev. A* **1988**, *36*, 3098.
[17] A. Schäfer, H. Horn, R. Ahlrichs, *J. Chem. Phys.* **1992**, *9*, 2571.
[18] D. Andrae, U. Haeussermann, M. Dolg, H. Stoll, H. Preuss, *Theor. Chim. Acta* **1990**, *77*, 123.
[19] K. Eichkorn, F. Weigend, O. Treutler, R. Ahlrichs, *Theor. Chem. Acc.* **1997**, *97*, 119.
[20] K. Eichkorn, O. Treutler, H. Oehm, M. Häser, R. Ahlrichs, *Chem. Phys. Lett.* **1995**, *240*, 283.
[21] R. Ahlrichs, M. Bär, M. Häser, H. Horn, C. Cölmel, *Chem. Phys. Lett.* **1989**, *162*, 165.

Received March 23, 2004
Early View Article
Published Online September 9, 2004

 © 2004 Wiley-VCH Verlag GmbH & Co. KGaA, Weinheim

Solid-State Reactions of AgAc with $TabHPF_6$ at Room Temperature − Isolation and Structural Characterisation of an Unusual Octadecanuclear Silver Thiolate Cluster $[Ag_9(Tab)_8(MeCN)_8]_2(PF_6)_{18}\cdot 4MeCN$ [Tab = 4-(trimethylammonio)benzenethiolate]

Jin-Xiang Chen,[a] Qing-Feng Xu,[a] Ying Xu,[a] Yong Zhang,[a] Zhong-Ning Chen,[b] and Jian-Ping Lang*[a]

Keywords: Solid-state reactions / Thiolates / Silver / Clusters

The room-temperature solid-state reaction of silver acetate with $TabHPF_6$ [Tab = 4-(trimethylammonio)benzenethiolate] followed by recrystallization from MeCN afforded a unique octadecanuclear silver thiolate complex $[Ag_9(Tab)_8(MeCN)_8]_2(PF_6)_{18}\cdot 4MeCN$ (**1**). An X-ray analysis of **1** revealed that the structure of $[Ag_9(Tab)_8(MeCN)_8]_2^{18+}$ contains an unprecedented tubular motif in which one central saddle-shaped Ag_6S_6 fragment and two identical Ag_5S_6 fragments are interconnected by a pair of Ag atoms and four Ag–S bonds. The solid-state product was assumed to be $[Ag_9(Tab)_8]_2(PF_6)_{18}$ and might have the $Ag_{18}S_{16}$ core structure of **1** based on elemental analysis, IR spectroscopy, ^1H NMR spectroscopy, luminescence spectra, XRD and TGA measurements.
(© Wiley-VCH Verlag GmbH & Co. KGaA, 69451 Weinheim, Germany, 2004)

Introduction

In recent years, silver thiolate complexes have been of intense interest due to their unique structures,[1−3] their relations to metallothioneins[4,5] and their potential applications in advanced materials [6−9] and antimicrobial drugs.[10] Usually, such complexes are prepared through routine solution reactions. Very few have been reported to have been prepared by solid-state reactions of silver salts with thiolates, especially at room temperature. On the other hand, we have been interested recently in the preparation of silver sulfide clusters from thiometallates with silver salts in the solid state.[11] In these reactions, the solid-state product must be extracted using certain solvents in order for structural characterisation to be carried out.[11a] One question may then arise: Does the solid-state product interact with solvent molecules when it is extracted? This is likely to be true because in the structure of the solid-state products, there are a number of metal atoms with vacant coordination sites which may be further coordinated by solvent molecules bearing donor atoms. However, isolation of such solvent-ligated products is difficult due to their instability arising from the weak coordination between the metal atoms and solvent molecules. In our continuing exploitation of solid-state syntheses of new metal thiolate clusters, we found that a zwitterionic thiolate $TabHPF_6$ [Tab = 4-(trimethylammonio)benzenethiolate][12] readily reacts with AgAc in the solid state at room temperature. When the resultant solid-state product was extracted with acentonitrile, an intriguing octadecanuclear silver thiolate cluster $[Ag_9(Tab)_8(MeCN)_8]_2(PF_6)_{18}\cdot 4MeCN$ (**1**) was formed in high yield. This represents an interesting example of the isolation of the solid-state product having solvent molecules coordinated and solvated. Herein we report its synthesis and structural characterisation.

Results and Discussion

Silver acetate (argenteous powder) and $TabHPF_6$ (white powder) were mixed in a molar ratio of 1:1 and firmly ground in an agate mortar at ambient temperature for about 0.5 h. During grinding, a strong smell of acetic acid was apparent while the colour of the mixture gradually became yellow. The liberation of the volatile acetic acid vapour might be the driving force for this solid-state reaction. The IR spectrum of the yellow powder showed the disappearance of the stretching vibration of the S−H group of $TabHPF_6$ at 2592 cm^{-1},[2f] implying completeness of the reaction. As shown in Scheme 1, the reaction yielded 1 equiv.

[a] Key Laboratory of Organic Synthesis of Jiangsu Province, School of Chemistry and Engineering, Suzhou University, 1 Shizi Street, Suzhou 215006, Jiangsu, P. R. China
Fax: (internat.) + 86-512-65224783
E-mail: jplang@suda.edu.cn
[b] State Key Laboratory of Structure Chemistry, Fujian Institute of Research on the Structure of Matter, Chinese Academy of Sciences, Fuzhou 350002, Fujian, P. R. China
Supporting information for this article is available on the WWW under http://www.eurjic.org or from the author.

of acetic acid and 1/9th of an equivalent of the zwitterionic Tab ligand which is very soluble in methanol. Consequently, we thoroughly washed the powder with MeOH and Et_2O and then dried the product in vacuo for 1 h to form a yellow solid **1a**. Subsequent extraction of **1a** with MeCN, followed by diffusion of Et_2O into the extract gave rise to colourless crystals of $[Ag_9(Tab)_8(MeCN)_8]_2(PF_6)_{18}\cdot 4MeCN$ (**1**) in 95% yield; the elemental analysis of **1** corresponds to this formula. The IR spectrum of **1** shows a C=N stretching vibration for MeCN at 2262 cm^{-1} and two strong characteristic peaks arising from PF_6 at 841 and 559 cm^{-1}. The ^1H NMR spectrum of **1** in $[D_6]$DMSO exhibits a single signal at $\delta = 2.07$ ppm for protons of the MeCN molecules, a singlet at $\delta = 3.34$ ppm for the NMe_3 groups and multiplets in the $\delta = 7.43-7.48$ ppm region for the phenyl groups. The identity of **1** was finally confirmed by a single-crystal X-ray diffraction study.

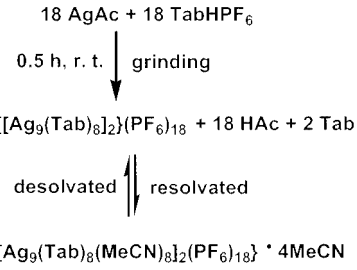

Scheme 1

Compound **1** crystallises in the triclinic space group $P\bar{1}$ and the asymmetric unit contains one-half of the discrete $[Ag_9(Tab)_8(MeCN)_8]_2^{18+}$ cation, ten $[PF_6]^-$ anions (two of them having an occupancy of 0.5) and two MeCN solvate molecules. Figure 1 shows the packing diagram of **1** in the unit cell. The $[Ag_9(Tab)_8(MeCN)_8]_2^{18+}$ cations are parallel to each other along the *c* axis. The associated $[PF_6]^-$ anions are located between the two tubular octadecacations. Except for the electrostatic forces between the octadecacations and the $[PF_6]^-$ anions, there are no other apparent interactions between the MeCN solvent molecules and the octadecacations or the $[PF_6]^-$ anions.

Figure 2 shows a perspective view of the $[Ag_9(Tab)_8(MeCN)_8]_2^{18+}$ ion while Figure 3 represents a side-view of the tubular structure of the octadecacation of **1**. Table 1 lists selected bond lengths and angles of **1**. Being a crystallographic centre of symmetry on the midpoint of Ag(1) and Ag(1′), the octadecacation of **1** contains 18 Ag atoms, 16 Tab moieties and 16 coordinated MeCN molecules. The $Ag_{18}S_{16}$ core of the octadecacation may be visualised as a long tubular structure which is composed of one central saddle-shaped Ag_6S_6 fragment and two identical Ag_5S_6 fragments bridged by a pair of Ag [Ag(3) and Ag(3′)] atoms and four Ag−S bonds [Ag(5)−S(5), Ag(4)−S(2), Ag(5′)−S(5′) and Ag(4′)−S(2′)]. The Ag_6S_6 fragment consists of two six-membered Ag_3S_3 rings, Ag(5)S(1′)Ag(1′)S(2′)Ag(2′)S(4′) and Ag(5′)S(1)Ag(1)S(2)Ag(2)S(4), which are held together by the Ag(1)−S(4′) and Ag(1′)−S(4) bonds. Each Ag_5S_5 fragment is composed of one six-membered Ag(9)S(7)Ag(7)S(3′)Ag(8)S(8) [or Ag(9′)S(7′)Ag(7′)S(3)Ag(8′)S(8′)] ring and one eight-membered Ag(9)S(7)Ag(7)S(6)Ag(6)S(5)Ag(4)S(8) [or Ag(9′)S(7′)Ag(7′)S(6′)Ag(6′)S(5′)Ag(4′)S(8′)] ring, sharing a group of Ag(9), S(7), Ag(7) and S(8) [or Ag(9′), S(7′), Ag(7′) and S(8′)] atoms. It is noteworthy that the coordination geometry of the 18 Ag atoms can be classified into three groups: distorted tetrahedral [Ag(1), Ag(1′), Ag(4), Ag(4′), Ag(5) and Ag(5′)], pyramidalised Y-shape [Ag(8) and Ag(8)] and trigonal planar [Ag(2), Ag(2′), Ag(3), Ag(3′), Ag(6), Ag(6′), Ag(7) Ag(7′) Ag(9) and Ag(9′)]. As can be seen in Table 1, most Ag···Ag contacts [3.011(3)−3.426(3) Å] are similar to those found in $\{[Ag_3(Tab)_4](PF_6)_3\cdot 2DMF\}_n$ [3.207(2) Å],[2f] but shorter than the sum of the van der Waals radii of two Ag atoms (3.44 Å), implying the possible existence of the silver−silver interactions.[13] Other relatively longer Ag···Ag separations such as Ag(3)···Ag(7′) = 3.667(3) Å and Ag(2)···Ag(8) = 3.758(3) Å may constitute weak nonbonding interactions. The sixteen sulfur atoms show doubly bridging [S(6), S(6′), S(7), S(7′)] and triply bridging [S(1) to S(5), S(1′) to S(5′), S(8), S(8′)] modes. The observed trend in the Ag−S bond lengths varying from 2.397(5) to 2.654(5) Å correlates with the coordination geometries of the Ag centres. The average Ag−S bond length of 2.512 Å is not unusual when compared with structures containing three-coordinate Ag^I such as $\{[Ag_3(Tab)_4](PF_6)_3\cdot 2DMF\}_n$ (2.529 Å),[2f] $[PPh_4]_2[Ag_4(SCH_2C_6H_4CH_2S)_3]$ (2.505 Å)[14] and $[PPh_4]_3[Ag_9(SCH_2CH_2S)_6]$ (2.579 Å).[15] Interestingly, as shown in Figure 1, except for Ag(7) and Ag(7′), the other sixteen Ag atoms are coordinated by sixteen MeCN molecules in an ordered way: 5 each on the right or left side and 3 each behind or before the tubular structure. Judging from the Ag−N bond lengths listed in Table 1, however, the strengths of the interactions between the Ag atoms and the MeCN molecules vary significantly. The longest Ag(3)−N(11) bond of 2.49(1) Å is 0.22 Å longer than that of the shortest Ag(9)−N(16) bond. This implies that some MeCN molecules may coordinate weakly at silver centres and some may bind tightly to silver atoms. This fact is con-

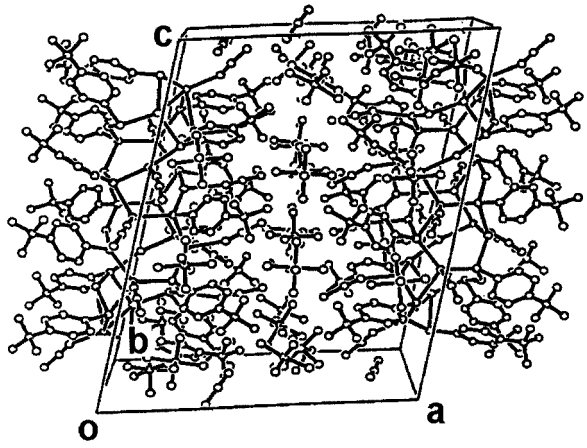

Figure 1. Cell packing diagram of **1** looking along the *b* axis; all hydrogen atoms have been omitted for clarity

 © 2004 Wiley-VCH Verlag GmbH & Co. KGaA, Weinheim

sistent with two stages for the loss of MeCN molecules as indicated by the TGA curves. This is discussed later in the paper.

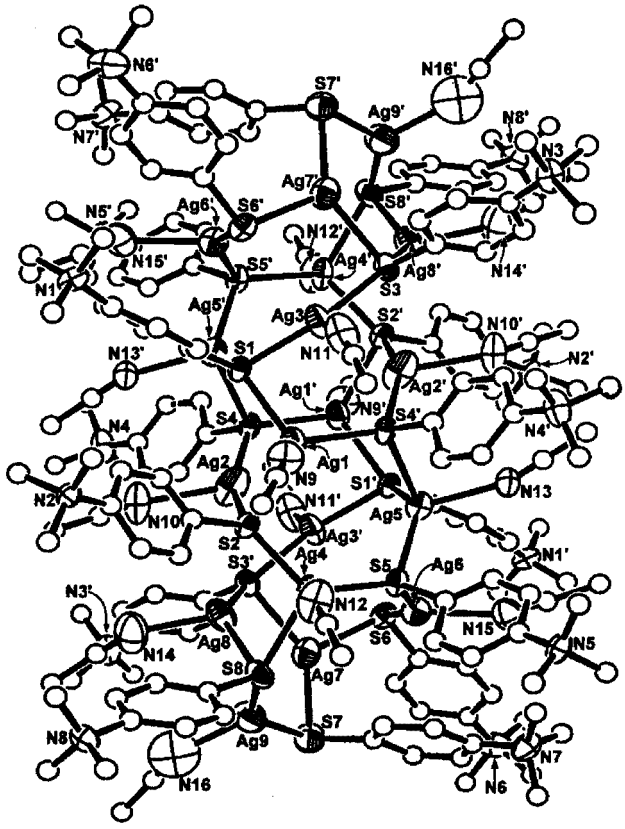

Figure 2. Perspective view of the $[Ag_9(Tab)_8(MeCN)_8]_2^{18+}$ ion of **1** including labelling scheme; thermal ellipsoids are shown at the 50% probability level; all hydrogen atoms have been omitted for clarity

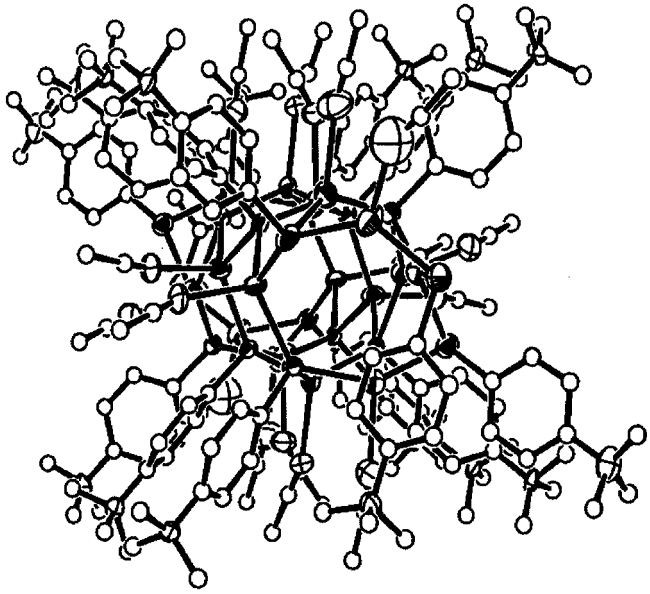

Figure 3. A side view of the tubular structure of the octadecacation of **1**, looking along the *c* axis

Table 1. Selected bond lengths [Å] and angles [°] for **1**

Ag(1)···Ag(2)	3.410(2)	Ag(1)···Ag(3)	3.426(2)
Ag(4)···Ag(8)	3.130(2)	Ag(5)···Ag(6)	3.195(2)
Ag(6)···Ag(7)	3.306(2)	Ag(7)···Ag(8)	3.424(2)
Ag(7)···Ag(9)	3.063(2)	Ag(8)···Ag(9)	3.011(3)
Ag(1)−S(1)	2.589(4)	Ag(1)−S(2)	2.654(5)
Ag(1)−S(4′)	2.503(5)	Ag(2)−S(2)	2.421(5)
Ag(2)−S(4)	2.410(5)	Ag(3)−S(1)	2.460(5)
Ag(3)−S(3)	2.455(6)	Ag(4)−S(2)	2.542(4)
Ag(4)−S(5)	2.486(5)	Ag(4)−S(8)	2.627(6)
Ag(5)−S(5)	2.531(6)	Ag(5)−S(1′)	2.537(5)
Ag(5)−S(4′)	2.638(4)	Ag(6)−S(5)	2.454(5)
Ag(6)−S(6)	2.399(5)	Ag(7)−S(6)	2.550(5)
Ag(7)−S(6)	2.553(6)	Ag(7)−S(7)	2.481(6)
Ag(7)−S(3′)	2.554(4)	Ag(8)−S(8)	2.530(5)
Ag(8)−S(3′)	2.526(5)	Ag(9)−S(7)	2.425(6)
Ag(9)−S(8)	2.455(6)	Ag(1)−N(9)	2.31(2)
Ag(2)−N(10)	2.49(2)	Ag(3)−N(11)	2.43(2)
Ag(4)−N(12)	2.35(2)	Ag(5)−N(13)	2.40(2)
Ag(6)−N(15)	2.44(2)	Ag(8)−N(14)	2.40(2)
Ag(9)−N(16)	2.27(4)		
S(1)−Ag(1)−S(2)	113.2(2)	S(1)−Ag(1)−N(9)	113.8(4)
S(2)−Ag(1)−N(9)	92.2(5)	S(4′)−Ag(1)−N(10)	116.0(4)
S(4′)−Ag(1)−S(1)	105.78(12)	S(2)−Ag(1)− S(4′)	116.2(1)
S(2)−Ag(2)−S(4)	151.6(2)	S(2)−Ag(2)−N(10)	94.9(5)
S(4)−Ag(2)−N(10)	108.5(5)	S(1)−Ag(3)−S(3)	143.5(2)
S(1)−Ag(3)−N(11)	108.8(6)	S(3)−Ag(3)−N(11)	107.7(6)
S(2)−Ag(4)−S(5)	111.2(2)	S(2)−Ag(4)−S(8)	107.3(2)
S(2)−Ag(4)−N(12)	114.5(5)	S(5)−Ag(4)−S(8)	115.9(2)
S(5)−Ag(4)−N(12)	111.3(5)	S(8)−Ag(4)−N(12)	96.0(6)
S(1′)−Ag(5)−N(13)	107.3(4)	S(4′)−Ag(5)−N(13)	93.7(4)
S(1′)−Ag(5)−S(4′)	99.28(5)	S(1′)−Ag(5)−S(5)	125.26(12)
S(4′)−Ag(5)−S(5)	111.80(11)	S(5)−Ag(5)−N(13)	114.1(4)
S(5)−Ag(6)−S(6)	143.8(2)	S(5)−Ag(6)−N(15)	97.0(4)
S(6)−Ag(6)−N(15)	116.5(4)	S(6)−Ag(7)−S(7)	114.9(2)
S(3′)−Ag(7)−S(6)	100.61(12)	S(3′)−Ag(7)−S(7)	91.5(6)
S(3′)−Ag(8)−S(8)	136.05(13)	S(3′)−Ag(8)−N(14)	102.2(6)
S(8)−Ag(8)−N(14)	109.8(6)	S(7)−Ag(9)−S(8)	132.5(2)
S(7)−Ag(9)−N(16)	106.7(8)	S(8)−Ag(9)−N(16)	120.0(8)
Ag(1)−S(1)−Ag(3)	85.4(1)	Ag(5′)−S(1)−Ag(3)	110.0(2)
Ag(5′)−S(1)−Ag(1)	127.2(2)	Ag(1)−S(2)−Ag(2)	84.3(2)
Ag(1)−S(2)−Ag(4)	106.0(2)	Ag(2)−S(2)−Ag(4)	135.4(2)
Ag(8′)−S(3)−Ag(7′)	84.7(1)	Ag(7′)−S(3)−Ag(3)	94.1(2)
Ag(8′)−S(3)−Ag(3)	134.9(2)	Ag(5′)−S(4)−Ag(2)	101.4(2)
Ag(1′)−S(4)−Ag(2)	119.9(2)	Ag(5′)−S(4)−Ag(1′)	112.0(2)
Ag(4)−S(5)−Ag(5)	119.0(2)	Ag(4)−S(5)−Ag(6)	124.1(2)
Ag(6)−S(5)−Ag(5)	79.7(2)	Ag(6)−S(6)−Ag(7)	83.7(2)
Ag(7)−S(7)−Ag(9)	76.2(2)	Ag(8)−S(8)−Ag(4)	74.7(2)
Ag(8)−S(8)−Ag(9)	74.3(2)	Ag(4)−S(8)−Ag(9)	130.0(2)

Interestingly, when crystals of **1** were heated in vacuo at 150 °C for 1 h, a yellow solid **1b** was formed and the liberation of MeCN was apparent by collection in a cold trap. When **1b** was immersed in MeCN, colourless crystals of **1** (identified by X-ray crystallography) were formed again in almost quantitative yield. What are the identities of **1a** and **1b**? We made numerous attempts to grow crystals of **1a** and **1b** in other solvents such as acetone and DMSO but were unsuccessful. Elemental analyses of **1a** and **1b** are in agreement with the formula $[Ag_9(Tab)_8]_2(PF_6)_{18}$. The FT-IR spectra of **1a** and **1b** are almost identical and display two strong peaks for PF_6 at 856 and 559 cm^{-1} but no C=N vibration at around 2262 cm^{-1} for **1**. The ^1H NMR spectra of both **1a** and **1b** in $[D_6]$DMSO exhibit only singlets at

 © 2004 Wiley-VCH Verlag GmbH & Co. KGaA, Weinheim

δ = 3.34 ppm for the NMe_3 groups and multiplets in the δ = 7.43−7.48 ppm region for phenyl groups but no resonances for the methyl groups of MeCN molecules in the region of δ = 2.07 ppm. Not surprisingly, the UV/Vis spectra of **1**, **1a** and **1b** in MeCN exhibit the same strong and broad absorbance band at 284 nm (see Supporting Information, for Supporting Informations see also the footnote on the first page of this article) which may overlap the possible absorption bands in the visible region for **1**, **1a** and **1b**.

Crystals of **1** quickly lose some of the solvated MeCN molecules as soon as they are taken out of the mother liquor at room temperature. The surfaces of the crystals were observed to crack within seconds under the microscope. As shown in Figure 2, the thermogravimetric analysis revealed that **1** underwent decomposition in three stages between 25 and 400 °C. As shown in Figure 4, the first stage caused a weight loss of 4.5% in the region of 25−90 °C which corresponds roughly to the loss of three solvate MeCN molecules and another six coordinated MeCN molecules. The second stage resulted in a weight loss of 5.1% in the region of 90−160 °C, consistent with the loss of the remaining ten MeCN molecules in **1**. In the first stage, one more solvate MeCN molecule may be missing during the sample preparation for TGA measurement. However, **1a** and **1b** were relatively stable in the range of 25−160 °C. On heating further to 250 °C, samples of **1**, **1a** and **1b** began to decompose with almost the same pattern.

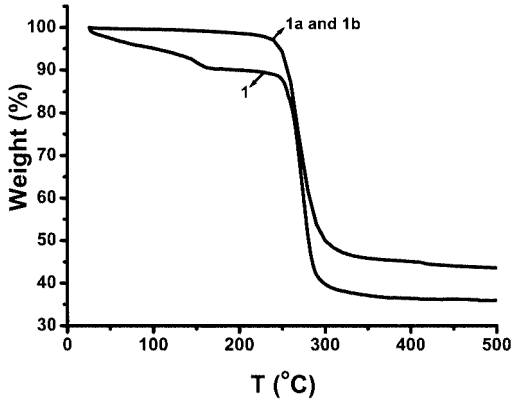

Figure 4. TGA curves for **1**, **1a** and **1b** under nitrogen

X-ray powder diffraction measurements for **1**, **1a** and **1b** gave data which was a little bit weak with a noisy baseline (see Supporting Information). However, the powder patterns of **1a** and **1b** resemble that of **1** which indicates that **1a** and **1b** may possess the $[Ag_{18}S_{16}]$ cluster core framework of **1**.

Compounds **1**, **1a** and **1b** exhibit luminescence in the solid state at ambient temperature. As shown in Figure 5, compound **1** exhibits an intense emission band at 625 nm (λ_{ex} = 450 and 507 nm) while **1a** and **1b** exhibit a similar emission band at 627 nm (λ_{ex} = 457 nm). As the free Tab ligand is not emissive in the solid state at ambient temperature, the possible origins of these emissions may be tentatively assumed to be MLCT from silver (4d) to the ligand (π^*) or an LC transition from S (nonbonding 3p) to the benzene ring (π^*) of the Tab ligands, though the metal-centred transition arising from the silver−silver contacts and transitions from surface S−Ar states cannot be ruled out.[2f,16]

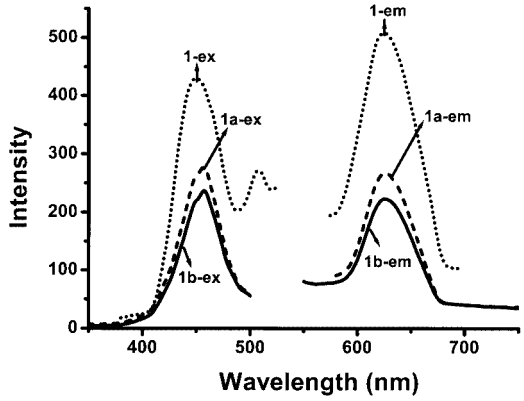

Figure 5. Excitation and emission spectra of **1**, **1a** and **1b** in the solid state at ambient temperature

Conclusions

In summary, we have successfully prepared a new silver thiolate complex from solid-state reactions between AgAc and $TabHPF_6$ at room temperature. When the solid-state product $[Ag_9(Tab)_8]_2(PF_6)_{18}$ was recrystallized from MeCN, it was solvated by MeCN molecules and some Ag atoms in its framework were coordinated by MeCN molecules, forming the unusual silver thiolate cluster **1**. The isolation of **1** provides convincing evidence that some solid-state products may have their structures altered, or at least experience changes in the coordination geometries of certain metal atoms in their structures when they are extracted with a solvent. The facile room-temperature solid-state synthesis reported in this paper is in accord with the current trend in green chemistry. Further investigation on the preparation of other metal/Tab complexes by this method is currently under way in our laboratory.

Experimental Section

General: $TabHPF_6$ was prepared according to a literature method.[12] Other chemicals and reagents were obtained from commercial sources and used as received. All solvents were pre-dried with activated molecular sieves and heated to reflux in the presence of appropriate drying agents under argon. IR spectra were recorded with a Nicolet MagNa-IR 550 instrument as KBr disk (4000−400 cm^{-1}). ^1H NMR spectra were recorded at ambient temperature with a Varian UNITYplus-400 spectrometer. ^1H NMR chemical shifts were referenced to the $[D_6]$DMSO signal. UV/Vis spectra were measured with a Hitachi U-2810 spectrophotometer. Elemental analyses for Ag and P were carried out by inductively coupled plasma atomic emission spectroscopy (Leeman PLA-SPECI ICP spectrophotometer). The elemental analyses for C, H and N were performed with an EA1110-CHNS elemental analyser. The thermal

 © 2004 Wiley-VCH Verlag GmbH & Co. KGaA, Weinheim

analysis was performed with a Perkin−Elmer TGA-7 thermogravimetric analyser at a heating rate of 10 °C/min and a flow rate of 100 cm^3/min (N_2). XRD spectra were recorded with a Rigaku D/MAX-IIIC X-ray diffractometer.

Preparation of $[Ag_9(Tab)_8(MeCN)_8]_2(PF_6)_{18}$·4MeCN (1): A mixture of argenteous AgAc powder (0.33 g, 2 mmol) and white $TabHPF_6$ powder (0.63 g, 2 mmol) was placed in an open agate mortar and ground at room temperature for 0.5 h. During this time, the mixture gradually became yellow and a strong smell of acetic acid was apparent. The mixture was washed with CH_3OH/Et_2O (3:1) and dried in vacuo to form 0.78 g of a yellow solid (**1a**). $C_{144}H_{208}Ag_{18}F_{108}N_{16}S_{16}P_{18}$ (7227.2): calcd. C 23.93, H 2.90, Ag 26.87, N 3.10, P 7.71; found C 24.12, H 3.28, Ag, 26.23, N 3.55, P, 7.58. IR (KBr disc): $\tilde{\nu}$ = 1624 (w), 1489 (s), 1126 (s), 1010 (m), 856 (s), 744 (s), 559 (m) cm^{-1}. UV/Vis (MeCN): $\lambda_{max.}$ (ε [M^{-1}·cm^{-1}]) = 282 (220000) nm. ^1H NMR (400 MHz, [D_6]DMSO): δ = 7.43−7.48 (m, 4 H, Ph), 3.34 (s, 9 H, NMe_3) ppm. Into a glass beaker containing **1a** (0.78 g) was added MeCN (10 mL) immediately forming a yellow solution. Colourless crystals of $[Ag_9(Tab)_8(CH_3CN)_8]_2(PF_6)_{18}$·$4CH_3CN$ (**1**) were isolated by layering diethyl ether (10 mL) onto the solution for one week. The crystals were collected by filtration and washed with $MeOH/Et_2O$ (1:4) Yield: 0.85 g (95%). $C_{184}H_{268}Ag_{18}F_{108}N_{36}P_{18}S_{16}$ (8048.3): calcd. C 27.46, H 3.36, Ag 24.13, N 6.26, P 6.93; found C 27.89, H 3.28, Ag 23.85, N 6.65, P 6.73. IR (KBr disc): $\tilde{\nu}$ = 2262 (w), 1628 (w), 1489 (s), 1126 (w), 1010 (w), 841 (s), 744 (w), 559 (m) cm^{-1}. UV/Vis (MeCN): $\lambda_{max.}$ (ε [M^{-1}·cm^{-1}]) = 283 (180000) nm. ^1H NMR (400 MHz, [D_6]DMSO): δ = 7.43−7.48 (m, 16 H, Ph), 3.34 (s, 36 H, NMe_3), 2.07 (s, 12 H, MeCN) ppm. Crystals of **1** suitable for X-ray analysis were obtained by recrystallization from MeCN.

De-solvation and Re-solvation Experiments: Colourless crystals of **1** (0.805 g, 0.1 mmol) were placed in a Pyrex glass tube which was connected to a cold trap. The tube was heated to 150 °C and allowed to stand at that temperature for 10 h. During this period, the colour of **1** gradually turned from white to yellow. After it was cooled to room temperature, 0.72 g of yellow solid **1b** had formed. To a glass beaker containing **1b** (0.3 g) was added MeCN (5 mL) forming a yellow solution. Similar workup generated colourless crystals of **1** (confirmed by X-ray crystallography) in 98% yield. **1b:** $C_{144}H_{208}Ag_{18}F_{108}N_{16}S_{16}P_{18}$ (7227.2): calcd. C 23.93, H 2.90, Ag 26.87, N 3.10, P 7.71; found C 23.62, H 2.56, Ag 26.45, N 3.42, P 7.60. IR (KBr disc): $\tilde{\nu}$ = 1620 (w), 1493 (s), 1126 (m), 1010 (m), 856 (s), 744 (s), 559 (m) cm^{-1}. UV/Vis (MeCN): $\lambda_{max.}$ (ε [M^{-1}·cm^{-1}]) = 282 (240000) nm. ^1H NMR (400 MHz, [D_6]DMSO): δ = 7.43−7.48 (m, 4 H, Ph), 3.34 (s, 9 H, NMe_3) ppm.

X-ray Crystal Structure Determination of 1: All measurements were carried out with a Rigaku Mercury CCD X-ray diffractometer (3 kV, sealed tube) using graphite-monochromated Mo-K_α radiation (λ = 0.71070 Å). A colourless single-crystal of **1** with dimensions of 0.30 × 0.30 × 0.30 mm was mounted at the top of a glass fibre and cooled to 193 K in a stream of gaseous nitrogen. Diffraction data were collected in the ω mode with a detector-to-crystal distance of 35 mm. Indexing was performed from 6 images each of which resulted from a 15 s exposure. Cell parameters were refined using the program CrystalClear (Rigaku and MSc, Ver. 1.3, 2001) on all observed reflections with θ between 3.0° and 27.5°. A total of 720 oscillation images were collected in the range 1.96° < 2θ < 54.9°. The collected data were reduced using the program CrystalStructure (Rigaku and MSC, Ver. 3.16, 2003) and an absorption correction (Multi-Scan) was applied which resulted in transmission factors ranging from 0.498 to 0.648. The data were also corrected for Lorentz and polarization effects. The structure of **1** was solved by direct methods[17] and refined by full-matrix least squares on *F*.[18] Non-hydrogen atoms except P(5) to P(10), F(1) to F(6), N(16) to N(18), C(7) to C(9), C(34) to C(36), C(52) to C(54) and C(87) to C(92) were refined anisotropically. The two PF_6^- anions bearing P(8) and P(10) were refined using restrained parameters as rigid groups with occupancy factors of 0.5. All hydrogen atoms were placed in calculated positions and refined in the final structure-factor refinement. There may be more than two free acetonitrile solvent molecules in the asymmetric unit. However, attempts to locate other acetonitrile molecules were unsuccessful. Besides, the relatively high thermal parameters of the F atoms of the PF_6^- anions of P(5) to P(10) and some carbon atoms [C(7) to C(9), C(34) to C(36), C(52) to C(54) and C(87) to C(92)] of the NMe_3 groups showed signs of disorder, but attempts to model these disorders did not succeed. The relatively high *R* values may be due to the quality of the crystal and the possible disorder of the methyl groups, part of the PF_6^- anions and part of the acetonitrile molecules. Neutral atom-scattering factors were taken from Cromer and Waber.[19] Anomalous dispersion effects were included in $F_{calcd.}$.[20] All calculations were performed with a Dell workstation using the CrystalStructure crystallographic software package. Crystal and data collection parameters for **1** are summarised in Table 2. CCDC-229000 (**1**) contains the supplementary crystallographic data for this paper. These data can be obtained free of charge at www.ccdc.cam.ac.uk/conts/retrieving.html [or from the Cambridge Crystallographic Data Centre, 12 Union Road, Cambridge CB2 1EZ, UK; Fax: + 44-1223-336-033; E-mail: deposit@ccdc.cam.ac.uk].

Table 2. Summary of the crystal data for **1**

Empirical formula	$C_{184}H_{268}Ag_{18}F_{108}N_{36}P_{18}S_{16}$
Formula mass	8048.32
Crystal system	triclinic
Space group	$P\bar{1}$
a [Å]	18.114(3)
b [Å]	18.311(3)
c [Å]	23.680(4)
α [°]	84.653(8)
β [°]	75.970(7)
γ [°]	89.252(9)
V [Å^3]	7586.3(21)
$D_{calcd.}$ [g·cm^{-3}]	1.762
Z	1
μ [cm^{-1}]	14.48
Reflections [$I > 3.00\sigma(I)$]	12874
Parameters	1488
R[a]	0.0890
R_w[b]	0.0940
GOF[c]	1.144
Largest residual peak/hole [e·Å^{-3}]	1.99/−1.14

[a] $R = \Sigma||F_o| - |F_c||/\Sigma|F_o|$. [b] $Rw = \{w\Sigma(|F_o| - |F_c|)^2/\Sigma w|F_o|^2\}^{1/2}$. [c] GOF = $\{\Sigma w(|F_o| - |F_c|)^2/(M - N)\}^{1/2}$, where *M* is the number of reflections and *N* is the number of parameters.

Acknowledgments

The authors thank the NNSF of China (No. 20271036), the NSF of the Education Committee of Jiangsu Province (No. 02KJB150001), the State Key Laboratory of Structural Chemistry of FJIRSM (030066), the Key Laboratory of Organic Synthesis of Jiangsu Province (JSK001), the Scientific Research Foundation for the Returned Overseas Chinese Scholars and the State Education Ministry of China for financial support.

 © 2004 Wiley-VCH Verlag GmbH & Co. KGaA, Weinheim

[1] [1a] I. Dance, *Polyhedron* **1986**, *5*, 1037−1104. [1b] I. Dance, K. Fisher, G. Lee, in *Metallothioneins: Synthesis, Structure and Properties of Metallothioneins, Phytohelatins, and Metal-Thiolate Complexes*, VCH, New York, **1992**, vol. 13, p. 284−345. [1c] *Metal Clusters in Chemistry* (Eds.: P. Braunstein, L. A. Oro, P. R. Raithby), Wiley-VCH, New York, **1999**, vols. 1−3.

[2] [2a] P. González-Duarte, J. Sola, J. Vives, X. Solans, *J. Chem. Soc., Chem. Commun.* **1987**, 1641−1642. [2b] I. Casal, P. Gonzalez-Duarte, J. Sola, J. Vives, M. Font-Bardia, X. Solans, *Polyhedron* **1990**, *9*, 769−771. [2c] W. P. Su, R. Cao, M. C. Hong, J. T. Chen, J. X. Lu, *Chem. Commun.* **1998**, 1389−1390. [2d] J. A. Garcia-Vazquez, J. Romero, A. Sousa-Pedrares, M. L. Louro, A. Soura, J. Zubieta, *J. Chem. Soc., Dalton Trans.* **2000**, 559−568. [2e] X. J. Wang, T. Langetape, C. Persau, B. S. Kang, G. M. Sheldrick, D. Fenske, *Angew. Chem. Int. Ed.* **2002**, *20*, 3818−3822. [2f] J. X. Chen, Q. F. Xu, Y. Zhang, Z. N. Chen, J. P. Lang, *J. Organomet. Chem.* **2004**, *689*, 1071−1077.

[3] [3a] K. L. Tang, X. L. Jin, Y. Q. Tang, *Reviews on Heteroatom Chemistry* (Ed.: S. Oae), MYU, Tokyo, **1996**, vol. 15, p. 83. [3b] K. L. Tang, X. J. Xie, Y. Zhang, X. Zhao, X. L. Jin, *Chem. Commun.* **2002**, 1024−1025.

[4] G. D. Pilar, S. Joan, V. Josep, S. Xavier, *J. Chem. Soc., Chem. Commun.* **1987**, 1641−1642.

[5] D. T. Jiang, Z. Q. Gui, S. M. Heald, T. K. Sham, M. J. Stillman, *Physica B* **1995**, *208−209*, 729−730.

[6] K. V. G. K. Murt, M. Venkataramanan, T. Pradeep, *Langmuir* **1998**, *14*, 5446−5456.

[7] S. H. Chen, T. Ida, K. Kimura, *J. Phys. Chem. B* **1998**, *102*, 6169−6176.

[8] M. Liang, N. Lackey, S. Carter, M. L. Norton, *J. Electrochem. Soc.* **1996**, *143*, 3117−3119.

[9] X. L. Jin, X. J. Xie, H. Qian, K. L. Tang, C. L. Liu, X. Wang, Q. H. Gong, *Chem. Commun.* **2002**, 600−601.

[10] K. Nomiya, S. Takahashi, R. Noguchi, *J. Chem. Soc., Dalton Trans.* **2000**, 2091−2098.

[11] [11a] J. P. Lang, X. Q. Xin, *J. Solid State Chem.* **1994**, *108*, 118−127. [11b] H. Yu, Q. F. Xu, Z. R. Sun, S. J. Ji, J. X. Chen, Q. Liu, J. P. Lang, K. Tatsumi, *Chem. Commun.* **2001**, 2614−2615.

[12] B. V. DePamphilis, B. A. Averill, T. Herskovitz, L. Que Jr., R. H. Holm, *J. Am. Chem. Soc.* **1974**, *96*, 4159−4167.

[13] N. Kaltsoyannis, *J. Chem. Soc., Dalton Trans.* **1997**, 1−12.

[14] G. Henkel, P. Betz, B. Krebs, *Angew. Chem. Int. Ed. Engl.* **1987**, *26*, 145−146.

[15] G. Henkel, B. Kreb, P. Betz, H. Fietz, K. Saatkamp, *Angew. Chem. Int. Ed. Engl.* **1988**, *27*, 1326−1329.

[16] [16a] S. Watae, M. Nakamoto, T. Kitamura, N. Kanehisa, Y. Kai, S. Yanagida, *J. Chem. Soc., Dalton Trans.* **2000**, 3585−3590. [16b] F. Sabin, C. K. Ryu, P. C. Ford, A. Vogler, *Inorg. Chem.* **1992**, *31*, 1941−1945. [16c] V. W. W. Yam, K. K. W. Lo, K. M. C. Wong, *J. Organomet. Chem.* **1999**, *578*, 3−30. [16d] V. W. W. Yam, K. K. W. Lo, *Chem. Soc. Rev.* **1999**, *28*, 323−334.

[17] G. M. Sheldrick, *SHELXS-97: Program for the Solution of Crystal Structures*, University of Göttingen, Germany, **1997**.

[18] P. T. Beurskens, G. Admiral, G. Beurskens, W. P. Bosman, R. de Gelder, R. Israel, J. M. M. Smits, *DIRDIF-94: The DIRDIF-94 program system*, Technical Report of the Crystallography Laboratory, University of Nijmegen, The Netherlands, **1992**.

[19] D. T. Cromer, J. T. Waber, *International Tables for X-ray Crystallography*, The Kynoch Press, Birmingham, England, **1974**, vol. IV, Table 2.2 A.

[20] J. A. Ibers, W. C. Hamilton, *Acta Crystallogr.* **1964**, *17*, 781−782.

Received March 10, 2004
Early View Article
Published Online August 26, 2004

 © 2004 Wiley-VCH Verlag GmbH & Co. KGaA, Weinheim

A Novel Hybrid Supramolecular Network Assembled from Perfect π−π Stacking of an Anionic Inorganic Layer and a Cationic Hydronium-Ion-Mediated Organic Layer

Tzuoo-Tsair Luo,[a,b] Yen-Hsiang Liu,[b] Hui-Lien Tsai,[c] Chan-Cheng Su,[a] Chuen-Her Ueng,*[a] and Kuang-Lieh Lu*[b]

Keywords: Coordination polymers / Hydrogen bonds / Self-assembly / Stacking interactions

The synthesis and characterization of a three-dimensional inorganic-organic hybrid network $[\{Cu_2(CA)_3\}\{(H_3O)_2(phz)_3\}\cdot G]_n$ (**1**; H_2CA = chloranilic acid, phz = phenazine; G = $2CH_3COCH_3\cdot 2H_2O$) is described. The crystal structure of **1** shows that the 3D network assembly is based on a combination of two types of grid-building sub-units of (6,3) topology: an anionic metal-organic coordination honeycomb grid, and a cationic hydronium-ion-mediated organic honeycomb grid. The inorganic and organic honeycomb nets are perfectly π–π-stacked, creating an infinite number of open-end channels (channel size about 8 Å in diameter). The solid framework of **1** retains its rigidity upon removal of the guest molecules under high vacuum to form compound $[\{Cu_2(CA)_3\}\{(H_3O)_2(phz)_3\}]_n$ (**2**) as revealed by a single-crystal X-ray diffraction analysis. Compounds $[\{M_2(CA)_3\}\{(H_3O)_2(phz)_3\}\cdot G]_n$ (M = Cd, **3**; M = Zn, **4**; M = Co, **5**; G = $2CH_3COCH_3\cdot 2H_2O$) were also prepared and characterized as isostructures of **1** [crystal data for **1**: $Cu_2(CA)_3(H_3O)_2(phz)_3\cdot G$, trigonal, space group $P\bar{3}1m$, formula mass = 1478.86, a = 13.7593(2) Å, c = 9.1869(2) Å, V = 1506.22(5) Å^3, Z = 1; crystal data for **2**: $Cu_2(CA)_3(H_3O)_2(phz)_3$, trigonal, space group $P\bar{3}1m$, formula mass = 1326.62, a = 13.7565(4) Å, c = 9.1544(5) Å, V = 1500.3(1) Å^3, Z = 1]. The magnetic-exchange coupling between the copper centers for compound **1** was analyzed on the basis of the Curie–Weiss expression and a dinuclear magnetic model. The negative values of the Weiss constant and the magnetic-exchange coupling constant indicate an antiferromagnetic interaction between the copper centers.
(© Wiley-VCH Verlag GmbH & Co. KGaA, 69451 Weinheim, Germany, 2004)

Introduction

The use of noncovalent interactions, (e.g. metal−ligand coordination, hydrogen bonding, π−π stacking, etc.) to arrange molecular building blocks has evolved into one of the most useful and flexible strategies for the crystal-engineering design of extended networks that have versatile functions.[1−14] Successful examples of this method include highly porous metal-organic frameworks with controllable pore sizes and channel properties,[15−25] porous magnetic networks with guest-tunable magnetism,[26,27] chiral porous networks with enantioselective catalytic properties,[28−32] and guest-responsive dynamic frameworks.[33,34] Inorganic-organic hybrid materials that have potential hybrid properties are of great importance in crystal engineering design due to their possible applications.[35−37] Typically, however, it is difficult to prepare a crystalline material containing more than two components as the entropy effect may induce unpredictable crystal structures.[38] However, it is a route to the generation of materials that have novel properties which are not characteristic of the individual components.

It is known that the chloranilate (CA) ligand and its homologues, which contain two chelating coordination sites, are capable of bridging metal centers to form monomeric molecules, chains, sheets, or 3D structures.[37,39−47] Studies based on CA-containing magneto-networks have also been carried out with respect to the propagation of magnetic superexchange interactions between the paramagnetic metal centers through the CA bridges.[37,39−47] The benefits derived from the phenazine ligand are twofold. First, it contains two pyridine donor sites capable of participation in coordination and hydrogen-bonding interactions, and second, the three fused aromatic rings of the phenazine ligand facilitate π−π stacking interactions. As part of our continuous efforts in the design and synthesis of functional crystalline materials,[13,48−51] we report herein on new supramolecular extended networks, $[\{M_2(CA)_3\}\{(H_3O)_2(phz)_3\}]_n$ (M = Cu, Cd, Zn, and Co), assembled from the

[a] Department of Chemistry, National Taiwan Normal University, Taipei 116, Taiwan
[b] Institute of Chemistry, Academia Sinica, Taipei 115, Taiwan
Fax: (internat.) + 886-2-2783-1237
E-mail: lu@chem.sinica.edu.tw
[c] Department of Chemistry, National Cheng Kung University, Tainan 701, Taiwan

perfect π−π stacking of alternate inorganic and organic 2D hexagonal grid (6,3) nets.[11] The chloranilate and phenazine ligands play key roles in the formation of the inorganic and the organic honeycomb building subunits as well as in the construction of unusually robust ionic 3D networks which contain neutral nanoscale 1D channels.

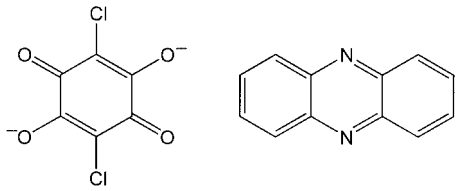

CA phz

Results and Discussion

Synthesis

The ligand CA was chosen as a bridging ligand and phenazine as a π-stacking moiety. Compound **1** was obtained as dark-purple crystals in a mixed-solvent system at room temperature (Scheme 1) and formulated as $[\{Cu_2(CA)_3\}\{(H_3O)_2(phz)_3\}\cdot G]_n$ (**1**; G = $2CH_3COCH_3\cdot 2H_2O$) by elemental and TG analyses. The self-assembly of **1** was achieved by the combination of two types of grid-building sub-units of a (6,3) topology: an anionic metal-organic coordinated honeycomb grid, and a cationic hydronium-ion-mediated organic honeycomb grid. Compound **1** is insoluble in most common solvents such as water, ethanol, acetonitrile, THF, DMF, acetone, etc. $[\{Cu_2(CA)_3\}\{(H_3O)_2(phz)_3\}]_n$ (**2**) was obtained by removing the guest molecules from **1** under vacuum and identified by X-ray single-crystal diffraction techniques and TG analysis. According to a similar synthetic strategy, compounds $[\{M_2(CA)_3\}\{(H_3O)_2(phz)_3\}\cdot G]_n$ (M = Cd, **3**; M = Zn, **4**; M = Co, **5**; G = $2CH_3COCH_3\cdot 2H_2O$) were also synthesized from $Cd(NO_3)_2\cdot 4H_2O$, $Zn(ClO_4)_2\cdot 6H_2O$ and $Co(NO_3)_2\cdot 6H_2O$, respectively.

$$Cu(NO_3)_2\cdot 4H_2O + H_2CA + phz \longrightarrow [Cu_2(CA)_3][(H_3O)_2(phz)_3]\cdot G$$

1, G = $2CH_3COCH_3\cdot 2H_2O$

$$[Cu_2(CA)_3][(H_3O)_2(phz)_3]\cdot G \xrightarrow[24\ h]{vacuum} [Cu_2(CA)_3][(H_3O)_2(phz)_3]$$

1 **2**

Scheme 1

Structural Analysis

A single-crystal X-ray analysis reveals that **1** exists in a trigonal crystal lattice (space group $P\bar{3}1m1$) with a formula of $[Cu_2(CA)_3(H_3O)_2(phz)_3]\cdot G$ (G = $2CH_3COCH_3\cdot 2H_2O$). The results of the X-ray analysis of **2** were similar to those for **1** except for the absence of the guests. Crystals of compounds **3**−**5** were also grown and characterized by X-ray diffraction analysis. Selected interatomic bond lengths and angles for **1** and **2** are given in Table 1. An analysis of the local site symmetry reveals that each Cu^{II} center is positioned on a special symmetry site containing a mutually perpendicular threefold rotation axis and a twofold rotation axis. The Cu^{II} center is chelated by three CA ligands that are related by the site symmetry to form a propeller-like arrangement, resulting in an octahedral CuO_6 coordination environment (Figure 1).

Table 1. Selected bond lengths [Å] and angles [°] for **1** and **2**[a]

1		**2**	
Cu(1)−O(1)	2.088(3)	Cu(1)−O(1)	2.088(2)
Cl(1)−C(2)	1.734(4)	Cl(1)−C(2)	1.734(3)
C(1)−O(1)	1.247(4)	C(1)−O(1)	1.251(2)
C(1)−C(2)	1.394(4)	C(1)−C(2)	1.395(2)
C(1)−C(1)#1	1.536(6)	C(1)−C(1)#1	1.531(4)
C(3)−N(1)	1.344(4)	C(3)−N(1)	1.341(2)
O(2)−H(3)	0.92(8)	O(2)−H(3)	1.08(7)
O(1)#1−Cu(1)−O(1)	77.6(1)	O(1)#1−Cu(1)−O(1)	77.76(7)
O(1)−Cu(1)−O(1)#2	175.4(1)	O(1)−Cu(1)−O(1)#2	175.37(8)
O(1)−Cu(1)−O(1)#3	98.90(9)	O(1)−Cu(1)−O(1)#3	98.76(5)
O(1)−Cu(1)−O(1)#5	84.8(1)	O(1)−Cu(1)−O(1)#5	84.87(9)

[a] Symmetry transformations used to generate equivalent atoms: #1: $-x + y + 1, y, -z$; #2: $-y + 1, -x + 1, -z$; #3: $-y + 1, x - y, z$; #4: $-x + y + 1, -x + 1, z$; #5: $x, x - y, -z$; #6: $x - y, -y, z$; #7: y, x, z; #8: $-y + 1, -x + 1, -z - 1$.

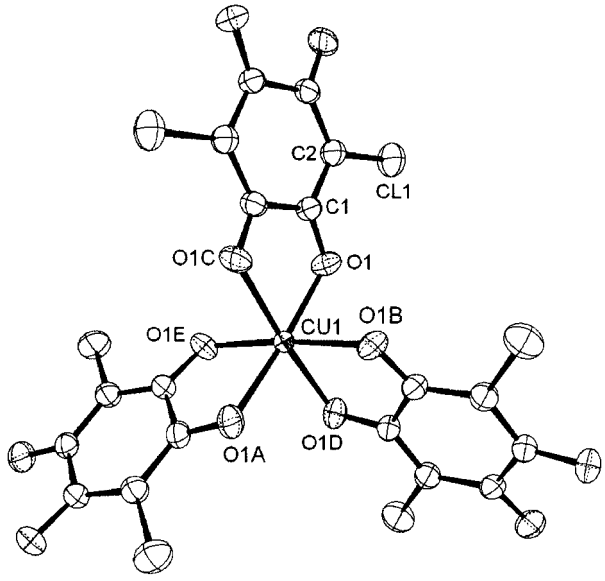

Figure 1. Coordination environment of the Cu^{II} center of compound **1** with atom numbering scheme

The oxygen atom of the hydronium ion also positioned at an identical type of symmetry site as the Cu^{II} ion, which is translated 4.593 Å (half the *c* axis) from the copper centers. The three hydrogen atoms of the hydronium ion are related by site symmetry, and form a strong O−H···N hydrogen-bonding interaction with three phz ligands [O···N distance of 2.583(3) Å, O−H distance of 0.921(0) Å and O−H···N angle of 180.0(1)°] (Figure 2). The short O···N distances between the hydronium ion and the phz ligands cause the phz ligands to assume a propeller-like arrangement.

 © 2004 Wiley-VCH Verlag GmbH & Co. KGaA, Weinheim

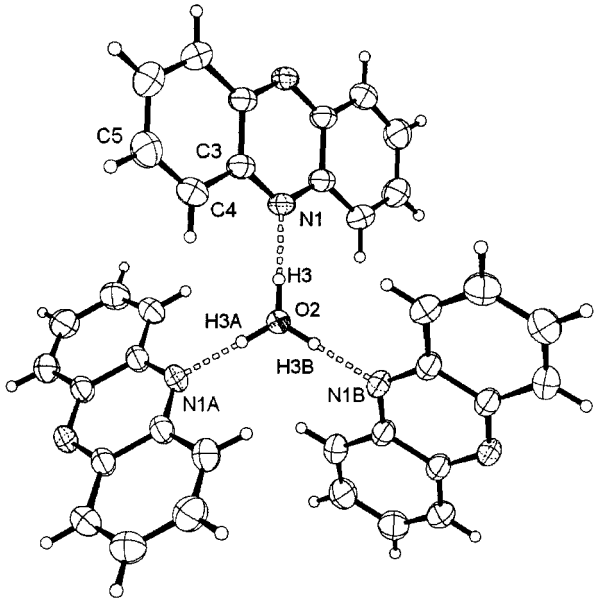

Figure 2. Propeller-like arrangement of hydronium ion and phenazine ligands of compound **1**

Based on the Cu−CA coordination and H_3O−phz hydrogen-bonding interactions, the self-assembly of the two types of two-dimensional grid building subunits with a (6,3) topology occurs. As shown in Figure 3a and 3b, a twelve-membered-ring pore is formed in both the anionic $[Cu_2(CA)_3]^{2-}$ metal-organic coordination layer and the cationic $[(H_3O)_2(phz)_3]^{2+}$ organic hydrogen-bonding layer. Infinite tubular channels with a pore diameter of about 8 Å are observed along the [001] direction (Figure 3c), which can be attributed to the alternate π−π stacking of the two types of grid-building subunits (Figure 3d) with a very short interplanar distance of 3.29 Å.[47] The propeller-like arrangement around the copper and hydronium ion centers is responsible for this perfect-layer π−π-stacking mechanism. The crystal-packing diagrams are shown in Figure 4. The results of an X-ray diffraction analysis of compounds **3**−**5**

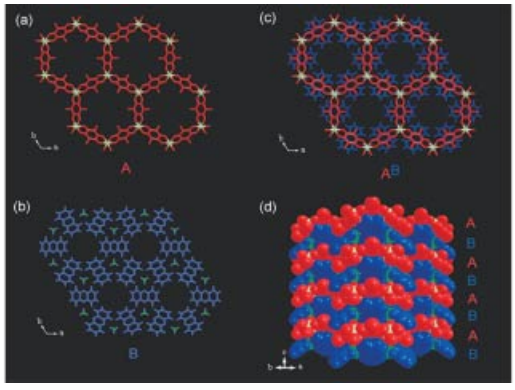

Figure 3. Perspective view of: (a) twelve-membered rings in the $[Cu_2(CA)_3]^{2-}$ metal-organic coordination layers; (b) twelve-membered rings in the $[(H_3O)_2(phz)_3]^{2+}$ organic hydrogen-bonding layers; (c) top-view and (d) side-view of the tubular channel formed by the alternate π−π stacking of the $[Cu_2(CA)_3]^{2-}$ (red) and $[(H_3O)_2(phz)_3]^{2+}$ (blue) grid-building subunits (channel size about 8 Å in diameter); the Cu^{II} ion is yellow, and the hydronium oxygen atom is green

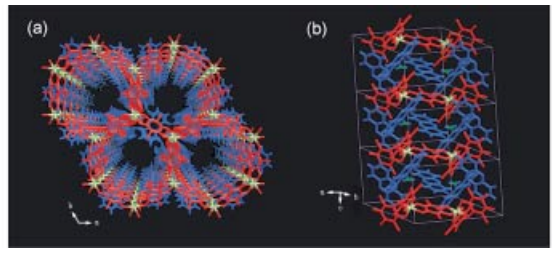

Figure 4. Crystal packing diagrams of **1** showing the perfect π−π stacking and (a) the honeycomb channels along the [001] direction and (b) the arrangement of Cu^{2+} (pale-yellow) and H_3O^+ (green)

reveal that these compounds are isomorphous with **1**. It is noteworthy that a considerable residual density of guest molecules is observed within the channels. However, attempts to resolve these disordered solvent molecules were not successful.

A weight loss of about 9.5%, corresponding to guest molecules, is observed in the TGA diagram of **1** (Figure 5). The alternating charged layers accommodate neutral guest molecules, which enter the extra-framework area in situ during the self-assembly of the framework. After the removal of the guest molecules from the channels under high vacuum for 24 h, the structural integrity of the guest-free network **2** was maintained (vide infra). We conclude that the size of the channels is sufficiently large to contain some diffused solvents, although the diffused portions of the crystal could not be determined clearly by X-ray diffraction analysis. The elemental analysis and thermogravimetric analysis support the assignment of the guest molecules as $2CH_3COCH_3{\cdot}2H_2O$. On the other hand, the acetone, water or THF content of the guests probably varies from crystal to crystal.

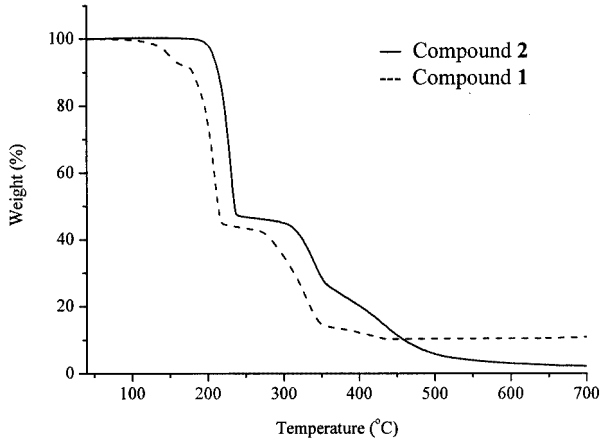

Figure 5. Thermogravimetric-analysis diagrams of **1** and **2**

Removal of Guests

Water, acetone or THF molecules occupy the one-dimensional channels of **1**, which have an estimated diameter of 8 Å (Figures 3 and 4). Attempts were made to remove the guests to form $[\{Cu_2(CA)_3\}\{(H_3O)_2(phz)_3\}]_n$ (**2**) by placing a single crystal of **1** under high vacuum for 24 h. The structure of **2** remained intact, even after the removal of the guest, as evidenced by the single-crystal X-ray analysis

 © 2004 Wiley-VCH Verlag GmbH & Co. KGaA, Weinheim

(Table 2). A TGA diagram of the desolvated compound **2** shows no weight loss until 190 °C (Figure 5), indicating that guest molecules can be removed under vacuum. Soaking crystals of **2** in benzene, chlorobenzene, *n*-hexane, or chloroform gave new inclusion compounds, which were characterized by single-crystal X-ray analysis. Surprisingly, the frameworks of these compounds are stable, but the issue of disordered guests remains unresolved.

Magnetic Studies

The magnetic susceptibility (χ_M) and effective moment (μ_B) per mol of copper for complex **1** are given in Figure 6. The effective moment per mol of copper is approximately 1.94 μ_B at 300 K and decreases slowly with decreasing temperature to 30 K. It then decreases sharply at temperatures below 20 K. This behavior indicates a typical weak antiferromagnetically coupled magnetic pair. As a first approximation, we applied the Curie−Weiss law [Equation (1)] to the magnetic-susceptibility data to measure the magnetic coupling interaction; N, g, β, and k_B have their usual meaning and J is the exchange interaction between metal ions.[52]

$$\chi = \frac{Ng^2\beta^2 S(S+1)}{3k_BT - 3JS(S+1)} = \frac{C_M}{T-\theta} \quad (1)$$

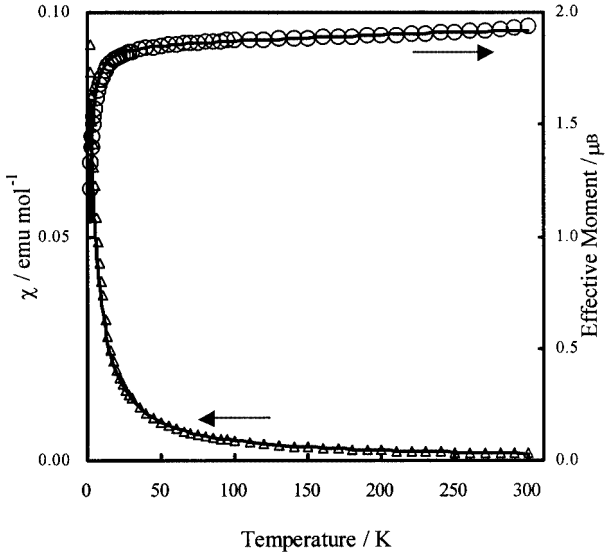

Figure 6. Plots of magnetic susceptibility (χ_M) and the effective magnetic moment (μ_B) per mol of copper versus temperature; the solid line of the magnetic susceptibility is from the fitting results of the Curie−Weiss law and the solid line of the effective magnetic moments is from the fitting results of the dinuclear magnetic equation

The temperature dependency of the magnetic susceptibility of complex **1** in the range 2.0−300 K was fit to the Curie−Weiss expression with a C_M value of 0.464 emu K/mol and a θ value of −3.80 K, which were determined by least-squares fitting in order to minimize the R agreement factor, defined as $R = \Sigma[(\chi_M)_i^{obs} - (\chi_M)_i^{calc}]^2/\Sigma[(\chi_M)_i^{obs}]^2$ (1.94×10^{-2}). The negative θ value is indicative of antiferromagnetic coupling between the metal sites. The effective moment $\mu_{eff} = (8 \times C_M)^{1/2}$ and exchange coupling constant $J/k_B = \theta/[S(S + 1)]$ were calculated to be 1.93 μ_B and −5.06 K, respectively, for complex **1**. The value of μ_{eff} is larger than the spin-only value of 1.73 μ_B; the corresponding g value of 2.22 commonly observed for Cu^{2+} centers is due to the spin-orbital coupling.[53] The magnetic coupling constant J/k_B is around −5.06 K, indicating a weak antiferromagnetic coupling between the copper centers via the CA ligands.

In order to analyze the magnetic exchange coupling interactions between the copper atoms, the susceptibility data of the complex were analyzed using the Bleaney−Bowers dinuclear magnetic equation [Equation (2)], with $H = -2JS_1 \cdot S_2$ as the Heisenberg exchange Hamiltonian,[54] where *TIP* is the temperature-independent paramagnetism of the Cu^{2+} ion.

$$\chi = \frac{2Ng^2\beta^2}{k_BT}\frac{1}{3+\exp(\frac{-2J}{k_BT})} + TIP \quad (2)$$

A reasonable fitting result for the magnetic susceptibility data with $TIP = 200 \times 10^{-6}$ emu/mol was found to be g = 2.14, J = −2.22 K (−1.58 cm^{-1}) for complex **1**, with an agreement factor R of 1.05×10^{-2}. The absolute value of J is much smaller than the value for $[Cu(CA)]_n$ ($J = -12.3\ cm^{-1}$), and is similar to the value for $[\{Cu(CA)(H_2O)\}(L)]_n$ (L = H_2O, dmpyz, phz).[41] Since this antiferromagnetic interaction is very weak, the maximum peak (T_N) of the magnetic susceptibility data would not be observed above 2.0 K. This very weak antiferromagnetic exchange interaction can be attributed to intrinsic structural aspects: because of the site symmetry (D_3) around the copper atom, the magnetic orbital is no longer pure $d_{x^2-y^2}$ and is mixed with the d_{z^2} orbital. This induces a reversal of 90° around the O−Cu−O axis of the magnetic orbital, and, consequently, reduces the extent of the antiferromagnetic interactions. Because of the weak antiferrromagnetic interactions within complex **1**, the Curie−Weiss law and the Bleaney−Bowers expression for the dimer both give reasonable fitting results. However, the values of the exchange coupling parameter J obtained from the two approximations are slightly different, which is due to the fact that both are not complete expressions of the honeycomb structure.

Conclusion

A novel robust supramolecular network $[\{Cu_2(CA)_3\}\{(H_3O)_2(phz)_3\}]_n$ has been synthesized and analyzed. The perfect π−π stacking of an alternating anionic inorganic layer and a cationic organic layer leads to an infinite number of one-dimensional, open-ended channels. The alternating charged layers are able to contain guests within the channels; these guests can be removed under high vacuum. This type of compound may have potential for use in vivo as guest adsorption/desorption and micro-reaction vessels for catalysts. The results of the magnetic study indicate the presence of an antiferromagnetic network.

 © 2004 Wiley-VCH Verlag GmbH & Co. KGaA, Weinheim

Experimental Section

General Remarks: Chloranilic acid, phenazine and metal nitrate salts were purchased commercially and used as received without further purification. Thermogravimetric analyses were performed under nitrogen with a Perkin−Elmer TGA-7 analyzer. Powder-diffraction measurements were recorded with a Siemens D-5000 diffractometer at 40 kV (30 mA) with Cu-K_α radiation (λ = 1.5406 Å), with a step size of 0.02° in θ and a scan speed of 1 s per step size. Variable-temperature dc magnetic susceptibility data were collected for a polycrystalline sample of complex **1** in an applied field of 1.0 kG in the temperature range 2.0−300.0 K with a SQUID magnetometer (Quantum Design, MPMS-7). The sample was embedded in eicosane wax to prevent any torquing of the polycrystalline material in the magnetic field. Pascal's constants were used to estimate the diamagnetic corrections.[55]

$[\{Cu_2(CA)_3\}\{(H_3O)_2(phz)_3\}\cdot G]_n$ (1; G = $2CH_3COCH_3\cdot 2H_2O$): The synthesis of **1** was carried out at ambient temperature by carefully layering a solution of H_2CA (0.6 mmol) in acetone (6 mL) on top of a solution of phenazine (0.6 mmol) in THF (2 mL, middle), and a solution of $Cu(NO_3)_2\cdot 4H_2O$ (0.4 mmol) in H_2O (2.5 mL, bottom). After the solutions had been allowed to stand for about one week, dark-purple, hexagonal-shaped crystals were formed in 65% yield based on H_2CA, along with a black amorphous powder of unknown composition. The bulk product was washed with deionized water and ethanol, and separated by suction filtration. Hexagonal-shaped crystals, suitable for crystallographic analysis, were separated mechanically from the dark powder and dried in a desiccator at ambient temperature. A powder X-ray diffraction pattern of the isolated crystals was in good agreement with the pattern simulated from single-crystal data (vide infra). $[\{Cu_2(CA)_3\}\{(H_3O)_2(phz)_3\}\cdot 2CH_3COCH_3\cdot 2H_2O]_n$ = $C_{60}H_{46}Cl_6Cu_2N_6O_{18}$ (1478.81): calcd. C 48.73, H 3.14, N 5.68; found C 49.24, H 2.94, N 5.55.

$[\{Cu_2(CA)_3\}\{(H_3O)_2(phz)_3\}]_n$ (2): A single crystal of **2** was obtained by mounting a single crystal of **1** on a glass fiber and keeping it sealed in a Schlenk tube under vacuum (10^{-3} Torr) for 24 h. The resulting crystal was sealed to prevent contact with moisture from the air during the single-crystal X-ray diffraction analysis.

$[\{M_2(CA)_3\}\{(H_3O)_2(phz)_3\}\cdot G]_n$ (M = Cd, 3; M = Zn, 4; M = Co, 5; G = $2CH_3COCH_3\cdot 2H_2O$): Cd, Zn, and Co analogs of **1** were synthesized under similar reaction conditions using $Cd(NO_3)_2\cdot 4H_2O$, $Zn(ClO_4)_2\cdot 6H_2O$, and $Co(NO_3)_2\cdot 6H_2O$, respectively, as starting materials. These hexagonal-shaped crystals of the products were small and formed in low yield, along with a black amorphous powder of unknown composition. Crystals with good quality could be selected easily for single-crystal X-ray diffraction analysis. Nevertheless, we were not able to obtain sufficient amounts of pure products for other analyses.

X-ray Crystallographic Study: A hexagonal single crystal of **1** with dimensions of 0.38 × 0.38 × 0.18 mm was mounted on the tip of a glass fiber and placed onto the goniometer head for indexing and intensity data collection using a Bruker Smart CCD diffractometer (Mo-K_α = 0.71073 Å). The raw frame data for **1** were integrated into SHELX format reflection files and corrected for Lorentz and polarization effects with the Denzo program.[56] Corrections for incident- and diffracted-beam absorption effects were applied with the Multiscan method.[57] The structure of **1** was solved by direct methods and refined against F^2 by the full-matrix least-squares technique, using the WINGX,[58] PLATON,[59] and SHELX[60] software packages. The hydrogen atoms of the hydronium ion were located from the difference map and refined isotropically. The remaining hydrogen atoms were calculated and refined as riding atoms; all non-hydrogen atoms were refined with anisotropic displacement parameters. The minimum and maximum residual density of −0.45 and 1.25 e/Å^3 indicated that some guest molecules could be assigned from the difference maps. Nevertheless, attempts to resolve these disordered solvent molecules failed. No further attempts to resolve these diffusion regions were made. To analyze compound **2**, a newly selected crystal of good quality of **1** with dimensions of 0.28 × 0.28 × 0.18 mm was first held under a vacuum and then sealed. A crystallographic determination procedure similar to that described above was then performed. Crystallographic details for compounds **1** and **2** are given in Table 2 and selected bond lengths and angles are shown in Table 1. Compounds **3**, **4** and **5** were also characterized by single-crystal X-ray diffraction analysis and their crystallographic details are also given in Table 2. CCDC-235466 (**1**), -235467 (**2**), -235468 (**3**), -235469 (**4**) and -235470 (**5**) contain the supplementary crystallographic data

Table 2. Crystal data collection and structure refinement

	1	**2**	**3**	**4**	**5**
Empirical formula	$C_{60}H_{46}Cl_6Cu_2N_6O_{18}$	$C_{54}H_{30}Cl_6Cu_2N_6O_{14}$	$C_{60}H_{46}Cd_2Cl_6N_6O_{18}$	$C_{60}H_{46}Cl_6N_6O_{18}Zn_2$	$C_{60}H_{46}Cl_6Co_2N_6O_{18}$
Formula mass	1478.81	1326.62	1576.58	1482.53	1469.92
Crystal system	trigonal	trigonal	trigonal	trigonal	trigonal
Space group	$P\bar{3}1m$	$P\bar{3}1m$	$P\bar{3}1m$	$P\bar{3}1m$	$P\bar{3}1m$
a [Å]	13.7593(2)	13.7565(4)	14.359(2)	13.7520(6)	13.7930(8)
c [Å]	9.1869(2)	9.1544(5)	8.651(2)	9.1950 (5)	9.1310(7)
V [Å^3]	1506.22(5)	1500.3(1)	1544.7(4)	1506.0(1)	1504.4(2)
Z	1	1	1	1	1
T [°C]	24(2)	24(2)	24(2)	24(2)	24(2)
λ [Å]	0.71073	0.71073	0.71073	0.71073	0.71073
$\rho_{calcd.}$ [g cm^{-3}]	1.630	1.468	1.695	1.635	1.723
μ [mm^{-1}]	1.052	1.042	1.013	1.129	0.884
R_1 [a] [$I > 2\sigma(I)$]	0.0522	0.0472	0.0477	0.0598	0.0669
wR_2 [b] [$I > 2\sigma(I)$]	0.1973	0.1502	0.1512	0.1862	0.1635
R_1 [a] (all data)	0.0585	0.0570	0.0582	0.0731	0.1158
wR_2 [b] (all data)	0.2017	0.1580	0.1602	0.1973	0.1907
GOF	1.290	1.127	1.137	1.195	1.021

[a] $R1 = \Sigma||F_o| - |F_c||/\Sigma|F_o|$. [b] $wR2 = \{\Sigma[w(F_o^2 - F_c^2)^2]/\Sigma[w(F_o^2)^2]\}^{1/2}$.

 © 2004 Wiley-VCH Verlag GmbH & Co. KGaA, Weinheim

for this paper. These data can be obtained free of charge at www.ccdc.cam.ac.uk/conts/retrieving.html [or from the Cambridge Crystallographic Data Centre, 12 Union Road, Cambridge CB2 1EZ, UK; Fax: (internat.) + 44-1223-336-033; E-mail: deposit@ccdc.cam.ac.uk].

Acknowledgments

We are grateful for funding from the Academia Sinica and the National Science Council of Taiwan.

[1] J.-M. Lehn, J. L. Atwood, J. E. D. Davies, D. D. MacNicol, F. Vögtle, *Comprehensive Supramolecular Chemistry*, Pergamon, Oxford, **1996**.
[2] M. J. Zaworotko, *Nature* **1999**, *402*, 242−243.
[3] G. R. Desiraju, *Crystal Engineering. The Design of Organic Solids*, Elsevier, Amsterdam, **1989**.
[4] S. Kitagawa, M. Kondo, *Bull. Chem. Soc. Jpn.* **1998**, *71*, 1739−1753.
[5] M. Eddaoudi, J. Kim, N. Rosi, D. Vodak, J. Wachter, M. O'Keeffe, O. M. Yaghi, *Science* **2002**, *295*, 469−472.
[6] B. J. Holliday, C. A. Mirkin, *Angew. Chem. Int. Ed.* **2001**, *40*, 2022−2043.
[7] G. F. Swiegers, T. J. Malefetse, *Chem. Rev.* **2000**, *100*, 3483−3537.
[8] F. A. Cotton, C. Lin, C. A. Murillo, *Acc. Chem. Res.* **2001**, *34*, 759−771.
[9] S. R. Batten, R. Robson, *Angew. Chem. Int. Ed.* **1998**, *37*, 1460−1494.
[10] B. Moulton, M. J. Zaworotko, *Chem. Rev.* **2001**, *101*, 1629−1658.
[11] R. Robson, *J. Chem. Soc., Dalton Trans.* **2000**, 3735−3744.
[12] G. Ferey, *Chem. Mater.* **2001**, *13*, 3084−3098.
[13] Y.-H. Liu, H.-C. Wu, H.-M. Lin, W.-H. Hou, K.-L. Lu, *Chem. Commun.* **2003**, 60−61.
[14] S. Ferlay, S. Koenig, M. W. Hosseini, J. Pansanel, A. De Cian, N. Kyritsakas, *Chem. Commun.* **2002**, 218−219.
[15] S. Noro, R. Kitaura, M. Kondo, S. Kitagawa, T. Ishii, H. Matsuzaka, M. Yamashita, *J. Am. Chem. Soc.* **2002**, *124*, 2568−2583.
[16] T. J. Prior, D. Bradshaw, S. J. Teat, M. J. Rosseinsky, *Chem. Commun.* **2003**, 500−501.
[17] M. Eddaoudi, D. B. Moler, H. Li, B. Chen, T. M. Reineke, M. O'Keeffe, O. M. Yaghi, *Acc. Chem. Res.* **2001**, *34*, 319−330.
[18] J. Kim, B. Chen, T. M. Reineke, H. Li, M. Eddaoudi, D. B. Moler, M. O'keeffe, O. M. Yaghi, *J. Am. Chem. Soc.* **2001**, *123*, 8239−8247.
[19] W. Mori, S. Takamizawa, *J. Solid State Chem.* **2000**, *152*, 120−129.
[20] S. S.-Y. Chui, S. M.-F. Lo, J. P. H. Charmant, A. G. Orpen, I. D. Williams, *Science* **1999**, *283*, 1148−1150.
[21] Y.-B. Dong, M. D. Smith, H.-C. zur Loye, *Angew. Chem. Int. Ed.* **2000**, *39*, 4271−4273.
[22] H. Li, M. Eddaoudi, M. O'Keeffe, O. M. Yaghi, *Nature* **1999**, *402*, 276−279.
[23] O. R. Evans, W. Lin, *Inorg. Chem.* **2000**, *39*, 2189−2198.
[24] K. Seki, *Chem. Commun.* **2001**, 1496−1497.
[25] M. Eddaoudi, H. Li, O. M. Yaghi, *J. Am. Chem. Soc.* **2000**, *122*, 1391−1397.
[26] M. Kurmoo, H. Kumagai, S. M. Hughes, C. J. Kepert, *Inorg. Chem.* **2003**, *42*, 6709−6722.
[27] G. J. Halder, C. J. Kepert, B. Moubaraki, K. S. Murray, J. D. Cashion, *Science* **2002**, *298*, 1762−1765.
[28] T. J. Prior, M. J. Rosseinsky, *Inorg. Chem.* **2003**, *42*, 1564−1575.
[29] Y. Cui, H. L. Ngo, P. S. White, W. Lin, *Chem. Commun.* **2003**, 994−995.
[30] U. Siemeling, I. Scheppelmann, B. Neumann, A. Stammler, H.-G. Stammler, J. Frelek, *Chem. Commun.* **2003**, 2236−2237.
[31] H. L. Ngo, W. Lin, *J. Am. Chem. Soc.* **2002**, *124*, 14298−14299.
[32] J. S. Seo, D. Whang, H. Lee, S. I. Jun, J. Oh, Y. J. Jeon, K. Kim, *Nature* **2000**, *404*, 982−986.
[33] Z. Wang, B. Zhang, H. Fujiwara, H. Kobayashi, M. Kurmoo, *Chem. Commun.* **2004**, 416−417.
[34] J. Y. Lu, A. M. Babb, *Chem. Commun.* **2002**, 1340−1341.
[35] J. W. Ko, K. S. Min, M. P. Suh, *Inorg. Chem.* **2002**, *41*, 2151−2157.
[36] M. P. Suh, K. S. Min, J. W. Ko, H. J. Choi, *Eur. J. Inorg. Chem.* **2003**, 1373−1379.
[37] K. Nagayoshi, M. K. Kabir, H. Tobita, K. Honda, M. Kawahara, M. Katada, K. Adachi, H. Nishikawa, I. Ikemoto, H. Kumagai, Y. Hosokoshi, K. Inoue, S. Kitagawa, S. Kawata, *J. Am. Chem. Soc.* **2003**, *125*, 221−232.
[38] J. D. Dunitz, *Chem. Commun.* **2003**, 545−548.
[39] S. Kitagawa, S. Kawata, *Coord. Chem. Rev.* **2002**, *224*, 11−34.
[40] M. Kawahara, M. K. Kabir, K. Yamada, K. Adachi, H. Kumagai, Y. Narumi, K. Kindo, S. Kitagawa, S. Kawata, *Inorg. Chem.* **2004**, *43*, 92−100.
[41] S. Kawata, S. Kitagawa, H. Kumagai, C. Kudo, H. Kamesaki, T. Ishiyama, R. Suzuki, M. Kondo, M. Katada, *Inorg. Chem.* **1996**, *35*, 4449−4461.
[42] M. K. Kabir, M. Kawahara, H. Kumagai, K. Adachi, S. Kawata, T. Ishii, S. Kitagawa, *Polyhedron* **2001**, *20*, 1417−1422.
[43] S. Kawata, S. Kitagawa, H. Kumagai, T. Ishiyama, K. Honda, H. Tobita, K. Adachi, M. Katada, *Chem. Mater.* **1998**, *10*, 3902−3912.
[44] Y.-T. Li, C.-W. Yan, Y.-J. Zheng, D.-Z. Liao, *Polyhedron* **1998**, *17*, 1423−1427.
[45] H. Kumagai, S. Kawata, S. Kitagawa, *Inorg. Chim. Acta* **2002**, *337*, 387−392.
[46] B. F. Abrahams, J. Coleiro, K. Ha, B. F. Hoskins, S. D. Orchard, R. Robson, *J. Chem. Soc., Dalton Trans.* **2002**, 1586−1594.
[47] A. Yoshino, H. Matsudaira, E. Asato, M. Koikawa, T. Shiga, M. Ohba, H. Okawa, *Chem. Commun.* **2002**, 1258−1259.
[48] Y.-H. Liu, Y.-L. Lu, H.-C. Wu, J.-C. Wang, K.-L. Lu, *Inorg. Chem.* **2002**, *41*, 2592−2597.
[49] Y.-H. Liu, H.-L. Tsai, Y.-L. Lu, Y.-S. Wen, J.-C. Wang, K.-L. Lu, *Inorg. Chem.* **2001**, *40*, 6426−6431.
[50] Y.-H. Liu, Y.-L. Lu, H.-L. Tsai, J.-C. Wang, K.-L. Lu, *J. Solid State Chem.* **2001**, *158*, 315−319.
[51] Y.-H. Liu, C.-S. Lin, S.-Y. Chen, H.-L. Tsai, C. -H Ueng, K.-L. Lu, *J. Solid State Chem.* **2001**, *157*, 166−172.
[52] O. Kahn, *Molecular Magnetism*, VCH, New York, **1993**.
[53] R. L. Carlin, *Magnetochemistry*, Springer-Verlag, New York, **1986**.
[54] S. Ferlay, G. Francese, H. W. Schmalle, S. Decurtins, *Inorg. Chim. Acta* **1999**, *286*, 108−113.
[55] E. A. Boudreaux, L. N. Mulay, *Theory and Application of Molecular Paramagnetism*, John Wiley & Sons, New York, **1976**.
[56] Z. Otwinowsky, W. Minor, "Processing of X-ray Diffraction Data Collected in Oscillation Mode", in *Methods in Enzymology* (Eds.: C. W. Carter, Jr., R. M. Sweet), Academic Press, New York, **1996**, vol. 276, p. 307.
[57] R. H. Blessing, *Acta Crystallogr., Sect. A* **1995**, *51*, 33−38.
[58] L. J. Farrugia, *J. Appl. Crystallogr.* **1999**, *32*, 837−838.
[59] A. L. Spek, *PLATON*, Utrecht University, Utrecht, The Netherlands, **2000**.
[60] G. M. Sheldrick, *SHELX-97* (including SHELXS and SHELXL), University of Göttingen, Germany, **1997**.

Received March 11, 2004
Early View Article
Published Online August 26, 2004

 © 2004 Wiley-VCH Verlag GmbH & Co. KGaA, Weinheim

The (Chloromethyl)dihalosilanes X_2HSiCH_2Cl (X = F, Cl, Br, I): Synthesis, Multinuclear NMR Spectroscopy and Rotational Isomerism Examined by Raman Spectroscopy

Karl Hassler,*[a] Reinhard Hummeltenberg,[a] and Günter Tekautz[a]

Keywords: Infrared spectroscopy / NMR spectroscopy / Raman spectroscopy / Silanes / Synthesis

(Chloromethyl)diphenylsilane Ph_2HSiCH_2Cl (**1**) was prepared from Ph_2SiHCl and $LiCH_2Cl$, in situ, and was then treated with CF_3SO_3H/LiCl and CF_3SO_3H/LiBr to give the (chloromethyl)dihalosilanes Cl_2HSiCH_2Cl (**2**) and Br_2HSiCH_2Cl (**3**). I_2HSiCH_2Cl (**4**) was formed quantitatively in a protodearylation reaction between liquid hydrogen iodide and **1**. Fluorination of **4** with ZnF_2 gave F_2HSiCH_2Cl (**5**), albeit in low yields. Compounds **1**–**5** were characterised by multinuclear NMR spectroscopy (^{29}Si, ^{13}C, ^{19}F) and vibrational spectroscopy. The temperature-dependent vibrational Raman spectra of **2**, **3** and **4** prove that they are mixtures of *gauche* and *anti* rotamers in the liquid state. Enthalpy differences, ΔH ($H_{anti} - H_{gauche}$), were determined for the liquids by applying the van't Hoff relation, with the *gauche* rotamer being lower in energy for **3** and **4**, and the *anti* rotamer for **2**. The vibrational spectra were assigned with the help of ab initio calculations of equilibrium geometries and harmonic fundamental frequencies. Harmonic symmetry force constants and potential energy distributions were calculated from the ab initio Hessian matrices.
(© Wiley-VCH Verlag GmbH & Co. KGaA, 69451 Weinheim, Germany, 2004)

Introduction

α-(Halomethyl)silanes are versatile starting materials for the synthesis of organosilicon compounds such as silylmethyllithium derivatives or main-group derivatives $M\text{-}CH_nX_{2-n}SiR_3$, where X is a halogen.[1] However, only a handful of methods, each one with its own limitations, can be used for their preparation. These comprise the direct chlorination of methylsilanes, $MeSiR_3$ with Cl_2 [2] or Cl_2SO_2,[3] a method which does not tolerate silyl, vinyl or aryl groups as the R substituent. Another synthetic approach uses silyllithiums, $LiSiR_3$ as precursors, treating them with, for instance, CH_2Cl_2 to form CH_2ClSiR_3.[4] However, this method is not widely applicable due to a lack of suitable silyllithiums. A third method with a wider range of applications is the alkylation of chlorosilanes by a (halomethyl)lithium $X_nH_{3-n}CLi$ (n = 1, 2, 3; X = halogen), which is usually generated in situ. Pannell and co-workers have prepared a considerable number of (chloromethyl)silanes with this method that contain functionalities such as SiH, SiCl, SiSi, Si-vinyl, Si-allyl and Si-phenyl.[5] The introduction of these functional groups was a major step forward, as they can be replaced by other substituents without affecting the halomethyl functionality.

We are interested in the synthesis and spectroscopic properties of silaethanes, silapropanes and disilapropanes bearing no other substituents but hydrogen and halogen atoms. They can be considered as the link between halogenated hydrocarbons and their heavier analogues the halogenated disilanes and trisilanes. The chemical behaviour of both the Si−Si bond and the Si−C bond is strongly influenced by the substituents at the molecular skeleton. Numerous experimental investigations show a weakening of the Si−C bond of carbosilanes (a term coined by Fritz[6] for compounds in which the molecular framework is exclusively built up by Si−C bonds) upon chlorination at the carbon atom, whereas chlorination at the silicon atom has the opposite effect, causing a bond strengthening. Ab initio studies of chlorinated silaethanes confirm these effects.[7] For instance, the bond-dissociation energies of $SiCl_3CH_3$, SiH_3CH_3, and SiH_3CCl_3 were calculated as 392, 369 and 314 kJ/mol, respectively. With disilanes, the bond strengths decrease in the order $SiCl_3SiCl_3 > SiH_3SiCl_3, > SiH_3SiH_3$, which is supported by experimental and ab initio Si−Si force constants and $^{29}Si,^{29}Si$ coupling constants, for instance.[8] The effect of Si chlorination can be rationalised by Bent's rule,[9] which states that bonds to electronegative substituents possess more p-character, thereby increasing the s-character of the bonds to electropositive atoms; more s-character usually means a stronger bond. Upon *C*-chlorination, Bent's rule should also be at work, but the effect is overridden by the repulsive force between the positive charges at the Si and C atoms due to the short Si−C distance. Moreover, the steric repulsion between the chlorine atoms at carbon — the Cl···Cl distance is in fact considerably shorter than the van der Waals distance — is reduced

[a] Institute of Inorganic Chemistry, University of Technology, Stremayrgasse 16, 8010 Graz, Austria
Fax: +43-316-873-8701
E-Mail: hassler@anorg.tu-graz.ac.at

in the free CCl_3 radical upon dissociation. This reduction of intramolecular repulsion energy certainly provides a further contribution to the weakening of the bond.

If chlorine is replaced by other halogens, the relative contributions of these two effects will certainly vary. Fluorine substitution is expected to increase the positive charge on the carbon atom, thereby also increasing the Si−C repulsion. Conversely, the nonbonding halogen−halogen repulsion will decrease. Substitution with bromine should decrease the positive charge and increase the nonbonding interactions, an effect which will be even more pronounced with iodine. For instance, no (triiodomethyl)silanes have been reported in the literature so far. C_2I_6 is also unstable and has not been prepared yet.

These properties of the Si−C bond should also influence the barriers to internal rotation and conformer stabilities. Our attention, therefore, is mainly focussed on silaethanes and silapropanes that can display rotational isomerism. The existence of at least two different conformers in silaethanes and silapropanes demands the presence of EH_2X or EHX_2 groups (X = halogen, E = C or Si) in the molecule. A literature search revealed that only a handful of these compounds have been prepared so far, such as ClH_2CSiCl_2H[10] and ClH_2CSiH_2X (X = F, Cl, Br);[11] no such compounds with iodine have been described. Moreover, the literature search revealed a complete absence of general procedures for the preparation of (halomethyl)silanes with SiH_2X or $SiHX_2$ groups. We have therefore set out to develop general synthetic methods suitable for the preparation of a wide range of (halomethyl)dihalosilanes.

Results and Discussion

Syntheses

Tetrachlorosilaethane, $CClH_2SiCl_3$, is readily obtained by direct chlorination of trichloromethylsilane with Cl_2.[12] However, it is difficult to transform it into $CClH_2SiCl_2H$ or $CClH_2SiClH_2$, as it is not easy to achieve a selective chlorination of the SiH_3 group. Recently, a two-step reaction sequence was reported[10] involving a reduction with $LiAlH_4$ and subsequent chlorination with $SnCl_4$.

$(ClH_2C)SiCl_3 + LiAlH_4 \rightarrow (ClH_2C)SiH_3$
$(ClH_2C)SiH_3 + SnCl_4 \rightarrow (ClH_2C)SiCl_2H$

Dichloro(chloromethyl)silane was prepared for vibrational spectroscopic purposes. No NMR shifts and physical data were reported, and the synthesis seems inappropriate for the preparation of larger quantities due to the volatility of $(ClH_2C)SiH_3$.

The introduction of aryl substituents into (chloromethyl)-silanes offers the possibility to replace them with Cl, Br or I by using either liquefied hydrogen halides HX or trifluoromethanesulfonic acid in combination with the lithium halides LiX. Both methods tolerate chloromethyl groups as well as Si−H and Si−Si functionalities, give good to excellent yields, and are widely applicable.

Si-aryl + HX → SiX + arylH (method 1)
Si-aryl + $CF_3SO_3H \rightarrow SiOSO_2CF_3$ + arylH
$SiOSO_2CF_3 + LiX \rightarrow SiX + Li^+[OSO_2CF_3]^-$ (method 2)

Method 1 usually gives better overall yields than 2.

From our experience with these two methods we expect that they can also be used successfully with (bromomethyl)-, (iodomethyl)- and even (fluoromethyl)silanes, though we have not yet tested them with these substrates.

The choice of which of the two methods to apply for a specific problem is dictated by practical considerations. If the desired carbosilane has a boiling point which is near that of the hydrocarbon arylH formed (which is the case for benzene and $CClH_2SiCl_2H$), purification becomes difficult. If one wishes to apply method 1 a larger aryl group can be introduced; for instance, phenyl groups can be replaced by tolyl or mesityl groups. Method 2 offers the advantage that phenyl groups still can be used as substituents, because benzene is easily separated from the trifluoromethanesulfonyloxysilane by evaporation in vacuo. Thus, commercially available phenylsilanes can be used as starting materials, reducing the time needed for the synthesis. As shown in Scheme 1, chlorodiphenylsilane was treated with CH_2ClLi, generated in situ from bromochloromethane and lithium at low temperatures,[13] forming (chloromethyl)diphenylsilane **1**. When a solution of **1** in toluene was treated with two equivalents of trifluoromethanesulfonic acid, the two phenyl groups were cleaved off, giving benzene and (chloromethyl)bis(trifluoromethanesulfonyloxy)silane (**1a**) without noticeable side reactions. Toluene and benzene were then removed by evaporation in vacuo, giving the pure (chloromethyl)sulfonyloxysilane as a colourless oily liquid. Upon addition of LiCl or LiBr, the (halomethyl)silanes **2** and **3** were formed in yields not exceeding 30%, presumably due to Si−C cleavage.

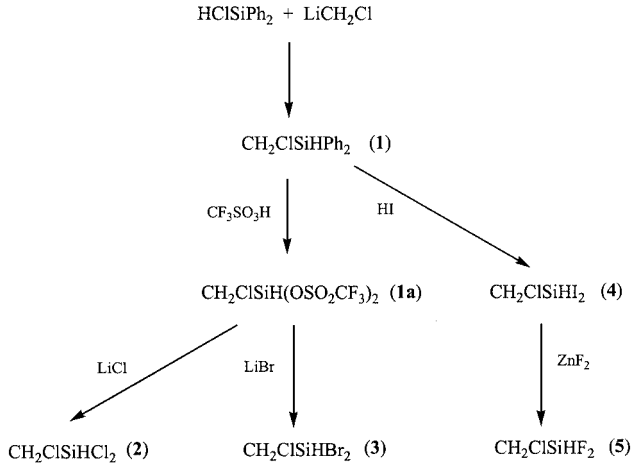

Scheme 1. Synthesis of (chloromethyl)dihalosilanes

Compound **4** was prepared by method 1, treating **1** with liquid HI. Dry gaseous hydrogen iodide was easily obtained from tetrahydronaphthalene and iodine as described in the literature,[14] and purified by trap-to-trap condensation. Scheme 1 summarises the syntheses of **1**−**5**. Fluorination

 © 2004 Wiley-VCH Verlag GmbH & Co. KGaA, Weinheim

of **4** with various fluorinating agents such as ZnF_2 turned out to be difficult due to extensive Si−C bond cleavage. The yields achieved were so small that only the NMR spectra of **5** could be obtained, albeit in good quality. We will therefore report on the fluorination of **5** in conjunction with the synthesis of (bromomethyl)halosilanes and (iodomethyl)halosilanes.

NMR Spectroscopy

Compounds **2**−**5** were characterised by multinuclear NMR spectroscopy (^{13}C, ^{19}F, ^{29}Si), and **1** by ^{29}Si NMR only. Table 1 summarises the chemical shifts and coupling constants that were obtained. In the proton-coupled ^{29}Si NMR spectra of **2**, **3** and **4**, the signal of the Si nucleus is split into a doublet of triplets due to one- and two-bond Si−H coupling. The ^{13}C NMR signal splits into a triplet of doublets. The ^{29}Si and ^{13}C NMR spectra of **5** are presented in Figure 1. The unusual appearance of the ^{29}Si NMR spectrum, which consists of two triplets and two quadruplets, results from the near equality of $^1J_{Si,H}$ and $^1J_{Si,F}$, the difference being almost equal to $^2J_{Si,H}$. Each quadruplet is therefore an overlap of two triplets. The ^{13}C NMR spectrum is composed of six triplets, as expected for a first-order spectrum.

Table 1. Chemical shifts[a] (ppm) and coupling constants (Hz) for the (chloromethyl)dihalosilanes **1**−**5**

	$\delta(^{29}Si)$	$\delta(^{13}C)$	$\delta(^{19}F)$	$^1J_{Si,H}$	$^2J_{Si,H}$	$^1J_{C,H}$	$^2J_{C,H}$	$^2J_{C,F}$	$^1J_{Si,F}$
1	−17.6			204.9	4.3				
1a	−30.3			335.6					
2	+0.9	29.9		300.0	4.3	144.0	16.0		
3	−13.4	29.6		299.0	4.3	146.0	15.0		
4	−85.2	28.1		292.0	4.3	146.0	11.0		
5	−29.1	23.8	−141.5	301.0	4.8	141.0	23.5	18.3	305.0

[a] $\delta(^{29}Si)$ and $\delta(^{13}C)$ are referenced against TMS; $\delta(^{19}F)$ is referenced against CCl_3F.

The ^{29}Si NMR chemical shifts of **1**−**5** do not follow a linear dependence on the electronegativities of the directly bonded halogens, which is not surprising, as it is known that ^{29}Si chemical shifts depend on the sum of the electronegativities of the substituents in a nonlinear manner.[15] The shift maximum for **2** can easily be explained on that basis.

One-bond Si−H coupling constants usually increase with increasing electronegativities (sum of the electronegativities) of the substituents, which can be interpreted in terms of isovalent hybridisation. Bonds to electronegative elements possess more p-character, which is balanced by more s-character in the Si−H bond. As the Fermi contact term dominates $^1J_{Si,H}$, the coupling constant increases. Interestingly, the values of $^1J_{Si,H}$ for **2**−**5** show only a slight increase by no more than 9 Hz with increasing electronegativity of the halogens. For the silanes H_2SiI_2 and H_2SiF_2, the difference is 7.4 Hz.[15]

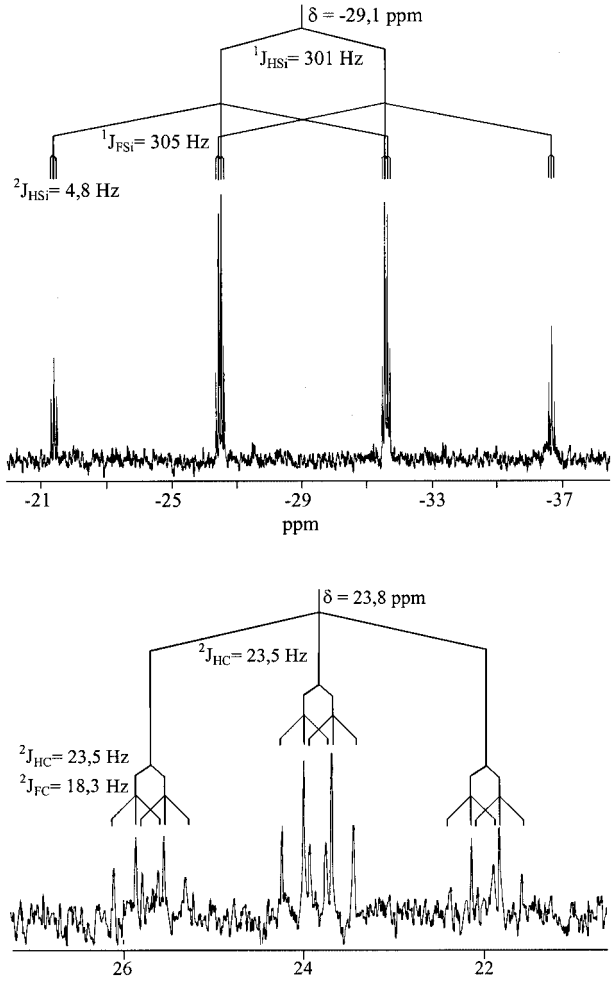

Figure 1. Splitting of the ^{29}Si (top) and the ^{13}C NMR signal (bottom) of CH_2ClSiF_2H due to indirect spin−spin coupling

Raman Spectroscopy and Rotational Isomerism

At ambient temperatures, the (chloromethyl)dihalosilanes **2**−**5** exist as mixtures of *gauche* [C_1 symmetry, ω(ClCSiH) ≈ 52°] and *anti* [C_s, ω(ClCSiH) = 180°] conformers, as illustrated in Figure 2 with the help of Newman projections.

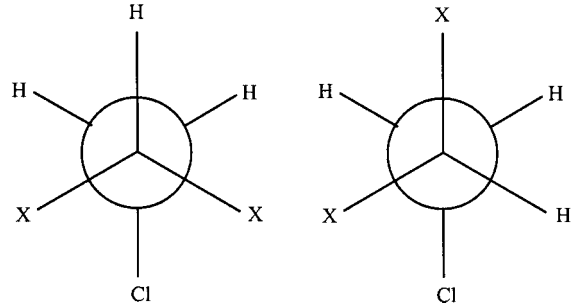

Figure 2. Newman projections of *anti* (left) and *gauche* (chloromethyl)dihalosilanes

As long as the barriers separating the two conformers are well above 2.5 kJ/mol (= RT at room temperature), they

 © 2004 Wiley-VCH Verlag GmbH & Co. KGaA, Weinheim

behave as distinct vibrating entities and can be identified by their IR and Raman vibrational spectra. For Si−C and Si−Si bonds this condition is usually fulfilled. For assigning bands to individual rotamers, a normal coordinate analysis based upon ab initio calculations of vibrational frequencies and force constants is normally carried out for both conformers.

The rotational isomerism of dichloro(chloromethyl)silane has been investigated recently by FT-IR spectroscopy on solutions in liquid xenon, with the more stable form being the *gauche* conformer ($\Delta H_{exp.} = 4.34 \pm 0.48$ kJ/mol).[10] The result is consistent with ab initio calculations at the MP2/6-31G(d) level of theory, but is also reproduced correctly at the Hartree−Fock level. Values for ΔH obtained on solutions in noble gases are supposed to differ only slightly from values in the gas phase.

For the present study, we have recorded the Raman spectra for the liquids of **2**, **3** and **4**. Figure 3 presents the Raman spectrum of **3** at two temperatures, illustrating the variations that occur upon cooling. In all cases we only obtained glassy solids at low temperatures that contained both conformers at the temperature of liquid nitrogen. No crystallisation was observed.

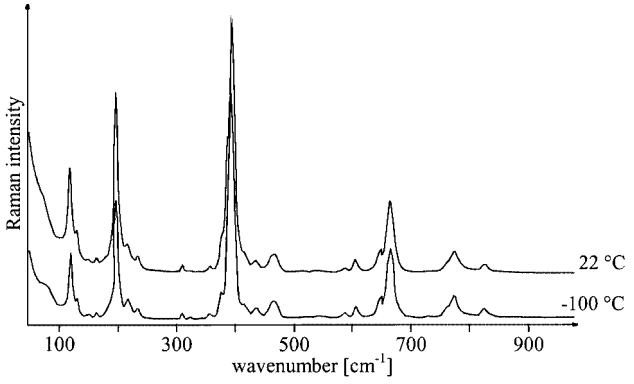

Figure 3. Raman spectrum of dibromo(chloromethyl)silane in the range 50−900 cm^{-1} at 22 °C and −100 °C.

To facilitate the identification of vibrational bands belonging to the various conformers, ab initio calculations of equilibrium geometries, harmonic frequencies and force constants (Hessian matrices) were performed at the Hartree−Fock level of theory for **2**−**5**. Inner filled electron shells were replaced by the electron core potentials (ECPs) reported by Stevens, Krauss and Basch.[16] A 6-31G** double-zeta basis set was used for the valence electrons. By use of the ECPs, relativistic corrections for the heavier halogens are taken into account. Table 2 summarises the most important geometric parameters for both conformers of **2**−**5** — *anti* and *gauche* — as well as the relative conformational energies predicted by the ab initio calculations. The Hessian matrices, which represent the force constants defined in Cartesian coordinates, were transformed into force fields defined with symmetry coordinates which are linear combinations of bond distortions and angle distortions. With the symmetry force fields, normal coordinate analyses were carried out which allow the description of the normal modes as group vibrations by use of the potential-energy distributions (PEDs). The program ASYM40[17] was used for these calculations. A factor of 0.92 was used to scale the calculated frequencies, and $(0.92)^2$ to scale the force constants. Table 3 and 4 summarise the wavenumbers in the Raman and IR spectra of **3** and **4**, the scaled and unscaled ab initio wavenumbers, and the descriptions of the modes as group vibrations based on calculated PEDs. The spectra of **2** are not repeated here as they have been reported previously.[10]

Table 2. Selected structural constants (pm, deg.) and relative energies (kJ/mol) for the conformers of **2**−**5** as predicted by the ab initio calculations

	$CClH_2SiF_2H$		$CClH_2SiCl_2H$		$CClH_2SiBr_2H$		$CClH_2SiI_2H$	
	anti	*gauche*	*anti*	*gauche*	*anti*	*gauche*	*anti*	*gauche*
CSi	187.8	187.8	188.9	188.8	189.3	189.1	189.9	189.7
SiH	147.2	146.7	147.4	146.9	147.6	147.1	147.7	147.3
SiX	158.1	158.6	205.2	206.2	222.2	223.2	245.4	246.5
		158.1		205.3		222.2		254.4
CSiH	111.5	114.2	109.3	112.4	108.8	112.3	107.9	111.5
CSiX	109.9	107.3	110.4	106.9	110.5	106.7	110.7	106.6
ClCSi	112.5	110.3	114.1	110.9	114.5	111.1	114.9	111.3
ClCSiH	180.0	52.2	180.0	52.2	180.0	52.0	180.0	52.3
E_{rel}	4.8	0.0	5.7	0.0	6.2	0.0	6.3	0.0

The value of the enthalpy difference can be determined from temperature-dependent vibrational spectra by applying the van't Hoff relationship, which is derived under the assumption that ΔH is independent of temperature

$$\ln(I_a/I_g) = -\Delta H/RT + \text{const.}$$

where I_a and I_g are the intensities of the Raman or IR bands for rotamer a and g, respectively. Plotting $\ln(I_a/I_g)$ versus $1/T$ thus results in a straight line whose slope is equal to $-\Delta H/R$. ΔH values were obtained by a least-squares fit from three line pairs for **2** and **3**, and from two pairs for **4**. As an example, two van't Hoff plots are presented in Figure 4.

Table 5 summarises the ΔH values together with the relevant band pairs and the statistical error. In these experiments, severe interference from overlapping with overtones or combination bands occur quite often. Fermi resonances between overtones and fundamentals are also encountered quite frequently. It is also a prerequisite of the method that the bands of the two conformers both have reasonably high intensity and are sitting on a flat baseline. These difficulties have been reviewed recently by Klaboe.[18]

The discrepancies between the experimental ΔH values obtained from the different band pairs can easily be explained on that basis. Average ΔH values of -0.57 ± 0.37, 0.21 ± 0.07 and 0.56 ± 0.50 were obtained for **2**, **3** and **4**, respectively, by neglecting the statistical uncertainties resulting from the least-squares fits. Due to the uncertainties mentioned above, the standard deviations are quite large.

Opposite to the gaseous state, the *anti* rotamer of $CH_2ClSiHCl_2$ is slightly more stable in the liquid. This can

 © 2004 Wiley-VCH Verlag GmbH & Co. KGaA, Weinheim

Table 3. Comparison of observed and calculated wavenumbers (cm^{-1}) for the fundamental vibrations of *anti* and *gauche* dibromo(chloromethyl)silane

Fundamental	Obsd.		anti		gauche	
	Ra(l)	Ir(l)	ab initio	scaled	ab initio	scaled
CH_2 antisymmetric stretch	2974 ms	2980 m	3302.4	3038	3320.9	3055
CH_2 symmetric stretch	2930 vs	2940 vs	3232.1	2974	3246.6	2987
SiH stretch	2216 vs	2220 s	2382.1	2192	2408.9	2216
CH_2 deformation	1377 w	1386 s	1532.4	1410	1534.0	1411
CH_2 wag	1171 vw	1177 ms	1322.5	1217	1320.2	1215
		1125 w				
CH_2 twist	1091 vw	1100 mw	1217.0	1120	1214.3	1117
SiH bend	826 w	823 vs	878.6	808	904.8	832
SiH bend		795 vs	875.2	805	837.8	771
CCl stretch	773 w,b	763 vs,b	863.3	794	851.4	783
CH_2 rock	666 m	667 vs	759.8	699	727.8	670
SiC stretch	649 sh				705.9	649
SiC stretch	606 w		641.5	590		
	587 w					
$SiBr_2$ antisymmetric stretch	466 w	463 vs			489.4	450
$SiBr_2$ antisymmetric stretch	435 w		483.9	445		
$SiBr_2$ symmetric stretch	397 vs	395 vs			419.4	386
$SiBr_2$ symmetric stretch	385 sh	380 sh	403.3	371		
$SiBr_2$ wag	309 w	307 mw	336.9	310		
ClSiC bend	234 w				222.7	205
	216 w					
$SiBr_2$ wag	197 vs				205.6	189
$SiBr_2$ twist	162 w		174.9	161		
$SiBr_2$ deformation	130 sh		132.5	122		
$SiBr_2$ deformation	119 s				120.8	111
$SiBr_2$ twist			96.3	89	106.2	98
torsion			52.4	48	60.2	55

Table 4. Comparison of observed and calculated wavenumbers (cm^{-1}) for the fundamental vibrations of *anti* and *gauche* (chloromethyl)diiodosilane

Fundamental	Obsd.		anti		gauche	
	Ra(l)	Ir(l)	ab initio	scaled	ab initio	scaled
CH_2 antisymmetric stretch	2975 ms	2983 m	3302.6	3039	3322.5	3057
CH_2 symmetric stretch	2928 vs	2942 ms	3231.3	2973	3246.6	2987
SiH stretch	2198 vs	2200 s	2371.6	2182	2397.3	2206
CH_2 deformation	1388 w	1390 s	1532.0	1409	1533.9	1412
CH_2 wag	1175 vw	1180 m	1319.5	1214	1318.9	1213
CH_2 twist	1090 vw	1180 m	1216.4	1119	1216.7	1119
CCl stretch	812 w	820 vs	870.2	801	845.9	778
SiH bend	789 w	795 vs	853.7	785	896.4	825
SiH bend	766 w		851.1	783		
SiH bend	724 w				810.1	745
CH_2 rock	687 vw		753.5	693		
CH_2 rock	653 m	660 vs			713.9	657
SiC stretch	636 sh				698.9	643
SiC stretch	596 w	590 w	632.0	581		
SiI_2 antisymmetric stretch	403 mw	403 vs	416.9	384	427.0	393
SiI_2 symmetric stretch	333 vs	333 ms	351.4	323	357.0	328
SiI_2 wag	280 m		302.6	278		
ClSiC bend	203 m				210.0	193
ClSiC bend	170 vs		167.5	154		
SiI_2 wag					177.2	163
SiI_2 twist			102.0	94	99.3	91
SiI_2 deformation			81.5	75	88.5	81
torsion			49.7	46	58.0	53

be explained by considering the dipole moments of the two rotamers, as the conformer with the larger dipole moment is normally stabilized in a polar solvent. The predicted dipole moments for *gauche* and *anti* $CH_2ClSiHCl_2$ are 1.53 and 3.22 D, respectively, and the latter is therefore stabilized in the liquid. *anti* $CH_2ClSiHBr_2$ and *anti* $CH_2ClSiHI_2$ are also

 © 2004 Wiley-VCH Verlag GmbH & Co. KGaA, Weinheim

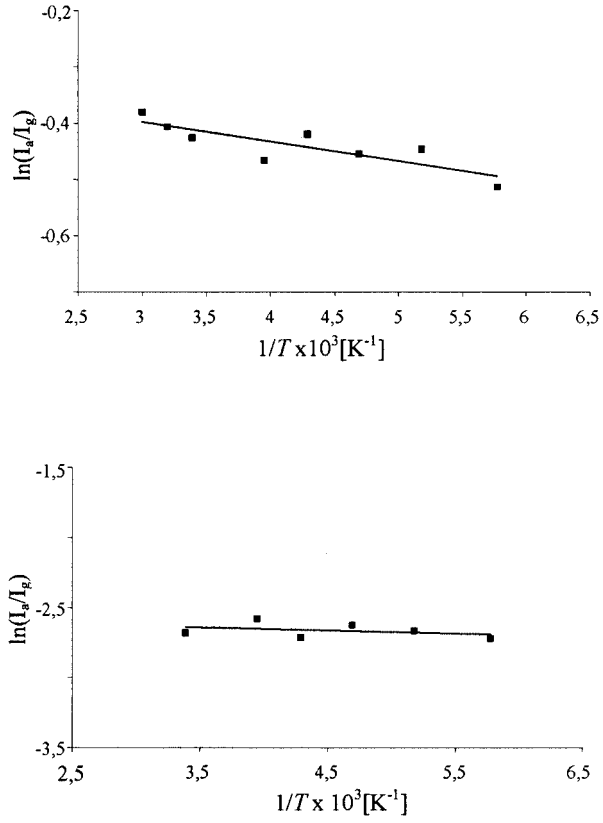

Figure 4. Van't Hoff plots for the line pairs 687/653 cm^{-1} of $ClCH_2SiHI_2$ (left) and 435/466 cm^{-1} of $ClCH_2SiHBr_2$ (right)

Table 5. Line pairs (cm^{-1}) and experimental ΔH values (kJ/mol; $\Delta H = H_{anti} - H_{gauche}$) obtained from least-square fits for **2**, **3** and **4**

$CH_2ClSiHCl_2$ line pair	ΔH	$CH_2ClSiHBr_2$ line pair	ΔH	$CH_2ClSiHI_2$ line pair	ΔH
508/495	−0.18±0.003	435/466	0.28±0.007	687/653	0.20±0.003
671/624	−0.92±0.006	387/396	0.19±0.005	596/636	0.91±0.008
680/624	−0.61±0.003	606/649	0.15±0.003		

stabilized, but due to the smaller dipole moments and the larger *gauche-anti* energy differences (Table 2) the stabilizing effect is not able to reverse the sign of ΔH.

It is also of some note that the SiC valence force constants calculated from the Hessian matrices by use of symmetry coordinates increase with increasing electronegativity of the halogen substituents. The calculated values for *gauche* **5**, **2**, **3** and **4** [N/cm, scaled by $(0.92)^2$] are: 2.87, 2.77, 2.73 and 2.67, respectively; the force constants for the *anti* conformers are smaller by 0.03−0.04 N/cm.

Experimental Section

General Remarks: All compounds except (chloromethyl)diphenylsilane are sensitive towards moisture; some of them, such as (chloromethyl)diiodosilane, are also sensitive towards oxygen. All syntheses and manipulations were therefore carried out under an atmosphere of dry, oxygen-free nitrogen using Schlenk techniques. Solvents were dried over sodium or potassium and distilled under N_2 prior to use.

Raman spectra were recorded with a Jobin−Yvon T64000 spectrometer equipped with a triple monochromator. A frequency-doubled Nd:YAG laser (20 mW) operating at 532 nm served as light source and a charge-coupled device (CCD) camera was used as detector. The samples were condensed into 1 mm capillary glass tubes that were sealed under nitrogen atmosphere. Variable-temperature Raman spectra were obtained by mounting the capillary on a copper block supplied with a heater and a thermocouple for temperature monitoring. Liquid nitrogen was used for cooling.

Infrared spectra in the range from 3000−250 cm^{-1} were measured with a Perkin−Elmer 883 spectrometer using a film of the pure liquid between CsBr plates

NMR spectra of **2**−**5** as solutions in $CDCl_3$ were obtained with a Bruker MSL 300 spectrometer.

(Chloromethyl)diphenylsilane (1): A solution of chlorodiphenylsilane (55.17 g, 250 mmol) and bromochloromethane (32.63 g, 250 mmol) in 500 mL of THF was cooled to −70 °C, and 138 mL of a 2 M solution of BuLi in pentane was added dropwise over a period of 2 h, whilst maintaining the temperature. After completion of the addition the mixture was stirred at −70 °C for another 2 h. It was then allowed to warm to room temperature and stirred overnight. After hydrolysis and extraction with n-hexane the organic layer was separated. Subsequently, the solvent is removed by evaporation in vacuo and the liquid residue was fractionated, giving 20.7 g (88.9 mmol, 35%) of **1** as a colourless liquid. $B.p._{0.1}$ = 125 °C. $C_{13}H_{13}ClSi$ (232.77): calcd. C 67.07, H 5.63; found C 66.98, H 5.6.

Dichloro(chloromethyl)silane (2): Triflic acid (6.46 g, 43.3 mmol) was added dropwise at a temperature of −30 °C to a solution of **1** (5.01 g, 21.5 mmol) in 20 mL of toluene. After completion the mixture was allowed to warm to room temperature and stirred for 5 h. The benzene formed in the reaction and the toluene were completely removed in vacuo, this process was controlled by IR spectroscopy. Diethyl ether and 3 g of LiCl (100% excess) were added and the mixture was then stirred at room temperature for 2 d. After this time all volatile substances were condensed off. The diethyl ether was removed very carefully from the mixture by distillation. The liquid residue was fractionated under slightly reduced pressure giving 0.9 g (6 mmol) of **2** (28.1%) as colourless liquid. $B.p._{200}$ = 42 °C. CH_3Cl_3Si (149.48).

Dibromo(chloromethyl)silane (3): Compound **3** was prepared using the same procedure as for **2**, except that LiBr was used instead of LiCl. The following amounts of starting materials were used: 5.67 g of **1** (24.36 mmol); 7.31 g of triflic acid and 5 g of LiBr. Fractionation in vacuo yielded**3** (1.4 g, 5.8 mmol; 24.1%) as a colourless liquid. $B.p._{20}$ = 43−45 °C. CH_3Br_2ClSi (238.38): calcd. Br 64.04; found Br 64.18.

(Chloromethyl)diiodosilane (4): Compound **1** (4.37 g) and an excess of HI were placed in a sealed glass tube and stored for one week at room temperature. After removal of the excess HI and the benzene formed during the reaction, the liquid residue was fractionated in vacuo to give 3.7 g (mmol) of **4** (59.3%) as a colourless liquid. $B.p._{0.1}$ = 33−35 °C. CH_3ClI_2Si (332.39): calcd. I 76.36; found I 76.15.

(Chloromethyl)difluorosilane (5): A solution of **4** (1.5 g, 4.5 mmol) in 15 mL of hexachlorobutadiene was added at a pressure of

 © 2004 Wiley-VCH Verlag GmbH & Co. KGaA, Weinheim

30 Torr to a suspension of 5.7 g of zinc fluoride (excess) in 60 mL of hexachlorobutadiene. The volatile products were continuously condensed into a flask cooled with liquid nitrogen. After completion of the addition the mixture was stirred at 90 °C for 5 h. The volatile products contained just a small amount of the desired product, as deduced from the NMR spectra. No further attempts to isolate these small quantities of CH_3F_2ClSi on a preparative scale were made.

[1] D. A. Armitage, in *Comprehensive Organometallic Chemistry* (Eds.: G. Wilkinson, F. G. A. Stone, E. W. Abel), Pergamon Press, Oxford U. K., **1995**, vol. 2, 1−44.
[2] J. D. Roberts, S. Dev, *J. Am. Chem. Soc.* **1951**, *73*, 1879−1880.
[3] M. Kumada, J. Nakajima, M. Ishikawa, Y. Yamamoto, *J. Org. Chem.* **1958**, *23*, 292−295.
[4] H. Gilman, D. J. Aoki, *J. Organomet. Chem.* **1964**, *1*, 449−463.
[5] T. Kobayashi, K. H. Pannell, *Organometallics* **1991**, *10*, 1960−1964.
[6] G. Fritz, E. Matern, *Carbosilanes: Syntheses and Reactions*, Springer, Berlin, Heidelberg, New York, **1987**.
[7] H. Schiffer, R. Ahlrichs, *Theor. Chim. Acta* **1989**, *75*, 99−110.
[8] K. Hassler, E. Hengge, F. Schrank, M. Weidenbruch, *Spectrochim. Acta* **1991**, *A37*, 57−62.
[9] H. A. Bent, *J. Chem. Educ.* **1960**, *37*, 616−624; H. A. Bent, *Chem. Rev.* **1961**, *61*, 275−311.
[10] G. A. Guirgis, C. Pan, J. R. Durig, *Spectrochim. Acta* **2002**, *A58*, 1839−1852.
[11] G. A. Guirgis, C. Pan, S. Shen, J. R. Durig, *Asian J. Spectrosc.* **2001**, *5*, 113−122; H. Bürger, P. Moritz, *Organometallics* **1993**, *12*, 4930−4939.
[12] F. Runge, W. Zimmermann, *Chem. Ber.* **1954**, *87*, 282−287.
[13] R. Tarhouni, B. Kirschleger, M. Rambaud, J. Villieras, *Tetrahedron Lett.* **1984**, *25*, 835−838.
[14] G. Brauer, *Handbuch der Präparativen Anorganischen Chemie*, Enke Verlag, Stuttgart, **1975**, vol. II, 299−302.
[15] H. Marsmann, in *NMR Basic Principles and Progress*, Springer Verlag, Berlin, Heidelberg, New York, **1981**, vol. 17, 65−235.
[16] W. J. Stevens, H. Basch, M. Krauss, *J. Chem. Phys.* **1984**, *81*, 6026−6033; W. J. Stevens, M. Krauss, H. Basch, P. G. Jasien, *Can. J. Chem.* **1992**, *70*, 612−630.
[17] L. Hedberg, I. A. Mills, *J. Mol. Spectrosc.* **1993**, *160*, 117−142.
[18] P. Klaboe, *Vib. Spectrosc.* **1995**, *9*, 3−17.

Received April 15, 2004
Early View Article
Published Online September 13, 2004

 © 2004 Wiley-VCH Verlag GmbH & Co. KGaA, Weinheim

The Effect of the Steric Bulk of the Ligand on the Geometry of the Species Self-Assembled from Co^{III} Bis(dioximates) and Boronic Acids

Renata Dreos,*[a] Giorgio Nardin,[a] Lucio Randaccio,*[a] Patrizia Siega,[a] Silvia Scagliola,[a] and Giovanni Tauzher[a]

Keywords: Boronic acid / Cobalt / Dioximes / Self-assembly / Solid-state structures

The synthesis and characterization of the products of the reactions between the bis(diphenylglyoximato)cobalt(III) complexes $[Co(CH_3)(dpgH)_2L]$ [L = py or H_2O; $dpgH_2$ = bis(diphenylglyoxime)] and 4-pyridinylboronic acid (**1**) and 3-aminophenylboronic acid (**2**) are described. The crystals of both **1** and **2** are built up by dimeric units arranged on a crystallographic symmetry center, so that the 4-pyridinyl (in **1**) or the 3-aminophenyl residue (in **2**) of one moiety coordinates to the Co atom of the symmetry-related unit. ^1H NMR spectra show that both **1** and **2** are stable in solution in aprotic solvents: they do not dissociate and are not in equilibrium with species having different nuclearity. The geometry of **1** is very similar to that of the species assembled from the corresponding bis(dimethylglyoximato)cobalt(III) complex and 4-pyridinylboronic acid. On the contrary, the replacement of the methyls by phenyls prevents the trimeric arrangement previously found in the supramolecular species assembled from methylcobaloxime and 3-aminophenylboronic acid and leads to the dimeric species **2**.

(© Wiley-VCH Verlag GmbH & Co. KGaA, 69451 Weinheim, Germany, 2004)

Introduction

Organobis(dimethylglyoximato)cobalt(III) complexes $[Co(CH_3)(dmgH)_2L]$ [$dmgH_2$ = bis(dimethylglyoxime)], also known as organocobaloximes (Scheme 1), have been widely studied as vitamin B_{12} models.[1] Their derivatives with either one or both of the intramolecular O−H···O bridges replaced by organoboryl groups are well known and have recently been reviewed.[2] In the last few years organocobaloximes have also been shown to be good building blocks for the assembly of supramolecular systems by reaction with functionalised aromatic boronic acids.[3−5] The $B(OH)_2$ group of the boronic acid reacts with the oxime bridge of one cobaloxime molecule, with simultaneous coordination of the donor atom to the cobalt of another cobaloxime. Products of different nuclearity and geometry have been obtained depending on the boronic acid used as linker (Scheme 1). Thus, the reaction of methylcobaloxime with 4- and 3-pyridinylboronic acid (L^1 and L^2, respectively) gave a dinuclear "molecular box"[4] and a dinuclear "molecular parallelogram",[3] respectively, whereas reaction with 3-aminophenylboronic acid (L^3) gave a trinuclear molecular triangle (Scheme 2).[5]

The substitution of Co by Rh in the reaction with 3-aminophenylboronic acid produced a dramatic structural change, leading to an inorganic polymer (Scheme 3), although both the geometry and the coordination properties of the $[Rh(CH_3)(dmgH)_2L]$ and $[Co(CH_3)(dmgH)_2L]$ moieties are very similar. These results suggest that slight variations in the geometry of the building blocks can strongly affect the structure of the assembled polynuclear systems. Therefore, we decided to study the effect of the increase in steric hindrance of the metal complex by substituting either one or both of the methyl groups of the equatorial bis(dimethylglyoximato) ligand by a phenyl group (Scheme 1). The synthesis and characterization of the products of the reactions between the organobis(diphenylglyoximato)cobalt(III) complexes $[Co(CH_3)(dpgH)_2L]$ and L^1, L^2 and L^3 are discussed in this paper, whereas the results concerning the reactions of organobis(methylphenylglyoximato)cobalt(III) complexes $[Co(CH_3)(mpgH)_2L]$ will be reported elsewhere.

Results and Discussion

Synthesis

The starting complex for the synthesis of **1**, $[Co(CH_3)(dpgH)_2py]$, was synthesized as described previously.[6,7] In the synthesis of **2**, $[Co(CH_3)(dpgH)_2(H_2O)]$ was used instead of $[Co(CH_3)(dpgH)_2py]$ to facilitate the replacement of the axial ligand by the amine nitrogen of

[a] Dipartimento di Scienze Chimiche, Università di Trieste, Via Licio Giorgieri 1, 34127, Trieste, Italy
Fax: +39-040-558-3903
E-mail: dreos@univ.trieste.it
randaccio@univ.trieste.it

Supporting information for this article is available on the WWW under http://www.eurjic.org or from the author.

 © 2004 Wiley-VCH Verlag GmbH & Co. KGaA, Weinheim **DOI: 10.1002/ejic.200400314**

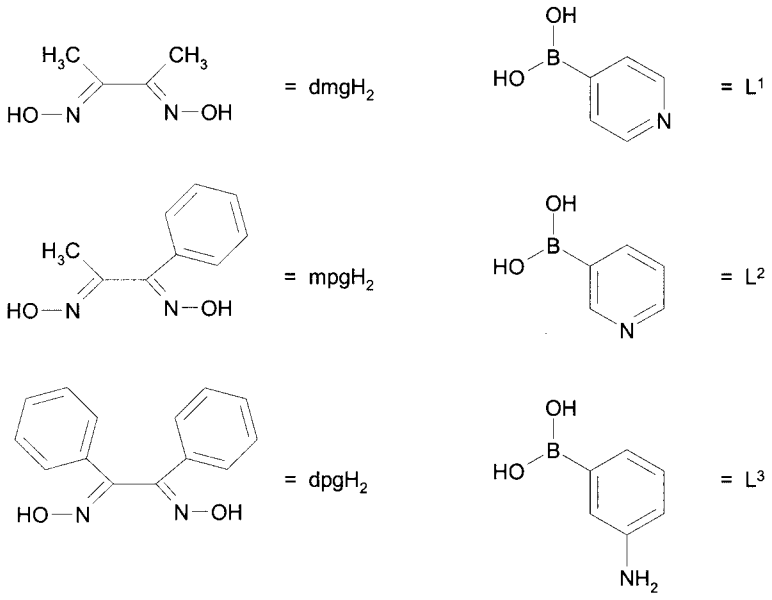

Scheme 1

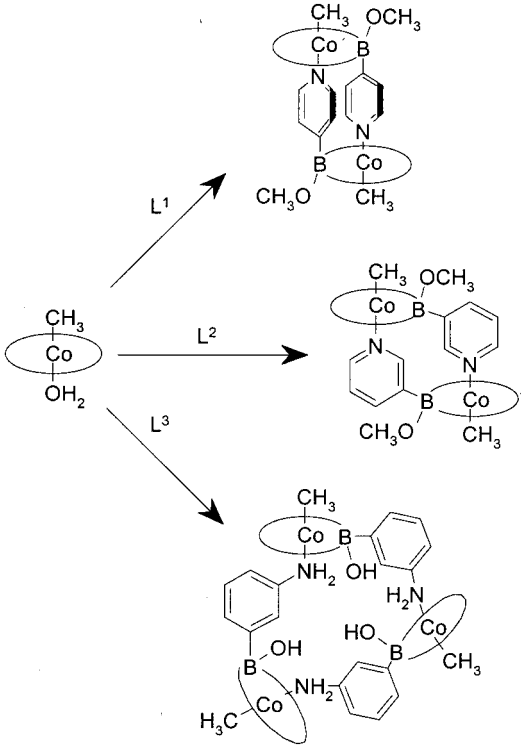

Scheme 2

the boronic acid. It has previously been shown that the products of the reactions of methylcobaloxime with L^1, L^2 and L^3 are strongly pH dependent,[4,5] because the boronic acids are zwitterionic species.[8] Indeed, the formation of the supramolecular species occurs by reaction of the complex with either the neutral or the zwitterionic form of the boronic acid.[4] The macroscopic pK_a values of the first and the second deprotonation are, respectively, 3.83 and 8.2 for L^1,[4] 4.0 and 8.2 for L^2,[8] and 4.56 and 9.14 for L^3.[5]

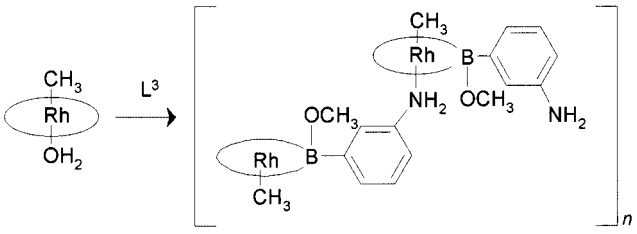

Scheme 3

Therefore the reactions were carried out within these pH ranges also in the present case. X-ray quality crystals of **1** and **2** were obtained from the reaction with L^1 and L^3, after one week and after four days, respectively. Only complicated mixtures of products were obtained from the reaction with L^2, despite several attempts carried out at different pH values and in different solvents, and they were not further characterized.

It should be noted that the reaction time for the formation of **1** and **2** is substantially longer than that required for the assembly of the corresponding systems starting from cobaloximes. This effect may be due to both electronic and to steric effects. In fact, the electron-withdrawing power of the phenyls decreases the electron density on the oxime oxygens with respect to cobaloximes and hinders the electrophilic attack of the sp^2-hybridized B atom of the boronic acid. Furthermore, the steric hindrance of the phenyls may also make the approach of L both to the oxime bridge and to the axial coordination position more difficult.

X-ray Crystal Structures

The crystal structure of $[Co(CH_3)(dpgH)\{dpgB(OMe)(4\text{-}Py)\}]_2$ (**1**) is built up from dimeric units arranged on a crystallographic symmetry center in such way that the 4-pyridi-

 © 2004 Wiley-VCH Verlag GmbH & Co. KGaA, Weinheim

nyl residue of one unit axially coordinates the Co atom of the symmetry-related unit (Figure 1). Four MeOH and two H_2O molecules were also located in the unit cell, all with half-occupancy factor. A series of H-bonds are formed between water and methanol [O1w···O7Me = 2.929 Å; O1w···O6Me = 2.422 Å] and between methanol and the B-methoxide residue [O6Me···O5 = 2.735 Å]. The dimer can be considered a rectangular box with the two equatorial moieties and the two pyridinyl groups as ideal sides. The Co···Co distance is 7.605(1) Å, whereas the Co···B distance is 3.240(4) Å, Co···B1 is 6.510(4) Å and the Co−B−Co′ and B−Co−B1 angles are 96.7(1)° and 82.9(9)°, respectively. The geometry of the dimer is very close to that found in $[Co(CH_3)(dmgH)\{dmgB(OMe)(4\text{-}Py)\}]_2$ (**1′**) in which the corresponding distances and angles are 7.592(3) Å, 3.20(1) Å, 6.51(1) Å, 97.1° and 82.9°, respectively (Scheme 4).[4] As in **1′**, the pyridinyl ligand is nearly perpendicular to the Co_2B_2 mean plane (85.4°) and oriented in such way as to nearly bisect the five-membered ring of the equatorial moiety. The two pyridinyl rings, related by a symmetry center, are nearly face to face at a distance of 3.38 Å (3.30 Å in **1′**).[4] The latter orientation of the axial planar ligand is typical of the iminocobaloximes (Costa's models)[1] and of bis(diphenylborylated) cobaloximes,[9−11] whereas the axial ligand is rotated by about 90° in the monomeric complexes $[CoR(dpgH)_2py]$ with R = CH_3,[6] CH_2SiMe_3,[7] CH_2CMe_3,[7] and CF_3,[7] where the pyridine ligand bisects the O···O vectors of the diphenylglyoximate ligands.

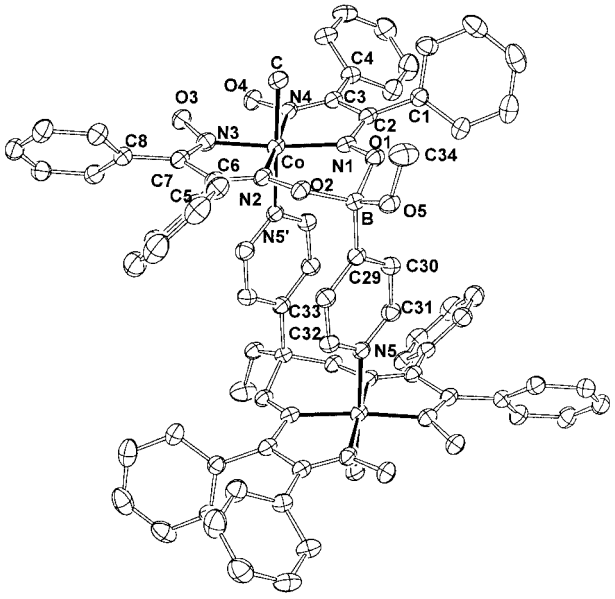

Figure 1. ORTEP drawing (thermal ellipsoids at 30% probability) and labeling scheme for the independent atoms in the dimer **1**; the crystallization solvent molecules have been removed

An ORTEP view of **2** is shown in Figure 2. The structure consists of dimeric units arranged around a crystallographic symmetry center so that the pendant 3-aminophenyl residue of one moiety coordinates the Co atom of the other unit in one axial position, as shown in Figure 2. The dimeric unit may be considered a molecular box, similar to that of **1**,

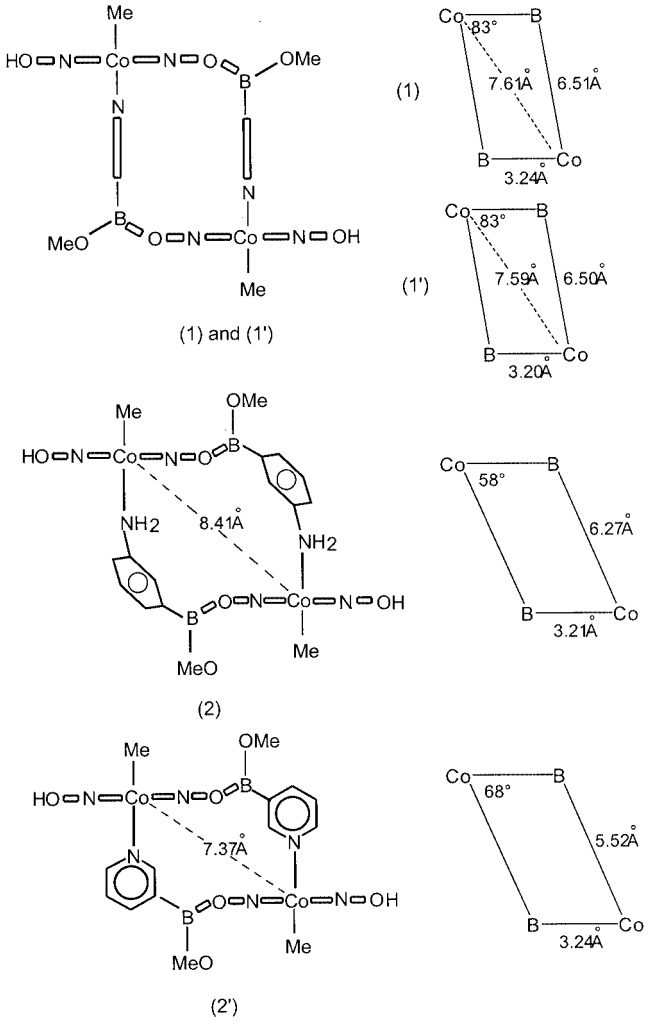

Scheme 4

but more distorted. In fact, the Co_2B_2 group, which forms a nearly regular rectangle in **1**, forms a distorted parallelogram in **2** (Scheme 4). This parallelogram is similar to that observed in $[Co(CH_3)(dmgH)\{dmgB(OMe)(3\text{-}Py)\}]_2$ (**2′**).[3] However, owing to the greater conformational freedom of the aminophenyl group with respect to that of the 3-pyridinyl one, a molecular box with the two phenyl groups oriented face to face is formed in **2**, whereas a "molecular parallelogram" is formed in **2′**.[3] In fact, in the latter the two pyridinyl residues are not faced but nearly coplanar. In **2**, the Co···Co distance of 8.410(2) Å is significantly longer than that observed in **2′** [7.365(4) Å]. The orientation of the axial aminophenyl residue with respect to the equatorial plane in **2** (dihedral angle Co′N5−C33C34 = 86.2°, interplanar angle 33.2°) is similar to that observed in the trimeric species $[Co(CH_3)(dmgH)\{dmgB(OH)(3\text{-}NH_2Ph)\}]_3$ (**3**; mean value 102.1°; interplanar mean angle 31.4°).[5] However, in the latter a trinuclear molecular triangle of cobalt atoms of about 9.47 Å side, was found. The difference between **2** and **3** can be ascribed to the replacement of the Me groups on the equatorial moiety by Ph groups. In fact, in **3** the closure of the Co triangle imposes the orientation of three methyl groups towards the centre of the Co tri-

 © 2004 Wiley-VCH Verlag GmbH & Co. KGaA, Weinheim

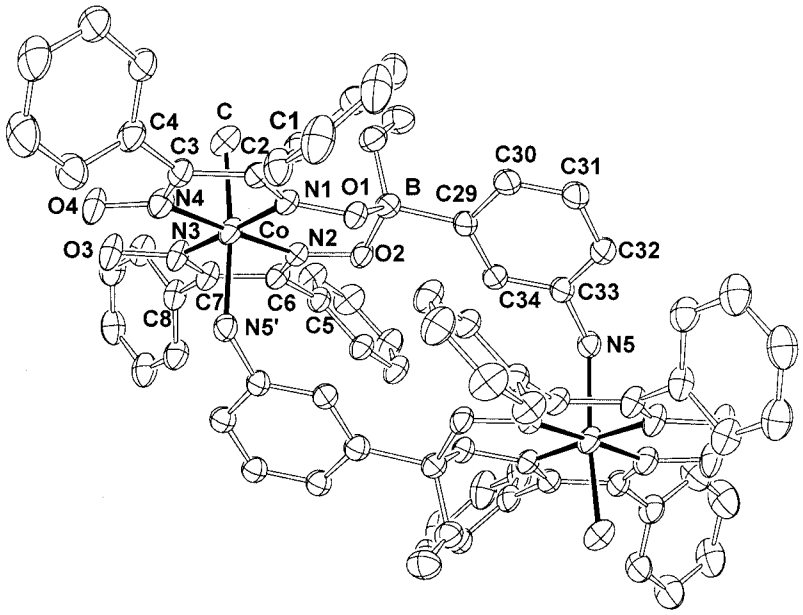

Figure 2. ORTEP drawing (thermal ellipsoids at 30% probability) and labeling scheme for the independent atoms in the dimer **2**; the crystallization solvent molecules have been removed

angle. Therefore the arrangement requires that the three C(Me) atoms are at about 3.89 Å (Scheme 5). When a phenyl group replaces the methyl group, the trimeric arrangement of **2** is prevented because of the steric hindrance between the phenyl groups.

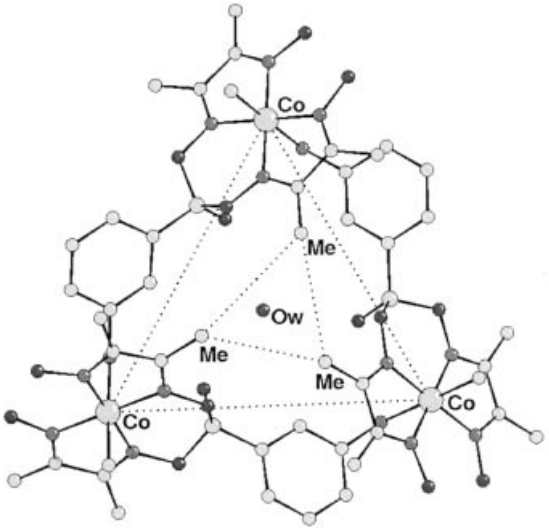

Scheme 5. A view of the molecular triangle **3**; the dotted lines indicate the Co···Co (mean value 9.47 Å) and the C(Me)···C(Me) (mean value 3.9 Å) distances

The coordination bond lengths in **1** and **2** are given in Table 1 and compared with those in **1′**, **2′** and **3**. As expected, the Co−N5′ (sp^2) distances in **1**, **1′**, and **2′** are essentially identical and shorter than the corresponding Co−N5′ (sp^3) distances in **2** and **3**.

Table 1. Selected bond lengths (Å) and angles (°) in **1**, **2**, and other similar models

	1	**1′**	**2**	**2′**	**3**
Co−N1	1.872(3)	1.85(1)	1.855(4)	1.868(8)	1.864(7)
Co−N2	1.884(3)	1.88(1)	1.881(4)	1.872(7)	1.869(6)
Co−N3	1.867(3)	1.86(1)	1.871(4)	1.872(7)	1.865(7)
Co−N4	1.894(3)	1.87(1)	1.877(4)	1.862(8)	1.873(7)
Co−C	2.013(4)	2.00(1)	1.997(6)	1.99(1)	1.987(8)
Co−N5′	2.068(3)	2.08(1)	2.085(4)	2.068(8)	2.102(6)
C−Co−N5′	178.6(1)	175.4(4)	174.2(2)	175.4(4)	178.2(4)
B···Co···B′	83.3(1)	82.9(9)	58.3(2)	68.2(3)	73.1(3)
Co···Co	7.605(1)	7.592(6)	8.410(2)	7.365(4)	9.474(4)
Co···B	3.240(4)	3.20(1)	3.207(6)	3.244(7)	3.221(7)
Co···B′	6.510(4)	6.51(1)	6.269(6)	5.515(7)	6.451(7)

^{1}H NMR Spectra

The ^{1}H NMR spectrum of **1** in $CDCl_3$ shows a single set of signals because of the presence of a symmetry center in the molecule. The axial methyl resonates at δ = 1.59 ppm, deshielded with respect to $[Co(CH_3)(dpgH)_2py]$ (δ = 1.44 ppm),[7] probably due to the electron-withdrawing effect of the boryl bridge. The singlet at δ = 3.27 ppm is due to the $BOCH_3$ protons. The *ortho* protons of the pyridinyl residue, assigned from a ^{1}H-^{1}H COSY experiment, resonate at δ = 7.35 ppm and the *meta* protons at δ = 6.75 ppm, considerably upfield shifted relative to those of $[Co(CH_3)(dpgH)_2py]$ (δ = 8.92 and 7.44 ppm, respectively), due to the shielding effect of the two faced pyridinyl rings.[7] The phenyl protons give rise to a multiplet in the range δ = 7.18−7.43 ppm.

 © 2004 Wiley-VCH Verlag GmbH & Co. KGaA, Weinheim

The ^1H NMR spectrum of **2** was recorded in C_6D_6 because the compound is almost insoluble in the most common deuterated solvents. The magnetic anisotropy of this solvent spreads the signals of the aromatic protons over a larger range, allowing an almost complete assignment. The axial methyl resonates at $\delta = 2.30$ ppm and the $BOCH_3$ group at $\delta = 3.20$ ppm. The NH_2 protons, which are diastereotopic as a consequence of the coordination, give rise to a doublet of doublets at $\delta = 3.32$ and 3.80 ppm. The protons of the four non-equivalent phenyls and the aminic protons resonate in the range $\delta = 6.20-8.01$ ppm.

These results are entirely consistent with the solid-state structures, suggesting that **1** and **2** are stable in solution in aprotic solvents: they do not dissociate and are not in equilibrium with species having different nuclearity.

Conclusion

The most interesting consequence of the increase of the steric hindrance in the equatorial ligand of the metal complex on going from bis(dimethylglyoximato) to bis(diphenylglyoximato), is the change in the nuclearity of the supramolecular species assembled from L^3. The molecular triangle **3** was obtained starting from bis(dimethylglyoximato) whereas the dimeric species **2** was obtained from bis(diphenylglyoximato). Assembly is still possible because of the conformational freedom of the boron bridge, which is directed toward the methyl group in **2**, whereas it is directed towards the opposite side in the triangle **3**; however, the trimeric arrangement is prevented because of the steric hindrance of the phenyl groups.

A further structural difference is the esterification of the B(OH) residual groups by methanol in **2**, which does not occur in **3**. In this case the esterification is probably hampered by the network of H-bonds between a water molecule lying approximately in the center of the triangle (Ow, Scheme 5) and the three boron OH groups.

Finally, both electronic and steric effects may be responsible for the longer time required for the assembly reaction in comparison with cobaloximes.

Experimental Section

General Remarks: NMR spectra were recorded on a Jeol EX-400 spectrometer with TMS as internal standard. Electrospray mass spectra were recorded in positive mode by using an API 1 mass spectrometer (Perkin−Elmer) at 60 V cone voltage. $[Co(CH_3)(dpgH)_2py]$ was prepared according to a literature procedure.[6,7] All other reagents were reagent grade and used without further purification.

Synthesis of $[Co(CH_3)(dpgH)_2(H_2O)]$: $[Co(CH_3)(dpgH)_2py]$ (0.10 g, 0.16 mmol) was dissolved in 10 mL of CH_2Cl_2 and 40 mL of CH_3OH. The solution was filtered to remove the undissolved residue and 0.30 g of the acidic cation exchange resin Dowex 50 W was added. The solution was heated at 50 °C for 2 h and then filtered and concentrated to half volume on a rotary evaporator. Red crystals of $[Co(CH_3)(dpgH)_2(H_2O)]$ were recovered from the solution after allowing it to stand. Yield: 63.7 mg (69%). $C_{29}H_{27}CoN_4O_5$ (570.48): calcd. C 61.06, H 4.77, N 9.82; found C 60.7, H 4.91, N

Table 2. Crystal data and structure refinement for **1** and **2**

	1	**2**
Empirical formula	$C_{36}H_{36}BCoN_5O_{6.5}$	$C_{38.5}H_{43}BCoN_5O_{7.5}$
Molecular mass	712.44	765.52
T (K)	150(2)	150(2)
λ (Å)	0.71069	0.71069
Crystal system, space group	triclinic, $P\bar{1}$	triclinic, $P\bar{1}$
a (Å)	10.543(4)	10.858(3)
b (Å)	12.445(4)	12.688(13)
c (Å)	13.937(6)	16.497(4)
α (°)	94.23(2)	106.75(2)
β (°)	103.53(2)	110.02(2)
γ (°)	94.95(2)	82.16(2)
V (Å^3)	1762.9(12)	1995.7(8)
Z	2	2
$\rho_{calcd.}$ (g cm^{-3})	1.342	1.274
$F(000)$	742	802
μ (mm^{-1})	0.540	0.484
Θ (°)	3−26	4−26
Reflections collected	10258	12001
Reflections observed	6319	7045
Criterion for obs.	$I > 2\sigma(I)$	$I > 2\sigma(I)$
Variables	450	466
Final R_{int} $[I > 2\sigma(I)]$	R_1 [a] = 0.070, wR_2 [b] = 0.191	$R_1 = 0.078$, $wR_2 = 0.212$
R_{int} (all data)	$R_1 = 0.083$, $wR_2 = 0.206$	$R_1 = 0.109$, $wR_2 = 0.239$
GOF	1.05	1.02
Max. resid. dens. (e/Å^3)	0.91	0.65

[a] $R_1 = \|F_o| - |F_c\|/|F_o|$. [b] $wR_2 = [w(|F_o^2| - |F_c^2|)^2/w|F_o^2|^2]^{1/2}$.

 © 2004 Wiley-VCH Verlag GmbH & Co. KGaA, Weinheim

9.60. ESI-MS (60 V, CH_3OH; m/z^+): calcd. for $CH_3Co(dpgH)_2H_2O$ 570.482; found 553.1 (100%) [$CH_3Co(dpgH)_2H_2O - H_2O$]. ^1H NMR ($CDCl_3$, 400 MHz, TMS): δ = 1.23 (s, 3 H, CH_3 ax.), 7.26 (m, 20 H, equatorial phenyls) ppm.

Synthesis of [Co(CH$_3$)(dpgH){dpgB(OMe)(4-Py)}]$_2$ (1): 4-Pyridinylboronic acid (0.012 g, 0.1 mmol) was added whilst stirring to a solution of [Co(CH$_3$)(dpgH)$_2$py] (0.03 g, 0.05 mmol) in a mixture of methanol (10 mL) and CH_2Cl_2 (2 mL). The resulting mixture was filtered and the pH was adjusted to 5 by addition of $HClO_4$ (70% w/w). X-ray quality crystals formed from the solution in 1 week. Yield: 0.014 g (40%). $C_{70}H_{62}B_2Co_2N_{10}O_{10}$ (1342.8): calcd. C 62.00, H 4.65, N 10.43; found C 61.8, H 4.69, N 10.18. ESI-MS (60 V, CH_2Cl_2/HCOOH 1%; m/z^+): calcd. for **1** 1342.8; found 1343.2. (43%) [**1** + H^+]. ^1H NMR ($CDCl_3$, 400 MHz, TMS): δ = 1.59 (s, 6 H, CH_3 ax.), 3.27 (s, 6 H, OCH_3), 6.72 (d, $^3J_{H,H}$ = 6.4 Hz, 4 H, *meta* of py), 7.18−7.43 (m, 40 H, equatorial phenyls), 7.35 (d, $^3J_{H,H}$ = 6.4 Hz, 4 H, *ortho* of py), 18.24 (s, 2 H, O···H···O) ppm.

Synthesis of [Co(CH$_3$)(dpgH){dpgB(OMe)(3-NH$_2$Ph)}]$_2$ (2): 3-Aminophenylboronic acid monohydrate(0.03 g, 0.18 mmol) was added whilst stirring to a solution of [Co(CH$_3$)(dpgH)$_2$(H$_2$O)] (0.10 g, 0.18 mmol) in methanol (100 mL). The resulting solution was filtered and the pH was adjusted to 8 by addition of $HClO_4$ (70% w/w). X-ray quality crystals formed from the solution within 4 days. Yield: 0.037 g (30%). $C_{72}H_{66}B_2Co_2N_{10}O_{10}$ (1370.8): calcd. C 63.08, H 4.85, N 10.22; found C 62.7, H 5.02, N 10.2. ^1H NMR (C_6D_6, 400 MHz, TMS): δ = 2.3 (s, 6 H, CH_3 ax.), 3.20 (s, 6 H, OCH_3), 3.32 (d, 2 H, NH_2), 3.80 (d, 2 H, NH_2), 6.21 (d, $^3J_{H,H}$ = 8.3 Hz, 1 H, *ortho*-C_6H_4-NH_2), 6.29 (t, 4 H, *meta*-Ph^I), 6.37 (d, $^3J_{H,H}$ = 7.8 Hz, 4 H, *ortho*-Ph^I), 6.67 (m, 2 H, *para*-Ph^I); 6.75 (t, 4 H, *meta*-Ph^{II}), 6.82 (m, 2 H, *para*-Ph^{II}), 7.10 (d, $^3J_{H,H}$ = 7.8 Hz, 4 H, *ortho*-Ph^{II}), 6.92 (m, 2 H, *para*-Ph^{IV}), 7.10 (t, 4 H, *meta*-Ph^{IV}), 7.91 (d, $^3J_{H,H}$ = 7.3 Hz, 4 H, *ortho*-Ph^{IV}), 6.95−7.05 (m, 6 H, *meta*- and *para*-Ph^{III}), 7.56 (d, $^3J_{H,H}$ = 7.3 Hz, 4 H, *ortho*-Ph^{III}), 7.25 (m, 2 H, *meta* -C_6H_4-NH_2), 7.43 (s, 2 H, *ortho*-C_6H_4-NH_2), 8.01 (d, $^3J_{H,H}$ = 7.3 Hz, 2 H, *para*-C_6H_4-NH_2), 19.50 (s, 2 H, O···H···O) ppm.

X-ray Crystallographic Study: Single crystals suitable for X-ray data collection,were obtained as reported above. X-ray diffraction data were collected at 150 K, with a Nonius DIP 1030 H System, using graphite-monochromated Mo-K_α radiation. For all compounds a total of 30 frames were collected, using the Xpress program,[12] over a half of reciprocal space with rotation of 6° about the φ axis. A Mac Science Image Plate (diameter = 300 mm) was used and the crystal-to-plate distance was fixed at 90 mm. The determination of unit-cell parameters, integration of reflection intensities and data scaling were performed using MOSFLM and SCALA from the CCP4 program suite.[13] Reflections, which were measured on previous and following frames, were used to scale the frames with each other, a procedure that partially eliminated absorption effects, taking into account also any crystal decay. The structures were solved by direct methods,[14] followed by Fourier syntheses and refined by full-matrix least-squares (on F^2) cycles.[15] Compound **1** crystallized with one water and two independent methanol molecules (all with occupancy factor 0.5), while **2** co-crystallized with three methanol molecules (one with o.f. 0.5). The solvent molecules were refined isotropically. The H-atoms were included at calculated positions in the final refinements. A suite of programs[5] was also used in the geometrical and final calculation. Crystal and refinement data of interest are given in Table 2.

CCDC-236499 (for **1**) and -236500 (for **2**) contain the supplementary crystallographic data for this paper. These data can be obtained free of charge at www.ccdc.cam.ac.uk/conts/retrieving.html [or from the Cambridge Crystallographic Data Centre, 12 Union Road, Cambridge CB2 1EZ, UK; Fax: +44-1223-336-033; E-mail: deposit@ccdc.cam.ac.uk].

Acknowledgments

This work was supported by MIUR (PRIN 2003 no. 2003037058) and Cofinlab CE00338925. We thank Dr. Fabio Hollan for recording mass spectra.

[1] L. Randaccio, *Comments Inorg. Chem.* **1999**, *21*, 327 and references cited therein.
[2] H. Höpfl, in *Structure & Bonding*, vol. 103 (D. M. P. Mingos, Ed.), Springer, Berlin, **2002**.
[3] R. Dreos, G. Nardin, L. Randaccio, G. Tauzher, S. Vuano, *Inorg. Chem.* **1997**, *36*, 2463.
[4] R. Dreos, G. Nardin, L. Randaccio, P. Siega, G. Tauzher, V. Vrdoljak, *Inorg. Chem.* **2001**, *40*, 5536.
[5] R. Dreos, G. Nardin, L. Randaccio, P. Siega, G. Tauzher, *Eur. J. Inorg. Chem.* **2002**, 2885.
[6] C. López, S. Alvarez, M. Font Bardía, X. Solans, *J. Organomet. Chem.* **1991**, *414*, 245.
[7] P. J. Toscano, L. Lettko, E. J. Schermerhorn, J. Waechter, K. Schufon, S. Liu, E. V. Dikarev, J. Zubieta, *Polyhedron* **2003**, *22*, 2809.
[8] F. C. Fischer, E. Havinga, *Recl. Trav. Chim. Pays Bas* **1974**, *93*, 21.
[9] F. Asaro, R. Dreos, G. Nardin, G. Pellizer, S. Peressini, L. Randaccio, P. Siega, G. Tauzher, C. Tavagnacco, *J. Organomet. Chem.* **2000**, *601*, 114.
[10] F. Asaro, R. Dreos, S. Geremia, G. Nardin, G. Pellizer, L. Randaccio, G. Tauzher, S. Vuano, *J. Organomet. Chem.* **1997**, *548*, 211.
[11] R. Dreos, G. Tauzher, S. Vuano, F. Asaro, G. Pellizer, G. Nardin, L. Randaccio, S. Geremia, *J. Organomet. Chem.* **1995**, *505*, 135.
[12] B. Schierbeek *Nonius*, Delft, The Netherlands, **1998**.
[13] Collaborative Computational Project, Number 4, *Acta Crystallogr., Sect. A* **1990**, *46*, 467.
[14] SIR92 − *A program for crystal structure solution:* A. Altomare, G. Cascarano, C. Giacovazzo, A. Guagliardi, *J. Appl. Crystallogr.* **1993**, *26*, 343.
[15] G. M. Sheldrick, SHELXL-97 − *Programs for Structure Refinement.* University of Göttingen, Göttingen, Germany, **1998**.

Received April 20, 2004
Early View Article
Published Online September 2, 2004

 © 2004 Wiley-VCH Verlag GmbH & Co. KGaA, Weinheim

The C_α-Deprotonated Iminophosphorane $Ph_2P(CH_2Py)(NSiMe_3)$ as an *N,N*-Chelating Ligand for Iron and Zinc

Alexander Murso[a] and Dietmar Stalke*[a]

Keywords: Chelates / Hypervalent compounds / Iminophosphoranes / Iron / N ligands

The iminophosphorane $Ph_2P(CH_2Py)(NSiMe_3)$ (Py = NC_5H_4) is deprotonated at the C_α-position in a reaction with $[M\{N(SiMe_3)_2\}_2]$ (M = Fe^{2+}, Zn^{2+}) to give metallaspirocycles in which the metal cations are *N,N*-chelated by the ring- and imino-nitrogen atoms of both monoanionic ligands. The molecular structures of $[M\{Ph_2P(CHPy)(NSiMe_3)\}_2]$ [M = Fe (**1**), Zn (**2**)] are discussed and general trends in the bonding of the $[Ph_2P(CHPy)(NSiMe_3)]^-$ anion on metal coordination are deduced.

(© Wiley-VCH Verlag GmbH & Co. KGaA, 69451 Weinheim, Germany, 2004)

Introduction

Iminophosphoranes of the general type R_3PNR' are valuable building blocks in organometallic and organic syntheses.[1] Their reactivity is mainly due to the inherent polarity of the phosphorus−nitrogen bond, which makes them reactive towards both electrophilic and nucleophilic reagents.[2] In silylated iminophosphoranes, $R_3PNSiMe_3$, the Si−N bond is cleaved in reactions with main-group[3] or transition-metal halides,[4] resulting in the $[R_3PN]^-$ building block, which has similar steric and electronic characteristics to the ubiquitous cyclopentadienyl ligand.[5] In addition, the incorporation of heteroaromatic substituents at the phosphorus centre instead of commonly used alkyl or phenyl groups alters and augments the reactivity and coordination modes of iminophosphoranes. In reactions of pyridyl-substituted iminophosphoranes and amino(imino)phosphoranes with organolithium compounds and lithium amides reduction of the phosphorus(V) centre by P−C or P−N bond cleavage is observed to give phosphanylamides or phosphanides.[6] Likewise, transiminations are observed when treating iminophosphoranes with imines.[7]

Additionally, *P*-alkyl-substituted iminophosphoranes can easily be deprotonated to give attractive building blocks for metallacycles.[8] The introduction of alkyl bridges between the phosphorus atom and the donating heterocycle in the ligand periphery of iminophosphoranes provides not only the opportunity of a higher geometrical adaptability by a wider bite but can also allow the formation of anionic species. Delocalisation of the carbanionic charge to the donating atoms would enable the ligand to respond to the various requirements of metal atoms with their different radii and polarisability. Recently, Leung et al. reported some main-group metal complexes of $iPr_2P(CH_2Py)(NSiMe_3)$ and [2,6-$(Me_3SiNPiPr_2CH_2)_2(cy\text{-}C_5H_3N)$], obtained by deprotonation with organolithium compounds, alkylmagnesium compounds or group-14 amides. Metathesis with group-14 halides gave 1,3-dimetallacyclobutanes (Scheme 1).[9,10]

In the literature the imino nitrogen atom is commonly described as a two-electron σ-donor with only minor π-acceptor properties.[1] However, we recently reported the syntheses and coordination modes of the iminophosphorane $Ph_2P(CH_2Py)(NSiMe_3)$ (Py = NC_5H_4) and its anion in alkali metal complexes and provided experimental evidence that the P=N bond in iminophosphoranes has to be regarded as a P^+-N^- single bond with high electrostatic contributions,[11] as already predicted from theoretical investigations.[12,13] Thus, we found both lone pairs at the sp^3-hybridized imino nitrogen atom in $[(Et_2O)Li\{Ph_2P(CHPy)(NSiMe_3)\}]$ to be directed towards the cation. Hence, the metal−imino nitrogen interactions cannot be regarded as simple 2e-donor bonds (Figure 1).

This bifurcated 4e-coordination pattern and the sidearm donation capability of the pyridyl nitrogen atom in the $[Ph_2P(CHPy)(NSiMe_3)]^-$ anion prompted us to investigate reactions of the iminophosphorane $Ph_2P(CH_2Py)(NSiMe_3)$ with transition metal amides $[M\{N(SiMe_3)_2\}_2]$. In this contribution we report the complexes of divalent iron and zinc (M = Fe, Zn).

Results and Discussion

Syntheses

The reaction of the iron(II) amide $[Fe\{N(SiMe_3)_2\}_2]_2$[14] with the iminophosphorane $Ph_2P(CH_2Py)(NSiMe_3)$[11] in a 1:2 ratio in polar solvents such as THF or Et_2O results, even at −78 °C, in dark-red to black solutions containing

[a] Institut für Anorganische Chemie der Universität Würzburg, Am Hubland, 97074 Würzburg, Germany
Fax: (internat.) + 49-931-888-4619
E-mail: dstalke@chemie.uni-wuerzburg.de

 © 2004 Wiley-VCH Verlag GmbH & Co. KGaA, Weinheim DOI: 10.1002/ejic.200400318

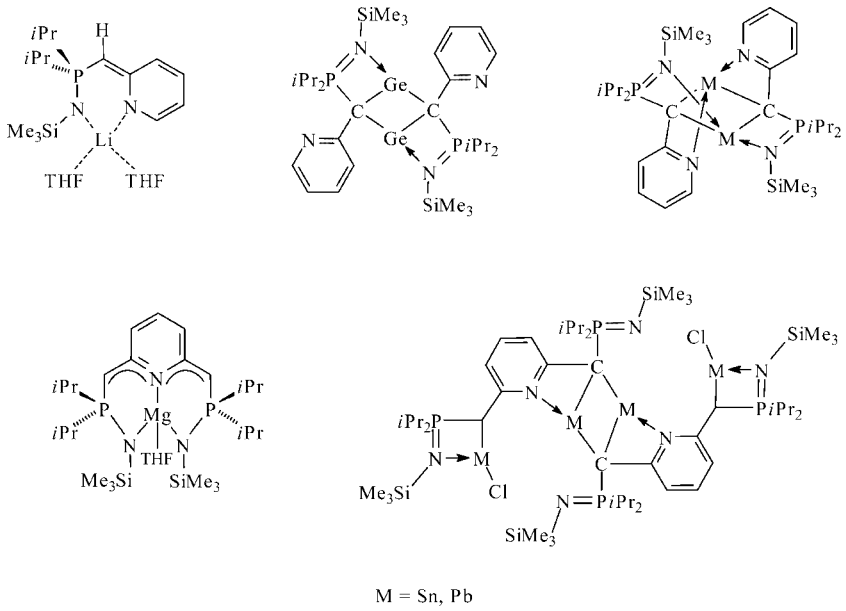

Scheme 1. Main-group metal complexes of $iPr_2P(CH_2Py)(NSiMe_3)$ (top) and $[2,6\text{-}(Me_3SiNPiPr_2CH_2)_2(cy\text{-}C_5H_3N)]$ (bottom)

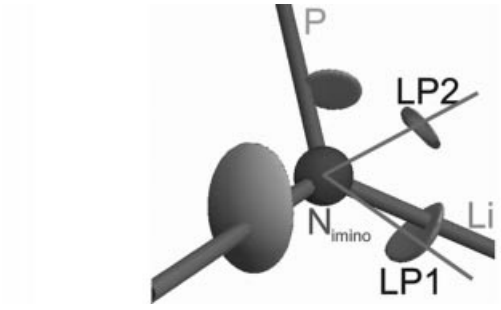

Figure 1. Bifurcated donation of the valence shell charge concentrations derived from experimental charge density studies of the imino nitrogen atom in $[(Et_2O)Li\{Ph_2P(CHPy)(NSiMe_3)\}]$

several products. In contrast, the addition of pure $[Fe\{N(SiMe_3)_2\}_2]_2$ to the solid iminophosphorane $Ph_2P(CH_2Py)(NSiMe_3)$ at room temperature gives immediately a red oily suspension of solid $[Fe\{Ph_2P(CHPy)(NSiMe_3)\}_2]$ (**1**) in liquid $HN(SiMe_3)_2$, formed by the C_α-deprotonation of the iminophosphorane (Scheme 2, left). A similar reaction of the iminophosphorane with $[Zn\{N(SiMe_3)_2\}_2]$[15] gives the isomorphous zinc derivative $[Zn\{Ph_2P(CHPy)(NSiMe_3)\}_2]$ (**2**; Scheme 2, right).

After workup, both complexes were isolated in high yields and their molecular structures determined by X-ray diffraction experiments. Both compounds **1** and **2** are insoluble in nonpolar solvents. The complexes were analysed by IR spectroscopy and elemental analysis. For the iron complex **1** no NMR spectroscopic data were available due to its paramagnetic nature. The NMR resonances for the zinc derivative **2** are given in the Exp. Sect.

Structure Discussion

The solid-state structure of **1** is depicted in Figure 2. The central iron(II) cation is chelated by the nitrogen atoms N1−N4 of the two ligands. The coordination sphere is best described as a distorted tetrahedron with the angles at the iron cation varying from 100.92(8) to 124.40(8)°. In the metallaspirocycle, the two six-membered FeN_2C_2P rings adopt a distorted boat conformation, each with the deprotonated carbon atoms C1 and C22 displaced by, on average, 45 pm

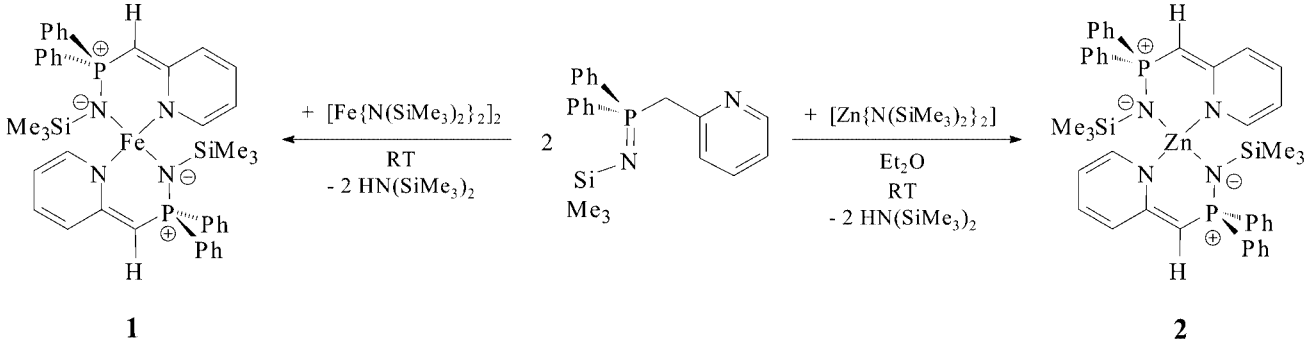

Scheme 2. Syntheses of $[Fe\{Ph_2P(CHPy)(NSiMe_3)\}_2]$ (**1**) and $[Zn\{Ph_2P(CHPy)(NSiMe_3)\}_2]$ (**2**) in the reaction of $Ph_2P(CH_2Py)(NSiMe_3)$ with the corresponding metal amide $[M\{N(SiMe_3)_2\}_2]_2$ (M = Fe, Zn)

 © 2004 Wiley-VCH Verlag GmbH & Co. KGaA, Weinheim

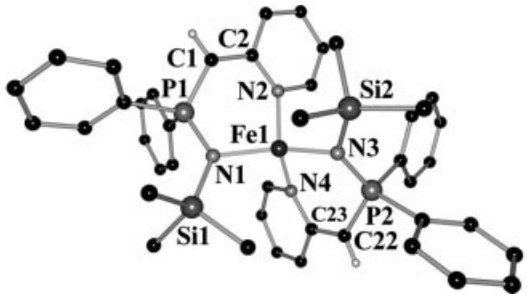

Figure 2. Solid-state structure of [Fe{$Ph_2P(CHPy)(NSiMe_3)$}$_2$] (**1**); selected bond lengths [pm] and angles [°]: Fe−N1 204.6(2), Fe−N3 204.2(2), Fe−N2 207.5(2), Fe−N4 207.9(2), P1−N1 161.2(2), P2−N3 161.3(2), N1−Si1 173.7(2), N3−Si2 173.7(2), P1−C1 172.5(2), P2−C22 172.7(2), P−C_{Ph} av. 182.2, C1−C2 139.4(3), C22−C23 140.3(3), C2−N2 137.9(3), C23−N4 137.5(3); P1−C1−C2 124.08(19), P2−C22−C23 123.42(19), P1−N1−Si1 132.07(12), P2−N3−Si2 129.83(12)

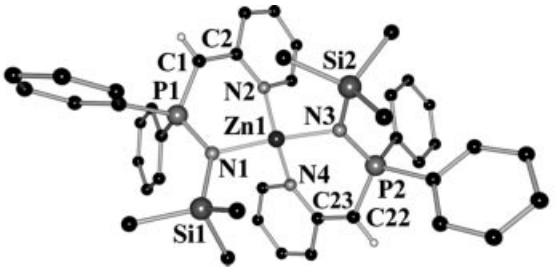

Figure 3. Solid-state structure of [Zn{$Ph_2P(CHPy)(NSiMe_3)$}$_2$] (**2**); selected bond lengths [pm] and angles [°]: Zn−N1 201.70(15), Zn−N3 201.15(16), Zn−N2 203.96(16), Zn−N4 203.88(16), P1−N1 160.92(16), P2−N3 161.43(16), N1−Si1 173.41(16), N3−Si2 173.43(16), P1−C1 172.1(2), P2−C22 172.28(19), P−C_{Ph} av. 181.6, C1−C2 138.9(3), C22−C23 139.6(3), C2−N2 137.5(2), C23−N4 137.5(2); P1−C1−C2 123.75(15), P2−C22−C23 123.35(15), P1−N1−Si1 131.10(10), P2−N3−Si2 128.80(10)

from the respective best N−P−C−N plane (29 pm for the Fe^{2+} cation).

The Fe−N_{imino} distances (av. 204.4 pm) are equal within their estimated standard deviations (esds). They are in the range typically found for iron(II) complexes in which the cation is coordinated to imino functions, for example in [Fe{(*o*-C_6H_4)$Ph_2PNSiMe_3$}$_2$] (211.1 pm),[16] [Fe{2-(R*N*PPh_2)-6-R′(*c*-C_5H_3N)}Cl_2] (R = 2,6-Me_2-C_6H_3, 2,6-*i*Pr_2-C_6H_3; R′ = Ph, H_2CPh, $SiMe_3$; 204.8−206.7 pm)[17] or in the 12 VE iron(II) complex [Fe(H_2CPh)-{HC(CMeNAr)$_2$}] (198.2 pm).[18] The Fe−N_{imino} distances in **1** are about 24.4 pm shorter than in the dibromoiron(II) compound [{2,6-($Ph_2PNSiMe_3$)Py}$FeBr_2$], where the Fe−N contacts are on average 228.8 pm,[19] reflecting the pronounced amidic character of the Fe−N_{imino} bonds.

It seems remarkable that the Fe−N_{py} distances in **1** (av. 207.7 pm) are only 3.3 pm longer than the Fe−N_{imino} contacts. They are much shorter than in the donor base coordinated complexes [(H_2NCH_2Py)Fe][Br]$_2$ (Fe−N_{py}: av. 222.3 pm),[20] [(Hpy)$_2$(H_2O)$_4$Fe][$MeCO_2$]$_2$ (221.3 pm)[21] or [Fe{2-(R*N*PPh_2)-6-R′(*cy*-C_5H_3N)}Cl_2] (R = 2,6-Me_2-C_6H_3, 2,6-*i*Pr_2-C_6H_3; R′ = Ph, H_2CPh, $SiMe_3$; 218.4−222.9 pm),[17] but similar to those in [Fe{C(H)(Si*t*$BuMe_2$)Py}$_2$]$_2$ (209.7 and 218.9 pm),[22] where the pyridyl nitrogen atom acts as a side-arm donor, like in **1**.

The solid-state structure of the isomorphous zinc derivative [Zn{$Ph_2P(CHPy)(NSiMe_3)$}$_2$] (**2**) is shown in Figure 3.

The central zinc cation is fourfold coordinated by the nitrogen atoms N1−N4 of the two anionic ligands. The coordination polyhedron around the Zn^{2+} ion is a nearly ideal tetrahedron [the angles vary from 103.70(6) to 111.31(6)°]. Like in **1**, both monoanionic [$Ph_2P(CHPy)(NSiMe_3)$]$^-$ units act as bidentate *N*,*N*-chelates and the two six-membered rings of the metallaspirocycle each show a distorted boat conformation. The displacement of the deprotonated carbon atoms and the metal centre from the best plane of the ligand (av. 45 pm for C1/C22 and 21 pm for Fe) is similar to **1**.

In **2**, the distances between the zinc atom and the imino nitrogen atoms N1 and N3 (av. 201.43 pm) are equal within the esds. In general, Zn−N contacts span a wide range from 182 pm for covalently bonded zinc amides to 231 pm for donor-base complexed dimethylzinc;[23] in **2** they are similar to Zn−N_{imino} interactions in the related zinc bis(iminophosphorane)methanides [Zn{HC(Ph_2PNR}$_2$X] [R = Mes, $SiMe_3$; X = Me, N($SiMe_3$)$_2$, $OCPh_3$], where the contacts vary from 198.6 to 208.3 pm.[24] In the *ortho*-deprotonated [Zn(*o*-$C_6H_4PPh_2NSiMe_3$)$_2$] the Zn−N contacts are 14.4 pm longer (215.8 pm).[25] Thus, the Zn1−N1/3 contacts in **2** are in the range for covalently bonded zinc amides. The Zn−N_{py} distances are identical (Zn1−N3/4: av. 203.92 pm) and only 2.5 pm longer than the Zn−N_{imino} interactions. The average value quoted for Zn−N_{py} contacts is 208.3 pm.[26] To judge the covalent or dative character of the Zn−N_{py} bonds, complex **2** is best compared with the bis(1,4-dihydropyridin-1-yl)bis(pyridine)zinc system:[27] the Zn−N_{py} distances in **2** are 4.4 pm longer than the covalent bonds in bis(1,4-dihydropyridin-1-yl)bis(pyridine)zinc (197 pm), but 11.6 pm shorter than the dative ones (213 pm), clearly emphasising the amidic character of the Zn−N_{py} interactions in **2**.

The geometrical parameters of the anionic ligands of both complexes **1** and **2** are almost equal. Thus, in the following discussion the averages are given; the exact parameters are listed in the captions of Figures 1 and 2, respectively.

The P1−C1 and P2−C22 bonds in **1** and **2** (av. 172.5 pm) are about 12 pm shorter than formal P−C single bonds (185 pm);[28] they are in the range found for ylidic P^+−C^- interactions (163−173 pm).[12,29] In addition, the C1/22−C2/23 contacts (av. 139.6 pm) are 10 pm shorter than the corresponding bond length in the neutral starting material $Ph_2P(CH_2Py)(NSiMe_3)$ (182.57 pm).[11] As a consequence, the C2−N2 and C23−N4 bonds in the pyridyl substituents (average 137.6 pm) are 4.4 pm longer than in the starting material (133.17 pm).[11] The sum of the angles at the imino nitrogen atoms in both complexes is about 360°, illustrating a planar coordination sphere at these atoms. For the pyridyl nitrogen atoms N2 and N4, a marginal pyramidal environment is observed, with a mean sum of the angles of 355.5° in **1** and 356.3° in **2**. All these parameters are very similar to those found in the alkali metal derivatives

 © 2004 Wiley-VCH Verlag GmbH & Co. KGaA, Weinheim

$[(Et_2O)Li\{Ph_2P(CHPy)(NSiMe_3)\}]$ and $[\{Ph_2P(CH_2Py)(NSiMe_3)\}M\{Ph_2P(CHPy)(NSiMe_3)\}]$ (M = Li, Na), containing the same anion,[11] and to the related $[(THF)Mg\{2,6\text{-}(Me_3SiNPiPr_2CH)_2(c\text{-}C_5H_3N)\}]$.[10] In the metallacyclobutanes $[\{2\text{-}[M\{C(iPr_2PNSiMe_3)\}]\text{-}6\text{-}[M\{HC(iPr_2PNSiMe_3)\}X]\}(c\text{-}C_5H_3N)]_2$ (M = Sn, X = Cl; M = Pb, X = $N(SiMe_3)_2$], which contain the mono- and dianionic derivative of $[2,6\text{-}(Me_3SiNPiPr_2CH_2)_2(c\text{-}C_5H_3N)]$, longer P−$C_\alpha$(H) (av. 178.6 pm) and C_α(H)−C_{Py} distances (av. 147.3 pm) are found than in **1** and **2** due to the observed [M]−C_α bonds in addition to the [M]−N contacts.[10] Whereas in the metallacyclobutanes the negative charge is accumulated at the deprotonated carbon centres, in **1** and **2** it is delocalised over the [HC−Py] backbone of the ligand, leading to a perturbation of the aromatic ring systems and charge accumulation at the pyridyl nitrogen atom. The increased electron density in the pyridyl substituents leads to a displacement of the metal cations from the ring plane towards the π-density of the pyridyl substituent, which explains the short M−N_{py} distances in **1** and **2**.

The P−N bonds in **1** and **2** are, on average, 161.2 pm long. They are at the upper end of the range found for P−N bonds in iminophosphoranes (147−162 pm)[30] and reflect the trend of P−N bond elongation on weakening the electrostatic P^+-N^- interaction because of the presence of the adjacent deprotonated C_α position and the additional *N*-metal coordination.[9,11,31] The Si−N distances in **1** and **2** are, on average, 173.6 pm long and are therefore about 5.5 pm longer than in the neutral iminophosphorane $Ph_2P(CH_2Py)(NSiMe_3)$ (168.08 pm).[11] Similar changes in Si−N bond lengths have been found in the alkali-metal derivatives of $Ph_2P(CH_2Py)(NSiMe_3)$[11] and in bis(iminophosphorane)methanides[32] with regard to the parent starting materials.[33] The long Si−N bonds found in **1** and **2** are a result of the strong interactions of the negatively charged imino nitrogen atoms with the doubly charged cations, reducing the electrostatic contributions in the Si−N interactions.

Spectroscopic Investigations

The IR spectra of **1** and **2** show signals at 1360 cm^{-1} for both complexes. These signals are in the range found for P−N stretching modes (1140−1370 cm^{-1}),[1,34] and are shifted 11 cm^{-1} to higher wavenumbers relative to the starting iminophosphorane (ν_{PN} = 1349 cm^{-1}). A similar shift to higher wavenumbers was detected unambiguously by DFT assignment earlier from the starting material $Ph_3PNSiMe_3$ (ν_{PN} = 1319 cm^{-1}) to the *ortho*-metallated $[(Et_2O)Li(o\text{-}C_6H_4PPh_2NSiMe_3)\}_2]$ (ν_{PN} = 1328 cm^{-1}).[35]

Due to the presence of a d^6 Fe^{II} centre in a tetrahedral coordination, no NMR spectroscopic data could be obtained for the paramagnetic iron complex **1**. In the ^{31}P NMR spectrum of **2**, the phosphorus nuclei resonate at δ = 26.4 ppm. Like for the alkali-metal derivatives of $Ph_2P(CH_2Py)(NSiMe_3)$,[11] deprotonation at the C_α atom results in a downfield shift from the resonance of the starting iminophosphorane (δ = −0.32 ppm). The negative charge and metal coordination at the *P*-bound nitrogen atom decrease the electron density at the phosphorus centre. The almost invariant ^{15}N NMR spectroscopic shift of the imino nitrogen atoms in **2** (δ = −348 ppm) and the iminophosphorane (δ = −343 ppm) indicate that the charge density at this nitrogen atom is less affected by the deprotonation. However, the ^{15}N NMR resonance for the pyridyl ring nitrogen atoms in the anionic ligands of **2** (δ = −182 ppm) differs remarkably from that of the parent iminophosphorane (δ = −61 ppm); it is considerably shifted to higher fields. This resonance is in the range observed earlier for the $[Ph_2P(CHPy)(NSiMe_3)]^-$ anion and is in accordance with charge accumulation at the pyridyl ring nitrogen atoms.[11]

Conclusion

Metal bis(trimethylsilyl)amides easily deprotonate the iminophosphorane $Ph_2P(CH_2Py)(NSiMe_3)$ at the methylene bridge to furnish *N*,*N*-chelating monoanionic ligands coordinating to the metal atom through the pyridyl and the imino nitrogen atoms. The negative charge is delocalised over the [HC−Py] backbone of the ligand, increasing the electron density in the pyridyl rings. Thus, the metal cations are shifted towards the π-density of the pyridyl rings. On metal coordination, the P−N and Si−N bonds in the ligands get simultaneously elongated, due to the decay of the electrostatic contributions in the P^+-N^- and Si^+-N^- bonds. Additionally, we found shorter M−N_{imino} contacts than expected for M←N donor bonds. These geometrical parameters show that the imino nitrogen atom cannot be regarded as a simple two-electron donor. The M−N_{imino} distances in complexes **1** and **2** reflect a high ionic contribution to the bonding. This leads to a description of the imino nitrogen atom between a monoanionic two- and four-electron donating centre.

Experimental Section

General Remarks: All manipulations were performed under dry N_2 with Schlenk techniques or in an argon-filled glovebox. All solvents were dried with Na/K alloy and distilled prior to use. IR spectroscopy was performed with a Bruker IFS 25 spectrometer. NMR spectra were recorded at room temperature with a Bruker DRX 300 spectrometer at 300.1 (^1H), 75.5 (^{13}C), 121.5 (^{31}P), 59.6 (^{29}Si) and 30.4 MHz (^1H,^{15}N HMBC). Chemical shifts are given as δ values relative to $[D_8]$toluene for ^1H, ^{13}C and to external formamide for ^1H,^{15}N HMBC NMR, H_3PO_4 (85%) for ^{31}P and to $SiMe_4$ for ^{29}Si NMR. Elemental analyses were performed by the Microanalytisches Labor der Universität Würzburg.

$[Fe\{Ph_2P(CHPy)NSiMe_3\}_2]$ (1): Pure, liquid $[Fe\{N(SiMe_3)_2\}_2]_2$ (0.26 g, 0.69 mmol) was added by syringe to solid $Ph_2P(CH_2Py)(NSiMe_3)$ (0.50 g, 1.37 mmol) in a drybox. The suspension turned red immediately. It was stirred at room temp. for 1 h, then 20 mL of hexane was added and the suspension was stirred for an additional 2 h. After evaporation of the solvent and formed $HN(SiMe_3)_2$ in vacuo, 0.99 g (1.27 mmol, 93%) of red solid **1** was isolated. To crystallise **1**, the red powder was dissolved in hexane/Et_2O (2:1). After 3 d, red blocks, suitable for an X-ray diffraction experiment, were obtained. IR: ν_{PN} = 1360 cm^{-1}. $C_{42}H_{48}FeN_4P_2Si_2$ (782.81): calcd.

 © 2004 Wiley-VCH Verlag GmbH & Co. KGaA, Weinheim

C 64.44, H 6.18, N 7.16; found C 64.36, H 6.21, N 7.12. M.p. (DTA) 258 °C.

[Zn{$Ph_2P(CHPy)NSiMe_3$}$_2$] (2): [Zn{$N(SiMe_3)_2$}$_2$] (0.29 g, 0.75 mmol) was dissolved in 10 mL of Et_2O and added slowly to a solution of $Ph_2P(CH_2Py)(NSiMe_3)$ (0.50 g, 1.37 mmol) in 25 mL of Et_2O at room temp. After stirring of the yellow solution for 2 h, the volume of the solvent was reduced. Storage of the solution at 4 °C overnight yielded 0.54 g (0.68 mmol, 91%) of **2** as yellow plates. IR: ν_{PN} = 1360 cm^{-1}. ^1H NMR: δ = 0.17 (s, 18 H, $SiMe_3$), 3.32 (d, $^2J_{P,H}$ = 20.9 Hz, 2 H, 1-H), 5.53 (dd, $^3J_{5,6}$ = 5.6, $^3J_{5,4}$ = 6.6 Hz, 2 H, 5-H), 6.28 (d, $^3J_{3,4}$ = 8.8 Hz, 2 H, 3-H), 6.56 (dd, $^3J_{4,3}$ = 8.8, $^3J_{4,5}$ = 6.6 Hz, 2 H, 4-H), 7.12 (d, $^3J_{6,5}$ = 5.6 Hz, 2 H, 6-H), 7.01−7.06 (m, 12 H, *m*-, *p*-PhH), 7.73−7.91 (m, 8 H, *o*-PhH) ppm. ^{13}C NMR: δ = 4.7 (d, $^3J_{Si,C}$ = 3.8 Hz, $SiMe_3$), 59.2 (d, C-1), 106.5 (s, C-5), 120.2 (d, C-3), 134.8 (s, C-4), 146.9 (s, C-6), 166.6 (d, C-2), 128.5 (*m*-PhC), 131.0 (*p*-PhC), 133.1 and 133.4 (*o*-PhC), 138.2 (*i*-PhC) ppm. ^{29}Si NMR: δ = 1.32 (d, $^2J_{Si,P}$ = 1.8 Hz) ppm. $^1H,^{15}N$-HMBC NMR: δ = −348 ($NSiMe_3$), −182 (PyN) ppm. ^{31}P NMR: δ = 26.4 (s) ppm. $C_{42}H_{48}N_4P_2Si_2Zn$ (792.33): calcd. C 63.67, H 6.11, N 7.07; found C 63.72, H 6.14, N 6.96. M.p. (DTA) 176 °C (dec.).

X-ray Crystallographic Study: All data were collected at 100(2) K[36] using graphite-monochromated Mo-K_α radiation (λ = 71.073 pm) with a Bruker D8 goniometer platform, equipped with a Smart Apex CCD detector. Cell parameters were determined and refined using the SMART software.[37] A series of ω-scans was performed at several φ settings. Raw frame data were integrated using the SAINT program.[38] Empirical absorption correction was carried out with SADABS 2.05.[39] The structures were solved by direct methods and refined by full-matrix least squares on F^2 using SHELXL.[40] *R* values defined as $R1 = \Sigma||F_o| - |F_c||/\Sigma|F_o|$, $wR2 = [\Sigma w(F_o^2 - F_c^2)^2/\Sigma w(F_o^2)^2]^{0.5}$, $w = [\sigma^2(F_o^2) + (g_1P)^2 + g_2P]^{-1}$, $P = 1/3[\max(F_o^2,0) + 2F_c^2]$. The positions of the hydrogen atoms H1 at C1 and H22 at C22 in **1** and **2** were taken from the difference Fourier map and refined freely. All other hydrogen atoms were refined using a riding model. The U_{iso} values for the hydrogen atoms of a CH_3 group were set to be 1.5 times and those of all other hydrogen atoms 1.2 times the U_{eq} values of the corresponding C atoms. All non-hydrogen atoms were refined anisotropically. The anisotropic displacement parameters (ADP) in the supplementary crystallographic data were drawn at the 50% probability level. **1:** $C_{42}H_{48}FeN_4P_2Si_2$, M_r = 782.81 g/mol, triclinic, space group $P\bar{1}$, a = 1028.83(6), b = 1081.12(6), c = 1836.20(11) pm, α = 85.8120(10), β = 81.1290(10), γ = 79.9010(10)°, V = 1.9845(2) nm^{-3}, Z = 2, $\rho_{calcd.}$ = 1.310 $Mg{\cdot}m^{-3}$, μ = 0.556 mm^{-1}, $F(000)$ = 824. Data were collected from θ = 2.03 to 25.35°. 30624 reflections measured, from which 7251 were unique, $R(int)$ = 0.0295, $wR2$(all data) = 0.1181, $R1[I > 2\sigma(I)]$ = 0.0414, for 7243 data and 474 parameters. **2:** $C_{42}H_{48}N_4P_2Si_2Zn$, M_r = 792.33 g/mol, triclinic, space group $P\bar{1}$, a = 1026.46(5), b = 1077.28(5), c = 1830.69(9) pm, α = 85.8180(10), β = 80.9470(10), γ = 79.7270(10)°, V = 1.96499(16) nm^{-3}, Z = 2, $\rho_{calcd.}$ = 1.339 $Mg{\cdot}m^{-3}$, μ = 0.803mm^{-1}, $F(000)$ = 832. Data were collected from θ = 2.04 to 26.44°. 42026 reflections measured, from which 8072 were unique, $R(int)$ = 0.0310, $wR2$(all data) = 0.0920, $R1[I > 2\sigma(I)]$ = 0.0347, for 8067 data and 474 parameters. CCDC-232887 (**1**) and -232888 (**2**) contain the supplementary crystallographic data for this paper. These data can be obtained free of charge at www.ccdc.cam.ac.uk/conts/retrieving.html [or from the Cambridge Crystallographic Data Centre, 12 Union Road, Cambridge CB2 1EZ, UK; Fax: (internat.) + 44 1223-336-033; E-mail: deposit@ccdc.cam.ac.uk].

Acknowledgments

This work was supported by the Deutsche Forschungsgemeinschaft (SFB 347 and the Graduiertenkolleg 690 *Electron Density − Theory and Experiment*).

[1] A. W. Johnson, *Ylides and Imines of Phosphorus*, Wiley, New York, **1993**.
[2] [2a] Y. G. Gololobov, I. N. Zhmurova, L. F. Kasukhin, *Tetrahedron* **1981**, *37*, 437. [2b] Y. G. Gololobov, L. F. Kasukhin, *Tetrahedron* **1992**, *48*, 1353.
[3] Review: K. Dehnicke, F. Weller, *Coord. Chem. Rev.* **1997**, *158*, 103.
[4] Review: K. Dehnicke, M. Krieger, W. Massa, *Coord. Chem. Rev.* **1999**, *182*, 19.
[5] [5a] T. V. Lubben, P. T. Wolczanski, G. D. van Duyne, *Organometallics* **1984**, *3*, 977. [5b] D. W. Stephan, J. C. Stewart, F. Guerin, R. E. v. Spence, W. Xu, D. G. Harrison, *Organometallics* **1999**, *17*, 1116. [5c] D. W. Stephan, F. Guerin, R. E. v. Spence, L. Koch, X. Gao, S. J. Brown, J. W. Swabey, Q. Wang, W. Xu, P. Zoricak, D. G. Harrison, *Organometallics* **1999**, *17*, 2046. [5d] K. Dehnicke, F. Weller, J. Strähle, *Chem. Soc. Rev.* **2001**, *30*, 125.
[6] [6a] S. Wingerter, M. Pfeiffer, A. Murso, C. Lustig, T. Stey, V. Chandrasekhar, D. Stalke, *J. Am. Chem. Soc.* **2001**, *123*, 1381. [6b] F. Baier, Z. Fei, H. Gornitzka, A. Murso, S. Neufeld, M. Pfeiffer, I. Rüdenauer, A. Steiner, T. Stey, D. Stalke, *J. Organomet. Chem.* **2002**, *661*, 111.
[7] [7a] S. A. Bell, S. J. Geib, T. Y. Meyer, *Chem. Commun.* **2000**, 1375. [7b] S. A. Bell, T. Y. Meyer, S. J. Geib, *J. Am. Chem. Soc.* **2002**, *124*, 10698. [7c] M. C. Burland, T. Y. Meyer, *Inorg. Chem.* **2003**, *42*, 3438.
[8] [8a] Review: A. Steiner, S. Zacchini, P. I. Richards, *Coord. Chem. Rev.* **2002**, *227*, 193. [8b] J. F. Bickley, M. C. Copsey, J. C. Jeffery, A. P. Leedham, C. A. Russell, D. Stalke, A. Steiner, T. Stey, S. Zacchini, *Dalton Trans.* **2004**, 989.
[9] W.-P. Leung, Z.-X. Wang, H.-W. Li, Q.-C. Yang, T. C. W. Mak, *J. Am. Chem. Soc.* **2001**, *123*, 8123.
[10] W.-P. Leung, Q. W.-Y. Ip, S.-Y. Wong, T. C. W. Mak, *Organometallics* **2003**, *22*, 4604.
[11] N. Kocher, D. Leusser, A. Murso, D. Stalke, *Chem. Eur. J.*, in press.
[12] Review: D. G. Gilheany, *Chem. Rev.* **1994**, *94*, 1339.
[13] [13a] A. Dobado, H. Martinez-García, J. M. Molina, M. R. Sundberg, *J. Am. Chem. Soc.* **1998**, *120*, 8461. [13b] D. B. Chesnut, *J. Phys. Chem. A* **2003**, *107*, 4307.
[14] [14a] R. A. Andersen, K. Faegri, J. C. Green, A. Haaland, M. F. Lappert, W. -P. Leung, K. Rypdal, *Inorg. Chem.* **1988**, *27*, 1782. [14b] M. M. Olmstead, P. P. Power, S. C. Shoner, *Inorg. Chem.* **1991**, *30*, 2547.
[15] H. Bürger, W. Sawdony, U. Wannagat, *J. Organomet. Chem.* **1965**, *3*, 113.
[16] S. Wingerter, M. Pfeiffer, T. Stey, M. Bolboacá, W. Kiefer, V. Chandrasekhar, D. Stalke, *Organometallics* **2001**, *20*, 2730.
[17] L. P. Spencer, R. Altwer, P. Wei, L. Gelmini, J. Gauld, D. W. Stephan, *Organometallics* **2003**, *22*, 3841.
[18] T. J. J. Sciarone, A. Meesma, B. Hessen, J. H. Teuben, *Chem. Commun.* **2002**, 1580.
[19] S. Al-Benna, M. J. Sarsfield, M. Thomton-Pett, D. L. Omsby, P. J. Maddox, P. Bres, M. Bochmann, *J. Chem. Soc., Dalton Trans.* **2000**, 4247.
[20] L. Wiehl, G. Kiel, C. P. Köhler, H. Spiering, P. Gütlich, *Inorg. Chem.* **1986**, *25*, 1565.
[21] B. Singh, J. R. Long, F. F. de Biani, D. Gatteschi, P. Stavropoulos, *J. Am. Chem. Soc.* **1997**, *119*, 7030.
[22] W.-P. Leung, H. K. Lee, L.-H. Weng, B.-S. Luo, Z. -Y. Zhou, T. C. W. Mak, *Organometallics* **1996**, *15*, 1785.
[23] [23a] A. Haaland, K. Hedberg, P. P. Power, *Inorg. Chem.* **1984**,

 © 2004 Wiley-VCH Verlag GmbH & Co. KGaA, Weinheim

23, 1972. [23b] J. Dekker, J. Boersma, L. Fernholt, A. Haaland, A. L. Speck, *Organometallics* **1987**, *6*, 1202.
[24] [24a] A. Kasani, R. McDonald, R. G. Cavell, *Organometallics* **1999**, *18*, 3775. [24b] M. S. Hill, P. B. Hitchcock, *J. Chem. Soc., Dalton Trans.* **2002**, 4694.
[25] S. Wingerter, H. Gornitzka, G. Bertrand, D. Stalke, *Eur. J. Inorg. Chem.* **1999**, 173.
[26] W. A. Herrmann, W. R. Thiel, J. G. Kuchler, J. Behm, E. Herdtweck, *Chem. Ber.* **1990**, *123*, 1963.
[27] [27a] A. J. de Koning, J. Boersma, G. J. M. van der Kerk, *J. Organomet. Chem.* **1980**, *186*, 159. [27b] A. L. Spek, *Cryst. Struct. Commun.* **1982**, *11*, 1621.
[28] P. Rademacher, in *Strukturen organischer Moleküle*, VCH, Weinheim, **1987**.
[29] [29a] J. C. J Bart, *J. Chem. Soc. B* **1969**, 350. [29b] H. Schmidbaur, A. Schlier, C. M. F. Frazao, G. Müller, *J. Am. Chem. Soc.* **1986**, *108*, 976. [29c] H. Schmidbaur, J. Jeong, A. Schier, W. Graf, D. L. Wilkinson, G. Müller, *New J. Chem.* **1989**, *13*, 341.
[30] [30a] A. F. Cameron, N. S. Hair, D. G. Norris, *Acta Crystallogr., Sect. B* **1974**, *30*, 221. [30b] E. Niecke, D. Gudat, *Angew. Chem.* **1991**, *103*, 251; *Angew. Chem. Int. Ed. Engl.* **1991**, *30*, 217. [30c] A. Steiner, D. Stalke, *Inorg. Chem.* **1993**, *32*, 1977. [30d] R. Fleischer, D. Stalke, *Inorg. Chem.* **1997**, *36*, 2413.
[31] [31a] V. Chandrasekhar, K. R. J. Thomas, *Struct. Bonding (Berlin, Ger.)* **1993**, *81*, 41. [31b] V. Chandrasekhar, K. R. Thomas, *J. Appl. Organomet. Chem.* **1993**, *7*, 1. [31c] V. Chandrasekhar, K. Vivekanandan, S. Nagendran, A. G. T. Senthil, N. R. Weathers, J. C. Yarbrough, A. W. Cordes, *Inorg. Chem.* **1998**, *37*, 6192.
[32] [32a] R. P. K. Babu, K. Aparna, R. McDonald, R. G. Cavell, *Inorg. Chem.* **2000**, *39*, 4981. [32b] M. T. Gamer, P. W. Roesky, *Z. Anorg. Allg. Chem.* **2001**, *627*, 877.
[33] Müller, M. Möhlen, B. Neumüller, N. Faza, W. Massa, K. Dehnicke, *Z. Anorg. Allg. Chem.* **1999**, *625*, 1748.
[34] [34a] R. B. King, J. C. Cloyd Jr., *Inorg. Chem.* **1975**, *14*, 1550. [34b] I. MacLeod, L. Manojlovic-Muir, D. Millington, K. W. Muir, D. W. A. Sharp, R. Walker, *J. Organomet. Chem.* **1975**, *97* C7. [34c] T. G. Appleton, M. A. Bennett, *Inorg. Chem.* **1978**, *17*, 738. [34d] S. Hietkamp, D. J. Stufkens, K. Vrieze, *J. Organomet. Chem.* **1979**, *169*, 107.
[35] [35a] M. Balboáca, M. Pfeiffer, D. Stalke, W. Kiefer, in *Eighteenth International Conference on Raman Spectroscopy (ICORS 2002)*, John Wiley & Sons New York, **2002**, p. 601. [35b] M. Pfeiffer, M. Balboáca, D. Stalke, W. Kiefer, in *Eighteenth International Conference on Raman Spectroscopy (ICORS 2002)*, John Wiley & Sons New York, **2002**, p. 657. [35c] M. Bolboaca, T. Stey, A. Murso, D. Stalke, W. Kiefer, *Appl. Spectrosc.* **2003**, *57*, 970.
[36] [36a] T. Kottke, D. Stalke, *J. Appl. Crystallogr.* **1993**, *26*, 615. [36b] T. Kottke, R. J. Lagow, D. Stalke, *J. Appl. Crystallogr.* **1996**, *29*, 465. [36c] D. Stalke, *Chem. Soc. Rev.* **1998**, *27*, 171.
[37] Bruker, *SMART-NT, Data Collection Software, Version 5.6*, Bruker Analytical X-ray Instruments Inc., Madison, Wisconsin, USA, **2000**.
[38] Bruker, *SAINT-NT, Data Reduction Software, Version 6*, Bruker Analytical X-ray Instruments Inc., Madison, Wisconsin, USA, **1999**.
[39] G. M. Sheldrick, *SADABS, Empirical Absorption Correction Program*, University of Göttingen, Germany, **2001**.
[40] Bruker, *SHELX-TL, Version 6*, Bruker Analytical X-ray Instruments Inc., Madison, Wisconsin, USA, **2000**.

Received April 21, 2004
Early View Article
Published Online September 7, 2004

 © 2004 Wiley-VCH Verlag GmbH & Co. KGaA, Weinheim

Structural Studies of Mono- and Dimetallic Mo^{VI} Complexes − A New Mechanistic Contribution in Catalytic Olefin Epoxidation Provided by Oxazoline Ligands

José A. Brito,[a] Montserrat Gómez,*[a] Guillermo Muller,[a] Helena Teruel,*[b] Jean-Claude Clinet,[c] Elisabet Duñach,[c] and Miguel A. Maestro[d]

Keywords: Molybdenum / Chiral oxazolines / Selective epoxidation / Oxo peroxo complexes / Catalysis

New seven-coordinate oxo(peroxo)molybdenum(VI) complexes with bidentate chiral oxazolines, anionic κ^2-*N*,*O* (**V**) and neutral κ^2-*N*,*N* (**VI**), have been prepared and fully characterised by NMR spectroscopy and single-crystal X-ray diffraction studies. Dimetallic dioxo(μ-oxo)molybdenum(VI) compounds containing oxazolinylpyridine ligands **II**–**IV** have also been synthesised. NMR studies showed the presence of several isomers (up to six species) due to the Mo–O–Mo bridge angle and the unsymmetrical nature of the N,N ligand. The roles of mono- (**I**, **V** and **VI**) and dimetallic (**II**) oxomolybdenum(VI) complexes in the catalytic epoxidation of cyclooctene, norbornene and (*R*)-limonene have been studied. The high activity of the oxomono(peroxo) precursor **V** containing the hemilabile oxazolinylphenolate, in contrast to the unexpected low activity for the oxobis(peroxo) species **VI**, could be justified by the inertness observed for the oxazolinylpyridine ligand. In addition, the dimetallic system **II** afforded high selectivity towards limonene epoxide formation (*trans*/*cis*-**10** ratio up to 9:1).

(© Wiley-VCH Verlag GmbH & Co. KGaA, 69451 Weinheim, Germany, 2004)

Introduction

High-valent oxometal species have demonstrated the ability to catalyse the oxidation of a variety of organic substrates by homogeneous as well as heterogeneous routes.[1,2] In particular, the Mo-catalysed alkene-to-epoxide conversion has received most attention due to its industrial interest. However, the oxygen transfer mechanism is still a controversial subject and three main hypotheses have dominated the discussion. Mimoun suggested that the olefin coordinates to the metal atom before subsequent insertion into the η^2-Mo−O_2 bond to form a five-membered alkyl peroxide metallacycle.[3,4] Coordination of the olefin to the metal centre makes the olefin electrophilic and thus ready for further reaction with a peroxo group acting as a nucleophile. On the other hand, Sharpless proposed a concerted reaction mechanism involving a direct attack by the olefin on the peroxo oxygen atom (with a three-membered ring intermediate).[5] In this case, the coordinated peroxo group is thought to have a sufficiently increased electrophilic character by decreasing the negative charge on the peroxo oxygen atoms. A "hybrid" mechanism was proposed by Jørgensen and Hoffman in which intramolecular slipping of the olefin after coordination to the metal atom, which depends on their relative orientation, was believed to form a three-membered metallacycle intermediate.[6,7]

In terms of the spectator part of the catalyst molecule, S-, N- and O-donor ligands have been mainly used because of their stability towards oxidation processes. However, under catalytic conditions, they frequently suffer partial decoordination.[8,9] This fact discourages their use as selective catalysts in certain organic processes.

Oxazolines have been used as stabilising agents for many transition metals based on their robustness under a variety of reaction conditions when coordinated.[10] Consequently, they have been frequently employed in asymmetric catalytic organic transformations.[11,12]

We have been carrying out research with dioxomolybdenum(VI) compounds (type-**I** complexes, Figure 1) and we herein describe the first examples of oxo(peroxo) and dioxodimetallic molybdenum complexes containing chiral bidentate oxazoline ligands (Figure 1). Both types of systems have been explored as catalytic precursors in olefin epoxid-

[a] Departament de Química Inorgànica, Universitat de Barcelona, Martí I Franquès 1−11, 08028 Barcelona, Spain
Fax: (internat.) + 34-934907725
E-mail: montserrat.gomez@qi.ub.es
[b] Departamento de Química, Universidad Simón Bolívar, Baruta 89000, Caracas 1081, Venezuela
[c] Laboratoire de Chimie Bioinorganique UMR 6001, Université de Nice-Sophia Antipolis, 06108 Nice Cédex 2, France
[d] Departamento de Química Fundamental, Universidade da Coruña, Campus da Zapateira, s/n, 15071 A Coruña, Spain

 © 2004 Wiley-VCH Verlag GmbH & Co. KGaA, Weinheim **DOI: 10.1002/ejic.200400331**

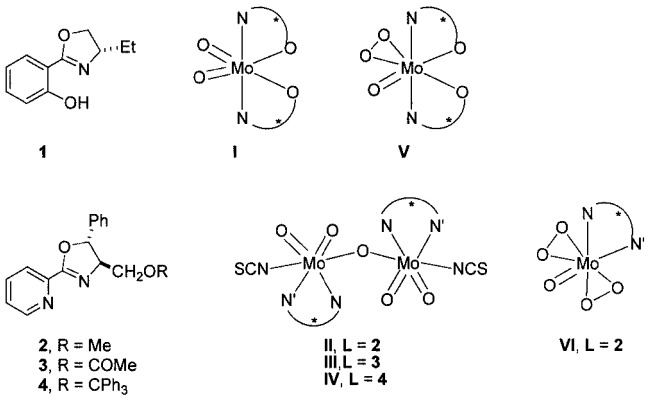

Figure 1. Oxazoline chiral ligands **1**−**4** and oxomolybdenum complexes **I**−**VI**

ation processes. Related structural studies, especially in solution, afforded new insight into the nature of the catalytic species involved.

Results and Discussion

Dimetallic Dioxomolybdenum Complexes II−IV

Dimetallic bis(oxazolinylpyridine)dioxo(μ-oxo)dimolybdenum(VI) complexes **II**−**IV** with oxazolinylpyridines of the general formula (μ-O)[MoO_2(NCS)(κ²-*N*,*N*-**L**)]₂ (**L** = **2**−**4**) were prepared according to the methodology previously described (Scheme 1, a).[13] A dichloromethane solution of the ligand **2**−**4** was added to an acidic aqueous solution of $Na_2MoO_4{\cdot}2H_2O$ and KSCN under phase-transfer conditions, affording the corresponding complexes in good yields (ca. 70%). Using the same conditions, the analogous complexes containing bis(oxazoline) ligands could not be isolated due to the oxazoline moiety decomposing to give amide derivatives. Modifications of the experimental conditions (higher pH values, different solution concentrations) were also unsuccessful.[14]

The IR spectra of **II**−**IV** show the characteristic functional group absorptions: a very strong band for NCS at ca. 2050 cm^{-1}, 1658 cm^{-1} for the oxazoline imine bond, two strong bands at 906 and 941 cm^{-1} for Mo=O as well as 772 cm^{-1} for the μ-oxo moiety (Mo−O−Mo). In the positive FAB-MS spectra, despite the absence of the parent ion, fragments such as $[Mo_2O_5(NCS)\mathbf{L}_2]^+$, $[Mo_2O_4(NCS)\mathbf{L}]^+$ and $[Mo_2O(NCS)\mathbf{L}]^+$ indicate the dimetallic nature of the complexes.

Efforts to grow single crystals were unsuccessful, probably due to the existence of some isomers (see below).

Studies in solution showed the presence of several species and the 2D NOESY spectra revealed exchange signals among them all. In the case of **II**, the signals were well enough separated to allow us to suggest the presence of at least six species (relative ratios 8.0:5.6:3.3:2.5:1.6:1) in $CDCl_3$. The most abundant isomer (ca. 40%) shows two equivalent oxazolinylpyridine fragments. The other isomers, however, show signals indicating that the two bidentate ligands are not chemically equivalent. In the case of symmetrical ligands, as in the 4,4′-disubstituted bipyridine compound (μ-O)[MoO_2(NCS)(4,4′-*tert*-butyl-2,2′-bpy)]₂, two isomers were formed depending on the Mo−O−Mo bridge angle (180° and ca. 156°, respectively, relative ratios 44:56).[13] The formation of more than two species would be expected for nonsymmetrical oxazolinylpyridines **2**−**4** and the major isomer exhibiting the symmetrical structure must correspond to the conformer with an Mo−O−Mo angle of 180°. In Figure 2, the arrangements of the three nonequivalent isomers are depicted with an Mo−O−Mo bridge angle of 180° and where the isocyanate ligand is opposite to the bridging oxygen atom. In addition, the corresponding isomers with an Mo−O−Mo angle less than 180°, could also be expected.

Monometallic Oxo(peroxo)molybdenum Complexes V, VI

New seven-coordinate monometallic oxo(peroxo)molybdenum(VI) complexes **V**, **VI** containing chiral oxazoline ligands were prepared by previously reported methods.[15] For the anion of **1**, an oxo(peroxo) compound with two bidentate N,O ligands, $[MoO(O_2)(\kappa^2\text{-}N,O\text{-}\mathbf{L})_2]$ (**V**), was isolated while for the oxazolinylpyridine **2**, the oxobis(peroxo)

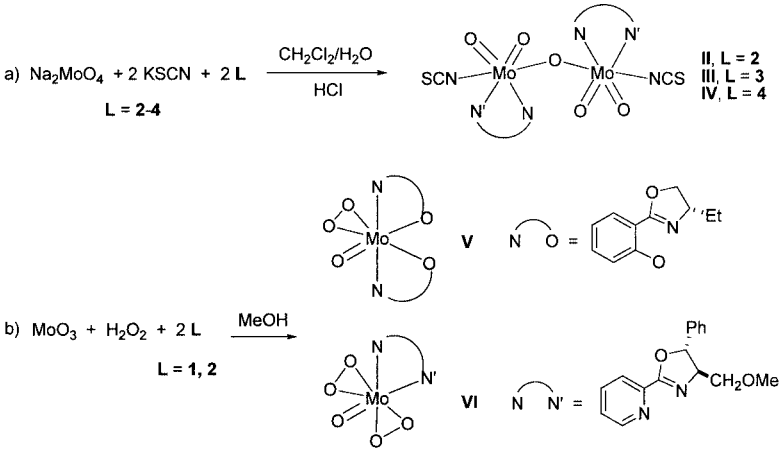

Scheme 1. Synthesis of dioxo(μ-oxo) dimetallic (**II**−**IV**) (a) and oxo(peroxo) monometallic (**V** and **VI**) (b) molybdenum(VI) complexes

 © 2004 Wiley-VCH Verlag GmbH & Co. KGaA, Weinheim

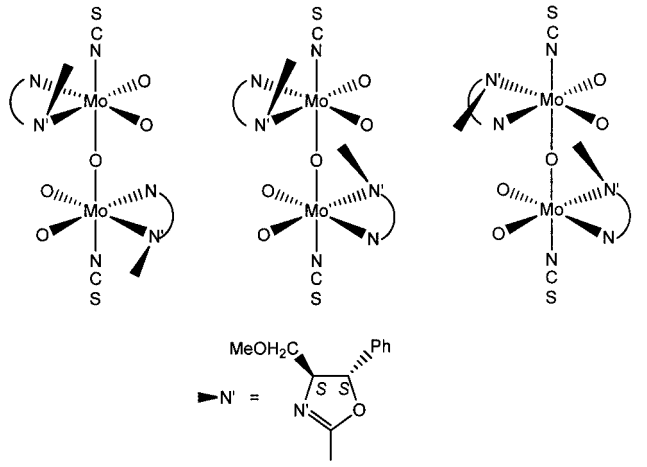

Figure 2. Isomers of dimetallic complex **II** containing the pure chiral oxazolinylpyridine ligand **2**, with an Mo−O−Mo angle of ca. 180°

complex $[MoO(O_2)_2(\kappa^2\text{-}N,N\text{-}\mathbf{2})]$ (**VI**) was produced (Scheme 1, b).

MoO_3 was dissolved in H_2O_2 (30%) to prepare an aqueous solution of $[Mo(O)(O_2)_2(H_2O)_2]$ (pH = 4). A methanol solution of the oxazoline **1**−**2** was then added and after addition of diethyl ether, **V** and **VI** were isolated as yellow solids, both stable in the solid state and in solution. No corresponding amide derivatives of the oxazolines were observed under these conditions. Attempts to isolate the oxo(peroxo) species **V** by perhydrolysis of **I** were unsuccessful.

In the solid state, the IR spectra of **V** and **VI** show two characteristic strong absorption bands at 962 (Mo=O) and 865−863 (O−O) cm^{-1}, as well as a very strong band at 1636−1630 (C=N) cm^{-1} corresponding to the oxazoline imine bond.

Single crystals of **V** and **VI** were obtained from dichloromethane/diethyl ether solutions (Figure 3). In Table 1, selected bond lengths and angles are collected. In **V**, the molybdenum atom is heptacoordinated by an oxo, a peroxo and two bidentate anionic phenolate oxazoline ligands. The geometry around the metal atom can be described as pseudo-pentagonal bipyramidal with the axial sites occupied by the oxo group O(1) and one of the phenolate oxygen atoms O(4). Thermal disorder is present around the Mo−oxo unit with high anisotropic parameters. The disorder was modelled with the two positions O(1A) and O(1B) having partial occupancies of 0.46(3) and 0.54(3), respectively. The peroxo bond O(2)−O(3) (1.3 Å) is shorter than usual (ca. 1.4−1.5 Å). This fact can be attributed to the relatively high thermal parameter for O(2) (anisotropic displacement parameter 0.148) compared with those of the phenolate and oxazolinyl oxygen atoms (0.05−0.07). Consequently, the distance is inaccurate. The remaining coordinating atoms are located in the equatorial plane in an almost coplanar arrangement, as indicated by the dihedral angles: N(1)−O(6)−N(2)−O(3) 4.60°, O(6)−N(2)−O(3)−O(2) 0.93°, N(2)−O(3)−O(2)−N(1) 5.43°, O(3)−O(2)−N(1)−O(6) 8.16° and O(2)−N(1)−O(6)−N(2) 6.11°. The other bond lengths and angles are similar to those in the only related published complex $[MoO(O_2)(8\text{-quinolate})_2]$.[16] In our case, the two nitrogen atoms are located almost opposite to each other [N(1)−Mo(1)−N(2) = 158.96°], while in the example reported in ref.[16], the two nitrogen atoms are vicinal (N−Mo−N = 81.91°).

In structure **VI**, the molybdenum atom is also heptacoordinated by an oxo group, two peroxo moieties and one bidentate oxazolinylpyridine **2** and the geometry around the metal atom can also be described as pseudo-pentagonal bipyramidal, with the axial sites occupied by the oxo group O(1) and the nitrogen atom from the pyridine moiety of the oxazoline ligand N(1). The remaining coordinating atoms are located in the equatorial plane in a nearly coplanar distribution, as indicated by the dihedral angles O(3)−O(2)−O(4)−O(5) 0.991°, N(2)−O(5)−O(4)−O(2) 1.596°, O(2)−O(3)−N(2)−O(5) 3.143° and O(3)−N(2)−O(5)−O(4) 2.460°. These angles are similar to other heptacoordinate oxobis(peroxo)molybdenum complexes containing bipyridine[17,18] and pyrazolylpyridine[19−21] derivatives. In the X-ray diffraction studies of the N,N-unsymmetrical ligands, the pyridine fragment is in an equatorial position while in **VI** it is axial. Intramolecular non-bonding O···H distances are longer than 3 Å.

The ^1H NMR spectrum of a freshly prepared solution of **V** in $CDCl_3$ revealed that the two anionic N,O-bidentate moieties are nonequivalent. A second set of signals appeared after approximately 12 h resulting in a relative ratio between the two molybdenum species of ca. 10:1. In deuterated acetone, the formation of the second species is favoured (relative ratio 4:1) and no changes were observed even after several days. This solvent dependence turned out to be similar to that observed for the analogous dioxomolybdenum complex **I** where partial decoordination of the oxazoline ligand takes place in coordinating solvents.[9]

For the major compound, important differences in the chemical shifts were observed. Compared with the free oxazoline [δ(H) = 4.10 ppm] the stereo-centre proton signal shifted remarkably downfield [δ(H) = 5.06 and 5.73 ppm]. This deshielding can be attributed to interaction with the oxo and peroxo groups, as shown by the average interatomic distances H(8A)···O=Mo and H(19A)···O_2−Mo from the crystallographic data, ca. 2.85 and 2.25 Å, respectively.

NMR studies of **VI** in solution clearly indicated only one compound in coordinating solvents. The chemical shifts of the oxazoline protons moved downfield (Δδ = 0.2−0.7 ppm) relative to those of the free oxazoline **2**. The coordination of the oxazolinylpyridine ligand is limited to the pyridine nitrogen atom located in an axial position opposite to the strong *trans*-directing oxo group in agreement with the X-ray study, although the thermodynamically favoured isomer should bear the poorer σ-donor moiety *trans* to the oxo group. In addition, the stereochemical behaviour is similar to that observed for oxobis(peroxo)molybdenum complexes with *N*,*N*-pyrazolylpyridines,[22] but oxazolinylpyridine dissociation was not observed.

 © 2004 Wiley-VCH Verlag GmbH & Co. KGaA, Weinheim

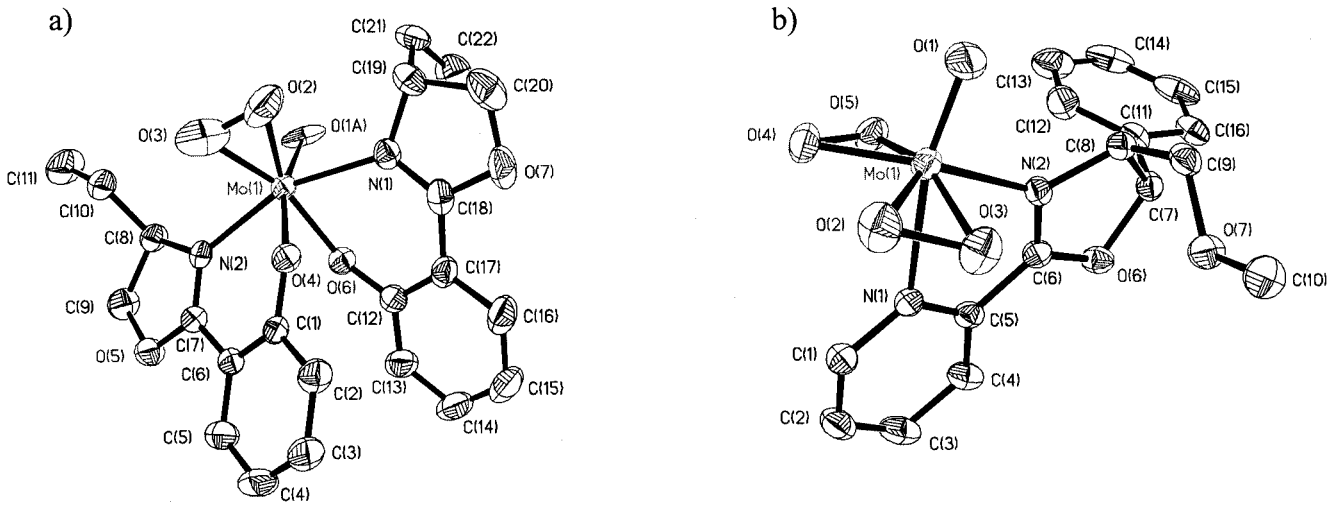

Figure 3. ORTEP diagrams of the molecular structures of **V** (a) and **VI** (b); hydrogen atoms are omitted for clarity

Table 1. Selected bond lengths [Å] and bond angles [°] for **V** and **VI** (with esds in parentheses)

	V	**VI**
Mo−O(1)	1.732(16)[a]	1.674(2)
Mo−O(2)	1.946(6)	1.912(2)
Mo−O(3)	1.979(7)	1.940(2)
Mo−O(4)	2.044(3)	1.928(2)
Mo−O(5)	–	1.9460(19)
Mo−O(6)	2.029(3)	–
Mo−N(1)	2.161(4)	2.427(2)
Mo−N(2)	2.167(3)	2.1524(18)
O(2)−O(3)	1.312(7)[b]	1.459(3)
O(4)−O(5)	–	1.474(3)
O(1)−Mo−O(4)	160.35(6)[a]	105.66(12)
O(1)−Mo−N(1)	105.3(5)[a]	164.45(10)
O(1)−Mo−N(2)	94.7(6)[a]	94.17(10)
O(1)−Mo−O(3)	101.7(4)[a]	102.96(11)
O(1)−Mo−O(5)	–	101.78(12)
N(1)−Mo−N(2)	158.96(13)	70.34(7)
O(4)−Mo−O(6)	81.16(12)	–
O(4)−Mo−O(5)	–	44.73(8)
O(6)−Mo−N(1)	80.23(14)	–
O(2)−Mo−O(1)	100.9(4)[a]	106.07(12)
O(2)−Mo−O(3)	39.1(2)	44.52(10)
N(1)−Mo−O(6)	80.34(13)	–
O(6)−Mo−N(2)	83.34(13)	–
N(2)−Mo−O(3)	80.4(2)	86.97(9)

[a] Average bond length and angle. [b] See X-ray discussion in the text.

Olefin Epoxidation Catalysed by Oxomolybdenum Complexes

The dioxo mono- and dimetallic complexes **I** and **II**, respectively, were tested as catalytic precursors for the epoxidation of cyclooctene (**5**), norbornene (**6**) and (*R*)-limonene (**7**), using *t*BuOOH in water as the oxidant at room temperature (Scheme 2). When reactions were performed using *t*BuOOH in decane, lower conversions were obtained. Catalytic reactions were carried out with and without solvent (toluene). Table 2 lists the catalytic results. In the case of **I**, activities were higher in the presence of solvent (Entries 1, 3, 5 and 6) but for **II** these differences were not significant (Entries 2, 4, 7 and 8). For both systems, cyclooctene oxide **8** and *exo*-norbornene oxide **9** were the only products obtained and the monometallic system **I** was more active (up to 57% conversion, Entry 3) than dimetallic **II** (Entries 1 and 3 versus 2 and 4). In the case of limonene oxidation, a mixture of products was detected, *trans*/*cis*-limonene oxide (**10**), the corresponding double epoxide (**11**) and alcohols (Scheme 2). Activity (substrate conversion) and chemoselectivity (ratio **10**/**11**) are almost the same for both catalytic systems (Entries 5−8). Ring epoxide opening to afford alcohols was lower for **I** than for **II** (alcohols/epoxide = 0−0.1 for **I** and 0.2−0.5 for **II**) (Entries 5 and 6 versus 7 and 8). An outstanding diastereoisomeric induction was observed for **10** when **II** was used (*trans*/*cis*-**10** up to 9:1 for 77% of olefin conversion, Entry 8) but no discrimination occurred with **I** (Entries 5 and 6).

The absence of exocyclic oxide formation suggests that the double epoxide **11** is probably produced by epoxidation of **10**. When *trans*/*cis*-**10** (ratio ca. 1:1) was used as the substrate and **II** as the catalyst, under the same experimental conditions, a 45% conversion to **11** and alcohols (**11**/alcohols ≈ 4:1) was obtained (Scheme 3). The remaining **10**, enriched in one of the diastereoisomers (relative ratio *trans*/*cis*-**10** > 98:2), indicates that *cis*-**10** reacts faster than *trans*-**10**. However, when monometallic complex **I** was used as a catalytic precursor, no kinetic resolution occurred.

Oxo(peroxo)molybdenum species are known key intermediates in epoxidation processes. The mono- and bis-

 © 2004 Wiley-VCH Verlag GmbH & Co. KGaA, Weinheim

Table 2. Results of epoxidation of olefins **5**−**7** with *t*BuOOH as an oxidant catalysed by molybdenum complexes **I**, **II**, **V** and **VI** (Scheme 2)

Entry[a]	Complex	Olefin	Conv. (%)[b]	**10** (%)[c] (*trans*/*cis*)	**11** (%)[d]	Alcohols (%)[d]	Alcohols/epoxides
1	**I**	**5**	52 (27) (41)	−	−	−	−
2	**II**	**5**	36 (40) (8)	−	−	−	−
3	**I**	**6**	57 (39) (40)	−	−	−	−
4	**II**	**6**	34 (20) (20)	−	−	−	−
5	**I**	(*R*)-**7**	62 (35)	54 (54:46)	2.0	6.0	0.1
6[e]	**I**	(*R*)-**7**	58 (35)	54 (60:40)	4.0	0	0
7	**II**	(*R*)-**7**	64 (46)	50 (80:20)	4.0	10.0	0.2
8[e]	**II**	(*R*)-**7**	77 (45)	45 (90:10)	6.0	26.0	0.5
9	**V**	**5**	95 (92) (83)	−	−	−	−
10	**VI**	**5**	15 (38)	−	−	−	−
11	**V**	(*R*)-**7**	79	62 (60:40)	2.0	15.0	0.2
12	**VI**	(*R*)-**7**	22	22 (50:50)	0	0	0

[a] Catalytic conditions: 0.025 mmol of Mo (complexes **I**, **II**, **V** and **VI**), 1 mmol olefin (**5**−**7**) and 1.5 mmol of *t*BuOOH (8 M in water) in 1 mL of toluene at room temp. for 22 h; 0.2−0.4 mmol of undecane (as external standard) was used to quantify the catalytic reaction. [b] Conversion percentage based on the substrate determined by GC; in parentheses is the conversion obtained without solvent; in italics the conversions obtained using *t*BuOOH in decane (5.5 M). [c] In parentheses, the ratio of *trans*/*cis* of endocyclic epoxide **10**. [d] Determined by GC. [e] Reaction carried out without solvent.

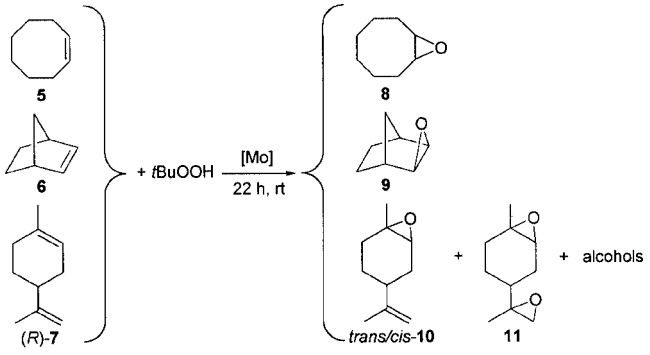

Scheme 2. Cyclooctene (**5**), norbornene (**6**) and (*R*)-limonene (**7**) epoxidation catalysed by **I**, **II**, **V** and **VI** using *t*BuOOH as an oxidant; olefin/*t*BuOOH/Mo = 40:60:1

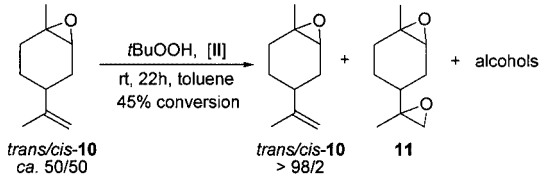

Scheme 3. *trans*/*cis*-Limonene oxide (**10**) epoxidation catalysed by **II** using *t*BuOOH as an oxidant; olefin/*t*BuOOH/Mo = 40:60:1

(peroxo) complexes **V** and **VI** were tested for oxidation of **5** and (*R*)-**7**. It was found that **V** was the most active of all systems studied (Entries 9 and 11) achieving 95% cyclooctene conversion (Entry 9). The higher activities observed for oxo(peroxo) species **V** than for the dioxo compound **I** suggest that the former is the catalytically active species and **I** is its precursor. On the contrary, **VI** gave the lowest conversions (Entries 10 and 12). Similar to the dioxo monometallic complex **I**, diastereoisomeric induction of (*R*)-limonene did not take place for either **V** or **VI**.

Mechanistic Aspects of Olefin Epoxidation

The structural studies carried out provided evidence of a certain relationship between the lability of the molybdenum centre and catalytic olefin epoxidation. Despite heptacoordinated oxobis(peroxo)molybdenum complexes having been reported to be fairly good epoxidation catalysts, the unexpected low activity [in the oxidation of cyclooctene and (*R*)-limonene] observed for **VI** can be attributed to the nonlability of the oxazolinylpyridine ligand, as observed by NMR spectroscopy (see above). However, in the case of **V**, the high activity obtained is in accordance with partial decoordination of the *N*,*O*-oxazolinylphenolate ligand, already observed for its precursor **I**[9] and for oxobis(peroxo) Thiel-type complexes.[19−22] The ability to generate a coordination vacancy at the molybdenum atom can then be responsible for the differences in the catalytic behaviour of **V** and **VI**. Furthermore, the remarkably higher activity obtained with **II** compared with **VI**, with both systems containing the nonlabile bidentate ligand **2**, is due to the facile formation of a vacant site in **II** by isothiocyanate dissociation. Thus, metallic species with unsaturated coordination environments will favour either the olefin or the oxidant to approach the metal. With regards to the equimolar *trans*/*cis*-**10** mixture obtained in the epoxidation of (*R*)-limonene using monometallic catalysts, the species directly coordinated to the molybdenum centre is probably *t*BuOOH instead of the olefin.

Information derived from NMR experiments and catalytic reactivity patterns allows us to propose the mechanism shown in Scheme 4. The oxo(peroxo)molybdenum species **V** can easily form a vacant site due to the hemilabile nature of the oxazolinylphenolate ligand (**A**). Further coordination of *t*BuOOH (**B**) leads to the formation of a transition state (**TS**), in which the olefin approaches towards the *tert*-butyl peroxide fragment, producing the epoxide and concomitant elimination of *tert*-butyl alcohol, the active catalytic species **V** being regenerated.

On the other hand, the unexpected selectivity observed with the dimetallic catalytic system **II** in both oxidations, (*R*)-limonene (**7**) (Entries 7 and 8, Table 2) and limonene epoxide **10** (Scheme 3), can only just be explained by the

 © 2004 Wiley-VCH Verlag GmbH & Co. KGaA, Weinheim

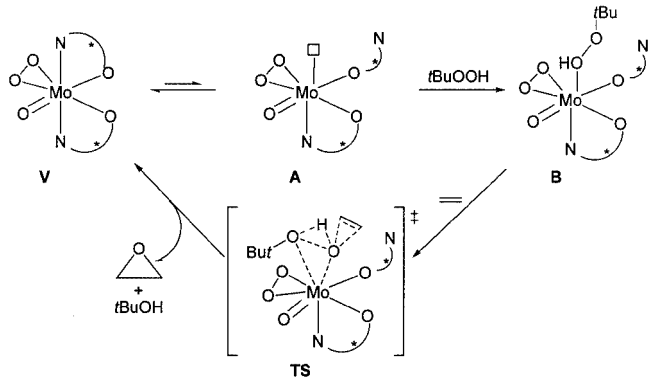

Scheme 4. Mechanistic proposal for olefin epoxidation catalysed by seven-coordinate molybdenum species containing hemilabile ligands

mechanism described. Nevertheless, as stated above, the nonlability of the oxazolinylpyridine ligand and the presence of a vacant site can favour the direct olefin coordination to the metal atom. Stereoselectivity control in the organic process is then possible.

Further reactivity studies with dimetallic molybdenum species involved in catalytic olefin epoxidations are in progress.

Experimental Section

General Remarks: Solvents were purified by standard procedures and distilled under nitrogen. $Na_2MoO_4{\cdot}2H_2O$ (Probus), MoO_3 (Strem), aqueous *t*BuOOH (8 M; Fluka), *t*BuOOH in decane solution (5.5 M; Fluka), cyclooctene (Fluka), norbornene (Aldrich) and (*R*)-limonene (Aldrich) were used as purchased. Ligands **1**,[23] **2**−**4**[24,25] and complex **I**[9] were prepared as described previously. NMR spectra (in $CDCl_3$) were recorded with Bruker Avance600, Varian XL-500, Varian Gemini or Bruker DRX 250 spectrometers. Chemical shifts are reported downfield from standards. IR spectra were recorded with a Nicolet 520 FT-IR or a Bruker IFS 55 FTIR spectrometer. FAB mass spectra were obtained with a Micromass VG-Quattro instrument. The GC-MS analyses were performed with a Hewlett−Packard 5890 Series II gas chromatograph (50 m Ultra 2 capillary column) interfaced with a Hewlett−Packard 5971 mass-selective detector. Elemental analyses were carried out by the Serveis Cientifico-Tècnics de la Universitat de Barcelona with an Eager 1108 microanalyser.

μ-Oxobis{[(3′*S*,4′*S*)-2-(3′,4′-dihydro-4′-methoxymethyl-2′-oxazolyl-3′-phenyl)pyridine-*N*,*N*](isothiocyanato)dioxomolybdenum(VI)} (II): HCl (1 M 1.7 mmol, 1.7 mL) was slowly added, with stirring, to a mixture of aqueous solutions (10 mL) of $Na_2MoO_4{\cdot}2H_2O$ (100 mg, 0.413 mmol) and KNCS (160 mg, 1.652 mmol). After 15 min, the oxazolinylpyridine **2** (110.8 mg, 0.413 mmol) in CH_2Cl_2 (20 mL) was added to the yellow solution and vigorously stirred for 45 min. The organic layer was extracted, washed with water (3 × 10 mL) and dried with Na_2SO_4. The solvent was removed under reduced pressure. The solid obtained was washed with diethyl ether (3 × 20 mL) and dried under vacuum. Yield: 0.161 g (77%). $C_{34}H_{32}Mo_2N_6O_9S_2$ (924.68): calcd. C 43.68, H 3.46, N 9.09, S 6.93; found C 43.62, H 3.29, N 8.90, S 6.84. MS (FAB positive): *m*/*z* = 867 [M − NCS]. IR (KBr): $\tilde{\nu}$ = 2045 (st, C=N_{NCS}), 1658 (st, C=N), 941 and 906 (Mo=O) cm^{-1}. ^1H NMR (600 MHz): δ_{major} = 8.87 (d, *J* = 4.8 Hz, 1 H), 8.18 (pt, *J* = 7.8 Hz, 1 H), 8.06 (d, *J* = 7.6 Hz, 1 H), 7.4−7.2 (m, 5 H), 6.02 (d, *J* = 7.0 Hz, 1 H), 4.45 (m, 1 H), 3.87 (m, 1 H), 3.78 (dd, *J* = 10.0, 3.4 Hz,1 H), 3.40 (s, 3 H) ppm.

μ-Oxobis{[(3′*S*,4′*S*)-2-(4′-acetoxymethyl-3′,4′-dihydro-2′-oxazolyl-3′-phenyl)pyridine-*N*,*N*](isothiocyanato)dioxomolybdenum(VI)} (III): An analogous procedure to that described for the preparation of **II** was used, replacing **2** with **3**.Yield: 0.443 g (75%). $C_{38}H_{36}Mo_2N_6O_{11}S_2$ (1008.37): calcd. C 44.02, H 3.48, N 8.11, S 6.18; found C 44.50, H 3.65, N 7.80, S 5.94. MS (FAB positive): *m*/*z* = 1010 [M], 922 [M − NCS − 2 O]. IR (KBr): $\tilde{\nu}$ = 2056 (st, C=N_{NCS}), 1658 (st, C=N) and, 940 and 910 (Mo=O) cm^{-1}.

μ-Oxobis{[(3′*S*,4′*S*)-2-(3′,4′-dihydro-2′-oxazolyl-3′-phenyl-4′-tritylmethyl)pyridine-*N*,*N*](isothiocyanato)dioxomolybdenum(VI)} (IV): An analogous procedure to that described for the preparation of **II** was used, replacing **2** with **4**. Yield: 0.302 g (68%). $C_{70}H_{56}Mo_2N_6O_9S_2$ (1381.26): calcd. C 60.87, H 4.06, N 6.09, S 4.64; found C 59.75, H 3.98, N 5.99, S 5.03. MS (FAB positive): *m*/*z* = 780 [M − NCS − 3 O − **4**]. IR (KBr): $\tilde{\nu}$ = 2043 (st, C=N_{NCS}), 1658 (st, C=N) and, 942 and 911 (Mo=O) cm^{-1}.

Bis[(4′*R*)-2-(4′-ethyl-3′,4′-dihydro-2′-oxazolyl)phenolato-*N*,*O*]oxo(peroxo)molybdenum(VI) (V): MoO_3 (0.285 g, 1.980 mmol) was added in portions to an aqueous H_2O_2 solution (30%, 5 mL) at room temperature. The mixture was stirred for 20 min and warmed to 40 °C for 40 min. The reaction mixture was filtered, the yellow solution was cooled to 10 °C and a solution of **1** (0.384 g, 2.00 mmol) in CH_3OH was added. The mixture was stirred at 20 °C for 30 min and then at 0 °C for 16 h. It was concentrated under reduced pressure to approximately 5 mL and diethyl ether was added (20 mL). The yellow precipitate obtained was filtered and recrystallized from CH_2Cl_2/diethyl ether (3:1). Yield: 0.405 g (39%). M.p. 197 °C. $C_{22}H_{24}MoN_2O_7$ (524.38): calcd. C 50.39, H 4.61, N 5.34; found C 50.34, H4.85, N 5.17. MS (FAB positive): *m*/*z* = 525. IR (KBr): $\tilde{\nu}$ = 1630 (st, C=N), 962 (st, Mo=O), 865 (st, O−O), 758 (asymm. st Mo−O), 582 (symm. st Mo−O) cm^{-1}. ^1H NMR (500 MHz): δ_{major} = 7.68 (dd, *J* = 8.5, 1.5 Hz, 1 H), 7.53 (dd, *J* = 8.0, 1.5 Hz, 1 H), 6.93 (m, 1 H), 6.88 (m, 1 H), 6.56 (m, 2 H), 6.04 (dd, *J* = 8.5, 0.5 Hz, 1 H), 5.77 (dd, *J* = 8.5, 0.5 Hz, 1 H), 5.73 (m, 1 H), 5.06 (m, 1 H), 4.92 (dd, *J* = 8.5, 6.5 Hz, 1 H), 4.88 (dd, *J* = 8.5, 5.5 Hz, 1 H), 4.60 (dd, *J* = 8.5, 5.5 Hz, 2 H), 4.52 (dd, *J* = 8.5, 6.5 Hz, 1 H), 2.45 (m, 1 H), 2.20 (m, 1 H), 2.15 (m, 1 H), 2.02 (m, 1 H); 1.07 (t, *J* = 7.5 Hz,, 3 H), 1.01 (t, *J* = 7.5 Hz, 3 H) ppm. ^{13}C NMR (75 MHz): δ = 167.6 (C=N), 167.4 (C=N), 166.2 (C), 164.0 (C), 135.4 (CH), 135.0 (CH), 129.1 (CH), 128.5 (CH), 120.9 (CH), 120.0 (CH), 117.8 (CH), 117.5 (CH), 112.7 (C−O), 111.3 (C−O), 73.1 (CH_2−O), 72.7 (CH_2−O), 70.0 (CH), 64.6 (CH), 28.1 (CH_2), 26.5 (CH_2), 9.1 (CH_3), 8.2 (CH_3) ppm. δ_{minor} = 8.08 (dd, *J* = 8, 1 Hz, 1 H), 7.78 (dd, *J* = 8 Hz, 1 H), 7.65 (m, 1 H), 7.50 (m, 1 H), 7.36 (pt, *J* = 7.5 Hz 1 H), 7.05 (m, 2 H), 6.11 (d *J* = 8.5 Hz, 1 H), 4.69 (pt, *J* = 10 Hz, 1 H), 4.44 (dd, *J* = 8.5, 5 Hz, 1 H), 4.28 (pt, *J* = 10 Hz, 1 H), 3.77 (dd, *J* = 5.0, 11. 5 Hz, 1 H), 1.90 (m, 2 H), 0.95 (t, *J* = 7.5 Hz, 3 H), 0.88 (t, *J* = 7.5 Hz, 3 H) ppm.

[(3′*S*,4′*S*)-2-(3′,4′-Dihydro-4′-methoxymethyl-2′-oxazolyl-3′-phenyl)pyridine-*N*,*N*]oxobis(peroxo)molybdenum(VI) (VI): MoO_3 (0.252 g, 1.75 mmol) was added in portions to an aqueous H_2O_2 solution (30%, 5 mL). The mixture was stirred for 20 min and warmed to 40 °C for 4 h. The reaction mixture was filtered and to the yellow solution was added **2** (0.470 g, 1.75 mmol) in CH_3OH (20 mL). The mixture was stirred at room temperature for 1 h and then concentrated under reduced pressure to 1 mL. Ethanol was

 © 2004 Wiley-VCH Verlag GmbH & Co. KGaA, Weinheim

Table 3. Crystal data for **V** and **VI**

	V	**VI**
Empirical formula	$C_{22}H_{24}MoN_2O_7$	$C_{16}H_{16}MoN_2O_7$
Formula mass	524.37	444.25
Crystal size [mm]	0.50 × 0.16 × 0.10	0.27 × 0.10 × 0.08
Temperature [K]	298(2)	298(2)
Crystal system	orthorhombic	monoclinic
Space group	*P*2(1)2(1)2(1)	*P*2(1)
a [Å]	6.7608(8)	7.2720(4)
b [Å]	9.9119(11)	14.6377(8)
c [Å]	33.456(4)	8.4005(4)
β [°]	90	90.6780(10)
V [Å^3]	2242.0(4)	894.13(8)
Z	4	2
Density (calculated) [Mg·m^{-3}]	1.554	1.650
Absorption coefficient [mm^{-1}]	0.631	0.774
θ range for data collection [°]	2.14−26.38	2.42−28.28
Reflections collected	12971	5751
Data/restraints/parameters	4560/0/299	3392/1/235
Independent reflections	4560 [*R*(int) = 0.0294]	3392 [*R*(int) = 0.0162]
Max./min. transmission	0.9396/0.7433	0.9407/0.8182
Final *R*(int) [$I > 2\sigma(I)$][a]	*R*1 = 0.0388, *wR*2 = 0.1020[b]	*R*1 = 0.0211, *wR*2 = 0.0526[b]
R int (all data)	*R*1 = 0.0482, *wR*2 = 0.107	*R*1 = 0.0227, *wR*2 = 0.0535
GOF on F^2	1.061	1.025
Absolute structure parameter	−0.02(5)	0.00(3)
Largest diff. peak/hole [e·Å^{-3}]	0.565/−0.481	0.201/−0.490

[a] $R1 = \Sigma||F_o| - |F_c||$ and $wR2 = \{\Sigma[w(F_o^2 - F_c^2)]/\Sigma[w(F_o^2)^2]\}^{1/2}$. [b] The weighting scheme employed was $w = [\sigma^2(F_o^2) + (aP)^2 + bP]^{-1}$ and $P = (|F_o|^2 + 2|F_c|^2)/3$.

added (2 × 20 mL) and removed each time. The yellow solid obtained was recrystallized from CH_2Cl_2/hexane (9:1). Yield: 0.234 g (30%). M.p. 146 °C. $C_{16}H_{16}MoN_2O_7$ (444.25): calcd. C 43.26, H 3.63, N 6.31; found C 47.28, H 5.05, N 6.31. MS (ES): *m*/*z* = 445 [M + 1], 415 [M − O_2]. IR (KBr): ṽ = 1636 (st, C=N), 962 (st, Mo=O), 863 (st, O−O), 769 (asymm. st Mo−O) and 581 (symm. st Mo−O) cm^{-1}. ^{1}H NMR (400 MHz): δ = 8.39 (pd, *J* = 5.2 Hz, 1 H), 7.94 (m, *J* = 1.6 Hz, 8 Hz, 2 H), 7.55 (m, *J* = 2 Hz, 1.6 Hz, 1 H), 7.49 (s, 5 H), 6.34 (d, *J* = 6.8 Hz, 1 H), 5.01 (m, 1 H), 4.30 (dd, *J* = 3.6 Hz; *J* = 10.8 Hz, 1 H), 3.98 (dd, *J* = 2.8 Hz; *J* = 10.8 Hz, 1 H), 3.57 (s, 3 H) ppm. ^{13}C NMR (75 MHz): δ = 169.8 (C=N), 148.0 (CH), 139.2 (CH), 139.1 (C), 135.9 (C), 130.4 (CH), 129.6 (CH), 129.3 (CH), 126.5 (CH), 124.6 (CH), 89.9 (CH), 73.4 (CH), 70.7 (CH_2−O), 59.6 (CH_3−O) ppm.

Molybdenum-Catalysed Olefin Epoxidation: The precursor (0.025 mmol of complex: 12.7 mg for **I**, 11.6 mg for **II**, 13.1 mg for **V** and 11.1 mg for **VI**) was dissolved in toluene (1 mL). The olefin (1 mmol, 110 mg for **5**, 94 mg for **6** and 139 mg for **7**) was added, followed by a *tert*-butyl hydroperoxide aqueous solution (8 M, 0.19 mL, 1.50 mmol). The mixture was stirred at room temperature for 22 h and then quenched by addition of ethyl acetate and filtered through silica. Undecane was added as an external standard (0.2−0.4 mmol). Analyses of organic products were performed by gas chromatography. Catalytic reactions were also performed without solvent according to the above mentioned experimental procedure.

X-ray Crystallographic Studies: Single crystals were grown by allowing diethyl ether to diffuse into a dichloromethane solution. The crystal data for **V** and **VI** were collected using a Bruker SMART CCD based diffractometer operating at room temperature. Intensities were collected with graphite-monochromated Mo-K_α radiation (λ = 0.71073 Å) generated at 50 kV and 30 mA, using the ω/2θ scan technique. A total of 1271 frames of intensity data were collected over a hemisphere of the reciprocal space by combination of three exposure sets. Each frame covered 0.3° in ω and the first 50 frames were recollected at the end of data collection to monitor crystal decay. The crystals used for the diffraction studies showed no decomposition during data collection. The crystallographic data for **V** and **VI** are summarised in Table 3. Absorption corrections were applied using the SADABS programme.[26] The structures were solved using the Bruker SHELXTL-PC software by direct methods and refined by full-matrix least-squares methods on F^2.[27] All non-hydrogen atoms were refined anisotropically. Hydrogen atoms were included in calculated positions and refined using the riding mode. CCDC-236207 (**V**) and -236208 (**VI**) contain the supplementary crystallographic data for this paper. These data can be obtained free of charge at www.ccdc.cam.ac.uk/conts/retrieving.html [or from the Cambridge Crystallographic Data Centre, 12, Union Road, Cambridge CB2 1EZ, UK; Fax: (internat.) + 44-1223-336-033; E-mail: deposit@ccdc.cam.ac.uk].

Acknowledgments

We would like to thank the Spanish Ministerio de Ciencia y Tecnología (BQU 2001-3358), Generalitat de Catalunya and the Decanato de Investigación y Desarrollo (Universidad Simón Bolívar) for financial support. The authors thank Dr. Xavier Santos for the GC analysis. J. B. thanks the Universitat de Barcelona for a two-year pre-doctoral grant.

[1] R. H. Holm, *Coord. Chem. Rev.* **1990**, *100*, 183−221 and references cited therein.
[2] R. C. Maurya, D. D. Mishra, S. N. Rao, R. Verma, N. N. Rao, *Ind. J. Chem.* **1997**, *36*, 599.
[3] H. Mimoun, I. Seree de Roch, L. Sajus, *Tetrahedron* **1970**, *26*, 37−50.

 © 2004 Wiley-VCH Verlag GmbH & Co. KGaA, Weinheim

[4] H. Mimoun, *Angew. Chem. Int. Ed. Engl.* **1982**, *21*, 734−750.
[5] K. B. Sharpless, J. M. Townsen, D. R. Williams, *J. Am. Chem. Soc.* **1972**, *94*, 295−296.
[6] K. A. Jørgensen, R. Hoffmann, *Acta Chem. Scand., Ser. B* **1986**, *40*, 411−419.
[7] P. Macchi, A. J. Schultz, F. K. Larsen, D. B. Iversen, *J. Phys. Chem. A* **2001**, *105*, 9231−9242.
[8] A. Hroch, G. Gemmecker, W. R. Thiel, *Eur. J. Inorg. Chem.* **2000**, 1107−1114.
[9] M. Gómez, S. Jansat, G. Muller, G. Noguera, H. Teruel, V. Moliner, E. Cerrada, M. Hursthouse, *Eur. J. Inorg. Chem.* **2001**, 1071−1076.
[10] M. Gómez, G. Muller, M. Rocamora, *Coord. Chem. Rev.* **1999**, *193−195*, 769−835.
[11] G. Helmchen, A. Pfaltz, *Acc. Chem. Res.* **2000**, *33*, 336−345.
[12] *Catalytic Asymmetric Synthesis* (Ed.; I. Ojima), 2nd ed., John Wiley & Sons, New York, **2000**.
[13] H. Arzoumanian, R. Bakhtchadjian, G. Agrifoglio, H. Krentzien, J.-C. Daran, *Eur. J. Inorg. Chem.* **1999**, 2255−2259.
[14] Bis(oxazolines) used were: 1,2-bis[(4*R*)-4-ethyl-Δ^2-1,3-oxazolin-2-yl)]benzene and 1,2-bis[(4*R*)-4-ethyl-Δ^2-1,3-oxazolin-2-yl)]ethane: M. Gómez, S. Jansat, G. Muller, M. A. Maestro, J. Mahía, M. Font-Bardía, X. Solans, *J. Chem. Soc., Dalton Trans.* **2001**, 1432−1439.
[15] R. J. Cross, P. D. Newman, R. D. Peacock, D. Stirling, *J. Mol. Catal. A: Chem.* **1999**, *144*, 273−284.
[16] R. Bandyopadhyay, S. Biswas, S. Guha, A. K. Mukherjee, R. Bhattacharyya, *Chem. Commun.* **1999**, 1627−1628.
[17] E. O. Schlemper, G. N. Schrauzer, I. A. Hugues, *Polyhedron* **1984**, *3*, 377−380.
[18] W. A. Herrmann, W. R. Thiel, J. G. Kuchlerf, J. Behm, E. Herdtweck, *Chem. Ber.* **1990**, *123*, 1963−1970.
[19] W. R. Thiel, M. Angstl, T. Preirmeier, *Chem. Ber.* **1994**, *127*, 2373−2379.
[20] W. R. Thiel, T. Preirmeier, *Angew. Chem. Int. Ed. Engl.* **1995**, *34*, 1737−1738.
[21] H. Glass, M. Spiegler, W. R. Thiel, *Eur. J. Inorg. Chem.* **1998**, 275−281.
[22] W. R. Thiel, J. Eppinger, *Chem. Eur. J.* **1997**, *3*, 696−705.
[23] M. Gómez, S. Jansat, G. Muller, D. Panyella, M. Font-Bardía, X. Solans, *J. Chem. Soc., Dalton Trans.* **1997**, 3755−3764.
[24] G. Balavoine, J. C. Clinet, I. Lellouche, *Tetrahedron Lett.* **1989**, *30*, 5141−5144.
[25] J. M. Canal, M. Gómez, F. Jiménez, M. Rocamora, G. Muller, E. Duñach, D. Franco, A. Jiménez, F. H. Cano, *Organometallics* **2000**, *19*, 966−978.
[26] G. M. Sheldrick, SADABS, *A Program for Empirical Absorption Correction of Area Detector Data*, University of Göttingen, Germany, **1996**, based on the method of Robert Blessing: R. H. Blessing, *Acta Crystallogr., Sect. A* **1995**, *51*, 33.
[27] G. M. Sheldrick, SHELXS-97, *A Program for Solving Crystal Structures and Crystal Structure Refinement*, University of Göttingen, Germany, **1997**.

Received April 26, 2004
Early View Article
Published Online August 26, 2004

 © 2004 Wiley-VCH Verlag GmbH & Co. KGaA, Weinheim

Formation of VN from VCl_4 and $NH(SiMe_3)_2$ by APCVD − a Potential Solar Control Coating

Anne Newport,[a] Claire J. Carmalt,[a] Ivan P. Parkin,*[a] and Shane A. O'Neill[a]

Keywords: Chemical vapour deposition / Nitrides / Solar control coatings

Vanadium nitride thin films have been synthesised by the reaction of vanadium(IV) chloride with hexamethyldisilazane (HMDS) under atmospheric pressure (AP)CVD conditions at 300–550 °C. The films deposited have good optical characteristics and low electrical resistivities. These films were not scratched off the glass substrate by a steel stylus and were not degraded by immersion in a range of solvents. X-ray diffraction showed an NaCl-type cubic cell with a = 4.102(1)–4.127(1) Å, dependent on the sample. X-ray photoelectron spectroscopy shows that the films have a V/N ratio close to unity. For comparison, films were also deposited by the APCVD reaction of $VOCl_3$ with HMDS. These films consist of mixed phases of vanadium oxynitride and V_2O_3. The VN films show properties suitable for use as solar control coatings.

(© Wiley-VCH Verlag GmbH & Co. KGaA, 69451 Weinheim, Germany, 2004)

Introduction

Vanadium nitride is a hard refractory material with metallic properties.[1] In its purest form it has a gold colour. Like the other transition metal nitrides it has many uses especially when deposited as a thin film.[2,3] Vanadium nitride has good metallic conductivity and stability to heat that makes it suitable as a barrier coating for microelectronic devices.[4] It is resistant to chemical attack by most solvents and reagents apart from hydrofluoric acid and aqua regia. The mechanical hardness of VN films has found application in wear-resistant parts.

Vanadium nitride films have been deposited under atmospheric pressure chemical vapour deposition (APCVD) conditions by reaction of vanadium chloride with nitrogen/hydrogen or ammonia[5] and reactions of vanadium amides {$[V(NR_2)_4]$; R = Me, Et}.[6] The former method evolved hydrogen chloride gas that is undesirable in the synthesis of films for microelectronic devices due to its corrosive nature.[5] The latter method yielded polycrystalline films with pinhole defects as result of rapid gas phase nucleation. This method also produced organic by-products.[7,8] Other methods of producing VN thin films include: N_2/H_2 plasma processing,[9] ion beam assisted deposition,[10] magnetron sputtering,[11] molecular organic CVD,[12] and pulsed laser deposition.[13]

Single-source CVD methods to prepare VN have also been reported using $[V(NR)Cl_3]$ (R = Me, C_6H_4Me, *t*Bu).[14] Unfortunately, the use of single-source precursors have so far yielded films with significant carbon contamination.[14] The presence of carbon can affect the optical properties of the film, whereas low amounts of oxygen seemingly do not.[15] It should be noted that in the case of VN, films have been classified as vanadium nitride with over 40 atom% carbon and oxygen contents. The decomposition of $[V(N\textit{t}Bu)Cl_3]$ gave films at temperatures as low as 250 °C that were shown to be vanadium carbonitride upon analysis.[14] Related precursors, $[V(NMe)Cl_3]$ and $[V(NC_6H_4Me)Cl_3]$, gave films with higher nitrogen content but only at temperatures above of 900 °C.[14]

We report here the dual-source CVD of vanadium nitride from vanadium(IV) chloride and hexamethyldisilazane (HMDS) under atmospheric pressure which yielded high-quality gold-coloured films of vanadium nitride. The reason for exploring HMDS as a nitrogen source was to try and avoid the problems in the conventional reaction of VCl_4 and NH_3 − which invariably lead to non-uniform films due to rapid gas-phase nucleation. Hexamethyldisilazane offers an alternative pathway by elimination of Me_3SiCl. The steric crowding in HMDS would also afford reduced rates of gas-phase combination and potentially better quality films. The VN films grown in this study show interesting properties that have potential to be used in glazing products for solar control applications.

Results

Vanadium(IV) Chloride with Hexamethyldisilazane (HMDS)

Synthesis

Reactions of vanadium(IV) chloride with hexamethyldisilazane (HMDS) under APCVD conditions at 300−550 °C yielded coatings of vanadium nitride on SiO_2-coated stand-

[a] University College London,
20 Gordon Street, London, WC1H 0AJ, UK

 © 2004 Wiley-VCH Verlag GmbH & Co. KGaA, Weinheim DOI: 10.1002/ejic.200400344

Table 1. Experimental conditions and analytical results for the APCVD reaction of VCl_4 and HMDS

Deposition temperature [°C]	VCl_4 flow [mol min^{-1}]	HMDS flow [mol min^{-1}]	N_2 carrier gas flow rate [Lmin^{-1}]	Lattice parameter (a [Å])	Electrical resistivity [μΩ cm]
550	0.02	0.05	1.0	4.102(1)	380
500	0.02	0.05	1.0	4.092(2)	650
450	0.02	0.05	1.0	4.13(2)	800
400	0.02	0.05	1.0	amorphous	900
300	0.02	0.05	1.0	amorphous	4000

ard float glass. The reaction could be expressed, in the idealised form, as shown in Equation (1). This idealised equation does not take into account the thermal stability of Me_3SiCl which would almost certainly decompose to other materials under the CVD conditions.

$$VCl_4 + 2\,(Me_3Si)_2NH \rightarrow VN + 4\,Me_3SiCl + 1/6\,N_2 + 2/3\,NH_3 \quad (1)$$

Flow rates of the precursor and plain nitrogen lines were varied. At total gas flow rates of 1.5 L min^{-1} or greater the films covered the whole substrate. However, at high carrier gas flow rates totalling over 3 L min^{-1} the deposition became non-uniform due to turbulence. For optimisation and coverage of all of the substrate in this particular APCVD setup, flow rates of 1 L min^{-1} for the plain nitrogen line and 0.3 L min^{-1} for the HMDS and 0.1 L min^{-1} for the VCl_4 line were used. This corresponds with molar flows of ca. 0.02 mol min^{-1} of VCl_4 and 0.05 mol min^{-1} of HMDS.

Characterisation

The films were analysed using glancing angle XRD, sheet resistance, SEM, EDAX, XPS, contact angle, Raman and UV/Vis reflectance and transmission measurements, selected data is given in Table 1. Film quality has been primarily correlated to deposition temperature and gas concentrations.

Films of uniform thickness were deposited over the entire substrate for a range of temperatures from 300 to 550 °C. The onset of deposition was noted at 300 °C as no film could be grown at 250 °C. The films were gold-coloured and free of pin-hole defects. The films could not be removed by rubbing with a tissue, soft cloth or scratched with a brass stylus or steel scalpel, indicating that they were extremely hard and typical of metal nitride films.[16] The vanadium nitride films were also unchanged by immersion in water, propan-2-ol, acetone, petroleum spirit and dilute (2 M) mineral acids for 48 h.

The glancing angle XRD analysis showed the presence of crystalline VN as the only detectable phase present in the films prepared at 450−550 °C.[17] The peaks were broad with the (2 0 0) peak being the most intense one, indicating a degree of preferred orientation. These films have a lattice constant from 4.09(2) to 4.13(2) Å (Table 1). This can be compared to the literature values where $VN_{1.00}$ films have a lattice constant recorded as a = 4.14(1) Å.[18] Bulk $VN_{0.92}O_{0.11}$ has an NaCl (*Fm3m*) structure and a lattice constant of a = 4.12 Å.[19] Previous work on the APCVD reaction of VCl_4 and NH_3 produced thin films of composition from $VN_{0.80}O_{0.18}$ to $VN_{0.68}O_{0.42}$ with lattice parameters of 4.078−4.072 Å. Notably in all of these studies the higher lattice constants were associated with the better nitrided products.

EDAX analysis confirmed the presence of vanadium and nitrogen in the films, although accurate quantitative data were not available due to the N peak being partially obscured by the vanadium. The EDAX measurements also showed breakthrough to the underlying substrate, thus making an accurate determination of any oxygen contaminant difficult. SEM analysis showed fine sub-micron spheroid particles of a uniform size distribution in the region of 250 nm (Figure 1). Growth rates as calculated from side-on SEM work were 175 nm min^{-1} at 450 °C and 250 nm min^{-1} at 550 °C.

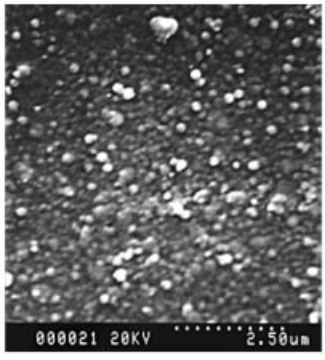

Figure 1. SEM of the films produced from the reaction of VCl_4 with HMDS at 550 °C

XPS analysis showed a small overlayer of oxide on all the VN samples, this was removed on Ar^+ etching. After the first few etchings the oxygen content was significantly reduced and the composition of the films prepared at 450, 500 and 550 °C had a V/N ratio of close to unity ($VN_{0.95(1)}$). This analysis also shows a surface N 1s binding energy shift at 396.9 eV and V 2p at 513.2 eV. These match previous measurements on VN.[20] the oxygen found in these films is a result of post CVD surface oxidation. This is because the oxygen content decreases with XPS sputtering depth and virtually disappears. This surface oxidation seems to be self-limiting as the VN films show no change in composition or in optical properties after storage in air for two years.

 © 2004 Wiley-VCH Verlag GmbH & Co. KGaA, Weinheim

The VN films are highly reflective and the spectra show a strong reflection in the NIR beyond 600 nm. This is more pronounced for films laid down at the higher deposition temperatures. These VN coatings prepared at 500 and 550 °C show good heat-mirror properties and suggest that these films have potential application as solar control coatings where visible light is transmitted but IR radiation is reflected. At deposition temperatures below 450 °C the films show little reflectance in the NIR. Films deposited at this temperature and below had a matte appearance and were not as shiny. The morphology of the films was identical to that grown at higher temperatures − it would seem that it is the lack of crystallinity that accounts for the observed changes in the reflection properties of the films. The transmission spectra of the films prepared at 450−550 °C showed few features transmitting light across the majority of the visible spectrum, (Figure 2). Notably no pin-hole defects were detected by optical microscopy or SEM in these films.

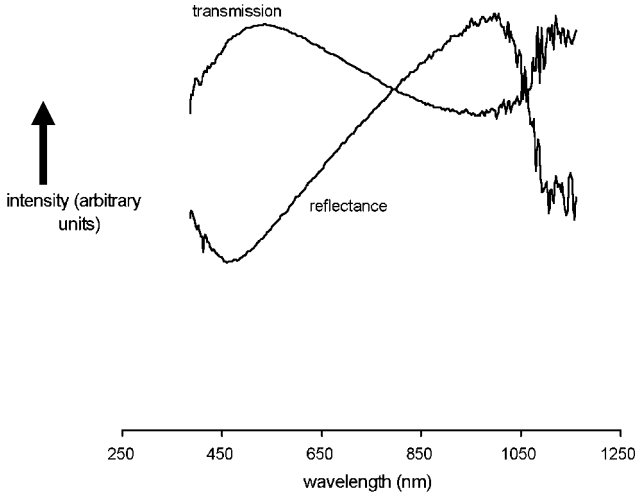

Figure 2. Transmission and reflectance spectra of films produced from the reaction of VCl_4 with HMDS at 550 °C

Raman analysis showed broad bands between 50 and 300 cm^{-1} that correspond to the region in which a powdered vanadium nitride standard gave a broad signal. Apart from this the Raman spectra were featureless. This indicates the absence of vanadium oxide phases (V_2O_5, VO_x, VO_2 and V_2O_3) and graphitic carbon in the films; as these are particularly strong Raman scatterers and would be expected to dominate the spectra even at low concentrations.

The electrical resistivity of the VN films was inversely proportional to the temperature of deposition. Post-treating the VN films with HMDS does not change the electrical resistivity of the film produced. The electrical resistivities of the films can be correlated with the powder XRD analysis − that is the resistance decreases with an increase in crystallite size (from amorphous at a deposition temperature of 300 °C to ca. 400 Å at 550 °C). The electrical resistivities measured of 380−4000 μΩ cm were similar to sputtered VN films (Table 1).[5]

The contact angles for water droplets of these films were calculated to be between 80 and 95° which indicates that the films were hydrophobic. The contact angle value for the silica-coated plain float glass was 75°.

Vanadium Oxychloride with Hexamethyldisilazane

Synthesis and Characterisation

Films produced from the reaction of vanadium(V) oxychloride with HMDS under APCVD conditions were dark-grey in colour. An idealised form of the reactions is given in Equation (2).

$$VOCl_3 + 2\,(Me_3Si)_2NH \rightarrow VN + 2\,Me_3SiCl + (Me_3Si)_2O + 1/2\,N_2 + HCl \quad (2)$$

Although some shiny areas were produced, the bulk of the films had a matte (lustreless) appearance. Substrate temperatures of 250−575 °C were employed in the deposition of these films in an attempt to improve uniformity of the surface and reduce the matte appearance. Despite this, most of the films were inhomogeneous and no correlations could be drawn as to what conditions favoured formation of the matte over shiny areas.

Powder XRD analysis of the films formed from $VOCl_3$ and HMDS showed slightly different data to the VCl_4 films. A cubic VN or oxynitride phase was identified and the measured lattice parameters *a* were from 4.07(9) to 4.08(0) Å. A second phase was also noted of V_2O_3.[21,22] This result is somewhat surprising as the analogous reaction of $VOCl_3$ and NH_3 yielded just a single-phase vanadium oxynitride material and not a biphasic mixture.

The XPS analysis gave a compositional ratio of $V_{3.0}N_{1.0}O_{4.0}$ for the film prepared from the reaction of $VOCl_3$ and HMDS at 600 °C which is consistent with the film consisting of two species V_2NO and V_2O_3. This correlates with the literature where treatment of V_2O_5 with ammonia at temperatures above 600 °C yielded a mixture of V_2NO and V_2O_3.[25] The V_2NO was reported to be black and have a cubic (*Fm3m*) structure which agrees with the XRD results.[23] Binding energy shifts for V 2p were at 513.5 eV, N 1s at 396.8 eV and O 1s at 530.7 eV which are in agreement with previous results.[17] The V 2p and O 1s peaks were much broader than that obtained for the XPS analysis of the films formed from VCl_4 and HMDS and was consistent with two environments (oxide and oxynitride).

The Raman spectra of the films formed from $VOCl_3$ and HMDS show a broad band at the lower wavenumbers similar to the samples produced from VCl_4 and HMDS. An additional broad band in the spectra was observed and assigned to the presence of a vanadium oxide phase reinforcing the XPS and XRD results (Figure 3). The additional Raman peaks associated with V_2O_3 were more defined in the matte area of the coatings.

 © 2004 Wiley-VCH Verlag GmbH & Co. KGaA, Weinheim

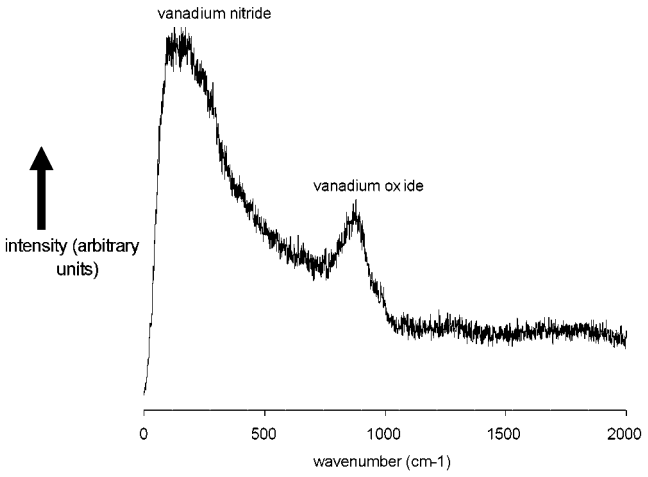

Figure 3. Raman spectrum of film produced from the reaction of $VOCl_3$ with HMDS

Reflectance spectra showed that certain of these samples reflect in the NIR although this extended across the visible as well. This was most apparent for the reflective areas of the films. The transmission spectra were noisy and, although they transmitted light across the visible, they also had transmission in the IR region showing that these films are not of sufficient quality for heat-mirror applications.

The majority of these films were conducting although their resistivity was an order of magnitude higher than the films formed from the reaction of VCl_4 with HMDS. There was difficulty in finding a correlation between deposition conditions and resistivity values of the film and few conclusions could be reached regarding the production of better quality deposition. The resistivity readings changed dependent on the area under analysis on the same film. Resistivity was noted to be greater on the matte regions of the film.

Contact angle measurements of these films for water droplets were contrasting depending on the area of film analysed. The shiny areas were measured in the region of 80° which is similar to that of the films from the reaction of VCl_4 with HMDS. However, values as low as 28° were recorded on the areas that were blackened, suggesting the presence of a vanadium oxide phase which has a lower contact angle. Measurements in these areas was not as simple as the shiny areas and open to error due to the presence of solid deposits on the surface of the films. Indeed, the irregular porous surface structure could be responsible for the lowered contact angle.

Discussion

Reaction of vanadium(IV) chloride with hexamethyldisilazane under APCVD conditions produced vanadium nitride films with good optical characteristics − free of pin-hole defects, reflecting in the NIR and transmitting in the visible. This demonstrates that these films have potential to be used as heat-mirror coatings on window glass. To be effective in this application the coating needs to have good transmission in the visible region whilst providing high reflectance in the IR.[24] This means that the heat mirror would enable a householder to see out of the window but not be subject to heat-gain from the IR part of the solar spectrum. Few materials have this combination of properties.

Less ideal reflectance and transmission spectra from the VN samples deposited at lower temperatures can be explained by lower crystallinity. This is confirmed by the resistivity measurements and the glancing angle XRD data, where samples deposited at temperatures above 450 °C gave an XRD pattern typical of a crystalline material and had considerably lower resistivity values. The SEM analysis shows that these films are composed of fine particles.

In comparison with films produced from the standard dual-source reaction of VCl_4 with ammonia, the films deposited from the APCVD reaction of VCl_4 with HMDS have superior qualities. In the former case, fast pre-reaction led to blockages of the pipework and gas-phase nucleation caused pin-hole defects in the films. Films formed from the dual-source reaction of VCl_4 with HMDS gave uniform coverage of the substrate and were free from pin-hole defects. These films were also gold-coloured whereas the VCl_4/NH_3 reaction under comparable conditions produced less reflective brown-yellow films. The reaction between VCl_4 and HMDS is probably less rapid than VCl_4 and NH_3 due to the size of the $SiMe_3$ groups. The absence of Si and C in these films suggests that the elimination of Me_3SiCl is facile, providing the driving force of the APCVD reaction [Equation (1)]. Notably a large excess of HMDS is not required to form VN films, just a slight excess over the gas-phase concentration of the vanadium tetrachloride (1:2.5). In nitride preparation from a metal halide and ammonia typically a hundredfold excess of ammonia would be used. The VN films formed in this work were superior in optical properties to those prepared from the analogous reaction with ammonia.

The films produced from the reaction of vanadium oxychloride and HMDS gave unexpected results. These were dark grey and, although the majority were conducting, the resistivity values were significantly higher than those of the samples produced from VCl_4. The reflectance and transmission spectra from these samples showed poorer heat-mirror properties and, although certain patches of these films were hard and adhered to the substrate, larger areas appeared to consist of powdery deposits and were more easily removed from the substrate. The Raman data shows that these films are contaminated with carbon and vanadium(III) oxide. This result was confirmed by XRD and by the compositional analysis by XPS. This suggests that significant amounts of oxygen remains bound with the vanadium from the vanadium oxychloride precursor during the reaction with HMDS. Interestingly, these results contrast with the reactions with $VOCl_3$ and NH_3 which formed a single-phase oxynitride product rather than a mixed-phase material.[15] This is probably a consequence of involv-

 © 2004 Wiley-VCH Verlag GmbH & Co. KGaA, Weinheim

ing the $SiMe_3$ as a leaving group in the reaction. However, further speculation is not warranted at this stage as to the detailed reaction mechanism.

Conclusion

Vanadium(IV) chloride reacts with hexamethyldisilazane under APCVD conditions to form uniform gold-coloured films that have optical properties suitable for heat-mirror applications. These films have a composition of $VN_{1.0}$. This has proved to be a novel and efficient method of producing VN films utilising existing technology. This method produces more uniform films free of pin-hole defects compared to the current method of treating VCl_4 with ammonia. It should also be noted that multi-precursor CVD normally requires a large excess of one of the reactants and by using hexamethyldisilazane as the nitrogen source this is overcome as a more complete reaction is occurring. Although a silicon-containing precursor is utilised in these depositions, no evidence of silicon is found in the resulting films.

The APCVD reaction of $VOCl_3$ with HMDS gave non-uniform grey-black films with a higher electrical resistivity than the gold-coloured VCl_4/HMDS films. These films consist of an oxynitride (V_2NO) and V_2O_3.

Experimental Section

Vanadium(IV) chloride, vanadium(V) oxychloride and 1,1,1,3,3,3-hexamethyldisilazane (HMDS) were purchased from Aldrich Chemical Company and used without further purification. The HMDS was loaded in one bubbler and the vanadium precursor was loaded into a second bubbler. Standard float glass with a silica diffusion barrier coating was used for the following deposition studies. The glass was cleaned thoroughly prior to use with water followed by propan-2-ol then dried at room temperature in a vertical position. Nitrogen (99.9% BOC) was used as the carrier gas after being passed through an oxygen removal column (CuH). The pipe assembly, bubbler and experimental setup are fully described elsewhere.[20,25] For this series of deposition experiments three independently controlled gas streams − the vanadium source, HMDS and nitrogen − are passed into a mixing chamber prior to entering the reaction chamber. The reactor is a cold-wall design similar to those reported by us previously.[18] The substrate is heated on a graphite-block containing a single Whatman cartridge-heater. The glass is coated in a horizontal position and has dimensions of 15 cm × 4 cm × 0.3 cm. The temperature of the glass substrate was recorded using an independent thermocouple and compared to the setting of the controlling thermocouple. It was found that there was a temperature variation across the surface of the glass substrate of ca. 40 °C. All temperatures recorded for the depositions in this report are those of the hottest central part of the glass substrate. Substrate temperatures ranged from 250 to 575 °C. All coatings were carried out at atmospheric pressure for 2 min. A range of flow rates for all three gas lines was used. Glancing angle X-ray diffraction analysis of the films was obtained using a Siemens D5000 diffractometer in the reflection mode (1.5° incidence) using Cu-K_α (1.5406 Å) radiation. SEM/EDAX was determined with a JEOL CR-37. XPS was performed with a VG ESCALAB 220i XL using focused (300 μm spot) monchromatic Al-K_α radiation at a pass energy of 20 eV. Scans were acquired with steps of 100 meV. A flood gun was used to control charging and the binding energies were referenced to an advantageous C 1s peak at 284.6 eV. Depth profiles were obtained by using an argon sputtering-gun. Reflectance and transmission spectra were recorded between 300 and 2600 nm with a U4000 spectrophotometer and between 300 and 1150 nm with a Zeiss miniture grating spectrometer. Raman spectra were obtained with a Renishaw 1000 spectrometer using an Ne excitation laser line. Contact angle measurements were determined by measuring the spread of a 1 μL^3 droplet of water. A powder sample of vanadium nitride (99%) was purchased from Aldrich Chemical Co. and used for comparison purposes for Raman spectroscopy.

Acknowledgments

The authors thank the EPSRC for financial support (GR/R16518). Pilkington glass are thanked for the gifts of glass substrates.

[1] C. H. Winter, V. C. Viejo, J. W. Proscia, *Mater. Res. Soc. Symp. Proc.* **1994**, *327*, 109−113.
[2] S. R. Kurtz, R. G. Gordon, *Thin Solid Films* **1986**, *140*, 277−290.
[3] C. G. Granquist, *Thin Solids Films* **1990**, *193/194*, 730−741.
[4] *The Chemistry of Transition Metal Carbides and Nitrides* (Ed.: S. T. Oyama), Blackie Academic and Professional, London, **1996**.
[5] H. E. Cheng, M. H. Hon, *J. Appl. Phys.* **1996**, *79*, 8047−53; I. P. Parkin, S. S. Elwin, *J. Mater. Chem.* **2001**, *11*, 3120−3125.
[6] I. J. Raaijmakers, *Thin Solid Films* **1994**, *247*, 85−93.
[7] R. Fix, R. G. Gordon, D. M. Hoffman, *Chem. Mater.* **1993**, *5*, 614−619.
[8] R. Fix, R. G. Gordon, D. M. Hoffman, *J. Am. Chem. Soc.* **1990**, *112*, 7833−35.
[9] A. M. Chaplanov, E. N. Shcherbakova, *Inorg. Mater.* **2001**, *37*, 233−6.
[10] C. H. Ha, J. H. Huang, H. Chen, *Surf. Coat. Technol.* **2000**, *133*, 289−294.
[11] R. Sanjines, P. Hoves, P. Levy, *Thin Solid Films* **1998**, *332*, 225−9.
[12] S. Abisset, F. Maury, *Surf. Coat. Technol.* **1998**, *109*, 200−5.
[13] Z. N. Dai, A. Miyashite, S. K. Yamamoto, H. Naramoto, *Thin Solid Films* **1999**, *347*, 117.
[14] F. Laurent, P. Michel, R. Feurer, R. Morancho, L. Valade, R. Choukroun, P. Cassoux, *J. Mater. Chem.* **1993**, *3*, 659 −63.
[15] G. C. Elwin, I. P. Parkin, *Chem. Vap. Deposition* **2000**, *6*, 59−63.
[16] F. Levy, P. Hones, P. E. Schmid, R. Sanjinés, M. Diserens, C. Wiemer, *Surf. Coat. Technol.* **1999**, *120−121*, 284−90.
[17] JC,PDS Data file number 25-1252, Swathmore, PA, **1990**.
[18] L. Soriano, M. Abbate, H. Pen, P. Prieto, J. M. Sanz, *Solid State Commun.* **1997**, *102*, 291−6.
[19] J. G. Zaninulin, *Zh. Neorg. Khim.* **1984**, *19*, 1770−72; L. G. Raskolenko, Y. M. Maksimov, *Inorg. Mater.* **1983**, *19*, 1770−72.
[20] I. P. Parkin, G. S. Elwin, *J. Mater. Chem.* **2001**, *11*, 3120−4.
[21] JC,PDS Data file number 43-1051, Swathmore, PA, **1990**.
[22] JC,PDS Data file number 39-0774, Swathmore, PA, **1990**.
[23] P. Wang, B. C. Chakoumakos, B. C. Sales, J. B. Bates, *J. Solid State Chem.* **1996**, *122*, 376.
[24] L. S. Price, I. P. Parkin, A. Hardy, R. J. H. Clark, Y. G. Hibbert, K. C. Molloy, *Chem. Mater* **1999**, *11*, 1792−9.
[25] A. Newport, C. J. Carmalt, I. P. Parkin, S. A. O'Niell, *J. Mater. Chem.* **2002**, *12*, 1906−9.

Received April 29, 2004
Early View Article
Published Online September 10, 2004

 © 2004 Wiley-VCH Verlag GmbH & Co. KGaA, Weinheim

Reactivity of a Thiolate-Bridged Dinuclear Ruthenium Complex with Nitrogenous Molecules: Spectroscopic Identification of a Labile Dinitrogen Complex[‡]

Dieter Sellmann,[a][†] Raju Prakash,*[a,b] and Frank W. Heinemann[a]

Dedicated to Prof. Dr. Joachim Sieler on the occasion of his 65th birthday

Keywords: N ligands / Nitrogenases / Nitrogen fixation / Ruthenium / S ligands

Reactions of the thiolate-bridged diruthenium complex $[Ru(py^{bu}S_4)]_2$ (**1**) {$py^{bu}S_4^{2-}$ = 2,6-bis[(3,5-di-*tert*-butyl-2-sulfanylphenyl)thiomethyl]pyridine(2–)} with small-molecule ligands L afforded the corresponding mononuclear complexes $[Ru(L)(py^{bu}S_4)]$ [L = H^- (**2**); CH_3CN (**3**); NH_3 (**4**); CO (**5**); N_2H_4 (**6**); PMe_3 (**7**); N_3^- (**8**)]. The molecular structures of **3**, **4**, and **5** exhibit pseudooctahedral geometry with two thiolate and two thioether donor atoms in a *trans* configuration. Complexes **2**–**8** exhibit a quasi-reversible, one-electron redox wave of the Ru^{II}/Ru^{III} couple in the region between $E_{1/2}$ = +0.214 and +0.460 V vs. NHE. Complex **1** reacts reversibly with N_2 (60 bar) at 40 °C to give the labile dinitrogen complex $[Ru(N_2)(py^{bu}S_4)]$ (**9**). Complex **9** can also be obtained from the reaction between **3** and N_2 (20 bar) at room temperature. Treatment of **4** with NO afforded the labile 19-valence-electron species $[Ru(NO)(py^{bu}S_4)]$ (**10**) in solution, which could subsequently be converted to **9** upon high-pressure reaction with N_2 (20 bar). In contrast, the analogous reaction of **4** with $NOBF_4$ results in the formation of the oxidized complex $[Ru(NH_3)(py^{bu}S_4)]BF_4$ (**11**), the structure of which was confirmed by X-ray structure analysis. The carbonyl complex $[Ru(CO)(py^{bu}S_4)]$ (**5**) could be reversibly protonated at the thiolate sulfur atom to give $[Ru(CO)(py^{bu}S_4H)]BF_4$ (**12**). UV irradiation of **5** and **12** under N_2 at –80 °C produced the short-lived species **9** and **13**, respectively, which were identified spectroscopically.
(© Wiley-VCH Verlag GmbH & Co. KGaA, 69451 Weinheim, Germany, 2004)

Introduction

Nitrogenases comprise sulfur-dominated polynuclear FeMo, FeV or FeFe cofactors as their active sites, which catalyze the transformation of dinitrogen to ammonia under mild conditions.[1] Coordination of N_2 to a sulfur-rich transition metal complex is thought to be an effective strategy towards nitrogen fixation.[2] Despite numerous intensive efforts,[3] metal−sulfur complexes that bind molecular nitrogen are very scarce.[4] However, it is believed that systematic in-depth studies on sulfur-rich transition metal complexes with biologically relevant molecules such as CO, NO, N_2H_2, N_2H_4, N_3^- etc. will shed light on this intriguing N_2 activation and its exploitation to produce ammonia under mild conditions. As part of our contribution in this field, we recently obtained the mononuclear and dinuclear dinitrogen complexes $[Ru(N_2)(PR_3)(N_2Me_2S_2)]$ and $[\mu\text{-}N_2\{Ru(PR_3)(N_2Me_2S_2)\}_2]$ [R = *i*Pr, Cy; $N_2Me_2S_2^{2-}$ = *N*,*N*′-dimethyl-1,2-ethanediamine-*N*,*N*′-bis(benzenethiolate)-(2−)] by direct reaction of $[Ru(CH_3CN)(PR_3)(N_2Me_2S_2)]$ with molecular nitrogen under very mild conditions.[5] However, attempts to reduce the coordinated N_2 in these complexes were unsuccessful due to decoordination of the N_2 ligand. Meanwhile, we developed the fragment $[M(pyS_4)]$ {M = Fe, Ru or Os; pyS_4^{2-} = 2,6-bis[(2-sulfanylphenyl)thiomethyl]pyridine(2−)}, which readily binds a number of small nitrogenase-relevant ligands. The resultant six-coordinate mononuclear complexes are redox-active and are formed diastereoselectively by maintaining the thiolate and thioether donors always *trans* to each other.[6] However, none of these metal fragments is capable of binding molecular nitrogen, even at elevated N_2 pressure (200 bar) and high temperature (100 °C).

[‡] Transition Metal Complexes with Sulfur Ligands, 166. Part 165: D. Sellmann, K. Hein, F. W. Heinemann, *Inorg. Chim. Acta*, in press.

[†] Deceased.
[a] Institut für Anorganische Chemie der Universität Erlangen-Nürnberg,
Egerlandstrasse 1, 91058 Erlangen, Germany
[b] Institut für Organische Chemie der Universität Erlangen-Nürnberg,
Henkestrasse 42, 91054 Erlangen, Germany
Fax: 49-9131-852-1165
E-mail: raju.prakash@chemie.uni-erlangen.de

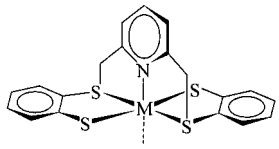

[M(pyS$_4$)] (M = Fe, Ru, Os)

Recently, we achieved the heterolytic cleavage of H_2 at room temperature using the thiolate-bridged diruthenium complex $[Ru(py^{bu}S_4)]_2$ (**1**) {$py^{bu}S_4^{2-}$ = 2,6-bis[(3,5-di-*tert*-butyl-2-sulfanylphenyl)thiomethyl]pyridine(2−)} to form the hydride protonated thiolate $[Ru(H)(py^{bu}S_4H)]$.[7] The latter species, in turn, reacts with a base to give the hydride $[Ru(H)(py^{bu}S_4)]^-$ by abstraction of the S−H proton. This remarkable result prompted us to further investigate the reactivity of **1** towards nitrogenase-relevant molecules. Herein we describe the synthesis and characterization of the mononuclear complexes $[Ru(L)(py^{bu}S_4)]$ (L = H^-, CO, NH_3, N_2H_4, CH_3CN, N_3^-, etc.) starting from complex **1**. The reaction of these complexes and of **1** with molecular nitrogen to form labile dinitrogen complexes is also reported.

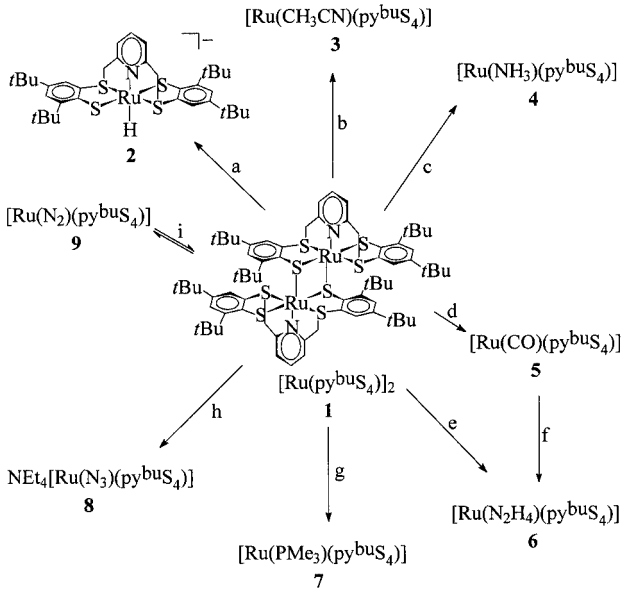

Scheme 1. Synthesis of $[Ru(L)(py^{bu}S_4)]$ complexes: (a) excess $NaAlH_4$, −78 to 20 °C, 2 h, THF; (b) CH_3CN, RF, 2 d; (c) excess NH_3, 20 h, THF; (d) excess CO, 15 h, THF; (e) excess N_2H_4, 70 °C, 1 d, THF; (f) excess N_2H_4, UV, −30 °C, 1 h, THF; (g) PMe_3, 2 h, THF; (h) excess NEt_4N_3, 2 d, THF; (i) N_2 (60 bar), 40 °C, 7 d, THF

Results and Discussion

Synthesis and Characterization of $[Ru(L)(py^{bu}S_4)]$ Complexes

The preparation of ruthenium complexes $[Ru(L)(py^{bu}S_4)]$ containing the σ or σ-π ligands L is a prerequisite for probing the influence of L on the potential coordination of the N_2 ligand. Scheme 1 summarizes the syntheses of $[Ru(L)(py^{bu}S_4)]$. The new complexes were prepared by the reaction of dinuclear complex **1** with nucleophiles L by the dissociation of the Ru−S bridges.

Treatment of complex **1** with a fivefold excess of $NaAlH_4$ in THF under argon yields extremely air- and moisture-sensitive $Na[Ru(H)(py^{bu}S_4)]$ (**2**), which can be isolated in the solid state conveniently at room temperature, and is obtained with much better yield (65%) than that of our previous method.[7] Refluxing of a suspension of **1** in CH_3CN continuously for 2 d affords $[Ru(CH_3CN)(py^{bu}S_4)]$ (**3**). In the course of the reaction, the pink suspension of **1** changes to an orange solution, from which **3** could be obtained in a reasonable yield (48%). Treatment of **1** with NH_3 or CO in THF under normal conditions leads to the formation of $[Ru(NH_3)(py^{bu}S_4)]$ (**4**) or $[Ru(CO)(py^{bu}S_4)]$ (**5**), respectively. In the former case, the pink suspension changes to a wine-red solution which exhibits the ν(NH) bands in the IR (THF) spectrum in the region of 3350−3000 cm^{-1}, whereas in the latter case the resulting yellow solution shows a strong carbonyl band at 1967 cm^{-1}. At 70 °C, compound **1** reacts with a tenfold excess of N_2H_4 to afford $[Ru(N_2H_4)(py^{bu}S_4)]$ (**6**) in an isolated yield of 67%. Alternatively, UV irradiation of the 18-valence-electron carbonyl complex **5** in the presence of an excess of N_2H_4 in THF at −30 °C proceeds efficiently with the extrusion of CO and subsequent coordination of the N_2H_4 molecule to afford **6** (91%). In the course of the reaction, the yellow solution changes to red. The ν(CO) band of **5** proved to be a good probe for monitoring the reaction by IR spectroscopy. The yellow-red complex $[Ru(PMe_3)(py^{bu}S_4)]$ (**7**) was formed instantaneously when a suspension of **1** in THF was treated with a slight excess of PMe_3. The labile azido complex $NEt_4[Ru(N_3)(py^{bu}S_4)]$ (**8**) can be obtained only after 2 d by vigorous stirring of the THF suspension of **1** with an excess of NEt_4N_3.

Most new complexes were isolated in analytically pure form, are soluble in THF, CH_2Cl_2, acetone, DMF or DMSO, and were characterized by IR and NMR spectroscopy, mass spectrometry and/or X-ray crystallography. The IR (KBr) spectra of the complexes exhibit a typical absorption pattern for the $[Ru(py^{bu}S_4)]$ fragment. In addition, the spectrum of **3** exhibits a sharp band at 2269 cm^{-1} for the CN stretching vibration of the CH_3CN ligand. The NH_3 and N_2H_4 ligands of **4** and **6**, respectively, gave rise to sharp ν(NH) bands in the region 3350−3000 cm^{-1}, whereas the $\nu(N_3)$ band of **8** appears at 2022 cm^{-1}. As judged by their well-resolved NMR spectra, the complexes are diamagnetic. The ^1H NMR spectra of all complexes show a characteristic splitting pattern for the $[Ru(py^{bu}S_4)]$ fragment, consisting of three doublets and a multiplet for the aromatic protons, two doublets for the bridging CH_2 groups, and two singlets for the *t*Bu groups. The number of ^1H and ^{13}C NMR signals for **2**−**8** (see Exp. Sect.) are consistent with a C_2 symmetry in solution, which has also been confirmed by the X-ray structure determinations of **3**, **4** and **5**. The cyclic voltammogram of **1** (Figure 1) shows two quasi-reversible one-electron waves at $E_{1/2}$ = +0.450 and +0.760 V for the $Ru^{II,II}/Ru^{II,III}$ and $Ru^{II,III}/$

 © 2004 Wiley-VCH Verlag GmbH & Co. KGaA, Weinheim

$Ru^{III,III}$ redox couples, respectively. All mononuclear complexes exhibit the quasi-reversible redox wave of the Ru^{II}/Ru^{III} couple in the region between $E_{1/2}$ = +0.214 and +0.460 V.

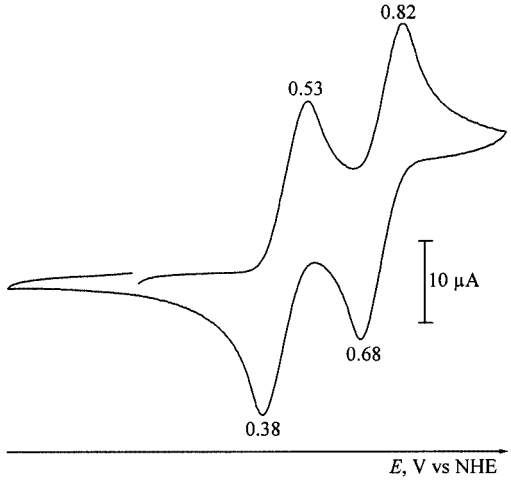

Figure 1. Cyclic voltammogram of **1** in THF (10^{-3} M; NBu_4PF_6, 10^{-1} M; ν = 50 mV s^{-1}; T = 25 °C)

The molecular structures of $[Ru(CH_3CN)(py^{bu}S_4)]\cdot 2CH_3CN$ (**3**·$2CH_3CN$), $[Ru(NH_3)(py^{bu}S_4)]\cdot CH_2Cl_2\cdot 0.5n$-pentane (**4**·$CH_2Cl_2$·0.5*n*-pentane) and $[Ru(CO)(py^{bu}S_4)]\cdot CH_3OH\cdot(CH_3)_2CO$ [**5**·CH_3OH·$(CH_3)_2CO$] were determined by single-crystal X-ray structure analysis. Figure 2 depicts the molecular structures and Table 1 lists selected distances and angles.

The unit cells of **3**−**5** contain one or more solvent molecules. In each compound the ruthenium center (Ru1) is surrounded by one N, four S, and one X (X = C, N or P) atoms in a pseudooctahedral geometry. The thioether and thiolate donors are *trans* to each other, with the pyridine N donor in an apical position such that a square-pyramidal $[RuNS_4]$ core results for the $[Ru(py^{bu}S_4)]$ fragment. The sixth position, *trans* to the pyridine N donor, is occupied by the X atom of the co-ligand L. The distances (except Ru−N1) and angles around the ruthenium atom are in the range usually found for diamagnetic six-coordinate Ru^{II} thiolate complexes.[8] The Ru−S(thiolate) distances (236−239 pm) are usually longer than the Ru−S(thioether) distances (229−231 pm). In particular, short distances are observed for Ru1−N1 *trans* to the coligands CH_3CN and NH_3 [203.3(6) pm in **3** and 203.6(3) in **4**]. These distances are distinctly shorter than the corresponding distance in **5** [212.1(6) pm], as well as those of $[Ru(L)(py^{bu}S_4)]$ (L = NO, HNO; 210−213 pm)[8,9] and $[Ru(L)(pyS_4)]$ (L = CO, PPh_3, DMSO; 209−212 pm),[10] indicating that in **3** and **4** a practically identical *trans* effect is imposed by the CH_3CN and NH_3 ligands.

Reactions with Dinitrogen

Treatment of **1** with N_2 under normal conditions did not result in any reaction. However, at 60 bar and 40 °C the

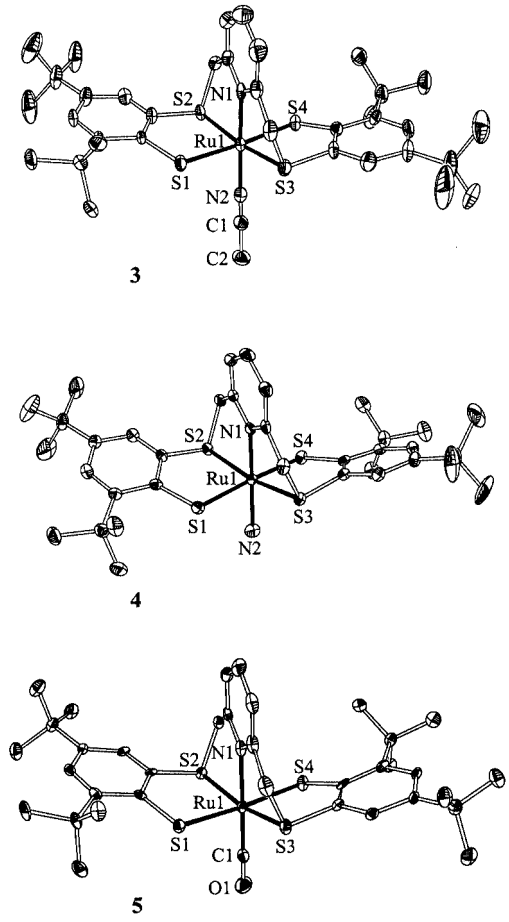

Figure 2. Thermal ellipsoid plots of $[Ru(CH_3CN)(py^{bu}S_4)]\cdot 2CH_3CN$ (**3**·$2CH_3CN$), $[Ru(NH_3)(py^{bu}S_4)]\cdot CH_2Cl_2\cdot 0.5n$-pentane (**4**·$CH_2Cl_2$·0.5*n*-pentane) and $[Ru(CO)(py^{bu}S_4)]\cdot CH_3OH\cdot(CH_3)_2CO$ [**5**·CH_3OH·$(CH_3)_2CO$] (50% probability ellipsoids; H atoms and solvent molecules omitted)

Table 1. Selected bond lengths [pm] and angles [°] for $[Ru(CH_3CN)(py^{bu}S_4)]\cdot 2CH_3CN$ (**3**·$2CH_3CN$), $[Ru(NH_3)(py^{bu}S_4)]\cdot CH_2Cl_2\cdot 0.5n$-pentane (**4**·$CH_2Cl_2$·0.5*n*-pentane), $[Ru(CO)(py^{bu}S_4)]\cdot CH_3OH\cdot(CH_3)_2CO$ [**5**·CH_3OH·$(CH_3)_2CO$], $[Ru(NH_3)(py^{bu}S_4)]BF_4\cdot CD_2Cl_2$ (**11**·CD_2Cl_2) and $[Ru(NH_3)(py^{bu}S_4\text{-}O_2)]BF_4\cdot CD_2Cl_2$ (**11a**·CD_2Cl_2)

	3	**4**	**5**	**11**	**11a**
Ru1−N1	203.3(6)	203.6(3)	212.1(6)	206.3(3)	206.3(3)
Ru1−N2	202.5(6)	215.8(3)	185.1(7)[a]	214.1(4)	214.1(4)
Ru1−S1	238.6(2)	236.5(1)	237.8(2)	229.6(1)	229.6(1)
Ru1−S2	229.4(2)	228.8(1)	231.3(2)	231.8(2)	231.8(2)
Ru1−S3	229.5(2)	229.5(1)	231.2(2)	229.9(2)	229.9(2)
Ru1−S4	237.5(2)	236.5(1)	239.6(2)	231.8(1)	231.8(1)
S4−O41	–	–	–	–	157(1)
S4−O42	–	–	–	–	142(1)
N1−Ru1−N2	178.8(2)	178.9(2)	179.4(3)[a]	178.1(2)	178.1(2)
N1−Ru1−S1	88.2(2)	91.77(8)	88.2(2)	89.99(9)	89.99(9)
S1−Ru1−S4	176.60(7)	174.85(4)	174.43(7)	178.69(4)	178.69(4)
S1−Ru1−S2	86.85(6)	86.51(3)	88.68(5)	87.25(4)	87.25(4)
S2−Ru1−S3	169.67(7)	167.53(3)	164.86(8)	168.79(4)	168.79(4)

[a] N2 = C1.

 © 2004 Wiley-VCH Verlag GmbH & Co. KGaA, Weinheim

labile mononuclear dinitrogen species $[Ru(N_2)(py^{bu}S_4)]$ (**9**) was formed after 4 d. In the course of the reaction, the pink suspension of **1** in THF changed to a clear red solution. The IR (THF) spectrum of the resulting solution showed the weak $\nu(N_2)$ band at 2139 cm^{-1}. This band gradually disappeared at room temperature over the course of 1 h to give **1**, as indicated by the formation of pink microcrystals from the solution, showing this conversion to be reversible. Identical results were obtained when similar reactions were carried out in CH_2Cl_2 or toluene. This suggests that the solvent medium has a negligible influence on the coordination of the N_2 ligand. Compound **9** was found to be stable at −80 °C for at least 24 h, although attempts to isolate it were unsuccessful.

^1H NMR spectroscopic monitoring of the reaction of **1** in $[D_8]$THF (or CD_2Cl_2 or $[D_8]$toluene) with N_2 (60 bar) in an autoclave specially constructed for the NMR tubes corroborated the IR spectroscopic data. Figure 3 shows the ^1H NMR spectra of **1** in $[D_8]$THF before and after pressurizing with N_2. The ^1H NMR spectrum of **1** under normal N_2 pressure is typical for a complex having C_1 symmetry (Figure 3a). When the suspension was pressurized with N_2 (60 bar) and allowed to react at 40 °C for 7 d, the ^1H NMR spectrum of the resulting red solution, recorded immediately after the release of the pressure, showed resonances that are characteristic of the mononuclear $[Ru(py^{bu}S_4)]$ fragment with C_2 symmetry (Figure 3b). The new resonances gradually disappeared and the spectrum of **1** reappeared over a period of 60 min when the solution was kept under N_2 (Figure 3c−e, only the CH_2 resonances are shown). ^1H NMR spectroscopic monitoring of the reaction at −80 °C indicated that the red solution is stable for at least 24 h.

These results show that compound **1** reacts with N_2 reversibly to give a mononuclear N_2 complex. It is reasonable that a moderate temperature and pressure are required to drive the reaction by breaking the Ru−S bridges.

Protonation reactions of metal hydride complexes under N_2 to form mononuclear or dinuclear dinitrogen complexes via the labile η^2-H_2 species are well known in the literature.[11] Unfortunately, protonation of **2** in CH_2Cl_2 (or THF) with HBF_4, CH_3COOH, H_2O, MeOH or HCl while bubbling N_2 instantaneously afforded only compound **1**. During ^1H NMR spectroscopic monitoring of the reaction in $[D_8]$THF at −80 °C, the RuH resonance of **2** at δ = −14.85 ppm disappeared and the spectrum of **1**, together with the resonance of H_2 at δ = 4.54 ppm, appeared. The analogous reaction of $[Ru(H)(PR_3)('S_4')]^-$ {$'S_4'^{2-}$ = 1,2-bis[(2-mercaptophenyl)thio]ethane(2−)} with H^+ afforded the short-lived species $[Ru(H_2)(PR_3)('S_4')]$.[8c] Such an intermediate could not be found in the reaction between **2** and H^+, probably owing to its extreme lability.

In another attempt, the substitution-labile acetonitrile complex **3** was treated with N_2. When N_2 was bubbled through a solution of **3** in THF for about 1 h, only **1** was formed, as indicated by the precipitation of pink-red microcrystals. The IR (THF) spectroscopic monitoring of the reaction inferred that the ν(CN) band of **3** at 2269 cm^{-1} is replaced by the ν(CN) band of free CH_3CN at 2251 cm^{-1}. In contrast, the analogous reaction performed in an autoclave with N_2 (30 bar) at 20 °C for 2 d produced the labile species **9**. In the course of the reaction, the solution color changed from orange to red, and the IR (THF) spectrum exhibited two bands at 2251 and 2139 cm^{-1} (Figure 4). The

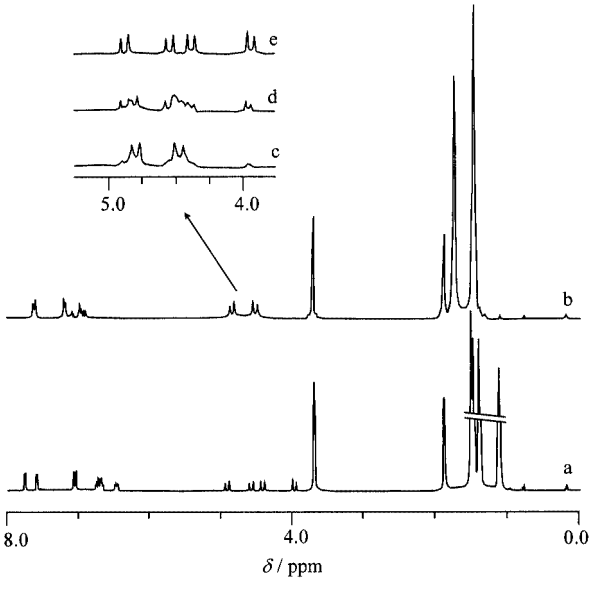

Figure 3. (a) ^1H NMR spectrum of **1** in $[D_8]$THF pressurized with N_2 (60 bar) at 40 °C for 7 d; the pressure was released and ^1H NMR spectra recorded at 20 °C after (b) 3 min, (c) 25 min, (d) 45 min, (e) 60 min

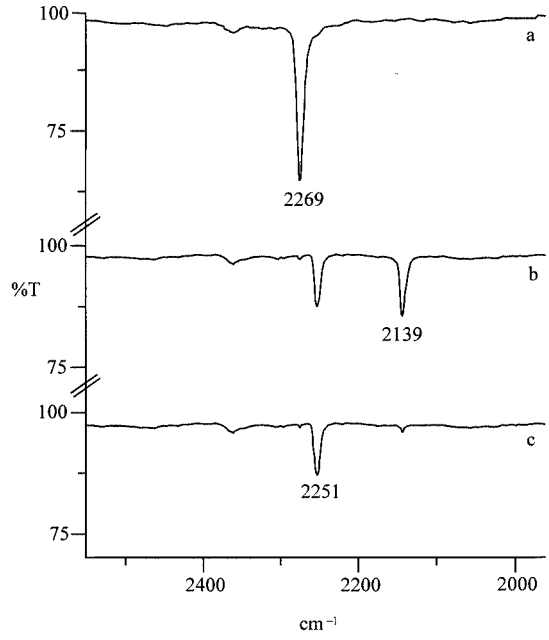

Figure 4. (a) IR spectrum of **3** in THF pressurized with N_2 (20 bar) at 20 °C for 2 d; the pressure was released and IR (THF) spectra recorded after (b) 2 min, (c) 60 min

 © 2004 Wiley-VCH Verlag GmbH & Co. KGaA, Weinheim

latter band, assigned to complex **9**, disappeared over the course of 1 h as the precipitate of **1** formed from the solution. The product isolated at −80 °C was found to be a mixture; however, it exhibits a weak, short-lived band in the IR (KBr) spectrum at 2134 cm^{-1}.

^1H NMR spectroscopic monitoring of the reaction of **3** in [D$_8$]THF (or CD_2Cl_2) with N_2 (20 bar) in a pressure tube complements the earlier results. The ^1H NMR spectrum of **3** under N_2 shows the methyl resonance of CH_3CN at δ = 2.18 ppm (see Exp. Sect.). After pressurizing the NMR tube with N_2 (20 bar), the signal at δ = 2.18 ppm decreased as the resonance of free CH_3CN at δ = 1.93 ppm increased over the course of 6 h. Apart from this, new resonances whose chemical shifts are identical to those of the previous high-pressure experiment appeared. The resonance at δ = 2.18 ppm vanished and the intensities of the new resonances increased over the course of 2 d. These new resonances were, in turn, gradually replaced by the spectrum of **1** when the N_2 pressure was released, showing this conversion to be reversible. These findings can be interpreted as follows: the primary step is the nucleophilic substitution of the CH_3CN ligand by N_2 to give the intermediate species **9** showing the $\nu(N_2)$ band at 2139 cm^{-1}. At normal pressure, compound **9** rapidly loses its N_2 ligand with subsequent formation of the stable compound **1** [Equation (1)].

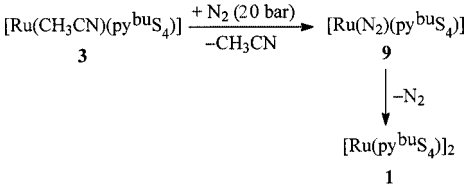

(1)

There are reports in the literature that the formation of dinitrogen complexes occurs in the reaction of NO with metal-bound ammonia.[12] Isotopic-tracer and kinetic studies imply that the mechanism involves attack of NO at metal-bound ammonia and subsequent dehydration.[13] Reaction of **4** with NO in THF yielded the 19-valence-electron neutral complex [Ru(NO)(py^{bu}S$_4$)] (**10**; IR: $\tilde{\nu}$ = 1640 cm^{-1}) as the major product; some traces of 18-valence-electron cationic [Ru(NO)(py^{bu}S$_4$)]$^+$ (IR: $\tilde{\nu}$ = 1886 cm^{-1}) and N_2O (IR: $\tilde{\nu}$ = 2224 cm^{-1}) were also found in solution. The solution of **10** is stable only under NO. Treatment of a solution of **10** with N_2 (50 bar) for 5 d caused the color of the solution to change from green to red; the resulting solution showed a weak band at 2139 cm^{-1} in the IR spectrum, indicating the formation of the N_2 species **9** in solution [Equation (2)]. In contrast to this, the analogous reaction of **4** with an equimolar amount of $NOBF_4$ resulted in the formation of the ruthenium(III) complex [Ru(NH$_3$)(py^{bu}S$_4$)]BF$_4$ (**11**), according to Equation (3). Figure 5 depicts the molecular structures of **11** and **11a**, and Table 1 lists selected bond lengths and angles.

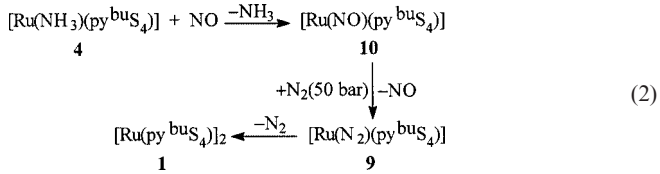

(2)

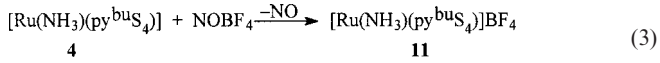

(3)

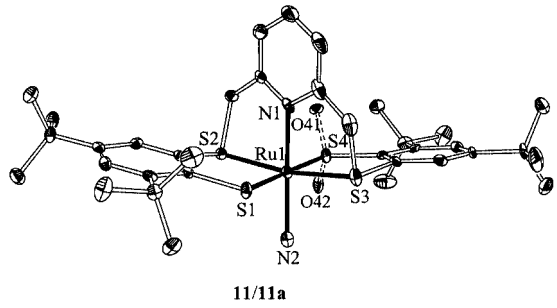

11/11a

Figure 5. Thermal ellipsoid plots of [Ru(NH$_3$)(py^{bu}S$_4$)]BF$_4$·CD_2Cl_2 (**11**·CD_2Cl_2) (without S−O bonds) and [Ru(NH$_3$)(py^{bu}S$_4$-O$_2$)]BF$_4$·CD_2Cl_2 (**11a**·CD_2Cl_2) (with S−O bonds) (50% probability ellipsoids; BF_4 counterion, H atoms and solvent molecules omitted)

The unit cell of **11** contains one molecule of CD_2Cl_2 per formula unit. The ruthenium(III) center is surrounded by two N and four S atoms in a pseudooctahedral geometry. The two thioether and two thiolate donors adopt *trans* positions, and the NH_3 ligand occupies the position *trans* to the pyridine N donor. The Ru−S(thiolate) and Ru−S(thioether) distances all lie in the range between 229 and 232 pm. This is in contrast to the corresponding distances of **4** as well as other [Ru^{II}(L)(py^{bu}S$_4$] complexes, where the Ru−S(thiolate) distances are usually longer than the Ru−S(thioether) distances.[8] The Ru−N(pyridine) distance in **11** is longer (by about 3 pm) than that of **4**. During crystallization of **11** complex **11a** is formed by aerial oxidation of **11**.

UV irradiation of complex **5** in CH_2Cl_2 while bubbling N_2 through the solution always yielded **1** as the final product. However, IR monitoring of this reaction suggested the formation of the intermediate species **9** in solution. The IR spectrum of the solution of **5** in CH_2Cl_2 shows the ν(CO) band at 1967 cm^{-1}. Irradiation of this solution at −80 °C for 10 min gave rise to a new weak band at 2138 cm^{-1}, and subsequently the intensity of the ν(CO) band decreased. On continuous irradiation, the intensity of both the bands decreased, and after 50 min microcrystals of **1** had precipitated.

Protonation of **5** with HBF_4 at −80 °C afforded the carbonyl protonated thiolate complex [Ru(CO)(py^{bu}S$_4$H)]BF$_4$ (**12**) according to Equation (4). The IR spectrum of **12** in CH_2Cl_2 exhibits the ν(CO) band at 2001 cm^{-1} and the

 © 2004 Wiley-VCH Verlag GmbH & Co. KGaA, Weinheim

ν(SH) band at 2486 cm^{-1}. The CO absorption of **12** is red-shifted by about 34 cm^{-1} compared to that in **5**, which is in good agreement with values reported for the protonation of thiolate groups.[6] Irradiation of **12**, analogous to **5**, initially gave rise to a band at 2172 cm^{-1}, which disappeared on further irradiation to give only an uncharacterizable red-brown solid. It is interesting to note that the difference in wavenumbers between the ν(CO) and ν(N_2) bands in the corresponding complex pairs of **5** and **12** are 168 and 169 cm^{-1}, respectively. These values are in good agreement with those reported for other CO and N_2 complexes.[3] Moreover, the frequency difference between the new bands formed during UV irradiation of **5** and **12** is 34 cm^{-1} for both complexes. These results indicate that the irradiation reactions of **5** and **12** in the presence of N_2 proceed by similar pathways; the first step may be the formation of the labile intermediate species [Ru(N_2)(py^{bu}S_4)] (**9**) and [Ru(N_2)(py^{bu}S_4H)]BF_4 (**13**), respectively. These species may either be subjected to irradiation or undergo simple decomplexation of the N_2 ligand to give the stable thiolate-bridged dimer or other products.

$$\underset{\mathbf{5}}{[Ru(CO)(py^{bu}S_4)]} + HBF_4 \underset{-50\ °C}{\overset{-78\ °C}{\rightleftharpoons}} \underset{\mathbf{12}}{[Ru(CO)(py^{bu}S_4H)]BF_4} \quad (4)$$

Taken together, these results demonstrate that the dinuclear complex **1** and the mononuclear complexes **3**, **5**, **10** and **12** are capable of coordinating molecular nitrogen under moderate pressures of N_2 to form the corresponding labile dinitrogen complexes, although attempts to isolate these species inevitably yielded only the more stable thiolate-bridged complex. Therefore, in an effort to stabilize the labile N_2 species, as well as to prevent the formation of Ru−S bridges, synthesis of a metal fragment containing electron-rich and sterically bulky substituent groups is in progress.

Conclusion

In the quest for transition metal−sulfur complexes that enable the modelling of the reactivity features and key intermediates of nitrogenases reactions, [Ru(L)(py^{bu}S_4] complexes were synthesized and completely characterized. The molecular structures of **3**, **4** and **5** were determined by X-ray structure analysis. All complexes exhibit a pseudooctahedral geometry. The central metal atom is surrounded by at least two thiolate and two thioether groups in mutual *trans* positions, and has a well-approximated C_2 symmetry. The reactivity of [Ru(py^{bu}S_4)]$_2$ and [Ru(L)(py^{bu}S_4] complexes towards molecular nitrogen was investigated. IR and NMR spectroscopic evidence for the formation of the labile mononuclear dinitrogen complexes has been found in the reactions between **1**, **3**, **5**, **10** or **12** and N_2. The reaction of **4** with NO results in the formation of the labile 19-valence-electron NO complex **10**, while treatment of **4** with $NOBF_4$ yielded only the (ammonia)ruthenium(III) complex **11**. Attempts to isolate compound **9** were unsuccessful.

Experimental Section

General: All reactions and manipulations were carried out under Ar or N_2 using standard Schlenk techniques. Solvents were freshly dried with appropriate drying agents and distilled before use. Most reactions were monitored by IR or NMR spectroscopy. Physical measurements were carried out with the following instruments: IR (KBr discs or CaF_2 cuvettes, solvent bands were compensated), Perkin−Elmer 983, 1620 FT-IR and 16PC FT-IR; NMR: Jeol JNM-GX 270, Jeol JNM-EX 270, and Lambda LA 400 with the residual signals of the deuterated solvent used as an internal reference, chemical shifts are quoted in the δ scale (downfield shifts are positive); MS: Jeol MSTATION 700 spectrometer; elemental analysis: Carlo Erba EA 1106 or 1108 analyzer; cyclic voltammetry (CV): EG&G potentiostat PAR model 264A and a conventional three-electrode assembly consisting of a glassy-carbon working electrode and Pt reference and counter electrodes, solutions: THF (10^{-3} M), supporting electrolyte: NBu_4PF_6 (10^{-1} M), internal standard: ferrocene with $E(F_c/F_c^+)$ = +0.4 V vs. NHE,[14] scan speed: 50 mV s^{-1}, T = 25 °C, the reversibility of the voltammograms and the number of electrons involved in the redox processes were determined as described in the literature.[15] $NaAlH_4$ (1 M solution in THF), N_2H_4 (1 M solution in THF) and NEt_4N_3 were purchased from either Aldrich or Fluka. The compounds [Ru(NO)(py^{bu}S_4)]Br and [Ru(py^{bu}S_4)]$_2$ (**1**) were prepared as described in the literature.[7,8b]

Na[Ru(H)(py^{bu}S_4)] (2): An excess of $NaAlH_4$ (4 mL, 1 M solution in THF, 4 mmol) was added to a pink-red suspension of **1** (500 mg, 0.35 mmol) in THF (20 mL) at −80 °C. Upon warming, the suspension changed to a red solution. The solution was stirred at 20 °C for 1 h, then the solvent was removed in vacuo. The resulting red residue was dissolved again in Et_2O (20 mL) and the insoluble colorless materials were removed by filtration. ***Caution:*** *The colorless precipitate is extremely pyrophoric and should be handled with care!* The filtrate was concentrated and treated with pentane to give red microcrystals of **2**. Yield: 336 mg (65%). ^{1}H NMR (269.7 MHz, [D$_8$]THF): δ = −14.85 (s, 1 H, RuH), 1.28 (s, 18 H, *t*Bu), 1.51 (s, 18 H, *t*Bu), 4.42 (d, $^2J_{H,H}$ = 15.3 Hz, 2 H, CH_2), 4.65 (d, $^2J_{H,H}$ = 15.3 Hz, 2 H, CH_2), 6.90−6.83 (m, 3 H, C_5H_3N), 6.99 (d, $^3J_{H,H}$ = 1.9 Hz, 2 H, C_6H_2), 7.51 (d, $^3J_{H,H}$ = 1.9 Hz, 2 H, C_6H_2) ppm. ^{13}C{^{1}H} NMR (67.8 MHz, [D$_8$]THF): δ = 30.0, 32.0, 34.8, 38.4 (*t*Bu), 62.4 (CH_2), 119.1, 122.5, 127.2, 129.7, 137.7, 142.2, 148.9, 154.9, 155.7 (C_6H_2/C_5H_3N) ppm. CV (vs. NHE): E = +0.235 V (Ru^{II}/Ru^{III}).

[Ru(CH_3CN)(py^{bu}S_4)] (3): A suspension of **1** (500 mg, 0.35 mmol) in CH_3CN (25 mL) was refluxed for 2 d. The resulting orange-red solution was filtered, concentrated (2 mL), and treated with pentane to give orange microcrystals of **3**. Yield: 254 mg (48%). $C_{37}H_{52}N_2ORuS_4$ (770.17): calcd. C 57.70, H 6.80, N 3.63, S 16.65; found C 57.87, H 7.14, N 3.80, S 16.18. IR (KBr): $\tilde{\nu}$ = 2269 cm^{-1} ν(CN). ^{1}H NMR (269.7 MHz, CD_3CN): δ = 1.31 (s, 18 H, *t*Bu), 1.54 (s, 18 H, *t*Bu), 2.18 (s, 3 H, CH_3CN), 4.53 (d, $^2J_{H,H}$ = 16.1 Hz, 2 H, CH_2), 4.68 (d, $^2J_{H,H}$ = 16.2 Hz, 2 H, CH_2), 6.93 (d, $^3J_{H,H}$ = 7.7 Hz, 2 H, C_5H_3N), 7.08 (t, $^3J_{H,H}$ = 2.0 Hz, 1 H, C_5H_3N), 7.18 (d, $^3J_{H,H}$ = 2.1 Hz, 2 H, C_6H_2), 7.58 (d, $^3J_{H,H}$ = 2.1 Hz, 2 H, C_6H_2) ppm. ^{13}C{^{1}H} NMR (67.8 MHz, CD_3CN): δ = 22.5 (CH_3CN), 29.6, 31.6, 34.9, 38.2 (*t*Bu), 57.5 (CH_2), 121.0, (C_6H_2), 124.3 (CH_3CN), 124.8, 127.9, 133.3, 134.4, 144.8, 149.2, 153.3,

 © 2004 Wiley-VCH Verlag GmbH & Co. KGaA, Weinheim

160.0 (C_6H_2/C_5H_3N) ppm. FD-MS (CH_3CN): m/z = 752 [$\mathbf{3}^+$], 1422 [$\mathbf{1}^+$]. CV (vs. NHE): E = +0.214 V (Ru^{II}/Ru^{III}).

[Ru(NH$_3$)(py^{bu}S$_4$)] (4): NH_3 gas was bubbled through the suspension of **1** (300 mg, 0.21 mmol) in THF (10 mL) for 15 min, and the mixture was then stirred under NH_3 for 20 h. The resulting solution was concentrated (2 mL) and treated with pentane to give red microcrystals of **4**. Yield: 278 mg (92%). $C_{35}H_{50}N_2RuS_4$ (728.13): calcd. C 57.74, H 6.92, N 3.85, S 17.62; found C 57.76, H 6.87, N 3.94, S 17.38. IR (KBr): $\tilde{\nu}$ = 3344, 3262, 3175, 3084 cm^{-1} $\nu(NH_3)$. ^{1}H NMR (269.7 MHz, [D$_8$]THF): δ = 1.30 (s, 18 H, *t*Bu), 1.59 (s, 18 H, *t*Bu), 1.71 (s, 3 H, NH_3), 4.45 (d, $^2J_{H,H}$ = 15.5 Hz, 2 H, CH_2), 4.65 (d, $^2J_{H,H}$ = 15.7 Hz, 2 H, CH_2), 6.95−6.80 (m, 3 H, C_5H_3N), 7.11 (d, $^3J_{H,H}$ = 1.7 Hz, 2 H, C_6H_2), 7.55 (d, $^3J_{H,H}$ = 1.8 Hz, 2 H, C_6H_2) ppm. ^{13}C{^{1}H} NMR (67.8 MHz, [D$_8$]THF): δ = 30.0, 31.9, 34.8, 38.4 (*t*Bu), 57.8 (CH_2), 119.9, 123.6, 127.3, 130.3, 135.2, 143.4, 149.1, 154.2, 159.7 (C_6H_2/C_5H_3N) ppm. FD-MS (THF): m/z = 728 [$\mathbf{4}^+$], 1422 [$\mathbf{1}^+$]. CV (vs. NHE): E = +0.252 V (Ru^{II}/Ru^{III}).

[Ru(CO)(py^{bu}S$_4$)] (5): CO gas was bubbled through the suspension of **1** (350 mg, 0.24 mmol) in THF (10 mL) for 30 min, and the mixture was then stirred under CO for 15 h. The resulting yellow solution was filtered, concentrated (2 mL), and treated with Et_2O to give yellow microcrystals of **4**. Yield: 337 mg (94%). $C_{36}H_{47}NORuS_4$ (739.11): calcd. C 53.93, H 5.99, N 1.70, S 15.56; found C 54.13, H 5.95, N 1.69, S 15.38. IR (KBr): $\tilde{\nu}$ = 1967 cm^{-1} ν(CO). ^{1}H NMR (269.7 MHz, [D$_6$]acetone): δ = 1.29 (s, 18 H, *t*Bu), 1.51 (s, 18 H, *t*Bu), 4.65 (d, $^2J_{H,H}$ = 16.2 Hz, 2 H, CH_2), 4.95 (d, $^2J_{H,H}$ = 16.3 Hz, 2 H, CH_2), 7.25 (d, $^3J_{H,H}$ = 2.0 Hz, 2 H, C_6H_2), 7.36 (d, $^3J_{H,H}$ = 7.7 Hz, 2 H, C_5H_3N), 7.53 (m, 1 H, C_5H_3N), 7.65 (d, $^3J_{H,H}$ = 2.0 Hz, 2 H, C_6H_2) ppm. ^{13}C{^{1}H} NMR (67.8 MHz, [D$_6$]acetone): δ = 29.9, 31.7, 35.0, 38.3 (*t*Bu), 59.2 (CH_2), 121.9, 125.0, 127.7, 133.9, 136.9 145.5, 149.8, 151.9, 156.9 (C_6H_2/C_5H_3N), 202.8 (CO) ppm. FD-MS (THF): m/z = 739 [$\mathbf{5}^+$]. CV (vs. NHE): E = +0.458 V (Ru^{II}/Ru^{III}).

[Ru(N$_2$H$_4$)(py^{bu}S$_4$)] (6). (a): N_2H_4 (3.5 mL, 1 M solution in THF, 3.5 mmol) was added to a suspension of **1** (250 mg, 0.17 mmol) in THF (15 mL), and was refluxed for 24 h. The red solution that resulted was filtered, reduced in volume and treated with pentane to give red microcrystals of **6**. Yield: 172 mg (67%). **(b):** A solution of **5** (300 mg, 0.21 mmol) and N_2H_4 (2 mL, 1 M solution in THF, 2 mmol) in THF (35 mL) was irradiated in a quartz immersion lamp apparatus with an Hg lamp (150 W) at −30 °C for 1 h. The resulting solution was filtered, reduced in volume and the product precipitated with pentane to give **6** as a red powder. Yield: 280 mg (91%). $C_{35}H_{51}N_3RuS_4$ (743.15): calcd. C 56.57, H 6.92, N 5.65, S 17.26; found C 56.59, H 7.14, N 5.38, S 17.08. IR (KBr): $\tilde{\nu}$ = 3334, 3202, 3101 cm^{-1} ν(NH). ^{1}H NMR (269.7 MHz, CD_2Cl_2): δ = 1.32 (s, 18 H, *t*Bu), 1.59 (s, 18 H, *t*Bu), 3.45 (b, 2 H, NH_2NH_2), 4.15 (m, 2 H, NH_2NH_2), 4.42 (d, $^2J_{H,H}$ = 15.8 Hz, 2 H, CH_2), 4.69 (d, $^2J_{H,H}$ = 16.0 Hz, 2 H, CH_2), 6.89 (d, $^3J_{H,H}$ = 7.6 Hz, 2 H, C_5H_3N), 6.94 (t, $^3J_{H,H}$ = 7.5 Hz, 1 H, C_5H_3N), 7.21 (d, $^3J_{H,H}$ = 2.0 Hz, 2 H, C_6H_2), 7.58 (d, $^3J_{H,H}$ = 2.0 Hz, 2 H, C_6H_2) ppm. ^{13}C{^{1}H} NMR (67.8 MHz, CD_2Cl_2): δ = 29.5, 31.6, 34.6, 38.0 (*t*Bu), 57.0 (CH_2), 120.0, 124.2, 127.2, 130.8, 134.0, 144.6, 149.3, 151.6, 158.9 (C_6H_2/C_5H_3N) ppm. FD-MS (THF): m/z = 743 [$\mathbf{6}^+$], 1422 [$\mathbf{1}^+$]. CV (vs. NHE): E = +0.284 V (Ru^{II}/Ru^{III}).

[Ru(PMe$_3$)(py^{bu}S$_4$)] (7): PMe_3 (52 mg, 0.68 mmol) was added to a suspension of **1** (250 mg, 0.17 mmol) in THF (10 mL) and stirred for 2 h. The resulting solution was filtered, reduced in volume and treated with pentane to give yellow-red microcrystals of **7**. Yield: 194 mg (71%). $C_{38}H_{56}NPRuS_4$ (787.181): calcd. C 57.98, H 7.17, N 1.78, S 16.29; found C 57.74, H 7.08, N 1.64, S 16.08. ^{1}H NMR (269.7 MHz, [D$_8$]THF): δ = 1.06 (s, 9 H, PMe_3), 1.28 (s, 18 H, *t*Bu), 1.56 (s, 18 H, *t*Bu), 4.41 (d, $^2J_{H,H}$ = 15.7 Hz, 2 H, CH_2), 4.62 (d, $^2J_{H,H}$ = 15.8 Hz, 2 H, CH_2), 6.90−6.75 (m, 3 H, C_5H_3N), 7.09 (d, $^3J_{H,H}$ = 1.7 Hz, 2 H, C_6H_2), 7.52 (d, $^3J_{H,H}$ = 1.8 Hz, 2 H, C_6H_2) ppm. ^{13}C{^{1}H} NMR (67.8 MHz, [D$_8$]THF): δ = 15.4 (PMe_3), 29.5, 31.3, 34.1, 38.2 (*t*Bu), 57.4 (CH_2), 119.4, 122.6, 127.1, 130.0, 134.7, 142.8, 148.3, 153.4, 158.7 (C_6H_2/C_5H_3N) ppm. ^{31}P{^{1}H} NMR (161.8 MHz, [D$_8$]THF): δ = 18.6 (PMe_3) ppm. FD-MS (THF): m/z = 787 [$\mathbf{4}^+$]. CV (vs. NHE): E = +0.243 V (Ru^{II}/Ru^{III}).

Et$_4$N[Ru(N$_3$)(py^{bu}S$_4$)] (8): NEt_4N_3 (100 mg, 0.58 mmol) was added to a suspension of **1** (200 mg, 0.14 mmol) in THF (10 mL) and stirred for 2 d. The resulting solution was filtered, concentrated, and treated with pentane to give pink-red microcrystals of **8**. Yield: 115 mg (47%). IR (KBr): $\tilde{\nu}$ = 2022 cm^{-1} $\nu(N_3)$. ^{1}H NMR (269.7 MHz, CD_3OD): δ = 0.50 (t, $^3J_{H,H}$ = 7.3 Hz, 12 H, NEt_4), 1.28 (m, 8 H, NEt_4), 1.34 (s, 18 H, *t*Bu), 1.60 (s, 18 H, *t*Bu), 4.47 (d, $^2J_{H,H}$ = 15.7 Hz, 2 H, CH_2), 4.68 (d, $^2J_{H,H}$ = 15.8 Hz, 2 H, CH_2), 6.90−6.75 (m, 3 H. C_5H_3N), 7.13 (d, $^3J_{H,H}$ = 1.7 Hz, 2 H, C_6H_2), 7.56 (d, $^3J_{H,H}$ = 1.8 Hz, 2 H, C_6H_2) ppm. ^{13}C{^{1}H} NMR (67.8 MHz, CD_3OD): δ = 8.2 (NEt_4), 29.5, 31.6, 34.6, 38.0 (*t*Bu), 52.4 (NEt_4), 56.6 (CH_2), 119.8, 124.5, 126.4, 130.8, 134.2, 146.6, 148.0, 151.8, 157.9 (C_6H_2/C_5H_3N) ppm. CV (vs. NHE): E = +0.293 V (Ru^{II}/Ru^{III}).

[Ru(NO)(py^{bu}S$_4$)] (10): NO gas was bubbled thorugh a solution of **4** (300 mg, 0.41 mmol) in THF (15 mL) for 3 min, The resulting green solution was filtered under NO. IR (THF): $\tilde{\nu}$ = 1640 cm^{-1} ν(NO).

[Ru(NH$_3$)(py^{bu}S$_4$)]BF$_4$ (11): $NOBF_4$ (35 mg, 0.30 mmol) was added to a solution of **4** (210 mg, 0.29 mmol) in THF (15 mL). The color of the solution changed instantaneously from red to green. K_2CO_3 (20.7 mg, 0.15 mmol) was added to this solution and stirred for 1 h. The solution was filtered, concentrated (2 mL) and treated with pentane to give green microcrystals of **10**. Yield: 202 mg (86%). $C_{35}H_{50}BF_4N_2RuS_4$ (814.94): calcd. C 51.59, H 6.18, N 3.44, S 15.74; found C 51.62, H 6.20, N 3.45, S 15.68. IR (KBr): $\tilde{\nu}$ = 3358, 3268, 3186, 3089 cm^{-1} $\nu(NH_3)$. FD-MS (THF): m/z = 728 [Ru(NH$_3$)(py^{bu}S$_4$)$^+$], 1422 [$\mathbf{1}^+$].

[Ru(CO)(py^{bu}S$_4$H)]BF$_4$ (12): HBF_4 (0.30 mL, 0.22 mmol) was added to a solution of **5** (300 mg, 0.21 mmol) in CH_2Cl_2 (10 mL) at −80 °C. The color of the solution changed from red-yellow to dark-green. IR (CH_2Cl_2): $\tilde{\nu}$ = 2001 cm^{-1} ν(CO), 2486 cm^{-1} ν(SH).

High-Pressure NMR Experiment in an Autoclave: In a special autoclave, an NMR tube containing a suspension of **1** (70 mg) in [D$_8$]THF (0.6 mL) was pressurized with N_2 (5.0 grade, 60 bar), and was kept at 40 °C for 7 d. The autoclave was cooled to room temperature, and the pressure was released. The resulting red solution was monitored by recording ^{1}H NMR spectra at various time intervals.

High-Pressure NMR Experiment: In a pressure NMR tube (524-PV-1,Wilmad, USA), a solution of **3** (50 mg) in [D$_8$]THF (0.6 mL) was pressurized with N_2 (5.0 grade, 20 bar). The reaction was monitored by recording ^{1}H NMR spectra at various time intervals for 2 d.[7,16]

High-Pressure Autoclave Experiment. (a): In an autoclave, a tube containing a suspension of **1** (350 mg) in THF (15 mL) was pressurized with N_2 gas (60 bar), and the suspension was stirred at 40 °C for 4 d. The autoclave was cooled to −80 °C and the pressure was released. IR (THF) spectra were recorded of the red solution at

 © 2004 Wiley-VCH Verlag GmbH & Co. KGaA, Weinheim

various time intervals. **(b):** In an autoclave, a tube containing an orange solution of **3** (200 mg) in THF (15 mL) was pressurized with N_2 gas (20 bar) and the solution was stirred at 20 °C for 2 d. The pressure was then released and IR (THF) spectra were recorded of the resulting red solution at various time intervals. **(c):** The pressure reaction was performed as in (b). The autoclave was frozen with liquid nitrogen and then the pressure was released. The temperature was raised to −80 °C, the red solution was filtered, and treated with cold pentane to give a red solid. IR (KBr): $\tilde{\nu}$ = 2134 cm^{-1} $\nu(N_2)$.

UV-Irradiation Reaction: At −80 °C and with vigorous N_2 bubbling, a solution of **5** (250 mg) or **12** (300 mg) in CH_2Cl_2 (35 mL) was irradiated in a quartz immersion lamp apparatus with an Hg lamp (150 W) for 1 h. The reaction was monitored by recording IR (CH_2Cl_2) spectra until a pink-red or brown precipitate had formed from the solution.

X-ray Structure Determination of [Ru(CH$_3$CN)(py^{bu}S$_4$)]·2CH$_3$CN (3·2CH$_3$CN), [Ru(NH$_3$)(py^{bu}S$_4$)]·CH$_2$Cl$_2$·0.5*n*-pentane (4·CH$_2$Cl$_2$·0.5*n*-pentane), [Ru(CO)(py^{bu}S$_4$)]·CH$_3$OH·(CH$_3$)$_2$CO [5·CH$_3$OH·(CH$_3$)$_2$CO], [Ru(NH$_3$)(py^{bu}S$_4$)]BF$_4$·CD$_2$Cl$_2$ (11·CD$_2$Cl$_2$) and [Ru(NH$_3$)(py^{bu}S$_4$-O$_2$)]BF$_4$·CD$_2$Cl$_2$ (11a·CD$_2$Cl$_2$): Over the course of 5 d, red plates of **3**·2CH_3CN crystallized from a saturated solution of **3** in CH_3CN at −25 °C. Red fragments of **4**·CH_2Cl_2·0.5*n*-pentane were grown from a concentrated CH_2Cl_2 solution of **4** layered with pentane at 4 °C over 2 d. Red crystals of **4**·0.5*n*-pentane were also formed from a solution of **4** in a THF/*n*-pentane mixture. Yellow plates of **5**·CH_3OH·$(CH_3)_2CO$ crystallized from a solution of **5** in acetone layered with CH_3OH at 4 °C. Green crystals of **11**/**11a**·CD_2Cl_2 were formed from a CD_2Cl_2 solution of **11** kept at room temperature for 3 d. Suitable single crystals were embedded in protective perfluoropolyether oil. Data were collected with a Bruker-Nonius KappaCCD diffractometer using Mo-K_α radiation (λ = 71.073 pm), and a graphite monochromator. A numerical absorption correction was performed for **3**·2CH_3CN. Absorption effects for the other compounds were corrected on a semiempirical basis with the help of multiple scans using either SORT AV[17a] [**5**·CH_3OH·$(CH_3)_2CO$ and 0.75**11**·0.25[Ru(NH_3)(py^{bu}S$_4$-O_2)]BF_4·CD_2Cl_2] or SADABS[17b] (**4**·CH_2Cl_2·0.5*n*-pentane). All structures were solved by direct methods, and full-matrix least-squares refinement was carried out on F^2 using SHELXTL NT 5.1 and NT 6.12.[18] All non-hydrogen atoms were refined anisotropically. The hydrogen atoms of **11**/**11a**·CD_2Cl_2 were located from a difference Fourier map, while in all other compounds the H atoms were geometrically positioned with isotropic displacement parameters being 1.5-times *U*(eq) of the parent C or N atom. One of the CH_3CN molecules of **3** is disordered, and two alternative sites were refined to 52(2)% (N4, C5, S6) and 48(2)% (N4′, C5′, S6′). Two alternative sites were refined for one of the *t*Bu groups of **4** to 66(2)% (C55−C57) and 34(2)% (C55′−C57′). In **11a**·CD_2Cl_2, the S4 atom is partially oxidized, with the two O atoms having occupancy factors of 25(1)% each. Selected crystallographic parameters and refinement details are summarized in Table 2. Crystallographic data for **4**·0.5*n*-pentane have only been deposited with the Cambridge Crystallographic Data Base.[20]

Acknowledgments

Financial support of these investigations by the Deutsche Forschungsgemeinschaft (SFB 583: Redoxaktive Metallkomplexe) is gratefully acknowledged. We thank Prof. Dr. Horst Kisch for helpful suggestions.

Table 2. Selected crystallographic data for [Ru(CH_3CN)(py^{bu}S$_4$)]·2CH_3CN (**3**·2CH_3CN), [Ru(NH_3)(py^{bu}S$_4$)]·CH_2Cl_2·0.5*n*-pentane (**4**·CH_2Cl_2·0.5*n*-pentane), [Ru(CO)(py^{bu}S$_4$)]·CH_3OH·$(CH_3)_2CO$ [**5**·CH_3OH·$(CH_3)_2CO$], [Ru(NH_3)(py^{bu}S$_4$)]BF_4·CD_2Cl_2 (**11**·CD_2Cl_2) and [Ru(NH_3)(py^{bu}S$_4$-O$_2$)]BF_4·CD_2Cl_2 (**11a**·CD_2Cl_2)

	3·2MeCN	**4**·CH_2Cl_2·0.5*n*-pentane	**5**·MeOH·Me_2CO	**11**·CD_2Cl_2/**11a**·CD_2Cl_2
Empirical formula	$C_{41}H_{56}N_4RuS_4$	$C_{38.5}H_{58}Cl_2N_2RuS_4$	$C_{40}H_{57}NO_3RuS_4$	$C_{36}H_{52}BCl_2F_4N_2O_{0.5}RuS_4$
M_r [g/mol]	834.21	849.08	829.18	907.82
Crystal system	monoclinic	triclinic	orthorhombic	monoclinic
Space group	$P2_1/n$	$P\bar{1}$	$Pna2_1$	$P2_1/n$
a [pm]	1757.5(2)	911.2(1)	3241.4(2)	1067.8(2)
b [pm]	1497.9(2)	1307.3(2)	952.54(8)	1400.0(2)
c [pm]	1776.8(1)	1818.8(2)	1320.43(8)	2745.8(3)
α [°]	90	93.775(7)	90.0	90
β [°]	111.92(1)	94.166(7)	90.0	94.826(8)
γ [°]	90	101.679(8)	90.0	90
V [nm^3]	4.3394(8)	2.1089(5)	4.0769(5)	4.0902(8)
Z	4	2	4	4
$d_{calcd.}$ [g/cm^3]	1.277	1.337	1.351	1.474
Temperature [*K*]	100(2)	100(2)	100(2)	100(2)
μ [mm^{-1}]	0.586	0.725	0.626	0.767
F (000)	1752	890	1744	1876
Crystal size [mm]	0.17 × 0.15 × 0.06	0.34 × 0.25 × 0.11	0.24 × 0.14 × 0.02	0.25 × 0.22 × 0.10
2θ range [°]	6.8−50.0	6.6−55.0	6.6−54.0	6.1−54.2
T_{min}/T_{max}	0.914/0.977	0.756/1.000	0.881/0.985	0.838/0.963
Measd. refl.	39123	37179	22814	74469
Indep. refl.	7631	9507	8252	8986
Obsd. refl.	4754	6523	4918	6099
Ref. parameter	495	493	444	625
*R*1 [$I > 2\sigma(I)$]	0.0665	0.0488	0.0570	0.0525
*wR*2 (all data)	0.1550	0.1110	0.1166	0.1057
$\Delta\rho_{max/min}$ [$Å^3$]	1.163/−0.676	0.859/−0.680	0.678/−0.557	0.584/−0.560
Absolute structure parameter[19]	−	−	0.01(4)	−

 © 2004 Wiley-VCH Verlag GmbH & Co. KGaA, Weinheim

[1] [1a] J. B. Howard, D. C. Rees, *Chem. Rev.* **1996**, *96*, 2965−2982. [1b] B. K. Burgess, D. J. Lowe, *Chem. Rev.* **1996**, *96*, 2983−3011. [1c] R. R. Eady, *Chem. Rev.* **1996**, *96*, 3013−3030. [1d] R. N. F. Thorneley, D. J. Lowe, *J. Biol. Inorg. Chem.* **1996**, *1*, 576−580. [1e] D. C. Rees, J. B. Howard, *Curr. Opin. Chem. Biol.* **2000**, *4*, 559−566. [1f] O. Einsle, F. A. Tezcan, S. L. A. Andrade, B. Schmid, M. Yoshida, J. B. Howard, D. C. Rees, *Science* **2002**, *297*, 1696−1700.

[2] [2a] H. Deng, R. Hofmann, *Angew. Chem.* **1993**, *105*, 1125−1128; *Angew. Chem. Int. Ed. Engl.* **1993**, *32*, 1062−1065. [2b] M. D. Fryzuk, S. A. Johnson, *Coord. Chem. Rev.* **2000**, *200−202*, 379−409. [2c] D. Sellmann, A. Fürsattel, J. Sutter, *Coord. Chem. Rev.* **2000**, *200−202*, 545−561.

[3] [3a] R. A. Henderson, C. J. Leigh, C. J. Pickett, *Adv. Inorg. Chem. Radiochem.* **1983**, *27*, 197−292. [3b] M. Hidai, Y. Mizobe, *Chem. Rev.* **1995**, *95*, 1115−1133. [3c] D. V. Yandulov, R. R. Schrock, *Science* **2003**, *301*, 76−78. [3d] B. A. MacKay, M. D. Fryzuk, *Chem. Rev.* **2004**, *104*, 385−401.

[4] [4a] Y. Yoshida, T. Adachi, M. Kamanica, T. Ueda, *J. Am. Chem. Soc.* **1988**, *110*, 4872−4873. [4b] R. H. Morris, J. M. Rassner, J. F. Sawyer, M. Shiralian, *J. Am. Chem. Soc.* **1984**, *106*, 3683−3684. [4c] J. Chatt, R. H. Crabtree, J. R. Dilworth, R. L. Richards, *J. Chem. Soc., Dalton Trans.* **1974**, 2358−2362. [4d] J. R. Dilworth, J. Hu, R. H. Thompson, D. L. Hughes, *J. Chem. Soc., Chem. Commun.* **1992**, 551−553; and references cited therein. [4e] M. B. O′Regan, A. H. Liu, W. C. Finck, R. R. Schrock, *J. Am. Chem. Soc.* **1990**, *112*, 4331−4338.

[5] [5a] D. Sellmann, B. Hautsch, A. Rösler, F. W. Heinemann, *Angew. Chem.* **2001**, *113*, 1553−1555; *Angew. Chem. Int. Ed.* **2001**, *40*, 1505−1508. [5b] D. Sellmann, A. Hille, F. W. Heinemann, M. Moll, A. Rösler, J. Sutter, G. Brehm, M. Reiher, B. A. Hess, S. Schneider, *Inorg. Chim. Acta* **2003**, *348*, 194−198.

[6] [6a] D. Sellmann, J. Utz, N. Blum, F. W. Heinemann, *Coord. Chem. Rev.* **1999**, *190−192*, 607−627. [6b] D. Sellmann, J. Sutter, *Prog. Inorg. Chem.* **2003**, *52*, 585−681.

[7] D. Sellmann, R. Prakash, F. W. Heinemann, M. Moll, M. Klimowicz, *Angew. Chem.* **2004**, *116*, 1913−1916; *Angew. Chem. Int. Ed.* **2004**, *43*, 1877−1880.

[8] [8a] D. Sellmann, J. Utz, F. W. Heinemann, *Inorg. Chem.* **1999**, *38*, 5314−5322. [8b] D. Sellmann, D. Häußinger, T. Gottschalk-Gaudig, F. W. Heinemann, *Z. Naturforsch., Teil B* **2000**, *55*, 723−729. [8c] D. Sellmann, T. Gottschalk-Gaudig, F. W. Heinemann, *Inorg. Chem.* **1998**, *37*, 3982−3988.

[9] D. Sellmann, T. Gottschalk-Gaudig, D. Häußinger, F. W. Heinemann, B. A. Hess, *Chem. Eur. J.* **2001**, *7*, 2099−2103.

[10] D. Sellmann, K. Engl, F. W. Heinemann, *Eur. J. Inorg. Chem.* **2000**, 423−429.

[11] *Recent Advances in Hydride Chemistry* (Eds.: M. Peruzzini, R. Poli), Elsevier, Amsterdam, **2001**, and references cited therein.

[12] [12a] S. D. Pell, J. N. Armor, *J. Am. Chem. Soc.* **1972**, *94*, 686−687. [12b] S. D. Pell, J. N. Armor, *J. Am. Chem. Soc.* **1973**, *95*, 7625−7633.

[13] J. D. Buhr, H. Taube, *Inorg. Chem.* **1980**, *19*, 2425−2434.

[14] [14a] H. M. Koepp, H. Wendt, H. Strehlow, *Z. Elektrochem.* **1960**, *64*, 483−491. [14b] G. Gritzner, J. Kuta, *Pure Appl. Chem.* **1984**, *56*, 461−466.

[15] A. J. Bard, L. R. Faulkner, *Electrochemical Methods, Fundamentals and Applications*, Wiley, New York, **1980**.

[16] [16a] D. Sellmann, R. Prakash, F. W. Heinemann, *Eur. J. Inorg. Chem.* **2004**, 1847−1858. [16b] D. Sellmann, R. Prakash, F. Geipel, F. W. Heinemann, *Eur. J. Inorg. Chem.* **2002**, 2138−2346.

[17] [17a] R. H. Blessing, *Acta Crystallogr., Sect. A* **1995**, *51*, 33−38. [17b] SADABS, *Bruker AXS*, Inc., Madison, WI, USA, **2002**.

[18] [18a] SHELXTL NT 5.1, *Bruker AXS*, Inc., Madison, WI, USA, **1998**. [18b] SHELXTL NT 6.12, *Bruker AXS*, Inc., Madison, WI, USA, **2002**.

[19] F. D. Flack, *Acta Crystallogr., Sect. A* **1983**, *39*, 876−881.

[20] CCDC-238008 (**3**·2CH_3CN), -238009 (**4**·CH_2Cl_2·0.5*n*-pentane), -238012 (**4**·0.5*n*-pentane), -238010 (**5**·CH_3OH·Me_2CO) and -238011 (**11/11a**·CD_2Cl_2) contain the supplementary crystallographic data for this paper. These data can be obtained free of charge at www.ccdc.cam.ac.uk/conts/retrieving.html [or from the Cambridge Crystallographic Data Centre, 12 Union Road, Cambridge CB2 1EZ, UK; Fax: + 44-1223-336-033; E-mail: deposit@ccdc.cam.ac.uk].

Received May 7, 2004
Early View Article
Published Online September 7, 2004

 © 2004 Wiley-VCH Verlag GmbH & Co. KGaA, Weinheim

A Calix[4]arene Monoalkyl Ether as a Model of a Tris(phenolate) Ligand with a Hemilabile Anisole Moiety: Syntheses, Molecular Structures and Bonding of Calix[4]arene Ether Supported Titanium Complexes and Their Catalytic Activity in Epoxidation Reactions

Andreas Friedrich[a] and Udo Radius*[a]

Keywords: Calixarenes / Density functional calculations / Epoxidation / Supported catalysts / Titanium

New mononuclear titanium complexes [TiCl(Rcalix)] [R = Me (**1**), Bz (**2**), $SiMe_3$ (**3**)] supported by *p-tert*-butylcalix[4]arene mono(organyl)ethers (Rcalix) were prepared in good yield from H_2R_2calix and $[TiCl_4(THF)_2]$. The crystallographically characterized complex [TiCl(Mecalix)] (**1**) reacts readily with NaCp and $LiNR_2$ to afford the complexes [TiCp(Mecalix)] (**4**) and [Ti(NR_2)(Mecalix)] [R = Me (**5**), Et (**6**), *i*Pr (**7**), Ph (**8**)], respectively. Reactions of [Ti(NR_2)(Mecalix)] (**5**) with alcohols, phenols and thiols proceed cleanly with amide exchange, as exemplified by the synthesis of [Ti(OR)(Mecalix)] [R = Me (**10**), *i*Pr (**11**), *t*Bu (**12**), 4-*t*BuC_6H_4 (**13**), 2,6-*i*$Pr_2C_6H_3$ (**14**)], and [Ti(S*t*Bu)(Mecalix)] (**15**). Depending on the steric demand of the ligand coordinated to the [Ti(Mecalix)] complex fragment these compounds are monomeric or dimeric in the solid state, as demonstrated by the molecular structures of monomeric [Ti(OC_6H_3-2,6-*i*Pr_2)(Mecalix)] (**14**) and [Ti(S*t*Bu)(Mecalix)] (**15**), or dimeric [{Ti(OMe)(Mecalix)}$_2$] (**10**). In all complexes the calix[4]arene ligand adopts an elliptically distorted cone conformation in which the distance of the titanium atom from the anisole oxygen atom varies between 2.342 Å and 2.438 Å for the structurally characterized complexes, with the exception of the Cp complex **4**. MP2 calculations on model complexes demonstrate that the titanium–anisole oxygen bond is weak, with a particularly shallow potential energy surface in the region between 2.30 Å and 2.80 Å. The Mecalix ligand system therefore might be described as a tris(phenolate) ligand with a hemilabile anisole group in the titanium compounds reported. Despite the labile anisole ether titanium bond, isomerization of the calix[4]arene ligand to a *paco* coordination mode, as described earlier for the Me_2calix complexes [Ti(OC_6H_4-4-R)$_2$(Me_2calix)], has not been observed in these complexes. Preliminary results on the catalytic epoxidation of cyclooctene with TBHP using calix[4]arene-stabilized titanium(iv) complexes are also briefly presented.

(© Wiley-VCH Verlag GmbH & Co. KGaA, 69451 Weinheim, Germany, 2004)

Introduction

Calix[*n*]arenes are macrocyclic molecules consisting of *n* phenol units connected by *ortho*-methylene groups.[1,2] Calix[4]arenes, with four phenolic residues in the macrocyclic ring, are the simplest and most common compounds of this family. These molecules and their derivatives have been extensively studied for their interesting properties, for example as hosts for cations, anions and neutral molecules, and for the formation of supramolecular assemblies.[3]

Because of the four phenoxy groups in the calix[4]arenes (*p-tert*-butylcalix[4]arene = H_4calix), reactions with transition metal complexes can produce metal phenolate compounds with substitution of up to four hydrogen atoms.[4] Calix[4]arenes have some unique geometrical peculiarities when acting as poly(phenolate) ligands. The fully deprotonated form of the parent calix[4]arene acts as a tetraanionic ligand and usually assumes a cone conformation, which keeps the set of oxygen donor atoms quasi-planar. Depending on the exact geometry adopted in the complex and on the presence of additional metal centers in the complex, this cone conformation readily distorts towards an elliptical cone conformation.[5]

The charge of the O_4 set can be tuned by etherification or esterification of the lower rim of the calix[4]arene, and the degree of functionalization of the metal atom can be controlled by alkylating or silylating the oxygen atom(s), which also offers steric protection. The [Me_2calix] homologues, in particular have received much attention in organotransition metal chemistry over the last 10 years, and a rich chemistry has emerged comprising mainly mononuclear group 4 and 5 metals. In these complexes, the $[R_2calix]^{2-}$ ligands usually provide two negatively charged phenolate oxygen donor atoms and two neutral anisole oxygen donors to a transition metal atom. If the calix[4]arene ethers coordinate in their elliptically distorted cone conformations, these ligands provide a robust and well-defined O_4 coordination environment, similar to other widely used sup-

[a] Institut für Anorganische Chemie, Universität Karlsruhe (TH)
Engesserstr., Geb. 30.45, 76128 Karlsruhe, Germany
Fax: + 49-721-608-7021
E-mail: radius@aoc1.uni-karlsruhe.de

 © 2004 Wiley-VCH Verlag GmbH & Co. KGaA, Weinheim **DOI: 10.1002/ejic.200400430**

porting dianionic ligands such as the O_2N_2 donor ligands of salen-type Schiff bases or N_4 donor ligands such as porphyrins and dibenzotetraaza[14]annulenes.[6−8]

In contrast to these nitrogen-containing ligand systems, the calix[4]arene dialkyl ethers are conformationally much more flexible. The coordination mode of calix[4]arene dialkyl ethers is largely determined by the nature of the ether group, the coordination number of the metal atom, and the nature of the co-ligands. The cavity of the macrocyclic ligand can therefore be influenced by other ligands in transition metal calix[4]arene complexes if strongly directing co-ligands such as oxo groups are used. We have shown that in the d^0-transition metal complex [$TiCl_2$(Me$_2$calix)] (**A**) the calix[4]arene ligand adopts an elliptically distorted cone conformation, whereas in the related d^0-transition metal complex [MoO_2(*paco*-Me$_2$calix)] (**B**) the metalated calix[4]-arene ligand is coordinated in the solid state as well as in solution in a form which is reminiscent of the partial cone (*paco*) conformation of calix[4]arene (see Scheme 1).[9] In these complexes, one of the methoxy groups of the ligand is located inside the cavity of the calix[4]arene complex.

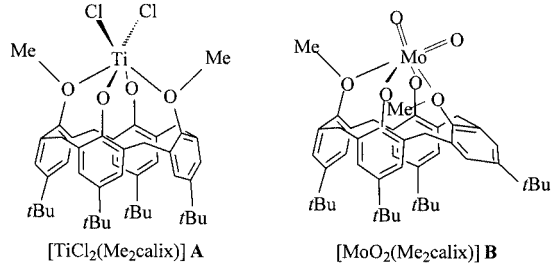

Scheme 1. Coordination modes of the calix[4]arene dimethyl ether ligand in [$TiCl_2$(Me$_2$calix)] (**A**) and [MoO_2(*paco*-Me$_2$calix)] (**B**)

In compound **B** the [Mo(Me$_2$calix)] complex fragment is further stabilized by two additional O^{2-} ligands, which exhibit a strong *trans* influence; density functional calculations on models of different isomers of **A** and **B** indicate that this phenomenon is mainly driven by the co-ligands employed in these complexes.

Furthermore, in compounds of the type [Ti(OC$_6$H$_4$-4-R)$_2$-(Me$_2$calix)] (R = Me or *t*Bu; **C**), both types of coordination mode have been observed.[10] These bis(phenolate) complexes have been isolated in good to excellent yields from the reaction of the imidotitanium complex [Ti(N*t*Bu)-(Me$_2$calix)] and 2 equiv. of the corresponding *para*-substituted phenol to afford complexes in which the calix[4]arene is coordinated in an elliptically distorted cone conformation. These complexes undergo elimination and/or rearrangement reactions in nonpolar solvents such as pentane and hexane. The metal-containing products of the elimination reactions are the dinuclear compounds [{Ti(OC$_6$H$_4$-4-R)(Mecalix)}$_2$] and the products of the rearrangement reaction are [Ti(OC$_6$H$_4$-4-R)$_2$(*paco*-Me$_2$calix)] (**C**). Density functional calculations on model compounds of [Ti(OC$_6$H$_5$)$_2$-(*cone*-Me$_2$calix)] and [Ti(OC$_6$H$_5$)$_2$(*paco*-Me$_2$calix)] reveal a slight thermodynamic preference for the *paco* isomer, but the pathway of this isomerization process is not yet clear. The rearrangement reaction is sensitive to changes of the sterics of the [M(OAr)$_2$] fragment; complexes [Ti(OC$_6$H$_3$-2,6-R$_2$)$_2$(Me$_2$calix)] with *ortho*-substituted phenolate ligands do not rearrange. We have also prepared the analogous zirconium complexes [Zr(OC$_6$H$_4$-4-Me)$_2$(Me$_2$calix)] and [Zr(OC$_6$H$_3$-2,6-Me$_2$)$_2$(Me$_2$calix)] from [Zr(NC$_6$H$_3$-2,6-*i*Pr$_2$)(Me$_2$calix)] and the corresponding phenol; they also do not undergo rearrangement or elimination reactions.[10] Furthermore, *paco* coordination was only observed for complexes of the calix[4]arene dimethyl ether in distorted octahedrally coordinated compounds of the type [MX$_2$-(Me$_2$calix)]. At this point we became interested in investigating the coordination behavior of calix[4]arene monomethyl ether complexes of the type [MX(Mecalix)]. In this contribution we report our results on titanium complexes of the type [TiX(Rcalix)], which are stabilized with the trianion of the calix[4]arene alkyl ether H_3Rcalix and different donor ligands X (Cl, NR_2, OR, SR).

Results and Discussion

Calix[4]arene Chlorotitanium Complexes

The preparation of [TiCl(Mecalix)] starting from H_2Me$_2$-calix and [$TiCl_4$(THF)$_2$] has already been published by Floriani and co-workers.[11] The outcome of this reaction depends critically upon the reaction conditions. The reaction of H_2Me$_2$calix and [$TiCl_4$(THF)$_2$] in toluene at 60 °C for 1 d affords the titanacalix[4]arene dimethyl ether [$TiCl_2$(Me$_2$-calix)],[9,10] whereas a prolonged reaction time in refluxing toluene leads to elimination of MeCl to give [TiCl(Mecalix)] [**1**; see Equation (1)]. Similarly, the reaction of H_2Bz$_2$calix[12] with [$TiCl_4$(THF)$_2$] in toluene at 80 °C for 1 h affords [TiCl(Bzcalix)] (**2**) in good yield. The elimination of BzCl seems to be more favorable than MeCl cleavage in [$TiCl_2$(Me$_2$calix)].

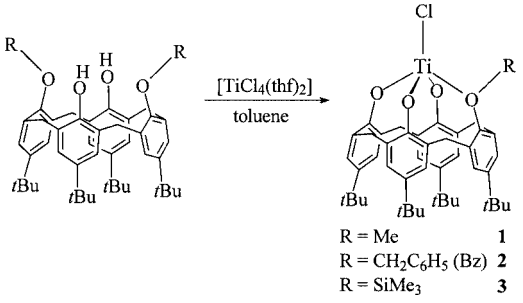

(1)

The bis(trimethylsilyl)ether H_2(Me$_3$Si)$_2$calix[13] also reacts readily with [$TiCl_4$(THF)$_2$] at room temperature to afford the titanacalix[4]arene [TiCl{(Me$_3$Si)calix}] (**3**). The thermal stability of the calixarene ether dichloro complexes [$TiCl_2$(R$_2$calix)] with respect to RCl elimination is $SiMe_3$ < Bz << Me, which reflects the stability of the radical species R — possible intermediates during the cleavage reaction — as well as the steric demand of the R group. On the other hand, formation of the dichloro complex

 © 2004 Wiley-VCH Verlag GmbH & Co. KGaA, Weinheim

$[TiCl_2\{(Me_3Si)_2calix\}]$ as a possible intermediate was not observed during the reaction of the silyl ether; NMR investigations of reaction mixtures of $H_2(SiMe_3)_2$calix and $[TiCl_4(THF)_2]$ have shown that **3** is formed within a few minutes. Therefore, it is likely that HCl as well as TMSCl elimination are involved in the first Ti−bond formation step. Raising the reaction temperature leads to further Me_3SiCl cleavage from **3** and formation of polynuclear calix[4]arene complexes.[14]

Compounds **1**−**3**, which were obtained as their toluene solvates, were characterized by elemental analysis, NMR spectroscopy and mass spectrometry. The ^1H NMR spectra of these compounds show signals typically found for calix[4]arene complexes with local C_s symmetry of the macrocyclic ligand. Three resonances were detected for the *t*Bu groups of the calix[4]arene ligand and four doublets for the methylene protons. The protons of the R substituents of [TiCl(Rcalix)] appear at δ = 3.84 (R = CH_3), 5.38 (R = CH_2Ph) and 0.49 (R = $SiMe_3$) ppm. Accurate integration of the signals confirms the cleavage of one ether group from the starting material. Furthermore, the signals are not significantly shifted to higher field, as observed previously for endohedrally located anisole ether groups, which suggests a distorted cone coordination mode of the calix[4]arene ligand. This was confirmed for **1** by X-ray analysis (Figure 1).

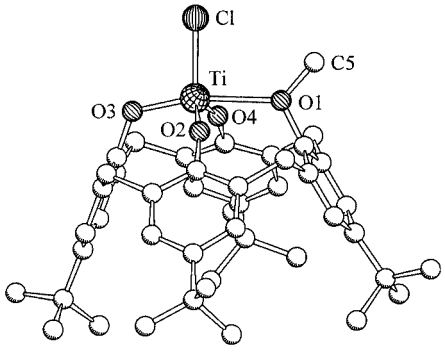

Figure 1. SCHAKAL plot of the molecular structure of [TiCl(Mecalix)] in **1**·1.5C_7H_8; H atoms and solvent molecules have been omitted for clarity; selected bond lengths [Å] and angles [°]: Ti−Cl 2.258(1), Ti−O(1) 2.424(2), Ti−O(2) 1.796(2), Ti−O(3) 1.813(2), Ti−O(4) 1.784(2); Cl−Ti−O(1) 90.1(1), Cl−Ti−O(2) 112.9(1), Cl−Ti−O(3) 103.4(1), Cl−Ti−O(4) 113.7(1), O(1)−Ti−O(2) 78.1(1), O(1)−Ti−O(3) 166.5(1), O(1)−Ti−O(4) 76.7(1), O(2)−Ti−O(3) 96.5(1), O(2)−Ti−O(4) 126.3(1), O(3)−Ti−O(4) 97.3(1), C(5)−O(1)−C(10) 112.8(2), Ti−O(1)−C(5) 129.7(2), Ti−O(1)−C(10) 117.4(2), Ti−O(2)−C(20) 156.5(2), Ti−O(3)−C(30) 121.9(2), Ti−O(4)−C(40) 159.4(2)

Single crystals of **1** were grown from saturated toluene solutions of the compound. This structure is identical, within experimental errors, with that published previously by Floriani and co-workers,[11] but it is nevertheless important to describe briefly its main features in the context of this paper for comparison with other structurally characterized complexes of the type [TiX(Mecalix)] reported here and the results of theoretical calculations described below.

Complex **1** crystallizes with an additional toluene molecule that is hosted inside the calixarene cavity and half of a toluene molecule in the asymmetric unit, which occupies a general position in the lattice. The X-ray crystal structure of **1** confirms the mononuclear character of the compound in the solid state, in which the calixarene is coordinated in an elliptically distorted cone conformation. The coordination polyhedron at the titanium atom can be described as a distorted trigonal bipyramid, in which the oxygen atoms O(1) and O(3) occupy the axial positions and Cl, O(2), and O(3) the equatorial sites. The angles Cl−Ti−O(3) [103.4(1)°] and O(2)−Ti−O(4) [126.3(1)°] reflect the significant distortions of the ideal polyhedron. The angle O(1)−Ti−O(3) between the mutually *trans*-oxygen atoms O(1) and O(3) [166.5(1)°] also reveals a deviation from a linear alignment of these atoms.

The Ti−Cl distance of 2.258(1) Å is approximately 0.10 Å shorter than that found in the distorted octahedral complex $[TiCl_2(Me_2calix)]$,[9] but it is similar to those observed in other pentacoordinated titanium complexes such as $[TiCl_2(mbmp)(THF)]$ ($[H_2mbmp$ = 2,2′-$CH_2\{6$-*t*Bu-4-$MeC_6H_2(OH)\}_2]$).[15] The Ti−O distances to the oxygen atoms O(2), O(3) and O(4) of the phenolate units [1.796(2) Å, 1.813(2) Å and 1.784(2) Å, respectively] are similar to those found in $[TiCl_2(Me_2calix)]$. The Ti−O(1) bond to the oxygen atom of the anisole unit [2.424(2) Å] is significantly longer (approximately 0.30 Å) than in $[TiCl_2(Me_2calix)]$. However, the sum of the Ti−O(1) and Ti−O(3) distances is almost identical to the sum of the corresponding Ti−O distances in $[TiCl_2(Me_2calix)]$ (4.234 Å vs. 4.237 Å), which reflects the geometrical constraint of the calix[4]arene ligand. In other words, the titanium atom moves from an ideal, central position between the anisole oxygen atoms in $[TiCl_2(Me_2calix)]$ towards the stronger phenolate oxygen donor atom O(3) in [TiCl(Mecalix)].

A Calix[4]arene Cyclopentadienyltitanium Complex

In the series [TiX(Mecalix)], Floriani et al. have already reported alkyl complexes of the type [TiR(Mecalix)] (R = Me, $CH_2C_6H_5$, 4-MeC_6H_4). In these compounds, the calix[4]arene binds in a distorted cone conformation to the [Ti−R] complex fragment, as was shown by NMR spectroscopy and a structural analysis of $[Ti(C_6H_4$-4-Me)(Mecalix)].[11] We were interested in coordinating the excellent σ,π-donor ligand $C_5H_5^-$ to the calix[4]arene titanium fragment. According to Equation (2), [TiCp(Mecalix)] (**4**) can be prepared in good yields from the reaction of **1** with NaCp.

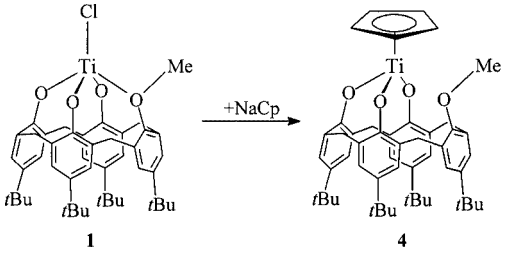

(2)

 © 2004 Wiley-VCH Verlag GmbH & Co. KGaA, Weinheim

Compound **4** was characterized by elemental analysis, mass spectrometry, and NMR spectroscopy. The NMR spectra are in accordance with a pseudo-C_s-symmetric structure of the complex in solution, as shown in Equation (2). The signals of the protons of the anisole methyl groups at δ = 3.89 ppm and of the Cp ligand at δ = 6.80 ppm, in the integration ratio 3:5, are sharp singlets at room temperature and do not change on cooling to −60 °C, which confirms the η^5-coordination mode of the Cp ligand. It is interesting to note that the chemical shifts of the protons of the anisole methyl groups at δ = 3.44 ppm in C_6D_6 and δ = 3.89 ppm in $CDCl_3$ are similar to the NMR shifts obtained for the uncomplexed ligand at δ = 3.49 ppm (C_6D_6) and δ = 3.93 ppm ($CDCl_3$). The resonances observed for **1** are significantly shifted to higher field compared to those of the uncomplexed ligand at δ = 3.84 ppm (C_6D_6) and δ = 4.26 ppm ($CDCl_3$). Similar observations have been made in the $^{13}C\{^1H\}$ NMR spectra of **4**, which points to an uncoordinated anisole group in solution. This probably reflects better electronic as well as steric shielding of the metal atom in **4** compared to the chloro complex **1**.

The molecular structure of **4** is shown in Figure 2. Complex **4** crystallizes in the space group $P2_1/c$ with one formula unit and two additional solvent molecules in the unit cell, which occupy general positions in the lattice. The titanium atom in **4** is tetrahedrally coordinated to the Cp ligand and three phenolate oxygen atoms of the calixarene. The Ti−O distances of 1.807(4) Å, 1.864(4) Å, and 1.809(4) Å are slightly longer than those observed in **1**, but similar to Ti−O bond lengths found in other stable complexes of the type $[TiCp(OR)_3]$, such as $[TiCp(OC_6H_3\text{-}2,6\text{-}i\text{Pr}_2)_3]$ [average 1.80(2) Å] and $[TiCp(OC_6F_4H)_3]$ [1.826(3) Å, 1.830(3) Å and 1.867(3) Å].[16] In comparison with the chloro complex **1**, the titanium atom is displaced further from the center of the calix[4]arene ligand; the Ti−O(1) distance of 3.498(6) Å can be regarded as nonbonding. Whereas the size of the C(50)−O(1)−C(10) angle [113.4(5)°] is similar to the corresponding angle C(5)−O(1)−C(10) [112.8(2)°] in **1**, a significant difference in the bonding of the fragments $[TiCl]^{3+}$ and $[Ti(\eta^5\text{-}C_5H_5)]^{3+}$ to the $[Mecalix]^{3-}$ ligand is also reflected in the Ti−O(1)−C(10) angles of 87.1(4)° in **4** and 117.4(1)° in **1**. As a consequence, the calixarene cavity is significantly influenced by the metal complex fragment bound at the lower rim of the ligand. The distance to the phenolate carbon atoms C(15) and C(35) in the *para* positions is 5.463 Å in the Cp complex, which is much smaller than the corresponding distance in the chloro compound **1** (7.685 Å); this distortion of the calix[4]arene ligand prevents inclusion of a solvent molecule inside the calixarene cavity.

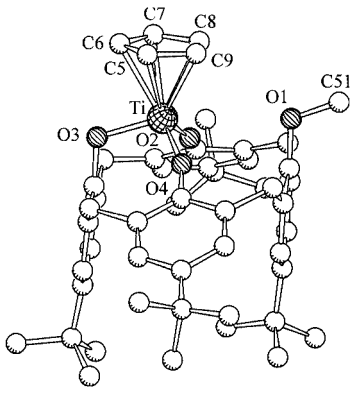

Figure 2. SCHAKAL plot of the molecular structure of [TiCp(Mecalix)] in $4{\cdot}2C_7H_8$; H atoms and solvent molecules have been omitted for clarity; selected bond lengths [Å] and angles [°]: Ti−O(1) 3.498(6), Ti−O(2) 1.807(4), Ti−O(3) 1.864(4), Ti−O(4) 1.809(4), Ti−Cp_{centr} 2.039(7), Ti−C(5) 2.365(7), Ti−C(6) 2.373(6), Ti−C(7) 2.359(7), Ti−C(8) 2.319(7), Ti−C(9) 2.327(7); Cp_{centr}−Ti−O(1) 88.5(2), Cp_{centr}−Ti−O(2) 119.6(2), Cp_{centr}−Ti−O(3) 108.1(2), Cp_{centr}−Ti−O(4) 119.5(2), O(1)−Ti−O(2) 69.4(4), O(1)−Ti−O(3) 163.4(4), O(1)−Ti−O(4) 70.2(4), O(2)−Ti−O(3) 100.98(17), O(2)−Ti−O(4) 104.84(17), O(3)−Ti−O(4) 100.68(17), Ti−O(1)−C(10) 87.1(4), Ti−O(1)−C(50) 158.4(3), C(50)−O(1)−C(10) 113.4(5), Ti−O(2)−C(20) 161.3(4), Ti−O(3)−C(30) 111.0(3), Ti−O(4)−C(40) 162.4(4)

Calix[4]arene Amidotitanium Complexes

Calix[4]arene-stabilized amidotitanium complexes of the type $[Ti(NR_2)(Mecalix)]$ with different substituents R = Me (**5**), Et (**6**), *i*Pr (**7**), Ph (**8**) are readily available by metathetical exchange of the chloro ligand in **1** with an equimolar amount of the corresponding lithium amide in toluene (see Scheme 2). These complexes can be isolated in good to reasonable yields as yellow to red powders. The mass spectra of these substances show peaks for the molecular ions as the base peaks at *m*/*z* = 751 (**5**), 779 (**6**), 807 (**7**), and 875 (**8**), which are in accordance with their formulation as mononuclear species. However, based on NMR spectroscopic data it is impossible to distinguish a monomeric complex from a possible dinuclear, amido-bridged complex of the composition $[\{Ti(\mu\text{-}NR_2)(Mecalix)\}_2]$.

The compounds $[Ti(NMe_2)(Mecalix)]$ (**5**) and $[Ti(NPh_2)(Mecalix)]$ (**8**) were structurally characterized. The molecular structures of these complexes are shown in Figures 3 and 4. All attempts to crystallize **5** from various solvents led to crystals unsuitable for X-ray diffraction. However, after prolonged storage as a THF solution, we obtained suitable crystals of complex **5** cocrystallized with its product of hydrolysis, $[\{Ti(Mecalix)\}_2(\mu\text{-}O)]$ (**9**). Complex **8** crystallizes with two independent molecules $[Ti(NPh_2)(Mecalix)]$ in the space group $P2_1/c$, which differ only slightly in their molecular structures. Since there are no significant differences between the two sets of bond lengths and angles we will refer specifically only to those from one of the molecules [at Ti(1)]; the parameters of the other molecule are given in the caption to Figure 4.

The results of the X-ray analyses confirm the mononuclear nature of **5** and **8** in the solid state, as postulated in Scheme 2. Typically, all calixarene ligands host a solvent molecule in their cavities. The coordination sphere at the metal atom in **5** and **8** is best described as distorted trigonal-bipyramidal, in which the oxygen atoms O(1) and O(3) occupy axial positions and the oxygen atoms O(2) and O(4), as well as the nitrogen atom of the amide ligand, span the equatorial plane. The oxygen atoms in the axial positions

 © 2004 Wiley-VCH Verlag GmbH & Co. KGaA, Weinheim

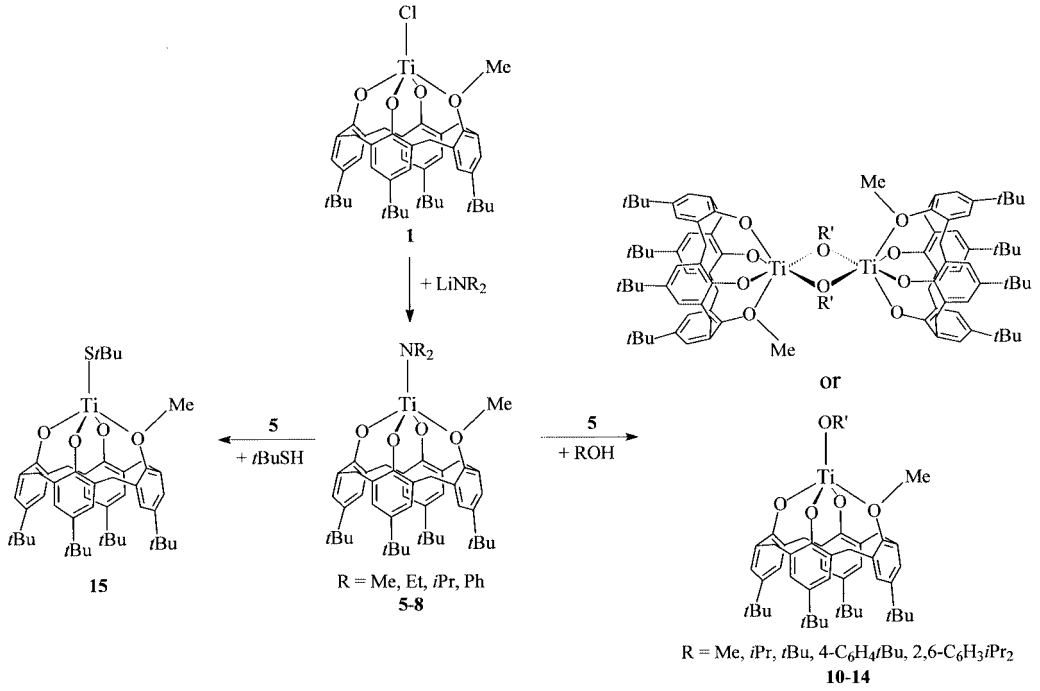

Scheme 2. Synthesis of Mecalix-stabilized amidotitanium alkoxide, phenolate, and thiolate complexes

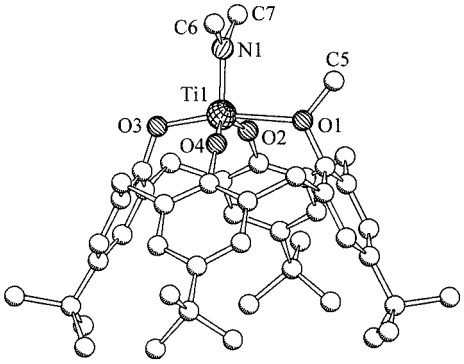

Figure 3. SCHAKAL plot of the molecular structure of [Ti(NMe_2)-(Mecalix)] (**5**) in **5**·**9**·5C_4H_8O; H atoms and solvent molecules have been omitted for clarity; selected bond lengths [Å] and angles [°]: Ti(1)−N(1) 1.846(5), Ti(1)−O(1) 2.342(4), Ti(1)−O(2) 1.818(4), Ti(1)−O(3), 1.874(4), Ti(1)−O(4) 1.814(5); Ti(1)−N(1)−C(6) 123.8(5), Ti(1)−N(1)−C(7) 123.3(5), C(6)−N(1)−C(7) 112.6(6), N(1)−Ti(1)−O(1) 90.6(2), N(1)−Ti(1)−O(2) 109.3(2), N(1)−Ti(1)−O(3) 103.3(2), N(1)−Ti(1)−O(4) 109.6(2), O(1)−Ti(1)−O(2) 79.5(2), O(1)−Ti(1)−O(3) 166.1(2), O(1)−Ti(1)−O(4) 79.5(2), O(2)−Ti(1)−O(3) 95.7(2), O(2)−Ti(1)−O(4) 135.6(2), O(3)−Ti(1)−O(4) 95.4(2), Ti(1)−O(1)−C(5) 125.9(4), Ti(1)−O(1)−C(10) 119.2(3), Ti(1)−O(2)−C(20) 150.9(4), Ti(1)−O(3)−C(30) 121.0(4), Ti(1)−O(4)−C(40) 151.7(4)

are almost linearly aligned, with O(1)−Ti−O(3) angles of 166.1(2)° (**5**) and 166.5(1)° (**8**). The N(1)−Ti−O(3) angles of 103.3(2)° (**5**) and 104.5(1)° (**8**), as well as the other bond angles in the equatorial plane, reflect a significant distortion from an ideal polyhedron. The metal atoms in **5** and **8** are dislocated from a central position in the trigonal bipyramid towards the phenolate oxygen donor atom O(3), as described above for the chloro complex **1**, but this distortion is not as pronounced as observed in the solid-state structure

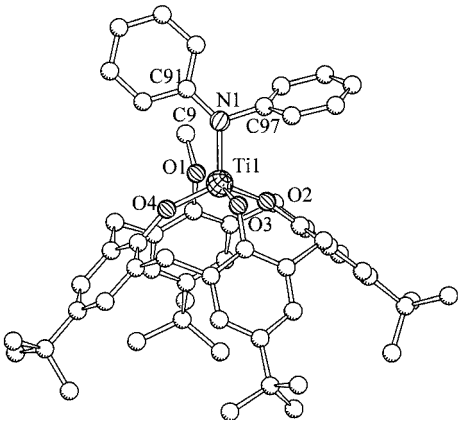

Figure 4. SCHAKAL plot of the molecular structure of [Ti(NPh_2)(Mecalix)]·(**8**) in **8**·8C_4H_8O·0.5C_6H_6; H atoms and solvent molecules have been omitted for clarity; selected bond lengths [Å] and angles [°]: Molecule 1: Ti(1)−N(1) 1.920(3), Ti(1)−O(1) 2.385(3), Ti(1)−O(2) 1.783(3), Ti(1)−O(3) 1.857(3), Ti(1)−O(4) 1.799(3); Ti(1)−N(1)−C(91) 1.338(3), Ti(1)−N(1)−C(97) 107.7(3), C(91)−N(1)−C(97) 118.0(3), N(1)−Ti(1)−O(1) 89.1(1), N(1)−Ti(1)−O(2) 111.4(1), N(1)−Ti(1)−O(3) 104.5(1), N(1)−Ti(1)−O(4) 115.5(1), O(1)−Ti(1)−O(2) 78.3(1), O(1)−Ti(1)−O(3) 166.5(1), O(1)−Ti(1)−O(4) 78.1(1), O(2)−Ti(1)−O(3) 95.6(1), O(2)−Ti(1)−O(4) 126.5(1), O(3)−Ti(1)−O(4) 96.4(1), Ti(1)−O(1)−C(9) 130.1(3), Ti(1)−O(1)−C(10) 116.8(2), Ti(1)−O(2)−C(20) 163.2(3), Ti(1)−O(3)−C(30) 120.2(2), Ti(1)−O(4)−C(40) 155.8(3), C(9)−O(1)−C(10) 113.0(3); Molecule 2: Ti(2)−N(2) 1.930(3), Ti(2)−O(5) 2.378(3), Ti(2)−O(6) 1.792(3), Ti(2)−O(7) 1.853(3), Ti(2)−O(8) 1.789(3); N(2)−Ti(2)−O(5) 89.88(12), N(2)−Ti(2)−O(6) 113.65(14), N(2)−Ti(2)−O(7) 103.96(13), N(2)−Ti(2)−O(8) 112.85(14), O(5)−Ti(2)−O(6) 78.48(11), O(5)−Ti(2)−O(7) 166.13(11), O(5)−Ti(2)−O(8) 77.65(11), O(6)−Ti(2)−O(8) 127.03(13), O(6)−Ti(2)−O(7) 96.43(13), O(7)−Ti(2)−O(8) 95.77(12), Ti(2)−O(5)−C(50) 117.1(2), Ti(2)−O(6)−C(60) 158.8(3), Ti(2)−O(7)−C(70) 121.1(2), Ti(2)−O(8)−C(80) 159.3(3), Ti(2)−O(5)−C(90) 129.0(3), Ti(2)−N(2)−C(103) 133.0(3), Ti(2)−N(2)−C(109) 108.6(2)

 © 2004 Wiley-VCH Verlag GmbH & Co. KGaA, Weinheim

of the Cp complex **4**. The sum of the X−Ti−Y angles of all atoms that are aligned in the equatorial plane [O(2), O(4), N/Cl/Cp_{centr}] is 352.9° in **1**, 354.5° in **5**, 353.4° in **8** and only 343.9° in **4**. They follow a similar trend as the Ti−O(1) bond lengths [2.424(2) Å (**1**), 2.342(4) Å (**5**), 2.38.5(3) Å (**8**), and 3.498(6) Å (**4**)], which indicates that the Ti−O(1) bond lengths do not follow only simple trends such as different steric hindrance or different electronic properties of the chloro, amido, and Cp ligands in this series.

The Ti−N distances [1.846(5) Å (**5**) and 1.920(3) Å (**8**)] are shorter than expected from the ionic radii (approximately 2.07 Å),[17] but are similar to the Ti−N bond lengths found in bis(amido)titanium complexes such as [$Ti(NMe_2)_2$-(OC_6H_3-2,6-tBu_2)$_2$] and [$Ti(NMe_2)_2(OC_6H_2$-2,4,6-$tBu_3)_2$], with values between 1.864 Å and 1.897 Å.[18] This can be attributed to π-donation of the amide ligand to the titanium atom, in which the nitrogen lone pair is involved in Ti−N bonding. Furthermore, the amido [NC_2] entity is almost planar, as revealed by the sum of the angles at the nitrogen atoms [359.7° (**5**) and 359.5° (**8**)]. The diorganylamido ligand in both complexes is oriented in such a way that the plane through the amido nitrogen atom and the N−C carbon atom is almost perpendicular to the plane through the atoms Ti, O(1) and O(3). These planes intersect each other with an angle of 89.9(10)° (**5**) and 74.8(6)° (**8**).

As mentioned above, the air- and moisture-sensitive amido complex **5** was cocrystallized with [{Ti(Mecalix)}$_2$(μ-O)] (**9**). Since the anisole methyl ether groups of **9** in **5·9**·$5C_4H_8O$ are disordered over two sites, the formation of complex **9** starting from the amido complex **5** was verified and its molecular structure was determined separately. Complex **9** crystallizes from saturated benzene solutions at room temperature in the form of thin plates in the space group $P2_1/n$ with two formula units and eight solvent molecules in the unit cell. The molecular structure of **9**, as found in **9**·$4C_6H_6$, is shown in Figure 5; selected bond lengths and angles are given in the figure caption.

The coordination sphere at the titanium atoms in **9** is also distorted trigonal-bipyramidal. The molecular unit of **9** as found in **5·9**·$5C_4H_8O$ has similar geometrical data. In this compound two $[Ti(Mecalix)]^+$ units are linked by a linear μ-O^{2-} ligand. The Ti−O−Ti′ angle (180.0°) in both molecular structures of **9** is superimposed by crystallographic symmetry, since the oxygen atoms are aligned in both cases on an inversion center. The Ti−O distances in the bridge are 1.798(1) Å in **9**·$4C_6H_6$ and 1.791(1) Å in **5·9**·$5C_4H_8O$; the Ti−O(1) bond length is 2.389(4) Å.

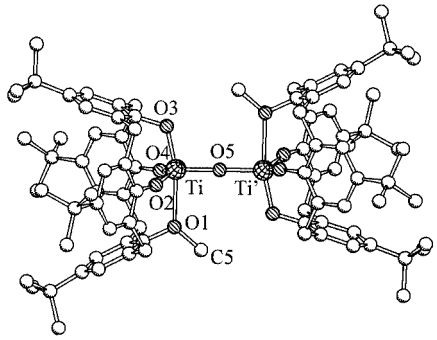

Figure 5. SCHAKAL plot of the molecular structure of [{Ti(Mecalix)}$_2$(μ-O)] in **9**·$4C_6H_6$; H atoms and solvent molecules have been omitted for clarity; selected bond lengths [Å] and angles [°]: Ti−O(1) 2.389(4), Ti−O(2) 1.784(4), Ti−O(3) 1.841(4), Ti−O(5) 1.798(1), Ti−O(4) 1.798(4); Ti−O(5)−Ti′ 180.0(1), O(1)−Ti−O(2) 77.2(2), O(1)−Ti−O(3) 166.7(1), O(1)−Ti−O(4) 79.1(2), O(1)−Ti−O(5) 91.2(1), O(2)−Ti−O(3) 95.2(2), O(2)−Ti−O(4) 126.0(2), O(2)−Ti−O(5) 115.5(1), O(3)−Ti−O(4) 97.2(2), O(3)−Ti−O(5) 102.0(1), O(4)−Ti−O(5) 112.8(1), Ti−O(1)−C(5) 129.9(3), Ti−O(1)−C(10) 115.9(3), Ti−O(2)−C(20) 167.3(4), Ti−O(3)−C(30) 119.0(3), Ti−O(4)−C(40) 151.2(3), C(5)−O(1)−C(10) 114.1(4)

Calix[4]arene Titanium Alkoxide, Phenoxide, and Thiolate Complexes

There are several ways to synthesize complexes of the type [Ti(OR)(Mecalix)]. The basic strategies are: (i) salt metathesis using [TiCl(Mecalix)] and an alkali metal alkoxide or phenolate; (ii) to introduce the calix[4]arene ligand into titanium alkoxide or phenolate complexes; and (iii) to introduce the alkoxide or phenolate by metathesis of more basic alkyl, aryl or amide ligands. The general route we chose for the preparation of such compounds is the reaction of equimolar amounts of alcohols or phenols with [Ti(N-Me_2)(Mecalix)] (**5**). These reactions afford the complexes [Ti(OR)(Mecalix)] (**10**; R = Me), (**11**; R = *i*Pr), (**12**; R = *t*Bu), (**13**; R = 4-*t*BuC_6H_4), and (**14**; R = 2,6-*i*$Pr_2C_6H_3$) in good yield (Scheme 2). Similarly, thiolate ligands can be introduced into the calixarene titanium system, as exemplified by the synthesis of [Ti(S*t*Bu)(Mecalix)] (**15**). Other routes are also viable, as was shown for the synthesis of compound **12** from the reaction of [TiCl(Mecalix)] with KO*t*Bu, or the synthesis of **11** starting from [Ti(O*i*Pr)$_4$] and 1 equiv. of H_3Mecalix. Whereas the latter approach is advantageous for the isopropoxide system, salt metathesis generally leads to lower yields and purities.

The composition of the resulting bright yellow metal complexes was verified by elemental analysis. In the mass spectra of these compounds, the molecular peaks for the mononuclear ions at m/z = 738 (**10**), 766 (**11**), 780 (**12**), 856 (**13**), 885 (**14**), and 796 (**15**) were found as base peaks. The ^{1}H and ^{13}C NMR spectra reveal signals typically found for pseudo-C_s-symmetrical calix[4]arene complexes. However, on the basis of NMR spectroscopic data a differentiation between monomeric and dimeric alkoxide-bridged species is not possible. The molecular structures of [Ti(OC_6H_4-4-*t*Bu)(Mecalix)] (**13**) and [Ti(OC_6H_4-4-Me)(Mecalix)] (**C**), synthesized previously from the reaction of [Ti(N*t*Bu)(Me_2-calix)] and the corresponding phenol, show that these complexes are dimers in the solid state.

In addition, X-ray analyses of the methoxide and diisopropylphenolate complexes **10** and **14** were performed. Crystals suitable for X-ray diffraction studies were grown from saturated toluene solutions. The molecular structures of these complexes are shown in Figures 6 and 7.

The methoxide complex **10** is a methoxy-bridged dimer in the solid state, in which two methoxide ligands bridge

 © 2004 Wiley-VCH Verlag GmbH & Co. KGaA, Weinheim

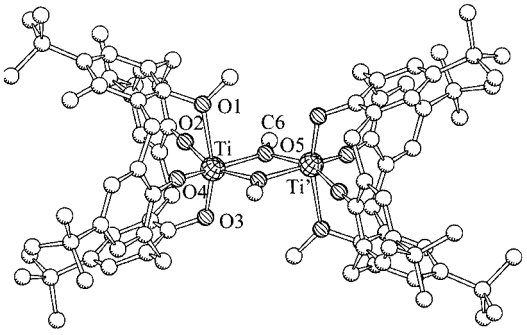

Figure 6. SCHAKAL plot of the molecular structure of $[\{Ti(OMe)(Mecalix)\}_2]$ in **10**·$6C_7H_8$; H atoms and solvent molecules have been omitted for clarity; selected bond lengths [Å] and angles [°]: Ti−O(1) 2.438(2), Ti−O(2) 1.808(2), Ti−O(3) 1.847(2), Ti−O(4) 1.800(2), Ti−O(5) 2.032(2), Ti−O(5′) 2.026(2); O(1)−Ti−O(2) 76.0(1), O(1)−Ti−O(3) 164.2(1), O(1)−Ti−O(4) 76.9(1), O(1)−Ti−O(5) 94.6(1), O(1)−Ti−O(5′) 90.0(1), O(2)−Ti−O(3) 94.4(1), O(2)−Ti−O(4) 104.2(1), O(2)−Ti−O(5) 158.8(1), O(2)−Ti−O(5′) 91.0(1), O(3)−Ti−O(4) 93.8(1), O(3)−Ti−O(5) 98.5(1), O(3)−Ti−O(5′) 103.0(1), O(3)−Ti−O(4) 76.9(1), O(4)−Ti−O(5) 91.8(1), O(4)−Ti−O(5′) 156.5(1), O(5)−Ti−O(5′) 69.8(1), O(1)−Ti−Ti′ 92.7(1), O(2)−Ti−Ti′ 125.4(1), O(3)−Ti−Ti′ 103.1(1), O(4)−Ti−Ti′ 125.2(1), O(5)−Ti−Ti′ 34.8(1), O(5′)−Ti−Ti′ 35.0(1), Ti′−O(5)−Ti 110.2(1), Ti−O(1)−C(5) 131.5(2), Ti−O(1)−C(10) 115.4(2), Ti−O(2)−C(20) 167.7(2), Ti−O(3)−C(30) 120.2(2), Ti−O(4)−C(40) 167.2(2), Ti−O(5)−C(6) 124.2(2), Ti′−O(5)−C(6) 125.3(2)

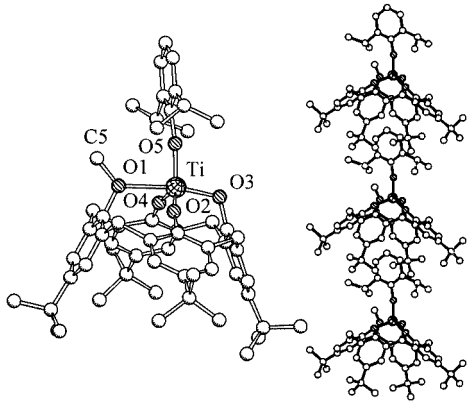

Figure 7. SCHAKAL plot of the molecular structure of $[Ti(OC_6H_3\text{-}2,6\text{-}i\text{Pr}_2)(Mecalix)]$ in **14**·$C_6H_3i\text{Pr}_2\text{OH}$; H atoms and solvent molecules have been omitted for clarity; (left) molecular unit; (right) plot of the columnar stacking of these molecular units to give a chain along the crystallographic *b* axis; selected bond lengths [Å] and angles [°]: Ti−O(1) 2.384(3), Ti−O(2) 1.768(3), Ti−O(3) 1.864(3), Ti−O(4) 1.785(3), Ti−O(5) 1.792(3); O(1)−Ti−O(2) 78.2(1), O(1)−Ti−O(3) 169.3(1), O(1)−Ti−O(4) 79.2(1), O(1)−Ti−O(5) 86.5(1), O(2)−Ti−O(3) 96.4(1), O(2)−Ti−O(4) 119.7(1), O(2)−Ti−O(5) 117.9(1), O(3)−Ti−O(4) 95.9(1), O(3)−Ti−O(5) 104.2(1), O(4)−Ti−O(5) 115.5(1), Ti−O(1)−C(10) 114.9(2), Ti−O(1)−C(5) 130.0(2), Ti−O(2)−C(20) 168.0(2), Ti−O(3)−C(30) 116.0(2), Ti−O(4)−C(40) 166.8(3), Ti−O(5)−C(50) 168.7(3)

two [Ti(Mecalix)] fragments. This complex has a crystallographically imposed inversion center at the center of the planar $[Ti_2O_2]$ four-membered ring. The coordination sphere at the titanium atom is distorted octahedral, and these two octahedra are connected by an common edge. The O−Ti−O and Ti−O−Ti′ angles within the four-membered ring are 69.8(1)° and 110.2(1)°, respectively. The Ti−Ti distance of 3.32.9(1) Å is nonbonding. The Ti−O(1) bond length to the oxygen atom of the anisole group of the calix[4]arene [2.438(2) Å] is similar to the distances found in the chloro and amido complexes. The distances of the bridging oxygen atoms from the titanium atoms are 2.032(2) Å and 2.026(2) Å, similar to other alkoxide-bridged compounds such as $[\{Ti(ONp)_4\}_2]$.[19]

In contrast to the dinuclear phenolate complexes $[Ti(OC_6H_4\text{-}4\text{-}t\text{Bu})(Mecalix)]$ (**13**) and $[Ti(OC_6H_4\text{-}4\text{-}Me)(Mecalix)]$ (**C**), the calixarene-stabilized diisopropylphenolate compound **14** is a monomer in the solid state, which is mainly due to the enhanced steric demand of the *ortho*-substituted phenolate ligand. The molecular structure of **14** is depicted on the left-hand side of Figure 7, with the stacking along the crystallographic *b* axis shown on the right. The coordination sphere around the titanium atom in this monomeric complex is best described as a distorted trigonal bipyramid, in which the oxygen atoms O(2), O(4) and O(5) occupy the equatorial positions. The O(2)−Ti−O(4), O(2)−Ti−O(5) and O(4)−Ti−O(5) angles [115.5(1)°−119.7(1)°] differ only slightly from their ideal value of 120°.

The distances between the titanium atom and the oxygen atoms O(2), O(4) and O(5) are in the narrow range of 1.768(3)−1.792(3) Å, whereas the Ti−O(3) distance of 1.864(3) Å is significantly longer. The Ti−O(1) distance of 2.384(3) Å, as well as the sum of the Ti−O distances to the oxygen atoms O(1) and O(3) (4.248 Å), are similar to the other calix[4]arene monomethyl ether complexes described in this paper.

Additional stabilization of the compound is provided by stacking of the molecular units. The right-hand side of Figure 7 shows the linear polymeric structure of **14** in the solid state. The aryl unit of the diisopropylphenolate ligand is oriented in the cavity of a neighboring calix[4]arene ligand with the plane defined by the aryl carbon atoms almost ideally aligned with the plane through the oxygen atoms O(2) and O(4) and the corresponding *ipso*-carbon atoms of the macrocyclic ligand [angle of intersection 8.9(4)°]. The closest distance between the carbon atoms of the diisopropylphenolate ligand and the carbon atoms of the calix[4]arene is 3.660(3) Å.

The thiolate complex **15** is also a monomer in the solid state, as can be seen from the molecular structure of **15** depicted in Figure 8. Crystals of this compound were obtained from saturated hexane solutions, from which the compound crystallizes in the monoclinic space group $P2_1/c$ with four molecular units and four solvent molecules in the unit cell. The titanium atom is in a distorted trigonal-bipyramidal coordination mode with the four oxygen atoms of the calix[4]arene ligand and the sulfur atom of the thiolate ligand. The oxygen atoms O(1) and O(3) occupy the axial positions. The Ti−O(1) bond length (to the oxygen atom of the anisole group) is 2.389(3) Å. The thiolate ligand in **15** is not linearly coordinated, with the Ti−S−C(6) angle of 110.8(2)° being close to the tetrahedral angle, which indicates that the sulfur lone pairs in **15** are not involved in Ti−S bonding. However, the Ti−S bond of 2.314(2) Å is

 © 2004 Wiley-VCH Verlag GmbH & Co. KGaA, Weinheim

significantly shorter than those in $[TiCp_2(StBu)_2]$ [2.416(1) Å].[20a] In more Lewis-acidic titanium thiolate complexes or in complexes with sterically less demanding ligands such as $[TiCp_2(SEt)_2]$ and $[Ti(diars)Cl_2(StBu)_2]$ [diars = 1,2-$(Me_2As)_2C_6H_4$], the Ti−S bond lengths are 2.387(3) Å and 2.398(3) Å (in the metallocene),[20b] and 2.332(3) Å (in the complex).[20c]

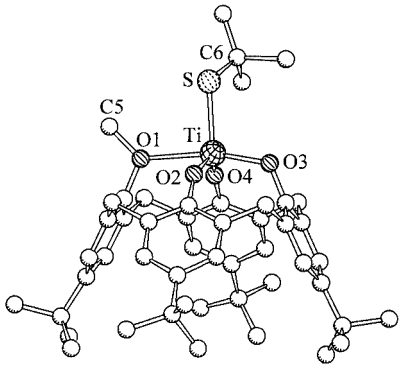

Figure 8. SCHAKAL plot of the molecular structure of [Ti(S*t*Bu)(Mecalix)] in **15**·C_6H_{14}; H atoms and solvent molecules have been omitted for clarity; selected bond lengths [Å] and angles [°]: Ti−S 2.314(2), Ti−O(1) 2.389(4), Ti−O(2) 1.793(4), Ti−O(3) 1.880(4), Ti−O(4) 1.787(3); S−Ti−O(1) 91.5(1), S−Ti−O(2) 108.1(1), S−Ti−O(3) 102.4(1), S−Ti−O(4) 115.9(1), O(1)−Ti−O(2) 79.2(2), O(1)−Ti−O(3) 166.1(2), O(1)−Ti−O(4), 79.2(1), O(2)−Ti−O(3) 96.9(2), O(2)−Ti−O(4) 131.1(2), O(3)−Ti−O(4) 93.8(2), Ti−S−C(6) 110.8(2), Ti−O(1)−C(5) 130.1(4), Ti−O(1)−C(10) 117.5(3), Ti−O(2)−C(20) 151.9(3), Ti−O(3)−C(30) 122.1(3), Ti−O(4)−C(40) 159.4(4)

Ab initio Calculations on Model Complexes

Ab initio and DFT calculations[21−24] were performed on model compounds to gain a better understanding of the main electronic and structural properties of the titanium complexes supported by the calix[4]arene methyl ether ligand. The aim of these calculations was to study the main features of the ligand in the titanium complexes described above as well as the frontier orbitals of the calix[4]arene titanium complex fragment, and their structural consequences.

Two models were considered in the calculations: A detailed model, [TiX(Mecalix^H)], in which the ligand has been slightly modified by a replacement of the *t*Bu groups with hydrogen atoms. In the second, more simplified model, $[TiX(OMe)_3(OMe_2)]$, the coordination environment at the titanium atom was maintained to resemble the main features of the ligand, but the aryl groups were replaced by methyl groups. Calculations on different detailed model complexes showed that DFT methods describe the geometry of the complexes rather poorly, especially the Ti−O(1) distance (anisole oxygen atom), which was overestimated (approximately 2.50 Å for different complexes [TiX(Mecalix^H)] and different functionals employed). Ab initio methods performed much better here, and all the results reported below are from MP2 calculations.

With the exception of $[Ti(OC_6H_3\text{-}2,6\text{-}iPr_2)(Mecalix)]$ (**14**), all the structures given above can be described in terms of the isolated molecular units present in the crystal, or their solvates, in which one of the additional solvent molecules is located inside the calix[4]arene cavity. The calculated geometries of [TiCl(Mecalix^H)] and its benzene solvate [TiCl(Mecalix^H)](C_6H_6) converge with almost identical geometries of the complex, the maximal deviation in the Ti−O distance and Ti−O−C angles are 0.006 Å and 1.23°, respectively, which are in good agreement with the experimentally observed geometry. The main structural features of the complex are therefore determined by coordination of the metal complex fragment $[TiX]^{3+}$ to the $[Mecalix]^{3-}$ ligand and are not significantly affected by lattice interactions or guest molecules in the calix[4]arene cages.

We were interested in learning more about the labile anisole ether coordination in the titanium complexes. The energy calculated for the removal of the OMe_2 group from the simplified model $[TiCl(OMe)_3(OMe_2)]$ is 45.2 kJ/mol, which indicates only weak bonding of the ether group to the titanium complex fragment. Moreover, the energy potential calculated for the elongation or compression of the Ti−O(ether) bond, which is shown in Figure 9, is very flat. The region between 2.30 Å and 2.80 Å lies within a narrow range of 5−6 kJ/mol, which indicates that the Ti−O(1) bond lengths are mainly determined by steric factors, that is, either interactions resulting from the ligand L with the anisole ether group or from an internal reorganization energy of the calix[4]arene ligand.

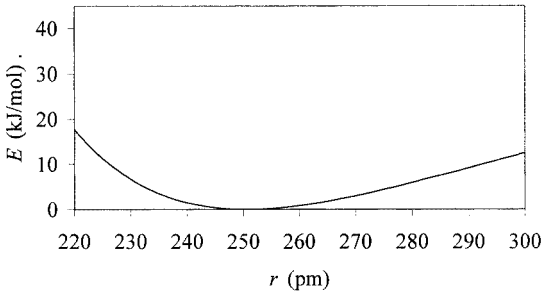

Figure 9. Potential energy curve calculated for the Ti−OMe_2 bond in $[TiCl(OMe)_3(OMe_2)]$

Geometry optimizations of the detailed model of the amido complex **5** confirmed the planar arrangement of the dimethylamido group and its perpendicular alignment with respect to the Ti−O(1) vector. A schematic FMO diagram of the interactions of an amido ligand $[NMe_2]^-$ with a calixarene metal fragment $[Ti(Mecalix)]^+$ is depicted on the right-hand side of Figure 10. The lowest metal-centered, unoccupied orbitals of the $[Ti(Mecalix)]^+$ fragment are shown on the left-hand side of the FMO scheme, while orbital plots of these relevant fragment orbitals drawn for the simplified model are given on the left-hand side of Figure 10.

The $[Ti(Mecalix)]^+$ orbitals responsible for binding of the calixarene-stabilized metal atom to a σ,π-donor ligand are three metal-centered, unoccupied orbitals. The lowest or-

 © 2004 Wiley-VCH Verlag GmbH & Co. KGaA, Weinheim

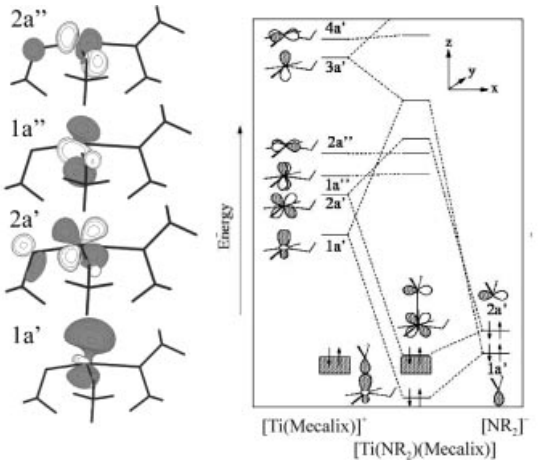

Figure 10. Schematic FMO diagram of the interaction of an amido ligand $[NMe_2]^-$ with the calixarene metal fragment $[Ti(Mecalix)]^+$ (right) and orbital plots of the relevant metal fragment orbitals of the simplified model $[Ti(OMe)_3(OMe_2)]^+$ (left)

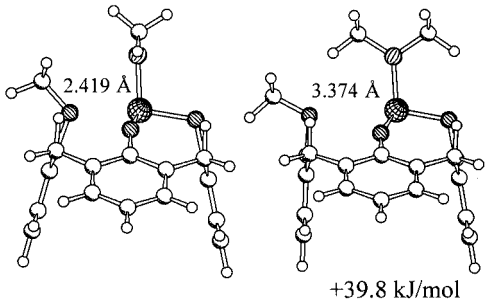

Figure 11. Geometry-optimized isomers of $[Ti(NMe_2)(Mecalix^H)]$ in which the amido ligand is oriented parallel (right) and perpendicular (left) to the Ti−O(1) vector

bital in energy, 1a′, is mainly d_z^2 in character and can be involved in Ti−L σ bonding. The 2a′ orbitals, which are mainly d_{xz}, and 1a′′, which has predominant contributions from Ti d_{yz}, are responsible for π interactions with the ligand. Dependent on the orientation of the amide ligand, 2a′ or 1a′′ are involved in Ti−N bonding, as shown schematically for the experimentally verified orientation of the amido ligand in the FMO diagram. However, a detailed analysis of the possible interactions of the nitrogen p orbital with either 2a′ or 1a′′ reveals only minor differences. This might be supported by the calculations using the simpler model and an NH_2 amido ligand. The experimentally observed geometry in this case is only 6.9 kJ/mol lower in energy than the model complex in which the NH_2 group is aligned along the Ti−O(1) vector. For the detailed models $[Ti(NMe_2)(Mecalix^H)]$ these two orientations optimize with a much larger difference in energy, as shown in Figure 11. The model that resembles the experimentally observed structure is 26.8 kJ/mol lower in energy than the other isomer, which also indicates that steric factors strongly influence the orientation of the amido ligand. This can be substantiated by a significant elongation calculated for the Ti−O(1) bond of the energetically disfavored molecule from 2.419 Å to 3.374 Å. Models in which the calixarene binds in a *paco* coordination mode are at least 75.4 kJ/mol higher in energy and should be experimentally unavailable by isomerization reactions.

Catalytic Epoxidation of Cyclooctene with TBHP

Titanium-containing synthetic zeolites such as titanium silicalite-1 (TS-1)[25] have received considerable attention in recent years because of their excellent catalytic properties.[26] TS-1 acts as a catalyst in a number of oxygen-transfer reactions utilizing hydrogen peroxide, including the epoxidation of alkenes, the oxidation of alcohols to aldehydes or ketones, the hydroxylation of aromatic compounds, and the oxidation of alkanes to alcohol/ketone mixtures. The application of these remarkable catalytic properties is limited by the pore size of the zeolite used, which was the basic motivation for research on titanium-silica mixed oxides[27] and amorphous forms of titania supported on silica.[28] These investigations led to the synthesis of zeolites with large[29] and "ultralarge"[30] pore sizes, in which titanium atoms can be located.

To gain a better understanding of the factors that determine the unique catalytic properties of these materials, special care was taken to clarify the nature of the catalytically active species.[31,32] An isolated tetrahedrally coordinated titanium complex was initially assumed to be the active species,[25,31] although further studies indicated the involvement of tripodally coordinated titanium sites. According to DFT calculations published by Rösch et al.,[33] both the reaction energy and the activation energy for the transition-metal-catalyzed epoxidation of ethene are identical, or more favorable, for the model complexes $[(HO)_3Ti(OOR)]$, $[(HO)_3Ti(OOR)(L)]$ or $[(HO)_3Ti(OOR)(L)_2]$ than models for the active species of methyltrioxorhenium (MTO)[34] or the Mimoun catalyst.[35] According to these calculations, titanium catalysts in which the $[(HO)_3Ti(OOR)]$ unit is stabilized by a further neutral ligand L (e.g. NH_3) are most favorable for epoxidation reactions using alkyl hydroperoxides.

One approach to model oxo surfaces that bind metal atoms on a molecular level is to employ ligands with a preorganized set of oxygen donor atoms in a quasiplanar arrangement, as provided, for example, by calixarenes. The titanium-containing calix[4]arene compounds [TiX(Mecalix)] exactly meet the requirements proposed by Rösch and co-workers.[33] The metal atom is threefold-coordinated by phenolate ligands and stabilized by an additional ether moiety. A fifth coordination site, occupied by a ligand X, may be used for the coordination of alkyl peroxides. Calix[4]arene complexes of the type [TiX(Rcalix)] (L = Cl, OR′, NR'_2) therefore might be able to transform the catalytic properties of titanasilicates to homogeneous catalytic systems.

We chose the titanium-catalyzed epoxidation of cyclooctene as a model reaction to test the catalytic properties of our calix[4]arene-stabilized titanium(IV) complexes in epoxidation reactions of olefins with TBHP. In a first experi-

 © 2004 Wiley-VCH Verlag GmbH & Co. KGaA, Weinheim

ment, the complexes were applied to a reaction using 5 mol % of the pre-catalyst and equimolar amounts of TBHP (see Figure 12).

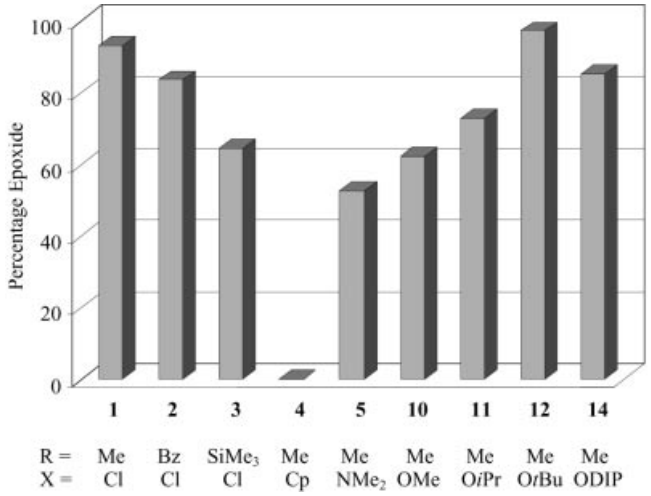

Figure 12. Conversion rate depending on the catalyst for the catalytic epoxidation of cyclooctene using 5 mol % pre-catalyst after a reaction time of 4 h; the formation of other oxidation products of cyclooctene were not observed

Whereas the Cp complex **4** is not an active catalyst, all other nine pre-catalysts tested show catalytic behavior. The best conversion rates were obtained for the complexes [TiCl(Mecalix)] (**1**; 93% conversion) and [Ti(O*t*Bu)(Mecalix)] (**12**; 97%), while the activity of the compounds [TiCl{($SiMe_3$)calix}] (**3**; 65%) and [Ti(NMe_2)(Mecalix)] (**5**; 53%) is significantly lower. The reason for the low catalytic activity of complex **3** is presumably due to silyl ether cleavage, which leads to the formation of catalytically ineffective calix[4]arene titanium complexes of higher nuclearity. Compound **11** is almost as active as **12** when it is used in its isolated form as a precatalyst. For the runs shown in Figure 12, **11** was generated in situ starting from [Ti(O*i*Pr)$_4$] and H_3Mecalix. The lower activity in this case reflects the autoretarding mechanism observed for the catalytic process (see below). Complex **5** also reveals an unexpectedly low catalytic activity compared to the other Mecalix complexes. In this case the formation of the catalytically active peroxide complex is suppressed by oxidation of the ligand and formation of a catalytically ineffective dimethylhydroxylaminato complex [Ti($ONMe_2$)(Mecalix)] (**16**).

Complex **16** was prepared independently from the reaction of the amide complex **5** and 1.1 equiv. of TBHP. The ^{1}H and ^{13}C{^{1}H} NMR spectra of **16** reveal local C_s symmetry of the calix[4]arene ligand. Compared with the amido complex **5**, the signals of the *N*-methyl protons are significantly shifted at δ = 2.92 ppm (δ = 3.59 ppm in **5**). The mass spectrum of **16** shows the molecular ion peak at *m*/*z* = 767 as the base peak of the spectrum.

According to kinetic measurements of the epoxidation reaction using [Ti(O*t*Bu)(Mecalix)] (**12**) as a catalyst, the process is neither of first nor of second order, in contrast to the findings of Abbenhuis and co-workers for the epoxidation of cyclooctene with TBHP using [{(*c*-$C_6H_{11}Si)_7O_{12}$}Ti(η^5-C_5H_5)].[36] For the calix[4]arene system the kinetics reveal an autoretarding mechanism. This autoretarding effect of the co-product *t*BuOH has been observed previously in a variety of homogeneous and heterogeneous titanium and vanadium catalysts.[37]

In the reaction mixtures of precatalyst, peroxide and substrate, we detected a new complex by NMR spectroscopy, which might be the catalytically active species [Ti(OO*t*Bu)(Mecalix)]. The resonances observed in the ^{1}H NMR spectra are four doublets for the methylene protons of the calix[4]arene ligand at δ = 4.43 and 3.37 ppm with a coupling constant of 13.7 Hz and at δ = 4.38 and 3.35 ppm with a coupling constant of 12.8 Hz, as well as a signal for the methoxy group at δ = 3.73 ppm. The resonances in the range of the *t*Bu groups could not be assigned unambiguously because this region also contains various other signals under the conditions of the catalysis. However, the calixarene signals do not belong to other possible species such as [Ti(O*t*Bu)(Mecalix)] or [{(Mecalix)Ti}$_2$O] or the Mecalix ligand. We have been unable so far to isolate this compound, but are currently exploring calixarene−titanium-catalyzed epoxidation and oxidation reactions further.

Conclusions

The complexes [TiCl(Rcalix)] **1**−**3** are easily accessible starting materials for studying the chemistry of calix[4]arene monoalkyl or silyl ether titanium complexes. For methyl ether stabilized calix[4]arene−titanium species, the dimethylamido complex **5** proved to be a convenient entry point. The results reported above show that the trianion [Mecalix]$^{3-}$ is a suitable ancillary ligand to stabilize titanium(IV) chloride, cyclopentadienyl amide, alkoxide, phenolate and thiolate functionalities. In all the complexes reported here the calix[4]arene ligand adopts an elliptically distorted cone conformation in which the anisole oxygen−titanium distance Ti−O(1) varies between 2.342 Å and 2.438 Å, with the exception of the Cp complex, for which a distance of almost 3.50 Å was observed. MP2 calculations reveal that the anisole oxygen−titanium bond is weak, particularly in the region between 2.30 Å and 2.80 Å, where the potential energy surface is very shallow. Thus, the Mecalix ligand system might be described as a tris(phenolate) ligand with a hemilabile anisole group. Despite the labile anisole oxygen−titanium bond, isomerization reactions of the calix[4]arene ligand to a *paco* coordination mode are not observed, and MP2 calculations reveal a considerable thermodynamic preference for the cone isomers. Most of the compounds are active catalysts in epoxidation reactions of cyclooctene using TBHP as an oxidant, the best results being observed for the complexes [Ti(O*t*Bu)(Mecalix)], [Ti(O*i*Pr)(Mecalix)], and [TiCl (Mecalix)].

 © 2004 Wiley-VCH Verlag GmbH & Co. KGaA, Weinheim

Experimental Section

General Remarks: All air/moisture-sensitive manipulations were performed using standard Schlenk-line (N_2) and dry-box (Ar) techniques. Solvents were pre-dried and refluxed in the presence of sodium, potassium or sodium/potassium alloy (1:3, w/w) (benzene, toluene, pentane, hexane, diethyl ether, THF), or P_2O_5 (acetonitrile, dichloromethane) under N_2. Solvents were distilled at atmospheric pressure prior to use. Deuterated solvents were dried with sodium (C_6D_6) or calcium hydride ($CDCl_3$, CD_2Cl_2) under N_2. ^1H and $^{13}C\{^1H\}$ NMR spectra were recorded with a Bruker AC 250 spectrometer at 298 K. Spectra are referenced internally to residual protonated-solvent resonances (^1H: $CDCl_3$: δ = 7.24 ppm; C_6D_6: δ = 7.15 ppm) or solvent resonances (^{13}C: $CDCl_3$: δ = 77.0 ppm; C_6D_6: δ = 128.0 ppm) and are reported relative to tetramethylsilane (δ = 0.00 ppm). Chemical shifts are quoted in δ (ppm) and coupling constants in Hz. Standard DEPT-135 experiments were recorded to distinguish CH_3 and CH carbon atoms from C and CH_2 carbon atoms in the ^{13}C NMR spectra. IR spectra were recorded with a Bruker IFS28 spectrometer as KBr pellets. All data are quoted in wavenumbers [cm^{-1}]. Mass spectra were recorded with a Finnigan MAT 900 XLT. All data are quoted as their mass/charge (*m*/*z*) ratios. Elemental analyses were carried out by the analytical laboratory of the Institute of Inorganic Chemistry of the University Karlsruhe (TH). The complexes isolated from toluene are usually solvate adducts, in which a toluene molecule is hosted inside the calix[4]arene cavity. The compound/solvent ratio was determined by integration of the appropriate peaks in the ^1H NMR spectra. This endohedrally hosted solvent molecule is usually displaced in the solvation process with the deuterated solvent (C_6D_6, $CDCl_3$) and is subtracted in the NMR spectra reported here. The mass spectra of these solvates show the peaks expected for the unsolvated species. CHN analyses were either performed on the solvates or on the unsolvated complexes as stated below. To obtain compounds free from additional solvent molecules, the complexes have to be dried vigorously or have to be recrystallized or suspended in nonpolar solvents such as pentane and hexane, filtered and dried in vacuo. No satisfactory elemental analysis was obtained for complexes **2** and **3** due to their ease of decomposition, or for **6** due to the compound's sensitivity. The composition of these complexes was verified by their mass spectra. H_4calix,[37] H_2Me_2calix,[12] H_2Bz_2calix[12] and $H_2(SiMe_3)_2$calix[38] were synthesized according to literature procedures. The synthesis of [TiCl(Mecalix)] has been reported previously,[13] but here we briefly report a modified version of this method for completeness.

[TiCl(Mecalix)]·C_7H_8 (1·C_7H_8): Toluene (180 mL) was added to a mixture of H_2Me_2calix (12.9 g, 19.1 mmol) and [$TiCl_4(THF)_2$] (6.37 g, 19.1 mmol) at room temperature. The resulting red suspension was refluxed for 48 h and the solution was concentrated to approximately 50 mL after cooling to room temperature. Hexane (130 mL) was added and, after stirring for 30 min, product **1**·C_7H_8 was isolated by filtration as a red solid, which was washed with two 15-mL portions of hexane and dried in vacuo (13.6 g, 81%). Crystals suitable for X-ray diffraction were grown from hot saturated toluene solutions of **1** $C_{45}H_{55}ClO_4Ti$·C_7H_8 (835.4): calcd. C 74.76, H 7.60; found C 74.92, H 7.60. MS: *m*/*z* (%) = 742 (100) [M^+], 727 (57) [M − CH_3]. IR: $\tilde{\nu}$ = 3055 m, 3024 m, 2962 vs br, 1603 m br, 1479 vs br, 1415 m, 1393 m, 1362 s, 1303 s br, 1254 vs, 1205 vs br, 1122 m, 1111 s, 1093 m, 1003 s br, 943 vs, 923 m, 876 vs, 831 s, 814 w, 797 vs, 763 m, 729 s, 695 w, 677 w, 647 w, 603 m, 585 vs, 568 m, 461 s, 446 s, 431 s, 401 m, 297 w cm^{-1}. ^1H NMR (C_6D_6): δ = 0.68 [s, 9 H, C(CH_3)$_3$], 0.77 [s, 9 H, C(CH_3)$_3$], 1.37 [s, 18 H, C(CH_3)$_3$], 3.13 (d, $^2J_{H,H}$ = 12.5 Hz, 2 H, CH_2), 3.22 (d, $^2J_{H,H}$ = 13.0 Hz, 2 H, CH_2), 3.84 (s, 3 H, OCH_3), 4.31 (d, $^2J_{H,H}$ = 12.5 Hz, 2 H, CH_2), 4.97 (d, $^2J_{H,H}$ = 13.0 Hz, 2 H, CH_2), 6.78 (s, 2 H, Aryl-H_m), 6.82 (s, 2 H, Aryl-H_m), 7.14 (s, 4 H, Aryl-H_m) ppm. ^{13}C NMR (C_6D_6): δ = 30.56, 30.88, 31.86 [C(*C*H$_3$)$_3$], 33.49, 33.65 (*C*H$_2$), 33.88, 34.30, 34.50 [*C*(CH$_3$)$_3$], 65.67 (O*C*H$_3$), 123.94, 125.29, 125.65, 127.22 (Aryl-C_m), 129.22, 131.47, 132.10, 132.23 (Aryl-C_o), 146.26, 146.38, 148.39 (Aryl-C_p), 151.82, 160.48, 162.97 (Aryl-C_i) ppm.

[TiCl(Bzcalix)]·C_7H_8·(2·C_7H_8): Toluene (20 mL) was added to a mixture of H_2Bz_2calix (1.00 g, 1.21 mmol) and [$TiCl_4(THF)_2$] (402 mg, 1.21 mmol). The reaction mixture immediately turned dark red and was stirred at 80 °C for 1 h. All volatiles were removed under reduced pressure and the dark red residue was suspended in 5 mL of hexane. The product was filtered off and [TiCl(Bzcalix)]·C_7H_8 (**2**·C_7H_8) was dried in vacuo (876 mg, 77%). MS: *m*/*z* (%) = 819 (26) [M^+], 818 (42) [M − H], 762 (12) [M − C(CH$_3$)$_3$] 728 (3) [M − Bz], 692 (8) [M − Bz − Cl]. ^1H NMR (C_6D_6): δ = 0.68 [s, 9 H, C(CH_3)$_3$], 0.76 [s, 9 H, C(CH_3)$_3$], 1.35 [s, 18 H, C(CH_3)$_3$], 2.92 (d, $^2J_{H,H}$ = 12.6 Hz, 2 H, CH_2), 3.22 (d, $^2J_{H,H}$ = 12.9 Hz, 2 H, CH_2), 4.08 (d, $^2J_{H,H}$ = 12.6 Hz, 2 H, CH_2), 4.96 (d, $^2J_{H,H}$ = 12.9 Hz, 2 H, CH_2), 5.38 (s, 2 H, Bz-CH_2), 6.77 (s, 2 H, Aryl-H_m), 6.81 (s, 2 H, Aryl-H_m), 7.11−7.05 (m, 7 H, Aryl-H_m), 7.37 (m, 2 H, Bz-Aryl-*H*) ppm. ^{13}C NMR (C_6D_6): δ = 30.57 [C(*C*H$_3$)$_3$], 30.88 [C(*C*H$_3$)$_3$], 31.84 [C(*C*H$_3$)$_3$], 33.60 (*C*H$_2$), 33.88 (*C*H$_2$), 34.46 [*C*(CH$_3$)$_3$], 81.13 (Bz-*C*H$_2$), 123.87, 125.18, 125.59, 127.06 (s, Aryl-C_m), 128.66, 129.21, 131.17 (Bz-*C*), 128.73, 131.86, 132.09, 132.87 (Aryl-C_o), 135.74 (Bz-C_i) 146.26, 146.46, 148.26 (Aryl-C_p), 149.85, 160.46, 163.04 (Aryl-C_i) ppm.

[TiCl{(Me$_3$Si)calix}]·3C_7H_8 (3·3C_7H_8): Toluene (15 mL) was added to a mixture of $H_2(SiMe_3)_2$calix (1.00 g, 1.26 mmol) and [$TiCl_4(THF)_2$] (421 mg, 1.26 mmol). The reaction mixture was stirred at room temperature for 2 h and its color changed from yellow to red. The red, cloudy solution was filtered through a pad of Celite and the filtrate concentrated to dryness to afford [TiCl{(Me$_3$Si)calix}]·3C_7H_8 as a red powder (990 mg, 72.9%). MS: *m*/*z* (%) = 801 (100) [M^+], 786 (23) [M − CH_3], 693 (6) [M − CH_3 − Si(CH$_3$)$_3$]. ^1H NMR (C_6D_6): δ = 0.49 [s, 9 H, Si(CH_3)$_3$], 0.70 [s, 9 H, C(CH_3)$_3$], 0.80 [s, 9 H, C(CH_3)$_3$], 1.40 [s, 18 H, C(CH_3)$_3$], 3.10 (d, $^2J_{H,H}$ = 12.4 Hz, 2 H, CH_2), 3.31 (d, $^2J_{H,H}$ = 13.0 Hz, 2 H, CH_2), 4.56 (d, $^2J_{H,H}$ = 12.4 Hz, 2 H, CH_2), 4.92 (d, $^2J_{H,H}$ = 13.0 Hz, 2 H, CH_2), 6.78 (s, 4 H, Aryl-H_m), 7.17 (s, 4 H, Aryl-H_m) ppm. ^{13}C NMR (C_6D_6): δ = 1.78 [Si(*C*H$_3$)$_3$], 30.59 [C(*C*H$_3$)$_3$], 30.91 [C(*C*H$_3$)$_3$], 31.84 [C(*C*H$_3$)$_3$], 33.51 (*C*H$_2$), 33.73 [*C*(CH$_3$)$_3$], 33.79 (*C*H$_2$), 34.48 [*C*(CH$_3$)$_3$], 123.94, 125.41, 126.48 (Aryl-C_m), 131.12, 131.77, 132.34 (Aryl-C_o), 146.12, 146.31, 146.77 (Aryl-C_p), 148.03, 159.80, 162.82 (Aryl-C_i) ppm.

[Ti(η^5-C_5H_5)(Mecalix)]·C_7H_8 (4·C_7H_8): A mixture of **1**·C_7H_8 (500 mg, 0.60 mmol) and [NaCp(THF)] (96.0 mg, 0.60 mmol) was suspended in 10 mL of toluene. The resulting suspension became orange after a few minutes and was stirred at room temperature for 12 h, filtered through a pad of Celite and the filtrate was concentrated to dryness. The orange product [Ti(η^5-C_5H_5)(Mecalix)]·C_7H_8 (**4**·C_7H_8) was dried in vacuo (342 mg, 66%). Crystals suitable for X-ray diffraction were grown from a saturated toluene solution at −30 °C. $C_{50}H_{60}O_4Ti$·C_7H_8 (865.0): calcd. C 79.14, H 7.92; found C 79.27, H 7.77. MS: *m*/*z* (%) = 772 (100) [M^+] 757 (22) [M − CH_3], 707 (14) [M − Cp]. IR: $\tilde{\nu}$ = 2962 vs br, 1603 w, 1580 w, 1467 vs br, 1392 w, 1362 m, 1301 s br, 1254 vs br, 1205 vs br, 1170 m, 1105 s br, 1019 vs br, 938 s, 922 m, 872 s, 861 vs, 822 s, 804 vs br, 752 s, 714 w, 676 m, 647 w, 603 m, 580 m, 562 s, 510 w br, 481 w, 455 m, 431 m cm^{-1}. ^1H NMR (C_6D_6): δ = 0.85 [s, 9 H, C(CH_3)$_3$], 1.07 [s, 9 H, C(CH_3)$_3$], 1.39 [s, 18 H, C(CH_3)$_3$],

 © 2004 Wiley-VCH Verlag GmbH & Co. KGaA, Weinheim

3.21 (d, $^2J_{H,H}$ = 12.9 Hz, 2 H, CH_2), 3.25 (d, $^2J_{H,H}$ = 12.9 Hz, 2 H, CH_2), 3.44 (s, 3 H, OCH_3), 4.46 (d, $^2J_{H,H}$ = 12.9 Hz, 4 H, CH_2), 6.57 (s, 5 H, C_5H_5), 6.70 (s, 2 H, Aryl-H_m), 6.88 (s, 2 H, Aryl-H_m), 7.18 (s, 2 H, Aryl-H_m), 7.21 (s, 2 H, Aryl-H_m) ppm. ^{13}C NMR (C_6D_6): δ = 31.17, 31.47, 31.88 [C(CH_3)$_3$], 32.06, 33.61 (CH_2), 33.86, 33.93, 34.22 [C(CH_3)$_3$], 61.78 (OCH_3), 117.28 (C_5H_5), 124.32, 125.02, 125.14, 125.46 (Aryl-C_m), 126.05, 131.49, 132.22, 133.09 (Aryl-C_o), 143.17, 144.32, 146.06 (Aryl-C_p), 153.70, 158.85, 162.00 (Aryl-C_i) ppm.

[Ti(NMe$_2$)(Mecalix)]·(5): A solution of **1**·C_7H_8 (2.00 g, 2.40 mmol) and LiNMe$_2$ (135 mg, 1.15 equiv., 2.64 mmol) in toluene (50 mL) was stirred for 12 h. During this time the red solution became orange and cloudy. It was then filtered through a pad of Celite and all volatiles of the filtrate were removed in vacuo. The residue was suspended in hexane (15 mL), and yellow [Ti(NMe$_2$)(Mecalix)] (**5**) was collected and dried in vacuo. A second fraction was obtained after concentrating the mother liquor to approximately 5 mL and cooling to −30 °C for 5 d (combined yield: 1.71 g, 95%). Crystals of **5** were grown from a saturated solution of **5** in THF after prolonged storage at room temperature. $C_{47}H_{61}NO_4Ti$ (751.9): calcd. C 75.08, H 8.18, N 1.24; found C 74.79, H 8.26, N 1.53. MS: *m*/*z* (%) = 751 (100) [M$^+$], 736 (30) [M − CH_3]. ^{1}H NMR (C_6D_6): δ = 0.74 [s, 9 H, C(CH_3)$_3$], 0.83 [s, 9 H, C(CH_3)$_3$], 1.44 [s, 18 H, C(CH_3)$_3$], 3.29 (d, $^2J_{H,H}$ = 12.1 Hz, 2 H, CH_2), 3.40 (d, $^2J_{H,H}$ = 12.3 Hz, 2 H, CH_2), 3.59 [s, 6 H, N(CH_3)$_2$], 3.48 (s, 3 H, OCH_3), 4.39 (d, $^2J_{H,H}$ = 12.1 Hz, 2 H, CH_2), 5.21 (d, $^2J_{H,H}$ = 12.3 Hz, 2 H, CH_2), 6.90 (s, 4 H, Aryl-H_m), 7.25 (d, $^4J_{H,H}$ = 2.4 Hz, 2 H, Aryl-H_m), 7.31 (d, $^4J_{H,H}$ = 2.4 Hz, 2 H, Aryl-H_m) ppm. ^{13}C NMR (C_6D_6): δ = 30.66 [s, C(CH_3)$_3$], 31.08 [s, C(CH_3)$_3$], 32.06 [s, C(CH_3)$_3$], 33.77 (s, CH_2), 33.88 (s, CH_2), 34.06 [s, C(CH_3)$_3$], 34.40 [s, C(CH_3)$_3$], 47.95 [s, N(CH_3)$_2$], 65.17 (s, OCH_3), 123.73, 125.39, 125.76, 127.02 (s, Aryl-C_m), 129.28, 129.94, 132.31, 132.58 (s, Aryl-C_o), 143.24, 144.05, 148.64 (s, Aryl-C_p), 150.40, 154.78, 159.62 (s, Aryl-C_i) ppm.

[Ti(NEt$_2$)(Mecalix)]·C_7H_8 (6·C_7H_8): A solution of **1**·C_7H_8 (1.00 g, 1.20 mmol) in 40 mL of toluene was added at room temperature to a solution of LiNEt$_2$ (100 mg, 1.27 mmol) in 25 mL of toluene. After 8 h of stirring at room temperature, all undissolved components of the cloudy, orange reaction mixture were filtered off through a pad of Celite and the filtrate was concentrated to dryness. The resulting greenish yellow powder of [Ti(NEt$_2$)(Mecalix)]·C_7H_8 (**6**·C_7H_8) was dried in vacuo (0.91 g, 87%). MS: *m*/*z* (%) = 779 (100) [M$^+$], 764 (50) [M − CH_3], 707 (62) [M − NEt$_2$], 677 (13) [M − 2 CH_3 − NEt$_2$]. IR: $\tilde{\nu}$ = 2963 vs br, 1603 w br, 1480 vs br, 1393 m, 1362 m, 1308 s br, 1261 m, 1208 vs br, 1095 s br, 1013 s br, 939 m, 920 m, 872 vs br, 798 vs, 756 m, 727 s, 694 w, 676 w, 584 s, 567 s, 552 s, 465 m, 428 m cm^{-1}. ^{1}H NMR (C_6D_6): δ = 0.74 [s, 9 H, C(CH_3)$_3$], 0.83 [s, 9 H, C(CH_3)$_3$], 1.44 [s, 18 H, C(CH_3)$_3$], 1.46 (t, $^3J_{H,H}$ = 7.1 Hz, 6 H, NCH$_2$CH_3), 3.31 (d, $^2J_{H,H}$ = 12.1 Hz, 2 H, CH_2), 3.40 (d, $^2J_{H,H}$ = 12.3 Hz, 2 H, CH_2), 3.56 (s, 3 H, OCH_3), 3.92 (q, $^3J_{H,H}$ = 7.1 Hz, 4 H, NCH_2CH$_3$), 4.42 (d, $^2J_{H,H}$ = 12.1 Hz, 2 H, CH_2), 5.16 (d, $^2J_{H,H}$ = 12.3 Hz, 2 H, CH_2), 6.90 (s, 2 H, Aryl-H_m), 6.91 (s, 2 H, Aryl-H_m), 7.25 (d, $^4J_{H,H}$ = 2.4 Hz, 2 H, Aryl-H_m), 7.30 (d, $^4J_{H,H}$ = 2.4 Hz, 2 H, Aryl-H_m) ppm. ^{13}C NMR (C_6D_6): δ = 15.77 (NCH$_2$CH_3), 30.67, 31.09, 32.06 [C(CH_3)$_3$], 33.53, 33.73 [C(CH_3)$_3$], 33.80, 33.99 (CH_2), 34.39 [C(CH_3)$_3$], 51.35 (NCH$_2$CH$_3$), 65.54 (OCH_3), 123.76, 125.42, 125.65, 127.00 (Aryl-C_m), 129.28, 130.03, 132.24, 132.47 (Aryl-C_o), 143.20, 143.93, 148.52 (Aryl-C_p), 150.66, 155.04, 159.75 (Aryl-C_i) ppm.

[Ti(N*i*Pr$_2$)(Mecalix)] (7): A solution of LiN*i*Pr$_2$ (69.0 mg, 0.64 mmol) in 10 mL of THF was slowly added at −30 °C to a solution of **1**·C_7H_8 (500 mg, 0.60 mmol) in 10 mL of THF. The initially red solution rapidly became orange, and the reaction mixture was allowed to reach room temperature during 8 h. At approximately +5 °C the orange solution turned brownish. Volatile components were evaporated in vacuo and the residue was extracted into 10 mL of toluene and filtered through a pad of Celite. The filtrate was concentrated to dryness and the remaining solid was suspended in 2 mL of hexane and filtered off to afford [Ti(N*i*Pr$_2$)(Mecalix)] (**7**) as a yellow powder (145 mg, 30%). $C_{51}H_{69}NO_4Ti$ (808.0): calcd. C 75.81 H 8.61 N 1.73; found C 75.86, H 9.01, N 1.56. MS: *m*/*z* (%) = 807 (29) [M$^+$], 792 (100) [M − CH_3], 707 (32) [M − N*i*Pr$_2$]. IR: $\tilde{\nu}$ = 2962 vs br, 1603 w br, 1480 vs br, 1393 w, 1362 m, 1308 s br, 1276 m sh, 1260 s, 1207 vs br, 1169 w br, 1123 m, 1113 m, 1104 m, 1014 m br, 941 m, 922 w, 873 s br, 815 m, 798 vs, 755 s, 730 s br, 646 w, 586 m, 567 m, 557 m cm^{-1}. ^{1}H NMR (C_6D_6): δ = 0.72 [s, 9 H, C(CH_3)$_3$], 0.80 [s, 9 H, C(CH_3)$_3$], 0.96 (d, $^3J_{H,H}$ = 6.2 Hz, 6 H, NCH(CH_3)$_2$], 1.43 [s, 18 H, C(CH_3)$_3$], 2.79 (sept, $^3J_{H,H}$ = 6.2 Hz, 1 H, NCH(CH$_3$)$_2$], 3.25 (d, $^2J_{H,H}$ = 12.8 Hz, 2 H, CH_2), 3.32 (d, $^2J_{H,H}$ = 12.6 Hz, 2 H, CH_2), 4.55 (s, 3 H, OCH_3), 4.71 (d, $^2J_{H,H}$ = 12.8 Hz, 2 H, CH_2), 5.04 (d, $^2J_{H,H}$ = 12.6 Hz, 2 H, CH_2), 6.86 (s, 2 H, Aryl-H_m), 6.92 (s, 2 H, Aryl-H_m), 7.20 (s, 2 H, Aryl-H_m), 7.23 (s, 2 H, Aryl-H_m) ppm. ^{13}C NMR (C_6D_6): δ = 23.64 [NCH(CH_3)$_2$], 30.66, 30.98, 32.04 [C(CH_3)$_3$], 33.61 [C(CH_3)$_3$], 33.72, 33.90 (CH_2), 34.21, 34.45 [C(CH_3)$_3$], 45.36 [NCH(CH_3)$_2$], 66.03 (OCH_3), 123.94, 125.11, 125.85, 127.84 (Aryl-C_m), 129.28, 130.96, 131.66, 132.65 (Aryl-C_o), 144.65, 144.95, 148.43 (Aryl-C_p), 151.88, 157.79, 161.24 (Aryl-C_i) ppm.

[Ti(NPh$_2$)(Mecalix)]·C_7H_8 (8·C_7H_8): A mixture of **1**·C_7H_8 (500 mg, 0.60 mmol) and LiNPh$_2$ (112 mg, 0.64 mmol) was suspended in 10 mL of toluene. After 8 h of stirring at room temperature, the resulting red suspension was filtered through a pad of Celite and the filtrate was concentrated to dryness to afford [Ti(NPh$_2$)(Mecalix)]·C_7H_8 (**8**·C_7H_8) as a dark-red powder (485 mg, 84%). Crystals suitable for X-ray analysis were obtained by diffusion of hexane into a saturated toluene solution of **8**. $C_{57}H_{65}NO_4Ti$·C_7H_8 (968.2): calcd. C 79.40, H 7.60, N 1.45; found C 78.97, H 7.51, N 1.54. MS: *m*/*z* (%) = 875 (100) [M$^+$], 860 (10) [M − CH_3], 707 (20) [M − NPh$_2$]. IR: $\tilde{\nu}$ = 2953 vs br, 1593 m br, 1478 vs br, 1415 w, 1392 w, 1361 m, 1306 s br, 1275 s, 1260 vs br, 1207 vs br, 1176 s, 1123 s, 1111 m, 1095 m, 1013 m br, 941 2, 932 s, 921 s, 873 vs br, 826 s, 797 vs, 748 s br, 695 s, 645 w, 634 w, 597 w, 585 m, 567 m, 556 m, 523 m, 503 w, 471 w, 445 w br cm^{-1}. ^{1}H NMR (C_6D_6): δ = 0.72 [s, 9 H, C(CH_3)$_3$], 0.80 [s, 9 H, C(CH_3)$_3$], 1.38 [s, 18 H, C(CH_3)$_3$], 3.27 (d, $^2J_{H,H}$ = 12.6 Hz, 2 H, CH_2), 3.30 (d, $^2J_{H,H}$ = 12.3 Hz, 2 H, CH_2), 3.68 (s, 3 H, OCH_3), 4.52 (d, $^2J_{H,H}$ = 12.3 Hz, 2 H, CH_2), 4.95 (d, $^2J_{H,H}$ = 12.6 Hz, 2 H, CH_2), 6.90−7.31 (Aryl-H of Mecalix and NPh) ppm. ^{13}C NMR (C_6D_6): δ = 30.63, 31.00, 31.96 [C(CH_3)$_3$], 33.58 [C(CH_3)$_3$], 33.71, 33.79 (CH_2), 34.14, 34.43 [C(CH_3)$_3$], 65.19 (OCH_3), 122.98 (Phenyl-C_m), 124.56 (Phenyl-C_p), 123.88, 125.47, 125.66, 127.13 (Aryl-C_m), 129.94 (Phenyl-C_o), 126.21, 130.54, 131.98, 132.21 (Aryl-C_o), 144.80 (Phenyl-C_i), 144.52, 148.39, 150.28 (Aryl-C_p), 151.51, 157.38, 161.26 (Aryl-C_i) ppm.

[{Ti(Mecalix)}$_2$(μ-O)] (9): Whilst stirring, 0.33 mL of a 1 M solution of H_2O in THF was added slowly to a solution of **5** (500 mg, 0.67 mmol) in toluene (10 mL). The initially yellow solution turned red for a moment and became orange after stirring at room temperature. After 30 min, the clear, orange solution was concentrated to dryness and the resulting orange powder was suspended in pentane (5 mL), filtered, and dried in vacuo to afford [{Ti(Mecalix)}$_2$(μ-O)] (**9**) as an orange powder (420 mg, 83%).

 © 2004 Wiley-VCH Verlag GmbH & Co. KGaA, Weinheim

Crystals suitable for X-ray analysis were obtained from saturated benzene solutions. $C_{90}H_{110}O_9Ti_2 \cdot 2C_7H_8$ (1615.9): calcd. C 75.51, H 7.74; found C 75.64, H 7.77. MS: *m*/*z* (%) = 1431 (98) [M^+], 1430 (100) [M − H], 1416 (18) [M − CH_3]. IR: $\tilde{\nu}$ = 2951 vs br, 1603 w br, 1582 w, 1482 vs br, 1393 w, 1362 m, 1301 s br, 1260 s, 1215 vs br, 1124 m, 1113 m, 1094 m, 1010 m br, 943 s, 921 s, 875 s, 815 s, 799 vs, 725 vs br, 676 m, 634 w, 601 s, 586 s, 567 s, 554 s, 508 w br, 449 m, 431 m cm^{-1}. ^{1}H NMR (C_6D_6): δ = 0.71 [s, 9 H, C(CH_3)$_3$], 0.79 [s, 9 H, C(CH_3)$_3$], 1.41 [s, 18 H, C(CH_3)$_3$], 3.25 (d, $^2J_{H,H}$ = 12.6 Hz, 2 H, CH_2), 3.30 (d, $^2J_{H,H}$ = 12.3 Hz, 2 H, CH_2), 4.48 (s, 3 H, OCH_3), 4.68 (d, $^2J_{H,H}$ = 12.3 Hz, 2 H, CH_2), 5.01 (d, $^2J_{H,H}$ = 12.6 Hz, 2 H, CH_2), 6.85 (s, 2 H, Aryl-H_m), 6.91 (s, 2 H, Aryl-H_m), 7.18 (d, $^4J_{H,H}$ = 2.4 Hz, 2 H, Aryl-H_m), 7.21 (d, $^4J_{H,H}$ = 2.4 Hz, 2 H, Aryl-H_m) ppm. ^{13}C NMR (C_6D_6): δ = 30.66 [s, C(*C*H_3)$_3$], 30.98 [s, C(*C*H_3)$_3$], 32.04 [s, C(*C*H_3)$_3$], 33.60 [s, *C*(CH$_3$)$_3$], 33.71 [s, *C*(CH$_3$)$_3$], 33.89 (s, *C*H$_2$), 33.94 (s, *C*H$_2$), 34.44 [s, *C*(CH$_3$)$_3$], 65.97 (s, O*C*H$_3$), 123.96, 125.12, 125.84, 127.23 (s, Aryl-C_m), 126.44, 130.96, 131.67, 132.66 (s, Aryl-C_o), 144.50, 144.88, 148.37 (s, Aryl-C_p), 152.04, 157.93, 161.30 (s, Aryl-C_i) ppm.

[Ti(OMe)(Mecalix)]·C_7H_8 (10·C_7H_8): Methanol (27.0 μL, 0.77 mmol) was added at room temperature to a solution of **5** (500 mg, 0.67 mmol) in toluene (10 mL). The initially yellow solution turned slightly orange and became cloudy. After 12 h of stirring at room temperature, the resulting yellow precipitate was isolated by filtration and dried in vacuo to afford [Ti(OMe)(Mecalix)]·C_7H_8 as a yellow solid. (357 mg, 64%). The product was recrystallized from refluxing toluene. $C_{46}H_{58}O_5Ti \cdot C_7H_8$ (831.0): calcd. C 76.79, H 7.78; found C 76.65, H 7.77. MS: *m*/*z* (%) = 738 (100) [M^+]; 723 (43) [M − CH_3]. IR: $\tilde{\nu}$ = 2952 vs br, 1602 w, 1580 w, 1480 vs br, 1393 w, 1362 m, 1315 s br, 1271 s br, 1238 w, 1209 vs br, 1170 w, 1122 m br, 1097 m, 1031 m br, 1004 s br, 939 s, 921 m, 874 vs, 865 s, 825 m, 795 s, 757 m, 731 s, 677 w, 646 w, 603 w, 586 s br, 537 vs br, 476 w, 457 m, 430 w cm^{-1}. ^{1}H NMR ($CDCl_3$): δ = 1.15 [s, 9 H, C(CH_3)$_3$], 1.16 [s, 9 H, C(CH_3)$_3$], 1.28 [s, 18 H, C(CH_3)$_3$], 3.28 (d, $^2J_{H,H}$ = 13.0 Hz, 4 H, CH_2), 4.13 (d, $^2J_{H,H}$ = 13.0 Hz, 2 H, CH_2), 4.39 (s, 3 H, TiOCH_3), 4.45 (s, 3 H, OCH_3), 4.73 (d, $^2J_{H,H}$ = 13.0 Hz, 2 H, CH_2), 6.96 (s, 2 H, Aryl-H_m), 6.98 (s, 2 H, Aryl-H_m), 7.16 (s, 2 H, Aryl-H_m), 7.17 (s, 2 H, Aryl-H_m) ppm. ^{13}C NMR ($CDCl_3$): δ = 31.23, 31.45, 31.73 [C(*C*H$_3$)$_3$], 33.96 [*C*(CH$_3$)$_3$], 34.08 (*C*H$_2$), 34.19 [*C*(CH$_3$)$_3$], 34.38 (*C*H$_2$), 34.85 [*C*(CH$_3$)$_3$], 62.07 (TiO*C*H$_3$), 65.30 (O*C*H$_3$), 123.79, 124.74, 125.17, 126.86 (Aryl-C_m), 127.06, 131.17, 132.59, 132.73 (Aryl-C_o), 142.81, 143.32, 147.11 (Aryl-C_p), 154.49, 162.09, 163.13 (Aryl-C_i) ppm.

[Ti(O*i*Pr)(Mecalix)]·C_7H_8 (11·C_7H_8): A solution of [Ti(O*i*Pr)$_4$] (0.90 mL, 859 mg, 3.02 mmol) in toluene (10 mL) was added at room temperature to a solution of H_3Mecalix (2.00 g, 3.02 mmol) in toluene (20 mL). The initially colorless solution turned yellow immediately after addition of the metal complex. After 2 h of stirring at room temperature, all volatile components were removed in vacuo to afford analytically pure, pale-yellow **11**·C_7H_8 (2.32 g, 89%). $C_{48}H_{62}O_5Ti \cdot C_7H_8$ (859.0): calcd. C 76.90, H 8.21; found C 76.67, H 8.15. MS: *m*/*z* (%) = 766 (100) [M^+], 751 (20) [M − CH_3]. IR: $\tilde{\nu}$ = 2963 vs br, 1599 w, 1580 w, 1480 vs br, 1393 w, 1361 m, 1307 s br, 1262 s br, 1206 s br, 1167 m, 1104 vs br, 1013 s br, 988 vs br, 939 m, 922 m, 864 vs br, 827 m, 797 vs, 759 m, 675 w, 627 w br, 598 w, 582 s, 567 m, 554 m, 465 w, 449 w, 430 w cm^{-1}. ^{1}H NMR (C_6D_6): δ = 0.74 [s, 9 H, C(CH_3)$_3$], 0.82 [s, 9 H, C(CH_3)$_3$], 1.42 [s, 18 H, C(CH_3)$_3$], 1.50 (d, $^3J_{H,H}$ = 6.1 Hz, 6 H, OCH(CH_3)$_2$], 3.27 (d, $^2J_{H,H}$ = 12.3 Hz, 2 H, CH_2), 3.34 (d, $^2J_{H,H}$ = 12.6 Hz, 2 H, CH_2), 3.76 (s, 3 H, OCH_3), 4.39 (d, $^2J_{H,H}$ = 12.3 Hz, 2 H, CH_2), 4.89 (sept, $^3J_{H,H}$ = 6.1 Hz, 1 H, OC*H*(CH$_3$)$_2$], 5.06 (d, $^2J_{H,H}$ = 12.6 Hz, 2 H, CH_2), 6.89 (s, 2 H, Aryl-H_m), 6.91 (s, 2 H, Aryl-H_m), 7.23 (s, 2 H, Aryl-H_m), 7.24 (s, 2 H, Aryl-H_m) ppm. ^{13}C NMR (C_6D_6): δ = 26.35 [OCH(*C*H$_3$)$_2$], 30.67, 31.03, 32.04 [C(*C*H$_3$)$_3$], 33.58, 33.72 [*C*(CH$_3$)$_3$], 33.79, 33.90 (*C*H$_2$), 34.40 [*C*(CH$_3$)$_3$], 65.02 (O*C*H$_3$), 80.39 [O*C*H(CH$_3$)$_2$], 123.91, 125.32, 125.79, 126.75 (Aryl-C_m), 127.10, 130.39, 131.56, 132.52 (Aryl-C_o), 144.11, 144.42, 148.39 (Aryl-C_p), 151.36, 156.18, 160.27 (Aryl-C_i) ppm.

[Ti(O*t*Bu)(Mecalix)]·C_7H_8 (12·C_7H_8): *t*BuOH (125 μL, 1.33 mmol) was added to a yellow solution of **5** (1.00 g, 1.33 mmol) in toluene (20 mL), and the reaction mixture was stirred for 8 h. All volatiles were evaporated under reduced pressure to give **12**·C_7H_8 (890 mg, 77%) as a pale-yellow powder, which was dried in vacuo. $C_{49}H_{64}O_5Ti \cdot C_7H_8$ (873.1): calcd. C 77.04, N 8.31; found C 76.76, H 8.26. MS: *m*/*z* (%) = 780 (100) [M^+], 765 (6) [M − CH_3], 724 (14) [M − *t*Bu], 709 (37) [M − *t*Bu − CH_3], 707 (8) [M − O*t*Bu]. IR: $\tilde{\nu}$ = 2963 vs br, 1603 w br, 1580 w, 1480 vs br, 1393 w, 1362 s, 1310 s br, 1280 m, 1262 s br, 1208 vs br, 1169 s br, 1123 m, 1112 m, 1095 m, 1013 vs br, 940 s br, 921 s, 873 vs br, 825 m, 798 vs, 757 m, 727 s, 694 w, 676 w, 646 w, 632 w, 599 m, 584 s, 568 m, 554 m, 506 w br, 464 w, 446 w, 428 w cm^{-1}. ^{1}H NMR (C_6D_6): δ = 0.74 [s, 9 H, C(CH_3)$_3$], 0.83 [s, 9 H, C(CH_3)$_3$], 1.42 [s, 18 H, C(CH_3)$_3$], 1.61 [s, 9 H, OC(CH_3)$_3$], 3.27 (d, $^2J_{H,H}$ = 12.3 Hz, 2 H, CH_2), 3.33 (d, $^2J_{H,H}$ = 12.6 Hz, 2 H, CH_2), 3.82 (s, 3 H, OCH_3), 4.40 (d, $^2J_{H,H}$ = 12.3 Hz, 2 H, CH_2), 5.04 (d, $^2J_{H,H}$ = 12.6 Hz, 2 H, CH_2), 6.88 (s, 2 H, Aryl-H_m), 6.91 (s, 2 H, Aryl-H_m), 7.23 (s, 2 H, Aryl-H_m), 7.24 (s, 2 H, Aryl-H_m) ppm. ^{13}C NMR (C_6D_6): δ = 30.67 [C(*C*H$_3$)$_3$], 31.04 [C(*C*H$_3$)$_3$], 32.04 [C(*C*H$_3$)$_3$],32.06 [OC(*C*H$_3$)$_3$], 33.58 [*C*(CH$_3$)$_3$], 33.72 [*C*(CH$_3$)$_3$], 33.79 (*C*H$_2$), 33.95 (*C*H$_2$), 34.39 [*C*(CH$_3$)$_3$], 65.29 (O*C*H$_3$), 85.59 [O*C*(CH$_3$)$_3$], 123.92, 125.32, 125.72, 127.08 (Aryl-C_m), 129.28, 130.38, 131.54, 132.54 (Aryl-C_o), 144.01, 144.36, 148.38 (Aryl-C_p), 151.41, 156.20, 160.23 (Aryl-C_i) ppm.

[Ti(OC$_6$H$_4$-4-*t*Bu)(Mecalix)}]·C_7H_8 (13·C_7H_8): Toluene (10 mL) was added at room temperature to a mixture of **5** (500 mg, 0.67 mmol) and *p*-*tert*-butylphenol (100 mg, 0.67 mmol) to give an orange, slightly cloudy solution. This solution was stirred at 100 °C for 24 h with formation of an orange precipitate. After cooling to room temperature, the precipitate was filtered off and dried in vacuo to afford **13**·C_7H_8 as an orange-red solid (518 mg, 81%). $C_{55}H_{68}O_5Ti \cdot C_7H_8$ (949.2): calcd. C 78.46; H 8.07; found C 77.95, H 8.09. MS: *m*/*z* (%) = 856 (100) [M^+], 841 (60) [M − CH_3]. IR: $\tilde{\nu}$ = 2968 vs br, 1603 w, 1504 s, 1480 vs br, 1435 vs br, 1415 w, 1392 w, 1361 w, 1319 m, 1300 s br, 1266 vs br, 1221 vs br, 1206 vs br, 1122 m, 1096 m, 1010 s, 940 s, 921 m, 874 vs br, 842 s, 824 s, 795 vs, 756 m, 728 m, 678 w, 582 vs br, 535 s br cm^{-1}. ^{1}H NMR ($CDCl_3$): δ = 1.17 [s, 9 H, C(CH_3)$_3$], 1.18 [s, 9 H, C(CH_3)$_3$], 1.25 [s, 18 H, C(CH_3)$_3$], 1.31 [s, 9 H, C(CH_3)$_3$], 3.31 (d, $^2J_{H,H}$ = 12.7 Hz, 4 H, CH_2), 3.32 (d, $^2J_{H,H}$ = 12.4 Hz, 4 H, CH_2), 4.10 (s, 3 H, OCH_3), 4.34 (d, $^2J_{H,H}$ = 12.4 Hz, 2 H, CH_2), 4.73 (d, $^2J_{H,H}$ = 12.7 Hz, 2 H, CH_2), 7.29−6.75 (m, 10 H, Aryl- and Phenyl-*H*) ppm. ^{13}C NMR ($CDCl_3$): δ = 31.14 [C(*C*H$_3$)$_3$], 31.37 [C(*C*H$_3$)$_3$], 31.56 [C(*C*H$_3$)$_3$], 31.67 [C(*C*H$_3$)$_3$], 33.42 (*C*H$_2$), 33.59 (*C*H$_2$), 34.19 [*C*(CH$_3$)$_3$], 65.54 (O*C*H$_3$), 123.66, 124.94, 126.25, 127.21 (Aryl-C_m), 126.89, 129.45, 130.13, 132.45 (Aryl-C_o), 144.46, 144.77, 148.59 (Aryl-C_p), 151.18, 158.73, 160.50 (Aryl-C_i) ppm.

[Ti(OC$_6$H$_3$-2,6-*i*Pr$_2$)(Mecalix)] (14): 2,6-Diisopropylphenol (123.2 μL, 0.67 mmol) was added to a solution of **5** (500 mg, 0.67 mmol) in toluene (10 mL). The resulting orange solution was stirred for 12 h and then concentrated to dryness. The viscous orange residue was suspended in hexane, and the precipitate was collected and dried in vacuo to give **14** as a yellow powder (269 mg, 45%). Crystals suitable for X-ray diffraction were obtained from a saturated

 © 2004 Wiley-VCH Verlag GmbH & Co. KGaA, Weinheim

toluene solution at room temperature. $C_{57}H_{72}O_5Ti$ (885.1): calcd. C 77.35; H 8.20; found C 77.19, H 8.32. MS: *m*/*z* (%) = 885 (100) [M^+], 870 (37) [M − CH_3]. IR: $\tilde{\nu}$ = 2975 vs br, 1601 w br, 1582 w br, 1483 vs br, 1430 s br, 1412 w, 1393 w, 1362 s, 1302 vs br, 1256 vs br, 1236 s, 1191 vs br, 1121 s br, 1096 m, 1048 w, 1017 m, 949 vs, 917 vs br, 881 vs br, 825 s, 798 vs, 757 s br, 716 m, 676 w, 605 m, 586 vs br, 551 s br, 505 w, 476 w, 445 m, 427 m cm^{-1}. ^1H NMR (C_6D_6): δ = 0.74 [s, 9 H, C(CH_3)$_3$], 0.83 [s, 9 H, C(CH_3)$_3$], 1.40 [s, 18 H, C(CH_3)$_3$], 1.46 [d, $^3J_{H,H}$ = 6.9 Hz, 12 H, OPh{CH(CH_3)$_2$}$_2$], 3.31 (d, $^2J_{H,H}$ = 12.3 Hz, 2 H, CH_2), 3.41 (d, $^2J_{H,H}$ = 12.7 Hz, 2 H, CH_2), 3.61 (s, 3 H, OCH_3), 4.18 [sept, $^3J_{H,H}$ = 6.9 Hz, 2 H, OPh{CH(CH$_3$)$_2$}$_2$], 4.49 (d, $^2J_{H,H}$ = 12.3 Hz, 2 H, CH_2), 5.12 (d, $^2J_{H,H}$ = 12.7 Hz, 2 H, CH_2), 6.91 (s, 2 H, Aryl-H_m), 6.92 (s, 2 H, Aryl-H_m), 7.02 (m, 1 H, DIP-H_p), 7.14 (m, 2 H, DIP-H_m), 7.25 (s, 2 H, Aryl-H_m), 7.26 (s, 2 H, Aryl-H_m) ppm. ^{13}C NMR (C_6D_6): δ = 23.16 [CH(*C*H$_3$)$_2$], 28.35 [*C*H(CH$_3$)$_2$], 30.65 [C(*C*H$_3$)$_3$], 31.00 [C(*C*H$_3$)$_3$], 31.99 [C(*C*H$_3$)$_3$], 33.65 [*C*(CH$_3$)$_3$], 33.74 (*C*H$_2$), 33.90 (*C*H$_2$), 34.46 [*C*(CH$_3$)$_3$], 64.57 (O*C*H$_3$), 123.01 (s, DIP-C_p), 124.01 (s, DIP-C_m), 123.78, 125.45, 125.93, 127.27 (s, Aryl-C_m), 126.19, 130.57, 131.58, 132.33 (s, Aryl-C_o), 138.12 (s, DIP-C_o), 144.74, 145.13, 148.49 (s, Aryl-C_p), 151.88 (s, DIP-C_i), 157.86, 161.21, 163.03 (s, Aryl-C_i) ppm.

[Ti(S*t*Bu)(Mecalix)] (15): *t*BuSH (75.5 μL, 0.67 mmol) was added to a solution of **5** (500 mg, 0.67 mmol) in toluene (10 mL) at −30 °C. The Schlenk flask was then removed from the cooling bath and the solution stirred at room temperature for 2 h until it turned orange. All volatiles were removed in vacuo and the orange residue was suspended in 3 mL of hexane, filtered off and dried in vacuo to afford **15** as an orange powder (272 mg, 58%). Crystals suitable for X-ray diffraction were obtained from a hexane solution saturated at 60 °C with **15**. $C_{49}H_{64}O_4STi$ (797.0): calcd. C 73.85; H 8.09; found C 73.58, H 8.21. MS: *m*/*z* (%) = 797 (58) [M^+], 796 (100) [M − H], 740 (53) [M − *t*Bu], 725 (14) [M − *t*Bu − CH_3], 707 (7) [M − S*t*Bu]. IR: $\tilde{\nu}$ = 2969 vs br, 1602 w br, 1580 w, 1481 vs br, 1393 w, 1362 s, 1301 s br, 1253 s br, 1208 vs br, 1157 s br, 1124 s, 1112 s, 1004 s, 942 s, 922 s, 874 vs br, 831 s, 798 vs, 760 s, 725 s, 676 w, 634 w, 585 s, 567 s, 554 m, 504 w br, 466 m, 445 m, 431 m cm^{-1}. ^1H NMR (C_6D_6): δ = 0.70 [s, 9 H, C(CH_3)$_3$], 0.80 [s, 9 H, C(CH_3)$_3$], 1.40 [s, 18 H, C(CH_3)$_3$], 2.03 [s, 9 H, SC(CH_3)$_3$], 3.24 (d, $^2J_{H,H}$ = 12.3 Hz, 2 H, CH_2), 3.34 (d, $^2J_{H,H}$ = 12.7 Hz, 2 H, CH_2), 3.95 (s, 3 H, OCH_3), 4.49 (d, $^2J_{H,H}$ = 12.3 Hz, 2 H, CH_2), 5.17 (d, $^2J_{H,H}$ = 12.7 Hz, 2 H, CH_2), 6.81 (s, 2 H, Aryl-H_m), 6.85 (s, 2 H, Aryl-H_m), 7.20 (s, 2 H, Aryl-H_m), 7.21 (s, 2 H, Aryl-H_m) ppm. ^{13}C NMR (C_6D_6): δ = 30.61, 30.97, 31.93 [C(*C*H$_3$)$_3$], 32.05, 32.22 [*C*(CH$_3$)$_3$], 33.58, 34.01 (*C*H$_2$), 34.47 [*C*(CH$_3$)$_3$], 36.48 [SC(*C*H$_3$)$_3$], 53.27 [S*C*(CH$_3$)$_3$], 66.99 (O*C*H$_3$), 124.00, 125.49, 125.56, 125.61 (Aryl-C_m), 127.03, 131.03, 132.12, 132.14 (Aryl-C_o), 145.20, 145.51, 148.30 (Aryl-C_p), 150.90, 157.54, 161.89 (Aryl-C_i) ppm.

[Ti(ONMe$_2$)(Mecalix)]·C$_7$H$_8$ (16·C$_7$H$_8$): A 5.5 M solution of *tert*-butyl hydroperoxide (1.1 equiv., 0.27 mL, 1.46 mmol) in decane was added to a yellow solution of **5** (1.00 g, 1.33 mmol) in toluene (20 mL). The solution turned red shortly after addition and became yellow while stirring at room temperature for 1 h. All volatiles were removed in vacuo to give **16**·C_7H_8 as a yellow powder (1.03 g, 90%). $C_{47}H_{61}NO_5Ti·C_7H_8$ (860.0): calcd. C 73.52, H 8.01, N 1.82; found C 73.48, H 7.94, N 1.67. MS: *m*/*z* (%) = 767 (100) [M^+] 752 (9) [M − CH_3], 723 (13) [M − N(CH$_3$)$_2$], 707 (12) [M − ON(CH$_3$)$_2$], 693 (12) [M − ON(CH$_3$)$_2$ − CH_3], 677 (12) [M − ON(CH$_3$)$_2$ − 2 CH_3]. IR: $\tilde{\nu}$ = 2962 vs br, 1603 w, 1580 w, 1480 vs br, 1393 w, 1362 s, 1309 s br, 1260 vs br, 1207 vs br, 1170 w, 1114 s br, 1096 s br, 1017 s br, 939 m, 921 m, 873 s, 797 vs, 756 m, 728 w, 676 w, 632 w br, 599 m, 584 m, 566 m, 508 w br, 478 w br cm^{-1}. ^1H NMR (C_6D_6): δ = 0.77 [s, 9 H, C(CH_3)$_3$], 0.86 [s, 9 H, C(CH_3)$_3$], 1.45 [s, 18 H, C(CH_3)$_3$], 2.92 [s, 6 H, ON(CH_3)$_2$], 3.28 (d, $^2J_{H,H}$ = 12.2 Hz, 2 H, CH_2), 3.37 (d, $^2J_{H,H}$ = 12.5 Hz, 2 H, CH_2), 3.79 (s, 3 H, OCH_3), 4.46 (d, $^2J_{H,H}$ = 12.2 Hz, 2 H, CH_2), 4.88 (d, $^2J_{H,H}$ = 12.5 Hz, 2 H, CH_2), 6.92 (s, 2 H, Aryl-H_m), 6.93 (s, 2 H, Aryl-H_m), 7.25 (s, 2 H, Aryl-H_m), 7.28 (s, 2 H, Aryl-H_m) ppm. ^{13}C NMR (C_6D_6): δ = 31.61 [s, C(*C*H$_3$)$_3$], 31.96 [s, C(*C*H$_3$)$_3$], 32.90 [s, C(*C*H$_3$)$_3$], 34.44 [s, *C*(CH$_3$)$_3$], 34.55 [s, *C*(CH$_3$)$_3$], 34.65 (s, *C*H$_2$), 34.85 (s, *C*H$_2$), 35.21 [s, *C*(CH$_3$)$_3$], 50.31 [s, N(*C*H$_3$)$_2$], 64.02 (s, O*C*H$_3$), 124.89, 126.13, 126.21, 127.51 (s, Aryl-C_m), 127.10, 132.08, 132.71, 133.33 (s, Aryl-C_o), 144.53, 144.71, 148.39 (s, Aryl-C_p), 153.12, 159.21, 161.87 (s, Aryl-C_i) ppm.

Epoxidation Reactions: In an NMR tube 0.029 mmol (based on monomeric units) of the precatalyst was layered with C_6D_6/TMS (0.30 mL) and frozen in liquid nitrogen. Cyclooctene (74.3 μL, 0.573 mmol) and a 5.5 M solution of *tert*-butyl hydroperoxide in decane (104.6 μL, 0.573 mmol) were then added. To determine the kinetics the samples were thawed and mixed shortly before they were placed into the NMR spectrometer. The ratio between substrate, product and catalyst was determined by integration of the resonances of the olefinic protons of the cyclooctene, the protons of the epoxide ring and the protons of the methoxy groups of the calixarene complexes relative to TMS. The entries in Figure 12 are averages of three runs.

Computational Details: All density functional and MP2 calculations reported were carried out by using the TURBOMOLE set of programs, developed by Ahlrichs and co-workers, within the RI-J approximation.[21,22] Standard SV(P) basis sets and auxiliary basis sets as implemented in the TURBOMOL package were used for all atoms.[22,23] The acronym SV(P) (split valence plus polarization) refers to TURBOMOLE split-valence basis sets, augmented by a shell of polarization functions. DFT calculations were performed including gradient corrections, Becke's nonlocal correction for exchange and Perdew's nonlocal correction for correlation to the local density approximation part of the density functional.[24]

Crystal Structure Determination of [TiCl(Mecalix)]·1.5C$_7$H$_8$, [Ti(η^5-C$_5$H$_5$)(Mecalix)]·3C$_7$H$_8$, [Ti(NMe$_2$)(Mecalix)]·[{Ti(Mecalix)}$_2$-(μ-O)]·5C$_4$H$_8$O, 2·[Ti(NPh$_2$)(Mecalix)]·8C$_4$H$_8$O·0.5C$_6$H$_6$, [{Ti(OMe)(Mecalix)}$_2$]·6C$_7$H$_8$, [Ti(OC$_6$H$_3$-2,6-*i*Pr$_2$)(Mecalix)]·C$_6$H$_3$*i*Pr$_2$OH, and [Ti(S*t*Bu)(Mecalix)]·C$_6$H$_{14}$: Crystal data collection and processing parameters are given in Tables 1 and 2. Crystals were immersed in a film of perfluoropolyether oil on a glass fiber and transferred to a Stoe-STADI 4 (Mo-K_α radiation for **1**·1.5C_7H_8) or Stoe-IPDS diffractometer (Ag-K_α radiation for the rest) equipped with an FTS AirJet low-temperature device. Data were collected at 203 K. The IPDS images were processed with the Stoe IPDS software package and equivalent reflections were merged. Corrections for Lorentz polarization effects and absorption were performed where necessary and the structures were solved by direct methods. Subsequent difference-Fourier syntheses revealed the positions of all other non-hydrogen atoms, and hydrogen atoms were included in calculated positions. Extinction corrections were applied as required. Crystallographic calculations were performed using SHELXS-97 and SHELXL-97.[39] For compound **4** the methyl carbon atoms of two of the calixarene *tert*-butyl groups [C(17) to C(19) and C(47) to C(49)] were disordered over two sites. These carbon atoms were refined in an isotropic approximation with occupancy factors of 70%/30% and 50%/50%, respectively. For **5·9**·5C_4H_8O the following carbon atoms of the calixarene *tert*-butyl groups were disordered over two sites and refined in an isotropic approximation with occupancy factors of 50% each: C(17), C(18),

 © 2004 Wiley-VCH Verlag GmbH & Co. KGaA, Weinheim

Table 1. X-ray data collection and processing parameters for **1**·1.5C_7H_8, **4**·2C_7H_8, **5·9**·5C_4H_8O and **8**·8C_4H_8O·0.5C_6H_6

	1·1.5C_7H_8	**4**·2C_7H_8	**5·9**·5C_4H_8O	**8**·8C_4H_8O·0.5C_6H_6
Empirical formula	$C_{55.5}H_{67}ClO_4Ti$	$C_{64}H_{76}O_4Ti$	$C_{112}H_{156}O_{13.5}Ti_2$	$C_{149}H_{197}N_2O_{16}Ti_2$
Formula mass	881.4	957.2	1828.18	2367.88
Crystal system	monoclinic	monoclinic	triclinic	monoclinic
Space group	*I*2/*a*	$P2_1/c$	$P\bar{1}$	$P2_1/c$
a [Å]	24.944(5)	16.561(1)	13.317(1)	26.366(2)
b [Å]	13.359(3)	14.970(1)	21.304(2)	20.525(1)
c [Å]	30.121(6)	23.676(2)	21.319(2)	27.381(2)
α [°]	90	90	100.944(8)	90
β [°]	94.77(3)	108.479(9)	100.244(8)	114.791(6)
γ [°]	90	90	100.196(8)	90
V [Å^3]	10003(3)	5566.9(7)	5702.7(7)	13451.6(12)
Z	8	4	2	4
μ [mm^{-1}]	0.268	0.111	0.108	0.102
Tot./indep. reflns.	9836/9836	31081/7485	26742/13513	80108/19065
Observed reflns.[a]	7718	3845	8652	13675
Parameters	574	602	1090	1440
Final *R*,[b] wR_2 [c] [d]	0.0611, 0.1521	0.0777, 0.1805	0.0976, 0.2746	0.0802, 0.2233

[a] Reflections with $I > 2\sigma(I)$. [b] $R = \Sigma||F_o| - |F_c||/\Sigma|F_o|$. [c] $wR_2 = \{\Sigma[w(F_o^2 - F_c^2)^2]/\Sigma[w(F_o^2)^2]\}^{1/2}$. [d] For data with $I > 2\sigma(I)$.

Table 2. X-ray data collection and processing parameters for **9**·4C_6H_6, **10**·6C_7H_8, **14**·C_6H_3·*i*Pr_2OH and **15**·C_6H_{14}

Empirical formula	**9**·4C_6H_6 $C_{114}H_{134}O_9Ti_2$	**10**·6C_7H_8 $C_{134}H_{164}O_{10}Ti_2$	**14**·C_6H_3·*i*Pr_2OH $C_{69}H_{90}O_6Ti$	**15**·C_6H_{14} $C_{55}H_{78}O_4Sti$
Formula mass	1744.0	2030.5	1063.3	813.1
Crystal system	monoclinic	monoclinic	monoclinic	monoclinic
Space group	$P2_1/n$	*C*2/*c*	$P2_1/c$	$P2_1/c$
a [Å]	1307.3(1)	28.472(6)	22.814(3)	1548.4(1)
b [Å]	17.612(1)	17.134(3)	10.570(3)	1666.4(1)
c [Å]	21.831(2)	2396.2(5)	24.710(4)	2167.1(1)
α [°]	90	90	90	90
β [°]	96.354(11)	91.11(3)	91.759(16)	106.676(6)
γ [°]	90	90	90	90
V [Å^3]	4995.6(7)	11687(4)	5956(2)	5356.5(5)
Z	2	4	4	4
μ [mm^{-1}]	0.120	0.109	0.109	0.130
Tot./indep. reflns.	15565/	45691/11128	23524/9321	29817/10096
Observed reflns.[a]	6003	7829	5962	5008
Parameters	536	605	702	538
Final *R*,[b] wR_2 [c] [d]	0.0609, 0.1082	0.0732, 0.2094	0.0692, 0.1843	0.0973, 0.2247

[a] Reflections with $I > 2\sigma(I)$. [b] $R = \Sigma||F_o| - |F_c||/\Sigma|F_o|$. [c] $wR_2 = \{\Sigma[w(F_o^2 - F_c^2)^2]/\Sigma[w(F_o^2)^2]\}^{1/2}$. [d] For data with $I > 2\sigma(I)$.

C(19), C(29), C(37), C(38), C(39), C(48), C(49), C(59), C(89). The anisole methyl group C(95) of the calixarene ligand of **9** was disordered in this structure over two sites at the oxygen atoms O(6) and O(8) and refined isotropically using equal occupancy. Furthermore, two methylene groups of one of the solvent molecules [C(109) and C(111)] were disordered and isotropically refined with occupancy factors of 50% each. For **8**·8C_4H_8O·0.5C_6H_6 the following carbon atoms of calixarene *tert*-butyl groups or THF molecules were disordered over two sites and refined in an isotropic approximation with occupancy factors of 50% each: C(19), C(49), C(122), C(129), C(130), C(131). The methylene carbon atoms C(132), C(133), C134), C(135), as well as C(137), C(138), C(144), C(145), C(147) of THF molecules were disordered over two sites. These carbon atoms were refined in an isotropic approximation with occupancy factors of 60%/40% and 70%/30%, respectively. The carbon atoms C(60) and C(61) of one of the isopropyl groups in **14**·C_6H_3 *i*Pr_2OH were disordered over two sites and refined in an isotropic approximation with occupancy factors of 45%/55%. For **15**·C_6H_{14} two of the *tert*-butyl groups of the calixarene ligand [C(27) to C(29) and C(37) to C(39)] and of the thiolate group [C(7) to C(9)] were disordered over two sites and refined in an isotropic approximation with occupancy factors of 65%/35%, 60%/40% and 50%/50%, respectively. CCDC-233967 to CCDC-233974 contains the supplementary crystallographic data for this paper. These data can be obtained free of charge at www.ccdc.cam.ac.uk/conts/retrieving.html [or from the Cambridge Crystallographic Data Centre, 12 Union Road, Cambridge CB2 1EZ, UK; Fax: + 44-1223-336-033; E-mail: deposit@ccdc.cam.ac.uk].

Acknowledgments

This work was supported by the Deutschen Forschungsgemeinschaft and the Fonds der Chemischen Industrie.

[1] [1a] *Calixarenes in Action* (Eds.: M. Lucinat, R. Ungaro), Imperial College Press, London, **2000**. [1b] G. J. Lumetta, R. D. Rogers, A. S. Gopalan, *Calixarenes for Separations*, American Chemical Society, Washington D.C., **2000**. [1c] C. D. Gutsche,

Calixarenes Revisited, Royal Society of Chemistry, Cambridge, **1998**. [1d] *Calixarenes 50th Anniversary: Commemorative Issue* (Eds.: J. Vicens, Z. Asfari, J. M. Harrowfield), Kluwer Academic Publishers, Dordrecht, **1994**. [1e] *Calixarenes: A Versatile Class of Macrocyclic Compounds* (Eds.: J. Vicens, V. Böhmer), Kluwer Academic Publishers, Dordrecht, **1991**. [1f] C. D. Gutsche, *Calixarenes*, Royal Society of Chemistry, Cambridge, **1989**.

[2] [2a] A. Ikeda, S. Shinkai, *Chem. Rev.* **1997**, *97*, 1713. [2b] V. Böhmer, *Angew. Chem.* **1995**, *107*, 785; *Angew. Chem. Int. Ed. Engl.* **1995**, *34*, 713. [2c] A. F. D. De Namor, R. M. Cleverly, M. L. Zapata-Ormachea, *Chem. Rev.* **1998**, *98*, 2485.

[3] [3a] A. Pochini, R. Ungaro, in *Comprehensive Supramolecular Chemistry*, vol. 2 (Ed.: F. Vögtle), Elsevier, Oxford, **1996**, p. 103. [3b] Y. K. Agrawal, S. Kunji, S. K. Menon, *Rev. Anal. Chem.* **1998**, *17*, 69. [3c] M. A. McKervey, F. Arnaud-Neu, M.-J. Schwing-Weill, in *Comprehensive Supramolecular Chemistry*, vol. 1 (Ed.: G. Gokel), Pergamon, Oxford, **1996**, p. 537.

[4] [4a] D. M. Roundhill, in *Comprehensive Coordination Chemistry II*, vol. 1 (Ed.: J. McCleverty, T. Meyer), Elsevier, Oxford, **2004**, p. 485. [4b] C. Floriani, R. Floriani-Moro, *Adv. Organomet. Chem.* **2001**, *47*, 167. [4c] C. Floriani, *Chem. Eur. J.* **1999**, *5*, 19. [4d] C. Wieser, C. B. Dieleman, D. Matt, *Coord. Chem. Rev.* **1997**, *165*, 93. [4f] D. M. Roundhill, *Prog. Inorg. Chem.* **1995**, *43*, 533.

[5] Assuming no additional metal centers, the calix[4]arene system retains its cone-like appearance in square-pyramidal complexes of the type [ML(Calix)], or in octahedral complexes [ML_2(Calix)], if both L ligands are oriented *trans* to each other. In mononuclear octahedral complexes with *cis*-oriented L ligands it has been found that the calix[4]arene usually binds in an elliptical cone conformation, in which the calix[4]arene oxygen atoms adopt *cis* and *trans* sites in octahedral [$CaxO_4ML_2$] complexes.[4] Additional metal centers in the complex may further influence the coordination behavior of calix[4]arenes, see for example: [5a] V. C. Gibson, C. Redshaw, W. Clegg, M. R. J. Elsegood, *Chem. Commun.* **1997**, 1605. [5b] K. Iwasa, T. Kochi, Y. Ishii, *Angew. Chem.* **2003**, *115*, 3786; *Angew. Chem. Int. Ed.* **2003**, *42*, 3658.

[6] [6a] M. Calligiaris, L. Ranaccio, in *Comprehensive Coordination Chemistry*, vol. 2 (Ed.: G. Wilkinson), Pergamon Press, Exeter, **1987**. [6b] C. Floriani, *Polyhedron* **1989**, *8*, 1717. [6c] D. E. Fenton, P. A. Vigato, *Chem. Soc. Rev.* **1988**, *17*, 69. [6d] J. Costamagna, J. Vargas, R. Latorre, A. Alvarado, G. Mena, *Coord. Chem. Rev.* **1992**, *119*, 67.

[7] [7a] *Porphyrins and Metalloporphyrins* (Ed.: K. M. Smith), Elsevier, New York, **1975**. [7b] *The Porphyrins* (Ed. D. Dolphin), Academic Press, New York, **1977−1979**. [7c] B. D. Berenzin, *Coordination Compounds of Porphyrins and Phthalocyanines*, Wiley, Chichester, **1981**. [7d] T. Mashiko, D. Dolphin, "Porphyrins, Hydroporphyrins, Azaporphyrins, Phthalocyanines, Corroles, Corrines and Related Macrocycles", in *Comprehensive Coordination Chemistry*, vol. 2 (Ed.: G. Wilkinson), Pergamon Press, Exeter, **1987**. [7e] K. Katylanasundaran, *Photochemistry of Polypyridine and Porphyrin Complexes*, Academic Press, London, **1992**. [7f] *Metalloporphyrins in Catalytic Oxidations* (Ed.: R. A. Sheldon), Marcel Dekker, New York, **1994**. [7g] *Metal Complexes with Tetrapyrrole Ligands* (Ed.: J. W. Buchler), Springer-Verlag, Berlin, **1995**. [7h] *The Colours of Life: An Introduction to the Chemistry of Porphyrin and Related Compounds* (Ed.: L. R. Milgram), Oxford University Press, Oxford, **1997**. [7i] H. Brand, J. Arnold, *Coord. Chem. Rev.* **1995**, *140*, 137.

[8] [8a] L. F. Lindoy, *The Chemistry of Macrocyclic Ligand Complexes*, Cambridge University Press, Cambridge, **1989**. [8b] F. A. Cotton, J. Czuchajowski, *Polyhedron* **1990**, *9*, 2663. [8c] P. Mountford, *Chem. Soc. Rev.* **1998**, *27*, 105.

[9] [9a] U. Radius, *Inorg. Chem.* **2001**, *40*, 6637. [9b] As pointed out by Harrowfield and co-workers, the classification based simply on four idealized conformers — the cone, partial cone, 1,2-alternate and 1,3-alternate species — has been eroded due to the number of factors which may influence the adoption of any conformation: J. M. Harrowfield, M. Mocerino, B. W. Skelton, C. R. Whitaker, A. H. White, *Aust. J. Chem.* **1994**, *47*, 1185. We use the term "paco" conformation here to emphasize the difference in calix[4]arene bonding to the usually observed (cone or elliptically distorted cone) conformations in transition metal complexes.

[10] [10a] U. Radius, A. Friedrich, *Z. Anorg. Allg. Chem.* **1999**, *625*, 2154. [10b] S. R. Dubberly, A. Friedrich, D. A. Willman, P. Mountford, U. Radius, *Chem. Eur. J.* **2003**, *9*, 3634.

[11] A. Zanotti-Gerosa, E. Solari, L. Giannini, C. Floriani, N. Re, A. Chiesi-Villa, C. Rizzoli, *Inorg. Chim. Acta* **1998**, *270*, 298.

[12] P. J. Dijkstra, J. A. J. Brunink, K. E. Bugge, D. N. Reinhoudt, S. Harkema, R. Ungaro, F. Ugozzoli, E. Ghidini, *J. Am. Chem. Soc.* **1989**, *111*, 7567.

[13] J. Zeller, S. Koenig, U. Radius, *Inorg. Chim. Acta* **2004**, *357*, 1813.

[14] [14a] A. Friedrich, U. Radius, unpublished results. For further calix[4]arene-stabilized titanium complexes see for example: [14b] M. M. Olmstead, G. Siegel, H. Hope, X. Xu, P. P. Power, *J. Am. Chem. Soc.* **1985**, *107*, 8087. [14c] X. Delaigue, M. W. Hosseini, E. Leize, S. Kieffer, A. van Dorsellaer, *Tetrahedron Lett.* **1993**, *34*, 7561. [14d] W. Clegg, M. R. J. Elsegood, S. J. Teat, C. Redshaw, V. C. Gibson, *J. Chem. Soc., Dalton Trans.* **1998**, 3037. [14e] O. V. Ozerov, F. T. Ladipo, B. O. Patrick, *J. Am. Chem. Soc.* **1999**, *121*, 7941. [14f] F. A. Cotton, E. V. Dikarev, C. A. Murillo, M. A. Petrukhina, *Inorg. Chim. Acta* **2002**, *332*, 41. [14g] A. J. Petrella, N. K. Roberts, C. L. Raston, M. Thornton-Pett, R. N. Lamb, *Chem. Commun.* **2003**, 1238.

[15] J. Okuda, S. Fokken, H.-C. Kang, W. Massa, *Chem. Ber.* **1995**, *128*, 221.

[16] [16a] A. V. Firth, D. W. Stephan, *Inorg. Chem.* **1998**, *37*, 4732. [16b] M. J. Sarsfield, S. W. Ewart, T. L. Tremblay, A. W. Roszak, M. C. Baird, *J. Chem. Soc., Dalton Trans.* **1997**, 3097.

[17] U. Müller, *Anorganische Strukturchemie*, Teubner-Verlag, Stuttgart, **1992**.

[18] [18a] V. Visciglio, P. E. Fanwick, I. P. Rothwell, *Acta Crystallogr., Sect. C* **1994**, *50*, 896. [18b] R. A. Jones, J. G. Hefner, T. C. Wright, *Polyhedron* **1984**, *3*, 1121.

[19] T. J. Boyle, T. M. Alam, E. R. Mechenbier, B. L. Scott, J. W. Ziller, *Inorg. Chem.* **1997**, *36*, 3293.

[20] [20a] F. Senocq, N. Viguier, A. Gleizes, *Eur. J. Solid State Inorg. Chem.* **1996**, *33*, 1185. [20b] M. J. Calhorda, M. A. A. F. de C. T. Carrondo, A. R. Dias, C. F. Farzao, M. B. Hursthouse, J. A. M. Simoes, C. Teixeira, *Inorg. Chem.* **1988**, *27*, 2513. [20c] R. A. Jones, S. T. Schwab, B. R. Whittlesey, *Polyhedron* **1984**, *3*, 505.

[21] [21a] R. Ahlrichs, "TURBOMOLE", in *Encyclopedia of Computational Chemistry* (Ed.: P. v. R. Schleyer), Wiley, Chichester, **1998**, vol. 5, p. 3123. [21b] R. Ahlrichs, M. v. Arnim, "TURBOMOLE, parallel implementation of SCF, density functional, and chemical shift modules", in *Methods and Techniques in Computational Chemistry* (Eds.: E. Clementi, G. Corongiu), STEF, Cagliary, **1995**.

[22] [22a] O. Treutler, R. Ahlrichs, *J. Chem. Phys.* **1995**, *102*, 346. [22b] K. Eichkorn, O. Treutler, H. Öhm, M. Häser, R. Ahlrichs, *Chem. Phys. Lett.* **1995**, *242*, 652. [22c] K. Eichkorn, F. Weigand, O. Treutler, R. Ahlrichs, *Theor. Chim. Acc.* **1997**, *97*, 119. [22d] M. v. Arnim, R. Ahlrichs, *J. Comp. Chem.* **1998**, *97*, 331. [22e] F. Weigend, A. Köhn, C. Hättig, *J. Chem. Phys.* **2002**, *116*, 3175. [22f] P. Deglmann, F. Furche, R. Ahlrichs, *Chem. Phys. Lett.* **2002**, *362*, 511. [22g] P. Deglmann, F. Furche, *J. Chem. Phys.* **2002**, *117*, 9535.

[23] [23a] F. Haase, R. Ahlrichs, *J. Comput. Chem.* **1993**, *14*, 907. [23b] F. Weigand, M. Häser, *Theor. Chem. Acc.* **1997**, *97*, 331. [23c] F. Weigand, M. Häser, H. Patzelt, R. Ahlrichs, *Chem. Phys. Lett.* **1998**, *294*, 143. [23d] A. Schäfer, H. Horn, R. Ahlrichs, *J. Chem. Phys.* **1992**, *97*, 2571.

[24] [24a] A. D. Becke, *Phys. Rev. A* **1988**, *38*, 3098. [24b] S. H. Vosko, L. Wilk, M. Nusair, *Can. J. Phys.* **1980**, *58*, 1200. [24c] J. P.

 © 2004 Wiley-VCH Verlag GmbH & Co. KGaA, Weinheim

Perdew, *Phys. Rev. B* **1986**, *33*, 8822; Erratum: J. P. Perdew, *Phys. Rev. B* **1986**, *34*, 7406.
[25] M. Taramasso, G. Perego, B. Notari, Snamprogetti S.p.A., US Pat. 4,410,510, **1983**; *Chem. Abstr.* **1981**, *95*, 206272k.
[26] [26a] G. Bellussi, M. S. Rigutto, *Stud. Surf. Sci. Catal.* **1994**, *85*, 177. [26b] B. Notari, *Catal. Today* **1993**, *18*, 163.
[27] [27a] R. J. Davies, Z. Liu, *Chem. Mater.* **1997**, *9*, 2311. [27b] R. Neumann, M. Levin-Elad, *J. Catal.* **1997**, *166*, 206. [27c] S. Klein, S. Thorimbert, W. F. Maier, *J. Catal.* **1996**, *163*, 476. [27d] R. Hutter, T. Mallat, A. Baiker, *J. Catal.* **1995**, *153*, 177. [27e] S. Imamura, T. Nakai, H. Kanai, T. Ito, *J. Chem. Soc., Faraday Trans.* **1995**, 1261.
[28] [28a] J. M. Fraile, J. L. Garcia, J. A. Mayoral, M. G. Proietti, M. C. Sanchez, *J. Phys. Chem.* **1996**, *100*, 19484. [28b] C. Cativiela, J. M. Fraile, J. L. Garcia, J. A. Mayoral, *J. Mol. Catal. A* **1996**, *112*, 259. [28c] E. Jorda, A. Tuel, R. Teissier, J. Kervennal, *J. Catal.* **1998**, *175*, 93. [28d] C. B. Khouw, C. B. Dartt, J. A. Labinger, M. E. Davies, *J. Catal.* **1994**, *149*, 195.
[29] [29a] T. Blasco, M. A. Camblor, A. Corma, P. Esteve, J. M. Guil, A. Martinez, J. A. Perdigón-Melón, S. Valencia, *J. Phys. Chem. B* **1998**, *102*, 75. [29b] C. B. Dartt, M. E. Davies, *Appl. Catal. A* **1996**, *143*, 53−73. [29c] M. S. Rigutto, R. de Ruiter, J. P. M. Niederer, H. van Bekkum, *Stud. Surf. Sci. Catal.* **1994**, *84*, 2245.
[30] [30a] A. Corma, M. T. Navarro, J. Perez-Pariente, *J. Chem. Soc., Chem. Commun.* **1994**, 147. [30b] W. Zhang, M. Fröba, J. Wang, P. T. Tanev, J. Wong, T. J. Pinnavaia, *J. Am. Chem. Soc.* **1996**, *118*, 9164. [30c] A. Corma, Q. Khan, F. Rey, *Chem. Commun.* **1998**, 579.
[31] [31a] J. Corker, F. Lefebvre, C. Lecuyer, V. Dufaud, F. Quignard, A. Choplin, J. Evans, J.-M. Basset, *Science* **1996**, *271*, 966. [31b] G. P. Niccolai, J.-M. Basset, *Appl. Catal. A* **1996**, *146*, 145. [31c] V. Vidal, A. Theolier, J. Thivolle-Cazat, J.-M. Basset, J. Corker, *J. Am. Chem. Soc.* **1996**, *118*, 4595.
[32] [32a] R. Murugavel, H. W. Roesky, *Angew. Chem.* **1997**, *109*, 491; *Angew. Chem. Int. Ed. Engl.* **1997**, *36*, 477. [32b] T. Maschmeyer, F. Rey, G. Sauhar, J. M. Thomas, *Nature* **1995**, *378*, 159. [32c] R. D. Oldroyd, P. A. MacFaul, T. Maschmeyer, J. M. Thomas, D. W. Snelgrove, K. U. Ingold, D. D. M. Wayner, *Angew. Chem.* **1996**, *108*, 2966; *Angew. Chem. Int. Ed. Engl.* **1996**, *35*, 2787. [32d] J. M. Thomas, *Angew. Chem.* **1999**, *111*, 3800; *Angew. Chem. Int. Ed.* **1999**, *38*, 3589. [32e] J. M. Thomas, *Chem. Eur. J.* **1997**, *3*, 1557. [32f] J. M. Thomas, G. Sankar, M. C. Klunduk, M. P. Attfield, T. Maschmeyer, B. F. G. Johnson, R. G. Bell, *J. Phys. Chem. B* **1999**, *103*, 8809.
[33] [33a] I. V. Yudanov, P. Gisdakis, C. Di Valentin, N. Rösch, *Eur. J. Inorg. Chem.* **1999**, 2135. [33b] P. Gisdakis, S. Antonczak, S. Köstlmeier, W. A. Herrmann, N. Rösch, *Angew. Chem.* **1998**, *110*, 2333; *Angew. Chem. Int. Ed.* **1998**, *37*, 2211. [33c] C. Di Valentin, P. Gisdakis, I. V. Yudanov, N. Rösch, *J. Org. Chem.* **2000**, *65*, 2996.
[34] [34a] W. A. Hermann, *J. Organomet. Chem.* **1995**, *500*, 149. [34b] W. A. Herrmann, F. E. Kühn, *Acc. Chem. Res.* **1997**, *30*, 169. [34c] C. C. Romao, F. E. Kühn, W. A. Herrmann, *Chem. Rev.* **1997**, *97*, 3197. [34d] W. A. Herrmann, R. W. Fischer, W. Scherer, M. U. Rauch, *Angew. Chem.* **1993**, *105*, 1209; *Angew. Chem. Int. Ed. Engl.* **1993**, *32*, 1157. [34e] J. Sundermeyer, *Angew. Chem.* **1993**, *105*, 1195; *Angew. Chem. Int. Ed. Engl.* **1993**, *32*, 1144.
[35] [35a] H. Mimoun, *Angew. Chem.* **1982**, *94*, 750; *Angew. Chem. Int. Ed. Engl.* **1982**, *21*, 734. [35b] K. A. Jørgensen, B. Schiøtt, *Chem. Rev.* **1990**, *90*, 1483.
[36] For the usage of epoxidation catalysts based on titanasilsesquioxanes see for example: [36a] H. C. L. Abbenhuis, S. Krijnen, R. A. van Santen, *Chem. Commun.* **1997**, 331. [36b] S. Krijnen, H. C. L. Abbenhuis, R. W. M. Hannsen, J. H. C. van Hooff, R. A. van Santen, *Angew. Chem.* **1998**, *110*, 374; *Angew. Chem. Int. Ed.* **1998**, *37*, 356. [36c] H. C. L. Abbenhuis, *Chem. Eur. J.* **2000**, *6*, 25. [36d] T. Maschmeyer, M. C. Klunduk, C. M. Martin, D. S. Shephard, J. M. Thomas, B. F. G. Johnson, *Chem. Commun.* **1997**, 1847. [36e] M. C. Klunduk, T. Maschmeyer, J. M. Thomas, B. F. G. Johnson, *Chem. Eur. J.* **1999**, *5*, 1481. [36f] B. F. G. Johnson, M. C. Klunduk, C. M. Martin, G. Sankar, S. J. Teate, J. M. Thomas, *J. Organomet. Chem.* **2000**, *596*, 221. [36g] P. P. Pescarmona, J. C. van der Waal, I. E. Maxwell, T. Maschmeyer, *Angew. Chem.* **2001**, *113*, 762; *Angew. Chem. Int. Ed.* **2001**, *40*, 740. [36h] M. Crocker, R. H. M. Herold, A. G. Orpen, *Chem. Commun.* **1997**, 2411. [36i] M. Crocker, R. H. M. Herold, A. G. Orpen, M. T. A. Overgang, *J. Chem. Soc., Dalton Trans.* **1999**, 3791.
[37] R. A. Sheldon, "Synthesis of Oxiranes", in *Applied Homogeneous Catalysis with Organometallic Compounds* (Eds.: B. Cornils, W. A. Herrmann), Wiley-VCH, Weinheim, **2000**, pp. 411−423.
[38] C. D. Gutsche, M. Iqbal, A. T. Watson, C. H. Heathcock, *Org. Synth.* **1989**, *68*, 234.
[39] [39a] G. M. Sheldrick, *SHELXS-97, Program for Crystal Structure Solution*, Universität Göttingen, **1997**. [39b] G. M. Sheldrick, *SHELXL-97, Program for Crystal Structure Refinement*, Universität Göttingen, **1997**.

Received May 24, 2004
Early View Article
Published Online September 17, 2004

 © 2004 Wiley-VCH Verlag GmbH & Co. KGaA, Weinheim

Synthesis, Structural Characterization and Properties of Copper(II) and Zinc(II) Coordination Polymers with a New Bridging Chelating Ligand

Guo-Ping Yong,[a] Zhi-Yong Wang,*[a] and Yong Cui[a]

Keywords: Coordination polymers / Copper / N,O ligands / Zinc

Two new coordination polymers $[Cu_3(cpida)_2(H_2O)_4]_n \cdot 4nH_2O$ (**1**) and $[Zn(Hcpida)]_n \cdot nH_2O$ (**2**) have been synthesized with a new bridging chelating ligand *N*-(4-carboxyphenyl)iminodiacetic acid (H_3cpida). X-ray diffraction analysis reveals that complex **1** consists of 1D parallelogram-shaped molecular-box chains constructed from unusual linear trinuclear Cu^{II} secondary building units (SBUs), which further extend into 2D layers by perfect parallel AA stacking. Complex **2** adopts a 2D framework comprised of tetrahedral Zn^{II} centres isolated from each other by the bridging bidentate carboxylate groups of the $Hcpida^{2-}$ ligands. Compound **2** possesses alternate open and closed channels along the *a* direction. The dehydation and rehydration experiments showed that compound **2** undergoes a reversible inclusion process to some extent. However, the removal of guest water molecules from **1** results in the collapse of the polymeric networks owing to the loss of the coordinated water molecules. Compound **2** also shows strong photoluminescence and may be a good candidate for a photoactive or porous material.

(© Wiley-VCH Verlag GmbH & Co. KGaA, 69451 Weinheim, Germany, 2004)

Introduction

Metal-organic coordination polymers built up from metallic clusters and multi-carboxylate building blocks have been widely studied in recent years due to their interesting topologies[1] and potential applications as functional materials.[2] The most commonly used strategy to obtain coordination polymers is to employ appropriate bridging ligands that are capable of binding to several metal centres through direct bond formation. Multi-carboxylate building blocks with special configurations can yield desired networks in metal-organic coordination polymers[3−5] because they can act as either bridging or chelating ligands. A chelating ligand provides stronger connectivity and enhances rigidity around the coordination centre, which results in higher stability of the resulting framework materials.[6] Thus, one of the most necessary tasks of current research is the synthesis of new bridging, chelating multi-carboxylate ligands because they have a pre-programmed tendency to form supramolecular motifs of defined geometry.[7−9] We are currently focusing our attentions on the design and synthesis of new bridging, chelating ligands and have recently obtained a new bridging, chelating multi-carboxylate ligand *N*-(4-carboxyphenyl)iminodiacetic acid (H_3cpida), which has two important features: (a) unlike rigid groups such as benzenetricarboxylate, the iminodiacetate group is more flexible and can adopt different coordination modes; (b) the introduced aromatic rings can offer additional π−π interactions which may stabilize the frameworks.[10]

We describe here the synthesis, structural characterization and properties of two new coordination polymers $[Cu_3(cpida)_2(H_2O)_4]_n \cdot 4nH_2O$ (**1**) and $[Zn(Hcpida)]_n \cdot nH_2O$ (**2**) obtained from the H_3cpida building block. Compound **1** is a rare 1D molecular-box chain constructed from unusual linear trinuclear Cu^{II} SBUs. Compound **2** is a new 2D framework constituted by tetrahedrally coordinated Zn^{II} with strong fluorescent emission.

Results and Discussion

Compound **1** was prepared by heating a mixture of basic copper carbonate and H_3cpida in water under steam bath conditions, while compound **2** was synthesized by treating $Zn(NO_3)_2 \cdot 6H_2O$ with H_3cpida in $KOH/CH_3OH/H_2O$ under hydrothermal conditions (Scheme 1Scheme 1). The presence of the characteristic band at 1703 cm^{-1} for compound **2** indicates that the deprotonation of H_3cpida ligand is incomplete, which is consistent with the crystal structure of **2**.

Description of Crystal Structures

$[Cu_3(cpida)_2(H_2O)_4]_n \cdot 4nH_2O$ (1)

The polymeric structure of **1** was confirmed by an X-ray single-crystal structure determination. The trinuclear entity of compound **1** with the atomic labelling scheme is shown

[a] Department of Chemistry, University of Science and Technology of China,
Hefei 230026, P. R. China
Fax: (internat.) + 86-551-363-1760
E-mail: zwang3@ustc.edu.cn

Supporting information for this article is available on the WWW under http://www.eurjic.org or from the author.

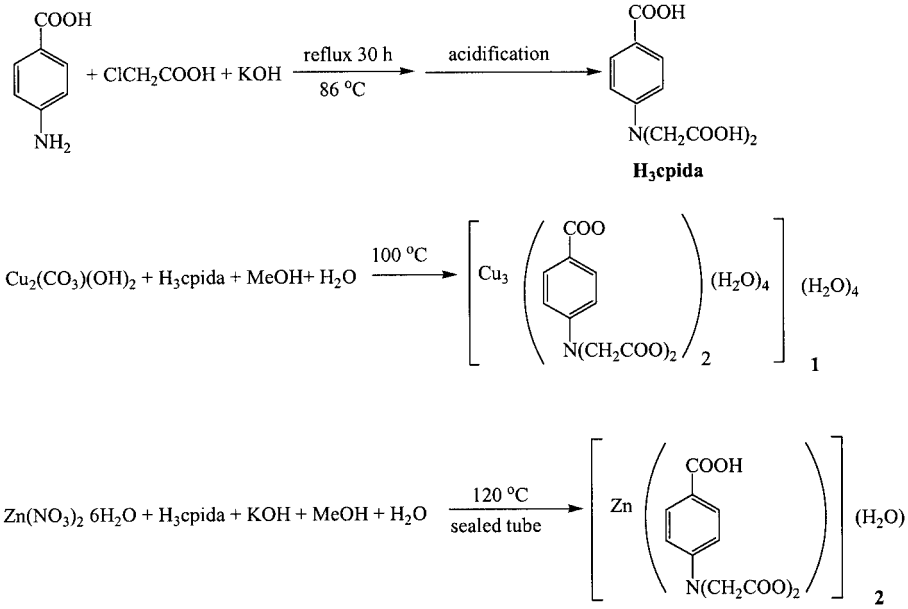

Scheme 1. Preparation of H_3cpida and complexes **1** and **2**

in Figure 1a. The two terminal Cu^{II} atoms (Cu1 and Cu1a) adopt a Jahn−Teller-distorted octahedral coordination environment, resulting in a longer axial Cu1−O6 bond [2.344(2) Å] from the coordinated water molecule and Cu1−N1 bond [2.496(2) Å] from the cpida^{3-} ligand. The equatorial plane is defined by four oxygen atoms, which come from the bridging monodentate (O1), the monodentate (O3) and the bridging bidentate (O7a) carboxylate groups of two deprotonated cpida^{3-} ligands, and the coordinated water molecule (O5). The bond lengths Cu1−O are in the range 1.947(2)−1.978(2) Å (Table 1). The central Cu2 atom presents a Jahn−Teller octahedral environment, resulting in very long axial Cu2−O6 bonds [2.608(2) Å] to the coordinated water molecule. The equatorial plane geometry is formed from the O1, O1a, O8 and O8a atoms of the bridging monodentate and bidentate carboxylate groups of four cpida^{3-} ligands [Cu2−O = 1.916(2) and 1.958 (2) Å].

The adjacent Cu^{II} centres are bridged by one oxygen atom of the monodentate carboxylate group and two oxygen atoms of the bidentate carboxylate groups of two cpida^{3-} ligands, leading to a linear trinuclear Cu^{II} SBU (Figure 1a). The three Cu^{II} atoms are arranged in a strictly linear fashion (Cu1−Cu2−Cu1a = 180°) with Cu2 at the inversion centre; the distance between Cu1 and Cu2 is 3.232 Å. Complex **1** is a rare example of a polynuclear metal cluster bridged by carboxylate groups from only one kind of ligand (cpida^{3-}). To the best of our knowledge, only a limited number of linear trinuclear Cu^{II} compounds have been reported,[11−13] and few metal-organic coordination frameworks containing a linear trinuclear Cu^{II} unit have been documented.[14] It is worth noting that **1** is the first linear trinuclear Cu^{II} compound in which the three Cu^{II} centres are linked by μ-carboxylato groups of only one type of ligand (cpida^{3-}); other reported examples[11−14] are mixed-

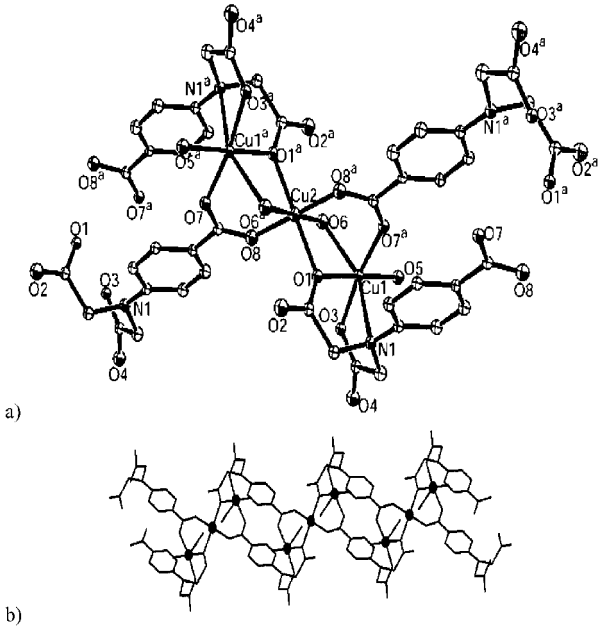

Figure 1. a) ORTEP diagram of the coordination environment around the linear trinuclear Cu^{II} unit in **1**; thermal ellipsoids are drawn at the 50% probability level; all hydrogen atoms are omitted for clarity; symmetry code: a: $-x$, $-y$, $-z$; b) 1D molecular-box chain of **1** along the *c* axis; the black spheres represent copper atoms

bridged compounds containing μ-hydroxo, μ-carboxylato, μ-acetato, etc.

Compound **1** possesses a 1D chain structure constructed from linear trinuclear Cu_3 SBUs. Interestingly, four Cu^{II} atoms of two Cu_3 SBUs are linked by two cpida^{3-} spacers in a head-to-tail mode leading to a parallelogram-shaped molecular box, as shown in Figure 1b. In each molecular box there are offset π−π stacking interactions between two cpida^{3-} aromatic rings (centroid···centroid = 4.32 Å). Each

 © 2004 Wiley-VCH Verlag GmbH & Co. KGaA, Weinheim

Table 1. Selected bond lengths [Å] and angles [°] for complexes **1** and **2**

1		**2**	
Cu(1)−O(1)	1.978(2)	Zn(1)−O(1A)	1.958(5)
Cu(1)−O(3)	1.973(2)	Zn(1)−O(2)	1.983(5)
Cu(1)−O(5)	1.952(2)	Zn(1)−O(3)	1.996(6)
Cu(1)−O(6)	2.344(2)	Zn(1)−O(4B)	2.002(5)
Cu(1)−O(7a)	1.947(2)	Zn(1)−N(1)	2.399(6)
Cu(2)−O(1)	1.958(2)		
Cu(2)−O(1a)	1.958(2)		
Cu(2)−O(8)	1.916(2)		
Cu(2)−O(8a)	1.916(2)		
O(1)−Cu(1)−O(3)	93.14(8)	O(1A)−Zn(1)−O(2)	100.7(2)
O(1)−Cu(1)−O(5)	177.87(9)	O(1A)−Zn(1)−O(3)	143.5(2)
O(1)−Cu(1)−O(6)	81.37(9)	O(1A)−Zn(1)−O(4B)	104.0(2)
O(1)−Cu(1)−O(7a)	92.67(9)	O(2)−Zn(1)−O(3)	110.0(2)
O(3)−Cu(1)−O(5)	85.94(10)	O(2)−Zn(1)−O(4B)	98.5(2)
O(3)−Cu(1)−O(6)	99.20(9)	O(3)−Zn(1)−O(4B)	90.8(2)
O(3)−Cu(1)−O(7a)	171.45(9)	O(1A)−Zn(1)−N(1)	90.7(2)
O(5)−Cu(1)−O(6)	100.67(10)	O(2)−Zn(1)−N(1)	79.1(2)
O(5)−Cu(1)−O(7a)	88.03(10)	O(3)−Zn(1)−N(1)	76.6(2)
O(6)−Cu(1)−O(7a)	87.86(9)	O(4B)−Zn(1)−N(1)	165.3(2)
O(1)−Cu(2)−O(1a)	180.00(14)		
O(1)−Cu(2)−O(8)	91.32(9)		
O(1)−Cu(2)−O(8a)	88.68(9)		
O(8)−Cu(2)−O(1a)	88.68(9)		
O(8)−Cu(2)−O(8a)	180.0(2)		
O(8a)−Cu(2)−O(1a)	91.32(9)		

parallelogram-shaped molecular box is then linked together by the bridging bidentate carboxylate groups, which results in the formation of a 1D molecular box coordination polymer. It is notable that the 1D molecular box chains propagate into 2D layers by an AA stacking pattern[15] in the *bc* plane, as shown in Figure 2.

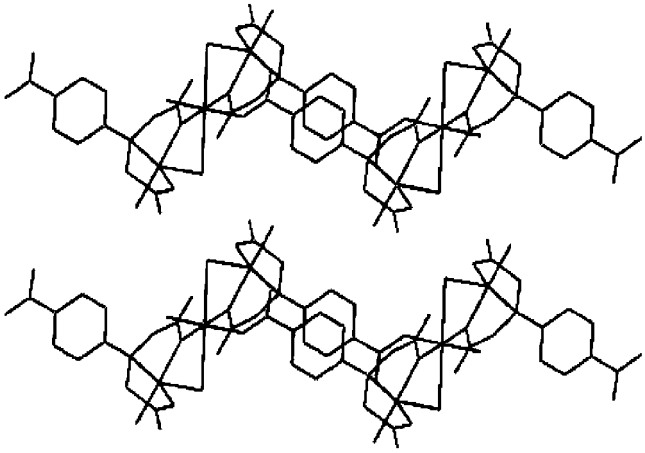

Figure 2. A view of the 2D layer of **1** down the *a* axis, showing the AA stacking pattern of the 1D molecular box chains

One guest water molecule (O9) forms a hydrogen bond with a coordinated water molecule (O9···O5 = 2.695Å), and another guest water molecule (O10) forms hydrogen bonds with the coordinated water molecule (O10···O5 = 2.576Å) and the noncoordinated carboxylate oxygen atom (O10···O2 = 2.725Å).

[Zn(Hcpida)]$_n$·nH$_2$O (2)

The asymmetric unit of **2** consists of one Zn^{II} atom, one $Hcpida^{2-}$ ligand and one guest water molecule. Each Zn^{II} centre is coordinated by two oxygen atoms (O1A, O4B) from the bridging bidentate carboxylate groups of two $Hcpida^{2-}$ ligands, and two oxygen atoms (O2, O3) from one chelating bidentate $Hcpida^{2-}$ ligand, leading to a distorted tetrahedral coordination geometry (Figure 3). The Zn−O bond lengths vary from 1.958(5) Å to 2.002(5) Å. The bond angles around the Zn^{II} centre range from 90.8(2)° to 143.5(2)°. There is an unusual structural feature around the Zn^{II} centre: the Zn^{II} centre has four nearest-neighboring oxygen atoms [d(Zn−O) < 2.002 Å] in an approximately tetrahedral arrangement, although the O1A−Zn1−O3 bond angle [143.5(2)°] is particularly obtuse. There is one nitrogen atom associated with the Zn atom [d(Zn−N) = 2.399 Å], which does not constitute a "bond" in any real sense. This association may be considered as a weak interaction.[16] The geometry at the Zn centre can be visualized as a mono-capped tetrahedron (Figure 3).[17] Because the Zn1−N1 bond (2.399 Å) is much longer than the Zn1−O4 bond (2.002 Å), the ZnO_4N unit should not be described as distorted trigonal-bipyramidal but as mono-capped tetrahedral. On the other hand, the Zn atom is displaced off-center by 0.317 Å, when the associated nitrogen atom is considered. These results support the validity of regarding this geometry as mono-capped tetrahedral.

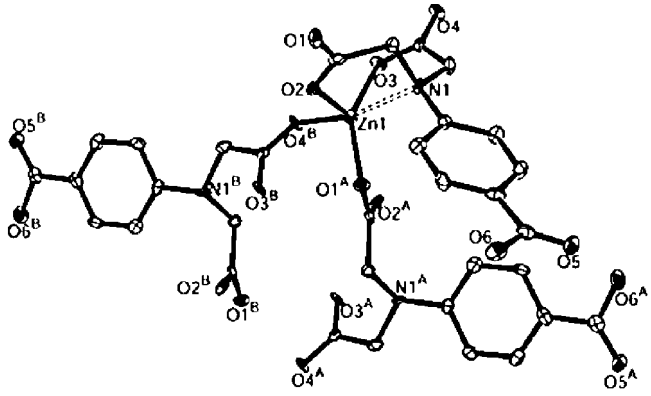

Figure 3. ORTEP diagram of the coordination environment around the Zn^{II} centre in **2**; thermal ellipsoids are drawn at the 50% probability level; all hydrogen atoms are omitted for clarity; symmetry code: A: x, $-y - 1/2$, $z - 1/2$; B: $-x$, $y + 1/2$, $-z + 1/2$

The coordinated H_3cpida ligand has an unchelated carboxylic group. The C−O bond [C11−O6 = 1.344(10) Å] is much longer than C−O [C11−O5 = 1.190(9) Å] in the carboxylic group, so C11−O5 can be assigned as the double bond and C11−O6 as the single bond. This shows that deprotonation of the H_3cpida ligand is incomplete.

The crystal structure of **2** consists of an infinite 2D network. The Zn1 centre is connected to four adjacent Zn centres through the bridging bidentate carboxylate groups of $Hcpida^{2-}$ ligands leading to a $Zn_4(Hcpida)_4$ unit, which further extends into a 2D polymeric network with alternate large and small pseudo-square grid motifs in the *bc* plane

 © 2004 Wiley-VCH Verlag GmbH & Co. KGaA, Weinheim

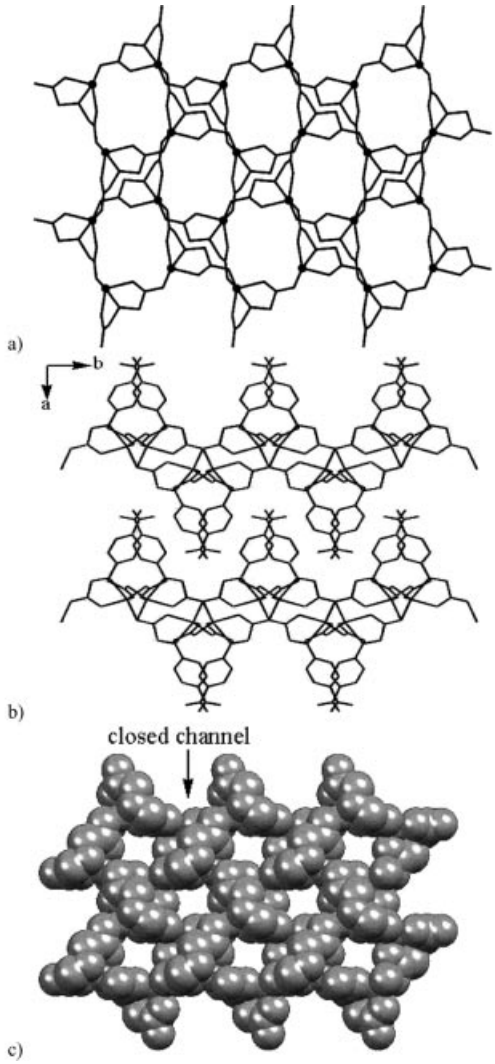

Figure 4. a) The 2D network of **2** as viewed down the *a* axis, showing alternate large and small pseudo-square grids (phenyl rings omitted for clarity); b) a view of the 2D wave-like layer of **2** down the *c* axis, showing the AA stacking pattern between the layers; c) a space-filling diagram showing alternate open and closed channels created perpendicularly to the *bc* plane; the alternate open channels are occupied by the guest water molecules, which have been omitted for clarity

(Figure 4a). In each large pseudo-square grid, the Zn−Zn separations are 4.90 and 5.20 Å, while the Zn−Zn−Zn angles are 80.73° and 99.27°. Each acetate group of the $Hcpida^{2-}$ ligand adopts a bidentate bridging mode to connect two Zn centres. Four Zn centres are connected together by μ_2-acetato groups to form a 2D grid network. However, according to the flexibility of the iminodiacetate groups of the $Hcpida^{2-}$ ligand, compound **2** does not adopt one kind of grid but alternate large and small grid motifs, as shown in Figure 5. The wave-like nature of the 2D layers of **2** can be clearly shown with a view of **2** down the *c* axis (Figure 4b). Interestingly, the 2D layers in **2** adopt an AA stacking pattern in the *ab* plane, and the convex phenylcarboxylic groups of $Hcpida^{2-}$ in one layer sit above or below the small grids of the adjacent layers along the *a* direction (Figure 4b). Thus, compound **2** possesses alternate open (large grids) and closed (small grids) channels that are perpendicular to the *bc* plane and parallel to the *a* axis (Figure 4c). Each alternate open channel is approximately 4.9 × 5.7 Å. The guest water molecules occupy the open channels resulting in the formation of the water columns along the *a* direction.[18] It should be noted that in the crystal packing there are offset π−π stacking interactions between two $Hcpida^{2-}$ aromatic rings (centroid···centroid = 4.10 Å), as shown in Figure 6. The guest water molecule (O7) forms hydrogen bonds with the coordinated carboxylate oxygen atoms (O7···O1 = 2.850 Å; O7···O4 = 2.961 Å) and the noncoordinated carboxylate oxygen atom (O7···O6 = 2.680 Å).

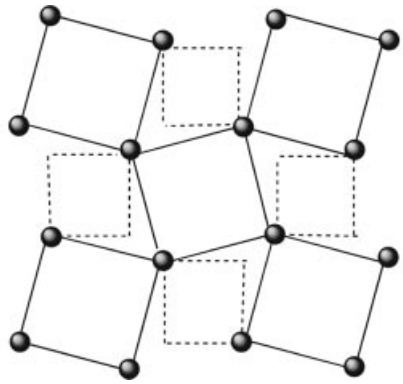

Figure 5. A topological illustration of the alternate large and small grids of compound **2**

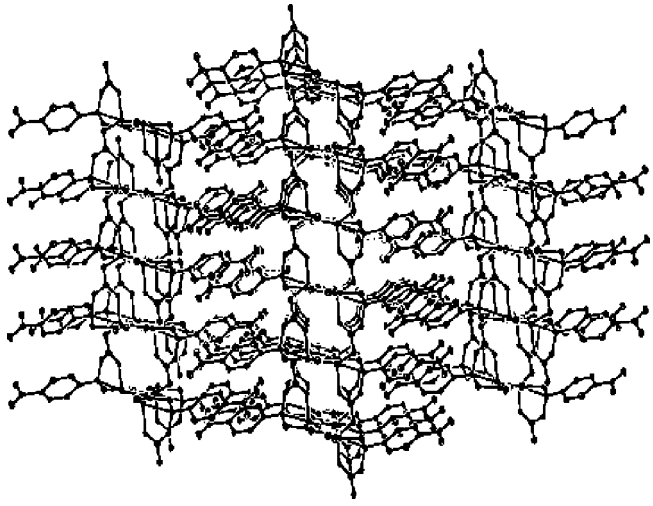

Figure 6. The 3D structure of **2** as viewed down the *b* axis, showing the offset π−π stacking interactions

Removal of the Guest Water Molecules: TGA and PXRD Studies

The X-ray single-crystal structures clearly indicate that compound **2** possesses alternate open channels along the *a* axis, and we became intrigued by the possibility of generating a cavity by removing the guest water molecules. The TGA curve of compound **1** exhibits a continuous weight

 © 2004 Wiley-VCH Verlag GmbH & Co. KGaA, Weinheim

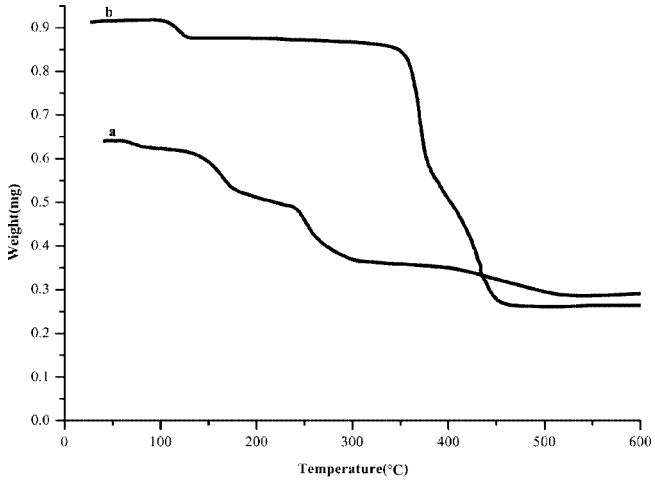

Figure 7. TGA curves for **1** (a) and **2** (b)

loss (curve a in Figure 7): the loss of the guest water molecules is accompanied by the loss of the coordinated water molecules, and the loss of the coordinated water molecules is accompanied by the loss of the ligands. As a result, it is difficult to give exact weight losses as a percentage for each weight-loss step in the TGA curve. The removal of the guest water molecules from **1** results in the collapse of the framework structure (see Supporting Information). The TGA curve of compound **2** exhibits an initial weight loss at an onset temperature of 120 °C (5.43%), corresponding to the removal of the guest water molecule (calcd. 5.38%). The second weight loss occurs between 340 and 480 °C (69.23%) and corresponds to the release of the $Hcpida^{2-}$ ligand (curve b in Figure 7). The remaining weight of 25.34% corresponds to the percentage of ZnO (calcd. 24.32%). Although the hydrogen bonds increase the difficulty of removing the guest water molecule (O7) from **2**,[19] the framework structure of the dehydrated sample is simlar to that of compound **2** in terms of their powder X-ray diffraction (PXRD) patterns (see Supporting Information). The rehydrated sample also exhibits a similar PXRD pattern to compound **2** (Supporting Information). In particular, the existence of the strongest peak at a 2θ value of 6.56° in the three PXRD patterns shows that the layer framework of **2** does not change upon dehydration and rehydration. Therefore, compound **2** not only maintains its 2D layer framework after dehydration but the inclusion process is reversible to some extent. This can be attributed to the absence of coordinated water molecules in compound **2** and the higher decomposition temperature (340 °C) of the $Hcpida^{2-}$ ligand.

Photoluminescence Properties of H_3cpida and 2

The solid-state photoluminescence spectra of H_3cpida and compound **2** at room temperature are depicted in Figure 8; H_3cpida exhibits a broad strong blue-fluorescent emission around 422 nm upon excitation at 332 nm (curve a in Figure 8). Interestingly, in the case of the metal-organic polymer **2**, a blue-shifted photoluminescence with the main emission at 366 nm and with a shoulder at about 480 nm upon excitation at 313 nm is observed (curve b in Figure 8). This emission arises from ligand-to-metal charge transfer (LMCT).[20] TGA indicated that **2** is thermally stable up to 340 °C. Thus, compound **2** may be a good candidate for highly thermally stable and solvent-resistant photoactive material because it is almost insoluble in common polar and nonpolar solvents.[4a] Compound **2** may also have potential as a porous material after removing the guest water molecules.

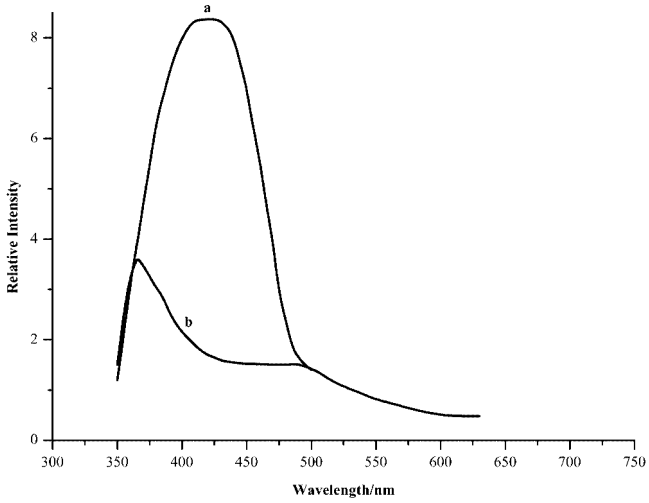

Figure 8. The emission spectra of the H_3cpida ligand (a) and compound **2** (b) in the solid state at room temperature

Conclusions

Two new metal-organic coordination polymers have been synthesised. Compound **1** is a linear trinuclear Cu^{II} compound in which the three Cu^{II} centres are linked only by μ-carboxylato groups of the same ligand ($cpida^{3-}$). A 1D parallelogram-shaped molecular-box chain is constructed from these unusual linear trinuclear Cu^{II} SBUs. Compound **2** possesses alternate open and closed channels and shows strong photoluminescence, thus it may be a good candidate for a photoactive or porous material.

Experimental Section

General Remarks: All commercially available chemicals were of reagent grade and used as received without further purification. Infrared spectra were recorded with a Bruker VECTOR-22 FT-IR spectrophotometer as KBr pellets. ^{1}H NMR spectra were measured with an Avance AV400 NMR spectrometer at room temperature. Powder X-ray diffraction (PXRD) patterns were obtained with an MXPAHF rotating-anode X-ray diffractometer. The luminescence spectra for the solid samples were recorded at room temperature with a Hitachi 850 fluorescence spectrophotometer. Thermogravimetric analyses (TGA) were performed under air with a heating rate of 10 °C·min^{-1} using a Shimadzu TGA-50H TG analyzer.

***N*-(4-Carboxyphenyl)iminodiacetic Acid (H_3cpida):** A solution of KOH (33.6 g, 0.6 mol) in water (100 mL) was added dropwise to a solution of chloroacetic acid (28.4 g, 0.3 mol) in water (100 mL). *p*-Aminobenzoic acid (13.7 g, 0.1 mol) was slowly added to the re-

 © 2004 Wiley-VCH Verlag GmbH & Co. KGaA, Weinheim

sulting alkaline solution, and the mixture was refluxed at 86 °C for 30 h. The reaction mixture was then cooled to room temperature and acidified with HCl (6 M) until the desired acid precipitated as a white solid (pH ≈ 2.5) (Scheme 1). This precipitate was collected by filtration, washed with water and recrystallised from water (yield: 32% based on *p*-aminobenzoic acid). IR (KBr): $\tilde{\nu}$ = 3458, 2919, 1714, 1612, 1530, 1462, 1388, 1239, 1192, 975, 771, 692 cm^{-1}. ^1H NMR (400 MHz, D_2O, 25 °C): δ = 7.84 (d, J = 8.9 Hz, AABB, 2 H), 6.58 (d, J = 8.9 Hz, AABB, 2 H), 4.23 (s, 4 H, CH_2-COO) ppm.

$[Cu_3(cpida)_2(H_2O)_4]_n \cdot 4nH_2O$ (1): This compound was prepared by a solvent evaporation method. A mixture of basic copper carbonate (0.111 g, 0.5 mmol) and H_3cpida (0.25 g, 1.0 mmol) in 15 mL of water was heated in a steam bath for 1 h, and then filtered. Methanol (5 mL) was then added to the filtrate (Scheme 1). Blue single crystals suitable for X-ray analysis were obtained by slow evaporation of the solvent from the filtrate at room temperature (yield: 72% based on Cu). IR (KBr): $\tilde{\nu}$ = 3418, 2919, 1645, 1605, 1538, 1412, 1260, 1217, 1170, 968, 925, 839, 778, 698, 643, 511 cm^{-1}.

$[Zn(Hcpida)]_n \cdot nH_2O$ (2): This compound was synthesized hydrothermally in a thick-walled Pyrex tube containing $Zn(NO_3)_2 \cdot 6H_2O$, H_3cpida, KOH, methanol and H_2O in a molar ratio of 3:2:1:78:222 under autogenous pressure. The tube was cooled in liquid N_2, sealed under vacuum, and placed inside an oven at 120 °C for 2 d (Scheme 1). The resulting colourless crystals were collected and washed with ethanol (yield: 58% based on Zn). IR (KBr): $\tilde{\nu}$ = 3491, 2977, 1703, 1573, 1518, 1460, 1412, 1352, 1308, 1262, 1197, 1146, 1122, 1016, 923, 851, 781, 755, 731, 699, 648, 585, 508 cm^{-1}.

X-ray Single-Crystal Structure Determination: Crystallographic data for **1** and **2** were collected at 173 K for **1** and 293 K for **2** with a Siemens Smart CCD diffractometer with Mo-K_α radiation (λ = 0.71073 Å). The structures were solved by direct methods using SHELXS-97[21] and refined by full-matrix least-squares method against F^2 (SHELXL-97).[22] All non-hydrogen atoms were refined anisotropically. Carbon-bound hydrogen atoms were placed in geometrically calculated positions; oxygen-bound hydrogen atoms were located in the difference Fourier map and kept fixed in that position. The crystallographic data for **1** and **2** are listed in Table 2; selected bond lengths and angles for **1** and **2** are presented in Table 1. CCDC-228511 (**1**) and -228512 (**2**) contain the supplementary crystallographic data for this paper. These data can be obtained free of charge at www.ccdc.cam.ac.uk/conts/retrieving.html [or from the Cambridge Crystallographic Data Centre, 12 Union Road, Cambridge CB2 1EZ, UK; Fax: (internat.) + 44-1223-336-033; E-mail: deposit@ccdc.cam.ac.uk].

Table 2. Crystal data and structure refinement for complexes **1** and **2**

	1	**2**
Empirical formula	$C_{22}H_{32}Cu_3N_2O_{20}$	$C_{11}H_{11}NO_7Zn$
Formula mass	835.12	334.56
Temperature [K]	173(2)	293(2)
Crystal system	triclinic	monoclinic
Space group	$P\bar{1}$	$P2_1/c$
a [Å]	8.5094(17)	13.900(3)
b [Å]	9.3206(19)	9.513(2)
c [Å]	10.392(2)	9.375(2)
α [°]	92.274(4)	90
β [°]	93.803(4)	101.136(5)
γ [°]	112.850(4)	90
V [Å^3]	756.0(3)	1216.4(5)
Z	1	4
μ [mm^{-1}]	2.183	2.041
Reflections collected	3991	5090
Independent reflections (R_{int})	3181 (0.0131)	1746 (0.0566)
Observed reflections	2614	1326
R_1, wR_2 [$I \geq 2\sigma(I)$]	0.0374, 0.0882	0.0634, 0.1481

Acknowledgments

The authors gratefully acknowledge the financial support of the National Natural Science Foundation of China (no. 50073021) and the Foundation of the Education Department of Anhui Province (2002kj330ZD).

[1] [1a] M. Eddaoudi, D. B. Moler, H. L. Li, B. Chen, T. Reineke, M. O'Keeffe, O. M. Yaghi, *Acc. Chem. Res.* **2001**, *34*, 319−330. [1b] S. R. Batten, R. Robson, *Angew. Chem. Int. Ed.* **1998**, *37*, 1460−1494. [1c] P. J. Hagrmann, D. Hagrman, J. Zubieta, *Angew. Chem. Int. Ed.* **1999**, *38*, 2638−2684. [1d] M. O'Keeffe, M. Eddaoudi, H. L. Li, T. Reineke, O. M. Yaghi, *J. Solid State Chem.* **2000**, *152*, 3−20. [1e] R. Robson, *J. Chem. Soc., Dalton Trans.* **2000**, 3735−3744. [1f] B. Moulton, M. J. Zaworotko, *Chem. Rev.* **2001**, *101*, 1629−1658.

[2] [2a] J. S. Seo, D. Whang, H. Lee, S. I. Jun, J. Oh, Y. J. Jeon, K. Kim, *Nature* **2000**, *404*, 982−986. [2b] O. Kahn, C. Martinez, *Science* **1998**, *279*, 44−48. [2c] O. R. Evans, R.-G. Xiong, Z.-Y. Wang, G.-K. Wong, W.-B. Lin, *Angew. Chem. Int. Ed.* **1999**, *38*, 536−538. [2d] W.-B. Lin, O. R. Evans, R.-G. Xiong, Z.-Y. Wang, *J. Am. Chem. Soc.* **1998**, *120*, 13272−13273.

[3] [3a] H. L. Li, M. Eddaoudi, M. O'Keeffe, O. M. Yaghi, *Nature* **1999**, *402*, 276−279. [3b] S. S.-Y. Chui, S. M.-F. Lo, J. P. H. Charmant, A. G. Orpen, I. D. Williams, *Science* **1999**, *283*, 1148−1150.

[4] [4a] J.-C. Dai, X.-T. Wu, Z.-Y. Fu, S.-M. Hu, W.-X. Du, C.-P. Cui, L.-M. Wu, H.-H. Zhang, R.-Q. Sun, *Chem. Commun.* **2002**, 12−13. [4b] J.-C. Dai, X.-T. Wu, Z.-Y. Fu, C.-P. Cui, S.-M. Hu, W.-X. Du, L.-M. Wu, H.-H. Zhang, R.-Q. Sun, *Inorg. Chem.* **2002**, *41*, 1391−1396.

[5] [5a] C. J. Kepert, T. J. Prior, M. J. Rosseinsky, *J. Am. Chem. Soc.* **2000**, *122*, 5158−5168. [5b] J. W. Wo, K. S. Min, M. P. Suh, *Inorg. Chem.* **2002**, *41*, 2151−2157. [5c] M. Du, X.-H. Bu, Y.-M. Guo, L. Zhang, D.-Z. Liao, J. Ribas, *Chem. Commun.* **2002**, 1478−1479. [5d] C. Ruiz-Pérez, J. Sanchiz, M. H. Molina, F. Lloret, M. Julve, *Inorg. Chem.* **2000**, *39*, 1363−1370.

[6] [6a] O. M. Yaghi, C. E. Davis, G. Li, H. L. Li, *J. Am. Chem. Soc.* **1997**, *119*, 2861−2868. [6b] O. Kristiansson, L.-E. Tergenius, *J. Chem. Soc., Dalton Trans.* **2001**, 1415−1420. [6c] M. Eddaoudi, J. Kim, N. Rosi, D. Vodak, J. Wachter, M. O'Keeffe, O. M. Yaghi, *Science* **2002**, *295*, 469−472.

[7] [7a] E. Brunet, M. T. Alonso, O. Juanes, O. Velasco, J. C. Rodriguez-Ubis, *Tetrahedron* **2001**, *57*, 3105−3116. [7b] G. Schwarzenbacher, R. Saf, R. Schitter, K. Hummel, *Synthetic Met.* **1999**, *101*, 143−144.

[8] [8a] M. Sirak, M. Mad'arova, J. Tatiersky, J. Marek, *Eur. J. Inorg. Chem.* **2003**, 2075−2081. [8b] D. Imbert, N. Fatin-Rouge, J. C. G. Bunzli, *Eur. J. Inorg. Chem.* **2003**, 1332−1339. [8c] S. Ulvenlund, A. S. Georgopoulou, D. M. P. Mingos, I. Baxter, S. E. Lawrence, A. J. P. White, D. J. Williams, *J. Chem. Soc., Dalton Trans.* **1998**, 1869−1878. [8d] R. Ruloff, R. Richter, L. Beyer, *Z. Anorg. Allg. Chem.* **1998**, *624*, 902−908.

[9] S. Burnet, A. K. Hall, J. M. Harrowfield, G. A. Koutsantonis, V. Sanford, D. Sauter, B. W. Skelton, A. H. White, *Supramol. Chem.* **2003**, *15*, 291−312.

[10] X.-M. Ouyang, D.-J. Liu, T. Okamura, H.-W. Bu, W.-Y. Sun, W.-X. Tang, N. Ueyama, *Dalton Trans.* **2003**, 1836−1845.

[11] [11a] G. A. van Albada, I. Mutikainen, U. Turpeinen, J. Reedijk, *Eur. J. Inorg. Chem.* **1998**, 547−549. [11b] G. A. van Albada, P. J. van Koningsbruggen, I. Mutikainen, U. Turpeinen, J. Reedijk, *Eur. J. Inorg. Chem.* **1999**, 2269−2275.

 © 2004 Wiley-VCH Verlag GmbH & Co. KGaA, Weinheim

[12] [12a] M. H. W. Lam, Y.-Y. Tang, K.-M. Fung, X.-Z. You, W.-T. Wong, *Chem. Commun.* **1997**, 957−958. [12b] T. C. Higgs, K. Spartalian, C. J. O'Connor, B. F. Matzanke, C. J. Carrano, *Inorg. Chem.* **1998**, *37*, 2263−2272.

[13] Y. F. Song, P. Gamez, O. Roubeau, M. Lutz, A. L. Spek, J. Reedijk, *Eur. J. Inorg. Chem.* **2003**, 2924−2928.

[14] [14a] L. Gutierrez, G. Alzuet, J. A. Real, J. Cano, J. Borrás, A. Castiñeiras, *Eur. J. Inorg. Chem.* **2002**, 2094−2102. [14b] M. González-Álvarez, G. Alzuet, J. Borrás, B. Macías, A. Castiñeiras, *Inorg. Chem.* **2003**, *42*, 2992−2998.

[15] W.-B. Lin, P. Ayyappan, *Polyhedron* **2003**, *22*, 3037−3042.

[16] T. A. Bowden, H. L. Milton, A. M. Z. Slawin, P. Lightfoot, *Dalton Trans.* **2003**, 936−939.

[17] M. G. Johnston, W. T. A Harrison, *Inorg. Chem.* **2001**, *40*, 6518−6520.

[18] R. Atencio, M. Chacón, T. González, A. Bricefio, G. Agrifoglio, A. Sierraalta, *Dalton Trans.* **2004**, 505−513.

[19] D.-F. Sun, R. Cao, Y.-Q. Sun, W.-H. Bi, X.-J. Li, Y.-Q. Wang, Q. Shi, X. Li, *Inorg. Chem.* **2003**, *42*, 7512−7518.

[20] [20a] J. Tao, M.-L. Tong, J.-X. Shi, X.-M. Chen, S. Ng, *Chem. Commun.* **2000**, 2043−2044. [20b] R. Bertoncello, M. Bettinelli, M. Vassrin, A. Gulino, E. Tondello, A. Vittadini, *Inorg. Chem.* **1992**, *31*, 1558−1565. [20c] J. Tao, J.-X. Shi, M.-L. Tong, X.-X. Zhang, X.-M. Chen, *Inorg. Chem.* **2001**, *40*, 6328−6330.

[21] G. M. Sheldrick, *SHELXS-97, Program for X-ray Crystal Structure Solution*, Göttingen University, Germany, **1997**.

[22] G. M. Sheldrick, *SHELXL-97, Program for X-ray Crystal Structure Refinement*, Göttingen University, Germany, **1997**.

Received March 19, 2004
Early View Article
Published Online August 26, 2004

 © 2004 Wiley-VCH Verlag GmbH & Co. KGaA, Weinheim

Synthesis, X-ray Characterisation and Studies of the New Ionic Complex [Bis(pyridin-2-yl) disulfide] Triiodide, Obtained by Oxidation of 2-Mercaptopyridine with I_2 − Implications in the Mechanism of Action of Antithyroid Drugs

Constantinos D. Antoniadis,[a] Sotiris K. Hadjikakou,*[a] Nick Hadjiliadis,*[a] Maciej Kubicki,[b] and Ian S. Butler[c]

Keywords: Bioinorganic chemistry / Iodine complexes / Polyiodides / S ligands / Crystal structures

The reaction of 2-mercaptopyridine (C_5H_5NS or PYSH) with diiodine in a molar ratio of 1:2 in dichloromethane led to the oxidation and dimerization of the ligand and formation of $[(PYS–PYSH)^+\cdot I_3^-]$. The compound was characterised by elemental analysis, DTA-TG, FT-Raman, FT-IR, UV/Vis and ^1H NMR spectroscopy. The crystal structure of the complex has been determined by X-ray diffraction at 293(2) K. The compound $[(C_5H_4NS–SNC_5H_5)I_3]$ is monoclinic with the space group $P2_1$ and a = 8.230(2) Å, b = 35.708(7) Å, c = 11.369(2) Å, β = 91.86(3)° and Z = 8. The results are discussed in relation to the mechanism of action of antithyroid drugs. The easy oxidation of PYSH by I_2 to form the monocationic disulfide complex $[(PYS–PYSH)^+\cdot I_3^-]$ is similar to the case of the antithyroid drug methimazole (MMI) and may indicate that PYSH might also possess antithyroid properties similar to those of MMI.
(© Wiley-VCH Verlag GmbH & Co. KGaA, 69451 Weinheim, Germany, 2004)

Introduction

Because of the effective antithyroid activity of thioamides, their interaction with diiodine has been thoroughly studied in recent years.[1−3] These thioamides include the antithyroid drugs methimazole (MMI) and 6-*n*-propyl-2-thiouracil (PTU)[1−3] and studies have aimed at drawing conclusions about their mechanism of action. It has been proposed that both MMI and PTU display both irreversible and reversible inhibition depending on the relative concentrations of the drug and iodine.[4] Nakataka et.al.[5] reported that the inhibition of tyrosil iodination by antithyroid drugs should be different in the cases of PTU and MMI; du Mont et.al.[6a] and Berry et al.[6b,6c] proposed that drugs such as PTU should, rather, interfere either with the formation of the thyroid peroxidase (TPO)−iodonium complex[4] or inhibit the activity of the iodothyronine deiodinase type I (ID-1), an enzyme containing selenocysteine in its active site which is responsible for the monodeiodination of the T4 prohormone to the T3 hormone.[6] Isaia et al.[3] have shown that MMI is readily oxidised by the TPO system to form MMI disulfide [bis(1-methylimidazol-2-yl disulfide], while activated iodine is simultaneously reduced to the iodide anion. We also recently demonstrated that PTU forms weak charge transfer complexes (CT) with diiodine.[2c] Thus, although it has been concluded[1−4] that thioamides inhibit the formation of thyroid hormones by preventing the incorporation of oxidised iodides into tyrosine, the precise mechanism of this trapping is still a matter for further investigation.

The perturbation of the I−I bond by heterocycles such as 2-mercaptopyridine (PYSH; Figure 1) can lead to novel complexes containing polyiodides.[7] With the aim of studying the interfering mechanism of thioamides in TPO-catalysed iodination reactions of tyrosil residues of thyroglobuline, we report here the isolation and study of the oxidation product of an I_2 complex with 2-mercaptopyridine of formula $[(PYS−PYSH)^+\cdot I_3^-]$ (**1**).

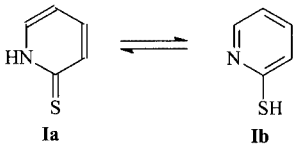

Ia **Ib**

Figure 1. Tautomeric forms of 2-mercaptopyridine (**I**) (thione **Ia**, thiol **Ib**)

[a] Section of Inorganic and Analytical Chemistry, Department of Chemistry, University of Ioannina
45110 Ioannina, Greece
Fax: (internat) + 30-26510-44831
E-mail: nhadjil@cc.uoi.gr
shadjika@cc.uoi.gr
[b] Department of Chemistry, A. Mickiewicz University, ul. Grunwaldzka 6, 60-780 Poznan, Poland
[c] Department of Chemistry, McGill University, 801 Sherbrooke, Montreal, Quebec H2A 2K6, Canada

 © 2004 Wiley-VCH Verlag GmbH & Co. KGaA, Weinheim **DOI: 10.1002/ejic.200400290**

Results and Discussion

PYSH reacts with I_2 in a molar ratio of 1:2 oxidizing the ligand to disulfide [Equation (1)].

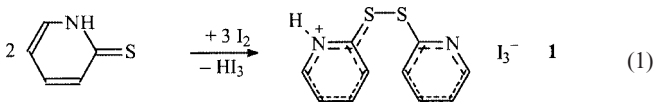

(1)

A thermal analysis in a flow of nitrogen showed that the compound decomposes in two stages. The TGA and DTA data curves show that the first stage of its decomposition (90−160 °C) is connected with an endothermic effect and involves a 42% mass loss consistent with the evolution of I_2 (calculated mass loss 42%). The second stage of its decomposition (204−234 °C) is connected with an endothermic effect and involves a 58% mass loss of (PYS−PYSH)I (calculated mass loss 58%). This indicates that I_3^- might be asymmetric of the $I^-\cdots I_2$ type[7b] which results in the easy breaking of this bond (see crystal structure).

The conductimetric titration of PYSH with I_2 in acetonitrile is shown in Figure 2.

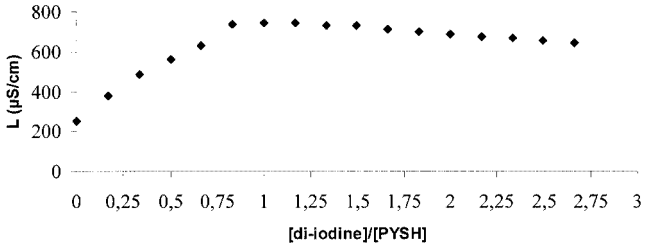

Figure 2. Conductivity titrations of PYSH (10^{-2} M) with I_2 in acetonitrile (T = 293 K)

At a zero I_2 concentration, the solution of PYSH in acetonitrile shows nonzero conductivity. Addition of I_2, increases the conductivity of the solution, with a maximum value attained at a molar ratio $[I_2]/[PYSH] = 0.83$, leading to a plateau in accordance with Equation (1).

Spectroscopy

(A) UV/Vis Spectroscopy

The UV/Vis spectra of dichloromethane solutions with constant concentrations of PYSH (10^{-4} M) and increasing quantities of diiodine are given in Figure 3. They exhibit one distinct absorption band at 495−505 nm which can be assigned to the "blue shift" band of I_2[2,8] occurring at 504 nm in free I_2 in CH_2Cl_2.[8e,8g]

The absorption band at 367 nm can be assigned to the I_3^- species (λ_{max} = 360 nm in free I_3^-).[9] I_3^- has one more absorption band at 295 nm, coinciding with the intra-ligand transition ($\pi^*\leftarrow\pi$) appearing at 292 nm in free PYSH.

No isosbestic points were observed, indicating that more than two species are present in solution (Figure 3). In the spectrophotometric titration curves of I_2/PYSH, the presence of the band at 367 nm, attributable to the I_3^- moiety, can be observed at low I_2/ligand ratios in accord with Equation (1) (see conductivity measurements).

(B) Vibrational Spectroscopy

The IR spectrum of the complex shows distinct vibrational bands at 1579 and 1452 cm^{-1} which can be assigned to ν(CN) vibrations (thioamide I and II bands) and at 1108 and 959 cm^{-1} attributable to the ν(CS) vibrations (thioamide III and IV bands). The new band appearing at 158 cm^{-1} in the FIR spectrum of the complex has been assigned to the ν(I−I) stretching vibration mode.[2a,2b,10]

Table 1 gives structural and Raman spectroscopic data of the complex and other complexes containing I_3^- in the region of 300−50 cm^{-1}.

Diiodine vapour gives a strong band at 216 cm^{-1} [ν(I−I)] which appears at 180 cm^{-1} in the solid state.[7b,11] This

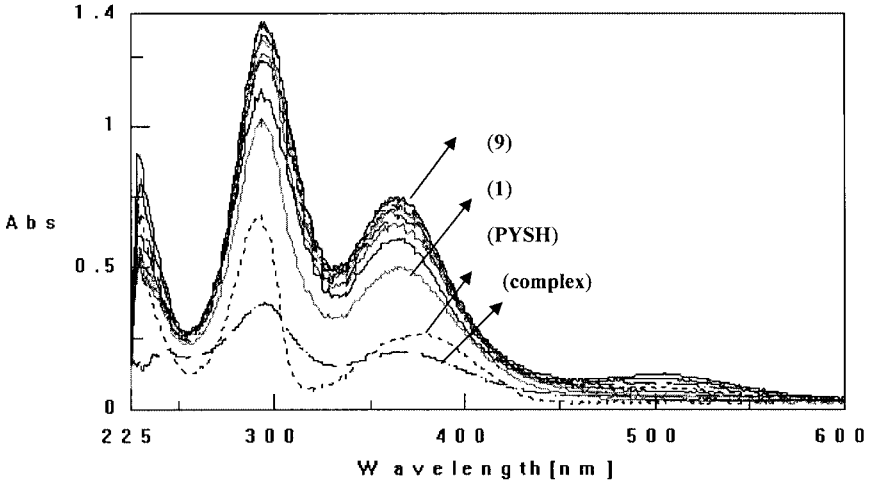

Figure 3. UV/Vis spectra of the complex (5×10^{-5} M) and the ligand (PYSH) (5×10^{-5} M) in dichloromethane; UV/Vis spectra of solutions with constant concentrations (10^{-4} M) of PYSH and increasing quantities of diiodine in dichloromethane ($[I_2]/[L]$: 1: 0.33; 2: 0.50; 3: 0.66; 4: 0.84; 5: 1.00; 6: 1.16; 7: 1.34; 8: 1.50; 9: 1.66)

 © 2004 Wiley-VCH Verlag GmbH & Co. KGaA, Weinheim

Table 1. Structural and Raman spectroscopic data of complex **1** and other known polyiodide adduct complexes

Compound	Iodine-containing counter part	Geometry	d(I−I) [Å]	n (bond order)	Raman data [cm^{-1}]	Ref.
[(PYS-PYSH)$^+$·I_3^-] [four molecules (**a**−**d**), see Figure 5)	I_3^-: I$^-$···I_2	linear asymmetric	**a**: 2.887(4), 2.944(3); **b**: 2.874(4), 2.957(3); **c**: 2.968(3), 2.862(4); **d**: 2.855(4), 2.927(3)	0.56, 0.48; 0.58, 0.46: 0.45, 0.59: 0.61, 0.50	162.4 vs, 154.7 vs	this work
[Et(NH$_2$)dtl] I_3^- [a]	I_3^-: I$^-$···I_2	linear asymmetric	2.74, 3.14	0.83, 0.28	167 s	[7b]
CsI_3	I_3^-: I$^-$···I_2	linear asymmetric	2.842, 3.038	0.63, 0.37	157 m, 148 s, 137 s, 102 s, 93 s	[7b]
UrBuI_3^- [b]	I_3^-: I$^-$−I$^+$−I$^-$	linear asymmetric	2.935, 2.889	0.49, 0.55	112 vs, 113 vs, 128 w	[7b]

[a] Et(NH$_2$)dtl = 3,5-bis(ethyllamino)-1,2-dithiolithium. [b] UrBu = *N*-butylurotropinium.

shifts to lower wavenumbers upon coordination to a donor atom, reflecting the reduction in the I−I bond order and the strengthening of the complex formed as well.[2,7b,8b,8c,12]

The Raman spectrum of the complex shows two strong bands at 162.4 and 154.7 cm^{-1}. It is worth mentioning that bands around 110 cm^{-1} are normally assigned to the ν_1 symmetric stretching of I_3^- which, being a symmetrical ion, normally exhibits only one Raman-active band.[2a,2b,7b] However, when a distortion of I_3^- occurs, the asymmetric stretching may become Raman-active and additional bands at higher (140−130 cm^{-1}) and at lower frequencies (80−70 cm^{-1}) can be observed[7b] and assigned to asymmetric stretching and deformation motions of asymmetric I_3^-, respectively.[7b,13] Thus, the complex should be a linear asymmetric I_3^- (I$^-$···I_2) complex (see crystal structure) (Table 1).[7b]

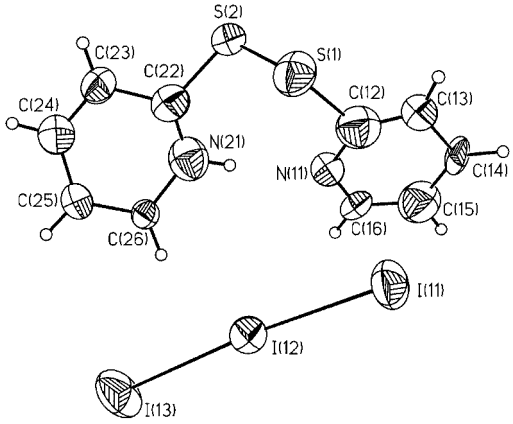

Figure 4. ORTEP diagram of the ionic components of compound **1** together with the atomic numbering scheme; thermal ellipsoids are shown at the 33% probability level, hydrogen atoms are depicted as the spheres of arbitrary radii; selected bond lengths are given in the text

Crystal and Molecular Structure of [(PYS−PYSH)$^+$·I_3^-]

Dark crystals of the complex suitable for a single-crystal X-ray analysis were grown by slow concentration of the filtrate obtained from the reaction of diiodine with the appropriate ligand in dichloromethane.

An ORTEP diagram of the compound is shown in Figure 4 with selected bond lengths and angles in Table 2. In the crystal there are four symmetry-independent cation/anion pairs (Figure 5). Figure 5 also shows the intermolecular or cation−anion interactions.

The structure of the compound consists of two residues, one cationic (PYS−PYSH)$^+$ containing the S−S bond linking the two 2-mercaptopyridine molecules, one of which is protonated, and one I_3^- counter anion. There are only a few crystal structures reported in the literature containing open-chain stable cations of DS−SD dimers. These include the monocation [{($C_4H_6N_2S$−$SN_2C_4H_5$)$_2$}$^{2+}$·(I_3^-)·(I_5^-)][3] ($C_4H_6N_2S$ = *N*-methylimidazole-2-thione) and dications such as [{($C_4H_6N_2S$−)$_2$}$^{2+}$·2I_3^-·I_2][3] ($C_4H_6N_2S$ = *N*-methylimidazole-2-thione), [{(*i*Pr$_2$timdt)$_2$}$^{2+}$·(IBr$_2^-$)$_2$][14a] (*i*Pr$_2$timdt = 1,3-diisopropylimidazolidine-2,4,5-trithione), and [{(H$_2$N)$_2$C−S−S−C(NH$_2$)$_2$}$^{2+}$·(2I$^-$)][14b] [(H$_2$N)$_2$C=S = thiourea], [(L)$_2^{2+}$·2(I_3^-)][14c] (L = 1,3-diisopropyl-4,5-dimethylimidazoldithiocarboxylate).

The mean value of the S−S bond length measured in the four symmetry-independent cation/anion pairs found in the structure is 2.032 Å [the individual bonds are S(1)−S(2) = 2.003(12) Å (**a**), S(3)−S(4) = 2.010(15) Å (**b**), S(5)−S(6) = 2.052(14) Å (**c**) and S(7)−S(8) = 2.062(14) (**d**), respectively] (Figure 5). These are among the shortest bonds of this type.[3,14] Examples include the monocation [{($C_4H_6N_2S$−$SN_2C_4H_5$)$_2$}$^{2+}$·(I_3^-)·(I_5^-)] ($C_4H_6N_2S$ = *N*-methylimidazole-2-thione) with S−S = 2.094(3) Å[3] and the dications, [{($C_4H_6N_2S$−)$_2$}$^{2+}$·2I_3^-·I_2] ($C_4H_6N_2S$ = *N*-methylimidazole-2-thione) with S−S = 2.085(2) Å,[3] [{(*i*Pr$_2$timdt)$_2$}$^{2+}$·(IBr$_2^-$)$_2$], (*i*Pr$_2$timdt = 1,3-diisopropylimidazolidine-2,4,5-trithione) with S−S = 2.071(7) Å,[18] [{(H$_2$N)$_2$C−S−S−C(NH$_2$)$_2$}$^{2+}$·(2I$^-$)] [(H$_2$N)$_2$C=S = thiourea] with S−S = 2.044 Å,[14b] and [(L)$_2^{2+}$·2(I_3^-)] (L = 1,3-diisopropyl-4,5-dimethylimidazoldithiocarboxylate) with S−S= 2.024(5) Å.[14c]

The two C−S bond lengths in the four symmetry-independent cation/anion pairs of the complex are unequal due to the monoprotonation of the aromatic ring of the disulfide [S(1)−C(12) = 1.85(3) and S(2)−C(22) = 1.77(3) Å (**a**), S(4)−C(42) = 1.78(3) and S(3)−C(32) = 1.75(3) Å (**b**), S(6)−C(62) = 1.65(2) and S(5)−C(52) = 1.77(3) Å (**c**), S(7)−C(72) = 1.71(2) and S(8)−C(82) = 1.69(3) Å (**d**), respectively] (Figure 5). The longer C−S distance corre-

 © 2004 Wiley-VCH Verlag GmbH & Co. KGaA, Weinheim

Table 2. Selected bond lengths [Å] and angles [°] for **1**

Bond lengths [Å]			
I(11)−I(12)	2.892(4)	S(3)−S(4)	2.010(15)
I(12)−I(13)	2.943(3)	S(3)−C(32)	1.78(3)
I(21)−I(22)	2.880(4)	S(4)−C(42)	1.75(3)
I(22)−I(23)	2.960(3)	S(5)−S(6)	2.052(14)
I(31)−I(32)	2.860(4)	S(5)−C(52)	1.65(2)
I(32)−I(33)	2.963(3)	S(6)−C(62)	1.77(3)
I(41)−I(42)	2.855(4)	S(7)−S(8)	2.062(14)
I(42)−I(43)	2.928(3)	S(7)−C(72)	1.71(2)
S(1)−S(2)	2.003(15)	S(8)−C(82)	1.69(3)
S(1)−C(12)	1.85(3)		
S(2)−C(22)	1.77(3)		
Angles [°]			
I(11)−I(12)−I(13)	174.92(12)	I(33)−I(32)−I(31)	176.17(11)
I(21)−I(22)−I(23)\tab	174.96(11)	I(41)−I(42)−I(43)	175.58(11)
C(12)−S(1)−S(2)−C(22)	90.4(15)	C(52)−S(5)−S(6)−C(62)	83.5(13)
C(32)−S(3)−S(4)−C(42)	−89.7(14)	C(72)−S(7)−S(8)−C(82)	−86.8(13)

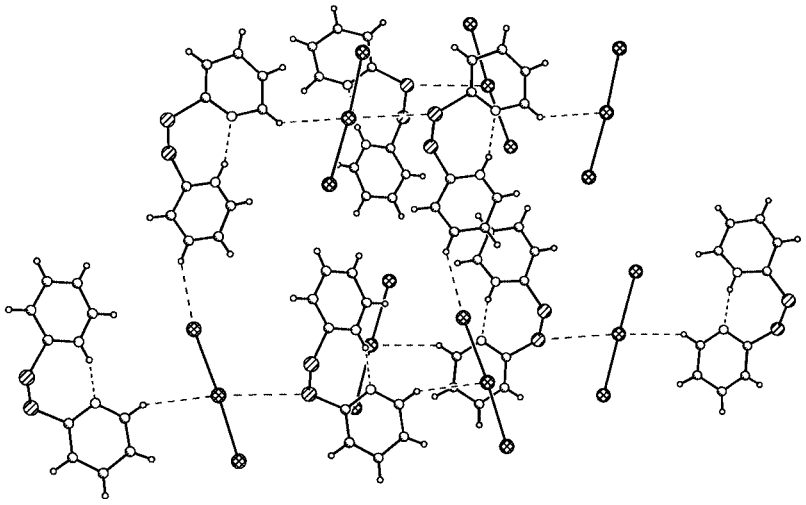

Figure 5. Crystal packing of **1** as seen approximately along the [100] direction, hydrogen bonds and S···I contacts are drawn as dashed lines

sponds to the nonprotonated ring and the shorter distance to the protonated one. The corresponding C−S bond lengths found in the monocation $[\{(C_4H_6N_2S-SN_2C_4H_5)_2\}^{2+}\cdot(I_3^-)\cdot(I_5^-)]$ ($C_4H_6N_2S$ = *N*-methylimidazole-2-thione)[3] are 1.744(9) Å and 1.700(11) Å. The C−S bond lengths found in the doubly protonated rings of the dications are almost equal, 1.748(5) and 1.735(5) Å in $[\{(C_4H_6N_2S-)_2\}^{2+}\cdot 2I_3^-\cdot I_2]$ ($C_4H_6N_2S$ = *N*-methylimidazole-2-thione),[3] 1.76(4) and 1.75(2) Å in $[\{(i\mathrm{Pr}_2\mathrm{timdt})_2\}^{2+}\cdot(\mathrm{IBr}_2^-)_2]$ (*i*Pr_2timdt = 1,3-diisopropylimidazolidine-2,4,5-trithione),[18] 1.76 and 1.78 Å in $[\{(H_2N)_2C-S-S-C(NH_2)_2\}^{2+}\cdot(2I^-)]$ $[(H_2N)_2C{=}S$ = thiourea],[14b] and 1.7281(2) Å in $[(L)_2{}^{2+}\cdot 2(I_3^-)]$ (L = 1,3-diisopropyl-4,5-dimethylimidazoldithiocarboxylate).[14c]

Both I−I bond lengths differ significantly from the corresponding I−I bond length of I_2 in the solid state (2.715 Å).[15] Thus, the two I−I bond lengths of I_3^- in the complex are I(11)−I(12) = 2.892(4) and I(12)−I(13) = 2.943(3) Å (**a**), I(21)−I(22) = 2.870(4) and I(22)−I(23) = 2.960(3) Å (**b**), I(31)−I(32) = 2.860(4) and I(32)−I(33) = 2.863(3) Å (**c**) and I(41)−I(42) = 2.855(4) and I(42)−I(43) = 2.928(3) Å (**d**), respectively (Figure 5), indicating a slight asymmetry of I_3^- in this complex (covalent linear asymmetric).[7b] In the following I_3^- adducts, however, the asymmetry seems to be stronger. Thus, in $[Et(NH_2)dtl]I_3^-$ [$Et(NH_2)$dtl = 3,5-bis(ethyllamino)-1,2-dithiolithium],[7b,16a] the I−I bond lengths are 2.74 and 3.14 Å, in CsI_3^- [7b,16b] 2.842 and 3.038 Å, in $Da_2I_3^-$ [7b,16c] (Da = 1,4-diazoniabicyclo[2.2.2]octane) 2.793 and 3.167 Å, and in [1-MethylcytosineH]I_3^- [7b,16d] 2.794 and 3.123 Å (see Table 1 and ref.[7b] for more examples).

According to Pauling,[17a] $d(\mathrm{I-I}) = d_o - 0.85\cdot\log(n)$ [Equation (2)], where d_o is the I−I bond length of I_2 in the gas phase, i.e. 2.67 Å,[17b] and *n* is the bond order. The calculated values of the bond orders for the I−I bonds of the complexes are listed in Table 1. Deplano et al.[7b] classi-

 © 2004 Wiley-VCH Verlag GmbH & Co. KGaA, Weinheim

fied triiodide adducts into two types: (a) the $I^-\cdots I_2$ adducts which have a linear asymmetric geometry with one strong I−I bond (bond orders > 0.63 e) and one weaker I−I bond (bond orders < 0.30 e) and (b) the covalent I−I−I complexes which have (i) a linear symmetric geometry with two equal I−I bonds and bond order values around 0.50 e and those with (ii) a linear asymmetric geometry which have two nonequivalent I−I bonds with bond order values around 0.50 e (a stronger bond with bond order > 0.50 e and a weaker with bond order < 0.50 e). Thus, according to the values of the I−I bond lengths and bond orders, the I_3^- in this complex can be classified as a linear asymmetric $I^-\cdots I_2$ complex.[7b]

The mean value of the I−I−I bond angle is 175.4(1)° [(11)−I(12)−I(13) = 174.92(12)° (**a**), I(21)−I(22)−I(23) = 174.96(11)° (**b**), I(33)−I(32)−I(31) = 176.17(11)° (**c**) and I(41)−I(42)−I(43) = 175.58(13)° (**d**), respectively] (Figure 5) indicative of the involvement of both terminal iodine atoms in the interaction with the disulfide. These differ only slightly from linearity. In particular, the mean C···I and S···I contact distances of the two terminal iodine atoms of I_3^- species in the four symmetry-independent cation/anion pairs are 3.842 Å and 3.943 Å, respectively. Similar angles were observed in $[\{(C_4H_6N_2S-)_2\}^{2+}\cdot 2I_3^-\cdot I_2]$ ($C_4H_6N_2S$ = *N*-methylimidazole-2-thione) [178.87(4)°][3] and in $[(L)_2^{2+}\cdot 2(I_3^-)]$ (L = 1,3-diisopropyl-(4,5-dimethylimidazolyl)dithiocarboxylate) [175.71(4)°].[14c]

Strong intramolecular hydrogen bonds between the imino NH proton and the nonprotonated nitrogen atom are formed in the complex (mean value of the N···N bond is 2.74 Å, mean value of H···N is 1.91Å and the mean value of the N−H···N angle is 163°). In the crystal structure, the weak C−H···I, S···I, and S···S interactions organise the cations and anions in alternate layers (Figure 5).

Conclusion

Recently, a mechanism for the transformation of MMI to MMI disulfide was proposed by Isaia et al.[3] and Po et al.[18] based on crystallographic and electrochemical data. The proposed redox process involves the formation of a di- and a monocationic disulfide species of MMI prior to the full transformation of MMI to MMI disulfide. Thus, thioamides such as MMI[3] or tzdtH[2a] exhibiting antithyroidal activity against hyperthyroidism (Graves' disease) are either oxidised by the TPO-I system to form disulfides or act as strong donors towards diiodine forming iodonium salts, while activated iodine is reduced to the iodide anion simultaneously. On the other hand, thioamides such as PTU[2c] which are able to form weak charge transfer species with diiodine, interfere in other steps of the mechanism, either in the formation of thyroid peroxidase (TPO)−iodonium complex[4] or inhibit the activity of the iodothyronine deiodinase type I (ID-1), an enzyme responsible for the monodeiodination of the T4 prohormone to the T3 hormone[6] The easy oxidation of PYSH by I_2 to form the monocationic disulfide complex [(PYSPYSH)$^+\cdot I_3^-$] similar to the antithyroid drug methimazole (MMI)[3,18] may indicate that PYSH might also possess antithyroid properties like MMI.

Experimental Section

Materials and Instruments: All solvents used were reagent grade. Diiodine (Aldrich) and pyridine-2-thione (Merck) were used with no further purification. Elemental analyses for C, H, N, and S were carried out with a Carlo Erba EA model 1108 elemental analyser. Melting points were measured in open tubes with a Stuart scientific apparatus and are uncorrected. Infrared spectra in the region of 4000−370 cm^{-1} were obtained in KBr discs while far-infrared spectra in the region of 400−50 cm^{-1} were obtained in polyethylene discs with a Perkin−Elmer Spectrum GX FT-IR spectrophotometer. A Jasco UV/Vis/NIR V 570 series spectrophotometer was used to obtain the electronic absorption spectra. Conductivity titrations were carried out at 293 K in acetonitrile solutions with a WTF LF-91 conductivity meter.

Synthesis and Crystallisation: The complex was prepared by mixing a dichloromethane solution of diiodine with a suspension of 2-mercaptopyridine in dichloromethane in a 1:2 PYSH/I_2 molar ratio in air at 0 °C with continuous stirring for 5 h. The solution was then filtered and the resultant clear solution was kept in the refrigerator for several days. Dark crystals of the complex suitable for single-crystal X-ray analysis were obtained, yield 0.012 g (20%); m.p. 80−82 °C. $C_{10}H_9I_3N_2S_2$ (602.02): calcd. C 19.95, H 1.51, N: 4.65, S 10.65; found C 19.23, H 1.51, N 4.31, S 10.87. IR: $\tilde{\nu}$ = 3119 w, 1577 s, 1496 s, 1108 vs, 959 s, 765 vs, 731 s, 654 s, 463 s, 158 m, 112 m cm^{-1}. UV/Vis (CH_2Cl_2): λ_{max} (logε) = 500.5 (2.90), 367.5 (3.56), 292.5 (3.84) nm.

X-ray Structure Determination: Data were collected using the ω-scan technique in the range 2.90° < 2θ < 29.92° with a KUMA KM4CCD four-circle diffractometer[19a] with a CCD detector using graphite-monochromated Mo-K_α radiation (λ = 0.71073 Å) at 293(2) K. Cell parameters were determined by a least-squares fit.[19b] All data were corrected for Lorentz-polarisation and absorption effects.[19b,19c] The crystals of the compound were relatively poor in quality and the statistical indicators of the appropriate refinements are, therefore, not very good and the refinements were provided with constraints. Nevertheless, the quality of the data obtained allow for a reasonable discussion, especially of crystal packing and the constitution of the complex. The structure was solved by direct methods with SHELXS-97[19d] and refined by full-matrix least-squares procedures on F^2 with SHELXL-97.[19e] All non-hydrogen atoms were refined anisotropically, hydrogen atoms were located in calculated positions and refined using the "riding model" with isotropic thermal parameters fixed at 1.2 times the U_{eq} values of the appropriate carrier atom. $C_{10}H_9I_3N_2S_2$, MW = 602.020, monoclinic in $P2_1$, a = 8.230(2) Å, b = 35.708(7) Å, c = 11.369(2) Å, β = 91.86(3)°, V = 3339.3(12) Å^3, Z = 8, ρ(calcd.) = 2.395 g cm^{-3}, μ = 5.849 mm^{-1}, reflections collected 21199, Final R ($\Sigma||F_o| - |F_c||/\Sigma|F_o|$), $wR2$ $\{[\Sigma w(F_o^2 - F_c^2)^2/\Sigma w(F_o^2)^2]^{1/2}\}$ [$I > 2\sigma(I)$] indices 0.0872 and 0.2028, respectively. Crystallographic data (excluding structure factors) for the structure reported in this paper have been deposited with the Cambridge Crystallographic Data Centre as supplementary publication no. CCDC-230097 (**1**). Copies of the data can be obtained free of charge on application to CCDC, 12 Union Road, Cambridge CB2 1EZ, UK [Fax: + 44-1223-336-033; E-mail: deposit@ccdc.cam.ac.uk].

 © 2004 Wiley-VCH Verlag GmbH & Co. KGaA, Weinheim

Acknowledgments

This work was carried out in partial fulfilment of the requirements for an M.Sc. by C. D. A. within the graduate program EPEAEK in Bioinorganic Chemistry financed by the Ministry of Education of Greece and coordinated by Professor N. Hadjiliadis. The NATO grant awarded to N. H. and I. S. B. is also acknowledged.

[1] [1a] *MARTIDALE − The Extra Pharmacopoeia*, 28th ed. (Ed.: J. E. F. Raynolds), The Pharmaceutical Press, London **1982**, p. 356−359. [1b] C. Laurence, M. J. El Ghomari, J.-Y. Le Questel, M. Berthelot, R. Mokhlisse, *J. Chem. Soc., Perkin Trans. 2* **1998**, 1545−1551. [1c] C. Laurence, M. J. El Ghomari, M. Berthelot, *J. Chem. Soc., Perkin Trans. 2* **1998**, 1163−1166. [1d] C. Laurence, M. J. El Ghomari, M. Luçon, *J. Chem. Soc., Perkin Trans. 2* **1998**, 1159−1162.

[2] [2a] V. Daga, S. K. Hadjikakou, N. Hadjiliadis, M. Kubicki, J. H. Z. dos Santos, I. S. Butler, *Eur. J. Inorg. Chem.* **2002**, 1718−1728. [2b] J H. Z. dos Santos, I. S. Butler, V. Daga, S. K. Hadjikakou, N. Hadjiliadis, *Spectrochim. Acta, Part A* **2002**, *58*, 2725−2735. [2c] C. D. Antoniadis, G. Corban, S. K. Hadjikakou, N. Hadjiliadis, M. Kubicki, S. Warner, I. S. Butler, *Eur. J. Inorg. Chem.* **2003**, 1635−1640.

[3] M. C. Aragoni, M. Arca, F. Demartin, F. A. Devillanova, A. Garau, F. Isaia, V. Lippolis, G. o Verani, *J. Am. Chem. Soc.* **2002**, *124*, 4538−4539.

[4] [4a] A. Taurog, *Endocrinology*, chapter 25 ("Hormone Synthesis") (Ed.: L. DeGroot), Accademic Press, Inc., London, **1979**, vol. 1, p. 331. [4b] D. R. Morris, L. P Hager, *J. Biol. Chem.* **1966**, *241*, 3582−3589.

[5] A. Nakataka, H. Hidaka, *J. Clin. Endocrinol. Metab.* **1976**, *43*, 152−158.

[6] [6a] W. W. du Mont, G. Mugesh, C. Wismach, P. G. Jones, *Angew. Chem. Int. Ed.* **2001**, *40*, 2486−2489. [6b] M. J. Berry, J. D. Kieffer, J. W. Harney, P. R. Larsen, *J. Biol. Chem.* **1991**, *266*, 14155−14158. [6c] M. J. Berry, L. Banu, P. R. Larsen, *Nature* **1991**, *349*, 438−440.

[7] [7a] P. D. Boyle, S. M. Godfrey, *Coord. Chem. Rev.* **2001**, *223*, 265−299. [7b] P. Deplanova, J. R. Ferraro, M. L. Mercuri, E. F. Trogu, *Coord. Chem. Rev.* **1999**, *188*, 71−95. [7c] P. H. Svensson, L. Kloo, *Chem. Rev.* **2003**, *103*, 1649−1684.

[8] [8a] M. Esseffar, W. Bouab, A. Lamsabhi, J. L. M. Abboud, R. Notario, M. Yanez, *J. Am. Chem. Soc.* **2000**, *122*, 2300−2308. [8b] F. Bigoli, P. Deplano, A. Ienco, C. Mealli, M. L. Mercuri, M. A. Pellinghelli, G. Pintus, G. Saba, E. F. Trogu, *Inorg. Chem.* **1999**, *38*, 4626−4636. [8c] F. Bigoli, P. Deplano, M. L. Mercuri, M. A. Pellinghelli, A. Sabatini, E. F. Trogu, A. Vacca, *J. Chem. Soc., Dalton Trans.* **1996**, 3583−3598. [8d] F. Freeman, J. W. Zi1ler, H. N. Po, M. C. Keindl, *J. Am. Chem. Soc.* **1988**, *110*, 2586−2591. [8e] D. Arzei, P. Deplano, E. F. Trogu, F. Bigou, M. A. Pellinghelli, A. Vacca, *Can. J. Chem.* **1988**, *66*, 1483−1489. [8f] F. Cristiani, F. A. Devillanova, A. Diaz, G. Verani, *J. Chem. Soc., Perkin Trans.* **1984**, 1383−1386. [8g] F. A. Devillanova, G. Verani, *Tetrahedron* **1979**, *35*, 511−514.

[9] [9a] A. Suszuka, *J. Chem. Soc., Perkin Trans.* **1985**, 531−534. [9b] A. I. Popov, N. E. Skelly, *J. Am. Chem. Soc.* **1955**, *77*, 3722−3724.

[10] P. J. Hendra, N. Sadasivan, *Spectrochim. Acta* **1965**, *21*, 1127−1133.

[11] [11a] A. Anderson, T. S. Sun, *Chem. Phys. Lett.* **1970**, *6*, 611−616. [11b] P. Deplano, F. A. Devillanova, J. R. Ferraro, F. Isaia, V. Lippolis, M. L. Mercuri, *Appl. Spectrosc.* **1992**, *46*, 1625−1629.

[12] F. Demartin, P. Deplano, F. A. Devillanova, F. Isaia, V. Lippolis, G. Verani, *Inorg. Chem.* **1993**, *32*, 3694−3699.

[13] [13a] P. D. Boyle, J. Christie, T. Dyer, S. M. Godfrey, I. R. Howson, C. McArthur, B. Omar, R. G. Pritchard, G. R. Williams, *J. Chem. Soc., Dalton Trans.* **2000**, 3106−3112. [13b] F. H. Herbstein, W. Schwotzer, *J. Am. Chem. Soc.* **1984**, *106*, 2367−2373.

[14] [14a] F. Bigoli, P. Deplano, M. Mercuri, M. Pellinghelli, G. Pintus, E. F. Trogu, G. Zonnedda, H. H. Wang, J. M. Williams, *Inorg. Chim. Acta* **1998**, *273*, 175−183. [14b] O. Foss, J. Johnsen, O. Tvedten, *Acta Chem. Scand.* **1958**, *12*, 1782−1798. [14c] N. Kuhn, H. Bohnen, G. Henkel, *Z. Naturforsch., Teil B* **1994**, *49*, 1473−1480.

[15] F. Van Bolhuis, P. B. Koster, T. Migchelsen, *Acta Crystallogr.* **1967**, *23*, 90−91.

[16] [16a] R. Ambrosetti, G. Bellucci, R. Bianchini, F. Bigoli, P. Deplano, M. A. Pellinghelli, E. F. Trogu, *J. Chem. Soc., Perkin Trans. 2* **1991**, 339−345. [16b] J. Runsink, S. Swen-Walstra, T. Migchelsen, *Acta Crystallogr., Sect. B* **1972**, *28*, 1331−1335. [16c] P. K. Bakshi, M. A. James, T. S. Cameron, O. Knop, *Can. J. Chem.* **1996**, *74*, 559−573. [16d] M. Rossi, L. G. Marzilli, T. J. Kistenmacher, *Acta Crystallogr., Sect. B* **1978**, *34*, 2030−2033.

[17] [17a] L. Pauling, *The Nature of the Chemical Bond*, 3rd ed., Cornell University Press, Ithaca, New York, **1960**. [17b] H. B. Burgi, *Angew. Chem. Int. Ed. Engl.* **1975**, *14*, 460−473.

[18] H. N. Po, Z. Shariff, J. A. Masse, F. Freeman, M. C. Keindl-Yu, *Phosphorus, Sulfur, Silicon* **1991**, *63*, 1−12.

[19] [19a] KUMA KM-4CCD user manual, KUMA Diffraction, Wroclaw, Poland, **1999**. [19b] *CrysAlis, program for reduction of data from the KUMA CCD diffractometer*, KUMA Diffraction, Wroclaw, Poland, **1999**. [19c] R. H. Blessing, *J. Appl. Crystallogr.* **1989**, *22*, 396. [19d] G. M. Sheldrick, *Acta Crystallogr., Sect. A* **1990**, *46*, 467−477. [19e] G. M. Sheldrick, *SHELXL-97, Program for the Refinement of Crystal Structures*, University of Göttingen, Göttingen, Germany, **1997**.

Received April 8, 2004
Early View Article
Published Online September 7, 2004

 © 2004 Wiley-VCH Verlag GmbH & Co. KGaA, Weinheim

Homoleptic Rare-Earth Carbazolates and the Trends of Their $E_{Ln^{II/III}}$ Redox Potentials: Mixed-Valent Samarium in $^1_\infty[Sm_2(Cbz)_5](CbzH)$ (CbzH = carbazole) and Trivalent Thulium, Neodymium and Gadolinium in $[Ln_2(Cbz)_6]$

Klaus Müller-Buschbaum*[a] and Catharina C. Quitmann[a]

Keywords: Solvent-free synthesis / Lanthanides / Carbazolates / N ligands

The solvent-free melt reaction of carbazole (CbzH, $C_{12}H_8NH$) with samarium metal yields $^1_\infty[Sm_2(Cbz)_5](CbzH)$ (**1**), whilst the melt reactions with thulium, neodymium and gadolinium give $[Tm_2(Cbz)_6]$ (**2**), $[Nd_2(Cbz)_6]$ (**3**) and $[Gd_2(Cbz)_6]$ (**4**), respectively. Compounds **1** and **2** were obtained as single crystals and their crystal structures determined by single-crystal X-ray analysis, whilst **3** and **4** were obtained as powders. X-ray powder diffraction studies show that the gadolinium-containing complex **4** is isotypic to the thulium complex **2**, whereas the neodymium-containing complex **3** is not. Compound **1** contains alternating Sm^{II} and Sm^{III} cations in a chain structure. Complex **2** only exhibits dimeric units of Tm^{III}. Besides Ln–N coordination, the crystal structures of both compounds show η^6-π interactions with the phenyl rings of the carbazolate ligands. This leads to small coordination polyhedra, such as connected tetrahedra of two nitrogen atoms and two η^6-π-coordinated phenyl rings around Sm^{II}, and trigonal bipyramids of five nitrogen atoms around Sm^{III} for **1**, as well as tetrahedra of three nitrogen atoms and one η^6-π-phenyl interaction around Tm^{III} for **2**. From the trend of the $E_{Ln^{II/III}}$ redox potentials, the complexes of neodymium and gadolinium are also trivalent. For **1**–**4** the results of FIR, MIR and Raman spectroscopy as well as simultaneous DTA/TG analyses are also presented.
(© Wiley-VCH Verlag GmbH & Co. KGaA, 69451 Weinheim, Germany, 2004)

Introduction

Since the syntheses of the first cyclopentadienyl complexes[1] and metallocenes[2] solvent-containing reaction routes have come to dominate all fields of rare-earth-metal coordination chemistry.[3−7] Accordingly, the vast majority of structurally characterised compounds are solvates and are therefore heteroleptic[8] whenever the ligands do not meet certain criteria like multi-chelating, such as in the rare-earth-metal amide complexes.[8−11] The reactivity of rare-earth metals themselves has proven to be high enough to be able to react directly with amines, yielding homoleptic amides. Whilst initial work with substituted pyrazolate ligands made solvent recrystallisation[12,13] steps necessary in order to obtain crystalline products, we have systematically developed a type of solvent-free melt synthesis that allows the crystallisation of products under reaction conditions,[14−17] including the first homoleptic carbazolates of europium and ytterbium;[18] heteroleptic solvent-containing carbazolates have been reported previously.[19,20] Both europium and ytterbium carbazolates are divalent. Therefore, reactions of samarium, thulium, neodymium and gadolinium metal with carbazole were carried out, their reaction products $^1_\infty[Sm_2(Cbz)_5](CbzH)$ (**1**) and $[Ln_2(Cbz)_6]$ [Ln = Tm, Nd, Gd (**2**−**4**)] illuminating the trend of the $E_{Ln^{II/III}}$ redox potentials[21,22] (see Scheme 1) from Eu^{II} and Yb^{II} in $^1_\infty[Ln_2(Cbz)_4]$[18] to mixed-valent Sm^{II}/Sm^{III} and trivalent Tm^{III}, Nd^{III} and Gd^{III}. The results are compounds with different crystal structures that are unique in rare-earth-metal amide chemistry.

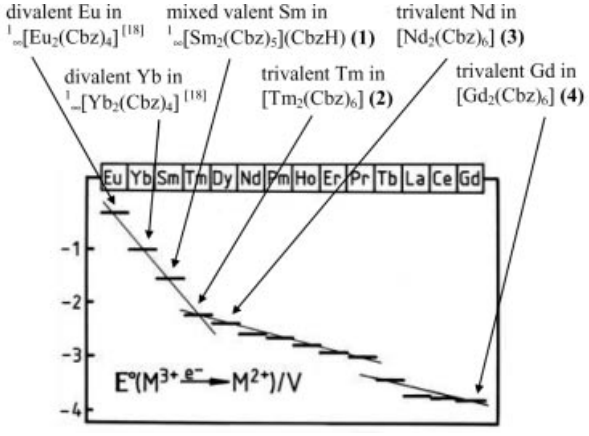

Scheme 1. Homoleptic rare-earth carbazolates and their $E_{Ln^{II/III}}$ redox potentials[21,22] (diagram taken from ref.[22] with permission of the author)

Results and Discussion

The solvent-free reactions of samarium, thulium, neodymium and gadolinium with carbazole were carried out in

[a] Institut für Anorganische Chemie, Universität zu Köln, Greinstrasse 6, 50939 Köln, Germany
E-mail: Klaus.Mueller-Buschbaum@Uni-Koeln.de

 © 2004 Wiley-VCH Verlag GmbH & Co. KGaA, Weinheim DOI: 10.1002/ejic.200400516

a melt of the amine in ampoules. The reaction with samarium metal yielded black, in thin layers dark red crystals of $^1_\infty[Sm_2(Cbz)_5](CbzH)$ (**1**) at 270 °C [Equation (1)]. Activation by amalgamation dropped the reaction temperature to 255 °C but decreased the crystallinity of the bulk product. No further reaction to the trivalent state was observed up to decomposition (see Figure 1), even when an excess of CbzH was used.

$$Ln + x\,HN(R_2) \rightarrow Ln(NR_2)_x + x/2\,H_2 \quad (1)$$

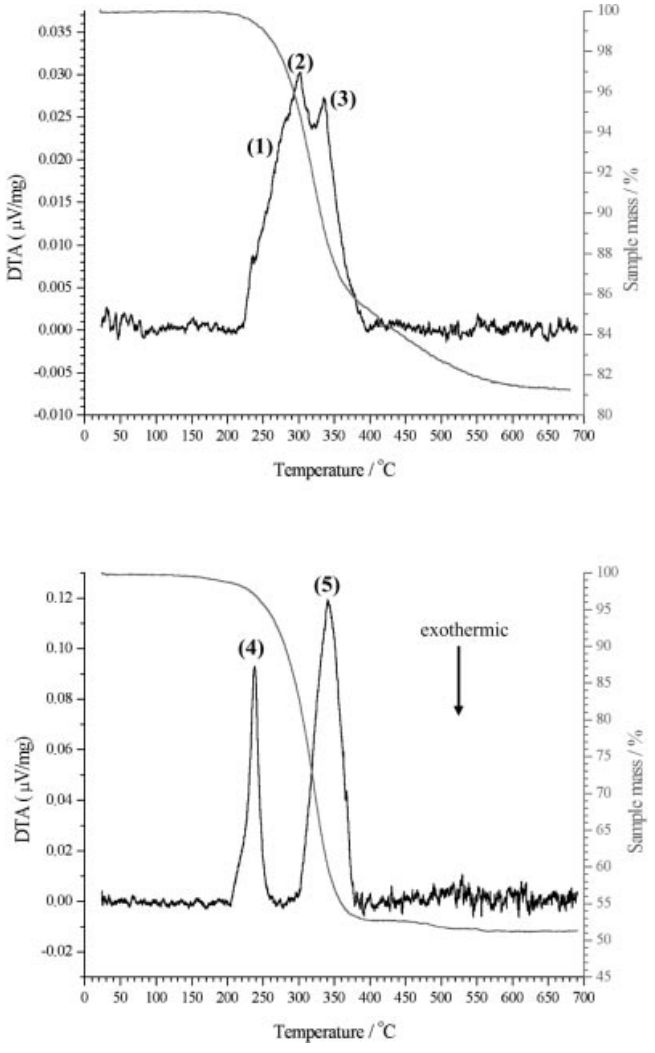

Figure 1. The thermal decompositions of $^1_\infty[Sm_2(Cbz)_5](CbzH)$ (**1**, top) and $[Tm_2(Cbz)_6]$ (**2**, bottom) investigated by simultaneous DTA/TG in the temperature range 20−700 °C; the plot of the bulk material of **1** exhibits the melting point of excess carbazole (1), release of uncoordinated carbazole from the structure (2) and the decomposition (3) of **1**; the thermal investigation of the bulk material of **2** exhibits the melting point (4) and the decomposition (5) of **2**; neither excess nor uncoordinated carbazole is observed for **2**

The reaction with thulium metal was also carried out under solvent-free conditions in a carbazole melt except that both amalgam activation of Tm and a reaction temperature of 280 °C were necessary to obtain orange to red crystals of $[Tm_2(Cbz)_6]$ (**2**).

Neodymium and gadolinium metal react with carbazole only as an amalgam containing at least one tenth of the amount of the rare-earth metal. A reaction temperature of 280 °C was also necessary to obtain $[Nd_2(Cbz)_6]$ (**3**) as a golden-yellow solid. $[Gd_2(Cbz)_6]$ (**4**) was formed upon annealing at 245 °C already, following activation at 280−290 °C, giving a poorly crystalline dark yellow solid.

The thermal decomposition of **1**−**4** was investigated by simultaneous DTA/TG.[23] This method has already proved its value for understanding comparable melt reactions with 2-(2-pyridyl)benzimidazole[15] and shows the decomposition path of the bulk product of the melt reaction. This analysis provides additional information regarding the completeness of the reaction and possible phase impurities.

$^1_\infty[Sm_2(Cbz)_5](CbzH)$ (**1**) is a molecular polymer formed at relatively high temperatures (255−270 °C). Accordingly, its thermal behaviour and stability must be different from the known heteroleptic carbazolates, and therefore the bulk product of the synthesis was studied. Although the thermogravimetric investigation displays no separated signals, the resolution of the differential thermoanalysis exhibits three different signals (Figure 1, top). The first signal in the heat flow was identified as the melting point of unchanged carbazole at 235 °C, followed by a slight mass loss of the excess carbazole (about 2%) displayed by a shoulder of an endothermic peak in the heat flow. At a reaction temperature of 270 °C, $^1_\infty[Sm_2(Cbz)_5](CbzH)$ slowly starts to decompose without melting and releases the uncoordinated CbzH (M = 167.1 g/mol; calcd. 12.9% of $M\{^1_\infty[Sm_2(Cbz)_5](CbzH)\}$; found 13%). At 290−300 °C another endothermic signal is observed that indicates further thermal decomposition of $^1_\infty[Sm_2(Cbz)_5]$ without the formation of defined decomposition products. The unseparated thermal signals indicate that the later processes begin before the earlier ones are completely finished. Although the thermal stability of $^1_\infty[Sm_2(Cbz)_5](CbzH)$ is high, it does not reach the stability of the homoleptic divalent rare-earth carbazolates.[18] One of the reasons for this behaviour could be the unsaturated coordination spheres of the samarium atoms. Considering the formation temperature of 270°C, the temperature frame to obtain the compound is very limited and it is neither likely that $^1_\infty[Sm_2(Cbz)_5]$ is obtained free of CbzH by the melt synthesis nor that $^1_\infty[Sm_2(Cbz)_5](CbzH)$ forms if the volatile CbzH is not forced to stay in the reaction mixture, as provided by the ampoule treatment.

The thermal decompositions of $[Ln_2(Cbz)_6]$ [Ln = Tm, Nd, Gd (**2**−**4**)] are relatively similar to each other, but different from **1** due to their different structures. All three compounds show sharp melting points of the products as well as one following endothermic decomposition step. Complexes **2**−**4** have much lower melting points (220 °C for **2**, 190 °C for **3** and 175 °C for **4**; see Figure 1 for Tm) than the polymeric carbazolates $^1_\infty[Ln_2(Cbz)_4]$ (Ln = Eu, Yb).[18] The melting points are identified by sharp endothermic peaks in the heat flow with no related mass loss.

 © 2004 Wiley-VCH Verlag GmbH & Co. KGaA, Weinheim

The subsequent decomposition step for **2** starts at 300 °C with release of 47% of the sample mass. For **3** the decomposition starts at 310 °C with release of 68% of the sample mass. This includes 15% of unchanged carbazole in the bulk sample, as identified by its melting point, and an additional endothermic signal in the heat flow. The behaviour of **4** is similar, its decomposition starting at 270 °C with 3% of unchanged carbazole being released prior to a mass loss of 51%. In contrast to **1**, **3** and **4** the bulk sample of **2** is free of unchanged carbazole, indicating complete reaction. Although the volatile products of the decompositions of **2**−**4** could not be defined, the decomposition pathways are likely to be similar for all three compounds because the released sample masses match the different molecular masses of Tm, Gd and Nd. The decomposition temperatures of **1**−**4** are distinctively lower than for the divalent compounds $^1_\infty[Ln_2(Cbz)_4]$ (Ln = Eu, Yb).[18] As for the rare-earth pyridylbenzimidazolates,[15] no periodic behaviour through the course of the rare earth elements is observable either for melting points or absolute thermal stability of rare earth carbazolates, although the influence of structural characteristics is clearly evident.

The FIR and Raman spectra of **1**−**4** show bands that cannot be identified with the ligand and thus represent the Ln−N stretching modes {$^1_\infty[Sm_2(Cbz)_5](CbzH)$ (**1**): FIR: $\tilde{\nu}$ = 231, 171, 123, 108 cm^{-1}; $[Tm_2(Cbz)_6]$ (**2**): FIR: $\tilde{\nu}$ = 251, 188, 158 cm^{-1}; Raman: $\tilde{\nu}$ = 251, 200, 170 cm^{-1}; $[Nd_2(Cbz)_6]$ (**3**): FIR: $\tilde{\nu}$ = 221, 145, 123 cm^{-1}; Raman: $\tilde{\nu}$ = 280, 230 cm^{-1}; $[Gd_2(Cbz)_6]$ (**4**): FIR: $\tilde{\nu}$ = 243, 231, 159 cm^{-1}; Raman: $\tilde{\nu}$ = 297, 258, 240 cm^{-1}}. The bands thereby match well with other Ln−N-containing compounds such as rare-earth porphyrin complexes,[24] dipyridylamides[16] or pyridylbenzimidazolates[14,15] regarding the coordination spheres, valences and ionic radii in **1** to **4**. They are also in good accordance with the homoleptic carbazolates of divalent Eu and Yb.[18] The ligand lattice stretching modes are reflected by rather broad bands (FIR: $\tilde{\nu}$ = 419, 145 cm^{-1}). The MIR and Raman spectra also contain vibrational bands of the carbazolate ligands that are independent of the rare-earth ion and can therefore be assigned to CbzH[18] (**1**: IR: $\tilde{\nu}$ = 3049, 1603, 1493, 1450, 1326, 1288, 1236, 1106, 750, 725, 574 cm^{-1}; **2**: IR: $\tilde{\nu}$ = 3050, 1602, 1493, 1450, 1327, 1287, 1239, 1108, 749, 726, 574 cm^{-1}; Raman: $\tilde{\nu}$ = 1483, 1450, 1316, 1015, 744 cm^{-1}; **3**: IR: $\tilde{\nu}$ = 3049, 1601, 1493, 1450, 1327, 1287, 1238, 1107, 748, 725, 574 cm^{-1}; Raman: $\tilde{\nu}$ = 1480, 1311, 1011, 741 cm^{-1}; **4**: IR: $\tilde{\nu}$ = 3050, 1603, 1492, 1450, 1327, 1237, 750, 726 cm^{-1}; Raman: $\tilde{\nu}$ = 1481, 1451, 1311, 1011, 742 cm^{-1}). The region between 1100 and 1400 cm^{-1} is well known to contain the bands of extended aromatic systems.[25] Other bands are shifted by about ten wavenumbers compared to the free ligand or show band splitting due to coordination to the metal centers (**1**: IR: $\tilde{\nu}$ = 1482, 1459, 1433, 1146, 912, 569, 430 cm^{-1}; **2**: IR: $\tilde{\nu}$ = 1481, 1458, 1430, 1148, 905, 749, 432 cm^{-1}; Raman: $\tilde{\nu}$ = 1620, 1570, 1248, 540, 310 cm^{-1}; **3**: IR: $\tilde{\nu}$ = 1456, 1426, 1139, 914, 564, 425 cm^{-1}; Raman: $\tilde{\nu}$ =

Table 1. Selected distances [pm] and angles [°] for $^1_\infty[Sm_2(Cbz)_5](Cbz-H)$ (**1**) and $[Tm_2(Cbz)_6]$ (**2**); estimated standard deviations are given in parentheses

$^1_\infty[Sm_2(Cbz)_5](Cbz-H)$ (**1**)			
Sm1−C[range C(25−30)[a]]	294(2)−338(2)	Sm1−N1	281.7(9)
Sm1−C[range C(43−47)[a]]	294(2)−320(2)	Sm2−N5	236(2)
Sm1−C[average C(25−30)[a]]	314(2)	Sm2−N3	239(1)
Sm1−C[average C(43−47)[a]]	308(2)	Sm2−N1	240.2(9)
Sm1−C12	300(2)	Sm2−N4	247(1)
Sm1−C24	294(2)	Sm2−N2	248.8(9)
Sm1−cent1[b]	275(2)	Sm1−Sm2	419.3(2)
Sm1−cent2[b]	274(2)	Sm1−Sm2[a]	577.6(2)
Sm1−N2	271.8(9)	N−C(range)	137(2)−143(2)
cent1−Sm1−cent2[b]	105	N1−Sm2−N3	114.0(4)
cent1−Sm1−N2[b]	105(1)	N1−Sm2−N4	105.9(4)
cent1−Sm1−N1[b]	142(1)	N2−Sm2−N3	99.2(4)
N1−Sm1−N2	67.7(3)	N2−Sm2−N5	128.7(8)
cent2−Sm1−N1[b]	102(1)	N2−Sm2−N4	175.4(4)
cent2−Sm1−N2[b]	138(1)	N3−Sm2−N4	81.6(4)
		N4−Sm2−N5	85.9(9)
$[Tm_2(Cbz)_6]$ (**2**)			
Tm−C[range C(31−36)]	274.9(4)−288.7(3)	Tm−N2	222.4(3)
Tm−C[average C(31−36)]	282.0(4)	Tm−N3	228.2(3)
Tm−cent3[b]	244.2(4)	Tm−Tm[c]	503.9(1)
Tm−N1	220.8(3)	N−C(range)	137.4(4)−141.1(5)
cent3−Tm−N3[b]	104.8(1)	N1−Tm−N2	108.1(1)
cent3−Tm−N2[b]	112.2(1)	N1−Tm−N3	90.0(1)
cent3−Tm−N1[b]	122.8(1)	N2−Tm−N3	117.4(1)

[a] $x, -y + 3/2, z - 1/2$. [b] cent1 = centroid of the phenyl rings with the C atoms C25 to C30; cent2 = centroid of the phenyl rings with the C atoms C43 to C47; cent3 = centroid of the phenyl rings with the C atoms C31 to C36. [c] $-x, y, -z + 3/2$.

 © 2004 Wiley-VCH Verlag GmbH & Co. KGaA, Weinheim

1625, 1573, 1260 cm^{-1}; **4**: IR: $\tilde{\nu}$ = 1471, 1448, 1430, 1426, 906, 750, 427 cm^{-1}; Raman: $\tilde{\nu}$ = 1624, 1570, 1261 cm^{-1}). A sharp ν(N−H) vibrational band[26] of CbzH in **1** can be observed at 3418 cm^{-1} and was confirmed by the MIR spectrum of the free ligand.[18] This band is only weak in the spectra of $[Ln_2(Cbz)_6]$ [Ln = Tm, Nd, Gd (**2**−**4**)], and here is due to excess carbazole only.

Although the formula of **1** differs by only one hydrogen atom from a formally trivalent compound like compounds **2**−**4**, the crystal structures of **1** and **2** are completely different from each other as well as from the carbazolates of divalent europium and ytterbium. Whilst the heteroleptic complexes $[Sm(Cbz)_2(THF)_4]$, $[Sm(Cbz)_2(N\text{-MeIm})_4]$[19] (N-MeIm = *N*-methylimidazole) and $[Eu(Cbz)_2(THF)_4]$[20] have monomeric structures due to solvent molecules saturating the coordination spheres, the homoleptic[27] rare-earth carbazolates exhibit larger building units in the crystal structures. Like the divalent compounds $^1_\infty[Ln_2(Cbz)_4]$ (Ln = Eu, Yb)[18] the crystal structure of $^1_\infty[Sm_2(Cbz)_5](CbzH)$ (**1**) consists of polymeric chains built of dimeric units with alternating Sm^{II} and Sm^{III} cations. Because of the mixed-valent character of **1** each dimeric unit contains 50% divalent and 50% trivalent samarium. The coordination spheres of Sm^{II} and Sm^{III} are very different so that the different valences can be clearly distinguished. The Sm^{II} atoms are surrounded by two nitrogen atoms and two η^6-coordinated π-systems resulting in a flattened tetrahedron. Distortion of the coordination polyhedron in $^1_\infty[Sm_2(Cbz)_5](CbzH)$ (**1**) can be seen in the deviations from the ideal value of 109.5° [centroid(1)−Sm^{II}−centroid(2): 105(1)°; N1−Sm^{II}−centroid(2): 102(1)°; N2−Sm^{II}−centroid(1): 105(1)°; N1−Sm^{II}−N2: 67.7(3)°]. The Sm^{II}−N distances are 271.8(9) and 281.7(9) pm, the differences being a result of asymmetric μ_2-bridging nitrogen atoms that link Sm^{II} to adjacent Sm^{III} atoms in the dimeric units. Such asymmetric bridges can also be found in $^1_\infty[Eu_2(Cbz)_4]$[18] or $[Yb_2(Cbz)_4(Phpip)_4](Phpip)_2$ (Phpip = phenylpiperazine).[28] The μ_2-coordination mode in **1** also explains the differences in Sm−N distances compared to $[Sm(Cbz)_2(THF)_4]$ and $[Sm(Cbz)_2(N\text{-MeIm})_4]$[19] with an average of 258 and 267 pm, respectively, or $\{[(CH_2)_5C(C_4H_3N)_2]Sm\}_4(THF)_2(N_2)[Na(THF)]_2{\cdot}2THF$ with 271−273 pm.[29] The distances from the Sm atoms to the π-systems of **1** are 274 pm on average (see Table 1 for detailed atom distances and bond angles of **1** and **2**). Although rarely observed, such η^6-phenyl π-interactions are known for the divalent homoleptic carbazolates[18] or for complexes like $[Me_2Si(C_5Me_4)(NPh)Yb(THF)_2]$[30] or the "ate" complex $[K(THF)_3]_2[Sm_2(C_{22}H_{28}N_4)_2](THF)_4$ ($C_{22}H_{28}N_4$ = TMTAT = tetramethyldibenzotetraaza[14]annulate)[10] The μ_2-bridging carbazolate ligands show a slight π-stacking towards the Sm^{II} center with relatively short Sm^{II}−C distances of 294(2) and 300(2) pm.

The Sm^{III} atoms are coordinated by five N atoms forming a distorted trigonal bipyramid. Two of the N atoms form μ_2 bridges to Sm^{II} centers, and two others belong to carbazolate ligands that coordinate in an η^6 fashion to another Sm^{II} center with one of their phenyl rings, thus forming the chain structure of **1**. The fifth nitrogen atom coordinated to Sm^{III} is not connected to any other samarium atom and is found in two disordered positions in the crystal structure. The Sm^{III}−N distances in $^1_\infty[Sm_2(Cbz)_5](CbzH)$ (**1**) range from 236(1) to 248.8(9) pm, the longer distances are located in the μ_2-bridges. Thus, **1** is similar to other trivalent Sm amides like $[(C_{11}H_{21}N_2)_2SmBr]$ ($C_{11}H_{21}N_2$ = 2-propylamino-4-propylimino-2-pentene) with Sm−N distances of 236−242 pm,[31] whilst homoleptic $[Sm(N\text{-MeIm})_8]I_3$ has longer Sm−N distances, averaging 260 pm, with the ligands having N-donor amine and not amide character.[31] The N−Sm^{III}−N angles in **1** are similar to those in an ideal trigonal bipyramid, with N1−Sm^{III}−N3 being 114.0(4)°, N2−Sm^{III}−N5 128.7(8)° and a stretched N2−Sm^{III}−N4 angle of 175.4(4)°. Figure 2 shows the dimeric building unit of **1** and the coordination spheres around Sm^{II} and Sm^{III}.

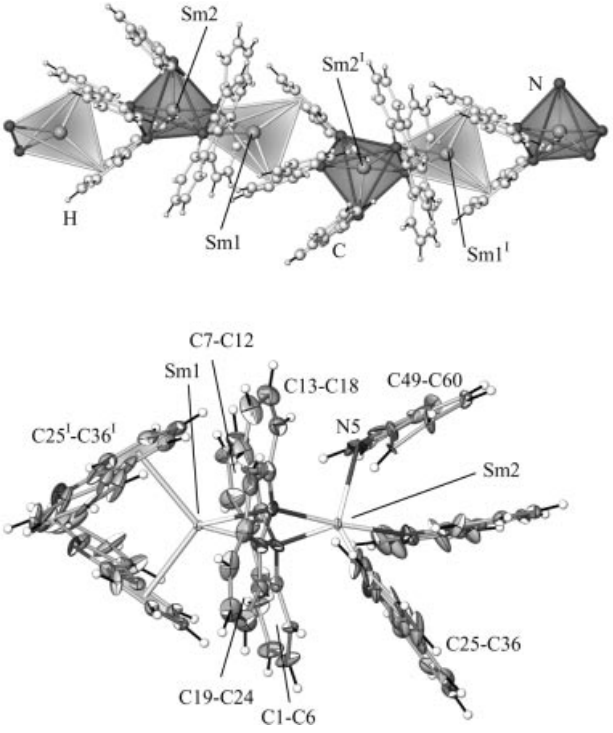

Figure 2. The coordination spheres around (top) and the dimeric building units of (bottom) divalent Sm1 and trivalent Sm2 in the chain structure of $^1_\infty[Sm_2(Cbz)_5](CbzH)$ (**1**); N−N connection lines mark only the coordination polyhedra and not bonds; π-interactions are marked by shaded planes and are represented by bonds towards centroids of the phenyl rings; the thermal ellipsoids here and in Figure 4 are scaled to a probability density of the atoms of 50%; symmetry operation: I: x, $-y + 3/2$, $z + 1/2$

The polymeric chains in the crystal structure of **1** leave tunnels between them, which are filled with carbazole molecules from the melt reaction. They are therefore not coordinated to the Sm centers and are released first in the thermal decomposition process. Figure 3 shows the crystal structure of $^1_\infty[Sm_2(Cbz)_5](CbzH)$ (**1**), including the chains

 © 2004 Wiley-VCH Verlag GmbH & Co. KGaA, Weinheim

and tunnels. The crystal structure of **1** is unique in amide chemistry.

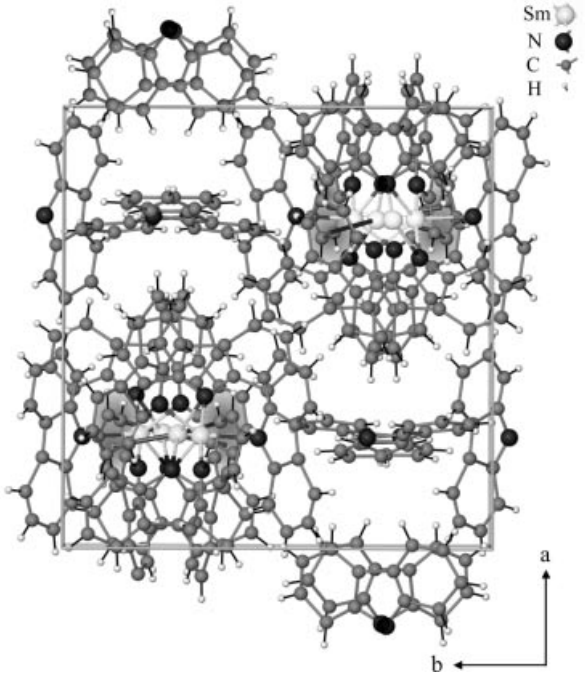

Figure 3. The crystal structure of $^{1}_{\infty}[Sm_2(Cbz)_5](CbzH)$ (**1**) with a view along the chain direction [00−1]; between the strands of $^{1}_{\infty}[Sm_2(Cbz)_5]$ run tunnels in which CbzH molecules are intercalated; η^6-interactions between Sm and phenyl rings are represented by bonds towards centroids and shaded rings

Despite the difference in stoichiometry, the dimeric building units of $[Tm_2(Cbz)_6]$ (**2**) resemble the divalent carbazolates $^{1}_{\infty}[Ln_2(Cbz)_4]$ (Ln = Eu, Yb).[18] Complex **2** also exhibits a tetrahedral coordination environment, with three nitrogen atoms and one η^6-coordinated phenyl ring. Contrary to the divalent carbazolates, however, the tetrahedra in the dimeric unit are not edge-connected by μ_2-bridging N atoms. With three carbazolate ligands coordinating each Tm atom, the linkage in the dimeric unit is formed by the N atoms of carbazolate ligands that use one of their phenyl rings to coordinate to the neighbouring Tm atom, similar to the coordination mode that forms the chains in $^{1}_{\infty}[Ln_2(Cbz)_4]$ (Ln = Eu, Yb)[18] as well as in **1**. As all the other carbazolate ligands in **2** do not connect further, Tm^{III} has a low coordination number of six and shows only dimers and no chains in the crystal structure. The dimeric units and coordination spheres around Tm^{III} in **2** are shown in Figure 4, while Figure 5 gives a view of the packing of the dimers in the crystal structure of **2**. The $Tm^{III}-N$ distances range from 220.8(3) to 228.2(3) pm, with the longest distance being found for the linking carbazolate ligands. These distances are in the region expected for the ionic radius of Tm^{III},[33] but shorter than in $[(Et_2C(C_4H_3N)_2]_3Tm][K(Tol)]_3$ (233−239 pm) or [(Et$_8$-calix[4]tetrapyrrole)Tm][K(DME)] [236−238 pm for the $Tm^{III}-N$(amide) bonds].[34] The Tm−centroid(3)distance to the π-coordinated phenyl rings in **2** is 244.2(4) pm, with Tm−π(C) bond lengths of 274.9(4)−288.7(3) ppm. The best comparable example to the η^6-phenyl−Tm interactions is found in $[Tm(DME)_2(\eta^2\text{-}C_{10}H_8)_2(\mu_2\text{-}\eta^4\text{:}\eta^4\text{-}C_{10}H_8)]$ with a Tm−π(C) distance of only 259−262 pm.[35] The coordination tetrahedron around Tm in **2** is more regular than in **1** [N1−Tm^{III}−N2: 108.1(1)°; N1−Tm−centroid(3): 122.8(1)°; N2−Tm−centroid(3): 112.2(1)°; see Table 1 for detailed atom distances and bond angles of **1** and **2**].

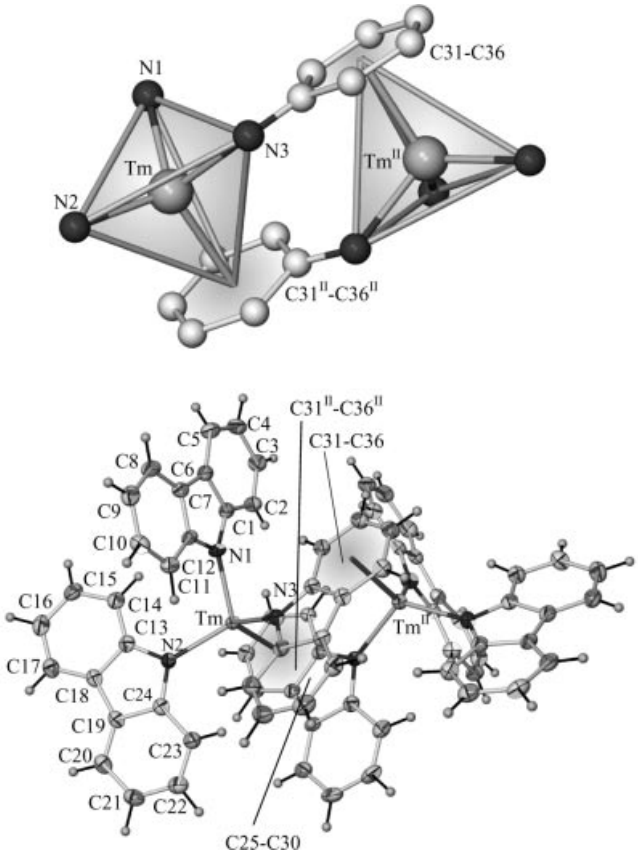

Figure 4. The coordination tetrahedra around Tm atoms (top) and the dimeric building units of $[Tm_2(Cbz)_6]$ (**2**, bottom); N−N connection lines mark only the coordination polyhedra and not bonds; π-interactions are marked by shaded planes and are represented by bonds towards centroids of the phenyl rings; symmetry operation: II: $-x, y, -z + 3/2$

The X-ray powder diffraction spectrum of $[Gd_2(Cbz)_6]$ (**4**) shows that the compound is isotypic to $[Tm_2(Cbz)_6]$ (**2**). Thus, the description of the crystal structure in the space group *Pbcn* is analogous to that of **2**. Because of the larger ionic radius of Gd^{III} compared to Tm^{III},[33] the unit cell is about 300×10^6 pm^3 larger than in **2**. $[Nd_2(Cbz)_6]$ (**3**) is not isotypic to **2**. The powder diffractogram of **3** can be indexed to give an orthorhombic cell of about half the size of the unit cell of **2**, with no unindexed lines. The large difference in the ionic radii of Nd^{III} and Tm^{III} is responsible for a different unit cell and thereby a different crystal structure. Considering this difference a tripled unit cell of **3** shows a volume increase of about 300×10^6 pm^3 compared to Gd^{III} in **4** or 600×10^6 pm^3 compared to Tm^{III} in **2**, and therefore is in good accordance with the radii increase throughout the series of rare-earth elements. Though the

 © 2004 Wiley-VCH Verlag GmbH & Co. KGaA, Weinheim

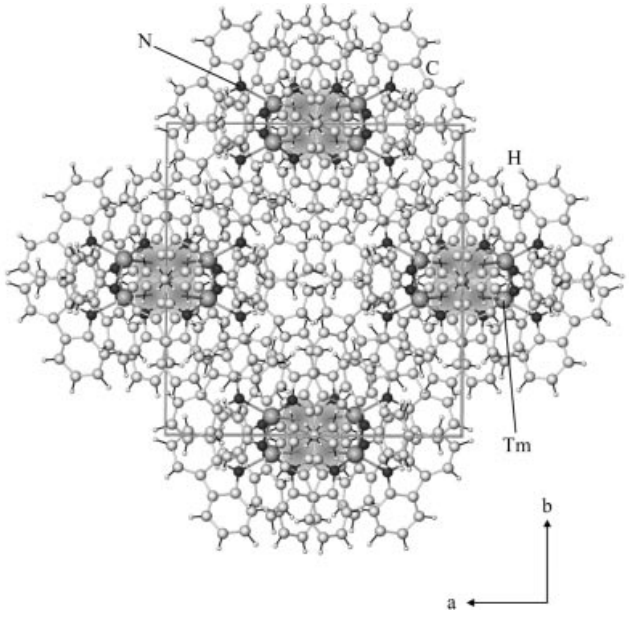

Figure 5. The crystal structure of $[Tm_2(Cbz)_6]$ (**2**) with a view of the unit cell along [001]; without further interaction between the dimeric units, the structure is a packing of dimers; η^6-interactions between Tm and phenyl rings are represented by bonds towards centroids and shaded rings

structure of **2** and **4** makes it likely that **3** also forms dimeric units, this remains unproven. Together with the results of microanalyses and the MIR and FIR spectra, the powder diffraction investigations of **3** and **4** confirm the trivalent character of neodymium and gadolinium as well as the absence of uncoordinated carbazole molecules in the structures.

Conclusions

The formation of **1**−**4** shows the possibility of obtaining homoleptic amides of the rare-earth elements that is an inherent feature of solvent-free melt synthesis methods. In the absence of any coordinating solvent the carbazolate ligands have no option but to completely saturate the coordination sphere around the large rare-earth ions. The results are structures that are unique in rare-earth amide chemistry and depend on additional η^6-π interactions as well as normal σ-N bonds. The course of the redox potentials from $E_{Eu^{II/III}} = 0.35$ V to $E_{Sm^{II/III}} = 1.57$ V and $E_{Tm^{II/III}} = 2.27$ V, $E_{Nd^{II/III}} = 2.62$ V up to $E_{Gd^{II/III}} = 3.9$ V[21,22] reflects the valences of the homoleptic carbazolates. Whilst divalent Eu and Yb compounds can be obtained,[18] Sm is mixed-valent in **1** with alternating Sm^{II} and Sm^{III}. Tm already gives pure trivalent **2**. Accordingly, all other rare-earth elements with redox potentials higher than Tm can also be expected to give trivalent compounds, as is shown by the neodymium and gadolinium carbazolates **3** and **4**. Due to the different stoichiometries, divalent, mixed-valent and trivalent homoleptic carbazolates, although having some common structural elements, have completely different crystal structures. Additional analytic methods like IR and Raman spectroscopy or thermal analysis support the results of the X-ray crystal-structure determinations.

Experimental Section

General: All reactions were carried out under argon using standard dry-box and Schlenk techniques due to the air and moisture sensitivity of **1**−**4**. Samarium, thulium, gadolinium (ChemPur), neodymium (STREM) and carbazole (Aldrich) were used as purchased. The IR spectra were recorded using a Bruker FTIR-IS66V-S spectrometer, and the Raman spectra using a Bruker FRA 106-S spectrometer. Probably because of its dark colour, **1** gave no Raman spectrum. KBr pellets were used for MIR investigations and PE pellets for FIR investigations, both under vacuum. The thermal decomposition of **1** was studied using simultaneous DTA/TG (NETZSCH STA-409). A 16.9 mg sample of the bulk of the Sm reaction was heated from 20 °C to 700 °C at a heating rate of 10 °C/min in a constant Ar flow of 60 mL/min. The thermal decomposition of **2** was studied on 17.0 mg of the bulk of the Tm reaction from 20 °C to 700 °C at a heating rate of 10 °C/min in a constant Ar flow of 60 mL/min. The thermal decomposition of **3** was studied on 38.8 mg of the bulk of the Nd reaction, and the thermal decomposition of **4** was studied on 24.3 mg of the bulk of the Gd reaction under analogous conditions to the investigations for **1** and **2**.

$^1_\infty[Sm_2(Cbz)_5](CbzH)$ (1): Samarium metal (150 mg, 1×10^{-3} mol) and carbazole (CbzH, $C_{12}H_8NH$; 501 mg, 3×10^{-3} mol) were sealed in an evacuated Duran glass ampoule. The reaction mixture was heated to 220 °C over 4 h and then to 265 °C in another 7 h. This temperature was maintained for 190 h. The melt was cooled to 200 °C over 70 h and then to room temperature over 24 h. Except for the excess of Sm metal and CbzH the reaction was complete giving a mixture of dark red to black microcrystals and black to dark red rod-shaped crystals of $^1_\infty[Sm_2(Cbz)_5](CbzH)$ with a length of 0.3 to 0.8 mm. Yield: 580 mg (89%). MIR: $\tilde{\nu}$ = 3418 s, 3049 m, 1615 m, 1603 m, 1585 m, 1580 msh, 1493 m, 1482 m, 1459 s, 1450s, 1433 s, 1336 s, 1326 m, 1288 m, 1273 s, 1262 ssh, 1236 m, 1146 m, 1118 m, 1106 m, 997 m, 927 m, 884 m, 844 m, 750 vs, 725 vs, 664 w, 569 w cm^{-1}. FIR: $\tilde{\nu}$ = 522 w, 508 w, 430 m, 424 m, 305 w, 231 m, 171 m, 146 w, 123 w, 108 w cm^{-1}. $C_{72}H_{49}N_6Sm_2$ (1298.9): calcd. C 66.63, H 3.78, N 6.48; found C 66.22, H 3.75, N 6.62.

$[Tm_2(Cbz)_6]$ (2): Thulium metal (85 mg, 5×10^{-4} mol), carbazole (334 mg, 2×10^{-3} mol) and Hg (0.2 g) were sealed in an evacuated Duran glass ampoule. The reaction mixture was heated to 240 °C over 4 h and then to 280 °C over another 3 h. This temperature was maintanied for 168 h. The melt was then cooled to 210 °C over 200 h and then to room temperature over 72 h. Except for a slight excess of Tm metal and CbzH, the reaction was complete, giving an orange crystalline bulk of crystals of $[Tm_2(Cbz)_6]$ with a length of 0.2 to 0.5 mm. Yield: 313 mg (94%). MIR: $\tilde{\nu}$ = 3419 w, 3049 m, 1618 w, 1602 m, 1493 m, 1458 ssh, 1450 vs, 1430 m, 1327 s, 1288 w, 1271 w, 1239 s, 1207 m, 1148 w, 1108 w, 1025 w, 1015 w, 932 m, 905 m, 848 w, 749 vs, 726 vs, 574 m cm^{-1}. FIR: $\tilde{\nu}$ = 432 m, 420 m, 343 w, 309 w, 251 m, 188 vw, 158 w, 143 w, 86 w cm^{-1}. Raman: $\tilde{\nu}$ = 3054 s, 1620 s, 1588 w, 1570 s, 1565 ssh, 1480 m, 1316 m, 1271 m, 1248 m, 1015 m, 744 m, 680 m, 310 w, 251 s, 200 w, 170 w, 157 w, 91 vs cm^{-1}. $C_{72}H_{48}N_6Tm_2$ (1335.1): calcd. C 64.77, H 3.62, N 6.29; found C 63.93, H 3.77, N 6.07.

$[Nd_2(Cbz)_6]$ (3): Neodymium metal (144 mg, 1×10^{-3} mol), carbazole (1032 mg, 6×10^{-3} mol) and Hg (0.2 g) were sealed in an

 © 2004 Wiley-VCH Verlag GmbH & Co. KGaA, Weinheim

evacuated Duran glass ampoule. The reaction mixture was heated to 230 °C over 8 h and then to 280 °C over another 5 h. The melt was cooled to 245 °C over 350 h and this temperature maintained for 168 h. The reaction mixture was then cooled to 210 °C over another 350 h and to room temperature over 72 h. Except for the excess CbzH, the reaction gave a golden yellow bulk of $[Nd_2(Cbz)_6]$. Yield: 548 mg (85%). MIR: $\tilde{\nu}$ = 3419 w, 3049 m, 1625 w, 1601 m, 1493 m, 1456 ssh, 1450 vs, 1426 w, 1394 w, 1336 m, 1327 s, 1286 w, 1238 s, 1205 w, 1138 w, 1106 w, 1009 w, 996 w, 928 m, 914 w, 857 w, 842 w, 748 vs, 725 vs, 574 s, 564 ssh cm^{-1}. FIR: $\tilde{\nu}$ = 440 m, 425 m, 352 w, 221 m, 145 m, 123 m, 102 w, 70 w cm^{-1}. Raman: $\tilde{\nu}$ = 3056 s, 1625 s, 1573 s, 1480 w, 1311 s, 1311 s, 1289 s, 1260 w, 1011 s, 741 m, 430 m, 280 m, 230 m, 104 s cm^{-1}. $C_{72}H_{48}N_6Nd_2$ (1291.1): calcd. C 66.98, H 3.72, N 6.51; found C 66.37, H 3.96, N 6.47.

$[Gd_2(Cbz)_6]$ (4): Gadolinium metal (157 mg, 1×10^{-3} mol), carbazole (668 mg, 4×10^{-3} mol) and Hg (0.2 g) were sealed in an evacuated Duran glass ampoule. The reaction mixture was heated to 200 °C over 6 h and to 280 °C over another 8 h for activation. The melt was cooled to 245 °C over 4 h and the temperature maintained for 336 h. The reaction mixture was then cooled to 210 °C over another 180 h and then to room temperature over 24 h. Except for the excess of CbzH the reaction gave a poorly crystalline dark yellow bulk of $[Gd_2(Cbz)_6]$. Yield: 526 mg (80%). MIR: $\tilde{\nu}$ = 3417 w, 3050 m, 1603 s, 1581 m, 1492 s, 1471 ssh, 1450 vs, 1426 m, 1407 s, 1325 vs, 1263 w, 1237 vs, 1207 msh, 1149 w, 1118 w, 1025 w, 1015 w, 930 w, 906 w, 750 vs, 726 vs, 569 m cm^{-1}. FIR: $\tilde{\nu}$ = 444 w, 430 m, 420 m, 363 w, 243 m, 231 wsh, 159 m, 148 wsh, 72 w cm^{-1}. Raman: $\tilde{\nu}$ = 3055 s, 1624 s, 1570 s, 1481 m, 1311 s, 1288 m, 1261 m, 1011 s, 742 m, 429 m, 297 m, 258 m, 240 w, 101 s cm^{-1}. $C_{72}H_{48}N_6Gd_2$ (1317.1): calcd. C 65.65, H 3.64, N 6.38; found C 65.74, H 3.70, N 6.39.

X-ray Crystal-Structure Determination: The data collection for single-crystal X-ray determinations of **1** and **2** were carried out with an IPDS-II diffractometer (STOE). Structure solutions: SHELXS-86;[36] structure refinements: SHELXL-97.[37] Integrity of symmetry and geometry: PLATON.[38] All non-hydrogen atoms were refined anisotropically. The hydrogen atoms of **2** were found in the Fourier map while the hydrogen atoms of **1** were placed in calculated positions and assigned to an isotropic displacement parameter of 1.2-times the size of the isotropic displacement parameter of the parent carbon atom. The nonlinking Cbz anion of **1** is disordered over two positions in a ratio of about 1:1. The crystal of **1** used for data collection shows another small crystalline individual grown on the surface (RECIPE).[39] The two individuals were separated (TWIN)[39] and refined individually. Compounds **3** and **4** were investigated on powder samples in sealed capillaries with a STOE STADI P transmission diffractometer (Cu-$K_{\alpha 1}$ radiation λ = 1.540598 Å, focussed single crystal germanium monochromator). Because **3** and **4** lose their crystallinity upon grinding, samples of both compounds had to be made only roughly homogeneous. Both were investigated in 0.5 mm capillaries, though this led to a higher background due to absorption phenomena of the rare-earth atoms. The diffraction patterns of the neodymium (**3**) and the gadolinium (**4**) compounds were compared with simulated diffractograms of **1** and **2** as well as the divalent europium and ytterbium carbazolates.[18] The cell constants of **3** were refined on 11 reflections with the best possible resolution leading to an orthorhombic unit cell without un-indexed lines and an average $\delta(2\Theta)$ of 0.018° [T = 293(2) K, a = 1899(2) pm, b = 1118.5(9), c = 920(1) pm, V = 1953.5(26) 10^6 pm^3]. The cell constants of **4** were refined on 23 reflections with the best possible resolution without un-indexed lines and an average $\delta(2\Theta)$ of 0.016° [T = 293(2) K, a = 1723(1) pm, b = 1888(1), c = 1710.5(9) pm, V = 5569.7(32) 10^6 pm^3], indicating that $[Gd_2(Cbz)_6]$ is isotypic with $[Tm_2(Cbz)_6]$ (**2**).[40] Crystallographic data for $C_{72}H_{49}N_6Sm_2$ (**1**): Monoclinic, $P2_1/c$, Z = 4, T = 170(1) K, a = 1835.3(2), b = 1657.0(2), c = 1937.9(2) pm, β = 112.138(8)°, V = 5458.8(1)·10^6 pm^3, μ = 21.8 cm^{-1} (Mo-K_α), 3.34° ≤ 2θ ≤ 50.0°, −21 ≤ h ≤ 20, −19 ≤ k ≤ 19, 0 ≤ l ≤ 23, F(000) = 2584, R_1 = 0.0745 for 4644 reflections [$I > 2\sigma(I)$], R_1 = 0.1288 and wR_2 = 0.1208 for all 9545 unique reflections, GOOF on F^2 = 0.886. Crystallographic Data for $C_{72}H_{48}N_6Tm_2$ (**2**): Orthorhombic, $Pbcn$, Z = 4, T = 170(1) K, a = 1712.2(2) pm, b = 1802.5(2) pm, c = 1699.7(2) pm, V = 5245.9(9)·10^6 pm^3, μ = 34.1 cm^{-1} (Mo-K_α), 3.28° ≤ 2θ ≤ 54.64°, −21 ≤ h ≤ 21, −23 ≤ k ≤ 23, −18 ≤ l ≤ 21, F(000) = 2640, R_1 = 0.0249 for 4147 reflections [$I > 2\sigma(I)$], R_1 = 0.0430 and wR_2 = 0.0581 for all 5831 unique reflections, GOOF on F^2 = 0.926. CCDC-220967 (**1**) and -241797 (**2**) contain the supplementary crystallographic data for this paper. These data can be obtained free of charge at www.ccdc.cam.ac.uk/conts/retrieving.html [or from the Cambridge Crystallographic Data Centre, 12 Union Road, Cambridge CB2 1EZ, UK; Fax: + 44 1223-336-033; E-mail: deposit@ccdc.cam.ac.uk].

Acknowledgments

We are grateful to the Fonds der Chemischen Industrie and Prof. Dr. Gerd Meyer for financial support.

[1] G. Wilkinson, J. M. Birmingham, *J. Am. Chem. Soc.* **1954**, *76*, 6210.
[2] R. G. Hayes, J. L. Thomas, *J. Am. Chem. Soc.* **1969**, *91*, 6876.
[3] H. Schumann, *Angew. Chem.* **1984**, *96*, 475−493; *Angew. Chem. Int. Ed. Engl.* **1984**, *23*, 474−492.
[4] R. Kempe, *Angew. Chem.* **2000**, *112*, 478−504; *Angew. Chem. Int. Ed.* **2000**, *39*, 468−494.
[5] H. Schumann, J. A. Meese-Marktscheffel, L. Esser, *Chem. Rev.* **1995**, *95*, 865−986.
[6] S. Arndt, J. Okuda, *Chem. Rev.* **2002**, *102*, 1953−1976.
[7] W. J. Evans, B. L. Davis, *Chem. Rev.* **2002**, *102*, 2119−2136.
[8] Cambridge Crystallographic Data Centre, CCDC, 12 Union Road, Cambridge CB2 1EZ, Great Britain.
[9] A. de Cian, M. Moussavi, J. Fischer, R. Weiss, *Inorg. Chem.* **1985**, *24*, 3162.
[10] J. Magull, A. Simon, *Z. Anorg. Allg. Chem.* **1992**, *618*, 81−86.
[11] R. Kempe, H. Noss, T. Irrgang, *J. Organomet. Chem.* **2002**, *647*, 12−20.
[12] G. B. Deacon, A. Gitlits, B. W. Skelton, A. H. White, *Chem. Commun.* **1999**, 1213−1214.
[13] G. B. Deacon, A. Gitlits, P. W. Roesky, M. R. Bürgstein, K. C. Lim, B. W. Skelton, A. H. White, *Chem. Eur. J.* **2001**, *7*, 127−138.
[14] K. Müller-Buschbaum, *Z. Anorg. Allg. Chem.* **2002**, *628*, 2731−2737.
[15] K. Müller-Buschbaum, C. C. Quitmann, *Inorg. Chem.* **2003**, *42*, 2742−2750.
[16] K. Müller-Buschbaum, *Z. Anorg. Allg. Chem.* **2003**, *629*, 2127−3132.
[17] K. Müller-Buschbaum, C. C. Quitmann, *Z. Anorg. Allg. Chem.* **2004**, *630*, 131−136.
[18] K. Müller-Buschbaum, C. C. Quitmann, *Z. Anorg. Allg. Chem.* **2003**, *629*, 1610−1616.
[19] W. J. Evans, G. W. Rabe, J. W. Ziller, *Organometallics* **1994**, *13*, 1641−1645.
[20] G. B. Deacon, C. M. Forsyth, B. M. Gatehouse, P. A. White, *Aust. J. Chem.* **1990**, *43*, 795−806.
[21] L. R. Morss, *Chem. Rev.* **1976**, *76*, 827−841.
[22] G. Meyer, *Chem. Rev.* **1988**, *88*, 93−107.
[23] W. F. Hemminger, H. K. Cammenga, *Methoden der Thermischen Analyse*, Springer Verlag, **1989**.

 © 2004 Wiley-VCH Verlag GmbH & Co. KGaA, Weinheim

[24] G. Ostendorp, H. W. Rotter, H. Homborg, *Z. Anorg. Allg. Chem.* **1996**, *622*, 235−244.
[25] B. Schrader, *Raman/Infrared Atlas of Organic Compounds*, 2nd ed., Wiley-VCH, Weinheim, **1989**.
[26] J. Weidlein, U. Müller, K. Dehnicke, *Schwingungsfrequenzen II, Nebengruppenelemente*, Georg Thieme Verlag, Stuttgart, **1986**.
[27] P. C. Davidson, M. F. Lappert, R. Pearce, *Acc. Chem. Res.* **1974**, *7*, 209−217.
[28] C. C. Quitmann, K. Müller-Buschbaum, *Z. Anorg. Allg. Chem.* **2004**, *630*, in press.
[29] T. Dube, M. Ganesan, S. Conoci, S. Gambarotta, G. P. A. Yap, *Organometallics* **2000**, *19*, 3716−3721.
[30] Z. Hou, T. Koizumi, M. Nishiura, Y. Wakatsuki, *Organometallics* **2001**, *20*, 3323−3328.
[31] W. J. Evans, G. W. Rabe, J. W. Ziller, *Inorg. Chem.* **1994**, *33*, 3072−3078.
[32] D. Drees, J. Magull, *Z. Anorg. Allg. Chem.* **1995**, *621*, 948−952.
[33] R. D. Shannon, *Acta Crystallogr., Sect. A* **1976**, *32*, 751−767.
[34] I. Korobkov, G. Aharonian, S. Gambarotta, G. P. A. Yap, *Organometallics* **2002**, *21*, 4899−4901.
[35] M. N. Bochkarev, I. L. Fedushkin, A. A. Fagin, H. Schumann, J. Demtschuk, *Chem. Commun.* **1997**, 1783−1784.
[36] G. M. Sheldrick, *SHELXS-86, Program for the resolution of crystal structures*, Göttingen, **1986**.
[37] G. M. Sheldrick, *SHELXL-97, Program for the refinement of crystal structures*, Göttingen, **1997**.
[38] A. L. Spek, *PLATON-99, A Multipurpose Crystallographic Tool*, Utrecht, **1999**.
[39] *STOE Software Package*, version 1.16, *RECIPE, Program for the identification of crystalline individuals* and *TWIN, Program for the separation of crystalline individuals*, Wiesbaden, **2001**.
[40] *STOE WINXPOW, Program package for the operation of powder diffractometers and analysis of powder diffractograms*, version 1.04, Darmstadt, **1999**.

Received June 15, 2004
Early View Article
Published Online August 26, 2004

 © 2004 Wiley-VCH Verlag GmbH & Co. KGaA, Weinheim

EurJIC
European Journal of Inorganic Chemistry

Issue 22/2004

Pages 4339–4532

Papers available ahead of print in Early View at www.interscience.wiley.com

Earliest available Table of Contents:
Automatically, free of charge by e-mail through
www.interscience.wiley.com/alerts

COVER PICTURE

The cover picture shows the reaction pathways available to $Ru_3(CO)_{10}$(dppe) in the catalytic hydrogenation of diphyenylacetylene, as elucidated by parahydrogen-assised NMR spectroscopy. The cluster leads to catalytic hydrogenation via a detected vinyl hydride intermediate, but fragments in low polarity solvents. Details are discussed in the article by S. B. Duckett et al. on p. 4381ff. We thank Universities UK (ORS award), Bruker Biospin UK and The University of York for financial support.

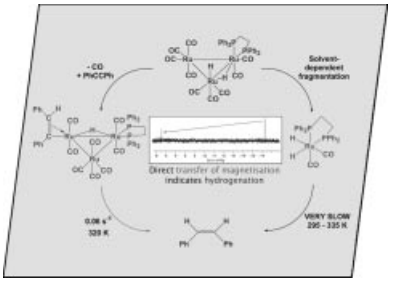

MICROREVIEW

Contents

4353 **A. Bousseksou,* G. Molnár, G. Matouzenko**

Switching of Molecular Spin States in Inorganic Complexes by Temperature, Pressure, Magnetic Field and Light: Towards Molecular Devices

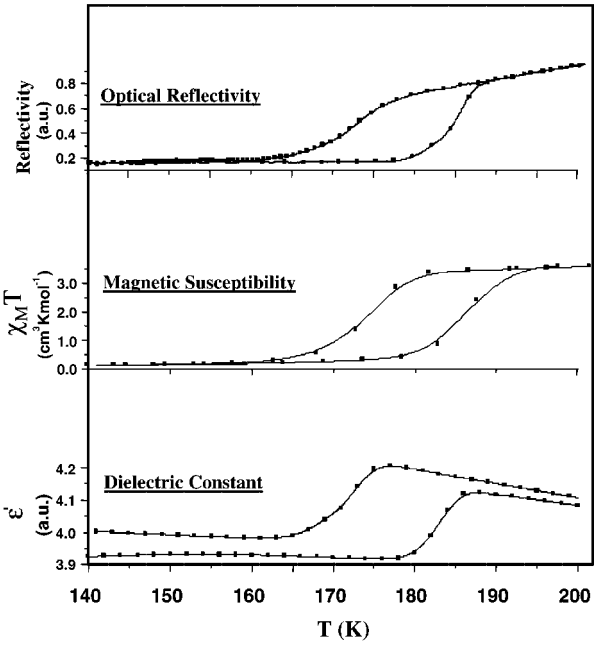

Keywords: Spin crossover / Metastability / Hysteresis loop / Pressure / Magnetic field / Dielectric properties / Ising-like model

 © 2004 Wiley-VCH Verlag GmbH & Co. KGaA, Weinheim

Short Communications

4371 **U. Darbost, X. Zeng, M.-N. Rager, M. Giorgi, I. Jabin,* O. Reinaud***

X-ray and Solution Structures of the First Zn Funnel Complex Based on a Calix[6]azacryptand

Keywords: Calixarenes / Cryptands / Host-guest systems / Supramolecular chemistry / Zinc

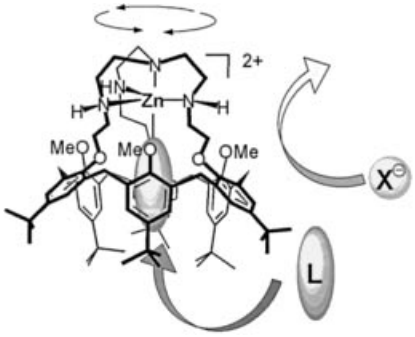

4375 **F.-T. Xie, L.-M. Duan, J.-Q. Xu,* L. Ye, Y.-B. Liu, X.-X. Hu, J.-F. Song**

Solvothermal Syntheses and Structural Characterisation of Three Isostructural 3D Metal-Malate Coordination Polymers: $\{[M(C_4H_4O_5)(H_2O)]\cdot H_2O\}_n$ (M = Co^{II}, Ni^{II}, Co^{II}/Ni^{II})

Keywords: Malate bridges / Solvothermal synthesis / Coordination polymer / Quinque-dentate ligand

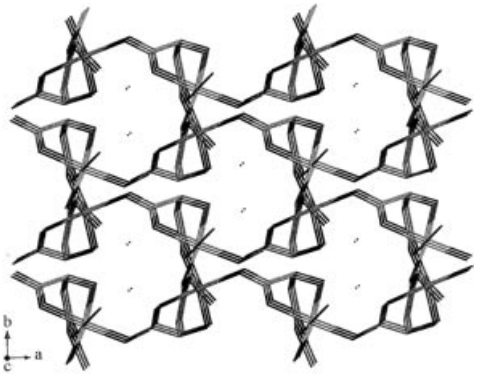

Full Papers

4381 **T. G. Prestwich, D. Blazina, S. B. Duckett,* P. J. Dyson**

A Parahydrogen Study of Catalytic Hydrogenation by Diphosphane-Substituted Triruthenium Clusters

Keywords: Homogeneous catalysis / Cluster compounds / NMR spectroscopy / Parahydrogen / Ruthenium

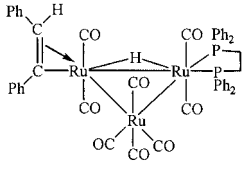

Active catalyst

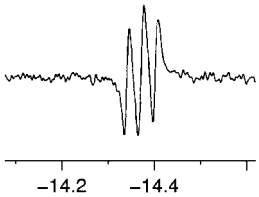

4388 **K. K. Pandey,* G. Frenking***

The Nature of the M≡E Bond: Theoretical Investigation of the Molecules $[(RO)_3M{\equiv}E]$ (M = Mo, W; E = N, P, As, Sb, Bi; R = H, Me) and $[(Me_3CO)_3Mo{\equiv}P]$

Keywords: Nitrido complexes / Bonding analysis / Density functional calculations / Metal−ligand triple bond / Pnicogens

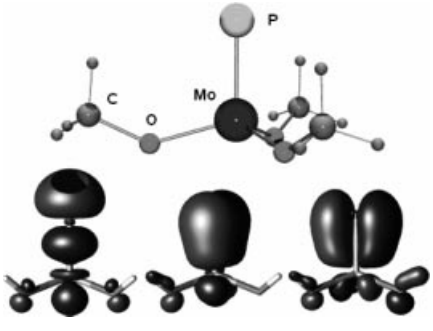

4396 **A. A. Trifonov,* E. A. Fedorova, G. K. Fukin, M. N. Bochkarev**

Post-Metallocene Hydridolanthanide Chemistry: $[Lu\{(Me_3Si)_2NC(NiPr)_2\}_2(\mu\text{-}H)]_2$ – A Novel Lanthanide Hydride in a Non-Cyclopentadienyl Coordination Environment; Synthesis, Structure and Catalytic Activity in Olefin Polymerization

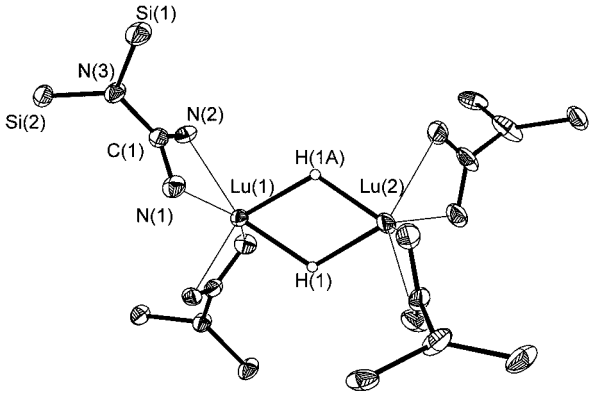

Keywords: Alkyl complexes / Homogeneous catalysis / Hydride ligands / Lanthanides / N ligands

4402 **J. Hausmann, S. Käss, S. Klod, E. Kleinpeter, B. Kersting***

Binucleating Aza-Sulfonate and Aza-Sulfinate Macrocycles – Synthesis and Coordination Chemistry

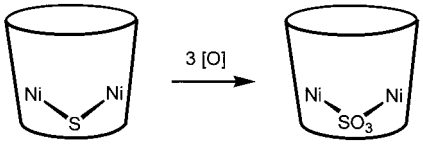

Keywords: Cavitands / Macrocyclic ligands / Nickel / S ligands

4412 **E. Budzisz,* B. K. Keppler, G. Giester, M. Wozniczka, A. Kufelnicki, B. Nawrot**

Synthesis, Crystal Structure and Biological Characterization of a Novel Palladium(II) Complex with a Coumarin-Derived Ligand

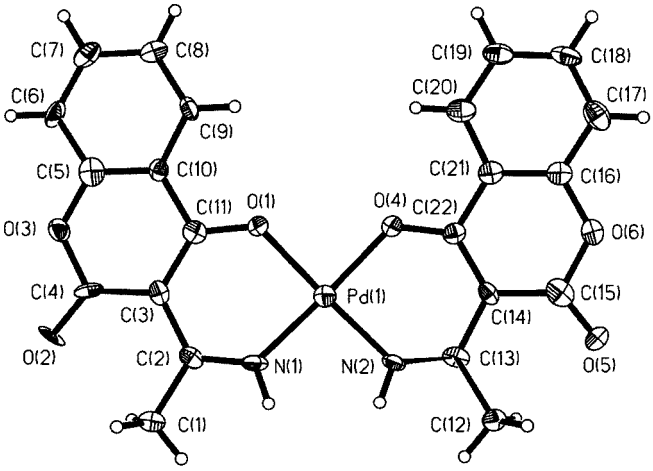

Keywords: Circular dichroism / Cytotoxicity / DNA / Palladium / Protonation constants

4420 **É. Fournier, A. Decken, P. D. Harvey***

Small Metal-Containing Oligomers Using $M_2(dmpm)_x$ and $M_2(dmb)_y$ Luminescent Building Blocks (M = Cu, Ag; x = 2, 3; y = 1, 2)

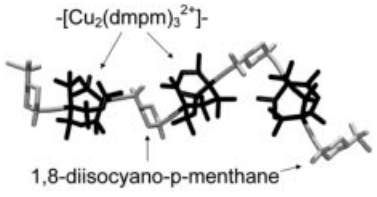

Keywords: Coordination polymers / Oligomers / Silver / Copper / Luminescence

4430 **G. Aullón,* S. Alvarez**

Formation of Sulfur–Sulfur Bonds in Copper Complexes

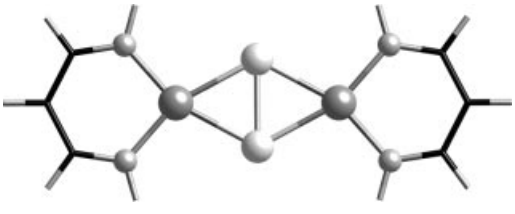

Keywords: Copper-sulfur complexes / Ligand–ligand bonds / Density functional calculations / Through-ring bonding / Electronic structure

 © 2004 Wiley-VCH Verlag GmbH & Co. KGaA, Weinheim

4439 V. Passarelli,* P. Zanella

Unsymmetrically Substituted Dimethyldiaminosilanes as Ligands towards Zirconium(IV)

Keywords: Zirconium / N ligands / Chelates / Silicon

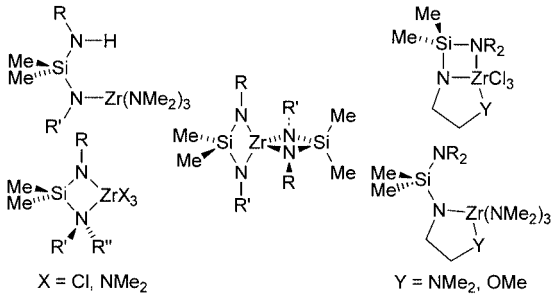

4447 Q.-X. Li, Q.-H. Luo,* Y.-Z. Li,* Z.-Q. Pan, M.-C. Shen

Studies on Manganese(II) Complexes of *N*-Benzimidazole-Functionalized 1,4,7-Triazacyclononane: Crystal Structures, Properties and Combined Superoxide Dismutase and Catalase Functions

Keywords: Enzyme models / Manganese / N ligands / Superoxide dismutase

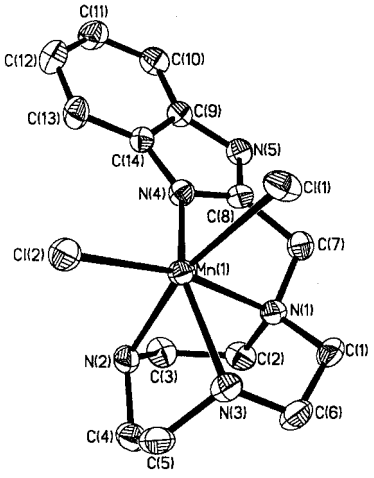

4457 Y. Xu, L. Han, Z.-Z. Lin, C.-P. Liu, D.-Q. Yuan, Y.-F. Zhou, M.-C. Hong*

Oxidation-State and Coordination-Site Specificity Influencing Dimensional Extension and Properties of Two Iron Complexes with Similar Helical Chains

Keywords: Iron / Helical chains / Coordination polymer / Oxidation state

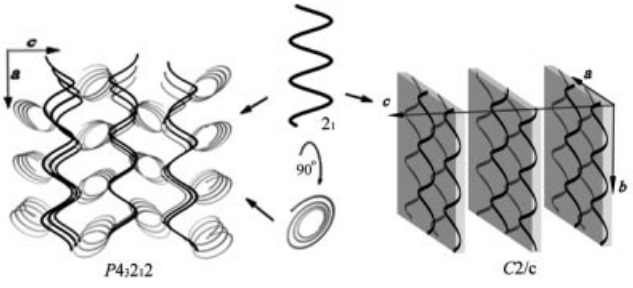

4463 T. Tsukuda, M. Ogita, T. Suzuki, S. Kaizaki*

Anomalous Diamagnetic Behaviour of the ^{1}H NMR Spectra of a Coordinated Imino Nitroxide Radical in Diamagnetic and Paramagnetic Lanthanide(III) Complexes

Keywords: ^{1}H NMR / Imino nitroxide radical / Lanthanide complexes / LIS analysis / Diamagnetic NMR behaviour

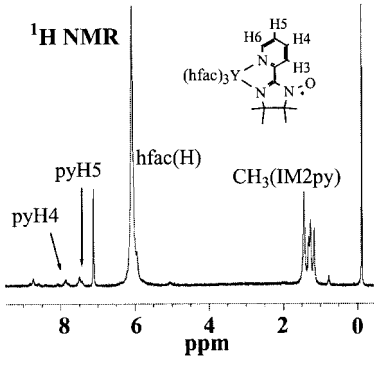

 © 2004 Wiley-VCH Verlag GmbH & Co. KGaA, Weinheim

4470 **C. J. Carmalt,* E. S. Peters, I. P. Parkin, T. D. Manning, A. L. Hector**

Chemical Vapor Deposition of Niobium Disulfide Thin Films

Keywords: Niobium disulfide / Thin films / Chemical vapor deposition

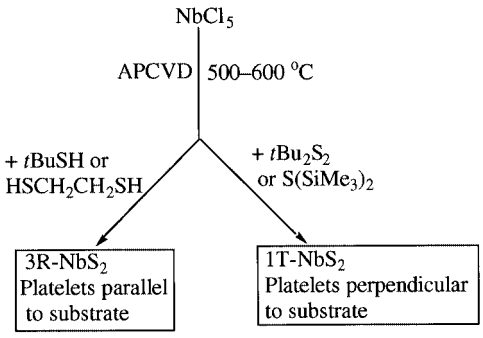

4477 **C. Crestini,* A. Pastorini, P. Tagliatesta**

The Immobilized Porphyrin-Mediator System Mn(TMePyP)/clay/HBT (clay-PMS): A Lignin Peroxidase Biomimetic Catalyst in the Oxidation of Lignin and Lignin Model Compounds

Keywords: Clays / Lignin models / Oxidation / Porphyrins / Supported catalysts

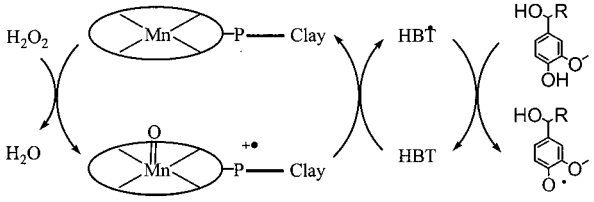

4484 **A. Zucca,* M. A. Cinellu, G. Minghetti, S. Stoccoro, M. Manassero***

Dinuclear, Tricyclometallated Platinum(II) Derivatives − Substitution Reactions and Reactivity of the Platinum−Carbon Bonds

Keywords: Cyclometallated compounds / N ligands / Platinum / X-ray diffraction

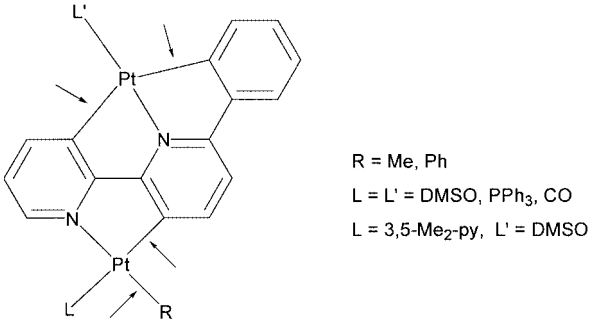

4491 **M. C. Barral, R. González-Prieto, R. Jiménez-Aparicio,* J. L. Priego, M. R. Torres, F. A. Urbanos**

Synthesis, Properties, and Structural Characterization of Bromo- and Iodotetracarboxylatodiruthenium(II,III) Compounds

Keywords: Carboxylate ligands / Metal-metal interactions / Multiple bonds / Ruthenium / Solvatochromism

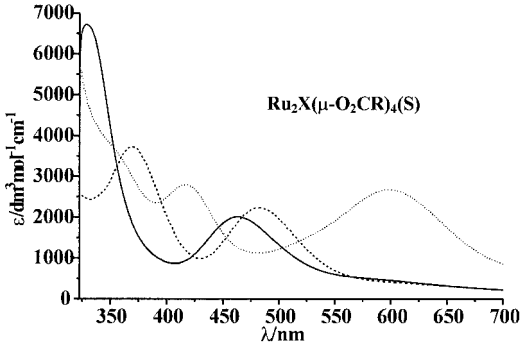

 © 2004 Wiley-VCH Verlag GmbH & Co. KGaA, Weinheim

4502 **T. Arliguie,* P. Thuéry, M. Fourmigué, M. Ephritikhine**

Monocyclooctatetraenyl(dithiolene)uranium Compounds

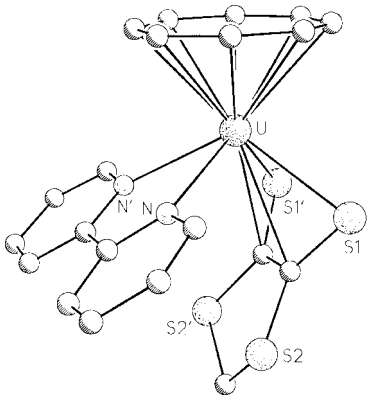

Keywords: Cyclooctatetraenyl ligands / Lewis bases / S ligands / Uranium

4510 **S. Dey, L. B. Kumbhare, V. K. Jain,* T. Schurr, W. Kaim,* A. Klein,* F. Belaj**

Structural Variety and Multiple Isomerism in 1-(Dimethylamino)propyl-2-chalcogenolate and 2-(Dimethylamino)propyl-1-chalcogenolate Complexes of Palladium(II) and Platinum(II): Synthesis, Spectroscopy and Structures

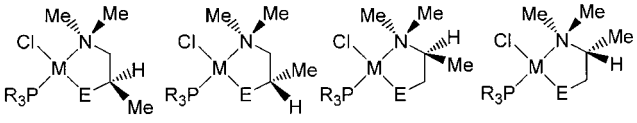

Keywords: Chalcogens / Isomers / N ligands / Palladium / Platinum

4521 **G. Zou, Z. Liu, D. Wang, C. Jiang, Y. Qian***

Selected-Control Solvothermal Synthesis of Nanoscale Hollow Spheres and Single-Crystal Tubes of PbTe

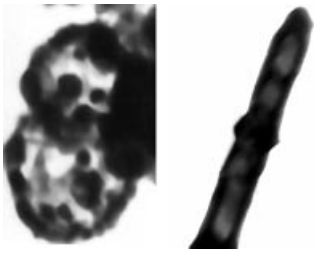

Keywords: Nanostructures / Semiconductors / Nanotubes

4525 **O. Mendoza, F.-J. K. Rehmann, L. P. Cuffe, M. Tacke***

Cocondensation Reactions of Five-Membered Heterocycles with Lithium Atoms at 77 K

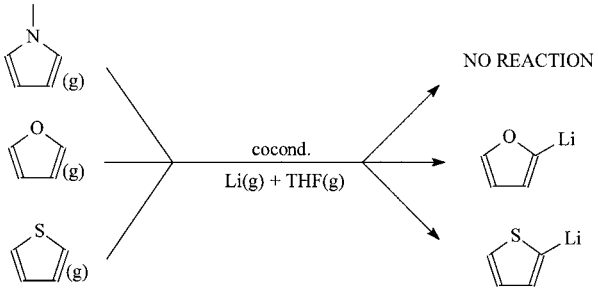

Keywords: Lithium / Heterocycles / C−H bond activation / Cocondensation / DFT

 © 2004 Wiley-VCH Verlag GmbH & Co. KGaA, Weinheim

Switching of Molecular Spin States in Inorganic Complexes by Temperature, Pressure, Magnetic Field and Light: Towards Molecular Devices

Azzedine Bousseksou,*[a] Gábor Molnár,[a] and Galina Matouzenko[b]

Keywords: Spin crossover / Metastability / Hysteresis loop / Pressure / Magnetic field / Dielectric properties / Ising-like model

The spin crossover phenomenon in molecular inorganic compounds is one of the most spectacular examples of bistability phenomena leading to a switching between the high-spin and the low-spin states of the molecule by several means such as temperature, pressure, light and magnetic field (multi-property molecular switching). In the present microreview we report our most important findings, both experimental results and theoretical approaches, and discuss possible technological applications for each switching method as well as the recent synthesis of new spin crossover molecular materials.

(© Wiley-VCH Verlag GmbH & Co. KGaA, 69451 Weinheim, Germany, 2004)

1. Introduction

Certain (pseudo)octahedral transition metal complexes are known to display a molecular bistability of the high-spin (HS) and low-spin (LS) electron configurations which can be distinguished by different occupations of the antibonding e_g and the nonbonding t_{2g} d orbitals of the central metal ion.[1,2] The electronic ground state of these spin crossover (SCO) complexes may be reversibly interchanged by an external stimulus such as temperature, pressure, magnetic field or light irradiation. This phenomenon was discovered by Cambi et al. as part of a study of iron(III) dithio-

[a] Laboratoire de Chimie de Coordination, UPR 8241 CNRS, 205 route de Narbonne, 31077 Toulouse, France
E-mail: boussek@lcc-toulouse.fr
[b] Laboratoire de Chimie (UMR CNRS and ENS-Lyon No. 5182), Ecole Normale Supérieure de Lyon, 46, allée d'Italie, 69364 Lyon, France

Azzedine Bousseksou was born in 1964 in Algiers, Algeria, and received his Ph.D. in solid state physics from the University of Paris 6 (Pierre et Marie Curie) in 1992. He was a Research Associate at the University of Paris 6 with the group of François Varret (Physics Research Department) for one year. In 1993 he received a permanent position as a "Chargé de Recherche" at the CNRS. In 1997 he joined the Laser Laboratory and Raman spectroscopy group of Prof. John McGarvey in N. Ireland for 18 months. In 1997, he was promoted to first class of "Chargé de Recherche-CNRS". He presently leads the team "Molecular Physics Properties" at the Laboratoire de Chimie de coordination CNRS Toulouse. His field of research includes molecular bistability and molecular spin-crossover phenomena, experimental and theoretical approaches, thin films, and nanostructures and devices; he published approximately 80 articles, 2 patents, 3 book chapters and organised several workshops, he is a member of the national comity of the CNRS (2000−2004). He was awarded the 2003 prize for the Coordination Chemistry Division of the French Chemical Society.

Gábor Molnár was born in Szolnok (Hungary) in 1973. He received his M.Sc. degree in 1996 from the Eötvös Loránd University (Budapest, Hungary). He prepared his Ph.D. thesis under the supervision of P. Iacconi (University of Nice, France) and J. Borossay (Eötvös University) in the field of thermoluminescent dosimeter materials. He held a postdoctoral position for 8 months at the IMRA-Europe company (Sophia Antipolis, France) and worked on photovoltaic materials. He then joined the group of J. J. McGarvey as a Marie Curie fellow for 12 months at the Queens University of Belfast (U.K.) to develop a new high-pressure Raman spectroscopy setup. In 2002, he became Research Associate ("poste rouge") at the CNRS Laboratoire de Chimie de Coordination (Toulouse, France) where he later received a permanent position with the group of A. Bousseksou. His current research focuses on molecular bistability and molecular spin-crossover phenomena.

Galina Matouzenko obtained her undergraduate degree at Kishinev University (USSR) and her Ph.D. degree from the Institute of Chemistry, Moldavian Academy of Sciences working with Professor A. V. Ablov, one of the leading Soviet coordination chemists. Her thesis focused on the synthesis, magnetic properties and magneto-structural correlations in new exchange-coupled polynuclear complexes of transition metals. After coming to France, in 1992 she joined the Laboratory of Chemistry, UMR (Unité Mixte de Recherche) of the CNRS and Ecole Normale Supérieure de Lyon. Her current interests lie in the field of the design of new mono- and polymeric spin-transition systems.

MICROREVIEWS: This feature introduces the readers to the authors' research through a concise overview of the selected topic. Reference to important work from others in the field is included.

carbamate compounds in the early 1930s.[3] The first Fe^{II} complexes $[Fe(phen)_2(NCS)_2]$ and $[Fe(bipy)_2(NCS)_2]$ (phen = 1,10-phenanthroline, bipy = 2,2-bipyridine) with "unusual magnetic behaviour" were reported only about 30 years later.[4] Their careful reinvestigation by König[5] has shown that they represent the first examples of iron(II) SCO compounds and this marked a starting point for further extensive developments of the field, chiefly in the framework of the European TOSS TMR network coordinated by P. Gütlich.[6] Although the SCO phenomenon may occur for octahedral compounds with d^4-d^7 configurations, it is most commonly observed for iron(II) complexes with nitrogen donor atoms. Currently, about two hundred spin transition systems are known.

The SCO phenomenon has been studied by a variety of physical methods such as magnetic susceptibility and heat capacity measurements, Mössbauer, Raman, UV/Vis, IR and EPR spectroscopy and also X-ray diffraction and dielectric constant measurements.[1,2] These methods combined with temperature, pressure, high magnetic field and light irradiation provided a firm basis for the theoretical modelling of the SCO. In our group (Toulouse, France) we are particularly interested in the application of an external perturbation in the macroscopic metastable states of SCO materials leading to an irreversible switching of their magnetic, optical and electrical properties. Experiments under different external stimuli will be discussed in the second part of this paper together with a theoretical treatment of experimental data.

Concerning synthetic methods, two approaches are currently employed for designing new cooperative SCO systems, namely supramolecular and polymeric approaches. These two strategies will be illustrated in the third part of the paper using several examples of mononuclear and polymeric compounds recently synthesised at ENS Lyon (France).

2. Switching of Spin States by External Perturbations

The SCO phenomenon is one of the most spectacular examples of molecular bistability which means that SCO molecules may exist in two different electronic states within a certain range of external perturbations.[7] Most notably, the existence of a thermal hysteresis in certain SCO complexes (in the solid state) confers a memory effect on these systems. This bistability is accompanied by a marked change in various physical properties. Besides the well-known magnetic and optical responses, we have recently shown that the dielectric constant can also be used to read the state of the bistable system[8] leading to the first prototype of an electronic component for information storage.[9]

According to the pioneering ideas of O. Kahn, several compounds have been designed for which room temperature falls within the hysteresis loop.[10] Using local warming and cooling for writing and erasing, O. Kahn and his colleagues have promoted devices based on SCO materials for different applications such as temperature sensors and active elements in displays and memory devices.[7] In our group, we have pursued these ideas and proposed the use of pulsed perturbations in the hysteresis loop temperature range (macroscopic metastable states) to switch the spin state of the system (Figure 1). In the first experiments we used a pulsed magnetic field to trigger an LS → HS transition.[11] Later, we showed that a pressure pulse leads to a "mirror effect" when compared with a pulsed magnetic field.[12] Recently, other groups reported the first results of the application of a laser pulse in the hysteresis loop.[13] In this chapter we discuss the effect of different external perturbations (temperature, magnetic field and pressure) on the spin state of SCO materials from an experimental and theoretical point of view. A brief summary of light pulse induced effects completes this part. Finally, an example is given to illustrate the response functions (optical, magnetic and electric) associated with the bistability.

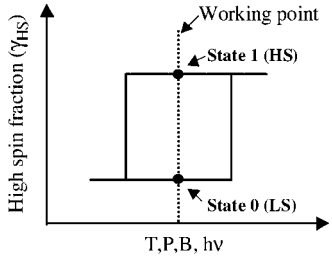

Figure 1. Schematic representation of the memory effect; the switching may be obtained by temperature, pressure, magnetic field or light irradiation

2.1. Thermally Induced Spin State Change

The thermally induced spin state change is the oldest spin-switching channel so far discovered in the field of molecular SCO compounds. The thermal spin transition curves, i.e. plots of HS fraction (γ_{HS}) vs. temperature, may take different forms such as gradual, abrupt or two-step and with or without hysteresis (see part 3 of the paper for examples). Several phenomena contribute to this different kind of behaviour, the most important being the interactions between the SCO molecules. The microscopic origins of the cooperative interactions have been extensively studied in the past and it is now generally accepted that the main contribution arises from elastic interactions between the molecules undergoing spin change. A detailed treatment of the elasticity theory was given by Spiering et al.[14]

To describe the thermally induced spin state change, in 1992 we adapted the Wajnflasz and Pick model[15] to a two-level system (HS and LS levels in our case) which we called the Ising-like model.[16] In our approach, a fictitious spin σ is associated with the HS and LS states for each molecule *i*. The Hamiltonian of the system is expressed as a function of the energy gap between the two levels of an isolated molecule (Δ_0) and a phenomenological parameter (J_{ij}) describing the interactions between the molecules *i* and *j*:

$$\bar{\mathbf{H}}_i = \frac{\Delta_0}{2}\bar{\sigma}_i - \sum_{j\neq i} J_{ij}\bar{\sigma}_i\bar{\sigma}_j$$

 © 2004 Wiley-VCH Verlag GmbH & Co. KGaA, Weinheim

where $\hat{\sigma}$ is a fictitious spin operator with eigenvalues of +1 or −1 for the HS and LS states, respectively. Each level in this model represents an effective level including the electronic configuration and the vibrational density of states. In the mean field approximation, where the interaction energy of the neighbouring molecules is averaged as $J\langle\hat{\sigma}\rangle$:

$$\sum_{j\neq i} J_{ij}\hat{\sigma}_i\hat{\sigma}_j \rightarrow J\langle\hat{\sigma}\rangle\hat{\sigma}_i,$$

the magnetisation of the system, proportional to the mean value of $\sigma = \langle\hat{\sigma}\rangle$ is a self-consistent equation and the fraction of HS molecules takes the form:

$$\gamma_{HS}(T) = \frac{r}{r+\exp\frac{\Delta_0 - 2J(2\gamma_{HS}-1)}{k_BT}}$$

with $r = g^{HS}/g^{LS}$ being the degeneracy ratio of the HS and LS levels including the vibrational contributions. The equilibrium temperature $T_{1/2}$ (obtained for $\gamma_{HS} = \gamma_{LS} = 1/2$) takes the form:

$$T_{1/2} = \frac{\Delta_0}{k_B \ln r}$$

In the case where the cooperative interaction exceeds a critical value ($J > T_{1/2}$), one observes a discontinuity in the first derivative of the free energy F of the system, leading to a first-order spin transition. In this case we observed a hysteresis loop. By introducing two kinds of cooperative interactions, namely "ferro-like" (positive) and "antiferro-like" (negative), this model reproduces the main thermal SCO behaviour observed experimentally: one-step or two-step transitions, with or without hysteresis loops.[16] Figure 2 shows four examples of theoretically calculated curves.

It is now well established that the HS form is stabilised at higher temperatures due to its higher entropy (electronic and vibrational in origin) when compared with the LS form. The prominent role of the entropy difference between the HS and LS states (ΔS_{HL}) in driving the thermal spin crossover was first considered by Sorai and Seki.[17] These authors studied the heat capacity of the compound $[Fe(phen)_2(NCS)_2]$ as a function of temperature and found a heat capacity anomaly around the spin crossover temperature (176 K). The entropy change associated with the spin transition was then estimated to be $\Delta S_{HL} = (49.0\pm0.7)$ $J\cdot K^{-1}\cdot mol^{-1}$. Since the entropy change measured by Sorai and Seki is significantly larger than the electronic entropy change, they proposed that the main contribution to ΔS_{HL} arises from the coupling of the electronic state to the phonons of the system. In a first approach, this effect can be explained by the increase in the number of antibonding e_g electrons upon an LS → HS crossover of the central metal ion. This electronic change significantly weakens the metal−ligand bonds leading to lower vibrational frequencies. For example the metal−ligand stretching frequencies, which are those most influenced by the spin state change, were found to decrease by a factor of 1.5−1.8. In other words, the density of vibrational states shifts to the low frequency range when going from the LS to the HS state. Since the contribution of low-frequency modes to the vibrational entropy will be higher, this phenomenon leads to a more entropic HS state.

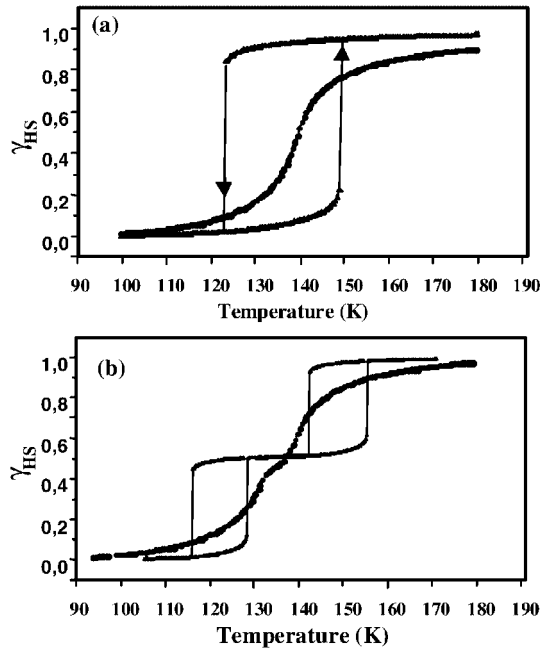

Figure 2. Calculated thermal variation of γ_{HS} using the Ising-like model: (a) one-step spin crossover: gradual ($J < T_{1/2}$) and abrupt with hysteresis loop ($J > T_{1/2}$); (b) two-step spin crossover: gradual and abrupt with two hysteresis loops

We have studied the effects of molecular vibrations on the SCO phenomenon using vibrational spectroscopic methods as experimental tools and by including the molecular vibrations in our Ising-like theoretical model.[16d,18] The vibrational spectra, even recorded by a variety of methods (Raman, IR, nuclear inelastic scattering), cannot provide the complete vibrational spectrum. For these reasons, theoretical treatments incorporating vibrational effects must inevitably rely on various approximations.

The Raman spectra of $[Fe(phen)_2(NCS)_2]$ have been analysed[18a] by making the assumption of an average frequency representative of the idealised FeN_6 octahedron. An average frequency ratio of 1.35 was obtained which is in good agreement with the result (1.5) of recent DFT calculations on the same compound.[19] Using this value, an estimated vibrational contribution to the entropy change from the coordination core of 20 $J\cdot K^{-1}\cdot mol^{-1}$ was obtained. This result supports the proposition of Sorai and Seki[17] that the intramolecular vibrations represent a prominent contribution to the overall entropy change.

The inherent limitations of the average frequency approach have been addressed by summing the entropy terms associated with the distinct vibrational modes.[18b,18c] A family of coordination polymers of formulae $[Fe(pyridine)_2(M(CN)_4)]$ and $[Fe(pyrazine)(M(CN)_4)]\cdot 2H_2O$ (M = Ni, Pd, or Pt), displaying comparatively clear-cut low-fre-

 © 2004 Wiley-VCH Verlag GmbH & Co. KGaA, Weinheim

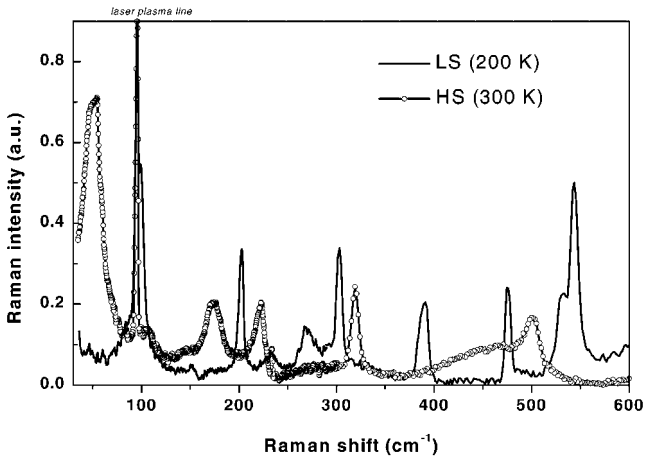

Figure 3. Raman spectra of the [Fe(pyrazine)(Pd(CN)$_4$)]·2H$_2$O spin crossover complex in the HS (300 K) and LS (200 K) states[18c]

quency vibrational spectra (Figure 3), has recently been studied by using this approach.[18c] It was shown that the spin state change in these compounds influences not only the vibrations which can be described as Fe^{II}−ligand modes but all other low-frequency modes of the polymeric network (below ca. 600 cm^{-1}). It was concluded that alongside a major contribution from the metal−ligand vibrations (ca. 60 %) other intra- and intermolecular vibrations can also make nonnegligible contributions to the entropy change (ca. 40 %). The underlying reason may involve either coupling with the Fe^{II}−ligand vibrations or with the lattice contraction/expansion that accompanies the spin transition. High pressure,[18f] isotopic substitution[18d] and metal dilution[18g] techniques combined with Raman spectroscopy and calorimetry measurements revealed that in this family of compounds, ΔS_{HL} decreases upon isotope exchange and metal dilution but does not change much with the lattice contraction. These observations suggest, therefore, that the vibrational couplings have a significant effect on the entropy change.

Thus, both infrared and Raman spectroscopy reveal a pronounced change in the molecular vibrational modes. We have also studied theoretically the effect of intramolecular vibrations on the spin crossover phenomenon for independent molecules involving a set of harmonic oscillators.[16d] Each two-level molecule is associated with p harmonic oscillators having two possible frequencies, ω_{LS} and ω_{HS} (p = 15 for an octahedral symmetry). For each oscillator of frequency ω_i, the vibrational partition function can be written:

$$z_i(\omega_i,T) = 1/[\exp(h\omega_i/kT) - 1]$$

The contribution of oscillator (i) to the total entropy is then derived from the free energy expression ($F_i = -kT\ln z_i$; $S_i = -\partial F_i/\partial T$) leading to:

$$S_i(\omega_i,T) = h\omega_i/2T\cdot\tanh(h\omega_i/2kT) - k\cdot\ln[2\sinh(h\omega_i/2kT)]$$

The total entropy of the system can be calculated by summing the contributions of the different vibrational modes. The decrease in the frequencies upon LS → HS crossover results in an entropy increase that can be expressed by:

$$\Delta S_{HL}(T) = S_{HS}(T) - S_{LS}(T)$$

The frequency dependence of the contribution of a given mode on the total entropy change calculated according to the above equations is shown in Figure 4 at different temperatures. The higher the frequency and the lower the temperature, the less the mode contributes to $\Delta S_{HL}(T)$.

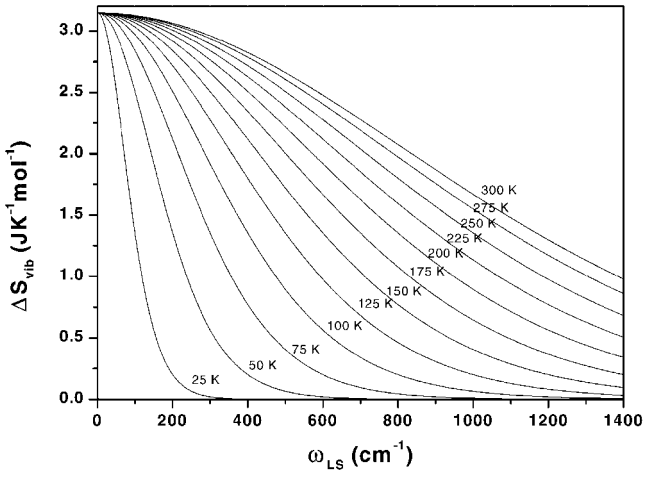

Figure 4. Vibrational entropy change of a harmonic oscillator upon spin transition as a function of the vibrational frequency; the curves were calculated with $\omega_{HS} = \omega_{LS}/1.5$ for different values of T_c [18c]

Interesting behaviour occurs due to the intramolecular vibrations when the system is in an "equi-energetic" situation. This situation corresponds to the case where $\Delta_{eff} = \Delta_{elec} - p\bar{h}(\omega_{LS} - \omega_{HS})/2 \approx 0$, i.e. when the contribution of the molecular vibrations is of the same order of magnitude as the electronic gap between the HS and LS states. In this case, the HS state will be the ground state at low temperature and one may observe, as illustrated in Figure 5, a partial SCO phenomenon with particular thermal behaviour.[16d] To date, three examples of such "equi-energetic" situations have been reported,[20] the first two examples coming from our group in 1996 and 1998.

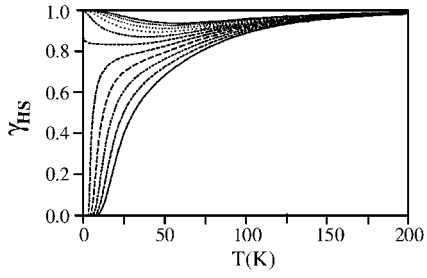

Figure 5. Theoretical thermal variation of γ_{HS} in the vicinity of the "equi-energetic" (HS, LS) situation ($\Delta_{eff} = \Delta_{elec} - p\bar{h}(\omega_{LS} - \omega_{HS})/2 \approx 0$)[16e]

 © 2004 Wiley-VCH Verlag GmbH & Co. KGaA, Weinheim

2.2. Magnetic Field Induced Spin State Change

Keeping in mind that (i) a magnetic field stabilises the highest spin-state of the molecule through the Zeeman effect, (ii) the spin crossover phenomenon is a dynamic process and (iii) it is possible to generate high pulsed magnetic fields[21] (LNCMP/CNRS, Toulouse, France: 32 Tesla in 2000 and 60 Tesla currently), the idea of applying a pulsed magnetic field in the hysteresis loop was developed.

Historically, the first study using a static magnetic field of 5.5 Tesla, reported by Y. Qi et al. on $[Fe(phen)_2(NCS)_2]$, revealed a shift of the thermal spin transition by −0.12 K.[22] In the second study with cobalt complexes under a static field of 20 Tesla, J. Lejay et al. measured a shift of $T_{1/2}$ by −0.6 K.[23a] In 2000, we reported the first study of the effect of a high and pulsed magnetic field (32 Tesla) on the spin state of $[Fe(phen)_2(NCS)_2]$ and a partial triggering of the SCO was demonstrated with at least a 15 % HS fraction created in an irreversible process (Figure 6).[11a]

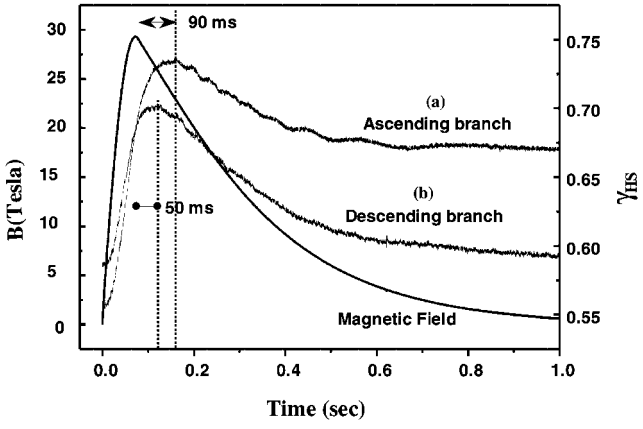

Figure 6. Magnetic pulse effect on $Fe(phen)_2(NCS)_2$; the time dependencies of $\gamma_{HS}(t)$ for two initial states belonging to the ascending (a) and descending (b) branches of the thermal hysteresis loop; for comparison, the time dependence of the magnetic field pulse is also shown[11a]

In a quasi-static approach, we modelled the observed effects under a magnetic field introduced in the Ising-like model.[11e] The magnetic field, through the Zeeman effect, removes the electronic degeneracies of the HS and LS levels and the new Hamiltonian can be written as:

$$\hat{\mathbf{H}}_i(m_S) = \frac{\Delta_0}{2}\hat{\sigma}_i + \sum_{j\neq i} J_{ij}\hat{\sigma}_i\hat{\sigma}_j + g_L\mu_B B\hat{S}_Z\frac{\hat{\sigma}_i+1}{2}$$

where μ_B is the Bohr magneton, g_L is the Landé factor, B is the magnetic field strength and S_z is the projection of the spin moment operator along the field direction. The latter can take any of the $2S + 1$ values $m_S = -S, -S + 1, ..., S$. The system can now be described by its spin state σ_i and also by m_S. In order to solve analytically the Hamiltonian of the system, we use the mean-field approximation. By explicit calculation of the mean value of $\hat{\sigma}$ we obtain for γ_{HS}:

$$\gamma_{HS}(B) = \frac{r(B)}{r(B)+\exp\frac{\Delta_0 - 2J(2\gamma_{HS}-1)}{k_BT}}$$

$$with \quad r(B) = \frac{g_{HS,vib}\,g(B,S_{HS})}{g_{LS,vib}\,g(B,S_{LS})} \quad and \quad g(B,S) = \frac{\sinh\left(\frac{(2S+1)g_L\mu_BB}{2k_BT}\right)}{\sinh\left(\frac{g_L\mu_BB}{2k_BT}\right)}$$

and for $T_{1/2}$:

$$T_{1/2} = \frac{\Delta_0}{k_B\ln\left\{\frac{g_{HS,vib}}{g_{LS,vib}}\cdot\frac{\sinh\left[\frac{(2S_{HS}+1)g_L\mu_BB}{2k_BT_{1/2}}\right]}{\sinh\left[\frac{(2S_{LS}+1)g_L\mu_BB}{2k_BT_{1/2}}\right]}\right\}}$$

where $g_{HS,vib}$ and $g_{LS,vib}$ are the vibrational degeneracies of the HS and LS states, respectively.

The exact solution of these self-consistent equations can only be obtained numerically. Figure 7 represents the resolution of the $\gamma_{HS}(T,B)$ equation using the Newton numerical method. This resolution was carried out in the case of a gradual conversion between the diamagnetic ($S_{LS} = 0$) and the paramagnetic ($S_{HS} = 2$) spin states with the parameter set as $\Delta_0 = 700$ K, $J = 139$ K, $g_{HS,vib}/g_{LS,vib} = 30$ and for different strengths of the applied magnetic field. It can be noted that for an applied magnetic field above 18 T, a first-order phase transition appears accompanied by a thermal hysteresis. This effect has also been shown qualitatively in ref.[23b] In fact, the magnetic field decreases the transition temperature but the condition for a first-order transition $J/k_BT_c > 1$ remains unchanged. This condition is illustrated in Figure 8, where, for $J = 139$ K, the first-order phase transition appears above 18 T.

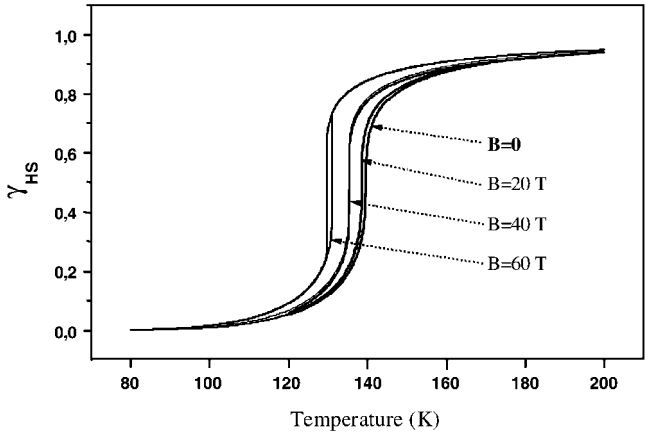

Figure 7. Calculated thermal variation of $\gamma_{HS}(T,B)$ under a static magnetic field using the Ising-like model,[11e] for selected values $B = 0$, 20 T, 40 T and 60 T; a thermal hysteresis loop (first-order phase transition) is obtained for $B = 60$ T

As described in ref.[11a] we can also obtain an analytical expression for the variation of $T_{1/2}$ as a function of the applied magnetic field strength from the Landau free energy in the presence of a field and in thermodynamic equilibrium. For an isothermal process and in the high-temperature approximation (paramagnetic Curie law), the magnetic molar free energy can be written as:

 © 2004 Wiley-VCH Verlag GmbH & Co. KGaA, Weinheim

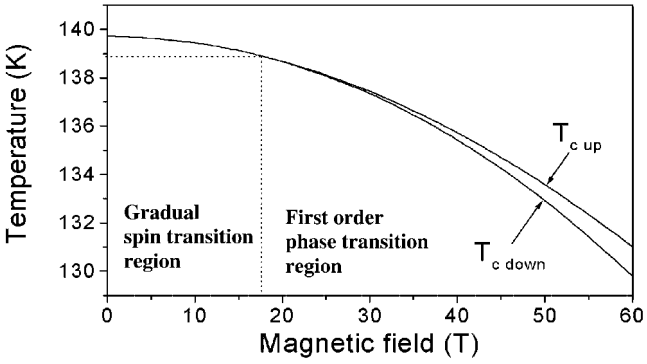

Figure 8. (B,T) phase diagram calculated using the Ising-like model (with $S_{LS} = 0$, $S_{HS} = 2$, $\Delta_0 = 700$ K, $J = 139$ K, $g_{HS,vib}/g_{LS,vib} = 30$)[11e]

$$\Delta G = G_{HS} - G_{LS} = \Delta H(0) - T\Delta S(0) - (\chi_{HS} - \chi_{LS})B^2/2\mu_0$$

where $\Delta H(0)$ and $\Delta S(0)$ refer to the properties in the absence of an external field. Accounting for the paramagnetic properties of the HS state, for a spin $S = 0 \rightarrow S = 2$ transition we obtain:[11a,11g]

$$\delta T_{1/2} = -\frac{4(\mu_B B)^2}{k_B \Delta_0}$$

and

$$\delta(\Delta) = \Delta(B) - \Delta(0) = -4(\ln g)(\mu_B B)^2/\Delta(0)$$

For a spin crossover between two paramagnetic states ($S = 1/2 \rightleftarrows S = 3/2$) the equilibrium temperature shift takes the form:[11d,11e]

$$\delta T_{1/2} = -\frac{2(\mu_B B)^2}{k_B \Delta_0}$$

The negative sign for both the equilibrium temperature and the energy gap between the HS and the LS states due to coupling to the magnetic field leads, as expected, to the stabilisation of the HS form.

Newton numerical resolution of $T_{1/2}$ obtained in the Ising-like model has been described in ref.[11e] It appears, as expected, that the transition temperature decreases quadratically with the magnetic field B and the two approaches (Ising-like and thermodynamic) are equivalent for weak magnetic fields but diverge for strong fields.

The dynamic aspects of the pulsed magnetic experiments are very interesting. In Figure 6 the peak value of the applied magnetic field (32 T) corresponds to a computed shift of the transition temperature $\Delta T_{1/2} \approx -1.8$ K which is sufficient for a complete triggering to be expected in the quasi-static regime. Therefore, the incompleteness of the spin switch can be associated with the kinetic part of the pulsed field experiment.

Subsequently, using the metal-diluted complexes $Fe_xNi_{(1-x)}(btr)_2(NCS)_2 \cdot H_2O$ [btr = 4′,4′-bis(1,2,4-triazole)], we observed a clear correlation between the cooperativity of the thermal transition and the dynamics of the triggering process. In particular, the delay between the excitation (magnetic pulse maximum) and the response increases exponentially with increasing cooperativity (J) (Figure 9).[11c,11f]

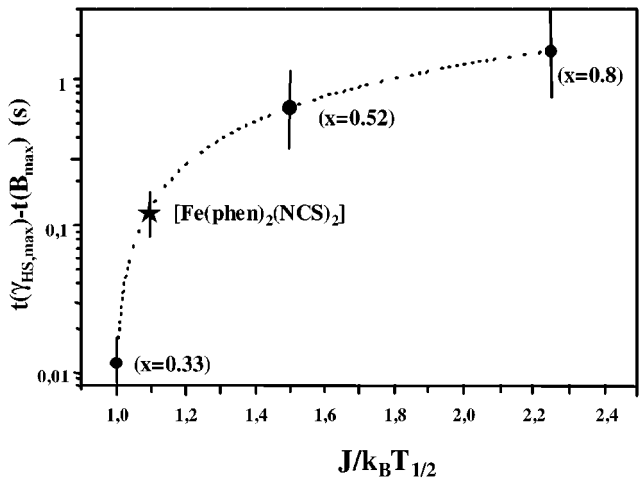

Figure 9. The time delay between $B^{max}(t)$ and $n_{HS}^{max}(t)$ on the ascending branch of the hysteresis loop (for initial temperatures corresponding to a molecular fraction $\gamma \cong {}^0_{HS} = 0.4$) for different samples of $[Fe_xNi_{(1-x)}(btr)_2(NCS)_2]\cdot H_2O$ mixed crystals as a function of J/k_BT_c;[11c] the point obtained with $Fe(Phen)_2(NCS)_2$ is also reported[11a]

This work prompted us to study, under a magnetic field, a system with a low energy barrier between the (macroscopic) LS and HS states and with a paramagnetic LS state in order to observe a complete spin-state switching. For this aim we selected the compound $Co^{II}[H_2(fsa)_2en](py)_2$.[11d] As shown in Figure 10, applying a magnetic field of 32 T to this system, initially being in the ascending branch of the hysteresis loop, leads to an irreversible and quasi-complete $S = 1/2 \rightarrow S = 3/2$ transition.

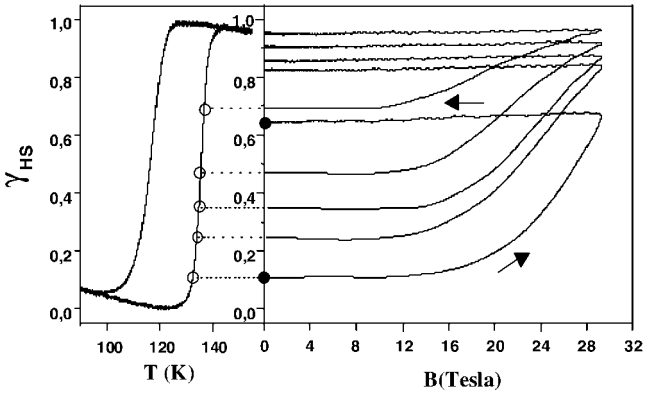

Figure 10. Magnetic pulse effect on $[Co\{H_2(fsa)_2en\}(py)_2]$; set of isotherms $\gamma_{HS}(T,B)$ showing the irreversible triggering of the LS → HS transition for an applied pulsed magnetic field in the ascending branch of the hysteresis loop;[11d] the pathway of the increase in the proportion of high-spin molecules as function of magnetic field is shown by the arrows

 © 2004 Wiley-VCH Verlag GmbH & Co. KGaA, Weinheim

The kinetic aspects of the spin crossover triggering by pulsed magnetic fields were modelled through dynamic treatments of the Ising-like model.[11d] This requires a stochastic description based on the following master equation:

$$\frac{d}{dt}p(\{\sigma\},t) = \sum_j W_j(-\sigma_j)p(\{\sigma_j\},-\sigma_j;t) - \sum_j W_j(\sigma_j)p(\{\sigma_j\},\sigma_j;t)$$

where $p(\{\sigma\},t)$ is the probability of observing the system in the configuration $\{\sigma\} = (\sigma_1, \sigma_2, ..., \sigma_N)$ at time t and $\{\sigma\}_j$ denotes the configuration of all spins, except σ_j. $W_j(\sigma_j)$ which are the transition rates of the spin flip $\sigma_j \rightarrow -\sigma_j$, induced by the thermal bath which are constrained in order to respect the microscopic detailed balance condition.

In the mean-field approximation, we obtained the following nonlinear differential equation for the HS fraction of molecules $\gamma_{HS} = (1 + m)/2$:

$$\frac{d\gamma_{HS}}{dt} = -\frac{2}{\tau_0}\gamma_{HS}e^{-\beta\varepsilon^+}e^{-2\beta qJ\gamma_{HS}} + \frac{2}{\tau_0}(1-\gamma_{HS})e^{-\beta\varepsilon^-}e^{2\beta qJ\gamma_{HS}}$$

$$\text{with } \varepsilon^{\pm} = \pm E_a^0 \mp \frac{\Delta_0}{2} \mp qJ \pm \frac{kT}{2}\ln 2\frac{g_{HS}}{g_{LS}} \pm 2\frac{(\mu B(t))^2}{kT}.$$

Figure 11 represents the solution of the equation for $\gamma_{HS}(t,T)$ in the ascending and descending branches of the thermal hysteresis loop: this model is (i) qualitatively in good agreement with the experimental behaviour and (ii) reproduces the nonreversible/reversible character of the triggering in the ascending/descending modes, respectively.

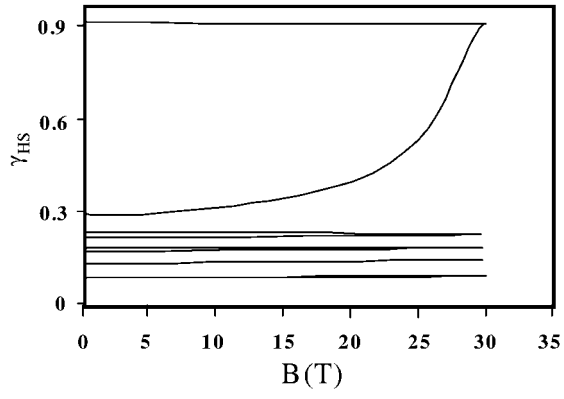

Figure 11. Calculated HS fraction as a function of the pulsed magnetic field B in the ascending branch of the hysteresis loop;[11d] no significant effects of magnetic field are observed for initial values of $\gamma_{HS} < 0.3$ (lower section of the figure)

As a summary of the main findings associated with the effects of intense and pulsed magnetic fields we refer to the following points:

1. In the first experiments with $Fe(phen)_2(NCS)_2$:[11a]

a) In the ascending (metastable) branch of the thermal hysteresis loop, a partial irreversible triggering of the spin crossover was obtained (15% of the LS molecules) by applying a 32 T pulsed magnetic field. In other words, in the ascending branch we succeeded in triggering the "first-order" (in the nonequilibrium sense) magnetic field induced spin transition.

b) In contrast to the situation with the ascending branch, reversible triggering was obtained in the descending branch (i.e. in this branch, the system cannot reach a metastable state in a magnetic field.)

c) Dynamic effects of the phenomenon are evidenced by the delay between the excitation (application of magnetic field) and the response (increase of high spin fraction) measured at 50 ms and 90 ms for the ascending and descending branches of the thermal hysteresis loop, respectively.

2. In a second series of experiments with the $Fe_xNi_{(1-x)}(btr)_2(NCS)_2{\cdot}H_2O$ family of complexes:[11c]

a) Similar effects were obtained with $x = 0.33$, 0.52, 0.8 in the ascending/descending branches of the hysteresis loops.

b) The delay between the excitation and the response increased exponentially with increasing cooperativity.

3. In a third series of experiments on $[Co(H_2(fsa)_2en)py_2]$, a quasi-total triggering of the SCO was observed[11d] and was attributed to the low energy barrier ($\Delta = 442$ cm^{-1}) between the HS and LS forms and to the paramagnetic character of the LS state ($S = 1/2$).

4. A dynamic Ising-like model, including a magnetic field, reproduced well the experimental observations.[11d]

2.3. Pressure-Induced Spin State Change

The LS → HS spin state change of the central metal ion in a molecule brings about a significant increase in the metal−ligand bond lengths and, as a result, an increase of the unit cell volume. This volume change associated with the SCO may reach several percent of the unit cell volume in iron(II) complexes as determined from X-ray diffraction data.[1,2] In the case of complexes with an $Fe^{II}N_6$ core, ΔV_{HL} is typically around 20 Å^3/iron atom.[24k,24l]

Externally applied pressure stabilises the LS state (i.e. with a smaller volume). Pressure thus has the effect of shifting the thermal spin transition towards higher temperatures.[24] It also speeds up the relaxation back to the LS state at a given temperature.[24g−24i,25a] For complexes with an $Fe^{II}N_6$ core, the shift in the transition temperature was found, in general, to be around 15 K/kbar, though in certain cases a few exceptions were also found.[24e,24f,24k]

The pressure effects on the SCO can be modelled within the Ising-like model using the mean-field approximation and by taking into account only a direct coupling between the HS fraction and the pressure through the work term which increases the energy gap ($\Delta_p = \Delta_0 + p\Delta V_{HL}$).[11g,24j,25] In this case the shift of the transition temperature with pressure is given as:

$$\delta T_{1/2}/\delta p = \Delta V_{HL}/\Delta S_{HL}$$

where ΔS_{HL} is the total entropy change upon SCO and ΔV_{HL} is the volume change. The positive sign of both ΔS_{HL}

 © 2004 Wiley-VCH Verlag GmbH & Co. KGaA, Weinheim

and ΔV_{HL} leads to a positive shift of $T_{1/2}$ with increasing pressure.

In the case of a first-order phase transition, the spin crossover is usually accompanied by a hysteresis loop. The hysteresis loop can be obtained from the Ising-like model if the condition $J > T_{1/2}$ is fulfilled.[16] The surface of the hysteresis loop is proportional to the difference between the cooperativity of the system and the equilibrium temperature [$S \sim (J - T_{1/2})$].[26] The positive sign of the shift of the equilibrium temperature obtained by the Ising-like model thus leads to a vanishing of the hysteresis loop upon increasing pressure.

The pressure-induced spin switching around room temperature can be illustrated by the example of the polymeric spin crossover compound $[Fe(Atrz)_3](NO_3)_2 \cdot nH_2O$ (Atrz = 4-amino-1,2,4-triazole). Mössbauer spectroscopic measurements have been carried out under pressure at 325 K, i.e. in the temperature range of the thermal hysteresis loop of this compound. Figure 12 shows Mössbauer spectra of this complex obtained at 325 K at low pressure (50 bar), under compression (1000 bar) and after decompression (50 bar). At low pressure the spectrum consists of a main doublet (80 %) with hyperfine parameters characteristic of Fe^{II} in the HS state (IS = 1.00 mms^{-1}, QS = 2.54 mms^{-1}) and a small (20 %) doublet (IS = 0.41 mms^{-1}, QS = 0.14 mms^{-1}) which can be assigned to LS Fe^{II} species. By application of 1000 bar, the system can be converted completely to the LS state as shown by the Mössbauer spectra. Since at the temperature of the experiment the system is in the hysteresis region of the phase diagram, after decompression it remains in the LS state, i.e. the piezo-switch is irreversible.

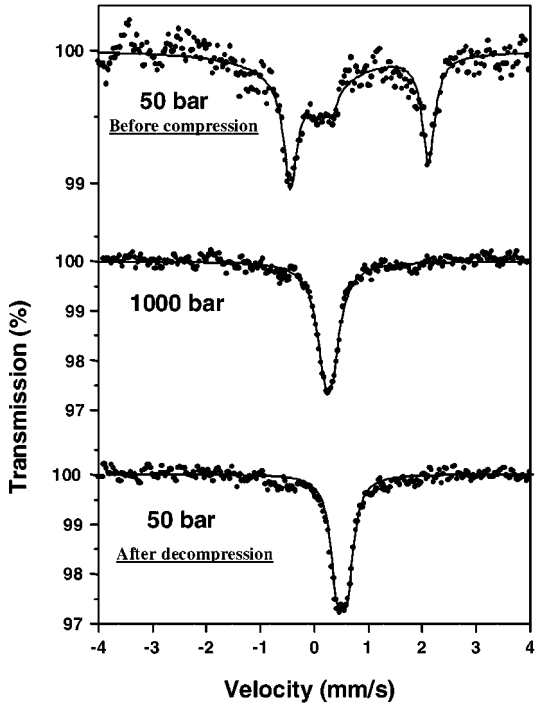

Figure 12. Pressure-induced spin switching in $[Fe(Atrz)_3](NO_3)_2 \cdot nH_2O$ at 325 K detected by Mössbauer spectroscopy

Since the early stages of SCO research, several authors have discussed interest in the influence of pressure on SCO systems.[24] However, pressure effects on these molecular materials have been found to be relatively complex. For example, pressure was often found to induce changes in the crystal structure.[27] For this reason, we decided to probe the pressure effects on SCO systems using a spectroscopic technique (Raman spectroscopy).

The spin states of a series of cyanide-bridged iron(II) spin-crossover coordination polymers of formulae $Fe(pyrazine)[M(CN)_4] \cdot 2H_2O$ (M = Ni, Pd, or Pt) have been studied by recording their solid state Raman spectra at room temperature as a function of pressure (Figure 13).[25b] For the first time, a reproducible piezo-hysteresis loop has been observed at room temperature for the Ni complex with characteristic spin transition pressures of $P_{1/2}\uparrow$ = 1350 bar and $P_{1/2}\downarrow$ = 650 bar upon compression and decompression, respectively. The fascinating feature here is the use of a perturbation other than the temperature to obtain a memory effect (piezo-hysteresis loop). Using the Ising-like model described above, we simulated piezo-hysteresis curves and we were able to show that the condition required to obtain a discontinuous pressure loop can be written as $J > T_{1/2}(p = 0) + P_{1/2}\Delta V(p)/\Delta S(p)$. Since the second term is always positive, piezo hysteresis can be expected only for complexes displaying thermal hysteresis at atmospheric pressure. Moreover, the piezo-hysteresis vanishes with increasing temperature (Figure 14). For the Pd and Pt complexes, the spin-state change occurs at higher pressures (1.8 and 3.5 kbar, respectively) and without hysteresis. The unexpectedly high value of $P_{1/2}$ in the case of the Pt complex was puzzling but Raman spectroscopy revealed that in this complex, a structural phase transition takes place at relatively low pressures (100−900 bar). The pressure-induced phase could be identified as a low-symmetry HS phase. This new HS phase transforms to the LS form only at higher pressures.

Using Raman spectroscopy in conjunction with a diamond anvil cell technique, a spin state change for the complex $Fe(pyridine)_2[Ni(CN)_4]$ could be observed at around

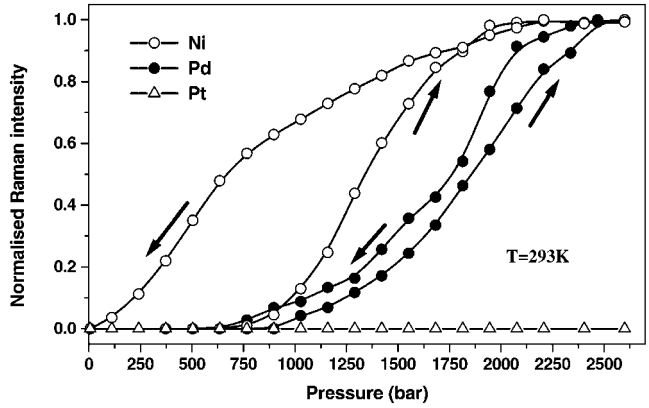

Figure 13. Intensity of the 675 cm^{-1} LS marker band as a function of pressure for the complexes $Fe(pyrazine)[M(CN)_4] \cdot 2H_2O$ (M = Ni, Pd, or Pt) at room temperature (arrows indicate the increase and subsequent decrease of the pressure)[25b]

 © 2004 Wiley-VCH Verlag GmbH & Co. KGaA, Weinheim

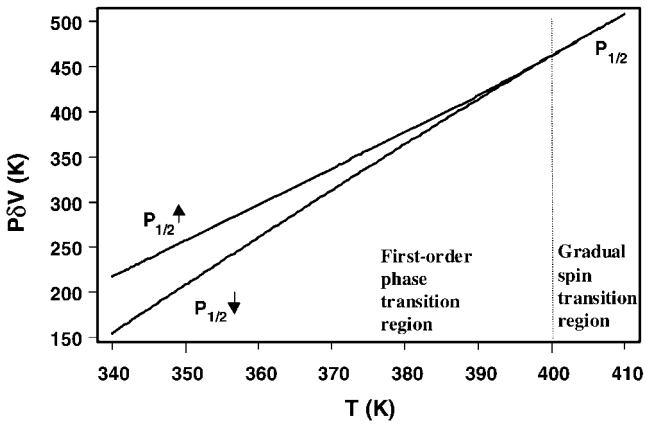

Figure 14. Calculated (P,T) phase diagram using the Ising-like model (with $g_{HS}/g_{LS} = 100$, $\Delta = 1380$ K, $J = 400$ K)[25b]

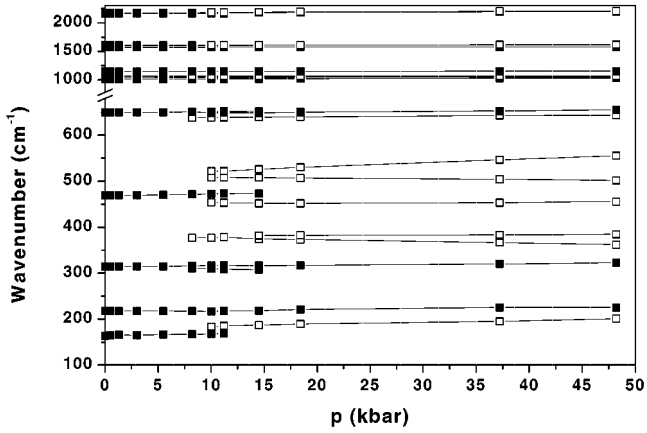

Figure 15. The pressure dependence of Raman frequencies in Fe(pyridine)$_2$[Ni(CN)$_4$]; symbols: black squares/open squares represent modes assigned to the HS/LS phase, respectively; lines are inserted to guide the eye[18f]

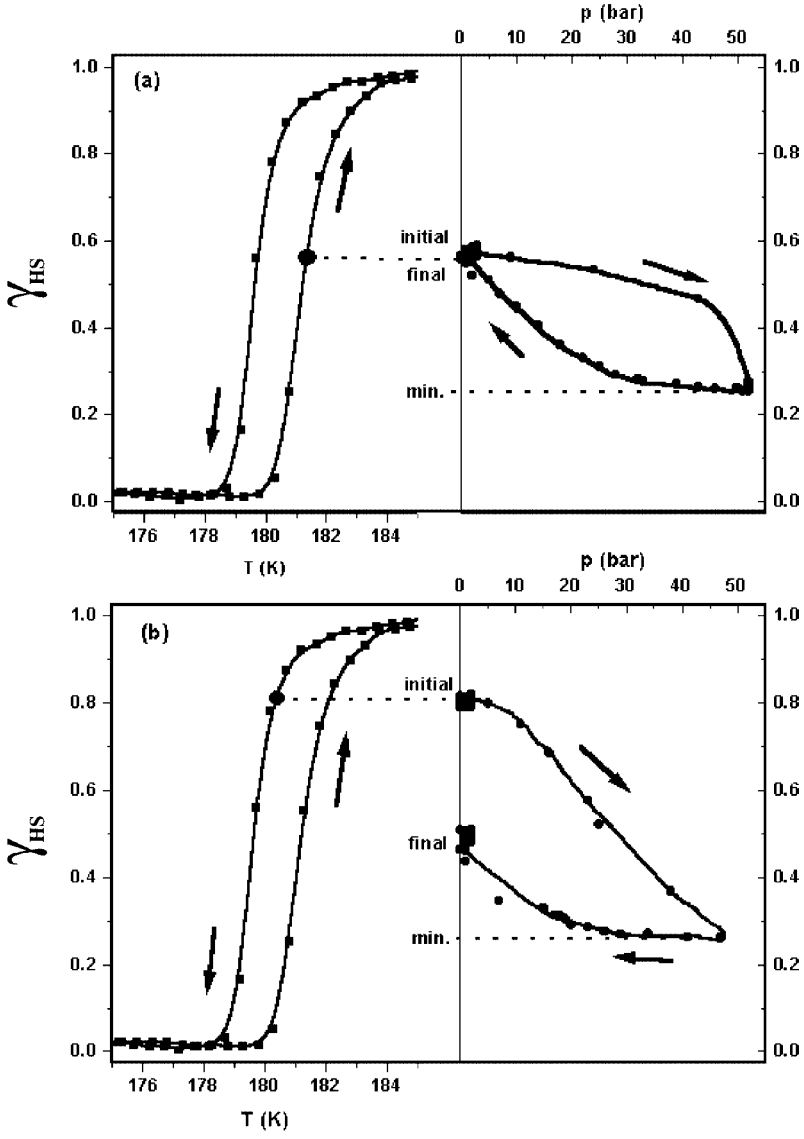

Figure 16. Pressure effect on the HS fraction $\gamma_{HS}(T,p)$ in Fe(phen)$_2$(NCS)$_2$ in the ascending (a) and descending (b) branches of the thermal hysteresis loop[12]

 © 2004 Wiley-VCH Verlag GmbH & Co. KGaA, Weinheim

10 kbar.[18f] The aim of this work was to study the effect of the lattice contraction on the vibrational frequencies in the HS and LS states, generated by externally applied pressure up to 50 kbar. This question has already been brought up in several previous European discussions (TOSS network) and in theoretical investigations.[16d,28] In fact, the expansion/contraction of the lattice upon spin crossover must induce a vibrational entropy change due to the anharmonicity of vibrations. In general, this pressure-induced entropy change is neglected in the treatment of the free energy of the system, though no experimental data are available. We have determined the pressure coefficients ($d\omega/dp$) of vibrational modes in $Fe(pyridine)_2[Ni(CN)_4]$ in both the HS and LS states down to 150 cm^{-1} (Figure 15). The pressure dependence of the Raman modes was found to vary between 0.1 and 0.4 $cm^{-1}\cdot kbar^{-1}$ in the investigated frequency range for both HS and LS frequencies. We therefore concluded that at moderate applied pressures ($< 10-15$ kbar) the lattice contraction induced entropy change is small and can be in fact neglected.[18f]

Besides the static effects of pressure on the SCO we have also studied the effects of a pressure pulse in the temperature range of the thermal hysteresis loop for the compound $Fe(phen)_2(NCS)_2$.[12] During the dynamic pressure pulse, a decrease in γ_{HS} can be observed with an irreversible (reversible) character in the descending (ascending) branch of the hysteresis loop (Figure 16). In this respect, pressure has a "mirror effect" compared with the application of an intense and pulsed magnetic field for which an increase in γ_{HS} is observed with an irreversible (reversible) character in the ascending (descending) branch of the hysteresis loop. This observation can be explained by the fact that an applied magnetic field stabilises the HS state through the Zeeman effect while external pressure stabilises the LS state due to its smaller volume. If one compares the theoretical shift of the transition temperature under quasi-static external pressure with that due to a magnetic field, it appears that the effect of 1 T is roughly the opposite of the shift caused by 2.5 bar. The fact that a pressure as low as 200 bar triggered a complete crossover between the two spin-states suggests that piezo effects might be implemented in devices for addressing SCO materials (e.g. pressure sensors).

2.4. Light Pulse Induced Spin State Change

A photo-induced technique for the study of SCO in Fe^{II} complexes was first reported by McGarvey and Lawthers in 1982 in a paper describing the use of a pulsed laser to perturb the equilibrium between the singlet (^1A) and quintuplet (^5T) states in several Fe^{II} complexes in solution.[29] Then, in 1984, Descurtins et al. reported that light irradiation of a solid Fe^{II} spin crossover complex at low temperature induced a transition from the LS to a metastable HS state.[30] Subsequently, this so-called Light-Induced Excited Spin-State Trapping (LIESST) effect was intensely studied by Hauser et al. and its main elements are considered today to be well understood.[31] Though the LIESST effect is potentially interesting for use in optical devices, the low relaxation temperatures of the metastable HS species strongly limits such applications.[32]

On the other hand, recent reports suggest that it is possible to realise a photoinduced spin-state change at relatively high temperatures when exciting the solid material with a short laser pulse in the thermal hysteresis loop region. This phenomenon was first demonstrated on the complex $Fe(PM\text{-}BiA)_2(NCS)_2$.[13a] In the hysteresis loop temperature range (around 170 K), an increase of the HS fraction was obtained using single laser pulse (5 ns, ca. 1 mJ). Similar phenomena have been reported on Prussian blue analogues exhibiting thermal hysteresis loops associated with valence tautomerism.[13b] It should be emphasised that, contrary to the LIESST effect, in these experiments the *macroscopic* metastable phase (HS or LS) is photo-transformed into the thermodynamically stable phase. It was suggested that such a phenomenon could occur if the concentration of locally photo-excited states exceeds a threshold value.

These preliminary photo-switching experiments represent interesting perspectives, especially if they prove to be effective on SCO compounds exhibiting hysteresis around room temperature. However, further experiments and theoretical work are necessary to confirm the origins of these observations.

2.5. The Promising Properties for Devices

Information processing is based on the ability to modify and retrieve a particular physical property of a material such as its electrical, magnetic or optical response. In the case of spin crossover complexes, changes of magnetic and optical properties are well documented.[1] The magnetic properties change between a paramagnetic and a diamagnetic state (Fe^{II} and Co^{III} ions) or between two different paramagnetic states (Fe^{III}, Co^{II}, Mn^{II}). The change in optical properties occurs in the visible and near-IR spectroscopic regions depending strongly on the particular complex in question. Both charge transfer (MLCT) and ligand field absorption bands contribute to these spectroscopic changes.

Though optical reading has some potential applications, it is more desirable to base these on electronic functions. In fact, the use of electronic properties offers much wider scope, particularly in the context of addressing the issue of miniaturisation through the "bottom up" (i.e. molecular level) approach. In this respect, we have recently reported results demonstrating a link between the dielectric constant and the SCO phenomenon. In fact, the real part of the dielectric constant (ε') showed a significant variation at the spin transition temperature for different iron(II) spin crossover complexes.[8] The frequency dependence of ε' was found to be negligible up to 1 MHz. As far as the origin of the dielectric constant change is concerned, one can assume to a first approximation that it results from the higher polarisability of the HS ions when compared with the LS form. Indeed, for most of the complexes, we have found a higher value of ε' in the HS state. However, in the case of the complexes $Fe[5NO_2\text{-}sal\text{-}N(1,4,7,10)]$ (sal = salicylaldehyde)

 © 2004 Wiley-VCH Verlag GmbH & Co. KGaA, Weinheim

and $[Fe(bpp)_2](BF_4)_2$ [bpp = 2,6-bis(pyrazol-3-yl)pyridine], ε' decreases when going from the LS to the HS state indicating that the interpretation of these changes might be more complex especially if one considers the possible existence of crystallographic phase transitions in these compounds.

As a recent example of bistability in three properties of the same compound (magnetic, optical and dielectric) the example of $[Fe(DAPP)(abpt)](ClO_4)_2$ {DAPP = [bis(3-aminopropyl)(2-pyridylmethyl)amine], abpt = 4-amino-3,5-bis(pyridin-2-yl)-1,2,4-triazole} is shown in Figure 17. The changes in all three physical channels occur as first-order phase transitions with 10 K wide hysteresis loops centred around 176 K. The high-temperature state shows a paramagnetic Curie temperature dependence of the magnetic susceptibility, with an effective magnetic moment (μ_{eff}) of 5.5 B.M. This magnetic moment corresponds to HS Fe^{II} ions with $S = 2$. Upon cooling, μ_{eff} decreases sharply around the spin transition temperature and the paramagnetism is almost completely quenched (μ_{eff} = 0.15 B.M.) at low temperatures, in agreement with a pure diamagnetic state of Fe^{II} ions ($S = 0$). The optical reflectivity measured at 632 nm also shows hysteresis. The reflectivity is higher in the HS form indicating that the optical absorption at this wavelength is lower in this state. The dielectric constant measured at 10 kHz shows an increase of ca. 8 % upon going from the LS to the HS state. The memory effect operates around 176 K by the storage of a high or low capacitance state. No significant frequency effect has been observed on ε' in the range of 10^2-10^7 Hz.

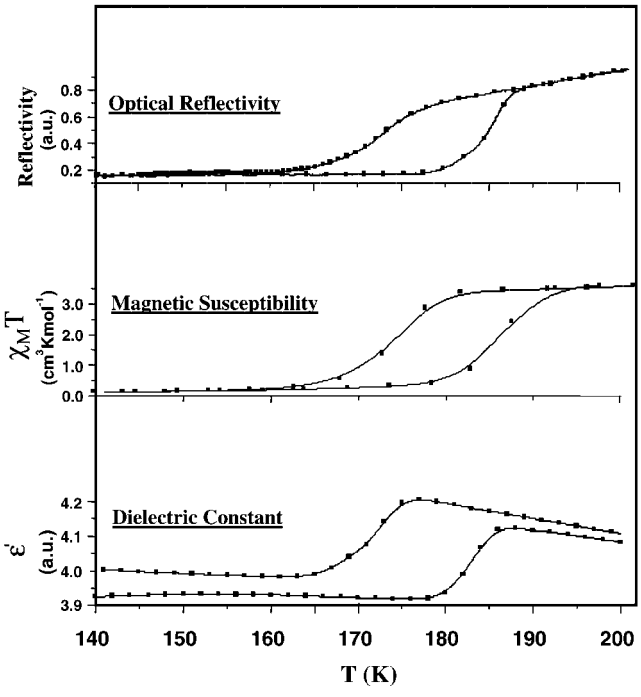

Figure 17. Thermal hysteresis loop for optical, magnetic and dielectric properties in the *same* spin crossover complex $[Fe(DAPP)(abpt)](ClO_4)_2$

3. Engineering Spin Crossover Materials

The prerequisite for the occurrence of a spin crossover is the proximity of the HS and LS electronic states. The energy gap between two states can be tuned in a relatively predictable fashion by variation of the ligand field strength. Several synthetic strategies used in the synthesis of spin transition complexes have been summarised in a recent volume of "Topics in Current Chemistry".[1] One of the possible approaches for engineering spin transition systems, applied by our group, is the use of ligands containing both aliphatic and aromatic nitrogen donor atoms. The combination of nitrogen atoms of a different nature in the same ligand can be expected to generate an intermediate ligand field, favouring spin-state interconversion. On the basis of this strategy, numerous complexes of polydentate ligands containing different types of nitrogen binding sites have been designed.[2c][2f] On the other hand, the involvement of amino and pyridyl groups in the same ligand may exert a favourable effect on the generation of intermolecular H-bonding and/or π-stacking interactions, leading to cooperative effects. Moreover, the variation of the aliphatic to aromatic nitrogen atoms ratio in the same ligand is also a convenient tool for the fine-tuning of the ligand field strength. However, the ligand field splitting is not the only factor which determines the existence and character of a spin transition. The interplay of the spin pairing energy and the ligand field strength is very sensitive to small structural perturbations in the metal environment. They may result from the existence of sterically demanding ligands and/or from minor crystal packing changes associated with the nature of the counter ions or even the presence of a solvent of crystallisation. As has been noted,[2f] even more subtle changes such as the number of chelate rings and/or the replacement of five- with six-membered cycles can also affect the spin state of the resultant iron(II) complex. Thus, in the framework of a general synthetic approach the spin transition behaviour is not generally readily predictable.

3.1. Mononuclear Complexes

In this context, in order to study the influence on the spin transition process of small perturbations in the ligand structure, several tetradentate ligands with mixed aliphatic and aromatic nitrogen atom functions were prepared (Figure 18) and their mononuclear iron(II) complexes were investigated. The new spin transition compound $[Fe(DPEA)(NCS)_2]$ [DPEA = 2-aminoethylbis(2-pyridylmethyl)amine] was isolated and its structure, magnetic properties and Mössbauer spectra were investigated.[33] This complex displays a *cis* configuration for the two NCS groups and a *mer* arrangement of two pyridyl rings of the DPEA ligand (Figure 19). The DPEA ligand, coordinated to the metal atom by two pyridine nitrogen atoms in apical positions and two aliphatic amino groups in adjacent positions in the $[FeN_6]$ octahedron, forms three 5-membered metallocycles. The X-ray analysis revealed the existence of an important distortion of the $[FeN_6]$ core from O_h symmetry, attribu-

 © 2004 Wiley-VCH Verlag GmbH & Co. KGaA, Weinheim

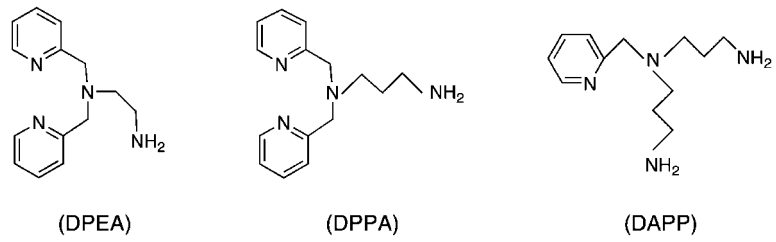

Figure 18. Representation of the DPEA, DPPA and DAPP ligands

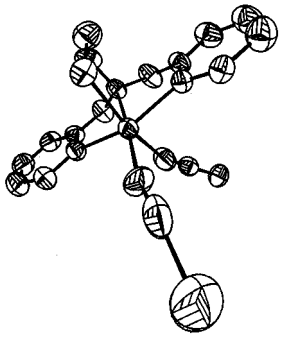

Figure 19. Molecular structure of [Fe(DPEA)(NCS)$_2$]

table to steric constraints due to the tetradentate ligand. The sharp spin conversion observed in the complex at 138 K is close to a first-order transition (Figure 20) and we anticipated that suitable changes in the structure of the ligand, which would release some strain, could modify the magnetic properties and possibly lead to a spin transition with hysteresis.

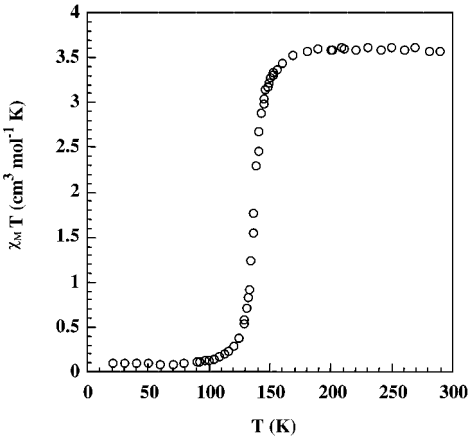

Figure 20. Thermal variation of χ_MT for [Fe(DPEA)(NCS)$_2$]

This idea was realised with the new DPPA ligand [DPPA = (3-aminopropyl)bis(2-pyridylmethyl)amine] (Figure 18) which differs from DPEA by the presence of an additional methylene unit in the amino aliphatic chain.[34] Upon coordination to iron(II), DPPA can form one 6-membered and two 5-membered chelate rings. However, during the preparation of the DPPA−iron(II) complex [Fe(DPPA)(NCS)$_2$], we isolated not a single crystalline form but four different species. Certainly, the enlargement of one of the three metallocycles leads to enhanced molecular flexibility and results in this greater variety of species. Three of these species were defined as polymorphic modifications (A, B, and C) and the fourth was a solvated complex. Only a few manifestations of polymorphism are known among spin transition systems.[35] For polymorph A, variable-temperature magnetic susceptibility measurements (Figure 21) as well as Mössbauer spectroscopy have revealed the occurrence of a rather gradual spin transition without hysteresis, centred at about 176 K. The polymorph B is paramagnetic over the temperature range 4.2−295 K, whereas polymorph C exhibits a very abrupt $S = 2 \rightleftarrows S = 0$ transition with hysteresis. The hysteresis width is 8 K, the transitions being centred at $T_c\downarrow = 112$ K for decreasing and $T_c\uparrow = 120$ K for increasing temperatures. The solvated complex [Fe(DPPA)(NCS)$_2$]·EtOH displays a rather gradual spin transition centred near 220 K. An X-ray analysis has shown that in the three polymorphs, the asymmetric units are almost identical and consist of one chiral complex molecule with the same configuration and conformation. The distorted [FeN$_6$] octahedron is formed by four nitrogen atoms belonging to DPPA and two provided by the *cis* thiocyanate groups. Contrary to our expectations, the two pyridine rings of DPPA are in the *fac* position, whereas the *mer* configuration has been isolated for [Fe(DPEA)(NCS)$_2$]. This circumstance, which made a direct comparison of the effect of metallocycle strain on magnetic properties irrelevant, offered instead a valuable opportunity to focus on the consequences of polymorphism on the magnetic properties of the same complex. The main differences between the structures of the three polymorphs are found in their crystal packings. The stabilisation of the high-spin ground state of poly-

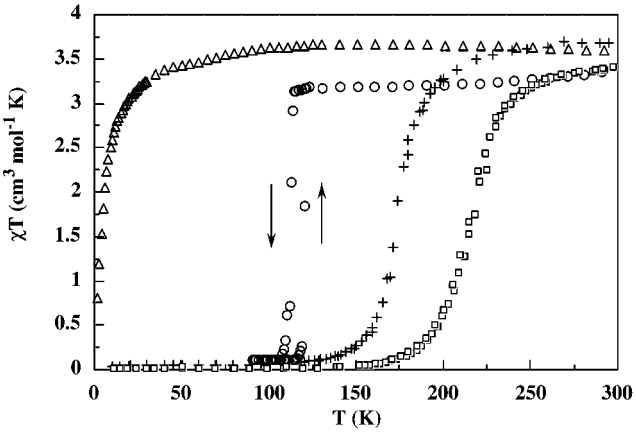

Figure 21. Thermal variation of $\chi_M T$: for *fac*-[Fe(DPPA)(NCS)$_2$] in polymorph A (+++), in polymorph B (open triangles), in polymorph C (open circles) and for [Fe(DPPA)(NCS)$_2$]EtOH (open squares)

 © 2004 Wiley-VCH Verlag GmbH & Co. KGaA, Weinheim

morph B can be tentatively explained by the presence of two centres of steric strain in the crystal lattice, resulting in the elongation of the Fe−N(aromatic) distance. The observed hysteresis in polymorph C seems to be due to the existence of an array of intermolecular contacts in the crystal lattice making the spin transition more cooperative than in polymorph A. The [Fe(DPPA)$(NCS)_2$] complex provides a new and particularly striking example of polymorphism leading to qualitatively different magnetic properties in a spin transition system.

This latter example shows that the crystal structure plays a major role in the shaping of spin transitions. Packing effects appear as a small perturbation on the interplay between the ligand field and the interelectronic interactions. Besides, they determine the propagation pattern of the cooperative interactions in the solid. Unfortunately, the influence of packing effects on the spin state of the complex is neither predictable nor controllable. Another alternative, connected with the packing effects, arises when several crystallographically independent iron(II) sites co-exist in the same unit cell and structural distinctions among iron(II) complexes can result in their different magnetic behaviour.[36] This latter situation can be illustrated by the recently reported mononuclear complex [Fe(DPEA)(bim)]-$(ClO_4)_2$·$0.5H_2O$ with the DPEA ligand and bim = 2,2-bis-(imidazole).[37] Variable-temperature magnetic susceptibility measurements (77−295 K) have shown the occurrence of a two-step spin transition (Figure 22). Two steps on the magnetic curve are separated by an inflection point at 200 K, corresponding to about 50 % of the molecules having undergone a thermal spin transition. The first step is centred at 171 K and the second at 218 K. Mössbauer spectroscopy, calorimetric measurements and X-ray analyses have shown that the profile of the magnetic curve is a consequence of the presence of two nonequivalent iron(II) ions in the crystal lattice. The crystal structure was resolved in the HS and LS forms at 293 and 123 K, respectively. The main differences between both spin-state isomers were found in the geometry of the [FeN_6] core which exhibits the shorter of the Fe−N distances at lower temperatures. Two inequivalent HS molecules at two crystal lattice sites successively undergo a thermal spin transition. The attribution of the two steps of the spin transition to the inequivalent lattice sites was performed through the analysis of the mean Fe−N distances for functionally different nitrogen donor atoms. At 10 K the light-induced excited spin-state trapping (LIESST) effect was observed (Figure 23). Two critical temperatures T(LIESST) have been recorded (36 and 21 K) and attributed to the two nonequivalent iron(II) lattice sites.

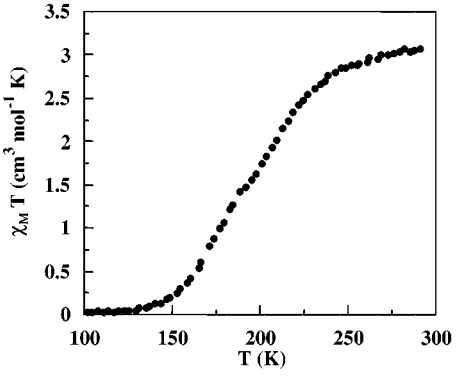

Figure 22. Thermal variation of $\chi_M T$ for [Fe(DPEA)(bim)]$(ClO_4)_2$·$0.5H_2O$

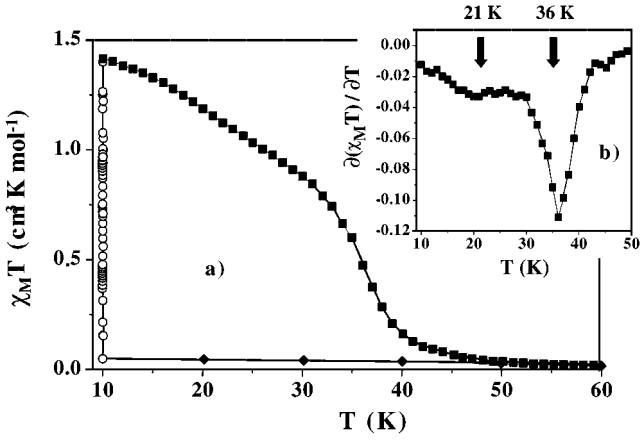

Figure 23. a) Temperature dependence of $\chi_M T$ for [Fe(DPEA)(bim)]$(ClO_4)_2$·$0.5H_2O$: data recorded in the cooling mode without irradiation (solid diamonds); data recorded with irradiation at 10 K for 2 h (open circles); data recorded in the warming mode (0.3 K min^{-1}) after the light irradiation had been applied for 2 h, then removed (solid squares); b) derivative $\partial(\chi_M T)/\partial T$

Following the study of how strain effects arising from the size of chelate rings could modify the spin-crossover regime of iron(II) complexes, the tetradentate DAPP ligand {DAPP = [bis(3-aminopropyl)(2-pyridylmethyl)amine]} (Figure 18) was then synthesised.[38] When coordinated to iron(II), DAPP can form one five-membered and two six-membered chelate rings. However, the isolated analogous complex [Fe(DAPP)$(NCS)_2$] displays only the HS state. This is certainly in line with the decrease of the ligand field strength in DAPP due to the substitution of one aliphatic nitrogen atom for an aromatic one in the DPPA ligand, resulting in an aliphatic/aromatic ratio of 3:1 in the former compared with 2:2 in the latter. Another bidentate ligand, 4-amino-3,5-bis(pyridin-2-yl)-1,2,4-triazole (abpt) was chosen to complete the octahedral coordination sphere of iron(II) and to reinforce the total ligand field strength needed for the occurrence of spin crossover. The isolated mononuclear complex [Fe(DAPP)(abpt)]$(ClO_4)_2$ displays an abrupt spin transition with a hysteresis loop of 10 K, the transition being centred at $T_c\downarrow$ = 171 K for decreasing and $T_c\uparrow$ = 181 K for increasing temperatures (Figure 24). The explanation for the pronounced cooperativity in this case was sought in the intrinsic structural features of the complex. The crystal structure was resolved in the high-spin (293 and 183 K) and low-spin (123 K) states. The X-ray analysis revealed that the cooperative spin transition results from a branched network of intermolecular interactions in the crystal lattice provided by two modes of π-stacking and numerous hydrogen bonds. The thermal spin transition is accompanied by a considerable change in the lattice param-

 © 2004 Wiley-VCH Verlag GmbH & Co. KGaA, Weinheim

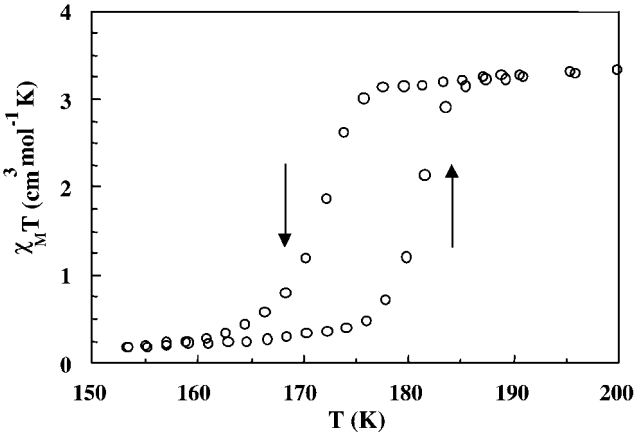

Figure 24. Thermal variation of $\chi_M T$ for [Fe(DAPP)(abpt)]$(ClO_4)_2$ in the heating mode and cooling mode

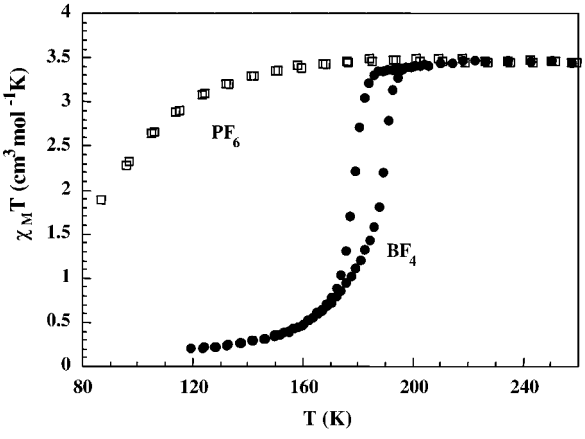

Figure 25. Thermal variation of $\chi_M T$ for (solid circles) [Fe(DAPP)(abpt)]$(BF_4)_2$ and (open squares) [Fe(DAPP)(abpt)]$(PF_6)_2$

eters (e.g. 7.5% for the *c* axis at 123 K) which in turn impose modifications on the molecular crystal packing and, accordingly, in the system of intermolecular interactions. In connection with this, the pronounced hysteresis in this complex, without any crystallographic phase transition, can be assumed to originate from the dramatic change of the unit cell parameters and rearrangement of the topology of the cooperative interactions. The second striking result of this study is the occurrence of two order-disorder transitions (in the counter anion and in the DAPP ligand) which accompany the spin change. The role of order-disorder phenomena has been discussed in the spin-crossover literature for a long time[39] and the ordering was suggested to be related to the nature of the spin transition. So far, only the disorder of species that are not coordinated to the iron(II) such as counter anions and solvent molecules, has been observed in spin transition complexes. [Fe(DAPP)(abpt)]$(ClO_4)_2$ is, to the best of our knowledge, the first example of a spin-crossover system with an order-disorder transition involving the ligand directly coordinated to the iron(II) site. In line with previous studies, the order-disorder phenomena and spin transition in [Fe(DAPP)(abpt)]$(ClO_4)_2$ seem to be internally interrelated. One may suppose that both tuning of the ligand field strength by the DAPP ligand and reinforcement of the cooperative interactions due to the thermal ordering in the perchlorate ions provide an intrinsic impulse for the initiation of the spin transition in [Fe(DAPP)(abpt)]$(ClO_4)_2$.

To examine the role of counter ions capable of giving rise to different crystal packings, we also prepared the compounds [Fe(DAPP)(abpt)]X_2 with X = BF_4, PF_6. Their magnetic behaviour (Figure 25) shows that the nature of the counter ion plays an important role in the spin-transition regime of [Fe(DAPP)(abpt)]X_2. The complex with the tetrahedral BF_4^- anion (as in the case of ClO_4^-) displays rather similar magnetic behaviour to [Fe(DAPP)(abpt)]$(ClO_4)_2$, with the hysteresis loop slightly displaced toward higher temperatures. In contrast, the complex with the octahedral PF_6^- anion shows a gradual spin transition, shifted towards lower temperatures, without hysteresis.

3.2. Coordination Polymers

The polymeric approach to designing SCO systems exhibiting strong cooperativity was only introduced quite recently[40] and therefore the number of such compounds still remains limited. The most extensively studied family includes iron(II) complexes with 1,2,4-triazole-type ligands.[41] Some of the complexes from this family, namely $[Fe(trz)_3]A_2{\cdot}nH_2O$ (trz = 4-substituted-1,2,4-triazole; A = a monovalent anion), exhibit abrupt spin transitions with a thermal hysteresis width up to ca. 40 K.[10b] The structural information for this complex has been deduced only from EXAFS spectroscopy.[42] The structure consists of linear chains in which the iron(II) atoms are triply bridged by triazole ligands. Unfortunately, structural information on the intermolecular interactions in the crystal lattice is not available. The cooperativity in these systems can be assumed to arise from a very short Fe−Fe intersite spacing and a rigid Fe−N−N−Fe linkage favouring the efficient spreading of the intersite interactions.

Several polymeric spin-crossover complexes have been synthesised using the self-assembly of rigid bifunctional N-donating spacer ligands and iron(II) ions.[20c,43] Recently, using this approach, we synthesised a new spin-crossover compound of formula $[Fe(pyim)_2(bpy)](ClO_4)_2{\cdot}2C_2H_5OH$ [pyim = 2-(2-pyridyl)imidazole and bpy = 4,4′-bipyridine].[44] It represents the first structurally characterised example of an iron(II) coordination polymer with an infinite zigzag chain undergoing the spin-crossover phenomenon. Variable-temperature magnetic susceptibility measurements revealed the occurrence of a relatively gradual spin transition centred at 205 K (Figure 26). The crystal structure was resolved at 293 K (HS form) and at 173 K (LS form). The complex assumes a 1D zigzag chain structure in which the iron(II) active sites are linked to each other by a chemical bridge such as the rigid rod-like 4,4′-bipyridine molecule. The polymeric chains which extend along the *c* axis are stacked in the *b* direction, forming 2D sheets of bound molecules (Figure 27). The sheets are linked together by several intermolecular hydrogen bonds in the *a* direction.

 © 2004 Wiley-VCH Verlag GmbH & Co. KGaA, Weinheim

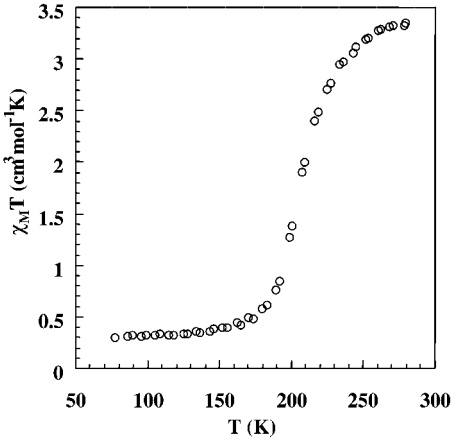

Figure 26. Thermal variation of $\chi_M T$ for $[Fe(pyim)_2(bpy)](ClO_4)_2 \cdot 2C_2H_5OH$

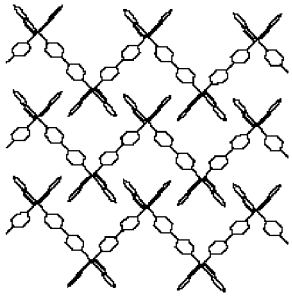

Figure 27. Projection of the molecular structure along the *a* axis for $[Fe(pyim)_2(bpy)](ClO_4)_2 \cdot 2C_2H_5OH$ showing the π−π stacking arrangement at 293 K

The ensemble of structural features of the complex, potentially leading to the cooperativity, provides a basis for strong interactions. However, they are not strong enough in comparison with the HS−LS energy gap and result in a relatively gradual spin transition for the complex. This example shows that the simple linking of active sites in the polymeric network is not in itself a sufficient condition to generate systems with the cooperative character of a spin transition. The presence of effective intermolecular interactions such as hydrogen bonding and/or π-stacking, favouring the efficient spreading of the intermolecular interactions, as well as the rigidity and conjugated nature of the chemical bridges, can contribute to the cooperativity.

4. Conclusions and Perspectives

To date, one of the most exciting perspectives in molecular science concerns the use of molecules or molecular assemblies as the active elements in devices for signal processing and information storage systems. Spin crossover and, in general, molecular bistability offer prospects for sensitivity and selectivity levels that cannot be reached with conventional solid-state materials. However, many fundamental questions remain to be answered. In particular, we need to study the effect of size reduction on the hysteresis behaviour and analyse the parameters determining the switching process (the origin of energy barriers, the mechanism of structural relaxation on both the molecular and macroscopic scales, etc.). From a chemical point of view, challenges in this field involve the problem of size-reduction and optimisation of the photo/piezo/magneto-excitation efficiency.

Acknowledgments

We deeply thank all our collaborators for their help in the realisation of the results reviewed in this paper, namely M.-L. Boillot, K. Boukheddaden, C. Consejo, P. Demont, L. Dubrovinsky, M. Goiran, J. Haasnoot, T. Kitazawa, J.-F. Létard, J. Linares, J. J. McGarvey, H. Paulsen, J.-A. Real, L. Salmon, K. Tanaka, J.-P. Tuchagues, F. Varret, C. Vieu and A. Zwick.

[1] "Topics in Current Chemistry", *Spin Crossover in Transition Metal Compounds I.-III.* (Eds.: P. Gütlich, H.A. Goodwin), **2004**, vol. 233−235.
[2] [2a] P. Gütlich, A. Hauser, H. Spiering, *Angew. Chem. Int. Ed. Engl.* **1994**, *33*, 2024. [2b] P. Gütlich, *Struct. Bonding (Berlin)* **1981**, *44*, 83. [2c] H. A. Goodwin, *Coord. Chem. Rev.* **1976**, *18*, 293. [2d] E. König, *Struct. Bonding (Berlin)* **1991**, *76*, 51. [2e] O. Kahn, *Molecular magnetism*, VCH, New York, **1993**. [2f] H. Toftlund, *Coord. Chem. Rev.* **1989**, *94*, 67. [2g] J. A. Real, in: *Transition Metals in Supramolecular Chemistry* (Ed.: J. P. Sauvage), Wiley, New York, **1999**, p. 54.
[3] [3a] L. Cambi, A. Cagnasso, *Atti Accad. Naz. Lincei* **1931**, *13*, 809. [3b] L. Cambi, L. Szegö, *Ber. Dtsch. Chem. Ges.* **1931**, *64*, 259.
[4] W. A. Baker, H. M. Bobonich, *Inorg. Chem.* **1964**, *3*, 1184.
[5] E. König, K. Madeja, *J. Chem. Soc., Chem. Commun.* **1966**, 61.
[6] http://iacgu7.chemie.uni-mainz.de/toss/ [Philipp Gütlich (Mainz, Germany), Wolfgang Linert (Wien, Austria), François Varret (Versailles, France), Olivier Kahn (Bordeaux, France), Jaap G. Haasnoot (Leiden, The Netherlands), Jose A. Real (Valencia, Spain), John J. McGarvey (Belfast, UK), Alfred X. Trautwein (Lübeck, Germany), Hans Toftlund (Odense, Danmark), Andreas Hauser (Genève, Switzerland)].
[7] [7a] O. Kahn, C. J. Martinez, *Science* **1998**, *279*, 44. [7b] O. Kahn, J.-P. Launay, *Chemtronics* **1988**, *3*, 140. [7c] O. Kahn, *Curr. Opin. Solid State Mater. Sci.* **1996**, *1*, 547. [7d] O. Kahn, J. Kröber, C. Jay, *Adv. Mater.* **1992**, *11*, 718.
[8] A. Bousseksou, G. Molnár, P. Demont, J. Menegotto, *J. Mater. Chem.* **2003**, *13* 2069.
[9] A. Bousseksou, C. Vieu, J.-F. Letard, P. Demont, J.-P. Tuchagues, L. Malaquin, J. Menegotto, *Molecular Memory with Spin Crossover Complexes*, French Patent filling, no. 01/11328 (31/08/2001), International extension PCT/FR02/02961, August 29, **2002**.
[10] [10a] J. Kröber, E. Codjovi, O. Kahn, F. Groliere, C. Jay, *J. Am. Chem. Soc.* **1993**, *115*, 9810. [10b] J. Krober, J. P. Audiere, R. Claude, E. Codjovi, O. Kahn, J. Haasnoot, F. Groliere, C. Jay, A. Bousseksou, J. Linares, F. Varret, A. Gonthier-Vassal, *Chem. Mater.* **1994**, *6*, 1404.
[11] [11a] A. Bousseksou, N. Negre, M. Goiran, L. Salmon, J. P. Tuchagues, M. L. Boillot, K. Boukhedaden, F. Varret, *Eur. Phys. J. B* **2000**, *13*, 451. [11b] N. Negre, M. Goiran, A. Bousseksou, J. G. Haasnoot, K. Boukheddaden, S. Askenazy, F. Varret, *Synth. Met.* **2000**, *115*, 289. [11c] N. Nègre, C. Consejo, M. Goiran, A. Bousseksou, F. Varret, J.-P. Tuchagues, R. Barbaste,

 © 2004 Wiley-VCH Verlag GmbH & Co. KGaA, Weinheim

S. Askénazy, J. G. Haasnot, *Physica B* **2001**, *294/295*, 91. [11d] A. Bousseksou, K. Bokheddaden, M. Goiran, C. Consejo, M. L. Boillot, J. P. Tuchagues, *Phys. Rev. B* **2002**, *65*, 172412. [11e] C. Conséjo, G. Molnár, M. Goiran, A. Bousseksou, *Polyhedron* **2003**, *22*, 2441. [11f] A. Bousseksou, K. Boukheddaden, M. Goiran, J. P. Tuchagues, F. Varret, "Spin Crossover in Transition Metal Compounds III", in *Top. Curr. Chem.* **2004**, *235*, 65. [11g] F. Varret, S. Arun Salunke, K. Boukheddaden, A. Bousseksou, É. Codjovi, C. Enachescu, J. Linares, *C. R. Chim.* **2003**, *6*, 385.

[12] A. Bousseksou, G. Molnar, J. P. Tuchagues, N. Menendez, E. Codjovi, F. Varret, *C. R. Chim.* **2003**, *6*, 329.

[13] [13a] S. Montant, G. Chastanet, S. Létard, S. Marcen, J. F. Létard, E. Freysz, *7th Spin Crossover Family Meeting*, Seeheim, Germany, March 1, **2002**. [13b]H. W. Liu, K. Matsuda, Z. Z. Gu, K. Takahashi, A. L. Cui, R. Nakajima, A. Fujishima, O. Sato, *Phys. Rev. Lett.* **2003**, *90*, 167403.

[14] [14a] H. Spiering, E. Meissner, H. Köppen, E. W. Müller, P. Gütlich, *Chem. Phys.* **1982**, *68*, 65. [14b] N. Willenbacher, H. Spiering, *J. Phys. C: Solid State Phys.* **1988**, *21*, 1423. [14c] H. Spiering, N. Willenbacher, *J. Phys.: Condens. Matter* **1989**, *1*, 10089. [14d] J. Jung, G. Schmitt, L. Wiehl, A. Hauser, K. Knorr, H. Spiering, P. Gütlich, *Z. Phys. B: Condens. Matter* **1996**, *100*, 523.

[15] J. Wajnflasz, R. Pick, *J. Phys.* **1971**, *32*, C1-91.

[16] [16a] A. Bousseksou, J. Nasser, J. Linares, K. Boukheddaden, F. Varret, *J. Phys. I* **1992**, *2*, 1381. [16b] A. Bousseksou, F. Varret, J. Nasser, *J. Phys. I* **1993**, *3*, 1463. [16c] A. Bousseksou, J. Nasser, J. Linares, K. Boukheddaden, F. Varret, *Mol. Crys. Liq. Cryst.* **1993**, *234*, 269. [16d] A. Bousseksou, H. Constant-Machado, F. Varret, *J. Phys. I* **1995**, *5*, 747. [16e] A. Bousseksou, J. Nasser, F. Varret, *J. Magn. Magn. Mater.* **1995**, *140−144*, 1511.

[17] M. Sorai, S. Seki, *J. Phys. Chem. Solids* **1974**, *35*, 555.

[18] [18a] A. Bousseksou, J. J. McGarvey, F. Varret, J. A. Real, J. P. Tuchagues, A. C. Dennis, M. L. Boillot, *Chem. Phys. Lett.* **2000**, *318*, 409. [18b] N. Moliner, L. Salmon, L. Capes, M. C. Munoz, J. F. Létard, A. Bousseksou, J. P. Tuchagues, J. J. McGarvey, A. C. Dennis, M. Castro, R. Burriel, J. A. Real, *J. Phys. Chem. B* **2002**, *106*, 4276. [18c] G. Molnár, V. Niel, A. B. Gaspar, J.-A. Real, A. Zwick, A. Bousseksou, J. J. McGarvey, *J. Phys. Chem. B* **2002**, *106*, 9701. [18d] K. Hosoya, T. Kitazawa, M. Takahashi, M. Takeda, J. F. Meunier, G. Molnar, A. Bousseksou, *Phys. Chem. Chem. Phys.* **2003**, *5*, 1682. [18e] J. P. Tuchagues, A. Bousseksou, G. Molnar, J. J. Mc Garvey, F. Varret, in "Spin Crossover in Transition Metal Compounds III", *Top. Curr. Chem.* **2004**, *235*, 85. [18f] G. Molnar, T. Kitazava, L. Dubrovinsky, J. J. McGarvey, A. Bousseksou, *J. Phys.: Condens. Matter* **2004**, *16*, S1129−S1136. [18g] T. Tayagaki, A. Galet, M. Carmen Muñoz, G. Molnár, A. Zwick, K. Tanaka, J.-A. Real, A. Bousseksou, *J. Phys. Chem. B.*, submitted.

[19] [19a] G. Baranovic, D. Babic, *Spectrochim. Acta A* **2004**, *60*, 1013. [19b] G. Brehm, M. Reiher, S. Schneider, *J. Phys. Chem. A* **2002**, *106*, 12024. [19c] H. Paulsen, A. X. Trautwein, *Top. Curr. Chem.* **2004**, *235*, 197.

[20] [20a] A. Bousseksou, M. Verelst, H. Constant-Machado, G. Lemercier, J.-P. Tuchagues, F. Varret, *Inorg. Chem.* **1996**, *35*, 110. [20b] A. Bousseksou, L. Salmon, F. Varret, J.-P. Tuchagues, *Chem. Phys. Lett.* **1998**, *282*, 209. [20c] N. Moliner, M. Muñoz, S. Létard, L. Salmon, J.-P. Tuchagues, A. Bousseksou, J.-A. Real, *Inorg. Chem.* **2002**, *41*, 6997.

[21] S. Askénazy, C. Fert, J. Marquez, P. Bellan, P. Wallace, F. Herlach, *Rev. Phys. Appl.* **1986**, *21*, 563.

[22] Y. Qi, E. W. Muller, H. Spiering, P. Gütlich, *Chem. Phys. Lett.* **1982**, *93*, 567.

[23] [23a] J. Lejay, A. G. W. Jansen, P. Wyder, *Phys. Rev. B* **1991**, *43*, 8196. [23b] Y. Garcia, O. Kahn, J.-P. Ader, A. Buzdin, Y. Meurdesoif, M. Guillot, *Phys. Lett. A* **2000**, *271*, 145.

[24] [24a] C. P. Slichter, H. G. Drickamer, *J. Chem. Phys.* **1971**, *56*, 2142. [24b] J. R. Ferraro, *Coord. Chem. Rev.* **1979**, *29*, 1. [24c] E. Meissner, H. Köppen, C. P. Kohler, H. Spiering, P. Gütlich, *Hyperfine Interact.* **1986**, *28*, 799. [24d] P. Adler, H. Spiering, P. Gütlich, *J. Phys. Chem. Solids* **1989**, *50*, 587. [24e] V. Ksenofontov, G. Levchenko, H. Spiering, P. Gütlich, J.-F. Létard, Y. Bouhedja, O. Kahn, *Chem. Phys. Lett.* **1998**, *294*, 545. [24f] V. Ksenofontov, H. Spiering, A. Schreiner, G. Levchenko, H. A. Goodwin, P. Gütlich, *J. Phys. Chem. Solids* **1999**, *60*, 393. [24g] S. Schenker, A. Hauser, W. Wang, I. Y. Chan, *Chem. Phys. Lett.* **1998**, *297*, 281. [24h] A. Hauser, H. Romstedt, J. Jeftic, *J. Phys. Chem. Solids* **1996**, *57*, 1743. [24i] J. Jeftic, A. Hauser, *J. Phys. Chem. B* **1997**, *101*, 10262. [24j] E. Codjovi, N. Menéndez, J. Jeftic, F. Varret, *C. R. Acad. Sci., Ser. IIc: Chim.* **2001**, *4*, 181. [24k] V. Ksenofontov, A. B. Gaspar, P. Gütlich, *Top. Curr. Chem.* **2004**, *235*, 23. [24l] T. Granier, B. Gallois, J. Gaultier, J. A. Real, J. Zarembowitch, *Inorg. Chem.* **1993**, *32*, 5305. [24m] J. J. McGarvey, I. Lawthers, K. Heremans, H. Toftlund, *J. Chem. Soc. Chem. Comm.* **1984**, 1575.

[25] [25a] F. Varret, A. Bleuzen, K. Boukheddaden, A. Bousseksou, E. Codjovi, C. Enachescu, A. Goujon, J. Linares, N. Menendez, M. Verdaguer, *Pure Appl. Chem.* **2002**, *74*, 2159. [25b] G. Molnar, V. Niel, J. A. Real, L. Dubrovinsky, A. Bousseksou, J. J. Mc-Garvey, *J. Phys. Chem. B* **2003**, *107*, 3149.

[26] A. Bousseksou, L. Tommasi, G. Lemercier, F. Varret, J.-P. Tuchagues, *Chem. Phys. Lett.* **1995**, *243*, 493.

[27] M. L. Boillot, J. Zarembowitch, J. P. Itié, A. Polian, E. Bourdet, J. Haasnot, *New J. Chem.* **2002**, *26*, 313.

[28] R. Zimmermann, E. König, *J. Phys. Chem. Solids* **1977**, *38*, 779.

[29] J. J. McGarvey, I. Lawthers, *J. Chem. Soc., Chem. Commun.* **1982**, 906.

[30] S. Decurtins, P. Gütlich, C. P. Köhler, H. Spiering, A. Hauser, *Chem. Phys. Lett.* **1984**, *105*, 1.

[31] [31a] A. Hauser, *J. Chem. Phys.* **1991**, *94*, 2741. A. Hauser, *Coord. Chem. Rev.* **1991**, *111*, 275. [31b] A. Hauser, J. Jeftic, H. Romstedt, R. Hinek, H. Spiering, *Coord. Chem. Rev.* **1999**, *190−192*, 491. [31c] A. Hauser, *Top. Curr. Chem.* **2004**, *234*, 155. [31d] F. Varret, K. Boukheddaden, E. Codjovi, C. Enachescu, J. Linarès, *Top. Curr. Chem.* **2004**, *234*, 199.

[32] J.-F. Létard, P. Guionneau, L. Goux-Capes, *Top. Curr. Chem.* **2004**, *235*, 221.

[33] G. S. Matouzenko, A. Bousseksou, S. Lecocq, P. J. van Koningsbruggen, M. Perrin, O. Kahn, A. Collet, *Inorg. Chem.* **1997**, *36*, 2975.

[34] G. S. Matouzenko, A. Bousseksou, S. Lecocq, P. J. van Koningsbruggen, M. Perrin, O. Kahn, A. Collet, *Inorg. Chem.* **1997**, *36*, 5869.

[35] [35a] E. König, K. Madeja, *Inorg. Chem.* **1967**, *6*, 48. [35b] E. König, K. Madeja, K. J. Watson, *J. Am. Chem. Soc.* **1968**, *90*, 1146. [35c] A. Ozarowski, B. R. MacGarvey, A. B. Sarkar, E. Drake, *Inorg. Chem.* **1988**, *27*, 627.

[36] [36a] P. Poganiuch, S. Decurtins, P. Gütlich, *J. Am. Chem. Soc.* **1990**, *112*, 3270. [36b] L. Wiehl, *Acta Crystallogr., Sect. B* **1993**, *49*, 289. [36c] R. Hinek, H. Spiering, D. Schollmeyer, P. Gütlich, A. Hauser, *Chem. Eur. J.* **1996**, *2*, 1427. [36d] G. Matouzenko, G. Vériot, J. P. Dutasta, A. Collet, J. Jordanov, F. Varret, M. Perrin, S. Lecocq, *New J. Chem.* **1995**, *19*, 881. [36e] Y. Garcia, O. Kahn, L. Rabardel, B. Chansou, L. Salmon, J. P. Tuchagues, *Inorg. Chem.* **1999**, *38*, 4663.

[37] G. S. Matouzenko, J.-F. Letard, S. Lecocq, A. Bousseksou, L. Capes, L. Salmon, M. Perrin, O. Kahn, A. Collet, *Eur. J. Inorg. Chem.* **2001**, 2935.

[38] G. S. Matouzenko, A. Bousseksou, S. A. Borshch, M. Perrin, S. Zein, L. Salmon, G. Molnar, S. Lecocq, *Inorg. Chem.* **2004**, *43*, 227.

[39] [39a] M. Mikami, M. Konno, Y. Saito, *Chem. Phys. Lett.* **1979**, *63*, 566. [39b] E. König, G. Ritter, S. K. Kulshreshtha, J. Waigel, L. Sacconi, *Inorg. Chem.* **1984**, *23*, 1241. [39c] C.-C. Wu, J. Jung, P. K. Gantzel, P. Gütlich, D. N. Hendrickson, *Inorg. Chem.* **1997**, *36*, 5339.

[40] [40a] O. Kahn, E. Codjovi, *Philos. Trans. R. Soc. London, Ser. A* **1996**, *354*, 359. [40b] O. Kahn, Y. Garcia, J.-F. Letard, C. Mathonière, *NATO ASI Ser., Ser. C* **1998**, *518*, 127.

[41] [41a] L. G. Lavrenova, V. N. Ikorskii, V. A. Varnek, I. M. Oglez-

 © 2004 Wiley-VCH Verlag GmbH & Co. KGaA, Weinheim

neva, S. V. Larionov, *Koord. Khim.* **1986**, *12*, 207. [41b] L. G. Lavrenova, V. N. Ikorskii, V. A. Varnek, I. M. Oglezneva, S. V. Larionov, *Koord. Khim.* **1990**, *16*, 654. [41c] W. Vreugdenhil, J. H. van Diemen, R. A. G. de Graaff, J. G. Haasnoot, J. Reedjik, A. M. van der Kraan, O. Kahn, J. Zarembowitch, *Polyhedron* **1990**, *9*, 2971.

[42] [42a] A. Michalowitch, J. Moscovici, J. Ducourant, D. Cracco, O. Kahn, *Chem. Mater.* **1995**, *7*, 1833. [42b] A. Michalowitch, J. Moscovici, O. Kahn, *J. Phys. IV* **1997**, *7*, C2-633.

[43] [43a] J. A. Real, E. Andrés, M. C. Munoz, M. Julve, T. Granier, A. Bousseksou, F. Varret, *Science* **1995**, *268*, 265. [43b] N. Moliner, C. Munoz, S. Létard, X. Solans, N. Menéndez, A. Goujon, F. Varret, J. A. Real, *Inorg. Chem.* **2000**, *39*, 5390.

[44] G. S. Matouzenko, G. Molnar, N. Bréfuel, M. Perrin, A. Bousseksou, S. A. Borshch, *Chem. Mater.* **2003**, *15*, 550.

Received July 1, 2004

 © 2004 Wiley-VCH Verlag GmbH & Co. KGaA, Weinheim

X-ray and Solution Structures of the First Zn Funnel Complex Based on a Calix[6]aza-cryptand

Ulrich Darbost,[a] Xianshun Zeng,[a] Marie-Noëlle Rager,[b] Michel Giorgi,[c] Ivan Jabin,*[a] and Olivia Reinaud*[d]

Keywords: Calixarenes / Cryptands / Host-guest systems / Supramolecular chemistry / Zinc

First insights into the coordinative behavior of a calix[6]tren ligand are presented. Reaction with zinc perchlorate led to a dicationic complex with the metal ion strongly bound to the tren cap. It presents a unique coordination site accessible for a small coordinating molecule that is controlled by the calixarene cavity. Hence, X-ray analysis and solution ^{1}H NMR studies evidenced a five-coordinate complex thanks to the coordination of a guest ligand, MeCN, included deep inside the calixarene cavity. Interestingly, the metal ion is bound in an asymmetrical environment in both the solid state and in solution. It is also particularly reluctant, and resistant, to anion binding.
(© Wiley-VCH Verlag GmbH & Co. KGaA, 69451 Weinheim, Germany, 2004)

Introduction

In nature, the control of the reactivity of a metallo site is performed by the structuring of the protein backbone in order to not only preorganize the coordination site for the metal ion, but also provide a cavity and a corridor connecting it to the bulk that controls the binding of exogeneous molecules and the reactivity of the metal ion.[1] Whilst exploring these supramolecular aspects of bioinorganic chemistry, we have developed a calixarene-based system that models mononuclear metallo-enzyme active sites.[2−4] In these systems, the binding of a zinc ion to a calix[6]arene bearing three nitrogenous arms allows the shaping of the molecular receptor. As a result, the first examples of stable tetrahedral dicationic Zn complexes were obtained. These so-called funnel complexes display unrivalled host/guest behavior toward neutral organic molecules due to the control exerted by the calixarene structure on the second coordination sphere of the metal ion and on the access to the metal center.[2] The highly flexible calix-based N_3 system appears, however, to suffer from two weaknesses: i) although highly disfavored, external binding of small molecules is not totally precluded, as evidenced in some particular cases,[4,5] and ii) the addition of a base such as triethylamine to the complex leads to decoordination and precipitation of metal hydroxides, particularly in an aprotic solvent, due to a weak chelate effect (two coordinating nitrogen centers are separated by 15 atoms). We have recently described the synthesis of a novel calix[6]aza-cryptand, namely calix[6]tren,[6] which appears to be a good candidate to remedy the weaknesses of the N_3-calix system (Scheme 1). Indeed, the tren structure offers a strong chelate effect and its tertiary nitrogen atom, which caps the narrow rim of the calixarene, closes the access in the *trans* position of the cavity for an exogenous molecule. This paper describes the first member of the calix-cryptand metal complexes family that fulfills both desired improvements of the supramolecular biomimetic system.

Results and Discussion

Complexation of zinc by calix[6]tren (**1**) was performed in a CH_2Cl_2/MeOH (1:1) mixture by reacting stoichiometric amounts of zinc perchlorate and the N_4 ligand. Under these conditions, the calix-tren Zn complex **2**⊃L (L = MeOH) was isolated in 69% yield (Scheme 1).

X-ray quality crystals of **2**⊃MeCN were grown by slow diffusion of diethyl ether into an acetonitrile solution of the complex. The crystal structure is displayed in Figure 1. As

[a] URCOM, Université du Havre, Faculté des Sciences et Techniques,
25 rue Philippe Lebon, BP 540, 76058 Le Havre cedex, France
Fax: (internat.) +33-232744391
E-mail: ivan.jabin@univ-lehavre.fr
[b] Service de RMN, Ecole Nationale Supérieure de Chimie de Paris (ENSCP),
11 rue Pierre et Marie Curie, 75231 Paris Cedex 05, France
[c] Laboratoire de Cristallochimie,
Université Paul Cézanne (Aix-Marseille III),
Faculté des Sciences et Techniques
av. Escadrille Normandie-Niemen, 13397 Marseille cedex 20, France
[d] Laboratoire de Chimie et Biochimie Pharmacologiques et Toxicologiques, UMR CNRS 8601, Université René Descartes,
45 rue des Saints Pères, 75270 Paris cedex 06, France
Fax: (internat.) +33-142862183
E-mail: Olivia.Reinaud@univ-paris5.fr
Supporting information for this article is available on the WWW under http://www.eurjic.org or from the author.

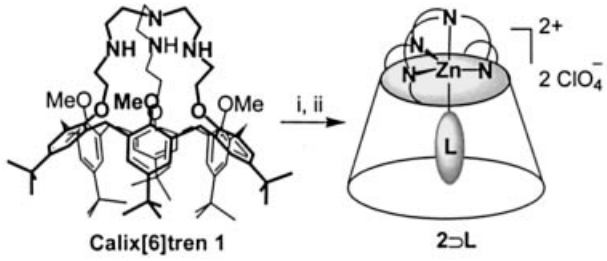

Scheme 1. Zn complexation of calix[6]tren **1**: i) $Zn(ClO_4)_2(H_2O)_6$, CH_2Cl_2/MeOH (L = MeOH); ii) MeCN (L = MeCN)

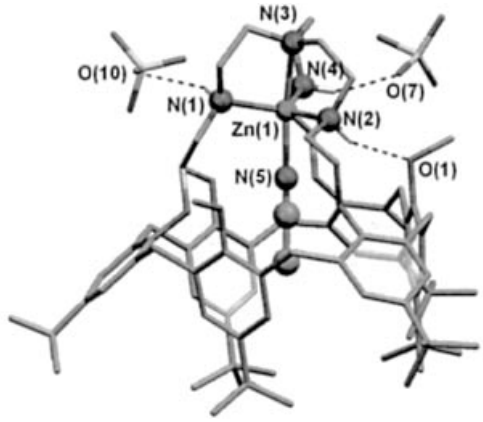

Figure 1. Crystal structures of **2**⊃MeCN; the location of the hydrogen atoms of the amino groups was calculated; other hydrogen atoms and solvents of crystallization have been omitted for clarity; selected bond lengths (Å) and angles (°): Zn(1)−N(4) 2.053(7), Zn(1)−N(2) 2.078(7), Zn(1)−N(1) 2.080(7), Zn(1)−N(5) 2.107(9), Zn(1)−N(3) 2.197(6); N(4)−Zn(1)−N(2) 124.8(3), N(4)−Zn(1)−N(1) 112.7(3), N(2)−Zn(1)−N(1) 118.0(3), N(4)−Zn(1)−N(5) 102.0(3), N(2)−Zn(1)−N(5) 89.4(3), N(1)−Zn(1)−N(5) 100.2(3), N(4)−Zn(1)−N(3) 84.4(3), N(2)−Zn(1)−N(3) 81.0(3), N(1)−Zn(1)−N(3) 83.6(3), N(5)−Zn(1)−N(3) 170.4(3); hydrogen bonding: N(1)···O(10) 3.07, N(4)···O(7) 3.01, N(2)···O(1) 3.07; N(1)···H···O(10) 131, N(4)···H···O(7) 157, N(2)···H···O(1) 156

attested by the presence of two counteranions, the Zn complex is dicationic. The metal ion is encapsulated in the calix[6]cryptand thanks to its coordination to the N_4 core of the tren cap and to a guest ligand (MeCN). The geometry is trigonal bipyramidal with some tetragonal distortion (τ = 0.76).[7] The average Zn−N distance for the trigonal base of the pyramid is 2.070 Å. This is slightly longer than found in the related tetrahedral calix-N_3 complexes,[2] in agreement with a decrease of the Zn Lewis acidity for a five-coordinate species compared to a four-coordinate one. In the axial position, the tertiary N atom capping the system is even more loosely bound to the metal ion [$d(Zn_1-N_3)$ = 2.197 Å] than the MeCN ligand [$d(Zn_1-N_5)$ = 2.107 Å]. The guest is deeply buried in the heart of the calixarene structure, with its methyl group pointing towards an aromatic ring at a perpendicular distance (3.8 Å) typical of CH-π interactions. Interestingly, weak hydrogen bonds are present between the capping secondary amino groups and either a perchlorate anion or a phenoxyl oxygen atom. Finally, the three amino arms wrapping the Zn ion do not form a helix, but adopt an asymmetric conformation with two coordinated arms presenting a relative helical orientation opposite to each other with opposite configurations at the nitrogen atoms.

The dicationic Zn complex **2**⊃MeCN has also been characterized in solution. When **2**⊃MeOH was dissolved in CD_3CN, a dissymmetrical ^1H NMR spectrum was obtained (Figure 2). Thanks to the sharpness of the spectrum, most resonances could be attributed by 2D NMR analyses (see the Exp. Sect. and Supporting Information). Compared to the free ligand, the methoxy protons are shifted downfield, which indicates that they have been expelled from the cavity by a coordinating guest. The dissymmetry of the NMR spectrum is due to the asymmetric conformation adopted by the cap due to the different configurations of the NH stereocenters, as depicted by the X-ray structure of **2**⊃MeCN.[8] When **2**⊃MeOH was dissolved in a non-coordinating solvent such as $CDCl_3$, in the presence of CH_3CN, the NMR spectrum was similar to that recorded in CD_3CN, although with an additional highfield-shifted singlet at δ = −1.11 ppm (220 K), thereby confirming the intra-cavity binding of the acetonitrile molecule. Increasing the temperature to above room temperature led to the coalescence of the calixarene resonances. At 390 K, in $Cl_2CDCDCl_2$, a C_{3v}-symmetric spectrum was obtained (see the Supporting Information). This phenomenon is explainable by the fast pyramidal inversion of the coordinated nitrogen atoms at high temperature, leading to an average C_{3v}-symmetrical conformation.

Finally, the nitrilo complex was not affected by the presence of chloride ions[9] nor by hydroxide.[10] This shows that the Zn ion is much more strongly coordinated by the calix-cryptand than it is by the calix-N_3 ligands. It also emphasizes the reluctance of these funnel complexes to bind anionic ligands due to repulsive interactions with the phenoxyl units of the calixarene structure.

Conclusion

We have described the first member of a novel family of biomimetic complexes based on an N_4-calix-cryptand. In this system, the Zn ion is strongly coordinated by the three tren NH moieties in an asymmetrical environment with the tren tertiary nitrogen atom capping the edifice. As a result, the calix-tren ligand forces the metal ion to complete its coordination sphere through the binding of a guest ligand that is deeply included in the calixarene cavity, leaving no access for an external binding in the position *trans* to the guest. The strong chelate effect provided by the tren cap confers on the complex an increased robustness compared to the parent calix-N_3 system as it does not collapse under strongly basic conditions. Hence, this calix-cryptand exerts a remarkable control on the first and second coordination sphere of the metal ion.

 © 2004 Wiley-VCH Verlag GmbH & Co. KGaA, Weinheim

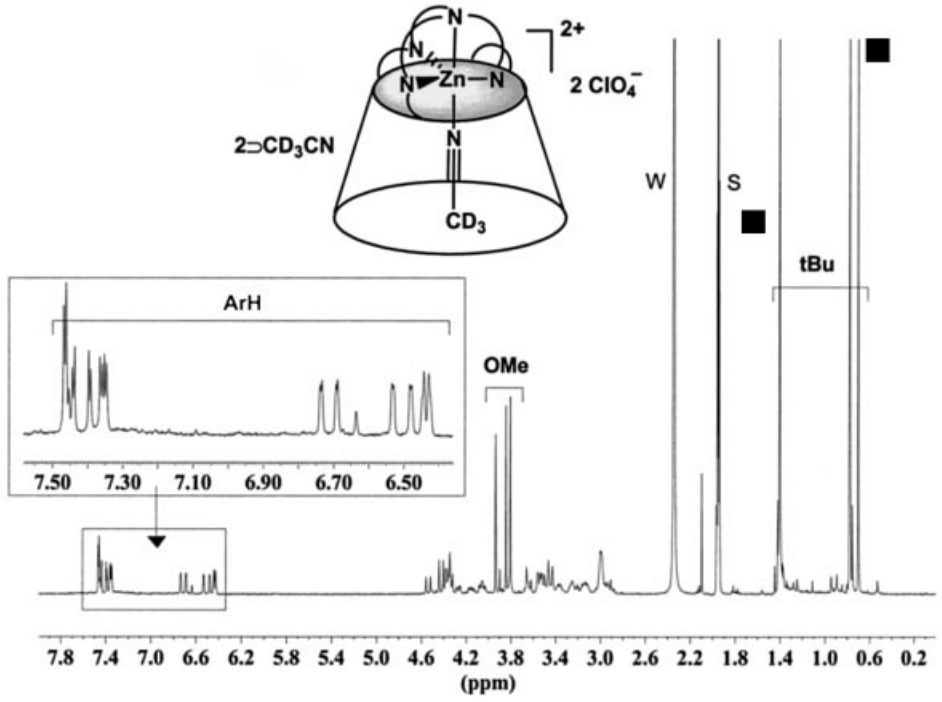

Figure 2. ^{1}H NMR spectrum (400 MHz, room temp., CD_3CN) of complex **2**⊃CD_3CN; residual solvent and water peaks have been labeled "S" and "W" respectively

Experimental Section

General Remarks: CH_2Cl_2 was distilled from CaH_2 under argon. ^{1}H and ^{13}C NMR spectra were recorded either with a Bruker Avance 400 or a Bruker Avance 300 specrtometer. Traces of residual solvent or poly(dimethylsiloxane) (R) were used as internal standard. ^{1}H and ^{13}C resonances corresponding to anisole moieties are labelled with a superscripted 1 (e.g. tBu^1, ArH^1, C$^1_{Ar}$) and the others are are labelled with a superscripted 2. They were assigned by HMBC and HMQC experiments. IR spectra were recorded on a Perkin−Elmer IRFT Paragon 1000 apparatus. Elemental analyses were performed at the Service de Microanalyse, (I.C.S.N., Gif sur Yvette, France).

Safety Note: ***Caution!*** *Although we have not encountered any problem, it is noted that perchlorate salts of metal complexes with organic ligands are potentially explosive and should be handled only in small quantities with appropriate precautions.*

Zn-calix[6]tren Complex 2: Methanol (2.5 mL), dichloromethane (3 mL) and triethylamine (0.011 mL, 0.082 mmol) were added to a flask containing $Zn(ClO_4)_2(H_2O)_6$ (30.6 mg, 0.082 mmol) and calix[6]tren (**1**; 102 mg, 0.082 mmol) under an inert atmosphere. The reaction mixture was stirred at room temperature for 30 min. After concentration to a third of the volume by bubbling argon through the solution, a crystalline product was obtained. It was separated from the solvent by centrifugation, washed with cold methanol and dried under vacuum to give **2**⊃MeOH (88 mg, 69%) as a white solid. M.p. 275 °C (decomp.). ^{1}H NMR (400 MHz, CD_3CN, room temp.): δ = 0.70 (s, 9 H, tBu^1), 0.77 (s, 9 H, tBu^1), 0.78 (s, 9 H, tBu^1), 1.40 (s, 27 H, tBu^2), 2.90−3.66 (m, 24 H, NHCH_2CH$_2$N + NHCH$_2$CH_2N + OCH$_2$CH_2N + Ar-αCH$_{eq}$), 3.80 (s, 3 H, OCH$_3$), 3.84 (s, 3 H, OCH$_3$), 3.93 (s, 3 H, OCH$_3$), 4.02−4.55 (m, 12 H, OCH_2CH$_2$NH + Ar-αCH$_{ax}$), 6.43 (br. s, 1 H, ArH^1), 6.44 (br. s, 1 H, ArH^1), 6.48 (d, J = 2 Hz, 1 H, ArH^1), 6.53 (d, J = 2 Hz, 1 H, ArH^1), 6.69 (d, J = 2 Hz, 1 H, ArH^1), 6.73 (d, J = 2 Hz, 1 H, ArH^1), 7.35 (d, J = 2 Hz, 1 H, ArH^2), 7.36 (d, J = 2 Hz, 1 H, ArH^2), 7.39 (d, J = 2 Hz, 1 H, ArH^2), 7.44 (d, J = 2 Hz, 1 H, ArH^2), 7.46 (d, J = 2 Hz, 1 H, ArH^2) ppm. ^{1}H NMR (300 MHz, 390 K, $Cl_2CDCDCl_2$): δ = 0.69 (s, 27 H, tBu^1), 1.33 (s, 27 H, tBu^2), 3.00−3.40 (m, 24 H, CH_2N + CH_2O), 3.47 (d, J = 15 Hz, 6 H, Ar-αCH$_{eq}$), 3.86 (br. s, 9 H, OCH$_3$), 4.31 (d, J = 15 Hz, 6 H, Ar-αCH$_{ax}$), 6.53 (s, 6 H, ArH), 7.25 (s, 6 H, ArH) ppm. ^{13}C NMR (75 MHz, CD_3CN, room temp.): δ = 29.4, 29.5, 30.0, 30.3, 30.7, 31.0 (Ar-αCH_2); 31.5, 31.6 [C^1(CH_3)$_3$]; 31.8 [C^2(CH_3)$_3$]; 34.5(5), 34.5(7), 34.6(2) [C^1(CH$_3$)$_3$]; 34.9(4), 34.9(8) [C^2(CH$_3$)$_3$]; 46.9, 48.5, 48.9 (NHCH_2CH_2N); 49.6, 51.1, 51.5 (OCH$_2$$CH_2$NH); 51.7, 52.0, 52.3 (NHCH$_2$$CH_2$N); 61.4, 61.5, 62.1 (OCH$_3$); 71.7, 73.4(6), 73.5(0) (OCH_2CH$_2$NH); 123.0, 123.3, 123.9(8), 124.0(2), 124.7, 125.2 (C$^1_{Ar}$H); 129.1(0), 129.1(4), 129.2, 129.4, 129.9, 130.1 (C$^2_{Ar}$H); 132.0, 132.6, 132.9, 133.3, 133.6, 133.8, 133.9, 134.0, 135.3(5), 135.4(1) (C_{Ar}CH$_2$); 146.4, 146.5, 146.6 (C$^1_{Ar}$); 147.6, 147.8, 147.9 (C$^2_{Ar}$); 152.8 (C$^2_{Ar}$O + C$^1_{Ar}$O), 153.2 (C$^1_{Ar}$O + C$^2_{Ar}$O), 153.4 (C$^1_{Ar}$O), 154.4 (C$^2_{Ar}$O) ppm. IR (KBr): $\tilde{\nu}$ = 1637, 1482, 1120, 624 (Cl−O) cm^{-1}. [Zn($C_{81}H_{114}N_4O_6$)(CH$_3$OH)]-(ClO_4)$_2$·0.5H_2O (1545.1): calcd. C 63.74, H 7.76, N 3.63; found C 63.69, H 7.65, N 3.46.

X-ray Crystallographic Study: X-ray quality crystals of **2**⊃MeCN were grown by slow diffusion of diethyl ether into an acetonitrile solution. M_w = 1545.1, monoclinic, colorless crystal (0.5 × 0.3 × 0.3 mm^3), a = 33.7660(6) Å, b = 14.7500(3) Å, c = 37.6960(9) Å, β = 97.255(7)°, V = 18624.1(7) Å^3, space group $C2/c$, Z = 8, ρ = 1.102 g·cm^{-3}, μ(Mo-K_α) = 3.79 cm^{-1}, 9382 reflections measured at 193 K (Bruker-Nonius KappaCCD diffractometer[11]) in the 0.54−27.83° θ range, 8901 unique, 969 parameters refined on F^2

 © 2004 Wiley-VCH Verlag GmbH & Co. KGaA, Weinheim

using 8901 reflections [Shelxl][12] to final indices $R[F^2 > 4\sigma F^2] = 0.1292$, $wR = 0.4056$ [$w = 1/[\sigma^2(F_o^2) + (0.35P)^2 + 40.0P]$ where $P = (F_o^2 + 2F_c^2)/3$]. Some remaining densities outside the calixarene complex were attributed to diffused and highly disordered water molecules. One of the two perchlorate counteranions was found to be disordered and was split on two sites with occupancies equal to 0.5. One *tert*-butyl group was treated in the same way. All hydrogen atoms were introduced in theoretical positions, included in the calculations but not refined. The last residual Fourier positive and negative peaks were equal to 0.930 and −0.933 respectively.

CCDC-244803 contains the supplementary crystallographic data for this paper. These data can be obtained free of charge at www.ccdc.cam.ac.uk/conts/retrieving.html [or from the Cambridge Crystallographic Data Centre, 12, Union Road, Cambridge CB2 1EZ, UK; fax: +44-1223-336-033; E-mail: deposit@ccdc.cam.ac.uk].

Supporting Information: See also the footnote on the first page of this article. ^{1}H NMR spectra of **2** (recorded at 293 K, 330 K, 360 K and 390 K in $Cl_2CDCDCl_2$). ^{13}C NMR, COSY and HMQC spectra of complex **2**⊃CD_3CN (recorded at room temp. in CD_3CN) and ^{1}H NMR spectra of **2**⊃CH_3CN (recorded at 290 K and 220 K in $CDCl_3$).

Acknowledgments

We thank the Région Haute-Normandie and the French Ministry of Research and New Technologies for financial support.

[1] Review: *Chem. Rev.* **1996**, *96*, 2237−3042 (theme: "Bioinorganic Enzymology").

[2] For leading references with Zn^{II}, see: [2a] O. Sénèque, M.-N. Rager, M. Giorgi, O. Reinaud, *J. Am. Chem. Soc.* **2000**, *122*, 6183−6189. [2b] Y. Rondelez, O. Sénèque, M.-N. Rager, A. F. Duprat, O. Reinaud, *Chem. Eur. J.* **2000**, *6*, 4218−4226. [2c] O. Sénèque, M.-N. Rager, M. Giorgi, O. Reinaud, *J. Am. Chem. Soc.* **2001**, *123*, 8442−8443. [2d] O. Sénèque, M. Giorgi, O. Reinaud, *Chem. Commun.* **2001**, 984−985. [2e] O. Sénèque, M. Giorgi, O. Reinaud, *Supramol. Chem.* **2003**, *15*, 573−580.

[3] For leading references with Cu^{I}, see: [3a] S. Blanchard, L. Le Clainche, M.-N. Rager, B. Chansou, J.-P. Tuchagues, A. F. Duprat, Y. Le Mest, O. Reinaud, *Angew. Chem. Int. Ed.* **1998**, *37*, 2732−2735. [3b] Y. Rondelez, G. Bertho, O. Reinaud, *Angew. Chem. Int. Ed.* **2002**, *41*, 1044−1046. [3c] Y. Rondelez, M.-N. Rager, A. F. Duprat, O. Reinaud, *J. Am. Chem. Soc.* **2002**, *124*, 1334−1340.

[4] For five-coordinate complexes, see: [4a] L. Le Clainche, M. Giorgi, O. Reinaud, *Inorg. Chem.* **2000**, *39*, 3436−3437. [4b] L. Le Clainche, Y. Rondelez, O. Sénèque, S. Blanchard, M. Campion, M. Giorgi, A. F. Duprat, Y. Le Mest, O. Reinaud, *Comptes Rendus Acad. Sci., Chimie, Série IIc* **2000**, *3*, 811−819. [4c] O. Sénèque, M. Campion, B. Douziech, M. Giorgi, Y. Le Mest, O. Reinaud, *Dalton Trans.* **2003**, 4216−4218. [4d] O. Sénèque, M. Campion, M. Giorgi, Y. Le Mest, O. Reinaud, *Eur. J. Inorg. Chem.* **2004**, 1817−1826.

[5] O. Sénèque, M. Campion, B. Douziech, M. Giorgi, E. Rivière, Y. Journaux, Y. Le Mest, O. Reinaud, *Eur. J. Inorg. Chem.* **2002**, 2007−2014.

[6] I. Jabin, O. Reinaud, *J. Org. Chem.* **2003**, *68*, 3416−3419.

[7] A. W. Addison, T. N. Rao, J. Reedijk, J. van Rijn, G. C. Verschoor, *J. Chem. Soc., Dalton Trans.* **1984**, 1349−1356.

[8] The use of $Zn(OTf)_2$ or $Zn(picrate)_2$ salts led also to a similar dissymmetrical ^{1}H NMR spectrum in CD_3CN. In the case of the zinc picrate complex, integration of the picrate signal confirmed the presence of two equivalents of anion versus calixtren.

[9] When $ZnCl_2$ was added to a CD_3CN solution of **1**, the ^{1}H NMR spectrum of the resulting Zn complex was identical to the one obtained from Zn perchlorate. The same procedure with the previously reported calix-N_3 system[2] led to the formation of dimeric species (unpublished data). With Cu, the presence of chloride gave rise to a tetranuclear complex.[5]

[10] The addition of four equivalents of tetrabutylammonium hydroxide (0.1 M solution in toluene/methanol) or a large excess of TEA (up to 126 equiv.) did not affect the NMR spectrum of the complex, even in $CDCl_3$. With the classical calix-N_3 based complexes,[2] addition of hydroxides or TEA in $CDCl_3$ led to instantaneous precipitation of $Zn(OH)_2$.

[11] Bruker-Nonius (**1998**), Kappa CCD Reference Manual, Nonius B.V., P. O. Box 811, 2600 Av, Delft, The Netherlands.

[12] G. M. Sheldrick (**1997**), *SHELXL-97. Program for the refinement of crystal structures*, Univ. of Göttingen, Germany.

Received July 16, 2004

 © 2004 Wiley-VCH Verlag GmbH & Co. KGaA, Weinheim

Solvothermal Syntheses and Structural Characterisation of Three Isostructural 3D Metal-Malate Coordination Polymers: $\{[M(C_4H_4O_5)(H_2O)]\cdot H_2O\}_n$ ($M = Co^{II}$, Ni^{II}, Co^{II}/Ni^{II})

Feng-Tong Xie,[a,b] Li-Mei Duan,[a] Ji-Qing Xu,*[a] Ling Ye,[c] Ya-Bing Liu,[a] Xi-Xue Hu,[a] and Jiang-Feng Song[a]

Keywords: Malate bridges / Solvothermal synthesis / Coordination polymer / Quinque-dentate ligand

Three isostructural coordination polymers with the general formula $\{[M(C_4H_4O_5)(H_2O)]\cdot H_2O\}_n$ [M = Co^{II} (**1**), Ni^{II} (**2**) and $1/3Co^{II} + 2/3Ni^{II}$ (**3**), $C_4H_4O_5$ = $Hmal^{2-}$, malate dianion] have been designed and synthesised via solvothermal routes. In these compounds, the malate acts as the unique quinque-dentate ligand with all five oxygen atoms participating in the coordination. The M^{II} ions are interconnected via α- and β-carboxyl groups from the malate ligands to generate zigzag chains and planes which are further linked together by the β-carboxyl groups leading to the 3D open frameworks. Variable temperature magnetic susceptibility measurements indicate the occurrence of antiferromagnetic (**1**), ferromagnetic (**2**) and ferrimagnetic (**3**) interactions between the M^{II} ions mediated by the *skew-skew* carboxylate bridges.
(© Wiley-VCH Verlag GmbH & Co. KGaA, 69451 Weinheim, Germany, 2004)

Introduction

Considerable effort has been made towards the construction of metal-organic frameworks by employing various organic linkers such as carboxylates, bipyridyl and other multifunctional ligands. The use of di- and polycarboxylates can generate a large number of coordination complexes composed of chains, sheets and 3D networks with an enormous variety of intriguing structural topologies. Such systems have received considerable attention due to their fascinating properties as well as their potential applications in many fields. A survey of the synthetic procedures attempted reveals that some of them deal with rigid bridging ligands such as benzenedi-,[1] benzenetri-,[2] benzenetetra-[3] and benzenehexacarboxylates[4] or nitrogen-containing heterocyclic dicarboxylates[5] while others employ flexible aliphatic dicarboxylates as bridging ligands such as malonate,[6] succinate,[7] maleate,[8] fumarate,[8,9] glutarate[10] and adipate.[11] However, the hydroxyl polycarboxylates (HPCs) such as malate, citrate and tartrate have been less studied as building blocks in the construction of metal-organic frameworks though they can display versatile coordination modes. In contrast to the aliphatic dicarboxylate compounds, the presence of the hydroxyl group in HPCs allows the formation of five- and six-membered rings which can stabilise the solid networks. In the metal-HPC systems, much attention has been focused on the compounds of V, Mo or W because malic or citric acid often act as a substitute for homocitric acid in synthetic model studies of nitrogenase and the extended networks of M-HPCs systems have not been further explored.

The malate ligand, besides two terminal carboxyl groups, contains a hydroxyl group in the α-position which can potentially provide an additional coordination site. In all known malate-bridged compounds, the oxygen atoms of the alkoxy or hydroxyl groups participate in coordination along with the α-carboxyl and/or β-carboxyl groups. As well as being an important biological ligand, malate has been found to be a versatile ligand in coordination chemistry. Structurally characterised metal-malate compounds include monomers,[12] dimers,[13] tetramers[14] and polymeric chain compounds[15] as well as a 3D coordination polymer based on copper ions and ternary mixed ligands.[16] To the best of our knowledge, no higher-dimensional network containing malate and water molecules as ligands has been constructed up to now. In addition, similar to the aliphatic dicarboxylates such as malonate or fumarate,[17] malate can also act as a suitable candidate for engineering the design of molecular magnets.

Our exploration of the solvothermal chemistry of the M-HPC systems has resulted in the discovery of some new

[a] State Key Laboratory of Inorganic Synthesis and Preparative Chemistry, Jilin University,
Changchun, 130023, P. R. China
Fax: (internat.) + 86-431-8923907
E-mail: xjq@mail.jlu.edu.cn
[b] The Institute of Product Quality and Metrology Inspection of Tongliao City,
Tongliao, 028000, P. R. China
[c] Key Laboratory of Supramolecular Structure and Materials of the Ministry of Education, Jilin University,
Changchun 130023, P. R. China
Supporting information for this article is available on the WWW under http://www.eurjic.org or from the author.

compounds with unusual coordination modes. Herein we report the solvothermal syntheses, crystal structures and magnetic behaviour of three isostructural compounds $\{[M(C_4H_4O_5)(H_2O)]\cdot H_2O\}_n$ [$C_4H_4O_5$ = $Hmal^{2-}$ (malate dianion), M = Co^{II} (**1**), Ni^{II} (**2**) and $1/3Co^{II} + 2/3Ni^{II}$ (**3**)] in which the coordination mode is unique and has not been previously reported.

Results and Discussion

Solvothermal reactions of the corresponding mixtures of cobalt(II) (or/and nickel) acetate (or chloride), malic acid, 4,4-bipyridine (4,4-bipy) and KOH in an alcohol-water medium yielded crystals of the title compounds. At first we try to synthesise the coordination polymers containing both malate and 4,4-bipy as bridging ligands. However, only the title compounds without 4,4-bipy were obtained under the selected reaction conditions. We also substituted the cobalt salts with iron dichloride to attempt to synthesise iron analogues of the title compounds under similar conditions but this was not successful.

Single-crystal X-ray structural analyses reveal that the metal centres M^{II} (Co^{II}, Ni^{II} and Co^{II}/Ni^{II}) in the title compounds are in distorted octahedral environments coordinated by three different malate ligands and one water molecule as shown in Figure 1. In each case three coordination positions are occupied by O(1), O(4) and O(3) coming from the α-carboxyl, β-carboxyl and hydroxyl groups of the same malate ligand, respectively. Two other coordination sites are occupied by O(2) and O(5) from the α-carboxyl and β-carboxyl groups from two different malato ligands and the sixth coordination site is occupied by OW(1) from a water molecule. The MO_6 polyhedra are severely distorted from idealised octahedral symmetry, the Co−O distances range from 2.0646(18) to 2.1126(19) Å with an average value of 2.0913(19) Å for compound **1**. The O−Co−O angles between neighbouring oxygen atoms range from 86.48(8) to 95.74(8)° except for two smaller angles [O(1)−Co−O(3), 79.04(7)°; O(3)−Co−O(4), 81.59(8)°] caused by the hydroxyl-oxygen atom. This is due to the formation of five- and six-membered chelate rings. For compound **2**, the Ni−O distances range from 2.035(2) to 2.088(2) Å with an average value of 2.056(2) Å. The O−Ni−O angles between neighbouring oxygen atoms range from 85.58(10) to 95.58(9)° except for the angles O(1)−Ni−O(3) [80.95(9)°] and O(3)−Ni−O(4) [82.38(9)°]. The corresponding bond lengths and angles of compound **3** are close to those in **1** and **2**.

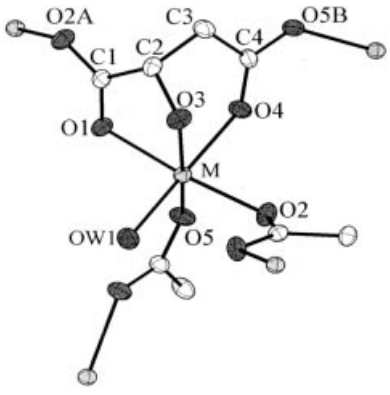

Figure 1. The coordination environment of M^{II} in **1**, **2** and **3**

The malate dianion coordinates to one M^{II} ion and acts as a tridentate ligand via its hydroxyl, α-carboxyl and β-carboxyl groups in a *face*-mode, while the α-carboxyl and β-carboxyl groups further coordinate in a monodentate fashion to the other M^{II} ions in the position trans to the hydroxyl group. The β-carboxyl groups bend back to chelate the M^{II} ions and the C(2)−C(3)−C(4) angles are reduced to 115.9(2)°, 115.7(3)° and 115.5(3)° for **1**, **2** and **3**, respectively. The angles of O(1)−C(1)−O(2A) are 125.1(2)°, 124.8(3)° and 125.3(3)°, and O(4)−C(4)−O(5B) are 123.4(2)°, 123.3(3)° and 124.1(3)° for compounds **1**, **2** and **3**, respectively. Both α-carboxyl and β-carboxyl groups adopt nonplanar *skew-skew* coordination modes and two bridged metal atoms on opposite sides of the carboxylate plane[18] and the corresponding torsion angles of compound **1** are as follow: Co−O(1)−C(1)−C(2) 8.12(29)°, Co−O(2A)−C(1)−C(2) 153.63(17)°; Co−O(4)−C(4)−C(3) 14.33(43)°, Co−O(5B)−C(4)−C(3) 164.53(20)°.

In the title compounds, each μ_3-malate dianion adopts a quinque-dentate coordination mode and all of the five oxygen atoms participate in the coordination towards three metal centres. It follows that each M atom in the crystal structure is attached to three different malate groups. As shown in Figure 2, the M^{II} ions are connected through α- and β-carboxyl groups to form zigzag chains in the [100] direction and the corresponding zigzag layers are further linked together by β-carboxyl groups of malate ligands roughly in the [010] direction leading to the formation of the 3D open frameworks (Figure 3). Figure 2 also shows the distribution of coordinated and lattice water molecules in the [001] direction. The OW(2) atoms of lattice water molecules form

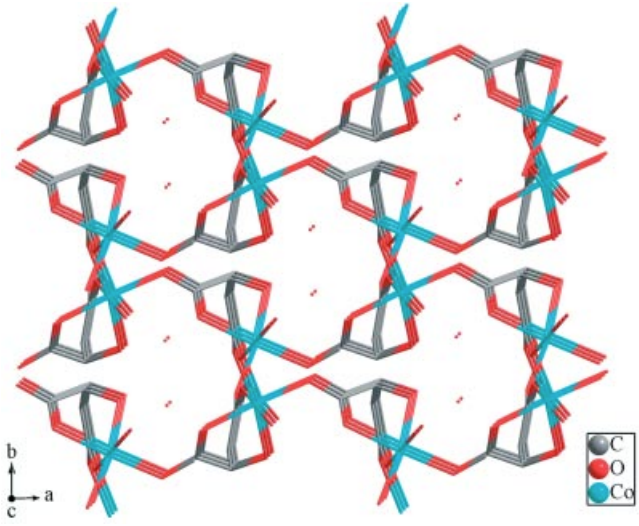

Figure 2. View of the network structure in the [001] direction, hydrogen atoms have been omitted for clarity

 © 2004 Wiley-VCH Verlag GmbH & Co. KGaA, Weinheim

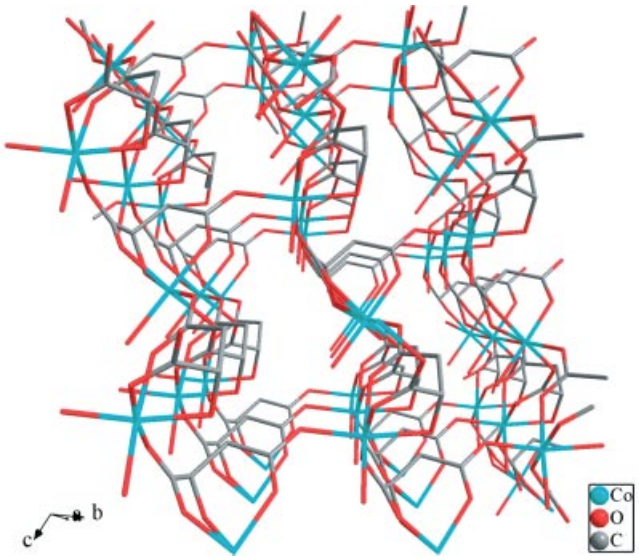

Figure 3. The packing diagram of compound **1** showing the 3D structure, hydrogen atoms and lattice water molecules have been omitted for clarity

hydrogen bonds with O(2) (symmetry mode: x, $-1 + y$, z) and the OW(2)···O(2) distance is 2.918(3) Å. The rhombic 16-membered channels consisting of M−O−C−O−M vectors along the [010] direction can be seen in Figure 4. The adjacent M···M distances are about 5.2 Å (through α-carboxyl groups) and 5.3 Å (through β-carboxyl groups).

The magnetic properties of compounds **1**, **2** and **3** were studied as a function of temperature (2−300 K) in a fixed magnetic field (5000 Oe). As the temperature is lowered, the χ_m values increase slowly until around 50 K in **1** and 20 K in **2** and **3**. They then dramatically increase at lower temperatures still. The data above 50 K can be fitted with Curie−Weiss functions with a Weiss constant $\theta = -20.21$ K and a Curie constant $c = 2.92$ cm^3·K·mol^{-1} for compound **1**, and $\theta = +2.38$ K and $c = 1.32$ cm^3·K·mol^{-1} for **2**. These are characteristic of overall antiferromagnetic (**1**) and ferromagnetic (**2**) interactions, respectively.

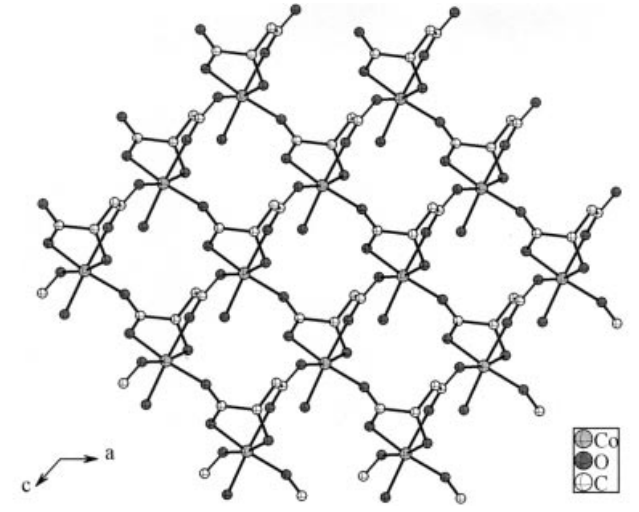

Figure 4. View of the network structure showing the channels in the [010] direction, hydrogen atoms and lattice water molecules have been omitted for clarity

Plots of μ_{eff} (the effective magnetic moment) versus T are shown in Figure 5 (compounds **1** and **2**). The μ_{eff} values of **1** decrease slowly from 4.65 μ_B at 300 K to 4.10 μ_B at 50 K and then decrease rapidly reaching 2.67 μ_B at 2 K. The μ_{eff} value of 4.65 μ_B at 300 K for compound **1** is larger than the spin-only value for high-spin cobalt(II) (3.87 μ_B per cobalt(II) ion with $g = 2.0$) and consistent with that expected for an octahedral cobalt(II) with an important orbital contribution.[19] For compound **2**, the μ_{eff} value of 3.18 μ_B at 300 K is close to the expected spin-only value (3.11 μ_B per nickel(II) with $g = 2.2$). Upon cooling, and in contrast to compound **1**, the μ_{eff} values of **2** increase slowly reaching 3.32 μ_B at 50 K and 3.42 μ_B at 30 K, then increase rapidly at low temperature. For compound **3**, as the temperature decreases, the μ_{eff} values (3.90 μ_B, 300 K) decrease slowly reaching steady values between 3.75 μ_B and 3.73 μ_B from 50 K to 24 K. This is then followed by a sharp increase below 24 K which is characteristic of ferrimagnetic behaviour.

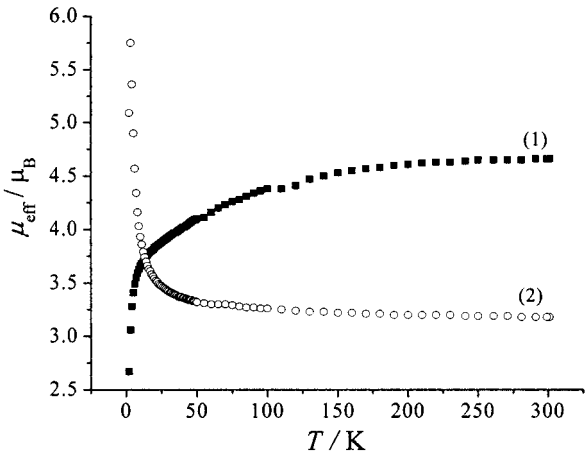

Figure 5. Thermal variations of μ_{eff} for compounds **1** and **2**

It should be noted that the magnetic coupling between the Co^{II} and/or Ni^{II} ions through the carboxylate-malate are antiferromagnetic, ferromagnetic and ferrimagnetic for compounds **1**, **2** and **3**, respectively. Different electronic configurations of the metal ions involving three (**1**) and two (**2**) unpaired electrons could account for this. The ferromagnetic couplings in **2** are very weak but the presence of one unpaired electron in a t_{2g} type orbital of Co^{II} in **1** would increase the possibility of net overlap between the magnetic orbitals,[19,20a] thus enhancing the antiferromagnetic contributions in **1** and the ferromagnetic terms would be overcome. Ferromagnetic interactions between the nickel(II) ions have been observed in some compounds involving *anti-syn* carboxylate bridged nickel(II).[20] The magnetic behaviour of the title compounds is related to their metal centres and the carboxylate-malate bridges. Detailed magnetic analyses are currently being carried out.

 © 2004 Wiley-VCH Verlag GmbH & Co. KGaA, Weinheim

The assignment of oxidation states for the cobalt and nickel atoms in the three compounds is consistent with their coordination geometries and bond valence sum calculations[21] and is also confirmed by the results of XPS measurements. The electronic binding energies of $Co2p_{3/2}$ for **1** (Figure S1 in the Supporting Information) and $Ni2p_{3/2}$ for **2** (Figure S2) are 783.2 and 856.1 eV, respectively, indicating that the oxidation states of both Co and Ni are +2. For compound **3**, the peaks at 782.4 and 855.3 eV (Figure S3) are also in the range of the electronic binding energies for $Co2p_{3/2}$ in Co^{II} and $Ni2p_{3/2}$ in Ni^{II}, respectively, which confirms the coexisistence of Co^{II} and Ni^{II}.

The thermal behaviour of compounds **1**, **2** and **3** was studied from 30 to 800 °C in air. The TGA curves indicate that the three compounds have similar thermal properties (Figure S4, see Supporting Information). Taking compound **2** as an example, the sample slowly loses one lattice water molecule and one coordinated water from 120 to 330 °C with the weight-loss of 16.2% being consistent with the calculated value of 15.9%. Upon further heating, the sample decomposes rapidly and the occurrence of an exothermic process is very clear. The decomposition is complete by about 440 °C and the residue is most probably nickel(II) oxide.

Conclusion

In this work we have, for the first time, synthesised under solvothermal conditions three isostructural coordination polymers, $\{[M(C_4H_4O_5)(H_2O)]\cdot H_2O\}_n$, [M = Co^{II} (**1**), Ni^{II} (**2**) and $1/3Co^{II}$ +$2/3Ni^{II}$ (**3**)], based on bridging malate groups and water molecules. Compared with other metal-malate compounds, the most remarkable features of the title compounds are: (a) The malate acts as the unique quinquedentate ligand and all of the five oxygen atoms participate in the coordination. (b) Three isostructural compounds show antiferromagnetic, ferromagnetic and ferrimagnetic interactions in **1**, **2** and **3**, respectively, and this interesting magnetic behaviour is related to the nature of the metal centre and the carboxylate-malate bridges in each case. In the future, it would be worthwhile exploring the relationship between the structures and properties of extended networks based on transition metals and HPCs.

Experimental Section

Syntheses of 1, 2 and 3: The three compounds were prepared in an analogous manner and the detailed synthetic procedures are as follows. Compound **1** was prepared from a weakly acidic mixture of cobalt(II) acetate tetrahydrate (0.75 g, 3.0 mmol), malic acid (0.40 g, 3.0 mmol), 4,4-bipyridine dihydrate (0.20 g, 1.0 mmol), KOH (0.18 g, 3.2 mmol), distilled water (10 mL) and anhydrous alcohol (10 mL). The mixture was stirred for ca. 1 h. and was then heated under autogenous pressure at 160 °C for three days in a 30 mL Teflon-lined stainless steel vessel and finally cooled to room temperature. The purplish-red crystals were filtered, washed with distilled water and dried at ambient temperature. Yield: 0.46 g (67%, based on cobalt). X-ray quality crystals of **2** in the form of green blocks were prepared by the procedure detailed above for **1** but using nickel(II) acetate tetrahydrate instead of the cobalt(II) salt. Yield: 0.51 g (74%, based on nickel). Dark purple crystals of **3** were isolated by following the procedure detailed above for **1** but using cobalt(II) acetate tetrahydrate (0.30 g) and nickel(II) acetate tetrahydrate (0.50 g) instead of the cobalt(II) salt. Yield: 0.57 g (70%, based on cobalt). Analyses for **1, 2** and **3:**

1: $C_4H_8CoO_7$ (227.03): calcd. Co 25.96, C 21.16, H 3.55; found Co 25.47, C 21.45, H 3.38. Main IR features (KBr disk): $\tilde{\nu}$ = 3514.4 m, 3432.9 m, 2807.4 w, 1617.5 s, 1577.7 s, 1546.6 s, 1434.8 s, 1398.7 s, 1321.4 w, 1291.0 s, 1260.9 w, 1208.5 w, 1088.1 m, 1038.0 m, 806.2 m, 669.2 m, 609.5 m, 583.1 m, 545.8 m, 331.0 w cm^{-1}.

2: $C_4H_8NiO_7$ (226.81): calcd. Ni 25.88, C 21.18, H 3.56; found Ni 25.14, C 21.33, H 3.62. Main IR features (KBr disk): $\tilde{\nu}$ = 3511.1 m, 3426.4 m, 2806.9 w, 1609.2 s, 1579.8 s, 1541.4 s, 1435.0 s, 1400.0 s, 1321.8 w, 1292.1 s, 1261.6 w, 1207.1 w, 1087.7 m, 1039.1 m, 834.3 m, 680.9 m, 616.7 m, 588.9 m, 552.4 m, 355.7 w cm^{-1}.

3: $C_4H_8Co_{0.33}Ni_{0.67}O_7$ (226.89): calcd. Co 8.57, Ni 17.33, C 21.17, H 3.55; found Co 8.13, Ni 16.75, C 20.86, H 3.69. Main IR features (KBr disk): $\tilde{\nu}$ = 3509.0 m, 3428.4 m, 2807.1 w, 1609.2 s, 1573.4.8 s, 1541.9 s, 1434.5 s, 1399.5 s, 1321.6 w, 1291.7 s, 1261.3 w, 1207.3 w, 1087.8 m, 1038.7 m, 835.3 m, 678.3 m, 614.1 m, 586.6 m, 550.1 m, 349.4 w cm^{-1}.

X-ray Crystallographic Studies

Compound 1: $C_4H_8CoO_7$, M_r = 227.03, dimensions 0.299 × 0.229 × 0.100 mm, monoclinic, space group *Cc*, a = 13.211(3) Å, b = 7.564(2) Å, c = 9.758(2) Å, β = 130.83(3)°, V = 737.7(3) Å^3, Z = 4, D_c = 2.044 g/cm^3, μ(Mo-K_α) = 2.325 mm^{-1}. X-ray data were collected on Rigaku RAXIS-RAPID diffractometer at 293 K in the range of 3.4 < θ < 27.5°. Unique reflections were used to solve the structure by direct methods using SHELXS-97 which was then refined on F^2 by full-matrix least-squares methods, converging at R = 0.0237 [$I > 2\sigma(I)$] with a goodness-of-fit on F^2 of 1.149 for 110 parameters and 1600 reflections, 1600 unique reflections.

Compound 2: $C_4H_8NiO_7$, M_r = 226.81, dimensions 0.594 × 0.393 × 0.353 mm, monoclinic, space group *Cc*, a = 13.103(3) Å, b = 7.526(2) Å, c = 9.629(2) Å, β = 130.88(3)°, V = 718.0(2) Å^3, Z = 4, D_c = 2.098 g/cm^3, μ(Mo-K_α) = 2.701 mm^{-1}. X-ray data were collected on Rigaku RAXIS-RAPID diffractometer at 293 K in the range of 3.4 < θ < 27.5°. Unique reflections were used to solve the structure by direct methods using SHELXS-97 which was then refined on F^2 by full-matrix least-squares methods, converging at R = 0.0269 [$I > 2\sigma(I)$] with a goodness-of-fit on F^2 of 1.094 for 110 parameters and 1550 reflections, 1550 unique reflections.

Compound 3: $C_4H_8Co_{0.33}Ni_{0.67}O_7$, M_r = 226.89, dimensions 0.462 × 0.434 × 0.359 mm, monoclinic, space group *Cc*, a = 13.137(3) Å, b = 7.536(2) Å, c = 9.676(2) Å, β = 130.91(3)°, V = 724.0(2) Å^3, Z = 4, D_c = 2.082 g/cm^3, μ(Mo-K_α) = 2.576 mm^{-1}. X-ray data were collected on Rigaku RAXIS-RAPID diffractometer at 293 K in the range of 3.4 < θ < 27.3°. Unique reflections were used to solve the structure by direct methods using SHELXS-97 which was then refined on F^2 by full-matrix least-squares methods, converging at R = 0.0278 [$I > 2\sigma(I)$] with a goodness-of-fit on F^2 of 1.064 for 119 parameters and 1528 reflections, 1528 unique reflections.

CCDC-241829 (for **1**), -241830 (for **2**) and -241831 (for **3**) contain the supplementary crystallographic data for this paper. These data can be obtained free of charge at www.ccdc.cam.ac.uk/conts/

 © 2004 Wiley-VCH Verlag GmbH & Co. KGaA, Weinheim

retrieving.html [or from the Cambridge Crystallographic Data Centre, 12, Union Road, Cambridge CB2 1EZ, UK; fax: +44-1223-336-033; E-mail: deposit@ccdc.cam.ac.uk].

Acknowledgments

This work was supported by the State Key Basic Research Project of China (No. 2001CB108906) and the National Natural Science Foundation of China (No. 20333070 and 20271021).

[1] [1a] O. M. Yaghi, C. E. Davis, G. Li, H. Li, *J. Am. Chem. Soc.* **1997**, *119*, 2861−2868. [1b] S. A. Bourne, J. Lu, A. Mondal, B. Moulton, M. J. Zaworotko, *Angew. Chem. Int. Ed.* **2001**, *40*, 2111−2113. [1c] K. Barthelet, J. Marrot, G. Férey, D. Riou, *Chem. Commun.* **2004**, 520−521.

[2] [2a] S. S. Y. Chui, S. M. F. Lo, J. P. H. Charmant, A. G. Orpen, I. D. Williams, *Science* **1999**, *283*, 1148−1150. [2b] O. M. Yaghi, H. Li, T. L. Groy, *J. Am. Chem. Soc.* **1996**, *118*, 9096−9101.

[3] [3a] D. Q. Chu, J. Q. Xu, L. M. Duan, T. G. Wang, A. Q. Tang, L. Ye, *Eur. J. Inorg. Chem.* **2001**, 1135−1137. [3b] S. O. H. Gutschke, D. J. Price, A. K. Powell, P. T. Wood, *Eur. J. Inorg. Chem.* **2001**, 2739−2741. [3c] C. D. Wu, C. Z. Lu, W. B. Yang, S. F. Lu, H. H. Zhuang, J. S. Huang, *Eur. J. Inorg. Chem.* **2002**, 797−800.

[4] S. S.-Y. Chui, A. Siu, X. Feng, Z. Y. Zhang, T. C. W. Mak, I. D. Williams, *Inorg. Chem. Commun.* **2001**, *4*, 467−470.

[5] [5a] X. J. Zhang, L. P. Jin, S. Z. Lu, *Eur. J. Inorg. Chem.* **2002**, 3356−3363. [5b] L. Pan, X. Y. Huang, J. Li, Y. G. Wu, N. W. Zheng, *Angew. Chem. Int. Ed.* **2000**, *39*, 527−530. [5c] M. L. Tong, L. J. Li, K. Mochizuki, H. C. Chang, Y. Li, S. Kitagawa, *Chem. Commun.* **2003**, 428−429.

[6] [6a] J. M. Li, H. Q. Zeng, J. H. Chen, Q. M. Wang, X. T. Wu, *Chem. Commun.* **1997**, 1213−1214. [6b] F. S. Delgado, J. Sanchiz, C. Ruiz-Pérez, F. Lloret, M. Julve, *Cryst. Eng. Comm.* **2003**, *5*, 280−284.

[7] [7a] C. Livage, C. Egger, G. Férey, *Chem. Mater.* **1999**, *11*, 1546−1550. [7b] P. M. Forster, A. K. Cheetham, *Angew. Chem. Int. Ed.* **2002**, *41*, 457−459.

[8] Z. Shi, L. Zhang, S. Gao, G. Yang, J. Hua, L. Gao, S. Feng, *Inorg. Chem.* **2000**, *39*, 1990−1993.

[9] S. Dalai, P. S. Mukherjee, E. Zangrando, F. Lloret, N. R. Chaudhuri, *Dalton Trans.* **2002**, 822−823.

[10] R. Vaidhyanathan, S. Natarajan, C. N. R. Rao, *Dalton Trans.* **2003**, 1459−1464.

[11] [11a] V. Kiritsis, A. Michaelides, S. Skoulika, S. Golhen, L. Ouahab, *Inorg. Chem.* **1998**, *37*, 3407−3410. [11b] A. Dimos, D. Tsaousis, A. Michaelides, S. Skoulika, S. Golhen, L. Ouahab, C. Didierjean, A. Aubry, *Chem. Mater.* **2002**, *14*, 2616−2622. [11c] L. S. Long, Y. R. Wu, R. B. Huang, L. S. Zheng, *Inorg. Chem.* **2004**, *43*, 3798−3800.

[12] Z. Z. Zhou, G. F. Wang, S. Y. Hou, H. L. Wan, K. R. Tsai, *Inorg. Chim. Acta* **2001**, *314*, 184−188.

[13] [13a] M. Kaliva, T. Giannadaki, A. Salifoglou, *Inorg. Chem.* **2001**, *40*, 3711−3718. [13b] M. Biagioli, L. Strinna-Erre, G. Micera, A. Panzanelli, M. Zema, *Inorg. Chim. Acta* **2000**, *310*, 1−9.

[14] Z. Z. Zhou, W. B. Yan, H. L. Wan, K. R. Tsai, *Chinese J. Struct. Chem.* **1995**, *14*, 255−260.

[15] [15a] A. T. Reed, A. Karipides, *Acta Crystallogr., Sect. B* **1976**, *35*, 2085−2088. [15b] A. Karipides, A. T. Reed, *Inorg. Chem.* **1976**, *15*, 44−47. [15c] Z. H. Zhou, J. J. Ye, Y. F. Deng, G. Wang, J. X. Gao, H. L. Wan, *Polyhedron* **2003**, *21*, 787−790.

[16] N. Lah, I. K. Cigić, I. Leban, *Inorg. Chem. Commun.* **2003**, *6*, 1441−1444.

[17] [17a] Y. Rodríguez-Martín, M. Hernández-Molina, F. S. Delgado, J. Pasán, C. Ruiz-Pérez, F. Lloret, M. Julve, *Cryst. Eng. Comm.* **2002**, *4*, 522−535. [17b] S. Konar, P. S. Mukherjee, E. Zangrando, F. Lloret, N. R. Chaudhuri, *Angew. Chem. Int. Ed.* **2002**, *41*, 1561−1563. [17c] N. Guillou, S. Pastre, C. Livage, G. Férey, *Chem. Commun.* **2002**, 2358−2359.

[18] X. M. Chen, T. C. W. Mak, *Inorg. Chim. Acta* **1991**, *189*, 3−5.

[19] [19a] R. L. Carlin, *Magnetochemistry*, Springer, New York, **1986**. [19b] O. Kahn, *Molecular Magnetism*, VCH Verlagsgesellschaft, Weinheim, **1993**.

[20] [20a] F. S. Delgado, M. Hernández-Molina, J. Sanchiz, C. Ruiz-Pérez, Y. Rodríguez-Martín, T. López, F. Lloret, M. Julve, *Cryst. Eng. Comm.* **2004**, *6*, 106−111. [20b] T. Whitfield, L. M. Zheng, X. Wang, A. J. Jacobson, *Solid State Sci.* **2001**, *3*, 829−835.

[21] I. D. Brown, D. Altermatt, *Acta Crystallogr., Sect. B* **1985**, *41*, 244−247.

Received June 26, 2004

 © 2004 Wiley-VCH Verlag GmbH & Co. KGaA, Weinheim

A Parahydrogen Study of Catalytic Hydrogenation by Diphosphane-Substituted Triruthenium Clusters

Tom G. Prestwich,[a] Damir Blazina,[a] Simon B. Duckett,*[a] and Paul J. Dyson[b]

Keywords: Homogeneous catalysis / Cluster compounds / NMR spectroscopy / Parahydrogen / Ruthenium

The diphosphane-substituted clusters $[Ru_3(CO)_{10}(dppe)]$ and $[Ru_3(CO)_8(dppe)_2]$ [dppe = 1,2-bis(diphenylphosphanyl)ethane] are shown to catalytically hydrogenate diphenylacetylene. This process is highly solvent-dependent with fragmentation dominating in low-polarity solvents, which indicates that the dppe ligand does not stabilise the cluster under catalytic conditions. In solvents of higher polarity, the clusters are active hydrogenation catalysts of lower activity than their monodentate phosphane analogues $[Ru_3(CO)_{10}(L)_2]$ (L = PPh_3, PMe_2Ph, PMe_3, PCy_3).
(© Wiley-VCH Verlag GmbH & Co. KGaA, 69451 Weinheim, Germany, 2004)

Introduction

Catalysis by transition metal clusters is of considerable interest due to the ability of these species to act as homogeneous catalysts with properties that lie between those of mononuclear complexes and colloidal/nanoparticle catalysts, whilst also representing fragments of a metal surface.[1] The study of clusters is, however, complicated by the wide variety of reaction pathways available to them, and in particular their tendency to fragment to mononuclear metal complexes. One way to circumvent this problem might be to utilise clusters with supporting ligand scaffolds, such as bidentate phosphanes, which could potentially stabilise the cluster under catalytic conditions and hence minimise fragmentation.

Phosphane-substituted triruthenium clusters have been shown to exhibit significantly greater catalytic activity than their comparatively unreactive homoleptic parent $[Ru_3(CO)_{12}]$.[1] Compounds containing bidentate phosphane ligands have previously been studied in an effort to preclude cluster fragmentation. For example, it is well established that diphosphane-substituted triruthenium clusters react with unsaturated organic molecules,[2] yielding species that may correspond to intermediates in a catalytic cycle. It has also been shown that the 1,2-bis(diphenylphosphanyl)-methane (dppm) substituted species $[Ru_3(CO)_{10}(dppm)]$ and $[Ru_3(CO)_8(dppm)_2]$, as well as their arsanyl (dpam) analogues, react with hydrogen to form stable hydride clusters.[3] These phosphane-containing species were subsequently shown to be active catalysts for the isomerisation and hydrogenation of 1-hexene, with turnover frequencies being taken to be indicative of catalysis by an intact cluster.[4] Analogous species containing bulky cyclohexyl and pentafluorophenyl substituents on the bidentate phosphane ligand have been shown to catalyse hydroformylation reactions,[5] but exact mechanistic information about these processes remains elusive.

Consequently, we set out to explore the mechanism of catalysis by diphosphane-substituted triruthenium clusters by using the parahydrogen-induced polarisation (PHIP) effect.[6] This technique is applicable to mechanistic studies since it yields substantially enhanced resonances in ^1H NMR spectra. The extent of enhancement available has recently been shown to approach a factor of 28500,[7] making this technique ideal for the detection of transient species or those present in low concentration, such as reaction intermediates. PHIP has already been successfully used to study H_2 addition to,[8] and hydride migration on,[9] a number of triruthenium and triosmium clusters, as well as yielding unprecedented insights into catalytic hydrogenation by the tertiary phosphane (L) containing cluster family $[Ru_3(CO)_{12-x}(L)_x]$ (L = PPh_3, PMe_2Ph, PMe_3, PCy_3; x = 1−3).[10] It was discovered that isomers of $[Ru_3(H)(\mu\text{-}H)(CO)_9(L)_2]$ play a kinetically significant role in the hydrogenation of alkyne substrates such as diphenylacetylene. This catalytic transformation proceeds by initial CO loss, with each isomer exhibiting different rates for H_2 transfer to the hydrogenation product *cis*-stilbene. In addition, a less significant secondary reaction involving loss of L was detected, yielding a detectable product that contained both a pendant vinyl unit and a bridging hydrido ligand. Competing pathways involving fragmentation to form $[Ru(H)_2$-

[a] Department of Chemistry, University of York, Heslington, York YO10 5DD, United Kingdom, Fax: + 44-1904-432564
E-mail: sbd3@york.ac.uk
[b] Institut des Sciences et Ingénierie Chimiques, Ecole Polytechnique Fédérale de Lausanne, EPFL-BCH, 1015 Lausanne, Switzerland
Supporting information for this article is available on the WWW under http://www.eurjic.org or from the author.

$(CO)_2(L)(alkene)$] were also observed and shown to be favoured by nonpolar solvents. Furthermore, it has very recently been reported that the presence of a stabilising phosphido group can stabilise the metal cluster framework under catalytic conditions, such that only cluster-based active species are observed with p-H_2, even in nonpolar solvents.[11]

In this paper, PHIP is utilised to investigate catalytic hydrogenation by the clusters $[Ru_3(CO)_{10}(dppe)]$ (**1**) and $[Ru_3(CO)_8(dppe)_2]$ (**2**) [dppe = 1,2-bis(diphenylphosphanyl)-ethane]. Our aim was to confirm mechanistically by the direct observation of key dihydride species whether the presence of the bidentate ligand exerts a stabilising influence on the cluster core whilst still allowing enough flexibility for catalytic transformations to take place, as well as to compare the stabilising effect of the diphosphane ligand to that of the phosphido ligand used in an earlier study.[11]

Results and Discussion

Hydrogen Addition to $[Ru_3(CO)_{10}(dppe)]$ (1)

The literature solid-state structure of **1**,[12] with the bidentate phosphane ligand located in the equatorial plane and bridging two metal centres, is consistent with the solution-state ^1H and ^{31}P NMR spectral features at 295 K (Table 1), which indicate the presence of only one ^{31}P environment. In addition, only one broad resonance is observed in the carbonyl region of the ^{13}C NMR spectrum at $\delta = 210.4$ ppm. This is indicative of rapid carbonyl exchange around the cluster framework under these conditions. Such effects have been reported in triiron clusters containing dppe ligands where evidence has been presented to support exchange by a merry-go-round mechanism[13] rather than the alternative mechanism of cluster core libration within the ligand polyhedron.[14]

On addition of p-H_2 to a $CDCl_3$ solution of **1** at 295 K, a new species, **3**, was formed, which yielded two mutually coupled enhanced hydride resonances at $\delta = -12.87$ and -14.74 ppm (Figure 1, Table 1). Based on previous work, it is suggested that the lower-field resonance corresponds to a terminal hydride (H_t), while the higher field resonance corresponds to a bridging hydride (H_b).[3,10] On careful examination, the resonance corresponding to H_b was found to appear as a doublet of doublets of antiphase doublets, indicative of coupling to two ^{31}P nuclei. The associated $^2J_{H,P}$ values of 9 Hz (to P_a signal at $\delta = 63.6$ ppm; by

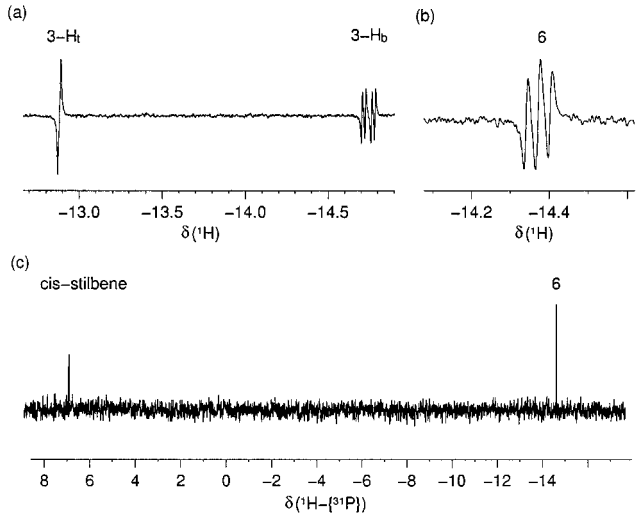

Figure 1. Selected regions of ^1H NMR spectra of **1** with p-H_2 in $CDCl_3$: (a) hydride region of **3** at 295 K; (b) in the presence of PhC≡CPh at 315 K, showing the bridging hydride resonance for **6**; (c) EXSY spectrum with a mixing time of 600 ms and selective irradiation of the hydride ligand yielding the $\delta = -14.36$ ppm signal, showing direct transfer of magnetisation from this site in **6** into *cis*-stilbene, the hydrogenation product

Table 1. NMR spectroscopic data for complexes **1**–**6** detected in $CDCl_3$ at 295 K unless otherwise indicated; H_t indicates terminal hydride and H_b bridging hydride, and the ^{31}P nuclei are labelled according to Figure 2

Compound	δ (^1H)	δ (^{31}P-{^1H})	δ (^{13}C-{^1H})
1	1.69 (d, $J_{H,P}$ = 12 Hz)	41.5 (s)	210.4 (br)
2	1.6–2.1 (m)	32.3 (m), 33.6 (m), 35.0 (m), 39.7 (m)	212 (br)
3	−12.87 [dd, $J_{H,P}$ = 3 Hz (P_b), $J_{H,H}$ = −7 Hz, H_t], −14.74 [ddd, $J_{H,P}$ = 9 Hz (P_a), 23 Hz (P_b), $J_{H,H}$ = −7 Hz (H_b)]	63.6 (s, P_a), 57.4 (s, P_b)	
4	−13.38 (t, $J_{H,P}$ = 12 Hz)	38.4 (s)	211.0 (br)
5a[a]	−4.93 [dd, $J_{H,P}$ = 12 Hz (P_a), $J_{H,H}$ = −7 Hz, H_t], −14.29 [tdd, $J_{H,P}$ = 30 Hz (P_a and P_b), 18 Hz (P_c), $J_{H,H}$ = −7 Hz, H_b]	51.08 (d, $J_{P,P}$ = 123 Hz, P_a), 51.12 (dd, $J_{P,P}$ = 123, 33 Hz, P_b), 49.03 (d, $J_{P,P}$ = 33 Hz, P_c)	
5b[a]	−5.02 (dd, $J_{H,P}$ = 14, $J_{H,H}$ = −7 Hz, H_t), −14.31 [tdd, $J_{H,P}$ = 31 Hz (P_a and P_b), 16 Hz (P_c), $J_{H,H}$ = −7 Hz, H_b]	49.16 (d, $J_{P,P}$ = 72 Hz, P_a), 48.58 (dd, J_{pp} = 72, 18 Hz, P_b), 50.30 (d, $J_{P,P}$ = 18 Hz, P_c)	
6[b]	−14.36 (td, $J_{H,P}$ = 12, $J_{H,H}$ = −4 Hz, H_b), +7.25 (d, $J_{H,H}$ = −4 Hz)	38.1 (s)	

[a] At 273 K. [b] At 315 K.

 © 2004 Wiley-VCH Verlag GmbH & Co. KGaA, Weinheim

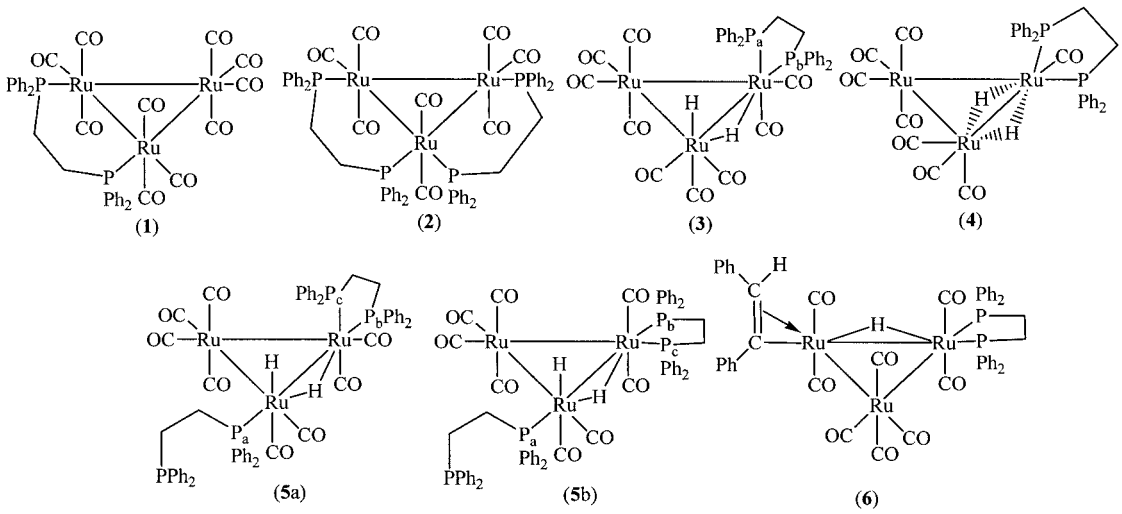

Figure 2. Structures of clusters **1**−**6**; **1** and **2** are from the literature,[12] the others were determined in this study

HMQC methods) and 23 Hz (to P_b signal at $\delta = 57.4$ ppm) indicate that H_b is *cis* to P_a and *trans* to P_b, as shown in Figure 2.[15] Both these ^{31}P centres were detected as simple singlets (vide infra). The resonance for H_t, meanwhile, appeared as a simple antiphase doublet. However, ^{31}P decoupling experiments revealed the presence of a small (3 Hz) coupling between H_t and P_b. In view of the very small size of the coupling between H_t and P_b, as well as the larger couplings from H_b to P_b and P_a, it is suggested that both the ^{31}P centres of the dppe ligand are located on the same Ru centre, which also coordinates the bridging hydride. The small phosphorus coupling between H_t and P_b therefore corresponds to a weak three-bond coupling, which is relayed through the Ru−Ru bond that is *trans* to P_b.

In view of the distinct *trans* and *cis* H_b-P coupling constants observed here, it is suggested that the dppe ligand occupies one axial and one equatorial centre on this metal centre. Previous reports indicate that ^{31}P centres in adjacent equatorial sites can exchange position rapidly on the NMR time scale.[10b] The observed singlet peak profile for the ^{31}P signals of the two sites could therefore be due to the occurrence of site exchange,[10,15] although it may arise because of mutual cancellation of the $^2J_{P,P}$ coupling through the metal centre and the $^3J_{P,P}$ coupling through the backbone of the dppe ligand. These two couplings would be expected to have opposite signs. Unfortunately, the need for *p*-H_2 amplification to detect **3** precluded the direct investigation of this process by ^{31}P EXSY methods, but the lack of any visible ^{13}C-^{31}P couplings in the associated NMR spectra of the precursor species **1** and **2** clearly demonstrates the presence of fluxionality in these systems. The proposed structure of **3** is shown in Figure 2.

Upon addition of 1 atm of CO to the sample, the hydride resonances for **3** were no longer visible at 315 K. This observation confirms that **3** is formed by loss of CO rather than the dissociation of an arm of the dppe ligand, a result which is not unexpected for a μ_2-phosphane, and further supports the proposed structure of **3**.

We have previously reported that oxidative addition of H_2 to clusters of the type $[Ru_3(CO)_{10}(L)_2]$, where L is a monodentate tertiary phosphane such as PPh_3, leads to three isomeric products of $[Ru_3(H)(\mu\text{-}H)(CO)_9(L)_2]$. One of these isomers matches the structure of **3** where both phosphane ligands are on the same metal centre but it is the least preferred of the three. The major isomer with L = PPh_3 has both phosphane ligands in equatorial locations on separate ruthenium centres spanned by the bridging hydride. Such an arrangement is not observed in the case of **3**, but would require both the dppe ligand and a hydride to bridge the same Ru−Ru bond, a situation that might be sterically unfavoured due to the elongated nature of the Ru−H−Ru bond.[16]

The hydrido ligands of $[Ru_3(H)(\mu\text{-}H)(CO)_9(L)_2]$ proved to be highly fluxional, undergoing both site exchange, interisomer exchange and reductive coupling to form H_2.[10b] The fluxional behaviour of the hydrido ligands in **3** was probed by the same EXSY methodology (Supporting Information). At 295 K, exchange between the two hydrido ligands proceeded at a rate of 3.4 s^{-1}; exchange with free H_2, which must be occurring in view of the enhanced hydride resonances exhibited by **3**, was not evident on this time scale. This behaviour is similar to that reported for $[Ru_3(H)(\mu\text{-}H)(CO)_9(L)_2]$, although it should be noted that with monodentate phosphane species, the rate of hydride interchange in the analogous isomer was slower under identical reaction conditions.

Over prolonged reaction times, the hydride resonances for **3** disappeared as the *p*-H_2 enhancement was depleted, and a stable resonance, assigned to species **4**, built up slowly at $\delta = -13.38$ ppm. This signal was split into a triplet by a 12 Hz coupling to two equivalent ^{31}P nuclei resonating at $\delta = 38.4$ ppm in the corresponding ^{31}P NMR spectrum. Since *p*-H_2 enhancement in these spectra would be quenched by a species with unpaired electrons, this resonance must correspond to two chemically equivalent hydrides, while its chemical shift is indicative of bridging hy-

 © 2004 Wiley-VCH Verlag GmbH & Co. KGaA, Weinheim

dride coordination. In the view of the configuration of the dppe ligand in **3** and of the apparent equivalence of the ^{31}P nuclei in **4**, the structure of **4** shown in Figure 2 is proposed. ^{31}P NMR investigations revealed that **4** is still a very minor product; after 18 h under H_2, the ratio of **1**/**4** was determined to be 20:1. ^{13}C NMR revealed that the carbonyl ligands in this product are highly fluxional at room temperature, with only one broad carbonyl signal being observed. According to the proposed structure, cluster **4** is an unsaturated, 46-electron species. This is not completely unexpected, since stable 46-electron dihydride clusters of the iron group, such as the osmium cluster $[Os_3(\mu\text{-}H)_2(CO)_{10}]$, are known.[17] It should, however, be noted that the ruthenium analogue $[Ru_3(\mu\text{-}H)_2(CO)_{10}]$ is unstable and can only be prepared by prolonged photolysis[18] in contrast to **4** which is stable and thermally accessible, albeit in small amounts. We further note that the hydride resonance for **4** disappears on venting the H_2.

Surprisingly, on changing the solvent to $[D_8]$toluene and warming with *p*-H_2, no cluster-containing hydrides were observed, and the only species evident was the known mononuclear complex $[Ru(CO)_2(dppe)(H)_2]$, characterised by enhanced hydride resonances at $\delta = -6.32$ and -7.55 ppm.[19] This contrasts with the situation observed with the $[Ru_3(CO)_{12-x}(L)_x]$ systems ($x = 1-3$), where the corresponding cluster-based dihydrides are observed under these conditions[10] and indicates that the dppe ligand makes the triruthenium cluster more susceptible to solvent effects than is the case with monodentate phosphanes.

Hydrogen Addition to $[Ru_3(CO)_8(dppe)_2]$ (2)

The ^{31}P NMR spectroscopic data for **2** (Table 1) indicate the presence of multiple isomers in solution, a feature already established for clusters containing multiple bidentate phosphanes;[3,5] the proposed structure of **2** is illustrated in Figure 2. When a sample of **2** was treated with *p*-H_2 in $CDCl_3$ at 295 K, two enhanced hydride signals were detected in the corresponding ^1H NMR spectrum at $\delta = -4.93$ and -5.02 ppm, due to terminal hydrides, and further two at $\delta = -14.29$ and -14.31 ppm, assigned to bridging hydrides. COSY investigations revealed that the resonances at $\delta = -4.93$ and -14.29 ppm correspond to one product (due to protons **5a**-H_t and **5a**-H_b, respectively) while those at $\delta = -5.02$ and -14.31 ppm correspond to another (due to protons **5b**-H_t and **5b**-H_b, respectively); the similarity between this situation and that previously observed for $[Ru_3(H)(\mu\text{-}H)(CO)_9(L)_2]$ (L = monodentate phosphane)[10] suggests that **5a** and **5b** correspond to two isomeric dihydride products. Characterisation of these species was complicated by hydride signal overlap, but the terminal hydride resonances could be resolved by cooling the sample to 273 K (Figure 3). The resonance for **5a**-H_t showed one coupling of 12 Hz to a single *cis*-^{31}P centre that was located at $\delta = 51.08$ ppm (P_a; Figure 2) by HMQC methods in addition to a -7 Hz H-H coupling. The analogous signal for **5b**-H_t also showed an interaction with a single ^{31}P nucleus, resonating at $\delta = 49.16$ ppm ($J_{H,P}$ = 14 Hz, P_a). It can therefore be concluded that the ruthenium centre to which the terminal hydride is coordinated also binds one phosphorus atom in both products.

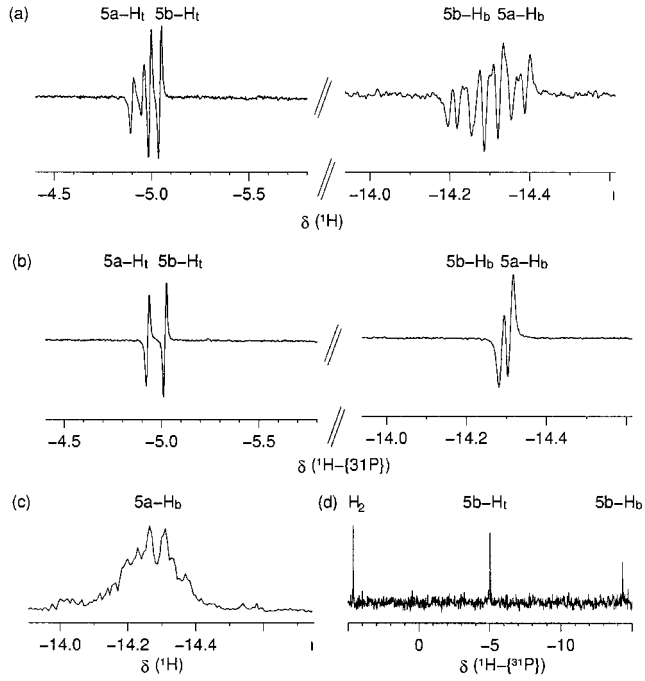

Figure 3. Selected regions of NMR spectra of **2** obtained with *p*-H_2 in $CDCl_3$ at 273 K: (a) ^1H spectrum showing the hydride resonances for **5a** and **5b**; (b) ^1H spectrum with $\{^{31}P\}$ decoupling; (c) cross-section of a 2D ^1H-^{31}P HMQC spectrum with retention of ^{31}P couplings, showing that the signal for **5a**-H_b is a triplet of doublets due to $^2J_{H,P}$ couplings; (d) cross-section of a 2D EXSY spectrum recorded at 285 K with a mixing time of 500 ms, showing exchange from **5b**-H_t into the bridging position on the same isomer and into free H_2, while exchange into **5a** is absent

As already stated, the bridging hydride signals for **5a** and **5b** show extensive overlap due to the presence of multiple ^1H-^{31}P couplings. However, they were successfully analysed by comparison of multiple high-resolution ^1H-^{31}P HMQC experiments where the ^{31}P couplings were either retained or decoupled (Figure 3). Careful examination of the two resonances in the ^1H dimension, revealed that **5a**-H_b appeared as a doublet of triplets due to two $^2J_{H,P}$ couplings of 30 Hz (to P_a at $\delta = 51.08$ ppm and to P_b at $\delta = 51.12$ ppm) and an 18 Hz coupling to P_c ($\delta = 49.03$ ppm). This suggests that P_a and P_b are *trans* to the bridging hydride, while P_c is *cis* to it. Furthermore, P_a and P_b showed a mutual ^{31}P coupling of 123 Hz, which is attributed to their *trans* arrangement across a metal−metal vector.[5,20]

P_b and P_c also coupled to each other, but with a smaller constant of 33 Hz. It can therefore be deduced that P_b and P_c are *cis* to each other and bound to the same metal centre. Since P_a is located on the Ru centre that binds the terminal hydride, the observed coupling patterns signify that the other two phosphorus nuclei must bind to the metal atom that coordinates the bridging hydride, as shown in Figure 2. In addition, since the structures of **3** and **4** suggest that the dppe ligand and the hydride do not bridge the same metal centre, P_b and P_c can be deduced to originate from the same phosphane ligand. It should also be noted that no "arti-

 © 2004 Wiley-VCH Verlag GmbH & Co. KGaA, Weinheim

facts'' arising from double and triple quantum coherences were detected in these HMQC spectra,[21] and it was therefore concluded that only single quantum transitions were being observed.

The resonance for proton **5b**-H_b was analysed in a similar way (Table 1, Figure 2). In brief, this resonance contains a 31 Hz *trans* triplet splitting to two phosphanes [$\delta = 49.16$ (P_a) and $\delta = 48.58$ (P_b) ppm] as well as a 16 Hz *cis* splitting due to P_c ($\delta = 50.30$ ppm). Nuclei P_a and P_b now exhibit a 72 Hz coupling, while P_b and P_c couple with a $^2J_{P,P}$ value of 18 Hz. Therefore, once again, P_b and P_c originate from the same dppe ligand and bind to the same ruthenium centre, which also coordinates the bridging hydride.

The structural difference between **5a** and **5b** thus stems from the orientation of the dppe ligand that contains P_b and P_c. In view of previous reports in related triosmium systems, which found that the coupling between an axial and an equatorial ligand is larger than that between two equatorial ligands,[15] it is suggested that in **5a**, P_b is an equatorial site and P_c is axial, whereas in **5b** both the phosphorus atoms are in equatorial locations. The small difference in chemical shift between axial and equatorial ^{31}P centres is in agreement with previous observations.[15] It should be noted that although the proposed structures for **3** and **5a** contain identical ligand arrangements on one ruthenium centre (a dppe ligand bridging between an axial and equatorial sites), P-P couplings are only observed in the spectra of **5a**. This indicates that the presence of the second dppe ligand on this species slows down dppe site interchange.

When these experiments were repeated in the presence of 1 atm of CO, there was no decrease in the signal intensities observed for **5a** and **5b**. It is therefore reasonable to assume that H_2 addition to **2** proceeds by a change in the coordination mode of one of the dppe ligands (in both cases, the one that contains P_a) from η^2 to η^1 (Figure 2). H_2 addition to triruthenium clusters by initial de-coordination of chelating phosphane ligands has been reported previously.[22] This mechanism also parallels the situation observed with related $[Ru_3(CO)_9(L)_3]$ systems, which undergo H_2 addition by loss of phosphane.[10d] Because of the need for p-H_2 amplification, the uncoordinated ^{31}P centres in these species could not be detected directly. Magnetisation transfer experiments have been used here to detect signals for key heteronuclei that couple directly to the hydrides, but this is not the case for the hydrides and the uncoordinated phosphorus centres of **5a** and **5b**. Attempts to detect the uncoordinated ^{31}P centres therefore proved unsuccessful but there can be no doubt of their presence.

When **5a** and **5b** were investigated by EXSY methods at 285 K, intra-isomer hydride exchange and H_2 elimination were detected in both cases (Figure 3 and Supporting Information). The rate constant for hydride self-exchange was determined to be 4.8 s^{-1} for **5a** and 4.6 s^{-1} for **5b**, while the rates for H_2 elimination were 1.5 s^{-1} for both isomers. The similarity of the intra-isomer hydride ligand exchange rates agrees with the very similar structures and relative abundances of the two isomers. Interestingly, inter-isomer exchange is not observed. These observations contrast those made on related $[Ru_3(H)_2(CO)_9(L)_2]$ systems, which exhibit both intra- and inter-isomer exchange under similar conditions.[10] Intra-isomer hydride exchange in $[Ru_3(H)_2(CO)_9(PPh_3)_2]$, under these conditions, occurs at the slower rate of 1.6 s^{-1}, and elimination of H_2 is also slow on the NMR time-scale.[10] The bidentate phosphane therefore facilitates hydride site exchange and H_2 elimination in these clusters.

At prolonged reaction times, the enhanced hydride signals corresponding to **5a** and **5b** disappeared as the extent of p-H_2 enrichment fell. However, no new stable dihydride species were detected at this point with only **2** being evident in the corresponding ^1H and ^{31}P NMR spectra. This indicates that the η^1-dppe ligand is able to re-coordinate with concurrent H_2 elimination. Repeating the investigation in [D_8]toluene once again yielded enhanced hydride resonances for the known mononuclear species $[Ru(CO)_2(dppe)(H)_2]$,[19] and no cluster based hydride products were observed.

Catalytic Hydrogenation of Diphenylacetylene

In order to examine the catalytic activity of these systems towards the hydrogenation of diphenylacetylene, samples of **1** and **2** were monitored in $CDCl_3$ in the presence of p-H_2 and a 100-fold excess of the substrate. When **1** was examined in this way, the formation of **3** was totally suppressed and a new species, **6**, was detected at 315 K and above (NMR spectroscopic data: Table 1). This species yielded two enhanced ^1H resonances at $\delta = -14.36$ and $+7.25$ ppm in the corresponding ^1H NMR spectrum, which were shown to couple by COSY experiments. The hydride resonance appeared as a triplet of antiphase doublets (Figure 1), due to coupling to two identical phosphorus centres (J_{PH} = 12 Hz) and the vinyl proton ($J_{H,H} = -4$ Hz). On the basis of similarity of these spectral features to those reported previously,[10,11] **6** is suggested to correspond to a vinyl hydride cluster, where the sign of the $J_{H,H}$ coupling indicates that the vinyl group occupies the two equatorial locations on a single ruthenium centre (Figure 2). In order for the ^{31}P centres to appear equivalent at these elevated temperatures, the dppe ligand must be located on the opposite metal centre to the vinyl group, occupying the two equatorial sites (cf. **4** and **5b**). Phosphane ligands in such arrangements are able to undergo rapid exchange, which would make them appear equivalent to the bridging hydride.[10b]

These spectra also contained an enhanced resonance for *cis*-stilbene, the hydrogenation product of diphenylacetylene. EXSY investigations revealed direct magnetisation transfer from **6** into *cis*-stilbene was occurring (Figure 1) and thereby confirmed that **6** is an active intermediate involved in catalytic hydrogenation by **1**. The hydrogenation process was then investigated in a quantitative manner in $CDCl_3$ at 320 K and the resulting data were analysed by simulation (Supporting Information).[10,23] The rate of elimination of *cis*-stilbene from **6** was determined to be 0.06 s^{-1}; this is slower than the rates exhibited by mononuclear phosphane analogues {for instance, species derived from

 © 2004 Wiley-VCH Verlag GmbH & Co. KGaA, Weinheim

$[Ru_3(CO)_{10}(PPh_3)_2]$ and $[Ru_3(CO)_{10}(PMe_2Ph)_2]$ exhibit pseudo-first-order hydrogenation rates between 0.07 and 0.18 s^{-1} at the lower temperature of 301 K} and hence the dppe-containing species is a less active hydrogenation catalyst.

Since **3** was not detected in these catalytic experiments, it can be concluded that either **6** is formed from **1** at the expense of **3**, or that **3** converts rapidly into **6** in the presence of diphenylacetylene. When the experiment was repeated in the presence of only a fivefold excess of substrate, **6** was still the only species detected. As **6** still contains the dppe ligand, its formation must proceed by loss of CO. This was confirmed by the addition of 1 atm of CO to the system, which quenched both the formation of **6** and the catalytic hydrogenation. Further experiments were then completed where the $[H_2]$ was varied from 1 to 4 atm. It was discovered that the rate of stilbene elimination is independent of $[H_2]$, which indicates that although H_2 is required to generate **6**, it is not required for stilbene elimination. Elimination of stilbene from **6** will therefore afford an unsaturated species, viz. $[Ru_3(CO)_8(dppe)]$, which may be stabilised by the solvent. The existence of such a stabilising influence has already been proposed by Fontal et al. for the analogous dppm systems.[4] The unsaturated species will subsequently be able to re-coordinate both H_2 and substrate in order to repeat the catalytic process, as illustrated in Scheme 1.

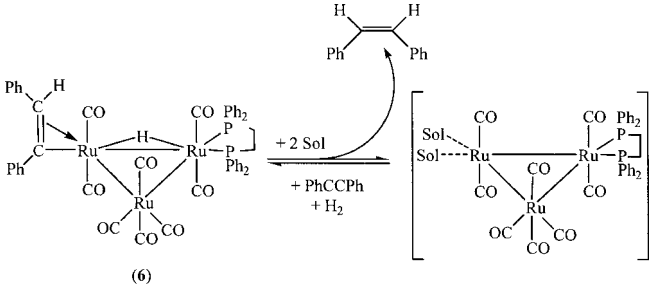

(6)

Scheme 1. Catalytic hydrogenation of diphenylacetylene by **6**

When **2** was employed as the catalytic precursor, **5a** and **5b** were observed at the same relative intensity as in the absence of substrate. No new hydride-containing species were observed, but a gradual build-up of normal ^1H resonances corresponding to *cis*-stilbene was evident at temperatures above 315 K. Since no *p*-H_2 activity is observed in the stilbene product, the rate of its formation must be sufficiently slow for normal signals to be observed; **2** is thus a poorer catalytic precursor than **1** in this reaction.

The lower catalytic activity of the dppe-containing clusters when compared with monodentate phosphane analogues of the type $[Ru_3(CO)_{10}(L)_2]$ indicates that the dppe ligand impedes substrate binding and hence slows down catalytic hydrogenation. This is supported by the significantly lower catalytic activity of **2** when compared to **1**. The same trend was observed by Fontal et al. for dppm-substituted analogues, based on reaction yields and catalytic turnover.[4]

When the catalytic investigations on **1** and **2** were repeated using $[D_8]$toluene as the solvent, no cluster-based hydrides could be observed and the only detected hydride product was the known mononuclear species $[Ru(CO)_2(dppe)(H)_2]$.[19] Hydrogenation was evident by the observation of a very slow build-up of normal signals corresponding to *cis*-stilbene at temperatures above 335 K. This again indicates that the dppe-substituted triruthenium clusters are highly susceptible to solvent effects, in agreement with literature observations for dppm analogues,[4] and demonstrates directly that they undergo significant fragmentation to less active mononuclear species in low-polarity solvents. Thus, the bidentate ligand is unable to stabilise the cluster framework under catalytic conditions.

Finally, it is interesting to compare the influence of the dppe ligand on the cluster core with that exerted by the phosphido group.[11] In solvents of moderate polarity, such as $CDCl_3$, the dppe-substituted cluster **1** is a superior catalyst compared to the phosphido-containing cluster $[Ru_3(\mu\text{-}H)(\mu\text{-}PPh_2)(CO)_9]$; at 315 K, **1** leads to catalytic hydrogenation at a rate of 0.06 s^{-1}, whereas $[Ru_3(\mu\text{-}H)(\mu\text{-}PPh_2)(CO)_9]$ becomes active only at 340 K. However, in low-polarity solvents such as toluene, the phosphido group is able to exert a stabilising influence on the cluster, such that only cluster-based species are observed under catalytic conditions; in contrast, fragmentation dominates in the case of dppe-substituted clusters **1** and **2**. These results also indicate that stabilising the cluster framework can result in lower catalytic activity. Therefore, the exact nature of the stabilising group, as well as the exact reaction conditions, are clearly of crucial importance if cluster fragmentation under catalytic conditions is to be precluded.

Conclusion

The clusters $[Ru_3(CO)_{10}(dppe)]$ (**1**) and $[Ru_3(CO)_8(dppe)_2]$ (**2**) have been shown to lead to catalytic hydrogenation of diphenylacetylene. This process is solvent-dependent, with fragmentation dominating in low-polarity solvents, indicating that the dppe ligand does not stabilise the cluster under catalytic conditions; this is in contrast to $[Ru_3(\mu\text{-}H)(\mu\text{-}PPh_2)(CO)_9]$, where only cluster-based active species are observed under such conditions. In solvents of higher polarity, clusters **1** and **2** are active catalysts, but exhibit lower activity than their monodentate phosphane analogues $[Ru_3(CO)_{10}(L)_2]$ (L = PPh_3, PMe_2Ph, PMe_3, PCy_3), which is indicative of the dppe ligand impeding substrate binding. The exact nature of the phosphane ligand is thus of great importance in the effort to preclude cluster fragmentation during catalytic transformations.

Experimental Section

General: All synthetic manipulations were carried out under dry nitrogen using standard Schlenk or glove-box techniques. Subsequent purifications were carried out without precautions to exclude air. THF was dried and distilled prior to use, whilst all other

 © 2004 Wiley-VCH Verlag GmbH & Co. KGaA, Weinheim

solvents were used as received. $[Ru_3(CO)_{12}]$ (Strem), dppe, benzophenone (Aldrich) and sodium (Fluka) were also used as received. The clusters $[Ru_3(CO)_{10}(dppe)]$ (**1**) and $[Ru_3(CO)_8(dppe)_2]$ (**2**) were prepared using a literature method[12] and purified by recrystallisation from hexane/dichloromethane. Characterisation was achieved by comparison of characteristic solution IR (ν_{CO}) and FAB MS with the literature data. NMR measurements were made using NMR tubes fitted with J. Young Teflon valves and solvents (dried and degassed) were added by vacuum transfer in a high-vacuum line. For the PHIP experiments, hydrogen enriched in the *para* spin state was prepared by cooling H_2 to 18 K over activated charcoal. The studies were carried out with sample concentrations of approximately 1 μM and spectra were recorded with a Bruker DRX-400 spectrometer with ^1H at 400.1 MHz, ^{13}C at 100.1 MHz and ^{31}P at 162.0 MHz, respectively. ^1H NMR chemical shifts are reported in ppm relative to residual ^1H signals in the deuterated solvents ([D_7]toluene: δ = 2.13 ppm; $CHCl_3$: δ = 7.27 ppm), ^{13}C NMR in ppm relative to $CDCl_3$ (δ = 77.05 ppm), and ^{31}P NMR in ppm downfield of an external 85% solution of phosphoric acid. Modified COSY, HMQC and EXSY pulse sequences were used as described previously.[24] In the exchange and hydrogenation studies, EXSY spectra were acquired immediately after exposing the sample to *p*-H_2 and introducing it into the NMR probe. The results were modelled for hydride exchange and hydride transfer into free H_2, or for hydride transfer into the hydrogenation product, applying published procedures.[10,23] The rate constants obtained in this way were multiplied by two to take into account the analysis method.[25]

Supporting Information: Lists of raw and simulation data and details of the analysis method are available for hydride exchange and H_2 elimination in species **3**, **5a** and **5b**, as well as for catalytic hydrogenation by **6** (footnote on first page of this article).

Acknowledgments

We are grateful to Bruker Biospin and the University of York for financial support. University scholarships from the ORS award scheme (D. B.) and Pfizer Central Research (T. G. P.) are gratefully acknowledged. We also thank Profs. R. N. Perutz, R. Eisenberg, B. F. G. Johnson for helpful discussions.

[1] For example, see: [1a] *Catalysis by di- and polynuclear metal cluster complexes* (Eds.: R. D. Adams, F. A. Cotton), Wiley-VCH, New York, **1998**. [1b] P. J. Dyson, J. S. McIndoe, *Transition metal carbonyl cluster chemistry*, Gordon and Breach, Amsterdam, **2000**.

[2] For example, see: [2a] M. I. Bruce, P. A. Humphrey, B. W. Skelton, A. H. White, *J. Organomet. Chem.* **1996**, *522*, 259−263. [2b] M. I. Bruce, P. A. Humphrey, B. W. Skelton, A. H. White, *J. Organomet. Chem.* **1996**, *526*, 85−97. [2c] M. I. Bruce, B. W. Skelton, A. H. White, N. N. Zaitseva, *J. Organomet. Chem.* **1998**, *558*, 197−207.

[3] G. Lavigne, N. Lugan, J. J. Bonnet, *Organometallics* **1982**, *1*, 1040−1050.

[4] [4a] B. Fontal, M. Reyes, T. Suarez, F. Bellandi, J. C. Diaz, *J. Mol. Catal. A: Chem.* **1999**, *149*, 75−85. [4b] B. Fontal, M. Reyes, T. Suarez, F. Bellandi, N. Ruiz, *J. Mol. Catal. A: Chem.* **1999**, *149*, 87−97.

[5] E. L. Diz, A. Neels, H. Stoeckli-Evans, G. Süss-Fink, *Polyhedron* **2001**, *20*, 2771−2780.

[6] [6a] J. Natterer, J. Bargon, *Prog. Nucl. Magn. Reson. Spectrosc.* **1997**, *31*, 293−315. [6b] S. B. Duckett, C. J. Sleigh, *Prog. Nucl. Magn. Reson. Spectrosc.* **1999**, *34*, 71−92. [6c] S. B. Duckett, D. Blazina, *Eur. J. Inorg. Chem.* **2003**, 2901−2912.

[7] M. S. Anwar, D. Blazina, H. A. Carteret, S. B. Duckett, T. K. Halstead, J. A. Jones, C. M. Kozak, R. J. K. Taylor, *Phys. Rev. Lett.* **2004**, *93*, 040501 .

[8] [8a] S. Aime, R. Gobetto, D. Canet, *J. Am. Chem. Soc.* **1998**, *120*, 6770−6773. [8b] S. Aime, W. Dastru, R. Gobetto, A. Russo, A. Viale, D. Canet, *J. Phys. Chem. A* **1999**, *103*, 9702−9705.

[9] [9a] B. Bergman, E. Rosenberg, R. Gobetto, S. Aime, L. Milone, F. Reineri, *Organometallics* **2002**, *21*, 1508−1511. [9b] R. Gobetto, L. Milone, F. Reineri, L. Salassa, A. Viale, E. Rosenberg, *Organometallics* **2002**, *21*, 1919−1924.

[10] [10a] C. J. Sleigh, S. B. Duckett, R. J. Mawby, J. P. Lowe, *Chem. Commun.* **1999**, 1223−1224. [10b] D. Blazina, S. B. Duckett, P. J. Dyson, B. F. G. Johnson, J. A. B. Lohman, C. J. Sleigh, *J. Am. Chem. Soc.* **2001**, *123*, 9760−9768. [10c] D. Blazina, S. B. Duckett, P. J. Dyson, J. A. B. Lohman, *Angew. Chem. Int. Ed.* **2001**, *40*, 3874−3877. [10d] D. Blazina, S. B. Duckett, P. J. Dyson, J. A. B. Lohman, *Chem. Eur. J.* **2003**, *9*, 1046−1061.

[11] D. Blazina, S. B. Duckett, P. J. Dyson, J. A. B. Lohman, *Dalton Trans.* **2004**, 2108−2114.

[12] M. I. Bruce, T. W. Hambley, B. K. Nicholson, M. R. Snow, *J. Organomet. Chem.* **1982**, *235*, 83−91.

[13] [13a] H. Adams, S. C. M. Agustinho, B. E. Mann, S. Smith, *J. Organomet. Chem.* **2000**, *607*, 175−181. [13b] H. Adams, S. C. M. Agustinho, K. Chomka, B. E. Mann, S. Smith, S. E. Spey, *Can. J. Chem.* **2001**, *79*, 760−774.

[14] B. F. G. Johnson, Y. V. Roberts, *J. Chem. Soc., Dalton Trans.* **1993**, 2945−2950.

[15] S. Aime, R. Gobetto, E. Valls, *Inorg. Chim. Acta* **1998**, *275−276*, 521−527.

[16] [16a] M. I. Bruce, E. Horn, O. bin Shawakataly, M. R. Snow, E. R. T. Tiekink, M. L. Williams, *J. Organomet. Chem.* **1986**, *316*, 187−211. [16b] M. A. Churchill, R. A. Lashewicz, J. R. Shapley, S. I. Richter, *Inorg. Chem.* **1980**, *19*, 1277−1285. [16c] P. Homanen, R. Persson, M. Haukka, T. A. Pakkanen, E. Nordlander, *Organometallics* **2000**, *19*, 5568−5574.

[17] For example, see: [17a] S. Aime, W. Dastru, R. Gobetto, J. Krause, L. Matas, A. Viale, *Organometallics* **1996**, *15*, 4967−4970. [17b] S. Aime, W. Dastru, R. Gobetto, F. Reineri, A. Russo, A. Viale, *Organometallics* **2001**, *20*, 2924−2927.

[18] N. E. Leadbeater, J. Lewis, P. R. Raithby, *J. Organomet. Chem.* **1997**, *543*, 251−253.

[19] D. Schott, C. J. Sleigh, J. P. Lowe, S. B. Duckett, R. J. Mawby, M. G. Partridge, *Inorg. Chem.* **2002**, *41*, 2960−2970.

[20] [20a] N. Lugan, J. J. Bonnet, J. A. Ibers, *Organometallics* **1988**, *7*, 1538−1545. [20b] S. M. Waterman, M. G. Humphrey, J. Lee, G. E. Ball, D. C. R. Hockless, *Organometallics* **1999**, *18*, 2440−2451.

[21] [21a] B. T. Heaton, J. A. Iggo, I. S. Podkorytov, D. J. Smawfield, S. P. Tunik, R. Whyman, *J. Chem. Soc., Dalton Trans.* **1999**, 1917−1919. [21b] D. S. Z. Sabounchei, B. T. Heaton, J. A. Iggo, C. Jacob, I. S. Podkorytov, *J. Clust. Sci.* **2001**, *12*, 339−348.

[22] For example, see: [22a] M. I. Bruce, P. A. Humphrey, B. W. Skelton, A. H. White, M. L. Williams, *Aust. J. Chem.* **1985**, *38*, 1301−1305. [22b] N. Lugan, J. J. Bonnet, J. A. Ibers, *J. Am. Chem. Soc.* **1985**, *107*, 4484−4491. [22c] C. Bergounhou, J. J. Bonnet, P. Fompeyrine, G. Lavigne, N. Lugan, F. Mansilla, *Organometallics* **1986**, *5*, 60−66.

[23] W. D. Jones, G. P. Rosini, J. A. Maguire, *Organometallics* **1999**, *18*, 1754−1760.

[24] [24a] B. A. Messerle, C. J. Sleigh, M. G. Partridge, S. B. Duckett, *J. Chem. Soc., Dalton Trans.* **1999**, 1429−1435. [24b] S. A. Colebrooke, S. B. Duckett, J. A. B. Lohman, *Chem. Commun.* **2000**, 685−686. [24c] P. Hubler, J. Bargon, *Angew. Chem. Int. Ed.* **2000**, *39*, 3701−3703.

[25] M. L. H. Green, L. L. Wong, A. Sella, *Organometallics* **1992**, *11*, 2660−2668.

Received May 31, 2004
Early View Article
Published Online September 2, 2004

 © 2004 Wiley-VCH Verlag GmbH & Co. KGaA, Weinheim

The Nature of the M≡E Bond: Theoretical Investigation of the Molecules $[(RO)_3M{\equiv}E]$ (M = Mo, W; E = N, P, As, Sb, Bi; R = H, Me) and $[(Me_3CO)_3Mo{\equiv}P]$

Krishna K. Pandey*[a] and Gernot Frenking*[b]

Keywords: Nitrido complexes / Bonding analysis / Density functional calculations / Metal−ligand triple bond / Pnicogens

The electronic and molecular structures of the metal-pnicogen complexes $[(RO)_3M{\equiv}E]$ (M = Mo, W; E = N, P, As, Sb, Bi; R = H, Me) and $[(Me_3CO)_3M{\equiv}P]$ have been investigated at the DFT level using the exchange correlation functionals B3LYP and BP86. The nature of the M≡E interactions was analyzed with charge and energy decomposition methods. The bonding analyses show that the metal-pnicogen bonds are genuine triple bonds containing a σ- and a degenerate π-bond. The M–E σ-bonds are always polarized towards the pnicogen atom E, particularly for the nitrogen complexes. The M–N π-bonds are also polarized towards nitrogen, while the π-bonds of the heavier pnicogens P–Bi show a small polarization towards the metal atom. The M–E σ-bonds at the pnicogen E are sp^n-hybridized; the p character is always > 80% of the total AO contribution. The hybridization of the metal atoms in the nitrido complexes is approximately sd^2 and that in the heavier homologues, approximately sd. The ratio of the energy contributions of the σ- and π-orbitals to the covalent bonding in $[(HO)_3M{\equiv}E]$ is about 50:50 for all pnicogen atoms E. The metal–nitrido bonds in $[(HO)_3M{\equiv}N]$ are more covalent than electrostatic. The covalent character becomes smaller when the pnicogen atom becomes heavier with the trend N >> P > As > Sb > Bi. The $[(HO)_3M{\equiv}E]$ tungsten complexes have stronger bonds that are slightly less covalent than the molybdenum complexes, the π-bonding contribution in the former species is slightly larger than in the latter.

(© Wiley-VCH Verlag GmbH & Co. KGaA, 69451 Weinheim, Germany, 2004)

Introduction

Triple bonding between transition metals is a feature commonly encountered in several classes of dinuclear complexes.[1] Molecules that have a σ- and a degenerate π-bond are also known to form between transition metals and main group elements as exemplified in carbyne,[2−9] nitrido,[10−20] and germylyne[21−25] complexes. The coordination chemistry of transition metal complexes with a terminal nitrido ligand has blossomed in the last 25 years, during which much knowledge of their properties has been obtained.[10−20]

For the heavier group 15 elements P, As, Sb, and Bi there are only a small number of complexes with a terminal phosphorus atom as a ligand known from the literature.[26−32] An intermediate metal phosphido complex [(O-*t*Bu)3 W≡P] was first suggested in 1985 by Becker et al.[33] from the reaction of [W2(O-*t*Bu)6] with t-BuC≡P. In 1987, Chisholm and coworkers proposed the formation of an intermediate phosphido complex [(NpO)3 W≡P] (Np = neopentyl).[34] The existence of metal-arsenido complexes [Cp(CO)2M≡As] (M = Mo, W] as intermediates was suggested by Ziegler et al.[35] Rheingold and coworkers reported on metal-stibido complexes $[(CO)_nM{\equiv}Sb]$ (n = 4, M = Cr, Mo, W; n = 3, M = Fe) as intermediates.[36]

Until ten years ago, no examples of stable, fully characterized complexes with a terminal M≡E bond (E = P, As, Sb, Bi) were known. In 1995, the groups of Cummins[37] and Schrock[38] independently reported representative examples of complexes containing metal−phosphorus triple bonds in $[(ArRN)_3Mo{\equiv}P]$, $[(R_2N)_3Mo{\equiv}P]$ {R = $C(CD_3)_2(CH_3)$, Ar = 3,5-$C_6H_3Me_2$} and $[(N_3N)M{\equiv}P]$ {M = Mo, W; N_3N = $(Me_3SiNCH_2CH_2)_3N$}. Schrock et al. also isolated the first examples of metal-arsenido complexes $[(N_3N)M{\equiv}As]$ (M = Mo, W).[38,39] Scheer and coworkers synthesized $[(N_3N)W{\equiv}E]$ (E = P, As) by a different synthetic route.[40] Recently, Cummins et al. reported on the phosphido complex $[(RO)_3Mo{\equiv}P]$ (R = 1-methylcyclohexyl).[41]

Several theoretical studies on metal nitrido complexes have been published[14−20] but little theoretical work has been performed on the heavier homologues. Four computational investigations on phosphido complexes have been reported. Wagener and Frenking optimized the geometries of the model compounds $[(H_2N)_3M{\equiv}P]$, $[(H_2N)3(NH_3)M{\equiv}P]$, $[(HNCH_2CH_2)_3M{\equiv}P]$ (M = Mo, W) at the HF, MP2, and B3LYP levels of theory[42] ^{31}P NMR

[a] School of Chemical Sciences, Devi Ahilya University Indore, Indore, 452017 India
[b] Fachbereich Chemie, Philipps-Universität Marburg, 35037 Marburg, Germany

chemical shielding calculations for phosphido complexes were carried out by Morokuma et al.[43] and by Cummins et al.[41] Geometries of $[(N_3N)W{\equiv}E]$ (E = P, As) were optimized at the DFT/BP86/SVP level of theory by Scheer et al.[40] Ab initio MP2 calculations on the $[(CO)_4Mo{\equiv}Sb]^-$ anion were reported by Rheingold et al.[36] A comparative study of complexes with terminal metal−pnicogen triple bonds $L_nM{\equiv}E$ has not been published until now.

In this paper, 21 metal-pnicogen complexes $[(RO)_3M{\equiv}E]$ (M = Mo, W; E = N, P, As, Sb, Bi; R = H, Me) and $[(Me_3CO)_3M{\equiv}P]$ have been investigated using density functional theory at the B3LYP and BP86 levels of theory. We report on the charge and energy decomposition analysis of the metal−pnicogen triple bonds in $[(MeO)_3M{\equiv}E]$ (M = Mo, W; E = N, P, As, Sb, Bi), which gives, for the first time, the energies that are associated with the M→E σ-donation and M←E π-bonding. The relative strength of the electrostatic and covalent contributions to the bond strength will be also reported. The following questions are addressed in this work: (i) how are the M≡E σ- and π-bonds polarized, and what is the hybridization at the metal and pnicogen atoms; (ii) how strong are the contributions of the M−E σ-bonding and M−E π-bonding to the total M≡E bonding energy; (iii) what are the relative strengths of the covalent and electrostatic interactions?

Computational Methods

Calculations on all complexes have been performed using the hybrid B3LYP density functional method, which uses Becke's 3-parameter nonlocal exchange functional[44] mixed with the exact (Hartree−Fock) exchange functional and Lee−Yang−Parr's nonlocal correlation functional.[45] The geometries of the molecules were optimized without any symmetry restrictions with standard 6−311G(d) basis sets[46] for H, C, O, N and P atoms. For As, Sb, Bi, Mo and W, quasi-relativistic effective core potentials (ECP) determined by Hay−Wadt have been used.[47] The valence basis sets for Mo and W have triple-ζ quality (10s10p4d1f/3s3p3d1f), which include $(n+1)$p functions[48] that were augmented by an additional set of f orbitals with an exponent of 1.043 for Mo and 0.823 for W.[49] For As, Sb and Bi, the standard (3s4p1d/2s3p1d) valence basis functions of Hay and Wadt have been used.[50] This basis set is denoted TZP. Frequency calculations were performed at B3LYP/TZP to determine whether the optimized geometries were minima on the potential energy surface. The electronic structures of the complexes were examined by NBO analysis.[51] The B3LYP/TZP calculations were carried out with the Gaussian98 program.[52] All MO pictures were made by using the MOLDEN program.[53]

Calculations on the model complexes $[(HO)_3M{\equiv}E]$ have also been performed at the nonlocal DFT level of theory using the exchange functional of Becke[54] and the correlation functional of Perdew[55] (BP86). Scalar relativistic effects have been considered using the ZORA formalism.[56] Uncontracted Slater-type orbitals (STOs) using triple-ζ basis sets augmented by two sets of polarization functions were employed for the SCF calculations.[57] The $(1s)^2$ core electrons of carbon and nitrogen, $(1s2s2p)^{10}$ core electrons of phosphorus, $(1s2s2p3s3p)^{18}$ core electrons of arsenic, $(1s2s2p3s3p3d)^{28}$ core electrons of molybdenum, $(1s2s2p3s3p3d4s4p)^{36}$ core electrons of antimony, and $(1s2s2p3s3p3d4s4p4d)^{46}$ core electrons of bismuth and tungsten were treated by the frozen-core approximation.[58] An auxiliary set of s, p, d, f and g STOs was used to fit the molecular densities, and to present the coulomb and exchange potentials accurately in each SCF cycle.[59] A numerical integration accuracy of INTEGRATION = 10 was used throughout. The geometries of $[(HO)_3M{\equiv}E]$ were optimized at BP86/TZ2P with C_3 symmetry. The latter calculations were performed utilizing the program package ADF-2002.01.[60]

The binding interactions in the complexes $[(HO)_3M{\equiv}E]$ between the fragment radicals in the electronic quadruplet states ($^4A_1$) $[(HO)_3Mo]$ and ($^4\Sigma^-$) E have been analyzed with C_3 symmetry using the energy decomposition scheme of ADF, which is based on the methods of Morokuma,[61] and Ziegler and Rauk.[62] According to the ETS method, the bond energy ΔE between the $[(HO)_3Mo]$ and E fragments is:

$$\Delta E = \Delta E_{int} + \Delta E_{prep} \quad (1)$$

Here, ΔE_{prep} is the energy required to promote the structures of the free fragments from their equilibrium structure in the electronic ground state to the geometry and electronic state that they take up in the molecule:

$$\Delta E_{prep} = E_{total}(\text{distorted fragments}) - E_{total}(\text{fragments in the equilibrium structure}) \quad (2)$$

ΔE_{int} in Equation (1) is the instantaneous interaction energy between the two fragments in the molecule. It is comprised of three main components as shown in Equation (3).

$$\Delta E_{int} = \Delta E_{elstat} + \Delta E_{Pauli} + \Delta E_{orb} \quad (3)$$

ΔE_{elstat} describes the classical Coulomb interaction between the fragments, which is attractive in most cases. The term ΔE_{Pauli}, which is called exchange repulsion or Pauli repulsion, takes into account the destabilizing two-orbital three- or four-electron interactions between occupied orbitals of both fragments. ΔE_{Pauli} is calculated by enforcing the Kohn−Sham determinant of the molecule, which results from superimposing both fragments, to obey the Pauli principle through antisymmetrization and renormalization. The last term ΔE_{orb} in Equation (1) gives the stabilizing orbital interactions between occupied and virtual orbitals of the two fragments. ΔE_{orb} can be further partitioned into contributions from the orbitals that belong to different irreducible representations of the point group of the system. It

 © 2004 Wiley-VCH Verlag GmbH & Co. KGaA, Weinheim

has been suggested that the covalent and electrostatic character of a bond is given by the ratio $\Delta E_{elstat}/\Delta E_{orb}$.[23,63−65]

Results and Discussion

Geometries

Figure 1 shows the optimized geometries of $[(RO)_3Mo{\equiv}P]$ (R = H, Me, CMe_3). Table 1 gives the most important bond lengths and angles that have been computed for the eleven molybdenum-pnicogen complexes $[(RO)_3Mo{=}E]$ (R = H, Me; M = Mo; E = N, P, As, Sb, Bi) and $[(Me_3CO)_3Mo{=}P]$. The geometrical data for the ten tungsten-pnicogen complexes $[(RO)_3W{=}E]$ (R = H, Me; M = W; E = N, P, As, Sb, Bi) are presented in Table 2.

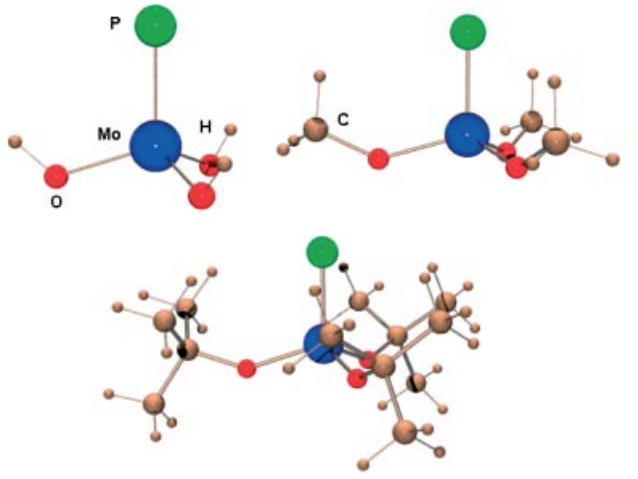

Figure 1. Optimized geometries of $[(RO)_3Mo{\equiv}P]$ (R = H, Me, CMe_3)

Experimental values are available for a large number of stable nitrido complexes of molybdenum and tungsten. From these structural data, the M≡N triple bond lengths are between 1.6−1.7 Å.[10−20] The calculated Mo≡N and W≡N bond lengths at B3LYP/TZP in $[(HO)_3Mo{\equiv}N]$ (1.634 Å), $[(MeO)_3Mo{\equiv}N]$ (1.639 Å), $[(HO)_3W{\equiv}N]$ (1.665 Å), and $[(MeO)_3W{\equiv}N]$ (1.670 Å) agree quite well with the experimental values. The calculated Mo≡P and W≡P bond lengths in $[(HO)_3Mo{\equiv}P]$ (2.094 Å), $[(MeO)_3Mo{\equiv}P]$ (2.102 Å), $[(Me_3CO)_3Mo{\equiv}P]$ (2.112 Å), $[(HO)_3W{\equiv}P]$ (2.118 Å) ,and $[(MeO)_3W{\equiv}P]$ (2.126 Å) are also very close to experimental values found by X-ray diffraction for $[(ArRN)_3Mo{\equiv}P]$ [2.119(4) Å], $[(RO)_3Mo{\equiv}P]$ [2.1144(16) Å], and $[(N_3N)W{\equiv}P]$ [2.162(4) Å]. We note that as the size of R increases, the M≡E bond lengthens. In arsenido complexes, the calculated M≡As bond lengths in $[(HO)_3Mo{\equiv}As]$ (2.217 Å), $[(MeO)_3Mo{\equiv}As]$ (2.224 Å), $[(HO)_3W{\equiv}As]$ (2.237 Å), and $[(MeO)_3W{\equiv}As]$ (2.245 Å) are slightly shorter than those found by X-ray diffraction for $[(N_3N)Mo{\equiv}As]$ [2.252(3) Å] and $[(N_3N)W{\equiv}As]$ [2.2903(11) Å]. The BP86/TZ2P values are very similar to the B3LYP/TZP data.

There are no experimental data for the length of M≡Sb and M≡Bi triple bonds. A bond length of 2.55 Å in $[(CO)_4Mo{\equiv}Sb]^-$ has been calculated at the MP2 level.[36] Using the relationship between bond order and bond lengths suggested by Pauling,[66] we find the estimated Mo≡E (Mo≡N = 1.81 Å, Mo≡P = 2.12 Å, Mo≡As = 2.25 Å, Mo≡Sb = 2.44 Å, and Mo≡Bi = 2.49 Å) and W≡E bond lengths (W≡N = 1.82 Å, W≡P = 2.13 Å, W≡As = 2.26 Å, W≡Sb = 2.45 Å, and W≡Bi = 2.50 Å) for triple bonds from the M−E single bond lengths based on covalent radii predictions (covalent radius, Mo = 1.40 Å, W = 1.41 Å, N = 0.75 Å, P = 1.06 Å, As = 1.19 Å, Sb = 1.38 Å, Bi = 1.43 Å).[67] It is interesting to note that the calculated M≡E bond lengths in the calculated molyb-

Table 1. Selected optimized geometrical parameters for the $[(RO)_3Mo{\equiv}E]$ (R = H, Me; E = N, P, As, Sb, Bi) complexes; distances are in Å and angles are in degrees

E =	N			P				As			Sb			Bi		
R =	H		Me	H		Me	$C(Me)_3$	H		Me	H		Me	H		Me
	B3LYP	BP86	B3LYP	B3LYP	BP86	B3LYP	B3LYP	B3LYP	BP86	B3LYP	B3LYP	BP86	B3LYP	B3LYP	BP86	B3LYP
Bond lengths																
Mo−E	1.634	1.657	1.639	2.094	2.117	2.102	2.112	2.217	2.226	2.224	2.429	2.443	2.436	2.484	2.523	2.488
Mo−O	1.902	1.906	1.893	1.893	1.893	1.881	1.889	1.893	1.893	1.880	1.892	1.891	1.878	1.893	1.893	1.879
O−H	0.963	0.973		0.962	0.971			0.962	0.971		0.962	0.971		0.962	0.971	
O−C			1.415			1.413	1.443			1.413			1.411			1.411
Bond angles																
E−Mo−O	106.2	107.1	105.3	107.1	107.8	105.5	107.9	107.2	107.8	105.5	107.3	107.7	105.2	107.2	107.9	104.9
O−Mo−O	112.5	111.8	113.3	111.8	111.0	113.1	111.1	111.7	111.1	113.1	111.5	111.2	113.4	111.6	111.1	113.6
M−O−H	122.5	119.9		124.9	122.1			125.2	121.8		125.7	121.8		125.9	122.1	
M−O−C			134.2			139.3	144.2			140.0			141.5			141.6

 © 2004 Wiley-VCH Verlag GmbH & Co. KGaA, Weinheim

Table 2. Selected optimized geometrical parameters for the [(RO)$_3$W≡E] (R = H, Me; E = N, P, As, Sb, Bi) complexes; distances are in Å and angles are in degrees

E =	N			P			As			Sb			Bi		
R =	H		Me	H		Me	H		Me	H		Me		H	Me
	B3LYP	BP86	B3LYP	B3LYP	BP86	B3LYP	B3LYP	BP86	B3LYP	B3LYP	BP86	B3LYP	B3LYP	BP86	B3LYP
Bond lengths															
Mo−E	1.665	1.686	1.670	2.118	2.133	2.126	2.237	2.237	2.245	2.446	2.448	2.455	2.502	2.539	2.508
Mo−O	1.888	1.907	1.878	1.877	1.898	1.865	1.876	1.896	1.863	1.876	1.892	1.860	1.876	1.894	1.861
O−H	0.962	0.971		0.961	0.970		0.961	0.970		0.961	0.970		0.961	0.970	
O−C			1.420			1.418			1.418			1.417			1.417
Bond angles															
E−Mo−O	106.4	106.7	105.5	107.6	107.7	106.3	107.6	107.7	106.4	108.0	107.7	106.4	107.9	107.8	106.1
O−Mo−O	112.9	112.1	113.1	111.3	111.1	112.5	111.3	111.2	112.3	110.9	111.2	112.4	111.0	111.1	112.6
M−O−H	124.9	119.4		127.1	121.7		127.1	121.8		128.2	121.6		128.2	121.7	
M−O−C			135.3			140.2			141.0			142.5			143.2

denum-pnicogen and tungsten-pnicogen complexes correspond to a Pauling bond order of approximately 3.

Bonding Analysis of M≡E Bonds

We begin the analysis of the bonding situation in the pnicogen complexes [(MeO)$_3$M≡E] (M = Mo, W; E = N, P, As, Sb, Bi) with a discussion on the conventional indices that are frequently used in order to characterize the bonding situation in molecules, i.e. bond orders and atomic charges. Table 3 gives the Wiberg bond indices (WBI)[68] and the results of the natural bond orbital (NBO) analysis.

Table 3 shows that the WBI values of the M≡E bonds in the pnicogen complexes are significantly higher (2.47−2.65) than the WBI values of the M−O single bond (0.81−0.85).

Table 3. Wiberg bond indices and results of the NBO analysis of the [(RO)$_3$M≡E] (M = Mo, W; E = N, P, As, Sb, Bi) complexes

	Mo							W				
E =	N	P			As	Sb	Bi	N	P	As	Sb	Bi
R =	Me	H	Me	CMe_3	Me	Me	Me	Me	Me	Me	Me	Me
Wiberg bond indices												
M−E	2.65	2.59	2.53	2.48	2.51	2.49	2.47	2.58	2.56	2.55	2.54	2.54
M−O	0.81	0.85	0.83	0.83	0.83	0.83	0.84	0.81	0.84	0.84	0.84	0.83
O−C	0.92		0.91	0.86	0.91	0.91	0.91	0.90	0.89	0.89	0.89	0.89
C−H	0.93		0.93	0.92	0.93	0.93	0.93	0.93	0.93	0.93	0.93	0.93
NBO charges												
M	1.63	1.07	1.09	1.14	1.03	0.99	1.06	1.94	1.39	1.33	1.25	1.29
E	−0.46	0.02	−0.01	−0.09	0.02	0.08	0.01	−0.66	−0.23	−0.18	−0.10	−0.10
O	−0.72	−0.87	−0.69	−0.70	−0.69	−0.69	−0.69	−0.77	−0.74	−0.74	−0.74	−0.74
Me	0.33		0.33		0.34	0.33	0.33	0.34	0.35	0.36	0.36	0.34
M−E σ bond												
Occupancy	1.871	1.869	1.837	1.831	1.840	1.835	1.849	1.918	1.898	1.900	1.899	1.905
M												
%[a]	37.13	43.16	41.35	39.77	42.19	42.96	41.49	33.98	41.20	42.84	45.48	44.22
%s	30.51	50.86	48.84	48.00	51.53	55.14	54.73	32.50	50.33	52.43	85.87	59.51
%p	0.37	0.81	0.14	0.40	0.69	1.49	1.63	0.49	0.16	0.72	1.73	1.66
%d	68.59	48.21	50.80	51.36	47.69	43.24	43.51	66.68	49.38	46.76	42.34	42.37
E												
%[a]	62.87	54.86	58.65	60.23	57.81	57.04	58.51	66.02	58.80	57.16	54.52	55.78
%s	16.86	10.29	13.10	14.22	12.42	10.96	8.82	19.08	14.63	13.66	11.73	9.78
% p	82.87	89.26	86.44	85.34	87.11	88.64	90.96	80.64	84.85	85.83	87.85	90.02
% d	0.27	0.45	0.46	0.44	0.47	0.40	0.22	0.28	0.52	0.51	0.24	0.20
M−E π bond												
Occupancy	1.988	1.975	1.981	1.969	1.981	1.981	1.978	1.983	1.975	1.975	1.974	1.882
M												
%[a]	45.81	56.06	56.13	55.09	56.42	58.12	57.13	42.49	51.03	52.03	53.00	50.28
% p	0.42	1.23	1.08	1.08	1.04	1.24	1.27	0.73	1.51	1.45	1.86	12.39
% d	99.47	98.74	98.90	98.89	98.94	98.75	98.27	99.16	98.46	98.54	98.13	87.09
E												
%[a]	54.19	43.94	43.87	44.91	43.58	41.88	42.87	57.51	48.97	47.97	47.00	49.72
% p	99.72	99.39	99.45	99.48	99.54	99.76	99.90	99.70	99.49	99.55	99.76	99.89
% d	0.28	0.61	0.55	0.52	0.46	0.24	0.10	0.30	0.51	0.45	0.24	0.11

[a] The % values give the polarization of the M−E bonds.

 © 2004 Wiley-VCH Verlag GmbH & Co. KGaA, Weinheim

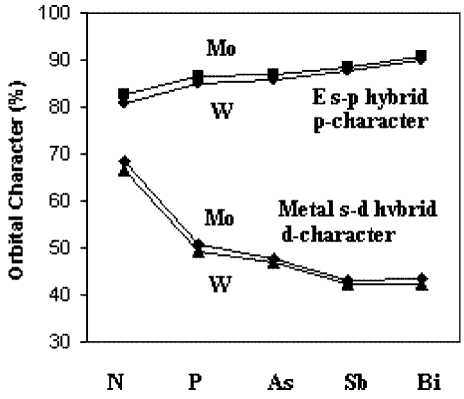

Figure 2. Metal s-d hybrid and E s-p hybrid orbitals for M≡E σ-bond in $[(MeO)_3M{\equiv}E]$ (M = Mo, W; E = N, P, As, Sb, Bi)

The latter values are approximately one third of the WBI values of the M≡E bonds. This is a first hint that the M−E bonds have a substantial degree of multiple bonding. The calculated NBO charge distribution indicates that the metal atoms always carry a large positive charge. Note that tungsten is always more positively charged than molybdenum. Nitrogen carries a significant negative charge in the nitrido complexes, while the heavier pnicogen ligands have only a small negative charge or, in cases of some molybdenum species, are slightly positive.

A more definitive picture of M≡E bonding is obtained through NBO analysis of the delocalized Kohn−Sham orbitals. The characteristics of the M≡E bonding orbitals are listed in Table 3. The M−E σ-bonding orbitals are always polarized towards the pnicogen atoms E, particularly for

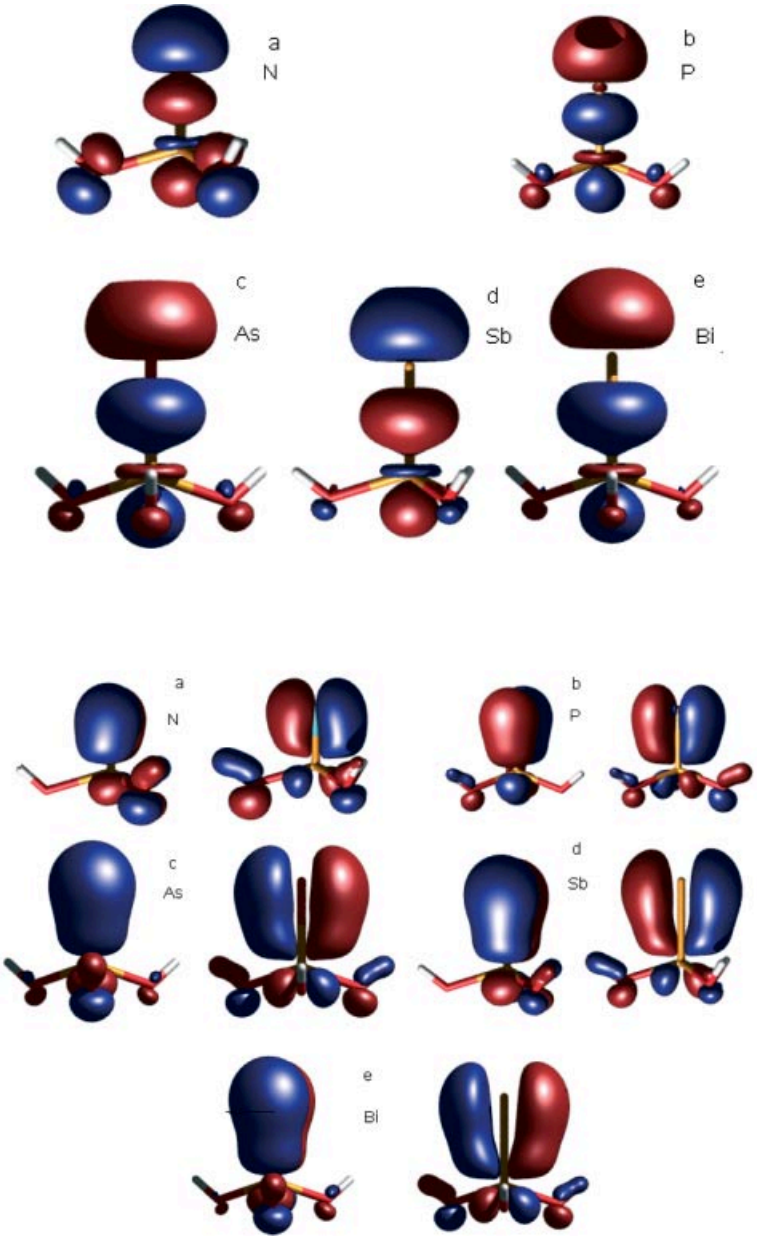

Figure 3. Plot of Mo≡E σ- (top) and π- (bottom) molecular orbitals of $[(HO)_3Mo{\equiv}E]$ (E = N, P, As, Sb, Bi)

 © 2004 Wiley-VCH Verlag GmbH & Co. KGaA, Weinheim

the nitrogen complexes. The M−N π-bonds are also polarized towards nitrogen, albeit less so than the σ-bonds, while the heavier pnicogen M−E π-bonds show a small polarization towards the metal atom. The hybridization of the M−E σ-bonds at the pnicogen atoms has a large p character, which is always >80% of the total AO contribution. The hybridization of the metal atoms in the metal−nitrido bonds is approximately sd^2, while the s and d contributions in the heavier metal−pnicogen σ-bonds are more balanced. The trend of the sp^n and sd^n character of the pnicogen and metal atoms of the σ-bonds is shown in Figure 2. It becomes obvious that the %d contribution at the metal atom of the σ-bonds for the heavier pnicogens is much lower than that for nitrogen. The strong triple-bond character of the M≡E bonds becomes visible by the envelope plots of the calculated σ- and π-orbitals of the model compounds $[(HO)_3Mo{\equiv}E]$ (E = N, P, As, Sb, Bi), which are shown in Figure 3.

Besides the charge decomposition analysis using the NBO method, we also carried out an energy decomposition analysis of the metal−pnicogen bonds in $[(HO)_3M{\equiv}E]$. The results are given in Table 4.

The calculated data in Table 4 show that the M≡E bonds are rather strong. The theoretically predicted BDEs of the nitrido bonds are 163.6 kcal/mol for $[(HO)_3Mo{\equiv}N]$ and 179.2 kcal/mol for $[(HO)_3W{\equiv}N]$. The heavier pnicogen complexes have significantly weaker bonds. The calculated bond energies are between 122.6 kcal/mol for $[(HO)_3W{\equiv}P]$ and 64.3 kcal/mol for $[(HO)_3Mo{\equiv}Bi]$. The bond energies show the expected trend for the BDE of the pnicogens, N >> P > As > Sb > Bi. The tungsten complexes have stronger bonds than the molybdenum complexes.

The breakdown of the metal−pnicogen interaction energies into the different energy terms shows that the M≡N bond has a larger covalent character (about 60%) than electrostatic character (Table 4). The covalent contribution to the M≡E bonds becomes significantly smaller than the electrostatic contribution for the heavier pnicogens. The trend for the covalent character for the pnicogens is N >> P > As > Sb > Bi. The trend is graphically shown in Figure 4. The ratio of σ- to π-bonding in the covalent M≡E bond is almost 50:50.

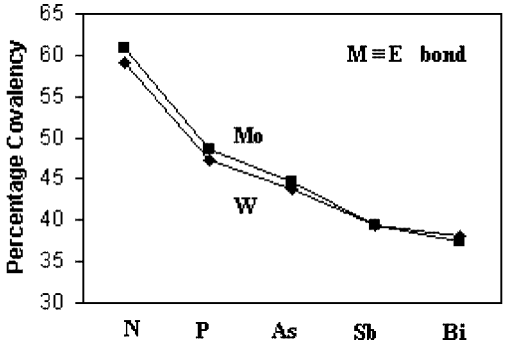

Figure 4. Trends of the covalent contributions to the M≡E bonding interactions in $[(HO)_3M{\equiv}E]$ (M = Mo, W; E = N, P, As, Sb, Bi)

Summary and Conclusion

The results of the bonding analysis of the title compounds show that the metal−pnicogen bonds are genuine triple bonds containing a σ- and a degenerate π-bond. The questions that have been addressed in the introduction can be answered as follows. (i) The M−E σ-bonds are always polarized towards the pnicogen atom E, particularly for the nitrogen complexes. The M−N π-bonds are also polarized towards nitrogen, while the π-bonds of the heavier pnicogens (P−Bi) show a small polarization towards the metal atom. The M−E σ-bonds at the pnicogen E are sp^n-hybridized; the p character is always > 80% of the total AO contribution, while the hybridization of the metal atoms in the nitrido complexes is approximately sd^2 and in the heavier homologues, approximately sd. (ii) The ratio of the energy contributions of the σ- and π-orbitals to the covalent bonding in $[(HO)_3M{\equiv}E]$ is about 50:50 for all pnicogen atoms E. (iii) The metal−nitrido bonds in $[(HO)_3M{\equiv}N]$ are more covalent than electrostatic in character. The covalent

Table 4. Energy decomposition analysis of $[(HO)_3M{\equiv}E]$ at BP86/TZ2P; energy contributions in kcal/mol

	Mo					W				
Term	N	P	As	Sb	Bi	N	P	As	Sb	Bi
ΔE_{int}	−175.2	−119.0	−106.1	−86.0	−76.5	−192.4	−136.9	−123.4	−102.2	−91.7
ΔE_{Pauli}	462.4	300.2	281.5	244.8	241.0	475.2	320.8	302.3	264.6	250.5
ΔE_{elstat}	−249.4	−215.8	−214.7	−200.2	−198.7	−272.3	−241.7	−239.4	−222.5	−212.0
ΔE_{orb} [a]	−388.3	−203.4	−172.8	−130.7	−119.1	−395.3	−215.9	−186.3	−144.3	−130.2
	(60.9%)	(48.5%)	(44.6%)	(39.5%)	(37.5%)	(59.3%)	(47.2%)	(43.8%)	(39.3%)	(38.0%)
a_1	−204.2	−101.4	−87.1	−66.9	−63.1	−205.7	−105.4	−91.2	−70.9	−66.4
a_2	0.0	0.0	0.0	0.0	0.0	0.0	0.0	0.0	0.0	0.0
e [b]	−184.1	−102.0	−85.7	−63.8	−56.0	−189.6	−110.5	−95.1	−73.4	−63.8
	(47.4%)	(50.1%)	(49.6%)	(48.8%)	(47.0%)	(48.0%)	(51.2%)	(51.0%)	(50.9%)	(49.0%)
ΔE_{prep}	11.6	12.3	12.2	11.9	12.2	13.2	14.3	14.2	14.0	14.3
$\Delta E(-D_e)$	−163.6	−106.7	−93.9	−74.1	−64.3	−179.2	−122.6	−109.2	−88.2	−83.4

[a] The values in parentheses are the percentage contribution to the total attractive interactions reflecting the covalent character of the bond. [b] The values in parentheses are the percentage π-contribution to the total orbital interactions, ΔE_{orb}.

 © 2004 Wiley-VCH Verlag GmbH & Co. KGaA, Weinheim

character becomes smaller when the pnicogen atom becomes heavier, following the trend N >> P > As > Sb > Bi. (iv) The $[(HO)_3M{\equiv}E]$ tungsten complexes have stronger bonds, which are slightly less covalent than the molybdenum complexes. The π-bonding contribution in the former species is slightly larger than in the latter.

[1] F. A. Cotton, R. A. Walton, *Multiple Bonds between Metal Atoms*, 2nd ed.; Clarendon, Oxford, **1993**. M. H. Chisholm, *Acc. Chem. Res.* **1990**, *23*, 419.
[2] W. A. Nugent, J. M. Meyer, *Metal-Ligand Multiple Bonds*, John Wiley & Sons, New York, **1988**.
[3] H. Fischer, P. Hofmann, F. R. Kreisal, R. R. Schrock, U. Schubert, K. Weiss, Carbyne Complexes; VCH Publishers, New York, **1988**.
[4] *Transition Metal Carbyne Complexes*, F. R. Kreisal, Ed.; Kluwer: Dordrecht, The Netherlands, **1993**.
[5] A. M. LaPoint, R. R. Schrock, W. M. Davis, *J. Am. Chem. Soc.* **1995**, *117*, 4802.
[6] S. F. Vyboishchikov, G. Frenking, *Chem. Eur. J.* **1998**, *4*, 1439.
[7] G. Frenking, N. Fröhlich, *Chem. Rev.* **2000**, *100*, 717.
[8] S. K. Cho, Y. S. Gal, S. H. Jin, H. K. Kim, *Chem. Rev.* **2000**, *100*, 1645.
[9] J. W. Herndon, *Coord. Chem. Rev.* **2002**, *227*, 1.
[10] F. A. Cotton, G. Wilkinson, C. A. Murillo, M. Bochmann, *Advanced Inorganic Chemistry*, 6th ed.; Wiley, New York, **1999**.
[11] K. Dehnicke, J. Strähle, *Angew. Chem. Int. Ed. Engl.* **1992**, *31*, 955.
[12] M. Scheer, *Angew. Chem. Int. Ed. Engl.* **1995**, *34*, 1947.
[13] C.-M. Ho, T.-C. Lau, H.-L. Kwong, W.-T. Wong, *J. Chem. Soc., Dalton Trans.* **1999**, 2411.
[14] [14a] A. Neuhaus, A. Veldkamp, G. Frenking, *Inorg. Chem.* **1994**, *33*, 5278. [14b] S. F. Vyboichshikov, G. Frenking, *Theor. Chem. Acc.* **1999**, *102*, 300. [14c] P. Spuhler, M. Lein, G. Frenking, *Z. Allg. Anorg. Chem.* **2003**, *629*, 803.
[15] K. L. Kunze, J. F. Harrison, *J. Am. Chem. Soc.* **1990**, *112*, 3812.
[16] J. F. Harrison, *J. Chem. Phys.* **1996**, *100*, 3513.
[17] A. Fiedler, S. Iwata, *Chem. Phys. Lett.* **1997**, *271*, 143.
[18] A. Daoudi, S. Elkhattabi, G. Berthiar, J. P. Flament, *Chem. Phys.* **1998**, *230*, 31.
[19] S. Elkhattabi, A. Daoudi, J. P. Flament, G. Berthiar, *Chem. Phys.* **1999**, *241*, 257.
[20] [20a] T. R. Cundari, *Chem. Rev.* **2000**, *100*, 807. [20b] J. F. Harrison, *Chem. Rev.* **2000**, *100*, 679 and references cited therein.
[21] R. S. Simons, P. P. Power, *J. Am. Chem. Soc.* **1996**, *118*, 11966.
[22] L. Pu, B. Twamley, S. T. Haubrich, M. M. Olmstead, B. V. Mork, R. S. Simons, P. P. Power, *J. Am. Chem. Soc.* **2000**, *122*, 650.
[23] A. C. Filippou, A. I. Philippoupolos, P. Portius, D. U. Neumann, *Angew. Chem. Int. Ed.* **2000**, *39*, 2778.
[24] A. C. Filippou, P. Portius, A. I. Philippoupolos, *Organometallics* **2002**, *21*, 635.
[25] K. K. Pandey, M. Lein, G. Frenking, *J. Am. Chem. Soc.* **2003**, *125*, 1660.
[26] M. Scheer, *Coord. Chem. Rev.* **1997**, *163*, 271.
[27] A. T. Termaten, H. Aktas, M. Schakel, A. W. Ehlers, M. Lutz, A. L. Spek, K. Lammertsma, *Organometallics* **2003**, *22*, 1827.
[28] B. T. Sterenberg, K. A. Udachin, A. J. Carty, *Organometallics* **2003**, *22*, 3927.
[29] A. W. Ehlers, E. J. Baerends, K. Lammertsma, *J. Am. Chem. Soc.* **2002**, *124*, 2831.
[30] J. Sanchez-Nieves, B. T. Sterenberg, K. A. Udachin, A. J. Carty, *J. Am. Chem. Soc.* **2003**, *125*, 2404.
[31] F. Basuli, J. Tomaszewski, J. C. Huffman, D. J. Mindiola, *J. Am. Chem. Soc.* **2003**, *125*, 10170.
[32] F. Basuli, B. C. Bailey, J. C. Huffman, M.-H. Baik, D. J. Mindiola, *J. Am. Chem. Soc.* **2004**, *126*, 1924.
[33] G. Becker, W. Becker, R. Knebl, H. Schmidt, U. Weber, M. Westerhausen, *Nova Acta Leopoldina* **1985**, *59*, 55.
[34] M. H. Chisholm, J. C. Huffman, J. W. Pasterczyk, *Inorg. Chim. Acta* **1987**, *133*, 17.
[35] M. L. Ziegler, H.-P. Neumann, *Chem. Ber.* **1989**, *112*, 25.
[36] A. R. Arnold, D. P. Ridga, A. L. Rheingold, *J. Am. Chem. Soc.* **1995**, *117*, 4427.
[37] C. E. Laplaza, W. N. Davis, C. C. Cummins, *Angew. Chem. Int. Ed. Engl.* **1995**, *34*, 2042.
[38] R. R. Schrock, N. C. Zanetti, W. N. Davis, *Angew. Chem. Int. Ed. Engl.* **1995**, *34*, 2044.
[39] J. A. Johnson-Carr, N. C. Zanetti, R. R. Schrock, M. D. Hopkins, *J. Am. Chem. Soc.* **1996**, *118*, 11305.
[40] M. Scheer, J. Müller, M. Häser, *Angew. Chem. Int. Ed. Engl.* **1996**, *35*, 2492.
[41] F. H. Stephens, J. S. Figueroa, P.-L. Diaconescu, C. C. Cummins, *J. Am. Chem. Soc.* **2003**, *125*, 9264.
[42] T. Wagener, G. Frenking, *Inorg. Chem.* **1998**, *37*, 1805.
[43] G. Wu, D. Rovnyak, M. J. A. Johnson, N. C. Zanetti, D. G. Musaev, K. Morokuma, R. R. Schrock, R. G. Griffin, C. C. Cummins, *J. Am. Chem. Soc.* **1996**, *118*, 10654.
[44] C. Lee, W. Yang, R. G. Parr, *Phys. Rev. B* **1988**, *37*, 785.
[45] D. Becke, *J. Chem. Phys.* **1993**, *98*, 5648.
[46] [46a] K. Raghavachari, J. S. Binkley, R. Seeger, J. A. Pople, *J. Chem. Phys.* **1980**, *72*, 650. [46b] A. D. McClean, G. S. Chandler, *J. Chem. Phys.* **1980**, *72*, 5639.
[47] M. Couty, M. B. Hall, *J. Comput. Chem.* **1996**, *17*, 1359.
[48] A. W. Ehlers, M. Böhme, S. Dapprich, A. Gobbi, A. Höllwarth, V. Jonas, K. F. Köhler, R. Stegmann, A. Veldkamp, G. Frenking, *Chem. Phys. Lett.* **1993**, *208*, 111.
[49] P. J. Hay, W. R. Wadt, *J. Chem. Phys.* **1985**, *82*, 299.
[50] W. R. Wadt, P. J. Hay, *Chem. Phys.* **1985**, *82*, 284.
[51] A. E. Reed, L. A. Curtiss, F. Weinhold, *Chem. Rev.* **1988**, *88*, 899.
[52] M. J. Frisch, G. W. Trucks, H. B. Schlegel, G. E. Scuseria, M. A. Robb, J. R. Cheeseman, B. G. Zarzewski, J. A. Montgomery, R. E. Startmann, J. C. Burant, S. Dapprich, J. M. Millam, A. D. Daniels K. N. Kudin, M. C. Straiin, O. Farkas, J. Tomasi, V. Barone, M. Cossi, R. Cammi, B. Mennucci, C. Pomelli, C. Adamo, S. Clifford, J. Ochteriski, G. A. Petersson, P. Y. Ayala, Q. Cui, K. Morokuma, P. Salvador, J. J. Dannenberg, D. K. Malick, A. D. Rabuck, K. Raghavachari, J. B. Foresman, J. Cioslowski, J. V. Ortiz, A. G. Baboul B. B. Stefanov, G. Liu, A. Liashenko, P. Piskorz, I. Komaromi, R. Gomperts, R. L. Martin, D. J. fox, T. Keith, M. A. Al-Laham, C. Y. Peng, A. Nanayakkara, M. Challacombe, P. M. W. Gill, B. G. Johnson, W. Chen. M. W. Wong, J. L. Andres, C. Gonzalez, M. Head-Gordon, E. S. Replogle, J. A. Pople, Gaussian98; Gussain, Inc., Pittsburgh PA, **1998**.
[53] G. Schaftenaar, MOLDEN3.4 CAOSCAMM Center, The Netherlands, **1998**.
[54] A. D. Becke, *Phys. Rev. A* **1988**, *38*, 3098.
[55] J. P. Perdew, *Phys. Rev. B* **1986**, *33*, 8822.
[56] [56a] C. Chang, M. Pelissier, Ph. Durand, *Phys. Scr.* **1986**, *34*, 394. [56b] J.-L. Heully, I. Lindgren, E. Lindroth, S. Lundquist, A.-M. Martensson-Pendrill, *J. Phys. B* **1986**, *19*, 2799. [56c] E. van Lenthe, E. J. Baerends, J. G. Snijders, *J. Chem. Phys.* **1993**, *99*, 4597. [56d] E. van Lenthe, E. J. Baerends, J. G. Snijders, *J. Chem. Phys.* **1996**, *105*, 6505. [56e] E. van Lenthe, R. van Leeuwen, E. J. Baerends, J. G. Snijders, *Int. J. Quantum Chem.* **1996**, *57*, 281. [56f] E. van Lenthe, A. W. Ehlers, E. J. Baerends, *J. Chem. Phys.* **1999**, *110*, 8943.
[57] J. G. Snijders, E. J. Baerends, P. Vernooijs, *At. Data Nucl. Data Tables* **1982**, *26*, 483.
[58] E. J. Baerends, D. E. Ellis, P. Ros, *Chem. Phys.* **1973**, *2*, 41.
[59] J. Krijn, E. J. Baerends, *Fit Functions in the HFS-Method*, Internal Report (in Dutch), Vrije University Amsterdam, The Netherlands, **1984**.
[60] E. J. Baerends, J. A. Autschbach, A. Berces, C. Bo, P. M. Boerrigter, L. Cavallo, D. P. Chong, L. Deng, R. M. Dickson, D.

 © 2004 Wiley-VCH Verlag GmbH & Co. KGaA, Weinheim

E. Ellis, L. Fan, T. H. Fischer, C. Fonseca Guerra, S. J. A. van Gisbergen, J. A. Groeneveld, O. V. Gritsenko, M. Grüning, F. E. Harris, P. van den Hoek, H. Jacobsen, G. van Kessel, F. Kootstra, E. van Lenthe, V. P. Osinga, S. Patchkovskii, P. H. T. Philipsen, D. Post, C. C. Pye, W. Ravenek, P. Ros, P. R. T. Schipper, G. Schreckenbach, J. G. Snijders, M. Sola, M. Swart, D. Swerhone, G. te Velde, P. Vernooijs, L. Versluis, O. Visser, E. Wezenbeek, G. Wiesenekker, S. K. Wolff, T. K. Woo, T. Ziegler, ADF **2002**−01, Scientific Computing & Modelling NV, The Netherlands.

[61] [61a] K. Morokuma, *J. Chem. Phys.* **1971**, *55*, 1236. [61b] K. Morokuma, *Acc. Chem. Res.* **1977**, *10*, 294.

[62] [62a] T. Ziegler, A. Rauk, *Theor. Chim. Acta* **1977**, *46*, 1. [62b] T. Ziegler, A. Rauk, *Inorg. Chem.* **1979**, *18*, 1558. [62c] T. Ziegler, A. Rauk, *Inorg. Chem.* **1979**, *18*, 1755.

[63] A. Diefenbach, M. B. Bickelhaupt, G. Frenking, *J. Am. Chem. Soc.* **2000**, *122*, 6449.

[64] J. Uddin, G. Frenking, *J. Am. Chem. Soc.* **2001**, *123*, 1683.

[65] K. K. Pandey, *Inorg. Chem.* **2003**, *42*, 6764.

[66] L. Pauling *The Nature of the Chemical Bond*, 3rd ed., Cornell University Press, New York, 1960, p. 239: The relationship of bond order to length is given by $d_n = d_1 - 0.71 \log n$ *where n is the bond order,* d_1 *and* d_n *are the lengths of bonds with bond order 1 and n, respectively.*

[67] [67a] A. F. Wells, *Structural Inorganic Chemistry*, 5th ed.; Clarendon: Oxford, 19**84**. [67b] L. Pauling, *The Nature of the Chemical Bond*, 3rd ed.; Cornell University Press: Ithaca, NY, **1960**.

[68] K. A. Wiberg, *Tetrahedron* **1968**, *24*, 1083.

Received April 30, 2004
Early View Article
Published Online September 16, 2004

 © 2004 Wiley-VCH Verlag GmbH & Co. KGaA, Weinheim

Post-Metallocene Hydridolanthanide Chemistry: $[Lu\{(Me_3Si)_2NC(NiPr)_2\}_2(\mu\text{-}H)]_2$ — A Novel Lanthanide Hydride in a Non-Cyclopentadienyl Coordination Environment; Synthesis, Structure and Catalytic Activity in Olefin Polymerization

Alexander A. Trifonov,*[a] Elena A. Fedorova,[a] Georgy K. Fukin,[a] and Mikhail N. Bochkarev[a]

Keywords: Alkyl complexes / Homogeneous catalysis / Hydride ligands / Lanthanides / N ligands

The reaction of anhydrous $LuCl_3$ with a twofold molar excess of lithium guanidinate $[Li\{(Me_3Si)_2NC(NiPr)_2\}]$, obtained in situ from the amide $[LiN(SiMe_3)_2(Et_2O)]$ and 1,3-diisopropylcarbodiimide in THF, yields the bis(guanidinate) "ate" complex $[Lu\{(Me_3Si)_2NC(NiPr)_2\}_2(\mu\text{-}Cl)_2Li(THF)_2]$ (**1**). The alkyllutetium derivative $[Lu\{(Me_3Si)_2NC(NiPr)_2\}_2(CH_2SiMe_3)]$ (**2**) was synthesized by a metathesis reaction of **1** with $LiCH_2SiMe_3$ in toluene. The treatment of **2** with an equimolar amount of $PhSiH_3$ in hexane at room temperature results in the first known dimeric lanthanide hydride in a bis(guanidinate) coordination environment, $[Lu\{(Me_3Si)_2NC(NiPr)_2\}_2(\mu\text{-}H)]_2$ (**3**). The crystal structures of complexes **1** and **3** have been determined by X-ray crystallography. The hydrido complex **3** was found to catalyze polymerization of ethylene, propylene and styrene.

(© Wiley-VCH Verlag GmbH & Co. KGaA, 69451 Weinheim, Germany, 2004)

Introduction

Mono- and bis(cyclopentadienyl) and -hydridolanthanide compounds have a very rich and unique chemistry[1–5] and have been found to be efficient catalysts or precatalysts in a wide range of transformations of unsaturated substrates.[6–10] Since the chemical properties of these compounds are known to be profoundly influenced by the nature of the ancillary ligands coordinated to the lanthanide atom,[11–13] related complexes in a stabilizing environment different from cyclopentadienyl one seem to be challenging targets for the exploration of stoichiometric and catalytic performance. In contrast to the well-developed chemistry of cyclopentadienyl-derived alkyl and hydrido complexes of lanthanides, their non-cyclopentadienyl analogues still remain extremely poorly investigated.[14–18] We decided to focus on the tetrasubstituted guanidinate ligand system[19] because its electronic and steric properties can be easily modified to provide stability and a high degree of unsaturation of the coordination sphere of the lanthanide atom due to the bulky substituents at the nitrogen atoms. Several examples of alkyl complexes of rare earth metals coordinated by guanidinate ligands have been reported recently.[20–22] We employed the advantages of the $\{(Me_3Si)_2NC(NiPr)_2\}^-$ ligand for the stabilization of lanthanide hydride, and report here the synthesis of the first complex of this type — $[Lu\{(Me_3Si)_2NC(NiPr)_2\}_2(\mu\text{-}H)]_2$ — and its structure and catalytic activity in olefin polymerization.

Results and Discussion

The monochloro bis(guanidinate) derivative of lutetium, $[Lu\{(Me_3Si)_2NC(NiPr)_2\}_2(\mu\text{-}Cl)_2Li(THF)_2]$ (**1**), was synthesized by a metathesis reaction of a twofold molar excess of the lithium guanidinate $[Li\{(Me_3Si)_2NC(NiPr)_2\}]$, obtained in situ from the amide $[Li\{N(SiMe_3)_2\}(Et_2O)]$ and 1,3-diisopropylcarbodiimide in THF, with anhydrous $LuCl_3$ at room temperature (Scheme 1).

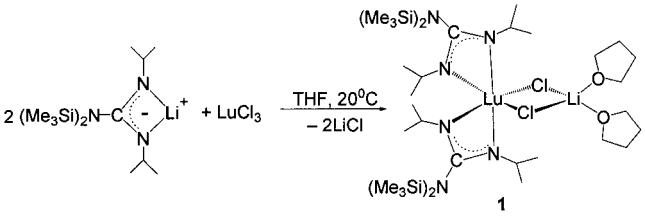

Scheme 1

Complex **1** was isolated in an analytically pure form as a colorless air- and moisture-sensitive crystalline solid by recrystallization from hexane in 76% yield. It is worth noting that the reaction of YCl_3 with 2 equiv. of

[a] G. A. Razuvaev Institute of Organometallic Chemistry of the Russian Academy of Sciences,
Tropinina 49, 603950 Nizhny Novgorod, GSP-445, Russia
Fax: + 7-8312-661-497
E-mail: trif@imoc.sinn.ru

 © 2004 Wiley-VCH Verlag GmbH & Co. KGaA, Weinheim **DOI: 10.1002/ejic.200400425**

$[Li\{(Me_3Si)_2NC(NiPr)_2\}]$ in diethyl ether resulted, after the same treatment, in the isolation of the neutral solvent-free dinuclear guanidinate complex $[Y\{(Me_3Si)_2NC(NiPr)_2\}_2(\mu\text{-}Cl)]_2$;[21] formation of the analogous "ate" complexes $[Ln\{(Me_3Si)_2NC(NiPr)_2\}_2(\mu\text{-}Cl)_2Li(THF)_2]$ (Ln = Y,[21] Yb[22]) has been reported when the reactions are carried out in THF. Complex **1** is soluble in ethers and aromatic and aliphatic hydrocarbons. The ^1H and ^{13}C NMR spectra of **1** in C_6D_6 at 20 °C do not have any notable features and reflect the equivalence of the two guanidinate ligands, with the expected single set of resonances indicating an increased rate of fluctionality compared to the more rigid dinuclear framework of $[Y\{(Me_3Si)_2NC(NiPr)_2\}_2(\mu\text{-}Cl)]_2$.[21] Both sets of THF methylene protons appear in the ^1H NMR spectrum of **1** as broad singlets, indicating their lability.

Clear, colorless single-crystals of **1** suitable for an X-ray crystal-structure determination were obtained by slow concentration of its hexane solution. An ORTEP diagram of **1** is presented in Figure 1; crystal and structural refinement data are listed in the Exp. Sect. The X-ray diffraction study revealed that **1** is a monomeric heterodimetallic "ate" complex that is isomorphous to the previously described $[Yb\{(Me_3Si)_2NC(NiPr)_2\}_2(\mu\text{-}Cl)_2Li(THF)_2]$.[22]

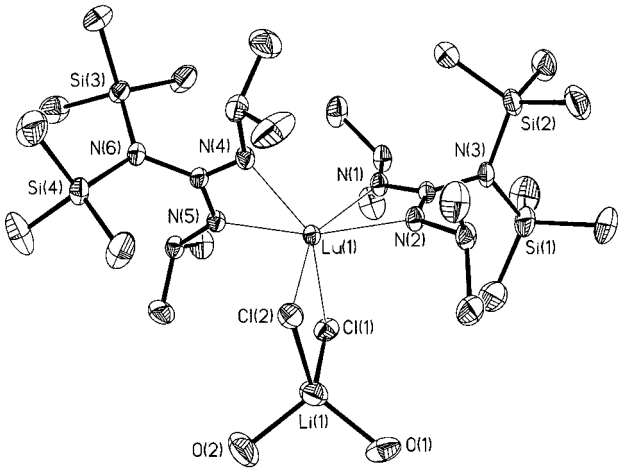

Figure 1. Molecular structure of **1**; the hydrogen atoms are omitted as well as the carbon atoms of the THF molecules; selected bond lengths [Å] and angles [°]: Lu(1)−N(1) 2.285(1), Lu(1)−N(4) 2.290(2), Lu(1)−N(5) 2.329(2), Lu(1)−N(2) 2.346(2), Lu(1)−Cl(1) 2.600(1), Lu(1)−Cl(2) 2.623(1), Lu(1)−C(14) 2.739(2), Lu(1)−C(1) 2.745(2); N(4)−Lu(1)−N(5) 57.87(6), N(1)−Lu(1)−N(2) 57.86(6), C(14)−Lu(1)−C(1) 132.30(6)

The coordination environment of the lutetium atom in **1** is defined by four nitrogen atoms of the bidentate guanidinate ligands, and two chlorine atoms, which form μ^2-bridges to the lithium atom. The lithium atom is also bonded to oxygen atoms of the two THF molecules. The formal coordination number of the lutetium atom is six, which is rather low for lanthanide derivatives.[1] The luthetium−nitrogen bonds in **1** have very similar lengths, which fall in the region 2.285(1)−2.346(1) Å. These bonds are much shorter than the coordination bonds in $[Lu(\eta^8\text{-}C_8H_8)\{o\text{-}C_6H_4CH_2N(CH_3)_2\}(THF)]$ [2.479(6) Å][23] and $[Lu\{o\text{-}C_6H_4CH_2N(CH_3)_2\}_3]$ [2.468(6), 2.4588(5) Å],[24] but similar to the length of the covalent bond in the anionic compound $[\{Li(THF)_4\}\{Lu(C_5H_5)_2(NPh_2)_2\}]$ [2.290(7), 2.293(7) Å].[25] The Lu−Cl distances in **1** [2.600(1) 2.622(1) Å] are very close to the values reported for the Cp analogue $[LuCp_2(\mu\text{-}Cl)_2Li(TMEDA)]$.[26] The Yb−N [2.295(3)−2.332(3) Å] and Yb−Cl [2.608(1), 2.631(1) Å] distances in an isomorphous Yb complex[22] are close to the analogous distances in **1**.

The alkylation of **1** with $LiCH_2SiMe_3$ in toluene yielded the solvent-free alkyl complex $[Lu\{(Me_3Si)_2NC(NiPr)_2\}_2(CH_2SiMe_3)]$ (**2**; Scheme 2), which was isolated as a colorless amorphous powder in 71% yield after extraction with hexane.

The air- and moisture-sensitive complex **2** is highly soluble in organic solvents. The presence of the CH_2SiMe_3 group in **2** is proved by a high-field-shifted singlet at $\delta = -0.49$ ppm in the ^1H NMR spectrum, corresponding to the two protons of the methylene group attached to the lutetium atom, and by a singlet at $\delta = 0.37$ ppm corresponding to the protons of the Me_3Si group. The carbon atoms of these groups produce resonances at $\delta = 40.0$ and 4.9 ppm, respectively, in the ^{13}C NMR spectrum of **2**.

The alkyl complex **2** was treated with an equimolar amount of phenylsilane in hexane at room temperature to yield the dimeric hydride $[Lu\{(Me_3Si)_2NC(NiPr)_2\}_2(\mu\text{-}H)]_2$ (**3**; Scheme 3).

Complex **3** was isolated in 84% yield as a colorless microcrystalline solid after recrystallization from hexane and drying in vacuo. Complex **3** is an air- and moisture-sensitive compound that is sparingly soluble in hexane and aromatic hydrocarbons. Crystallization of **3** by slow cooling of a warm (40 °C) saturated hexane solution to 20 °C resulted in the formation of single crystals of $[Lu\{(Me_3Si)_2NC(NiPr)_2\}_2(\mu\text{-}H)]_2(C_6H_{14})$. An X-ray crystal structure analysis revealed that **3** adopts a dimeric structure. Each of the two metal centres are coordinated by the four nitrogen atoms of the two guanidinate ligands and by two bridging hydrido ligands (Figure 2).

The two lutetium atoms and the two hydrido ligands are coplanar. The Lu−H [2.12(4), 2.04(4) Å] and Lu−Lu [3.577(1) Å] distances in the Lu_2H_2 core are similar to those in other dimeric μ^2-hydrido-bridged lutetium complexes with bis(cyclopentadienyl) and amido(cyclopentadienyl) ancillary ligation.[27,28] The dihedral angles between the planar four-membered cycles Lu(1)N(1)C(1)N(2) and Lu(1)N(1A)C(1A)N(2A), and Lu(2)C(14)N(4)N(5) and Lu(2)C(14A)N(4A)N(5A), are 66.8(1) and 60.6(1)°, respectively. Remarkably, the disposition of the two $Lu\{(Me_3Si)_2NC(NiPr)_2\}_2$ groups is such that the C(1)Lu(1)C(1A) and C(14)Lu(2)C(14A) planes are nearly orthogonal [86.90(11)°], which allows a reduction of the steric hindrance in the coordination sphere of the Lu atoms. A particularity of the structure of **3** is the difference of the bonding parameters within the $Lu\{(Me_3Si)_2NC(NiPr)_2\}_2$ fragments of the dimer, which results in their inequivalence. In one moiety the Lu(1)−N(1) and Lu(1)−N(2) distances are nearly similar [2.304(3) and 2.315(3) Å], while in the other one they differ noticeably [Lu(2)−N(4): 2.266(3) Å; Lu(2)−N(5): 2.372(5) Å]. The shortest Lu−N bond in **3** is

 © 2004 Wiley-VCH Verlag GmbH & Co. KGaA, Weinheim

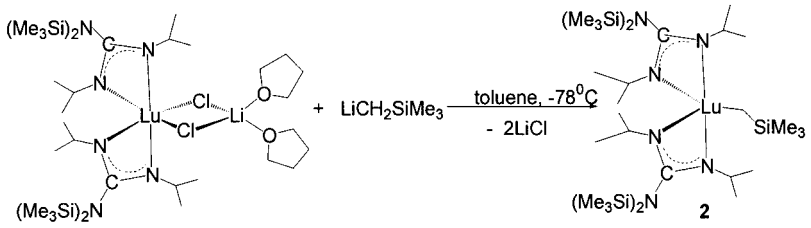

Scheme 2

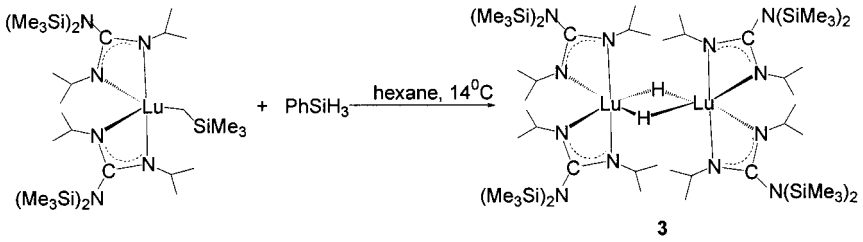

Scheme 3

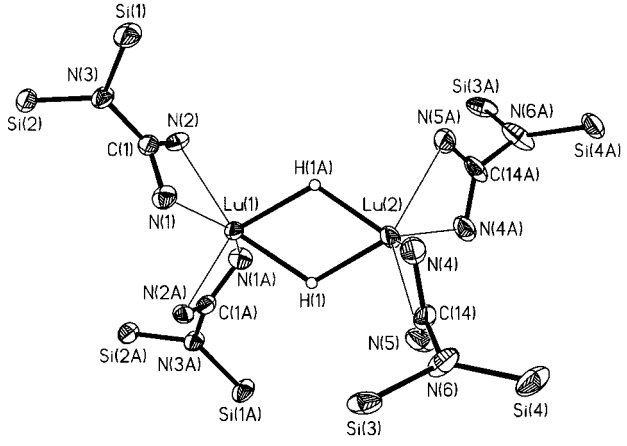

Figure 2. Molecular structure of **3**; the hydrogen atoms as well as methyl radicals of Me_3Si groups and isopropyl groups are omitted; selected bond lengths [Å] and angles [°]: Lu(1)−H(1) 2.12(4), Lu(2)−H(2) 2.03(4), Lu(1)−N(1) 2.304(3), Lu(1)−N(2) 2.315(3), Lu(1)−C(1) 2.747(3), Lu(1)−Lu(2) 3.5767(3), Lu(2)−N(4) 2.266(3), Lu(2)−N(5A) 2.372(3), Lu(2)−C(14) 2.733(3); N(1A)−Lu(1)−N(1) 144.71(16), N(1A)−Lu(1)−N(2A) 58.02(10), N(1)−Lu(1)−N(2A) 101.14(11), N(1)−Lu(1)−N(2) 58.02(10)

nevertheless significantly longer than the covalent Lu−N bond in the complex $[Lu\{Me_2Si(C_9H_5Me)_2\}\{N(SiMe_3)_2\}]$,[29] whereas the longest one is shorter than the coordination bonds in the above-mentioned complexes $[Lu(\eta^8\text{-}C_8H_8)(o\text{-}C_6H_4CH_2N(CH_3)_2(THF)]$[23] and $[Lu\{o\text{-}C_6H_4CH_2N(CH_3)_2\}_3]$.[24] The bonding situation within the NCN fragments does not indicate a significant difference of the π-system delocalization in the guanidinate ligands or the presence of different resonance forms. Such a structure obviously results from a steric repulsion of the bulky trimethylsilyl and isopropyl groups in the adjacent moieties and demonstrates the flexibility of coordination of guanidinate ligands. The strong geometry distortion in **3**, compared to the related dinuclear yttrium chloride bis(guanidinate) $[Y\{(Me_3Si)_2NC(N\mathit{i}Pr)_2\}_2(\mu\text{-}Cl)]_2$,[21] may suggest a greater steric encumbrance of the metal coordination sphere in the lutetium compound, resulting from the smaller ion sizes of Lu and H compared to those of Y and Cl.[30]

The hydrido ligands appear in the ^1H NMR spectrum of **3** as a singlet at $\delta = 12.96$ ppm, which is at substantially lower field than the respective signals of previously reported lutetium hydrides.[11,13,27,28,31−34] This observation is consistent with the enhanced electron-withdrawing properties of guanidinate ligands compared to those of cyclopentadienyl ligands. The ^1H and ^{13}C NMR spectra of **3** indicate that the guanidinate ligands remain inequivalent in solution (20 °C, C_6D_6). The methyl and methyne protons of the isopropyl groups appear in the ^1H NMR spectrum of **3** as complex multiplets, rather than the expected doublet and septuplet, respectively.

The catalytic reactions of **3** with ethylene (20 °C, 0.48 bar) and propylene (0 °C, 0.75 bar) in toluene were monitored by recording the absorption of the monomers. The polymerization of ethylene was rather slow; the catalyst retained similar activity during 3 d, and the reaction was stopped after this time (activity: 0.1 g polyethylene/mmol Lu·h·bar). The polyethylenes obtained with this catalyst are highly crystalline, with a melting temperature of 124 °C. Most of the lanthanide complexes which readily polymerize ethylene are inactive in propylene polymerization. On the contrary, **3** catalyzes propylene polymerization. The reaction proceeds much faster than in the case of ethylene, but the catalyst loses activity 1 h after the beginning of the process (activity: 3.9 g polypropylene/mmol Lu·h·bar). The solid polymer formed in this reaction is insoluble in organic solvents. Complex **3** also catalyzes polymerization of styrene (room temperature, neat styrene, 5% of **3**). A conversion of 90% was reached after 6 d, and the polystyrene obtained

 © 2004 Wiley-VCH Verlag GmbH & Co. KGaA, Weinheim

has a high molecular weight (M_n = 811000 g mol^{-1}; M_w = 1250000 g mol^{-1}), a narrow molecular weight distribution (M_w/M_n = 1.54), and a melting temperature of 255−260 °C.

Conclusion

The bis(guanidinate) ligand has been demonstrated to be a suitable alternative to the cyclopentadienyl ligand for the stabilization of hydridolanthanide complexes. Due to the bulky substituents on the nitrogen atoms this coordination environment provides a high solubility of the lanthanide derivatives and a low coordination number at the metal atom. The first hydridolanthanide complex with a bis(guanidinate) coordination environment was synthesized and structurally characterized. This complex demonstrates modest activity in olefin polymerization. Studies on the synthesis of hydrido bis(guanidinate) derivatives of other lanthanide metals and investigation of their properties in catalysis of olefin polymerization and hydrosilylation are currently in progress.

Experimental Section

General Remarks: All procedures were performed under vacuum using standard Schlenk-tube techniques. After drying with KOH, THF was distilled from sodium benzophenone ketyl prior to use. Hexane and toluene were purified by distillation from sodium/triglyme benzophenone ketyl. Deuterated benzene was dried with sodium and vacuum-transferred. Diisopropylcarbodiimide was purchased from Acros and purified by distillation. Anhydrous $LuCl_3$ [35] and [Li{N(SiMe$_3$)$_2$}(Et$_2$O)][36] were prepared according to literature procedures. All other commercially available chemicals were used after the appropriate purification. NMR spectra were recorded with a Bruker DPX 200 spectrometer (^{1}H, 200 MHz; ^{13}C, 50 MHz) in C_6D_6 at 20 °C, unless otherwise stated. Chemical shifts for ^{1}H and ^{13}C NMR spectra were referenced internally to the residual solvent resonances and are reported relative to tetramethylsilane. IR spectra were recorded with a Specord M80 instrument as Nujol mulls. Molecular weights and molecular-weight distributions were determined against polystyrene standards by gel-permeation chromatography (GPC) with a Knauer apparatus with Phenogel columns (10 μm, Linear 2) using chloroform as the eluent. Lanthanide metal analysis was carried out by complexometric titration. Elemental analysis was performed by the Microanalytical Laboratory of this institute.

Synthesis of [Lu{(Me$_3$Si)$_2$NC(N*i*Pr)$_2$}$_2$(μ-Cl)$_2$Li(THF)$_2$] (1): Diisopropylcarbodiimide (0.99 g, 7.90 mmol) was slowly added to a solution of [Li{N(SiMe$_3$)$_2$}(Et$_2$O)] (1.91 g, 7.90 mmol) in THF (30 mL) at 20 °C and the reaction mixture was stirred for 45 min. $LuCl_3$ (1.11 g, 3.95 mmol) was added and the reaction mixture was stirred overnight. The solution was filtered, the solvent was evaporated in vacuo and the solid residue was extracted with toluene (2 × 20 mL). The toluene extracts were filtered and toluene was evaporated in vacuo. The off-white solid was dissolved in hot hexane (30 mL). The solution was slowly concentrated at room temperature to one quarter of its volume, cooled to −30 °C and left overnight. The crystalline precipitate was washed with cold hexane and dried in vacuo at room temperature for 20 min. Complex **1** was obtained as a colorless crystalline solid (2.91 g, 76%). $C_{34}H_{80}Cl_2LiLuN_6O_2Si_4$ (970.21): calcd. C 42.09, H 8.24, Lu 18.03; found C 41.80, H 8.69, Lu 17.88. ^{1}H NMR (200 MHz, [D$_6$]benzene): δ = 0.49 [s, 36 H, Si(C*H*$_3$)$_3$], 1.46 (br. s, 8 H, β-C*H*$_2$, THF), 1.61 [d, $^3J_{H,H}$ = 4.8 Hz, 24 H, (C*H*$_3$)$_2$CH], 3.76 (br. s, 8 H, α-C*H*$_2$, THF), 4.15 (sept, $^3J_{H,H}$ = 6.2 Hz, 4 H, C*H*Me$_2$) ppm. ^{13}C{^{1}H} NMR (50 MHz, [D$_6$]benzene): δ = 2.8 [(NSi*C*H$_3$)$_2$], 25.2 (β-*C*H$_2$, THF), 26.9 [(*C*H$_3$)$_2$CH], 46.1 (*C*HMe$_2$), 68.5 (α-*C*H$_2$, THF), 168.4 (*C*N$_3$) ppm. IR (nujol, KBr): $\tilde{\nu}$ = 1630 (s), 1310 (s), 1250 (s), 1200 (s), 1050 (m), 940 (s), 860 (m), 820(s) cm^{-1}.

Synthesis of [Lu{(Me$_3$Si)$_2$NC(N*i*Pr)$_2$}$_2$(CH$_2$SiMe$_3$)] (2): A solution of Me$_3$SiCH$_2$Li (0.14 g, 1.48 mmol) in toluene (5 mL) was slowly added at −78 °C to a solution of **1** (1.44 g, 1.48 mmol) in toluene (25 mL). The reaction mixture was allowed to warm to room temperature and stirred for 3 h. The pale-yellow solution was filtered and toluene was evaporated in vacuo. The residue was extracted with hexane (2 × 10 mL), the extracts were filtered, and hexane was removed in vacuo to give **2** as an off-white amorphous powder (0.83 g, 71%). $C_{30}H_{75}LuN_6Si_5$ (834.74): calcd. C 43.16, H 8.98, Lu 20.96; found C 42.70, H 9.33, Lu 20.74. ^{1}H NMR (200 MHz, [D$_6$]benzene): δ = −0.49 (s, 2 H, LuC*H*$_2$), 0.29 [s, 36 H, NSi(C*H*$_3$)$_3$], 0.37 [s, 9 H, CH$_2$Si(C*H*$_3$)$_3$], 1.29 [d, $^3J_{H,H}$ = 6.4 Hz, 24 H, (C*H*$_3$)$_2$CH], 3.92 (sept, $^3J_{H,H}$ = 6.4 Hz, 4 H, C*H*Me$_2$) ppm. ^{13}C{^{1}H} NMR (50 MHz, [D$_6$]benzene): δ = 2.2 (NSi*C*H$_3$)$_2$], 4.8 (CH$_2$Si*C*H$_3$), 27.1 [(*C*H$_3$)$_2$CH], 40.0 (Lu*C*H$_2$), 46.0 (*C*HMe$_2$), 168.9 (*C*N$_3$) ppm. IR (nujol, KBr): $\tilde{\nu}$ = 1630 (s), 1300 (w), 1250 (s), 1200 (s), 1210 (m), 950 (s), 930 (m), 820(s) cm^{-1}.

Synthesis of [Lu{(Me$_3$Si)$_2$NC(N*i*Pr)$_2$}$_2$(μ-H)]$_2$ (3): A solution of PhSiH$_3$ (0.12 g, 1.08 mmol) in hexane (2 mL) was added at room temperature to a solution of **2** (0.86 g, 1.08 mmol) in hexane (10 mL). The reaction mixture was stirred for 45 min and then concentrated in vacuo to approximately one third of its initial volume. When crystallization started, the solution was cooled to −30 °C and kept at that temperature overnight. The mother liqueur was decanted, the solid was washed with cold hexane and dried in vacuo at room temperature for 45 min to give **3** as a colorless microcrystalline solid (0.68 g, 84%). $C_{52}H_{130}Lu_2N_{12}Si_8$ (1497.2): calcd. C 41.71, H 8.68, Lu 23.37; found C 41.18, H 8.39, Lu 23.71. ^{1}H NMR (200 MHz, [D$_6$]benzene): δ = 0.45 [s, 72 H, NSi(C*H*$_3$)$_3$], 1.53 [m, 48 H, (C*H*$_3$)$_2$CH], 4.10 (m, 8 H, C*H*Me$_2$), 12.96 (s, 2 H, Lu*H*) ppm. ^{13}C{^{1}H} NMR (50 MHz, [D$_6$]benzene): δ = 3.1, 3.3 [N(Si*C*H$_3$)$_2$], 27.1, 28.2, 28.6 [(*C*H$_3$)$_2$CH], 46.5, 46.6 (*C*HMe$_2$), 168.7, 170.8 (CN$_3$) ppm. IR (Nujol, KBr): $\tilde{\nu}$ = 1630 (s), 1605 (m), 1320 (s), 1250 (s), 1205 (s), 1050 (s), 950 (s), 820(s) cm^{-1}.

Ethylene Polymerization: Ethylene polymerization tests were carried out in a constant-volume glass vessel connected to a Hg manometer (20 °C, $p_{monomer}$ = 0.48 bar). A solution of **3** (0.088 g, 0.0588 mmol) in toluene (5 mL) was loaded into the reaction vessel, which was then charged with ethylene, and the reaction mixture stirred. The reaction was monitored by the absorption of ethylene. After 72 h, the reaction vessel was disconnected and methanol was added (ca. 20 mL). The polymer was collected by filtration, washed with a 15% solution of HCl, then with methanol, and dried in vacuo to a constant weight; 0.192 g of polyethylene was isolated.

Propylene Polymerization: Propylene polymerization tests were carried out in a constant-volume glass vessel connected to a Hg manometer (0 °C, $p_{monomer}$ = 0.75 bar). A solution of **3** (0.053 g, 0.0353 mmol) in toluene (5 mL) was loaded into the reaction vessel, which was charged with propylene, and the reaction mixture stirred. The reaction was monitored by the absorption of the monomer. After 1 h, the reaction vessel was disconnected and methanol

 © 2004 Wiley-VCH Verlag GmbH & Co. KGaA, Weinheim

Table 1. Crystallographic data and structure refinement details for **1** and **3**

	1	**3**
Empirical formula	$C_{34}H_{80}Cl_2LiLuN_6O_2Si_4$	$C_{58}H_{144}Lu_2N_{12}Si_8$
Formula mass	970.21	1534.37
T [K]	100(2)	100(2)
λ [Å]	0.71073	0.71073
Crystal system	triclinic	trigonal
Space group	$P\bar{1}$	$P3_221$
Unit cell dimensions	a = 9.8860(8) Å	a = 14.7379(4) Å
	b = 14.7621(12) Å	b = 14.7379(4) Å
	c = 18.2178(15) Å	c = 32.7706(19) Å
	α = 75.231(2)°	α = 90°
	β = 86.632(2)°	β = 90°
	γ = 79.344(2)°	γ = 120°
Volume [Å^3]	2526.3(4)	6164.3(4)
Z	2	3
$D_{calcd.}$ [g/cm^3]	1.275	1.240
Absorption coefficient [mm^{-1}]	2.187	2.542
F(000)	1012	2394
Crystal size [mm]	0.08 × 0.08 × 0.02	0.45 × 0.40 × 0.32
θ range for data collection [°]	1.45−29.09	1.86−28.06
Index ranges	$-9 \le h \le 13$	$-19 \le h \le 19$
	$-19 \le k \le 18$	$-19 \le k \le 19$
	$-24 \le l \le 24$	$-43 \le l \le 43$
Reflections collected	18359	51913
Independent reflections	12927 (R_{int} = 0.0190)	9959 (R_{int} = 0.0377)
Completeness to θ	29.09°, 95.4%	28.06°, 99.5%
Data/restraints/parameters	12927/6/471	9959/59/422
Goodness-of-fit on F^2	1.030	1.101
Final R_{int} [$I > 2\sigma(I)$]	$R1$ = 0.0313, $wR2$ = 0.0766	$R1$ = 0.0338, $wR2$ = 0.0823
R_{int} (all data)	$R1$ = 0.0363, $wR2$ = 0.0790	$R1$ = 0.0361, $wR2$ = 0.0834
Largest diff. peak/hole [e·Å^3]	2.542/−1.603	1.454/−1.698

was added (ca. 20 mL). The polymer was collected by filtration, washed with a 15% solution of HCl, then with methanol, and dried in vacuo to a constant weight; 0.105 g of polypropylene was isolated.

Styrene Polymerization: Complex **3** (0.045 g, 0.0300 mmol) was added to styrene (1 mL) and the reaction mixture was stirred at room temperature. After 6 d, the volatiles were evaporated in vacuo. The polymer was washed with methanol (2 × 10 mL), HCl (10%, 10 mL), dissolved in toluene (20 mL), filtered, and precipitated into methanol (100 mL). The polymer was collected by filtration, washed with methanol, and dried in vacuo to a constant weight; 0.815 g of polystyrene was isolated.

X-ray Crystallographic Study: Single crystals of **1** and **3** for X-ray structure analysis were obtained from hexane solutions. The data were collected with a Bruker AXS SMART APEX diffractometer (graphite-monochromated Mo-K_α-radiation, φ/ω-scan technique, λ = 0.71073 Å). The intensity data were integrated with the SAINT program.[37] The structures were solved by direct methods and refined on F^2 using all reflections with SHELXL-97.[38] All non-hydrogen atoms were refined anisotropically. The hydrogen atoms in **1** and **3** were placed in calculated positions and refined in the "riding-model". Only the hydride atom H(1) in **3** was found from Fourier synthesis and refined isotropically with fixed U_{iso} (0.08 Å^2). The crystal of **3** contained a solvate disordered molecule of hexene. SADABS[39] was used to perform area-detector scaling and absorption corrections. The details of crystallographic, collection and refinement data are shown in Table 1. CCDC-235927 (**1**) and -235926 (**3**) contain the supplementary crystallographic data for this paper. These data can be obtained free of charge at www.ccdc.cam.ac.uk/const/retrieving.html [or from the Cambridge Crystallographic Data Centre, 12 Union Road, Cambridge CB2 1EZ, UK; Fax: + 44-1223-336-033; E-mail: deposit@ccdc.cam.ac.uk].

Acknowledgments

This work was supported by the Russian Foundation of Basic Research (Grant no. 02-03-32112). We gratefully acknowledge Dr. Yu. A. Kurskii for recording the NMR spectra, and Dr. V.N. Glushakova and Mrs. N. A. Skorodumova for assistance with polymerization tests.

[1] M. N. Bochkarev, L. N. Zakharov, G. N. Kalinina, *Organo Derivatives of Rare Earth Elements*, Kluwer Academic Publishers, Dordrecht, **1995**.
[2] H. Schumann, J. A. Meese-Marktscheffel, L. Esser, *Chem. Rev.* **1995**, *95*, 865−893.
[3] S. Arndt, J. Okuda, *Chem. Rev.* **2002**, *102*, 1953−1976.
[4] M. Ephritikhine, *Chem. Rev.* **1997**, *97*, 2193−2242.
[5] J. Okuda, *Dalton Trans.* **2003**, 2367−2378.
[6] G. A. Molander, J. A. C. Romero, *Chem. Rev.* **2002**, *102*, 2161−2185.
[7] Z. Hou, Y. Wakatsuki, *Coord. Chem. Rev.* **2002**, *231*, 1−22.
[8] T. E. Mueller, M. Beller, *Chem. Rev.* **1998**, *98*, 675−703.
[9] H. Yasuda, *J. Organomet. Chem.* **2002**, *647*, 128−138.
[10] G. A. Molander, E. C. Dowdy, *Top. Organomet. Chem.* **1999**, *2*, 119−155.
[11] G. Jeske, H. Lauke, H. Mauermann, P. N. Swepston, H. Schumann, T. J. Marks, *J. Am. Chem. Soc.* **1985**, *107*, 8091−8103.
[12] G. Jeske, L. E. Schock, P. N. Swepston, H. Schumann, T. J. Marks, *J. Am. Chem. Soc.* **1985**, *107*, 8103−8110.

 © 2004 Wiley-VCH Verlag GmbH & Co. KGaA, Weinheim

[13] D. Stern, M. Sabat, T. J. Marks, *J. Am. Chem. Soc.* **1990**, *112*, 9558−9575.
[14] F. T. Edelmann, D. M. M. Freckmann, H. Schumann, *Chem. Rev.* **2002**, *102*, 1851−1896.
[15] F. T. Edelmann, *Coord. Chem. Rev.* **1994**, *137*, 403−481.
[16] W. E. Piers, D. J. H. Emslie, *Coord. Chem. Rev.* **2002**, *233−234*, 131−155.
[17] P. Mountford, B. D. Ward, *Chem. Commun.* **2003**, 1797−1803.
[18] T. Dubé, S. Gambarotta, G. Yapp, *Organometallics* **2000**, *19*, 121−126.
[19] P. J. Bailey, S. Pace, *Coord. Chem. Rev.* **2001**, *214*, 91−141.
[20] Y. Zhou, G. P. A. Yapp, D. S. Richeson, *Organometallics* **1998**, *17*, 4387−4391.
[21] Z. Lu, G. P. A. Yapp, D. S. Richeson, *Organometallics* **2001**, *20*, 706−712.
[22] Y. Luo, Y. Yao, Q. Shen, K. Yu, L. Weng, *Eur. J. Inorg. Chem.* **2003**, 318−323.
[23] A. L. Wayda, R. D. Rogers, *Organometallics* **1985**, *4*, 1440−1444.
[24] A. L. Wayda, J. L. Atwood, W. E. Hunter, *Organometallics* **1984**, *3*, 939−941.
[25] H. Schumann, E. Palamidis, J. Loebel, *J. Organomet. Chem.* **1990**, *390*, 45−52.
[26] V. K. Belsky, S. Ya. Knyazhansky, B. M. Bulychev, G. L. Soloveitchik, *Metalloorg. Khim.* **1989**, *2*, 754−756.
[27] H. Schumann, W. Genthe, E. Hahn, M. B. Hossain, D. Van Der Helm, *J. Organomet. Chem.* **1986**, *299*, 67−84.
[28] S. Arndt, P. Voth, T. P. Spaniol, J. Okuda, *Organometallics* **2000**, *19*, 4690−4700.
[29] J. Eppinger, M. Spiegler, W. Hieringer, W. A. Herrmann, R. Anwander, *J. Am. Chem. Soc.* **2000**, *122*, 3080−3096.
[30] S. S Batsanov, *Russ. J. Inorg. Chem.* **1991**, *36*, 1694−1706.
[31] A. Z. Voskoboynikov, I. N. Parshina, A. K. Shestakova, K. P. Butin, I. P. Beletyskaya, L. G. Kuz'mina, J. A. K. Howard, *Organometallics* **1997**, *16*, 4041−4055.
[32] Y. K. Gun'ko, B. M. Bulychev, G. L. Soloveichik, V. K. Bel'skii, *J. Organomet. Chem.* **1992**, *24*, 289−300.
[33] P. W. Roesky, U. Denninger, C. L. Stern, T. J. Marks, *Organometallics* **1997**, *16*, 4886−4492.
[34] O. Tardif, M. Nishiura, Z. Hou, *Tetrahedron* **2003**, *59*, 10525−10539.
[35] M. D. Taylor, C. P. Carter, *J. Inorg. Nucl. Chem.* **1962**, *24*, 387−393.
[36] L. E. Manzer, *Inorg. Chem.* **1978**, *17*, 1552−1558.
[37] Bruker, *SAINTPlus Data Reduction and Correction Program*, v. 6.02a, Bruker AXS, Madison, Wisconsin, USA, **2000**.
[38] G. M. Sheldrick, *SHELXTL, Structure Determination Software Suite*, v. 6.12, Bruker AXS, Madison, Wisconsin, USA, **2000**.
[39] G. M. Sheldrick, *SADABS, Bruker/Siemens Area Detector Absorption Correction Program*, v.2.01, Bruker AXS, Madison, Wisconsin, USA, **1998**.

Received May 21, 2004
Early View Article
Published Online September 7, 2004

 © 2004 Wiley-VCH Verlag GmbH & Co. KGaA, Weinheim

Binucleating Aza-Sulfonate and Aza-Sulfinate Macrocycles — Synthesis and Coordination Chemistry

Julia Hausmann,[a][‡] Steffen Käss,[a] Sabrina Klod,[b] Erich Kleinpeter,[b] and Berthold Kersting*[a]

Keywords: Cavitands / Macrocyclic ligands / Nickel / S ligands

The preparation and ligating properties of S-oxygenated derivatives of a macrobinucleating hexaazadithiophenolate macrocycle H_2L^1 of the Robson type towards nickel(II) and zinc(II) ions are reported. Nickel complexes of the hexaazadiphenylsulfonate ligand $(L^2)^{2-}$ $[(L^2)Ni^{II}_2(\mu\text{-}L)]^+$ (L = *m*-Cl-OBz$^-$ (**3**), Cl$^-$ (**4**) and OAc$^-$ (**6**)] are readily obtained in high yields by oxidation of the respective $[(L^1)Ni^{II}_2(\mu\text{-}L)]^+$ parent complexes [L = *m*-Cl-OBz$^-$ (**2**), Cl$^-$ (**1**), OAc$^-$ (**5**)] with *meta*-chloroperoxybenzoic acid or hydrogen peroxide. Decomposition of the sulfonate complexes gives the free macrocycle H_2L^2 which, upon treatment with $Zn(OAc)_2{\cdot}2H_2O$, produces the diamagnetic zinc complex $[(L^2)Zn^{II}_2(OAc)]^+$ (**8**). A dinuclear Cu^{II} complex of the hexaazadisulfinate derivative $(L^{3'})^{2-}$, $[(L^3)Cu^{II}_2]^{2+}$ (**9**), is formed rather unexpectedly by air oxidation of $(L^1)^{2-}$ in the presence of Cu^{I}. The crystal-structure determinations of the perchlorate or tetraphenylborate salts of **2**, **3**, and **4** show that the new ligands support the formation of binuclear complexes with bowl-shaped, calixarene-like binding cavities. NMR spectroscopic studies of **8** show that the complexes retain their solid-state structures in solution. A crystal-structure determination of **9** reveals two five-coordinate Cu^{II} ions bridged by the two sulfinate functions of $(L^3)^{2-}$.

(© Wiley-VCH Verlag GmbH & Co. KGaA, 69451 Weinheim, Germany, 2004)

Introduction

The development of ligand systems that support the formation of metal complexes with confined environments about active coordination sites is currently attracting much interest.[1−3] This is mainly due to the fact that such assemblies improve the ability to control the rate and selectivity of substrate transformations.[4−8] Such aggregates also allow for the construction of more-effective enzyme mimics.[9] Consequently, a large number of bowl-shaped supporting ligands have been reported and their ligating properties towards the 3d elements have been investigated. While most of these ligands form mononuclear complexes, as, for instance, the calixarenes,[10] the cyclodextrins,[11] and some tripod ligands,[12−14] there are only a few reports of ligand systems that impose calixarene-like structures about dinuclear cores.[15−17] We have recently shown that N-functionalized hexaazadithiophenolate macrocycles[18,19] of the Robson type[20−23] are suitable for the construction of such species.[24] The unique features of the corresponding complexes[25] led us to investigate potential routes to S-oxygenated derivatives of H_2L^1 and to examine the ligating properties of these hitherto unknown ligand systems (Scheme 1). Herein we report the synthesis of the binucleating hexaazasulfonate ligand $(L^2)^{2-}$ and demonstrate its ability to form dinuclear transition-metal complexes with bowl-shaped binding cavities. The synthesis and crystal structure of a dinuclear copper(II) complex of the related hexaazasulfinate ligand $(L^3)^{2-}$ are also reported.

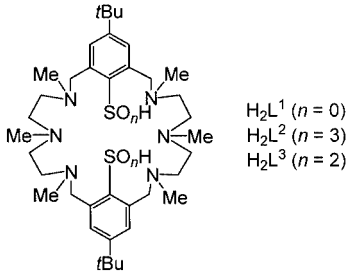

Scheme 1. Structures of the ligands H_2L^1, H_2L^2 and H_2L^3 (see Scheme 2 for numbering of complexes)

Results and Discussion

The compounds synthesized in this paper are collected in Scheme 2. Of these, the nickel and zinc complexes **1**, **5**, and **7** have been reported previously.

[a] Institut für Anorganische und Analytische Chemie, Universität Freiburg
Albertstr. 21, 79104 Freiburg, Germany
Fax: (internat.) + 49-761-203-5987
E-mail: berthold.kersting@ac.uni-freiburg.de
[b] Institut für Chemie, Universität Potsdam
P. O. Box 601553, 14415 Potsdam, Germany
[‡] Present address: Department of Chemistry, University of Otago
P. O. Box 56, Dunedin, New Zealand
Supporting information for this article is available on the WWW under http://www.eurjic.org or from the author.

 © 2004 Wiley-VCH Verlag GmbH & Co. KGaA, Weinheim **DOI: 10.1002/ejic.200400460**

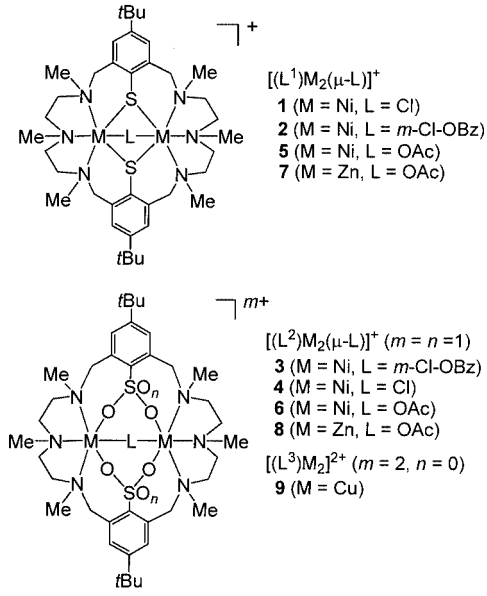

Scheme 2. Synthesized complexes and their labels (see Scheme 1 and ref. 31 for ligand abbreviations)

Attempts to *S*-oxygenate the free hexaazadithiophenol H_2L^1 invariably proved unsuccessful, presumably due to the formation of amine *N*-oxides. The oxidation of dinickel complexes of $(L^1)^{2-}$ was attempted next, since this has recently been demonstrated to be a versatile method for the preparation of sulfonate complexes,[26] even for complexes of labile transition-metal ions such as nickel(II).[27–29] In a preliminary experiment the *meta*-chlorobenzoato-bridged species **2**[30] was treated with six equivalents of *meta*-chloroperoxybenzoic acid (MCPBA) at 0 °C (Scheme 3).[31] This resulted in the rapid and almost quantitative formation of the desired aminosulfonate complex **3**. The facile formation of **3** is somewhat remarkable given that S-oxygenation of bridging thiolate functions has not been observed previously in nickel thiolate chemistry.[32,33]

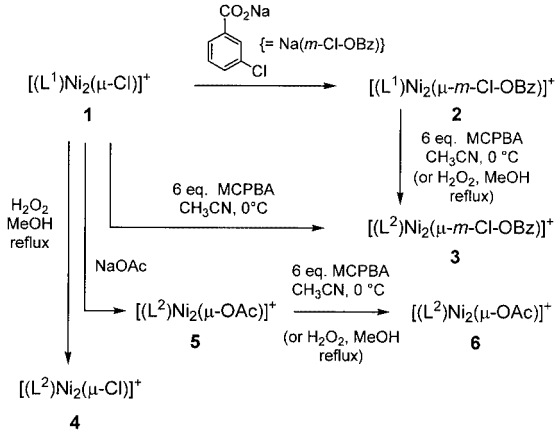

Scheme 3. Synthesis of compounds **2**–**6**

In light of these results the oxidation of the chloro- and acetato-bridged species **1** and **5**, respectively, was examined next (Scheme 3). The oxidation of the chloro complex **1** by MCPBA was expected to give the μ-Cl compound **4**, but the infrared spectrum (vide infra) revealed the presence of the μ-*meta*-chlorobenzoate-containing complex **3**, showing that this transformation is accompanied by a substitution of the bridging chloride ion by the *meta*-chlorobenzoate group (which is produced upon reduction of MCPBA). In contrast, the oxidation of **5** yields the acetato-bridged complex **6** as the sole product. Thus, in this case an exchange of the encapsulated acetate moiety by the external *meta*-chlorobenzoate does not occur, despite it being present in a sixfold molar excess.

In the course of our work it was found that the aminosulfonate complexes **3** and **6** can also be prepared by oxidation of their respective parent complexes with hydrogen peroxide (Scheme 3). This prompted us to test whether complex **4** would be similarly accessible by H_2O_2 oxidation of **1**. Indeed, treatment of **1** with a large excess of H_2O_2 resulted in the formation of a pale-green solution, from which the desired μ-chloro complex **4**·ClO_4 could be obtained upon addition of an excess of $LiClO_4$. Nevertheless, the thiolate complexes are very resistant towards oxidation by H_2O_2. In the case of **2** and **5**, for example, a large excess and prolonged heating was required to obtain the respective oxidation products **3** and **6** in good yields.

As noted above, the direct oxidation of H_2L^1 failed to provide the macrocyclic hexaazadisulfonic acid H_2L^2, and so another route had to be developed. We have previously observed that binuclear complexes of the aminothiolate ligand $(L^1)^{2-}$ decompose under acidic conditions to give the free aminothiol H_2L^1 as its hexahydrochloride salt.[34] Accordingly, the decomposition of the perchlorate salt **3**·ClO_4 with hydrochloric acid was attempted (Scheme 4). The aminosulfonate complex was found to be very stable under acidic conditions, but with concentrated hydrochloric acid complete hydrolysis occurred, such that the desired ligand H_2L^2·6HCl could be isolated in good yields. The identity of H_2L^2·6HCl was confirmed by IR, ^1H and ^{13}C NMR spectroscopy (see below), and by the successful regeneration of complex **6**. Thus, treatment of H_2L^2·6HCl with two equivalents of $Ni(OAc)_2$·$6H_2O$ resulted in a pale-green solution, from which the known complex **6**·ClO_4 could be isolated in excellent yields upon addition of $LiClO_4$.

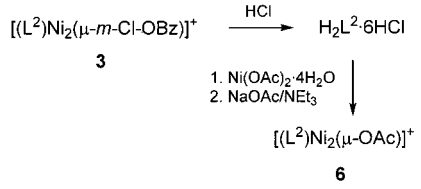

Scheme 4. Synthesis of compounds H_2L^2·6HCl and **6**

In order to get some preliminary information on the solution structures of the new complexes, the synthesis of diamagnetic zinc complexes was devised. The acetato-bridged dizinc complex **8** was selected as the target compound. All attempts to access **8** by oxidation of its parent complex **7** were unsuccessful, but, similar to **6**·ClO_4, this complex

 © 2004 Wiley-VCH Verlag GmbH & Co. KGaA, Weinheim

could be readily prepared by the complexation of the free macrocycle with $Zn(OAc)_2 \cdot 2H_2O$ (Scheme 5). Thus, the reaction of $H_2L^2 \cdot 6HCl$ with two equivalents of $Zn(OAc)_2 \cdot 2H_2O$ resulted in a colourless solution, from which the colourless perchlorate salt $[(L^2)Zn_2(\mu\text{-}OAc)]ClO_4$ ($\mathbf{8} \cdot ClO_4$) was obtained in the form of large crystals in nearly quantitative yield upon addition of $LiClO_4$.

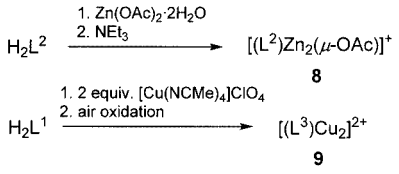

Scheme 5. Synthesis of compounds **8** and **9**

Finally, we were also able to prepare a dinuclear complex of the aminosulfinate ligand $(L^3)^{2-}$, the dicopper(II) complex **9**. This complex was obtained rather unexpectedly from attempts to prepare mixed-valent Cu^ICu^{II} complexes of $(L^1)^{2-}$. Attempts to access this compound by air oxidation of a methanolic solution of the dicopper(I) complex $[(L^1)Cu^I_2]^{2-}$ (prepared in situ from H_2L^1, $[Cu^I(CH_3CN)_4](ClO_4)$ and NEt_3), however, resulted in the formation of the sulfinate complex **9** instead. The dark-green perchlorate salt $[(L^3)Cu^{II}_2](ClO_4)_2$ [$\mathbf{9} \cdot (ClO_4)_2$] was reproducibly obtained as a dark-green microcrystalline solid in about 45% yield.

All new complexes are stable in air, both in solution and in the solid state. The perchlorate salts are very soluble in a range of common organic solvents. The solubility of the complexes of the hexaazadisulfonate macrocycle is particularly good in polar protic solvents such as ethanol, methanol, and even 25% aqueous methanol. In contrast to the aminothiolate complexes, the sulfonate complexes are stable over a wide pH range. They can be isolated from acidic or basic methanolic solution (pH 1 to 10) without any noticeable decomposition or exchange of the bridging coligands L. The new compounds gave satisfactory elemental analyses and were characterized by spectroscopic methods (IR, UV/Vis, ^1H and ^{13}C NMR spectroscopy) and compounds $\mathbf{2} \cdot BPh_4 \cdot 1.25MeCN$, $\mathbf{3} \cdot BPh_4 \cdot 4EtOH \cdot 2H_2O$, $\mathbf{4} \cdot BPh_4 \cdot EtOH \cdot 0.5CH_3CN$, and $\mathbf{9} \cdot (ClO_4)_2 \cdot H_2O$ also by X-ray structure analysis.

Infrared and UV/Vis Spectroscopy

Table 1 summarizes selected analytical data for compounds **1**−**9**. In agreement with the formulation of **3** the IR spectrum displays a strong band at 1220 cm^{-1} for the sulfonate group $\nu(RSO_3^-)$[35] and two absorptions at 1563 [$\nu_{as}(RCO_2^-)$] and 1410 cm^{-1} [$\nu_s(RCO_2^-)$] for the *meta*-chlorobenzoate coligand.[36] The latter two values are very similar to those of the parent complex **2**, suggesting that the *meta*-chlorobenzoate moiety in **3** is also in the $\mu_{1,3}$-bridging mode. Similarly, the IR spectrum of the acetato-bridged complex **6** shows distinct IR bands for bridging acetate (1597 and 1411 cm^{-1}) and sulfonate groups (1202 cm^{-1}). Unfortunately, the sulfonate stretching frequencies overlap with the bands of the $[(L^2)Ni^{II}_2]^{2+}$ fragment[37] and the counterions (ClO_4^- or BPh_4^-), such that the coordination mode of the RSO_3^- functions could not be deduced from the IR data. The IR spectra of the homologous nickel and zinc complexes **5** and **7** (and **6** and **8**) are identical. Finally, the IR spectrum of the copper complex **9** shows two absorptions at 1052 and 950 cm^{-1}, which can be attributed to the stretching frequencies of the sulfinate functions.[38] Again, the coordination mode of the sulfinate groups could not be inferred from the IR data.

All new complexes were further characterized by UV/Vis spectroscopy. The UV/Vis data of **1**, **2** and **5** have been reported previously.[24,25] The electronic absorption spectra of the new complexes were recorded in the range 300−1600 nm in acetonitrile solution at ambient temperature (Table 1). The spectra of the pale-green nickel complexes **3**, **4**, and **6** are similar but not identical. In agreement with the oxidation of the thiophenolate sulfur atoms, there are no intense $RS^- \rightarrow Ni^{II}$ charge-transfer transitions in the 300 to 400 nm region.[39] Each compound displays three weak absorption bands. The first band is seen around 400 nm, the second one appears in the 670 to 690 nm range, and the third one is observed between 1120 and 1130 nm. These absorptions can be attributed to the three spin-allowed d-d-transitions ν_3 [$^3A_{2g}(F) \rightarrow {}^3T_{1g}(P)$], ν_2 [$^3A_{2g}(F) \rightarrow$

Table 1. Selected analytical data of compounds **2**−**9**[a]

Compound	IR bands (cm^{-1}) and assignments	UV/Vis λ_{max} [nm] (ε [$M^{-1} \cdot cm^{-1}$])
1		390 (2830), 625 (58), 941 (56)[b]
2	1566, 1423; ν_{as}, $\nu_s(RCO_2^-)$	385 (2400), 651 (26), 1116 (65)
3	1563, 1410; ν_{as}, $\nu_s(RCO_2^-)$; 1220 $\nu_s(RSO_3^-)$	400 (47), 674 (14), 1126(15)
4	1202, $\nu_s(RSO_3^-)$	396 (33), 686 (15), 1124 (17)
5	1588, 1426; ν_{as}, $\nu_s(RCO_2^-)$[c]	395 (2640), 649 (28), 1134(55)[c]
6	1597, 1411; ν_{as}, $\nu_s(RCO_2^-)$; 1202 $\nu_s(RSO_3^-)$	398 (55), 670 (25), 1122 (47)
$H_2L^{Me\prime} \cdot 6HCl$	1228, $\nu(RSO_3H)$	
7	1585, 1428; ν_{as}, $\nu_s(RCO_2^-)$[c]	
8	1595, 1411; ν_{as}, $\nu_s(RCO_2^-)$; 1202 $\nu_s(RSO_3^-)$	
9	1052, 950; $\nu_s(RSO_2^-)$	668 (430), 947 (153)

[a] The complexes were isolated as their ClO_4^- or BPh_4^- salts. [b] Ref.[24a] [c] Ref.[25]

 © 2004 Wiley-VCH Verlag GmbH & Co. KGaA, Weinheim

$^3T_{1g}(F)$], and ν_1 [$^3A_{2g}(F) \rightarrow {}^3T_{2g}(F)$], respectively, of an octahedral d^8 nickel(II) ion. The higher energy features below 300 nm result from π-π* transitions within the $(L^2)^{2-}$ ligand. The slight differences in the position of the d-d transitions indicate that each complex retains its coligand in the solution state. Finally, the dark-green dicopper(II) complex displays a single absorption band at 668 nm. This is a typical value for square-pyramidal $Cu^{II}N_3O_2$ complexes.[40]

NMR Spectroscopy

To investigate the solution structures, the zinc complex **8** was characterized by ^1H and ^{13}C NMR spectroscopy. The NMR spectroscopic properties of the zinc complex **7** have been reported previously.[25] The ^1H NMR spectrum of **8** in CD_3CN solution displays only one set of signals, indicating that **8** exists as a single isomer in solution. The four aromatic protons, the methyl protons on the benzylic nitrogens, the methyl protons on the central amine nitrogen of the linking diethylene triamine units, and the *tert*-butyl protons all appear as singlets. This is indicative of a C_{2v} symmetric solution structure for the $[(L^2)Zn_2(\mu\text{-OAc})]^+$ cation. In agreement with this assumption the $[(L^2)Zn_2]^{2+}$ fragment gives rise to only eleven ^{13}C NMR signals (seven for the aliphatic and four for the aromatic carbon atoms). The appearance of a ^1H NMR signal at $\delta = 0.59$ ppm, which can be assigned to the methyl protons of the bridging acetate ion, is worthy of note. The observed high-field shift [**8**: $\Delta\delta = -1.24$ ppm, relative to NaOAc ($\delta = 1.83$ ppm)] can be explained by the ring current. As can be seen from Figure S1,[41] the methyl protons of the coordinated acetate group are positioned above the center of the two phenyl rings in the shielding region. The angle between the phenyl rings in **8** (41.6°)[42] is more acute than in **7** (80.0°) and hence the shielding effect is less pronounced in the latter (**7**: $\Delta\delta = -0.92$ ppm, relative to NaOAc). This is also supported by preliminary chemical shielding calculations using Gaussian 98 ($\Delta\delta_{calc} = -1.92$ ppm for **8** vs. -1.25 ppm for **7**; see Exp. Sect. for details).

X-ray Crystallography

Although the formulations of the new compounds were reasonably substantiated by the above spectroscopic data, further confirmation was provided by X-ray diffraction studies. Single crystals of X-ray quality were obtained for the perchlorate or tetraphenylborate salts of complexes **2**, **3**, **4**, and **9**. The crystal structures of complexes **1**, **5**, and **7** have been reported previously.[24,25] All data collections were performed at 210 K. A common labeling scheme for the $[(L^1)Ni_2]^{2+}$ and $[(L^2)Ni_2]^{2+}$ units has been used to facilitate structural comparisons. Selected bond lengths and angles are given in Table 2 and 3.

Table 3. Selected bond lengths (Å) and angles (°) in complex **9**; symmetry code used to generate equivalent atoms (′): $-x, -y, -z$

Cu(1)−O(1)	2.002(2)	Cu(1)−O(2′)	1.968(2)
Cu(1)−N(1)	2.258(3)	Cu(1)−N(2)	2.056(3)
Cu(1)−N(3)	2.041(3)	S(1)−O(1)	1.504(2)
S(1)−O(2)	1.510(3)	Cu(1)···Cu(1′)	4.993(1)
O(2′)−Cu(1)−O(1)	95.91(10)	O(2′)−Cu(1)−N(1)	96.36(11)
O(2′)−Cu(1)−N(3)	89.81(12)	O(1)−Cu(1)−N(1)	88.38(11)
O(1)−Cu(1)−N(3)	154.03(11)	N(3)−Cu(1)−N(1)	116.20(12)
O(2′)−Cu(1)−N(2)	175.42(12)	N(2)−Cu(1)−N(1)	85.12(13)
O(1)−Cu(1)−N(2)	88.45(12)	O(1)−S(1)−O(2)	109.46(14)
N(3)−Cu(1)−N(2)	85.65(12)		

The structure of **2** (Figure 1) reveals the presence of discrete dinuclear $[(L^1)Ni_2(m\text{-Cl-OBz})]^+$ cations, tetraphenylborate anions and acetonitrile molecules of solvent of crystallization. The macrocycle $(L^1)^{2-}$ adopts a conical calixarene-like conformation, which is typical for carboxylato-

Table 2. Selected bond lengths (Å) and angles (°) in complexes **2**, **3**, and **4**

2[a]		**3**		**4**[a]	
Ni(1A)−O(1A)	2.010(3) [2.028(3)]	Ni(1)−O(1)	2.111(5)	Ni(1A)−Cl(1A)	2.439(1) [2.482(2)]
Ni(1A)−N(1A)	2.282(3) [2.281(3)]	Ni(1)−N(1)	2.230(7)	Ni(1A)−N(1A)	2.160(4) [2.183(4)]
Ni(1A)−N(2A)	2.176(4) [2.158(3)]	Ni(1)−N(2)	2.136(6)	Ni(1A)−N(2A)	2.146(4) [2.132(4)]
Ni(1A)−N(3A)	2.222(4) [2.239(3)]	Ni(1)−N(3)	2.265(6)	Ni(1A)−N(3A)	2.320(4) [2.264(4)]
Ni(1A)−S(1A)	2.504(2) [2.512(1)]	Ni(1)−O(5)	2.073(5)	Ni(1A)−O(1A)	2.064(3) [2.048(3)]
Ni(1A)−S(2A)	2.406(2) [2.396(1)]	Ni(1)−O(7)	2.040(5)	Ni(1A)−O(4A)	2.051(3) [2.095(3)]
Ni(2A)−O(2A)	2.020(3) [2.016(3)]	Ni(2)−O(2)	2.102(5)	Ni(2A)−Cl(1A)	2.453(1) [2.449(1)]
Ni(2A)−N(4A)	2.207(4) [2.216(3)]	Ni(2)−N(4)	2.266(6)	Ni(2A)−N(4A)	2.180(4) [2.254(4)]
Ni(2A)−N(5A)	2.170(4) [2.172(3)]	Ni(2)−N(5)	2.131(7)	Ni(2A)−N(5A)	2.120(4) [2.132(4)]
Ni(2A)−N(6A)	2.307(4) [2.311(3)]	Ni(2)−N(6)	2.254(7)	Ni(2A)−N(6A)	2.286(4) [2.195(4)]
Ni(2A)−S(1A)	2.484(2) [2.501(2)]	Ni(2)−O(4)	2.109(5)	Ni(2A)−O(2A)	2.057(3) [2.043(4)]
Ni(2A)−S(2A)	2.401(2) [2.398(1)]	Ni(2)−O(8)	2.009(5)	Ni(2A)−O(5A)	2.098(3) [2.084(3)]
Ni−N[b]	2.227(3) [2.230(3)]		2.214(7)		2.202(4) [2.193(4)]
Ni−O[b]	2.015(3) [2.022(3)]		2.074(5)		2.068(3) [2.068(3)]
Ni−S[b]	2.449(2) [2.451(1)]				
C(4)···C(20)	9.489 [9.563]		7.958		9.471 [9.370]
Ph/Ph[c]	93.6 [92.2]		44.5		72.2 [69.8]
Ni···Ni	3.460(1) [3.457(1)]		4.584(2)		4.063(2) [4.086(2)]

[a] There are two crystallographically independent molecules A and B in the unit cell. Values in square brackets refer to the corresponding bond lengths of the second molecule. [b] Average values. [c] Angle between the normals of the planes of the two aryl rings.

 © 2004 Wiley-VCH Verlag GmbH & Co. KGaA, Weinheim

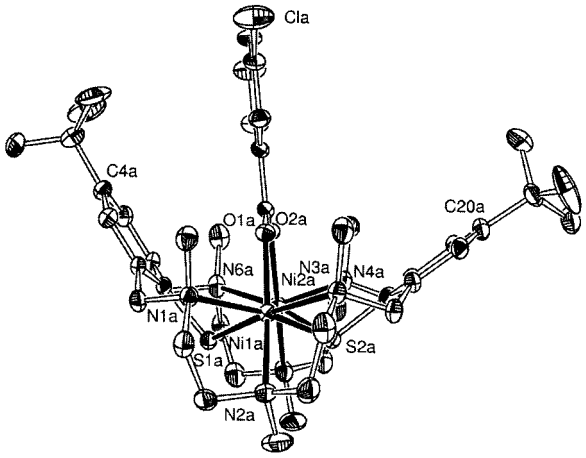

Figure 1. Molecular structure of the cation **2**; thermal ellipsoids are drawn at the 30% probability level; hydrogen atoms are omitted for clarity.

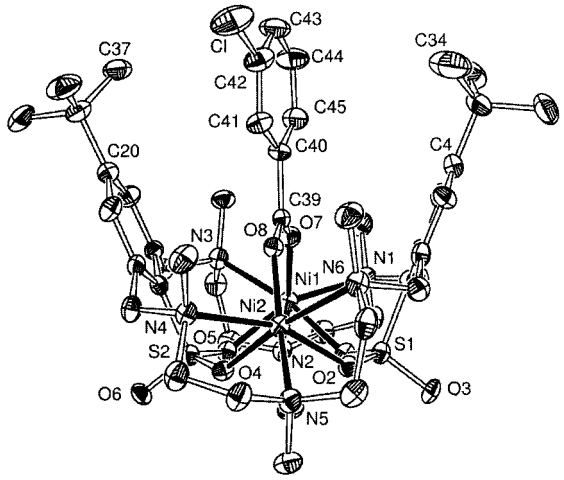

Figure 2. Molecular structure of the cation **3**; thermal ellipsoids are drawn at the 30% probability level; hydrogen atoms are omitted for clarity

bridged complexes of this ligand.[43] In this approximately C_{2v}-symmetric structure, the two nickel(II) ions are coordinated in a square-pyramidal fashion by the two *fac*-N_3(μ-$S)_2$ donor sets of the macrocycle. Upon coordination of the *meta*-chlorobenzoate group, both nickel atoms reach distorted octahedral coordination environments at a metal−metal distance of 3.460(1) Å. As in previously reported carboxylato-bridged nickel complexes of $(L^1)^{2-}$, the Ni−N bond lengths involving the four benzylic nitrogen donors are invariably longer (by ca. 0.10−0.12 Å) than the ones comprising the central nitrogen atoms of the linking diethylenetriamine units. The individual Ni−S distances also vary considerably. These distortions are almost certainly a consequence of the steric constraints of the macrocycle.

The dimensions of the bowl-shaped binding cavity of the $[(L^1)Ni_2]^{2+}$ fragment can be described by the intramolecular distance between the two opposing aryl ring carbon atoms C(4) and C(20) and by the angle between the planes through the phenyl rings. For the present structure, the corresponding values are 9.489(1) Å and 93.6°, respectively. As we will show below, these values decrease considerably upon oxygenation of the thiophenolate sulfur atoms.

The crystal-structure determination of **3**·BPh_4 unambiguously confirmed **3** to be a bioctahedral dinickel complex of the new hexaazadiphenylsulfonate ligand $(L^2)^{2-}$ (see Figure 2). The two sulfonate groups and the *meta*-chlorobenzoate ion bridge the two Ni^{II} ions in symmetrical $\mu_{1,3}$-modes, at a distance of 4.584(1) Å. The amine nitrogens of $(L^2)^{2-}$ occupy the remaining positions and complete the pseudo-octahedral N_3O_3 coordination spheres of the metal ions. Precedents for this type of $\mu_{1,3}$-bridging RSO_3^- functions exist in the literature,[44] albeit not incorporated into a macrobinucleating ligand. A comparison with the structure of the parent complex **2** reveals a significant compression of the binding pocket. Thus, in **3** the best planes through the phenyl rings intersect at an angle of 44.6°. This value is much more acute than in **2** (93.6°). As a consequence the *meta*-chlorobenzoate ion becomes tightly embraced by the tertiary butyl groups of $(L^2)^{2-}$, as evidenced by a very short C(4)···C(20) distance of 7.958 Å. The short distances between the coligand and the *t*Bu protons [H(37a)···C(43) 3.230 Å; H(34c)···C(43) 3.311 Å] are indicative of intramolecular van der Waals interactions between the host and its guest. This is also supported by the wider binding pocket in the μ-Cl species **4** (see below).

Crystals of **4**·BPh_4·EtOH·0.5CH_3CN are composed of discrete, dinuclear $[(L^2)Ni_2(\mu\text{-}Cl)]^+$ cations, tetraphenylborate anions and ethanol and acetonitrile molecules of solvent of crystallization (see Figure 3). Similar to **3**, the aminosulfonate ligand in **4** assumes a calixarene-like conformation such that the bridging halide ion is deeply buried in the binding cavity of the $[(L^2)Ni_2]^{2+}$ fragment. This ligand conformation is different from the "partial cone"-like conformation seen in its parent **1**.[24] The corresponding Ni−O and Ni−N bond lengths in **3** and **4**, respectively, are very similar. In both structures the Ni−N bond lengths involving the four benzylic nitrogen donors are invariably longer (by ca. 0.1 Å) than the ones comprising the central nitrogen atoms of the linking diethylenetriamine units; the Ni−O distances also vary considerably. These distortions can be traced back to the steric constraints of the macrocycle. The main differences between the structures of **3** and **4** concern the Ni···Ni distances (4.063 Å in **4**, 4.584 Å in **3**) and the angle between the phenyl rings (72.2° in **4**, 44.5° in **3**). While the differences in the Ni···Ni distances can be traced back to the different ligating properties of the coligands, the more pronounced clipping of the phenyl rings in **3** is presumably due to attractive van der Waals interactions between the apolar CH function of the bowl-shaped host and its guest. Such secondary interactions are of importance as they can confer unusual binding modes on the coligands.[45]

Finally, the crystal structure determination of **9**·$(ClO_4)_2$·H_2O reveals the dication **9** to be a dicopper(II) complex of the new hexaazadiphenylsulfinate ligand $(L^3)^{2-}$. The complex dication exhibits a center of inversion such that the asymmetric unit consists of only one half of the

 © 2004 Wiley-VCH Verlag GmbH & Co. KGaA, Weinheim

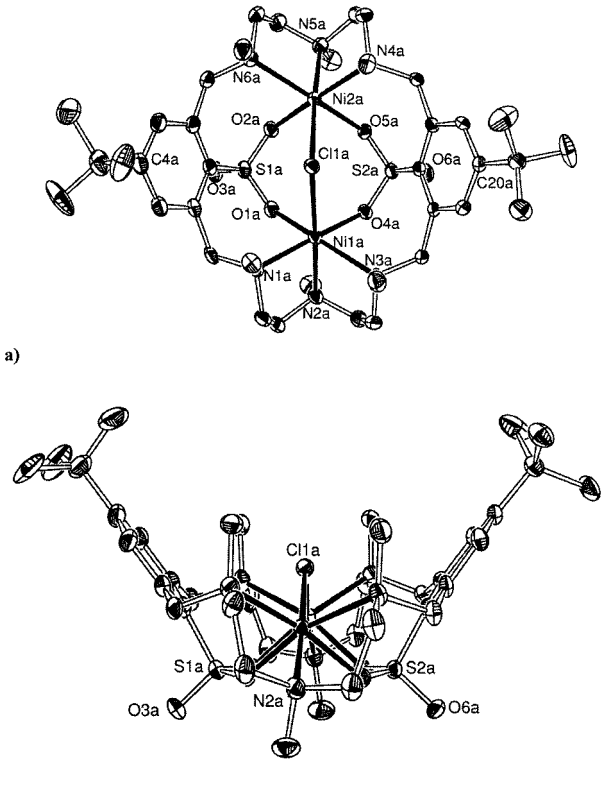

Figure 3. Two views of the molecular structure of the cation **4**; thermal ellipsoids are drawn at the 30% probability level; hydrogen atoms are omitted for clarity

formula unit. As can be seen from Figure 4 the two sulfinate functions bridge the two Cu^{II} ions in symmetrical $\mu_{1,3}$-modes, at a Cu···Cu distance of 4.993(1) Å. The amine nitrogens of $(L^3)^{2-}$ occupy the remaining positions and complete the pseudo-square-pyramidal N_3O_2 coordination spheres of the metal ions. The mean Cu−N and Cu−O distances of 2.118 and 1.985 Å show no unusual features and compare well with those in related $Cu^{II}N_3O_2$ complexes.[46]

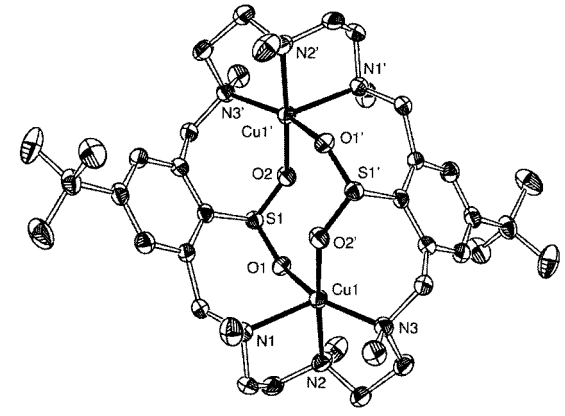

Figure 4. Molecular structure of the dication **9**; thermal ellipsoids are drawn at the 50% probability level; hydrogen atoms are omitted for clarity

Conclusion

The main findings of the present work can be summarized as follows: a) S-oxygenated derivatives of binucleating hexaazadithiophenolate macrocycles of the Robson type can be readily prepared by oxidation of dinuclear nickel complexes of the parent hexaazadithiophenolate macrocycles followed by decomposition of the oxidation products in acidic solution. b) The new hexaazadisulfonate macrocycle $(L^2)^{2-}$ is an effective dinucleating ligand that supports the formation of dinuclear complexes of the type $[(L^2)M_2(\mu\text{-}L)]^+$ with a bowl-shaped, calixarene-like structure. c) The $[(L^2)M_2]^{2+}$ fragment is capable of binding different coligands. d) The $[(L^2)M_2(\mu\text{-}L)]^+$ complexes retain their solid-state structures in the solution state. e) The more pronounced clipping of the phenyl rings in the $[(L^2)M_2(\mu\text{-}L)]^+$ complexes is presumably due to attractive van der Waals interactions between the ligand matrix of the complex and the encapsulated coligand. f) The sulfonate complexes are stable over a wider pH range and oxidizing conditions. Thus, the reactivity of the encapsulated coligands can now also be examined under these more forcing conditions.

Experimental Section

General: Unless otherwise noted the preparations of the metal complexes were carried out under an argon atmosphere by using standard Schlenk techniques. The compounds $H_2L^1\cdot 6HCl$, $[(L^1)Ni_2(Cl)]ClO_4$ (**1**·ClO_4), $[(L^1)Ni_2(OAc)]ClO_4$ (**5**·ClO_4), and $[(L^1)Zn_2(OAc)]ClO_4$ (**7**·ClO_4) were prepared as described in the literature.[25] All other compounds and reagents were purchased from Aldrich. Melting points were determined in capillaries and are uncorrected. ^1H and ^{13}C NMR spectra were recorded on a Bruker AVANCE DPX-200 or a Varian 300 unity spectrometer. Elemental analyses were performed on a Vario EL analyzer (Elementaranalysensysteme GmbH). All compounds crystallize with solvent molecules (see crystal structures of **3**·$BPh_4\cdot 2EtOH\cdot 0.5CH_3CN$ and **4**·$BPh_4\cdot 2EtOH\cdot 0.5CH_3CN$), but the compounds slowly lose their solvent molecules of crystallization upon standing in air. This is why the observed microanalytical data do not fit exactly with the calculated values (for the solvent-free compounds). IR spectra were recorded on a Bruker VECTOR 22 FT-IR spectrophotometer as KBr pellets. Electronic absorption spectra were recorded on a Jasco V-570 UV/Vis/near IR spectrophotometer.

Safety note! *Perchlorate salts of transition-metal complexes are hazardous and may explode. Only small quantities should be prepared and great care taken. We have not encountered any problems with the ClO_4 salts of the present complexes (hammer test), and have for this reason not prepared the BF_4 complexes.*

$[(L^1)Ni^{II}_2$(*m*-Cl-OBz)$]ClO_4$ (2·ClO_4): A solution of sodium *meta*-chlorobenzoate (26.8 mg, 0.150 mmol) in methanol (5 mL) was added to a solution of $[(L^1)Ni_2(Cl)]ClO_4$ (92 mg, 0.10 mmol) in methanol (30 mL). The mixture was stirred for 2 h, during which time the color of the solution turned from yellow to pale green. A solution of $LiClO_4\cdot 3H_2O$ (400 mg, 2.50 mmol) in methanol (2 mL) was then added. The resulting pale-green microcrystalline solid was isolated by filtration, washed with methanol, and dried in air. This material was recrystallized once from a mixed ethanol/acetonitrile (1:1) solvent system. Yield: 78 mg (75%). M.p. 348−350 °C (de-

 © 2004 Wiley-VCH Verlag GmbH & Co. KGaA, Weinheim

comp.). UV/Vis (CH_3CN): λ_{max} (ε) = 385 (2400), 651 (26), 1116 nm (65 $M^{-1}cm^{-1}$). IR (KBr): $\tilde{\nu}$ = 1598 cm^{-1}, 1566 s [$\nu_{as}(RCO_2^-)$], 1423 s [$\nu_s(RCO_2^-)$], 1098 vs [$\nu(ClO_4^-)$]. The tetraphenylborate salt [$(L^1)Ni^{II}_2$(*m*-Cl−OBz)]BPh_4 (**2**·BPh_4) was prepared by adding $NaBPh_4$ (342 mg, 1.00 mmol) to a solution of **2**·ClO_4 (104 mg, 0.100 mmol) in methanol (40 mL). The resulting green solid was recrystallized from a mixed ethanol/acetonitrile solution. Yield: 101 mg (80%). M.p. 298−300 °C (decomp.). UV/Vis (CH_3CN): λ_{max} (ε) = 385 (2500), 649 (34), 1115 nm (68 $M^{-1}cm^{-1}$). IR (KBr): $\tilde{\nu}$ = 1601 s cm^{-1}, 1580 w, 1564 s [$\nu_{as}(RCO_2^-)$], 1423 [$\nu_s(RCO_2^-)$], 732, 703 (BPh_4^-). $C_{69}H_{88}BClN_6Ni_2O_2S_2$ (1261.3): calcd. C 65.71, H 7.03, N 6.66, S 5.08; found C 65.26, H 7.23, N 6.55, S 5.04. The tetraphenylborate salt **2**·BPh_4 was additionally characterized by X-ray crystallography.

[$(L^2)Ni_2$(*m*-Cl-OBz)]ClO_4 (3·ClO_4). Method A (Oxidation with *meta*-Chloroperoxybenzoic acid, MCPBA): A solution of *meta*-chloroperoxybenzoic acid (121 mg, 0.700 mmol) in acetonitrile (2 mL) was added dropwise to a solution of the perchlorate salt **2**·ClO_4 (104 mg, 0.100 mmol) in acetonitrile (30 mL). During the addition the temperature was kept at 0 °C. After stirring for 2 h, a solution of $LiClO_4$·$3H_2O$ (500 mg, 3.12 mmol) in ethanol (40 mL) was added. The product precipitated during evaporation of the solvent (the final amount of solvent was 3−4 mL). The pale-green microcrystalline material was isolated by filtration and dried in air. Yield: 95 mg (84%). M.p. 348−350°C (decomp.). UV/Vis (CH_3CN): λ_{max} (ε) = 400 (47), 674 (16), 1126 nm (15 $M^{-1}cm^{-1}$). IR (KBr): $\tilde{\nu}$ = 1606 cm^{-1}, 1563 s [$\nu_{as}(RCO_2^-)$], 1410 s [$\nu_s(RCO_2^-)$], 1220 vs [$\nu(RSO_3^-)$], 1091 vs [$\nu(ClO_4^-)$]. $C_{45}H_{68}Cl_2N_6Ni_2O_{12}S_2$·$2H_2O$·EtOH (1137.5 + 82.1): calcd. C 45.61, H 6.52, N 6.79, S 5.18; found C 46.00, H 6.82, N 6.89, S 4.77. The tetraphenylborate salt [$(L^2)Ni_2$(*m*-Cl−OBz)]BPh_4 (**3**·BPh_4) was prepared by adding $NaBPh_4$ (342 mg, 1.00 mmol) to a solution of **3**·ClO_4 (114 mg, 0.100 mmol) in methanol (40 mL). The resulting pale-green solid was recrystallized from a mixed ethanol/acetonitrile solution. Yield: 128 mg (94%). M.p. 340−344°C (decomp.). IR (KBr): $\tilde{\nu}$ = 1608 cm^{-1}, 1565 s [$\nu_{as}(RCO_2^-)$], 1410 w [$\nu_s(RCO_2^-)$], 1218 vs [$\nu(RSO_3^-)$], 732, 705 s [$\nu(BPh_4^-)$]. $C_{69}H_{88}BClN_6Ni_2O_8S_2$·$2H_2O$ (1357.3 + 36.0): calcd. C 59.48, H 6.66, N 6.03, S 4.60; found C 59.47, H 6.92, N 5.82, S 3.97.

Method B (Oxidation with Hydrogen Peroxide): Hydrogen peroxide (1.00 mL, 35 wt.-% solution in water, 11.7 mmol) was added to a solution of **2**·ClO_4 (104 mg, 0.10 mmol) in methanol (30 mL). The reaction mixture was refluxed for 5 h to give a pale-green solution. After cooling to room temperature, a solution of $LiClO_4$·$3H_2O$ (0.500 g, 3.12 mmol) in ethanol (40 mL) was added. The product precipitated during evaporation of the solvent (the final amount of solvent was 3−4 mL). The pale-green microcrystalline material was isolated by filtration and dried in air. Yield: 70 mg (60%). The analytical data of this material are identical to those of compound **3**·ClO_4 prepared by method A. The tetraphenylborate salt was additionally characterized by X-ray crystallography.

[$(L^2)Ni_2$(Cl)]ClO_4 (4·ClO_4): H_2O_2 (1.00 mL, 35 wt.-% solution in water, 11.7 mmol) was added to a solution of **1**·ClO_4 (92 mg, 0.10 mmol) in methanol (30 mL). The reaction mixture was refluxed for 4 h to give a pale-green solution. After cooling to room temperature, a solution of $LiClO_4$·$3H_2O$ (0.250 g, 1.56 mmol) in ethanol (40 mL) was added. The product precipitated during evaporation of the solvent (the final amount of solvent was 3−4 mL). The pale-green microcrystalline material was isolated by filtration and dried in air. Yield: 63 mg (62%). An analytical sample was obtained by recrystallization from acetonitrile/ethanol. M.p. 318−320°C (decomp.). UV/Vis (CH_3CN): λ_{max} (ε) = 396 (33), 686 (15), 1124 nm (17 $M^{-1}cm^{-1}$). IR (KBr): $\tilde{\nu}$ = 1202vs cm^{-1} [$\nu(RSO_3^-)$], 1092s [$\nu(ClO_4^-)$]. $C_{38}H_{64}Cl_2N_6Ni_2O_{10}S_2$·$2H_2O$·EtOH (1017.4 + 82.1): calcd. C 43.70, H 6.78, N 7.64, S 5.83; found C 43.35, H 6.98, N 7.88, S 5.47. The tetraphenylborate salt [$(L^2)Ni_2$(Cl)]BPh_4 (**4**·BPh_4) was prepared by adding $NaBPh_4$ (342 mg, 1.00 mmol) to a solution of **4**·ClO_4 (105 mg, 0.100 mmol) in methanol (40 mL). The resulting green solid was recrystallized from a mixed ethanol/acetonitrile solution. Yield: 111 mg (90%). M.p. 330−334°C (decomp.). IR (KBr): $\tilde{\nu}$ = 1203 vs cm^{-1} [$\nu(RSO_3^-)$]. $C_{62}H_{84}BClN_6Ni_2O_6S_2$·EtOH (1237.2 + 46.1): calcd. C 59.90, H 7.07, N 6.55, S 5.00; found C 60.27, H 6.86, N 6.61, S 4.96. The tetraphenylborate salt was additionally characterized by X-ray crystallography. The oxidation of **1**·ClO_4 by *meta*-chloroperoxybenzoic acid yields **3**·ClO_4 (vide supra).

[$(L^2)Ni_2$(OAc)]ClO_4 (6·ClO_4). Method A (Oxidation with *meta*-Chloroperoxybenzoic Acid): A solution of the acetato-bridged complex **5**·ClO_4 (94 mg, 0.10 mmol) in acetonitrile (30 mL) was added slowly to a solution of *meta*-chloroperoxybenzoic acid (0.12 g, 0.70 mmol) in acetonitrile (2 mL). During the addition the temperature was kept at 0 °C. After stirring for 30 min, a solution of $LiClO_4$·$3H_2O$ (0.500 g, 3.12 mmol) in ethanol (40 mL) was added. The product precipitated during evaporation of the solvent (the final amount of solvent was 3−4 mL). The pale-green microcrystalline material was isolated by filtration and dried in air. Yield: 87 mg (84%). M.p. 344−348°C (decomp.). UV/Vis (CH_3CN): λ_{max} (ε) = 398 (55), 670 (25), 1122 nm (47 $M^{-1}cm^{-1}$). IR (KBr): $\tilde{\nu}$ =1611 sh cm^{-1}, 1597 s [$\nu_{as}(RCO_2^-)$], 1411 w [$\nu_s(RCO_2^-)$], 1202 vs [$\nu(RSO_3^-)$], 1092 s [$\nu(ClO_4^-)$]. $C_{40}H_{67}ClN_6Ni_2O_{12}S_2$·$4H_2O$ (1041.0 + 72.1): calcd. C 43.16, H 6.79, N 7.55, S 5.76; found C 43.73, H 6.94, N 7.43, S 5.34.

Method B (Oxidation by Hydrogen Peroxide): Hydrogen peroxide (1.00 mL, 35 wt.-% solution in water, 11.7 mmol) was added to a solution of **5**·ClO_4 (94 mg, 0.10 mmol) in methanol (30 mL). The reaction mixture was refluxed for 5 h to give a pale-green solution. After cooling to room temperature, a solution of $LiClO_4$·$3H_2O$ (0.500 g, 3.12 mmol) in ethanol (40 mL) was added. The product precipitated during evaporation of the solvent (the final amount of solvent was 3−4 mL). The pale-green microcrystalline material was isolated by filtration and dried in air. Yield: 56 mg (50%). The analytical data of this material are identical to those of compound **6**·ClO_4 prepared by method A.

Method C (from the Free Ligand H_2L^2·6HCl): The reaction of $Ni(OAc)_2$·$4H_2O$ with H_2L^2·6HCl in the presence of a base also gives **6**·ClO_4. The procedure is detailed below for the corresponding zinc complex **8**.

H_2L^2·6HCl: Hydrochloric acid (12 M, 100 mL) was added to a suspension of complex **3**·ClO_4 (3.50 g, 3.08 mmol) in methanol (300 mL) and the reaction mixture was stirred vigorously at 50 °C for 24 h. The resulting solution was then concentrated at reduced pressure (final volume ca 40 mL) and the pH adjusted to 13 with 5 M aqueous potassium hydroxide solution. The resulting green suspension was allowed to cool to room temperature, and the aqueous phase was extracted with dichloromethane (5 × 100 mL). The organic fractions were combined and the dichloromethane was distilled off at reduced pressure to give a colorless solid. The residue was redissolved in ethanol (100 mL), acidified to pH 1 with conc. hydrochloric acid (ca. 3−4 mL), and the resulting solution quickly filtered off from an insoluble white solid (KCl). Evaporation of the solvent gave H_2L^2·6HCl as a colorless voluminous solid. M.p. 240−242°C (dec.). Yield: 2.63 g (85%). This material was pure enough for metal-complex synthesis. IR (KBr): $\tilde{\nu}$ = 3023 w cm^{-1}, 2962 m, 2591 br. s, 1634, 1602, 1464 s, 1228 vs [$\nu(RSO_3H)$], 1074

 © 2004 Wiley-VCH Verlag GmbH & Co. KGaA, Weinheim

s, 1019 s, 688 s, 662 s. $C_{38}H_{72}Cl_6N_6O_6S_2$ $(H_2O)_3$ (985.86 + 54.05): calcd. C 43.89, H 7.65, N 8.08, S 6.17; found C 44.02, H 7.37, N 7.75, S 5.91. ^{1}H NMR (200 MHz, D_2O, 330 K): δ = 7.87 (s, 4 H, ArH), 4.86 (s, 8 H, $ArCH_2$), 3.72 (t, ^3J, 5.6 Hz, 8 H, CH_2), 3.33 (t, ^3J, 5.6 Hz, 8 H, CH_2), 3.02 (s, 12 H, $BzNCH_3$), 2.45 (s, 6 H. NCH3), 1.47 [s, 18 H, $C(CH_3)_3$] ppm. ^{13}C{^{1}H} NMR (50 MHz, D_2O): δ = 30.9 [$C(CH_3)_3$], 35.4 [$C(CH_3)_3$] 41.5 (CH_3), 52.5 (CH_2), 52.9 (CH_2), 60.9 (CH_2), 128.6, 136.0 (CH), 142.2, 157.4 ppm; one aliphatic carbon signal was not observed.

[(L^2)Zn_2(OAc)](ClO_4) (8·ClO_4): $Zn(O_2CCH_3)_2$·$2H_2O$ (44 mg, 0.20 mmol) and triethylamine (61 mg, 0.60 mmol) were added to a solution of H_2L^2·6HCl (99 mg, 0.10 mmol) in methanol (25 mL). After stirring the reaction mixture for 2 d at room temperature, solid $LiClO_4$·$3H_2O$ (321 mg, 2.00 mmol) was added. The mixture was then stirred for a further 12 h. The resulting white precipitate was collected by filtration and recrystallized from an acetonitrile/ethanol mixed-solvent system. Yield: 96 mg (91%). M.p. 360−364°C (decomp.). IR (KBr): $\tilde{\nu}$ = 1595s cm^{-1} [$\nu_{as}(RCO_2^-)$], 1411 w [$\nu_s(RCO_2^-)$], 1202 vs [$\nu(RSO_3^-)$], 1090 s [$\nu(ClO_4^-)$]. ^{1}H NMR (200 MHz, CD_3OD): δ = 7.26 (s, 4 H, ArH), 4.58 (d, ^2J = 12.4 Hz, 4 H, $ArCH_2$), 3.00 (d, ^2J = 12.4 Hz, 4 H, $ArCH_2$), 2.95−2.75 (m, 16 H, CH_2), 2.68 (s, 6 H, NCH_3), 2.47 (s, 12 H, NCH_3), 1.26 [s, 18 H, $C(CH_3)_3$], 0.59 (s, 3 H, CH_3) ppm. ^{13}C{^{1}H} NMR (50 MHz, $CDCl_3$): δ = 173.1, 153.2, 143.5, 133.3, 132.5, 64.4, 57.1, 52.8, 45.3, 44.7, 35.08, 30.9, 23.3 ppm. $C_{40}H_{67}ClN_6O_{12}S_2Zn_2$·$4H_2O$ (1054.4 + 72.1): calcd. C 42.65, H 6.71, N 7.46, S 5.69; found C 42.58, H 6.74, N 7.36, S 5.20.

[(L^3)Cu_2](ClO_4)$_2$ (9·2ClO_4): $[Cu(CH_3CN)_4]ClO_4$ (65 mg, 0.20 mmol) and triethylamine (81 mg, 0.80 mmol) were added successively to a suspension of H_2L^1·6HCl (89 mg, 0.10 mmol) in methanol (40 mL). The colorless reaction mixture was stirred for 24 h and was then exposed to air to give a dark-green solution. A solution of $LiClO_4$·$3H_2O$ (160 mg, 1.00 mmol) in methanol was added. The mixture was then filtered and stored in an open vessel for five days. The resulting green crystals were isolated by filtration and dried in air. Yield: 45 mg (45%). M.p. 350−352°C (decomp.). IR (KBr): $\tilde{\nu}$ = 1058 cm^{-1}, 970 [$\nu(RSO_2^-)$], 1090 s [$\nu(ClO_4^-)$]. UV/Vis (CH_3CN): λ_{max} (ε) = 668 (430), 947 sh nm (153 $M^{-1}cm^{-1}$). $C_{38}H_{64}Cl_2Cu_2N_6O_8S_2$ (995.08): calcd. C 45.87, H 6.48, N 8.45, S 6.44; found C 45.66, H 6.53, N 8.33, S 6.22. This compound was additionally characterized by X-ray crystallography.

Crystal Structure Determinations: Single crystals of **2**·BPh_4·1.25CH_3CN, **3**·BPh_4·4EtOH·$2H_2O$, and **4**·BPh_4·2EtOH·0.5CH_3CN suitable for X-ray structure analysis were grown from an acetonitrile/ethanol (1:1) mixed-solvent system. Crystals of **9**·$(ClO_4)_2$·H_2O were grown from methanolic solution. The crystals were mounted on glass fibers in perfluoropolyether oil. Intensity data were collected at 210(2) K, using a Bruker SMART CCD diffractometer. Graphite-monochromated Mo-K_α radiation (λ = 0.71073 Å) was used throughout. The data were processed with SAINT and corrected for absorption using SADABS[47] (transmission factors: 1.00−0.89 for **2**, 1.00−0.58 for **3**, 1.00−0.85 for **4**, and 1.00−0.91 for **9**). The structures were solved by direct methods using the program SHELXS-86[48] and refined by full-matrix least-squares techniques against F^2 using SHELXL-97.[49] The ShelXTL version 5.10 program package was used for the structure solutions and refinements.[50] PLATON was used to search for higher symmetry.[51] Ortep3 was used for the artwork of the structures.[52] Unless otherwise noted all non-hydrogen atoms were refined anisotropically. Hydrogen atoms were assigned to idealized positions and given isotropic thermal parameters 1.2-times (1.5-times for CH_3 groups) the thermal parameter of the atoms to which they are attached. Selected details of the data collection and refinement are given in Table 4.

In the crystal structure of **2** two *tert*-butyl groups were found to be disordered over two positions. A split-atom model was applied for the disordered *t*Bu groups. The site occupancies of the two orientations were refined as 0.70(1)/0.30(1) [for C(32a/c), C(33a/c), C(34a/c)] and 0.62(1)/0.38(1) [for C(36a/c), C(37a/c), C(38a/c)]. All non-hydrogen atoms were refined anisotropically, except the nitro-

Table 4. Crystallographic data for **2**·BPh_4·1.25MeCN, **3**·BPh_4·4EtOH·$2H_2O$, **4**·BPh_4·EtOH·0.5CH_3CN, and **9**·$(ClO_4)_2$·H_2O

Compound	**2**·BPh_4·1.25MeCN	**3**·BPh_4·4EtOH·$2H_2O$	**4**·BPh_4·EtOH·0.5CH_3CN	**9**·$(ClO_4)_2$·H_2O
Formula	$C_{71.5}H_{91.75}BClN_{7.25}Ni_2O_8S_2$	$C_{77}H_{116}BClN_6Ni_2O_{14}S_2$	$C_{65}H_{91.5}BClN_{6.5}Ni_2O_7S_2$	$C_{38}H_{68}Cl_2Cu_2N_6O_{14}S_2$
M_r (g/mol)	1312.57	1577.56	1303.75	1095.08
Space group	$P\bar{1}$	$C2/c$	$P2_1/c$	$P2_1/c$
a (Å)	13.003(3)	31.604(6)	19.960(4)	12.688(3)
b (Å)	15.939(3)	16.444(4)	19.772(4)	9.131(2)
c (Å)	33.871(7)	34.628(6)	33.322(7)	20.780(4)
α (°)	77.22(3)	90.00	90.00	90.00
β (°)	82.06(3)	111.02(2)	93.514(5)	106.25(3)
γ (°)	82.75(3)	90.00	90.00	90.00
V (Å^3)	6747(2)	16798(6)	13126(5)	2311.3(9)
Z	4	8	8	2
$d_{calcd.}$ (g/cm^3)	1.292	1.248	1.319	1.574
Cryst. size (mm^3)	0.30 × 0.30 × 0.30	0.20 × 0.26 × 0.31	0.30 × 0.30 × 0.20	0.20 × 0.20 × 0.20
μ(Mo-K_α) (mm^{-1})	0.710	0.591	0.734	1.197
2θ limits (deg)	2.64−58.14	1.52−57.66	3.10−57.76	3.34−56.60
Measured refl.	61676	42079	81701	14432
Independent refl.	31611	18414	31159	5571
Observed refl.[a]	12737	5500	12272	3025
No. parameters	1608	802	1519	289
$R1$[b] ($R1$ all data)	0.0533 (0.1054)	0.0783 (0.1996)	0.0554 (0.1378)	0.0446 (0.0969
$wR2$[c] ($wR2$ all data)	0.1639 (0.1410)	0.2458 (0.2737)	0.1696 (0.1784)	0.1032 (0.1153)
Max., min. peaks (e/Å^3)	0.724, −0.831	1.309, −1.219	1.237, −1.160	0.591, −0.565

[a] Observation criterion: $I > 2\sigma(I)$. [b] $R1 = \Sigma||F_o| - |F_c||/\Sigma|F_o|$. [c] $wR2 = \{\Sigma[w(F_o^2 - F_c^2)^2]/\Sigma[w(F_o^2)^2]\}^{1/2}$.

 © 2004 Wiley-VCH Verlag GmbH & Co. KGaA, Weinheim

gen and carbon atoms [N(9), C(51), C(52)] of one half-occupied acetonitrile solvent molecule. No hydrogen atoms were calculated for the methyl carbon atom C(52). In the crystal structure of **3**, the C and O atoms of the ethanol and water molecules of solvent of crystallization were found to exhibit very large thermal parameters indicative of severe disorder. This disorder could not be modeled by using split-atom models, therefore the coordinates of the respective atoms were fixed at their initial positions and given a common isotropic thermal parameter of 0.20. No problems were encountered with the refinement of the $[(L^2)Ni_2(m\text{-Cl-OBz})]^+$ cation. The relatively large *R* value is due to the disorder of the solvent molecules. In the crystal structure of **4**, one *tert*-butyl group and the two ethanol molecules of crystallization were found to be disordered over two positions. A split atom model was applied to account for this disorder. The site occupancies of the two orientations were refined as 0.53(1)/0.47(1) [for C(32a/b), C(33a/b), C(34a/b)], 0.71(1)/0.29(1) [for O(5a/b), C(39a/b), C(40a/b)], and 0.78(1)/0.22(1) [for O(7a/b), C(41a/b), C(42a/b)]. The disorder of the acetonitrile molecule of solvent of crystallization could not be modeled by using a split-atom model, therefore the coordinates of the C and N atoms were fixed at their initial positions and given a common isotropic thermal parameter of 0.20. No hydrogen atoms were calculated for the solvate molecules. In the crystal structure of $\mathbf{9}\cdot(ClO_4)_2(H_2O)$ no hydrogen atoms were calculated for the H_2O molecule.

CCDC-239553 (for **2**), -239554 (for **3**), -239555 (for **4**) and -239556 (for **9**) contain the supplementary crystallographic data for this paper. These data can be obtained free of charge via www.ccdc.cam.ac.uk/conts/retrieving.html (or from the Cambridge Crystallographic Data Centre, 12 Union Road, Cambridge CB2 1EZ, UK (fax: +44-1223-336-033; or deposit@ccdc.cam.ac.uk).

Calculation of Ring-Current Effects: All ab initio calculations were performed on an SGI Octane and an SGI Origin 2000 using the program Gaussian 98.[53] Geometry optimization was carried out using HF/6-31G* without restrictions.[54] The chemical shieldings in the surrounding of the molecules were calculated based on the idea of NICS (nucleus-independent chemical shift) by Schleyer.[55] The molecule was placed in the center of a grid of "ghost atoms" ranging from −10.0 to +10.0 Å in all three dimensions with a step width of 0.5 Å. This resulted in a cube of 68921 ghost atoms. The chemical-shielding calculations were done with the GIAO (gauge-independent atomic orbital) method using HF/6-31G*.[56] Since GIAO is a coupled HF method that uses gauge-independent atom orbitals for the calculation of shielding values it can be applied in the calculation of NICS. From the GIAO calculations the coordinates and isotropic shielding values of the ghost atoms were extracted. After the transformation of the tabulated chemical shieldings into a SYBYL contour file, the ring-current effects of the two isolated phenyl rings in the complexes can be visualized as iso chemical-shielding surfaces (ICSS).[57] Thus, it is possible to map both spatial extension and sign of the ring current effects of the two phenyls on the methyl protons at each position.[58]

The chemical shielding values at the positions of the three methyl protons of the bridging acetate ions in **7** and **8** (atomic coordinates were taken from the crystal structures) were calculated as follows: **7**: $\Delta\delta$ = −1.56, −1.08, −1.12 ppm (mean value = −1.25 ppm, in the gas phase); **8**: $\Delta\delta$ = −2.32, −1.59, −1.85 ppm (mean value = −1.92 ppm). The observed chemical shielding values (relative to NaOAc at δ = 1.83 ppm in CD_3OD) are as follows: **7** δ(μ-OAc) = 0.86 ppm ($\Delta\delta$ = −0.97 ppm); **8**: δ(μ-OAc) = 0.59 ppm ($\Delta\delta$ = −1.24 ppm). The differences between the calculated and the experimental values are most likely due to solvation effects.

Supporting Information Available: Figures S1 and S2 (see also the footnote on the first page of this article). The calculated chemical shielding values at the positions of the three methyl protons of the bridging acetate ions in **7** and **8**.

Acknowledgments

We are particularly grateful to Prof. Dr. H. Vahrenkamp for providing facilities for NMR and X-ray crystallographic measurements. Financial support of this work from the Deutsche Forschungsgemeinschaft (Priority programme "Sekundäre Wechselwirkungen", KE 585/3-1,2) and by the Wissenschaftliche Gesellschaft in Freiburg is gratefully acknowledged.

[1] J. W. Canary, B. C. Gibb, *Prog. Inorg. Chem.* **1997**, *45*, 1−83.
[2] C. Wieser, C. B. Dieleman, D. Matt, *Coord. Chem. Rev.* **1997**, *165*, 93−161.
[3] S. Hecht, J. M. J. Fréchet, *Angew. Chem.* **2001**, *113*, 76−94; *Angew. Chem. Int. Ed.* **2001**, *40*, 74−91.
[4] [4a] M. T. Reetz, S. R. Waldvogel, *Angew. Chem.* **1997**, *109*, 870−873; *Angew. Chem. Int. Ed. Engl.* **1997**, *36*, 865−867. [4b] M. T. Reetz, *Catal. Today* **1998**, *42*, 399.
[5] E. Engeldinger, D. Armspach, D. Matt, *Angew. Chem.* **2001**, *113*, 2594−2597; *Angew. Chem. Int. Ed.* **2001**, *40*, 2526−2529.
[6] V. F. Slagt, J. N. H. Reek, P. C. J. Kramer, P. W. N. M. van Leeuwen, *Angew. Chem.* **2001**, *113*, 4401−4404; *Angew. Chem. Int. Ed.* **2001**, *40*, 4271−4274.
[7] M. Yoshizawa, Y. Takeyama, T. Kusukawa, M. Fujita, *Angew. Chem.* **2002**, *114*, 1403−1405; *Angew. Chem. Int. Ed.* **2002**, *41*, 1347−1349.
[8] T. Ooi, Y. Kondo, K. Maruoka, *Angew. Chem.* **1998**, *110*, 3213−3215; *Angew. Chem. Int. Ed.* **1998**, *37*, 3039−3041.
[9] [9a] S. Blanchard, L. Le Clainche, M.-N. Rager, B. Chansou, J.-P. Tuchagues, A. F. Duprat, Y. Le Mest, O. Reinaud, *Angew. Chem.* **1998**, *110*, 2861−2864; *Angew. Chem. Int. Ed.* **1998**, *37*, 2732−2735. [9b] Y. Rondelez, G. Bertho, O. Reinaud, *Angew. Chem.* **2002**, *114*, 1086−1088; *Angew. Chem. Int. Ed.* **2002**, *41*, 1044−1046. [9c] Y. Rondelez, M.-N. Rager, A. Duprat, O. Reinaud, *J. Am. Chem. Soc.* **2002**, *124*, 1334−1340. [9d] O. Seneque, M.-N. Rager, M. Giorgi, O. Reinaud, *J. Am. Chem. Soc.* **2001**, *123*, 8442−8443. [9e] O. Seneque, M.-N. Rager, M. Giorgi, O. Reinaud, *J. Am. Chem. Soc.* **2000**, *122*, 6183−6189.
[10] B. R. Cameron, S. J. Loeb, G. P. A. Yap, *Inorg. Chem.* **1997**, *36*, 5498−5504.
[11] For reviews of cyclodextrins, see *Chem. Rev.* **1998**, *98*, 1741−2076 (special issue).
[12] [12a] N. Kitajima, W. B. Tolman, *Prog. Inorg. Chem.* **1995**, *43*, 419−531. [12b] S. Trofimenko, *Scorpionates: The Coordination Chemistry of Polypyrazolylborate Ligands*, Imperial College Press, London, U.K., **1999**. [12c] H. Vahrenkamp, *Acc. Chem. Res.* **1999**, *32*, 589−596.
[13] P. Chaudhuri, K. Wieghardt, *Prog. Inorg. Chem.* **1988**, *35*, 329−436.
[14] B. S. Hammes, D. Ramos-Maldonado, G. P. A. Yap, L. Liable-Sands, A. L. Rheingold, V. G. Young Jr., A. S. Borovik, *Inorg. Chem.* **1997**, *36*, 3210−3211.
[15] A. J. Atkins, D. Black, A. J. Blake, A. Marin-Becerra, S. Parsons, L. Ruiz-Ramirez, M. Schröder, *Chem. Commun.* **1996**, 457−464.
[16] J. B. Fontecha, S. Goetz, V. McKee, *Angew. Chem.* **2002**, *114*, 4735−4738; *Angew. Chem. Int. Ed.* **2002**, *41*, 4553−4556.
[17] T. Kajiwara, H. Wu, T. Ito, N. Iki, S. Miyano, *Angew. Chem.* **2004**, *116*, 1868−1871; *Angew. Chem. Int. Ed.* **2004**, *43*, 1832−1835.
[18] [18a] A. J. Atkins, A. J. Blake, M. Schröder, *J. Chem. Soc., Chem. Commun.* **1993**, 1662−1665. [18b] N. D. J. Branscombe, A. J. Blake, A. Marin-Becerra, W.-S. Li, S. Parsons, L. Ruiz-Ramirez, M. Schröder, *Chem. Commun.* **1996**, 2573−2574.

 © 2004 Wiley-VCH Verlag GmbH & Co. KGaA, Weinheim

[19] [19a] S. Brooker, P. D. Croucher, *J. Chem. Soc., Chem. Commun.* **1995**, 1493−1494. [19b] S. Brooker, P. D. Croucher, *J. Chem. Soc., Chem. Commun.* **1995**, 2075−2076. [19c] S. Brooker, P. D. Croucher, F. M. Roxburgh, *J. Chem. Soc., Dalton Trans.* **1996**, 3031−3037. [19d] S. Brooker, P. D. Croucher, *Chem. Commun.* **1997**, 459−460. [19e] S. Brooker, P. D. Croucher, T. C. Davidson, G. S. Dunbar, A. J. McQuillan, G. B. Jameson, *Chem. Commun.* **1998**, 2131−2132.

[20] N. H. Pilkington, R. Robson, *Aust. J. Chem.* **1970**, *23*, 2225−2236.

[21] [21a] P. A. Vigato, S. Tamburini, D. Fenton, *Coord. Chem. Rev.* **1990**, *106*, 25−170. [21b] D. Fenton, *Chem. Soc., Rev.* **1999**, *28*, 159−168.

[22] [22a] H. Okawa, H. Furutachi, D. E. Fenton, *Coord. Chem. Rev.* **1998**, *174*, 51−75. [22b] M. Shinoura, S. Kita, M. Ohba, H. Okawa, H. Furutachi, M. Suzuki, *Inorg. Chem.* **2000**, *39*, 4520−4526.

[23] [23a] C. Fraser, L. Johnston, A. L. Rheingold, B. S. Haggerty, G. K. Williams, J. Whelan, B. Bosnich, *Inorg. Chem.* **1992**, *31*, 1835−1844. [23b] B. Bosnich, *Inorg. Chem.* **1999**, *38*, 2554−2562. [23c] A. L. Gavrilova, C. J. Qin, R. D. Sommer, A. L. Rheingold, B. Bosnich, *J. Am. Chem. Soc.* **2002**, *124*, 1714−1722.

[24] [24a] B. Kersting, G. Steinfeld, *Chem. Commun.* **2001**, 1376−1377. [24b] M. H. Klingele, G. Steinfeld, B. Kersting, *Z. Naturforsch., Teil B* **2001**, *56*, 901−907. [24c] B. Kersting, G. Steinfeld, *Inorg. Chem.* **2002**, *41*, 1140−1150.

[25] B. Kersting, *Angew. Chem.* **2001**, *113*, 4109−4112; *Angew. Chem. Int. Ed.* **2001**, *40*, 3987−3990.

[26] I. K. Adzamli, K. Libson, J. D. Lydon, R. C. Elder, E. Deutsch, *Inorg. Chem.* **1979**, *18*, 303−311.

[27] [27a] C. A. Grapperhaus, M. Y. Darensbourg, *Acc. Chem. Res.* **1998**, *31*, 451−459. [27b] R. M. Buonomo, I. Font, M. J. Maguire, J. H. Reibenspies, T. Tuntulani, M. Y. Darensbourg, *J. Am. Chem. Soc.* **1995**, *117*, 963−973.

[28] S. A. Mirza, M. A. Pressler, M. Kumar, R. O. Day, M. J. Maroney, *Inorg. Chem.* **1993**, *32*, 977−987.

[29] [29a] V. E. Kaasjager, E. Bouwman, S. Gorter, J. Reedijk, C. A. Grapperhaus, J. H. Reibenspies, J. J. Smee, M. Y. Darensbourg, A. Derecskei-Kovacs, L. M. Thomson, *Inorg. Chem.* **2002**, *41*, 1837−1844. [29b] R. K. Henderson, E. Bouwman, A. L. Spek, J. Reedijk, *Inorg. Chem.* **1997**, *36*, 4616−4617.

[30] The absence of sharp ^{1}H NMR resonances in the δ = 0−10 ppm region indicates that the nickel complexes **1**−**6** are paramagnetic in solution. For complexes **2** and **5** this is further supported by temperature-dependent magnetic susceptibility measurements.[45] We anticipate performing a more detailed study of the electronic structures of the other compounds by temperature-dependent susceptibility measurements.

[31] Abbreviations: MCPBA = *meta*-chloroperoxybenzoic acid (*m*-Cl-C_6H_4-CO_3H), *m*-Cl-OBz = *m*-Cl-C_6H_4-CO_2^-, OAc^- = $CH_3CO_2^-$).

[32] N. D. J. Branscombe, A. J. Atkins, A. Marin-Becerra, E. J. L. McInnes, F. E. Mabbs, J. McMaster, M. Schröder, *Chem. Commun.* **2003**, 1098−1099.

[33] S. A. Mirza, R. O. Day, M. J. Maroney, *Inorg. Chem.* **1996**, *35*, 1992−1995.

[34] G. Steinfeld, V. Lozan, B. Kersting, *Angew. Chem.* **2003**, *115*, 2363−2365; *Angew. Chem. Int. Ed.* **2003**, *42*, 2261−2263.

[35] M. Y. Darensbourg, T. Tuntulani, J. H. Reibenspies, *Inorg. Chem.* **1995**, *34*, 6287−6294.

[36] K. Nakamoto, *Infrared and Raman Spectra of Inorganic and Coordination Compounds*, 5th ed., Wiley-VCH, New York, **1997**.

[37] For a complete listing of these IR absorptions see: Exp. Sect., complex **2**.

[38] P. J. Farmer, T. Solouki, D. K. Mills, T. Soma, D. H. Russell, J. H. Reibenspies, M. Y. Darensbourg, *J. Am. Chem. Soc.* **1992**, *114*, 4601−4605.

[39] The nickel complex **5** and other carboxylato-bridged dinickel complexes of $(L^1)^{2-}$ all display an intense absorption in the 380 to 400 nm region ($\varepsilon \approx 2500$ $M^{-1}\cdot cm^{-1}$) in CH_3CN solution.

[40] M. Duggan, N. Ray, B. Hathaway, G. Tomlinson, P. Brint, K. Pelin, *J. Chem. Soc., Dalton Trans.* **1980**, 1342−1348.

[41] See Supporting Information.

[42] A preliminary crystal structure determination of **8**·BPh_4 revealed the structure of the complex cation **8** to be very similar to that of **3**, with a Zn···Zn distance of 4.542(2) Å and an acute angle (41.6°) between the phenyl rings. However, due to severe disorder of the solvent molecules, the *R* value is very low and the structure cannot be published yet.

[43] B. Kersting, *Z. Anorg. Allg. Chem.* **2004**, *630*, 765−780.

[44] F. A. Cotton, G. Wilkinson, C. A. Murillo, M. Bochmann, *Advanced Inorganic Chemistry*, 6th ed., John Wiley & Sons, New York, **1999**, p. 492.

[45] J. Hausmann, M. H. Klingele, V. Lozan, G. Steinfeld, D. Siebert, Y. Journaux, J. J. Girerd, B. Kersting, *Chem. Eur. J.* **2004**, *10*, 1716−1728.

[46] J. Ackermann, F. Meyer, E. Kaifer, H. Pritzkow, *Chem. Eur. J.* **2002**, *8*, 247−258.

[47] SADABS, An empirical absorption correction program part of the SAINTPlus NT version 5.10 package, BRUKER AXS, Madison, WI, **1998**.

[48] G. M. Sheldrick, *Acta Crystallogr., Sect. A* **1990**, *46*, 467−473.

[49] G. M. Sheldrick, *SHELXL-97*, Computer *program for crystal structure refinement*, University of Göttingen, Göttingen, Germany, **1997**.

[50] ShelXTL version 5.10: Bruker AXS, Madison, WI, **1998**.

[51] A. L. Spek, *PLATON − A Multipurpose Crystallographic Tool*; Utrecht University, Utrecht, The Netherlands, **2000**.

[52] L. J. Farrugia, *J. Appl. Cryst.* **1997**, *30*, 565.

[53] Gaussian 9*8, Revision A.11.3:* M. J. Frisch, G. W. Trucks, H. B. Schlegel, G. E. Scuseria, M. A. Robb, J. R. Cheeseman, V. G. Zakrzewski, J. A. Montgomery, Jr., R. E. Stratmann, J. C. Burant, S. Dapprich, J. M. Millam, A. D. Daniels, K. N. Kudin, M. C. Strain, O. Farkas, J. Tomasi, V. Barone, M. Cossi, R. Cammi, B. Mennucci, C. Pomelli, C. Adamo, S. Clifford, J. Ochterski, G. A. Petersson, P. Y. Ayala, Q. Cui, K. Morokuma, N. Rega, P. Salvador, J. J. Dannenberg, D. K. Malick, A. D. Rabuck, K. Raghavachari, J. B. Foresman, J. Cioslowski, J. V. Ortiz, A. G. Baboul, B. B. Stefanov, G. Liu, A. Liashenko, P. Piskorz, I. Komaromi, R. Gomperts, R. L. Martin, D. J. Fox, T. Keith, M. A. Al-Laham, C. Y. Peng, A. Nanayakkara, M. Challacombe, P. M. W. Gill, B. Johnson, W. Chen, M. W. Wong, J. L. Andres, C. Gonzalez, M. Head-Gordon, E. S. Replogle, J. A. Pople, Gaussian, Inc., Pittsburgh PA, **2002**.

[54] W. J. Hehre, L. Radom, P. v. R. Schleyer, J. A. Pople, *Ab initio Molecular Orbital Theory*, Wiley New York, **1986**.

[55] P. v. R. Schleyer, C. Maerker, A. Dansfeld, H. Jiao, N. J. R. v. E. Hommes, *J. Am. Chem. Soc.* **1996**, *118*, 6317−6318.

[56] [56a] J. R. Ditchfield, *Mol. Phys.* **1974**, *27*, 789−807. [56b] J. P. Cheeseman, G. W. Trucks, T. A. Keith, M. J. Frisch, *J. Chem. Phys.* **1996**, *104*, 5497−5509.

[57] *SYBYL 6.9:* Tripos Inc., St. Louis MO 63144, S. Hanley Road 303, **2002**.

[58] S. Klod, E. Kleinpeter, *J. Chem. Soc., Perkin Trans. 2* **2001**, 1893−1898.

Received June 2, 2004
Early View Article
Published Online October 7, 2004

 © 2004 Wiley-VCH Verlag GmbH & Co. KGaA, Weinheim

Synthesis, Crystal Structure and Biological Characterization of a Novel Palladium(II) Complex with a Coumarin-Derived Ligand

Elzbieta Budzisz,*[a] Bernhard K. Keppler,[b] Gerald Giester,[c] Magdalena Wozniczka,[d] Aleksander Kufelnicki,[d] and Barbara Nawrot[e]

Keywords: Circular dichroism / Cytotoxicity / DNA / Palladium / Protonation constants

Methyl 2-methyl-4-oxo-4*H*-chromene-3-carboxylate (**1**) was treated with 25% aqueous ammonia to give 3-(1-aminoethylidene)-2*H*-chromene-2,4(3*H*)-dione (**2**). Compound **2** was used as a ligand for the formation of a palladium(II) complex. The structures of the ligand and its palladium complex **3** were determined by IR and ^{1}H NMR spectroscopy, FAB mass spectrometry and elemental analysis. The single-crystal X-ray structure of **3** was also solved. Ligand **2** in 20% dioxane solution shows two protonation constants — $\log \beta_{11} = 4.28 \pm 0.01$ and $\log \beta_{12} = 7.66 \pm 0.03$. In complex **3** two ligand molecules chelate to the Pd ion through their N and O donors, giving a four-coordinate Pd^{II} center with a *cis*-N_2O_2 donor set. The coordination geometry at Pd^{II} is square-planar with typical values for the distances from the Pd atom to the coordinated atoms. The cytotoxicity of compound **3** was determined on three cancer cell lines. IC_{50} values of 9.7, 7.8 and 7.8 nM were found for A546, HeLa and K562 cells, respectively, which is notably lower than carboplatin, which shows corresponding IC_{50} values of 105.98, 73.49 and 60.92 μM. Double-stranded DNA treated with **3** shows a significant increase in the Δε value in the CD spectra, as well as a lower electrophoretic mobility than parent DNA.
(© Wiley-VCH Verlag GmbH & Co. KGaA, 69451 Weinheim, Germany, 2004)

Introduction

Since the discovery by Rosenberg[1] that cisplatin exhibits antitumour activity, extensive studies on platinum complexes with various ligands as potential antitumor agents have been performed. It has been shown that cisplatin [*cis*-diamminedichloroplatinum(II)] is active against several human malignant diseases, such as neck and head, ovarian, testicular, lung, and bladder cancers.[2] It is generally accepted that cisplatin exerts its therapeutic activity by binding directly to DNA, deactivating it as a template for the transcription process and inhibiting in that way the protein biosynthesis.[3] However, cisplatin has several disadvantages, among which are its severe nephrotoxicity, neurotoxicity and emetogenesis.[4] The toxic side-effects of cisplatin therefore limit the doses that can be applied to patients.[5] The clinical application of the second-generation drug diammine[1,1-cyclobutanedicarboxylato(2−)-*O*,*O*′]platinum(II) (carboplatin; Figure 1) resulted in significant decrease of the toxic side-effects. These differences were attributed to the greater pharmokinetic stability of carboplatin due to the presence of the bidentate bis(carboxylato) ligand.[6] Studies on the interaction of carboplatin with DNA indicate that the mechanism involves carboplatin ring-opening and subsequent platinum binding to DNA nucleobases.[7]

Taking into account the structural analogy between Pt^{II} and Pd^{II} complexes, a variety of studies on Pd^{II} complexes have been performed, including their cytotoxicity[8] and antitumor activity.[9−11] Pd complexes with β-carboline alkaloids,[12−14] pyrazoles[15] and DMSO[16] have been tested against solid-tumor cell lines, and in some cases exhibited remarkable activity. It has been suggested that their biological activity depends on the nature of the ligand, the type of the counterion used and the configuration of the complex.

Coumarin and its derivatives are biologically important compounds with spasmolytic, antiarrhythmic, cardiotonic,

[a] Faculty of Pharmacy, Medical University of Lodz,
Muszyńskiego 1, 90-151 Lodz, Poland
Fax: + 48-42-678-83-98
E-mail: elora@ich.pharm.am.lodz.pl
[b] Institute of Inorganic Chemistry of the University of Vienna,
Währingerstr. 42, 1090 Vienna, Austria
E-mail: keppler@ap.univie.ac.at
[c] Institute of Mineralogy and Crystallography of the University of Vienna,
Althanstr. 14, 1090 Vienna, Austria
E-mail: gerald.giester@univie.ac.at
[d] Laboratory of Physical and Biocoordination Chemistry, Faculty of Pharmacy, Medical University of Lodz,
Muszyńskiego 1, 90-151 Lodz, Poland
Fax: + 48-42-678-83-98
E-mail: akuf@ich.pharm.am.lodz.pl
[e] Department of Bioorganic Chemistry, Centre of Molecular and Macromolecular Studies, Polish Academy of Sciences,
Sienkiewicza 112, 90-363 Lodz, Poland
Fax: + 48-42-681-54-83
E-mail: bnawrot@bio.cbmm.lodz.pl

 © 2004 Wiley-VCH Verlag GmbH & Co. KGaA, Weinheim **DOI: 10.1002/ejic.200400483**

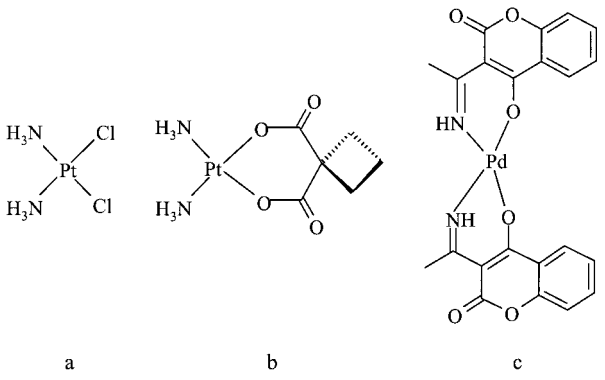

Figure 1. The structures of cisplatin (a), carboplatin (b) and complex **3** (Pd^{II} complex of ligand **2**) (c)

photodynamic[17] and antitumor properties.[18,19] Metal complexes of coumarin reveal anticoagulant action[20,21] and possess antitumor activity.[22,23] In particular, complexes of coumarin with cerium(III), zirconium(IV), copper(II), zinc(II), bismuth(III) and cadmium(II) have shown promising cytotoxic activity in vitro.[24,25]

Here, we describe the synthesis, structure and properties of a novel coumarin ligand **2** and its palladium(II) complex **3** (Figure 1). Spectral data and protonation constants are given for the ligand **2**. The structure of complex **3** is confirmed by spectral and X-ray analysis. Its biological properties are evaluated, including alkylating activity, cytotoxicity against selected cell lines as well as its interaction with double-stranded DNA monitored by circular dichroism (CD) spectroscopy and agarose-gel electrophoresis.

Results and Discussion

Synthesis and Structure of Ligand 2

The reaction of methyl 2-methyl-4-oxo-4*H*-chromene-3-carboxylate[26] (**1**) with an equimolar amount of 25% aqueous ammonia in methanol afforded product **2** in 94% yield (Scheme 1). This compound was previously synthesized by Somogyi and co-workers[27] in a multistep reaction with a total yield of 23% starting from 3-acetyl-4-hydroxycoumarin. Our approach is based upon a one-step, high-yield transformation of chromone **1** into 3-substituted coumarin **2** by the reaction of **1** with ammonia or an alkylamine.[28]

The structure of compound **2** was confirmed by spectroscopic methods (^1H and ^{13}C NMR, IR, EI-MS) as well as by elemental analysis. The first report of this compound by Somogyi et al. suggested that compound **2** exists in two tautomeric forms **2** and **2a** (Scheme 1), with proton magnetic resonances at δ = 10.01 (NH) and 12.04 (OH) ppm, respectively. These data were confirmed by our investigations, as two signals at δ = 9.99 and 12.32 ppm are observed in the ^1H NMR spectrum of **2** taken in DMSO. These signals disappear after proton exchange with D_2O, which directly confirms the presence of both tautomeric forms in DMSO solution. However, *N*-alkyl-substituted derivatives of **2** exist exclusively in the keto form in the solid state and in solution.[29–31] Thus, the presence of a β-amino group in the α,β-unsaturated carbonyl system ensures the accessibility of both terminal centers for metal-ion complexation.

Determination of the Protonation Constant of Ligand 2

Potentiometric experiments within the pH range 2.5–5.5 showed that the ligand behaves as a diprotonated molecule with one hydroxy (OH) and one imino (NH) proton. The measured protonation constants $\log \beta_{11} = 4.28 \pm 0.01$ and $\log \beta_{12} = 7.66 \pm 0.03$ are in reasonable agreement with those obtained from theoretical calculations[32] ($\log \beta_{11} = 4.50 \pm 0.20$ and $\log \beta_{12} = 7.71 \pm 0.20$, respectively). The statistical parameters $\sigma = 3.52$ and $\chi^2 = 15.64$ only slightly exceed the critical values of 3.00 and 12.60 at a confidence level of 0.95 as regarding the comprehensive file consisting of four titration data, but they are satisfactory in the particular titrations.

The two protonation constants indicate the presence of two potential donors, the 4-O and 3-N atoms. According to our results, the stepwise protonation constants are 4.28 and 3.38. An exemplary speciation diagram is shown in Figure 2.

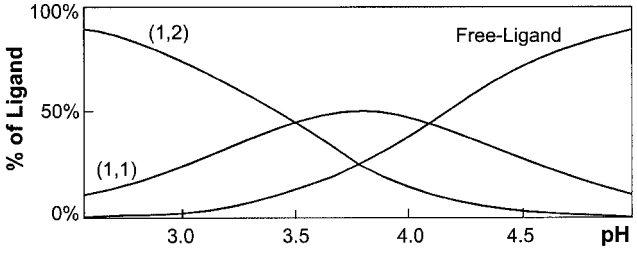

Figure 2. Species distribution of L = 4-hydroxy-3-(1-iminoethyl)-2*H*-chromen-2-one in 20% dioxane; (1,1) and (1,2) denote the mono- and diprotonated forms of L^{2-} (free ligand); $C_L = 6.21 \times 10^{-3}$ mol·dm^{-3}; $\sigma = 1.75$; $\chi^2 = 9.58$

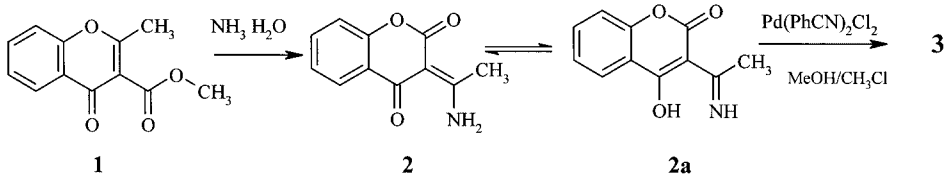

Scheme 1. Synthesis of the ligand **2** and its Pd complex **3**

 © 2004 Wiley-VCH Verlag GmbH & Co. KGaA, Weinheim

Synthesis and Structure of Complex 3

The palladium(II) complex of ligand **2** was synthesized by mixing **2** and bis(benzonitrile)dichloropalladium(II) in a 1:2 molar ratio in chloroform/methanol (1:2.5) solution at room temperature for 24 h (Scheme 1). The resulting solid shows an FAB-MS signal at $m/z = 510$, characteristic for PdL_2. This complex composition was confirmed by elemental analysis. In the ^1H NMR spectrum of the complex, one of the exchangeable protons, attributed to the enol OH group (at $\delta = 12.32$ ppm) of **2a**, is not present. The IR spectrum excludes the presence of chloride groups (no signals at 350 cm^{-1}). Instead, two bands were found at 508 and 437 cm^{-1}, which could be assigned to the M−O and M−N vibrations.[33] Moreover, the band assigned to the NH vibrations in **2** (3260 cm^{-1}) is shifted to higher energy (3310 cm^{-1}), indicating that the nitrogen atom is involved in the coordination (Table 1). At this stage we could not assign the complex geometry. It is known that palladium(II) complexes adopt predominantly *trans* conformations,[34] and only a few examples of *cis* conformers are known.[35]

Table 1. IR frequencies ($\tilde{\nu}$ [cm^{-1}]) for the ligand and its palladium complex

	NH/OH	C=O	C=N	M−N	M−O
2	3261	1708 1665	1609	–	–
3	3310 3265	1702 1670	1606	437	508

Our attempts to obtain a platinum(II) complex of ligand **2** failed, despite trying various solvent systems (aqueous methanol, aqueous acetone, aqueous dioxane, chloroform/methanol), various Pt^{II} substrates {K_2PtCl_4 or *cis*-$[PtCl_2(PhCN)_2]$} and various temperature conditions (room temperature, 60 °C). A black powder, identified as platinum, was the only solid product of this reaction. In contrast, a phosphorus analogue of coumarin (2-ethanimidoyl-2-methoxy-2*H*-1,2-benzoxaphosphinin-4-ol 2-oxide) forms complexes with Pt^{II} and Pd^{II} with a structure analogous to **3**.[36] We cannot offer any explanation why the Pt^{II} complex of ligand **2** is not formed or is too unstable to be isolated.

X-ray Structure of 3

The X-ray diffraction study of **3** (Figure 3) shows that in the PdL_2 molecule two L^- ligands chelate to the Pd ion through their N and O donors, giving a four-coordinate Pd^{II} center with a *cis*-N_2O_2 donor set. The coordination geometry at Pd^{II} is square-planar, with standard values for the distances from the metal atom to the coordinated atoms [Pd−N1: 1.965(6); Pd−N2: 1.951(6); Pd−O1: 1.972(5); Pd−O4: 1.990(5) Å]. The Pd^{II} ion lies in the least-squares plane of the coordinated atoms, deviating by ±0.023 Å. While the C2−N1 and C13−N2 bonds in the six-membered chelate rings possess the character of a localized double bond that deviates only marginally from the ideal value of 1.28 Å,[37] a substantial lengthening of the C11−O1 and C22−O4 bonds is observed when compared to the localized double bonds C4−O2 and C15−O5 (Table 2). The distribution of the bond lengths over the fragments C2−C3−C11 and C13−C14−C22 indicates significant delocalization of the electron density (Table 2).

Table 2. Bond lengths [Å] and angles [°] for compound **3**

Pd(1)−N(2)	1.951(6)	C(11)−O(1)−Pd(1)	128.1(4)
Pd(1)−N(1)	1.965(6)	C(5)−O(3)−C(4)	123.1(6)
Pd(1)−O(1)	1.972(5)	C(22)−O(4)−Pd(1)	127.1(4)
Pd(1)−O(4)	1.990(5)	C(16)−O(6)−C(15)	122.8(6)
N(2)−Pd(1)−N(1)	92.8(3)	C(2)−N(1)−Pd(1)	131.5(5)
N(2)−Pd(1)−O(1)	177.0(2)	C(2)−N(1)−H(1)	114.2
N(1)−Pd(1)−O(1)	89.6(2)	Pd(1)−N(1)−H(1)	114.2
N(2)−Pd(1)−O(4)	89.6(2)	C(13)−N(2)−Pd(1)	131.5(5)
N(1)−Pd(1)−O(4)	177.5(2)	C(13)−N(2)−H(2)	114.3
O(1)−Pd(1)−O(4)	88.1(2)	Pd(1)−N(2)−H(2)	114.3

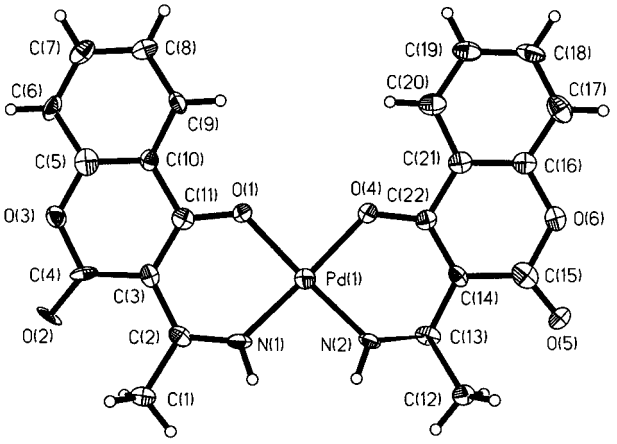

Figure 3. ORTEP drawing of the molecule of **3** with thermal ellipsoids depicted at 50% probability

The molecular structure of **3** shows stacked pairs with an interplanar "face-to-back" separation of 3.28 Å; the Pd1···Pd1′ distance is 3.775 Å. The shortest contact observed is Pd1···O4′ at 3.566 Å and the angle O4′···Pd1′···Pd1 is 80.1°. These pairs, which are slightly slipped with respect to each other, form columns with separations between pairs of 3.37 Å and a Pd1···Pd1′′ separation of 6.736 Å.

Biological Characterization of 3

Alkylating Properties

Cisplatin and carboplatin are nonclassical alkylating agents. These drugs interact with cellular DNA according to the same mechanism[38,39] — alkylation of nucleobases of both DNA strands. An effective drug concentration for carboplatin is 4−7 times higher than for cisplatin, and the former is also less toxic.[40] The alkylating activity of complex **3** was determined according to the Preussmann test.[41] The level of alkylation of 4-(4′-nitrobenzyl)pyridine (NBP) was quantified spectrophotometrically at 560 nm. The molar

 © 2004 Wiley-VCH Verlag GmbH & Co. KGaA, Weinheim

absorbance (A) for complex **3** is 0.3584, while for ligand **2** it is significantly lower (Table 3). Interestingly, cisplatin in this test has an A value of 0.300[42] and carboplatin alkylates NBP with an A value of 0.2312. According to the Preussmann scale (described in a footnote to Table 3), complex **3** and both cisplatin and carboplatin exhibit moderate alkylating activity in this test.

Table 3. Alkylating activity of compound **2** and its Pd complex **3** determined by the Preussmann test

Compound	Absorbance (A)[a] λ_{max} 560 nm	Alkylation activity[b]
2	0.0508	+
3	0.3584	++
Cisplatin[c]	0.3000	++
Carboplatin	0.2312	++

[a] Means of three determinations. [b] According to Preussmann: (+) A = 0.05−0.1, (++) A = 0.1−0.5. [c] According to Zyner.[42]

Cytotoxicity

The cytotoxicity of **2** and **3** was determined in a concentration range from 10^{-10} to 10^{-3} M using three human cell lines — A549, HeLa and K562 — with carboplatin as reference. The activity is expressed as the concentration required for reducing the cell survival fraction to 50% after 72 h exposure of the cells to the compounds (IC_{50}; Table 4). The responses of A549, HeLa and K562 cells to continuous exposure to **2** and **3** at various concentrations for 24, 48 and 72 h are presented in Figure 4. From these figures, a time-dependent response can be observed for complex **3** in all three cell lines. Interestingly, compound **3** exhibits very high cytotoxicity against A549, HeLa and K562 cells, with IC_{50} values of 0.0097, 0.0078 and 0.0078 μM, respectively, which are superior to those of the reference carboplatin (105.98, 73.49 and 60.92 μM). The ligand was not toxic for the test cell lines even after 72 h exposure.

Table 4. IC_{50} values of compounds **2**, **3** and carboplatin after 72 h

Compound	A549 IC_{50} [μM][a]	HeLa IC_{50} [μM][a]	K562 IC_{50} [μM][a]
2	> 1000[b]	> 1000[b]	> 1000[b]
3	0.0097 ± 0.0017	0.0078 ± 0.0003	0.0078 ± 0.0007
Carboplatin	105.98 ± 6.79	73.49 ± 6.03	60.92 ± 13.64

[a] Mean values of IC_{50} (in μM) ± standard deviation from four experiments are presented. [b] At this concentration of compound **2** reduction in cell growth was less than 50%.

Interaction of 3 with Double-Stranded DNA

CD Analysis

The influence of complex **3** on the geometry of double-stranded DNA was investigated by CD spectroscopy. The CD spectra of the control samples (DNA in PBS buffer and DNA in PBS buffer/10% DMSO) were compared with the spectra of DNA incubated at room temperature for 18 h with increasing amounts of complex **3** (Figure 5). For DNA in PBS buffer the maximum intensity of the positive band at 281 nm was found at $\Delta\varepsilon$ = 6.2; for DNA in PBS/10% DMSO solution this value was 7.0. The spectra of the control samples do not differ significantly, indicating that at this concentration (10%) DMSO has no influence on the DNA structure. However, changes are observed in the spectra of DNA incubated with complex **3**. While the λ_{max} value of the positive band is not shifted, the $\Delta\varepsilon$ value is lowered

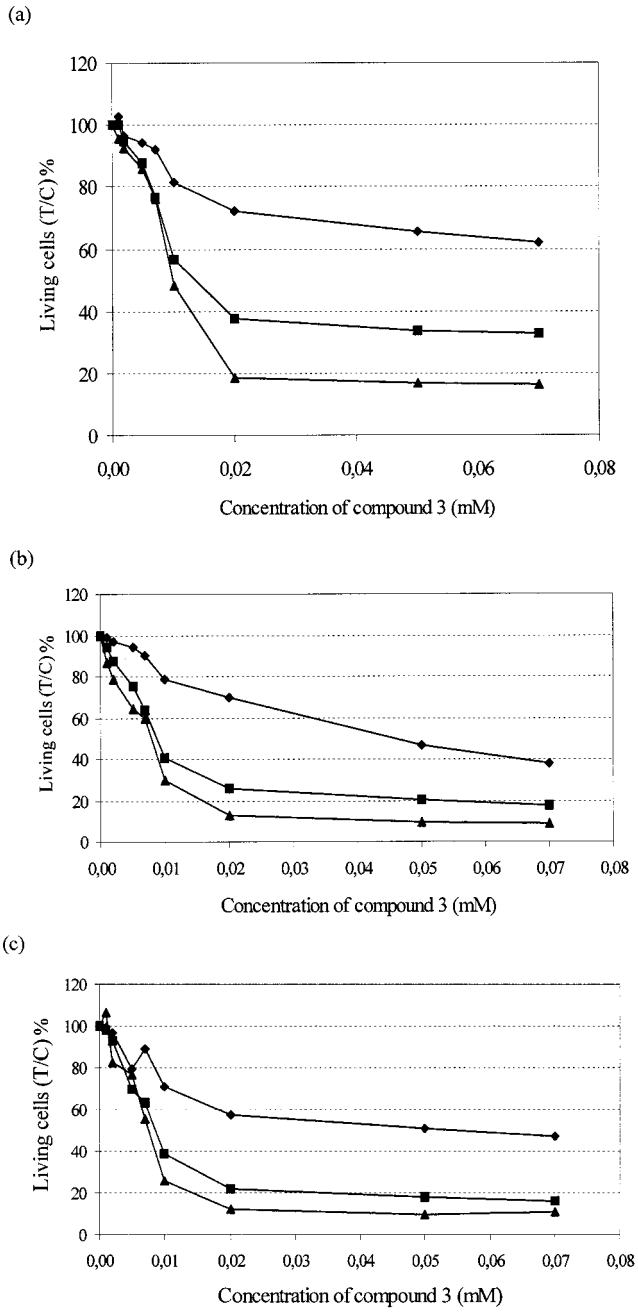

Figure 4. Cytotoxic effect of complex **3** on (a) A549, (b) HeLa, and (c) K562 cell lines after 24 (diamonds), 48 (squares) and 72 h (triangles) measured by MTT assay

 © 2004 Wiley-VCH Verlag GmbH & Co. KGaA, Weinheim

by 0.8 units for DNA interacting with complex **3** at r_i = 1.3. At r_i = 2.6 and r_i = 3.9 (r_i is the molar ratio of **3** to nucleotides) the $\Delta\varepsilon$ values increase to 19 and 34 units, respectively, with only a 2 nm shift of the λ_{max} value to long wavelength, which suggests that structural changes are produced on DNA by complex **3**. These changes may originate from several sources, such as intercalation of the palladium compound into double-stranded DNA[43] or interhelical alkylation of nucleobases.[44] Such a significant increase of band intensity accompanied by the shift of the long-wavelength crossover by about 3 nm is characteristic for denatured DNA structures.[45] It is also known that dehydration of DNA, which induces $B \rightarrow A$ conformational changes, results in an increase of the band intensity in the region between 250 and 300 nm.[45] However, dehydration of DNA is not likely here since the concentration of complex **3** (r_i = 3.9) and DMSO (10%) is much lower than the conditions required to induce such conformational changes (> 60% ethanol).

DMSO (%)	–	–	10	20	30	10	20	30
Preincubation	–	+	+	+	+	+	+	+
Complex **3** [μg]	–	–	–	–	–	0.1	0.2	0.3
r_i						0.2	0.4	0.6
Lane M	1	2	3	4	5	6	7	8

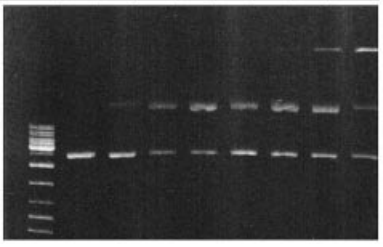

Figure 5. Interaction of **3** with double-stranded DNA monitored by 3% agarose gel electrophoresis; plasmid DNA (pUC, 2749 bp) was incubated with increasing amounts of complex **3**/DMSO in 3 × diluted PBS buffer containing 10 mM $MgCl_2$; M: mass marker; lanes 1 and 2: DNA in PBS buffer without and with 18 h, incubation; lanes 3–5: DNA in PBS buffer with increasing amounts of DMSO (as described above); lanes 6–8: DNA in PBS with increasing amounts of complex **3** and DMSO (data given above figure)

Agarose-Gel Electrophoresis

Plasmid DNA samples dissolved in triply diluted PBS/10 mM $MgCl_2$ buffer were incubated for 18 h at room temperature with increasing amounts of complex **3** (DMSO solution). As controls, plasmid DNA in PBS buffer and in PBS/DMSO buffer (containing 10, 20 or 30% of DMSO) were used. Samples were analyzed by agarose-gel electrophoresis (Figure 6). At first we checked the impact of incubation on DNA structure. After 18 h of incubation, we observed more of the superhelical form (90%) and only a very small amount of the circular form of DNA (10%) (lane 2 versus lane 1). In the plasmid samples incubated with increasing amounts of DMSO, the ratio of both forms of DNA was almost identical (lanes 3–5). However, when DNA was treated with increasing amounts of complex **3**, we observed a new band of very low electrophoretic mobility, tentatively attributed to a high-molecular-weight DNA/**3** adduct which contains 13.2% and 48.6% of the total DNA (lanes 7 and 8, respectively). The observed lowered mobility might result from intercalation of the planar compound **3** into the double-stranded plasmid DNA.

Conclusions

Coumarin-derived palladium(II) complex **3** is an interesting analogue of carboplatin. Its very high cytotoxicity toward three cancer-cell lines, with IC_{50} values in the nanomolar range (four orders of magnitude lower than that for the reference carboplatin), speaks for the need for further biological evaluations. At the present stage we can conclude that **3**, similarly to cisplatin and carboplatin, shows moderate alkylating activity toward aromatic amine (NBP), a compound that mimics the nucleobases in DNA. Complex

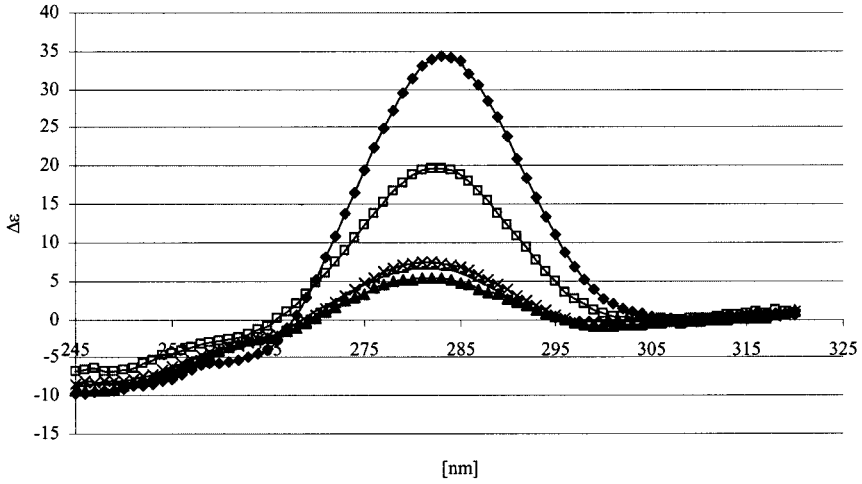

Figure 6. CD spectra of control double-stranded DNA (20 bp duplex of sequence given in Exp. Sect.) in PBS buffer (-) and in PBS/10% DMSO buffer (×), and adducts of DNA with increasing amount of complex **3** r_i = 1.3 (triangles), r_i = 2.6 (empty squares) and r_i = 3.9 (diamonds)

 © 2004 Wiley-VCH Verlag GmbH & Co. KGaA, Weinheim

3 probably also binds to double-stranded DNA, enforcing in that way structural changes of short duplex DNA and reducing the electrophoteric mobility of plasmid DNA.

Experimental Section

General: The melting points were determined using an Electrothermal 1A9100 apparatus and are uncorrected. The IR spectra were recorded with a Pye-Unicam 200G Spectrophotometer in KBr and CsI. The ^{1}H NMR spectra were registered at 300 MHz with a Varian Mercury spectrometer. The MS data were obtained with a LKB 2091 mass spectrometer (70 eV ionisation energy). The MS-FAB data were determined with a Finnigan Matt 95 mass spectrometer (NBA, Cs^+ gun operating at 13 keV). For the new compounds satisfactory elemental analyses (±0.3% of the calculated values) were obtained using a Perkin−Elmer PE 2400 CHNS analyser. Methyl 2-methyl-4-oxo-4*H*-chromene-3-carboxylate (**1**) was prepared according to a published method.[26]

Synthesis of 3-(1-Aminoethylidene)-2*H*-chromene-2,4(3*H*)-dione (2): A 25% aqueous ammonia solution (0.31 mL, 2 mmol) in methanol (0.5 mL) was added at room temperature to a solution of methyl 2-methyl-4-oxo-4*H*-chromene-3-carboxylate (**1**; 0.44 g, 2 mmol) in methanol (5 mL). After several minutes, the solid crude product precipitated. The product was filtered off, dried, and crystallized from acetone (5 mL). Pure compound **2** was obtained as a white solid (382 mg, 94.0%); m.p. 234.5−234.9 °C. ^{1}H NMR ([D$_6$]DMSO): δ = 2.58 (s, 3 H, CH$_3$), 7.23−7.94 (m, 4 H, aromat. H), 9.99 (s, 1 H, NH), 12.32 (s, 1 H, OH) ppm. ^{13}C NMR ([D$_6$]DMSO): δ = 24.57 (C−CH$_3$), 95.57, 116.15, 120.24, 123.43, 125.59, 133.83, 152.95, 161.79, 177.06, 179.36 (C=O) ppm. MS: *m*/*z* (%) = 204 (100) [M$^+$], 124 (1.75). $C_{11}H_9NO_3$ (203.19): calcd. C 65.02, H 4.46, N 6.89; found C 65.05, H 4.45, N 7.07.

Palladium Complex 3: A methanolic solution of **2** (0.5 mmol, 101.6 mg in 5 mL) was added to a chloroform/methanol (1:1, v/v; 5 mL) solution of [PdCl$_2$(C$_6$H$_5$CN)$_2$] (95.9 mg, 0.25 mmol). The mixture was stirred at room temperature. After 2 h, the resulting light yellow crystals were filtered off, washed with diethyl ether, and dried in vacuo over anhydrous silica gel overnight. Yield 126.3 mg (43.3%); m.p. 330 °C (dec.). ^{1}H NMR ([D$_6$]DMSO): δ = 2.64 (s, 6 H, CH$_3$), 7.29−8.16 (m, 8 H, aromat. H), 9.43 (s, 2 H, NH) ppm. MS-FAB: *m*/*z* = 511.2. $C_{22}H_{16}N_2O_6Pd$ (510.72): calcd. C 51.73, H 3.16, N 5.48; found C 51.69, H 3.16, N 5.29.

Potentiometric Studies of the Ligand: The protonation constants of the ligand were determined by pH-metric titration of 4-mL samples at a temperature of 25 ± 0.1 °C. The total concentration of the ligand in each sample ranged from 6.0×10^{-3} to 2.0×10^{-2} M. Owing to the very low solubility in pure water a mixed 20% (v/v) 1,4-dioxane/water solvent was used. The titrations were carried out with a carbonate-free NaOH solution of known concentration (0.5 mol/L). The value of pK_w = 13.77 was obtained from our acid/base calibrations in the same solvent. The pH was measured with a Molspin Ltd. (Newcastle upon Tyne, England) automatic titration set and combined OSH 10-10 electrode (Metron, Poland). The total volume of the Hamilton microsyringe in the autoburette was 250 μL; the volume increments amounted to 0.0025 mL. The experiments were performed using MOLSPIN.EXE software. The electrode was calibrated in the −log [H$^+$] scale by titration of 0.005 M HNO$_3$ (in 20% dioxane) with 0.5 M NaOH at 25 °C. Then overall protonation constants $\beta_{lh} = [L_lH_h]/[L]^l[H]^h$ were calculated with the SUPERQUAD computer program.[46]

X-ray Crystallographic Structure Determination:[47] X-ray diffraction measurements were performed with a Nonius Kappa CCD diffractometer at 120 K. A colorless single crystal was positioned at 30 mm from the detector and 137 frames were measured, each for 200 s over a 2° scan. The data were processed using Denzo-SMN software.[48] Crystal data, data collection parameters, and structure refinement details for **3** are given in Table 5. The structure was solved by direct methods and refined by full-matrix least-squares techniques. Non-hydrogen atoms were refined with anisotropic displacement parameters. The H atoms were placed in calculated positions and allowed to ride. Computer programs: structure solution SHELXS-97;[49] refinement SHELXL-97;[50] molecular diagrams ORTEP;[51] computer: Pentium II; scattering factors were taken from the literature.[52]

Table 5. Crystal data and details of data collection for **3**

	3
Empirical formula	$C_{22}H_{16}N_2O_6Pd$
Formula mass	510.77
Space group	$P2_1/n$
a [Å]	9.384(2)
b [Å]	11.241(2)
c [Å]	18.306(4)
β [°]	103.38(3)
V [Å^3]	1878.6(7)
Z	4
λ [Å]	0.71073
$\rho_{calcd.}$ [g cm^{-3}]	1.806
Crystal size [mm]	0.025 × 0.025 × 0.3
T [K]	120
μ [cm^{-1}]	10.34
*R*1[a]	0.0376
*wR*2[b]	0.0942
GOF[c]	1.002

[a] $R1 = \Sigma||F_o| - |F_c||/\Sigma|F_o|$. [b] $wR2 = \{\Sigma[w(F_o^2 - F_c^2)^2]/\Sigma[w(F_o^2)^2]\}^{1/2}$. [c] GOF = $\{\Sigma[w(F_o^2 - F_c^2)^2]/(n - p)\}^{1/2}$, where *n* is the number of reflections and *p* is the total number of parameters refined.

Cell Lines and Culture Conditions: Three human cell lines were used for cytotoxicity experiments: A549 (lung carcinoma, human), HeLa (cervix epithelial carcinoma, human), K562 (chronic myelogenous leukemia, human). Cells were cultured in RPMI 1640 medium supplemented with 10% heat-inactivated fetal calf serum, streptomycin (100 μg/mL) and penicillin (100 U/mL) at 37 °C in 5% CO_2/95% air.

Drug Cytotoxicity: Exponentially growing cells were seeded at $5-7 \times 10^3$ in 200 μL of the complete culture medium per well of a 96-well plate (Nunc). After 24 h, the cells were exposed to compounds **2**, **3** and carboplatin (used as a reference) at 37 °C in 5% CO_2/95% air for 24 h, 48 h and 72 h. Cytotoxicity was estimated for a concentration range from 10^{-10} to 10^{-3} M. The cell number relative to the control was then determined by the colorimetric MTT [3-(4,5-dimethylthiazol-2-yl)-2,5-diphenyltetrazolium bromide, Sigma][53] method. The values of IC_{50} (concentration of compounds required to reduce the cell survival fraction to 50% of the control) were calculated from dose-response curves and used as a measure of cellular sensitivity to a given treatment. Each experiment was performed in quadruplicate and evaluation was based on means.

Determination of Alkylating Properties: The test compound (0.005 mmol) was dissolved in 2-methoxyethanol (1 mL) and a solution of 4-(4′-nitrobenzyl)pyridine (NBP) in 2-methoxyethanol

 © 2004 Wiley-VCH Verlag GmbH & Co. KGaA, Weinheim

(5% solution, 1 mL) was added. The sample was heated at 100 ± 0.5 °C for 1 h and then quickly cooled to 20 °C. 2-Methoxyethanol (2.5 mL) and piperidine (0.5 mL) were added to the sample to give a total volume of 5 mL. The final concentration of the test compound was 1×10^{-3} M. After 90 s, the absorbance was measured at λ_{560} nm in a glass cell (1 cm). 2-Methoxyethanol was used as a reference solvent.

CD Spectra of Complex 3 with Double-Stranded DNA: CD measurements of complex **3** with double-stranded DNA were performed with a Jobin Yvon CD6 (France) dichrograph. The double-stranded DNA was obtained by annealing of 5′-TCTTCAAGAATTCAGGACTA-3′ and 5′-TAGTCCTGAATTCTTGAAGA-3′. Samples of double-stranded DNA (4.6×10^{-6} M, 200 μL) were dissolved in PBS buffer (700 μL, 155 mM NaCl, 4.2 mM KH_2PO_4/Na_2HPO_4, pH = 7.2), to which the complex **3** in a solution of DMSO (1.9×10^{-3} M, 25, 50 or 75 μL) was added. DMSO was added to each sample up to 10% of total volume (including solvent of the complex **3**). The molar ratio of compound **3** to nucleotides is expressed as r_i. Each sample of a total volume of 1 mL was incubated at room temperature for 18 h and then scanned twice between 245 and 320 nm at 25 °C. The data are expressed as the mean of Δε (in $°\cdot cm^{-1}\cdot M^{-1}$).

Electrophoretic Mobility of Plasmid DNA in the Presence of Complex 3: Plasmid DNA (pUC19, 2749 bp) (0.2 μg) was incubated at 37 °C for 18 h in a mixture of triply diluted PBS/10 mM $MgCl_2$ buffer and DMSO (10%, 20% or 30%, v/v) that either contained complex **3** (0.1, 0.2 or 0.3 μg) or no complex **3** at all. Electrophoretic analysis was done on 3% agarose gel containing ethidium bromide. Quantification of the bands in the gel was done by densitometry and Image Quant analysis.

Acknowledgments

Financial support from Medical University of Lodz (grant no. 502-13-287 to E. B. and project no. 503-314-2 to the Laboratory of Physical and Biocoordination Chemistry) is gratefully acknowledged. We thank Mrs. Maria Maszewska for help in the determination of the cytotoxicity of the investigated compounds. We also thank Mrs. Agnieszka Zdolska for skilful experimental assistance.

[1] B. Rosenberg, L. Van Camp, J. E. Trosko, H. V. Mansour, *Nature* **1969**, *222*, 385−386.
[2] P. J. Loeherer, L. H. Einhorn, *Ann. Inter. Med.* **1984**, *100*, 704−713.
[3] L. A. Zwelling, *Cancer Chemother.* **1986**, *8*, 97−116.
[4] M. A. Jakupec; M. Galanski, B. K. Keppler, *Rev. Physiol. Biochem. Pharmacol.* **2003**, *146*, 1−53.
[5] J. Reedijk, *Chem. Commun.* **1996**, *7*, 801−806.
[6] M. E. Heim, in *Metal Complexes in Cancer Chemotherapy* (Ed.: B. K. Keppler), VCH, Weinheim, **1993**, p. 9.
[7] M. R. Shehata, *Trans. Met. Chem.* **2001**, *26*, 198−204.
[8] M. Curic, Lj. Tusek-Bozic, D. Vikic-Topic, S. V. A. Furlani, J. Balzarini, E. De Clercq, *J. Inorg. Biochem.* **1996**, *63*, 129−142.
[9] S. Kirschner, Y. K. Wei, D. Francis, J. S. Bergman, *Med. Chem.* **1966**, *9*, 369−372.
[10] A. A. Grinberg, J. S. Warschavski, M. J. Gelfman, N. W. Kisseleva, D. B. Smolenskaya, *Z. Neorg. Khim.* **1968**, *13*, 803−813.
[11] J. D. Higgins, L. Neely, S. Fricker, *J. Inorg. Biochem.* **1993**, *49*, 149−156.
[12] T. A. Al-Allaf, L. J. Rashan, *Boll. Chim. Farmac.* **2001**, *140*, 205−210.
[13] T. A. Al-Allaf, M. T. Ayoub, L. J. Rashan, *J. Inorg. Biochem.* **1990**, *38*, 47−56.
[14] T. A. Al-Allaf, L. J. Rashan, *Eur. J. Med. Chem.* **1998**, *33*, 817−820.
[15] T. A. Al-Allaf, L. J. Rashan, R. F. Khuzaie, W. F. Halseh, *Asian J. Chem.* **1997**, *9*, 239−246.
[16] T. A. Al-Allaf, L. J. Rashan, A. S. Abu-Surrah, R. Fawzi, M. Steimann, *Trans. Met. Chem.* **1998**, *23*, 403−406.
[17] I. Malonov, I. Kostova, T. Netzeva, S. Konastantinov, M. Karaivanova, *Archiv. Pharm. Pharm. Med. Chem.* **2000**, *333*, 93−98.
[18] T. Patonay, G. Litkei, R. Bognar, J. Erdei, G. Miszti, *Pharmazie* **1984**, *39*, 84−91.
[19] U. S. Weber, B. Steffen, C. Sigers, *Res. Commun. Mol. Pathol. Pharmacol.* **1998**, *99*, 193−206.
[20] D. Jiang, R. Deng, J. Wu, *Wuji Huaxue* **1989**, *5*, 21−28.
[21] R. Deng, J. Wu, L. Long, *Bull. Soc. Chim. Belg.* **1992**, *101*, 439−443.
[22] I. Kostova, I. Manolov, S. Konstantinov, M. Karaivanova, *Eur. J. Med. Chem.* **1999**, *34*, 63−68.
[23] I. Manolov, I. Kostova, T. Netzeva, S. Konstantinov, M. Karaivanova, *Arch. Pharm. Pharm. Med. Chem.* **2000**, *333*, 93−98.
[24] I. Kostova, I. Malonov, M. Karaivanova, *Archiv. Pharm. Pharm. Med. Chem.* **2001**, *334*, 157−162.
[25] V. D. Karaivanova, I. Malonov, M. L. Minassyan, N. D. Danchev, S. M. Samurova, *Pharmazie* **1994**, *49*, 856−857.
[26] G. M. Coppola, R. W. Dodsworth, *Synthesis* **1981**, *7*, 523−524.
[27] L. Somogyi, P. Sohar, *Liebigs Ann.* **1995**, 1903−1906.
[28] E. Budzisz; E. Brzezinska, U. Krajewska, M. Rozalski, *Eur. J. Med. Chem.* **2003**, *38*, 597−603.
[29] M. Malecka, E. Budzisz, *Acta Crystallogr., Sect. C* **2001**, *57*, 929−931.
[30] E. Budzisz, E. Nawrot, M. Malecka, *Arch. Pharm. Pharm. Med. Chem.* **2001**, *334*, 381−387.
[31] S. Grabowski, M. Malecka, E. Budzisz, *Chem. Phys.* **2004**, *297*, 235−244.
[32] Advanced Chemistry Development (ACD) Software Solaris V4.67, **1994−2003**.
[33] C. G. Van Kralingen, J. K. De Ridder, J. Reedijk, *Inorg. Chim. Acta* **1979**, *36*, 69−77.
[34] J. H. K. A. Acquaye, M. F. Richardson, *Inorg. Chim. Acta* **1992**, *201*, 101−107.
[35] L. D. Petit, M. Bezer, *Coord. Chem. Rev.* **1985**, *61*, 97−114.
[36] E. Budzisz, U. Krajewska, M. Rozalski, *Pol. J. Pharmacol.,* in press.
[37] I. N. Levine, *J. Chem. Phys.* **1963**, *38*, 2326−2328.
[38] A. Lacko, P. Hudziec, G. Mazur, *Nowotwory* **2000**, *50*, 609−614.
[39] S. Rajski, R. M. Williams, *Chem. Rev.* **1998**, *98*, 2723−2795.
[40] R. J. Knox, F. Friedlos, F. D. A. Lydall, *Cancer Res.* **1986**, *46*, 1972−1979.
[41] R. Preussmann, H. Schneider, F. Epple, *Arzneim. Forsch.* **1969**, *19*, 1059−1073.
[42] E. Zyner, J. Graczyk, J. Ochocki, *Pharmazie* **1999**, *54*, 945−946.
[43] S. Lee, S. H. Jeon, B. J. Kim, S. W. Han, H. G. Jang, S. K. Kim, *Biophys. Chem.* **2001**, *92*, 35−45.
[44] A. G. Quiroga, J. M. Perez, I. Lopez-Solera, J. R. Masaguer, A. Lique, P. Roman, A. Edwrds, C. Alonso, C. Navarro-Ranninger, *J. Med. Chem.* **1998**, *41*, 1399−1408.
[45] D. M. Gray, R. L. Ratliff, M. R. Vaughan, *Methods in Enzymo*logy, Academic Press, Inc., **1992**, vol. 211, p. 389−405.
[46] A. Sabatini, A. Vacca, P. Gans, *Coord. Chem. Rev.* **1992**, *120*, 389−405.
[47] CCDC-229585 contains the supplementary crystallographic data for this paper. These data can be obtained free of charge at www.ccdc.cam.ac.uk/conts/retrieving.html [or from the Cambridge Crystallographic Data Centre, 12 Union Road, Cambridge CB2 1EZ, UK; Fax: + 44-1223-336-033; E-mail: deposit@ccdc.cam.ac.uk].
[48] *Denzo-SMN*, Nonius B.V., **2003**.

 © 2004 Wiley-VCH Verlag GmbH & Co. KGaA, Weinheim

[49] G. M. Sheldrick, *SHELXS-97, Program for Crystal Structure Solution*, University Göttingen, Germany, **1997**.
[50] G. M. Sheldrick, *SHELXL-97, Program for Crystal Structure Refinement*, University Göttingen, Germany, **1997**.
[51] C. K. Johnson, *Rep. ORNL-5138*, OAK Ridge National Laboratory, OAK Ridge, TN, **1976**.
[52] *International Tables for X-ray Crystallography*, Kluwer Academic Press, Dordrecht, The Netherlands, **1992**, vol. C, Tables 4.2.6.8 and 6.1.1.4.
[53] M. B. Hansen, S. E. Nilsen, K. J. Berg, *J. Immunol. Methods* **1989**, *119*, 203−210.

Received June 7, 2004
Early View Article
Published Online September 9, 2004

 © 2004 Wiley-VCH Verlag GmbH & Co. KGaA, Weinheim

Small Metal-Containing Oligomers Using $M_2(dmpm)_x$ and $M_2(dmb)_y$ Luminescent Building Blocks (M = Cu, Ag; x = 2, 3; y = 1, 2)

Éric Fournier,[a] Andreas Decken,[b] and Pierre D. Harvey*[a]

Keywords: Coordination polymers / Oligomers / Silver / Copper / Luminescence

The luminescent binuclear complexes $M_2(dmpm)_3^{2+}$ [M = Cu, Ag; dmpm = bis(dimethylphosphanyl)methane], $Ag_2(dmpm)_2^{2+}$ and $Cu_2(dmpm)_3(CN\text{-}tBu)_2^{2+}$ (as BF_4^- salts), as well as the oligomers described as $\{Cu_2(dmpm)_3(dmb)_{1.33}^{2+}\}_3$ and $\{Ag_2(dmpm)_2(dmb)_{1.33}^{2+}\}_3$ (dmb = 1,8-diisocyano-*p*-menthane), have been prepared and fully characterized in the solid state. These compounds exhibit emission maxima ranging from 445 to 485 nm with emission lifetimes in the μs time scale. The X-ray structures for the $M_2(dmpm)_3^{2+}$ (M = Cu, Ag) and $Cu_2(dmpm)_3(CN\text{-}tBu)_2^{2+}$ complexes, XRD patterns (X-ray powder diffraction), DSC (differential scanning calorimetry), TGA (thermal gravimetric analysis), and the solid-state IR spectra have been examined in order to characterize these complexes and oligomers.
(© Wiley-VCH Verlag GmbH & Co. KGaA, 69451 Weinheim, Germany, 2004)

Introduction

The synthesis and characterization of transition-metal-containing coordination and organometallic oligomers and polymers built with phosphane and isocyanide assembling ligands is becoming a topic of increasing interest in the quest for new materials and applications.[1−14] In this respect, our group has recently reported the syntheses and characterizations of 1-D polymers of the type $\{M(dmb)_2^+\}_n$ [15,16] and the mixed-ligand polymers $\{M_2(dppm)_2(dmb)_2^{2+}\}_n$ [17] (M = Cu, Ag; dmb = 1,8-diisocyano-*p*-menthane in its *U*- or *Z*-conformation; dppm = bis(diphenylphosphanyl)-methane; Scheme 1). The chromophores are the $M(C{\equiv}NR)_4^+$ centers (M = Cu, Ag), which are separated by 5 Å (Ag···Ag distance) in $\{Ag(dmb)_2^+\}_n$,[15] and the $M(C{\equiv}NR)_2(P)_2^+$ units, which are separated by 4.03 and 9.61 Å in $\{Ag_2(dppm)_2(dmb)_2^{2+}\}_n$.[17]

The average polymer length for the $\{Ag(dmb)_2^+\}_n$ materials in solution was determined to be approximately 8 units by T_1/NOE measurements,[18] whereas the amorphous Cu analogue had an average polymer length of 300 units, as determined by light scattering.[15] This difference is explained by the greater lability of the dmb ligand in the Ag^I complexes, which was convincingly verified by the interconversion observed between the *U*- and *Z*-isomers of the $\{Ag(dmb)_2^+\}_n$ polymers, but not for the Cu analogues.[19] Ligand dissociation has also been established in previous works on the $\{Pd_4(dmb)_4(dmb)^{2+}\}_n$ [6] and $\{Pt_4(dmb)_4(diphos)^{2+}\}_n$ [7] polymers [diphos = $Ph_2P(CH_2)_mPPh_2$; m = 4−6; 84000 < MW_n < 307000; Scheme 2]. There are also some differences in the photophysical data, in particular the emission lifetimes, between the polymers and the corresponding building blocks [here $M_4(dmb)_4^{2+}$ (M = Pd, Pt)].

More recently, a new series of amorphous polymeric materials of the type $\{M(diphos)(dmb)^+\}_n$ (M = Cu, Ag),[22] $\{Pd_2(diphos)_2(dmb)^{2+}\}_n$ (diphos = dppe, dppp),[22] $\{Pd_2(dmb)_2Cl_2\}_n$,[23] and $\{Pd_2(dmb)_2(diphos')^{2+}\}_n$ (diphos′ = dppb, dpppen, dpph)[23] (Scheme 3) were prepared and characterized. It was clearly demonstrated that polymers in the solid state dissociated to give oligomers in solution (8−16 units).

We now wish to report the syntheses and characterizations of new Cu^I and Ag^I binuclear and oligomeric complexes using the bridging diisocyanide dmb and electron-rich diphosphane dmpm ligands. By changing the nature of the assembling ligands and building blocks, one can hope not only to change the distance between the building blocks, but also to change the number of units. These oligomers are composed of the following building blocks: $M_2(dmpm)_3^{2+}$,[24−26] $Ag_2(dmpm)_2^{2+}$,[24−26] $M_2(dmb)_2^{2+}$ (M = Ag, Cu),[27−29] and $Ag_2(dmb)^{2+}$ [15−16] (Scheme 4).

Results and Discussion

The $M_2(dmpm)_x^{2+}$ Building Blocks

The binuclear $M_2(dmpm)_3^{2+}$ complexes [M = Cu (**1**), Ag (**2**)] are synthesized by the direct reaction between dmpm and the desired metal cationic species in the appropriate stoichiometric ratio. In a 1:1 stoichiometric ratio, the dmpm ligand also reacts with $AgBF_4$ to form the dicoordinated

[a] Département de Chimie, Université de Sherbrooke, Sherbrooke J1K 2R1, PQ., Canada
Fax: (internat.) + 1 819-821-8017
E-mail: p.harvey@Usherbrooke.ca
[b] Department of Chemistry, University of New Brunswick, Fredericton E3B 6E2, New Brunswick, Canada
E-mail: adecken@unb.ca

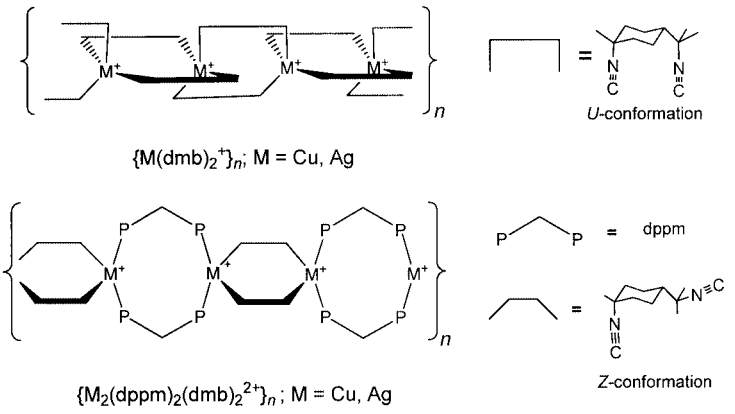

Scheme 1

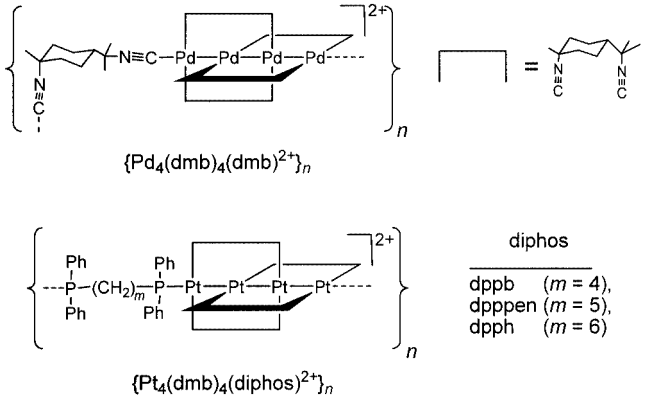

Scheme 2

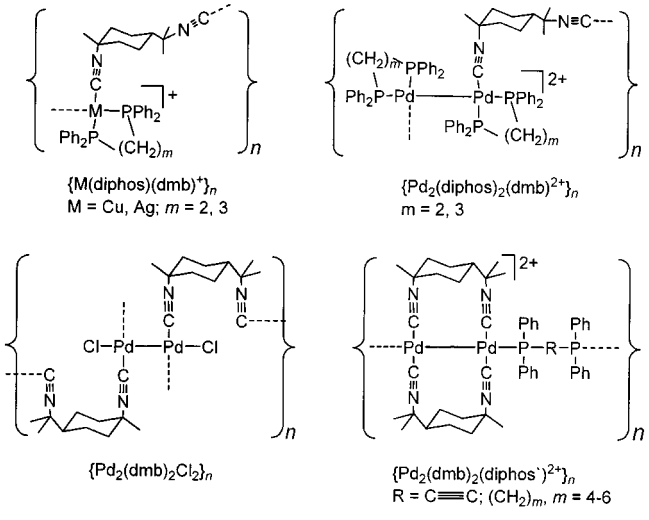

Scheme 3

dimer $Ag_2(dmpm)_2^{2+}$ (**3**). Complexes **2** and **3** can be distinguished by their sensitivity to light (**3** turns gray with time) and by ^{31}P NMR spectroscopy.

Crystals suitable for X-ray single-crystal analysis were obtained for **1** and **2**. (Figures 1 and 2, Table 1 and Table 7). The complexes exhibit two nearly trigonal planar coordinated metal atoms positioned face-to-face, and separated by 2.9265(3) and 2.9893(2) Å, for **1** and **2**, respectively. The separation in **1** is significantly shorter than that in the $[Cu_2(dmpm)_3](ClO_4)_2$ salt [3.021(2)Å],[26] and the distances for **1** and **2** fall short in comparison with the isostructural $Au_2(dmpm)_3^{2+}$ analogue (3.040 and 3.050 Å).[30] The average M···M distances follow the trend of their respective ionic radii (Cu^I, 0.91 Å < Ag^I, 1.29 Å < Au, 1.51 Å).[31] The Ag_2 and Au_2 distances are shorter than the sum of the van der Waals radii (3.4 Å)[31] indicating the presence of M_2 interactions, but this is not the case for the Cu_2 distance in **1** (2.8 Å).[31] The average PCuCu angle is not 90°, but slightly bent inward (88.3°), which may suggest the presence of weak M_2 interactions in this case. In addition, the AgP distances (average 2.434 Å) are longer than the CuP and AuP distances (Table 2), and do not follow the change in ionic radii. This is perfectly consistent with the findings of Schmidbaur et al., which state that Ag is larger than Au due to relativistic effects[32] but the M···M data presented above do not support this argument. The aurophilicity may be more important than the argentophilicity in this case.

The neutral isoelectronic $M_2(dppm)_3$ dimers (M = Pd,[33] Pt[34]) exhibit M_2 distances similar to their neighboring atoms in the periodic table (Pd ~ Ag^+; Pt ~ Au^+), but the cationic systems show slightly longer M_2 distances (Table 2), most likely reflecting internuclear electrostatic repulsion. Remarkably, the $d(Ag_2)$ value for $[Ag_2(dmpm)_2](PF_6)_2$ [3.041(1)Å][35] is longer than that found in **2**, indicating that the third dmpm ligand applies some extra restoring force. This is further exemplified in the $Cu_2(dmpm)_2(O_2CMe)^+$ complex, in which the shorter bite distance of the acetate ligand forces the Cu atoms to lie closer to one another [2.7883(11)Å][36] in comparison with **1**.

The model compound **4** was prepared by the direct reaction between **1** and 2 equivalents of *t*BuNC. Despite the poor quality of the single crystals [a = 24.935(4), b = 10.5070(15), c = 19.266(3) Å, β = 111.034(2)°, V =

 © 2004 Wiley-VCH Verlag GmbH & Co. KGaA, Weinheim

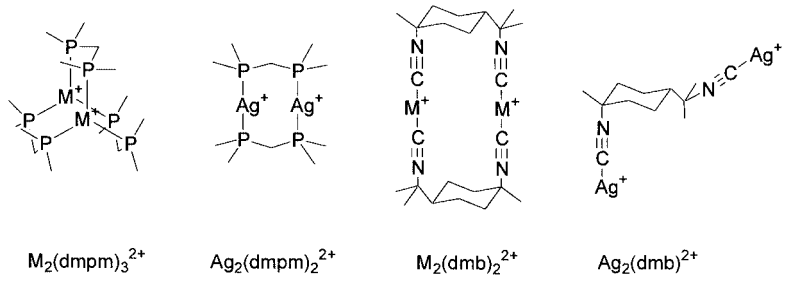

Scheme 4

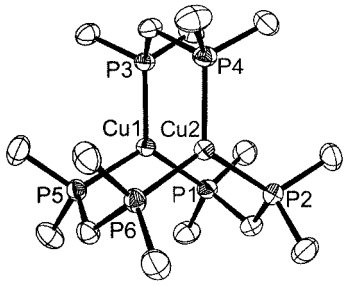

Figure 1. Thermal ellipsoid plots for **1**; the ellipsoids are shown with 30% probability; the H atoms and BF_4^- ions are not shown for clarity

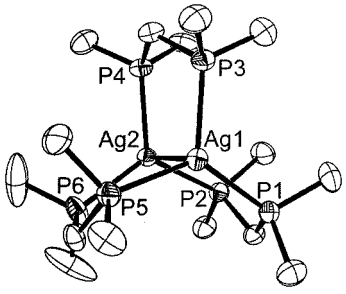

Figure 2. Thermal ellipsoid plots for **2**; the ellipsoids are shown with 30% probability; the H atoms and BF_4^- ions are not shown for clarity

Table 1. Selected bond lengths [Å] and angles [°] for **1** (left) and **2** (right)

Cu(1)−Cu(2)	2.9265(3)	Ag(1)−Ag(2)	2.9893(2)
Cu(1)−P(1)	2.2484(5)	Ag(1)−P(1)	2.4415(5)
Cu(1)−P(3)	2.2519(5)	Ag(1)−P(3)	2.4537(5)
Cu(1)−P(5)	2.2463(5)	Ag(1)−P(5)	2.4774(5)
Cu(2)−P(2)	2.2329(5)	Ag(2)−P(2)	2.4403(5)
Cu(2)−P(4)	2.2392(5)	Ag(2)−P(4)	2.4246(5)
Cu(2)−P(6)	2.2378(5)	Ag(2)−P(6)	2.4378(5)
P(5)−Cu(1)−P(1)	120.12(2)	P(1)−Ag(1)−P(5)	120.298(18)
P(5)−Cu(1)−P(3)	118.11(2)	P(3)−Ag(1)−P(5)	113.530(18)
P(1)−Cu(1)−P(3)	121.67(2)	P(1) −Ag(1)−P(3)	126.122(18)
P(2)−Cu(2)−P(6)	118.74(2)	P(2)−Ag(2)−P(6)	117.882(18)
P(2)−Cu(2)−P(4)	121.19(2)	P(4)−Ag(2)−P(2)	119.69(2)
P(6)−Cu(2)−P(4)	119.53(2)	P(4)−Ag(2)−P(6)	122.16(2)
P(5)−Cu(1)−Cu(2)	92.475(15)	P(5)−Ag(1)−Ag(2)	89.931(13)
P(1)−Cu(1)−Cu(2)	89.760(16)	P(1)−Ag(1)−Ag(2)	92.317(13)
P(3)−Cu(1)−Cu(2)	90.888(15)	P(3)−Ag(1)−Ag(2)	85.399(14)
P(2)−Cu(2)−Cu(1)	93.963(16)	P(2)−Ag(1)−Ag(2)	88.852(13)
P(6)−Cu(2)−Cu(1)	90.983(15)	P(6)−Ag(1)−Ag(2)	91.912(13)
P(4)−Cu(2)−Cu(1)	92.386(15)	P(4)−Ag(1)−Ag(2)	94.312(14)

4711.2(12) Å^3, $Z = 8$, $d = 2.061$ Mg/m^3, $R_1 = 0.22$; $wR_2 = 0.55$] both the spectra and crystallographic data are consistent with the addition of 2 *t*BuNC ligands at the axial positions of the $Cu_2(dmpm)_3^{2+}$ skeleton (Scheme 5).

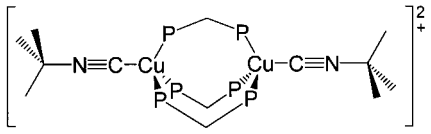

$Cu_2(dmpm)_3(CN\text{-}tBu)_2^{2+}$

Scheme 5

The Cu···Cu separation is found to be 4.011 Å, where no Cu···Cu interaction is noted. The structure exhibits similarities with the d^{10}-d^{10} complex $Pt_2(dppm)_3(PPh_3)$,[37] in which one Pt atom adopts a tetracoordinate geometry causing an increase in the Pt···Pt distance with respect to $Pt_2(dppm)_3$.[33,34]

Table 2. Comparison of selected structural data for d^{10}-d^{10} $M_2(dmpm)_3^{2+}$ and $M'_2(dppm)_3$ dimers

	$d(M_2)$ [Å]	$2r_{vdw}$ [Å]	d[(MP)$_{av}$] [Å]	Approx. point group	Refs.
$Cu_2(dmpm)_3^{2+}$ (BF_4^-)	2.9265(3)	2.80	2.243(10)	C_s	this work
$Cu_2(dmpm)_3^{2+}$ (ClO_4^-)	3.021(2)	2.80	2.245(6)	C_s	[26]
$Ag_2(dmpm)_3^{2+}$	2.9893(2)	3.40	2.434(31)	C_s	this work
$Au_2(dmpm)_3^{2+}$	3.040(1) 3.050(1)	3.40	2.358	C_s	[40]
$Pd_2(dppm)_3$	2.956(1)	3.20	2.310(10)	C_3	[42]
$Pt_2(dppm)_3$	3.022(3)	3.50	2.265(3)	C_3	[43][44]

 © 2004 Wiley-VCH Verlag GmbH & Co. KGaA, Weinheim

No attempt was made to synthesize the $\{Ag_2(dmpm)_2(CN\text{-}tBu)_2\}^{2+}$ complex, as the crystallographically characterized $[Ag_2(dppm)_2(CN\text{-}tBu)_2](ClO_4)_2$ complex was recently reported by us (Scheme 6).[17] The structure consists of two face-to-face tricoordinate Ag^I atoms bridged by two dppm ligands, where one CN-*t*Bu ligand binds each of the metals, similar to that in $Ag_2(dmpm)_3^{2+}$ with the difference that one diphosphane ligand is replaced by two isocyanide groups.

Synthesis and Characterization of the Oligomers

Compound **1** and dmb reaction ratios varying from 1:1 to 1:2, invariably forming an oligomeric material best described as $[Cu_6(dmpm)_9(dmb)_4](BF_4)_6$ or $\{[Cu_2(dmpm)_3(dmb)_{1.33}](BF_4)_2\}_2$ (**5**). This formulation, $[Cu_2(dmpm)_3(dmb)^{2+}]_x(dmb)$ ($x = 3$), is unambiguously established from the reproducible chemical analyses, integration of the ^1H NMR data (dmpm vs. dmb), and TGA data (Table 3). It is possible that traces of shorter and longer oligomers ($x = 1$, 2 and $x > 3$) exist, but the product distribution must be very narrow since the oligomer is very small, and all three techniques above indicate the same results. If such oligomers exist, their concentration must be very low. The XRD spectra indicate the presence of a highly crystalline material, which is consistent with the oligomeric nature of the material, but also support the hypothesis for a very narrow product distribution. The chemical yield is modest, indicating some losses during the attempts to obtain pure samples. The short oligomeric nature of the material is also confirmed by the observed ν(N≡C) absorption for uncoordinated isocyanides at 2132 cm^{-1} in the solid-state IR spectra (Figure 3), indicating that its relative presence is important in comparison with the coordinated ones (2161 cm^{-1}). Long chains ending with dmb ligands would exhibit very weak absorption due to uncoordinated isocyanides relative to the coordinated ones.

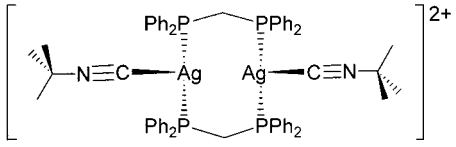

Scheme 6

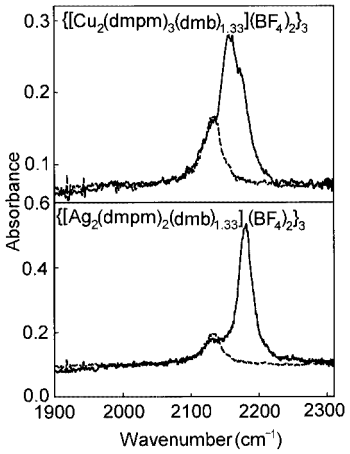

Figure 3. Solid state FT-IR spectra of **5** (top) and **6** (bottom) in the ν(N≡C) region (−) in comparison with free dmb (- - - -), emphasizing evidence of non-coordinated −N≡C groups in the oligomers

The corresponding $Ag_2(dmpm)_3^{2+}$ complex does not react with dmb even in excess. This behavior may reflect the fact that dmpm is a strong σ-donor, which renders the Ag^I atoms significantly more electron-rich. As a result, the monodentate RNC ligands become very labile. Conversely, the $Ag_2(dmpm)_2^{2+}$ complex reacts with dmb in a 1:1 ratio to generate another oligomeric material, identified as $[Ag_6(dmpm)_6(dmb)_4](BF_4)_6$ or $\{[Ag_2(dmpm)_2(dmb)_{1.33}](BF_4)_2\}_3$ (**6**) by reproducible chemical analysis, ^1H NMR spectroscopy and TGA. Oligomer **6** is also a crystalline solid (XRD). The MALDI-TOF spectra for both **5** and **6** are very complex, where fragment peaks show evidence for M−P, P−C, and C−N bond cleavage. In both cases, the molecular ion was not observed. Size-exclusion chromatography was also inadequate, as the compounds tended to stay trapped in the column, despite the use of different column materials. Both oligomeric materials crystallize to form long needle-shaped crystals, a shape that is common for dmb-containing polymers, but the thickness of these needles was inadequate for X-ray analysis. IR characteristics similar to those described for **5** above are depicted in the spectra of **6**, where a weak absorption associated to free ν(N≡C) is observed (Figure 3). It is interesting to note that both oligomers **5** and **6** (6 metal atoms) exhibit a lower degree of oligomerization than that reported for $\{[Ag(dmb)_2]BF_4\}_n$ in solution ($n = 7-8$).[18]

Table 3. TGA data for **1**, **4**, **5**, and **6**

Compounds		Weight loss 1[a]			Weight loss 2[a]			Residue	
		Temp. Range (°C)	Exp. %	Theor. %	Temp. Range (°C)	Exp. %	Theor. %	Exp. %	Theor. %
1	$[Cu_2(dmpm)_3](BF_4)_2$	−	−	−	320−390	86	81	14	19
4	$[Cu_2(dmpm)_3(CN\text{-}tBu)_2](BF_4)_2$	120−190	19	19	320−390	66	66	15	15
5	$\{[Cu_2(dmpm)_3(dmb)_{1.33}](BF_4)_2\}_3$	210−230	27	26	300−390	60	61	13	13
6	$\{[Ag_2(dmpm)_2(dmb)_{1.33}](BF_4)_2\}_3$	180−210	28	29	290−345	46	48	26	23

[a] Weight loss 1 is due to the loss of *t*BuNC or dmb; weight loss 2 is due to the loss of dmpm and BF_4; the uncertainties are ±2% based on the small drift of the baseline.

 © 2004 Wiley-VCH Verlag GmbH & Co. KGaA, Weinheim

No glass transition (or other thermal phenomenon) was observed between −20 °C and 100 °C in the DSC traces for any of the investigated compounds. The result is consistent with the nonpolymeric nature of the materials.

Modeling

In the absence of X-ray data, the model compounds $Ag_2(dmpm)_2(CN\text{-}tBu)_2^{2+}$ and $Cu_4(dmpm)_6(dmb)_2(CN\text{-}tBu)^{4+}$ were computed to address two specific questions. Is the Ag···Ag distance in $Ag_2(dmpm)_2(CN\text{-}tBu)_2^{2+}$ (model compound for **6**) similar to $Ag_2(dmpm)_3^{2+}$ (explaining some similarities in the electronic spectra), and what distance separates the different dimer units in **5** (and ultimately in **6** as well)?

The methodology has been tested on the X-ray data for **1**, **2**, and the related binuclear complex $[Ag_2(dppm)_2(CN\text{-}tBu)_2](ClO_4)_2$[17] (Table 4) in order to provide a degree of confidence in the results. The M···M and M···P distances are computed within an uncertainty of 0.05−0.06 Å, which is acceptable in the context of this work. The Ag−C bond length gives the worst agreement, with a difference of approximately 0.3 Å from the experimental value, and is taken into account.

The computed model structure for $Ag_2(dmpm)_2(CN\text{-}tBu)_2^{2+}$ (Figure 4) exhibits an Ag···Ag separation of 2.94 Å, similar to that for **2** (2.9265 Å, X-ray), and a CAgAgC twisted angle of 18°. The first conclusion is that if this structure is correct, as suggested by the $Ag_2(dppm)_2(CN\text{-}tBu)_2^{2+}$ X-ray data, the UV/Vis $d\sigma^* \rightarrow p\sigma$ signature should be present at the same wavelength for both **2** and **6** (see section below). The second point is that the replacement of CN-*t*Bu by dmb should not induce great ring stress or angle torsion.

The computed structure for $Cu_4(dmpm)_6(dmb)_2(CN\text{-}tBu)^{4+}$ exhibits a central bridging dmb ligand adopting a *Z*-conformation (Figure 5). The *U*-form is unfavorable because of important steric hindrance between the Cu_2 units. The M···M distance in the M−dmb−M unit is 9.112 Å, which may be slightly overevaluated by 2 × 0.3 Å, as indicated above. The calculated triply bridged Cu···Cu distance is 4.35 Å, predictably longer than that found in **1**, and more similar to the X-ray data for **4** (≈ 4.011 Å). Similarly, the computed NC···CN and N···N distances in the *Z*-dmb are 7.064 and 5.755 Å, respectively. These M···M, C···C, and N···N distances compare favorably to those reported for the crystallographically characterized polymer $\{[Pd_4(dmb)_4(dmb)](MeCO_2)_2\}_n$ (i.e. 9.241, 6.801, and 5.549 Å, respectively).[20]

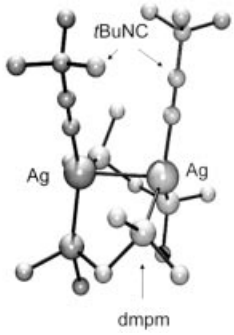

Figure 4. Computed structure for the model compound $Ag_2(dmpm)_2(CN\text{-}tBu)_2^{2+}$; the calculated distances are 2.94, 2.02, 1.20, and 2.47 Å, for the Ag···Ag separation, the AgC, C≡N, and AgP bond lengths, respectively

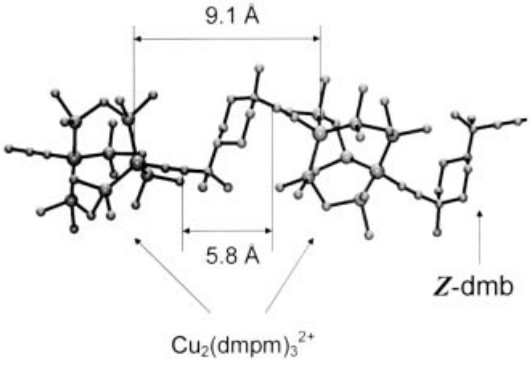

Figure 5. Computed structure for the model compound $Cu_4(dmpm)_6(dmb)_2(CN\text{-}tBu)^{4+}$; the calculated distances are 4.35, 1.83, 1.20, and 2.36 Å, for the Cu···Cu separation, the CuC, C≡N and CuP bond lengths, respectively

Electronic Spectra

The absorption spectra of compounds **1** and **2** (Figure 6) exhibit an absorption band at about 250 nm. These unstructured bands are due to the $d\sigma^* \rightarrow p\sigma$ transition; an electronic transition that is well-documented for cofacial d^{10}-d^{10} species such as $Au_2(dmpm)_3^{2+}$,[38] $Au_2(dcpm)_2^{2+}$ (dcpm = bis(dicyclohexylphosphanyl)-methane),[39] $Au_2(dmpm)_2^{2+}$,[40−42] $M_2(dppm)_3$ (M = Pd, Pt),[43,44] and $Ag_2(dmpm)_2^{2+}$.[45] In order to confirm this assignment, the absorption spectra were also recorded at 77 K in butyronitrile. At this temperature, the bandwidth decreases, in a somewhat similar manner to that of $Pd_2(dppm)_3$[43,44] and $Ag_2(dmpm)_2^{2+}$ [45] (Figure 7). This well-known phenom-

Table 4. Comparison between X-ray data and MMX computations[a]

	X-ray			MMX		
	d(M···M)	*d*(M−P)	*d*(M−C)	*d*(M···M)	*d*(M−P)	*d*(M−C)
1	2.9265	2.243	−	2.978	2.267	−
2	2.9893	2.434	−	2.974	2.463	−
$Ag_2(dppm)_2(CN\text{-}tBu)_2^{2+}$	3.223	2.428	2.334	3.216	2.473	2.024

[a] All the distances are in Å.

 © 2004 Wiley-VCH Verlag GmbH & Co. KGaA, Weinheim

enon has been fully described by Gray et al. and others.[46−52] The absorption maxima for the dσ*→pσ bands compare favorably with those of $Au_2(dmpm)_3^{2+}$ rather than with those of other related triply bridged d^{10}-d^{10} species (Table 5). No obvious trend is seen along the Cu, Ag, Au series, perhaps reflecting two opposite effects; lengthening of the M···M distance disfavors the M···M interactions, while an increase in atomic radii favors them. The data for **1** agree with that for $[Cu_2(dmpm)_3](ClO_4)_2$ (λ_{max} = 264 nm; ε = 7380 $M^{-1}cm^{-1}$ in acetonitrile at 298 K).[26]

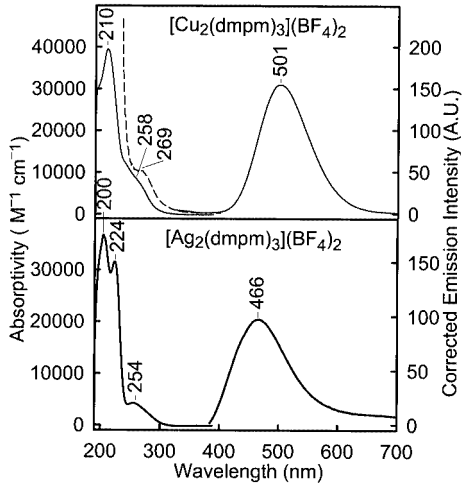

Figure 6. Comparison of the UV/Vis absorption (left) and emission (right) spectra for **1** (top) and **2** (bottom) in acetonitrile at 298 K; the broken line is an example of an excitation spectrum, here for **1**

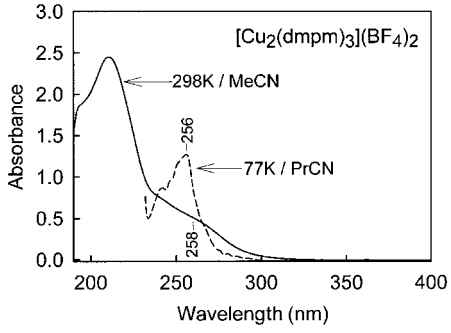

Figure 7. Comparison of the UV/Vis spectra of **1** at 298 K (−) and 77 K (- - -). The lowest wavelength possible is 240 nm at 77 K, because of absorption by the solvent glass

The absorption spectra for **4** and **5** are almost identical to each other, where strong absorptions are observed at 212 and 236, and at 210 and 236 nm, respectively. As anticipated for the noninteracting Cu···Cu systems, the dσ*→pσ absorption is absent. The lowest energy absorption is assigned to the spin-allowed $t_2(d\sigma^*) \rightarrow t_2(\pi^*, p\sigma^*)$ transition.[53,54] Oligomer **6** in acetonitrile exhibits an absorptivity of 10200 $M^{-1}cm^{-1}$ per Ag_2 unit for the dσ*→pσ band (λ_{max} = 254 nm).

Emission

The compounds are luminescent in solution at 298 and 77 K (Figures 6 and 8, Table 6), as well as in the solid state. The excitation spectra measured in solution confirm the authenticity of the emission, and the μs timescale for the lifetimes is consistent with a phosphorescence process. Compounds **1** and **2** exhibit luminescence of modest intensity in solution at 298 K at 500 and 471 nm, respectively. The energy gaps between the absorption and emission (18800cm^{-1} for **1**; 17300 cm^{-1} for **2**) are somewhat large. This phenomenon has also been observed for $Au_2(dmpm)_3^{2+}$ by Che, Miskowski et al. ,[38] who have suggested that the emission arises from $^3(d(x^2\text{-}y^2), xy \rightarrow p\sigma)$ excitation, in agreement with Mason's former proposal.[55] The similarity in the absorption maxima and emission lifetimes for **2** and **6** in the solid state strongly suggests that this assignment also applies for oligomer **6**.

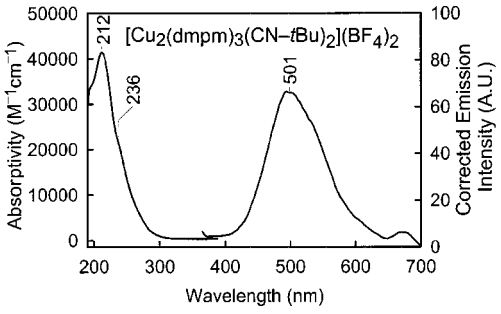

Figure 8. Absorption (left) and emission (right) spectra for **4** in acetonitrile at 298 K

In solution, the emission bands for all compounds are shifted to the red from about 446 nm to 466−520 nm. This range falls in the same region as that for the tetracoordinate Cu species (474−502 nm), and suggests that the emission arising from the tricoordinate Ag species in solution may

Table 5. Comparison of the dσ*→pσ absorption data at 298 K for various $M_2(diphos)_3$ complexes

	λ (±1 nm)	$\tilde{\nu}$ [cm^{-1}]	ε [$M^{-1}cm^{-1}$]	Refs.
$[Cu_2(dmpm)_3](BF_4)_2/CH_3CN/298K$	258	38800	8500	this work
$[Ag_2(dmpm)_3](BF_4)_2/CH_3CN/298K$	254	39400	4300	this work
$[Au_2(dmpm)_3](ClO_4)_2/H_2O/298K$	256	39000	18500	[30]
$Pd_2(dppm)_3$/2MeTHF/77K	440	22700	33800	[33]
$Pt_2(dppm)_3$/2MeTHF/77K	488	20500	27400	[33]

 © 2004 Wiley-VCH Verlag GmbH & Co. KGaA, Weinheim

Table 6. Comparison of the emission spectroscopy and photophysical data (the reported lifetimes are those obtained from the ESM method)

Compounds		Solid, 298 K		Solution,[a] 298 K			Solution,[b] 77 K	
		λ_{emi} [nm]	τ_{em} [μs]	λ_{emi} [nm]	τ_e [μs][c]	Φ_e	λ_{emi} [nm]	τ_e [μs]
1	$[Cu_2(dmpm)_3](BF_4)_2$	Not measured		500	16.5	0.020	505	840
4	$[Cu_2(dmpm)_3(CN\text{-}t\text{Bu})_2](BF_4)_2$	476	291	501	3.8	0.0043	502	712
5	$\{[Cu_2(dmpm)_3(dmb)_{1.33}](BF_4)_2\}_3$	482	257	500	< 2	0.0013	474	523
2	$[Ag_2(dmpm)_3](BF_4)_2$	445	41	466	3.0	0.0031	482	6300
6	$\{[Ag_2(dmpm)_2(dmb)_{1.33}](BF_4)_2\}_3$	447	31	520	≈ 2	0.0014	500	542

[a] In acetonitrile. [b] In butyronitrile. [c] The detection limit of the instrument is 2 μs, so the accuracy is poor near this limit.

be due to tetracoordinate solvent/anion exciplexes.[39] For the formally tetracoordinate **4** and **5**, the assignment of the emissive state is $^3([t_2(d\sigma^*)]^5[t_2(\pi^*,p\sigma^*)]^1)$ in agreement with that of $M(diphos)_2$ (M = Pd, Pt; diphos = dppe, dppp)[53] and that of $M(CN\text{-}t\text{Bu})_4^+$ (M = Cu, Ag).[15]

The emission lifetime data show two trends (Table 6). First, emission lifetimes predictably increase with the rigidity of the medium, and decrease as the temperature increases. Second, emission lifetimes and quantum yields decrease as the size of the molecule increases. The latter is due to the well-known "loose bolt" effect,[56] where the number of vibrational levels favoring internal conversion increases with the number of groups around the chromophores, as well as with their sizes. It is noteworthy that emission lifetimes for **2** and **6** are significantly longer than those reported for solid $Ag_2(dcpm)_2^{2+}$ at 298 K (λ_{emi} = 420 nm; τ_e = 0.5 μs),[57] and for $Ag_2(dmpm)_2^{2+}$ in ethanol at 77 K (λ_{emi} = 371 nm; τ_e = 49 μs),[45] the latter being dicoordinated.

Conclusion

The use of an electron-rich phosphane, which renders the metal center more electron-rich, increases the lability of the ligands, in particular that of the isocyanide ligand in this work. This property has a significant effect on the length of the oligomeric materials. This general approach may provide another strategic tool to make the polymer chain shorter for cases where the material would exhibit undesirable properties such as low solubility, preventing easier characterization, and amorphous character in the solid state.

Experimental Section

Materials: 1,8-diisocyano-*p*-menthane[58] was synthesized according to literature procedures. $[Cu(CH_3CN)_4]BF_4$ was freshly prepared before use, following the published procedure.[59] All solvents were purified by standard procedures.[60,61] The following materials were purchased from commercial suppliers: acetone (Fisher), acetonitrile and Cu(m) (Anachemia), petroleum ether and dichloromethane (ACP), ethanol (Les Alcools de Commerce Inc.), dinitrogen and argon (Praxair), $AgBF_4$, $Cu(BF_4)_2{\cdot}xH_2O$ and *tert*-butyl isocyanide (Aldrich Chemicals Co); bis(dimethylphosphanyl)methane (Strem Chemicals Co). Unless otherwise stated, all materials were handled under argon or dinitrogen using standard Schlenk techniques, high-vacuum manifolds and an inert-atmosphere glove box.

$[Cu_2(dmpm)_3](BF_4)_2$ (1): $[Cu(CH_3CN)_4]BF_4$ (370.0 mg, 1.18 mmol) was dissolved in acetone (20 mL). The ligand dmpm (0.35 mL, 2.21 mmol) was added dropwise using a microsyringe. The reaction mixture was stirred for 1 h prior to the addition of diethyl ether (80 mL). A white precipitate appeared, which was filtered and dried in a glove box. Yield 60% (315 mg). ^1H NMR (CD_3CN): δ = 2.02 (m, 6 H, PCH_2P), 1.36 (s, 36 H, PCH_3) ppm. $^{31}P\{^1H\}$ NMR (CD_3CN): δ = −25.36 ppm. $^{13}C\{^1H\}$ NMR (CD_3CN): δ = 32.12, 16.12 ppm. UV/Vis (CH_3CN): λ (ε) = 210 (39500), 248 nm (8500 $M^{-1}cm^{-1}$). $C_{15}H_{42}B_2Cu_2F_8P_6$ (709.04): calcd. C 25.41, H 5.97; found C 25.45, H 5.90.

$[Ag_2(dmpm)_3](BF_4)_2$ (2): $AgBF_4$ (259.6 mg, 1.33 mmol) was dissolved in acetone (15 mL). The resulting solution was filtered prior to use. The ligand dmpm (0.35 mL, 2.21 mmol) was added dropwise with a microsyringe. The solution was stirred for 1 h, and diethyl ether (70 mL) was added to precipitate the white product, which was filtered and dried in vacuo. Yield 90% (478 mg). ^1H NMR (CD_3COCD_3): δ = 2.45 (m, 6 H, PCH_2P), 1.60 (s, 36 H, PCH_3) ppm. $^{31}P\{^1H\}$ NMR (CD_3COCD_3): δ = −13.98, −15.39, −16.86 ppm. $^{13}C\{^1H\}$ NMR (CD_3COCD_3): δ = 31.63, 16.41 ppm. UV/Vis (CH_3CN): λ (ε) = 200 (47400), 224 (31400), 254 nm (4300 $M^{-1}cm^{-1}$). $C_{15}H_{42}Ag_2B_2F_8P_6$ (797.68): calcd. C 22.59, H 5.31; found C 22.08, H 5.20.

$[Ag_2(dmpm)_2](BF_4)_2$ (3): $AgBF_4$ (53.4 mg, 0.274 mmol) was dissolved in acetone (15 mL). The ligand dmpm (37.5 mg, 0.275 mmol) was added dropwise using a microsyringe. The solution was stirred for 1 h, prior to adding diethyl ether (70 mL). The white precipitate was filtered and dried under an inert atmosphere. Yield 76% (90.6 mg). ^1H NMR (CD_2Cl_2): δ = 2.31 (m, 4 H, PCH_2P), 1.61 (s, 24 H, PCH_3) ppm. $^{31}P\{^1H\}$ NMR (CD_2Cl_2): δ = −12.99 (br d, J(AgP) = 560 Hz) ppm. $^{13}C\{^1H\}$ NMR (CD_3CN): δ = 30.01, 14.46 ppm. UV/Vis (CH_3CN): λ (ε) = 202 (48000), 256 nm (23400 $M^{-1}cm^{-1}$). $C_{10}H_{28}Ag_2B_2F_8P_4$ (661.57): calcd. C 18.15, H 4.27; found C 18.24, H 4.32.

$[Cu_2(dmpm)_3(CN\text{-}t\text{Bu})_2](BF_4)_2$ (4): Compound **1** (102.1 mg, 0.144 mmol) was dissolved in degassed acetone (30 mL). *t*BuNC (0.1 mL, 0.88 mmol) was added dropwise using a microsyringe. The solution was stirred for 1 h prior to being concentrated in vacuo to a volume of 5 mL. Dimethyl ether (25 mL) was added to precipitate a white solid, which was filtered and dried in vacuo. Yield 86% (108 mg). ^1H NMR (CD_3COCD_3): δ = 2.26 (m, 6 H, PCH_2P): 1.59 [s, 18 H, $(CH_3)_3C$], 1.45 (s, 36 H, PCH_3) ppm. $^{31}P\{^1H\}$ NMR (CD_3COCD_3): δ = −25.41ppm. $^{13}C\{^1H\}$ NMR (CD_3COCD_3): δ = 58.38, 33.03, 30.20, 17.84 ppm. IR (KBr): 1052 (ν_{BF}), 2177

 © 2004 Wiley-VCH Verlag GmbH & Co. KGaA, Weinheim

($\nu_{C\equiv N}$) cm^{-1}. Raman (solid): 2176 ($\nu_{C\equiv N}$) cm^{-1}. UV/Vis (CH_3CN): λ (ε) = 212 (39500), 236 (sh.) nm (22200 $M^{-1}cm^{-1}$). $C_{25}H_{60}B_2Cu_2F_8N_2P_6$ (875.30): calcd. C 34.30, H 6.91, N 3.20; found C 34.03, H 6.74, N 3.02.

{[Cu_2(dmpm)$_3$(dmb)$_{1.33}$][$(BF_4)_2$}$_3$ (5): Compound **1** (106.2 mg, 0.150 mmol) was dissolved in degassed acetone (20 mL). The ligand dmb (100.0 mg, 0.525 mmol) was dissolved separately in a round-bottom flask containing degassed acetone (150 mL). This solution was added dropwise and slowly to the former solution, and the mixture was stirred for 4 h prior to being concentrated in vacuo to a volume of 15 mL. Diethyl ether (150 mL) was added. A white product precipitated, which was filtered and dried. Yield 52% (86.9 mg). ^1H NMR (CD_3CN): δ = 2.08−2.02 (m, 8 H, dmb), 2.01 (m, 18 H, PCH_2P), 1.87−1.83 (m, 8 H, dmb), 1.61−1.56 (m, 12 H, dmb), 1.51 (s, 20 H, dmb), 1.45 (s, 24 H, dmb), 1.35 (s, 108 H, CH_3P) ppm. $^{31}P\{^1H\}$ NMR (CD_3CN): δ = −25.55 ppm. $^{13}C\{^1H\}$ NMR (CD_3CN): δ = 60.45, 63.18, 45.32, 37.10, 32.55, 29.11, 26.05, 23.32, 7.18 ppm. IR (KBr): $\tilde{\nu}$ = 1052 (ν_{BF}), 2161 ($\nu_{C\equiv N}$) cm^{-1}. Raman (solid): 2160 ($\nu_{C\equiv N}$) cm^{-1}. UV/Vis (CH_3CN): λ (ε) = 210 (51100), 236 (sh.) nm (26500 $M^{-1}cm^{-1}$). $C_{93}H_{198}B_6Cu_6F_{24}N_8P_{18}$ (2888.25): calcd. C 38.67, H 6.91, N 3.88; found C 38.64, H 6.79, N 4.02.

{[Ag_2(dmpm)$_2$(dmb)$_{1.33}$][$(BF_4)_2$}$_3$ (6): Compound **3** (59.1 mg, 0.089 mmol) was dissolved in degassed acetone (45 mL). The ligand dmb (53 mg, 0.279 mmol) was dissolved separately in a round-bottom flask containing degassed acetone (60 mL). This solution was added dropwise and slowly to the former solution, and the mixture was stirred for 3 h prior to being concentrated in vacuo to a volume of 15 mL. Diethyl ether (120 mL) was added to precipitate the white product, which was filtered and dried in vacuo. Yield 99% (76.1 mg). ^1H NMR (CD_2Cl_2): δ = 2.16 (m, 12 H, PCH_2P), 2.03−1.85 (m, 16 H, dmb) 1.53 (s, 88 H, CH_3P + dmb) 1.50−1.43 (m, 40 H, dmb) ppm. $^{31}P\{^1H\}$ NMR (CD_2Cl_2): δ = −15.68 (m) ppm. $^{13}C\{^1H\}$ NMR (CD_3COCD_3): δ = 64.12, 61.21, 43.78, 36.92, 31.96, 28.25, 27.21, 22.88, 16.44, 15.56 ppm. IR (KBr): $\tilde{\nu}$ = 1051 (ν_{BF}), 2181 ($\nu_{C\equiv N}$) cm^{-1}. Raman (solid): 2182 ($\nu_{C\equiv N}$) cm^{-1}. UV/Vis (CH_3CN): λ (ε) = 198 (40300), 254 nm (10200 $M^{-1}cm^{-1}$). $C_{78}H_{156}Ag_6B_6F_{24}N_8P_{12}$ (2745.85): calcd. C 34.12, H 5.73, N 4.08; found C34.29, H 5.32, N 3.96.

Apparatus: All NMR spectra were acquired using a Bruker AC-300 spectrometer (^1H 300.15 MHz, ^{13}C 75.48 MHz, ^{31}P 121.50 MHz) using the solvent as the chemical shift standard, except for ^{31}P NMR, where the chemical shifts are relative to external D_3PO_4 85% in D_2O. IR spectra were acquired on a Bomem FT-IR MB series spectrometer equipped with a baseline-diffused reflectance. UV/Vis spectra were acquired using a Hewlett Packard diode array 8452A spectrophotometer . Continuous wave emission and excitation spectra were obtained using a SPEX Fluorolog II spectrometer. Emission lifetimes were measured with a nanosecond N_2 laser system (PTI) model GL-3300 pumping a dye laser model GL-302. The excitation wavelength was 311 nm for all the measurements. MALDI-TOF mass spectra were acquired on a Bruker Proflex III linear mode spectrometer with a nitrogen laser (337 nm) at the Université de Bourgogne in Dijon (France) using a dithranol matrix. Glass transition temperatures (T_g) were measured with a Perkin−Elmer 5A DSC7 equipped with a thermal controller 5B TAC 7/DS. Calibration standards were water and indium. FT-Raman spectra were acquired on a Bruker RFS 100/S spectrometer. XRD were acquired on a Rigaku/USA Inc with a copper lamp operating under a 30 mA current and a 40 kV tension. TGA were acquired on a TGA 7 of Perkin−Elmer between 50 and 650 °C at 3°C/minute under N_2.

Crystallography: Crystals of [Ag_2(dmpm)$_3$][$(BF_4)_2$ (**2**) were grown by vapor diffusion using acetonitrile/*tert*-butylmethyl ether at 23 °C, crystals of [Cu_2(dmpm)$_3$][$(BF_4)_2$ (**1**) were grown by vapor diffusion using acetone/*tert*-butylmethyl ether at 23 °C (data see Table 7). Single crystals were coated with Paratone-N oil, mounted on a glass fiber and frozen in the cold nitrogen stream of the goniometer. A hemisphere of data was collected on a Bruker AXS P4/SMART 1000 diffractometer using ω and θ scans with a scan width of 0.3° and 10 s exposure times. The detector distance was 5 cm. The data were reduced (SAINT)[62] and corrected for absorption (SADABS).[63,64] The structure was solved by direct methods and refined by full-matrix least-squares on F[63,64] (SHELXTL).[63,64] All non-hydrogen atoms were refined anisotropically. Hydrogen atoms were found in Fourier difference maps and refined isotropically. Thermal ellipsoid plots are at the 30% probability level. In some plots, hydrogen atoms have been omitted for clarity.

Table 7. Crystal data for **1** and **2**

	[Cu_2(dmpm)$_3$][$(BF_4)_2$	[Ag_2(dmpm)$_3$][$(BF_4)_2$
Empirical formula	$C_{15}H_{42}B_2Cu_2F_8P_6$	$C_{15}H_{42}Ag_2B_2F_8P_6$
Molecular mass	709.01	797.67
Temperature [K]	198(1)	198(1)
Wavelength [Å]	0.71073	0.71073
Crystal system	monoclinic	orthorhombic
Space group	$P2_1/c$	*Pbca*
a [Å]	16.9960(9)	13.9467(7)
b [Å]	11.0485(5)	14.6460(8)
c [Å]	16.9515(9)	31.6720(17)
β [°]	99.258(1)	90
Volume [$Å^3$]	3141.7(3)	6469.4(6)
Z	4	8
d (calcd) [Mg/m^3]	1.499	1.638
Reflections collected	22019	43787
Independent reflections	7131	7391
Goodness-of-fit	1.085	1.037
*R*1[a]	0.0299	0.0202
*wR*2[a]	0.0824	0.0499

[a] $R1 = \||F_o| - |F_c|\| / |F_o|$; $wR2 = \{[w(F_o^2-F_c^2)^2]/[F_o^4]\}^{1/2}$; (**1**): weight = $1/[\sigma^2(F_o^2) + (0.0528P)^2 + (0.9190P)]$ and (**2**): weight = $1/[\sigma^2(F_o^2) + (0.0463P)^2 + (1.7267P)]$, where $P = [\max(F_o^2, 0) + 2F_c^2]/3$.

Procedures: The emission quantum yields were measured using 9,10-diphenylanthracene as the standard (Φ_F = 1.00 for degassed solutions).[65] The emission lifetimes were analyzed in two ways. The first way was the common deconvolution method allowing for analysis of the raw data using models with 1−4 exponential decays. The second way was the ESM (Exponential Series Method),[66,67] which gave a distribution of lifetimes instead of a single value, and the maximum of the distribution was retained. Both methods gave the same results, but ESM gave better fits. The quality of the fit between the experimental and calculated curves was addressed using the parameter χ (goodness of fit), and by the analysis of the residual.

Computer Modeling: The calculations were performed using the commercially available PC-Model from Serena Software (version 7.0), which uses the MMX empirical model. Comparisons between literature X-ray structures and computed models are provided in the text. The R−N≡C groups are replaced by R−C≡C^- because PC Model does not model C≡N^+− fragments, as strongly bent

 © 2004 Wiley-VCH Verlag GmbH & Co. KGaA, Weinheim

structures had to be calculated. Instead −C≡C− is used securing a more linear and realistic frame for the ligand.

CCDC-245030 (for **2**) and -245031 (for **1**) contain the supplementary crystallographic data for this paper. These data can be obtained free of charge at www.ccdc.cam.ac.uk/conts/retrieving.html [or from the Cambridge Crystallographic Data Centre, 12 Union Road, Cambridge CB2 1EZ, UK; Fax: (internat.) +44-1223-336-033; E-mail: deposit@ccdc.cam.ac.uk].

Acknowledgments

This research was supported by the Natural Sciences ad Engineering Research Council of Canada (NSERC). P.D.H. thanks Dalila Samar for technical assistance.

[1] S. L. James, *Chem. Soc. Rev.* **2003**, *32*, 276−288.
[2] E. Lozano, M. Nieuwenhuyzen, S. L. James, *Chem. Eur. J.* **2001**, *7*, 2644−2651.
[3] F. Mohr, M. C. Jennings, R. J. Puddephatt, *Angew. Chem. Int. Ed.* **2004**, *43*, 969−971.
[4] R. J. Puddephatt, *Coord. Chem. Rev.* **2001**, *216−217*, 313−332.
[5] P.-S. Kim, M.-C. Brandys, Y. Hu, R. J. Puddephatt, T.-K. Sham, *J. Luminescence* **2003**, *105*, 21−26.
[6] T. J. Burchell, D. J. Eisler, M. C. Jennings, R. J. Puddephatt, *Chem. Commun.* **2003**, 2228−2229.
[7] R. J. Puddephatt, *Macromol. Symp.* **2003**, *196*, 137−144.
[8] W. J. Hunks, M. C. Jennings, R. J. Puddephatt, *Chem. Commun.* **2002**, 1834−1835.
[9] M.-C. Brandys, R. J. Puddephatt, *J. Am. Chem. Soc.* **2002**, *124*, 3946−3950.
[10] A. Adolf, M. Gonsior, I. Krossing, *J. Am. Chem. Soc.* **2002**, *124*, 7111−7116.
[11] S.-M. Kuang, Z.-Z. Zhang, Q.-G. Wang, T. C. W. Mak, *Chem. Commun.* **1998**, 581−582.
[12] I. Ino, J. C. Zhong, M. Manukata, T. Kudora-Sowa, M. Maekawa, M. Suenaga, Y. Kitamori, *Inorg. Chem.* **2000**, *39*, 4273−4279.
[13] P. D. Harvey, *Polymer Preprint* **2004**, *45*, 433−434.
[14] P. D. Harvey, *Macromol. Symp.* **2004**, *209*, 81−95.
[15] D. Fortin, M. Drouin, M. Turcotte, P. D. Harvey, *J. Am. Chem. Soc.* **1997**, *119*, 531−541.
[16] D. Perreault, M. Drouin, A. Michel, P. D. Harvey, *Inorg. Chem.* **1992**, *31*, 3688−3689.
[17] É. Fournier, F. Lebrun, A. Decken, P. D. Harvey, *Inorg. Chem.* **2004**, *43*, 3127−3135.
[18] M. Turcotte, P. D. Harvey, *Inorg. Chem.* **2002**, *41*, 2971−2974.
[19] D. Fortin, M. Drouin, P. D. Harvey, *J. Am. Chem. Soc.* **1998**, *120*, 5351−5352.
[20] T. Zhang, M. Drouin, P. D. Harvey, *Inorg. Chem.* **1999**, *38*, 1305−1315.
[21] T. Zhang, M. Drouin, P. D. Harvey, *Inorg. Chem.* **1999**, *38*, 957−963.
[22] É. Fournier, S. Sicard, A. Decken, P. D. Harvey, *Inorg. Chem.* **2004**, *43*, 1491−1501.
[23] S. Sicard, J.-F. Bérubé, D. Samar, A. Massaoudi, F. Lebrun, J.-F. Fortin, D. Fortin, A. Decken, P. D. Harvey, *Inorg. Chem.* **2004**, *43*, in press.
[24] P. A. Dean, J. J. Vittal, R. S. Srivastava, *Can. J. Chem.* **1987**, *65*, 2628−2633.
[25] D. Perreault, M. Drouin, A. Michel, V. M. Miskowski, W. P. Schaefer, P. D. Harvey, *Inorg. Chem.* **1992**, *31*, 695−702.
[26] Z. Mao, H.-Y. Chao, Z. Hui, C.-M. Che, W.-F. Fu, K.-K. Cheung, N. Zhu, *Chem. Eur. J.* **2003**, *9*, 2885−2894.
[27] P. D. Harvey, *Coord. Chem. Rev.* **2001**, *219−221*, 17−52.
[28] D. Fortin, M. Drouin, P. D. Harvey, F. G. Herring, D. A. Summers, R. C. Thompson, *Inorg. Chem.* **1999**, *38*, 1253−1260.
[29] D. Perreault, M. Drouin, A. Michel, P. D. Harvey, *Inorg. Chem.* **1993**, *32*, 1903−1912.
[30] W. Bensch, M. Prelati, W. Ludwig, *J. Chem. Soc., Chem. Commun.* **1986**, 1762−1763.
[31] F. A. Cotton, G. Wilkinson, P. Gaus, *Basic Inorganic Chemistry*, Wiley, New York, **1995**, p.61.
[32] U.M. Tripathi, A. Bauer, H. Schmidbaur, *J. Chem. Soc., Dalton Trans.* **1997**, 2865.
[33] R. V. Kirss, R. Eisenberg, *Inorg. Chem.* **1989**, *28*, 3372−3380.
[34] L. J. Manojlovic-Muir, K. W. Muir, M. C. Grossel, M. P. Brown, C. D. Nelson, A. Yavari, E. Kallas, R. P. Moulding, K. R. Seddon, *J. Chem. Soc., Dalton Trans.* **1986**, 1955−1963.
[35] H. H. Karsch, U. Schubert, *Z. Naturforsch., Teil B* **1982**, *37*, 186−189.
[36] P. D. Harvey, M. Drouin, T. Zhang, *Inorg. Chem.* **1997**, *36*, 4998−5005.
[37] S. S. M. Ling, I. R. Jobe, A. J. McLennan, L. J. Manojlovic-Muir, K. W. Muir, R. J. Puddephatt, *J. Chem. Soc., Chem. Commun.* **1985**, 566−567.
[38] K. H. Leung, D. L. Phillips, Z. Mao, C.-M. Che, V. M. Miskowski, C.-M. Chan, *Inorg. Chem.* **2002**, *41*, 2054−2059.
[39] H.-X. Zhang, C.-M. Che, *Chem. Eur. J.* **2001**, *7*, 4887−4893.
[40] W.-F. Fu, K.-C. Chan, K.-K. Cheung, C.-M. Che, *Chem. Eur. J.* **2001**, *7*, 4656−4664.
[41] K. H. Leung, D. L. Phillips, M.-C. Tse, C.-M. Che, V. M. Miskowski, *J. Am. Chem. Soc.* **1999**, *121*, 4799−4803.
[42] W.-F. Fu, K.-C. Chan, V. M. Miskowski, C.-M. Che, *Angew. Chem. Int. Ed.* **1999**, *38*, 2783−2785.
[43] P. D. Harvey, H. B. Gray, *J. Am. Chem. Soc.* **1988**, *110*, 2145−2147.
[44] P. D. Harvey, R. F. Dallinger, W. H. Woodruff, H. B. Gray, *Inorg. Chem.* **1989**, *28*, 3057−3059.
[45] D. Piché, P. D. Harvey, *Can. J. Chem.* **1994**, *72*, 705−713.
[46] V. M. Miskowski, T. P. Smith, T. M. Loehr, H. B. Gray, *J. Am. Chem. Soc.* **1985**, *107*, 7925−7934.
[47] R. A. Levenson, H. B. Gray, *J. Am. Chem. Soc.* **1975**, *97*, 6042−6047.
[48] M. S. Wrighton, D. S. Ginley, *J. Am. Chem. Soc.* **1975**, *97*, 4246−4251.
[49] H. B. Abrahamson, C. C. Frazier, D. S. Ginley, H. B. Gray, J. Lilienthal, D. R. Tyler, M. S. Wrighton, *Inorg. Chem.* **1977**, *16*, 1554−1556.
[50] D. R. Tyler, R. A. Levenson, H. B. Gray, *J. Am. Chem. Soc.* **1978**, *100*, 7888−7893.
[51] J. Markham, *J. Rev. Mod. Phys.* **1959**, *31*, 956−989.
[52] P. D. Harvey, Z. Murtaza, *Inorg. Chem.* **1993**, *32*, 4721−4729.
[53] P. D. Harvey, W. P. Schaefer, H. B. Gray, *Inorg. Chem.* **1988**, *27*, 1101−1104.
[54] A. A. Orio, B. B. Chastain, H. B. Gray, *Inorg. Chim. Acta* **1969**, *3*, 8−10.
[55] M. M. Savas, W. R. Mason, *Inorg. Chem.* **1987**, *26*, 301−307.
[56] N. J. Turro, *Modern Molecular Photochemistry*, Benjamen/Cummings Pub. Co., Menlo Park, **1978**, p. 235.
[57] C.-M. Che, M.-C. Tse, M. C. W. Chan, K.-K. Cheung, D. L. Phillips, K. H. Leung, *J. Am. Chem. Soc.* **2000**, *122*, 2464−2468.
[58] W. D. Weber, G. W. Gokel, I. K. Ugi, *Angew. Chem. Int. Ed. Engl.* **1972**, *11*, 530−531.
[59] B. J. Hathaway, D. G. Holah, J. D. Postlethwaite, *J. Chem. Soc.* **1961**, 3215−3218.
[60] D. D. Perrin, W. L. F. Armarego, D. R. Perrin, *Purifications of Laboratory Chemicals*, Pergamon, Oxford, **1966**.
[61] A. J. Gordon, R. A. Ford, *The Chemist's Companion, a Handbook of Practical Data, Techniques, and References*, Wiley, New York, **1972**, p. 436.
[62] *SAINT 6.02*, Bruker AXS, Inc., Madison, Wisconsin, **1997−1999**.
[63] *SADABS*, George Sheldrick, Bruker AXS, Inc., Madison, Wisconsin, **1999**.

 © 2004 Wiley-VCH Verlag GmbH & Co. KGaA, Weinheim

[64] *SHELXTL 5.1*, George Sheldrick, Bruker AXS, Inc., Madison, Wisconsin, **1997**.
[65] E. C. Lim, J. D. Laposa, J. M. H. Yu, *J. Mol. Spectrosc.* **1966**, *19*, 412−420.
[66] A. Siemiarczuk, B. D. Wagner, W. R. Ware, *J. Phys. Chem.* **1990**, *94*, 1661−1666.
[67] A. Siemiarczuk, W. R. Ware, *Chem. Phys. Lett.* **1989**, *160*, 285−290.

Received June 20, 2004
Early View Article
Published Online September 9, 2004

 © 2004 Wiley-VCH Verlag GmbH & Co. KGaA, Weinheim

Formation of Sulfur−Sulfur Bonds in Copper Complexes

Gabriel Aullón*[a] and Santiago Alvarez[a]

Keywords: Copper-sulfur complexes / Ligand−ligand bonds / Density functional calculations / Through-ring bonding / Electronic structure

The recently reported dinuclear complexes [$Cu_2(\mu\text{-}S_2)$(diketiminato)$_2$] that have short S–S distances across their Cu_2S_2 rings are theoretically studied with the help of density functional calculations and a topological analysis of the electron density. The possibility of obtaining the isomeric form without a S–S bond is explored by comparing the structure and bonding with its oxo analogue. A study of the influence of several terminal-chelating ligands on the relative stability of the sulfido- and the disulfido-bridged forms is also presented. The only way to stabilize a sulfido-bridged isomer is found to be via two-electron reduction, whereas chemical substitutions are not able to produce the cleavage of the S–S bond.
(© Wiley-VCH Verlag GmbH & Co. KGaA, 69451 Weinheim, Germany, 2004)

Introduction

The rich chemistry of copper-oxygen compounds is dramatically modified when we move to the sulfur analogues, limited to a few examples in biological chemistry, such as cupredoxins[1] and metallothioneins.[2] An example is provided by the so-called Cu_A dinuclear center, active in electron transfer processes, and present in heme-copper oxidases and also nitrous oxide reductases.[3] Its basic unit is a Cu_2S_2 ring in which two cysteine ligands bridge the two copper atoms, whose coordination sphere is completed with two terminal histidine and methionine residues. In such compounds both the oxidation states I and II are available for the metal atoms.

A recently reported reaction of a β-diketiminato Cu^{II} complex with $(TMS)_2S$ or a Cu^{I} analog with S_8 yields the disulfido Cu^{II} complexes of type **1a**.[4] One can in principle expect an alternative structure for the same compounds, schematically represented in **1b**, formally a sulfido/Cu^{III} complex with a long through-ring S···S distance, similar to what is found for oxygen-bridged copper complexes, for which equilibria between the peroxo and oxo-bridged forms have been well characterized.[5,6] We asked ourselves two questions that we tried to answer by performing a theoretical study: Could the sulfido-bridged Cu^{III} isomer **1b** be isolated? What could be made to favor the formation of that isomer? These compounds belong to a wider family represented by **2a** and **2b**, and challenge our understanding of the electronic structure and bonding of double bridged dinuclear complexes, since the framework electron counting rules[7,8] predict it to present the regular ring structure **2b**, with no S−S bonding interactions across the ring, in clear disagreement with the experimental result. Therefore, understanding the structural preferences of these compounds is a relevant task considering the importance of copper complexes in several biological processes.[9]

1a

1b

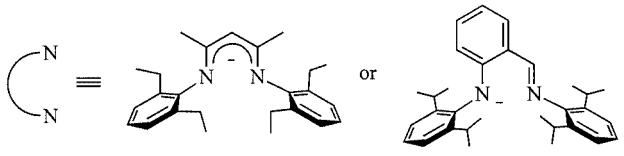

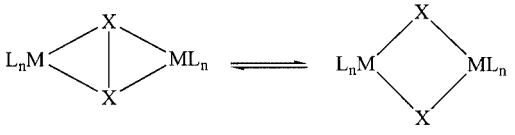

2a **2b**

To the best of our knowledge, the only structurally characterized copper compound with unsubstituted bridging sulfur atoms is the disulfido-bridged complex [$Cu_2(\mu\text{-}S_2)$(HB{3,5-*i*Prpz}$_3$)$_2$], which also has a rather short S−S

[a] Departament de Química Inorgànica and Centre de Recerca en Química Teòrica, Universitat de Barcelona, Avda. Diagonal 647, 08028 Barcelona, Spain
Supporting information for this article is available on the WWW under http://www.eurjic.org or from the author.

 © 2004 Wiley-VCH Verlag GmbH & Co. KGaA, Weinheim **DOI: 10.1002/ejic.200400206**

distance (2.07 Å) across the $\{Cu_2S_2\}^{2+}$ unit.[10] Other Cu_2S_2 cores either correspond to thiolato bridges or belong to cubane-type Cu_4S_4 structures. Examples of square-planar complexes of d^8 ions of the type $[L_2M(\mu\text{-}XR_n)_2ML_2]$, with dialkylphosphido or thioether bridges (XR_n = PR_2, SR_2) are known and they all have regular M_2X_2 rings without bonding interactions across the diamond (2.82−2.90 and 2.92−3.06 Å, respectively), whereas a silylene bridged compound (XR_n = SiR_2) has a short Si···Si distance (≈ 2.6 Å).[7] Recently, we have studied the possibility of ring isomers for $[M_2(\mu\text{-}X)_2(PR_3)_4]$ complexes with square-planar metals, where M and X are group 10 and 16 elements, respectively.[11]

We attempt here to extend these theoretical studies to copper-sulfur complexes in order to understand their structural behavior and to compare them with the important analogous oxo-bridged compounds.[8,12] In particular we would like to find out whether the alternative structure **1b** for a copper-sulfur core could be obtained by an adequate choice of terminal ligands. To that end, we report calculations based on density functional theory for $[Cu_2(\mu\text{-}O)_2(dki)_2]$ and $[Cu_2(\mu\text{-}S)_2(dki)_2]$, as well as for the reduced species $[Cu_2(\mu\text{-}S)_2(dki)_2]^{2-}$ and for several related complexes $[Cu_2(\mu\text{-}S)_2(chel)_2]$, where chel stands for a variety of bidentate ligands and dki represents a β-diketiminato ligand.

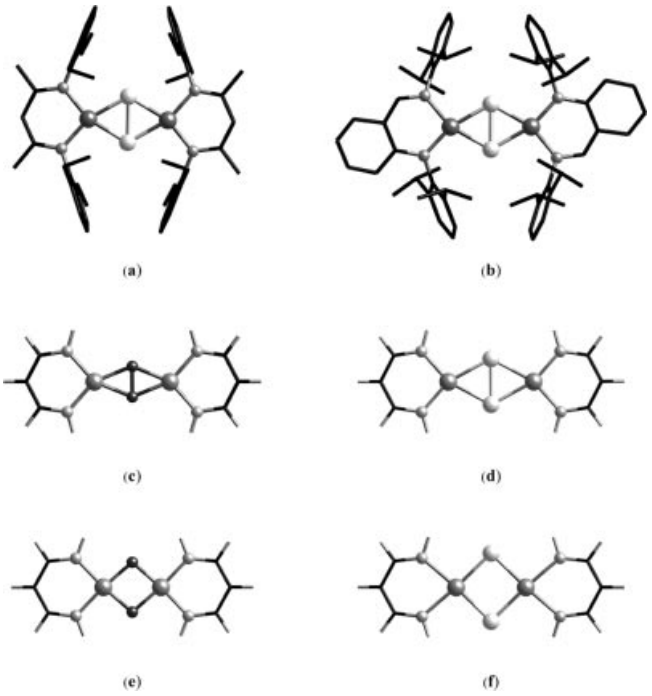

Figure 1. Experimental structures[4] of $[Cu_2(\mu\text{-}S_2)(dki)_2]$ (**a** and **b**), and optimized structures of $[Cu_2(\mu\text{-}O_2)(dki)_2]$ (**c**), $[Cu_2(\mu\text{-}S_2)(dki)_2]$ (**d**), $[Cu_2(\mu\text{-}O)_2(dki)_2]$ (**e**) and $[Cu_2(\mu\text{-}S)_2(dki)_2]^{2-}$ (**f**)

Results and Discussion

Optimized Structures: The main results of our DFT calculations for complexes of formula $[Cu_2(\mu\text{-}X)_2(chel)_2]$ (X = O or S) are reported in Table 1 and the optimized structures are shown in Figure 1. The atomic coordinates of structures corresponding to calculated energy minima are supplied as Supporting Information (see footnote on the first page of this article). We discuss here the diketiminato complexes and defer the analysis of the results with other terminal ligands to a later section. For $[Cu_2(\mu\text{-}O)_2(dki)_2]$, two minima are found that correspond to different through-ring O−O distances (2.36 and 1.44 Å, respectively), in agreement with previous results for a related simpler model $[Cu_2(\mu\text{-}O)_2(NH_3)_6]$[12] and with the existence of structurally characterized compounds with either structure (Table 2). The existence of an energy minimum at a long O−O distance agrees well with the prediction of the FEC rules for d^8 transition metals with square-planar coordination and O^{2-} as bridging ligands. Other optimized structural data (e.g., O···O and Cu−O distances of 2.36 Å and 1.81 Å, respectively) are in good agreement with experimental results for related complexes (2.26−2.35 and 1.80−1.86 Å, respectively, see Table 2) and for the infinite chains of CuO_2^- present in solid state compounds (2.45−2.51 and 1.82−1.85 Å). All these data for the isomers of type **2b** are consistent with their formulation as Cu^{III} compounds[13] for which planar rings can be expected.[14]

A geometry of the type **2a**, such as that with a short O−O distance found here for $[Cu_2(\mu\text{-}O)_2(dki)_2]$, has recently been analyzed in related compounds of group 10 metals.[11] In that study, the isoelectronic oxo complexes having Pd_2O_2 and Pt_2O_2 cores always produce the two minima that

Table 1. Optimized data for the two isomers (**2a** and **2b**) of diketiminate complexes with $Cu_2(\mu\text{-}X)_2$ core (X = O or S). Distances in Å, angles in degrees and energies in kcal·mol^{-1}.

Compound	Isomer	X···X	Cu−X	Cu−L	X−Cu−X	L−Cu−L	Energy
$[Cu_2(\mu\text{-}O)_2(dki)_2]$	**2a**	1.443	1.944	1.933	43.6	96.7	+0.7
	2b	2.359	1.808	1.897	81.4	92.3	0.0
$[Cu_2(\mu\text{-}S)_2(dki)_2]$	**2a**	2.178	2.313	1.928	56.2	97.2	0.0
	2b	3.238[a]	2.307	1.924	89.1	92.9	+21.4
$[Cu_2(\mu\text{-}S)_2(dki)_2]^{2-}$	**2a**	2.178[a]	2.516	2.103	51.3	87.6	+7.0
	2b	3.238	2.321	2.142	88.5	81.0	0.0

[a] Parameter frozen in the geometry optimization.

 © 2004 Wiley-VCH Verlag GmbH & Co. KGaA, Weinheim

Table 2. Main structural parameters for experimental structures of $[Cu_2(\mu-X)_2L_4]$ complexes (X = O, S) and of inorganic solids of formula $ACuX_2$ (A = alkaline cation)

Compound	X···X	Cu−X	X−Cu−X	Cu−L	L−Cu−L	Ref.	Code[a]
Isomer **2a**							
$[Cu_2S_2(N,N'\text{-Ar-NC}_6H_4CH{=}N)_2]$	2.166	2.206	58.8	1.901	97.7	[4]	–
$[Cu_2S_2(N,N'\text{-Ar-1,3-Me-dki})_2]$	2.201	2.195	60.2	1.908	99.3	[4]	–
$[Cu_2S_2(HB\{3,5\text{-}i\text{Pr-pz}\}_3)_2]$ [b]	2.072	2.265	54.5	2.018	93.3	[10]	LEJBOR
$[Cu_2O_2(HB\{3,5\text{-}i\text{Pr-pz}\}_3)_2]$ [b]	1.413	1.913	43.3	1.997	92.6	[15]	KECZEK10
$[Cu_2O_2(\{6\text{-Me-py}_2CHpy\}_2C_2H_4)]^{2+}$ [b]	1.486	1.908	45.8	1.995	91.6	[16]	GUGPUT
Isomer **2b**							
$[Cu_2O_2(N,N'\text{-Ar-1,3-Me-dki})(C_3H_6\{NMe_2\}_2)]^{2+}$	2.259	1.818	76.8	1.943	98.7	[17]	OGIXAD
$[Cu_2O_2(9ane\text{-}BzN_3)_2]^{2+}$ [b]	2.287	1.806	78.6	1.986	88.9	[18]	ZOSXIO10
$[Cu_2O_2(\{pyCH_2\}\{6\text{-Me-py}CH_2\}_2N)_2]^{2+}$ [b]	2.323	1.803	80.2	1.940	87.0	[19]	QIDBUA
$[Cu_2O_2(\{9ane\text{-}i\text{PrN}_3\}_2C_2H_4)]^{2+}$ [b]	2.352	1.827	80.1	1.991	88.0	[20]	RENZEP
$[Cu_2O_2(C_6H_{10}\{NMeEt\}_2)_2]^{2+}$	2.344	1.807	80.8	1.938	89.6	[21]	NUWDAK
$[Cu_2O_2(t\text{Bu}_2P\{NSiMe_3\}_2)_2]$	2.339	1.865	77.7	1.978	77.4	[22]	WOMVOJ
$LiCuO_2$	2.469	1.836	84.5	1.836	84.5	[23]	074978
$NaCuO_2$	2.446	1.839	83.4	1.839	83.4	[24−26]	203080
$KCuO_2$	2.460	1.829	84.5	1.829	84.5	[26−28]	203081
$RbCuO_2$	2.500	1.845	85.3	1.845	85.3	[27]	015096
$CsCuO_2$	2.511	1.849	85.5	1.849	85.5	[27]	015097

[a] Alphanumerical code for CSD[29] or ICSD[30]. [b] The terminal ligand acts as tridentate.

we have also observed for Cu. This second isomer can be formulated as either having two d^{10} transition metal atoms bridged by a side-on bridging dioxygen molecule (**3a**), or two d^9 Cu^{II} ions, side-on bridged by a peroxo group (**3b**). As found earlier,[11] the Cu−O edges of the diamonds in the complex with structure **2a** (1.94 Å) are significantly longer than in the **2b** isomer (1.81 Å). Such distances, as well as the O−O one (1.44 Å) are in excellent agreement with those experimentally found in complexes that present this structural motif (≈ 1.91 and 1.41−1.49 Å, respectively, see Table 2).

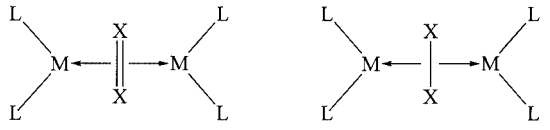

3a

3b

When oxygen atoms are replaced by sulfur, an important change is produced,[12] since only one minimum with a short S−S distance (2.18 Å) is found for $[Cu_2(\mu\text{-S})_2(dki)_2]$. Such a distance is consistent with the experimental values (2.16 and 2.20 Å) in the complexes prepared by Tolman et al.[4] and somewhat longer than in the other known compound with bare sulfur atom bridges, $[Cu_2(\mu\text{-S}_2)(HB\{3,5\text{-}i\text{Prpz}\}_3)_2]$ (2.07 Å).[10] This behavior is remarkably different from that found earlier for isoelectronic complexes of group 10 metals with sulfur bridging atoms, since the two minima (**2a** and **2b**) were found for the Pd_2S_2 core, whereas Ni_2S_2 and Pt_2S_2 compounds are predicted to only have structure **2b**.[11]

Since it is well known that $\{Cu_2(\mu\text{-O})_2\}^{2+}$ species acting as mild two-electron oxidants are reduced to $\{Cu_2(\mu\text{-O})_2\}^{0}$,[5,31] it seemed interesting to explore the hypothetical reduced sulfur complex $[Cu_2(\mu\text{-S})_2(dki)_2]^{2-}$. For this compound the **2b** isomer appears to correspond to an energy minimum (see Figure 1). The structural data (e.g., S···S = 3.24, Cu···Cu = 3.34 and Cu−S ca. 2.32 Å) are in excellent agreement with those in two structurally characterized isoelectronic Cu^{II} compounds with thiolato bridges (Cu···Cu = 3.34 and Cu−S = 2.33 Å).[32] It is remarkable that the Cu−N distances increase upon reduction from 1.93 to 2.14 Å, in contrast with what happens with the Cu−S distances, that are practically unaltered. Other bond lengths are practically unaffected by reduction, except for a decrease of the bite distance (N···N) of the bidentate dki ligand (≈ 0.1 Å shorter) concomitant with the increased Cu−N distance. Alternatively, in agreement with the framework electron counting rules,[7] a second structure for the reduced complex $[Cu_2(\mu\text{-S})_2(dki)_2]^{2-}$ with tetrahedrally coordinated copper atoms and a short S−S distance (2.31 Å) is found as an energy minimum, only a few kcal·mol^{-1} above the **2b** isomer. Given the small energy difference between alternative geometries, one can anticipate that both could be obtained experimentally.

Cross sections of the potential energy surfaces for the O- and S-bridged complexes $[Cu_2(\mu\text{-X})_2(dki)_2]$ are presented in Figure 2, where the calculated energy is plotted as a function of the normalized X···X distance. For the Cu_2S_2 core the minimum is found at a normalized distance of 1.07 (i.e., a S−S distance that is practically twice the sulfur atomic radius[12]). Upon reduction, the minimum is shifted to 1.59 (**2b**), a geometry that is 21 kcal·mol^{-1} above the minimum for the neutral species. For the analogous complex with a

 © 2004 Wiley-VCH Verlag GmbH & Co. KGaA, Weinheim

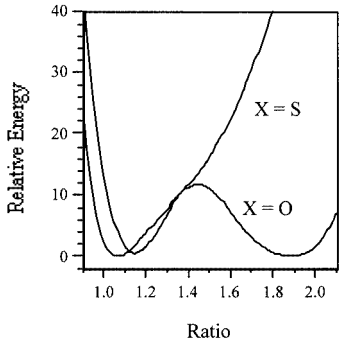

Figure 2. Relative energy (in kcal·mol^{-1}) as a function of the normalized X···X distance for complexes $[Cu_2(\mu\text{-}X)_2(dki)_2]$ (X = O or S). The normalized distance is defined as the ratio between the X···X distance and twice the atomic radius of X

Cu_2O_2 core, two nearly isoenergetic minima appear with O···O distances at 1.15 and 1.87 times the atomic radii sum and the transition state can be estimated to appear near 1.45 with an approximate barrier of 11.8 kcal·mol^{-1}. These results are in agreement with the equilibrium between two isomers recently proposed for the activation of O_2 by β-diketiminatocopper(I),[33] but the evaluation of the energy difference between the oxo- and peroxo-bridged forms of copper complexes is not straightforward and the reader is referred to a recent study by P. Siegbahn[34] for a more detailed discussion.

Orbital Analysis: In an attempt to understand the different behaviors of the oxo and sulfido-bridged complexes, we report here on an analysis of the corresponding molecular orbitals. In the oxo isomer with a regular ring **2b**, the bonding within the $\{Cu_2X_2\}^{2+}$ core can be associated with four framework bonding molecular orbitals (a_g, b_{1u}, b_{2g} and b_{3u} in Figure 3). For the Cu^{III}/O^{2-} compound, these four orbitals are occupied, whereas the framework antibonding orbitals (only two out of four are shown as the uppermost orbitals in Figure 3: $2b_{2g}$ and $2b_{3u}$).

As the rhombus distorts and the two oxygen atoms approach each other, the energies of the framework orbitals change due to the interplay of the through-ring σ overlap and the metal-bridging ligand overlap. Since two occupied framework orbitals are stabilized and two are destabilized upon distortion, two minima appear, separated by a low barrier resulting from the crossing between the two b_{3u} orbitals. Additionally, an important change in composition of the framework orbitals is induced by the approach of the two oxygen atoms, the occupied bonding b_{3u} combination becoming localized at the Cu atoms and the empty antibonding one at the bridging O atoms.[7,8,11,12] The outcome of such an orbital localization is that the two b_{3u} electrons

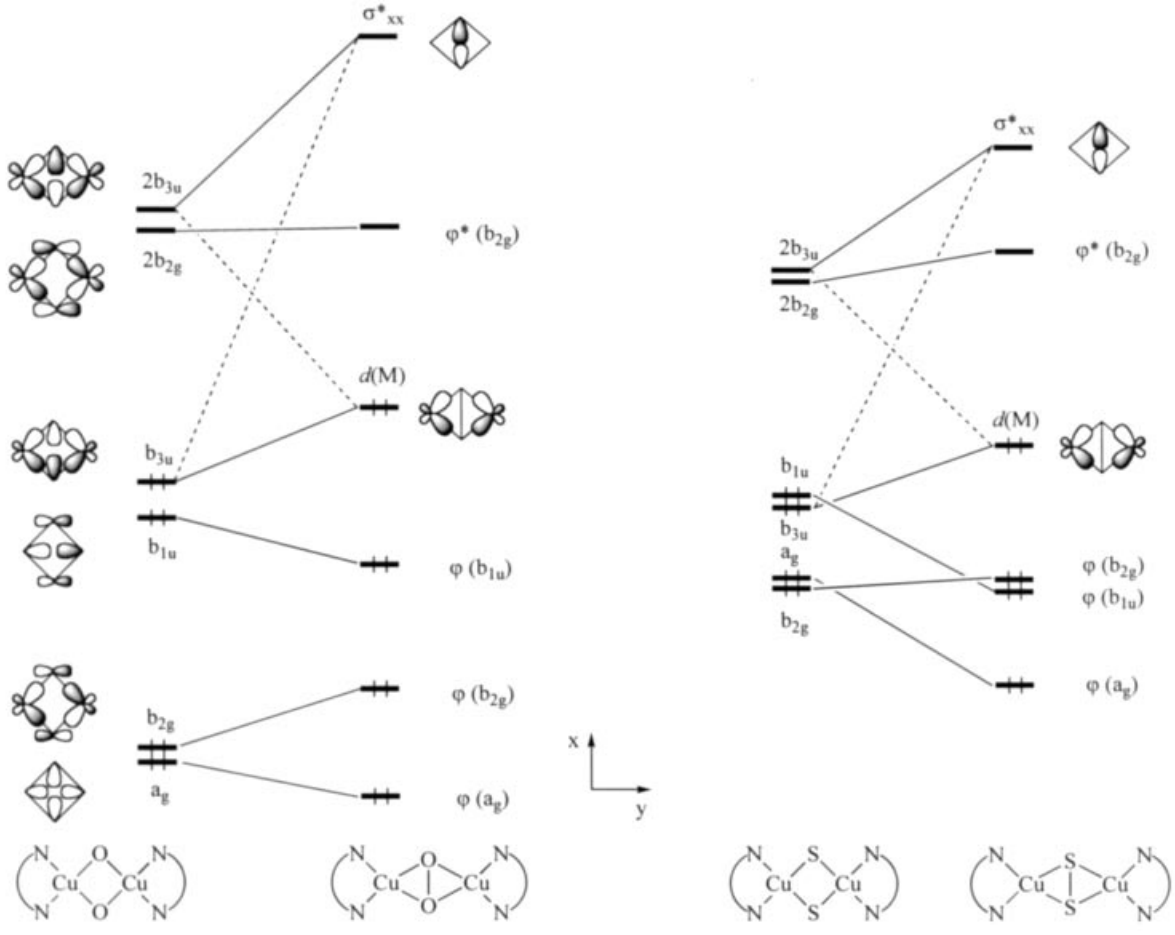

Figure 3. Simplified orbital diagram for the compounds $[Cu_2(\mu\text{-}O)_2(dki)_2]$ (left) and $[Cu_2(\mu\text{-}S)_2(dki)_2]$ (right)

 © 2004 Wiley-VCH Verlag GmbH & Co. KGaA, Weinheim

are transferred from the Cu_2O_2 framework to the metal d orbitals, the copper atoms becoming formally Cu^{II} and the bridging oxo ions forming a peroxo bridge (notice the loss of σ* character of the occupied b_{3u} orbital in the **2a** form), which is the reason why the framework electron counting rule[7,8,11,12] fails. It must be noted that a strong antiferromagnetic coupling should be expected between the two Cu^{II} ions.[35] Such a description of the electronic structure of the **2a** form is consistent with the results of a natural bond order (NBO)[36] analysis, that indicates a net charge transfer of about 0.4 e^- from each sulfur atom to copper and the terminal ligands when going from **2b** to **2a**. It is also seen that such a charge transfer occurs mainly between the p_x orbitals of the bridges and the d_{xy} orbitals of the copper atoms, as would be expected from the change in the composition of the b_{3u} framework orbital.

For the analogous sulfur complex, a similar orbital picture should apply (Figure 3), but in fact we find only the disulfido-bridged compound **1a**, both theoretically and experimentally. The main difference between the two Walsh diagrams can be found in the occupied b_{2g} orbital, which is significantly stabilized when the two bridges are taken apart for X = O, but is practically insensitive to the bridge-bridge distance for X = S. The analysis of the composition of that orbital (Figure 4) clearly shows that in the sulfido-bridged compound there is little contribution from the metal to this molecular orbital, thus accounting for its nearly constant energy throughout the **2a** ⇆ **2b** interconversion path. It is likely that the lesser mixing of the metal xy and the sulfur p orbitals in b_{2g} for the sulfido bridges compared with the oxo ones should be attributed to the less electronegative character of sulfur. A similar effect was previously observed for isoelectronic square-planar Pt complexes with XH_2 bridges,[7] for which increasing orbital localization and decreasing through-ring X···X distances (S > P > Si) were found for different bridging atoms. Since the degree of mixing is likely to be affected by the basis set used, this finding could provide a rationale for the strong effect that the basis set has on the calculated relative energies of isomers **2a** and **2b** in other cases, as recently reported by Siegbahn.[34] Also the different behavior of related Ni, Pd and Pt complexes found recently by us[11] might be related to this subtle orbital effect.

Upon two-electron reduction of the sulfido complex, the structure is dramatically modified and the regular Cu_2S_2 ring with a long S···S distance is obtained. From Figure 3 it is clear that such a geometry change must be associated with the occupation of the high lying (framework antibonding) b_{3u} orbital. The proximity of b_{2g} and b_{3u} suggests an open shell ground state for this compound. Indeed our broken symmetry calculations indicate open shell singlet and triplet states to be close in energy, with the former being more stable (by 240 cm^{-1}), indicating antiferromagnetic coupling of the two Cu^{II} ions, in good agreement with the observed line broadening in the ^1H NMR spectrum and the EPR-silent nature of the experimentally known analogues.[32] All these results are consistent with the formal description of the reduced compound as Cu^{II}/S^{2-}, although the increase in Cu−N distances upon reduction is indicative of significant delocalization throughout the $\{Cu_2S_2\}$ core.

Analysis of the Electron Density: To further characterize the electronic structure of the studied compounds, we carried out a topological analysis of the electron density ρ(*r*) for the optimized geometries, according to the "Atoms in Molecules" theory.[37] According to Bader, the main properties of the electron density can be summarized in terms of critical points. A bond critical point corresponding to two negative and one positive curvatures, is also referred to as a (3, −1) critical point, and is taken as an indication of the presence of a chemical bond. On the other hand, ring

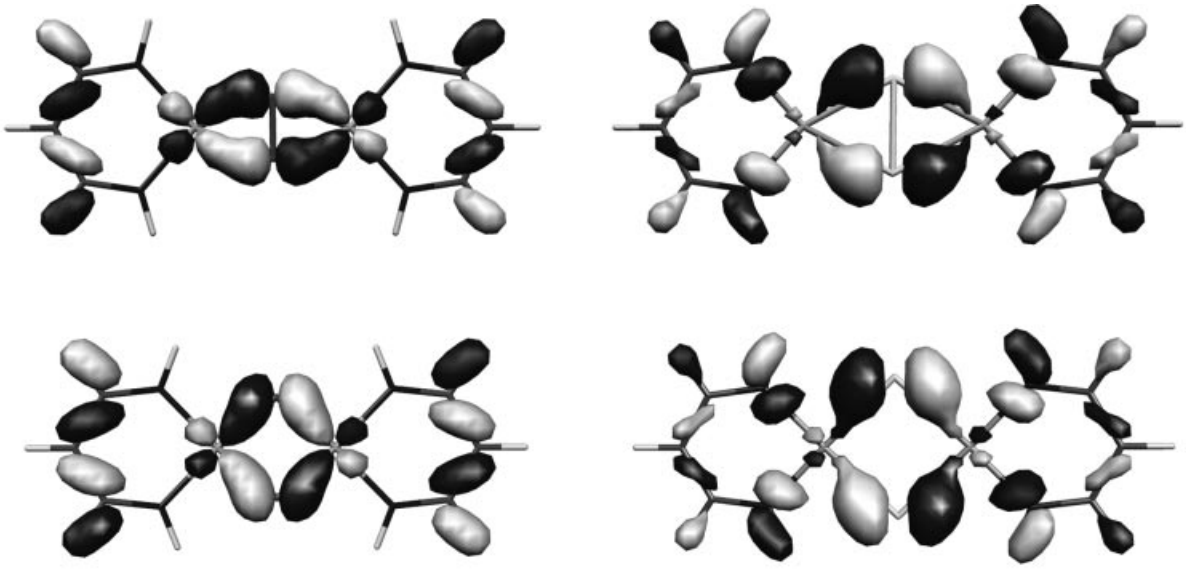

Figure 4. Composition of the occupied b_{2g} molecular orbital in the $[Cu_2(\mu\text{-}X)_2(dki)_2]$ complexes with X = O (left) and S (right) in the **2a** (top) and **2b** (bottom) geometries

 © 2004 Wiley-VCH Verlag GmbH & Co. KGaA, Weinheim

critical points (3, +1) are characterized by a single negative curvature and are taken as an indication of a cyclic path of chemical bonds around it.

For the $[Cu_2(\mu\text{-}X)_2(dki)_2]$ compounds (X = S, O) with geometries **2a** and **2b** we have found four bond critical points between each Cu−X pair (Figure 5), consistent with the presence of four Cu−X single bonds, according to their ellipticities ($\varepsilon < 0.06$ for X = S and $\varepsilon < 0.10$ for X = O). The positive values of $\nabla^2\rho(r)$ (≈ 0.20 and 0.55−0.65 for sulfur and oxygen complexes, respectively), point to shared interactions characteristic of donor-acceptor Cu−X bonds and indicate a stronger covalent character for the Cu−S bonds compared to the Cu−O ones.

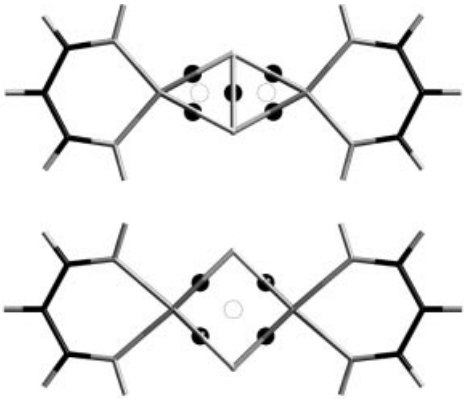

Figure 5. Localization of the critical points in Cu_2S_2 diamonds of the optimized complexes $[Cu_2(\mu\text{-}S_2)(dki)_2]$ (top) and $[Cu_2(\mu\text{-}S)_2(dki)_2]^{2-}$ (bottom). The bond critical points (3,-1) are represented by black circles, ring critical points by white circles

The optimized structures **2a** present an extra (3, −1) bond critical point between the two bridging atoms, consistent with the existence of X−X bonds (Figure 5, top). The negative value of $\nabla^2\rho(r)$ at this critical point indicates their covalent nature, and its ellipticity ($\varepsilon \approx 0.2$) shows a weak π character due to the non-negligible contribution of the Cu^I/S_2 alternative description.[11] As expected, two (3, +1) ring critical points are also found at the center of each CuS_2 ring in this case. In contrast, for structures **2b** (optimized for X = O, frozen for X = S) of $[Cu_2(\mu\text{−}X)_2(dki)_2]$, only one (3, +1) ring critical point appears at the center of the Cu_2X_2 core, consistent with the absence of through-ring bonding interactions. Similarly, the reduced sulfido bridged complex $[Cu_2(\mu\text{-}S)_2(dki)_2]^{2-}$ has, in its optimized structure, a ring critical point at the center of the Cu_2S_2 ring, as shown in Figure 5 (bottom).

Effect of the Peripheral Ligands

Now that we know, from calculations, that $[Cu_2(\mu\text{-}S)_2(dki)_2]$ is unlikely to have the **1b** structure, we wish to explore the possibility of stabilizing a Cu_2S_2 core with that geometry by using different peripheral ligands in which we can vary the nature of the donor atoms and bite of the bidentate ligand (see Scheme 1). The results (Table 3) reveal the following trends: (*a*) two minima appear for $\{Cu_2O_2\}^{2+}$ cores whereas only the **2a** isomer is found to correspond to an energy minimum for the related $\{Cu_2S_2\}^{2+}$ complexes;[12] (*b*) changes in the L−Cu−L bite angles within the 66−107° range do not significantly stabilize the sulfido-bridged structure; (*c*) the negatively charged ligands stabilize isomer **2b** relative to **2a** to a certain extent, the former appearing some 30−40, 21−31 and 11−18 kcal·mol^{-1} higher for neutral, monoanionic and dianionic ligands, respectively; (*d*) the tridentate macrocyclic ligands explored destabilize isomer **2a** and show a marked preference for a pseudotetrahedral coordination sphere of the copper atoms, with the sulfur-sulfur bond occupying one of the coordination sites at short S−S distances,[8,12,38] as observed in the experimental compounds cited in the introductory section.

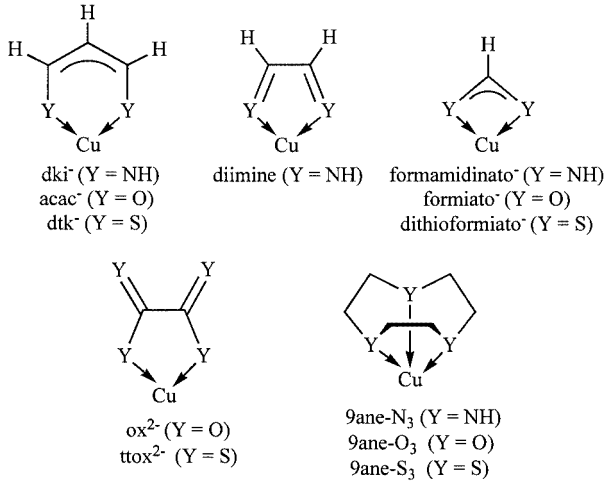

Scheme 1

It is noteworthy that the sulfido-bridged complexes with tridentate terminal ligands (Table 3, last three entries) all give rather short S−S distances (2.06−2.13 Å), as does the tris(pyrazolyl)borato complex of Kitajima (2.07 Å). This is probably an indication of the important contribution of the Cu^I/S_2 form (**3a**), which is favored in the pseudotetrahedral environment provided by a tridentate ligand and the side-on bonded S_2 molecule.[12]

Conclusions

A theoretical study on $[Cu_2(\mu\text{-}X)_2(dki)_2]$ complexes (X = O, S) indicates that two isomers are attainable for X = O, corresponding to peroxo- and oxo-bridged structures **2a** and **2b**, in agreement with the experimental structural data available for a variety of copper-oxygen compounds. The compound with X = S, in contrast, seems to give only the disulfido-bridged isomer **2a**. The reason for the different behavior has been found to be the different mixing of the atomic $p_y(X)$ and $d_{xy}(Cu)$ orbitals in the framework bonding orbital of B_{2g} symmetry, that is stabilized in the oxo-bridged form **2b** with an O−Cu−O bond angle of 44°, but

 © 2004 Wiley-VCH Verlag GmbH & Co. KGaA, Weinheim

Table 3. Optimized data for the two isomers (**2a** and **2b**) of complexes with $Cu_2(\mu\text{-}X)_2$ core (X = O or S) and bidentate terminal ligands shown in Scheme 1; distances in Å, angles in degrees and energies in kcal·mol^{-1}

Compound	X···X	Cu−X	Cu−L[a]	L−Cu−L[a]	Energy
$[Cu_2(\mu\text{-}O)_2(acac)_2]$	1.443	1.936	1.927	99.0	
	2.190	1.804	1.908	96.1	+11.7
$[Cu_2(\mu\text{-}O)_2(dtk)_2]$	1.435	1.967	2.276	106.7	
	2.380	1.821	2.278	100.2	+12.5
$[Cu_2(\mu\text{-}S)_2(acac)_2]$	2.175	2.312	1.929	99.5	
	3.238[b]	2.313	1.933	96.7	+28.5
$[Cu_2(\mu\text{-}S)_2(dtk)_2]$	2.146	2.372	2.281	107.7	
	3.238[b]	2.321	2.315	99.6	+26.5
$[Cu_2(\mu\text{-}S)_2(diimine)_2]^{2+}$	2.134	2.330	2.025	81.8	
	3.238[b]	2.309	2.010	81.2	+37.2
$[Cu_2(\mu\text{-}S)_2(ox)_2]^{2-}$	2.225	2.312	1.921	88.4	
	3.238[b]	2.309	1.916	87.0	+17.5
$[Cu_2(\mu\text{-}S)_2(ttox)_2]^{2-}$	2.204	2.368	2.303	91.9	
	3.238[b]	2.304	2.326	87.4	+11.2
$[Cu_2(\mu\text{-}S)_2(HC\{NH\}_2)_2]$	2.173	2.301	2.002	67.2	
	3.238[b]	2.282	2.004	66.6	+24.4
$[Cu_2(\mu\text{-}S)_2(HCO_2)_2]$	2.166	2.308	2.046	65.9	
	3.238[b]	2.296	2.039	65.9	+30.1
$[Cu_2(\mu\text{-}S)_2(HCS_2)_2]$	2.172	2.339	2.384	76.8	
	3.238[b]	2.293	2.393	75.1	+22.9
$[Cu_2(\mu\text{-}S)_2(9ane\text{-}N_3)_2]^{2+}$	2.133	2.353	2.063, 2.180	87.6, 84.7	
	3.238[b]	2.324	2.051, 2.222	86.8, 82.7	+31.3
$[Cu_2(\mu\text{-}S)_2(9ane\text{-}O_3)_2]^{2+}$	2.059	2.443	2.086, 2.152	80.8, 79.2	
	3.238[b]	2.352	2.065, 2.200	80.3, 77.3	+37.8
$[Cu_2(\mu\text{-}S)_2(9ane\text{-}S_3)_2]^{2+}$	2.100	2.407	2.376, 2.477	94.4, 91.9	
	3.238[b]	2.338	2.399, 2.569	91.6, 87.8	+39.9

[a] Parameter frozen in the geometry optimization. [b] For tridentate ligands, the first value corresponds to the basal distance or angle, the second value to the apical one.

not in the sulfido-bridged analogue. The use of other terminal ligands with different donor atoms and a variety of bite angles proved theoretically not to be a good strategy to stabilize the sulfido-bridged isomer in dinuclear copper complexes. The use of tridentate terminal ligands results in shorter S−S distances, due to an enhanced contribution of the Cu^I/S_2 resonance form. Two-electron reduction of the disulfido-bridged complex results in the cleavage of the S−S bond and a Cu^{II}/S^{2-} dinuclear complex.

Appendix

Computational Details: Density functional calculations were carried out using the GAUSSIAN98 package[39] with the UB3LYP hybrid method that applies the Becke three parameters exchange functional[40] and the Lee−Yang−Parr correlation functional.[41] The basis set of valence double-ζ quality and effective core potentials to represent the innermost electrons of the metal atoms (LANL2DZ) was used for Cu atoms.[42] A similar description was used for S atoms,[43] supplemented with extra d-polarization functions.[44] The light elements were described with the 6−31G (C and H of ligands[45]) and 6−31G* (N and O directly attached to the metal[46]) basis sets. Since it has been recently shown that in Cu complexes with two bridges such as those studied here the choice of basis set for the bridging atoms may strongly influence the calculated relative energies of the two isomers,[34] we have performed a series of tests with different basis sets for $[Cu_2(\mu\text{-}S)_2(dki)_2]^{2-}$. The use of the same basis set described above without polarization functions gave a S−S bond length (2.66 Å) that was too long when compared with the experimental value (2.20 Å), and similar results were obtained with a 6−31G* basis set that includes polarization functions for all atoms (2.60 Å). On the other hand, both the triple-ζ TZV basis set and the one discussed in the previous paragraph were found to give excellent agreement with the experimental S−S distance for the new compound (2.23 and 2.18 Å, respectively), and the calculated energy difference between the two isomers was also similar in both cases (18.3 and 21.4 kcal/mol, respectively). These tests allowed us to conclude that the basis set chosen, with a polarization function only for those atoms directly attached to the metal, provide a description of the electronic structure practically as good as a triple-ζ basis set. For the dinuclear Cu^{II} complex $[Cu_2(\mu\text{-}S)_2(dki)_2]^{2-}$, the evaluation of the singlet-triplet energy gap has been carried out by using nonprojected DFT calculations using the methodology described elsewhere.[47] The reported exchange coupling constant corresponds to the spin hamiltonian $H = -J\, S_1 \cdot S_2$. For the topological analysis of the electron density, critical points have been generated with the *Xaim* routine.[48]

Structural Analysis: The structural data were retrieved with the help of the Cambridge Structural Database (Version 5.25, November 2003),[29] including in our search all

 © 2004 Wiley-VCH Verlag GmbH & Co. KGaA, Weinheim

compounds with Cu_2X_2 cores, X being a group 16 element. Additional crystallographic data has been obtained from the Inorganic Crystal Structure Database (Release 2003),[30] searching for ternary compounds of general formula $ACuX_2$. When more than one structure determination was available for the same compound, the one with the lowest *R* factor was selected.

Acknowledgments

Financial support for this work was provided by the Dirección General de Investigación Científica (MCyT) through grant BQU2002−04033-C02−01 and by Comissionat per a Universitats i Recerca (Generalitat de Catalunya) through grant 2001SGR-0044. The computing resources at the Centre de Supercomputació de Catalunya (CESCA) were made available in part through a grant of Fundació Catalana per a la Recerca (FCR) and Universitat de Barcelona. G. A. thanks a Ramón y Cajal research contract. The authors thank W. Tolman for providing them with experimental information prior to publication and for helpful discussions, and C. Bo (URV) for the Xaim graphical interface.

[1] Y. Lu, in *Comprehensive Coordination Chemistry II* (Ed.: T. J. Meyer), Elsevier, Amsterdam, **2004**, vol. 8, pp. 91−122.
[2] P. González-Duarte, in *Comprehensive Coordination Chemistry II* (Eds.: J. A. McCleverty, T. J. Meyer), Elsevier, Amsterdam, **2004**, vol. 8, pp. 213−228.
[3] B. G. Malmstrom, P. Wittung-Stafshede, *Coord. Chem. Rev.* **1999**, *185/186*, 127−140.
[4] E. C. Brown, N. W. Aboelella, A. M. Reynolds, G. Aullón, S. Alvarez, W. B. Tolman, *Inorg. Chem.* **2004**, *43*, 3335−3337.
[5] W. B. Tolman, *Acc. Chem. Res.* **1997**, *30*, 227−237.
[6] A. G. Blackman, W. B. Tolman, *Struct. Bonding (Berlin)* **2000**, *97*, 179−211.
[7] G. Aullón, P. Alemany, S. Alvarez, *J. Organomet. Chem.* **1994**, *478*, 75−82.
[8] S. Alvarez, A. A. Palacios, G. Aullón, *Coord. Chem. Rev.* **1999**, *185/186*, 431−450.
[9] [9a] N. Kitajima, *Adv. Inorg. Chem.* **1992**, *39*, 1−77. [9b] E. I. Solomon, M. J. Baldwin, M. D. Lowery, *Chem. Rev.* **1992**, *92*, 521−542. [9c] S. Fox, J. A. Potenza, S. Knapp, H. J. Schugar, in *Bioinorganic Chemistry of Copper* (Ed.: Z. Tyeklar), Chapman & Hall, New York, **1993**, pp. 34−47.
[10] K. Fujisawa, Y. Moro-oka, N. Kitajima, *J. Chem. Soc., Chem. Commun.* **1994**, 623−624.
[11] G. Aullón, M. Hamidi, A. Lledós, S. Alvarez, *Inorg. Chem.* **2004**, *43*, 3702−3714.
[12] X.-Y. Liu, A. A. Palacios, J. J. Novoa, S. Alvarez, *Inorg. Chem.* **1998**, *37*, 1202−1212.
[13] J. L. DuBois, P. Mukherjee, A. M. Collier, J. M. Mayer, E. I. Solomon, B. Hedman, T. D. P. Stack, K. O. Hodgson, *J. Am. Chem. Soc.* **1997**, *119*, 8578−8579.
[14] G. Aullón, G. Ujaque, A. Lledós, S. Alvarez, P. Alemany, *Inorg. Chem.* **1998**, *37*, 804−813.
[15] [15a] N. Kitajima, K. Fujisawa, Y. Moro-oka, *J. Am. Chem. Soc.* **1989**, *111*, 8975−8976. [15b] N. Kitajima, K. Fujisawa, C. Fujimoto, Y. Moro-oka, S. Hashimoto, T. Kitagawa, K. Toriumi, K. Tatsumi, A. Nakamura, *J. Am. Chem. Soc.* **1992**, *114*, 1277−1291.
[16] M. Kodera, K. Katayama, Y. Tachi, K. Kano, S. Hirota, S. Fujinami, M. Suzuki, *J. Am. Chem. Soc.* **1999**, *121*, 11006−11007.
[17] N. W. Aboelella, E. A. Lewis, A. M. Reynolds, W. W. Brennessel, C. J. Cramer, W. B. Tolman, *J. Am. Chem. Soc.* **2002**, *124*, 10660−10661.
[18] [18a] J. A. Halfen, S. Mahapatra, E. C. Wilkinson, S. Kaderli, V. G. Young Jr., L. Que Jr., A. D. Zuberbühler, W. B. Tolman, *Science* **1996**, *271*, 1397−1400. [18b] S. Mahapatra, J. A. Halfen, E. C. Wilkinson, G. Pan, X. Wang, V. G. Young Jr., C. J. Cramer, L. Que Jr., W. B. Tolman, *J. Am. Chem. Soc.* **1996**, *118*, 11555−11574.
[19] H. Hayashi, S. Fujinami, S. Nagatomo, S. Ogo, M. Suzuki, A. Uehara, Y. Watanabe, T. Kitagawa, *J. Am. Chem. Soc.* **2000**, *122*, 2124−2125.
[20] S. Mahapatra, V. G. Young Jr., S. Kaderli, A. D. Zuberbühler, W. B. Tolman, *Angew. Chem. Int. Ed. Eng.* **1997**, *36*, 130−133.
[21] V. Mahadevan, Z. Hou, A. P. Cole, D. E. Root, T. K. Lal, E. I. Solomon, T. D. P. Stack, *J. Am. Chem. Soc.* **1997**, *119*, 11996−11997.
[22] B. F. Straub, F. Rominger, P. Hofmann, *Chem. Commun.* **2000**, 1611−1612.
[23] R. Berger, L.-E. Tergenius, *J. Alloys. Compd.* **1994**, *203*, 203−207.
[24] K. Hestermann, R. Hoppe, *Z. Allg. Anorg. Chem.* **1969**, *367*, 261−269.
[25] J. Pickardt, W. Paulus, M. Schmalz, R. Schöllhorn, *J. Solid St. Chem.* **1990**, *89*, 308−314.
[26] N. E. Brese, M. O′Keeffe, R. B. von Dreele, V. G. Young Jr., *J. Solid St. Chem.* **1989**, *83*, 1−7.
[27] K. Hestermann, R. Hoppe, *Z. Allg. Anorg. Chem.* **1969**, *367*, 249−260.
[28] M. T. Weller, D. R. Lines, *J. Solid St. Chem.* **1989**, *82*, 21−29.
[29] F. H. Allen, O. Kennard, *Chem. Des. Autom. News* **1993**, *8*, 31−37.
[30] *ICSD*, Gmelin-Institut für Anorganische Chemie and Fachinformationzentrum (FIZ), Karlsruhe, **1995**.
[31] [31a] V. Mahadevan, J. L. DuBois, B. Hedman, K. O. Hodgson, T. D. P. Stack, *J. Am. Chem. Soc.* **1999**, *121*, 5583−5584. [31b] S. Itoh, in *Comprehensive Coordination Chemistry II* (Eds.: J. A. McCleverty, T. J. Meyer), Elsevier, Amsterdam, **2004**, vol. 8, pp. 369−393.
[32] [32a] R. P. Houser, J. A. Halfen, V. G. Young Jr., N. J. Blackburn, W. B. Tolman, *J. Am. Chem. Soc.* **1995**, *117*, 10745−10746. [32b] Y. Ueno, Y. Tachi, S. Itoh, *J. Am. Chem. Soc.* **2002**, *124*, 12428−12429.
[33] X. Dai, T. H. Warren, *Chem. Commun.* **2001**, 1998−1999.
[34] P. Siegbahn, *J. Biol. Inorg. Chem.* **2003**, *8*, 577−585.
[35] P. K. Ross, E. I. Solomon, *J. Am. Chem. Soc.* **1990**, *112*, 5871−5872.
[36] A. E. Reed, L. A. Curtiss, F. Weinhold, *Chem. Rev.* **1988**, *88*, 899−926 and references cited therein.
[37] [37a] R. F. W. Bader, *Chem. Rev.* **1991**, *91*, 893−928. [37b] R. F. W. Bader, *Atoms in Molecules: A Quantum Theory*, Clarendon Press, Oxford, **1995**.
[38] P. L. Holland, W. B. Tolman, *Coord. Chem. Rev.* **1999**, *190−192*, 855−869.
[39] *Gaussian 98 (Revision A.7)*: M. J. Frisch, G. W. Trucks, H. B. Schlegel, G. E. Scuseria, M. A. Robb, J. R. Cheeseman, V. G. Zakrzewski, J. A. Montgomery, R. E. Stratmann, J. C. Burant, S. Dapprich, J. M. Millam, A. D. Daniels, K. N. Kudin, M. C. Strain, O. Farkas, J. Tomasi, V. Barone, M. Cossi, R. Cammi, B. Mennucci, C. Pomelli, C. Adamo, S. Clifford, J. Ochterski, G. A. Petersson, P. Y. Ayala, Q. Cui, K. Morokuma, D. K. Malick, A. D. Rabuck, K. Raghavachari, J. B. Foresman, J. Cioslowski, J. V. Ortiz, B. B. Stefanov, G. Liu, A. Liashenko, P. Piskorz, I. Komaromi, R. Gomperts, R. L. Martin, D. J. Fox, T. Keith, M. A. Al-Laham, C. Y. Peng, A. Nanayakkara, C. Gonzalez, M. Challacombe, P. M. W. Gill, B. Johnson, W. Chen, M. W. Wong, J. L. Andres, C. Gonzalez, M. Head-Gordon, E. S. Replogle, J. A. Pople, Gaussian Inc., Pittsburgh, PA, **1998**.
[40] A. D. Becke, *J. Chem. Phys.* **1993**, *98*, 5648−5652.
[41] C. Lee, W. Yang, R. G. Parr, *Phys. Rev. B* **1988**, *37*, 785−789.

 © 2004 Wiley-VCH Verlag GmbH & Co. KGaA, Weinheim

[42] P. J. Hay, W. R. Wadt, *J. Chem. Phys.* **1985**, *82*, 299−310.
[43] W. R. Wadt, P. J. Hay, *J. Chem. Phys.* **1985**, *82*, 284−298.
[44] A. Höllwarth, M. Böhme, S. Dapprich, A. W. Ehlers, A. Gobbi, V. Jonas, K. F. Köhler, R. Stegman, A. Veldkamp, G. Frenking, *Chem. Phys. Lett.* **1993**, *208*, 237−240.
[45] W. J. Hehre, R. Ditchfield, J. A. Pople, *J. Chem. Phys.* **1972**, *56*, 2257−2261.
[46] [46a] P. C. Hariharan, J. A. Pople, *Theoret. Chim. Acta* **1973**, *28*, 213−222. [46b] M. M. Francl, W. J. Pietro, W. J. Hehre, J. S. Binkley, M. S. Gordon, D. J. Defrees, J. A. Pople, *J. Chem. Phys.* **1982**, *77*, 3654−3665.
[47] [47a] E. Ruiz, P. Alemany, S. Alvarez, J. Cano, *J. Am. Chem. Soc.* **1997**, *119*, 1297−1303. [47b] E. Ruiz, J. Cano, S. Alvarez, P. Alemany, *J. Comput. Chem.* **1999**, *20*, 1391 − 1400. [47c] E. Ruiz, S. Alvarez, A. Rodríguez-Fortea, P. Alemany, Y. Pouillon, C. Massobrio, in *Magnetism: Molecules to Materials* (Eds.: J. S. Miller, M. Drillon), Wiley-VCH, Weinheim, **2001**, vol. 2, pp. 227−279.
[48] *Xaim*; J. C. Ortiz, C. Bo, Departament de Química Física i Inorgànica (Universitat Rovira i Virgili), Tarragona (Spain), **1998**.

Received March 15, 2004
Early View Article
Published Online September 23, 2004

 © 2004 Wiley-VCH Verlag GmbH & Co. KGaA, Weinheim

Unsymmetrically Substituted Dimethyldiaminosilanes as Ligands towards Zirconium(IV)

Vincenzo Passarelli*[a][‡] and Pierino Zanella[a]

Keywords: Zirconium / N ligands / Chelates / Silicon

Unsymmetrically substituted dimethyldiaminosilanes of the general formula $SiMe_2(NR_2)(NR'_2)$ have been prepared by treating $LiNR_2$ with $SiMe_2Cl(NR'_2)$ (NR_2, NR'_2 = NMe_2, NC_4H_8, NH*i*Pr, NH*t*Bu, $NHCH_2CH_2NMe_2$ or $NHCH_2CH_2OMe$). Their ligating properties towards zirconium(IV) have been investigated as a function of the nitrogen substituents and the syntheses of the binary compound $Zr[SiMe_2(N{\it i}Pr)(N{\it t}Bu)]_2$ and of the zirconium derivatives $ZrX_3(L)$ [X = Cl, NMe_2; L = $SiMe(NR)(NR'_2)$, NR = N*i*Pr, N*t*Bu, $NCH_2CH_2NMe_2$, NCH_2CH_2OMe; NR'_2 = NMe_2, NC_4H_8, NH*i*Pr, NH*t*Bu] are also reported. The solution structures and dynamics of the compounds have been elucidated by 1D/2D multinuclear NMR spectroscopy.

(© Wiley-VCH Verlag GmbH & Co. KGaA, 69451 Weinheim, Germany, 2004)

Introduction

The discovery of novel nonmetallocene polymerisation catalysts[1] has raised new interest in amido metal chemistry. As far as silylamides are concerned, a large number of data exist on SiR_3 *N*-substituted amido ligands (see refs.[1a−1c] for examples) but only a few papers[2−8] describe the synthesis, starting from diaminosilanes, of coordination compounds (Scheme 1, **I**−**II**).

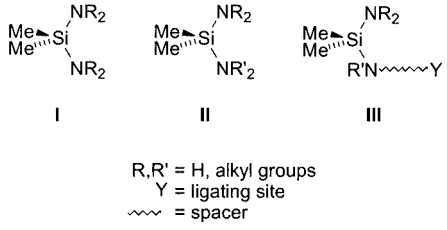

Scheme 1

Nevertheless diaminosilanes appear to be flexible ligands, their coordination mode strongly depending on the nature of the nitrogen substituents. Examples of the zirconium systems include, i) $Zr(NMe_2)_4$ reacts with $SiMe_2(NHR)_2$ yielding $Zr(NMe_2)_3(NHMe_2)[SiMe_2(N{\it t}Bu)(NH{\it t}Bu)]$[3] or $Zr(NMe_2)_2(NHMe_2)[SiMe_2(NPh)_2]$ (Ph = 2,6-$Me_2C_6H_3$);[4] ii) the binary amido derivative $Zr[SiMe_2(NR)_2]_2$ is a dimer when R = *i*Pr[3] and a monomer when R = *t*Bu.[5]

Moreover, as a consequence of the different structures, different physical and/or chemical properties are observed and expected for the metal derivatives. For instance, the above mentioned *tert*-butyl derivative $Zr[SiMe_2(N{\it t}Bu)_2]_2$ is volatile,[5] while the isopropyl analogue decomposes at about 430 K without subliming.[3]

Based on this background, it seemed interesting to enlarge the class of dimethyldiaminosilanes and their metal complexes and, since little[6−8] is known about the ligating ability of unsymmetrically substituted diaminosilanes, we have pursued a) the synthesis of novel compounds of this class (eventually containing additional ligating sites) (Scheme 1, **II**−**III**) and b) the investigation of their ligating properties towards zirconium(IV).

Results and Discussion

Synthesis of $SiMe_2XY$ (X = NR_2, Y = Cl, NR'_2)

According to the literature procedures,[7,9] the following general route to $SiMe_2(NR_2)(NR'_2)$ was followed (Scheme 2): a) ligand exchange reactions between $SiMe_2Cl_2$ and $SiMe_2(NR_2)_2$;[10] b) treatment of the resultant $SiMe_2Cl(NR_2)$ with $LiNR'_2$.

The ^1H and ^{13}C NMR spectra of **1**−**11** show high field resonances for $SiMe_2$, while the signals of the NR_2 moieties can be observed in the range δ = 1−4 ppm (^1H) and 20−80 ppm (^{13}C). In addition, note that the nature of the amido group and the degree of substitution of the $SiMe_2$ core affect δ_{Si} (cf. ESI).

[a] ICIS−CNR,
Corso Stati Uniti 4, 35127 Padova, Italy
Fax (internat.): +39-049-8702911
E-mail: passarel@dcci.unipi.it
[‡] Present address: Università degli Studi di Pisa, Dipartimento di Chimica e Chimica Industriale,
Via Risorgimento 35, 56126 Pisa, Italy

Supporting information for this article is available on the WWW under http://www.eurjic.org or from the author.

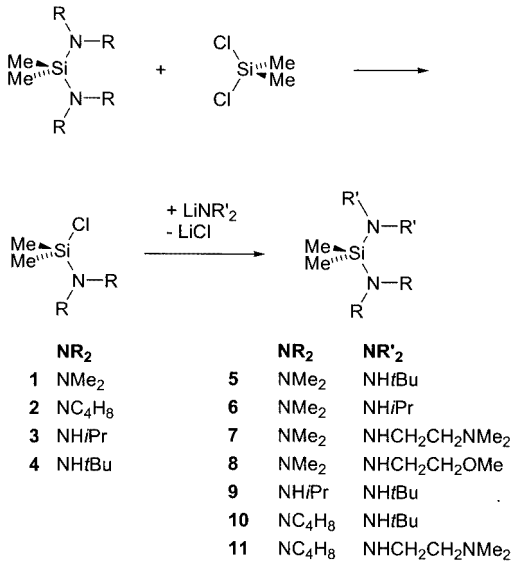

	NR_2		NR_2	NR'_2
1	NMe_2	**5**	NMe_2	NH*t*Bu
2	NC_4H_8	**6**	NMe_2	NH*i*Pr
3	NH*i*Pr	**7**	NMe_2	$NHCH_2CH_2NMe_2$
4	NH*t*Bu	**8**	NMe_2	$NHCH_2CH_2OMe$
		9	NH*i*Pr	NH*t*Bu
		10	NC_4H_8	NH*t*Bu
		11	NC_4H_8	$NHCH_2CH_2NMe_2$

Scheme 2

Synthesis of $Zr[SiMe_2(NtBu)(NiPr)]_2$

As alluded to in the introduction, the binary species $Zr[SiMe_2(NR)_2]_2$ adopts a different molecular structure (both in the solid state and in solution) depending on the identity of R (R = *i*Pr, dimer;[3] R = *t*Bu, monomer[5]) and elsewhere[3] we proposed that the different steric hindrances of *i*Pr and *t*Bu should be responsible for this observation. Therefore, elucidation of the molecular structure of $Zr[SiMe_2(NtBu)(NiPr)]_2$ (**12**) appeared interesting. Compound **12** was prepared by treating $ZrCl_4$ with $Li_2[SiMe_2(NiPr)(NtBu)]$ (1:2 molar ratio) and it was obtained as a pure material after crystallisation from an Et_2O/pentane solution at 243 K, Equation (1).

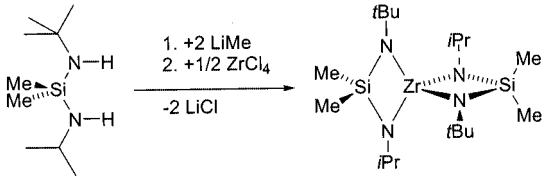

9 **12** (1)

Despite a large number of attempts, we were unable to obtain suitable crystals for a single-crystal X-ray diffraction study of the structure. Nevertheless, ^1H, ^{13}C and ^{29}Si NMR spectroscopy allowed at least the solution molecular structure to be elucidated. Provided that the ^{29}Si chemical shifts reported for ZrL_2 are −40.5 [L = $SiMe_2(NtBu)_2$,[5] chelating], −38.0 [L = $SiMe_2(NiPr)_2$,[3] chelating] and −12.2 ppm [L = $SiMe_2(NiPr)_2$,[3] bidentate bridging], the only ^{29}Si resonance of **12** at −40.5 ppm indicates that two equivalent ligands are present and that they are both chelating. In addition, the ^1H and ^{13}C spectra show only one kind of *i*Pr and *t*Bu group even at 200 K, thus suggesting an approximately tetrahedral arrangement of the donor atoms around the zirconium centre. Finally, the two methyls of each $SiMe_2$ moiety are nonequivalent, i.e. two ^1H and two ^{13}C signals have been observed for the $SiMe_2$ group. Thus, the solution molecular structure of **12** should be similar to that of $Zr[SiMe_2(NtBu)_2]_2$.

Synthesis of $ZrCl_3(L)$

Treatment of $ZrCl_4$ with LiL (prepared in situ by treating LiMe with HL, 1:1 molar ratio; HL = **7**, **8**, **10** and **11**) yielded the trichloro derivatives $ZrCl_3(L)$ (Scheme 3).

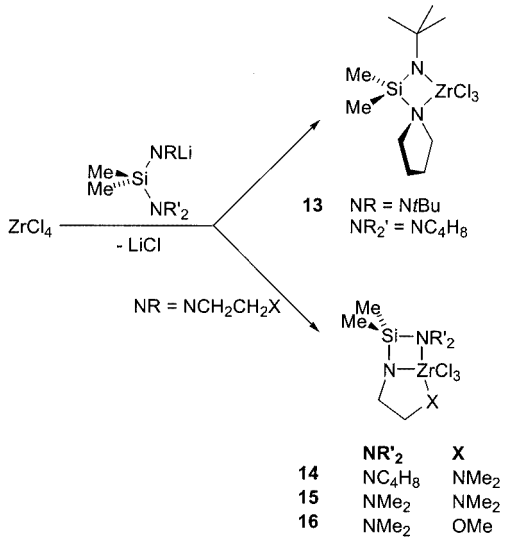

	NR'_2	X
14	NC_4H_8	NMe_2
15	NMe_2	NMe_2
16	NMe_2	OMe

Scheme 3

For convenience, **13** will be discussed separately from the other compounds in order to illustrate in detail, the correlation between the spectroscopic data and the proposed molecular structure.

The ^1H and ^{13}C NMR spectra of **13** show high field resonances for $SiMe_2$ (^1H, δ = 0.18 ppm; ^{13}C, 1.4 ppm), the signals of the hydrocarbyl moieties being observed in the range 1−3.5 ppm (^1H) and 20−60 ppm (^{13}C). As far as the CH_2NCH_2 moiety (pyrrolidinide) is concerned, i) the ^{13}C and ^1H ^{13}C HMQC spectra show that the two carbons are equivalent (54.0 ppm) and that two nonequivalent methylene protons (δ_H = 3.49, 3.35 ppm) are bonded to each carbon; ii) a negative crosspeak was observed in the ^1H NOESY spectrum of **13** between the resonances at δ = 3.35 and 0.18 ppm ($SiMe_2$) and iii) the ^{13}C resonances of CH_2NCH_2 are shifted with respect to the uncomplexed ligand (Table 1), thus suggesting that **13** contains $SiMe_2(NtBu)(NC_4H_8)$ as a bidentate ligand.

 © 2004 Wiley-VCH Verlag GmbH & Co. KGaA, Weinheim

Table 1. Shifts of the ^{13}C resonances of the CH_xNCH_x moiety in $ZrX_3(SiMe_2YZ)$ (X = Cl, NMe_2) ($\Delta\delta_C = \delta_C^{ZrX3(L)} - \delta_C^{HL}$), cf. Schemes 3 and 4

Compound	Y	Z	$\Delta\delta_C$ X = Cl
13	N*t*Bu	$N(CH_2CH_2)_2$	7.3
14	$N(CH_2)_2NMe_2$	$N(CH_2CH_2)_2$	3.0
15	$N(CH_2)_2NMe_2$	NMe_2	7.4
16	$N(CH_2)_2OMe$	NMe_2	6.6
			X = NMe_2
17	$N(CH_2)_2NMe_2$	$N(CH_2CH_2)_2$	0.7
18	$N(CH_2)_2OMe$	NMe_2	0.8
19	$N(CH_2)_2NMe_2$	NMe_2	0.7
20	N*t*Bu	$N(CH_2CH_2)_2$	4.8
21	N*i*Pr	NMe_2	4.8
22	N*t*Bu	NMe_2	5.2

Similar to **13**, the ^1H and ^{13}C spectra of **14**−**16** show high field resonances for the $SiMe_2$ moiety (^1H, about δ = 0.3 ppm; ^{13}C, about −2.2 ppm) and signals of the hydrocarbyl groups in the range 2−4.5 ppm (^1H) and 20−80 ppm (^{13}C). In addition, i) the downfield shift of the ^1H and ^{13}C resonances of the amino NMe_2 moieties in **14** and **15** and of the ethereal OMe group in **16** with respect to the uncomplexed ligands, and ii) the equivalent methylene protons of the ethylene chain, even at 190 K, indicate that the NMe_2 and the OMe groups coordinate to the metal centre and that a mirror plane containing the $ZrNC_2X$ moiety should exist in the molecule (X = OMe, NMe_2).

Moreover, similar to **13**, the observed ^{13}C shifts for the pyrrolidinide $CH_2N(Si)CH_2$ moiety in **14** and for the $SiNMe_2$ group in **15** and **16** (Table 1) suggest that the $SiNR_2$ moiety is also coordinated to the metal centre, making the silane ligands tridentate.[3]

As far as **14** is concerned, further comments are appropriate. In contrast with the proposed coordination of the $SiNC_4H_8$, the two faces of the pyrrolidinide ring appear equivalent at room temperature, i.e. one ^1H resonance is observed for each NCH_2 and NCH_2CH_2 proton set. In order to further elucidate this feature, we undertook a variable temperature NMR investigation and we observed that at 213 K i) the ^1H NCH_2 (pyrrolidinide) signal broadened and appeared unresolved and the NCH_2CH_2 (pyrrolidinide) resonance split into two signals at δ = 1.86 and 1.54 ppm (1:1 molar ratio) ii) in the ^1H NOESY spectrum a negative cross-speak was observed only between the NCH_2CH_2 resonance at 1.54 and the signal at δ = 0.39 ppm ($SiMe_2$) and iii) the carbon responsible for the resonance at δ = 25.1 ppm is bonded to the protons which yield the resonances at δ = 1.86 and 1.54 ppm (^1H ^{13}C HMQC). Therefore, the proposed coordination of the $SiNC_4H_8$ moiety is confirmed and it appears that the two faces of the pyrrolidinide ring are nonequivalent at 213 K and exchange at room temperature.

Synthesis of $Zr(NMe_2)_3(L)$

Compounds **5**−**11** readily react with $Zr(NMe_2)_4$ displacing one NMe_2 group as $NHMe_2$ and yielding the mixed amido derivatives $Zr(NMe_2)_3(L)$ (**17**−**24**) (Scheme 4).

The NMR spectra of **17**−**19** show i) ^{13}C chemical shifts of the $CH_xN(Si)CH_x$ (x = 2, 3) moiety similar to the uncomplexed ligands (Table 1) and ii) downfield shifted $CH_2N(CH_3)_2$ and CH_2OCH_3 resonances (^1H and ^{13}C), thus suggesting that **17**−**19** should contain the diaminosilane as a bidentate ligand coordinating to the metal centre through the amido $SiNCH_2$ nitrogen atom and the amino NMe_2 or the ethereal OMe moieties, while the $SiNR_2$ group is un-

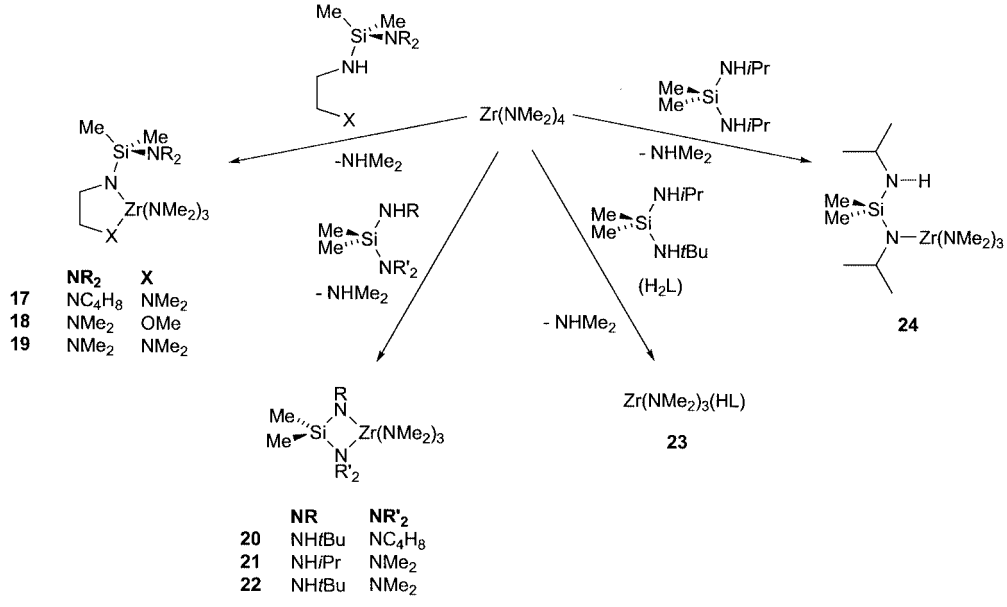

Scheme 4

 © 2004 Wiley-VCH Verlag GmbH & Co. KGaA, Weinheim

complexed. As confirmation, the ^{1}H methylene NC_4H_8 resonances of **17** appear as unique multiplets even at 190 K (cf. **13** and **14**).

As far as **20**−**22** are concerned, since the ^{13}C $CH_xN(Si)CH_x$ resonances are noticeably shifted with respect to those of the uncomplexed ligand (Table 1) and the two faces of the pyrrolidinide ring of **20** appear nonequivalent at 200 K (^{1}H NMR), the mixed amido derivatives **20**−**22** should contain the SiN_2 core coordinated to the metal centre.

The microcrystalline powder obtained from the reaction of $Zr(NMe_2)_4$ with $SiMe_2(NHiPr)(NHtBu)$ (H_2L) was identified as $Zr(NMe_2)_3(HL)$ (**23**) and the NMR spectra of a C_6D_6 solution indicated that two isomers were present in solution, namely $Zr(NMe_2)_3[SiMe_2(NiPr)(NHtBu)]$ (**23′**) and $Zr(NMe_2)_3[SiMe_2(NtBu)(NHiPr)]$ (**23′′**) [Eqn. (2)]. In fact, the ^{29}Si NMR spectrum shows two signals (−2.8, −5.9 ppm) and the ^{1}H COSY and ^{1}H ^{13}C HMQC spectra indicate two nonequivalent $SiMe_2$, *i*Pr and *t*Bu moieties (vide infra, cf. Exp. Sect.).

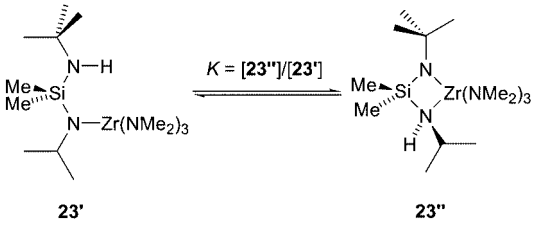

23′ **23′′** (2)

As far as **23′** is concerned, the ^{1}H and ^{13}C NMR resonances are little affected by the temperature (188−298 K) and the signal of the *tert*-butyl quaternary ^{13}C nucleus is slightly shifted with respect to the uncomplexed ligand, thus indicating that the NH*t*Bu moiety is probably not complexed and that we are dealing with the mono-hapto $SiMe_2(NiPr)(NHtBu)$ ligand [Equation (2)].

On the other hand the ^{1}H and ^{13}C signals of **23′′** are strongly affected by the temperature. At 188 K, one ^{29}Si resonance and two nonequivalent methyls both in the $SiMe_2$ and the *i*Pr moiety (^{1}H, ^{13}C) suggest that the SiNH*i*Pr unit is coordinated. For confirmation, and relevant to the molecular structure elucidation, the following comments can be made i) the ^{1}H COSY spectrum shows correlation peaks between the two isopropyl methyl groups (δ = 0.86, 0.72 ppm) and the methyne resonance (δ = 2.79 ppm), confirming that we are dealing with one isopropyl group containing two nonequivalent methyls; ii) both the $SiCH_3$ resonances are correlated (^{1}H NOESY) with the *tert*-butyl CH_3, confirming that only one $SiMe_2$ moiety is present with the methyls in different chemical environments; iii) a strong correlation (^{1}H NOESY) exists between the $SiMe_2$ methyl at δ = 0.29 ppm and the isopropyl methyl groups, suggesting that this methyl and the *i*Pr group are in a *syn* configuration with respect to the SiN_2Zr ring (Table 2). Finally, at 188 K, three nonequivalent $ZrNMe_2$ groups (δ_H, δ_C = 3.36, 45.97; 3.12, 46.00; 3.04, 45.2 ppm) were observed for **23′′** as a consequence of the asymmetric zirconium coordination sphere.

Table 2. Proposed assignment of ^{1}H and ^{13}C signals of $Zr(NMe_2)_3$-$[SiMe_2(NtBu)(NHiPr)]$ (**23′′**)

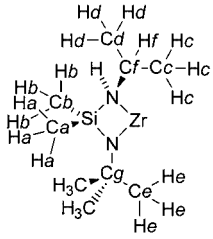

δ_H (188 K)	δ_C (188 K)
0.29 (H*a*)	7.20 (C*a*)
0.33 (H*b*)	1.29 (C*b*)
0.72 (H*c*)	27.3 (C*c*)
0.86 (H*d*)	25.0 (C*d*)
1.40 (H*e*)	35.3 (C*e*)
2.79 (H*f*)	45.7 (C*f*)
−	54.7 (C*g*)

The equilibrium constants K = [**23′′**]/[**23′**] [Equation (2)] at different temperatures [198−293 K] were calculated from the integrals of the $SiCH_3$ ^{1}H NMR resonances and the van't Hoff plot yielded ΔH_r = −3.4±0.4 kJ·mol^{-1} and ΔS_r = −7.3±1.8 J·mol^{-1}·K^{-1}. Reasonably, the negative ΔS_r results from the loss of entropy due to the chelation of the SiN_2 system and the negative ΔH_r should be related to a) the different basicities of the SiN*i*Pr and SiN*t*Bu moieties, b) the formation of a novel Zr−N bond and c) the reorganisation of the zirconium coordination sphere. Reasonably, the difference between the two Brønsted sites is negligible and the enthalpy contribution of Zr−N bond formation (esothermic) is higher with respect to that of the reorganisation of the donor atoms set on increasing the zirconium coordination number (endothermic). Nevertheless, the small absolute value of ΔH_r clearly indicates that the above mentioned effects are comparable.

For comparison (vide infra), the mixed amido derivative $Zr(NMe_2)_3[SiMe_2(NiPr)(NHiPr)]$ (**24**) was prepared (Scheme 4) and its solution molecular structure elucidated. Only one ^{29}Si resonance was observed and the ^{1}H and ^{13}C NMR spectra show one resonance for the $SiMe_2$ and two nonequivalent *i*Pr moieties (i.e. two nonequivalent CH_3 and two nonequivalent CH proton sets). Moreover, the ^{1}H and ^{13}C signals of the $SiMe_2$ and *i*Pr moieties are little affected by the temperature and appear as single well-shaped resonances even at 188 K. Finally, at room temperature, *positive* crosspeaks between both the CH_3 and the CH resonances of the two nonequivalent *i*Pr groups were observed in the ^{1}H NOESY spectrum and the coalescences of the CH and CH_3 ^{1}H resonances occur above 370 K. Therefore, the SiNH*i*Pr group is not coordinated and the chemical exchange between the two halves of $SiMe_2(NHiPr)(NiPr)$ op-

 © 2004 Wiley-VCH Verlag GmbH & Co. KGaA, Weinheim

erates with the consequent 1,3-shift of the NH proton (Scheme 5).

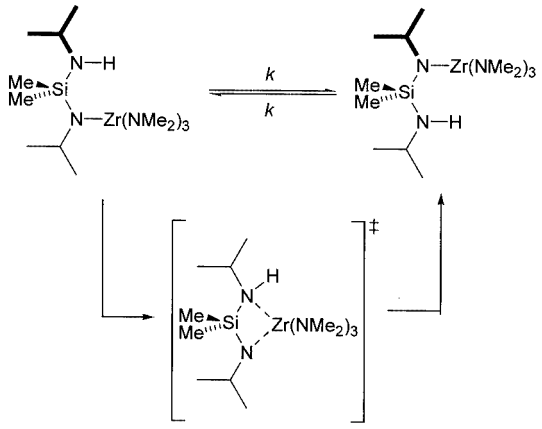

Scheme 5

This phenomenon has been investigated by variable temperature ^{13}C NMR spectroscopy in the range of 298−358 K and a line shape analysis of the isopropyl methyl resonances enabled us to calculate the kinetic constant k (Scheme 5) at different temperatures and to determine the activation parameters using the Eyring plot (ΔH_{act} = 47.1±1.2 kJ·mol^{-1}; ΔS_{act} = −73.8±3.8 J·mol^{-1}·K^{-1}). The negative value of ΔS_{act} suggests that the mechanism should be concerted, the 1,3-shift of the $Zr(NMe_2)_3$ fragment being reasonably the rate determining step (Scheme 5), yielding a **23′′**-type transition state. In this respect, the positive ΔH_{act} is reasonably indicative of the kinetic influence of the proposed rate-determining labilisation of the amido Zr−N(Si)*i*Pr bond.

Finally, a comparison among compounds **20**−**24** throws light on the influence of the nitrogen substituents on the coordination mode of L in $Zr(NMe_2)_3(L)$ [HL = **5**, **6**, **9**, **10**, $SiMe_2(NH{i}Pr)_2$]. Provided that the coordination of the SiNHR moiety (R = *i*Pr, *t*Bu) is observed only in **23′′** and not in **23′** or in **24**, we propose that the steric hindrance of SiNHR is hardly relevant in determining its ligating ability and that the steric interactions within the SiN(R)Zr group should be decisive, i.e. the more sterically demanding *t*Bu group in **23′′** encourages the chelation. This could reasonably be due to the consequent reduction of unfavourable steric interactions within the SiN(*t*Bu)Zr fragment itself. Conversely, compounds **20**−**22** contain $SiMe_2(NR)(NR'_2)$ as a chelating ligand, regardless of the nature of R (R = *i*Pr, *t*Bu), thus suggesting that the $SiNR'_2$ moieties, namely $SiNMe_2$ and $SiNC_4H_8$, have better ligating abilities with respect to SiNH*i*Pr and SiNH*t*Bu (in **23′** and **24**).

Conclusions

The ligating ability of $SiMe_2(NR_2)(NR'_2)$ towards zirconium(IV) is affected by the nitrogen substituents and eventually by the zirconium ancillary ligands. As far as the binary derivatives ZrL_2 are concerned, in contrast to $\{Zr[SiMe_2(N{i}Pr)_2]_2\}_2$ (Scheme 6, A) and similar to $Zr[SiMe_2(N{t}Bu)_2]_2$ (Scheme 6, B), $Zr[SiMe_2(N{i}Pr)(N{t}Bu)]_2$ is mononuclear indicating that the formal substitution of one methyne proton with CH_3 in each silane ligand of $\{Zr[SiMe_2(N{i}Pr)_2]_2\}_2$ makes the ligand itself too bulky to be accommodated in the dimer frame.

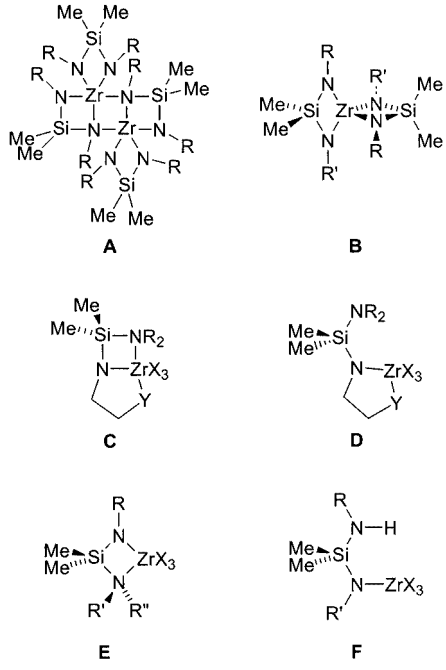

Scheme 6

The coordination mode of $SiMe_2(NR')(NR_2)$ (NR_2 = NMe_2 or NC_4H_8; NR′ = N*i*Pr, N*t*Bu, $NCH_2CH_2NMe_2$ or NCH_2CH_2OMe) to the ZrX_3 moiety (X = Cl, NMe_2) is strictly determined by the ancillary ligands. In fact, $SiMe_2(NR_2)(NCH_2CH_2Y)$ (NR_2=NMe_2 or NC_4H_8; Y = NMe_2 or OMe) is tridentate when X = Cl (Scheme 6, C) and bidentate when X = NMe_2 (Scheme 6, D). This could reasonably be due to the higher steric hindrance of the amido NMe_2 with respect to Cl and to the ability of NMe_2 to act as a π-donor. In addition, when X = NMe_2, the formation of the more stable five membered ring $ZrNC_2Y$ (Y = NMe_2, OMe) can be observed rather than the four membered SiN_2Zr one. On the other hand, $SiMe_2(NR')(NR_2)$ (R′ = *i*Pr or *t*Bu; NR_2 = NMe_2 or NC_4H_8) exhibit similar ligating properties towards ZrX_3 (X = Cl, NMe_2) regardless of the nature of X and the formation of chelates is always observed (Scheme 6, E).

Finally, the hapticity of the silane ligand in $Zr(NMe_2)_3$-$[SiMe_2(NR)(NHR')]$ is related to the steric hindrance of the nitrogen substituent R. As a matter of fact, the chelation of $SiMe_2(N{t}Bu)(NH{i}Pr)$ (Scheme 6, E) in $Zr(NMe_2)_3[SiMe_2(N{t}Bu)(NH{i}Pr)]$ and the mono-hapto coordination of $SiMe_2(N{i}Pr)(NHR)$ (Scheme 6, F) in $Zr(NMe_2)_3[SiMe_2(N{i}Pr)(NHR)]$ (R = *i*Pr, *t*Bu) indicate that the release of

 © 2004 Wiley-VCH Verlag GmbH & Co. KGaA, Weinheim

some steric congestion within the amido moiety SiN(R)Zr is decisive.

Experimental Section

All operations were carried out in a glove-box under dinitrogen. Elemental analyses (C, H, N) were performed using a Fisons Instruments analyser (Mod. EA 1108). The chlorine content in the samples was determined by potentiometric titration using a standard solution of silver nitrate (Aldrich). NMR spectra were recorded with a BRUKER AMX 300 spectrometer (300 MHz for ^{1}H). ^{1}H, ^{13}C and ^{29}Si NMR spectra are referred to TMS. The multiplicity is indicated as s (singlet), d (doublet), t (triplet), dt (doublet of triplets), q (quadruplet), sp (septet), ds (doublet of septets), m (multiplet) and br. was used to indicate broad signals.
The mass spectra (100−800 amu) were recorded with a Thermo-Finnigan Trace GC-MS instrument equipped with an accessory for the direct introduction of the sample into the source. The probe temperature was initially maintained at 373 K for 10 min, then raised to 473 K (50 K/min) and finally maintained at 473 K for 10 min. The source temperature was 473 K.
Zirconium tetrachloride ($ZrCl_4$, Fluka) was washed with boiling toluene then with pentane, dried in vacuo and stored under dinitrogen. *tert*-Butylamine ($C_4H_{11}N$, Aldrich), isopropylamine (C_3H_9N, Aldrich) and *N*,*N*-dimethylethylenediamine ($C_4H_{12}N_2$, Aldrich) were refluxed over BaO for one day, then distilled and stored under dinitrogen. Dichlorodimethylsilane ($SiMe_2Cl_2$, Aldrich), 2-methoxyethyleneamine (C_3H_9NO, Aldrich), LiMe (Et_2O solution, 1.6 M, Aldrich) and dimethylamine (C_2H_7N, Aldrich) were used as received. $SiMe_2(NR_2)_2$ [3,9] (NR_2 = NH*i*Pr, NH*t*Bu, NMe_2 or NC_4H_8) and $Zr(NMe_2)_4$ [11] were prepared according to the published procedures. The lithium amides $LiNR_2$ (NR_2 = NH*i*Pr, NH*t*Bu, $NHCH_2CH_2NMe_2$ or $NHCH_2CH_2OMe$) were prepared by treating NHR_2 with LiMe in Et_2O (1:1 molar ratio) and the resultant mixture was used without isolating the product.

Synthesis of $SiMe_2Cl(NR_2)$ (NR_2 = NH*i*Pr, NH*t*Bu, NMe_2 or NC_4H_8)

Only the synthesis of $SiMe_2Cl(NMe_2)$ is described in detail, the others being similar except for the reaction time (vide infra).
A solution of $SiMe_2(NMe_2)_2$ (1.20 g, 8.20 mmol) in pentane (50 mL) was treated with $SiMe_2Cl_2$ (1.07 g, 8.29 mmol). After 10 min stirring volatiles were removed in vacuo yielding a colourless liquid material, identified as $SiMe_2Cl(NMe_2)$ (**1**).

$SiMe_2Cl(NMe_2)$ (1): 2.15 g, 95% yield. $C_4H_{12}ClNSi$ (137.68): calcd. C 34.9, H 8.8, Cl 25.7, N 10.2; found C 34.8, H 8.9, Cl 25.5, N 10.1. ^{1}H NMR (C_6D_6, 298 K): δ = 2.28 (s, 1 H, NCH_3), 0.28 (s, 1 H, $SiCH_3$) ppm. ^{13}C NMR (C_6D_6, 298 K): δ = 37.1 (NCH_3), 1.32 ($SiCH_3$) ppm. ^{29}Si NMR (C_6D_6, 298 K): δ = 13.9 ppm.

$SiMe_2Cl(NC_4H_8)$ (2): Reaction time: 10 min, colourless liquid, 96% yield. $C_6H_{14}ClNSi$ (163.72): calcd. C 44.0, H 8.6, Cl 21.7, N 8.6; found C 44.2, H 8.8, Cl 21.7, N 8.4. ^{1}H NMR (C_6D_6, 298 K): δ = 2.85 (m, 2 H, NCH_2), 1.53 (m, 2 H, NCH_2CH_2), 0.33 (s, 3 H, $SiCH_3$) ppm. ^{13}C NMR (C_6D_6, 298 K): δ = 46.5 (NCH_2), 26.9 (NCH_2CH_2), 1.82 ($SiCH_3$) ppm. ^{29}Si NMR (C_6D_6, 298 K): δ = 10.1 ppm.

$SiMe_2Cl(NHiPr)$ (3): Reaction time: 18 h, colourless liquid, 92% yield. $C_5H_{14}ClNSi$ (151.71): calcd. C 39.6, H 9.3, N 9.2; found C 39.7, H 9.1, N 9.0. ^{1}H NMR (C_6D_6, 298 K): δ = 3.00 (ds, $^3J_{H,H}$ = 10.7, 1 H, CH, 6.4 Hz), 0.95 (d, $^3J_{H,H}$ = 6.4 Hz, 6 H, $CHCH_3$), 0.74 (br., 1 H, NH), 0.27 (s, 6 H, $SiCH_3$) ppm. ^{13}C NMR (C_6D_6, 298 K): δ = 43.3 (CH), 27.1 ($CHCH_3$), 2.07 ($SiCH_3$) ppm. ^{29}Si NMR (C_6D_6, 298 K): δ = 8.4. ppm

$SiMe_2Cl(NHtBu)$ (4): Reaction time: 80 h, colourless liquid, 91% yield. $C_6H_{16}ClNSi$ (165.74): calcd. C 43.5, H 9.7, Cl 21.4, N 8.5; found C 43.2, H 10.0, Cl 21.3, N 8.2. ^{1}H NMR (C_6D_6, 298 K): δ = 1.14 (s, 9 H, CCH_3), 0.55 (br., 1 H, NH), 0.34 (s, 6 H, $SiCH_3$) ppm. ^{13}C NMR (C_6D_6, 298 K): δ = 50.3 (C), 33.2 (CCH_3), 4.52 ($SiCH_3$) ppm. ^{29}Si NMR (C_6D_6, 298 K): δ = 5.6 ppm.

Synthesis of $SiMe_2(NR_2)(NR'_2)$: Only the synthesis of $SiMe_2(NMe_2)(NHtBu)$ is reported in detail, the others being similar. A solution of $SiMe_2Cl(NMe_2)$ (**1**, 900 mg, 6.54 mmol) in Et_2O (30 mL) was treated with an Et_2O suspension of LiNH*t*Bu (4.1 mL of an Et_2O solution, 1.6 M, 6.6 mmol of LiMe +485 mg, 6.63 mmol of NH_2tBu) and the resultant suspension stirred for 3 h. The colourless solid was filtered (270 mg) and the solvent was removed in vacuo from the filtrate yielding a pale yellow liquid identified as $SiMe_2(NMe_2)(NHtBu)$ (**5**).

$SiMe_2(NMe_2)(NHtBu)$ (5): 1.05 g, 92% yield. $C_8H_{22}N_2Si$ (174.36): calcd. C 55.1, H 12.7, N 16.1; found C 55.1, H 12.9, N 16.0. ^{1}H NMR (C_6D_6, 298 K): δ = 2.41 (s, 6 H, $SiNCH_3$), 1.12 (s, 9 H, CCH_3), 0.53 (br., 1 H, NH), 0.10 (s, 6 H, $SiCH_3$) ppm. ^{13}C NMR (C_6D_6, 298 K): δ = 48.8 (C), 37.6 ($SiNCH_3$), 33.5 (CCH_3), −0.08 ($SiCH_3$) ppm. ^{29}Si NMR (C_6D_6, 298 K): δ = −10.8 ppm.

$SiMe_2(NMe_2)(NHiPr)$ (6): Colourless liquid, 90% yield, from $SiMe_2Cl(NMe_2)$ (**1**) + LiNH*i*Pr. $C_7H_{20}N_2Si$ (160.33): calcd. C 52.4, H 12.6, N 17.5; found C 52.0, H 12.5, N 17.3. ^{1}H NMR (C_6D_6, 298 K): δ = 2.99 (ds, $^3J_{H,H}$ = 10.2, 6.3 Hz, 1 H, CH), 2.49 (s, 6 H, $SiNCH_3$), 1.00 (d, $^3J_{H,H}$ = 6.3 Hz, 6 H, $CHCH_3$), 0.29 (br., 1 H, NH), 0.07 (s, 6 H, $SiCH_3$) ppm. ^{13}C NMR (C_6D_6, 298 K): δ = 42.6 (CH), 37.5 ($SiNCH_3$), 27.8 ($CHCH_3$), −1.96 ($SiCH_3$) ppm. ^{29}Si NMR (C_6D_6, 298 K): δ = −7.5 ppm.

$SiMe_2(NMe_2)(NHCH_2CH_2NMe_2)$ (7): Colourless liquid, 91% yield, from $SiMe_2Cl(NMe_2)$ (**1**) + $LiNHCH_2CH_2NMe_2$. $C_8H_{23}N_3Si$ (189.37): calcd. C 50.7, H 12.2, N 22.2; found C 51.0, H 11.9, N 22.1. ^{1}H NMR (C_6D_6, 298 K): δ = 2.74 (dt, $^3J_{H,H}$ = 6.9, 6.2 Hz, 2 H, $SiNCH_2$), 2.48 (s, 6 H, $SiNCH_3$), 2.18 (t, $^3J_{H,H}$ = 6.2 Hz, 2 H, CH_2NCH_3), 2.08 (s, 6 H, CH_2NCH_3), 1.15 (br., 1 H, NH), 0.04 ($SiCH_3$) ppm. ^{13}C NMR (C_6D_6, 298 K): δ = 63.2 (CH_2NCH_3), 45.5 (CH_2NCH_3), 39.2 ($SiNCH_2$), 37.7 ($SiNCH_3$), −2.38 ppm. ^{29}Si NMR (C_6D_6, 298 K): δ = −5.3 ppm.

$SiMe_2(NMe_2)(NHCH_2CH_2OMe)$ (8): Colourless liquid, 95% yield, from $SiMe_2Cl(NMe_2)$ (**1**) + $LiNHCH_2CH_2OMe$. $C_7H_{20}N_2OSi$ (176.33): calcd. C 47.7, H 11.4, N 15.9; found C 47.7, H 11.0, N 15.8. ^{1}H NMR (C_6D_6, 298 K): δ = 3.19 (t, $^3J_{H,H}$ = 5.6 Hz, 2 H, OCH_2), 3.13 (s, 3 H, OCH_3), 2.87 (dt, $^3J_{H,H}$ = 7.7, 5.6 Hz, 2 H, $SiNCH_2$), 2.48 (s, 6 H, $SiNCH_3$), 0.99 (br., 1 H, NH), 0.06 (s, 6 H, $SiCH_3$) ppm. ^{13}C NMR (C_6D_6, 298 K): δ = 76.0 (OCH_2), 58.4 (OCH_3), 41.3 ($SiNCH_2$), 37.6 ($SiNCH_3$), −2.38 ($SiCH_3$) ppm. ^{29}Si NMR (C_6D_6, 298 K): δ = −5.0 ppm.

$SiMe_2(NHiPr)(NHtBu)$ (9): Colourless liquid, 88% yield, from $SiMe_2Cl(NHiPr)$ (**3**) + LiNH*t*Bu. $C_9H_{24}N_2Si$ (188.39): calcd. C 57.4, H 12.8, N 14.9; found C 57.3, H 12.8, N 14.7. ^{1}H NMR (C_6D_6, 298 K): δ = 3.13 (ds, $^3J_{H,H}$ = 10.4, 6.3 Hz, 1 H, CH), 1.19 (s, 9 H, CCH_3), 1.04 (d, $^3J_{H,H}$ = 6.3 Hz, 6 H, $CHCH_3$), 0.56 (br., 1 H, NH), 0.24 (br., 1 H, NH), 0.12 (s, 6 H, $SiCH_3$) ppm. ^{13}C NMR (C_6D_6, 298 K): δ = 49.1 (C), 42.6 (CH), 33.8 (CCH_3), 28.0 ($CHCH_3$), 1.74 ($SiCH_3$) ppm. ^{29}Si NMR (C_6D_6, 298 K): δ = −15.0 ppm.

 © 2004 Wiley-VCH Verlag GmbH & Co. KGaA, Weinheim

$SiMe_2(NC_4H_8)(NHtBu)$ (10): Colourless liquid, 92% yield, from $SiMe_2Cl(NC_4H_8)$ (**2**) + LiNH*t*Bu. $C_{10}H_{24}N_2Si$ (200.40): calcd. C 59.9, H 12.1, N 14.0; found C 60.0, H 12.0, N 14.1. ^1H NMR (C_6D_6, 298 K): δ = 2.97 (m, 4 H, NCH_2), 1.61 (m, 4 H, NCH_2CH_2), 1.14 (s, 9 H, CCH_3), 0.58 (br., 1 H, NH), 0.12 (s, 6 H, $SiCH_3$) ppm. ^{13}C NMR (C_6D_6, 298 K): δ = 48.9 (C), 46.7 (NCH_2), 33.7 (CCH_3), 27.2 (NCH_2CH_2), 0.14 ($SiCH_3$) ppm. ^{29}Si NMR (C_6D_6, 298 K): δ = −14.4 ppm.

$SiMe_2(NC_4H_8)(NHCH_2CH_2NMe_2)$ (11): Colourless liquid, 90% yield, from $SiMe_2Cl(NC_4H_8)$ (**2**) + $LiNHCH_2CH_2NMe_2$. $C_{10}H_{25}N_3Si$ (215.41): calcd. C 55.8, H 11.7, N 19.5; found C 55.6, H 11.5, N 19.5. ^1H NMR (C_6D_6, 298 K): δ = 2.99 (m, 4 H, NCH_2CH_2), 2.81 (dt, $^3J_{H,H}$ = 7.0, 6.2 Hz, 2 H, $SiNHCH_2$), 2.21 (t, $^3J_{H,H}$ = 6.2 Hz, 2 H, CH_2NCH_3) 2.09 (s, 6 H, NCH_3), 1.61 (m, 4 H, NCH_2CH_2), 1.18 (br., 1 H, NH), 0.13 (s, 6 H, $SiCH_3$) ppm. ^{13}C NMR (C_6D_6, 298 K): δ = 63.4 (CH_2NCH_3), 46.8 (NCH_2CH_2), 45.5 (NCH_3), 39.4 ($SiNHCH_2$), 27.3 (NCH_2CH_2), −2.05 ($SiCH_3$) ppm. ^{29}Si NMR (C_6D_6, 298 K): δ = −8.9 ppm.

Synthesis of $Zr[SiMe_2(NiPr)(NtBu)]_2$: An Et_2O solution of SiMe(NH*i*Pr)(NH*t*Bu) (**9**, 1.25 g, 6.64 mmol) was treated with LiMe (Et_2O solution, 1.6 M, 8.3 mL, 13.3 mmol), stirred for 1.5 h and then cooled to 243 K. $ZrCl_4$ (780 mg, 3.35 mmol) was added and after 2 h stirring at 243 K the mixture was warmed to the room temperature and the solid was filtered (540 mg). The pale yellow solution was partially evaporated, pentane was added and $Zr[SiMe_2(NiPr)(NtBu)]_2$ (**12**) was finally obtained as a microcrystalline powder on cooling the resultant solution to 240 K overnight (985 mg, 64% yield). $C_{18}H_{44}N_4Si_2Zr$ (463.96): calcd. C 46.6, H 9.6, N 12.1; found C 46.4, H 9.4, N 12.0. ^1H NMR (C_6D_6, 298 K): δ = 3.35 (sp, $^3J_{H,H}$ = 6.2 Hz, 1 H, CH), 1.32 (s, 9 H, CCH_3), 1.24 (d, $^3J_{H,H}$ = 6.2 Hz, 6 H, $CHCH_3$), 0.44 (s, 3 H, $SiCH_3$), 0.43 (s, 3 H, $SiCH_3$) ppm. ^{13}C NMR (C_6D_6, 298 K): δ = 55.6 (C), 50.6 (CH), 36.2 (CCH_3), 31.2 ($CHCH_3$), 4.3 ($SiCH_3$), 4.1 ($SiCH_3$) ppm. ^{29}Si NMR (C_6D_6, 298 K): δ = −40.5 ppm.

Synthesis of $ZrCl_3(L)$: Only the procedure for L = $SiMe_2(NMe_2)(NCH_2CH_2NMe_2)$ is described in detail, the others being similar. A solution of $SiMe_2(NMe_2)(NHCH_2CH_2NMe_2)$ (**7**, 780 mg, 4.12 mmol) in Et_2O (40 mL) was treated with LiMe (Et_2O solution, 1.6 M, 2.6 mL, 4.2 mmol). After gas evolution ceased, the solution was cooled to 243 K and $ZrCl_4$ (960 mg, 4.12 mmol) was added. The suspension was stirred at 243 K for 3 h and was then warmed to the room temperature and stirred overnight. The resultant suspension was filtered (165 mg of colourless solid) and the filtrate was evaporated yielding a sticky material which was recrystallized from Et_2O/pentane yielding a microcrystalline powder, identified as **$ZrCl_3[SiMe_2(NMe_2)(NCH_2CH_2NMe_2)]$ (15):** Colourless solid, 1.35 mg, 85% yield. MS: *m*/*z* (%) = 368 (9) [$M^{+\cdot}$ − CH_3], 332 (100) [$M^{+\cdot}$ − CH_3 − H − Cl]. $C_8H_{22}Cl_3N_3SiZr$ (385.95): calcd. C 24.9, H 5.7, Cl 27.6, N 10.9; found C 25.0, H 5.5, Cl 27.5, N 11.0. ^1H NMR ($CDCl_3$, 298 K): δ = 3.51 (t, $^3J_{H,H}$ = 5.6 Hz, 1 H, $SiNCH_2$), 3.00 (t, $^3J_{H,H}$ = 5.6 Hz, 1 H, CH_2NMe_2), 2.71 (s, 3 H, $SiNCH_3$), 2.70 (s, 3 H, CH_2NCH_3), 0.35 (s, 3 H, $SiCH_3$) ppm. ^{13}C NMR ($CDCl_3$, 298 K): δ = 67.1 (CH_2NMe_2), 50.5 (CH_2NCH_3), 47.8 ($SiNCH_2$), 45.1 ($SiNCH_3$), −2.5 ($SiCH_3$) ppm.

$ZrCl_3[SiMe_2(NC_4H_8)(NtBu)]$ (13): Colourless solid, 70% yield. $C_{10}H_{23}Cl_3N_2SiZr$ (396.97): calcd. C 30.3, H 5.8, Cl 26.8, N 7.1; found C 30.0, H 5.6, Cl 27.2, N 7.2. ^1H NMR ($CDCl_3$, 298 K): δ = 3.49 (br., 2 H, NCH_2), 3.35 (br., 2 H, NCH_2), 1.48 (s, 9 H, CCH_3), 1.01 (br., 4 H, NCH_2CH_2), 0.18 (s, 6 H, $SiCH_3$) ppm. ^{13}C NMR ($CDCl_3$, 298 K): δ = 58.2 (C), 54.0 (NCH_2), 34.1 (CCH_3), 24.9 (NCH_2CH_2), 1.4 ($SiCH_3$) ppm.

$ZrCl_3[SiMe_2(NC_4H_8)(NCH_2CH_2NMe_2)]$ (14): Colourless solid, 91% yield. MS: *m*/*z* (%) = 339 (17.8) [$M^{+\cdot}$ − $NCH_2CH_2CH_2CH_2$], 332 (75.3) [$M^{+\cdot}$ − $CH_2CH_2CH_2$ − Cl]. $C_{10}H_{24}Cl_3N_3SiZr$ (411.98): calcd. C 29.2, H 5.9, N 10.2; found C 29.3, H 5.8, N 10.1. ^1H NMR ($CDCl_3$, 298 K): δ = 3.48 (t, $^3J_{H,H}$ = 5.5 Hz, 1 H, $SiNCH_2$), 3.36 (m, 2 H, NCH_2 pyrrolidinide), 2.98 (t, $^3J_{H,H}$ = 5.5 Hz, 1 H, CH_2NMe_2), 2.72 (s, 3 H, NCH_3), 1.61 (m, 2 H, NCH_2CH_2 pyrrolidinide), 0.31 (s, 3 H, $SiCH_3$) ppm. ^{13}C NMR ($CDCl_3$, 298 K): δ = 66.6 (CH_2NMe_2), 53.3 (NCH_3), 49.8 (NCH_2 pyrrolidinide), 47.5 ($SiNCH_2$), 25.1 (NCH_2CH_2 pyrrolidinide), −2.14 ($SiCH_3$) ppm.

$ZrCl_3[SiMe_2(NMe_2)(NCH_2CH_2OMe)]$ (16): Colourless solid, 88% yield. MS: *m*/*z* (%) = 355 (15.9) [$M^{+\cdot}$ − CH_3], 319 (29.4) [$M^{+\cdot}$ − CH_3 − H − Cl]. $C_7H_{19}Cl_3N_2OSiZr$ (372.91): calcd. C 22.5, H 5.1, Cl 28.5, N 7.5; found C 22.3, H 5.0, Cl 28.8, N 7.6. ^1H NMR ($CDCl_3$, 298 K): δ = 4.24 (t, $^3J_{H,H}$ = 5.3 Hz, 2 H, OCH_2), 3.94 (s, 3 H, OCH_3), 3.56 (t, $^3J_{H,H}$ = 5.3 Hz, 2 H, NCH_2), 2.74 (s, 6 H, NCH_3), 0.32 (s, 6 H, $SiCH_3$) ppm. ^{13}C NMR ($CDCl_3$, 298 K): δ = 81.5 (OCH_2), 65.4 (OCH_3), 47.5 (NCH_2), 44.2 (NCH_3), −2.16 ($SiCH_3$) ppm.

Synthesis of $Zr(NMe_2)_3(L)$: Only the procedure for L = $SiMe_2(NiPr)(NMe_2)$ is reported in detail, the others being similar except for the reaction time (vide infra). A solution of $SiMe_2(NHiPr)(NMe_2)$ (**6**, 540 mg, 3.37 mmol) in toluene (20 mL) was treated with $Zr(NMe_2)_4$ (900 mg, 3.36 mmol). After 3 h stirring, the solution was evaporated yielding a pale yellow solid which was identified as $Zr(NMe_2)_3[SiMe_2(NiPr)(NMe_2)]$ (**21**).

$Zr(NMe_2)_3[SiMe_2(NiPr)(NMe_2)]$ (21): Colourless solid, 1.20 g, 93% yield. $C_{13}H_{37}N_5SiZr$ (382.78): calcd. C 40.8, H 9.7, N 18.3; found C 40.5, H 9.9, N 18.5. ^1H NMR (C_6D_6, 298 K): δ = 3.53 (sp, $^3J_{H,H}$ = 6.4 Hz, 1 H, CH), 3.04 (s, 18 H, $ZrNCH_3$), 2.24 (s, 6 H, $SiNCH_3$), 1.23 (d, $^3J_{H,H}$ = 6.4 Hz, 6 H, $CHCH_3$), 0.14 ($SiCH_3$) ppm. ^{13}C NMR (C_6D_6, 298 K): δ = 50.2 (CH), 43.2 ($ZrNCH_3$), 42.3 ($SiNCH_3$), 28.9 ($CHCH_3$), 0.67 ($SiCH_3$) ppm. ^{29}Si NMR (C_6D_6, 298 K): δ = 3.2 ppm.

$Zr(NMe_2)_3[SiMe_2(NC_4H_8)(NCH_2CH_2NMe_2)]$ (17): Reaction time: 3 h, colourless solid, 90% yield. $C_{16}H_{42}N_6SiZr$ (437.86): calcd. C 43.9, H 9.7, N 19.2; found C 44.0, H 9.5, N 19.0. ^1H NMR (C_6D_6, 298 K): δ = 3.26 (t, $^3J_{H,H}$ = 5.6 Hz, 1 H, $SiNCH_2$), 3.07 (m, 2 H, NCH_2 pyrrolidinide), 2.99 (s, 9 H, $ZrNCH_3$), 2.42 (t, $^3J_{H,H}$ = 5.6 Hz, 1 H, CH_2NMe_2), 1.96 (s, 3 H, NCH_3), 1.68 (m, 2 H, NCH_2CH_2 pyrrolidinide), 0.28 (s, 3 H, $SiCH_3$) ppm. ^{13}C NMR (C_6D_6, 298 K): δ = 61.0 (CH_2NMe_2), 47.5 (NCH_2 pyrrolidinide), 46.4 ($SiNCH_2$), 46.2 (CH_2NCH_3), 43.4 ($ZrNCH_3$), 27.3 (NCH_2CH_2 pyrrolidinide), −0.7 ($SiCH_3$) ppm. ^{29}Si NMR (C_6D_6, 298 K): δ = −5.9 ppm.

$Zr(NMe_2)_3[SiMe_2(NMe_2)(NCH_2CH_2OMe)]$ (18): Reaction time: 3 h, colourless solid, 92% yield. $C_{13}H_{37}N_5OsiZr$ (398.78): calcd. C 39.2, H 9.4, N 17.6; found C 39.0, H 9.4, N 17.5. ^1H NMR (C_6D_6, 298 K): δ = 3.31 (t, $^3J_{H,H}$ = 5.4 Hz, 2 H, CH_2O), 3.19 (t, $^3J_{H,H}$ = 5.4 Hz, 2 H, $SiNCH_2$), 3.05 (s, 18 H, $ZrNCH_3$), 2.98 (s, 3 H, OCH_3), 2.56 (s, 6 H, $SiNCH_3$), 0.24 (s, 6 H, $SiCH_3$) ppm. ^{13}C NMR (C_6D_6, 298 K): δ = 79.2 ($SiNCH_2$), 59.2 (OCH_3), 46.5 (CH_2O), 43.2 ($ZrNCH_3$), 38.4 ($SiNCH_3$), −1.0 ($SiCH_3$) ppm. ^{29}Si NMR (C_6D_6, 298 K): δ = −3.9 ppm.

$Zr(NMe_2)_3[SiMe_2(NMe_2)(NCH_2CH_2NMe_2)]$ (19): Reaction time: 3 h, colourless solid, 87% yield. $C_{14}H_{40}N_6SiZr$ (411.82): calcd. C 40.8, H 9.8, N 20.4; found C 41.0, H 10.0, N 20.0. ^1H NMR (C_6D_6, 298 K): δ = 3.21 (t, 1 H, $SiNCH_2$, $^3J_{H,H}$ = 5.9 Hz), 3.02 (s, 18 H, $ZrNCH_3$), 2.62 (s, 3 H, $SiNCH_3$), 2.36 (t, $^3J_{H,H}$ = 5.9 Hz, 1 H, CH_2NMe_2), 1.90 (s, 3 H, CH_2NCH_3), 0.32 (s, 3 H, $SiCH_3$) ppm.

 © 2004 Wiley-VCH Verlag GmbH & Co. KGaA, Weinheim

^{13}C NMR (C_6D_6, 298 K): δ = 60.7 (CH_2NMe_2), 46.5 ($SiNCH_2$), 46.0 (CH_2NCH_3), 43.3 ($ZrNCH_3$), 38.4 ($SiNCH_3$), −0.93 ($SiCH_3$) ppm.

$Zr(NMe_2)_3[SiMe_2(NtBu)(NC_4H_8)]$ (20): Reaction time: 30 h, colourless solid, 85% yield. $C_{16}H_{41}N_5SiZr$ (422.84): calcd. C 45.5, H 9.8, N 16.6; found C 45.7, H 9.5, N 16.5. ^{1}H NMR (C_6D_6, 298 K): δ = 3.04 (s, 18 H, $ZrNCH_3$), 2.74 (m, 4 H, NCH_2), 1.37 (m, 4 H, NCH_2CH_2), 1.33 (s, 9 H, CCH_3), 0.23 ($SiCH_3$) ppm. ^{13}C NMR (C_6D_6, 298 K): δ = 55.1 (C), 51.5 (NCH_2), 43.9 ($ZrNCH_3$), 35.5 (CCH_3), 24.7 (NCH_2CH_2), 3.5 ($SiCH_3$) ppm. ^{29}Si NMR (C_6D_6, 298 K): δ = −2.7 ppm.

$Zr(NMe_2)_3[SiMe_2(NtBu)(NMe_2)]$ (22): Reaction time: 28 h, colourless solid, 88% yield. $C_{14}H_{39}N_5SiZr$ (396.80): calcd. C 42.4, H 9.9, N 17.6; found C 42.3, H 10.0, N 17.8. ^{1}H NMR (C_6D_6, 298 K): δ = 3.04 (s, 18 H, $ZrNCH_3$), 2.19 (s, 6 H, $SiNCH_3$), 1.33 (s, 9 H, CCH_3), 0.20 (s, 6 H, $SiCH_3$) ppm. ^{13}C NMR (C_6D_6, 298 K): δ = 54.8 (C), 43.8 ($ZrNCH_3$), 42.8 ($SiNCH_3$), 35.4 (CCH_3), 3.4 ($SiCH_3$) ppm. ^{29}Si NMR (C_6D_6, 298 K): δ = 1.0 ppm.

When $Zr(NMe_2)_4$ was reacted with $SiMe_2(NHiPr)(NHtBu)$ (**9**, H_2L) (1:1 molar ratio) a microcrystalline powder was obtained which was analytically identified as $Zr(NMe_2)_3(HL)$ (**23**).

$Zr(NMe_2)_3(HL)$ (23): Colourless sticky material, 95% yield. $C_{15}H_{41}N_5SiZr$ (410.83): calcd. C 43.9, H 10.1, N 17.1; found C 44.0, H 10.2, N 17.4. The ^{1}H, ^{13}C and ^{29}Si NMR spectra (298 K, C_6D_6) indicated the presence of two isomers, namely $Zr(NMe_2)_3[SiMe_2(NiPr)(NHtBu)]$ (**23′**) and $Zr(NMe_2)_3[SiMe_2(NHiPr)(NtBu)]$ (**23″**) (**23′**/**23″** molar ratio about 0.7). **$Zr(NMe_2)_3[SiMe_2(NiPr)(NHtBu)]$ (23′):** ^{1}H NMR (C_6D_6, 298 K): δ = 3.38 (sp, $^3J_{H,H}$ = 6.4 Hz, 1 H, CH), 3.07 (s, 18 H, $ZrNCH_3$), 1.23 (d, $^3J_{H,H}$ = 6.4 Hz, 6 H, $CHCH_3$), 1.05 (s, 9 H, CCH_3), 0.25 (s, 6 H, $SiCH_3$) ppm. ^{13}C NMR (C_6D_6, 298 K): δ = 52.0 (C), 50.3 (CH), 43.7 ($ZrNCH_3$), 32.1 (CCH_3), 29.0 ($CHCH_3$), 3.6 ($SiCH_3$) ppm. ^{29}Si NMR (C_6D_6, 298 K): δ = −4.6 ppm.

$Zr(NMe_2)_3[SiMe_2(NHiPr)(NtBu)]$ (23″): ^{1}H NMR (C_6D_6, 298 K): δ = 2.93 (sp, $^3J_{H,H}$ = 6.1 Hz, 1 H, CH), 3.06 (s, 18 H, $ZrNCH_3$), 1.32 (s, 9 H, CCH_3), 0.88 (d, $^3J_{H,H}$ = 6.1 Hz, 6 H, $CHCH_3$), 0.32 (s, 6 H, $SiCH_3$) ppm. ^{13}C NMR (C_6D_6, 298 K): δ = 54.9 (C), 45.9 (CH), 43.3 ($ZrNCH_3$), 35.5 (CCH_3), 26.6 ($CHCH_3$), 4.6 ($SiCH_3$) ppm. ^{29}Si NMR (C_6D_6, 298 K): δ = −5.9 ppm.

$Zr(NMe_2)_3[SiMe_2(NiPr)(NHiPr)]$ (24): Colourless solid, 95% yield. $C_{14}H_{39}N_5SiZr$ (396.80): calcd. C 42.4, H 9.9, N 17.6; found C 42.7, H 9.8, N 18.0. ^{1}H NMR (C_6D_6, 298 K): δ = 3.45 (sp, $^3J_{H,H}$ = 6.4 Hz, 1 H, CH), 3.08 (s, 18 H, $ZrNCH_3$), 2.92 (sp, $^3J_{H,H}$ = 6.4 Hz, 1 H, CH), 2.0 (br., 1 H, NH), 1.23 (d, $^3J_{H,H}$ = 6.4 Hz, 6 H, $CHCH_3$), 0.89 (d, $^3J_{H,H}$ = 6.4 Hz, 6 H, $CHCH_3$), 0.22 (s, 6 H, $SiCH_3$) ppm. ^{13}C NMR (C_6D_6, 298 K): δ = 50.2 (CH), 45.6 (CH), 43.4 ($ZrNCH_3$), 29.0 ($CHCH_3$), 26.6 ($CHCH_3$), 1.7 ($SiCH_3$) ppm. ^{29}Si NMR (C_6D_6, 298 K): δ = −2.8 ppm.

Acknowledgments

V. P. is indebted to Dr. Sergio Tamburini (ICIS−CNR, Padova) for meaningful comments and insightful discussions. The authors thank Ms. Anna Rosa Moresco (ICIS−CNR, Padova) for the elemental analysis and Prof. G. Paolucci and Dr. L. Sperini (Università di Venezia) for the MS measurements.

[1] [1a] R. Kempe, *Angew. Chem. Int. Ed.* **2000**, *39*, 468. [1b] L. H. Gade, *Chem. Commun.* **2000**, 173. [1c] G. J. P. Britovsek, V. C. Gibson, D. F. Wass, *Angew. Chem. Int. Ed.* **1999**, *38*, 428.

[2] [2a] D. W. von Beiersdorf, D. J. Brauer, H. Bürger, *Z. Anorg. Allg. Chem.* **1981**, *475*, 56. [2b] H. Bürger, W. Geschwandtner, G. R. Liewald, *J. Organomet. Chem.* **1983**, *259*, 145. [2c] R. A. Jones, M. H. Seeberger, J. L. Atwood, W. E. Hunter, *J. Organomet. Chem.* **1983**, *247*, 1. [2d] D. J. Brauer, H. Bürger, W. Geschwandtner, G. R. Liewald, C. Krüger, *J. Organomet. Chem.* **1983**, *248*, 1. [2e] F. Preuss, E. Fuchslocher, W. S. Sheldrick, *Z. Naturforsch., Teil B* **1985**, *40*, 1040. [2f] M. Veith, H. Lange, A. Belo, O. Recktenwald, *Chem. Ber.* **1985**, *118*, 1600. [2g] D. J. Brauer, H. Bürger, G. R. Liewald, *J. Organomet. Chem.* **1986**, *307*, 177. [2h] D. J. Brauer, H. Bürger, G. R. Liewald, J. Wilke, *J. Organomet. Chem.* **1986**, *310*, 317. [2i] M. Veith, W. Frank, F. Töllner, H. Lange, *J. Organomet. Chem.* **1987**, *326*, 315. [2j] M. Veith, L. Stahl, V. Huch, *J. Chem. Soc., Chem. Commun.* **1990**, 359. [2k] M. Veith, M. Noetzel, L. Stahl, V. Huch, *Z. Anorg. Allg. Chem.* **1994**, *620*, 1264. [2l] A. D. Horton, J. de With, *Organometallics* **1997**, *16*, 5424. [2m] S.-J. Kim, I. N. Jung, B. R. Yoo, S. H. Kim, J. Ko, D. Byun, S. O. Kang, *Organometallics* **2001**, *20*, 2136. [2n] M. S. Hill, P. B. Hitchcock, *Organometallics* **2002**, *21*, 3258. [2o] S.-J. Kim, Y.-J. Lee, S. H. Kim, J. Ko, S. Cho, S. O. Kang, *Organometallics* **2002**, *21*, 5358. [2p] V. Passarelli, F. Benetollo, P. Zanella, *Eur. J. Inorg. Chem.* **2004**, 1714.

[3] V. Passarelli, F. Benetollo, P. Zanella, G. Carta, G. Rossetto, *Dalton Trans.* **2003**, 1411.

[4] V. C. Gibson, B. S. Kimberley, A. J. P. White, D. J. Williams, P. Howard, *Chem. Commun.* **1998**, 313.

[5] D. J. Brauer, H. Bürger, E. Essig, W. Geschwandtner, *J. Organomet. Chem.* **1980**, *190*, 343.

[6] R. Buheitel, W. Milius, W. Schnick, *Z. Naturforsch., Teil B* **1996**, *51*, 1141.

[7] F. J. Schattenmann, R. R. Schrock, W. M. Davis, *Organometallics* **1998**, *17*, 989.

[8] H. Schumann, J. Gottfriedsen, S. Dechert, F. Girgsdies, *Z. Anorg. Allg. Chem.* **2000**, *626*, 747.

[9] U. Wannagat, G. Schreiner, *Monatsh. Chem.* **1965**, *96*, 1889.

[10] The rate of the reaction is strongly affected by the nature of R. In fact Cl/NR_2 exchange occurs within the mixing time when NR_2 = NMe_2, NC_4H_8, whereas the reaction is markedly slower when NR_2 = NhiPr or NH*t*Bu, the conversion being complete after 12 h for NR_2 = NH*i*Pr and 70 h for NR_2=NH*t*Bu.

[11] D. C. Bradley, I. M. Thomas, *J. Chem. Soc.* **1960**, 3857.

Received January 17, 2004
Early View Article
Published Online September 23, 2004

 © 2004 Wiley-VCH Verlag GmbH & Co. KGaA, Weinheim

Studies on Manganese(II) Complexes of *N*-Benzimidazole-Functionalized 1,4,7-Triazacyclononane: Crystal Structures, Properties and Combined Superoxide Dismutase and Catalase Functions

Qing-Xiang Li,[a,b] Qin-Hui Luo,*[a] Yi-Zhi Li,*[a] Zhi-Quan Pan,[a,b] and Meng-Chang Shen[a]

Keywords: Enzyme models / Manganese / N ligands / Superoxide dismutase

Two new manganese(II) complexes $[MnL^1Cl_2]$ and $[MnL^2Cl]ClO_4$·MeOH were synthesized [L^1 = 1-(benzimidazol-2-ylmethyl)-1,4,7-triazacyclononane; L^2 = 1,4-bis(benzimidazol-2-ylmethyl)-1,4,7-triazacyclonone) and characterized by standard physical methods. The new complexes have better stability than the parent complex due to the introduction of benzimidazole groups on the backbone of tacn. The complexes were studied as superoxide dismutase (SOD) mimics by the riboflavin photoreduction method at pH 7.4. In basic or weakly basic solutions, the complexes decompose hydrogen peroxide catalytically, and possess the combined functions of SOD and catalase.
(© Wiley-VCH Verlag GmbH & Co. KGaA, 69451 Weinheim, Germany, 2004)

Introduction

Superoxide dismutase (SOD) efficiently catalyzes the dismutation of superoxide anion ($O_2^{\cdot-}$) to oxygen and hydrogen peroxide,[1,2] which is subsequently disproportionated into water and oxygen by catalase[3] (CAT).

$$O_2^{\cdot-} + 2\,H^+ + e^- \rightarrow H_2O_2$$
$$2\,H_2O_2 \rightarrow 2\,H_2O + O_2$$

Both SOD and CAT play important roles in the protection of cells against the toxicity of oxygen.[3] Manganese is involved in many biological processes,[4] such as hydrogenperoxide decomposition and superoxide dismutation etc., and is found at the active centers of MnSOD[5,6] and MnCAT.[5]

In MnSOD the manganese has a trigonal-bipyramidal coordination environment with three histidine groups and one monodentate carboxylate group,[6] whereas MnCAT may effectively catalyze the disproportionation of H_2O_2 by using a μ-oxo/hydroxo-bis(μ-carboxylate)dimanganese structural unit as the active site.[5,7,8] Recently, various dinuclear manganese-based catalase mimics[9] that decompose hydrogen peroxide have been screened as catalysts for low-temperature bleaching[10] and for organic syntheses.[11] The manganese complexes used as mimics of MnSOD are more suitable than Cu_2Zn_2SOD because manganese has a lower toxicity in mammalian systems.[12] Recently, various mononuclear manganese complexes have been selected for pharmaceutical uses,[13] such as manganese complexes with Schiff-base ligands,[14] porphyrins, 1,4,7,10,13-pentazacylic pentadecane derivatives,[15,16] and so on.[17] Among these, a class of complexes with combined SOD and catalase functions have attracted many people's attention: complexes such as [Mn(salen)Cl] and [Mn(vanl)Cl] (salen and vanl are the [1+2] condensates of ethylenediamine with salicyladehyde or vanillin, respectively) exhibit both SOD and catalase activities, catalytically destroying both superoxide anion and hydrogen peroxide. Due to their novel combined functions, they have been suggested to serve as therapeutic agents.[18–20]

An attractive property of the tridentate macrocycle 1,4,7-triazacyclonone (tacn) is its ability to form thermodynamically stable redox-active manganese complexes.[21,22] In this paper, this ligand has been further modified. Two new manganese(II) complexes $[MnL^1Cl_2]$ **1** and $[MnL^2Cl]ClO_4$·MeOH **2** [L^1 = 1-(benzimidazol-2-yl-methyl)-1,4,7-tacn, L^2 = 1,4-bis(benzimidazol-2-yl-methyl)-1,4,7-tacn] have been synthesized and characterized by stndard physical methods. Interestingly, the two complexes exhibit SOD activities, catalytically dismutating $O_2^{\cdot-}$, and possess the combined functions of SOD and catase.

Results and Discussion

Characterization

Both complexes possess similar spectroscopic features. In the IR spectra the strong bands at 3415 and 3384 cm^{-1} are

[a] Coordination Chemistry Institute, State Key Laboratory of Coordination Chemistry,
Nanjing 210093, P. R. China
E-mail: qhluo@jlonline.com
[b] School of Chemical engineering & Pharmacy, Wuhan Institute of Chemical Technology
430073, P. R. China

due to the N−H stretching vibration of complexes **1** and **2**, respectively. The medium-strong bands at about 750 cm^{-1} are designated as skeleton stretching of the aromatic ring. Complex **2** exhibits a strong band at 1107 cm^{-1}, showing the presence of ClO_4^-.

In the electronic spectra, the absorptions of the two complexes in the range of 279−272 nm and at 244 nm are characteristic of the B band and E_2(K) band of *o*-phenylene, respectively. The values of the molar conductivities indicate that both complexes are 1:1 electrolytes in MeCN solution.

The magnetic susceptibilities of the two complexes show that the manganese in each complex has a high-spin, d^5 configuration.

The EPR spectra of complex **2** in MeOH solution at room temperature and 110 K are shown in Figure 1. Figure 1 (see a) exhibits a six-line spectrum, typical of mononuclear Mn^{II}, centered at 3496 G, with $g = 1.999$ and a hyperfine coupling constant, A, of 88×10^{-4} cm^{-1} associated with the $I = 5/2$ nuclear spin of ^{55}Mn. This signal results from allowed transitions ($\Delta m_s = \pm 1$, $\Delta m_I = 0$). In the spectrum at 110 K (see b in Figure 1) it is possible to see the weak, forbidden transition signals between the six intense signals.

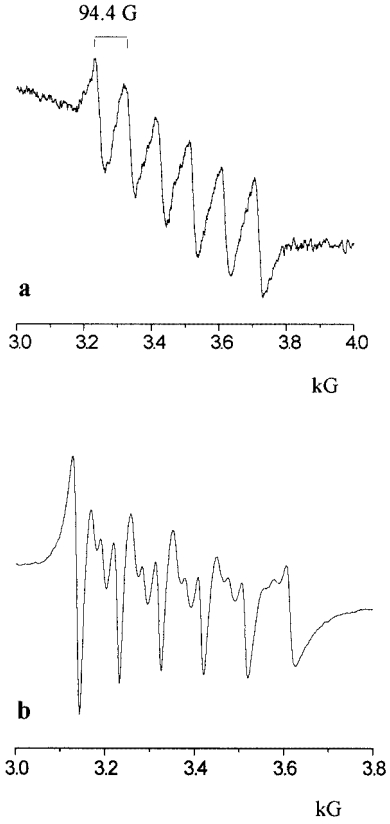

Figure 1. EPR spectra of the complex $[MnL^2Cl]ClO_4 \cdot MeOH$ in methanol (1.0×10^{-2} mol·dm^{-3}): (a) at room temperature; (b) at 110 K; microwave frequency: 948 GHz; microwave power: 20 mW; gain: 1.0×10^5; scan range: 2000 G; time constant: 100 s; scan time: 100 s

The positive-ion electrospray (ES) mass spectra of $[MnL^1Cl_2]$ **1** and $[MnL^2Cl]ClO_4 \cdot MeOH$ **2** in MeOH solution were also recorded. The results are listed in Table 1. These peaks are due to loss of one or two chloride anions, formation of dinuclear Mn^{II} species with two chloride anions as bridging ligands, or binding of solvent molecules. The loss of chloride anions shows the weak interaction between the Cl^- ion and manganese(II), which would favor the attack of species with low molecular weight, such as superoxide anion. No peaks of ligands or their fragments were found in the mass spectra of the two complexes, and their simplicity is attributed to the thermodynamic stability and kinetic inertness of the two complexes.[22] No peaks were found due to the loss of Mn^{2+} ion or the pendant arm. This indicates that both complexes are stable under the experimental conditions.

Electrochemical Properties

The redox behavior of **1** and **2** was studied by cyclic voltammetry in aqueous solution and in MeOH solution for **1** and **2**, respectively. During scanning from −0.3 V to +0.8 V the CV diagram of **1** in aqueous solution displays one pair of anodic and cathodic peaks with peak potentials of $E_{pa} = 0.411$ V and $E_{pc} = -0.109$ V (vs. SCE) respectively. The value of the half-wave potential, $E_{1/2}$, was calculated to be 0.151 V. The anodic peak current (i_p) is almost equal to the cathodic one. In the same range of potential scan rate (v), the $i_p/v^{1/2}$ ratio is kept constant. The peak separation between the anodic and cathodic peaks at a scan rate 50 mV·s^{-1} is 520 mV. These features are indicative of a quasi-reversible M^{II}/Mn^{III} redox process. Other redox peaks were not found at a more negative potential, implying that the macrocycle effect stabilizes the Mn^{III} oxidation state. Complex **2** shows two pairs of quasi-reversible anodic and cathodic peaks with $E^1_{1/2} = 0.527$ V for first pair of peaks and $E^2_{1/2} = 0.697$ V for the second pair of peaks (Figure 2); they are assigned to the Mn^{III}/Mn^{II} and Mn^{IV}/Mn^{III} couples, respectively.

According to the redox potential of $\cdot O_2^-$ in neutral solution

$O_2 + e^- \rightarrow \cdot O_2^-$; $E^o_{pH7} = -0.16$ V (vs. NHE)
$\cdot O_2^- + 2\,H^+ + e^- \rightarrow H_2O_2$; $E^o_{pH7} = +0.89$ V (vs. NHE)

in order to act as a catalyst of $\cdot O_2^-$ disproportionation, the complexes must have a half-wave potential falling between two values. The half-wave potentials for complex **1** [$E_{1/2} = 0.392$ V (vs. NHE)] and complex **2** [$E^1_{1/2} = 0.769$ V (vs. NHE)] both fall between −0.16 V and +0.89 V (see Equation 3 and 4[23]), therefore both complexes can be oxidized by $\cdot O_2^-$ and their oxidized form can be re-reduced by $\cdot O_2^-$ to finish the catalytic cycles, as follows:

$Mn^{II} + \cdot O_2^- + 2H^+ \rightarrow Mn^{III} + H_2O_2$
$Mn^{III} + \cdot O_2^- \rightarrow Mn^{II} + O_2$

For the second pair of peaks of complex **2**, the half-wave potential is higher than +0.89 V [$E^2_{1/2} = 0.939$ V (NHE)], indicating that $\cdot O_2^-$ cannot oxidize Mn^{III} to Mn^{IV} in this

 © 2004 Wiley-VCH Verlag GmbH & Co. KGaA, Weinheim

Table 1. Peak assignments of complexes **1** and **2**

$[MnL^1Cl_2]$ (**1**)		$[MnL^2Cl]ClO_4$·MeOH (**2**)	
349.2 (100)[a]	$[MnL^1Cl]^+$	479.2 (100)	$[MnL^2Cl]^+$
172.9 (22)	$[MnL^1 + MeOH]^{2+}$	222.2 (24)	$[MnL^2]^{2+}$
732.9 (13)	$[Mn_2L^1{}_2Cl_2 + 0.5MeOH + OH^-]^+$	609.2 (13)	$[MnL^2 + 4MeOH]^+$
		237.7 (9)	$[MnL^2 + MeOH]^{2+}$

[a] The relative abundance is given in parentheses.

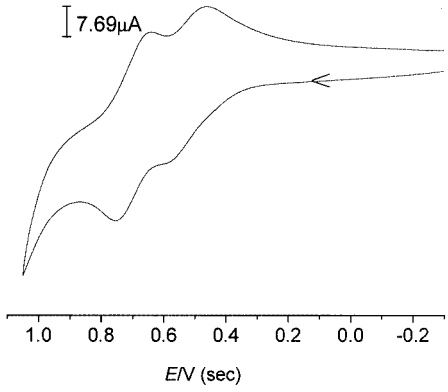

Figure 2. Cyclic voltammogram of complex **2** in MeOH solution; concentration: 1.0×10^{-3} mol·dm^3 (scan rate 100 mV·s^{-1})

complex. Therefore the catalytic cycle occurs only between Mn^{II} and Mn^{III}; this is similar to MnSOD.

pH Titration

The coordinating ability of the ligands towards Mn^{2+} was studied by means of pH titration of a solution containing L^1·3HCl (or L^2·3HCl) and $Mn(NO_3)_2$ in equimolar amounts. To avoid precipitation of manganese(II) complexes of L^2 in aqueous solution during titration by NaOH, the experiments were carried out in dioxane/water (7:3, v/v). The titration curves of ligand L^1·3HCl (1) and L^1·3HCl plus Mn^{2+} ion (2) in aqueous solution are shown in Figure 3. The first inflexions of the two curves are at about $a = 1$ (a denotes the number of mols of NaOH added per mol of ligand), showing that one mol of the acid was titrated by base. For curve (2) in Figure 3 a very long buffer region at about $a = 1-3$, indicates the formation of the dominant species $[Mn(L^1)]^{2+}$, after which a slow inflexion occurs corresponding to the coexistence of $[MnL^1(OH)]^+$ and $[MnL^1(OH)_2]$ species, implying that the hydroxyl ions are bound to the unoccupied coordination sites. Assuming the coexistence of $[Mn(L^1)]^{2+}$, $[MnL^1(OH)]^+$ and $[MnL^1(OH)_2]$, the equilibrium constants (Table 2) were obtained by a curve fitting procedure. Comparing the equilibrium constants of complexes **1** and **2** with those of their parent complexes, which have no benzimidazole groups on the tacn backbone, we can see that the species $[MnL]^{2+}$ for 1 and 2 have better stability than the parent complex. The species-distribution curves of curve (2) are shown in Figure 4. The distribution curves of complexes **1** and **2** show that, at physiological pH (7.4), an $[MnL^1(OH)]^+$ species still predominates for both L^1 and L^2, implying that the vacant site at Mn^{II} atom is suitable for the coordination of hydroxyl ion. The percentage of free Mn^{2+} is less than 0.07% and 0.08% for L^1 and L^2, respectively. This means that the ligands have a relatively strong coordinating ability to manganese(II).

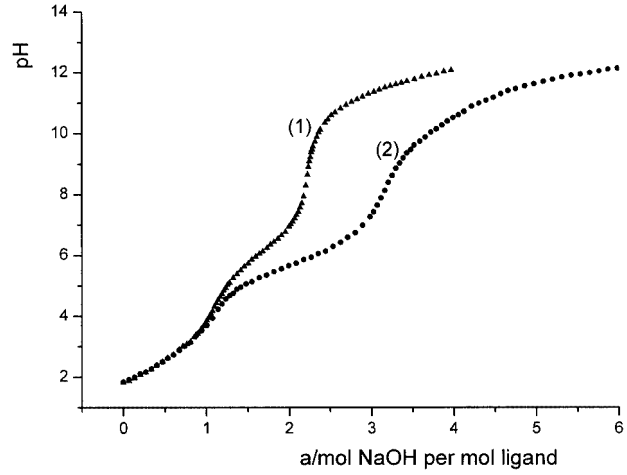

Figure 3. pH Titration curves in aqueous solutions: (1) $[L^1·3HCl] = 0.002496$ mol·dm^{-3}; (2) $[L^1·3HCl] = [Mn^{2+}] = 0.002504$ mol·dm^{-3}; $I = 0.1$ mol·dm^{-3} (KNO_3), 25 °C

Crystal Structures of the Complexes

[MnL¹Cl₂]

The crystal data of complexes **1** and **2** are listed in the Exp. Sect. The structure of the $[MnL^1Cl_2]$ is shown in Figure 5 (a), and selected bond lengths and angles are given in Table 3. In complex **1**, each Mn^{II} atom is coordinated by four nitrogen atoms of the triazacycle [N(1), N(2), N(3)], with average bond lengths of 2.292 Å, one benzimidazole nitrogen atom N(4), and two chloride ions. The Mn−N(4) bond length is 2.214 Å, and is the shortest of the Mn−N bonds. This indicates that the nitrogen atom of the benzimidazole group has a stronger coordination ability to Mn^{II} than the nitrogens of the triazacycle and plays an important role in increasing the stability of the complex. The two Mn−Cl bond lengths [2.5298(11) Å for Cl (1) and 2.4067 Å for Cl (2)] are longer than the Mn−N bond lengths, therefore these Cl^- anions are able to be detached from the Mn^{II} atom in solution, as proved by the ES-MS experiment.

 © 2004 Wiley-VCH Verlag GmbH & Co. KGaA, Weinheim

Table 2. Equilibrium constants at 25 °C; I = 0.20 mol·dm^{-3} (KNO_3)

Reaction	L^1	L^2 [a]	[9]aneN$_3$ [21c]
$L + H^+ \rightleftarrows [HL]^+$	11.01± 0.02	9.16 ± 0.01	10.42
$[HL]^+ + H^+ \rightleftarrows [H_2L]^{2+}$	5.74 ± 0.01	3.39 ± 0.02	6.82
$[H_2L]^{2+} + H^+ \rightleftarrows [H_3L]^{3+}$	3.50 ± 0.02	1.02 ± 0.01	very small
$Mn^{2+} + L \rightleftarrows [MnL]^{2+}$	9.95 ± 0.01	6.52 ± 0.01	5.8
$Mn^{2+} + L + OH^- \rightleftarrows [MnL(OH)]^+$	3.50 ± 0.02	2.69 ± 0.02	3.6
$Mn^{2+} + L + 2OH^- \rightleftarrows [MnL(OH)_2]$	−5.52 ± 0.03	−6.73 ± 0.02	

[a] Experiments for L^2 were carried out in dioxane/water solution (7:3, v/v).

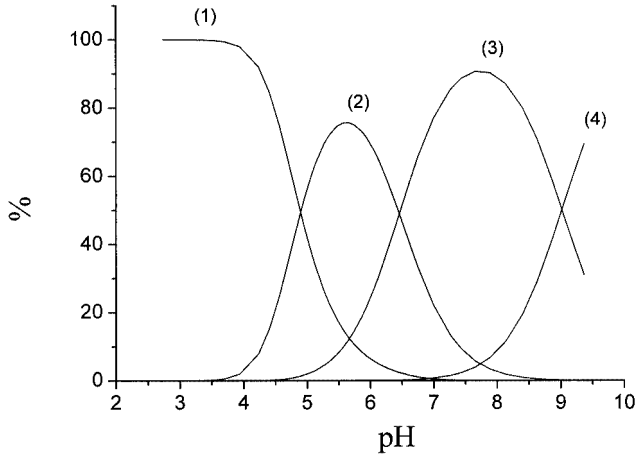

Figure 4. Species distribution curves for curve (2) of Figure 3: (1) Mn^{2+}; (2) $[Mn(L^1)]^{2+}$; (3) $[MnL^1(OH)]^+$; (4) $[MnL^1(OH)_2]$

The Mn^{II} is located at the center of a distorted octahedron, with the Cl(1) and N(2) atoms located in the axial direction and Cl(2), N(1), N(3) and N(4) located in the equatorial plane. The Cl(1)−Mn−N(2) angle is 164.45(7)°. The least-squares plane is composed of Cl(2), N(1), N(3), and N(4), with the Mn^{II} atom lying 0.6973 Å out of this plane. The dihedral angle between the benzimidazole plane and the equatorial plane is 11.5°.

Table 3. Selected bond lengths (Å) and angles (°) of complex **1**

Mn(1)−Cl(1)	2.5298(11)	Mn(1)−N(1)	2.389(2)
Mn(1)−N(2)	2.304(2)	Mn(1)−N(3)	2.261(3)
Mn(1)−N(4)	2.214(3)	Mn(1)−Cl(2)	2.4067(11)
Cl(1)−Mn(1)−N(1)	91.25(6)	Cl(1)−Mn(1)−N(2)	164.45(7)
Cl(1)−Mn(1)−N(3)	94.57(9)	Cl(1)−Mn(1)−N(4)	89.70(7)
Cl(1)−Mn(1)−Cl(2)	99.95(4)	Cl(2)−Mn(1)−N(1)	167.53(7)
Cl(2)−Mn(1)−N(2)	93.73(7)	Cl(2)−Mn(1)−N(3)	98.18(7)
Cl(2)−Mn(1)−N(4)	111.34(8)	N(1)−Mn(1)−N(2)	74.49(9)
N(1)−Mn(1)−N(3)	75.30(9)	N(1)−Mn(1)−N(4)	73.88(10)
N(2)−Mn(1)−N(3)	76.07(10)	N(2)−Mn(1)−N(4)	92.18(10)
N(3)−Mn(1)−N(4)	148.96(10)		

[MnL^{2}Cl]ClO$_4$·MeOH

The structure of the complex cation $[MnL^2Cl]^+$ is shown in Figure 5 (b); selected bond lengths and angles are given in Table 4. The coordination environment of **2** is very similar to that of **1**, except that one chloride anion has been replaced by a nitrogen atom of another benzimidazol-2-yl-

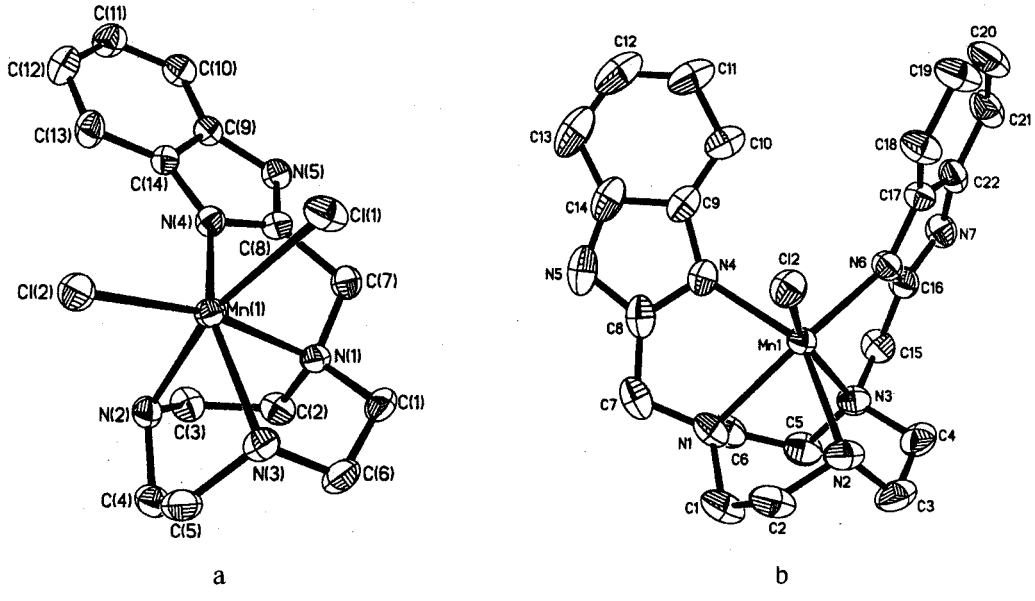

Figure 5. Crystal structure of $[MnL^1Cl_2]$ (a) and the $[MnL^2Cl]^+$ cation (b)

 © 2004 Wiley-VCH Verlag GmbH & Co. KGaA, Weinheim

Table 4. Selected bond lengths (Å) and angles (°) of complex **2**

Mn(1)−Cl(2)	2.4668(7)	Mn(1)−N(1)	2.407(2)
Mn(1)−N(2)	2.228(2)	Mn(1)−N(3)	2.376(2)
Mn(1)−N(4)	2.202(2)	Mn(1)−N(6)	2.1723(19)
Cl(2)−Mn(1)−N(1)	116.20(7)	Cl(2)−Mn(1)−N(2)	88.04(7)
Cl(2)−Mn(1)−N(3)	158.13(6)	Cl(2)−Mn(1)−N(4)	92.82(6)
Cl(2)−Mn(1)−N(6)	101.17(6)	N(1)−Mn(1)−N(2)	75.00(8)
N(1)−Mn(1)−N(3)	74.15(8)	N(1)−Mn(1)−N(4)	72.38(8)
N(1)−Mn(1)−N(6)	141.65(8)	N(2)−Mn(1)−N(3)	75.80(8)
N(2)−Mn(1)−N(4)	143.96(8)	N(2)−Mn(1)−N(6)	116.55(8)
N(3)−Mn(1)−N(4)	108.94(8)	N(3)−Mn(1)−N(6)	74.00(7)
N(4)−Mn(1)−N(6)	98.64(8)		

methyl ligand. The Mn−Cl bond length is 2.4668(7) Å. The Mn^{II} atom is also located at the center of a distorted octa5-hedron as in **1**. The atoms N(1), N(2) and N(3) of the aza-macrocycle constitute a face of the octahedron, and two nitrogen atoms [N(4), N(6)] of the two benzimidazol-2-yl-methyls and the Cl^- anion compose the opposite face. Cl(2) and N(3) are located in the axial direction with a Cl(2)−Mn−N(3) angle of 158.13(6)°. The equatorial plane is composed of N(1), N(2), N(4) and N(6), and the Mn^{II} atom is 0.3893 Å out of this plane. The dihedral angle between the equatorial plane and one of the benzimidazole planes [N(4), N(5), C(8)−C(14)] is 164.2°, and that between the equatorial plane and the other benzimidazole plane [N(6), N(7), C(16)−C(22)] is 89.3°. The dihedral angle between the two benzimidazole planes is 76.1°. The two benzimidazole groups encapsulate Mn^{II} to form a hydrophobic packet with a channel.

SOD Activities of the Complexes

The SOD activities of the complexes were studied in aqueous solutions of phosphate buffer (pH 7.4) by the riboflavin photoreduction method.[24] Both complexes inhibit the reduction of nitroblue tetrazolium chloride, depending on their concentrations. The activity was obtained by plotting the percentage of inhibiting NBT reduction, *f* (%), against the concentration of the complex, *C*. The plot for complex **2** is shown in Figure 6. The activities of complexes **1** and **2**, together with those for $Mn(ClO_4)_2$ and Cu_2Zn_2SOD determined under the same conditions, are listed in Table 5. The activities of **1** and **2** are of the same order of magnitude as that of Mn^{2+} ion, but these high activities are not due to free Mn^{2+} ion produced by dissociation of the complexes. The free Mn^{2+} ion can be ignored in solution, as proved by the pH titration. The activities of the complexes are about 1% of that of Cu_2Zn_2SOD.

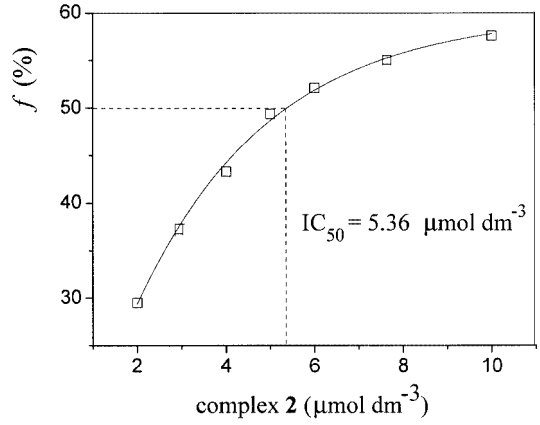

Figure 6. A plot of inhibition percentage (*f*%) vs. concentration for complex **2**

The complexes were also studied by the addition of various concentrations of bovine serum albumin (BSA) to the tested solutions in order to further prove the stability of the complexes under protein conditions. It was found that the concentration of BSA has no effect on the activities of the two complexes until it reached a value of 0.2 mg/mL. The ES mass spectra and X-ray structural analyses of the two complexes show that the binding of chloride anions to the Mn^{II} center is rather weak, and therefore it is likely that the Cl^- could become partially detached in solution. As the concentration of $^{\cdot}O_2^-$ in the solution much higher than that of OH^- at pH 7.4, the vacant coordination sites are open to attack by $^{\cdot}O_2^-$. The benzimidazole groups are similar to the hydrophobic residues of MnSOD. In complex **2**, with two benzimidazole groups, the benzimidazole groups surround the metal ion to form a hydrophobic channel which favors the attack of $^{\cdot}O_2^-$; complex **2** therefore displays higher SOD activity.

Reactivity with Hydrogen Peroxide

The catalytic activity of complexes **1** and **2** towards hydrogen peroxide was investigated in methanol/water solutions (1:5, v/v) and in aqueous solutions, respectively. The evolution of dioxygen was followed manometrically as a function of time at room temperature. The O_2-evolution curve for complex **1** is shown in Figure 7. In the absence of NaOH, the complex decomposes hydrogen peroxide very slowly (Figure 7, curve 1) corresponding to the self-decomposition of H_2O_2. After 15 min only 7.0% of the total H_2O_2 had been decomposed. Previous authors have re-

Table 5. The activities of complexes **1** and **2**

Compounds	**1**	**2**	$Mn(ClO_4)_2{\cdot}6H_2O$	Cu_2Zn_2SOD
IC_{50} (μmol·dm^{-3})	8.33 (8.41)[a]	5.36 (5.88)[a]	3.56	0.06
Relative activity (%)	0.7	1.1	1.7	100

[a] The numbers in parentheses are the activities assayed upon addition of a further 0.2 mg/L of BSA.

 © 2004 Wiley-VCH Verlag GmbH & Co. KGaA, Weinheim

Table 6. The kinetic data of H_2O_2 decomposition by the complexes at 25 °C

Complex	Solvent	$C_{complex}$ ($\times 10^4$ mol·dm^{-3})	$C_{H^2O^2}$ (mol·dm^{-3})	C_{NaOH} ($\times 10^3$ mol·dm^{-3})	υ_0 ($\times 10^4$ mol·min^{-1})	υ' (s^{-1})	Turnover (t = 15 min)	H_2O_2 (%) (t = 15 min)
1	MeOH/H_2O	8.45	0.535	4.84	4.24	5.58	606	95.7%
2	MeOH/H_2O	8.50	0.535	5.69	1.55	2.03	609	96.8%
1	H_2O	9.89	0.487	5.43	6.63	6.70	483	98.2%

ported that the addition of an organic base accelerates significantly the catalytic decomposition of hydrogen peroxide by manganese complexes.[25] However, in this experiment organic bases such as pyridine, imidazole and acetate anion did not increase the rate of O_2 evolution. Interestingly, the rate of O_2 evolution increased with an increase of the concentration of NaOH, and at a molar ratio of NaOH to complex **1** of 1.68 (pH 7.38), the percentage of decomposed H_2O_2 reached 90% after 15 min. When the molar ratio of NaOH to complex **1** was equal to 5.73 (pH 11.03), we obtained an initial turnover rate, υ' of 5.58 mol H_2O_2/mol catalyst·s^{-1} and a turnover number (number of mols of H_2O_2 decomposed per mol catalyst) of 606 (after the reaction stopped). The kinetic data for H_2O_2 decomposition by the complexes are listed in Table 6, where it can be seen that the value of υ' of complex **1** is higher than that of complex **2** in MeOH/water solvent, although its turnover is lower, because the formation of a dinuclear manganese complex as the active species (see below) is difficult for complex **2** due to the steric hindrance of the two benzimidazole groups, however, the turnover of complex **2** is higher because the active species of **2** does not easily decompose. In aqueous solution, complex **1** has a higher value of υ' and a lower turnover number than in mixed solvent, probably because both H_2O_2 and the active species of complex **1** have a low stability in aqueous solution, resulting in a high catalytic activity and a low turnover. The υ' values of complex **1** in aqueous solution and mixed solvent are close to that of the dinuclear manganese complex with the *N*,*N*′,*N*′′-trimethyl-1,4,7-triazacyclononane ligand[26] (υ' = 5.55 s^{-1}), although the turnover is lower. To date, the dinuclear manganese complexes reported[4] have rate values that range from 0.013[28] to 50 s^{-1}.[27] The values of υ' for complexes **1** and **2** therefore fall at the high end of the range of those reported previously.

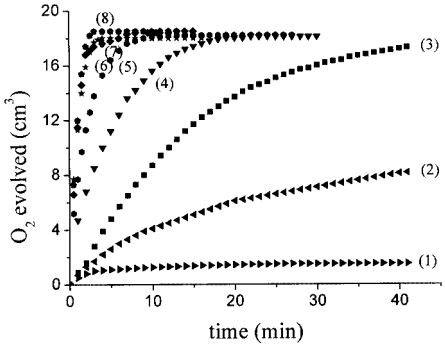

Figure 7. Curves of oxygen evolution for the catalytic disproportionation of H_2O_2 by $[MnL^1Cl_2]$ (**1**) in methanol/water solution (1:5, v/v); $C_{complex}$: 8.45 × 10^{-4} mol·dm^{-3}; C_{NaOH}: (1) 0 (pH 4.71); (2) 5.12 × 10^{-4} (pH 5.06); (3) 7.11 × 10^{-4} (pH 6.02); (4) 1.42 × 10^{-3} (pH 7.38); (5) 1.99 × 10^{-3} (pH 8.31); (6) 3.42 × 10^{-3} (pH 9.44); (7) 4.27 × 10^{-3} (pH 10.57); (8) 4.84 × 10^{-3} (pH 11.03)

Active Intermediates

A number of the dinuclear manganese complexes with oxygen or hydroxyl bridges reported previously exhibit significant rate enhancement for the disproportionation of hydrogen peroxide in the presence of an exogenous base. It has been proposed that this effect is due to the base-facilitated deprotonation of H_2O_2 in the course of the coordination of hydrogen peroxide to the manganese center. In our experiment, however, this is not the case as the concentration of H_2O_2 is very much higher (several hundred times) than those of complex and NaOH. Therefore, the main function of the added NaOH is not capturing a proton from H_2O_2.

The active intermediates in the catalytic decomposition reactions of hydrogen peroxide by the manganese complexes could not be isolated from the solutions. Therefore, in order to trap the active species, the ES mass spectrum of complex **1** plus H_2O_2 and NaOH in MeOH solution was recorded (Figure 8). The peak assignments are shown in Table 7, in which all species derived from complex **1** are oxygen-bridged or hydroxyl-bridged binuclear complex cations and the oxidation state of manganese is +2 or +3. According to these results, a possible mechanism of hydrogen peroxide dismutation is suggested in Scheme 1.

In step 1 the Cl^- ligand in complex 1 is substituted by water molecules, and in step 2 complexes containing one or two hydroxyl-bridged units are formed in basic solution. In step 3 the water molecules are replaced by H_2O_2, followed by an intramolecular electron transfer (step 4). Finally, the intermediate reacts further with H_2O_2 and the catalytic cycle is completed (step 5).

For complex **2**, the ES mass spectrum obtained under the same conditions as **1** is different (Table 8) as only a few molecules of complex **2** are changed into hydroxyl-bridged or oxygen-bridged binuclear manganese units due to the steric hindrance of the two benzimidazole groups; the manganese therefore exists in the Mn^{II}, Mn^{III} and Mn^{IV} oxidation states. The variation of oxidation state for complexes **1** and **2** during the disproportionation of hydrogen peroxide is in agreement with the results obtained by cyclic voltammetry.

It is remarkable that irrespective of whether they are dissolved in MeOH/water or only in water at about pH 7.3,

 © 2004 Wiley-VCH Verlag GmbH & Co. KGaA, Weinheim

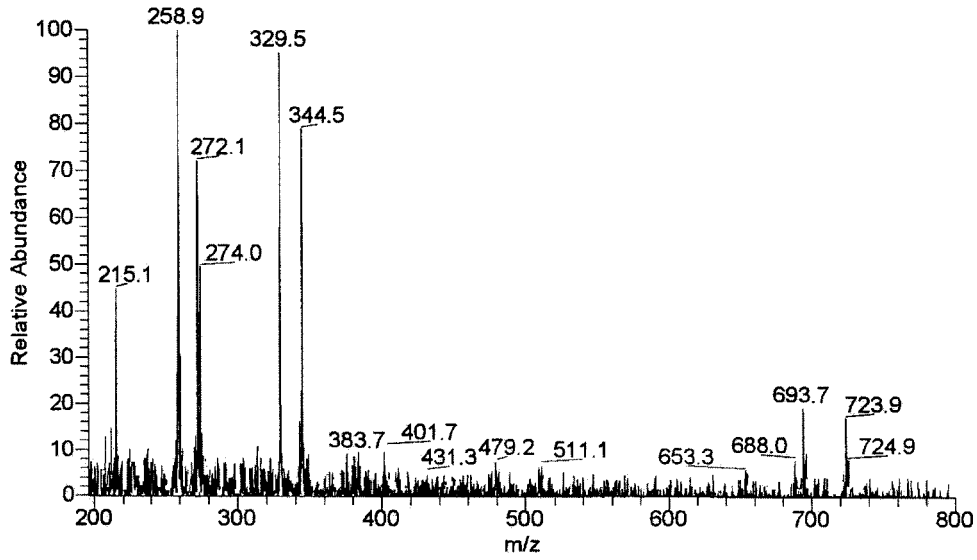

Figure 8. ES-MS of complex **1** in the presence of NaOH and H_2O_2 in methanol; $[MnL^1Cl_2]/NaOH/H_2O_2$ = 1:2:8

Table 7. Peak assignment of complex **1** in the presence of NaOH and H_2O_2 in MeOH; $[MnL^1Cl_2]/NaOH/H_2O_2$ = 1:2:8

m/z (%)	Species
258.9 (100)	$[L^1{}_2Mn^{II}{}_2(\mu\text{-}OH)_2 + H_2O + MeOH + H^+]^{3+}$
329.5 (95)	$[L^1{}_2Mn^{III}{}_2(\mu\text{-}O)_2]^{2+}$
344.5 (78)	$[L^1{}_2Mn^{II}{}_2(\mu\text{-}OH)_2 + 1.5H_2O]^{2+}$
272.1 (72)	$[L^1{}_2Mn^{III}{}_2(\mu\text{-}OH)_2 + 3Cl^- + 2.5H_2O + 2H^+]^{3+}$
215.1 (45)	$[L^1{}_2Mn^{II}{}_2(\mu\text{-}OH)]^{3+}$
693.7 (18)	$[L^1{}_2Mn^{II}{}_2(\mu\text{-}OH)(\mu\text{-}O) + MeOH]^+$
723.9 (17)	$[[L^1{}_2Mn^{II}Mn^{III}(\mu\text{-}O)_2 + 2MeOH]^+$

Table 8. Peak assignments for complex **2** in the presence of NaOH and H_2O_2 in MeOH; $[MnL^2Cl]ClO_4{\cdot}MeOH/NaOH/H_2O_2$ = 1:2:8

m/z (%)	Species
177.1 (100)	$[L^2Mn^{II} + 3H_2O + MeOH + H^+]^{3+}$
418.0 (76)	$[L^2{}_2Mn^{III}{}_2(\mu\text{-}OH) + 2ClO_4^- + 3MeOH + 3H_2O]^{3+}$
287.3 (65)	$[L^2Mn^{IV}(OH)_2 + 3MeOH]^{2+}$
404.3 (32)	$[L^2{}_2Mn^{III}{}_2(\mu\text{-}OH)_2 + 2ClO_4^- + 5H_2O + H^+]^{3+}$
319.1(24)	$[L^2{}_2Mn^{III}Mn^{IV}(\mu\text{-}OH)\ (\mu\text{-}O) + Cl^-]^{3+}$
215.1 (24)	$[L^2Mn^{III} + 2ClO_4^- + 2H^+]^{3+}$
386.1 (19)	$[L^2{}_2Mn^{III}Mn^{IV}(\mu\text{-}O) + 2ClO_4^- + 3H_2O]^{3+}$

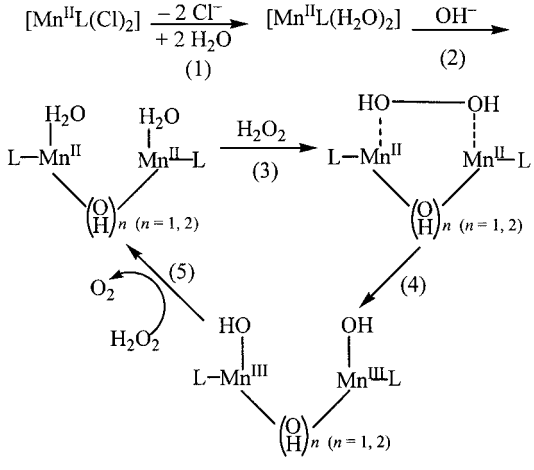

Scheme 1. The mechanism of hydrogen peroxide dismutation by complex **1**

which is close to physiological conditions, complexes **1** and **2** decompose 90% of H_2O_2 during the first 15 min (Figure 7). Therefore, we consider that at physiological pH values the complexes are able to dismutase $^{\cdot}O_2^-$ and are also able to decompose H_2O_2, depending on the concentration of $^{\cdot}O_2^-$. The SOD activities of the complexes are not high, and this is probably due to the fact that some of the species are hydroxylated or bridged. The mechanism for this and its biological relevance need to be studied further.

Conclusion

Two manganese(II) complexes of 1,4,7-tacn with benzimidazole groups, $[MnL^1Cl_2]$ and $[MnL^2Cl]ClO_4{\cdot}MeOH$, were synthesized and characterized. pH titration was used to investigate their stabilities in solution. The introduction of benzimidazole groups on the backbone of tacn increases the stability of the new complexes relative to the parent, unsubstituted complex. The redox potentials of the complexes obtained from cyclic voltammetry show that they are able to dismutase $^{\cdot}O_2^-$. The oxidation state for manganese of the two complexes changes from +2 to +3, and then from +3 to +2, implying that the catalytic mechanism is just a "ping-pong" reaction. ES mass spectrometric and X-ray structure analyses indicated that the binding of Cl^- with Mn^{II} in the complexes is relatively weak, therefore Cl^- can be attacked by $^{\cdot}O_2^-$. The complexes can also be converted into OH- or O-bridged dinuclear manganese(III) or manga-

 © 2004 Wiley-VCH Verlag GmbH & Co. KGaA, Weinheim

nese(IV) complexes, which act as active species to decompose H_2O_2 catalytically.

Experimental Section

Materials: L^1 [1-(benzimidazol-2-ylmethyl)-1,4,7-triazacyclononane] and L^2 [1,4-bis(benzimidazol-2-ylmethyl)-1,4,7-triazacyclonone] were prepared by the reported method.[29] Carbonate-free NaOH for pH titration was obtained by Powell's method.[30] $Mn(NO_3)_2{\cdot}6H_2O$ (Analytic Reagent) was recrystallized from doubly distilled water and the stock solutions were standardized by titration with EDTA. In SOD activity experiments, nitroblue tetrazolium nitrate (NBT) (Biochemical Reagent) and L-methionine (Biochemical Reagent) were used and the solutions were prepared using doubly distilled water. The purity of riboflavin was determind by the literature method.[31] The concentration of stock solution of hydrogen peroxide for catalysis activity assay was measured by titration with standardized $KMnO_4$ solution.

Physical Measurements: Elemental analysis was performed using a Perkin−Elmer 240c analytical instrument. IR spectra were measured as KBr discs using a Nicolet 5DX FT-IR spectrophotometer. Electronic spectra were recorded on a UV-3100 spectrophotometer. X-band EPR spectra were measured on an EMX spectrometer in 1.0×10^{-2} mol·dm^{-3} MeOH solution. The electrical conductivity of solutions was measured with a BSD-A conductometer (Jiangsu, P. R. China) with a solution concentration of about 1.0×10^{-3} mol·dm^{-3} in MeCN at 25 ± 0.1 °C. The electrospray mass spectra were determined on a Finnigan LCQ mass spectrograph. The samples (about 0.1 mmol·dm^{-3} in MeOH) were electrosprayed at a flow rate of 5×10^{-6} mol·min^{-1} with a needle voltage of +4.5 kV. The temperature of the heated capillary at the interface was 200 °C and a fused-silica sprayer was used. The mobile phase was an aqueous solution of methanol (1:1, v/v). The samples were run in the positive-ion mode.

Electrochemical Measurements: The cyclic voltammogram experiments were carried out on a PAR Model 273 potentiostat coupled to a PAR Model 175 universal programmer under highly pure nitrogen at 25 ± 0.1 °C. A glassy-carbon electrode was employed as working electrode, a saturated calomel electrode (SCE) as reference electrode, and a platinum wire as auxiliary electrode. The concentration of complex 1 was 1.0×10^{-3} mol·dm^{-3} in 0.1 mol·dm^{-3} $NaClO_4$ aqueous solution and that of complex 2 was 1.0×10^{-3} mol·dm^{-3} in 0.1 mol·dm^{-3} TBAP (tetrabutylammonium perchlorate) MeOH solution. The solutions were deaerated for about 15 min before applying the voltage. The half-wave potentials, $E_{1/2}$, were calculated approximately from $(E_{pa} + E_{pc})/2$ and the measured errors were ±2 mV. Unless otherwise stated, all potentials reported are referenced to the saturated calomel electrode.

pH Titration: Protonation constants of the ligands and stability constants of the complexes were determined by using a Corning pH meter with a glass/silver/silver chloride combination electrode with a precision of ±0.001 pH units. The electrode was standardized against buffer solutions of potassium hydrogen phthalate and sodium borate. The concentrations of ligands ($L^1{\cdot}3HCl$ or $L^2{\cdot}3HCl$) was about 0.0025 mol·dm^{-3}, and the molar ratio of $L^1{\cdot}3HCl$ or $L^2{\cdot}3HCl$ to $Mn(NO_3)_2$ was 1:1. The experimental solutions were titrated with carbonate-free 0.0825 mol·dm^{-3} NaOH by using a microsyringe with a precision of ±2 μL under a nitrogen atmosphere in a sealed jacketed vessel at 25 °C. The ionic strength was kept at 0.1 mol·dm^{-3} by adding KNO_3. For the L^2 systems a dioxane/water mixture (7:3) was used as the solvent and 0.1 mol·dm^{-3} KNO_3 as the support electrolyte as the formed product was not soluble in water.

The equilibria in the systems can be represented by Equation (1)

$$qM + pH + rL \rightleftarrows M_qH_pL_r, \text{ where } \beta_{pqr} = [M_qH_pL_r]/[M]^q[H]^p[L]^r \quad (1)$$

where q, p, and r denote the number of metal ions (M), hydrogen ions (H) and ligand molecules (L) bound in the complex, respectively. A negative p value shows that hydrogen ion is released during coordination. The protonation constants of the ligands were calculated with the PKAS program.[31] Applying the law of mass action to each experimental point i (i = 1, 2, 3...n) gives Equations (2)−(4):

$$C_{Hi} = [H]_i + \sum_{j=1}^{m} p_j \beta_{pjqjrj} [H]_i^{pj} [M]_i^{qj} [L]_i^{rj} \quad (2)$$

$$C_{Mi} = [M]_i + \sum_{j=1}^{m} q_j \beta_{pjqjrj} [H]_i^{pj} [M]_i^{qj} [L]_i^{rj} \quad (3)$$

$$C_{Li} = [L]_i + \sum_{j=1}^{m} r_j \beta_{pjqjrj} [H]_i^{pj} [M]_i^{qj} [L]_i^{rj} \quad (4)$$

where j denotes the ordinal number of complexes (j = 1, 2...m) and C_{Hi}, C_{Mi}, and C_{Li} denote the total concentrations of hydrogen ions, metal ions and ligands in solution, respectively, at each experimental point i.

The equilibrium constants of the complexes were calculated by using the program LEMIT,[32] which is based on the Newton−Raphson and Gauss−Newton method for minimizing U in Equation (5), where C_{Hi}^{calc} and C_{Hi}^{expt} denote the calculated and experimental values of H^+ concentration at the ith point.

$$U = \sum_{i}^{n} (C_{Hi}^{calc} - C_{Hi}^{expt})^2 \quad (5)$$

Crystal-Structure Determination: X-ray intensity data for the manganese(II) complexes were collected on a SMART-CCD area-detector diffractometer. Data reduction and cell refinement were performed with the programs SMART and SAINT.[33] The absorption corrections were carried out by an empirical method. The structures were solved by direct methods (Bruker Shelxtl) and refined on F^2 by full-matrix least-squares (Bruker Shelxtl) using all unique data.[34] The non-H atoms in the structures were subjected to anisotropic refinement. Hydrogen atoms were located geometrically and treated with the riding mode. In $[MnL^2Cl]{\cdot}ClO_4{\cdot}CH_3OH$, the ClO_4^- anion was disordered.

CCDC-233744 (**1**) and -233743 (**2**) contain the supplementary crystallographic data for this paper. These data can be obtained free of charge at www.ccdc.cam.ac.uk/conts/retrieving.html or from the Cambridge Crystallographic Data Centre, 12 Union Road, Cambridge CB2 1EZ, UK [Fax: +44-1223-336-033; E-mail: deposit@ccdc.cam.ac.uk].

Assay of Superoxide Dismutase Activity: The activities were assayed by photoreduction of riboflavin.[24] The solutions contained riboflavin (3.4×10^{-6} mol·dm^{-3}), methionine (0.01 mol·dm^{-3}), nitroblue tetrazolium nitrate (NBT; 4.66×10^{-5} mol·dm^{-3}) and the complexes of various concentrations were prepared with phosphate buffer (pH 7.4). They were illuminated by a fluorescent lamp with a constant light intensity at 25 °C. The optical absorbance (A) of the solutions at 560 nm were measured with various illumination periods (t). Each solution was measured in two parallel tests. Inhibition percentage (I%) was calculated according to the reported

 © 2004 Wiley-VCH Verlag GmbH & Co. KGaA, Weinheim

method.[35] The activity (IC_{50}) was defined as the necessary concentration to inhibit 50% reduction of NBT.

Disproportionation of Hydrogen Peroxide:[25,26] An aqueous solution of H_2O_2 (0.5 mL, 3.08 mol·dm^{-3}) was added to a flask containing an aqueous solution of complex **1** or a solution of complex **2** (2.0 mL, 1.22×10^{-3} mol·dm^{-3}) in a methanol/water mixture (1:5). The mixture was stirred and thermostatted at 25 °C, and the O_2 evolved was followed manometrically. To investigate the effect of basicity on the disproportionation of H_2O_2, NaOH solutions of various concentration were added to the flask, the total volumes of solutions were kept to be 2.88 mL for each experiment.

[MnL^{1}Cl$_2$] (1): Manganese(II) acetate (91 mg, 0.34 mmol) was added to a methanol solution (20 mL) of L^1·3HCl·MeOH (125 mg, 0.31 mmol) in 10 mL of methanol. The mixture was stirred for 5 h at room temperature and then filtered. Slow evaporation of the solution gave a pink crystalline compound. Crystals suitable for X-ray diffraction were obtained by diffusion of diethyl ether into an MeCN solution over one week. Yield: 72 mg (61%). $C_{14}H_{21}Cl_2MnN_5$: calcd. C 43.65, H 5.50, N 18.18; found C 43.97, H 5.97, N 18.45. IR (KBr): $\tilde{\nu}$ = 3415 [s, ν(N−H)], 755 cm^{-1} [m, δ(Ph−H)]. UV/Vis (MeOH): λ_{max} = 279 nm (9469 dm^3·mol^{-1}·cm^{-1}), 272 (9150), 268 (8654), 243 (6704). Ω_m (MeCN, 298.2 K): 96.60 S·cm^2·mol^{-1}. μ (290.3 K): 5.63 μ_B.

[MnL^{2}Cl]·ClO$_4$·CH$_3$OH (2): Manganese(II) perchlorate (83 mg, 0.23 mmol) was added to a methanol solution (20 mL) of L^2·3HCl·H$_2$O·1.5EtOH (120 mg, 0.21 mmol) in 10 mL of methanol. Under stirring, the mixture was adjusted to pH 5.0 by addition of a methanol solution of sodium hydroxide. After refluxing for 2 h, the mixture was cooled and filtered. Yellow crystals were isolated from the solution. Yield 69 mg (55%). $C_{23}H_{31}Cl_2MnN_7O_5$: calcd. C 43.13, H 4.93, N 15.17; found C 43.18, H 5.11, N 15.87. IR (KBr): $\tilde{\nu}$ = 3384 cm^{-1} [s, ν(N−H)]; 1108 [s, ν(ClO$_4^-$)], 748 [m, δ(Ph−H)]. UV/Vis (CH_3CN): λ_{max} = 311 nm (416 dm^3·mol^{-1}·cm^{-1}), 279 (12365), 272 (11654), 244 (9846). Ω_m (MeCN, 298.2 K): 100.45 S·cm^2·mol^{-1}. μ (290.3 K): 5.75 μ_B. Crystals suitable for X-ray diffraction analysis were obtained by diffusion of diethyl ether into an MeCN solution over two weeks. Crystallographic data are given in Table 9.

Table 9. Crystal data of complexes **1** and **2**

Complexes	[MnL^{1}Cl$_2$]	[MnL^{2}Cl]ClO$_4$·MeOH
Empirical formula	$C_{14}H_{21}Cl_2MnN_5$	$C_{23}H_{31}Cl_2MnN_7O_5$
Mol. mass	385.20	611.39
Crystal system	monoclinic	monoclinic
Space group	$P2_1/c$	$P2_1/c$
a (Å)	11.208(2)	12.3140(10)
b (Å)	7.6500(10)	14.6130(10)
c (Å)	20.817(3)	15.9340(10)
α (°)	90	90
β (°)	104.900(10)	99.07(2)
γ (°)	90	90
U (Å^3), Z	1724.9(5), 4	2831.4(4), 4
D_c (g·cm^{-3})	1.483	1.434
2θ range (°)	4.0−50	4.4-50
T (K)	293	293
μ(Mo-K_α) (mm^{-1})	1.078	0.701
F(000)	796	1268
Reflections collected	8534	14224
Independent reflections	3020	4978
R indices	0.050	0.021
Observed data [$I > 2\sigma(I)$]	1824	3975
S	0.97	1.03
Final $R1$, $wR2$ [$I > 2\sigma(I)$]	0.0426, 0.0610	0.0527, 0.1481
(all data)	0.0729, 0.0633	0.0641, 0.1535

Acknowledgments

This project was supported by the National Natural Science Foundation of China.

[1] [1a] R. Krämer, *Angew. Chem. Int. Ed.* **2000**, *39*, 4469. [1b] M. McCord, I. Fridovich, *J. Biol. Chem.* **1969**, *244*, 6049.
[2] M. Pick, I. Roboni, J. Fridovich, *J. Am. Chem. Soc.* **1974**, *96*, 7329.
[3] R. Hage, *Recl. Trav. Chem. Pays-Bas.* **1996**, *115*, 385.
[4] V. L. Pecoraro, M. J. Baldwin, A. Gelasco, *Chem. Rev.* **1994**, *94*, 807.
[5] K. Wieghardt, *Angew. Chem. Int. Ed. Engl.* **1989**, *28*, 1153.
[6] W. C. Stallings, K. A. Pattridge, R. A. Strong, M. L. Ludwig, *J. Biol. Chem.* **1985**, 1624.
[7] V. V. Barynin, A. I. Grebenko, *Dokl. Akad. Nauk. SSR.* **1986**, *285*, 1100.
[8] G. C. Dismukes, *Chem. Rev.* **1996**, *96*, 2909.
[9] [9a] C. E. Dube, D. W. Wright, W. H. Armstrong, *Angew. Chem. Int. Ed.* **2000**, *39*, 2169. [9b] A. Gelasco, S. Bensiek, V. L. Pecoraro, *Inorg. Chem.* **1998**, *37*, 3301.
[10] [10a] J. F. Boe, J. J. Girerd, C. Guignard, J. L. Seŕis, J. B. Verlhac, patent no 94/00234, **1994**. [10b]R. Hage, J. E. Iburg, J. Kerschner, J. H. Koek, E. J. M. Lempers, R. J. Martens, U. S. Racherla, S. W. Russell, T. Swarthaff, M. R. P. vanvliet, J. B. Warnaar, L. Van der wolf, B. Krijnen, *Nature* **1994**, *369*, 637.
[11] G. B. Sulpin, G. V. Nizova, Y. N. Kozlov, I. G. Pechenkina, *New J. Chem.* **2002**, *26*, 1238.
[12] D. P. Riley, *Chem. Rev.* **1999**, *99*, 2573.
[13] [13a] D. Salvemini, Z.-Q. Wang, J. L. Zweier, A. Samouilov, H. Macarthur, T. P. Misko, M. G. Currie, S. Cuzzocrea, J. A. Sikorski, D. P. Riley, *Science* **1999**, *286*, 209−210. [13b] D. Riley, K. Udipi, R. Ornberg, *Chem. Brit.* **2000**, 43−44.
[14] [14a] M. Baudry, S. Etienne, A. Bruce, M. Palucki, E. Jacobsen, B. Malfroy, *Biochem. Biophys. Res. Commun.* **1993**, *192*, 964. [14b] Z.-X. Liu, G. B. Robinson, E. M. Gregory, *Arch. Biochem. Biophys.* **1994**, *315*, 74.
[15] [15a] R. F. Pasternack, A. Banth, J. M. Pasternack, C. S. Johnson, *J. Inorg. Biochem.* **1981**, *15*, 261. [15b] L. Batinic-Haberie, L. Benov, I. Spasojevic, I. Fridovich, *J. Biol. Chem.* **1998**, *273*, 2452. [15c] S. Cuzzocrea, B. Zingarelli, G. Castantino, A. P. Caputi, *Free Radic. Biol. Med.* **1999**, *26*, 26.
[16] [16a] D. P. Riley, P. J. Lennon, L. Neumann, R. H. Weiss, *J. Am. Chem. Soc.* **1997**, *119*, 6522. [16b] D. P. Riley, S. L. Henke, P. J. Lennon, K. Aston, *Inorg. Chem.* **1999**, *39*, 1908.
[17] [17a] C. Policar, S. Durot, F. Lambert, M. Cesario, F. Ramiandrasoa, I. Morgenstern-Badarau, *Eur. J. Inorg. Chem.* **2001**, 1807. [17b] D. Salvemini, C. Muscoli, D. P. Riley, S. Cuzzocrea, *Pulm. Thera.* **2002**, *15*, 439.
[18] [18a] R. Bianca, N. Wayman, M. McDonald, A. Pinto, M. Shape, P. Chatterjee, C. Thiemermann, *Med. Sci. Monit.* **2002**, *8*, 1−7. [18b] K. Pong, Y. Rong, S. R. Doctrow, M. Baudry, *Bran Res.* **2002**, *950*, 218. [18c] S. Melov, J. Ravenscroft, S. Malik, M. S. Gill, D. W. Walker, P. E. Clayton, D. C. Wallace, B. Malfroy, S. R. Doctrow, G. J. Lithgow, *Science* **2000**, *289*, 1567.
[19] [19a] S. R. Doctrow, K. Huffman, C. B. Marcus, W. Muslch, A. Bruce, M. Baudry, B. Malfroy, *Adv. Pharmacol.* **1997**, *38*, 247. [19b] K. Baker, C. B. Marcus, K. Huffman, *J. Pharmacol. Exp. Ther.* **1998**, *284*, 215.
[20] C. Jung, Y. Rong, S. Doctrow, M. Baudry, B. Malfroy, Z. Xu, *Neurosci. Lett.* **2001**, *304*, 157.
[21] [21a] S. J. Brudenell, L. Spiccia, A. M. Bond, G. D. Fallon, D. C. R. Hockless, G. Lazarev, P. J. Mahon, E. R. T. Tiekink,

 © 2004 Wiley-VCH Verlag GmbH & Co. KGaA, Weinheim

Inorg. Chem. **2000**, *39*, 881. [21b] P. Chaudhuri, K. Wieghardt, *Prog. Inorg. Chem.* **1987**, *35*, 329. [21c] P. V. Bernhardt, G. A. Lawrance, *Coord. Chem. Rev.* **1990**, *104*, 297.
[22] Z. L. Wang, Q. H. Luo, C. Y. Duan, C. Y. Shen, Y. Z. Li, *Dalton Trans.* **2004**, 1104.
[23] D. T. Sawyer, J. S. Valentine, *Acc. Chem. Res.* **1981**, *14*, 393.
[24] C. Beauchamp, I. Fridovich, *Anal, Biochem.* **1971**, *44*, 276.
[25] J.-J. Zhang, Q.-H. Luo, C.-Y. Duan, Z.-L. Wang, Y.-H. Mei, *J. Inorg. Biochem.* **2001**, *86*, 573.
[26] [26a] J.-J. Zhang, Y.-Y. Tang, Q.-H. Luo, C.-Y. Duan, Z.-L. Wang, Y.-H. Mei, *Polyhedron* **2001**, *20*, 2285. [26b] A. E. M. Boelrijk, G. C. Dismukes, *Inorg. Chem.* **2000**, *39*, 3020.
[27] E. J. Larson, V. L. Pecoraro, *J. Am. Chem. Soc.* **1991**, *113*, 3810.
[28] U. Bossek, M. Saher, T. Weyhermuller, K. Wieghardt, *J. Chem. Soc., Chem. Commun.* **1992**, 1780.
[29] Y. Naruta, K. Maruyama, *J. Am. Chem. Soc.* **1991**, *113*, 3595.
[30] Q.-X. Li, Q.-H. Luo, Y.-Z. Li, C.-Y. Duan, Q.-Y. Tu. *Inorg. Chim. Acta*, in press.
[31] J. E. Powell, M. A. Hiller, *J. Chem. Educ.* **1957**, *34*, 330.
[32] A. E. Martell, R. J. Motekaitis, *Determination and Use of Stability Constants*, 2nd ed., VCH Publishers, New York, **1992**, 129.
[33] [33a] Q.-H. Luo, M.-C. Shen, Y. Ding, X.-L. Bao, A.-B. Dai, *Talanta* **1990**, *37*, 357. [33b] J. J. Zhang, Q.-H. Luo, D.-L. Long, J.-T. Chen, F.-M. Li, A.-D. Liu, *J. Chem. Soc., Dalton Trans.* **2000**, 1893.
[34] *SMART and SAINT. Area Detector Control and Integration Software. Siemens Analytical X-ray Systems*, Inc., Madison, Wisconsin, USA, **1996**.
[35] G. M. Sheldrick, *SHELXTL V5.1 Software Reference Manual, Bruker AXS*, Inc., Madison, Wisconsin, USA, **1997**.
[36] Q.-H. Luo, Q. Lu, A.-B. Dai, L.-G. Huang, *J. Inorg. Biochem.* **1993**, *51*, 655.

Received February 25, 2004
Early View Article
Published Online September 23, 2004

 © 2004 Wiley-VCH Verlag GmbH & Co. KGaA, Weinheim

Oxidation-State and Coordination-Site Specificity Influencing Dimensional Extension and Properties of Two Iron Complexes with Similar Helical Chains

Ying Xu,[a] Lei Han,[a] Zheng-Zhong Lin,[a] Cai-Ping Liu,[a] Da-Qiang Yuan,[a] You-Fu Zhou,[a] and Mao-Chun Hong*[a]

Keywords: Iron / Helical chains / Coordination polymer / Oxidation state

Two new iron coordination frameworks, $\{[NH_2(CH_3)_2]_2Fe^{II}(pydc)_2\}_n$ (**1**) and $\{[NH_2(CH_3)_2]Fe^{III}(pydc)_2\}_n$ (**2**) (pydc = 2,5-pyridinedicarboxylate), have been synthesized through the reaction of $FeCl_3$ with H_2pydc in dimethylformamide (DMF). **1** crystallizes in an achiral space group $C2/c$, while **2** crystallizes in a chiral space group $P4_32_12$. Both crystal structures consist of 2_1 helices with similar units: $[Fe^{II}(pydc)_2]^{2-}$ and $[Fe^{III}(pydc)_2]^-$, respectively. The iron oxidation states have been confirmed by means of ESR spectra and bond valence calculations. Quantum chemistry calculations and thermogravimetric analysis have demonstrated their energy and thermal stability. Magnetic studies have revealed that **1** and **2** show weak antiferromagnetic and ferromagnetic interactions between the metal centers, respectively.
(© Wiley-VCH Verlag GmbH & Co. KGaA, 69451 Weinheim, Germany, 2004)

Introduction

Metal-organic coordination networks are the largest class of engineered crystal structures. They expand coordination in diverse dimensions by means of polydentate organic ligands coordinating to metal atoms.[1] Much work has been done towards understanding the molecular packing[2−4] and the relationship between inner structure and collective properties.[5,6] The selection or design of suitable ligands containing certain features, such as functionality and versatile binding modes, plays an important role in determining the topologies and properties of coordination networks.[7−11] Metal atoms, especially their metal oxidation state, also significantly affect the structural extension and properties of coordination networks.[12,13] However, the influence of the metal oxidation state has been comparatively less well investigated.[14,15] Our efforts have focused on constructing coordination networks by assembling multidentate ligand H_2pydc and multiple oxidation state iron atoms. Herein, we report the syntheses and characterizations of two new iron coordination frameworks with 2_1 helical chains: $\{[NH_2(CH_3)_2]_2Fe^{II}(pydc)_2\}_n$ (**1**) and $\{[NH_2(CH_3)_2]Fe^{III}(pydc)_2\}_n$ (**2**), assembled from iron ions and pydc in different coordination modes (Scheme 1).

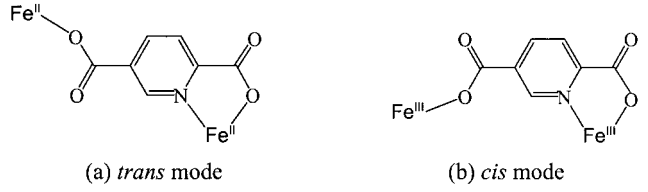

(a) *trans* mode (b) *cis* mode

Scheme 1. Coordination modes of pydc in (a) **1** and (b) **2**

Results and Discussion

Syntheses

Although the formation mechanisms are poorly understood, solvothermal synthesis under mild conditions ($T <$ 200 °C, autogenous pressure) is a good way of generating complexes with interesting structures or functional materials, as the nature of organic solvent may drastically effect the formation of compounds.[16−19] In this respect, DMF is a good polar, aprotic solvent with a high boiling point. Consequently, we carried out the solvothermal reaction of iron(III) chloride and H_2pydc (1:2 molar ratio) in DMF, which was used to remove the carboxylate group protons and to avoid coordination between the iron atoms and water solvent molecules. Two kinds of well-shaped crystals, dark red blocks for **1** and light yellow dipyramids for **2**, were separated with a moderate yield for **1** and a very low yield for **2**. To obtain a higher yield of **2**, 0.1 mL of H_2O_2 (30%) was added to the reaction system, only compound **2** was isolated (44% yield). The formulae of $\{[NH_2(CH_3)_2]_2Fe^{II}(pydc)_2\}_n$ for **1** and $\{[NH_2(CH_3)_2]Fe^{III}(pydc)_2\}_n$ for **2** were revealed by X-ray single-crystal diffraction analy-

[a] State Key Laboratory of Structural Chemistry, Fujian Institute of the Research on the Structure of Matter, Chinese Academy of Sciences,
Fuzhou, Fujian 350002, China
Fax: (internat.) + 86-591-8371-4946
E-mail: hmc@fjirsm.ac.cn

ses and elemental analyses. Clearly, some Fe^{III} was reduced to Fe^{II} as part of a redox reaction. Earlier reports show that the reaction of aromatic N ligands such as pyridine or imidazole derivatives with a transition-metal salt can result in spontaneous metal ion reduction.[20−23] The presence of $[NH_2(CH_3)_2]^+$ in the two compounds results from the decomposition of DMF. No crystals or precipitation were obtained when using *N*,*N*-dimethylacetamide instead of DMF.

Crystal Structures

$\{[NH_2(CH_3)_2]_2Fe^{II}(PYDC)_2\}_n$ (1)

Single-crystal X-ray diffraction analysis reveals that complex **1** has a two-dimensional layer structure and crystallizes in a monoclinic space group *C*2/*c*. Figure 1 (a) shows a perspective view of the local coordination environment around the Fe^{II} atom of **1**. The iron atom is hexacoordinate in an N_2O_4 environment with a distorted octahedral geometry. Two pyridyl nitrogen donors from different pydc ligands are in an L-shaped arrangement with the central iron atom at the corner; the Fe−N bond length and N(1)−Fe−N(1B) bond angle are 2.170(2) Å and 102.77(14)°, respectively. Four oxygen atoms from different pydc ligands complete its coordination sphere. Fe−O(1) and Fe−O(4A) are 2.098(2) and 2.084(2) Å, respectively. A pydc ligand bridges two Fe^{II} atoms in a *trans* mode through the pyridyl nitrogen atom and an adjacent carboxylate oxygen atom, forming a five-membered chelate ring, while one oxygen atom of the second carboxylate group coordinates another Fe^{II} atom in *trans* position (Scheme 1, a). Thus, an extended two-dimensional layer structure is formed (Figure 2, b) that contains rhombic grids with four Fe^{II} atoms at the corners, with pydc ligands as linkers. The lateral Fe···Fe distances of the Fe_4 rhombus are 8.602 Å, the diagonal Fe···Fe distances are 15.066 Å and 8.305 Å.

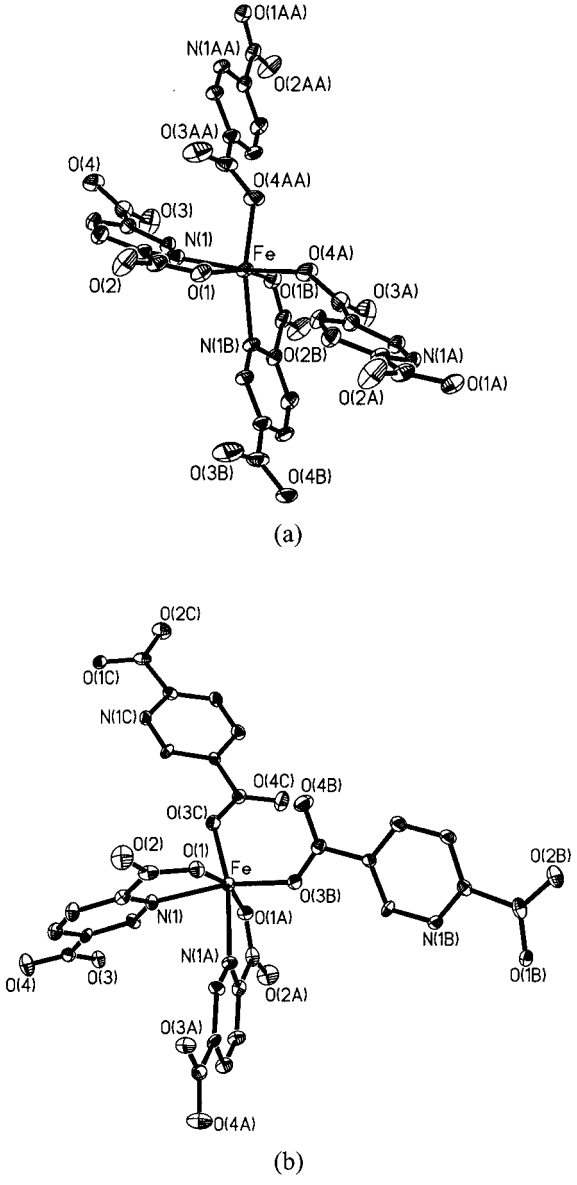

Figure 1. Coordination environments of **1** (a) and **2** (b); ellipsoids are shown at 30% probability

In **1**, the 2D layer $\{[Fe^{II}(pydc)_2]^{2-}\}_n$ can also be considered as arising from 2_1 helices (Figure 2, a). The helix winds along the *b* axis and the pitch of the helix is the length of *b* (8.305Å). All the helices extend along the same direction, generating a 2D layer structure (Figure 2, b). The layers are parallel to the *ab* plane with a C_2 symmetry for neighboring 2_1 helices. All layers are stacked on top of each other along the *c* axis, with a separation of one half of the *c* length. However, adjacent layers arranged in antiparallel orientation lead to an overall centrosymmetric structure with an achiral space group *C*2/*c* (Figure 2, c). The $[NH_2(CH_3)_2]^+$ cations, omitted in the figures for clarity, lie between the layers to balance charges.

$\{[NH_2(CH_3)_2]Fe^{III}(PYDC)_2\}_n$ (2)

Single-crystal X-ray diffraction analysis reveals that complex **2** has a three-dimensional structure and crystallizes in the tetragonal chiral space group $P4_32_12$. Figure 1 (b) gives a perspective view of the local coordination environment around the Fe^{III} atom of **2**. As in **1**, the iron atom is hexacoordinate in an N_2O_4 environment with a distorted octahedral geometry. Two pyridyl nitrogen donors from different pydc ligands form an L-shaped arrangement with the central iron atom at the corner. The Fe−N(1) bond length and N(1)−Fe−N(1A) bond angle are 2.201(5) Å and 79.8(3)°, respectively. Four oxygen atoms from different pydc ligands complete its coordination sphere. Fe−O(1) and Fe−O(3B) are 1.983(4) and 1.954(4) Å, respectively. Unlike **1**, a pydc ligand bridges two Fe^{III} atoms in a *cis* mode (Scheme 1, b) through the pyridyl nitrogen atom and an adjacent carboxylate oxygen atom, forming a five-membered chelate ring, and one oxygen atom of the second carboxylate group coordinating another Fe^{III} atom on the same side as the chelate ring. Thus, a helical polymer chain is formed that is similar to that in **1** (Figure 2, a; Figure 3, a).

Compound **2** contains 2_1 helices along the *a* or *b* axis with the pitch being 8.896 Å (Figure 3, a). In contrast to **1**,

 © 2004 Wiley-VCH Verlag GmbH & Co. KGaA, Weinheim

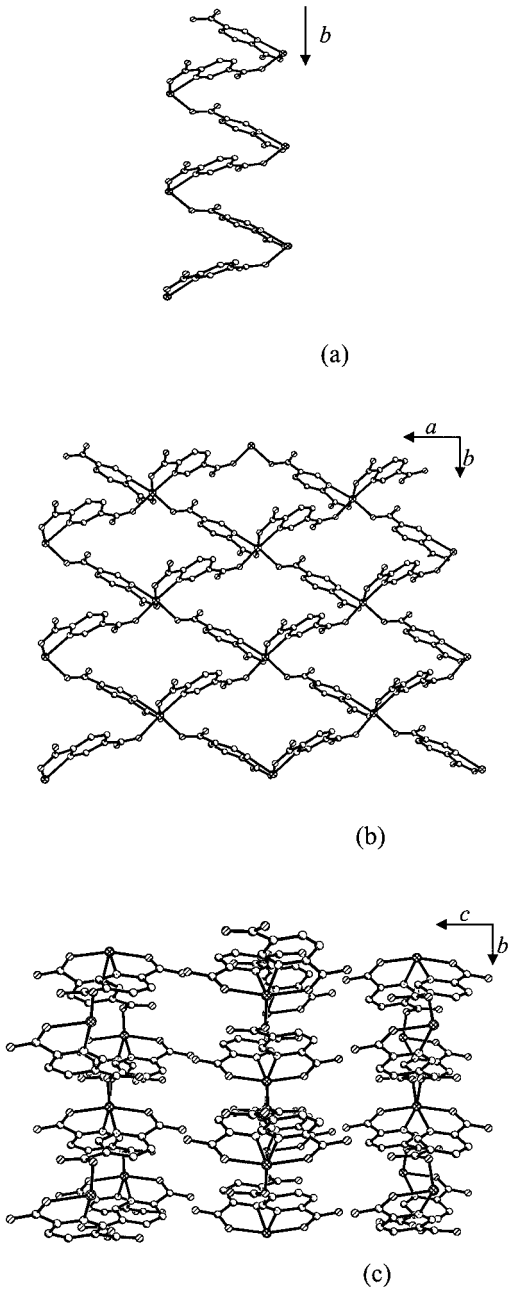

Figure 2. (a) Section of the 2_1 helical polymer chain along the *b* axis in **1**; (b) 2D layer structure along the *ab* plane in **1**; (c) the stacking 2D layers viewed from the *a* axis in **1**; dimethylamine cations omitted for clarity

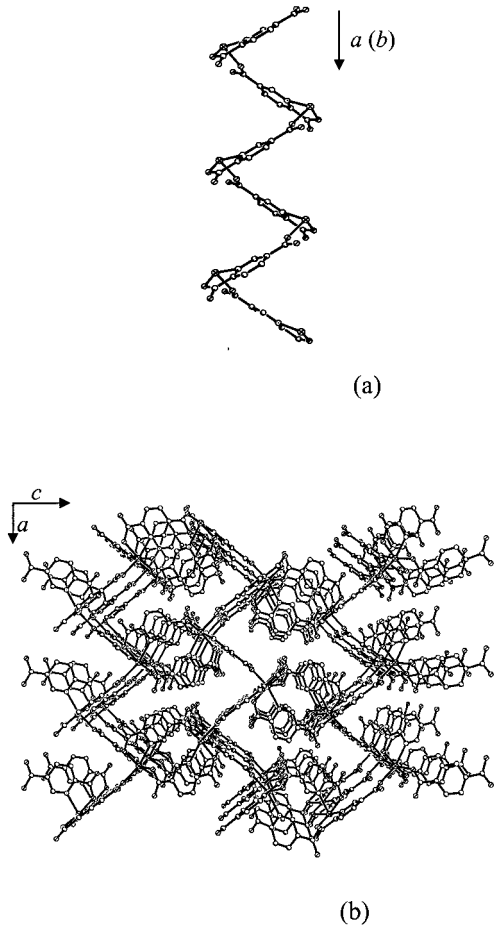

Figure 3. (a) Section of the 2_1 helical polymer chain along the *a* or *b* axis in **2**; (b) packing diagram of **2** viewed from the *b* axis; dimethylamine cations omitted for clarity

all the helices in **2** are arranged parallel to or perpendicular with the metal atoms as the connective nodes, and so compound **2** has noncentrosymmetry for the overall structure (Figure 3, b). Infinite 3D networks with 4_3 helices along the *c* axis are formed with the chiral space group $P4_32_12$. $[NH_2(CH_3)_2]^+$ cations lie within the networks to balance charges (omitted from the figures for clarity).

We also found that Fe^{II} atoms coordinated to pydc ligands in a *trans* mode, whereas Fe^{III} atoms coordinated in a *cis* mode, even though both ions underwent the same reaction − the oxidation state of the iron atom might affect the coordination modes of the pydc ligand. Thus, the oxidation state of iron atoms together with the coordination site of pydc ligands specifically influence the dimensional extensions of the two iron compounds. Scheme 2 illustrates the packing, which features two different kinds of inner structures for **1** and **2**.

Bond Valence Calculation and ESR Spectrum

According to X-ray analyses, element analyses and charge-balance requirements, the bond valence of the Fe atoms in **1** and **2** should be +2 and +3, respectively. This is verified through X-band ESR spectra recorded on polycrystalline samples at room temperature. As expected, **1** is ESR-silent due to non-Kramer spin states ($S = 2$) of the Fe^{II} ion, as a result of either large zero-field splitting or fast relaxation processes.[24] Compound **2** gave a strong, typical response of high-spin Fe^{III} with $g = 3.6615$. Typical low-spin Fe^{III} species have *g* values around 2.[25] Furthermore, bond valence calculations carried out for the FeN_2O_4 octahedrons gave bond valence sums (bvs) of +2.39 and +2.92 valence unit (v.u.) for iron atoms in **1** and **2**, respectively. The calculations used reported bond valence parameters for Fe−O and Fe−N bonds.[26] Similar bond valence calcu-

 © 2004 Wiley-VCH Verlag GmbH & Co. KGaA, Weinheim

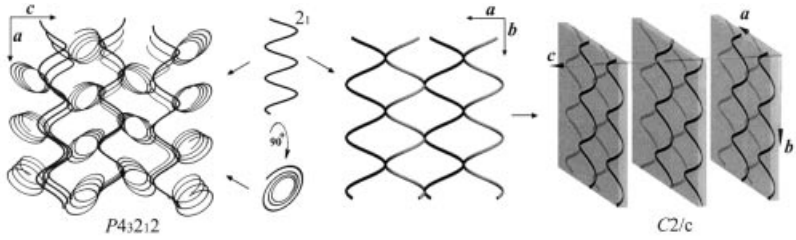

Scheme 2. Arrangement models of 2_1 helices in complexes **1** and **2**: for **1**, 2_1 helices along the *b* axis form the 2D layer structure in the *ab* plane, and the adjacent antiparallel layers produce a centrosymmetric achiral space group *C*2/*c*; for **2**, 2_1 helices along the *a* or *b* axis perpendicular or parallel to each other construct a 3D network with the chiral space group $P4_32_12$

lations have been used successfully for a polyoxovanadate complex.[27]

Single-Point Energy Calculations and TGA

The organic ligand adopts *trans* and *cis* coordination patterns in **1** and **2**, respectively. Taking account of the energy distinction between the two octahedral coordination units (Figure 1, a, b), single-point energy calculations for them were carried out using the unrestricted Hartree−Fock (UHF) method. For Fe atoms the Los Alamos ECP plus DZ basis set (Lanl2dz)[28] was used, and for C, N, O and H atoms the 6-31G* basis set was employed. Calculations were completed using the Gaussian 98 program.[29] Computational values of −2596.10205193 and −2605.17304136 Hartrees were obtained for **1** and **2**, respectively. These single-point energy calculations show that the energy of the central atom of the octahedral unit in **2** (Figure 1, b) is lower, by ca. 9 Hartrees, than that of the unit in **1** (Figure 1, a), indicating that **2** is thermodynamically slightly more stable than **1**. In agreement, TGA analysis revealed decomposition temperatures of 264 and 315 °C for **1** and **2**, respectively.

Magnetic Properties

Magnetic measurements were performed for polycrystalline samples of **1** and **2** in the temperature range 270−2 K. For both complexes, as the temperature is lowered to around 35 K, χ_M increases gradually, and then increases dramatically (Figures 4 and 5). The measured effective magnetic moments μ_{eff} per iron atom in **1** and **2** are ca. 4.92 μ_B and 5.80 μ_B, respectively, at 270 K, in agreement with the 4.90 μ_B for free-ion Fe^{II} in high spin ($S = 2$) and 5.91μ_B for high-spin Fe^{III} ($S = 5/2$). The results confirm that the oxidation state of iron atoms in **1** and **2** are +2 and +3, respectively.

The magnetic behavior of **1** over the whole temperature range (270−2 K) can be well expressed using Equation (1) derived by Fisher,[30] based on the Hamiltonian $H = -J\Sigma S_iS_{i+1}$ for local spin values $S = 2$, where J is the exchange coupling between two adjacent paramagnetic centers.

$$\chi_M = \{[Ng^2\beta^2S(S+1)]/3kT\}\cdot[(1+u)/(1-u)]$$
$$u = \coth\{[JS(S+1)]/kT\} - kT/[JS(S+1)] \quad (1)$$

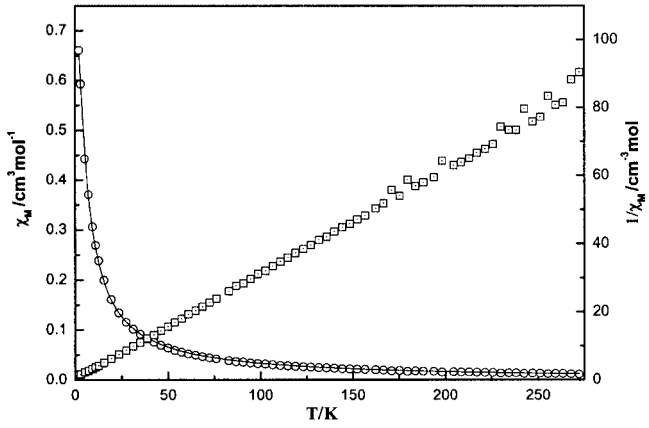

Figure 4. χ_M vs. T (open circles) and $1/\chi_M$ vs. T (open squares) for **1**; for clarity, only 50% of the recorded data is shown; the line through the symbols (open circles) corresponds to the calculated data of χ_M for **1** with $g = 2.14$ and $J = -0.36$ cm^{-1}

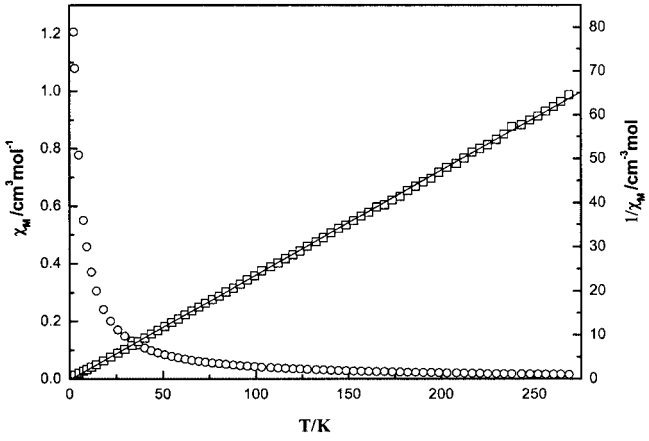

Figure 5. χ_M vs. T (open circles) and $1/\chi_M$ vs. T (open squares) for **2**; for clarity, only 50% of the recorded data is shown; the line through the symbols (open squares) correspond to the calculated data of $1/\chi_M$ for **2** with calcd. $C = 4.17$ cm^3·mol^{-1}·K and $T_p = 1.75$ K

For **1**, the best fit parameters are $J = -0.36$ cm^{-1}, $g = 2.14$ and $R = 7.66 \times 10^{-6}$, where $R = \Sigma[(\chi_M)_i^{exp} - (\chi_M)_i^{calcd.}]^2/\Sigma[(\chi_M)_i^{exp.}]^2$, illustrating the very weak $Fe^{II}-Fe^{II}$ antiferromagnetic interactions in **1** bridged by pydc ligands. However, the case in **2** is much more complicated, as the network has a three-dimensional extension, and we were

 © 2004 Wiley-VCH Verlag GmbH & Co. KGaA, Weinheim

unable to model the experimental data. Thus, the $1/\chi_M$ data of **2** was fitted to a Curie−Weiss law [$\chi_M = C/(T - T_P)$], with $C = 4.17$ cm^3·mol^{-1}·K, $T_p = 1.75$ K and relation factor 0.9997. The small positive Weiss temperature indicates the presence of a weak $Fe^{III}-Fe^{III}$ ferromagnetic interaction, although a detailed elucidation of the magnetic interaction in **2** is awaited.

Decomposition of DMF

X-ray diffraction analyses revealed the presence of dimethylamine cations $[NH_2(CH_3)_2]^+$ in both **1** and **2**, which result from the decomposition of DMF. IR spectra of **1** and **2** further confirm the presence of $-NH_2^+$ and $-CH_3$ groups. Broad bands in the range of 2700−2250 cm^{-1}, together with a weak peak at ca. 2000 cm^{-1}, correspond to N−H vibration modes of the $-NH_2^+$ group. In addition, peaks at ca. 2967 and 1460 cm^{-1} indicate C−H stretching and bending modes, respectively, of $-CH_3$ groups. Moreover, elemental analyses are also consistent with the presence of $[NH_2(CH_3)_2]^+$ cations. The decomposition of solvent DMF has been used previously to develop a synthesis of gallium compounds.[19] The product of DMF decomposition could be taken as the unique source of a structure-directing agent for the formation of coordination networks.[19] In fact, dimethylamine, triethylamine, etc. appear to be suitable agents, under solvo(hydro)thermal conditions, to maintain a relatively stable pH and to serve as a mineralizer.[19,31,32−34]

Conclusion

Two iron complexes with diverse metal oxidation states and coordination patterns of organic ligand have been synthesized by solvothermal reaction. Our focus on the variations in molecular packing, which lead to different dimensional extensions, demonstrates that both the metal oxidation state and the coordination-site of ligands are important in the formation of these compounds.

Experimental Section

Materials and Methods: All reagents and solvents were purchased from commercial sources and used as received. Elemental analyses were determined with an Elementar Vario ELIII elemental analyzer. IR spectra were measured as KBr pellets with a Nicolet Magna 750 FT-IR spectrometer in the range of 200−4000 cm^{-1}. ESR spectra were recorded as powder samples at the X-band frequency with a Bruker ER420 spectrometer at room temperature. TGA was recorded with a NETZSCH STA 449C instrument, with samples under nitrogen (15 mL/min), at a heating rate of 15 °C/min. Temperature-dependent magnetic measurements were determined with a Quantum Design SQUID-XL7 magnetometer in an external field of 20 kG.

Syntheses of Complexes: Complexes **1** and **2** were obtained from the solvothermal reactions of iron(III) chloride (16.2 mg, 0.1 mmol) and 2,5-pyridinedicarboxylic acid ($C_7H_5NO_4$, 99%, denoted H_2pydc) (33.4 mg, 0.2 mmol) in dimethylformamide as solvent (C_3H_7NO, 99.8%, denoted DMF) (14 mL). Reactions were performed in Teflon-lined stainless steel Parr bombs (23 mL) under autogenous pressure for 3 d. After cooling the reaction system at a rate of 13 °C/h to 30 °C, dark red crystals (**1**) and light yellow crystals (**2**) were separated, with yields of 36 mg (75%) for **1** and 2 mg (5%) for **2**. To increase the yield of **2**, H_2O_2 (30%, 0.1 mL) was added to the system; only compound **2** was obtained, with a higher yield of 19 mg (44%).

$\{[NH_2(CH_3)_2]_2Fe^{II}(pydc)_2\}_n$ (1): $C_{18}H_{22}FeN_4O_8$ (478.25): calcd. C 45.21, N 11.72, H 4.64; found C 44.88, N 11.29, H 4.50. IR (KBr pellet, cm^{-1}): $\tilde{\nu}$ = 3437 (br., m), 3145 (m), 3029 (m), 2967 (m), 2761 (br., m), 2452 (br., m), 2349 (w), 2000 (w), 1892 (w), 1620(s), 1475 (m), 1455 (m), 1386(s), 1341(s), 1275 (w), 1246 (w), 1165 (w), 1098 (w), 1032 (w), 887 (w), 822 (m), 769 (m), 694 (w), 512 (w). Decomposition temperature: 264 °C.

$\{[NH_2(CH_3)_2]Fe^{III}(pydc)_2\}_n$ (2): $C_{16}H_{14}FeN_3O_8$(432.15): calcd. C 44.47, H 3.27, N 9.72; found C 43.82, H 3.39, N 9.68. IR (KBr pellet, cm^{-1}): $\tilde{\nu}$ = 3436 (br., m), 3105 (m), 3074 (m), 2960 (m), 2799 (br., m), 2465 (br., w), 2014 (w), 1902 (w), 1778 (w), 1648(s), 1574 (m), 1462 (w), 1391 (m), 1322(s), 1277 (m), 1257 (m), 1233 (m), 1164 (w), 1143 (m), 1117 (w), 1034 (m), 1005 (w), 887 (w), 862 (w), 827 (m), 761 (m), 688 (w), 658 (w), 589 (m), 538 (m), 520 (w). Decomposition temperature: 315 °C.

X-ray Crystallographic Study: Crystal data collections were performed at 293 K with a Siemens Smart-CCD diffractometer with graphite-monochromated Mo-K_α radiation (λ = 0.71073 Å). Empirical absorption corrections were applied using the SADABS program.[35] Structures were solved with direct methods and refined by full-matrix least squares.[36] Non-hydrogen atoms were refined anisotropically, and the hydrogen atoms were positioned with idealized geometry. All calculations were performed using the SHELXTL program.[37] Crystallographic data and other pertinent

Table 1. Crystal data collection and refinement parameters for $\{[NH_2(CH_3)_2]_2Fe^{II}(pydc)_2\}_n$ (**1**) and $\{[NH_2(CH_3)_2]Fe^{III}(pydc)_2\}_n$ (**2**)

Complex	**1**	**2**
Empirical formula	$C_{18}H_{22}FeN_4O_8$	$C_{16}H_{14}FeN_3O_8$
Formula mass	478.25	432.15
a [Å]	15.0657(9)	8.8956(6)
b [Å]	8.3054(5)	8.8956(6)
c [Å]	17.0198(10)	21.905(2)
β [°]	100.851(2)	90
V [Å^3]	2091.6(2)	1733.4(2)
Z	4	4
Crystal system	monoclinic	tetragonal
Space group	$C2/c$	$P4_32_12$
λ [Å]	0.71073	0.71073
ρ [g·cm^{-3}]	1.519	1.656
μ [cm^{-1}]	7.74	9.23
T [K]	293(2)	293(2)
Number of data collected	3048	4254
Number of unique data collected	1836	1514
R_{int}	0.0210	0.0851
Data/restraints/parameters	1836/0/141	1514/0/128
R_1[a] [$I > 2\sigma(I)$]	0.0443	0.0607
wR_2 [a] [$I > 2\sigma(I)$]	0.1105	0.1166
R_1 [a] (all data)	0.0560	0.1054
wR_2 [a] (all data)	0.1208	0.1342
GOF	1.036	1.157
$\Delta\rho_{min.}$ [e·Å^{-3}]	−0.464	−0.337
$\Delta\rho_{max.}$ [e·Å^{-3}]	0.363	0.401

[a] $R_1 = \Sigma||F_o| - |F_c||/\Sigma|F_o|$, $wR_2 = [\Sigma w(F_o^2 - F_c^2)^2/\Sigma w(F_o^2)^2]^{1/2}$.

 © 2004 Wiley-VCH Verlag GmbH & Co. KGaA, Weinheim

Table 2. Selected bond lengths [Å] and angles [°] for **1** and **2**

Complex **1**			
Fe−N(1)	2.170(2)	Fe−O(1)	2.098(2)
Fe−O(4A)	2.084(2)	Fe−O(4AA)	2.084(2)
Fe−O(1B)	2.098(2)	Fe−N(1B)	2.170(2)
O(4AA)−Fe−O(4A)	87.38(14)	O(4AA)−Fe−O(1B)	92.27(11)
O(4A)−Fe−O(1B)	99.34(11)	O(4AA)−Fe−O(1)	99.34(11)
O(4A)−Fe−O(1)	92.27(11)	O(1B)−Fe−O(1)	163.95(14)
O(4AA)−Fe−N(1B)	165.95(11)	O(4A)−Fe−N(1B)	86.13(10)
O(1B)−Fe−N(1B)	76.53(9)	O(1)−Fe−N(1B)	93.36(9)
O(4AA)−Fe−N(1)	86.13(10)	O(4A)−Fe−N(1)	165.95(11)
O(1B)−Fe−N(1)	93.36(9)	O(1)−Fe−N(1)	76.53(9)
N(1B)−Fe−N(1)	102.77(14)		
Complex **2**			
N(1)−Fe	2.201(5)	O(1)−Fe	1.983(4)
Fe−O(3C)	1.954(4)	Fe−O(3B)	1.954(4)
Fe−O(1A)	1.983(4)	Fe−N(1A)	2.201(5)
O(3C)−Fe−O(3B)	109.2(3)	O(3C)−Fe−O(1)	96.04(18)
O(3B)−Fe−O(1)	93.24(18)	O(3C)−Fe−O(1A)	93.24(18)
O(3B)−Fe−O(1A)	96.04(18)	O(1)−Fe−O(1A)	164.0(3)
O(3C)−Fe−N(1A)	162.95(19)	O(3B)−Fe−N(1A)	86.16(19)
O(1)−Fe−N(1A)	90.31(19)	O(1A)−Fe−N(1A)	77.33(19)
O(3C)−Fe−N(1)	86.16(19)	O(3B)−Fe−N(1)	162.95(19)
O(1)−Fe−N(1)	77.33(19)	O(1A)−Fe−N(1)	90.31(19)
N(1A)−Fe−N(1)	79.8(3)		

Symmetry codes: (A) = $x + 1/2, y - 1/2, z$; (B) = $-x, y, -z + 1/2$; (AA) = $-x - 1/2, y - 1/2, -z + 1/2$ for **1**; (A) = $y, x, -z$; (B) = $-y + 1/2, x + 1/2, z - 1/4$; (C) = $x + 1/2, -y + 1/2, -z + 1/4$ for **2**

information are summarized in Table 1; selected bond lengths and angles for the two complexes are given in Table 2. CCDC-226709 and -226710 contain the supplementary crystallographic data for this paper. These data can be obtained free of charge at www.ccdc.cam.ac.uk/conts/retrieving.html [or from the Cambridge Crystallographic Data Centre, 12 Union Road, Cambridge CB2 1EZ, UK; Fax: (internat.) + 44-1223-336-033; E-mail: deposit@ccdc.cam.ac.uk].

Acknowledgments

This work was supported by grants from the NNSF of China (No. 20031020) and NSF of Fujian Province. We also thank Professor Song Gao for the magnetism data collection.

[1] D. Braga, *Chem. Commun.* **2003**, 2751−2754.
[2] E. Pidcock, W. D. S. Motherwell, *Chem. Commun.* **2003**, 3028−3029.
[3] J. D. Dunitz, *Chem. Commun.* **2003**, 545−548.
[4] P. A. Maggard, C. L. Stern, K. R. Poeppelmeier, *J. Am. Chem. Soc.* **2001**, *123*, 7742−7743.
[5] O. R. Evans, W. B. Lin, *Acc. Chem. Res.* **2002**, *35*, 511−522.
[6] T. F. Liu, D. Fu, S. Gao, Y. Z. Zhang, H. L. Sun, G. Su, Y. J. Liu, *J. Am. Chem. Soc.* **2003**, *125*, 13976−13977.
[7] S. S.-Y. Chui, S. M.-F. Lo, J. P. H. Charmant, A. G. Orpen, L. D. Williams, *Science.* **1999**, *283*, 1148−1150.
[8] M. C. Hong, Y. J. Zhao, W. P. Su, R. Cao, M. Fujita, Z. Y. Zhou, A. S. C. Chan, *J. Am. Chem. Soc.* **2000**, *122*, 4819−4820.
[9] M. Eddaoudi, J. Kim, N. Rosi, D. Vodak, J. Wachter, M. O'Keeffe, O. M. Yaghi, *Science.* **2002**, *295*, 469−472.
[10] B. F. Abrahams, S. R. Batten, H. Hamit, B. F. Hoskins, R. Robson, *Angew. Chem. Int. Ed. Engl.* **1996**, *35*, 1690−1691.
[11] R. H. Wang, M. C. Hong, D. Q. Yuan, Y. Q. Sun, L. J. Xu, J. H. Luo, R. Cao, A. S. C. Chan, *Eur. J. Inorg. Chem.* **2004**, 37−43.
[12] M.-L. Tong, L.-J. Li, K. Mochizuki, H.-C. Chang, X.-M. Chen, Y. Li, S. Kitagawa, *Chem. Commun.* **2003**, 428−429.
[13] J. Tao, Y. Zhang, M.-L. Tong, X.-M. Chen, T. Yuen, C. L. Lin, X.-Y. Huang, J. Li, *Chem. Commun.* **2002**, 1342−1343.
[14] J. C. Liu, G. C. Guo, J. S. Huang, X. Z. You, *Inorg. Chem.* **2003**, *42*, 235−243.
[15] L. P. Wu, Y. Yamagiwa, I. Ino, K. Sugimoto, T. Kuroda-Sowa, T. Kamikawa, M. Munakata, *Polyhedron* **1999**, *18*, 2047−2053.
[16] D. M. Low, E. K. Brechin, M. Helliwell, T. Mallah, E. Riviere, E. J. L. Mclnnes, *Chem. Commun.* **2003**, 2330−2331.
[17] D. M. Low, L. F. Jones, A. Bell, E. K. Brechin, T. Mallah, E. Rivière, S. J. Teat, E. J. L. Mclnnes, *Angew. Chem. Int. Ed.* **2003**, *42*, 3781−3784.
[18] H. Kominami, J. Kato, S. Murakami, Y. Ishii, M. Kohno, K. Yabutani, T. Yamamoto, Y. Kera, M. Inoue, T. Inui, B. Ohtani, *Catal. Today* **2003**, *84*, 181−189.
[19] C. Paulet, T. Loiseau, G. Férey, *J. Mater. Chem.* **2000**, *10*, 1225−1229.
[20] J. Y. Lu, A. M. Babb, *Inorg. Chem.* **2002**, *41*, 1339−1341.
[21] H. Sugiyama, G. Aharonian, S. Gambarotta, G. P. A. Yap, P. H. M. Budzelaar, *J. Am. Chem. Soc.* **2002**, *124*, 12268−12274.
[22] G. Stupka, L. Gremaud, G. Bernardinelli, A. F. Williams, *Dalton Trans.* **2004**, 407−412.
[23] C.-F. Wang, E.-Q. Gao, H. Zheng, C.-H. Yan, *Chem. Commun.* **2004**, 720−721.
[24] X. S. Tan, J. Chen, Z. N. Chen, P. J. Zheng, W. X. Tang, *Inorg. Chim. Acta* **1995**, *234*, 27−33.
[25] S. J. Lippard, J. M. Berg, *Principles of Bioinorganic Chemistry*, University Science Books, Mill Valley, CA, **1994**.
[26] N. E. Brese, M. O'Keeffe, *Acta Crystallogr., Sect. B* **1991**, *47*, 192−197.
[27] X. Q. Wang, L. M. Liu, G. Zhang, A. J. Jacobson, *Chem. Commun.* **2001**, 2472−2473.
[28] P. J. Hay, W. R. Wadt, *J. Chem. Phys.* **1985**, *82*, 299−310.
[29] M. J. Frisch, G. W. Trucks, H. B. Schlegel, G. E. Scuseria, M. A. Robb, J. R. Cheeseman, V. G. Zakrzewski, J. A. Montgomery, R. E. Stratmann, J. C. Burant, S. Dapprich, J. M. Millam, A. D. Daniels, K. N. Kudin, M. C. Strain, O. Farkas, J. Tomasi, V. Barone, M. Cossi, R. Cammi, B. Mennucci, C. Pomelli, C. Adamo, S. Clifford, J. Ochterski, G. A. Petersson, P. Y. Ayala, Q. Cui, K. Morokuma, D. K. Malick, A. D. Rabuck, K. Raghavachari, J. B. Foresman, J. Cioslowski, J. V. Ortiz, B. B. Stefanov, G. Liu, A. Liashenko, P. Piskorz, I. Komaromi, R. Gomperts, R. L. Martin, D. J. Fox, T. Keith, M. A. Al-Laham, C. Y. Peng, A. Nanayakkara, C. Gonzalez, M. Challacombe, P. M. W. Gill, B. G. Johnson, W. Chen, M. W. Wong, J. L. Andres, M. Head-Gordon, E. S. Replogle, J. A. Pople, Gaussian 98, revision A.5, Gaussian, Inc., Pittsburgh, PA, **1998**.
[30] M. E. Fisher, *Am. J. Phys.* **1964**, *32*, 343−346.
[31] M. H. Zeng, S. Gao, X.-L. Yu, X.-M. Chen, *New J. Chem.* **2003**, *27*, 1599−1602.
[32] R. M. Barrer, *Hydrothermal Chemistry of Zeolites*, Academic Press, London, **1982**.
[33] S.-H. Feng, R.-R. Xu, *Acc. Chem. Res.* **2001**, *34*, 239−247.
[34] Y.-P. Zhang, C. J. O'Connor, A. Clearfield, R. C. Haushalter, *Chem. Mater.* **1996**, *8*, 595−597.
[35] G. M. Sheldrick, *SADABS, Program for Empirical Absorption Correction of Area Detector Data*, University of Göttingen, Germany, **1996**.
[36] G. M. Sheldrick, *SHELXS 97, Program for Crystal Structure Solution*, University of Göttingen, Germany, **1997**.
[37] G. M. Sheldrick, *SHELXTL 97, Program for Crystal Structure Refinement*, University of Göttingen, Germany, **1997**.

Received March 29, 2004
Early View Article
Published Online October 1, 2004

 © 2004 Wiley-VCH Verlag GmbH & Co. KGaA, Weinheim

Anomalous Diamagnetic Behaviour of the ^{1}H NMR Spectra of a Coordinated Imino Nitroxide Radical in Diamagnetic and Paramagnetic Lanthanide(III) Complexes

Toshiaki Tsukuda,[a] Masahiro Ogita,[a] Takayoshi Suzuki,[a] and Sumio Kaizaki*[a]

Keywords: ^{1}H NMR / Imino nitroxide radical / Lanthanide complexes / LIS analysis / Diamagnetic NMR behaviour

Diamagnetic lanthanide(III) complexes with an imino nitroxide radical IM2py [2-(2′-pyridyl)-4,4,5,5-tetramethyl-4,5-dihydro-1*H*-imidazol-1-oxyl], [Ln(hfac)$_3$(IM2py)] (Ln = Y and Lu; hfac = hexafluoroacetylacetonate), exhibit ^{1}H NMR chemical shifts for the pyridyl protons of the coordinated IM2py suggesting it behaves as if it were diamagnetic. To a series of paramagnetic lanthanide complexes of this type, the structural analyses of the lanthanide induced shifts (LIS) of the hfac 3-proton and pyridyl protons in IM2py were successfully applied, showing not only the diamagnetic behaviour of the pyridyl protons in the IM2py group, but also the dominant dipolar contribution and isostructural nature with apparent or effective axial symmetry in solution irrespective of the asymmetry in the solid state.
(© Wiley-VCH Verlag GmbH & Co. KGaA, 69451 Weinheim, Germany, 2004)

Introduction

There have been a large number of studies of lanthanide complexes and/or radical complexes with much concomitant interest in their potential applications in luminescent probes[1,2] or as building blocks for molecular-based magnetic materials.[3,4] The lanthanide−radical complexes have been mainly investigated in order to reveal the magnetic properties in solid state or absorption and emission spectra.[4,5] Our recent magneto-optical investigations on the nitroxide radical metal complexes were concerned not only with transition metal ions, but also lanthanide(III) ions.[6−12] For the imino nitroxide radical lanthanide complexes, [Ln(hfac)$_3$(IM2py)] [IM2py = 2-(2′-pyridyl)-4,4,5,5-tetramethyl-4,5-dihydro-1*H*-imidazol-1-oxyl],[11] we examined the solution spectroscopic properties as well as the magnetic interaction between Gd^{III} and the IM2py radical which is antiferromagnetic, in contrast to the ferromagnetic case[4] of (NIT2py)- and related (NIT)Gd^{III} complexes [NIT2py = 2-(2′-pyridyl)-4,4,5,5-(tetramethyl)-4,5-dihydro-1*H*-imidazolin-1-oxyl 3-oxide]. On the other hand, there have been many NMR studies of lanthanide complexes which have been utilised as lanthanide shift reagents (LSR) with the advantage of bringing about high resolution of complicated NMR spectral patterns of diamagnetic organic compounds, e.g. chiral discrimination and as biological probes since their introduction by Hinckley in 1969.[13] More recently, much attention has been paid to Gd^{III} complexes as contrast agents for magnetic resonance imaging (MRI) due to the short relaxation times encountered in ^{1}H NMR spectroscopy.[14] However, there have been no reports on the NMR spectra of Ln^{III} complexes containing a radical ligand. There have been a number of scattered reports on paramagnetic metal complexes with radical ligands mainly with a limited focus on the coordination effects on the radical ligands with the metal ions.[15,16] In our recent study, the chemical shifts in the ^{1}H NMR spectra of (NIT2py)Ni^{II} complexes were found to correlate with magnetic interactions between paramagnetic Ni^{II} and the NIT2py radical.[6a] In this context, when the diamagnetic complexes or paramagnetic metal complexes are magnetically weakly coupled with a nitroxide radical, the effect of coordination on the NMR spectra or the simple NMR spectroscopic patterns consisting of the original unperturbed signals of the radical and the auxiliary nonradical coligands can be predicted. In the course of the characterisation of Co^{III} or Ln^{III} complexes with IM3py and IM4py [3- and -4-(2′-pyridyl)-4,4,5,5-tetramethyl-4,5-dihydro-1*H*-imidazol-1-oxyl] or IM2py (Scheme 1), we observed unprecedented and apparently diamagnetic ^{1}H NMR behaviour for the imino nitroxide radical ligands in diamagnetic Co^{III} or Y^{III} and Lu^{III} complexes.

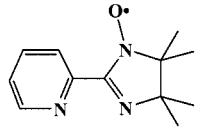

Scheme 1. IM2py

In this study, the NMR spectra of (IM2py)Ln^{III} complexes were examined in order to substantiate the diamag-

[a] Department of Chemistry, Graduate School of Science, Osaka University,
Toyonaka, Osaka 560-0043, Japan
Supporting information for this article is available on the WWW under http://www.eurjic.org or from the author.

netic NMR behaviour. Lanthanide induced paramagnetic shift (LIS) data of the paramagnetic Ln^{III} complexes will be analysed in terms of the classical crystal field dependent and the recently developed crystal field independent methods. The resultant analyses will be compared with the influence of the imino radical on the diamagnetic behaviour as well as the solution structure.

Results and Discussions

Magnetic Properties in Solution

The magnetic moments of [Y(hfac)$_3$(IM2py)] and [Lu(hfac)$_3$(IM2py)] in the solid state at 300 K are 1.81 and 1.90 μ_B, respectively, and those in $CDCl_3$ solution are 2.17 and 2.20 μ_B, respectively. The theoretical value is 1.73 μ_B. The corresponding Yb^{III} complex has values of 5.07 and 4.80 μ_B in the solid state and in solution, respectively, which are close to the theoretical value of 4.80 μ_B. These facts support the existence of the IM2py radical in the solid state and solution, in accordance with the UV/Vis spectra in solution.[11a]

In addition, the solution EPR spectrum of [Y(hfac)$_3$(IM2py)] displays hyperfine splittings to the Y^{III} ion and both nitrogen atoms [N(1) for IM−N and N(2) for IM−N−O] of the IM moiety (Figure 1) where the unpaired electron resides. The coupling of Y^{III} and N(1) is a result of the coordination. These hyperfine coupling constants were estimated by comparing them with the simulated spectra. The nitrogen hyperfine splittings are 4.9 G [N(1) and 7.8 G [N(2)] for [Y(hfac)$_3$(IM2py)]. These values are in contrast to 4.25 G [N(1)] and 9.25 G [N(2)] for free IM2py.[17] This change is due to electron delocalisation from the ligand toward the Y^{III} ion. With ^{89}Y having a nuclear spin of I = 1/2, the expected hyperfine splitting resulting from delocalisation onto the Y ion is only 0.4 G.

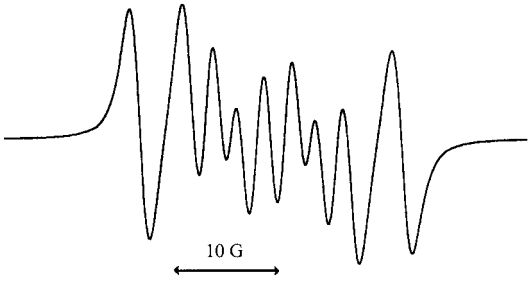

Figure 1. X-band (9.31 GHz) ESR spectrum at 296 K of [Y(hfac)$_3$(IM2py)]

As previously reported,[11a] the UV/Vis spectroscopic changes with the variation of mixing ratios also revealed the stability of the radical Ln^{III} complexes. In view of these results, it is certain that [Y(hfac)$_3$(IM2py)] remains paramagnetic due to the IM2py radical, even in solution.

^{1}H NMR Spectra of the Diamagnetic Ln^{III} Complexes Containing the IM2py Radical

The ^{1}H NMR spectra of [Y(hfac)$_3$(IM2py)] and [Lu(hfac)$_3$(IM2py)] should exhibit additive patterns consisting of the signals for the methine proton of hfac (hfac-H) at the diamagnetic Ln^{III} centre and those for the paramagnetic radical IM2py ligand, as if it were a mixture only of the Ln(hfac)$_3$ and IM2py moieties. However, the ^{1}H NMR spectra of [Y(hfac)$_3$(IM2py)] and [Lu(hfac)$_3$(IM2py)] appear like those of diamagnetic species. As shown in Figure 2 (a, b), the ^{1}H NMR spectra of [Y(hfac)$_3$(IM2py)] and [Lu(hfac)$_3$(IM2py)] appear in the diamagnetic region (δ = 0 to +10 ppm) associated with line-broadening, whereas no splitting by spin-spin coupling was observed. There is no signal for these Ln complexes in the paramagnetic range at $\delta \approx +20$ or −20 ppm, where the paramagnetic IM2py radical itself exhibits a typical paramagnetic NMR spectroscopic pattern [Figure 2 (c)]. A broad signal at $\delta \approx -15$ ppm is due to the IM methyl groups and the signals at δ = +22, +13 and ca. +4 ppm are due to the pyridyl protons as inferred from the assignments for NIT radicals (4,4,5,5-tetramethyl-4,5-dihydro-1*H*-imidazolyl-3-oxide-1-oxyl).[18]

The signals from δ = +7.5 to +8.5 ppm of the (IM2py)Y and -Lu complexes can be assigned to the pyridyl protons on the basis of the ^{1}H-^{1}H COSY spectrum. This exhibits two kinds of cross peaks for the pyridyl protons (Figure 3). There is a discrimination between two pairs of signals corresponding to each proton which are coupled with three ($\delta \approx$ +7.6, +7.9 and +8.5 ppm) and two protons ($\delta \approx$ +8.5 and +8.7 ppm), respectively. Apparently, the former two are due to the 4- and 5-protons of py (py-H4 and py-H5, respectively), the latter two to the 3- and 6-protons of py (py-H3 and py-H6, respectively) (Scheme 2). Since the signal at δ = +8.5 ppm is relatively broader than that at δ = +8.7 ppm, this can be assigned to py-H3 which is closer to the N−O radical moiety. Accordingly, the signals at δ = +7.91 and +7.62 ppm can be assigned to py-H4 and py-H5, respectively. A group of signals at $\delta \approx +1.5$ ppm arises from the methyl protons of the imidazole ring in IM2py. These assignments are in accordance with the chemical shifts of the analogous diamagnetic complex, *trans*-[Co(acac)(NO$_2$)$_2$(IMH2py)], where IMH2py [2-(2′-pyridyl)-4,4,5,5-tetramethyl-1-hydroxyimidazoline] is a diamagnetic one electron reduced IM2py group.[9] The broad signal at δ = 6.0 ppm should be due to the methine proton of the hfac (hfac-H) function in the (IM2py)Y complex, since its position is close to that in the nonradical [Y(hfac)$_3$(bpy)] complex. The ^{1}H NMR line widths in [Y(hfac)$_3$(IM2py)] are similar to those of an equimolar mixture of [Y(hfac)$_3$(bpy)] and IM2py, both of which are about five times as large as those of the diamagnetic complex [Y(hfac)$_3$(bpy)]. Therefore, it can be observed that the relaxation times of the hfac methine proton as well as the py protons and imidazole methyl protons of IM2py become shorter by through-space or outer-sphere dipolar interactions with the proximate molecules in solution, substantiating the existence of the IM2py radical in solution.

Since the ^{89}Y NMR spectrum of [Y(hfac)$_3$(IM2py)] gives only a sharp singlet at δ = 72.5 ppm (Figure 1S, Supporting Informations; for Supporting Informations see footnote on the first page of this article), the Y^{III} ion exists only as one

 © 2004 Wiley-VCH Verlag GmbH & Co. KGaA, Weinheim

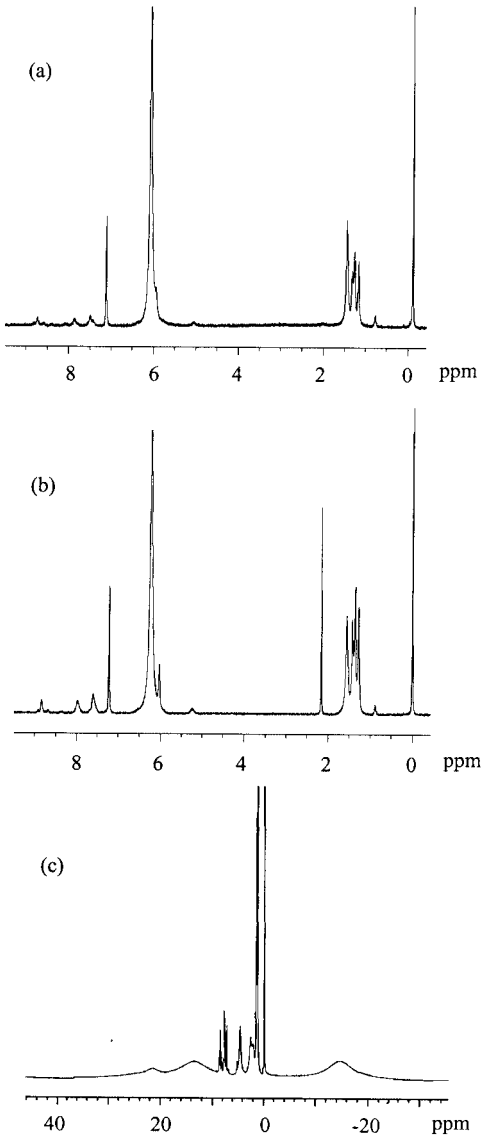

Figure 2. ^1H NMR spectra of (a) $[Y(hfac)_3(IM2py)]$, (b) $[Lu(hfac)_3(IM2py)]$ and (c) free IM2py

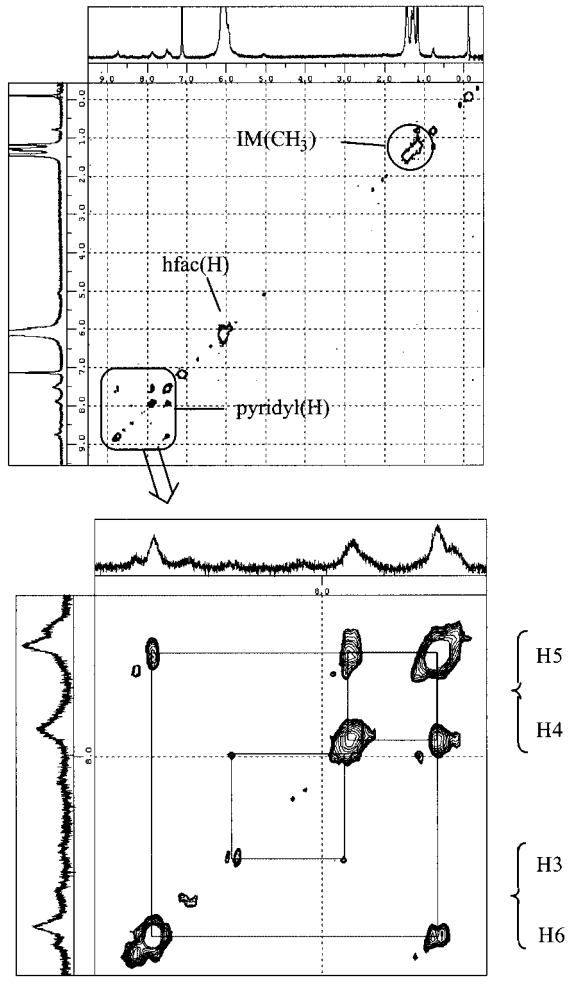

Figure 3. ^1H-^1H COSY spectrum of $[Y(hfac)_3(IM2py)]$

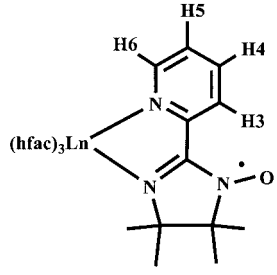

Scheme 2. $Ln(hfac)_3(IM2py)$ with atom numberings of the pyridyl ring

species coordinated by IM2py. Thus, the ^1H and ^{89}Y NMR spectroscopic behaviour originates from the radical complex itself, but not from complexes containing decomposed nonradical ligands such as $[Y(hfac)_3(H_2O)]$ and/or $[Y(hfac)_3(IMH2py)]$. It is clear that the protons in the IM2py moiety show diamagnetic ^1H NMR behaviour with respect to chemical shift but remain paramagnetic in line-width due to the outer-sphere interaction.

In the ^1H NMR spectra of diamagnetic *trans*-$[Co(acac)_2(NO_2)(IM3py$ or $IM4py)]$, only the methine and methyl proton signals of the acac ligand were previously considered when making the assessment of the geometrical structures. The coordinated pyridyl and imidazole protons of the IM*n*py group were not considered.[10] A re-examination of the ^1H NMR spectra of these Co^{III} complexes revealed the existence of the signals at $\delta \approx +8$ ppm and $\delta \approx +1.5$ ppm, respectively, which correspond to the diamagnetic pyridyl and imidazole protons both in terms of chemical shift and splitting pattern as in *trans*-$[Co(acac)(NO_2)_2(IMH2py)]$ and [Y- or $Lu(hfac)_3(IM2py)]$ [Figure 2 (a, b)]. Thus, it is from the *coordination* in the complexes containing diamagnetic metal ions that the diamagnetic NMR behaviour of IM radicals arises, but it does *not* necessarily depend on whether the coordination mode is monodentate or bidentate. The paramagnetic radicals coordinated in diamagnetic lanthanide and/or diamagnetic transition metal ions may hamper paramagnetic shifting of the ^1H NMR signals in the radical compounds or make them behave as if they were diamagnetic. This gives the appearance of complete disappearance

 © 2004 Wiley-VCH Verlag GmbH & Co. KGaA, Weinheim

of the unpaired electron around the protons in the IM radicals with respect to the ^{1}H NMR chemical shifts.

^{1}H NMR Spectra of the Paramagnetic Ln^{III} Complexes Containing the IM2py Radical

The ^{1}H NMR spectra of the paramagnetic lanthanide complexes [Ln(hfac)$_3$(IM2py)] deserve examination in relation to the diamagnetic NMR behaviour of the coordinated IM2py ligand in the complexes. Slightly broad NMR signals were observed for [Yb(hfac)$_3$(IM2py)] with the chemical shifts ranging from $\delta = +60$ to -30 ppm [Figure 4 (a)]. If there were little or no magnetic interaction between Yb^{III} and IM2py, the ^{1}H NMR spectra would appear as a sum of each paramagnetically shifted signal due to the Yb^{III} ion and IM2py. This is in contrast to the case of the paramagnetic Ni^{II} complexes, [Ni(β-diketonato)$_2$(NIT2py)], where the chemical shifts of the β-diketonato methine protons are given by a product of the NMR contact shifts of the nonradical Ni^{II} complexes and the fractional contribution to the Ni^{II} moiety arising from the magnetic interaction between the Ni^{II} ion and the NIT2py radical.[6a] By analogy with the diamagnetic ^{1}H NMR behaviour of [Y(hfac)$_3$(IM2py)] and [Lu(hfac)$_3$(IM2py)], it can be assumed that one unpaired electron of IM2py has no influence to the paramagnetic shift of Ln^{III}. In other words, the ^{1}H NMR signals of the IM2py coordinated to paramagnetic Yb^{III} suggest it might behave as a *diamagnetic* ligand in the complex. In order to assess this assumption, the ^{1}H NMR spectra could be analysed in the same manner as a series of isostructural paramagnetic lanthanide(III) complexes with diamagnetic ligands. The methine protons of the hfac (hfac-H) moiety can be assigned readily by comparison with the ^{1}H NMR spectra of the analogous nonradical complexes [Ln(hfac)$_3$(bpy)]. The NMR signals of the pyridyl protons of the IM2py group can be assigned in comparison with those of [Yb(hfac)$_3$(IM4- or -5Me2py)] (IM4- or -5Me2py = methyl-substituted pyridyl at the 4- or 5-position in IM2py). Though the ^{1}H NMR spectra of the (IM4Me2py)- and (IM5Me2py)-Yb^{III} complexes [Figure 4 (b, c)] are similar, on the whole, to that of [Yb(hfac)$_3$(IM2py)], the py-H4 and py-H5 signals of [Yb(hfac)$_3$(IM2py)] disappear in the NMR spectra of the (IM4Me2py)- and (IM5Me2py)Yb^{III} complexes, respectively. In the same manner, the assignments of the py-H4 and py-H5 signals for other paramagnetic Ln^{III} complexes were also made. The chemical shifts for py-H4 and -H5 in [Yb(hfac)$_3$(IM*n*Me2py)] are entirely different from those of free IM2py [Figure 4 (a)], whereas those of hfac-H in the (IM*n*Me2py)Yb^{III} complexes at $\delta \approx -10$ ppm are mostly unshifted relative to those of the corresponding nonradical Yb^{III} complex as shown in Figure 4 (b, c). In view of the latter behaviour, there is little influence on the hfac-H signal from the IM2py unpaired electron in the coordinated IM2py, whereas a large magnetic interaction between the paramagnetic Yb^{III} and the IM2py radical may be inferred from the significant change in the IM2py signals. This contradicts the fact that the magnetic interactions are very small, as deduced from the examination of the variable-temperature magnetic susceptibility measurements.[11] This discrepancy may be resolved by assuming that the ^{1}H NMR spectra of the coordinated IM2py ligands are affected by the paramagnetism of the Yb^{III} ion or the lanthanide induced shifts (LIS). In order to examine the ^{1}H NMR spectroscopic behaviour of the IM2py moiety in the paramagnetic Ln^{III} complexes, it is appropriate to make a quantitative structural analysis for the LIS of the NMR spectroscopic data on the basis of the above-mentioned assignments. The LIS, δ_{ij}^{LIS}, is given as the difference between the chemical shifts (δ^{para}) in the paramagnetic Ln^{III} complexes and those (δ^{dia}) of the corresponding diamagnetic Y^{III} complexes [Equation (1)].

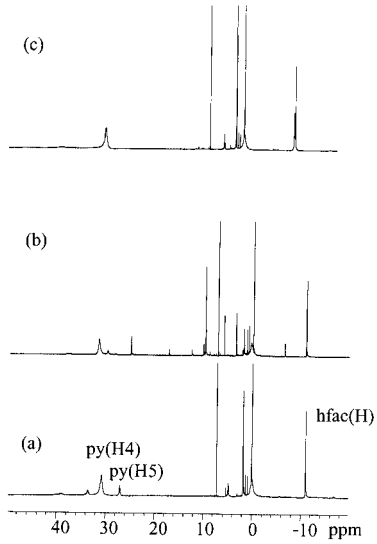

Figure 4. ^{1}H NMR spectra of (a) [Yb(hfac)$_3$(IM2py)], (b) [Yb(hfac)$_3$(IM4Me2py)] and (c) [Yb(hfac)$_3$(IM5Me2py)]

$$\delta_{ij}^{LIS} = \delta^{para} - \delta^{dia} \quad (1)$$

As a result of the dipolar and contact interactions between the electron spins on the Ln^{III} and the proton nuclear spin of the ligand, the chemical shifts of a given proton are shifted from the position observed in the corresponding diamagnetic environment [Equation (2)].

$$\delta_{ij}^{LIS} = \delta(\text{contact}) + \delta(\text{dipolar}) \quad (2)$$

The dipolar interaction contains the information on the geometrical positions in space of the ligand nuclei [Equation (3)], where F_i is the hyperfine coupling constant of the nucleus (i) in the ligand independent of Ln^{III} ions (j),[20] $\langle S_z \rangle_j$ is the spin expectation value for Ln ions (j),[22] D_j is a magnetic constant proportional to Bleaney's constant C_i which is characteristic of a given Ln^{III} ion, $\langle B_2^0 \rangle = \langle A_2^0(r^2) \rangle$ is a crystal field coefficient of the Ln^{III} complex and G_i is a geometric function of the ligand nu-

 © 2004 Wiley-VCH Verlag GmbH & Co. KGaA, Weinheim

cleus which is equal to $(3\cos^2\theta - 1)/r^3$ assuming the axial symmetric magnetic susceptibility.[19−21]

$$\delta_{ij}^{LIS} = F_i\langle S_z\rangle_j + \langle B_2^0\rangle D_j \cdot G_i \quad (3)$$

In order to obtain the dipolar and contact parts from the experimental LIS, the graphical separation methods or classical one-nucleus crystal field dependent methods are given [Equations (4) and (5)].[19,20]

$$\delta_{ij}^{LIS}/\langle S_z\rangle_j = F_i + \langle B_2^0\rangle G_i \cdot D_j/\langle S_z\rangle_j \quad (4)$$

$$\delta_{ij}^{LIS}/D_j = F_i\langle S_z\rangle_j/D_j + \langle B_2^0\rangle G_i \quad (5)$$

If the lanthanide complexes were isostructural, a plot of $\delta_{ij}^{LIS}/\langle S_z\rangle$ against $D_j/\langle S_z\rangle_j$ according to Equation (4) would be linear for a particular nucleus (i) of the ligand in the corresponding complexes across the entire Ln series. A linear plot of Equations (4) and (5) can be assumed for the dominant dipolar and constant contribution, respectively. In the case of multi-spin systems such as $[Ln(hfac)_3(IM2py)]$, the magnetic interaction between unpaired spins of Ln^{III} and IM2py must be taken into consideration. This could be significantly large, unless the plots were linear. Thus, the intramolecular magnetic interaction in the $(IM2py)Ln^{III}$ complexes may be tested by the application of the LIS analysis for nonradical complexes to the NMR spectroscopic data of $[Ln(hfac)_3(IM2py)]$ (Table 1S, Supporting Information). In view of the correlation coefficients (r) in Figure 5, the linearity was found to be excellent for hfac-H and fairly good for py-H5 and py-H4 in the IM2py moiety for a series of Ln^{III} complexes according to Equation (4). According to Equation (5), however, the plots deviate significantly from linearity for py-H4 (r = 0.72) and hfac-H (r = 0.76) but not for py-H5 (r = 0.97). This suggests that the LIS for three protons are more dominantly contributed from the dipolar contribution than the contact one. The slopes for the two neighbouring protons (py-H4 and py-H5) in the plots of Equation (4) are similar to each other and have the same sign which is opposite to that of hfac-H, reflecting the differences in the geometrical dispositions of the three protons. The agreement factors $\{AF_i = [\Sigma(\delta^{LIS} - \delta^{calcd.})^2/\Sigma(\delta^{LIS})^2]^{1/2}\}$ were found to be 0.1, 0.6 and 0.48 for hfac-H, py-H4 and py-H5, respectively, from the plots of Equation (4). The small AF value for hfac-H shows no significant influence from the IM2py radical. The fairly large AF values for py-H4 and py-H5 may result from less invariance in the crystal field coefficient and/or the influence of the unpaired electron of the IM2py group.

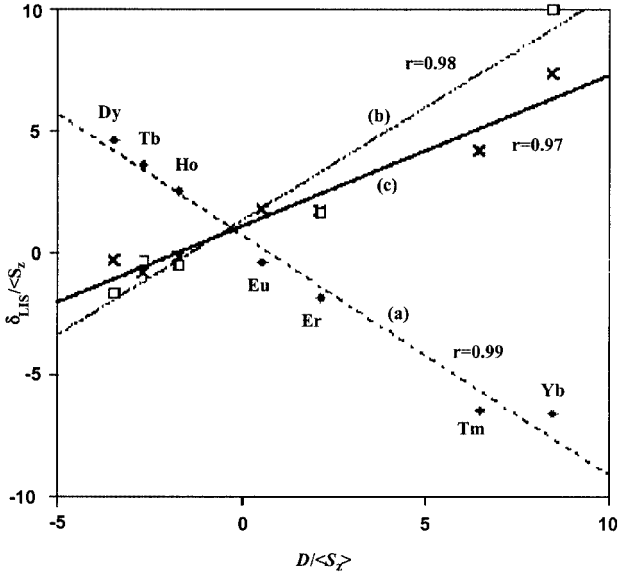

Figure 5. Plots of $\delta_i^{LIS}/\langle S_z\rangle$ versus $D_j/\langle S_z\rangle$ according to Equation (4) ($\delta_i^{LIS}/\langle S_z\rangle = F_i + G_iB_2^0D_j/\langle S_z\rangle$); hfac-H (a), py-H4 (b) and py-H5 (c)

In order to examine these causes, the two- and three-nuclei crystal field independent separation methods[23] were applied to the LIS. These are represented by Equation (6)[22] and Equation (7)[23], respectively.

$$\delta^{LIS}(pyH_i)/\langle S_z\rangle = (F_{py\text{-}Hi} - F_{hfac\text{-}H}R_i) + R_i\delta^{LIS}(hfac\text{-}H)/\langle S_z\rangle \quad (6)$$

where $R_i = G_{py\text{-}Hi}/G_{hfac\text{-}H}$

$$\delta^{LIS}(py\text{-}H_i)/\delta^{LIS}(hfac\text{-}H) = \alpha\delta^{LIS}(py\text{-}H_j)/\delta^{LIS}(hfac\text{-}H) + \beta \quad (7)$$

where $\alpha = (F_{py\text{-}Hi}/F_{hfac\text{-}H} - R_i)/(F_{py\text{-}Hj}/F_{hfac\text{-}H} - R_j)$ and $\beta = [(F_{py\text{-}Hi}/F_{hfac\text{-}H})R_i - (F_{py\text{-}Hi}/F_{hfac\text{-}H})R_j]/(F_{py\text{-}Hj}/F_{hfac\text{-}H} - R_j)$

The plots for $\delta^{LIS}(py\text{-}H_i)/\langle S_z\rangle$ versus $\delta^{LIS}(hfac\text{-}H)/\langle S_z\rangle$ according to Equation (6) for the two-nuclei crystal field independent analysis show fairly good linearity with high r values (r = 0.95 for py-H4 and 0.93 for py-H5). In addition, the three-nuclei crystal field independent analysis given by a plot of $\delta^{LIS}(py\text{-}H4)/\delta^{LIS}(hfac\text{-}H)$ versus $\delta^{LIS}(py\text{-}H5)/\delta^{LIS}(hfac\text{-}H)$ in terms of Equation (7) exhibits good linearity (r = 0.93), confirming the invariance of the crystal field coefficient and the isostructural nature of the Ln^{III} complexes. Moreover, in order to check the invariance in the hyperfine coupling constant and the geometric factor, a crystal field independent method was employed according to Equations (8) and (9). This is based on the shift modulation, Y, using Yb^{III} as the reference Ln complex as defined in Equations (8) and (9).[20d,25]

$$Y_{Ln,j} = \delta^{LIS}{}_{Yb,j}\langle S_z\rangle_{Ln}/\langle S_z\rangle_{Yb} - \delta^{LIS}{}_{Ln,j} \quad (8)$$

$$Y_{Ln,py\text{-}Hi} = Y_{Ln,hfac\text{-}H}G_{py\text{-}Hi}/G_{hfac\text{-}H} \quad (9)$$

The plots of $Y_{Ln,py\text{-}Hi}$ of py-H4 and py-H5 with reference to $Y_{Ln,hfac\text{-}H}$ of hfac-H give excellent conformities (Figure 6). Internal conformity for the F_i and $R = G_{py\text{-}Hi}/G_{hfac\text{-}H}$ values was also found from Equations (4), (6) and (7) (Table 2S, Supporting Information), reconfirming the invariance of the parameters and isostructural pattern. From

 © 2004 Wiley-VCH Verlag GmbH & Co. KGaA, Weinheim

these structural analyses of the LIS, no change in the geometrical structures or isostructure with axial symmetry in solution was found and little or negligible magnetic interactions between Ln and IM2py were observed through the Ln series. This fact means that there is little effect on the ^{1}H NMR properties from the unpaired electron spin in the IM2py radical. Accordingly, the paramagnetic shifts of the IM2py ligand in the paramagnetic Ln^{III} ions are induced only by unpaired 4f electrons in the Ln^{III} ions and are hardly affected by the unpaired spin in IM2py. The present LIS analyses suggest that there is a difference in symmetry between the solid-state and solution structures of the complexes. That is, the present complexes in the solid state do not have actual axial symmetry as revealed by the X-ray analysis[11] and they exhibit no effect due to the magnetic asymmetry in solution. This can be re-emphasized from the fairly good linear relationships [r = 0.80 (py-H4), 0.86 (py-H5), and 0.98 (hfac-H)] in terms of the structural analyses according to plots of δ^{LIS}/D' versus D/D' derived from Equation (10), where D and G are given in Equation (3) and D' is an asymmetric magnetic constant and $G' = (\sin^2\theta\cos 2\varphi)r^{-3}$.[26]

$$\delta^{LIS}/D' = D/D'G + G' \quad (10)$$

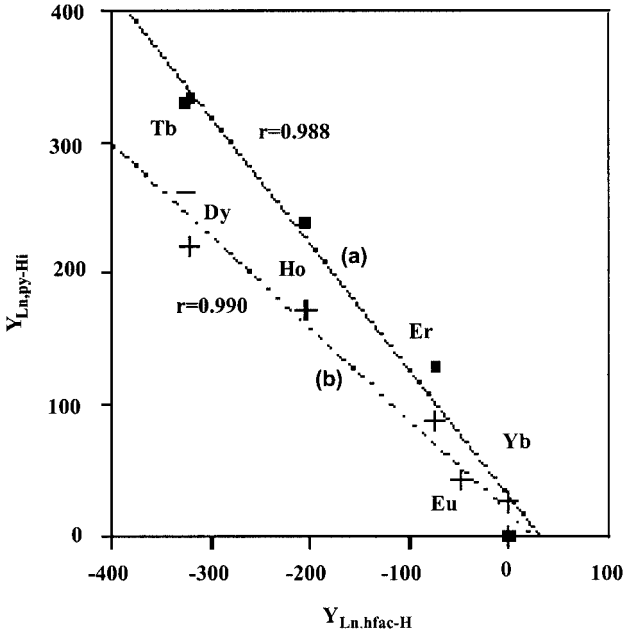

Figure 6. Plots of $Y_{Ln,pynH}$ versus $Y_{Ln,hfacH}$ according to Equation (9); py-H4 (a) and py-H5 (b)

The evidence for the effective magnetic axial symmetry of the Ln complexes can be accounted for by the intramolecular motions and/or rearrangements leading to the dynamic averaging on a faster time scale than that of NMR spectroscopy. This dynamic aspect is consistent with the observation of only one NMR signal for hfac-H, revealing the equivalence of three hfac ligands which are not symmetrically correlated in the solid state as found by the X-ray analysis.[11]

Conclusions

It has been found that the ^{1}H NMR spectra for the (IM2-py)Ln^{III} complexes behave as if the IM2py radical was diamagnetic. For the diamagnetic Ln^{III} complexes, the ^{1}H NMR signals of the coordinated IM2py radical come in the range observed for the diamagnetic compounds, whereas in the paramagnetic Ln^{III} complexes their chemical shifts exhibit only shifts induced by the lanthanide ion's unpaired 4f electron spin(s) and not by the IM2py radical spin. In order to elucidate the peculiar diamagnetic behaviour of the coordinated IM2py ligand, more NMR spectroscopic data are needed for the coordinated radicals in diamagnetic and/or paramagnetic metal complexes.

Experimental Section

General: All chemicals were reagent grade and were used without purification. Lanthanide or yttrium trichloride hexahydrate and Hhfac were purchased from Wako Pure Chemical Industries Ltd. and Tokyo Chemical Industry Co. Ltd., respectively. The radical ligands IM2py, methyl-substituted pyridyl ligands IM*n*Me2py[27] and the complexes [Ln(hfac)$_3$(IM2py)][11] were prepared by previously reported methods.

Measurements: Magnetic susceptibility data of solids and solutions were measured using a magnetic balance (Sherwood Scientific, MSB-AUTO) and the Evans method[28] (^{1}H NMR spectra), respectively, at 23 °C. Pascal's constants were used to determine the constituent atom diamagnetism. The EPR spectrum was measured using a JES-RE1X ESR spectrometer at 296 K in CH_2Cl_2 and was analysed with WinFonia EPR Spectrum Simulation Software Ver. 1.25 (Bruker Analytische Messtechnik GmbH, Germany, **1996**). ^{1}H NMR spectra were recorded with a JEOL EX-270 spectrometer in $CDCl_3$ at 23 °C with concentrations of about 15 mM. The internal standard of tetramethylsilane (TMS) was assigned a chemical shift of δ = 0 ppm. ^{89}Y NMR spectra were recorded with a JEOL Lambda-500 spectrometer in $CDCl_3$ at 30 °C, where the external standard of $Y(NO_3)_3$ in D_2O was assigned a chemical shift of δ = 0 ppm.

Supporting Information: See footnote on the first page of this article. Table 1S with lists of the chemical shifts and LIS values for the IM2py complexes; Table 2S with F, B_2^0G, R, $(F_i - RF_i)$, α, β. Figure 1S with Y NMR spectra.

[1] J.-C. G. Bünzli, in *Lanthanide Probes in Life, Chemical and Earth Sciences, Theory and Practice*, Elsevier, New York, **1989**, p. 219.
[2] [2a] C. Lescop, D. Luneau, G. Bussière, M. Triest, C. Reber, *Inorg. Chem.* **2000**, *39*, 3740. [2b] C. Lescop, D. Luneau, P. Ray, G. Bussière, C. Reber, *Inorg. Chem.* **2002**, *41*, 5566. [2c] R. Beauiac, G. Bussière, C. Reber C. Lescop, D. Luneau, *New J. Chem.* **2003**, *27*, 1200.
[3] [3a] O. Kahn, *Adv. Inorg. Chem.* **1995**, *43*, 179. [3b] C. Benelli, A. J. Blake, P. E. Y. Milne, J. M. Rawson, R. E. P. Winpenny, *Chem. Eur. J.* **1995**, *1*, 614.
[4] [4a] C. Benelli, A. Caneschi, D. Gatteschi, L. Pardi, *Inorg. Chem.* **1992**, *31*, 741. [4b] C. Benelli, A. Caneschi, D. Gatteschi, R. Sessoli, *Inorg. Chem.* **1993**, *32*, 4797. [4c] M. L. Kahn, J. -P. Sutter, S. Golhen, P. Guionneau, L. Ouahab, O. Kahn, D. Chasseau, *J. Am. Chem. Soc.* **2000**, *122*, 3413. [4d] M. L. Kahn,

 © 2004 Wiley-VCH Verlag GmbH & Co. KGaA, Weinheim

R. Ballou, P. Porcher, O. Kahn, J. -P. Sutter, *Chem. Eur. J.* **2002**, *8*, 525. [4e] C. Benelli, D. Gatteschi, *Chem. Rev.* **2002**, *102*, 2369.

[5] [5a] C. Lescop, D. Luneau, G. Bussiére, M. Triest, C. Reber, *Inorg. Chem.* **2000**, *39*, 3740. [5b] C. Lescop, E. Belorizky, D. Luneau, P. Rey, *Inorg. Chem.* **2002**, *41*, 3375. [5c] C. Lescop, D. Luneau, P. Rey, G. Bussiére, C. Reber, *Inorg. Chem.* **2002**, *41*, 5566. [5d] R. Beaulac, G. Bussiére, C. Reber, C. Lescop, D. Luneau, *New J. Chem.* **2003**, *27*, 1200.

[6] [6a] T. Yoshida, S. Kaizaki, *Inorg. Chem.* **1999**, *38*, 1054. [6b] T. Yoshida, K. Kanamori, S. Takamizawa, W. Mori, S. Kaizaki, *Chem. Lett.* **1997**, 603. [6c] T. Yoshida, T. Suzuki, K. Kanamori, S. Kaizaki, *Inorg. Chem.* **1999**, *38*, 1059.

[7] [7a] Y. Yamamoto, T. Suzuki, S. Kaizaki, *J. Chem. Soc., Dalton Trans.* **2001**, 1566. [7b] Y. Yamamoto, T. Suzuki, S. Kaizaki, *J. Chem. Soc., Dalton Trans.* **2001**, 2943.

[8] [8a] Y. Tsukahara, A. Iino, T. Yoshida, T. Suzuki, S. Kaizaki, *Dalton Trans.* **2002**, 181. [8b] Y. Tsukahara, T. Kamatani, A. Iino, T. Suzuki, S. Kaizaki, *Inorg. Chem.* **2002**, *41*, 4363. [8c] Y. Tsukahara, H. Nakata, S. Kaizaki, *Inorg. Chem.* **2004**, *43*, 4383.

[9] T. Ishida, T. Suzuki, S. Kaizaki, *Inorg. Chim. Acta* **2004**, *357*, 3134.

[10] M. Ogita, Y. Yamamoto, T. Suzuki, S. Kaizaki, *Eur. J. Inorg. Chem.* **2002**, 886.

[11] [11a] T. Tsukuda, T. Suzuki, S. Kaizaki, *Dalton Trans.* **2002**, 1721. [11b] T. Tsukuda, T. Suzuki, S. Kaizaki, *Mol. Cryst. Liq. Cryst.* **2002**, *379*, 159. [11c] T. Tsukuda, T. Suzuki, S. Kaizaki, *Inorg. Chim. Acta*, in press.

[12] S. Kaizaki, *Bull. Chem. Soc. Jpn.* **2003**, *76*, 673.

[13] [13a] C. C. Hinckley, *J. Am. Chem. Soc.* **1969**, *114*, 1908. [13b] A. F. Cockerhill, G. L. Davies, R. C. Harden, D. M. Rackham, *Chem. Rev.* **1973**, *73*, 553.

[14] S. Aime, M. Botta, M. Fasano, E. Terreno, *Chem. Soc. Rev.* **1998**, *27*, 19.

[15] [15a] W. Beck, K. Schmidtner, H. J. Keller, *Chem. Ber.* **1967**, *100*, 503. [15b] D. Wilbur, R. Kreilick, *J. Chem. Phys.* **1970**, *52*, 1643. [15c] R. A. Zelonka, M. C. Baird, *J. Am. Chem. Soc.* **1971**, *93*, 6066. [15d] R. Z. Sagdeev, Yu. N. Molin, R. A. Sadikov, L. B. Volodarsky, G. A. Kutikova, *J. Mag. Res.* **1973**, *9*, 13.

[16] [16a] P. F. Richardson, R. Kreilick, *J. Am. Chem. Soc.* **1977**, *99*, 8183. [16b] P. F. Richardson, R. Kreilick, *Chem. Phys. Lett.* **1977**, *50*, 333. [16c] P. F. Richardson, R. Kreilick, *J. Mag. Reson.* **1978**, *29*, 285. [16d] P. F. Richardson, R. Kreilick, *J. Phys. Chem.* **1978**, *82*, 1149.

[17] J. N. Helbert, P. W. Kopf, E. H. Poindexter, B. E. Wagner, *J. Chem. Soc., Dalton Trans.* **1975**, 998.

[18] H. Heise, F. H. Köhler, F. Mota, J. J. Novoa, J. Veciana, *J. Am. Chem. Soc.* **1999**, *121*, 9659.

[19] I. Bertini, C. Luchinat, *NMR of Paramagnetic Molecules in Biological Sytems*, The Benjamin/Cummings Publishing Company, Inc., Menlo Park, California, **1986**, p. 273 and references therein.

[20] [20a] C. P. Iglesias, E. Mourad, M. Hollenstein, J. -C. G. Bünzli, C. Piguet, *J. Chem. Soc., Dalton Trans.* **2000**, 2031. [20b] S. Rigault, C. Piguet, J. -C. G. Bünzli, *J. Chem. Soc., Dalton Trans.* **2000**, 2045. [20c] S. Floquet, N. Quali, B. Bocquet, G. Bernardinelli, D. Imbert, J. -C. G. Bünzli, G. Hopfgartner, C. Piguet, *Chem. Eur. J.* **2003**, *9*, 1560. [20d] N. Quali, B. Bocquet, S. Rigault, P-Y. Morgantini, J. Weber, C. Piguet, *Inorg. Chem.* **2002**, *41*, 1436.

[21] R. M. Golding, M. P. Halton, *Aust. J. Chem.* **1972**, *25*, 2577.

[22] A. A. Pinkerton, M. Rossier, S. Spiliadis, *J. Magn. Reson.* **1985**, *64*, 430.

[23] [23a] C. C. F. G. C. Geraldes, S. Zhang, C. Platas, T. Rodríguez-Blas, A. de Blas, A. D. Sherry, *J. Alloys Compd.* **2001**, *323/324*, 824. [23b] J. Ren, S. Zhang, A. D. Sherry, C. F. G. C. Geraldes, *Inorg. Chim. Acta* **2002**, *339*, 272. [23c] C. F. G. C. Geraldes, A. D. Sherry, S. Zhang, *Inorg. Chim. Acta* **2004**, *357*, 381.

[24] C. Platas, F. Avecilla, A. de Blas, C. F. G. C. Geraldes, T. Rodríguez-Blas, H. Adams, J. Mahia, *Inorg. Chem.* **1999**, *38*, 3190.

[25] J. Reuben, *J. Magn. Reson.* **1982**, *50*, 233; J. Ren, A. D. Sherry, *J. Magn. Reson.* **1996**, *B111*, 178.

[26] J. Reuben, G. A. Elgavish, *J. Magn. Reson.* **1980**, *39*, 421.

[27] [27a] E. F. Ullman, J. H. Osiecki, D. G. B. Boocock, R. Darcy, *J. Am. Chem. Soc.* **1974**, *94*, 7049. [27b] E. F. Ullman, L. Call, J. H. Osiecki, *J. Org. Chem.* **1970**, *35*, 3623. [27c] T. Akita, Y. Mazaki, K. Kobayashi, N. Koga, H. Iwamura, *J. Org. Chem.* **1995**, *60*, 2092.

[28] [28a] D. F. Evans, *J. Chem. Soc.* **1959**, 2003. [28b] C. Piguet, *J. Chem. Educ.* **1997**, *74*, 815.

Received March 31, 2004
Early View Article
Published Online October 1, 2004

 © 2004 Wiley-VCH Verlag GmbH & Co. KGaA, Weinheim

Chemical Vapor Deposition of Niobium Disulfide Thin Films

Claire J. Carmalt,*[a] Emily S. Peters,[a] Ivan P. Parkin,[a] Troy D. Manning,[a] and Andrew L. Hector[b]

Keywords: Niobium disulfide / Thin films / Chemical vapor deposition

Atmospheric pressure chemical vapor deposition (APCVD) of niobium sulfide coatings was achieved on glass substrates from the reaction of $NbCl_5$ and $S(SiMe_3)_2$, tBu_2S_2, *t*BuSH, or $HSCH_2CH_2SH$ at 250–600 °C. The niobium sulfide films grown at temperatures above 500 °C were crystalline, and powder X-ray diffraction showed that two polytypes of NbS_2 were produced. The sulfur precursor used is fundamental to the polytype of NbS_2 obtained; films that are grown from the APCVD reaction of $NbCl_5$ and $S(SiMe_3)_2$ or tBu_2S_2 at 500–600 °C crystallize into the 1T structure, whereas those grown from the APCVD reaction of $NbCl_5$ and *t*BuSH or $HSCH_2CH_2SH$ at 500–600 °C crystallize into the 3R structure. Energy dispersive X-ray analysis (EDXA) studies gave elemental ratios close to the expected 1:2 ratio for Nb:S. Scanning electron microscopy (SEM) revealed surface morphologies consistent with an island growth mechanism. The films were also characterized using Raman and X-ray photoelectron spectroscopy, both of which showed differences consistent with the formation of the two polytypes, 1T and 3R-NbS_2.

(© Wiley-VCH Verlag GmbH & Co. KGaA, 69451 Weinheim, Germany, 2004)

Introduction

Niobium sulfides are part of the family of transition metal dichalcogenide layered materials, which gives rise to a host of interesting properties and facilitates intercalation into the van der Waals gap between these layers.[1] This function of transition metal dichalcogenides has been exploited for use as the cathode material in secondary batteries.[1] The layer structure also gives rise to unique optical and magnetic properties, which have been widely studied.[2−4] Niobium disulfide (NbS_2) has found uses as hydrodesulfurization and hydrodenitrogenation catalysts for hydrotreatment reactions in the purification of petroleum.[5] In addition, NbS_2 has been shown to be an effective humidity sensor.[6] However, the development of new applications has been hampered by difficulty in forming thin-films of NbS_2.

There are two known phases of NbS_2, termed 2H and 3R, both of which can also form nonstoichiometric phases with $Nb_{1+x}S_2$ compositions.[7,8] 2H-NbS_2 is a superconductor with a transition range of 5−6.3 K, whereas 3R-NbS_2 has a superconducting transition temperature of 1.7 K.[9,10] The stoichiometry of the niobium sulfide obtained is very sensitive to pressure, making identification of the polytype difficult due to the formation of substoichiometric compounds and mixtures.[9] The formation of niobium sulfides with high surface areas, such as in thin-film form, is particularly important in battery, gas sensing and catalyst applications.[1,5,10] However, there have been relatively few reports on thin-film formation of NbS_2, a possible consequence of the difficulty in isolating a single polytype.[11,12] Physical deposition processes for the preparation of NbS_2 films have been reported.[11] However, chemical vapor deposition (CVD) routes to niobium sulfide films are limited and involve the use of the single-source precursors $[NbCl_4(S_2\text{-}i\text{Pr}_2)][NbCl_6]$[12] and $[Nb(S\text{-}2,6\text{-}Me_2C_6H_3)_5]$,[13] resulting in thin-films of Nb_2O_5/NbS_2 and NbS, respectively.

In this paper we report the atmospheric pressure (AP)CVD reaction of $NbCl_5$ with $S(SiMe_3)_2$, tBu_2S_2, *t*BuSH or $HSCH_2CH_2SH$. The formation of a new trigonal polytype 1T-NbS_2 is described and the effect of the sulfur precursor on the phase of the NbS_2 film formed is discussed.[14]

Results and Discussion

Films have been deposited on glass from the dual source APCVD reaction of $NbCl_5$ with a range of sulfur sources [$S(SiMe_3)_2$, tBu_2S_2, *t*BuSH and $HSCH_2CH_2SH$]. The onset of deposition varied from 250−600 °C, a consequence of the sulfur-bonding environment in the precursor [onset of deposition: $S(SiMe_3)_2$ 600 °C; tBu_2S_2 400 °C; *t*BuSH 250 °C; $HSCH_2CH_2SH$ 350 °C]. At temperatures above 500 °C, deposition was localized towards the front of the substrate, at lower temperatures complete coverage was observed. The

[a] Department of Chemistry, Christopher Ingold Laboratories, University College London,
London, WC1H OAJ, UK
Fax: (internat.) + 44-2076797463
E-mail: c.j.carmalt@ucl.ac.uk
[b] School of Chemistry, University of Southampton,
Highfield, Southampton, SO17 1BJ, UK

 © 2004 Wiley-VCH Verlag GmbH & Co. KGaA, Weinheim **DOI: 10.1002/ejic.200400308**

films produced from $NbCl_5$ and $S(SiMe_3)_2$ or tBu_2S_2 at 500 °C or above had a gold color, and the lower temperature (< 500 °C) films were reflective. The reflectance and transmission spectra indicate that all the films have good reflectance and minimal transmission in the region 400−1000 nm. APCVD of $NbCl_5$ and *t*BuSH or $HSCH_2CH_2SH$ produced dark brown, reflective films at all temperatures. All the films produced, regardless of the sulfur precursor used or temperature of the reaction, were adhered to the substrate, passing the Scotch tape test. However, they were readily scratched by a brass or stainless steel stylus. The films were chemically robust to toluene, dichloromethane, THF and acetone, showing no visible changes after 2 weeks of immersion. Concentrated nitric acid digested the films within 1 min of immersion, whereas concentrated hydrochloric acid dissolved the films after 2 hours.

The niobium sulfide films were characterized by a range of techniques. Composition analysis of the films was determined by EDAX analysis, which shows niobium to sulfur ratios close to the expected 1:2 for NbS_2 (Table 1). Some slight deviations from this composition were noted; however, this tended to be for thinner films where breakthrough to the underlying glass was observed, which interfered with accurate compositional analysis. No evidence of carbon or chlorine contamination was found, within the detection limit of the instrument (1 atom%). Interestingly, the films produced from $NbCl_5$ and $HSCH_2CH_2SH$ at 350−400 °C were slightly rich in sulfur (Table 1). Scanning electron microscopy (SEM) shows that each film grew by a Volmer−Webber type growth mechanism. However the morphology of the films varied depending on the sulfur precursor employed in the APCVD reaction (Figure 1).

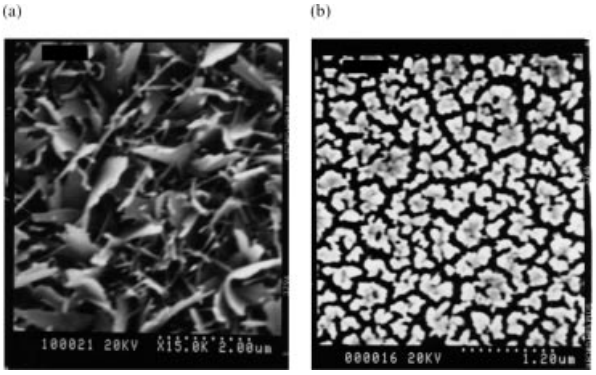

Figure 1. Scanning electron microscopy image of the film prepared from (a) APCVD of $NbCl_5$ and tBu_2S_2 at 550 °C and (b) APCVD of $NbCl_5$ and $HSCH_2CH_2SH$ at 550 °C

SEM of the films grown from $NbCl_5$ and $S(SiMe_3)_2$ or tBu_2S_2 show platelets (approximately 2 μm at 550 °C) that are orientated largely perpendicular to the substrate (Figure 1, a). In contrast, SEM of films produced from $NbCl_5$ and *t*BuSH or $HSCH_2CH_2SH$ display a crazy paving type morphology with particle sizes of 0.6 μm at 550 °C (Figure 1, b) and 0.25 μm at 400 °C. Edge-on SEM photographs allowed for the determination of film thickness. For example, films grown at 600 °C from $NbCl_5/S(SiMe_3)_2$ or tBu_2S_2 were 16 μm thick, whereas films from $NbCl_5/t$BuSH or $HSCH_2CH_2SH$ (at the same growth temperature) were

Table 1. Deposition conditions and analysis of the films grown from the APCVD of $NbCl_5$ and $S(SiMe_3)_2$, tBu_2S_2, *t*BuSH or $HSCH_2CH_2SH$

Substrate temp. (°C); sulfur precursor	Deposition time (min)	EDXA	Raman (cm^{-1})	XRD / 2θ	Contact angle (°)
600; $S(SiMe_3)_2$	5	$NbS_{1.8}$	1T-NbS_2	1T-NbS_2	95.1
600; tBu_2S_2	5	$NbS_{1.9}$	1T-NbS_2	1T-NbS_2	6.0
550; tBu_2S_2	5	$NbS_{1.8}$	1T-NbS_2	1T-NbS_2	3.5
500; tBu_2S_2	5	$NbS_{2.1}$	1T-NbS_2	1T-NbS_2	9.2
450; tBu_2S_2	5	$NbS_{2.1}$	90, 224, 285, 417, 604, 924	–[a]	87.3
400; tBu_2S_2	5	$NbS_{1.7}$	93, 226, 282, 418, 605, 924	–[a]	8.4
600; *t*BuSH	5	$NbS_{1.6}$	3R-NbS_2	3R-NbS_2	3.2
550; *t*BuSH	5	$NbS_{1.7}$	3R-NbS_2	3R-NbS_2	3.1
500; *t*BuSH	5	$NbS_{1.7}$	3R-NbS_2	3R-NbS_2	3.5
450; *t*BuSH	5	$NbS_{1.9}$	3R-NbS_2	3R-NbS_2	4.8
400; *t*BuSH	5	$NbS_{1.7}$	3R-NbS_2	3R-NbS_2	2.4
350; *t*BuSH	5	$NbS_{2.0}$	3R-NbS_2	3R-NbS_2	4.1
300; *t*BuSH	5	$NbS_{2.0}$	169, 241, 372	X-ray amorphous	4.1
250; *t*BuSH	5	$NbS_{2.0}$	187, 294, 328, 549	X-ray amorphous	14.5
600; $HSCH_2CH_2SH$	5	$NbS_{2.1}$	3R-NbS_2	3R-NbS_2	54
550; $HSCH_2CH_2SH$	5	$NbS_{1.2}$	3R-NbS_2	3R-NbS_2	87
500; $HSCH_2CH_2SH$	5	$NbS_{1.8}$	3R-NbS_2	3R-NbS_2	90
500; $HSCH_2CH_2SH$	4	$NbS_{1.9}$	3R-NbS_2	X-ray amorphous	105
500; $HSCH_2CH_2SH$	3	$NbS_{1.8}$	195, 260, 328, 383	X-ray amorphous	48
450; $HSCH_2CH_2SH$	5	$NbS_{2.0}$	186, 260, 331, 381, 535	Nanocrystalline NbS_2	95
400; $HSCH_2CH_2SH$	5	$NbS_{2.4}$	197, 239, 299, 334, 535	X-ray amorphous	95
350; $HSCH_2CH_2SH$	5	$NbS_{2.3}$	187, 242, 298, 332, 544	X-ray amorphous	21

[a] Film too thin.

 © 2004 Wiley-VCH Verlag GmbH & Co. KGaA, Weinheim

0.4 μm thick. This indicated that typical growth rates were 3.2 μm·min^{-1} [$NbCl_5$/$S(SiMe_3)_2$ or tBu_2S_2] and 0.1 μm·min^{-1} ($NbCl_5$/*t*BuSH or $HSCH_2CH_2SH$).

The niobium sulfide films grown at 500−600 °C (from $NbCl_5$ and $S(SiMe_3)_2$, tBu_2S_2 or $HSCH_2CH_2SH$) or 350−600 °C (from $NbCl_5$/*t*BuSH) were crystalline (Table 1). NbS_2 is known to form with two structure types, which have been classified as 3R and 2H. However, powder X-ray diffraction (XRD) of the crystalline films shows that two different polytypes of NbS_2 are produced (3R- and 1T-NbS_2), as shown in Scheme 1.

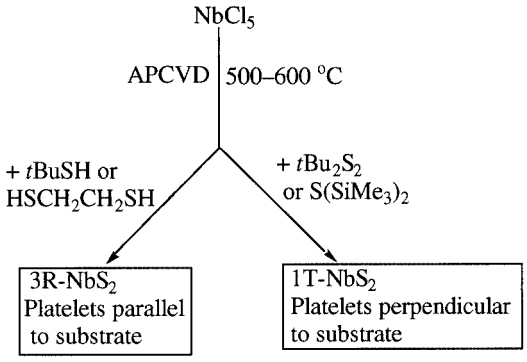

Scheme 1

Thus, films grown from $NbCl_5$/*t*BuSH or $HSCH_2CH_2SH$ formed nanocrystalline 3R-NbS_2, whereas $NbCl_5$/$S(SiMe_3)_2$ or tBu_2S_2 gave crystalline 1T-NbS_2. The XRD patterns for the nanocrystalline 3R-NbS_2 films formed from $NbCl_5$/*t*BuSH or $HSCH_2CH_2SH$ are shown in Figure 2.

The XRD patterns obtained for films that were grown from $NbCl_5$/$S(SiMe_3)_2$ or tBu_2S_2 at 600 °C indicate that the 3R-NbS_2 structure does not match the data well. Although the 2H-NbS_2 structure gives a similar diffraction pattern to the observed data, the 1T structure, as adopted by some other transition metal dichalcogenides (e.g. TaS_2),[7,15] is also a close match. The 2H structure comprises close packed sulfur atoms with an AABB repeating unit, with Nb located in half of the trigonal prismatic sites. The double layer repeating unit is shown in Figure 3, the structure in the *xy* plane shows edge-linked NbS_2 trigonal prisms. In contrast, the 1T structure consists of hexagonal close packed sulfur atoms (AB repeat unit) with Nb filling half of the octahedral holes in every other layer. Hence the structure shows edge-linked NbS_2 octahedra, two layers of the repeating unit are shown in Figure 3.

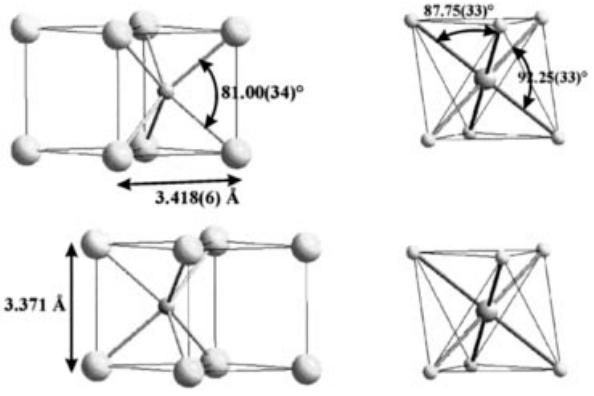

Figure 3. 2H (left) and 1T (right) NbS_2 structures; distances and angles shown are as refined from the NbS_2 thin films by XRD; thermal ellipsoids are shown at the 50% probability level

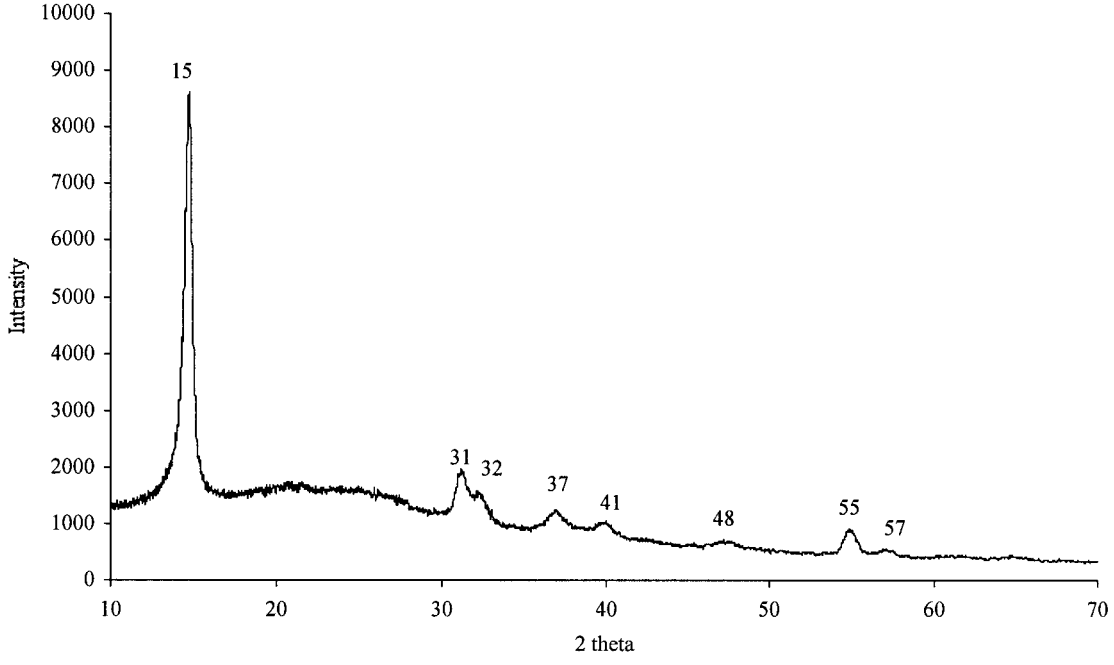

Figure 2. X-ray powder diffraction pattern for a 3R-NbS_2 film produced from the APCVD reaction of $NbCl_5$ and *t*BuSH at 550 °C

 © 2004 Wiley-VCH Verlag GmbH & Co. KGaA, Weinheim

Rietveld refinements using the 2H and 1T structure models were performed with the GSAS package,[16] both were stable and converged. A cosine Fourier series (GSAS #2) with 6 terms was used to model the background and lattice parameters, zero point and scale factor were allowed to refine. Using profile function #2, the Gaussian terms were fixed at the values obtained with the Cu standard. The particle size broadening term was refined but no strain broadening was found. Transparency was also refined to a fairly high value (this is not surprising since the glass substrate was observed in the data, hence the offset in the tick marks on the fit diagrams). Particle size in Å is defined as $p = 18000\ K\lambda/\pi X$,[17] where K is the Scherrer constant and X is the particle size associated Lorentzian term from the Rietveld refinement. X is refined to 38 and 36 for the 2H and 1T structures, respectively, corresponding to an average crystallite size of around 180 Å. The preferred orientation ratio along 001 is refined to values of 1.18 (2H) and 1.27 (1T). Growth of the platelets perpendicular to the substrate is reflected in the apparent preferential *c*-axis growth in the diffraction data. The fit statistics are better for the 1T structure to a significant degree (Table 2). Furthermore, the 2H structure should have extra reflections, compared with the 1T structure, at 26.5° (101) and 32.5° (103) since it has a doubled *c* axis and these are not observed. The Nb thermal parameter in the 1T structure is slightly high but the S thermal parameter in the 2H structure is very high. The space group is $P\bar{3}m1$ (No. 164) and refined lattice parameters are $a = 3.420(6)$ Å and $c = 5.938(1)$ Å ($Z = 1$) (Figure 4). Prior to this work, there were no reports of NbS_2 crystallizing into the 1T structure.[14]

Table 2. Refined crystallographic parameters for NbS_2 with the 1T and 2H structure models.

	1T Structure	2H Structure
Space group	$P\bar{3}m1$ (No. 164)	$P6_3/mmc$ (No. 194)
Lattice constants *a*, *c* (Å)	3.420(6), 5.938(11)	3.418(6), 11.860(23)
Cell volume (Å^3)	60.16(19)	120.0(4)
Nb site	1a	2b
x, *y*, *z*	0, 0, 0	0, 0, $^1/_4$
U_{iso} (Å^2 × 100)	3.5(4)	2.4(3)
S site	2d	4f
x, *y*, *z*	$^1/_3$, $^2/_3$, 0.2491(29)	$^1/_3$, $^2/_3$, 0.1079(16)
U_{iso} (Å^2 × 100)	1.6(6)	7.8(7)
χ^2	1.893	2.363
R_{wp}	6.52%	7.29%
R_p	5.20%	5.67%
Nb–S (Å)	2.467(11)	2.595(13)
Nb–S–Nb (°)	87.8(5)	82.4(5)

Raman microscopy was used to investigate all of the films. The Raman spectra of the thin films that were grown from $NbCl_5$/*t*BuSH or $HSCH_2CH_2SH$ correspond well with that reported previously for 3R-NbS_2 [18] (Figure 5). Thus peaks at 322, 386, and 462 cm^{-1} are assigned to E_2, A_1 and A_2 modes, respectively. Other peaks were observed at approximately 190 and 258 cm^{-1}.

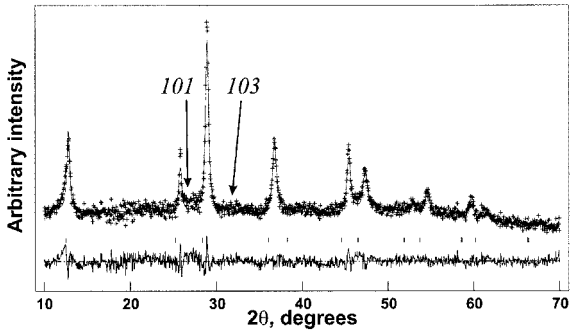

Figure 4. X-ray powder diffraction pattern for NbS_2 film produced from the APCVD reaction of $NbCl_5$ and tBu_2S_2 at 550 °C

It was noted that there was a slight shift in the Raman bands between samples that were sulfur-rich ($NbS_{2.3-2.4}$), fully stoichiometric (NbS_2) and sulfur-deficient ($NbS_{1.6-1.9}$). The formation of 1T-NbS_2 from $NbCl_5$/$S(SiMe_3)_2$ or tBu_2S_2 was further supported by the Raman spectra obtained for the films (Figure 6). It was found that the Raman spectra of the 1T-NbS_2 films is markedly different from those reported previously for 2H- and 3R-NbS_2,[18] but did show similarities with the 1T-TaS_2 pattern.[19]

X-ray photoelectron spectroscopy (XPS) shows that the surface of the films had been partially oxidized (depth of about 50 nm). The oxide surface layer was removed by sputtering to leave the bulk of the film consisting of niobium and sulfur. No evidence of chloride contamination (1–2% detection limit) was observed. XPS of films that were grown from $NbCl_5$ and *t*BuSH gave Nb $3d_{3/2}$, Nb $3d_{5/2}$, and S 2p binding energy shifts of 210.4, 207.5, and 162.3 eV, respectively. These are in good agreement with previous literature measurements for bulk NbS_2 (Nb $3d_{5/2}$ 207.7 eV).[20] XPS of the films that were grown from $NbCl_5$/$HSCH_2CH_2SH$ at temperatures > 400 °C also suggest the formation of 3R-NbS_2. However, XPS of films that were grown from $NbCl_5$/$HSCH_2CH_2SH$ at 350–400 °C show slight deviations (Nb $3d_{5/2}$ 207.4 eV, S 2p 162.3 eV) from the literature measurements of bulk NbS_2. As discussed above, the films that were grown from $NbCl_5$/$HSCH_2CH_2SH$ at 350–400 °C are shown by EDAX to be slightly sulfur-rich ($NbS_{2.3-2.4}$), which could result in shifts in the binding energies. Only one sulfur environment was found by XPS in all samples and this corresponds to the S^{2-} anion showing that these sulfur-rich samples are not a mixture of NbS_2 and NbS_3 (which would also contain the S_2^{2-} anion). It is also worth noting that $NbSe_2$ shows a phase change from 2H-$NbSe_2$ to 4H-$NbSe_2$ between 600–700 °C, which is slightly rich in selenium, 2H being the higher temperature phase.[21] Therefore, it is possible that a different phase to 3R-NbS_2 has been formed. Indeed, XPS of films that were grown from $NbCl_5$/$S(SiMe_3)_5$ or tBu_2S_2 at 500–600 °C gave Nb $3d_{3/2}$, Nb $3d_{5/2}$, and S 2p binding energy shifts of 209.4, 206.3, and 161.8 eV, respectively. The Nb $3d_{5/2}$ value is different from that for bulk NbS_2[20] and 3R-NbS_2 films (from $NbCl_5$/*t*BuSH). However, the binding energy shifts compare well with those published for a mixed transition metal disul-

 © 2004 Wiley-VCH Verlag GmbH & Co. KGaA, Weinheim

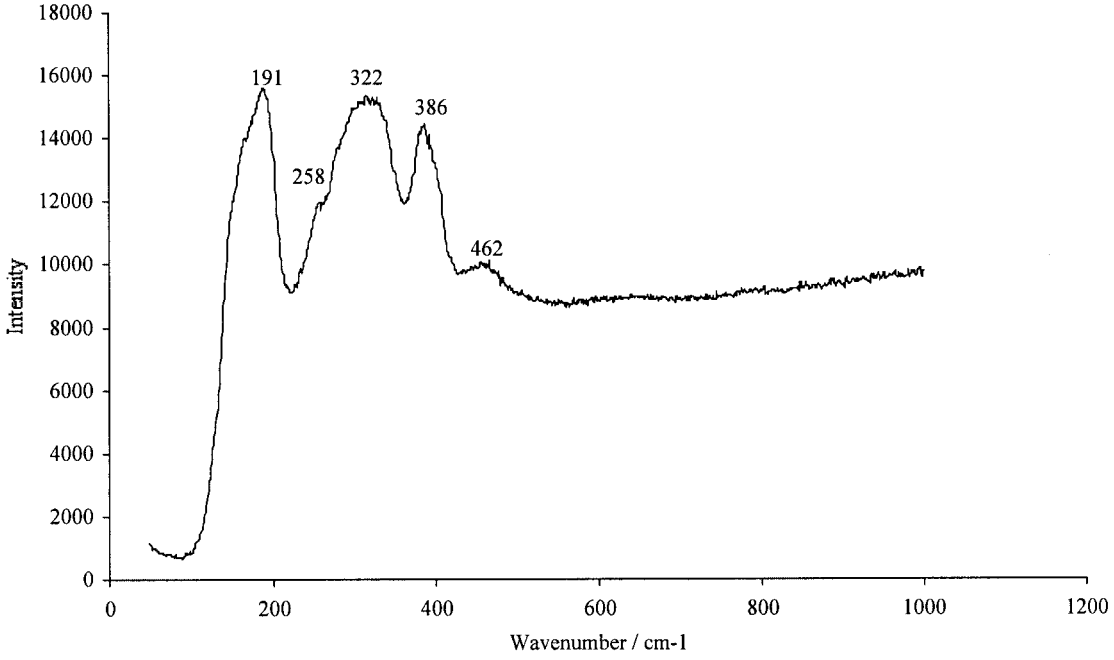

Figure 5. Raman spectrum of a NbS_2 film deposited on glass from $NbCl_5$ and *t*BuSH at 550 °C

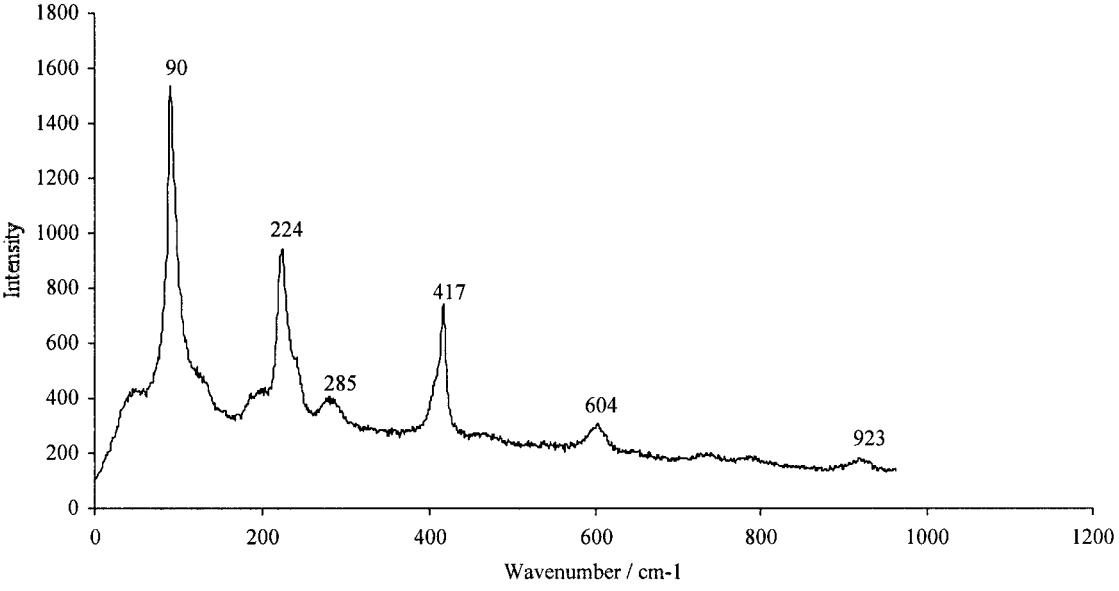

Figure 6. Raman spectrum of a NbS_2 film deposited on glass from $NbCl_5$ and tBu_2S_2 at 550 °C

fide system, 1T-$Nb_{1-x}Ir_xS_2$, which crystallizes into the 1T structure (Nb $3d_{5/2}$ about 206 eV; S 2p 162 eV).[22] These binding energy shifts suggest that the APCVD of $NbCl_5$ and $S(SiMe_3)_2$ or tBu_2S_2 at 500−600 °C results in the formation of a new trigonal polytype 1T-NbS_2, and this is further supported by the powder XRD and Raman spectra for the films.

A wide range of contact angles for water droplets on the NbS_2 films produced were obtained (Table 1). The contact angle measurements are valuable in the glass industry in assessing whether films have self-cleaning properties. Low contact angles arising from hydrophilic films lead to the spreading of the water across the surface, and hence the washing away of any loose dirt. For example, niobium(V) oxide films have been shown to generate low contact angle measurements (about 10°) under photo-irradiation.[23] Some of the niobium sulfide films obtained had contact angles >50° indicating that the films are hydrophobic. However, a number of films had very low contact angles between 2.4° and 14.5° suggesting a degree of hydrophilicity. The contact angles did not change upon photo-irradiation suggesting that this low contact angle is not due to some form of photo-induced hydrophilicity. Thus, the low contact angle is most likely due to a high-porosity within the films. Furthermore, these measurements indicate that the niobium sulfide films are unlikely to be oxide sur-

 © 2004 Wiley-VCH Verlag GmbH & Co. KGaA, Weinheim

face terminated since if niobium(v) oxide was present a drop in contact angle on photo-irradiation would be observed.[23] Four-point probe measurements show that the niobium sulfide films are metallic conductors at room temperature, as is expected. Accurate measurements could not be obtained as the films were scratched by the probe, which led to the fluctuation of the reading.

The deposition of NbS_2 films worked best at substrate temperatures between 500 and 600 °C. These results suggest that temperatures in excess of 400 °C are required for the precursors to react completely and form a film. However, nanocrystalline NbS_2 films were obtained from $NbCl_5$ and *t*BuSH at temperatures as low as 350 °C. The lack of chlorine contamination in the resulting films, despite the use of $NbCl_5$ indicates that a clean decomposition pathway is available. This probably occurs via species such as *t*BuCl and Me_3SiCl when tBu_2S_2 and $S(SiMe_3)_2$ are used, respectively. It is also possible that the reactions proceed via the formation of gas phase adducts, for example $[NbCl_5(tBuSH)_x]$.

The calculated growth rate for the formation of 1T-NbS_2 from $NbCl_5/S(SiMe_3)_2$ or tBu_2S_2 at 600 °C is 3.2 μm min^{-1}. This is faster than that for the formation of 3R-NbS_2 from $NbCl_5$/*t*BuSH or $HSCH_2CH_2SH$ at the same growth temperature (0.1 μm min^{-1}). The XPS, Raman, and XRD results suggest that 1T-NbS_2 is the kinetic product ,and this metastable phase forms due to the rapid growth rate. The formation of 1T-NbS_2 when using the sulfur precursors, $S(SiMe_3)_2$ and tBu_2S_2, may also be a result of the faster reaction chemistry relative to *t*BuSH or $HSCH_2CH_2SH$. In addition, it is also possible that $S(SiMe_3)_2$ and tBu_2S_2 do not have low energy decomposition pathways, for example, to yield H_2S, whereas *t*BuSH and $HSCH_2CH_2SH$ could rapidly afford H_2S on thermolysis. However, precursor volatility is also likely to contribute to the phase of NbS_2 obtained. Further studies into the reaction chemistry are required in order to obtain a more definite mechanism for the reaction. The formation of 1T-NbS_2 from $NbCl_5/S(SiMe_3)_2$ or tBu_2S_2 at 600 °C is markedly different from that of $NbSe_2$, where the 1T phase is only stable above 980 °C.[21]

Conclusion

APCVD of $NbCl_5$ and $S(SiMe_3)_2$ or tBu_2S_2 at 500−600 °C form crystalline 1T-NbS_2 thin films on glass. The XRD pattern of these films are not consistent with that of 3R-NbS_2, and appear to have missing reflections when compared with 2H-NbS_2. However, the XRD pattern obtained for the niobium sulfide films compares well with the reported pattern for 1T-TaS_2. The formation of the 1T-NbS_2 phase is further supported by the Raman spectra and XPS data obtained for the films. The dual-source CVD reaction of $NbCl_5$ and *t*BuSH or $HSCH_2CH_2SH$ produced 3R-NbS_2 films. All the films are free from contamination by carbon, oxygen, and chlorine (to detection limits about 0.5 atom%). They show good surface coverage, adhesion, and uniformity.

Experimental Section

Nitrogen (99.99%) was obtained from BOC and used as supplied. $NbCl_5$, $S(SiMe_3)_2$, tBu_2S_2, *t*BuSH, and $HSCH_2CH_2SH$ were supplied by Aldrich and used without further purification. Coatings were obtained on float glass substrates (90 mm × 45 mm × 4 mm) with a ca. 50 nm thick blocking layer of SiCO (to limit diffusion of ions from the glass) on a purpose built reactor.[24] A graphite block containing a Whatman cartridge heater was used to heat the glass substrate. The temperature of the substrate was monitored by a Pt-Rh thermocouple. The rig was designed so that four separate gas lines could be used, all of which were made of 1/4-in. diameter stainless steel, except for the inlet to the reaction chamber and the exhaust line from the reaction chamber which was 1/2-in. diameter. The nitrogen carrier gas was preheated to 157 °C by passing along 2 m lengths of coiled stainless steel tubing inside a tube furnace. Gas temperatures were monitored in situ by Pt-Rh thermocouples. The $NbCl_5$ and sulfur sources were placed into individual bubblers and heated through a heating jacket ($NbCl_5$, 220 °C; $S(SiMe_3)_2$, 90 °C; tBu_2S_2, 170 °C; *t*BuSH, 55 °C; $HSCH_2CH_2SH$, 85 °C). The vapors produced were introduced into a stream of hot nitrogen and transported to the mixing chamber. Flow rates were kept constant for all experiments ($NbCl_5$, 2.0 L·min^{-1}; $S(SiMe_3)_2$, 0.3 L·min^{-1}; tBu_2S_2, 0.3 L·min^{-1}; *t*BuSH, 0.2 L·min^{-1}; $HSCH_2CH_2SH$, 0.2 L·min^{-1}). All systems were investigated over a range of temperatures from the onset of deposition up to 600 °C. The exhaust from the reactor was passed through three bleach bubblers and vented directly into the extraction system of a fume cupboard. Deposition experiments were timed by stopwatch for typically 60 s. At the end of the deposition the bubbler line was closed, and nitrogen was passed over the substrate. The glass substrate was allowed to cool to ca. 60 °C before it was removed. The large substrates were cut into ca. 4 cm × 1 cm strips for analysis by SEM, XPS, Raman, UV/Vis spectroscopy and contact angle studies. 3 cm × 2 cm strips were used for X-ray diffraction. Film adherence to the glass was assessed using the Scotch tape test and by scratching the surface using brass and steel.

X-ray powder diffraction patterns were measured on a Siemens D5000 diffractometer using monochromated Cu-$K_{\alpha 1}$ radiation (λ_1 = 1.5406 Å) with glancing incident radiation (1.5°) or using synchrotron radiation (λ_1 = 1.2982 Å) on beamline 2.3 at the UK Synchrotron Radiation Source. The data contained a large glass background, and this was removed by subtracting a heavily smoothed and normalized data set collected on a glass substrate. Data collected with a copper standard was used to obtain an instrumental Gaussian peak shape, this was then kept fixed when fitting the NbS_2 data. EDXA was obtained with a JEOL 35CF, and SEM was obtained with a Hitachi S570 instrument using the KEVEX system. X-ray photoelectron spectra were recorded with a VG ESCALAB 220i XL instrument using focused (300 μm spot) monochromatic Al-K_α radiation at a pass energy of 20 eV. Scans were acquired with steps of 50 meV. A flood gun was used to control charging, and the binding energies were referenced to an adventitious C 1s peak at 284.8 eV. Depth profile measurements were obtained by using argon beam sputtering. UV/Vis spectra were recorded in the range 190−1100 nm with a Helios double beam instrument. Reflectance and transmission spectra were recorded between 300 and 1200 nm by a Zeiss miniature spectrometer. Reflectance measurements were standardized relative to a rhodium mir-

 © 2004 Wiley-VCH Verlag GmbH & Co. KGaA, Weinheim

ror and transmission relative to air. Raman spectra were acquired with a Renishaw Raman System 1000 using a helium-neon laser of wavelength 632.8 nm. The Raman system was calibrated against the emission lines of neon. Contact angle measurements of selected glass samples were determined by measuring the spread of a 7.5 μL droplet of water. Electrical conductivity was determined with a four-probe measurement.

Caution! It should be noted the APCVD reaction of $NbCl_5$ and $S(SiMe_3)_2$, tBu_2S_2, tBuSH or $HSCH_2CH_2SH$ could conceivably produce H_2S. Care should be taken to conduct all experiments in a fume cupboard and pass the exhaust gases through a series of bleach scrubbers.

Acknowledgments

E. S. P. thanks the EPSRC for a studentship. I. P. P. thanks the EPSRC for purchase of the Renishaw Raman microscope (GR/M82592). CCLRC is thanked for beamtime at the SRS at Daresbury (40056). A. L. H. is supported by a Royal Society University Research Fellowship.

[1] P. Lavela, J. Morales, L. Sanchez, J. L. Tirado, *J. Power Sources* **1997**, *68*, 704−707.
[2] Z. -M. Li, B. Bergersen, *J. Phys. C: Solid State Phys.* **1986**, *19*, 7281−7290.
[3] C. Liu, R. F. Frindt, *Phys. Rev. B* **1985**, *31*, 4086−4088.
[4] Z. -M. Li, B. Bergersen, P. Palffy-Muhovay, D. Beigie, *Can. J. Phys.* **1988**, *66*, 228−232.
[5] J. Afonso, M. Breysse, N. Allali, M. Danot, *Catal. Today* **1996**, *28*, 23−30.
[6] W. M. R. Divigalpitiya, R. F. Frindt, S. R. Morrison, *J. Phys. D: Appl. Phys.* **1990**, *23*, 966−970.
[7] F. Jellinek, G. Brauer, H. Müller, *Nature* **1960**, *185*, 376−377.
[8] A. Meerschaut, C. Deudon, *Mater. Res. Bull.* **2001**, *36*, 1721−1727.
[9] W. G. Fisher, M. J. Sienko, *Inorg. Chem.* **1980**, *19*, 39−43.
[10] K. Motizuki, Y. Nishio, M. Shirai, N. Suzuki, *J. Phys. Chem. Solids* **1996**, *57*, 1091−1096.
[11] W. M. R. Divigalpitiya, R. F. Frindt, S. R. Morrison, *J. Phys. D: Appl. Phys.* **1990**, *23*, 966−970.
[12] P. J. McKarns, M. J. Heeg, C. H. Winter, *Inorg. Chem.* **1998**, *37*, 4743−4747.
[13] C. J. Carmalt, C. W. Dinnage, I. P. Parkin, A. J. P. White, D. J. Williams, *Inorg. Chem.* **2002**, *41*, 3668−3672.
[14] A communication of part of this work relating to the preparation of NbS_2 thin-films has appearec, see: C. J. Carmalt, T. D. Manning, I. P. Parkin, E. S. Peters, A. L. Hector, *J. Mater. Chem.* **2004**, *14*, 290−291.
[15] A. Spijkerman, J. L. de Boer, A. Meetsma, G. A. Wiegers, S. van Smaalen, *Phys. Rev. B* **1997**, *56*, 13757−13767.
[16] R. B. von Dreele, A. C. Larson, *GSAS: general structure analysis system* Neutron Scattering Centre, MS-H805, Los Alamos National Laboratory, Los Alamos, NM (**2001**).
[17] GSAS technical manual.
[18] W. G. McMullan, J. C. Irwin, *Solid State Commun.* **1983**, *45*, 557−560.
[19] T. Hirata, F. S. Ohuchi, *Solid State Commun.* **2001**, *117*, 361−364.
[20] G. E. McGuire, G. K. Schweitzer, T. A. Carlson, *Inorg. Chem.* **1973**, *12*, 2450−2453.
[21] F. Kadijk, F. Jellinek, *J. Less-Common Met.* **1971**, *23*, 437−441.
[22] M. Shimakawa, K. Kawachi, S. Nishikawa, K. Hayashi, *J. Solid State Chem.* **1997**, *129*, 242−249.
[23] S. A. O′Neill, I. P. Parkin, A. Mills, N. Elliott, *J. Mater. Chem.* **2003**, *13*, 2952−2956.
[24] C. J. Carmalt, I. P. Parkin, E. S. Peters, *Polyhedron* **2003**, *22*, 1499−1505.

Received April 15, 2004
Early View Article
Published Online September 9, 2004

 © 2004 Wiley-VCH Verlag GmbH & Co. KGaA, Weinheim

The Immobilized Porphyrin-Mediator System Mn(TMePyP)/clay/HBT (clay-PMS): A Lignin Peroxidase Biomimetic Catalyst in the Oxidation of Lignin and Lignin Model Compounds

Claudia Crestini,*[a] Alessandra Pastorini,[a] and Pietro Tagliatesta[a]

Keywords: Clays / Lignin models / Oxidation / Porphyrins / Supported catalysts

A biomimetic system for lignin peroxidase (LiP) was designed by using a cationic porphyrin, [Mn(TMePyP)OAc_5], supported on the smectitic clay montmorillonite [Mn(TMePyP)/clay]. The natural role of the polypeptidic pocket of LiP was mimicked by the clay. The possibility to use low-molecular-weight redox mediators as active readily diffusible oxidizing species has been investigated. This assembly — a sort of "synthetic enzyme" — can be defined as an immobilized porphyrin-mediator system (clay-PMS). The clay-PMS was found to be a stable, recyclable, and efficient catalyst for the environmentally friendly H_2O_2-catalyzed oxidation of different lignins and representative lignin model compounds. The clay-PMS showed a higher reactivity than Mn(TMePyP)/clay alone due to an effective role of the redox mediator on the oxidation.

(© Wiley-VCH Verlag GmbH & Co. KGaA, 69451 Weinheim, Germany, 2004)

Introduction

Lignin peroxidase (ligninase, LiP) is an enzyme isolated from ligninolytic cultures of *Phanerochaete chrysosporium*[1] that performs a one-electron oxidation of the lignin aromatic moieties in the presence of hydrogen peroxide.[2] The catalytic cycle consists of a two-electron oxidation of Fe^{III} protoporphyrin IX (high spin) to give a highly reactive (oxo)iron(IV)−protoporphyrin IX π-cation radical, the LiP compound I.[3] LiP compound I is then reduced to the initial state by two different one-electron reductions by the substrate (Figure 1).[4]

In nature, the ligninolitic activity of LiP is enhanced by the presence of veratryl alcohol (VA), which acts as a diffusible redox mediator in lignin oxidation.[5] Thus, the oxidative potential can be transferred from the enzyme to the bulk of the polymer avoiding a kinetic barrier for the heterogeneous reaction.

Unfortunately, the use of LiP for delignification processes is not economically convenient with respect to inorganic catalysts, mainly due to the costs of enzyme purification. Moreover, LiP is inactivated when exposed to an excess of hydrogen peroxide (more than 20 equiv.), to give the inactive form LiP III (Figure 1).[6] Novel LiP biomimetic catalysts resistant to peroxide inactivation might be of pivotal importance for the design of environmentally friendly and economically feasible lignin degradation processes.

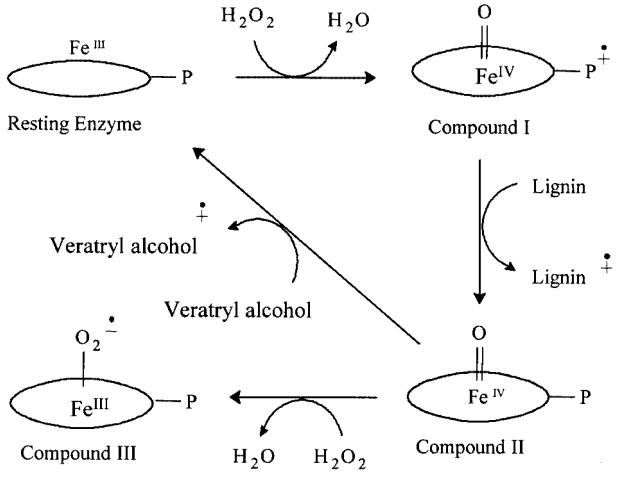

Figure 1. Catalytic cycle of lignin peroxidase

Metalloporphyrins are well-known biomimetic model compounds for protoporphyrin IX and have been extensively studied in the oxidative degradation of monomeric, dimeric, and oligomeric lignin model compounds.[7] The design of heterogeneous porphyrin systems that might be used in several cycles of transformations is a crucial point for their industrial application. In this context, a heterogenation technique based on the anchorage of the active catalyst onto appropriate inert and low-cost supports appears to be highly promising.[8] Smectite clay minerals, such as montmorillonite, have been used as support for the cationic manganese *meso*-tetrakis(tetramethylpyridinio)porphyrin pentaacetate [Mn(TMePyP)$(OAc)_5$] by use of ion-exchange methods.[9] This heterogeneous catalyst [named Mn(TMe-

[a] Dipartimento di Scienze e Tecnologie Chimiche Università di Tor Vergata,
Via della Ricerca Scientifica, 00133 Rome, Italy
Fax: (internat.) + 39-06-7259-4754
E-mail: crestini@uniroma2.it

PyP)/clay] is highly efficient in the oxidation of monomeric and dimeric lignin model compounds. Nevertheless, it is not suitable for lignin oxidation mainly due the presence of a kinetic barrier to the approach of the polymeric substrate.[10] With the aim of solving this problem, we report here our results on the oxidation of lignins and lignin model compounds with the Mn(TMePyP)/clay system in the presence of veratryl alcohol (VA) and 1-hydroxybenzotriazole (HBT) as low-molecular-weight redox mediators. This novel biomimetic system of LiP — a clay/porphyrin mediator system (clay-PMS) — was able to efficiently degrade lignin model compounds resembling the fundamental bonding pattern in lignin. The degradation of milled wood and technical softwood lignins, carefully studied by ^{31}P NMR spectroscopy after phosphitylation of the oxidized samples, was also effective.[11]

Results and Discussion

Oxidation of Lignin Model Compounds

The reactivity of some aromatic model compounds resembling the most representative lignin bonding patterns is of pivotal interest in order to rationalize the oxidative behavior of the polymer. Thus, an array of monomeric and dimeric, phenolic and nonphenolic lignin model compounds was selected in order to clarify the reactivity of clay-PMS with lignin subunits.

4-(1-Hydroxyethyl)-2-methoxyphenol (apocinol; **1**), the β-*O*-4-phenolic model 1-(4-hydroxy-3-methoxyphenyl)-2-(2-methoxyphenoxy)propane-1,3-diol (**7**), the non-phenolic models 1-(3,4-dimethoxyphenyl)ethanol (**14**), and 1-(4-ethoxy-3-methoxyphenyl)-2-(2-methoxyphenoxy)propane-1,3-diol (**16**) were oxidized as representative lignin model compounds. The reactions were carried out by treating the appropriate substrate (50 μmol) in the presence of a catalytic amount (2% mol/mol) of clay-PMS (0.27 mmol of active catalyst/g of support) using H_2O_2 (10% aqueous solution) as primary oxidant and HBT as redox mediator. HBT is known to generate long-lived radical intermediates with an electrostatic potential (1.04 V vs. NHE) high enough for the oxidation of either phenolic or non-phenolic lignin model compounds.[12] Oxidations with homogeneous $Mn(TMePyP)(OAc)_5$ in the presence or absence of HBT and with Mn(TMePyP)/clay were also performed as references. Irrespective of the experimental conditions used for the oxidation a low mass balance with respect to isolated products was observed. In accord with results previously reported in the literature, the loss of material from the reaction mixture might be due to formation of highly polar hydrophilic overoxidation products not recovered by usual workup procedures.[7] HBT, present as an oxidation mediator, was quantitatively recovered at the end of the reaction in all the experiments performed, as shown by GC quantitative measurements.

The reactivity of the catalysts toward lignin model compound degradation was studied by measuring the conversion of substrate after 30 min and 4 h for the oxidation of phenolic model compounds, and after 4 h for the oxidation of the more stable nonphenolic lignin model compounds (vide infra). All reaction products were characterized by means of GC-MS analysis after silylation with *N*,*O*-bis(trimethylsilyl)trifluoroacetamide (BSTFA) and by ^1H and ^{13}C NMR spectroscopy. Control experiments in the absence of the catalysts were performed as previously reported in a study dealing with the activity of montmorillonite-immobilised porphyrins.[10] In this specific case, in order to clarify the role of the oxidation mediator, it is significant to consider the reactions performed in the absence of HBT (and in the presence of catalyst) as reference blank experiments.

Acetophenone **2** was the only recovered product after 30 min reaction time with all the catalysts used for the oxidation of **1**, with a substrate conversion that ranged from 24.5 to 44.3% (Scheme 1, Table 1). It is noteworthy that the clay-PMS system was found to be more reactive than Mn(TMePyP)/clay alone, showing the important role of HBT in the oxidation. This effect was not revealed when the reaction was performed under homogeneous conditions. In fact, the reactivity of $[Mn(TMePyP)OAc_5]$ under identical experimental conditions decreased in the presence of the redox mediator (Table 1). A similar behavior was observed after 4 h reaction time. In this latter case, products of side-chain fragmentation to aldehyde (compounds **3** and **6**), demethylation (**6**) and formation of a benzoquinone de-

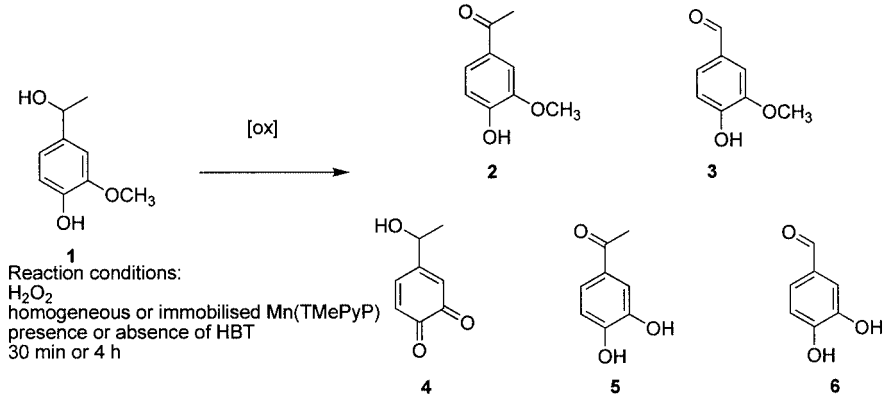

Scheme 1

 © 2004 Wiley-VCH Verlag GmbH & Co. KGaA, Weinheim

Table 1. Substrate conversion in the [Mn(TMePyP)OAc_5] and Mn(TMePyP)/clay, Mn(TMePyP)OAc_5/HBT and clay-PMS catalysed H_2O_2 oxidation of phenolic lignin models **1** and **7**

Catalyst	Monomeric model **1**		β-*O*-4 model **7**	
	Reaction time	Conv. (%)	Reaction time	Conv. (%)
[Mn(TMeTPyP)OAc_5]	30 min	35.4	30 min	44.7
[Mn(TMeTPyP)OAc_5]	4 h	59.0	4 h	59.6
Mn(TMeTPyP)-clay	30 min	39.5	30 min	41.1
Mn(TMeTPyP)-clay	4 h	51.5	4 h	59.2
[Mn(TMePyP)OAc_5]/HBT	30 min	24.5	30 min	34.4
[Mn(TMePyP)OAc_5]/HBT	4 h	53.7	4 h	72.1
Clay-PMS[a]	30 min	44.3	30 min	57.1
Clay-PMS[a]	4 h	56.4	4 h	73.9

[a] Mn(TMePyP) immobilized on clay + HBT.

rivative (compound **4**; Scheme 1) were characterized in the reaction mixture. In a test for checking the leaching of catalyst, the oxidation of **1** with clay-PMS was stopped at about 50% conversion. After centrifugation, the colourless solution had lost its catalytic activity. Table 2 shows that the clay-PMS system is stable enough to perform at least five recycling experiments with similar conversion and selectivity.

Table 2. Apocinol (**1**) conversion after recycling of the clay-PMS system[a]

Cycle[a]	**1** (% conv.)
1	59.0
2	58.2
3	58.8
4	57.3
5	54.0

[a]Reaction conditions: substrate 50 μmol, active catalyst 1 μmol, hydrogen peroxide 10% in 0.5 mL of dioxane/buffer citrate phosphate pH = 6 (100 mM) (1:4, v/v), 60 °C, reaction time 4 h.

The oxidation of compound **7**, an aromatic phenolic β-*O*-4 model that represents the most diffuse bonding network in lignin, showed a reactivity pattern close to that observed for apocinol (**1**). The clay-PMS system was again the most active catalyst at both 30 min and 4 h reaction time (Table 1). On the other hand, HBT decreased the reactivity of the homogeneous catalyst [Mn(TMePyP)OAc_5]. Compounds of side-chain oxidation (**8**, **10**), demethylation (**9**), benzoquinone formation (**11** and **13**), and side-chain fragmentation (**12**; Scheme 2) were obtained. On the basis of these data some further considerations are needed. The novel porphyrin-mediator system, clay-PMS, was the most active catalyst in the oxidative degradation of phenolic monomeric and dimeric lignin model compounds. The reaction proceeds mainly by side-chain oxidation and/or fragmentation, demethylation of alkyl aryl ether moieties, and aromatic ring oxidation to *ortho*- and *para*-benzoquinones. The minor reactivity observed for Mn(TMePyP)/clay in the absence of a redox mediator is probably due to the presence of a kinetic barrier for the approach of the substrate to the catalyst when it is embedded and surrounded by the polymeric environment. Thus, the presence of HBT in the

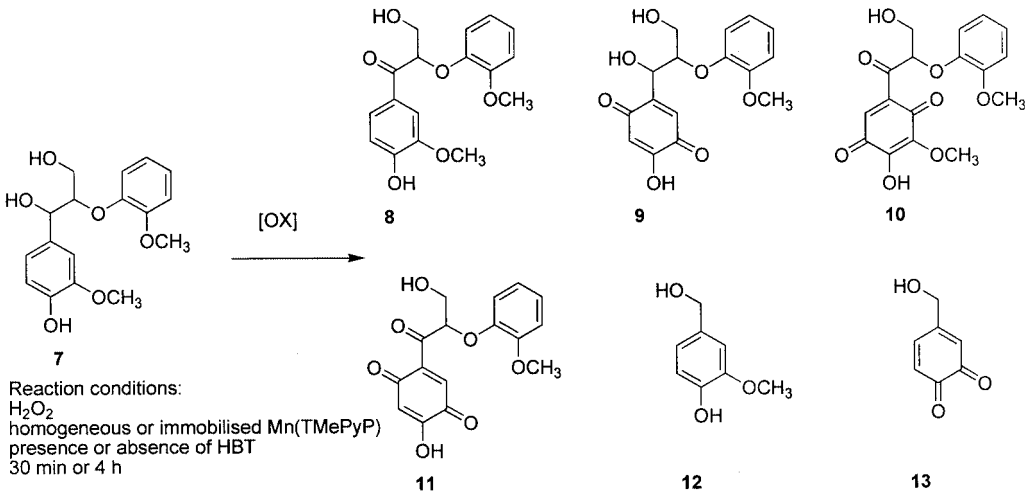

Scheme 2

 © 2004 Wiley-VCH Verlag GmbH & Co. KGaA, Weinheim

reaction mixture increases the reactivity of the metalloporphyrin towards the phenolic lignin model compounds by acting as a diffusible oxidation carrier. This effect might be switchable depending on the homogeneous or heterogeneous character of the catalyst. In fact, the presence of HBT decreased the reactivity of [Mn(TMePyP)OAc_5] under homogeneous conditions. Although we have not studied the mechanism of the reaction in detail, it is reasonable to suggest that under homogeneous conditions HBT might compete with the substrate in the H_2O_2-catalysed oxidation.

Oxidation of Non-Phenolic Lignin Model Compounds

Next we turned our attention to the oxidation of non-phenolic lignin model compounds. They represent the inner lignin chain bonding network rather than the terminal units of the polymer. The redox potential of non-phenolic lignin model compounds is higher than that of the corresponding phenolic ones, therefore their oxidation is more difficult, and they are usually resistant to biological treatments.

First we considered the monomeric model, 1-(3,4-dimethoxyphenyl)ethanol (**14**; Scheme 3). Treatment of compound **14** under previously reported experimental conditions gave, after 4 h of reaction time, the corresponding acetophenone derivative **15** as the only recovered product with a substrate conversion that ranged from 24.9 to 50.5% (Table 3). Again, the porphyrin-mediator system clay-PMS was found to be more reactive than heterogeneous Mn(TMePyP)/clay and homogeneous [Mn(TMePyP)OAc_5] systems (Table 3). In this case, HBT also increased the reactivity of the catalysts under homogeneous conditions, and [Mn(TMePyP)OAc_5] showed a higher conversion of substrate in the presence of the redox mediator than in its absence (Table 3).

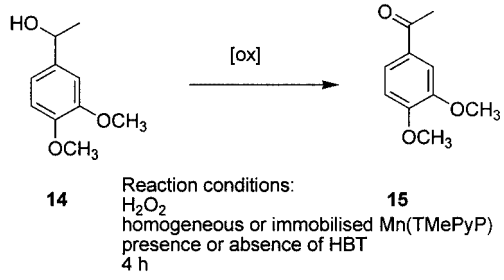

Scheme 3

Table 3. Substrate conversion in the [Mn(TMePyP)OAc_5], Mn(TMePyP)/clay, Mn(TMePyP) immobilized on clay + HBT, and clay-PMS catalysed H_2O_2 oxidation of nonphenolic lignin models **14** and **16**

Treatment	Substrate **14** (conv. %)	Substrate **16** (conv. %)
[Mn(TMePyP)OAc_5]	24.9	81.0
Mn(TMePyP)-clay	47.8	80.4
[Mn(TMePyP)OAc_5]/HBT	33.1	85.2
Clay-PMS[a]	50.5	86.3

[a] Mn(TMePyP) immobilized on clay + HBT.

A similar trend was observed upon oxidation of the dimeric lignin model compound 1-(4-ethoxy-3-methoxyphenyl)-2-(2-methoxyphenoxy)propane-1,3-diol (**16**; Scheme 4). In this case, both Mn(TMePyP)/clay and [Mn(TMePyP)OAc_5] were more reactive in the presence of HBT than alone (Table 3), with clay-PMS being the best catalyst. As reported in Table 3 the conversion of substrate ranged from 80.4% [Mn(TMePyP)/clay] to 86.3% (clay-PMS). A complex mixture of reaction products was recovered after GC-MS analysis and chromatographic purification. Among them, products of side-chain oxidation (ketone derivative **17**), side-chain fragmentation (compounds **18**, **19** and **22**), and side-chain fragmentation/demethylation (compounds **20** and **21**) were unambiguously identified by GC-MS analysis; their low yields showed the high efficiency of the oxidative degradation. All of these transformations are potentially useful for delignifying processes. It is noteworthy that even though HBT is always efficient in the reactions catalysed by the porphyrin mediator system clay-PMS, it shows a different effect in the oxidation of non-phenolic lignin model compounds with respect to phenolic ones when the reactions are performed in the presence of homogeneous catalyst. In fact, the reactivity of [Mn(TMePyP)$(OAc)_5$] was increased by HBT only in the case of non-phenolic compounds.

Both [Mn(TMePyP)OAc_5] and Mn(TMePyP)-clay are able to oxidize HBT to benzotriazol *N*-oxide radical (HBT$^{\cdot}$). In turn, HBT$^{\cdot}$ can oxidize the model compound presumably by a side-chain hydrogen atom abstraction (HAT) process.[13]

The reaction of metalloporphyrins with lignin model compounds is thought to occur by electron transfer.[14] One might hypothesize that, in the presence of [Mn(TMePyP)(OAc_5)] the direct reaction of porphyrin with phenolic model compounds could be faster than the hydrogen atom abstraction process by HBT$^{\cdot}$. When non-phenolic substrates are used, the oxidation of HBT to HBT$^{\cdot}$ and further side-chain oxidation of the model by HAT could be faster than the direct oxidation both in homogeneous and heterogeneous phase.

Oxidation of Lignins

Lignin is a complex tridimensional phenylpropanoic polymer whose units are connected by an array of interunit bondings that makes its chemical characterization extremely difficult. An efficient method to study the modifications induced by the chemical treatment of lignin polymers is ^{31}P NMR spectroscopy; ^{31}P-based magnetic resonance analysis of lignin is capable of detecting and quantitatively determining all functional groups in lignin that possess reactive hydroxy groups — aliphatic OH groups, the various forms of phenolic OH groups, and carboxylic acid groups. More specifically, it allows the unambiguous quantification of the amount of condensed phenolic structures of lignin. Oxidative processes with lignin depolymerization and/or oxidative coupling typically induce a decrease in the number of aliphatic OH groups and noncondensed phenolic subunits and an increase in the number of carboxylic acid

 © 2004 Wiley-VCH Verlag GmbH & Co. KGaA, Weinheim

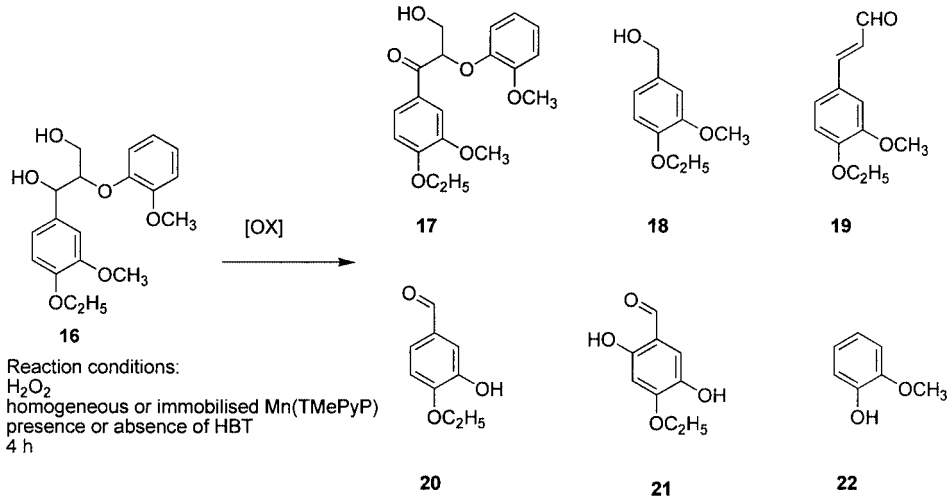

Scheme 4

groups.[15] The number of condensed phenolic OH groups is usually greater after oxidative coupling treatment. Furthermore, condensed lignin subunits are resistant to most of the oxidation treatments. Thus, an increase in these groups indicates the occurrence of oxidative coupling together with side-chain oxidation, while their decrease is identificative of efficient delignification processes.

In order to verify the activity of the clay-PMS on bulky polymeric substrates we selected Black Spruce (BS) milled wood (MWL) and residual kraft lignins (RKL). The oxidations were carried out with an excess of hydrogen peroxide (10% aqueous solution) in buffer citrate phosphate (pH = 6) in the presence of a catalytic amount of the appropriate porphyrin catalyst and, where necessary, HBT. In this case, with the aim of mimicking LiP, VA was also evaluated as a redox mediator for the reaction. Lignin samples recovered from the reaction mixture after usual workup procedures were phosphitylated and then subjected to quantitative ^{31}P NMR analysis in the presence of a suitable amount of cholesterol as an internal standard. The assignment of the different signals was carried out on the basis of earlier work.[11] Table 4 shows the quantitative distribution of the OH groups as revealed by ^{31}P NMR spectroscopy. In agreement with data previously recovered on the side-chain oxidation of phenolic and non-phenolic lignin model compounds, the treatment of MWL with the porphyrin-mediator systems clay-PMS-HBT and clay-PMS-VA yielded an appreciable decrease in the number of aliphatic OH groups (Table 4). The reference systems [Mn(TMePyP)OAc_5] and Mn(TMePyP)/clay were not efficient catalysts under these experimental conditions. Moreover, the reaction performed with HBT was more efficient than that with VA, probably because of the higher stability of the first redox mediator intermediate (Table 4).

BS MWL contains a small amount of condensed OH groups. Irrespective of the experimental conditions used in the oxidation, this did not vary significantly during the treatment of MWL. Thus, oxidative coupling reactions are not operative side-processes. In agreement with the data reported above for the oxidation of lignin model compounds, the number of guaiacyl OH groups decreased after oxidation showing a depolymerization process. It is noteworthy that the number of carboxylic acid groups, which arise from lignin oxidation of both side-chains and aromatic rings, increased after treatment of MWL with clay-PMS-HBT more than with clay-PMS-VA. This different behavior could be due to the longer lifetime of HBT radical with respect to veratryl alcohol radical cation.

Table 4. Distribution of aliphatic, phenolic and carboxylic hydroxy groups in MWL and RKL (mmol/g of lignin) after metalloporphyrin- and PMS-catalyzed oxidations as obtained by quantitative ^{31}P NMR spectroscopy

Sample/catalyst	Aliphatic OH	Condensed OH [mmol/g]	Guaiacyl OH	COOH
Black spruce MWL	4.59	0.05	0.75	0.15
MWL/[Mn(TMePyP)OAc_5]	4.57	0.05	0.63	0.16
MWL/Mn(TMePyP)-Clay	4.55	0.05	0.65	0.12
MWL/clay-PMS-HBT[a]	3.93	0.04	0.68	0.17
MWL/clay-PMS-VA[b]	4.14	0.04	0.73	0.19
Black spruce RKL	1.94	0.92	1.27	0.27
RKL/[Mn(TMePyP)OAc_5]	1.64	0.91	1.09	0.65
RKL/Mn(TMePyP)-Clay	1.39	0.80	0.78	0.27
RKL/clay-PMS-HBT[a]	1.19	0.63	0.52	0.17

[a] Mn(TMePyP) immobilized on clay + HBT. [b] Mn(TMePyP) immobilized on clay + veratryl alcohol.

 © 2004 Wiley-VCH Verlag GmbH & Co. KGaA, Weinheim

Residual kraft lignin (RKL) is the lignin fraction that can be isolated by acidolysis of kraft pulps. This lignin is severely altered with respect to native and milled wood lignins and contains higher amounts of condensed subunits.[16] In order to clarify the ability of the PMS to oxidize these units, we performed experiments of oxidation of a sample of black spruce RKL with [Mn(TMePyP)(OAc_5)], Mn(TMePyP)-clay and the HBT-clay-PMS (Table 4). While [Mn(TMePyP)(OAc_5)] was not able to degrade condensed OH groups and Mn(TMePyP)-clay induced a modest decrease, HBT-clay-PMS reduced their amount by 32%. The guaiacyl units were reduced to 79% and the aliphatic OH groups were reduced to 61% of their initial content (Table 4). These data are a clear indication of the extensive degradation induced by the clay-PMS on a resistant polymer such as RKL.

Conclusion

An advanced biomimetic system for lignin peroxidase has been designed and realized. When using such systems, the application of the "mediator" concept avoids kinetic problems due to the solid nature of the substrate and of the heterogeneous catalyst, and opens the way to advanced biomimetic ligninase mediator systems (porphyrin mediator systems). Phenolic and non-phenolic, monomeric and β-*O*-4-lignin model compounds were efficiently oxidized with the occurrence of side-chain and aromatic ring oxidation reactions. Oxidation of BS MWL and RKL revealed the occurrence of efficient delignification processes and absence of significant coupling reactions. The porphyrin mediator systems represent the last step in the development of a "synthetic enzyme" for the pulp and paper transformations.

Experimental Section

General: ^1H, ^{13}C and ^{31}P NMR spectra were recorded with a Bruker AM 400 spectrometer. Mass spectrometry (MS) was performed with a GC Shimadzu GC-17A and a mass-selective detector QP 6000. All solvents were ACS reagent grade and were redistilled and dried according to standard procedures. Chromatographic purifications were performed on columns packed with Merck silica gel 60, 230−400 mesh for flash technique. Thin-layer chromatography was carried out using Merck platten Kieselgel 60 F254. Lignin model compounds **1**, **7**, **14** and **16** were synthesized according to literature procedures.[17]

Catalyst Preparation: The manganese porphyrin [Mn(TMePyP)(OAc_5)] was synthesized according to a literature procedure.[18] [Mn(TMePyP)(OAc_5)} was immobilized on montmorillonite as previously reported by refluxing in the presence of Na^+-saturated montmorillonite.[9] The determination of the content of metalloporphyrin supported on the clay was performed spectrophotometrically, as reported previously.[9]

Lignin Isolation: Milled lignin was prepared from ultraground extractive free powder according to Bjorkman's procedure. Extractive free powders were ultraground for three weeks in a rotatory ball mill. The ML fraction was then extracted with dioxane/water (96:4, v/v). The residue was concentrated under reduced pressure and freeze-dried. Purification was performed by dissolving the lignin in 90% acetic acid. The solution was then added dropwise to stirred water. The precipitated lignin was centrifuged and freeze-dried. It was then dissolved again in a mixture of 1,2-dichloroethane/ethanol (2:1, v/v) and precipitated by addition of diethyl ether.[19] Residual kraft lignin was isolated from kraft pulp using a slightly modified acidolysis procedure. The yield was 38%, and the purity was confirmed by UV and klason lignin content measurements.[16,20]

General Procedure for the Oxidation of Lignin Model Compounds: Hydrogen peroxide (10%) was added with stirring at 60 °C as 20-μL aliquots every hour to a solution of the porphyrin catalyst (1 μmol) in 0.5 mL of dioxane/buffer citrate phosphate pH = 6 (100 mM) (1:4, v/v) containing 50 μmol of substrate and 5 μmol of HBT. As an example, the amount of active catalyst corresponds to 12% (w/w) in the case of the monomeric model compound **1** and to 6% (w/w) for the dimeric model **7**. After 4 h, the reaction mixtures were extracted with CH_2Cl_2 in the presence of saturated aqueous NaCl solution. The organic layer was dried with $MgSO_4$ and concentrated under reduced pressure. The residues were dissolved in 20 μL of pyridine in the presence of 3,4-dimethoxytoluene as an internal standard for GC-MS analysis. The mixture was than silylated by addition of *N*,*O*-bis(trimethylsilyl)trifluoroacetamide (BSTFA).

Oxidation of Lignin. General Procedure: Oxidation of black spruce and cypress MWL, and black spruce residual kraft lignin were carried out in buffer citrate phosphate pH = 6 (100 mM) (10 mL) at 90 °C in the presence of 100 mg of lignin, 10 mg of active catalyst, 50 μmol of HBT or veratryl alcohol, and 200 μL of 10% H_2O_2. Aliquots of H_2O_2 (200 μL) were added every hour for 6 h. The reaction mixture was washed with water several times, centrifuged and freeze-dried. The samples obtained were submitted to quantitative ^{31}P NMR analysis (see below).

Characterization of Products: Gas chromatography and gas chromatography/mass spectrometry of the reaction products were performed using a DB1 column (30 m × 0.25 mm and 0.25 mm film thickness), and an isothermal temperature profile of 100 °C for the first 2 min, followed by a 20 °C/min temperature gradient to 300 °C and finally an isothermal period at 300 °C for 10 min. The injector temperature was 280 °C. Chromatography-grade helium was used as the carrier gas. The identification of **2**, **3**, **5**, **6**, **8**, **12**, **15**, **17**, **18**, **19**, **20** and **22** was carried out by comparison with samples of authentic products. Compounds **5**, **13** and **21** were assigned by comparison with the fragmentation spectra of original compounds. Products **9**, **10** and **11** were tentatively identified on the basis of the fragmentation spectra. The fragmentation patterns are shown in Table 5. Quantitative ^{31}P NMR spectra were obtained using methods identical to those described by Argyropoulos et al.[11] The chemical shifts were referenced to phosphoric acid. Derivatization of the lignin samples with 2-chloro-4,4,5,5-tetramethyl-1,3,2-dioxaphospholane were performed as described previously.[11] The ^{31}P NMR spectroscopic data reported in this effort are averages of three phosphitylation experiments followed by quantitative ^{31}P NMR acquisitions. The maximum standard deviation of the reported data was 2×10^{-2} mmol/g, while the maximum standard error was 1×10^{-2} mmol/g.

Acknowledgments

The Italian National Council of Research (CNR) is acknowledged for financial support.

 © 2004 Wiley-VCH Verlag GmbH & Co. KGaA, Weinheim

Table 5. Mass spectrometric data

Product	Derivative[a]	*m/z* (%)
2	$Si(CH_3)_3$	238 (41) [M^+], 223 (35), 209 (9), 193 (23), 91 (10), 73 (100)
3	$Si(CH_3)_3$	224 (45) [M^+], 209 (15), 193 (22), 177 (5), 137 (8), 73 (100)
4	$Si(CH_3)_3$	224 (18) [M^+], 209 (10), 193 (15), 179 (31), 151 (9), 73 (100)
5	$Si(CH_3)_3$	296 (8) [M^+], 224 (30), 209 (10), 193 (23), 151(84), 73 (100)
6	$Si(CH_3)_3$	282 (8) [M^+], 223 (40), 207 (6), 192 (35), 177 (6), 73 (100)
8	$Si(CH_3)_3$	224 (15), 209 (10), 194 (5), 166 (12), 150 (76), 73 (100)
9	$Si(CH_3)_3$	297 (12), 223 (5), 181 (5), 166 (6), 109 (8), 73 (100)
10	$Si(CH_3)_3$	252 (9), 209 (5), 166 (8), 124 (7), 103 (12), 73 (100)
11	$Si(CH_3)_3$	224 (9), 209 (6), 194 (8), 166 (10), 150 (45), 73 (100)
12	$Si(CH_3)_3$	298 (13) [M^+], 283 (6), 268 (9), 209 (9), 179 (6), 73 (100)
13	$Si(CH_3)_3$	210 (12) [M^+], 179 (18), 136 (20), 147 (10), 105 (8), 73 (100)
14	–	182 (42) [M^+], 167 (64), 139 (100), 124 (30), 108 (21), 77 (45)
15	–	180 (45) [M^+], 165 (100), 137 (17), 122 (10), 107 (8), 77 (26)
16	–	330 (16) [$M^+ - 18$], 206 (17), 179 (26), 151 (33), 109 (47), 77 (100)
17	–	328 (17) [$M^+ - 18$], 207 (35), 179 (100), 151 (63), 137 (7), 123 (21)
18	–	180 (50) [M^+], 154 (38), 137 (40), 122 (48), 109 (21), 65 (100)
19	–	206 (33) [M^+], 179 (8), 151 (100), 123 (18), 77 (24), 55 (90)
20	–	180 (37) [M^+], 151 (100), 109 (17), 95 (10), 81 (20), 65 (25)
21	–	196 (22) [M^+], 181 (37), 153 (30), 135 (33), 125 (51), 93 (100)
22	–	124 (65) [M^+], 109 (100), 81 (89), 65 (15), 77 (21), 53 (55)

[a] – = underivatized; $Si(CH_3)_3$ = trimethylsilylated with *N*,*O*-bis(trimethylsilyl)trifluoroacetamide.

[1] M. Tien, T. K. Kirk, *Science* **1983**, *221*, 661. J. K. Glenn, M. A. Morgan, M. B. Mayfield, M. Kuwahara, M. H. Gold, *Biochem. Biophys. Res. Commun.* **1983**, *114*, 1077.

[2] T. K. Kirk, R. L. Farrell, *Ann. Rev. Microbiol.* **1987**, *41*, 465–505.

[3] B. Chance, *Arch. Biochem. Biophys.* **1952**, *41*, 416–424. Khindaria, S. D. Aust, *Biochemistry* **1996**, *35*, 13107–13111.

[4] P. J. Harvey, H. E. Shoemaker, J. M. Palmer, *FEBS Lett.* **1986**, *195*, 242–246. H. Wariishi, M. H. Gold, *FEBS Lett.* **1989**, *243*, 165–168. H. Wariishi, M. H. Gold, *J. Biol. Chem.* **1990**, *265*, 2070–2077.

[5] R. S. Koduri, M. Tien, *Biochemistry* **1994**, *33*, 4225–4230; and references cited therein.

[6] M. S. A. Leisola, D. C. Ulmer, R. Waldner, A. Fiechter, *J. Biotechnol.* **1984**, *1*, 331–339. D. C. Ulmer, M. S. A. Leisola, A. Fiechter, *J. Biotechnol.* **1984**, *1*, 13–24.

[7] C. Crestini, P. Tagliatesta, in *The Porphyrin Handbook II* (Eds.: K. M. Kadish, K. M. Smith, R. Guilard), Academic Press, New York, **2003**, vol. 11, chapter 66, pp. 161–203. C. Crestini, P. Tagliatesta, R. Saladino, in *Oxidative Delignification Chemistry – Fundamentals and Catalysis* (Ed.: D. S. Argyropoulos), ACS Symposium Series 785, Washington DC, **2001**, pp. 212–225. B. Meunier, in *Metalloporphyrin-Catalyzed Oxidations* (Ed.: F. Montanari, L. Casella), Kluwer Academic Publishers, Dordrecht, **1994**, p. 11–19.

[8] T. Habe, M. Shimada, T. Okamoto, B. Panijpan, T. Higuchi, *J. Chem. Soc., Chem. Commun.* **1985**, 1323. G. Labat, B. J. Meunier, *J. Org. Chem.* **1989**, *54*, 5008–5011.

[9] T. J. Pinnavia, *Science* **1983**, *220*, 3659. L. Barloy, P. Battioni, D. J. Mansuy, *J. Chem. Soc., Chem. Commun.* **1990**, 1365.

[10] C. Crestini, A. Pastorini, P. Tagliatesta, *J. Mol. Catal. A.: Chem.* **2004**, *208*, 195. C. Crestini, P. Tagliatesta, *Sixth European Workshop on Lignocellulosics and Pulps*, Bordeaux, France, **2000**.

[11] A. Granata, D. S. Argyropoulos, *J. Agric. Food Chem.* **1995**, *33*, 375. Z. H. Jiang, D. S. Argyropoulos, A. Granata, *Magn. Res. Chem.* **1995**, *43*, 1538.

[12] H. Potthast, K. Koch, K. Fisher, *Proc. ISWPC* **1997**, F2-1/4.

[13] M. Fabbrini, C. Galli, P. Gentili, *J. Mol. Catal. B: Enzyme* **2002**, *16*, 231–24; F. D'Acunzo, M. Fabbrini, C. Galli, P. Gentili, *Seventh European Workshop on Lignocellulosics and Pulps*, Turku, Finland, **2002**

[14] I. Artaud, K. Ben-Aziza, D. Mansuy, *J. Org. Chem.* **1993**, *58*, 3373.

[15] C. Crestini, R. Saladino, P. Tagliatesta, T. Boschi, *Bioorg. Med. Chem.* **1999**, *7*, 1897–1905. C. Crestini, L. Jurasek, D. S. Argyropoulos, *Chem. Eur. J.* **2004**, *9*, 5371.

[16] Z. Jiang, D. S. Argyropoulos, *J. Pulp Paper Sci.* **1994**, *20*, 183.

[17] C. Crestini, M. D'Auria, *Tetrahedron* **1997**, *53*, 7877.

[18] G. Bernadou, G. Pratviel, F. Bennis, M. Girardet, B. Meunier, *Biochemistry* **1989**, *28*, 7268.

[19] R. Obst, K. T. Kirk, "Isolation of Lignin", in *Methods in Enzymology* (Eds.: W. A. Wood, S. T. Kellogg), Academic Press, Inc., New York, **1988**, vol. 161, p. 6–8.

[20] J. M. Pepper, P. E. T. Baylis, E. Adler, *Can. J. Chem.* **1959**, *37*, 1241.

Received April 30, 2004
Early View Article
Published Online September 23, 2004

 © 2004 Wiley-VCH Verlag GmbH & Co. KGaA, Weinheim

Dinuclear, Tricyclometallated Platinum(II) Derivatives − Substitution Reactions and Reactivity of the Platinum−Carbon Bonds

Antonio Zucca,*[a] Maria Agostina Cinellu,[a] Giovanni Minghetti,[a] Sergio Stoccoro,[a] and Mario Manassero*[b]

Keywords: Cyclometallated compounds / N ligands / Platinum / X-ray diffraction

In the recently reported dinuclear cyclometallated species $[Pt_2(R)(L)(DMSO)_2]$ [H_3L = 6-phenyl-2,2′-bipyridine; R = Me (**1a**), Ph (**1b**)] the threefold deprotonated ligand L links the two platinum atoms acting as an N′,C(3) and a C,N,C donor. Aspects of their reactivity have been studied first with regards to the substitution of the two DMSO ligands, which are coordinated to the platinum atom *trans* to a nitrogen and a carbon atom, respectively. Substitution of DMSO with neutral two-electron donors affords several new species, all having the same bridging ligand L: $[Pt_2(R)(L)(L')_2]$ [L′ = PPh_3 (**2a**, **2b**), CO (**3a**, **3b**)] and $[Pt_2(R)(L)(L')(DMSO)]$ [L′ = 3,5-Me_2-py (**4a**)]. The potentially bidentate diphosphane $Ph_2P(CH_2)_3PPh_2$ (dppp) gives a more complex species having both chelating and bridging dppp ligands [{Pt(Me)(L)(dppp)}$_2$(μ-dppp)] (**5a**). The reactivity of the platinum–carbon bonds with HCl has been studied in complexes **1a**, **1b** and **2a**, **2b** and found to be strongly dependent on the nature of the ancillary ligands. To discern the most labile of the four metal–carbon bonds, the reaction has been carried out with 1 equiv. of HCl under mild conditions. Although the reaction is not selective and minor species are formed, cleavage of the Pt–Me (**1a**) and Pt–Ph (**1b**) bonds is favoured — $[Pt_2(L)Cl(DMSO)_2]$ (**6**) can be isolated and spectroscopically characterised from the reaction with either **1a** or **1b**. Substitution of PPh_3 for DMSO in **6** gives $[Pt_2(L)Cl(PPh_3)_2]$ (**7**) as the thermodynamically stable isomer having a *trans* Cl–Pt–C arrangement. The structure of complex **7** has been solved by X-ray crystallography. In contrast, reaction of **2a** or **2b** with HCl proceeds by another route: even with excess HCl the Pt–Me and Pt–Ph bonds are unaffected whereas one of the Pt–C bonds of the pincer-like C,N,C system is cleaved to selectively give $[Pt_2(R)(HL)Cl(PPh_3)_2]$ [R = Me (**8a**), Ph (**8b**)]. The same bond is cleaved also in **1a** and **1b** by excess HCl to give $[Pt_2(HL)(Cl)_2(DMSO)_2]$ (**9**).

(© Wiley-VCH Verlag GmbH & Co. KGaA, 69451 Weinheim, Germany, 2004)

Introduction

Cyclometallated platinum(II) complexes containing substituted pyridines and 2,2′-bipyridines are well documented.[1] They comprise mono- and dimetallated species (**I**−**IV**) with various donor sequences.[2−5]

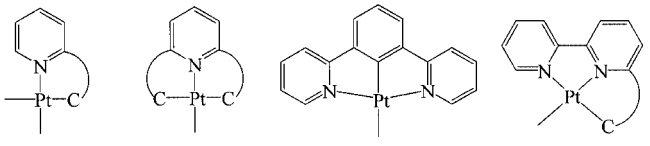

I **II** **III** **IV**

Both five- and six-membered rings are known, and both Pt−C(sp^2) and Pt−C(sp^3) bonds have been reported, the former being more common. The variety of possible coordination modes allows one to obtain species with different properties and an array of potential applications. In particular, it is worth noting that species of type **II**,[3] with a *trans* C−Pt−C arrangement, are still rare and often cannot be obtained by direct activation of a C−H bond.

Recently, a new type of cyclometallation, which entails activation of a C−H bond of a pyridine ring, has been described: reaction of 6-substituted 2,2′-bipyridines with *cis*-$[Pt(R)_2(DMSO)_2]$ (R = Me, Ph) gave a series of "rollover" cyclometallated species (**V**).[6]

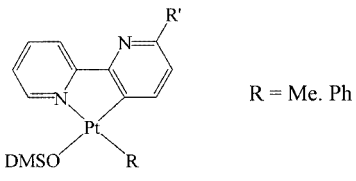

R = Me. Ph

V

[a] Dipartimento di Chimica, Università di Sassari,
Via Vienna 2, 07100 Sassari, Italy
E-mail: zucca@uniss.it
[b] Dipartimento di Chimica Strutturale e Stereochimica Inorganica, Università di Milano, Centro CNR,
Via Venezian 21, 20133 Milano, Italy
E-mail: m.manassero@istm.cnr.it

 © 2004 Wiley-VCH Verlag GmbH & Co. KGaA, Weinheim **DOI: 10.1002/ejic.200400371**

In the case of 6-phenyl-2,2′-bipyridine (6-Ph-2,2′-bipy), further reaction of complexes of type **V** with *cis*-$[Pt(R)_2(DMSO)_2]$ allowed us to isolate the dinuclear complexes **1a** (R = Me) and **1b** (R = Ph).[7]

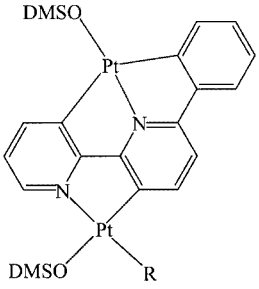

1a, R = Me
1b, R = Ph

Compounds **1a** and **1b** were fully characterised by means of NMR spectroscopy and FAB mass spectrometry, and, in the case of **1b**, by X-ray crystallography. They are rare examples of multiple C−H bond activation: indeed 6-Ph-2,2′-bipy displays an unprecedented behaviour, acting as a threefold deprotonated ligand. Compounds **1a** and **1b** are unique in several aspects, having (i) three five-membered rings assembled in the same molecule, (ii) a ten-electron bridging ligand, and (iii) a rare C,N,C sequence of donor atoms. Furthermore, in each of the two molecules a pincer-like system with a *trans* C−Pt−C arrangement coexists with an N′−C(3) cycle having two *cis* platinum−carbon bonds. Due to these interesting features, we deemed it worthwhile to synthesise analogous species by substitution of neutral ligands for DMSO and to study some aspects of the reactivity of the four different platinum−carbon bonds assembled in each of these unusual molecules.

Results and Discussion

Reaction with Neutral Ligands

We have recently reported that the reaction of *cis*-$[Pt(Me)_2(DMSO)_2]$ and *cis*-$[Pt(Ph)_2(DMSO)_2]$ with 6-Ph-2,2′-bipy gives compounds **1a** and **1b**, respectively, in fairly good yields (ca. 60−65%).[7]

The neutral ligands PPh_3 and CO easily displace both the DMSO molecules, whereas only one DMSO is substituted by a nitrogen donor such as 3,5-dimethylpyridine (3,5-Me_2-py; Scheme 1). With PPh_3 the reaction proceeds under mild conditions to give the disubstituted complexes $[Pt_2(R)(L)(PPh_3)_2]$ [R = Me (**2a**), Ph (**2b**)] in high yields (ca. 90%).

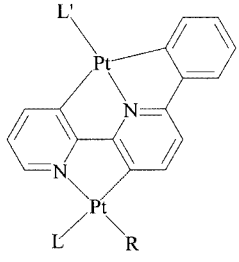

compd.	R	L	L'
1a	Me	DMSO	DMSO
1b	Ph	DMSO	DMSO
2a	Me	PPh_3	PPh_3
2b	Ph	PPh_3	PPh_3
3a	Me	CO	CO
3b	Ph	CO	CO
4a	Me	3,5-Me_2-py	DMSO

Scheme 1

$$[Pt_2(R)(L)(DMSO)_2] + 2\ PPh_3 \longrightarrow [Pt_2(R)(L)(PPh_3)_2] + 2\ DMSO$$

With 1 equiv. of PPh_3 a mixture of starting material and mono- and disubstituted products is obtained, indicating nonselective DMSO substitution.

Compounds **2a**,**b** were characterised by analytical and spectroscopic methods: in particular the $^{31}P\{^1H\}$ NMR spectra show two resonances [e.g. δ = 26.52 and 32.44 ppm (**2a**)] with very different ^{195}Pt-^{31}P coupling constants (3931 and 2412 Hz) in agreement with phosphorus atoms *trans* to donors with a low (N) and high (C) *trans* influence, respectively.[8] In the ^1H NMR spectrum of **2a** the Me group, which is slightly shielded with respect to **1a**, appears as a doublet due to coupling with a ^{31}P nucleus ($^3J_{P,H}$ = 7.6 Hz), suggesting a PPh_3 ligand in a *cis* position.

The coordinated DMSO can also be easily displaced from **1a** and **1b** by CO at atmospheric pressure. In this case, however, the reaction products, compounds **3a** and **3b**, are almost insoluble in common organic solvents, hampering their characterisation by NMR spectroscopy. Analytical and spectroscopic data fit the formulation $[Pt_2(R)(L)(CO)_2]$: in particular the IR spectra show two bands in the region of terminal carbonyl ligands (2050, 2063 cm^{-1} for **3a** and 2066, 2073 cm^{-1} for **3b**) supporting substitution of both the DMSO ligands. To completely rule out the possibility of the coordination of only one CO ligand, compound **3a** was treated with PPh_3 in a 1:1 Pt/P molar ratio. The almost insoluble complex **3a** reacts immediately with loss of gas (CO): the ^1H NMR spectrum of the solution shows the formation of complex **2a**, and no free or coordinated DMSO is detected.

With a nitrogen donor such as 3,5-Me_2-py, only one of the DMSO ligands is substituted, yielding $[Pt_2(Me)(L)(DMSO)(3,5\text{-}Me_2\text{-py})]$ (**4**). The ^1H NMR spectra give evidence for a DMSO coordinated *trans* to a nitrogen atom (δ = 3.63, $J_{Pt,H}$ = 25.6 Hz);[9] only the more labile DMSO *trans* to the carbon atom is displaced. Even with excess 3,5-Me_2-py or at higher temperature the disubstituted product is not obtained. The low affinity of the nitrogen donor for platinum(II) likely accounts for this behaviour.

Displacement of the DMSO ligands from **1a** was also attained by reaction with a bidentate phosphane such as 1,3-bis(diphenylphosphanyl)propane (dppp). The outcome of the reaction, however, was unexpected: the analytical values point to a species, **5a**, with a Pt/dppp molar ratio of 4:3. The ^1H NMR spectrum shows, in the aliphatic region, a methyl resonance at δ = 0.30 ppm, at high field with respect to **1a**, coupled to ^{195}Pt ($^2J_{Pt,H}$ = 67 Hz) and to two phosphorus nuclei ($^3J_{P,H}$ = 8.0 Hz and 6.7 Hz). The $^{31}P\{^1H\}$ spectrum exhibits a singlet at δ = 17.71 ppm ($^1J_{Pt,P}$ = 3913 Hz) and two doublets at δ = −0.31 ppm

 © 2004 Wiley-VCH Verlag GmbH & Co. KGaA, Weinheim

($^1J_{Pt,P}$ = 1918, $^2J_{P,P}$ = 22.9 Hz) and δ = 1.35 ppm ($^1J_{Pt,P}$ = 2106, $^2J_{P,P}$ = 22.9 Hz). Coupling of the methyl group to two ^{31}P nuclei indicates an endobidentate diphosphane whereas the chemical shift of the singlet, δ = 17.71 ppm, and the absence of a P-P coupling, suggests a bridging dppp ligand. The high value of $^1J_{Pt,P}$ (3913 Hz) observed for the latter resonance is consistent with a phosphorus atom *trans* to a nitrogen atom. In the absence of X-ray data, a plausible description of **5a** which accounts for the experimental, analytical and spectroscopic data is shown in Figure 1.

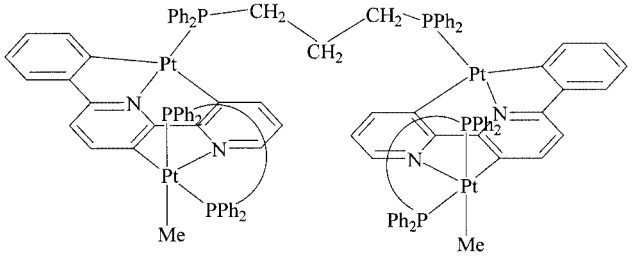

Figure 1. A plausible description of complex **5a**

The small differences between the two $^3J_{P,H}$ coupling constants (8.0, 6.7 Hz), makes a pentacoordinate arrangement more likely than a square-planar one. In the latter geometry, which entails the cleavage of the Pt−N bond of the chelated N′,C(3) ring, the phosphorus atoms of the chelated dppp should be *cis* and *trans*, respectively, to the methyl group.

It seems, therefore, that a variety of molecules with ancillary ligands having different electronic and steric properties can be synthesised from compounds **1** by substitution reactions without disruption of the dinuclear cyclometallated core of the system. All the new species **2**−**5** exhibit high thermal stability.

Reaction with Acids

Compounds **1a** and **1b** have four Pt−C bonds: in **1a** one of them is a C(sp^3)−Pt bond, whereas in **1b** all of them are C(sp^2)−Pt bonds. Regardless of the presence of two Pt−C(sp^2) bonds in mutual *trans* positions, the trimetallated compounds are stable in air both in solution and in the solid state. With the aim of investigating the reactivity of these platinum−carbon bonds, we have studied the behaviour of **1a** and **1b** toward HCl, an acid having a coordinating anion. To detect the most labile of the Pt−C bonds, the reaction was first carried out under mild conditions with a 1:1 L/HCl molar ratio. Under these conditions the platinum−methyl and the platinum−phenyl bond in **1a** and **1b**, respectively, were preferentially cleaved. The reaction is not selective and other species are also formed; however, according to their ^1H NMR spectra none of them contains an Me or a Ph group bound to the metal atom. One product could be isolated in pure form by chromatography, albeit in low yield. It was fully characterised and the analytical and spectroscopic data agree with the formulation [$Pt_2Cl(L)(DMSO)_2$] (**6**). In particular, a band at 292 cm^{-1} in the IR spectrum supports the thermodynamically favoured isomer having the chlorine atom *trans* to a carbon atom.[10]

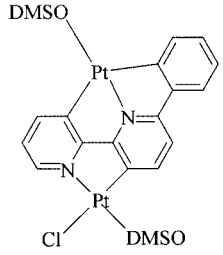

6

Reaction of complex **6** with PPh_3 under mild conditions leads to substitution of the DMSO ligands to give [$Pt_2Cl(L)(PPh_3)_2$] (**7**) for which crystals suitable for an X-ray structure determination were obtained.

The structure consists of the packing of **7** and $CHCl_3$ molecules in the molar ratio 2:3. An ORTEP view of **7** is shown in Figure 2 and principal bond parameters are listed in Table 1. The two platinum atoms are essentially square-planar coordinated with slight square-pyramidal distortions. For Pt(1) the maximum distances from the best plane are +0.041(1) and −0.055(4) Å for Pt(1) and N(2), respectively. For Pt(2) the maximum distances from the best plane are +0.017(1) and −0.021(3) Å for Pt(2) and N(1), respectively. The dihedral angle between these two least-squares planes is 7.5(2)°, a value which shows that the overall planarity of the $Pt_2ClP_2N_2C_{16}$ moiety is less rigorous than that of the analogous $Pt_2S_2N_2C_{17}$ fragment of [$Pt_2Ph(L)(DMSO)_2$],[7] where the analogous dihedral angle

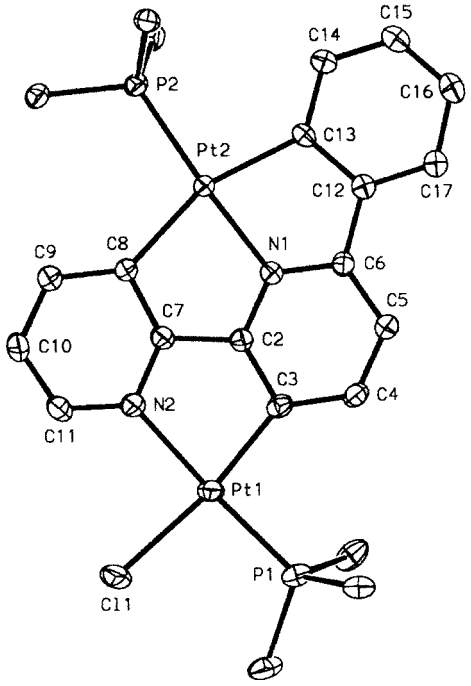

Figure 2. ORTEP view of **7**; ellipsoids are drawn at the 30% probability level; only the first carbon atoms of the phosphane phenyl rings are shown for clarity

 © 2004 Wiley-VCH Verlag GmbH & Co. KGaA, Weinheim

Table 1. Selected distances [Å] and angles [°] in **7**·1.5$CHCl_3$ with estimated standard deviations in parentheses

Pt(1)−Cl(1)	2.347(1)	Pt(1)−P(1)	2.225(1)
Pt(1)−N(2)	2.119(3)	Pt(1)−C(3)	2.010(4)
Pt(2)−P(2)	2.231(1)	Pt(2)−N(1)	2.024(3)
Pt(2)−C(8)	2.103(4)	Pt(2)−C(13)	2.071(4)
Cl(1)−Pt(1)−P(1)	94.1(1)	Cl(1)−Pt(1)−N(2)	89.6(1)
Cl(1)−Pt(1)−C(3)	171.3(1)	P(1)−Pt(1)−N(2)	173.9(1)
P(1)−Pt(1)−C(3)	94.5(1)	N(2)−Pt(1)−C(3)	81.8(1)
P(2)−Pt(2)−N(1)	175.7(1)	P(2)−Pt(2)−C(8)	103.3(1)
P(2)−Pt(2)−C(13)	97.3(1)	N(1)−Pt(2)−C(8)	80.6(1)
N(1)−Pt(2)−C(13)	78.8(1)	C(8)−Pt(2)−C(13)	159.4(1)

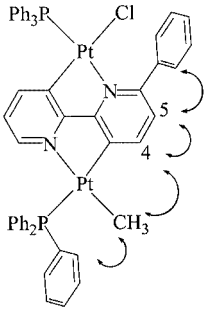

Figure 3. Complex **8a** with selected NOE contacts

is 1.7(6)°. The Pt(1)−N(2) bond length [2.119(3) Å] is normal for a Pt−N bond *trans* to phosphorus.[11] The Pt(2)−N(1) distance [2.024(3) Å], however, is much shorter. This shortness is a common feature of the central bonds of bicyclic systems: see, for instance, the Pt−N bond length [1.937(7) Å] in [PtCl(L′)] (HL′ = 6-*tert*-butyl-2,2′-bipyridine).[5c] Similarly, the C(8)−Pt(2)−C(13) angle [159.4(1)°] is very far from 180° because of the relative rigidity of the tricyclic ligand. All the other bond lengths and angles are as expected if the *trans* influence of the carbon atoms is taken into account.

The reaction with HCl was also studied in the case of complexes **2a** and **2b**. In contrast with the behaviour of **1a**, in the case of **2a** the platinum−methyl bond is not cleaved, even with an excess of HCl. The ^{1}H NMR spectrum of the reaction product **8a** [δ = 0.68 (d, $^2J_{Pt,H}$ = 80.8, $^3J_{P,H}$ = 7.3 Hz, Me) ppm] indicates that the N′,C(3) chelated part of the complex does not undergo substantial changes. In agreement, in the ^{31}P{^{1}H} spectrum one of the resonances, assignable to a phosphorus atom *trans* to a carbon atom (δ = 33.07 ppm, $^1J_{Pt,P}$ = 2405 Hz) is observed at a value very close to that of complex **2a** (δ = 32.44 ppm, $^1J_{Pt,P}$ = 2412 Hz) as well as to that of the analogous mononuclear species [Pt(Me)(H_2L)(PPh_3)] (δ = 33.01 ppm, $^1J_{Pt,P}$ = 2233 Hz).[6] However, the environment of the platinum atom coordinated by the C,N,C pincer part of the bridging ligand is significantly modified. (e.g. ^{31}P NMR: δ = 13.14 vs. δ = 26.53 ppm in **2a**), suggesting that one of the Pt−C bonds of the strained [5+5] fused-ring system has been cleaved. A ^{1}H 2D-COSY spectrum allowed us to ascribe three spin systems, with three, two and five protons, respectively, to the bridging ligand, the latter being assignable to a monosubstituted phenyl ring [δ = 8.56 (d, 2 H, H_{ortho}), 7.86 (m, 2 H, H_{meta}), 7.71 (t, 1 H, H_{para}) ppm]. A ^{1}H NOE difference spectrum shows contacts between the Pt−Me group, the *ortho* protons of the coordinated PPh_3 ligand, and the 4-H proton, as well as between the 4-H and the 5-H protons and between 5-H and the doublet at δ = 8.56 ppm ascribed to the *ortho* protons of the phenyl ring. On the whole the ^{1}H NMR spectra taken together with the ^{31}P{^{1}H}NMR spectra provide evidence for complex **8a** being [Pt_2Cl(Me)(HL)(PPh_3)$_2$] (Figure 3).

Complex **2b** reacts with HCl in a similar manner to **2a**, to give **8b**, as shown, in particular, by the ^{31}P NMR spectrum, which is similar to that of **8a**. In this case the two platinum−carbon bonds — Pt−Ph and Pt−C(sp^2) — in the five-membered N′,C(3) cycle are unaffected.

Finally, it is worth noting that the same platinum−carbon bond of the pincer C,N,C ligand can also be broken in complexes **1a** and **1b** upon addition of excess HCl to give [Pt_2Cl_2(HL)(DMSO)$_2$] (**9**). The ^{1}H NMR spectrum is consistent with a species having two DMSO ligands *trans* to nitrogen atoms [δ = 3.47 ($^3J_{Pt,C}$ ≈ 24.5 Hz), 3.64 ($^3J_{Pt,C}$ ≈ 22 Hz) ppm] and ten aromatic protons with a pattern similar to that of compound **8**.

The reactions of compound **1** (a and b) and **2** (a and b) with HCl are summarised in Scheme 2. The reactivity of the Pt−C bonds appears to be strongly dependent on the nature of the spectator ligands. Substitution of PPh_3 for

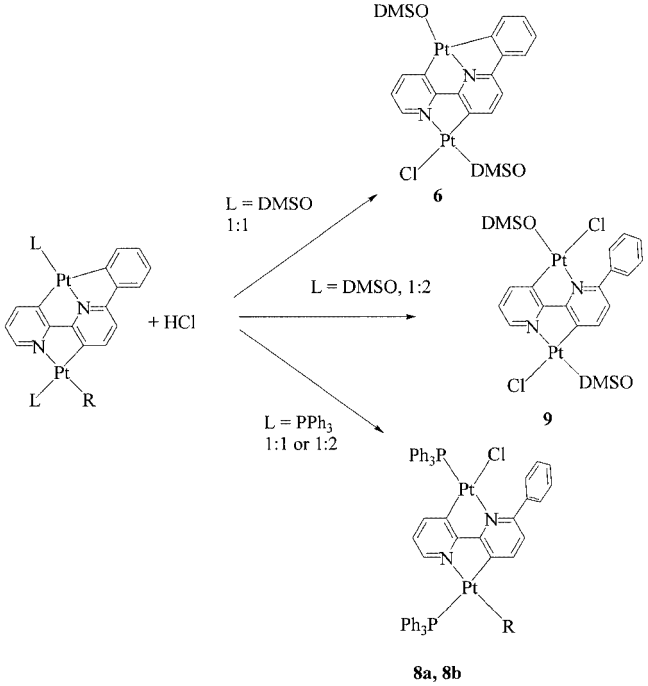

Scheme 2

 © 2004 Wiley-VCH Verlag GmbH & Co. KGaA, Weinheim

DMSO makes the Pt−Me (or Pt−Ph) bond less prone to cleavage by HCl. Indeed, even in the related mononuclear "rollover" derivatives [Pt(R)(H_2L)(DMSO)] the reaction with HCl gives selective and fast attack at the Pt−Me and Pt−Ph centres, respectively, whereas [Pt(Me)(H_2L)(PPh_3)] reacts slowly. After 4 h, about half of the starting compound is recovered unchanged, and prolonged reaction times are required to achieve quantitative attack at the Pt−Me bond. A more marked effect is observed in the case of the dinuclear species: the methyl group of compound **2a** is not cleaved even with excess HCl, suggesting a non-negligible degree of electronic communication between the two platinum atoms through the unsaturated bridging ligand.

Experimental Section

General: All the reactions were carried out under argon. The solvents were purified and dried according to standard methods.[12] Elemental analyses were performed with a Perkin−Elmer Elemental Analyser 240B by Mr. A. Canu (Dipartimento di Chimica, Università di Sassari). Infrared spectra were recorded with a Perkin−Elmer 983 spectrometer as Nujol mulls. ^{1}H, ^{13}C{^{1}H} and ^{31}P{^{1}H} NMR spectra were recorded with a Varian VXR 300 spectrometer operating at 300.0, 75.4 and 121.4 MHz, respectively. Chemical shifts are given in ppm relative to internal TMS (^{1}H, ^{13}C) or external 85% H_3PO_4 (^{31}P). 2D-COSY and NOE difference spectra were performed by means of standard pulse sequences. The mass spectrometric measurements were performed with a VG 7070EQ instrument, equipped with a PDP 11-250J data system and operating under positive ion fast atom bombardment (FAB) conditions with 3-nitrobenzyl alcohol as supporting matrix. *cis*-[Pt(Me)$_2$(DMSO)$_2$] and *cis*-[Pt(Ph)$_2$(DMSO)$_2$] were prepared according to literature procedures,[13] as were the ligand HL[14] and complexes **1a** and **1b**.[7]

[Pt_2(Me)(L)(PPh_3)$_2$] (2a): PPh_3 (84.9 mg, 0.324 mmol) was added, under vigorous stirring, to a solution of **1a** (125.0 mg, 0.158 mmol) in CH_2Cl_2 (15 mL). The solution was stirred for 2 h, then concentrated to a small volume and treated with hexane (15 mL). The precipitate formed was filtered and washed with hexane to give the analytical sample as a yellow solid. Yield: 90% (169.0 mg), m.p. 210 °C. $C_{53}H_{42}N_2P_2Pt_2\cdot 1/3C_6H_{14}$ (1187.7) calcd. C 55.62, H 3.96, N 2.36; found C 55.48, H 3.95, N 2.37. IR (Nujol): $\tilde{\nu}$ = 1097 (s), 1557 (w) cm^{-1}. ^{1}H NMR (CD_2Cl_2): δ = 0.62 (d, $^2J_{Pt,H}$ = 76.2, $^3J_{P,H}$ = 7.6 Hz, 3 H, CH_3Pt, 5.95 (m, 2 H), 6.28 (d, $J_{H,H}$ = 7.3 Hz, 1 H), 6.59 (m, 1 H), 6.88 (m, 1 H), 6.98 (m, 1 H), 7.26−7.50 (m, 20 H), 7.68−7.77 (m, 6 H), 7.80−7.89 (m, 6 H), 8.07 (dd, $^4J_{P,H}$ = 4.8, $^3J_{H,H}$ = 7.7, $^3J_{Pt,H}$ = 38 Hz, 1 H, 4-H) ppm. ^{31}P NMR (CD_2Cl_2): δ = 26.52 (s, $^1J_{P,Pt}$ = 3931 Hz, P *trans* N), 32.44 (s, $^1J_{P,Pt}$ = 2412 Hz, P *trans* C) ppm. MS (FAB$^+$): *m/z* = 1143 [M − CH_3]$^+$, 895 [M − PPh_3 − H]$^+$, 801 [M −PPh_3 − C_6H_6 − CH_3 − 2 H]$^+$, 725 [M − PPh_3 − 2 C_6H_6 − CH_3]$^+$. Compound **2a** can be obtained in almost quantitative yield also by reaction of [Pt_2(CO)$_2$(CH_3)(L)] with PPh_3 in a 1:2 molar ratio.

[Pt_2(Ph)(L)(PPh_3)$_2$] (2b): Complex **2b** was obtained as for complex **2a**, using **1b** instead of **1a**. Yield: 88%; m.p. > 260 °C. $C_{58}H_{44}N_2P_2Pt_2\cdot 2H_2O$ (1257.1): calcd. C 55.41, H 3.85, N 2.23; found C 55.69, H 3.91, N 2.25. IR (Nujol): $\tilde{\nu}$ = 1096 (s), 1560 (w) cm^{-1}. ^{1}H NMR ($CDCl_3$): δ = 5.94 (m, 2 H), 6.19 (d, J_{H-H} = 7.1 Hz, 1 H), 6.59 (m, 4 H), 6.84 (t, J_{H-H} = 7.4 Hz, 1 H), 6.93−7.44 (m, 24 H), 7.48−7.55 (m, 6 H), 7.82−7.89 (m, 6 H) ppm. ^{31}P NMR ($CDCl_3$): δ = 26.86 (s, $^1J_{P,Pt}$ = 3937 Hz, P *trans* N), 30.58 (s, $^1J_{P,Pt}$ = 2363 Hz, P *trans* C) ppm.

[Pt_2(Me)(L)(CO)$_2$] (3a): CO (1 atm) was bubbled for 1 h through a solution containing **1a** (63.5 mg, 0.080 mmol) in 20 mL of CH_2Cl_2. The precipitate formed was filtered and washed with Et_2O (3 × 5 mL), to give the analytical sample as an orange-yellow solid. Yield: 82% (45.4 mg); m.p. 245 °C (dec.). $C_{19}H_{12}N_2O_2Pt_2$ (690.5): calcd. C 33.05, H 1.74, N 4.06; found C 33.07, H 1.34, N 3.93. IR (Nujol): $\tilde{\nu}$ = 1037 (w), 1127 (m), 1558 (m), 1580 (m), 2050 (s), 2063 (s) cm^{-1}.

[Pt_2(Ph)(L)(CO)$_2$] (3b): Complex **3b** was obtained as for **3a** using **1b** instead of **1a**. Yield: 64%; m.p. 235 °C (dec.). $C_{24}H_{14}N_2O_2Pt_2$ (752.5): calcd. C 38.30, H 1.88, N 3.72; found C 37.94, H 1.80, N 4.02. IR (Nujol): $\tilde{\nu}$ = 1024 (w),1065 (w), 1560 (m), 1575 (m), 2066 (s), 2073 (s) cm^{-1}.

[Pt_2(Me)(L)(3,5-Me_2-py)DMSO] (4a): 3,5-Dimethylpyridine (3,5-Me_2-py; 42 mg, 0.39 mmol) was added, under vigorous stirring, to a solution of **1a** (58 mg, 0.073 mmol) in CH_2Cl_2 (20 mL) The solution, whose colour changed immediately to orange yellow, was stirred for 30 min, then concentrated to a small volume and treated with Et_2O (10 mL). The precipitate formed was filtered and washed with Et_2O (3 × 5 mL) to give an analytical sample as a yellow solid. Yield: 45% (26.9 mg); m.p. > 250 °C. $C_{26}H_{27}N_3OPt_2S$ (819.7): calcd. C 38.10, H 3.32, N 5.13; found C 38.26, H 3.46, N 5.17. ^{1}H NMR ($CDCl_3$): δ = 1.00 (s, $^2J_{Pt,H}$ = 85.7 Hz, 3 H, CH_3Pt), 2.38 (s, 6 H, CH_3 of 3,5-Me_2-py), 3.63 (s, $^3J_{Pt,H}$ = 25.6 Hz, 6 H, CH_3 of DMSO), 6.88−7.49 (m, 8 H), 7.93 (d, $^3J_{H,H}$ = 8.0 Hz, 1 H, 4-H), 8.17 (dd, $^3J_{H,H}$ = 7.6 Hz, 1 H), 8.48 (s, $^3J_{Pt,H}$ = 22.7 Hz, 2 H, 2-H of 3,5-Me_2-py) ppm.

[{Pt_2(Me)(L)(dppp)$_2$}$_2$(μ-dppp)] (5a): dppp (97.2 mg, 0.236 mmol) was added, under vigorous stirring, to a solution of **1a** (88.3 mg; 0.112 mmol) in CH_2Cl_2 (20 mL). The solution, whose colour changed immediately from yellow to orange-yellow, was stirred for 90 min, then concentrated to a small volume and treated with hexane (15 mL). The precipitate formed was filtered off and washed with hexane (3 × 5 mL) to give the analytical sample as a yellow solid. Yield 43% (60.6 mg); m.p. 211−214 (dec.). $C_{115}H_{102}N_4P_6Pt_4$ (2506.2): calcd. C 55.11, H 4.10, N 2.24; found C 54.80, H 4.14, N 2.28. IR (Nujol): $\tilde{\nu}$ = 1100 (m), 1549 (w), 1569 (w) cm^{-1}. ^{1}H NMR ($CDCl_3$): δ = 0.30 (dd, $^2J_{Pt,H}$ = 67, $^3J_{P,H}$ = 6.7, 8.0 Hz, 6 H, CH_3Pt), 2.06−2.94 [br. m, 18 H, CH_2 (dppp)], 6.32−8.21 (m, 78 H, aromatic H) ppm. ^{31}P NMR ($CDCl_3$): δ = −0.31 (d, $^1J_{P,Pt}$ = 1918, $^2J_{P,P}$ = 22.9 Hz, 2 P), 1.35 (d, $^1J_{P,Pt}$ = 2106, $^2J_{P,P}$ = 22.9 Hz, 2 P), 17.71 (s, $^1J_{P,Pt}$ = 3913 Hz, 2 P) ppm.

[Pt_2(Cl)(L)(DMSO)$_2$] (6): Aqueous 0.1 M HCl (2.0 mL) was added, under vigorous stirring, to a solution of **1a** (152.3 mg, 0.193 mmol) in acetone (25 mL). The mixture was stirred for 2 h, then concentrated to a small volume. The brick-red precipitate formed was filtered and washed with EtOH (3 × 5 mL) and Et_2O (3 × 5 mL). The crude product thus obtained was purified by chromatography on silica gel (Merck, 230−400 mesh; eluent: benzene/acetone, 2:1) to give an analytical sample as a yellow solid. Yield: 25% (39.0 mg); m.p. 206 (dec.). $C_{20}H_{21}ClN_2O_2Pt_2S_2$ (811.1): calcd. C 29.61, H 2.61, N 3.45; found C 30.52, H 2.33, N 3.82. IR (Nujol): $\tilde{\nu}$ = 292 (m) cm^{-1}. ^{1}H NMR ($CDCl_3$): δ = 3.61 (s, $J_{Pt,H}$ not resolved, 6 H, CH_3 of DMSO), 3.63 (s, $J_{Pt,H}$ not resolved, 6 H, CH_3 of DMSO), 7.03−7.44 (m, 6 H), 8.23 (dd, $^3J_{H,H}$ = 7.3, $^4J_{H,H}$ = 1.2 Hz, 1 H, 4′-H), 8.32 (d, $^3J_{H,H}$ = 8.3 Hz, 1 H, 4-H), 8.77 (d, $^3J_{H,H}$ = 5.7, $^4J_{H,H}$ = 1.2 Hz, 1 H, 6′-H) ppm. MS (FAB$^+$): *m/z* = 811 [MH]$^+$, 810 [M]$^+$, 775 [M − Cl]$^+$, 732 [M − DMSO]$^+$, 697 [M − DMSO − Cl]$^+$, 654 [M − 2 DMSO]$^+$, 619 [M − 2 DMSO − Cl]$^+$.

 © 2004 Wiley-VCH Verlag GmbH & Co. KGaA, Weinheim

[Pt_2(Cl)(L)(PPh_3)$_2$] (7): PPh_3 (0.020 mmol) was added to an NMR tube containing a solution of **6** (8.1 mg, 0.010 mmol) in $CDCl_3$. The reaction was monitored by ^1H and ^{31}P NMR spectroscopy, showing a fast reaction that produced complex **7** almost quantitatively. A slow evaporation of the solvent gave crystals suitable for an X-ray analysis. ^1H NMR ($CDCl_3$): δ = 6.12 (d, J_{H-H} = 7.5 Hz, 1 H), 6.24 (d, J_{H-H} = 8.1 Hz, 1 H), 6.58 (m, 2 H), 6.80 (t, broad, 1 H), 7.13 (d, J_{H-H} = 7.1 Hz, 1 H), 7.30−7.49 (m, 22 H), 7.74−7.90 (m, 10 H), 8.88 (m, 1 H, 6′-H) ppm. ^{31}P NMR ($CDCl_3$): δ = 25.93 (s, $^1J_{Pt,P}$ = 4146 Hz, P *trans* N), 18.32 (s, $^1J_{Pt,P}$ = 3952 Hz, P *trans* N) ppm.

[Pt_2(Me)(HL)(Cl)(PPh_3)$_2$] (8a): Aqueous 0.1 M HCl (1.7 mL, 0.17 mmol, molar ratio 1:2), was added, under vigorous stirring, to a solution of **2a** (67.4 mg, 0.085 mmol) in acetone (20 mL). The solution became pale yellow and was stirred for 16 h. The precipitate formed was filtered and washed with $(CH_3)_2CO$ (3 × 5 mL). From the filtered solution a second pale-yellow sample was obtained by concentration and filtration. The filtered precipitate was washed with $(CH_3)_2CO$ and Et_2O and added to the first sample. Yield: 89% (94.6 mg); m.p. 215 (dec.). $C_{53}H_{43}N_2ClP_2Pt_2\cdot 3H_2O$ (1249.5): calcd. C 50.94, H 3.95, N 2.24; found C 50.27, H 3.51, N 2.28. IR (Nujol): $\tilde{\nu}$ = 1097 (s),1292 (s), 1585 (m), 1595 (m), 1715 (s), 296 m, 305 (m) cm^{-1}. ^1H NMR ($CDCl_3$): δ = 0.68 (d, $^2J_{Pt,H}$ = 80.8 Hz $^3J_{P,H}$ = 7.3 Hz, 3 H, CH_3Pt), 5.98 (dd, $^3J_{H,H}$ = 7.9, $^3J_{H,H}$ = 5.2 Hz, 1 H, 5′-H), 6.94−7.00 (m, 6 H), 7.16−7.26 (m, 10 H), 7.38−7.46 (m, 9 H), 7.47 (d, 1 H, 4′-H or 6′-H), 7.54−7.69 (m, 5 H), 7.71 (t, J_{H-H} = 7.8 Hz, 1 H, H_{para}, Ph bipy), 7.78 (d, $^3J_{H,H}$ = 8.0 Hz, 1 H, 5-H), 7.86 (t, $^3J_{H,H}$ = 7.8 Hz, 2 H, H_{meta}, Ph bipy), 8.01 (d, $^3J_{H,H}$ = 7.9 Hz, 1 H, 6′-H or 4′-H), 8.56 (d, $^3J_{H,H}$ = 7.8 Hz, 2 H, H_{ortho}, Ph bipy), 8.74 (dd, $^3J_{H,H}$ = 8.0, $^4J_{P,H}$ = 5.7, $^3J_{Pt,H}$ = 52 Hz, 1 H, 4-H) ppm. ^{31}P NMR ($CDCl_3$): δ = 33.07 (s, $^1J_{P,Pt}$ = 2405 Hz, P *trans* C), 13.14 (s, $^1J_{P,Pt}$ = 4580 Hz, P *trans* N) ppm.

[Pt_2(Ph)(HL)(Cl)(PPh_3)$_2$] (8b): Aqueous 0.1 M HCl (0.7 mL, 0.07 mmol) was added, under vigorous stirring, to a solution of **2b** (81.7 mg, 0.067 mmol) in acetone (20 mL). The solution became yellow and was stirred for 13 h. The precipitate formed was filtered and washed with acetone (3 × 5 mL) to give the analytical sample as a yellow solid. Yield: 55% (47.3 mg); m.p. 205 °C. $C_{58}H_{45}N_2ClP_2Pt_2\cdot H_2O$ (1275.6): calcd. C 54.61, H 3.71, N 2.20; found C 54.75, H 3.53, N 2.28. IR (Nujol): $\tilde{\nu}$ = 700 (s), 750 (s), 1100 (s), 1550 (m) cm^{-1}. ^1H NMR ($CDCl_3$): δ = 5.99 (m, 1 H, 5′-H), 6.62−7.75 (m, 39 H), 7.83 (t, J_{H-H} = 7.5 Hz, 2 H, H_{meta}, Ph bipy), 8.01 (d, J_{H-H} = 8.3 Hz, 1 H, 6′-H or 4′-H), 8.47 (d, J_{H-H} = 7.5 Hz, 2 H, H_{ortho}, Ph bipy) ppm. ^{31}P NMR ($CDCl_3$) = 30.68 (s, $^1J_{P,Pt}$ = 2352 Hz, P *trans* C), 13.10 (s, $^1J_{P,Pt}$ = 3725 Hz, P *trans* N) ppm.

[Pt_2(HL)($Cl)_2$($DMSO)_2$] (9): Aqueous 0.1 M HCl (0.65 mL, 0.065 mmol) was added, under vigorous stirring, to a solution of **1b** (52.3 mg, 0.061 mmol) in acetone (20 mL). After 4 h, a second quantity of HCl was added (1.35 mL). The mixture was stirred for 15 h, then concentrated to dryness and crystallised from CH_2Cl_2/Et_2O to give an analytical sample as a yellow solid. Yield: 46% (24.0 mg); m.p. 215−218 °C (dec.). $C_{20}H_{22}Cl_2N_2O_2Pt_2S_2$ (847.6):calcd. C 28.34, H 2.62, N 3.31; found C 28.09, H 2.33, N 3.24. ^1H NMR ($CDCl_3$): δ = 3.47 (s, $J_{Pt,H} \approx$ 24.5 Hz, 6 H, CH_3 of DMSO), 3.64 (s, $^3J_{Pt,H} \approx$ 22 Hz, 6 H, CH_3 of DMSO), 7.07 (dd, J_{H-H} = 5.6 Hz, J_{H-H} = 7.8 Hz, 1 H, 5′-H), 7.18 (d, J_{H-H} = 8.1 Hz, 1 H, 5-H), 7.42−7.48 (m, 3 H, H_{meta} and H_{para}), 7.73 (d, J_{H-H} = 8.1 Hz, 2 H, H_{ortho}), 8.63−8.69 (m, 2 H, 4′-H and 4-H), 8.98 (dd, J_{H-H} = 5.6 Hz, J_{H-H} = 1.2 Hz, 1 H, 6′-H) ppm.

X-ray Data Collection and Structure Determination: Crystal data are summarised in Table 2. The diffraction experiment was carried out with a Bruker SMART CCD area-detector diffractometer at 223 K. No crystal decay was observed, therefore no time-decay correction was needed. The collected frames were processed with the software SAINT,[15] and an empirical absorption correction was applied (SADABS)[16] to the collected reflections. The calculations were performed using the Personal Structure Determination Package[17] and the physical constants tabulated therein.[18] The structure was solved by direct methods (SHELXS)[19] and refined by full-matrix least squares using all reflections and minimising the function $\Sigma w(F_o^2 - kF_c^2)^2$ (refinement on F^2). One of the two chloroform solvent molecules is disordered around a twofold axis and its atoms have been given occupancy factors of 0.50. All the non-hydrogen atoms were refined with anisotropic thermal factors. The hydrogen atoms were placed in their ideal positions (C−H = 0.97 Å), with the thermal parameter B set to 1.10-times that of the carbon atom to which they are attached, and not refined. In the final Fourier map the maximum residual was 3.86(20) e·Å^{-3} at 0.62 Å from Pt(1). CCDC-236975 contains the supplementary crystallographic data for this paper. These data can be obtained free of charge at www.ccdc.cam.ac.uk/conts/retrieving.html [or from the Cambridge Crystallographic Data Centre, 12 Union Road, Cambridge CB2 1EZ, UK; Fax: + 44-1223-336-033; E-mail: deposit@ccdc.cam.ac.uk].

Table 2. Crystallographic data of **7**·1.5$CHCl_3$

Empirical formula	$C_{53.5}H_{40.5}Cl_{5.5}N_2P_2Pt_2$
Formula mass	1358.55
Colour	yellow
Crystal system	monoclinic
Space group	*C*2/*c*
a [Å]	31.238(3)
b [Å]	17.779(2)
c [Å]	18.688(2)
β [°]	110.48(1)
V [Å^3]	9723(2)
Z	8
F(000)	1284
$D_{calcd.}$ [g cm^{-3}]	1.856
T [K]	223
Crystal dimensions [mm]	0.338 × 0.450 × 0.507
μ(Mo-K_α) [cm^{-1}]	62.2
Min./max. transmission factors	0.759/1.000
Scan mode	ω
Frame width [°]	0.30
Time per frame [s]	15
No. of frames	2750
Detector−sample distance [cm]	4.00
θ range [°]	3−28
Reciprocal space explored	full sphere
No. of reflections (total/independent)	89654/14815
R_{int}	0.0326
Final R_2 and R_{2w} indices[a] (F^2/all reflections)	0.053/0.110
Conventional R_1 index[b][$I > 2\sigma(I)$]	0.036
Reflections with $I > 2\sigma(I)$	11770
No. of variables	604
Goodness of fit[c]	1.29

[a] $R_2 = [\Sigma(|F_o^2 - kF_c^2|/\Sigma F_o^2]$, $R_{2w} = [\Sigma w/(F_o^2 - kF_c^2)^2/\Sigma w(F_o^2)^2]^{1/2}$. [b] $R_1 = [\Sigma(|F_o - k|F_c||/\Sigma F_o)$. [c] $[\Sigma w(F_o^2 - kF_c^2)^2/(N_o - N_v)]^{1/2}$, where $w = 4F_o^2/\sigma(F_o^2)^2$, $\sigma(F_o^2) = [\sigma^2(F_o^2) + (pF_o^2)^2]^{1/2}$, where N_o is the number of observations, N_v the number of variables, and p, the ignorance factor (0.06).

 © 2004 Wiley-VCH Verlag GmbH & Co. KGaA, Weinheim

Acknowledgments

Financial support from Università di Sassari and Ministero dell'Istruzione, dell'Università e della Ricerca (MIUR) is gratefully acknowledged.

[1] G. R. Newkome, W. E. Puckett, V. K. Gupta, G. E. Kiefer, *Chem. Rev.* **1986**, *86*, 451−489.

[2] Type **I**, NC species: [2a] T. J. Giordano, P. G. Rasmussen, *Inorg. Chem.* **1975**, *14*, 1628. [2b] G. Matsubayashi, Y. Kondo, T. Tanaka, S. Nishigaki, K. Nakatsu, *Chem. Lett.* **1979**, 375. [2c] L. Chassot, E. Muller, A. von Zelewsky, *Inorg. Chem.* **1984**, *23*, 4249. [2d] G. R. Newkome, K. J. Theriot, F. R. Fronczek, B. Villar, *Organometallics* **1989**, *8*, 2513. [2e] C. Deuschel-Cornioley, H. Stoeckli-Evans, A. von Zelewsky, *J. Chem. Soc., Chem. Commun.* **1990**, 121. [2f] G. Minghetti, A. Zucca, S. Stoccoro, M. A. Cinellu, M. Manassero, M. Sansoni, *J. Organomet. Chem.* **1994**, *481*, 195. [2g] V. M. Mdleleni, J. S. Bridgewater, R. J. Watts, P. C. Ford, *Inorg. Chem.* **1995**, *34*, 2334. [2h] P. Kvam, T. Engebretsen, K. Maartmann-Moe, J. Songstad, *Acta Chem. Scand.* **1996**, *50*, 107. [2i] S.-W. Lai, M. C.-W. Chan, S.-M. Peng, C.-M. Che, *Angew. Chem. Int. Ed.* **1999**, *38*, 669. [2j] G. Minghetti, A. Doppiu, A. Zucca, S. Stoccoro, M. A. Cinellu, M. Manassero, M. Sansoni, *Chem. Heteroatom Compd.* **1999**, 1127. [2k] S. Tollari, S. Cenini, A. Penoni, G. Granata, G. Palmisano, F. Demartin, *J. Organomet. Chem.* **2000**, *608*, 34. [2l] J. DePriest, G. Y. Zheng, N. Goswami, D. M. Eichhorn, C. Woods, D. P. Rillema, *Inorg. Chem.* **2000**, *39*, 1955. [2m] J.-C. Shi, H.-Y. Chao, W.-F. Fu, S.-M. Peng, C.-M. Che, *J. Chem. Soc., Dalton Trans.* **2000**, 3128. [2n] A. Doppiu, G. Minghetti, M. A. Cinellu, S. Stoccoro, A. Zucca, M. Manassero, *Organometallics* **2001**, *20*, 1148. [2o] T. Okada, I. M. El-Mehasseb, M. Kodaka, T. Tomchiro, K. Okamoto, H. Okuno, *J. Med. Chem.* **2001**, *44*, 4661. [2p] G. Minghetti, A. Doppiu, S. Stoccoro, A. Zucca, M. A. Cinellu, M. Manassero, M. Sansoni, *Eur. J. Inorg. Chem.* **2002**, 431. [2q] A. D. Ryabov, I. M. Panyashkina, V. A. Polyakov, A. Fischer, *Organometallics* **2002**, *21*, 1633.

[3] Type **II**, C,N,C systems: [3a] C. Cornioley-Deuschel, T. Ward, A. von Zelewsky, *Helv. Chim. Acta* **1988**, *71*, 130−133. [3b] G. W. V. Cave, N. W. Alcock, J. P. Rourke, *Organometallics* **1999**, *18*, 1801. [3c] G. W. V. Cave, F. P. Fanizzi, R. J. Deeth, W. Eddington, J. P. Rourke, *Organometallics* **2000**, *19*, 1355. [3d] W. Lu, M. C. W. Chan, K.-K. Cheung, C.-M. Che, *Organometallics* **2001**, *20*, 2477. [3e] C. P. Newman, G. W. V. Cave, M. Wong, W. Errington, N. W. Alcock, J. P. Rourke, *J. Chem. Soc., Dalton Trans.* **2001**, 2678. [3f] V. W.-W. Yam, R. P.-L. Tang, K. M.-C. Wong, X.-X. Lu, K.-K. Cheung, N. Zhu, *Chem. Eur. J.* **2002**, *8*, 4066.

[4] Type **III**, NC,N systems: [4a] D. J. Cardenas, A. M. Echavarren, M. C. Ramirez de Arellano, *Organometallics* **1999**, *18*, 3337. [4b] M. A. Albrecht, G. van Koten, *Angew. Chem. Int. Ed.* **2001**, *40*, 3750−3781.

[5] Type **IV**, NN,C systems: [5a] G. Minghetti, M. A. Cinellu, G. Chelucci, S. Gladiali, F. Demartin, M. Manassero, *J. Organomet. Chem.* **1986**, *307*, 107. [5b] E. C. Constable, R. P. G. Henney, T. A. Leese, D. A. Tocher, *J. Chem. Soc., Chem. Commun.* **1990**, 513. [5c] G. Minghetti, M. A. Cinellu, S. Stoccoro, A. Zucca, M. Manassero, *J. Chem. Soc., Dalton Trans.* **1995**, 777. [5d] F. Neve, A. Crespini, S. Campagna, *Inorg. Chem.* **1997**, *36*, 6150. [5e] M.-C. Tse, K.-K. Cheung, M. C. W. Chan, C.-M. Che, *Chem. Commun.* **1998**, 2295. [5f] K.-H. Wong, M. C. Chang, C.-M. Che, *Chem. Eur. J.* **1999**, *5*, 2845. [5g] S.-W. Lai, M. C.-W. Chan, K.-K. Cheung, C.-M. Che, *Organometallics* **1999**, *18*, 3327. [5h] J. H. K. Yip, Suwarno, J. J. Vittal, *Inorg. Chem.* **2000**, *39*, 3537. [5i] G. Sanna, G. Minghetti, A. Zucca, M. I. Pilo, R. Seeber, F. Laschi, *Inorg. Chim. Acta* **2000**, *305*, 189−205. [5j] W. Lu, N. Zhu, C.-M. Che, *Chem. Commun.* **2002**, 900. [5k] W. Lu, B.-X. Mi, M. C. W. Chan, Z. Hui, N. Zhu, S.-T. Lee, C.-M. Che, *Chem. Commun.* **2002**, 206. [5l] S.-W. Lai, H.-W. Lam, W. Lu, K.-K. Cheung, C.-M. Che, *Organometallics* **2002**, *21*, 226. [5m] A. Zucca, S. Stoccoro, M. A. Cinellu, G. Minghetti, M. Manassero, M. Sansoni, *Eur. J. Inorg. Chem.* **2002**, 3336.

[6] G. Minghetti, S. Stoccoro, M. A. Cinellu, B. Soro, A. Zucca, *Organometallics* **2003**, *22*, 4770−4777.

[7] A. Zucca, A. Doppiu, M. A. Cinellu, G. Minghetti, S. Stoccoro, M. Manassero, *Organometallics* **2002**, *21*, 783−785.

[8] P. S. Pregosin, R. W. Kunz, ^{31}P *and* ^{13}C *NMR of Transition Metal Phosphane Complexes*, Springer, Berlin, **1978**.

[9] [9a] R. Romeo, L. Monsù Scolaro, N. Nastasi, B. E. Mann, G. Bruno, F. Nocolò, *Inorg. Chem.* **1996**, *35*, 7691−7698. [9b] C. Eaborn, K. Kundu, A. Pidcock, *J. Chem. Soc., Dalton Trans.* **1981**, 933.

[10] K. Nakamoto, *Infrared and Raman Spectra of Inorganic and Coordination Compounds*, 3rd ed., Wiley, New York, **1978**.

[11] [11a] G. Minghetti, A. Zucca, S. Stoccoro, M. A. Cinellu, M. Manassero, M. Sansoni, *J. Organomet. Chem.* **1994**, *481*, 195−204. [11b] A. Albinati, F. Lianza, B. Muller, P. S. Pregosin, *Inorg. Chim. Acta* **1993**, *208*, 119.

[12] *Vogel's Textbook of Practical Organic Chemistry*, 5th ed., Longman Scientific and Technical, Harlow, **1989**.

[13] [13a] C. Eaborn, K. Kundu, A. Pidcock, *J. Chem. Soc., Dalton Trans.* **1981**, 933. [13b] R. Romeo, L. Monsù Scolaro, *Inorg. Synth.* **1998**, *32*, 153.

[14] T. Kauffmann, J. König, A. Woltermann, *Chem. Ber.* **1976**, *109*, 3864−3868.

[15] *SAINT Reference manual*, Siemens Energy and Automation, Madison, WI, **1994−1996**.

[16] G. M. Sheldrick, *SADABS, Empirical Absorption Correction Program*, University of Göttingen, **1997**.

[17] B. A. Frenz, *Comput. Phys.* **1988**, *2*, 42.

[18] *Crystallographic Computing 5*, Oxford University Press, Oxford, U. K., **1991**, chapter 11, p. 126.

[19] G. M. Sheldrick, *SHELXS 86, Program for the solution of crystal structures*, University of Göttingen, Germany, **1985**.

Received May 5, 2004
Early View Article
Published Online September 13, 2004

 © 2004 Wiley-VCH Verlag GmbH & Co. KGaA, Weinheim

Synthesis, Properties, and Structural Characterization of Bromo- and Iodotetracarboxylatodiruthenium(II,III) Compounds

M. Carmen Barral,[a] Rodrigo González-Prieto,[a] Reyes Jiménez-Aparicio,*[a] J. Luis Priego,[a] M. Rosario Torres,[b] and Francisco A. Urbanos[a]

Keywords: Carboxylate ligands / Metal-metal interactions / Multiple bonds / Ruthenium / Solvatochromism

The synthesis and characterization of the compounds $[Ru_2X(\mu\text{-}O_2CPh)_4]_n$ [X = Br (**1**), I (**2**)] and $[Ru_2X(\mu\text{-}O_2CC_6H_4\text{-}p\text{-}OMe)_4(H_2O)]$ [X = Br (**3**) and I (**4**)] is described. The structures of these compounds were determined by single-crystal X-ray diffraction. The molecular structures of $[Ru_2Br(\mu\text{-}O_2CCMePh_2)_4(EtOH)\cdot 0.5EtOH]$ (**5**·0.5EtOH) and $[Ru_2I(\mu\text{-}O_2CCMePh_2)_4(MeOH)\cdot 0.5H_2O]$ (**6**·0.5H_2O) are also reported. Complexes **1** and **2** show a zigzag polymeric arrangement with the diruthenium units linked by bromide and iodide ligands, respectively. The molecular nature of compounds **3** and **4** shows the influence of the axial ligand in the arrangement in the solid state, which contrasts with the polymeric structure found in all chlorodiruthenium(II,III) derivatives with arenecarboxylate bridging ligands. The Ru–Ru bond lengths for all complexes range from 2.2756(17) to 2.2906(7) and 2.273(3) to 2.2965(6) Å for the bromide and iodide derivatives, respectively. This study demonstrates that the nature of the axial ligand plays an important role in the arrangement in the solid state and in the electronic properties of the halotetracarboxylatodiruthenium(II,III) complexes. Thus, the iodo derivatives show an intense solvatochromism, whereas the solvatochromism is slight in the bromo derivatives and is not observed in the chloro complexes.

(© Wiley-VCH Verlag GmbH & Co. KGaA, 69451 Weinheim, Germany, 2004)

Introduction

The synthesis and properties of the diruthenium(II,III) complexes of formula $[Ru_2Cl(\mu\text{-}O_2CR)_4]$ (R = alkyl, aryl) have attracted much attention, mainly due to the interest in their electronic and magnetic properties.[1−3] The use of these complexes as building blocks in the formation of supramolecular species has increased this interest.[4] Much effort has been devoted to the assembly of dinuclear units and a wide variety of oligomers and polymers have been isolated. These new materials containing diruthenium units may display novel conductive, optical, and magnetic properties.[1−4] In $[Ru_2Cl(\mu\text{-}O_2CR)_4]$ compounds the ruthenium atoms are strongly bonded by four bridging carboxylate ligands, with one axial position occupied by a chloride ion.[1−3] The chloride ligand of the $[Ru_2Cl(\mu\text{-}O_2CR)_4]$ molecule is usually bonded to the free axial position of a neighboring diruthenium unit leading to zigzag or linear chains.[4−15] However, a neutral ligand can also coordinate to the free axial position giving discrete dinuclear molecules.[16−19] Both discrete molecules and polymeric species with 2,2-diphenylpropionate and axial chloride ligands have been reported.[11,19] Thus, the influence of the carboxylate bridging group on the properties of these chlorocarboxylate derivatives has been studied. However, the role of the axial halogen ligand has been little explored. To the best of our knowledge, only one crystal structure of a bromo derivative, which contains zigzag chains, has been described.[20] We have recently published[19] the first crystal structure of an iododiruthenium derivative showing a cation/anion arrangement $[Ru_2(\mu\text{-}O_2CCH_2CH_2OPh)_4(H_2O)_2]$-$[Ru_2I_2(\mu\text{-}O_2CCH_2CH_2OPh)_4]$ in the solid state. The crystal structure of the diiodotetrabenzamidinatodiruthenium(III) complex $[Ru_2(DMBA)_4I_2]$ (DMBA = *N*,*N*′-dimethylbenzamidinate) has been reported very recently.[21]

In this paper we analyse the role of the axial halogen ligand on the properties of the halotetracarboxylatodiruthenium(II,III) complexes. Tetrabenzoate- and tetra-*p*-methoxybenzoatediruthenium(II,III) compounds have been used in this study. The preparation and structural characterization of new bromo and iodo derivatives are described. The synthesis of the bromo and iodo complexes with 2,2-diphenylpropionate has been reported in a previous paper[19] but the structural determination of both complexes is reported here. These complexes show an intense solvatochromism in several solvents, which is also explored.

[a] Departamento de Química Inorgánica, Universidad Complutense
Ciudad Universitaria, 28040 Madrid, Spain
Fax: +34-91-394-4352
E-mail: qcmm@quim.ucm.es
[b] Centro de Asistencia a la Investigación de Rayos X, Facultad de Ciencias Químicas, Universidad Complutense
Ciudad Universitaria, 28040 Madrid, Spain

Results and Discussion

The reaction of $[Ru_2Cl(\mu\text{-}O_2CR)_4]$ (R = Ph, C_6H_4-*p*-OMe) with $AgBF_4$ in THF leads to the complexes $[Ru_2(\mu\text{-}O_2CR)_4(THF)_2]BF_4$, which were treated in ethanol with an aqueous solution of KBr or KI to give $[Ru_2X(\mu\text{-}O_2CPh)_4]_n$ [X = Br (**1**), I (**2**)] and $[Ru_2X(\mu\text{-}O_2CC_6H_4\text{-}p\text{-}OMe)_4(H_2O)]$ [X = Br (**3**) and I (**4**)]. Crystals of **1** and **2** were grown by layering an ethanol solution of $[Ru_2(\mu\text{-}O_2CR)_4(THF)_2]BF_4$ onto an aqueous solution of KX (X = Br, I). An analogous procedure allowed us to isolate single crystals of $[Ru_2Br(\mu\text{-}O_2CCMePh_2)_4(EtOH)]\cdot 0.5EtOH$ (**5**·0.5EtOH). The hydrate $[Ru_2Br(\mu\text{-}O_2CCMePh_2)_4(H_2O)]$ and unsolvated $[Ru_2Br(\mu\text{-}O_2CCMePh_2)_4]$ have been isolated previously, although the growth of single crystals was not possible.[19] The slow evaporation of an ethanol/water solution of compound **3** gave crystals of **3**·H_2O. Crystals of **4**·H_2O were obtained by cooling a methanol solution of **4** to −18 °C. Single crystals of $[Ru_2I(\mu\text{-}O_2CCMePh_2)_4(MeOH)]\cdot 0.5H_2O$ (**6**·0.5H_2O) were grown from a methanol/water solution containing the cation $[Ru_2(\mu\text{-}O_2CCMePh_2)_4]^+$ and tetraphenylphosphonium iodide over 48 h.

The unsolvated $[Ru_2X(\mu\text{-}O_2CR)_4]$ complexes were prepared by heating the solvated complexes under vacuum.

All compounds are thermally stable in air and can be manipulated without decomposition for long periods of time. They are soluble in methanol, DMSO and THF, but insoluble in hexane or toluene, and are 1:1 electrolytes in methanol and DMSO but non-electrolytes in acetone, THF and acetonitrile solutions.[22]

The IR spectra of all compounds exhibit the typical pattern for bridging carboxylate ligands in the CO_2 stretching region.[1−3] Other bands attributable to aryl or alkyl groups of the carboxylate ligands are also observed in all cases. For **3** and **4** bands corresponding to coordinated water molecules also appear.

The base peak in all mass spectra (ESI+) corresponds to the ion $[Ru_2(\mu\text{-}O_2CR)_4]^+$ or $[Ru_2(\mu\text{-}O_2CR)_4(DMSO)]^+$. The $[Ru_2X(\mu\text{-}O_2CR)_4]^+$ ion is only observed in compound **1**. In complex **5**, the molecular peak associated with a DMSO molecule $[Ru_2Br(\mu\text{-}O_2CCMePh_2)_4(DMSO)]^+$ is detected. All spectra in ESI negative mode show the peak corresponding to the ion $[Ru_2X_2(\mu\text{-}O_2CR)_4]^-$.

Crystal Structures of $[Ru_2Br(\mu\text{-}O_2CPh)_4]$ (1), $[Ru_2Br(\mu\text{-}O_2CC_6H_4\text{-}p\text{-}OMe)_4(H_2O)]\cdot H_2O$ (3·H_2O), and $[Ru_2Br(\mu\text{-}O_2CCMePh_2)_4(EtOH)]\cdot 0.5EtOH$ (5·0.5EtOH)

The crystal structures of these complexes are depicted below. Selected bond lengths and angles are given in Table 1. These complexes have two Ru atoms linked by four carboxylate bridging ligands. The Ru−Ru distances are 2.2906(7), 2.2756(17), and 2.2849(14) Å, respectively. These distances are of the same order as those found in other carboxylatodiruthenium(II,III) compounds.[1−3]

The structure of **1** (Figure 1) consists of $[Ru_2(\mu\text{-}O_2CPh)_4]^+$ units connected by bromide ions to give zigzag chains. The Ru−Br−Ru angle of 117.00(3)° is similar to those found in other polymeric complexes,[5,7,9,10,12,15] and in the sole previously described bromo derivative $[Ru_2Br(\mu\text{-}O_2CH)_4]_n$.[20] Figure 2 shows the packing of the zigzag chains in the solid state. No significant interactions are seen between the chains of $[Ru_2Br(\mu\text{-}O_2CPh)_4]_n$.

Table 1. Selected bond lengths (Å) and angles (°) for $[Ru_2Br(\mu\text{-}O_2CPh)_4]$ (**1**), $[Ru_2Br(\mu\text{-}O_2CC_6H_4\text{-}p\text{-}OMe)_4(H_2O)]\cdot H_2O$ (**3**·H_2O), and $[Ru_2Br(\mu\text{-}O_2CCMePh_2)_4(EtOH)]\cdot 0.5EtOH$ (**5**·0.5EtOH); symmetry transformations used to generate equivalent atoms: #1: $-x+2, -y+1, -z$; #2: $-x+2, y, z+1/2$.

1		**3**·H_2O		**5**·0.5EtOH	
Ru(1)−Ru(1)#1	2.2906(7)	Ru(1)−Ru(2)	2.2756(17)	Ru(1)−Ru(2)	2.2849(14)
Ru(1)−Br(1)	2.6700(5)	Ru(1)−Br(1)	2.671(2)	Ru(1)−Br(1)	2.6108(17)
Ru(1)−O(1)	2.014(3)	Ru(1)−O(1)	2.002(10)	Ru(1)−O(2)	2.027(9)
Ru(1)−O(2)	2.025(3)	Ru(1)−O(4)	2.014(10)	Ru(1)−O(4)	2.033(8)
Ru(1)−O(3)	2.018(3)	Ru(1)−O(5)	1.989(9)	Ru(1)−O(7)	2.013(9)
Ru(1)−O(4)	2.023(3)	Ru(1)−O(8)	2.028(11)	Ru(1)−O(9)	2.018(9)
Br(1)−Ru(1)#2	2.670(5)	Ru(2)−O(2)	1.996(9)	Ru(2)−O(1)	2.296(8)
Ru(1)#1−Ru(1)−Br(1)	174.94(3)	Ru(2)−O(3)	1.973(10)	Ru(2)−O(3)	2.024(9)
Ru(1)#2−Br(1)−Ru(1)	117.00(3)	Ru(2)−O(6)	2.017(10)	Ru(2)−O(5)	2.011(9)
O(1)−Ru(1)−Ru(1)#1	89.73(8)	Ru(2)−O(7)	1.998(10)	Ru(2)−O(6)	2.016(8)
O(2)−Ru(1)−Ru(1)#1	89.86(8)	Ru(2)−O(9)	2.292(11)	Ru(2)−O(8)	2.012(9)
O(3)−Ru(1)−Ru(1)#1	86.44(8)	Ru(2)−Ru(1)−Br(1)	177.64(8)	Ru(2)−Ru(1)−Br(1)	178.48(8)
O(4)−Ru(1)−Ru(1)#1	90.42(8)	Ru(1)−Ru(2)−O(9)	177.6(3)	Ru(1)−Ru(2)−O(1)	177.5(3)
		O(1)−Ru(1)−Ru(2)	88.7(3)	O(2)−Ru(1)−Ru(2)	88.9(2)
		O(4)−Ru(1)−Ru(2)	89.0(3)	O(4)−Ru(1)−Ru(2)	88.0(2)
		O(5)−Ru(1)−Ru(2)	89.4(3)	O(7)−Ru(1)−Ru(2)	88.6(2)
		O(8)−Ru(1)−Ru(2)	89.4(3)	O(9)−Ru(1)−Ru(2)	88.8(2)
		O(2)−Ru(2)−Ru(1)	89.7(3)	O(3)−Ru(2)−Ru(1)	89.9(2)
		O(3)−Ru(2)−Ru(1)	90.4(3)	O(5)−Ru(2)−Ru(1)	90.3(2)
		O(6)−Ru(2)−Ru(1)	90.4(3)	O(6)−Ru(2)−Ru(1)	89.8(2)
		O(7)−Ru(2)−Ru(1)	89.8(3)	O(8)−Ru(2)−Ru(1)	89.7(2)
				C(61)−O(1)−Ru(2)	134.5(10)

 © 2004 Wiley-VCH Verlag GmbH & Co. KGaA, Weinheim

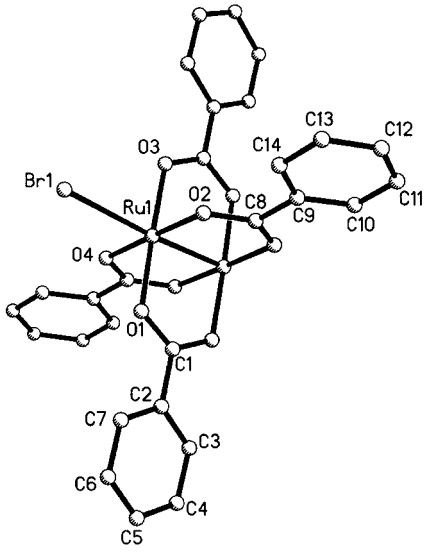

Figure 1. PLUTO view of $[Ru_2Br(\mu\text{-}O_2CPh)_4]$ (**1**); hydrogen atoms have been omitted for clarity

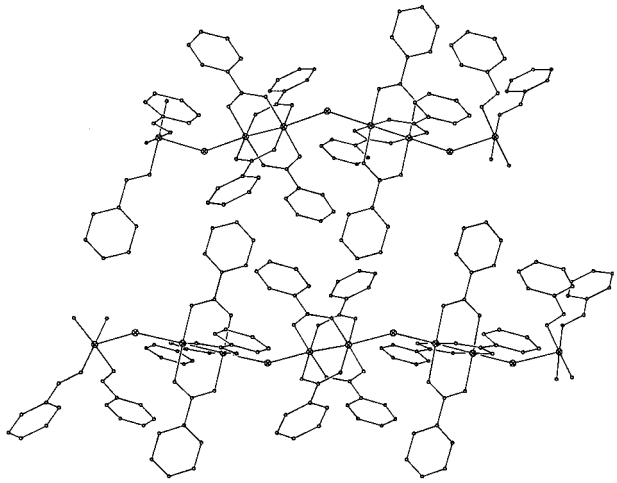

Figure 2. Packing of the polymeric complex **1**

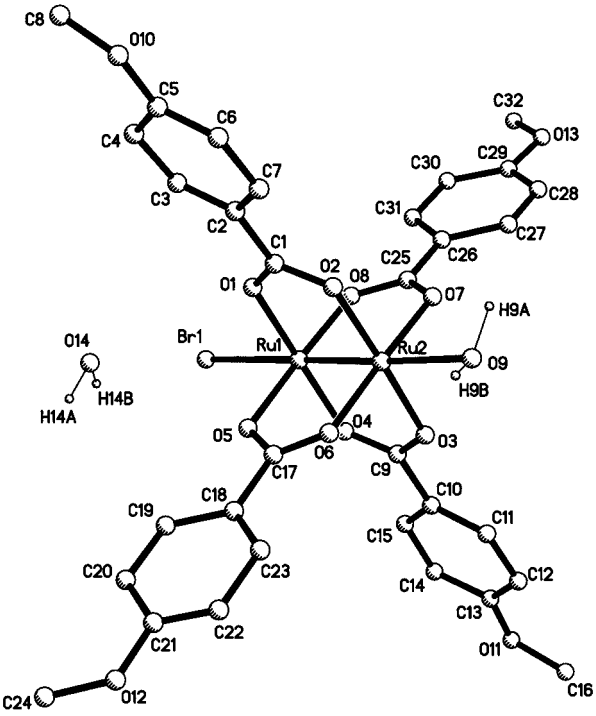

Figure 3. PLUTO view of $[Ru_2Br(\mu\text{-}O_2CC_6H_4\text{-}p\text{-}OMe)_4(H_2O)]\cdot H_2O$ (**3**·H_2O); hydrogen atoms, except in water molecules, have been omitted for clarity

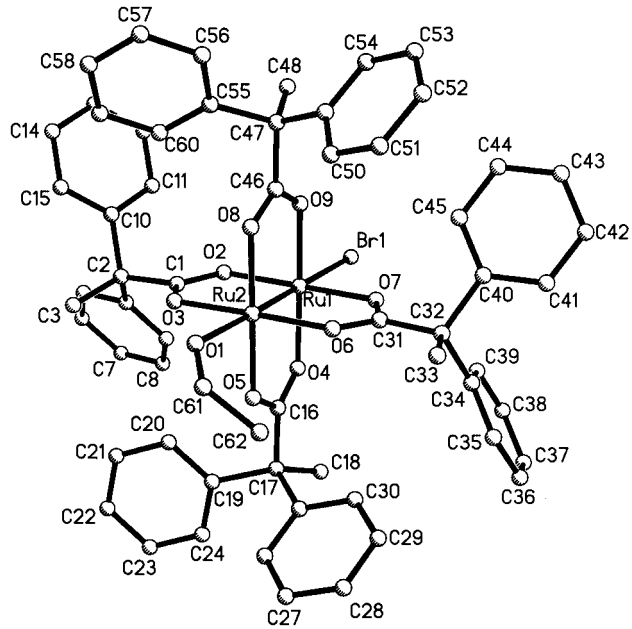

Figure 4. PLUTO view of $[Ru_2Br(\mu\text{-}O_2CCMePh_2)_4(EtOH)]\cdot 0.5EtOH$ (**5**·0.5EtOH); crystallization solvent molecules and hydrogen atoms have been omitted for clarity

The molecular structures of complexes **3**·H_2O (Figure 3) and **5**·0.5EtOH (Figure 4) consists of discrete dinuclear molecules of $[Ru_2Br(\mu\text{-}O_2CR)_4(S)]$ (S = solvent molecule). The dinuclear unit of **3**·H_2O has one bromide atom and one water molecule in the axial positions. The crystallisation water molecule is hydrogen bonded to the coordinated water of a dinuclear unit and to the bromide ligand of another dimetallic molecule. The molecular structure of **5**·0.5EtOH is similar, with one of the axial positions occupied by an ethanol molecule instead of a water molecule. In this compound, the possible presence of hydrogen bonds could not be established due to the low quality of the crystal.

The molecular nature of these bromo derivatives contrasts with the polymeric chains found in the formate derivative[20] and with the above-described benzoate complex **1**. The formation of discrete dinuclear molecules in **3**·H_2O

 © 2004 Wiley-VCH Verlag GmbH & Co. KGaA, Weinheim

in the solid state is more surprising because all chloro derivatives with arenecarboxylate ligands,[1−3] including the *p*-methoxybenzoate complex[9] $[Ru_2Cl(\mu\text{-}O_2CC_6H_4\text{-}p\text{-}OMe)_4]_n$, have a polymeric structure. Complexes **3**·H_2O and **5**·0.5EtOH are the first examples of halotetraarenecarboxylatodiruthenium(II,III) compounds with a nonpolymeric arrangement. This molecular nature indicates that the axial ligands play a key role in the arrangement of these diruthenium(II,III) complexes in the solid state.

The Ru−Br bond lengths for **1**, **3**·H_2O, and **5**·0.5EtOH are 2.6700(5), 2.671(2), and 2.6108(17) Å, respectively. In the molecular complex **5**·0.5EtOH the Ru−Br bond length is shorter than in the polymeric compound **1** and in $[Ru_2Br(\mu\text{-}O_2CH)_4]_n$ [2.7170(8)−2.7313(9) Å].[20] This fact is consistent with the variation observed in the Ru−Cl distances in the analogous molecular and polymeric chlorotetracarboxylatodiruthenium(II,III) complexes.[4−19] However, the Ru−Br distance in the molecular compound **3**·H_2O is slightly longer than in polymeric **1**.

Crystal Structures of $[Ru_2I(\mu\text{-}O_2CPh)_4]$ (2), $[Ru_2I(\mu\text{-}O_2CC_6H_4\text{-}p\text{-}OMe)_4(H_2O)]\cdot H_2O$ (4·H_2O), and $[Ru_2I(\mu\text{-}O_2CCMePh_2)_4(MeOH)]\cdot 0.5H_2O$ (6·0.5H_2O)

Figure 5 shows a PLUTO view of the dinuclear unit of **2**. Selected bond lengths and angles are collected in Table 2. The arrangement in the solid state — zigzag chains with an iodide ligand linking the $[Ru_2(\mu\text{-}O_2CPh)_4]^+$ units — is similar to that found in **1**. The chains are separated by normal van der Waals forces. The Ru−I−Ru angle is 114.246(18)° and the Ru−I distance [2.8562(4) Å] is longer than the Ru−Br distance [2.6700(5) Å] in **1**. This large bond length is in accordance with the size of the axial ligand. The Ru−Ru distance [2.2965(6) Å] is longer than those observed in the chloro derivatives [2.267(1)−2.292(7) Å]. It is independent of the type of arrangement in the solid state[4−19] and is similar to that found[19] in $[Ru_2(\mu\text{-}O_2CCH_2CH_2OPh)_4(H_2O)_2][Ru_2I_2(\mu\text{-}O_2CCH_2CH_2OPh)_4]$ [2.310(2) Å].

Complexes **4**·H_2O (Figure 6) and **6**·0.5H_2O (Figure 7) have molecular structures analogous to those of **3**·H_2O and **5**·0.5EtOH. Selected bond lengths and angles are listed in Table 2. The structural parameters of the $[Ru_2(\mu\text{-}O_2C)_4]$ units are similar in the four complexes. In compounds **4**·H_2O and **6**·0.5H_2O one axial position is occupied by an iodide ligand and the other one is occupied by a water molecule or a MeOH ligand, respectively. In complex **4**·H_2O the water molecule of crystallization is hydrogen bonded to the coordinated water of a dinuclear unit and to the bromide ligand of another dimetallic molecule, similarly to **3**·H_2O. The Ru−I bond lengths in **4**·H_2O and **6**·0.5H_2O are 2.831(4) and 2.8055(10) Å, respectively, which are shorter than that observed for compound **2**. The Ru−I distances in these tetracarboxylatodiruthenium(II,III) derivatives are also shorter than those found in the benzamidinatediruthenium(III) complex[21] $[Ru_2I_2(DMBA)_4]$ [2.917(1) and 2960(1) Å].

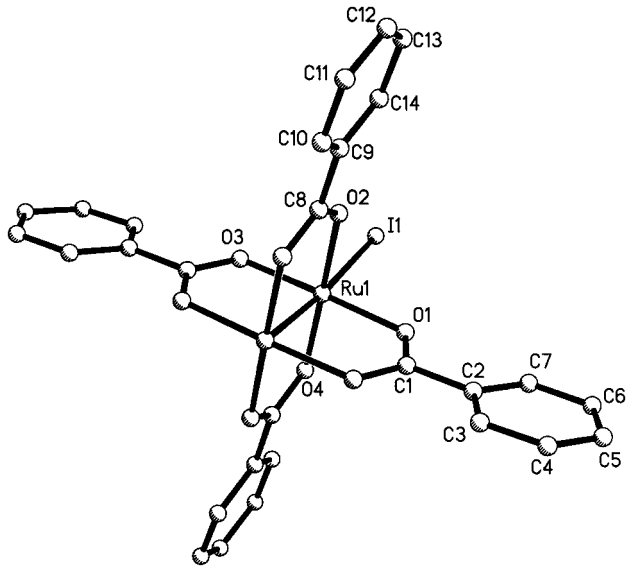

Figure 5. PLUTO view of $[Ru_2I(\mu\text{-}O_2CPh)_4]$ (**2**); hydrogen atoms have been omitted for clarity

Magnetic Properties

Magnetic measurements of the compounds show magnetic moments at room temperature of 4.09−4.36 μ_B in all cases. These values correspond to the presence of three unpaired electrons per dimer unit, in accordance with the ground-state configuration $\sigma^2\pi^4\delta^2(\pi^*\delta^*)^3$ proposed by Norman et al.[23] In all cases the molar magnetic susceptibility increases with decreasing temperature and no maximum is observed. The magnetic moments of these complexes decrease with temperature. This behaviour is usual in this type of complexes and has been ascribed[11,13,15,19,24−27] to a large zero-field splitting (ZFS) and some degree of antiferromagnetic coupling between the dimetallic units. The zero-field splitting effect on the susceptibility can be quantified by considering the Hamiltonian $H_D = S\cdot D\cdot S$, as described by O'Connor.[28] The perturbation of a weak antiferromagnetic coupling over the zero-field splitting system can be considered by using the molecular field approximation.[28] Thus, for an $S = 3/2$ spin system the magnetic suscpetibility can be expressed as:

$$\chi' = \chi'_M/[1 - (2zJ/Ng^2\beta^2)\chi'_M]$$

where χ'_M includes the temperature independent paramagnetism (TIP)

$$\chi'_M = \chi_M + \text{TIP}$$

and

$\chi_M = (\chi_\parallel + 2\chi_\perp)/3$,
$\chi_\parallel = (Ng^2\beta^2/kT)(1 + 9e^{-2D/kT})/4(1 + e^{-2D/kT})$ and
$\chi_\perp = (Ng^2\beta^2/kT)[4 + (3kT/D)(1 - e^{-2D/kT})]/4(1 + e^{-2D/kT})$.

Finally, the consideration of a paramagnetic impurity (P) leads to the expression

$$\chi'_{mol} = [(1 - P)\chi'] + [PNg^2_{mo}\beta^2/4kT]$$

which has been used previously[13,15,19] in the fits of similar diruthenium complexes.

 © 2004 Wiley-VCH Verlag GmbH & Co. KGaA, Weinheim

Table 2. Selected bond lengths (Å) and angles (°) for $[Ru_2I(\mu\text{-}O_2CPh)_4]$ (**2**), $[Ru_2I(\mu\text{-}O_2CC_6H_4\text{-}p\text{-}OMe)_4(H_2O)]\cdot H_2O$ (**4**·H_2O), and $[Ru_2I(\mu\text{-}O_2CCMePh_2)_4(MeOH)]\cdot 0.5H_2O$ (**6**·$0.5H_2O$); symmetry transformations used to generate equivalent atoms: #1: $-x + 1, -y + 1, -z + 1$; #2: $-x + 1, y, -z + 1/2$.

2		**4**·H_2O		**6**·$0.5H_2O$	
Ru(1)−Ru(1)#1	2.2965(6)	Ru(2)−Ru(1)	2.273(3)	Ru(1)−Ru(2)	2.2902(11)
Ru(1)−I(1)	2.8562(4)	Ru(1)−I(1)	2.831(4)	Ru(2)−I(1)	2.8055(10)
Ru(1)−O(1)	2.018(3)	Ru(1)−O(1)	2.00(2)	Ru(1)−O(1)	2.010(6)
Ru(1)−O(2)	2.023(2)	Ru(1)−O(4)	2.032(19)	Ru(1)−O(4)	2.021(6)
Ru(1)−O(3)	2.021(3)	Ru(1)−O(5)	2.007(19)	Ru(1)−O(6)	1.999(6)
Ru(1)−O(4)	2.023(2)	Ru(1)−O(8)	1.987(19)	Ru(1)−O(7)	2.014(6)
I(1)−Ru(1)#2	2.8562(4)	Ru(2)−O(2)	1.99(2)	Ru(1)−O(17)	2.314(8)
Ru(1)#1−Ru(1)−I(1)	174.71(2)	Ru(2)−O(3)	2.00(2)	Ru(2)−O(2)	2.042(6)
Ru(1)−I(1)−Ru(1)#2	114.246(18)	Ru(2)−O(6)	1.970(18)	Ru(2)−O(3)	2.038(6)
O(1)−Ru(1)−Ru(1)#1	89.70(8)	Ru(2)−O(7)	1.964(17)	Ru(2)−O(5)	2.039(6)
O(2)−Ru(1)−Ru(1)#1	88.51(8)	Ru(2)−O(9)	2.288(19)	Ru(2)−O(8)	2.050(6)
O(3)−Ru(1)−Ru(1)#1	88.45(8)	Ru(2)−Ru(1)−I(1)	176.87(15)	Ru(1)−Ru(2)−I(1)	176.68(4)
O(4)−Ru(1)−Ru(1)#1	89.81(8)	O(9)−Ru(2)−Ru(1)	178.0(5)	Ru(2)−Ru(1)−O(17)	177.64(19)
		O(1)−Ru(1)−Ru(2)	88.1(6)	O(1)−Ru(1)−Ru(2)	90.31(19)
		O(4)−Ru(1)−Ru(2)	87.8(6)	O(4)−Ru(1)−Ru(2)	90.18(19)
		O(5)−Ru(1)−Ru(2)	87.3(6)	O(6)−Ru(1)−Ru(2)	89.37(19)
		O(8)−Ru(1)−Ru(2)	90.4(6)	O(7)−Ru(1)−Ru(2)	90.5(2)
		O(2)−Ru(2)−Ru(1)	90.3(6)	O(2)−Ru(2)−Ru(1)	87.59(19)
		O(3)−Ru(2)−Ru(1)	88.8(7)	O(3)−Ru(2)−Ru(1)	88.2(2)
		O(6)−Ru(2)−Ru(1)	90.7(6)	O(5)−Ru(2)−Ru(1)	88.53(19)
		O(7)−Ru(2)−Ru(1)	90.7(6)	O(8)−Ru(2)−Ru(1)	87.68(19)
				C(121)−O(17)−Ru(1)	125.5(8)

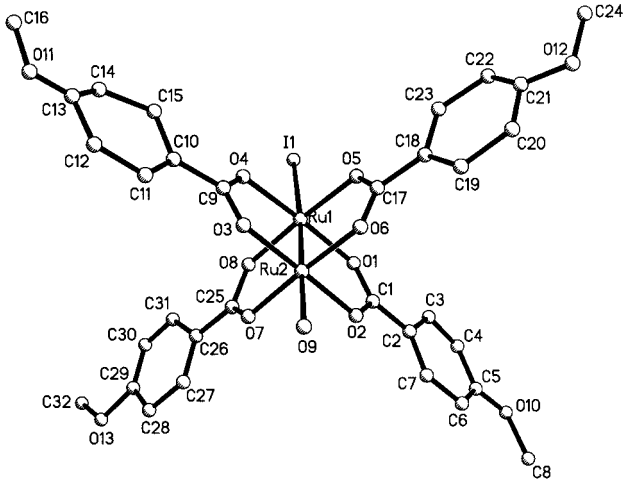

Figure 6. PLUTO view of $[Ru_2I(\mu\text{-}O_2CC_6H_4\text{-}p\text{-}OMe)_4(H_2O)]\cdot H_2O$ (**4**·H_2O); crystallization solvent molecules and hydrogen atoms have been omitted for clarity

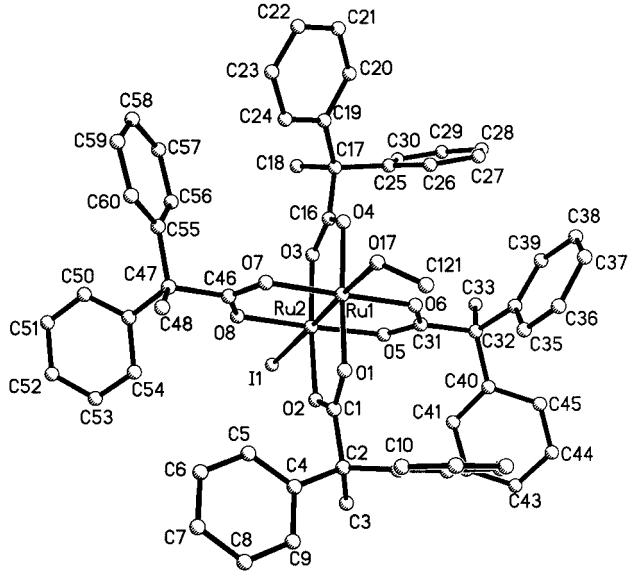

Figure 7. PLUTO view of $[Ru_2I(\mu\text{-}O_2CCMePh_2)_4(MeOH)]\cdot 0.5H_2O$ (**6**·$0.5H_2O$); crystallization solvent molecules and hydrogen atoms have been omitted for clarity

The magnetic parameters obtained in the fit of the magnetic data of complexes **1**−**4** using this model are collected in Table 3. The magnetic properties of complexes **5**·0.5EtOH and **6**·$0.5H_2O$ are analogous to those described previously[19] for $[Ru_2X(\mu\text{-}O_2CCMePh_2)_4(H_2O)]$ (X = Br, I).

A very good agreement between the experimental and calculated curves of the magnetic moment and the molar susceptibility for complexes **1**−**4** was observed. Figure 8 shows the experimental and calculated curves for complex **1** using the above-mentioned model. Similar curves have been obtained for the other complexes, with *D* values ranging from 63.4 to 71.5 cm^{-1}. Similar *D* values have been calculated for other tetracarboxylato complexes.[13,15,19] These large *D* values are a consequence of the presence of two second row transition metal atoms and the existence of several vacant energy levels near the HOMO level in the diruthenium unit, as described by Norman et al.[23] The *zJ* values for complexes **3** and **4** are low as is expected from their molecular nature. Low *zJ* values are also observed in **1** and **2,** as expected for polymeric complexes with Ru−X−Ru angles lower than 125°.[13,15,19] The higher *zJ* value of the bromo complex **1** with respect to the iodo complex **2** could

 © 2004 Wiley-VCH Verlag GmbH & Co. KGaA, Weinheim

Table 3. Magnetic parameters obtained in the fits of the magnetic moment as a function of temperature

Compound	g	D (cm^{-1})	zJ (cm^{-1})	TIP (mL/mol)	P (%)	$\sigma^{2[a]}$
1	2.16	63.4	−1.37	$3.46\ 10^{-4}$	0.08	8.80×10^{-6}
2	2.15	71.5	−0.03	$<10^{-6}$	2.67×10^{-3}	3.27×10^{-5}
3·H_2O	2.30	70.0	−0.04	$<10^{-6}$	0.03	8.10×10^{-4}
4·H_2O	2.35	70.0	−0.04	$<10^{-6}$	8.80×10^{-3}	4.93×10^{-4}

[a] $\sigma^2 = \Sigma(\mu_{eff.calcd.} - \mu_{eff.exp.})^2/\Sigma\mu_{eff.exp.}^2$.

be due to the better overlap between the π-type lone-pair orbital of the bromo ligand and the π*(Ru−Ru) orbital as the overlapping of the π-type halogen and ruthenium orbitals in these complexes becomes smaller for the heavier halide ligand.

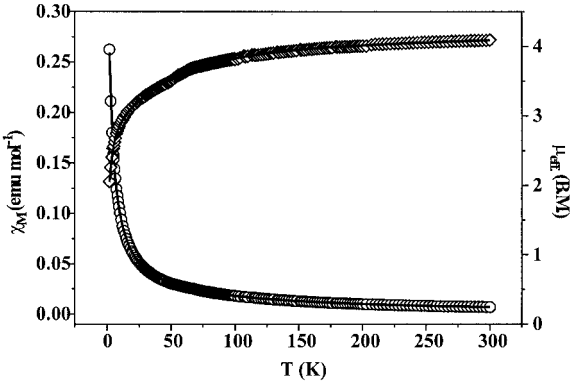

Figure 8. Temperature dependence of the molar susceptibility χ_M (circles) and $\mu_{eff.}$ (rhombs) for complex **1**; solid lines are the product of a least-squares fit to the model indicated in the text

Electronic Properties

The absorption data in the visible-UV−NIR range for solutions of complexes **1**−**6** in several solvents are given in Table 4.

The electronic spectra of the complexes in methanol solution mainly show two bands in the visible-UV range at about 430 and 330 nm. The major absorption band in the visible range (430 nm) is unambiguously assigned to a π(RuO,Ru_2) → π*(Ru_2) transition according to Norman et al.[23] and Miskowski and Gray.[29] The metal-metal character ($Ru_2 \rightarrow Ru_2$) of this transition has been well established by resonance Raman studies[29,30] although the amount of ligand to metal charge transfer (LMCT) (RuO → Ru_2) seems to be questionable. The band observed at ca. 330 nm could be assigned to a ligand-to-metal charge transfer π(axial ligand) → π*(Ru_2) transition. This assignment is in accordance with that described previously for other tetracarboxylatodiruthenium(II,III) complexes.[1,3,29]

The complexes **1**−**6** are 1:1 electrolytes in MeOH and DMSO solutions. As a consequence, the cation [Ru_2(μ-O_2CR)$_4$(S)$_2$]$^+$ (S = solvent) is present in solution and no dependence on the nature of the halogen is observed. However, the conductivity measurements in acetone, acetonitrile and THF indicate that these complexes are nonelectrolytes and the monoadducts [Ru_2X(μ-O_2CR)$_4$(S)] must exist in solution.

In order to compare the electronic spectra of this series of chloro-, bromo-, and iodotetracarboxylatodiruthenium(II,III) derivatives, the UV/Vis-NIR data of the chloro compounds [Ru_2Cl(μ-O_2CR)$_4$] (R = C_6H_4-*p*-OMe, $CMePh_2$) were also recorded (Table 4). However, the spectra of the chlorotetrabenzoate complex was not measured due to its insolubility.

The first absorption band observed in the chloro complexes in the range 317−339 nm could be assigned to an LMCT π(axial ligand) → π*(Ru_2) transition similar to that described above for the [Ru_2(μ-O_2CR)$_4$(MeOH)$_2$]$^+$ species. This band is shifted to 340−400 nm and to 409−445 nm in the bromo and iodo complexes, respectively. This assignment is in accordance with the sensibility of this transition to the axial ligand and with the strong, systematic red shift predicted for the change from chloro to iodo. An analogous shift has been described in the UV/Vis spectra of the dibromo and diiodo complexes[29] (Bu_4N)[Ru_2Br_2(μ-O_2CPr)$_4$] and (Bu_4N)[Ru_2I_2(μ-O_2CPr)$_4$]. The first high-intensity absorption observed in the iodo complexes in the range 344−383 nm could be assigned to an LMCT σ(axial ligand) → σ*(Ru_2) transition, in agreement with those described[29] for the 307 nm band observed in the diodo anion [Ru_2I_2(μ-O_2CR)$_4$]$^-$.

The second absorption band observed in the chloro complexes in the range 464−467 nm is assigned to the π(RuO,Ru_2) → π*(Ru_2) transition. This absorption is slightly red-shifted in the bromo derivatives (476−494 nm), whereas in the iodo compounds it is strongly shifted (564−625 nm). This absorption should be only very weakly sensitive to the nature of the axial ligand,[1,3,29] although it has been described that in the diiodo complex (Bu_4N)-[Ru_2I_2(μ-O_2CPr)$_4$] it is strongly perturbed. This perturbation could be due to the mixing of this transition with the π(axial ligand) → π*(Ru_2) charge transfer.[29] Figure 9 shows the electronic spectra of the 2,2-diphenylpropionato derivatives [Ru_2X(μ-O_2CC$Me Ph_2$)$_4$] (X = Cl, Br, I) in acetone.

The chloro and bromo derivatives also display a very weak shoulder in the range 553−622 nm which is shifted to 712−754 nm in the iodo compounds. This band could be assigned to a σ(Ru-axial ligand) → π*(Ru_2) transition in accordance with the very weak and poorly defined band at ca. 560 nm observed in some chloro complexes [Ru_2Cl(μ-O_2CR)$_4$].[8,23,29]

All the complexes show a weak absorption band in the range 981−1166 nm in the NIR region due to the δ → δ* transition.

 © 2004 Wiley-VCH Verlag GmbH & Co. KGaA, Weinheim

Table 4. Electronic spectra data for $[Ru_2X(\mu\text{-}O_2CR)_4]$

Compound R	X		λ (nm) (ε; $dm^3 \cdot mol^{-1} \cdot cm^{-1}$) σ(axial ligand) → σ*($Ru_2$)	π(axial ligand) → π*(Ru_2)	π(RuO,Ru_2) → π*(Ru_2)	σ(axial ligand) → π*(Ru_2)	δ(Ru_2) → δ*(Ru_2)
			MeOH				
Ph	Br	**1**		335 sh (3032)	434 (743)	523 sh (118)	1040 (52)
	I	**2**		333 sh (3074)	433 (715)	522 sh (188)	1012 (49)
C_6H_4-*p*-OMe	Cl	[a]		385 sh (1233)	427 (786)		1092 (48)
	Br	**3**		358 sh (1637)	427 (552)		1108 (31)
	I	**4**		372 sh (2076)	425 (1125)		1105 (69)
$CMePh_2$	Cl	[b]		335 (1325)	425 (983)	533 sh (263)	987 (34)
	Br	**5**		336 sh (1024)	425 (807)	531 sh (200)	988 (32)
	I	**6**		335 sh (1024)	425 (850)	531 sh (254)	986 (52)
			DMSO				
Ph	Br	**1**		336 sh (4239)	438 (1011)	564 (528)	994 (84)
	I	**2**		333 sh (5355)	437 (1020)	561 (493)	995 (52)
C_6H_4-*p*-OMe	Cl	[a]		386 sh (1469)	444 (930)	562 sh (293)	1137 (32)
	Br	**3**		384 sh (1579)	439 (982)	542 sh (364)	1125 (37)
	I	**4**		370 sh (2515)	441 (1251)	552 sh (397)	1166 (53)
$CMePh_2$	Cl	[b]		324 (2261)	438 (1104)	562 (553)	1040 (47)
	Br	**5**		320 sh (2153)	438 (1081)	557 (379)	1033 (46)
	I	**6**		320 sh (2191)	438 (1050)	557 (344)	986 (35)
			Acetone				
Ph	Br	**1**	insoluble				
	I	**2**	344 sh (5056)	419 (2071)	593 (2142)	737 sh (373)	1153 (106)
C_6H_4-*p*-OMe	Cl	[a]	insoluble				
	Br	**3**	insoluble				
	I	**4**	383 sh (2605)	412 sh (2282)	579 (2027)	712 sh (363)	1153 (96)
$CMePh_2$	Cl	[b]		329 (6718)	464 (2012)	595 sh (468)	1065 (105)
	Br	**5**		370 (3722)	483 (2230)	602 sh (407)	1097 (157)
	I	**6**	349 sh (3849)	418 (2796)	599 (2673)	718 sh (726)	1102 (228)
			THF				
Ph	Br	**1**		377 (3127)	492 (1772)	619 sh (182)	981 (50)
	I	**2**	347 sh (10252)	409 sh (3086)	625 (1577)	738 sh (360)	960 sh (83)
C_6H_4-*p*-OMe	Cl	[a]			467 (2376)	581 sh (433)	1169 (83)
	Br	**3**		366 (4359)	490 (1884)	604 sh (274)	1160 (54)
	I	**4**	354 sh (7680)	418 sh (3016)	612 (2510)	754 sh (395)	1000 (82)
$CMePh_2$	Cl	[b]		339 (3521)	465 (1182)	577 sh (249)	1073 (106)
	Br	**5**		381 (3367)	494 (2512)	622 sh (256)	1093 (59)
	I	**6**	366 (5351)	444 sh (1230)	614 (400)		1113 (35)
			CH_3CN				
Ph	Br	**1**	insoluble				
	I	**2**	348 (6065)		573 (1861)		
C_6H_4-*p*-OMe	Cl	[a]	insoluble				
	Br	**3**		347 sh (4634)	476 (1241)	576 sh (453)	1161 (61)
	I	**4**	348 sh (4399)	445 sh (1145)	564 (1413)		1151 (92)
$CMePh_2$	Cl	[b]		317 (4659)	464 (1215)	553 sh (664)	
	Br	**5**		363 (2731)	477 (1479)	565 sh (532)	1102 (64)
	I	**6**	356 (4396)	409 sh (2075)	585 (1517)		1108 (67)

[a] $[Ru_2Cl(\mu\text{-}O_2CC_2H_4\text{-}p\text{-}OMe)_4]$. [b] $[Ru_2Cl(\mu\text{-}O_2CCMePh_2)_4]$.

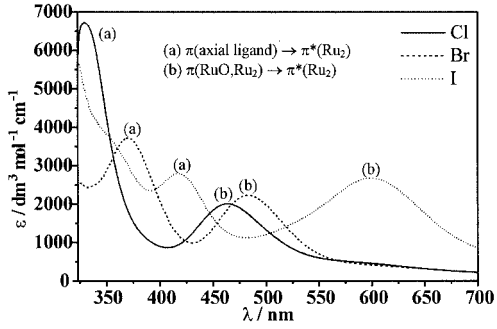

Figure 9. Electronic spectra of $[Ru_2X(\mu\text{-}O_2CCMePh_2)_4]$ in acetone

The variations in the absorption bands imply important colour changes of the solutions of the complexes. All compounds are yellow in methanol or DMSO solutions, due to the existence of the π(RuO,Ru_2) → π*(Ru_2) transition in the visible range. The acetonitrile, acetone, and THF solutions of the chloro derivatives have a similar yellow-brown colour and the bromo derivatives show a little solvatochromism, whose colours change from yellow-orange to pink. However, the iodo derivatives in acetone, acetonitrile and THF are blue, violet, and green respectively. The $[Ru_2I(\mu\text{-}O_2CR)_4(S)]$ complexes display two transitions in the visible range, but the colour changes seems to be related mainly

 © 2004 Wiley-VCH Verlag GmbH & Co. KGaA, Weinheim

with the presence, position, and intensity of the second band, in which the axial ligands have a great influence. In summary, the electronic data of the halotetracarboxylatodiruthenium(II,III) complexes indicate that the solvatochromism of these complexes can be ascribed to the combined influence of the halide and the solvent molecule bonded to the axial positions.

Conclusions

In this work we have found that complexes of the type $[Ru_2X(\mu\text{-}O_2CR)_4]$ (X = Br, I) give polymeric zigzag chains with R = Ph and discrete dinuclear molecules with R = C_6H_4-*p*-OMe or $CMePh_2$ ligands. These examples represent the first nonpolymeric complexes with arenecarboxylate bridging ligands, and indicate that the polymeric or molecular nature of this type of compounds is due to the influence of the equatorial and axial ligands. The presence of chloride, bromide or iodide as axial ligand in the diruthenium complexes produce a shift of the LMCT bands to lower energy. In the iodo derivatives a strong shift of the $\pi(RuO,Ru_2) \rightarrow \pi^*(Ru_2)$ transition is also induced, thereby producing solvatochromism for these complexes.

Experimental Section

General Remarks: All reactions were carried out under an inert atmosphere, using standard Schlenk techniques. Ruthenium trichloride, carboxylic acids and solvents were obtained from commercial sources and used without previous purification. The complexes $[Ru_2Cl(\mu\text{-}O_2CR)_4]$ (R = C_6H_4-*p*-OMe, $CMePh_2$, Ph) were prepared by literature procedures.[9,11,31] IR spectra were recorded as KBr discs on a Nicolet Magna-FTIR 550 spectrophotometer. Elemental analysis of C and H were performed by the Microanalytical Service of the Complutense University of Madrid. Electronic spectra in the range 250−1300 nm were recorded on a Cary 5G spectrophotometer in 10^{-4} M solutions in methanol, DMSO, acetone, THF, or acetonitrile. The variable-temperature magnetic susceptibility data were measured on a Quantum Design MPMSXL SQUID (Superconducting Quantum Interference Device) susceptometer over a temperature range of 2 to 300 K. Each raw data point was corrected for the diamagnetic contribution of both the sample holder and the compound to the susceptibility. The molar diamagnetic corrections for the complexes were calculated on the basis of Pascal's constants. The fits of experimental data were carried out using the commercial MATLAB V.5.1.0.421 program. Mass spectra were obtained on a Bruker Esquire-LC with Electrospray Ionization (ESI) using chloroform, methanol, THF, or DMSO as solvent. Nominal molecular masses and isotopic distributions of all peaks were calculated with the MASAS[32] computer program,

Table 5. Crystal data for $[Ru_2Br(\mu\text{-}O_2CPh)_4]$ (**1**), $[Ru_2Br(\mu\text{-}O_2CC_6H_4\text{-}p\text{-}OMe)_4(H_2O)]\cdot H_2O$ (**3**·H_2O), and $[Ru_2Br(\mu\text{-}O_2CCMePh_2)_4(EtOH)]\cdot 0.5EtOH$ (**5**·0.5EtOH)

	1	**3**·H_2O	**5**·0.5EtOH
Empirical formula	$C_{28}H_{20}BrO_8Ru_2$	$C_{32}H_{32}BrO_{14}Ru_2$	$C_{63}H_{60}BrO_{9.5}Ru_2$
Molecular mass	766.49	922.63	1251.16
Crystal system	monoclinic	tetragonal	monoclinic
Space group	*C*2/*c*	$P4_32_12$	$P2_1/n$
a (Å)	20.9722(16)	15.8370(6)	14.6671(11)
b (Å)	10.9455(9)	15.8370(6)	23.2288(18)
c (Å)	13.1733(10)	30.2980(15)	17.7816(13)
a (°)	90	90	90
β (°)	108.9060(10)	90	103.364(2)
γ (°)	90	90	90
Volume (Å^3)	2860.8(4)	7599.1(6)	5894.1(8)
Z	4	8	4
$D_{calcd.}$ (g cm^{-3})	1.780	1.613	1.410
μ (mm^{-1})	2.499	1.908	1.245
F(000)	1500	3672	2548
Crystal size (mm^3)	0.06 × 0.11 × 0.13	0.10 × 0.34 × 0.37	0.07 × 0.15 × 0.20
θ range (°)	2.05 to 25.00	1.45 to 25.00	1.47 to 25.00
Index ranges	$-24 \le h \le 13$	$-18 \le h \le 16$	$-17 \le h \le 15$
	$-13 \le k \le 12$	$16 \le k \le 18$	$27 \le k \le 27$
	$-15 \le l \le 15$	$36 \le l \le 35$	$21 \le l \le 18$
Collected reflections	7310	40017	30716
Independent reflections	2500 [*R*(int) = 0.0521]	6706 [*R*(int) = 0.1394]	10358 [*R*(int) = 0.1270]
Completeness to θ = 25.00° (%)	99.5	100.0	99.7
Absorption correction	none	none	none
Refinement method	full-matrix least-squares on F^2	full-matrix least-squares on F^2	full-matrix least-squares on F^2
Data/restraints/parameters	2500/0/177	6706/0/438	10358/8/258
Goodness-of-fit on F^2	0.910	1.048	0.993
Final *R* values [$I > 2\sigma(I)$]	*R*1 = 0.0320, *wR*2 = 0.0549	*R*1 = 0.0645, *wR*2 = 0.1686	*R*1 = 0.0908, *wR*2 = 0.2470
R values (all data)	*R*1 = 0.0529, *wR*2 = 0.0597	*R*1 = 0.1628, *wR*2 = 0.2164	*R*1 = 0.2053, *wR*2 = 0.2983
Largest diff. peak/hole (e·Å^{-3})	0.516 and −0.497	1.785 and −0.633	1.925 and −1.092

 © 2004 Wiley-VCH Verlag GmbH & Co. KGaA, Weinheim

using a polynomial expansion based on natural abundances of the isotopes.

Preparation of [$Ru_2Br(\mu\text{-}O_2CPh)_4$] (1): Silver tetrafluoroborate (0.07 g, 0.35 mmol) was added to a suspension of [$Ru_2Cl(\mu\text{-}O_2CPh)_4$] (0.25 g, 0.35 mmol) in THF (30 mL). The reaction mixture was stirred for 24 h, giving a solid precipitate of AgCl and a brown solution. The precipitate was filtered through celite and the solution was pumped to dryness. The solid was dissolved in ethanol (10 mL) and treated with a water solution (10 mL) of KBr (0.42 g, 3.50 mmol) giving a light brown precipitate, which was filtered off, washed with water (3 × 20 mL) and dried under vacuum. Single crystals were obtained by slow interdiffusion of the above-mentioned ethanol solution and the aqueous solution of KBr. Yield 0.16 g (59%). $C_{28}H_{20}BrO_8Ru_2$ (766.52): calcd. C 43.88, H 2.63; found C 43.80, H 2.69. IR (KBr): $\tilde{\nu}$ = 3067 w, 3050 w, 1600 m, 1495 m, 1465 s, 1408 vs, 1177 w, 1143 w, 1081 w, 1002 w, 845 w, 715 s, 689 s, 531 m cm^{-1}. $\mu_{eff.}$ = 4.09 μ_B at room temperature. MS in DMSO/MeOH (ESI^+): *m*/*z* = 767 [M^+], 688 [$M^+ - Br$]; (ESI^-): *m*/*z* = 848 [$M^- + Br$].

Preparation of [$Ru_2I(\mu\text{-}O_2CPh)_4$] (2): The reaction was carried out as mentioned above for **1**, using KI (0.58 g, 3.50 mmol) instead of KBr. Yield 0.16 g (57%). $C_{28}H_{20}IO_8Ru_2$ (813.51): calcd. C 41.34, H 2.48; found C 41.20, H 2.45. IR (KBr): $\tilde{\nu}$ = 3066 w, 1600 m, 1495 m, 1464 s, 1408 vs, 1176 w, 1143 w, 1071 w, 1002 w, 845 w, 715 s, 689 s, 529 m cm^{-1}. $\mu_{eff.}$ = 4.16 μ_B at room temperature. MS in THF/$CHCl_3$ (ESI^+): *m*/*z* = 688 [$M^+ - I$]; (ESI^-): *m*/*z* = 942 [$M^- + I$].

Preparation of [$Ru_2Br(\mu\text{-}O_2CC_6H_4\text{-}p\text{-}OMe)_4(H_2O)$] (3): The reaction was carried out as described above for **1**, using [$Ru_2Cl(\mu\text{-}O_2CC_6H_4\text{-}p\text{-}OMe)_4$] (0.29 g, 0.35 mmol). The solid isolated was characterized as **3**. Single crystals of **3**·H_2O were obtained by evaporation in air of a solution of **3** in methanol. Yield 0.22 g (69%). $C_{32}H_{30}BrO_{13}Ru_2$ (904.64): calcd. C 42.49, H 3.34; found C 42.40, H 3.27. IR (KBr): $\tilde{\nu}$ = 3447 w, 3015 w, 2960 w, 2935 w, 2838 w, 1605 s, 1583 w, 1442 m, 1396 vs, 1315 w, 1304 w, 1261 s, 1172 s, 1109 w, 1025 w, 849 w, 773 m, 702 w, 649 m, 527 w, 511 w, 459 w cm^{-1}. $\mu_{eff.}$ = 4.12 μ_B at room temperature. MS in $CHCl_3$ (ESI^+): *m*/*z* = 808 [$M^+ - Br - H_2O$]; (ESI^-): *m*/*z* = 968 [$M^- + Br - H_2O$].

Preparation of [$Ru_2I(\mu\text{-}O_2CC_6H_4\text{-}p\text{-}OMe)_4(H_2O)$] (4): The reaction was carried out as described above for **2**, using [$Ru_2Cl(\mu\text{-}O_2CC_6H_4\text{-}p\text{-}OMe)_4$] (0.29 g, 0.35 mmol). The brown-violet solid obtained in this way was characterized as **4**. Single crystals of **4**·H_2O were obtained by dissolving **4** in hot methanol (20 mL) and allowing this solution to stand at room temperature and then at −18 °C. Yield 0.21 g (64%). $C_{32}H_{30}IO_{13}Ru_2$ (951.63): calcd. C 40.39, H 3.18; found C 40.26, H 3.08. IR (KBr): $\tilde{\nu}$ = 3447 w, 3078 w, 3013 w, 2961 w, 2934 w, 2837 w, 1605 vs, 1583 m, 1442 s, 1393 vs, 1315 m, 1303 m, 1260 vs, 1172 vs, 1109 w, 1026 m, 849 m, 773 s, 702 w, 668 m, 649 m, 529 w, 511 w, 458 w cm^{-1}. $\mu_{eff.}$ = 4.36 μ_B at room

Table 6. Crystal data for [$Ru_2I(\mu\text{-}O_2CPh)_4$] (**2**), [$Ru_2I(\mu\text{-}O_2CC_6H_4\text{-}p\text{-}OMe)_4(H_2O)$]·$H_2O$ [**4**·H_2O], and [$Ru_2I(\mu\text{-}O_2CCMePh_2)_4(MeOH)$]·0.5$H_2O$ [**6**·0.5H_2O].

	2	**4**·H_2O	**6**·0.5H_2O
Empirical formula	$C_{28}H_{20}IO_8Ru_2$	$C_{32}H_{28}IO_{14}Ru_2$	$C_{63}H_{60}BrO_{9.50}Ru_2$
Molecular weight	813.48	965.58	1251.16
Crystal system	monoclinic	tetragonal	monoclinic
Space group	*C*2/*c*	$P4_32_12$	$P2_1/n$
a (Å)	20.7489(15)	15.8723(10)	14.6671(11)
b (Å)	11.1708(8)	15.8723(10)	23.2288(18)
c (Å)	13.6401(10)	30.180(3)	17.7816(13)
α (°)	90	90	90
β (°)	109.1690(10)	90	103.364(2)
γ (°)	90	90	90
Volume ($Å^3$)	2986.2(4)	7603.2(9)	5894.1(8)
Z	4	8	4
$D_{calcd.}$ (g cm^{-3})	1.809	1.687	1.410
μ (mm^{-1})	2.090	1.668	1.245
F(000)	1572	3784	2548
Crystal size (mm^3)	0.04 × 0.08 × 0.29	0.04 × 0.09 × 0.11	0.07 × 0.15 × 0.20
θ range (°)	2.08 to 28.84	1.45 to 25.00	1.47 to 25.00
Index ranges	$-19 \le h \le 27$	$-18 \le h \le 17$	$-17 \le h \le 15$
	$14 \le k \le 13$	$13 \le k \le 18$	$27 \le k \le 27$
	$18 \le l \le 17$	$35 \le l \le 35$	$21 \le l \le 18$
Collected reflections	9428	40480	30716
Independent reflections	3623 [*R*(int) = 0.0491]	6708 [*R*(int) = 0.3321]	10358 [*R*(int) = 0.1270]
Completeness to θ (%)	92.6 to 28.84	100.0 to 25.00	99.7 to 24.71
Absorption correction	none	none	none
Refinement method	full-matrix least-squares on F^2	full-matrix least-squares on F^2	full-matrix least-squares on F^2
Data/restraints/parameters	3623/0/177	6708/0/447	10358/8/258
Goodness-of-fit on F^2	0.768	0.877	0.993
Final *R* values [$I > 2\sigma(I)$]	*R*1 = 0.0327, *wR*2 = 0.0600	*R*1 = 0.0890, *wR*2 = 0.2112	*R*1 = 0.0908, *wR*2 = 0.2470
R values (all data)	*R*1 = 0.0663, *wR*2 = 0.0716	*R*1 = 0.3155, *wR*2 = 0.3000	*R*1 = 0.2053, *wR*2 = 0.2983
Largest diff. peak/hole (e·$Å^{-3}$)	0.847 and −0.417	1.611 and −1.138	1.925 and −1.092

 © 2004 Wiley-VCH Verlag GmbH & Co. KGaA, Weinheim

temperature. MS in $CHCl_3$ (ESI^+): m/z = 808 [$M^+ - I - H_2O$]; (ESI^-): m/z = 1062 [$M^- + I - H_2O$].

Preparation of [$Ru_2Br(\mu\text{-}O_2CCMePh_2)_4(EtOH)$] (5): This complex was prepared by a literature procedure.[19] Single crystals of **5**·0.5EtOH were obtained by the procedure described for complex **1**. MS in DMSO/MeOH (ESI^+): m/z = 1261 [M^+ + DMSO], 1182 [M^+ + DMSO − Br]; (ESI^-): m/z = 1264 [M^- + Br].

Preparation of [$Ru_2I(\mu\text{-}O_2CCMePh_2)_4(MeOH)$] (6): This complex was prepared by a literature procedure.[19] Single crystals of **6**·0.5H_2O were obtained by the following procedure: A solution of [$Ru_2Cl(\mu\text{-}O_2CCMePh_2)_4$] (0.11 g, 0.10 mmol) in MeOH (15 mL), was treated with a water solution of $AgNO_3$ (0.017 g, 0.10 mmol). The solution was filtered and treated with an excess of PPh_4I (0.23 g, 0.50 mmol). Single crystals of **6**·0.5H_2O grew from this solution in 48 h. MS in $CHCl_3$/MeOH (ESI^+): m/z = 1104 [M^+ − I]; (ESI^-): m/z = 1358 [M^- + I].

X-ray Crystallographic Study: Details of the data collection and crystal structure refinement correction for **1**, **2**, **3**·H_2O, **4**·H_2O, **5**·0.5EtOH, and **6**·0.5H_2O are summarised in Table 5 and 6. Suitable crystals were mounted on a Bruker Smart-CCD diffractometer equipped with graphite-monochromated Mo-K_α (λ = 0.71073 Å) radiation. Data were collected at 293(2) K over a quadrant of the reciprocal space by combination of two exposure sets. Each exposure of 20 s covered 0.3 in ω. The cell parameters were refined by least-squares fit of all reflections collected. The structures were solved by Patterson (Ru atoms, SHELXS[33]) and conventional Fourier techniques and refined by full-matrix least-squares on F^2 (SHELXL) (except **6**·0.5H_2O which was refined by full-cycle).[34] Final mixed refinements were undertaken with anisotropic thermal parameters for the nonhydrogen atoms. The hydrogen atoms were included with fixed isotropic contributions at their positions calculated geometrically. Elevated final R values were obtained for **3**·H_2O and **5**·0.5EtOH due to the low quality of these crystals.
CCDC-236884−236889 (for **1**, **2**, **3**·H_2O, **4**·H_2O, **5**·0.5EtOH, and **6**·0.5H_2O, respectively) contain the supplementary crystallographic data for this paper. These data can be obtained free of charge at www.ccdc.cam.ac.uk/conts/retrieving.html [or from the Cambridge Crystallographic Data Centre, 12 Union Road, Cambridge CB2 1EZ, UK; Fax: +44-1223-336033; E-mail: deposit@ccdc.cam.ac.uk].

Acknowledgments

We are grateful to the Ministerio de Ciencia y Tecnología (Dirección General de Investigación, project no. BQU 2000-0643) and the Universidad Complutense de Madrid (project PR3/04-12426) for financial support.

[1] F. A. Cotton, R. A. Walton, *Multiple Bonds Between Metal Atoms*, 2nd edition, Oxford University Press, Oxford, U.K., **1993**.
[2] M. C. Barral, R. Jiménez-Aparicio, J. L. Priego, E. C. Royer, F. A. Urbanos, *An. Quim. Int. Ed.* **1997**, *93*, 277−283.
[3] M. A. S. Aquino, *Coord. Chem. Rev.* **1998**, *170*, 141−202.
[4] [4a] M. W. Cooke, T. S. Cameron, K. N. Robertson, J. C. Swarts, M. A. S. Aquino, *Organometallics* **2002**, *21*, 5962−5971. [4b] C. S. Campos-Fernández, L. M. Thomson, J. R. Galán-Mascarós, X. Ouyang, K. R. Dunbar, *Inorg. Chem.* **2002**, *41*, 1523−1533. [4c] M. Rusjan, B. Donnio, B. Heinrich, F. D. Cukiernik, D. Guillon, *Langmuir* **2002**, *18*, 10116−10121. [4d] H. Miyasaka, R. Clérac, C. S. Campos-Fernández, K. R. Dunbar, *J. Chem. Soc., Dalton Trans.* **2001**, 858−861. [4e] H. Miyasaka, R. Clérac, C. S. Campos-Fernández, K. R. Dunbar, *Inorg. Chem.* **2001**, *40*, 1663−1671. [4f] H. Miyasaka, C. S. Campos-Fernández, R. Clérac, K. R. Dunbar, *Angew. Chem. Int. Ed.* **2000**, *39*, 3831−3835. [4g] Y. Sayama, M. Handa, M. Mikuriya, I. Hiromitsu, K. Kasuga, *Bull. Chem. Soc. Jpn.* **2000**, *73*, 2499−2504. [4h] M. Handa, D. Yoshioka, Y. Sayama, K. Shioni, M. Mikuriya, I. Hiromitsu, K. Kasuga, *Chem. Lett.* **1999**, 1033−1034. [4i] Y. Sayama, M. Handa, M. Mikuriya, I. Hiromitsu, K. Kasuga, *Chem. Lett.* **1999**, 453−454. [4j] M. Handa, Y. Sayama, M. Mikuriya, R. Nukada, I. Hiromitsu, K. Kasuga, *Bull. Chem. Soc. Jpn.* **1998**, *71*, 119−125. [4k] J. L. Wesemann, M. H. Chisholm, *Inorg. Chem.* **1997**, *36*, 3258−3267. [4l] X. Ouyang, C. Campana, K. R. Dunbar, *Inorg. Chem.* **1996**, *35*, 7188−7189.
[5] M. J. Bennett, K. G. Caulton, F. A. Cotton, *Inorg. Chem.* **1969**, *8*, 1−6.
[6] A. Bino, F. A. Cotton, T. R. Felthouse, *Inorg. Chem.* **1979**, *18*, 2599−2604.
[7] T. Togano, M. Mukaida, T. Nomura, *Bull. Chem. Soc. Jpn.* **1980**, *53*, 2085−2086.
[8] D. S. Martin, R. A. Newman, L. M. Vlasnik, *Inorg. Chem.* **1980**, *19*, 3404−3407.
[9] B. K. Das, A. R. Chakravarty, *Polyhedron* **1991**, *10*, 491−494.
[10] M. McCann, A. Carvill, P. Guinan, P. Higgings, J. Campbell, H. Ryan, M. Walsh, G. Ferguson, J. Gallagher, *Polyhedron* **1991**, *10*, 2273−2281.
[11] F. A. Cotton, Y. Kim, T. Ren, *Polyhedron* **1993**, *12*, 607−611.
[12] M. C. Barral, R. Jiménez-Aparicio, J. L. Priego, E. C. Royer, F. A. Urbanos, U. Amador, *Inorg. Chem.* **1998**, *37*, 1413−1416.
[13] F. D. Cukiernik, D. Luneau, J. C. Marchon, P. Maldivi, *Inorg. Chem.* **1998**, *37*, 3698−3704.
[14] M. C. Barral, R. Jiménez-Aparicio, D. Pérez-Quintanilla, E. Pinilla, J. L. Priego, E. C. Royer, F. A. Urbanos, *Polyhedron* **1998**, *18*, 371−376.
[15] M. C. Barral, R. Jiménez-Aparicio, D. Pérez-Quintanilla, J. L. Priego, E. C. Royer, M. R. Torres, F. A. Urbanos, *Inorg. Chem.* **2000**, *39*, 65−70.
[16] M. C. Barral, R. Jiménez-Aparicio, E. C. Royer, C. Ruiz-Valero, M. J. Saucedo, F. A. Urbanos, *Inorg. Chem.* **1994**, *33*, 2692−2694.
[17] M. C. Barral, R. Jiménez-Aparicio, J. L. Priego, E. C. Royer, M. J. Saucedo, F. A. Urbanos, U. Amador, *J. Chem. Soc., Dalton Trans.* **1995**, 2183−2187.
[18] M. C. Barral, R. Jiménez-Aparicio, J. L. Priego, E. C. Royer, F. A. Urbanos, U. Amador, *J. Chem. Soc., Dalton Trans.* **1997**, 863−868.
[19] M. C. Barral, R. González-Prieto, R. Jiménez-Aparicio, J. L. Priego, M. R. Torres, F. A. Urbanos, *Eur. J. Inorg. Chem.* **2003**, 2339−2347.
[20] T. Kimura, T. Sakurai, M. Shima, T. Togano, M. Mukaida, T. Nomura, *Bull. Chem. Soc. Jpn.* **1982**, *55*, 3927−3928.
[21] W. Z. Chen, T. Ren, *Inorg. Chem.* **2003**, *42*, 8847−8852.
[22] W. J. Geary, *Coord. Chem. Rev.* **1971**, *7*, 81−122.
[23] G. J. Norman, G. E. Renzoni, D. A. Case, *J. Am. Chem. Soc.* **1979**, *101*, 5256−5267.
[24] F. A. Cotton, E. Pedersen, *Inorg. Chem.* **1975**, *14*, 388−391.
[25] J. Telser, R. S. Drago, *Inorg. Chem.* **1984**, *23*, 3114−3120.
[26] G. Estiú, F. D. Cukiernik, P. Maldivi, O. Poizat, *Inorg. Chem.* **1999**, *38*, 3030−3039.
[27] R. Jiménez-Aparicio, F. A. Urbanos, J. M. Arrieta, *Inorg. Chem.* **2001**, *40*, 613−619.
[28] C. J. O'Connor, *Prog. Inorg. Chem.* **1982**, *29*, 232 and 244.
[29] [29a] V. M. Miskowski, M. D. Hopkins, J. R. Winkler, H. B. Gray, *Multiple Metal-Metal Bonds*, 343−402, in *Inorganic Electronic Structure and Spectroscopy, Volume II: Applications and Case Studies* (Eds.: E. I. Solomon, A. B. P. Lever), J. Wiley &

 © 2004 Wiley-VCH Verlag GmbH & Co. KGaA, Weinheim

Sons, New York, **1999**. [29b] V. M. Miskowski, H. B. Gray, *Inorg. Chem.* **1988**, *27*, 2501−2506. [29c] V. M. Miskowski, T. M. Loehr, H. B. Gray, *Inorg. Chem.* **1987**, *26*, 1098−1108.
[30] [30a] R. J. H. Clark, M. L. Franks, *J. Chem. Soc., Dalton Trans.* **1976**, 1825−1828. [30b] R. J. H. Clark, L. T. H. Ferris, *Inorg. Chem.* **1981**, *20*, 2759−2766.
[31] M. Mukaida, T. Nomura, T. Ishimori, *Bull. Chem. Soc. Jpn.* **1972**, *45*, 2143−2147.
[32] F. A. Urbanos, Program MASAS V 3.1, **2002**.
[33] G. M. Sheldrick, SHELXS-97, Program for the solution of Crystal Structures, University of Göttingen, Germany, **1997**.
[34] G. M. Sheldrick, SHELXL-97, Program for the solution of Crystal Structures, University of Göttingen, Germany, **1997**.

Received May 7, 2004
Early View Article
Published Online October 1, 2004

 © 2004 Wiley-VCH Verlag GmbH & Co. KGaA, Weinheim

Monocyclooctatetraenyl(dithiolene)uranium Compounds

Thérèse Arliguie,*[a] Pierre Thuéry,[a] Marc Fourmigué,[b] and Michel Ephritikhine[a]

Keywords: Cyclooctatetraenyl ligands / Lewis bases / S ligands / Uranium

The neutral mononuclear dithiolene compounds [U(cot)(dithiolene)(tppo)$_2$] [cot = η-C_8H_8; dithiolene = dddt (**9**), dmio (**10**), mdt (**11**)], [U(cot)(dithiolene)(hmpa)$_2$] [dithiolene = dddt (**12**), dmio (**13**), mdt (**14**)], [U(cot)(mdt)(bipy)] (**15**) and [U(cot)(mdt)(terpy)] (**16**) were obtained by treating the dimeric complexes [{U(cot)(dithiolene)}$_2$] [dithiolene = dddt (**3**), dmio (**4**), mdt (**5**)] (dddt = 5,6-dihydro-1,4-dithiine-2,3-dithiolate; dmio = 1,3-dithiole-2-one-4,5-dithiolate; mdt = 1,3-dithiole-4,5-dithiolate) with the corresponding Lewis base [triphenylphosphine oxide (tppo), hexamethylphosphoramide (hmpa), 2,2′-bipyridine (bipy), or 2,2′:6′,2′′-terpyridine (terpy)]. Complexes **9**·2THF, **11**·2THF, **12**, **13**, **14**, **15** and **16**·1.5py have been crystallographically characterized. The crystal structures show a significant interaction between the C=C double bond of the dithiolene ligand and the metal centre. The ^{1}H NMR spectra reveal the fluxional behaviour of the compounds in solution in relation to the facile inversion of the dithiolene ring. The variation of the activation energies of the inversion process reflects the steric congestion of the complexes.
(© Wiley-VCH Verlag GmbH & Co. KGaA, 69451 Weinheim, Germany, 2004)

Introduction

Dithiolene complexes of the d-block transition metals have received much attention for their remarkable structural features and physicochemical properties, finding applications in the elaboration of novel conducting and magnetic materials.[1] In contrast, such compounds of the f-block elements have been practically neglected,[2] mainly due to the presumption that this type of complex should be unstable. In fact, lanthanides and actinides have proved to have a strong affinity for sulfur,[3−12] and the synthesis of their dithiolene complexes is worth considering since their coordination flexibility, paramagnetism and redox behaviour could favour the emergence of interesting structures and electronic interactions. For these reasons we have started studies on organouranium−dithiolene compounds, in particular bis(pentamethylcyclopentadienyl) and monocyclooctatetraenyl derivatives, for comparison with the heteroleptic cyclopentadienyl/dithiolene complexes of the metals of groups 4−6[13,14] and with the uranium bis(thiolate) complexes [U(cp*)$_2$(SR)$_2$][11] and [{U(cot)(SR)$_2$}$_2$][7] (cp* = η-C_5Me_5; cot = η-C_8H_8). The dithiolene ligands selected for this work are represented in Scheme 1.

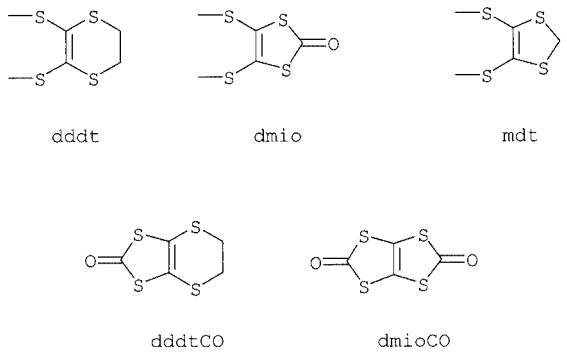

Scheme 1. The dithiolene ligands and dithiocarbonates (dddt = 5,6-dihydro-1,4-dithiine-2,3-dithiolate; dmio = 1,3-dithiole-2-one-4,5-dithiolate; mdt = 1,3-dithiole-4,5-dithiolate)

We recently reported that anionic bis(dithiolene) derivatives could be obtained from the metathesis reaction of the uranium bis(borohydride) complex [U(cot)(BH_4)$_2$] with 2 mol-equiv. of Na_2dddt in THF, affording, in the presence of 18-crown-6, red crystals of a THF solvate of [Na(18-crown-6)(THF)$_2$]$_2$[U(cot)(dddt)$_2$] (**1**). Complex **1** was a unique example of a dianionic monocyclooctatetraenyluranium compound, although the [U(cot)X_3]$^-$ anions were found to be stable in the presence of an excess of X^- (X = SR,[7] NR_2,[15] BH_4 [16]). Its oxidation with $AgBPh_4$ in THF afforded the corresponding monoanionic compound [Na(18-crown-6)(THF)][U(cot)(dddt)$_2$] (**2**), which was structurally characterized.[17] Complex **2** was the first uranium(v) compound with metal−sulfur bonds and, after the cycloheptatrienyl sandwich compound [K(18-crown-

[a] Service de Chimie Moléculaire, DSM, DRECAM, CNRS URA 331, CEA/Saclay,
91191 Gif-sur-Yvette, France
E-mail: arliguie@drecam.cea.fr
[b] Laboratoire de Chimie Inorganique, Matériaux et Interfaces (CIMI), FRE 2447 CNRS-Université d'Angers,
2 Bd. Lavoisier, 49045 Angers, France

 © 2004 Wiley-VCH Verlag GmbH & Co. KGaA, Weinheim **DOI: 10.1002/ejic.200400403**

6)][U(η-C_7H_7)$_2$],[18] a new example of an anionic organouranium(v) derivative.

We also disclosed that the same borohydride, [U(cot)(BH_4)$_2$], could act as a hydride reagent in the reductive fission of dithiocarbonates, affording a series of neutral dimetallic dithiolene complexes [{U(cot)(dithiolene)}$_2$] [dithiolene = dddt (**3**), dmio (**4**), mdt (**5**)].[19] Upon dissolution in pyridine, those dimeric compounds could be transformed into the mononuclear complexes [U(cot)(dithiolene)(py)$_2$] [dithiolene = dddt (**6**), dmio (**7**), mdt (**8**)]. The crystal structure of **8** revealed a significant interaction between the dithiolene ligand and the metal centre.[19] With the aim of understanding and controlling this interaction, we have studied the complexation of **3**−**5** with various Lewis bases, such as triphenylphosphine oxide (tppo) or hexamethylphosphoramide (hmpa), and chelating pyridines such as bipyridine or terpyridine.

Here we report the synthesis of a series of adducts of general formula [U(cot)(dithiolene)(L)$_n$] (n = 1 and L = bipy or terpy; n = 2 and L = tppo or hmpa). We describe the X-ray crystal structures of the complexes, paying special attention to the interaction between the dithiolene ligand and the metal centre, and we present the ^{1}H NMR spectra, which reveal the dynamic behaviour of the complexes in solution, related to the facile ring-inversion process of the dithiolene ligand.[17,19]

Results and Discussion

The bis adducts [U(cot)(dithiolene)(tppo)$_2$] [dithiolene = dddt (**9**), dmio (**10**), mdt (**11**)] and [U(cot)(dithiolene)(hmpa)$_2$] [dithiolene = dddt (**12**), dmio (**13**), mdt (**14**)] were obtained by treatment of **3**−**5** with 2 mol-equiv. of tppo or hmpa in THF (Scheme 2). With the exception of **10**, these complexes could also be prepared in a one-pot reaction from [U(cot)(BH_4)$_2$], L and the dithiocarbonates dddtCO or dmioCO, which are the protected forms of the corresponding dithiolene ligands (dddtCO = 5,6-dihydro-1,3-dithiolo[4,5-*b*][1,4]dithiine-2-one; dmioCO = 1,3,4,6-tetrathiapentalene-2,5-dione). In the presence of 2,2′-bipyridine (bipy) or 2,2′:6′,2″-terpyridine (terpy) in THF, **5** was transformed into [U(cot)(mdt)(bipy)] (**15**) and [U(cot)(mdt)(terpy)] (**16**), respectively. Complexes **6**−**16** were isolated as red to dark-brown crystals or powders with yields from 65 to 95%.

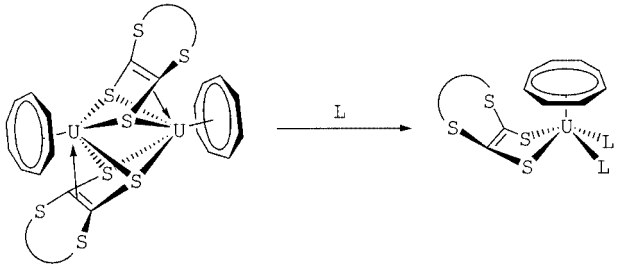

dithiolene	
dddt	**3**
dmio	**4**
mdt	**5**

dithiolene \ L	py	tppo	hmpa
dddt	**6**	**9**	**12**
dmio	**7**	**10**	**13**
mdt	**8**	**11**	**14**

Scheme 2. Synthesis of the mononuclear compounds **6**−**14**

At least one example of each type of the Lewis-base adducts of **3**−**5** with tppo or hmpa (**11**, **12** and **13**) was characterized by elemental analysis, as were **15** and **16** , and the X-ray crystal structures of **9**·2THF, **11**·2THF, **12**, **13**, **14**, **15** and **16**·1.5py were also determined.

Crystal Structures of the Complexes

The crystal structure of the dinuclear compound **5** (Figure 1) has already been described in a preliminary report;[19] only the main geometrical features will be recalled for comparison with its congeners.

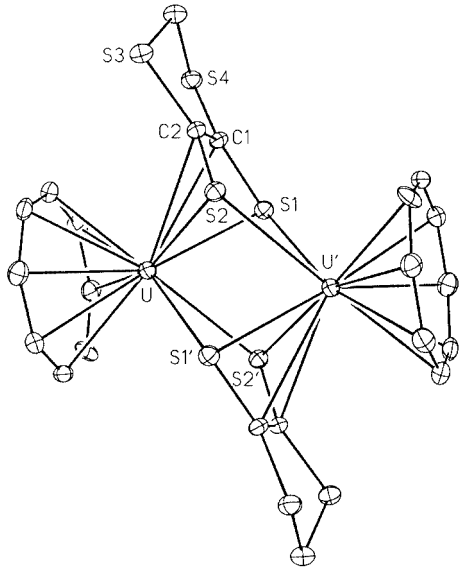

Figure 1. View of the complex [{U(cot)(mdt)}$_2$] (**5**); the hydrogen atoms have been omitted for clarity; the displacement ellipsoids are drawn at the 30% probability level; symmetry code: ′ = − x, 1 − y, − z

The Lewis-base adducts of general formula [U(cot)(dithiolene)(L)$_2$] adopt a four-legged piano-stool configuration, the base of which is defined by the S(1) and S(2) atoms of the dithiolene ligand and the two oxygen [O(1) and O(2)] or the two nitrogen [N(1) and N(2)] atoms of the Lewis base. The structures of **9** (Figure 2), **14** (Figure 3) and **15** (Figure 4), which are representatives of the series, are shown below; selected bond lengths and angles in the complexes [U(cot)(dithiolene)(L)$_2$] are listed in Table 1. Complex **15** has crystallographic mirror symmetry.

 © 2004 Wiley-VCH Verlag GmbH & Co. KGaA, Weinheim

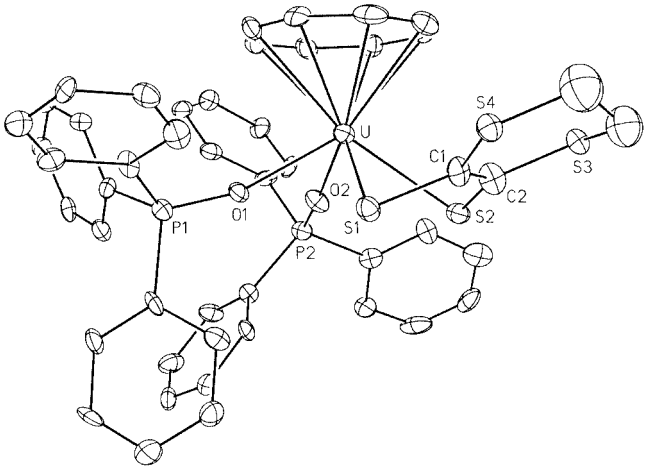

Figure 2. View of the complex [U(cot)(dddt)(tppo)$_2$] (**9**); the hydrogen atoms have been omitted for clarity; the displacement ellipsoids are drawn at the 30% probability level

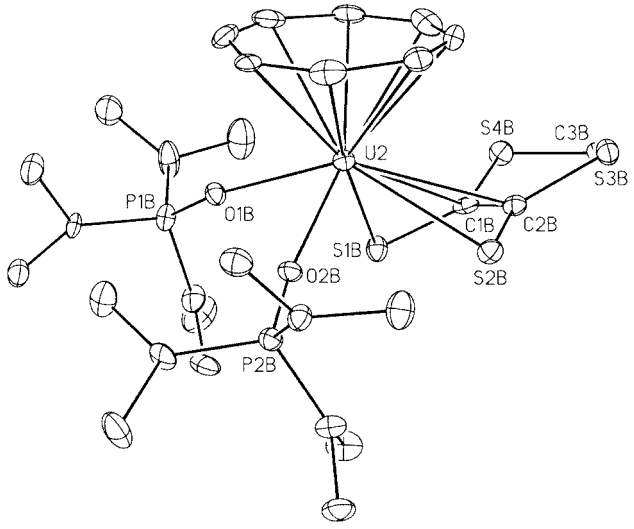

Figure 3. View of one of the two independent molecules of [U(cot)(mdt)(hmpa)$_2$] (**14**); the hydrogen atoms have been omitted for clarity; the displacement ellipsoids are drawn at the 30% probability level

The cot ligand in all the complexes is planar within ±0.09 Å. The average U−C(cot) distances in the Lewis-base adducts [U(cot)(dithiolene)(L)$_2$], with a typical value of 2.71 Å, are longer than that of 2.640(2) Å in **5**, and are at the upper limit of the range of U−C(cot) bond lengths in monocyclooctatetraenyluranium(IV) compounds, which vary from 2.62(2) Å in the bis(thiolate) complex [{U(cot)(S*i*Pr)$_2$}$_2$][7] to 2.71(4) Å in [U(cot)(NEt$_2$)-(THF)$_3$][BPh$_4$].[20]

In the tppo and hmpa adducts, the U−O distances vary from 2.302(8) Å in **13** to 2.444(8) Å in **14** and are unexceptional; they are similar to those of 2.27(1) Å in [U(cot)-(BH$_4$)$_2$(tppo)][21] and 2.461(8) Å in [U(cot)(Cp*)(hmpa)].[22] The U−N distance in **15** [2.555(4) Å] can be compared with those in **8** [2.636(9) and 2.691(10) Å], [U(cot)Cl$_2$(py)$_2$] [2.639(5) and 2.644(6) Å],[23] and to the average U−N(bipy)

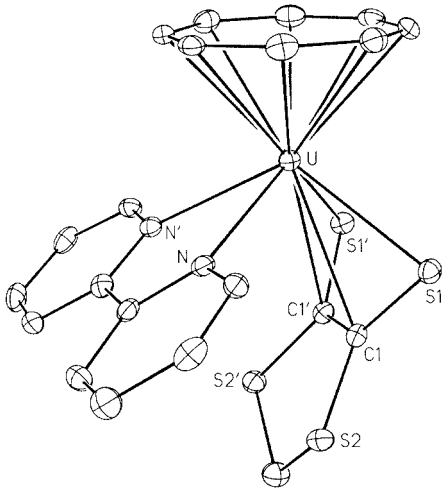

Figure 4. View of the complex [U(cot)(mdt)(bipy)] (**15**); the hydrogen atoms have been omitted for clarity; the displacement ellipsoids are drawn at the 30% probability level; symmetry code: $' = x, 0.5 - y, z$

distance of 2.63(2) Å in [NEt$_4$][U(NCS)$_5$(bipy)$_2$],[24] which is the other uranium(IV)−bipy complex to have been crystallographically characterized. The O(1)−U−O(2) or N(1)−U−N(2) angles are quite similar, with an average value of 75(1)°, except for the N−U−N angle of the bidentate bipy ligand, which is equal to 63.12(19)°.

The U−S distances in the series of [U(cot)(dithiolene)(L)$_2$] complexes vary from 2.720(3) Å in **8** to 2.859(3) Å in **13** and are larger than the U−S bond lengths in the monomeric uranium(IV) thiolate compounds, which range between 2.61(5) Å in [U(S*i*Pr)$_2$(hmpa)$_4$][BPh$_4$][9] and 2.744(2) Å in [Na(18-crown-6)][U(Cp*)$_2$(S)(S*t*Bu)].[10] However, as expected for terminal SR ligands, these distances are shorter than the mean bridging SR bond length of 2.88(8) Å in the dimeric compound **5**. The S(1)−U−S(2) angles in the mononuclear compounds are close to 75°, while they are slightly smaller in **5**, with values of 68.29(6) and 71.98(6)°.

In all the complexes, the characteristics of the dithiolene ligands, such as the average C(sp^2)−S distances, which vary from 1.720(13) Å in **14** to 1.796(17) Å in **9**, and the C=C distances, which lie between 1.343(10) Å in **12** and 1.394(17) Å in **14**, are consistent with those found in [Mo(cp)$_2$(dddt)] [1.76(1) and 1.33(1) Å],[25] [NEt$_4$]$_2$[Ni(dmio)$_2$] [1.75(1) and 1.34(1) Å][26] and [NBu$_4$][Ni(mdt)$_2$] [1.74(2) and 1.36(2) Å].[27]

Special attention should be paid to the folding of the metallacycle as this reflects the interaction of the dithiolene ligand with the metal centre. The S$_4$C$_2$ fragment of the dithiolene ligands is planar within ±0.06 Å and forms a dihedral angle, θ, with the corresponding S−U−S plane. Scheme 3 shows the variation of this folding angle and the distinct conformations of the dithiolene ligands in the complexes. Previous studies on dithiolene compounds of the d-block transition metals have shown that θ increases upon lowering the electron density at the metal atom, reflecting the strength of the interaction of an empty metal orbital

 © 2004 Wiley-VCH Verlag GmbH & Co. KGaA, Weinheim

Table 1. Selected bond lengths [Å] and angles [°] in the neutral mononuclear complexes **8**, **9** and **11**−**15**

	8[19]	**9**[a]	**11**[a]	**12**	**13**	**14**[b]	**15**
U−C(cot)	2.70(3)	2.70(2)	2.703(17)	2.716(17)	2.71(3)	2.71(2); 2.72(3)	2.686(7)
U−S(1)	2.720(3)	2.745(5)	2.773(2)	2.736(2)	2.801(3)	2.791(3); 2.739(3)	2.7511(14)
U−S(2)	2.751(3)	2.782(5)	2.781(2)	2.793(2)	2.859(3)	2.751(3); 2.821(3)	
U−C(1)	2.889(11)	3.089(15)	3.086(9)	3.181(8)	3.679(15)	3.146(10); 2.969(11)	2.879(5)
U−C(2)	2.965(11)	3.11(2)	3.081(8)	3.179(8)	3.674(14)	3.154(13); 3.020(11)	
U−O(1) or		2.398(10)	2.354(5)	2.363(5)	2.327(8)	2.354(8); 2.444(8)	
U−N(1)	2.691(10)						2.555(4)
U−O(2) or		2.376(12)	2.424(5)	2.353(5)	2.302(8)	2.367(8); 2.312(8)	
U−N(2)	2.636(9)						
C(1)−C(2)[c]	1.389(16)	1.35(2)	1.363(12)	1.343(10)	1.378(16)	1.348(16); 1.394(17)	1.374(10)
C(1)−S(1)	1.732(12)	1.796(17)	1.740(8)	1.757(7)	1.742(15)	1.732(12); 1.720(13)	1.748(5)
C(1)−S(4)[c]	1.781(12)	1.772(19)	1.765(9)	1.774(8)	1.754(14)	1.795(11); 1.762(12)	1.768(6)
C(2)−S(2)	1.749(11)	1.72(2)	1.742(9)	1.757(8)	1.722(14)	1.733(12); 1.742(12)	
C(2)−S(3)	1.749(13)	1.79(2)	1.772(8)	1.774(8)	1.762(13)	1.795(13); 1.772(12)	
S(1)−U−S(2)	77.08(10)	73.67(15)	75.74(7)	73.74(6)	73.89(9)	75.26(9); 75.48(9)	77.13(6)
O(1)−U−O(2) or		74.1(4)	74.2(2)	74.78(19)	77.1(3)	76.1(3); 74.8(3)	
N(1)−U−N(2)	74.3(3)						63.12(19)
θ[d]	75.6(3)	71.89(12)	71.32(6)	65.97(6)	20.93(19)	66.98(9); 75.97(9)	80.60(5)

[a] Complexes **9** and **11** crystallize with two THF molecules. [b] Values are given for the two independent molecules. [c] C(1)−C(2) and C(1)−S(4) are C(1)−C(1′) and C(1)−S(2) in complex **15**. [d] θ is the folding angle as defined in the text.

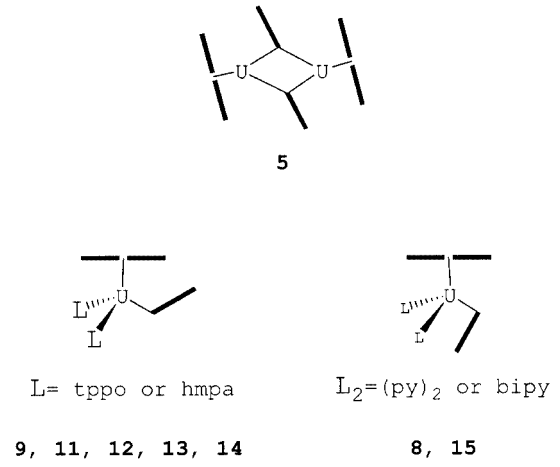

Scheme 3. Conformation of the dithiolene ligands

with the HOMO of the dithiolene ligand.[13,28] For example, in the series of $[M(Cp^*)(dmit)_2]^{-1,0}$ compounds, the d^2 complexes $[M(Cp^*)(dmit)_2]^{-1}$ (M = Mo, W) adopt an *exo-exo* conformation, and the d^0 derivative $[Ti(Cp^*)(dmit)_2]^{-1}$ is found in an *exo-endo* conformation, while the geometry of the d^1 complex $[M(Cp^*)(dmit)_2]^{\cdot}$ (M = Mo, W) compounds is intermediate between those of the Mo^{IV} or W^{IV} and Ti^{IV} analogues.[29]

In the series of Lewis-base adducts [U(cot)(dithiolene)$(L)_2$], the dithiolene ligand is found in the *exo* conformation, except in the pyridine and bipyridine derivatives **8** and **15**. The lower steric hindrance of these nitrogen ligands, in comparison with tppo and hmpa, permits the folding of the US_2C_2 fragment towards the *endo* position, with θ being equal to 75.6(3) and 80.60(5)° in **8** and **15**, respectively; the C(1) and C(2) atoms approach the metal centre at less than 3 Å. With the exception of **14**, the folding angles in the tppo and hmpa adducts are smaller than 75°, and are probably limited by the steric interaction between the dithiolene and cot ligands. One of the two independent molecules of **14** presents a θ angle of 75.97(9)° despite the *exo* conformation of the dithiolene ligand. The low value of θ in the dmio complex **13** [20.93(19)°] seems peculiar since the complexes $[Ti(Cp)_2$(dithiolene)] (dithiolene = dddt, dmio or dmit) exhibit quite similar θ angles of 47−50°.[13,14] However, this distinct feature of **13** might be ascribed to the presence in the crystal structure of weak intermolecular O(3)···H−C interactions[30−32] with four H atoms of the hmpa or cot groups of two neighbouring molecules, with O(3)···H distances in the range 2.621−2.893 Å. The structures of the other neutral dithiolene complexes exhibit weak intermolecular C−H···S contacts, shorter than 3 Å and as low as 2.70 Å; such interactions have been observed in a large number of tetrathiafulvalene derivatives.[33]

The crystal structure of the terpy adduct **16** is shown in Figure 5; selected bond angles and distances are given in Table 2. Complex **16** is a unique example of a distorted octahedral monocyclooctatetraenyluranium compound; the apical positions are occupied by the centroid of the cot ring and the S(2) atom, while S(1) and the three nitrogen atoms of the terpy ligand define the equatorial plane, with a mean deviation of ±0.002 Å. This plane is almost parallel to the planar cot ligand, with a dihedral angle of 4.38(13)°, and the U atom is located between the two planes at a distance of 0.8687(13) and 2.0148(15) Å, respectively. The planar dithiolene ligand is practically perpendicular to both the cot ring and equatorial plane, with dihedral angles of 88.93(7) and 84.72(5)°, respectively. The long U−S distances of 2.8203(10) and 2.8304(10) Å and the small folding angle, θ, of 20.40(4)° reflect the electronic and steric saturation of

 © 2004 Wiley-VCH Verlag GmbH & Co. KGaA, Weinheim

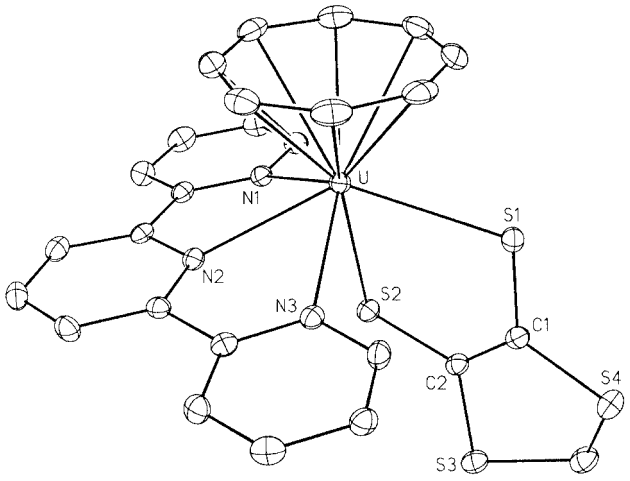

Figure 5. View of the complex [U(cot)(mdt)(terpy)] (**16**); the hydrogen atoms and solvent molecules have been omitted for clarity; the displacement ellipsoids are drawn at the 30% probability level

the complex. The average U−N distance of 2.589(9) Å can be compared with that of 2.63(3) Å in the U^{III} cation $[U(terpy)_3]^{3+}$, the other terpyridine uranium complex to have been crystallographically characterized.[34]

Dynamic Behaviour of the Complexes in Solution

The ^{1}H NMR spectroscopic data of the complexes are reported in Table 3. Complex **9** is not soluble in THF, while **15** and **16** are not soluble in THF or pyridine; their NMR spectra could therefore not be recorded. The spectra of the tppo and hmpa adducts in pyridine are more complicated, showing partial substitution of the L ligands by solvent molecules. At 20 °C, the cot ligand in all the complexes gives rise to a signal at $\delta \approx -30$ ppm, characteristic of monocyclooctatetraenyluranium compounds.[7,15,21,35] Two signals of equal intensities corresponding to the magnetically non-equivalent methylene protons of the dddt and mdt ligands in the Lewis-base adducts [U(cot)(dithiolene)$(L)_2$] are visible at 20 °C, or at lower temperature in the case of **12**, as already observed for **6** and **8**.[19] Coalescence of these resonances occurred upon increasing the temperature, and the fast limit spectrum was obtained for complex **12**.

The dynamic behaviour of the complexes can be ascribed to the dithiolene ring inversion represented in Scheme 4; a similar fluxionality has been observed in a variety of [M$(Cp)_2$(dithiolene)] compounds.[13,14] The ring inversion should proceed via the trigonal bipyramidal intermediate (**A** in Scheme 4) which renders the methylene protons equivalent. It is conceivable that, for the sterically less saturated complexes **6** and **8**, the octahedral intermediate [U(cot)(di-

Table 2. Selected bond lengths [Å] and angles [°] in [U(cot)(mdt)(terpy)]·1.5py (**16**·1.5py)

<U−C(cot)>	2.72(2)	U−S(1)	2.8203(10)	U−S(2)	2.8304(10)
U−N(1)	2.582(3)	U−N(2)	2.585(3)	U−N(3)	2.599(3)
C(1)−S(1)	1.743(4)	C(1)−S(4)	1.771(4)	C(2)−S(2)	1.746(4)
C(2)−S(3)	1.783(4)	C(1)−C(2)	1.336(5)		
S(1)−U−S(2)	71.06(3)	N(1)−U−N(2)	62.57(10)	N(1)−U−N(3)	119.58(10)
N(2)−U−N(3)	61.94(10)	S(1)−U−N(1)	125.45(7)	S(1)−U−N(2)	134.27(7)
S(1)−U−N(3)	81.48(7)	S(2)−U−N(1)	64.23(7)	S(2)−U−N(2)	77.15(7)
S(2)−U−N(3)	81.96(7)	cot−U−N(1)[a]	107.9	cot−U−N(2)	113.0
cot−U−N(3)	114.0	cot−U−S(1)	106.3	cot−U−S(2)	163.6

[a] cot is the centroid of the C_8H_8 ring.

Table 3. ^{1}H NMR spectroscopic data of the complexes[a]

Compound	T [°C]	cot ligand[b]	Dithiolene ligand	L ligands or 18-crown-6[c]
[U(cot)(dddt)$(py)_2$] (**6**)[19]	+20	−30.98 (12 Hz)	10.87 (33 Hz, 4 H)	
	−40	−38.75 (12 Hz)	20.2 and 15.1 (500 Hz, 2 × 2 H)	
[U(cot)(dddt)$(hmpa)_2$] (**12**)	+60	−26.13 (6 Hz)	−3.6 (140 Hz, ca 3 H)	1.30 (36 H)
	−80	−45.2 (130 Hz)	1.33 and −5.10 (35 Hz, 2 × 2 H)	−1.60 (36 H)
[U(cot)(dmio)$(py)_2$] (**7**)[19]	+20	−32.07 (12 Hz)		
[U(cot)(dmio)$(tppo)_2$] (**10**)	+20	−31.46 (15 Hz)		7.11 (6 H), 6.73 (12 H) 5.30 (45 Hz, 12 H)
[U(cot)(dmio)$(hmpa)_2$] (**13**)	+20	−30.44 (12 Hz)		1.93 (36 H)
[U(cot)(mdt)$(py)_2$] (**8**)[19]	+90	−24.82 (8 Hz)	11.21 (35 Hz, 2 H)	
	−30	−37.51 (3 Hz)	17.08 (45 Hz, 1 H)[d]	
[U(cot)(mdt)$(tppo)_2$] (**11**)	+20	−29.52 (4 Hz)	5.22 and −2.74 (20 Hz, 2 × 1 H)	7.07 (6 H), 6.68 (12 H) 3.78 (45 Hz, 12 H)
[U(cot)(mdt)$(hmpa)_2$] (**14**)	+20	−28.78 (4 Hz)	3.29 and −4.79 (35 Hz, 2 × 1 H)	0.07 (36 H)

[a] In [D_8]THF; **6**, **7** and **8** in [D_5]pyridine. The half-height width and the relative integral of the singlet signal are given in parentheses. [b] The cot signal integrates for 8 H. [c] When not specified, the half-height width is between 10 and 30 Hz. [d] The other signal of the mdt ligand is masked by the solvent resonances.

 © 2004 Wiley-VCH Verlag GmbH & Co. KGaA, Weinheim

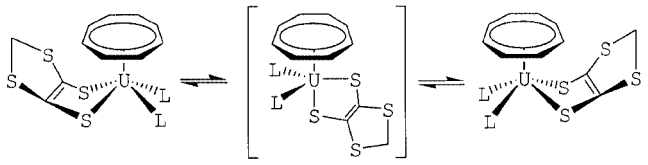

A

Scheme 4. Ring inversion process of the dithiolene ligand

thiolene)(py)$_3$], with a structure similar to that of the terpy adduct **16**, should be involved in the reaction. However, such an associative mechanism is not likely for the other Lewis-base adducts, since addition of tppo or hmpa has no influence on the fluxional process. The coalescence temperatures, T_c, and the activation energies, $\Delta G^{\ddagger}$, for the dithiolene ring inversion process are given in Table 4. The values of $\Delta G^{\ddagger}$ are in the range of those calculated for the [Ti(Cp)$_2$(dithiolene)] compounds, which vary from 40.5 to 69 kJ·mol^{-1} when the dithiolene is $S_2C_2(CN)_2$ and mdt, respectively;[14] they can also be compared with those measured for the metallacyclopentene ring inversion in bis(cyclopentadienyl)diene complexes of group 4 metals and actinides.[36] In the (dithiolene)titanium compounds, a correlation was found between the activation energy $\Delta G^{\ddagger}$ and the folding angle θ.[14] However, in the [U(cot)(dithiolene)(L)$_2$] derivatives, the variation of $\Delta G^{\ddagger}$ seems better related to the steric congestion of the complex and the difficulty of the ligands to rearrange around the metal centre. The lower barrier in the dddt compounds **6** and **12**, by comparison with the mdt analogues **8** and **14**, respectively, would correspond to a greater steric interaction between the dithiolene and L ligands in the ground state of the complex.

Table 4. Coalescence temperatures and activation energies for the ring-inversion process

Compound	T_c [°C]	$\Delta G^{\ddagger}$ [kJ·mol^{-1}]
[U(cot)(dddt)(py)$_2$] (**6**)[19]	−30	43(1)
[U(cot)(dddt)(hmpa)$_2$] (**12**)	+20	53(1)
[U(cot)(mdt)(py)$_2$] (**8**)[19]	+30	50(1)
[U(cot)(mdt)(tppo)$_2$] (**11**)	+80	63(1)
[U(cot)(mdt)(hmpa)$_2$] (**14**)	+80	63(1)

Conclusion

We have prepared a series of Lewis-base adducts of general formula [U(cot)(dithiolene)(L)$_n$] (n = 1, L = bipy or terpy and dithiolene = mdt; n = 2, L = tppo or hmpa and dithiolene = dddt, dmio, mdt). Crystallographic and NMR studies revealed that the solid-state structure and dynamic behaviour of these dithiolene complexes of an f-block element are similar to those of the d-block transition metal analogues, in particular the mixed cyclopentadienyl/dithiolene derivatives. The interaction between the dithiolene ligand and the metal centre observed in the solid state is favoured with the sterically less demanding Lewis bases which allow an *endo* conformation of the ligand. Still, the characteristics of the dithiolene ligands, such as the average C(sp^2)−S and C=C distances, are not greatly influenced by the nature of the Lewis base. In the whole series, the variable temperature ^{1}H NMR spectra show the fluxionality of the complexes due to the facile dithiolene ring inversion.

Experimental Section

General Remarks: All reactions were carried out under argon (<5 ppm oxygen or water) using standard Schlenk and vacuum-line techniques or in a glove box. Solvents were dried by standard methods and distilled immediately before use. The ^{1}H NMR spectra were recorded with a Bruker DPX 200 instrument and referenced internally using the residual protio solvent resonances relative to tetramethylsilane (δ = 0 ppm). Elemental analyses were performed by Analytische Laboratorien at Lindlar (Germany). [U(cot)(BH$_4$)$_2$],[21] [U(cot)I$_2$(THF)$_2$],[37] dddtCO,[38] dmioCO[39] and Na$_2$dddt[13] were prepared by published methods. The syntheses of **3**, **4**, **5** and **8** were described in our previous paper.[19]

Synthesis of [U(cot)(dddt)(py)$_2$] (6) and [U(cot)(dmio)(py)$_2$] (7): These complexes were obtained by dissolving **3** and **4**, respectively, in pyridine. After concentration to dryness, a dark-red powder of **6** and a brown powder of **7** were obtained in almost quantitative yield.

Synthesis of [U(cot)(dddt)(tppo)$_2$] (9): An NMR tube was charged with **3** (5.0 mg, 4.6 μmol) and tppo (2.6 mg, 9.2 μmol) in [D$_8$]THF (0.4 mL). Upon standing at 50 °C for 2−3 d, red crystals of **9** suitable for X-ray analysis were deposited.

Synthesis of [U(cot)(dmio)(tppo)$_2$] (10): An NMR tube was charged with **4** (5.0 mg, 4.8 μmol) and tppo (5.3 mg, 19.1 μmol) in [D$_8$]THF (0.4 mL). After 1 h at 20 °C, the spectrum of the brown solution showed the quantitative formation of **10**.

Synthesis of [U(cot)(mdt)(tppo)$_2$] (11). (a): An NMR tube was charged with **5** (5.0 mg, 4.9 μmol) and tppo (5.5 mg, 19.6 μmol) in [D$_8$]THF (0.4 mL). After standing at 65 °C for 3 h, brown crystals of **11** suitable for X-ray analysis were deposited. **(b):** A flask was charged with [U(cot)(BH$_4$)$_2$(THF)] (113 mg, 0.254 mmol) and tppo (142 mg, 0.51 mmol) in THF (25 mL). The reaction mixture was stirred at 20 °C for 15 min and a solution of dmioCO (53 mg, 0.254 mmol) in THF (10 mL) was added to the flask. After refluxing for 3 h, the solution was filtered and the solvents were evaporated to dryness, leaving a brown powder of **11** (276 mg, 90%). **11**·2THF, $C_{55}H_{56}O_4P_2S_4U$ (1209.3): calcd. C 54.63, H 4.67, S 10.61; found C 54.45, H 4.50, S 10.78.

Synthesis of [U(cot)(dddt)(hmpa)$_2$] (12): An NMR tube was charged with **3** (5.0 mg, 4.8 μmol) in [D$_8$]THF (0.4 mL) and hmpa (3.3 μL, 19.1 μmol) was introduced with a microsyringe. After 1 h at 20 °C, the spectrum of the red solution showed the quantitative formation of **12**. After standing at 20 °C overnight, red crystals of **12** suitable for X-ray analysis were deposited. $C_{24}H_{48}N_6O_2P_2S_4U$ (880.93): calcd. C 32.72, H 5.49, S 14.56; found C 32.59, H 5.51, S 14.41.

 © 2004 Wiley-VCH Verlag GmbH & Co. KGaA, Weinheim

Synthesis of [U(cot)(dmio)(hmpa)$_2$] (13): A flask was charged with [U(cot)(BH$_4$)$_2$(THF)] (208 mg, 0.56 mmol) and hmpa (201 mg, 1.12 mmol) in THF (30 mL) and dmioCO (233 mg, 1.12 mmol) was added to the solution. After stirring at 20 °C for 24 h, the solution was filtered and the solvents were evaporated to dryness. The dark-red powder of **13** was washed with diethyl ether (50 mL), THF (20 mL) and dried under vacuum (460 mg, 93%). $C_{23}H_{44}N_6O_3P_2S_4U$ (880.88): calcd. C 31.36, H 5.03, S 14.56; found C 31.13, H 5.03, S 14.39.

Synthesis of [U(cot)(mdt)(hmpa)$_2$] (14): An NMR tube was charged with **5** (5.0 mg, 4.9 μmol) in [D$_8$]THF (0.4 mL) and hmpa (3.4 μL, 19.6 μmol) was introduced with a microsyringe. After 1 h at 65 °C, the spectrum of the brown solution showed the quantitative formation of **14**. After standing at 65 °C overnight, the tube was allowed to cool to room temperature and red crystals of **14** suitable for X-ray analysis were deposited.

Synthesis of [U(cot)(mdt)(bipy)] (15): An NMR tube was charged with **5** (21.0 mg, 20.6 μmol) and bipy (6.4 mg, 41.2 μmol) in [D$_8$]THF (0.4 mL). After standing at 5 °C overnight, dark brown crystals of **15** suitable for X-ray analysis were deposited. $C_{21}H_{18}N_2S_4U$ (664.68): calcd. C 37.95, H 2.73, S 19.30; found C 38.10, H 2.85, S 19.05.

Synthesis of [U(cot)(mdt)(terpy)] (16): An NMR tube was charged with **5** (10.0 mg, 9.8 μmol) and terpy (4.6 mg, 19.6 μmol) in [D$_8$]THF (0.4 mL). After standing at 5 °C overnight, dark-brown crystals of **16** suitable for X-ray analysis were deposited. $C_{26}H_{21}N_3S_4U$ (741.76): calcd. C 42.10, H 2.85, S 17.29; found C 41.92, H 2.96, S 17.06.

X-ray Crystallography: The data were collected at 100(2) K with a Nonius Kappa-CCD area-detector diffractometer[40] using graphite-monochromated Mo-K_α radiation (λ = 0.71073 Å). The crystals were placed inside glass capillaries with a protecting "Paratone-N" oil (Hampton Research) coating. The unit-cell parameters were determined from ten frames, then refined on all data. A 180° φ-range was scanned with 2° steps during data collection, with a crystal-to-detector distance fixed at 28 mm, giving complete data sets up to an angle, θ_{max}, of 25.7°. The data were processed with DENZO-SMN.[41] The structures were solved by direct methods with SHELXS-97 and subsequent Fourier-difference synthesis and refined by full-matrix least squares on F^2 with SHELXL-97.[42] Absorption effects were corrected empirically with the program DELABS from PLATON.[43] The correct enantiomorph in compound **13** was determined from the Flack parameter [−0.020(10)].[44] Three compounds crystallize as solvates: **9** and **11** with two tetrahydrofuran molecules and **16** with 1.5 pyridine molecules. A second form of compound **11**, with only one tetrahydrofuran solvent molecule, has been isolated and characterized [crystal data: $C_{51}H_{48}O_3P_2S_4U$, M = 1137.10, triclinic, space group $P\bar{1}$, a = 12.5818(13), b = 12.7381(13), c = 16.4223(14) Å, α = 71.253(6)°, β = 72.669(6)°, γ = 72.573(4)°, V = 2318.0(4) Å^3, Z = 2, D_c = 1.629 g·cm^{-3}, μ = 3.793 mm^{-1}, F(000) = 1128]. As it is essentially similar to the first form, it is not further described here. Some disorder is present in several complexes. In **9**·2THF, the atoms C(3) and C(4) of the dithiolene ligand may be disordered, but the different positions are not resolved and these atoms have been refined with restraints on bond lengths and displacement parameters. In **16**·1.5py, one pyridine solvent molecule is disordered around a symmetry centre and the nitrogen atom has not been located. All non-hydrogen atoms were refined with anisotropic displacement parameters, with some restraints on bond lengths and/or displacement parameters for some disordered or badly behaving atoms, particularly in the solvent molecules. Hydrogen atoms were introduced at calculated positions and were treated as riding atoms with

Table 5. Crystal data and structure refinement details

	9·2THF	**11**·2THF	**12**	**13**	**14**	**15**	**16**·1.5py
Empirical formula	$C_{56}H_{58}O_4P_2S_4U$	$C_{55}H_{56}O_4P_2S_4U$	$C_{24}H_{48}N_6O_2P_2S_4U$	$C_{23}H_{44}N_6O_3P_2S_4U$	$C_{23}H_{46}N_6O_2P_2S_4U$	$C_{21}H_{18}N_2S_4U$	$C_{33.5}H_{28.5}N_{4.5}S_4U$
M [g mol^{-1}]	1223.23	1209.21	880.89	880.85	866.87	664.64	860.38
Crystal system	monoclinic	monoclinic	monoclinic	orthorhombic	triclinic	monoclinic	monoclinic
Space group	$P2_1/c$	$P2_1/c$	$P2_1/n$	$P2_12_12_1$	$P\bar{1}$	$P2_1/m$	$P2_1/n$
a [Å]	17.4062(10)	17.8541(9)	11.2254(8)	10.3673(6)	10.7430(6)	7.4304(5)	14.1685(4)
b [Å]	11.2254(5)	10.8390(5)	16.2142(17)	15.8278(15)	16.2499(10)	14.4901(9)	14.9404(4)
c [Å]	26.2282(17)	25.8930(12)	18.7509(18)	20.0597(18)	20.5468(10)	10.0511(7)	15.3685(5)
α [°]	90	90	90	90	67.938(3)	90	90
β [°]	91.459(5)	91.377(3)	92.248(6)	90	86.563(3)	109.787(4)	105.399(2)
γ [°]	90	90	90	90	87.829(3)	90	90
V [Å^3]	5123.1(5)	5009.4(4)	3410.2(5)	3291.6(5)	3317.8(3)	1018.28(12)	3136.46(16)
Z	4	4	4	4	4	2	4
$D_{calcd.}$ [g cm^{-3}]	1.586	1.603	1.716	1.777	1.735	2.168	1.822
μ(Mo-K_α) [mm^{-1}]	3.440	3.517	5.130	5.317	5.271	8.391	5.474
F(000)	2448	2416	1744	1736	1712	628	1668
Reflections collected	28649	33582	21645	19862	22784	7023	20975
Ind. reflections	9533	9466	6432	6128	11554	2006	5908
Obsd. reflections [$I > 2\sigma(I)$]	3607	6356	4471	4979	8411	1757	4911
R_{int}	0.093	0.094	0.088	0.129	0.074	0.068	0.054
Parameters refined	604	595	364	364	704	130	388
R_1	0.087	0.053	0.050	0.056	0.070	0.030	0.027
wR_2	0.135	0.106	0.094	0.129	0.154	0.059	0.055
S	0.933	1.019	1.019	1.013	1.104	1.023	1.017
$\Delta\rho_{min}$ [e·Å^{-3}]	−1.00	−1.02	−1.03	−1.23	−2.02	−0.91	−0.78
$\Delta\rho_{max}$ [e·Å^{-3}]	0.90	1.24	0.89	1.15	4.41	0.62	0.74

 © 2004 Wiley-VCH Verlag GmbH & Co. KGaA, Weinheim

a displacement parameter equal to 1.2 (CH, CH_2) or 1.5 (CH_3) times that of the parent atom. Some short H···H contacts in **11**·2THF involve the protons of disordered parts or of badly behaving solvent molecules. Some short intramolecular contacts in **14** and **16**·1.5py (lower value 2.98 Å), which involve carbon atoms of the cot moiety and S, O or N donor atoms, are likely the result of the steric congestion in these molecules. The large positive and negative residual electron density peaks in **14** are located at 1.32 and 0.95 Å, respectively, from the uranium atom U(1) and may result from an imperfect absorption correction. Crystal data and structure refinement details are given in Table 5. The molecular plots were drawn with SHELXTL.[45] All calculations were performed with a Silicon Graphics R5000 workstation. CCDC-238470 (**9**·2THF), -238471 (**11**·2THF), -238472 (**12**), -238473 (**13**), -238474 (**14**), -238475 (**15**), -238476 (**16**·1.5py) and -238477 (**11**bis) contain the supplementary crystallographic data for this paper. These data can be obtained free of charge at www.ccdc.cam.ac.uk/conts/retrieving.html [or from the Cambridge Crystallographic Data Centre, 12 Union Road, Cambridge CB2 1EZ, UK; Fax: + 44-1223-336-033; E-mail: deposit@ccdc.cam.ac.uk].

[1] [1a] P. Cassoux, L. Valade, H. Kobayashi, A. Kobayashi, R. A. Clark, A. E. Underhill, *Coord. Chem. Rev.* **1991**, *110*, 115−160. [1b] R. M. Olk, B. Olk, W. Dietzsch, R. Kirmse, E. Hoyer, *Coord. Chem. Rev.* **1992**, *117*, 99−131.

[2] Y. Tang, X. Gan, M. Tan, X. Zheng, *Polyhedron* **1998**, *17*, 429−432.

[3] D. A. Wrobleski, D. T. Cromer, J. V. Ortiz, T. B. Rauchfuss, R. R. Ryan, A. P. Sattelberger, *J. Am. Chem. Soc.* **1986**, *108*, 174−175.

[4] K. Tatsumi, T. Amemiya, H. Kawaguchi, K. Tani, *J. Chem. Soc., Chem. Commun.* **1993**, 773−774.

[5] B. Cetinkaya, P. B. Hitchcock, M. F. Lappert, R. G. Smith, *J. Chem. Soc., Chem. Commun.* **1992**, 932−934.

[6] K. Tatsumi, I. Matsubara, Y. Inoue, A. Nakamura, R. E. Cramer, G. J. Tagoshi, J. A. Golen, J. W. Gilje, *Inorg. Chem.* **1990**, *29*, 4928−4938.

[7] P. C. Leverd, T. Arliguie, M. Lance, M. Nierlich, J. Vigner, M. Ephritikhine, *J. Chem. Soc., Dalton Trans.* **1994**, 501−504.

[8] P. C. Leverd, M. Lance, M. Nierlich, J. Vigner, M. Ephritikhine, *J. Chem. Soc., Dalton Trans.* **1994**, 3563−3567.

[9] P. C. Leverd, M. Lance, J. Vigner, M. Nierlich, M. Ephritikhine, *J. Chem. Soc., Dalton Trans.* **1995**, 237−244.

[10] L. Ventelon, C. Lescop, T. Arliguie, P. C. Leverd, M. Lance, M. Nierlich, M. Ephritikhine, *Chem. Commun.* **1999**, 659−660.

[11] C. Lescop, T. Arliguie, M. Lance, M. Nierlich, M. Ephritikhine, *J. Organomet. Chem.* **1999**, *580*, 137−144.

[12] T. Arliguie, C. Lescop, L. Ventelon, P. C. Leverd, P. Thuéry, M. Nierlich, M. Ephritikhine, *Organometallics* **2001**, *20*, 3698−3703.

[13] [13a] F. Guyon, C. Lenoir, M. Fourmigué, J. Larsen, J. Amaudrut, *Bull. Soc. Chim. Fr.* **1994**, *131*, 217−226. [13b] B. Domercq, C. Coulon, M. Fourmigué, *Inorg. Chem.* **2001**, *40*, 371−378.

[14] M. Fourmigué, *Coord. Chem. Rev.* **1998**, *180*, 823−864.

[15] C. Boisson, J. C. Berthet, M. Lance, J. Vigner, M. Nierlich, M. Ephritikhine, *J. Chem. Soc., Dalton Trans.* **1996**, 947−953.

[16] T. Arliguie, D. Baudry, J. C. Berthet, M. Ephritikhine, J. F. Le Maréchal, *New J. Chem.* **1991**, *15*, 569−590.

[17] T. Arliguie, M. Fourmigué, M. Ephritikhine, *Organometallics* **2000**, *19*, 109−111.

[18] T. Arliguie, M. Lance, M. Nierlich, J. Vigner, M. Ephritikhine, *J. Chem. Soc., Chem. Commun.* **1995**, 183−184.

[19] T. Arliguie, P. Thuéry, M. Fourmigué, M. Ephritikhine, *Organometallics* **2003**, *22*, 3000−3003.

[20] C. Boisson, J. C. Berthet, M. Ephritikhine, M. Lance, M. Nierlich, *J. Organomet. Chem.* **1996**, *522*, 249−257.

[21] D. Baudry, E. Bulot, M. Ephritikhine, M. Nierlich, M. Lance, J. Vigner, *J. Organomet. Chem.* **1990**, *388*, 279−287.

[22] S. M. Cendrowski-Guillaume, G. Le Gland, M. Nierlich, M. Ephritikhine, *Eur. J. Inorg. Chem.* **2003**, 1388−1393.

[23] T. R. Boussie, R. M. Moore, A. Streitwieser, A. Zalkin, J. Brennan, K. Smith, *Organometallics* **1990**, *9*, 2010−2016.

[24] O. Wiley, R. B. Von Dreele, T. M. Brown, *Inorg. Chem.* **1980**, *19*, 3351−3356.

[25] M. Fourmigué, C. Lenoir, C. Coulon, F. Guyon, J. Amaudrut, *Inorg. Chem.* **1995**, *34*, 4979−4985.

[26] S. Sun, B. Zhang, P. J. Wu, D. B. Zhu, *J. Chem. Soc., Dalton Trans.* **1997**, 277−282.

[27] Y. S. J. Veldhuizen, N. Veldman, A. L. Spek, P. Cassoux, R. Carlier, M. J. J. Mulder, J. G. Haasnoot, J. Reedijk, *J. Chem. Soc., Dalton Trans.* **1998**, 2989−2994.

[28] J. W. Lauher, R. Hoffman, *J. Am. Chem. Soc.* **1976**, *98*, 1729−1742.

[29] [29a] M. Fourmigué, C. Coulon, *Adv. Mater.* **1994**, *6*, 948−952. [29b] B. Domercq, C. Coulon, P. Feneyrou, V. Dentan, P. Robin, M. Fourmigué, *Adv. Funct. Mater.* **2002**, *12*, 359−366.

[30] T. Steiner, *Chem. Commun.* **1997**, 727−734.

[31] F. M. Raymo, M. D. Bartberger, K. N. Houk, J. F. Stoddart, *J. Am. Chem. Soc.* **2001**, *123*, 9264−9267.

[32] [32a] J. L. Wardell, S. M. S. V. Wardell, J. M. S. Skakle, J. N. Low, C. Glidewell, *Acta Crystallogr., Sect. C* **2002**, *58*, 428−430. [32b] E. M. Mohamed, S. Muralidharan, K. Panchanatheswaran, R. Ramesh, J. N. Low, C. Glidewell, *Acta Crystallogr., Sect. C* **2003**, *59*, 367−369.

[33] M. Fourmigué, P. Batail, *J. Chem. Soc., Chem. Commun.* **1991**, 1370−1372.

[34] J. C. Berthet, Y. Miquel, P. B. Iveson, M. Nierlich, P. Thuéry, C. Madic, M. Ephritikhine, *J. Chem. Soc., Dalton Trans.* **2002**, 3265−3272.

[35] J. C. Berthet, C. Boisson, M. Lance, J. Vigner, M. Nierlich, M. Ephritikhine, *J. Chem. Soc., Dalton Trans.* **1995**, 3027−3033.

[36] G. M. Smith, H. Suzuki, D. C. Sonnenberger, D. C. Day, V. W. Day, T. J. Marks, *Organometallics* **1986**, *5*, 549−561.

[37] J. C. Berthet, J. F. Le Maréchal, M. Ephritikhine, *J. Organomet. Chem.* **1994**, *480*, 155−161.

[38] [38a] J. Larsen, C. Lenoir, *Synthesis* **1989**, 134−134. [38b] J. Larsen, C. Lenoir, *Org. Synth.* **1993**, *72*, 265−273.

[39] R. R. Schumaker, V. Y. Lee, E. M. Engler, *J. Org. Chem.* **1984**, *49*, 564−566.

[40] *Kappa-CCD Software*, Nonius BV, Delft, The Netherlands, **1998**.

[41] Z. Otwinowski, W. Minor, *Methods Enzymol.* **1997**, *276*, 307−326.

[42] G. M. Sheldrick, *SHELXS-97*, *SHELXL-97*, University of Göttingen, Germany, **1997**.

[43] A. L. Spek, *PLATON*, University of Utrecht, The Netherlands, **2000**.

[44] H. D. Flack, *Acta Crystallogr., Sect. A* **1983**, *39*, 876−881.

[45] G. M. Sheldrick, *SHELXTL*, Version 5.1, Bruker AXS Inc., Madison, WI, USA, **1999**.

Received May 14, 2004
Early View Article
Published Online September 7, 2004

 © 2004 Wiley-VCH Verlag GmbH & Co. KGaA, Weinheim

Structural Variety and Multiple Isomerism in 1-(Dimethylamino)propyl-2-chalcogenolate and 2-(Dimethylamino)propyl-1-chalcogenolate Complexes of Palladium(II) and Platinum(II): Synthesis, Spectroscopy and Structures

Sandip Dey,[a] Liladhar B. Kumbhare,[a] Vimal K. Jain,*[a] Thilo Schurr,[b] Wolfgang Kaim,*[b] Axel Klein,*[b] and Ferdinand Belaj[c]

Keywords: Chalcogens / Isomers / N ligands / Palladium / Platinum

Isomeric dichalcogenides $[Me_2NCH(Me)CH_2E]_2$ $[(N^{\frown}E^{**})_2]$ and $[Me_2NCH_2CH(Me)E]_2$ $[(N^{\frown}E^{*})_2]$ (E = S, Se, Te) have been obtained by the reactions of NaSH or M'_2E_2 (M′ = Na or K) with $Me_2NCH_2CHMeCl$. The former reaction affords mainly $(N^{\frown}E^{**})_2$ (E = S) while from the latter mixtures of $(N^{\frown}E^{**})_2$ and $(N^{\frown}E^{*})_2$ [referred to as $(N^{\frown}E)_2$, E = S, Se, Te] were isolated, the ratios in the mixtures depending on the chalcogen. Reactions of $(N^{\frown}E)Na$ with $[M_2Cl_2(\mu\text{-}Cl)_2(PR_3)_2]$ gave complexes $[MCl(N^{\frown}E)(PR_3)]$ (M = Pd or Pt). These chiral, mixed-ligand complexes have been characterised by elemental analysis, IR, UV/Vis and NMR (^1H, ^{13}C, ^{31}P, ^{77}Se, ^{125}Te, ^{195}Pt) spectroscopy, and, in part, by X-ray structure analysis. The complexes display a typical pattern of mutually *trans*-oriented neutral (P and N) and anionic (Cl and E) donor atoms in an approximately square-planar environment. In contrast to the platinum(II) analogues, the X-ray structures of the complexes $[PdCl(N^{\frown}E)(PMePh_2)]$ (E = S or Se) revealed both a conformational isomerism of the five-membered chelate ring and, for Se, the co-crystallisation of complexes with both the $N^{\frown}E^{*}$ and $N^{\frown}E^{**}$ isomeric ligands. The thermal behaviour of some complexes has been investigated.

(© Wiley-VCH Verlag GmbH & Co. KGaA, 69451 Weinheim, Germany, 2004)

Introduction

The chemistry of metal chalcogenolates continues to be an active area of research. Their emerging application as single-source precursors for low-decomposition-temperature synthesis of solid-state chalcogenide materials has provided a further momentum to this activity.[1−4] The chemistry of the heavier metal chalcogenolates is dominated by thiolate complexes, which are often isolated as non-volatile, insoluble (or sparingly soluble) polymers.[5] One of the strategies to suppress polymerisation has been to use internally functionalised ligands.[3] Among such ligands are (aminoalkyl)chalcogenolate ions $R_2N(CR_2')_nE^-$. While the chemistry of mercaptoalkylamines is now fairly well documented,[6−12] the heavier analogues containing Se and Te have been more recently developed and investigated by us.[13−17] Subtle variations in either the carbon chain length of the ligand or in the auxiliary ligands at the metal centre have led to the isolation of complexes with quite varied structural patterns. Some of these complexes also provided an opportunity to study metal-mediated donor−acceptor interactions between coordinated ligands.[14,15]

A new series of (aminoalkyl)chalcogenolate ligands with asymmetrically substituted carbon atoms in the alkyl chain was conceived for the following reasons: (i) chiral thiolate complexes such as the recently reported $[PdCl\{SCH_2CH(COOEt)NH_2\}(PPh_3)]$ are useful asymmetric homogeneous catalysts;[12,18−20] (ii) the cleavage of secondary chalcogenolates often proceeds more cleanly than that of primary or tertiary analogues;[21] (iii) the influence of electron-releasing methyl groups on donor−acceptor interactions in metal complexes can be studied.[14,15]

In this perspective, 2-[(dimethylamino)propyl]-1-chalcogenolate ($N^{\frown}E^{**}$) (**A**) and 1-[(dimethylamino)propyl]-2-chalcogenolate ($N^{\frown}E^{*}$) (**B**) ligands have been synthesised, and their chemistry with palladium(II) and platinum(II) has been explored. The results of this work are described in this paper.

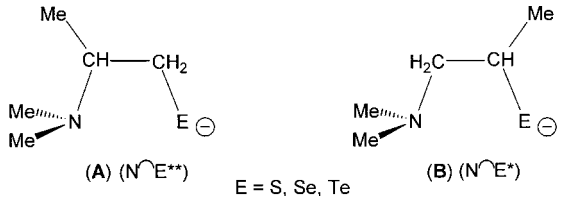

[a] Novel Materials & Structural Chemistry Division, Bhabha Atomic Research Centre (BARC)
Mumbai 400085, India
E-mail: jainvk@apsara.barc.ernet.in
[b] Institut für Anorganische Chemie, Universität Stuttgart, Pfaffenwaldring 55, 70569, Stuttgart, Germany
E-mail: aklein@uni-stuttgart.de
kaim@iac.uni-stuttgart.de
[c] Institut für Chemie, Karl-Franzens-Universität Graz, Schubertstrasse 1, 8010 Graz, Austria
Supporting information for this article is available on the WWW under http://www.eurjic.org or from the author.

 © 2004 Wiley-VCH Verlag GmbH & Co. KGaA, Weinheim **DOI: 10.1002/ejic.200400524**

Results and Discussion

Synthesis of Dichalcogenides

Two general reactions [Equations (1) and (2)] have been employed for the synthesis of the dichalcogenides. The disulfide formed by the reaction according to Equation (1) was isolated mainly as a single rearranged product $[Me_2NCH(Me)CH_2S]_2$ $(N^{\cap}E^{**})_2$, whereas the raction according to Equation (2) gave a mixture of $[Me_2NCH(Me)CH_2E]_2$ $(N^{\cap}E^{**})_2$ (E = S, Se, Te) and $(Me_2NCH_2CH(Me)E]_2$ $(N^{\cap}E^{*})_2$ (E = S, Se, Te). The relative amounts of $(N^{\cap}E^{**})_2$ and $(N^{\cap}E^{*})_2$ are chalcogen-dependent: the ratios were 1:2 for E = S, approx. 1:1 for E = Se, and 5:1 for E = Te (from ^{1}H NMR integration).

$$Me_2N\text{-}CH_2\text{-}CHMeCl \xrightarrow[-\ NaCl]{+\ NaSH} Me_2N\text{-}CHMe\text{-}CH_2\text{-}SH$$

$$\xrightarrow[-\ 1/2\ H_2O]{+\ 1/4\ O_2} 1/2\ (Me_2N\text{-}CHMe\text{-}CH_2S)_2 \qquad (1)$$

$$2\ Me_2N\text{-}CH_2\text{-}CHMeCl \xrightarrow[-\ NaCl\ /\ KCl]{+\ Na_2E_2\ /\ K_2Te_2} (Me_2N\text{-}CHMe\text{-}CH_2\text{-}E)_2 + (Me_2N\text{-}CH_2\text{-}CHMe\text{-}E)_2 \qquad (2)$$

Several factors have been identified which influence the product formation in nucleophilic substitution reactions of alkyl halides. In the present case, the participation of a nucleophilic neighbouring group (NMe_2) is believed to play an essential role to produce the *C*-methylaziridinium species **C** as a possible intermediate. In **C**, the less substituted carbon atom (i.e. the CH_2 group) seems to be the preferred site of attack by a nucleophile such as HS^- in the reaction according to Equation (1) as it is sterically less encumbered and electronically more positive. Accordingly, an isomerized product $[Me_2NCH(Me)CH_2S]_2$ (type **A**) could be isolated from the reaction according to Equation (1). The reaction according to Equation (2) is carried out using M_2E_2 in DMF. The nucleophiles E_2^{2-} and RE_2^- as intermediates in a solvent such as DMF may attack either of the carbon centres (CH_2 or CHMe) leading to the formation of different products. Their formation in different ratios reflects the differing nucleophilic character of anionic S, Se, or Te. Cyclic intermediates similar to **C** with various heteroatoms (e.g, N, O, S) are commonly invoked in organic reactions. The cleavage of the N−C bond in C-substituted aziridines or aziridinium ions frequently leads to isomerized products.[22]

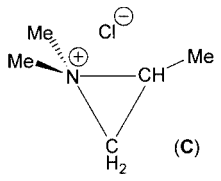

(C)

The ^{1}H and ^{13}C NMR spectra of the disulfide obtained from reaction according to Equation (1) display only one set of resonances attributable to $[Me_2NCH(Me)CH_2S]_2$ $(N^{\cap}S^{**})_2$. However, the spectra of the dichalcogenides prepared from the reaction according to Equation (2) exhibit two sets of resonances which can be assigned to mixtures [referred to as $(N^{\cap}E)_2$].

The corresponding ^{77}Se (Figure 1) and ^{125}Te NMR spectra show eight and four lines, respectively. The molecules R_2E_2 (E = O, S, Se, Te) have a "skew" structure and can show restricted rotation about the E−E bond. For the molecules $(N^{\cap}E^{**})_2$ and $(N^{\cap}E^{*})_2$ three stereoisomers — (*R*,*R*), (*S*,*S*) and a *meso* form — are expected. Thus, each molecule is expected to display two resonances [(*R*,*R*)/(*S*,*S*) and *meso*] for the chalcogen atom in the ^{77}Se or ^{125}Te NMR spectrum. The resonances at $\delta = -791$ and -559 ppm and $\delta = -870$ and -659 ppm in the ^{125}Te NMR spectra may be assigned to molecules $(N^{\cap}Te^{*})_2$ and $(N^{\cap}Te^{**})_2$. Similarly, resonances at $\delta \approx 226$ and 357 ppm and $\delta \approx 286$ and 415 ppm in the ^{77}Se NMR spectra can be attributed to $(N^{\cap}Se^{*})_2$ and $(N^{\cap}Se^{**})_2$. However, each signal in the ^{77}Se NMR spectrum appears as two closely spaced lines (ca. 1 ppm separation). The presence of intramolecular interactions between nitrogen and selenium atoms may lead to the magnetic nonequivalence of the two selenium atoms in each molecule, resulting in two separate but closely spaced resonances. Recently, intramolecular Se···N interactions have been reported in several diselenides.[23−25] The Se···N distances of about 2.8 Å in these compounds are longer than the sum of the covalent radii, but significantly shorter than the sum of the corresponding van der Waals radii (ca. 3.5 Å).[23−25] For instance, the atomic distances Se(1)−N(1) and Se(2)−N(2) in **D** are 2.819(5) and 2.705(5) Å, respectively.[24] For the same reasons one would anticipate an analogous pattern for the ^{125}Te NMR spectrum. However, relatively large line widths [ca. 100 Hz (1 ppm)] for the ^{125}Te resonances appear to preclude a visible separation of closely spaced signals.

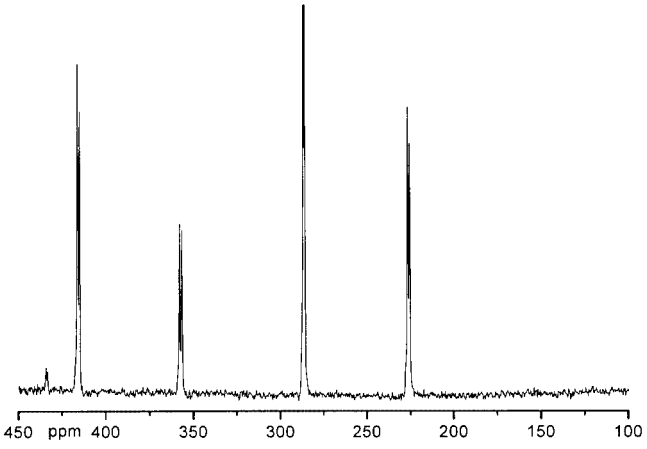

Figure 1. ^{77}Se{^{1}H} NMR spectrum of $(N^{\cap}Se)_2$ [mixture of $(N^{\cap}Se^{**})_2$ and $(N^{\cap}Se^{*})_2$] in $CDCl_3$

 © 2004 Wiley-VCH Verlag GmbH & Co. KGaA, Weinheim

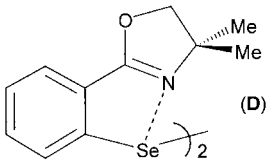

(D)

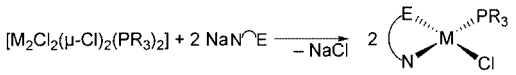

M = Pd or Pt; PR_3 = P*n*Bu_3, P*n*Pr_3, PEt_3, PMe_2Ph, $PMePh_2$ or PPh_3. (3)

Synthesis of Palladium(II) and Platinum(II) Complexes

Treatment of $[M_2Cl_2(\mu\text{-}Cl)_2(PR_3)_2]$ with N∩ENa in methanol/dichloromethane readily gave coloured complexes of the general formula $[MCl(N\cap E)(PR_3)]$ [Equation (3)].

NMR Spectroscopy of Complexes $[MCl(N\cap E)(PR_3)]$

The ^1H NMR spectra (Table 1) of the thiolate complexes $[MCl(SCH_2CHMeNMe_2)(PR_3)]$ as prepared from the N∩S** (**A**) ligand display only one set of signals. The NMe_2

Table 1. ^1H and ^{31}P NMR spectroscopic data of palladium and platinum complexes $[MCl(N\cap E)(PR_3)]$[a]

	^1H	$^{31}P\{^1H\}$[b]
$[PdCl(N\cap S^{**})(P\mathit{n}Pr_3)]$	1.06 (t, J = 7.1 Hz, $PCH_2CH_2\mathit{Me}$), 1.16 (d, J = 6 Hz, $CH\mathit{Me}$), 1.60−1.67 (m, $PCH_2\mathit{CH_2}$), 1.78−1.83 (m, $PC\mathit{H_2}$), 2.51 (br., s), 2.76 (br., s) $N\mathit{Me_2}$, 2.56−2.70 (m, $SC\mathit{H_2}$), 2.86−2.96 (m, $NC\mathit{H}$)	23.8
$[PdCl(N\cap S^{**})(PEt_3)]$	1.15−1.29 (m, $PCH_2\mathit{Me}$, $NCH\mathit{Me}$), 1.83−2.00 (m, $PC\mathit{H_2}$), 2.53 (d, J = 2.5 Hz), 2.78 (d, J = 2.8 Hz) $N\mathit{Me_2}$, 2.57−2.73 (m, $SC\mathit{H_2}$), 2.92 (m, $NC\mathit{H}$)	34.5
$[PdCl(N\cap S^{**})(PMe_2Ph)]$	1.15 (d, J = 6.5 Hz $NCH\mathit{Me}$), 1.79 (d, J = 11.6 Hz), 1.83 (d, J = 11.7 Hz, $P\mathit{Me_2}$), 2.52 (d, J = 3.0 Hz), 2.80 (d, J = 3.3 Hz) $N\mathit{Me_2}$, 2.46−2.66 (m, $SC\mathit{H_2}$), 2.98 (m, $NC\mathit{H}$), 7.41−7.44 (m), 7.70−7.75 (m) $P\mathit{Ph}$	7.0
$[PdCl(N\cap S^{**})(PMePh_2)]$	1.15 (d, J = 6.5 Hz $NCH\mathit{Me}$), 2.16 (d, J = 11.4 Hz, $P\mathit{Me}$), 2.37−2.64 (m, $SC\mathit{H_2}$), 2.59 (d, J = 3.0 Hz), 2.86 (d, J = 3.3 Hz) $N\mathit{Me_2}$, 3.04 (m, $NC\mathit{H}$), 7.34−7.44 (m), 7.55−7.62 (m), 7.70−7.77 (m) $P\mathit{Ph}$	21.0
$[PdCl(N\cap S^{*})(PMePh_2)]$	1.21 (d, J = 6.5 Hz, $SCH\mathit{Me}$), 2.11 (d, J = 11 Hz, $P\mathit{Me}$) 2.70, 2.78 (d, J = 2.5 Hz, $N\mathit{Me_2}$), 2.62 (br., $SC\mathit{H_2}$), 2.74 (m, $NC\mathit{H_2}$), 3.38 (m, $C\mathit{H}S$), 7.39−7.81 (m, $P\mathit{Ph}$).	19.6
$[PdCl(N\cap S^{**})(PPh_3)]$	1.20 (d, J = 6.4 Hz $SCH\mathit{Me}$), 2.66 (d, J = 3.0 Hz), 2.93 (d, J = 3.2 Hz) $N\mathit{Me_2}$, 2.45−2.85 (m, $SC\mathit{H_2}$), 3.15 (m, $NC\mathit{H}$), 7.38−7.49, 7.71−7.78 (m, $P\mathit{Ph}$)	34.2
$[PtCl(N\cap S^{**})(P\mathit{n}Bu_3)]$	0.94 (t, J = 7.3 Hz, $PCH_2CH_2CH_2\mathit{Me}$), 1.22 (d, J = 6.5 Hz, $NCH\mathit{Me}$), 1.39−1.59 (m, $PCH_2C\mathit{H_2}C\mathit{H_2}$), 1.80−1.89 (m, $PC\mathit{H_2}$), 2.39−2.53 (m, $SC\mathit{H_2}$), 2.58, 2.88 (each d, J = 2.7 Hz, $N\mathit{Me_2}$ with Pt satellites), 2.83 (br., $NC\mathit{H}$)	−1.7 [3468]
$[PtCl(N\cap S^{**})(P\mathit{n}Pr_3)]$	1.04 (t, J = 7.3 Hz, $PCH_2CH_2\mathit{Me}$), 1.21 (d, J = 6.5 Hz, $NCH\mathit{Me}$), 1.57−1.66 (m, $PCH_2C\mathit{H_2}$), 1.78−1.87 (m, $PC\mathit{H_2}$), 2.58, 2.88 (each d, J = 2.7 Hz, $N\mathit{Me_2}$ with Pt satellites, 2.48−2.54 (m, $SC\mathit{H_2}$), 2.82 (br., $NC\mathit{H}$)	−2.4 [3472]
$[PtCl(N\cap S^{**})(PEt_3)]$	1.15 (dt, J = 7.6, 16.7 Hz, $PCH_2\mathit{Me}$), 1.22 (d, J = 6.7 Hz, $NC\mathit{H}$), 1.83−1.94 (m, $PC\mathit{H_2}$), 2.59, 2.89 (each d, J = 2.2 Hz; $J_{Pt,H}$ = 17 Hz, $N\mathit{Me_2}$), 2.82 (br., $NC\mathit{H}$), 2.43−2.54 (m, $SC\mathit{H_2}$)	6.2 [3468]
$[PtCl(N\cap S^{**})(PMe_2Ph)]$	1.22 (d, J = 6.5 Hz, $NCH\mathit{Me}$), 1.83, 1.87 (each d, J = 11 Hz, $P\mathit{Me_2}$), 2.38−2.58 (m, $SC\mathit{H_2}$), 2.62, 2.93 (each d, J = 2.9 Hz, $N\mathit{Me_2}$ with Pt satellites), 2.86 (br., $NC\mathit{H}$), 7.42, 7.74−7.81 (m, $P\mathit{Ph}$)	−18.7 [3548]
$[PtCl(N\cap S^{**})(PMePh_2)]$	1.20 (d, J = 6.5 Hz, $NCH\mathit{Me}$), 2.19 (d, J = 11 Hz, $P\mathit{Me}$), 2.64, 2.97 (each d, J = 3 Hz, $N\mathit{Me_2}$), 2.52 (m, $C\mathit{H_2}S$), $NC\mathit{H}$ merged in $N\mathit{Me_2}$, 7.40−7.70 (m, $P\mathit{Ph}$)	−4.3 [3616]
$[PdCl(N\cap Se)(PEt_3)]$	1.08−1.14 (m, $PCH_2\mathit{CH_3}$), 1.18 (d, J = 6.4 Hz, $CH\mathit{Me}$, N∩E**), 1.36 (d, J = 6.7 Hz, $CH\mathit{Me}$, N∩E*), 1.75−1.89 (m, $PC\mathit{H_2}$), 2.48, 2.51, 2.66, 2.70 (each, d, J = 2.5 Hz $J_{P,H}$, $N\mathit{Me_2}$, N∩E* + N∩E**), 2.55 ($NC\mathit{H_2}$, N∩E*, merged in $N\mathit{Me_2}$), 2.92−2.97 (m, $C\mathit{H_2}Se$, N∩E**), 3.42−3.50 (m, $C\mathit{H}Se$, N∩E*)	31.3 (s), 31.2 (s)
$[PdCl(N\cap Se)(PMe_2Ph)]$	1.19 (d, J = 6.4 Hz, $CH\mathit{Me}$, N∩E**), 1.35 (d, J = 6.6 Hz, $CH\mathit{Me}$, N∩E*), 1.79 (d, J = 13 Hz, $P\mathit{Me_2}$), 1.87 (d, J = 11.5 Hz, $P\mathit{Me_2}$), 2.53 (d, J = 3.0 Hz), 2.58 (d, J = 2.6 Hz, 2.72 (d, J = 3.5 Hz), 2.78 (d, J = 3 Hz) $N\mathit{Me_2}$, N∩E*+ N∩E**) $NC\mathit{H}$, $NC\mathit{H_2}$, merged in $N\mathit{Me_2}$, 3.01−3.08 (m, $C\mathit{H_2}Se$, N∩E**, 3.44−3.52 (m, $C\mathit{H}Se$, N∩E*), 7.40−7.43 (m), 7.66−7.73 (m) $P\mathit{Ph}$	2.5 (s)[c]

 © 2004 Wiley-VCH Verlag GmbH & Co. KGaA, Weinheim

Table 1 *(continued)*

	^{1}H	^{31}P{^{1}H}[b]
[PdCl(N∩Se)(PMePh$_2$)]	1.21 (d, J = 6.4 Hz, CH*Me*, N∩E**), 1.29 (d, J = 6.6 Hz, CH*Me*, N∩E*), 2.18 (d, J = 11.3 Hz minor), 2.21 (d, J = 11.4 Hz, major, P*Me*), 2.53 (AB pattern, NCH_2), NC*H* merged with NMe_2, 2.60 (d, J = 3.1 Hz), 2.66 (d, J = 2.5 Hz), 2.77 (d, J = 3.4 Hz), 2.85 (d, J = 3.0 Hz) (NMe_2, N∩E*+ N∩E**), 3.07−3.16 (m, CH_2Se, N∩E*), 3.46 (m C*H*Se, N∩E*), 7.33−7.44 (m), 7.49−7.80 (m) P*Ph*[b]	16.7 (s)
[PdCl(N∩Se)(PPh$_3$)]	1.27 (d, J = 6.4 Hz), 1.30 (d, J = 6.5 Hz, NMe_2), 2.66, 2.92, 2.72, 2.84 (each d, J = 3 Hz) NMe_2, 2.52−2.61 (m, NC*H*), 2.95−3.30 (m, CH_2Se, NCH_2), 3.50 (m, C*H*Se) 7.19−7.80 (m, P*Ph*)	29.6, 29.8
[PtCl(N∩Se)(PnBu$_3$)]	0.80 (t, J = 7.1 Hz, PCHCH$_2$CH$_2$*Me*), 1.13 (d, J = 6.3 Hz, CH*Me*, N∩E*), 1.25−1.45 (m, PCH$_2$CH_2CH_2 + doublet due to CH*Me*, N∩E*), 1.59−1.78 (m, PCH_2), 2.15, 2.40 (AB pattern, NCH_2), 2.49 (d, J = 2.4 Hz), 2.70 (d, J = 2.5 Hz), 2.74 (d, J = 2.6 Hz) ($J_{P,H}$, NMe_2, N∩E* + N∩E** merged with CH_2Se N∩E**), 3.08−3.20 (m, SeC*H*, N∩E*)	−4.0 [3431], −4.3 [3416]
[PtCl(N∩Se)(PEt$_3$)]	1.06−1.20 (m, PCH$_2$CH_3), 1.24 (d, J = 6.3 Hz, CH*Me*, N∩E**), 1.48 (d, J = 6.6 Hz, CH*Me*, N∩E*), (3:2 ratio), 1.78−1.92 (m, PCH_2), 2.25 (quadruplet, NC*H*, N∩E**), 2.49 (AB pattern, NCH_2, N∩E*), 2.61 (d, $J_{P,H}$ = 2.6, $J_{Pt,H}$ = 14.5 Hz), 2.81 (d, $J_{P,H}$ = 2.5 Hz), 2.86 (d, $J_{P,H}$ = 2.8 Hz) NMe_2, N∩E*+ N∩E**, (br., CH_2Se, N∩E**), 3.26 (m, C*H*Se, N∩E*)	4.3[d] [3435], 4.6[e] [3450]
[PtCl(N∩Se)(PMe$_2$Ph)]	1.24 (d, J = 6.4 Hz, CH*Me*, N∩E**), 1.45 (d, J = 6.7 Hz, CH*Me*, N∩E*), 1.89 (d), 1.86, 1.83 (each d, J = 11 Hz, PMe_2), 2.27 (AB, NCH_2), 2.43 (AB, NC*H* and NCH_2), 2.64, 2.66 (each d, J = 2.5 Hz), 2.88, 2.90 (each d, J = 3 Hz) (NMe_2, N∩E* + N∩E**), 3.26 (m, SeC*H*, N∩E*), 7.38−7.48 (m), 7.70−7.77 (m) P*Ph*	−22.2[d] [3476], −21.9[e] [3489]
[PdCl(N∩Te)(PnPr$_3$)][f]	1.02 (t, J = 7 Hz, PCH$_2$CH$_2$*Me*), 1.25 (d, J = 6.1 Hz, CH*Me*, N∩E**), 1.52−1.63 (m, PCH$_2$CH_2 + CH*Me*, N∩E*), 1.77−1.84 (m, PCH_2), 2.15−2.21 (m, NCH_2), 2.68 (d, J = 2.7 Hz), 2.73 (d, J = 2.0 Hz) NMe_2, 2.55, 2.86 (m, NCH_2),	−6.9 [3373], −7.2 [3350]
[PdCl(N∩Te**)(PPh$_3$)][g]	1.33 (d, J = 6.0 Hz, CH*Me*), 2.63 (d, J = 3.0 Hz), 2.90 (d, J = 1.8 Hz) NMe_2, 3.10 (br., NC*H*), 3.48 (br., TeCH_2), 7.36−7.86 (m, P*Ph*)	21.6 (s)
[PdCl(N∩Te*)(PPh$_3$)][g]	1.41 (d, J = 6.8 Hz CH*Me*), 2.81 (d, J = 3.2 Hz), 2.98 (br) NMe_2, 2.70 (br., NCH_2), 3.80 (m, TeC*H*), 7.36−7.86 (m, P*Ph*)	22.4 (s)
[PtCl(N∩Te**)(PPh$_3$)]	1.12 (d, J = 6.4 Hz, CH*Me*), 2.57, 3.27 (each br, NMe_2), 3.10 (m, NC*H*), 3.21 (br., TeCH_2), 7.32−7.87 (m, P*Ph*).	8.7 [3742]
[PtCl(N∩Te*)(PPh$_3$)]	1.27 (br., CH*Me*), 2.80 (d, J = 2.9 Hz), 2.94 (d, J = 2.2 Hz) NMe_2, 2.63 (br., NCH_2), 3.90 (br., TeC*H*), 7.32−7.87 (m, P*Ph*)	0.4 [3538]

[a] Measured in CDCl3. [b] ^1J(^{195}Pt,^{31}P) in Hz in parentheses. [c] Separate signals not resolved. [d] Minor product. [e] Major product. [f] The ^{31}P NMR spectrum shows an additional small resonance at δ = −1.3 ppm ($^1J_{Pt,P}$ = 3103 Hz). [g] The ^{31}P NMR spectrum shows an impurity of [PdCl$_2$(PPh$_3$)$_2$] at δ = 23.8 ppm (ca. 10%).

proton resonances appear as two doublets of equal intensity due to $^4J_{P,H}$ coupling. However, the spectra of those complexes synthesised with ligands obtained from the reaction according to Equation (2) show two sets of resonances for the organochalcogenolate fragments and for the phosphane methyl protons (if present). Each set of resonances can be assigned to N∩E** (**A**) and N∩E* (**B**) ligand protons. The NMe_2 proton signals for both isomers appear as two separate doublets with $^4J_{P,H} \approx 3$ Hz. The appearance of two doublets for the NMe_2 protons suggests that the methyl groups are diastereotopic in both the isomers, possibly due to the asymmetric carbon centre in the chalcogenolate moiety. In contrast, the complexes [MCl(ECH$_2$CH$_2$NMe$_2$)(PR$_3$)] show only one doublet for the NMe_2 protons.[13−15]

The ^{31}P{^{1}H} (Figure 2), ^{77}Se{^{1}H} (Figure 3) and ^{195}Pt{^{1}H} NMR spectra (Figure 4) of compounds [MCl(N∩E)(PR$_3$)] (E = Se or Te; Tables 1 and 2) and the thiolate complex [PdCl(N∩S)(PMePh$_2$)], display two sets of resonances. For the (*R*) and (*S*) forms (**E**−**H**) of each stereoisomer one set of resonances is observed. The $^1J_{Pt,P}$ coupling constants for the two resonances (from ^{31}P and ^{195}Pt NMR spectra) are of the same magnitude and are thus indicative of a similar configuration. The magnitude of $^1J_{Pt,P}$ for the platinum complexes suggests that the phosphane ligand is *trans* to the nitrogen atom. The values of $^1J_{Pt,P}$ can be compared with those observed for analogous complexes derived from achiral ligands.[13−15] The two sets of resonances in the

 © 2004 Wiley-VCH Verlag GmbH & Co. KGaA, Weinheim

Table 2. $^{77}Se\{^1H\}$ and ^{195}Pt NMR spectroscopic data of selected $[MCl(N^{\cap}E)(PR_3)]$ complexes[a]

	$^{77}Se\{^1H\}$	$^{195}Pt\{^1H\}$ [$^1J^{195}_{Pt,}{}^{31}_{P}$ in Hz]
$[PdCl(N^{\cap}Se)(PEt_3)]$	201 (s), 351 (s)	–
$[PdCl(N^{\cap}Se)(PMePh_2)]$	282 (s), 425 (s)	–
$[PtCl(N^{\cap}Se)(PEt_3)]$	–	−4211 (d) [3445] (40%), −4315 (d) [3432] (60%)
$[PtCl(N^{\cap}Se)(P\mathit{n}Bu_3)]$	88 (s), 244 (s)	−4286 (d) [3426], −4182 (d) [3419]
$[PtCl(N^{\cap}Se)(PMe_2Ph)]$	113 (s), 263 (s)	−4165 (d) [3452] (minor), −4267 (d) [3478] (major)
$[PtCl(N^{\cap}Te)(P\mathit{n}Pr_3)]$	–	−4425 (d) [3362], −4569 (d) [3371]

[a] Measured in $CDCl_3$.

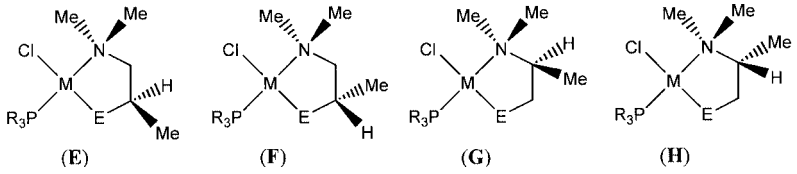

^{31}P, ^{77}Se, and ^{195}Pt NMR spectra are assigned to complexes containing the $N^{\cap}E^*$ and $N^{\cap}E^{**}$ ligand moieties.

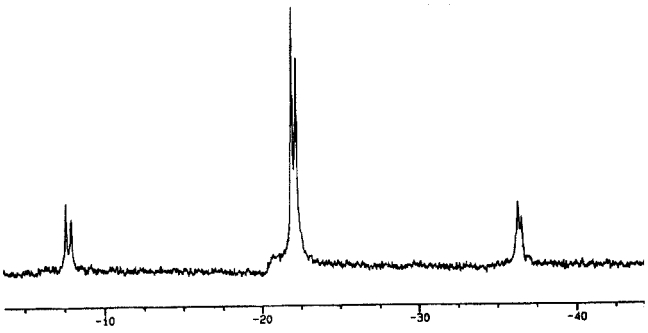

Figure 2. $^{31}P\{^1H\}$ NMR spectrum of $[PtCl(N^{\cap}Se)(PMe_2Ph)]$ in $CDCl_3$

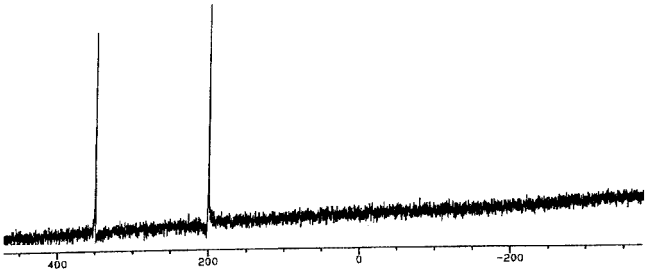

Figure 3. $^{77}Se\{^1H\}$ NMR spectrum of $[PdCl(N^{\cap}Se)(PEt_3)]$ in $CDCl_3$

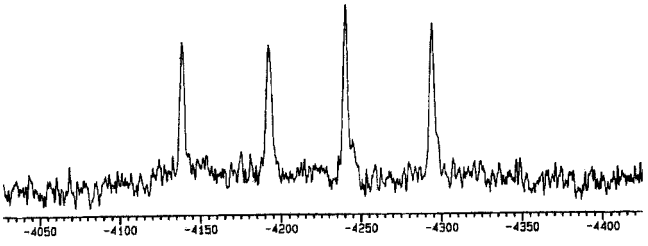

Figure 4. $^{195}Pt\{^1H\}$ NMR spectrum of $[PtCl(N^{\cap}Se)(PMe_2Ph)]$ in $CDCl_3$

Electronic Spectra

Like the analogous achiral derivatives,[14,15,27] the absorption spectra (Table 3) of the complexes $[MCl(N^{\cap}E)(PR_3)]$ display very weak long-wavelength bands. These absorptions are slightly red-shifted when compared with the corresponding achiral complexes. While the absorptions of the platinum complexes are blue-shifted in comparison to the palladium analogues, the selenium- and especially the tellurium-containing compounds absorb at lower energies than the corresponding sulfur analogues. Replacement of a methyl substituent by a phenyl group in PR_3 leads to a bathochromic shift.

Table 3. UV/Vis absorption data for $[MCl(N^{\cap}E)(PR_3)]$ complexes in CH_2Cl_2

Complex	λ_{max} (ε)[a]
$[PdCl(N^{\cap}S^{**})(P\mathit{n}Pr_3)]$	277 (2730), 325 (1780), 407 (br., 440)
$[PdCl(N^{\cap}S^{**})(PMe_2Ph)]$	329 (2150), 462 (90)
$[PdCl(N^{\cap}S^{**})(PMePh_2)]$	331 (1980), 474 (70)
$[PdCl(N^{\cap}S)(PMePh_2)]$[b]	327 (2000), 459 (90)
$[PdCl(N^{\cap}S^{**})(PPh_3)]$	337 (3340)
$[PtCl(N^{\cap}S^{**})(PEt_3)]$	282 (3000), 325 (780)
$[PtCl(N^{\cap}S^{**})(PMe_2Ph)]$	281 (2600), 396 (80)
$[PtCl(N^{\cap}S^{**})(PMePh_2)]$	289 (2130), 404 (70)
$[PdCl(N^{\cap}Se)(PEt_3)]$	338 (1830), 476 (80)
$[PdCl(N^{\cap}Se)(PMe_2Ph)]$	339 (2780), 483 (90)
$[PdCl(N^{\cap}Se)(PMePh_2)]$	255 (2860), 345 (2580), 495 (90)
$[PtCl(N^{\cap}Se)(PEt_3)]$	284 (3980), 406 (110)
$[PtCl(N^{\cap}Se)(PMe_2Ph)]$	285 (6380), 412 (180)
$[PdCl(N^{\cap}Te)(PPh_3)]$	392 (4280), 616 (110)

[a] Wavelengths, λ_{max}, at the absorption maxima in nm; molar extinction coefficients, ε, in $M^{-1}\cdot cm^{-1}$ (in parentheses). [b] Ligand prepared by the Na_2S_2 route.

Such weak long-wavelength absorptions have been attributed for similar complexes to ligand (E) to ligand (PR_3) charge-transfer (L′LCT) transitions, based on DFT calculations.[14,15] The results presented here are fully in line with this assignment.[14,15,26]

 © 2004 Wiley-VCH Verlag GmbH & Co. KGaA, Weinheim

Crystal Structure Analysis

The molecular structures of [PdCl(N∩S**)(PMePh$_2$)], [PtCl(N∩S**)(PMe$_2$Ph)], the isostructural complex [PtCl(N∩Se**)(PMe$_2$Ph)] and two molecules from a crystal of [PdCl(N∩Se)(PMePh$_2$)] were unambiguously established by single-crystal X-ray diffraction analyses.

The compounds were found to crystallise in the space group $P2_1$ with the exception of [PdCl(N∩S**)(PMePh$_2$)] ($P\bar{1}$). The quality of the obtained data was excellent for [PdCl(N∩S**)(PMePh$_2$)], [PtCl(N∩S**)(PMe$_2$Ph)] and [PtCl(N∩Se**)(PMe$_2$Ph)] and moderate for [PdCl(N∩Se)(PMePh$_2$)] (see Exp. Sect.). No significant intermolecular contacts were found in any of the crystal structures. Selected bond lengths and angles for the molecules are given in Table 4, crystallographic and refinement data are given in Table 5.

The coordination environments around the central metal atom in each molecule are approximately square-planar, defined by the P, Cl, N and E atoms. The strong donor atoms E and P are oriented *cis* to each other to avoid an unfavourable *trans* interaction. Such a configuration with *trans*-oriented neutral (P and N) and anionic (Cl and E) donor atoms has also been reported for several related achiral complexes.[13−15,26]

The five-membered chelate rings exhibit a twist conformation which, combined with the presence of the methyl substituent, gives rise to two conformations, **I** and **J**, with different configurations at the asymmetric carbon [(*R*) for **I** and (*S*) for **J**]. For three compounds — both platinum complexes and [PdCl(N∩S**)(PMePh$_2$)] — the crystals analysed contained exclusively Me$_2$NCH(Me)CH$_2$E (E = S or Se) ligands (N∩E**), whereas complexes with both isomeric ligands N∩Se* and N∩Se** had co-crystallised in [PdCl(N∩Se)(PMePh$_2$)]. The crystals of [PdCl(N∩S**)-(PMePh$_2$)] (Figures 5 and 6) contain two crystallographically independent molecules, both of which show a disorder according to the conformations **I** and **J**. The structure was best refined using 45% and 55% occupancy for the two conformers, respectively (see Figure 6). For the platinum

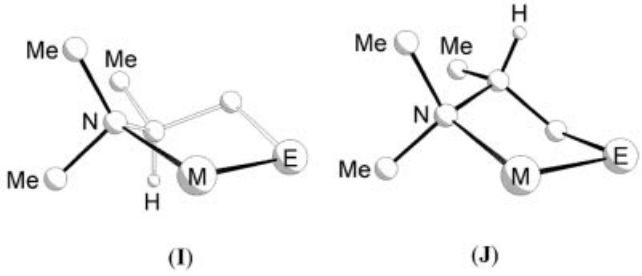

Figure 5. Molecular structure of [PdCl(N∩S**)(PMePh$_2$)]; one of two independent molecules in one possible orientation is shown (for disorder **I/J**, see text) with 30% thermal ellipsoids; H atoms have been omitted for clarity

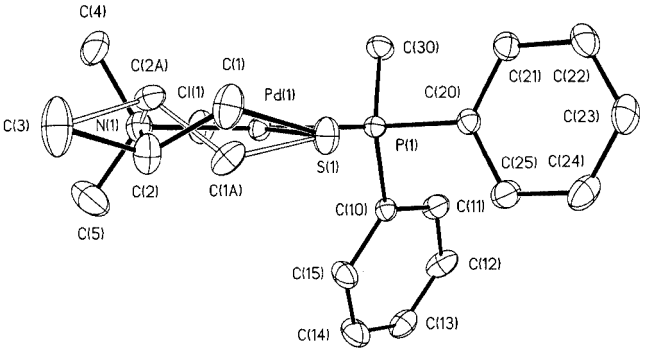

Figure 6. View of [PdCl(N∩S**)(PMePh$_2$)] showing one of two independent molecules with conformation disorder **I/J** (30% thermal ellipsoids; H atoms have been omitted for clarity)

Table 4. Selected bond lengths [Å] and bond angles [°] of complexes [MCl(N∩E)(PR$_3$)][a]

	[PdCl(N∩S**)(PMePh$_2$)] Pd1	Pd2	[PtCl(N∩S**)(PMe$_2$Ph)]	[PdCl(N∩Se)(PMePh$_2$)] Pd1(N∩E**)	Pd2(N∩E*)	[PtCl(N∩Se**)(PMe$_2$Ph)]
M−E	2.2560(10)	2.2521(11)	2.235(2)	2.323(3)	2.322(4)	2.3860(11)
M−Cl	2.3676(10)	2.3639(10)	2.403(3)	2.332(6)	2.360(8)	2.348(3)
M−P	2.2399(10)	2.2409(9)	2.247(2)	2.195(6)	2.184(6)	2.193(2)
M−N	2.172(2)	2.169(2)	2.130(9)	2.149(18)	2.127(17)	2.220(8)
N−M−P	177.58(7)	177.32(7)	176.2(3)	174.2(6)	177.7(6)	177.4(3)
N−M−Cl	93.40(7)	93.95(7)	91.1(2)	97.0(5)	93.5(6)	89.43(10)
N−M−E	87.33(7)	87.10(7)	88.6(2)	84.0(5)	87.6(6)	86.6(2)
P−M−Cl	88.60(3)	88.71(3)	86.95(10)	87.1(2)	86.8(2)	91.6(2)
Cl−M−E	177.83(3)	176.33(4)	179.40(13)	176.8(2)	176.6(2)	177.81(9)
P−M−E	90.72(3)	90.27(3)	93.29(9)	91.78(14)	92.22(18)	92.42(7)

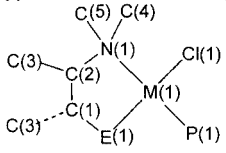

[a] Numbering scheme employed in figures and text is shown below the table.

 © 2004 Wiley-VCH Verlag GmbH & Co. KGaA, Weinheim

homologue [PtCl(N∩S**)(PMe$_2$Ph)] only one kind of molecule with conformation **J** (see Figure 7) was found in the crystal. The C(1) atom in this molecule shows some distortion according to a possible disorder. However, attempts to introduce the same disorder as observed for the palladium analogue or refining the structure in triclinic space groups failed. The C(2) atom does not show any sign of disorder; the extended thermal ellipsoid of C(1) can thus be attributed to a molecular vibration.

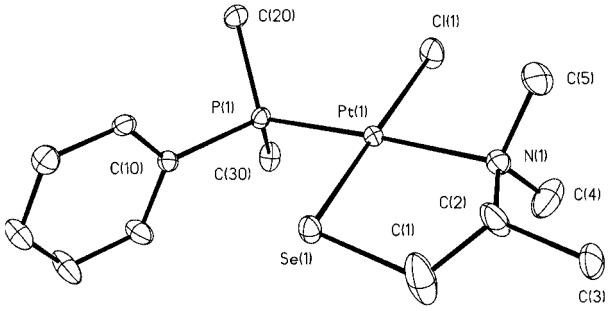

Figure 7. Molecular structure of [PtCl(N∩Se**)(PMe$_2$Ph)] with 30% thermal ellipsoids; H atoms have been omitted for clarity; the sulfur analogue [PtCl(N∩S**)(PMe$_2$Ph)] looks essentially the same

The crystals of [PtCl(N∩Se**)(PMe$_2$Ph)] also contain only one molecule, which clearly shows conformation **J** (Figure 7). In contrast, the palladium derivative [PdCl(N∩Se)(PMePh$_2$)] was found to contain both isomeric ligands N∩Se* and N∩Se**. One of the two independent molecules found in the unit cell contains the ligand Me$_2$NCH(Me)CH$_2$Se$^-$ (N∩Se**) and exhibits the disorder described by conformations **I** and **J** (Figure 8). This has also been observed for the sulfur analogue. The other complex molecule, which contains the isomeric ligand Me$_2$NCH$_2$CH(Me)Se$^-$ (N∩Se*; Figure 9), exists exclusively

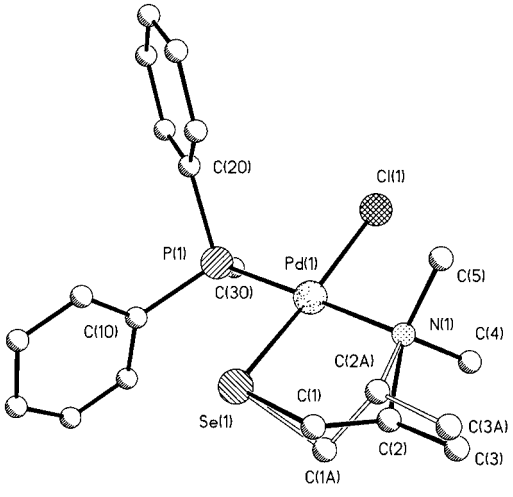

Figure 8. Molecular structure of the disordered (**I**/**J**) molecule 1 in [PdCl(N∩Se)(PMePh$_2$)] (N∩Se** isomer)

as one conformer (similar to **J**). Attempts to introduce disorder models to this molecule were unsuccessful.

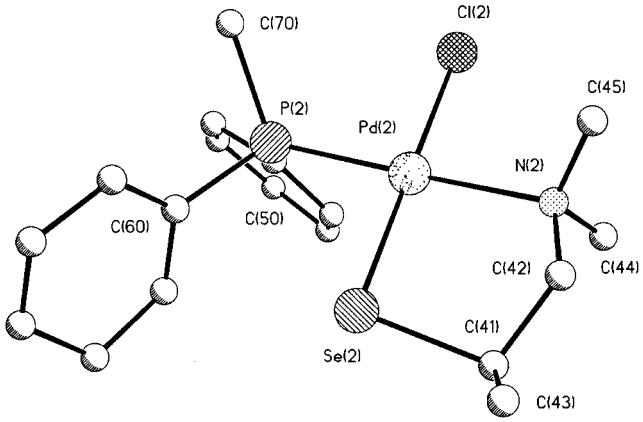

Figure 9. Molecular structure of molecule 2 in [PdCl(N∩Se)(PMePh$_2$)] (N∩Se* isomer)

The coordination planes around the metal atoms in these complexes exhibit only small tilt angles (N−M−E/Cl−M−P), ranging between 2.5 and 4.9°. The N−M−P and Cl−M−E angles are only slightly below 180° (Table 4). The metal−ligand distances are all longer for the palladium complexes than for the platinum homologues. This has also been found in related studies[14,27−29] and is attributed to the lanthanide contraction and relativistic effects.[29] The M−N and M−Cl distances are slightly longer than those reported in [M$_2$Cl$_2$(μ-Me$_2$pz)$_2$(PR$_3$)$_2$][30,31] owing to the strong *trans* influence of PR$_3$ and E (E = S or Se) donors. The M−E, M−P, M−N and M−Cl distances and various angles around the metal centre are similar to those reported for [MCl(ECH$_2$CH$_2$NMe$_2$)(PR$_3$)] complexes.[13−15,26]

In summary, it is remarkable that the two crystallised platinum complexes both contain exclusively the same conformer **J** [(*S*) enantiomer]; the two palladium derivatives are nonselective in this respect, showing disorder in the chelate ring according to both conformers in the crystal. For the selenium derivative [PtCl(N∩Se**)(PMe$_2$Ph)] multiple selectivity is observed for the molecules in the crystal: (i) regioselectivity of the ligands Se, Cl, P and N around the metal atom; (ii) the crystal contains only one regioisomer (N∩Se**) although the compound was prepared using regioisomeric mixed ligands; (iii) from the two possible conformers arising from the twist of the chelate ring only one conformer (enantiomer) is found in the crystal.

Thermal Studies

The thermal behaviour of some of the complexes has been evaluated to assess their suitability as molecular precursors for the synthesis of metal chalcogenides. The TG curve of [PdCl(N∩S**)(PMePh$_2$)] (Figure 10) shows a three-step decomposition, finally leading to Pd$_4$S at 374 °C. The first two stages are overlapping steps which account for 70% of the weight loss. This weight loss can be attributed to elimination of phosphane, organic residue and the chloride ligand with the formation of PdS. There is further loss of

 © 2004 Wiley-VCH Verlag GmbH & Co. KGaA, Weinheim

sulfur at 374 °C, resulting in the formation of Pd_4S which remains stable up to 500 °C. To prepare bulk quantities, a sufficient amount of [PdCl(N∩S**)(PMePh$_2$)] (128 mg) was heated at 400 °C in a furnace and the residue (35 mg, 30 mg calcd. for Pd_4S) was annealed for 2 h. The X-ray powder pattern of this residue corresponds to that of Pd_4S[32] (JC,PDS-10-335; analysis: found C 4.7, H ca. 0.2, N ca. 0.2%). Decomposition of [PdCl(N∩Se)(PMePh$_2$)] (107 mg) at 350 °C in a furnace gave a bulk residue (35 mg, 37 mg calcd. for $Pd_{17}Se_{15}$), identified as $Pd_{17}Se_{15}$ from the XRD pattern (JC,PDS-29-1427; analysis: found C 2.6, H ca. 0.2, N ca. 0.2%). The TG curve of [PtCl(N∩S**)(PMe$_2$Ph)] shows a two-step decomposition, the first step occurring at 265 °C being attributed to the loss of the phosphane ligand by the weight loss (obsd. 26%, calcd. 28%). The second step leads to the formation of PtS at 374 °C.

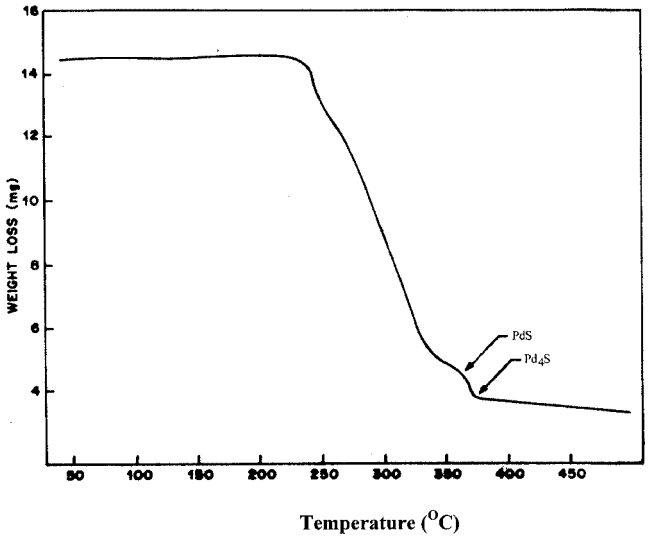

Figure 10. TG curve of [PdCl(N∩S**)(PMePh$_2$)]

Conclusion

This report illustrates how, by NMR spectroscopy and partial crystal structure analysis, the attempts to obtain aminochalcogenolate chelate ligands with an asymmetrically substituted carbon atom lead to regioisomeric dichalcogenide precursor molecules. In the chiral metal complexes [MCl(N∩E)(PR$_3$)] (M = Pt, Pd) the neutral (P and N) and charged donor atoms (Cl and E) were invariably found *trans* to each other. Further conformational isomerism in these complexes results from the twisted chelate rings. Whereas the two crystallised platinum complexes [PtCl(N∩S**)-(PMe$_2$Ph)] and [PtCl(N∩Se**)(PMe$_2$Ph)] exhibit exclusively one conformer (enantiomer), the palladium derivatives were nonselective, showing disorder in the chelate ring according to both conformers in the crystal. The regio- and enantioselectivity in the case of the selenium derivative [PtCl(N∩Se**)(PMe$_2$Ph)] is highly remarkable since the compound was prepared using a regioisomerically mixed ligand. Despite these various possibilities of constitutional, positional and conformational isomerism the isolated compounds were found to be sufficiently stable to be used as molecular precursors for metal chalcogenide phases.

Experimental Section

General: The complexes [M$_2$Cl$_2$(μ-Cl)$_2$(PR$_3$)$_2$] (M = Pd or Pt; PR$_3$ = P*n*Bu$_3$, P*n*Pr$_3$, PEt$_3$, PMe$_2$Ph, PMePh$_2$, PPh$_3$) were prepared according to literature methods.[33] The phosphanes (Strem Chemicals) and Me$_2$NCH$_2$CH(Me)Cl·HCl (Fluka Chemika, Cat. No. 24367) were obtained from commercial sources. All reactions were carried out under nitrogen in dry and distilled analytical grade solvents. Microanalyses were carried out in the Analytical Chemistry Division of BARC. ^{1}H, ^{13}C{^{1}H}, ^{31}P{^{1}H}, ^{77}Se{^{1}H}, ^{125}Te{^{1}H} and ^{195}Pt{^{1}H} NMR spectra were recorded with a Bruker DPX-300 NMR spectrometer operating at 300, 75.47, 121.49, 57.24, 94.86 and 64.52 MHz, respectively. Chemical shifts are relative to the internal chloroform peak at δ = 7.26 ppm for ^{1}H and δ = 77.0 ppm for ^{13}C, external 85% H$_3$PO$_4$ for ^{31}P, Me$_2$Se for ^{77}Se, [Te(dtc)$_2$] (dtc = *N*,*N*-diethyldithiocarbamate) for ^{125}Te, and Na$_2$[PtCl$_6$] in D$_2$O for ^{195}Pt. A 90° pulse was used in every case. The IR spectra were recorded as Nujol mulls between CsI plates with a Bomem MB-102 FT-IR spectrometer. UV/Vis absorption spectra were recorded with a JASCO V-530 spectrometer. Thermogravimetric analysis (TGA) was carried out with a NETZSCH STA 449C instrument calibrated with $CaC_2O_4.H_2O$. The TG curves were recorded at a heating rate of 10 °C·min^{-1} under a flow of argon. X-ray powder diffraction patterns were measured using Cu-K_α radiation.

Preparation of [Me$_2$NCH(Me)CH$_2$S]$_2$ [(N∩S)$_2$]:** Sodium hydrogensulfide was prepared by bubbling an excess of hydrogen sulfide into an ethanolic solution (150 mL) of sodium ethoxide (from 14.02 g Na metal) for 4 h until a pale yellow solid began to separate. Freshly distilled Me$_2$NCH$_2$CH(Me)Cl (59.34 g, 488 mmol) [obtained by neutralising an aqueous solution of Me$_2$NCH$_2$CH(Me)Cl·HCl with 10% sodium hydroxide, extracting with diethyl ether, drying with anhydrous CaCl$_2$ and distilling at 120−122 °C as a colourless liquid; ^{1}H NMR (CDCl$_3$): δ = 1.49 (d, *J* = 6.6 Hz, CH*Me*), 2.26 (s, NMe$_2$), 2.48 (doublet of AB pattern, NCH$_2$), 4.02 (m, 6.5 Hz, C*H*Cl) ppm; ^{13}C{^{1}H} NMR (CDCl$_3$): δ = 23.2 (s, CH*Me*), 45.8 (s, N*Me*$_2$), 55.1 (s, N*C*H$_2$), 68.0 (s, *C*HCl) ppm] was added dropwise to this solution, whereupon a white precipitate formed. The reaction mixture was heated to reflux under nitrogen for 2 h, and, after cooling, the mixture was filtered. The filtrate was concentrated in vacuo, leaving behind a pale-yellow solid [Me$_2$NCH(Me)CH$_2$SH] which was found to be contaminated by disulfide. Oxygen was bubbled through an ethanol solution (50 mL) of the residue until a yellow liquid was obtained. The solvent was stripped off and the residue was distilled in vacuo at 120−125 °C/1 Torr to give a yellow oil (30.2 g, 53%). ^{1}H NMR (CDCl$_3$): δ = 1.00 (d, *J* = 6.5 Hz, CH*Me*), 2.19 (s, N*Me*$_2$), 2.52 (m, C*H*$_2$S), 2.77−2.92 (m, NC*H*) ppm. ^{13}C{^{1}H} (CDCl$_3$): δ = 12.7 (s, CH*Me*), 40.0 (s, N*Me*$_2$), 42.4 (s, N*C*H), 58.2 (*C*H$_2$S) ppm. The NMR spectra showed resonances attributable to traces (less than 1%) of [Me$_2$NCH$_2$CH(Me)S]$_2$.

Preparation of (N∩S)$_2$. [Me$_2$NCH(Me)CH$_2$S]$_2$ [(N∩S)$_2$] and [Me$_2$NCH$_2$CH(Me)S]$_2$ [(N∩S*)$_2$]:** Finely powdered yellow sulfur (3.20 g, 100 mmol) and sodium metal (2.37 g, 103 mmol) were allowed to react in liquid ammonia (100 mL) at −78 °C. The resulting yellow solution was stirred for 90 min and the ammonia

 © 2004 Wiley-VCH Verlag GmbH & Co. KGaA, Weinheim

was evaporated by leaving the flask to stand at room temperature. The yellow residue (Na_2S_2) was dried under vacuum and dissolved in DMF (200 mL) with stirring. Freshly distilled $Me_2NCH_2CH(Me)Cl$ (10.5 g, 86 mmol) in DMF (100 mL) was added dropwise. The mixture was stirred at room temperature for 18 h whereupon the green colour of the solution changed to yellow. The reaction was quenched with water (300 mL) and the product was extracted with diethyl ether (3 × 60 mL). The ether extracts were dried with $CaCl_2$. The solvent was stripped off and the residue was distilled in vacuo (100−105 °C/0.5 Torr) to give a mixture of $(N^{\cap}S^{**})_2$ and $(N^{\cap}S^{*})_2$ as a yellow liquid (7.9 g, 77%). Attempts to separate the two isomers by vacuum distillation were unsuccessful. ^{1}H NMR ($CDCl_3$): δ = 1.01 [d, J = 6.5 Hz, $(N^{\cap}S^{**})_2$], 1.26 [d, J = 6.5 Hz, $(N^{\cap}S^{*})_2$] (CH*Me*) (ratio 1:2), 2.18 [s, N*Me*$_2$, $(N^{\cap}S^{*})_2$], 1.20 [s, N*Me*$_2$, $(N^{\cap}S^{**})_2$], 2.26−2.95 (m, NC*H*, C*H*$_2$S, NC*H*$_2$, C*H*S) ppm. ^{13}C{^{1}H} NMR ($CDCl_3$): $(N^{\cap}S^{*})_2$: δ = 18.6 (s, N*Me*$_2$), 43.9 (s, N*C*H$_2$), 45.3 (s, N*Me*$_2$), 64.8 (s, *C*HS) ppm; $(N^{\cap}S^{**})_2$: δ = 12.7 (s, CH*Me*), 40.1 (s, N*Me*$_2$), 42.4 (s, N*C*H), 58.2 (s, *C*H$_2$S) ppm [$(N^{\cap}S^{*})_2$ and $(N^{\cap}S^{**})_2$ in 2:1 ratio from ^{1}H NMR integration].

Preparation of $(N^{\cap}Se)_2$. $[Me_2NCH(Me)CH_2Se]_2$ $[(N^{\cap}Se^{**})_2]$ and $[Me_2NCH(Me)CH_2Se]_2$ $[(N^{\cap}Se^{*})_2]$: A mixture of $(N^{\cap}Se)_2$ was prepared (in 54% yield) in an analogous manner to the sulfur analogue as described above, from $Me_2NCH_2CH(Me)Cl$ and Na_2Se_2. The orange liquid was fractionally distilled at 130−138 °C/2 Torr. ^{1}H NMR ($CDCl_3$): δ = 1.08 [dd, J = 6.3, 2 Hz, $(N^{\cap}Se^{**})_2$], 1.47 [d, J = 6.2 Hz, $(N^{\cap}Se^{*})_2$ (CH*Me*)], 2.22 [br., NC*H*, $(N^{\cap}Se^{**})_2$], 2.24 $(N^{\cap}Se^{**})_2$, 2.25 $(N^{\cap}Se^{*})_2$ (each s, N*Me*$_2$), 2.48 [AB pattern with doublet NCH$_2$, $(N^{\cap}Se^{*})_2$], 2.89 (m, C*H*$_2$Se), 3.25 [m, CHSe, $(N^{\cap}Se^{*})_2$] ppm. ^{13}C{^{1}H} NMR ($CDCl_3$): δ = [$(N^{\cap}Se^{*})_2$] 20.8 (s, CH*Me*), 36.8 (N*C*H$_2$), 45.6 (N*Me*$_2$), 67.0 (Se*C*H) ppm; [$(N^{\cap}Se^{**})_2$]: δ = 13.7 (s, CH*Me*), 35.8 (N*C*H$_2$), 40.5 (N*Me*$_2$), 60.3 (Se*C*H) ppm. ^{77}Se{^{1}H} NMR ($CDCl_3$): δ = 225.4, 226.6, 286.0, 286.8, 356.5, 357.9, 415.1, 416.2 ppm.

Preparation of $(N^{\cap}Te)_2$. $[Me_2NCH(Me)CH_2Te]_2$ $[(N^{\cap}Te^{**})_2]$ and $[Me_2NCH_2CH(Me)Te]_2$ $[(N^{\cap}Te^{*})_2]$: $(N^{\cap}Te)_2$ was synthesised in a similar manner to the corresponding selenium analogue from $Me_2NCH_2CH(Me)Cl$ and K_2Te_2 (prepared from potassium and tellurium powder in liquid ammonia). The brown-red liquid was dissolved in hexane, passed through a Florisil column and dried under vacuum (yield 68%). The compound was contaminated by $(Me_2NCH_2CHMe)_2Te$; attempted vacuum distillation resulted in excessive decomposition. ^{1}H NMR ([D$_6$]acetone): δ = 1.01 [d, J = 6.5 Hz, $(N^{\cap}Te^{**})_2$], 1.66 [d, J = 6.5 Hz, $(N^{\cap}Te^{*})_2$] (CH*Me*), 2.23 [s, N*Me*$_2$, $(N^{\cap}Te^{**})_2$], 2.25 [s, N*Me*$_2$ minor, $(N^{\cap}Te^{*})_2$], 2.75 (m, C*H*), 3.12−3.49 (m, C*H*$_2$) ppm. ^{13}C NMR ([D$_6$]acetone): [$(N^{\cap}Te^{*})_2$]: δ = 14.9 (s, CH*Me*), 35.0 (s, N*C*H$_2$), 45.5 (s, N*Me*$_2$), 68.7 (s, Te*C*H) ppm; $(N^{\cap}Te^{**})_2$: δ = 13.7 (each s, CH*Me*), 31.6 (s, N*C*H), 40.4 (s, N*Me*$_2$), 61.4 (s, Te*C*H) ppm. ^{125}Te{^{1}H} NMR ([D$_6$]acetone): δ = −870 (very small), −791, −639 (very small), −559 ppm; peaks at δ = −455, −461 and −504 (integrating to about 7%) are due to partial decomposition of the ligand.

Synthesis of Palladium(II) and Platinum(II) Complexes: All preparations involving thiolate were carried out using $Me_2NCH(Me)CH_2S^-$ ($N^{\cap}S^{**}$) unless otherwise stated. For the preparation of selenolate and tellurolate complexes, $(E^{\cap}N)_2$ was employed. NMR spectroscopic data for complexes $[MCl(E^{\cap}N)(PR_3)]$ are collected in Tables 1 and 2. Yields, recrystallisation solvents and analytical data for all complexes are provided in the Supporting Information.

Thiolate Complexes: As an example for the thiolate complexes the synthesis of $[PdCl(N^{\cap}S^{**})(PMe_2Ph)]$ is described. A dichloromethane solution (40 mL) of $[Pd_2Cl_2(\mu\text{-}Cl)_2(PMe_2Ph)_2]$ (156 mg, 0.25 mmol) was added to a freshly prepared methanol solution of $NaSCH_2CH(Me)NMe_2$, prepared by treating $(N^{\cap}S^{**})_2$ (58 mg, 0.25 mmol) with $NaBH_4$ (19 mg, 0.51 mmol). The reaction mixture was stirred at room temperature for 4 h. After solvent evaporation in vacuo, the brown residue was extracted with dichloromethane (20 mL). The solution was passed through a Florisil column and the solvent was removed in vacuo. The residue was recrystallised from a acetone/hexane mixture to give reddish crystals. Other thiolate complexes with M = Pd and P*n*Pr$_3$, PEt$_3$, PMe$_2$Ph, PMePh$_2$ or PPh$_3$ and M = Pt and P*n*Bu$_3$, P*n*Pr$_3$, PEt$_3$, PMe$_2$Ph or PMePh$_2$ were prepared similarly.

Selenolate Complexes: As an example for the selenolate complexes the synthesis of $[PdCl(N^{\cap}Se)(PMe_2Ph)]$ is described. An acetone suspension (20 mL) of $[Pd_2Cl_2(\mu\text{-}Cl)_2(PMe_2Ph)_2]$ (180 mg, 0.29 mmol) was added to a freshly prepared methanol solution (5 mL) of $N^{\cap}SeNa$, prepared from $(N^{\cap}Se)_2$ (96 mg, 0.29 mmol) and $NaBH_4$ (23 mg, 0.61 mmol). The reaction mixture was stirred for 4 h. The solvents were evaporated in vacuo, the residue was washed with hexane and extracted with toluene (3 × 8 mL). The extracts were passed through a Florisil column. The solvent was reduced to 2 mL and a few drops of hexane were added which, on cooling to −5 °C, gave pink crystals (156 mg, 62%). Analogously, complexes of the type $[MCl(N^{\cap}Se)(PR_3)]$ (M = Pd with PEt$_3$, PMe$_2$Ph, PMePh$_2$ or PPh$_3$ and M = Pt with P*n*Bu$_3$, PEt$_3$, PMe$_2$Ph) were prepared.

Tellurolate Complexes: As an example for the tellurolate complexes the synthesis of $[PdCl(N^{\cap}Te)(PPh_3)]$ is described. To a freshly prepared solution of $N^{\cap}TeNa$, prepared from $(N^{\cap}Te)_2$ (127 mg, 0.30 mmol) and $NaBH_4$ (24 mg, 0.63 mmol) in methanol (10 mL), an acetone suspension (25 mL) of $[Pd_2Cl_2(\mu\text{-}Cl)_2(PPh_3)_2]$ (261 mg, 0.30 mmol) was added with vigorous stirring which continued for 3 h. The solvents were removed under vacuum and the residue was washed with hexane and extracted with acetone (3 × 6 cm^3). The volume of the acetone was reduced to 8 mL which on cooling gave a brown powder (142 mg, 39% yield). $[PtCl(N^{\cap}Te)(PnPr_3)]$ and $[PtCl(N^{\cap}Te)(PPh_3)]$ were prepared similarly.

X-ray Crystallography: Single crystals of $[PdCl(N^{\cap}S^{**})(PMePh_2)]$ and $[PtCl(N^{\cap}S^{**})(PMe_2Ph)]$ were obtained at −10 °C from CH_2Cl_2/hexane and at room temperature from acetone/hexane mixtures, while single crystals of $[PdCl(N^{\cap}Se)(PMePh_2)]$ and $[PtCl(N^{\cap}Se^{**})(PMe_2Ph)]$ were obtained from toluene/hexane mixtures at room temperature and −10 °C, respectively. The X-ray data of these complexes were collected at 173(2) K or 178(2) K with Siemens (P4 or P3) or Stoe diffractometers, using graphite-monochromated Mo-K_α radiation (λ = 0.71073 Å) and employing Wyckoff scans. Further details are given in Table 5. All structures were solved by the Patterson method using the SHELXTL package while refinement was carried out with SHELXL-97 employing full-matrix least-squares methods on F^2 with $F_o^2 = -2\sigma(F_o^2)$.[34] All non-hydrogen atoms were refined anisotropically, except for the disordered C and N atoms in the chelate ligand of $[PdCl(N^{\cap}Se^{**})(PMePh_2)]$. The same atoms had to be refined using DFIX restraints. Hydrogen atoms were introduced using appropriate riding models. Empirical absorption correction was performed using XABS2.[35] CCDC-235479 for $[PdCl(N^{\cap}S^{**})(PMePh_2)]$, -235480 for $[PtCl(N^{\cap}S^{**})(PMe_2Ph)]$, -235481 for $[PdCl(N^{\cap}Se)(PMePh_2)]$ and -235482 for $[PtCl(N^{\cap}Se^{**})(PMe_2Ph)]$ contain the supplementary crystallographic data for this paper. These data can be obtained free of charge at www.ccdc.cam.ac.uk/conts/retrieving.html [or from the Cambridge Crystallographic Data Centre, 12 Union

 © 2004 Wiley-VCH Verlag GmbH & Co. KGaA, Weinheim

Table 5. Crystallographic and structure refinement data of complexes [MCl(N∩E)(PR_3)]

	[PdCl(N∩S**)($PMePh_2$)]	[PtCl{N∩S**}(PMe_2Ph)]	[PdCl{N∩Se} ($PMePh_2$)]	[PtCl{N∩Se**}(PMe_2Ph)]
Empirical formula	$C_{18}H_{25}ClNPPdS$	$C_{13}H_{23}ClNPPtS$	$C_{18}H_{25}ClNPPdSe$	$C_{13}H_{23}ClNPtSe$
Formula mass	460.27	486.89	507.17	533.79
Crystal system	triclinic	monoclinic	monoclinic	monoclinic
Space group	$P\bar{1}$	$P2_1$	$P2_1$	$P2_1$
a [Å]	11.434(2)	5.8519(12)	11.480(2)	5.8716(12)
b [Å]	13.023(3)	12.932(3)	14.025(3)	13.005(3)
c [Å]	13.932(3)	11.030(2)	12.850(3)	11.132(2)
α [°]	91.75(3)	90	90	90
β [°]	92.88(3)	98.76(3)	102.42(3)	100.24(3)
γ [°]	108.37(3)	90	90	90
V [Å^3]/Z	1964.0(7)/4	825.0(3)/2	2020.5(7)/4	836.5(3)/2
$\rho_{calcd.}$ [g·cm^{-3}]	1.557	1.960	1.667	2.119
μ [mm^{-1}]/F(000)	1.267/936	8.874/468	2.930/1008	10.802/504
Limiting indices	$-1 \le h \le 17$	$0 \le h \le 7$	$-14 \le h \le 13$	$0 \le h \le 8$
	$-16 \le k \le 15$	$0 \le k \le 17$	$-1 \le k \le 17$	$0 \le k \le 17$
	$-17 \le l \le 17$	$-15 \le l \le 14$	$0 \le l \le 15$	$-15 \le l \le 14$
Refl.collected/unique	8992/8581	2083/1910	4364/4364	2259/2086
R_{int}	0.0270	0.0214	0.0693	0.0284
Data/restr./param.	8581/0/457	1910/0/168	4364/11/407	2086/1/168
Goof on F^2	1.317	1.177	1.128	1.058
Final R_1, wR_2 indices	0.0322, 0.0735	0.0321, 0.0786	0.0715, 0.1439	0.0271, 0.0677
R_1, wR_2 (all data)	0.0443, 0.0771	0.0346, 0.0799	0.1074, 0.1619	0.0287, 0.0685
Largest diff. peak/hole [e·Å^{-3}]	0.631/−0.685	2.248/−1.553	0.998/−0.913	1.138/−0.962

Road, Cambridge CB2 1EZ, UK; Fax: + 44-1223-336-033; E-mail: deposit@ccdc.cam.ac.uk].

Supporting Information (see also footnote on the first page of this article): Further tables with analytical data for all new complexes and structural details of [PdCl(N∩S**)($PMePh_2$)], [PtCl(N∩S**)-(PMe_2Ph)], [PdCl(N∩Se)($PMePh_2$)] and [PtCl(N∩Se**)(PMe_2Ph)] are available. Further figures illustrating the crystal and molecular structures are also provided.

Acknowledgments

We thank Drs. J. P. Mittal, T. Mukherjee and S. K. Kulshreshtha for encouragement of this work. We are also grateful to Dr. M. Sudershanan, Head, Analytical Chemistry Division, BARC for providing microanalyses of the complexes. Dr. M. Bader (University of Stuttgart) is thanked for collecting single crystal XRD data, as is Dr. Rudolph Pietschnig (University of Graz) for collecting NMR spectroscopic data. Support for this work under the Indo-German bilateral program from the BMBF (Project No. IND 99/060) is gratefully acknowledged.

[1] M. Bochmann, *Chem. Vap. Deposition* **1996**, *2*, 85.
[2] A. Singhal, V. K. Jain, R. Misra, B. Varghese, *J. Mater. Chem.* **2002**, 1121.
[3] [3a] S. Dey, V. K. Jain, J. Singh, V. Trehan, K. K. Bhasin, B. Varghese, *Eur. J. Inorg. Chem.* **2003**, 744. [3b] S. Dey, V. K. Jain, *Platinum Met. Rev.* **2004**, *48*, 16.
[4] A. M. Malik, P. O' Brien, N. Revaprasadu, *J. Mater. Chem.* **2002**, *12*, 92.
[5] [5a] I. G. Dance, *Polyhedron* **1986**, *5*, 1037. [5b] P. J. Blower, J. R. Dilworth, *Coord. Chem. Rev.* **1987**, *76*, 121.
[6] J. Sola, R. Yanez, *J. Chem. Soc., Dalton Trans.* **1986**, 2021.
[7] M. Capdevila, P. Gonzalez-Duarte, C. Foces-Foces, F. H. Cano, M. Martinez-Ripoll, *J. Chem. Soc., Dalton Trans.* **1990**, 143.
[8] J. A. Ayllon, P. Gonzalez-Duarte, C. Miravittles, E. Molins, *J. Chem. Soc., Dalton Trans.* **1990**, 1793.
[9] M. Capdevila, W. Clegg, P. Gonzalez-Duarte, I. Mira, *J. Chem. Soc., Dalton Trans.* **1992**, 173.
[10] M. Capdevila, W. Clegg, P. Gonzalez-Duarte, B. Harris, I. Mira, J. Sola, I. C. Taylor, *J. Chem. Soc., Dalton Trans.* **1992**, 2817.
[11] S. Marchal, V. Moreno, G. Aullon, S. Alvarez, M. Quiros, M. Font-Bardia, X. Solans, *Polyhedron* **1999**, *18*, 3675.
[12] J. Real, M. Pages, A. Polo, J. F. Pinella, A. Alvarez-Larena, *Chem. Commun.* **1999**, 277.
[13] S. Dey, V. K. Jain, S. Chaudhury, A. Knoedler, F. Lissner, W. Kaim, *J. Chem. Soc., Dalton Trans.* **2001**, 723.
[14] S. Dey, V. K. Jain, A. Knoedler, A. Klein, W. Kaim, S. Zalis, *Inorg. Chem.* **2002**, *41*, 2864.
[15] S. Dey, V. K. Jain, A. Knoedler, W. Kaim, S. Zalis, *Eur. J. Inorg. Chem.* **2001**, 2965.
[16] S. Dey, V. K. Jain, A. Knoedler, W. Kaim, *Inorg. Chim. Acta* **2003**, *349*, 104.
[17] S. Dey, V. K. Jain, A. Klein, W. Kaim, *Inorg. Chem. Commun.* **2004**, *7*, 601.
[18] T. Konno, T. Yoshimura, K. Aoki, K. Okamoto, M. Hirotsu, *Angew. Chem. Int. Ed.* **2001**, 1765.
[19] H. Honda, T. Yoshimura, M. Hirotsu, T. Kawamoto, T. Konno, *Inorg. Chem.* **2002**, *41*, 2229.
[20] T. Konno, H. Honda, Y. Chikamoto, T. Kawamoto, T. Yoshimura, M. Hirotsu, *Chem. Lett.* **2002**, 472.
[21] J. Cheon, S. D. Talaga, J. I. Zink, *Chem. Mater.* **1997**, *9*, 1208.
[22] [22a] D. Burton, W. D. Ollis, *Comprehensive Organic Chemistry*, Pergamon Press, Oxford, **1979**, vol. 2, pp. 52−55. [22b] A. K. Katritzky, O. Meth-Cohn, C. W. Rees, *Comprehensive Organic Functional Group Transformations* Pergamon Press, Oxford, **1995**, vols. 1 and 2.
[23] R. Kaur, H. B. Singh, R. P. Patel, *J. Chem. Soc., Dalton Trans.* **1996**, 2719.
[24] G. Mugesh, A. Panda, H. B. Singh, N. S. Punekar, R. J. Butcher, *Chem. Commun.* **1998**, 2227.
[25] G. Mugesh, A. Panda, H. B. Singh, R. J. Butcher, *Chem. Eur. J.* **1999**, *5*, 1411.

 © 2004 Wiley-VCH Verlag GmbH & Co. KGaA, Weinheim

[26] S. Dey, V. K. Jain, A. Knoedler, W. Kaim, *Indian J. Chem.* **2003**, *42A*, 2339.
[27] P. P. Phadnis, V. K. Jain, A. Klein, M. Weber, W. Kaim, *Inorg. Chim. Acta* **2003**, *346*, 119.
[28] P. P. Phadnis, V. K. Jain, A. Klein, T. Schurr, W. Kaim, *New J. Chem.* **2003**, 1584.
[29] K. Herbst, B. Rink, L. Dahlenburg, M. Brorson, *Organometallics* **2001**, *20*, 3655.
[30] V. K. Jain, S. Kannan, E. R. T. Tiekink, *J. Chem. Soc., Dalton Trans.* **1993**, 3625.
[31] V. K. Jain, S. Kannan, E. R. T. Tiekink, *J. Chem. Soc., Dalton Trans.* **1992**, 2231.
[32] F. Gronvold, E. Rost, *Acta Crystallogr.* **1962**, *15*, 11.
[33] F. R. Hartley, *The Chemistry of Platinum and Palladium*, John Wiley & Sons, New York, **1973**.
[34] [34a] G. M. Sheldrick, *SHELXTL*, Bruker Analytical X-ray Systems, Madison, Wisconsin, USA, **1998**. [34b] G. M. Sheldrick, *SHELXL-97: A program for Crystal Structure Determination*, Universität Göttingen, Göttingen, Germany, **1997**.
[35] XABS2: S. Parkin, B. Moezzi, H. Hope, *J. Appl. Crystallogr.* **1995**, *28*, 53.

Received June 16, 2004
Early View Article
Published Online September 9, 2004

 © 2004 Wiley-VCH Verlag GmbH & Co. KGaA, Weinheim

Selected-Control Solvothermal Synthesis of Nanoscale Hollow Spheres and Single-Crystal Tubes of PbTe

Guifu Zou,[a,b] Zhaopin Liu,[b] Debao Wang,[b] Changlong Jiang,[b] and Yitai Qian*[a,b]

Keywords: Nanostructures / Semiconductors / Nanotubes

For the first time, hollow PbTe nanospheres with diameters of 80–140 nm have been prepared in an ether/glycerol microemulsion system and PbTe single-crystalline nanotubes with diameters of 60–80 nm have been synthesised in a homogeneous ethanol/glycerol system. They can be facilely controlled via a solvothermal process without any additional catalysts and templates. Two different template mechanisms are discussed herein. The Raman and far infrared spectra of the samples have been investigated at room temperature.

(© Wiley-VCH Verlag GmbH & Co. KGaA, 69451 Weinheim, Germany, 2004)

Introduction

In recent years, one of the important goals of material scientists has been to tailor the structures of materials to obtain special nanomorphologies because the properties of nanomaterials are strongly dependent on the their sizes and shapes.[1−5] Among specific morphologies, hollow nanoscale spheres and tubes have drawn more and more attention.[6,7] Three-dimensional hollow spheres are interesting in the fields of medicine, material science and catalysis due to their hollow structures which make them particularly applicable for drug delivery, medical imaging, protein and enzyme transplantation, encapsulation of products (cosmetics, inks and dyes) and contaminated waste removal.[8] So far, various hollow spheres (SiC, ZnS, CdS, Ag_2S and polymers) have been synthesised by different methods.[9−12] Meanwhile, one-dimensional nanotubes have also attracted attention because of their unique optical, electronic and mechanical properties resulting in promising applications in electrical and optoelectronic nanodevices. Many tubular structures have been fabricated for compounds with layered structures such as C, MoS_2 and BN with the assistance of catalysts. Moreover, there have been many tubular materials without layered structures produced by physical template methods.[13] However, the introduction of templates or catalysts to the reaction system means a much more complicated process involving the preparation of catalysts or the selection of templates and may introduce impurities into the final product. Therefore, it is always a challenge for the tubular materials to be prepared by a simple wet chemical route.

PbTe has been intensively studied for more than forty years because it has interesting physical properties which can be applied in many fields such as IR detection, photoconductivity and thermoelectric materials.[14] PbTe nanocrystals have been prepared by various methods.[15] To the best of our knowledge, however, there are no reports regarding hollow PbTe nanospheres and nanotubes. We have successfully synthesised hollow PbTe spheres and nanotubes by a wet chemical method, simply using ether and ethanol as the reaction solvents, respectively. In the solvothermal process, neither physical templates nor catalysts are required. In addition, two different template mechanisms are discussed.

Results and Discussion

The typical XRD patterns of the products are shown in Figure 1. All the peaks can be indexed as face-centred cubic

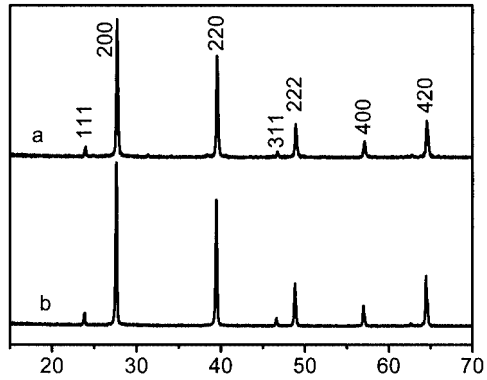

Figure 1. XRD patterns of (a) hollow spheres and (b) tubular PbTe

[a] Structure Research Laboratory, University of Science and Technology of China,
Hefei, Anhui 230026, PR China
Fax: (internat.) + 86-551-3607402
E-mail: ytqian@ustc.edu.cn
[b] Department of Chemistry, University of Science and Technology of China,
Hefei, Anhui 230026, PR China

PbTe (JCPDS, 38-1435). No peaks of any other impurities are detected, indicating the high purity of the products. In addition, the strong and sharp reflection peaks suggest that the products are highly crystalline.

Figure 2 (see a and b) shows the TEM images of the samples prepared by the process using ether as the solvent. The strong contrast between the dark edge and pale centre is evidence of its hollow nature. Figure 2 clearly displays many hollow PbTe spheres prepared in the products. The proportion of hollow spheres in the samples was estimated to be 25−30% using large numbers of TEM observations. Their external diameter and wall thickness are ca. 80−140 nm and 15−30 nm, respectively. Close observations indicate that the hollow spheres consist of PbTe nanoparticles. The inset of Figure 2 (see b) shows the selected area electron diffraction (SAED) pattern of the hollow PbTe spheres. The SAED exhibits diffuse polycrystalline ring patterns and agrees well with the XRD peaks of the products. It also further confirms that the hollow spheres are constructed from highly crystalline PbTe nanoparticles. In addition, it could be shown that the hollow spheres are sensitive to beam irradiation during TEM examination. This may be related to their thin and porous walls. A similar phenomenon can be also found in former reports concerning hollow spheres.[6,16] In addition to the hollow spheres, some cubes are also present in the samples (Figure 2, c).

Figure 2 (see d−g) shows tubular PbTe prepared in the process using ethanol as the solvent. The yield of the nanotubes in the sample was about 20%. The external diameter and wall thickness of the nanotubes are ca. 70 nm and 15 nm, respectively. Their lengths are about several hundred nanometers. Most nanotubes have closed ends and a few have open ends. The microstructure of tubular PbTe was further characterised by HRTEM and SAED. The HRTEM images looking down onto the wall and open end of the nanotubes are given in Figure 2 (see f−h), where the inset is the corresponding open end ED pattern. The regular spacing of the observed lattice planes is ca. 0.32 nm which is consistent with the separation of the (200) planes of c-PbTe. It shows that the nanotube is single-crystalline, structurally uniform and dislocation free. Moreover, the SAED patterns taken from various regions of an individual nanotube are essentially the same. It can also be concluded that the nanotubes synthesised using the present procedure are single-crystalline in structure. According to the HRTEM images and the SAED pattern, it can be concluded that the nanotubes grow along the [100] direction.

To investigate the reaction process, a series of experiments was carried out. When $Pb(NO_3)_2$ was not added to the reaction system, only Te nanocrystals formed. On the other hand, Pb was not produced when Na_2TeO_4 was left out of the reaction system. Moreover, a large amount of Te mixed with some PbTe was obtained when the reaction proceeded for a short time and then more PbTe and less Te were produced when the reaction time was continually increased. Based on the above results and the former reports,[15,17,18] all the reactions can be described according to part A in Scheme 1. Firstly, the Na_2TO_4 was reduced

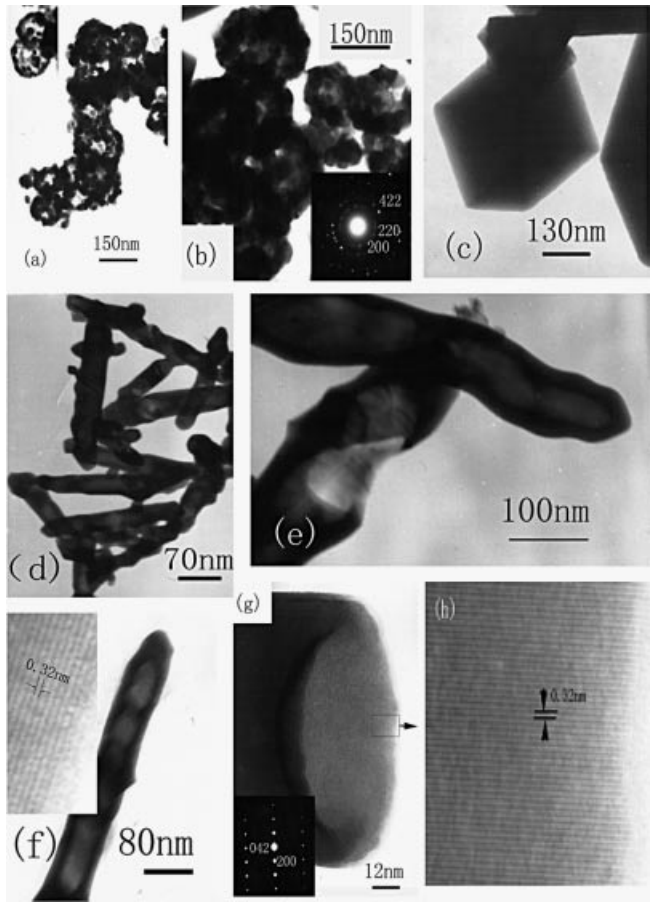

Figure 2. TEM images of (a) and (b) hollow PbTe spheres and (c) a few cubes, the inset shows the hollow sphere ED patterns; (d) Tubular PbTe TEM images and (e) their magnification images. (f) HRTEM images of the wall and (g) the open end of the nanotubes, the inset show the corresponding ED patterns

to Te by hydrazine. Secondly, the PbTe was formed slowly through a redox reaction between $Pb(C_3H_6O_3)$, Te and hydrazine. Here, glycerol was used as the complexing reagent to form a complex, $Pb(C_3H_6O_3)$. The complex served to reduce the speed of reaction (2) because the $Pb(C_3H_6O_3)$ sharply decreased the free Pb^{2+} concentration in the solution. It is well-known that a slow reaction rate is favourable for crystallisation as well as separating the growth step from the nucleation step.[19] Thus, highly crystalline PbTe was obtained in our experiments and the ED, XRD and HRTEM of the products also confirmed this. For the detailed formation process of the hollow spheres, we assume the process to be a template-interface route. Because the ether was insoluble in the glycerol, the whole system can be described as a microemulsion state. The ether could form stable microscale oil droplets in glycerol at a moderate temperature. When Te nanoparticles were formed through reaction (1) in an ether/glycerol system, many Te particles accumulated on the surface of the oil droplets and formed a template-interface. The reaction then progressed according to Equation (2). Finally the shell-core structure formed. Moreover, the hollow spheres can be obtained when the ether is removed

 © 2004 Wiley-VCH Verlag GmbH & Co. KGaA, Weinheim

by washing and drying of the product. The whole process can be described diagrammatically as in part B of Scheme 1.

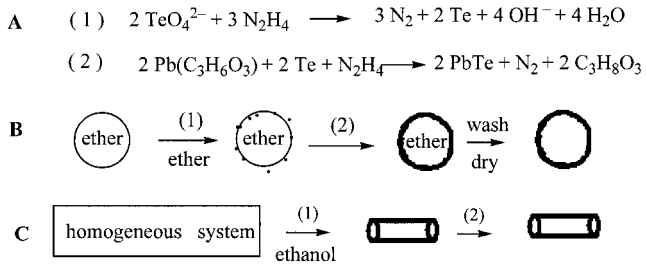

Scheme 1. A) Illustration of the hollow spheres formation process by a template-interface route B) Illustration of the nanotube formation process by a self-generated template route C

In order to discuss the formation mechanism of PbTe nanotubes, some experiments were carried out. Te nanotubes could be obtained in the products (the images not shown here) when $Pb(NO_3)_2$ was not added to the ethanol/glycerol reaction system. This phenomenon can also be found in the literature.[17,18] Moreover, more PbTe and less Te were obtained when the reaction time was continually increased. In addition, it is worth noting that the diameter of the Te nanotubes obtained was almost the same as that of the PbTe nanotubes. Based on these results, we propose a self-generated template process. Firstly, some Te nanotubes were produced according to reaction (1) in the ethanol/glycerol homogeneous system and then according to reaction (2) considerable tubular PbTe formed using the Te nanotubes as the templates. Some similar template syntheses have been reported.[20–22] Accordingly, we are inclined to describe the formation process of the PbTe nanotubes as a self-generated template route. It can be described according to part C in Scheme 1. However, the detailed mechanism needs to be further studied.

The room temperature Raman and far infrared spectra of the hollow PbTe nanospheres are shown in Figure 3. Peaks at 121, 137 and 154 cm^{-1} are observed as indicated in Figure 3 (a). Among them, the peaks marked with asterisks are related to the vibrational modes of a thin TeO_2 layer on the PbTe nanocrystals.[23,24] The wide band with the peak at ca. 154 cm^{-1} corresponds to the mixed plasmon-phonon modes of the PbTe nanoparticles forming hollow nanospheres. It is worth noting that the frequency is lower than that for bulk PbTe. This can be explained by the effect of dimensional quantization as the average PbTe nanocrystal radius decreases. This phenomenon has also been observed by others.[25] Figure 3 (b) shows the far infrared spectrum of the hollow PbTe nanospheres. The peaks (marked with asterisks) at 81 and 110 cm^{-1} are related to two TeO_2 infrared active modes.[26] The other peaks in part b of Figure 3 corresponded to the infrared active modes of the hollow PbTe nanospheres.[25] Here, the wide band from 50 to 70 cm^{-1} is split into two bands appearing at 57 and

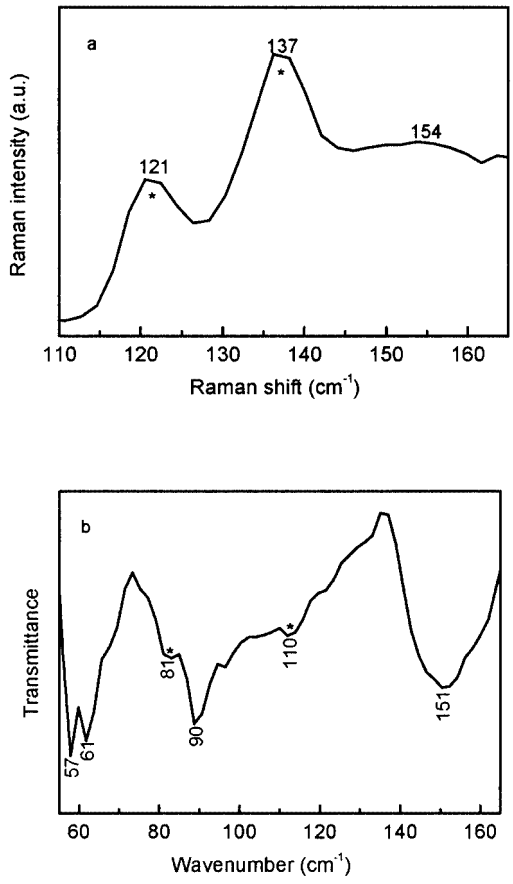

Figure 3. (a) the Raman and (b) far infrared spectra of the hollow PbTe nanospheres

61 cm^{-1}. A similar phenomenon has been reported in the literature.[27] From Figure 3 (see a and b), it can be also shown that the frequency of the mixed plasmon-phonon mode (at 154 cm^{-1}) in the Raman spectrum of the hollow PbTe nanospheres is almost same as that (at 151cm^{-1}) in the infrared spectrum. Additionally, the Raman and far infrared spectra (not shown here) of the PbTe nanotubes were similar to the above Raman and far infrared spectra of the hollow PbTe nanospheres, respectively.

Conclusion

In conclusion, hollow nanoscale spheres and single-crystal tubular PbTe have been synthesised via facile solvothermal processes for the first time. Two different models, template-interface and self-generated template routes, have been proposed to explain the formation mechanism of hollow PbTe nanospheres and nanotubes. The present study will not only open up great opportunities for novel morphologies of PbTe and their applications to be investigated, but might also be extended to the synthesis of hollow spheres and nanotubes of other materials.

 © 2004 Wiley-VCH Verlag GmbH & Co. KGaA, Weinheim

Experimental Section

All chemical reagents in this work, such as $Pb(NO_3)_2$, $Na_2TO_4{\cdot}2H_2O$, ether, ethanol, glycerol and hydrazine were of A.R. grade and were purchased from the Shanghai Chemical Company, China. They were used as received without further purification.

Preparation of Hollow Nanoscale Spheres and Tubular PbTe: In a typical procedure, $Pb(NO_3)_2$ (0.5 mmol) and $Na_2TO_4{\cdot}2H_2O$ (0.5 mmol) were added to a mixture of ether (18 mL) and glycerol (18 mL). The mixture was then stirred vigorously to form a microemulsion phase. After this, hydrazine (10 mL) was added to the microemulsion system and stirring was continued for 10 min. Finally, the mixture was transferred into a 60 mL Teflon-lined autoclave and the autoclave was sealed and heated at 160 °C for 20 h. The autoclave was then allowed to cool to room temperature without assistance. The grey precipitate was filtered and washed several times with distilled water and absolute ethanol to remove impurities and was then dried in vacuo at 60 °C for 4 h. Finally the product (PbTe hollow spheres) was obtained. The whole method, appropriate for the preparation of PbTe nanotubes, was similar to the above process except for the use of ethanol instead of ether as the reaction solvent.

Sample Characterisation: The X-ray diffraction (XRD) patterns for the products were recorded on a Philips X'pert diffractometer with Cu-K_{a1} radiation (λ = 1.54178 Å). The morphologies and structures of the products were examined by transmission electron microscopy (TEM) using a Hitachi H-80 instrument. The high-resolution TEM study was carried out using a JEOL 2010 microscope. The samples used for characterisation were dispersed in absolute ethanol and were ultrasonicated before TEM and HRTEM. The Raman spectrum was recorded with a LABRAM-HR Confocal Laser MicroRaman Spectrometer with 514.5 nm radiation from a 10-mW argon ion laser at room temperature. The far infrared spectroscopic measurements were performed with a Nicolet Nexus 870 spectrometer. The powders were dispersed in silicon oil and were studied at room temperature.

Acknowledgments

The project was supported by the Chinese Natural Science Foundation. The 973 project of China and the State key project of fundamental research for nanomaterials and nanostructures are gratefully acknowledged. The authors gratefully acknowledge informative discussions with Professor Jian Zuo.

[1] N. G. Chopra, R. J. Luyken, K. Cherrey, V. H. Crespi, M. L. Cohen, S. G. Louie, A. Zettl, *Science* **1995**, *269*, 966−967.
[2] S. Lijma, *Nature* **1991**, *354*, 56−58.
[3] W. Huynh, X. Peng, A. P. Alivsatos, *Adv. Mater.* **1999**, *11*, 923−925.
[4] W. C. W. Chan, S. M. Nie, *Science* **1998**, *281*, 2016−2018.
[5] A. P. Alivisatos, *Science* **1996**, *271*, 933−937.
[6] Y. R. Ma, L. M. Qi, J. M. Ma, H. M. Cheng, W. Shen, *Langmuir* **2003**, *19*, 9079−9085.
[7] Y. D. Li, X. L. Li, R. R. He, J. Zhu, Z. X. Deng, *J. Am. Chem. Soc.* **2002**, *124*, 1411−1412.
[8] L. J. Zhang, M. X. Wan, *Adv. Funct. Mater.* **2003**, *13*, 815−820.
[9] K. P. Velikov, A. V. Blaaderen, *Langmuir* **2001**, *17*, 4779−4786.
[10] J. X. Huang, Y. Xie, B. Li, Y. Liu, Y. T. Qian, S. Y. Zhang, *Adv. Mater.* **2000**, *12*, 808−811.
[11] Q. Lu, F. Gao, D. Zhao, *Chem. Phys. Lett.* **2002**, *360*, 355−357.
[12] M. Kuang, H. W. Duan, J. Wang, D. Y. Chen, M. Jiang, *Chem. Commun.* **2003**, 496−497.
[13] X. Y. Kong, Z. L. Wang, J. S. Wu, *Adv. Mater.* **2003**, *15*, 1445−1449.
[14] A. M. Samoylov, M. K. Sharov, S. A. Buchnev, A. M. Khoviv, E. A. Dolgopolova, *J. Crystal Growth* **2002**, *240*, 340−346.
[15] C. Wang, G. Zhang, S. Fan, Y. Li, *J. Phys. Chem. Solids* **2001**, *62*, 1957−1960.
[16] C. R. Wang, K. B. Tang, Q. Yang, J. Q. Hu, Y. T. Qian, *J. Mater. Chem.* **2002**, *12*, 2426−2429.
[17] B. Mayers, Y. N. Xia, *Adv. Mater.* **2002**, *14*, 279−283.
[18] Z. P. Liu, S. Li, Y. You, Z. K. Hu, S. Peng, J. B. Liang, Y. T. Qian, *New J. Chem.* **2003**, *27*, 1748−1752.
[19] Z. P. Liu, S. Li, Y. Yang, S. Peng, Z. K. Hu, Y. T. Qian, *Adv. Mater.* **2003**, *15*, 1946−1958.
[20] B. Gates, Y. Y. Wu, Y. D. Yin, P. D. Yang, Y. N. Xia, *J. Am. Chem. Soc.* **2001**, *123*, 11500−11501.
[21] X. C. Jiang, B. Mayers, T. Herricks, Y. N. Xia, *Adv. Mater.* **2003**, *15*, 1740−1744.
[22] B. J. Yang, M. S. Mo, H. M. Hu, C. Li, X. G. Yang, Q. W. Li, Y. T. Qian, *Eur. J. Inorg. Chem.* **2004**, *9*, 1785−1787.
[23] A. P. Mirgorodsky, T. Merle-Mejean, J.-C. Champarnaud, P. Thomas, B. Frit, *J. Phys. Chem. Solids* **2000**, *61*, 501−509.
[24] A. S. Pine, G. Dresselhaus, *Phys. Rev. B* **1972**, *5*, 4087−4090.
[25] A. I. Belogorokhov, L. I. Belogorokhova, D. R. Khokhlov, S. V. Lemeshko, *Semiconductors* **2002**, *36*, 663−669.
[26] D. M. Korn, A. S. Pine, G. Dresselhaus, T. B. Reed, *Phys. Rev. B* **1973**, *8*, 768−771.
[27] C. R. Wang, K. B. Tang, Q. Yang, Y. T. Qian, *Chem. Phys. Lett.* **2002**, *357*, 371−375.

Received May 14, 2004
Early View Article
Published Online October 1, 2004

 © 2004 Wiley-VCH Verlag GmbH & Co. KGaA, Weinheim

Cocondensation Reactions of Five-Membered Heterocycles with Lithium Atoms at 77 K

Oscar Mendoza,[a] Franz-Josef K. Rehmann,[a] Laurence P. Cuffe,[a] and Matthias Tacke*[a]

Keywords: Lithium / Heterocycles / C−H bond activation / Cocondensation / DFT

Lithium atoms were cocondensed with eight aromatic five-membered heterocycles in the presence of THF at 77 K. In the case of the oxygen- and sulfur-containing heterocycles (furans and thiophenes), the reaction resulted in C–H bond activation and led to the corresponding aryllithium compound. The other heterocycles (pyrroles) failed to react with lithium atoms in the presence of THF. A special case was found when oxazole was reacted under these cocondensation conditions; here a dilithiated product was obtained. DFT (B3LYP/6-31G**) calculations were carried out in order to interpret the pathways of the reactions and the possible intermediates. For all the reactions π- and σ-complexes between lithium clusters and the heterocycles were found as stable intermediates.
(© Wiley-VCH Verlag GmbH & Co. KGaA, 69451 Weinheim, Germany, 2004)

Introduction

The activation of carbon−hydrogen bonds has been a major topic of research for the last thirty years.[1,2,3] Numerous methods have been developed to perform these reactions. Most of these have centred on the oxidative addition of the hydrocarbon moiety to a highly sub-coordinated metal complex as shown below.[4,5]

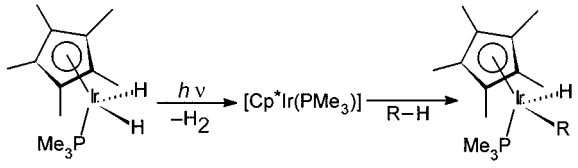

However, C−H bond activation is not limited just to transition metal chemistry. Another commonly used method is σ-bond metathesis using extremely electrophilic lanthanide centres as outlined below.[6]

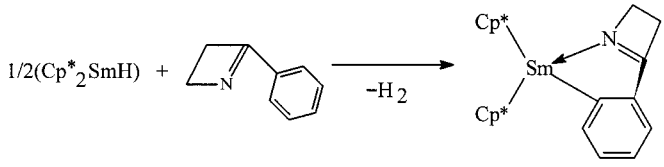

To date there has been very little preparative-scale work using metal atoms to perform oxidative addition reactions. Many metals are known to activate methane in a matrix under photochemical conditions.[3,7] However, these types of reactions are of no use in preparative-scale metal vapour synthesis (MVS). For example, iron atoms react with methane to form CH_3FeH at 10 K when photolysed in an argon matrix.[8]

$$Fe + CH_4 \xrightarrow[Ar,\ 10K]{h\nu} HFeCH_3$$

Work performed by this group in the nineties showed that lithium atoms could selectively activate the C−H bond of benzene and toluene in the presence of THF without photochemical excitation.[9,10,11] This result led to the direct preparation of aryllithium compounds on a synthetic scale.

$$8\ Li(g) + 4\ PhH(g) + 4\ THF(g) \xrightarrow[77K]{cocond.} \left[\text{C}_6\text{H}_5\text{Li(THF)}\right]_4 + 4\ LiH(s)$$

One of the key intermediates in this reaction is a Li_2-benzene π-complex. This complex is capable of undergoing two single-electron transfers from the Li_2 cluster to the LUMO of the aromatic ring, resulting in the activation of the aromatic C−H bond.

$$2\ Li(g) + 4\ PhH(g) \xrightarrow[77K]{cocond.} \left[Li{-}Li{\leftarrow}PhH\right] \longrightarrow \left[H\begin{smallmatrix}Li\\Li\end{smallmatrix}Ph\right] \longrightarrow LiH(s) + PhLi(s)$$

[a] Chemistry Department, Centre for Synthesis and Chemical Biology (CSCB), Conway Institute of Biomolecular and Biomedical Research University College Dublin,
Belfield, Dublin 4, Ireland
E-mail: matthias.tacke@ucd.ie
Supporting information for this article is available on the WWW under http://www.eurjic.org or from the author.

The work has been expanded to +I-substituted (CMe_3, $SiMe_3$, *o*- and *m*-xylene) and donor-substituted (OMe, NMe_2, SMe) benzene derivatives recently.[12]

The aim of this paper was to perform cocondensation reactions with furans, thiophenes, pyrroles and oxazole in order to find similarities to and differences from benzene derivatives.

Results

1. Experimental Studies

A variety of five-membered heterocyclic compounds were cocondensed with lithium atoms at 77 K in the presence of THF.

When methylpyrrole, furan and thiophene were cocondensed, a reaction was observed in the case of furan and thiophene only. The products of these reactions were monolithiated compounds[13,14] in which the heterocyclic ring showed a C−H activation in the *ortho* position as shown in Scheme 1. In the case of furan and thiophene, the yields were 35% (2.15 g) and 55% (3.55 g) respectively.

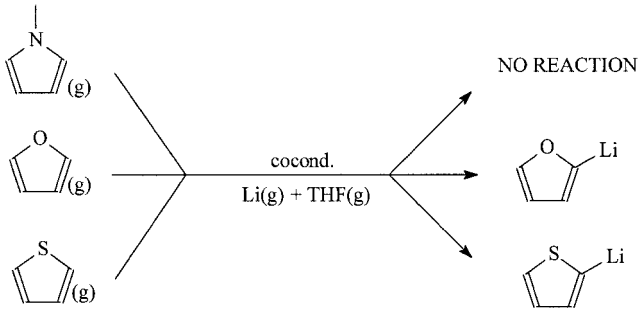

Scheme 1. Cocondensation reaction of lithium atoms with heterocycles at 77 K

A derivatisation reaction with Me_3SiCl was carried out, yielding products stable in air in order to identify the position of the lithium in the aromatic ring. The TMS-substituted compound was identified from NMR spectroscopic data and GC-MS data.[15,16]

A similar reaction series was carried out with the *ortho* position blocked. Methyl groups were placed in the *ortho* positions of the aromatic rings, and cocondensation experiments were carried out.

1,2,5-Trimethylpyrrole, 2,5-dimethylfuran and 2,5-dimethylthiophene were condensed with lithium at 77 K, and lithiated products were obtained in the case of 2,5-dimethylfuran and 2,5-dimethylthiophene.[17] As shown in Scheme 2, in this case C−H activation was observed in the *meta* position with respect to the heteroatom. Again, no reaction was observed for the pyrrole compound. The lithiated compound was identified from the TMS-substituted derivative.[18]

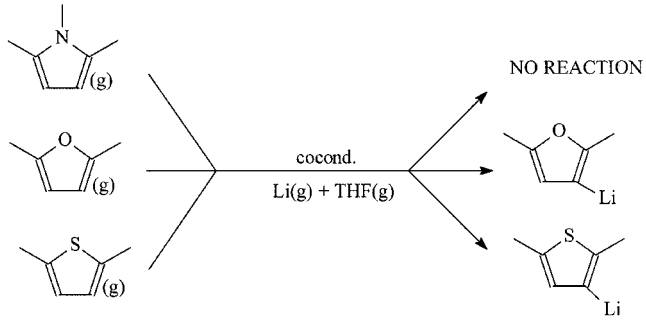

Scheme 2. Cocondensation reaction of lithium atoms with *ortho*-dimethyl heterocycles at 77 K

Earlier reports showed that lithium atoms were able to activate aromatic hydrocarbons selectively under these cocondensation conditions.[9,10,11] When a methoxy group was added to the aromatic hydrocarbons, activation was always found in an *ortho* position with respect to the methoxy group.[12] Thus methoxy groups can be considered as useful tools to activate the *ortho* position on hydrocarbon aromatic rings.

When a methoxy group was placed on a heterocycle, the same behaviour was observed. 2-Methoxyfuran was used for this reaction and a C−H activation was observed in an *ortho* position with respect to the methoxy group instead of the heteroatom.

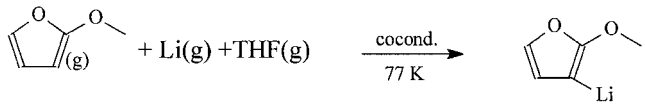

Scheme 3. Cocondensation reaction of lithium atoms with 2-methoxyfuran

Oxazole presents a special case. When oxazole was cocondensed with lithium atoms the reaction yielded a dilithiated compound. In this unusual reaction sequence two lithium atoms were able to activate two C−H bonds in this compound, both in an *ortho* position with respect to the oxygen.

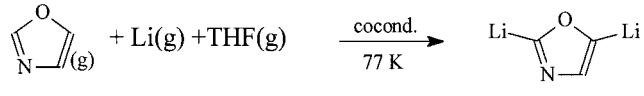

Scheme 4. Cocondensation reaction of lithium atoms with oxazole

In order to facilitate an overview, all cocondensation reactions are summarised in Scheme 5.

2. Theoretical Studies

The aim of this work was to identify, by calculation, plausible intermediate species for all these heterocycle cocondensation reactions, thereby identifying the reaction

 © 2004 Wiley-VCH Verlag GmbH & Co. KGaA, Weinheim

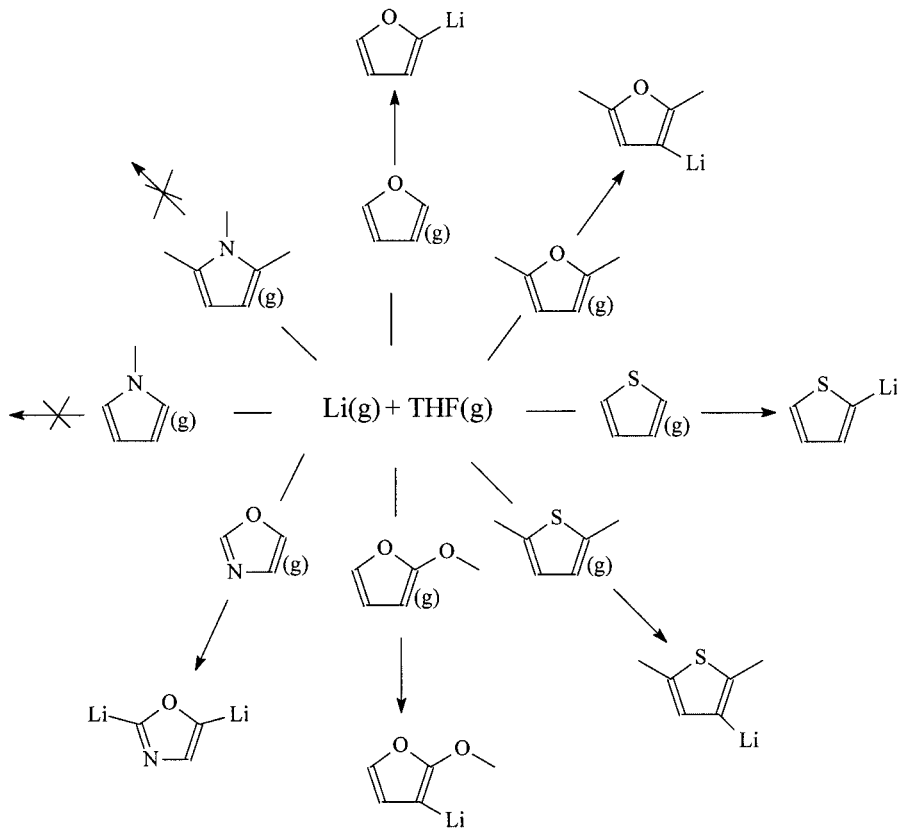

Scheme 5. Summary of the reactions of lithium atoms with five-membered heterocycles in the presence of THF at 77 K

mechanism. Calculations were performed using the GAUSSIAN 98[19] and the B3LYP DFT functional with the 6−31G** set basis.

The C−H activation involves at least two steps, the coordination of the lithium cluster with the aromatic compound, and then the insertion of the Li_2 cluster into the C−H bond by a double electron transfer via the aromatic system.[9,10]

Two different possibilities were found for the coordination of the dilithium cluster (Figure 1). Please note that in some cases the lines on the diagrams only have topological significance. The first possibility is the coordination of the Li_2 cluster to the aromatic system to form a π-complex, and the second possibility is η^1-coordination of the Li_2 cluster to the heteroatom in the ring.[12]

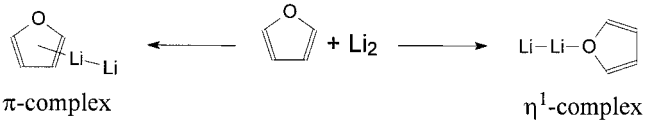

Figure 1. Principal coordination modes of the dilithium cluster to a heterocyclic aromatic compound like furan

When furan is used the preferred pathway is via the η^1-complex. An energy difference of 2.7 kcal/mol was found between the two complexes, showing that the η^1-complex is more stable than the π-complex. The strong interaction between the lithium cluster and the oxygen results in a short Li−O distance of 197.4 pm and supports this pathway. As described previously, the next step is a double electron transfer step from the Li_2 cluster to the LUMO of the aromatic ring. For the furan cocondensation, this step has a larger reaction enthalpy of −29.0 kcal/mol and there is still a strong interaction between the lithium and the oxygen in the second intermediate [*d*(LiO):184.5 pm]. The optimised structure of this second intermediate shows an elongation in the C−O bond of the lithiated carbon. In uncoordinated furan the distance is 136.4 pm; in the second intermediate this distance is 145.7 pm.

When methyl groups are placed in the two *ortho* positions in the furan, a similar situation is found. The η^1-complex is the more stable intermediate with a small energy difference of 2.7 kcal/mol from the π-complex. Furan gives a similar energy for the first step, while there is a less exothermic second step (−18.7 kcal/mol instead of −29.9 kcal/mol found in furan). The distance between the Li_2 and the oxygen in the η^1-complex is the same in both complexes (196.9 pm).

For heterocycles containing sulfur, like thiophene or 2,5-dimethylthiophene, the situation changes and the favoured pathway is via the π-complex.

In the thiophene calculation, a difference in energy of 5.7 kcal/mol in favour of the π-complex was found between the π- and the η^1-coordinated intermediates.

 © 2004 Wiley-VCH Verlag GmbH & Co. KGaA, Weinheim

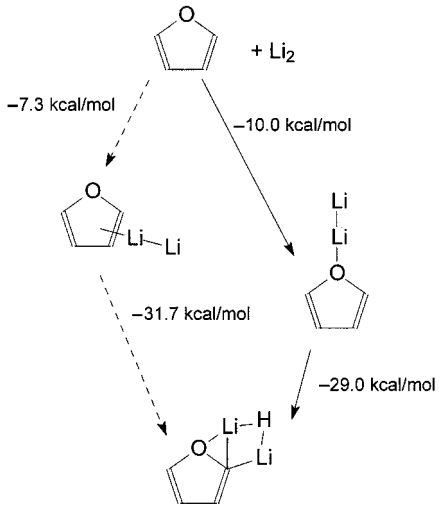

Figure 2. Calculated reaction mechanism for the cocondensation of lithium atoms with furan

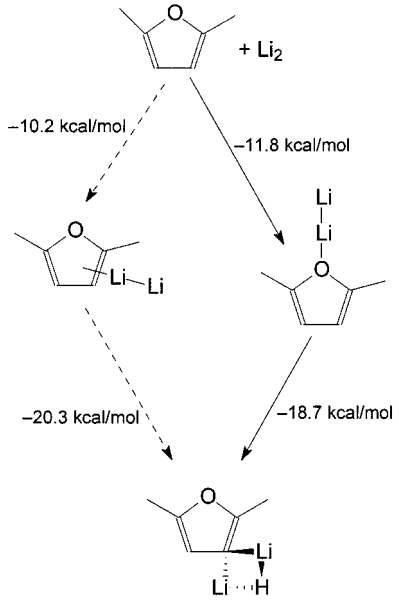

Figure 3. Calculated reaction mechanism for the cocondensation of lithium atoms with 2,5-dimethylfuran

As shown in Figure 4, the C−H activation step for thiophene is a highly exothermic process, as was also the case for furan. There is no interaction between the sulfur and the lithium in the second intermediate and the Li_2H plane is found to be perpendicular to the thiophene plane. The corresponding intermediate in the furan calculation is almost planar (Figure 5). There is a small elongation in the C−S bond by 2.9 pm compared to the uncoordinated thiophene. In furan, the extra coordination to the oxygen atom in the C−H-activated second intermediate leads to an elongation of the C−O bond by 9.3 pm compared to the uncoordinated furan.

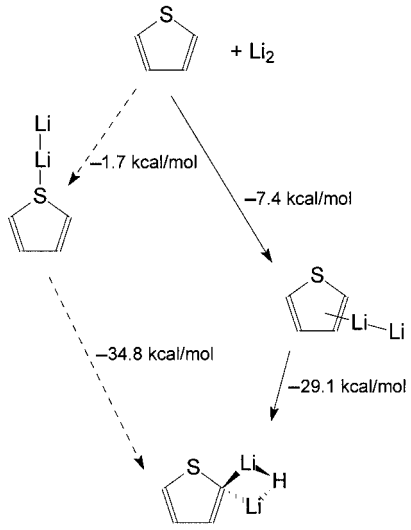

Figure 4. Calculated reaction mechanism for the cocondensation of lithium atoms with thiophene

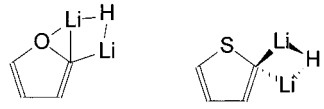

Figure 5. Second intermediate calculations for furan and thiophene

A similar theoretical study was performed on 2,5-dimethylthiophene where a π-complex pathway was shown to be more stable as well. As shown in Figure 6, there is a difference of 7.5 kcal/mol between the η^1- and the π-complex, favouring the latter.

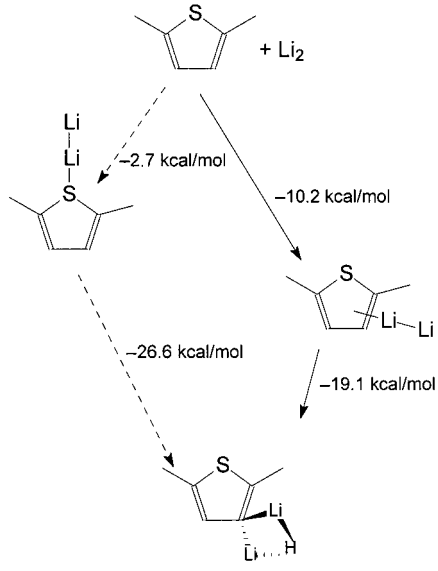

Figure 6. Calculated reaction mechanism for the cocondensation of lithium atoms with 2,5-dimethylthiophene

When there is a methoxy substituent on the aromatic ring functioning as an additional Lewis base, the reaction pathway is more complicated. A theoretical study of 2-meth-

 © 2004 Wiley-VCH Verlag GmbH & Co. KGaA, Weinheim

oxyfuran was carried out, and two different pathways were found.

The first possibility is the formation of a π-complex, as found in the previous calculations. The second pathway involves the coordination of the Li_2 cluster to the methoxy group. A third possibility can be ruled out, since the coordination of the Li_2 cluster to the oxygen in the furan forming an η^1-complex does not lead to a stable intermediate on the energy hypersurface of this system.

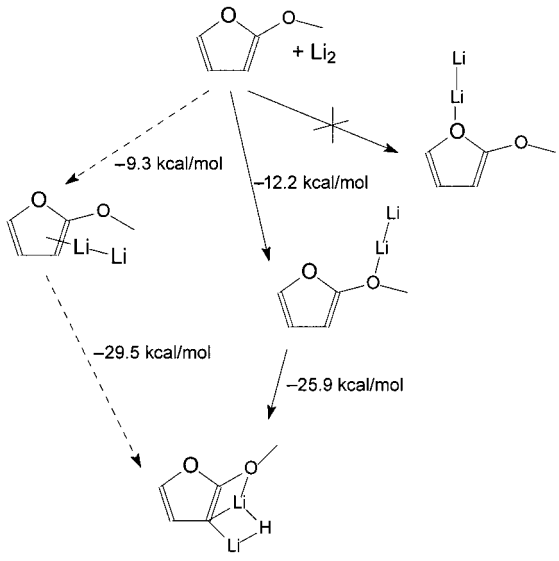

Figure 7. Calculated reaction mechanism for the cocondensation of lithium atoms with 2-methoxyfuran

As Figure 7 shows, the preferred pathway is via an η^1-complex involving the methoxy group. The η^1-complex is more stable than the π-complex by 2.9 kcal/mol. This η^1-complex shows a strong interaction between the lithium and the oxygen in the methoxy group, resulting in a Li–O bond length of 193.1 pm. As in previous mechanisms the next step is a double electron transfer from the Li_2 cluster to the LUMO of the aromatic ring forming a hydride and a carbanion. In this second intermediate a strong bond is still present between oxygen and lithium (194.0 pm).

The theoretical study of the oxazole reaction pathway presents a special case. The presence of two heteroatoms gives oxazole the possibility of forming two η^1-complexes: one in which the lithium cluster is bonded to the nitrogen and one in which it is bonded to the oxygen. The cocondensation reaction of oxazole in the presence of THF gives a dilithiated product; however, only the formation of the monolithiated oxazole is considered in this calculation.

In the first step, the η^1-complex is the more stable intermediate when nitrogen is the donor. The η^1-complex with the oxygen is also a stable intermediate, but in this case the reaction is about 9 kcal/mol less exothermic, as shown in Figure 8. No stable π-complex was found.

Both η^1-complexes lead to a C–H-activated second intermediate where the interaction between the heteroatom and the lithium is still present. These second steps are

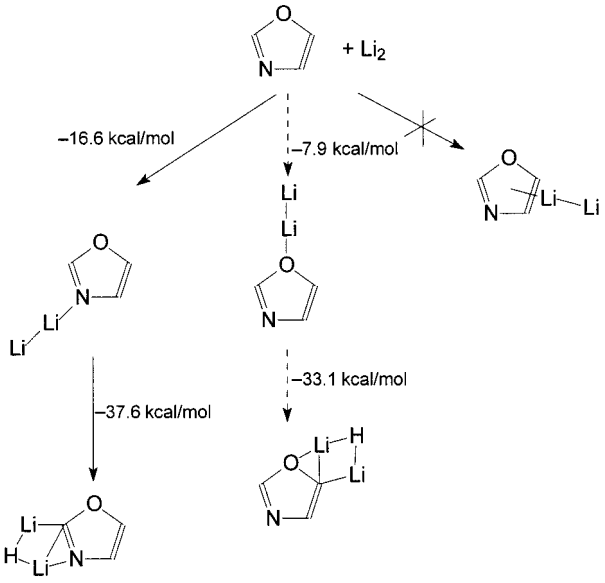

Figure 8. Calculated reaction mechanism for the first lithiation of oxazole

highly exothermic processes, both for the nitrogen η^1-complex (–37.6 kcal/mol) and for the oxygen η^1-complex (–33.1 kcal/mol).

Discussion

Previous research in this area showed that aromatic hydrocarbons react with lithium atoms in the presence of THF under cocondensation conditions.[9,10] The isolated products were identified as monolithiated aromatic compounds. This study examines the effect of heteroatoms introduced into the aromatic rings on the C–H activation reactions.

A delicate balance between enhancing complex formation ability and lowering LUMO energy, which allows reductive cleavage of the aromatic C–H bond, is needed for a successful C–H activation. As shown in Scheme 6, the electron-deficient Li_2 cluster **1** accepts electron density from the aromatic system to form an unusual main group element π-complex **2**, or from the heteroatom to form an η^1-complex **3**. C–H activation follows this step, leading to **4**.

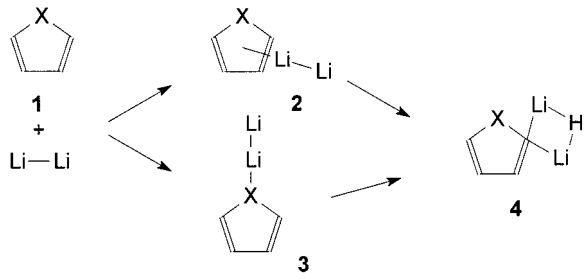

Scheme 6. Key mechanistic steps in heteroaromatic C–H bond activation using lithium atoms

 © 2004 Wiley-VCH Verlag GmbH & Co. KGaA, Weinheim

When the heteroatom in the aromatic ring donates electron density to the lithium cluster, the interaction between the two lithium atoms is strengthened. This can be observed by comparing the calculated Li−Li bond lengths for the π- and η^1-complexes as shown in Table 1. For example, the biggest difference is observed in the case of 2,5-dimethylthiophene, where the Li−Li distance decreases from 277.5 pm to 273.7 pm, whereas for furan there is only a decrease of 0.9 pm. However, when the heterocycle contains sulfur, as in thiophene and 2,5-dimethylthiophene, the π-complex is found to be more stable than the η^1-complex. In all other cases the opposite behaviour is found.

Table 1. Selected Li−Li bond lengths for all calculated intermediates; the calculated Li−Li bond length for free Li_2 is 272.3 pm

	d(LiLi) [pm] π-complex	*d*(LiLi) [pm] η^1-complex	*d*(LiLi) [pm] C−H-activated intermediate
furan	275.2	274.3	238.5
2,5-dimethylfuran	276.3	275.7	228.4
thiophene	276.0	272.9	231.4
2,5-dimethylthiophene	277.5	273.7	229.1
2-methoxyfuran	276.5	275.2	236.0
oxazole		(N) 276.4	254.5
		(O) 273.3	

The next mechanistic step is crucial. It involves the double electron transfer from the π- or η-complex-bonded Li_2 cluster (**2**,**3**) to the LUMO of the aromatic ring. If the LUMO energy is too high, as it is for pyrroles (as outlined in Table 2), it is impossible to place electron density into it, thereby preventing the C−H-activation reaction from occurring. It can be seen in Schemes 1 and 2 that lithium does not react with 1-methylpyrrole or 1,2,5-trimethylpyrrole. If the LUMO energy is low enough, as in furan or thiophene (as shown in Table 2) the reaction proceeds to give an aryllithium compound and lithium hydride.

Table 2. LUMO energies of selected reactants calculated with B3LYP/6-31G**

	LUMO (eV)	Reaction
1-methylpyrrole	1.44	no reaction
1,2,5-trimethylpyrrole	1.27	
2-methoxyfuran	0.94	C−H activation
2,5-dimethylfuran	0.76	
furan	0.51	
2-lithiooxazole	0.21	
5-lithiooxazole	0.12	
2,5-dimethylthiophene	0.00	
oxazole	−0.03	
thiophene	−0.22	

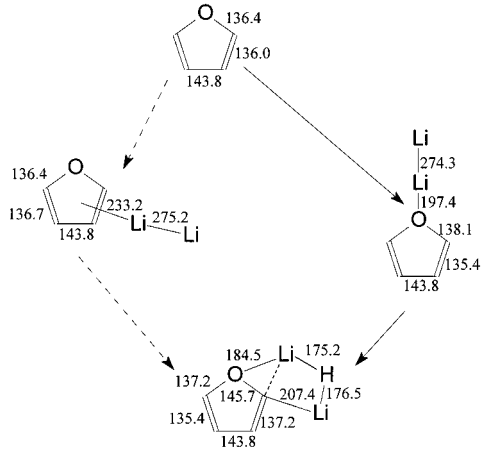

Scheme 7. Bond lengths in pm for furan reaction intermediates

Scheme 7 shows all the bond lengths of the calculated species in the furan study. The formation of the first intermediate does not change the structure of the furan ring significantly. The Li−Li distance is slightly elongated. In the uncoordinated dilithium species *d*(Li−Li) is 272.3 pm, which changes to 274.3 and 275.2 pm in the η^1-complex and π-complex.

The formation of the second intermediate changes the structure of the ring. The distance between the activated carbon and the oxygen is elongated by 9.3 pm by the formation of a three-membered ring involving lithium. Furan, methoxyfuran and oxazole show a clear interaction between the heteroatom and one lithium in this second intermediate, which can be seen from the short bond lengths of 184.5, 194.0 and 192.4 pm, respectively.

For 2,5-dimethylfuran, 2,5-dimethylthiophene and thiophene the second intermediates exhibit a symmetrical four-membered CLi_2H ring, as shown in Table 3.

Table 3. Bond lengths for C−Li−H rings on second intermediates

	2,5-Dimethylfuran	Thiophene	2,5-Dimethylthiophene
C−Li	210.1	211.7	210.6
Li−H	177.5	177.2	176.8

When an oxygen-donor group is placed in the heterocyclic ring, as in the case of methoxyfuran, the NMR spectroscopic data indicate an *ortho* lithiated product with respect to the methoxy group. In furan and 2,5-dimethylfuran, the η^1-complex is a more stable first intermediate than the π-complex, but, in contrast, the Li−Li is bonded to the methoxy group in the η^1-complex formed.

For the reaction of oxazole with lithium atoms in the presence of THF, a different reaction sequence with respect to the other heterocyclic compounds was observed. The ability to develop a second lithiation reaction, as shown in

 © 2004 Wiley-VCH Verlag GmbH & Co. KGaA, Weinheim

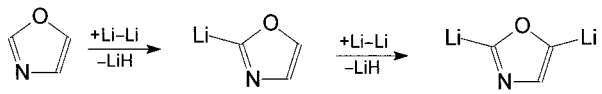

Scheme 8. Reaction of oxazole with lithium atoms in the presence of THF

Scheme 8, is the governing factor here. The first intermediate is characterised by the nitrogen, which is able to stabilise the Li−Li cluster more than the oxygen η^1-complex. However, no π-complex was found as a stable intermediate.

Once the first C−H activation has occurred, the monolithiated oxazole is still able to react further. As Scheme 8 shows, this second lithium is also observed in an *ortho* position with respect to the oxygen.

From the calculated LUMO energies of the reactants (Table 2), a comparison can be made in relation to the dilithiated species. The calculation of LUMO energies of the monolithiated compounds was carried out considering solvent interaction with the lithium. For this purpose, three molecules of ammonia were taken to fill the coordination sphere of lithium instead of THF, in order to simplify the process. The calculated LUMO energies for the monolithiated species 2-lithiooxazole and 5-lithiooxazole are 0.21 and 0.12 eV respectively. These LUMO energies can be considered within the range of species that can be activated. It follows that a further activation with addition of lithium to the lithiated oxazole can readily occur during the cocondensation reaction.

Conclusion

Lithium atoms are able to activate heterocyclic aromatic compounds like furan and thiophene, which have a relatively low-lying LUMO energy. The only product of this selective C−H-activation process is 2-lithiofuran or 2-lithiothiophene. If the LUMO energy is considerably higher as in pyrrole, no C−H activation can be observed. If the normally activated *ortho* position is blocked, as in 2,5-dimethylfuran or thiophene, the cocondensation reaction in the presence of THF leads to a selective monolithiation at the *meta* position. The corresponding 1,2,5-trimethylpyrrole fails to react because of its high-lying LUMO energy. Interestingly, oxazole cocondensed with lithium atoms results in 2,5-dilithiooxazole in a novel reaction variation, but the exact mechanism of the dilithiation of oxazole remains unclear. For all the furans in this study and the oxazole, an η^1-complex was calculated to be the most stable intermediate in the early phase of the C−H activation reaction, while thiophenes preferred π-complexes with the intermediate dilithium cluster.

Experimental Section

General: All experimental procedures were performed using standard Schlenk techniques under dry argon. THF was dried and distilled from sodium/benzophenone under argon. Furan, thiophene, 1-methylpyrrole, 2,5-dimethylfuran, 2,5-dimethylthiophene, 1,2,5-trimethylpyrrole, 2-methoxyfuran and oxazole were dried and distilled from calcium dihydride under argon. All solvents were then degassed by three freeze-pump-thaw cycles. Celite was stored in an oven at 120 °C overnight and was dried under vacuum for three hours before use. For each filtration, a plug of approximately 6 cm of Celite was used and each filtration was performed under the vigorous exclusion of air and moisture. ^{1}H and ^{13}C NMR spectra were obtained with either a Varian 300 MHz or a Varian 500 MHz NMR machine. All chemical shifts are reported in ppm and are referenced to TMS. All GC-MS samples were run as liquid samples in ethyl acetate on a Finnigan Trace GC-MS, equipped with an RTX-5MS 15 m column.

A Typical Cocondensation Experiment: Lithium metal (0.53 g, 0.076 mol) was vapourised from an alumina crucible protected by a stainless-steel inlet at around 800 °C over 90 minutes and cocondensed with a mixture of the aromatic compound (15 mL) and THF (80 mL, 1.12 mol). The solution was filtered through a plug of Celite in order to remove the solid lithium hydride by-product and unchanged lithium metal. After removal of the solvent mixture in vacuo, a solid was isolated and washed with THF (20 mL). The lithiated aromatic compound was identified by derivatisation with Me_3SiCl.

A Typical Derivatisation of the Lithiated Aromatic with Me_3SiCl: Me_3SiCl in THF solution was added dropwise with vigorous stirring to a solution of the lithiated aromatic compound (about 0.25 g) in THF (20 mL) at room temperature. The reaction was judged to be finished when a colour change from dark red-yellow to pale yellow occurred. Water (10 mL) was added to this solution, and the organic phase was separated. The aqueous phase was washed three times with dichloromethane (10 mL). The combined organic extracts were dried with $MgSO_4$ and then the solvent was removed under reduced pressure, affording the derivative. GC-MS, ^{1}H and ^{13}C NMR were used to identify the product.

Theoretical Methods Used in This Study: DFT calculations were performed with B3LYP and the 6−31G** basis set for C, H, O, N, S, and Li. For this purpose the program GAUSSIAN 98[19] was used on a Dell workstation running Red Hat Linux. Harmonic vibrational frequencies, calculated at the same level, characterised stationary points and gave the zero-point energy. The difference in the sum of the electronic and the zero-point energies were interpreted as reaction enthalpies at 0 Kelvin. LUMO energies for each aromatic compound were obtained from geometry-optimised structures using B3LYP/6-31G**.

2,5-Dimethyl-3-(trimethylsilyl)furan: The general procedure applied to 2,5-dimethylfuran gave 3-lithio-2,5-dimethylfuran (red) in 25% yield (0.8 g), identified as its TMS derivative. ^{1}H NMR ($CDCl_3$): δ = 5.7 (s), 2.1 (s) ppm. ^{13}C NMR ($CDCl_3$): δ = 151.0, 106.9, 99.8, 14.5, 12.1, 2.9 ppm.

2,5-Dimethyl-3-(trimethylsilyl)thiophene: The general procedure applied to 2,5-dimethylthiophene gave 3-lithio-2,5-dimethylthiophene (brown) in 45% yield (5.8 g), identified as its TMS derivative. ^{1}H NMR ($CDCl_3$): δ = 6.5 (s), 2.4 (s) ppm. ^{13}C NMR ($CDCl_3$): δ = 137.0, 126.0, 123.7, 14.2, 13.0, 2.1 ppm.

2-Methoxy-3-(trimethylsilyl)furan: The general procedure applied to 2-methoxyfuran gave 3-lithio-2-methoxyfuran (red) in 35% yield (2.7 g), identified as its TMS derivative. ^{1}H NMR ($CDCl_3$): δ = 7.5 (d, J = 5.3 Hz), 6.1 (d, J = 5.3 Hz), 3.7 (s) ppm. ^{13}C NMR ($CDCl_3$): δ = 172.7, 151.8, 120.6, 98.0, 67.0, 0.9 ppm.

 © 2004 Wiley-VCH Verlag GmbH & Co. KGaA, Weinheim

2,5-Bis(trimethylsilyl)oxazole: The general procedure applied to oxazole gave 2,5-dilithiooxazole (red/orange) in 29% yield (1.5 g), identified as its TMS derivative. ^{1}H NMR ($CDCl_3$): δ = 7.2 (s) ppm. ^{13}C NMR ($CDCl_3$): δ = 149.0, 137.5, 125.9, 2.0 ppm.

Supporting Information: Coordinates, electronic and zero-point energies of all optimised species.

Acknowledgments

The authors want to thank the Higher Education Authority (HEA) and the Centre for Synthesis and Chemical Biology (CSCB) for funding through the HEA PRTLI cycle 3 and the UCD Science Faculty for a PhD stipend for O. M.

[1] A. E. Shilov, G. B. Shul'pin, *Chem. Rev.* **1997**, *97*, 2905.
[2] B. A. Arndtsen, R. G. Bergmann, T. A. Mobley, T. H. Petersen, *Acc. Chem. Res.* **1995**, *28*, 154.
[3] R. H. Crabtree, *Chem. Rev.* **1995**, *95*, 987.
[4] A. H. Janowicz, R. G. Bergman, *J. Am. Chem. Soc.* **1982**, *104*, 352.
[5] A. H. Janowicz, R. G. Bergman;, *J. Am. Chem. Soc.* **1983**, *154*, 3929.
[6] N. S. Radu, S. L. Buchwald, B. Scott, C. J. Burns, *Organometallics* **1996**, *15*, 3913.
[7] R. H. Hauge, J. L. Margrave, *Reactions of First-Row Transition Metal Atoms and Small Clusters in Matrices*, in *Chemistry and Physics of Matrix-Isolated Species* (Eds.: L. Andrews, M. Moskowits), North Holland, Amsterdam, **1989**, pp. 277−302.
[8] W. E. Billups, M. M. Konars, R. H. Hauge, J. L. Margrave, *J. Am. Chem. Soc.* **1980**, *102*, 7393.
[9] M. Tacke, *Chem. Ber.* **1995**, *128*, 91.
[10] M. Tacke, *Chem. Ber.* **1996**, *129*, 1369.
[11] M. Tacke, *Eur. J. Inorg. Chem.* **1998**, 537.
[12] J. P. Dunne, M. Bockmeyer, M. Tacke, *Eur. J. Inorg. Chem.* **2003**, 458.
[13] W. Touce, E. Wellisch, *J. Am. Chem. Soc.* **1952**, *74*, 5177.
[14] M. Tiecco, L. Testaferri, L. Bagnoli, F. Marini, A. Temperini, C. Tomassini, C. Santi, *Tetrahedron* **2000**, *56*, 3255.
[15] H. J. Wu, C. H. Yen, C. T. Chuang, *J. Org. Chem.* **1998**, 5064.
[16] E. Lukevits, O. Pudova, Y. Popelis, N. P. Erchak, *J. Gen. Chem. USSR.* **1981**, *51*, 102.
[17] T. Frejd, *J. Heterocyclic Chem.* **1977**, *14*, 1085.
[18] S. Gronowitz, A. B. Hornfeldt, E. Lukevics, O. Pudova, *Synthesis* **1994**, *1*, 40.
[19] GAUSSIAN 98, Revision A.11.3, Gaussian Inc., Carnegie Office Park, Building 6, Suite 230, Carnegie, PA 15106, USA.

Received May 20, 2004
Early View Article
Published Online October 1, 2004

 © 2004 Wiley-VCH Verlag GmbH & Co. KGaA, Weinheim

EurJIC
European Journal of Inorganic Chemistry

Issue 23/2004

Pages 4533–4724

Papers available ahead of print in Early View at www.interscience.wiley.com

Earliest available Table of Contents:
Automatically, free of charge by e-mail through
www.interscience.wiley.com/alerts

COVER PICTURE

The cover picture shows DFT-optimized models of a non-heme high-spin iron(IV)-oxo intermediate and of Collins' stable high-spin Fe^{IV} complex. A. Ghosh, P. R. Taylor and co-workers show in their article on p. 4555ff. that these species, although both are high-spin Fe^{IV}, exhibit radically different electronic configurations and spin density profiles (green). Moreover, the authors present some of the first high-level ab initio calculations aimed at benchmarking the triplet-quintet energy difference for Fe^{IV} species.

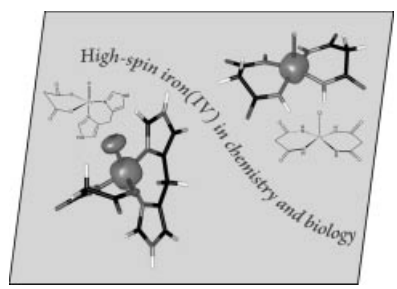

SHORT COMMUNICATIONS

Contents

4547 **Y. Xu,* W. Fan, S. P. Elangovan, M. Ogura, T. Okubo***

$[Ge_9O_{14}(OH)_{12}](C_6N_2H_{16})_2 \cdot H_2O$: A Novel Germanate with Ge–O Helical Chains Formed by Hydrothermal Synthesis that Can Separate *trans* and *cis* Isomers in Situ

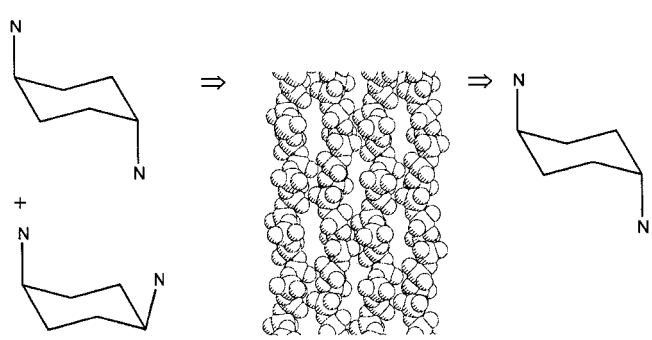

Keywords: Germanium / Helical structures / Hydrothermal synthesis / Isomers

 © 2004 Wiley-VCH Verlag GmbH & Co. KGaA, Weinheim

4550 **H. Sugimoto,* H. Tsukube, K. Tanaka**

Immobilization of a High-Valent Rhenium Complex on an Indium-Doped Tin-Oxide Electrode: Enhanced Catalytic Activity of a *trans*-Dioxorhenium(V) Complex in Electrochemical Oxidation of Alcohols

Keywords: Surface analysis / Cyclic voltammetry / Immobilization / Rhenium / Oxidation

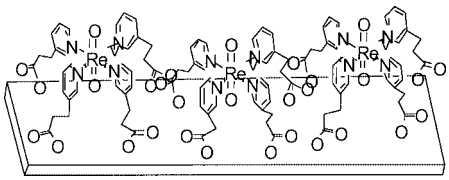

FULL PAPERS

4555 **A. Ghosh,* E. Tangen, H. Ryeng P. R. Taylor***

Electronic Structure of High-Spin Iron(IV) Complexes

Keywords: High-spin species / Nonheme / Iron / Oxo ligand / Diamond core / Quantum chemistry

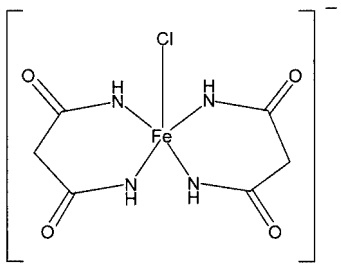

4561 **S. Di Bella,* N. Leonardi, G. Consiglio, S. Sortino,* I. Fragalà**

Fluorescent Self-Assembled Monolayers of Bis-(salicylaldiminato)zinc(II) Schiff-Base Complexes

Keywords: Fluorescence / Monolayers / Schiff bases / Zinc

4566 **Y. F. Song, C. Massera, M. Quesada, I. A. Koval, P. Gamez, A. M. Manotti Lanfredi, J. Reedijk***

A New Trinuclear Linear Copper(II) Complex: Unusual Crystal Structure with Semi-Coordinated Thiophene Moieties and Weak Antiferromagnetic Coupling Through the Bridging Imidazolate Rings

Keywords: Copper / Trinuclear complexes / EPR / Thiophene / N,S ligands / Imidazole

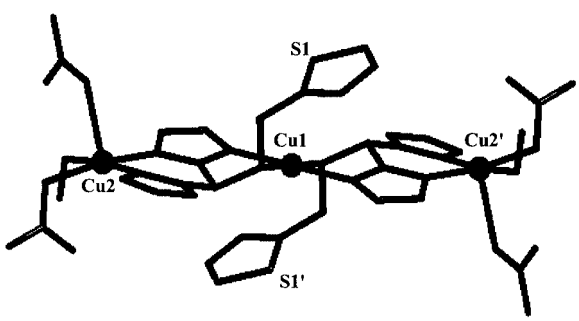

 © 2004 Wiley-VCH Verlag GmbH & Co. KGaA, Weinheim

4572 **S. Tanase, E. Bouwman, G. J. Long, A. M. Shahin, A. M. Mills, A. L. Spek, J. Reedijk***

Acid-Base Self-Assembly Chemistry and Hydrogen Bonding Interactions Resulting in the Formation of a Tetranuclear Aggregate Containing Four Crystallographically Non-Equivalent Fe^{III} Centers

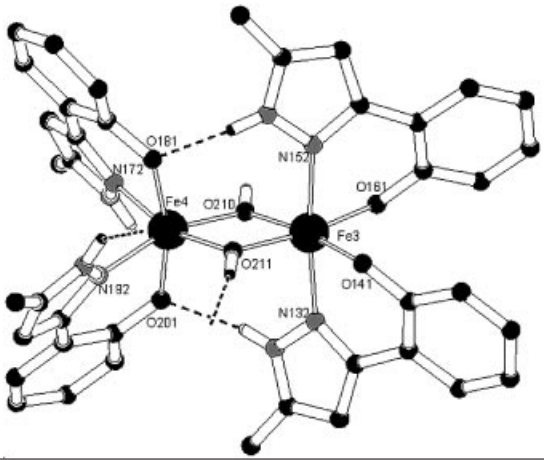

Keywords: Iron / Pyrazole ligands / Hydroxo-bridge / Mössbauer

4579 **J. Kontrec, D. Kralj,* L. Brečević, G. Falini, S. Fermani, V. Noethig-Laslo, K. Mirosavljević**

Incorporation of Inorganic Anions in Calcite

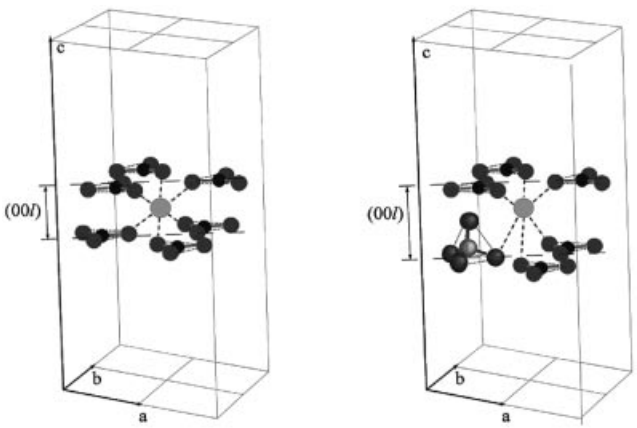

Keywords: Anions / Calcite / Calcium carbonate / Crystal growth / EPR spectroscopy

4586 **P. Liptau, D. Carmona,* L. A. Oro,* F. J. Lahoz, G. Kehr, G. Erker***

Facile [N]C−H Activation by a (*P,N*)-Chelate [3]Ferrocenophane−Ruthenium System

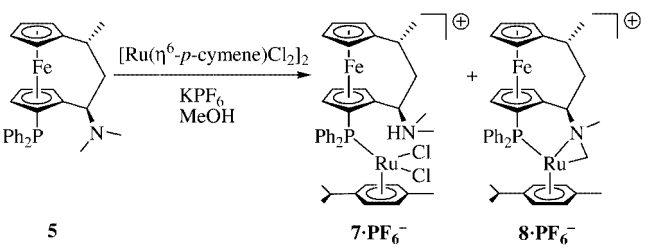

Keywords: (*P,N*)-Chelate ligands / Ruthenium / Ferrocenophane / C−H activation

4591 **D. Sellmann, S. Y. Shaban,* F. W. Heinemann**

Syntheses, Structures and Reactivity of Electron-Rich Fe and Ru Complexes with the New Pentadentate Ligand $Et_2NpyS_4-H_2$ {4-(Diethylamino)-2,6-bis[(2-mercaptophenyl)thiomethyl]-pyridine}

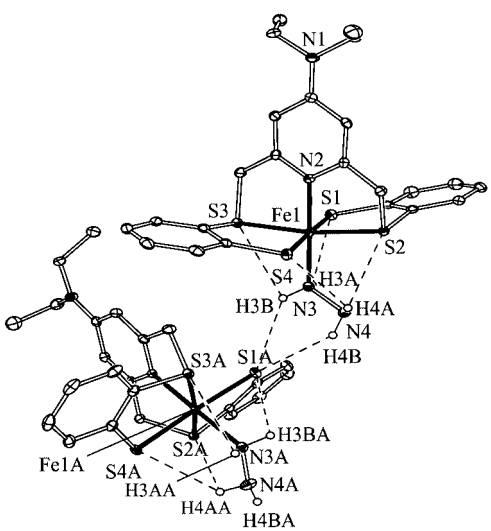

Keywords: Electron density / Iron / Nitrogenase / Ruthenium / S ligand

 © 2004 Wiley-VCH Verlag GmbH & Co. KGaA, Weinheim

4602 **P. Kuhn, C. Jeunesse, D. Sémeril, D. Matt,* P. Lutz, R. Welter**

Coordination Chemistry of Large Diphosphanes − Directional Properties of a Calix[4]arene Proximally Substituted by Two $-OCH_2PPh_2$ Podand Arms

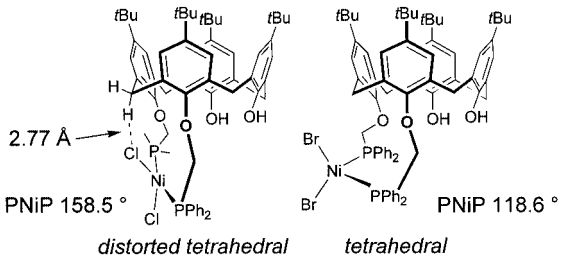

Keywords: Calixarenes / Large diphosphanes / Nickel complexes / Ethylene oligomerisation

4608 **Y.-B. Jiang, H.-Z. Kou,* R.-J. Wang, A.-L. Cui**

(Schiff-base)Cu^{II} Complexes with Phenolate-Oxygen/Chloro or -Oxygen/Azido Mixed Bridges − Syntheses, Crystal Structures and Magnetic Properties

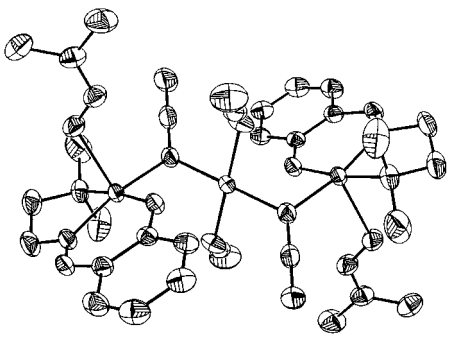

Keywords: Chloro bridges / Azido bridges / Magnetic properties / Cu^{II} ions / Crystal structures

4616 **Y.-H. Lo, Y.-C. Lin,* G.-H. Lee, Y. Wang**

Synthesis of (Vinylidene)- and (Cyclopropenyl)-ruthenium Complexes Containing a Tris-(pyrazolyl)borato (Tp) Ligand

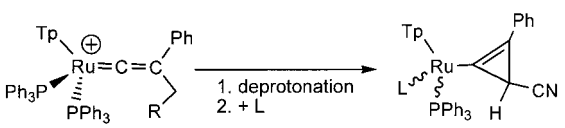

Keywords: Cyclopropenyl / N ligands / Ruthenium / Vinylidene ligands

4624 **C. Villiers,* P. Thuéry, M. Ephritikhine***

A Comparison of Analogous 4f- and 5f-Element Compounds: Syntheses, X-ray Crystal Structures and Catalytic Activity of the Homoleptic Amidinate Complexes $[M\{MeC(NCy)_2\}_3]$ (M = La, Nd or U)

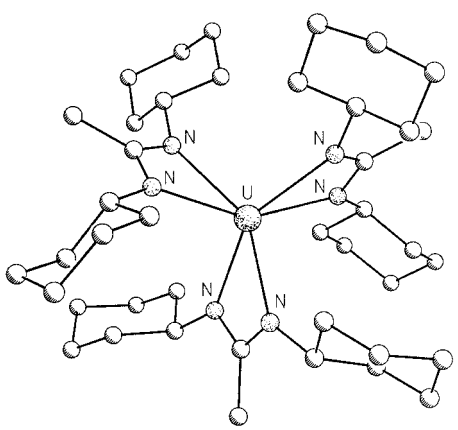

Keywords: ε-Caprolactone / Lanthanides / N ligands / Polymerization / Uranium

 © 2004 Wiley-VCH Verlag GmbH & Co. KGaA, Weinheim

4633 **S. Sarkar, A. Mondal, J. Ribas, M. G. B. Drew, K. Pramanik, K. K. Rajak***

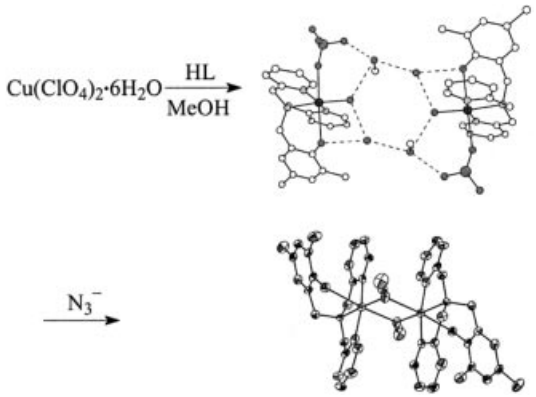

Synthesis, Structure and Properties of a Mononuclear and an End-On Double Azido-Bridged Copper(II) Complex Incorporating an N,N,N,O-Coordinating Tripodal Ligand

Keywords: Azide ligands / Copper / Hydrogen bonds / Magnetic properties / Tripodal ligands

4640 **P. Comba,* M. Kerscher, A. Roodt**

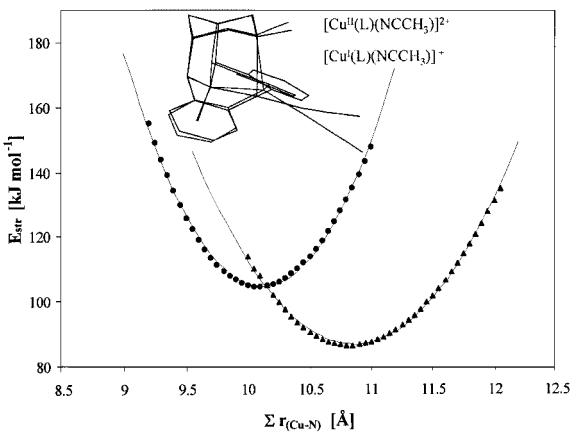

Slow Electron Self-Exchange in Spite of a Small Inner-Sphere Reorganisation Energy – The Electron-Transfer Properties of a Copper Complex with a Tetradentate Bispidine Ligand

Keywords: Marcus theory / Kinetics / Molecular mechanics / Outer-sphere electron transfer / Cross reaction

4646 **Y. Sakai, Y. Kitakoga, K. Hayashi, K. Yoza, K. Nomiya***

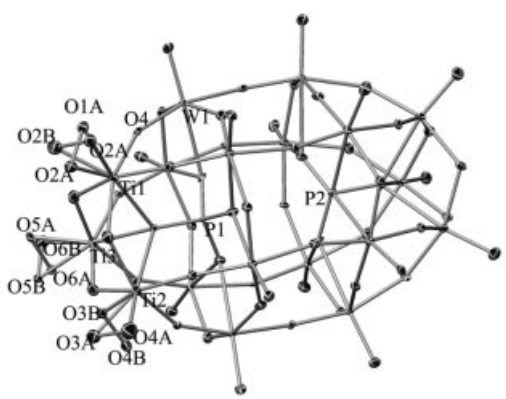

Isolation and Molecular Structure of a Monomeric, Tris[peroxotitanium(IV)]-Substituted α-Dawson Polyoxometalate Derived from the Tetrameric Anhydride Form Composed of Four Tris[titanium(IV)]-Substituted α-Dawson Substructures and Four Bridging Titanium(IV) Octahedral Groups

Keywords: Titanium(IV) / Peroxo complexes / Polyoxometalates

 © 2004 Wiley-VCH Verlag GmbH & Co. KGaA, Weinheim

4653 **S. Xu, H. Wang, J.-J. Zhu,* X.-Q. Xin, H.-Y. Chen**

An in situ Template Route for Fabricating Metal Chalcogenide Hollow Spherical Assemblies Sonochemically

Keywords: Sonochemistry / Nanostructures / Self-assembly / Metal chalcogenides / Hollow spheres

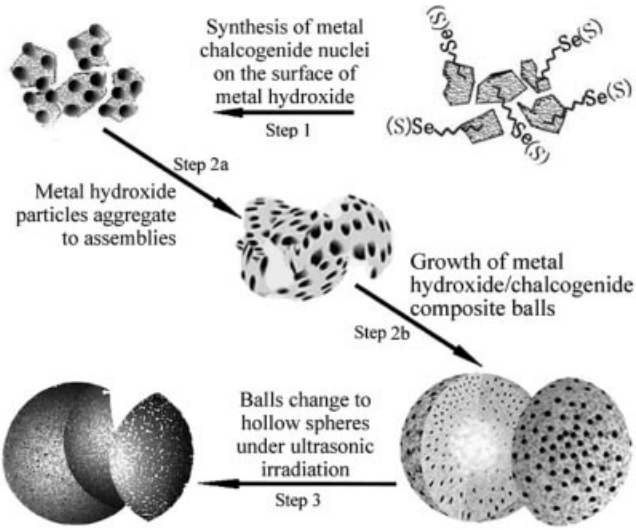

4660 **M. C. Aragoni, M. Arca, M. B. Carrea, F. Demartin, F. A. Devillanova, A. Garau, F. Isaia,* V. Lippolis, G. Verani**

Reaction of Mercury(0) with the I_2 Adduct of Tetraphenyldithioimidodiphosphinic Acid $(SPPh_2)_2NH$ (HL) − Crystal Structures of $[Hg(HL)I_2]$ and HgL_2

Keywords: Bridging ligands / Coordination chemistry / Density functional calculations / Iodine / Mercury / S ligands

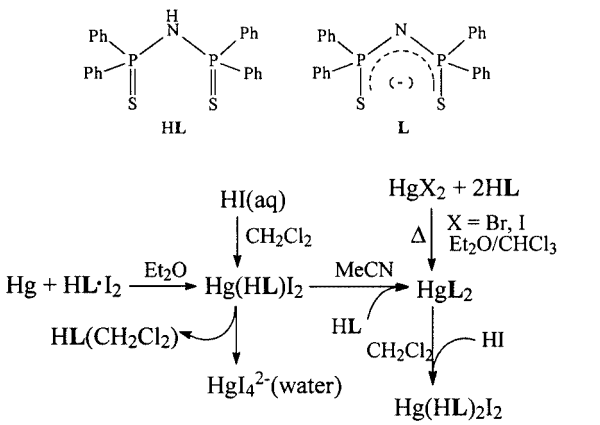

4669 **C. Jiang, Z. Yu, C. Jiao, S. Wang, J. Li, Z. Wang,* Y. Cui***

Luminescent Zn and Cd Coordination Polymers

Keywords: N ligands / Coordination polymers / Hydrothermal synthesis / Tubular structures / Fluorescence

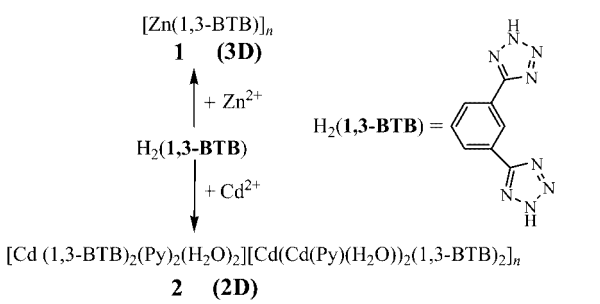

4675 **P. S. Mukherjee, D. Ghoshal, E. Zangrando,* T. Mallah, N. Ray Chaudhuri***

Use of Different Unsaturated Dicarboxylates Toward the Design of New 3D and 2D Networks of Copper(II)

Keywords: Coordination polymers / Copper / Magnetic properties / Weak interaction / Dicarboxylate ligands

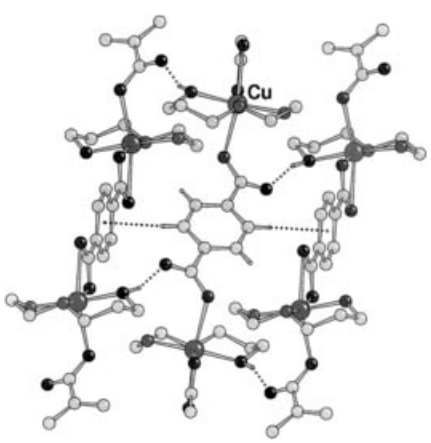

 © 2004 Wiley-VCH Verlag GmbH & Co. KGaA, Weinheim

4681 **E. C. E. Rosenthal,* H. Cui, K. C. H. Lange, S. Dechert**

Synthesis, Molecular Structure, and Olefin Polymerisation Activity of an Oxovanadium(V) Alkoxide with Unprecedented Chloride Bridging Ligands

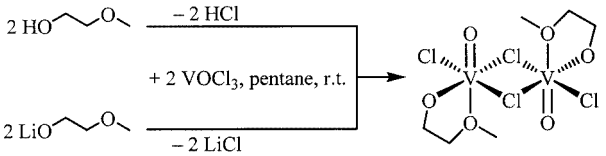

Keywords: Chelates / O ligands / Oxo ligands / Polymerisation / Vanadium

4686 **A. D. Burrows,* A. S. Donovan, R. W. Harrington, M. F. Mahon**

Backbone Flexibility and Counterion Effects on the Structure and Thermal Properties of Di(thiourea)zinc Dicarboxylate Coordination Polymers

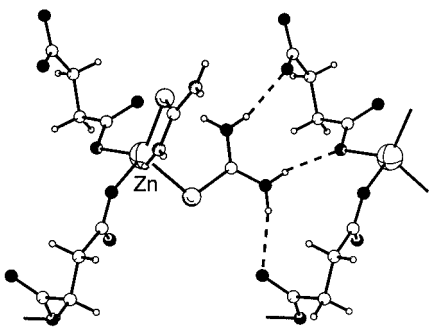

Keywords: Crystal engineering / Coordination polymers / Helical structures / Hydrogen bonds / Zinc

4696 **H.-L. Hu, C.-W. Yeh, J.-D. Chen***

Synthesis and Structural Characterisation of Ag^{I} Complexes with *N*,*N*′-Bis(2-pyridyl)oxalamide and the Anion of *N*-(2-Pyridyl)oxalamic Acid

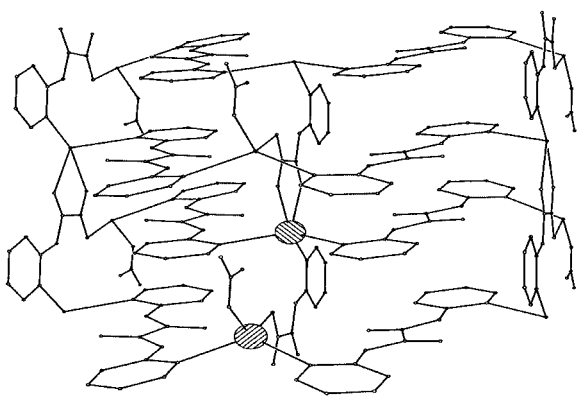

Keywords: Silver / Coordination polymer / *N*-(2-Pyridyl)oxalamic acid / *N*,*N*-Bis(2-pyridyl)-oxalamide

4702 **K. V. Axenov, M. Klinga, M. Leskelä, V. Kotov, T. Repo***

[Bis(amido)cyclodiphosph(III)azane]dichlorozirconium Complexes for Ethene Polymerization

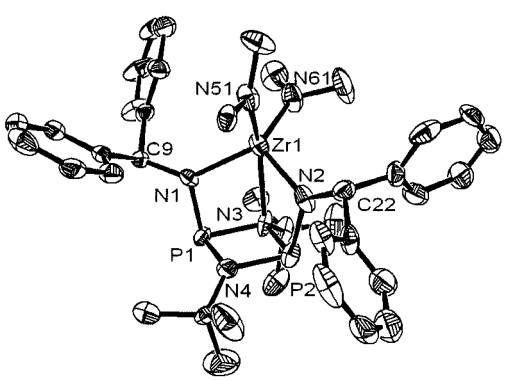

Keywords: Zirconium / Polymerization / Homogeneous catalysis

 © 2004 Wiley-VCH Verlag GmbH & Co. KGaA, Weinheim

4710 **E. Rotondo,* A. Rotondo, F. Nicoló, M. L. Di Pietro, M. A. Messina, M. Cusumano**

NMR Study of L-Shaped (Quinoxaline)-platinum(II) Complexes − Crystal Structure of $[Pt(DMeDPQ)(bipy)](PF_6)_2$

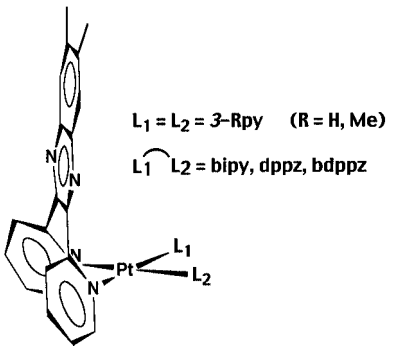

Keywords: DNA recognition / N ligands / Nitrogen heterocycles / NMR spectroscopy / Platinum

4718 **S. G. Sreerama, S. Pal***

A Triiron Complex Containing the Carboxylate-Free $\{Fe_3(\mu_3\text{-}O)\}^{7+}$ Core and Distorted Pentagonal-Bipyramidal Metal Centres

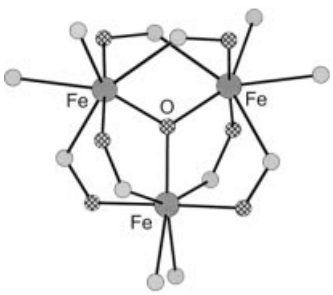

Keywords: Trinuclear iron(III) complex / Crystal structure / Magnetic properties / Redox properties

 © 2004 Wiley-VCH Verlag GmbH & Co. KGaA, Weinheim

$[Ge_9O_{14}(OH)_{12}](C_6N_2H_{16})_2{\cdot}H_2O$: A Novel Germanate with Ge−O Helical Chains Formed by Hydrothermal Synthesis that Can Separate *trans* and *cis* Isomers in Situ

Yan Xu,*[a] Wei Fan,[a] S. P. Elangovan,[a] Masaru Ogura,[a] and Tatsuya Okubo*[a]

Keywords: : Germanium / Helical structures / Hydrothermal synthesis / Isomers

A novel germanate $[Ge_9O_{14}(OH)_{12}](C_6N_2H_{16})_2{\cdot}H_2O$ (**1**; UTM-4) has been synthesized under hydrothermal conditions and its structure characterized by X-ray crystallography [a = 9.293(2), b = 12.164(2), c = 14.564(3) Å, β = 94.96(3)°, V = 1640.1(6) Å^3, Z = 2, monoclinic, space group $P2_1/c$]. The structure consists of Ge–O layers of helical chains, which are linked by hydrogen bonds to form a soft, open framework that exhibits a selectivity for *cis*-1,4-diaminocyclohexane during the synthesis.
(© Wiley-VCH Verlag GmbH & Co. KGaA, 69451 Weinheim, Germany, 2004)

Introduction

Great efforts have been made to synthesize germanium frameworks, as germanium is the closest analog to silicon and is therefore an attractive element to build open-frameworks in zeolite chemistry.[1−9] In germanates, Ge can adopt different Ge/O radius ratios to form polyhedra with a coordination number of four (tetrahedron), five (square bipyramid) or six (octahedron). The Ge−O distances are also significantly longer than the Si−O bond in silicates. Therefore, the flexibility of the polyhedral structure for germanium allows the formation of various open-framework structures with an extra-large pore, such as FDU-4[7a] and ASU-16.[7b] Recent research in the field of materials chemistry has focused on the synthesis of inorganic materials with helical pores or chains as they are desirable for selective enantiotopic separation and catalysis.[4d,10−14] Among the open-framework materials reported so far, only a limited number of phosphates and germanates[2c,4d] have such structural features. For examples, the zinc phosphate $[NH_3(C_2H_4)NH_2(C_2H_4)NH_3][Zn_4(PO_4)_3(HPO_4)]{\cdot}H_2O$[10] possesses intersecting helical chains, UCSB-7 has cross-linked helical pores,[4d] and the vanadophosphate $[(CH_3)_2NH_2]K_4[V_{10}O_{10}(H_2O)_2(OH)_4(PO_4)_7]$[11] contains interpenetrating double helices. Some other examples include aluminum phosphates, gallium phosphates, boron phosphates, and zinc phosphates.[12,13] Here we report the hydrothermal synthesis and structural characterization of a novel germanate $[Ge_9O_{14}(OH)_{12}](C_6N_2H_{16})_2{\cdot}H_2O$ (**1**) with a particularly interesting structure containing helical Ge−O chains that is selective for *cis*-1,4-diaminocyclohexane during the synthesis.

[a] Department of Chemical System Engineering, The University of Tokyo,
7-3-1 Hongo, Bunkyo-ku, Tokyo 113-8656, Japan
Fax: + 81-3-5800-3806
E-mail: yanxu@chemsys.t.u-tokyo.ac.jp
okubo@chemsys.t.u-tokyo.ac.jp

Results and Discussion

Germanate **1** was synthesized by a hydrothermal method from an organic-rich gel consisting of germanium dioxide, a mixture of *cis*- and *trans*-1,4-diaminocyclohexane, HF, pyridine, and H_2O in a 25-mL, Teflon-lined autoclave at 175 °C for 7 d. The crystalline product was characterized by thermal analysis (TG-DTA), powder X-ray diffraction (XRD) and single-crystal XRD.

The structural analysis revealed that the novel Ge−O layers are linked by hydrogen bonds to form a three-dimensional structure, and that only *cis*-1,4-diaminocyclohexane is present in **1**. As shown in Figure 1, the Ge−O (or OH) layer is constructed from three units, namely $\{[GeO_3(OH)_2]-(GeO_4)-[GeO_4(OH)]\}_n$ helical chains, $[Ge(OH)_2]^{2+}$ fragments connected by different chains, and $[Ge(OH)_3]^+$ fragments bonded by three bridging O-atoms from one chain that stabilize the helical chains. In the helical chain, GeO_4OH and GeO_3OH_2 trigonal bipyramids share their edges, and they are linked by corner-sharing GeO_4 tetrahedra. The central axis for every Ge−O helical chain is a twofold screw axis (symmetry: $-x$, 0.5 + y, 0.5 − z). Two bridging O atoms from adjacent GeO_4 and GeO_3OH_2 units in the helical Ge−O chain coordinate to another germanium of $[Ge(OH)_2]^{2+}$, generating a three-membered $[Ge_3O_3]$ ring. These three-membered rings link the right- and left-handed helical Ge−O chains (Figure 1b) to produce a Ge−O layer in the 011 plane (Figure 1a). Adjacent Ge−O layers are connected by hydrogen bonds

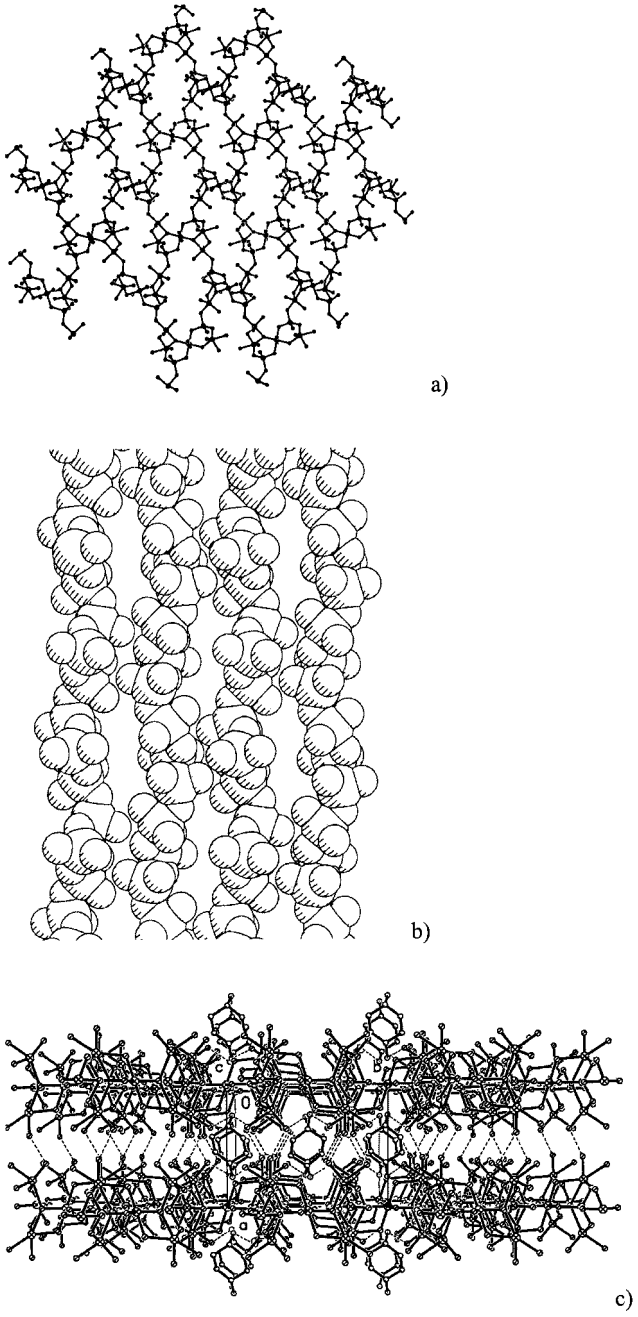

Figure 1. a) View of the Ge−O layer [$Ge(OH)_3^+$ fragments have been omitted]; b) helical Ge−O chains; c) three-dimensional, hydrogen-bonded structure (*cis*-1,4-diaminocyclohexane has been omitted for clarity)

through terminal OH groups to form a three-dimensional structure (Figure 1c).

The Ge in $[Ge(OH)_2]^{2+}$ is located at the symmetric center and, therefore, is constrained by symmetry to adopt an octahedral coordination (bonded by four bridging oxygen atoms and two hydroxyl groups), while the Ge of $[Ge(OH)_3]^+$ is chelated by three bridging oxygen atoms from a helical Ge−O chain, and shares one bridging OH with $[Ge(OH)_2]^{2+}$, to stabilize the helical chains and layers. There are three unique germanium sites in the helical chains: one regular tetrahedrally coordinated germanium (GeO_4) is bonded to four oxygen atoms, and two kinds of five-coordinate germanium sites [$GeO_3(OH)_2$ and $GeO_4(OH)$] are coordinated by O atoms and OH groups. Some terminal OH groups are involved in hydrogen-bond interactions between adjacent layers. The shortest O···O distance in the two layers is 2.96(2) Å. The Ge−OH distances for these OH groups are 2.038(8) and 2.094(8) Å, which are much longer than the other reported Ge−OH bond lengths. This can be ascribed to the hydrogen bonds between adjacent layers. All the Ge−O bond lengths for the tetrahedral germanium center vary from 1.712(4) to 1.752(5) Å [mean 1.730(4) Å)], and are very similar to the reported value for the quartz modification of GeO_2 [1.741(3) Å]. The Ge−O bond lengths for the five- and six-coordinate germanium centers range from 1.683(10) to 2.344(8) Å. These values are in agreement with those observed for known germanates.

A particularly interesting aspect of this reaction is the selectivity for *cis*-1,4-diaminocyclohexane (Figure 2) in the synthesis of germanate **1**. The separation of isomers is, in general, very difficult because of their similar physical and chemical properties. For example, the boiling point of both *trans*- and *cis*-1,4-diaminocyclohexane is 197 °C. Here we found that *cis*-1,4-diaminocyclohexane was successfully recovered from the mixture. In order to separate the isomers, a mixture of *trans*- and *cis*-1,4-diaminocyclohexane (approx. 1:1) was used as the reactant in a separation experiment. After hydrothermal synthesis, *cis*-1,4-diaminocyclohexane was found to be concentrated in the Ge−O layers as a guest molecule, with both N-atoms of the organic amine binding to the helical Ge−O chains through N-H···O hydrogen-bond interactions, while *trans*-1,4-diaminocyclohexane remained in solution. We analyzed the structures of four different crystals of germanate **1** but did not find any *trans*-1,4-diaminocyclohexane.

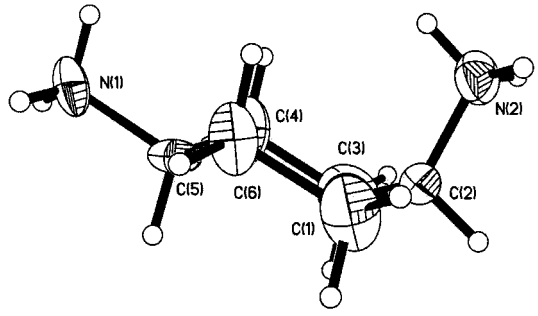

Figure 2. *cis*-1,4-Diaminocyclohexane was selected by germanate **1**

Significant changes in the powder X-ray diffraction patterns and TG curve were seen after germanate **1** was stirred in a 1 m solution of $NaNO_3$ at 50 °C. These ion-exchange results indicate that part of the structure-directing agents (SDAs) can be exchanged.

Thermal analysis of germanate **1** under a 10% O_2 (Ar balance) atmosphere reveals a weight loss of 1.3% between 60 and 226 °C, followed by a further weight loss of 26.7% between 226 and 700 °C. The calculated weight losses for

 © 2004 Wiley-VCH Verlag GmbH & Co. KGaA, Weinheim

water (1.35%) and combustion of the SDA and OH (28.6%) are in agreement with these results.

In conclusion, a novel germanate with helical Ge−O chains has been synthesized. This compound can separate *cis*- and *trans*-1,4-diaminocyclohexane in situ during the hydrothermal synthesis. The present work has great significance for germanium chemistry and isomer separation.

Experimental Section

1: Colorless, plate-like crystals of $[Ge_9O_{14}(OH)_{12}](C_6N_2H_{16})_2{\cdot}H_2O$ were prepared by a hydrothermal method from an organic-rich solution consisting of GeO_2, SiO_2, a mixture of *trans*- and *cis*-1,4-diaminocyclohexane, HF, pyridine, and H_2O in a molar ratio of 1:1:7.5:4.5:51:75. To avoid the formation of $Ge_7O_{14}F_3{\cdot}[H_2DACH]_{1.5}{\cdot}2H_2O$[15] ($H_2DACH$ = diaminocyclohexane) SiO_2 was added to induce the formation of germanate **1**. GeO_2 (0.12 g) and SiO_2 (0.60 g) were added to a mixture of pyridine (4.66 g), 1,4-diaminocyclohexane (1.05 g, mixture of *trans* and *cis* isomers), and water (1.55 g). Thereafter, this gel was stirred at room temperature overnight. Finally, a 47% HF solution (0.10 g) was added. The mixture was kept in a 25-mL, Teflon-lined autoclave at 170 °C for 7 d. The product was then washed with deionized water and ethanol, and dried at room temperature for 24 h (0.07 g; yield 41% based on Ge). Germanate **1** can also be synthesized under the same conditions but without SiO_2 powder. $C_{12}H_{46}Ge_9N_4O_{27}$: calcd. C 10.81, H 3.45, N 4.20; found C 10.10, H 3.67, N 3.91. X-ray powder diffraction analysis was performed on an M03X-HF (MAC Science) diffractometer, with Cu-K_α radiation, at 40 kV and 20 mA at a scanning rate of 4°/min with a step of 0.02°. Thermogravimetric (TG) analysis of germanate **1** was carried out under an O_2/Ar atmosphere on a Thermoplus TG 8120 (Rigaku) analyzer from 25 to 750 °C, at a heating rate of 10 °C/min.

X-ray Crystallographic Study: $C_{12}H_{46}Ge_9N_4O_{27}$, monoclinic, $P2_1/C$ (no.14), a = 9.293(2), b = 12.164(2), c = 14.564(3) Å, β = 94.96(3)°, V = 1640.1(6) Å^3, Z = 2, μ(Mo-K_α) = 8.237 mm^{-1}. Dimensions: 0.12 × 0.11 × 0.05 mm. 3661 Reflections with $I > 2\sigma(I_0)$ and 268 parameters gave $R1$ (wR) = 0.0729 (0.1223). The occupancy factors are 0.5 for O8, O8a, O12, O12a, O13, and O13a. Diffraction data were collected on a Rigaku R-AXIS RAPID IP diffractometer at 20 °C in the range $2.76° < \theta < 27.44°$. An empirical absorption correction was applied. The structure was solved by direct methods and refined by full-matrix least-squares on F^2. All non-hydrogen atoms were refined anisotropically. The oxygen atoms O5, O10, O11, O12, O12a, O13, and O13a are terminal and correspond to OH, as in other reported germanates. The half-occupied O8 and O8a atoms also belong to OH, because of their low thermal parameters and longer bond distances than other doubly bridging O-atoms.

CCDC-233622 contains the supplementary crystallographic data for this paper. These data can be obtained free of charge at www.ccdc.cam.ac.uk/conts/retrieving.html [or from the Cambridge Crystallographic Data Centre, 12 Union Road, Cambridge CB2 1EZ, UK; Fax: + 44-1223-336-033; E-mail: deposit@ccdc.cam.ac.uk].

Acknowledgments

This work was supported by the Japan Society for the Promotion of Science (JSPS). The authors thank Dr. Kazuhiro Uehara, Dr. Shirou Hikichi, and Prof. Noritaka Mizuno for the collection of single-crystal diffraction data.

[1] [1a] J. Cheng, R. Xu, *J. Chem. Soc., Chem. Commun.* **1991**, 483−485. [1b] J. Cheng, R. Xu, G. Yang, *J. Chem. Soc., Dalton Trans.* **1991**, 1537−1540. [1c] R. H. Jones, J. Chen, J. M. Thomas, A. George, M. B. Hursthouse, R. Xu, S. Li, Y. Lu, G. Yang, *Chem. Mater.* **1992**, *4*, 808−812.

[2] [2a] C. Cascales, E. Gutiérrez-Puebla, M. A. Monge, C. Ruíz-Valero, *Angew. Chem. Int. Ed.* **1998**, *37*, 129−131. [2b] C. Cascales, B. Gomez-Lor, E. Gutierrez-Puebla, M. Iglesias, M. A. Monge, C. Ruiz-Valero, N. Snejko, *Chem. Mater.* **2002**, *14*, 677−681. [2c] M. E. Medina, M. Iglesias, N. Snejko, E. Gutiérrez-Puebla, M. A. Monge, *Chem. Mater.* **2004**, *16*, 594−599.

[3] [3a] H. Li, M. Eddaoudi, D. A. Richardson, O. M. Yaghi, *J. Am. Chem. Soc.* **1998**, *120*, 8567−8568. [3b] H. Li, O. M. Yaghi, *J. Am. Chem. Soc.* **1998**, *120*, 10569−10570. [3c] H. Li, M. Eddouadi, O. M. Yaghi, *Angew. Chem. Int. Ed.* **1999**, *38*, 653−655. [3d] M. O'Keeffe, O. M. Yaghi, *Chem. Eur. J.* **1999**, *5*, 2796−2801. [3e] H. Li, M. Eddaoudi, J. Plévert, M. O'Keeffe, O. M. Yaghi, *J. Am. Chem. Soc.* **2000**, *122*, 12409−12410.

[4] [4a] P. Feng, X. Bu, G. D. Stucky, *Chem. Mater.* **1999**, *11*, 3025−3027. [4b] X. Bu, P. Feng, G. D. Stucky, *Chem. Mater.* **2000**, *12*, 1505−1507. [4c] X. Bu, P. Feng, G. D. Stucky, *J. Am. Chem. Soc.* **1998**, *120*, 11204−11205. [4d] T. E. Gier, X. Bu, P. Feng, G. D. Stucky, *Nature* **1998**, *395*, 154−157.

[5] T. Conradsson, M. S. Dadachov, X. D. Zou, *Microporous Mesoporous Mater.* **2000**, *41*, 183−191.

[6] L. Beitone, T. Loiseau, G. Férey, *Inorg. Chem.* **2002**, *41*, 3962−3966.

[7] [7a] Y. Zhou, H. Zhu, Z. Chen, M. Chen, Y. Xu, H. Zhang, D. Zhao, *Angew. Chem. Int. Ed.* **2001**, *40*, 2166−2168. [7b] J. Plévert, T. M. Gentz, A. Laine, H. Li, V. G. Young, O. M. Yaghi, M. O'Keeffe, *J. Am. Chem. Soc.* **2001**, *123*, 12706−12707.

[8] [8a] Y. Xu, W. Fan, N. Chino, K. Uehara, S. Hikichi, N. Mizuno, M. Ogura, T. Okubo, *Chem. Lett.* **2004**, *33*, 74−75. [8b] Y. Xu, M. Ogura, T. Okubo, *Microporous Mesoporous Mater.* **2004**, *70*, 1−6.

[9] D. Pitzschke, W. Bensch, *Angew. Chem. Int. Ed.* **2003**, *42*, 4389−4391.

[10] V. Soghomonian, Q. Chen, R. C. Haushalter, J. Zubieta, C. J. O'Connor, *Science* **1993**, *259*, 1596−1599.

[11] S. Neeraj, S. Natarajan, C. N. R. Rao, *Chem. Commun.* **1999**, 165−166.

[12] [12a] R. Kniep, H. G. Will, I. Boy, C. Röhr, *Angew. Chem. Int. Ed. Engl.* **1997**, *36*, 1013−1014. [12b] A. Yilmaz, X. Bu, M. Kizilyalli, G. D. Stucky, *Chem. Mater.* **2000**, *12*, 3243−3245.

[13] Z. Shi, S. Feng, S. Gao, L. Zhang, G. Yang, J. Hua, *Angew. Chem. Int. Ed.* **2000**, *39*, 2325−2327.

[14] Y. Wang, J. Yu, M. Guo, R. Xu, *Angew. Chem. Int. Ed.* **2003**, *42*, 4089−4092.

[15] J. Plévert, T. M. Gentz, T. L. Groy, M. O'Keeffe, O. M. Yaghi, *Chem. Mater.* **2003**, *15*, 714−718.

Received June 29, 2004

 © 2004 Wiley-VCH Verlag GmbH & Co. KGaA, Weinheim

Immobilization of a High-Valent Rhenium Complex on an Indium-Doped Tin-Oxide Electrode: Enhanced Catalytic Activity of a *trans*-Dioxorhenium(V) Complex in Electrochemical Oxidation of Alcohols

Hideki Sugimoto,*[a] Hiroshi Tsukube,[a] and Koji Tanaka[b]

Keywords: Surface analysis / Cyclic voltammetry / Immobilization / Rhenium / Oxidation

A high-valent *trans*-dioxorhenium(V) complex containing pyridine ligands was successfully immobilized on an ITO (indium-doped tin-oxide) electrode. The complex formed a monolayer structure on the electrode surface and promoted electrochemical catalytic oxidation of 1-phenylethanol to acetophenone in CH_2Cl_2. Oxidation hardly occurred in CH_2Cl_2 solution containing the free rhenium(V) complex. Immobilization of other high-valent metal complexes will present opportunities for design of functional electrodes with high activities.
(© Wiley-VCH Verlag GmbH & Co. KGaA, 69451 Weinheim, Germany, 2004)

Introduction

One of the most effective strategies in the development of novel molecular devices such as sensors and nanosized catalysts is to immobilize redox- and photo-active metal complexes on semiconductor electrodes by utilizing their well-defined structure.[1] Several ferrocene derivatives[2] and Re^{I},[3] Os^{II},[4] and Ru^{II} [5] complexes have already been immobilized on electrodes and have effectively mediated electron- and charge-transfer processes. Although most of the metal complexes operating in previous electrode systems were limited to those of low oxidation numbers, a few studies have immobilized high-valent compounds.

trans-$[Re^{V}O_2(pys)_4]^+$ (pys = pyridine derivatives) complexes have interesting features as redox- and photo-active catalysts, such as: 1) one-electron oxidation of the $Re^{V}O_2$ complexes affords higher-valent $Re^{VI}O_2$ cores;[6] 2) the two oxygen atoms attached to the Re center are responsible for electrochemical oxidation of organic molecules;[7] and 3) they exhibit microsecond long-lived luminescence based on d-d transitions in the visible region.[7] We have prepared the novel complex *trans*-$[ReO_2(L)_4]PF_6$ [**1**]PF_6 (L = 3-pyridinecarboxylic acid) containing free carboxylic acid groups (Figure 1). Such high-valent Re^{V} complexes have rarely been immobilized. Herein we investigate the immobilization of a series of Re^{V} complexes on ITO (indium-doped tin-oxide) electrodes and their catalytic activity in the oxidation of 1-phenylethanol and related alcohols (Scheme 1).

[a] Department of Chemistry, Graduate School of Science, Osaka City University,
Sumiyoshi-ku, Osaka, 558-8585, Japan
Fax: (internat.) + 81-6-6605-2522
E-mail: sugimoto@sci.osaka-cu.ac.jp
[b] Institute for Molecular Science,
Higashiyama, Okazaki, 444-8787, Japan

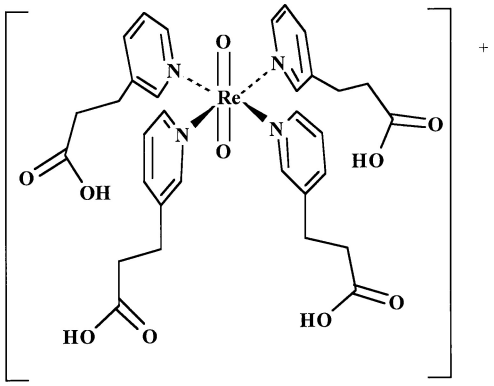

[**1**]$^+$

Figure 1. Suggested structure of [**1**]$^+$

Results and Discussion

In electrochemical experiments, complex [**1**]$^+$ shows a reversible redox wave assignable to a $Re^{VI/V}$ couple at 0.90 V vs. Fc/Fc^+ in CH_3CN. The complex was immobilized on ITO[8] electrodes by three different methods. Electrode **A** was modified by dipping the ITO electrode into a CH_3CN solution of the [**1**]PF_6 complex (2×10^{-4} M) for several days. Electrodes **B** and **C** were modified by combining the [**1**]PF_6 complex with aminoethyl- and aminomethylphosphonic acids by inserting them into the space between the surface of the electrodes and the [**1**]PF_6 complex. In electrode **A**, [**1**]$^+$ can connect with the ITO surface through carboxylate ester bonds [Sn−O−C(O)-] and hydrogen bonds [Sn=O···HO-C(O)-], as observed for the adsorption of ruthenium complexes containing free carboxylic acids

 © 2004 Wiley-VCH Verlag GmbH & Co. KGaA, Weinheim DOI: 10.1002/ejic.200400546

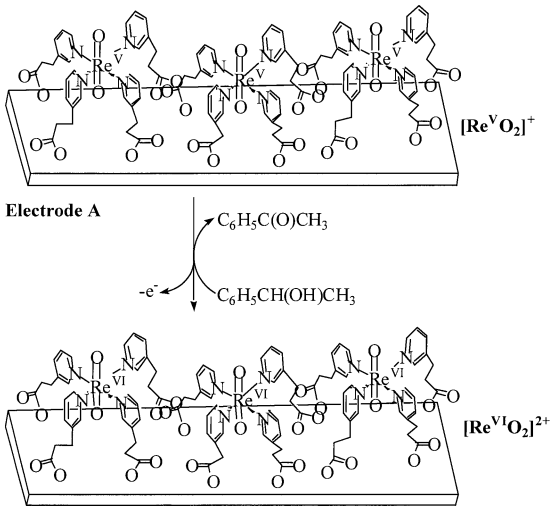

Scheme 1. *trans*-Dioxorhenium complex $[\mathbf{1}]^{+/2+}$ immobilized on an ITO electrode and electrochemical oxidation of 1-phenylethanol to acetophenone

onto metal oxides such as SnO_2, TiO_2, and In_2O_3.[5h] In electrodes **B** and **C**, however, $[\mathbf{1}]^+$ can connect with the amino groups of the spacer compounds through peptide bonds [−NH−C(O)-], and these units, in turn, connect with the ITO surface through phosphate ester bonds [Sn−O−P(O)-], as reported for the adsorption of ruthenium complexes containing free phosphonic acids onto these metal oxides.[5f,5g,9] The only difference between electrodes **B** and **C** is the length of the methylene chain: P−CH_2−CH_2−N for electrode **B** and P−CH_2−N for electrode **C**. The electrode performances were characterized by cyclic voltammetry. The three electrodes **A**−**C** exhibit the same redox potential, $E_{1/2}$, of $Re^{VI/V}$, but with different peak-to-peak separations ($\Delta E_p = E_{pa} - E_{pc}$). Electrode **A** shows a somewhat larger peak separation of 0.11 V than electrodes **B** and **C** (ΔE_p = 0.05 V). The electrodes also exhibit somewhat different surface stabilities. After the electrodes were rinsed for one hour, the current intensity of $Re^{VI/V}$ decreased by 15% for electrode **A**, but decreased by only 5% for electrodes **B** and **C**.

The electron-transfer process of electrode **B**, as characterized by cyclic voltammetry, was typical (Figure 2). The intensities of the anodic and cathodic currents are directly proportional to the increase in scan rate up to 300 mV·s^{-1}; they gradually saturate as the rate increases above 350 mV·s^{-1}. Since electrodes **A** and **C** show similar electrochemical behaviors despite their different construction, the redox processes in these systems must be confined to the surface. The surface coverages of the complexes were calculated by coulometric measurements at 1.2 V. The surface areas were estimated as 2.5×10^{-10} mol/cm^2 for electrode **A**, 1.9×10^{-10} mol/cm^2 for electrode **B**, and 1.8×10^{-10} mol/cm^2 for electrode **C**. Although the crystal structure of $[\mathbf{1}]PF_6$ is not available, the limiting surface coverage was roughly estimated as 2.9×10^{-10} mol/cm^2 by assuming that spheres based on the bond lengths and angles reported for *trans*-$[ReO_2(4\text{-picoline})_4]ReO_4$ are packed on a flat surface, and neglecting counteranions.[10] Similar surface coverages have been reported for monolayered electrodes with Ru complexes: $[Ru(2,2'\text{-bipyridyl})_2(2,2'\text{bipyridyl-4,4'-dicarboxylic acid})]^{2+} = 1.5 \times 10^{-10}$ mol/cm^2;[9] and $[Ru(2,2'\text{-bipyridyl})_2(2,2'\text{bipyridyl-4,4'-diphosphonic acid})]^{2+} = 2.5 \times 10^{-10}$ mol/cm^2.[9] Thus, the employed Re^V complex $[\mathbf{1}]^+$ is believed to form a monolayer structure on the ITO electrode surface.

The modified electrodes exhibit interesting catalytic behavior in the electrochemical oxidation of 1-phenylethanol. As shown in Figure 3, the intensity of the oxidation current corresponding to $Re^{VI/V}$ increases in the presence of 8.2 mM 1-phenylethanol (see b in Figure 3). Further addition of the alcohol substrate (total 24.5 mM) led to a further increase in the oxidation current, and a corresponding decrease in the reduction current (see c in Figure 3). Electrolysis was carried out at 1.2 V until no oxidation current was observed, and the reaction mixtures were then characterized by GC-MS and HPLC methods, which indicated that 1-phenylethanol had been converted into acetophenone. Electrochemical oxidation of this alcohol hardly occurred in CH_2Cl_2 solution containing the free complex $[\mathbf{1}]^+$, in which a glassy carbon electrode having the same surface area as

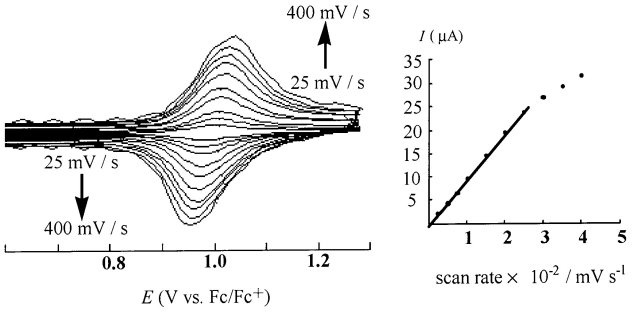

Figure 2. Cyclic voltammetry of modified electrode **B**: scan-rate dependence at 25, 50, 75, 100, 150, 200, 250, 300, 350, and 400 mV·s^{-1} (left) and linear correlation of current against scan rate recorded in CH_2Cl_2 containing 0.1 M Bu_4NPF_6 (right)

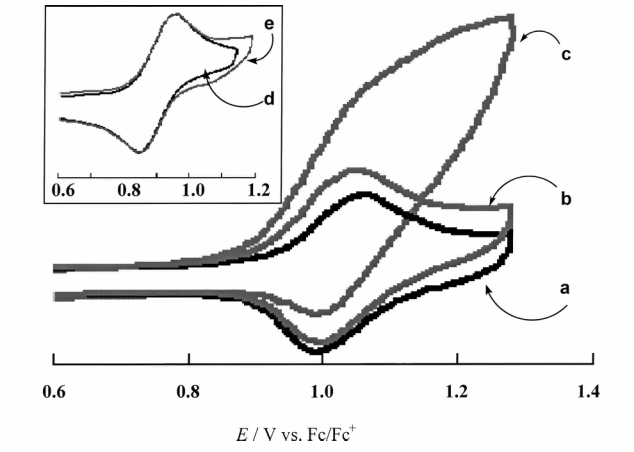

Figure 3. Cyclic voltammetry changes of modified electrode **B** in CH_2Cl_2 upon addition of 1-phenylethanol (**a**: 0 mM, **b**: 8.2 mM, **c**: 24.5 mM), and complex $[\mathbf{1}]PF_6$ in CH_2Cl_2 upon addition of 1-phenylethanol (inset, **d**: 0 mM, **e**: 810 mM)

 © 2004 Wiley-VCH Verlag GmbH & Co. KGaA, Weinheim

the employed ITO electrode was used. Also, the current intensity only increased slightly, even in the presence of a large excess of 1-phenylethanol (810 mM) (see inset e in Figure 3). Electrodes **B** and **C** exhibit higher turnover numbers (TON) and current efficiencies in the oxidation of 1-phenylethanol than electrode **A**. Table 1 compares the catalytic profiles of the three modified electrodes. The spacer insertion enhances the catalytic activity of the *trans*-dioxorhenium(V) complexes.

Table 1. Catalytic oxidation of 1-phenylethanol by modified electrodes **A**−**C**

Modified electrode	**A**	**B**	**C**
TON[a]	900	1300	1200
Current efficiency[b]	65	85	80

[a] Turnover number (product mol/complex mol). [b] $2e^-$ per substrate.

The rate constants for the system $v = k[Re^V$ on electrodes][1-phenylethanol] of electrodes **A**−**C** were roughly determined to be about 1 M^{-1} s^{-1} using Equation (1)

$$i = nFAk\Gamma_p C_A \quad (1)$$

where n = number of electrons, F = Faraday constant, A = surface area, Γ_p = surface coverage, k = rate constant, and C_A = concentration of substrate, which has been previously applied to heterogeneous systems.[11] The current intensities independent of the scan rates were entered as i in this equation. Since these three electrodes have almost identical surface coverages and rate constants, their catalytic activities must depend on the presence, or absence, and nature of the spacers introduced between the electrode surface and complex $[\mathbf{1}]^+$.

These electrodes also catalyze the oxidation of 1-heptanol and 2-propanol to give 1-heptanealdehyde and acetone, respectively. Although the detailed mechanism is unclear,[12] the catalytic cycles may contain redox and acid-base reactions of the *trans*-ReO_2 unit as suggested in a *trans*-$[ReO_2(py)_4]^+$ system,[7] in which the active Re^{VI} state was significantly involved (Scheme 1).

Conclusion

We have presented the first example of high-valent metal complexes immobilized on an electrode surface. The *trans*-dioxorhenium(V) complexes immobilized on the electrode surface enable catalytic oxidation of 1-phenylethanol to acetophenone with high turnover and high current efficiency. A combination of high-valent metal complexes with electrodes could provide a new generation of electrochemical catalysts.

Experimental Section

***trans*-$[ReO_2(L)_4]PF_6$ ($[\mathbf{1}]PF_6$; L = 3-pyridinecarboxylic acid):** A suspension containing $[ReOCl_3(PPh_3)_2]$ (0.50 g, 0.60 mmol) and 3-pyridinecarboxylic acid (1.80 g, 12 mmol) in acetone/H_2O (20:1 v/v) was refluxed for 90 minutes to give an orange solution. After filtration, the orange solution was concentrated to 5 mL. After silica-gel column chromatography (CH_3OH eluent), addition of NH_4PF_6 (300 mg, 1.80 mmol) in H_2O (10 mL) gave an orange powder. The collected powder was dried in air (yield: 126 mg, 22%). $C_{32}H_{36}F_6N_4O_2PRe$ (967.84): calcd. C 39.71, H 3.75, N 5.79. found C 39.79, H 3.89, N 5.42. ESI-MS: m/z = 823 $[M - PF_6]^+$. IR: $\tilde{\nu}$ = 799 cm^{-1} $\nu_{(O=Re=O)}$. ^1H NMR (300 MHz, $[D_6]$DMSO): δ = 2.52 (t, J = 7.7 Hz, 8 H, CH_2), 2.81 (t, J = 7.4 Hz, 8 H, CH_2), 7.49 (t, J = 5.8 Hz, 4 H, py), 7.74 (d, J = 7.7 Hz, 4 H, py), 8.84 (d, J = 5.8 Hz, 4 H, py), 8.92 (s, 4 H, py) ppm. UV/Vis (CH_3CN): λ = 430 nm (ε = 1250 $M^{-1}\cdot cm^{-1}$), 346 (19800), 254 (15600).

Preparation of ITO Electrodes: Before surface modification, each ITO electrode was washed with a 5:1:1 solution of H_2O, H_2O_2, and NH_4OH and thoroughly rinsed with purified water. After heating at 120 °C for 60 minutes, the electrode was cooled and stored under dry N_2.

ITO Electrode A: The dried ITO electrode was dipped in a CH_3CN solution of $[\mathbf{1}]PF_6$ (2×10^{-4} M) for several days. The electrode was then rinsed in ethanol to remove the adsorbed salt.

ITO Electrodes B and C: The dried ITO electrode was dipped in a CH_3CN solution of aminoethyl- or aminomethylphosphonic acid; after 24 hours, the electrode was picked up from the solution. The electrode on which the phosphonic acid was immobilized was again dipped in a solution of complex $[\mathbf{1}]PF_6$ (2×10^{-4} M) in the presence of four equivalents of DCC (1,3-dicyclohexylcarbodiimide) as a coupling agent for 3−4 days. The electrodes were then rinsed in ethanol to remove the adsorbed salt; in the absence of DCC the complex was not immobilized.

Acknowledgments

This work was partly supported by the Joint Studies Program (2004) of the Institute for Molecular Science, Japan, and by CREST of the Japan Science and Technology Agency. The authors are grateful to Prof. Akio Ichimura of Osaka City University for helpful discussion and to Central Glass Co., Ltd., Japan, for supplying the ITO electrodes.

[1] [1a] *Interfacial Electrochemistry: Theory, Experiment, and Applications* (Ed.: A. Wieckowski), Marcel Dekker, New York, **1999**. [1b] E. Palomares, R. Vilar, J. R. Durrant, *Chem. Commun.* **2004**, 362−363. [1c] J. Garcia-Canadas, A. P. Meacham, L. M. Peter, M. D. Ward, *Angew. Chem. Int. Ed.* **2003**, *42*, 3011−3014.
[2] [2a] C. E. D. Chidsey, *Science* **1991**, *251*, 919−922. [2b] J. J. Hickman, *Science* **1991**, *252*, 688−691.
[3] R. Argazzi, C. A. Bignozzi, T. A. Heimer, G. J. Meyer, *Inorg. Chem.* **1997**, *26*, 2−3.
[4] C. Kleverlaan, M. Alebbi, R. Argazzi, C. A. Bignozzi, G. M. Hasselmann, G. J. Meyer, *Inorg. Chem.* **2000**, *39*, 1342−1343.
[5] [5a] J.-K. Lee, S.-H. Lee, M. Kim, H. Kim, D.-H. Kim, W.-Y. Lee, *Chem. Commun.* **2003**, 1602−1603. [5b] B. O'Regan, M. Gratzel, *Nature* **1991**, *353*, 737−740. [5c] S. A. Trammell, J. C. Wimbish, F. Odobel, L. A. Gallagher, P. M. Narula, T. J. Meyer, *J. Am. Chem. Soc.* **1998**, *120*, 13248−13249. [5d] M. K. Nazeeruddin, P. Pechy, T. Renouard, S. M. Zakkeruddin, R. H-Baker, P. Comte, P. Liska, L. Cevey, E. Costa, V. Shklover, L. Spiccia, G. B. Deacon, C. A. Bignozzi, M. Gratzel, *J. Am.*

 © 2004 Wiley-VCH Verlag GmbH & Co. KGaA, Weinheim

Chem. Soc. **2001**, *123*, 1613−1624. [5e] K. Wang, M. Haga, M. D. Hossain, H. Shindo, K. Hasebe, H. Monjushiro, *Langmuir* **2002**, *18*, 3528−3536. [5f] B. M. Nakhle, S. A. Trammell, K. M. Sigel, T. J. Meyer, B. W. Erickson, *Tetrahedron* **1999**, *55*, 2835−2846. [5g] S. M. Zakeeruddin, M. K. Nazeeruddin, P. Pechy, F. P. Rotzinger, R. Humphry-Baker, K. Kalyanasundaram, M. Gratzel, *Inorg. Chem.* **1997**, *36*, 5937−5946. [5h] T. J. Meyer, G. J. Meyer, B. W. Pfenning, J. R. Schoonover, C. J. Timpson, J. F. Wall, C. Kobusch, X. Chen, B. M. Peek, C. G. Wall, W. Ou, B. W. Erickson, C. A. Bignozzi, *Inorg. Chem.* **1994**, *33*, 3952−3964.

[6] M. S. Ram, L. M. Skeens-Jones, C. S. Johnson, X. L. Zhang, C. Stern, D. I. Yoon, D. Selmarten, J. T. Hupp, *J. Am. Chem. Soc.* **1995**, *117*, 1411−1421.

[7] [7a] J. R. Winkler, H. B. Gray, *J. Am. Chem. Soc.* **1983**, *105*, 1373−1374. [7b] H. H. Thorp, J. V. Houten, H. B. Gray, *Inorg. Chem.* **1989**, *28*, 889−892.

[8] ITO-coated glasses of 10 Ω/cm^2 were used in this study.

[9] S. A. Trammell, J. A. Moss, J. C. Yang, B. M. Nakhle, C. A. Slate, F. Odobel, M. Sykora, B. W. Erickson, T. J. Meyer, *Inorg. Chem.* **1999**, *38*, 3665−3669.

[10] J. W. Johnson, J. F. Brody, G. B. Ansell, S. Zentz, *Inorg. Chem.* **1984**, *24*, 2415−2418.

[11] A. J. Bard, L. R. Faulkner, *Electrochemical Methods 2nd ed*, John Wiley & Sons, New York, **2001**.

[12] There are two possibilities of hydrogen transfer and hydride transfer processes (see ref.[7]).

Received June 22, 2004

 © 2004 Wiley-VCH Verlag GmbH & Co. KGaA, Weinheim

Electronic Structure of High-Spin Iron(IV) Complexes

Abhik Ghosh,*[a] Espen Tangen,[a] Hege Ryeng,[a] and Peter R. Taylor*[b]

Keywords: High-spin species / Nonheme / Iron / Oxo ligand / Diamond core / Quantum chemistry

High-spin (S = 2) iron(IV) species are rare but increasingly recognized as reactive intermediates in the catalytic cycles of several nonheme iron enzymes. A question of some interest, therefore, concerns how much higher in energy the low-spin (S = 1) state is for these species. With the use of density functional theory (DFT) and high-level ab initio calculations [CASPT2 and CCSD(T)], we have attempted to answer this question for the so-called Collins complex, a square-pyramidal Fe^{IV} complex with a tetraamido-*N* equatorial ligand set, a chloride axial ligand, and an S = 2 ground state. The calculations suggest that relative to the ground state, the low-spin state is higher in energy by at least 0.3 eV and possibly as much as 0.7 eV. Using DFT calculations, a broad quantum chemical survey of high-spin $Fe^{IV}O$ intermediates was also undertaken. A key finding is that the Fe–O distance and O spin population are quite similar across all mononuclear $Fe^{IV}O$ species studied, regardless of the heme versus nonheme environment and of the S = 1 versus 2 spin state, reflecting the essential similarity of the Fe(d_π)–O(p_π) orbital interactions in all the species studied. However, the spin density profiles of high-spin $Fe^{IV}O$ species, currently believed to be known only as a nonheme iron enzyme (TauD) intermediate, are predicted to be very different from that of Collins' high-spin Fe^{IV} complex. Our calculations further suggest that with the help of sterically hindered ligands such as 6-me_3-tpa, it might be possible to generate synthetic high-spin $Fe^{IV}O$ models of the unique TauD intermediate. Finally, our calculations confirm the aptness of describing the [(6-me_3-tpa)Fe^{III}(μ-O)$_2$$Fe^{IV}$(6-$me_3$-tpa)]$^{3+}$ cation as a flexible diamond core and indicate the presence of a fairly discrete high-spin $Fe^{IV}O$ unit within the dinuclear core.

(© Wiley-VCH Verlag GmbH & Co. KGaA, 69451 Weinheim, Germany, 2004)

Introduction

Although high-spin iron(IV) species are believed to be involved in the catalytic cycles of a number of nonheme iron enzymes,[1,2] they are exceedingly rare in a traditional inorganic context. This is not surprising given that high oxidation states are generally favored by strongly basic ligands, which in turn normally favor low-spin states of the coordinated transition metal ion. Indeed, a square-pyramidal Fe^{IV} complex with a macrocyclic tetraamido-*N* equatorial ligand and a chloride axial ligand, reported by Collins and coworkers more than a decade ago, serves as the only well-characterized high-spin Fe^{IV} species known.[3] At least three enzymatic high-spin Fe^{IV} species have been spectroscopically characterized but until now they have not lent themselves to X-ray crystallographic analysis. Perhaps the most celebrated example of a high-spin Fe^{IV} species is the critical methane-hydroxylating intermediate **Q** of sMMO.[4] There is strong evidence indicating that **Q** features an [Fe^{IV}_2(μ-O)$_2$]$^{4+}$ diamond core with antiferromagnetically coupled local high-spin Fe^{IV} centers.[2,4] A related $Fe^{III}Fe^{IV}$ species called intermediate **X** produces the catalytically essential tyrosyl radical in the R2 protein of ribonucleotide reductase to initiate the process of ribonucleotide reduction in DNA biosynthesis.[5] On the modeling front, Que and co-workers have reported synthetic [Fe_2(μ-O)$_2$]$^{3+}$ intermediates with localized high-spin Fe^{III} and Fe^{IV} centers, the high-spin character of the metal centers reflecting the relatively weak-field nature of the capping ligands, which are based on sterically hindered 2,6-dialkylpyridine units.[6,7] Finally and very recently, a high-spin Fe^{IV} intermediate of the mononuclear nonheme iron enzyme TauD (taurine/α-ketoglutarate dioxygenase) has been spectroscopically detected.[8] Given our longstanding interest in the electronic structures of high-valent transition metal species,[9] we have initiated a broad quantum chemical exploration of the electronic structures of various known high-spin Fe^{IV} species, this being our first report on the subject.

We present our results in two parts. In the first part, we present our efforts to model the well-characterized Collins species mentioned above,[3] focusing on benchmarking the relative energies of the high- and low-spin states using density functional theory (DFT) and ab initio CASPT2 and

[a] Department of Chemistry, University of Tromsø, 9037 Tromsø, Norway
Fax: (internat.) + 47-77644765
E-mail: abhik@chem.uit.no
[b] Department of Chemistry, University of Warwick, Coventry, UK
Fax: (internat.) + 44-2476-523258
E-mail: p.r.taylor@warwick.ac.uk
Supporting information for this article is available on the WWW under http://www.eurjic.org or from the author.

CCSD(T) calculations.[10] The results emphasize the difficulty of the problem − an issue that is largely overlooked in modern quantum chemical studies of bioinorganic problems − but that said, the DFT results are not bad at all, and DFT is clearly indicated as the method of choice for a broad survey of high-spin Fe^{IV} species. In the second part of this paper, we present such a survey, focusing on high-spin $Fe^{IV}O$ species, including a model of the TauD intermediate.

The Collins Complex

Before undertaking a broad quantum chemical survey of high-spin $Fe^{IV}O$ species, it seemed worthwhile to obtain a feel for the suitability of DFT for such a study. While DFT has emerged as the almost universal method of choice for bioinorganic modeling studies, a number of cases have been documented in which DFT apparently does a poor job of describing the relative energetics of the low-lying states of transition metal complexes.[10] Indeed, based on the somewhat limited data available, Fe^{III} complexes appear to be particularly problematic; for example, DFT (PW91, B3LYP) does not exhibit a clear preference for a sextet ground state for (porphyrin)Fe^{III} chloride, as expected on the basis of experimental data, whereas CASPT2 and CCSD(T) calculations clearly yield the correct ground state and a substantial sextet-quartet splitting of about 0.7 eV.[11] In a recent review article,[10] we have summarized much of what has been accomplished so far in terms of benchmarking the energetics of key spin states of transition metal species of bioinorganic relevance. As the only well-characterized high-spin Fe^{IV} complex, the Collins complex appeared to be an ideal candidate for our benchmarking studies.

To address the essence of the benchmarking problem, there seemed little to be gained by dealing with the relatively complex macrocyclic tetraamido-*N* ligand used in the experimental study.[3] We have therefore used the smaller C_{2v} model complex **1** shown in Figure 1, which captures the key structural features of the synthetic complex.[3] Geometry optimizations were carried out for the $S = 1$ and 2 states of the model complex with both the PW91 and B3LYP functionals.[12] CASPT2 and CCSD(T) calculations[13] were carried out at both the PW91 and B3LYP optimized geometries. The CASPT2 calculations were carried out with two high-quality basis sets, denoted BS1 and BS2, the latter being significantly larger than the former.[14] Basis set BS1 was used for the CCSD(T) calculations. Table 1 lists selected geometry parameters for the PW91 and B3LYP structures as well as the PW91 Mulliken spin populations for selected atoms.[15,16] The agreement between the optimized and experimental[3] geometry parameters may be regarded as generally very good.[15] The triplet-quintet splitting turned out to be essentially zero with the PW91 functional and 0.21 eV (with the triplet higher in energy) with B3LYP DFT calculations, which clearly emphasized the need for benchmarking with more elaborate, correlated methods such as CASPT2 and CCSD(T).

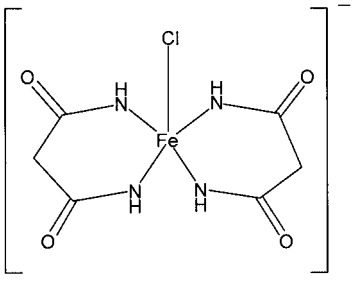

Figure 1. Simplified C_{2v} model **1** of the complex used in this study

Table 1. Selected geometry parameters (Å, °) and Mulliken spin populations[15]

	$S = 1$		$S = 2$	
	PW91	B3LYP	PW91	B3LYP
Geometry parameters[a][b]				
Fe−N	1.893	1.896	1.927	1.925
Fe−Cl	2.164	2.198	2.331	2.349
Fe−N_4	0.343	0.345	0.372	0.376
N−Fe−Cl	100.44	100.48	101.12	101.25
Mulliken spin populations[c]				
Fe	1.632		3.149	
N	0.043		0.074	
Cl	0.059		0.330	
C(CO)	0.002		−0.003	
O(CO)	0.036		0.050	

[a] In general, the PW91 and B3LYP geometry parameters are in excellent agreement, better than ±0.01 Å and ±0.05°. The only exception is the Fe−Cl distance, for which a somewhat larger difference is observed between the two functionals. [b] The symbol Fe−N_4 refers to the distance of the Fe atom from the plane containing the four nitrogen atoms. [c] The version of Turbomole used for the B3LYP optimizations does not report atomic spin populations.

At the CASPT2/BS1 level and with B3LYP optimized geometries, the triplet-quintet splitting was found to be 0.66 eV, or 0.56 eV if Fe 3s3p correlation was excluded. With the larger basis set BS2 and B3LYP geometries, the CASPT2 triplet-quintet splitting was 0.69 eV, or 0.58 eV if Fe 3s3p correlation was excluded. CCSD(T) calculations including 3s3p correlation were too large for our computational resources: the triplet-quintet splitting at the CCSD(T)/BS1 level without Fe 3s3p correlation, with B3LYP optimized geometries, was found to be 0.26 eV. Thus, agreement between the CASPT2 and CCSD(T) energetics is only fair, with a difference of about 0.3 eV between the two predictions when Fe 3s3p correlation is excluded. This discrepancy is as large as the splitting itself predicted by DFT [or by CCSD(T)] and begs the question as to which results (if any) are to be relied on.[17] On a more positive note, the triplet-quintet splitting obtained with B3LYP energetics is not bad and essentially the same as the CCSD(T) result, indicating the suitability of DFT for a broader exploration of high-spin Fe^{IV} intermediates; we have indeed carried out such a study and the results are outlined below.

 © 2004 Wiley-VCH Verlag GmbH & Co. KGaA, Weinheim

High-Spin $Fe^{IV}O$ Intermediates

A question of longstanding interest concerns the possible involvement of $Fe^{IV}O$ intermediates in the catalytic cycles of *mononuclear* nonheme iron enzymes such as the pterin-dependent enzyme phenylalanine hydroxylase and the α-ketoglutarate-dependent enzyme prolyl hydroxylase.[1] However, as mentioned above, only very recently has the first such species been spectroscopically characterized: this is an intermediate of the mononuclear nonheme iron enzyme TauD (taurine/α-ketoglutarate dioxygenase), for which Mössbauer spectroscopic studies suggest a unique high-spin Fe^{IV} formulation.[8] While the ligation state of the iron center is not known, mechanistic considerations suggest that this may be an $Fe^{IV}O$ species, which would make it the first *mononuclear* high-spin $Fe^{IV}O$ intermediate − enzymatic or synthetic − to be spectroscopically characterized.

Considerable progress has also been made on the synthetic modeling front. Thus, the groups of Wieghardt[18] and Que[19,20] have synthesized and spectroscopically characterized a number of mononuclear nonheme $Fe^{IV}O$ intermediates.[1] One of these intermediates, $Fe^{IV}(O)(me_4cyclam)(CH_3CN)$, has also lent itself to a high-quality crystallographic analysis.[21] However, none of these species, which are $S = 1$, faithfully mimic the $S = 2$ TauD intermediate. In contrast, a formally dinuclear but "flexible" diamond-core intermediate formulated as $[(6\text{-}me_3\text{-}tpa)Fe^{III}-O-Fe^{IV}(6\text{-}me_3\text{-}tpa)=O]^{3+}$ and containing antiferromagnetically coupled, localized high-spin Fe^{III} and Fe^{IV} centers, reported by Que and co-workers, may provide the closest synthetic mimic of a mononuclear $S = 2$ $Fe^{IV}O$ intermediate.[22] Given the well-documented ability of sterically hindered 6-alkylated tpa ligands to enforce high-spin states of coordinated Fe^{III} and Fe^{IV} ions,[23,24] it is natural to consider $(6\text{-}me_3\text{-}tpa)Fe^{IV}(O)(L)$ (where L is an, as yet, undefined ligand) species as attractive synthetic models for the $S = 2$ TauD intermediate. We have done so in this study, and indeed a high-spin ground state appears likely for such species. Also presented are the first results of our attempts to model the flexible diamond core mentioned above.

The optimized structures of the $S = 1$ species $Fe^{IV}(O)(L)_2(PhCN)$ (**2**: L = en; **3**: L = tmen) and of $Fe^{IV}(O)(P)(PhCN)$ (**4**), shown in Figure 2, provide a comparison of the electronic character of the $Fe^{IV}O$ unit in heme with nonheme environments.[25] Figure 2 shows that for a particular *trans* ligand (PhCN in all these cases), the Fe−O bond lengths are nearly identical in all three species and very similar to that observed experimentally for $Fe^{IV}(O)(me_4cyclam)(CH_3CN)$.[21] As long known for (porphyrin)$Fe^{IV}O$ derivatives (peroxidase compound II analogues),[26,27] the electron spin density is almost completely localized on the FeO unit for all three species **2**−**4** and also partitioned rather similarly between the Fe and O atoms.

The TauD iron site has a 2-His-1-carboxylate ligand environment,[8] which we have chosen to model with chelating bis(2-imidazolyl)methane and malonate ligands to provide some conformational rigidity to the optimized species. A number of stereoisomers were examined, and species **5**, a

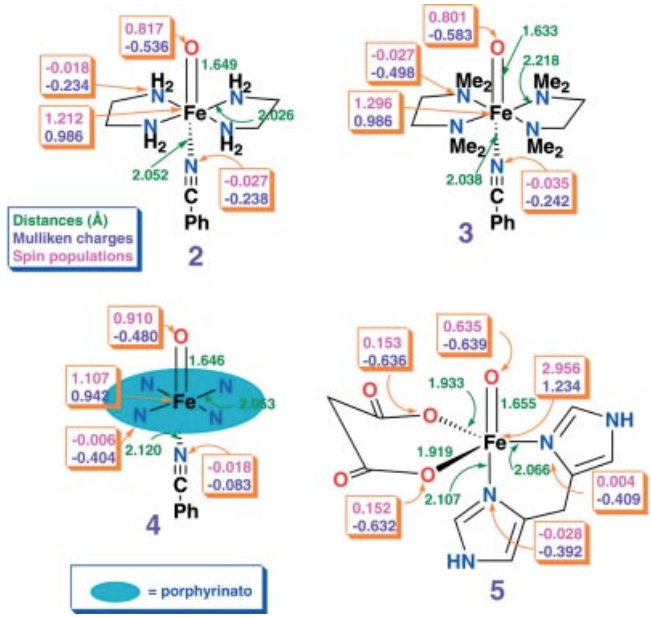

Figure 2. Selected optimized distances, Mulliken charges and spin populations for $Fe^{IV}O$ model complexes **2**−**5**; complexes **2**−**4** are $S = 1$, while **5** is $S = 2$

five-coordinate trigonal-bipyramidal species shown in Figure 1, was found to have the lowest energy. Perhaps not surprisingly in view of its trigonal-bipyramidal structure, an $S = 2$ spin state was favored over lower-spin states by several tenths of an eV. As shown in Figure 1, the Fe−O distance and O spin population for **5** are strikingly similar to those for the low-spin species **2**−**4**, indicating that the low- versus high-spin character of the $Fe^{IV}O$ unit has relatively little effect on the $Fe(d_\pi)-O(p_\pi)$ orbital interactions (which are largely responsible for the oxygen spin populations).

A comparison of the spin density profiles of **5** and of the Collins model complex **1** proved enlightening. If we define the Fe=O axis of **5** and the FeCl axis of **1** as the z direction, simple crystal field theory arguments (which are confirmed by our calculations) suggest that **5** should have a d_{z^2} hole, while **1** should have a $d_{x^2-y^2}$ hole. Thus, if we describe the local symmetries of the iron centers in **5** and **1** as approximately C_{3v} and C_{4v}, then their ground states may be described as $^5A_1$ and $^5B_2$, respectively. Further, we have already seen that the spin density profile of **5** is strongly affected by $Fe(d_\pi)-O(p_\pi)$ orbital interactions, for which there is no analogue in **1**. These considerations suggest that species **5** and **1** should exhibit significantly different spin density profiles, an expectation that is confirmed by Figure 3, which plots the spin density profiles for the two species. This may be seen as qualitatively consistent with the fact that the TauD intermediate and Collins' complex exhibit dramatically different Mössbauer spectroscopic parameters,[3,8] although these remain to be explicitly determined with DFT calculations.

Without question, the discovery of a high-spin Fe^{IV} intermediate for TauD has galvanized biochemists and synthetic chemists alike to seek additional nonheme $Fe^{IV}O$ intermedi-

 © 2004 Wiley-VCH Verlag GmbH & Co. KGaA, Weinheim

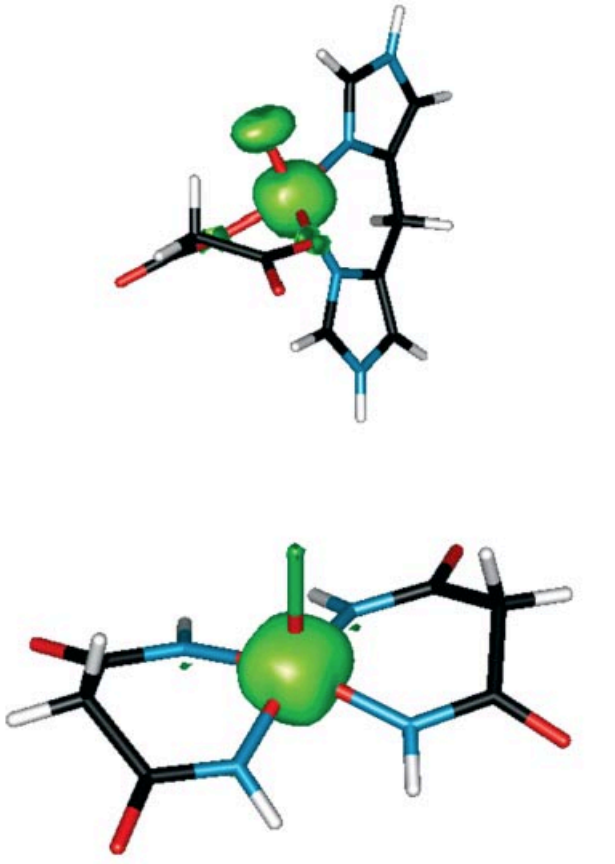

Figure 3. Comparison of the spin density profile of **5** (top) with that of a model (**1**, bottom) of Collins' $S = 2$ Fe^{IV} complex, $[Fe^{IV}(pmd\text{-}N,N)_2Cl]^-$ (pmd-*N*,*N* = propanediamidato-*N*,*N*); color code for atoms: calcd. C black, N blue, O red, H grey/white, and Cl green

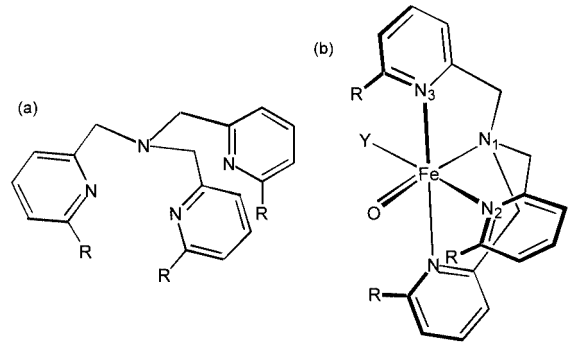

Figure 4. (a) Ligands used in calculations summarized in Table 2; tpa, R = H, 6-me_3-tpa, R = CH_3; (b) note the notation of the N_1, N_2, N_3 and Y atoms/groups, which are mentioned in Table 2

ates. What might be a good strategy for the synthetic chemist? As alluded to above,[6,7,23,24] the use of 6-alkylated tpa ligands seems like a promising strategy, which led us to carry out geometry optimizations for both $S = 1$ and $S = 2$ states for the following four species: $[Fe^{IV}(O)(X)(Y)]^+$, where X = tpa and 6-me_3-tpa and Y = F and OH (Figure 4). Table 2 lists key geometry parameters and atomic spin populations, but these essentially lead to the same generalizations as made above for **2**−**5**, namely that the Fe−O distance and the O spin population are rather similar across all the species studied, regardless of spin state.

Table 2 shows that the PW91 calculations predict $S = 1$ ground states for $[Fe^{IV}(O)(tpa)(Y)]^+$, consistent with the experiment, but the preference for $S = 2$ ground states for $[Fe^{IV}(O)(6\text{-}me_3\text{-}tpa)(Y)]^+$ is less clear. The B3LYP calculations clearly favor $S = 2$ ground states for $[Fe^{IV}(O)(6\text{-}me_3\text{-}tpa)(OH)]^+$, but also for $[Fe^{IV}(O)(tpa)(OH)]^+$, albeit by a very slight margin. Elsewhere, we have documented that PW91 calculations exhibit a greater preference for low-spin states than B3LYP results.[10] Thus, at least certain of these calculations deserve to be repeated with more definitive but far more computationally demanding CASPT2 calculations. These uncertainties notwithstanding, the energetics data shown in Table 1 suggest that there is a good chance that $[Fe^{IV}(O)(6\text{-}me_3\text{-}tpa)(Y)]^+$ species may exhibit $S = 2$ ground states and, therefore, are attractive targets for synthetic modeling studies.

Finally, we have examined the question of whether Que's "flexible diamond core" may be viewed as one containing a high-spin $Fe^{IV}{=}O$ unit.[22] For simplicity, we have only studied the ferromagnetically coupled $S = 9/2$ state of the $[(6\text{-}me_3\text{-}tpa)Fe^{III}(\mu\text{-}O)_2Fe^{IV}(6\text{-}me_3\text{-}tpa)]^{3+}$ cation. The calculation employed a diamond-core-like starting geometry but only a C_s symmetry constraint to allow for spontaneous desymmetrization of the $Fe_2(\mu\text{-}O)_2$ core, which indeed took place;[28] selected geometry parameters and Mulliken spin populations for the two spin states are shown in Figure 5.

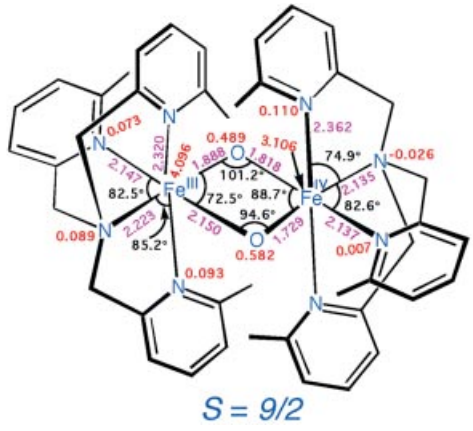

Figure 5. Selected PW91/TZP optimized distances (Å, magenta), angles (°, black) and Mulliken spin populations (red) for the ferromagnetically coupled $S = 9/2$ state of the $[(6\text{-}me_3\text{-}tpa)Fe^{III}(\mu\text{-}O)_2Fe^{IV}(6\text{-}me_3\text{-}tpa)]^{3+}$ cation

The geometrical asymmetry of the Fe_2O_2 unit (which seems consistent with its flexible nature, as emphasized in the experimental study[22]) and the spin density profile clearly indicate the presence of localized high-spin Fe^{III} and Fe^{IV} centers for both spin states. Thus, the Fe^{IV} center has a short Fe−O bond of about 1.73 Å, consistent with a high-spin $Fe^{IV}{=}O$ unit. Note that the nitrogen atom *trans* to this

 © 2004 Wiley-VCH Verlag GmbH & Co. KGaA, Weinheim

Table 2. Selected results on mononuclear tpa and 6-me$_3$-tpa complexes: distances (Å), Mulliken spin populations, and relative energies (E_{rel}, eV); in general, the results refer to PW91/TZP calculations, while those shown in italics refer to single-point B3LYP/6-311G(d,p) calculations on PW91/TZP optimized geometries

Compound	S	Distances					Mulliken spin populations						E_{rel}
		FeO	FeL	FeN	FeN_2	FeN_3	Fe	O	Y	N_1	N_2	N_3	
$[(tpa)Fe(O)(F)]^+$	1	1.65	1.84	2.13	2.00	1.98	1.26	0.79	0.01	−0.01	−0.01	−0.01	0.00
$[(tpa)Fe(O)(F)]^+$	2	1.65	1.81	2.19	2.09	2.24	2.97	0.66	0.15	−0.02	0.01	0.08	0.50
$[(tpa)Fe(O)(OH)]^+$	1	1.65	1.90	2.15	2.03	1.98	1.29	0.78	−0.01	−0.01	0.00	−0.01	0.00
	1						*1.33*	*0.78*	*−0.03*				*0.00*
$[(tpa)Fe(O)(OH)]^+$	2	1.65	1.83	2.26	2.09	2.26	2.88	0.68	0.25	−0.01	0.00	0.07	0.29
	2						*3.05*	*0.66*	*0.17*				*−0.07*
$[(6\text{-}me_3\text{-}tpa)Fe(O)(F)]^+$	1	1.65	1.85	2.10	2.08	2.08	1.24	0.79	0.00	−0.02	−0.00	−0.01	0.00
$[(6\text{-}me_3\text{-}tpa)Fe(O)(F)]^+$	2	1.64	1.82	2.14	2.16	2.32	2.97	0.67	0.14	−0.02	0.01	0.08	0.08
$[(6\text{-}me_3\text{-}tpa)Fe(O)(OH)]^+$	1	1.64	1.90	2.12	2.12	2.08	1.27	0.78	−0.03	−0.02	0.01	−0.01	0.12
	1						*1.35*	*0.76*	*−0.06*				*0.54*
$[(6\text{-}me_3\text{-}tpa)Fe(O)(OH)]^+$	2	1.65	1.84	2.18	2.16	2.37	2.89	0.70	0.24	−0.02	0.01	0.07	0.00
	2						*3.13*	*0.56*	*0.20*				*0.00*

group has a small negative spin population, unlike all the other nitrogen atoms, but consistent with the expectation that the metal d_{z^2} orbital that lies along the Fe^{IV}=O unit is formally unoccupied.

Summary

The main conclusions of this study may be enumerated as follows.

(1) We began this study by an attempt to benchmark the relative energies of the high- and low-spin states for a well-characterized high-spin Fe^{IV} complex. Based on the CCSD(T) and CASPT2 results on model complex **1**, we would like to assert that the triplet-quintet splitting is likely to be larger than 0.3 eV and perhaps as large as 0.7 eV. Obviously, we wish we could have narrowed down this range somewhat, but that seems impossible with currently available technology. If this range is correct, then the DFT values are on the low side, consistent with the known tendency of DFT to favor low-spin states.[10] On a more positive note, DFT does not perform badly and does emerge as the practical tool of choice for a broad survey of high-spin Fe^{IV} species.

(2) The Fe−O distance and O spin population are quite similar across all mononuclear $Fe^{IV}O$ species studied, regardless of the heme versus nonheme environment and of the $S = 1$ versus 2 spin state, reflecting the essential similarity of the $Fe(d_\pi)-O(p_\pi)$ orbital interactions in all these species.

(3) A significant insight from this study is that a high-spin Fe^{IV} center does not correspond to a unique type of electron spin density profile. Thus, the TauD intermediate and Collins' high-spin Fe^{IV} complex feature dramatically different spin density profiles, qualitatively consistent with their very different Mössbauer spectroscopic parameters.

(4) The sterically hindered 6-me$_3$-tpa ligand and related ligands provide a promising recipe for generating synthetic $S = 2$ $Fe^{IV}O$ intermediates.

(5) Lastly, our calculations indicate the presence of a fairly discrete high-spin Fe^{IV}=O unit in the mixed-valent, so-called "flexible diamond-core" intermediate.

Supporting Information: Optimized Cartesian coordinates for the different molecules studied are provided.

Acknowledgments

This work was supported by a grant of computer time by the Research Council of Norway.

[1] For a recent review, see: M. Costas, M. P. Mehn, M. P. Jensen, L. Que, Jr., *Chem. Rev.* **2004**, *104*, 939−986.
[2] For a recent review, see: E. Y. Tshuva, S. J. Lippard, *Chem. Rev.* **2004**, *104*, 987−1011.
[3] K. L. Kostka, B. G. Fox, M. P. Hendrich, T. J. Collins, C. E. F. Rickard, L. J. Wright, E. Münck, *J. Am. Chem. Soc.* **1993**, *115*, 6746−6757.
[4] L. Shu, J. C. Nesheim, K. Kauffmann, E. Münck, J. D. Lipscomb, L. Que, Jr., *Science* **1997**, *275*, 515−518.
[5] P. J. Riggs-Gelasco, L. Shu, S. Chen, D. Burdi, B. H. Huynh, L. Que, Jr., J. Stubbe, *J. Am. Chem. Soc.* **1998**, *120*, 849−860.
[6] Y. Dong, L. Que, Jr., K. Kauffmann, E. Münck, *J. Am. Chem. Soc.* **1995**, *117*, 11377−11378.
[7] H. Zheng, S. J. Yoo, E. Münck, L. Que, Jr., *J. Am. Chem. Soc.* **2000**, *122*, 3789−3790.
[8] J. C. Price, E. W. Barr, B. Tirupati, J. M. Bollinger, Jr., C. Krebs, *Biochemistry* **2003**, *42*, 7497. Addition/Correction: *Biochemistry* **2004**, *43*, 1134−1134.
[9] For a review, see: A. Ghosh, E. Steene, *J. Biol. Inorg. Chem.* **2001**, *6*, 739−752.
[10] For a critical review of high-level ab initio calculations on systems of bioinorganic interest, see: A. Ghosh, P. R. Taylor, *Curr. Opin. Chem. Biol.* **2003**, *7*, 113−124.
[11] Despite the popularity of DFT, the suitability of DFT for such unusual species as high-spin Fe^{IV} intermediates is hardly a foregone conclusion. Thus, DFT does not do a good job of pre-

 © 2004 Wiley-VCH Verlag GmbH & Co. KGaA, Weinheim

dicting the energy ordering of the low-lying spin states for some (porphyrin)Fe^{III} derivatives: A. Ghosh, B. J. Persson, P. R. Taylor, *J. Biol. Inorg. Chem.* **2003**, *8*, 507−511.

[12] The PW91 calculations were carried out using the ADF program system, using Slater-type TZP basis sets and a fine mesh for numerical integration of matrix elements. The B3LYP calculations were carried out using the program Turbomole and Gaussian basis sets of TZP quality. Adequately tight convereg-ence criteria for geometry optimizations were used in all the calculations.

[13] For the CASPT2 calculations, the CASSCF active space comprised eight electrons in eight orbitals: the five Fe 3d orbitals and three equatorial ligand orbitals, including two of a_1 symmetry and one of a_2. The a_1 symmetry equatorial ligand orbitals would be the π HOMO and LUMO if the ligands were exactly planar. The a_2 symmetry ligand orbital is a combination of the N lone-pairs. The CASPT2 calculations were performed using the program Molcas 5.2 and the CCSD(T) calculations with Molpro 2002.

[14] BS1 consisted of Dunning's cc-pVDZ basis sets on C, N O, and H, the aug-cc-pVDZ basis on Cl (T. H. Dunning, *J. Chem. Phys.* **1989**, *90*, 1007−1023), and a [6s5p4d3f2g] atomic natural orbital (ANO) basis on Fe (B. J. Persson, P. R. Taylor, unpublished results). BS2 consisted of Dunning's cc-pVTZ basis sets on C, N O, and H, the aug-cc-pVTZ basis on Cl (T. H. Dunning, *J. Chem. Phys.* **1989**, *90*, 1007−1023), and a [7s6p5d4f3g] ANO basis on Fe (B. J. Persson, P. R. Taylor, unpublished results). The Fe ANO basis sets are optimized for calculations that include Fe 3s3p correlation, the effects of which are not negligible here.

[15] At present, there is extensive evidence (see, for example: P. E. M. Siegbahn, M. R. A. Blomberg, *Chem. Rev.* **2000**, *100*, 421−437) that DFT provides generally good results for geometries, spin density profiles, and a variety of other molecular properties for transition metal complexes. We believe that this generalization also holds for the species studied here and therefore largely refrain from commenting on the data presented in Table 1. However, one point worth noting is the relatively small amounts of spin density on the equatorial ligand set. By this criterion, the ligands may be described as relatively innocent, even though they must be extremely σ-donating.

[16] For a discussion of population analyses, see: C. J. Cramer; *Essentials of Computational Chemistry: Theories and Models*, Wiley, Hoboken, NJ, USA, **2002**, pp. 278−291.

[17] A few more technical comments may be worthwhile. Examining the CASSCF and CASPT2 results suggests that the wavefunctions for both states are somewhat multiconfigurational in character, but not exceptionally so. In this situation we would typically expect much closer agreement between CASPT2 and CCSD(T). We know that DFT (certainly with the functionals used here) tends to favour low-spin states; CASPT2 in its simplest implementation also tends to favour low-spin states but here we have used a modified Hamiltonian which gives a much better balanced treatment of different spin states, with no obvious preference for high or low spin. The 8-in-8 CASSCF/BS1 calculation itself gives 0.69 eV for the splitting (quintet lower), whereas a Hartree−Fock calculation gives 2.16 eV, again with the quintet lower. From the Hartree−Fock value we infer that electron correlation makes a substantial contribution to the splitting, which is expected; from the CASSCF value we can infer further that much of this correlation contribution is non-dynamical correlation. We must also recognize that the basis sets used here for the CCSD(T) calculations, though large, are far from complete and the contribution of dynamical correlation may well be larger in a more complete basis set.

[18] C. A. Grapperhaus, B. Mienert, E. Bill, T. Weyhermüller, K. Wieghardt, *Inorg. Chem.* **2000**, *39*, 5306−5317.

[19] M. H. Lim, J.-W. Rohde, A. Stubna, M. R. Bukowski, M. Costas, R. Y. N. Ho, E. Münck, W. Nam, L. Que, Jr., *Proc. Natl. Acad. Sci. U. S. A.* **2003**, *100*, 3665−3670.

[20] J. Kaizer, E. J. Klinker, N. Y. Oh, J.-U. Rohde, W. J. Song, A. Stubna, J. Kim, E. Munck, W. Nam, L. Que, Jr., *J. Am. Chem. Soc.* **2004**, *126*, 472−473.

[21] J.-W. Rohde, J.-H. In, M. H. Lim, W. W. Brennessel, M. R. Bukowski, A. Stubna, E. Münck, W. Nam, L. Que, Jr., *Science* **2003**, *299*, 1037−1039.

[22] H. Zheng, S. J. Yoo, E. Münck, L. Que, Jr., *J. Am. Chem. Soc.* **2000**, *122*, 3789−3790.

[23] Y. Zang, Y. Dong, L. Que, Jr., K. Kauffmann, E. Münck, *J. Am. Chem. Soc.* **1995**, *117*, 1169−1170.

[24] Y. Zang, J. Kim, Y. Dong, E. C. Wilkinson, E. H. Appelman, L. Que, Jr., *J. Am. Chem. Soc.* **1997**, *119*, 4197−4205.

[25] We used the PhCN ligand, instead of CH_3CN, to exploit C_{2v} symmetry for species **2**−**4**.

[26] See e. g. the first DFT calculation on an (porphyrin)$Fe^{IV}O$: A. Ghosh, J. Almlöf, L. Que, Jr., *J. Phys. Chem.* **1994**, *98*, 5576−5579. The same effect (i. e. the complete localization of the spin density on the Fe and O atoms) was also noted in the first studies of high-valent iron diamond core intermediates A. Ghosh, J. Almlöf, L. Que, Jr., *Angew. Chem. Int. Ed. Engl.* **1996**, *35*, 770−772.

[27] H. Kuramochi, L. Noodleman, D. A. Case, *J. Am. Chem. Soc.* **1997**, *119*, 11442−11451.

[28] For a recent DFT study of valence-delocalized $[Fe_2(\mu\text{-}O)_2]^{3+,4+}$ diamond-core species, see: A. Ghosh, E. Tangen, E. Gonzalez, L. Que, Jr., *Angew. Chem. Int. Ed.* **2004**, *43*, 834−838.

Received May 4, 2004
Early View Article
Published Online September 7, 2004

 © 2004 Wiley-VCH Verlag GmbH & Co. KGaA, Weinheim

Fluorescent Self-Assembled Monolayers of Bis(salicylaldiminato)zinc(II) Schiff-Base Complexes

Santo Di Bella,*[a] Nicoletta Leonardi,[a] Giuseppe Consiglio,[b] Salvatore Sortino,*[a] and Ignazio Fragalà[a]

Keywords: Fluorescence / Monolayers / Schiff bases / Zinc

The synthesis and fluorescence properties of novel bis(salicylaldiminato)zinc(II) Schiff-base complexes is reported. Self-assembled monolayers (SAMs) of these complexes are obtained by reaction of coupling layers, functionalized quartz substrates and a derivatized precursor complex. A comparison between the integrated emission intensity of the SAM films and that of a suitable model compound in solution indicates molecular fluorescence retention of the Zn^{II} Schiff bases on going from the solution phase to the monolayer. This is consistent with the absence of significant self-quenching processes, as expected on the basis of the relatively high estimated surface coverage.
(© Wiley-VCH Verlag GmbH & Co. KGaA, 69451 Weinheim, Germany, 2004)

Introduction

Nanostructured functional molecular materials are attracting growing interest in the expanding field of molecular electronics and optoelectronics,[1] where molecular organization in defined assemblies and its control on a molecular scale represents one of the most interesting issues.

Molecular self-assembly is one of the most efficient methods to achieve well-defined and organized molecular architectures covalently anchored to various substrates.[2] Among various functional molecular systems, self-assembled monolayers (SAMs) of fluorescent molecules are attractive for a variety of potential applications,[3] including molecular electronics and optoelectronics.[4]

Recently, Schiff base bis(salicylaldiminato)metal complexes have been widely investigated for their properties and applications in different fields, such as catalysis[5] and materials chemistry.[6] For example, metal complexes possess distinct second-order nonlinear optical[6,7] and fluorescent[8,9] properties that are closely related to the coordinated metal centre. In fact, as far as the luminescent properties are concerned, while the free Schiff-base ligands are non-emissive, their complexes with metal ions such as Zn^{II}, Al^{III} and Mg^{II} exhibit an appreciable fluorescence.[9]

In this paper we report the synthesis and spectroscopic properties of novel bis(salicylaldiminato)zinc(II) Schiff-base complexes and related self-assembled monolayers on quartz substrates.

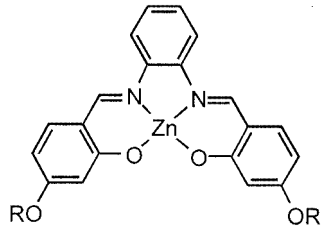

R = H **1**
R = CH_3 **2**

Results and Discussion

Synthesis and Spectroscopic Properties of Zn^{II} Schiff-Base Complexes

In order to compare the spectroscopic properties of the self-assembled monolayer of the complex **1** (SAM-**1**) with a suitable model compound, the 4,4′-methoxy derivative **2** was synthesized. Both the 4,4′-dihydroxy-substituted Zn^{II} Schiff-base precursor complex **1** and the model compound **2** were synthesized by standard methods.[7] The complexes were characterized by mass spectrometry, ^1H NMR spectroscopy, and satisfactory microanalysis.

Figure 1 shows the absorption and emission spectra of **2** in CH_2Cl_2 solution. The absorption is characterized by two bands at 310 and 374 nm and a shoulder at about 420 nm. The fluorescence emission exhibits an unstructured band with a maximum at 508 nm. Based on the overlap of the fluorescence emission with the lowest energy absorption

[a] Dipartimento di Scienze Chimiche, Università di Catania and INSTM UdR di Catania,
95125 Catania, Italy,
Fax: (internat.) +39-095-580-138
E-mail: sdibella@unict.it
ssortino@unict.it
[b] Dipartimento di Metodologie Fisiche e Chimiche per l'Ingegneria, Università di Catania,
95125 Catania, Italy

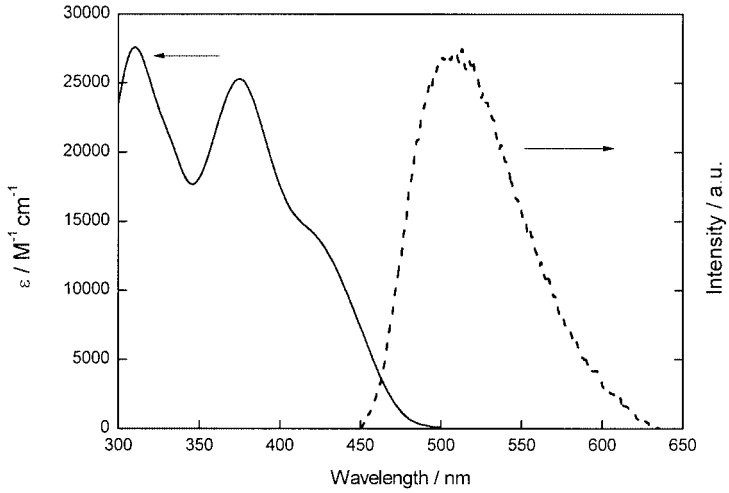

Figure 1. Absorption and fluorescence spectra of **2** in CH_2Cl_2 solution

band, the lowest excited singlet state can be experimentally located at about 260 kJ·mol^{-1}.

The fluorescence quantum yield, Φ_f, is found to be about 0.05 in CH_2Cl_2. This value is almost unaffected on going to more polar solvents such as THF and CH_3CN. The fluorescence lifetime in the above solvents lies in the sub-nanosecond time domain. These photophysical properties are consistent with those recently found for analogous Zn^{II} Schiff-base complexes.[8]

Preparation and characterization of SAM-1

The derivatization of the molecular precursor with appropriate end-groups represents the initial step for the self-assembly process. It should consist of an accessible and efficient chemistry so that the derivatized group can easily react with the substrate or with an appropriate derivatized substrate, the so-called coupling layer. In our case the 4,4′-dihydroxy-substituted Zn^{II} Schiff-base complex **1** was used as precursor. Actually, given their acid nature, 4-hydroxyl groups can readily be transformed into the related phenoxides **1a**, which, in turn, are nucleophilic species for a variety of substitution reactions.

SAM-**1** was obtained by a two-step approach (Scheme 1), which involves chemisorption of the $Br(CH_2)_3SiCl_3$ (CP-Br) coupling layer onto hydroxylated quartz substrates followed by grafting of **1** by a nucleophilic-substitution reaction between the alkyl bromide of the silylated surface and the derivatized salt **1a**.

The first step was carried out with standard procedures.[10] It leads to the formation of densely packed, sil-

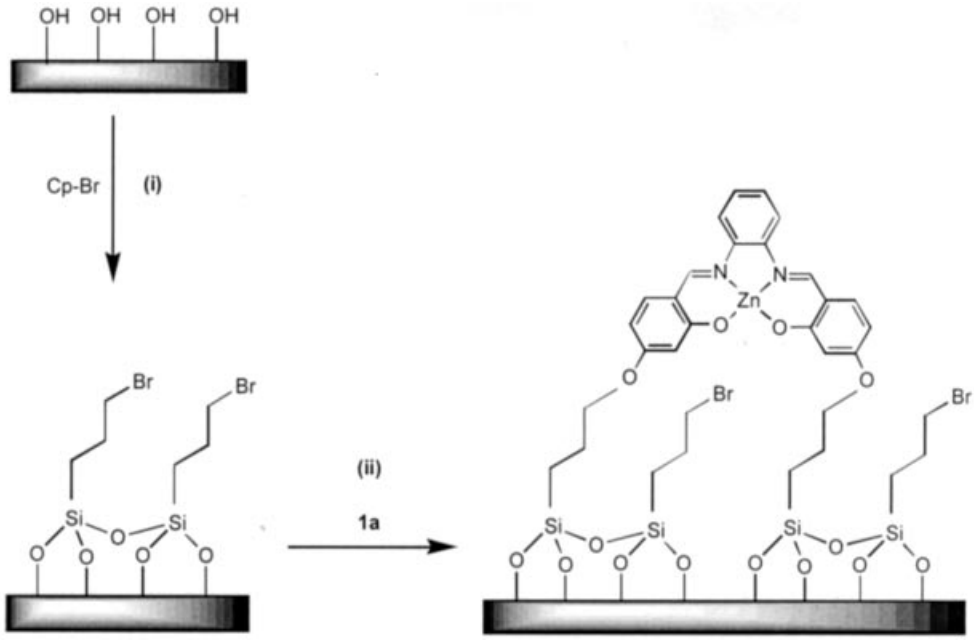

Scheme 1. Preparation of fluorescent self-assembled monolayers of the Zn^{II} Schiff-base complex

 © 2004 Wiley-VCH Verlag GmbH & Co. KGaA, Weinheim

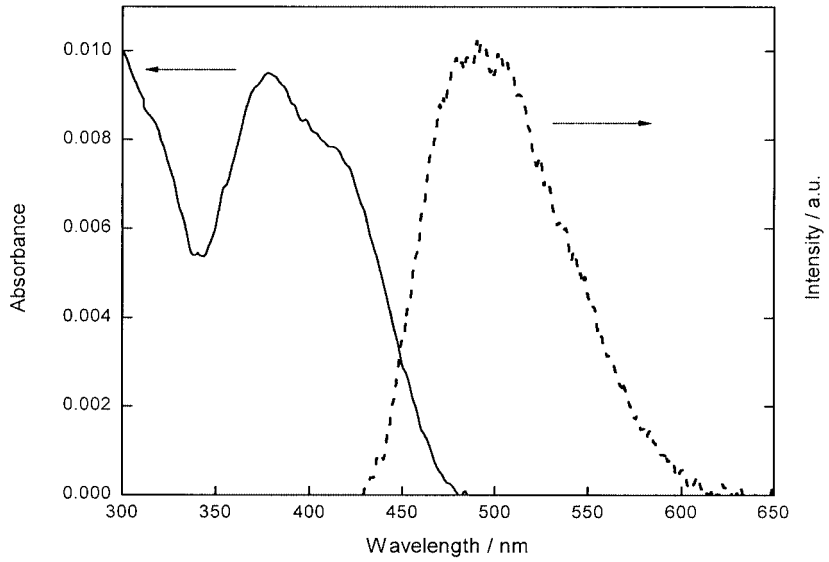

Figure 2. Absorption and fluorescence spectra of SAM-**1**

ane-based coupling layers bound to the quartz surface through a siloxane linkage. The typical advancing aqueous contact-angle (θ_a) values (ca. 68°) confirmed the complete silylation of the surface.

The second step was achieved by immersion of substrates terminated with the coupling layer in an anhydrous DMF solution of the derivatized complex **1a** for 20 h at 80 °C. The substrates were then washed and sonicated with DMF and acetone to remove any physisorbed material on the surface. Aqueous contact-angle measurements after the second step indicated that θ_a changes from 66−68° for the substrate terminated with the coupling layer to 78−80° for SAM-**1**. This is consistent with an increased surface hydrophobicity due to the relatively apolar Zn^{II} complex headgroup.[11]

SAM-**1** was characterized by UV/Vis absorption and emission spectroscopy (Figure 2). It shows an optical absorption band at 378 nm and a shoulder at about 416 nm. These features are similar to those of the model complex **2** in CH_2Cl_2 (Figure 1), except for a slight shift. It should be noted that the observed absorbance is related to two monolayers, one for each side of the quartz slide. These absorbance values allow an estimation of the surface coverage (Γ_{surf}) of the functional Zn^{II} complex by the relation $\Gamma_{surf} = A\varepsilon^{-1}$, where A is the absorbance of the SAM-**1** and ε is the molar extinction coefficient of the chemisorbed species.[12] Using the extinction coefficient of the model compound **2** (λ_{max} = 374 nm; ε_{max} = 25300 $M^{-1}\cdot cm^{-1}$ in CH_2Cl_2) and a monolayer absorbance of about 0.005, the estimated surface density of the Zn^{II} derivative is about 1.2×10^{14} molecules/cm^2 or about 1.2 molecules/100 $Å^2$. These surface coverage values for the bulky complex **1** are within the range commonly observed for analogous systems.[2,13]

The fluorescence spectrum of SAM-**1** (Figure 2) is characterized by a shape similar to that observed in solution for the model compound **2** (Figure 1), although the emission maximum is somewhat blue-shifted (by about 16 nm). A comparison between the integrated emission intensity of SAM-**1** and that of a solution of **2** having the same absorbance at the excitation wavelength reveals that the fluorescence efficiency of the monolayer is similar to that of the model compound **2**. This result indicates molecular fluorescence retention of the Zn^{II} Schiff base complex on going from the solution phase to the monolayer. This is consistent with the absence of significant self-quenching processes, as expected on the basis of the relatively high surface coverage estimated above. Quenching of fluorescence is actually quite common in more densely packed monolayers as a result of effective inter-chromophore interactions.[14]

In summary, we have presented a simple, efficient route to fluorescent self-assembled monolayers of novel Zn^{II} Schiff-base complexes. They may be appealing systems in the perspective of molecular optical devices.

Experimental Section

Materials and General Procedures: Zinc acetate dihydrate, 2,4-dihydroxybenzaldehyde, 2-hydroxy-4-methoxybenzaldehyde, sodium methoxide, (3-bromopropyl)trichlorosilane [$Br(CH_2)_3SiCl_3$], and anhydrous DMF (Aldrich) were used without purification. 1,2-Phenylenediamine (Aldrich) was purified by sublimation in vacuo. Pentane and heptane (Aldrich) were distilled from Na/K alloy before use. The coupling layer formation was performed in a dry box (under nitrogen atmosphere; <1 ppm O_2 and <3 ppm H_2O).

Physical Measurements: Elemental analyses were performed on a Carlo Erba 1106 elemental analyzer. ^1H NMR spectra were recorded on a Varian Inova 500 spectrometer, using TMS as internal standard. The absorption and fluorescence spectra were recorded with a Beckman DU 650 spectrophotometer and a Spex Fluorolog-2 (mod. F-111) spectrofluorimeter, respectively, and λ_{max} values are considered accurate to ±1 nm. The fluorescence quantum yield was

 © 2004 Wiley-VCH Verlag GmbH & Co. KGaA, Weinheim

obtained using quinine sulfate in 1 N H_2SO_4 as standard. The absorbance value of the samples at the excitation wavelength were lower than 0.15 for a 1-cm path length. The fluorescence lifetimes in air-equilibrated solutions were determined by means of a time-correlated single-photon counting system. A nitrogen-filled lamp was used for excitation at 337 nm. Fluorescence measurements on SAM-**1** were carried out by aligning the quartz slide sample at an angle of 60° with respect to the excitation beam. Reflection of the excitation from the sample was to the opposite side of the emission detection. ESI mass spectra were recorded on an Agilent 1100 Series ESI/MSD spectrometer. Experimental conditions were as follows: capillary voltage, 3.5 kV; fragmentor, 100 V; source temperature, 350 °C; drying gas, N_2 (10 L/min); carrier solvent, methanol (0.4 mL/min). Advanced aqueous contact angles were measured using a goniometer (KERNCO) under ambient conditions.

[1,2-Phenylenebis(iminomethyl)bis(4-hydroxy-2-phenolato]zinc(II) (1): 2,4-Dihydroxybenzaldehyde (1.106 g, 8.00 mmol) was added, whilst stirring, to a solution of 1,2-phenylenediamine (0.433 g, 4.00 mmol) in methanol (25 mL) at room temperature. Zinc acetate dihydrate (0.878 g, 4.00 mmol), dissolved in methanol (20 mL), was added to the resulting solution, and the mixture was heated at reflux for 2 h. After cooling, the precipitate was collected by filtration, washed with water, and dried. The yellow solid was crystallized from a THF/*n*-hexane mixture. Yield: 1.556 g (94%). $C_{20}H_{14}N_2O_4Zn$ (411.73): calcd. C 58.34, H 3.43, N 6.80; found C 58.05, H 3.38, N 6.90. ESI MS: *m*/*z* (%) = 433 (50) $[M + Na]^+$. ^1H NMR (500 MHz, [D$_6$]DMSO): δ = 6.03 (m, 4 H, Ar*H*), 7.19 (d, J_{ortho} = 9.0 Hz, 2 H, Ar*H*), 7.24 (m, 2 H, Ar*H*), 7.75 (m, 2 H, Ar*H*), 8.79 (s, 2 H, C*H*=N), 9.71 (s, 2 H, O*H*) ppm. UV/Vis (DMF): λ_{max} = 308, 388, 426 (sh) nm.

Disodium Zincate 1a: Compound **1** (1.556 g, 3.78 mmol) was added, with stirring, to a solution of sodium methoxide (1.73 mL of a 25% w/w methanol solution, 7.56 mmol), and the mixture heated at 50 °C for 1 h under a nitrogen atmosphere. The solution was then concentrated under vacuum. The precipitate product was collected and washed with anhydrous THF. A yellow-brown solid was obtained (1.583 g, 92%). $C_{20}H_{12}N_2Na_2O_4Zn$ (455.69): calcd. C 52.71, H 2.65, N 6.15; found C 52.40, H 2.60, N 6.09.

Zinc(II) Complex 2: Zinc acetate dihydrate (0.094 g, 0.43 mmol) was added to a solution of *N*,*N*′-bis(4-methoxy-2,4-dihydroxybenzylidene)-1,2-phenylenediamine[7c] (0.116 g, 0.43 mmol) in methanol (30 mL). The resulting yellow solution was heated at reflux for 2 h. After cooling, the precipitate was collected by filtration, washed with water and dried. The yellow solid was crystallized from THF (1.60 g, 85%). $C_{22}H_{18}N_2O_4Zn$ (439.78): calcd. C 60.08, H 4.13, N 6.37; found C 59.62, H 4.09, N 6.43. ESI MS: *m*/*z* (%) = 461 (100) $[M + Na]^+$. ^1H NMR (500 MHz, [D$_6$]DMSO): δ = 3.75 (s, 6 H, C*H*$_3$), 6.15 (dd, J_{ortho} = 9.0, J_{meta} = 2.5 Hz, 2 H, Ar*H*), 6.19 (d, J_{meta} = 2.5 Hz, 2 H, Ar*H*), 7.29 (m, 4 H, Ar*H*), 7.79 (m, 2 H, Ar*H*), 8.86 (s, 2 H, C*H*=N) ppm. UV/Vis (CH_2Cl_2): λ_{max} ($\varepsilon \times 10^4$) = 310 (2.75), 374 (2.53), 420 (sh) nm (1.40).

Preparation of SAMs

Substrate Cleaning: Substrates were cleaned by standard procedures.[15] Quartz slides (0.5 × 1 cm) were cleaned by immersion in "piranha" solution (H_2SO_4/30% H_2O_2 = 70:30 v/v) at 80 °C for 1 h (***warning****: piranha is an extremely strong oxidising reagent; it should be handled with caution because it can detonate unexpectedly*).[16] After cooling to room temperature, the substrates were repeatedly rinsed with deionized water and then cleaned with a (H_2O/30% H_2O_2/28% NH_3 = 5:1:1 v/v/v) solution, at room temperature for 40 min. The substrates were then washed with a large amount of deionized water and dried under vacuum at room temperature.

Coupling Layer Formation: Substrate silylation was performed by immersion of freshly cleaned quartz substrates in a 1:100 (v/v) solution of $Br(CH_2)_3SiCl_3$ (CP-Br) in dry heptane for 40 min, at room temperature. The substrates were first rinsed with dry heptane, then with dry pentane, sonicated in acetone for 1 min, and dried at room temperature. Advancing contact angle: CP−Br, $\theta_a(H_2O)$ = 68°.

Monolayer Formation: Under a dry nitrogen atmosphere the freshly silylated substrates were immersed in a 3.0 mM solution of salt **1a** in anhydrous DMF at 80 °C for 20 h, whilst stirring. After cooling to room temperature, the substrates were rinsed with DMF, sonicated in DMF for 1 min, and washed with acetone. Advancing contact angle: SAM-**1**, $\theta_a(H_2O)$ = 80°. UV/Vis: SAM-**1**, λ_{max} = 378 nm (A = 0.095).

Acknowledgments

We thank the MIUR (PRIN and FIRB research programs) for financial support. We are indebted to Dr. F. Ortica (University of Perugia) for fluorescence lifetime measurements.

[1] See, for example: R. L. Carrol, C. B. Gorman, *Angew. Chem. Int. Ed.* **2002**, *41*, 4378−4400; C. Joachim, J. K. Gimzewski, A. Aviram, *Nature* **2000**, *408*, 541−548; M. A. Ratner, *Mater. Today* **2002**, *5*, 20−27; M. A. Ratner, *Nature* **2000**, *404*, 137−138.

[2] See, for example: *Organized Monolayers and Assemblies: Structure, Processes, and Function* (Eds.: D. Möbius, R. Miller), Elsevier, Amsterdam, **2002**; A. Ulman, *Chem. Rev.* **1996**, *96*, 1533−1554; A. Ulman, *An Introduction to Ultrathin Organic Films: From Langmuir-Blodgett to Self-Assembly*, Academic Press, New York, **1991**.

[3] See, for example: E. A. McArthur, T. Ye, J. P. Cross, S. Petoud, E. Borguet, *J. Am. Chem. Soc.* **2004**, *126*, 2260−2261; S. A. Levi, A. Mourran, J. P. Spatz, F. C. J. M. van Veggel, D. N. Reinhoudt, M. Möller, *Chem. Eur. J.* **2002**, *8*, 3808−3814; L. A. J. Chrisstoffels, A. Adronov, J. M. J. Fréchet, *Angew. Chem. Int. Ed.* **2000**, *39*, 2163−2166; S. Flink, F. C. J. M. van Veggel, D. N. Reinhoudt, *Chem. Commun.* **1999**, 2229−2230.

[4] See, for example: M. W. Holman, R. Liu, D. M. Adams, *J. Am. Chem. Soc.* **2003**, *125*, 12649−12654; H. Yamada, H. Imahori, Y. Nishimura, I. Yamazaki, T. K. Ahn, S. K. Kim, D. Kim, S. Fukuzumi, *J. Am. Chem. Soc.* **2003**, *125*, 9129−9139.

[5] See, for example: M. J. Sabater, M. Alvaro, H. Garcia, E. Palomares, J. C. Scaiano, *J. Am. Chem. Soc.* **2001**, *123*, 7074−7080; L. Canali, D. C. Sherrington, *Chem. Soc., Rev.* **1999**, *28*, 85−93.

[6] S. Di Bella, *Chem. Soc. Rev.* **2001**, *30*, 355−366; P. G. Lacroix, *Eur. J. Inorg. Chem.* **2001**, 339−348.

[7] [7a] S. Di Bella, I. Fragalà, *New J. Chem.* **2002**, *26*, 285−290. [7b] S. Di Bella, I. Fragalà, I. Ledoux, J. Zyss, *Chem. Eur. J.* **2001**, *7*, 3738−3743. [7c] S. Di Bella, I. Fragalà, I. Ledoux, M. A. Diaz-Garcia, T. J. Marks, *J. Am. Chem. Soc.* **1997**, *119*, 9550−9557.

[8] K. E. Splan, A. M. Massari, G. A. Morris, S.-S. Sun, E. Reina, S. T. Nguyen, J. T. Hupp, *Eur. J. Inorg. Chem.* **2003**, 2348−2351.

[9] P. G. Cozzi, L. S. Dolci, A. Garelli, M. Montalti, L. Prodi, N. Zaccheroni, *New J. Chem.* **2003**, *27*, 692−697.

[10] For a recent contribution see: A. Facchetti, A. Abbotto, L. Beverina, M. E. van der Boom, P. Dutta, G. Evmenenko, G. A. Pagani, T. J. Marks, *Chem. Mater.* **2003**, *15*, 1064−1072, and references cited therein.

 © 2004 Wiley-VCH Verlag GmbH & Co. KGaA, Weinheim

[11] M. W. J. Beulen, F. C. J. M. van Veggel, D. N. Reinhoudt, *Isr. J. Chem.* **2000**, *40*, 73−80.
[12] C. T. Buscher, D. McBranch, D. Li, *J. Am. Chem. Soc.* **1996**, *118*, 2950−2953.
[13] D. Li, B. I. Swanson, J. M. Robinson, M. A. Hoffbauer, *J. Am. Chem. Soc.* **1993**, *115*, 6975−6980.
[14] See, for example: F. J. Kampas, M. Gouterman, *J. Lumin.* **1978**, *17*, 439−447; M. Miller, W. Knoll, H. Moehwald, A. Ruaudel-Teixer, *Thin Solid Films* **1985**, *133*, 83−91; N. Kobayashi, A. P. B. Lever, *J. Am. Chem. Soc.* **1987**, *109*, 7433−7441.
[15] W. Lin, W. Lin, G. K. Wong, T. J. Marks, *J. Am. Chem. Soc.* **1996**, *118*, 8034−8042.
[16] D. A. Dobbs, R. G. Bergman, K. H. Theopold, *Chem. Eng. News* **1990**, *68*, 2; C. V. Erikson, *Chem. Eng. News*, **1990**, *68*, 2.
Received June 7, 2004
Early View Article
Published Online October 14, 2004

 © 2004 Wiley-VCH Verlag GmbH & Co. KGaA, Weinheim

A New Trinuclear Linear Copper(II) Complex: Unusual Crystal Structure with Semi-Coordinated Thiophene Moieties and Weak Antiferromagnetic Coupling Through the Bridging Imidazolate Rings

Yufei F. Song,[a] Chiara Massera,[b] Manuel Quesada,[a] Iryna A. Koval,[a] Patrick Gamez,[a] Anna Maria Manotti Lanfredi,[b] and Jan Reedijk*[a]

Keywords: Copper / Trinuclear complexes / EPR / Thiophene / N,S ligands / Imidazole

A trinuclear copper(II) complex, $[Cu_3(imthio)_2(NO_3)_4(MeOH)_2]$ [where Himthio is 1,1-bis(imidazol-2-yl)-3-(thiophen-2-yl)-2-azapropane], has been synthesized by the reaction of Himthio with $Cu(NO_3)_2{\cdot}3H_2O$ in MeOH. The structure of the copper complex is centrosymmetric and contains a linear trinuclear array of copper atoms. The central copper(II) ion, Cu1, which lies on an inversion centre, is equatorially coordinated by four nitrogen atoms from two anionic imthio ligands and axially by two semicoordinated thiophene sulfur atoms to give an octahedral environment (Cu1–S1 3.136 Å). The Himthio ligand bridges Cu1 and the terminal copper(II) ions through imidazole nitrogen atoms. The coordination around the external ions is completed by the oxygen atoms from two nitrate groups and by a methanol molecule in a distorted square-pyramidal geometry. The two terminal copper(II) complexes can be considered to be chelating ligands for the central Cu^{II} ion. The EPR spectrum of the complex in MeOH at 77 K shows two mononuclear species, as is fully confirmed by EPR simulation. Magnetic susceptibility of the complex shows weak antiferromagnetic behaviour (J = –71.37 cm^{-1}) caused by the overlapping of the magnetic orbitals of the copper atoms and the bridging imidazolate rings. (© Wiley-VCH Verlag GmbH & Co.. KGaA, 69451 Weinheim, Germany, 2004)

Introduction

Copper complexes are widely known in nature and play an essential part as biological redox catalysts in most life forms. Current interest in copper complexes focuses on the design and synthesis of mimics of active sites for their potential use in catalysis and molecular-based magnets.[1] Models of the active sites of multicopper proteins such as ascorbate oxidase,[2] cerpulasmin[3] and laccase[4] have been studied extensively, and many efforts have been made to synthesize and investigate multinuclear copper complexes with various bridges between the metal centres.[5] The commonly used ligands are based on pyrazole, benzimidazole, and pyridine moieties.[6] Due to the presence of histidine as a ligand to copper ions in most copper proteins, copper complexes with the biologically more relevant imidazolyl donors are increasingly being studied as model compounds of copper proteins' active sites.[7,8]

Sulfur-donor compounds are known to be good ligands for low-oxidation-state copper atoms. It is well known that sulfur coordination to copper plays a very important role in metalloenzyme chemistry,[9] especially in the control of the redox potentials. In copper proteins such as azurin[10] or plastocyanin,[11] thioether sulfur, thiolate and heterocyclic nitrogen atoms are coordinated to the copper atoms at the active site, and the redox reaction occurs by outer-sphere electron-transfer processes requiring a coordination-sphere reorganisation around the copper atom.[12] Long Cu–S (methionine) contacts in the range 2.7–3.2 Å, considered to be semicoordination, are of particular current interest, as protein engineering studies suggest that, notwithstanding an appreciable effect on the redox and spectroscopic properties of the active site,[13] in most cases no coordination of the S atom to the Cu^{II} ion appears to be involved.[14,15]

In the course of our research on developing relatively simple copper compounds as mimics of copper metalloenzymes, we synthesized the asymmetric tripodal ligand 1,1-bis(imidazol-2-yl)-3-(thiophen-2-yl)-2-aza-propane (Himthio) with S and N donor atoms (Figure 1).

The weak thiophene donor appears to be a good candidate for examining the semicoordination of the sulfur atom.[15] Surprisingly, the reaction of Himthio with $Cu(NO_3)_2$ in methanol results in a trinuclear copper(II) complex in which three copper ions are linearly bridged by two ligands. The crystal structure shows that the thiophene sulfur atoms are semicoordinated to the central Cu^{II} atom,

[a] Leiden Institute of Chemistry, Gorlaeus Laboratories, Leiden University,
P. O. Box 9502, 2300 RA Leiden, The Netherlands.
Fax: (internat.) + 31-71-5274671
E-mail: reedijk@chem.leidenuniv.nl
[b] Dipartimento di Chimica Generale ed Inorganica, Chimica Analitica, Chimica Fisica, Universita' degli Studi di Parma, Parco Area delle Scienze 17/A, 43100 Parma, Italy

 © 2004 Wiley-VCH Verlag GmbH & Co. KGaA, Weinheim **DOI: 10.1002/ejic.200400196**

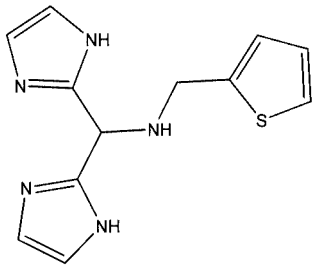

Figure 1. Molecular structure of the Himthio ligand

and such S−Cu^{II} interactions are quite rare, as analysis of the Cambridge Structural database shows. No other examples of trinuclear copper(II) complex in which the central Cu^{II} atom is coordinated by sulfur atoms have been found in the literature, it therefore represents the first example of a trinuclear linear copper(II) complex with semicoordination of thiophene moieties. The complex has been fully characterized by XRD, UV/Vis, EPR, and magnetic susceptibility measurement.

Results and Discussion

Synthesis of the Ligand and the Coordination Complex

The bis(imidazol-2-yl)amine unit[16] is a very interesting synthetic building block and can be prepared in five steps by a ring-opening and double ring-closure reaction. The Himthio ligand was synthesized by incorporating the thiophene group by nucleophilic substitution of a nitro group (see Exp. Sect.). The trinuclear copper complex, with the formula $[Cu_3(imthio)_2(NO_3)_4(MeOH)_2]$, was obtained by the reaction of 1 equiv. of imthio with 1 equiv. of copper(II) nitrate in methanol. Slow concentration of the solution at room temperature led to the formation of green, square crystals suitable for X-ray analysis. An ORTEP view of the complex, together with the atomic labelling scheme, is shown in Figure 2.

Crystal Structure of the Complex $[Cu_3(Imthio)_2(NO_3)_4(MeOH)_2]$

The structure consists of a centrosymmetric trinuclear linear molecular complex in which the central copper(II) atom occupies the inversion centre. In the $[Cu_3(imthio)_2]^{4+}$ moiety, each ligand is coordinated by four nitrogen atoms to two different copper ions. One of the two imidazolyl groups of Himthio is deprotonated and bridges the central and terminal ions through the N2 and N3 atoms.

Each of the two terminal copper atoms, Cu2 and Cu2′, is coordinated by two imidazole nitrogen atoms (N3 and N4), by two oxygen atoms from the NO_3^- anions (O1 and O4) and by the oxygen atom of the methanol (O1s); Cu2−O1 is the longest of these bonds [2.309(4) Å], so that the coordination around the metal atom can be described as a slightly distorted square pyramid, elongated towards the apex (N_2O_3 donor set, $\tau = 0.052$, where $\tau = 0$ and 1 are for perfect square-pyramidal and trigonal-bipyramidal geometries, respectively[17]).

The central Cu1 ion is coordinated by four nitrogen atoms (two amine nitrogen atoms, N1 and N1′; two imidazole nitrogen atoms, N2 and N2′) belonging to two centrosymmetric imthio ligands, thus giving origin to a CuN_4 chromophore in the equatorial plane [Cu1−N1 and Cu1−N2 distances are 2.064(3) and 1.933(3) Å, respectively].

The interatomic contact distance between Cu1 and the thiophene sulfur atoms is 3.136(2) Å. Other S−Cu distances reported in the literature range from 3.012 Å for a Cu^{II}−S containing system[18] to 2.90 Å and 3.16 Å for Cu^{I}−S,[19] which is believed to contain thiophene-*S* coordination to the Cu atom. Some Cu−O distances reported by Yates et al.[20] fall into the same range. The distance from Cu1 to the gravity centre of the thiophene ring (S1−C3−C4−C5−C6) is 3.620 Å. The angle between the Cu−S bond and the least-squares plane passing through

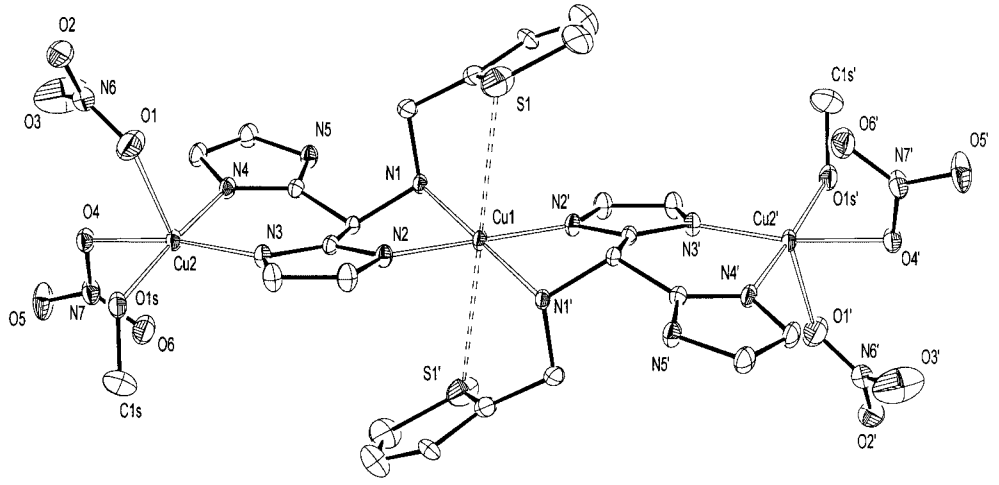

Figure 2. Thermal ellipsoid plot (20% probability level) of the trinuclear copper complex $[Cu_3(imthio)_2(NO_3)_4(MeOH)_2]$; hydrogen atoms have been omitted for clarity; selected bond lengths and angles: Cu1−N1 2.064(3), Cu1−N2 1.933(3), Cu1−S1 3.136 Å, Cu2−O1 2.309(4), Cu2−O1s 2.002(4), Cu2−O4 2.013(3), Cu2−N3 1.939(3), Cu2−N4 1.973(3) Å; N1−Cu1−N2 81.29(11), N1−Cu1−N2′ 98.71(11), S1−Cu−N1 81.3, S1−Cu1−N2 93.98, S1−Cu1−N1a 98.7, S1−Cu1−N2a 86.02, O1−Cu2−O1s 84.52(15), O1−Cu2−O4 93.53(13), O1−Cu2−N3 94.67(13), O1−Cu2−N4 101.57(13), O1s−Cu2−O4 87.05(13), O1s−Cu2−N3 89.25(15), O1s−Cu2−N4 173.77(14), O4−Cu2−N3 170.64(12), O4−Cu2−N4 91.24(11), N3−Cu2−N4 91.53(13)°

 © 2004 Wiley-VCH Verlag GmbH & Co. KGaA, Weinheim

the thiophene ring is 123.38(17)° (the angle between the vector of Cu1 to the centre of gravity of the thiophene ring and the normal to the ring plane is 43.76°). The geometry around the central Cu^{2+} ion can be described as a tetragonally distorted octahedral environment, resulting from the long axial Cu1−S1 (and consequently Cu1−S1′) bond (S1−Cu1−N1: 81.3°; S1−Cu1−N2: 93.98°; S1−Cu1−N1′: 98.7°; S1−Cu1−N2′: 86.02°).

The crystal packing exhibits some π-stacking and face-to-face interactions with the shortest intramolecular ring−ring distances of 3.807(4) Å between the thiophene ring (S1−C3−C4−C5−C6) and one of the imidazole rings (N2−N3−C7−C8−C9). The dihedral angle between them is 23.97°. In the crystal the different units interact with each other through the imidazole and amine nitrogen atoms, which form intermolecular N−H···O hydrogen bonds involving the oxygens of the nitrate groups and of the methanol molecule (Figure 3). Very weak intermolecular C−H···O interactions [C1···O5 = 3.216(6) Å; C11···O3 = 3.237(6) Å] between −CH groups and nitrate oxygen atoms also contribute to the crystal packing.

Crystal structures of copper complexes with related ligands reported previously, for example 1,1-bis(imidazol-2-yl)-3-(pyridin-2-yl)-2-azapropane (Im-2Py), consist of two copper ions in distorted square-pyramidal environments.[8,21] Compared with those systems, the significant structural alteration induced by the substitution of pyridine rings by thiophene moieties and the semicoordination of thiophene sulfur atoms in the complex can be considered to have thermodynamic and/or kinetic consequences for redox reactivity.[20] It should be noted that, to the best of our knowledge, the title compound represents the first example to date of a linear trinuclear copper(II) complex in which the central Cu^{II} atom is semicoordinated with the thiophene sulfur atoms. Moreover, two lateral copper complexes can be considered as chelating ligands on the central Cu^{II} atom in the crystal structure.

Ligand-Field and UV/Vis Measurement

The ligand-field diffuse-reflectance spectrum of the crystalline powder of the complex shows a peak at $17.1\cdot10^3$ cm^{-1}, which is due to a d-d transition and is a normal ligand-field transition for a $CuN_2O_2(x)$ chromophore.[22,23] A strong absorption band at $28.3\cdot10^3$ cm^{-1} and a shoulder peak at $32.8\cdot10^3$ cm^{-1} can be attributed to the charge transfer from the N, O, or S to Cu^{II}. An absorption band at $37.3\cdot10^3$ cm^{-1} is associated with ligand π-π* transition.[24] The UV/Vis spectrum recorded in MeOH shows absorption bands as shoulder peaks at approximately 281 nm (ε = 2 054 $M^{-1}cm^{-1}$) and 372 nm (ε = 1 240 M^{-1} cm^{-1}), due to the LMCT transition from N and O to Cu^{II}.[25] The transition in the visible region of the electronic spectra is a much less intense absorption at 636 nm, which is assigned to d-d transitions.[23] The difference between the solid-state spectrum and the solution measurement suggests a change in geometry upon dissolution. The complex may therefore partially dissociate in solution.

EPR Measurements

The EPR spectra of the polycrystalline powder of the complex were recorded at room temperature and at 77 K. The complex shows axial spectra with $g_{//}$ =2.28, $g_{\perp}$ = 2.07 and $A_{//}$ = 165 G at room temperature. When the solid sample is measured at 77 K (liquid nitrogen), the signals become sharper with the same g and A values.

The EPR spectrum of the complex recorded in frozen solution at 77 K in MeOH shows an overlapping of two well-resolved axial signals with superhyperfine splitting superimposed on the axial and equatorial absorptions. The

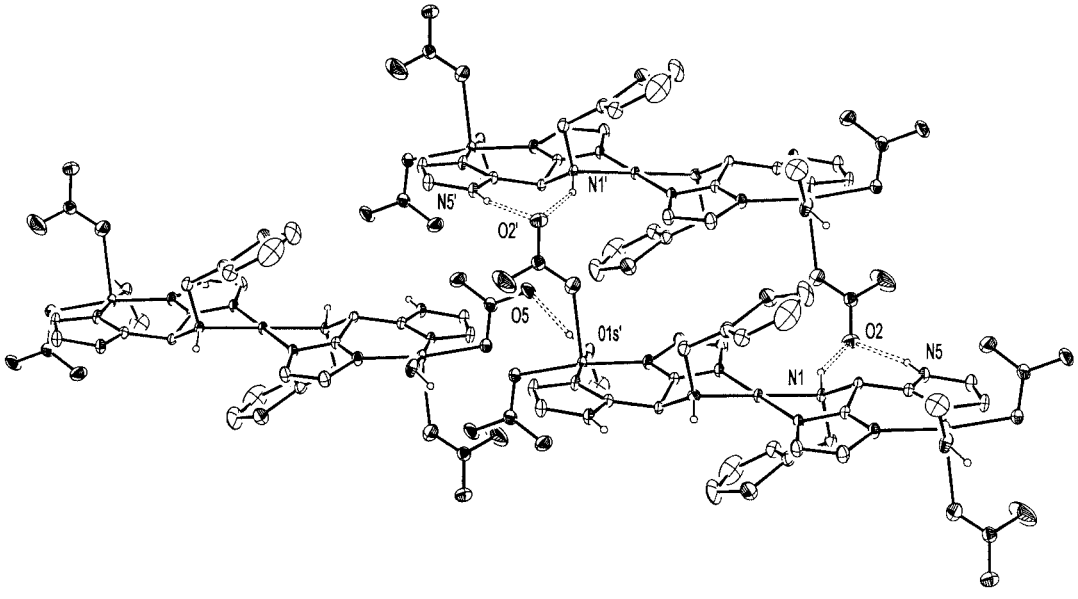

Figure 3. Perspective view showing the relevant hydrogen bonds connecting three different molecular complexes; intermolecular (D−H···A [Å]): N1−H1···O2 2.885(4), N5−H5···O2 2.848(5), O1s−H1s···O5 2.708(6)

 © 2004 Wiley-VCH Verlag GmbH & Co. KGaA, Weinheim

spectrum clearly indicates the presence of two mononuclear species in solution, suggesting the dissociation of the trinuclear core. No half-field splitting signals, usually observed in the case of dinuclear species, are found. The equatorial coordination by four nitrogen donors around Cu1 in the complex results in the expected nine superhyperfine lines ($A_{N\perp}$ = 12.0 G). The spectrum was simulated satisfactorily[26] (see Figure 4) by using two noninteracting mononuclear Cu^{II} species in a ratio of 2.1:1.1. The reliability factor, defined as $R = n^{-1}[\Sigma(\chi_{obs} - \chi_{cal})^2/(\chi_{cal})^2]$ (n = number of data points), was $8.58 \cdot 10^{-4}$. The best simulating parameters for the species 1 were $g_x = 2.02$, $g_y = 2.05$ and $g_z = 2.25$, with $A_z = 198$ G (other A values set at 0). These values are reasonably close to those reported in the literature for CuN_4 chromophores. For species 2, the following values were obtained: $g_x \approx g_y = 2.06$ and $g_z = 2.33$, with $A_{//} = 175$ G (other A value set at 0).

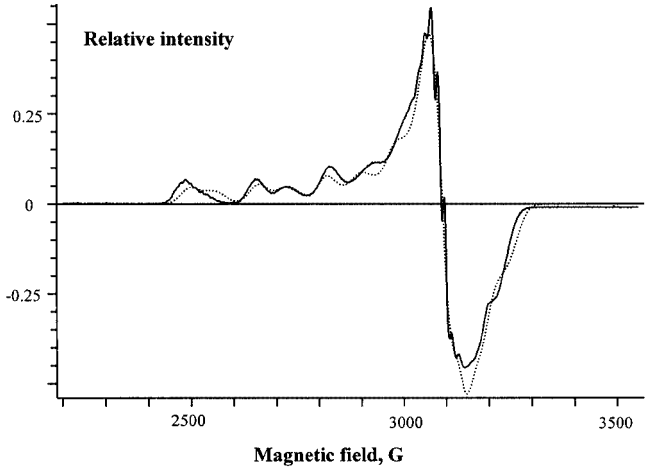

Figure 4. X-band EPR spectrum of the complex recorded at 77 K in MeOH; experimental curve (solid line) and simulated curve (dashed line) spectra of the complex (see text for further details)

Magnetic Susceptibility Measurement

The temperature-dependent magnetic susceptibility of the imidazolato-bridged trinuclear copper complex shows weak antiferromagnetic behaviour through the whole range of temperature (5−300 K). At 300 K the magnetic susceptibility has a value of 0.9725 cm^3mol^{-1}, a little bit lower than expected for three independent copper atoms (1.125 cm^3mol^{-1}). The decrease of the value of χT upon cooling is gradual and becomes slightly steeper at around 100 K, finally reaching a value of 0.2505 cm^3mol^{-1} at 5 K (Figure 5). This behaviour is typical for compounds with weak antiferromagnetism and was modelled using the spin Hamiltonian presented below:

$$H = g\beta S_z H - J_1(S_1 \cdot S_2 + S_{1a} \cdot S_2) - J_2(S_1 \cdot S_{1a}) - zJ' \langle S_z \rangle S_z$$

The first term of this Hamiltonian corresponds to the Zeeman term, for which only one isotropic g tensor has been considered for the two different Cu^{II} ions. The second and third terms are the isotropic nearest-neighbour and next-nearest-neighbour interactions, respectively; J_1 represents the exchange parameter between neighbouring Cu^{II} ions and J_2 the exchange parameter between terminal Cu^{II} ions. The latter has been neglected ($J_2 = 0$), as can be done when the compound is completely linear and the main interaction is antiferromagnetic. The last term takes into account the intermolecular interactions between the trinuclear arrays in the mean field approximation, in which J' is the intermolecular exchange interaction and z the number of trimeric neighbours (in this case 4). Considering the *TIP* (temperature-independent paramagnetism) and p as paramagnetic impurities, the resulting expression is:

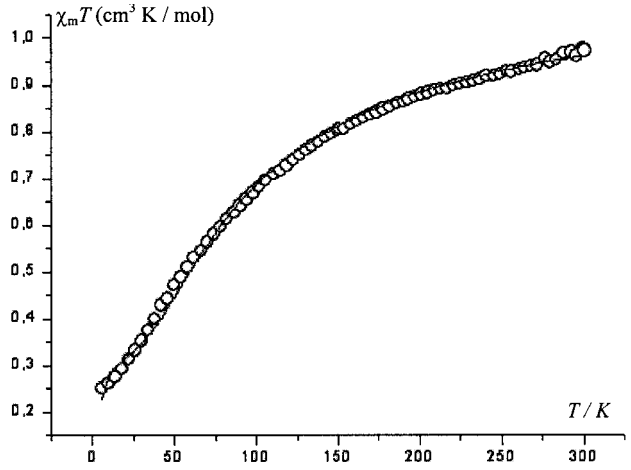

Figure 5. $\chi_m T$ vs. T plot for $[Cu_3(imthio)_2(NO_3)_4(MeOH)_2]$; the solid line is the best fit obtained with a nearest-neighbour interaction of -71.37 cm^{-1} (see text)

$$\chi_m T = \{(N_a g^2 \beta^2 F(T)/4k_B[T - zJ'F(T)]\}(1 - p) + (N_a g^2 \beta^2/2kT)p + TIP$$

$$F(T) = [1 + \exp(J_1/k_B T) + 10\exp(3J_1/2k_B T)]/[1 + \exp(J_1/k_B T) + 2\exp(3J_1/2K_B T)]$$

The best-fit parameters were $g = 2$, $J_1 = -71.37$, $zJ' = -4.03$ and $p = 0$ and the *TIP* is $60 \cdot 10^{-3}$ cm^3mol^{-1}, with an R value of $1.2 \cdot 10^{-4}$. The J_1 value is in good agreement with the expected value for imidazolato-bridged copper complexes reported previously.[27] Indeed, the Cu−Cu separation is large (Cu−Cu = 5.676 Å), obviously indicating that no direct exchange mechanism is likely to contribute to the magnetic coupling. Therefore, the antiferromagnetic coupling in the compound is ascribed solely to superexchange mechanisms between the magnetic orbitals of copper(II) ions ($d_{x^2-y^2}$) through the bridging imidazolate rings. The quite high value of the intertrinuclear superexchange interaction can be explained by the hydrogen-bonding network and π-π interactions between the trinuclear units in the lattice.

Conclusions

In summary, the Himthio ligand allows the preparation of a homometallic, trinuclear complex, $[Cu_3(imthio)_2(NO_3)_4$-

 © 2004 Wiley-VCH Verlag GmbH & Co. KGaA, Weinheim

$(MeOH)_2$]. As Cu1 occupies an inversion centre, the resulting Cu2−Cu1−Cu2′ array is linear by symmetry. The molecular structure results in two different coordination sites within the same molecular complex, i.e. an N_4S_2 octahedral site and two N_2O_3 distorted square-pyramidal sites. The Cu−S distance is around 3.136 Å, which indicates moderate interactions between sulfur atoms and Cu^{II} atoms and results in the distortion of the ligand in the complex. Since only a limited number of linear trinuclear compounds have been reported as yet,[25,28] this trinuclear complex, with semicoordination of the thiophene sulfur atoms with Cu^{II} atoms, is unique. The crystal packing of the complex is stabilized by several hydrogen bonds and the interactions between aromatic rings. The EPR spectrum at 77 K in MeOH shows well-resolved superfine splitting signals, which are satisfactorily simulated with two mononuclear species. The magnetic susceptibility measurement of the complex indicates weak antiferromagnetic behaviour between copper(II) ions by a superexchange mechanism through the bridging imidazolate moieties. The studies not only present an unusual trinuclear copper(II) complex with semicoordinated thiophene moieties, but also provide more information about the magnetic and structural data for imidazolato-bridged complexes.

Experimental Section

General Remarks: All reagents and solvents were purchased from commercial sources and used as received. Elemental analyses (C, H N, S) were carried out with a Perkin−Elmer 2400 series II analyser. Infrared spectra were recorded with a Perkin−Elmer Paragon 1000 spectrophotometer equipped with a Golden Gate Diamond ATR device, using the diffuse reflectance technique. X-band EPR spectra were recorded at room temperature and at 77 K with a Jeol RE2X electron spin resonance spectrometer using diphenylpicrylhydrazyl (DPPH) (g = 2.0036) as a standard. The UV/Vis spectra of the compound were recorded in the 250−800 nm range with a Cary 50 Varian UV/Vis/NIR spectrometer. The cyclic voltammetry measurements were performed with an Autolab PGstat10 potentiostat controlled by GPES4 software. A three-electrode system was used, consisting of a glassy carbon (GC) working electrode, a platinum (Pt) auxiliary electrode and an Ag/AgCl reference electrode. All potentials are given versus Ag/AgCl. The experiments were carried out in MeOH solution at room temperature under argon. Magnetic susceptibility measurements (5−300 K) were carried out using a Quantum Design MPMS-5S SQUID magnetometer, in a 1 kG applied field. Data were corrected for the experimentally determined contribution of the sample holder. Corrections for the diamagnetic responses of the complex, as estimated from Pascal's constants, were applied.[29]

Preparation of the 1,1-Bis(imidazol-2-yl)-3-(thiophen-2-yl)-2-azapropane (Himthio) Ligand: 2-(Aminomethyl)thiophene (0.50 g, 4.37 mmol) in water (10 mL) was added to a solution of the hydrochloride salt of bis(imidazol-2-yl)nitromethane[16] (1.0 g, 4.37 mmol) in sodium hydroxide solution (2.0 M, 5 mL) . The solution was stirred at 80 °C for 2 h, during which the product crystallised from the reaction mixture (if not, the solution was left at room temperature, until precipitation of the compound occurred). After cooling to room temperature, the reaction mixture was filtered and washed with water, ethanol and diethyl ether in air. Yield: 0.74 g, 65%. ^{1}H NMR (200 MHz, CD_3OD, 25 °C, 0−10 ppm): δ = 7.30 (t, 1 H, Thio-*H*), 7.02 (s, 4 H, Im-*H*), 6.92 (d, 2 H, Thio-*H*), 5.18 (s, 1 H, C*H*), 3.87 (s, 2 H, CH_2) ppm. MS: m/z = 259.9 $[M + H]^+$.

Preparation of the Copper Complex $[Cu_3(imthio)_2(NO_3)_4(MeOH)_2]$: A solution of the Himthio ligand (20.72 mg, 0.08 mmol) in methanol (10 mL) was added to a solution of $Cu(NO_3)_2{\cdot}3H_2O$ (19.3 mg, 0.08 mmol) in methanol (5 mL). The reaction mixture was stirred at room temperature for 30 min and filtered. The solution was left alone at room temperature for several weeks, and green crystals suitable for X-ray analysis were produced. Yield: 9.5 mg, 35%. $C_{26}H_{32}Cu_3N_{14}O_{14}S_2$ (1019.40): calcd. C 30.6, H 3.2, N 19.2, S 6.3; found C 30.9, H 2.7, N 18.7, S 6.8. IR (solid): $\tilde{\nu}$ = 1564.9, 1484.6, 1373.3, 1329.2, 1300.2, 1140.2, 1030.5, 926.1, 825.7, 750.0, 724.1, 651.2, 431.8 cm^{-1}.

X-ray Crystallographic Study: The molecular structure of $[Cu_3(imthio)_2(NO_3)_4(MeOH)_2]$ was determined by single-crystal X-ray diffraction methods. Crystallographic and experimental details for the structure are summarized in Table 1. Intensity data and cell parameters were recorded at room temperature (25 °C) with a Bruker AXS Smart 1000 single-crystal diffractometer (Mo-K_α radiation) equipped with a CCD area detector. The data reduction was performed using the SAINT and SADABS programs.[30] The structure was solved by Direct Methods using the SIR97 program[31] and refined on F_o^2 by full-matrix least-squares procedures, using the SHELXL-97 program.[32] All non-hydrogen atoms were refined with anisotropic atomic displacements. The hydrogen atoms were included in the refinement at idealised geometry (C−H 0.95 Å) and refined "riding" on the corresponding parent atoms, with the exception of H1S4, which was located in the difference Fourier map. The weighting scheme used in the last cycle of refinement was

Table 1. Crystallographic data for $Cu_3(imthio)_2(NO_3)_4(MeOH)_2$

Empirical formula	$C_{26}H_{32}Cu_3N_{14}O_{14}S_2$
Formula mass	1019.40
Crystal system	triclinic
Space group	$P\bar{1}$
a [Å]	9.176(5)
b [Å]	9.180(5)
c [Å]	12.804(5)
α [°]	89.718(5)
β [°]	76.847(5)
γ [°]	69.140(5)
V [Å^3]	978.0(8)
Z	1
$D_{calcd.}$ [g cm^{-3}]	1.731
Linear absorption coeff. [mm^{-1}]	1.805
F(000)	517
Crystal size [mm]	0.11 × 0..14 × 0.23
Index ranges	$-11 \le h \le 11$, $-11 \le k \le 11$, $-16 \le l \le 16$
θ range for data collection [°]	1.64−27.01
Reflections collected	10634
Independent reflections	4173 (R_{int} =0.0345)
Observed reflections [$I > 2\sigma(I)$]	2714
Data/restraints/parameters	4173/1/277
Goodness-of-fit on F^2 [a]	0.889
Final R indices (obsd. data)[b]	R_1 = 0.0407, wR_2=0.0920
R indices (all data)[b]	R_1 = 0.0735, wR_2=0.0992
Largest diff. peak /hole [e/Å^{-3}]	0.631/−0.532

[a] Goodness-of-fit $S = [\Sigma w(F_o^2 - F_c^2)^2/(n-p)]^{1/2}$, where n is the number of reflections and p the number of parameters. [b] $R_1 = \Sigma F_o - F_c/\Sigma F_o$, $wR_2 = [\Sigma w(F_o^2 - F_c^2)^2/\Sigma wF_o^4]^{1/2}$.

 © 2004 Wiley-VCH Verlag GmbH & Co. KGaA, Weinheim

$w = 1/[\sigma^2 F_o^2 + (0.0544P)^2]$ [where $P = (F_o^2 + 2F_c^2)/3$]. Molecular geometry calculations were carried out using the PARST97 program[33]. Drawings were obtained by ORTEP3 in the WinGX suite.[34] All calculations were carried out with a DIGITAL Alpha Station 255 computer. Crystallographic data (excluding structure factors) for the structure reported have been deposited with the Cambridge Crystallographic Data Centre as supplementary publication no. CCDC-233200 and can be obtained free of charge on application to the CCDC, 12 Union Road, Cambridge CB2 1EZ, UK [Fax: (internat.) + 44-1223-336-033; E-mail: deposit@ccdc.cam.ac.uk].

Acknowledgments

The work described here has been supported by the Leiden University Study group Werkgroep Fundamenteel-Materialen Onderzoek (WFMO). Support from the NRSC Catalysis (a research school combination of HRSMC and NIOK) is kindly acknowledged. The project is supported financially by the Dutch Economy, Ecology, Technology (EET) program, a joint program of the Ministry of Economic Affairs, the Ministry of Education, Culture and Science and the Ministry of Housing, Spatial Planning and the Environment.

[1] J. Reedijk, E. Bouwman (Eds.), *Bioinorganic Catalysis*, Marcel Dekker **1999**; E. I. Solomon, U. M. Sundaram, T. E. Machonkin, *Chem. Rev.* **1996**, *96*, 2563; K. D. Karlin, Z. Tyeklar, *Bioinorganic Chemistry of Copper*, Chapman & Hall, New York, **1993**; W. B. Tolman, *Acc. Chem. Res.* **1997**, *30*, 227.
[2] A. Messerschmidt, A. Rossi, R. Ladenstein, R. Huber, M. Bolognesi, G. Gatti, A. Marchesini, R. Petruzzelli, A. Finazziagro, *J. Mol. Biol.* **1989**, *206*, 513.
[3] P. Kyritsis, A. Messerschmidt, R. Huber, G. A. Salmon, A. G. Sykes, *J. Chem. Soc., Dalton Trans.* **1993**, 731.
[4] R. Huber, *Angew. Chem. Int. Ed. Engl.* **1989**, *28*, 848.
[5] L. Gutierrez, G. Alzuet, J. A. Real, J. Cano, J. Borras, A. Castineiras, *Inorg. Chem.* **2000**, *39*, 3608; I. Riggio, G. A. van Albada, D. D. Ellis, A. L. Spek, J. Reedijk, *Inorg. Chim. Acta* **2001**, *313*, 120; G. A. van Albada, M. E. Quiroz-Castro, I. Mutikainen, U. Turpeinen, J. Reedijk, *Inorg. Chim. Acta* **2000**, *298*, 221.
[6] N. K. Kitajima, K. Fujisabbla, Y. Moro-oka, *J. Mol. Catal. A.* **1992**, *74*, 143; I. Sanyal, M. Mahroof-Tahir, M. S. Nasir, P. Ghosh, B. Cohen, Y. Gulthey, R. W. Cruse, A. Farooq, K. D. Karlin, S. Liu, J. Zubieta, *Inorg. Chem.* **1992**, *31*, 4322.
[7] C. J. Campbell, W. L. Driessen, J. Reedijk, W. Smeets, A. L. Spek, *J. Chem. Soc., Dalton Trans.* **1998**, 2703; M. C. Mimmi, F. Micciche, H. Kooijman, A. L. Spek, S. T. Warzeska, E.. Bouwman, *Inorg. Chim. Acta* **2002**, *340*, 197; G. A. van Albada, W. J. J. Smeets, A. L. Spek, J. Reedijk, *J. Coord. Chem.* **1999**, *48*, 375.
[8] G. J. A. A. Koolhaas, P. M. v. Berkel, S. C. v. d. Slot, G. Mendoza-Diaz, W. L. Driessen, J. Reedijk, H. Kooijman, N. Veldman, A. L. Spek, *Inorg. Chem.* **1996**, *35*, 3525.
[9] E. T. Adman, *Adv. Protein Chem.* **1991**, *42*, 145.
[10] G. E. Norris, B. F. Anderson, E. N. Baker, *J. Am. Chem. Soc.* **1986**, *108*, 2784.
[11] J. M. Guss, H. C. Freeman, *J. Mol. Biol.* **1983**, *169*, 521.
[12] C. Beguin, P. Chautemps, A. E. Marzouki, J. L. Pierre, S. M. Refaif, G. Serratrice, E. Saintaman, P. Rey, *J. Chem. Soc., Dalton Trans.* **1995**, 1939.
[13] G. W. Canters, G. Gilardi, *FEBS Lett.* **1993**, *325*, 39.
[14] E. Danielsen, R. Bauer, L. Hemmingsen, M. L. Andersen, M. J. Bjerrum, T. Butz, W. Troger, G. W. Canters, C. W. G. Hoitink, G. Karlsson, O. Hansson, A. Messerschmidt, *J.. Biol. Chem.* **1995**, *270*, 573.
[15] M. G. B. Drew, C. J. Harding, O. W. Howarth, Q. Lu, D. J. Marrs, F. F. Morgan, V. McKee, J. Nelson, *J. Chem. Soc., Dalton Trans.* **1996**, 3021.
[16] M. Joseph, T. Leigh, M. L. Swain, *Synthesis.* . **1977**, 459.
[17] A. W. Addison, T. N. Rao, J. Reedijk, J. van Rijn, G. C. Verschoor, *J. Chem. Soc., Dalton Trans.* **1984**, 1349.
[18] C. R. Lucas, S. Liu, M. J. Newlands, J. P. Charland, E. J. Gabe, *Can. J. Chem.* **1989**, *67*, 639.
[19] G. C. van Stein, G. van Koten, K. Verieze, A. L. Spek, E. A. Klop, C. Brevard, *Inorg. Chem.* **1985**, *24*, 1367.
[20] P. C. Yates, M. G. B. Drew, J. Trochagrimshaw, K. P. McKillop, S. M. Nelson, P. T. Ndifon, C. A. McAuliffe, J. Nelson, *J. Chem. Soc., Dalton Trans.* **1991**, 1973.
[21] G. J. A. A. Koolhaas, PhD Thesis, Leiden University, **1996**.
[22] G. A. van Albada, M. T. Lakin, N. Veldman, A. L. Spek, J. Reedijk, *Inorg. Chem.* **1995**, *34*, 4910.
[23] B. J. Hathaway, *Comprehensive Coordination Chemistry*, Pergamon Press, Oxford, **1987**, vol. 5.
[24] L. Casella, O. Carugo, M. Gullotti, S. Garofani, P. Zanello, *Inorg. Chem.* **1993**, *32*, 2056.
[25] M. H. W. Lam, Y. Y. Tang, K. M. Fung, X. Z. You, W. T. Wong, *Chem. Commun.* **1997**, *21*, 957.
[26] F. Neese, *The program EPR, a modeling approach, Version 1.0*, University of Konstanz, **1993**.
[27] G. J. A. A. Koolhaas, W. L. Driessen, P. J. Van Koningsbruggen, J. Reedijk, A. L. Spek, *J. Chem. Soc., Dalton Trans.* **1993**, 3803; N. Matsumoto, S. Yamashita, A. Ohyoshi, S. Kohata, H. Okawa, *J. Chem. Soc., Dalton Trans.* **1988**, 1943; O. Kahn, *Molecular Magnetism*, Wiley-VCH, New York, **1993**.
[28] G. A. van Albada, I. Mutikainen, O. Roubeau, U. Turpeinen, J. Reedijk, *Inorg. Chim. Acta* **2002**, *331*, 208; Y. F. Song, P. Gamez, A. F. Stassen, M. Lutz, A. L. Spek, J. Reedijk, *Eur. J. Inorg. Chem.* **2003**, 4073; T. C. Higgs, K. Spartalian, C. J. O′Connor, B. F. Matzanke, C. J. Carrano, *Inorg. Chem.* **1998**, *37*, 2263.
[29] I. M. Kolthoff, P. J. Elving, *Treatise on Analytical Chemistry*, Interscience Publ., New York **1963**, vol. 4.
[30] SAINT, *Software Users Guide, Version 6.0*, Bruker Analytical X-ray Systems, Madison, WI, **1999**; G. M. Sheldrick, *SADABS v2.03: Area-Detector Absorption Correction*, University of Göttingen, Germany, **1999**.
[31] A. Altomare, M. C. Burla, M. Camalli, G. L. Cascarano, C. Giacovazzo, A. Guagliardi, A. G. G. Moliterni, G. Polidori, R. Spagna, *J. Appl. Crystallogr.* **1999**, *32*, 115.
[32] G. M. Sheldrick, *SHELXL-97, Program for Crystal Structure Refinement*, University of Göttingen, Germany, **1997**.
[33] M. Nardelli, *J. Appl. Crystallogr.* **1995**, *28*, 659.
[34] L. J. Farrugia, *J. Appl. Crystallogr.* **1997**, *30*, 565.

Received March 10, 2004
Early View Article
Published Online October 14, 2004

 © 2004 Wiley-VCH Verlag GmbH & Co. KGaA, Weinheim

Acid-Base Self-Assembly Chemistry and Hydrogen Bonding Interactions Resulting in the Formation of a Tetranuclear Aggregate Containing Four Crystallographically Non-Equivalent Fe^{III} Centers

Stefania Tanase,[a] Elisabeth Bouwman,[a] Gary J. Long,[b] Ahmed M. Shahin,[b] Allison M. Mills,[c] Anthony L. Spek,[c] and Jan Reedijk*[a]

Keywords: Iron / Pyrazole ligands / Hydroxo bridge / Mössbauer

The synthesis and characterization of a mononuclear iron(III) complex [Fe(Hphpz)Cl(CH_3OH)] (**1**) and a tetranuclear assembly of a bis(μ-hydroxo)-bridged dinuclear iron(III) complex [{Fe(Hphpz)$_2$(OH)}$_2$][Fe(Hphpz)$_3$]$_2$ (**2**) with the ligand 3(5)-methyl-5(3)-(2-hydroxyphenyl)pyrazole (H_2phpz) is reported. Compound **1** is converted into **2** in a methanol solution and in the presence of a base. The asymmetric unit of **2** consists of two independent [Fe(Hphpz)$_3$] molecules and one dinuclear complex [Fe(Hphpz)$_2$(OH)]$_2$ containing two crystallographically non-equivalent iron(iii) ions; the three units are linked by N–H···O and O–H···O hydrogen bonding and stacking interactions to form a cluster with an approximate C_2-symmetry. The Mössbauer spectra of [{Fe(Hphpz)$_2$-(OH)}$_2$][Fe(phpz)$_3$]$_2$ have been measured at 295 and 78 K and indicate the presence of four crystallographically distinct, but chemically similar iron(III) sites. The magnetic properties of this compound originate from the weak antiferromagnetic interaction between the Fe^{III} ions of the [Fe(phpz)$_2$(OH)]$_2$ dimer ($J = -2.8$ cm^{-1}).

(© Wiley-VCH Verlag GmbH & Co. KGaA, 69451 Weinheim, Germany, 2004)

Introduction

The chemistry of dinuclear iron(III) complexes bridged by carboxylato residues and/or by a single water-derived ligand (such as hydroxo or oxo) continues to be of great interest because of their implication in the active site of a number of metalloproteins, such as hemerytin (Hr),[1] ribonucleotide reductase (RR),[2] methane monooxygenase (MMO),[3] and purple acid phosphatase (PAPs).[4] At various stages of the enzymatic cycle, the type of the bridge and water-derived ligands may vary depending on the protein. The coordination spheres of the two iron centers play important roles in providing selective substrate binding, control of the iron oxidation states and stereochemical control of the intermediates in the enzymatic cycle. The functions performed by these metalloproteins and their significance have inspired a range of biomimetic studies, studies which suggest that bio-inspired catalytic oxidations might represent a valuable approach for the development of new and more environmentally friendly catalysts for industrial applications. Because spectroscopy plays a key complementary role in obtaining molecular-level insight into the catalytic mechanism that occurs at the active site of metalloproteins, the synthesis of small molecule model compounds has remained a challenging field.

As part of a programme of synthesizing dinuclear iron complexes which model the active sites of metalloproteins, we have chosen to work with nitrogenous and oxygenous ligands and, in particular, with pyrazole-containing ligands.[5] Pyrazole-containing ligands provide an interesting alternative to the often used pyridine ligands for the design of model complexes that can mimic active sites containing imidazole groups from histidine bound to an iron center.[6,7] Especially the lower pK_a values of the pyrazoles and the availability of an acid N−H group as possible hydrogen-bond donor, provide an interesting possibility for new structural features. So, these ligands might even be preferred in the field of biomimetic chemistry, both because they are good structural analogues for the size and electronic properties of histidine and because of their relative ease of preparation as compared to imidazole ligands. In this regard and because of the occurrence of tyrosinase radicals in metalloproteins involved in oxygen-dependent enzymatic radical catalysis,[8] we have been interested in the assembly of discrete diiron(III) cores from 3(5)-methyl-5(3)-(2-

[a] Leiden Institute of Chemistry, Gorlaeus Laboratories, Leiden University
P. O. Box 9502, 2300 RA Leiden, The Netherlands
Fax: + 31 71-527-4671
E-mail: reedijk@chem.leidenuniv.nl
[b] Department of Chemistry, University of Missouri-Rolla, Rolla, MO 65409-0010, USA
[c] Bijvoet Center for Biomolecular Research, Utrecht University, Padualaan 8, 3584 CH Utrecht, The Netherlands

Supporting information for this article is available on the WWW under http://www.eurjic.org or from the author.

 © 2004 Wiley-VCH Verlag GmbH & Co. KGaA, Weinheim **DOI: 10.1002/ejic.200400609**

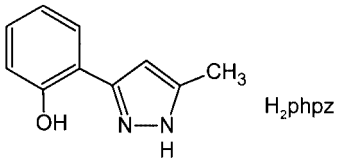

Scheme 1

hydroxyphenyl)pyrazole (H_2phpz, Scheme 1) and simple donors, such as hydroxide, formate, acetate, and benzoate. We report herein the synthesis, structural, spectroscopic and magnetic characterization of $[\{Fe(Hphpz)_2(OH)\}_2][Fe(phpz)_3]_2$, a compound which contains a $Fe_2(\mu\text{-}OH)_2$ core and is extensively stabilized by hydrogen bonding and stacking interactions between the lattice components.

Results and Discussion

Synthesis and Characterization of Iron Complexes of H_2phpz

The procedure for synthesizing the H_2phpz ligand[10] has been reported previously; for the mono-anionic Hphpz, only the mononuclear complex $[Fe(Hphpz)(MeOH)_2](NO_3)$ has so far been reported.[9] In the present study, the reaction of H_2phpz with $Fe(NO_3)_3$, and with other iron(III) salts in various solvents has been extensively investigated. However, elemental analysis and ligand field spectra reveal that mixtures of compounds are obtained in all cases. Therefore, a more specific systematic study had to be undertaken. The reaction of the ligand H_2phpz with $FeCl_2$ (2:1) in the presence of two equiv. of base in methanol leads to a dark purple crystalline product with the tentative formula $[Fe(Hphpz)_2Cl(MeOH)]$ (**1**) as suggested by elemental analysis (Scheme 2). The positive ion mass spectrum of a fresh solution of **1** in either methanol or CH_2Cl_2 exhibits a prominent signal at $m/z = 433$ (relative intensity $I = 100\%$ in the range $m/z = 200-1000$). This signal matches very well with the calculated isotopic distribution for $[Fe(Hphpz)_2(MeOH)]^+$. The effective magnetic moment of **1** at room temperature (5.84 μ_β) is close to the spin-only value expected for a high-spin iron(III) center ($S = {}^5/_2$, $\mu_{eff} = 5.92\ \mu_\beta$); the variable temperature solid-state magnetic susceptibility of **1** has been investigated in the range 5−300 K and it displays strict Curie−Weiss behaviour consistent with the presence of an isolated paramagnetic iron(III) ion. No single crystals were obtained however.

Coordination of 3(5)-methyl-5(3)-(2-hydroxyphenyl)pyrazole with the iron(III) ion is indicated in the infrared spectrum by a shift of the ν_{C-O} stretch from 1654 cm^{-1} in the free ligand to 1599 cm^{-1} in complex **1** and of the $\nu_{C=N}$ stretch from 1636 cm^{-1} in the free ligand to 1557 cm^{-1} in the complex. A sharp peak observed at 3259 cm^{-1} can be assigned to the ν_{N-H} stretch of the pyrazole ring. The absence of any absorption in the range 3300−3600 cm^{-1} indicates that the phenolic proton is lost on coordination.

The main feature of the UV/Vis spectrum of **1** in the solid state is a low-energy band with a maximum at 568 nm that gives rise to the purple colour and which is ascribed to the charge-transfer transition from the p_π orbitals of the phenolic oxygens to the d_π* orbitals of the iron(III) ions.[9,11] A second charge-transfer band occurs at 369 nm and has been assigned to a $p_\pi \rightarrow d_\sigma$* type transition.[11] Electronic absorption spectra of **1** have also been recorded in methanol and dichloromethane, and both show spectroscopic features that are similar to that in the solid state consisting of two absorption bands with maxima at 359 nm and 547 nm, respectively and it suggests that the chloride ion is not replaced by methanol.

The cyclic voltammogram of **1** recorded at room temperature in CH_2Cl_2 shows an irreversible cathodic wave at 0.83 V vs. Ag/AgCl, which is ascribed to the reduction of iron(III) to iron(II). The relatively high reduction potential suggests that **1** is stabilized by the coordination of the chloride anion. This stabilization is also confirmed by the absence of any oxidation peak when scanning the potential up to 1.2 V, a potential at which free chloride ions may be detected.

When a purple-colored methanol solution of **1** is stored in a closed inert atmosphere it gradually changes to red over a number of days. Ligand field spectra would suggest that the new species is a mixture of $[Fe(Hphpz)_2Cl(MeOH)]$, $[Fe(Hphpz)_2(OH)]_2$ and $[Fe(Hphpz)_3]$. Addition of 2 equiv. of base to a fresh methanol solution of **1** results in the immediate appearance of an intense red coloration, accompanied by significant spectroscopic changes (Figure 1). The absorption maximum at 490 nm suggest the presence of a bis(μ-hydroxo) dimer.[12] The function of the added base appears to be to provide the medium required for the formation of the $Fe_2(\mu\text{-}OH)_2$ core. Vapor diffusion of ethyl acetate into this solution yields a red microcrystalline solid, for which elemental analysis indicates the formula $[\{Fe(Hphpz)_2(OH)\}_2][Fe(Hphpz)_3]_2$ (**2**). Thus, it appears that compound **2** is a decomposition product of **1**. Although we were unsuccessful in growing crystals large enough to carry out an X-ray structural study of **1**, we were successful in growing crystals of **2**. The yield of compound **2** has been optimized via acid-base self assembly chemistry (Scheme 2), by mixing

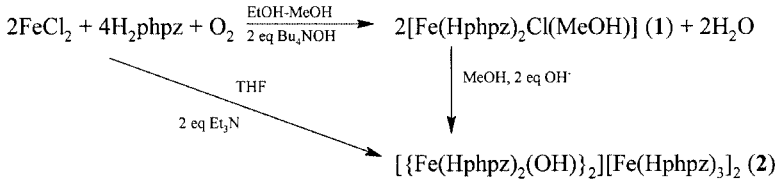

Scheme 2. Reaction pathways for the synthesis of compounds **1** and **2**

 © 2004 Wiley-VCH Verlag GmbH & Co. KGaA, Weinheim

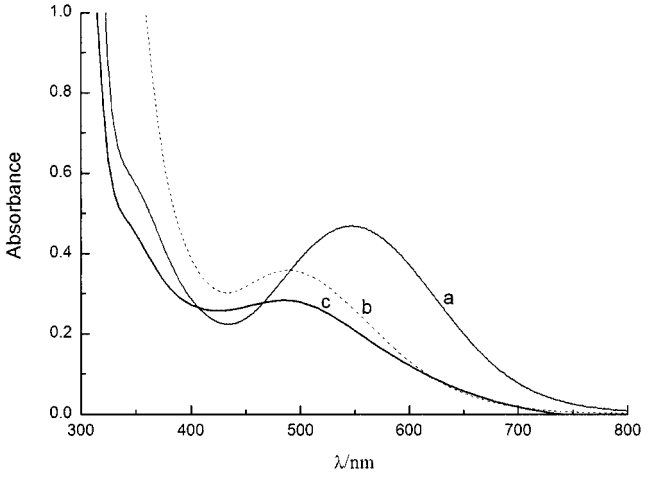

Figure 1. UV/Vis spectra of a methanol solution of $[Fe(Hphpz)_2Cl(MeOH)]$ (a), after the addition of 2 equiv. of Bu_4NOH to **1** (b), and $[\{Fe(Hphpz)_2(OH)\}_2][Fe(Hphpz)_3]_2$ redissolved in methanol (c)

$FeCl_2{\cdot}4H_2O$ with H_2phpz under air in the presence of triethylamine as base.

The infrared spectrum of **2** exhibits the bands expected for the ligand Hphpz and it is similar to that of the compound **1**. Unfortunately, it is not possible to definitely identify the Fe−O−Fe vibrational bands, because of the complexity of the infrared spectrum in the 500−800 cm^{-1} range. The ligand field spectrum of **2** displays the features typical of bis(μ-hydroxo)-bridged iron(III) compounds: an intense absorption band at 495 nm with a lower energy shoulder at 586 nm, bands that may be assigned to ligand-to-iron(III) charge-transfer transitions.[13] A weak-intensity absorption band that occurs at 997 nm is attributed to the d-d transitions involving forbidden states of the high-spin iron(III) ion.[14]

X-ray Crystal Structure of $[\{Fe(Hphpz)_2(OH)\}_2][Fe(Hphpz)_3]_2$

Perspective views of the molecular entities of **2** are shown in Figure 2 along with the atom-labeling scheme. The asymmetric unit of **2** contains two independent *mer*-$[Fe(Hphpz)_3]$ molecules and one dinuclear complex $[Fe(Hphpz)_2(OH)]_2$. Selected bond lengths and angles pertaining to the iron(III) coordination spheres are given in Table 1.

Each of the two independent $[Fe(Hphpz)_3]$ molecules consists of an iron(III) ion coordinated to three $phpz^-$ ligands (Figure 2, a and b). The distorted octahedral-based FeN_3O_3 chromophores both have a meridional (*mer*) configuration. The bond lengths and angles at the iron center are similar in both entities and indicate an extensive deviation from octahedral symmetry (Table 1, Supplementary material). The largest deviations from ideal octahedral symmetry are observed for the *trans* O21−Fe1−O61 = 162.10(14)° and O81−Fe2−O121 = 161.67(15)° angles. The least-square phenyl rings and pyrazole rings in the $Hphpz^-$ ligand containing N32 and N92 nitrogen atoms make dihedral angles of 8.2(3) and 2.1(3)°. Although a planar molecule is expected, the $Hphpz^-$ ligand may also bind in a twisted conformation because the conjugation of the phenyl−pyrazole bond is flexible. Due to the aromaticity of the pyrazole ring the lone pair of the nitrogen, and therefore the coordinated metal ion all are expected to lie in a nearly perfect plane. In the case of the pyrazole ring containing N32 and the one containing N92, however, the iron atoms lie 0.8−1.0 Å above the least-squares plane of the pyrazole ring. This implies that the pyrazole ring is bound to the iron atoms in a rather acute angle of 19.41° and 20.59°. The hydrogen bonding interactions from N−H to a neighboring oxygen atoms and the π-π interactions clearly enforce the deviation from the planarity of distorted $Hphpz^-$ ligands (see below). The $Fe-N_{pz}$ and $Fe-O_{ph}$ bond lengths are very similar to those found in the dinuclear species $[Fe(Hphpz)_2(OH)]_2$.

The dinuclear $[Fe(Hphpz)_2(OH)]_2$ unit contains two crystallographically non-equivalent iron(III) ions that are bridged by two hydroxyl groups (Figure 2, c). The nitrogen and oxygen donors of two molecules of the H_2phpz ligand in its mono-dehydronated form ($Hphpz^-$) occupy four coordination sites of each iron(III) ion. At Fe3 the nitrogen donors of the two ligands are mutually *trans*, whereas at Fe4 they are positioned *cis* with respect to one another. The two remaining sites are filled by the bridging hydroxyl ions. Therefore, each iron(III) ion has a N_2O_4 donor set in a distorted octahedral coordination geometry. All *cis* and *trans* angles deviate from 90 and 180°; in particular, the angles N192−Fe4−O210 = 162.48(14)° and N172−Fe4−O211 = 162.56(14)° are considerably kinked. In the four-membered $Fe_2(\mu\text{-}OH)_2$ core, the two metal centers are separated by 3.1492(9) Å and have two slightly different bridging angles of Fe3−O210−Fe4 = 105.45(14)° and Fe3−O211−Fe4 104.97(14)°. Each of the hydroxyl ions bridges the metal centers asymmetrically; the Fe3−OH distances are somewhat shorter than those for Fe4, which may be related to the *trans* effect of the nitrogen donors and to the steric requirements of the Hphpz ligands. All of the $Fe^{III}-\mu$-OH bond lengths, as well as the Fe−OH−Fe bridge angles, are in the range of those observed for similar $Fe_2(\mu\text{-}OH)_2$ complexes.[15−18] The $Fe-N_{pz}$ and $Fe-O_{ph}$ bond lengths are also comparable to those reported for related complexes.[9,19]

An interesting feature of the crystal structure of **2** is the presence of multiple intra- and intermolecular hydrogen bonds, as well as intermolecular π···π stacking interactions, interactions which play an important role in the stabilization of the observed molecular configuration (Figure 3 and Table S1 in the Supporting Information). Two strong intramolecular N−H···O hydrogen bonds (N−H···O = 2.803 Å) link $Hphpz^-$ ligands on different iron centres in the $[Fe(Hphpz)_2(OH)]_2$ unit. In each of the $[Fe(Hphpz)_3]$ molecules, two intramolecular N−H···O hydrogen bonds are established between two of the anionic $Hphpz^-$ ligands. The third anionic $phpz^-$ molecule of each mononuclear entity is involved in two intermolecular N−H···O hydrogen bonds with $Hphpz^-$ ligands of the dinuclear

 © 2004 Wiley-VCH Verlag GmbH & Co. KGaA, Weinheim

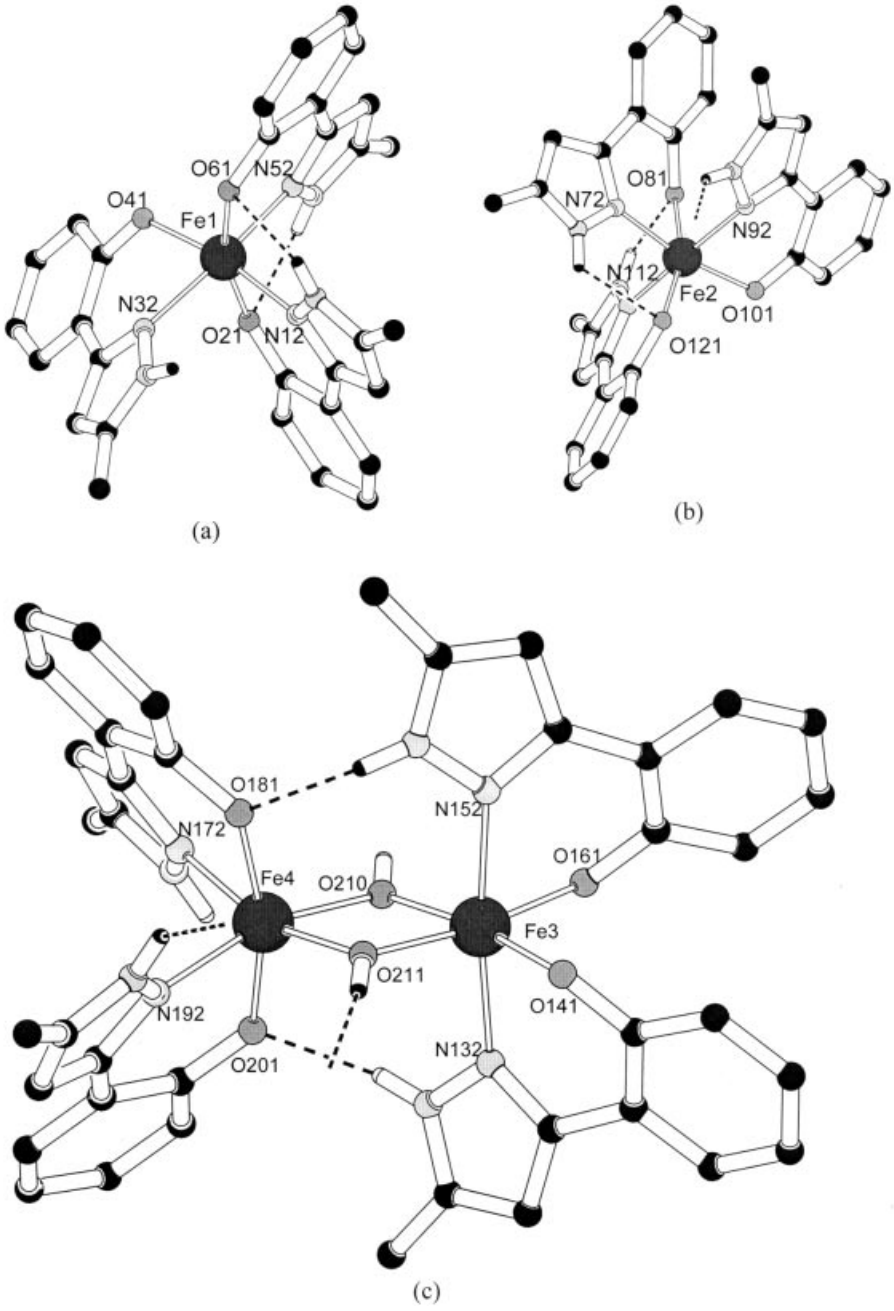

Figure 2. Pluton projections and labeling scheme of the three molecules of the asymmetric unit of $[\{Fe(Hphpz)_2(OH)\}_2][Fe(Hphpz)_3]_2$ (**2**) including the hydrogen bond interactions

$[Fe(Hphpz)_2(OH)]_2$. Two strong O−H···O hydrogen bonds occur between the hydroxo-bridges of $[Fe(Hphpz)_2(OH)]_2$ and the O donor of one $Hphpz^-$ ligand from each $[Fe(Hphpz)_3]$ monomer. Thus, the three molecules are linked by N−H···O and O−H···O hydrogen bonding interactions to form a tetranuclear assembly with approximate C_2-symmetry. Several intermolecular π···π stacking interactions involving aromatic rings of the of the $Hphpz^-$ ligands of the three iron complexes further reinforce the tetranuclear assembly (Table S2 in the Supporting Information). An additional inter − tetranuclear assembly π···π interaction occurs between peripheral pyrazole rings of inversion-related tetranuclear assemblies. The optimization of these packing interactions leads to $Hphpz^-$ ligand conformations varying from nearly planar to considerably twisted; the dihedral angles between the phenyl and pyrazole ring planes within the ligands range from 1.6(3) to 23.0(4)°. In the three-dimensional structure of $[\{Fe(Hphpz)_2(OH)\}_2]$-$[Fe(Hphpz)_3]_2$, the assemblies are separated by large voids filled with disorded THF solvent molecules.

Mössbauer Spectroscopic Results

To study the four different species in more detail, Mössbauer spectroscopy was applied with fitting pro-

 © 2004 Wiley-VCH Verlag GmbH & Co. KGaA, Weinheim

Table 1. Selected bond lengths (Å) and angles (°) for $[\{Fe(Hphpz)_2(OH)\}_2][Fe(Hphpz)_3]_2$

Bond lengths			
Fe1−O21	1.942(3)	Fe3−O141	1.990(3)
Fe1−O41	1.942(3)	Fe3−O161	1.986(3)
Fe1−O61	1.960(3)	Fe3−O210	1.968(3)
Fe1−N12	2.099(4)	Fe3−O211	1.979(3)
Fe1−N32	2.156(4)	Fe3−N132	2.117(4)
Fe1−N52	2.109(4)	Fe3−N152	2.118(4)
Fe2−O81	1.952(3)	Fe4−O181	1.971(3)
Fe2−O101	1.945(3)	Fe4−O201	1.968(3)
Fe2−O121	1.941(3)	Fe4−O210	1.990(3)
Fe2−N72	2.122(5)	Fe4−O211	1.991(3)
Fe2−N92	2.157(4)	Fe4−N172	2.119(4)
Fe2−N112	2.109(4)	Fe4−N192	2.134(4)
Bond angles			
O21−Fe1−O41	94.67(13)	O141−Fe3−O161	94.14(13)
O21−Fe1−O61	162.12(13)	O141−Fe3−O210	169.71(14)
N32−Fe1−N52	172.32(15)	O141−Fe3−O211	95.33(13)
N12−Fe1−N32	88.30(15)	O161−Fe3−O211	169.88(12)
O41−Fe1−N32	81.43(13)	O161−Fe3−N152	83.20(13)
O61−Fe1−N32	102.08(13)	O210−Fe3−N152	92.94(13)
O41−Fe1−N12	169.61(14)	N132−Fe3−N152	173.50(15)
O61−Fe1−N52	82.75(13)	O210−Fe3−O211	75.16(13)
O81−Fe2−O101	95.75(15)	O181−Fe4−O201	165.28(12)
O81−Fe2−O121	161.65(15)	O181−Fe4−O210	104.84(12)
O121−Fe2−N92	102.2(14)	O181−Fe4−O211	86.72(12)
N92−Fe2−N112	172.22(16)	O201−Fe4−O211	105.29(12)
O101−Fe2−N92	80.88(14)	O210−Fe4−O211	74.42(13)
O81−Fe2−N72	82.87(17)	O210−Fe4−N192	162.48(14)
O101−Fe2−N72	167.15(16)	N172−Fe4−N192	99.16(15)
N72−Fe2−N112	99.19(16)	O211−Fe4−N172	162.57(14)

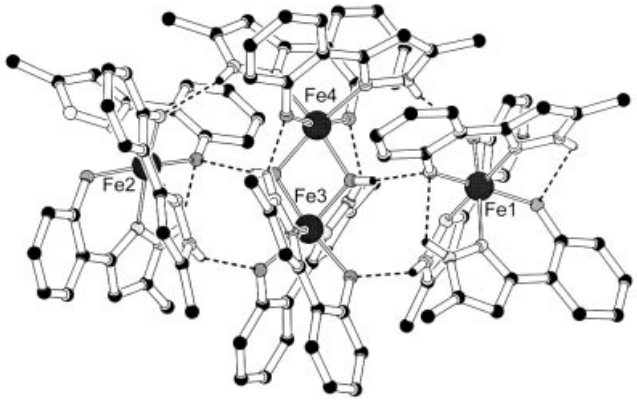

Figure 3. View of **2** showing the hydrogen-bonded network. Hydrogen atoms not involved in hydrogen bonding are omitted for clarity

cedures. The Mössbauer spectra of $[\{Fe(Hphpz)_2(OH)\}_2][Fe(Hphpz)_3]_2$ measured at 295 and 78 K are shown in Figure 4. As might be expected for a compound containing four crystallographically distinct, but chemically similar iron sites, the observed spectra do not show spectral resolution of the four different iron sites. Because of the four crystallographically different iron sites found in $[\{Fe(Hphpz)_2(OH)\}_2][Fe(Hphpz)_3]_2$, the Mössbauer spectra have been fitted with four symmetric quadrupole doublets whose relative areas were constrained to 25 percent each; the resulting hyperfine parameters are given in Table 2.

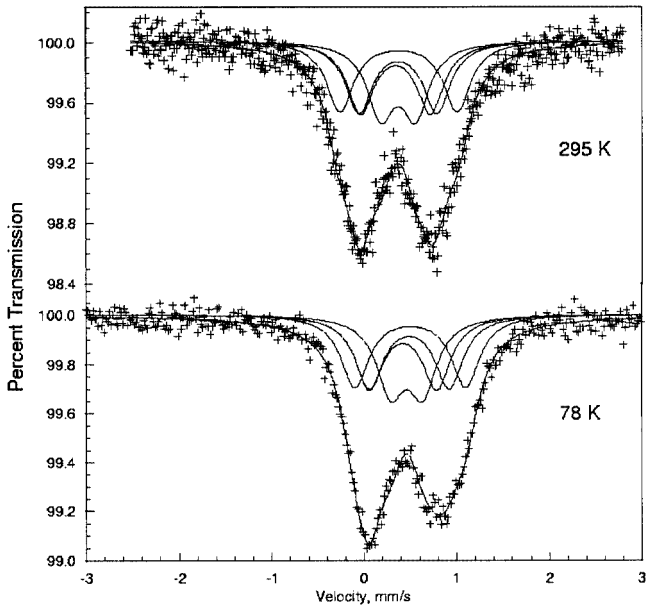

Figure 4. The Mössbauer spectra of **2** obtained at 78 K and 295 K together with the fits for four different species

Table 2. Mössbauer spectral hyperfine parameters of $[\{Fe(Hphpz)_2(OH)\}_2][Fe(Hphpz)_3]_2$

T [K]	δ[a] [mm/s]	ΔE_Q [mm/s]	Γ [mm/s]	Area [%]	Site assignment[b]
295	0.37	0.38	0.36	25	Fe(3)
	0.33	0.74	0.36	25	Fe(1)
	0.38	0.85	0.36	25	Fe(2)
	0.38	1.27	0.36	25	Fe(4)
average	0.365	0.81	0.36	−	
78	0.46	0.35	0.37	25	Fe(3)
	0.42	0.73	0.37	25	Fe(1)
	0.49	0.86	0.37	25	Fe(2)
	0.50	1.19	0.37	25	Fe(4)
average	0.47	0.78	0.37	−	

[a] The isomer shifts are given relative to room temperature α-iron foil. [b] Based on the degree of the octahedral distortions.

It should be noted that the 78 K spectrum shown in Figure 4 was obtained over an ca. ±5 mm/s range in order to detect the presence of any high-spin iron(II) spectral impurities. As expected none was observed and, as a consequence, the 295 K spectrum was obtained over an ca. ±2.5 mm/s range under different spectrometer geometric and electronic conditions. This difference accounts for the unexpected increase in the percentage transmission observed upon warming from 78 to 295 K and may also account for the small, but unexpected, increase in the quadrupole splitting observed upon warming.

Although the fits depicted in Figure 4 may not be unique, the average values of the hyperfine parameters are characteristic of $[\{Fe(Hphpz)_2(OH)\}_2][Fe(Hphpz)_3]_2$ and are typical of those expected of iron(III) in a distorted octahedral coordination environment.[5,20−22] In an attempt to assign

 © 2004 Wiley-VCH Verlag GmbH & Co. KGaA, Weinheim

the different spectral components shown in Figure 4 the average bond angle distortion parameter, d, as defined[23] by

$$d = \frac{100}{n} \bullet \sum_{i=1}^{n} \frac{|a_i - a_m|}{a_m},$$

where n is the number of bonds, a_m is the mean angle, and a_i is an individual bond angle, has been calculated for each of the four different iron sites. The resulting bond angle distortions are 6.53, 7.09, 5.17, and 8.33% for sites Fe(1) to Fe(4), respectively. Because the quadrupole splitting observed at an iron(III) site will increase with increasing distortion of the coordination environment and hence the distortion of the octahedral bond angles, these parameters were used to make the assignments of the sites given in Table 2. However, it should be noted that these assignments are tentative, as the fits may not be unique.

Magnetic Properties

The variable temperature solid-state magnetic susceptibility of complex **2** is shown in the form of χ_m versus T and μ_{eff} versus T plots (Figure 5). The effective magnetic moment decreases as the temperature is lowered from 300 to 5 K. This variation indicates an overall antiferromagnetic behaviour for compound **2**. The temperature dependence of χ_m could be simulated by using the Van Vleck equation derived from the Heisenberg exchange Hamiltonian for two interacting spins $S_1 = S_2 = {}^5/_2$, modified in order to take into account the two isolated Fe^{III} ions.[24] The temperature-independent paramagnetism (TIP = $400 \cdot 10^{-6}$ $cm^3 \cdot K \cdot mol^{-1}$ for each iron ion) was taken into account. Using this approach, the best fit parameters were $J = -2.8$ cm^{-1}, $g = 2.03$. The exchange coupling parameter, J, is known to have values between -5 and -11 cm^{-1} in the case of bis(μ-hydroxo)-bridged iron(III) complexes and the low electron density of the hydroxo-bridge is likely to be responsible for the observed weak antiferromagnetic coupling.[15,25] In the present case, the remarkable dissymmetry of the $Fe_2(\mu\text{-}OH)_2$ core geometry accounts for the weaker antiferromagnetic coupling, as compared with related bis(μ-hydroxo)-bridged iron(III) compounds.

Conclusion

Two iron complexes of the ligand 3(5)-methyl-5(3)-(2-hydroxyphenyl)pyrazole, namely $[Fe(Hphpz)_2Cl(MeOH)]$ (**1**) and $[\{Fe(Hphpz)_2(OH)\}_2][Fe(Hphpz)_3]_2$ (**2**), have been synthesized and characterized by various spectroscopic measurements. Compound **2**, which appears to be a decomposition product of **1** was structurally characterized by X-ray diffraction; its asymmetric unit contains two independent $[Fe(Hphpz)_3]$ molecules and one dinuclear complex $[Fe(Hphpz)_2(OH)]_2$ with two crystallographically nonequivalent iron(III) ions. The remarkable dissymmetric dinuclear $[Fe(Hphpz)_2(OH)]_2$ unit is highly stabilized through π donation of the OH^- bridge and through N−H···O and O−H···O hydrogen bonds. Further attempts to isolate (μ-oxo)(μ-carboxylato)diiron(III) complexes based on $[Fe(Hphpz)_2]^+$ units are underway. The influence of different pyrazole derivatives on the stability of the $Fe_2(OH)_2$ core will also be investigated.

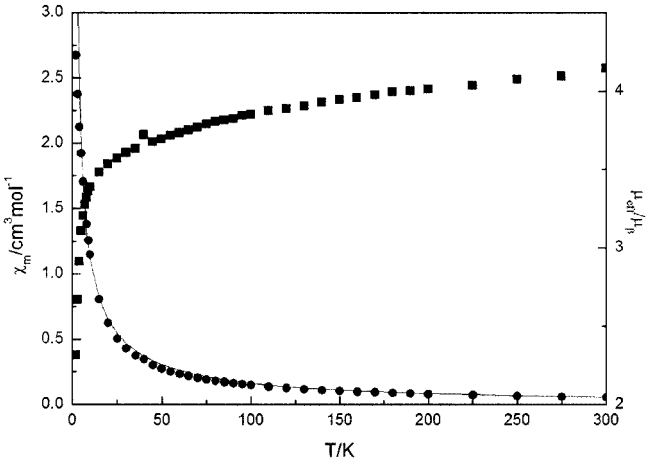

Figure 5. Plots of χ_m and μ_{eff} vs. temperature for compound **2**: (dots) experimental values; (−) calculated values for $J = -2.8$ cm^{-1} and $g = 2.03$

Experimental Section

General Remarks: All chemicals were of reagent grade, and were used as received. 3(5)-methyl-5(3)-(2-hydroxyphenyl)pyrazole (H_2phpz) was prepared by condensation of hydrazine and salicoylacetone as reported previously.[10] All experiments were carried out in air, unless stated otherwise.

Physical Measurements: Elemental analyses for C, H, and N were performed on a Perkin−Elmer 2400 Series II analyzer. Infrared spectra (4000−300 cm^{-1}) were recorded on a Perkin−Elmer Paragon 1000 FTIR spectrometer equipped with a Golden Gate ATR device, using the reflectance technique. UV/Vis spectra were obtained on a Perkin−Elmer Lambda 900 spectrophotometer using the diffuse reflectance technique, with MgO as a reference. Magnetic susceptibility measurements (5−300 K) were carried out at 0.1 T using a Quantum Design MPMS-5 5T SQUID magnetometer. Data were corrected for magnetization of the sample holder and for diamagnetic contributions, which were calculated from the Pascal constants. Mössbauer spectra were measured on a constant-acceleration spectrometer that utilized a room temperature rhodium matrix cobalt-57 source and was calibrated at room temperature with α-iron foil.

$[Fe(Hphpz)_2Cl(MeOH)]$ (1) was synthesized by adding an ethanolic solution containing 3(5)-methyl-5(3)-(2-hydroxyphenyl)pyrazole (0.322 g, 2 mmol) and Bu_4NOH (2 mmol, solution in methanol) to an ethanolic solution of $FeCl_2 \cdot 4H_2O$ (0.198 g, 1 mmol) and stirring for one hour. The resulting dark purple precipitate was collected by filtration, washed with diethyl ether and dried under vacuum. Yield: 72%. $C_{21}H_{22}ClFeN_4O_3$ (469.73): calcd. C 53.70, H 4.72, N 11.93; found C 54.04, H 4.51, N 12.29. IR ($\tilde{\nu}$/cm^{-1}): 3259 s, 2971 m, 2889 m, 1599 m, 1557 s, 1456 m, 1310 s, 1243 m, 1119 m, 1063 m, 982 w, 865 s, 784 s, 747 s, 656 m, 628 m, 583 m, 553 s, 438 m, 386 m. UV/Vis/NIR, $\lambda_{?max}$/nm (ε/m$M^{-1}cm^{-1}$): 264, 369, 568; 359 (3.9), 547(3.5) in methanol solution.

$[\{Fe(Hphpz)_2(OH)\}_2][Fe(Hphpz)_3]_2$ (2) was obtained by slow diffusion of hexane into a tetrahydrofuran solution containing

 © 2004 Wiley-VCH Verlag GmbH & Co. KGaA, Weinheim

$FeCl_2 \cdot 4H_2O$ (0.397 g, 2 mmol) and 3(5)-methyl-5(3)-(2-hydroxyphenyl)pyrazole (0.644 g, 4 mmol) in the presence of 4 equiv. of triethylamine. The resulting red crystals were collected by filtration, washed with diethyl ether and dried under vacuum. Yield: 65% based on iron. $C_{100}H_{92}Fe_4N_{20}O_{12}$ (1989.34): calcd. C 60.38, H 4.66, N 14.08; found C 60.04, H 4.51, N 14.29. IR ($\tilde{\nu}$/cm^{-1}): 3183 m, 2918 m, 2817 m, 1597 m, 1557 m, 1457 s, 1290 m, 1254 m, 1117 m, 1040 m, 972 w, 848 s, 788 m, 751 s, 602 m, 563 m, 481 m. UV/Vis/NIR, $\lambda_{?max}$/nm (ε/mM^{-1}cm^{-1}): 255, 311, 495, 997; 490(3.2) in methanol solution.

X-ray Crystallographic Study: Intensity data for a single crystal of **2** were collected using Mo-K_α radiation (λ = 0.71073 Å) on a Nonius KappaCCD diffractometer. A correction for absorption was considered unnecessary. The structure was solved by automated Patterson methods using SHELXS-97[26] and was refined on F^2 by least-squares procedures using SHELXL-97.[27] The crystal structure contains voids (799.3 A^3/unit cell) filled with disordered THF solvent molecules. Their contribution to the structure factors was ascertained using PLATON/SQUEEZE (206 e/unit cell).[28] All non-hydrogen atoms were refined with anisotropic displacement parameters. The hydroxyl hydrogen atoms were positively identified in a difference Fourier map, and their positions were refined with the restraint that the O−H distances be similar. All other hydrogen atoms were constrained to idealized geometries and allowed to ride on their carrier atoms. The hydrogen atoms of some methyl groups are disordered over two sets of positions. All hydrogen atoms were refined with an isotropic displacement parameter related to the equivalent displacement parameter of their carrier atoms. Structure validation and molecular graphics preparation were performed with the PLATON package.[28] CCDC-244433 contains the supplementary crystallographic data for this paper. These data can be obtained free of charge at www.ccdc.cam.ac.uk/conts/retrieving.html [or from the Cambridge Crystallographic Data Centre, 12 Union Road, Cambridge CB2 1EZ, UK; Fax: +44-1223-336-033; E-mail: deposit@ccdc.cam.ac.uk].

Acknowledgments

This work was financially supported by the Dutch Economy, Ecology, Technology (EET) programme, a joint programme of the Ministry of Economic Affairs, the Ministry of Education, Culture and Science, and the Ministry of Housing, Spatial Planning and the Environment. We would like to acknowledge Dr. R. Hage (Unilever, The Netherlands) for useful discussions.

[1] R. E. Stenkamp, *Chem. Rev.* **1994**, *94*, 715−726.
[2] D. T. Logan, X. D. Su, A. Aberg, K. Regnstrom, J. Hajdu, H. Eklund, P. Nordlund, *Structure* **1996**, *4*, 1053−1064.
[3] A. C. Rosenzweig, C. A. Frederick, S. J. Lippard, P. Nordlund, *Nature* **1993**, *366*, 537−543.
[4] T. Klabunde, N. Sträter, B. Krebs, H. Witzel, *FEBS Lett.* **1995**, *367*, 56−60.
[5] S. Tanase, E. Bouwman, G. J. Long, A. M. Shahin, R. de Gelder, A. M. Mills, A. L. Spek, J. Reedijk, *Polyhedron*, manuscript submitted.
[6] R. Mukherjee, *Coord. Chem. Rev.* **2000**, *203*, 151−218.
[7] H. Toftlund, *Coord. Chem. Rev.* **1989**, *94*, 67−108.
[8] R. H. Holm, P. Kennepohl, E. I. Solomon, *Chem. Rev.* **1996**, *96*, 2239−2314.
[9] E. W. Ainscough, A. M. Brodie, J. E. Plowman, K. L. Brown, A. W. Addison, A. R. Gainsford, *Inorg. Chem.* **1980**, *19*, 3655−3663.
[10] A. W. Addison, P. J. Burke, *J. Heterocyclic Chem.* **1981**, *18*, 803−805.
[11] B. P. Gaber, V. Miskowski, T. G. Spiro, *J. Am. Chem. Soc.* **1974**, *96*, 6868−6873.
[12] E. J. Enemark, T. D. P. Stack, *Inorg. Chem.* **1996**, *35*, 2719−2720.
[13] J. A. Bertrand, P. G. Eller, *Inorg. Chem.* **1974**, *13*, 927−934.
[14] A. B. P. Lever, *Inorganic Electronic Spectroscopy*, Elsevier Science B. V., Amsterdam, **1986**.
[15] E. I. Solomon, T. C. Brunold, M. I. Davis, J. N. Kemsley, S. K. Lee, N. Lehnert, F. Neese, A. J. Skulan, Y. S. Yang, J. Zhou, *Chem. Rev.* **2000**, *100*, 235−349.
[16] V. L. MacMurdo, H. Zheng, L. Que, *Inorg. Chem.* **2000**, *39*, 2254−2255.
[17] D. Lee, J. Du Bois, D. Petasis, M. P. Hendrich, C. Krebs, B. H. Huynh, S. J. Lippard, *J. Am. Chem. Soc.* **1999**, *121*, 9893−9894.
[18] D. W. Lee, S. J. Lippard, *J. Am. Chem. Soc.* **1998**, *120*, 12153−12154.
[19] S. K. Dutta, K. K. Nanda, U. Florke, M. Bhadbhade, K. Nag, *J. Chem. Dalton-Trans.* **1996**, 2371−2379.
[20] G. J. Long, J. T. Wrobleski, R. V. Thundathil, D. M. Sparlin, E. O. Schlemper, *J. Am. Chem. Soc.* **1980**, *102*, 6040−6046.
[21] W. M. Reiff, G. J. Long, W. A. Baker, *J. Am. Chem. Soc.* **1968**, *90*, 6347−6351.
[22] J. A. Bertrand, J. L. Breece, A. R. Kalyanaraman, G. J. Long, W. A. Baker, *J. Am. Chem. Soc.* **1970**, *92*, 5233−5234.
[23] B. Renner, G. Lehmann, *Z. Krist.* **1986**, *175*, 43−59.
[24] O. Kahn, *Molecular Magnetism*, VCH Publishers, New York, **1993**.
[25] W. Rudiger, S. Ostrovsky, K. Griesar, W. Haase, *Inorg. Chim. Acta* **2001**, *326*, 78−88.
[26] G. M. Sheldrick, *SHELXS-97. Program for Crystal Structure solution*, University of Göttingen, Germany, **1997**.
[27] G. M. Sheldrick, *SHELXL-97. Program for Crystal Structure refinement*, University of Göttingen, Germany, **1997**.
[28] A. L. Spek, *PLATON, A Multi-purpose Crystallographic Tool*, Utrecht University, The Netherlands, **2003**.

Received July 14, 2004
Early View Article
Published Online October 14, 2004

 © 2004 Wiley-VCH Verlag GmbH & Co. KGaA, Weinheim

Incorporation of Inorganic Anions in Calcite

Jasminka Kontrec,[a] Damir Kralj,*[a] Ljerka Brečević,[a] Giuseppe Falini,[b] Simona Fermani,[b] Vesna Noethig-Laslo,[c] and Krunoslav Mirosavljević[c]

Keywords: Anions / Calcite / Calcium carbonate / Crystal growth / EPR spectroscopy

A number of analytical methods and techniques (X-ray diffraction, FT-IR and electron paramagnetic resonance spectroscopy, ionic chromatography, scanning electron microscopy, etc.) have been used to study the mode and sites of incorporation of some common inorganic anions (SO_4^{2-}, NO_3^- and Cl^-) in the calcite crystal lattice. Calcite, the thermodynamically stable calcium carbonate polymorph under standard conditions, was prepared by spontaneous precipitation from calcium hydroxide and carbonic acid solutions. The particular co-anion was added into the carbonic acid solution in the form of a calcium salt before mixing the reactants. The system prepared in such a way is particularly suitable for investigating the mode of foreign anion incorporation into the crystal lattice of calcite. Apart from the constituent ions and the products of water protolysis, this system contains only the co-anion examined. In order to study the local environment in the calcite crystal lattice by EPR spectroscopy, Mn^{2+} was used as a paramagnetic substitute for Ca^{2+}. The experiments were performed at 25 °C and the samples for analyses were taken after a predetermined ageing time of 20 min. It was found that the co-anions, when added in the concentrations examined, did not affect the morphology of the calcite crystals but were incorporated into the calcite structure. The largest distortion of the calcite structure was obtained when sulfate ions were added. The measured parameters of the calcite unit cell are given, the results obtained are discussed and a model that explains the possible mode and sites of sulfate incorporation is presented.
(© Wiley-VCH Verlag GmbH & Co. KGaA, 69451 Weinheim, Germany, 2004)

Introduction

In a previous paper, a whole range of different thermodynamic and hydrodynamic parameters that could influence physical-chemical properties of the precipitated calcium carbonate was investigated.[1] Different processes were involved in its formation and different products (polymorphs) were obtained. Thus, even in the systems in which calcite was found to be the only solid phase after the predetermined period of time, its formation was the result either of the recrystallisation of the precursor phase(s) (amorphous calcium carbonate, vaterite) or the crystallisation. As a consequence, the calcite crystals appeared with a range of different physical properties (morphology, size etc.). The influence of foreign ions, primarily Mg^{2+}, in conjunction with some common anions (SO_4^{2-}, NO_3^- and Cl^-) on the physical and chemical properties of calcium carbonate precipitate was also described. The aim of these investigations was principally to study the effects of both the cation and the anions on the morphology of calcite. This work showed that incorporation of magnesium into the calcite crystal lattice depends on the nature of the co-anion present in the system. It was also shown that there is a clear relation between the morphological properties of calcites containing magnesium and the concentration of the corresponding anion, as well as the amount of Mg^{2+} incorporated into calcite lattice. Besides, it was found that the addition of sulfate ions only, caused the formation of spherical aggregates of the originally rhombohedral calcite crystals. Calcite was chosen because it is the only thermodynamically stable polymorph of calcium carbonate under standard conditions to which the other two less stable polymorphs (aragonite and vaterite) gradually transform. Moreover, extensive data relating to calcite exist in the literature. These data are the source of valuable information necessary for our findings to be explained and for the model proposed, in which small inorganic anions are incorporated into the calcite lattice. In addition, calcite is of great interest because of its wide use in industry (pigment and filler in paper, rubber, plastics, paints etc.) and also because of its widespread occurrence in the natural environment (biomineralisation, geological scales). It also has significant impact on energy production and water treatment (scaling). In all these instances, the crystal size distribution and morphology of the crystals are of great significance, as well as their chemical composition

[a] Laboratory for Precipitation Processes, Division of Materials Chemistry, Ruđer Bošković Institute,
P. O. Box 180, 10002 Zagreb, Croatia
Fax: (internat.) + 385-1-4680098
E-mail: kralj@rudjer.irb.hr
[b] Dipartimento di Chimica "G. Ciamician", Università degli Studi,
via Selmi 2, 40126 Bologna, Italy
[c] Laboratory for Magnetic Resonance, Division of Physical Chemistry, Ruđer Bošković Institute,
P. O. Box 180, 10002 Zagreb, Croatia

(degree of the additive incorporation into the crystal lattice). Additives and impurities of both an inorganic and an organic nature play an important role. In recent years, the most intensively investigated additives concerning this matter were soluble polymeric and special functional low molecular weight additives,[2−7] as well as the protein macromolecules isolated from some living organisms.[8−11] Among the inorganic ions and small molecules, the effects of Mg^{2+} and some organic acids[12−19] on the formation and morphology of calcium carbonate polymorphs were studied much more than the effects of anions and other cations.[1,20−23] Only a few papers[1,20,22] have considered anions as a possible way of controlling the calcite morphology. The anions studied in our previous investigations and in the present work were chosen because they are the possible impurities in any precipitation system and some of them, such as SO_4^{2-} in seawater, can be present in rather high concentrations.

In order to investigate the role of anions separately from the foreign cations in the calcium carbonate precipitation system in this investigation, calcite was precipitated from a system in which calcium hydroxide and carbonic acid solutions were used as reactants. Thus, any possible effects of ions other than the constituent ions or products of autoprotolysis of water (Ca^{2+}, CO_3^{2-}, HCO_3^-, H_3O^+, OH^-) on the precipitation of calcite were avoided. Calcite prepared in such a way can be used as a reference material for a number of different studies. After that, foreign anions were added to the precipitation system in the form of calcium salts [$CaSO_4$, $Ca(NO_3)_2$ and $CaCl_2$] and a relatively narrow range of the co-anion concentrations was investigated at a relatively low initial supersaturation.

The aim of the present work was to shed more light upon the mode and sites of incorporation of these anions into the calcite lattice. For this purpose X-ray powder diffraction (XRD), FT-IR and electron paramagnetic resonance (EPR) spectroscopy, scanning electron microscopy (SEM) and ion chromatography (IC) were used. In order to study the local environment in the calcite crystal lattice by EPR spectroscopy, Mn^{2+} was used as a paramagnetic substitute for Ca^{2+}. Mn^{2+} is a particularly appropriate probe for such a study because it readily substitutes for Ca^{2+} in the calcite structure and gives a strong EPR signal at room temperature providing abundant information even in the solid state.[13,24−29]

Results and Discussion

All experiments were performed on the precipitation system in which the total initial concentrations of calcium and carbonate ions in solution were, respectively, $c_i(Ca^{2+}) = 5.0 \times 10^{-3}$ mol·dm^{-3} and $c_i(CO_3^{2-}) = 9.0 \times 10^{-3}$ mol·dm^{-3} and the initial pH was approximately 8.7. The initial supersaturation of this system $S = (\Pi/K_{sp}^{o})^{1/2}$, defined as relative supersaturation, S-1, where Π is the ion activity product $\Pi = a(Ca^{2+})\cdot a(CO_3^{2-})$ and K_{sp}^{o} is the thermodynamic equilibrium constant of calcite dissolution ($K_{sp}^{o} = 3.313 \times 10^{-9}$ at 25 °C), was calculated to be S-1 = 10.38. The detailed calculation procedure, which takes into account the respective protolytic equilibria and equilibrium constants as well as the charge and mass balance equations, has been given previously.[1,30]

Figure 1 (a) shows typical crystal size distributions of calcite precipitated in a pure system. A relatively narrow distribution was obtained exhibiting a maximum at about 7 μm. This is consistent with the previous findings[1] according to which the crystals obtained at relatively low supersaturations [(S-1) < 20], formed by heterogeneous nucleation and slow crystal growth, are small in size and considerably monodispersed. This also confirms the observation that the crystal size distribution depends primarily on supersaturation and not on the initial molar ratios $c_i(Ca^{2+})/c_i(CO_3^{2-})$, since such distributions are obtained regardless of carbonate or calcium ions being in excess in the system. The presence of a co-anion (sulfate, nitrate, chloride), added in the system in concentrations mentioned above, did not change the size distribution significantly. Figure 1 (b) shows such a distribution obtained when the highest of the $CaSO_4$ concentrations examined in this work ($c_i = 1.0 \times 10^{-3}$ mol·dm^{-3}) was added into the precipitation system. Slight differences between the distribution curves shown in Figure 1 (a and b) reflect the appearance of a certain portion of smaller calcite crystals obtained in the system with the additive.

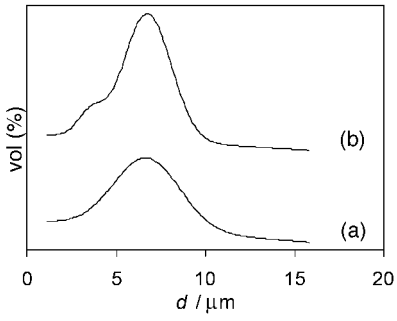

Figure 1. Volume distributions of calcite crystals obtained in the precipitation system $c_i(Ca^{2+}) = 5.0 \times 10^{-3}$ mol·dm^{-3}, $c_i(CO_3^{2-}) = 9.0 \times 10^{-3}$ mol·dm^{-3} at 25 °C, containing $CaSO_4$: a) 0 mol·dm^{-3}; b) 1.0×10^{-3} mol·dm^{-3}

Rather uniformly shaped crystals were obtained with or without the addition of the co-anions. As an example, Figure 2 shows scanning electron micrographs of calcite crystals obtained in the systems with increasing concentrations of sulfate ions. At the highest concentration of sulfate ions, a slight tendency towards the formation of aggregates of smaller rhombohedral calcite crystals, as shown in Figure 2 (d), could be sporadically observed. This is consistent with the findings represented in Figure 1. It should be noted that the effect of sulfate ions on the calcite morphology is more pronounced in the precipitation systems, in which the initial supersaturation, and consequently the growth rate and the aggregation tendency is much higher (S-1 > 30, pH_i > 10.5). In such cases, the formation of spherical aggregates

 © 2004 Wiley-VCH Verlag GmbH & Co. KGaA, Weinheim

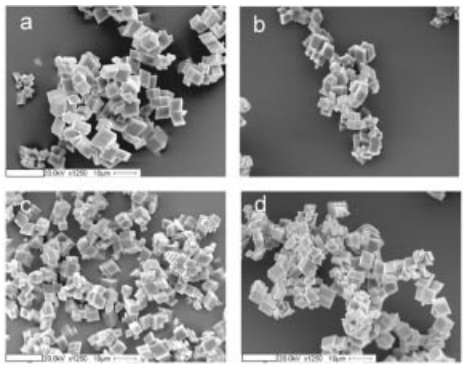

Figure 2. Scanning electron micrographs of calcite crystals isolated from the system $c_i(Ca^{2+}) = 5.0 \times 10^{-3}$ mol·dm^{-3}, $c_i(CO_3^{2-}) = 9.0 \times 10^{-3}$ mol·dm^{-3} at 25 °C, to which the following concentrations of $CaSO_4$ were added: (a) 1.0×10^{-4} mol·dm^{-3}, (b) 3.0×10^{-4} mol·dm^{-3}, (c) 6.0×10^{-4} mol·dm^{-3} and (d) 1.0×10^{-3} mol·dm^{-3}

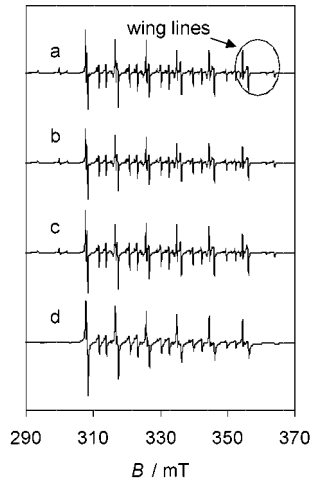

Figure 3. EPR spectra of $^{55}Mn^{2+}$ in (a) pure calcite (the "wing lines" are denoted) and calcites prepared in the presence of 1.0×10^{-3} mol·dm^{-3}: (b) NO_3^-, (c) Cl^- and (d) SO_4^{2-}; the measured parameters of the spectra are given in Table 1

of the originally rhombohedral calcite crystals could be obtained.[1] In order to minimise the influence of the kinetic factors, a relatively narrow range of the co-anion concentrations was investigated at a relatively low initial supersaturation. Such precautions were necessary since changes in nucleation and/or crystal growth rates can cause changes in the growth mechanisms and, consequently, influence the mode and extent of the co-anion incorporation. Therefore, the initial supersaturations in the systems with and without the addition of co-anions were also kept approximately the same.

In order to establish the possible incorporation of sulfate into the calcite lattice and to find out the possible sites and mode of their incorporation, the samples were analysed by EPR spectroscopy, IC and XRD. Figure 3 shows a comparison of an EPR spectrum of Mn^{2+}-doped pure calcite (spectrum a) with the EPR spectra of Mn^{2+}-doped calcite samples obtained when the highest concentration of co-anions used in this work were added to the precipitation system, i.e. 1.0×10^{-3} mol·dm^{-3} NO_3^- (spectrum b), 1.0×10^{-3} mol·dm^{-3} Cl^- (spectrum c) or 1.0×10^{-3} mol·dm^{-3} SO_4^{2-}, (spectrum d). The lines in spectrum b remain similar in structure and linewidth to those in spectrum a. Spectra c and d exhibit broader lines and a larger broadening of the wing lines. Results of the EPR spectroscopic analyses are summarised in Table 1. It can be seen that the addition of Cl^- or SO_4^{2-} is reflected in the spectra as an increase in the parameter D' from 1.7 mT to 1.8 mT. On the other hand, the addition of NO_3^- did not show any effect of this kind. Parameter D' reflects the distortion of the calcite lattice from axial symmetry. The increase of D' may be accompanied by the uniaxial strain of the threefold axis, expressed in the EPR spectra by broadening of the wing lines (*RH* parameter). Uniaxial strain is produced by defects in the crystal lattice due to the different charges or sizes of the impurity ions, the co-anions in this case. Any of these cannot affect the spectroscopic hyperfine linewidths (ΔW). The *RH* parameters measured in the samples to which SO_4^{2-}, Cl^- or NO_3^- were added are displayed in Figure 4 as a function of the co-anion initial concentrations. A pronounced increase in the *RH* parameter upon the addition of SO_4^{2-} suggests that although these anions match the charge of the calcite CO_3^{2-} groups, they produce

Table 1. EPR spectroscopic parameters [axial unit cell distortion, D'; parallel ($\Delta W_\parallel$) and perpendicular ($\Delta W_\perp$) hyperfine linewidths of $m_{Mn} = -5/2$; "wing lines" broadening, *RH*] of pure calcite and calcite samples prepared with the addition of different concentrations of Cl^-, NO_3^- and SO_4^{2-} ions

	c [mol·dm^{-3}]	D' [mT]	$\Delta W_\parallel$ [mT]	$\Delta W_\perp$ [mT]	P	Q	$RH = P/Q$
	0	1.72 ± 0.02	0.17 ± 0.02	0.24 ± 0.03	1853.0	290.3	6.4
Chloride	0.0010	1.80 ± 0.05	0.20 ± 0.03	0.26 ± 0.03	1760.8	221.2	8.0
	0.0006	1.80 ± 0.05	0.15 ± 0.03	0.23 ± 0.03	1681.4	233.5	7.2
	0.0003	1.80 ± 0.05	0.16 ± 0.03	0.22 ± 0.03	1189.8	182.3	6.5
Nitrate	0.0010	1.71 ± 0.02	0.19 ± 0.02	0.25 ± 0.03	990.0	158.2	6.3
	0.0006	1.79 ± 0.02	0.20 ± 0.02	0.26 ± 0.03	978.0	163.8	6.0
	0.0003	1.71 ± 0.02	0.18 ± 0.02	0.24 ± 0.03	1550.0	240.6	6.4
	0.0001	1.74 ± 0.02	0.15 ± 0.02	0.25 ± 0.03	1161.4	192.0	6.0
Sulfate	0.0010	1.82 ± 0.05	0.24 ± 0.03	0.41 ± 0.03	577.4	11.1	52.0
	0.0006	1.82 ± 0.05	0.24 ± 0.03	0.35 ± 0.03	530.0	15.2	34.9
	0.0003	1.80 ± 0.05	0.18 ± 0.03	0.27 ± 0.03	635.6	32.4	19.6
	0.0001	1.71 ± 0.03	0.21 ± 0.03	0.24 ± 0.03	962.0	84.2	11.4

 © 2004 Wiley-VCH Verlag GmbH & Co. KGaA, Weinheim

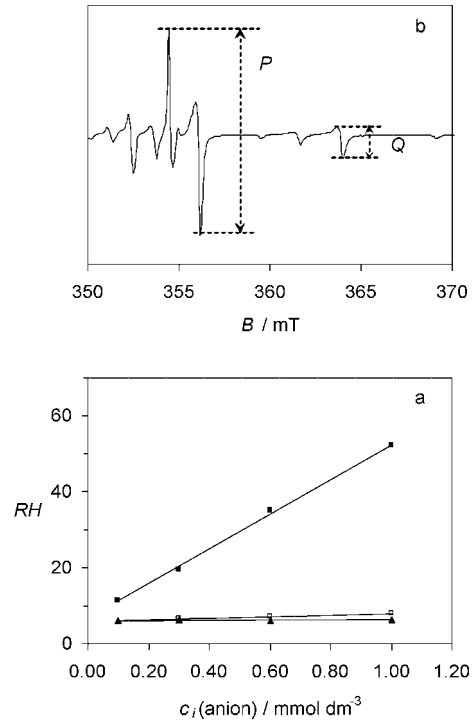

Figure 4. Plots of the *RH* parameter, broadening of the wing lines in the EPR spectrum, as a function of co-anion concentration (a): sulfate (solid squares), chloride (open squares) and nitrate (solid triangles); the *P* and *Q* parameters are denoted on the magnified image of the wing lines shown in Figure 3 (b); from these parameters $RH = P/Q$ was calculated

larger uniaxial strain than NO_3^- or Cl^-. As uniaxial strain has its effect on the threefold axis of the crystal symmetry alone, one would expect it to have a larger effect on the symmetry of only one of the crystal axes, that is, along the *c* axis of the calcite lattice.

Figure 5 compares the X-ray diffraction pattern of pure calcite with those of the samples prepared with the addition of the highest concentration (1.0×10^{-3} mol·dm^{-3}) of co-anions examined in this work. All the diffraction patterns reveal the presence of calcite as the unique calcium carbonate crystalline phase. It is evident that the presence of nitrate ions in the precipitation system does not have an effect on the diffraction pattern of the precipitated calcite which is similar to that of pure calcite. The presence of chloride ions also has no effect on the diffraction peak positions but results in a slight increase of the diffraction peak full width half maxima (FWHM) as the co-anion concentration increases. Since this effect indicates a reduction in the overall crystallinity, it could be related to the incorporation of chloride ions into the calcite structure. The effect of sulfate ions is more pronounced. These ions are not only incorporated in the calcite structure but, at the same time, they induce a reduction in the phase crystallinity. Although the differences among the diffraction patterns presented are minimal, they can be considered as relevant because the trend in the increase of line broadening follows the increase of the initial co-anion concentration in solution.

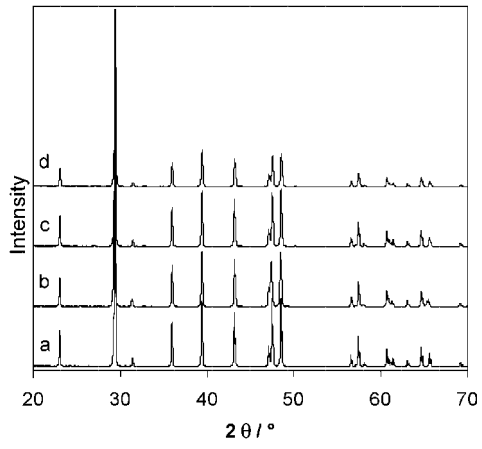

Figure 5. Powder X-ray diffraction pattern of (a) pure calcite and calcites prepared in the presence of 1.0×10^{-3} mol·dm^{-3}: (b) sulfate, (c) nitrate and (d) chloride

Additional support to the previous conclusions is provided by the differential thermal analyses (DTA) of the samples. An endothermic peak at 810 °C was obtained for pure calcite, denoting its decomposition by loss of CO_2. The samples prepared with the addition of 1.0×10^{-3} mol·dm^{-3} $CaSO_4$ showed a shift in this peak by 15 °C toward lower temperatures. These observations suggest that such a shift could be induced by incorporation of sulfate ions in the calcite structure causing a destabilising effect.

Since SO_4^{2-} showed the largest effect on the calcite crystal symmetry, most emphasis will be given to this anion in the following discussion.

Figure 6 shows the content of sulfate ions in the calcite crystals, determined by ion chromatography, as a function of the initial concentration of sulfate ions in the precipitation systems. The incorporation of sulfate ions in the solid phase increases linearly with the increase in the amount of $CaSO_4$ added. This is consistent with the XRD measurements of the calcite unit cell parameters (i.e. *a*, *c* and unit cell volume), as shown in Table 2. The changes in the *a* and *c* axes are also linearly dependent on the quantity of sulfate ions added to the precipitation systems, the change in the *c* axis being larger than that in *a* axis. Figure 7 shows these changes as a relative scale, i.e. as $(a_{sample}/a_{reference}) \times 100$.

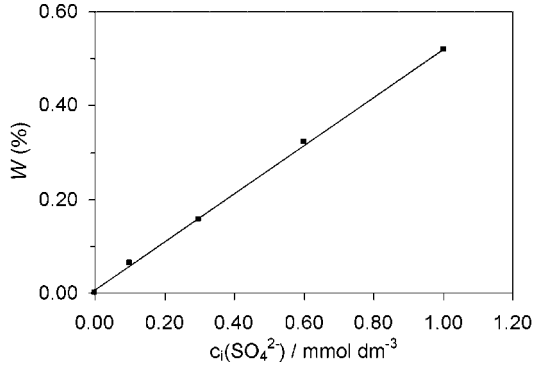

Figure 6. Sulfate ion content in the calcite crystals, determined by ion chromatography, as a function of the initial concentration of sulfate ions added as $CaSO_4$ in the precipitation systems

 © 2004 Wiley-VCH Verlag GmbH & Co. KGaA, Weinheim

Table 2. Calcite unit cell parameters and full width half maxima (FWHM) of two diffraction peaks as a function of sulfate ion concentration added to the precipitation system

Sample	$c_i(SO_4^{2-})$ [mmol·dm^{-3}]	a [Å]	c [Å]	V [Å^3]	FWHM (006)[a] (2θ)	FWHM (300)[a] (2θ)
Ref. data[31]		4.989	17. 062	367.78		
00[b]	0.00	4.9917(2)	17.069(9)	368.34(3)	0.09	0.10
S 01	0.10	4.9899(1)	17.085(5)	368.43(1)	0.12	0.10
S 02	0.30	4.9931(2)	17.081(8)	368.8(3)	0.12	0.10
S 03	0.60	4.99258(7)	17.10(1)	369.2(9)	0.13	0.11
S 04	1.00	4.996(4)	17.11(1)	370.0(5)	0.15	0.13

[a] Miller index of the calcite structure according to a rhombohedral unit cell.[31] [b] Pure calcite obtained from the precipitation system.

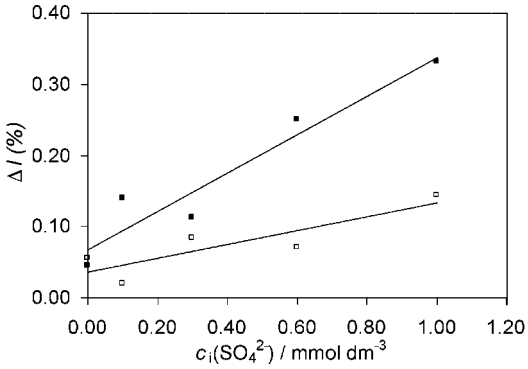

Figure 7. Relative changes of calcite crystal cell *a* (open squares) and *c* (solid squares) axes shown as a function of the initial concentration of sulfate ions added as $CaSO_4$, in the precipitation systems

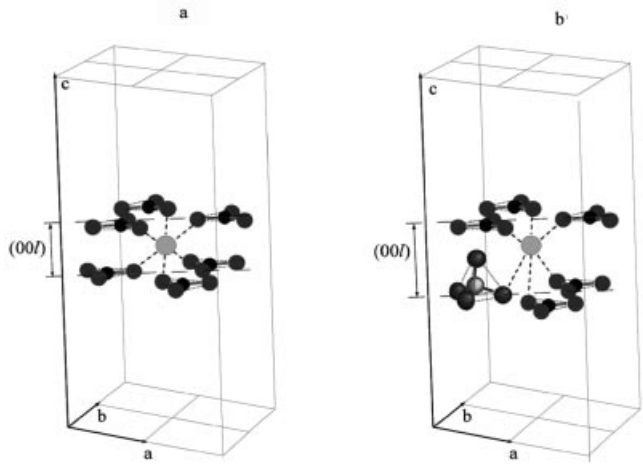

Figure 8. Schematic representation of the model showing: (a) the calcite crystal lattice cell and (b) the possible mode and site of sulfate ion incorporation

The observed similarity in the crystal size distributions (Figure 1) and morphologies (Figure 2) of the investigated systems, as well as the linear dependence of the amount of anion incorporated in the calcite crystals on its concentration in solution (Figure 6), give additional assurance that the extent and mode of anion incorporation (SO_4^{2-} in particular) are predominantly functions of thermodynamic factors (e.g. chemical nature of the ions, ionic radii, coordination properties, hydration free energy etc.).

Based on the results of EPR spectroscopic, IC and particularly the XRD analyses, a simplified model can be proposed which attempts to explain the mode and site of sulfate incorporation in the calcite crystal lattice. A schematic presentation of a calcite crystal lattice, in which one calcium ion is coordinated with six carbonate ions, is shown in Figure 8 (a). If a planar carbonate is replaced by a sulfate ion, three of the sulfate's apical oxygen atoms in the tetrahedral structure could be accommodated in the place of the planar trigonal carbonate, as shown in Figure 8 (b). In this case, the sulfur and the fourth oxygen atom of the sulfate are out of the carbonate plane which induces an increase in the calcite *c* axis. A small increase in the *a* axis can also be expected, since the three apical oxygen atoms of the sulfate occupy a slightly larger surface (256.4 Å^2) in the plane compared with the carbonate ion (212.1 Å^2). In accordance with the proposed model, the effect of distortion of the calcite structure, caused by sulfate substitution, should be more evident along the *c* axis. At the highest isomorphic substitution of sulfate ions obtained, the distortion of the unit cell axes, with respect to the pure calcite, was about 0.05 Å (0.3%) and 0.01 Å (0.1%) for the *c* and *a* axes, respectively. The XRD broadening of peaks, detected in the calcite samples prepared with the additions of sulfate ions, confirms the crystal lattice disorder induced by the presence of sulfate ions (Table 2). This effect, related to the size of the crystalline domains, is quite evident in the (00*l*) reflections but is smaller in the (*h*00) reflections. This suggests a higher degree of disorder induced in the calcite structure by sulfate ions along the *c* direction.

These crystallographic observations agree well with the EPR spectroscopy and provide evidence of the importance of the sulfate ions in destabilising the calcite structure.

Conclusions

The extent and mechanism of incorporation of some common inorganic anions (SO_4^{2-}, Cl^-, NO_3^-) into the calcite crystal lattice and their influence on the physical and chemical properties of the precipitate were investigated in the precipitation system under conditions of a moderate relative initial superstaturation (S-1 = 10.4) at 25 °C.

In order to avoid the presence of any undesirable chemical species (except Ca^{2+}, CO_3^{2-} and the products of their hydrolysis, as well as H^+ and OH^-) the precipitation was

 © 2004 Wiley-VCH Verlag GmbH & Co. KGaA, Weinheim

initiated by mixing calcium hydroxide ($c_i = 5.0 \times 10^{-3}$ mol·dm^{-3}) and carbonic acid ($c_i = 9.0 \times 10^{-3}$ mol·dm^{-3}) solutions. For the same reasons, no pH or ionic strength adjustments were made.

Under the given experimental conditions, calcite crystals were formed by heterogeneous nucleation and were small in size and considerably monodispersed.

The co-anions (chloride, nitrate or sulfate) were added into the system in the form of an appropriate calcium salt and the addition of any of the co-anions did not cause significant changes in the physical or chemical properties of the precipitate.

According to the X-ray diffraction, ion chromatographic and EPR spectroscopic analyses of the calcite samples, the respective co-anions were incorporated into the calcite crystal lattice to a certain extent, the incorporation of sulfate ions being the most extensive.

A model of sulfate incorporation into the calcite lattice can be proposed: carbonate ions are partially substituted by sulfate ions, thus causing a distortion of the calcite unit cell. The degree of disorder along the *c* axis is much higher than along the other two crystallographic directions as a consequence of substitution of the tetrahedral sulfate for the planar carbonate ions.

Experimental Section

Materials: All solutions used were prepared from analytically pure chemicals and deionised water of high quality (conductivity < 0.1 μS·cm^{-1}). For the experiments, a thermostatted double-walled glass vessel of 400 mL capacity was used. Precipitation of calcite was initiated by pouring 150 mL of carbonic acid solution into the same volume of calcium hydroxide solution of the appropriate concentration. During precipitation, the system was continuously stirred at a constant rate by means of a flat-bladed stirrer with two perpendicular blades and the extent of the reaction was determined by measuring the pH of the solution. All experiments were performed at 25 °C.

The carbonic acid stock solution was prepared by bubbling a high-grade carbon dioxide stream into water until the apparent constancy of the pH was obtained. The exact concentrations of freshly prepared carbonic acid stock solutions were determined by potentiometric titration using a standard NaOH solution ($c = 0.10$ mol·dm^{-3}). The calcium hydroxide stock solution was prepared by adding an excess of calcium hydroxide into water. The suspension was then filtered through a 0.22 μm membrane filter and the saturated solution was kept under nitrogen. The exact concentration was determined by potentiometric titration using a standard HCl solution ($c = 0.10$ mol·dm^{-3}) and the total calcium content was additionally checked by complexometric titration with EDTA. Foreign anions were added to the system in the form of a calcium salt (calcium sulfate, calcium nitrate or calcium chloride). The required amount of the foreign anion was always added into the freshly prepared carbonic acid solution of known concentration [$c_i(CO_3^{2-}) = 9.0 \times 10^{-3}$ mol·dm^{-3}, diluted from the stock solution] and the total initial concentration of the foreign anion in the system was varied [c_i(anion) = 1.0×10^{-4}, 3.0×10^{-4}, 6.0×10^{-4} or 1.0×10^{-3} mol·dm^{-3}]. The total initial calcium concentration in the system was kept the same [$c_i(Ca^{2+}) = 5.0 \times 10^{-3}$ mol·dm^{-3}] in all experiments.

The samples for analyses were taken after a predetermined ageing time of 20 min, when the total volume of suspension was filtered through a 0.22 μm membrane filter, thoroughly washed with small portions of water and dried at 105 °C. In the system in which no additive was added [$c_i(Ca^{2+}) = 5.0 \times 10^{-3}$ mol·dm^{-3} and $c_i(CO_3^{2-}) = 9.0 \times 10^{-3}$ mol·dm^{-3}], the precipitate consisted entirely of calcite crystals and the amount of crystals obtained in one preparation was just sufficient for all types of analyses to which the solid phase was subjected to.

Methods: The precipitate composition was characterised by a combination of FT-IR spectroscopic (Mattson), thermogravimetric (Mettler TG 50 thermobalance with TC 11 TA processor), differential thermal (Netzsch differential thermal analyzer), and scanning electron microscopic (Philips XL-20) analyses. TGA and DTA were carried out with a heating rate of 20 °C/min and 10 °C/min, respectively, and Al_2O_3 was used as the reference substance for DTA. For the SEM observations, the dried samples were glued by a carbon tape on an aluminium stub and were gold-coated.

Crystal number and size distributions were determined by means of an electronic counting device (Coulter Electronics Ltd.) fitted with a 50-μm orifice tube. This aperture-size diameter enabled crystals in the size range between about 1 and 30 μm to be measured. The instrument was calibrated with standard latex spheres (13.3 μm in diameter). The total content of calcium and sulfate ions in the solid phase was determined by means of an ionic chromatography system (Dionex DX100 fitted with a CD20 conductivity detector). The chromatographic data were collected and processed with the Dionex Peaknet 5.1 program.

The possible incorporation of the co-anion into the calcite structure was evaluated by measuring the calcite unit-cell parameters by XRD. The sample for the X-ray data collection was manually ground in an agate mortar. The powder was mounted on a 1.5 mm thick flat Al holder using the front loading technique and the data collection was performed using a powder diffractometer (Philips PW 1050/81 equipped with a secondary graphite monochromator; Cu-K_α radiation at 40 kV and 40 mA). The instrument was configured with a 1° divergence and 0.2 mm receiving slits. The presence of impurities was checked and excluded by a preliminary qualitative analysis of the X-ray powder pattern. The phase identification was possible using the ICDD-PDF-2 database.[32] The unit cell parameters and their standard deviations were calculated using the CellSize computer program.[33] The number of significant figures of the data obtained depends on the material crystallinity. The diffraction peak full width half maxima (FWHM) were calculated using the computer program WinFit.[34]

Apart from XRD, the interaction of foreign anions with the calcite crystals was also studied by EPR spectroscopy (Varian E-9 spectrometer equipped with a dual microwave resonant cavity). In this case, the local environment of Ca^{2+} in the crystal lattice of calcite was studied using Mn^{2+} ions as a paramagnetic substitute for Ca^{2+}. The calcite crystals were prepared by adding carbonic acid solution (150 mL of 9.0×10^{-3} mol·dm^{-3}) into an equal volume of calcium hydroxide solution (5.0×10^{-3} mol·dm^{-3}). Manganese (2.0×10^{-7} mol·dm^{-3}) was added into the carbonic acid solution prior to mixing the reactants, so that the Mn^{2+} substitution for Ca^{2+} took place during the precipitation of calcite.[13] After the initial mixing of the reactants, the system was agitated mechanically with a flat-bladed stirrer for 20 min at a constant rate and then aged for 30 d without further stirring. The calcite thus obtained was filtered, washed several times with small portions of water, dried at 105 °C and stored in a desiccator. The EPR spectrum of such Mn^{2+}-doped calcite crystals was used as a reference. The uptake of Mn^{2+} by such a method (as determined by IC) was approxi-

 © 2004 Wiley-VCH Verlag GmbH & Co. KGaA, Weinheim

mately 0.005 mol%.[13] This amount does not cause any measurable change in the unit cell parameters of calcite. This was established by our own XRD analyses and has also been reported by other researchers.[29] A qualitative interpretation of the EPR spectroscopic parameters proposed by Angus et al.[29] was applied. These authors reported that the axial distortion parameter D' of the calcite unit cell depends on temperature, pressure and the concentration and nature of the impurity ions incorporated into calcite. In a magnetic field and in the absence of any ligands, Mn^{2+} ions give six lines in the EPR spectrum due to the hyperfine interaction of the high-spin electron state of five electrons, $S = 5/2$, with the nuclear spin of $^{55}Mn^{2+}$ nuclei, $I = 5/2$. The crystal field of the CO_3^{2-} ligands in the calcite unit cell splits these spectral lines further, giving rise to a multi-line EPR spectrum. Thus, the spectrum contains information about the CO_3^{2-} symmetry in the calcite lattice. Any axial distortion of the CO_3^{2-} ligands around Mn^{2+} in the calcite lattice changes the crystal field parameter D' in the spectrum. This parameter is best regarded as a measure of the separation of the parallel and perpendicular components of each of the six main hyperfine lines in the EPR spectrum of calcite and is largest for the high-field hyperfine line $m_{Mn} = -5/2$. The line shapes, ΔW, of the Mn^{2+} spectra are expected to be Lorenzian because of homogeneous line-broadening. Deviations from these ideal line shapes, giving rise to an inhomogeneous line broadening, can be caused by many factors. As suggested by Barberis et al.,[28] a random distribution of oxygen atoms of the CO_3^{2-} groups about their equilibrium positions in the calcite lattice can be induced by the impurity ions. In the EPR spectra, this is reflected as a broadening of all spectral lines and is measured by the parallel ($\Delta W_{\|}$) and perpendicular ($\Delta W_{\perp}$) linewidths of the hyperfine line $m_{Mn} = -5/2$ at half-height from the baseline. On the other hand, the compression along the threefold axis, or random electric fields produced by impurities with different charges or sizes, cannot affect the linewidth of the main lines but does broaden the outer so called "wing lines".[29] This is expressed as the so-called *RH* parameter.

Acknowledgments

This research has been sponsored by the Ministry of Science, Education and Sport of the Republic of Croatia (Project No. 0098061).

[1] D. Kralj, J. Kontrec, Lj. Brečević, G. Falini, V. Nöthig-Laslo, *Chem. Eur. J.* **2004**, *10*, 1647−1656.
[2] J. M. Didymus, P. Oliver, S. Mann, A. L. DeVries, P. V. Hauschka, P. Westbroek, *J. Chem. Soc., Faraday Trans.* **1993**, *89*, 2891−2900.
[3] L. A. Gower, D. A. Tirrel, *J. Cryst. Growth* **1998**, *191*, 153−160.
[4] S. K. Zhang, K. E. Gonsalves, *Langmuir* **1998**, *14*, 6761−6766.
[5] G. Xu, N. Yao, I. A. Aksay, J. T. Groves, *J. Am. Chem. Soc.* **1998**, *120*, 11977−11985.
[6] K. Naka, Y. Tanaka, Y. Chujo, Y. Ito, *Chem. Commun.* **1999**, 1931−1932.
[7] J. García-Carmona, J. Gómez-Morales, J. Fraile-Sainz, R. Rodrígez-Clemente, *Powder Technol.* **2003**, *130*, 307−315.
[8] G. Falini, S. Albeck, S. Weiner, L. Addadi, *Science* **1996**, *271*, 67−69.
[9] N. Wada, K. Yamasita, T. Umegaki, *J. Colloid Interface Sci.* **1999**, *212*, 357−364.
[10] A. M. Belcher, X. H. Wu, R. J. Christensen, P. K. Hansma, G. D. Stucky, D. E. Morse, *Nature* **1996**, *381*, 56−58.
[11] J. Aizenberg, J. Hanson, T. F. Koetzle, S. Weiner, L. Addadi,, *J. Am. Chem. Soc.* **1997**, *119*, 881−886.
[12] G. Falini, M. Gazzano, A. Ripamonti, *J. Cryst. Growth* **1994**, *137*, 577−584.
[13] Lj. Brečević, V. Nöthig-Laslo, D. Kralj, S. Popović, *J. Chem. Soc., Faraday Trans.* **1996**, *92*, 1017−1022.
[14] G. Falini, S. Fermani, M. Gazzano, A. Ripamonti, *J. Mater. Chem.* **1998**, *8*, 10611065.
[15] K. J. Davis, P. M. Dove, J. J. De Yoreo, *Science* **2000**, *290*, 1134−1137.
[16] F. C. Meldrum, S. T. Hyde, *J. Cryst. Growth* **2001**, *231*, 544−558.
[17] M. Kitamura, *J. Colloid Interface Sci.* **2001**, *236*, 318−327.
[18] C. A. Orme, A. Noy, A. Wierzbicki, M. T. McBride, M. Grantham, H. H. Teng, P. M. Dove, J. J. De Yoreo, *Nature* **2001**, *411*, 775−779.
[19] E. Loste, R. M. Wilson, R. Seshadri, F. C. Meldrum, *J. Cryst. Growth* **2003**, *254*, 206−218.
[20] B. W. H. van Beest, G. J. Kramer, R. A. van Santen, *Phys. Rev. Lett.* **1990**, *64*, 1955−1958.
[21] V. Noethig-Laslo, Lj. Brečević, *J. Chem. Soc., Faraday Trans.* **1998**, *94*, 2005−2009.
[22] S. L. Tracy, D. A. Williams, H. M. Jennings, *J. Cryst. Growth* **1998**, *193*, 382−388.
[23] V. Nöthig-Laslo, Lj. Brečević, *Phys. Chem. Chem. Phys.* **1999**, *1*, 3697−3700.
[24] F. K. Hurd, M. Suchs, W. D. Hershberger, *Phys. Rev.* **1954**, *93*, 373−380.
[25] H. M. McConnell, *J. Chem. Phys.* **1956**, *24*, 904−905.
[26] C. Kikuchi, L. M. Matarrese, *J. Chem. Phys.* **1960**, *33*, 601−606.
[27] D. J. J. Kinsman, H. D. Holland, *Geochim. Cosmochim. Acta* **1969**, *33*, 1−17.
[28] G. Barberis, R. Calvo, H. G. Maldonado, C. E. Zarate, *Phys. Rev. B* **1975**, *12*, 853−860.
[29] J. G. Angus, J. B. Raynor, M. Robson, *Chem. Geol.* **1979**, *27*, 181−205.
[30] D. Kralj, Lj. Brečević, J. Kontrec, *J. Crystal Growth* **1997**, *177*, 248−257.
[31] F. Swanson, *Natl. Bur. Stand. (US)* **1953**, *51*, 359.
[32] *Powder Diffraction File 2*, International Centre for Diffraction Data, Newtown Square, Pennnsylvania, USA, **2002**.
[33] David Hay, *CELSIZ*, CSIRO Division of Material Science and Technology, Clayton, Australia.
[34] *Winfit − A Computer Program for X-ray Diffraction Line Profile Analysis*: S. Krumm, *Acta Univ. Carol., Geol.* **1994**, *38*, 253−261.

Received April 2, 2004
Early View Article
Published Online October 7, 2004

 © 2004 Wiley-VCH Verlag GmbH & Co. KGaA, Weinheim

Facile [N]C−H Activation by a (*P*,*N*)-Chelate [3]Ferrocenophane−Ruthenium System

Patrick Liptau,[a] Daniel Carmona,*[b] Luis A. Oro,*[b] Fernando J. Lahoz,[b] Gerald Kehr,[a] and Gerhard Erker*[a]

Keywords: (*P*,*N*)-Chelate ligands / Ruthenium / Ferrocenophane / C−H activation

The chelate ligand **5** was prepared from the corresponding (dimethylamino)[3]ferrocenophane by directed *ortho*-lithiation with *n*-butyllithium followed by treatment with $ClPPh_2$. The rigid (*P*,*N*)-chelate ligand reacts with [Ru(η^6-*p*-cymene)Cl_2] dimer in the presence of KPF_6 in methanol to afford two products in an almost equimolar ratio. Instead of the simple addition product of the [Ru(*p*-cymene)Cl]$^+$ cation reagent to the chelate, selective C–H abstraction at an N–CH_3 moiety occurs with the formation of the "metallaaziridinium"-type product **8** (isolated as its PF_6^- salt). The liberated equivalent of HCl is trapped by the putative (*P*,*N*)-chelate [RuCl]$^+$ complex intermediate to form the corresponding internal hydrochloride complex **7**. The starting material **5** and the products **8** and **7** were characterised by single-crystal X-ray diffraction studies.

(© Wiley-VCH Verlag GmbH & Co. KGaA, 69451 Weinheim, Germany, 2004)

Introduction

The activation of aliphatic C−H bonds by transition metal complexes in a homogeneous phase has continued to attract considerable attention.[1] C−H activation in a position α to a nitrogen atom is of interest for carbon−carbon coupling reactions as well as because of its participation in hydrodenitrogenation of petroleum feedstocks.[2,3] This is commonly observed with early transition metals[4] (see Scheme 1). In the case of late transition metals, only a few examples have been reported.[5] Here, C−H activation mostly takes place next to a phosphorus atom,[6] but a much smaller number of examples of [N]C−H activation has been reported. Weissensteiner et al. have recently described the formation of the stable cationic chelate complex **4** which was obtained by treatment of the ferrocene-derived (*P*,*N*)-chelate ligand **3** with [Ru(η^6-cymene)Cl_2] dimer and a chloride abstractor.[7] We have now employed a related, more rigid [3]ferrocenophane (*P*,*N*)-ligand in a similar reaction and observed markedly different behaviour which is characterised by rapid C−H activation adjacent to nitrogen.

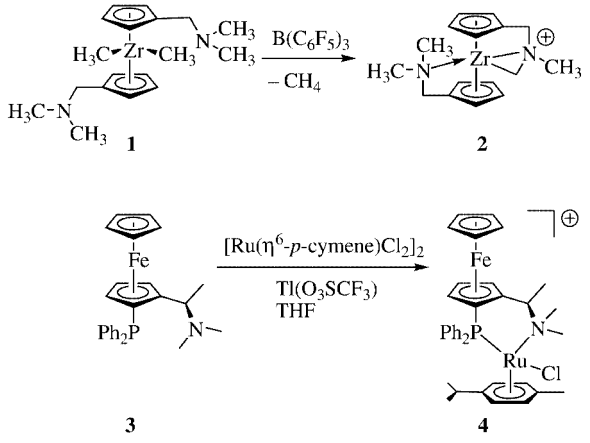

Scheme 1

Results and Discussion

The [3]ferrocenophane-based (*P*,*N*)-chelate ligand system **5** was prepared as described previously by us.[8] Treatment of 1,1′-diacetylferrocene with dimethylamine/$TiCl_4$ resulted in an intramolecular Mannich-type condensation reaction to generate the C_3 bridge. Subsequent catalytic hydrogenation (Pd/C) then gave an approximately 1:7 mixture of the corresponding saturated *cis*- and *trans*-disubstituted [3]ferrocenophane derivatives. The major *trans* isomer **5** was then treated with *n*-butyllithium to bring about directed *o*-lithiation at the Cp ring. Treatment with $ClPPh_2$ then gave the [3]ferrocenophane (*P*,*N*)-chelate ligand **5** in good yield.

Single crystals of the racemate (*rac*-**5**) were obtained from pentane at −18 °C. In the crystal, the enantiomers (*R*)-**5** (6*R*,8*R*,R_{pl}) and (*S*)-**5** (6*S*,8*S*,S_{pl}, see Scheme 2) were found as crystallographically independent molecules. The molecu-

[a] Organisch-Chemisches Institut der Universität Münster, Corrensstrasse 40, 48149 Münster, Germany
Fax: (internat.) + 49-251-8336503
[b] Departamento de Química Inorgánica, Instituto de Ciencia de Materiales de Aragón, Universidad de Zaragoza, C.S.I.C., 50009 Zaragoza, Spain
Fax: (internat.) + 34-976-761143

 © 2004 Wiley-VCH Verlag GmbH & Co. KGaA, Weinheim DOI: 10.1002/ejic.200400400

lar structure of the (*R*)-**5** enantiomer is depicted in Figure 1. The structure features an almost undistorted central ferrocene unit. The C_3 bridge that spans between the pair of almost parallel Cp ring systems attains a typically folded

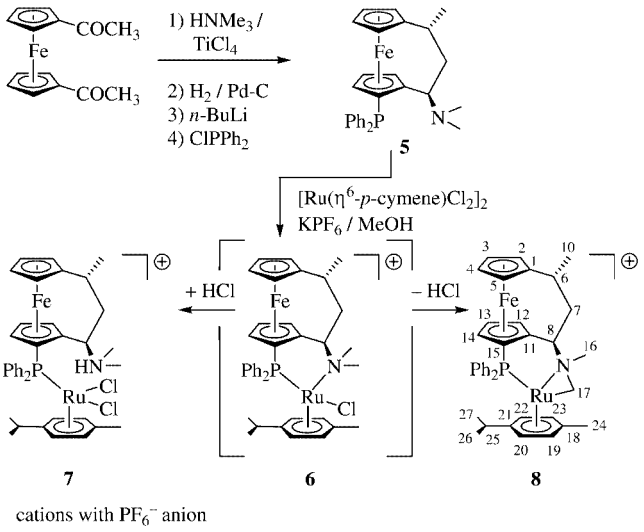

Scheme 2

conformation. At this [3]ferrocenophane framework, the methyl substituent is found in a pseudoaxial orientation whereas the apparently more bulky NMe_2 group is attached pseudo-equatorially. This results in a strong deviation of the P1−C23−C27−C36−N1 chelate pincer from planarity. Inside this framework, the C23−P1 and C36−N1 vectors are found close to a *gauche* arrangement.

Ligand **5** was treated with $[Ru(\eta^6\text{-}p\text{-cymene})Cl_2]_2$ (*p*-cymene = 4-isopropyl-1-methylbenzene) and KPF_6 as a chloride abstractor in methanol at room temperature. The ^{31}P NMR spectra of the crude reaction mixture indicated the formation of two main products. Instead of the expected cationic (*P*,*N*)-chelate compound **6** the hydrochloride **7** and the cyclometallated species **8** were obtained (Scheme 2).

In the solid state, both **7** and **8** show the ruthenium centre as formally hexacoordinate with similar three-legged pianostool environments. Both cationic complexes exhibit an η^6-coordination of the *p*-cymene ring and the *P*-bonded metallo-ligand. In **7**, two chloride ligands with similar but statistically different Ru−Cl bond lengths [2.4102(8) and 2.3942(8) Å] complete the Ru coordination sphere. The molecular structure of complex **8** can be related to that of **7** if we assume the formal substitution of the two halogen atoms by an η^2-bonded CH_2N moiety (Figures 2 and 3).

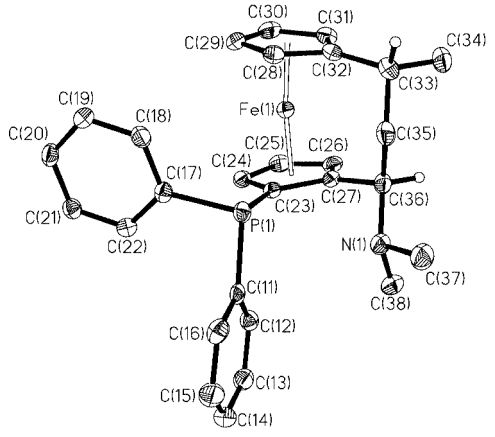

Figure 1. Molecular structure of *rac*-**5** [only the structure of the (*R*)-**5** enantiomer is depicted]; selected bond lengths [Å] and bond and torsional angles [°] [values of the (*S*)-**5** enantiomer in brackets]: Fe−G(2) 1.6307(10) [1.6278(9)], Fe−G(3) 1.6342(10) [1.6314(10)], P−C(11) 1.840(2) [1.836(2)], P−C(17) 1.847(2) [1.841(2)], P−C(23) 1.824(2) [1.820(2)], N−C(36) 1.478(3) [1.482(2)], N−C(37) 1.454(3) [1.453(3)], N−C(38) 1.464(3) [1.454(3)], C(27)−C(36) 1.511(3) [1.515(3)], C(32)−C(33) 1.504(3) [1.510(3)], C(33)−C(35) 1.551(3) [1.547(3)], C(35)−C(36) 1.546(3) [1.538(3)], G(2)−Fe−G(3) 172.47(5) [172.94(5)], C(11)−P−C(17) 99.56(9) [103.00(9)], C(11)−P−C(23) 102.46(9) [100.13(9)], C(17)−P−C(23) 99.03(9) [99.59(9)], C(36)−N−C(37) 115.14(18) [114.62(17)], C(36)−N−C(38) 109.43(17) [110.31(17)], C(37)−N−C(38) 109.17(18) [108.36(17)], C(32)−C(33)−C(35) 112.65(18) [113.32(17)], C(33)−C(35)−C(36) 116.59(19) [116.30(17)], N−C(36)−C(27) 106.20(17) [106.56(16)], N−C(36)−C(35) 111.62(18) [111.67(16)], C(27)−C(36)−C(35) 113.56(17) [113.30(17)], C(23)−C(27)−C(36)−C(35) −69.9(3) [69.8(2)], C(28)−C(32)−C(33)−C(35) 52.3(3) [−50.0(3)], C(32)−C(33)−C(35)−C(36) 69.1(3) [−70.2(2)], C(33)−C(35)−C(36)−C(27) −60.2(2) [60.0(2)], C(33)−C(35)−C(36)−N 179.81(18) [−179.68(16)], C(35)−C(36)−N−C(37) −42.5(2) [47.4(2)], C(35)−C(36)−N−C(38) −165.86(18) [170.01(17)]; G(2) and G(3) represent the centroids of the substituted Cp ligands

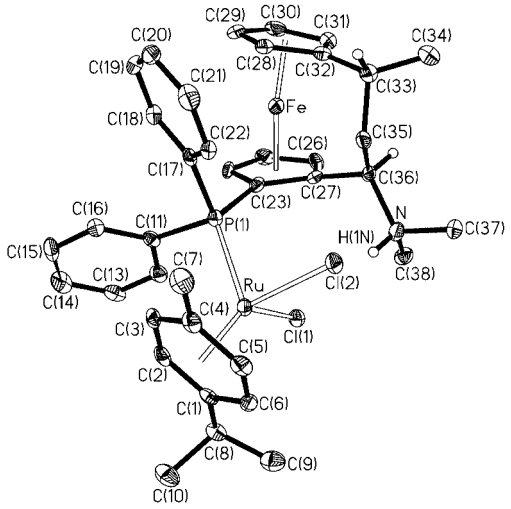

Figure 2. Molecular structure of complex **7** (only the cation is depicted); selected bond lengths [Å] and bond and torsional angles [°]: Ru−Cl(2) 2.4102(8), Ru−Cl(1) 2.3942(8), Ru−P 2.4011(9), Ru−G(1) 1.6964(13), Fe−G(2) 1.6352(14), Fe−G(3) 1.6552(15), P−C(11) 1.834(3), P−C(17) 1.819(3), P−C(23) 1.865(3), N−C(36) 1.527(4), N−C(37) 1.497(4), N−C(38) 1.489(3), C(27)−C(36) 1.520(4), C(32)−C(33) 1.522(4), C(33)−C(35) 1.551(4), C(35)−C(36) 1.521(4), Cl(2)−Ru−P 93.09(3), Cl(1)−Ru−P 83.61(3), Cl(2)/Ru−Cl(1) 87.96(3), G(2)−Fe−G(3) 172.54(8), Ru−P−C(11) 103.31(10), Ru−P−C(17) 117.25(11), Ru−P−C(23) 123.63(10), C(11)−P−C(17) 103.39(15), C(11)−P−C(23) 101.79(14), C(17)−P−C(23) 104.50(13), C(36)−N−C(37) 111.9(2), C(36)−N−C(38) 111.6(2), C(37)−N−C(38) 108.6(3), C(32)−C(33)−C(35) 111.3(3), C(33)−C(35)−C(36) 113.7(3), N−C(36)−C(27) 111.5(2), N−C(36)−C(35) 114.3(2), C(27)−C(36)−C(35) 113.5(3), C(23)−C(27)−C(36)−C(35) −39.0(4), C(28)−C(32)−C(33)−C(35) 75.2(4), C(32)−C(33)−C(35)−C(36) 59.4(3), C(33)−C(35)−C(36)−C(27) −82.8(3), C(33)−C(35)−C(36)−N 147.7(3), C(35)−C(36)−N−C(37) −52.7(3), C(35)−C(36)−N−C(38) −174.7(2); G(1) denotes the centroid of the *p*-cymene ring

 © 2004 Wiley-VCH Verlag GmbH & Co. KGaA, Weinheim

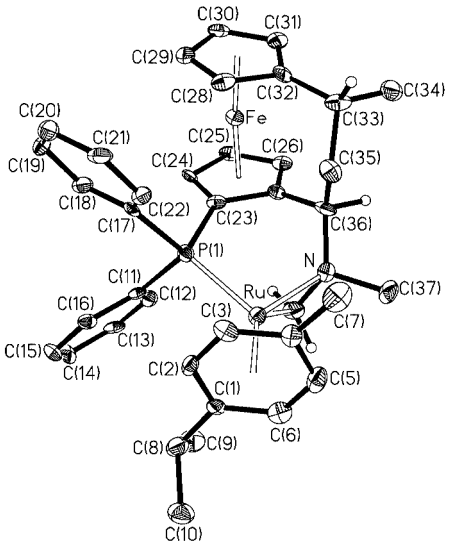

Figure 3. View of the molecular geometry of complex **8** (only the cation is depicted); selected bond lengths [Å] and bond and torsional angles [°]: Ru−N 2.120(4), Ru−C(38) 2.068(5), Ru−P 2.3133(15), Ru−G(1) 1.738(2), Fe−G(2) 1.624(2), Fe−G(3) 1.630(2), P−C(11) 1.827(5), P−C(17) 1.836(5), P−C(23) 1.806(5), N−C(36) 1.481(6), N−C(37) 1.488(6), N−C(38) 1.417(6), C(27)−C(36) 1.468(7), C(32)−C(33) 1.489(7), C(33)−C(35) 1.544(6), C(35)−C(36) 1.567(6), N−Ru−P 93.03(13), C(38)−Ru−P 85.11(16), N−Ru−C(38) 39.55(15), G(2)−Fe−G(3) 173.78(13), Ru−P−C(11) 111.47(16), Ru−P−C(17) 121.60(18), Ru−P−C(23) 112.94(18), C(11)−P−C(17) 101.7(2), C(11)−P−C(23) 101.6(2), C(17)−P−C(23) 105.2(2), C(36)−N−Ru 122.6(3), C(37)−N−Ru 116.4(3), C(38)−N−Ru 68.3(2), C(36)−N−C(37) 109.7(4), C(36)−N−C(38) 120.2(5), C(37)−N−C(38) 114.3(4), C(32)−C(33)−C(35) 113.0(4), C(33)−C(35)−C(36) 115.3(4), N−C(36)−C(27) 113.2(4), N−C(36)−C(35) 108.8(4), C(27)−C(36)−C(35) 113.5(4), C(23)−C(27)−C(36)−C(35) −71.4(7), C(28)−C(32)−C(33)−C(35) 46.2(6), C(32)−C(33)−C(35)−C(36) 72.0(5), C(33)−C(35)−C(36)−C(27) −60.1(6), C(33)−C(35)−C(36)−N 172.8(4), C(35)−C(36)−N−C(37) −78.7(4), C(35)−C(36)−N−C(38) 145.8(4)

The bond lengths within this three-membered metallacycle being Ru−N 2.120(4), Ru−C(38) 2.068(5) and N−C(38) 1.417(6) Å. From these structural parameters an intermediate situation, slightly closer to $(sp^3)C-NR_2$ between a methylene ammonium salt [the $(sp^2)C=N^+R_2$ mean distance in CSD is 1.334 Å] and an aza-metallacyclopropane system [$(sp^3)C-NR_2$ mean distance 1.469 Å] seems to be present. A relevant structural feature of **7** seems to be the presence of a bifurcated asymmetric hydrogen bond between the dimethylammonium group and the two chloride ligands [N···Cl(1) 3.143(3) and N···Cl(2) 3.203(3) Å, see Figure 2]. This may account for the conformational modification observed for the bridging C_3 chain in **7** from the free ligand **5** [torsion angles C(28)−C(32)−C(33)−C(35) 52.3(3)° (in **5**) and 75.2(4)° (in **7**); C(23)−C(27)−C(36)−C(35) −69.9(3)° (**5**) and −39.0(4)° (**7**)]. Interestingly, the strain of this presumably enforced conformation is released when **8** is formed, as confirmed by the values detected for its torsion angles [46.2(6)° and −71.4(7)°] which are very similar to those observed in **5**. Both compounds crystallise in centrosymmetric space groups with only one independent molecule in the unit cell. This feature implies the presence of racemic mixtures of **7** and **8** in the crystals.

As mentioned above, the Ru/N/C ring in **8** can be described as an iminium salt coordinated to the metal atom or as an aza-metallacyclopropane system. We measured direct NMR coupling constants ^1J(C,H) as a method of estimating the s-character of the corresponding C−H bond. For the CH_2 group of the ring, the obtained values of 167 and 176 Hz fall in the range of aziridine (168 Hz) and oxirane (176 Hz). For an iminium salt, larger values would be expected. These data, together with the determined structural parameters, seem to indicate a more accurate description of the metallacycle as an aza-metallacyclopropane ring.[4]

To explain the formation of **7** and **8** it is reasonable to assume that an intermediate (*P*,*N*)-chelate complex [Ru(*p*-cymene)(Cl)(**5**)]·[PF_6] (**6**, Scheme 2) is initially formed. Subsequent cleavage of a C−H methyl bond and cyclometallation lead to **8**, liberating 1 equiv. of HCl. This HCl then may react with a second equivalent of the (*P*,*N*)-chelate complex to yield the hydrochloride **7** (see Scheme 2).

Complex **8** was obtained as a single diastereoisomer. It is likely that this results from a diastereoselective formation of the intermediate **6** which may be efficiently controlled by the rigid framework of this special (*P*,*N*)-chelate ligand. An inspection of molecular models revealed that the (pro-*S*)-*N*-methyl group may be oriented almost coplanar with the Ru−Cl vector. This may possibly have favoured the selective C−H activation[9] at this $N-CH_3$ group to form the observed product **8**. It is likely that such conformational features may have caused the observed differences in the behaviour of the systems described here from the open, more flexible system **4** which was described previously in the literature (see Scheme 1).[7,10]

Experimental Section

General Remarks: All reactions were carried out under dry argon in Schlenk-type glassware or in a glove-box. Solvents were dried and distilled prior to use. NMR spectra were recorded with a Bruker AC 200 P (^{31}P, 81.0 MHz), Varian UNITY 300 (^{31}P, 121.5 MHz) or Varian UNITYplus 600 (^{1}H, 599.9 MHz; ^{13}C, 150.8 MHz; ^{31}P, 242.5 MHz) spectrometer. Most assignments were confirmed using 2D spectra.[11] Exact masses were determined with a Micromass Quattro LC-Z electrospray mass spectrometer. The following instruments were used for additional physical characterisation: IR spectroscopy: Nicolet 5DXC FT-IR spectrometer; melting points: DSC 2010 (TA instruments); elemental analyses: Foss Heraeus CHN-O-Rapid. Compound *rac*-**5** was prepared in an analogous manner previously described by us for the (*R*)-**5** and (*S*)-**5** enantiomers.[8]

X-ray Structure Determinations: Data for **5**, **7** and **8** were collected at low temperature (100 K) with a Bruker SMART APEX diffractometer equipped with a CCD area detector using graphite-monochromated Mo-K_α radiation (λ = 0.71073 Å). Data were measured through the use of CCD recording of ω-rotation frames

 © 2004 Wiley-VCH Verlag GmbH & Co. KGaA, Weinheim

(0.3° each). Data were integrated with the Bruker SAINT program (*SAINT*+, version 6.01; Bruker AXS, Inc., Madison, WI, **2001** and SAINT, version 6.02) and corrected for Lorentz and polarisation effects. Absorption corrections were applied using the SADABS routine (SADABS: Area-Detector Absorption Correction, **1996**; Bruker-AXS within SAINT+ package, v. 6.01). Structures were solved by direct methods and completed by subsequent difference Fourier techniques. Refinement on F^2 was carried out by full-matrix least squares (SHELXL-97) (G. M. Sheldrick, *SHELXL-97 Program for Crystal Structure Refinement*, University of Göttingen, Göttingen, Germany, **1997**). All non-hydrogen atoms were refined with anisotropic displacement parameters. In **5** and **7**, hydrogen atoms were found from difference Fourier maps and refined with positional parameters riding on carbon atoms and free thermal parameters. Hydrogen atoms in **8** were analogously refined except a terminal methyl group for which hydrogen atoms were included in calculated positions.

Preparation of 5: To a solution of the corresponding amino[3]ferrocenophane (714 mg, 2.52 mmol) in Et_2O (10 mL) at 4 °C was added *n*-butyllithium (1.9 mL, 1.6 M, 3.02 mmol, 1.2 equiv.). The cooling bath was removed and the solution stirred for 3 h, during which the colour changed from light orange to dark orange. Afterwards, the mixture was cooled to 4 °C and chlorodiphenylphosphane (0.54 mL, 3.02 mmol, 1.2 equiv.) was added dropwise. The cooling bath was removed and the resultant suspension stirred at room temperature for 12 h. The reaction was quenched with saturated $NaHCO_3$ solution (10 mL) and the aqueous phase extracted with pentane (3 × 10 mL). The combined organic phases were washed with water and brine and dried with $MgSO_4$. Column chromatography on silica (SiO_2; pentane/ethanol, 6:1) yielded **5** as a yellow solid (0.547 g, 1.17 mmol, 46%), m.p. 156.1 °C (DSC). IR (KBr): $\tilde{\nu}$ = 3104 (w), 3072 (w), 2993 (m), 2953 (m), 2854 (m), 2808 (m), 2751 (s), 1643 (m), 1617 (m), 1466 (m), 1446 (s), 1308 (m), 1143 (m), 1038 (s), 755 (s), 702 (s), 531 (m) cm^{-1}. ^1H NMR (599.9 MHz, $CDCl_3$, 25 °C): δ = 1.22 [d, $^3J_{H,H}$ = 7.3 Hz, 3 H, C(10)−H], 1.79 [s, 6 H, C(16), C(17)−H], 2.31 [m, 1 H, C(7)−H_{trans}], 2.68 [pd, 1 H, C(8)−H], 2.84 [m, 1 H, C(6)−H], 3.16 [m, 1 H, C(7)−H_{cis}], 3.68 [m, 2 H, C(2−5)−H, C(12−14)−H], 3.85 [m, 1 H, C(2−5)−H], 4.11 [m, 1 H, C(2−5)−H], 4.14 [m, 2 H, C(12−14)−H], 4.41 [m, 1 H, C(2−5)−H], 7.22−7.47 (m, 10 H, phenyl−H) ppm. $^{13}C\{^1H\}$ NMR (150.8 MHz, $CDCl_3$, 25 °C): δ = 16.7 [C(10)], 27.7 [C(6)], 44.2 [C(16), C(17)], 45.3 [C(7)], 59.1 [C(8)], 67.5 [C(2−5)], 68.6 [C(2−5)], 68.9 [C(12−14)], 70.2 [C(2−5)], 72.2 [C(2−5)], 73.9 [C(12−14)], 74.1 [C(12−14)], 75.2 [d, $^1J_{C,P}$ = 12.0 Hz, C(15)], 91.4 [br., C(11)], 93.3 [C(1)], 127.5, 127.7, 128.1, 133.1, 133.4 (d, $J_{C,P}$ = 19.0 Hz), 134.2, (d, $J_{C,P}$ = 19.0 Hz), 138.9, 139.4 (all broad, phenyl−C) ppm. $^{31}P\{^1H\}$ NMR (121.5 MHz, $CDCl_3$, 25 °C): δ = −21.6 ppm. $C_{28}H_{30}FeNP$ (467.375): calcd. C 71.96, H 6.47, N 3.00; found C 71.74, H 6.07, N 2.96.

Crystal Data for *rac*-5: Crystals suitable for the X-ray structure analysis were grown from a pentane solution at −18 °C. $C_{28}H_{30}FeNP$ (467.35), triclinic, $P\bar{1}$ (no.2), a = 8.8320(5), b = 14.6260(8), c = 18.0284(10) Å, α = 98.110(1), β = 93.210(1), γ = 96.919(1)°, V = 2282.4(2) Å^3, Z = 4, $\rho_{calcd.}$ = 1.360 Mg·m^{-3}, μ = 0.747 mm^{-1}, F(000) = 984, crystal size 0.30 × 0.27 × 0.15 mm. θ range for data collection 1.42 to 28.58° (−11 ≤ h ≤ 11, −19 ≤ k ≤ 19, −22 ≤ l ≤ 23), reflections collected/unique 26891/10615 [R(int) = 0.0361], max. and min. transmission 0.876172 and 0.667727, data/parameters 10615/619, S (on F^2) = 0.924, final R_{int} [$I > 2\sigma(I)$]: $R1$ = 0.0397, $wR2$ = 0.0799, R_{int} (all data): $R1$ = 0.0543, $wR2$ = 0.0847, largest diff. peak and hole 0.513 and −0.387 e·Å^{-3}.

Preparation of the Complexes 7 and 8: A solution of **5** (762 mg, 1.63 mmol), [Ru(η^6-*p*-cymene)Cl_2]$_2$ (500 mg, 0.81 mmol) and KPF_6 (300 mg, 1.63 mmol) in MeOH (48 mL) was stirred at room temperature for 12 h. The hydrochloride **7** which precipitated was collected by filtration and washed with MeOH to yield an orange solid (520 mg, 0.56 mmol, 34%), m.p. 207 °C (dec., DSC). The combined filtrates were concentrated in vacuo to yield **8** in two crops as an orange solid (286 mg, 0.33 mmol, 20%), m.p. 261 °C (DSC). **Metallacycle 8:** Crystals suitable for the X-ray structure analysis were grown by slow diffusion of Et_2O into an MeOH solution. IR (KBr): $\tilde{\nu}$ = 3058 (w), 2966 (m), 2920 (m), 2868 (w), 1630 (w), 1492 (m), 1446 (m), 1097 (m), 1018 (m), 841 (s), 755 (m), 702 (m), 564 (m) cm^{-1}. ^1H NMR (599.9 MHz, $CDCl_3$, 25 °C): δ = 1.00 [d, $^3J_{H,H}$ = 6.8 Hz, 3 H, C(10)−H], 1.11 [d, $^3J_{H,H}$ = 6.7 Hz, 3 H, C(26)/C(27)−H], 1.14 [d, $^3J_{H,H}$ = 7.2 Hz, 3 H, C(26)/C(27)−H], 1.90 [m, 1 H, C(5)−H], 2.01 [m, 1 H, C(25)−H], 2.04 [m, 1 H, C(7)−H], 2.15 [s, 3 H, C(24)−H], 2.42 [m, 1 H, C(7)−H], 2.54 [m, 1 H, C(6)−H], 2.77 [d, $^3J_{H,H}$ = 11.8 Hz, 1 H, C(17)−H], 3.05 [s, 3 H, C(16)−H], 3.40 [dd, $^3J_{H,H}$ = 2.1, 11.6 Hz, 1 H, C(8)−H], 3.45 [m, 1 H, C(17)−H], 3.47 [m, 1 H, C(2−4)−H], 3.77 [m, 1 H, C(2−4)−H], 4.00 [m, 1 H, C(2−4)−H], 4.09 [m, 1 H, C(12−14)−H], 4.26 [m, 2 H, C(12−14)−H], 4.41 [d, $^3J_{H,H}$ = 5.1 Hz, 1 H, C(19)/C(20)/C(22)/C(23)−H], 4.72 [d, $^3J_{H,H}$ = 5.8 Hz, 1 H, C(19)/C(20)/C(22)/C(23)−H], 5.58 [d, $^3J_{H,H}$ = 5.6 Hz, 1 H, C(19)/C(20)/C(22)/C(23)−H], 5.74 [d, $^3J_{H,H}$ = 5.8 Hz, 1 H, C(19)/C(20)/C(22)/C(23)−H], 6.98 (m, 2 H, phenyl−H), 7.27 (m, 3 H, phenyl−H), 7.68 (m, 3 H, phenyl−H), 8.22 (m, 2 H, phenyl−H) ppm. $^{13}C\{^1H\}$ NMR (150.8 MHz, $CDCl_3$, 25 °C): δ = 16.4 [C(26)/C(27)], 18.9 [C(24)], 23.4 [C(26)/C(27)], 23.8 [C(10)], 27.0 [C(6)], 31.3 [C(25)], 46.3 [d, $J_{C,P}$ = 9.5 Hz, C(17)], 50.7 [C(7)], 57.6 [C(16)], 60.7 [C(8)], 67.8 [d, $J_{C,P}$ = 42.2 Hz, C(15)], 68.4 [C(2−4)], 68.9 [C(2−4)], 69.3 [d, $J_{C,P}$ = 5.2 Hz, C(12−14), 71.1 [C(2−4)], 71.4 [d, $J_{C,P}$ = 8.3 Hz, C(12−14)], 72.6 [C(5)], 74.2 [C(12−14)], 83.4 [d, $J_{C,P}$ = 18.8 Hz, C(11)], 84.9 [C(19)/C(20)/C(22)/C(23)], 88.2 [d, $J_{C,P}$ = 4.4 Hz, C(19)/C(20)/C(22)/C(23)], 89.5 [d, $J_{C,P}$ = 3.6 Hz, C(19)/C(20)/C(22)/C(23)], 92.7 [d, $J_{C,P}$ = 2.0 Hz, C(19)/C(20)/C(22)/C(23)], 92.8 [C(1)], 128.2 (d, $J_{C,P}$ = 9.9 Hz, *ortho*/*meta*-phenyl C), 128.4 (d, $J_{C,P}$ = 10.3 Hz, *ortho*/*meta*-phenyl C), 129.4 (*para*-phenyl C), 130.3 (d, $J_{C,P}$ = 9.5 Hz, *ortho*/*meta*-phenyl C), 131.6 (*para*-phenyl C), 134.9 (d, $J_{C,P}$ = 12.9 Hz, *ortho*/*meta*-phenyl C), 135.8 (d, $^1J_{C,P}$ = 49.1 Hz, *ipso*-phenyl C), 141.4 (d, $^1J_{C,P}$ = 53.6 Hz, *ipso*-phenyl C) ppm. $^{31}P\{^1H\}$ NMR (121.5 MHz, $CDCl_3$, 25 °C): δ = −145.1 (sept, $^1J_{F,P}$ = 716.6 Hz, PF_6), 37.1 ppm. Exact mass ($C_{38}H_{43}FeNPRu$): calcd. 702.1519, found 702.1511. **Hydrochloride 7:** Crystals suitable for the X-ray structure analysis were grown by slow concentration of an acetone solution. IR (KBr): $\tilde{\nu}$ = 3651 (m), 3045 (s), 2973 (m), 2874 (m), 1630 (w), 1485 (s), 1439 (s), 1393 (m), 1328 (m), 913 (s), 854 (s), 702 (s), 564 (s) cm^{-1}. ^1H NMR (599.9 MHz, $CDCl_3$, 25 °C): δ = 1.01 [d, $^3J_{H,H}$ = 6.9 Hz, 3 H, C(26)/C(27)−H], 1.13 [d, $^3J_{H,H}$ = 6.9 Hz, 6 H, C(26)/C(27)−H, C(10)−H], 1.83 [s, 3 H, C(24)−H], 1.85 [m, 1 H, C(5)−H], 2.26 [m, 1 H, C(7)−H], 2.37 [sept, $^3J_{H,H}$ = 6.8 Hz, 1 H, C(25)−H], 2.45 [m, 1 H, C(6)−H], 2.51 [m, 1 H, C(7)−H], 2.92 [s, 6 H, C(16), C(17)−H], 3.72 [m, 1 H, C(8)−H], 3.74 [m, 2 H, C(2−4)−H], 4.16 [m, 2 H, C(12−14)−H, C(19)/C(20)/C(22)/C(23)−H], 4.25 [m, 1 H, C(2−4)−H], 4.28 [m, 1 H, C(12−14)−H], 4.48 [bm, 1 H, C(19)/C(20)/C(22)/C(23)−H], 4.74 [m, 1 H, C(12−14)−H], 5.08 [bm, 1 H, C(19)/C(20)/C(22)/C(23)−H], 5.31 [d, $^3J_{H,H}$ = 5.3 Hz, 1 H, C(19)/C(20)/C(22)/C(23)−H], 7.42 (m, 6 H, phenyl H), 7.64 (m, 4 H, phenyl H), 8.12 (br., 1 H, N−H) ppm. $^{13}C\{^1H\}$ NMR (150.8 MHz, $CDCl_3$, 25 °C): δ = 15.6 [C(10)], 17.9 [C(24)], 21.3 [C(26)/C(27)],

 © 2004 Wiley-VCH Verlag GmbH & Co. KGaA, Weinheim

23.1 [C(26)/C(27)], 28.3 [C(6)], 30.5 [C(25)], 42.6 [C(16)/C(17)], 44.9 [C(7)], 45.3 [C(16)/C(17)], 66.3 [C(8)], 68.9 [C(2−4)], 69.7 [C(2−4)], 70.1 [C(12−14)], 71.5 [C(2−4)], 75.0 [C(5)], 77.0 [d, $^1J_{C,P}$ = 14.8 Hz, C(15)], 78.3 [d, $J_{C,P}$ = 16.3 Hz, C(12−14)], 82.0 [C(12−14)], 83.3 [d, $J_{C,P}$ = 25.0 Hz, C(11)], 84.6, 86.9, 87.0, 93.4 [C(19)/C(20)/C(22)/C(23)], 94.6 [C(1)], 97.4 [C(18)], 109.4 [C(21)], 128.1 (d, $J_{C,P}$ = 8.7 Hz, *ortho*/*meta*-phenyl C), 128.4 (br., *ortho*/*meta*-phenyl C), 128.5 (br., *ortho*/*meta*-phenyl C), 130.1 (*para*-phenyl C), 131.9 (br., *ortho*/*meta*-phenyl C), 132.3 (*para*-phenyl C), 136.7 (d, $^1J_{C,P}$ = 41.4 Hz, *ipso*-phenyl C), 142.2 (d, $^1J_{C,P}$ = 47.5 Hz, *ipso*-phenyl C) ppm. $^{31}P\{^1H\}$ NMR (121.5 MHz, $CDCl_3$, 25 °C): δ = −145.1 (sept, $^1J_{F,P}$ = 716.6 Hz, PF_6), 13.3 ppm. $C_{38}H_{45}Cl_2F_6FeNP_2Ru$ (919.544): calcd. C 49.64, H 4.93, N 1.52; found C 49.61, H 4.73, N 1.31.

Crystal Data for 7: $C_{41}H_{51}Cl_2F_6FeNOP_2Ru$ (977.59), monoclinic, $P2_1/c$ (no. 14), a = 14.5842(12), b = 15.6498(13), c = 17.5933(14) Å, β = 95.272(2)°, V = 3998.5(6) Å^3, Z = 4, $\rho_{calcd.}$ = 1.624 Mg·m^{-3}, μ = 1.017 mm^{-1}, F(000) = 2000, crystal size 0.22 × 0.16 × 0.13 mm. θ range for data collection 1.74 to 28.52° (−15 ≤ h ≤ 19, −20 ≤ k ≤ 20, −22 ≤ l ≤ 23) reflections collected/unique 25996/9345 [R_{int} = 0.0486], max. and min. transmission 0.887895 and 0.735866, data/parameters 9345/547, S (on F^2) = 0.916, R_{int} [$I > 2\sigma(I)$]: $R1$ = 0.0420, wR^2 = 0.0622, R_{int} (all data): $R1$ = 0.0637, wR^2 = 0.0656, largest diff. peak and hole 1.170 and −0.823 e·Å^{-3}.

Crystal Structure of 8: $C_{38}H_{43}F_6FeNP_2Ru$ (846.59), orthorhombic, *Pbca* (no. 61), a = 16.7411(15), b = 18.9689(17), c = 21.6800(18) Å, V = 6884.7(10) Å^3, Z = 8, $\rho_{calcd.}$ = 1.634 Mg·m^{-3}, μ = 1.016 mm^{-1}, F(000) = 3456, crystal size 0.14 × 0.13 × 0.96 mm. θ range for data collection 1.87 to 26.00° (−20 ≤ h ≤ 20, −23 ≤ k ≤ 19, −23 ≤ l ≤ 26), reflections collected/unique 39041/6769 [R(int) = 0.1310], max. and min. transmission 0.916497 and 0.806607, data/parameters 6769/484, S (on F^2) 0.733, final R_{int} [$I > 2\sigma(I)$]: $R1$ = 0.0464, wR^2 = 0.0601, R_{int} (all data): $R1$ = 0.1061, wR^2 = 0.0686, largest diff. peak and hole 1.004 and −0.640 e·Å^{-3}.

CCDC-237957 to -237959 contain the supplementary crystallographic data for this paper. These data can be obtained free of charge at www.ccdc.cam.ac.uk/conts/retrieving.html [or from Cambridge Crystallographic Data Centre, 12 Union Road, Cambridge CB2 1EZ, UK; Fax: (internat.) + 44-1223-336-033; E-mail: deposit@ccdc.cam.ac.uk].

Acknowledgments

Financial support from the Deutsche Forschungsgemeinschaft, the Fonds der Chemischen Industrie and from MCYT (projects BQU2003-1096 and BQU2002-1729) is gratefully acknowledged. P. L. gratefully acknowledges the support of a Marie Curie stipend (HPMT-CT-2000-00200).

[1] [1a] R. H. Crabtree, *J. Chem. Soc., Dalton Trans.* **2001**, 2437−2450. [1b] S. Niu, M. B. Hall, *Chem. Rev.* **2000**, *100*, 353−405. [1c] M. Torrent, M. Solà, G. Frenking, *Chem. Rev.* **2000**, *100*, 439−493. [1d] G. Dyker, *Angew. Chem.* **1999**, *111*, 1808−1822; *Angew. Chem. Int. Ed.* **1999**, *38*, 1699−1712. [1e] Y. Guari, S. Sabo-Etienne, B. Chaudret, *Eur. J. Inorg. Chem.* **1999**, 1047−1055. [1f] A. E. Shilov, G. B. Shul'pin, *Chem. Rev.* **1997**, *97*, 2879−2932. [1g] R. H. Crabtree, *Chem. Rev.* **1995**, *95*, 987−1007. [1h] A. D. Ryabov, *Chem. Rev.* **1990**, *90*, 403−424. [1i] R. H. Crabtree, *Chem. Rev.* **1985**, *85*, 245−269. [1j] A. E. Shilov, G. B. Shul'pin, *Activation and Catalytic Reactions of Saturated Hydrocarbons in the Presence of Metal Complexes*, Kluwer, Dordrecht, **2000**. [1k] *Activation of Unreactive Bonds and Organic Synthesis* (Ed.: S. Murai), Springer, Berlin, **1999**. [1l] G. A. Olah, A. Molnar, *Hydrocarbon Chemistry*, John Wiley & Sons, New York, **1995**.

[2] [2a] S. Doye, *Angew. Chem.* **2001**, *113*, 3455−3457; *Angew. Chem. Int. Ed.* **2001**, *40*, 3351−3353. [2b] S. Sakaguchi, T. Kubo, Y. Ishii, *Angew. Chem.* **2001**, *113*, 2602−2604; *Angew. Chem. Int. Ed.* **2001**, *40*, 2534−2536. [2c] N. Chatani, T. Asaumi, T. Ikeda, S. Yorimitsu, Y. Ishii, F. Kakiuchi, S. Murai, *J. Am. Chem. Soc.* **2000**, *122*, 12882−12883.

[3] [3a] A. Meli, F. Vizza, C. Bianchini, *Eur. J. Inorg. Chem.* **2001**, 43−68. [3b] K. J. Weller, P. A. Fox, S. D. Gray, D. E. Wigley, *Polyhedron* **1997**, *16*, 3139−3163.

[4] [4a] A. Bertuleit, C. Fritze, G. Erker, R. Fröhlich, *Organometallics* **1997**, *16*, 2891−2899. [4b] A. Bertuleit, M. Könemann, L. Duda, G. Erker, R. Fröhlich, *Top. Catal.* **1999**, *7*, 37−44. [4c] J. Pflug, A. Bertuleit, G. Kehr, R. Fröhlich, G. Erker, *Organometallics* **1999**, *18*, 3818−3826. [4d] J. Pflug, G. Erker, G. Kehr, R. Fröhlich, *Eur. J. Inorg. Chem.* **2000**, 1795−1801. [4e] S. Venne-Dunker, G. Kehr, R. Fröhlich, G. Erker, *Organometallics* **2003**, *22*, 948−958. [4f] D. W. Ovenall, S. J. Holmes, W. A. Nugent, *Organometallics* **1983**, *2*, 161−162.

[5] [5a] A. W. Holland, R. G. Bergman, *Organometallics* **2002**, *21*, 2149−2152. [5b] S.-W. Jean, H.-J. Wang, K.-B. Shiu, *Organometallics* **1997**, *16*, 114−119. [5c] R. Crabtree, *Angew. Chem.* **1993**, *105*, 828−845; *Angew. Chem. Int. Ed. Engl.* **1993**, 789−806.

[6] [6a] K. Mauthner, C. Slugovc, K. Mereiter, R. Schmid, K. Kirchner, *Organometallics* **1997**, *16*, 1956−1961. [6b] I. C. M. Wehman-Ooyevaar, I. F. Luitwieler, K. Vatter, D. M. Grove, W. J. J. Smeets, E. Horn, A. L. Spek, G. van Koten, *Inorg. Chim. Acta* **1996**, *252*, 55−69. [6c] R. Kuhlman, K. Folting, K. G. Caulton, *Organometallics* **1995**, *14*, 3188−3195.

[7] C. Standfest-Hauser, C. Slugovc, K. Mereiter, R. Schmid, K. Kirchner, L. Xiao, W. Weissensteiner, *J. Chem. Soc., Dalton Trans.* **2001**, 2989−2995.

[8] [8a] S. Knüppel, R. Fröhlich, G. Erker, *J. Organomet. Chem.* **1999**, *586*, 218−222, **2000**, *595*, 307−312. [8b] P. Liptau, S. Knüppel, G. Kehr, O. Kataeva, R. Fröhlich, G. Erker, *J. Organomet. Chem.* **2001**, *637−639*, 621−630. [8c] P. Liptau, T. Seki, G. Kehr, A. Abele, R. Fröhlich, G. Erker, S. Grimme, *Organometallics* **2003**, *22*, 2226−2232. [8d] P. Liptau, L. Tebben, G. Kehr, B. Wibbeling, R. Fröhlich, G. Erker, *Eur. J. Inorg. Chem.* **2003**, 3590−3600; 4261. [8e] P. Liptau, L. Tebben, G. Kehr, R. Fröhlich, G. Erker, F. Hollmann, B. Rieger, *Eur. J. Org. Chem.* submitted. [8f] L. Tebben, G. Kehr, R. Fröhlich, G. Erker, *Synthesis* **2004**, 1971−1976.

[9] [9a] Y. Guari, S. Sabo-Etienne, B. Chaudret, *Eur. J. Inorg. Chem.* **1999**, 1047−1055. [9b] A. D. Ryabov, *Chem. Rev.* **1990**, *90*, 403−424.

[10] [10a] F. W. B. Einstein, A. C. Willis, *Acta Crystallogr., Sect. B* **1980**, *36*, 39−43. [10b] T. Hayashi, K. Yamamoto, M. Kumada, *Tetrahedron Lett.* **1974**, *49−50*, 4405−4408.

[11] S. Braun, H.-O. Kalinowski, S. Berger, *150 and More Basic NMR Experiments*, Wiley-VCH, Weinheim, **1995**.

Received May 14, 2004
Early View Article
Published Online October 7, 2004

 © 2004 Wiley-VCH Verlag GmbH & Co. KGaA, Weinheim

Syntheses, Structures and Reactivity of Electron-Rich Fe and Ru Complexes with the New Pentadentate Ligand $Et_2NpyS_4-H_2$ {4-(Diethylamino)-2,6-bis[(2-mercaptophenyl)thiomethyl]pyridine}

Dieter Sellmann,[a][†] Shaban Y. Shaban,*[a] and Frank W. Heinemann[a]

Keywords: Electron density / Iron / Nitrogenase / Ruthenium / S ligand

The new pentadentate thioether thiolate ligand $Et_2NpyS_4^{2-}$ {= 4-(diethylamino)-2,6-bis[(2-mercaptophenyl)thiomethyl]-pyridine(2–)} has been synthesised from dimethyl 4-bromopyridine-2,6-dicarboxylate by treatment with Et_2NH followed by reduction and tosylation. The tosylated product was subsequently used for the template alkylation of $[Ni(S_2C_6H_4)_2]^{2-}$ to give $[\{Ni(Et_2NpyS_4)\}_2]$ (**4**). Acidic hydrolysis of **4** resulted in the formation of the ligand $Et_2NpyS_4–H_2$·HCl (**5**). The dianion $Et_2NpyS_4^{2-}$ reacted with $FeCl_2$·H_2O to afford the dinuclear high-spin species $[\{Fe(Et_2NpyS_4)\}_2]$ (**6**) [μ_{eff} (297 K) = 5.15 μ_B]. Aerial oxidation of dinuclear **6** afforded the sulfinato complex $[\{Fe(Et_2NpyS_4–O_2)\}_2]$ (**7**). Complex **6** proved to be a good precursor for the syntheses of $[Fe(L)(Et_2NpyS_4)]$ [L = CO (**8**), CNCy (**9**), NO (**11**) and N_2H_4 (**12**)] and $[Fe(NO)(Et_2NpyS_4)]BF_4$ (**10**). Protonation or alkylation of the thiolate donor atoms resulted in a series of complexes $[Fe(CO)(Et_2NpyS_4–R)]BF_4$ [R = H (**8a**), Et (**8b**)] and $[Fe(CO)(Et_2NpyS_4–Et_2)](BF_4)_2$ (**8c**) but no labilisation of the Fe–CO bond was observed. Only in complex **8** could the CO coligand be exchanged by NO^+ to give $[Fe(NO)(Et_2NpyS_4)]BF_4$ (**10**). Reduction of **10** using N_2H_4, NH_3 or N_3^- afforded the 19 valence electron species $[Fe(NO)(Et_2NpyS_4)]$ (**11**). $[Ru(NO)(Et_2NpyS_4)]Br$ (**13**) was synthesised by template alkylation of $Bu_4N[Ru(NO)(S_2C_6H_4)_2]$ using $Et_2Npy(CH_2Br)_2$ (**3**). Under reducing conditions, **13** releases the NO coligand to give $[\{Ru(Et_2NpyS_4)\}_2]$ (**14**), while in the presence of N_2H_4, $[Ru(N_2H_4)(Et_2NpyS_4)]$ (**15**) was formed. The complexes were well characterised including the solid-state structures in most cases. X-ray structural analyses of **7**, **8**, **9**, **10**, **12** and **15** revealed that all complexes exhibit *trans*-thiolate donors irrespective of the σ–π- or σ-ligand character of L.
(© Wiley-VCH Verlag GmbH & Co. KGaA, 69451 Weinheim, Germany, 2004)

Introduction

Transition metals in sulfur-dominated coordination spheres form the active centres of numerous oxidoreductases such as nitrogenases, hydrogenases and CO dehydrogenases.[1] In the search for low-molecular weight compounds that combine structural and reactivity features of these [MS] enzymes, we have found that transition metal complexes containing $[M(pyS_4)]$ fragments [pyS_4^{2-} = 2,6-bis(2-mercaptophenylthiomethyl)pyridine(2−)] (M = Fe, Ru) bind many nitrogenase-relevant molecules such as CO, NO, N_2H_4, N_2H_2 and NH_3, although not N_2 (Scheme 1).[2]

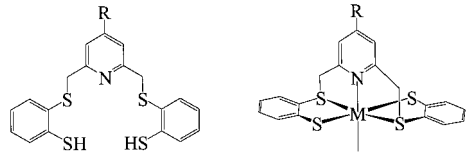

Scheme 1. Schematic structures of $RpyS_4-H_2$ ligands and $[M(RpyS_4)]$ fragments (M = Fe, Ru; R = H, Et_2N)

As was pointed out earlier,[3] and even more so for the syntheses of the first pair of mono- and dinuclear N_2 complexes $[Ru(N_2)(PiPr_3)(N_2Me_2S_2)]$[4] and $[\mu\text{-}N_2\{Ru(PiPr_3)(N_2Me_2S_2)\}_2]$[5] [$N_2Me_2S_2^{2-}$ = *N*,*N*′-dimethyl-1,2-ethanediamine-*N*,*N*′-bis(2-benzenethiolate)(2−)] which formed directly from N_2 and sulfur−metal complex fragments under mild conditions, a major factor for the binding of N_2 can be considered to be a high electron density at the metal centres. Although the position of the ν(CO) bands in $[Fe(CO)(pyS_4)]$ (1963 cm^{-1})[6] and $[Ru(CO)(pyS_4)]$ (1954 cm^{-1})[2g] indicate a relatively high electron density at the metal centres, no N_2 complexes could be obtained. It is possible that the electron density is not high enough to enable

[‡] Transition Metal Complexes with Sulfur Ligands, 166. Part 165: D. Sellmann, K. Hein, F. W Heinemann, *Inorg. Chem. Acta* **2004**, *357*, 3739−3745.

[a] Institut für Anorganische Chemie der Universität Erlangen-Nürnberg,
Egerlandstraße 1, 91058 Erlangen, Germany
Fax: (internat.) + 49-9131-8527367
E-mail: shaban@anorganik.chemie.uni-erlangen.de

[†] Deceased.

 DOI: 10.1002/ejic.200400404 © 2004 Wiley-VCH Verlag GmbH & Co. KGaA, Weinheim

the coordination of N_2. Numerous efforts have been made to increase the electron density in [M(pyS$_4$)] fragments by modifying the benzene ring substituents with electron-donating groups but these have remained unsuccessful.[2d,6] Apparently, the electronic changes in the benzene rings are not transmitted beyond the sulfur donor atoms to the metal centres. These findings prompted us to start a systematic study of the influence of the pyridine ring substituents on the electron density at the metal centres and the reactivity of the resultant complexes. We describe herein the syntheses of the new $Et_2NpyS_4-H_2$ ligand and some related iron and ruthenium complexes. The similarities and differences between [M(Et_2NpyS_4)] and [M(pyS$_4$)] complexes (M = Ru and Fe) are discussed in detail.

Results and Discussions

Synthesis of the New Ligand $Et_2NpyS_4-H_2$

The target ligand $Et_2NpyS_4-H_2$·HCl (**5**) was synthesised according to the route indicated in Scheme 2.

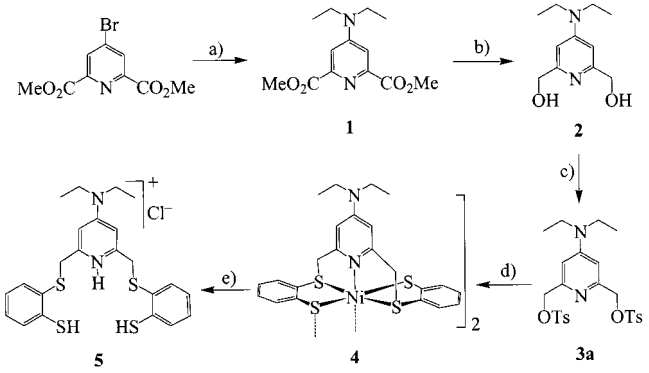

Scheme 2. Synthesis of the target $Et_2NpyS_4-H_2$·HCl ligand **5**: a) + Et_2NH, K_2CO_3, DMSO, 55 °C; b) + $NaBH_4$, EtOH, reflux, 16 h; c) + tosyl chloride, KOH, THF; d) + $Na_2[Ni(S_2C_6H_4)_2]$, THF, MeOH, 60 °C, 2 h; e) $HCl_{aq.}$, CH_2Cl_2

Treatment of dimethyl 4-bromopyridine-2,6-dicarboxylate[7] with excess Et_2NH and K_2CO_3 in DMSO at 55 °C for 28 h afforded dimethyl 4-diethylaminopyridine-2,6-dicarboxylate (**1**). The resultant ester **1** was reduced with $NaBH_4$ and continuously extracted with $CHCl_3$ at 45 °C for 72 h to yield 4-(diethylamino)-2,6-bis(hydroxymethyl)-pyridine (**2**). Treatment of **2** with either HBr or tosyl chloride afforded 2,6-bis(bromomethyl)-4-(diethylamino)pyridine (**3**) or 4-(diethylamino)-2,6-bis(tosyloxymethyl)pyridine (**3a**), respectively. Compound **3a** was subsequently used for the template alkylation of $[Ni(S_2C_6H_4)_2]^{2-}$[8] to give [{Ni(Et_2NpyS_4)}$_x$] (**4**). Complex **4** is paramagnetic with μ_{eff} (293 K) = 2.25 μ_B which is consistent with two unpaired electrons per Ni centre. A solution of **4** in CH_2Cl_2 was readily hydrolysed when treated with aqueous concentrated HCl to afford $Et_2NpyS_4-H_2$ as its HCl salt.

Syntheses and Reactions of Complexes

Schemes 3 and 4 summarise the syntheses and reactions of $Et_2NpyS_4^{2-}$ complexes.

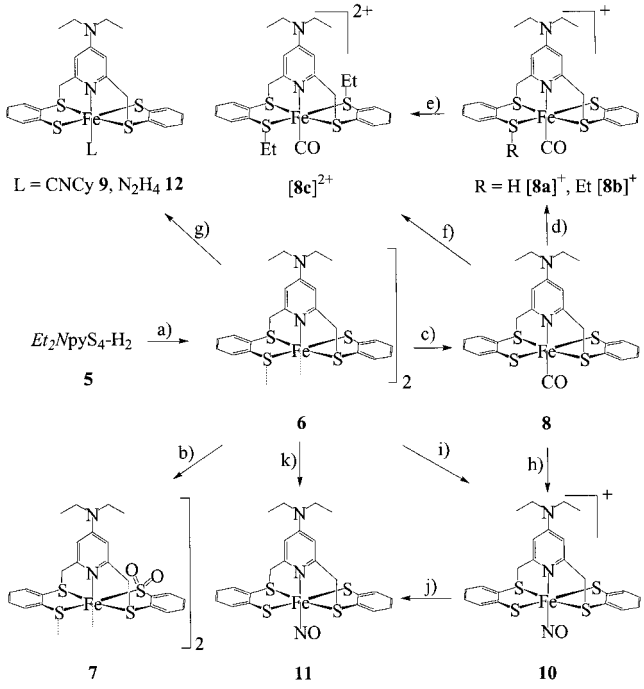

Scheme 3. Synthesis and reactions of iron complexes: a) + $FeCl_2$·4 H_2O, THF, room temp.; b) + air, $CHCl_3$, 72 h; c) + CO, THF, room temp.; d) + HBF_4, CH_2Cl_2, −78 °C or Et_3OBF_4, room temp.; e) + Et_3OBF_4, CH_2Cl_2; f) 2 Et_3OBF_4, CH_2Cl_2; g) + L (CNCy or N_2H_4)/THF; h) + $NOBF_4$, CH_2Cl_2, 0 °C; room temp.; i) + $NOBF_4$, CH_2Cl_2, room temp.; j) + N_2H_4, MeOH or DMF; k) NO, CH_2Cl_2.

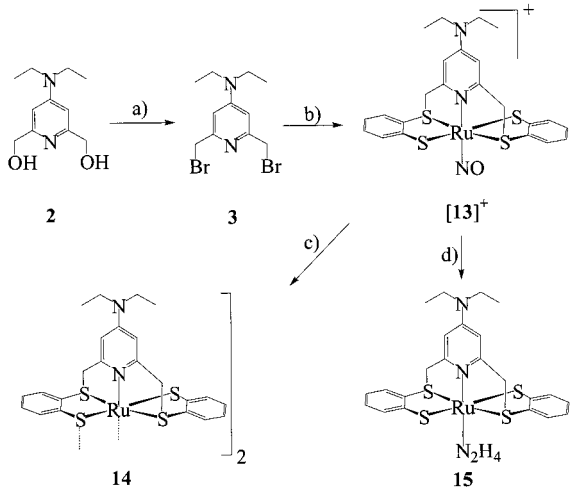

Scheme 4. Synthesis and reactions of ruthenium complexes: a) +HBr/H_2O, reflux, 16 h; b) + $Bu_4N[Ru(NO)(S_2C_6H_4)_2]$, THF, 60 °C, 2 h; c) + NH_3, MeOH, 1 h; d) + N_2H_4, THF, 2 h, room temp.

The reaction between $FeCl_2$·4H_2O and the $Et_2NpyS_4^{2-}$ anion resulting from deprotonation of **5** with 3 equiv. of LiOMe afforded yellow paramagnetic [{Fe(Et_2NpyS_4)}$_x$] (**6**) [μ_{eff} (293 K) = 5.15 μ_B]. The solid-state structure of **6** has not yet been determined. However, *x* is probably 2. Aer-

 © 2004 Wiley-VCH Verlag GmbH & Co. KGaA, Weinheim

ial oxidation of **6** afforded the sulfinato complex [{Fe($Et_2NpyS_4-O_2$)}$_2$] (**7**) showing $\nu_a(SO_2)$ and $\nu_s(SO_2)$ IR (KBr) bands at 1238, 1185, 1133 and 983 cm^{-1}.[9] An X-ray structure determination established that **7** is dinuclear and exhibits a *trans*-thiolate structure. A possible reason for this mild thiolate oxidation could be the high basicity of the thiolate donors originating from the presence of the Et_2N substituent. Dinuclear **6** readily coordinates CO or CNCy to give the C_2-symmetric and diamagnetic mononuclear complexes [Fe(CO)(Et_2NpyS_4)] (**8**) and [Fe(CNCy)(Et_2NpyS_4)] (**9**), respectively, indicating that **6** partially dissociates in solution into two unsaturated monomers. Complexes **8** and **9** exhibit characteristic ν(CO) (1948 cm^{-1}) and ν(CNCy) (2105 cm^{-1}) bands in their IR (KBr) spectra. The ν(CO) of **8** is low when compared with that of [Fe(CO)(pyS_4)] (1963 cm^{-1}),[6] indicating a high electron density at the Fe centre which in turn results in a strong Fe−CO bond. Complex **8** could also be obtained directly from $FeCl_2{\cdot}4H_2O$ and $Et_2NpyS_4^{2-}$ in the presence of CO.

During attempts to diminish the inertness of [Fe(CO)(Et_2NpyS_4)] (**8**) towards substitution, the thiolate donor atoms were protonated or alkylated using either HBF_4 or Et_3OBF_4, affording the thioether derivatives [Fe(CO)(Et_2NpyS_4-R)]BF_4 [R = H (**8a**), Et (**8b**)] and [Fe(CO)($Et_2NpyS_4-Et_2$)]$(BF_4)_2$ (**8c**). Complexes **8a**−**c** were completely characterised and each shows a characteristic ν(CO) band in the 1975−2016 cm^{-1} range but they proved as inert towards substitution as their precursor **8**. For example, **8a** is deprotonated in solvents such as Et_2O, H_2O, MeOH, DMF or THF to regenerate **8** indicating that the protonation is reversible and does not lead to CO cleavage. This is in contrast to the parent complex [Fe(CO)(pyS_4-H)]BF_4, in which the CO ligand is labile and undergoes elimination to give [{Fe(pyS_4-H)}$_2$]$(BF_4)_2$.[6] One possible reason for the stability of the Fe−CO bond in **8a** may be the higher electron density at the iron centre. A comparison of the ν(CO) bands (in KBr) of [Fe(CO)(Et_2NpyS_4-H)]BF_4 (**8a**) and [Fe(CO)(pyS_4-H)]BF_4 (1975 cm^{-1} vs. 1996 cm^{-1})[6] shows that the iron centres in the [Fe(Et_2NpyS_4)] fragments have a higher electron density than in the [Fe(pyS_4)] fragments, thus favouring bonding of the good π-acceptor CO. The low ν(CO) frequency of **8** prompted us to attempt to obtain an [Fe(Et_2NpyS_4)] dinitrogen complex. For this purpose, a solution of **8** was UV-irradiated under N_2 for a prolonged period of time at different temperatures. However, the CO coligand dissociated and dinuclear **6** formed. Complex **8** was found to react only with $NOBF_4$ at 0 °C to afford the 18 valence electron (VE) complex [Fe(NO)(Et_2NpyS_4)]BF_4 (**10**). Complex **10** could also be obtained directly from **6** and $NOBF_4$.

The relatively high ν(NO) frequency of **10** (1882 cm^{-1} in KBr) made the $[\mathbf{10}]^+$ cation a candidate for attempts to convert the NO into an N_2 ligand by addition of nitrogen nucleophiles to the nitrosyl N atom.[10] For this purpose, **10** was treated with NH_3, N_2H_4 or N_3^-. However, in none of these cases did a nucleophilic addition to the NO coligand take place and, rather, the nucleophiles acted as reductants yielding the neutral 19 VE complex [Fe(NO)(Et_2NpyS_4)] (**11**), showing a ν(NO) band at 1637 cm^{-1} in its IR (KBr) spectrum. Subsequent experiments revealed that even N_2H_4 or solvents such as MeOH or DMF could reduce the cationic $[\mathbf{10}]^+$ to give neutral **11**. Alternatively, **11** could be synthesised directly from **6** and an equimolar amount of NO gas. Complex **11** is highly reactive and can be oxidised to give the $[\mathbf{10}]^+$ cation.

Treatment of an equimolar amount of **6** with N_2H_4 afforded the hydrazine complex [Fe(N_2H_4)(Et_2NpyS_4)] (**12**). Complex **12** is stable and could be isolated as a solid and completely characterised. This is in contrast to the analogous [Fe(N_2H_4)(pyS_4)][2a] which is highly labile towards N_2H_4 elimination and could be isolated in crystalline form only in the presence of excess N_2H_4. One possible reason for this high stability could be that all N_2H_4 hydrogen atoms are involved in both intra- and intermolecular hydrogen bonding as found for solid **12** in the solid state.

The unsuccessful attempts to obtain an [Fe(Et_2NpyS_4)] dinitrogen complex prompted us to also study ruthenium complexes which could be expected to be less labile (Scheme 4).

As a first target complex [Ru(NO)(Et_2NpyS_4)]Br (**13**) was prepared. It was obtained by template alkylation of Bu_4N[Ru(NO)($S_2C_6H_4$)$_2$][11] with $Et_2Npy(CH_2Br)_2$ (**3**) in boiling THF. Complex **13** exhibits a low ν(NO) frequency (1858 cm^{-1} in KBr) compared with the related complex [Ru(NO)(pyS_4)]Tos (1892 cm^{-1}).[2e] This again indicates a higher electron density at the ruthenium centre. Attempts to obtain an [Ru(Et_2NpyS_4)] dinitrogen complex from the reaction of **13** with NH_3 in MeOH resulted in the formation of the thiolate bridged dinuclear [{Ru(Et_2NpyS_4)}$_2$] (**14**). Monitoring of the reaction by solution IR spectroscopy showed that at first **13** [ν(NO) = 1880 cm^{-1} in MeOH] is reduced to give the 19 VE electron species [Ru(NO)(Et_2NpyS_4)] [ν(NO) = 1640 cm^{-1} in MeOH][2b] which is highly labile and releases NO to give dinuclear **14**. Complex **14** is practically insoluble in all common solvents and inert towards cleavage reactions. When a red brown THF suspension of **13** was treated with N_2H_4, a green solution was formed from which the hydrazine complex [Ru(N_2H_4)(Et_2NpyS_4)] (**15**) was isolated. Complex **15** is stable over prolonged periods of time in both the solid state and solution.

Characterization and General Properties of the Complexes

As far as possible, all complexes have been characterised by common spectroscopic methods and elemental analyses and, with the exception of **6** and **11**, they are all diamagnetic. All complexes, except the dinuclear species **6** proved to be soluble in THF, CH_2Cl_2 and DMF. The IR (KBr) spectra show a typical pattern for the [M(Et_2NpyS_4)] fragment besides the characteristic bands of the coligands. For example, the ν(CNCy) band at 2105 cm^{-1} indicates coordination of the CNCy ligand in **9**. Characteristic strong ν(CO) bands were observed for **8** (1948 cm^{-1}), **8a** (1974 cm^{-1}), **8b** (1980 cm^{-1}) and **8c** (2007 cm^{-1}), while weak ν(N−H) bands at 3318, 3285 and 3237, and 3318, 3242 and

 © 2004 Wiley-VCH Verlag GmbH & Co. KGaA, Weinheim

3100 cm^{-1} appeared for the hydrazine complexes **12** and **15**, respectively. Strong ν(NO) bands at 1882, 1637 and 1858 cm^{-1} characterise the nitrosyl complexes **10**, **11** and **13**, respectively.

The mass spectra in all cases exhibited peaks corresponding to either the molecular ion or ions resulting from loss of the coligands. The $^{13}C\{^1H\}$ NMR spectra proved particularly helpful in establishing the diastereomeric purity of the complexes and the twofold symmetry of the $[M(Et_2NpyS_4)]$ fragments. ^1H and $^{13}C\{^1H\}$ NMR spectra corroborated the C_2 symmetry of complexes **8**, **8c**, **9**, **10**, **12**, **13** and **15**, and the C_1 symmetry of complex **8b**. The hydrazine complex **12** gave rise to a broad singlet at $\delta = 2.9$ pm which can be attributed to *Fe*-bound and terminal NH_2 groups, while **15** gave rise to two doublets at $\delta = 4.2$ and 4.4 ppm which can be attributed to an *Ru*-bound NH_2 group and a multiplet at $\delta = 3.3$ ppm which can be assigned to the terminal NH_2 group.

Benzene and Pyridine Ring Substituent Effects

In the search for complexes which exhibit electron-rich metal centres, we have found that the benzene ring substituents have no significant influence on the electron density at the metal centres. In other words, the electronic changes in the benzene rings cannot be transmitted beyond the sulfur donors to the metal centres.[6,12] The ν(CO) or ν(NO) frequencies which sensitively reflect electronic changes at the metal centres are practically identical in the corresponding complexes (Table 1). It was therefore of interest to examine whether such an electron-donating effect of the pyridine ring Et_2N substituent would reach and be detectable at the metal centres of the homologous complexes.

Table 1. The ν(CO) and ν(NO) frequencies of $[Fe(NS_4)]$ cores with electron-donating benzene and pyridine ring substituents

Complex	ν(CO)[a]	Complex	ν(NO)[a]
$[Fe(CO)(pyS_4)]$	1963[6]	$[Fe(NO)(pyS_4)]^+$	1893[6]
$[Fe(CO)(pybuS_4)]$	1969[6]	$[Fe(NO)(Et_2NpyS_4)]^+$ (**10**)	1882[b]
$[Fe(CO)(Et_2NpyS_4)]$ (**8**)	1948[b]	$[Fe(NO)(pyS_4)]$	1648[6]
		$[Fe(NO)(Et_2NpyS_4)]$ (**11**)	1637[b]

[a] In KBr [cm^{-1}]. [b] This work.

Table 1 demonstrates that all iron complexes with $[Fe(Et_2NpyS_4)]$ cores show significant shifts of the ν(CO) and ν(NO) bands to lower wave numbers by about 11−22 cm^{-1} indicating that the electron donation of the pyridine ring substituents increases the electron density. This conclusion is supported by the high basicity of the sulfur donor atoms which form strong hydrogen bonds as found in the solid-state structures of **12**, **15** and **15**·N_2H_4. Further supporting observations include the cyclic voltammograms of the isoelectronic iron complexes $[Fe(CO)(Et_2NpyS_4)]$ (**8**) and $[Fe(CO)(pyS_4)]$[6] as well as the nitrosylruthenium complexes $[Ru(NO)(Et_2NpyS_4)]Br$ (**13**) and $[Ru(NO)(Et_2NpyS_4)]Tos$[2e] (Figure 1, Table 2). A comparison of the redox potentials of the carbonyliron complexes $[Fe(CO)(Et_2NpyS_4)]$ (**8**) and $[Fe(CO)(pyS_4)]$[6] (+361 mV vs. +514 mV in CH_2Cl_2) indicates the electron-donating nature of the Et_2N substituent which makes oxidation easier. On the other hand, the redox potentials of the nitrosylruthenium cations $[Ru(NO)(Et_2NpyS_4)]^+$ (**13**) and $[Ru(NO)(Et_2NpyS_4)]$[2e] (−467, −1524 mV vs. −275, −1200 mV in DMF) indicate that the Et_2N substituent renders cationic complexes with $[Fe(Et_2NpyS_4)]$ fragments more difficult to reduce. Keeping all these observations in mind, we can conclude that the Et_2N substituent has a significant influence on the electron density in $[M(Et_2NpyS_4)]$ cores.

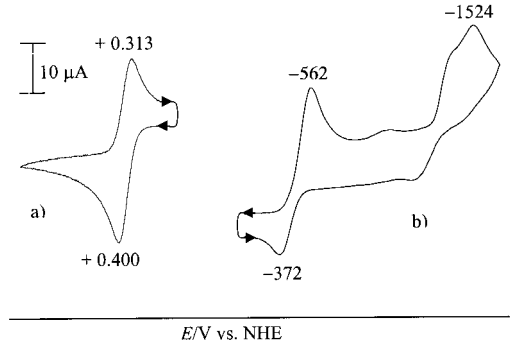

Figure 1. Cyclic voltammograms of a) $[Fe(CO)(Et_2NpyS_4)]$ (**8**) in CH_2Cl_2, b) $[Ru(NO)(Et_2NpyS_4)]Br$ (**13**) in DMF (10^{-3} M, 10^{-1} Bu_4NPF_6, $v = 50$ mV/s, potentials given in mV)

X-ray Crystal Structure Determinations

The crystal structures of the complexes $[\{Fe(Et_2NpyS_4-O_2)\}_2]\cdot 8CDCl_3$ (**7**·8$CDCl_3$), $[Fe(CO)(Et_2NpyS_4)]\cdot CDCl_3$ (**8**·$CDCl_3$), $[Fe(CNCy)(Et_2NpyS_4)]\cdot 2THF$ (**9**·2THF), $[Fe(NO)(Et_2NpyS_4)]BF_4\cdot CH_2Cl_2$ (**10**·CH_2Cl_2), $[Fe(N_2H_4)(Et_2NpyS_4)]$ (**12**), $[Ru(N_2H_4)(Et_2NpyS_4)]$ (**15**) and $[Ru(N_2H_4)(Et_2NpyS_4)]\cdot N_2H_4$ (**15**·N_2H_4) were determined by X-ray crystallography. Figures 2−4 depict the molecular structures of the complexes. Tables 3 and 4 list selected bond lengths and angles.

Table 2. Redox potentials of carbonyl and nitrosyl complexes with $[M(NS_4)]$ cores

Complex	Redox potentials in CH_2Cl_2 [mV][a]	Complex	Redox potentials in DMF [mV][a]
$[Fe(CO)(pyS_4)]$	+ 514[6]	$[Ru(NO)(pyS_4)]^+$	− 275, − 1200[2e]
$[Fe(CO)(Et_2NpyS_4)]$ (**8**)	+ 361[b]	$[Ru(NO)(Et_2NpyS_4)]^+$ (**13**)	− 467, − 1524[b]

[a] Related to NHE. [b] This work.

 © 2004 Wiley-VCH Verlag GmbH & Co. KGaA, Weinheim

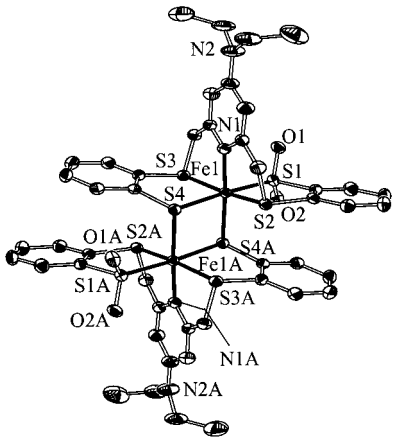

7

Figure 2. Molecular structure of $[\{Fe(Et_2NpyS_4-O_2)\}_2]\cdot 8CHCl_3$ (**7**·$8CHCl_3$) (50% probability ellipsoids, all solvate molecules, anions and C-bound H atoms omitted)

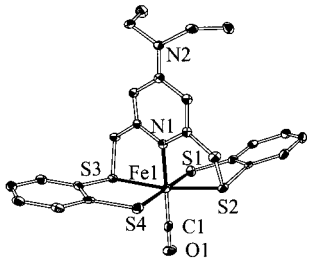

8

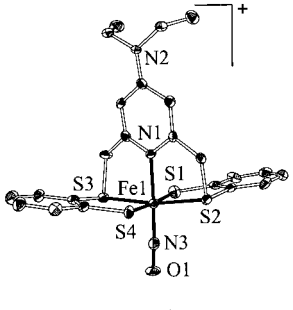

$[\mathbf{10}]^+$

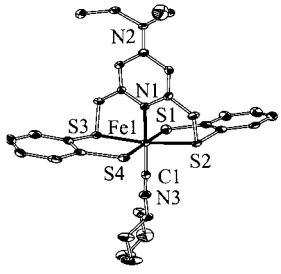

9

Figure 3. Molecular structures of $[Fe(CO)(Et_2NpyS_4)]\cdot CDCl_3$ (**8**·$CDCl_3$), $[Fe(CNCy)(Et_2NpyS_4)]\cdot 2THF$ (**9**·2THF) and $[Fe(NO)(Et_2NpyS_4)]BF_4\cdot CH_2Cl_2$ (**10**·CH_2Cl_2) (50% probability ellipsoids, all solvate molecules, anions and C-bound H atoms omitted)

The Et_2NpyS_4 ligand acts as a square-pyramidal coordination cap and the overall geometry around the iron centre is pseudo-octahedral. The pyridine N1 donor and the coligand L or the bridging S donor of a second Fe fragment as well as the two thiolate and the two thioether donor atoms of the $Et_2NpyS_4^{2-}$ ligand occupy corresponding *trans* positions and thus provide the steric rigidity of the $py(CH_2)_2$ backbone. A comparison of the geometrical parameters of **8**·$CDCl_3$, **9**·2THF and **10**·CH_2Cl_2 demonstrates that the Fe−donor distances in all cases lie in the usual

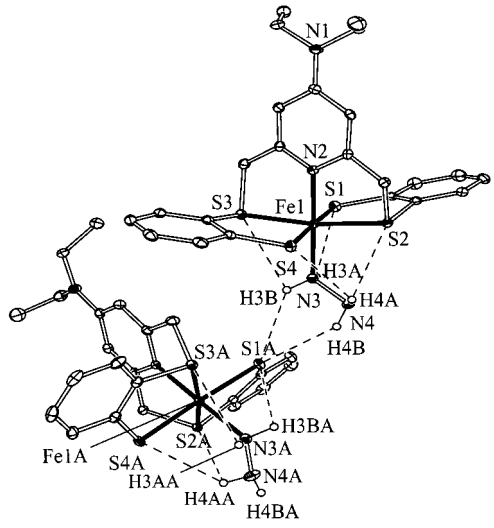

12

Figure 4. Molecular structure and hydrogen bonds (dashed lines) observed for $[Fe(N_2H_4)(Et_2NpyS_4)]$ (**12**) (50% probability ellipsoids, *C*-bound H atoms omitted)

Table 3. Selected bond lengths [pm] and angles [°] for $[\{Fe(Et_2NpyS_4-O_2)\}_2]\cdot 8CDCl_3$ (**7**·$8CDCl_3$), $[Fe(CO)(Et_2NpyS_4)]\cdot CDCl_3$ (**8**·$CDCl_3$), $[Fe(CNCy)(Et_2NpyS_4)]\cdot 2THF$ (**9**·2THF), $[Fe(NO)(Et_2NpyS_4)]BF_4\cdot CH_2Cl_2$ (**10**·CH_2Cl_2) and $[Fe(N_2H_4)(Et_2NpyS_4)]$ (**12**)

	7·$8CDCl_3$	**8**·$CDCl_3$	**9**·2THF	**10**·CH_2Cl_2	**12**
Fe(1)−N(1)	198.8(3)	201.5(2)	200.9(4)	199.2(4)	197.1(2)
Fe(1)−S(1)	218.8(2)	231.3(9)	231.1(2)	230.6(2)	230.46(6)
Fe(1)−S(2)	221.6(2)	224.0(1)	221.9(2)	224.9(2)	222.78(5)
Fe(1)−S(3)	223.3(2)	222.7(1)	221.6(2)	224.5(2)	223.22(6)
Fe(1)−S(4)	229.9(2)	229.8(1)	230.6(2)	231.3(2)	229.42(5)
Fe(1)−L	233.4(2)	176.5(3)	183.4(5)	163.8(5)	203.73(2)
N(1)−Fe(1)−S(1)	89.7(1)	91.42(7)	89.8(2)	88.3(2)	90.73(5)
N(1)−Fe(1)−S(2	86.1(2)	83.33(7)	84.7(2)	85.1(2)	84.59(5)
N(1)−Fe(1)−S(3)	84.8(2)	84.34(7)	84.7(2)	85.0(2)	85.26(5)
N(1)−Fe(1)−S(4)	93.1(1)	89.32(7)	90.8(2)	87.6(2)	92.08(5)
N(1)−Fe(1)−L	176.8(1)	178.9(2)	178.6(2)	177.4(2)	178.59(7)

range observed for diamagnetic $[FeNS_4]$ cores.[2a,2b,2e,6] The Fe−S(thiolate) distances (average 230 pm) are slightly longer than the Fe−S(thioether) distances (average 223 pm).

In complex **7**·$8CDCl_3$, the oxygenation causes a significant effect in the Fe−S(sulfinate) distance while the other Fe−S and Fe−N distances remain practically unchanged. The Fe−S(sulfinate) distance decreases by about 12 pm [218(2) pm for **7**·$8CDCl_3$ vs. 230 pm (average) for **8**·$CDCl_3$, **9**·2THF and **12**]. An explanation could be that the Fe−S distances are governed by three factors: 1) the σ-donor ability, expected to be best in the thiolate which decreases with increasing oxygenation, 2) a contraction in the size of the sulfur atoms as the formal oxidation state of the sulfur atoms changes from −2 (for Fe−S in complexes **8**·$CDCl_3$, **9**·2THF and **10**) to +2 [for Fe−S(sulfinate) in complex **7**·$8CDCl_3$], and 3) the destabilisation of the Fe−S bond due

 © 2004 Wiley-VCH Verlag GmbH & Co. KGaA, Weinheim

Table 4. Selected bond lengths [pm] and angles [°] for $[Ru(N_2H_4)(Et_2NpyS_4)]$ (**15**) and $[Ru(N_2H_4)(Et_2NpyS_4)]\cdot N_2H_4$ (**15**·N_2H_4)

	15	**15**·N_2H_4		**15**	**15**·N_2H_4
Ru(1)−(N1)	205.6(3)	205.4(3)	N(1)−Ru(1)−S(1)	90.33(8)	90.54(9)
Ru(1)−S(1)	237.51(9)	239.2(2)	N(1)−Ru(1)−S(2)	83.21(8	83.60(9)
Ru(1)−S(2)	230.49(9)	230.7(1)	N(1)−Ru(1)−S(3)	83.71(8)	84.29(9)
Ru(1)−S(3)	231.06(9)	228.6(1)	N(1)−Ru(1)−S(4)	91.81(8)	90.63(9)
Ru(1)−S(4)	237.23(9)	237.9(2)	N(1)−Ru(1)−N(3)	179.09(11)	176.6(2)
Ru(1)−N(3)	213.70(3)	213.7(4)	Ru(1)−N(3)−N(4)	115.90(2)	118.3(3)
N(3)−N(4)	146.40(4)	144.6(5)			
N(5)−N(6)	−	139.6(6)			

to a repulsive interaction between the filled d orbital of the metal atom and two lone pairs of the thiolate sulfur atom.[9a,13]

The crystal structures of the complexes **12**, **15** and **15**·N_2H_4 deserve special interest because all types of hydrazine hydrogen atoms are involved in a system of inter- and intramolecular N−H···S and N−H···N hydrogen bonding with the sulfur donors (thiolate, thioether) as well as the solvate hydrazine N atoms. The hydrogen bonds are indicated by both the N−H···S and N−H···N vectors as well as the distances which are shorter than the sum of the corresponding van der Waals radii (r_H = 120 pm, r_S = 185 pm).[14] Figure 3 shows the molecular structures and the hydrogen bonding geometry for **12** and **15**·N_2H_4. The parameters of the hydrogen bonds are collected in Table 5.

The crystal lattices of **12** and **15** contain chains of molecules which are connected by intermolecular N−H···S(thiolate) hydrogen bonds and each molecule exhibits additional intramolecular N−H···S hydrogen bonds. The type of bonds, bond lengths and bond angles in the two complexes are very similar, only **12** contains an additional N−H···S bond. The crystal lattice of **15**·N_2H_4 additionally contains intermolecular N−H···N hydrogen bonds between the solvate hydrazine and the coordinated hydrazine. This system of hydrogen bonds is of interest because it contributes significantly to the stabilisation of the N_2H_4 coligand and a similar effect may stabilise the intermediate diazene complex which is assumed to be essential for N_2 fixation.[2c]

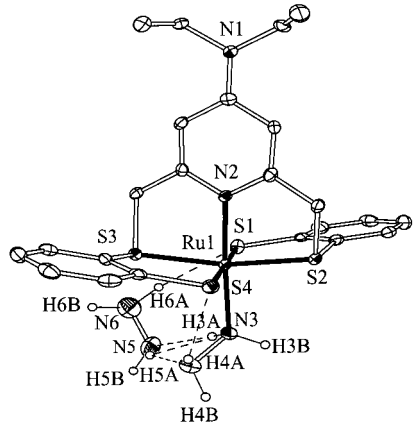

15 · N_2H_4

Figure 5. Molecular structure and hydrogen bonds (dashed lines) observed for $[Ru(N_2H_4)(Et_2NpyS_4)]\cdot N_2H_4$ (**15**·N_2H_4) (50% probability ellipsoids, *C*-bound H atoms omitted)

Conclusion

The new pentadentate $Et_2NpyS_4-H_2$ ligand has been synthesised with the aim of preparing transition metal com-

Table 5. Hydrogen bond parameters [pm and °] for $[Fe(N_2H_4)(Et_2NpyS_4)]$ (**12**), $[Ru(N_2H_4)(Et_2NpyS_4)]$ (**15**) and $[Ru(N_2H_4)(Et_2NpyS_4)]\cdot N_2H_4$ (**15**·N_2H_4)

D−H···A	*d*(D···A)		*d*(D−H)		*d*(H···A)		ν(DHA)	
	12	**15**	**12**	**15**	**12**	**15**	**12**	**15**
N(3)−H(3A)···S(1A)[a]	344.1(2)	335.3(3)	89(3)	99	277(3)	260	134(2)	132
N(3)−H(3A)···S(3)	311(2)	−	89(3)	−	300(3)	−	88(2)	−
N(3)−H(3B)···S(1)	304.5(2)	316.8(3)	90(3)	82	268(3)	288	105(2)	103
N(4)−H(4A)···S(4)	348.1(2)	359.9(3)	88(3)	88	292(3)	301	123(2)	126
N(4)−H(4A)···S(2)	316.3(2)	327.7(3)	88(3)	88	285(3)	291	103(2)	107
N(4)−H(4B)···S(1A)[a]	340.1(2)	337.3(3)	88(3)	83	265(3)	266	144(2)	145
15·N_2H_4								
N(3)−H(3A)···N(5)	323.6(6)		102		227		157	
N(4)−H(4A)···S(1)	337.2(4)		104		256		135	
N(5)−H(5A)···N(4)	314.9(6)		106		218		151	
N(5)−H(5A)···N(3)	323.6(6)		106		259		119	
N(6)−H(6A)···S(4)	366.7(5)		105		264		157	

[a] Symmetry transformations used to generate equivalent atoms: $x + 1/2$, y, $-z - 1/2$.

 © 2004 Wiley-VCH Verlag GmbH & Co. KGaA, Weinheim

plexes which exhibit electron-rich metal centres, possess a core configuration with thiolate, thioether and amine donors related to the structure of [M(pyS_4)] fragments (M = Fe and Ru), and bind biologically relevant small molecules. This goal was achieved as evidenced by the low ν(CO) frequency of [Fe(CO)(Et_2NpyS_4)] (1948 cm^{-1}) compared with the analogous [Fe(CO)(pyS_4)] (1963 cm^{-1}). The [M(Et_2NpyS_4)] fragments (M = Fe, Ru) were found to bind and stabilise many nitrogenase-relevant molecules such as CO, NO, NO^+, CNCy and N_2H_4. The results also revealed that the Et_2N substituent not only increases the electron density at the metal centres but also at the sulfur donor atoms which leads to highly basic sulfur donors. This high basicity influences the reactivity of the M−L bonds. For example, the protonated complex [Fe(CO)(Et_2NpyS_4-H)]-BF_4 is deprotonated only in solution to give [Fe(CO)-(Et_2NpyS_4)], while the related complex [Fe(CO)-(pyS_4-H)]BF_4 is labile and undergoes CO elimination to give [{Fe(pyS_4-H)}$_2$](BF_4).

The X-ray structural analyses of [Fe(N_2H_4)(Et_2NpyS_4)] and [Ru(N_2H_4)(Et_2NpyS_4)] revealed that such complexes can form intra- and intermolecular N−H···S and N−H···N hydrogen bonds. This stabilises the hydrazine complex [Fe(N_2H_4)(Et_2NpyS_4)] and makes it isolable and stable in the solid state. This is in contrast to the parent complex [Fe(N_2H_4)(pyS_4)] which was highly labile with respect to elimination of the N_2H_4 coligand and could not be isolated.

Experimental Section

General: Unless noted otherwise, all procedures were carried out under nitrogen using Schlenk techniques. Stringently dried solvents were used. As far as possible, reactions were monitored by IR or NMR spectroscopy. Spectra were recorded with the following instruments: IR (KBr discs or CaF_2 corvettes, solvent bands were compensated): Perkin−Elmer 983, 1620 FT-IR, and 16PC FT-IR. NMR: Jeol-JNM-GX 270, EX 270, and Lambda LA 400 with the proton solvent signals used as an internal reference. Spectra were recorded at 25 °C. MS: Jeol MSTATION 700 spectrometer. Elemental analyses: Carlo Erba EA 1106 or 1108 analyser. Magnetic susceptibility: Johnson Matthey susceptibility balance. Cyclic voltammograms were recorded using an EG&G potentiostat PAR model 264A and a conventional three-electrode configuration consisting of a glassy carbon working electrode, a platinum auxiliary electrode and a platinum reference electrode. Ferrocene was used as an internal reference, $E(Fc/Fc^+)$ = +400 mV (vs. NHE).[15] The reversibility of the voltammograms and the number of electrons involved in the redox processes at 25°C were determined as described in the literature.[16] "S_2"−H_2 (1,2-benzenedithiol),[17] dimethyl 4-bromo-pyridine-2,6-dicarboxylate[7] and Bu_4N[Ru(NO)($S_2C_6H_4$)$_2$][11] were prepared as described in the literature. Anhydrous hydrazine was obtained by twofold distillation of N_2H_4·H_2O from KOH under reduced pressure.

$Et_2Npy(CO_2Me)_2$ (1): Anhydrous K_2CO_3 (4.15 g, 30 mmol) and diethylamine (20 mL, 192.5 mmol) were added to a white suspension of dimethyl 4-bromo-pyridine-2,6-dicarboxylate (6.89 g, 25.1 mmol) in DMSO (200 mL). The resultant yellow-brown mixture was heated at 55−60 °C for 48 h. The resultant orange-brown suspension was cooled to room temperature and poured onto ice-cold water (250 mL). A yellow solid formed which was separated by filtration, washed with water and dried in vacuo. Yield: 6.32 g of **1** (34%). ^{1}H NMR ($CDCl_3$, 269.60 MHz): δ = 1.20 (t, 6 H, $2CH_2CH_3$), 3.44 (q, 4 H, $2CH_2CH_3$), 3.95 (s, 6 H, $2COOCH_3$), 7.45 (s, 2 H, H_β, pyridine) ppm. IR (KBr): $\tilde{\nu}$ = 1748, 1708, (vs, C=O) cm^{-1}. MS (FD^+, $CHCl_3$): m/z = 266 [M^+]. $C_{13}H_{18}N_2O_4$ (266.29): calcd. C 58.63, H 6.81, N 10.52; found C 58.44, H 6.92, N 10.37.

$Et_2Npy(CH_2OH)_2$ (2): $NaBH_4$ (2.96 g, 40 mmol) was added portionwise to **1** (4.05 g, 16 mmol) in ethanol (200 mL). The mixture was kept at room temperature for 1.5 h and was then heated to reflux for 16 h. The solvent was evaporated, the residue treated with a saturated solution of $NaHCO_3$ (50 mL) and heated to reflux for 1.5 h. H_2O (100 mL) was added and the aqueous phase was extracted continuously with $CHCl_3$ (500 mL) over 2 d. The $CHCl_3$ was evaporated to give a colourless solid. Yield 2.83 g of **2** (88%). ^{1}H NMR ([D_6]DMSO, 269.60 MHz): δ = 1.10 (t, $^3J_{H,H}$ = 7.1 Hz, 6 H, CH_2CH_3), 3.33 (q, 4 H, CH_2CH_3), 4.35 (d, $^2J_{H,H}$ = 5.5 Hz, 4 H, $2CH_2$), 5.14 (t, $^3J_{H,H}$ = 5.8 Hz, 2 H, 2O*H*), 6.51 (s, 2 H, H_β pyridine) ppm. MS (FD, DMSO): m/z = 210 [M^+].

$Et_2Npy(CH_2Br)_2$ (3): A solution of **2** (400 mg, 1.9 mmol) in 40% aqueous HBr (50 mL) was heated to reflux for 16 h. The aqueous phase was extracted with $CHCl_3$ (3 × 100 mL). The $CHCl_3$ extract was dried with $MgSO_4$ and the solvent removed in vacuo to give a white solid residue. Yield: 400 mg of **3**·0.16THF (62%). ^{1}H NMR ($CDCl_3$, 269.60 MHz): δ = 1.21 (t, 6 H, $2CH_2CH_3$), 3.41 (q, 4 H, $2CH_2CH_3$), 4.50 (s, 4 H, $2CH_2$), 6.55 (s, 2 H, H_β pyridine), ^{13}C{^{1}H} NMR ($CDCl_3$, 67.83 MHz): δ = 12.27 (CH_2CH_3), 33.43 (CH_2CH_3), 44.31 (CH_2Br), 105.24, 154.02, 156.01 [*C*(aryl)] ppm. IR (KBr): $\tilde{\nu}$ = 3033, 2969 (m, C−H) cm^{-1}. FD MS: m/z: 336 [M^+]. $C_{11.7}H_{17.3}Br_2N_2O_{0.17}$ (348.10): calcd. C 40.26, H 5.02, N 8.05; found C 40.12, H 5.13, N 8.13.

[{Ni(Et_2NpyS_4)}$_2$] (4). a): A solution of **2**·0.75MeOH (1.17 g, 5.34 mmol) in THF (30 mL) was combined with KOH (0.9 g, 17.80 mmol) and cooled to 0 °C. Tosyl chloride (2.43 g, 10.68 mmol) in THF (20 mL) was added dropwise and the resultant suspension was stirred at 0 °C for 5 h and at room temperature for 14 h. The resultant solid was removed by filtration and washed with THF (30 mL). The washings and the filtrates were dried in vacuo, yielding a light brown viscous residue. Yield 2.6 g of $Et_2Npy(CH_2OTs)_2$ (**3a**) (90%) which was used without further purification. **b):** Sodium (453 mg, 19.67 mmol) was dissolved in methanol (40 mL) and combined with 1,2-benzenedithiol (1.12 mL, 9.83 mmol) and a solution of Ni(ac)$_2$·4H_2O (1.22 g, 4.92 mmol) in MeOH (50 mL). Addition of $Et_2Npy(CH_2OTs)_2$ (**3a**) (2.55 g, 4.92 mmol) in THF (70 mL) to the dark-brown solution resulted in a brown precipitate which was isolated after 3 h, washed with THF and MeOH (30 mL each) and dried in vacuo. Yield: 2.0 g of [{Ni(Et_2NpyS_4)}$_2$]·1.5MeOH (**4**·1.5MeOH) (76%). IR (KBr): $\tilde{\nu}$ = 3050, 2968, ν(C−H) cm^{-1}. MS (FD^+, MeOH): m/z = 514 [Ni(Et_2NpyS_4)]$^+$, 1028 [{Ni(Et_2NpyS_4)}$_2$]$^+$. $C_{23}H_{24}N_2NiS_4$ (515.40): calcd. C 52.22, H 5.36, N 5.00; found C 52.66, H 5.16, N 5.12. μ_{eff} = 2.25 μ_B (297 K).

$Et_2NpyS_4-H_2$·HCl (5): Concentrated hydrochloric acid (15.14 mL) was added to a suspension of **4**·1.5MeOH (4.86 g, 9.60 mmol) in CH_2Cl_2 (200 mL) and the mixture was stirred for 30 min. The CH_2Cl_2 phase was separated from the aqueous green phase, dried with anhydrous Na_2SO_4 and the solvents were evaporated to dryness yielding a grey-green solid. Yield 1.7 g of **5**·2CH_3OH (32%). ^{1}H NMR (CD_2Cl_2, 269.60 MHz): δ = 0.94 (t, $^3J_{H,H}$ = 7.2 Hz, 6 H, $2CH_2CH_3$), 3.14 (q, 4 H, $2CH_2CH_3$), 4.38 (s, 2 H, 2S*H*), 4.40

 © 2004 Wiley-VCH Verlag GmbH & Co. KGaA, Weinheim

(s, 4 H, 2CH_2), 5.92 (s, 2 H, H_β, pyridine), 7.04−7.38 (m, 8 H, C$_6H_4$), 7.78 (d, $^2J_{H,H}$ = 6.5 Hz, 1 H, N*H*) ppm. IR (KBr): $\tilde{\nu}$ = 3414, 3255, 3070 (w, N−H), 2412 (w, S−H) cm^{-1}. MS (FD$^+$, CH_2Cl_2): *m*/*z* = 495 [M]$^+$. $C_{25}H_{35}ClN_2O_2S_4$ (559.3): calcd. C 53.69, H 6.31, N 5.01; found C 53.94, H 5.91, N 4.69.

[{Fe(Et$_2$NpyS$_4$)}$_2$] (6): Solid $FeCl_2{\cdot}4H_2O$ (77 mg, 0.39 mmol) was added to a light yellow solution of **5**·H_2O (220 mg, 0.39 mmol) and LiOMe (1.17 mL of a 1 M solution in MeOH) in THF (20 mL). A yellow precipitate resulted which was separated by filtration after 30 min, washed with THF (20 mL) and dried in vacuo. Yield: 105 mg of **6** (53%). IR (KBr): $\tilde{\nu}$ = 3050, 2966 (s, C−H) cm^{-1}. MS (FD$^+$, DMF): *m*/*z* = 512 [Fe(Et$_2$NpyS$_4$)]$^+$, 1024 [Fe(Et$_2$NpyS$_4$)]$_2^+$. $C_{23}H_{24}FeN_2S_4$ (513.55): calcd. C 53.90 H 4.72, N 5.47, S 25.02; found C 53.65, H 5.11, N 5.46, S 24.86. μ_{eff} = 5.15 μ_B (297 K).

[{Fe(Et$_2$NpyS$_4$−O$_2$)}$_2$] (7): A yellow suspension of **6** (120 mg, 0.12 mmol) in $CHCl_3$ (30 mL) was stirred in air for 24 h. The resultant red-brown fine crystals were isolated, washed with $CHCl_3$ then H_2O (30 mL each) and dried in vacuo. Yield: 80 mg of **7**·3$CHCl_3{\cdot}H_2O$ (23%). IR (KBr): $\tilde{\nu}$ = 2960 (s, C−H), 1238, 1185, 1133, 983 (s, SO_2) cm^{-1}. MS (FD$^+$, $CHCl_3$): *m*/*z* = 512 [Fe(Et$_2$NpyS$_4$)]$^+$, 1024 [{Fe(Et$_2$NpyS$_4$)}$_2$]$^+$, 1088 [{Fe(Et$_2$NpyS$_4$−O$_2$)}$_2$]$^+$. $C_{49}H_{53}Cl_9Fe_2N_4O_5S_8$ (1459.77): calcd. C 40.17, H 3.65, N 3.82, S 17.51; found C 40.12, H 4.09, N 3.84, S 17.85.

[Fe(CO)(Et$_2$NpyS$_4$)] (8): A stream of CO was passed through a yellow suspension of **6** (70 mg, 0.14 mmol) in THF (20 mL) for 10 min during the course of which a red solution formed which was kept under CO for a further 12 h, filtered and reduced in volume to about 2 mL. Addition of Et_2O (20 mL) precipitated a red solid which was separated by filtration and dried in vacuo. Yield 62 mg of **8**·0.7H_2O (84%). ^{1}H NMR (CD_2Cl_2, 269.60 MHz): δ = 1.06 (t, $^3J_{H,H}$ = 7.05 Hz, 6 H, 2CH_2CH_3), 3.22 (q, $^4J_{H,H}$ = 6.20 Hz, 4 H, 2CH_2CH$_3$), 4.34 (d, $^2J_{H,H}$ = 16.2 Hz, 2 H, CH_2), 4.86 (d, $^2J_{H,H}$ = 16.2 Hz, 2 H, CH_2), 6.39 (s, 2 H, H_β, pyridine), 6.93 (m, 4 H, C$_6H_4$), 7.41 (d, $^2J_{H,H}$ = 6.5 Hz, 2 H, C$_6H_4$), 7.56 (d, $^2J_{H,H}$ = 6.5 Hz, 2 H, C$_6H_4$) ppm. ^{13}C{^{1}H} NMR (CD_2Cl_2, 67.83 MHz): δ = 9.6 (CH_2CH_3), 41.9 (CH_2CH$_3$), 53.8 (CH_2), 101.2, 119.7, 126.2, 127.9, 129.5, 131.0, 149.4, 153.9, 155.2 [*C*(aryl)], 214.4 (*C*O) ppm. IR (KBr): $\tilde{\nu}$ = 1948 (vs, CO), 2966 (m, C−H) cm^{-1}. MS (FD$^+$, CH_2Cl_2): *m*/*z* = 512 [Fe(Et$_2$NpyS$_4$)]$^+$, 1024 [{Fe(Et$_2$NpyS$_4$)}$_2$]$^+$. $C_{24}H_{25.4}FeN_2O_{1.7}S_4$ (552.02): calcd. C 52.17, H 4.62, N 5.07, S 23.21; found C 52.21, H 4.76, N 5.01, S 23.00.

[Fe(CO)(Et$_2$NpyS$_4$−H)]BF$_4$ (8a): At −78 °C, (0.013 mL, 0.1 mmol) HBF_4 (54% in Et_2O) was added to a red suspension of **8**·0.7H_2O (50 mg, 0.1 mmol) in CH_2Cl_2 (15 mL). After 1 h of stirring, during the course of which the resultant grey solution was reduced in volume to about 3 mL at −78 °C, addition of *n*-hexane (15 mL) precipitated a grey solid which was isolated and dried in vacuo. Yield: 40 mg (69%) of **8a**. IR (KBr): $\tilde{\nu}$ = 2503 (w, S−H), 1974 (vs, CO) cm^{-1}. MS (FD$^+$, CH_2Cl_2): *m*/*z* = 512 [Fe(Et$_2$NpyS$_4$)]$^+$, 1024 [{Fe(Et$_2$NpyS$_4$)}$_2$]$^+$. $C_{24.5}H_{26}FeBClF_4N_2OS_4$ (670.49): C 43.86, H 3.91, N 4.17; found C 43.66, H 3.79, N 3.91.

[Fe(CO)(Et$_2$NpyS$_4$-Et)]BF$_4$ (8b): A red solution of **8**·0.7H_2O (90 mg, 0.17 mmol) in CH_2Cl_2 (10 mL) was combined with a 1 M Et_3OBF_4 solution in CH_2Cl_2 (0.17 mL, 0.17 mmol). The resultant brown solution was reduced in volume to 3 mL. Addition of Et_2O (20 mL) precipitated a brown solid which was separated by filtration, washed with Et_2O (20 mL) and dried in vacuo. Yield 85 mg of **8b**·0.3CH_2Cl_2 (76%). ^{1}H NMR (CD_2Cl_2, 269.60 MHz): δ = 0.98 (m, 6 H, 2CH_2CH_3), 1.46 (m, 3 H, CH_2CH_3), 3.12 (m, 6 H, 3CH_2CH$_3$), 4.48 (m, 2 H, CH_2), 4.90 (m, 2 H, CH_2), 6.43 (d, 2 H, H_β, pyridine), 7.00 (m, 2 H, C$_6H_4$), 7.32 (d, 1 H, C$_6H_4$), 7.61−7.51 (m, 3 H, C$_6H_4$), 7.74 (m, 1 H, C$_6H_4$), 8.09 (m, 1 H, C$_6H_4$) ppm. ^{13}C{^{1}H} NMR (CD_2Cl_2, 67.83 MHz): δ = 12.33 (CH_2CH_3), 13.34 (CH_2CH_3), 41.51 (CH_2CH_3), 44.97 (CH_2CH_3), 55.80, 55.90 (CH_2), 105.38, 105.64, 124.03, 129.69, 129.95, 130.57, 132.22, 132.38, 132.78, 133.61, 133.90, 135.75, 137.14, 152.90, 154.14, 155.48, 156.58 [*C*(aryl)], 213.24 (*C*O) ppm. IR (KBr): $\tilde{\nu}$ = 1980 (vs, CO), 1055 (vs, B−F) cm^{-1}. MS (FD$^+$, CH_2Cl_2): *m*/*z* = 512 [Fe(Et$_2$NpyS$_4$)]$^+$, 1024 [{Fe(Et$_2$NpyS$_4$)}$_2$]$^+$. $C_{26.3}H_{29.6}FeBCl_{0.6}F_4N_2OS_4$ (684.74): C 46.19, H 4.37, N 4.09; found C 46.39, H 4.73, N 4.04.

[Fe(CO)(Et$_2$NpyS$_4$−Et$_2$)](BF$_4$)$_2$ (8c): Et_3OBF_4 (0.40 mL, 0.40 mmol of a 1 M solution in CH_2Cl_2) was added to a red solution of **8**·0.7H_2O (110 mg, 0.20 mmol) in CH_2Cl_2 (15 mL). The colour immediately changed from red to brown. After 24 h, the reaction mixture was reduced in volume to 3 mL. Addition of Et_2O (30 mL) precipitated a brown solid which was separated by filtration, washed with Et_2O (20 mL) and dried in vacuo. Yield 120 mg of **8c**·0.5CH_2Cl_2 (72%). ^{1}H NMR (CD_3OD, 269.60 MHz): δ = 1.02−0.97 (t, $^3J_{H,H}$ = 7.2 Hz, 6 H, 2CH_2CH_3), 1.53−1.62 (t, $^3J_{H,H}$ = 7.2 Hz, 6 H, 2CH_2CH_3), 3.21−3.34 (m, 4 H, 2CH_2CH$_3$), 3.35−3.49 (m, 4 H, CH_2CH$_3$), 4.79−4.82 (d, $^2J_{H,H}$ = 16.69 Hz, 2 H, CH_2), 5.17−5.23 (d, $^2J_{H,H}$ = 16.70 Hz, 2 H, CH_2), 6.77 (s, 2 H, H_β, pyridine), 7.65 (t, $^3J_{H,H}$ = 7.4 Hz, 3 H, C$_6H_4$), 7.77 (t, $^3J_{H,H}$ = 7.20/7.60 Hz, 3 H, C$_6H_4$), 7.97 (d, $^2J_{H,H}$ = 7.64 Hz, 2 H, C$_6H_4$), 8.32 (d, $^2J_{H,H}$ = 7.83 Hz, 2 H, C$_6H_4$) ppm. ^{13}C{^{1}H} NMR (CD_3OD, 67.83 MHz): δ = 12.01 (CH_2CH_3), 13.09 (CH_2CH_3), 41.41 (CH_2CH_3), 44.59 (CH_2CH_3), 54.74 (CH_2), 107.23, 133.47, 134.15 134.20, 134.83, 135.42, 136.42, 154.96, 158.00 [*C*(aryl)], 210.00 (*C*O) ppm. IR (KBr) : $\tilde{\nu}$ = 2007 (vs, CO), 1056 (vs, B−F) cm^{-1}. MS (FD$^+$, CH_3OH): *m*/*z* = 512 [Fe(Et$_2$NpyS$_4$)]$^+$, 1024 [{Fe(Et$_2$NpyS$_4$)}$_2$]$^+$. $C_{28.5}H_{35}FeB_2ClF_8N_2OS_4$ (814.77): C 42.00, H 4.33, N 3.44, S 15.74; found C 41.68, H 4.57, N 3.64, S 15.98.

[Fe(CNCy)(Et$_2$NpyS$_4$)] (9): Cyclohexyl isocyanide (0.032 mL, 0.30 mmol) was added to a yellow suspension of **6** (100 mg, 0.20 mmol) in THF (20 mL). A red solution resulted which was stirred for 12 h, filtered and reduced in volume to about 5 mL. Addition of Et_2O (20 mL) precipitated a red-orange solid which was separated by filtration and dried in vacuo. Yield: 60 mg of **9** (57%). ^{1}H NMR ([D$_8$]toluene, 269.60 MHz): δ = 0.39 (t, 6 H, 2CH_2CH_3), 0.93 (t, 10 H, C$_6H_{11}$), 7.85 (m, 1 H, C$_6H_{11}$), 2.35 (m, 4 H, 2CH_2CH$_3$), 3.98−3.92 (d, 2 H, CH_2), 4.85−4.80 (d, 2 H, CH_2), 5.68 (s, 2 H, H_β, pyridine), 6.68−6.83 (m, 4 H, C$_6H_4$), 7.53−7.24 (m, 2 H, C$_6H_4$), 7.80 (d, 2 H, C$_6H_4$) ppm. IR (KBr): $\tilde{\nu}$ = 2105 (vs, CN), 2969, 2932 (m, C−H) cm^{-1}. MS (FD$^+$, toluene): *m*/*z* = 512 [Fe(Et$_2$NpyS$_4$)]$^+$, 620 [Fe(CNCy)(Et$_2$NpyS$_4$)]$^+$, 1024 [{Fe(Et$_2$NpyS$_4$)}$_2$]$^+$. $C_{30}H_{35}FeN_3S_4$ (621.73): calcd. C 57.95, H 5.67, N 6.76, S 20.63; found C 57.34, H 6.21, N 6.77, S 20.43.

[Fe(NO)(Et$_2$NpyS$_4$)]BF$_4$ (10). a) From 8: Solid $NOBF_4$ (5 mg, 0.04 mmol) was added to a red solution of **8**·0.7H_2O (20 mg, 0.04 mmol) in CH_2Cl_2 (10 mL). During the course of 10 min, a yellow-green solution resulted which was filtered and reduced in volume to about 5 mL. Addition of Et_2O (20 mL) precipitated a yellow-green solid which was separated by filtration and dried in vacuo. Yield: 15 mg of **10**·$CH_2Cl_2{\cdot}Et_2O$ (65%). **b) From 6:** At 0 °C, solid $NOBF_4$ (5 mg, 0.04 mmol) was added to a yellow suspension of **6** (20.5 mg, 0.04 mmol) in CH_2Cl_2 (10 mL). After stirring at 0 °C for 70 min and at room temperature for 30 min, the resultant yellow-green mixture was filtered, reduced in volume to about 5 mL and combined with Et_2O (20 mL). The resultant green solid was separated by filtration and dried in vacuo. Yield: 18 mg **10**·$CH_2Cl_2{\cdot}Et_2O$ (82%). ^{1}H NMR (CD_2Cl_2, 269.60 MHz): δ = 1.05

 © 2004 Wiley-VCH Verlag GmbH & Co. KGaA, Weinheim

(t, 6 H, $2CH_2CH_3$), 3.25 (q, 4 H, $2CH_2CH_3$), 4.46 (d, 2 H, CH_2), 5.00 (m, 2 H, CH_2), 6.46 (s, 2 H, H_β?, pyridine), 7.28 (m, 4 H, C_6H_4), 7.45 (m, 2 H, C_6H_4), 7.65 (d, 2 H, C_6H_4) ppm. $^{13}C\{^1H\}$ NMR (CD_2Cl_2, 67.83 MHz): δ = 11.9 (CH_2CH_3), 45.1 (CH_2CH_3), 55.1 (CH_2), 106.2, 126.26, 128.1, 129.5, 131.1, 132.1, 151.3, 152.7, 156.65 [*C*(aryl)] ppm. IR (KBr): $\tilde{\nu}$ = 1882 (vs, NO), 1081 (vs, B−F) cm^{-1}. MS (FD^+, CH_2Cl_2): *m*/*z* = 512 $[Fe(Et_2NpyS_4)]^+$, 1024 $[\{Fe(Et_2NpyS_4)\}_2]^+$. $C_{28}H_{36}BCl_2F_4FeN_3OS_4$ (788.42): calcd. C 42.65, H 4.60, N 5.33, found C 42.68, H 4.21, N 5.76.

[Fe(NO)(Et_2NpyS_4)] (11): By means of a syringe, NO gas (5 mL, 0.21 mmol) was injected into a stirred yellow suspension of **6** (80 mg, 0.158 mmol) in CH_2Cl_2 (20 mL). A brown mixture resulted which was stirred for 24 h, filtered and reduced in volume to about 5 mL. Addition of Et_2O (20 mL) precipitated a brown solid which was separated by filtration and dried in vacuo. Yield: 78 mg **11**·0.5CH_2Cl_2 (92%). IR (KBr): $\tilde{\nu}$ = 1637 (s, NO) cm^{-1}. MS (FD^+, CH_2Cl_2): *m*/*z* = 512 $[Fe(Et_2NpyS_4)]^+$, 544 $[Fe(NO)(Et_2NpyS_4)]^+$, 1024 $[\{Fe(Et_2NpyS_4)\}_2]^+$. $C_{23.5}H_{25}ClFeN_3OS_4$ (565.15): calcd. C 48.25, H 4.31, N 7.18; found C 48.77, H 4.49, N 7.11.

[Fe(N_2H_4)(Et_2NpyS_4)] (12): N_2H_4 (0.032 mL, 1.0 mmol) was added to a yellow suspension of **6** (100 mg, 0.20 mmol) in CH_2Cl_2 (15 mL). During the course of 48 h, a deep red solution resulted which was filtered and reduced in volume to about 2 mL. Addition of Et_2O (20 mL) precipitated a brown solid which was separated by filtration and dried in vacuo. Yield: 60 mg of **12**·0.25Et_2O (55%). ^1H NMR ([D$_8$]THF, 269.60 MHz): δ = 0.85 (t, 6 H, $2CH_2CH_3$), 2.90 (br., N_2H_4), 3.32 (m, 4 H, $2CH_2CH_3$), 4.50 (m, 4 H, $2CH_2$), 6.56 (s, 2 H, H_β, pyridine), 7.44 (m, 2 H, C_6H_4), 7.94 (m, 2 H, C_6H_4), 9.72 (m, 4 H, C_6H_4) ppm. IR (KBr): $\tilde{\nu}$ = 3318, 3285, 3237 (m, N−H) cm^{-1}. MS (FD^+, THF): *m*/*z* = 512 $[Fe(Et_2NpyS_4)]^+$, 1024 $[\{Fe(Et_2NpyS_4)\}_2]^+$. $C_{24}H_{30.5}FeN_4OS_4$ (563.13): calcd. C 51.19, H 5.46, N 9.95; found C 50.82, H 5.71, N 9.55.

[Ru(NO)(Et_2NpyS_4)]Br (13): Over the course of 1 h, a solution of $Bu_4N[Ru(NO)(S_2C_6H_4)_2]$ (2.5 g, 3.82 mmol) in THF (30 mL) was added dropwise to a boiling solution of **3**·0.16 THF (1.52 g, 4.52 mmol) in THF (30 mL). The mixture was heated to reflux for a further 1 h and cooled to room temperature. After 2 h, the precipitated red solid was separated by filtration, washed with THF (30 mL), ether (20 mL) and dried in vacuo. Yield 2 g of **13**·0.3THF (77%). ^1H NMR ([D$_6$]DMSO, 269.60 MHz): δ = 0.92 (t, 6 H, $2CH_2CH_3$), 3.20 (q, 4 H, $2CH_2CH_3$), 4.94 (d, 2 H, CH_2), 5.25 (d, 2 H, CH_2), 6.67 (s, 2 H, H_β, pyridine), 7.28 (m, 4 H, C_6H_4), 7.52 (d, 2 H, C_6H_4), 7.99 (d, 2 H, C_6H_4) ppm. $^{13}C\{^1H\}$ NMR (CD_2Cl_2, 67.83 MHz): δ = 13.85 (CH_2CH_3), 44.00 (CH_2CH_3), 54.83 (CH_2), 104.62, 124.96, 128.51, 129.73, 130.72, 132.87, 149.86, 151.80, 156.19 [*C*(aryl)] ppm. IR (KBr): $\tilde{\nu}$ = 1858 (vs, NO) cm^{-1}. MS (FD^+, CH_2Cl_2): *m*/*z* = 558 $[Ru(Et_2NpyS_4)]^+$, 585 $[Ru(NO)(Et_2NpyS_4)]^+$, 1116 $[\{Ru(Et_2NpyS_4)\}_2]^+$. $C_{24.3}H_{28.6}BrN_3O_2RuS_4$ (704.3): calcd. C 41.49, H 4.10, N 5.97; found C 41.37, H 4.48, N 6.18.

[$\{$Ru(Et_2NpyS_4)$\}_2$] (14): NH_3 gas was bubbled through a red solution of **13**·0.3THF (110 mg, 0.16 mmol) in MeOH (10 mL) for 1 h. The green solid which precipitated was separated by filtration, washed with MeOH (10 mL), Et_2O (10 mL) and dried in vacuo. Yield 140 mg, **14**·H_2O (42%). IR (KBr): $\tilde{\nu}$ = 2967, 2923 (m, C−H) cm^{-1}. MS (FD^+, DMSO): *m*/*z* = 1116 $[\{Ru(Et_2NpyS_4)\}_2]^+$. $C_{46}H_{50}N_4ORuS_8$ (1115.53): C 48.74, H 4.44, N 4.94; found C 48.70, H 4.14, N 4.85.

[Ru(N_2H_4)(Et_2NpyS_4)] (15): N_2H_4 (0.5 mL, 16 mmol) was added to a red-brown suspension of **13**·0.3THF (110 mg, 0.16 mmol) in THF (10 mL). Gas evolved and a red solution formed which was concentrated in volume to 3 mL. Addition of MeOH (10 mL) led to precipitation of a red microcrystalline solid which was separated, washed with MeOH (10 mL) and ether (20 mL) then dried in vacuo. Yield 40 mg of **15**·0.3 N_2H_4·0.6H_2O (41%). ^1H NMR ([D$_6$]DMSO, 269.60 MHz): δ = 1.02−0.83 (t, 6 H, $2CH_2CH_3$), 3.10−2.99 (m, 4 H, $2CH_2CH_3$), 3.30 (m, 1 H, NH_2), 4.24−4.22 (d, 1 H, NH_2), 4.31−4.28 (d, 2 H, CH_2), 4.37 (d, 2 H, CH_2), 4.42 (d, 1 H, N*H*), 6.19 (s, 2 H, H_β, pyridine), 6.67−6.59 (m, 4 H, C_6H_4), 7.37−7.35 (m, 2 H, C_6H_4), 7.50−7.47 (m, 2 H, C_6H_4) ppm. $^{13}C\{^1H\}$ NMR (DMF-d$_7$, 67.83 MHz): δ = 12.02 (CH_2CH_3), 43.25 (CH_2CH_3), 56.69 (CH_2), 102.93, 119.93, 130.61, 132.19, 132.98, 149.98, 158.28 [*C*(aryl)] ppm. IR (KBr): $\tilde{\nu}$ = 3318, 3242, 3100 (m, N−H) cm^{-1}. MS (FD^+, CH_2Cl_2): *m*/*z* = 558 $[Ru(Et_2NpyS_4)]^+$, 590 $[Ru(N_2H_4)(Et_2NpyS_4)]^+$, 1116 $[\{Fe(Et_2NpyS_4)\}_2]^+$. $C_{23}H_{29.7}N_{3.3}O_{0.6}RuS_4$ (611.5): calcd. C 45.17, H 4.89, N 10.69, S 20.97; found C 45.16, H 5.07, N 10.53, S 20.63.

X-ray Structure Determination of [$\{$Fe($Et_2NpyS_4-O_2$)$\}_2$]·8$CDCl_3$ (7·8$CDCl_3$), [Fe(CO)(Et_2NpyS_4)]·$CDCl_3$ (8·$CDCl_3$), [Fe(CNCy)(Et_2NpyS_4)]·2THF (9·2THF), [Fe(NO)(Et_2NpyS_4)]BF_4·CH_2Cl_2 (10·CH_2Cl_2), [Fe(N_2H_4)(Et_2NpyS_4)] (12), [Ru(N_2H_4)(Et_2NpyS_4)] (15) and [Ru(N_2H_4)(Et_2NpyS_4)]·N_2H_4 (15·N_2H_4): Red-brown blocks of 7·8$CDCl_3$ were grown at room temperature from a saturated $CDCl_3$ solution of **7** over one week. Red blocks of **8**·$CDCl_3$ were grown at room temperature from a saturated $CDCl_3$ solution of **8** over 3 d. Red single-crystals of **9**·2THF were grown at −27 °C from a saturated THF solution of **9** over 5 weeks. Brown blocks of **10**·CH_2Cl_2 were obtained from a saturated CH_2Cl_2 solution at room temperature over 4 weeks. Brown single-crystals of **12** were grown at room temperature from a saturated CD_2Cl_2 solution over 2 weeks. Red prisms of **15** were grown at room temperature from a saturated THF solution over one week. Orange single crystals of **15**·N_2H_4 were grown at room temperature from a saturated THF solution of **15** over one week in the presence of excess hydrazine. Suitable single-crystals were embedded in protective perfluoropolyether oil. Data were collected either with a Siemens P4 (**7**·8$CDCl_3$) or a Nonius-KappaCCD diffractometer (**8**·$CDCl_3$, **9**·2THF, **10**·CH_2Cl_2, **12**, **15** and **15**·N_2H_4) using Mo-K_α radiation (λ = 71.073 pm, graphite monochromator). Intensity data were corrected for absorption effects using either ψ-scans[18] (**7**·8$CDCl_3$) or multiple scans of equivalent reflections (SADABS[19] for **9**·2THF and SORTAV[20] for **8**·$CDCl_3$, **12**, **15** and **15**·N_2H_4) while for **10**·CH_2Cl_2 absorption effects were neglected. The structures were solved by direct methods and refined on F^2 using full-matrix least-squares procedures (SHELXTL NT 5.10[21] for **7**·8$CDCl_3$ **8**·$CDCl_3$, **9**·2THF, **12**, **15** and **15**·N_2H_4 or SHELXTL NT 6.12[22] for **10**·CH_2Cl_2). Hydrogen atoms were either located in a difference Fourier map and refined with a common fixed isotropic displacement parameter (**7**·8$CDCl_3$ **8**·$CDCl_3$, **12**), kept fixed in their positions with a common fixed isotropic displacement parameter (**15**, **15**·N_2H_4), or were geometrically positioned (**9**·2THF, **10**·CH_2Cl_2). The solvate molecules in the structures of **7**·8$CDCl_3$ **8**·$CDCl_3$, **9**·2THF and **10**·CH_2Cl_2 are partly disordered. Table 6 lists selected crystallographic data. CCDC-238453 (**7**·8$CDCl_3$), -238454 (**8**·$CDCl_3$), -238455 (**9**·2THF), -238456 (**10**·CH_2Cl_2), -238457 (**12**), -238458 (**15**) and -238459 (**15**·N_2H_4) contain the supplementary crystallographic data for this paper. These data can be obtained free of charge at www.ccdc.cam.ac.uk/conts/retrieving.html [or from the Cambridge Crystallographic Data Centre, 12 Union Road, Cambridge CB2 1EZ, UK; Fax: (internat.) + 44-1223-336-033; E-mail: deposit@ccdc.cam.ac.uk]

 © 2004 Wiley-VCH Verlag GmbH & Co. KGaA, Weinheim

Table 6. Crystallographic data and structure refinement details for [{Fe(Et_2NpyS$_4$-$(O_2)_2$]$_2$]·8$CHCl_3$ (**7**·8$CHCl_3$), [Fe(CO)(Et_2NpyS$_4$)]·$CDCl_3$ (**8**·$CDCl_3$), [Fe(CNCy)(Et_2NpyS$_4$)]·2THF (**9**·2THF), [Fe(NO)(Et_2NpyS$_4$)]BF_4·CH_2Cl_2 (**10**·CH_2Cl_2), [Fe(N_2H_4)(Et_2NpyS$_4$)] (**12**) [Ru(N_2H_4)(Et_2NpyS$_4$)] (**15**) and [Ru(N_2H_4)(Et_2NpyS$_4$)]·N_2H_4 (**15**·N_2H_4)

	7·8$CDCl_3$	**8**·$CDCl_3$	**9**·2THF	**10**·CH_2Cl_2	**12**	**15**	**15**·N_2H_4
Empirical formula	$C_{54}H_{48}Cl_{24}D_8Fe_2N_4O_4S_8$	$C_{25}H_{24}Cl_3DFeN_2OS_4$	$C_{38}H_{51}FeN_3O_2S_4$	$C_{24}H_{26}BCl_2F_4FeN_3OS_4$	$C_{23}H_{28}FeN_4S_4$	$C_{23}H_{28}N_4RuS_4$	$C_{23}H_{32}N_6RuS_4$
M_r [g mol^{-1}]	2052.06	569.91	756.91	714.28	544.58	589.80	621.86
Crystal size [mm]	0.50 × 0.28 × 0.15	0.20 × 0.15 × 0.05	0.49 × 0.28 × 0.10	0.20 × 0.07 × 0.05	0.25 × 0.21 × 0.14	0.38 × 0.22 × 0.12	0.17 × 0.17 × 0.04
F(000)	1028	1352	1624	728	2272	2416	1280
Crystal system	triclinic	monoclinic	monoclinic	triclinic	orthorhombic	orthorhombic	monoclinic
Space group	$P\bar{1}$	$P2_1/n$	$P2_1/n$	$P\bar{1}$	$Pbca$	$Pbca$	$P2_1/n$
a [pm]	1168.6(1)	1286.76(3)	1595.4(2)	933.94(5)	1194.52(2)	1199.83(3)	1091.05(8)
b [pm]	1305.7(1)	1316.25(3)	1320.8(2)	1208.46(7)	1899.01(3)	1922.54(4)	1312.29(8)
c [pm]	1521.6(1)	1642.96(4)	1799.0(3)	1417.81(7)	2111.16(4)	2105.70(4)	1806.19(8)
α [°]	99.91(1)	90	90	82.880(4)	90	90	90
β [°]	111.80(1)	96.347(2)	101.088(7)	75.627(4)	90	90	96.562(5)
γ [°]	98.77(1	90	90	67.638(4)	90	90	90
V [nm^3]	2.0632(3)	2.7656(2)	3.7201(9)	1.4328(2)	4.7890(2)	4.8573(2)	2.5691(3)
Z	1	4	4	2	8	8	4
$\rho_{calcd.}$ [g cm^{-3}]	1.652	1.585	1.368	1.656	1.511	1.613	1.608
μ [mm^{-1}]	1.375	1.161	0.668	1.057	0.999	1.009	0.961
T [K]	210	100	100	100	100	100	100
θ range [°]	1.9−26.01	3.34−29.00	3.46−25.68	3.15−25.00	6.01−30.00	3.3−30	3.47−27.50
Measured reflections	9209	46227	35439	18296	33984	47848	24316
Unique reflections	7971	7346	6961	5037	6926	7017	5867
R_{int}	0.0392	0.1189	0.1036	0.1415	0.0808	0.1335	0.1031
Observed reflections	5274	4691	4587	3507	5040	716	4038
σ criterion	$I > 2\sigma(I)$	$I > 2\sigma(I)$	$I > 2\sigma(I)$	$I > 2\sigma(I)$	$I > 2\sigma(I)$	$I > 2\sigma(I)$	$I > 2\sigma(I)$
Refined parameters	551	419	509	389	373	289	307
R_1 [$I > 2\sigma$ (I)]	0.0518	0.0468	0.0592	0.0651	0.0384	0.0445	00451
wR_2 (all data)	0.1084	0.1092	0.1472	0.1871	0.0871	0.0892	0.0897
Absorption correction $T_{min.}/T_{max.}$	0.505/0.613	0.850/0.957	0.795/1.000	−	0.723/0.937	0.807/0.885	0.888/0.972

Acknowledgments

We thank Prof. Dr. Horst Kisch and Prof. Dr. Andreas Grohman for their helpful suggestions. Financial support for this work from the Deutsche Forschungsgemeinschaft (SFB, 583: "Redoxaktive Metallkomplexe") and the Fonds der Chemischen Industrie is gratefully acknowledged.

[1] [1a] B. K. Burgess, in "Molybdenum Enzymes, Cofactors and Model Systems" (Eds.: E. I. Stiefel, D. Coucouvanis, W. E. Newton), *ACS Symp. Ser.* **1993**, *535*, 144−170. [1b] D. J. Lowe, R. N. F. Thorneley, B. E. Smith, in *Metalloproteins*, part 1 ("Metal Proteins with Redox Roles") (Ed.: P. Harrison), Verlag Chemie, Weinheim, **1985**. [1c] R. R. Eady, in *Perspectives in Bioinorganic Chemistry* (Eds.: R. W. Hay, J. R. Dilworth, K. B. Nolan), JAI Press, London, **1991**, p. 225.

[2] [2a] D. Sellmann, N. Blum, F. W. Heinemann, *Z. Naturforsch., Teil B* **2001**, *56*, 581−588. [2b] D. Sellmann, N. Blum, F. W. Heinemann, B. A. Hess, *Chem. Eur. J.* **2001**, *7*, 1874−1880. [2c] D. Sellmann, J. Utz, N. Blum, F. W. Heinemann, *Coord. Chem. Rev.* **1999**, *190−192*, 607−627. [2d] D. Sellmann, D. Häußinger, T. Gottschalk-Gaudig, F. W. Heinemann, *Z. Naturforsch., Teil B* **2000**, *55*, 723−729. [2e] D. Sellmann, K. Engl, F. W. Heinemann, *Eur. J. Inorg. Chem.* **2000**, 423−429. [2f] D. Sellmann, J. Utz, F. W. Heinemann, *Inorg. Chem.* **1999**, *38*, 5314−5322. [2g] D. Sellmann, K. Hein, F. W. Heinemann, *Eur. J. Inorg. Chem.* **2004**, 3136−3146.

[3] [3a] R. A. Henderson, G. J. Leigh, C. J. Pickett, *Adv. Inorg. Chem. Radiochem.* **1983**, *27*, 197−292. [3b] H. Kandler, C. Gauss, W. Bidell, S. Rosenberger, T. Bürgi, I. L. Eremenko, D. Veghini, O. Orama, P. Burger, H. Berke, *Chem. Eur. J.* **1995**, *1*, 541−548. [3c] J. Chatt, A. J. Pearman, R. L. Richards, *J. Organomet. Chem.* **1975**, *101*, 45−47.

[4] D. Sellmann, B. Hautsch, A. Rösler, F. W. Heinemann, *Angew. Chem.* **2001**, *113*, 1553−1555; *Angew. Chem. Int. Ed.* **2001**, *40*, 1505−1507.

[5] D. Sellmann, A. Hille, F. W. Heinemann, M. Moll, A. Rösler, J. Sutter, G. Brehm, M. Reiher, B. A. Hess, S. Schneider, *Inorg. Chim. Acta* **2003**, *348*, 194−198.

[6] N. Blum, PhD Dissertation, University of Erlangen-Nürnberg, **2000**.

[7] H. Takato, J. Kankare, *Acta Chem. Scand., Ser. B* **1987**, *41*, 219−221.

[8] [8a] M. J. Baker-Hawkes, D. Billig, H. B. Gray, *J. Am. Chem. Soc.* **1966**, *88*, 4870−4875. [8b] D. Sellmann, S. Fünfgelder, G. Pohlmann, F. Knoch, M. Moll, *Inorg. Chem.* **1990**, *29*, 4772−4778. [8c] D. Sellmann, S. Fünfgelder, F. Knoch, M. Moll, *Z. Naturforsch., Teil B* **1991**, *46*, 1601−1608. [8d] D.

 © 2004 Wiley-VCH Verlag GmbH & Co. KGaA, Weinheim

Sellmann, P. Bail, F. Knoch, M. Moll, *Chem. Ber.* **1995**, *128*, 653−663. [8e] D. Sellmann, P. Bail, F. Knoch, M. Moll, *Inorg. Chim. Acta* **1995**, *237*, 137−141.
[9] [9a] A. T. Laurie, C. N. Juan, M. O. Marilyn, K. M. Pradip, *Inorg. Chem.* **1998**, *38*, 616−617. [9b] C. A. Ghilardi, S. Midollini, S. Moneti, *J. Organomet. Chem.* **1981**, *217*, 391−401. [9c] K. Manoj, C. J. Gerard, R. O. Day, J. M. Michael, *J. Am. Chem. Soc.* **1989**, *111*, 8323−8325.
[10] [10a] F. Bottomley, *Acc. Chem. Res.* **1978**, *11*, 158−163. [10b] J. A. McCleverty, *Chem. Rev.* **1979**, *79*, 53−76.
[11] D. Sellmann, G. Binker, *Z. Naturforsch., Teil B* **1987**, *42*, 341−347.
[12] [12a] D. Sellmann, K. P. Peters, F. W. Heinemann, *Eur. J. Inorg. Chem.* **2004**, 581−590. [12b] D. Sellmann, J. Sutter, *Inorg. Chem.* **2004**, *52*, 587−681.
[13] P. L. Bogdan, M. Sabat, S. A. Sunshine, C. Woodcock, D. F. Shriver, *Inorg. Chem.* **1988**, *27*, 1904−1910.
[14] L. Pauling, *Die Natur der chemischen Bindung*, VCH Verlagsgesellschaft, Weinheim, **1973**, p. 249.
[15] R. R. Gagne, C. A. Koval, G. C. Linsensky, *Inorg. Chem.* **1980**, *19*, 2855−2857.
[16] A. J. Bond, L. R. Faulkner, *Electrochemical Methods, Fundamentals and Applications*, Wiley, New York, **1980**.
[17] J. Degani, R. Fochi, *Synthesis* **1976**, *7*, 471−472.
[18] A. C. T. North, D. C. Phillips, F. S. Mathews, *Acta Crystallogr., Sect. A* **1968**, *24*, 351−359.
[19] R. H. Blessing, *Acta Crystallogr., Sect. A* **1995**, *51*, 33−38.
[20] SADABS: Bruker AXS, Inc., Madison, WI, USA, **2002**.
[21] SHELXTL NT 5.10: Bruker AXS, Inc., Madison, WI, USA, **1998**.
[22] SHELXTL NT 6.12: Bruker AXS, Inc., Madison, WI, USA, **2002**.

Received May 14, 2004
Early View Article
Published Online October 20, 2004

 © 2004 Wiley-VCH Verlag GmbH & Co. KGaA, Weinheim

Coordination Chemistry of Large Diphosphanes − Directional Properties of a Calix[4]arene Proximally Substituted by Two $-OCH_2PPh_2$ Podand Arms

Pierre Kuhn,[a] Catherine Jeunesse,[a] David Sémeril,[a] Dominique Matt,*[a] Pierre Lutz,[b] and Richard Welter[c]

Dedicated to Professor Jean-Pierre Sauvage on the occasion of his 60th birthday

Keywords: Calixarenes / Large diphosphanes / Nickel complexes / Ethylene oligomerisation

The proximally-functionalised calixarene 5,11,17,23-tetra-*tert*-butyl-25,26-bis(diphenylphosphanylmethoxy)-27,28-dihydroxycalix[4]arene (**1**), a large diphosphane in which the P^{III} centres are separated by 10 bonds, behaves as a chelating ligand towards NiX_2 moieties (X = Cl, Br). As shown by three X-ray studies carried out on complexes of the type [NiX_2·**1**], the diphosphane is able to accommodate either tetrahedral or strongly distorted tetrahedral coordination geometries, but not a square planar one. In all structures, the ligand positions the nickel atom away from the calixarene axis. In the presence of methylaluminoxane (MAO), [$NiCl_2$·**1**] effectively catalyses the oligomerisation of ethylene, affording C_4–C_{12} oligomers.

(© Wiley-VCH Verlag GmbH & Co. KGaA, 69451 Weinheim, Germany, 2004)

Introduction

Calix[4]arenes locked in the cone conformation are remarkable building blocks for the preparation of multifunctional ligands.[1−5] They are frequently used as preorganising platforms allowing control of the orientation of podands anchored to one of the rims and hence for imposing a particular coordination geometry upon a complexed metal ion.[6,7] Depending upon their nature, length and flexibility, convergent binding sites tethered at the same rim may not only result in high complexation selectivities but also produce metal complexes with unconventional catalytic properties.[8−18] In a recent paper, we reported the coordination chemistry of the diphosphane **1** and have shown that this conical calixarene,[19] as well as some derivatives,[20,21] forms square planar Pt^{II} chelate complexes (**A**) exclusively in the *cis* configuration in which the P-M vectors are oriented away from the calixarene axis, thus positioning the metal outside the conical domain defined by the macrocycle. The ligand bite angle in *cis*-[$PtCl_2$·**1**], as revealed by an X-ray study, is 103.4(1)°. In order to further substantiate the directional properties of this diphosphane, we have now investigated its coordination behaviour towards $NiCl_2$ and $NiBr_2$ units, two versatile fragments known to form either tetrahedral or square planar [NiX_2(phosphane)$_2$] metal complexes. The present study describes the syntheses and structures of three paramagnetic nickel(II) complexes based on **1** and illustrates that the ligand bite angle may undergo major variation, hence enabling the metal centre to approach closer to the calixarene core.

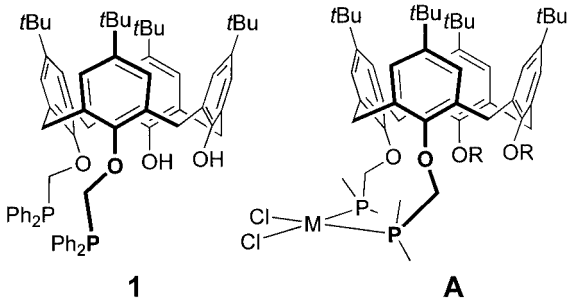

Results and Discussion

From our previous study it appears that despite its considerable length, diphosphane **1** is sufficiently preorganised to readily form chelate complexes with the $PtCl_2$ moiety.[19] Complexation of this fragment results in formation of a compound in which the platinum atom is oriented outwards from the cone defined by the calixarene. The same com-

[a] Université Louis Pasteur, Laboratoire de Chimie Inorganique Moléculaire,
UMR 7513 CNRS,
1 rue Blaise Pascal, 67008 Strasbourg Cedex, France
E-mail: dmatt@chimie.u-strasbg.fr
[b] Institut Charles Sadron, UPR 22 CNRS,
6 rue Boussingault, 67083 Strasbourg Cedex, France
[c] DECMET, UMR 7513,
4 rue Blaise Pascal, 67070 Strasbourg Cedex, France

 © 2004 Wiley-VCH Verlag GmbH & Co. KGaA, Weinheim **DOI: 10.1002/ejic.200400411**

plexation behaviour towards $PtCl_2$ was observed when using analogues of **1** in which the phenol rings bear substituents.[19,21] Inverting the orientation of the P lone pairs is a challenging goal that would lead to complexes where the metal is brought closer to the calixarene axis, thus favouring interactions between the coordination centre and the bulky calixarene core. In order to study whether **1** gives access to such structures, we decided to investigate the coordination properties of **1** towards the nickel(II) centre which has a greater stereoflexibility than platinum(II).

The preparation of complex **2** required a two-step procedure consisting of (*i*) dissolution of anhydrous $NiCl_2$ in small amounts of EtOH to form an unidentified species which, unlike $NiCl_2$, is soluble in CH_2Cl_2 and (*ii*) treatment of the thus formed species with a solution of **1** in CH_2Cl_2 (Equation 1). A direct synthesis in CH_2Cl_2 was impossible due to the insolubility of $NiCl_2$ in this solvent, while attempted synthesis in pure EtOH did not result in phosphane coordination. We found that the best $EtOH/CH_2Cl_2$ ratio was ca. 1:10.

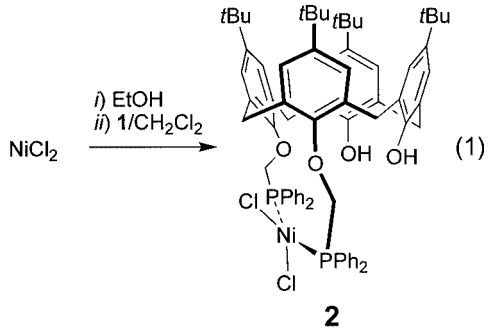

The dark blue complex **2** is paramagnetic and was characterised by elemental analysis and an X-ray diffraction study. Its molecular structure is shown in Figure 1. The shape of the calixarene core deviates only slightly from an ideal cone. Thus, the "centroid-centroid" separations between the distal phenol units are 6.45 and 6.93 Å, respectively, while the dihedral angles between the calixarene reference plane [defined as the mean plane of the bridging C atoms, here C(12), C(23), C(34), C(45)] and those of the four phenol rings are 115° (C2), 103° (C18), 134° (C29) and 124° (C40). Hydrogen bonds involving the hydroxy groups and the neighbouring phenolic oxygen atoms may contribute to this structure, as indicated by the rather short O(1)···O(3) [2.78(2) Å], O(2)···O(4) [2.87(2) Å] and O(3)···O(4) [2.67(2) Å] separations (cf. O(1)···O(2) 3.46(2) Å]. The compound crystallises with two dichloromethane molecules, one of them lying inside the calixarene basket. The shortest contacts of the latter with the aromatic walls are between H(71b) and C(27) (2.83 Å), and H(71b) and C(28) (2.84 Å). Note, considerably shorter contacts have been found in other calixarenes with CH_2Cl_2 guests.[22] The Ni atom is slightly bent towards the exterior of the cavity and its coordination geometry may be regarded as being between square planar and tetrahedral. By considering the PNiP and ClNiCl angles of 158.45(3)° and 158.29(4)°, one gets the impression that the ligand is attempting unsuccessfully to behave as a *trans* spanning ligand. Clearly, complexation results in a strained chelate ring, as shown by the C(1)P(1)Ni and C(46)P(2)Ni angles of 109.9(1)° and 108.1(1)°, respectively, which are about 10° smaller than the other CPNi angles. It should be remembered here that, as shown in previous studies, calix[4]arenes having at least two proximal $-OCH_2PPh_2$ units display a marked propensity to form *cis*-chelated structures, no *trans* complexes having been reported to date. The NiP bond lengths [2.220(1), 2.247(1) Å] lie in the range found for complexes of the general formula *trans*-$[NiCl_2(PPh_2R)_2]$.[23–25]

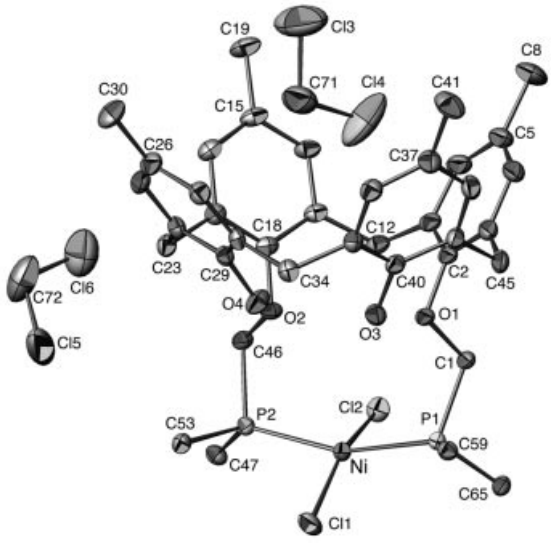

Figure 1. Molecular structure of the blue complex $[NiCl_2 \cdot \mathbf{1}] \cdot 2CH_2Cl_2$ ($\mathbf{2} \cdot 2CH_2Cl_2$); only the C_{ipso} atoms of the P-phenyl rings are shown; the *t*Bu groups are not shown in full

Complexes **3** and **4** were obtained as a binary mixture, but could be separated mechanically after crystallisation. They were prepared similarly to the method outlined above for **2**, but starting from anhydrous $NiBr_2$ (Equation 2). Crystallisation from dichloromethane/heptane afforded a mixture of crystals of turquoise **3** and red-brown **4**.

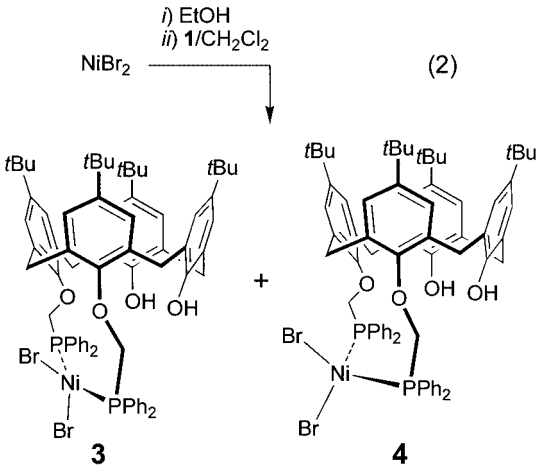

 © 2004 Wiley-VCH Verlag GmbH & Co. KGaA, Weinheim

Obtaining this crystal mixture is easily reproducible. It appears likely that both compounds exist in equilibrium in solution, since dissolving crystals of either of them afforded the same green solution (toluene or CH_2Cl_2). The two molecular structures were determined by single-crystal X-ray diffraction studies (Figure 2 and 3). Again, both calixarenes adopt the shape of a cone having a "circular" cross section and both cavities host a dichloromethane molecule. As found in **2**, hydrogen bonds involving the hydroxy groups appear to stabilise the whole calixarene geometry (Table 1). The coordination geometry of **3** is close to that found in **2**, as can be seen from the PNiP and BrNiBr angles of 158.58(3)° and 152.19(2)°, respectively. In contrast, **4** has a conventional tetrahedral stereochemistry with considerably smaller PNiP [118.6(3)°] and BrNiBr [138.55(5)°] angles. Incidentally, the metallomacrocyclic unit of **4** is less strained than those of **2** and **3**. For example, the values of the $NiPC_\alpha$ angles in this unit are 119.0(1)° and 117.6(1)°. We note that in all three complexes, the Ni atom is orientated away from the calixarene axis. In each structure, a halogen atom approaches the axial H(12) atom but weak interactions with this methylene H are likely to occur in **2** and **3** [$H_{axial}(12)\cdots X$ distances (Å): 2.77, 2.84 and 3.00, respectively, for **2**, **3** and **4**]. These weak interactions could explain why the Ni−X(2) bonds of **2** and **3** are slightly but significantly longer than the corresponding Ni−X(1) bonds. Involvement of $ArCH_{axial}$ hydrogen atoms in weak bonding have recently been found in other calixarenes, in particular in some agostic CH···M interactions.[21] Finally, it is noteworthy that there is no indication in the syntheses outlined above of oligomer formation, illustrating the high degree of preorganisation of calixarene **1**.

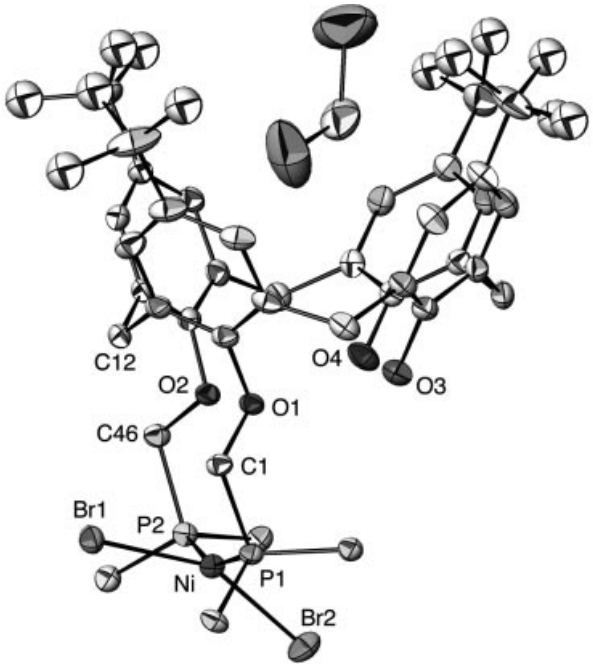

Figure 2. Molecular structure of the turquoise complex [$NiBr_2$·**1**]·$2CH_2Cl_2$ (**3**·$2CH_2Cl_2$); for clarity, only the C_{ipso} atoms of the P-phenyl rings are shown; the *t*Bu groups are not shown in full

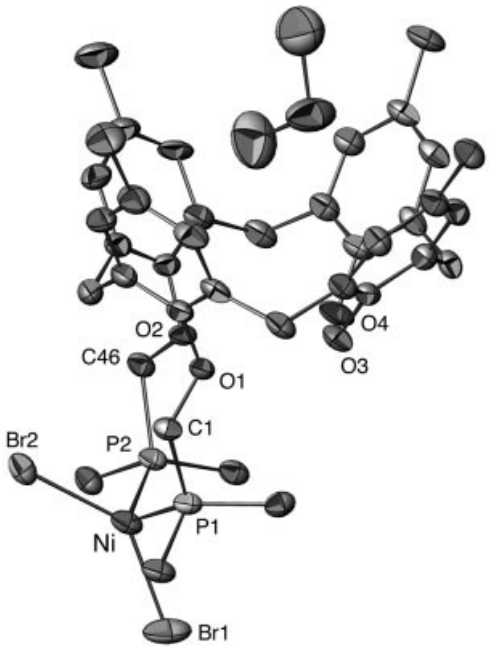

Figure 3. Molecular structure of the red brown complex [$NiBr_2$·**1**]·$1.75CH_2Cl_2$ (**4**·$1.75CH_2Cl_2$); for clarity, only the C_{ipso} atoms of the P-phenyl rings are shown; the *t*Bu groups are not shown in full

Table 1. Relevant structural parameters for **2**, **3** and **4** in the solid state

	2	**3**	**4**
Distances (Å)			
O1···O2	3.46(2)	3.47(2)	3.30(2)
O1···O3	2.78(2)	2.78(2)	2.74(2)
O1···O4	3.96(2)	3.98(2)	4.11(2)
O2···O3	4.33(2)	4.33(2)	4.14(2)
O2···O4	2.87(2)	2.89(2)	3.05(2)
O3···O4	2.67(2)	2.68(2)	2.63(2)
Ni−P1	2.247(1)	2.235(1)	2.290(9)
Ni−P2	2.220(1)	2.215(1)	2.303(9)
Ni−X1	2.150(2)	2.286(1)	2.320(6)
Ni−X2	2.168(2)	2.308(1)	2.338(6)
Angles (°)			
PNiP	158.45(3)	158.58(3)	118.6(3)
XNiX	158.29(4)	152.19(2)	138.55(5)
Dihedral angles (°) between the phenol rings and the calixarene reference plane	**2**	**3**	**4**
(C2)	115(1)	115(1)	114(1)
(C18)	103(1)	104(1)	110(1)
(C29)	134(1)	136(1)	122(1)
(C40)	124(1)	124(1)	133(1)

It is well known that [$NiCl_2$(phosphane)$_2$] complexes constitute good precatalysts for the oligomerisation or polymerisation of olefins, the outcome of the reaction being strongly dependent on the nature of the phosphane.[26,27] Thus for example, [$NiCl_2(PCy_3)_2$] activated with $AlEt_2Cl$ becomes a highly selective ethylene dimerisation catalyst.[28] A typical activity for this complex is 1600 mol(C_2H_4)·mol(Ni)$^{-1}$·h^{-1}.[29] Other complexes, for instance

 © 2004 Wiley-VCH Verlag GmbH & Co. KGaA, Weinheim

Table 2. Ethylene oligomerisation with **2** (conditions: complex **2** (6 μmol), MAO (0.500 g), toluene (20 mL), initial temperature 25 °C)

$P(C_2H_4)$ (bar)	α (°)	TOF (mol C_2H_4)/(mol [Ni]·h)	Activity g C_2H_4/(mmol [Ni]·h·bar)	Olefin distribution (wt.-%)					
				C_4	C_6	C_8	C_{10}	C_{12}	C_{14}
10	0.18	3100	8.7	73.9	19.9	4.8	1.1	0.3	/
30	0.22	9800	9.1	68.4	22.6	6.6	1.8	0.5	0.1

$[NiBr_2\{Ar_2PN(Me)PAr_2\}]$ (Ar = *o*-*i*PrC_6H_4), display a high ethylene polymerisation activity [with activities as high as 79000 mol(C_2H_4)·mol(Ni)$^{-1}$·h^{-1}] producing high molecular weight polymers.[30] Recent work on $[NiCl_2(chelate)]$ complexes has clearly underlined that a subtle combination of backbone rigidity and partial steric protection of the nickel centre is the determining factor for product distribution control.[31,32] It is also worth mentioning that to date, long chain diphosphanes having a backbone containing more than six carbon atoms have not been studied in olefin oligomerisation/polymerisation systems.[27,33] Reports dealing with generic calix[4]arenes that were employed in olefin polymerisation have appeared in the literature, but these remain scarce.[34−37]

In view of the fact that ligand **1** possesses a flexible bite angle, we decided to assess the role of complex **2** in ethylene oligomerisation. The runs were performed in toluene ([catalyst] = 0.3 mmol/dm^3) using methylaluminoxane (MAO) (1500 equiv.) as the activator. Operating under an ethylene pressure of 10 bar and stopping the reaction after 1 h, produced C_4 to C_{12} oligomers. The observed activity was 3100 mol(C_2H_4)·mol(Ni)$^{-1}$·h^{-1}. The product distribution is typically of the Schulz−Flory type, with α about 0.2 (Table 2).

Applying a pressure of 30 bar increased the activity up to 9800 mol(C_2H_4)·mol(Ni)$^{-1}$·h^{-1} without modifying the product distribution. Interestingly, no catalyst deactivation was observed during these 1 h experiments. As shown by the study outlined above, diphosphane **1** is able to undergo large bite angle variations but this has only little impact on the catalyst activity. For comparison, in terms of activity and selectivity, the catalyst performance compares with that of $[NiCl_2(Ph_2PCH_2PPh_2)]$, a complex in which the chelating unit is much more strained than that in **2**.[38] The structural studies revealed that, whatever the coordination geometry of nickel complexes containing **1**, the bulky calixarene core is remote from the nickel centre, resulting in a rather uncrowded metal environment and hence facilitating reductive elimination steps.

Conclusion

In this study we have shown that in the presence of NiX_2 moieties the large diphosphane **1** straightforwardly forms chelate complexes, thus confirming the good preorganisation of the ligand. While previous studies have shown that **1** and its congeners act exclusively as *cis*-chelators towards the $PtCl_2$ moiety, we have discovered that **1** is also able to adapt to various tetrahedral coordination geometries, some of them being extremely distorted. Thus, **1** gives access to bite angles lying in the range 103.4°−158.6°. The fact that to date no complex could be synthesised in which **1** behaves as a genuine *trans* chelator obviously arises from the rigidity of the spacer that links the P^{III} atoms as well as the shortness of the two phosphorus arms. The present work further demonstrates that ligand **1** is able to bring the metal centre closer to the calixarene axis than was previously observed in Pt^{II} complexes, although the PM vectors remain oriented outwards. Activation of **2** with MAO afforded a good ethylene oligomerisation catalyst resulting selectively in C_4−C_{12} oligomers. The formation of short oligomers suggests that during catalysis the nickel environment is slightly encumbered hence favouring reductive elimination over chain propagation. The formation of polymers could possibly be forced by orientating the PM vectors towards the calixarene axis so as to ensure partial protection of the metal. Further studies are aimed at exploiting the bite angle flexibility of diphosphane **1** in catalytic reactions.

Experimental Section

General Conditions: Solvents were dried with suitable reagents and freshly distilled under dry nitrogen before use. All reactions were carried out using modified Schlenk techniques under a dry nitrogen atmosphere. Elemental analyses were performed by the Service de Microanalyse, Centre de Recherche Chimie, Université Louis Pasteur, Strasbourg. 5,11,17,23-Tetra-*tert*-butyl-25,26-bis(diphenylphosphanylmethoxy)-27,28-dihydroxycalix[4]arene (**1**) was prepared according to the previously reported method.[19] MAO 10 wt.-% (Aldrich) was used as a white powder which was obtained after evaporation of the solvent (60 °C, 3 h). This treatment reduces the amount of residual trimethylaluminium to ca. 3%.

Synthesis of Dichloro-{5,11,17,23-tetra-*tert*-butyl-25,26-bis(diphenylphosphanylmethoxy)-27,28-dihydroxycalix[4]arene}nickel(II) (2): Anhydrous $NiCl_2$ (0.019 g, 0.15 mmol) was dissolved in hot ethanol (0.5 mL) whereupon a solution of **1** (0.153 g, 0.15 mmol) in CH_2Cl_2 (5 mL) was added. During addition the pale yellow solution turned deep blue. After 0.25 h, the solvent was removed in vacuo. The residue was treated with a small volume of pentane (5 mL) and the resultant suspension filtered through a glass frit. Cooling to −30 °C precipitated a dark blue powder which was dried in vacuo. Yield: 0.070 g, 40%. $C_{70}H_{78}Cl_2NiO_4P_2$ (M_r = 1174.93): calcd. C 71.56, H 6.69; found C 71.66, H 6.90. Single-crystals suitable for X-ray diffraction were obtained by slow diffusion at room temperature of hexane into a CH_2Cl_2 solution of the complex.

 © 2004 Wiley-VCH Verlag GmbH & Co. KGaA, Weinheim

Table 3. Crystal and structure refinement data for **2**, **3** and **4**

Formula	$C_{70}H_{78}Cl_2NiO_4P_2\cdot 2CH_2Cl_2$	$C_{70}H_{78}Br_2NiO_4P_2\cdot 2CH_2Cl_2$	$C_{70}H_{78}Br_2NiO_4P_2\cdot 1.75CH_2Cl_2$
Molecular mass	1344.73	1433.65	1387.97
Crystal system	triclinic	triclinic	monoclinic
Space group	$P\bar{1}$	$P\bar{1}$	$P2_1/n$
a (Å)	12.7590(10)	12.736(5)	18.868(2)
b (Å)	16.7150(10)	16.895(5)	14.1060(10)
c (Å)	18.4130(10)	18.441(5)	29.853(3)
α (°)	110.11(5)	110.599(5)	90
β (°)	104.31(5)	104.026(5)	105.62(5)
γ (°)	100.36(5)	100.257(5)	90
V (Å^3)	3418(2)	3448.8(19)	7651.8(12)
Z	2	2	4
D(calcd.) (g·cm^{-3})	1.307	1.380	1.205
μ(Mo-K_α) (mm^{-1})	0.612	1.688	1.470
F(000)	1412	1484	2882
Crystal size (mm)	0.08 × 0.10 × 0.13	0.05 × 0.07 × 0.08	0.06 × 0.07 × 0.08
Temperature (K)	173	173	173
Radiation, λ (Mo-K_α) (Å)	0.71069	0.71069	0.71069
$\Theta_{min.,max.}$ (°)	1.3, 30.0	1.8, 30.0	1.0, 30.0
Data set (h; k; l)	−17/17; −23/22; 0/25	−17/17; −23/23; −25/24	−21/26; −19/19; −34/42
Total, unique data, R(int.)	19905, 19905, 0.035	41543, 20069, 0.050	36106, 20421, 0.073
Obsd. data with $I > 2.0\sigma(I)$	14740	15013	10790
$N_{reflections}$, $N_{parameters}$	19905, 766	20069, 766	20421, 748
$R1$, $wR2$, S	0.0712, 0.1863, 1.05	0.0663, 0.1496, 1.03	0.0989, 0.3089, 1.02
Min., max. residual electron density (e·Å^{-3})	−1.07, 1.17	−1.13, 1.29	−1.25, 1.56

Synthesis of Dibromo-{5,11,17,23-tetra-*tert*-butyl-25,26-bis(diphenylphosphanylmethoxy)-27,28-dihydroxycalix[4]arene}nickel(II), Isomers 3 and 4: Anhydrous $NiBr_2$ (0.041 g, 0.19 mmol) was dissolved in hot ethanol (0.5 mL) resulting in a pale orange solution. A solution of **1** (0.200 g, 0.19 mmol) in CH_2Cl_2 (5 mL) was then added and the mixture turned green. After 0.25 h, the solution was evaporated to dryness. The residue was redissolved in CH_2Cl_2 (ca. 1 mL), whereupon pentane was added to precipitate a pale green powder which was recovered by filtration. Yield: 0.197 g, 82%. The green powder was then dissolved in CH_2Cl_2. Slow diffusion of heptane into the resultant intense green solution afforded crystals of **3** (turquoise colour) and **4** (red brown) which were separated mechanically. Elemental analyses were carried out on both isomers after drying in high vacuum: $C_{70}H_{78}Br_2NiO_4P_2$ (M_r = 1263.83): calcd. C 66.53, H 6.22; found for **3**: C 66.22; H 5.75; found for **4**: C 66.50; H 6.42.

Crystal Structure Determination of 2·2CH$_2$Cl$_2$: Single crystals of **2** suitable for X-ray diffraction analysis were obtained by slow diffusion of hexane into a CH_2Cl_2 solution of the complex. Data were collected with a Nonius KappaCCD diffractometer (graphite-monochromated Mo-K_α radiation, λ = 0.71073 Å). The structure was solved by direct methods using the SHELXS-97 program and refined by full-matrix least-squares techniques (SHELXL-97) on F^2.[39] Hydrogen atoms were located using the geometric method. The crystal data and structural refinement details are listed in Table 3. The compound was found to crystallise with two molecules of dichloromethane, one of them lying inside the cavity. CCDC-234357 contains the supplementary crystallographic data for this structure. These data can be obtained free of charge at www.ccdc.cam.ac.uk/conts/retrieving.html [or from the Cambridge Crystallographic Data Centre, 12, Union Road, Cambridge CB2 1EZ, UK; Fax: +44-1223-336-033; E-mail: deposit@ccdc.cam.ac.uk].

Crystal Structure Determination of 3·2CH$_2$Cl$_2$ and 4·1.75CH$_2$Cl$_2$: Single crystals of **3** and **4** were obtained simultaneously by slow diffusion of heptane into a solution of [$NiBr_2$·**1**]. Data collection and structure solution were carried out as above for **2** (Table 3). The poorer quality of the structure of **4** is due to disordered solvent molecules, whether they lie inside or outside the cavity. CCDC-234358 (for **3**) and CCDC-234359 (for **4**). These data can be obtained free of charge at www.ccdc.cam.ac.uk/conts/retrieving.html [or from the Cambridge Crystallographic Data Centre, 12, Union Road, Cambridge CB2 1EZ, UK; Fax: +44-1223-336-033; E-mail: deposit@ccdc.cam.ac.uk].

Oligomerisation of Ethylene: The catalytic runs were carried out in a 100 mL glass-lined stainless steel autoclave containing a magnetic stirring bar. In a typical run, a solution of complex **2** (0.007 g, 6 μmol) in toluene (15 mL) was introduced under nitrogen into the autoclave whereupon a solution of MAO (0.500 g) in toluene (5 mL) was added. After stirring for ca. 1 min the autoclave was pressurised with ethylene and the pressure (10 or 30 bar) was maintained at a constant value. During the runs described in this work, the temperature raised from 25 °C to 37 °C when operating at 10 bar and up to 42 °C under 30 bar. After 1 h, the autoclave was cooled to 7 °C and then depressurised over a period of 1 h. Heptane (200 μL), which serves as internal reference for the GC analysis, was then added to the reaction mixture. The liquid phase was analysed with a VARIAN 3900 gas chromatograph equipped with a WCOT fused silica column (25 m, 0.32 mm inside diameter, 0.25 mm film thickness).

Acknowledgments

We thank the Ministère de l'Education Nationale et de la Recherche Scientifique for a grant to P. K.

 © 2004 Wiley-VCH Verlag GmbH & Co. KGaA, Weinheim

[1] V. Böhmer, *Angew. Chem. Int. Ed. Engl.* **1995**, *34*, 713−745.
[2] C. D. Gutsche, *Calixarenes Revisited, Monographs in Supramolecular Chemistry* (Ed.: J. F. Stoddart), The Royal Society of Chemistry, Cambridge, **1998**.
[3] P. J. A. Kenis, O. F. J. Noordman, H. Schönherr, E. G. Kerver, B. H. M. Snellink-Ruël, G. J. van Hummel, S. Harkema, C. van der Vorst, J. Hare, S. J. Picken, J. F. J. Engbersen, N. F. van Hulst, G. J. Vancso, D. N. Reinhoudt, *Chem. Eur. J.* **1998**, *4*, 1225−1234.
[4] *Calixarenes in Action* (Ed.: L. Mandolini, R. Ungaro), Imperial College Press, **2000**.
[5] S. Steyer, C. Jeunesse, D. Armspach, D. Matt, J. Harrowfield, in *Calixarene 2001* (Eds.: Z. Asfari, V. Böhmer, J. Harrowfield, J. Vicens), Kluwer, Dordrecht, pp. 513−535.
[6] C. Wieser, C. Dieleman, D. Matt, *Coord. Chem. Rev.* **1997**, *165*, 93−161.
[7] P. D. Harvey, *Coord. Chem. Rev.* **2002**, *233−234*, 289−309.
[8] C. Wieser, D. Matt, J. Fischer, A. Harriman, *J. Chem. Soc., Dalton Trans.* **1997**, 2391−2402.
[9] R. Paciello, L. Siggel, M. Röper, *Angew. Chem. Int. Ed.* **1999**, *38*, 1920−1923.
[10] C. J. Cobley, D. D. Ellis, A. G. Orpen, P. G. Pringle, *J. Chem. Soc., Dalton Trans.* **2000**, 1109−1112.
[11] C. J. Cobley, D. D. Ellis, A. G. Orpen, P. G. Pringle, *J. Chem. Soc., Dalton Trans.* **2000**, 1101−1107.
[12] F. J. Parlevliet, C. Kiener, J. Fraanje, K. Goubitz, M. Lutz, A. L. Spek, P. C. J. Kamer, P. W. N. M. van Leewen, *J. Chem. Soc., Dalton Trans.* **2000**, 1113−1122.
[13] C. Jeunesse, C. Dieleman, S. Steyer, D. Matt, *J. Chem. Soc., Dalton Trans.* **2001**, 881−892.
[14] X. Fang, B. L. Scott, J. G. Watkin, C. A. G. Carter, G. J. Kubas, *Inorg. Chim. Acta* **2001**, *317*, 276−281.
[15] C. Kunze, D. Selent, I. Neda, M. Freytag, P. G. Jones, R. Schmutzler, W. Baumann, A. Börner, *Z. Anor. Allg. Chem.* **2002**, *628*, 779−787.
[16] S. Steyer, C. Jeunesse, D. Matt, R. Welter, M. Wesolek, *Dalton Trans.* **2002**, 4264−4274.
[17] F. Plourde, K. Gilbert, J. Gagnon, P. D. Harvey, *Organometallics* **2003**, *22*, 2862−2875.
[18] M. Frank, G. Maas, J. Schatz, *Eur. J. Org. Chem.* **2004**, 607−613.
[19] C. B. Dieleman, C. Marsol, D. Matt, N. Kyritsakas, A. Harriman, J.-P. Kintzinger, *J. Chem. Soc., Dalton Trans.* **1999**, 4139−4148.
[20] C. Dieleman, S. Steyer, C. Jeunesse, D. Matt, *J. Chem. Soc., Dalton Trans.* **2001**, 2508−2517.
[21] C. Dieleman, C. Jeunesse, D. Matt, *Z. Kristallog. NCS* **2001**, *216*, 435−438.
[22] C. Dieleman, D. Matt, P. G. Jones, H. Thönnessen, *Acta Crystallogr., Sect. C* **2003**, *59*, o247−o249.
[23] P. Braunstein, D. Matt, D. Nobel, F. Balegroune, S.-E. Bouaoud, D. Grandjean, J. Fischer, *J. Chem. Soc., Dalton Trans.* **1988**, 353−361.
[24] J. Sletten, J. A. Kovacs, *J. Crystallogr. Spectrosc. Res.* **1993**, *23*, 239.
[25] S. J. Coles, P. Faulds, M. B. Hursthouse, D. G. Kelly, G. C. Ranger, N. M. Walker, *J. Chem. Res.* **1999**, *418*, 1811.
[26] S. Muthukumaru Pillai, M. Ravindranathan, S. Sivaram, *Chem. Rev.* **1986**, *86*, 353−399.
[27] V. C. Gibson, S. K. Spitzmesser, *Chem. Rev.* **2003**, *103*, 283−315.
[28] D. Commereuc, Y. Chauvin, G. Léger, J. Gaillard, *Rev. Inst. Fr. Pet.* **1982**, *37*, 639−649.
[29] F. Speiser, P. Braunstein, L. Saussine, *Organometallics* **2004**, *23*, 2625−2632.
[30] N. A. Cooley, S. M. Green, D. F. Wass, K. Heslop, A. G. Orpen, P. G. Pringle, *Organometallics* **2001**, *20*, 4769−4771.
[31] M. Sauthier, F. Leca, R. F. de Souza, K. Bernardo-Gusmão, L. F. Trevisan Queiroz, L. Toupet, R. Réau, *New J. Chem.* **2002**, 630−635.
[32] C. Bianchini, L. Gonsalvi, W. Oberhauser, D. Sémeril, P. Brüggeller, R. Gutman, *Dalton Trans.* **2003**, 3869−3875.
[33] P.-G. Lassahn, V. Lozan, B. Wu, A. S. Weller, C. Janiak, *Dalton Trans.* **2003**, 4437−4450.
[34] R. A. Kemp, D. S. Brown, M. Lattman, J. Li, *J. Mol. Cat. A: Chem.* **1999**, *149*, 125−133.
[35] V. C. Gibson, C. Redshaw, M. R. J. Elsegood, *J. Chem. Soc., Dalton Trans.* **2001**, 767−769.
[36] C. Capacchione, P. Neri, A. Proto, *Inorg. Chem. Commun.* **2003**, *6*, 339−342.
[37] C. Huang, J. Ahn, S. Kwon, J. Kim, J. Lee, Y. Han, H. Kim, *Applied Catal. A* **2004**, *258*, 173−181.
[38] C. Bianchini, unpublished results.
[39] G. M. Sheldrick, *SHELXL-97, Program for Crystal Structure Refinement*, University of Göttingen: Göttingen, Germany, **1997**.

Received May 18, 2004
Early View Article
Published Online October 13, 2004

 © 2004 Wiley-VCH Verlag GmbH & Co. KGaA, Weinheim

(Schiff-base)Cu^{II} Complexes with Phenolate-Oxygen/Chloro or -Oxygen/Azido Mixed Bridges − Syntheses, Crystal Structures and Magnetic Properties

Yun-Bo Jiang,[a] Hui-Zhong Kou,*[a] Ru-Ji Wang,[a] and Ai-Li Cui[a]

Keywords: Chloro bridges / Azido bridges / Magnetic properties / Cu^{II} ions / Crystal structures

Four new Cu^{II} complexes of formulae $[Cu_3(SE)_2(H_2O)_2Cl_3]Cl{\cdot}6H_2O$ (**1**), $Cu_3(SE)_2(N_3)_4(DMF)_2$ (**2**), $Cu(SE)N_3{\cdot}DMF$ (**3**) and $Cu(SE)N_3{\cdot}Cu(SE)N_3$ (**4**) with tridentate Schiff-base ligands SE^-, derived from condensation of *N*,*N*-dimethylethylenediamine with salicylaldehyde, have been synthesised and characterised by IR spectroscopy, X-ray structural analyses and variable-temperature magnetic susceptibility measurements. Complex **1** has an alternating phenoxy- and chloro-bridged 1D chain structure. Complex **2** possesses trinuclear units in which the Cu^{II} ions are bridged by single end-on (μ-1,1) azido ligands. Uniformly spaced 1D chains with end-to-end (μ-1,3) azido bridges are found in **3** and **4**. As expected, complexes **1** and **2** exhibit antiferromagnetic and ferromagnetic exchange, respectively. Compounds **3** and **4** show unusual ferromagnetic coupling though the 1,3-azido pathways. Theoretical simulations have been carried out in order to evaluate the magnitude of the magnetic exchange and the magneto-structural correlation has been investigated.
(© Wiley-VCH Verlag GmbH & Co. KGaA, 69451 Weinheim, Germany, 2004)

Introduction

During the past decade, particular interest has been directed towards the investigation of copper(II) complexes with halogen bridging ligands as well as pseudohalogens, due to their correlative structures and ability to transmit magnetic interactions.[1−24] Among the ligands examined, the chloride anion has the capability of acting as either a bridging or a terminal ligand, occupying either axial or equatorial coordination positions. As a result, mono- or polynuclear complexes as well as 1D chain-like compounds have been obtained.[1−6] In addition, the azide ion is a versatile and popular pseudohalogen ligand due to its functionality as a bridging bi-, tri- and tetradentate ligand and its rich coordination behaviour, e.g. end-on (μ-1,1 and μ-1,1,1) or end-to-end (μ-1,3). These bridging ligands have yielded plenty of metal complexes with a wide variety of coordination geometries including tetrahedral or square-planar, trigonal-bipyramidal or square-pyramidal and octahedral, the geometry being dependent upon the coligands and the counterions.[8−24]

It has been reported that {*N*-[2-(dimethylamino)ethyl]-salicylaldiminato}copper(II) chloride, Cu(SE)Cl, can be synthesised in an anhydrous methyl/isopropyl alcohol medium.[7] A trinuclear complex $[Cu_3(\mu_3\text{-}OH)(SE)_3](ClO_4)_2(H_2O)_{0.5}$ containing a partially cubic Cu_3O_4 core was obtained from the reaction of $Cu(ClO_4)_2$ with SE^- in a methanol/water solution.[6] We have found, in the absence of ClO_4^-, the reaction between $CuCl_2$ and SE^- in a 1:1 molar ratio did not produce the expected 1:1 complex. Instead, a chain-like complex with the empirical formula $Cu_3(SE)_2(H_2O)_8Cl_4$ (**1**) was obtained which can be regarded as a mixture of $Cu(H_2O)_2Cl_2$ and Cu(SE)Cl (molar ratio = 1:2). It is worth noting that this complex exhibits an interesting and very rare structure, namely a 1D polymeric chain containing mixed bridges and hexa- and pentacoordinate copper atoms. The replacement of the bridging chloro ligands by azido ligands yields complexes with different structural types depending upon the solvents used (see Scheme 1). One example is the end-on azido-bridged trinuclear structure **2** $[Cu_3(SE)_2(N_3)_4(DMF)_2]$. $Cu(SE)N_3{\cdot}DMF$ (**3**) possesses a uniformly spaced end-to-end azido-bridged copper(II) chain while $Cu(SE)N_3{\cdot}Cu(SE)N_3$ (**4**) displays a chain structure similar to that of **3** with a cocrystallised mononuclear $Cu(SE)N_3$ unit. Herein, we report the syntheses, structural characterisation and magnetic properties of the four complexes.

Results and Discussion

Synthesis and General Characterisation

The trinuclear complex $[Cu_3(OH)(SE)_3](ClO_4)_2(H_2O)_{0.5}$ was always found to be the product from the reaction of $Cu(ClO_4)_2{\cdot}6H_2O$ with SE^- (molar ratio = 1:1).[6] We have observed that the employment of $CuCl_2{\cdot}2H_2O$ instead of $Cu(ClO_4)_2{\cdot}6H_2O$ results in the formation of the 1D chain complex $Cu_3(SE)_2(H_2O)_8Cl_4$ (Cu/SE^-, 3:2). The loss of the SE^- ligand around a Cu^{II} ion may be due to the partial hydrolysis of the Schiff base while in anhydrous solvent environments 1:1 complexes were formed, as previously re-

[a] Department of Chemistry, Tsinghua University, Beijing 100084, China
Fax: (internat.) + 86-10-62795477
E-mail: kouhz@mail.tsinghua.edu.cn

 © 2004 Wiley-VCH Verlag GmbH & Co. KGaA, Weinheim DOI: 10.1002/ejic.200400449

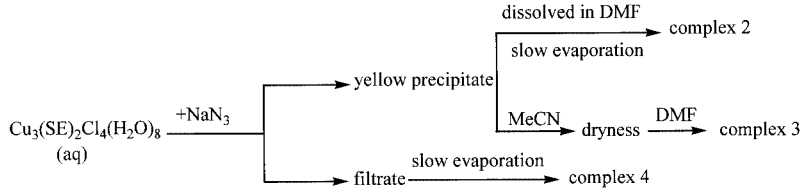

Scheme 1. Formation of Cu^{II} compounds

ported.[6,7] This observation indicates that the structures of Cu^{II}-SE$^-$ complexes vary with the synthetic conditions and counteranions used. Several complexes were obtained from the reaction of complex **1** with NaN_3.

The IR spectra of the complexes are similar and show peaks for the ν(C=N) bands at 1647 cm^{-1} in **1** and 1635 cm^{-1} in **2**, **3** and **4**, suggesting the presence of a Schiff base. The peaks at 1655 cm^{-1} in **2** and **3** can be reasonably attributed to the ν(C=O) of DMF. The appearance of a broad strong absorption at 3434 cm^{-1} in **1** indicates the presence of water molecules, consistent with the single-crystal X-ray diffraction results. Peaks at 2070 and 2031 cm^{-1} in the IR spectrum of **2** are due to the stretching of the μ-1,1 azide while the appearance of absorptions at 2074 and 2047 cm^{-1} in **3** and **4** is due to the asymmetric stretching of the μ-1,3 azide anions.

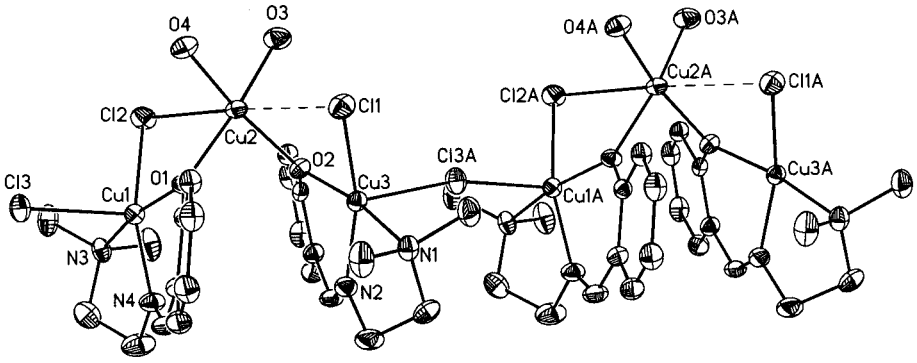

Figure 1. ORTEP representation of the cationic polymeric chain for **1** − 2.5H_2O with the atom labelling scheme showing 30% probability thermal ellipsoids; hydrogen atoms, solvent molecules and counterions have been omitted for clarity

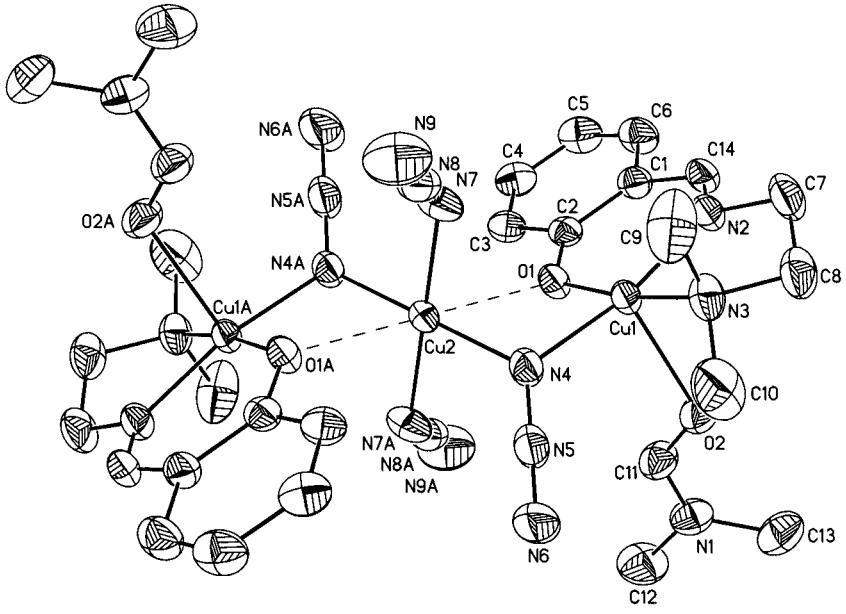

Figure 2. ORTEP representation of the trinuclear unit for **2** with the atom labelling scheme showing 30% probability thermal ellipsoids; for clarity hydrogen atoms have been omitted

 © 2004 Wiley-VCH Verlag GmbH & Co. KGaA, Weinheim

Crystal Structures

The structures of **1**−**4** are displayed in Figures 1−4, respectively. Selected bond lengths and angles for complexes **1** − 2.5H_2O, **2**, **3** and **4** are listed in Tables 1−4, respectively.

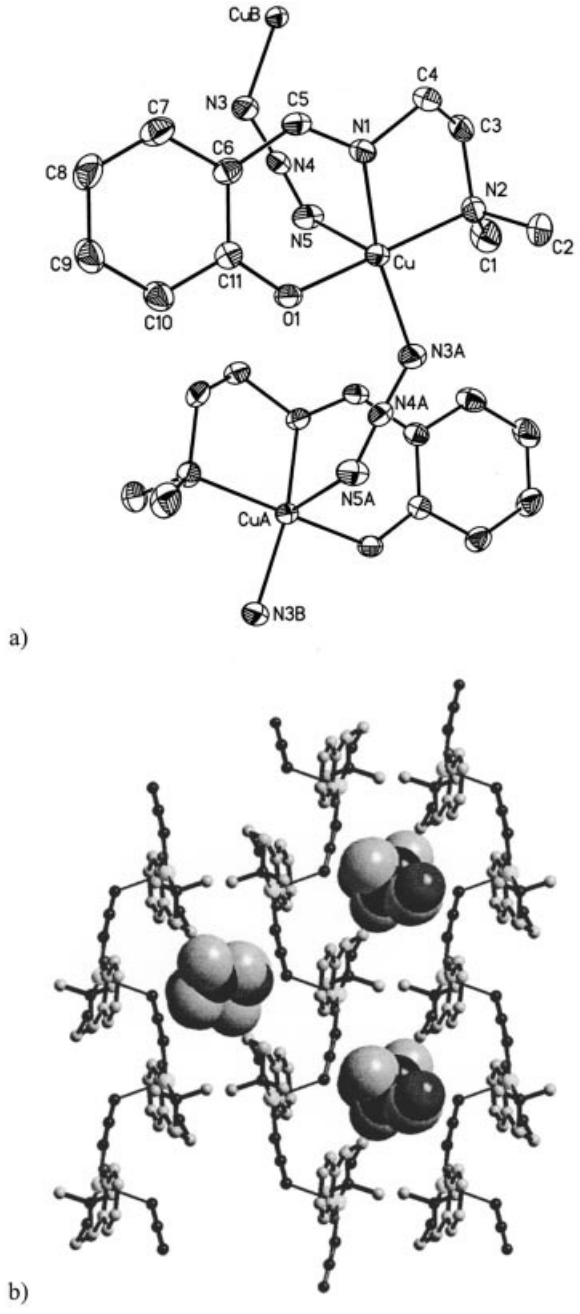

Figure 3. a) ORTEP representation of the 1D polymeric chain for **3** with the atom labelling scheme showing 30% probability thermal ellipsoids; for clarity hydrogen atoms and solvent DMF molecules have been omitted; b) view of the packing of the 1D chains in complex **3** (DMF was displayed in space-filling diagram)

The structure of **1** − 2.5H_2O consists of trinuclear cationic $[Cu_3(SE)_2(H_2O)_2Cl_3]_n^{n+}$ chains along the *a* axis formed by the chloro and phenolate oxygen bridges of SE^- (Figure 1), discrete Cl^- counteranions and solvated water molecules.

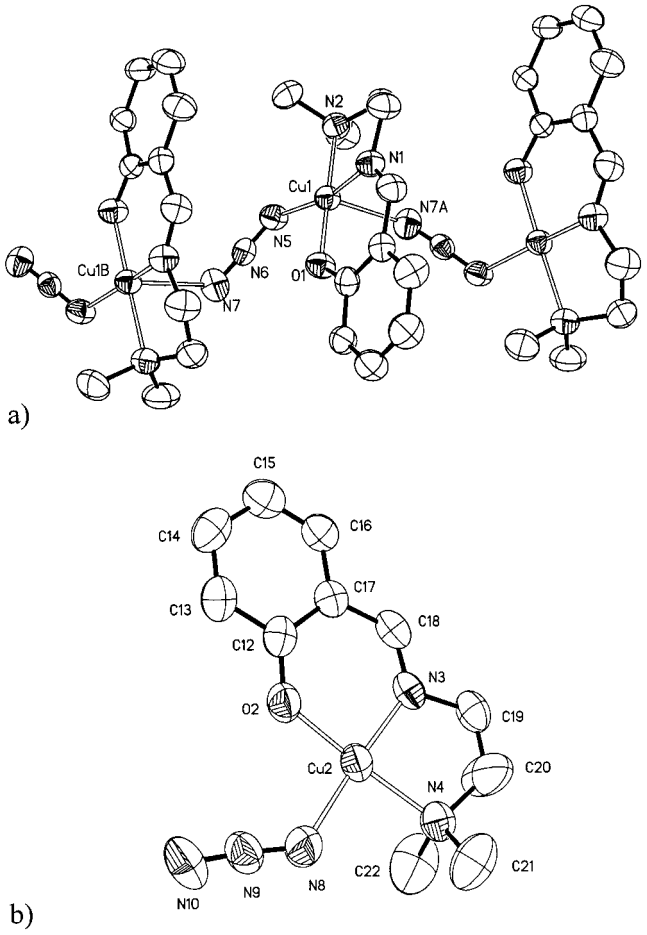

Figure 4. ORTEP representations of the structure of **4**: (a) the 1D chain, (b) the monomer with ellipsoids drawn at 30% probability level; for clarity hydrogen atoms have been omitted

Two of the copper atoms are pentacoordinate while the other is six-coordinate in the independent trinuclear fragment. Cu(1) and Cu(3) have slightly distorted square-pyramidal geometries as ascertained by the Reedijk factors τ of 0.113 and 0.132, respectively.[30] Cu(2) is in an elongated octahedral environment, being coordinated to two bridged chloro atoms [Cl(1) and Cl(2)] and four oxygen atoms, two of these being from water molecules [O(3) and O(4)] and two from the SE^- ligands [O(1) and O(2)]. For Cu(2), the Cu−Cl bonds [2.7176(15) and 2.7890(15) Å] are longer than Cu−O bonds [2.010(3), 1.984(4), 1.981(3) and 1.966(3) Å]. The elongated octahedron shares two equator-to-apex edges with the bases of two other square pyramids. The neighbouring pyramids share an apex occupied by a bridged chloro atom, yielding a 1D chain. Their basal planes, defined by N, N, O and Cl, are not coplanar and exhibit a dihedral angle of 21.1°, while the angles between these planes and the octahedral equatorial plane [O(1),O(2),O(3),O(4)] are 100° and 99.2°, respectively. Within the chain, the Cu(1)−Cu(2) distance is 3.257(7) Å, similar to the Cu(2)−Cu(3) distance of 3.223(7) Å, while the Cu(3)−Cu(1A) separation [5.161(14) Å] is very large.

Complex **2** contains a hexacoordinate and two pentacoordinate Cu^{II} ions which are bridged by the two end-on

 © 2004 Wiley-VCH Verlag GmbH & Co. KGaA, Weinheim

Table 1. Selected bond lengths [Å] and angles [°] for **1** − 2.5H_2O

Cu(1)−N(5)	1.954(4)	Cu(1)−O(1)	1.994(3)
Cu(1)−N(3)	2.057(4)	Cu(1)−Cl(2)	2.2524(14)
Cu(1)−Cl(3)	2.5961(14)	Cu(2)−O(4)	1.966(3)
Cu(2)−O(2)	1.981(3)	Cu(2)−O(3)	1.984(4)
Cu(2)−O(1)	2.010(3)	Cu(2)−Cl(2)	2.7176(15)
Cu(2)−Cl(1)	2.7890(15)	Cu(3)−N(2)	1.958(4)
Cu(3)−O(2)	1.976(3)	Cu(3)−N(1)	2.071(4)
Cu(3)−Cl(1)	2.2577(15)	Cu(3)−Cl(3a)	2.5974(14)
N(5)−Cu(1)−O(1)	90.13(15)	N(5)−Cu(1)−N(3)	84.44(17)
O(1)−Cu(1)−N(3)	170.15(15)	N(5)−Cu(1)−Cl(2)	163.20(14)
O(1)−Cu(1)−Cl(2)	87.38(9)	N(3)−Cu(1)−Cl(2)	95.45(12)
N(5)−Cu(1)−Cl(3)	96.26(14)	O(1)−Cu(1)−Cl(3)	94.05(10)
N(3)−Cu(1)−Cl(3)	94.70(12)	Cl(2)−Cu(1)−Cl(3)	100.49(5)
O(4)−Cu(2)−O(2)	166.03(15)	O(4)−Cu(2)−O(3)	89.75(16)
O(2)−Cu(2)−O(3)	92.04(15)	O(4)−Cu(2)−O(1)	92.55(15)
O(2)−Cu(2)−O(1)	88.57(13)	O(3)−Cu(2)−O(1)	167.99(15)
O(4)−Cu(2)−Cl(2)	91.50(12)	O(2)−Cu(2)−Cl(2)	102.24(10)
O(3)−Cu(2)−Cl(2)	92.94(12)	O(1)−Cu(2)−Cl(2)	75.23(9)
N(2)−Cu(3)−O(2)	89.65(14)	N(2)−Cu(3)−N(1)	84.65(16)
O(2)−Cu(3)−N(1)	170.86(14)	N(2)−Cu(3)−Cl(1)	163.06(13)
O(2)−Cu(3)−Cl(1	88.47(10)	N(1)−Cu(3)−Cl(1)	94.90(12)
N(2)−Cu(3)−Cl(3a)	92.80(13)	O(2)−Cu(3)−Cl(3a)	92.79(10)
N(1)−Cu(3)−Cl(3a)	94.62(11)	Cl(1)−Cu(3)−Cl(3a)	104.10(5)
Cu(2)−Cl(1)−Cu(3)	78.60(13)	Cu(1)−Cl(2)−Cu(2)	81.38(4)
Cu(1)−O(1)−Cu(2)	108.99(13)	Cu(2)−O(2)−Cu(3)	109.05(14)

Symmetry operation: a: 1 − x, −y, 1 − z.

Table 2. Selected bond lengths [Å] and angles [°] for **2**

Cu(1)−O(1)	1.927(2)	Cu(1)−N(2)	1.941(3)
Cu(1)−N(4)	2.001(3)	Cu(1)−N(3)	2.050(3)
Cu(1)−O(2)	2.326(3)	Cu(2)−N(7a)	1.976(3)
Cu(2)−N(7)	1.976(3)	Cu(2)−N(4)	2.042(3)
Cu(2)−N(4a)	2.042(3)	Cu(2)−O(1)	2.468(3)
Cu(2)−O(1a)	2.468(3)		
O(1)−Cu(1)−N(2)	92.33(11)	O(1)−Cu(1)−N(4)	86.62(11)
N(2)−Cu(1)−N(4	169.19(13)	O(1)−Cu(1)−N(3)	172.15(12)
N(2)−Cu(1)−N(3)	84.33(13)	N(4)−Cu(1)−N(3	95.33(13)
O(1)−Cu(1)−O(2)	95.29(11)	N(2)−Cu(1)−O(2)	94.61(12)
N(4)−Cu(1)−O(2)	96.20(12)	N(3)−Cu(1)−O(2)	92.06(12)
N(7a)−Cu(2)−N(4)	91.60(15)	N(7)−Cu(2)−N(4)	88.40(15)
N(7)−Cu(2)−N(4a)	91.60(15)	Cu(1)−N(4)−Cu(2)	102.34(13)
N(6)−N(5)−N(4)	178.5(6)	Cu(2)−O(1)−Cu(1)	90.70(15)

Symmetry operation: a: −1 + x, y, z.

Table 3. Selected bond lengths [Å] and angles [°] for **3**

Cu−O(1)	1.9126(19)	Cu−N(1)	1.948(2)
Cu−N(3a)	1.974(3)	Cu−N(2)	2.067(2)
Cu−N(5)	2.474(2)		
O(1)−Cu−N(1)	92.76(9)	O(1)−Cu−N(3a)	92.42(10)
N(1)−Cu−N(3a)	167.08(10)	O(1)−Cu−N(2)	173.71(8)
N(1)−Cu−N(2)	84.05(10)	N(3a) −Cu−N(2)	89.63(11)
O(1)−Cu−N(5)	94.72(9)	N(1)−Cu−N(5)	88.81(9)
N(3a)−Cu−N(5)	102.55(10)	N(2)−Cu−N(5)	90.64(9)
N(5)−N(4)−N(3)	176.4(3)		

Symmetry operation: a: 0.5 + x, 1.5 − y, 2 − z.

Table 4. Selected bond lengths [Å] and angles [°] for **4**

Cu(1)−O(1)	1.905(4)	Cu(1)−N(1)	1.955(6)
Cu(1)−N(5)	1.972(7)	Cu(1)−N(2)	2.068(6)
Cu−N(7a)	2.604(6)	Cu(2)−O(2)	1.891(6)
Cu(2)−N(3)	1.926(6)	Cu(2)−N(8)	1.946(9)
Cu(2)−N(4)	2.072(7)		
O(1)−Cu(1)−N(1)	93.4(2)	O(1)−Cu(1)−N(5	92.4(2)
N(1)−Cu(1)−N(5)	164.8(3)	O(1)−Cu(1)−N(2)	177.2(2)
N(6a)−N(7a)−Cu(1)	124.4(3)	N(6)−N(5)−Cu(1)	121.0(5)
O(2)−Cu(2)−N(3)	93.2(3)	O(2)−Cu(2)−N(8)	92.0(4)
N(3)−Cu(2)−N(8)	173.2(5)	O(2)−Cu(2)−N(4)	176.3(3)
N(3)−Cu(2)−N(4)	84.3(3)	N(8)−Cu(2)−N(4)	90.7(4)
N(7)−N(6)−N(5)	177.1(8)	N(10)−N(9)−N(8)	177.0(12)

Symmetry operation: a: 0.5 − x, y, z − 0.5.

azido ligands (Figure 2). The central copper atom has an elongated octahedral coordination geometry with four azido nitrogen atoms (two terminal ligands, two end-on dicoordinated bridging ligands) in equatorial positions [Cu−N 1.976(3)−2.042(3) Å] and two phenoxy oxygen atoms from the SE^- ligands in the axial positions (Cu−O 2.469 Å). Alternatively, the trinuclear structure of **2** is composed of two $[Cu(SE)(DMF)]^+$ cations connected by a $[Cu(N_3)_4]^{2-}$ anion through two azido ligands. Similar to complex **1**, the elongated octahedron shares two equator-to-vertex edges with the bases of two other square pyramids. With a τ factor of 0.048, the basal plane of the slightly distorted square pyramid is defined by N(2)−N(3)−N(4)-O(1) and the copper atom Cu(1) is 0.1570(5) Å above the basal plane towards the apical oxygen atom O(5) of the DMF molecule. The Cu−N−Cu angle is 102.34(13)°. It is evident that the basal planes of the square pyramids are perfectly coplanar, while the angle between these planes and the equatorial plane of the central copper ion is 70°. The intramolecular Cu(1)−Cu(2) distance is 3.150(5) Å.

The structure of **3** consists of end-to-end azido-bridged 1D infinite uniformly spaced chains with DMF molecules situated in the spaces between the chains (Figure 3). In the chain, each copper atom is coordinated by an SE^- ligand and two azido ligands in a slightly distorted square-pyramidal arrangement (τ = 0.110). The basal plane is defined by N(1)−N(2)−N(3A)−O(1) and the copper atom is 0.1482(4) Å above the basal plane towards N(5) in the apical position. The angles between the copper ions and the azido ligands are 119.1(2)° [Cu−N(5)−N(4)] and 127.0(2)° [Cu−N(3A)−N(4A)] and the Cu−N_3−Cu torsion angle is 81.5°. The intrachain Cu−Cu distance is 5.530(4) Å, while the closest interchain Cu−Cu distance is 7.671(5) Å. Interstitial DMF molecules occupy interchain spaces and connect neighbouring 1D chains through van der Waals interactions and hydrogen bonds.

Complex **4** contains 1D chains similar to complex **3** with discrete Cu(SE)N_3 monomers beside the chains (Figure 4). In the chains, each copper atom is in a slightly distorted square-pyramidal arrangement with a τ factor of 0.200. The basal plane of the square pyramid is defined by N(1)−N(2)−N(5)−O(1) and Cu^{2+} is 0.1264(8) Å above the

 © 2004 Wiley-VCH Verlag GmbH & Co. KGaA, Weinheim

basal plane towards the bridging azido nitrogen atom N(7A) in the apical position. The bond angles between copper ions and azido ligands are 124.4(5)° [Cu(1)−N(7A)−N(6A)] and 121.0(5)° [Cu(1)−N(5A)−N(6A)] and the torsion angle (Cu−N_3−Cu) is 80.2°. The intrachain Cu−Cu distance is 5.392(2) Å. The copper atom in the monomer is in a square-planar arrangement and is tetracoordinated by SE^- and one terminal azido ligand. The chains and monomers form a complicated network by hydrogen bonds and van der Waals interactions.

Magnetic Properties

The $\chi_M T$ value at 300 K for **1** is 1.229 emu·K·mol^{-1} and this decreases slowly with decreasing temperature. The Weiss constant derived from the χ_m^{-1} vs. T plot is equal to −12.8 K with the Curie constant of 1.26 emu·K·mol^{-1} being close to the calculated value of 1.125 emu·K·mol^{-1} (g = 2.0) per Cu_3 unit. The overall behaviour of **1** corresponds to a weak antiferromagnetically coupled system. To evaluate the strength of the intermetallic exchange constants of **1**, we used an approximate approach similar to that previously used for 1D and quasi-2D complexes.[32] On the basis of the crystal data, for simplicity, the two coupling constants between Cu(1) and Cu(2) and between Cu(3) and Cu(2) which are bridged by the phenoxy and chloro bridges were assumed to be equal. The single axis-to-axis Cu−Cl−Cu coupling constants were considerably small compared with the coupling through the phenolate oxygen and the equator-to-vertex chloro bridges. Therefore, the 1D chain can be treated as being composed of weakly interacting trimers. The magnetic susceptibility data were fitted using the following expansion [Equation (1)] in which intertrimer and interchain exchanges were included in the parameter θ:

$$\chi_{trimer} = \frac{Ng^2\beta^2}{4kT}\left[\frac{1+\exp(-2J/kT)+10\exp(J/kT)}{1+\exp(-2J/kT)+2\exp(J/kT)}\right] \quad (1)$$

$$\chi_M = \chi_{trimer}\frac{T}{T-\theta}$$

The results of the best fit, shown as the solid lines in Figure 5, are J = −4.89 cm^{-1}, g = 2.02 and θ = −0.69 K with the agreement factor $R = \Sigma[(\chi_M T)_{obsd.} - (\chi_M T)_{calcd.}]^2/\Sigma[(\chi_M T)^2_{obsd.}]$ of 6.7 × 10^{-4}.

Generally speaking, oxygen-bridging exchange interactions are much stronger than those involving halogens. On the basis of the structural data of **1**, the chloro-bridging conformation involves equator-to apex linkages [Cl(1) and Cl(2)] and axis-to-axis linkages [Cl(3)] while oxygen atoms occupy equator-to-equator positions. As a result, strong magnetic coupling with a large value ($|J|$ > 100 cm^{-1}) can be expected via the oxygen bridge. In our case, however, the observed superexchange interaction (J = −4.89 cm^{-1}) is smaller than expected. We have ascribed the low superexchange to the small overlap of neighbouring Cu^{II} $d_{x^2-y^2}$ magnetic orbitals. If the $d_{x^2-y^2}$ orbitals interact in the same plane, strong coupling can be observed. In complex **1**, there are large dihedral angles of 100° and 99.2° between the oxygen-bridging copper orbital planes. The delocalisation is poor due to the small overlap and, consequently, the low superexchange can be understood.

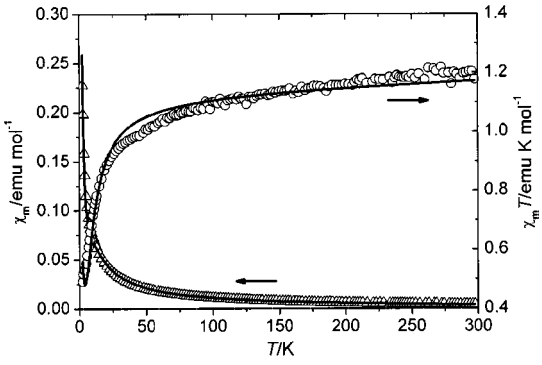

Figure 5. Plot of χ_M vs. T (open triangles) and $\chi_M T$ vs. T (open circles) for **1**; the solid lines represent the theoretical values based on the parameters described in the text

The temperature dependence of the magnetic susceptibility of complex **2** illustrated in Figure 6 suggests the presence of ferromagnetic coupling between the adjacent Cu^{II} ions. The Weiss constant derived from the χ_m^{-1} vs. T plot is equal to +12.1 K and the Curie constant of 1.31 emu·K·mol^{-1} is close to the calculated value of 1.125 emu·K·mol^{-1} (g = 2.0) per trimer. According to the crystal structure data, complex **2** has a symmetrical trinuclear entity which requires only one coupling constant. Similar to complex **1**, the magnetic susceptibility data can be successfully fitted using Equation (1) while intertrimeric exchange was included in the parameter θ. The best fit results, shown as the solid lines in Figure 6, are J = +32.6 cm^{-1}, g = 2.07 and θ = −0.44 K with R = 1.6 × 10^{-4}.

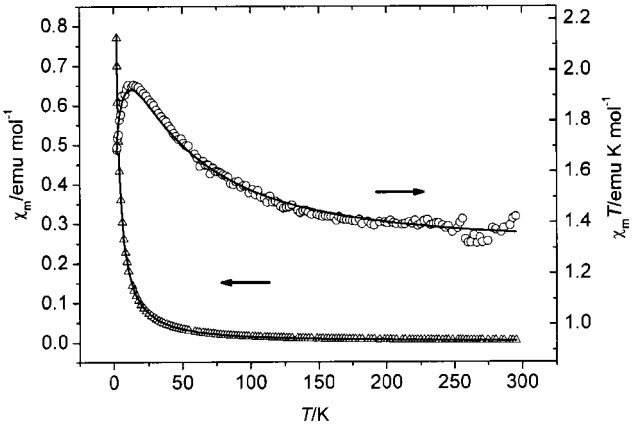

Figure 6. Plot of χ_M vs. T (open triangles) and $\chi_M T$ vs. T (open circles) for **2**; the solid lines represent the theoretical values based on the parameters described in the text.

Most of the $\mu_{1,1}$-azido bridged complexes are ferromagnetic as determined by the spin distribution in the spin triplet ground states according to the spin polarisation mechanism.[25,26] It has been widely cited that the superexchange

 © 2004 Wiley-VCH Verlag GmbH & Co. KGaA, Weinheim

interactions via the end-on azido bridges become antiferromagnetic at higher Cu−N−Cu angles.[8−13] From the density functional study by Ruiz et al., the critical angle is 104°.[8] Also, Thompson et al. suggested that the realm of ferromagnetic coupling ceases for angles greater than 108°.[9] However, an unprecedented low Cu−N−Cu angle of 89.1° was recently reported with an actual antiferromagnetic coupling.[13] This has been assumed to be due to minimal orbital overlap in a basal-axial fashion and a Cu−N distance (2.505 Å) longer than the cutoff distance (2.05 Å) for ferromagnetic interactions. In our case, the ferromagnetic coupling is in agreement with a Cu−N−Cu angle of 102.4° which is lower than the critical angle of 104° and the Cu−N distances [2.001(3) and 2.042(3) Å] are shorter than 2.05 Å. Generally speaking, the basal-to-basal coordination suggests a strong exchange coupling parameter and the actual value of +32.6 cm^{-1} for **2** can be understood in spite of the moderately large dihedral angle (70°) between the neighbouring Cu basal $d_{x^2-y^2}$ orbital planes. It should be mentioned that we have not considered the possible interaction through phenolate oxygen groups. Obviously, the superexchange interaction is negligible due to its basal-to-axial orientation and a long Cu−O distance [2.469(3) Å].

The gradual increase of $\chi_M T$ values with decreasing T for compounds **3** and **4** clearly indicates the existence of intrachain ferromagnetic interactions (Figures 7 and 8). The magnetic susceptibilities above 20.0 K obey the Curie−Weiss law with positive Weiss constants (θ) of +9.68 K for **3** and +6.3 K for **4**, suggesting the existence of ferromagnetic coupling between the adjacent Cu^{II} ions. The Curie constant (C) is equal to 0.355 emu·K·mol^{-1} for **3** which is close to the expected value of 0.375 emu K mol^{-1} and g = 2.0, while the Curie constant of 0.747 emu K mol^{-1} for **4** is in good agreement with the calculated value of 0.75 emu·K·mol^{-1} (g = 2.0). On the basis of the structural data for complex **3**, the magnetic susceptibility data were fitted using the 1D S = 1/2 expression based on the Hamiltonian $\hat{H} = -J\Sigma S_i S_{i+1}$. According to Kahn, no analytical expression has yet been proposed for the ferromagnetic Cu^{II} 1D system. However, a high-temperature series expansion, valid for both positive and negative J values, has been proposed.[27,28]

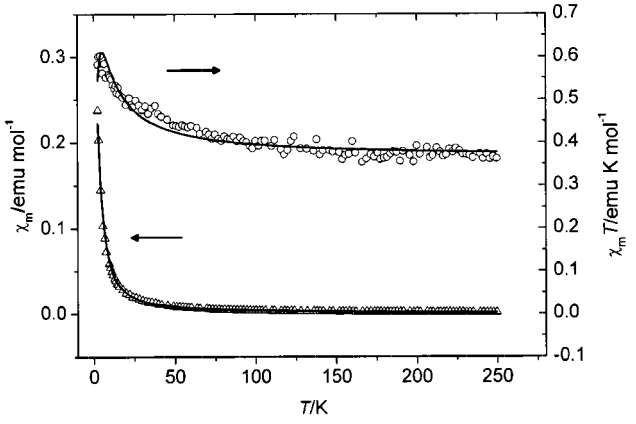

Figure 7. Plot of χ_M vs. T (open triangles) and $\chi_M T$ vs. T (open circles) for **3**; the solid lines represent the theoretical values based on the parameters described in the text

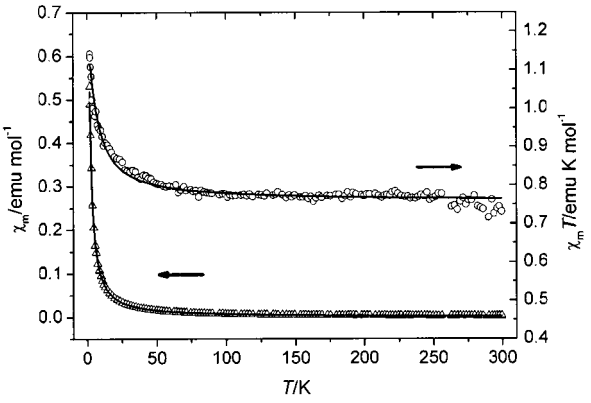

Figure 8. Plot of χ_M vs. T (open triangles) and $\chi_M T$ vs. T (open circles) for **4**; the solid lines represent the theoretical values based on the parameters described in the text

This expansion is:

$$\chi_{chain} = \frac{Ng^2\beta^2}{4kT}\left[\frac{A}{B}\right]^{2/3}$$

with $A = 1 + 5.7979916 \times x + 16.902653 \times x^2 + 29.376885 \times x^3 + 29.832959 \times x^4 + 14.036918 \times x^5$; $B = 1 + 2.7979916 \times x + 7.008678 \times x^2 + 8.6538644 \times x^3 + 4.5743114 \times x^4$ and $x = J/2kT$.

With the consideration of the interchain interactions:[29]

$$\chi_M = \frac{\chi_{chain}}{1-\chi_{chain}(2zJ'/Ng^2\beta^2)}$$

the best-fit results were obtained as J = +6.7 cm^{-1}, g = 2.0, zJ' = −1.3 cm^{-1} with $R = 1.5 \times 10^{-3}$.

Because complex **4** has a 1D chain similar to that in complex **3**, the magnetic susceptibilities of **4** were similarly simulated based on the chain model. The magnetic contribution of the discrete Cu(SE)N_3 monomer was added separately. All the non-intrachain interactions were included in the parameter zJ' using the molecular-field approximation.[29] This expansion is:

$$\chi_{chain} = \frac{Ng^2\beta^2}{4kT}\left[\frac{A}{B}\right]^{2/3}$$

$$\chi_{monomer} = \frac{Ng^2\beta^2}{4kT}$$

$$\chi_M = \frac{\chi_{chain} + \chi_{monomer}}{1-(\chi_{chain} + \chi_{monomer})(2zJ'/Ng^2\beta^2)}$$

The best fit results, as shown in Figure 8, are J = +4.64 cm^{-1}, g = 2.01 and zJ' = −0.30 cm^{-1} with $R = 2.6 \times 10^{-4}$.

For the end-to-end bridging mode of the azide, superexchange is generally antiferromagnetic in nature.[14,15,21−26] Recently, a few compounds have been reported to show a weak ferromagnetic interaction through the 1,3-bridging azido pathway.[16−20] It was found that in these unusual

 © 2004 Wiley-VCH Verlag GmbH & Co. KGaA, Weinheim

Cu^{II} complexes, the bridging azido ligand involves an equatorial linkage to one Cu^{II} ion and an axial coordination to another Cu^{II} ion in the square-pyramidal or elongate octahedral geometry.[16] It is known that for the copper(II) ions, the unpaired electrons occupy the $d_{x^2-y^2}$ orbitals while the d_{z^2} orbitals are filled with the paired electrons. Since the azido σ- and π-orbitals mainly overlap the full d_{z^2} orbitals via the axial interaction, there is almost no coupling between them and thus magnetic coupling is expected to be weak. Furthermore, the 1,3-azido pathway superexchange coupling mainly depends on the Cu−N−N angle α and the Cu−N−N−N−Cu torsion angle θ. Large α and θ values may strongly reduce the antiferromagnetic component of superexchange. In our examples, the effects of the Cu−N−N angles were not drastic (below 104°), so the effect of torsion angles should be dominant. The antiferromagnetic component decreases with increasing θ and becomes zero when $\theta = 90°$ due to accidental orthogonality. The antiferromagnetic interactions then increase until reaching the maximum when $\theta = 180°$.[31] The Cu−N−N−N−Cu torsion angles of 81.5° for **3** and 80.2° for **4** (close to 90°) nullify the antiferromagnetic component and, as a result, net weak ferromagnetic interactions can be observed and explained on the basis of the above arguments.

Conclusion

The present report describes the syntheses, X-ray crystal structures and magneto-structural correlations of four novel phenoxy/chloro- and phenoxy/azido-bridged Cu^{II} complexes. The syntheses of the four compounds are intriguing and the final products are strongly dependent on the synthetic conditions. The $\chi_M T$ data for **1** and **2** were simulated using a trinuclear model, while the data for **3** and **4** were treated using a 1D infinite chain model for $S = 1/2$. The unusual ferromagnetic behaviour of the two $\mu_{1,3}$-N_3-bridged 1D complexes has been rationalised qualitatively on the basis of the axial-equatorial bridging mode as well as the Cu−N_3−Cu torsion angles.

Experimental Section

General Remarks: Elemental analyses (C, H, N) were carried out with an Elementar Vario EL instrument. Infrared spectroscopy was performed with a Magna-IR 750 spectrophotometer in the 4000−400 cm^{-1} region. The TGA measurement of **1** was performed in the temperature range 20−300 °C under nitrogen with a Universal V2.6D TA instrument. Magnetic measurements were performed with a few single crystals (ca. 46 mg for **1**, 32.6 mg for **2**, 11.9 mg for **3** and 33.5 mg for **4**) using a MagLab 2000 magnetometer in a field of 10 kOe (**1**, **2** and **4**) or 20 kOe (**3**) from 2 to 300 K. The experimental susceptibilities were corrected for the diamagnetism of the constituent atoms (Pascal's Tables).

Caution! Although not encountered in our experiments, azido complexes of metal ions are potentially explosive. Only small amounts of the materials should be prepared and they should be handled with care.

Synthesis of 1: *N*,*N*-Dimethylethylenediamine (5.5 mL, 50 mmol) in methanol (10 mL) was mixed with salicylaldehyde (7.605 g, 50 mmol) in methanol (10 mL). $CuCl_2 \cdot 2H_2O$ (8.525 g, 50 mmol) in water (50 mL) was then added slowly and the mixture was heated to reflux for 0.5 h. The resultant dark green solution was reduced to 50 mL by rotary evaporation. Dark green needle-shaped single crystals suitable for X-ray analysis separated after several days. Yield: 4.44 g (31%). $C_{22}H_{46}Cl_4Cu_3N_4O_{10}$ (828.03): calcd. C 30.76, H 5.40, N, 6.52; found C 30.98, H 5.26, N 6.63. IR (KBr): $\tilde{\nu}$ = 3434 (O−H, H_2O), 1647 (C=N) cm^{-1}. The water content of **1** was confirmed by thermogravimetric analysis.

Syntheses of 2, 3 and 4: A slight excess of sodium azide (57 mg, 0.88 mmol), dissolved in a minimum amount of water, was added to an aqueous solution (10 mL) of **1** (170.2 mg, 0.2 mmol) with continuous stirring. This gave an immediate yellowish-brown precipitate which was collected by filtration and used for the following synthesis. Dark green platelet crystals of **4** were obtained by concentration of the filtrate at room temperature. Yield: 33.5 mg (30%). $C_{11}H_{15}CuN_5O$ (593.64): calcd. C 44.51, H 5.09, N 23.59; found C 44.26, H 5.07, N 24.20. IR (KBr): $\tilde{\nu}$ = 2074, 2048 (N_3), 1635(C=N) cm^{-1}. The yellow brown precipitate was directly dissolved in DMF (10 mL). Black block-shaped crystals suitable for X-ray analysis were formed by slow concentration at room temperature over several weeks. Pure **2** was obtained by manual separation under a microscope. Yield: 32.6 mg (19%). $C_{28}H_{44}Cu_3N_{18}O_4$ (887.43): calcd. C 37.90, H 5.00, N 28.41; found C 37.12, H 4.94, N 27.82. IR (KBr): $\tilde{\nu}$ = 2070, 2031 (N3), 1655 (C=O, DMF), 1636 (C=N) cm^{-1}. The yellow-brown precipitate was at first dissolved in MeCN (10 mL). After concentration to dryness, the resultant microcrystalline solid was collected and dissolved in DMF (10 mL). Slow concentration of the DMF solution gave bluish-green crystals of **3** suitable for X-ray analysis. Yield: 11.9 mg (8%). $C_{14}H_{22}CuN_6O_2$ (369.92): calcd. C 45.46, H 5.99, N 22.72; found C 44.16, H 5.73, N 23.16. IR (KBr): $\tilde{\nu}$ = 2074, 2047 (N_3), 1655 (C=O, DMF), 1634 (C=N) cm^{-1}.

X-ray Crystallographic Study: The data collections for **1** − $2.5H_2O$, **2**, **3** and **4** were made with a Bruker Smart CCD (293 K) and a Siemens Bruker P4 diffractometer, respectively. Intensity data were corrected for Lorentz and polarisation factors. Absorption corrections were applied using SADABS (Bruker 2000) (complexes **1** − $2.5H_2O$, **3** and **4**) and ψ-scan (complex **2**). The structures were solved by direct methods (SHELXS-97) and refined by full-matrix least squares (SHELXL-97) on F^2. Hydrogen atoms attached to the C and N atoms were added geometrically and refined using the riding model. In complex **1** − $2.5H_2O$, considerable disorder of the interstitial water molecules was observed and a split model was employed during the refinement. The crystal data are summarised in Table 5. CCDC-239759 to -239762 contain the supplementary crystallographic data for this paper. These data can be obtained free of charge at www.ccdc.cam.ac.uk/conts/retrieving.html [or from the Cambridge Crystallographic Data Centre, 12 Union Road, Cambridge CB2 1EZ, UK; Fax: + 44-1223-336-033; E-mail: deposit@ccdc.cam.ac.uk].

Acknowledgments

This work was supported by the National Natural Science Foundation of China (project nos. 20201008 and 50272034). We are grateful to Prof. Song Gao for the magnetic measurements.

 © 2004 Wiley-VCH Verlag GmbH & Co. KGaA, Weinheim

Table 5. Crystal data for complexes **1** − 2.5H_2O, **2**, **3** and **4**

	1 − 2.5H_2O	**2**	**3**	**4**
Empirical formula	$C_{23}H_{43}Cl_4Cu_3N_4O_{7.5}$	$C_{28}H_{44}Cu_3N_{18}O_4$	$C_{14}H_{22}CuN_6O_2$	$C_{22}H_{30}Cu_2N_{10}O_2$
Formula mass	828.03	887.43	369.92	593.64
Space group	$P2_1/n$	$P2_1/c$	$P2_12_12_1$	$Pca2_1$
a [Å]	9.154(2)	10.7026(13)	9.3270(19)	21.783(3)
b [Å]	19.589(5)	17.4369(15)	12.049(2)	11.927(3)
c [Å]	18.371(5)	11.1640(15)	15.321(3)	10.207(2)
β [°]	94.677(6)	111.572(8)	90	90
V [A^3]	3283.2(15)	1937.5(4)	1721.8(6)	2651.8(8)
Z	4	2	4	4
$\rho_{calcd.}$ [g cm^{-3}]	1.675	1.521	1.427	1.487
μ(Mo-K_α) [mm^{-1}]	2.298	1.690	1.286	1.643
Data/restraint/parameters	5760/1/393	3412/0/241	6317/0/208	4193/1/325
GOF	1.064	1.006	1.158	0.992
$R1$ [$I > 2\sigma(I)$]	0.0458	0.0388	0.0552	0.0468
$wR2$ (all data)	0.1183	0.1135	0.0981	0.1582

[1] S. Haddad, R. D. Willett, *Inorg. Chem.* **2001**, *40*, 2457−2460.
[2] M. Y. Wei, R. D. Willett, *Inorg. Chem.* **1996**, *35*, 6381−6385.
[3] R. Bhattacharya, A. Ghosh, M. S. Ray, L. Righi, G. Bocelli, S. Chaudhuri, R. D. Willett, J. M. Clemente-Juan, E. Coronado, C. J. Goméz-Garicia, *Eur. J. Inorg. Chem.* **2002**, 4253−4259.
[4] M. Hernández-Molina, J. González-Platas, C. Ruiz-Pérez, F. Lloret, M. Julve, *Inorg. Chim. Acta* **1999**, *284*, 258−265.
[5] A. M. Schuitema, A. F. Stassen, W. L. Driessen, J. Reedijk, *Inorg. Chim. Acta* **2002**, *337*, 48−52.
[6] H.-D. Bian, J.-Y. Xu, W. Gu, S.-P. Yan, P. Cheng, D.-Z. Liao, Z.-H. Jiang, *Polyhedron* **2003**, *22*, 2927−2932.
[7] E. W. Hatfield, F. L. Bunger, *Inorg. Chem.* **1968**, *8*, 1194−1195.
[8] E. Ruiz, J. Cano, S. Alvarez, P. Alemany, *J. Am. Chem. Soc.* **1998**, *120*, 11122−11129.
[9] S. S. Tandon, L. K. Thompson, M. E. Manuel, I. N. Bridson, *Inorg. Chem.* **1994**, *33*, 5555−5570.
[10] L. K. Thompson, S. S. Tandon, M. E. Manuel, *Inorg. Chem.* **1995**, *34*, 2356−2366.
[11] P. S. Mukherjee, T. K. Maji, G. Mostafa, T. Mallah, N. R. Chaudhuri, *Inorg. Chem.* **2000**, *39*, 5147−5150.
[12] E.-Q. Gao, S.-Q. Bai, C.-F. Wang, Y.-F. Yue, C.-H. Yan, *Inorg. Chem.* **2003**, *42*, 8456−8464.
[13] S. Koner, S. Saha, T. Mallah, K.-I. Okamoto, *Inorg. Chem.* **2004**, *43*, 840−842.
[14] C. G. Pierpont, D. N. Hendrickson, D. M. Duggan, F. Wagner, E. K. Barefield, *Inorg. Chem.* **1975**, *14*, 604−610.
[15] A. Escuer, R. Vicente, J. Ribas, M. S. El Fallah, X. Solans, *Inorg. Chem.* **1993**, *32*, 1033−1035.
[16] C. S. Hong, Y. Do, *Angew. Chem. Int. Ed.* **1999**, *38*, 193−195.
[17] P. S. Mukherjee, S. Dalai, E. Zangrando, F. Lloret, N. R. Chaudhuri, *Chem. Commun.* **2001**, 1444−1445.
[18] [18a] P. S. Mukherjee, T. K. Maji, A. Escuer, R. Vicente, J. Ribas, G. Rosair, F. A. Mautner, N. R. Chaudhuri, *Eur. J. Inorg. Chem.* **2002**, 943−949. [18b] S. Dalai, P. S. Mukherjee, M. G. B. Drew, T.-H. Lu, N. R. Chaudhuri, *Inorg. Chim. Acta* **2002**, *335*, 85−90. [18c] S. Dalai, P. S. Mukherjee, T. Mallah, M. G. B. Drew, N. R. Chaudhuri, *Inorg. Chem. Commun.* **2002**, *5*, 472−474. [18d] T. K. Maji, P. S. Mukherjee, G. Mostafa, T. Mallah, J. Cano-Boquera, N. R. Chaudhuri, *Chem. Commun.* **2001**, 1012−1013. [18e] P. S. Mukherjee, S. Dalai, G. Mostafa, T.-H. Lu, E. Rentschler, N. R. Chaudhuri, *New J. Chem.* **2001**, *25*, 1203−1207.
[19] L.-C. Li, D.-Z. Liao, Z.-H. Jiang, S.-P. Yan, *Inorg. Chem.* **2002**, *41*, 1019−1021.
[20] B. Woodard, R. D. Willett, S. Haddad, B. Twamley, C. J. Gomez-Garcia, E. Coronado, *Inorg. Chem.* **2004**, *43*, 1822−1824.
[21] C. R. Choudhuri, S. K. Dey, R. Karmakar, C.-D. Wu, C.-Z. Lu, M. S. El Fallah, S. Mitra, *New J. Chem.* **2003**, *27*, 1360−1366.
[22] S. K. Dey, N. Mondal, M. S. El Fallh, R. Vicente, A. Escuer, X. Solans, M. Font-Bardfa, T. Matsushita, V. Gramlich, S. Mitra, *Inorg. Chem.*, in press.
[23] S. S. Tandon, L. K. Thompson, D. O. Miller, *J. Chem. Soc., Chem. Commun.* **1995**, 1907−1908.
[24] L. K. Thompson, S. S. Tandon, F. Lloret, J. Cano, M. Julve, *Inorg. Chem.* **1997**, *36*, 3301−3306.
[25] J. Comarmond, P. Plumere, J.-M. Lehn, Y. Agnus, R. Louis, R. Weiss, O. Kahn, I. Morgenstern-Badarau, *J. Am. Chem. Soc.* **1982**, *104*, 6330−6340.
[26] M.-F. Charlot, O. Kahn, M. Chaillet, C. Larried, *J. Am. Chem. Soc.* **1986**, *108*, 2574−2581.
[27] O. Kahn, *Molecular Magnetism*, VCH, Weinheim, **1993**, chapter 6.
[28] G. A. Baker, G. S. Rushbrooke, H. E. Gilbert, *Phys. Rev.* **1964**, *135*, A1272.
[29] C. J. O′Conner, *Prog. Inorg. Chem.* **1982**, *29*, 203.
[30] A. W. Addison, T. N. Rao, J. Reedijk, J. V. Rijin, G. C. Verschoor, *J. Chem. Soc., Dalton Trans.* **1984**, 1349.
[31] A. Escuer, R. Vicente, J. Ribas, M. S. El Fallah, X. Solans, M. Font-Bardia, *Inorg. Chem.* **1993**, *32*, 3727−3732.
[32] [32a] S. G. Kang, K. Ryu, S.-K. Jung, J. Kim, *Inorg. Chim. Acta* **1999**, *293*, 140. [32b] B. Chiari, A. Cinti, O. Piovesana, P. F. Zanazzi, *Inorg. Chem.* **1995**, *34*, 2652−2657.

Received May 282004
Early View Article
Published Online October 7, 2004

 © 2004 Wiley-VCH Verlag GmbH & Co. KGaA, Weinheim

Synthesis of (Vinylidene)- and (Cyclopropenyl)ruthenium Complexes Containing a Tris(pyrazolyl)borato (Tp) Ligand

Yih-Hsing Lo,[a] Ying-Chih Lin,*[a] Gene-Hsiang Lee,[a] and Yu Wang[a]

Keywords: Cyclopropenyl / N ligands / Ruthenium / Vinylidene ligands

A convenient high-yield route to [Ru(C≡C–Ph)(Tp)(PPh_3)$_2$] [**2**; Tp = HB(pz)$_3$, pz = pyrazolyl] has been found through the intermediacy of [$RuCl_2$(Hpz)$_2$(PPh_3)$_2$] (**1**). This complex is readily obtained on treatment of [$RuCl_2(PPh_3)_3$] with 2 equiv. of pyrazole in boiling THF. The molecular structures of complexes **1** and **2** have been confirmed by single-crystal X-ray diffraction analysis. A number of new cationic vinylidene complexes [Ru{=C=C(Ph)CH_2R}(Tp)(PPh_3)$_2$]$^+$ [**3a**, R = CN; **3b**, R = HC=CH_2; **3c**, R = CH=C(CH_3)$_2$; **3d**, R = Ph; **3e**, R = C(O)OMe] have been prepared by electrophilic addition of organic halides to complex **2**. The deprotonation reaction of **3a** yields the cyclopropenyl complex **4a**. One phosphane ligand of **4a** is remarkably labile, being replaced by donor ligands L to yield diastereomeric mixtures of the cyclopropenyl complexes **5a**–**5d** mostly in an approximate 4:1 ratio. The cyclopropenyl rings in **4a** and **5a** are susceptible to ring opening by I_2. In addition, treatment of **4a** with *n*BuNC in the presence of MeOH results in substitution of a phosphane ligand by *n*BuNC followed by protonation of the three-membered ring by MeOH. This is then followed by addition of methoxide to give the vinyl ether complex [Ru{C(OMe)=C(Ph)CH_2CN}(Tp)(PPh_3)(*n*BuNC)] (**8a**).
(© Wiley-VCH Verlag GmbH & Co. KGaA, 69451 Weinheim, Germany, 2004)

Introduction

The hydrotris(pyrazol-1-yl)borate (Tp) ligand has been used to stabilize a wide variety of transition-metal complexes since its discovery by Trofimenko,[1] and the development of Tp chemistry within group VIII, in particular, has accelerated recently.[1c,1d] Tp is often compared with Cp (η^5-C_5H_5) due to the same charge and number of electrons donated, although their differences in size and electronic properties are obvious. Thus, the cone angle of Tp (close to 180°) is well above the value of 100° calculated for Cp. The steric bulkiness of the Tp ligand appears to disfavor higher coordination numbers or bulky metal fragment. Much of the chemistry of the [CpRu(PPh_3)$_2$]$^+$ fragment can be traced to the strongly π-basic nature of the ruthenium center. Replacing Cp with Tp increases the basicity of the metal center further, and it has been claimed that it also leads to more ideally octahedral hybridization.[2] The chemistry of (vinylidene)transition-metal complexes has attracted increasing attention in recent years especially because of their application as key intermediates in stoichiometric and catalytic transformations of organic molecules.[3] Representative examples of ruthenium-based catalysis involving vinylidene complexes have been reported for the cyclization of dienylalkynes,[4a] the dimerization of HC≡C*t*Bu,[4b] and the tandem cyclization/reconstructive addition of propargyl alcohols with allyl alcohols.[4c] A key characteristic of vinylidene complexes appears to be the electrophilicity of the α-carbon atom, which adds, often easily, amines,[5] alcohols,[6,7] phosphanes,[8] and even fluoride.[6a]

The reactions of metal complexes with cyclopropenes often generate interesting chemistry, mainly due to the large amount of strain energy (ca. 50 kcal/mol) in the three-membered ring.[9] This molecule has played a crucial role in the development of the important concept of aromaticity, and its chemical reactivity has been extensively explored.[10] The syntheses of cyclopropenyl-containing metal derivatives in which the metal atom is bonded to the sp^3-hybridized carbon atom of the cyclopropene ring have been reported in the literature.[11] However, only a few examples of such derivatives in which the metal atom is bonded to the sp^2-carbon atom of the three-membered ring have been reported.[12] A few structurally different (cyclopropenylidene)-transition-metal complexes, mostly prepared from dichlorocyclopropene,[13] and a number of π-cyclopropene complexes,[14] are also known.

During the course of our investigations into (vinylidene)ruthenium chemistry, we previously studied the formation of several interesting neutral cyclopropenyl complexes.[6] For example, the cationic complex [RuCp{=C=C(Ph)CH_2CN}(PPh_3)$_2$]$^+$ was found to undergo deprotonation to afford the yellow cyclopropenyl complex. The cationic nature of the vinylidene complex, along with the presence of an electron-withdrawing functionality such as a CN group at C-γ of the vinylidene ligand, play a role in enhancing the acidity of the proton next to the CN group. Thus, addition of a base successfully brings about an intra-

[a] Department of Chemistry, National Taiwan University, Taipei, Taiwan 106, Republic of China

 © 2004 Wiley-VCH Verlag GmbH & Co. KGaA, Weinheim DOI: 10.1002/ejic.200400467

molecular cycloaddition leading to the formation of a neutral cyclopropenyl complex. To elaborate the breadth of such a system, we set out to study analogous ruthenium complexes containing a Tp ligand. Herein, we report the synthesis of a series of new cationic vinylideneruthenium complexes and new neutral cyclopropenyl complexes in high yields. The reaction of the cyclopropenyl complex with I_2 to give a new vinylidene complex is also reported.

Results and Discussion

Preparation of (Tp)metal Acetylide Complexes

We have previously reported[6b] that $[RuCl(Tp)(PPh_3)_2]$ reacts with phenylacetylene in the presence of NaOMe to afford the acetylide complex $[Ru(C{\equiv}C{-}Ph)(Tp)(PPh_3)_2]$ (**2**). However, complex **2**, prepared using this method, is persistently contaminated with the starting material because of incomplete conversion. Therefore, a new synthetic approach to prepare **2** has been developed (Scheme 1). This new, convenient, high-yield route to **2** proceeds through the intermediacy of $[RuCl_2(Hpz)_2(PPh_3)_2]$ (**1**) (Hpz = pyrazole). This compound is readily obtained as an air-sensitive yellow solid in 97% yield upon treatment of $[RuCl_2(PPh_3)_3]$ with 2 equiv. of pyrazole in boiling THF for 1 h. Complex **1** is soluble in $CHCl_3$, CH_2Cl_2, MeOH, CH_3CN and THF but insoluble in hexane, and was characterized by a combination of elemental analysis and ^1H and $^{13}C\{^1H\}$ NMR spectroscopy. Characteristic ^1H NMR spectroscopic data for **1** include a singlet at $\delta = 11.67$ ppm assignable to the proton of the pyrazole ligand. In addition, the solid-state structure was determined by a single-crystal X-ray diffraction study. An ORTEP diagram is shown in Figure 1 (with selected bond lengths and angles). The coordination geometry of **1** is approximately octahedral with both pyrazole ligands *N*-bonded. The ruthenium atom is at the center, with the nitrogen atoms of the two pyrazole ligands and two PPh_3 ligands occupying the equatorial positions and the axial positions being occupied by two *trans*-chlorine atoms. The Ru−N(1) and Ru−N(3) bond lengths are 2.133(5) and 2.127(5) Å, respectively. The two Ru−Cl bonds of 2.428(2) and 2.426(2) Å are similar to those found in other (pyrazole)ruthenium complexes, such as 2.427(2) and 2.392(2) Å in $[RuCl_2(HPz)(DMSO)_3]$ and 2.427(1) and 2.397(1) Å in $[RuCl_2(HPz)_2(DMSO)_2]$.[15] Pyrazoles and their deprotonated form (pyrazolate anions) are attractive ligands that exhibit a rich coordination chemistry.[16] Pyrazoles and substituted pyrazoles usually behave as monodentate ligands[17] and these monodentate pyrazoles may give rise to interesting processes such as prototropic equilibrium or reversible metal−ligand binding, which are relevant to biological systems.[18]

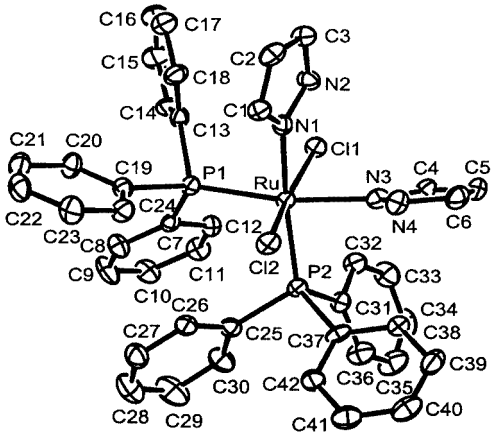

Figure 1. ORTEP drawing of complex **1** (30% probability ellipsoids); selected bond lengths [Å] and angles [°]: Ru−P(1) 2.3423(20), Ru−P(2) 2.3421(20), Ru−N(1) 2.133(5), Ru−N(3) 2.127(5), Ru−Cl(1) 2.4283(19), Ru−Cl(2) 2.4261(19); N(1)−Ru−N(3) 83.24(20)

The one-pot reaction of **1** with NaTp and phenylacetylene in the presence of NaOMe gives the ruthenium acetylide complex $[Ru(C{\equiv}C{-}Ph)(Tp)(PPh_3)_2]$ (**2**). The yield of this one-pot reaction was higher than the yield obtained from the previously reported reaction that required several steps.[6b] The ν(B−H) vibration of **2** is found at 2489 cm^{-1}, which is characteristic of Tp bound to a metal center in a terdentate (N,N,N) manner. Yellow crystals of **2** were obtained by slow diffusion of hexane into a $CHCl_3$ solution of **2** at room temperature for 3 d. The molecular structure of **2** was determined by an X-ray diffraction study. An ORTEP diagram is shown in Figure 2 (with selected bond lengths and angles). The coordination geometry of complex **2** is approximately octahedral. The Ru−C(1) bond length of 2.006(6) Å is typical of an Ru−C single bond. The Ru−C(1)−C(2) bond angle of 173.9(5)° and C(1)−C(2) bond length of 1.205(8) Å are characteristic of a ruthenium acetylide complex.

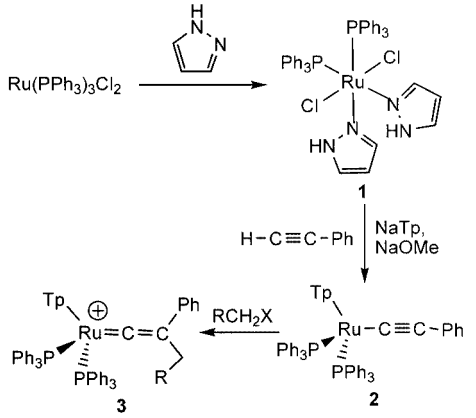

Scheme 1

Cationic (Tp)(vinylidene)metal Complexes

Treatment of **2** with ICH_2CN affords the cationic vinylidene complex $[Ru\{{=}C{=}C(Ph)CH_2CN\}(Tp)(PPh_3)_2]I$ (**3a**) in 90% yield (Scheme 1).[9b] In the presence of excess NH_4PF_6 the counteranion is replaced by PF_6^-. Similarly,

 © 2004 Wiley-VCH Verlag GmbH & Co. KGaA, Weinheim

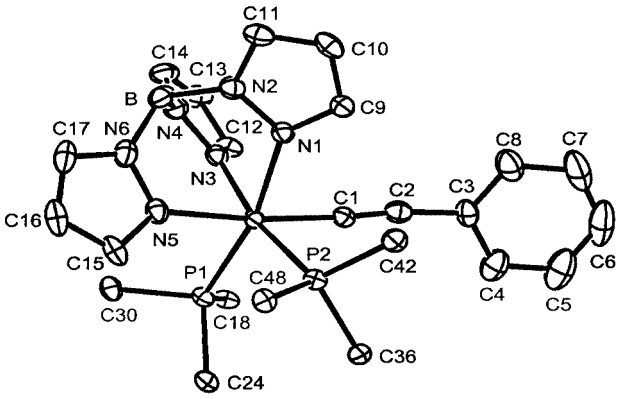

Figure 2. ORTEP drawing of complex **2** (30% probability ellipsoids); the carbon atoms of the phenyl groups (except the *ipso*-carbon atoms) on the triphenylphosphane have been eliminated for clarity; selected bond lengths [Å] and angles [°]: Ru−C(1) 2.006(6), C(1)−C(2) 1.205(8), C(2)−C(3) 1.439(9); Ru−C(1)−C(2) 173.9(5), C(1)−C(2)−C(3) 167.8(6)

the preparation of other vinylidene complexes $[Tp(PPh_3)_2Ru{=}C{=}C(Ph)CH_2R]^+$ [**3b**, R = CH=CH_2; **3c**, R = CH=$C(CH_3)_2$; **3d**, R = Ph; **3e**, R = C(O)OMe] was accomplished by treating **2** with the corresponding halides; they were all isolated in high yields. With the exception of **3e**, all the vinylidene complexes mentioned above were prepared in CH_2Cl_2 at room temperature; mild heating was required for the synthesis of **3e**, and a mixture of CH_2Cl_2/$CHCl_3$ (3:1, v/v) was used as solvent in order to achieve a slightly higher reaction temperature. Complexes **3a**−**3e** are all soluble in polar solvents such as $CHCl_3$, CH_2Cl_2, MeOH and CH_3CN but insoluble in acetone, diethyl ether and hexane. These complexes are green in the solid state. Characteristic spectroscopic data of theses vinylidene complexes consist of a strongly deshielded C-α resonance as a triplet at $\delta = 370 \pm 5$ ppm in the ^{13}C NMR spectrum and a singlet ^{31}P NMR resonance at $\delta = 36 \pm 1$ ppm in $CDCl_3$ at room temperature; this is due to the fluxional behavior of the vinylidene ligand.[19] The spectroscopic data of the Cp analogues are similar; the triplet C-α resonance appears at $\delta = 340 \pm 5$ ppm in the ^{13}C NMR spectrum and a singlet ^{31}P NMR resonance is observed at $\delta = 42 \pm 1$ ppm. The newly formed carbon−carbon bond of these vinylidene complexes is easily cleaved in the presence of acid. Complexes **3a**−**3d** are all stable at room temperature for a period of 3 d, after which they decomposed to give unidentified products.

(Cyclopropenyl)(Tp)metal Complexes

The neutral complex $[Ru\{C{=}C(Ph)CH(CN)\}(Tp)(PPh_3)_2]$ (**4a**) can be readily prepared in high yield by deprotonation of **3a** at 0 °C in CH_2Cl_2 (Scheme 2). However, no deprotonation was observed for the other vinylidene complexes **3b**−**3d**, even in the presence of NaOMe, nBu_4NF (1 M in THF), DBU (1,8-diazabicyclo[5.4.0]undecene) or KOH (dissolved in a minimum amount of H_2O) at room temperature for 24 h. We have previously prepared neutral cyclopropenyl complexes containing a Cp ligand by deprotonation of the cationic vinylidene precursors.[19] Cyclopropenyl complexes with substituents such as vinyl, dimethylvinyl, phenyl and methyl ester groups are all achievable. The chemistry of the $[CpRu(PPh_3)_2]^+$ fragment can be traced to the strongly π-basic nature of the ruthenium center. Replacing Cp with Tp increases the basicity of the metal center and reduces the cationic character of the vinylidene complexes. Complexes **3b**−**3e** all lack enough cationic character to lead to intramolecular cycloaddition. We thus believe that the facile deprotonation of cationic vinylidene complexes may be ascribed to the combined effect of the cationic character and the presence of the electron-withdrawing substituent of the vinylidene complex.

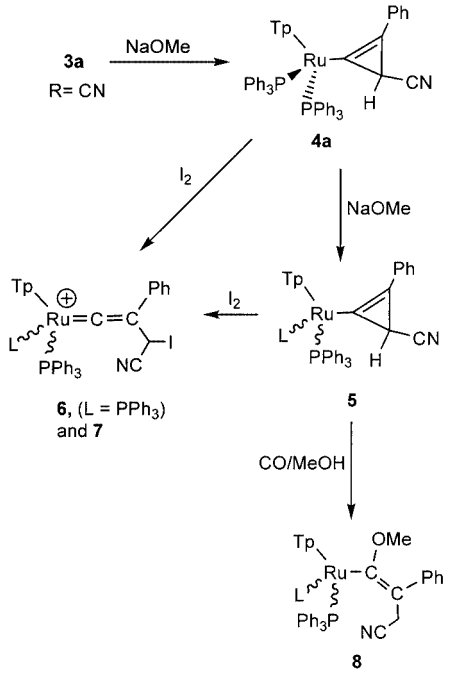

Scheme 2

The analogous Cp complex of **4a** is stable with respect to ligand substitution — the phosphane ligand binds strongly to the ruthenium center, making the coordination site unavailable for an incoming substrate. In contrast, the Tp complex **4a** is susceptible to ligand substitution under relatively mild conditions. This may be attributed to the increased steric bulkiness of the Tp ligand relative to Cp. For example, when 2 equiv. of PhCN, *p*-$CF_3C_6H_4CN$, *n*BuNC or *t*BuNC were added at room temperature to a CH_2Cl_2 solution of **4a** a smooth reaction ensued over 1 h which afforded good yields of the bright-yellow (cyclopropenyl)ruthenium complexes $[Ru\{C{=}C(Ph)CH(CN)\}(Tp)(PPh_3)(L)]$ (**5a**, L = *n*BuNC; **5b**, L = *t*BuNC; **5c**, L = *p*-$CF_3C_6H_4CN$; **5d**, L = PhCN), respectively (Scheme 2). Significantly, when these reactions were repeated using only 1 equiv. of L much lower yields (ca. 8%) were obtained.

Complexes **5a**−**5d** all contain two diastereomers in a 4:1 ratio. The ^1H NMR resonances of **5a** attributed to the CHCN moiety of the three-membered rings of the major and the minor isomers appear at $\delta = 0.93$ and 1.16 ppm,

 © 2004 Wiley-VCH Verlag GmbH & Co. KGaA, Weinheim

respectively. In the $^{13}C\{^1H\}$ NMR spectrum, singlet ^{13}C resonances at δ = 3.8 and 3.5 ppm and doublet resonances at δ = 128.7 and 128.8 ppm, with $^2J_{P,C}$ coupling constants of 11.6 and 11.5 Hz, are assigned to the CHN and the ruthenium-bonded C-α carbon atoms of the major and the minor isomers, respectively. Interestingly, in the cases of **5c** and **5d** the major isomer is more stable than the minor isomer; the minor isomer decomposes within about 3 h.[6b] In the $^{13}C\{^1H\}$ NMR spectrum of **5c**, the singlet resonance at δ = 4.10 ppm and the doublet resonance at δ = 132.6 ppm, with a $^2J_{P,C}$ coupling of 12.3 Hz, are assigned to the CHN and the ruthenium-bonded C-α carbon atoms of the major isomer; the ^{13}C NMR spectrum of the minor isomer was not obtained because of its lower stability. Complexes **5a** and **5b** are stable in diethyl ether and THF, but in $CHCl_3$ compounds **5b**, **5c**, **5d** are less stable than **5a**. Furthermore, **5b** decomposes in $CHCl_3$ producing [RuCl(Tp)(PPh_3)(*t*BuNC)] and some unidentified organic products. Decomposition of **5c** and **5d** produces complicated mixtures. The stability of the substituted cyclopropenyl complexes was found to decrease in the order *n*BuNC > *t*BuNC > *p*-$CF_3C_6H_4CN$ > PhCN.

Opening of the Three-Membered Ring by Electrophiles

Treatment of **4a** with I_2 at 0 °C afforded the cationic vinylidene complex [Ru{=C=C(Ph)CH(I)(CN)}(Tp)(PPh_3)$_2$]I (**6**) in 79% yield (Scheme 2). Complex **6** is a green solid and its spectroscopic data display the features of a vinylidene complex. The pattern of two-doublet resonances at δ = 34.3 and 33.6 ppm, with a $J_{P,P}$ coupling of 26.9 Hz, in the ^{31}P NMR spectrum arises from the stereogenic C-γ center. In the ^1H NMR spectrum of **6** the resonance at δ = 3.23 ppm is assigned to the CHICN group, and in the $^{13}C\{^1H\}$ spectrum the triplet resonance at δ = 374.5 ppm, with a $^2J_{P,C}$ coupling of 15.1 Hz, is assigned to the vinylidene C-α atom. Similarly, treatment of **5a** with I_2 affords the addition product [Ru{=C=C(Ph)CH(I)(CN)}(Tp)(PPh_3)(*n*BuNC)]I (**7**) in high yield. Interestingly, only one diastereoisomer is observed for **7**. The ^1H NMR spectrum of **7** displays one singlet resonance at δ = 3.56 ppm, assigned to the CHICN group; the doublet resonance at δ = 367.3 ppm, with a $^2J_{P,C}$ coupling of 16.4 Hz, in the ^{13}C NMR spectrum is assigned to the vinylidene C-α atom. Formation of these vinylidene complexes occurs by selective cleavage of the cyclopropenyl single bond near the metal center. No alkylation is observed when **4a** is treated with CH_3I, CH_3CH_2I, CH_2=$CHCH_2Br$, CH≡$CHCH_2Br$ or ICH_2CN.

Reaction of 4a with nBuNC in the Presence of MeOH

Reaction of **4a** with *n*BuNC in the presence of MeOH causes substitution of a phosphane ligand by *n*BuNC. This is followed by protonation of the three-membered ring to give a vinylidene intermediate and addition of MeO^- to give the vinyl ether complex [Ru{C(OMe)=C(Ph)CH_2CN}(Tp)(PPh_3)(*n*BuNC)] (**8a**). Similarly, the reaction of **4a** with *t*BuNC in the presence of MeOH gives the vinyl ether product [Ru{C(OMe)=C(Ph)CH_2CN}(Tp)(PPh_3)(*t*BuNC)] (**8b**) in lower yield, which may be due to steric effects. The ^1H NMR spectrum of **8a** displays an AB pattern for the CH_2CN moiety, with two doublets centered at δ = 3.86 and 2.79 ppm with a coupling constant of 16.4 Hz. The characteristic $^{13}C\{^1H\}$ NMR spectroscopic features of **8a** and **8b** comprise downfield resonances at δ = 179.1 and 182.2 ppm, respectively, assignable to the vinyl C-α atom. In the absence of MeOH these reactions give the simple substitution products **5a** and **5b**, respectively. The reaction proceeds with substitution as the first step, followed by opening of the cyclopropenyl ring by MeOH to give the vinylidene ligand. This was confirmed by a separate experiment where **5** was allowed to react with MeOH, resulting in protonation followed by a nucleophilic attack of methoxide at C-α of the vinylidene ligand to give the final product. In our previous paper we reported that MeOH is able to open three-membered rings in some cases.[6]

Concluding Remark

The (cyclopropenyl)ruthenium complex **4a**, containing a Tp ligand, has been prepared by deprotonation of the vinylidene precursor **3a**. No deprotonation was observed in the reaction of **3b**−**3e** with NaOMe or nBu_4NOH which may be attributed to the reduced cationic character of vinylidene complexes caused by the presence of the Tp ligand. Unlike its Cp analogue, complex **4a** undergoes a facile phosphane substitution reaction with several two-electron donor molecules. This property was taken advantage of to prepare novel complexes of Ru. For example, *n*BuNC readily displaces one of the phosphane ligands of **4a** to give a mixture of diastereomers **5** in a 4:1 ratio. Reaction of **4a** with *n*BuNC in the presence of MeOH gives the vinyl ether product **8a**, which results from a displacement reaction followed by nucleophilic addition of the MeO^- group at C-α.

Experiment Section

General Procedures: All manipulations were performed under nitrogen using vacuum-line, drybox, and standard Schlenk techniques. CH_3CN and CH_2Cl_2 were distilled from CaH_2 and diethyl ether and THF from Na/benzophenone ketyl. All other solvents and reagents were of reagent grade and were used without further purification. NMR spectra were recorded with Bruker AC-200 and AM-300WB FT NMR spectrometers at room temperature (unless stated otherwise) and are reported in δ units with residual protons in the solvent as an internal standard [$CDCl_3$: δ = 7.24 ppm; CD_3CN: δ = 1.93 ppm; $CD_3C(O)CD_3$: δ = 2.04 ppm]. FAB mass spectra were recorded with a JEOL SX-102A mass spectrometer. Elemental analyses and X-ray diffraction studies were carried out at the Regional Center of Analytical Instrument at the National Taiwan University. The complexes [$RuCl_2(PPh_3)_3$][20] and **4a**[6] were prepared according to literature methods.

Synthesis of [$RuCl_2(C_3H_3NNH)_2(PPh_3)_2$] (1): Pyrazole (0.38 g, 5.60 mmol) was added to a solution of [$RuCl_2(PPh_3)_3$] (2.45 g,

 © 2004 Wiley-VCH Verlag GmbH & Co. KGaA, Weinheim

2.80 mmol) in 20 mL of THF, and the reaction mixture was heated to 60 °C for 1 h. After cooling and removal of the solvent under reduced pressure, the residue was dissolved in CH_2Cl_2. Addition of hexane afforded a bright yellow precipitate, which was filtered off, washed with hexane and dried under vacuum to give **1** (2.12 g, 91% yield). ^{1}H NMR ($CDCl_3$): δ = 5.91 (t, $J_{H,H}$ = 2.3 Hz, 3 H, Tp), 7.32−6.91 (m, Ph, Tp), 8.09 (d, $J_{H,H}$ = 2.1 Hz, 3 H, Tp), 11.67 (s, 2 H, NH) ppm. ^{31}P NMR ($CDCl_3$): δ = 40.8 ppm. MS (FAB): *m*/*z* = 832.1 [M^+], 764.2 [M^+ − HPz], 502.2 [M^+ − HPz − PPh_3]. $C_{42}H_{38}BCl_2N_4P_2Ru$ (832.68): calcd. C 60.58, H 4.60, N 6.73; found C 60.46, H 4.54, N 6.65.

Preparation of [Ru(C≡C−Ph)(Tp)(PPh$_3$)$_2$] (2): An excess of phenylacetylene (4.17 mL, 36.1 mmol) and NEt_3 (6.3 mL, 36.1 mmol) were added to 50 mL of an MeOH solution of **1** (3.00 g, 3.61 mmol), and the solution was heated to reflux for 90 min. The yellow precipitate thus formed was filtered off and washed with MeOH and hexane. The product was dried under vacuum and was subsequently identified as compound **2** (3.43 g, 97% yield). Yellow crystals of **2** were obtained by slow diffusion of hexane into a $CHCl_3$ solution of **2** at room temperature. ^{1}H NMR ($CDCl_3$): δ = 5.20 (d, $J_{H,H}$ = 1.8 Hz, 1 H, Tp), 5.31 (t, $J_{H,H}$ = 2.1 Hz, 1 H, Tp), 5.54 (t, $J_{H,H}$ = 2.3 Hz, 2 H, Tp), 7.24−6.91 (m, Ph, Tp), 7.40 (d, $J_{H,H}$ = 2.0 Hz, 2 H, Tp), 7.58 (d, $J_{H,H}$ = 2.1 Hz, 1 H, Tp) ppm. ^{13}C NMR [$CD_3C(O)CD_3$]: δ = 122.7 (C-β), 135.8 (t, $J_{C,P}$ = 12.3 Hz, C-α), 145.7−127.2 (Ph, Tp) ppm. ^{31}P NMR ($CDCl_3$): δ = 48.6 ppm. MS (FAB): *m*/*z* = 940.1 [M^+], 678.1 [M^+ − PPh_3], 577.1 [M^+ − PPh_3 − C_2Ph], 363.0 [M^+ − PPh_3 − C_2Ph − Tp]. $C_{53}H_{44}BN_6P_2Ru$ (938.75): calcd. C 67.81, H 4.72, N 8.95; found C 67.94, H 4.59, N 8.91.

Synthesis of [Ru{=C=C(Ph)CH$_2$(CH=CH$_2$)}(Tp)(PPh$_3$)$_2$]I (3b): $ICH_2{=}CH_2$ (0.46 mL, 3.5 mmol) was added to a Schlenk flask charged with complex **2** (1.41 g, 1.50 mmol) in 50 mL of CH_2Cl_2. The clear solution was stirred for 16 h and then the volume of solvent was reduced to about 5 mL. This mixture was slowly added to 90 mL of vigorously stirred diethyl ether. The green precipitate thus formed was filtered off and washed with diethyl ether and hexane to give compound **3b** (1.33 g, 77%). ^{1}H NMR ($CDCl_3$): δ = 3.05 (d, $J_{H,H}$ = 5.5 Hz, 2 H, CH_2), 4.95 (dd, $J_{H,H}$ = 15.3, 2.7 Hz, 1 H, =CH), 5.05 (dd, $J_{H,H}$ = 10.3, 2.7 Hz, 1 H, =CH), 5.38 (d, $J_{H,H}$ = 1.9 Hz, 1 H, Tp), 5.53 (m, 1 H, CH=), 5.56 (t, $J_{H,H}$ = 1.9 Hz 1 H, Tp), 5.61 (t, $J_{H,H}$ = 2.1 Hz, 2 H, Tp), 6.59−7.42 (m, Ph), 7.57 (d, $J_{H,H}$ = 2.2 Hz, 2 H, Tp), 7.84 (d, $J_{H,H}$ = 1.9 Hz 1 H, Tp) ppm. ^{13}C NMR ($CDCl_3$): δ = 14.0 (CH_2), 105.8 (=CH_2), 118.4 (C-β), 105.9−146.2 (m, Ph, Tp), 153.8 (=CH), 377.5 (t, $J_{C,P}$ = 16.3 Hz, C-α) ppm. ^{31}P NMR ($CDCl_3$): δ = 37.8 ppm. MS (FAB): *m*/*z* = 981.3 [M^+ − I], 719.3 [M^+ − I − PPh_3], 577.1 [M^+ − I − PPh_3 − $C_2PhCH_2CH{=}CH_2$]. $C_{56}H_{50}BIN_6P_2Ru$ (1107.7): calcd. C 60.71, H 4.55, N 7.59; found C 60.62, H 4.43, N 7.63.

[Ru{=C=C(Ph)CH$_2$CH=C(Me)$_2$}(Tp)(PPh$_3$)$_2$]Br (3c): Yield 1.36 g, in 83%; prepared in a similar manner from 1.43 g (1.52 mmol) of **2** and excess $BrCH_2CH{=}C(Me)_2$ (3.7 mmol) at room temperature. ^{1}H NMR ($CDCl_3$): δ = 1.18 (s, 3 H, Me), 1.62 (s, 3 H, Me), 3.12 (d, $J_{H,H}$ = 5.1 Hz, 2 H, CH_2), 4.90 (m, 1 H, CH=), 5.42 (t, $J_{H,H}$ = 1.9 Hz, 1 H, Tp), 5.54 (t, $J_{H,H}$ = 2.2 Hz, 2 H, Tp), 6.41 (d, $J_{H,H}$ = 2.1 Hz, 1 H, Tp), 6.45 (d, $J_{H,H}$ = 2.0 Hz, 2 H, Tp), 6.96−7.42 (m, Ph) 7.66 (d, $J_{H,H}$ = 2.0 Hz, 2 H, Tp), 7.83 (d, $J_{H,H}$ = 2.1 Hz, 1 H, Tp) ppm. ^{13}C NMR ($CDCl_3$): δ = 18.1 (CH_2), 21.2 (Me), 25.6 (Me), 118.3 (C-β), 104.3−146.5 (Ph, Tp), 379.8 (t, $J_{C,P}$ = 15.8 Hz, C-α) ppm. ^{31}P NMR ($CDCl_3$): δ = 37.9 ppm. MS (FAB): *m*/*z* = 1009.3 [M^+ − Br], 747.3 [M^+ − Br − PPh_3], 577.1 [M^+ − Br − PPh_3 − $C_2PhCH_2CH{=}CMe_2$]. $C_{58}H_{54}BBrN_6P_2Ru$ (1088.8): calcd. C 63.98, H 5.00, N 7.72; found C 63.87, H 4.91, N 7.81.

[Ru{=C=C(Ph)CH$_2$Ph}(Tp)(PPh$_3$)$_2$]I (3d): Yield 1.45 g, in 87%; prepared in a similar manner from 1.50 g (1.59 mmol) of **2** and excess $BrCH_2Ph$ (0.40 mL, 3.0 mmol) at room temperature. ^{1}H NMR ($CDCl_3$): δ = 3.90 (s, 2 H, CH_2), 5.29 (br, 1 H, Tp), 5.34 (br, 1 H, Tp), 5.39 (br, 1 H, Tp), 5.54 (t, $J_{H,H}$ = 2.0 Hz, 2 H, Tp), 7.73−6.59 (m, Ph, Tp), 7.86 (d, $J_{H,H}$ = 2.1 Hz, 1 H, Tp) ppm. ^{13}C NMR ($CDCl_3$): δ = 16.0 (CH_2), 147.3−108.4 (Ph, Tp), 378.5 (t, $J_{C,P}$ = 15.8 Hz, C-α) ppm. ^{31}P NMR ($CDCl_3$): δ = 37.4 ppm. MS (FAB): *m*/*z* = 1031.4 [M^+ − Br], 769.5 [M^+ − Br − PPh_3], 577.1 [M^+ − Br − PPh_3 − C_2PhCH_2Ph]. $C_{60}H_{52}BBrN_6P_2Ru$ (1110.8): calcd. C 64.87, H 4.72, N 7.57; found C 64.91, H 4.67, N 7.41.

Preparation of [Tp(PPh$_3$)$_2$Ru=C=C(Ph)CH$_2$COOMe]Br (3e): A mixture of complex **2** (2.80 g, 3.10 mmol) and $BrCH_2COOMe$ (0.5 mL, 5.10 mmol) in 40 mL of CH_2Cl_2/CH_3Cl (3:1) was heated to reflux for 6 h. The workup procedure was the same as that for **3d**. Purification by recrystallization from CH_2Cl_2/hexane (1:5) gave **3e** (1.45 g, 87% yield). ^{1}H NMR ($CDCl_3$): δ = 3.10 (s, 2 H, CH_2), 3.59 (s, 3 H, OMe), 5.45 (br, 1 H, Tp), 5.53 (br, 1 H, Tp), 5.61 (br, 1 H, Tp), 5.77 (t, $J_{H,H}$ = 2.0 Hz, 2 H, Tp), 6.32 (br, 2 H, Tp), 7.57−6.59 (m, Ph, Tp), 7.65 (d, $J_{H,H}$ = 1.9 Hz, 2 H, Tp), 7.79 (d, $J_{H,H}$ = 2.0 Hz, 1 H, Tp) ppm. ^{13}C NMR ($CDCl_3$): δ = 19.1 (CH_2), 57.1 (CH_3), 106.4−145.6 (Ph, Tp), 171.4 (COO), 378.5 (t, $J_{C,P}$ = 15.6 Hz, C-α) ppm. ^{31}P NMR ($CDCl_3$): δ = 38.4 ppm. MS (FAB): *m*/*z* = 1013.3 [M^+ − Br], 751.2 [M^+ − Br − PPh_3], 577.4 [M^+ − Br − PPh_3 − C_2PhCH_2COOMe]. $C_{56}H_{50}BBrN_6O_2P_2Ru$ (1092.7): calcd. C 61.55, H 4.61, N 7.69; found C 61.61, H 4.51, N 7.82.

Synthesis of 5a: Complex **4a** (0.50 g, 0.51 mmol) was dissolved in CH_2Cl_2 (20 mL), and *n*BuNC (0.05 mL, 0.51 mmol) was added. The mixture was stirred for 50 min to afford a bright-yellow solution. The solvent was then removed under vacuum and the solid residue was extracted with 20 mL of diethyl ether. The extract was filtered through Celite, and the filtrate was dried to give a bright-yellow solid, which was washed with hexane (2 × 10 mL), and dried under vacuum to give a mixture of diastereoisomers of **5a** (0.327 g, 80.3% yield). ^{1}H NMR [$CD_3C(O)CD_3$]: major isomer: δ = 0.75 (t, $J_{H,H}$ = 7.5 Hz, 3 H, CH_3), 0.93 (s, 1 H, C*H*), 1.23 (m, 2 H, CH_2), 1.53 (m, 2 H, CH_2), 3.72 (t, $J_{H,H}$ = 6.6 Hz, 2 H, CH_2), 5.88 (t, $J_{H,H}$ = 2.2 Hz, 1 H, Tp), 5.96 (t, $J_{H,H}$ = 2.1 Hz, 1 H, Tp), 6.01 (t, $J_{H,H}$ = 1.8 Hz, 1 H, Tp), 6.76 (br, 1 H, Tp), 6.78 (br, 1 H, Tp), 6.86 (br, 1 H, Tp), 7.69 (d, $J_{H,H}$ = 2.0 Hz, 1 H, Tp), 7.07−7.40 (m, Ph), 7.81 (d, $J_{H,H}$ = 2.0 Hz, 1 H, Tp), 7.88 (d, $J_{H,H}$ = 2.1 Hz, 1 H, Tp) ppm; minor isomer: δ = 0.77 (t, $J_{H,H}$ = 7.4 Hz, 3 H, CH_3), 1.16 (s, 1 H, C*H*CN), 1.26 (m, 2 H, CH_2), 1.55 (m, 2 H, CH_2), 3.84 (t, $J_{H,H}$ = 6.7 Hz, 2 H, CH_2), 6.14 (t, $J_{H,H}$ = 2.2 Hz, 1 H, Tp), 6.21 (t, $J_{H,H}$ = 2.1 Hz, 1 H, Tp), 6.34 (t, $J_{H,H}$ = 2.0 Hz, 1 H, Tp), 6.76 (br, 1 H, Tp), 6.94 (br, 2 H, Tp), 7.40 −7.07 (m, Ph), 7.71 (d, $J_{H,H}$ = 2.1 Hz, 1 H, Tp), 7.92 (d, $J_{H,H}$ = 1.9 Hz, 1 H, Tp), 8.12 (d, $J_{H,H}$ = 2.0 Hz, 1 H, Tp) ppm. ^{13}C NMR [$CD_3C(O)CD_3$]: major isomer: δ = 3.8 (CH), 13.5 (*C*H_3), 20.2 (*C*H_2), 32.3 (*C*H_2), 44.8 (*C*H_2), 116.3 (CN), 128.7 (d, $J_{C,P}$ = 11.6 Hz, C-α), 146.9 −129.3 (Ph, Tp), 160.1 (d, $J_{C,P}$ = 22.5 Hz, *C*N) ppm; minor isomer: δ = 3.5 (CH), 13.5 (*C*H_3), 20.2 (*C*H_2), 32.2 (*C*H_2), 44.7 (*C*H_2), 115.2 (CN), 128.8 (d, $J_{C,P}$ = 11.6 Hz, C-α), 129.3−146.9 (Ph, Tp), 163.2 (d, $J_{C,P}$ = 21.3 Hz, *C*N) ppm. ^{31}P NMR [$CD_3C(O)CD_3$]: δ = 54.1, 52.7 (4:1) ppm. MS (FAB): *m*/*z* = 800.3 [M^+], 660.3 [M^+ − $C_2PhCHCN$], 577.2 [M^+ − $C_2PhCHCN$ − *n*BuNC]. $C_{42}H_{40}BN_8PRu$ (799.65): calcd. C 63.08, H 5.04, N 14.01; found C 62.98, H 4.96, N 13.89.

Synthesis of 5b: Complex **4a** (1.01 g, 1.03 mmol) was dissolved in CH_2Cl_2 (30 mL), and *t*BuNC (0.11 mL, 1.03 mmol) was added.

 © 2004 Wiley-VCH Verlag GmbH & Co. KGaA, Weinheim

The mixture was stirred at room temperature to afford a bright-yellow solution. The solvent was then removed under vacuum, and the solid residue was extracted with 20 mL of diethyl ether. The extract was filtered, and the filtrate was dried to give a bright-yellow solid, which was washed with hexane (2 × 10 mL) and dried under vacuum to give a diastereomeric mixture of **5b** (0.62 g, 79.1% yield). ^{1}H NMR [$CD_3C(O)CD_3$]: major isomer: δ = 0.96 (s, 1 H, C*H*), 1.47 (s, 9 H, Me), 5.81 (t, $J_{H,H}$ = 2.1 Hz, 1 H, Tp), 5.97 (t, $J_{H,H}$ = 2.1 Hz, 1 H, Tp), 6.11 (t, $J_{H,H}$ = 1.9 Hz, 1 H, Tp), 6.71 (br, 1 H, Tp), 6.74 (br, 1 H, Tp), 6.83 (br, 1 H, Tp), 7.46 −7.07 (m, Ph), 7.73 (d, $J_{H,H}$ = 2.1 Hz, 1 H, Tp), 7.80 (d, $J_{H,H}$ = 2.2 Hz, 1 H, Tp), 7.82 (d, $J_{H,H}$ = 2.0 Hz, 1 H, Tp) ppm; minor isomer: δ = 1.08 (s, 1 H, C*H*), 1.48 (s, 9 H, Me), 6.13 (t, $J_{H,H}$ = 2.1 Hz, 1 H, Tp), 6.20 (t, $J_{H,H}$ = 2.0 Hz, 1 H, Tp), 6.32 (t, $J_{H,H}$ = 2.2 Hz, 1 H, Tp), 6.72 (br, 1 H, Tp), 6.99 (br, 2 H, Tp), 7.42−7.17 (m, Ph), 7.67 (d, $J_{H,H}$ = 2.0 Hz, 1 H, Tp), 7.92 (d, $J_{H,H}$ = 2.1 Hz, 1 H, Tp),8.11 (d, $J_{H,H}$ = 2.0 Hz, 1 H, Tp) ppm. ^{13}C NMR [$CD_3C(O)CD_3$]: major isomer: δ = 3.8 (CH), 32.1 (C*Me*$_3$), 58.7 (*C*Me$_3$), 119.2 (CN), 126.5 (d, $J_{C,P}$ = 12.1 Hz, C-α), 141.9 −129.3 (Ph, Tp), 163.4 (d, $J_{C,P}$ = 21.4 Hz, *C*N) ppm; minor isomer: δ = 3.5 (CH), 31.2 (*Me*$_3$), 55.3 (*C*Me$_3$), 118.9 (CN), 127.1 (d, $J_{C,P}$ = 11.2 Hz, C-α), 129.3−146.9 (Ph, Tp), 164.1 (d, $J_{C,P}$ = 20.1 Hz, *C*N) ppm. ^{31}P NMR [$CD_3C(O)CD_3$]: δ = 52.9, 53.9 (4:1) ppm. MS (FAB): *m*/*z* = 801.1 [M$^+$ + 1], 660.3 [M$^+$ − C_2PhCHCN], 577.2 [M$^+$ − C_2PhCHCN − *t*BuNC]. $C_{42}H_{40}BN_8PRu$ (799.65): calcd. C 63.08, H 5.04, N 14.01; found C 63.12, H 5.10, N 13.97.

Synthesis of 5c: An excess of PhCN (0.21 mL, 2.02 mmol) was added to a solution of **4a** (1.00 g, 1.02 mmol) in 20 mL of CH_2Cl_2. The solution was stirred at room temperature (the color changed from yellow to brown) and then the solvent was removed under vacuum. The solid residue was extracted with diethyl ether, and the extract was filtered. The volume of the resulting solution was reduced to 5 mL and 40 mL of hexane was added to form an orange precipitate, which was filtered and washed twice with 10 mL of hexane. The product was dried under vacuum (0.60 g, 72% yield). ^{1}H NMR [$CD_3C(O)CD_3$]: major isomer: δ = 1.13 (s, 1 H, C*H*CN), 5.90 (t, $J_{H,H}$ = 2.0 Hz, 1 H, Tp), 6.02 (t, $J_{H,H}$ = 2.1 Hz, 1 H, Tp), 6.06 (br, 1 H, Tp), 6.78 (br, 1 H, Tp), 6.97 (br, 1 H, Tp), 7.69−7.03 (m, Ph),7.91 (d, $J_{H,H}$ = 2.2 Hz, 2 H, Tp) ppm; minor isomer: δ = 0.79 (s, 1 H, C*H*), 5.92 (t, $J_{H,H}$ = 2.1 Hz, 1 H, Tp), 6.01 (t, $J_{H,H}$ = 1.9 Hz, 1 H, Tp), 6.05 (d, $J_{H,H}$ = 2.0 Hz, 2 H, Tp), 6.43 (d, $J_{H,H}$ = 1.9 Hz, 2 H, Tp), 6.96 (d, $J_{H,H}$ = 2.1 Hz, 2 H, Tp), 7.64 −7.01 (m, Ph), 7.93 (d, $J_{H,H}$ = 2.0 Hz, 2 H, Tp) ppm. ^{13}C NMR [$CD_3C(O)CD_3$] major isomer: δ = 4.1 (CH), 116.1 (NCPh), 119.2 (CN), 132.6 (d, $J_{C,P}$ = 12.3 Hz, C-α), 147.9 −123.1 (Ph, Tp) ppm. ^{31}P NMR [$CD_3C(O)CD_3$]: δ = 54.5, 54.8 (4:1) ppm. MS (FAB): *m*/*z* = 821.4 [M$^+$ + 1], 718.4 [M$^+$ + 1 − PhCN], 577.1 [M$^+$ + 1 − PhCN − C_2PhCHCN]. $C_{44}H_{36}BN_8PRu$ (819.64): calcd. C 64.47, H 4.43, N 13.69; found C 64.49, H 4.44, N 13.63.

Synthesis of 5d: An excess of $CF_3C_6H_4CN$ (0.14 mL, 2.04 mmol) was added to a solution of **4a** (1.00 g, 1.02 mmol) in 20 mL of CH_2Cl_2. The solution was stirred for 50 min (the color changed from yellow to brown) and then the solvent was removed under vacuum. The solid residue was extracted with diethyl ether, and the extract was filtered. The volume of the resulting solution was reduced to 5 mL and 40 mL of hexane was added to form a orange precipitate, which was filtered and washed twice with 10 mL of hexane. The product was dried under vacuum (0.70 g, 77% yield). ^{1}H NMR [$CD_3C(O)CD_3$] major isomer: δ = 1.08 (s, 1 H, C*H*), 5.85 (t, $J_{H,H}$ = 2.2 Hz, 1 H, Tp), 5.98 (t, $J_{H,H}$ = 2.1 Hz, 1 H, Tp), 6.02 (t, $J_{H,H}$ = 1.8 Hz, 1 H, Tp), 6.76 (br, 1 H, Tp), 6.78 (br, 1 H, Tp), 6.86 (br, 1 H, Tp), 7.07−7.40 (m, Ph), 7.69 (d, $J_{H,H}$ = 2.0 Hz, 1 H, Tp), 7.81 (d, $J_{H,H}$ = 2.2 Hz, 1 H, Tp), 7.85 (d, $J_{H,H}$ = 2.2 Hz, 1 H, Tp) ppm; minor isomer: δ = 0.82 (s, 1 H, C*H*), 5.91 (t, $J_{H,H}$ = 2.0 Hz, 1 H, Tp), 6.05 (t, $J_{H,H}$ = 1.9 Hz, 1 H, Tp), 6.07 (d, $J_{H,H}$ = 2.1 Hz, 2 H, Tp), 6.46 (d, $J_{H,H}$ = 2.0 Hz, 2 H, Tp), 6.89 (d, $J_{H,H}$ = 2.0 Hz, 2 H, Tp), 7.01−7.64 (m, Ph), 7.97 (d, $J_{H,H}$ = 2.1 Hz, 2 H, Tp) ppm. ^{13}C NMR [$CD_3C(O)CD_3$]: major isomer: δ = 5.1 (CH), 110.6 (q, $J_{C,F}$ = 282.0 Hz, *C*F$_3$), 111.2 (NCPh), 118.1 (CN), 131.7 (d, $J_{C,P}$ = 11.9 Hz, C-α), 148.2−126.6 (Ph, Tp) ppm. ^{31}P NMR [$CD_3C(O)CD_3$]: δ = 53.6, 54.3 (4:1) ppm. MS (FAB): *m*/*z* = 888.4 [M$^+$ + 1], 718.4 [M$^+$ + 1 − $CF_3C_6H_4CN$], 577.1 [M$^+$ + 1 − $CF_3C_6H_4CN$ − C_2PhCHCN]. $C_{45}H_{35}BF_3N_8PRu$ (887.63): calcd. C 60.88, H 3.97, N 12.62; found C 60.78, H 4.08, N 12.51.

Synthesis of [Ru{=C=C(Ph)CH(I)CN}(Tp)(PPh$_3$)$_2$]I (6): CH_2Cl_2 (30 mL) was added to a solid mixture of **4a** (0.51 g, 0.52 mmol) and I_2 (0.13 g, 0.52 mmol) at 0 °C. The mixture was stirred for 2 min whereupon the color changed from yellow to green; the solvent was then removed under vacuum. The residual solid was extracted twice with 20 mL of diethyl ether and, after filtration, the solvent was removed under vacuum to give complex **6** (0.45 g, 69% yield). ^{1}H NMR [$CD_3C(O)CD_3$]: δ = 3.23 (s, 1 H, C*H*), 5.43 (t, $J_{H,H}$ = 2.1 Hz, 1 H, Tp), 5.55 (t, $J_{H,H}$ = 2.0 Hz, 1 H, Tp), 5.76 (d, $J_{H,H}$ = 2.0 Hz, 1 H, Tp), 5.65 (d, $J_{H,H}$ = 2.1 Hz, 1 H, Tp), 6.79 (d, $J_{H,H}$ = 1.9 Hz 1 H, Tp), 7.56−7.11 (m, Tp, Ph), 7.73 (m, 2 H, Tp), 7.98 (d, $J_{H,H}$ = 2.1 Hz, 1 H, Tp) ppm. ^{13}C NMR ($CDCl_3$): δ = 26.1 (CH), 119.4 (CN), 106.8−147.2 (Ph, Tp, C-β), 374.5 (t, $J_{C,P}$ = 15.1 Hz, C-α) ppm. ^{31}P NMR [$CD_3C(O)CD_3$]: δ = 33.6, 34.3 (AB, $J_{P,P}$ = 26.9 Hz) ppm. MS (FAB): *m*/*z* = 1107.1 [M$^+$ − I], 980.3 [M$^+$ − 2I], 839.2 [M$^+$ − 2 I − C_2PhCHCN], 577.1 [M$^+$ − 2 I − C_2PhCHCN − PPh_3]. $C_{55}H_{47}BI_2N_7P_2Ru$ (1233.6): calcd. C 53.55, H 3.84, N 7.95; found C 53.46, H 4.01, N 8.03.

Synthesis of [Ru{=C=C(Ph)CH(I)CN}(Tp)(PPh$_3$)(*n*BuNC)]I (7): CH_2Cl_2 (30 mL) was added to a solid mixture of **5a** (0.17 g, 0.21 mmol) and I_2 (0.054 g, 0.17 mmol). The mixture was stirred for 5 min and the solvent was then removed under vacuum. The residual solid was extracted twice with 20 mL of diethyl ether and, after filtration, the solvent was removed under vacuum to give **7** (0.14 g, 78% yield). ^{1}H NMR [$CD_3C(O)CD_3$]: δ = 0.73 (t, $J_{H,H}$ = 7.4 Hz, 3 H, CH_3), 1.03 (m, 2 H, C*H*$_2$), 1.94 (m, 2 H, C*H*$_2$), 3.46 (t, $J_{H,H}$ = 6.2 Hz, 2 H, C*H*$_2$), 3.56 (s, 1 H, C*H*), 5.96 (t, $J_{H,H}$ = 2.3 Hz, 1 H, Tp), 6.10 (t, $J_{H,H}$ = 2.1 Hz, 1 H, Tp), 6.36 (d, $J_{H,H}$ = 2.1 Hz, 1 H, Tp), 6.43 (d, $J_{H,H}$ = 2.1 Hz, 1 H, Tp), 7.39−7.01 (m, Tp, Ph), 7.67 (d, $J_{H,H}$ = 2.1 Hz, 1 H, Tp), 7.69 (d, $J_{H,H}$ = 2.3 Hz, 1 H, Tp), 7.75 (d, $J_{H,H}$ = 2.1 Hz, 1 H, Tp) ppm. ^{13}C NMR [$CD_3C(O)CD_3$]: δ = 14.2 (*C*H$_3$), 20.0 (*C*H$_2$), 25.4 (CH), 35.2 (*C*H$_2$), 44.1 (*C*H$_2$), 126.3 (CN), 108.4−148.9 (Ph, Tp), 167.2 (d, $J_{C,P}$ = 22.9 Hz, *C*N), 367.3 (d, $J_{C,P}$ = 16.4 Hz, C-α) ppm. ^{31}P NMR [$CD_3C(O)CD_3$]: δ = 45.9 ppm. MS (FAB): *m*/*z* = 926.3 [M$^+$ − I], 800.1 [M$^+$ − 2 I], 660.2 [M$^+$ − 2 I − C_2PhCHCN], 577.2 [M$^+$ − 2 I − C_2PhCHCN − *n*BuNC]. $C_{42}H_{40}BI_2N_8PRu$ (1053.5): calcd. C 47.88, H 3.83, N 10.64; found C 47.81, H 4.02, N 10.70.

Synthesis of [Ru{C(OMe)=C(Ph)CH$_2$CN}(Tp)(PPh$_3$)(*n*BuNC)] (8a): A solution of **4a** (1.50 g, 1.53 mmol) was dissolved in methanol and *n*BuNC (0.30 mL, 3.06 mmol) was added. After stirring for 10 min, the yellow solution became bright yellow. The solution was filtered through Celite and the solvent was removed under vacuum to give **8a** (1.01 g, 85% yield). ^{1}H NMR [$CD_3C(O)CD_3$]: δ = 0.70 (t, $J_{H,H}$ = 7.5 Hz, 3 H, CH_3), 0.86 (m, 2 H, C*H*$_2$), 1.88 (m, 2 H, C*H*$_2$), 2.79 (d, $J_{H,H}$ = 16.4 Hz, 1 H, C*H*), 3.63 (t, $J_{H,H}$ = 6.4 Hz, 2 H, C*H*$_2$), 3.86 (d, $J_{H,H}$ = 16.4 Hz, 1 H, CH*H*), 5.63 (t, $J_{H,H}$ = 1.8 Hz, 1 H, Tp), 6.05 (br, 1 H, Tp), 6.11 (br, 1 H, Tp), 7.00 (br, 1 H, Tp), 7.60−7.02 (m, Ph, Tp), 7.81 (d, $J_{H,H}$ = 2.0 Hz, 1 H, Tp) ppm. ^{13}C NMR [$CD_3C(O)CD_3$]: δ = 13.5 (*C*H$_3$), 21.1 (*C*H$_2$), 22.4

 © 2004 Wiley-VCH Verlag GmbH & Co. KGaA, Weinheim

(CH_2), 31.1 (CH_2), 43.1 (CH_2), 55.4 (OMe), 115.5 (CN), 123.4−147.6 (Ph), 162.1 (d, $J_{C,P}$ = 23.1 Hz, *C*N),179.1 (d, $J_{C,P}$ = 15.3 Hz, C-α) ppm. ^{31}P NMR [$CD_3C(O)CD_3$]: δ = 46.9 ppm. MS (FAB): *m*/*z* = 832.3 [M^+], 660.1 [M^+ − (OMe)C=C(Ph)(CH_2CN)], 577.1 [M^+ − (OMe)C=C(Ph)(CH_2CN) − *n*BuNC]. $C_{43}H_{44}BN_8OPRu$ (831.69): calcd. C 62.08, H 5.33, N 13.47; found C 62.16, H 5.40, N 13.35.

Synthesis of [Ru{C(OMe)=C(Ph)CH_2CN}Tp(PPh_3)(*t*BuNC)] (8b): Complex **4a** (0.5 g, 0.51 mmol) was dissolved in CH_3OH (20 mL), and *t*BuNC (0.30 mL, 3.02 mmol) was added. The mixture was stirred for 50 min to afford a bright-yellow solution. The solvent was then removed under vacuum and the solid residue was extracted with diethyl ether. The extract was filtered, and the filtrate was dried under vacuum to give a bright-yellow solid, which was washed with hexane (2 × 10 mL), and dried to give **8b** (0.327 g, 80.3% yield). ^1H NMR [$CD_3C(O)CD_3$]: δ = 1.44 (s, 9 H, C*Me*$_3$), 2.84, 3.87 (2d, $J_{H,H}$ = 15.3 Hz, 1 H, CH_2CN), 5.61 (br, 1 H, Tp), 6.15 (br, 1 H, Tp), 6.21 (br, 1 H, Tp), 6.43 (br, 1 H, Tp), 6.96−7.56 (m, Ph, Tp), 7.78 (d, $J_{H,H}$ = 2.2 Hz, 1 H, Tp) ppm. ^{13}C NMR [$CD_3C(O)CD_3$]: δ = 32.7 (C*Me*$_3$), 55.4 (OMe), 113.2 (CN), 123.4−147.6 (Ph), 182.2 (d, $J_{C,P}$ = 16.1 Hz, C-α) ppm. ^{31}P NMR [$CD_3C(O)CD_3$]: δ = 46.8 ppm. MS (FAB): *m*/*z* = 832.2 [M^+], 660.1 [M^+ − (OMe)C=C(Ph)(CH_2CN)], 577.1 [M^+ − (OMe)C=C(Ph)(CH_2CN) − *t*BuNC]. $C_{43}H_{44}BN_8OPRu$ (831.69): calcd. C 62.08, H 5.33, N 13.47; found C 62.11, H 5.34, N 13.51.

X-ray Diffraction Analysis: Dark-yellow crystals of **1** suitable for an X-ray diffraction study were grown directly from CH_2Cl_2. A suitable single crystal of dimensions 0.10 × 0.40 × 0.50 mm was glued to a glass fiber and mounted on a Nonius CD4 diffractometer. The data were collected using Mo-K_α radiation (at 298 K). The data were processed and the structure was solved and refined with the SHELXTL program. The structure was solved by direct methods and confirmed by Patterson methods. Hydrogen atoms were placed geometrically using the riding model with thermal parameters set to 1.2-times that of the atom to which they are attached (1.5-times for the methyl hydrogen atoms). Yellow crystals of **2** suitable for an X-ray diffraction study were obtained as above. A suitable single crystal of dimensions 0.05 × 0.10 × 0.15 mm was mounted on a SMART CCD diffractometer. The data were collected using 3-kW sealed-tube Mo-K_α radiation (at 298 K). The exposure time was 5 s per frame. SADABS (Siemens area detector absorption) absorption correction was applied, and decay was negligible. Data were processed with the SHELXTL program.[21] The structure was solved by direct methods refining on intensities of all data. Hydrogen atoms were placed geometrically using the riding model. Crystal data for **1** and **2** are listed in Table 1.

Table 1. Crystal data and structure refinement for **1** and **2**

	1	**2**
Empirical formula	$C_{42}H_{38}Cl_2N_4P_2Ru$ CH_2Cl_2	$C_{53}H_{45}BN_6P_2Ru$
Formula mass	917.64	939.77
T [K]	295(2)	296(2)
Crystal system	triclinic	triclinic
Space group	$P\bar{1}$	$P\bar{1}$
a [Å]	9.827(3)	10.277(2)
b [Å]	13.163(3)	11.930(3)
c [Å]	17.0307(20)	20.164(6)
α [°]	81.404(13)	93.57(2)
β [°]	78.311(16)	99.82(2)
γ [°]	78.289(19)	111.54(2)
V [Å^3]	2098.9(7)	2244.6(10)
Z	2	2
ρ(calcd.) [Mg/m^3]	1.452	1.390
F(000)	935	968
GOF	1.50	0.929
*R*1, *wR*2 [$I > 2\sigma(I)$][a]	0.048, 0.042	0.0491, 0.1195
(all data)	0.0888, 0.1417	0.0830, 0.1480

[a] $R1 = \Sigma||F_o| - |F_c||/\Sigma|F_o|$; $wR2 = [\Sigma w(F_o^2 - F_c^2)^2/\Sigma w(F_o^2)^2]^{1/2}$.

Acknowledgments

We thank the National Science Council of Taiwan for financial support.

[1] [1a] S. Trofimenko, *Chem. Rev.* **1993**, *93*, 943. [1b] N. Kitajima, W. B. Tolman, *Prog. Inorg. Chem.* **1995**, *43*, 419. [1c] C. Slugovc, R. Schmid, K. Kirchner, *Coord. Chem. Rev.* **1999**, *185/186*, 109. [1d] S. Hikichi, M. Akita, Y. Moro-oka, *Coord. Chem. Rev.* **2000**, *198*, 61. [1e] N. Marques, A. Sella, J. Takats, *Chem. Rev.* **2002**, *102*, 2137.

[2] M. D. Curtis, K. B. Shiu, W. M. Butler, *Organometallics* **1983**, *2*, 1475.

[3] [3a] Y. Fukumoto, H. Masaoka, T. Dohi, N. Chatani, S. Murai, *Organometallics* **2002**, *21*, 19. [3b] Y. Wang, M. G. Finn, *J. Am. Chem. Soc.* **1995**, *117*, 8045. [3c] C. Bruneau, P. H. Dixneuf, *Chem. Commun.* **1997**, 507. [3d] M. I. Bruce, *Chem. Rev.* **1991**, *91*, 197. [3e] B. M. Trost, *Angew. Chem.* **1995**, *107*, 285; *Angew. Chem. Int. Ed. Engl.* **1995**, *34*, 259. [3f] C. Bianchini, M. Peruzzini, A. Romerosa, F. Zanobini, *Organometallics* **1995**, *14*, 3152. [3g] C. Bianchini, P. Innocenti, M. Peruzzini, A. Romerosa, F. Zanobini, *Organometallics* **1996**, *15*, 272. [3h] H. Werner, R. Wiedmann, P. Steinert, J. Wolf, *Chem. Eur. J.* **1997**, *3*, 127. [3i] B. M. Trost, J. A. Flygare, *J. Am. Chem. Soc.* **1992**, *114*, 5476. [3j] B. M. Trost, G. Dyker, R. Kulawiec, *J. Am. Chem. Soc.* **1990**, *112*, 7809.

[4] [4a] C. A. Meric, M. E. Pauly, *J. Am. Chem. Soc.* **1996**, *118*, 11319. [4b] Y. Wakatsuki, H. Yamazaki, N. Kumegawa, T. Satoh, J. Y. Satoh, *J. Am. Chem. Soc.* **1991**, *113*, 9604. [4c] B. M. Trost, G. Dyker, R. Kulawiec, *J. Am. Chem. Soc.* **1992**, *114*, 5476.

[5] [5a] M. I. Bruce, A. G. Swincer, R. C. Wallis, *J. Organomet. Chem.* **1979**, *171*, C5. [5b] C. Bianchini, J. A. Casares, M. Peruzzini, A. Romerosa, F. Zanobini, *J. Am. Chem. Soc.* **1996**, *118*, 4585.

[6] [6a] P. C. Ting, Y. C. Lin, G. H. Lee, M. C. Cheng, Y. Wang, *J. Am. Chem. Soc.* **1996**, *118*, 6433. [6b] Y. H. Lo, Y. C. Lin, G. H. Lee, Y. Wang, *Organometallics* **1999**, *18*, 982. [6c] Y. C. Lin, *J. Organomet. Chem.* **2001**, 617−618, 141. [6d] C. C. Huang, Y. C. Lin, S. L. Huang, Y. H. Liu, Y. Wang, *Organometallics* **2003**, *22*, 1512.

[7] [7a] G. M. Barreett, N. E. Carpenter, *Organometallics* **1987**, *6*, 2249. [7b] P. Normbel, N. Lugan, R. Mathieu, *J. Organomet. Chem.* **1995**, *503*, C22.

[8] D. R. Senn, A. Wong, A. T. Patton, M. Marsi, C. E. Strouse, J. A Gladysz, *J. Am. Chem. Soc.* **1988**, *110*, 6096.

[9] [9a] Special issue on strained organic compounds: *Chem. Rev.* **1989**, *89*. [9b] J. F. Liebman, A. Greenberg, *Strained Organic Molecules*, Wiley, New York, **1978**, p. 91.

[10] [10a] J. F. Liebman, A. Greenberg, *Chem. Rev.* **1976**, *76*, 311. [10b] B. Halton, M. G. Banwell, in *The Chemistry of the Cyclopropnyl group, Part 2* (Eds.: S. Patai, Z. Rappoport), Wiley, Chichester, **1987**, chapter 21, p. 1223.

[11] [11a] R. Gompper, E. Bartmann, *Angew. Chem. Int. Ed. Engl.* **1978**, *17*, 456. [11b] D. M. Desimone, P. J. Desrosiers, R. P.

 © 2004 Wiley-VCH Verlag GmbH & Co. KGaA, Weinheim

Hughes, *J. Am. Chem. Soc.* **1982**, *104*, 4842. [11c] R. P. Hughes, W. A. Donaldson, *J. Am. Chem. Soc.* **1982**, *104*, 4846.
[12] R. Gompper, E. Bartmann, *Angew. Chem. Int. Ed. Engl.* **1985**, *24*, 209.
[13] [13a] U. Kirchassner, H. Piana, U. Schubert, *J. Am. Chem. Soc.* **1991**, *113*, 228. [13b] S. Miki, T. Ohno, H. Iwasaki, Z-I. Yoshida, *J. Phys. Org. Chem.* **1998**, *1*, 333.
[14] [14a] R. R. Schrock, *Acc. Chem. Res.* **1986**, *19*, 342. [14b] R. P. Hughes, W. J. Reisch, A. L. Rheingold, *Organometallics* **1985**, *4*, 1754. [14c] C. Mealli, S. Midollini, S. Moneti, L. Sacconi, J. Silvestre, T. A. Albright, *J. Am. Chem. Soc.* **1982**, *104*, 59.
[15] T. Khan, N. H. Khan, R. I. Kureshy, K. Venkatasubramanian, *Polyhedron* **1992**, *4*, 431.
[16] [16a] S. Trofimenko, *Prog. Inorg. Chem.* **1986**, *34*, 115. [16b] J. P. Steel, *Coord. Chem. Rev.* **1990**, *106*, 227. [16c] J. E. Cosgriff, G. B. Deacon, *Angew. Chem. Int. Ed.* **1998**, *37*, 286. [16d] G. B. Deacon, E. E. Delbridge, B. W. Skelton, A. H. White, *Angew. Chem. Int. Ed.* **1998**, *37*, 2251.
[17] [17a] G. López, J. Ruiz, C. Vicent, J. M. Martí, G. García, P. A. Chaloner, P. B. Hitchcock, R. M. Harrison, *Organometallics* **1992**, *11*, 4090. [17b] M. P. García, M. A. Esteruelas, M. Martín, L. A. Oro, *J. Organomet. Chem.* **1994**, *467*, 151. [17c] M. Cano, J. A. Campo, J. V. Heras, J. Lafuente, C. Rivas, E. Pinilla, *Polyhedron* **1995**, *14*, 1139.
[18] [18a] J. A. Cowan, *Inorganic Biochemistry, An Introduction*, VCH, New York, **1993**. [18b]N. Kitajama, W. Tolman, *Prog. Inorg. Chem.* **1995**, *43*, 419. [18c] B. Govind, T. Satyanarayana, K. Veera-Reddy, *Polyhedron* **1995**, *15*, 1009.
[19] [19a] D. L. Allen, V. C. Gison, M. L. Green, T. F. Skinner, J. Bashikin, P. D. Grebenik, *J. Chem. Soc., Chem. Commum.* **1985**, 895. [19b] G. Consiglio, F. Morandini, *Chem. Rev.* **1987**, *87*, 761.
[20] T. A. Stephenson, G. Wilkinson, *J. Inorg. Nucl. Chem.* **1996**, *28*, 945.
[21] G. M. Sheldrick, *SHELXTL PLUS User's Manual*, revision 4.1, Nicolet XRD Corporation, Madison, WI, **1991**.

Received June 3, 2004
Early View Article
Published Online October 7, 2004

 © 2004 Wiley-VCH Verlag GmbH & Co. KGaA, Weinheim

A Comparison of Analogous 4f- and 5f-Element Compounds: Syntheses, X-ray Crystal Structures and Catalytic Activity of the Homoleptic Amidinate Complexes [M{MeC(NCy)$_2$}$_3$] (M = La, Nd or U)

Claude Villiers,*[a] Pierre Thuéry,[a] and Michel Ephritikhine*[a]

Keywords: ε-Caprolactone / Lanthanides / N ligands / Polymerization / Uranium

Reaction of UCl_4 with [Li{RC(NCy)$_2$}(THF)]$_2$ (R = Me, **1a**; R = *n*Bu, **1b**) in THF gave the tris(amidinate) compounds [U{RC(NCy)$_2$}$_3$Cl] (R = Me, **2a**; R = *n*Bu, **2b**) which were reduced with lithium powder in THF to the homoleptic complexes [U{RC(NCy)$_2$}$_3$] (R = Me, **3a**; R = *n*Bu, **3b**). Complexes **1a**, **1b**, **2a** and **3a** have been crystallographically characterized. Comparison of the crystal structure of **3a** with those of the lanthanide analogues [Ln{MeC(NCy)$_2$}$_3$] (Ln = La, **4**; Ln = Nd, **5**; Ln = Yb, **6**) shows that the average U–N distance is shorter than expected from a purely ionic bonding model. The uranium complex **3a** is much less efficient than its lanthanide counterparts in the catalytic polymerization of ε-caprolactone because of its rapid oxidation into U^{IV} species.

(© Wiley-VCH Verlag GmbH & Co. KGaA, 69451 Weinheim, Germany, 2004)

Introduction

Amidinate complexes of main group and d-block transition metals are currently receiving a great deal of interest, especially for use in the catalytic polymerization of alkenes and lactides.[1] Homoleptic metal amidinates were also recently found to be useful precursors for atomic layer deposition of thin films.[2] A major advantage of the bidentate [RC{NR′}$_2$]$^-$ anions, which are considered as alternatives to the ubiquitous cyclopentadienyl-based ligands, is the easy modification of both their steric bulk and electronic properties through changes to the R and R′ substituents. In this context, special attention has been paid during the last decade to the bis(benzamidinate) complexes of group 3 metals and lanthanides as they exhibit catalytic activities similar to those of the corresponding metallocenes.[3] More recently, homoleptic tris(amidinate) lanthanide complexes have proved to be efficient catalysts for the ring-opening polymerization of ε-caprolactone.[4]

The amidinate ligand was introduced into 5f-element chemistry by Edelmann et al. who synthesized a series of bis- and tris(benzamidinate) compounds of thorium(IV) and uranium(IV), [M{ArC(NSiMe$_3$)$_2$}$_3$Cl] and [M{ArC(NSiMe$_3$)$_2$}$_2$Cl$_2$] (M = Th, U) and their derivatives,[5] the uranium(V) complex [U{(C$_6$H$_4$Me)C(NSiMe$_3$)$_2$}$_2$Cl$_3$][6] and the uranyl compound [UO$_2$\{PhC(NSiMe$_3$)$_2$\}$_2$].[7] Another complex, [{UCl(μ-Cl)(L)(NSiMe$_3$)}$_2$][UCl$_2$(L)(L′)]$_2$, in which L is a β-diketiminate and L′ a benzamidinate ligand, can be considered either as a [{U^{VI}}$_2$][U^{III}]$_2$ or a [{U^{IV}}$_2$][U^{V}]$_2$ mixed-valence salt.[8] Here we report on the first well-characterized uranium(III) amidinate complexes, [U{RC(NCy)$_2$}$_3$] (R = Me, *n*Bu), which were prepared by reduction of the chloride precursors [U{RC(NCy)$_2$}$_3$Cl]. We describe the crystal structures of these U^{III} and U^{IV} compounds, as well as those of the lithium amidinates [Li{RC(NCy)$_2$}(THF)]$_2$, and finally we present the activity of the homoleptic complexes in ε-caprolactone polymerization, and we compare the structural features and catalytic properties of [U{MeC(NCy)$_2$}$_3$] with those of the lanthanide analogues.

Results and Discussion

The Lithium Amidinate Complexes [Li{RC(NCy)$_2$}(THF)]$_2$ (R = Me, *n*Bu)

Addition of MeLi or *n*BuLi to *N*,*N*′-dicyclohexylcarbodiimide in THF, according to Equation (1), led to the formation of the lithium amidinates [Li{RC(NCy)$_2$}(THF)]$_2$ (R = Me, **1a**; R = *n*Bu, **1b**) which were isolated as colorless crystals in almost quantitative yield.

$$\text{Cy–N=C=N–Cy} + \text{RLi} \xrightarrow{\text{THF}} 0.5\,[\text{Li}\{\text{RC(NCy)}_2\}(\text{THF})]_2 \quad \text{R = Me, 1a; R = } n\text{Bu, 1b} \tag{1}$$

The two compounds were characterized by ^{1}H NMR spectroscopy (Table 1) and an X-ray crystal structure. A

[a] Service de Chimie Moléculaire, DSM, DRECAM, CNRS, URA 331, CEA-Saclay,
91191 Gif-sur-Yvette, France
E-mail: villiers@drecam.cea.fr
ephri@drecam.cea.fr

 © 2004 Wiley-VCH Verlag GmbH & Co. KGaA, Weinheim DOI: 10.1002/ejic.200400491

Table 1. ^{1}H NMR spectra of the amidinate complexes[a]

Compound	R group (Me or *n*Bu)	Cyclohexyl group
[Li{MeC(NCy)$_2$}(THF)]$_2$ (**1a**)	2.89 (s, 3 H)	1.47−1.07 (m, 22 H)
[Li{*n*BuC(NCy)$_2$}(THF)]$_2$ (**1b**)	2.91, 2.15 and 1.47 (m, 3 × 2 H), 0.82 (t, 3 H)	1.56−1.08 (m, 22 H)
[U{MeC(NCy)$_2$}$_3$Cl] (**2a**)	3.32 (3 H)	1.47−1.07 (m, 16 H), −0.51 (m, 2 H), −2.6 (br., $w_{1/2}$ = 250 Hz, 4 H)
[U{*n*BuC(NCy)$_2$}$_3$Cl] (**2b**)	5.69, 4.19 and 2.72 (m, 3 × 2 H), 1.70 (t, 3 H)	1.50−1.00 (m, 16 H), −0.50 (m, 2 H), −2.0 (br., $w_{1/2}$ = 300 Hz, 4 H)
[U{MeC(NCy)$_2$}$_3$] (**3a**)	11.79 (3 H)	25.10 (2 H), −0.82 (6 H), −1.29 (4 H), −2.22 (4 H), −3.61 (2 H), −11.20 (4 H)
[U{*n*BuC(NCy)$_2$}$_3$] (**3b**)	14.82, 8.00 and 4.90 (m, 3 × 2 H), 2.98 (t, 3 H)	27.48 (2 H), 0.80 (6 H), 0.90 (4 H), −1.17 (4 H), −4.50 (2 H), −12.50 (4 H)
[La{MeC(NCy)$_2$}$_3$] (**4**)	3.22 (3 H)	2.12−1.24 (m, 22 H)
[Nd{MeC(NCy)$_2$}$_3$] (**5**)	12.64 (3 H)	20.25 (2 H), 0.31 (6 H), −0.38 (4 H), −1.26 (4 H), −3.22 (2 H), −10.93 (4 H)

[a] At 23 °C in [D$_8$]THF; when not specified, the signals are singlets with a half-height width between 10 and 50 Hz.

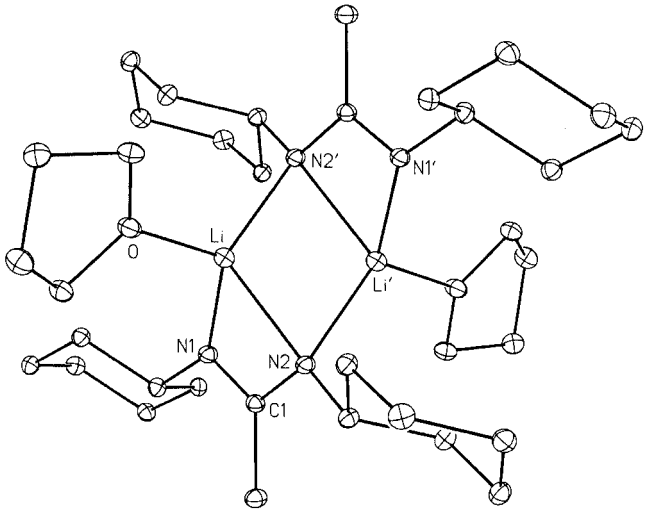

Figure 1. View of the complex [Li{MeC(NCy)$_2$}(THF)]$_2$ (**1a**) with displacement ellipsoids drawn at the 20% probability level; hydrogen atoms have been omitted for clarity; primed atoms are related to the unprimed ones by the symmetry centre

Table 2. Selected distances [Å] and angles [°] in the lithium amidinate complexes

	[Li{MeC(NCy)$_2$}(THF)]$_2$ (**1a**)	[Li{*n*BuC(NCy)$_2$}(THF)]$_2$ (**1b**)[a]
Li−N(1)	2.008(3)	1.987(6); 1.992(8)
Li−N(2)	2.143(3)	2.251(6); 2.201(9)
Li−N(2′)	2.066(3)	2.093(6); 2.085(8)
Li−O	1.936(3)	1.947(6); 1.950(9)
Li···C(1)	2.417(3)	2.459(6); 2.423(8)
N(1)−Li−N(2)	66.14(10)	64.59(19); 65.0(3)
N(2)−Li−N(2′)	110.01(14)	112.1(3); 112.7(4)
Li−N(2)−Li′	69.99(14)	67.9(3); 67.3(4)
N(1)−C(1)	1.322(2)	1.328(4); 1.316(5)
N(2)−C(1)	1.347(2)	1.350(4); 1.344(4)
<N−C(1)>	1.335(18)	1.335(15)
N(1)−C(1)−N(2)	116.35(14)	116.4(3); 116.4(3)

[a] Individual values are given for the two independent complex molecules, mean values include both of them. Primed atoms are related to the unprimed ones by the symmetry centre.

view of **1a** is shown in Figure 1; selected bond lengths and angles are listed in Table 2. Both **1a** and **1b** are centrosymmetric dimers which adopt a ladder-type structure similar to that determined for several lithium amidinate complexes.[9] The lithium atoms are bound to the two nitrogen atoms of one amidinate ligand, one nitrogen atom of the other ligand and the oxygen atom of a THF molecule. The two nearly planar four-membered Li−N(1)−C(1)−N(2) rings [maximum deviations: 0.102(1) Å in **1a** and 0.121(2) and 0.135(3) Å in **1b**] are connected on either side of the planar central Li_2N_2 ring. These central and side planes form dihedral angles of 59.99(17)° and 56.3(4)° in **1a** and **1b**, respectively, with the usual *transoid* arrangement. The Li−N bond lengths, which range from 1.987(6) to 2.251(6) Å, indicate some asymmetry in the bonding of the bidentate ligand, with Li−N(1) shorter than Li−N(2) by 0.135 Å in **1a** and 0.209−0.264 Å in **1b**; the third bond length, Li−N(2′), is intermediate but closer to the former. The N(1)−C(1) and N(2)−C(1) bond lengths in both compounds are similar, with mean values of 1.322(6) and 1.347(3) Å, indicating uniform π delocalisation throughout the amidine moiety. The environment of the lithium atom is tetrahedral, but strongly distorted owing to the small bite angle of the bidentate amidinate. The Li···C(1) contacts, with a mean value of 2.43(2) Å, are larger than the usual values in such compounds, which are in the range 2.30−2.42 Å.[9b] The Li−O(THF) bond lengths are in perfect agreement with the mean value of 1.94(6) Å from the Cambridge Structural Database.[10]

The Uranium(IV) Amidinate Complexes [U{RC(NCy)$_2$}$_3$Cl] (R = Me, *n*Bu)

Treatment of UCl_4 with **1a** in THF gave the tris(amidinato)uranium chloride [U{MeC(NCy)$_2$}$_3$Cl] (**2a**), according to Equation (2); extraction in toluene and crystallization from this solvent afforded pale-green crystals of **2a** in 85% yield. A similar reaction with **1b** led to the quantitative formation of **2b** (NMR-tube experiment). The ^{1}H NMR sig-

 © 2004 Wiley-VCH Verlag GmbH & Co. KGaA, Weinheim

nals corresponding to the R and Cy substituents of the amidinate ligands are visible at lower and higher field, respectively (Table 1), as previously observed for the resonances of the R and R′ groups in the series of $[U\{RC(NR'_2)_2\}_3Cl]$ complexes (R = C_6H_4X with X = H, Me, OMe, CF_3; R′ = $SiMe_3$).[5b]

$$UCl_4 + 1.5\ [Li\{RC(NCy)_2\}(THF)]_2 \xrightarrow{THF} \underset{\mathbf{1}}{} [U\{RC(NCy)_2\}_3Cl] + 3\ LiCl \quad (2)$$

R = Me, **2a**; R = *n*Bu, **2b**

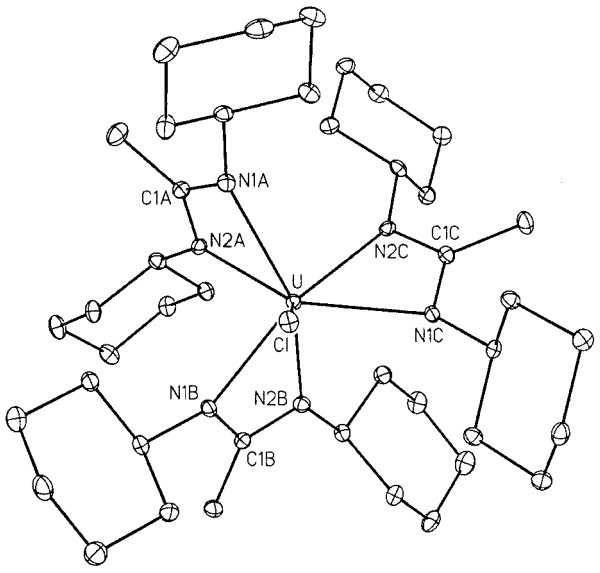

Figure 2. View of the complex $[U\{MeC(NCy)_2\}_3Cl]$ (**2a**) with displacement ellipsoids drawn at the 20% probability level; hydrogen atoms have been omitted for clarity

The molecular structure of **2a**, represented in Figure 2, is devoid of any imposed crystallographic symmetry, but possesses a pseudo C_3 axis defined by the U and Cl atoms; the three amidinate ligands are arranged in a propeller shape around this axis (the position of some cyclohexyl rings does not match this pseudo-trigonal symmetry). The structure of **2a** resembles that of the two tris(benzamidinate) compounds $[U\{ArC(NSiMe_3)_2\}_3Cl]$ (Ar = Ph, $C_6H_4CF_3$) which have been crystallographically characterized.[5b] The mean U−N bond length [2.43(4) Å] matches that in the above-mentioned complexes [2.44(5) Å], and for each of the three ligands (denoted A, B and C), the U−N(1) distance is shorter than the U−N(2) distance by 0.032−0.097 Å (Table 3). The atoms N(1A), N(1B) and N(1C), which are on the side of the complex on which the chlorine atom is located, are farther apart from each other than N(2A), N(2B) and N(2C); the steric strain between the cyclohexyl rings bound to the latter may explain the larger U−N(2) bond lengths. The three four-membered U−N(1)−C(1)−N(2) rings are planar, with a maximum deviation of 0.07 Å, the carbon atom always being the more displaced one. The mean U···C(1) distance [2.870(10) Å] is somewhat larger than its counterpart in the tris(benzamidinate) derivatives [2.84(2) Å], which is in agreement with smaller N(1)−C(1)−N(2) angles [mean value 114.3(8)° compared with 117(1)° in the latter]. Electronic delocalisation throughout the amidinate ligands is reflected by the identical N−C(1) bond lengths in the range 1.330(5)−1.337(5) Å. The uranium atom is displaced by 0.707(2) Å from the plane defined by the three atoms C(1A), C(1B) and C(1C) (on the same side as the chlorine atom), and the C(1A)···U···C(1B), C(1A)···U···C(1C) and C(1B)···U···C(1C) angles are 107.29(11)°, 114.50(12)° and 120.46(11)°, respectively; the C(1)···U−Cl angles vary from 102.14(8)° to 106.18(8)°. These values are similar to those of the ring centroid−U−ring centroid and ring centroid−U−Cl angles in the series of tris(cyclopentadienyl)[11] and tris(indenyl)uranium(IV)[12] complexes, which adopt a pseudo-tetrahedral configuration.

Interestingly, complex **2a** has the second longest U−Cl bond [2.6783(10) Å] in the series of 13 uranium(IV) complexes $[UL_3Cl]$ which have been crystallographically characterized and which include five cyclopentadienyl,[11a−11d,13] three indenyl,[12] three amidinate,[5b] including **2a**, one phospholyl,[14] and one imidophosphinate[15] derivatives (Table 4). The U−Cl bond lengths in this series lie in the range 2.559−2.90 Å. The shortest bond belongs to the first known organometallic uranium compound $[U(C_5H_5)_3Cl]$[11a] while the longest one, 2.90 Å, appears as a peculiar case since it corresponds to a chlorine atom disordered over two positions in $[U(C_5Me_5)_3Cl]$;[13] apart from this case, the twelve other U−Cl bond lengths define a relatively narrow range (0.12 Å). The lengthening of the U−Cl bond in each of the cyclopentadienyl, indenyl and amidinate families can be related to the increasing steric bulk and electron-donating capacity of the substituted ligands. Substitution of the cyclopentadienyl ring by methyl groups gives rise to an amazing gap in the variation of the U−Cl bond lengths, with a major influence of the fifth methyl group on the lengthening of the bond. In reference to $[U(C_5H_5)_3Cl]$,[11a] the complexes $[U(C_5Me_4H)_3Cl]$[11d] and $[U(C_5Me_5)_3Cl]$[13] exhibit variations in their U−Cl bond lengths of 0.08 Å and 0.26 Å, respectively, and, in contrast to the other tris(cyclopentadienyl)uranium chlorides, $[U(C_5Me_5)_3Cl]$ does not adopt a pseudo-tetrahedral structure; the ring centroid−U−ring centroid angles are equal to 120°. The long U−Cl bond in **2a** is in agreement with the electron richness of the $[U\{RC(NCy)_2\}_3]$ moiety, which is manifest in its redox reactions (vide infra).

The Uranium(III) and Lanthanide(III) Amidinate Complexes $[U\{RC(NCy)_2\}_3]$ (R = Me, nBu) and $[Ln\{MeC(NCy)_2\}_3]$ (Ln = La, Nd)

In contrast to $[U(C_5H_5)_3Cl]$, which is reduced with Na/Hg in THF to give $[U(C_5H_5)_3(THF)]$,[16] complexes **2** do not react with sodium amalgam. The synthesis of the uranium(III) amidinate $[U\{MeC(NCy)_2\}_3]$ (**3a**) therefore required a stronger reducing agent. Treatment of **2a** with lithium powder in THF cleanly afforded **3a** which, after extraction

 © 2004 Wiley-VCH Verlag GmbH & Co. KGaA, Weinheim

Table 3. Selected distances [Å] and angles [°] in the uranium, lanthanum and neodymium amidinate complexes

	[U{MeC(NCy)$_2$}$_3$Cl] (**2a**)	[U{MeC(NCy)$_2$}$_3$] (**3a**)	[La{MeC(NCy)$_2$}$_3$] (**4**)	[Nd{MeC(NCy)$_2$}$_3$] (**5**)[a]
M−N(1A)	2.388(3)	2.493(4)	2.531(6)	2.459(3); 2.464(2)
M−N(2A)	2.485(3)	2.501(4)	2.521(6)	2.471(2); 2.471(3)
M−N(1B)	2.380(3)	2.487(4)	2.538(6)	2.458(3); 2.480(3)
M−N(2B)	2.436(3)	2.497(4)	2.545(6)	2.473(3); 2.454(2)
M−N(1C)	2.418(3)	2.481(4)	2.512(6)	2.468(3); 2.455(3)
M−N(2C)	2.450(3)	2.477(4)	2.521(6)	2.445(3); 2.469(3)
<M−N>	2.43(4)	2.489(9)	2.528(12)	2.464(10)
M−Cl	2.6783(10)			
M···C(1A)	2.881(4)	2.939(5)	2.979(7)	2.899(3); 2.908(3)
M···C(1B)	2.865(4)	2.942(5)	2.971(8)	2.900(3); 2.907(3)
M···C(1C)	2.863(4)	2.940(5)	2.989(7)	2.897(3); 2.904(3)
<M···C(1)>	2.870(10)	2.9403(15)	2.980(9)	2.903(5)
N(1A)−M−N(2A)	54.70(11)	53.85(14)	53.2(2)	54.59(8); 54.45(9)
N(1B)−M−N(2B)	55.12(11)	53.23(14)	53.0(2)	54.56(9); 54.44(9)
N(1C)−M−N(2C)	55.08(10)	53.99(14)	53.3(2)	54.61(9); 54.53(9)
<N(1)−M−N(2)>	55.0(2)	53.7(4)	53.1(2)	54.5(7)
<N−C(1)>	1.333(3)	1.335(11)	1.341(16)	1.335(4)
<N(1)−C(1)−N(2)>	114.3(8)	114.8(8)	115.1(17)	115.4(2)

[a] Individual values are given for the two independent complex molecules, mean values include both of them; the second values correspond to amidinate groups D, E and F in place of A, B and C, respectively.

with pentane and crystallization from this solvent, was isolated as dark-green crystals in 80% yield [Equation (3)]. Similarly, **2b** was quantitatively transformed into **3b** (NMR-tube experiment). The paramagnetic ^{1}H NMR resonances corresponding to the cyclohexyl substituents of **3** are more shifted than those of **2**, with one signal at high field and the others at low field (Table 1).

$$\underset{\mathbf{2}}{[U\{RC(NCy)_2\}_3Cl]} + Li \xrightarrow{THF} \underset{R = Me,\ \mathbf{3a};\ R = n\text{Bu},\ \mathbf{3b}}{[U\{RC(NCy)_2\}_3]} + LiCl \qquad (3)$$

Monitoring of the **2** → **3** transformation by NMR spectroscopy showed that the signals of the two complexes were distinct and not shifted during the reduction process, indicating the absence of electron-transfer or ligand-exchange reactions similar to those occurring during the reduction of [U(C$_5$H$_5$)$_3$Cl], where the intermediate formation of the bridged species [{U(C$_5$H$_5$)$_3$}$_2$(μ-Cl)]$^{n-}$ (n = 0 or 1) was observed.[16] These results, with the more difficult reduction of **2**, can be explained by the greater electron density on the metal atom.

In order to compare their crystal structures and reactions with those of **3a**, the lanthanum and neodymium analogues [Ln{MeC(NCy)$_2$}$_3$] [Ln = La (**4**) or Nd (**5**)] were prepared by treatment of LaI$_3$ or NdCl$_3$ with **1a** in THF; colorless (**4**) or pale blue-purple (**5**) crystals were obtained from a pentane solution. Contrary to previous reports[4] the ^{1}H NMR spectrum of **5** is well resolved; it is similar to that of **3a** (Table 1). The crystal structure of the ytterbium counterpart [Yb{MeC(NCy)$_2$}$_3$] (**6**) has been reported previously.[4]

Complexes **3a**, **4** and **6** are isomorphous. The crystal structure of **3a** is shown in Figure 3; selected bond lengths and angles are listed in Table 3. The complex possesses a pseudo-trigonal symmetry axis, with the three ligands in a propeller-like arrangement. As usual with six-coordinate compounds with three identical small-bite bidentate ligands, the environment of the central metal atom is intermediate between octahedral and trigonal prismatic.[17] The uranium atom is located at 1.013(3) and 0.979(2) Å from the planes defined by N(1A), N(1B), N(1C) and N(2A), N(2B), N(2C), respectively, which form a dihedral angle of 0.77(15)°. In contrast with what has been observed in **2a**, these two sets of nitrogen atoms are not located differently with respect to the metal atom and, as a consequence, the U−N distances span a relatively narrow range [2.477(4)−2.501(4) Å]. The average U−N distance of 2.489(9) Å is larger than that in **2a** by about 0.06 Å, in fair agreement with a difference of about 0.075 Å in ionic radii between seven-coordinate U^{IV} and six-coordinate U^{III};[18] this distance is longer than that of 2.320(4) Å in the homoleptic tris(amide) uranium(III) compound [U(N{SiMe$_3$}$_2$)$_3$].[19] The three U−N(1)−C(1)−N(2) rings in **3a** define mean planes with a maximum deviation of 0.020(3) Å at most, the carbon atom being the farthest from the plane. The U···C(1) distances, with a mean value of 2.9403(15) Å, follow the same trend as the U−N bond lengths when passing from U^{IV} to U^{III}, since the N(1)−C(1)−N(2) angle remains approximately constant. The N−C(1) bond lengths span the range 1.317(7)−1.348(7) Å, wider than in **2a** and equivalent to that in the lithium complexes, the mean value being constant in all cases. The metal atom is displaced by 0.030(3) Å from the mean plane defined by atoms C(1A), C(1B) and C(1C) and the three angles C(1A)···U···C(1B), C(1A)···U···C(1C) and C(1B)···U···C(1C) are 123.25(14)°, 117.75(14)° and 118.96(14)°, respectively, with a sum equal

 © 2004 Wiley-VCH Verlag GmbH & Co. KGaA, Weinheim

Table 4. Variation of the U−Cl bond length among the $[UL_3Cl]$ complexes

Ligand L		U–Cl [Å]	Ref.
Cyclopentadienyl		2.559(16)	[11a]
Indenyl	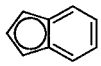	2.593(3)	[12a]
1,4,7-Trimethylindenyl	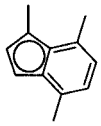	2.601(3)	[12b]
1,3-Bis(trimethylsilyl)cyclopentadienyl	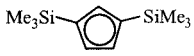	2.614(2)	[11b]
1,2,4,5,6,7-Hexamethylindenyl	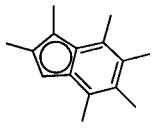	2.621(1)	[12c]
Tetraphenylimidophosphinato	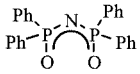	2.624(3)	[15]
Benzylcyclopentadienyl	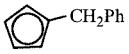	2.627(2)	[11c]
N,*N*′-Bis(trimethysilyl)-4-trifluoromethylbenzamidinato	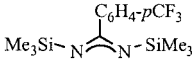	2.634(2)	[5b]
Tetramethycyclopentadienyl	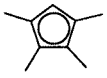	2.637	[11d]
N,*N*′-Bis(trimethysilyl)benzamidinato	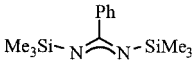	2.660(9)	[5b]
Tetramethylphospholyl	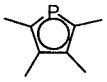	2.67(1)	[14]
N,*N*′-Bis(cyclohexyl)methylamidinato		2.6783(10)	this work
Pentamethylcyclopentadienyl	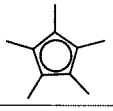	2.90(1)	[13]

to 359.96°. The geometry around the metal atom can thus be described as trigonal-planar if each bidentate amidinate ligand is considered to occupy a single coordination site. This arrangement is reminiscent of that adopted by the three cyclopentadienyl ligands in sterically encumbered trivalent metallocenes such as $[U(C_5H_5SiMe_3)_3]$,[20] $[U(C_5Me_5H)_3]$[21] and $[U(C_5Me_5)_3]$,[22] and reinforces the analogy which has been established between the amidinate and cyclopentadienyl ligands.

Complexes **3a**, **4**, **5** and **6** are isostructural but not isomorphous since the neodymium derivative **5** crystallizes in a different system and space group, with two independent molecules in the asymmetric unit (corresponding to ligands A, B, C and D, E, F; Figure 4). The Nd−N bond lengths are in the range 2.445(3)−2.480(3) Å, with a mean value of 2.464(10) Å, which is identical to that found in the homoleptic guanidinate compounds $[Nd\{iPr_2NC(NR)_2\}_3]$ (R = Cy or *i*Pr),[23a] and is slightly shorter than that of 2.49(3) Å determined in the other neodymium amidinates.[23b,23c] The Nd−N(1)−C(1)−N(2) four-membered rings define mean planes with maximum deviations of 0.032(2) Å for the carbon atoms, the latter being at a mean distance of 2.903(5) Å from the metal centres. The N−C(1) bond lengths are in the range 1.330(4)−1.340(4) Å, the mean value being identical to that in the other complexes. The two independent neodymium atoms are displaced by 0.021(2) and 0.034(2) Å from the mean planes defined by the atoms C(1) of the three ligands in each molecule, and the angles defined by the atoms C(1) around Nd are in the range 117.80(9)−121.76(9)°, nearly identical to those in **3a**, **4** and **6**.

The plot of the average Ln−N distances versus the ionic radii $r(Ln^{III})$ of the six-coordinate Yb^{III}, Nd^{III} and La^{III} ions (Figure 5) shows the usual almost perfect linear relationship, with a correlation coefficient of 0.998. However, the average U−N distance is shorter by 0.025 Å than that expected from a purely ionic bonding model; the same trend is observed when considering the U···C(1) distances. Although this difference is smaller than three times the value of the standard deviation for the measured distances (0.01 Å), it seems significant, as the average distances are calculated from six M−N distances and the values are

 © 2004 Wiley-VCH Verlag GmbH & Co. KGaA, Weinheim

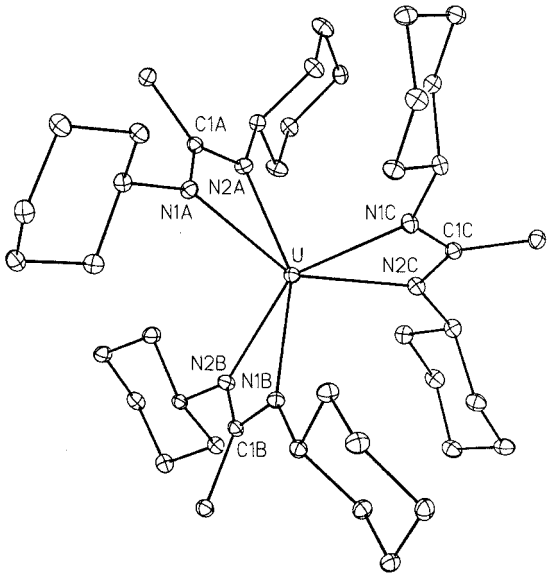

Figure 3. View of the complex [U{MeC(NCy)$_2$}$_3$] (**3a**) with displacement ellipsoids drawn at the 10% probability level; hydrogen atoms have been omitted for clarity

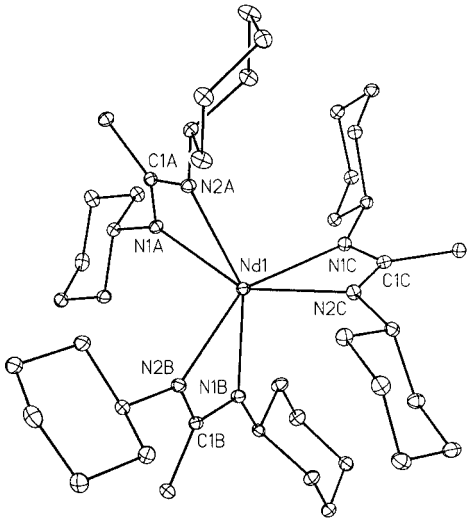

Figure 4. View of one molecular unit in the complex [Nd{MeC(NCy)$_2$}$_3$] (**5**) with displacement ellipsoids drawn at the 10% probability level; hydrogen atoms have been omitted for clarity

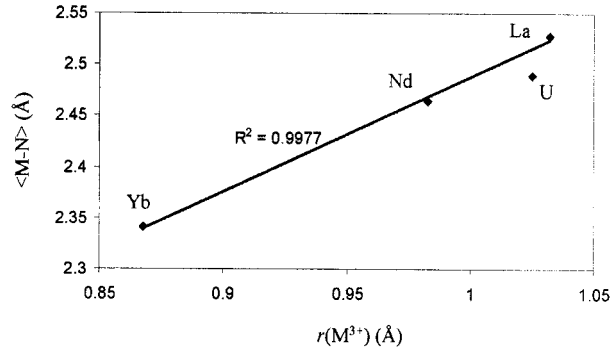

Figure 5. Average M−N distances as a function of the metal ionic radii in the complexes [M{MeC(NCy)$_2$}$_3$]

identical for each of the two independent [Nd{MeC(NCy)$_2$}$_3$] molecules. The shortening of the U−N distances with respect to the Ln−N distances in the series of isostructural compounds **3a**, **4**, **5** and **6** could reflect a stronger interaction between the actinide and the amidinate ligand, in relation with the more covalent character of the bond. The better affinity of neutral nitrogen, phosphorous and sulfur ligands or anionic cyclopentadienyl and iodide groups for U^{III} than for Ln^{III} ions has been similarly assessed from the crystal structures of analogous complexes, by measuring the deviations, Δ, between the differences [<U−X> − <Ln−X>] and [$r(U^{III})$ − $r(Ln^{III})$].[24] These deviations are generally equal to 0.02−0.05 Å, as found, for example, in [MI$_3$(bipy)(C$_5$H$_5$N)] (M = Ce or U; bipy = 2,2′-bipyridine),[24a] [M(C$_5$H$_4$R)$_3$(L)] (M = Ce or U; R = *t*Bu or SiMe$_3$; L = pyridine, picoline, lutidine, pyrimidine and 3,5-dimethylpyrazine),[24b] [MI$_2$(OPPh$_3$)$_4$]I (M = Nd, Ce, La, U),[24c] [M(terpy)$_3$]I$_3$ (M = La, Ce, Nd or U; terpy = 2,2′:6′,2′′-terpyridine)[24d] and [MI$_3$(1,4,7-trithiacyclononane)(MeCN)$_2$] (M = La or U).[24e] In the phosphorus-containing complexes [M(C$_5$H$_4$Me)$_3$(L)] [M = Ce or U; L = PMe$_3$ or P(OCH$_2$)$_3$CEt][24f] and in the tris(btp) compounds [M(btp)$_3$]I$_3$ [M = La, Ce, Sm or U; btp = 2,6-dialkyl-1,2,4-triazin-3-yl)pyridine],[24d] Δ is equal to 0.1 Å; this deviation has been explained by the softer character and better π-accepting ability of the phosphane, phosphite and btp ligands. In agreement with these arguments, the low value of Δ for the series of compounds **3a**, **4**, **5** and **6**, if significant, would result from the lower softness of the nitrogen atoms and the energetically less accessible π* orbitals of the amidinate ligand.[25]

Polymerization of ε-Caprolactone

Homoleptic amidinate lanthanide complexes show extremely high activity in the ring-opening polymerization of ε-caprolactone (CL) at room temperature.[4] Thus, in the presence of 0.5% mol-equiv. of the neodymium complex **5** in toluene, polymerization of CL was achieved in less than 2 min, giving a viscous gel of poly(ε-caprolactone), which was characterized by its ^{1}H NMR spectrum.[26] It is likely that the mechanism of this reaction is similar to that proposed for the polymerization of CL catalyzed by guanidino-[23a] or amidolanthanide[27] compounds, in which the initial step is the nucleophilic attack of a nitrogen atom at the carbonyl carbon atom of the lactone, followed by acyl-bond cleavage and formation of an alkoxide complex. Under the same conditions, when using the uranium(III) counterpart **3a** in place of **5**, polymerization of CL was very much slower, requiring 5 d to go to completion. In view of the poor catalytic activity of **3a**, the properties of the polyester obtained were not analyzed further. However, the ^{1}H NMR spectra showed that **3a** reacts immediately with 0.5 mol-equiv. of CL to give a mixture of unidentified compounds, while the colour of the solution turned from green to yellow; these observations suggest that **3a** is oxidized to U^{IV} derivatives by CL. The ability of CL to oxidize low-valent f-element complexes was previously noted during its polymerization by means of a variety of Sm^{II} initiators,

 © 2004 Wiley-VCH Verlag GmbH & Co. KGaA, Weinheim

like $[Sm(OAr)_2(THF)_3]$ (Ar = $C_6H_2tBu_2$-2,6-Me-4),[28a] $[Sm\{N(SiMe_3)_2\}_2(THF)_2]$ and $[Sm(C_5Me_5)_2(THF)_x]$,[28b] which were initially transformed into the true, uncharacterized Sm^{III} catalysts. It is possible that one of the products resulting from oxidation of **3a** is the dinuclear species $[U]-O(CH_2)_5CO-[U]$ ($[U] = \{MeC(NCy)_2\}_3$), by analogy with the compound $[U(C_5H_5)_3-O(CH_2)_5CO-U(C_5H_5)_3]$ (**7**), which is readily obtained by treating $[U(C_5H_5)_3(THF)]$ with CL in toluene.[29] Complex **7** exhibits the same activity as the oxidation product(s) of **3a** in the catalytic polymerization of CL. The much lower performances of these compounds, by comparison with those of the lanthanide amidinates, can be explained by the more difficult insertion of the lactone monomer into a $U^{IV}-O$ bond than into an $Ln^{III}-N$ or $Ln^{III}-O$ bond; this difference can be compared with that previously noted between titanium(IV)[30] and lanthanide(III)[26a] alkoxides in their reactions with CL.

Conclusion

After the benzamidinate compounds $[U\{ArC(NSiMe_3)_2\}_3Cl]$ (Ar = C_6H_5 or 4-$CF_3C_6H_4$), the complexes $[U\{RC(NCy)_2\}_3Cl]$ (R = Me or *n*Bu) are new examples of tris(amidinato)uranium chlorides. Their reduction with lithium metal affords the first homoleptic tris(amidinate) compounds of uranium(III). Comparison of the crystal structure of $[U\{MeC(NCy)_2\}_3]$ with those of the lanthanide analogues shows that the average U−N distance is shorter than expected from a purely ionic bonding model. This U^{III} complex was found to be much less efficient than the lanthanide counterparts in the catalytic polymerization of ε-caprolactone because of its rapid oxidation into poorly active U^{IV} species.

Experimental Section

General: All preparations and experiments were carried out under argon (< 5 ppm oxygen or water) using standard Schlenk-vessel and vacuum-line techniques, or in a glove box. Solvents were thoroughly dried and deoxygenated by standard methods and distilled immediately before use; deuterated toluene and THF (Eurisotop) were distilled from Na/K alloy and stored over molecular sieves (3 Å). UCl_4 was prepared by a published method.[31] LaI_3, $NdCl_3$, *N*,*N*′-dicyclohexylcarbodiimide, ε-caprolactone, MeLi (1.6 M in diethyl ether) and *n*BuLi (2.0 M in hexanes) were purchased from Aldrich and used without further purification. The ^1H NMR spectra were recorded with a Bruker DPX 200 instrument and referenced internally using the residual protonated solvent resonances relative to tetramethylsilane ($\delta = 0$ ppm); the spectra of the amidinate complexes are reported in Table 1. Elemental analyses were performed by Analytische Laboratorien at Lindlar (Germany).

Synthesis of $[Li\{MeC(NCy)_2\}(THF)]_2$ (1a): A flask was charged with *N*,*N*′-dicyclohexylcarbodiimide (330 mg, 1.6 mmol) and THF (10 mL) was condensed into it under vacuum at −78 °C. MeLi (1.0 mL of a 1.6 M solution in diethyl ether, 1.6 mmol) was added with a syringe at room temperature. After 2 h, evaporation of the solvent gave colorless crystals which were dried under vacuum (447 mg, 93%).

Synthesis of $[Li\{nBuC(NCy)_2\}(THF)]_2$ (1b): This compound was prepared by using the same procedure as for **1a**, from *N*,*N*′-dicyclohexylcarbodiimide (330 mg, 1.6 mmol) and *n*BuLi (0.8 mL of a 2.0 M solution in hexanes, 1.6 mmol). Colorless crystals were obtained after drying (498 mg, 91%).

Synthesis of $[U\{MeC(NCy)_2\}_3Cl]$ (2a): A flask was charged with UCl_4 (152 mg, 0.4 mmol) and **1a** (360 mg, 0.6 mmol), and THF (10 mL) was condensed into it under vacuum at −78 °C. The reaction mixture was stirred at room temperature for 2 h. The solvent was evaporated and the residue extracted with toluene (10 mL). The solution was filtered and concentrated to dryness, leaving pale-green crystals of **2a** (318 mg, 85%). $C_{42}H_{75}ClN_6U$ (937): calcd. C 53.80, H 8.06, N 8.96; found C 53.92, H 8.15, N 9.08.

Synthesis of $[U\{nBuC(NCy)_2\}_3Cl]$ (2b): An NMR tube was charged with UCl_4 (11.4 mg, 0.030 mmol) and **1b** (30.9 mg, 0.045 mmol) in $[D_8]$THF (0.3 mL). The NMR spectrum showed the immediate and almost quantitative formation of **2b**.

Synthesis of $[U\{MeC(NCy)_2\}_3]$ (3a): A flask was charged with **2a** (281 mg, 0.29 mmol) and Li powder (2.1 mg, 0.29 mmol), and THF (10 mL) was condensed into it under vacuum at −78 °C. The reaction mixture was stirred at room temperature for 2 h. The solvent was evaporated to dryness and the residue extracted with pentane (10 mL). The solution was filtered and concentrated to dryness, leaving dark-green crystals of **3a** (219 mg, 80%). $C_{42}H_{75}N_6U$ (902): calcd. C 55.92, H 8.38, N 9.32; found C 55.68, H 8.44, N 9.22.

Synthesis of $[U\{nBuC(NCy)_2\}_3Cl]$ (3b): An NMR tube was charged with **2b** (29.7 mg, 0.030 mmol) and Li powder (0.2 mg, 0.030 mmol) in $[D_8]$THF (0.3 mL). The pale-green solution progressively turned dark blue, and after 2 h at room temperature the NMR spectrum showed the quantitative formation of **3b**.

Synthesis of $[Ln\{MeC(NCy)_2\}_3]$ [Ln = La (4) or Nd (5)]: These complexes were prepared by modifying a published procedure.[4] A flask was charged with LaI_3 (51.9 mg, 0.1 mmol) and **1a** (90 mg, 0.15 mmol) and THF (5 mL) was condensed into it under vacuum at −78 °C. The reaction mixture was stirred at room temperature for 24 h. The solvent was evaporated and the residue extracted with pentane (5 mL). The solution was filtered and concentrated to dryness, leaving colorless crystals of **4** (60 mg, 75%). Compound **5** was similarly prepared from $NdCl_3$ (100.2 mg, 0.4 mmol) and **1a** (360 mg, 0.6 mmol) and isolated as pale blue-purple crystals (298 mg, 92%).

Polymerization of ε-Caprolactone (CL). a) With $[Nd\{MeC(NCy)_2\}_3]$ (5): An NMR tube was charged with **5** (0.80 mg, 0.0010 mmol) in $[D_8]$toluene (0.6 mL) and CL (22 μL, 0.20 mmol) was introduced with a microsyringe. After 2 min at 20 °C, a viscous gel was obtained and the spectrum showed that CL had completely polymerized. ^1H NMR: $\delta = 1.29$ (m, 2 H, γ-CH_2), 1.54 (m, 4 H, β- and δ-CH_2), 2.20 (t, $J = 7$ Hz, 2 H, ε-CH_2), 3.94 (t, $J = 7$ Hz, 2 H, α-CH_2) ppm; α, β, γ, δ and ε are the positions of the carbon atoms of the polyester chain with respect to the oxygen atom. **b) With $[U\{MeC(NCy)_2\}_3]$ (3a) or $[U(C_5H_5)_3(THF)]$:** An NMR tube was charged with **3a** (0.9 mg, 0.0010 mmol) in $[D_8]$toluene (0.6 mL) and CL (22 μL, 0.20 mmol) was introduced with a microsyringe. The NMR spectra showed the slow formation of the polyester, which required 5 d at 20 °C to go to completion. The same observations were made upon replacing **3a** with $[U(C_5H_5)_3(THF)]$.

 © 2004 Wiley-VCH Verlag GmbH & Co. KGaA, Weinheim

Table 5. Crystal data and structure refinement details

	1a	**1b**	**2a**	**3a**	**4**	**5**
Empirical formula	$C_{36}H_{66}Li_2N_4O_2$	$C_{42}H_{78}Li_2N_4O_2$	$C_{42}H_{75}ClN_6U$	$C_{42}H_{75}N_6U$	$C_{42}H_{75}LaN_6$	$C_{42}H_{75}N_6Nd$
M [g mol^{-1}]	600.81	684.96	937.56	902.11	802.99	808.32
Crystal system	monoclinic	monoclinic	monoclinic	triclinic	triclinic	monoclinic
Space group	$P2_1/c$	$P2_1/c$	$P2_1/c$	$P\bar{1}$	$P\bar{1}$	$P2_1/c$
a [Å]	9.8074(5)	21.6623(12)	12.1285(3)	11.6077(10)	11.6688(12)	11.5709(3)
b [Å]	10.9431(7)	17.5871(15)	17.3182(7)	12.8671(10)	12.8558(18)	32.5180(10)
c [Å]	17.3307(11)	11.1983(9)	21.5602(9)	16.2289(10)	16.278(2)	22.4268(8)
α [°]	90	90	90	104.222(5)	104.358(7)	90
β [°]	105.731(3)	95.137(5)	105.398(3)	90.740(5)	90.650(9)	90.727(2)
γ [°]	90	90	90	115.175(4)	115.035(8)	90
V [Å^3]	1790.32(19)	4249.2(6)	4366.0(3)	2107.3(3)	2124.5(5)	8437.7(5)
Z	2	4	4	2	2	8
$\rho_{calcd.}$ [g cm^{-3}]	1.115	1.071	1.426	1.422	1.255	1.273
μ(Mo-K_α) [mm^{-1}]	0.067	0.064	3.814	3.886	1.040	1.266
F(000)	664	1520	1912	922	852	3432
No. of data collected	13809	32315	29703	14463	13811	57209
No. of unique data	3322	7810	8113	7357	7262	15852
Observed data [$I > 2\sigma(I)$]	2493	5114	6547	6183	5794	11905
R_{int}	0.060	0.096	0.066	0.040	0.076	0.055
Parameters	200	493	454	445	445	889
R_1	0.049	0.088	0.030	0.037	0.074	0.033
wR_2	0.120	0.263	0.063	0.088	0.198	0.082
S	1.048	1.065	1.031	1.014	1.024	1.017
$\Delta\rho_{min}$ [e Å^{-3}]	−0.23	−0.61	−0.52	−1.03	−0.82	−0.62
$\Delta\rho_{max}$ [e Å^{-3}]	0.19	0.91	0.45	1.23	1.58	1.35

X-ray Crystallography of 1a, 1b, 2a, 3a, 4 and 5: Data collections were carried out at 100(2) K with a Nonius Kappa-CCD area-detector diffractometer[32] using graphite-monochromated Mo-K_α radiation (λ = 0.71073 Å). The crystals were introduced into glass capillaries with a protecting Paratone-N oil (Hampton Research) coating. The unit-cell parameters were determined from ten frames, then refined on all data. A 180° φ range was scanned with 2° steps during data collection, with a crystal-to-detector distance fixed at 28 mm. The data were processed with DENZO-SMN.[33] The structures were solved by direct methods or Patterson map interpretation with SHELXS-97 and subsequent Fourier difference synthesis and refined by full-matrix least squares on F^2 with SHELXL-97.[34] Absorption effects of the uranium and neodymium complexes were corrected empirically with the program DELABS from PLATON.[35] In one of the two independent molecules in compound **1b** (unit B), the terminal carbon atom of the *n*-butyl chain and three carbon atoms of the tetrahydrofuran molecule were found disordered over two positions, which were refined with occupancy parameters constrained to sum to unity and some restraints on bond lengths and displacement parameters for the atoms of the tetrahydrofuran molecule. The hydrogen atoms were introduced at calculated positions, except in the disordered parts (when present), and were treated as riding atoms with a displacement parameter equal to 1.2- (CH, CH_2) or 1.5-times (CH_3) that of the parent atom. All non-hydrogen atoms were refined with anisotropic displacement parameters. Crystal data and structure refinement parameters are given in Table 5. The molecular plots were drawn with SHELXTL.[36] CCDC-240952 to -240957 (for **1a**, **1b**, **2a**, **3a**, **4** and **5**, respectively) contain the supplementary crystallographic data for this paper. These data can be obtained free of charge at www.ccdc.cam.ac.uk/conts/retrieving.html [or from the Cambridge Crystallographic Data Centre, 12 Union Road, Cambridge CB2 1EZ, UK; Fax: + 44-1223-336-033; E-mail: deposit@ccdc.cam.ac.uk].

[1] [1a] V. Volkis, E. Nelkenbaum, A. Lisovskii, G. Hasson, R. Semiat, M. Kapon, M. Botoshansky, Y. Eishen, M. S. Eisen, *J. Am. Chem. Soc.* **2003**, *125*, 2179−2194. [1b] B. J. O'Keefe, M. A. Hillmyer, W. B. Tolman, *J. Chem. Soc., Dalton Trans.* **2001**, 2215−2224. [1c] K. C. Jayaratne, L. R. Sita, *J. Am. Chem. Soc.* **2001**, *123*, 10754−10755. [1d] A. Little, N. Sleiman, C. Bensimon, D. S. Richeson, G. P. A. Yap, S. J. Brown, *Organometallics* **1998**, *17*, 446−451. [1e] R. Gomez, R. Duchateau, A. N. Chernega, J. N. Teuben, F. T. Edelmann, M. L. H. Green, *J. Organomet. Chem.* **1995**, *491*, 153−158.

[2] B. S. Lim, A. Rahtu, J. S. Park, R. G. Gordon, *Inorg. Chem.* **2003**, *42*, 7951−7958.

[3] F. T. Edelmann, D. M. M. Freckmann, H. Schumann, *Chem. Rev.* **2002**, *102*, 1851−1896 and references herein.

[4] Y. Luo, Y. Yao, Q. Shen, J. Sun, L. Weng, *J. Organomet. Chem.* **2002**, *662*, 144−149.

[5] [5a] M. Wedler, F. Knösel, F. T. Edelmann, U. Behrens, *Chem. Ber.* **1992**, *125*, 1313−1318. [5b] M. Wedler, F. Knösel, M. Noltemeyer, F. T. Edelmann, U. Behrens, *J. Organomet. Chem.* **1990**, *388*, 21−45. See also [5c] M. Müller, V. C. Williams, L. H. Doerrer, M. A. Leech, S. A. Mason, M. L. H. Green, K. Prout, *Inorg. Chem.* **1998**, *37*, 1315−1323.

[6] M. Wedler, M. Noltemeyer, F. T. Edelmann, *Angew. Chem. Int. Ed. Engl.* **1992**, *31*, 72−73.

[7] M. Wedler, H. W. Roesky, F. Edelmann, *J. Organomet. Chem.* **1988**, *345*, C1−C3.

[8] P. B. Hitchcock, M. F. Lappert, D. S. Liu, *J. Organomet. Chem.* **1995**, *488*, 241−248.

[9] [9a] C. Knapp, E. Lork, P. G. Watson, R. Mews, *Inorg. Chem.* **2002**, *41*, 2014−2025. [9b] C. L. Boyd, B. R. Tyrrell, P. Mountford, *Acta Crystallogr., Sect. E* **2002**, *58*, m597−m598. [9c] C. F. Caro, P. B. Hitchcock, M. F. Lappert, M. Layh, *Chem. Commun.* **1998**, 1297−1298. [9d] J. R. Hagadorn, J. Arnold, *Inorg. Chem.* **1997**, *36*, 132−133. [9e] J. Barker, D. Barr, N. D. R. Barnett, W. Clegg, I. Cragg-Hine, M. G. Davidson, R. P. Davies, S. M. Hodgson, J. A. K. Howard, M. Kilner, C. W. Lehmann,

 © 2004 Wiley-VCH Verlag GmbH & Co. KGaA, Weinheim

I. Lopez-Solera, R. E. Mulvey, P. R. Raithby, R. Snaith, *J. Chem. Soc., Dalton Trans.* **1997**, 951−955. [9f] D. Stalke, M. Wedler, F. T. Edelmann, *J. Organomet. Chem.* **1992**, *431*, C1−C3.
[10] F. H. Allen, *Acta Crystallogr., Sect. B* **2002**, *58*, 380−388.
[11] [11a] C. H. Wong, T. M. Yen, T. Lee, *Acta Crystallogr.* **1965**, *18*, 340−345. [11b] P. C. Blake, M. A. Edelman, P. B. Hitchcock, J. Hu, M. F. Lappert, S. Tian, G. Müller, J. L. Atwood, H. Zhang, *J. Organomet. Chem.* **1998**, *551*, 261−270. [11c] J. Leong, K. O. Hodgson, K. N. Raymond, *Inorg. Chem.* **1973**, *12*, 1329−1335. [11d] F. G. N. Cloke, S. A. Hawkes, P. B. Hitchcock, P. Scott, *Organometallics* **1994**, *13*, 2895−2897.
[12] [12a] J. H. Burns, P. G. Laubereau, *Inorg. Chem.* **1971**, *10*, 2789−2792. [12b] J. Meunier-Piret, M. van Meerssche, *Bull. Soc. Chim. Belg.* **1984**, *93*, 299−305. [12c] M. R. Spirlet, J. Rebizant, S. Bettonville, J. Goffart, *Acta Crystallogr., Sect. C* **1992**, *48*, 1221−1223.
[13] W. J. Evans, G. W Nyce, M. A. Johnston, J. A. Ziller, *J. Am. Chem. Soc.* **2000**, *13*, 12019−12020.
[14] P. Gradoz, C. Boisson, D. Baudry, M. Lance, M. Nierlich, J. Vigner, M. Ephrithikine, *J. Chem. Soc., Chem. Commun.* **1992**, 1720−1721.
[15] M. R. A. Carvallo, V. Garcia-Montalvo, A. Domingos, R. Cea-Olivares, N. Marques, A. Pires de Matos, *Polyhedron* **2000**, *19*, 1699−705.
[16] J. F. Le Maréchal, C. Villiers, P. Charpin, M. Nierlich, M. Lance, J. Vigner, M. Ephritikhine, *J. Organomet. Chem.* **1989**, *379*, 259−269.
[17] D. L. Kepert, *Inorganic Stereochemistry*, Springer-Verlag, Heidelberg, **1982**.
[18] R. D. Shannon, *Acta Crystallogr., Sect. A* **1976**, *32*, 751−767.
[19] J. L. Stewart, R. A. Andersen, *Polyhedron* **1998**, *17*, 953−958.
[20] A. Zalkin, J. G. Brennan, R. A. Andersen, *Acta Crystallogr., Sect. C* **1988**, *44*, 2104−2106.
[21] M. del Mar Conejo, J. S. Parry, E. Carmona, M. Schultz, J. G. Brennan, S. M. Beshouri, R. A. Andersen, R. D Rogers, S. Coles, M. Hursthouse, *Chem. Eur. J.* **1999**, *5*, 3000−3009.
[22] W. J. Evans, K. J. Forrestal, J. W. Ziller, *Angew. Chem. Int. Ed. Engl.* **1997**, *36*, 774−776.
[23] [23a] J. L. Chen, Y. M. Yao, Y. J. Luo, L. Y. Zhou, Y. Zhang, Q. Shen, *J. Organomet. Chem.* **2004**, *689*, 1019−1024. [23b] Y. Luo, Y. Yao, Q. Shen, K. Yu, L. Weng, *Eur. J. Inorg. Chem.* **2003**, 318−323. [23c] A. Recknagel, F. Knösel, H. Gornitzka, M. Noltemeyer, F. T. Edelmann, *J. Organomet. Chem.* **1991**, *417*, 363−375.
[24] [24a] C. Rivière, M. Nierlich, M. Ephritikhine, C. Madic, *Inorg. Chem.* **2001**, *40*, 4428−4435. [24b] T. Mehdoui, J. C. Berthet, P. Thuéry, M. Ephritikhine, *Dalton Trans.* **2004**, 579−590. [24c] J. C. Berthet, M. Nierlich, M. Ephritikhine, *Polyhedron* **2003**, *22*, 3475−3482. [24d] J. C. Berthet, Y. Miquel, P. B. Iveson, M. Nierlich, P. Thuéry, C. Madic, M. Ephritikhine, *J. Chem. Soc., Dalton Trans.* **2002**, 3265−3272. [24e] L. Karmazin, M. Mazzanti, J. Pécaut, *Chem. Commun.* **2002**, 654−655. [24f] J. G. Brennan, S. D. Stults, R. A. Andersen, A. Zalkin, *Organometallics* **1988**, *7*, 1329−1334.
[25] A. Singhal, V. K. Jain, M. Nethaji, A. G. Samuelson, D. Jayaprakash, R. J. Butcher, *Polyhedron* **1998**, *17*, 3531−3540.
[26] [26a] C. E. Martin, P. Dubois, R. Jérôme, *Macromolecules* **2003**, *36*, 5934−5941. [26b] S. M. Guillaume, M. Schappacher, A. Soum, *Macromolecules* **2003**, *36*, 54−60.
[27] K. C. Hultzsch, T. P. Spaniol, J. Okuda, *Organometallics* **1997**, *16*, 4845−4856.
[28] [28a] M. Nishiura, Z. Hou, T. Koizumi, T. Imamoto, Y. Wakatsuki, *Macromolecules* **1999**, *2*, 8245−8251. [28b] W. J. Evans, H. Katsumata, *Macromolecules* **1994**, *27*, 2330−2332.
[29] C. Villiers, M. Ephritikhine, unpublished results.
[30] [30a] D. Takeuchi, T. Nakamura, T. Aida, *Macromolecules* **2000**, *33*, 725−729. [30b] J. Okuda, I. L. Rushkin, *Macromolecules* **1993**, *26*, 5530−5532.
[31] J. A. Hermann, J. F. Suttle, *Inorg. Synth.* **1957**, *5*, 143−145.
[32] *Kappa-CCD Software*, Nonius BV, Delft, The Netherlands, **1998**.
[33] Z. Otwinowski, W. Minor, *Methods Enzymol.* **1997**, *276*, 307−326.
[34] G. M. Sheldrick, *SHELXS-97* and *SHELXL-97*, University of Göttingen, Germany, **1997**.
[35] A. L. Spek, *PLATON*, University of Utrecht, The Netherlands, **2000**.
[36] G. M. Sheldrick, *SHELXTL*, Version 5.1, Bruker AXS Inc., Madison, WI, USA, **1999**.

Received June 9, 2004
Early View Article
Published Online October 7, 2004

 © 2004 Wiley-VCH Verlag GmbH & Co. KGaA, Weinheim

Synthesis, Structure and Properties of a Mononuclear and an End-On Double Azido-Bridged Copper(II) Complex Incorporating an N,N,N,O-Coordinating Tripodal Ligand

Sumana Sarkar,[a] Amrita Mondal,[a] Joan Ribas,[b] M. G. B. Drew,[c] Kausikisankar Pramanik,[a] and Kajal Krishna Rajak*[a]

Keywords: Azide ligands / Copper / Hydrogen bonds / Magnetic properties / Tripodal ligands

The blue coloured complex $[Cu(HL)(H_2O)(ClO_4)]ClO_4{\cdot}H_2O{\cdot}MeOH$ (**1**·H_2O·MeOH) has been synthesised in excellent yields by reacting $Cu(ClO_4)_2{\cdot}6H_2O$ with *N*,*N*-bis(2-methylpyridyl)(3,5-dimethyl-2-hydroxybenzyl)amine (HL) in methanol. The same reaction, when carried out in the presence of sodium azide, afforded a dark-blue complex of formula $[Cu_2(HL)_2(\mu\text{-}1,1\text{-}N_3)_2](ClO_4)_2$ (**2**). The crystal and molecular structures of the complexes have been solved. Variable-temperature magnetic susceptibility data in the range of 2–300 K for **2** reveal the existence of an antiferromagnetic interaction through an end-on azido linker. Temperature-dependent susceptibility studies for **2** were fitted using the Bleaney–Bowers expression, which led to the parameters $J = -3.2\ cm^{-1}$, $g = 2.12$ and $R = 2.14 \times 10^{-4}$.
(© Wiley-VCH Verlag GmbH & Co. KGaA, 69451 Weinheim, Germany, 2004)

Introduction

The existence of copper-containing enzymes and proteins and the potent biological activity of copper have increased recent interest in the coordination chemistry of copper with *O*,*N*-coordinating ligands.[1−6] It is well known that the azide ion inhibits the activity of metalloproteins,[1c,1d,1e,3e,7] thus metal azide complexes of such proteins have been studied extensively[8] in order to investigate the role of the metal ion in biological processes. The chemistry of azido-bridged copper(II) compounds has also received a great deal of attention for the understanding of magneto-structural correlations and for developing new functional-molecule-based materials.[9]

Among the many bridging ligands known, the azide ion can act not only as a monodentate ligand[10] but also link the metal ions in μ-1,1 (end-on) or μ-1,3 (end-to-end) bridging coordination modes, depending on the steric and electronic demands of the co-ligand. It has been widely found that the end-to-end bridging mode predominantly leads to antiferromagnetic coupling[11] and the end-on mode to ferromagnetic exchange;[12] instances of antiferromagnetic coupling in the case of end-on azido-bridged complexes are rare.[13] This has prompted us to undertake the task of designing diazido-bridged copper(II) species by using an *N*,*N*,*N*,*O*-coordinating tripodal ligand.

Here we describe the synthesis and characterisation of a mononuclear copper(II) species and a double asymmetric μ-1,1 azido-bridged Cu^{II} complex incorporating an *N*,*N*,*N*,*O*-coordinating tripodal ligand. The solid and solution structures of the complexes, as well as their properties, were probed by X-ray diffractometry and spectroscopic and electrochemical methods. The variable-temperature magnetic moment was measured for the dinuclear species.

Results and Discussion

The tripodal ligand HL is used in this present work; it was synthesised by a reported procedure.[14]

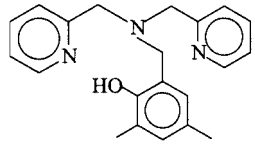

HL

[a] Inorganic Chemistry Section, Department of Chemistry, Jadavpur University,
Kolkata, 700 032, India
E-mail: kajalrajak@hotmail.com
[b] Department de Química Inorgánica, Universitat de Barcelona, Diagonal 6487, 08028 Barcelona, Spain
E-mail: joan.ribase@qi.ub.es
(for correspondence related to magnetic studies)
[c] School of Chemistry, The University of Reading, P. O. Box 224, Whiteknights, Reading, UK RG6 6AD

The stoichiometric reaction of $Cu(ClO_4)_2 \cdot 6H_2O$ with HL, in methanol, afforded the blue complex $[Cu(HL)(H_2O)(ClO_4)]ClO_4$ (**1**) in excellent yields. The same reaction, when carried out in the presence of an excess of sodium azide, yielded the dark-blue complex of formula $[Cu_2(HL)_2(\mu\text{-}1,1\text{-}N_3)_2](ClO_4)_2$ (**2**) [Equation (1)].

$$Cu(ClO_4)\cdot 6H_2O \xrightarrow[MeOH]{HL} [Cu(HL)(H_2O)(ClO_4)]ClO_4$$

$$\xrightarrow{N_3^-} [Cu_2(HL)_2(\mu\text{-}1,1\text{-}N_3)_2](ClO_4)_2 \quad (1)$$

In the IR spectra of complexes **1** and **2** the characteristic perchlorate stretches occur at 600 cm^{-1} and 1100 cm^{-1}, respectively, and the hydrogen-bonded phenolic OH appears as a broad peak near 3250 cm^{-1}.[5c] The Cu−N_3 stretch is observed at 2100 cm^{-1} in **2**.

In solution the complexes exhibit a relatively weak band in the 590 nm region of the UV/Vis spectrum. This transition is logically assigned as the ligand-field excitation.[15] An allowed intense band observed near 390 nm for complex **2** may be assigned as the $N_3^- \rightarrow Cu^{II}$ transition.[16]

All the complexes are electroactive at a platinum electrode in acetonitrile solution. Cyclic voltammetric reduction potential data are given in the Exp. Sect. and the voltammograms are shown in Figure 1. In both cases an anodic response occurs near 1.5 V, believed to be due to $Cu^{II} \rightarrow Cu^{III}$ oxidation; the oxidized complex is too reactive to survive for the cathodic scan. The complexes also display a quasireversible peak near 0.0 V corresponding to the Cu^{II}/Cu^{I} reduction couple. The low oxidation and reduction potentials for **2** compared to those of **1** may be due to the azide chelation.

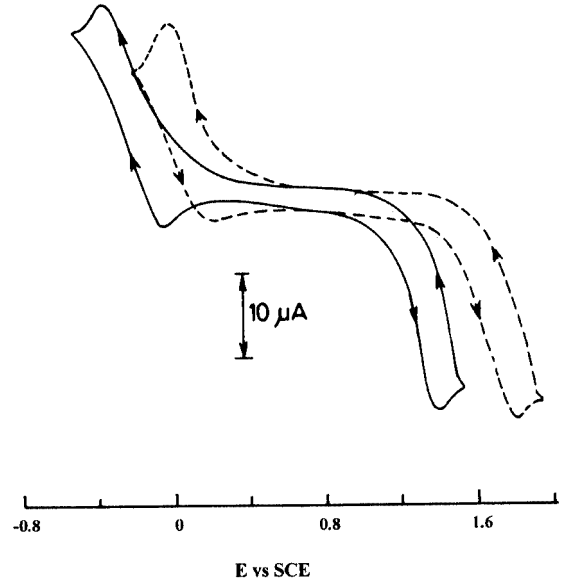

Figure 1. Cyclic voltammograms of ca. 10^{-3} M solutions of $[Cu(HL)(H_2O)(ClO_4)]ClO_4$ (----) and $[Cu_2(HL)_2(\mu\text{-}1,1\text{-}N_3)_2](ClO_4)_2$ (−) in acetonitrile

X-ray Crystallography

The crystal structures of $[Cu(HL)(H_2O)(ClO_4)]ClO_4 \cdot H_2O \cdot MeOH$ (**1**·H_2O·MeOH) and $[Cu_2(HL)_2(\mu\text{-}1,1\text{-}N_3)_2](ClO_4)_2$ (**2**) have been determined. Molecular views excluding the hydrogen atoms and the solvent molecules are shown in Figure 2 and 3, respectively. Selected bond parameters are listed in Table 1.

In both complexes the three nitrogen atoms of the tripodal ligand are disposed meridionally forming two five-membered chelate rings, whereas the phenolic oxygen atom is coordinated axially, forming a six-membered chelate ring. The two pyridine rings (NC_5H_5) of the ligand are planar (mean deviation about 0.02 Å) and the dihedral angle be-

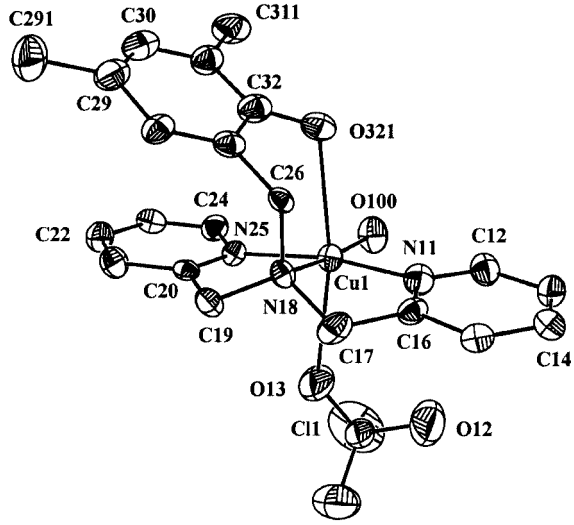

Figure 2. Perspective view and atom-labelling scheme for $[Cu(HL)(H_2O)(ClO_4)]ClO_4$ (**1**); all non-hydrogen atoms (excluding solvent molecules) are represented by 30% thermal probability ellipsoids

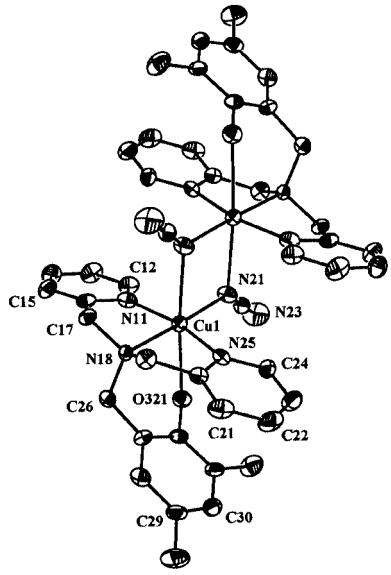

Figure 3. Perspective view and atom-labelling scheme of $[Cu_2(HL)_2(\mu\text{-}1,1\text{-}N_3)_2](ClO_4)_2$ (**2**): all non-hydrogen atoms (excluding perchlorate ions) are represented by 30% thermal probability ellipsoids

 © 2004 Wiley-VCH Verlag GmbH & Co. KGaA, Weinheim

Table 1. Selected bond lengths (Å) and angles (°) for **1**·H_2O·MeOH and **2**

	1·H_2O·MeOH	**2**
Cu(1)−N(11)	1.949(10)	1.993(7)
Cu(1)−N(18)	2.051(8)	2.065(6)
Cu(1)−N(25)	1.975(8)	2.009(7)
Cu(1)−N(21)		1.972(7)
Cu(1)−N(21A)		2.563(8)
Cu(1)−O(13)	2.491(10)	
Cu(1)−O(100)	1.996(8)	
Cu(1)−O(321)	2.506(9)	2.578(9)
N(21)−N(22)		1.175(9)
N(22)−N(23)		1.154(10)
Cu···Cu		3.452(8)
N(11)−Cu(1)−N(18)	82.70(4)	81.70(3)
N(11)−Cu(1)−N(25)	164.50(4)	165.30(3)
N(18)−Cu(1)−N(25)	83.80(3)	83.50(3)
N(18)−Cu(1)−N(21)		177.10(3)
N(21)−Cu(1)−N(11)		97.70(3)
N(21)−Cu(1)−N(25)		97.00(3)
N(11)−Cu(1)−N(21A)		90.24(4)
N(18)−Cu(1)−N(21A)		95.42(5)
N(21)−Cu(1)−N(21A)		81.69(3)
N(25)−Cu(1)−N(21A)		91.34(5)
N(11)−Cu(1)−O(13)	89.67(5)	
N(18)−Cu(1)−O(13)	90.28(6)	
N(25)−Cu(1)−O(13)	82.84(4)	
N(11)−Cu(1)−O(100)	96.80(4)	
N(18)−Cu(1)−O(100)	174.70(3)	
N(25)−Cu(1)−O(100)	97.40(3)	
N(11)−Cu(1)−O(321)	101.45(6)	93.98(5)
N(18)−Cu(1)−O(321)	88.10(5)	87.16(6)
N(25)−Cu(1)−O(321)	85.62(4)	85.07(5)
N(21)−Cu(1)−O(321)		95.76(4)
N(21A)−Cu(1)−O(321)		175.34(6)
O(13)−Cu(1)−O(100)	95.12(6)	
O(13)−Cu(1)−O(321)	168.45(5)	
O(100)−Cu(1)−O(321)	86.70(6)	
Cu(1)−N(21)−Cu(1A)		98.31(8)
N(21)−N(22)−N(23)		177.00(10)

tween these two planes is 5.6° in **1**·H_2O·MeOH and 18.4° in **2**.

$[Cu(HL)(H_2O)(ClO_4)]ClO_4·H_2O·MeOH$ (**1**·H_2O·MeOH)

The structure of **1**·H_2O·MeOH consists of a monomeric $[Cu(HL)(H_2O)(ClO_4)]ClO_4·H_2O·MeOH$ unit. The geometry around the metal centre of **1**·H_2O·MeOH appears to be distorted octahedral and is characterised by an O−Cu−O bond angle of 168.45°, which deviates significantly from the ideal value of 180°. In a distorted CuN_3O_3 octahedral environment, the fourth equatorial position *trans* to the tripodal nitrogen atom is occupied by the oxygen atom of a water molecule and the sixth axial position by the perchlorate oxygen atom. The copper atom is displaced by 0.01 Å towards the phenolic oxygen atom from the equatorial plane (mean deviation 0.105 Å) defined by N(11), N(18), N(25) and O(100). The three basal Cu−N bond lengths are unequal; the longest distance is the bond to the tripodal nitrogen and the shortest is that to the pyridine nitrogen. The latter is due to the sp^2 character of the pyridine nitrogen. The axial Cu−O and Cu−N bond lengths are longer because of the pseudo Jahn−Teller effect.

$[Cu_2(HL)_2(\mu\text{-}1,1\text{-}N_3)_2](ClO_4)_2$ (**2**)

Two centrosymmetrically related Cu(HL)(μ-1,1-N_3) units are linked by the azide ion in an end-on fashion forming a doubly asymmetric bridged dimeric complex. The coordination geometry around the copper ion is distorted octahedral. Four nitrogen atoms (two pyridine, one tripodal and one azide nitrogen) form the square plane (mean deviation 0.023 Å) and the copper atom is displaced by 0.026 Å towards the coordinated phenolic oxygen atom from this plane. The remaining apical position of the octahedron is occupied by the bridging azide nitrogen atom of the other unit. The Cu−N distances and N−Cu−N bond angles in the basal plane range from 1.972 Å to 2.065 Å and 97.0° to 177.1° respectively. The long axial Cu−N (ca. 2.563 Å) distance can be attributed to a pseudo Jahn−Teller distortion. The intra-dimer Cu···Cu bond length is 3.452 Å. The azide ion is quasilinear, with an N−N−N bond angle of 177.0(10)°; the N−N bond lengths are 1.175(9) Å and 1.154(10) Å, respectively. In the end-on bridging moiety, the Cu−N−Cu bond angle is 98.31(8)°.

Hydrogen Bonding

In complex **1**·H_2O·MeOH the coordinated water molecule, the oxygen atom of the coordinated perchlorate ion and the phenolic oxygen atom of the ligand are extensively involved in hydrogen bonding with lattice water and methanol molecules. The lattice water molecule is held by water(lattice)···water(coordinated) [O···O = 2.718(14) Å] and water(lattice)··· oxygen(phenolic) [2.883(12) Å] hydrogen bonds. The methanol molecule in the lattice is also engaged in such bonding with the oxygen atom of the coordinated perchlorate ion and the coordinated water molecule, with O···O bond lengths of 2.831(13) Å and 2.782 (12) Å, respectively. The most striking feature is that two such molecules are linked by water···methanol hydrogen bonds [2.713(12) Å] forming a six-membered ring as depicted in

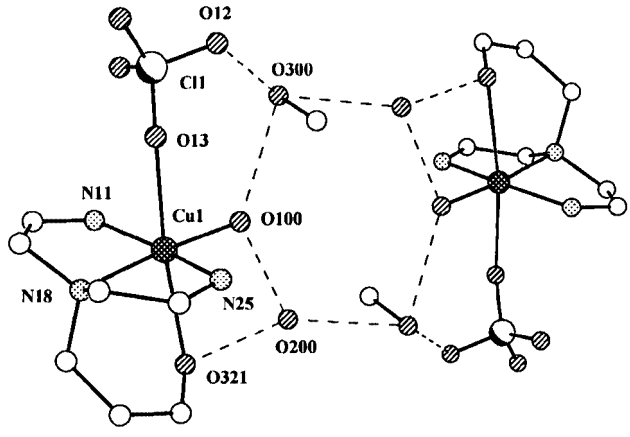

A

 © 2004 Wiley-VCH Verlag GmbH & Co. KGaA, Weinheim

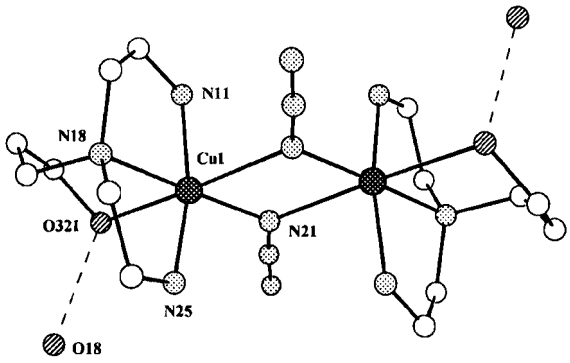

B

A. In the case of **2** the oxygen atom of the perchlorate ion is hydrogen bonded to the phenolic oxygen atom, with an O···O bond length of 2.650(10) Å as depicted in **B**.

Magnetic Studies

Variable-temperature magnetic susceptibility measurements were performed in the range of 2−300 K. The plot of $\chi_M T$ versus T for complex **2** is shown in Figure 4.

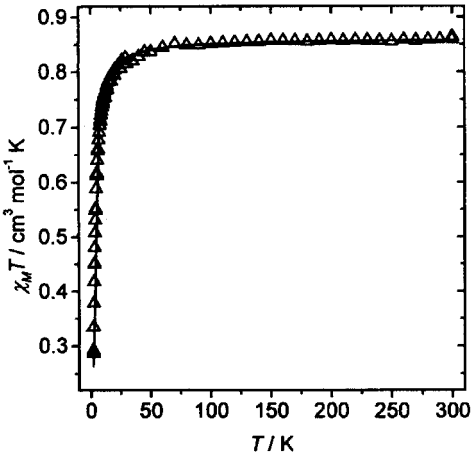

Figure 4. $\chi_M T$ versus T for **2**; open points are the experimental data and the solid line represents the best fit obtained

In **2**, the magnetic data are for two copper(II) ions as the complex is a dinuclear system. The experimental $\chi_M T$ value at 300 K is 0.86 emu·cm^{-1}·K, as expected for two quasi-isolated spin doublets. This value remains almost constant up to 50 K but decreases rapidly to 0.28 emu·cm^{-1}·K at 2 K. This feature is characteristic of a weak antiferromagnetic interaction. The reduced molar magnetisation at 2 K (Figure 5) clearly corroborates that the antiferromagnetic coupling is very small.

The magnetic susceptibility data were fitted by applying the Bleaney−Bowers formula with the Hamiltonian[9d]

$H = -JS_1 \cdot S_2$

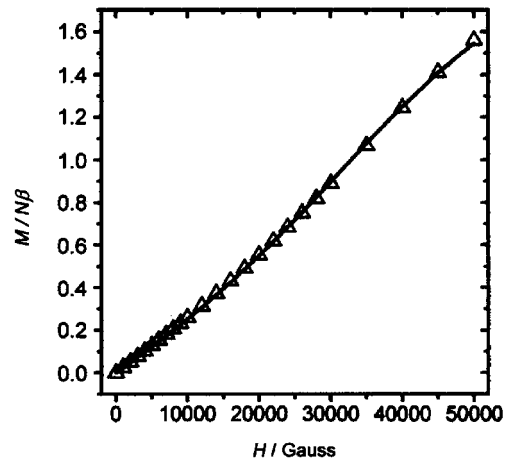

Figure 5. Plot of the reduced magnetisation, $M/N\beta$, versus H for **2**; open points are the experimental data and the solid line represents the best fit obtained.

The best-fit parameters obtained are $J = -3.2 \pm 0.1$ cm^{-1}, $g = 2.12 \pm 0.01$ and $R = 2.1 \times 10^{-4}$. Very similar J and g values were obtained by a full-diagonalisation from the curve of the magnetisation at 2 K. In this case, the best-fit parameters are $J = -3.0 \pm 0.1$ cm^{-1}, $g = 2.12 \pm 0.01$ and $R = 5.1 \times 10^{-5}$. Thus, the two methods give almost identical results. It is well documented that end-on double azido-bridged copper(II) dimers are usually ferromagnetic[12] but here the measurement clearly indicates that the coupling between the two Cu^{II} ions is antiferromagnetic which is very unusual.

In copper(II) systems with an end-on coordination of the azide ion, the exchange interaction will be strong when the magnetic orbitals involved are of the $d_{x^2-y^2}$ type. However, a low magnetic coupling should be expected when the interaction is between axial-equatorial coordination sites because the atomic orbitals involved are $d_{x^2-y^2}$ and d_{x^2} respectively. In complex **2**, the nitrogen atom of the unsymmetrically bridged azide ion belongs to the basal plane of one copper ion and also occupies one elongated apical position of the other metal centre. An exactly analogous situation occurs for the other centrosymmetrically related azide bridge. Consequently, the interaction between the magnetic orbitals is expected to be very weak, leading to a small exchange-coupling parameter. Moreover, the Cu−N(apical) bond is significantly longer than the distance required for a ferromagnetic interaction.[17] These two factors are most probably responsible for the weak antiferromagnetic coupling.

EPR Spectra

Both complexes show axial EPR spectra typical for monomeric copper(II) species with a $d_{x^2-y^2}$ ground-state doublet ($g_\parallel > g_\perp > 2.0$) in the solid state and in solution.[18] The spectroscopic data are listed in Table 2. From the spectrum of **2** it is clear that there is no significant interaction between the copper centres (Figure 6) in the solid state. The EPR spectra of **1**·H_2O·MeOH and **2** are practically

 © 2004 Wiley-VCH Verlag GmbH & Co. KGaA, Weinheim

identical with very similar $g_{\|}$ (range = 2.219−2.234), $g_{\perp}$ (range = 2.039−2.042) and $A_{\|}$ (range = 171−176 G) values.

Table 2. X-Band EPR data for 1·H_2O·MeOH and 2((Author: There appears to be data missing from this table. Please check))

	Matrix	g_{av}	A_{av} (G)	$g_{\|}$	$g_{\perp}$	$A_{\|}$ (G)
1·H_2O·MeOH	DMF/toluene, 77 K	2.122	120	2.235	2.042	171
	solid, 77 K					
	DMF/toluene, 77 K	2.115	120	2.219	2.039	175
2	solid, 77 K					

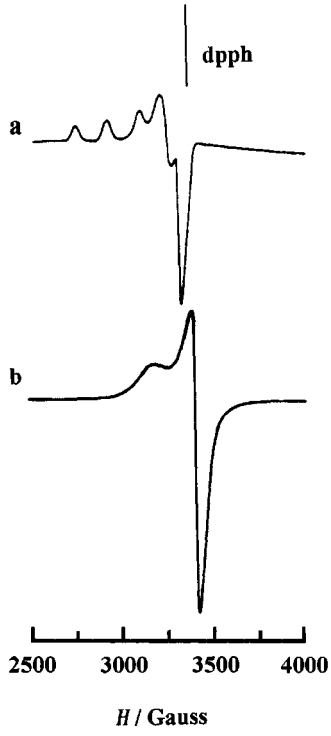

Figure 6. X-band EPR spectra of (a) $[Cu_2(HL)_2(\mu\text{-}1,1\text{-}N_3)_2](ClO_4)_2$ in DMF/ toluene at 77 K, and (b) $[Cu_2(HL)_2(\mu\text{-}1,1\text{-}N_3)_2](ClO_4)_2$ in the solid state at 77 K; instrument settings: power 30 db; modulation 100 kHz; sweep centre 3200 G

Conclusions

The synthesis and structural characterisation of copper(II) complexes incorporating *N*,*N*-bis(2-methylpyridyl)(3,5-dimethyl-2-hydroxybenzyl)amine (HL) has been successfully achieved. The parent species $[Cu(HL)(H_2O)(ClO_4)]ClO_4$ was prepared by the reaction of HL with $Cu(ClO_4)_2{\cdot}6H_2O$ in methanol. This complex reacts with sodium azide to afford the complex $[Cu_2(HL)_2(\mu\text{-}1,1\text{-}N_3)_2](ClO_4)_2$. To the best of our knowledge $[Cu_2(HL)_2(\mu\text{-}1,1\text{-}N_3)_2](ClO_4)_2$ is the first example of an end-on diazido-bridged octahedral copper(II) complex showing antiferromagnetic character. A search for new copper(II) complexes with different tetradentate ligand systems is in progress.

Experimental Section

Materials: All the starting chemicals were analytically pure and used without further purification. The ligands were prepared according to the literature procedure.[14]

Caution! *Perchlorate salts are highly explosive, and should be handled with care and in small amounts.*

Physical Measurements: UV/Vis spectra were recorded on a Perkin−Elmer LAMBDA EZ-301 spectrophotometer and IR spectra were measured with a Perkin−Elmer L-0100 spectrometer. Electrochemical measurements were performed on acetonitrile solutions of the complexes on a CH 620 A electrochemical analyzer using a platinum electrode. Tetraethylammonium perchlorate (TEAP)[19] was used as the supporting electrolyte and the potentials are referenced to the standard calomel electrode (SCE) without junction correction. EPR spectra were recorded on a Varian E-109C X-band spectrometer. Magnetic measurements were carried out on polycrystalline samples with a Quantum Design MPMS XL SQUID susceptometer operating at a magnetic field of 0.1 T between 2 and 3 K. The diamagnetic corrections were evaluated from Pascal's constants. Elemental analyses (C, H, N) were performed on a Perkin−Elmer 2400 Series II elemental analyzer.

$[Cu(HL)(H_2O)(ClO_4)]ClO_4$ (1): HL (0.168 g, 0.5 mmol) was added to a solution of copper(II) perchlorate hexahydrate (0.186 g, 0.5 mmol) in methanol (10 mL) and the resulting blue solution was stirred for 0.5 h at room temperature. Slow evaporation of the solution yielded a blue, crystalline product. Yield: 0.210 g (70%). $C_{21}H_{25}ClCuN_3O_{10}$ (610.5): calcd. C 42.32, H 4.20, N 7.05; found C 42.08, H 4.04, N 6.94. UV/Vis (CH_3CN): λ_{max} (ε) = 590 nm (107 $M^{-1}cm^{-1}$). IR (KBr): $\nu(ClO_4^-)$ 1100, 620; ν(OH) 3250 cm^{-1}. E_{pa} (Cu^{III}/Cu^{II} couple): 1.8 V (irr.); $E_{1/2}$ (Cu^{II}/Cu^{I} couple): 0.15 V (ΔE_p, 200 mV).

$[Cu_2(HL)_2(\mu\text{-}1,1\text{-}N_3)_2](ClO_4)_2$ (2): HL (0.168 g, 0.5 mmol) and sodium azide (0.046 g, 0.7 mmol) were added to a methanolic solution (10 mL) of copper(II) perchlorate hexahydrate (0.186 g, 0.5 mmol). The resulting blue solution was stirred for 0.5 h at room temperature. Slow evaporation of the solution yielded a blue, crystalline product. Yield: 0.140 g (70%). $C_{21}H_{23}N_6ClCuO_5$ (538.44): calcd. C 46.84, H 4.28, N 15.61; found C 46.56, H 4.12, N 15.44. UV/Vis (CH_3CN): λ_{max} (ε) = 392 nm (2368 $M^{-1}cm^{-1}$), 590 (293). IR (KBr): $\nu(N_3^-)$ 2100; $\nu(ClO_4^-)$ 1100, 640; ν(OH) 3240 cm^{-1}. E_{pa} (Cu^{III}/Cu^{II} couple): 1.5 V (irr.); $E_{1/2}$ (Cu^{II}/Cu^{I} couple): −0.2 V (ΔE_p, 200 mV).

Crystallographic Studies: Crystals of $[Cu(HL)(H_2O)(ClO_4)]ClO_4$ and $[Cu_2(HL)_2(\mu\text{-}1,1\text{-}N_3)_2](ClO_4)_2$ were grown by slow evaporation of the solvents from their methanolic solution. Data were measured with Mo-K_α radiation using an MA Research Image Plate System. The crystals were positioned 70 mm from the Image Plate. 100 Frames were measured at 2° intervals with a counting time of 5 min. Data analyses were carried out with the XDS program[20] and the structures were solved by direct methods with the Shelx-86 program.[21] Non-hydrogen atoms were refined with anisotropic thermal parameters. One of the perchlorate ions of complex 1·H_2O·MeOH and that of **2** are highly disordered. The hydrogen atoms bonded to carbon were included in geometric positions and given thermal parameters equivalent to 1.2-times those of the atom to which they are attached. Empirical absorption corrections were applied using DIFABS[22] and the structures were refined on F^2 using Shelxl.[23] Significant crystal data are given in Table 3.
CCDC-240990 (for 1·H_2O·MeOH) and -240991 (for **2**) contain the supplementary crystallographic data for this paper. The CIF files

 © 2004 Wiley-VCH Verlag GmbH & Co. KGaA, Weinheim

for $[Cu(L^1)(N_3)(ClO_4)]$, $[Cu(L^2)(N_3)(ClO_4)]_2$ and $[Cu(L^3)(N_3)]_n(ClO_4)_n$ have also been deposited. These data can be obtained free of charge at www.ccdc.cam.ac.uk/conts/retrieving.html [or from the Cambridge Crystallographic Data Centre, 12 Union Road, Cambridge CB2 1EZ, UK; Fax: +44-1223-336-033; E-mail: deposit@ccdc.cam.ac.uk].

Table 3. Crystal data and structure-refinement parameters for **1**·H_2O·MeOH and **2**

	1·H_2O·MeOH	**2**
Formula	$C_{22}H_{28}Cl_2N_3O_{12}Cu$	$C_{21}H_{23}ClN_6O_5Cu$
Mol. mass	660.5	538.44
Crystal system	monoclinic	monoclinic
Space group	$P2_1/c$	$P2_1/n$
a (Å)	8.360(11)	8.185(9)
b (Å)	21.690(2)	12.573(14)
c (Å)	15.256(17)	22.70(2)
β (°)	92.272(10)	90.913(10)
V (Å^3)	2765(6)	2336(4)
Z	4	4
$D_{calcd.}$, [mg m^{-3}]	1.547	1.531
μ(Mo-K_α) (mm^{-1})	1.046	1.095
θ (°)	2.61 to 25.79	1.85 to 26.11
Measured reflections	7872	3996
Unique reflections (R_{int})	4000/ 0.1025	3996/ 0.0000
Temperature (K)	293	293
$R1$,[a] $wR2$[b][$I > 2\sigma(I)$]	0.1029, 0.2330	0.0976, 0.2601
GOF on F^2	1.059	1.057

[a] $R1 = |F_o| - |F_c|/|F_o|$. [b] $wR2 = [w(F_o^2 - F_c^2)^2/w(F_o^2)^2]^{1/2}$.

Acknowledgments

Financial support from the Council of Scientific and Industrial Research, New Delhi, India, and from the Department of Science and Technology, New Delhi, India, are gratefully acknowledged. Joan Ribas acknowledges financial support from the Spanish Government (grant BQU2000/0791).

[1] [1a] F. A. Cotton, G. Wilkinson, C. A. Murillo, *Advanced Inorganic Chemistry*, Wiley, New York, **1999**. [1b] M. E. Cuff, K. I. Miller, K. E. van Holde, W. A. Hendrickson, *J. Mol. Biol.* **1998**, *278*, 855. [1c] E. I. Solomon, U. M. Sundaram, T. E. Machonkin, *Chem. Rev.* **1996**, *96*, 2563. [1d] N. Kitajima, Y. Moro-oka, *Chem. Rev.* **1994**, *94*, 737. [1e] K. A. Magnus, H. Ton-That, J. E. Carpenter, *Chem. Rev.* **1994**, *94*, 727. [1f] N. Kitajima, *Adv. Inorg. Chem.* **1992**, *39*, 1.

[2] [2a] R. H. Holm, P. Kennepohl, E. I. Solomon, *Chem. Rev.* **1996**, *96*, 2239. [2b] E. T. Adam, *Adv. Protein Chem.* **1991**, *92*, 145. [2c] S. K. Chapman, *Perspectives on Bioinorganic Chemistry* (Eds.: R. W. Hay, J. R. Dilworth, K. B. Nolan), JAI Press, London, **1991**, p. 95.

[3] [3a] K. D. Karlin, A. D. Zuberbhuler, in *Bioinorganic Catalysis*, 2nd. ed. (Eds.: J. Reedijk, E. Bouwman), Marcel Dekker, New York, **1999**, p. 469. [3b] H. C. Liang, M. Dahan, K. D. Karlin, *Curr. Opin. Chem. Biol.* **1999**, *3*, 168. [3c] S. Fox, K. D. Karlin, in *Active Oxygen in Biochemistry* (Eds.: J. S. Valentine, C. S. Foote, A. Greenberg, J. F. Liebman), Blackie Academic and Professional, Glasgow, Scotland, **1995**, p. 188. [3d] K. D. Karlin, N. Wei, B. Jung, S. Kaderli, P. Niklaus, A. D. Zuberbuehler, *J. Am. Chem. Soc.* **1993**, *115*, 9506. [3e] *Bioinorganic Chemistry of Copper* (Eds.: K. D. Karlin, Z. Tyekler), Chapman & Hall, New York, **1993**. [3f] K. D. Karlin, *Science* **1993**, *261*, 701.

[4] [4a] S. Schindler, *Eur. J. Inorg. Chem.* **2000**, 2311. [4b] D. E. Wilcox, *Chem. Rev.* **1996**, *96*, 2435. [4c] A. L. Feig, S. J. Lippard, *Chem. Rev.* **1994**, *94*, 759. [4d] E. I. Solomon, F. Tuczek, D. E. Root, C. A. Brown, *Chem. Rev.* **1994**, *94*, 827. [4e] T. N. Sorell, *Tetrahedron* **1989**, *45*, 3.

[5] [5a] B. K. Santra, P. A. N. Reddy, M. Nethaji, A. R. Chakravarty, *J. Chem. Soc., Dalton Trans.* **2001**, 3553. [5b] M. Schatz, M. Becker, F. Thaler, F. Hampel, S. Schindler, R. R. Jacobson, Z. Tyeklár, N. N. Murthy, P. Ghosh, Q. Chen, J. Zubieta, K. D. Karlin, *Inorg. Chem.* **2001**, *40*, 2312. [5c] S. Torelli, C. Belle, I. Gautier-Luneau, J. L. Pierre, E. Saint-Aman, J. M. Latour, L. Le Pape, D. Luneau, *Inorg. Chem.* **2000**, *39*, 3526. [5d] H. Decker, R. Dillinger, F. Tuczek, *Angew. Chem. Int. Ed.* **2000**, *39*, 1591. [5e] A. G. Blackman, W. B. Tolman, *Structure and Bonding: Metal Oxo and Metal Peroxo Species* (Ed.: B. Meunier), Springer, Berlin, **2000**, vol. 97, pp. 179. [5f] L. L. Koh, J. O. Ranford, W. T. Robinson, J. O. Svensson, A. L. C. Tan, D. Wu, *Inorg. Chem.* **1996**, *35*, 6466.

[6] [6a] R. C. Holz, J. M. Bradshaw, B. Bennett, *Inorg. Chem.* **1998**, *37*, 1219 and references cited therein. [6b] J. Reim, B. Krebs, *J. Chem. Soc., Dalton Trans.* **1997**, 3793. [6c] Y.-H. Chung, H.-H. Wei, H.-Y. Liu, G.-H. Lee, Y. Wang, *J. Chem. Soc., Dalton Trans.* **1997**, 2825. [6d] W. Kaim, J. Rall, *Angew. Chem. Int. Ed. Engl.* **1996**, *35*, 43. [6e] J. Ling, L. P. Nestor, R. S. Czernuszewicz, T. G. Spiro, R. Fraczkiewicz, K. D. Sharma, T. M. Loehr, J. Sanders-Loehr, *J. Am. Chem. Soc.* **1994**, *116*, 7682. [6f] K. Lerch, *Life Chem. Rep.* **1987**, *5*, 221.

[7] [7a] T. G. Spiro, *Copper Proteins*, Wiley, New York, **1981**. [7b] B. Reinhammer, *Copper Proteins and Copper Enzymes*, CRC, Boca Raton, FL, **1984**, vol. 3, pp. 1−35. [7c] E. I. Solomon, M. J. Baldwin, M. D. Lowery, *Chem. Rev.* **1992**, *92*, 521. [7d] E. I. Solomon, *Metal Clusters in Proteins* (Ed.: L. Que), American Chemical Society, Washington D.C., **1988**, pp. 116. [7e] M. Trémolières, J. G. Bieth, *Phytochemistry* **1984**, *23*, 501. [7f] A. Rompel, H. Fisher, K. Büldt-Karentzopoulos, D. Miewes, F. Zippel, H. F. Nolting, C. Hermes, B. Krebs, H. Witzel, *J. Inorg. Biochem.* **1995**, *59*, 715.

[8] [8a] J. L. Cole, P. A. Clark, E. I. Solomon, *J. Am. Chem. Soc.* **1990**, *112*, 9534. [8b] J. L. Cole, L. Avigliano, L. Morpurgo, E. I. Solomon, *J. Am. Chem. Soc.* **1991**, *113*, 9080.

[9] [9a] P. Manikandan, R. Muthukumaran, K. R. Justin Thomas, B. Varghese, G. V. R. Chandramouli, P. T. Manoharan, *Inorg. Chem.* **2001**, *40*, 2378. [9b] K.-S. Bürger, P. Chaudhuri, K. Weighardt, *Inorg. Chem.* **1996**, *35*, 2704. [9c] *Magnetism: A Supramolecular Function* (Ed.: O. Kahn), NATO ASI Series, No. C484; Kluwer Academic Publishers, Dordrecht, The Netherlands, **1996**. [9d] O. Kahn, *Molecular Magnetism*, VCH Publishers, New York, **1993**. [9e] *Magnetism: Molecules to Materials* (Eds.: J. Miller, M. Drilon), Wiley-VCH, Weinheim, **2002**.

[10] R. Kurtaran, C. Arici, S. Durmu, D. Ülkü, O. Atakol, *Anal. Sci.* **2003**, *19*, 335.

[11] [11a] Y. Agnus, R. Louis, J. P. Gisselbrecht, R. Weiss, *J. Am. Chem. Soc.* **1984**, *106*, 93. [11b] V. Mckee, M. Zvagulis, J. V. Dagdigian, M. G. Patch, C. A. Reed, *J. Am. Chem. Soc.* **1984**, *106*, 4765.

[12] [12a] O. Kahn, S. Sikorav, J. Gouteron, S. Jeannin, Y. Jeannin, *Inorg. Chem.* **1983**, *22*, 2877. [12b] J. Comarmond, P. Plumere, J. M. Lehn, Y. Agnus, R. Louis, R. Weiss, O. Kahn, I. Morgenstern-Badarau, *J. Am. Chem. Soc.* **1982**, *104*, 6330. [12c] I. B. Waksman, M. L. Boillot, O. Kahn, S. Sikorav, *Inorg. Chem.* **1984**, *23*, 4454. [12d] J. Cabrero, C. de Graaf, E. Bordas, R. Caballol, J.-P. Malrieu, *Chem. Eur. J.* **2003**, *9*, 2307.

[13] [13a] M. Sinha Ray, A. Ghosh, R. Bhattacharya, G. Mukhopadhyay, M. G. B. Drew, J. Ribas, *Dalton Trans.* **2004**, 252. [13b] S. Koner, S. Saha, T. Mallah, K.-I. Okamoto, *Inorg. Chem.* **2004**, *43*, 840.

[14] R. Kannappan, R. Mahalakshmy, T. M. Rajendiram, R. Venk-

 © 2004 Wiley-VCH Verlag GmbH & Co. KGaA, Weinheim

atesan, P. Sambasiva Rao, *Proc. Indian Acad. Sci. (Chem. Sci.)* **2003**, *115*, 1−14.
[15] J. M. Rowland, M. M. Olmstead, P. K. Mascharak, *Inorg. Chem.* **2000**, *39*, 5326.
[16] M. E. Winkler, K. Lerch, E. I. Solomon, *J. Am. Chem. Soc.* **1981**, *103*, 7001.
[17] E. Ruiz, J. Cano, S. Alvarez, P. Alemany, *J. Am. Chem. Soc.* **1998**, *120*, 11122.
[18] B. J. Hathaway, *Comprehensive Coordination Chemistry* (Eds.: G. Wilkinson, R. D. Gillard, J. A. McCleverty), Pergamon Press, Oxford, U. K., **1987**, vol. 5, p. 668.
[19] G. K. Lahiri, S. Bhattacharya, B. K. Ghosh, A. Chakravorty, *Inorg. Chem.* **1987**, *26*, 4324.
[20] W. Kabsh, *J. Appl. Crystallogr.* **1988**, *21*, 916.
[21] G. M. Sheldrick, *SHELXL-86, Acta Crystallogr., Sect. A* **1990**, *46*, 467.
[22] N. Walker, D. Stuart, DIFABS program, *Acta Crystallogr., Sect. A* **1983**, *39*, 158.
[23] G. M. Sheldrick, *SHELXL*; University of Göttingen, **1993**.

Received June 6, 2004
Early View Article
Published Online October 20, 2004

 © 2004 Wiley-VCH Verlag GmbH & Co. KGaA, Weinheim

Slow Electron Self-Exchange in Spite of a Small Inner-Sphere Reorganisation Energy − The Electron-Transfer Properties of a Copper Complex with a Tetradentate Bispidine Ligand

Peter Comba,*[a] Marion Kerscher,[a] and Andreas Roodt[b]

Keywords: Marcus theory / Kinetics / Molecular mechanics / Outer-sphere electron transfer / Cross reaction

The electron self-exchange rate of $[Cu(L)(OH_2)]^{2+/1+}$, k_{11}^{exp}(298.13 K) = 15 ± 11 $m^{-1}s^{-1}$ {L = dimethyl 3,7-dimethyl-9-oxo-2,4-bis(2-pyridyl)-3,7-diazabicyclo[3.3.1]nonane-1,5-dicarboxylate}, was determined by a cross reaction. The analysis, based on classical Marcus theory, indicates that this relatively slow rate is to a large extent due to enthalpic terms ($\Delta G_{11}^{\ddagger,exp}$ = 62.8 ± 3.5 kJ·mol^{-1}, $\Delta H_{11}^{\ddagger,exp}$ = 36.0 ± 2.7 kJ·mol^{-1} and $\Delta S_{11}^{\ddagger,exp}$ = –92 ± 10 J·mol^{-1}K^{-1}). The activation entropy is significant but not unusually large and the calculated outer-sphere reorganization energy, $\Delta G_{out}^{\ddagger,calc}$ = 20.5 kJ·mol^{-1}, is at least of the same order of magnitude as the calculated inner-sphere reorganisation energy $\Delta G_{in}^{\ddagger,calc}$ = 18.6 kJ·mol^{-1}, i.e. the deformation of the solvent sheath is a major reason for the slow electron transfer rate. This is believed to be due to the highly elastic coordination geometry which leads to little strain upon distortion enforced by the electron transfer but to comparably large structural changes and, hence, to a large outer-sphere reorganisation term.
(© Wiley-VCH Verlag GmbH & Co. KGaA, 69451 Weinheim, Germany, 2004)

Introduction

Transition metal complexes of bispidine-type ligands {Figure 1 shows the tetradentate ligand L = dimethyl 3,7-dimethyl-9-oxo-2,4-bis(2-pyridyl)-3,7-diazabicyclo[3.3.1]-nonane-1,5-dicarboxylate} have a number of unique properties: (i) Due to the comparably high degree of preorganisation and complementarity[1] they lead to very stable complexes (e.g., for Cu^{II} complexes, stabilities are in the same range as those with macrocyclic ligands[2−4]). (ii) L enforces a square pyramidal configuration upon Cu^{II} with a monodentate co-ligand in plane with two co-planar pyridines and a tertiary amine (N3), and with a tertiary amine (N7) as an apical donor.[4] This unique configuration for Cu^{II} leads to strong copper-substrate binding and interesting reactivities.[5−8] (iii) Most relevant for the present study is that while the bispidine ligands are rigid, the coordination sphere is elastic.[1] This follows from experimental structural data[9] and from empirical force field calculations[1,9−11] which indicate that metal ions of quite different sizes fit into the bispidine cavity without inducing much steric strain in the ligand, i.e. the structure of the ligand backbone is practically constant while the metal donor bonds vary in the expected ranges.[6,9] Another interesting observation based on experimental structural data and related to the elasticity of the coordination geometry is that there are various structurally different positions within the bispidine cavity.[9] For pentadentate derivatives of L we recently isolated and structurally characterised isomers along a Jahn−Teller-active vibrational mode.[12] Similar observations have also been made of a tetradentate derivative of L where the pyridine donors are 6-methyl-substituted.[10]

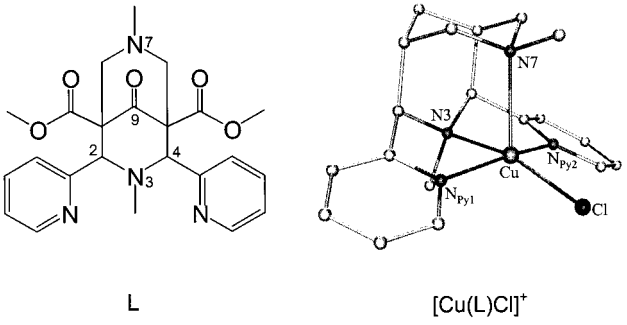

Figure 1. Diagram of the bispidine ligand L and a structural plot of the bispidine complex

The conclusion from all these observations is that the potential energy surface of metal-bispidine complexes is flat and has various shallow minima. Therefore, the inner-sphere reorganisation energy accompanying an electron self-exchange process should be small. Indeed, molecular-

[a] Anorganisch-Chemisches Institut der Universität Heidelberg, INF 270,
69120 Heidelberg, Germany
Fax: (internat.) + 49-6221-546617
E-mail: peter.comba@aci.uni-heidelberg.de
[b] Department of Chemistry and Biochemistry, Rand Afrikaans University,
P. O. Box 524, Auckland Park 2006, Johannesburg, South Africa
Supporting information for this article is available on the WWW under http://www.eurjic.org or from the author.

 © 2004 Wiley-VCH Verlag GmbH & Co. KGaA, Weinheim **DOI: 10.1002/ejic.200400518**

mechanics-derived potential energy surface scans of $[Cu^{I}(L)(X)]^{n+}$ and $[Cu^{II}(L)(X)]^{n+1}$ indicate that the inner-sphere reorganisation energy ΔG^{*}_{in} is around only 10−20 kJ·mol^{-1} (see Figure 2 and below). Does that mean that electron self-exchange is fast as, for example, in blue copper proteins?

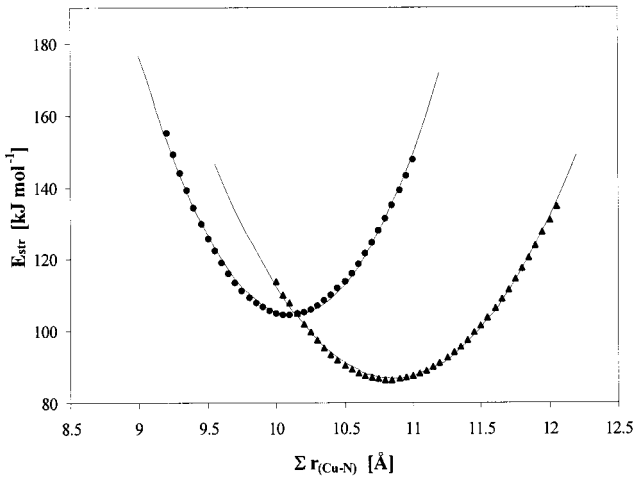

Figure 2. Potential energy scans for $[Cu^{II}(L)(NH_3)]^{2+}$ (filled circles) and $[Cu^{I}(L)(NH_3)]^{+}$ (filled triangles) (based on sum-constraints,[41] implemented with MOMEC97[42] and using a published parameterisation Scheme)[43]; the corresponding curves were obtained as least square fits to the equation $E = 0.5f(r - r_0)^2 + E_0$ (see below)

Results and Discussion

Experimentally Determined Electron Self-Exchange Parameters

Initial ^{1}H NMR line-broadening studies (CD_3CN, 298 K) indicated that electron self-exchange for the $[Cu^{II/I}(L)(NCCD_3)]^{2+/1+}$ couple is much slower than might have been expected (20 m^{-1}s^{-1} ≤ k_{11} ≤ 120 m^{-1}s^{-1}; see Supporting Information). Therefore, no accurate values are available from NMR titrations and the approximate range of the rate given here was only used as an estimate for the range of the electron self-exchange rate which was itself determined via a cross reaction using $[Co(sep)](NO_3)_2$ (sep = 1,3,6,8,10,13,16,19-octaazabicyclo[6.6.6]icosane) as a reducing agent [Equation (1), see Figure 3]. This was measured in water because the published electron self-exchange rate of the Co^{II} reductant has been obtained in aqueous solution (see below). Note that the change of solvent (CD_3CN, H_2O) implies that the two rates (NMR, cross reaction) are not directly comparable (different redox potential, different co-ligands and possible subtle changes in the mechanism). Indeed, there are examples where electron self-exchange rate constants of $Cu^{II/I}$ couples measured in H_2O and CH_3CN differ by as much as two orders of magnitude.[13] In other examples they are virtually identical.[14] Therefore, the only implication of the (inaccurate) rate of the NMR experiment is that electron self-exchange in the $[Cu^{II/I}(L)(solvent)]^{2+/1+}$ couple is slow.

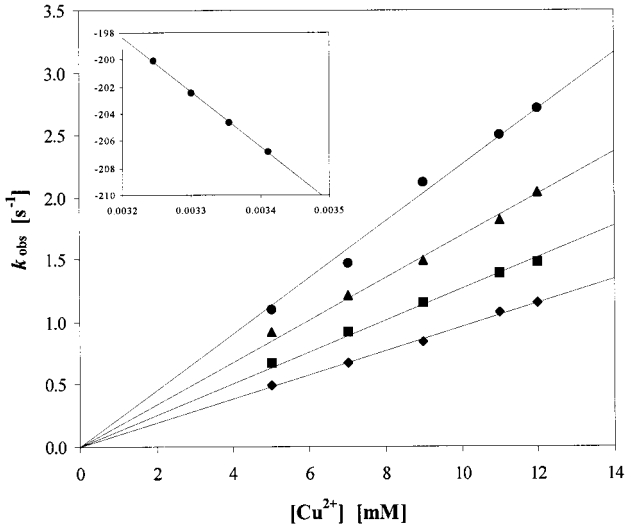

Figure 3. Plots of the pseudo-first-order rate constants k_{obs} for reaction (1) as a function of $[\{Cu^{II}(L)(OH_2)\}^{2+}]$ at 293.13 K (filled diamonds), 298.13 K (filled squares), 303.13 K (filled triangles) and 308.13 K (filled circles) in water (μ = 0.25 m, KNO_3), $[Co^{II}(sep)]_0$ = 5×10^{-4} m); inset: Eyring plot $[R\ln(k_{12}h/k_BT)$ [J·mol^{-1}·K^{-1}] vs. $1/T$ [K^{-1}]); k_{12} (298.13 K) = 126.9 ± 1.7 m^{-1}s^{-1}; $\Delta G^{\ddagger}_{12}$ (298.13 K) = 61.0 ± 1.2 kJ·mol^{-1}; $\Delta H^{\ddagger}_{12}$ = 40.3 ± 0.8 kJ·mol^{-1}; $\Delta S^{\ddagger}_{12}$ = −69.4 ± 2.8 J·mol^{-1}·K^{-1}

$$[Cu(L)(OH_2)]^{2+} + [Co(sep)]^{2+} \rightleftharpoons [Cu(L)(OH_2)]^{+} + [Co(sep)]^{3+} \quad (1)$$

The electron self-exchange rate, determined by the cross reaction, was obtained from the experimental data using the Marcus equations [Equation (2)−(6)[15,16] where Z is, as usual, 10^{11} m^{-1}s^{-1}]. The centre to centre distance in the precursor complex a_{ij} was obtained as the sum of the radii of the isolated complexes (a_j = $r([Co(sep)]^{3+/2+})$ = 4.5 ± 0.6 Å, identical to the published value.[17] a_i = $r([Cu(L)(NCCH_3)]^{2+/1+})$ = 6.3 ± 1.5 Å and both were calculated as $(a_x a_y a_z)^{1/3}$. The molecular dimensions along the three principal directional axes (a_x,a_y,a_z) were calculated using an established method.[16,18] The value K_{12} = 66.9 was derived from the redox potentials, measured under the same conditions as those used for the kinetic experiments [$E^0([Cu(L)(OH_2)]^{2+/1+})$ = −383 mV, $E^0([Co(sep)]^{3+/2+}$ = −491 mV, vs. Ag/AgCl]. The rate constant for the cross reaction k_{12} = 126.9 ± 1.7 m^{-1}s^{-1} was obtained from the experimental data (see Figure 3) and the electron self-exchange rate of the reductant is k_{22} = 5.1 ± 0.3 m^{-1} s^{-1}.[19] The self-exchange rate for the $[Cu^{I}(L)(OH_2)]^{+}$/$[Cu^{II}(L)(OH_2)]^{2+}$ couple is therefore k_{11} (298.13 K) = 15 ± 11 m^{-1}s^{-1},[20] i.e. as expected from the preliminary NMR experiments and a number of orders of magnitude slower than that of blue copper proteins which are in the range of

 © 2004 Wiley-VCH Verlag GmbH & Co. KGaA, Weinheim

$k_{11} = 10^3-10^8$ $m^{-1}s^{-1}$ [21,22] and in the area of "slow" $Cu^{II/I}$ couples.[23−26]

$$k_{12} = \sqrt{k_{11}k_{22}K_{12}f_{12}}\ W_{12} \tag{2}$$

$$\ln f_{12} = \frac{1}{4}\frac{\left(\ln K_{12} + \frac{w_{12}-w_{21}}{RT}\right)^2}{\ln\frac{k_{11}k_{22}}{Z^2} + \frac{w_{11}+w_{22}}{RT}} \tag{3}$$

$$W_{12} = \exp\frac{-w_{12}-w_{21}+w_{11}+w_{22}}{2RT} \tag{4}$$

$$w_{ij} = \frac{z_i z_j e^2 N}{D_s a_{ij}\left(1+\beta a_{ij}\sqrt{\mu}\right)} \tag{5}$$

$$\text{with}\quad \beta = \sqrt{\frac{8\pi N e^2}{1000\, D_s k_B T}} \tag{6}$$

The activation parameters of the electron self-exchange reaction were determined by using Equations (7)−(10).[27] ΔS^0_{12} emerges from the reaction entropies of the redox couples [$\Delta S^0_{12} = \Delta S^0_{rc}(Cu^{II}) - \Delta S^0_{rc}(Co^{II})$,[28] $\Delta S^0_{rc}(Co^{II}) = 79.5$ $J\cdot mol^{-1}\cdot K^{-1}$,[29] $\Delta S^0_{rc}(Cu^{II}) = 130.3 \pm 1.8$ $J\cdot mol^{-1}\cdot K^{-1}$ (temperature dependence of the redox potential) i. e. $\Delta S^0_{12} = 50.8 \pm 1.8$ $J\cdot mol^{-1}\cdot K^{-1}$]. The activation parameters for the $[Co(sep)]^{3+/2+}$ self-exchange are from the literatures, i.e. $\Delta G^{\ddagger}_{22} = 68.8 \pm 3.2$ $kJ\cdot mol^{-1}$, $\Delta H^{\ddagger}_{22} = 40.2 \pm 2.1$ $kJ\cdot mol^{-1}$ and $\Delta S^{\ddagger}_{22} = -96 \pm 8$ $J\cdot mol^{-1}\cdot K^{-1}$ [19] and those for the cross reaction are $\Delta G^{\ddagger}_{12} = 61.0 \pm 1.2$ $kJ\cdot mol^{-1}$, $\Delta H^{\ddagger}_{12} = 40.3 \pm 0.8$ $kJ\cdot mol^{-1}$ and $\Delta S^{\ddagger}_{12} = -69.4 \pm 2.8$ $J\cdot mol^{-1}\cdot K^{-1}$, derived from the experiment (see Figure 3). The resultant experimental activation parameters for the $[Cu(L)(OH_2)]^{2+/1+}$ self-exchange are, therefore, $\Delta G^{\ddagger}_{11} = 62.8 \pm 3.5$ $kJ\cdot mol^{-1}$, $\Delta H^{\ddagger}_{11} = 36.0 \pm 2.7$ $kJ\cdot mol^{-1}$ and $\Delta S^{\ddagger}_{11} = -92 \pm 10$ $J\cdot mol^{-1}\cdot K^{-1}$.

$$\Delta G^{\ddagger}_{12} = \frac{\Delta G^{\ddagger}_{11}}{2} + \frac{\Delta G^{\ddagger}_{22}}{2} + \frac{\Delta G^{o}_{12}}{2}(1+\alpha) \tag{7}$$

$$\Delta S^{\ddagger}_{12} = \left(\frac{\Delta S^{\ddagger}_{11}}{2} + \frac{\Delta S^{\ddagger}_{22}}{2}\right)\left(1-4\alpha^2\right) + \frac{\Delta S^{o}_{12}}{2}(1+2\alpha) \tag{8}$$

$$\Delta H^{\ddagger}_{12} = \left(\frac{\Delta H^{\ddagger}_{11}}{2} + \frac{\Delta H^{\ddagger}_{22}}{2}\right)\left(1-4\alpha^2\right) + \frac{\Delta H^{o}_{12}}{2}(1+2\alpha) \tag{9}$$

$$\text{with}\quad \alpha = \frac{\Delta G^{o}_{12}}{4\left(\Delta G^{\ddagger}_{11} + \Delta G^{\ddagger}_{22}\right)} \tag{10}$$

Calculated Electron Self-Exchange Parameters

Three methods were used to calculate the inner-sphere reorganisation energy: (i) From the crossing point of the molecular-mechanics-derived energy surface scans [Figure 2, Equation (11)].[30] This method has some deficiencies and may only be considered as an upper limit.[25,31] (ii) From a free energy perturbation-type approach [Equation (12)], where $E^{*}_{str,Cu(I)}$ is the strain energy of the Cu^{II} structure, determined with the Cu^{I} force field and vice versa.[25] (iii) From the force constants of the Cu^{II} and Cu^{I} breathing modes, derived from the energy surface scans shown in Figure 2 (solid lines) and Equations 13−15[16] in which $n = 5$ is the number of donors and f_i is the averaged reduced force constant which approximately takes account of the asymmetry and rigidity of the ligand. The inner-sphere reorganisation energy, derived from the three approaches leads to similar values and these are, as expected, small: (i) $\Delta G^{*}_{in} = 18.6$ $kJ\cdot mol^{-1}$, (ii) $\Delta G^{*}_{in} = 13.4$ $kJ\cdot mol^{-1}$ and (iii) $\Delta G^{*}_{in} = 12.2$ $kJ\cdot mol^{-1}$. The three methods are based on the assumption that the Cu^{I} and Cu^{II} chromophores are similar, i.e. pentacoordinate. Published experimental data indicate that, as expected for Cu^{I}, there is a fast equilibrium between four- and five-coordinate structures (dissociation of one of the pyridine donors).[6,32] However, ^1H NMR spectra in D_2O indicate that the five-coordinate species is the major component in water and this is similar to earlier observations in acetonitrile.[6,32] Also, recent structural studies[33] indicate that, in addition to the published four- and five-coordinate Cu^{I} structures, there is a "pseudo-4-coordinate" Cu^{I} species with a short (2.0 Å) and a long (2.9 Å) $Cu-N_{pyridine}$ bond (pyridine lone-pair on the $Cu\cdots N_{py}$ axis) and a coordinated co-ligand ($NCCH_3$). This is also supported by DFT calculations[34] and is further evidence for the flat energy surface and validates the approximation of similar Cu^{I} and Cu^{II} chromophores. The three values for ΔG^{*}_{in} are all based on molecular mechanics calculations and, therefore, depend on the accuracy of the force field and on the model used (replacement of substituents at C1, C5, C9 of the bispidine backbone by hydrogen atoms, NH_3 instead of $NCCH_3$ as co-ligand; while chemically these changes might be unreasonable, in terms of the molecular mechanics model, which does not include any electronic effects, these are believed to be uncritical). The suitability of molecular mechanics for the computation of the inner-sphere reorganisation energy was therefore also confirmed by preliminary DFT calculations.[35]

$$\Delta G^{*}_{in} = 2E^{*}_{str} - E_{str,Cu(I)} - E_{str,Cu(II)} \tag{11}$$

The outer-sphere reorganisation energy can be obtained on the basis of a two-sphere (Equation 16) or an ellipsoid model (Equations 17−19).[16] The outer-sphere reorganisation energy, using the probably more accurate ellipsoid model, $\Delta G^{*}_{out,ellipsoid} = 20.5$ $kJ\cdot mol^{-1}$ ($\Delta G^{*}_{out,sphere} = 15.2$ $kJ\cdot mol^{-1}$) is of at least a similar magnitude to the inner-sphere reorganisation energy. The term derived from the

 © 2004 Wiley-VCH Verlag GmbH & Co. KGaA, Weinheim

formation of the precursor complex (w_r = 2.80 ± 0.47 kJ·mol^{-1}) is significantly smaller.

$$\lambda_{in} = E^*_{str,Cu(I)} + E^*_{str,Cu(II)} - E_{str,Cu(I)} - E_{str,Cu(II)}$$

$$\Delta G^*_{in} = \frac{\lambda_{in}}{4} \quad (12)$$

$$\lambda_{in} = n\, f_i (\Delta a_0)^2 \quad (13)$$

$$\text{with} \quad f_i = \frac{2 f_{Cu(I)} f_{Cu(II)}}{f_{Cu(I)} + f_{Cu(II)}} \quad (14)$$

$$\text{and} \quad \Delta G^*_{in} = \frac{\lambda_{in}}{4} \quad (15)$$

$$\lambda_{out} = Ne^2 \left(\frac{1}{2a_1} + \frac{1}{2a_2} - \frac{1}{r} \right) \left(\frac{1}{D_{op}} - \frac{1}{D_s} \right) \quad (16)$$

$$\lambda_{out} = \frac{Ne^2 r^2}{2 I_a I_b^2} \left(\frac{1}{D_{op}} - \frac{1}{D_s} \right) S(\lambda_0) \quad (17)$$

$$\text{with} \quad S(\lambda_0) = \sum_{n=1,3,5\ldots}^{\infty} \frac{(2n+1)\lambda_0 (\lambda_0^2 - 1) Q_n(\lambda_0)}{P_n(\lambda_0)} \quad (18)$$

$$\text{and} \quad \lambda_0^2 = \frac{I_a^2}{I_a^2 - I_b^2} \quad (19)$$

The calculated rate, using the computed activation parameters, is k_{11}^{calc} = 4.5 10^3 m^{-1}s^{-1}, i.e. approx. 2 orders of magnitude too large (k_{11}^{obs} = 15 ± 11 m^{-1}s^{-1}, see above). An important point here is that the ΔG^* values in Equation (20) are not corrected for entropy effects. The inner-sphere reorganisation energy [Equation (11)] has been shown to have a linear dependence on the strain energies.[30] For a series of Co(III/II) hexamine couples this resulted in a $T\Delta S^*$ term (T = 298.13 K) of 20 kJ·mol^{-1}. This value is of a similar magnitude to the herein experimentally determined activation entropy at 298.13 K of $T\Delta S^{\ddagger}_{obs}$ = 27.4 kJ·mol^{-1}. With this 20 kJ·mol^{-1} added to ΔG^*_{calc} in Equation (21), k_{11}^{calc} = 1.5 m^{-1}s^{-1} is obtained which is in reasonable agreement with the experimentally determined self-exchange rate of k_{11}^{obs} (298.13 K) = 15 ± 11 m^{-1}s^{-1}. Note, however, that $\Delta S^{\ddagger}_{11}$ is the total transition state activation entropy and not the reorganisational entropy,[36] i.e. part of $\Delta S^{\ddagger}$ is included in the pre-exponential factor in the commonly used Equation (22) (which is a combination of Equations 20 and 21). Another possible reason for a reduction of Z (i.e. for a smaller value of the computed self-exchange rate) is reduced electronic coupling, i.e. nonadiabicity.

$$\Delta G^*_{calc} = w_r + \Delta G^*_{in} + \Delta G^*_{out} - RT \ln \frac{hZ}{k_B T} \quad (20)$$

$$k_{11}^{calc} = \frac{k_B T}{h} \exp \frac{-\Delta G^*}{RT} \quad (21)$$

$$k_{11}^{calc} = Z \exp\left(- \frac{w_r + \Delta G^*_{in} + \Delta G^*_{out}}{RT} \right) \quad (22)$$

Conclusions

As suggested by structural studies, the rearrangement of the coordination sphere of the copper-bispidine complex with L is a low energy process and ΔG^*_{in} = 18.6 kJ·mol^{-1} is overestimated rather than underestimated. Our analysis suggests that the experimentally determined slow electron self-exchange rate is to a large extent the result of a comparably high outer-sphere reorganisation energy barrier. A significant contribution to the activation entropy term and nonadiabicity might also be responsible for the relatively slow self-exchange rate. While our experimental and computational results do not yet allow a thorough and unambiguous assignment of the ratio of the various terms to the high activation barrier, it is clear that while the flat energy surface of transition metal bispidine complexes with L leads to a high elasticity and hence to a minimal loss of energy upon distortions enforced by the electron transfer, the elasticity also allows for large structural changes and this results in a significant perturbation of the solvation sheath (note that structural elasticity and solvation in small coordination compounds are both not directly comparable to those in proteins).[21,37,38] While this is a very specific result for the highly elastic Cu$^{II/I}$-bispidine system, the interesting but not unexpected general conclusion is that small inner-sphere reorganisation energies do not necessarily lead to fast electron transfer rates. This is in contrast to a common but naive interpretation of the Cu$^{II/I}$ electron self-exchange in blue copper proteins and a further argument in the discussion on entatic states.[39] Experiments and calculations which might help to answer some of the remaining questions, include kinetic studies with other bispidine derivatives and other bispidine redox couples (e.g., Co$^{III/II}$, Ru$^{III/II}$) and extensive DFT calculations. Some of these will be carried out in due course.

Experimental Section

Syntheses: Ligand L was synthesised as described in the literature.[40] The Cu^{II} complex as its triflate salt was obtained by addition of a hot solution of $Cu(CF_3SO_3)_2$ in dry CH_3CN to an equimolar suspension of L in dry CH_3CN. The resultant solution was stored in a diethyl ether diffusion bath to give $[Cu(L)(NCCH_3)(O\text{-}SO_2CF_3)]CF_3SO_3$ as deep blue crystals. $C_{27}H_{29}CuF_6N_5O_{11}S_2$ (841.22): calcd. C 38.55, H 3.47, N 8.33, S 7.62; found C 38.51, H 3.50, N 8.30, S 7.58. All solutions of the Cu^{II} complex were prepared with deionised and deoxygenated water and KNO_3 to keep

 © 2004 Wiley-VCH Verlag GmbH & Co. KGaA, Weinheim

the ionic strength at 0.25 m. The Cu^{I} complex was obtained as described previously.[32]

$[Co(sep)]Cl_3$ (Aldrich) was converted into its nitrate salt by treatment of an aqueous solution of 1 equivalent of $[Co(sep)]Cl_3$ with 3 equivalents of $AgNO_3$. After filtration, solid KNO_3 was added slowly to the filtrate until precipitation of the orange $[Co(sep)](NO_3)_3$ was complete. This was recrystallised from a small amount of warm water and the precipitate was dried in vacuo. A solution of $[Co(sep)](NO_3)_3$ of the appropriate concentration and desired ionic strength (0.25 m, KNO_3) in deionised and deoxygenated water was then treated with an excess of zinc dust under Ar until the complex was fully reduced (approx. 4 h, colourless solution). The solution was used for kinetic measurements within 3 h after preparation.

Measurements: Redox potentials were measured by cyclic voltammetry using a BAS-100B electrochemical analyser with a scan rate of 100 mV/s. The electrode setup consisted of a glassy/carbon working electrode, a platinum auxiliary electrode and an aqueous Ag/AgCl reference electrode. The concentrations of the solutions were 10^{-3} m for the $Co^{III/II}$(sep) couple and 10^{-2} m for the $Cu^{II/I}$(L) couple, μ = 0.25 m (KNO_3). The temperature of the solutionswas maintained using a circulating water bath (Haake K 20).

^{1}H NMR Spectra: (60 mm $[Cu^{I}(L)]$, 0−28 mm $[Cu^{II}(L)]$, CD_3CN, T = 193 K) were obtained on a Bruker AS 300 spectrometer (300.13 MHz). Chemical shifts (δ, ppm) are relative to the solvent. Note that in addition to the electron self-exchange there is a dynamic process between two different structures of $[Cu^{I}(L)(NCCD_3)]^+$ (four- and five-coordinate).[6,32] ^{1}H NMR spectroscopy suggests that this process is much faster than the electron self-exchange reaction and that the five-coordinate complex is the major species in solution. This also emerges for the corresponding aqua complexes measured in aqueous solution and it is in agreement with preliminary DFT calculations.[34]

Kinetics: Measurements were performed on an Applied Photophysics SX.18MV-R stopped-flow spectrophotometer. The temperatures of the solutions were maintained (± 0.1 °C) using a circulating water bath (Haake K20). The cross reactions were carried out under pseudo-first-order conditions (Cu^{II} in at least 10-fold excess) and the rates were monitored at 474 nm. The kinetic data were analysed using the !SX.18MV Kinetic Spectrometer Workstation Software v4.46.

Supporting Information: Details of the determination of $K_{Cu\text{-}Cl}$, the NMR line-broadening studies, the experimentally measured entropy of the redox potential and the calculations of the electron transfer rates are given as Supporting Information (see also footnote on the first page of this article)

Acknowledgments

Generous financial support by the Deutsche Forschungsgemeinschaft (DFG) is gratefully acknowledged. A.R. would like to thank the Research Fund of the RAU and the South African NRF for financial support.

[1] P. Comba, W. Schiek, *Coord. Chem. Rev.* **2003**, *238−239*, 21.
[2] log $K_{Cu(II)(L)}$ = 20.0, measured potentiometrically at 298.13 K in dioxane/water (2:3), at 0.1 m ionic strength (KCl), using 1 equivalent of ligand and 0.8 equivalents of Cu^{II}.[3]
[3] P. Comba, S. Kuwata, G. A. Lawrance, work in progress.
[4] P. Comba, A. Lienke, *Inorg. Chem.* **2001**, *40*, 5206.
[5] H. Börzel, P. Comba, H. Pritzkow, *Chem. Commun.* **2001**, 97.
[6] H. Börzel, P. Comba, K. S. Hagen, M. Kerscher, H. Pritzkow, M. Schatz, S. Schindler, O. Walter, *Inorg. Chem.* **2002**, *41*, 5440.
[7] P. Comba, M. Merz, H. Pritzkow, *Eur. J. Inorg. Chem.* **2003**, 1711.
[8] The stability constant of $[Cu(L)(Cl)]^+$ (Cl^- binding to $[Cu(L)]^{2+}$, K_{CuCl}, measured spectrophotometrically (water, 298.13 K, ionic strength = 1.0 m ($NaClO_4$), $[Cu(L)_{aq}]^{2+}$ = 10^{-3} m) at 300 nm and 330 nm, is: K_{CuCl} = 18.7 ± 0.9 (complete experimental data are available as Supporting Information).
[9] P. Comba, M. Kerscher, M. Merz, V. Müller, H. Pritzkow, R. Remenyi, W. Schiek, Y. Xiong, *Chem. Eur. J.* **2002**, *8*, 5750.
[10] P. Comba, B. Martin, A. Prikhod′ko, H. Pritzkow, H. Rohwer, *Comptes Rendus Chimie* (Special Issue on Integrated Experimental, Spectroscopic and Theoretical Aspects of Inorganic Chemistry, (Ed.: Carlo Mealli), accepted.
[11] C. Bleiholder, H. Börzel, P. Comba, A. Heydt, M. Kerscher, S. Kuwata, G. Laurenczy, G. A. Lawrance, A. Lienke, B. Martin, M. Merz, B. Nuber, H. Pritzkow, submitted.
[12] P. Comba, A. Hauser, M. Kerscher, H. Pritzkow, *Angew. Chem.* **2003**, *115*, 4675; *Angew. Chem. Int. Ed.* **2003**, *42*, 4536.
[13] H. Doine, Y. Yano, T. W. Swaddle, *Inorg. Chem.* **1989**, *28*, 2319.
[14] B. C. Dunn, C. W. Ochrymowycz, D. B. Rorabacher, *Inorg. Chem.* **1995**, *34*, 1954.
[15] R. A. Marcus, N. Sutin, *Biochim. Biophys. Acta* **1985**, *811*, 265.
[16] N. Sutin, *Prog. Inorg. Chem.* **1983**, *104*, 441.
[17] B. Brunschwig, C. Creutz, D. Maeartney, T.-K. Sham, N. Sutin, *Faraday Discuss. Chem. Soc.* **1982**, *74*, 113.
[18] B. Martin, J. Schaumberger, P. Gedeck, T. Schindler, M. Hennemann, A. H. C. Horn, T. Clark, *in preparation*.
[19] I. I. Creaser, R. J. Geue, J. M. Harrowfield, A. J. Herlt, A. M. Sargeson, M. R. Snow, J. Springborg, *J. Am. Chem. Soc.* **1982**, *104*, 6016.
[20] All error limits given are the result of the experimental standard deviations and calculated error propagation.
[21] S. J. Lippard, J. M. Berg, *''Principles of Bioinorganic Chemistry''*, University Science Books, **1994**.
[22] C. Buning, G. W. Canters, P. Comba, C. Dennison, L. Jeuken, M. Melter, J. Sanders-Loehr, *J. Am. Chem. Soc.* **2000**, *122*, 204.
[23] A. G. Lappin, *Redox mechanisms in inorganic chemistry* (Ed.: J. Burgess), Ellis Horwood Ltd., Chichester, **1994**.
[24] B. C. Dunn, L. A. Ochrymowycz, D. B. Rorabacher, *Inorg. Chem.* **1997**, *36*, 3253.
[25] B. Xie, T. Elder, L. J. Wilson, D. M. Stanbury, *Inorg. Chem.* **1999**, *38*, 12.
[26] E. A. Ambundo, Q. Yu, L. A. Ochrymowycz, D. B. Rorabacher, *Inorg. Chem.* **2003**, *42*, 5267.
[27] R. A. Marcus, N. Sutin, *Inorg. Chem.* **1975**, *14*, 213.
[28] M. J. Weaver, E. L. Ya, *Inorg. Chem.* **1980**, *11*, 1936.
[29] S. Sahami, M. J. Weaver, *J. Electroanal. Chem.* **1981**, *122*, 171.
[30] P. Comba, A. F. Sickmüller, *Inorg. Chem.* **1997**, *36*, 4500.
[31] P. Comba, T. W. Hambley, *''Molecular Modeling of Inorganic Compounds, 2nd edition with a tutorial, based on MOMEClite''*, Wiley-VCH, **2001**.
[32] H. Börzel, P. Comba, K. S. Hagen, C. Katsichtis, H. Pritzkow, *Chem. Eur. J.* **2000**, *6*, 914.
[33] P. Comba, M. Kerscher, *Cryst. Eng.* **2004**, *6*, 197.
[34] P. Comba, H. Rohwer, work in progress.
[35] The approach used was identical to (ii) [Equation (12)]. The Cu^{II} and Cu^{I} structures ($NCCH_3$ as co-ligand, five-coordinate (global minimum also for the Cu^{I} structure)) were refined with Gaussian98, B3LYP, 6−31G*. Single point energy calculations with Cu^{I} and Cu^{II} each in both optimised structures (B3LYP, TZV) resulted in E^* = 24.9 kJ·mol^{-1} (see ref.[33]).

 © 2004 Wiley-VCH Verlag GmbH & Co. KGaA, Weinheim

[36] L. W. Ungar, M. D. Newton, G. A. Voth, *J. Phys. Chem. B* **1999**, *103*, 7367.
[37] Note that our approach neglects further effects due to the second coordination sphere [see ref. 38].
[38] F. P. Rotzinger, *Dalton Trans.* **2002**, 719.
[39] P. Comba, *Coord. Chem. Rev.* **2000**, *200−202*, 217.
[40] U. Holzgrabe, E. Ericyas, *Arch. Pharm. (Weinheim, Germany)* **1992**, *325*, 657.
[41] P. Comba, N. Okon, R. Remenyi, *J. Comput. Chem.* **1999**, *20*, 781.
[42] P. Comba, T. W. Hambley, G. Lauer, M. Melter, N. Okon, *''MOMEC97, a molecular modeling package for inorganic compounds''*, University of Heidelberg, **1997**.
[43] P. Comba, H. Jakob, *Helv. Chim. Acta* **1997**, *80*, 1983.

Received June 15, 2004
Early View Article
Published Online October 20, 2004

 © 2004 Wiley-VCH Verlag GmbH & Co. KGaA, Weinheim

Isolation and Molecular Structure of a Monomeric, Tris[peroxotitanium(IV)]-Substituted α-Dawson Polyoxometalate Derived from the Tetrameric Anhydride Form Composed of Four Tris[titanium(IV)]-Substituted α-Dawson Substructures and Four Bridging Titanium(IV) Octahedral Groups

Yoshitaka Sakai,[a] Yuh Kitakoga,[a] Kunihiko Hayashi,[a] Kenji Yoza,[b] and Kenji Nomiya*[a]

Keywords: Titanium(IV) / Peroxo complexes / Polyoxometalates

The isolation and structural characterisation of a novel tris-[peroxotitanium(IV)]-substituted α-Dawson polyoxometalate (POM), [α-1,2,3-$P_2W_{15}(TiO_2)_3O_{56}(OH)_3]^{9-}$ (**1a**), containing side-on coordination (i.e. η^2-coordination) of the peroxo group to the titanium(IV) atom are described. A water-soluble, completely inorganic compound of the monomeric POM Na_9[α-1,2,3-$P_2W_{15}(TiO_2)_3O_{56}(OH)_3]\cdot 16H_2O$ (**1**), obtained as analytically pure, homogeneous orange crystals, was obtained from a reaction in aqueous solution of an excess of 30% aqueous hydrogen peroxide with {[α-1,2,3-$P_2W_{15}Ti_3O_{59}(OH)_3]_4[\mu_3$-$Ti(OH)_3]_4Cl\}^{33-}$ (**2a**). The latter has been recently shown to be a giant "tetrapod"-shaped, tetrameric anhydride formed from the tris[titanium(IV)]-substituted Dawson substructures with four bridging Ti octahedral groups. Compound **1** could not be obtained from the reaction with another giant tetrapod POM, {[α-1,2,3-$P_2W_{15}Ti_3O_{57.5}(OH)_3]_4Cl\}^{25-}$ (**3a**), which does not contain the bridging octahedral Ti groups. The molecular structure of **1a** was successfully determined by a single-crystal X-ray diffraction study and was shown to be a monomeric α-Dawson POM derived from the tris[peroxotitanium(IV)] species. Bond valence sum (BVS) calculations suggest that the μ_2-oxo sites of the three Ti–O–Ti bridges in the Ti_3 cap of the Dawson unit are protonated. Characterisation of **1** was also accomplished by complete elemental analysis, TG/DTA, FTIR and solution (^{31}P and ^{183}W) NMR spectroscopy.
(© Wiley-VCH Verlag GmbH & Co. KGaA, 69451 Weinheim, Germany, 2004)

Introduction

Polyoxometalates (POMs) are molecular metal oxide clusters. They are of current interest as soluble metal oxides and because of their applications in catalysis, medicine and materials science.[1] Site-selective substitution of the W^{VI} atoms in POMs with Ti^{IV} atoms is particularly interesting because of the multicentre active sites formed with corner- and/or edge-sharing TiO_6 octahedra and the water-soluble molecular modelling studies of titanium(IV) oxides as an effective semiconductor and photocatalysts.[2]

Many H_2O_2-based oxidation reactions catalysed by titanium(IV)-substituted POMs have been described in which the peroxotitanium(IV) and/or hydroperoxotitanium(IV) species have been proposed as the active intermediates in such reactions.[3] Thus, the synthesis and structural characterisation of peroxotitanium(IV)-substituted POMs would constitute an intriguing project. Only a few structure determinations of peroxotitanium(IV) complexes have been conducted and these have been for the mono[peroxotitanium(IV)]-substituted Keggin POM $[PW_{11}(TiO_2)O_{39}]^{5-}$ species,[4] whereas related examples from the Dawson POM family have not been reported so far.

Very recently, we reported the two tetrameric anhydride forms of tri-Ti^{IV}-substituted Dawson POMs, i.e. {[α-1,2,3-$P_2W_{15}Ti_3O_{59}(OH)_3]_4[\mu_3$-$Ti(OH)_3]_4Cl\}^{33-}$ (**2a**, tetrapod-shaped POM with the four bridging octahedral Ti^{IV} groups and with one encapsulated Cl^- ion)[5a] and {[α-1,2,3-$P_2W_{15}Ti_3O_{57.5}(OH)_3]_4Cl\}^{25-}$ (**3a**, tetrapod-shaped POM without the bridging octahedral Ti^{IV} groups and with one encapsulated Cl^- ion),[5b] both of which contain a giant, inorganic "tetrapod" molecule composed of four 1,2,3-tri-Ti^{IV}-substituted α-Dawson substructures.[6,7] Separately, Kortz et al. have also determined the molecular structure of the related tetrameric Dawson species without encapsulated chloride ions, $\{[P_2W_{15}Ti_3O_{57.5}(OH)_3]_4\}^{24-}$ (**4a**).[5c,6,7]

During our study of the formation of **2a** and **3a** in aqueous solution[8] and the reactivity of these species with hydrogen peroxide (see the Exp. Sect.), we unexpectedly obtained a monomeric and pure form of the tris[peroxotitanium(IV)]-substituted Dawson POM [α-1,2,3-

[a] Kanagawa University,
Tsuchiya 2946, Hiratsuka, Kanagawa 259-1293, Japan
Fax: (internat.) + 81-463-58-9684
E-mail: nomiya@chem.kanagawa-u.ac.jp
[b] Nihon Bruker AXS,
Kanagawa-ku, Moriyacho 3-9 A6F, Yokohama 221-0022, Japan
Supporting information for this article is available on the WWW under http://www.eurjic.org or from the author.

 © 2004 Wiley-VCH Verlag GmbH & Co. KGaA, Weinheim **DOI: 10.1002/ejic.200400628**

$P_2W_{15}(TiO_2)_3O_{56}(OH)_3]^{9-}$ (**1a**) from the reaction of **2a**. The reaction of **3a**, however, did not produce such a result. An X-ray structure analysis revealed that the peroxo groups on the Ti atoms are attached by side-on coordination, i.e. η^2-coordination. The bond valence sum (BVS) calculations of the oxygen atoms suggest that three protons are bound to the surface edge-sharing oxygen atoms of the Ti_3 cap in **1a**. The lack of any other protons in **1a** conclusively suggests that the peroxo group, but not the hydroperoxo group, is bound to the Ti atom. The X-ray structure determination of the POM-based tris[peroxotitanium(IV)] complex highlighted here is the first example of its type. Herein, we report full details of the synthesis and characterisation of the water-soluble sodium salt Na_9[**1a**]·$16H_2O$ (**1**) and the molecular structure of **1a**.

Results and Discussion

Synthesis, Isolation and Characterisation of 1

The water-soluble sodium salt of **1** was prepared in ca. 25% (0.53 g scale) yield by recrystallising the orange powder which was obtained from the reaction of the precursor **2** in aqueous solution with an excess of 30% aqueous H_2O_2. Of particular note is the fact that the reactivity of the two tetrameric Dawson POMs **2** and **3** with aqueous hydrogen peroxide was remarkably different. Compound **1** was successfully derived from the reaction of **2** with aqueous H_2O_2, but **3** did not behave in such a way. The formation of **1a** is shown in Equation (1).

$$\{[P_2W_{15}Ti_3O_{59}(OH)_3]_4[\mu_3\text{-}Ti(OH)_3]_4Cl\}^{33-}\ (\mathbf{2a}) + 12\ H_2O_2 \rightarrow 4\ [P_2W_{15}(TiO_2)_3O_{56}(OH)_3]^{9-}\ (\mathbf{1a}) + 4\ \{Ti(OH)_3\}^+ + Cl^- + 12H_2O \quad (1)$$

Compound **1** was characterised by complete elemental analysis, TG/DTA, FTIR, ^{31}P and ^{183}W NMR spectroscopy and a single-crystal X-ray diffraction study. The sample for elemental analysis was prepared by drying at room temperature under a vacuum of 10^{-3}–10^{-4} Torr overnight. All elements were observed, including oxygen, to a total analysis of 98.95 %. These data are consistent with a composition of Na_9[**1a**]·$4H_2O$. The weight loss observed during the course of drying before analysis was 4.93% which corresponded to 12–13 water molecules weakly bound or adsorbed in **1**. In contrast, TG/DTA measurements performed under atmospheric conditions showed a weight loss of 6.61% between 25 and 168 °C with endothermic points at 60 and 84 °C corresponding to the presence of 16 water molecules constituting both the intrinsic water of hydration and adsorbed water from the atmosphere. The number of water molecules (16) is consistent with the sum of the water molecules (4) found in the elemental analysis plus the water molecules (12–13) corresponding to the weight loss observed during the course of drying before analysis. Interestingly, bond-valence sum (BVS) calculations of the oxygen atoms in **1a** indicate that the μ_2-oxo sites of the three Ti–O–Ti bridges in the Dawson unit are protonated (see "Molecular Structure of **1a**").

TG/DTA measurements also showed the thermal stability of **1**. A weight loss of 4.12% observed from 167 °C up to ca. 400 °C with an endothermic point at 172 °C was due to decomposition of the coordinated peroxo groups. FTIR spectroscopic measurements of the samples after heating up to 150 °C (resulting in dehydration) and 200 °C (resulting in decomposition of the peroxo groups) showed that the Dawson POM framework was still intact. However, the IR measurements of the sample after heating up to 500 °C showed that the Dawson framework had been disrupted.

The solid-state FTIR spectrum of **1** (Figure 1, a; $\tilde{\nu}$ = 1083, 940, 923, 800 br cm^{-1}) measured as a KBr disk, showed the characteristic vibrational bands of the Dawson-type POM "$P_2W_{18}O_{62}^{6-}$" framework.[9] The lack of bands at around 650 cm^{-1} which would be due to an inter-Dawson unit Ti–O–Ti vibration suggests that **1** is a monomer and not an oligomer. The O–O stretching band which is known to appear around 900 cm^{-1} for monoperoxo complexes[10] was observed at 890 cm^{-1}.

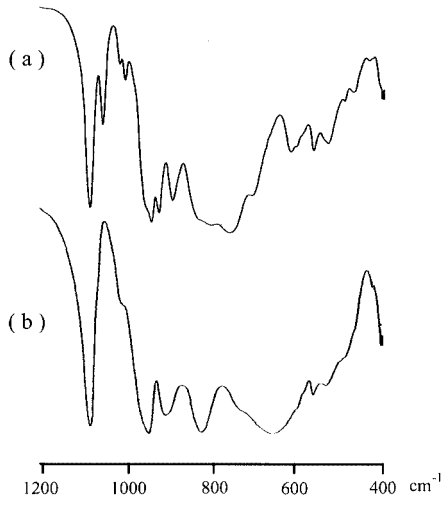

Figure 1. FTIR spectra in the polyoxoanion region (1200–400 cm^{-1}), measured as KBr disks, of a) Na_9[**1a**]·$16H_2O$ (**1**) {**1a** = [α-1,2,3-$P_2W_{15}(TiO_2)_3O_{56}(OH)_3]^{9-}$} and b) Na_xH_{33-x}[**2a**]·yH_2O (**2**) (x = 16–19, y = 60–70; **2a** = {[α-1,2,3-$P_2W_{15}Ti_3O_{59}(OH)_3]_4[\mu_3$-$Ti(OH)_3]_4Cl\}^{33-}$)

The ^{183}W NMR spectrum of **1** measured in D_2O at 20.7 °C (Figure 2, a) showed a three-line pattern with signals at δ = −156.5, −201.9 and −230.1 ppm with relative intensities of 1:2:2. This spectrum is in agreement with the presence of two tungsten belts consisting of six WO_6 octahedra and a tungsten cap of three WO_6 octahedra. The ^{31}P NMR spectrum of **1** in D_2O at 22.6 °C (Figure 3, a) showed a clean two-line pattern with signals at δ = −3.93 and −14.41 ppm, confirming its purity and single-product nature. The downfield resonance can be assigned to the phosphorus atom closest to the Ti_3 cap, whereas the upfield resonance is due to the phosphorus atom closer to the W_3 cap. It should be noted that the downfield signal is much more shifted to low-field compared with those of the tetrameric

 © 2004 Wiley-VCH Verlag GmbH & Co. KGaA, Weinheim

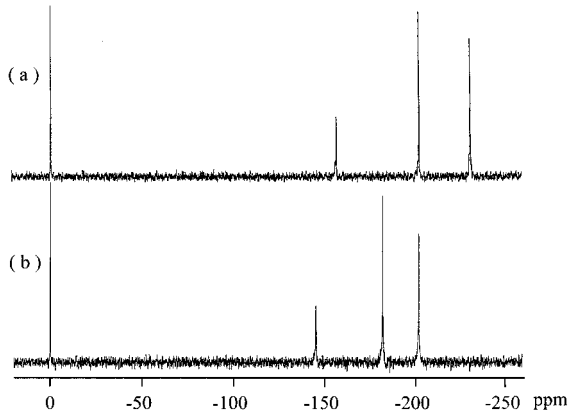

Figure 2. ^{183}W NMR spectra in D_2O of a) Na_9[**1a**]·$16H_2O$ (**1**) {**1a** = $[\alpha\text{-}1,2,3\text{-}P_2W_{15}(TiO_2)_3O_{56}(OH)_3]^{9-}$} and b) Na_xH_{33-x}[**2a**]·yH_2O (**2**) (x = 16−19, y = 60−70; **2a** = $\{[\alpha\text{-}1,2,3\text{-}P_2W_{15}Ti_3O_{59}(OH)_3]_4[\mu_3\text{-}Ti(OH)_3]_4Cl\}^{33-}$); the resonance at δ = 0.0 ppm is due to the external reference saturated Na_2WO_4/D_2O solution

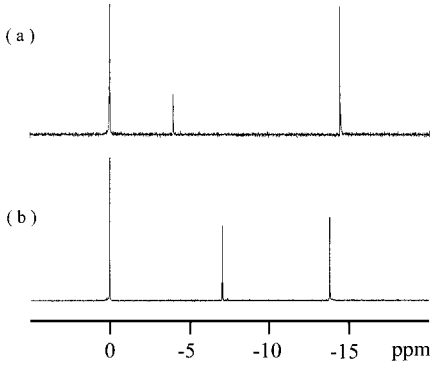

Figure 3. ^{31}P NMR spectra in D_2O of a) Na_9[**1a**]·$16H_2O$ (**1**) {**1a** = $[\alpha\text{-}1,2,3\text{-}P_2W_{15}(TiO_2)_3O_{56}(OH)_3]^{9-}$} and b) Na_xH_{33-x}[**2a**]·yH_2O (**2**) (x = 16−19, y = 60−70; **2a** = $\{[\alpha\text{-}1,2,3\text{-}P_2W_{15}Ti_3O_{59}(OH)_3]_4[\mu_3\text{-}Ti(OH)_3]_4Cl\}^{33-}$); the resonance at δ = 0.0 ppm is due to the external reference 25% H_3PO_4 in H_2O; in each case a very high level of purity is indicated (i.e., with respect to any other P-containing polyoxoanions or other materials)

Ti^{IV}-substituted Dawson POMs **2**−**4** listed in Table 1. Both the ^{183}W and ^{31}P NMR spectra are consistent with the solid-state structure.

Table 1. ^{31}P and ^{183}W NMR spectroscopic data of **1**−**4** in D_2O

Complex	δ (^{31}P NMR)	δ (^{183}W NMR)	Ref.
1	−3.93, −14.41	−156.5, −201.9, −230.1	this work
2	−7.04, −13.77	−145.0, −181.5, −201.4	[5a]
3	−7.6, −14.0	−148.3, −185.8, −211.2	[5b]
4	−7.3, −13.8		[5c]

Molecular Structure of 1a

The crystal of **1** contains discrete cluster anions, sodium cations and lattice water molecules, all in general positions in the monoclinic space group $P2_1/c$. The solid-state packing of the polyoxoanions of **1a** is shown in Figure S2 in the Supporting Information. The observed electron densities of the Ti and W atoms are quite different and the data unequivocally distinguish and define the Ti and W atoms. The 15 tungsten atoms, 3 titanium atoms and the 2 phosphorus atoms can be clearly identified. Thus, the main features of the molecular structure of the POM have been identified. However, the resolution obtained for the structure of the salt was limited by the poor quality of the available crystals and by the considerable disorder of the countercations and the solvent of crystallization. Such a problem is common in POM crystallography.[11]

The molecular structure of **1a** is composed of the monomeric Dawson POM unit "α-$P_2W_{15}Ti_3O_{62}$", in which the

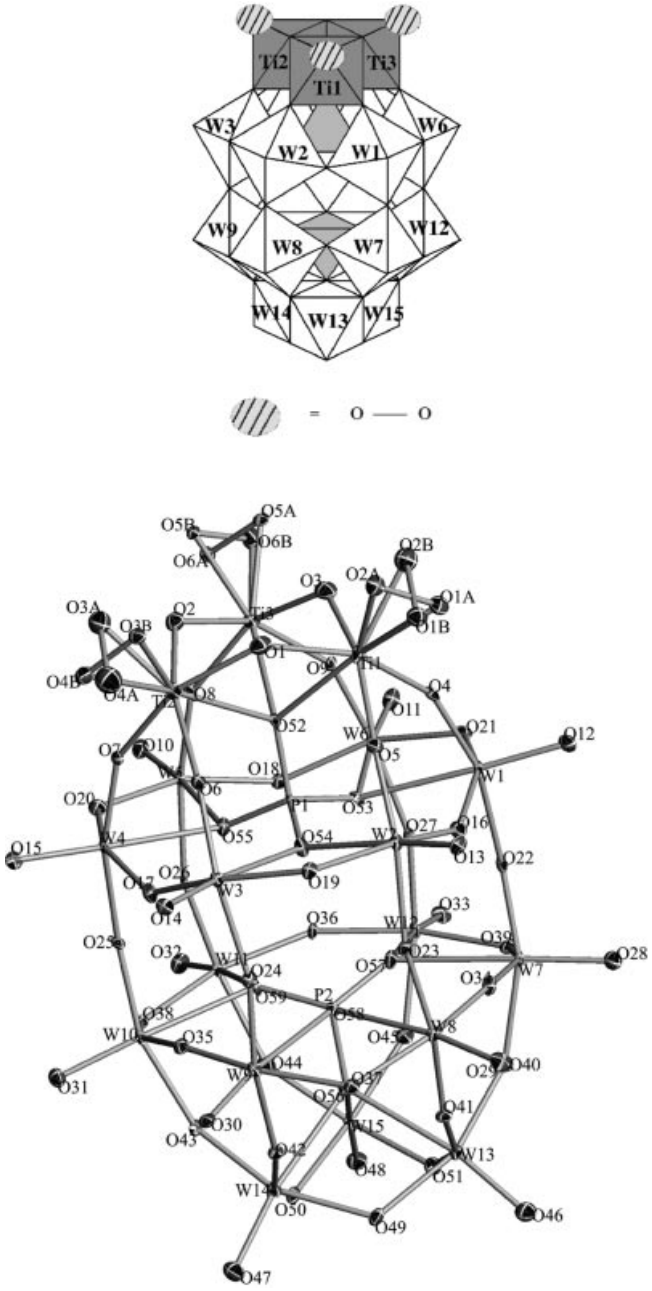

Figure 4. Top: polyhedral representation of the monomeric tris[peroxotitanium(IV)]-substituted Dawson POM [α-1,2,3-$P_2W_{15}(TiO_2)_3O_{56}(OH)_3]^{9-}$ (**1a**); bottom: molecular structure of **1a** with 50% probability ellipsoids

 © 2004 Wiley-VCH Verlag GmbH & Co. KGaA, Weinheim

three edge-sharing octahedral sites of the titanium(IV) atoms (Ti_3-cap site) in the "α-$P_2W_{15}Ti_3$" Dawson unit substitute the three edge-sharing octahedral sites of the tungsten(VI) atoms (W_3-cap site) of $[\alpha\text{-}P_2W_{18}O_{62}]^{6-}$. The 3 titanium atoms and 15 tungsten atoms in the Dawson unit all adopt conventional octahedral coordination polyhedra. The polyhedral representation and molecular structure of **1a** are shown in Figure 4 (top and bottom, respectively). In **1a**, the three terminal oxygen atoms of the Ti_3 cap are substituted by the side-on-coordinated peroxo groups (Figure 4, top). The peroxo groups coordinated to the titanium(IV) atoms are shown in two positions in Figure 4 (bottom) because of disorder. The site occupancy factors of the oxygen atoms in the peroxo group were fixed at 0.64 for those labelled A and 0.36 for those labelled B. Nevertheless, the three edge-sharing titanium(IV) octahedra were positively identified and have been more fully characterised, compared with the structures so far reported for other POM-based mono- and bis[peroxotitanium(IV)] complexes.[3,4]

Selected bond lengths and angles around the three titanium(IV) centres and average bond lengths and angles for the Dawson POM unit in **1a** are given in Tables 2and 3, respectively. The O−O distances of the peroxo groups [O1A−O2A 1.45(3), O3A−O4A 1.43(3), O5A−O6A 1.45(3) Å] indicate their single-bond nature.

The Ti−O distances in the Ti_3 cap (Ti1, Ti2, Ti3) are significantly influenced by the coordination of the peroxo group, whereas the W−O distances in the W_3 cap and the two W_6 belts, i.e. the W−Ot (Ot: terminal oxygen atom), W−Oe (Oe: edge-sharing oxygen atom), W−Oc (W belt) (Oc: corner-sharing oxygen atom) and W−Oa (Oa: oxygen atom coordinated to phosphorus atom) distances are in the normal ranges.[1b] The Dawson unit contains two central P atoms in almost regular tetrahedral PO_4 units, i.e. the PO_4 closest to the Ti_3 cap [P−O distances 1.520(11)−1.560(11) Å; O−P−O angles 107.4(6)−110.9(6)°] and the PO_4 closer to the W_3 cap [P−O distances 1.513(12)−1.575(11) Å; O−P−O angles 106.8(6)−112.2(6)°].

Table 2. Selected bond lengths [Å] and angles[°] around the Ti_3 cap for **1a**

Ti−O−Ti distances		Ti−O−W distances			
Ti1−O1	2.001(13)	Ti1−O4	1.984(11)	W1−O4	1.806(13)
Ti2−O1	1.980(13)	Ti1−O5	1.963(11)	W2−O5	1.810(10)
Ti2−O2	1.975(12)	Ti2−O6	1.974(11)	W3−O6	1.813(11)
Ti3−O2	1.962(12)	Ti2−O7	1.991(11)	W4−O7	1.816(10)
Ti3−O3	1.986(13)	Ti3−O8	2.000(11)	W5−O8	1.806(11)
Ti1−O3	1.957(13)	Ti3−O9	1.982(11)	W6−O9	1.821(10)
Ti−Oa distances		$Ti-O_{peroxo}$ distances			
Ti1−O52	2.360(11)	Ti1−O1A	1.84(2)	Ti2−O4A	1.88(2)
Ti2−O52	2.403(11)	Ti1−O2A	1.909(18)	Ti3−O5A	1.904(17)
Ti3−O52	2.372(11)	Ti2−O3A	1.92(2)	Ti3−O6A	1.894(17)
O−O distances					
O1A−O2A	1.45(3)	O3A−O4A	1.43(3)	O5A−O6A	1.45(3)
Angles					
Ti1−O1−Ti2	120.3(6)	Ti2−O7−W4	150.8(6)		
Ti2−O2−Ti3	123.0(6)	Ti3−O8−W5	151.5(7)		
Ti3−O3−Ti1	122.5(6)	Ti3−O9−W6	151.3(6)		
Ti1−O4−W1	152.3(6)	O1A−Ti1−O2A	45.5(8)		
Ti1−O5−W2	151.5(6)	O3A−Ti2−O4A	44.2(9)		
Ti2−O6−W3	152.7(6)	O5A−Ti3−O6A	44.8(8)		

Table 3. Average bond lengths [Å] and angles [°] for **1a**

	Cap W (13,14,15)	Cap Ti(1,2,3)
M−O(terminal)	1.707 (12) [1.705(12)−1.709(11)]	1.89(2) [1.84(2)−1.92(2)]
M−O(M cap)	1.937 (11) [1.918(11)−1.954(11)]	1.977(13) [1.957(13)−2.001(13)]
M−O(W belt)	1.870(11) [1.851(12)−1.890(11)]	1.982(11) [1.963(11)−2.000(11)]
M−O(P)	2.370(11) [2.352(11)−2.393(11)]	2.378(11) [2.360(11)−2.403(11)]
	Belt W(1−6)	Belt W(7−12)
W−O(terminal)	1.723(11) [1.698(12)−1.738(11)]	1.721(11) [1.706(12)−1.732(11)]
W−O(M cap)	1.812(11) [1.806(11)−1.821(10)]	1.985(11) [1.963(11)−2.002(10)]
W−O(W belt)[a]	1.921(11) [1.897(11)−1.952(11)]	1.914(11) [1.894(11)−1.929(11)]
W−O(W belt)[b]	1.899(11) [1.884(11)−1.917(11)]	1.891(11) [1.884(11)−1.904(11)]
W−O(W belt)[c]	2.002(10) [1.985(10)−2.031(10)]	1.822(10) [1.797(10)−1.834(10)]
W−O(P)	2.342(11) [2.322(11)−2.374(11)]	2.358(11) [2.323(10)−2.388(11)]
	W_3 cap side	Ti_3 cap side
P−O distance	1.537(11) [1.513(12)−1.575(11)]	1.541(11) [1.520(11)−1.560(11)]
O−P−O angle	109.4(6) [106.8(6)−112.2(6)]	109.5(6) [107.4(6)−110.9(6)]

[a] Edge-sharing, between octahedra. [b] Corner-sharing, same belt.[c] Corner-sharing, between belts.

 © 2004 Wiley-VCH Verlag GmbH & Co. KGaA, Weinheim

The calculated bond valence sums (BVS),[12] based on observed bond lengths in **1a**, are in the range of 6.042−6.320 for the 15 tungsten atoms and 4.937−4.982 for the two phosphorus atoms. These data reasonably correspond to the formal valences of W^{6+} and P^{5+}, respectively. Furthermore, the BVS calculations of the oxygen atoms are in the range of 1.2322−1.2880 for O1, O2 and O3, indicating that a total of three protons are bound to the surface edge-sharing oxygen atoms of the Ti_3 cap in **1a**. In relation to this fact, we re-investigated the protonation sites and the actual anionic charges for **2a** and **3a** using BVS calculations and confirmed the protonation of all Ti−O−Ti bridges within the Dawson unit.[6] Protonation of the μ_2-oxo sites of the Ti−O−Ti bridges in the Dawson unit was first proposed for **4a**.[5c] Thus, POM **1a** takes a total charge of −9, suggesting that a peroxo group, but not a hydroperoxo group, is attached to each Ti atom.

The average O−O and Ti−O_{peroxo} bond lengths (1.44 and 1.89 Å, respectively) in **1a** can be compared with those of the previously reported mono[peroxotitanium(IV)] complex, OEPTi(O_2) (OEP = 2,3,7,8,12,13,17,18-octaethylporphinato) which contains η^2-coordination of the peroxo group to the titanium(IV) atom [O−O bond length 1.445(5) Å and two Ti−O distances 1.872(4) and 1.822(4) Å].[10a] In comparison with other peroxo groups in the POM, the average O−O distance (1.44 Å) in **1a** is close to that in [α-$P_2W_{12}(NbO_2)_6O_{56}]^{12-}$ (average 1.43 Å),[13a] but shorter than that in [A,β-$PW_9(NbO_2)O_{37}]^{6-}$ (average 1.51 Å)[13b] and the noncoordinated O_2^{2-} group (average 1.49 Å).[13c]

The peroxo groups influence the average bond lengths around the Ti_3 cap moiety more significantly than those around the W_3 cap moiety as evidenced by (i) the peroxo groups attached to the Ti atoms in **1a**, (ii) the intermolecular Ti−O−Ti interaction through the octahedral Ti^{IV} bridging groups in **2a** and (iii) the intermolecular Ti−O−Ti interaction due to direct linkage of the Dawson units in **3a** (Table 4). This effect would be reflected in the ^{31}P and ^{183}W NMR resonances. In fact, the ^{31}P resonance closest to the Ti_3 cap and the ^{183}W resonance of the W_6 belt closer to the Ti_3 cap are considerably more shifted (Table 1). Thus, the molecular structure of **1a** is consistent with the results of solution (^{31}P and ^{183}W) NMR spectroscopy, suggesting that the tris[peroxotitanium(IV)] group containing Dawson structure is maintained in aqueous solution.

On standing at room temperature for a prolonged period of time (approximately a couple of weeks), an aqueous solution of **1a** formed new crystals. An X-ray structure analysis showed that the new crystals contain the tetrapod-shaped POM without the bridging octahedral Ti groups and without an encapsulated Cl^- ion, corresponding to the POM **4a** reported by Kortz et al.[5c] In relation to this fact, two control experiments were performed as follows: (1) A clear orange solution of 0.3 g (0.067 mmol) of **1**, dissolved in 10 mL of water, was heated to reflux. ^{31}P NMR spectra of the solution were measured after 1, 2, 12 and 19 h of heating at reflux. The orange colour of the solution remained for at least 3.5 h. After 12 h, the solution became colourless and a ^{31}P NMR spectrum showed signals (δ = −7.40 and −14.16 ppm) due only to the giant tetrapod-POM without the bridging groups, i.e. **4a**. No ^{31}P NMR signal for **1a** was observed. (2) The transformation of **1a** to **4a** was also confirmed by the reaction of **1a** (0.3 g, 0.067 mmol) with $NaHSO_3$ (0.5 g, 4.80 mmol) in aqueous solution at room temperature. Several minutes after mixing of **1a** with $NaHSO_3$, the solution became colourless. Compound **4a** had probably formed at this stage. After stirring overnight, the solution (which had been concentrated at 30 °C to about 2 mL) was added to 300 mL of EtOH and a white powder of **4**, showing ^{31}P NMR resonances at δ = −7.31 and −14.05 ppm, was collected.

The transformation of **1a** to **4a** is due to thermal decomposition of the coordinated peroxo groups and also indicates the potential of **1a** as a nanobuilding block for formation of POM-based giant molecules. The peroxo group attached to the Ti atoms was relatively stable and the catalytic activity of **1a** for 2-propanol oxidation with aqueous H_2O_2 was very low. Thus, POM **1a** can be expected to act as a building block for the preparation of POM-based giant molecules, rather than as an oxidation catalyst. It is likely that the catalytically active species will be the hydroperoxotitanium(IV) species rather than the peroxotitanium(IV) species.[3c]

Conclusion

In conclusion, the monomeric tris[peroxotitanium(IV)]-substituted α-Dawson POM [α-1,2,3-$P_2W_{15}(TiO_2)_3O_{56}$-

Table 4. Comparison of average bond lengths [Å] [range] around the Ti_3 caps for Dawson POM units in **1a**−**3a**

	1a	**2a**[a]
Ti−O(terminal)	1.89(2) [1.84(2)−1.92(2)]	1.78(2) [1.77(2)−1.79(2)]
Ti−O(Ti cap)	1.977(13) [1.957(13)−2.001(13)]	2.01(2) [1.98(2)−2.05(2)]
Ti−O(W belt)	1.982(11) [1.963(11)−2.000(11)]	1.89(2) [1.87(2)−1.94(2)]
Ti−O(P)	2.378(11) [2.360(11)−2.403(11)]	2.29(2) [2.27(2)−2.30(2)]
	3a[b]	
Ti−O(terminal)	1.823(15) [1.809(15)−1.845(15)]	
Ti−O(Ti cap)	1.934(15) [1.888(15)−1.955(14)]	
Ti−O(W belt)	1.959(15) [1.937(15)−1.982(16)]	
Ti−O(P)	2.267(14) [2.242(15)−2.307(14)]	

[a] Ref.[5a] [b] Ref.[5b].

 © 2004 Wiley-VCH Verlag GmbH & Co. KGaA, Weinheim

$(OH)_3]^{9-}$ (**1a**), showing η^2-coordination of the peroxo group, was obtained from the reaction of an excess of 30% aqueous H_2O_2 with the recently reported giant tetrapod-shaped POM $\{[\alpha\text{-}1,2,3\text{-}P_2W_{15}Ti_3O_{59}(OH)_3]_4[\mu_3\text{-}Ti(OH)_3]_4Cl\}^{33-}$ (**2a**) (FW ≈ 16000) with approximately T_d symmetry. The water-soluble compound isolated as Na_9[**1a**]·$16H_2O$ (**1**) can be expected to be suitable as a precursor for the synthesis of novel POM-based giant molecules.

Experimental Section

Materials: The following were used as received: $Na_2WO_4{\cdot}2H_2O$, 85% H_3PO_4, KCl, NaCl, $NaClO_4$, 12 M aqueous HCl solution (quantitative analysis grade), 30% aqueous H_2O_2 solution, $TiCl_4$ (all from Wako) and D_2O (Isotec). The synthesis and characterisation of the tetrameric precursor **2** have been reported elsewhere.[5a]

Instrumentation/Analytical Procedure: A complete elemental analysis was carried out by Mikroanalytisches Labor Pascher (Remagen, Germany). The sample was dried at room temperature at $10^{-3}-10^{-4}$ Torr overnight before analysis. IR spectra were recorded with a Jasco 300 FT-IR spectrometer in KBr disks at room temperature. Thermogravimetric (TG) and differential thermal analyses (DTA) were acquired with a Rigaku TG8101D and TAS 300 data processing system. TG/DTA measurements were carried out in air with a temperature ramp of 4 °C per min between 25 and 500 °C. ^{31}P NMR (161.70 MHz) spectra in D_2O were recorded in 5-mm outer-diameter tubes with a JEOL JNM-EX 400 FT NMR spectrometer and a JEOL EX-400 NMR spectroscopic data-processing system. ^{31}P NMR spectra were referenced to an external standard of 25% H_3PO_4 in H_2O in a sealed capillary. Chemical shifts were reported on the δ scale with resonances upfield of H_3PO_4 (δ = 0 ppm) as negative. ^{183}W NMR (16.50 MHz) spectra were recorded in 10-mm outer-diameter tubes with a JEOL JNM-EX 400 FT NMR spectrometer equipped with a JEOL NM-40T10 L low-frequency tuneable probe and a JEOL EX-400 NMR spectroscopic data-processing system. ^{183}W NMR spectra measured in D_2O were referenced to an external standard of saturated Na_2WO_4 in D_2O (δ = 0 ppm). Chemical shifts were reported as negative for resonances upfield of Na_2WO_4 (δ = 0 ppm).

Synthesis of 1 as a Powder: To a stirred, clear, colourless solution of the precursor **2**[5a,6] (2.1 g, ca. 0.12 mmol), dissolved in water (16 mL), was added 30% aq. H_2O_2 (1.0 mL, 12.7 mmol). The clear red solution was stirred for 1 h and NaCl (5.0 g, 86.0 mmol) was then added. After stirring for 1 h, a red-orange powder formed which was collected on a membrane filter (JG 0.2 μm), washed with ethanol (10 mL × 2) and diethyl ether (50 mL × 2). The crude product at this stage was obtained in a quantity of about 1.0 g. The yellow-orange powder was dissolved in water (10 mL). The clear red-orange solution was concentrated to ca. 3 mL using a rotary evaporator at 35 °C and the resultant solution was placed in a refrigerator at 5 °C. After 1 d, the orange crystalline compound **1** was collected on a membrane filter (JG 0.2 μm), washed with ethanol (10 mL × 2) and diethyl ether (50 mL × 2) and dried in vacuo for 2 h. A yellow-orange powder of **1** was obtained in ca. 25% (0.53 g) yield. Compound **1** is highly soluble in water but insoluble in diethyl ether and ethanol. $Na_9[P_2W_{15}(TiO_2)_3O_{56}(OH)_3]{\cdot}4H_2O$ = $H_{11}Na_9O_{69}P_2Ti_3W_{15}$ (4285.29): calcd. H 0.26, Na 4.83, O 25.76, P 1.45, Ti 3.35, W 64.35; found H 0.38, Na 4.61, O 25.5, P 1.40, Ti 3.36, W 63.5, Cl < 0.03; total 98.85%. A weight loss of 4.93% was observed during the course of drying at room temperature at $10^{-3}-10^{-4}$ Torr overnight before the elemental analysis. This suggests the presence of 12−13 water molecules weakly or adsorbed. Using TG/DTA under atmospheric conditions, a weight loss of 6.61% was observed below 167.4 °C with endothermic points at 60.2 and 83.9 °C; calcd. 6.44% for x = 16 in $Na_9[P_2W_{15}(TiO_2)_3O_{56}(OH)_3]{\cdot}xH_2O$. A weight loss of 4.12% observed from 167 °C up to ca. 400 °C with an endothermic point at 172 °C is due to decomposition of the coordinated peroxo groups. IR (KBr) (polyoxometalates region): $\tilde{\nu}$ = 1083 s, 1054 m, 1013 w, 1002 w, 940 vs, 923 vs, 891 s, 820 vs, br, 811 vs, br, 755 m, 707 m, 612 m, 599 m, 559 m, 527 m, 487 w, 465 w, 431 w cm^{-1}. ^{31}P NMR (21.3 °C, D_2O): δ = −3.93, −14.41 ppm. ^{183}W NMR (20.7 °C, D_2O): δ = −156.5 (3 W), −201.9 (6 W), −230.1 (6 W) ppm.

Crystallisation of 1: Compound **1** (1.89 g) was dissolved in water (20 mL) and filtered through a folded filter paper (Whatman No. 2). The clear orange filtrate was concentrated to ca. 3 mL using a rotary evaporator at 30 °C. The solution was divided into two portions and slow concentration of both at room temperature was allowed to occur. After 3 d, clear orange plate crystals formed. One portion was used for X-ray diffraction measurements and the other for characterisation purposes. The crystals of one portion (1.5 mL) amounted to 0.17 g (8.99% yield). The characterisation data of the crystals using TG/DTA, IR and ^{31}P NMR spectroscopy are in agreement with those of the powder sample, suggesting that the crystals were representative of the bulk sample.

X-ray Crystallography for 1: A clear orange plate crystal of **1** (0.26 × 0.16 × 0.06 mm) was picked up with a cryo loop™ (from Hampton Research) and coated with liquid paraffin to prevent its degradation. Data were collected with a Bruker SMART APEX CCD diffractometer at 90 K in the range $1.8° < 2\theta < 56.7°$. The intensity data were automatically corrected for Lorentz and polarisation effects during integration. The structure was solved by direct methods (SHELXS-97: G. M. Sheldrick, University of Göttingen, **1990**) followed by subsequent difference Fourier calculations and refined by full-matrix least-squares procedures (SHELXS-97: G. M. Sheldrick, University of Göttingen, **1997**). The site occupancy factors of the oxygen atoms in the peroxo group were fixed at 0.64 for those labelled A and 0.36 for those labelled B. Crystal data for $H_{35}Na_9O_{81}P_2Ti_3W_{15}$, M = 4501.58, monoclinic, space group $P2_1/c$ (no. 14), a = 23.118(3), b = 15.2478(19), c = 24.967(3) Å, β = 100.247(2)°, V = 8660.4(19) Å^3, Z = 4, $\rho_{calcd.}$ = 3.453 g·cm^{-3}, μ(Mo-K_α) = 20.28 mm^{-1}, R_{int} = 0.1912, $R1$ = 0.0643, $wR2$ = 0.1904, GOF = 1.054 [103259 total reflections, 21557 unique reflections were $I > 2\sigma(I)$] [$R1$ = 0.0845, $wR2$ = 0.2025 (for all data)]. The maximum and minimum residual densities (10.29 and −4.784, respectively) were located at 2.31 Å from O29 and 1.11 Å from W3, respectively. In the X-ray crystallography of **1** there are several points to be addressed. (1) Absorption correction: the product of μ and tmid is greater than 3. Since an oil was used for the diffraction measurements, numerical correction of the absorption is actually impossible. (2) In the structure analysis, disorder treatment was used. There are some short O−O distances (less than 1.5 Å), that is, distances between water molecules. This is necessary because the occupancy of O was set at less than 0.5. The positions of the hydrogen atoms of the water molecule could not be determined. (3) The larger residual electron density peaks still remain and a greater R_{int} (> 0.15) results. It is actually impossible to obtain high-quality diffraction data from the POM because of the disorder of the solvent in the crystal and the difficulties applying absorption corrections. Further details on the crystal structure investigation may be obtained from the Fachinformationzen-

 © 2004 Wiley-VCH Verlag GmbH & Co. KGaA, Weinheim

trum Karlsruhe, 76344 Eggenstein-Leopoldshafen, Germany [Fax: (internat.) + 49-7247-808-666; E-mail: crysdata@fiz-karlsruhe.de], on quoting the depository number CSD-413816 (formula/code: yos20mo).

Reactivity of 2a and 3a with Aqueous Hydrogen Peroxide: The reaction of the giant tetrapod-shaped POM **2a** with hydrogen peroxide gave a pure form of the peroxo species **1a** within 30 min. In contrast, the reaction of another giant tetrapod-shaped POM (**3a**) with hydrogen peroxide, which was monitored by ^{31}P NMR spectroscopy, did not react in the same way. To a colourless solution of **3** (0.52 g, 0.029 mmol), dissolved in water (5 mL), was added 30% aqueous H_2O_2 (0.25 mL, 3.18 mmol). The colour of the solution became clear yellow after 30 min, yellow-orange after 9 h and orange after 35 h. A ^{31}P NMR spectrum of the solution, measured after 30 min, showed only a two-line spectrum with resonances $\delta = -7.70$ and -13.97 ppm due to **3a** itself, indicating that no peroxo species was formed. After 9 h, the two ^{31}P NMR signals at $\delta = -4.24$ and -14.16 ppm, assignable to the peroxo species **1a**, began to appear but the large signals (at $\delta = -7.70$, -13.97 ppm) of **3a** still remained and smaller peaks due to at least three other species (at $\delta = -5.18$, -5.38, -6.90 and -14.23 ppm) could also be observed. After 35 h, the ^{31}P NMR signals due to the peroxo species **1a** at $\delta = -4.15$ and -14.06 ppm, as well as other peaks due to at least three species (at $\delta = -5.09$, -5.30, -6.80, -13.81, -14.14 ppm), became larger, whereas only the two signals due to **3a** (at $\delta = -7.62$ and -13.88 ppm) became less intense. After a prolonged reaction time of **3a**, the formation of the peroxo species **1a** was definitely confirmed. However, **1a** was not the only species formed. Thus, with hydrogen peroxide, the reactivity of compound **3a** was quite different from that of **2a**.

Supporting Information: Figures S1 and S2; see also the footnote on the first page of this article

Acknowledgments

This work was supported by a Grant-in-Aid for Scientific Research and also by a High-tech Research Centre Project, both from the Ministry of Education, Culture, Sports, Science and Technology, Japan. We thank Akira Shinohara for evaluation of the catalytic activity of **1a** for 2-propanol oxidation with 30% aqueous hydrogen peroxide.

[1] [1a] M. T. Pope, A. Müller, *Angew. Chem. Int. Ed. Engl.* **1991**, *30*, 34. [1b] M. T. Pope, *Heteropoly and Isopoly Oxometalates*, Springer-Verlag, New York, **1983**. [1c] V. W. Day, W. G. Klemperer, *Science* **1985**, *228*, 533. [1d] C. L. Hill, *Chem. Rev.* **1998**, *98*, 1. [1e] T. Okuhara, N. Mizuno, M. Misono, *Adv. Catal.* **1996**, *41*, 113. [1f] C. L. Hill, C. M. Prosser-McCartha, *Coord. Chem. Rev.* **1995**, *143*, 407. [1g] A series of 34 recent papers in a volume devoted to poloxoanion in catalysis: C. L. Hill, *J. Mol. Catal.* **1996**, *114*, 1. [1h] R. Neumann, *Prog. Inorg. Chem.* **1998**, *47*, 317. [1i] *Polyoxometalate Chemistry from Topology via Self-Assembly to Applications* (Eds: M. T. Pope, A. Müller), Kluwer Academic Publishers, Netherlands, **2001**. [1j] *Polyoxometalate Chemistry for Nano-Composite Design* (Eds: T. Yamase, M. T. Pope), Kluwer Academic Publishers, Netherlands, **2002**. [1k] M. T. Pope, "Polyoxo anions: synthesis and structure", in *Comprehensive Coordination Chemistry II* (Ed.: A. G. Wedd), Elsevier Science, New York, **2004**, vol. 4, p. 635.

[2] [2a] U. Müller, *Inorganic Structural Chemistry*, Wiley, New York, **1993**. [2b] A. L. Linsenbigler, G. Lu, J. T. Yates, Jr., *Chem. Rev.* **1995**, *95*, 735. [2c] T. Kawahara, Y. Konishi, H. Tada, N. Tohge, J. Nishii, S. Ito, *Angew. Chem. Int. Ed.* **2002**, *41*, 2811.

[3] [3a] F. Gao, T. Yamase, H. Suzuki, *J. Mol. Catal. A: Chem.* **2002**, *180*, 97. [3b] T. Yamase, E. Ishikawa, Y. Asai, S. Kanai, *J. Mol. Catal. A: Chem.* **1996**, *114*, 237. [3c] O. A. Kholdeeva, G. M. Maksimov, R. I. Maksimovskaya, L. A. Kovaleva, M. A. Fedotov, V. A. Grigoriev, C. L. Hill, *Inorg. Chem.* **2000**, *39*, 3828.

[4] T. Yamase, T. Ozeki, S. Motomura, *Bull. Chem. Soc. Jpn.* **1992**, *65*, 1453.

[5] [5a] Y. Sakai, K. Yoza, C. N. Kato, K. Nomiya, *Chem. Eur. J.* **2003**, *9*, 4077. [5b] Y. Sakai, K. Yoza, C. N. Kato, K. Nomiya, *Dalton Trans.* **2003**, 3581. [5c] U. Kortz, S. S. Hamzeh, A. Nasser, *Chem. Eur. J.* **2003**, *9*, 2945. [5d] K. Nomiya, Y. Arai, Y. Shimizu, M. Takahashi, T. Takayama, H. Weiner, T. Nagata, J. A. Widegren, R. G. Finke, *Inorg. Chim. Acta* **2000**, *300–302*, 285.

[6] Abbreviation of compounds **1**–**4**: Previous formulae of **2** and **2a**[5a] as well as **3** and **3a**[5b] were revised by considering the protonation sites in the Dawson unit found with BVS calculations of the oxygen atoms; (1) tris[peroxotitanium(IV)]-substituted Dawson POM Na_9[**1a**]·$16H_2O$ (**1**) {**1a** = [α-1,2,3-$P_2W_{15}(TiO_2)_3O_{56}(OH)_3]^{9-}$}, (2) giant tetrapod-POM with the bridging Ti octahedral groups Na_xH_{33-x}[**2a**]·yH_2O (**2**) (x = 16–19, y = 60–70; **2a** = {[α-1,2,3-$P_2W_{15}Ti_3O_{59}(OH)_3]_4$[$\mu_3$-$Ti(OH)_3]_4Cl\}^{33-}$), (3) giant tetrapod-POM without the bridging groups K_4Na_{21}[**3a**]·yH_2O (**3**) (y = 60–70; **3a** = {[α-1,2,3-$P_2W_{15}Ti_3O_{57.5}(OH)_3]_4Cl\}^{25-}$), and (4) giant tetrapod-POM without the bridging groups and without the encapsulated Cl^- ion $K_4(NH_4)_{20}$[**4a**]·$77H_2O$ (**4**) {**4a** = $[P_2W_{15}Ti_3O_{57.5}(OH)_3]_4^{24-}$}.[5c]

[7] At present, we can consider at least four giant tetrapod-shaped POMs with regard to the presence of the bridging Ti octahedral groups and/or the presence of an encapsulated chloride ion. Three of them (**2a**, **3a** and **4a** have been confirmed.[5a–5c] The encapsulated chloride ion in **3a** can be removed from the POM by recrystallisation from an aqueous solution containing KCl and HCl.[5d]

[8] Formation conditions of the two tetrameric Dawson POMs **2a** and **3a** were examined by ^{31}P NMR measurements in aqueous solution (Figure S1, see Supporting Information, see also the footnote on the first page of this article). One key for their formation is the concentration of the titanium(IV) ion used in the reaction. POM **3a** was formed in solution at a 3:1 molar ratio of $Ti(SO_4)_2·4H_2O/Na_{12}[B\text{-}α\text{-}P_2W_{15}O_{56}]·19H_2O$, while POM **2a** was formed in solution at a 10:1 molar ratio.

[9] C. Rocchiccioli-Deltcheff, R. Thouvenot, *Spectrosc. Lett.* **1979**, *12*, 127.

[10] [10a] R. Guilard, J-M. Latour, C. Lecomte, J-C. Marchon, J. Protas, D. Ripoll, *Inorg. Chem.* **1978**, *17*, 1228. [10b] P. E. Esser, U. Englert, W. Keim, *Chem. Ber.* **1996**, *129*, 833.

[11] [11a] T. J. R. Weakley, R. G. Finke, *Inorg. Chem.* **1990**, *29*, 1235. [11b] Y. Lin, T. J. R. Weakley, B. Rapko, R. G. Finke, *Inorg., Chem.* **1993**, *32*, 5095. [11c] T. Yamase, T. Ozeki, H. Sakamoto, S. Nishiya, A. Yamamoto, *Bull. Chem. Soc. Jpn.* **1993**, *66*, 103. [11d] K. Nomiya, M. Takahashi, K. Ohsawa, J. A. Widegren, *J. Chem. Soc., Dalton Trans.* **2001**, 2872. [11e] K. Nomiya, M. Takahashi, J. A. Widegren, T. Aizawa, Y. Sakai, N. C. Kasuga, *J. Chem. Soc., Dalton Trans.* **2002**, 3679.

[12] [12a] I. D. Brown, D. Altermatt, *Acta Crystallogr., Sect. B* **1985**, *41*, 244. [12b] I. D. Brown, R. D. Shannon, *Acta Crystallogr., Sect. A* **1973**, *29*, 266.

[13] [13a] D. A. Judd, Q. Chen, C. F. Campana, C. L. Hill, *J. Am. Chem. Soc.* **1997**, *119*, 5461. [13b] M. K. Harrup, G-S. Kim, H. Zeng, R. P. Johnson, D. VanDerveer, C. L. Hill, *Inorg. Chem.* **1998**, *37*, 5550. [13c] L. Vaska, *Acc. Chem. Res.* **1976**, *9*, 175.

Received July 19, 2004
Early View Article
Published Online October 18, 2004

 © 2004 Wiley-VCH Verlag GmbH & Co. KGaA, Weinheim

An in situ Template Route for Fabricating Metal Chalcogenide Hollow Spherical Assemblies Sonochemically

Shu Xu,[a] Hui Wang,[a] Jun-Jie Zhu,*[a] Xin-Quan Xin,[a] and Hong-Yuan Chen[a]

Keywords: Sonochemistry / Nanostructures / Self-assembly / Metal chalcogenides / Hollow spheres

An ultrasound-assisted in situ template approach has been developed for fabricating a series of nanoscale metal chalcogenides in the form of well-defined hollow spherical assemblies. These hollow spherical assemblies have well-controlled dimensions and are composed of uniform nanoparticles. Initially, metal hydroxide particles self-assemble into spherical templates generated in situ, and subsequent surface crystal growth leads to hollow spherical structures. Ultrasound irradiation plays a critical role both in the formation of the intermediate templates and in the crystal-growth process. This approach provides a convenient and efficient one-step pathway to the large-scale fabrication of hollow spherical nanostructures. It also represents a new demonstration of sonochemical effects on the formation and assembly of crystalline particles on the nanometer scale.

(© Wiley-VCH Verlag GmbH & Co. KGaA, 69451 Weinheim, Germany, 2004)

Introduction

Much attention has been devoted lately to developing methods for preparing, connecting, and assembling semiconductor nanocrystals. The well-ordered assemblies, unlike nanoparticles or single crystals, have new properties suitable for building fine powders or other functional materials. Over the last decades the novel properties and applications of these materials, including mesoporous structures, networks, core−shell spherical materials, and a series of wire- or rod-like assemblies have been exhibited.[1−9] Especially the assembled hollow spherical materials are important because of their many potential applications in various fields of chemistry, biotechnology, and materials science. For example, they can be used for the transport, controlled storage, and release of chemical and biological products such as drugs, for the protection of biologically active macromolecules, and in the field of catalysis and waste removal.[10−13] Until now, most methods for the fabrication of inorganic materials with hollow spherical structures were based on a number of well-developed techniques, such as the nozzle reaction system, emulsion/water extraction, layer-by-layer (LBL) self-assembly, and sacrificial core−shell techniques.[5,14−21]

Currently, the template-directed assembly of nanodimensional materials is arousing increasing interest due to its unique advantages in the control over shape, orientation, and crystal growth. It usually takes three steps to prepare hollow spherical assemblies: first, a colloidal core consisting of a polymer or some other material is prepared as a template; then, assembly is carried out on the surface of the core to obtain a core−shell structure; finally, the core is removed to form the hollow structure. A widely adopted and quickly developed template method is the LBL self-assembly technique, which is based on the use of electrostatic interactions or hydrogen bonding between alternate layers of materials deposited on a surface. This technique can be applied to the coating of colloids.[5,18,19] However, only a few hollow spheres of silica, zeolite, and other magnetic materials have been fabricated by using this strategy because of the difficulty in the removal of the template cores. For this reason, we are still trying to find some new methods with the goal of avoiding the disassembly of the shell in the process of removing the cores to produce the final hollow spherical materials, or of even generating hollow spherical structures directly without a core−shell step (Scheme 1).

Ultrasound waves that are intense enough to produce cavitations can drive chemical reactions such as oxidation, reduction, dissolution, decomposition, and polymerization.[22−33] Ultrasound irradiation has also been employed to prepare a series of polymer core/metal oxide shell particles and a cadmium selenide hollow spherical material.[9,22,26,34−36] In recent years, the sonochemical method has been proven to be convenient and effective in the fabrication of porous structures. It has been discovered that the ultrasound wave has a strong effect on the congregation and self-assembly of nanoparticles. Gedanken's group has established this procedure as a route to produce some tubular assemblies and a variety of mesoporous oxide materials.[37−39] The advantage of the application of ultrasound irradiation to the synthesis of mesoporous materials

[a] State Key Laboratory of Coordination Chemistry, Department of Chemistry, Nanjing University,
Nanjing 210093, P. R. China
E-mail: jjzhu@nju.edu.cn

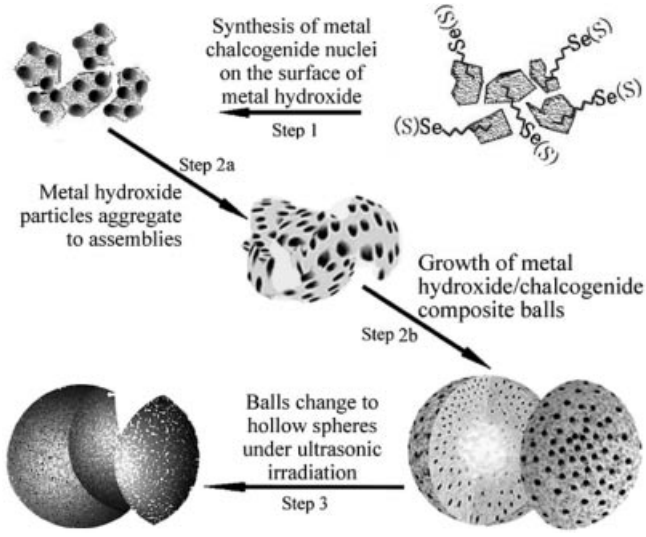

Scheme 1. Proposed mechanism for the synthesis of hollow-sphere materials

is the significant reduction in fabrication time and the possibility to induce the aggregation of nanoparticles into porous structures without destroying the micellar structure. Hence, this method provides an effective surface assembly route for the controllable synthesis of spatially structured materials.

We have extended the sonochemical method to the synthesis of hollow spherical nanostructural materials.[40] An in situ template route was developed for fabricating a series of metal chalcogenide hollow spherical assemblies in an aqueous system. It is a general approach for fabricating hollow spherical materials directly, which makes it possible to avoid the step of removing the template core.

Results and Discussion

Characterization of Hollow-Sphere Assemblies

Cadmium selenide, cadmium sulfide, and copper sulfide hollow spherical assemblies were prepared. To study the properties and morphology of the products, characterization techniques including powder XRD, TEM, XPS, SAED, UV/Vis absorption and fluorescence spectroscopy were employed.

XRD, XPS Studies, and TEM Observations

The X-ray diffraction patterns for the products are shown in Figure 1. The diffraction peak in pattern (a) indicates that the CdSe particles are crystallized in the pure cubic phase (JCPDS No. 19-191), pattern (b) corresponds to the pure cubic phase CdS (JCPDS No.75-0581), and pattern (c) belongs to pure CuS crystals (JCPDS No. 03-1090). No peaks of any other impurities were detected, indicating the high purity of the products. According to the Debye−Scherrer equation,[41] the average sizes of the CdSe, CdS, and CuS particles were estimated to be about 7 nm, 7 nm, and 10 nm, respectively.

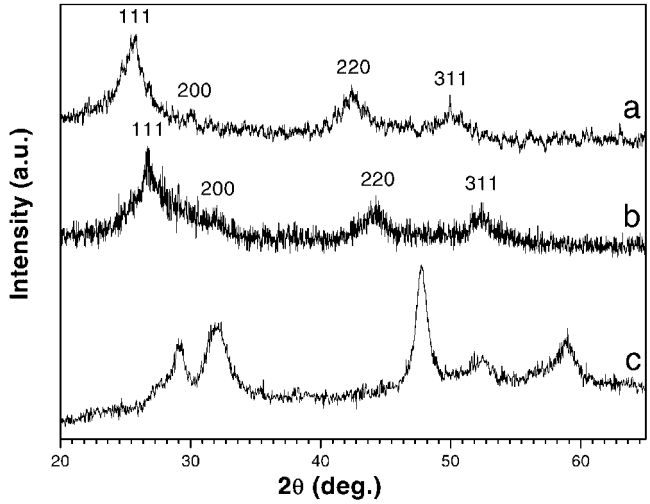

Figure 1. Powder XRD pattern of hollow spherical assemblies: (a) CdSe; (b) CdS; (c) CuS

XPS measurements supply further evidence for the composition and purity of the products. All peaks were calibrated by using C(1s) (284.6 eV) as the reference. The two peaks located at 405.5 eV and 412.3 eV were assigned to Cd(3d). The peaks at 54.5 eV, 162.2 eV, and 932 eV correspond to Se(3d), S(2p), and Cu(2p), respectively. According to the measurements, the ratio Cd/Se is approximately 6:4, which shows that the sample of the CdSe assembly is rich in cadmium at the surface. The measurements also show that the ratio Cd/S is approximately 6:4 and the ratio Cu/S is approximately 1.1:1.

In the TEM images (Figure 2, a, b), uniform hollow CdSe spheres with an average diameter of 120 nm are observed. These hollow spheres consist of spherical nanoparticles about 5 nm in size. The HRTEM image (Figure 2, c) of a single hollow sphere exhibits the clear crystalline lattice of CdSe particles on the spherical surface and the hollow inside can also be observed clearly. The SAED (Figure 2, d) recorded on a CdSe hollow sphere shows the presence of clear diffraction rings, which correspond to the cubic phase of CdSe with polycrystalline nature. In Figure 3, uniform hollow CdS spheres with an average diameter of 120 nm are observed. The surface structure of the CdS spheres is the same as that of the hollow CdSe spheres assembled from nanoparticles about 5 nm in size. Figure 4 shows the TEM image of the CuS hollow spheres with diameters ranging from 150 to 300 nm. These spheres are made up of CuS nanoparticles about 8 nm in size. The shell of the CuS sphere is thinner than that of the hollow CdSe and CdS spheres, so the hollow space inside is very distinct. The TEM images confirm that all the spheres for all three compounds are hollow.

 © 2004 Wiley-VCH Verlag GmbH & Co. KGaA, Weinheim

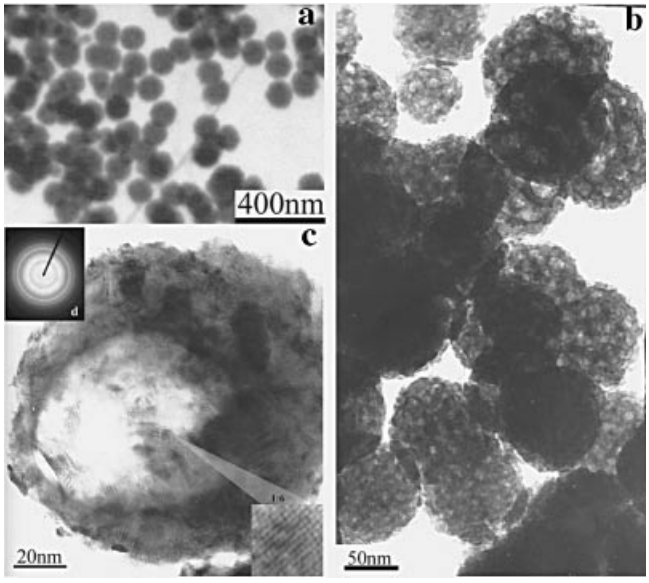

Figure 2. TEM and HRTEM images of the CdSe assemblies in the presence of ammonia after sonication for 30 min (concentration of NH_3: 0.8 mol/L): (a, b) TEM images of the product, (c) HRTEM image of an individual CdSe hollow-spherical assembly, (d) [inset in (c)] SAED pattern recorded on the hollow sphere shown in (c)

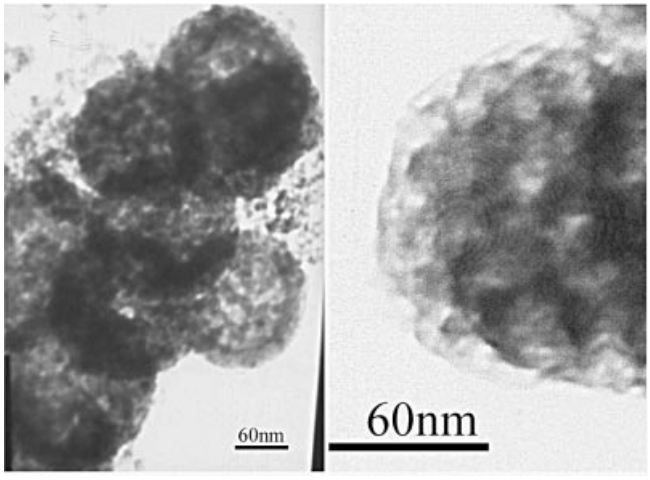

Figure 3. TEM images of the CdS assemblies in the presence of ammonia after sonication for 30 min (concentration of NH_3: 0.8 mol/L)

Optical Characterization

The UV/Vis absorbance spectra of the prepared hollow spherical materials were measured and their correlative optical band gaps were calculated according to the following Equation, where A is a constant, α is the absorption coefficient, and $m = 3$ for a direct and $m = 1$ for an indirect transition.[42]

$$\alpha(\nu) = A\cdot[h\nu/(2 - E_g)]^{m/2}$$

The CdSe assembly has its absorbance peak at 350 nm. Its direct band gap is calculated to be 2.7 eV, which is much larger than the reported value for bulk CdSe (E_g = 1.7 eV).[43] This band-gap value, which indicates the quantum size effect of this sample, equals that of the 7 nm quantum CdSe nanoparticles prepared. It offers further evidence that these spherical assemblies are made up of smaller nanoparticles. The direct band gap of the hollow CdS assemblies is calculated to be 2.11 eV. The equation with $m = 1$ is used for the indirect transition to the copper sulfide nanoparticles, since copper sulfide is a typical indirect semiconductor.[44] The calculated band gap of this CuS assembly is 2.02 eV, which equals that of 8 nm CuS nanoparticles.

We also investigated the fluorescent absorbance spectra of the prepared materials and compared them with those of the dispersed particles. The excitation and emission wavelengths of the hollow CdSe spheres were 485 nm and 730 nm, respectively; the fluorescence spectrum was the same as that of dispersed 5 nm CdSe nanoparticles. The emission peak of CdS was at 570 nm when an excitation wavelength of 430 nm was selected. The CuS sphere had a strong emission peak at 362 nm when the excitation wavelength was 220 nm.

Discussion of the Reaction Procedure

A study of the reaction processes showed that metal hydroxide was an in situ template in the reaction and directed the formation of hollow spherical structures. We propose a probable reaction mechanism to explain the formation of hollow spherical materials in accordance with our experimental results. The effect of ultrasound irradiation, release rate of Se^{2-} and S^{2-} ions, pH value and ligands on the reaction were also investigated.

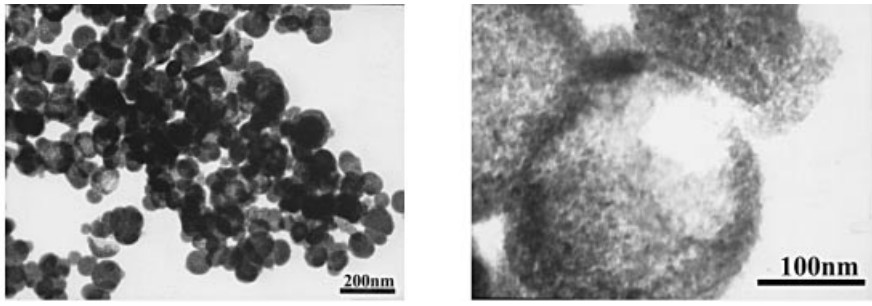

Figure 4. TEM images of the CuS assemblies in the presence of TEA after sonication for 30 min (concentration of TEA: 0.8 mol/L)

 © 2004 Wiley-VCH Verlag GmbH & Co. KGaA, Weinheim

Microscopic Monitoring of the Reaction Process

The structures of the assemblies at various stages of the growth process were characterized using TEM. We collected the products every 5 min during the reaction. The precursor, the intermediate structure formed during the sonochemical reaction, and the final structure are shown in Figure 5. These TEM images indicate the tendency to form a hollow spherical structure from the metal hydroxide particles. To begin with, ammonia or triethylamine was added to an aqueous solution of metal ions to form a metal hydroxide colloidal solution. The metal hydroxide particles were made up of many very irregular slices and some blocks, as shown in Figure 5 (a). Initially, the metal hydroxide particles reacted with selenium or sulfur ions, giving rise to metal chalcogenide nanoparticles on their surface, and formed metal hydroxide/chalcogenide composites. In the medial stage (Figure 5, b), we could observe that some slices and blocks were interconnected and enwrapped to form balls or multilayered spheres. At the final stage (Figure 5, c), the balls had grown into regular hollow spheres. Furthermore, when the ultrasound intensity was lower than 15 W/cm^2, the products were inclined to form irregular hollow spheres or balls, whereas an intensity higher than 30 W/cm^2 lead to the formation of dispersed particles. All the experiments showed that ultrasound waves had a critical effect on the fabrication of the special structures.

We also investigated some contrastive experiments and compared the morphology of the products in different stages of the reaction process with that in the process of fabricating hollow spheres. In the thermal process, in which sonication was replaced by heating and stirring, the metal hydroxide and chalcogenide particles continuously congregated to form large irregular assemblies instead of spheres. These assemblies were also composed of 7−10 nm metal chalcogenide nanoparticles. On the other hand, when metal hydroxide particles alone were sonicated, they formed rodlike crystals or assemblies. When metal hydroxide particles alone were heated, their congregation was much slower and more irregular. Figure 6 exhibits the morphology of a sample of cadmium hydroxide sonicated for 30 min and a cadmium sulfide aggregate prepared by the thermal process. None of these reactions produced a sphere-like structure.

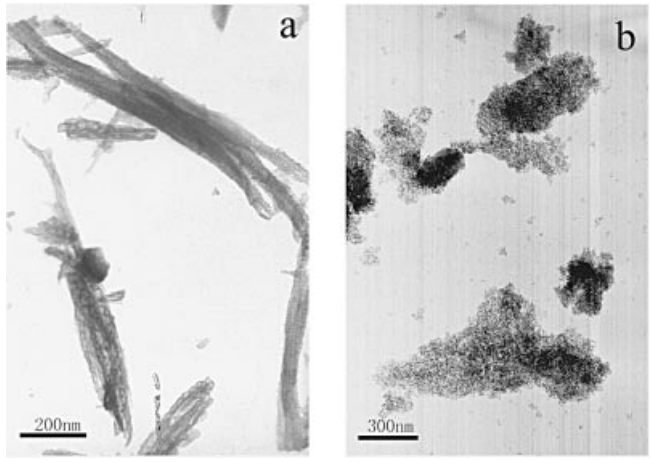

Figure 6. TEM images: (a) cadmium hydroxide nanorods prepared (cadmium hydroxide was sonicated for 30 min in the presence of ammonia); (b) cadmium sulfide particles prepared by the thermal process (cadmium hydroxide reacted with Na_2SeSO_3 at 90 °C for 30 min in the presence of ammonia)

Probable Reaction Mechanism

In a typical reaction, ultrasound irradiation induces the assembly of the metal hydroxide particles into both balls and hollow spherical structures and the growth of cadmium chalcogenide crystals on the template surface.

The elevated temperatures and pressures inside the collapsing bubbles cause water to vaporize and to further pyrolyze into H$^{\cdot}$ and OH$^{\cdot}$ radicals during an aqueous sonochemical process.[22] The H$^{\cdot}$ and OH$^{\cdot}$ radicals can react with sodium selenosulfate and thiourea to release Se^{2-} and S^{2-}. The dangling bonds on the surface of the metal hydroxide particles provide some active spots for the formation of me-

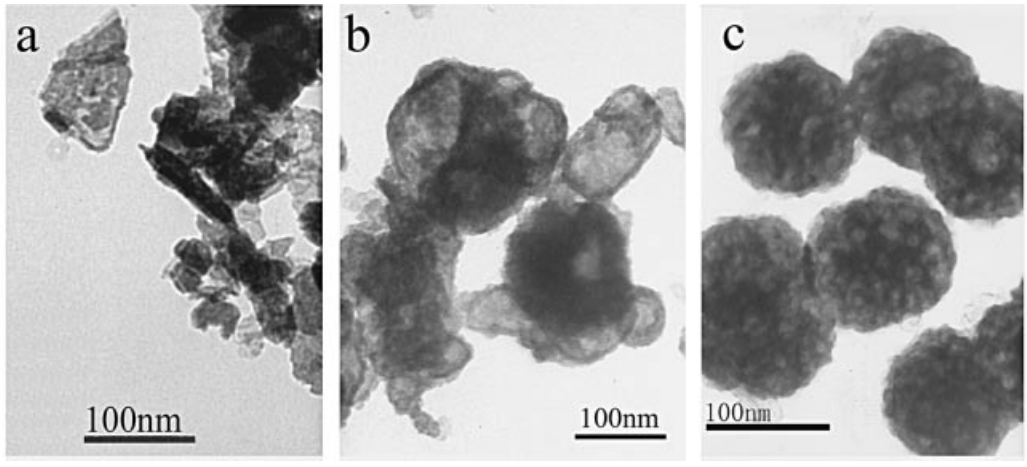

Figure 5. TEM images of the products at different stages of fabricating CdSe hollow spheres (sonic intensity is 20 W/cm^2): (a) cadmium hydroxide particles at the initial stage (immediately after precipitation); (b) after 15 min reaction; (c) after 30 min reaction

 © 2004 Wiley-VCH Verlag GmbH & Co. KGaA, Weinheim

tal chalcogenide nuclei. The probable reaction sequence for the sonochemical formation of the metal chalcogenide nanoparticles can be summarized as shown in Equations (1)−(6).

$$H_2O \xrightarrow{\text{sonication}} H^{\cdot} + HO^{\cdot} \quad (1)$$

$$2\,H^{\cdot} + SeSO_3^{2-} \rightarrow Se^{2-} + 2\,H^{+} + SO_3^{2-} \quad (2)$$

$$H^{\cdot} + OH^{\cdot} + CS(NH_2)_2 \rightarrow (NH_2)_2C(OH)-SH$$
$$H^{\cdot} + OH^{\cdot} + (NH_2)_2C(OH)-SH \rightarrow (NH_2)_2C(OH)_2 + H_2S \quad (3)$$
$$(NH_2)_2C(OH)_2 \rightarrow (NH_2)_2C{=}O + H_2O$$

$$H^{\cdot} + OH^{\cdot} + CH_3CSNH_2 \rightarrow CH_3C(NH_2)(OH)-SH$$
$$H^{\cdot} + OH^{\cdot} + CH_3C(NH_2)(OH)-SH \rightarrow CH_3C(NH_2)(OH)_2 + \quad (4)$$
$$H_2S\,CH_3C(NH_2)(OH)_2 \rightarrow CH_3CO(NH_2) + H_2O$$

$$M(OH)_2 + Se^{2-}\ (S^{2-}) \rightarrow MSe\ (MS) + 2\,OH^{-}\ (M = Cd, Cu) \quad (5)$$

$$n\,MSe\ (or\ MS) \rightarrow (MSe)_n\ or\ (MS)_n\ (M = Cd, Cu) \quad (6)$$

The freshly born nuclei will grow into large particles until they become stable finally. It is well known that the Gibbs free energy of the surface of small-sized nanoparticles is usually very high due to the large surface/volume ratio and the existence of dangling bonds on the surface. These small particles have the tendency to aggregate, to decrease the Gibbs free energy of the surface and to make the surface state stable. In most cases, the smaller nanoparticles result in more easy aggregation. In our experiments, the particles grown on the metal hydroxide were also inclined to conglomeration. The kinetics of the thermal process enables the formation of Se and S ions and the growth of metal chalcogenide nanoparticles, which induce congregation. Since this kind of congregation is not directional assembly, the final product consists of big irregular particles as shown in part b of Figure 6.

On the other hand, in the sonication process, cavitation resulting in bubble collapse will launch shock waves out into the liquid. The strength of the waves can even result in the breakage of the bonds in the polymer chain. When these shock waves pass over metal hydroxide and metal oxide particles, they can also cause the rapid impact of the liquid on the surface of the particles and promote the rupture of the bonds.[25] Ultrasound studies have indicated that a large number of dangling bonds and defects will appear especially at the edge of sheetlike particles as a result of the impingements of the microjets created by ultrasonic waves.[22,45] Gedanken's group has produced a kind of tubular titania assembly using this mechanism.[39] If only metal hydroxide particles were under sonication, the many dangling Cd−O−Cd bonds on the edges of the sheetlike particles would connect to form a layer-like structure which continuously rolls into rods or tubes as the structure observed in Figure 6 (a).

However, in our system, the metal hydroxide particles were not merely assembled through the dangling Cd−O−Cd bonds or the metal chalcogenide nuclei on the surface. Once the chalcogenide nuclei were formed on the surface of the hydroxide particles, the effect resulted in the assembly both on the edge by the connection of the dangling Cd−O−Cd bonds, and on the surface by the congregation of the chalcogenide nanoparticles. The two kinds of assembly lead to intermediate products with ball-like or multilayered hollow-spherical structures, as observed in the TEM images (see b in Figure 3).

After the formation of the intermediate structure, the growth of the metal chalcogenide particles only on the surface of the metal hydroxide/chalcogenide composite spheres continually consumed the inner metal hydroxide. These freshly born nuclei grew into large particles until they finally became stable.[46] The product was a regular hollow sphere. The metal chalcogenide particles thus formed were held together by van der Waals forces. Since these forces are not very strong, the rapid impact of the liquid would promote the dispersion of the assemblies, which would crack into small particles and disperse further in the presence of the strong ultrasound shock wave. Hence, a high sonic intensity could not be used in the experiments. When the aggregation and dispersion were balanced, the metal hydroxides could aggregate to form the desired assemblies; then the reaction could be carried out to fabricate the hollow-sphere structures described in Equations (5) and (6). At a sonic intensity of 20 W/cm^2, a good balance was observed, and an appropriate growth rate could be obtained.

Effect of the Release Rate of Chalcogen Ions

In our further studies, we determined that the growth rate of metal chalcogenide nuclei had a strong effect on the fabrication process. This effect depended on the release rate of Se^{2-} and S^{2-}. With a high release rate, many metal chalcogenide nuclei and particles would grow on the surface of the metal hydroxide particles before their assembly. In this case, the number of the remaining metal hydroxide particles was not enough for crystal growth on the surface to form hollow structures and aggregation neutralized the dispersive effect of ultrasound. The result was ball-like metal chalcogenide aggregation instead of hollow spherical assemblies. In contrast, a low release rate would make the dispersive effect of ultrasound so strong that the particles would break away from the surface. This resulted in incompact hollow spheres or dispersed particles.

In the presence of ultrasonic irradiation, the release rates of Se^{2-} and S^{2-} from different selenium and sulfur sources are different. Our study on the growth of CdS spheres proved the importance of selecting the appropriate sulfur source. When thiourea was the sulfur source, the release rate of S ions was slow, and the white turbid suspension began to turn yellow after 10 min of reaction. After 30 min of reaction, the product consisted almost completely of dispersed particles, and only a few hollow spheres were observed. Alternatively, when thioacetamide was selected as

 © 2004 Wiley-VCH Verlag GmbH & Co. KGaA, Weinheim

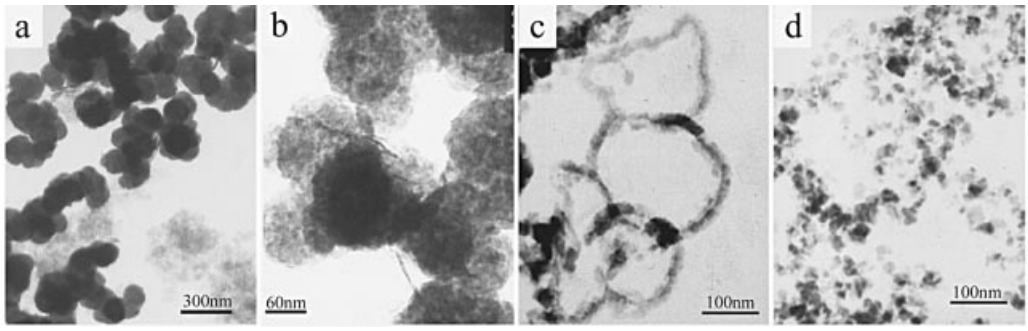

Figure 7. TEM images of the CdS particles obtained with different thiourea/thioacetamide ratios as the sulfur source (sonic intensity: 20 W/cm^2; sonication time: 30 min): (a) thioacetamide as the sulfur source; (b) with a 1:1 ratio of thiourea/thioacetamide; (c) with a 4:1 ratio of thiourea/thioacetamide; (d) thiourea as the sulfur source

the sulfur source, the release rate of S^{2-} was quick enough to form the yellow turbidity immediately. After 30 min of reaction, all of the product was ball-like and no hollow spherical structure was observed. Only when the ratio thiourea/thioacetamide was in an appropriate range would the hollow spherical structure be fabricated. The TEM images in Figure 7 show a series of structures ranging from ball, hollow sphere, circle-like to dispersed particles. It seemed that the dispersed particles were decomposed from the circles. The relation between the structures was strong evidence for the dispersive effect of sonication. In the preparation of cadmium selenide, the experimental results showed that the release rate of Se^{2-} from sodium selenosulfate was acceptable in the fabrication of CdSe hollow spheres.

Effect of the Ligands on the Reaction

Se^{2-} and S^{2-} need to be released in an alkaline environment; otherwise the release rate will be too slow to fabricate the assemblies. In our experiments, the pH value of the reaction system was kept at about 10 by adjusting the ligands and the reactants in the solution. The ligands in the solution were also important in the control of both the formation of metal chalcogenide nuclei and the crystal-growth rate. According to our experiments, in the absence of the ligands or with ligands having weak complexing ability, the products would be dispersed particles or irregular assemblies. Some unidentate and chelating ligands with strong complexing capability and steric effects would strongly decrease the growth of the nanoparticles and lead to monodispersed particles or even prevent the metal ions from combining with the Se^{2-} and S^{2-} ions. This observation proved the protection effect of the ligands. Through the complexing action between metal ions and ligands that lead to the formation of the complexes, the ligands could protect the metal ions from reacting with Se^{2-} and S^{2-} directly and provided a stable reaction rate. Here we selected ammonia and tetraethylammonium (TEA) as the ligands because they had a moderate complexing ability for the metal ions in the alkaline environment. In addition, the concentration of the ligands had to be limited to a certain range; otherwise the ligands in excess would dissolve all the metal hydroxide particles. Actually, in the reaction system the ligands were adsorbed on the surface of the metal hydroxide stoichiometrically. The steric effect enhanced the stability of the surface structure and controlled the rate of combination of Se^{2-} and S^{2-} with the metal ions.

Conclusion

A general sonochemical approach for the fabrication of hollow spherical assemblies composed of metal chalcogenide nanoparticles has been successfully established. In this reaction, we make the best use of the balance between the conglomeration of the particles and the dispersive effect of ultrasound to direct the growth of the assemblies. As we have demonstrated in this article, the effect of ultrasound on the metal hydroxide balls directs the formation of the in situ template, and the growth on the surface leads to the fabrication of the final hollow-sphere assemblies. The sonochemical method provides a mild, energy-efficient, and environment-friendly approach to hollow-sphere assemblies of nanodimensional metal chalcogenides. Furthermore, a major advantage is that it circumvents the disassembly of the shell in the process of removing the cores and produces the hollow metal chalcogenide spheres conveniently. It promises to be useful in the fabrication of other hollow assemblies composed of metal, alloy, oxide, and similar nanoparticles.

Experimental Section

General: All reagents used were of analytical purity. Na_2SeSO_3 solution (0.2 M) was prepared by stirring Se (0.2 M) and Na_2SO_3 (0.5 M) at about 70 °C for 24 h. The XRD patterns were recorded with a Shimadzu XD-3 A X-ray diffractometer (Cu-K_α radiation, $\lambda = 0.15418$ nm). The TEM and SAED examinations were carried out with a JEOL JEM-200CX transmission electron microscope, with an accelerating voltage of 200 kV. The surface of the products was studied by X-ray photoelectron spectroscopy with an ESCALAB MK II X-ray photoelectron spectrometer, taking nonmonochromatized Mg-K_α X-ray as the excitation source and choosing C(1s) (284.6 eV) as the reference line. A Ruili 1200 spectrophotometer (Peking Analytical Instrument Co.) was used to record the UV/Vis absorption spectra of the CdSe, CdS and CuS assemblies.

 © 2004 Wiley-VCH Verlag GmbH & Co. KGaA, Weinheim

Preparation of Hollow CdSe Spheres: $CdCl_2$ (0.5 g) was dissolved in distilled water (50 mL), and then ammonia (5 mL, 30% NH_3) or TEA (11 mL) was added. A white colloid appeared immediately in the solution. This solution, Na_2SeSO_3 (10 mL, 0.2 M), and the amount of distilled water to make the total volume 100 mL were transferred into a 150-mL round-bottom flask. This mixture was irradiated with a high-intensity ultrasonic horn (Xinzhio C, China, Ti horn, 20 kHz, 60 W/cm^2) under ambient conditions in air for 30 min, and a dark red precipitate was obtained. After being cooled to room temperature, the precipitate was centrifuged, washed with distilled water followed by acetone, and then dried in air.

Preparation of Hollow CdS Spheres: Thiourea (0.15 g) and thioacetamide (0.05 g) were dissolved in distilled water (50 mL) and mixed with the $CdCl_2$/ammonia colloid solution. The final product was a yellow precipitate.

Preparation of Hollow CuS Spheres: $CuSO_4$ (0.35 g) was dissolved in distilled water (50 mL), and then TEA (10 mL) was added. A green colloid was observed. After adding thiourea (0.15 g), the product was a black precipitate.

Preparation of Dispersed Nanoparticles: The reaction for preparing CdSe and CdS nanoparticles was the same as that for hollow spheres, with the difference that the TEA ligand was used in excess. No ligand was used in the reaction for preparing CuS nanoparticles.

Acknowledgments

This work was supported by the National Natural Science Foundation of China (No. 20325516, 90206037).

[1] *Characterization of Nanophase Materials* (Ed.: Z. L. Wang), Wiley-VCH, Weinheim, **2000**.
[2] W. Schartl, *Adv. Mater.* **2000**, *12*, 1899−1908.
[3] W. U. Huynh, J. J. Dittmer, A. P. Alivisatos, *Science* **2002**, *295*, 2425−2427.
[4] Z. Y. Tang, N. A. Kotov, M. Giersig, *Science* **2002**, *297*, 237−240.
[5] F. Caruso, R. A. Caruso, H. Mohwald, *Science* **1998**, *282*, 1111−1114.
[6] M. Brust, C. J. Kiely, *Colloids Surf., A* **2002**, *202*, 175−186.
[7] S. A. Davis, M. Breulmann, K. H. Rhodes, B. Zhang, S. Mann, *Chem. Mater.* **2001**, *13*, 3218−3226.
[8] M. deWild, S. Berner, H. Suzuki, L. Ramoino, A. Baratoff, T. A. Jung, *Chimia* **2002**, *56*, 500−505.
[9] D. N. Srivastava, N. Perkas, G. A. Seisenbaeva, Y. Koltypin, V. G. Kessler, A. Gedanken, *Ultroson. Sonochem.* **2003**, *10*, 1−9.
[10] D. L. Wilcox, M. Berg, T. Bernat, D. Kellerman, J. K. Cochran, *Hollow and Solid Spheres and Microspheres: Science and Technology Associated with Their Fabrication and Application, Materials Research Society Proceedings*, Materials Research Society, Pittsburgh, **1995**, vol. 372.
[11] H. Y. Huang, E. E. Remsen, *J. Am. Chem. Soc.* **1999**, *121*, 3805−3806.
[12] T. K. Mandal, M. S. Fleming, D. R. Walt, *Chem. Mater.* **2000**, *12*, 3481−3487.
[13] F. Caruso, X. Y. Shi, R. A. Caruso, A. Susha, *Adv. Mater.* **2001**, *13*, 740−744.
[14] J. K. Cochran, *Curr. Opin. Solid State Mater. Sci.* **1998**, *3*, 474.
[15] G. Decher, *Science* **1997**, *277*, 1232−1237.
[16] Z. Y. Zhong, Y. D. Yin, B. Gates, Y. N. Xia, *Adv. Mater.* **2000**, *12*, 206−209.
[17] H. P. Lin, Y. R. Cheng, C. Y. Mou, *Chem. Mater.* **1998**, *10*, 3772−3776.
[18] F. Caruso, *Chem. Eur. J.* **2000**, *6*, 413−419.
[19] X. D. Wang, W. L. Yang, Y. Tang, Y. J. Wang, S. K. Fu, Z. Gao, *Chem. Commun.* **2000**, 2161−2162.
[20] J. X. Huang, Y. Xie, B. Li, Y. Liu, Y. T. Qian, S. Y. Zhang, *Adv. Mater.* **2000**, *12*, 808−811.
[21] X. C. Jiang, Y. Xie, J. Y. Lu, L. Zhu, W. He, X. M. Liu, *Can. J. Chem.* **2002**, *80*, 263−268.
[22] K. S. Suslick, *Ultrasound: Its Chemical, Physical, and Biological Effects*, VCH Verlagsgesellschaft, Weinheim, **1988**.
[23] K. S. Suslick, D. A. Hammerton, R. E. Cline, *J. Am. Chem. Soc.* **1986**, *108*, 5641−5642.
[24] K. S. Suslick, S. B. Choe, A. A. Cichowlas, M. W. Grinstaff, *Nature* **1991**, *353*, 414−416.
[25] T. Hyeon, M. Fang, K. S. Suslick, *J. Am. Chem. Soc.* **1996**, *118*, 5492−5493.
[26] K. S. Suslick, G. J. Price, *Ann. Rev. Mater. Sci.* **1999**, *29*, 295−326.
[27] N. A. Dhas, A. Gedanken, *J. Phys. Chem. B* **1997**, *101*, 9495−9503.
[28] R. V. Kumar, Y. Diamant, A. Gedanken, *Chem. Mater.* **2000**, *12*, 2301.
[29] J. J. Zhu, Y. Koltypin, A. Gedanken, *Chem. Mater.* **2000**, *12*, 73−78.
[30] R. Kerner, O. Palchik, A. Gedanken, *Chem. Mater.* **2001**, *13*, 1413−1419.
[31] H. Wang, J. J. Zhu, J. M. Zhu, H. Y. Chen, *J. Phys. Chem. B* **2002**, *106*, 3848−3854.
[32] H. Wang, J. J. Zhu, J. M. Zhu, X. H. Liao, S. Xu, T. Ding, H. Y. Chen, *Phys. Chem. Chem. Phys.* **2002**, *4*, 3794−3799.
[33] J. J. Zhu, H. Wang, S. Xu, H. Y. Chen, *Langmuir* **2002**, *18*, 3306−3310.
[34] O. Palchik, G. Kataby, Y. Mastai, A. Gedanken, *Adv. Mater.* **1999**, *11*, 1289−1292.
[35] M. L. Breen, A. D. Dinsmore, R. H. Pink, S. B. Qadri, B. R. Ratna, *Langmuir* **2001**, *17*, 903−907.
[36] X. W. Zheng, Y. Xie, L. Y. Zhu, X. C. Jiang, A. H. Yan, *Ultroson. Sonochem.* **2002**, *9*, 311−316.
[37] A. Gedanken, X. H. Tang, Y. Q. Wang, N. Perkas, Y. Koltypin, M. V. Landau, L. Vradman, M. Herskowitz, *Chem. Eur. J.* **2001**, *7*, 4546−4552.
[38] Y. Q. Wang, L. X. Yin, A. Gedanken, *Ultroson. Sonochem.* **2002**, *9*, 285−290.
[39] Y. C. Zhu, H. L. Li, Y. Koltypin, Y. R. Hacohen, A. Gedanken, *Chem. Commun.* **2001**, 2616−2617.
[40] J. J. Zhu, S. Xu, H. Wang, J. M. Zhu, H. Y. Chen, *Adv. Mater.* **2003**, *15*, 156−160.
[41] *X-ray Diffraction Procedures* (Eds.: H. Klug, L. Alexander), Wiley, New York, **1962**.
[42] S. Tsunekawa, T. Fukuda, A. J. Kasuya, *Appl. Phys.* **2000**, *87*, 1318−1321.
[43] K. R. Patil, D. V. Paranjape, S. D. Sathaye, A. Mitra, S. R. Padalkar, A. B. Mandale, *Mater. Lett.* **2000**, *46*, 81−85.
[44] L. Reijnen, B. Meester, A. Goossens, J. Schoonman, *J. Mater. Sci. Eng. C 2002, 19, 311−314.*
[45] S. Andersson, A. D. Wadsley, *Acta Crystallogr.* **1961**, *14*, 1245−1249.
[46] W. Chen, Z. G. Wang, Z. J. Lin, L. Y. Lin, *J. Appl. Phys.* **1997**, *82*, 3111−3115.

Received March 26, 2004
Early View Article
Published Online October 7, 2004

 © 2004 Wiley-VCH Verlag GmbH & Co. KGaA, Weinheim

Reaction of Mercury(0) with the I_2 Adduct of Tetraphenyldithioimidodiphosphinic Acid $(SPPh_2)_2NH$ (HL) − Crystal Structures of $[Hg(HL)I_2]$ and HgL_2

M. Carla Aragoni,[a] Massimiliano Arca,[a] M. Bonaria Carrea,[a] Francesco Demartin,[b] Francesco A. Devillanova,[a] Alessandra Garau,[a] Francesco Isaia,*[a] Vito Lippolis,[a] and G. Verani[a]

Keywords: Bridging ligands / Coordination chemistry / Density functional calculations / Iodine / Mercury / S ligands

The complex $[Hg(HL)I_2]$ (**1**) has been synthesised by reacting liquid Hg(0) in Et_2O under mild reaction conditions with the I_2 adduct of HL, $HL{\cdot}I_2$, while HgL_2 (**2**) has been obtained from the reaction of compound **1** with HL in CH_3CN. A single-crystal X-ray investigation of **1** shows four independent molecules in the asymmetric unit, each of which contains an Hg^{II} ion coordinated to two iodine atoms and two sulfur atoms of one bidentate neutral ligand in a distorted tetrahedral coordination geometry. Compound **2** consists of two anionic ligands coordinated to an Hg^{II} ion, which again displays a distorted tetrahedral coordination sphere. The reaction of **2** with HI (55 wt.-% in water) affords $[Hg(HL)_2](I)_2$ (**3**). Compounds **1**, **2**, and **3** have been characterised by FT-IR and ^{31}P NMR spectroscopy. Density functional calculations suggest that compound **3** should feature a distorted tetrahedral coordination around the metal centre, with unequal Hg–S bond lengths.

(© Wiley-VCH Verlag GmbH & Co. KGaA, 69451 Weinheim, Germany, 2004)

Introduction

The oxidation/complexation reaction of metal powders by diiodine adducts of phosphane and polyfunctional thione donors has been investigated thoroughly in recent years. Numerous papers on this subject have shown this synthetic route to be a useful tool for obtaining coordination compounds with unusual geometries, stoichiometries, and oxidation numbers at the metal centre. In fact, owing to the majority use of $R_3E{\cdot}X_2$ adducts (R = alkyl, aryl; E = P, As, Sb; $X_2 = I_2$, Br_2, IBr), novel metal tertiary phosphane, arsane, and stibine complexes have been prepared by McAuliffe and co-workers.[1] Recently, another class of powerful oxidation reagents based on the I_2 and IBr adducts of *N*,*N*′-dimethylperhydrodiazepine-2,3-dithione has been employed successfully to oxidise gold metal in a one-step reaction under mild conditions. This reaction has found potential industrial applications in the fields of electronics and the recovery of precious metals from waste materials.[2]

Thanks to our extensive experience in the area of I_2 adducts of sulfur- and selenium-containing donors,[3] mainly aimed at improving our understanding of the nature of donor-I_2 bonding, we have recently decided to investigate the metal activation reaction by using tetraphenyldithioimidodiphosphinic acid $HN(Ph_2PS)_2$ (HL), which contains both group 15 and 16 elements, as the donor/complexing agent. Our choice was driven both by the donor ability of phosphane-sulfide compounds[4] towards I_2 and by the well-known intrinsic ability of L to give chelation and to favour the preferred geometry required by the metal ion.[5,6] Generally, the reaction of HL with metal ions leads to the formation of the anion L, which has the negative charge delocalised over the SPNPS moiety, and is capable of coordinating a metal centre through the two sulfur atoms, to form six-membered $MSSP_2N$ metallacycles.[5,6]

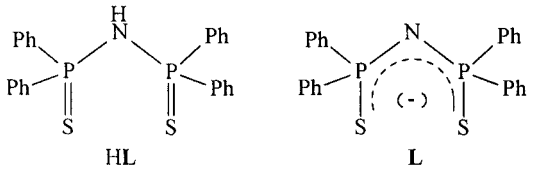

In this context, the I_2 adduct of HL, $HL{\cdot}I_2$, has shown an interesting potential in the oxidation/complexation of zerovalent metals in a low-polar solvent, as demonstrated by the results described above. Antimony(0) powder, for example, has been easily oxidised to Sb^{III} in a single step to give the unusual, X-ray characterised, dinuclear complex

[a] Dipartimento di Chimica Inorganica ed Analitica, Università di Cagliari,
S. S. 554 bivio per Sestu, 09042 Cagliari, Italy
E-mail: isaia@unica.it
[b] Dipartimento di Chimica Strutturale e Stereochimica Inorganica, Università di Milano,
Via G. Venezian 21, 20133 Milano, Italy

 © 2004 Wiley-VCH Verlag GmbH & Co. KGaA, Weinheim **DOI: 10.1002/ejic.200400279**

[LSb(μ-S)(μ-I)$_2$SbL].[7] Similarly, the adduct HL·I_2 reacts with palladium and cobalt powders to produce the complexes PdL_2 [8] and CoL_2.[9]

Since there is a current interest in the chemistry of mercury, which stems from its widespread industrial use as well as its inherent toxicity and hazardous effects on human health,[10,11] and considering the promising results obtained with this synthetic route for other zero-valent metals, we report here on the reaction of HL·I_2 with liquid mercury with a view to opening new perspectives for the recovery of mercury(0) from industrial waste materials.[12]

Results and Discussion

Synthesis and X-ray Crystal-Structure Determination of [Hg(HL)I_2] and HgL_2

The reaction between equimolar quantities of the adduct HL·I_2 (generated in situ) and Hg ([HL·I_2] = 2.22 × 10^{-3} M, 25 °C) was carried out under nitrogen and anhydrous conditions in diethyl ether solution. The dark-red colour of the reaction mixture, due to the HL·I_2 charge-transfer adduct, disappeared almost completely within six hours with formation of an insoluble whitish precipitate. At this stage of the reaction, the concentration of HL·I_2 in the mixture is negligible, as determined from the very low intensity of the blue-shifted band of iodine[13] at 460 nm; moreover, no phosphorus-containing species was detectable by ^{31}P NMR spectroscopy. Elemental analysis of the separated solid and ^{31}P NMR spectroscopy confirmed the formation of [Hg(HL)I_2] (**1**) with the ligand in its neutral form. In this reaction, the zero-valent mercury is oxidised to Hg^{II} according to Equation (1).

$$Hg + HL{\cdot}I_2 \xrightarrow{Et_2O} Hg(HL)I_2 \quad (1)$$

Complexes containing metal ions coordinated to undissociated HL are very scarce in the literature since anything less than strictly anhydrous reaction conditions or the use of polar solvents always provokes imido-proton dissociation and the consequent formation of the deprotonated ligand L.[5a,6e] In this respect, in the case of the reactions with cobalt(0) and palladium(0) we were able to isolate the species [Co(HL)I_2] and [Pd(HL)I_2], but not to obtain suitable crystals since crystallization attempts always led to the formation of complexes CoL_2 [8] and PdL_2.[9]

The reaction in Equation (1) was also carried out in the presence of an excess of the adduct (1:2 Hg:HL·I_2 molar ratio) in order to synthesise complexes with a different stoichiometry. In addition to the formation of complex **1**, a small amount of white crystals of stoichiometry HgL_2 (**2**) was obtained after concentration of the reaction solution. Although complex **2** has been reported previously,[6e] its crystal structure has not been solved, and the complex has only partly been investigated. Moreover, since no structurally characterised complexes bearing HL have been reported in the literature, and due to the current interest in mercury complexes with dichalcogenoimidodiphosphinate derivatives,[14a−14c] we expanded our study on **1** and **2** by characterising the complexes by X-ray single-crystal diffractometry and ^{31}P NMR and FT-IR spectroscopy; DFT calculations on the simplified model complexes [Hg{N(H$_2$PS)$_2$}$_2$] and [Hg{HN(H$_2$PS)$_2$}$_2$I$_2$], and on the ion [Hg{HN(H$_2$PS)$_2$}$_2$]$^{2+}$ were carried out as well.

The X-ray structures of **1** and **2** are reported in Figure 1 and 2, respectively; selected bond lengths and angles are given in Table 1. The asymmetric unit of compound **1** contains four independent [Hg(HL)I_2] molecules with the metal centres labelled Hg(1), Hg(2), Hg(3), and Hg(4), respectively. Each molecule consists of an Hg^{II} ion coordinated to two iodide ions and one HL ligand, with the metal ion showing a very distorted tetrahedral coordination geometry [X−Hg−X angles (X = I, S) in the range 91.14(8)−135.66(4)°]. The HgSPNPS metallacycle displays a pseudo-boat conformation similar to that found in other metal complexes containing the anionic ligand L,[5] with a

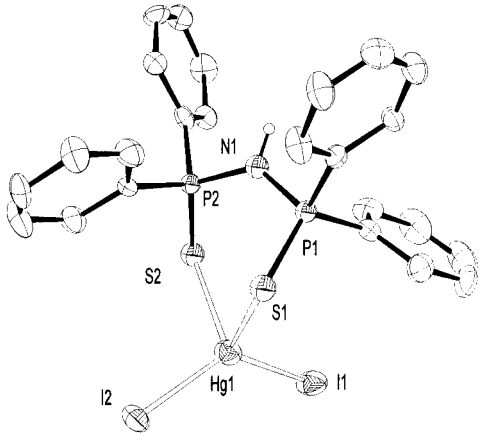

Figure 1. ORTEP plot of one of the crystallographically independent molecules of [Hg(HL)I_2] (**1**); thermal ellipsoids are shown at 50% probability; hydrogen atoms, except for the one bonded to the nitrogen, have been omitted for clarity

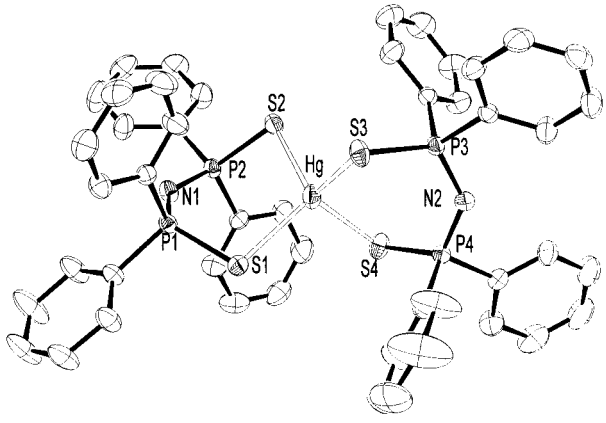

Figure 2. ORTEP plot of [Hg(L)$_2$] (**2**); thermal ellipsoids are depicted at 50% probability; hydrogen atoms have been omitted for clarity

 © 2004 Wiley-VCH Verlag GmbH & Co. KGaA, Weinheim

Table 1. Selected interatomic distances (Å) and angles (°) in the structures of **1** and **2**

[Hg(HL)I$_2$] (**1**)			
Hg(1)−I(1)	2.662(1)	Hg(2)−I(3)	2.683(1)
Hg(1)−I(2)	2.691(1)	Hg(2)−I(4)	2.676(1)
Hg(1)−S(1)	2.692(3)	Hg(2)−S(3)	2.660(4)
Hg(1)−S(2)	2.709(3)	Hg(2)−S(4)	2.681(4)
S(1)−P(1)	1.960(4)	S(3)−P(3)	1.966(4)
S(2)−P(2)	1.970(4)	S(4)−P(4)	1.983(5)
P(1)−N(1)	1.674(9)	P(3)−N(2)	1.645(9)
P(2)−N(1)	1.686(9)	P(4)−N(2)	1.687(9)
Hg(3)−I(5)	2.681(1)	Hg(4)−I(7)	2.694(1)
Hg(3)−I(6)	2.678(1)	Hg(4)−I(8)	2.656(1)
Hg(3)−S(5)	2.665(4)	Hg(4)−S(7)	2.715(3)
Hg(3)−S(6)	2.679(4)	Hg(4)−S(8)	2.681(3)
S(5)−P(5)	1.964(5)	S(7)−P(7)	1.962(4)
S(6)−P(6)	1.980(5)	S(8)−P(8)	1.969(4)
P(5)−N(3)	1.650(9)	P(7)−N(4)	1.659(9)
P(6)−N(3)	1.691(10)	P(8)−N(4)	1.672(9)
I(1)−Hg(1)−S(1)	118.79(8)	S(5)−Hg(3)−I(6)	118.46(9)
I(1)−Hg(1)−I(2)	134.00(3)	S(5)−Hg(3)−S(6)	96.96(10)
S(1)−Hg(1)−I(2)	91.45(8)	I(6)−Hg(3)−S(6)	95.24(8)
I(1)−Hg(1)−S(2)	95.07(8)	S(5)−Hg(3)−I(5)	94.55(7)
S(1)−Hg(1)−S(2)	96.27(9)	I(6)−Hg(3)−I(5)	128.49(5)
I(2)−Hg(1)−S(2)	116.54(8)	S(6)−Hg(3)−I(5)	120.29(9)
S(3)−Hg(2)−I(4)	117.32(9)	I(8)−Hg(4)−S(8)	117.43(8)
S(3)−Hg(2)−S(4)	97.31(11)	I(8)−Hg(4)−I(7)	135.66(4)
I(4)−Hg(2)−S(4)	95.65(9)	S(8)−Hg(4)−I(7)	91.14(8)
S(3)−Hg(2)−I(3)	95.45(8)	I(8)−Hg(4)−S(7)	96.17(8)
I(4)−Hg(2)−I(3)	129.42(5)	S(8)−Hg(4)−S(7)	95.87(9)
S(4)−Hg(2)−I(3)	118.43(9)	I(7)−Hg(4)−S(7)	114.92(8)
HgL$_2$ (**2**)			
Hg−S(1)	2.5167(8)	S(1)−P(1)	2.0221(9)
Hg−S(2)	2.5436(7)	S(2)−P(2)	2.0221(9)
Hg−S(3)	2.5430(7)	S(3)−P(3)	2.0157(9)
Hg−S(4)	2.5569(8)	S(4)−P(4)	2.0135(9)
P(1)−N(1)	1.587(2)	P(3)−N(2)	1.590(2)
P(2)−N(1)	1.583(2)	P(4)−N(2)	1.585(2)
S(1)−Hg−S(2)	112.13(2)	S(2)−Hg−S(3)	111.44(3)
S(1)−Hg−S(3)	108.93(3)	S(2)−Hg−S(4)	104.42(3)
S(1)−Hg−S(4)	108.30(3)	S(3)−Hg−S(4)	111.54(2)

P and an S atom of the ring acting as the stern and bow of the boat. Two out of the four independent complex molecules, Hg(2) and Hg(3), conform to an almost exact C_2 symmetry, the twofold axis passing through the Hg and N atoms and the puckering of the HgSPNPS metallacycle having the same absolute configuration. As regards the other two [those containing Hg(1) and Hg(4)] the conformation of the ring is much more distorted and the absolute configuration is the opposite of that found in the former two complex molecules (see Figure 3a and 3b). Such distortions, together with some variability in the length of chemically equivalent interactions, are due to packing effects, which play an important role in determining the actual symmetry of the crystal. The P−S distances are, on average, only slightly, although significantly, longer than those found in the uncoordinated ligand HL[15] [1.969(5) vs. 1.937(1)−1.959(1) Å]. Conversely, no significant variation is detected for the P−N bonds [average 1.670(9) vs. 1.672(2)−1.683(2) Å].

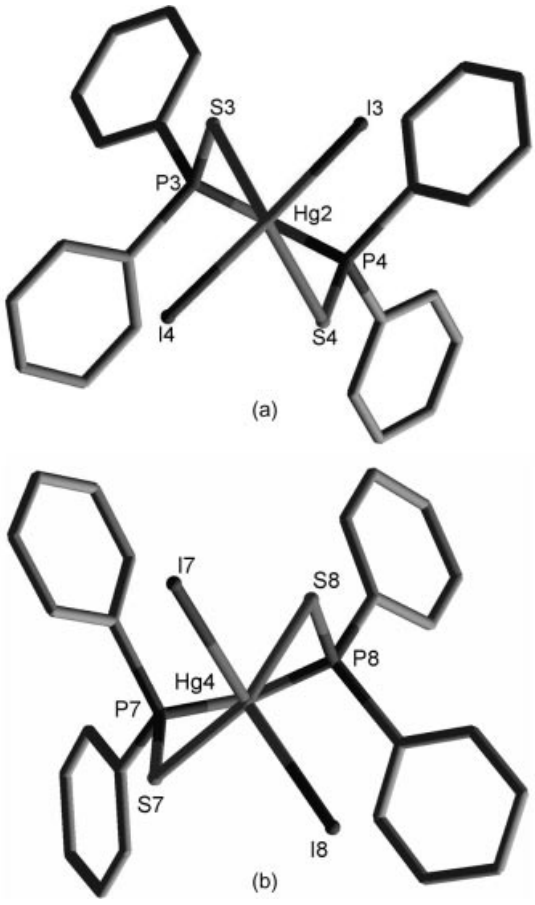

Figure 3. View along the axis connecting Hg(2)−N(2) (a) and Hg(4)−N(4) (b) in complex **1**

Compound **2** consists of two anionic L ligands coordinated to an Hg^{II} ion, which displays tetrahedral coordination geometry. Distortion from the idealized tetrahedral geometry is less pronounced than in complex **1**, the S−Hg−S angles ranging from 104.42(3)° to 112.13(2)°. Each of the two pseudo-boat metallacycles arising from coordination of the anionic ligand to the metal ion displays an almost exact C_2 symmetry, with the twofold axis joining the metal and the N atoms. However, the two rings have opposite configurations within the same molecule. As a result of deprotonation and coordination, the P−S distances increase from 1.937(1)−1.950(1) Å in the free ligand to 2.0135(9)−2.0221(9) Å in **2** and, accordingly, the P−N bond lengths decrease from 1.672(2)−1.683(2) to 1.583(2)−1.590(2) Å.

Complexes **1** and **2** are easily distinguishable by IR spectroscopy since, upon coordination, HL and L have a different π-electron delocalisation over the chelating ring HgSPNPS. The ν_{asym}(PNP) stretching band, which is the most sensitive to metal coordination,[6e] occurs in HL as a strong absorption at 922 cm^{-1}; this increases by about 300 cm^{-1} when the imido proton is removed. As regards the ν(P−S) stretching frequencies, a 30−60 cm^{-1} and 50−80 cm^{-1} decrease is expected upon metal-ion chelation of HL and L, respectively. The IR spectra of **1** and **2** support these findings: the ν(P−S) stretching frequencies measured in

 © 2004 Wiley-VCH Verlag GmbH & Co. KGaA, Weinheim

complex **1** (606 and 592 cm^{-1}) and in complex **2** (576 and 561 cm^{-1}) agree with a lower P−S bond order than the free ligand HL (645 and 622 cm^{-1} for the antisymmetric and symmetric stretching modes, respectively);[6d,6e] the ν_{asym}(PNP) stretching frequency (922 cm^{-1} in HL)[6d,6e] appears at 916 cm^{-1} in **1** and 1239 and 1219 cm^{-1} in **2**; these values are within the expected frequency range for single-bonded P−N and double-bonded P=N stretching regions, respectively.

The ^{31}P CP MAS NMR spectrum of complex **1** shows the presence of a single broad resonance at δ = 59.5 ppm with a spectral line-width of 300 Hz, suggesting that the eight phosphorus atoms in the asymmetric unit have a very similar environment. Conversely, the ^{31}P CP MAS NMR spectrum of **2** shows the presence of three resonances at δ = 40.0 ($\Delta\nu_{1/2}$ = 155 Hz), 37.8 ($\Delta\nu_{1/2}$ = 163 Hz), and 33.9 ppm ($\Delta\nu_{1/2}$ = 148 Hz), with a relative intensity ratio of approximately 1:1:2. Evidently, small bond-length differences in the anionic ligands L imply a different charge distribution over the SPNPS fragment and lead to a significant effect on the phosphorus chemical shifts. This effect is not observed for complex **1**, where the neutral ligand HL is involved in the metal coordination. The ^{31}P NMR spectrum (in CH_2Cl_2) of **1** exhibits a single resonance at δ = 57.8 ppm ($\Delta\nu_{1/2}$ = 8.1 Hz), which confirms the presence of the ligand in the complex in its neutral form when in solution too, since deprotonation/complexation of the ligand results in a high-field shift of the ^{31}P NMR signal of about 20−30 ppm. The corresponding chemical shift for HL in the same solvent is δ = 56.6 ppm ($\Delta\nu_{1/2}$ = 3.6 Hz), and the small change caused by coordination is in keeping with the structural similarities between the free and bound ligand in the solid state. The absence of any Hg/P coupling suggests that, at room temperature, the ligand HL is labile on the NMR timescale. In fact, as increasing amounts of HL are added to the solution of the complex up to a 3:1 molar ratio, only one phosphorus resonance is observed, although the chemical shift decreases towards the value of δ = 56.6 ppm as a consequence of the weighted average of the individual shifts of the contributing species **1** and free HL. Low-temperature measurements were carried out to as low as −70 °C, the lowest temperature for which ^{31}P NMR spectroscopic data were recordable, with no Hg/P coupling or significant shifts in the position of the resonance being observed. The broadening of the signal with decreasing temperature (25 °C, $\Delta\nu_{1/2}$ = 8.1 Hz; −70 °C, $\Delta\nu_{1/2}$ = 10.4 Hz) is indicative of the expected slowing of the chemical-exchange process. Obviously, we were not able to achieve the temperature at which the complex is "frozen out" on the NMR timescale.

In the case of complex **2**, the ^{31}P NMR spectrum (CH_2Cl_2) shows only one resonance at δ = 39.7 ppm ($\Delta\nu_{1/2}$ = 6 Hz) flanked by mercury satellites with a $^2J_{(^{199}Hg-^{31}P)}$ coupling of 101 Hz. Thus, in solution at room temperature, unlike the situation found in the solid state, the four phosphorus atoms in the complex are equivalent, indicating that the three resonances found in the solid state are due to solid-state effects. Addition of an equimolar amount of HL to a solution of **2** ([**2**] = 1.1 × 10^{-2} M; CH_2Cl_2, 25 °C) gives a ^{31}P NMR spectrum with two resonances, one due to the free ligand and one due to the complex. Variable-temperature NMR experiments were carried out to as low as −80 °C, the lowest temperature for which ^{31}P NMR spectroscopic data were recordable, with no significant change in the spectra, suggesting the presence of different conformers.

Reaction Chemistry of $[Hg(HL)I_2]$ and HgL_2

The attempts to synthesise new complexes by reacting $[Hg(HL)I_2]$ (**1**) with increasing amounts of HL proved unsuccessful ([**1**] = 2.5 × 10^{-3} M; HL to **1** molar ratio 3:1; CH_2Cl_2, 25 °C). However, the same reaction carried out in a more polar solvent like CH_3CN (HL to **1** molar ratio 1:1; 25 °C) leads to the quantitative formation of complex **2**, thus confirming that in polar solvents HL is prone to lose the imido proton when complexed to a metal.[6e,8,9]

The reaction of complex **1** with hydroiodic acid (55 wt.-% in water) was also evaluated since it may prove useful in freeing the ligand from the complex. Examination of the equimolar reaction between HI and compound **1** (CH_2Cl_2, 25 °C) by ^{31}P NMR spectroscopy revealed only one signal at δ = 57.3 ppm, which is only slightly high-field shifted with respect to the resonance of complex **1**; conversely, when a twentyfold excess of HI is employed the resonance is found at δ = 56.6 ppm, indicating the presence of free HL in the solution [Equation (2)]. Raman spectra carried out on the organic phase confirmed the presence of free HL, whereas in the water phase a peak at 121 cm^{-1} is indicative of the formation of the anion $[HgI_4]^{2-}$.[16]

$$Hg(HL)I_2 + 2HI(aq) \xrightarrow{CH_2Cl_2} HL + 2H^+(aq) + HgI_4^{2-}(aq) \quad (2)$$

Equation (1) and (2) could obviously be very important as far as a recovery process is concerned, since they allow not only an easy oxidation of mercury(0) to mercury(II), but also the possibility to free the metal from the complex **1** and to recover the ligand HL.

Reaction of **2** with hydroiodic acid (55 wt.-% in water) in a 1:2 molar ratio in CH_2Cl_2 results in a considerable change in the ^{31}P NMR spectrum of the complex (Figure 4a and 4b). Indeed, the signal of **2** at δ = 39.5 ppm disappears completely and a new signal is observed at low field (δ = 57.6 ppm). The shift of the signal and its value, which is similar to that of complex **1** (δ = 57.8 ppm, CH_2Cl_2), strongly indicate the successful protonation of the anionic ligand in the complex. Slow concentration of the dichloromethane solution afforded a white powder, whose microanalysis suggests a stoichiometry $[Hg(HL)_2](I)_2$ (**3**). The ^{31}P CP MAS NMR spectrum of **3** shows a broad band at δ = 59.1 ppm ($\Delta\nu_{1/2}$ = 494 Hz), confirming the presence of the ligands in their neutral form in the complex. IR bands at 565 cm^{-1} [ν(P−S)], 922 cm^{-1} [ν(P−N)], and 2631 cm^{-1}, which originates from the first overtone of the δ(N−H) bending vibration[6e] at 1325 cm^{-1}, further support coordination of HL to the metal in **3**. In addition, the molar con-

 © 2004 Wiley-VCH Verlag GmbH & Co. KGaA, Weinheim

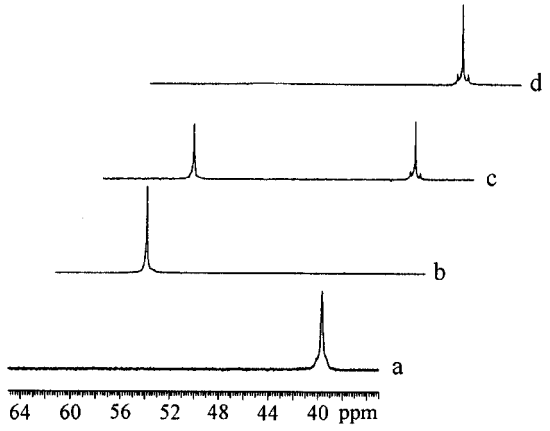

Figure 4. ^{31}P NMR spectra in CH_2Cl_2 (25 °C) of: (a) **2** (3.58×10^{-3} M); (b) solution of **2** after addition of HI (55 wt.-% in H_2O; **2**/HI 1:2 molar ratio); (c) the solution from (b) after addition of DMAN (**2**/HI/DMAN 1:2:1 molar ratio); (d) the solution from (c) after addition of more DMAN (**2**/HI/DMAN 1:2:2 molar ratio)

ductivity of **3** (660 $\mu S \cdot cm^2 \cdot mol^{-1}$, CH_2Cl_2, 25 °C) is considerably higher than that of **2** (93 $\mu S \cdot cm^2 \cdot mol^{-1}$, CH_2Cl_2, 25 °C). The protonation reaction is reversibl. A very strong base such as 1,8-bis(dimethylamino)naphthalene (DMAN) was added to a solution of **3** in CH_2Cl_2 in order to obtain 1:1 and 1:2 molar ratios of complex **3**/DMAN. In the former case the neutral complex **2** is partly regenerated (Figure 4c) and in the latter fully regenerated (see d in Figure 4), as shown by the ^{31}P NMR peak at $\delta = 39.5$ ppm. The reactions involving complexes **2** and **3** in CH_2Cl_2 are summarised in Scheme 1.

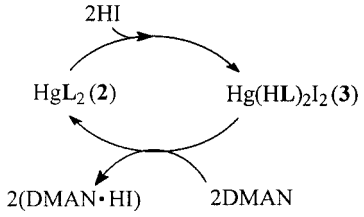

Scheme 1

Quantum-Chemical Calculations

In the light of the novelty of complex **1**, and in order to provide further insight into the electronic properties of the title compounds, we performed hybrid-DFT calculations on complexes **1** and **2**. We also determined the geometrical features of complex **3**. Theoretical calculations were performed on the model complexes $[Hg\{N(H_2PS)_2\}_2]$ (**4**) and $[Hg\{HN(H_2PS)_2(I)_2\}]$ (**5**), in which the phenyl groups have been replaced by hydrogen atoms, and subsequently on the model complex $[Hg\{HN(H_2PS)_2\}_2]^{2+}$ (**6**). As previously reported by us for similar model complexes, hybrid-DFT calculations have given reliable results in understanding both the structural and electronic features of the model complexes $[Pd\{N(H_2PS)_2\}_2]$[8] (**7**) and $[In\{N(H_2PS)_2\}I_2]$[9b] (**8**). Encouraged by our recent results,[17] the mPW1PW[18] functional was preferred to the B3LYP functional,[19] which was previously employed for **7** and **8**. As regards the ligand atoms, the pVDZ basis set of Schafer et al.[20,21] was used. The basis set for the metal atom is more difficult to choose since, due to the high atomic number of mercury, relativistic effects have to be taken into account. Thus, for **4** and **5**, we used the SBKJC with effective core potentials (ECP),[21,22] since the LanL2DZ basis set previously used successfully for Pd and In in **7** and **8** is not available for Hg. Geometry optimizations on **4** and **5**, performed starting from the structural data of **2** and **1**, respectively, show a very good agreement with the experimental data. Thus, in both complexes, the central mercury atom is coordinated by the ligand donor atoms in a distorted tetrahedral arrangement with average Hg−S bond lengths of 2.611 Å (experimental 2.543 Å).[23] Analogously, in the case of **5**, the average Hg−S and Hg−I bond lengths (2.889 and 2.743 Å, respectively) are very close to the experimental values determined for **1** (2.700 and 2.688 Å, respectively). In agreement with the experimental structures of **1** and **2**, a comparison of the optimized structural features of the ligand moiety in **4** and **5** shows that, upon protonation, we obtain a lengthening of the P−N bond lengths (1.606 and 1.709 Å in **4** and **5**, respectively) and a shortening of the P−S bond lengths (2.031 and 1.959 Å in **4** and **5**, respectively). In order to better understand the interaction between the metal ion and the ligands, a qualitative interpretation can be obtained from the fragment molecular orbital approach (FMO) within the formalism of the extended Hückel theory (EHT).[24] The interaction diagram between the 6s and 6p atomic orbitals of the Hg^{2+} ion and those of the ligands is shown in Figure 5, calculated at the DFT-optimised geometries. For both **4** and **5**, the Kohn−Sham HOMOs are nonbonding orbitals built from the p atomic orbitals of the donor atoms with a small contribution from the filled $5d_{xy}$ and $5d_{xz}$ orbitals of the central metal atom. The LUMOs are nonbonding in nature and they are made up of a combination of the 6s atomic orbital of the Hg ion σ-interacting with the p-orbitals of the donor atoms pointing towards the central metal ion. Confident in the agreement between the calculated geometries of **4** and **5** and their parent complexes, we extended our DFT calculations at the same level of theory to **6** so as to acquire information on the geometrical features of the parent cationic complex **3**. In this case the Hg ion is also coordinated by the two ligand units in a distorted tetrahedral fashion. In agreement with what emerges from the comparison of the calculated structural features of **4** and **5**, upon imido protonation, model **6** shows an increase in the Hg−S (average value 2.628 Å) and the P−N (average value 1.698 Å) bond lengths compared to those calculated for **4**, while the P−S bond lengths are slightly shortened (average value 1.993 Å). Since **4** and **6** are isoelectronic, their frontier orbitals are very similar in shape and composition. In particular, the Kohn−Sham HOMOs of **4** and **6** (see a in Figure 6) are slightly antibonding orbitals built from the p atomic orbitals of the donor atoms with a small contribution from the filled $5d_{xy}$ and $5d_{xz}$ orbitals of the central metal atom. On the other hand, in the case of **5** (c in Figure 5), the HOMO and the HOMO−1 are almost entirely centered on the iodides, and

 © 2004 Wiley-VCH Verlag GmbH & Co. KGaA, Weinheim

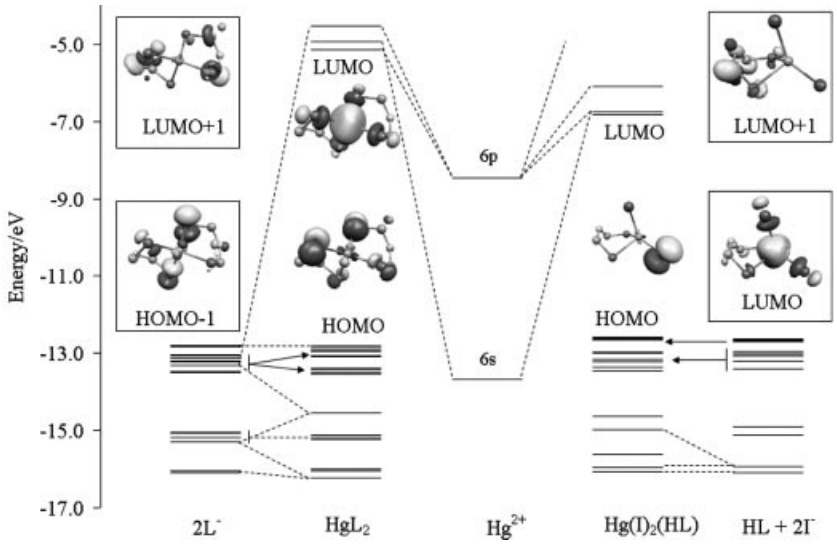

Figure 5. EHT-interaction diagram showing the interaction between the empty atomic orbitals of the Hg^{2+} central ion and the filled ones of the ligands HL in the model complexes **4** and **5** [HL = $H_2P(S)-NH-P(S)H_2$]; the dashed lines connect FMOs which contribute at least 15% to the formation of molecular orbitals; the hybrid-DFT frontier orbitals are also depicted (contour value 0.05)

they are therefore nonbonding in nature. The LUMOs of the three complexes are all antibonding in nature, and are due to the combination of the 6s atomic orbitals of the Hg ion σ-interacting with the p-orbitals of the donor atoms pointing towards the central metal ion (see b and d in Figure 5 for **4** and **5**, respectively).

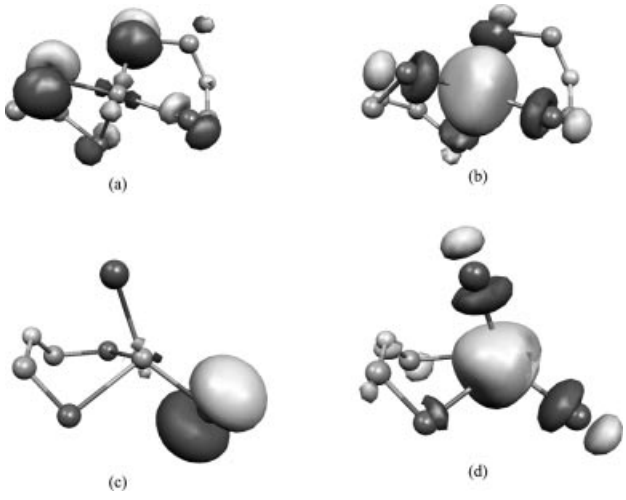

Figure 6. Sketches of Kohn−Sham HOMOs and LUMOs calculated for **4** (a and b, respectively), and **5** (c and d, respectively)

Conclusion

The oxidizing ability of the adduct $HL{\cdot}I_2$ in Et_2O towards liquid Hg(0) leads to the synthesis of the air stable complex $[Hg(HL)I_2]$ (**1**) in a single oxidation step. To the best of our knowledge, this complex represents the first example of a structurally characterised complex of HL. The reaction of **1** with an excess of HL in MeCN affords the neutral air stable complex $[Hg(L)_2]$ (**2**), which can also be obtained from the reaction of HgX_2 (X = Br, I) with HL. The reaction of **2** with concentrated HI leads to the species $[Hg(HL)_2](I)_2$ (**3**; see Scheme 2). X-ray diffraction analyses and DFT calculations on simplified model complexes have been performed to elucidate the structural and electronic properties of **3**. Complex **1** readily reacts with an excess of HI to yield the anion $[HgI_4]^{2-}$ with the release of HL, which can be re-utilised, hopefully opening new perspectives for the recovery of Hg(0) from mercury-containing waste materials.

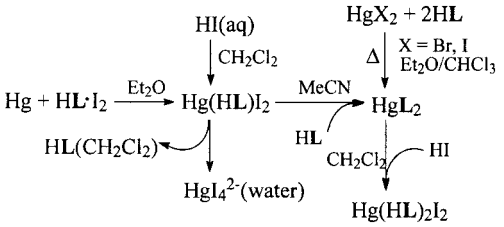

Scheme 2

Experimental Section

Materials and Instrumentation: All reagents were used as purchased from Aldrich. Diethyl ether was distilled from over $LiAlH_4$ shortly before use. CH_2Cl_2 was distilled from P_2O_5 and stored under N_2. All reactions were carried out under an atmosphere of dry nitrogen. $^{31}P\{^1H\}$ NMR spectra were recorded on a Varian Unity Inova 400 MHz operating at 161.9 MHz. The ^{31}P chemical shifts are referenced to an external standard of 85% H_3PO_4 (δ = 0.0 ppm). ^{31}P NMR CP MAS NMR spectra were calibrated indirectly from the H_3PO_4 peak (δ = 0.0 ppm). Variable temperature ^{31}P NMR spectroscopic data on compound **1** were collected from a 1.1×10^{-2} M solution in CH_2Cl_2 [temp. (°C), δ, $\Delta\nu_{1/2}$: 25, 57.7, 8.1; 0, 57.9, 8.6; −20, 58.1, 10.0; −40, 58.3, 10.2; −60, 58.3, 10.5, −70, 58.4, 10.4]. ^{31}P NMR data for compound **2** were collected from a 1.2×10^{-2} M solution in CH_2Cl_2 [temp. (°C), δ, $\Delta\nu_{1/2}$: 25, 39.5, 6.1; −20, 39.5,

 © 2004 Wiley-VCH Verlag GmbH & Co. KGaA, Weinheim

9.0; −40, 39.5, 9.5; −70, 39.1, 12.9, −80, 39.2, 14.0]. IR spectra were measured as KBr (4000−400 cm^{-1}) or polyethylene pellets (400−50 cm^{-1}) on a Bruker IFS 55 FT-IR spectrometer. FT Raman spectra were recorded on a Bruker FRS 100 Fourier-transform Raman spectrometer, operating with a diode-pumped Nd:YAG exciting laser at 1064 nm. Conductometric measurements were carried out at 25 °C.

Synthesis: HL was prepared according to ref. 25. The adduct $HL{\cdot}I_2$ was prepared in situ in distilled Et_2O just before use from equimolar amounts of HL and I_2.

[Hg(HL)I$_2$] (1): A mixture of HL (0.100 g, 0.222 mmol) and I_2 (0.0565 g, 0.223 mmol) in Et_2O (100 mL) was stirred at room temperature under N_2 until complete dissolution of the reagents. Liquid mercury (0.0236 g, 0.222 mmol) was then added while stirring. This reaction was continued at room temperature under N_2 for about one day. The resulting air-stable whitish solid was isolated by suction filtration, washed with diethyl ether, and dried in vacuo, to give 0.172 g of **1** (0.211 mmol; yield 95%). Stable colourless crystals were obtained upon dissolution of **1** in anhydrous CH_2Cl_2 and subsequent slow evaporation of the solvent. $C_{24}H_{21}HgI_2NP_2S_2$ (903.87): calcd. C 31.89, H 2.34, N 1.55, S 7.09; found C 32.0, H 2.5, N 1.6, S 7.4. IR (KBr): $\tilde{\nu}$ = 3054w cm^{-1}, 2966w, 2924w, 2855w, 2606brw, 1435vs, 1384m, 1303m, 1184m, 1107vs, 916s, 804m, 782s, 733vs, 720vs, 685vs, 622w, 606ms, 592s, 506m, 487m, 464m, 441w. ^{31}P NMR (CH_2Cl_2): δ = 57.8 ppm. M.p. 228−230 °C (dec.).

[Hg(L)$_2$] (2). Method a: A mixture of HL (0.100 g, 0.222 mmol) and [Hg(HL)I_2] (0.200 g, 0.222 mmol) in CH_3CN (100 mL) was stirred at room temperature for 4 h. The solid white product was collected by filtration and then dissolved in hot CH_2Cl_2. The resulting solution was allowed to evaporate in air to yield a white solid. Yield: 0.230 g (0.210 mmol, 95%). **Method b:**[6e] A solution of HL (0.125 g, 2.774. mmol) in $CHCl_3$ (10 mL) was added to a solution of $HgBr_2$ (0.050 g, 1.387 mmol) in Et_2O (10 mL). The reaction mixture was stirred for 1 h at room temperature and then refluxed for 20 min. The solid product was separated by filtration, washed twice with a 1:1 acetone/diethyl ether mixture, and dried under vacuum to give 0.136 g of **2** (89% yield). $C_{48}H_{40}HgN_2P_4S_4$ (1097.5): calcd. C 52.32, H 3.67, N 2.55, S 11.68; found C 53.0, H 3.9, N 2.6, S 12.0. IR (KBr): $\tilde{\nu}$ = 3054m cm^{-1}, 2918w, 2846w, 1475w, 1436s, 1384w, 1239s, 1219s, 1174s, 1103s, 1025w, 997w, 786w, 742m, 714s, 698vs, 618w, 576s, 561vs, 514s, 495m. ^{31}P NMR (CH_2Cl_2): δ = 39.7 ppm. M.p. > 255 °C

[Hg(HL)$_2$](I)$_2$ (3): A dichloromethane solution (10 mL) of **2** (0.020 g, 0.018 mmol) and a hydroiodic acid solution (55 wt.-% in water; 0.0092 g, 0.04 mmol) were vigorously stirred for 1 h at 25 °C. The colourless two-phase mixture was then passed through a phase-separation filter (Whatman, Phase Separator 1PS) to remove the water. After concentration of the solution to about 5 mL, *n*-hexane (5 mL) was added dropwise and a white solid precipitated. This was washed with *n*-hexane and dried to give 0.018 g of **3** (74% yield). $C_{48}H_{42}HgI_2N_2P_4S_4$ (1353.4): calcd. C 42.60, H 3.13, N 2.07, S 9.48; found C 43.0, H 3.2; N 2.2, S 10.0. IR (KBr): $\tilde{\nu}$ = 2631w cm^{-1}, 1436vs, 1325m, 1218m, 1106s, 922s, 785s, 741s, 716s, 688vs, 649m, 561s, 513m. ^{31}P NMR (CH_2Cl_2): δ = 57.6 ppm. M.p. 203−204 °C

X-ray Crystallography: Crystal data and refinement details for structure determinations of both compounds are reported in Table 2. Intensity data were acquired at room temperature on a SMART CCD diffractometer (ω scans). All data sets were corrected for Lorentz-polarisation effects and for absorption using the SADABS routine.[26] The structures were solved by direct methods using the SHELXS 97 program,[27] followed by difference Fourier synthesis, and refined by full-matrix least-squares procedures on F^2 using the SHELXL-97 program.[28] All non-H atoms were refined anisotropically and H atoms were introduced at calculated positions and thereafter incorporated into a riding model with $U_{iso}(H) = 1.2U_{eq}(C)$. For compound **1** the search for an alternative symmetry other than the triclinic one reported in Table 2 was done using Le Page's MISSYM (PLATON) routine.[29] The check revealed that the triclinic unit cell can be transformed metrically into an almost-monoclinic C-centred unit cell with a = 24.485(3), b = 24.506(3), c = 19.230(3) Å, α = 90.42(1), β = 103.25(1), γ = 89.61(1)°. However, with this choice, the agreement between equivalent reflections was poor (R_{int} = 0.434) thus ruling out the possibility of the symmetry being monoclinic.
CCDC-228871 (for **1**) and -228872 (for **2**) contain the supplementary crystallographic data for this paper. These data can be obtained free of charge at www.ccdc.cam.ac.uk/conts/retrieving.html [or from the Cambridge Crystallographic Data Centre, 12 Union Road, Cambridge CB2 1EZ, UK; Fax: +44-1223-336033; E-mail: deposit@ccdc.cam.ac.uk].

Table 2. Crystal data and details of refinements for [Hg(HL)I_2] and HgL_2

Compound	[Hg(HL)I_2] (**1**)	HgL_2 (**2**)
Formula	$C_{24}H_{21}HgI_2NP_2S_2$	$C_{48}H_{40}HgN_2P_4S_4$
Mol. mass (amu)	903.87	1097.53
Crystal system	triclinic	triclinic
Space group	$P\bar{1}$ (no. 2)	$P\bar{1}$ (no. 2)
a (Å)	17.262(2)	13.626(1)
b (Å)	17.380(2)	13.794(1)
c (Å)	19.230(3)	14.336(1)
α (°)	99.59(1)	82.21(1)
β (°)	99.05(1)	66.10(1)
γ (°)	90.05(1)	69.44(1)
U (Å^3)	5616(1)	2306.6(4)
Z	8	2
ρ_{calcd} (Mg·m^{-3})	2.138	1.580
μ(Mo-K_α) (mm^{-1})	7.957	3.692
Transmission factors	0.602−1.000	0.735−1.000
Unique refl. with $I > 2\sigma(I)$	9240	8871
Final R and $wR2$ indices	0.0496, 0.1225	0.0243, 0.0613

Computations: Quantum-chemical DFT calculations were carried out with the Gaussian 98 (rev. A11)[30] suite of programs on the model complexes [Hg{N($H_2PS)_2$}$_2$] (**4**), [Hg{N($H_2PS)_2$}I_2] (**5**), and [Hg{HN($H_2PS)_2$}$_2$]$^{2+}$ (**6**), with Adamo and Barone's mPW1PW functional[18] and pVDZ Schafer, Horn and Ahlrichs pVDZ basis sets for H, N, P, and S.[20,21] For Hg and I, the SBKJC basis set with effective core potentials was used.[22] In the case of **4**, the calculations were also performed with the Stuttgart RLC ECP basis set for Hg.[23] Integration was performed numerically using a total of 7500 points for each atom (Finegrid option). The geometry optimizations of **4**, **6** and **5** were performed starting from the experimental geometries determined for **1** and **2**, avoiding introducing any symmetry constraint. DFT calculations were performed on an SGI Origin 3800 equipped with 128 GByte of RAM. The results of the calculations were analysed with the Molekel 4.3[32a] and Molden 3.9[32b] programs. The quantum mechanically optimised structure was verified by normal-mode harmonic frequency analysis. Harmonic frequencies were obtained using the second derivatives of the DFT energy, computed by numerical differentiation of the DFT energy gradients. The qualitative EHT analyses were obtained with the CACAO (Computer Aided Composition of

 © 2004 Wiley-VCH Verlag GmbH & Co. KGaA, Weinheim

Atomic Orbitals) program package[32c] on the hybrid-DFT-optimised geometry. The interaction diagram was generated using the fragment molecular orbital (FMO) approach.[32d] Parameters used in EHT calculations were taken from the standard database of CACAO.

Acknowledgments

This research was financially supported by the "Regione Autonoma della Sardegna". We are grateful to CINECA (Consorzio Interuniversitario per il Calcolo Automatico dell'Italia Nord Orientale) for providing computational facilities.

[1] [1a] S. M. Godfrey, C. A. McAuliffe, R. G. Pritchard, J. M. Sheffield, *Inorg. Chim. Acta* **1999**, *292*, 213−219. [1b] S. M. Godfrey, N. Ho, C. A. McAuliffe, R. G. Pritchard, *Angew. Chem. Int. Ed. Engl.* **1996**, *33*, 2344−2345. [1c] C. A. McAuliffe, S. M. Godfrey, A. G. Mackie, R. G. Pritchard, *Angew. Chem. Int. Ed. Engl.* **1992**, *31*, 919−921, and references cited therein.

[2] [2a] L. Cau, P. Deplano, L. Marchiò, M. L. Mercuri, L. Pilia, A. Serpe, E. F. Trogu, *Dalton Trans.* **2003**, 1969−1974. [2b] F. Bigoli, P. Deplano, M. L. Mercuri, M. A. Pellinghelli, G. Pintus, A. Serpe, E. F. Trogu, *J. Am. Chem. Soc.* **2001**, *123*, 1788−1789. [2c] F. Bigoli, P. Deplano, M. L Mercuri, M. A. Pellinghelli, G. Pintus, M. A. Serpe, E. F. Trogu, *Chem. Commun.* **1998**, 2351−2352. [2d] F. Bigoli, P. Deplano, F. A. Devillanova, V. Lippolis, M. L. Mercuri, M. A. Pellinghelli, E. F. Trogu, *Inorg. Chim. Acta* **1998**, *267*, 115−121.

[3] [3a] M. C. Aragoni, M. Arca, F. Demartin, F. A. Devillanova, A. Garau, F. Isaia, V. Lippolis, G. Verani, *Trends Inorg. Chem.* **1999**, *6*, 1−18. [3b] M. C. Aragoni, M. Arca, F. Demartin, F. A. Devillanova, A. Garau, F. Isaia, V. Lippolis, G. Verani, *Coord. Chem. Rev.* **1999**, *184*, 271−290. [3c] M. C. Aragoni, M. Arca, A. J. Blake, F. A. Devillanova, W.-W. du Mont, A. Garau, F. Isaia, V. Lippolis, G. Verani, C. Wilson, *Angew. Chem. Int. Ed.* **2001**, *40*, 4229−4232.

[4] [4a] M. Arca, F. A. Devillanova, A. Garau, F. Isaia, V. Lippolis, G. Verani, F. Demartin, *Z. Anorg. Allg. Chem.* **1998**, *624*, 745−749. [4b] M. Arca, F. Demartin, F. A. Devillanova, A. Garau, F. Isaia, V. Lippolis, G. Verani, *J. Chem. Soc., Dalton Trans.* **1999**, 3069−3073.

[5] [5a] I. Haiduc, *Comprehensive Coordination Chemistry II*, vol 1 (Ed.: A. B. P. Lever), Elsevier Pergamon, Amsterdam, Oxford, **2004**, p. 323−347. [5b]C. Silvestru, J. E. Drake, *Coord. Chem. Rev.* **2001**, *223*, 117−216. [5c] T. Q. Ly, J. D. Woollins, *Coord. Chem. Rev.* **1998**, *176*, 451−481, and references cited therein.

[6] [6a] C. G. Pernin, J. A. Ibers, *Inorg. Chem.* **2000**, *39*, 1216−121. [6b] C. G. Pernin, J. A. Ibers, *Inorg. Chem.* **2000**, *39*, 1222−1226. [6c] O. Siiman, C. P. Huber, M. L. Post, *Inorg. Chim. Acta* **1977**, *25*, L11−L14. [6d] O. Siiman, J. Vetuskey, *Inorg. Chem.* **1980**, *19*, 1672−1680. [6e] G. P. McQuillan, I. A. Oxton, *Inorg. Chim. Acta* **1978**, *29*, 69−75.

[7] M. Arca, F. A. Devillanova, A. Garau, F. Isaia, V. Lippolis, G. Verani, G. L. Abbati, A. Cornia, *Z. Anorg. Allg. Chem.* **1999**, *625*, 517−520.

[8] G. L. Abbati, M. C. Aragoni, M. Arca, A. C. Fabretti, F. A. Devillanova, A. Garau, F. Isaia, V. Lippolis, G. Verani, *J. Chem. Soc., Dalton Trans.* **2001**, 1105−1110.

[9] [9a] M. C. Aragoni, M. Arca, A. Garau, F. Isaia, V. Lippolis, G. L. Abbati, A. C. Fabretti, *Z. Anorg. Allg. Chem.* **2000**, *626*, 1454−1459. [9b] G. L. Abbati, M. C. Aragoni, M. Arca, F. A. Devillanova, A. C. Fabretti, A. Garau, F. Isaia, V. Lippolis, G. Verani, *Dalton Trans.* **2003**, 1515−1519.

[10] W. Kaim, B. Schwedersky, *Bioinorganic Chemistry: Inorganic Elements in the Chemistry of Life, an introduction and Guide*, Wiley-Interscience, New York **1991**, chapter 17, p. 338−343.

[11] H. G. Seiler, H. Sigel, A. Sigel, *Handbook on Toxicity of Inorganic Compounds*, Marcel Dekker, Inc., New York and Basel, **1988**, chapter 35, p. 419−436.

[12] The largest source of recycled mercury-containing products is the spent catalysts used in the production of chlorine and caustic soda, followed by electrical apparatus, dental amalgams, batteries, and other instruments such as thermometers. See: L. G. Twidwell, R. J. Thompson, *JOM-J. Miner. Met. Mater. Soc.* **2001**, *53*, 15−17.

[13] K. F. Purcell, J. C. Kotz, *Inorganic Chemistry*, W. B. Saunders Company, **1977**, chapter 5, p. 209−212.

[14] [14a] V. Garcia-Montalvo, J. Novosad, P. Kilian, A. M. Z. Slawin, P. Garcia y Garcia, M. Lopez-Cardoso, G. Espinosa-Perez, R. Cea-Olivares, *J. Chem. Soc., Dalton Trans.* **1997**, 1025−1029. [14b] O. Bumbu, A. Silvestru, C. Silvestru, J. E. Drake, M. B. Hursthouse, M. E. Light, *J. Organomet. Chem.* **2003**, *687*, 118−124. [14c] D. J. Crouch, P. M. Hatton, M. Helliwell, P. O'Brien, J. Raftery, *Dalton Trans.* **2003**, 2761−2766.

[15] S. Husebye, K. Maartmann-Moe, *Acta Chem. Scand., Ser. A* **1983**, *37*, 439−441.

[16] M. L. Delwaulle, *Bull. Soc. Chim. Fr.* **1955**, *247*, 1294−1299.

[17] [17a] M. C. Aragoni, M. Arca, C. Denotti, F. A. Devillanova, E. Grigiotti, F. Isaia, F. Laschi, V. Lippolis, L. Pala, A. M. Z. Slawin, P. Zanello, J. D. Woollins, *Eur. J. Inorg. Chem.* **2003**, 1291−1295. [17b] M. C. Aragoni, M. Arca, F. Demartin, F. A. Devillanova, F. Isaia, F. Lelj, V. Lippolis, A. Mancini, L. Pala, *Eur. J. Inorg. Chem.* **2004**, 3099−3109.

[18] C. Adamo, V. Barone, *J. Chem. Phys.* **1998**, *108*, 664−675.

[19] [19a] A. D. Becke, *J. Chem. Phys.* **1993**, *98*, 1372−1377. [19b] A. D. Becke, *J. Chem. Phys.* **1993**, *98*, 5648−5652. [19c] C. Lee, W. Yang, R. G. Parr, *Phys. Rev. B* **1988**, *37*, 785−789.

[20] A. Schafer, H. Horn, R. Ahlrichs, *J. Chem. Phys.* **1992**, *97*, 2571−2577.

[21] [21a] W. J. Stevens, M. Krauss, H. Basch, P. G. Jasien, *Can. J. Chem.* **1992**, *70*, 612−630. [21b] T.R. Cundari, W. J. Stevens, *J. Chem. Phys.* **1993**, 5555−5565.

[22] Basis sets were obtained from the Extensible Computational Chemistry Environment Basis Set Database, Version 6/19/03, as developed and distributed by the Molecular Science Computing Facility, Environmental and Molecular Sciences Laboratory which is part of the Pacific Northwest Laboratory, P.O. Box 999, Richland, Washington 99352, USA, and funded by the U.S. Department of Energy. The Pacific Northwest Laboratory is a multi-program laboratory operated by Battelle Memorial Institute for the U.S. Department of Energy under contract DE-AC06−76RLO 1830.

[23] The same calculation on **4** has also been performed with the larger Stuttgart RLC ECP basis set for the mercury atom. The calculated molecular orbital composition as well as the geometrical features are very close to those calculated with the SBKJC ECP basis set. Calculated Hg−S distances: 2.583, 2.564, 2.637, and 2.666 Å.

[24] R. Hoffmann, W. N. Lipscomb, *J. Chem. Phys.* **1962**, *36*, 2179−2189.

[25] A. Schmidpeter, R. H. Bohm, H. Groenger, *Angew. Chem.* **1964**, *76*, 860−861.

[26] SADABS Area-Detector Absorption Correction Program, Bruker AXS, Inc. Madison, WI, USA (2000).

[27] SHELXS-97; G. M. Sheldrick, *Acta Crystallogr., Sect. A* **1990**, *46*, 467−473.

[28] G. M. Sheldrick, SHELXL-97, *Program for Crystal Structure Refinement*, Universität Göttingen, Germany, **1997**.

[29] A. L. Spek, *Acta Crystallogr., Sect. A* **1990**, *46*, supplement C34, MS-02.01.05.

[30] M. J. Frisch, G. W. Trucks, H. B. Schlegel, G. E. Scuseria, M. A. Robb, J. R. Cheeseman, V. G. Zakrzewski, J. A. Montgomery, R. E. Stratmann, J. C. Burant, S. Dapprich, J. M. Millam, A. D. Daniels, K. N. Kudin, M. C. Strain, O. Farkas, J. Tomasi, V. Barone, M. Cossi, R. Cammi, B. Mennucci, C. Pomelli, C. Adamo, S. Clifford, J. Ochterski, G. A. Petersson, P. Y. Ayala, Q. Cui, K. Morokuma, D. K. Malick, A. D. Rabuck, K. Raghavachari, J. B. Foresman, J. Cioslowski, J. V. Ortiz, B. B.

 © 2004 Wiley-VCH Verlag GmbH & Co. KGaA, Weinheim

Stefanov, G. Liu, A. Liashenko, P. Piskorz, I. Komaromi, R. Gomperts, R. L. Martin, D. J. Fox, T. Keith, M. A. Al-Laham, C. Y. Peng, A. Nanayakkara, C. Gonzalez, M. Challacombe, P. M. W. Gill, B. G. Johnson, W. Chen, M. W. Wong, J. L. Andres, M. Head-Gordon, E. S. Replogle, J. A. Pople, GAUSSIAN 98 (Revision A 11), Gaussian, Inc., Pittsburgh, PA, **1998**.
[31] [31a] W. Kuechle, M. Dolg, H. Stoll, H. Preuss, *Mol. Phys.* **1991**, *74*, 1245−1263. [31b] A. E. Reed, L. A. Curtiss, F. Weinholt, *Chem. Rev.* **1988**, *88*, 899−926.
[32] [32a] MOLEKEL 4.3, P. Flükiger, H.P. Lüthi, S. Portmann, J. Weber, Swiss Center for Scientific Computing, Manno (Switzerland), **2000**. [32b] G. Schaftenaar, J. H. Noordik, MOLDEN 3.6: a pre- and post-processing program for molecular and electronic structures, *J. Comp.-Aided Mol. Design* **2000**, *14*, 123−124. [32c] C. Mealli, D. M. Proserpio, *J. Chem. Educ.* **1990**, *67*, 399−402. [32d] R. Hoffmann, *J. Chem. Phys.* **1963**, *39*, 1397−1412.

Received April 5, 2004
Early View Article
Published Online October 18, 2004

 © 2004 Wiley-VCH Verlag GmbH & Co. KGaA, Weinheim

Luminescent Zn and Cd Coordination Polymers

Chao Jiang,[a] Zhaopeng Yu,[a] Chao Jiao,[a] Sujing Wang,[a] Jiaming Li,[a] Zhiyong Wang,*[a] and Yong Cui*[a]

Keywords: N ligands / Coordination polymers / Hydrothermal synthesis / Tubular structures / Fluorescence

The hydrothermal reactions of $Zn(ClO_4)_2{\cdot}6H_2O$ and $Cd(ClO_4)_2{\cdot}6H_2O$ with 1,3-bis(2*H*-tetrazol-5-yl)benzene in an aqueous ethanol and an aqueous methanol/pyridine medium, respectively, yielded a 3D and a 2D metal-organic coordination framework [Zn(1,3-BTB)] (**1**) and [Cd(1,3-BTB)$_2$(Py)$_2$(H$_2$O)$_2$] [Cd[Cd(Py)(H$_2$O)]$_2$(1,3-BTB)$_2$] (**2**) (1,3-BTB = 1,3-ditetrazolylbenzene, Py = pyridine), respectively. Species **1** possesses an open network structure with no guest molecules residing in its small cavities. The structural characterisation of **2** shows a 2D layered framework consisting of nano-sized polytube structures which are stacked one on top of another in the (110) plane giving small channels along the *b* and *c* axes. Additionally, compounds **1** and **2** exhibit strong fluorescence at room temperature in the solid state.
(© Wiley-VCH Verlag GmbH & Co. KGaA, 69451 Weinheim, Germany, 2004)

Introduction

Molecular-based tubular structures have received much attention because of their potential to selectively accommodate ions and molecules and catalyse specific chemical transformations.[1] The potential uses of such architectures largely depend on the size and type of their cavities which are mainly controlled by the ligands and appropriate metal ions.[2] There still remains difficulty in predicting the nature of the cavities in the polymer frameworks because of the frequent occurrence of interpenetration of the networks.[3] This problem could be solved, in principle, by designing organic ligands which disfavour interpenetration. In this respect, the use of a panel-like ligand[4] such as 1,3-ditetrazolylbenzene is promising because its coordination assembly is supposed to give polytube structures[5] without the possibility of interpenetration. Because of the aromaticity and multiple N-donor atoms, tetrazolate is also as excellent an N-donor group as pyridyl[6] and nitrile[7] with potential applications in the construction of coordination frameworks.[8] Most importantly, it is an anionic group like carboxylate which may potentially result in neutral polymeric structures which may not accommodate anions in their cavities, in contrast to those formed from neutral donor ligands. Moreover, it was found that the tetrazole functional group has a wide range of applications as a ligand in coordination chemistry, in medicinal chemistry as a metabolically stable surrogate for a carboxylic acid group and in various materials science applications involving high density energy materials and speciality explosives.[9] Here we show, that upon treatment with zinc or cadmium, 1,3-ditetrazolylbenzene can be assembled into a 3D open network structure and a 2D layered framework with a nano-sized polytube structure. No organic guests were found in the small cavities of [Zn(1,3-BTB)] (**1**), while coordinated pyridine molecules resided in the nano-sized tubes of [Cd(1,3-BTB)$_2$Py$_2$(H$_2$O)$_2$][Cd(CdPyH$_2$O)$_2$(1,3-BTB)$_2$] (**2**). Their fluorescence spectra were investigated in the solid state. The present report is concerned with the syntheses, crystal structures and luminescent properties of compounds **1** and **2**.

[a] Department of Chemistry, University of Science and Technology of China,
Hefei, 230026, Anhui, P. R. China
Fax: (internat.) + 86-551-3631760
E-mail: zwang3@ustc.edu.cn or ycui@ustc.edu.cn
Supporting information for this article is available on the WWW under http://www.eurjic.org or from the author.

Results and Discussion

Complex **1** was prepared by treating $Zn(NO_3)_2{\cdot}6H_2O$ with 1,3-ditetrazolylbenzene in water and ethanol at 90 °C under hydrothermal conditions (Scheme 1).[10] Complex **2** was prepared by treating $Cd(ClO_4)_2{\cdot}6H_2O$ with 1,3-ditetrazolylbenzene in methanol, water and pyridine at 120 °C under hydrothermal conditions. The observed tetrazolate stretching frequencies (1442 and 1396 cm^{-1} in **1**, and 1448 and 1428 cm^{-1} in **2**) of these compounds are consistent with those of other tetrazolate-based assemblies in previous reports.[8] An IR peak over 3100 cm^{-1} in **2** indicated the presence of coordinated water. The thermogravimetric analysis (TGA) of **1** showed it to be stable up to ca. 300 °C without any weight loss (see Supporting Information; see also the footnote on the first page of this article). The TGA of **2** showed that there were consecutive processes, namely loss of the coordinated water and pyridine molecules as well as ligand pyrolysis.

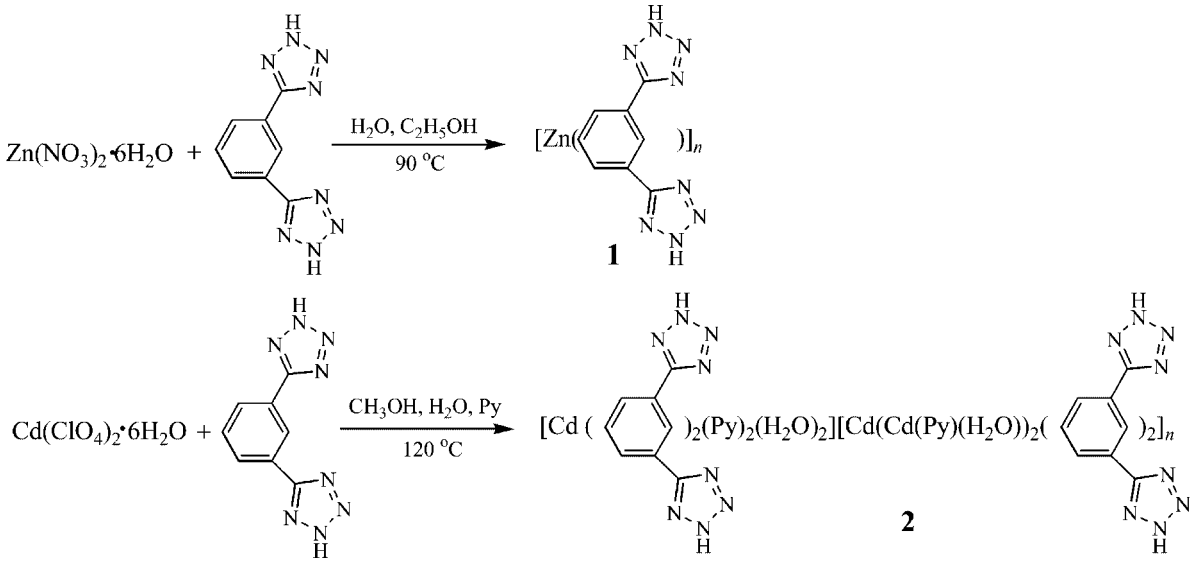

Scheme 1

Structural Description

[Zn(1,3-BTB)] (1): Compound **1** has a 3D-open network structure. The asymmetric unit comprises one Zn atom and one 1,3-BTB ligand. Each Zn atom is bound to four tetrazoles from four different 1,3-BTB ligands to adopt a highly distorted tetrahedral geometry (Figure 1). The N−Zn−N angles vary from 101.69(7) to 121.31(7)°. All donor atoms form strong bonds with the zinc atom [from 1.986(0) to 2.003(4) Å]. Each 1,3-BTB ligand coordinates through the 1,3 nitrogen atoms (N1, N3) of one tetrazole and the 1,4 nitrogen atoms (N5, N8) of the other tetrazole to four zinc atoms. Zinc atoms are connected by the 1,3 nitrogen atoms of one tetrazole along the *a* axis and by the 1,4 nitrogen atoms of the other tetrazoles along the *c* axis to form 2D sheets (Figure 2). The 1,3-BTB ligands then link parallel sheets together along the *b* axis giving rise to a 3D network (Figure 3). A preliminary inspection of the topology suggests that the zinc centre and the 1,3-BTB ligand both serve as 4-connecting centres. The overall topology appears to be that of the Al net in $SrAl_2$.[11] Small cavities can be seen along the *a* axis. No guest molecules are encapsulated in the cavities because of space restrictions.

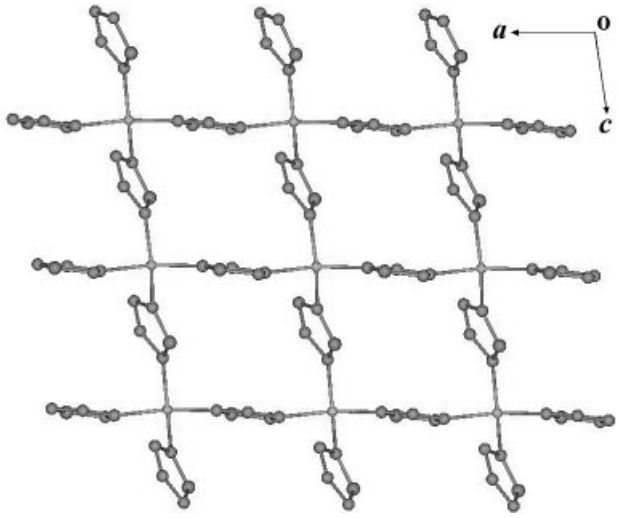

Figure 2. The 2D sheet composed of zinc atoms and tetrazolyl units in **1** (The phenyl ring and the other tetrazolyl ring in the ligand are omitted for clarity)

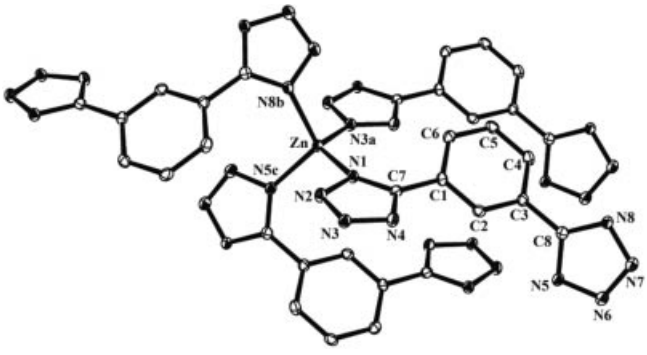

Figure 1. The local coordination geometry around the Zn centre in **1**

[Cd(1,3-BTB)$_2$(Py)$_2$(H$_2$O)$_2$][Cd[Cd(Py)(H$_2$O)]$_2$(1,3-BTB)$_2$] (2): Compound **2** is composed of 2D frameworks, the structure being a little more complicated than that of **1**. The asymmetric unit of **2** consists of one Cd atom and two half Cd atoms, two 1,3-BTB ligands, two water molecules and two pyridines. There are three unique cadmium atoms and all of their coordination geometries may be best described as distorted octahedral. Cd1 is bound to four tetrazoles from four 1,3-BTB ligands, one water molecule and one pyridine, the bond angles around the central Cd1 atom and the *cis* ligands range from 82.5° to 99.4° (Figure 4). Cd2 is

 © 2004 Wiley-VCH Verlag GmbH & Co. KGaA, Weinheim

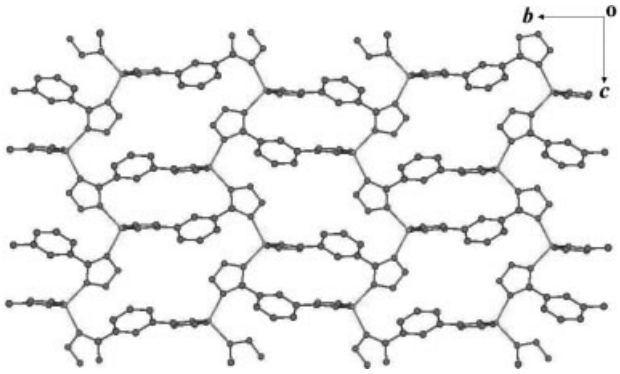

Figure 3. The 3D structure of **1** viewed along the *a* axis

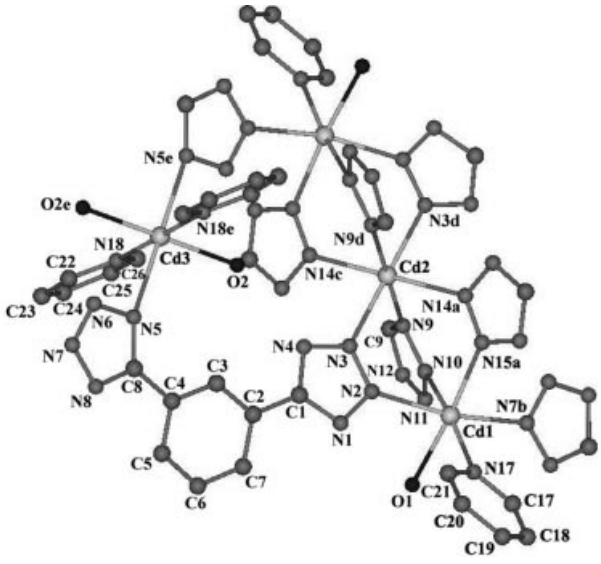

Figure 4. Part of the structure of **2** showing the local coordination geometry around the three unique Cd centres

bound to six tetrazoles from six 1,3-BTB ligands, the bond angles around the central Cd2 atom and the *cis* ligands range from 86.5° to 93.5°. Cd3 is bound to two *trans* tetrazoles from two 1,3-BTB ligands, two *trans* water molecules and two *trans* pyridines, the bond angles around the central Cd3 atom and the *cis* ligands range from 80.9° to 99.1°. The lengths of the majority of the Cd−N bonds vary from 2.265(6) to 2.415(6) Å, while Cd3−N5 is 2.503(6) Å which is a little longer than the ususal value. The two Cd−O bond lengths are 2.317(4) and 2.406(5) Å, while the latter value is somewhat long and indicates weak bonding. The two unique 1,3-BTB ligands have different coordination modes: one coordinates through the 1,3 nitrogen atoms (N5, N7) and the 2,3 nitrogen atoms (N2, N3) of its two tetrazoles, the other coordinates through the 1,2 nitrogen atoms (N9, N10) and the 2,3 nitrogen atoms (N14, N15) of its two tetrazoles.

To clearly understand the 2D framework in **2**, we first consider two Cd1 atoms, one Cd2 atom, two water molecules and two pyridines as a four-connected node. Secondly, we take two 1,3-BTB ligands as one bridge and take one Cd3, two 1,3-BTB ligands, two water molecules and two pyridines as the other bridge. A two-dimensional (4, 4) layer structure is then obtained as can be seen from Figure 5. As a result, the polytube structure is formed with the approximate dimensions of 10.0 × 9.2 Å (Figure 6). Each tube is self-assembled from six units of 1,3-BTB and is mainly lined with phenyl groups which accommodate two coordinated pyridine molecules. The 2D layers pack together in the crystallographic (011)-plane, resulting in channel formation along both the *b*-axis and the *c*-axis (Supporting Information). These 2D frameworks are stabilised by hydrogen bonding (O1···N11, 2.740 Å) (Figure 7).

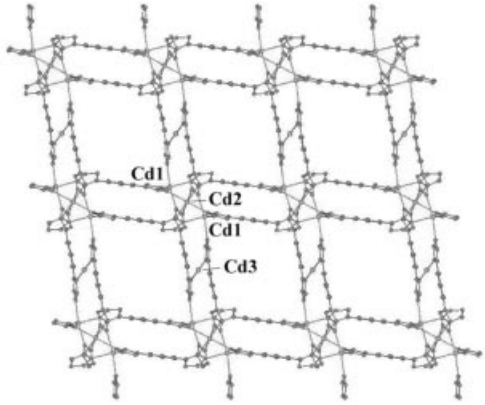

Figure 5. The 2D framework in **2** (coordinated water and pyridine molecules are omitted for clarity)

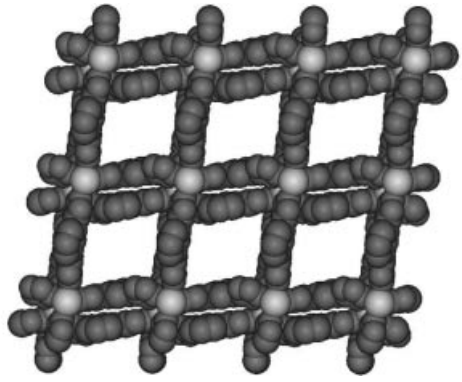

Figure 6. Space filling representation of the nano-sized tubes in the crystal structure of **2** (Coordinated water and pyridine molecules are omitted for clarity)

Fluorescent Properties

Coordination frameworks are promising luminescent materials owing to their higher thermal stability than the pure organic ligand and the ability to affect the emission wavelength of the organic material by metal coordination. The combination of organic spacers and transition-metal centres in the coordination frameworks can be viewed as an efficient method for obtaining new types of electroluminescent materials for potential applications, e.g. as light-emitting diodes (LEDs).[12] The luminescent properties of 1,3-BTB and compounds **1** and **2** were investigated in the solid

 © 2004 Wiley-VCH Verlag GmbH & Co. KGaA, Weinheim

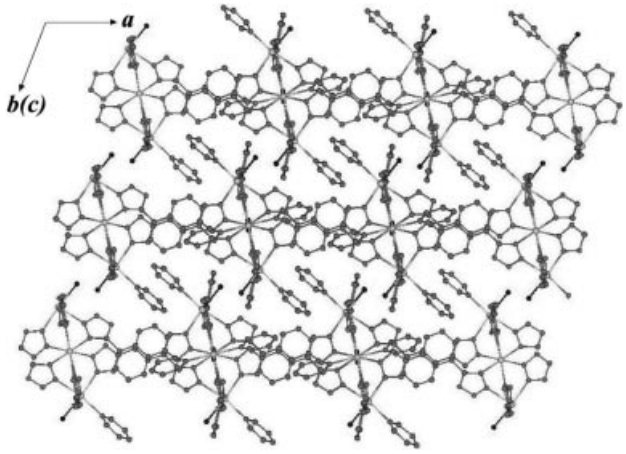

Figure 7. The packing view of the 2D framework in **2**

state. The fluorescence spectrum of 1,3-BTB is shown in Figure 8 and exhibits an emission maximum at 471 nm. The emission spectra of **1** and **2**, also shown in Figure 8, are equally blue-shifted to 323 nm. However, no enhancement in the fluorescence intensity is realised, in fact the fluorescence intensity of **2** is virtually weakened. The emission colour of free 1,3-BTB was significantly affected by its incorporation into the Zn- and Cd-containing polymeric frameworks of **1** and **2**, as evidenced by the large shift in the emission. The emissions that occurred in compounds **1** and **2** can still be assigned to free ligand photoluminescence and the large blue-shift may be due to bad conjugation effects compared with those in the free ligand.[12] In general, compounds **1** and **2** reported herein are unusual examples of room-temperature luminescent Zn- and Cd-containing polymeric compounds.

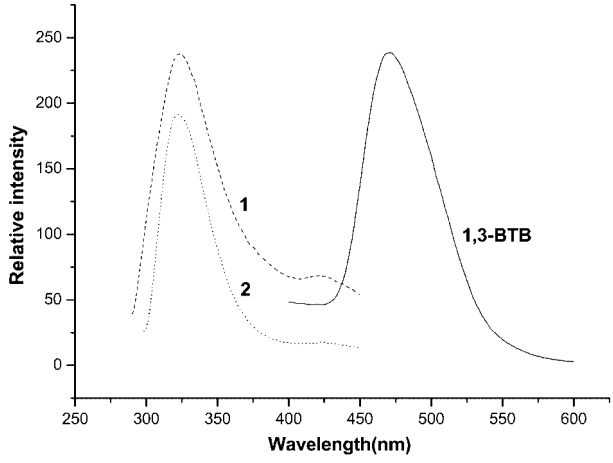

Figure 8. The emission spectra of 1,3-BTB (solid line), **1** (dashed line) and **2** (dotted line) in the solid state at room temperature

Conclusions

In summary, we have prepared two new coordination framework polytube structures from 1,3-ditetrazolylbenzene. The structural features of complexes **1** and **2** demonstrate the coordination flexibility of the tetrazolate group. The luminescent properties of **1** and **2** indicate that the metal coordination and formation of the coordination framework can affect the emission wavelength and the intensity of the organic material.

Experimental Section

General Remarks: 1,3-Ditetrazolylbenzene was prepared from NaN_3 and *m*-dicyanobenzene in 84% yield.[13] Cadmium perchlorate hexahydrate was prepared from the reaction of cadmium hydroxide with perchloric acid.[14] ***Caution:*** $Cd(ClO_4)_2·6H_2O$ is potentially explosive and should be used with care! All other chemicals were of AR grade. Elemental analyses (C, H, N) were performed with an Elementar Vario ELIII elemental analyser. IR spectra as KBr discs were recorded with a Bruker VECTOR-22 FT-IR spectrophotometer. Thermal gravimetric analyses were performed with a Shimadzu TGA-50H Thermal Gravimetric Analyser with a heating rate of 5 °C min^{-1}. Excitation and emission spectra were recorded with a Perkin−Elmer LS55 luminescence spectrometer.

Preparation of 1: Hydrothermal treatment of $Zn(NO_3)_2·6H_2O$ (30 mg, 0.1 mmol), 1,3-ditetrazolylbenzene (21 mg, 0.1 mmol), water (0.8 mL) and ethanol (0.2 mL) for 12 h at 90 °C yielded colourless plate crystals (0.012 g, 44%, only one pure phase). $C_8H_4N_8Zn$ (277.56): calcd. C 34.62, H 1.45, N 40.37; found C 35.04, H 1.39, N 40.85. IR spectrum (KBr): $\tilde{\nu}$ = 3444 (w), 1614 (m), 1524 (m), 1441 (s), 1396 (s), 1345 (m), 1251 (m), 1207, 1174, 1127 (m), 1106 (m), 1080 (m), 1064 (m), 1022 (m), 911 (m), 820 (s), 780 (s), 766 (m), 746 (s), 700 (s), 662 (m), 596 (m), 527 (m), 456 (m), 439 (m) cm^{-1}.

Preparation of 2: Hydrothermal treatment of $Cd(ClO_4)_2·6H_2O$ (41 mg, 0.1 mmol), 1,3-ditetrazolylbenzene (21 mg, 0.1 mmol), methanol (0.4 mL), water (0.2 mL) and pyridine (0.1 mL) at 120 °C for 12 h yielded colourless plate crystals (0.029 g, 68%, only one pure phase). $C_{52}H_{44}Cd_4N_{36}O_4$ (1686.79): calcd. C 37.03, H 2.63, N 29.89; found C 37.94, H 2.32, N 30.25. IR spectrum (KBr): $\tilde{\nu}$ = 3384 (w), 1638 (m), 1604 (s), 1447 (s), 1428 (s), 1363 (m), 1327 (m), 1221 (m), 1170 (m), 1155 (m), 1133 (m), 1069 (m), 1040 (m), 1012 (m), 914 (m), 831 (m), 810 (m), 780 (m), 761 (m), 750 (s), 698 (s), 630 (m), 506 (m), 417 (m) cm^{-1}.

X-ray Crystallographic Studies: Crystal data and details of the structure refinements are presented in Table 1. Intensity data were collected using Mo-K_α radiation (λ = 0.71073 Å) at 173 K for compound **1** and 100 K for compound **2**. The structure solutions and refinements were carried out using SHELXS-96[15] and SHELXL-97.[16] All hydrogen atoms were identified from difference maps and were included in the successive refinement cycles. All non-hydrogen atoms (including those of solvent water molecules) were refined anisotropically. CCDC-232821 (for **1**) and -232822 (for **2**) contain the supplementary crystallographic data for this paper. These data can be obtained free of charge at www.ccdc.cam.ac.uk/conts/retrieving.html [or from the Cambridge Crystallographic Data

 © 2004 Wiley-VCH Verlag GmbH & Co. KGaA, Weinheim

Centre, 12 Union Road, Cambridge CB2 1EZ, UK; Fax: (internat.) + 44-1223-336-033; E-mail: deposit@ccdc.cam.ac.uk].

Table 1. Crystallographic data and refinement details for **1** and **2**

	1	**2**
Empirical formula	$C_8H_4N_8Zn$	$C_{52}H_{44}Cd_4N_{36}O_4$
M	277.56	1686.79
Crystal system	monoclinic	triclinic
Space group	$P2_1/c$	$P\bar{1}$
a / Å	5.6038(10)	11.457(5)
b / Å	18.304(3)	12.210(5)
c / Å	9.9544(17)	12.935(5)
α / °	90	66.206(8)
β / °	98.199(3)	73.384(9)
γ / °	90	82.799(9)
V / Å^3	1010.6(3)	1586.4(11)
Z	4	1
D_c / g·cm^{-3}	1.824	1.472
μ (Mo-K_α) / mm^{-1}	2.419	1.373
F(000)	552	692
T / K	173(2)	100(2)
Total data	5615	6965
Unique data	2372	4533
R_{int}	0.0230	0.0356
Data $I > 2\sigma(I)$	2088	3245
$R1$[a] $[I > 2\sigma(I)]$	0.0301	0.0447
$wR2$[a] $[I > 2\sigma(I)]$	0.0719	0.0762
GOF[b]	1.026	0.863
Residuals / e·Å^{-3}	0.536, −0.366	0.827, −0.723

[a] $R1 = \Sigma| |F_o| - |F_c| |/\Sigma|F_o|$, $wR2 = [\Sigma w(F_o^2 - F_c^2)^2/\Sigma w(F_o^2)^2]^{1/2}$. [b] GOF $= \{\Sigma[w(F_o^2 - F_c^2)2]/(n - p)\}^{1/2}$.

Acknowledgments

We acknowledge financial support from the National Natural Science Foundation of China (No. 50073021) and the Education Department of Anhui Province (2002kj330ZD). We thank the referees for their useful suggestions regarding the descriptions of the crystal structures.

[1] [1a] S. Iijima, *Nature* **1991**, *354*, 56−58. [1b] A. Harada, J. Li, M. Kamachi, *Nature* **1992**, *356*, 325−327. [1c] A. Harada, J. Li, M. Kamachi, *Nature* **1993**, *364*, 516−518. [1d] J. D. Hartgerink, T. D. Clark, M. R. Ghadiri, *Chem. Eur. J.* **1998**, *3*, 1367−1372. [1e] T. Shimizu, M. Kogiso, M. Masuda, *Nature* **1996**, *383*, 487−488. [1f] N. Kimizuka, T. Kawasaki, K. Hirata, T. Kunitake, *J. Am. Chem. Soc.* **1995**, *117*, 6360−6361. [1g] Z. R. Qu, H. Zhao, Y. P. Wang, X. S. Wang, Q. O. Ye, Y. H. Li, R. G. Xiong, B. F. Abrahams, Z. G. Liu, Z. L. Xue, X. Z. You, *Chem. Eur. J.* **2004**, *10*, 54−60. [1h] R. G. Xiong, X. Z. You, B. F. Abrahams, Z. L. Xue, C. M. Che, *Angew. Chem. Int. Ed.* **2001**, *40*, 4422−4425.

[2] [2a] B. F. Abrahams, P. A. Jackson, R. Robson, *Angew. Chem. Int. Ed.* **1998**, *37*, 2656−2659. [2b] M. R. Ghadiri, J. R. Granja, R. A. Milligan, D. E. McRee, N. Khazanovich, *Nature* **1993**, *366*, 324−327. [2c] M. Scherer, D. L. Caulder, D. W. Johnson, K. N. Raymond, *Angew. Chem. Int. Ed.* **1999**, *38*, 1588−1592.

[3] [3a] T. M. Reineke, M. Eddaoudi, M. O'Keeffe, O. M. Yaghi, *Angew. Chem. Int. Ed.* **1999**, *38*, 2590−2594. [3b] K.-J. Lin, *Angew. Chem. Int. Ed.* **1999**, *38*, 2730−2732. [3c] S. S.-Y. Chui, S. M.-F. Lo, J. P. H. Charmant, A. G. Orpen, I. D. Williams, *Science* **1999**, *283*, 1148−1150. [3d] H. Gudbjartson, K. Biradha, K. M. Poirier, M. J. Zaworotko, *J. Am. Chem. Soc.* **1999**, *121*, 2599−2600. [3e] C. J. Kepert, M. J. Rosseinsky, *Chem. Commun.* **1999**, 375−376. [3f] M. Kondo, T. Okubo, A. Asami, S. Noro, T. Yoshitomi, S. Kitagawa, T. Ishii, H. Matsuzaka, K. Seki, *Angew. Chem. Int. Ed.* **1999**, *38*, 140−143. [3g] M. Tadokoro, K. Isobe, H. Uekusa, Y. Ohashi, J. Toyoda, K. Tashiro, K. Nakasuji, *Angew. Chem. Int. Ed.* **1999**, *38*, 95−98. [3h] O. R. Evans, R.-G. Xiong, Z. Wang, G. K. Wong, W. Lin, *Angew. Chem. Int. Ed.* **1999**, *38*, 536−538.

[4] M. Aoyagi, K. Biradha, M. Fujita, *J. Am. Chem. Soc.* **1999**, *121*, 7457−7458.

[5] [5a] K. Biradha, M. Aoyagi, M. Fujita, *J. Am. Chem. Soc.* **2000**, *122*, 2397−2398. [5b] M. Hong, Y. Zhao, W. Su, R. Cao, M. Fujita, Z. Zhou, A. S. C. Chan, *Angew. Chem. Int. Ed.* **2000**, *39*, 2468−2470.

[6] [6a] R. W. Gable, B. F. Hoskins, R. Robson, *J. Chem. Soc., Chem. Commun.* **1990**, 1677−1678. [6b] B. F. Abrahams, B. F. Hoskins, D. M. Michail, R. Robson, *Nature* **1994**, *369*, 727−729. [6c] L. R. MacGillivray, S. Subramanian, M. J. Zaworotko, *J. Chem. Soc., Chem. Commun.* **1994**, 1325−1326. [6d] J. A. Real, E. Andres, M. C. Munoz, M. Julve, T. Granier, A. Bousseksou, F. Varret, *Science* **1995**, *268*, 265−267. [6e] J. S. Seo, D. Whang, H. Lee, S. I. Jun, J. Oh, Y. J. Jeon, K. Kim, *Nature* **2000**, *404*, 982−986.

[7] [7a] B. F. Abrahams, S. J. Egan, B. F. Hoskins, R. Robson, *Chem. Commun.* **1996**, 1099−1100. [7b] K. A. Hirsch, D. Venkataraman, S. R. Wilson, J. S. Moore, S. Lee, *J. Chem. Soc., Chem. Commun.* **1995**, 2199−2200.

[8] [8a] R.-G. Xiong, X. Xue, H. Zhao, X.-Z. You, B. F. Abrahams, Z. Xue, *Angew. Chem. Int. Ed.* **2002**, *41*, 3800−3803. [8b] X. Xue, X.-S. Wang, L.-Z. Wang, R.-G. Xiong, B. F. Abrahams, X.-Z. You, Z. Xue, C.-M. Che, *Inorg. Chem.* **2002**, *41*, 6544−6546. [8c] L.-Z. Wang, Z.-R. Qu, H. Zhao, X.-S. Wang, R.-G. Xiong, Z. Xue, *Inorg. Chem.* **2003**, *42*, 3969−3971. [8d] Z.-R. Qu, H. Zhao, X.-S. Wang, Y.-H. Li, Y.-M. Song, Y. Liu, Q. Ye, R.-G. Xiong, B. F. Abrahams, Z. Xue, X.-Z. You, *Inorg. Chem.* **2003**, *42*, 7710−7712.

[9] [9a] S. J. Wittenberger, *Org. Prep. Proced. Int.* **1994**, *26*, 499−531. [9b] J. V. Duncia, M. E. Pierce, J. B. Santella III, *J. Org. Chem.* **1991**, *56*, 2395−2400. [9c] D. P. Curran, S. Hadida, S.-Y. Kim, *Tetrahedron* **1999**, *55*, 8997−9006. [9d] H. Singh, A. S. Chawla, V. K. Kapoor, D. Paul, R. Malhotra, *Prog. Med. Chem.* **1980**, *17*, 15. [9e] V. A. Ostrovskii, M. S. Pevzner, T. P. Kofmna, M. B. Shcherbinin, I. V. Tselinskii, *Targets Heterocycl. Syst.* **1999**, *3*, 467. [9f] M. Hiskey, D. E. Chavez, D. L. Naud, S. F. Son, H. L. Berghout, C. A. Bome, *Proc. Int. Pyrotech. Semin.* **2000**, *27*, 3.

[10] [10a] C. Jiang, Z. P. Yu, X. Zhu, Z. Y. Wang, *Inorg. Chem. Commun.* **2003**, *6*, 706−709. [10b] C. Jiang, Z. Y. Wang, *Polyhedron* **2003**, *22*, 2953−2959. [10c] C. Jiang, Z.-P. Yu, J.-M. Li, C. Jiao, S.-J. Wang, Z.-Y. Wang, Y. Cui, *Eur. J. Inorg. Chem.* **2004**, 0000−0000.

[11] M. O'Keeffe, B. G. Hyde, *Crystal Structures I: Patterns and Symmetry*, Am. Mineral. Assoc., Washington, DC, **1996**, figure 7.17 on page 306.

[12] [12a] M. Altmann, U. H. F. Bunz, *Angew. Chem. Int. Ed. Engl.* **1995**, *34*, 569−571. [12b] U. H. F. Bunz, *Chem. Rev.* **2000**, *100*, 1605−1644. [12c] Y.-B. Dong, G.-X. Jin, M. D. Smith, R.-Q. Huang, B. Tang, H.-C. zur Loye, *Inorg. Chem.* **2002**, *41*, 4909−4914. [12d] Y. X. Li, Y. H. Li, X. R. Zeng, R. G. Xiong, X. Z. You, H. K. Fun, *Inorg. Chem. Commun.* **2003**, *6*, 1144−1147. [12e] J. Zhang, Y. R. Xie, Q. Ye, R. G. Xiong, Z. L. Xue, X. Z. You, *Eur. J. Inorg. Chem.* **2003**, 2572−2577. [12f] Z. F. Chen, R. G. Xiong, J. Zhang, X. T. Chen, Z. L. Xue, X. Z. You, *Inorg. Chem.* **2001**, *40*, 4075. [12g] H. K. Fun, S. S. S. Raj, R. G. Xiong, J. L. Zuo, Z. Yu, X. Z. You, *J. Chem. Soc., Dalton Trans.* **1999**, 1915−1916. [12h] R. G. Xiong, J. L. Zuo, X. Z. You, B. F. Abrahams, Z. P. Bai, C. M. Che, H. K. Fun, *Chem. Commun.* **2000**, 2061−2062.

 © 2004 Wiley-VCH Verlag GmbH & Co. KGaA, Weinheim

[13] H. Detert, D. Schollmeier, *Synthesis* **1999**, 999−1004.
[14] The Chemical Society of Japan, *Handbook of Inorganic Compounds Synthesis*, Chemical Industry Press, Beijing, **1986**, vol. 2, p. 480.
[15] G. M. Sheldrick, *SHELXS-96, Program for Crystal Structure Solution*, University of Göttingen, Germany, **1996**.
[16] G. M. Sheldrick, *SHELXL-97, Program for Crystal Structure Refinement*, University of Göttingen, Germany, **1997**.

Received April 21, 2004
Early View Article
Published Online October 7, 2004

 © 2004 Wiley-VCH Verlag GmbH & Co. KGaA, Weinheim

Use of Different Unsaturated Dicarboxylates Toward the Design of New 3D and 2D Networks of Copper(II)

Partha Sarathi Mukherjee,[a] Debajyoti Ghoshal,[a] Ennio Zangrando,*[b] Talal Mallah,[c] and Nirmalendu Ray Chaudhuri*[a]

Keywords: Coordination polymers / Copper / Magnetic properties / Weak interaction / Dicarboxylate ligands

Two new polymeric complexes of copper(II), $[Cu(L1)(\mu\text{-fum})(\mu\text{-}H_2O)]_n$ (**1**) (fum = fumarate dianion; L1 = *N*,*N*′-dimethylethane-1,2-diamine) and $[Cu(L2)(\mu\text{-tp})]_n$ (**2**) [tp = terephthalate dianion; L2 = *N*-(2-aminoethyl)-3-amino-1-propanol], have been synthesized. The molecular structures are determined by X-ray crystallography. Complex **1** is a fumarato-bridged zig-zag 1D chain of Cu^{II}–L1, which is extended to a 3D coordination polymer through bridging water molecules. Complex **2** is a chain of Cu^{II} in which the terephthalate anions bridge in alternate bis(bidentate) and bis(monodentate) fashions. The coexistence of such types of bridging modes of terephthalate ions in a single molecule is unprecedented. The chelating terephthalate ion is linked to an equatorial and an axial site of consecutive metal ions, while the other terephthalate ion is axially linked to Cu^{II} centers. Both the complexes are characterized by variable-temperature susceptibility measurements at room temperature down to 4 K. Fitting of the magnetic data reveals the existence of weak antiferromagnetic interactions through the bridging dicarboxylate pathways.
(© Wiley-VCH Verlag GmbH & Co. KGaA, 69451 Weinheim, Germany, 2004)

Introduction

Construction of molecules with covalent and noncovalent motifs has recently become a rapidly growing area of research as it pursues to establish principles that will ultimately lead to the development of new state-of-the-art functional materials.[1−6] Among the noncovalent motifs, hydrogen bonding[2,3] and π-π stacking[7] have been employed as synthetic paradigms to rationally design superstructures. Recent progress in this area has generated examples in which the design of network structures has produced crystals with (a) one-dimensional (1D) molecular networks composed of hydrogen bonding,[8,9] metal−ligand coordination,[10,11] or a combination of these and other interactions, referred to as hybrid interactions;[12] (b) 2D networks comprising either hydrogen bonding[13]/metal−ligand coordination[14] or hybrid interactions; and (c) 3D networks composed of hydrogen bonding[15] or metal−ligand coordination.[16] These approaches seek to establish structural relationships between the molecular and supramolecular networks and look for molecular features, such as functional groups, that can interfere and modify the arrangements of molecules in crystals, a task that remains a considerable challenge at present.

Recently, di- and polycarboxylates have become one of the most demanding spacers to the material chemist, and especially to the inorganic chemist, for the synthesis of compounds that have potential useful applications as molecular-based magnetic materials as well as materials that mimick zeolite with host-guest behavior.[17−19] Different types of dicarboxylates like terephthalate, malonate, succinate, and oxalates are widely used by these chemists, but use of fumarate is relatively less frequent due to poor solubility of its coordination complexes in common solvents. We have reported a new method of crystallization of Cu^{II} complexes of fumarate that uses ammonia as solvent.[20] With this procedure we have already obtained and reported on some interesting molecular architectures.[20,21] We are currently exploring the design of molecules that use suitable metal ions and ligands capable of forming H-bonds as well as π-π interactions as directional motifs to extend the dimensionality of the molecule. The present article contributes to the synthesis, crystal structure, and variable-temperature magnetic behavior of two Cu^{II} complexes with unsaturated dicarboxylate as bridging ligands, namely $[Cu(L1)(\mu\text{-fum})(\mu\text{-}H_2O)]_n$ (**1**) and $[Cu(L2)(\mu\text{-tp})]_n$ (**2**) [fum = fumarate dianion; tp = terephthalate dianion; L1 = *N*,*N*′-dimethylethane-1,2-diamine; L2 = *N*-(2-aminoethyl)-3-amino-1-pro-

[a] Department of Inorganic Chemistry, Indian Association for the Cultivation of Science,
Jadavpur, Kolkata 700032, India
Fax: (internat.) + 91-33-24732805
E-mail: icnrc@iacs.res.in
[b] Dipartimento di Scienze Chimiche, University of Trieste, 34127 Trieste, Italy
[c] Laboratoire de Chimie Inorganique, UMR CNRS 8613, Universite de Paris-Sud, 91405 Orsay, France

panol]. The results of the structural analysis of complex **1** reveals a 3D network and that of **2** a chain with alternating bis(bidentate) and bis(monodentate) bridging modes of terephthalate, which results in a molecule with a unique topology. The coexistence of terephthalate ligands with different bridging fashions inside a single molecule has not been reported earlier. These unsaturated dicarboxylates are chosen as spacers because of the following reasons: (i) fumarate and terephthalate show versatile coordination modes (Scheme 1); (ii) they coordinate metal ions to form unidimensional coordination chains, which, in general, can enlarge the dimensionality through H-bonding; and (iii) they have ethylenic and phenyl moieties that are capable of forming π-π stacking as a directional motif (Scheme 2).

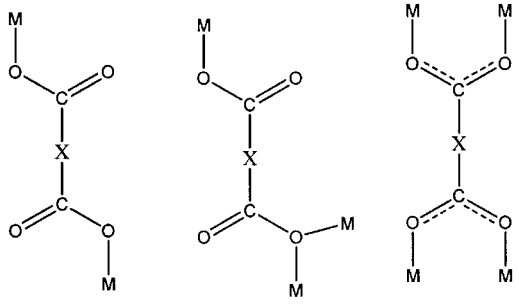

Scheme 1. [X = −CH=CH− or $-C_6H_4-$ (1,4)]

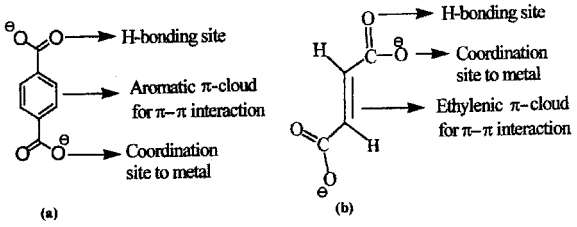

Scheme 2. Possible sites for coordination as well as supramolecular interaction in terephthalate (a) and fumarate (b)

Results and Discussion

Description of the Structures

[Cu(L1)(μ-fum)(μ-H_2O)]$_n$ (1)

The crystal structure of **1** consists of Cu^{II}(L1) units connected through bridging amphi-monodentate fumarate dianions to form polymeric chains with a zig-zag arrangement (Figure 1). Each copper atom is located on a twofold crystallographic axis with an elongated octahedral geometry that involves the diamine ligand donors N(1) and the carboxylic oxygen atom O(2) in the equatorial positions, and two water molecules as axial ligands. The former distances [Cu−O(2) 1.973(2), Cu−N(1) 2.022(2) Å] are significantly shorter than those involving the water molecule [2.481(2) Å]. A selection of bond lengths and angles is reported in Table 1. The dicarboxylate anion spans the metal atoms with a distance of 8.857 Å, a distance similar to those of 8.653 and 8.666 Å observed in two dinuclear fumarate-bridged Cu^{II} complexes.[22,23] It is worthwhile to note the

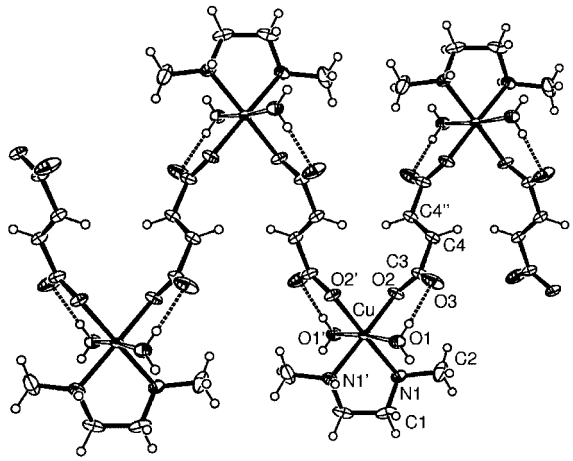

Figure 1. ORTEP drawing (thermal ellipsoid at 40% probability level) of the polymeric arrangement of **1** with atom labeling scheme; dotted lines indicate intrachain H-bonds

Table 1. Selected bond lengths [Å] and angles [°] for complex [Cu(L1)(μ-fum)(μ-H_2O)] (**1**)

Cu−O(2)	1.973(2)	O(2)−C(3)	1.265(3)
Cu−N(1)	2.022(2)	O(3)−C(3)	1.234(3)
Cu−O(1)	2.481(2)	C(4)−C(4′′)[a]	1.311(5)
O(2)−Cu−N(1′)[a]	174.88(8)	N(1′)−Cu−N(1)	85.4(1)
O(2)−Cu−N(1)	93.60(9)	N(1)−Cu−O(1)	90.13(8)
O(2)−Cu−O(1)	98.48(7)	N(1)−Cu−O(1′)	86.54(8)
O(2)−Cu−O(1′)	84.80(7)	O(2)−Cu−O(2′)	87.9(1)
O(1′)−Cu−O(1)	175.5(2)	C(3)−O(2)−Cu	123.3(2)

[a] Symmetry operations: (′): 1.25 − x, 0.25 − y, z; (′′): 1 − x, −y, 1 − z.

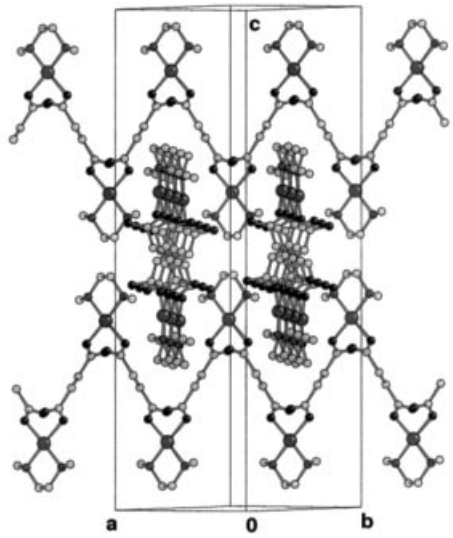

Figure 2. Perspective view of the packing of **1** showing the intersecting Cu(L1)(fum) chains (water molecules not shown for clarity)

 © 2004 Wiley-VCH Verlag GmbH & Co. KGaA, Weinheim

packing shown by the X-ray structural analysis, in which the coordination polymers present an intersecting arrangement (Figure 2). The dimensionality of the network is enlarged to 3D through the axially coordinated water molecules that bridge consecutive metal ions as depicted in Figure 3. These $-(Cu-H_2O)_n-$ chains are characterized by a metal−metal separation of 4.512 Å and a Cu−OH$_2$−Cu′′ bond angle of 130.6(1)°. The dicarboxylate skeleton is not coplanar, and instead, a O(3)−C(3)−C(4)−C(4′′) torsion angle of 145.0(4)° is observed. This conformational feature is likely assumed in order to favor the intrachain H-bond formation between the coordinated water molecule and the fumarate oxygen atom O(3) (Figure 3; O−O 2.651 Å). However, the C(4)−C(4′′) bond length of 1.311(5) Å still indicates a larger double-bond character relative to that of the C(3)−C(4) bond [1.491(3) Å].

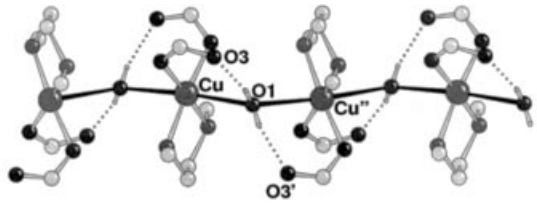

Figure 3. Bridging water molecules connecting the coordination polymers to form a 3D network in **1**; dotted lines indicate H-bonds [O(3′) at 1.75 − *x*, *y*, 0.75 − *z*; Cu′′ at 0.5 + *x*, 0.25 − *y*, 0.75 − *z*]

[Cu(L2)(μ-tp)]$_n$ (2)

The structure of complex **2** consists of 1D polymeric chains formed by Cu(L2) moieties [L2 = *N*-(2-aminoethyl)-3-amino-1-propanol] bridged by terephthalate anions. The polymeric motifs, together with the atom numbering scheme, is shown in Figure 4, and a selection of bond lengths and angles is given in Table 2. The metal environment can be described as a distorted octahedron in which the equatorial positions are occupied by the hydroxy-diamine ligand donors and by the carboxyl oxygen atom O(2), while the oxygen atoms O(4) and O(3) of different bridging terephthalate anions complete the coordination sphere. The latter distances [Cu−O(4) 2.300(4), Cu−O(3) 2.553(4) Å] are significantly longer with respect to those in the basal plane [range 1.971(4)−2.027(5) Å]. The distortions from the octahedral geometry are indicated by the small bite angle of the carboxylate group O(2)−Cu−O(3) [56.7(2)°] and by the O(4)−Cu−O(3) angle [153.3(1)°]. The four equatorial donors are coplanar ±0.086(3) Å, with the metal atom slightly displaced by 0.164(3) Å from their mean plane towards O(4). Thus, along the chain, two terephthalate anions, both having the phenyl ring located about a crystallographic symmetry center, connect Cu(L2) units, alternatively in a bis(monodentate) and a chelating bis(bidentate) fashion (Figure 4). The simultaneous presence of terephthalate ligands with different bridging fashions gives rise to an unprecedented coordination chain. The dihedral angle formed by the anions with the equatorial coordination plane is 45.9(1) and 80.3(2)°, the latter indicating a nearly perpendicular orientation for the bis(bidentate) terephthalate. The respective *intra*molecular Cu−Cu distances spanned by the anions are 10.998(5) and 10.830(3) Å; the small difference appears to be caused by the ligand coordination mode. In fact, making allowance for packing and for the different ligands bound at the metal atom, distances of about 11.0 Å were found for copper ions bridged by bis(monodentate) terephthalate anions,[24−26] while a separation of 10.710 Å was reported in [(CuL")$_2$tp](ClO$_4$)$_2$ (L" = pentaethyldiethylenetriamine)[27] in which the anion bridges in a chelating bis(bidentate) fashion. The carboxylate group C(6)/O(2)/O(3) is nearly coplanar with the phenyl ring [4.9(3)°], while C(10)/O(4)/O(5) exhibits a tilt of 24.0(5)°. This dihedral angle was tentatively taken into account to assess the magnetic exchange coupling with structural parameters in transition metal ions bridged by a tp ligand.[28] The described polymers are held together through strong hydrogen bonds that occur between the hydroxy group O(1)−H and the carboxylate oxygen atom O(5) [2.678 Å, O(1)−H···O(5) 159.07°] to yield a layered structure (Figure 5) in which the shortest *inter*chain Cu−Cu distance is 5.532(1) Å. Moreover, the phenyl groups of the bis(bidentate) terephthalate are not coplanar with

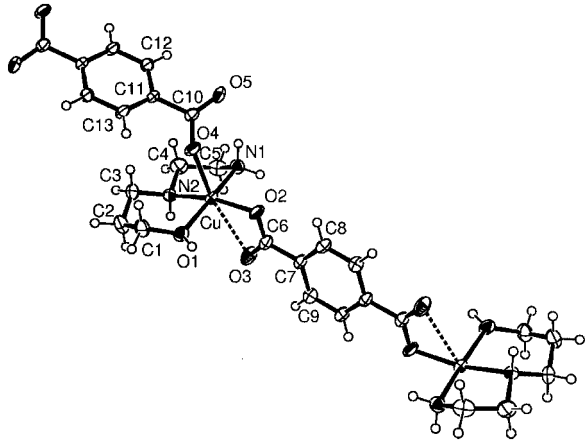

Figure 4. ORTEP drawing (thermal ellipsoid drawn at 40% probability level) of the polymeric chain of **2** with atom labeling scheme; the broken lines indicate the weak interaction between the copper and carboxyl oxygen O(3) atoms

Table 2. Selected bond lengths [Å] and angles [°] of [Cu(L2)(μ-tp)] (**2**)

Cu−O(1)	2.006(4)	Cu−O(4)	2.300(4)
Cu−O(2)	1.971(4)	O(2)−C(6)	1.273(7)
Cu−N(1)	1.997(5)	O(3)−C(6)	1.231(7)
Cu−N(2)	2.027(5)	O(4)−C(10)	1.265(7)
Cu−O(3)	2.553(4)	O(5)−C(10)	1.246(7)
O(1)−Cu−O(2)	89.4(2)	N(1)−Cu−N(2)	84.6(2)
O(1)−Cu−N(1)	172.6(2)	N(1)−Cu−O(3)	95.7(2)
O(1)−Cu−N(2)	89.2(2)	N(1)−Cu−O(4)	94.1(2)
O(1)−Cu−O(3)	82.6(2)	N(2)−Cu−O(3)	109.1(2)
O(1)−Cu−O(4)	90.5(2)	N(2)−Cu−O(4)	96.4(2)
O(2)−Cu−N(1)	95.7(2)	O(4)−Cu−O(3)	153.3(1)
O(2)−Cu−N(2)	165.7(2)	C(10)−O(4)−Cu	128.7(4)
O(2)−Cu−O(3)	56.7(2)	C(6)−O(2)−Cu	102.8(4)
O(2)−Cu−O(4)	97.7(2)	C(6)−O(3)−Cu	76.9(3)

 © 2004 Wiley-VCH Verlag GmbH & Co. KGaA, Weinheim

aromatic rings of neighboring chains, but are perpendicular. As a consequence, the phenyl centroid of the latter is at a distance of 2.66 Å from the H−C group of the adjacent aromatic ring leading to a C−H···π interaction (Figure 5).

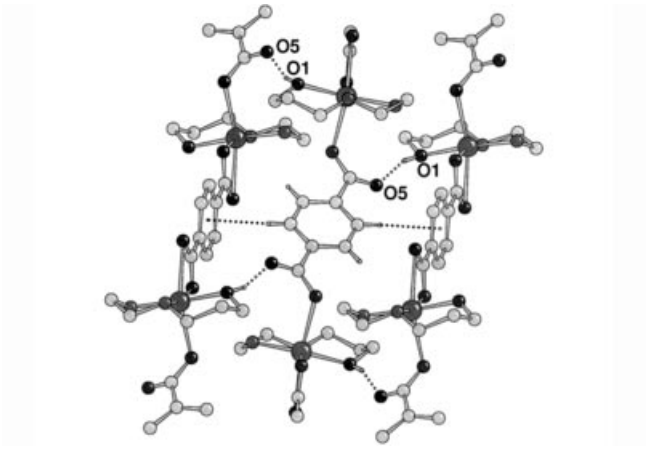

Figure 5. Perspective view of the layered structure in **2** (along axis *a*) showing the interchain H-bonding scheme and the C−H···π interactions

Magnetic Properties

[Cu(L1)(μ-fum)(μ-H_2O)]$_n$ (1)

The magnetic behavior of complex **1** was investigated using a SQUID magnetometer in the temperature region 280−4 K within an applied magnetic field of 5 kOe. The $\chi_M T$ product first decreases smoothly and then abruptly when cooling down from $T = 280$ K. It reaches a value close to zero at $T = 4$ K. The $\chi_M = f(T)$ plot is shown in Figure 6. These magnetic data are consistent with the presence of a weak antiferromagnetic interaction between the Cu^{II} ions within the compound even though the shorter Cu−Cu distance is larger than 6 Å. The susceptibility data, using the 1D chain model of the Cu^{II} system, was fitted, resulting in a J value of $-2.6\ cm^{-1}$. This value is satisfactory, since it is of the same order of magnitude as that from a previously reported communication in which a 3D interlocked network of Cu^{II} ions has a bridging fumarate ion that is linked in a similar manner to that in the present complex.[21] From a structural point of view, each copper atom, located on a twofold crystallographic axis, shows an elongated octahedral geometry involving the diamine ligand donors and a carboxylic oxygen atom in the equatorial positions, and two water molecules at the axial sites. Due to this axially elongated geometry of Cu^{II} centers, the magnetically active unpaired electron on each Cu^{II} atom is located on the basal $d_{x^2-y^2}$ orbital, whereas the d_{z^2} orbital is occupied by paired electrons. Since each bridging water is bound to the d_{z^2} (nonmagnetic) orbital of two Cu^{II} centers, the coupling interaction through the aqua bridging pathway may be considered to be zero. Therefore, in the fitting, we did not consider the coupling interaction through the water bridging pathway, and rather, for magnetic study, the compound was considered as a 1D coordination chain.

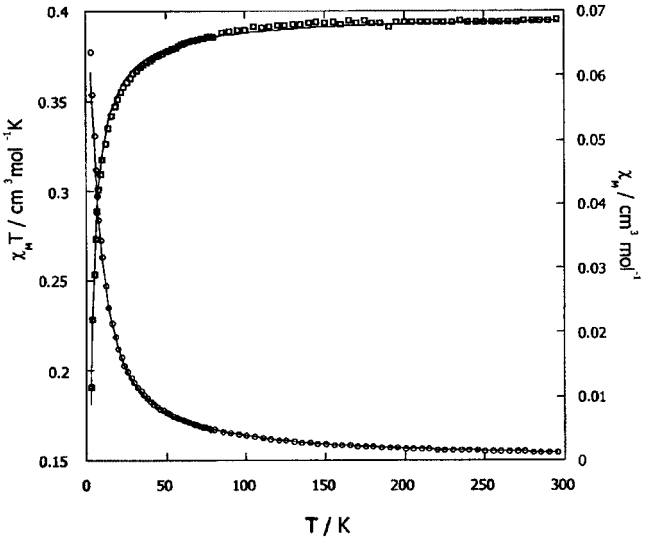

Figure 6. Plot of $\chi_M T$ vs. T (squares) and χ_M vs. T (circles) data; solid lines show the best fit obtained considering a uniform chain of $S = 1/2$ local spin states

[Cu(L2)(μ-tp)] (2)

The structural analysis reveals a 1D chain with dicarboxylate anions in a different alternating bridging mode. We have considered that an axial−axial bridging terephthalate ion has no influence on magnetic coupling since the unpaired electron on the Cu^{II} atom is not concentrated in axial orbital regions. The $\chi_M T$ vs. T plot shows a gradual decrease in $\chi_M T$ values with decreasing temperature (Figure 7), which indicates the existence of antiferromagnetic interactions within the complex. The $\chi_M T$ vs. T data are fitted using the Bleaney−Bowers formula[29] of the Cu^{II} local spin state. The results of the best fit are $J = -6\ cm^{-1}$, $\rho = 0.007$, $g = 2.01$, $R = 1.8 \cdot 10^{-5}$, which are similar to those previously reported for a similar type of bridging tp core.[25]

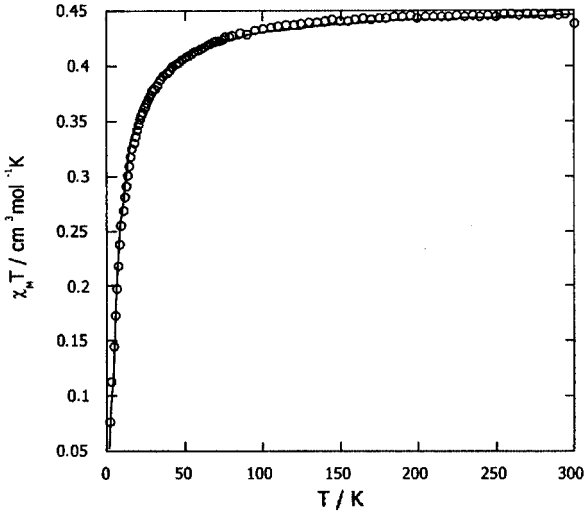

Figure 7. Fitting of $\chi_M T$ vs. T data using the dimeric model of $S = {}^1/_2$ local spins; solid line shows the best fit obtained

 © 2004 Wiley-VCH Verlag GmbH & Co. KGaA, Weinheim

Conclusions

This article presents the synthesis, single-crystal structure, and magnetic behavior of two dicarboxylate-bridged metal complexes. Complex **1** is a 3D network of Cu^{II} in which both a fumarate ion and a water molecule function as a bridging ligand. Cu−fumarate zig-zag chains are involved in the bridging by water molecules to form a 3D network. On the other hand, complex **2** is a 1D chain of Cu^{II}−terephthalate in which the dicarboxylate is alternately bridged in a bis(bidentate) and a bis(monodentate) fashion in an axial−axial and equatorial−equatorial mode to form a unique molecule since such an alternate coordination fashion has not been reported earlier for terephthalate systems. Furthermore, the solid-state structure of complex **2** is stabilized by C−H···π interactions. Here, the role of the chemically different dicarboxylates upon the formation of the superstructure is a crucial aspect open to theoretical speculations. Low-temperature magnetic susceptibility data of **1** were fitted to the equation of a chain of $S = {}^1/_2$ local spins, which reveal the existence of weak antiferromagnetic interactions along the fumarate pathway. In the case of **2**, the variable-temperature magnetic data were fitted to a dimeric formula of $S = {}^1/_2$ spin state, which indicates a weak antiferromagnetic interaction along the terephthalate pathway.

Experimental Section

Synthesis of Cu(L1)(μ-fum)(μ-H_2O)] (1): 1 mmol of *N*,*N*′-dimethylethane-1,2-diamine was slowly added drop by drop to an aqueous solution of $CuCl_2{\cdot}2H_2O$ (5 mL, 1 mmol, 0.1705 g), resulting in a deep blue solution. An aqueous solution of Na_2−fumarate (10 mL, 1 mmol, 0.160 g) was added with continuous stirring and the stirring continued for 40 min and then filtered. Suitable blue single crystals for X-ray analysis were obtained after 15 d on keeping the deep blue filtrate in a refrigerator. $C_8H_{16}CuN_2O_5$ (283.77): calcd. C 33.80, H 5.63, N 9.86; found C 32.17, H 5.73, N 10.14. IR: ν(COO^-) = 1392, 1562 cm^{-1}; ν(N−H) = 3000 cm^{-1}; ν(O−H) = 3450−3370 cm^{-1}.

Synthesis of [Cu(L2)(μ-tp)] (2): A methanolic solution of a mixture of terephthalic acid (1 mmol) and triethylamine (2 mmol) was layered on a blue aqueous solution of $Cu(ClO_4)_2{\cdot}6H_2O$ (1 mmol) and *N*-(2-aminoethyl)-3-amino-1-propanol (1 mmol). After a month, a microcrystalline blue complex with suitable single crystals for X-ray diffraction were obtained. The crystals were separated by a needle. $C_{13}H_{18}CuN_2O_5$ (345.83): calcd. C 45.10, H 5.20, N 8.09; found C 44.87, H 5.33, N 9.84. IR: ν(COO^-) = 1372, 1543 cm^{-1}; ν(N−H) = 3050 cm^{-1}; ν(O−H) = 3400−3350 cm^{-1}.

Physical Measurements: IR spectra were recorded with a Nicolet 520 FTIR spectrometer using KBr pellets. Magnetic measurements were carried out on a polycrystalline sample with a SQUID magnetometer operating in the 2−300 K temperature range with an applied field of 5 kOe. Diamagnetic corrections were estimated from Pascal constants.

Crystal Data Collection and Refinement: The data set for **1** and **2** were collected at room temperature using the ω-2θ scan technique with an Enraf−Nonius MACH 3 and a CAD4 Enraf−Nonius single-crystal diffractometer, respectively, equipped with a graphite monochromator and Mo-K_α radiation (λ = 0.71073 Å). Three standard reflections, measured at regular intervals throughout the data collection, showed no noticeable variation in intensity. An absorption correction based on the ψ-scan method was applied (max./min. T = 0.9988/0.8316 for **1** and 0.9971/0.8035 for **2**). The structure was solved by conventional Patterson and Fourier analyses and refined on F^2 by full-matrix anisotropic least-squares method using the SHELXL-97 package.[30] All the calculations were performed using the WinGX System, Ver 1.63.[31] Crystal data and refinement details are given in Table 3. X-ray crystallographic data in CIF format for the structures reported in this paper have been deposited with the Cambridge Crystallographic Data Centre. CCDC-236904 and -236905 contain these data, which can be obtained free of charge at www.ccdc.cam.ac.uk/conts/retrieving.html [or from the Cambridge Crystallographic Data Centre, 12 Union Road, Cambridge CB2 1EZ, UK [Fax: (internat.) + 44-1223-336-033; E-mail: deposit@ccdc.cam.ac.uk].

Table 3. Crystal data and structure refinement for complexes [Cu(L1)(μ-fum)(μ-H_2O)] (**1**) and [Cu(L2)(μ-tp)] **(2)**

	1	**2**
Empirical formula	$C_8H_{16}CuN_2O_5$	$C_{13}H_{18}CuN_2O_5$
M	283.77	345.83
T [K]	293(2)	293(2)
Crystal system	orthorhombic	monoclinic
Space group	*Fddd* (choice 2)	$P2_1/n$
a [Å]	9.016(4)	7.437(3)
b [Å]	16.322(6)	9.367(2)
c [Å]	30.908(8)	20.103(5)
β [°]	90.00	94.07(4)
V [Å^3]	4548(4)	1396.8(7)
Z	16	4
$D_{calcd.}$ [g cm^{-1}]	1.685	1.644
μ(Mo-K_α) [mm^{-1}]	1.929	1.587
Reflections collected	4929	4307
Unique reflections	1316	3976
R(int)[a]	0.0689	0.0638
$R1$	0.0322	0.0633
$wR2$	0.0720	0.1709
GOF	1.016	1.207
Residuals [e·Å^{-3}]	0.281/−0.427	1.483/−0.742

[a] $R = \|\|F_o\| - |F_c\|\|/|F_o|$; $Rw = \{[w(F_o^2 - F_c^2)^2]/[w(F_o^2)^2]\}^{1/2}$.

Acknowledgments

Funding for the work described here was provided by the Council of Scientific and Industrial Research, New Delhi (grant to NRC), and they are gratefully acknowledged. We also thank Dr. S. Pal, School of Chemistry, University of Hyderabad, India for X-ray data collection.

[1] D. Braga, F. Grepioni, A. G. Orpen, *Crystal Engineering: From Molecules and Crystals to Materials*, NATO Science Series, Mathematical and Physical Sciences, vol. 538, Kluwer Academic Publishers, Dordrecht, The Netherlands, **1999**.
[2] R. K. Seddon, M. Zaworotko, *Crystal Engineering: The Design and Application of Functional Solids*, NATO Science Series,

 © 2004 Wiley-VCH Verlag GmbH & Co. KGaA, Weinheim

Mathematical and Physical Sciences, vol. 539, Kluwer Academic Publishers, Dordrecht, The Netherlands, **1999**.
[3] G. R. Desiraju, *Crystal Engineering: The Design of Organic Solids*, Elsevier Science Publishers, Amsterdam, The Netherlands, **1989**.
[4] D. N. Chin, J. A. Zerkowski, J. C. MacDonald, G. M. Whitesides, *Organized Molecular Assemblies in the Solid State*, John Wiley and Sons, New York, **1999**, pp. 185−253.
[5] M. Fujita, *Molecular Self-Assembly − Organic versus Inorganic Approaches*, Structure and Bonding, vol. 96, Springer-Verlag, Berlin, Heidelberg, Germany, **2000**.
[6] J. M. Lehn, *Supramolecular Chemistry − Concepts and Perspectives*, VCH, Weinheim, Germany, **1995**.
[7] [7a] I. G. Dance, in: *The Crystals as a Supramolecular Entity* (Ed.: G. R. Desiraju), John Wiley, NewYork, **1996**. [7b]D. J. Hill, M. J. Mio, R. B. Prince, T. S. Hughes, J. S. Moore, *Chem. Rev.* **2001**, *101*, 3893. [7c] D. Ghoshal, T. K. Maji, G. Mostafa, T. H. Lu, N. Ray Chaudhuri, *Cryst. Growth Des.* **2003**, *3*, 9. [7d] A. K. Ghosh, D. Ghoshal, T. H. Lu, G. Mostafa, N. Ray Chaudhuri, *Cryst. Growth Des.* **2004**, *4*, 851. [7e] D. Ghoshal, T. K. Maji, G. Mostafa, S. Sain, J. Ribas, E. Zangrando, T. H. Lu, N. Ray Chaudhuri, *Dalton Trans.* **2004**, 1687.
[8] [8a] S. Palacin, D. N. Chin, E. E. Simanek, J. C. MacDonald, G. M. Whitesides, M. T. McBride, G. T. R. Palmore, *J. Am. Chem. Soc.* **1997**, *119*, 11807. [8b] K. E. Schwiebert, D. N. Chin, J. C. MacDonald, G. M. Whitesides, *J. Am. Chem. Soc.* **1996**, *118*, 4018.
[9] Y. L. Chang, M. A. West, F. W. Fowler, J. W. Lauher, *J. Am. Chem. Soc.* **1993**, *115*, 5991.
[10] S. L. James, *Chem. Soc., Rev.* **2003**, *32*, 276.
[11] B. Moulton, M. J. Zaworotko, *Chem. Rev.* **2001**, *101*, 1629.
[12] C. K. Kuehl, F. M. Tabellion, A. M. Arif, P. J. Stang, *Organometallics* **2001**, *20*, 1956.
[13] S. S. Kuduva, D. Bläser, R. Boese, G. R. Desiraju, *J. Org. Chem.* **2001**, *66*, 1621.
[14] R. H. Groeneman, L. R. MacGillivray, J. L. Atwood, *Chem. Commun.* **1998**, 2735.
[15] K. T. Holman, A. M. Pivotar, J. A. Swift, M. D. Ward, *Acc. Chem. Res.* **2001**, *34*, 107.
[16] T. J. Prior, M. J. Rosseinsky, *Chem. Commun.* **2001**, 495.
[17] [17a] M. Eddaoudi, H. Li, O. M. Yaghi, *J. Am. Chem. Soc.* **2000**, *122*, 1391. [17b] M. Eddaoudi, D. B. Moler, H. Li, B. Chen, T. M. Reineke, M. O'Keeffe, O. M. Yaghi, *Acc. Chem. Res.* **2001**, *34*, 319.
[18] T. M. Reineke, M. Eddaoudi, M. Fehr, D. Kelley, O. M. Yaghi, *J. Am. Chem. Soc.* **1999**, *121*, 1651.
[19] S. S.-Y. Chui, S. M.-F. Lo, J. P. H. Charmant, A. G. Orpen, I. D. Williams, *Science* **1999**, *283*, 1148.
[20] P. S. Mukherjee, T. K. Maji, G. Mostafa, T. Mallah, N. Ray Chaudhuri, *Inorg. Chem.* **2000**, *39*, 5147.
[21] P. S. Mukherjee, S. Dalai, G. Mostafa, E. Zangrando, G. Rogez, T. Mallah, N. Ray Chaudhuri, *Chem. Commun.* **2001**, 1346.
[22] P. Charpin, G. Chevrier, M. Lance, D. Vigner, *Acta Crystallogr., Sect. C* **1987**, *43*, 216.
[23] C. E. Xanthopoulos, M. P. Sigalas, G. A. Katsoulos, C. A. Tsipis, A. Terzis, A. Hountas, *Inorg. Chim. Acta* **1993**, *214*, 153.
[24] P. Chaudhuri, K. Oder, K. Wieghardt, S. Gehring, W. Haase, B. Nuber, J. Weiss, *J. Am. Chem. Soc.* **1988**, *110*, 3657.
[25] E. G. Bakalbassis, A. P. Bozopoulos, J. Mrozinski, P. J. Rentzeperis, C. A. Tsipis, *Inorg. Chem.* **1988**, *27*, 529.
[26] E. Bakalbassis, C. Tsipis, A. Bozopoulos, W. Dreissig, H. Hartl, J. Mrozinski, *Inorg. Chim. Acta* **1991**, *186*, 113.
[27] M. Verdaguer, J. Gouteron, S. Jeannin, Y. Jeannin, O. Kahn, *Inorg. Chem.* **1984**, *23*, 4291.
[28] J. Cano, G. De Munno, J. L. Sanz, R. Ruiz, J. Faus, F. Lloret, M. Julve, A. Caneschi, *J. Chem. Soc., Dalton Trans.* **1997**, 1915.
[29] [29a] B. Bleaney, K. D. Bowers, *Proc. R. Soc., London, Ser. A* **1952**, *214*, 415. [29b] O. Kahn, *Molecular Magnetism*, VCH, Heidelberg, **1993**.
[30] G. M. Sheldrick, *SHELXL 97, Program for the Solution of Crystal Structure*, University of Göttingen, Germany, **1997**.
[31] WinGX − A Windows Program for Crystal Structure Analysis: L. J. Farrugia, *J. Appl. Crystallogr.* **1999**, *32*, 837.

Received April 23, 2004
Early View Article
Published Online October 13, 2004

 © 2004 Wiley-VCH Verlag GmbH & Co. KGaA, Weinheim

Synthesis, Molecular Structure, and Olefin Polymerisation Activity of an Oxovanadium(v) Alkoxide with Unprecedented Chloride Bridging Ligands

Esther C. E. Rosenthal,*[a] Huiling Cui,[a] Katharina C. H. Lange,[a] and Sebastian Dechert[b]

Keywords: Chelates / O ligands / Oxo ligands / Polymerisation / Vanadium

The reaction of 2-methoxyethanol or (2-methoxyethanolato)-lithium with $VOCl_3$ yields the chloro-bridged dinuclear complex $[VOCl_2(OCH_2CH_2OCH_3)]_2$, which has been characterised spectroscopically and structurally by single-crystal X-ray diffraction analysis. This is the first reported structure of a neutral dinuclear oxovanadium complex connected by bridging chloro ligands. The orange complex is a precatalyst for the polymerisation of ethene and the oligomerisation of styrene.

(© Wiley-VCH Verlag GmbH & Co. KGaA, 69451 Weinheim, Germany, 2004)

Introduction

Oxovanadium complexes are known to act as catalysts for oxidation[1] and polymerisation reactions, for example.[2,3] As part of our investigations aimed at vanadium-based catalysts our interest is primarily concerned with the synthesis and characterisation of vanadium(v) compounds stabilised by alkoxyalkoxide ligands. While a significant number of oxovanadium(v) alkoxides and aryloxides derived from various alcohols have been synthesised,[4] the majority of (alkoxo- or aryloxo)chloro(oxo)vanadium compounds structurally characterised to date contain vanadium in the oxidation state +4.[5−10] The main feature of these complexes is that the alkoxide or aryloxide ligands predominantly act as bridging groups.[7−13] Monomeric derivatives have been reported with very bulky aryloxo groups,[14] intramolecular donor stabilisation[5,6,9,15] or additional donor ligands.[16−18] As far as we are aware, there are no examples of vanadium alkoxides in which chloro ligands appear as bridging units.

Previously we have reported the reaction of 2-phenoxyethanol with $VOCl_3$, which gives the mononuclear complex $[VOCl_2(OCH_2CH_2OPh)]$ and which is still the only structurally characterised dichlorooxovanadium(v) alkoxide.[19] The presence of the remaining chloro ligands in the complex makes the metal atom functionalisable, for example by the introduction of alkyl groups. Chloro ligands, either in the catalyst or in the co-catalyst, are essential for olefin polymerisation.[3]

Herein we show that in the field of vanadium alkoxides, the variation of substituents on the ligands can have large effects on the complex structure and possibly on their catalytic behaviour.

Results and Discussion

Synthesis and Structure

Bis[(μ-chloro)chloro(η^2-2-methoxyethanolato)oxovanadium(v)] was prepared by two different strategies: HCl elimination and a salt metathesis reaction. The equimolar reaction of $VOCl_3$ with 2-methoxyethanol in *n*-pentane gave the dinuclear vanadium(v) species only in very low yields due to significant quantities of reduction products. Such a reduction process has been observed previously when Hovnanian and co-workers obtained the vanadium(iv) complex $[VOCl\{OCH(CH_3)CH_2OCH_3\}]_2$ from a vanadium(v) starting material.[7] Employing the lithium salt instead of the pure alcohol minimised the amount of reduction. The reaction proceeds smoothly under ambient conditions in hydrocarbon solvents, which were chosen with the intention to obtain intramolecularly stabilised complexes instead of additional solvent coordination.

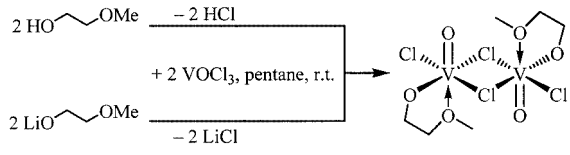

[a] Institut für Chemie, Fakultät II − Mathematik und Naturwissenschaften, Technische Universität Berlin
Sekr. C 2, Straße des 17. Juni 135, 10623 Berlin, Germany
Fax: + 49-30-314-22168
E-mail: rosenthal@chem.tu-berlin.de
[b] Institut für Anorganische Chemie, Georg-August-Universität Göttingen
Tammannstraße 4, 37077 Göttingen, Germany
Fax: + 49-551-393-063
E-mail: Sebastian.Dechert@chemie.uni-goettingen.de

The orange diamagnetic crystalline solid $[VOCl_2(OCH_2CH_2OCH_3)]_2$ slowly decomposes at ambient temperatures both in solution, where it forms blue vanadium(IV), and as a solid, where it forms a black crystalline material. Unfortunately, the black material contained no crystals suitable for X-ray diffraction; it is insoluble in inert solvents like hydrocarbons, dichloromethane or toluene and attempts to recrystallise it from pyridine led to $[VOCl_2(py)_2]$,[20] which was identified by an X-ray structure determination. The title compound can be stored for weeks under an inert gas at −30 °C in the dark without any appreciable decomposition. It dissolves in dichloromethane and toluene and decomposes in water, tetrahydrofuran, diethyl ether, and alcohols. The compound has a ^{51}V NMR chemical shift of $\delta = -259$ ppm in C_6D_6 and $\delta = -262$ ppm in $CDCl_3$. A minor peak is observed at $\delta = -279$ ppm in C_6D_6 and $\delta = -282$ ppm in $CDCl_3$. As a decrease of the coordination number on going, for example, from an octahedral to a tetrahedral arrangement is usually accompanied by an increase of shielding, this signal may be ascribed to the presumably tetrahedral monomer. This chemical shift is also in good agreement with that of other tetrahedrally coordinated dichloro(oxo)vanadium alkoxides in solution.[19,21]

The ^1H and $^{13}C\{^1H\}$ NMR spectra of the title compound show the expected number of signals for the coordinated 2-methoxyethanolato ligand as well as the 1:1 relative intensity proton pattern for the methylene peaks in the ^1H NMR spectrum. The signals at lower field at $\delta \approx 4.6$ ppm in C_6D_6 and $\delta \approx 5.7$ ppm in $CDCl_3$ are due to the $VOCH_2$ protons while those at $\delta \approx 2.8$ ppm in C_6D_6 and $\delta \approx 3.9$ ppm in $CDCl_3$ are assigned to the CH_2OMe methylene protons. The $^{13}C\{^1H\}$ NMR resonance for the carbon atom adjacent to the alcohol moiety shifts approximately 30 ppm downfield upon vanadylation. As for the corresponding proton resonances this shift may be ascribed to the deshielding of this carbon atom due to transfer of electron density to the metal atom. The signals of all other carbon atoms shift very little.

The dimeric nature of the compound is supported by mass spectrometric data, which exhibit no molecular ion but $[VOCl(OCH_2CH_2OCH_3)]_2$, formed by loss of two chlorine atoms and containing two vanadium atoms, as the fragment with the highest molecular mass. The same is true for IR spectroscopy, which indicates both terminal and bridging V−Cl bonds. The intense bands at 464 and 434 cm^{-1} arise from terminal V−Cl and bridging V−Cl stretching vibrations, respectively. The sharp bands at 1028 cm^{-1} in nujol and 1024 cm^{-1} in CS_2, associated with the V=O moiety, are characteristic of $VOCl_2(OR)$ compounds.[9,19,21]

Single crystals of the complex, suitable for X-ray diffraction, were obtained from cold *n*-hexane solutions. An ORTEP drawing of the molecule is shown in Figure 1, and selected bond lengths and angles are given in the caption. The structural analysis revealed the (alkoxyalkoxo)vanadium compound to be a dimer with two bridging chlorine atoms. The two halves of the dimer are related by a centre of inversion. Thus, oxo groups and terminal chlorine atoms adopt an *anti* orientation while the V=O groups are orientated perpendicular and the chlorine atoms coplanar with respect to the bridging plane, which is spanned by the $V_2(\mu\text{-}Cl)_2$ core.[22] Each vanadium atom possesses a distorted octahedral geometry which is similar to that in other hexacoordinate vanadium(V) complexes.[23−25] The vanadium atom is displaced by 0.296(1) Å from the plane formed by the equatorial atoms Cl(1), Cl(2), O(2), and Cl(1′) towards the oxo oxygen atom. It is unusual, and we believe unique, in having the two VO_3Cl_3 octahedra joined by chlorine atoms. Hitherto structurally characterised examples of dimeric chloro(oxo)vanadium complexes containing an $[OV(\mu\text{-}Cl)_2VO]^{n+}$ ($n = 2, 4$) core have only been reported for the purely inorganic vanadium(IV) anions $[\{VOCl_2(OH_2)\}_2(\mu\text{-}Cl)_2]^{2-}$ and $[V_2O_2Cl_6]^{2-}$.[26,27] So far if alkoxo or aryloxo ligands are involved they function as bridging units instead of chlorine atoms.[7−13]

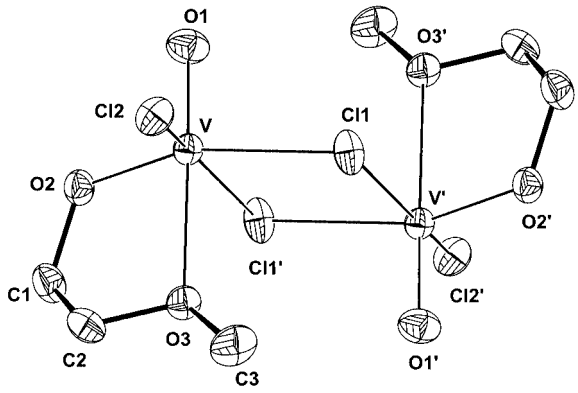

Figure 1. ORTEP view of $[VOCl_2(OCH_2CH_2OMe)]_2$; displacement ellipsoids are drawn at the 50% probability level; hydrogen atoms are omitted for clarity; selected bond lengths [Å] and angles [°]: V−Cl(1) 2.4321(6), V−Cl(1′) 2.4172(6), V−Cl(2) 2.2581(6), V−O(1) 1.5827(16), V−O(2) 1.7697(15), V−O(3) 2.3120(15); Cl(1)−V−Cl(1′) 79.33(2), V−Cl(1)−V′ 100.67(2), Cl(1)−V−O(1) 97.15(7), Cl(1′)−V−O(1) 95.23(6), Cl(2)−V−O(1) 99.40(6), O(1)−V−O(2) 99.08(8), O(1)−V−O(3) 175.88(7)

As in $[\{VOCl_2(OH_2)\}_2(\mu\text{-}Cl)_2]^{2-}$, both vanadium atoms are part of a planar $V_2(\mu\text{-}Cl)_2$ four-membered ring,[26] in which the angles at the vanadium atom are 79.33(2)° and those at μ-Cl are 100.67(2)°. The two chlorine atoms bridge the two vanadium atoms in an almost symmetric fashion: both bonds have approximately the same length [2.4321(6) Å and 2.4172(6) Å for V−Cl(1) and V−Cl(1′), respectively] and are similar to those in the $[V_2O_2Cl_6]^{2-}$ ion.[27] The distances of the vanadium atom to the terminal chlorine atoms are 2.2581(6) Å, which are very similar to those observed for $[\{HB(pz)_3\}VOCl(O\textit{i}Pr)]$[18] and $[VOCl\{OC(CH_3)_2C(CH_3)_2O\}]_2$.[12]

Three different vanadium−oxygen bonds are present. The vanadium−oxo distance is in the normal range for such a bond [V−O(1) = 1.5827(16) Å].[5−15,17−21,23−27] The V−O distance for the alkoxide oxygen atom O(2) is only about 0.2 Å longer, which is in agreement with some degree of π-donation from O(2) to the metal atom and is typical for vanadium alkoxide moieties.[5,9,13,15,17−19,21,23] Owing to the fact that the oxygen atom O(3) of the methoxy group encounters the *trans* influence of the doubly bonded oxygen

 © 2004 Wiley-VCH Verlag GmbH & Co. KGaA, Weinheim

atom O(1), its distance to the vanadium atom is, as expected, the longest [2.3120(15) Å].

In contrast to the monomeric vanadium(v) complex $[VOCl_2(OCH_2CH_2OPh)]$ and the dimeric vanadium(iv) complexes $[VOCl\{OCH(CH_3)CH_2OCH_3\}]_2$ and $[VOCl\{OCH_2(C_4H_7O)\}]_2$, where the aryloxy- and alkoxyalkoxides are pendant or bridging, respectively,[7,8,19] both groups in the compound reported here coordinate directly to a single vanadium centre. Although $[VOCl_2(OCH_2CH_2OPh)]$ was obtained by the corresponding reactions with 2-phenoxyethanol, both dichloro(oxo)vanadium compounds differ completely in their structures.[19] As there are no steric reasons for this phenomenon the origin of this difference is probably due to the lower Lewis basicity of the phenyl ether than the methyl one.

Catalytic Activity

The catalytic activity of the title compound for the polymerisation of styrene, 1-decene, and ethene was examined. Polymerisation studies were conducted employing a polymerisation catalyst prepared by adding the vanadium compound to a toluene solution of methylaluminoxane (MAO) as the co-catalyst. The low molecular masses given in Table 1 show that only oligomers are obtained for styrene with methyl trichloroacetate (MTCA) as promoter. The catalytic activity decreases with rising temperatures and is highest at room temperature, with quantitative conversion of styrene, while the polydispersity (D) has values of around 2.

Under the same conditions the activity for styrene oligomerisation is ten times higher than that for 1-decene conversion and is independent of the nuclearity of the precatalyst employed (Table 2). The molecular mass and polydispersity of styrene oligomers are in the same range as for the mononuclear (M_n = 2700 g/mol, M_w = 4100 g/mol, D = 1.8) and the dinuclear complex (M_n = 3200 g/mol, M_w = 5000 g/mol, D = 1.5).

Table 1. Oligomerisation of styrene with $[VOCl(OCH_2CH_2OCH_3)]_2$[a]

T [°C]	Yield [%]	M_w [g/mol]	M_n [g/mol]	M_w/M_n
20	99.6	2900	1200	2.3
40	85.3	3000	1500	2.0
50	71.1	2700	1600	1.7

[a] Reaction conditions: V catalyst/styrene/MAO/MTCA = 0.01:13:1:1, 20 h; solvent: toluene.

Table 2. Activity (kg per mol vanadium atom per h) of olefin conversions with vanadium(v) compounds[a]

Precatalyst	Styrene	1-Decene
$[VOCl_2(OCH_2CH_2OMe)]_2$	27.7	2.5
$[VOCl_2(OCH_2CH_2OPh)]$	27.9	2.7

[a] Reaction conditions: V catalyst/monomer/MAO/MTCA = 0.01:17:1:1, 90 min at 23 °C; solvent: toluene.

The ethene polymerisation catalysts were prepared by treating the vanadium compound either with MAO or chlorodiethylaluminium as the co-catalyst. The results of ethene polymerisation are shown in Table 3. Even at atmospheric pressure and room temperature the title compound displays a reasonable activity (100 kg PE/mol[V] h) for ethene polymerisation with MTCA as promoter in the presence of MAO; without MTCA the activities are negligible. The conditions have been optimised for MAO to give highest activities at an Al/V ratio of 400 (300 kg PE/mol[V] h bar). Et_2AlCl, with almost double the activity (560 kg PE/mol[V] h bar), is the best co-catalyst for the system, as has been found previously for other vanadium procatalysts.[3] For comparison, under similar conditions, the best result for a catalyst based on $VOCl_3$ was 360 kg PE/mol[V] h bar after activation with Et_2AlCl. In the range investigated the activities drop if the Al/V ratio is lowered. During the polymerisation reaction the catalyst is stable and the activities decrease only after 30 min. GPC analyses showed that the product molecular mass distribution is very broad. With MAO as co-catalyst the system forms polyethene with a higher molecular mass than with Et_2AlCl. The molecular mass distribution of all polymers formed is bimodal.

Table 3. Data for polymerisation of ethene

Entry	Precatalyst	Co-catalyst	$[V]_0$ [a]	[Al]/[V] [n/n]	Activity[a]	10^{-3} M_w [g/mol]	10^{-3} M_n [g/mol]	M_w/M_n
1[b]	$[VOCl_2(OCH_2CH_2OMe)]_2$	MAO	0.2	80	100	954	87	11.0
2[c]	$[VOCl_2(OCH_2CH_2OMe)]_2$	MAO	0.1	100	6	1084	119	9.9
3[c]	$[VOCl_2(OCH_2CH_2OMe)]_2$	MAO	0.02	400	300	1414	168	8.4
4[c]	$[VOCl_2(OCH_2CH_2OMe)]_2$	MAO	0.02	1000	15	1169	155	8.5
5[c]	$VOCl_3$	MAO	0.02	400	3	[d]	[d]	[d]
6[c]	$[VOCl_2(OCH_2CH_2OMe)]_2$	Et_2AlCl	0.1	100	560	586	66	8.9
7[c]	$[VOCl_2(OCH_2CH_2OMe)]_2$	Et_2AlCl	0.1	20	320	696	110	6.3
8[c]	$VOCl_3$	Et_2AlCl	0.1	100	360	390	34	11.4

[a] $[V]_0$ [mmol/L]; activity [kg PE/mol[V] h bar]. [b] Schlenk tube; p(ethene) = 1 bar, 30 min at 22 °C; solvent: toluene. [c] Glass autoclave; p(ethene) = 2 bar, 30 min at 30 °C; solvent: toluene. [d] Entry 5 contained a substantial amount of insoluble material resulting in very poor data detection.

 © 2004 Wiley-VCH Verlag GmbH & Co. KGaA, Weinheim

Conclusion

In summary, the synthesis of $[VOCl_2(OCH_2CH_2OCH_3)]_2$ has resulted in the first dinuclear chloride-bridged oxovanadium alkoxide to be structurally characterised. The two bridging chloro ligands build the sharing edge of two VO_3Cl_3 octahedra, which incorporate a five-membered chelate ring. This structural feature may give rise to altered reactivities as polymerisation catalyst or oxidation reagent compared to mononuclear or alkoxide-bridged oxovanadium sites. The title compound shows catalytic activity in ethene polymerisation and styrene oligomerisation. Further catalytic studies besides polymerisation, including the oxidation properties, as well as comparative synthetic investigations concerning other alkoxyalkoxides are currently underway.

Experimental Section

General Remarks: All experiments were performed under nitrogen using standard Schlenk techniques in dry, oxygen-free solvents. Commercial $VOCl_3$ (Aldrich) was used as received. 2-Methoxyethanol, MTCA and styrene were dried with molecular sieves (4 Å). 1-Decene was distilled from CaH_2 followed by treatment with molecular sieves. The ethene gas (Messer Griesheim, 99.995%) was passed through an Oxiclear gas purifier before being passed into the reactor. The IR spectrum was recorded using a Nicolet Magna IR spectrometer 750. NMR spectra were recorded at ambient temperatures with a Bruker ARX 200 or ARX 400 spectrometer. All chemical shifts are reported in ppm relative to the ^1H and ^{13}C residue of the deuterated solvents. For ^{51}V NMR $VOCl_3/CDCl_3$ (2:1) was used as external standard. The mass spectrum (EI) was obtained using a Varian MAT 311 A instrument. Elemental analyses were performed with a Perkin−Elmer Series II CHNS/O Analyzer 2400. GPC data of styrene oligomers were obtained with a Waters model 150 LC/GPC in THF solvent running at ambient temperature and were calibrated using polystyrene standards. GPC measurements of polyethene samples were carried out by high-temperature GPC at 140 °C, using 1,2,4-trichlorobenzene as solvent and narrow polystyrene standard sample as reference. The measurements were performed with a PL-GPC210 with 4 PL-Gel Mixed A columns, with triple detection: RALLS detector (Precision Detector, PD2040 at 800 nm), H502 viscometer (Viscotek), refractive detector and DM400 datamanager (Viscotek).

$[VOCl_2(OCH_2CH_2OCH_3)]_2$. Method A: $VOCl_3$ (3.0 mL, 32 mmol) was added to a colourless mixture of $HOCH_2CH_2OCH_3$ (2.5 mL, 32 mmol) in *n*-pentane (150 mL). The reaction mixture turned brown immediately and was stirred at room temperature for 1 h. In order to complete the evolution of HCl gas, the mixture was heated in a warm-water bath. The resulting orange solution was concentrated and stored at 0 °C. Orange crystals separated overnight. Yield: 0.82 g (12%). M.p. 65 °C. **Method B:** *n*-Hexane (100 mL) and a 1 M solution of $VOCl_3$ (10 mL, 1.73 g, 10 mmol) in *n*-pentane were added to $LiOCH_2CH_2OCH_3$ (0.83 g, 10 mmol). The reaction mixture was stirred at room temperature for 12 h. The orange solution was decanted from the brown residue and stored at −30 °C. Orange crystals separated. Yield: 0.83 g (39%). IR (KBr, nujol mull): $\tilde{\nu}$ = 1255 m, 1224 m, 1192 m, 1156 w, 1102 s (V−O−C), 1081 vs (C−O), 1028 vs (V=O), 994 vs, 897 vs (C−O−C), 825 s, 629 s (V−OR), 577 w, 464 vs (V−Cl), 434 s (V−Cl−V) cm^{-1}. IR (KBr, CS_2): $\tilde{\nu}$ = 1127 s (V−O−C), 1108 w, 1090 w, 1047 vs (C−O), 1024 vs (V=O), 1001 m, 919 m (C−O−C), 644 w (V−OR), 484 s (V−Cl), 439 m (V−Cl−V) cm^{-1}. ^1H NMR (400 MHz, C_6D_6): δ = 4.61 (br. s, 4 H, VOCH_2), 2.94 (s, 6 H, CH_3), 2.81 (br. s, 4 H, CH_2OMe) ppm. ^1H NMR (400 MHz, $CDCl_3$): δ = 5.71 (t, $^3J_{H,H}$ = 4.5 Hz, 4 H, VOCH_2), 3.86 (t, $^3J_{H,H}$ = 4.5 Hz, 4 H, CH_2OMe), 3.50 (s, 6 H, CH_3) ppm. $^{13}C\{^1H\}$ NMR (100.64 MHz, C_6D_6): δ = 90.6 (VOCH_2), 71.3 (CH_2OMe), 58.8 (CH_3) ppm. $^{13}C\{^1H\}$ NMR (50.32 MHz, $CDCl_3$): δ = 90.7 (VOCH_2), 71.7 (CH_2OMe), 59.2 (CH_3) ppm. ^{51}V NMR (105.19 MHz, C_6D_6): δ = −259 (> 99%), −279 (< 1%) ppm. ^{51}V NMR (105.19 MHz, $CDCl_3$): δ = −262 (> 98%), −282 (< 2%) ppm. MS (70 eV, 150 °C): *m*/*z* (%) = 354 (25) [M^+ − 2 Cl], 319 (5) [M^+ − 3 Cl], 318 (7) [M^+ − 2 Cl − HCl], 279 (11) [M^+ − 2 Cl − $OCH_2CH_2OCH_3$], 274 (10), 217 (39), 45 (100) $[CH_2OCH_3]^+$. $C_6H_{14}Cl_4O_6V_2$ (425.86): calcd. C 16.92, H 3.31; found C 16.93, H 3.49.

X-ray Crystallographic Study: $C_6H_{14}Cl_4O_6V_2$, M = 425.86, orange plate, 0.46 × 0.36 × 0.08 mm, monoclinic, space group $P2_1/n$ (no. 14), a = 6.9487(2), b = 17.6924(5), c = 6.9663(2) Å, β = 117.514(1)°, V = 759.57(4) Å^3, d = 1.862 g/cm^3, T = 173(2) K, Z = 2, μ = 1.944 mm^{-1}, 2.30° < θ < 27.50°, 5617 measured reflections, 1731 independent reflections, R_{int} = 0.0372, $R1$ [$I > 2\sigma(I)$] = 0.0288, $wR2$ (all data) = 0.0688. X-ray data were collected with a Siemens SMART CCD diffractometer (graphite-monochromated Mo-K_α radiation, λ = 0.71073 Å) fitted with an area-detector by use of ω scans. The structure was solved by direct methods using SHELXS-97[28] and refined on F^2 using all reflections with SHELXL-97.[29] All non-hydrogen atoms were refined anisotropically. The hydrogen atoms were placed in calculated positions and assigned an isotropic displacement parameter of 0.08 Å^2. SADABS[30] was used to perform area-detector scaling and absorption corrections (max./min. transmission factors: 0.8911/0.6151). CCDC-232374 contains the supplementary crystallographic data for this paper. These data can be obtained free of charge at www.ccdc.cam.ac.uk/conts/retrieving.html [or from the Cambridge Crystallographic Data Centre, 12 Union Road, Cambridge CB2 1EZ, UK; Fax: + 44-1223-336-033; E-mail: deposit@ccdc.cam.ac.uk].

Polymerisation Studies: Styrene and 1-decene polymerisation reactions were performed in a 50-mL Schlenk flask and an external temperature-controlled bath on a Schlenk line. In a typical procedure, toluene (10 mL) and MAO (2 mmol) were loaded into the Schlenk flask. The vanadium compound (0.05 mmol based on vanadium atoms) was then added as a toluene solution (0.01 M) and the mixture was stirred at room temperature for 5 min. After the external bath temperature had stabilised, MTCA (2 mmol) and the monomer were added with a syringe. The polymerisation was terminated by addition of acidic methanol (MeOH/HCl = 10:1; 3 mL). The product was precipitated into ethanol (200 mL), filtered off, and dried under vacuum. The molecular mass and the molecular mass distribution were determined by GPC. The polymerisation of ethene was carried out either in a Schlenk tube or in a glass autoclave (1 L) equipped with a stirrer. For Schlenk tube polymerisation, toluene (50 mL), MAO (0.8 mmol), $[VOCl_2(OCH_2CH_2OCH_3)]_2$ (5 μmol), and MTCA (0.8 mmol) were stirred for 10 min. Afterwards, ethene was polymerised at room temperature at an ethene pressure of 1 bar. Toluene (200 mL), MAO, and MTCA (MAO/MTCA = 1:1) were injected sequentially into the autoclave at 30 °C, and the mixture stirred for 15 min. The vanadium precatalyst was then injected into the reactor and allowed to interact with MAO for 10 min. In the case of Et_2AlCl the co-catalyst solution was divided into two parts: one half was injected into the autoclave

 © 2004 Wiley-VCH Verlag GmbH & Co. KGaA, Weinheim

together with MTCA (MTCA/$Et_2AlCl \geq 1:1$) and the other half was used to activate the sample of precatalyst solution for 15 min prior to injection into the reactor. The ethene pressure in the autoclave was kept at 2 bar during all polymerisations. Polymerisations were quenched with a 5% solution of HCl in ethanol (150 mL). The mixtures were poured into water (150 mL) and stirred for 30 min. The white precipitate was collected by filtration, washed with ethanol and dried at 60 °C to a constant weight. Molecular masses and polydispersities were determined by GPC.

Acknowledgments

We are grateful to Prof. B. Hessen (University of Groningen) for his help in running the GPCs of polyethene samples. We thank A. Steffens for GPC measurements and interpretation of styrene oligomers. This work was financially supported by the Deutsche Forschungsgemeinschaft (Graduiertenkolleg "Synthetische, mechanistische und reaktionstechnische Aspekte von Metallkatalysatoren").

[1] [1a] T. Hirao, *Chem. Rev.* **1997**, *97*, 2707−2724. [1b] A. G. J. Ligtenbarg, R. Hage, B. L. Feringa, *Coord. Chem. Rev.* **2003**, *237*, 89−101. [1c] C. Bolm, *Coord. Chem. Rev.* **2003**, *237*, 245−256. [1d] T. Hirao, *Coord. Chem. Rev.* **2003**, *237*, 271−279.
[2] C. Janiak, P. G. Lassahn, *J. Mol. Catal. A* **2001**, *166*, 193−209.
[3] H. Hagen, J. Boersma, G. van Koten, *Chem. Soc., Rev.* **2002**, *31*, 357−364.
[4] See for example: [4a] E. M. Page, S. A. Wass, *Encyclopedia of Inorganic Chemistry*, John Wiley & Sons, Chichester, **1994**, vol. 8. [4b] F. A. Cotton, G. Wilkinson, C. A. Murillo, M. Bochmann, *Advanced Inorganic Chemistry*, 6th ed., John Wiley & Sons, New York, **1999**.
[5] D. Wang, M. Ebel, C. Schulzke, C. Grüning, S. K. S. Hazari, D. Rehder, *Eur. J. Inorg. Chem.* **2001**, 935−942.
[6] H. Hagen, A. Barbon, E. E. van Faassen, B. T. G. Lutz, J. Boersma, A. L. Spek, G. van Koten, *Inorg. Chem.* **1999**, *38*, 4079−4086.
[7] G. Foulon, J.-D. Foulon, N. Hovnanian, *Polyhedron* **1993**, *12*, 2507−2511.
[8] Z. Janas, P. Sobota, M. Klimowicz, S. Szafert, K. Szczegot, L. B. Jerzykiewicz, *J. Chem. Soc., Dalton Trans.* **1997**, *20*, 3897−3901.
[9] H. Glas, K. Köhler, E. Herdtweck, P. Maas, M. Spiegler, W. R. Thiel, *Eur. J. Inorg. Chem.* **2001**, 2075−2080.
[10] [10a] K.-H. Thiele, H. Görls, W. Imhof, W. Seidel, *Z. Anorg. Allg. Chem.* **1999**, *625*, 1927−1933. [10b] J. Salta, J. Zubieta, *Inorg. Chim. Acta* **1997**, *257*, 83−88. [10c] S. Kitagawa, M. Munakata, M. Ueda, T. Yonezawa, *Inorg. Chim. Acta* **1990**, *175*, 3−4.
[11] D. C. Crans, R. W. A. Marshman, M. S. Gottlieb, O. P. Anderson, M. M. Miller, *Inorg. Chem.* **1992**, *31*, 4939−4949.
[12] D. C. Crans, R. A. Felty, M. M. Miller, *J. Am. Chem. Soc.* **1991**, *113*, 265−269.
[13] [13a] D. C. Crans, R. A. Felty, O. P. Anderson, M. M. Miller, *Inorg. Chem.* **1993**, *32*, 247−248. [13b] Y. Chang, Q. Chen, M. I. Khan, J. Salta, J. Zubieta, *J. Chem. Soc., Chem. Commun.* **1993**, 1872−1874.
[14] P. J. Toscano, E. J. Schermerhorn, C. Dettelbacher, D. Macherone, J. Zubieta, *J. Chem. Soc., Chem. Commun.* **1991**, 933.
[15] H. Hagen, C. Bezemer, J. Boersma, H. Kooijman, M. Lutz, A. L. Spek, G. van Koten, *Inorg. Chem.* **2000**, *39*, 3970−3977.
[16] A. J. Tasiopoulos, A. N. Troganis, A. Evangelou, C. P. Raptopoulou, A. Terzis, Y. Deligiannakis, T. A. Kabanos, *Chem. Eur. J.* **1999**, *5*, 910−920.
[17] [17a] K. D. Soulti, A. Troganis, A. Papaioannou, T. A. Kabanos, A. D. Keramidis, Y. G. Deligiannakis, C. P. Raptopoulou, A. Terzis, *Inorg. Chem.* **1998**, *37*, 6785−6794. [17b] H. Glas, E. Herdtweck, G. R. J. Artus, W. R. Thiel, *Inorg. Chem.* **1998**, *37*, 3644−3646. [17c] F. Wolff, C. Lorber, R. Choukroun, B. Donnadieu, *Inorg. Chem.* **2003**, *42*, 7839−7845.
[18] C. J. Carrano, M. Mohan, S. M. Holmes, R. de la Rosa, A. Butler, J. M. Charnock, C. D. Garner, *Inorg. Chem.* **1994**, *33*, 646.
[19] E. C. E. Rosenthal, F. Girgsdies, *Z. Anorg. Allg. Chem.* **2002**, *628*, 1917−1920.
[20] A. Hills, D. L. Hughes, G. F. Leigh, R. Prieto-Alcón, *J. Chem. Soc., Dalton Trans.* **1993**, 3609−3617.
[21] W. Priebsch, D. Rehder, *Inorg. Chem.* **1990**, *29*, 3013−3019.
[22] W. Plass, *Angew. Chem.* **1996**, *108*, 699−703; *Angew. Chem. Int. Ed. Engl.* **1996**, *35*, 627−631.
[23] [23a] K. Nakajima, M. Kojima, K. Toriumi, K. Saito, J. Fujita, *Bull. Chem. Soc. Jpn.* **1989**, *62*, 760−767. [23b] R. Fulwood, H. Schmidt, D. Rehder, *J. Chem. Soc., Chem. Commun.* **1995**, 1443−1444. [23c] S. Mondal, S. P. Rath, K. K. Rajak, A. Chakravorty, *Inorg. Chem.* **1998**, *37*, 1713−1719. [23d] S. Mondal, S. P. Rath, S. Dutta, A. Chakravorty, *J. Chem. Soc., Dalton Trans.* **1996**, 99−103.
[24] C. R. Cornman, K. M. Geiser-Bush, J. W. Kampf, *Inorg. Chem.* **1999**, *38*, 4303−4308.
[25] K. K. Rajak, S. Mondal, S. P. Rath, *Polyhedron* **2000**, *19*, 931−936.
[26] W. Priebsch, C. Weidemann, D. Rehder, J. Kopf, *Z. Naturforsch., Teil B* **1986**, *41*, 834−838.
[27] F. A. Cotton, M. W. Extine, L. R. Falvello, D. Beck Lewis, G. E. Lewis, C. A. Murillo, W. Schwotzer, M. Tomas, J. M. Troup, *Inorg. Chem.* **1986**, *25*, 3505−3512.
[28] G. M. Sheldrick, *SHELXS-97*, Universität Göttingen, **1990**.
[29] G. M. Sheldrick, *SHELXL-97*, Universität Göttingen, **1997**.
[30] G. M. Sheldrick, *SADABS*, Universität Göttingen, **1996**.

Received May 28, 2004
Early View Article
Published Online October 14, 2004

 © 2004 Wiley-VCH Verlag GmbH & Co. KGaA, Weinheim

Backbone Flexibility and Counterion Effects on the Structure and Thermal Properties of Di(thiourea)zinc Dicarboxylate Coordination Polymers

Andrew D. Burrows,*[a] Adele S. Donovan,[a] Ross W. Harrington,[a] and Mary F. Mahon[a]

Keywords: Crystal engineering / Coordination polymers / Helical structures / Hydrogen bonds / Zinc

The reaction between $[Zn(tu)_4]Cl_2$ and the appropriate sodium dicarboxylate has been shown to give the coordination polymers $[Zn(tu)_2(\mu\text{-succinate})]_n$ (**7**), $[Zn(tu)_2(\mu\text{-itaconate})]_n$ (**8**), $[Zn(tu)_2(\mu\text{-ethylmalonate})]_n$ (**9**), $[Zn(tu)_2(\mu\text{-1,3-phenylenediacetate})]_n$ (**10**) and $\{[Zn(tu)_2(\mu\text{-mesaconate})]\cdot 2H_2O\}_n$ (**11**), all of which have been crystallographically characterised. The crystal structures of **7**–**9** demonstrate that these compounds form helical structures in which the dicarboxylates adopt conformations with the relative positions of the carboxylate groups similar to those in constrained anions such as phthalate. The role of the chloride counterion in the starting material has been explored by investigating the reactions of $[Zn(tu)_4](NO_3)_2$ with a range of dicarboxylates. Although in the majority of cases the counterion was shown to have no effect, in the case of fumarate, a hydrated coordination polymer $\{[Zn(tu)_2(\mu\text{-fumarate})]\cdot 2H_2O\}_n$ (**12**) was observed in addition to the anhydrous product $[Zn(tu)_2(\mu\text{-fumarate})]_n$ (**1**), which was formed as the sole product from $[Zn(tu)_4]Cl_2$. Thermogravimetric analyses are reported for compounds **1**–**12**. The compounds $\{[Zn(tu)_2(\mu\text{-isophthalate})]\cdot H_2O\}_n$ **3** and **12** lose their included water before 140 °C, whereas the compounds $\{[Zn(tu)_2(\mu\text{-maleate})]\cdot H_2O\}_n$ **6** and **11** only lose their water molecules at higher temperatures with the onset of decomposition. This difference in behaviour can be related to the structural role of the water molecules.

(© Wiley-VCH Verlag GmbH & Co. KGaA, 69451 Weinheim, Germany, 2004)

Introduction

The majority of crystal engineering studies employ one of two strategies to engender structural predictability. Hydrogen bonds, especially in systems involving two or more such interactions between the same molecules or ions, have proved effective in both organic and inorganic systems.[1−3] In the latter, bifunctional ligands containing both coordination sites and hydrogen-bonding faces are used to include metal centres.[4] A number of examples of bifunctional ligands have been reported recently, including bis(imidazolates),[5] amidinoureas[6] and oxalurates.[7] Inorganic crystal engineering has also exploited coordination bonds in the formation of metal-organic frameworks.[8−10] This approach relies on the use of polytopic ligands that are able to bridge between metal centres. Bridging coordination modes are encouraged through rigidity in the ligand, which makes chelation geometrically impossible.

We have been interested in the interplay between the hydrogen bond and coordination bond approaches, and have focussed attention on systems in which both types of aggregation are possible and potentially in competition.[11−13] We recently reported the reactions of $[Zn(tu)_4]Cl_2$ with the appropriate sodium dicarboxylates to give the coordination polymers $[Zn(tu)_2(\mu\text{-fumarate})]_n$ (**1**), $[Zn(tu)_2(\mu\text{-malonate})]_n$ (**2**), $\{[Zn(tu)_2(\mu\text{-isophthalate})]\cdot H_2O\}_n$ (**3**), $[Zn(tu)_2(\mu\text{-phthalate})]_n$ (**4**), $[Zn(tu)_2(\mu\text{-citraconate})]_n$ (**5**) and $\{[Zn(tu)_2(\mu\text{-maleate})]\cdot H_2O\}_n$ (**6**).[14] In all cases, the coordination polymers are interconnected through hydrogen bonds, and these are dominated by interactions involving the thiourea face containing two parallel NH groups. Similar observations on zinc and cadmium dicarboxylates have been reported by Zhang and co-workers.[15−17]

In this paper we extend the reaction between $[Zn(tu)_4]Cl_2$ and dicarboxylate to a further five anions. In three of these − succinate, itaconate and 1,3-phenylenediacetate − there is much greater conformational flexibility due to the inclusion of one or more sp^3-hybridised carbon atoms between the carboxylate groups. Ethylmalonate and mesaconate were chosen to determine the structural effects of alkyl substituents by comparison with the previously reported malonate and fumarate compounds. We report herein the crystal structures of the products $[Zn(tu)_2(\mu\text{-succinate})]_n$ (**7**), $[Zn(tu)_2(\mu\text{-itaconate})]_n$ (**8**), $[Zn(tu)_2(\mu\text{-ethylmalonate})]_n$ (**9**), $[Zn(tu)_2(\mu\text{-1,3-phenylenediacetate})]_n$ (**10**) and $\{[Zn(tu)_2(\mu\text{-mesaconate})]\cdot 2H_2O\}_n$ (**11**), and compare their supramolecular structures with those previously reported for compounds **1**−**6**. The role of the counterion in the starting material has also been explored by investigating the reactions of $[Zn(tu)_4](NO_3)_2$ with a range of dicarboxylates. This has led to the structural characterisation of $\{[Zn(tu)_2(\mu$-

[a] Department of Chemistry, University of Bath, Claverton Down, Bath BA2 7AY, UK
Fax: (internat.) + 44-1225-386231
E-mail: a.d.burrows@bath.ac.uk

Supporting information for this article is available on the WWW under http://www.eurjic.org or from the author.

 © 2004 Wiley-VCH Verlag GmbH & Co. KGaA, Weinheim **DOI: 10.1002/ejic.200400502**

fumarate)]·2H_2O}$_n$ (**12**). The dicarboxylates relevant to this paper are illustrated in Scheme 1.

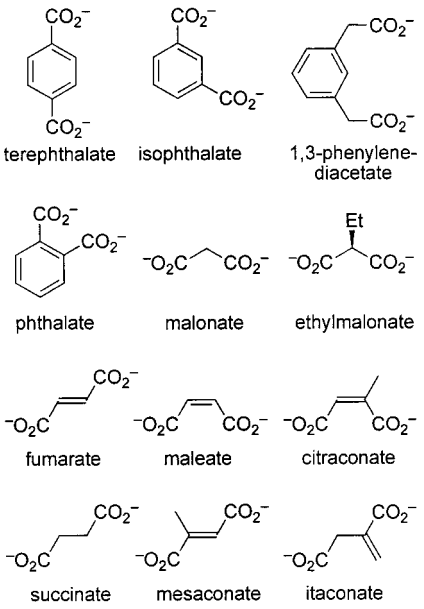

Scheme 1. Dicarboxylates incorporated in compounds **1**−**12** or mentioned in the text

Syntheses of Compounds 7−11

Compounds **7**−**11** were prepared from the reaction between [Zn(tu)$_4$]Cl$_2$ and the appropriate sodium dicarboxylate in water; crystallisation typically occurred over a period of a week. Yields were in the range 51−78%. In each case, crystals suitable for single-crystal analysis were obtained and the representative nature of the single crystals chosen for analyses to the bulk materials were confirmed by comparison of the X-ray powder diffraction pattern with that predicted from the single-crystal data. The compounds were identified as [Zn(tu)$_2$(μ-succinate)]$_n$ (**7**), [Zn(tu)$_2$(μ-itaconate)]$_n$ (**8**), [Zn(tu)$_2$(μ-ethylmalonate)]$_n$ (**9**), [Zn(tu)$_2$(μ-1,3-phenylenediacetate)]$_n$ (**10**) and {[Zn(tu)$_2$(μ-mesaconate)]·2H_2O}$_n$ (**11**). The structures of **7**−**11** are all based on coordination polymers, and the Zn(tu)$_2$ centres are bridged by dicarboxylate ligands. In all cases, the zinc centres adopt distorted tetrahedral coordination geometries. However, variation in the relative orientations of the carboxylate groups within the individual dicarboxylates leads to differences in the conformations of the polymer chains and in the manner in which they interact with each other. Selected bond lengths and angles for compounds **7**−**11** are given in Tables 1 and 2.

Table 2. Selected bond lengths and angles for compound **10**; primed atoms generated by the symmetry transformation $-x$, $y - {}^1/_2$, $-z + {}^1/_2$; double-primed atoms generated by the symmetry transformation $-x + 1$, $y - {}^1/_2$, $-z + {}^1/_2$

Zn(1)−S(1)	2.3268(7)	Zn(2)−S(3)	2.3374(7)
Zn(1)−S(2)	2.3337(7)	Zn(2)−S(4)	2.3047(6)
Zn(1)−O(2)	1.9833(17)	Zn(2)−O(6)	1.9686(17)
Zn(1)−O(4)′	1.9629(17)	Zn(2)−O(8)"	1.9849(18)
S(1)−Zn(1)−S(2)	102.96(2)	S(3)−Zn(2)−S(4)	117.55(2)
S(1)−Zn(1)−O(2)	108.50(5)	S(3)−Zn(2)−O(6)	107.63(5)
S(1)′−Zn(1)−O(4)′	110.56(6)	S(3)−Zn(2)−O(8)"	104.06(5)
S(2)−Zn(1)−O(2)	106.52(5)	S(4)−Zn(2)−O(6)	111.24(5)
S(2)−Zn(1)−O(4)′	132.79(5)	S(4)−Zn(2)−O(8)"	118.60(5)
O(2)−Zn(1)−O(4)′	93.49(7)	O(6)−Zn(2)−O(8)"	95.08(7)
Zn(1)−S(1)−C(12)	107.62(9)	Zn(2)−S(3)−C(23)	108.91(9)
Zn(1)−S(2)−C(11)	114.06(9)	Zn(2)−S(4)−C(24)	110.33(8)

The Structures of [Zn(tu)$_2$(μ-succinate)]$_n$ (7), [Zn(tu)$_2$(μ-itaconate)]$_n$ (8) and [Zn(tu)$_2$(μ-ethylmalonate)]$_n$ (9)

Compounds **7**, **8** and **9** each crystallise in space group $P2_12_12_1$ with lattice parameters within a narrow range. As their structures are broadly similar, they can be treated together. Compounds **7**−**9** all form helical coordination polymers, which propagate along the crystallographic *b* axes. The helices pack in hexagonal arrays, and within each structure, the chains all display the same handedness. In each case, intrachain hydrogen bonding between thiourea NH groups and carboxylate oxygen atoms is observed around the zinc centres. In compounds **7** and **8** there are two hydrogen bonds around each zinc centre, one involving a coordinated oxygen atom and the other involving an uncoordi-

Table 1. Selected bond lengths and angles for compounds **7**, **8**, **9**, **11** and **12**

	7[a]	**8**[b]	**9**[c]	**11**	**12**
Zn(1)−S(1)	2.3054(13)	2.3249(15)	2.313(2)	2.3329(12)	2.3322(12)
Zn(1)−S(2)	2.3269(14)	2.2948(15)	2.352(2)	2.3196(12)	2.3452(13)
Zn(1)−O(1)	1.999(3)	2.008(3)	1.985(5)	1.987(3)	1.980(3)
Zn(1)−O(3)	2.001(3)	1.999(4)	1.993(5)	2.002(3)	1.963(3)
S(1)−Zn(1)−S(2)	117.49(6)	119.51(6)	117.15(11)	117.68(5)	106.26(5)
S(1)−Zn(1)−O(1)	112.02(10)	119.58(11)	115.71(16)	104.36(10)	108.32(10)
S(1)−Zn(1)−O(3)	104.66(12)	103.49(10)	109.20(17)	107.64(10)	113.74(11)
S(2)−Zn(1)−O(1)	117.60(11)	108.21(11)	102.90(17)	105.83(10)	103.33(11)
S(2)−Zn(1)−O(3)	106.60(10)	108.25(11)	94.57(16)	116.74(11)	107.97(10)
O(1)−Zn(1)−O(3)	94.67(14)	93.79(15)	115.6(3)	102.73(13)	116.26(14)
Zn(1)−S(1)−C(1)	109.73(17)	107.95(19)	105.6(3)	109.84(16)	108.26(17)
Zn(1)−S(2)−C(2)	107.0(2)	108.14(19)	110.5(3)	109.20(17)	106.7(2)

[a] O(1) generated by the symmetry transformation $-x + 1$, $y + {}^1/_2$, $-z + {}^1/_2$. [b] O(3) generated by the symmetry transformation $-x + 1$, $y + {}^1/_2$, $-z + {}^3/_2$. [c] O(1) generated by the symmetry transformation $-x + 1$, $y - {}^1/_2$, $-z + {}^1/_2$.

 © 2004 Wiley-VCH Verlag GmbH & Co. KGaA, Weinheim

nated oxygen atom. These hydrogen bonds give rise to S(6) and S(8) motifs, respectively, using graph set notation[18] (Figure 1). In both cases, the hydrogen bond leading to the six-membered ring involves the shorter N···O distance. The two Zn−S distances differ significantly (Table 1); the bond length involving the sulfur atom of the S(6) ring is longer than that of the S(8) ring. In compound **9**, there are also two hydrogen bonds present around each zinc centre, although in this case, both involve coordinated oxygen atoms as acceptors and consequently both result in the formation of S(6) rings.

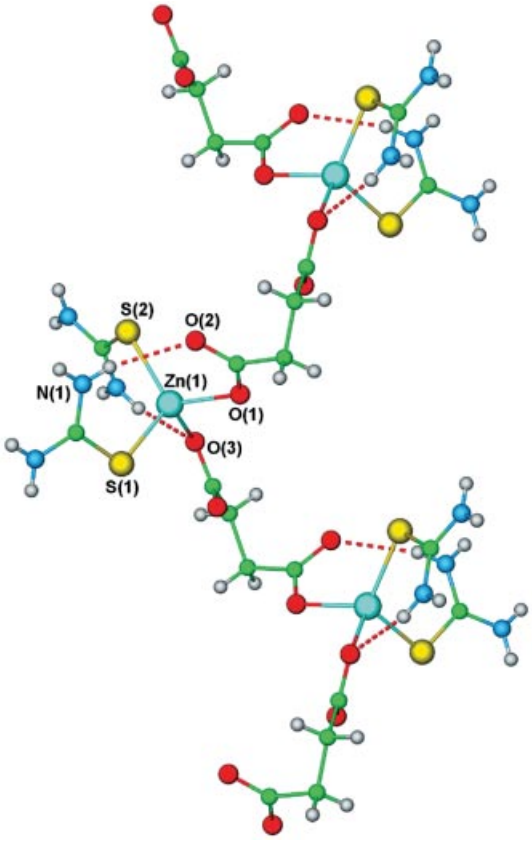

Figure 1. Intrachain hydrogen bonding in $[Zn(tu)_2(\mu\text{-succinate})]_n$ (**7**); selected hydrogen-bond lengths (Å) and angles (°) N(1)···O(2) 3.149, H(1B)···O(2) 2.33, N(1)−H(1B)···O(2) 161; and N(3)···O(3) 2.870, H(3B)···O(3) 2.20, N(3)−H(3B)···O(3) 165

In the helices, the Zn···Zn···Zn angles lie in a narrow range spanning 93° to 101°, and the Zn···Zn distances are 7.36 Å for **7**, 7.62 Å for **8** and 7.40 Å for **9**. Surprisingly the closest Zn···Zn distance occurs in the succinate compound **7** rather than its ethylmalonate analogue **9**, which has one less carbon atom between the carboxylate groups.

Further similarities between the three structures are evident with respect to the manner in which the helices interact together. In **7** and **8** the interactions are identical, occurring in two directions, corresponding to the crystallographic *a* and *c* axes. In each direction there are three independent hydrogen bonds, two of these involving the parallel NH groups on a thiourea ligand. A DD−AA interaction involving two hydrogen bonds between the parallel NH groups and two oxygen atoms generates $R_2^2(11)$ rings in the *a* direction (Figure 2). The two hydrogen-bond acceptors lie on the same dicarboxylate; one is coordinated and the other is uncoordinated. A further hydrogen bond involving an uncoordinated oxygen atom on a second dicarboxylate, generating a second $R_2^2(11)$ ring, completes the hydrogen bonding in this direction. The hydrogen bonding in the *c* direction is somewhat different as a single uncoordinated oxygen atom acts as acceptor to the two parallel NH groups, generating a $R_2^1(6)$ ring, although one of these interactions is relatively long in **7**. The final hydrogen bond in this direction involves a coordinated oxygen atom of a second dicarboxylate as acceptor, and generates a $R_2^2(11)$ ring motif. In each case, the hydrogen bonding is reciprocal along the crystallographic *a* axis, whereby each chain acts as a hydrogen-bond donor *and* acceptor to each adjacent chain, whereas along the crystallographic *c* axis the chains act as either hydrogen-bond donors *or* acceptors to each adjacent chain.

The interactions in **9** are broadly similar to those in **7** and **8**, although there are subtle differences. In the *a* direction, the acceptors for the parallel NH groups are both uncoordinated, generating a $R_2^2(10)$ motif, whereas the third hydrogen bond is to a coordinated oxygen atom leading to a $R_2^2(12)$ ring. In the *c* direction the $R_2^1(6)$ motif observed for **7** and **8** is not present, as the comparative oxygen atom acts as acceptor to only one NH group, while the parallel NH group forms a weak bifurcated hydrogen bond with both a sulfur atom and a second uncoordinated oxygen atom on a separate ethylmalonate. The third hydrogen bond is to a coordinated oxygen atom in a third ethylmalonate, and leads to the formation of a $R_2^2(10)$ motif.

The similarities in the hydrogen bonding within these three compounds can be related to the angle between the carboxylate group planes and the distance between the hydrogen-bond acceptors, which are similar for the three compounds. The angle θ between the carboxylate groups is 87° for **7**, 87° for **8** and 88° for **9**, whereas the distance between the oxygen atoms involved in the $R_2^2(10)$ or $R_2^2(11)$ motifs is 3.28 Å for **7**, 3.45 Å for **8** and 3.18 Å for **9**.

The structures adopted by compounds **7**−**9** possess a number of features in common with those previously reported for $[Zn(tu)_2(\mu\text{-phthalate})]_n$ (**4**) and $[Zn(tu)_2(\mu\text{-citraconate})]_n$ (**5**).[14] All of these compounds form helical coordination polymers, which are interlinked by hydrogen bonding in two directions. This is a reflection of the equivalent relative arrangements of the carboxylate within each anion. In **4** and **5**, the carboxylate orientations are determined by the presence of the double bond or benzene ring, and by the steric interactions that prevent co-planarity of the functionalities. In **7**−**9**, the observed carboxylate arrangements are similar to those in **4** and **5**, but in these cases are not dictated by the ligand geometry. Succinate, itaconate and ethylmalonate all contain one or two sp^3-hybridised carbon atoms between the carboxylates, and therefore have the potential of adopting a range of conformations. A search of the Cambridge Structural Database[19] reveals that of the 211 independent $O_2CCH_2CH_2CO_2$ units, 141 (67%) adopt

 © 2004 Wiley-VCH Verlag GmbH & Co. KGaA, Weinheim

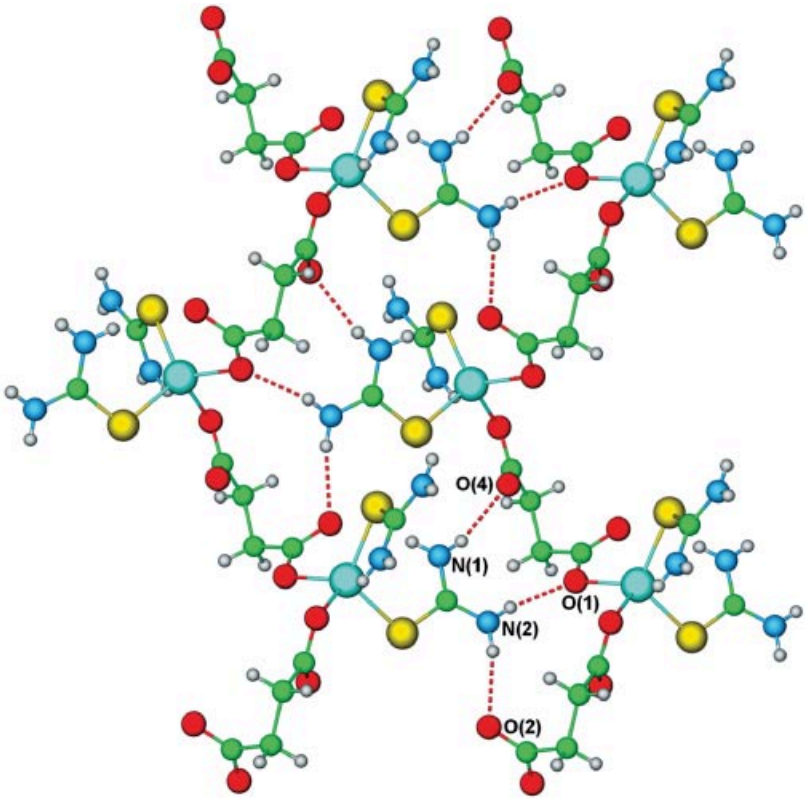

Figure 2. Interchain hydrogen bonding in $[Zn(tu)_2(\mu\text{-succinate})]_n$ (**7**) along the crystallographic *a* axis; selected hydrogen-bond lengths (Å) and angles (°) N(1)···O(4) 3.021, H(1A)···O(4) 2.19, N(1)−H(1A)···O(4) 162; N(2)···O(1) 2.944, H(2A)···O(1) 2.10, N(2)−H(2A)···O(1) 166; and N(2)···O(2) 3.051, H(2B)···O(2) 2.20, N(2)−H(2B)···O(2) 168

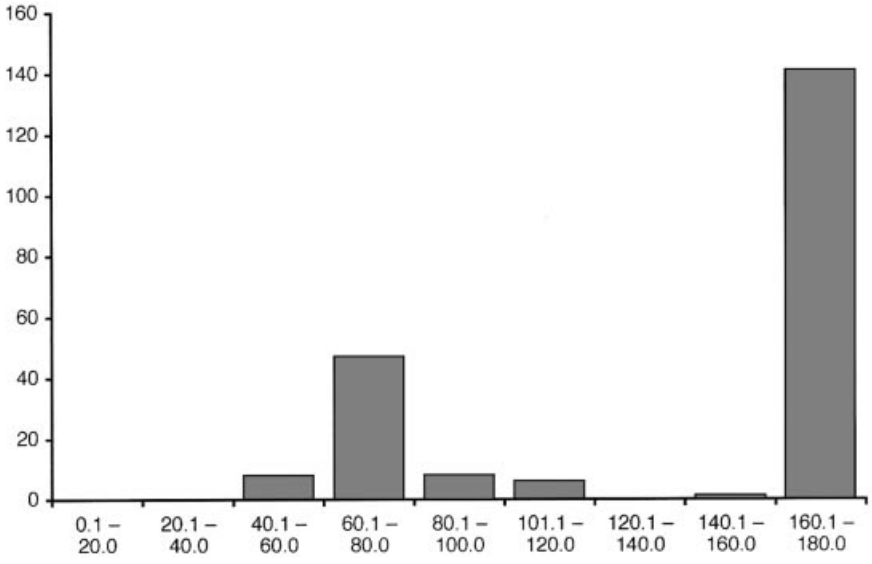

Figure 3. Distribution of CCCC torsion angles in compounds containing the $O_2CCH_2CH_2CO_2$ fragment

an *anti* conformation, with a CCCC torsion angle greater than 160° (Figure 3). In this conformation the O···O distances are all greater than 4.4 Å. In over half of the cases with an O···O distance less than 3.5 Å, this is a direct result of chelation. The observation of helical structures for **7**−**9**, similar to those for **4** and **5**, suggests that this arrangement is driven by the formation of the interhelix hydrogen bonds. The cadmium analogue of **7** has also been reported, and it too has a similar helical structure despite the inclusion of water in the lattice.[20]

The ethylmalonate compound **9** has a very different supramolecular structure to the malonate analogue $[Zn(tu)_2(\mu\text{-malonate})]_n$ (**2**).[14] These differences can be related to the different conformations adopted by the dicar-

 © 2004 Wiley-VCH Verlag GmbH & Co. KGaA, Weinheim

boxylates (Figure 4). The steric bulk of the ethyl group and the consequent unfavourable interchain interactions would appear to be the major factor that disfavours **9** from adopting a similar conformation to that observed in **2**.

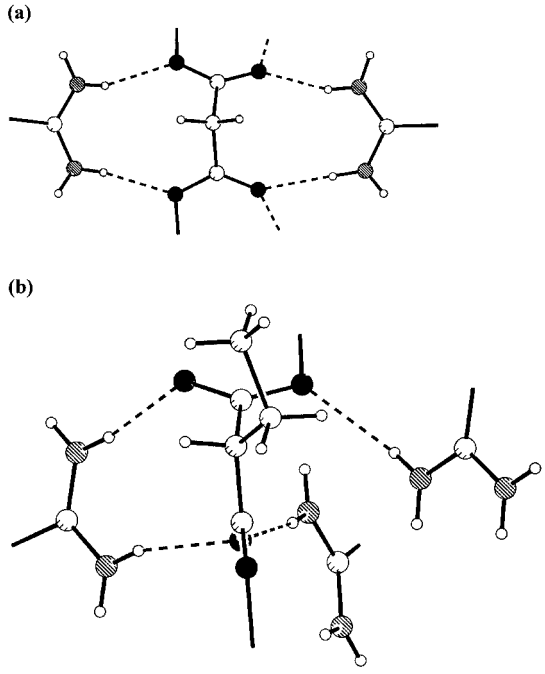

Figure 4. Conformations of and hydrogen bonds to (a) the malonate ligand in **5** and (b) the ethylmalonate ligand in **9**

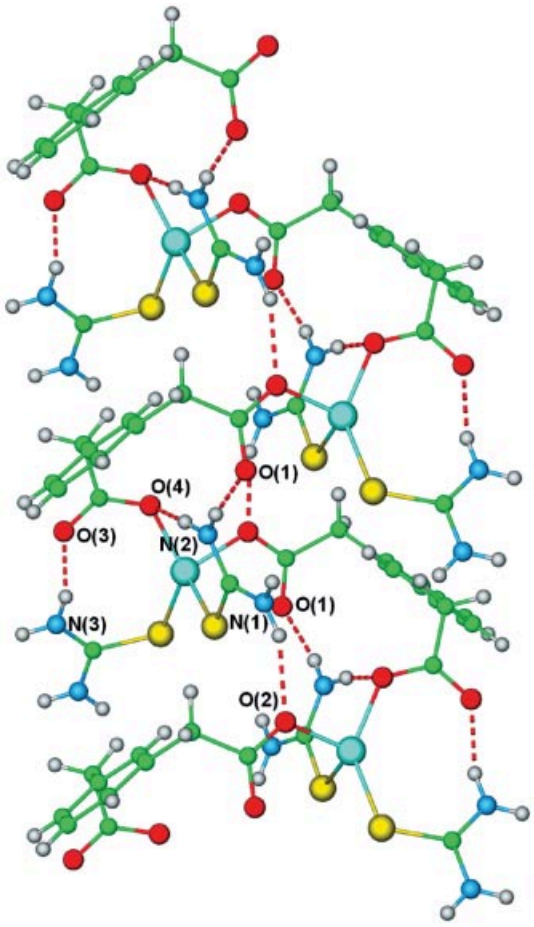

Figure 5. Intrachain hydrogen bonding in one of the independent chains in $[Zn(tu)_2(\mu\text{-}1,3\text{-phenylenediacetate})]_n$ (**10**); selected hydrogen-bond lengths (Å) and angles (°) N(1)···O(2) 2.943, H(1B)···O(2) 2.12, N(1)−H(1B)···O(2) 156; N(2)···O(1) 2.954, H(2A)···O(1) 2.08, N(2)−H(2A)···O(1) 173; N(2)···O(4) 3.011, H(2B)···O(4) 2.17, N(2)−H(2B)···O(4) 160; and N(3)···O(3) 2.756, H(3B)···O(3) 1.90, N(3)−H(3B)···O(3) 163

The Structure of $[Zn(tu)_2(\mu\text{-}1,3\text{-phenylenediacetate})]_n$ (10)

There are two independent helices in the structure of compound **10**, each containing only one of the two crystallographically independent zinc atoms, Zn(1) and Zn(2). Both helical chains contain two intrachain hydrogen bonds between the thiourea NH groups and carboxylate oxygen atoms around each of the zinc centres. These hydrogen bonds involve coordinated and uncoordinated oxygen atoms as acceptors, and give rise to S(6) and S(8) motifs, respectively. This intrachain hydrogen bonding is similar to that observed in **7** and **8**. The length and flexibility of the 1,3-phenylenediacetate ligand allows for additional intrachain hydrogen bonding to more remote thiourea groups. Thus, in each of the independent helices there are two further hydrogen bonds, involving the formation of S(14) and S(16) rings, respectively (Figure 5). One consequence of this additional hydrogen bonding is the increased tightness of the helices, which is reflected in the Zn···Zn···Zn angles, which are 72° and 74° for the two independent polymer chains (93° to 101° for **7**−**9**). The Zn···Zn distances are 6.80 and 6.92 Å for the two chains, shorter than those in **7**−**9**, and clearly illustrate the effect of the intrachain hydrogen bonding. This becomes more apparent when comparing the chains in **10** with those observed in $[Zn\{SC(NHMe)(NH_2)\}_2(\mu\text{-}1,3\text{-phenylenediacetate})]_n$,[21] as in this latter compound, substitution of a hydrogen atom for a methyl group prevents the extended intrachain hydrogen bonding from occurring. Consequently, the Zn···Zn separation is much larger (11.6 Å).

In **10**, the helices are packed in a square-based array rather than in a hexagonal array as observed for **7**−**9**. Each helix interacts, through hydrogen bonds, with helices in the *a* and *ac* directions. In both of these directions there are two hydrogen bonds from parallel NH groups to a single uncoordinated carboxylate oxygen atom, generating $R_2^1(6)$ rings, in addition to one further hydrogen bond, also to an uncoordinated oxygen atom (Figure 6). The hydrogen bonds in both directions link the Zn(1)-based chains to the Zn(2)-based chains. The presence of $R_2^1(6)$ rings with one hydrogen-bond acceptor to the parallel NH groups, as opposed to $R_2^2(n)$ rings with two oxygen atoms acting as acceptors, relates to the distance between oxygen atoms within each dicarboxylate ligand. This O···O distance ranges from 3.18 to 3.45 Å for **7**−**9** but is much longer (5.23 Å) for **10** as a consequence of the greater length of the linker between the carboxylate groups.

 © 2004 Wiley-VCH Verlag GmbH & Co. KGaA, Weinheim

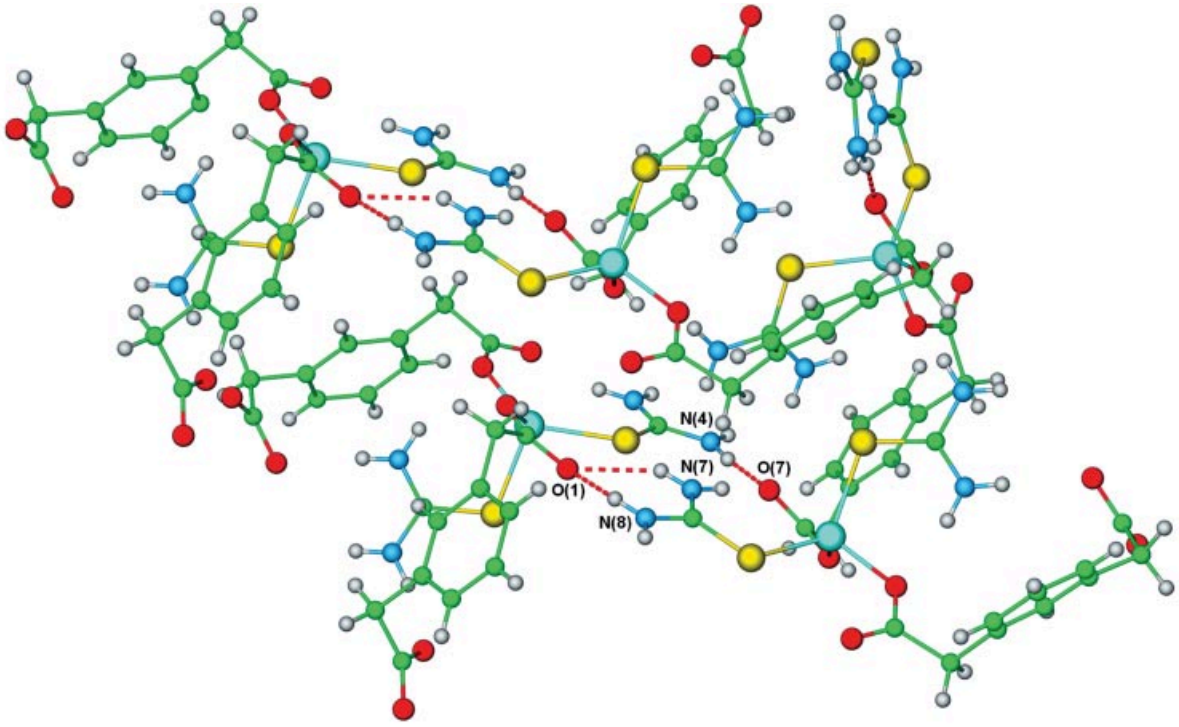

Figure 6. Interchain hydrogen bonding in $[Zn(tu)_2(\mu\text{-}1,3\text{-phenylenediacetate})]_n$ (**10**) along the crystallographic *a* axis; selected hydrogen-bond lengths (Å) and angles (°) N(4)···O(7) 2.935, H(4B)···O(7) 2.06, N(4)−H(4B)···O(7) 173; N(7)···O(1) 2.956, H(7A)···O(1) 2.19, N(7)−H(7A)···O(1) 145; and N(8)···O(1) 2.953, H(8A)···O(1) 2.19, N(8)−H(8A)···O(1) 145

The Structure of $\{[Zn(tu)_2(\mu\text{-mesaconate})]\cdot 2H_2O\}_n$ (11)

In contrast to compounds **7**−**10**, $[Zn(tu)_2(\mu\text{-mesaconate})]_n$ crystallises with two molecules of water per metal centre. Mesaconate has a *trans* arrangement of the carboxylate groups around the central double bond, and consequently the anion is flat. This means that the chains observed in $\{[Zn(tu)_2(\mu\text{-mesaconate})]\cdot 2H_2O\}_n$ (**11**) are not helices, but flat zig-zag chains with a Zn···Zn···Zn angle of 107° and Zn···Zn separations of 8.94 and 9.33 Å. Intrachain hydrogen bonding is observed, and both thiourea ligands are involved in S(6) rings. Only one of the acceptors is an oxygen atom, the other being a sulfur atom (Figure 7). The N−H···S hydrogen bond is, as expected, longer than the N−H···O hydrogen bond, and the Zn−S distance to the sulfur atom involved in the hydrogen bond is the shorter of the two Zn−S distances (Table 1).

Hydrogen bonds involving the two amino protons on a single amino group and an uncoordinated oxygen atom link the chains into a three-dimensional network through the formation of $R_4^2(8)$ rings. All other NH groups are involved in hydrogen bonds with the included water molecules with the exception of N(2)−H(2A), which is involved in a weak N−H···S interaction. The water oxygen atom O(5) acts as a linker between the chains along the crystallographic *b* direction, whereas the water oxygen atom O(6) fulfils the same role along the crystallographic *a* direction.

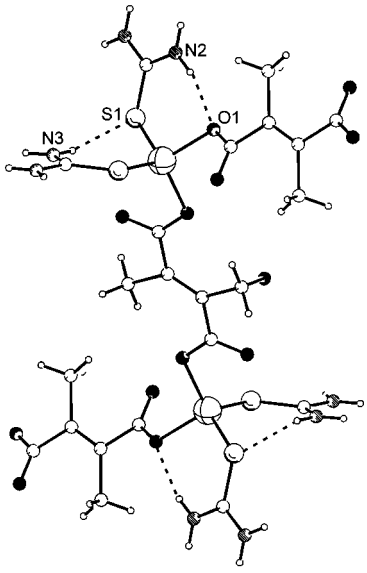

Figure 7. Intrachain hydrogen bonding in $\{[Zn(tu)_2(\mu\text{-mesaconate})]\cdot 2H_2O\}_n$ (**11**); selected hydrogen-bond lengths (Å) and angles (°) N(2)···O(1) 2.916, H(2B)···O(1) 2.06, N(2)−H(2B)···O(1) 163; N(3)···S(1) 3.409, H(3B)···S(1) 2.57, N(3)−H(3B)···S(1) 161; disordered methyl groups are shown in both available positions

Reactions of $[Zn(tu)_4](NO_3)_2$ with Dicarboxylates

The reaction of $[Zn(tu)_4](NO_3)_2$ with a dicarboxylate might be expected to give the same product as that from the reaction of $[Zn(tu)_4]Cl_2$ with the same dicarboxylate. After all, neither chloride nor nitrate is incorporated into the product. Attempts to prepare **1** with $[Zn(tu)_4](NO_3)_2$ suggested that things might not be this simple, and therefore the reactions between $[Zn(tu)_4](NO_3)_2$ and the series of dicarboxylates in Scheme 1 were explored. In the majority

 © 2004 Wiley-VCH Verlag GmbH & Co. KGaA, Weinheim

of cases, X-ray powder diffraction studies did indeed verify that the products derived from $[Zn(tu)_4]Cl_2$ and $[Zn(tu)_4](NO_3)_2$ were identical. However, there were two exceptions. The reaction of $[Zn(tu)_4](NO_3)_2$ with terephthalate had previously been reported to give $\{[Zn_2(tu)_2(\mu\text{-tu})(\mu\text{-terephthalate})_2]\cdot 4H_2O\}_n$.[22] In contrast, the analogous reaction with $[Zn(tu)_4]Cl_2$ gave $[Zn(OH_2)_2(\mu\text{-terephthalate})]_n$[23] as the only isolated product. The identity of this compound was confirmed by comparison of the powder X-ray diffraction pattern with that simulated from the single-crystal data. No evidence for thiourea-containing polymers was obtained for this reaction, which is surprising as coordination polymers containing the substituted thioureas $MeNHC(S)NH_2$ and MeNHC(S)NHMe have been prepared in good yield and structurally characterised.[21]

The reaction of $[Zn(tu)_4]Cl_2$ with sodium fumarate was previously reported to give $[Zn(tu)_2(\mu\text{-fumarate})]_n$ (**1**),[14] and this reaction was repeated to confirm **1** as the only product by X-ray powder diffraction. In contrast, the reaction of $[Zn(tu)_4](NO_3)_2$ with sodium fumarate was shown by powder diffraction to give two compounds, **1** and a previously unobserved material. Crystals of the new compound were manually separated from those of **1**, and a single-crystal analysis showed this material to be the hydrated compound $\{[Zn(tu)_2(\mu\text{-fumarate})]\cdot 2H_2O\}_n$ (**12**). Although the reaction with $[Zn(tu)_4]Cl_2$ does not give **12** under normal circumstances, **12** can be isolated as the major product from the reaction by seeding the solution of $[Zn(tu)_4]Cl_2$ and sodium fumarate with small crystals of **12**.

The Structure of $\{[Zn(tu)_2(\mu\text{-fumarate})]\cdot 2H_2O\}_n$ (12)

Like mesaconate, fumarate has a *trans* orientation around the central double bond, and as such the two carboxylate groups are co-planar. Consequently, the coordination polymers formed are flat zig-zag chains as in **11** rather than the helical chains observed for **7**−**10**. There are two intrachain hydrogen bonds around each zinc centre, both involving coordinated oxygen atoms and leading to the formation of S(6) rings (Figure 8). The chains are cross-linked into the three-dimensional structure by three N−H···O hydrogen bonds to carboxylate oxygen atoms and by other interactions involving the included water molecules. Two of the N−H···O hydrogen bonds are to the same acceptor − an uncoordinated oxygen atom − and lead to the generation of an $R_2^1(6)$ motif.

There are a number of key differences in the structures of **1** and **12** brought about by the inclusion of the solvent. The most obvious of these relates to the carboxylate coordination modes (Figure 9). In **1**, the fumarate coordinates in an *anti* coordination mode, which enables it to use the two parallel lone pairs to form DD−AA interactions. This coordination mode is unusual for a carboxylate group, and has not been observed in any other $[Zn(tu)_2(\mu\text{-dicarboxylate})]_n$ structure. In **12**, the carboxylate groups coordinate in the more common manner through *syn* lone pairs. This difference between **1** and **12** affects the distance be-

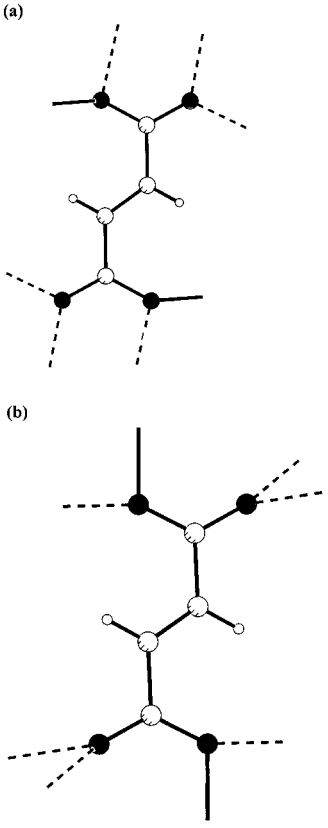

Figure 9. Coordination modes of and hydrogen bonding to the fumarate anions in (a) $[Zn(tu)_2(\mu\text{-fumarate})]_n$ (**1**) and (b) $\{[Zn(tu)_2(\mu\text{-fumarate})]\cdot H_2O\}_n$ (**12**)

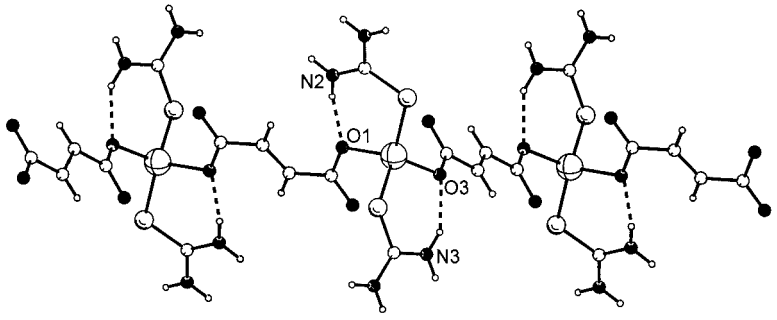

Figure 8. Intrachain hydrogen bonding in $\{[Zn(tu)_2(\mu\text{-fumarate})]\cdot 2H_2O\}_n$ (**12**); selected hydrogen-bond lengths (Å) and angles (°) N(2)···O(1) 2.821, H(2B)···O(1) 1.96, N(2)−H(2B)···O(1) 167; and N(3)···O(3) 2.906, H(3B)···O(3) 2.12, N(1)−H(3B)···O(3) 148

 © 2004 Wiley-VCH Verlag GmbH & Co. KGaA, Weinheim

tween Zn centres within the chain and leads to an increase in the Zn···Zn distance from 6.33 Å in **1** to 8.89 and 9.33 Å in **12**. The less favourable coordination mode in **1** is presumably driven by the accompanying DD−AA interactions allowed between the thiourea and carboxylate groups.

The intrachain hydrogen bonds in **1** and **12** also differ. In **1**, sulfur atoms act as acceptors, whereas this role is fulfilled by oxygen atoms in **12**. Both the differing coordination modes of the fumarate and the presence of the water molecules in **12** ensure that the supramolecular structures of **1** and **12** are completely different.

Thermogravimetric Analyses

The presence of the water molecules in compounds **3**, **6**, **11** and **12** begged the question of whether these included molecules could be removed without destruction of the metal-organic frameworks. Consequently, thermogravimetric analyses (TGAs) were carried out on the compounds. The TGA of {[Zn(tu)$_2$(μ-isophthalate)]·H$_2$O} (**3**) showed no mass loss up to 100 °C, followed by a mass loss of 4.5% between 100 °C and 140 °C. This mass loss corresponds to the loss of the water molecule (calcd. 4.51%). The anhydrous material was stable to further mass loss up until 200 °C, at which temperature decomposition started. The anhydrous material **3a** was generated in larger quantities by heating **3** at 150 °C for several hours. Compound **3a** no longer consisted of single crystals, and the X-ray powder diffraction pattern suggested a more fundamental change had occurred than the simple removal of water from the pores within the structure. Compound **3a** does not absorb atmospheric moisture, but can be reconverted into **3** by dissolution in water and reprecipitation. Attempts to prepare other solvates were unsuccessful.

The TGA of {[Zn(tu)$_2$(μ-maleate)]·H$_2$O} (**6**) showed no mass loss until 150 °C. A gradual loss of mass until 270 °C was then observed, followed by more rapid mass loss on destruction of the framework. Water comprises 5.1% of **6**, although a mass less than this had been lost up to 270 °C. The TGA of {[Zn(tu)$_2$(μ-mesaconate)]·2H$_2$O} (**11**) showed no mass loss until 120 °C and only a gradual loss of 2% until the start of decomposition of the framework at 250 °C. The TGA of {[Zn(tu)$_2$(μ-fumarate)]·2H$_2$O} (**12**) revealed a mass loss between 50 and 120 °C corresponding to the elimination of the included water molecules. The resulting anhydrous product was then stable up to 220 °C, after which it began to lose mass again. This second mass loss corresponds to the destruction of the metal-organic framework. The X-ray powder diffraction pattern of **12** changed markedly on solvent loss and is different from that of **1**.

These results imply a different structural role for the water molecules in **3** and **12** relative to that in **6** and **11**. The higher temperature at the onset of mass loss, combined with the absence of a clearly defined anhydrous compound for **6** and **11**, suggest that the water is an integral part of the supramolecular structure. This is consistent with the structural data that show the water as being part of the hydrogen-bonding networks in **6** and **11**. In contrast, water loss occurs at lower temperatures for **3** and **12**, and the anhydrous compounds are stable over a wide temperature range. This indicates that the water molecules play a less important structural role in these compounds. This is certainly true for **3**, in which the water molecules are disordered and lie within pores in the structure. In **12**, the water molecules lie within channels along the crystallographic 111 direction. The majority of the hydrogen bonding involves O−H···O and O−H···S interactions, which suggests that these water molecules are less well-bound than those in **11**, as confirmed by the TGA experiments.

TGA on the anhydrous compounds **1**, **4**−**5** and **7**−**10** showed no significant mass loss until the onset of decomposition of the framework between 180 °C and 230 °C. In contrast, [Zn(tu)$_2$(μ-malonate)]$_n$ **2** lost 9.5% of mass between 80 °C and 200 °C. This corresponds to a mass of 30, and it is difficult to rationalise such a mass loss at the current time.

Conclusions

The crystal structures for compounds **7**−**9** provide good evidence that the structures based on helical polymers interlinked by hydrogen bonding, previously observed for [Zn(tu)$_2$(μ-citraconate)]$_n$ and [Zn(tu)$_2$(μ-phthalate)]$_n$, represent recurrent motifs. This is a favourable product for cases in which the dicarboxylate can adopt an orientation with mutually perpendicular carboxylate planes, and O···O separations between 3 and 3.5 Å. The crystal structure for **12** is surprising as it demonstrates that the [Zn(tu)$_4$]X$_2$ anion, despite not being incorporated into the final product, plays a role in determining the nature of the product. The chloride compound exclusively gives [Zn(tu)$_2$(μ-fumarate)]$_n$ (**1**), whereas the nitrate analogue gives both **1** and {[Zn(tu)$_2$(μ-fumarate)]·H$_2$O}$_n$ (**12**). The chloride anion has a greater coordinating nature than the nitrate anion, and the previous observation of compounds such as [ZnCl$_2${SC(NHMe)(NMe$_2$)}$_2$] from the reaction of [Zn{SC(NHMe)(NMe$_2$)}$_4$]Cl$_2$ and a dicarboxylate,[24] suggests that the reactive species in solution from [Zn(tu)$_4$]Cl$_2$ may be [ZnCl$_2$(tu)$_2$] rather than [Zn(tu)$_4$]$^{2+}$. It is possible that this affects the solution concentration of intermediates such as [Zn(tu)$_2$(dicarboxylate)$_2$]$^{2-}$, which in turn may influence the crystallisation route adopted. However, no evidence for the intermediates was observed by NMR spectroscopy, and therefore such inferences should be regarded as speculative at this stage.

Experimental Section

General Remarks: Microanalyses (C, H and N) were carried out by Mr. Alan Carver (University of Bath Microanalytical Service). Infrared spectra were recorded with a Nicolet Nexus FT-IR spectrometer as KBr pellets, and thermogravimetric analyses were carried out with a Perkin−Elmer TGA 7 instrument. [Zn(tu)$_4$]Cl$_2$,[25] [Zn(tu)$_4$](NO$_3$)$_2$[26] and compounds **1**−**6**[14] were prepared as described in the literature. Sodium dicarboxylates were prepared by

 © 2004 Wiley-VCH Verlag GmbH & Co. KGaA, Weinheim

reaction of the appropriate dicarboxylic acid with either sodium hydroxide or sodium hydrogen carbonate.

Synthesis of [Zn(tu)$_2$(μ-succinate)]$_n$ (7): An aqueous solution of sodium succinate (0.037 g, 0.23 mmol) was added to an aqueous solution of [Zn(tu)$_4$]Cl$_2$ (0.10 g, 0.23 mmol), with no discernible change. After several days a colourless crystalline precipitate was observed, which was separated by filtration. Yield 0.059 g (78%). $C_6H_{12}N_4O_4S_2Zn$ (333.7): calcd. C 21.6, H 3.62, N 16.8; found C 21.6, H 3.63, N 17.0. IR: $\tilde{\nu}$ = ν(NH) 3454 s; ν(CO$_2$)/δ(NH$_2$) 1658 s, 1584 s, 1504 s cm^{-1}.

Compounds **8**−**11** were prepared in an analogous manner to **1** with [Zn(tu)$_4$]Cl$_2$ (0.10 g, 0.23 mmol) and one equivalent of the appropriate sodium dicarboxylate.

[Zn(tu)$_2$(μ-itaconate)]$_n$ (8): Yield 0.053 g (68%). $C_7H_{12}N_4O_4S_2Zn$ (345.7): calcd. C 24.3, H 3.50, N 16.2; found C 24.2, H 3.48, N 16.1. IR: $\tilde{\nu}$ = ν(NH) 3447 s, 3368 s, 3321 s, 3208 s (br); ν(CO$_2$)/δ(NH$_2$) 1644 s, 1577 m, 1511 s, 1384 m cm^{-1}.

[Zn(tu)$_2$(μ-ethylmalonate)]$_n$ (9): Yield 0.057 g (72%). $C_7H_{14}N_4O_4S_2Zn$ (347.7): calcd. C 24.2, H 4.06, N 16.1; found C 24.1, H 3.99, N 16.0. IR: $\tilde{\nu}$ = ν(NH) 3408 s (br), 3327 s (br), 3195 s (br); ν(CO$_2$)/δ(NH) 1637 s, 1584 s (br), 1358 m cm^{-1}.

[Zn(tu)$_2$(μ-1,3-phenylenediacetate)]$_n$ (10): Yield 0.049 g (53%). $C_{12}H_{16}N_4O_4S_2Zn$ (409.8): calcd. C 35.2, H 3.94, N 13.7; found C 35.1, H 3.90, N 13.5. IR: $\tilde{\nu}$ = ν(NH) 3311 s (br), 3197 s (br); ν(CO$_2$)/δ(NH$_2$) 1659 s, 1640 s, 1563 s, 1511 s, 1370 s (br) cm^{-1}.

{[Zn(tu)$_2$(μ-mesaconate)]·2H$_2$O}$_n$ (11): Yield 0.059 g (76%). $C_7H_{12}N_4O_4S_2Zn$ (345.7): calcd. C 24.3, H 3.50, N 16.2; found C 21.6, H 3.63, N 17.0. IR: $\tilde{\nu}$ = ν(NH) 3394 s (br), 3142 s (br); ν(CO$_2$)/δ(NH$_2$) 1644 s, 1557 s, 1511 s, 1438 s, 1345 m cm^{-1}.

Synthesis of {[Zn(tu)$_2$(μ-fumarate)]·2H$_2$O}$_n$ (12): An aqueous solution of sodium fumarate (0.032 g, 0.20 mmol) was added an aqueous solution of [Zn(tu)$_4$](NO$_3$)$_2$ (0.100 g, 0.20 mmol), with no discernible change. After several hours a colourless crystalline precipitate was observed, which was separated by filtration. Yield 0.058 g (78%). $C_6H_{10}N_4O_4S_2Zn$ (331.7): calcd. C 19.6, H 3.81, N 15.2; found C 19.6, H 3.52, N 15.1. IR: $\tilde{\nu}$ = ν(NH)/OH 3421 s, 3374 s, 3301 s, 3182 s, 3135 s; ν(CO$_2$)/δ(NH$_2$) 1624 s, 1565 d, 1511 s, 1371 s (br) cm^{-1}.

Single crystals of compounds **7**−**12** suitable for X-ray analysis were obtained by repeating the reactions on a smaller scale in a more dilute solution, allowing the crystals to grow over several days. Compounds **2**−**11** were also prepared from [Zn(tu)$_4$](NO$_3$)$_2$, and their identities confirmed by X-ray powder diffraction studies.

Crystallography: Single crystals of the compounds **7**, **8**, **9** and **11** were analysed with an Enraf−Nonius CAD4 diffractometer, while data for **10** and **12** were collected with a Nonius KappaCCD diffractometer. Graphite-monochromated Mo-K_α radiation was employed throughout. Details of the data collections, solutions and refinements are given in Table 3. The structures were solved using SHELXS-97[27] and refined using SHELXL-97.[28] Absorption corrections (semi-empirical from equivalent reflections) were applied to data for **10** and **12**. (Max./min. transmission factors 0.82, 0.62 and 1.000, 0.890, respectively). Hydrogen atoms were universally included at calculated positions except in solvent water molecules, where they were located in the penultimate difference Fourier electron-density maps and restrained at 0.89 Å from the relevant parent oxygen. Convergence was routine throughout, with the exception of the observations below.

Positional disorder (65:35) was observed in the ethyl group of the ethylmalonate ligand in **9**. In the final least-squares refinement, the ADPs for the alpha carbon partial atoms [C(6), C(6A)] were restrained to be similar, while those for C(7) and C(7A) were constrained to be identical. The asymmetric unit in **10** was seen to be based on two independent zinc centres.

The asymmetric unit in **11** contained two solvent water molecules for each zinc centre. The metal is sulfur-bound to two thiourea units and oxygen-bound to two crystallographically independent anion halves. The proximity of the anion halves to inversion centres means that the single methyl group contained in each is disordered in a 1:1 ratio between the two available positions for its location. The water hydrogen atoms on O(6) could not be reliably located, and hence were omitted from the refinement. The asymmetric unit for **12** closely parallels that for **11** insofar as it contains two solvent water molecules for each zinc centre. The coordination sphere around the metal is similar, and also consists of two anion halves

Table 3. Crystallographic information for compounds **7**−**12**

	7	**8**	**9**	**10**	**11**	**12**
Empirical formula	$C_6H_{12}N_4O_4S_2Zn$	$C_7H_{12}N_4O_4S_2Zn$	$C_7H_{14}N_4O_4S_2Zn$	$C_{24}H_{32}N_8O_8S_4Zn_2$	$C_7H_{15}N_4O_6S_2Zn$	$C_6H_{14}N_4O_6S_2Zn$
M	333.69	345.70	347.71	819.56	380.72	367.70
Crystal system	orthorhombic	orthorhombic	orthorhombic	monoclinic	triclinic	triclinic
Space group	$P2_12_12_1$	$P2_12_12_1$	$P2_12_12_1$	$P2_1/c$	$P\bar{1}$	$P\bar{1}$
a (Å)	8.3080(10)	8.327(2)	8.331(2)	18.8080(3)	7.1377(6)	7.7910(2)
b (Å)	11.2380(10)	11.742(2)	10.778(2)	8.1800(1)	8.616(1)	8.5230(2)
c (Å)	13.5350(10)	13.396(4)	15.209(6)	21.2960(4)	12.658(5)	10.9450(2)
a (°)	90	90	90	90	102.42(1)	91.105(1)
β (°)	90	90	90	98.197(1)	91.176(9)	102.602(1)
γ (°)	90	90	90	90	92.661(8)	97.949(1)
V (Å^3)	1263.7(2)	1309.7(5)	1365.6(7)	3242.91(9)	759.0(3)	701.53(3)
Z	4	4	4	4	2	2
μ (mm^{-1})	2.282	2.205	2.115	1.796	1.920	2.074
Reflections collected	1330	1264	1296	32037	2973	2852
Independent reflections	1288	1110	1209	7406	2652	2819
R(int.)	0.0105	0.0094	0.0076	0.0671	0.0131	0.0238
*R*1, *wR*2 [$I > 2\sigma(I)$]	0.0391, 0.0971	0.0277, 0.0735	0.0488, 0.1243	0.0348, 0.0723	0.0424, 0.1118	0.0464, 0.1247
R indices (all data)	0.0421, 0.0988	0.0332, 0.0764	0.0523, 0.1271	0.0533, 0.0794	0.0432, 0.1121	0.0467, 0.1248

 © 2004 Wiley-VCH Verlag GmbH & Co. KGaA, Weinheim

proximate to crystallographic inversion centres in addition to a pair of thiourea ligands. The hydrogen atoms in the water molecule based on O(5) in this structure could not be reliably located and were omitted from the refinement.

CCDC-241267 to -241272 for compounds **7**−**12** contains the supplementary crystallographic data for this paper. These data can be obtained free of charge at www.ccdc.cam.ac.uk/conts/retrieving.html [or from the Cambridge Crystallographic Data Centre, 12 Union Road, Cambridge CB2 1EZ, UK; Fax: +44-1223-336-033; E-mail: deposit@ccdc.cam.ac.uk].

Supporting Information: Figures showing the interchain hydrogen bonding in compounds **7**, **11** and **12** are available (see also footnote on the first page of this article).

Acknowledgments

The EPSRC is thanked for financial support.

[1] A. D. Burrows, *Struct. Bond.* **2004**, *108*, 55−95.
[2] T. Steiner, *Angew. Chem. Int. Ed.* **2002**, *41*, 48−76.
[3] C. B. Aakeröy, A. M. Beatty, *Aust. J. Chem.* **2001**, *54*, 409−421.
[4] A. D. Burrows, C.-W. Chan, M. M. Chowdhry, J. E. McGrady, D. M. P. Mingos, *Chem. Soc., Rev.* **1995**, *24*, 329−339.
[5] M. Tadokoro, H. Kanno, T. Kitajima, H. Shimada-Umemoto, N. Nakanishi, K. Isobe, K. Nakasuji, *Proc. Natl. Acad. Sci. USA* **2002**, *99*, 4950−4955.
[6] U. Suksangpanya, A. J. Blake, P. Hubberstey, C. Wilson, *CrystEngComm* **2002**, *4*, 638−643.
[7] L. R. Falvello, R. Garde, M. Tomás, *Inorg. Chem.* **2002**, *41*, 4599−4604.
[8] S. L. James, *Chem. Soc., Rev.* **2003**, *32*, 276−288.
[9] C. Janiak, *Dalton Trans.* **2003**, 2781−2804.
[10] R. Robson, *J. Chem. Soc., Dalton Trans.* **2000**, 3735−3744.
[11] A. D. Burrows, R. W. Harrington, M. F. Mahon, S. J. Teat, *Eur. J. Inorg. Chem.* **2003**, 766−776.
[12] J. E. V. Babb, A. D. Burrows, R. W. Harrington, M. F. Mahon, *Polyhedron* **2003**, *22*, 673−686.
[13] A. D. Burrows, R. W. Harrington, M. F. Mahon, S. J. Teat, *Cryst. Growth Des.* **2004**, *4*, 813−822.
[14] A. D. Burrows, R. W. Harrington, M. F. Mahon, C. E. Price, *J. Chem. Soc., Dalton Trans.* **2000**, 3845−3854.
[15] Y. Zhang, J. Li, J. Chen, Q. Su, W. Deng, M. Nishiura, T. Imamoto, X. Wu, Q. Wang, *Inorg. Chem.* **2000**, *39*, 2330−2336.
[16] Y. Zhang, J. Li, M. Nishiura, H. Hou, W. Deng, T. Imamoto, *J. Chem. Soc., Dalton Trans.* **2000**, 293−297.
[17] Y. Ke, J. Li, Y. Zhang, *Cryst. Res. Technol.* **2002**, *37*, 501−508.
[18] J. Bernstein, R. E. Davis, L. Shimoni, N.-L. Chang, *Angew. Chem. Int. Ed. Engl.* **1995**, *34*, 1555−1573.
[19] D. A. Fletcher, R. F. McMeeking, D. Parkin, *J. Chem. Inf. Comput. Sci.* **1996**, *36*, 746−749.
[20] Y. Zhang, J. Li, M. Nishiura, W. Deng, T. Imamoto, *Chem. Lett.* **1999**, 1287−1288.
[21] N. J. Burke, A. D. Burrows, A. S. Donovan, R. W. Harrington, M. F. Mahon, C. E. Price, *Dalton Trans.* **2003**, 3840−3849.
[22] A. D. Burrows, S. Menzer, D. M. P. Mingos, A. J. P. White, D. J. Williams, *J. Chem. Soc., Dalton Trans.* **1997**, 4237−4240.
[23] G. Guilera, J. W. Steed, *Chem. Commun.* **1999**, 1563−1564.
[24] A. D. Burrows, R. W. Harrington, M. F. Mahon, unpublished results.
[25] S. J. Ashcroft, *J. Chem. Soc., A* **1970**, 1020−1024.
[26] R. Vega, A. López-Castro, R. Márguez, *Acta Crystallogr., Sect. B* **1978**, *34*, 2297−2299.
[27] G. M. Sheldrick, *Acta Crystallogr., Sect. A* **1990**, *46*, 467−473.
[28] G. M. Sheldrick, *SHELXL-97, Computer Program for Crystal Structure Refinement*, University of Göttingen, **1997**.

Received June 10, 2004
Early View Article
Published Online October 14, 2004

 © 2004 Wiley-VCH Verlag GmbH & Co. KGaA, Weinheim

Synthesis and Structural Characterisation of Ag^{I} Complexes with *N*,*N*′-Bis(2-pyridyl)oxalamide and the Anion of *N*-(2-Pyridyl)oxalamic Acid

Hui-Ling Hu,[a] Chun-Wei Yeh,[b] and Jhy-Der Chen*[b]

Keywords: Silver / Coordination polymer / *N*-(2-Pyridyl)oxalamic acid / *N*,*N*-Bis(2-pyridyl)oxalamide

A series of silver(I) complexes of the type $\{[Ag_2(\mathbf{L})_2(\mathbf{L}')][X]\}_\infty$ [**L** = *N*,*N*′-bis(2-pyridyl)oxalamide; **L**′ = anion of *N*-(2-pyridyl)-oxalamic acid; X = BF_4^- (**1**), ClO_4^- (**2**), PF_6^- (**3**) and NO_3^- (**4**)] have been prepared from the reaction of AgX with **L** in $EtOH/H_2O$. All the complexes have been structurally characterised by X-ray crystallography confirming that complexes **1**–**4** are 2D coordination polymers. The Ag^{I} centres show two types of coordination geometries, i.e. distorted trigonal-bipyramidal and distorted tetrahedral which are linked by the **L** and **L**′ ligands, forming unique 2D doubly pleated rectangular grids. The anions BF_4^-, ClO_4^- and PF_6^- in complexes **1**–**3** are not coordinated to the Ag^{I} centres whereas the NO_3^- anions in **4** are coordinated to the metal centres through one of the three oxygen atoms. The transformation of **L** to **L**′ is also discussed.

(© Wiley-VCH Verlag GmbH & Co. KGaA, 69451 Weinheim, Germany, 2004)

Introduction

Recently, a great deal of effort has been devoted to the self-assembly of organic and inorganic molecules in the solid state because it extends the range of new solids which can be designed to have particular physical and chemical properties.[1,2] The range and variety of self-assembling inorganic structures that can be constructed relies on the presence of suitable metal−ligand interactions and supramolecular contacts, i.e., hydrogen bonds and other weak interactions.[3] Many topologically promising Ag^{I}-containing architectures have been constructed with bidentate building blocks containing nitrogen donors.[4] The polymers include 1D, 2D and 3D network structures.[4b]

In our continuing work on the preparation of complexes with new structural types,[5] we have reported[5b] a series of 1D coordination polymers, $\{[Ag(\mathbf{L})][NO_3]\}_\infty$, $\{[Ag(\mathbf{L})(CH_3CN)][ClO_4]\}_\infty$, $\{[Ag_2(\mathbf{L})_3(CH_3CN)_2][PF_6]_2\}_\infty$ and $[Ag_3(\mathbf{L})_4(CH_3CN)_4][BF_4]_3$ which were prepared by the reaction between AgX (X = NO_3^-, ClO_4^-, PF_6^- and BF_4^-) and the bidentate ligand *N*,*N*′-bis(2-pyridyl)oxalamide (**L**) in CH_3CN.

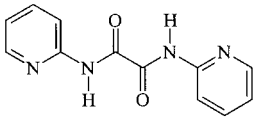

L

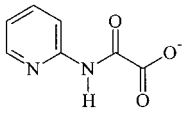

L'

[a] Department of Chemical Engineering, Nanya Institute of Technology,
Chung-Li, Taiwan, R.O.C.
[b] Department of Chemistry, Chung-Yuan Christian University, Chung-Li, Taiwan, R. O. C.

These complexes are capable of self-assembling into 2D molecular structures through a series of interactions involving Ag−O weak covalent bonds and self-complementary double N−H···O hydrogen bonds.[5b] It was also found that changing the counterion had a drastic effect on the structures of the Ag^{I} coordination polymers. Interestingly, when the reactions were carried out in $EtOH/H_2O$, transformation of the **L** ligand to the anion of *N*-(2-pyridyl)oxalamic acid (**L**′) was observed and the Ag^{I} ions were interlinked by both of the **L** and **L**′ ligands forming unique 2D doubly pleated rectangular grids. The syntheses and structural characterisation of complexes of the type $\{[Ag_2(\mathbf{L})_2(\mathbf{L}')][X]\}_\infty$ [**L** = *N*,*N*′-bis(2-pyridyl)oxalamide]; **L**′ = anion of *N*-(2-pyridyl)oxalamic acid; X = BF_4^-, ClO_4^-, PF_6^- and NO_3^-) form the subject of this report.

Results and Discussions

Syntheses

Complexes of the type $\{[Ag_2(\mathbf{L})_2(\mathbf{L}')][X]\}_\infty$ [**L** = *N*,*N*′-bis(2-pyridyl)oxalamide; **L**′ = anion of *N*-(2-pyridyl)oxalamic acid; X = BF_4^- (**1**), ClO_4^- (**2**), PF_6^- (**3**) and NO_3^- (**4**)] have been prepared by the reaction of AgX with **L** in $EtOH/H_2O$. The IR spectra show broad bands in the range from 3160 to 3184 cm^{-1} for complexes **1**−**4**, assignable to the N−H stretching vibrations. Two strong absorption bands at 1702 and 1685 cm^{-1} were observed for each of the complexes **1**−**4** which can be assigned to the C=O stretching of **L**′ and **L**, respectively. For complexes **1**−**4**, the IR spectra also exhibit strong bands at 1593−1595 cm^{-1} due

 © 2004 Wiley-VCH Verlag GmbH & Co. KGaA, Weinheim **DOI: 10.1002/ejic.200400101**

to the $\nu_{as}(COO^-)$ mode in addition to the other strong bands at 1304−1305 cm^{-1} associated with the $\nu_s(COO^-)$ mode which are consistent with the coordination of the carboxylate groups in these complexes. The formation of the carboxylate groups indicates the transformation of **L** to **L′** which was verified by their X-ray crystallographic structures.

The yields of the products were fully dependent on the length of time of crystallisation. Attempts to shorten the time by stirring or heating the reactants to reflux always led to the formation of a mixture of several compounds which, due to their insolubilities in common solvents, could not be separated. Preparation of the four complexes using solutions of **L** and **L′** in nonaqueous media in a 1:1 ratio is one of our research projects currently under investigation. Instead of **L′**, we have attempted several reactions using ligands such as **L** and nicotinic acid (Hnic) in CH_3OH or ethanol solution, but only a mixture of Ag(nic) and Ag(**L**)(X) was obtained.

Differential scanning calorimetry (DSC) experiments of complexes **1**−**4** show endothermic peaks in the curves and the values of the melting temperatures (T_m) for complexes **1**−**4** are 216.21, 215.65, 214.88 and 215.78 °C, respectively. These results indicate that the stabilities of the network structures of complexes **1**−**4** are similar and are not dependent one the nature of the anions.

Structures of Complexes 1−4

The crystal structures of complexes **1**−**4** belong to the space group *Pnma*. A representative asymmetric unit and ORTEP diagrams showing the geometries of Ag(1) and Ag(2) in complexes **1**−**3** are depicted in Figure 1 (a, b, and c, respectively), while the asymmetric unit and ORTEP diagram showing the geometry about Ag(2) in complex **4** are shown in Figure 2 (a and b, respectively). The geometry about Ag(1) in complex **4** is shown in Figure 2 (b). Tables 1 and 2 list the bond lengths and angles around Ag(1) and Ag(2), respectively, for complexes **1**−**4**. Two types of coordination geometries are observed for the metal centres. The Ag(1) atom which is coordinated by two pyridyl nitrogen atoms of different **L** ligands, one pyridyl nitrogen atom of **L′** and one carboxylate oxygen atom and one carbonyl oxygen atom of the same **L′** is distorted trigonal-bipyramidal. The Ag(2) atom which is coordinated by two pyridyl nitrogen atoms of different **L** ligands and the two carboxylate oxygen atoms of the **L′** ligand is distorted tetrahedral. The structural difference between complexes **1**−**3** and **4** is that the anions in **1**−**3** link the metal centres through weak interactions while the NO_3^- anion in complex **4** coordinates to the metal centre through its oxygen atom [Ag(2)−O(6): 2.494(8) Å]. It can be seen form Tables 1 and 2 that the Ag−N distances to the Ag(1) atoms are all similar, while that to the Ag(2) atom in complex **4**, which is 2.432(4) Å, is significantly longer than those in the other three complexes. The Ag(1)−O distances to the carbonyl oxygen atoms of the **L′** ligand are all longer than those to the carboxylate oxygen atoms, while the Ag(2)−O distances in complexes **1**−**3** are all similar. The bond angles around the Ag(1) centres are normal for a distorted trigonal-bipyramidal geometry. Due to the chelation of the aceto group of the **L′** ligand, the O−Ag(2)−O angles for complexes **1**−**3** are 51.8(2), 51.6(3) and 52.05(19)°, respectively, while the other O−Ag−N and N−Ag−N angles are in the range from 103.0(2) to 127.0(2)°.

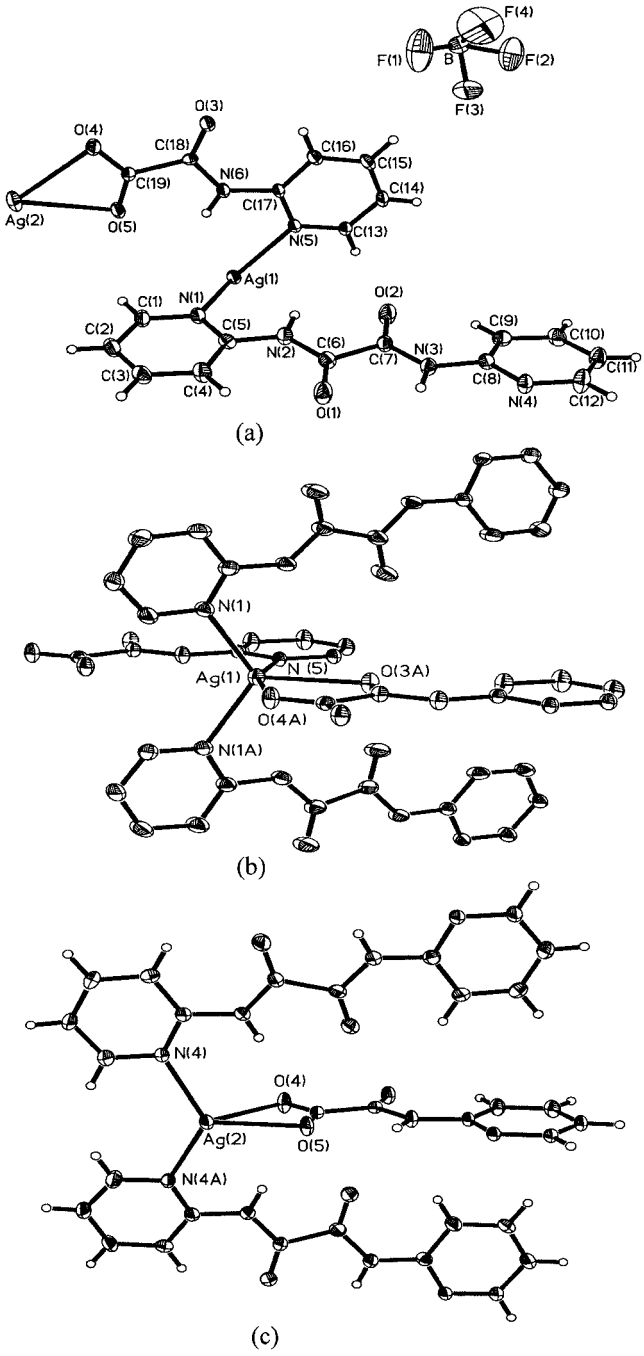

Figure 1. (a) Representative asymmetric unit of the cation in **1**−**3**; (b) ORTEP diagram showing the arrangement around Ag(1); (c) ORTEP diagram showing the arrangement around Ag(2)

The most remarkable feature of complexes **1**−**4** is that they are coordination polymers of $[Ag_2(\mathbf{L})_2(\mathbf{L}')][X]$, forming 2D doubly pleated rectangular grids (Figure 3, bot-

 © 2004 Wiley-VCH Verlag GmbH & Co. KGaA, Weinheim

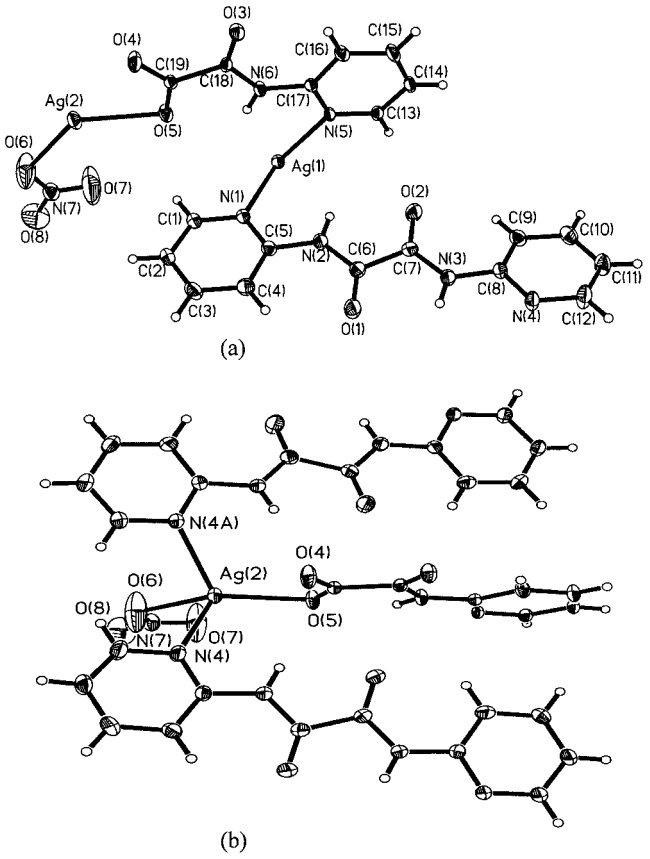

Figure 2. (a) Asymmetric unit of **4**; (b) ORTEP diagram showing the arrangement around Ag(2)

Table 1. Bond lengths [Å] and angles [°] around the Ag(1) centres for complexes **1**−**4**

	1	**2**	**3**	**4**
Distances:				
Ag(1)−N(5)	2.329(6)	2.327(9)	2.301(6)	2.372(4)
Ag(1)−N(1)	2.406(5)	2.410(6)	2.454(5)	2.394(3)
Ag(1)−O(3A)	2.524(6)	2.542(8)	2.551(6)	2.509(4)
Ag(1)−O(4A)	2.384(6)	2.379(8)	2.360(6)	2.415(4)
Angles:				
N(5)−Ag(1)−N(1)	105.85(14)	104.53(19)	104.03(13)	105.62(9)
N(5)−Ag(1)−O(4A)	158.2(2)	158.8(3)	159.6(2)	158.39(15)
N(5)−Ag(1)−O(3A)	89.8(2)	90.2(3)	91.4(2)	89.52(13)
N(1)−Ag(1)−O(3A)	114.50(14)	115.25(17)	114.70(12)	119.78(16)
N(1)−Ag(1)−N(1B)	120.6(2)	120.6(3)	121.5(2)	
O(4A)−Ag(1)−O(3A)	68.4(2)	68.5(3)	68.15(19)	68.86(13)
N(1)−Ag(1)−O(4B)				84.59(10)
N(1)−Ag(1)−O(4B)				89.59(10)
O(4A)−Ag(1)−N(1)	84.27(15)	85.5(2)	85.45(14)	

Symmetry transformations used to generate equivalent atoms: A: x, $-y + 1/2$, z; B: x, y, $z + 1$.

tom, for complexes **1**−**3**, while that of **4** is shown in Figure 4). The 2D doubly-pleated-grid structure can be regarded as interweaving of concavo-convex chains involving **L** ligands and zigzag chains involving **L′** ligands, as shown in Figure 3, top and center, respectively. The **L** ligand coordinates to the metal centres in a bidentate fashion through

Table 2. Bond lengths [Å] and angles [°] around the Ag(2) centres in complexes **1**−**4**

	1	**2**	**3**	**4**
Distances:				
Ag(2)−O(4)	2.535(6)	2.552(8)	2.495(6)	2.723
Ag(2)−O(5)	2.480(6)	2.463(8)	2.522(6)	2.428(4)
Ag(2)−O(6)				2.494(8)
Ag(2)−N(4C)	2.301(5)	2.300(7)	2.285(5)	2.432(4)
Angles:				
N(4C)−Ag(2)−N(4D)	124.7(2)	123.4(3)	127.0(2)	116.96(17)
N(4C)−Ag(2)−O(4)	104.50(15)	103.0(2)	108.50(13)	
N(4C)−Ag(2)−O(5)	117.52(12)	117.83(16)	116.29(12)	
O(5)−Ag(2)−O(4)	51.8(2)	51.6(3)	52.05(19)	128.5(2)
N(4C)−Ag(2)−O(6)				87.44(13)
O(5)−Ag(2)−N(4C)				115.83(8)
O(5)−Ag(2)−N(6)				128.5(2)

Symmetry transformations used to generate equivalent atoms: C: $-x$, $-y$, $-z + 2$; D: $-x$, $y + 1/2$, $-z + 2$.

the two pyridyl nitrogen atoms, while the **L′** ligand chelates and bridges three Ag^I atoms in a tetradentate bonding mode through all the three oxygen atoms and the pyridyl nitrogen atom. A schematic drawing of the 2D structures of complexes **1**−**4** is shown in Figure 5, where the Ag^I ions occupy the intersections. Two types of rectangles with the same lengths and different widths can be found for complexes **1**−**4** and Table 3 lists the sizes for these rectangles. The dihedral angles between the adjacent rectangles are listed in Table 4. It can be seen from Tables 3 and 4 that the sizes and dihedral angles for complexes **1**−**4** are similar, although slight differences have been found for complex **4**, indicating that changing the anions hardly affects the structures of the cations. Such a type of grid is unique and is in marked contrast to the regular grids found previously.[6] This 2D structure is also in marked contrast to our reported Ag^I complexes containing *N*,*N′*-bis(2-pyridyl)oxalamide ligands, where only 1D coordination polymers were obtained.[5b]

In complexes **1**−**4**, the 2D grids are further linked by the anions through Ag···X interactions (X = F or O) and/or C−H···X hydrogen bonds to form 3D structures (Ag···F−B 2.981, 3.070 Å, C−H···F−B 2.492−2.559 Å for **1**; Ag···O−Cl 2.926, 2.919 Å, C−H···O−Cl 2.528−2.580 Å for **2**; Ag···F−P 3.065−3.611 Å, C−H···F−P 2.405−2.527 Å for **3**; C−H···O−N 2.434 Å for **4**). Figure 6 shows a representative packing diagram for **2**. It can be seen that the molecules pack into layers of 2D cations which are separated by layers of the anions.

Transformation of L to L′

As shown in the structures of complexes **1**−**4**, a transformation of **L** to **L′** was observed. There are three possible reasons for this transformation. (1) The formation of **L′** could be due to the contamination of the by-product, *N*-(2-pyridyl)oxalamic acid, which may have been formed during the preparation of **L**. This possibility can be ruled out since all the spectroscopic data of **L** show that the ligand is pure

 © 2004 Wiley-VCH Verlag GmbH & Co. KGaA, Weinheim

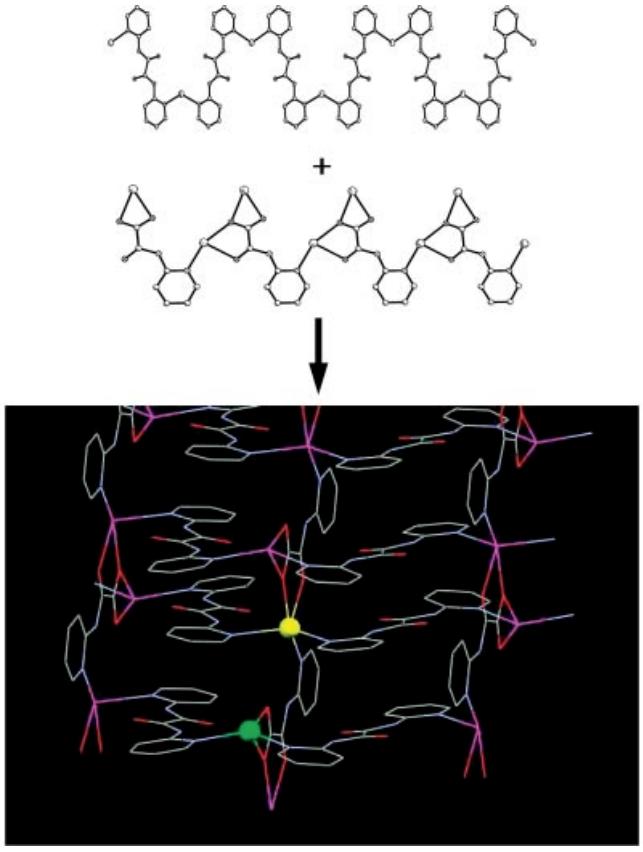

Figure 3. ORTEP drawings showing the concavo-convex chain involving **L** ligands (top), zigzag chain involving **L**′ ligands (center) and the 2D structure looking down the *a* axis (bottom)

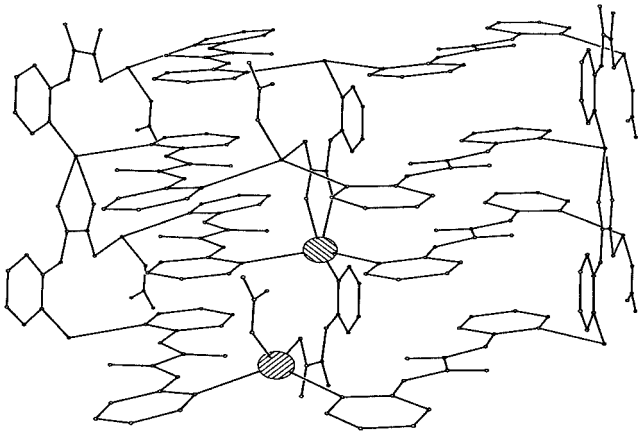

Figure 4. 2D structure of **4**

with no contamination of *N*-(2-pyridyl)oxalamic acid. (2) The **L** ligand decomposes to form *N*-(2-pyridyl)oxalamic acid during the crystallisation of complexes **1**−**4** in EtOH/H_2O. A blank test without addition of the metal salts had been carried out and no indication of *N*-(2-pyridyl)oxalamic acid was observed even under continuous stirring for more than two months. (3) The transformation is thus due to catalysis by Ag^+ in EtOH/H_2O. This shows that the metal centre plays an important role in converting **L** to **L**′.

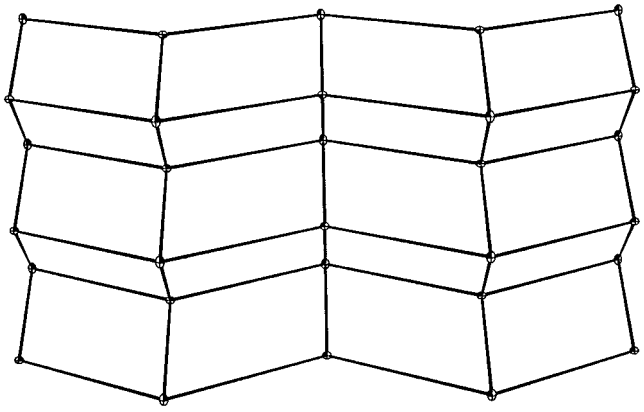

Figure 5. Schematic drawing for complexes **1**−**4**

Table 3. The sizes [Å] of small and large rectangles for complexes **1**−**4**

Complex	Small		Large	
	Length	Width	Length	Width
1	9.537	4.751	9.537	6.162
2	9.537	4.768	9.537	6.160
3	9.637	4.660	9.637	6.338
4	9.612	5.023	9.612	5.984

Table 4. Dihedral angles [°] between rectangles for complexes **1**−**4**

Complex	Large & large	Large & small	Small & small
1	37.7	86.1	48.9
2	39.1	86.1	47.7
3	38.2	86.3	47.2
4	40.7	85.9	48.4

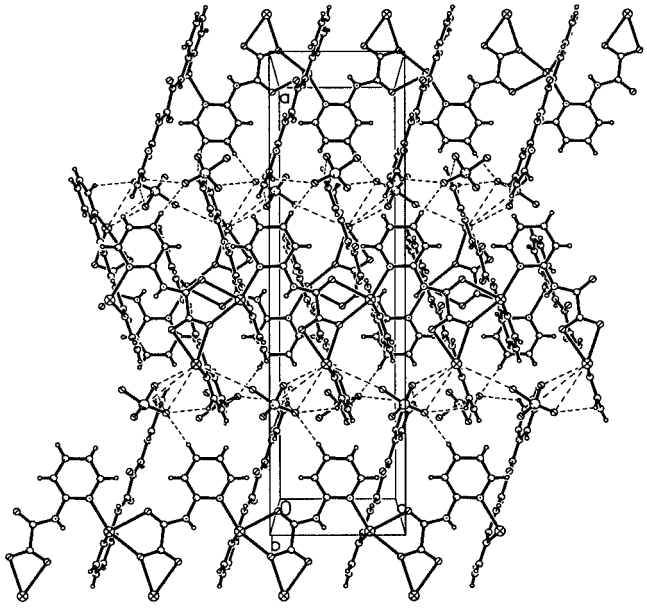

Figure 6. Packing diagram for **2** showing the interactions between the cations and the anions

 © 2004 Wiley-VCH Verlag GmbH & Co. KGaA, Weinheim

Stronger Lewis acids such as $AlCl_3$ have been used to investigate the conversion, but no positive results could be obtained. A mechanism describing the transformation pathways of **L** to **L′** is proposed in Scheme 1. The Ag^+ first coordinates to the carbonyl oxygen atom of **L′** followed by nucleophilic attack of a water molecule on the carbonyl carbon atom. A 2-aminopyridinium cation is lost to give Ag**L′** which then reacts with another **L** to afford complexes **1**−**4**.

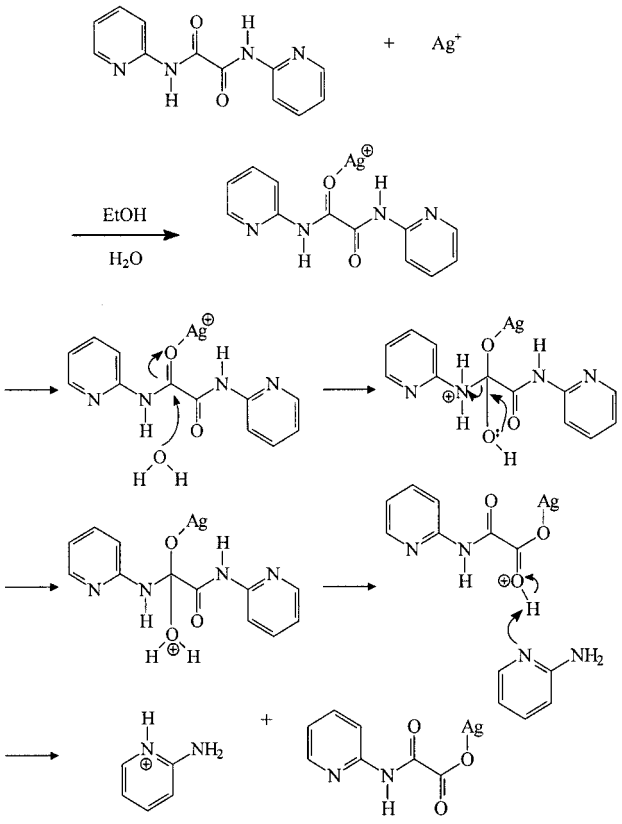

Scheme 1. Mechanism showing the transformation of **L** to **L′**

Concluding Remarks

In this study, the coordination chemistry of AgX (X = BF_4^-, ClO_4^-, PF_6^- and NO_3^-) with *N*,*N*′-bis(2-pyridyl)oxalamide (**L**) and the anion of *N*-(2-pyridyl)oxalamic acid (**L′**) was investigated. Unique 2D doubly-pleated-grid structures were seen in these complexes. During the crystallisation of the complexes, some of the **L** ligands were transformed to **L′** in the presence of Ag^I ions and water molecules. It has also been shown that the 2D pleated grids adopted by complexes **1**−**4** were hardly altered upon changing their counterions.

Experimental Section

General Procedures: All manipulations were carried out under air. The visible absorption spectra were recorded with a Hitachi U-2000 spectrophotometer. IR spectra were obtained with a Jasco FT/IR-460 plus spectrometer. Elemental analyses were obtained with a PE 2400 series II CHNS/O analyser or a HERAEUS VaruoEL analyser.

Materials: The reagents AgX (X = BF_4^-, ClO_4^-, PF_6^- and NO_3^-) were purchased from Aldrich Chemical Co. The ligand *N*,*N*′-bis(2-pyridyl)oxalamide was prepared according to a literature procedure.[7]

Syntheses: The complexes were synthesised by treatment of AgX (X = BF_4^-, ClO_4^-, PF_6^- and NO_3^-) with *N*,*N*′-bis(2-pyridyl)oxalamide in EtOH/H_2O.

1: *N*,*N*′-Bis(2-pyridyl)oxalamide (0.048 g, 0.20 mmol) in EtOH (5 mL) was layered onto a solution of $AgBF_4$ (0.020 g, 0.10 mmol) in H_2O (5 mL). The resultant solution was allowed to slowly diffuse for several weeks to give colourless crystals. Yield: 0.013 g, (27.0%). $C_{31}H_{27}Ag_2BF_4N_{10}O_8$ (**1**·H_2O; 970.16): calcd. C 38.38, H 2.81, N 14.44; found C 38.19, H 2.46, N 14.28. IR (KBr disk, cm^{-1}): $\tilde{\nu}$ = 3446 (w), 3172 [br., ν_s(N−H)], 1702 [s, ν_s(C=O)], 1685 [s, ν_s(C=O)], 1593 [br., $\nu_{as}(COO^-)$ + ν(C=N)], 1576 (s), 1499 (s), 1434 (s), 1305 [s, $\nu_s(COO^-)$], 1084 (w), 777 (m), 626 (w), 551 (w), 484 (w).

2: Prepared as described for **1**. Yield 0.015 g (28%). $C_{31}H_{27}Ag_2ClN_{10}O_{12}$ (**2**·H_2O; 982.80): calcd. C 37.89, H 2.77, N 14.25; found C 37.90, H 2.65, N 14.33. IR (KBr disk, cm^{-1}): $\tilde{\nu}$ = 3410 (w), 3180 [br., ν_s(N−H)], 1702 [s, ν_s(C=O)], 1685 [s, ν_s(C=O)], 1593 [br., $\nu_{as}(COO^-)$ + ν(C=N)], 1575 (s), 1498 (s), 1434 (s), 1305 [s, $\nu_s(COO^-)$], 1145 (s, ClO_4^-), 777 (m), 627 (w), 551 (w), 484 (w).

3: Prepared as described for **1**. Yield: 0.016 g (31%). $C_{31}H_{27}Ag_2F_6N_{10}O_8P$ (**3**·H_2O; 1028.32): calcd. C 36.21, H 2.65, N 13.62; found C 35.92, H 2.49, N 13.43. IR (KBr disk, cm^{-1}): $\tilde{\nu}$ = 3412 (w), 3160 (br., ν_s(N−H)], 1702 [s, ν_s(C=O)], 1685 [s, ν_s(C=O)], 1595 (br., $\nu_{as}(COO^-)$ + ν(C=N)], 1576 (s), 1498 (s), 1433 (s), 1304 [s, $\nu_s(COO^-)$], 837 (w), 770 (m), 626 (w), 551 (w), 483 (w).

4: Prepared as described for **1**. Yield: 0.013 g (28%). $C_{31}H_{27}Ag_2N_{11}O_{10}$ (**4**·H_2O; 929.36): calcd. C 40.06, H 2.93, N 16.58; found C 39.26, H 2.60, N 16.51. IR (KBr disk, cm^{-1}): $\tilde{\nu}$ = 3422 (w), 3184 [br., ν_s(N−H)], 1702 [s, ν_s(C=O)], 1685 [s, ν_s(C=O)], 1595 [br., $\nu_{as}(COO^-)$ + ν(C=N)], 1575 (s), 1498 (s), 1433 (s), 1384 (s, NO_3^-), 1304 [s, $\nu_s(COO^-)$], 770 (m), 626 (w), 551 (w), 483 (w).

X-ray Crystallography: The diffraction data of **1** were collected with a Bruker AXS diffractometer using graphite-monochromated Mo-K_α (K_α = 0.71073 Å) radiation. Data reduction was carried out using standard methods with the use of well-established computational procedures.[8] The structure factors were obtained after Lorentz and polarisation corrections. The positions of the heavy atoms, including the silver atoms, were located by direct methods. The remaining K_α (K_α = 0.71073 Å) radiation. Data reduction was carried out using and least-squares refinements.[9] The final residuals were R_1 = 0.0514, $wR2$ = 0.1309. The crystallographic procedures for **2**−**4** were similar to those for **1**. Basic information pertaining to crystal parameters and the structure refinements is summarized in Table 5. CCDC-230419 to -230422 contain the supplementary crystallographic data for this paper. These data can be obtained free of charge at www.ccdc.cam.ac.uk/conts/retrieving.html [or from the Cambridge Crystallographic Data Centre, 12 Union Road, Cambridge, CB2 1EZ, UK; Fax: (internat.) + 44-1223-336-033; E-mail: deposit@ccdc.cam.ac.uk].

 © 2004 Wiley-VCH Verlag GmbH & Co. KGaA, Weinheim

Table 5. Crystal data for compounds **1**−**4**

	1	**2**	**3**	**4**
Empirical formula	$C_{31}H_{25}Ag_2BF_4N_{10}O_7$	$C_{31}H_{25}Ag_2ClN_{10}O_{11}$	$C_{31}H_{25}Ag_2F_6N_{10}O_7P$	$C_{31}H_{25}Ag_2N_{11}O_{10}$
Formula mass	952.16	964.8	1010.32	927.36
Crystal system	orthorhombic	orthorhombic	orthorhombic	orthorhombic
Space group	*Pnma*	*Pnma*	*Pnma*	*Pnma*
a [Å]	27.469(2)	27.453(3)	27.884(3)	27.227(3)
b [Å]	16.426(2)	16.532(2)	16.681(2)	16.251(2)
c [Å]	7.4868(7)	7.511(2)	7.5763(12)	7.4935(7)
V [Å^3]	3378.0(6)	3409(1)	3523.9(8)	3315.6(5)
Z	4	4	4	4
$d_{calcd.}$ [gcm^{-3}]	1.872	1.897	1.904	1.823
Crystal size [mm]	0.1 × 0.2 × 0.7	0.1 × 0.2 × 0.4	0.1 × 0.2 × 0.8	0.1 × 0.2 × 0.7
μ(Mo-K_α) [mm^{-1}]	1.247	1.317	1.253	1.235
Temp. [°C]	22	22	22	22
Data/restraints/parameters	3057/0/289	3093/0/289	3200/0/338	3015/0/271
Quality-of-fit indicator[a]	1.048	1.005	1.012	1.013
Final *R* indices [$I > 2\sigma(I)$][b] [c]	$R_1 = 0.0514, wR_2 = 0.1309$	$R_1 = 0.0609, wR_2 = 0.1255$	$R_1 = 0.0496, wR_2 = 0.1236$	$R_1 = 0.0370, wR_2 = 0.0867$
R indices (all data)	$R_1 = 0.0691, wR_2 = 0.1422$	$R_1 = 0.1311, wR_2 = 0.1562$	$R_1 = 0.0703, wR_2 = 0.1389$	$R_1 = 0.0531, wR_2 = 0.0952$

[a] Quality-of-fit = $\{[\Sigma w||F_o^2| - |F_c^2||^2/N_{observed} - N_{parameters}]\}^{1/2}$. [b] $R_1 = \Sigma||F_o| - |F_c||/\Sigma|F_o|$. [c] $wR_2 = [\Sigma w(F_o^2 - F_c^2)^2/\Sigma w(F_o^2)^2]^{1/2}$. $w = 1/[\sigma^2(F_o^2) + (ap)^2 + (bp)]$, $p = [\max.(F_o^2 \text{ or } 0) + 2(F_c^2)]/3$. $a = 0.0694$, $b = 11.5112$ for **1**; $a = 0.0757$, $b = 0$ for **2**; $a = 0.0747$, $b = 8.7532$ for **3**; $a = 0.0482$, $b = 2.8985$ for **4**.

Acknowledgments

We are grateful to the National Science Council of the Republic of China for support.

[1] [1a] G. R. Desiraju, *Angew. Chem. Int. Ed. Engl.* **1995**, *34*, 2311−2327. [1b] G. R. Desiraju, *Chem. Commun.* **1997**, 1475−1482. [1c] J. M. Lehn, *Supramolecular Chemistry*, Wiley-VCH, Weinheim, **1995**.

[2] [2a] R. Robson, B. E. Abrahams, S. R. Batten, R. W. Gable, B. F. Hoskins, J. Lieu, *Supramolecular Architecture*, ACS publications, Washington, DC, **1992**. [2b] S. R. Batten, R. Robson, *Angew. Chem. Int. Ed.* **1998**, *37*, 1460−1494. [2c] O. M. Yaghi, H. Li, C. Davis, D. Richardson, T. L. Groy, *Acc. Chem. Res.* **1998**, *31*, 474−484. [2d] H. Gudbjartson, K. Biradha, K. M. Poirier, M. J. Zaworotko, *J. Am. Chem. Soc.* **1999**, *121*, 2599−2600. [2e] C. B. Aakeröy, K. R. Seddon, *Chem. Soc., Rev.* **1993**, 397−407. [2f] M. Fujita, K. Ogura, *Coord. Chem. Rev.* **1996**, *148*, 249−264. [2g] S.-I. Noro, R. Kitauta, M. Kondo, S. Kitagawa, T. Ishii, H. Matauzaka, M. Yamashita, *J. Am. Chem. Soc.* **2002**, *124*, 2568−2583. [2h] S. Kitagawa, M. Kondo, *Bull. Chem. Soc. Jpn.* **1998**, *71*, 1739−1753.

[3] [3a] R. P. Sijbesma, E. W. Meijer, *Curr. Opin. Colloid Interface Sci.* **1999**, *4*, 24−32. [3b] S. C. Zimmerman, P. S. Corbin, *Struct. Bonding* **2000**, *96*, 63−94. [3c] D. C. Sherrington, K. A. Taskinen, *Chem. Soc. Rev.* **2001**, *30*, 83−93. [3d] D. S. Lawrence, T. Jiang, M. Levett, *Chem. Rev.* **1995**, *95*, 2229−2260.

[4] [4a] A. J. Blake, N. R. Champness, P. Hubberstey, W.-S. Li, M. A. Withersby, M. Schröder, *Coord. Chem. Rev.* **1999**, *183*, 117−138. [4b] S. Muthu, J. H. K. Yip, J. J. Vittal, *Dalton Trans.* **2002**, 4561−4568, and references cited therein.

[5] [5a] C.-W. Su, C.-P. Wu, J.-D. Chen, L.-S. Liou, J.-C. Wang, *Inorg. Chem. Commun.* **2002**, *5*, 215−219. [5b] Y.-F. Hsu, J.-D. Chen, *Eur. J. Inorg. Chem.* **2004**, 1488−1493.

[6] [6a] S.-L. Zheng, M.-L. Tong, X.-L. Yu, X.-M. Chen, *J. Chem. Soc., Dalton Trans.* **2001**, 586−592. [6b] M. J. Zaworotko, *Chem. Commun.* **2001**, 1−9. [6c] J. Y. Lu, K. A. Runnels, C. Norman, *Inorg. Chem.* **2001**, *40*, 4516−4517. [6d] M. J. Plater, M. R. St J. Foreman, A. M. Z. Slawin, *J. Chem. Research (S)* **1999**, 74−75. [6e] J. Zhang, R.-G. Xiong, X.-T. Chen, Z. Xue, S.-M. Peng, X.-Z. You, *Organometallics* **2002**, *21*, 235−238. [6f] S. Sain, T. K. Maji, G. Mostafa, T.-H. Lu, M. Y. Chiang, N. R. Chaudhuri, *Polyhedron* **2002**, *21*, 2293−2299. [6g] J. Y. Lu, C. Norman, K. A. Abboud, A. Ison, *Inorg. Chem. Commun.* **2001**, *4*, 459−461. [6h] A. J. Blake, S. J. Hill, P. Hubberstey, W.-S. Li, *J. Chem. Soc., Dalton Trans.* **1997**, 913−914. [6i] K. Biradha, M. Fujita, *Chem. Commun.* **2001**, 15−16. [6j] R. H. Groeneman, L. R. MacGillivray, J. L. Atwood, *Chem. Commun.* **1998**, 2735−2736. [6k] J. T. Culp, J.-H. Park, M. W. Meisel, D. R. Talham, *Inorg. Chem.* **2003**, *42*, 2842−2848.

[7] M. C. Seidel, G. C. V. Tuyle, W. D. Weir, *J. Org. Chem.* **1970**, *35*, 1662−1664.

[8] *XSCANS, Release, 2.1*, Siemens Energy & Automation, Inc, Madison, Wisconsin, USA, **1995**.

[9] *SHELXTL 5.10*, Bruker Analytical X-ray Instruments Inc., Karlsruhe, Germany, **1997**.

Received February 8, 2004
Early View Article
Published Online October 1, 2004

 © 2004 Wiley-VCH Verlag GmbH & Co. KGaA, Weinheim

[Bis(amido)cyclodiphosph(III)azane]dichlorozirconium Complexes for Ethene Polymerization

Kirill V. Axenov,[a] Martti Klinga,[a] Markku Leskelä,[a] Vasily Kotov,[b] and Timo Repo*[a]

Keywords: Zirconium / Polymerization / Homogeneous catalysis

A series of new zirconium dichloride complexes bearing bulky *cis*-bis(amino)cyclodiphosph(III)azane ligands, $[(RN)_2(t\text{BuNP})_2]ZrCl_2$ [R = phenyl (**7**), diphenylmethyl (**8**), 2,6-diethylphenyl (**9**), 2,5-di-*tert*-butylphenyl (**10**), and 2,6-diisopropylphenyl (**11**)] were prepared in high yields by a two-step synthetic route. The structure of *cis*-$[(Ph_2CHN)(t\text{BuNP})]_2Zr(NMe_2)_2$ (**8a**), determined by X-ray analysis, shows that the zirconium atom has a distorted trigonal-bipyramidal configuration consisting of four equidistant metal–amido nitrogen bonds and an additional coordination between the metal and a nitrogen atom from the cyclodiphosph(III)azane ring. After methylaluminoxane activation, these complexes exhibit moderate to high activities in ethene polymerization and produce high molar mass polyethene (M_w up to 1100 kg/mol). Polymerization experiments reveal that the behavior of bis(amido)cyclodiphosph(III)azane-based Zr^{IV} catalysts depends on the nature and steric bulkiness of the amido substituents, reaction temperature, MAO/zirconium ratio, as well as monomer pressure.

(© Wiley-VCH Verlag GmbH & Co. KGaA, 69451 Weinheim, Germany, 2004)

Introduction

Group 4 metal complexes bearing bi- or tridentate[1−7] diamido ligands have attracted considerable attention as a new generation of early transition metal based polymerization catalysts.[8,9] After methylaluminoxane (MAO) activation, highly electrophilic 10-electron cationic species, $[(R_2N)_2ZrR]^+$, which serve as active catalytic sites, form.[8] This type of nonmetallocene complex has the advantage that the electronic character, geometry and steric hindrance of the catalytic center can be easily controlled through rational ligand design. To date, an impressive number of transition metal complexes have been synthesized[8,9] and applied for α-olefin polymerization,[10−13] in particular ethene polymerization.[14−17]

Recently, novel bis(amido) complexes of Group 4 metals based on the cyclodiphosph(III)azane framework were reported.[18−21] Due to the fact that these complexes possess a tetrahedral coordination of the metal center and the chloride ions are in a *cis* position, they can be considered as potential catalyst precursors for olefin polymerization. As an augmentation to our previous studies on nonmetallocene polymerization catalysts,[22−25] we have developed a straightforward synthesis towards new [bis(amido)cyclodiphosph(III)azane]Ti^{IV} complexes bearing sterically hindered aryl substituents and investigated them as ethene polymerization catalysts.[26] After MAO activation, these Ti complexes were able to polymerize ethene with moderate activity and produce polymers with high molar mass and narrow molar mass distribution (MMD). Here we describe an efficient synthetic route to the new [bis(amido)cyclodiphosph(III)azane]Zr complexes and report on the results of an investigation of their catalytic behavior in ethene polymerization as well as on the properties of the produced polymers.

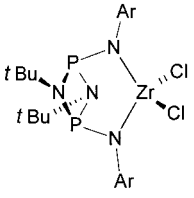

Results and Discussion

Synthesis of Ligand Precursors

A series of cyclodiphosph(III)azanes, **1**−**5**, were prepared in high yields by reaction of the appropriate anilines with dichlorocyclodiphosph(III)azane **a** in the presence of excess Et_3N, as was reported earlier (Scheme 1).[26] The X-ray

[a] Department of Chemistry, Laboratory of Inorganic Chemistry, University of Helsinki,
P. O. Box 55, 00014 Finland
Fax: (internat.) + 358 9-19150198
E-mail: timo.repo@helsinki.fi
[b] Department of Chemistry, CB#3290 Venable Hall, The University of North Carolina at Chapel Hill,
Chapel Hill, NC 27599-3290, USA
Supporting information for this article is available on the WWW under http://www.eurjic.org or from the author.

 © 2004 Wiley-VCH Verlag GmbH & Co. KGaA, Weinheim **DOI: 10.1002/ejic.200400296**

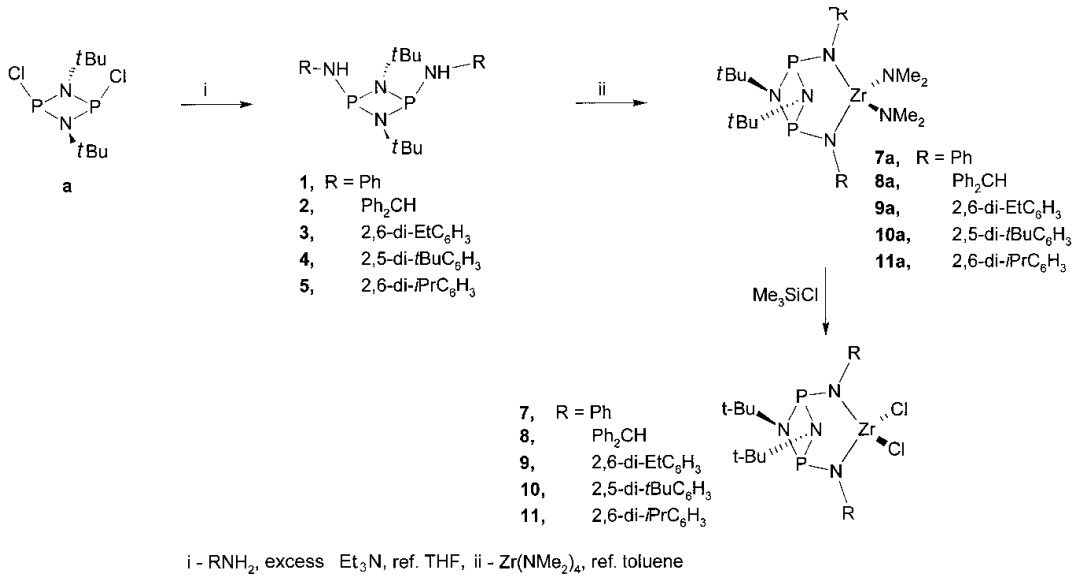

Scheme 1

analysis (solid state) and NMR spectroscopic data have shown that these compounds favor a *cis* conformation – the most desirable arrangement for coordination chemistry applications. The solid-state structure of *cis*-[(Ph_2CHNH)-(*t*BuNP)]$_2$ (**2**, Figure 1, Tables 1 and 2) also supports the previously observed *cis* orientation of the bulky amino substituents. However, this structure differs sharply from previously reported structures for *cis*-bis(amino)cyclodiphosph(III)azanes; according to X-ray crystallographic analysis, the NH groups in all other known cyclodiphosph(III)azanes[27,28] adopt the *endo* orientation relative to the P–N ring, while in **2** these substituents have the *exo*,*endo* orientation (Figure 1). Such an unusual structural feature has been reported earlier for *cis*-[(*t*BuNH)-(*t*BuNPS)]$_2$ with P^V only.[29] Furthermore, the distortion of the P–N ring is diminished as indicated by the P–N bond lengths and the planarity of the ring. It can be assumed that the reduced ring distortion is mainly a consequence of the unique *exo*,*endo* orientation.

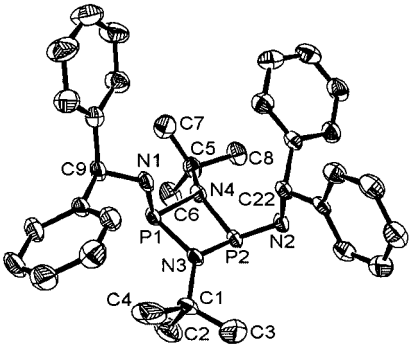

Figure 1. ORTEP plot of **2** with thermal ellipsoids drawn at 50% probability level; all hydrogen atoms are omitted for clarity

Table 1. Crystallographic data for **2** and **8a**

	2	**8a**
Empirical formula	$C_{34}H_{42}N_4P_2$	$C_{38}H_{52}N_6P_2Zr$
Formula mass	568.66	746.02
Space group	$P\bar{1}$	$P2_1/n$
a [Å]	10.449(1)	10.715(2)
b [Å]	12.419(1)	20.287(4)
c [Å]	13.493(1)	18.055(4)
α [°]	75.39(1)	
β [°]	73.57(1)	96.31(3)
γ [°]	74.65(1)	
V [Å^3]	1589.5(2)	3900.9(14)
$d_{calcd.}$ [g cm^{-3}]	1.188	1.270
Z	2	4
μ [cm^{-1}]	14.52	3.98
λ [Å]	1.54179	0.71073
T [K]	193(2)	173(2)
R[a]	0.053	0.0927
R_w[b]	0.1549	0.2060

[a] $R = \Sigma(F_o - F_c)/\Sigma F_o$ for observed reflections [$I > 2\sigma(I)$]. [b] $Rw = \{\Sigma[w(F_o^2 - F_c^2)^2]/\Sigma[w(F_o^2)^2]\}^{1/2}$ for all data.

Synthesis of Complexes

The most common synthetic route to the transition metal complexes that have an anionic ligand is a transmetalation reaction. According to this general strategy, *cis*-[(PhNH)(*t*BuNP)]$_2$ (**1**) and *cis*-[(2,6-di-*i*PrC_6H_3NH)$_2$(*t*-BuNP)$_2$] (**5**) ligands were first deprotonated with BuLi, and the obtained Li salts were then treated with $ZrCl_4$ in toluene at –78 °C. The resulting reaction mixtures were analyzed by ^{31}P NMR spectroscopy. When ligand **1** was used, only one product (δ_P = 145 ppm, see Supporting Information) was observed. The same transformation with ligand **5** leads to a complex mixture of unidentified products. According to data published previously, the signal at δ = 145 ppm is assigned to the Zr^{IV} complex that has two cyclodiphosph(III)azane ligands attached to the metal center.[20] In

 © 2004 Wiley-VCH Verlag GmbH & Co. KGaA, Weinheim

Table 2. Selected structural parameters for compounds **2** and **8a**

Compound **2**			
Distances [Å]		Angles [°]	
P1−N4	1.727(2)	N3−P1−N4	81.20(10)
P2−N3	1.722(2)	P1−N3−P2	97.52(11)
P2−N4	1.728(2)	P1−N4−P2	97.41(11)
P1−P2	2.5957(9)	C1−N3−P1	126.59(16)
P2−N2	1.677(2)	C5−N4−P1	123.57(16)
N3−C1	1.468(3)	N2−P2−N4	107.96(10)
N4−C5	1.486(3)	N2−P2−N3	105.13(10)
N1−C9	1.468(3)	C9−N1−P1	122.51(17)
		C22−N2−P2	126.99(16)
Compound **8a**			
Distances [Å]		Angles [°]	
P1−N3	1.773(7)	N61−Zr1−N51	100.0(3)
P1−N4	1.746(7)	N61−Zr1−N2	117.9(3)
P2−N2	1.702(7)	N51−Zr1−N1	106.7(2)
N3−C1	1.515(10)	N2−Zr1−N1	108.5(2)
N1−C9	1.467(9)	N61−Zr1−N3	104.8(3)
Zr1−N1	2.141(6)	N51−Zr1−N3	153.8(3)
Zr1−N2	2.113(7)	P2−N3−Zr1	92.0(3)
Zr1−N3	2.439(7)	N3−P2−P4	81.1(3)
Zr1−N51	2.046(7)	P1−N3−P2	97.9(4)
		C9−N1−P1	118.5(5)

fact, the salt metathesis route was unselective in the preparation of corresponding titanium(IV) bis(amido)complexes also, and alternative synthetic routes were therefore looked for.[26] As in the case of Ti^{IV}, the direct metalation of the ligand precursors by amine elimination[17] appeared to be the most efficient method. According to ^1H and ^{31}P NMR spectroscopic data, the reaction of $Zr(NMe_2)_4$ with **1**−**5** leads selectively to the bis(amido)complexes [(RN)-(*t*BuNP)]$_2$Zr(NMe$_2$)$_2$ (**7a**−**11a**) (Scheme 1).

However, it is well known that bis(amido) early transition metal complexes are less active catalyst precursors in polymerization of α-olefins than the corresponding dichloro derivatives. Treatment of bis(amido)[*cis*-bis(amido)cyclodiphosph(III)azane]zirconium complexes **7a**−**11a** with excess chlorotrimethylsilane in toluene selectively gave the desired dichlorozirconium derivatives **7**−**11** in high yields (Scheme 1). These complexes have been characterized by NMR spectroscopy, elemental analysis, and mass spectroscopic methods. According to the ^1H NMR spectra, the *cis*-[(RN)$_2$(*t*BuNP)$_2$]ZrCl$_2$ complexes show C_2 symmetry in solution and reveal the equivalence of all aromatic substituents.

X-ray structures of [*cis*-bis(amido)cyclodiphosph(III)azane]zirconium complexes are rather rare, and only one structure involving [bis(amido)cyclodiphosph(III)azane]-ZrX$_2$-type complexes, namely *cis*-[(*t*BuN)$_2$(*t*BuNP)$_2$]ZrX$_2$ (X = Cl, **6**),[18,20] has been reported. The crystals of *cis*-[(Ph$_2$CHN)$_2$(*t*BuNP)$_2$]Zr(NMe$_2$)$_2$ (**8a**) suitable for X-ray analysis were successfully grown from a saturated Et$_2$O solution at −20 °C. In the structure of **8a** the four amido N−Zr bonds and an additional coordination of the cyclodiphosph(III)azane ring nitrogen to the zirconium atom define a rather distorted trigonal-bipyramidal configuration of the metal center. The amido nitrogen atoms are located in the corners of a zirconium-centered tetrahedron (Figure 2). In general, all amido−zirconium bonds are equidistant (average 2.110 Å), while the Zr−N coordination bond is significantly longer (2.448 Å) (Tables 1 and 2). The N−M−N angles range from 100° to 123.19°. The geometry of the ligand moiety **2** is changed due to the coordination to the zirconium atom, and the P−N(amido) bonds adopt an *endo*,*endo* orientation relative to the cyclodiphosph(III)-azane ring. Overall, the Zr−N coordination is similar to those reported for *cis*-[(*t*BuN)$_2$(*t*BuNP)$_2$]ZrCl$_2$ and *cis*-[(PhN)$_2$(*t*BuNP)$_2$]$_2$Zr.[20]

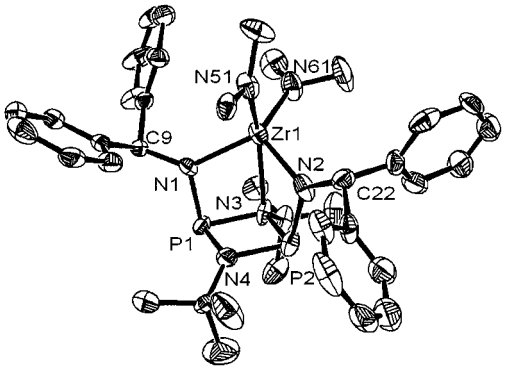

Figure 2. ORTEP plot of **8a** with thermal ellipsoids drawn at 50% probability level; all hydrogen atoms are omitted for clarity

Ethene Polymerization

Despite a certain interest in *cis*-bis(amido)cyclodiphosph(III)azane-based zirconium complexes, few preliminary reports concerning their polymerization properties have been published.[18−20] In order to evaluate the influence of the structure of the catalyst precursors on polymerization properties, we carried out a detailed ethene polymerization investigation. In general, MAO-activated zirconium complexes **6**−**11** reveal moderate to high catalytic activity and, according to obtained data, the size of the substituents at the amido nitrogen atoms has a significant effect on the catalytic behavior (Table 3).

Under the chosen polymerization conditions (50 °C and 3.8 bars), **6**/MAO bearing *tert*-butyl groups shows the highest average activity in the series of catalysts (Entry 1, Table 3). When ethene polymerization is conducted under the same conditions, there are two distinct differences in the behavior of catalyst **6**/MAO from that of its Ti^{IV} analog; the catalytic activity is significantly higher for **6**/MAO as it remains high during the whole polymerization reaction, while *cis*-[(*t*BuN)$_2$(*t*BuNP)$_2$]TiCl$_2$/MAO gives a remarkably high initial activity that decreases drastically after a few minutes. In addition, **6**/MAO produces polyethene with narrow polydispersity, whereas the corresponding Ti^{IV} catalyst is prone to produce polyethylene with bimodal MMD.[26] These facts indicate the higher stability of the [bis(amido)cyclodiphosph(III)azane]Zr catalytic species.

Replacement of the *tert*-butyl groups with diphenylmethyl (**8**) leads to dramatic changes in the catalyst

 © 2004 Wiley-VCH Verlag GmbH & Co. KGaA, Weinheim

Table 3. Ethene polymerization data for complexes **6**−**11**

Entry[a]	Catalyst	Concentration [μmol]	Reaction temp. [°C]	Time [min]	Yield [g]	Activity[b]	M_w [g/mol]	M_w/M_n	T_m [°C]
1	**6**	1.5	50	30	5.8	24058	228 000	2.17	134
2	**7**	10	50	30	1.63	1031	1 132 000	3.32	134
3	**8**	10	50	30	1.53	973	1 042 000	22.18	131
4	**9**	10	50	30	1.89	1181	1 039 000	3.41	138
5	**10**	10	50	30	2.93	2534	306 000	4.10	133
6	**11**	10	50	30	4.05	7000	672 000	2.84	136

[a] MAO (Al/M = 1000), 200 mL of toluene, 3.8 bar of ethylene. [b] kg PE/(mol_{cat} × [C_2H_4] × h).

behavior. The activity decreases substantially and the produced polyethene has a high M_w (1040 kg/mol) and bimodal MMD (see Supporting Information). The series of catalysts **7**/MAO, **9**/MAO, **10**/MAO, and **11**/MAO bearing phenyl, 2,6-diethylphenyl, 2,5-di-*tert*-butylphenyl, and 2,6-diisopropylphenyl groups, respectively, reveal a clear enhancement of activity with increased steric bulk on the arylamido substituents. The activity as well as the properties of the polymer material are strongly connected to the ligand design. The molar mass of polyethene varies between 230 and 1130 kg/mol and polymers with diverse MMDs and different modalities are obtained.

Reaction temperature as well as monomer concentration are the key factors, which define the activity of catalysts and also the properties of the polymers produced. Ethene was polymerized at 30, 50, 60, and 70 °C to evaluate the influence of polymerization temperature on the catalytic activity and polymer properties (Figure 3). The steric bulkiness of the amido substituents is crucial for the catalyst behavior, in particular, the polymerization activity, as well as the stability of these Zr catalysts. The *tert*-butyl substituents in **6**/MAO seem to create a highly propitious environment for the catalytically active center, and already at 30 °C a very high activity is observed. However, the activity decreases to one third when the temperature increases from 30 to 70 °C, whereas the molar mass of polyethene and the MMD are slightly enhanced (Figure 4). Polymerization activities of the other catalysts are much lower but not as sensitive to the temperature changes and show their highest values at temperatures between 50 and 60 °C. At higher temperatures deactivation of the catalytically active species occurs. Quite unexpectedly, the produced polyethene possesses maximum molar mass values at 50 °C. The decrease in M_w at higher temperatures is often explained by a change in relative rates of chain propagation and β-H elimination.[30] This seems to be a plausible explanation here as well. The lower M_w values at 30 °C remain unexplained but could be caused by another competing chain termination route, e.g. chain transfer to aluminum.

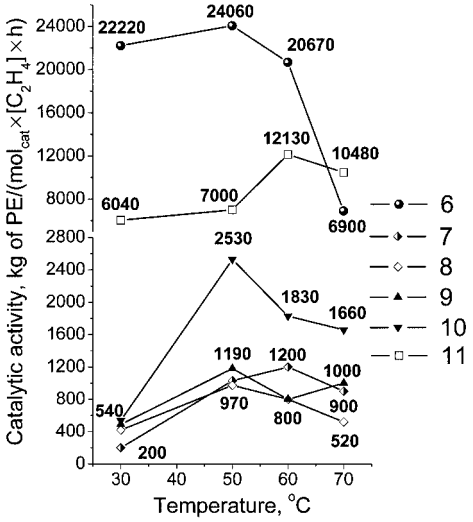

Figure 3. Catalytic activity as a function of polymerization temperature for [(*t*BuN)(*t*BuNP)]$_2$ZrCl$_2$ (**6**), [(PhN)(*t*BuNP)]$_2$ZrCl$_2$ (**7**), [(Ph_2CHN)(*t*BuNP)]$_2$ZrCl$_2$ (**8**), [(2,6-$Et_2C_6H_3$N)(*t*BuNP)]$_2$ZrCl$_2$ (**9**), [(2,5-$tBu_2C_6H_3$N)(*t*BuNP)]$_2$ZrCl$_2$ (**10**), and [(2,6-$iPr_2C_6H_3$N)(*t*BuNP)]$_2$ZrCl$_2$ (**11**) as catalyst precursors; the numeric values of the observed average activities are also given for the corresponding graph points; activity is expressed as kg of PE × (mol_{cat} × [C_2H_4] × h)$^{-1}$; experimental conditions used: MAO (Al/M = 1000), 3.8 bar of ethylene

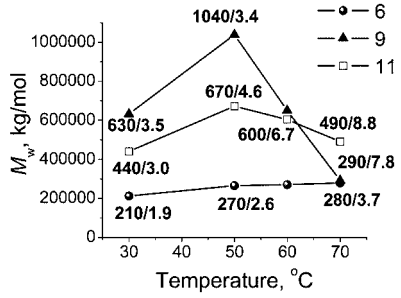

Figure 4. Molar mass of polyethene as a function of polymerization temperature with selected catalyst precursors [(*t*BuN)(*t*BuNP)]$_2$ZrCl$_2$ (**6**), [(2,6-$Et_2C_6H_3$N)(*t*BuNP)]$_2$ZrCl$_2$ (**9**), and [(2,6-$iPr_2C_6H_3$N)(*t*BuNP)]$_2$ZrCl$_2$ (**11**); the numeric values of M_w (in kg/mol) as well as polydispersities are given

All cyclodiphosph(III)azane catalysts were tested with ethene concentrations ranging from 0.15 to 0.8 mol/L (2−8 bar at 50 °C). The highest average productivity (calculated from the yield of polymer) is 22 800 kg of PE/mol_{cat} × h for **6**/MAO at 8 bar. The maximum catalytic activity for **6**−**10**/MAO is reached at low ethene concentrations (Fig-

 © 2004 Wiley-VCH Verlag GmbH & Co. KGaA, Weinheim

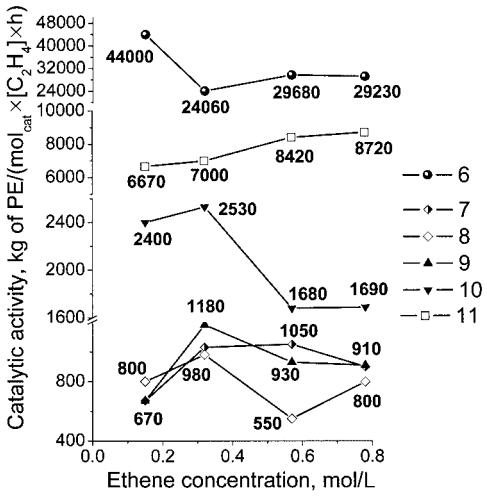

Figure 5. Catalytic activity of complexes as a function of ethene concentration for [(*t*BuN)(*t*BuNP)]$_2$ZrCl$_2$ (**6**), [(PhN)(*t*BuNP)]$_2$ZrCl$_2$ (**7**), [(Ph$_2$CHN)(*t*BuNP)]$_2$ZrCl$_2$ (**8**), [(2,6-Et$_2$C$_6$H$_3$N)(*t*BuNP)]$_2$ZrCl$_2$ (**9**), [(2,5-*t*Bu$_2$C$_6$H$_3$N)(*t*BuNP)]$_2$ZrCl$_2$ (**10**), and [(2,6-*i*Pr$_2$C$_6$H$_3$N)(*t*BuNP)]$_2$ZrCl$_2$ (**11**) as catalyst precursors; the numeric values of the observed average activities are also given for the corresponding graph points; activity is expressed as kg of PE × (mol$_{cat}$ × [C$_2$H$_4$] × h)$^{-1}$; experimental conditions used: MAO (Al/M = 1000), polymerization temperature 50 °C

ure 5). It has been suggested that at higher monomer concentrations, due to enhanced polymer formation, the active complex becomes quickly embedded in the swollen-gel-like polymer matrix, which leads to the diffusion-controlled reaction conditions.[31]

Despite the increased monomer pressure enhancing the productivity of catalysts (yield of polymer), the molar mass of polymers produced by **6**/MAO and **11**/MAO are slightly reduced (Figure 6). This fact indicates the presence of β-H transfer to the monomer as a major chain-termination mechanism. However, in the case of **10**/MAO, where aniline is unsymmetrically substituted with *tert*-butyl substituents, the dominating chain termination reaction changes from β-H transfer to the monomer to β-H transfer to the metal center as the molar mass of polyethene appreciably increases from 310 kg/mol at 3.8 bar of ethene to 1480 kg/mol at 8 bar.[32]

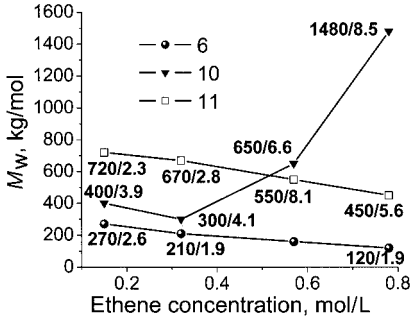

Figure 6. Molar mass of polyethene as a function of ethene concentration with selected catalyst precursors [(*t*BuN)(*t*BuNP)]$_2$ZrCl$_2$ (**6**), [(2,5-*t*Bu$_2$C$_6$H$_3$N)(*t*BuNP)]$_2$ZrCl$_2$ (**10**), and [(2,6-*i*Pr$_2$C$_6$H$_3$N)(*t*BuNP)]$_2$ZrCl$_2$ (**11**); the numeric values of M_w (in kg/mol) as well as polydispersities are given

Depending on the ligand structure, the catalysts have different responses to variations in MAO concentration e.g. the polymerization activity of **6**/MAO significantly decreases when the Al/Zr ratio increases (Figure 7). Even though **6**/MAO possesses a high polymerization activity, it is vulnerable to higher temperatures and MAO concentrations. Hence, we assume that the *tert*-butyl groups of **6**/MAO are not bulky enough to protect the catalytic center from deactivation. It has been proposed that the coordination of Lewis acidic MAO to the electron-pair-donating P^{III} atoms in the cyclodiphosph(III)azane ring can initiate the destruction of the catalyst during the polymerization process.[19]

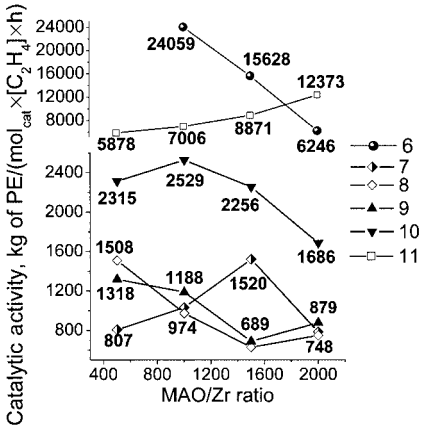

Figure 7. Catalytic activity of complexes as a function of MAO/Zr ratio for [(*t*BuN)(*t*BuNP)]$_2$ZrCl$_2$ (**6**), [(PhN)(*t*BuNP)]$_2$ZrCl$_2$ (**7**), [(Ph$_2$CHN)(*t*BuNP)]$_2$ZrCl$_2$ (**8**), [(2,6-Et$_2$C$_6$H$_3$N)(*t*BuNP)]$_2$ZrCl$_2$ (**9**), [(2,5-*t*Bu$_2$C$_6$H$_3$N)(*t*BuNP)]$_2$ZrCl$_2$ (**10**), and [(2,6-*i*Pr$_2$C$_6$H$_3$N)(*t*BuNP)]$_2$ZrCl$_2$ (**11**) as catalyst precursors; the numeric values of the observed average activities are also given for the corresponding graph points; activity is expressed as kg of PE × (mol$_{cat}$ × [C$_2$H$_4$] × h)$^{-1}$; experimental conditions used: 3.8 bar of ethylene, polymerization temperature 50 °C

According to the polymerization results, diphenylmethyl substituents are not able to provide a suitable surrounding for the highly active metal center and, in addition, **8**/MAO is sensitive to increased MAO concentrations. Increasing the size of substituents at the aniline moiety improves the shielding at the cationic metal center, and the activity of **10**/MAO, with 2,5-di-*tert*-butylphenyl groups, is enhanced up to an MAO/Zr ratio of 1000. In fact, the sterically most demanding 2,6-diisopropylphenyl groups in **11**/MAO efficiently protect the catalytically active site, and it is the only catalyst that gradually enhances the polymerization activity with increasing MAO/Zr ratio. While the bulky ligand protects the catalytic species from destructive side reactions, it also congests the actual polymerization site and the observed activity for **11**/MAO is thus lower than for **6**/MAO.

Published solid-state structures (Figure 2[18−20,26]) of [bis(amido)cyclodiphosph(III)azane]Zr and -Ti complexes show that the environment of the P atoms remains rather open regardless of the changes in the bulkiness of the amino substituents. It appears in this study that the observed correlation between the stability of the catalytically active species

 © 2004 Wiley-VCH Verlag GmbH & Co. KGaA, Weinheim

and the size of amido substituents could be better explained if destructive MAO interaction with metal−ligand bonding was the major decomposition pathway for the catalysts.

Conclusion

New [bis(amido)cyclodiphosph(III)azane]zirconium complexes $[(RN)(t\text{BuNP})]_2ZrCl_2$ (**7**−**11**) [R = Ph (**7**), Ph_2CH (**8**), 2,6-$Et_2C_6H_3$ (**9**), 2,5-$t\text{Bu}_2C_6H_3$ (**10**), 2,6-$i\text{Pr}_2C_6H_3$ (**11**)] were synthesized by reaction of the corresponding ligand precursors with $Zr(NMe_2)_4$. The amido complexes were successfully transformed into the dichloro derivatives $[(RN)(t\text{BuNP})]_2ZrCl_2$ (**7**−**11**) with excess Me_3SiCl. MAO-activated **7**−**11** display moderate to high activities in ethene polymerization. The catalyst behavior is dependent on the bulk of the ligand substituents. The nature and size of the amido substituents play a great role in defining the catalytic activity of the investigated Zr complexes as well as the polymer properties. From the series of catalysts studied here, only **11**/MAO revealed increased activity in the range 500−2000 for the MAO/Zr ratio as well as in the polymerization temperature range 30−60°C.

Experimental Section

General Remarks: All manipulations were performed under argon in a glovebox or using standard Schlenk techniques. Hydrocarbon and ether solvents were refluxed in the presence of sodium and benzophenone, distilled, and stored under an inert gas in the presence of sodium flakes. Dichloromethane was refluxed in the presence of CaH_2 powder and distilled before use. Mass spectra were measured with a JEOL SX102 spectrometer and the ^1H and ^{13}C NMR spectra were recorded with a Varian Gemini 200 MHz spectrometer. The ^1H and ^{13}C NMR spectra are referenced relative to $CHCl_3$ (δ = 7.24 ppm and 77.0 ppm, respectively) and C_6D_5H (δ = 7.15 ppm and 128.0 ppm, respectively). ^{31}P NMR spectra were collected with a Bruker AMX 400 spectrometer and phosphorus signals were referenced relative to an external 85% H_3PO_4 solution. Elemental analyses were performed by Analytische Laboratorien Prof. Dr. H. Malissa, G. Reuter GmbH, Lindlar, Germany. High-temperature gel permeation chromatography of polyethylene samples (GPC) was performed in 1,2,4-trichlorobenzene at 145 °C using a Waters HPLC 150C. *tert*-Butylamine and phosphorus trichloride were purchased from Merck and purified by distillation under argon ($t\text{BuNH}_2$ from sodium hydroxide). Arylamines and diphenylmethylamine were received from Aldrich and distilled in vacuo from sodium hydroxide before use. Chlorotrimethylsilane was purchased from Fluka and used as received. $Zr(NMe_2)_4$ was purchased from Aldrich and used as a toluene solution. Methylaluminoxane (MAO, 30 wt.% solution in toluene) was received from Borealis Polymers Oy.

Ligand Synthesis: *cis*-$[Cl(t\text{BuNP})]_2$ (**a**) was prepared according to modified literature procedures.[29] The cyclodiphosph(III)azane ligands *cis*-$[(PhNH)(t\text{BuNP})]_2$ (**1**), *cis*-$[(Ph_2CHNH)_2(t\text{BuNP})_2]$ (**2**), *cis*-$[(2,6\text{-di-Et}C_6H_3NH)_2(t\text{BuNP})_2]$ (**3**), *cis*-$[(2,5\text{-di-}t\text{Bu}C_6H_3NH)_2(t\text{BuNP})_2]$ (**4**), and *cis*-$[(2,6\text{-di-}i\text{Pr}C_6H_3NH)_2(t\text{BuNP})_2]$ (**5**) were prepared as described previously.[26] $[(t\text{BuN})_2(t\text{BuNP})_2]ZrCl_2$ (**6**) was prepared according to the literature.[18]

$[(PhN)_2(t\text{BuNP})_2]ZrCl_2$ (7): A solution of $Zr(NMe_2)_4$ (1.56 g, 5.86 mmol) in toluene (20 mL) was added with a syringe to a toluene solution of *cis*-$[(PhNH)_2(t\text{BuNP})_2]$ (2.28 g, 5.86 mmol, 30 mL) at 0 °C. The reaction mixture was then refluxed for 16 h, and the obtained bis(dimethylamido)zirconium complex $[(PhN)(t\text{BuNP})]_2Zr(NMe_2)_2$ (**7a**) was characterized by NMR spectroscopy. ^1H NMR (200 MHz, C_6D_6, 29°C): δ_H = 1.19 (s, 18 H, *t*Bu), 2.93 (s, 12 H, NMe_2), 6.81 (t, J = 6.6 Hz, 2 H, *o*-H), 7.26 (m, 8 H, Ph) ppm. $^{13}C\{^1H\}$ NMR (50.3 MHz, C_6D_6, 29°C): δ_C = 29.7 [t, $J_{P,C}$ = 6.87 Hz, $C(CH_3)_3$], 40.94 (Me_2NZr), 53.2 [t, $J_{P,C}$ = 12.5 Hz, $C(CH_3)_3$], 119.36 (Ph), 129.7 (Ph), 150.0 (Ph) ppm. $^{31}P\{^1H\}$ NMR (162 MHz, C_6D_6, 21°C): δ_P = 124 ppm. The bis(amido) complex $[(PhN)(t\text{BuNP})]_2Zr(NMe_2)_2$ was converted into the corresponding dichloro derivative **7** by reaction with excess Me_3SiCl (1.3 g, 1.5 mL, 11.7 mmol) at 0 °C. The obtained reaction mixture was stirred at room temperature overnight. The volatiles were removed in vacuo, and the residue was extracted with a mixture of hexane and CH_2Cl_2 (1:1). After filtration and evaporation of the solvents, the product was dried in vacuo to give a pale-yellow powder containing 1 equiv. of Me_2NH per Zr (2.03 g; 60%) $C_{20}H_{28}Cl_2N_4P_2Zr{\cdot}Me_2NH$ (593.6): calcd. C 44.51, H 5.94, N 11.80; found C 44.79, H 6.19, N 11.44. ^1H NMR (200 MHz, C_6D_6, 29°C): δ_H = 1.32 (s, 18 H, *t*Bu), 1.80 (br. s, Me_2NH), 6.82 (t, J = 7.7 Hz, 2 H, *p*-H), 7.09 (t, J = 7.7 Hz, 4 H, *m*-H), 7.50 (d, J = 7.7 Hz, 4 H, *o*-H) ppm. $^{13}C\{^1H\}$ NMR (50.3 MHz, C_6D_6, 29°C): δ_C = 28.65 [t, $J_{P,C}$ = 7.4 Hz, $C(CH_3)_3$], 32.2 (Me_2NH), 54.25 [t, $J_{P,C}$ = 9.15 Hz, $C(CH_3)_3$], 124.0, 129.5, 150.2 ppm. $^{31}P\{^1H\}$ NMR (162 MHz, C_6D_6, 21°C): δ_P = 145.03 (s) ppm. MS(EI): *m*/*z* (%) = 548 (10) [M^+], 503 (6) [M^+ − Cl], 388 (10) [ligand].

$[(Ph_2CHN)_2(t\text{BuNP})_2]ZrCl_2$ (8): A toluene solution of $Zr(NMe_2)_4$ (0.52 g, 1.97 mmol, 20 mL) was added with a syringe to a solution of *cis*-$[(Ph_2CHNH)_2(t\text{BuNP})_2]$ (1.12 g, 1.97 mmol) in toluene (10 mL) at 0 °C. The reaction mixture was then refluxed for 16 h, and the bis(dimethylamido)zirconium complex $[(Ph_2CHN)_2(t\text{BuNP})_2]Zr(NMe_2)_2$ (**8a**) was isolated according to a procedure described earlier. ^1H NMR (200 MHz, C_6D_6, 29°C): δ_H = 1.30 (s, 18 H, *t*Bu), 2.70 (12 H, NMe_2), 5.57 (dd, 2 H, Ph_2CH), 7.09 (m, 20 H, Ph-H) ppm. Crystals suitable for X-ray analysis were obtained by slow crystallization from saturated Et_2O solution at −20 °C. The bis(amido) complex $[(Ph_2CHN)_2(t\text{BuNP})_2]Zr(NMe_2)_2$ (**8a**) was converted into the corresponding dichloro derivative **8** by reaction with excess Me_3SiCl (2.31 g, 2.0 mL, 21.28 mmol) at 0 °C. The obtained reaction mixture was stirred at room temperature overnight. The volatiles were removed in vacuo, and the residue was extracted with a mixture of hexane and CH_2Cl_2 (1:1). The crude product was washed with cold pentane and dried under vacuum (yield 0.95 g). The remaining pentane solution was kept in a freezer at −20 °C for 3 d, and a second crop of product (0.27 g) was isolated as a white powder by removing the pentane with a syringe. Total yield 1.22 g, 85%. $C_{34}H_{40}Cl_2N_4P_2Zr$ (728.8): calcd. C 56.03, H 5.53, N 7.69; found C 55.85, H 6.30, N 7.50. ^1H NMR (200 MHz, C_6D_6, 29°C): δ_H = 1.21 (s, 18 H, *t*Bu), 6.08 (t, 2 H, Ph_2CH), 7.14−7.28 (m, 16 H, Ph), 7.68 (d, J = 7.0 Hz, 4 H, *p*-H) ppm. $^{13}C\{^1H\}$ NMR (50.3 MHz, C_6D_6, 29°C): δ_C = 30.88 [t, $J_{P,C}$ = 7.25 Hz, $C(CH_3)_3$], 51.88 [t, $J_{P,C}$ = 11 Hz, $C(CH_3)_3$], 98.4 (Ph_2CH), 126.85 (Ph), 128.6 (Ph), 150.8 (Ph) ppm. $^{31}P\{^1H\}$ NMR (162 MHz, C_6D_6, 21°C): δ_P = 102.0 (s) ppm. MS(EI): *m*/*z* (%) = 691 (5) [M^+ − Cl], 566 (60) [ligand].

$[(2,6\text{-}Et_2C_6H_3N)_2(t\text{BuNP})_2]ZrCl_2$ (9): A toluene solution of *cis*-$[(2,6\text{-}Et_2C_6H_3NH)_2(t\text{BuNP})_2]$ (1.5 g, 3.0 mmol, 20 mL) and $Zr(NMe_2)_4$ (0.8 g, 2.99 mmol) in toluene (10 mL) was treated as in the case of **8**. The bis(dimethylamido)zirconium complex [(2,6-

 © 2004 Wiley-VCH Verlag GmbH & Co. KGaA, Weinheim

$Et_2C_6H_3N)_2(t$BuNP$)_2]Zr(NMe_2)_2$ (**9a**) was isolated according to a previously described procedure. ^{1}H NMR (200 MHz, C_6D_6, 29°C): δ_H = 1.33 (s, 18 H, *t*Bu), 1.40 (t, 12 H, CH_3CH_2), 3.03 and 3.19 (2 s, 12 H, NMe_2), 3.08 (q, 8 H, CH_3CH_2), 7.16 (m, 6 H, Ar) ppm. Me_3SiCl (4.8 mL, 4.15 g, 38.2 mmol) was added with a syringe to a stirred solution of $[(2,6\text{-}Et_2C_6H_3N)_2(t$BuNP$)_2]Zr(NMe_2)_2$. The reaction mixture was stirred at room temperature overnight. The solvent was removed under vacuum. An orange residue was first extracted with hexane (30 mL) and then twice with a mixture of hexane (20 mL) and CH_2Cl_2 (7 mL). After solvent evaporation, the obtained dichloro complex was dried under vacuum to give the yellow-orange oil (1.6 g, 80.8%). $C_{28}H_{44}Cl_2N_4P_2Zr$ (660.8): calcd. C 50.90, H 6.71, N 8.48; found C 50.47, H 7.06, N 8.64. ^{1}H NMR (200 MHz, C_6D_6, 29°C): δ_H = 1.41 (s, 18 H, *t*Bu), 1.49 (t, 12 H, CH_3CH_2), 3.16 (q, J = 7.69 Hz, 8 H, CH_3CH_2), 7.20−7.33 (m, 6 H, Ar) ppm. ^{13}C{^{1}H} NMR (50.3 MHz, C_6D_6, 29°C): δ_C = 14.92 (t, J = 1.53 Hz, CH_3CH_2), 26.4 (d, J = 9.9 Hz, CH_3CH_2), 31.23 [t, $J_{P,C}$ = 6.48 Hz, $C(CH_3)_3$], 51.53 [t, $J_{P,C}$ = 14.5 Hz, $C(CH_3)_3$], 123.3 (Ar), 127.1 (Ar), 135.75 (Ar), 138.13 (t, J = 1.9 Hz, Ar) ppm. ^{31}P{^{1}H} NMR (162 MHz, C_6D_6, 21°C): δ_P = 115.6 (s) ppm. MS(EI): *m*/*z* (%) = 661 (1) [M^+], 626 (3) [M^+ − Cl], 500 (80) [ligand].

$[(2,5\text{-}t$Bu$_2C_6H_3N)_2(t$BuNP$)_2]ZrCl_2$ (10): A toluene solution of *cis*-$[(2,5\text{-}t$Bu$_2C_6H_3NH)_2(t$BuNP$)_2]$ (2.29 g, 3.74 mmol, 30 mL) was treated with $Zr(NMe_2)_4$ (1.0 g, 3.74 mmol) in toluene (10 mL) as in the case of **8**. The obtained bis(dimethylamido)zirconium complex $[(2,5\text{-}t$Bu$_2C_6H_3N)_2(t$BuNP$)_2]Zr(NMe_2)_2$ (**10a**) was characterized by NMR spectroscopy. ^{1}H NMR (200 MHz, C_6D_6, 29°C): δ_H = 1.44 (s, 36 H, *t*Bu*Ar*), 1.57 (s, 18 H, *t*Bu), 3.03−3.28 (12 H, NMe_2), 7.0 (dd, J_1 = 6.2, J_2 = 2.2 Hz, 2 H, 4-HPh), 7.35 (2 H, 3-HPh), 8.25 (dd, J_1 = 3.1, J_2 = 2.2 Hz, 2 H, 2-HPh) ppm. ^{13}C{^{1}H} NMR (50.3 MHz, C_6D_6, 29°C): δ_C = 31.0 [5-(CH_3)$_3$CAr], 31.34 [t, $J_{P,C}$ = 6.48 Hz, (CH_3)$_3$C], 31.54 [2-(CH_3)$_3$CAr], 33.11 [5-(CH_3)$_3$*C*Ar], 33.3 [2-(CH_3)$_3$*C*Ar], 43.8 (NMe_2), 51.7 [t, $J_{P,C}$ = 13.7 Hz, (CH_3)$_3$*C*], 113.85 (Ar), 114.5 (Ar), 117.17 (Ar), 127.0 (Ar), 141.9 (Ar), 150.0 (t, J = 1.15 Hz, Ar) ppm. ^{31}P{^{1}H} NMR (162 MHz, C_6D_6, 21°C): δ_P = 99.8 (s) ppm. Me_3SiCl (5.1 mL, 4.34 g, 40 mmol) was added with a syringe to a toluene solution of $[(2,5\text{-}t$Bu$_2C_6H_3N)_2(t$BuNP$)_2]Zr(NMe_2)_2$. The reaction mixture was stirred at room temperature overnight. All volatiles were removed under vacuum. The residue was extracted three times with a mixture of hexane (30 mL) and CH_2Cl_2 (20 mL). The extracts were combined and the solvent was removed in vacuo. The product, a yellow powder, was dried under vacuum. Yield 2.4 g, 83%. $C_{36}H_{60}Cl_2N_4P_2Zr$ (773.0): calcd. C 55.94, H 7.82, N 7.25; found C 55.16, H 8.52, N 7.96. ^{1}H NMR (200 MHz, C_6D_6, 29°C): δ_H = 1.44 (s, 36 H, *t*Bu*Ar*), 1.57 (s, 18 H, *t*Bu), 7.0 (dd, 2 H, J_1 = 6.22, J_2 = 2.2 Hz, 4-HPh), 7.36 (2 H, 3-HPh), 8.25 (2 H, J_1 = 3.3, J_2 = 2.2 Hz, 2-HPh) ppm. ^{13}C{^{1}H} NMR (50.3 MHz, C_6D_6, 29°C): δ_C = 31.0 [5-(CH_3)$_3$CAr], 31.34 [t, $J_{P,C}$ = 6.6 Hz, (CH_3)$_3$C], 31.54 [2-(CH_3)$_3$CAr], 33.1 [5-(CH_3)$_3$*C*Ar], 33.7 [2-(CH_3)$_3$*C*Ar], 51.7 [t, $J_{P,C}$ = 13.73 Hz, (CH_3)$_3$*C*], 113.8 (Ar), 114.5 (Ar), 117.15 (Ar), 136.95 (Ar), 140.7 (Ar), 150.0 (t, J = 1.53 Hz, Ar) ppm. ^{31}P{^{1}H} NMR (162 MHz, C_6D_6, 21°C): δ_P = 99.8 (s) ppm. MS(EI): *m*/*z* (%) = 772 (40) [M^+], 735 (20) [M^+ − Cl], 612 (90) [ligand].

$[(2,6\text{-}i$Pr$_2C_6H_3N)_2(t$BuNP$)_2]ZrCl_2$ (11): A toluene solution of *cis*-$[(2,6\text{-}i$Pr$_2C_6H_3NH)_2(t$BuNP$)_2]$ (1.91 g, 3.44 mmol, 20 mL) was treated with $Zr(NMe_2)_4$ (0.92 g, 3.44 mmol) in toluene (10 mL) as in the case of **8**. The bis(dimethylamido)zirconium complex $[(2,6\text{-}i$Pr$_2C_6H_3N)_2(t$BuNP$)_2]Zr(NMe_2)_2$ (**11a**) obtained was characterized by NMR spectroscopy. ^{1}H NMR (200 MHz, C_6D_6, 29°C): δ_H = 1.32 (s, 18 H, *t*Bu), 1.37 [d, 24 H, $(CH_3)_2CH$], 3.08−3.16 (m, 12 H, NMe_2), 3.92 [m, 4 H, $(CH_3)_2CH$], 7.0−7.3 (6 H, Ar) ppm. ^{31}P{^{1}H} NMR (162 MHz, C_6D_6, 21°C): δ_P = 115.45 (s) ppm. Me_3SiCl (4.5 mL, 3.8 g, 35 mmol) was added with a syringe to a toluene solution of $[(2,6\text{-}i$Pr$_2C_6H_3N)_2(t$BuNP$)_2]Zr(NMe_2)_2$ at 0 °C. The reaction mixture obtained was stirred at room temperature overnight. The product (yellow oil) was isolated as in the case of **9**. Yield 2.28 g, 92.3%. $C_{32}H_{52}Cl_2N_4P_2Zr$ (716.9): calcd. C 53.61, H 7.31, N 7.82; found C 53.50, H 7.17, N 7.80. ^{1}H NMR (200 MHz, C_6D_6, 29°C): δ_H = 1.37 (s, 18 H, *t*Bu), 1.42 [d, 24 H, $(CH_3)_2CH$], 3.97 [m, J = 6.96 Hz, 4 H, $(CH_3)_2CH$], 7.12−7.28 (6 H, Ar) ppm. ^{13}C{^{1}H} NMR (50.3 MHz, C_6D_6, 29°C): δ_C = 24.17 [t, J = 1 Hz, $(CH_3)_2CH$], 31.37 [t, $J_{P,C}$ = 6.7 Hz, $(CH_3)_3C$], 32.2 [d, J = 0.8 Hz, $(CH_3)_2CH$], 51.8 [t, $J_{P,C}$ = 14.6 Hz, $(CH_3)_3C$], 123.3 (Ar), 124.0 (Ar), 128.3 (Ar), 141 (Ar) ppm. ^{31}P{^{1}H} NMR (162 MHz, C_6D_6, 21°C): δ_P = 115.47 (s) ppm. MS(EI): *m*/*z* (%) = 716 (3) [M^+], 681 (2) [M^+ − Cl], 556 (20) [ligand].

Polymerization Experiments: A 1-L Büchi glass autoclave (or a steel autoclave at a pressure of 8 bar) was charged with dry toluene (200 mL), cocatalyst (MAO), and thermostatted to the required temperature. The autoclave was saturated with ethylene, and a desired amount of precatalyst solution was then injected. The monomer pressure (±50 mbar), temperature (±0.5 °C), and monomer consumption were controlled by real-time monitoring. Polymerization was quenched with 10% HCl solution in methanol, and the polymer precipitated quantitatively by pouring the solution into methanol (400 mL), acidified with a small amount of aqueous hydrochloric acid. The polymer materials obtained were washed several times with methanol and water, and dried at 60 °C. The polymerization activities were calculated as kg of PE × (mol_{cat} × $[C_2H_4]$ × h)$^{-1}$ from experimental data to adjust the changes in the ethene concentration in toluene. The values of $[C_2H_4]$ for different ethene pressures and polymerization temperatures were taken from ref.[33]

X-ray Crystallographic Study: The crystal data of *cis*-$[(Ph_2CHNH)_2(t$BuNP$)_2]$ (**2**) were collected with an Enraf−Nonius CAD-4 single-crystal diffractometer at 193(2) K using Cu-K_α radiation (graphite monochromator), λ = 1.54179 Å (scan type ω/2θ). Intensities were corrected for Lorentz and polarization effects and for absorption, XCAD4.[34−36] The crystal data of $[(Ph_2CHN)_2(t$BuNP$)_2]Zr(NMe_2)_2$ (**8a**) were collected with a Nonius KappaCCD area-detector diffractometer at 173(2) K using Mo-K_α radiation (graphite monochromator), λ = 0.71073 Å. Data reduction: COLLECT.[37] Absorption correction: SADABS.[38] Solution and refinement: SHELX-97,[39] direct methods. All non-hydrogen atoms were refined anisotropically. Hydrogen atoms were refined in calculated positions. The displacement factors of the H atoms were 1.2 × (1.5 ×) that of the host atom. Graphics: SHELXTL/PC.[40] CCDC-231525 and -231526 contain the supplementary crystallographic data for this paper. These data can be obtained free of charge at www.ccdc.cam.ac.uk/conts/retrieving.html [or from the Cambridge Crystallographic Data Centre, 12 Union Road, Cambridge CB2 1EZ, UK; Fax: + 44-1223-336-033; E-mail: deposit@ccdc.cam.ac.uk].

Acknowledgments

Support of this work by CIMO and Academy of Finland (decision no.: 0204408) is gratefully acknowledged.

[1] R. R. Schrock, F. Schattenmann, M. Aizenberg, W. M. Davis, *Chem. Commun.* **1998**, 199.
[2] A. D. Horton, J. de With, A. J. van der Linden, H. van de Weg, *Organometallics* **1996**, *15*, 2672.

 © 2004 Wiley-VCH Verlag GmbH & Co. KGaA, Weinheim

[3] R. R. Schrock, S. W. Seidel, Y. Schrodi, W. M. Davis, *Organometallics* **1999**, *18*, 428.
[4] L.-C. Liang, R. R. Schrock, W. M. Davis, *Organometallics* **2000**, *19*, 2526.
[5] R. R. Schrock, R. Baumann, S. M. Reid, J. T. Goodman, R. Stumpf, W. M. Davis, *Organometallics* **1999**, *18*, 3649.
[6] Y. Schrodi, R. R. Schrock, P. J. Bonitatebus Jr., *Organometallics* **2001**, *20*, 3560.
[7] L. P. Grocholl, V. Huch, P. Steinhart, A. Johnson, L. Stahl, R. J. Staples, *Inorg. Chem.* **1997**, *36*, 4451.
[8] G. J. P. Britovsek, V. C. Gibson, D. F. Wass, *Angew. Chem.* **1999**, *111*, 448; *Angew. Chem. Int. Ed.* **1999**, *38*, 428.
[9] V. C. Gibson, K. Spitzmesser, *Chem. Rev.* **2003**, *103*, 283.
[10] R. R. Schrock, P. J. Bonitatebus Jr., Y. Schrodi, *Organometallics* **2001**, *20*, 1056.
[11] J. T. Patton, S. G. Feng, K. A. Abboud, *Organometallics* **2001**, *20*, 3399.
[12] J. D. Scollard, D. H. McConville, J. J. Vittal, *Organomnetallics* **1997**, *16*, 4415.
[13] A. D. Horton, J. de With, *Chem. Commun.* **1996**, 1375.
[14] C. H. Lee, Y.-H. L, J. W. Park, *Organometallics* **2000**, *19*, 344.
[15] V. C. Gibson, B. S. Kimberley, A. J. P. White, D. J. Williams, P. Howard, *Chem. Commun.* **1998**, 313.
[16] R. M. Gauvin, J. Kress, *J. Mol. Cat. A: Chem.* **2002**, *182*, 411.
[17] F. Guerin, D. H. McConville, J. J. Vittal, *Organometallics* **1996**, *15*, 5586.
[18] L. P. Grocholl, L. Stahl, R. J. Staples, *Chem. Commun.* **1997**, 1465.
[19] D. F. Moser, C. J. Carrow, L. Stahl, R. J. Staples, *J. Chem. Soc., Dalton Trans.* **2001**, 1246.
[20] D. F. Moser, L. Grocholl, L. Stahl, R. J. Staples, *Dalton Trans.* **2003**, 1402.
[21] G. Bai, H. W. Roesky, H.-G. Schmidt, M. Noltemeyer, *Organometallics* **2001**, *20*, 2962.
[22] P. M. Castro, K. Lappalainen, M. Ahlgren, M. Leskelä, T. Repo, *J. Polym. Sci., Part A: Polym. Chem.* **2003**, *41*, 1380.
[23] A. S. Abu-Surrah, K. Lappalainen, U. Piironen, P. Lehmus, T. Repo, M. Leskelä, *J. Organomet. Chem.* **2002**, *648*, 55.
[24] T. V. Laine, U. Piironen, K. Lappalainen, M. Klinga, E. Aitola, M. Leskelä, *J. Organomet. Chem.* **2000**, *606*, 112.
[25] T. Repo, M. Klinga, P. Pietikäinen, M. Leskelä, A.-M. Uusitalo, T. Pakkanen, K. Hakala, P. Aaltonen, B. Löfgren, *Macromolecules* **1997**, *30*, 171.
[26] K. V. Axenov, V. V. Kotov, M. Klinga, M. Leskelä, T. Repo, *Eur. J. Inorg. Chem.* **2004**, 695.
[27] R. Jefferson, J. F. Nixon, T. M. Painter, *J. Chem. Soc., Dalton Trans.* **1973**, 1415.
[28] L. Stahl, *Coord. Chem. Rev.* **2000**, *210*, 203.
[29] T. G. Hill, R. C. Haltiwanger, M. L. Thompson, S. A. Katz, A. D. Norman, *Inorg. Chem.* **1994**, *33*, 1770.
[30] W. Kaminsky, M. Arndt, *Applied Homogeneous Catalysis with Organometallic Compounds* (Eds.: B. Cornils, W. A. Herrmann), VCH Weinheim, New York, Basel, Cambridge, Tokyo, **1996**, vols. 1 and 2.
[31] *Metallocenes* (Eds.: A. Togni, R. L. Halterman), Wiley-VCH, Weinheim, New York, Basel, Cambridge, Tokyo, **1998**, vol. 1, p. 577 and references therein.
[32] The dependency of the molar mass and monomer concentration has been elegantly demonstrated with metallocene catalysts and explained by Brintzinger at al.; see: U. Stehling, J. Diebold, R. Kirsten, W. Roell, H. H. Brintzinger, S. Juengling, R. Mülhaupt, F. Langhauser, *Organometallics* **1994**, *13*, 964.
[33] W. Hayduk, *Solubility Data Series*, Oxford University Press, Oxford, **1994**, vol. 57 (Ethene), p. 126−162.
[34] *CAD-4 Software (Updated 1998, Linux version)*, Enraf−Nonius, Delft, The Netherlands, **1985**.
[35] A. C. T. North, D. C. Phillips, F. C. Mathews, *Acta Crystallogr., Sect. A* **1968**, *24*, 351.
[36] K. Harms, *Program for the Lp-correction of Enraf−Nonius CAD-4 Diffractometer Data*, University of Marburg, Marburg, Germany, **1996**.
[37] Nonius, *COLLECT*, Nonius BV, Delft, The Netherlands, **2002**.
[38] G. M. Sheldrick, *SADABS*, University of Göttingen, Germany, **1996**.
[39] G. M. Sheldrick, *SHELX-97*, *Program for the Solution and Refinement of Crystal Structures*, University of Göttingen, Germany, **1997**.
[40] G. M. Sheldrick, *SHELXTL/PC*, Version 5.10. Bruker AXS, Inc., Madison, Wisconsin, USA, **1997**.

Received April 13, 2004
Early View Article
Published Online October 26, 2004

 © 2004 Wiley-VCH Verlag GmbH & Co. KGaA, Weinheim

NMR Study of L-Shaped (Quinoxaline)platinum(II) Complexes − Crystal Structure of $[Pt(DMeDPQ)(bipy)](PF_6)_2$

Enrico Rotondo,*[a] Archimede Rotondo,[a] Francesco Nicolò,[a] Maria Letizia Di Pietro,[a] Maria Anna Messina,[a] and Matteo Cusumano[a]

Keywords: DNA recognition / N ligands / Nitrogen heterocycles / NMR spectroscopy / Platinum

A ^1H and ^{13}C NMR study of nine Pt^{II} complexes of DMeDPQ [6,7-dimethyl-2,3-bis(2-pyridyl)quinoxaline] and BDPQ [2,3-bis(2-pyridyl)benzo[*g*]quinoxaline], and the crystal structure of one of them, are reported. The results are consistent with C_s symmetry of "L-shaped square-planar complexes". The rigid seven-membered chelated quinoxaline ligand holds the fused aromatic rings nearly perpendicular to the Pt^{II} coordination plane, generating the peculiar L-shaped structure. Ancillary ligands in the residual coordination sites are: a) bidentate flexible-planar 2,2′-bipyridine (bipy; complexes **1** and **2**); b) bidentate rigid-planar dipyrido[3,2-*a*:2′3′-*c*]phenazine (dppz) or benzo[*b*]dipyrido[3,2-*h*:2′,3′-*j*]phenazine (bdppz; complexes **3**–**6**); or c) 3-substituted monodentate pyridines (3-Rpy; complexes **7**–**9**). The L-shaped geometry has been exploited to gain insight into the steric and dynamic features that regulate the noncovalent interactions of these square-planar complexes with DNA. We have shown previously, for $[Pt(bipy)(n\text{-}Rpy)_2]^{2+}$, that bipy twisting can be frozen out on the NMR timescale below 260 K. Preservation of the C_s symmetry at low temperature indicates a lack of bipy fluxionality within these L-shaped structures. The static butterfly-like symmetric orientation of the quinoxaline pyridyl rings accounts for the hampered twisting of Pt(bipy), which is otherwise assisted by the synchronous "windscreen wiper" conrotatory rocking of the ancillary pyridine rings. The L-geometry can also be used to monitor the ancillary *n*-Rpy rotation by NMR spectroscopy. The quasi-vertical quinoxaline pyridyl rings alignment leave room in the coordination plane for the crossing of the opposite pyridine rings, thereby reducing their rotational barriers about the Pt–N bond.
(© Wiley-VCH Verlag GmbH & Co. KGaA, 69451 Weinheim, Germany, 2004)

Introduction

In the course of our interest in intercalative, noncovalent interaction of square-planar Pt^{II} complexes with DNA duplex, we have recently synthesised platinum(II) complexes of DMeDPQ and BDPQ. These ligands display a rather flexible metal-ion binding pattern often characterised by chelation through the pyrazine and pyridyl nitrogen atoms to form potentially dicompartmental five-membered ring ligands. Different coordination patterns, however, are also known. On the basis of literature reports three main coordination geometries can be envisaged for these ligands: (i) half-filled mononuclear;[1] (ii) completely filled dinuclear (the ligand acts as a two-metal bridge);[2] and (iii) a less-common seven-membered bis(pyridyl)metal chelate ring[3] (Scheme 1). One case of BDPQ three-coordination through two pyridyl nitrogen atoms and the deprotonated hydroxy oxygen atom of the hydrate ligand has also been reported.[4]

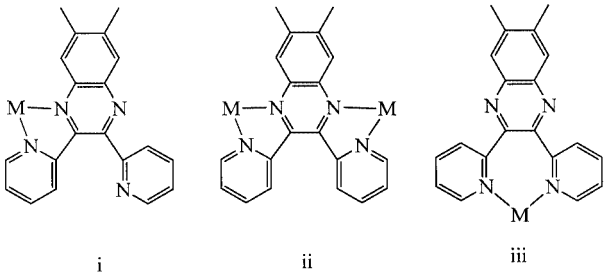

i ii iii

Scheme 1. Common coordination modes adopted by BDPQ and DMeDPQ

Most of the known DMeDPQ and BDPQ complexes were unambiguously characterised by X-ray crystallography as mononuclear and binuclear octahedral complexes, and very few tetracoordinate complexes have been reported so far.[5] We have recently found that in $[PdCl_2(DMeDPQ)]$[6] and $[Pt(BDPQ)(bipy)](PF_6)_2$ [7] the quinoxalines coordinate to the metal as seven-membered bis-pyridyl chelates. This binding holds the fused aromatic rings perpendicular to the coordination plane to give an angular "L-shaped" structure (Figure 1).

The same coordination geometry has been reported for $[PtCl_2(DMeDPQ)]$[8] and $[Pd(DPQ)_2](PF_6)_2$.[9] Saturation of

[a] Dipartimento di Chimica Inorganica, Chimica Analitica e Chimica Fisica, Facoltà di Scienze, Università di Messina
Salita Sperone 31, 98166 Messina, Italy
Fax: + 39-090-393-756
E-mail: rotondo@chem.unime.it

 © 2004 Wiley-VCH Verlag GmbH & Co. KGaA, Weinheim **DOI: 10.1002/ejic.200400421**

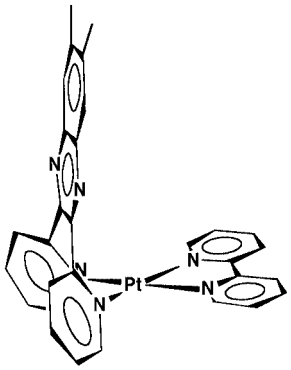

Figure 1. Schematic drawing of $[Pt(DMeDPQ)(bipy)]^{2+}$

the residual coordination sites of (quinoxaline)Pt^{II} substrates with flat bidentate ligands led to the six mixed complexes **1**−**6**, which bear two extended mutually orthogonal planar moieties, both of which are capable of undergoing intercalation as well as enantioselective DNA recognition. The ambintercalating character of these complexes has been investigated recently.[7] In this paper we report the ^1H and ^{13}C NMR spectroscopic characterisation of the ambintercalator complexes **1**−**6**, and their monodentate pyridine analogues **7**−**9** (see Scheme 2). The crystal structure of $[Pt(DMeDPQ)(bipy)](PF_6)_2$ (**1**) has also been resolved by X-ray diffraction. The unambiguous resonance assignment and structure determination are essential steps on the way toward intercalative mapping driven by magnetic perturbation of the nuclei upon insertion into the DNA double helix. Moreover, we designed the quinoxaline coordination geometry to gain insight into the structural and dynamic features regulating the noncovalent interactions of the square-planar complexes with DNA. Despite quinoxalines' versatility to act as a magnetic probe of the structural and dynamic features of the ancillary ligands, NMR studies of these L-shaped Pt^{II} complexes have, up to now, been largely neglected.

Results and Discussion

The syntheses of complexes **1**−**9** are discribed in the Exp. Sect.

Our experimental evidence is consistent with DMeDPQ and BDPQ acting as bidentate seven-membered dipyridyl chelates. The ancillary ligands in the residual coordination sites of the nine complexes studied here belong to three different classes: a) bidentate-planar with a certain degree of flexibility (bipy; complexes **1** and **2**); b) more rigid bidentate-planar phenazine (dppz and bdppz; complexes **3**−**6**); c) monodentate pyridines (3-Rpy, R = H, CH_3; complexes **7**−**9**). 2-D representations of the ligands and schematic formulae for complexes **1**−**9** are given in Scheme 2.

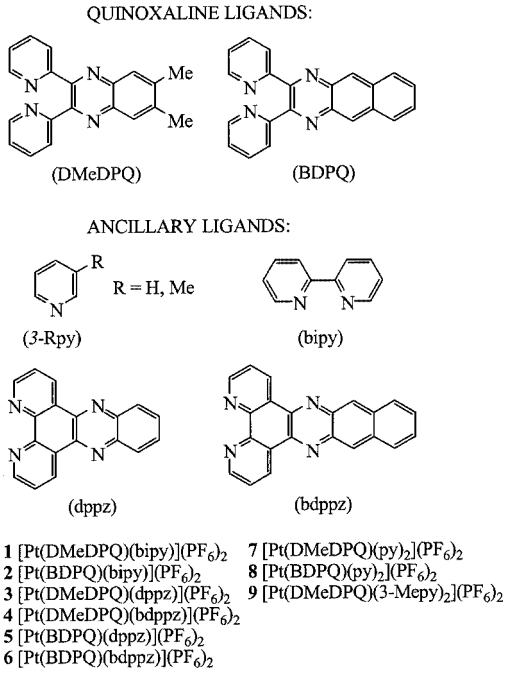

Scheme 2. 2D representation of ligands and schematic formulae **1**−**9**

The solid-state structure, solved by X-ray diffraction, unequivocally shows the L-shaped nature of **1**. The same coordination has previously been found for analogous substrates,[6−9] meaning that "L-shaped" is the preferred structure for square-planar (quinoxaline)Pt^{II} and -Pd^{II} complexes. This geometry has C_s symmetry due to a vertical mirror plane (σ_v) intersecting the metal atom. The high-resolution NMR spectra are consistent with this symmetry element, as single signals are detected for every pair of nuclei interchanged by the symmetry operation. Standard 1- and 2-D NMR techniques were employed for thorough resonance assignment (Tables 1 and 2).

Discrimination between the quinoxaline pyridyl and the 2,2′-bipyridine proton resonances of **1** and **2** was achieved by heteronuclear long-range C-7′/3′-H coupling, which allowed the assignment of 3′-H and thus the whole set of pyridyl resonances. Analogously, the phenazine pyridyl resonances could be assigned due to the heteronuclear long-range C-7/4-H coupling (C-7 signal at higher field than C-7′ signal). Together with other data, dipolar 10-H/4-H coupling of the planar phenazine protons, which is not found between 10′-H and 3′-H or 10′-H and 4′-H of the bent quinoxaline, confirmed the heteronuclear long-range coupling assignments of **3**−**6**. A peculiar, previously reported ^1H NMR spectral feature of $[Pt(bipy)(n\text{-}Rpy)_2]^{2+}$ is a strong diamagnetic shift experienced by the 6-H protons of the bipy ligand because of the anisotropic ring current of the quasi-perpendicular *n*-Rpy group.[10] We found a similar effect in **1** and **2**, where the seven-membered chelates hold the bis(pyridyl) vertical rings just above 6-H of bipy. This diamagnetic shift is less in rigidly planar phenazine complexes **3**−**6**, and even more so in the 3-Rpy derivatives **7**−**9**.

 © 2004 Wiley-VCH Verlag GmbH & Co. KGaA, Weinheim

Table 1. Selected ^{1}H NMR resonances of complexes **1**−**9** in [D$_6$]acetone at 298 K

	2-H	3-H	4-H	5-H	6-H	10-H	11-H	12-H	13-H	3′-H	4′-H	5′-H	6′-H	10′-H	12′-H	13′-H
1	–	8.67	8.53	7.83	8.18	–	–	–	–	8.29	8.57	8.14	9.46	8.05	2.58	–
2	–	8.65	8.53	7.85	8.22	–	–	–	–	8.39	8.61	8.18	9.52	8.98	8.34	7.78
3	–	–	10.01	8.33	8.71	8.47	8.21	–	–	8.36	8.63	8.21	9.60	8.05	2.54	–
4	–	–	9.88	8.29	8.65	8.92	–	8.14	7.55	8.39	8.65	8.23	9.62	8.09	2.54	–
5	–	–	9.99	8.33	8.73	8.43	8.17	–		8.45	8.66	8.29	9.65	8.96	8.31	7.73
6	–	–	9.86	8.29	8.66	8.88	–	8.11	7.52	8.48	8.68	8.29	9.67	9.00	8.29	7.71
7	8.92	7.62	8.07	7.62	8.92	–	–	–	–	8.21	8.37	7.86	9.24	8.19	2.70	–
8	8.94	7.62	8.07	7.62	8.94	–	–	–	–	8.31	8.40	7.91	9.29	9.12	8.46	7.88
9	8.80	–	7.86	7.47	8.71					8.19	8.35	7.86	9.22	8.20	2.70	–

Table 2. Selected ^{13}C{^{1}H} NMR resonances of complexes **1**−**9** in [D$_6$]acetone at 298 K

	C-2	C-3	C-4	C-5	C-6	C-7	C-2′	C-3′	C-4′	C-5′	C-6′	C-7′	C-9′	C-10′
1	157.5	125.6	143.7	129.8	150.9	–	158.8	131.0	143.9	130.2	153.2	147.4	145.2	129.2
2	157.6	125.6	143.9	129.8	150.9	–	158.6	131.3	144.0	130.4	153.3	148.7	138.4	129.6
3	151.1	131.7	139.5	129.3	152.9	143.7	159.0	131.2	143.9	130.3	153.4	147.6	145.5	129.2
4	151.5	131.8	139.4	129.6	152.9	140.0	159.0	131.2	144.0	130.4	153.5	147.6	145.6	129.1
5	151.1	131.6	139.5	129.5	152.9	143.7	158.8	131.4	144.1	130.6	153.5	148.6	138.3	129.3
6	151.4	131.8	139.4	129.5	152.9	140.0	158.8	131.5	144.1	130.6	153.6	148.6	138.4	129.5
7	152.7	128.8	142.5	128.8	152.7	–	158.6	130.9	143.2	128.9	152.1	147.6	145.2	129.5
8	152.7	128.8	142.6	128.8	152.7	–	158.5	131.1	143.4	129.1	152.3	148.7	138.9	129.7
9	152.0	139.2	142.6	127.7	149.5	17.9	158.3	130.5	142.9	128.5	151.8	147.5	145.2	129.3

Coordinated bipy is usually thought of as a perfectly flat fragment; however, we have previously proposed a slight propeller-like torsion of the ligand in [Pt(bipy)(*n*-Rpy)$_2$]$^{2+}$ cations on the basis of both low-temperature NMR spectra[10] and X-ray crystal structures.[11] Indeed, in order to minimize intramolecular bumping, these complexes undergo a slight bipy-propeller distortion concerted to an about 10° conrotation of the quasi-vertical *n*-Rpy. NMR spectra consistent with time-averaged C_{2v} symmetry are due to fast bipy twisting synchronous to windscreen wiper rocking of *n*-Rpy. Locked propeller structures can be witnessed by low-temperature resonance splitting observed for nonfluxional molecules devoid of C_2 symmetry axis.[10] In this sense the lack of C_2 symmetry and the static configuration makes the (DMeDPQ)Pt and (BDPQ)Pt fragments excellent NMR probes of the ancillary bipy distortion. Despite the presence of many nuclei suitably positioned for magnetic monitoring of bipy distortion, we could not detect any ^{1}H or ^{13}C resonance splitting at 210 K for solutions of **1** and **2** (or for any of the other complexes studied here). This is a strong indication of planar bipy, which is not allowed to break the L-shaped molecular C_s symmetry. In agreement with this, the X-ray diffraction data of **1** show a perfectly planar Pt(bipy) skeleton. The disparity between the coordinated bipy geometry and fluxionality can be attributed to a slight but crucial difference in the orientation adopted, respectively by the *n*-Rpy of [Pt(bipy)(*n*-Rpy)$_2$]$^{2+}$, and quinoxaline pyridyl rings of **1** and **2**. Molecular models based on crystallographic data show, in fact, that the symmetrically disrotated quinoxaline pyridyl wings of [Pt(DMeDPQ)(bipy)]$^{2+}$ and [Pt(BDPQ)(bipy)]$^{2+}$ (rigid butterfly-like configuration) hamper, unlike the conrotated pyridine rings of [Pt(bipy)(*n*-Rpy)$_2$]$^{2+}$, twisting of the opposite bipy (Figure 2). Therefore, the bipy moieties of the L-shaped cations are forced into the same rigid planar structure as dppz and bdppz. Indeed, low-temperature NMR spectra of [Pt(dppz)(*n*-Rpy)$_2$]$^{2+}$ and [Pt(dppz)(*n*-Rpy)$_2$]$^{2+}$, as the L-shaped cations, do not show resonance splitting.[12]

The monodentate 3-substituted pyridines 3-Rpy are the ancillary ligands in **7**−**9**. In **9** we introduced a methyl substituent on the pyridine ring to gain clues concerning geometry and monitoring of the dynamics, as hindered rotation of 3-Mepy would lead to an NMR-detectable *s-cis*/*s-trans* rotamer equilibrium.[10] Solutions of **9** actually show resonances of a single compound. This could either mean a much greater thermodynamic stability of one rotamer, or a low rotational barrier for 3-Rpy (fast exchange). Very accurate selective NOED spectra indicate a spatial 2-H/6-H connectivity attributable to the neighbouring pyridine rings. This excludes the unique presence of an *s-cis* rotamer, but is consistent with both a static *s-trans* rotamer and fast rotation. Positive NOEs for **9** were also detected between the quinoxaline 6′-H and both 2-H and 6-H of the pyridyl moieties. Indeed, dipolar couplings by themselves suggest 3-Mepy rotation leading to transient 2-H/6-H contacts between nuclei of the neighbouring 3-Mepy; and also 2-H and 6-H temporarily alternate their proximity to 6′-H of the static quinoxaline pyridyl rings (Figure 3). This conclusion is further supported by the ^{13}C-^{1}H relaxation-time constants of **7** and **9**. Under decoupling conditions, for a pure dipolar relaxation in the extreme narrowing limit (neglect-

 © 2004 Wiley-VCH Verlag GmbH & Co. KGaA, Weinheim

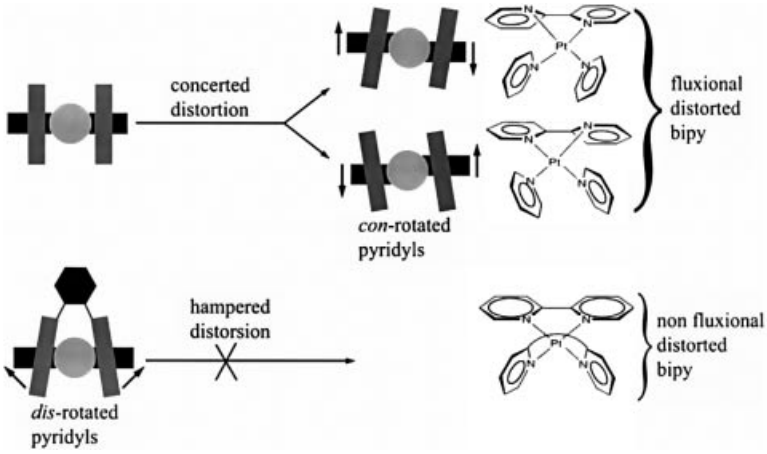

Figure 2. Allowed or hampered distortion of Pt(bipy) cations

ing contributions of unattached protons and considering the C−H distance to be constant), the aromatic ^{13}C-^{1}H relaxation time can be taken as a measure of the anisotropic spin diffusion.[13] The rotation of rings anchored to a bulk matrix slows down the relaxation rates of the *ortho*- and *meta*-carbon atoms without altering the *para*-carbon atom, whose proton-attached dependent local field is not affected by the rotational diffusion. The increased relaxation-time constants shown by the *ortho*- and *meta*-carbon atoms relative to the *para*-carbon atom are thus consistent with fast 3-Rpy rotation (Table 3).

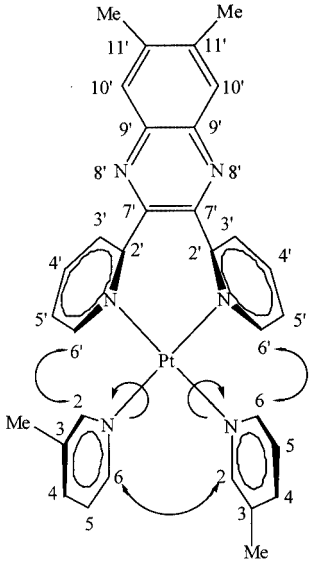

Figure 3. Remarkable dipolar couplings detected for **9** by NOESY NMR spectroscopy

The low-temperature NMR spectra of **9** in acetone at 210 K do not show evidence of 3-Mepy freezing, in agreement with a low rotational barrier of the pyridine ring. On the contrary, the corresponding $[Pt(bipy)(3\text{-}Mepy)_2]^{2+}$ cation shows *s-cis* and *s-trans* rotamers interconverting at 320 K with $\Delta G^{\#}$ of 68.5 kJ·mol^{-1}.[10] This difference can be attributed to the quasi-vertical orientation of quinoxaline

Table 3. Selected relaxation-time constants [s] of the aromatic ^{13}C-H carbon atoms in [D_6]acetone at 298 K; standard deviations are less than 5%

	DMeDPQ						3-Rpy			
	C-3′	C-4′	C-5′	C-6′	C10′	C-2	C-3	C-4	C-5	C-6
7	0.79	0.78	0.84	0.81	0.88	1.31	1.35	0.90	1.35	1.31
9	0.74	0.72	0.80	0.75	0.85	1.21	–	0.85	1.28	1.16

pyridyl rings which remove hindrance from the coordination plane. Analogous conclusions can be drawn from the NMR spectra of **7** and **8** showing, also at 210 K, three pyridine resonances (for the four *ortho*, four *meta* and two *para* nuclei, respectively) due to symmetry averaging about the coordination plane prompted by fast pyridine rotation.

Despite all our efforts we were not able to prepare 2-Mepy quinoxaline complexes. It is likely that coordination is inhibited by the steric hindrance between the *ortho*-methyl substituent and the hetroaromatic rings.

Molecular Structure of {[Pt(DMeDPQ)(bipy)][PF_6]$_2$}·0.5{(DMeDPQ)(CH_3OH)}

The 6,7-dimethyl-2,3-bis(2-pyridyl)quinoxaline ligand (DMeDPQ) crystallises with the platinum salt in a 3:2 ratio. The crystal contains a discrete complex $[Pt(DMeDPQ)(bipy)]^{2+}$ cation with the hexafluorophosphate ions as counterions (ratio 1:2), and co-crystallised uncoordinated ligand and methanol solvent (both in a 2:1 ratio). This solid-state aggregate is stabilized by strong π-stacking (3.6 Å) between the planar quinoxaline fragment of the alternate free and coordinated ligands along the *c* axis: the anions and the methanol molecules are retained between these parallel columns by hydrogen-bonding interactions. The 3-D packing arrangement is very ordered and shows an overall symmetry (expressed by the adopted crystallographic space group) higher than the single compound moieties, which causes an important symmetry disorder for the free ligand and one PF_6^- anion.

 © 2004 Wiley-VCH Verlag GmbH & Co. KGaA, Weinheim

The coordinated quinoxaline ligand shows the same arrangement as adopted in a previous Pd compound [$PdCl_2$(DMeDPQ)][6] showing a slight conjugation between the aromatic bicyclic system and the pyridine ring, as evidenced by the N2−C10−C11−C11′ torsion angles [−52.9(5)° vs. the average value of 57.5(4)°] that is similar to the corresponding value in the free disordered ligand [−48(1)°]. This typical butterfly arrangement, which allows the nitrogen lone pairs to be oriented out of the ligand plane towards the metal atom in the coordinated quinoxaline, is also observed in the uncoordinated ligand.[14] The steric requirements of the ligand bite may also be responsible for the significant deformations from planarity of the quinoxaline[15] and the enlargement of the pyridine substituent angles up to 130° (protonated free ligand).[16]

The pyridyl orientation causes the quinoxaline mean plane to be normal to the platinum coordination plane containing the bipyridyl ligand, with a dihedral angle between them of 81.09(9)°. The angle of 71.4(2)° between the quinoxaline pyridine rings and the Pt coordination plane may indicate a possible interaction of the π-orbitals of both rings with the d_{xz}, d_{yz} and d_{xy} orbitals of the metal atom.[17] The DMeDPQ and bipy Pt−N bond lengths are similar [2.027(4) vs. 2.013(3) Å, respectively], the angular distortion from the regular square-planar Pt coordination geometry being mainly due to the different bite size of the two ligands (Figure 4).

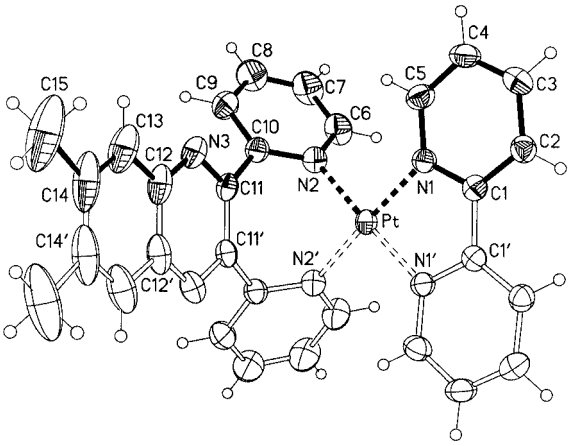

Figure 4. View of the cation of complex **1**, which lies on a mirror plane, with its labelling scheme; empty atoms represent the symmetric half moiety generated by the $x, -y + 1, z$ operation; anions, co-crystallised uncoordinated ligand and methanol moieties have been omitted for clarity; thermal ellipsoids are drawn at 30% probability while the hydrogen-atom size is arbitrary; selected bond lengths [Å] and angles [°]: Pt−N1 2.013(3), Pt−N2 2.027(4), N1−C1 1.365(5), C1−C1′ 1.457(8), N2−C10 1.341(5), C10−C11 1.480(6), C11−C11′ 1.425(9), C11−N3 1.330(5), N3−C12 1.368(6), C12−C12′ 1.42(1); N1−Pt−N2 97.0(1), N1′−Pt−N1 80.7(2), N2−Pt−N2′ 85.2(2), N1−C1−C1′ 114.9(2), C2−C1−C1′ 124.3(3), N3−C11−C10 113.4(4), C11′−C11−C10 124.9(2)

Conclusions

Quinoxalines lead to L-shaped Pt^{II} complexes of C_s local symmetry. The rigid butterfly-like structure gives these complexes stereochemical properties, which can be exploited for studying geometry and fluxionality of several ancillary ligands. The prochiral character of coordinated quinoxaline could pave the way to enantioselective synthesis and new classes of chiral compounds.

Experimental Section

General Remarks: ^1H and $^{13}C\{^1H\}$ NMR spectra were recorded with a Bruker ARX 300 spectrometer, at 300.13 and 75.47 MHz, respectively. The ^1H NMR spectra were calibrated against the residual proton signals of the solvent as internal reference ([D_6]acetone, δ = 2.04 ppm), the $^{13}C\{^1H\}$ spectra were calibrated against the septuplet signals of the solvent ([D_6]acetone δ = 29.80 ppm).

Synthesis: Complexes **1** and **2** were prepared by dissolving DMeDPQ (Aldrich) or BDPQ[18] (2.5 mmol), respectively, in 100 mL of CH_3OH, adding H_2O to give a 1:1 CH_3OH/H_2O mixture and suspending a slight excess (5%) of [$PtCl_2$(bipy)][19] with respect to the stoichiometric ratio in it. The mixture was then heated to boiling and kept refluxing for 1/2 h until almost complete dissolution of the platinum complex. After filtration to eliminate the traces of solid material, NH_4PF_6 was added and the resulting complexes **1** and **2** precipitated as yellow solids, which were recrystallised from CH_3OH. Yields: 75% (**1**), 83% (**2**).

Complexes **3**−**6** were synthesised starting from the corresponding phenazine (dppz[20] or bdppz[21]) dichloride, obtained as follows: The phenazine ligand (2.5 mmol) was dissolved in 100 mL of warm (ca. 50 °C) DMSO and added dropwise and with stirring to an equivalent amount of [$PtCl_2(DMSO)_2$],[22] also dissolved in 100 mL of warm DMSO. After a few minutes, the red (phenazine)platinum dichloride, initially yellow in the case of [$PtCl_2$(dppz)], precipitated. To facilitate its coagulation, the mixture was stirred for 1 h, then filtered, washed with H_2O and a few drops of CH_3OH to eliminate the DMSO, and air-dried. A slight excess of the dichloride thus obtained was then suspended in a CH_3OH/H_2O (2:1) mixture (300 mL) in which the quinoxaline ligand (DMeDPQ or BDPQ; 2.5 mmol) had been previously dissolved. To facilitate the dissolution of the sparingly soluble phenazine dichloride complex, a few drops of DMSO were added and the mixture was heated to boiling and kept refluxing for 3 d. After cooling, insoluble material was separated by centrifugation, and the final product precipitated from the coloured solution (yellow for the complexes with dppz and orange-red for the ones with bdppz) by addition of an excess of NH_4PF_6. Since the yield of the reaction was very low, especially for the two complexes with bdppz, it was necessary to recover the unchanged (dppz)- and (bdppz)platinum dichloride from the bottom of the test tubes, and to repeat 2−3 times, under the same conditions, the treatment with the corresponding quinoxaline ligand. The ivory [Pt(DMeDPQ)(dppz)]$(PF_6)_2$, the reddish [Pt(DMeDPQ)(bdppz)]$(PF_6)_2$, the orange-brown [Pt(BDPQ)(dppz)]$(PF_6)_2$ and the brick-red [Pt(BDPQ)(bdppz)]$(PF_6)_2$ were all recrystallised from CH_3CN. Yields: 61% (**3**), 27% (**4**), 69% (**5**), 20% (**6**).

For the synthesis of complexes **7**−**9** it was necessary to prepare the corresponding (DMeDPQ)- or (BDPQ)platinum dichloride. To this end, the quinoxaline ligand (2.5 mmol) was dissolved in warm (ca. 50 °C) DMSO (100 mL) and added dropwise with stirring to an equivalent amount of [$PtCl_2(DMSO)_2$],[22] also dissolved in DMSO (100 mL). After a few minutes, an off-white product, in the case of [$PtCl_2$(DMeDPQ)], or a deep yellow one, for [$PtCl_2$(BDPQ)],

 © 2004 Wiley-VCH Verlag GmbH & Co. KGaA, Weinheim

precipitated. Since the chloro complexes were very powdery and so very difficult to filter, after 5 h a few drops of H_2O were added to facilitate their coagulation and then filtered through a water pump. The product was washed with H_2O and a few drops of CH_3OH to eliminate the DMSO, and air-dried. The dichloride complex thus obtained was then suspended in H_2O in the presence of the appropriate pyridine (5% excess with respect to the stoichiometric 1:2 ratio) and heated to boiling. After dissolution of the complex, NH_4PF_6 was added and the resulting complexes **7**−**9** precipitated as light-yellow solids, which were washed with H_2O and a few drops of CH_3OH, and air-dried. The complexes were then recrystallised from CH_3OH. Yields: 67% (**7**), 70% (**8**), 68% (**9**).

All complexes were characterised by elemental analysis and ^1H and ^{13}C NMR spectroscopy (see Scheme 3 for atom numbering). The structure of $[Pt(DMeDPQ)(bipy)][PF_6)_2$ was determined by a single-crystal X-ray analysis of $\{[Pt(DMeDPQ)(bipy)][PF_6]_2\}\cdot 0.5\{(DMeDPQ)(CH_4O)\}$.

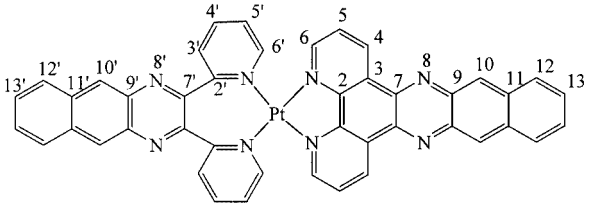

Scheme 3. General numbering scheme

[Pt(DMeDPQ)(bipy)](PF$_6$)$_2$ (1): ^1H NMR (300 MHz, [D$_6$]acetone): δ = 9.46 (d, ^3J = 5 Hz, 2 H, 6′-H), 8.67 (d, ^3J = 6 Hz, 2 H, 3-H), 8.57 (td, ^3J = 7, ^4J = 1 Hz, 2 H, 4′-H), 8.53 (td, ^3J = 7, ^4J = 1 Hz, 2 H, 4-H), 8.29 (d, ^3J = 6 Hz, 2 H, 3′-H), 8.18 (d, ^3J = 8 Hz, 2 H, 6-H), 8.14 (m, 2 H, 5′-H), 8.05 (s, 2 H, 10′-H), 7.83 (td, ^3J = 6, ^4J = 1 Hz 2 H, 5-H), 2.58 (s, 6 H, 12′-H) ppm. $^{13}C\{^1H\}$ NMR (75 MHz, [D$_6$]acetone): δ = 158.8 (2 C, C-2′), 157.5 (2 C, C-2), 153.2 (2 CH, C-6′), 150.9 (2 CH, C-6), 147.4 (2 C, C-7′), 145.2 (2 C, C-9′), 143.9 (2 CH, C-4′), 143.7 (2 CH, C-4), 141.5 (2 C, C-11′), 131.0 (2 CH, C-3′), 130.2 (2 CH, C-5′), 129.8 (2 CH, C-5), 129.2 (2 CH, C-10′), 125.6 (2 CH, C-3), 20.4 (2 CH$_3$, C-12′) ppm. $C_{30}H_{24}F_{12}N_6P_2Pt$ (954): calcd. C 37.79, H 2.54, N 8.81; found C 37.70, H 2.58, N 8.88.

[Pt(BDPQ)(bipy)](PF$_6$)$_2$ (2): ^1H NMR (300 MHz, [D$_6$]acetone): δ = 9.52 (d, ^3J = 5 Hz, 2 H, 6′-H), 8.98 (s, 2 H, 10′-H), 8.65 (d, ^3J = 8 Hz, 2 H, 3-H), 8.61 (td, ^3J = 7, ^4J = 1 Hz, 2 H, 4′-H), 8.53 (td, ^3J = 7, ^4J = 1 Hz, 2 H, 4-H), 8.39 (d, ^3J = 7 Hz, 2 H, 3′-H), 8.34 (m, 2 H, 12′-H), 8.22 (d, ^3J = 6 Hz, 2 H, 6-H), 8.18 (m, 2 H, 5′-H), 7.85 (m, 2 H, 5-H), 7.78 (m, 2 H, 13′-H) ppm. $^{13}C\{^1H\}$ NMR (75 MHz, [D$_6$]acetone): δ = 158.6 (2 C, C-2′), 157.6 (2 C, C-2), 153.3 (2 CH, C-6′), 150.9 (2 CH, C-6), 148.7 (2 C, C-7′), 144.0 (2 CH, C-4′), 143.9 (2 CH, C-4), 138.4 (2 C, C-9′), 136.2 (2 C, C-11′), 131.3 (2 CH, C-3′), 130.4 (2 CH, C-5′), 129.8 (2 CH, C-5), 129.6 (2 CH, C-10′), 129.4 (4 CH, C-13′, C-12′), 125.6 (2 CH, C-3) ppm. $C_{32}H_{22}F_{12}N_6P_2Pt$ (976): calcd. C 39.40, H 2.27, N 8.61; found C 39.21, H 2.38, N 8.56.

[Pt(DMeDPQ)(dppz)](PF$_6$)$_2$ (3): ^1H NMR (300 MHz, [D$_6$]acetone): δ = 10.01 (dd, ^3J = 8, ^4J = 1 Hz, 2 H, 4-H), 9.60 (d, ^3J = 6 Hz, 2 H, 6′-H), 8.71 (dd, ^3J = 5, ^4J = 1 Hz, 2 H, 6-H), 8.63 (td, ^3J = 8, ^4J = 1 Hz, 2 H, 4′-H), 8.47 (m, 2 H, 10-H), 8.36 (m, 2 H, 3′-H), 8.33 (dd, ^3J = 8, ^3J = 5 Hz, 2 H, 5-H), 8.21 (m, 4 H, 5′-H and 11-H), 8.05 (s, 2 H, 10′-H), 2.54 (s, 6 H, Me) ppm. $^{13}C\{^1H\}$ NMR (75 MHz, [D$_6$]acetone): δ = 159.0 (2 C, C-2′), 153.4 (2 CH, C-6′), 152.9 (2 CH, C-6), 151.1 (2 C, C-2), 147.6 (2 C, C-7′), 145.5 (2 C, C-9′), 143.9 (2 CH, C-4′), 143.7 (2 C, C-7), 141.4 (2 C, C-11′), 139.6 (2 C, C-9), 139.5 (2 CH, C-4), 134.0 (2 CH, C-11), 131.7 (2 C, C-3), 131.2 (2 CH, C-3′) 130.6 (2 CH, C-10) 130.3 (2 CH, C-5′), 129.3 (2 CH, C-5), 129.2 (2 CH, C-10′), 20.4 (2CH3, C-12′) ppm. $C_{38}H_{26}F_{12}N_8P_2Pt$ (1080): calcd. C 42.27, H 2.43, N 10.38; found C 42.13, H 2.45, N 10.26.

[Pt(DMeDPQ)(bdppz)](PF$_6$)$_2$ (4): ^1H NMR (300 MHz, [D$_6$]acetone): δ = 9.88 (d, ^3J = 9 Hz, 2 H, 4-H), 9.62 (d, ^3J = 5 Hz, 2 H, 6′-H), 8.92 (s, 2 H, 10-H), 8.65 (m overlapped, 4 H, 6-H and 4′-H), 8.39 (m, 2 H, 3′-H), 8.29 (m, 2 H, 5-H), 8.23 (m, 2 H, 5′-H), 8.14 (m, 2 H, 12-H), 8.09 (s, 2 H, 10′-H), 7.55 (m, 2 H, 13-H), 2.54 (s, 6 H, 12′-H) ppm. $^{13}C\{^1H\}$ NMR (75 MHz, [D$_6$]acetone): δ = 159.0 (2 C, C-2′), 153.5 (2 CH, C-6′), 152.9 (2 CH, C-6), 151.5 (2 C, C-2), 147.6 (2 C, C-7′), 145.6 (2 C, C-9′), 144.0 (2 CH, C-4′), 141.4 (2 C, C-11′), 140.0 (2 C, C-7), 139.4 (2 CH, C-4), 139.1 (2 C, C-9), 136.0 (2 C, C-11), 131.8 (2 CH, C-3), 131.2 (2 CH, C-3′), 130.4 (2 CH, C-5′), 129.6 (2 CH, C-5), 129.3 (2 CH, C-12, C-13), 129.2 (2 CH, C-10), 129.1 (2 CH, C-10′), 20.4 (2CH$_3$, C-12′) ppm. $C_{42}H_{28}F_{12}N_8P_2Pt$ (1130): calcd. C 44.65, H 2.50, N 9.92; found C 44.47, H 2.56, N 9.88.

[Pt(BDPQ)(dppz)](PF$_6$)$_2$ (5): ^1H NMR (300 MHz, [D$_6$]acetone): δ = 9.99 (dd, ^3J = 8, ^4J = 1 Hz, 2 H, 4-H), 9.65 (d, ^3J = 5 Hz, 2 H, 6′-H), 8.96 (s, 2 H, 10′-H), 8.73 (td, ^3J = 6, ^4J = 1 Hz, 2 H, 6-H), 8.66 (td, ^3J = 8, ^4J = 1 Hz, 2 H, 4′-H), 8.44 (m, overlapped 4 H, 3′-H and 10-H), 8.33 (m, 2 H, 5-H), 8.31 (m, 2 H, 12′-H), 8.29 (m, 2 H, 5′-H), 8.17 (dd, ^3J = 6, ^4J = 3 Hz, 2 H, 11-H), 7.73 (dd, ^3J = 6, ^4J = 3 Hz, 2 H, 13′-H) ppm. $^{13}C\{^1H\}$ NMR (75 MHz, [D$_6$]acetone): δ = 158.8 (2 C, C-2′), 153.5 (2 CH, C-6′), 152.9 (2 CH, C-6), 151.1 (2 C, C-2), 148.6 (2 C, C-7′) 144.1 (2 CH, C-4′), 143.7 (2 C, C-7), 139.6 (2 C, C-9), 139.5 (2 CH, C-4), 138.3 (2 C, C-9′), 136.2 (2 C, C-11′), 134.0 (2 CH, C-11), 131.6 (2 C, C-3), 131.4 (2 CH, C-3′), 130.6 (4 CH, C-10, C-5′), 129.5 (2 CH, C-5), 129.4 (2 CH, C-13′), 129.3 (4 CH, C-10′, C-12′) ppm. $C_{40}H_{24}F_{12}N_8P_2Pt$ (1102): calcd. C 43.61, H 2.20, N 10.17; found C 43.65, H 2.11, N 10.07.

[Pt(BDPQ)(bdppz)](PF$_6$)$_2$ (6): ^1H NMR (300 MHz, [D$_6$]acetone): δ = 9.86 (d, ^3J = 9 Hz, 2 H, 4-H), 9.67 (d, ^3J = 5 Hz, 2 H, 6′-H), 9.00 (s, 2 H, 10′-H), 8.88 (s, 2 H, 10-H), 8.68 (m, 2 H, 4′-H), 8.66 (d, ^3J = 6 Hz, 2 H, 6-H), 8.48 (d, ^3J = 9 Hz, 2 H, 3′-H), 8.29 (overlapped m, 6 H, 5-H, 5′-H, 12′-H), 8.11 (m, 2 H, 12-H), 7.71 (dd, ^3J = 6, ^4J = 3 Hz, 2 H, 13′-H), 7.52 (dd, ^3J = 6, ^4J = 3 Hz, 2 H, 13-H) ppm. $^{13}C\{^1H\}$ NMR (75 MHz, [D$_6$]acetone): δ = 158.8 (2 C, C-2′), 153.6 (2 CH, C-6′), 152.9 (2 CH, C-6), 151.4 (2 C, C-2), 148.6 (2 CH, C-7′), 144.1 (2 CH, C-4′), 140.0 (2 C, C-7), 139.4 (2 CH, C-4), 139.1 (2 C, C-9), 138.4 (2 C, C-9′), 136.2 (2 C, C-11′), 135.9 (2 C, C-11), 131.8 (2 C, C-3), 131.5 (2 CH, C-3′), 130.6 (2 CH, C-5′), 129.5 (6 CH, C-5, C-10′, C-12′), 129.4 (2 CH, C-13′), 129.3 (4 CH, C-10, C-12), 129.1 (2 CH, C-13) ppm. $C_{44}H_{26}F_{12}N_8P_2Pt$ (1152): calcd. C 45.88, H 2.28, N 9.73; found C 45.81, H 2.22, N 9.65.

[Pt(DMeDPQ)(py)$_2$](PF$_6$)$_2$ (7): ^1H NMR (300 MHz, [D$_6$]acetone): δ = 9.24 (d, ^3J = 6 Hz, 2 H, 6′-H), 8.92 (dd, ^3J = 7, ^4J = 2 Hz, 4 H, 2-H = 6-H), 8.37 (td, ^3J = 8, ^4J = 1 Hz, 2 H, 4′-H), 8.21 (dd, ^3J = 7, ^4J = 1 Hz, 2 H, 3′-H), 8.19 (s, 2 H, 10′-H), 8.07 (tt, ^3J = 7, ^4J = 2 Hz, 2 H, 4-H), 7.86 (td, ^3J = 8, ^4J = 1 Hz, 2 H, 5′-H), 7.62 (m, 4 H, 3-H = 5-H), 2.70 (s, 6 H, 12′-H). $^{13}C\{^1H\}$ NMR (75 MHz, [D$_6$]acetone): δ = 158.6 (2 C, C-2′), 152.7 (4 CH, C-2 = C-6), 152.1 (2 CH, C-6′), 147.6 (2 C, C-7′), 145.2 (2 C, C-9′), 143.2 (2 CH, C-4′), 142.5 (2 CH, C-4), 141.9 (2 C, C-11′), 130.9 (2 CH,

 © 2004 Wiley-VCH Verlag GmbH & Co. KGaA, Weinheim

C-3′), 129.5 (2 CH, C-10′), 128.9 (2 CH, C-5′), 128.8 (4 CH, C-3 to C-5), 20.6 (2 CH_3) ppm. $C_{30}H_{26}F_{12}N_6P_2Pt$ (956): calcd. C 37.71, H 2.74, N 8.79; found C 37.66, H 2.89, N 8.67.

[Pt(BDPQ)(py)$_2$](PF$_6$)$_2$ (8): ^{1}H NMR (300 MHz, [D$_6$]acetone): δ = 9.29 (d, ^3J = 6 Hz, 2 H, 6′-H), 9.12 (s, 2 H, 10′-H), 8.94 (dd, ^3J = 7, ^4J = 2 Hz, 4 H, 2-H = 6-H), 8.46 (dd, ^3J = 6, ^4J = 3 Hz, 2 H, 12′-H), 8.40 (dd, ^3J = 8, ^4J = 2 Hz, 2 H, 4′-H), 8.31 (dd, ^3J = 7, ^4J = 1 Hz, 2 H, 3′-H), 8.07 (m, 2 H, 4-H), 7.91 (m, 2 H, 5′-H), 7.88 (dd partially overlapped with 5′-H, ^3J = 6, ^4J = 3 Hz, 2 H, 13′-H), 7.62 (dd, ^3J = 7, ^4J = 2 Hz, 4 H, 3-H = 5-H) ppm. $^{13}C\{^1H\}$ NMR (75 MHz, [D$_6$]acetone): δ = 158.5 (2 C, C-2′), 152.7 (4 CH, C-2−C-6), 152.3 (2 CH, C-6′), 148.7 (2 C, C-7′), 143.4 (2 CH, C-4′), 142.6 (2 CH, C-4), 138.9 (2 C, C-9′), 136.3 (2 C, C-11′), 131.1 (2 CH, C-3′), 129.7 (4 CH, C-10′, C-12′), 129.4 (2 CH, C-13′), 129.1 (2 CH, C-5′), 128.8 (4 CH, C-3 = C-5) ppm. $C_{32}H_{24}F_{12}N_6P_2Pt$ (978): calcd. C 39.32, H 2.47, N 8.58; found C 39.17, H 2.41, N 8.67.

[Pt(DMeDPQ)(3-Mepy)$_2$](PF$_6$)$_2$ (9): ^{1}H NMR (300 MHz, [D$_6$]acetone): δ = 9.22 (d, ^3J = 6 Hz, 2 H, 6′-H), 8.80 (s, 2 H, 2-H), 8.71 (d, ^3J = 6 Hz, 2 H, 6-H), 8.35 (td, ^3J = 8, ^4J = 1 Hz, 2 H, 4′-H), 8.19 (m overlapped, 4 H, 10′-H and 3′-H), 7.86 (m overlapped, 4 H, 4-H and 5′-H), 7.47 (dd, ^3J = 8, ^3J = 6 Hz, 2 H, H- 5), 2.70 (s, 6 H, 12′-H), 2.26 (s, 6 H, 3-Me) ppm. $^{13}C\{^1H\}$ NMR (75 MHz, [D$_6$]acetone): δ = 158.3 (2 C, C-2′), 152.0 (2 CH, C-2), 151.8 (2 CH, C-6′), 149.5 (2 CH, C-6) 147.5 (2 C, C-7′), 145.2 (2 C, C-9′), 142.9 (2 CH, C-4′), 142.6 (2 CH, C-4), 141.8 (2 C, C-11′), 139.2 (2 C, C-3), 130.5 (2 CH, C-3′), 129.3 (2 CH, C-10′), 128.5 (2 CH, C-5′), 127.7 (2 CH, C-5), 20.2 (2 CH_3, C-12′), 17.9 (2 CH_3, 3-Mepy) ppm. $C_{32}H_{30}F_{12}N_6P_2Pt$ (984): calcd. C 39.07, H 3.07, N 8.54; found C 39.16, H 2.99, N 8.67.

X-ray Crystallographic Study of [Pt(DMeDPQ)(bipy)](PF$_6$)$_2$·0.5{(C$_{20}$H$_{16}$N$_4$)(CH$_4$O)}: Suitable crystals of the title complex were obtained by slow solvent evaporation from a methanol solution of **1**. Diffraction data were collected with a Siemens P4 automatic four-circle diffractometer. A summary of the crystallographic data and the structure refinement is reported in Table 4. No crystal deterioration was evidenced by monitoring of three standard reflection measurements. The reflection intensities were evaluated by a learnt-profile procedure[23] among 2θ shells and then corrected for Lorentz-polarisation effects. Absorption correction was applied by fitting a pseudo-ellipsoid to the azimuthal scan data (0−360° range by a 10° step) of 15 high reflections.[24] Data collection and reduction were performed with the SHELXTL[25] package. The diffraction data did not allow us to determine uniquely the crystal packing symmetry and the structure modellisation was carried out in all the three possible monoclinic space groups *C*2, *Cm* and *C*2/*m*. The refinement in the two acentric space groups was seriously hampered by several very strong parameter correlations (> 0.9) while the centrosymmetric one shows incompatibility between the crystallographic point symmetries and the compound moieties in special positions. The structure was solved in *C*2/*m* by a combination of standard direct methods[26] and Fourier synthesis, and refined by minimizing the function $\Sigma w(F_o^2 - F_c^2)^2$ with the full-matrix least-squares technique based on all independent *F*, with SHELXL-97.[27] All non-hydrogen atoms were refined anisotropically. Hydrogen atoms were included in the model refinement with the "riding model" method with the X−H bond geometry and isotropic displacement parameter depending on the parent atom X. The co-crystallised methanol and uncoordinated quinoxaline molecules were placed in crystallographic special positions having a higher symmetry than these molecules. This generates a significant symmetry disorder. Further, one hexafluorophosphate anion shows the usual rotational disorder evidenced by the overlap of two symmetric orientations related by the intersecting mirror plane. All attempts to represent the biggest ellipsoids as adjacent atomic partial occupancies were unsuccessful. The final geometrical calculations and drawings were carried out with the PARST program[28] and the XPW utility of the Siemens package, respectively. CCDC-237593 contains the supplementary crystallographic data for this paper. These data can be obtained free of charge at www.ccdc.cam.ac.uk/conts/retrieving.html [or from the Cambridge Crystallographic Data Centre, 12 Union Road, Cambridge CB2 1EZ, UK; Fax: + 44-1223-336-033; E-mail: deposit@ccdc.cam.ac.uk].

Table 4. Crystallographic data for **1**

Empirical formula	{[$C_{30}H_{24}N_6Pt$][PF_6]$_2$}·0.5{($C_{20}H_{16}N_4$)(CH_4O)}
Formula mass	1125.79
Crystal size	0.32 × 0.25 × 0.19 mm
Crystal colour, form	yellow, irregular
Crystal system	monoclinic
Space group	*C*2/*m* (no. 12)
Unit cell dimensions	*a* = 30.431(5) Å
	b = 12.637(2) Å
	c = 11.923(2) Å
	β = 90.84(1)°
V	4585(1) Å^3
Z	4
F(000)	2212
ρ_{calcd}	1.631 g/cm^3
μ	3.219 mm^{-1}
λ (graphite-monochromated)	0.71073 Å (Mo-K_α)
2Θ range	4.3−54°
No. of data collected (2θ-ω)	5294
No. of data independent (refined)	5197 (R_{int} = 0.0214)
No. of data observed	3931 [$I \geq 2\sigma(I)$]
No. of variables	344
Completeness to 2θ = 50°	0.987%
*R*1[a] (observed/refined data)[a]	0.0353/0.0782
*wR*2[b] (observed/refined data)	0.0544/0.0822
GOF[c] (observed/refined data)	0.951/0.951
Max. diff. peak and hole	0.752/−0.555 e·Å^{-3}
Max. and mean shift/esd	0.007/0.001

[a] $R = [\Sigma||F_o| - |F_c||]/\Sigma|F_o|$. [b] $R_w = \{\Sigma[w(F_o^2 - F_c^2)^2]/[\Sigma w(F_o^2)^2]\}^{1/2}$. [c] GOF = $\{\Sigma[w(F_o^2 - F_c^2)^2/(N_{obs} - N_{var})]\}^{1/2}$.

[1] A. Escuer, R. Vicente, T. Comas, J. Ribas, M. Gomez, X. Solans, D. Gatteschi, C. Zanchini, *Inorg. Chim. Acta* **1991**, *181*, 51−60.
[2] K. C. Gordon, A. H. R. Al-Obaidi, P. M. Jayaweera, J. J. McGarvey, J. F. Malone, S. E. J. Bell, *J. Chem. Soc., Dalton Trans.* **1996**, 1591−1596.
[3] A. Escuer, T. Comas, J. Ribas, R. Vicente, X. Solans, C. Zanchini, D. Gatteschi, *Inorg. Chim. Acta* **1989**, *162*, 97−103.
[4] G. Bandoli, T. I. A. Gerber, R. Jacobs, J. G. H. du Preez, *Inorg. Chem.* **1994**, *33*, 178−179.
[5] K. V. Goodwin, W. T. Pennington, J. D. Petersen, *Acta Crystallogr., Sect. C* **1990**, *46*, 898−900.
[6] F. Nicolò, M. Cusumano, M. L. Di Pietro, R. Scopelliti, G. Bruno, *Acta Crystallogr., Sect. C* **1998**, *54*, 485−487.
[7] M. Cusumano, M. L. Di Pietro, A. Giannetto, F. Nicolò, B. Nordén, P. Lincoln, *Inorg. Chem.* **2004**, *43*, 2416−2421.
[8] J. Granifo, M. E. Vargas, H. Rocha, M. T. Garland, R. Baggio, *Inorg. Chim. Acta* **2001**, *321*, 209−214.

 © 2004 Wiley-VCH Verlag GmbH & Co. KGaA, Weinheim

[9] J. Granifo, M. T. Garland, R. Baggio, *Inorg. Chim. Acta* **2003**, *348*, 263−270.
[10] E. Rotondo, G. Bruschetta, G. Bruno, A. Rotondo, M. L. Di Pietro, M. Cusumano, *Eur. J. Inorg. Chem.* **2003**, 2612−2618.
[11] [11a] Z. Qin, M. C. Jennings, R. J. Puddephatt, *Chem. Commun.* **2001**, 2676−2677. [11b] H.-Q. Liu, S.-M. Peng, C. M. Che, *J. Chem. Soc., Chem. Commun.* **1995**, 509−510.
[12] E. Rotondo, unpublished results.
[13] [13a] G. C. Levy, *J. Chem. Soc., Chem. Commun.* **1972**, 47−48. [13b] M. Fuss, H. U. Siehl, B. Olenyuk, P. J. Stang, *Organometallics* **1999**, *18*, 758−769.
[14] K. Wozniak, *Acta Crystallogr., Sect. C* **1991**, *47*, 1761−1763.
[15] S. C. Rasmussen, M. M. Richter, E. Yi, H. Place, K. J. Brewer, *Inorg. Chem.* **1990**, *29*, 3926−3932.
[16] K. Wozniak, T. M. Krygowski, E. Grech, *Pol. J. Chem.* **1994**, *68*, 1813−1817.
[17] A. Albinati, C. Arz, P. S. Pregosin, *Inorg. Chem.* **1987**, *26*, 508−513.
[18] L. M. Vogler, C. Franco, S. W. Jones, K. J. Brewer, *Inorg. Chim. Acta* **1994**, *221*, 55−59.
[19] G. T. Morgan, F. H. Burstall, *J. Chem. Soc.* **1934**, 965−971.
[20] J. E. Dickenson, L. A. Summers, *Aust. J. Chem.* **1970**, *23*, 1023−1027.
[21] P. Lincoln, A. Broo, B. Nordén, *J. Am. Chem. Soc.* **1996**, *118*, 2644−2653.
[22] Yu. N. Kukushkin, Yu. E. Vyaz′menskii, L. J. Zorina, Yu. L. Pazukhina, *Russ. J. Inorg. Chem.* **1968**, *13*, 1595−1599; *Chem. Abstr.* **1968**, *69*, 40851j.
[23] R. Diamond, *Acta Crystallogr., Sect. A* **1969**, *25*, 43−55.
[24] G. Kopfmann, R. Huber, *Acta Crystallogr., Sect. A* **1968**, *24*, 348−351.
[25] G. M. Sheldrick, *SHELXTL*, VMS version 5.05, Siemens Analytical X-ray Instruments Inc., Madison, Wisconsin, **1991**.
[26] A. Altomare, O. Cascarano, C. Giacovazzo, A. Guagliardi, M. C. Burla, G. Polidori, M. Camalli, *J. Appl. Crystallogr.* **1994**, *27*, 435−436.
[27] G. M. Sheldrick, *SHELXL-97, Program for Crystal Structure Refinement*, University of Göttingen, Germany, **1997**.
[28] M. Nardelli, *J. Appl. Chem.* **1995**, *28*, 659; locally modified version).

Received May 20, 2004
Early View Article
Published Online October 26, 2004

 © 2004 Wiley-VCH Verlag GmbH & Co. KGaA, Weinheim

A Triiron Complex Containing the Carboxylate-Free $\{Fe_3(\mu_3\text{-}O)\}^{7+}$ Core and Distorted Pentagonal-Bipyramidal Metal Centres

Subramanya Gupta Sreerama[a] and Samudranil Pal*[a]

Keywords: Trinuclear iron(III) complex / Crystal structure / Magnetic properties / Redox properties

The reaction of $Fe(ClO_4)_3\cdot 6H_2O$, 1,2-bis(biacetylmonoximeimino)ethane (H_2bamen) and triethylamine (1:1:2 mol ratio) in methanol affords a trinuclear complex with the formula $[Fe_3(\mu_3\text{-}O)(\mu_3\text{-bamen})_3]ClO_4\cdot 2H_2O$. The structure of the complex cation in this species shows a symmetric planar central $\{Fe_3(\mu_3\text{-}O)\}^{7+}$ unit coordinated to three N_4O_2 donor bridging (via oximate groups) ligands ($bamen^{2-}$). The N_4O_3 coordination sphere around each metal centre is very close to pentagonal-bipyramidal. Four N atoms of one $bamen^{2-}$ and the oxo group satisfy five coordination sites and form a pentagonal plane around the metal ion. The axial sites are occupied by two oximato O atoms from the other two $bamen^{2-}$ ligands. Thus, in addition to the μ_3-oxo group, two oximate groups provide two additional bridges between each pair of metal centres. In the crystal lattice, the water molecules exist as hydrogen-bonded dimers and these water dimers together with the perchlorate ions form a hydrogen-bond-supported helix. The complex cations form a chain via C–H···O interactions involving a methyl group and a metal-coordinated oximato O atom. The helix of $\{(H_2O)_2ClO_4^-\}$ units and the chain of $[Fe_3O(bamen)_3]^+$ cations are connected by O–H···O interactions which involve a water molecule and a second oximato O atom. In its cyclic voltammogram, the complex displays metal-centred oxidation as well as reduction responses. Variable-temperature magnetic susceptibility measurements revealed the presence of an antiferromagnetic interaction [J = –41.0(2) cm^{-1}] between the Fe^{III} centres in this complex.

(© Wiley-VCH Verlag GmbH & Co. KGaA, 69451 Weinheim, Germany, 2004)

Introduction

Trinuclear μ_3-oxo-bridged transition metal ion complexes have been of considerable interest for their molecular structures, magnetic properties and intramolecular electron transfer features in the mixed-valence variety. Such complexes are also useful precursors for the synthesis of higher nuclearity metal clusters. A number of complexes containing the $\{M_3(\mu_3\text{-}O)\}$ unit have been reported.[1–11] Essentially in all of them, the triangular metal ion core with the central oxo bridge is stabilised by six carboxylate groups (RCO_2^-) and three monodentate ligands (L). In these complexes of general formula $[M_3(\mu_3\text{-}O)(\mu_2\text{-}O_2CR)_6L_3]^{0/+}$, each metal ion is in a distorted octahedral coordination sphere. The O atoms of the bridging carboxylate groups constitute an O_4 square plane and the μ_3-O and the monodentate ligand L occupy the remaining two *trans* sites. The central $\{M_3(\mu_3\text{-}O)\}$ core is usually planar and has close to threefold symmetry. Complexes of $\{M_3(\mu_3\text{-}O)\}$ without carboxylate ligands are very rare although a few mixed-ligand complexes of this type are known.[12,13] However, in these complexes the $\{M_3(\mu_3\text{-}O)\}$ unit is asymmetric and pyramidal. Recently, we reported a carboxylate-free trinuclear complex containing the planar and symmetric $\{Mn_3(\mu_3\text{-}O)\}^{7+}$ core with a Schiff base (H_2bamen, two H represent the dissociable oxime protons) derived from 1 equiv. of ethylenediamine and 2 equiv. of biacetylmonoxime.[14] The metal ions in $[Mn_3(\mu_3\text{-}O)(\mu_3\text{-bamen})_3]^+$ are in a distorted pentagonal-bipyramidal N_4O_3 coordination sphere. A ferromagnetic interaction is operative between the metal ions in this complex. In contrast, the known μ_3-oxo-bridged trimanganese(III) complexes with carboxylate groups of formula $[Mn_3(\mu_3\text{-}O)(\mu_2\text{-}O_2CR)_6(py)_3]^+$ are antiferromagnetic.[3] Because of this variation, and also to examine whether the stabilisation of the $\{Mn_3(\mu_3\text{-}O)\}^{7+}$ unit by three $bamen^{2-}$ ligands is unique or can be extended to Fe^{III}, we attempted to synthesise the triiron(III) analogue of $[Mn_3(\mu_3\text{-}O)(\mu_3\text{-bamen})_3]^+$ and compare its structure and properties with the known $[Fe_3(\mu_3\text{-}O)(\mu_2\text{-}O_2CR)_6L_3]^+$ complexes. Indeed we were able to isolate the trinuclear μ_3-oxo-bridged Fe^{III} complex using H_2bamen. In the following account, we describe the synthesis, X-ray structure and physical properties of $[Fe_3(\mu_3\text{-}O)(\mu_3\text{-bamen})_3]ClO_4\cdot 2H_2O$.

Results and Discussion

Synthesis and Characterisation of $[Fe_3O(bamen)_3]ClO_4\cdot 2H_2O$

The complex was synthesised in good yield by allowing $Fe(ClO_4)_3\cdot 6H_2O$, H_2bamen and triethylamine to react in a

[a] School of Chemistry, University of Hyderabad, Hyderabad 500046, India
Fax: (internat.) + 91-40-2301-2460
E-mail: spsc@uohyd.ernet.in

 © 2004 Wiley-VCH Verlag GmbH & Co. KGaA, Weinheim DOI: 10.1002/ejic.200400427

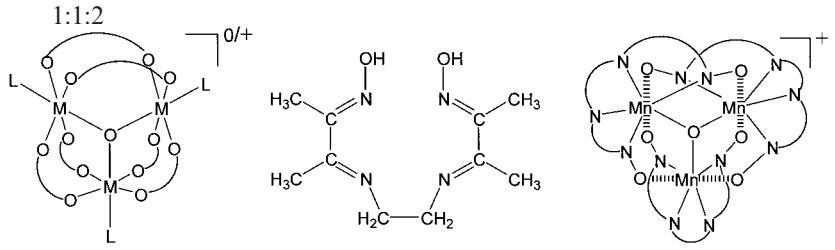

molar ratio in methanol under aerobic conditions. It precipitates as a brown solid from the reaction mixture. The elemental analysis data are satisfactory for the assigned molecular formula. In CH_3CN solution, the molar conductivity value of the complex (152 Ω^{-1} cm^2 M^{-1}) is consistent with 1:1 electrolytic behaviour.[15]

The infrared spectrum of the complex does not display any peak near 3000 cm^{-1}. The oxime OH groups of the ligands are therefore deprotonated. A broad peak centred at 3500 cm^{-1} is most likely due to the lattice water molecules. The presence of perchlorate is indicated by the bands at 1090 and 621 cm^{-1}. Two strong bands can be observed at 1641 and 1533 cm^{-1}. Comparable bands observed for complexes with dioxime ligands have been attributed to the coupled C···N and C···C stretching modes.[16] There is a 1:1 correlation between the infrared spectrum of this complex and that of $[Mn_3O(bamen)_3]ClO_4{\cdot}2H_2O$.[14] This observation, together with the elemental analysis and molar conductivity data, suggests that the present complex is most likely the Fe^{III} analogue of $[Mn_3O(bamen)_3]ClO_4{\cdot}2H_2O$.

The electronic spectrum of the complex in CH_3CN solution shows a weak absorption at 720 nm followed by three strong absorptions in the range of 383−248 nm. Weak absorptions observed for $[Fe_3O(O_2CR)_6(H_2O)_3]^+$ in the range of 980−625 nm have been assigned to d-d transitions and the large extinction coefficients which are unusual for spin-forbidden transitions can be attributed to the spin-exchange between the metal ions.[1] The higher energy intense absorptions are most likely due to ligand-to-metal and intraligand charge transfer transitions.[16]

Structure of $[Fe_3O(bamen)_3]^+$

An X-ray crystallographic study revealed that $[Fe_3O(bamen)_3]ClO_4{\cdot}2H_2O$ is isomorphous with the corresponding Mn^{III} analogue $[Mn_3O(bamen)_3]ClO_4{\cdot}2H_2O$.[13] Both species crystallise in the same space group with very similar unit cell dimensions. The structure of $[Fe_3O(bamen)_3]^+$ is illustrated in Figure 1. The cation contains three bridging N_4O_2 donor bamen^{2-} ligands, one μ_3-oxo group and three metal centres. The presence of one ClO_4^- anion per complex cation indicates that the oxidation state of each metal centre is +3. The C−N and N−O bond lengths in the oximate [−(CH$_3$)C=N−O$^-$] fragments are in the ranges 1.277(4)−1.288(4) Å and 1.337(4)−1.353(4) Å, respectively. These bond lengths are similar to the corresponding ones reported for deprotonated oxime functionalities.[14,17] All other intraligand bond parameters are unexceptional. The metal ions are heptacoordinated and each bamen^{2-} is coordinated to all three Fe atoms. Four N atoms coordinate one metal centre forming three five-membered chelate rings and the two oximato O atoms coordinate to the other two metal centres. As a result, each pair of iron centres is bridged by two oximate groups (=N−O$^-$) in a reciprocal fashion with respect to the N and O atom coordination. The seventh coordination site is satisfied by the μ_3-oxo atom. Thus, each metal ion has an N_4O_3 coordination sphere. The Fe−N_{imine} bond lengths [2.233(3)−2.250(3) Å] are significantly shorter than the Fe−$N_{oximate}$ bond lengths [2.302(3)−2.340(3) Å] (Table 1). This difference is possibly due to the bridging nature of the oximate groups and the rigidity of the N_4 fragment of the ligands.[14,18] The central $\{Fe_3(\mu_3\text{-}O)\}^{7+}$ core is essentially planar. The solid angle at the μ_3-O centre is 359.95° and its displacement from the Fe_3 plane is 0.024(2) Å. The Fe−μ_3-O bond lengths [1.898(2)−1.911(2) Å] and the Fe···Fe distances [3.2992(9)−3.3013(7) Å] are similar to the corresponding values reported for complexes containing the $\{Fe_3(\mu_3\text{-}O)\}^{7+}$ core.[6,9,11] The N_4O_3 coordination geometry around each Fe atom can be best described as pentagonal-bipyramidal. The four N atoms and the μ_3-O atom constitute the pentagonal plane and the two oximato O

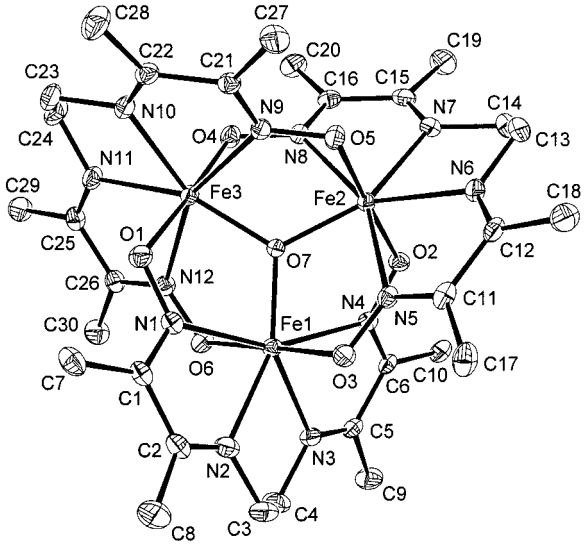

Figure 1. Structure of $[Fe_3(\mu_3\text{-}O)(\mu_3\text{-bamen})_3]^{3+}$ with the atom-labelling scheme; all atoms are represented by their 25% probability thermal ellipsoids; hydrogen atoms are omitted for clarity

 © 2004 Wiley-VCH Verlag GmbH & Co. KGaA, Weinheim

Table 1. Selected bond lengths [Å] and bond angles [°] for $[Fe_3O(bamen)_3]ClO_4{\cdot}2H_2O$

Fe(1)−N(1)	2.326(3)	Fe(2)−O(2)	1.987(2)
Fe(1)−N(2)	2.247(3)	Fe(2)−O(5)	1.983(2)
Fe(1)−N(3)	2.236(3)	Fe(2)−O(7)	1.908(2)
Fe(1)−N(4)	2.341(3)	Fe(3)−N(9)	2.334(3)
Fe(1)−O(3)	1.979(2)	Fe(3)−N(10)	2.251(3)
Fe(1)−O(6)	1.982(2)	Fe(3)−N(11)	2.236(3)
Fe(1)−O(7)	1.910(2)	Fe(3)−N(12)	2.311(3)
Fe(2)−N(5)	2.302(3)	Fe(3)−O(1)	1.997(2)
Fe(2)−N(6)	2.235(3)	Fe(3)−O(4)	1.989(2)
Fe(2)−N(7)	2.233(3)	Fe(3)−O(7)	1.898(2)
Fe(2)−N(8)	2.334(3)		
N(1)−Fe(1)−N(2)	67.57(11)	O(2)−Fe(2)−N(8)	94.72(10)
N(2)−Fe(1)−N(3)	72.31(12)	O(2)−Fe(2)−O(7)	90.85(10)
N(3)−Fe(1)−N(4)	67.28(11)	O(5)−Fe(2)−N(5)	91.75(10)
N(4)−Fe(1)−O(7)	77.48(10)	O(5)−Fe(2)−N(6)	80.73(10)
O(7)−Fe(1)−N(1)	78.43(10)	O(5)−Fe(2)−N(7)	98.73(11)
O(3)−Fe(1)−N(1)	93.53(10)	O(5)−Fe(2)−N(8)	87.04(10)
O(3)−Fe(1)−N(2)	81.43(11)	O(5)−Fe(2)−O(7)	90.92(10)
O(3)−Fe(1)−N(3)	96.64(11)	N(9)−Fe(3)−N(10)	67.00(10)
O(3)−Fe(1)−N(4)	86.04(10)	N(10)−Fe(3)−N(11)	72.47(11)
O(3)−Fe(1)−O(7)	90.74(10)	N(11)−Fe(3)−N(12)	68.15(11)
O(6)−Fe(1)−N(1)	84.22(10)	N(12)−Fe(3)−O(7)	78.17(10)
O(6)−Fe(1)−N(2)	96.12(11)	O(7)−Fe(3)−N(9)	77.28(10)
O(6)−Fe(1)−N(3)	83.88(10)	O(1)−Fe(3)−N(9)	94.17(10)
O(6)−Fe(1)−N(4)	96.71(10)	O(1)−Fe(3)−N(10)	82.03(11)
O(6)−Fe(1)−O(7)	90.48(10)	O(1)−Fe(3)−N(11)	95.20(11)
N(5)−Fe(2)−N(6)	68.24(11)	O(1)−Fe(3)−N(12)	83.45(10)
N(6)−Fe(2)−N(7)	72.52(12)	O(1)−Fe(3)−O(7)	92.02(10)
N(7)−Fe(2)−N(8)	67.48(11)	O(4)−Fe(3)−N(9)	87.01(10)
N(8)−Fe(2)−O(7)	77.21(10)	O(4)−Fe(3)−N(10)	96.08(11)
O(7)−Fe(2)−N(5)	77.99(10)	O(4)−Fe(3)−N(11)	82.20(11)
O(2)−Fe(2)−N(5)	87.24(10)	O(4)−Fe(3)−N(12)	96.56(11)
O(2)−Fe(2)−N(6)	97.02(11)	O(4)−Fe(3)−O(7)	90.75(10)
O(2)−Fe(2)−N(7)	80.69(10)		

atoms occupy the two axial sites. The mean deviations from the pentagonal $N_4(\mu_3\text{-}O)$ plane are in the range 0.21−0.22 Å. The $O_{oximate}$−Fe−N/O7 angles fall in the range 80.69(10)−98.73(11)° and the $O_{oximate}$−Fe−$O_{oximate}$ angles are within 177.17(10)−177.74(10)°.

Hydrogen Bonding and Crystal Packing

In the crystal lattice of $[Fe_3O(bamen)_3]ClO_4{\cdot}2H_2O$, the water molecules and the perchlorate ions exist in a helical fashion through hydrogen bonding interactions (Figure 2). Two water molecules form a linear dimer [O···O distance, 2.890(8) Å; O−H···O angle, 149.8°]. The hydrogen bond acceptor molecule in this water dimer is again hydrogen-bonded to one perchlorate oxygen atom [O···O distance, 3.119(8) Å; O−H···O angle, 142.8°]. The donor water molecule of the dimer in the $\{(H_2O)_2ClO_4^-\}$ unit is hydrogen-bonded with a perchlorate oxygen atom (O···O distance, 3.026(8) Å; O−H···O angle, 160.3°) of a symmetry-related $\{(H_2O)_2ClO_4^-\}$ unit. These three hydrogen bonding interactions lead to the helical arrangement of the water molecules and the perchlorate ions (Figure 2). Interestingly, the cations also exist in a chain-like arrangement via inter-cation C−H···O interactions [C···O distance, 3.346(5) Å; C−H···O angle, 147.4°] involving a methyl group (C17) and an oximato O atom (O6).[19−21] Another metal-coordinated oximato O atom (O1) and the O atom of the acceptor molecule in the water dimer present in the $\{(H_2O)_2ClO_4^-\}$ unit are within hydrogen bond lengths [O···O distance, 3.201(7) Å; O−H···O angle, 128.1°]. This is also reflected in the rather long Fe3−O1 bond [1.997(2) Å] compared with the other Fe−$O_{oximate}$ bonds [1.979(2)−1.989(2) Å]. Thus, the chain of cations and the helix of $\{(H_2O)_2ClO_4^-\}$ units are bridged by O−H···O interactions (Figure 3). There are no other inter-chain or inter-helix noncovalent interactions. The same packing arrangement of the water molecules, the perchlorates and the complex cations can be observed in the crystal lattice of $[Mn_3O(bamen)_3]ClO_4{\cdot}2H_2O$.[14]

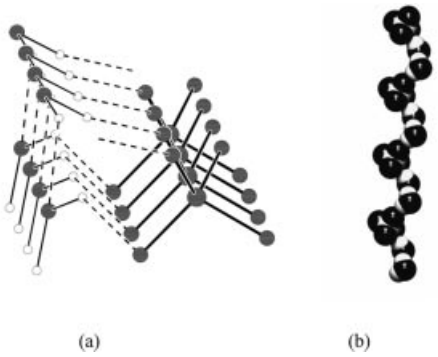

Figure 2 Helical arrangement of the $\{(H_2O)_2ClO_4^-\}$ units: (a) propagation of the helix through the hydrogen bonding interactions; (b) space-filling model of the helix

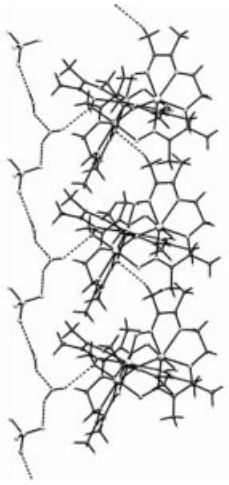

Figure 3. Ball-and-stick representation of the chain of complex cations and the helix of $\{(H_2O)_2ClO_4^-\}$ units connected by O−H···O interactions

Redox Properties

The electron transfer behaviour of $[Fe_3O(bamen)_3]ClO_4{\cdot}2H_2O$ in CH_3CN has been studied using cyclic voltammetry. The complex displays a reversible oxidation response at $E_{1/2}$ = 1.05 V (ΔE_p = 80 mV) and another reversible reduction response at $E_{1/2}$ = −1.05 V (ΔE_p = 60 mV) (Figure 4). The peak currents observed for these two responses are similar to the peak currents of known one-electron processes under identical conditions.[18,22] The depro-

 © 2004 Wiley-VCH Verlag GmbH & Co. KGaA, Weinheim

tonated ligand ($bamen^{2-}$) does not display any response in the potential range +2.1 to −2.1 V. Thus, the oxidation response can be assigned to the $Fe^{III}{}_2Fe^{IV}/Fe^{III}{}_3$ couple and the reduction response to the $Fe^{III}{}_3/Fe^{III}{}_2Fe^{II}$ couple. On the anodic side of the SCE, in addition to the reversible oxidation response, two more irreversible oxidation responses (E_{pa} = 1.41 and 1.75 V) can be observed. However, the peak current of the lower potential response is 1/3rd and that of the higher potential response is almost double the peak current of the reversible oxidation response. The corresponding Mn^{III} analogue displays two reversible and one irreversible metal-centred oxidations.[14] Thus, the irreversible oxidations observed for the present complex may perhaps involve the metal centres. However, the irreversible nature clearly indicates that the corresponding oxidised species are unstable in the cyclic voltammetric time scale. Similarly, on the cathodic side of the SCE, an irreversible reduction at −1.66 V having a peak current similar to that of the reversible reduction response was observed. This response may be due to the $Fe^{III}{}_2Fe^{II} \rightarrow Fe^{III}Fe^{II}{}_2$ process as the ligand is redox inactive at this potential. It is interesting to note that there are no reports of metal-centred oxidations displayed by $[M_3O(O_2CR)_6L_3]^+$ species containing first row metal ions. Normally for these species, metal-centred reductions are observed and very few of them display more than one reversible redox step.[9]

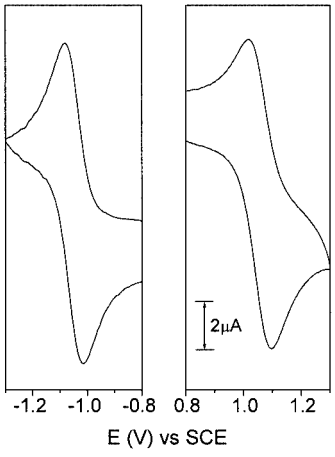

Figure 4. Cyclic voltammograms (scan rate 50 mV s^{-1}) of $[Fe_3O(bamen)_3]ClO_4{\cdot}2H_2O$ in acetonitrile (0.1 M TBAP) at a platinum electrode (298 K)

Magnetic Properties

A powdered sample of $[Fe_3O(bamen)_3]ClO_4{\cdot}2H_2O$ was used for the measurements of the magnetic susceptibilities at a fixed magnetic field of 5 kG in the temperature range 18−300 K. The effective magnetic moment of the complex at 300 K is 5.00 μ_B. The moment gradually decreases with the lowering of the temperature and reaches a value of 1.71 μ_B at 18 K. The nature of the curve obtained by plotting the moment against temperature (Figure 5) clearly indicates the antiferromagnetic character of the complex and the value of the moment at the lowest temperature is consistent with an S = 1/2 ground state. The data were fitted using an expression for χ_M vs. T obtained from the isotropic spin exchange Hamiltonian $H = -2J(S_1S_2 + S_2S_3 + S_3S_1)$ for a triangular triiron(III) complex in which all the metal ions are equivalent and have the same spin state $S_1 = S_2 = S_3 = 5/2$.[23] The best least-squares fit[24] was obtained with $J = -41.0(2)$ cm^{-1} and $g = 1.984(4)$ ($R = 1.50 \times 10^{-4}$). Complexes of formula $[Fe_3(\mu_3\text{-}O)(\mu_2\text{-}O_2CR)_6L_3]^+$ are known to be antiferromagnetic and the J values reported for such species span the range −15 to −33 cm^{-1}.[1,3−5,11] It has also been noted that the antiferromagnetic interaction decreases as the metal ion is changed from Fe^{III} to Mn^{III} in the acetate complexes of $\{M_3(\mu_3\text{-}O)\}^{7+}$. In this type of species, the metal ions are in a distorted octahedral coordination sphere. The unpaired electrons present in the σ-interacting e_g orbitals are involved in the antiferromagnetic exchange process. Thus, the decrease in the $-J$ value has been attributed to the decrease in the number of unpaired electrons in the e_g orbitals as one goes from high-spin Fe^{III} ($t_{2g}{}^3e_g{}^2$) to high-spin Mn^{III} ($t_{2g}{}^3e_g{}^1$).[3] Interestingly, the antiferromagnetic interaction in $[Fe_3O(bamen)_3]^+$ is noticeably higher than that in the $[Fe_3O(O_2CR)_6L_3]^+$ complexes and a ferromagnetic interaction [J = 22.3(1) cm^{-1}][14] is operative in $[Mn_3O(bamen)_3]^+$ rather than a weaker antiferromagnetic interaction as observed in $[Mn_3O(O_2CR)_6L_3]^+$. It is very likely that the change in the coordination geometry around the metal ions from octahedral in $[M_3O(O_2CR)_6L_3]^+$ to pentagonal-bipyramidal in $[M_3O(bamen)_3]^+$ is primarily responsible for the differences in the magnetic properties of these two types of complex containing the same $\{M_3(\mu_3\text{-}O)\}^{7+}$ core. It may be noted that in the pentagonal-bipyramidal coordination sphere the highest energy d_{z^2} orbital in the high-spin Fe^{III} species will have an unpaired electron but that in the high-spin Mn^{III} species will be empty. Thus, the alteration in the nature of the spin-coupling from ferromagnetic in $[Mn_3O(bamen)_3]^+$ to antiferromagnetic in $[Fe_3O(bamen)_3]^+$ is perhaps dictated by the absence or presence of an electron in the d_{z^2} orbital of the metal ion.

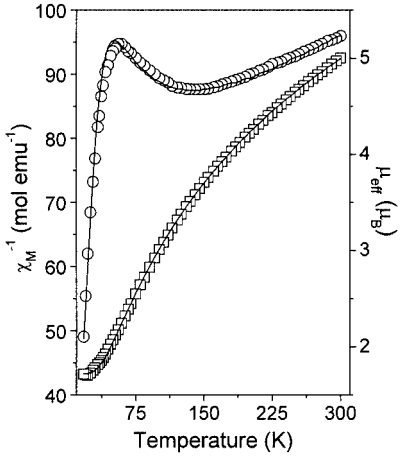

Figure 5. Temperature dependence of the inverse molar magnetic susceptibilities (open circles) and effective magnetic moments (open squares) of $[Fe_3O(bamen)_3]ClO_4{\cdot}2H_2O$; the continuous lines were generated from the best least-squares fit parameters given in the text

 © 2004 Wiley-VCH Verlag GmbH & Co. KGaA, Weinheim

Conclusion

Before we reported the cationic complex $[Mn_3O(bamen)_3]^+$ [14], examples of carboxylate-free complexes containing the symmetric $\{M^{III}{}_3(\mu_3\text{-}O)\}$ unit were nonexistent. Now, we have been able to isolate the Fe^{III} analogue of the above complex. As in the Mn^{III} species, the metal ions in $[Fe_3O(bamen)_3]^+$ are in a pentagonal-bipyramidal N_4O_3 coordination sphere assembled by the bridging hexadentate N_4O_2 donor $bamen^{2-}$ and the μ_3-oxo group. Thus, like carboxylates, three $bamen^{2-}$ ligands are fairly efficient at stabilising the planar triangular ensemble of Mn^{III} and Fe^{III} ions with the central oxo bridge. A comparison of the redox and magnetic properties of $[M_3O(O_2CR)_6L_3]^+$ in which the metal ions are octahedral, with that of $[M_3O(bamen)_3]^+$ (M = Mn^{III} and Fe^{III}], reveals some interesting differences. Both $[M_3O(bamen)_3]^+$ species exhibit several metal-centred redox steps uncommon for $[M_3O(O_2CR)_6L_3]^+$ complexes. The $[M_3O(O_2CR)_6L_3]^+$ species are antiferromagnetic. However, the antiferromagnetic exchange is weaker in the Mn^{III} complexes than in the Fe^{III} complexes. On the other hand, $[Mn_3O(bamen)_3]^+$ is ferromagnetic whereas the Fe^{III} analogue is antiferromagnetic. The extent of antiferromagnetic coupling in $[Fe_3O(bamen)_3]^+$ is noticeably larger than in the carboxylate complexes of $\{Fe_3(\mu_3\text{-}O)\}^{7+}$.

Experimental Section

Materials: The Schiff base H_2bamen was prepared according to a reported procedure.[25] All other chemicals and solvents were of commercially available analytical grade and were used as received.

Physical Measurements: Microanalytical (C, H, N) data were obtained with a Perkin−Elmer Model 240C elemental analyser. A Shimadzu 3101-PC UV/Vis/NIR spectrophotometer was used to record the electronic spectrum. The infrared spectrum was collected in a KBr pellet with a Jasco-5300 FT-IR spectrophotometer. The variable-temperature (18−300 K) magnetic susceptibility measurements were performed using the Faraday technique with a set-up consisting of a George Associates Lewis coil force magnetometer, a CAHN microbalance and an Air Products closed-cycle helium cryostat. $Hg[Co(NCS)_4]$ was used as the standard. Diamagnetic corrections (-468×10^{-6} emu mol^{-1} for $[Fe_3O(bamen)_3]ClO_4{\cdot}2H_2O$) calculated from Pascal's constants[26] were used to obtain the molar paramagnetic susceptibilities. The solution electrical conductivity was measured with a Digisun DI-909 conductivity meter. A CH-Instruments model 620A electrochemical analyser was used for cyclic voltammetric experiments with an acetonitrile solution of the complex containing tetrabutylammonium perchlorate (TBAP) as the supporting electrolyte. The three electrode measurements were carried out at 298 K under nitrogen with a platinum working electrode, a platinum wire auxiliary electrode and a saturated calomel reference electrode (SCE). The potentials reported in this work are uncorrected for junction contributions.

Synthesis of $[Fe_3O(bamen)_3]ClO_4{\cdot}2H_2O$: A methanol solution (20 mL) of $Fe(ClO_4)_3{\cdot}6H_2O$ (1.022 g, 2.21 mmol) was added to a suspension of H_2bamen (500 mg, 2.21 mmol) in methanol (20 mL). The colour of the reaction mixture immediately became brown. To this brown solution was added triethylamine (435 mg, 4.3 mmol, 0.6 mL) and the reaction mixture was stirred in air at room temperature (298 K) for 8 h. The brown solid which precipitated was collected by filtration, washed with ice-cold methanol and finally dried in air. Recrystallisation was performed by dissolving the complex in a methanol/xylene mixture (2:1). Yield, 460 mg (63%). $C_{30}H_{52}ClFe_3N_{12}O_{13}$ (991.84): calcd. C 36.33, H 5.28; N 16.95; found C 36.12, H 5.48, N 17.13. Selected IR bands [cm^{-1}]: $\tilde{\nu}$ = 3500 br, 1641 s, 1533 s, 1431 m, 1379 m, 1323 m, 1188 m, 1090 vs, 692 s, 621 m, 592 m, 505 s, 411 s. Electronic spectroscopic data in CH_3CN: $\lambda_{max.}$ [nm] (ε [$M^{-1}\,cm^{-1}$]) = 720 (115), 383 (11 900), 277sh (37 900), 248 (47 800). Molar conductivity (CH_3CN): Λ_M [$\Omega^{-1}\,cm^2\,M^{-1}$] = 152.

X-ray Crystallography: Single crystals were grown by slow concentration of a methanol/xylene (2:1) solution of the complex. A crystal of dimensions 0.48 × 0.40 × 0.24 mm was used for data collection with an Enraf−Nonius Mach-3 diffractometer using graphite-monochromated Mo-K_α radiation (λ = 0.71073 Å) by the ω-scan method at 298 K. Unit cell parameters were determined by a least-squares fit of 25 reflections having θ values in the range 9−11°. Intensities of three check reflections were measured every 1.5 h during the data collection to monitor the crystal stability and no decay was observed. The ψ-scans[27] of 6 reflections having θ and χ values within 1−21° and 80−86°, respectively, were used for an empirical absorption correction. The structure was solved by direct methods in the $P\bar{1}$ space group and refined on F^2 by full-matrix least-squares procedures. The asymmetric unit contains a molecule of $[Fe_3O(bamen)_3]ClO_4$ and two water molecules. All non-H atoms were refined using anisotropic thermal parameters. The H atoms of the water molecules were located in a difference map and refined with geometric restraints with $U_{iso}(H) = 1.5U_{eq}(O)$. The remainder of the H atoms were included in the structure factor calculation in idealised positions using the riding model but they were not refined. The programs of the WinGX package[28] were used for data reduction and the absorption correction. The structure solution and refinement were performed with the SHELX-97 programs.[29] The ORTEX6a[30] and the PLATON[31] packages were used for molecular graphics. Selected crystal and refinement data are summarised in Table 2. Crystallographic data have been deposited with the

Table 2. Crystallographic data for $[Fe_3O(bamen)_3]ClO_4{\cdot}2H_2O$

Empirical formula	$C_{30}H_{52}ClFe_3N_{12}O_{13}$
Formula mass	991.84
Crystal system	triclinic
Space group	$P\bar{1}$
a [Å]	8.6821(9)
b [Å]	14.7950(11)
c [Å]	16.586(2)
α [°]	84.404(13)
β [°]	82.13(2)
γ [°]	85.970(8)
V [Å^3]	2096.9(4)
Z	2
μ [mm^{-1}]	1.162
Reflections collected	7389
Reflections unique	7389
Reflections [$I \geq 2\sigma(I)$]	5346
Parameters	544
$R1$, $wR2$ [$I \geq 2\sigma(I)$]	0.0381, 0.0889
$R1$, $wR2$ (all data)	0.0670, 0.1005
Goodness-of-fit on F^2	1.014
Largest peak, hole [eÅ^{-3}]	0.479, −0.449

 © 2004 Wiley-VCH Verlag GmbH & Co. KGaA, Weinheim

Cambridge Crystallographic Data Centre (deposition number CCDC-239485). These data can be obtained from the CCDC, 12 Union Road, Cambridge, CB2 1EZ, UK; Fax: + 44-1233-336-033; E-mail: deposit@ccdc.cam.ac.uk.

Acknowledgments

Financial support for this work was provided by the Council of Scientific and Industrial Research (CSIR), New Delhi [Grant No. 01(1880)/03/EMR-II]. X-ray crystallographic data were obtained from the National Single Crystal Diffractometer Facility (established by the Department of Science and Technology, New Delhi) at the School of Chemistry, University of Hyderabad. Our sincere thanks are due to Prof. A. R. Chakravarty for providing the cryomagnetic data. We thank the University Grants Commission, New Delhi for the facilities provided under the Universities with Potential for Excellence program. S. G. S. thanks the CSIR for a research fellowship.

[1] G. J. Long, W. T. Robinson, W. P. Tappmeyer, D. L. Bridges, *J. Chem. Soc., Dalton Trans.* **1973**, 573.
[2] D. N. Hendrickson, S. M. Oh, T.-Y. Doug, T. Kambara, M. J. Cohn, M. F. Moore, *Comments Inorg. Chem.* **1985**, *4*, 329.
[3] J. B. Vincent, H.-R Chang, K. Folting, J. C. Huffman, G. Christou, D. N. Hendrickson, *J. Am. Chem. Soc.* **1987**, *109*, 5703.
[4] R. D. Cannon, U. A. Jayasooriya, R. Wu, S. K. Arapkoske, J. A. Stride, O. F. Nielsen, R. P. White, G. J. Kearly, D. Summerfield, *J. Am. Chem. Soc.* **1994**, *116*, 11869.
[5] R. D. Cannon, R. P. White, *Prog. Inorg. Chem.* **1988**, *36*, 195.
[6] R. Wu, M. Poyraz, F. E. Sowrey, C. E. Anson, S. Wocadlo, A. K. Powell, U. A. Jayasooriya, R. D. Cannon, T. Nakamoto, M. Katada, H. Sano, *Inorg. Chem.* **1998**, *37*, 1913.
[7] T. Fujihara, J. Aonahata, S. Kumakura, A. Nagasawa, K. Murakami, T. Ito, *Inorg. Chem.* **1998**, *37*, 3779.
[8] R. D. Cannon, U. A. Jayasooriya, F. E. Sowrey, C. Tilford, A. Little, J. P. Bourke, R. D. Rogers, J. B. Vincent, G. J. Kearley, *Inorg. Chem.* **1998**, *37*, 5675.
[9] A. M. Bond, R. J. H. Clark, D. G. Humphrey, P. Panayiotopoulos, B. W. Skelton, A. H. White, *J. Chem. Soc., Dalton Trans.* **1998**, 1845.
[10] C. P. Raptopoulou, V. Tangoulis, V. Psycharis, *Inorg. Chem.* **2000**, *39*, 4452.
[11] S. Supriya, S. K. Das, *New J. Chem.* **2003**, *27*, 1568.
[12] E. Bill, C. Krebs, M. Winter, M. Gerdan, A. X. Trautwein, U. Flörke, H.-J. Haupt, P. Chaudhuri, *Chem. Eur. J.* **1997**, *3*, 193.
[13] P. Chaudhuri, M. Hess, T. Weyhermüller, E. Bill, H.-J. Haupt, U. Flörke, *Inorg. Chem. Commun.* **1998**, *1*, 39.
[14] S. G. Sreerama, S. Pal, *Inorg. Chem.* **2002**, *41*, 4843.
[15] W. J. Geary, *Coord. Chem. Rev.* **1971**, *7*, 81.
[16] J. G. Mohanty, R. P. Singh, A. Chakravorty, *Inorg. Chem.* **1975**, *14*, 2178.
[17] F. Birkelbach, T. Weyhermüller, M. Lengen, M. Gerdan, A. X. Trautwein, K. Weighardt, P. Chaudhuri, *J. Chem. Soc., Dalton Trans.* **1997**, 4529.
[18] S. N. Pal, S. Pal, *J. Chem. Soc., Dalton Trans.* **2002**, 2102.
[19] G. R. Desiraju, *Angew. Chem. Int. Ed. Engl.* **1995**, *34*, 2328.
[20] M. G. Davidson, A. E. Goeta, J. A. K. Howard, S. Lamb, S. A. Mason, *New J. Chem.* **2000**, *24*, 477.
[21] S. N. Pal, K. R. Radhika, S. Pal, *Z. Anorg. Allg. Chem.* **2001**, *627*, 1631.
[22] S. N. Pal, S. Pal, *Eur. J. Inorg. Chem.* **2003**, 4244.
[23] K. Kambe, *J. Phys. Soc. Jpn.* **1950**, *5*, 48.
[24] G. V. R. Chandramouli, C. Balagopalakrishna, M. V. Rajasekharan, P. T. Manoharan, *Comput. Chem.* **1996**, *20*, 353.
[25] V. E. Uhlig, M. Friedrich, *Z. Anorg. Allg. Chem.* **1966**, *343*, 299.
[26] W. E. Hatfield, *Theory and Applications of Molecular Paramagnetism* (Eds.: E. A. Boudreaux, L. N. Mulay), Wiley, New York, **1976**, p. 491.
[27] A. C. T. North, D. C. Philips, F. S. Mathews, *Acta Crystallogr., Sect. A* **1968**, *24*, 351.
[28] L. J. Farrugia, *J. Appl. Crystallogr.* **1999**, *32*, 837.
[29] G. M. Sheldrick, *SHELX-97, Structure Determination Software*, University of Göttingen, Göttingen, Germany, **1997**.
[30] P. McArdle, *J. Appl. Crystallogr.* **1995**, *28*, 65.
[31] A. L. Spek, *PLATON, A Multipurpose Crystallographic Tool*, Utrecht University, Utrecht, The Netherlands, **2002**.

Received May 22, 2004
Early View Article
Published Online October 18, 2004

 © 2004 Wiley-VCH Verlag GmbH & Co. KGaA, Weinheim

EurJIC
European Journal of Inorganic Chemistry

Issue 24/2004

Pages 4725–4932

Papers available ahead of print in Early View at www.interscience.wiley.com

The editorial staff and the publishers thank all readers, authors, referees, and advertisers for their interest and support over the past year and wish them all a Happy New Year.

COVER PICTURE

The cover picture shows the stable and well-defined metallocene bis(trimethylsilyl)acetylene complexes $Cp_2M(L)(\eta^2\text{-}Me_3SiC_2SiMe_3)$ (M = Ti, without L; M = Zr, L = THF, pyridine), of the pentamethylcyclopentadienyl complexes $Cp^*_2M(\eta^2\text{-}Me_3SiC_2SiMe_3)$ (M = Ti, Zr) and the ethylene-bis(tetrahydroindenyl) complexes *rac*-(ebthi)$M(\eta^2\text{-}Me_3Si\text{-}C_2SiMe_3)$ (M = Ti, Zr). These form an essential basis for recent applications in chemistry. By using different Cp ligands (Cp, Cp*, ebthi), additional ligands (THF, pyridine), and metals (Ti, Zr), a fine-tuning of several stoichiometric and catalytic reactions was feasible. The latter complexes offer a number of compelling advantages over the widely used other similar metallocene reagents. As a metaphor, this piece of basic research stands "*solid as a rock in heavy seas*" (in the photo the Baltic Sea nearby Rostock-Warnemünde), alluding to the fact that fundamental preparative organometallic chemistry provides a solid foundation for attractive applications. Details of this chemistry are described in the Microreview by U. Rosenthal et al. on p. 4739 ff.

MICROREVIEW

Contents

4739 **U. Rosenthal,* V. V. Burlakov, P. Arndt, W. Baumann, A. Spannenberg, V. B. Shur**

Bis(trimethylsilyl)acetylene Complexes of Titanocenes and Zirconocenes: Their Recent Chemistry and Reactions with Lewis Acids

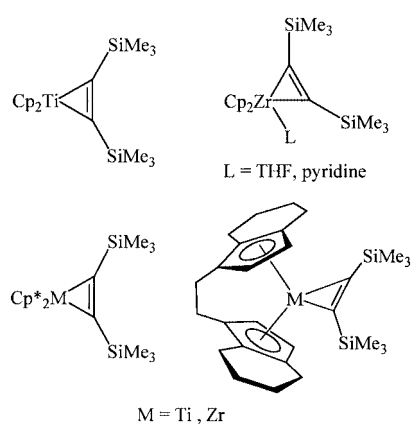

Keywords: Lewis acids / Metallocenes / Polymerization / Titanium / Zirconium

 © 2004 Wiley-VCH Verlag GmbH & Co. KGaA, Weinheim

SHORT COMMUNICATIONS

4751 **G. Lorusso, G. Boccaletti, N. G. Di Masi, F. P. Fanizzi, L. Maresca,* G. Natile**

Vinylic Deprotonation in the Coordination Sphere of Platinum(II): Regioselective Formation of Alkenyl Complexes

Keywords: Platinum / Alkenes / Brönsted acidity / Deprotonation reaction / (*E*)/(*Z*) isomerization

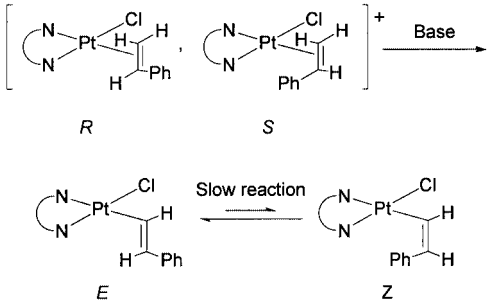

4755 **H. J. Deiseroth,* M. Wagener, E. Neumann**

$(AgI)_2Te_6$ and $(AgI)_2Se_6$: New Composite Materials with Cyclic Te_6 and Se_6 Molecules Stabilized in the "Solid Solvent" AgI

Keywords: Composite materials / Cyclic hexaselenium / Cyclic hexatellurium / Solid solvent silver iodide / Selenium / Tellurium

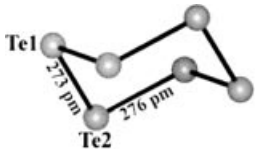

4759 **K. A. Rufanov,* B. Ziemer, M. Hummert, S. Schutte**

Synthesis of (Indenylidene)phosphoranes − A Novel Class of Ligand Precursors for Main-Group and Transition Metal Organometallics

Keywords: Bridging ligands / Constrained geometry catalysts / Cyclopentadienyl ligands / Isoelectronic analogues / Isolobal relationship / Phosphoranes / Phosphorus ylides / Indenyl / Sodium

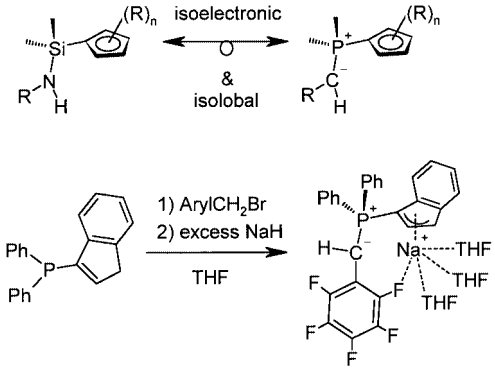

4764 **T. M. Klapötke,* B. Krumm, J. C. Gálvez-Ruiz, H. Nöth, I. Schwab**

Experimental and Theoretical Studies of Homoleptic Tellurium Cyanides $Te(CN)_x$: Crystal Structure of $Te(CN)_2$

Keywords: Cyanides / Structure elucidation / Tellurium / Ab initio calculations

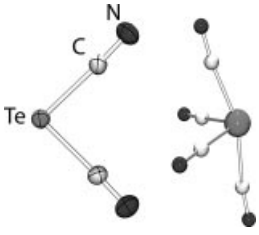

 © 2004 Wiley-VCH Verlag GmbH & Co. KGaA, Weinheim

4770 **A. B. Gaspar, V. Ksenofontov, V. Martinez, M. C. Muñoz, J. A. Real, P. Gütlich***

A Novel Dinuclear Fe^{II} Spin-Crossover Complex Based on a 2,2-Bipyrimidine Bridge Ligand: $[Fe(CH_3bipy)(NCS)_2]_2bpym$

Keywords: Spin crossover / Iron(II) bpym-bridged dinuclear compounds / Pressure-induced spin transition / Mössbauer spectroscopy

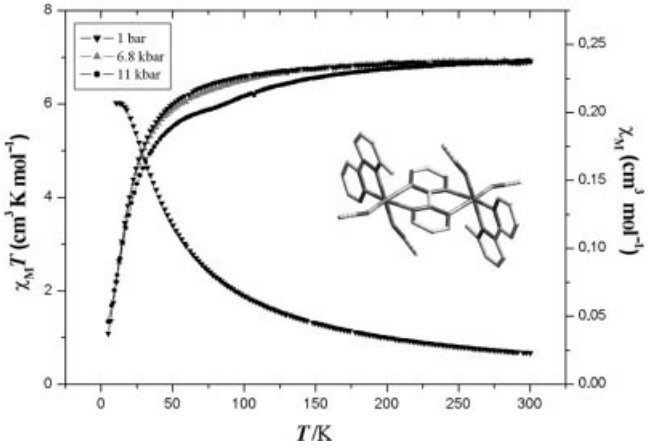

4774 **C.-M. Liu,* J.-L. Luo, D.-Q. Zhang,* N.-L. Wang, Z.-J. Chen, D.-B. Zhu***

Spin Glass Behaviour in a 1D Mixed Molybdenum-Vanadium Heteropolyoxometalate-Bridged Coordination Polymer

Keywords: Nickel / Hydrothermal synthesis / Polyoxometalate / Crystal structure / Magnetic properties

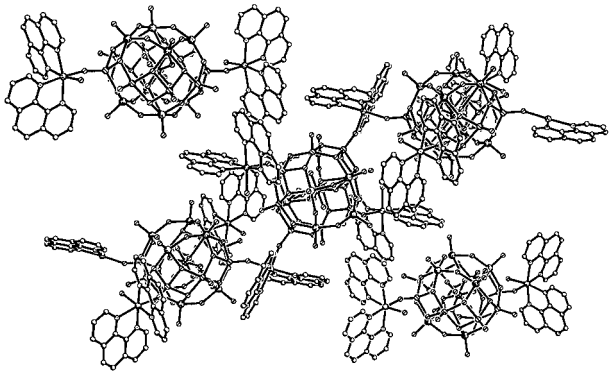

FULL PAPERS

4781 **K. K. Bhasin,* V. Arora, T. M. Klapötke, M.-J. Crawford**

One-Pot Synthesis of Pyridyltellurium Derivatives from a Reaction with Isopropylmagnesium Chloride and X-ray Crystal Structures of Various Pyridyl Ditellurides

Keywords: Grignard reaction / Pyridyl telluride / Tellurium / Transmetallation

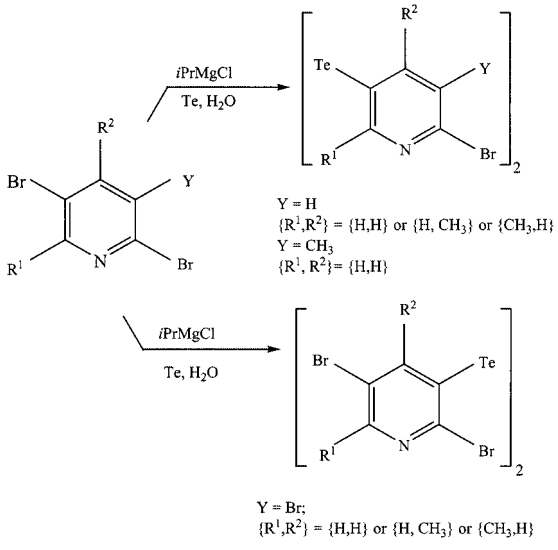

4789 **Q.-Y. Zhu, J. Dai,* D.-X. Jia, L.-H. Cao, H.-H. Lin**

Manganese(II) Complexes Coordinated by a New Derivative of Bipyridine: 9′-[4,5-Bis(methylthio)-1,3-dithiol-2-ylidene]-4′,5′-diazafluorene

Keywords: Diazafluorene / Manganese(II) complex / Crystal structure / Catalysis

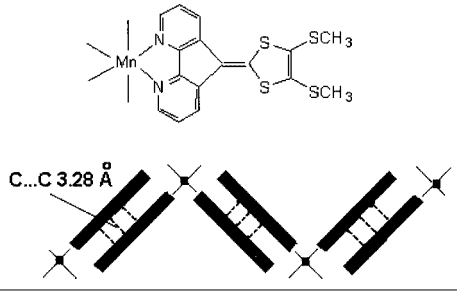

 © 2004 Wiley-VCH Verlag GmbH & Co. KGaA, Weinheim

4795 **K. O. Xavier, E. Smolensky, M. Kapon, S. M. Aucott, J. D. Woollins, M. S. Eisen***

Synthesis and Characterization of Lithium Complexes of 2-(Diphenylphosphanylamino)-pyridine and *N*,2-Bis(diphenylphosphanyl)benzeneamine

Keywords: Lithium complexes / (Diphenylphosphanylamino)pyridine / *N*,2-Bis(diphenylphosphanyl)benzeneamine / Hard-soft interactions / *N*,*N*-chelation / *N*,*P*-chelation / X-ray diffraction

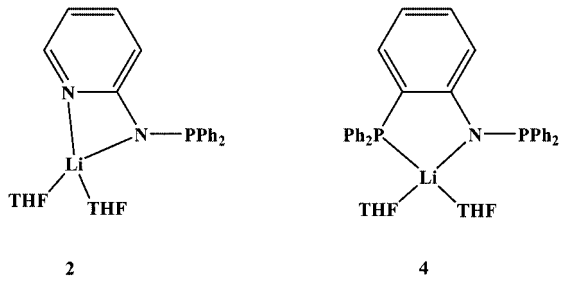

2 4

4803 **F. A. Kunrath, O. L. Casagrande Jr.,* L. Toupet, J.-F. Carpentier***

Thallium−Arene Contacts in a Rare Yttrium Tris(pyrazolyl)hydroborate "ate" Complex

Keywords: Arene ligands / N ligands / Noncovalent interactions / Thallium / Yttrium

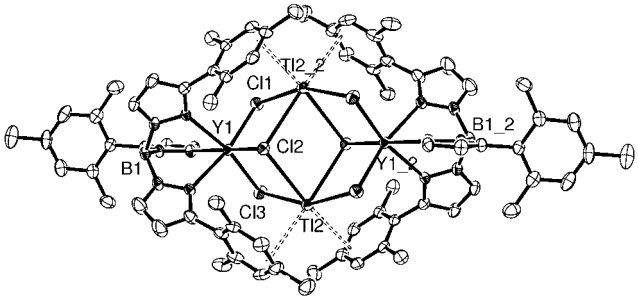

4807 **J. Chai, H. Zhu, Q. Ma, H. W. Roesky,* H.-G. Schmidt, M. Noltemeyer**

Synthesis and Structural Characterization of Three-Coordinate Mn^{II}, Fe^{II}, and Zn^{II} Complexes Containing a Bulky Diamide Ligand $[DippN(CH_2)_3NDipp]^{2-}$ (Dipp = 2,6-*i*$Pr_2C_6H_3$)

Keywords: Iron / Manganese / N ligands / Zinc

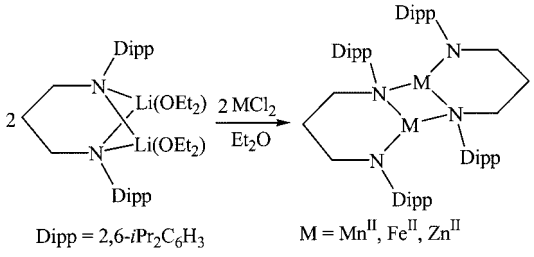

Dipp = 2,6-*i*$Pr_2C_6H_3$ M = Mn^{II}, Fe^{II}, Zn^{II}

4812 **S. Bolaño, J. Bravo,* S. García-Fontán***

Mono- and Dinuclear Rhenium Polyhydride Complexes Bearing the Chelating Ligand 1,2-Bis(dicyclohexylphosphanyloxy)ethane

Keywords: Rhenium / Hydrido ligands / P ligands / Fluxionality

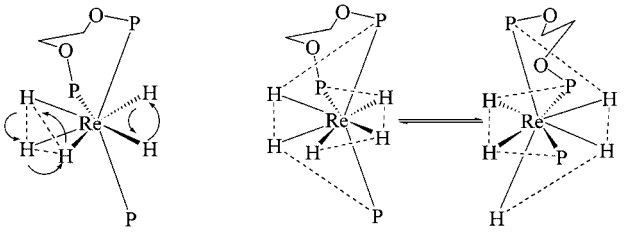

4820 **E. M. Barranco, O. Crespo, M. C. Gimeno,* P. G. Jones, A. Laguna**

The Role of Secondary Interactions in Group 11 Metal Complexes Containing the Ferrocene Ligand $FcCH_2NHpyMe$ in Supramolecular Structures

Keywords: Ferrocenyl derivatives / Group 11 compounds / Supramolecular chemistry / Aurophilic attractions / N ligands

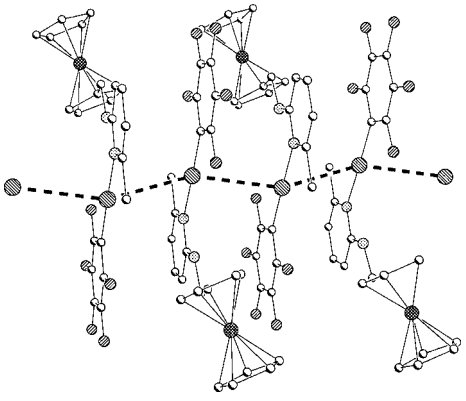

 © 2004 Wiley-VCH Verlag GmbH & Co. KGaA, Weinheim

4828 **S. Komeda, H. Yamane, M. Chikuma, J. Reedijk***

A Kinetic Study on the Reactions of Azolato-Bridged Dinuclear Platinum(II) Complexes with Guanosine 5′-Monophosphate

Keywords: Azoles / Platinum complexes / Cisplatin / Antitumor agents

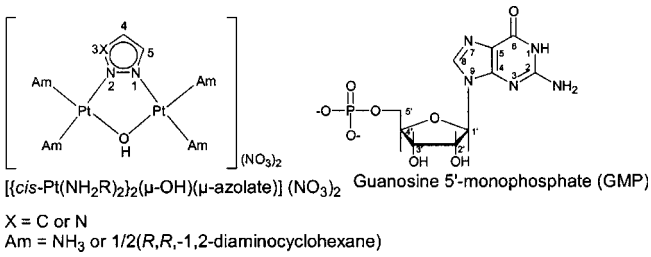

4836 **J. Carranza, H. Grove, J. Sletten,* F. Lloret, M. Julve,* P. E. Kruger, C. Eller, D. P. Rillema**

Synthesis, X-ray Crystal Structure and Magnetic Properties of Oxalato-Bridged Copper(II) Complexes with 2,3-Bis(2-pyridyl)pyrazine, 2,3-Bis(2-pyridyl)quinoxaline and 2,2′-Bipyrazine as Peripheral Ligands

Keywords: Copper / Magnetic properties / N ligands / Oxalate

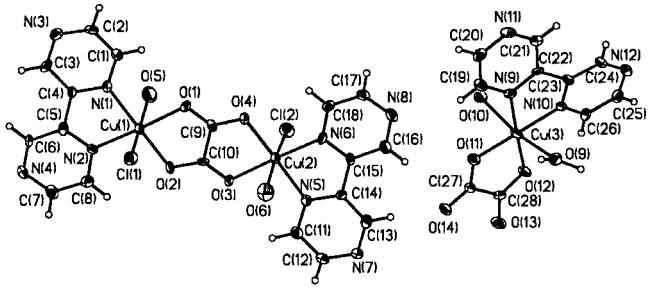

4849 **D. Drewes, E. M. Limanski, B. Krebs***

The Anderson-Type Anion $(TeMo_6O_{24})^{6-}$ – A Multidentate Ligand for Trivalent Rare Earth Cations

Keywords: Polyoxometalates / Molybdenum / Lanthanides / Tellurium / Self-assembly

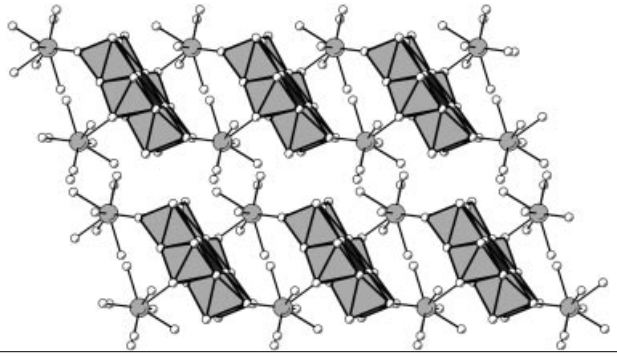

4854 **B. B. Dhar, R. Mukherjee, S. Mukhopadhyay,* R. Banerjee***

Mechanistic Investigation of the Oxidation of Glyoxylic and Pyruvic Acids by Tris(biguanide)-manganese(IV) in Weakly Acidic Aqueous Media

Keywords: Kinetics / Mechanism / Redox reaction / Manganese(IV) / Glyoxylic acid / Pyruvic acid

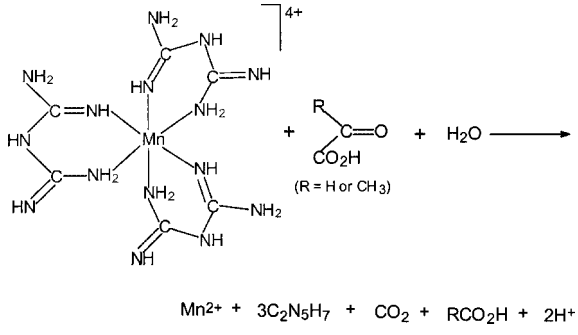

4859 **S. Dilsky, W. A. Schenk***

Diastereomeric Halfsandwich Rhenium Complexes Containing Hemilabile Phosphane Ligands

Keywords: Rhenium / Chiral complexes / Chiral P ligands / Hemilabile P ligands / Sandwich complexes

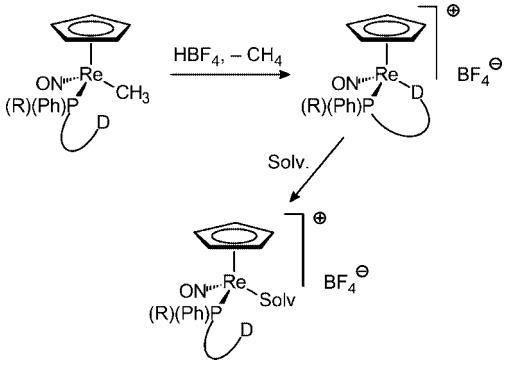

 © 2004 Wiley-VCH Verlag GmbH & Co. KGaA, Weinheim

4871 **J. Sola,* A. López, R. A. Coxall, W. Clegg***

Hydrogen-Bonded Network and Layered Supramolecular Structures Assembled from ClO_4^- Counterions with Unprecedented Monomeric $[AgL_2]^+$ and Chain Polymeric $[AgL_2]_n^{n+}$ Complex Cations (L = Thioamide or Thiourea-Like Ligands)

Keywords: X-ray diffraction / Silver / Supramolecular chemistry / S ligands / Bridging ligands

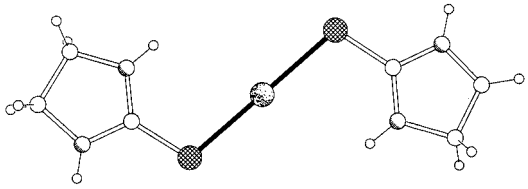

4882 **T. Sunahara, S. Onaka,* M. Ito, H. Imai, K. Inoue, T. Ozeki**

Construction of Nano-Channels Based on Zinc(II) Pyrazine-2-carboxylate Complexes

Keywords: Carboxylato ligands / Nanostructures / Self-assembly / Zinc

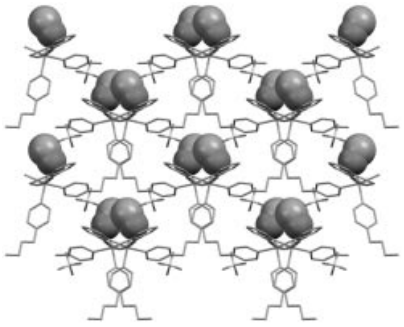

4891 **R.-Q. Fan, D.-S. Zhu, Y. Mu,* G.-H. Li, Y.-L. Yang, Q. Su, S.-H. Feng**

Syntheses, Structures, and Luminescent Properties of [Bis(iminoalkyl)pyridine]cadmium(II) Complexes

Keywords: Cadmium / Luminescence / N ligands / X-ray diffraction

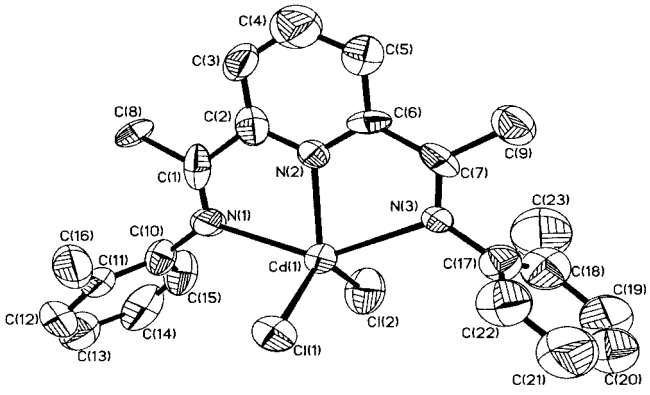

4898 **P.-C. Kuo, I.-C. Chen, J.-C. Chang, M.-T. Lee, C.-H. Hu, C.-H. Hung, H. M. Lee, J.-H. Huang***

Hydroalumination of Carbon Dioxide, Carbon Disulfide, and Phenyl Isocyanate with an Aluminum Ketiminate Compound

Keywords: Aluminum / Carbon dioxide / Hydrides / Hydroalumination/Insertion / N ligands

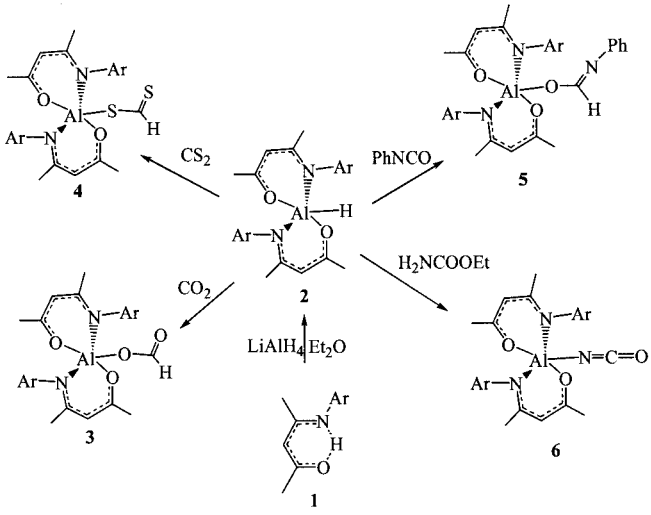

 © 2004 Wiley-VCH Verlag GmbH & Co. KGaA, Weinheim

4907 **S. Wang, G. Yang,* R. Li, Y. Wang, D. Liao**

Syntheses, Structures and Magnetic Properties of Novel Oxamido-Bridged Tetranuclear Complexes [Cu_3M] (M = Cu, Mn)

Keywords: Oxamido bridge / Tetranuclear / Macrocyclic complex / Magnetic property

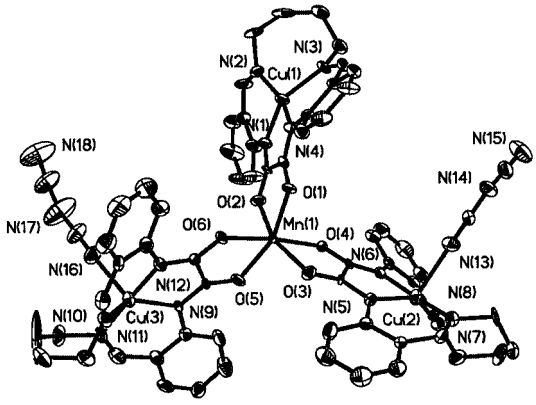

4914 **M. Abrantes, S. Gago, A. A. Valente, M. Pillinger, I. S. Gonçalves,* T. M. Santos, J. Rocha, C. C. Romão***

Incorporation of a (Cyclopentadienyl)molybdenum Oxo Complex in MCM-41 and Its Use as a Catalyst for Olefin Epoxidation

Keywords: Molybdenum / Sandwich complexes / Mesoporous materials / Supported catalysts / Epoxidation

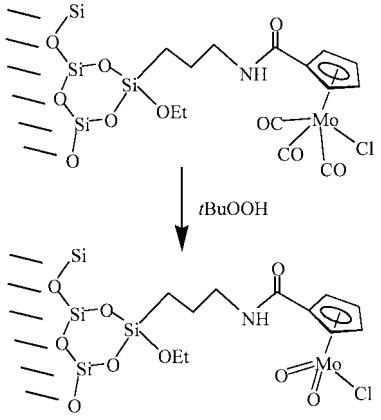

4921 **Index 2004**

 © 2004 Wiley-VCH Verlag GmbH & Co. KGaA, Weinheim

Bis(trimethylsilyl)acetylene Complexes of Titanocenes and Zirconocenes: Their Recent Chemistry and Reactions with Lewis Acids

Uwe Rosenthal,*[a] Vladimir V. Burlakov,[b] Perdita Arndt,[a] Wolfgang Baumann,[a] Anke Spannenberg,[a] and Vladimir B. Shur[b]

Dedicated to Prof. Dr. Dirk Walther on the occasion of his 65th birthday[‡]

Keywords: Lewis acids / Metallocenes / Polymerization / Titanium / Zirconium

The chemistry of the metallocene bis(trimethylsilyl)acetylene complexes [$Cp_2M(L)(\eta^2$-$Me_3SiC_2SiMe_3)$] [M = Ti, without L (**1**); M = Zr, L = THF (**2a**); M = Zr, L = pyridine (**2b**)], the pentamethylcyclopentadienyl complexes [$Cp^*_2M(\eta^2$-$Me_3SiC_2SiMe_3)$] [M = Ti (**3**), Zr (**4**)], and the ethylenebis(tetrahydroindenyl) (ebthi) complexes *rac*-[(ebthi)$M(\eta^2$-$Me_3SiC_2SiMe_3)$] [M = Ti (**5**), Zr (**6**)] has been described in several reviews. A fine-tuning of the reactions is possible by varying the Cp ligands (Cp, Cp*, ebthi), additional the co-ligands (THF, pyridine), and/or metals (Ti, Zr), and it has been pointed out that these complexes offer a number of compelling advantages over other, similar, widely used metallocene reagents. In this microreview recent (2000–2004) examples of the chemistry of complexes **1**–**6** are summarized, and some special interactions with Lewis acids are described. In these reactions the metallocene cores "Cp'_2Ti" and "Cp'_2Zr" (Cp′ = substituted Cp ligands) are mostly formed after dissociation of the alkyne. As examples of this, a new selective zirconocene coupling route to large, functionalized macrocycles has been established from **2b** and polyynes, complex **1** catalyses the first anti-Markovnikov hydroamination of terminal alkynes, complexes **1** and **3** selectively form polynuclear titanium complexes by C–C coupling of N-containing heterocycles, and complexes **1**, **2b**, **3**, and **6** promote selective C–H and C–F bond-cleavage reactions of fluorinated N-containing heterocycles. Beside this recent chemistry, this microreview also focuses on the reactions of the above-mentioned complexes with the Lewis acids diisobutylaluminum hydride and tris(pentafluorophenyl)borane. For example, complexes **1**, **2b**, and **6** react with iBu$_2$AlH to give heterodimetallic complexes containing tetracoordinate planar carbon atoms. The titanium complex **1** reacts with $B(C_6F_5)_3$ with elimination of the alkyne and gaseous hydrogen to give an electrophilic substitution of the Cp or Cp* ligand in which zwitterionic Ti^{III} complexes are formed. The zirconium complexes **4** and **6** do not liberate hydrogen in the reaction with $B(C_6F_5)_3$, although, after C–H activation of one methyl group of the Cp* or Cp part of the ebthi ligand and a B–C bond formation, zwitterionic complexes containing alkylidene groups with agostic interactions with the metal center are obtained. Complex **5** reacts with $B(C_6F_5)_3$ with Si–C bond cleavage of the alkyne and formation of an alkynylboranate $[Me_3SiC{\equiv}CB(C_6F_5)_3]^-$, which is complexed by the "*rac*-(ebthi)Ti" fragment to give a zwitterionic complex. Some of the formed heterodinuclear complexes and the zwitterionic complexes are active catalysts in the ring-opening polymerization of lactones, cyclic carbonates, and epoxides, as well as the polymerization of ethylene.

(© Wiley-VCH Verlag GmbH & Co. KGaA, 69451 Weinheim, Germany, 2004)

Introduction

Coordinatively and electronically unsaturated complex fragments are often required to realize stoichiometric and catalytic reactions of organometallic compounds. These core complexes coordinate to the substrates, activate them, and push them in the direction of the desired products. This is nicely illustrated in manifold reactions of the complex fragments titanocene "Cp_2Ti" and zirconocene "Cp_2Zr" as unstable 14-electron compounds with a d^2 configuration (M^{II}). The possible interactions between occupied and unoccupied orbitals explain why these "Cp_2M" metallocenes react with a variety of unsaturated compounds to form metallacycles, having with a high potential to undergo diverse conversions with further substrates. An important question in this context is what ligand can be used that sufficiently stabilizes the metallocene fragment but is re-

[a] Leibniz-Institut für Organische Katalyse an der Universität Rostock e.V.,
Buchbinderstr. 5−6, 18055 Rostock, Germany
Fax: + 49-381-466-9376
E-mail: uwe.rosenthal@ifok.uni-rostock.de
[b] A. N. Nesmeyanov Institute of Organoelement Compounds, Russian Academy of Sciences,
Vavilov St. 28, 117813 Moscow, Russia
Fax: + 7-095-135-5085
E-mail: vbshur@ineos.ac.ru

[‡] The authors are indebted to Prof. Dr. Dirk Walther who always advocated the tuning aproach detailed in this review.

leased under mild conditions to generate the unstable and very reactive metallocene core.

Many systems are known to generate titanocene "Cp_2Ti" or zirconocene "Cp_2Zr" very well. Selected examples are mixtures of $[Cp_2ZrCl_2]$ with *n*BuLi, which form $[Cp_2Zr(\pi$-n-butene$)]$ via $[Cp_2Zr(\sigma$-$nBu)_2]$, and the reaction of $[Cp_2ZrCl_2]$ with EtMgCl, which forms $[Cp_2Zr(\pi$-ethylene$)]$ via $[Cp_2Zr(\sigma$-$Et)_2]$. In some cases these complexes are stabilized by additional ligands, such as those found in the complexes $[Cp_2Zr(PR_3)(\pi$-*n*-butene$)]$ or $[Cp_2Ti(PMe_3)(\pi$-ethylene$)]$. Other complexes like $[Cp_2Ti(PMe_3)_2]$ and $[Cp_2Zr(\pi$-1,3-butadiene$)]$ can also be used. This chemistry has been summarized in a number of excellent reviews and various informative contributions in textbooks.[1−15]

The applicability and the success of these systems often depends on their preparative accessibility, on the selectivity of the conversions, and on the inertness of the stabilizing ligands. From this point of view, all of the above -mentioned systems have certain disadvantages. Nevertheless, they have been frequently and successfully used for organic synthesis over the few last years.

We have described the stable and well-defined metallocene bis(trimethylsilyl)acetylene complexes $[Cp_2M(L)(\eta^2$-$Me_3SiC_2SiMe_3)]$ [M = Ti, without L (**1**); M = Zr, L = THF (**2a**); M = Zr, L = pyridine (**2b**)], the pentamethylcyclopentadienyl complexes $[Cp^*_2M(\eta^2$-$Me_3SiC_2SiMe_3)]$ [M = Ti (**3**), Zr (**4**)], and the ethylenebis(tetrahydroindenyl) complexes *rac*-$[(ebthi)M(\eta^2$-$Me_3SiC_2SiMe_3)]$ [M = Ti (**5**), Zr (**6**)] as novel reagents for this type of chemistry (Scheme 1). All these complexes are synthesized under anaerobic conditions by the reaction of the corresponding dichlorides $[Cp'_2MCl_2]$ (Cp′ = substituted Cp; M = Ti, Zr) with magnesium in THF at room temperature in the presence of bis(trimethylsilyl)acetylene.[16−25]

The chemistry of these complexes, and particularly their bonding situation, their spectroscopic properties, their reactivity and mechanistic behavior etc., has been described in several reviews.[16−25] Variation of the Cp ligands (Cp, Cp*, ebthi), additional the co-ligands (THF, pyridine) and/or the metals (Ti, Zr) enables a fine-tuning of their reactivity. It has been pointed out that these complexes offer a number of compelling advantages over other widely used

Uwe Rosenthal, born in 1950 in the Altmark, Germany, studied chemistry (1968−1972), received his Ph.D. under the supervision of E. Kurras (1976), and completed his habilitation (1991) at the University of Rostock. He pursued postdoctoral work at the A. N. Nesmeyanov Institute of Organoelement Compounds of the Russian Academy of Sciences in Moscow with M. E. Vol'pin and V. B. Shur (1988) and became a visiting research scientist at the Max Planck Institute of Kohlenforschung in Mülheim/Ruhr with G. Wilke and K. Pörschke (1990−1991). He headed the Max Planck Research group "Complex Catalysis" (1992−1996) and became Professor of Inorganic Chemistry at the University of Rostock (1993). Today he is Vice Director of the Leibniz Institute of Organic Catalysis at the University of Rostock, a member of the Advisory Editorial Board of Organometallics and member of the reviewing board for "The Chemistry of Inorganic Molecules" of the Deutsche Forschungsgemeinschaft. His scientific interests are concentrated in organometallic chemistry (Cr, Ni, Ti, Zr, B, Al, Si) and complex catalysis (C−C single bond coupling and cleavage reactions and activation of small molecules, alkynes, diynes, and organosilicon compounds).

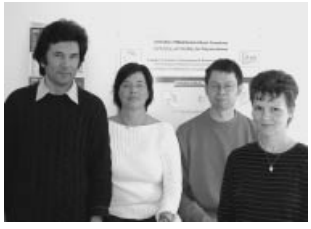

Vladimir V. Burlakov (left) was born in Moscow in 1955. He graduated from the M.V. Lomonosov Moscow Institute of Fine Chemical Technology in 1982. Since 1982, he has been working at the A. N. Nesmeyanov Institute of Organoelement Compounds of the Russian Academy of Sciences (Moscow). In 1995, he received his Ph.D. degree with M. E. Vol'pin and V. B. Shur. Since 1992, he has often been a visiting research scientist in Rostock, hosted by the Rosenthal group. His scientific interests are focused on the transformation of unsaturated hydrocarbons and small molecules mediated by metal complexes of Group IV.

Perdita Arndt (center left), born in 1953 in Stralsund, Germany, studied chemistry (1972−1976) and obtained her Diploma (1976) with U. Kibbel at the University of Rostock. From 1976−1991 she worked as research assistant in the Division of Complex Catalysis in Rostock, Institute of Organic Chemistry, Academy of Sciences with a six-month break working in the group of S. Pasynkiewicz at the Technical University of Warsaw (1978). In 1981 she graduated under supervision of E. Kurras at the University of Rostock (organochromium chemistry) and entered the Max Plank Research group "Complex Catalysis" at the University of Rostock (1992−1996) followed by scientific work at the Institute of Organic Catalysis Research (1997−2002) and the Leibniz Institute for Organic Catalysis at the University of Rostock (from 2003).

Wolfgang Baumann (center right), born in 1962 in Zweibrücken (Palatinate), studied chemistry at the University of Kaiserslautern (1982−1988), obtained his Diploma there in 1988, and did his doctoral work in the group of C. G. Kreiter (preparative organometallic chemistry: photochemistry of carbonyl-cyclopentadienyliron compounds). After graduation in 1990 he became "scientific coordinator" at the "Graduiertenkolleg" Chemical Reactivity and Molecular Order at the University of Siegen (1990−1991) and did postdoctoral work (organolithium chemistry, solid-state NMR) in the group of H. Günther (1991−1993). He has since worked in the Max Planck Research Group "Complex Catalysis" at the University of Rostock (1993−1996), the Institute of Organic Catalysis Research (1997−2002), and the Leibniz Institute of Organic Catalysis at the University of Rostock (from 2003).

Anke Spannenberg (right), born in 1967 in Rostock, Germany, studied chemistry and mathematics at the College of Education in Güstrow (1985−1990), graduated (Dr. rer. nat.) in 1994 under the supervision of H.-J. Holdt at the University of Rostock, and became a member of the Max Planck Research group "Complex Catalysis" at the University of Rostock (1995−1996). As a research scientist she has been working at the Institute of Organic Catalysis Research (1997−2002) and since 2003 at the Leibniz Institute for Organic Catalysis at the University of Rostock. Her scientific interests focus on X-ray crystal structure analysis.

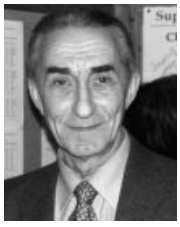

Vladimir B. Shur was born in Moscow in 1936. He graduated from the Moscow Institute of Chemical Technology in 1959. From 1959 to 1962, he worked in industry. Since 1962 he has been working at the A. N. Nesmeyanov Institute of Organoelement Compounds of the Russian Academy of Sciences (Moscow). In 1972, he received his Ph.D. degree with M. E. Vol'pin. From 1964 to 1989, he was head of the research group on nitrogen fixation in the Laboratory of Complex Organometallic Catalysts, headed by M. E. Vol'pin. In 1989, he received his degree of Doctor of Chemical Sciences. In the same year, he became head of the Laboratory of Metal Complex Activation of Small Molecules. Since 1991, he is Professor of Chemistry. His scientific interests focus on molecular nitrogen fixation, C−H bond activation, acetylene complexes of the Group IV metals, and coordination and catalytic chemistry of anticrowns.

MICROREVIEWS: This feature introduces the readers to the author's research through a concise overview of the selected topic. Reference to important work from others in the field is included.

 © 2004 Wiley-VCH Verlag GmbH & Co. KGaA, Weinheim

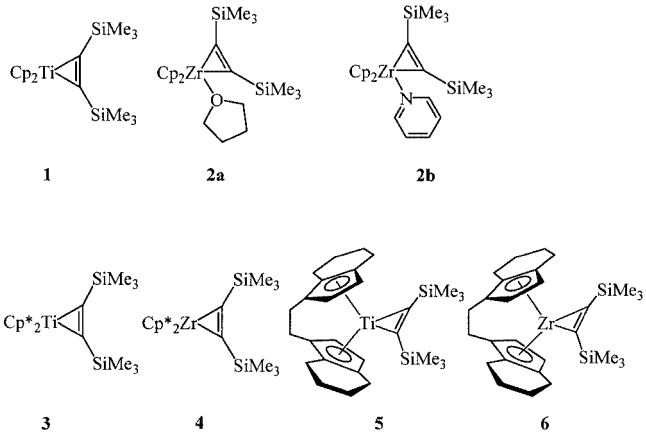

Scheme 1

systems that significantly expand the scope of metallocene-based coupling reactions.[18]

In this microreview recent (2000−2004) examples of the chemistry of complexes **1**−**6** are summarized, and some special interactions with Lewis acids are described.

New Reactions

Two different reaction pathways for complexes **1**−**6** — coupling and elimination of the bis(trimethylsilyl)acetylene — represent the two most commonly found types of reactions of these complexes, with the latter one being the most attractive because of the generation of metallocenes.[18] The formation of stable substituted titanocenes by elimination of bis(trimethylsilyl)acetylene from the corresponding alkyne complexes has been documented in some excellent papers by Mach and coworkers.[26,27]

The reaction of **2a**, **2b**, or **6** with norbornadiene or benzonorbornadiene proceeds with elimination of the alkyne (and THF or pyridine) to give zirconacyclopentanes bearing additional functional groups (Scheme 2).[28] Note that in almost all reaction schemes the elimination of co-ligands and/or bis(trimethylsilyl)acetylene is omitted for simplicity.

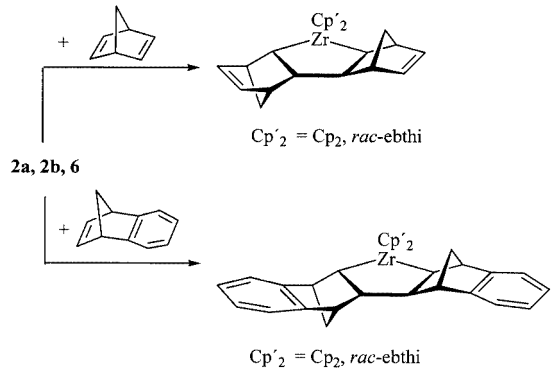

Scheme 2

Another substituted zirconacyclopentane has been isolated from the reaction of **6** with 2-vinylpyridine and norbornadiene. This complex is formed, via a 2-vinylpyridine complex intermediate,[29] by elimination of the bis(trimethylsilyl)acetylene and coupling of the coordinated pyridine and norbornadiene fragments (Scheme 3).[28]

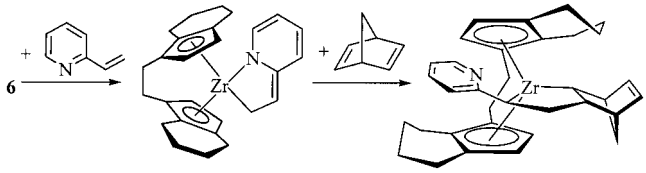

Scheme 3

Polar functionalized olefins also react with complexes **2b** and **6**, although in a different manner, to give either coupling products with the alkyne or substitution of the alkyne.[30] Complex **6** forms a novel 1,4-conjugated insertion product with methyl vinyl ketone, whereas mesityl oxide forms a zirconadihydrofuran by insertion of the carbonyl group (Scheme 4).

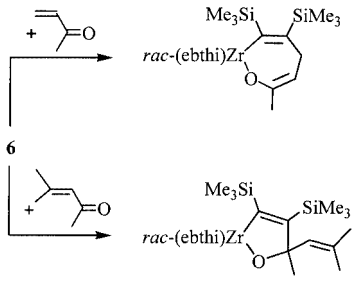

Scheme 4

In contrast, **2b** and methyl vinyl ketone, or **6** and *tert*-butyl acrylate, eliminate the alkyne to yield a different zirconadihydrofuran (Scheme 5).

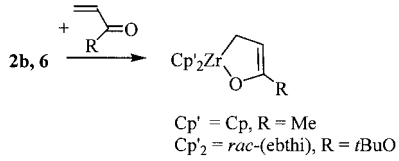

Scheme 5

It is well known that the five-membered titanacyclocumulenes (1-titanacyclopenta-2,3,4-trienes), which can be considered formally as mononuclear "*cis*-diyne" complexes, are formed in the reactions of **1** with 1,3-butadiynes.[17] These compounds react, in the case of titanium, with further complex **1** to yield the dinuclear "*trans*-diyne" complexes with "zigzag butadiyne ligands" — μ-η(1,3),η(2,4)-

 © 2004 Wiley-VCH Verlag GmbH & Co. KGaA, Weinheim

trans,trans-tetradehydrobutadiene moieties — between the two titanocene cores (Scheme 6).

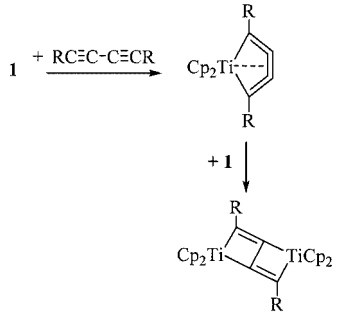

Scheme 6

The novel reaction of 2 equiv. of **1** with 1,4-dichloro-2-butyne gives, probably by the formation of 1,2,3-butatriene, $[Cp_2TiCl_2]$, and $Me_3SiC_2SiMe_3$, 1-titanacyclopent-3-yne, formally a "*cis*-triene" complex, which reacts with additional **1** to give a "*trans*-triene" complex with bridging "zigzag butatriene ligands" between the two titanium centers (Scheme 7).[23,31] Its structure is best described as a 2,5-dititanabicyclo[2.2.0]hex-1(4)-ene (**A**) rather than the resonance structures B — a μ-*trans*-butatriene-bridged π-complex — or C — a butynediyl-bridged σ-propargylic complex (Scheme 7).

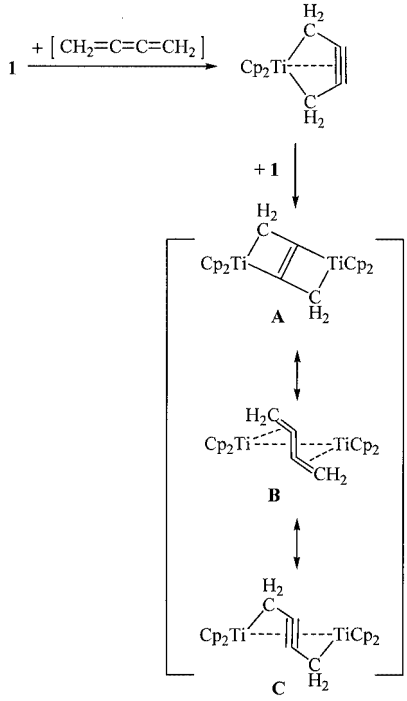

Scheme 7

Suzuki and coworkers have reported the complexation of 1,2,3-butatrienes with zirconocene with formation of the corresponding 1-zirconacyclopent-3-ynes.[32,33] Jemmis,[34] Lin,[35] and Jiao,[36] and their coworkers, have compared these rather exotic compounds by detailed calculations.

The zirconocene monofluoride *rac*-[(ebthi)Zr(F)-$(CH_2CH_2$-2-py)] and difluoride *rac*-[(ebthi)ZrF_2] have been obtained, via the 2-vinylpyridine complex *rac*-[(ebthi)Zr(2-vipy)], by reaction with triethylamine tris(hydrofluoride) (Scheme 8).[37]

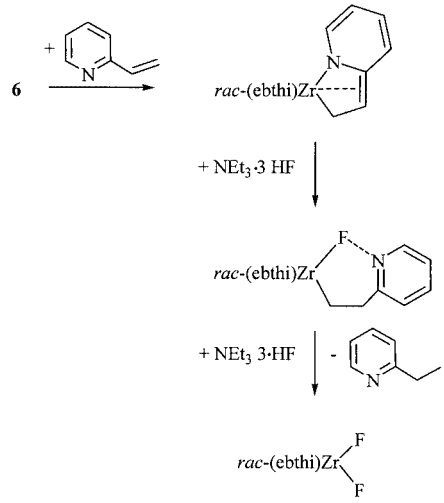

Scheme 8

This novel method for the synthesis of zirconocene difluorides and alkyl monofluorides via the 2-vinylpyridine complexes $[Cp'_2Zr(L)$(2-vipy)] has also been reported for other compounds of the type $[Cp'_2Zr(L)(\eta^2\text{-}Me_3SiC_2SiMe_3)]$ with different ligand Cp'_2 systems, such as $(thi)_2$ [bis(η^5-tetrahydroindenyl)], $Me_2Si(\eta^5\text{-}C_5H_4)_2$ [dimethylsilylbis(η^5-cyclopentadienyl)], and ebthi.

In the last few years several research groups have taken advantage of the above-mentioned complexes for stoichiometric and catalytic reactions. Tilley and coworkers have reported that the complex $[Cp_2Zr(pyridine)(\eta^2\text{-}Me_3SiC_2\text{-}SiMe_3)]$ (**2b**) is best suited for a new selective zirconocene-coupling reaction of polyynes to give large, functionalized macrocycles in which zirconacyclopentadienes are bridged by different groups.[38–40] Protolysis of these products gives the corresponding substituted butadienes. A large number of dimeric and trimeric bridged metallacycles have been synthesized by this method (Scheme 9) including, most recently, several substrates with fluoro substituents.[41]

Beller et al. have described the first anti-Markovnikov hydroamination of terminal alkynes with the complex $[Cp_2Ti(\eta^2\text{-}Me_3SiC_2SiMe_3)]$ (**1**) as a precatalyst (Scheme 10).[42]

This complex was subsequently compared to the corresponding substituted complexes $[Cp'_2Ti(\eta^2\text{-}Me_3SiC_2\text{-}SiMe_3)]$ [Cp′ = Cp* (**3**) and C_5H_4Et], which need a higher reaction temperature.[43] Detailed theoretical calculations by Jiao have revealed that the experimentally observed regioselectivity is determined by the relative stability of the postulated intermediate π-complexes "$[CpTi(NH_2)$-$(=NH)(\eta^2\text{-}HC{\equiv}CH)]$", in which the electrostatic substitution favors the Markovnikov product for aniline and the sterically repulsive destabilization disfavors the Markovnikov

 © 2004 Wiley-VCH Verlag GmbH & Co. KGaA, Weinheim

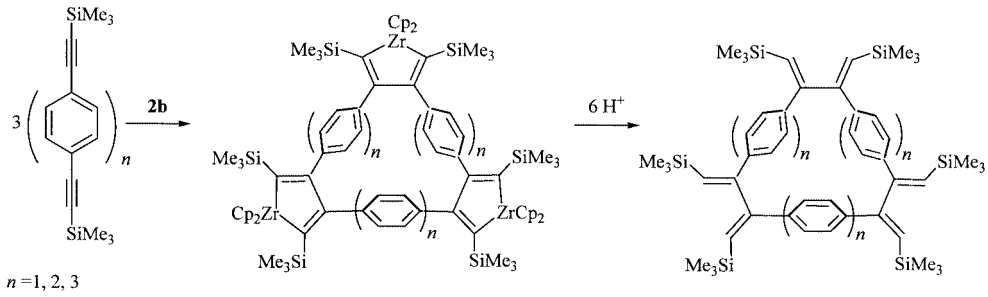

Scheme 9

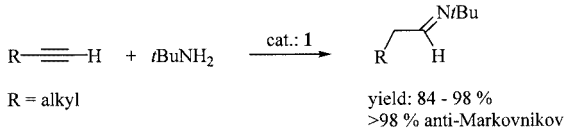

Scheme 10

product for *tert*-butylamine. The one-pot synthesis of several branched secondary aliphatic amines by the hydroamination of terminal alkynes with aliphatic primary amines in the presence of **3** gave the aldimines, in situ, which react with organolithium compounds to give the α-branched amines in high yields (Scheme 11).[44]

Odom and coworkers have compared the activity of complex **1** with a series of other titanium complexes as precata-

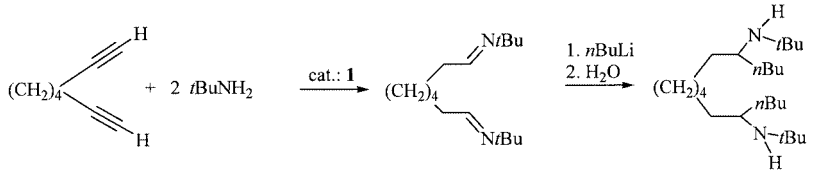

Scheme 11

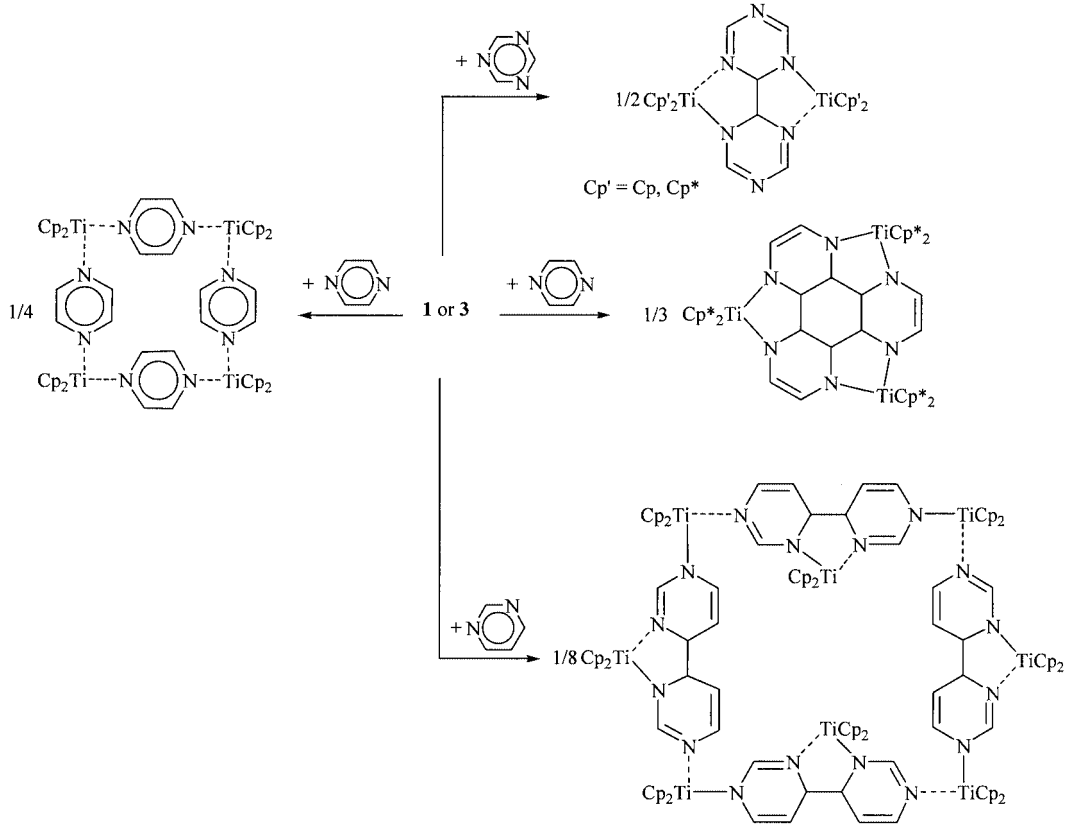

Scheme 12

 © 2004 Wiley-VCH Verlag GmbH & Co. KGaA, Weinheim

lysts for intermolecular alkyne hydroamination; they found that it has a lower activity than the commercially available $Ti(NMe_2)_4$.[45]

Beckhaus and coworkers have published very recently a series of excellent examples of molecular self-organization. The selective formation of polynuclear titanium complexes was realized in the reactions of **1** and **3** with different N-heterocyclic compounds[46,47] by directed reduction of six-membered nitrogen heterocycles and molecular self-organization (Scheme 12).

In these reactions, after dissociation of the bis(trimethylsilyl)acetylene from complexes **1** and **3**, the formed titanocene "Cp_2Ti" and permethyltitanocene "Cp^*_2Ti" moieties react in the same manner with triazine — by C−C bond coupling — to give dinuclear chelate complexes. However, different products were formed with pyrazine: a tetranuclear, pyrazine-bridged complex from **1**, and a trinuclear chelate complex, in a spontaneous threefold C−C coupling reaction, from **3**. Complex **1** gives an octanuclear complex with pyrimidine, whereas the reaction of **1** with triazine leads, by C−C coupling, to a dimeric chelate ligand.[46]

As discussed before for Tilley's reaction with [Cp_2Zr(pyridine)(η^2-$Me_3SiC_2SiMe_3$)] (**2b**),[38−41] the good solubility of the starting materials **1** and **3** allows a smooth separation of the in-most-cases sparingly soluble products. The bis(trimethylsilyl)acetylene formed from these reactions is soluble and volatile, and is thus easy to remove.

The crucial step of C−H activation has also been described by Beckhaus and coworkers for some reactions of complexes **1** and **3** with pyridine, fluorinated pyridines, and other N-containing heterocyclic compounds (Scheme 13).[47] Complex **1** and pyridine, for example, give a hydride-bridged dinuclear titanium fulvalene derivative after C−H activation, whereas monofluoropyridine reacts with **1**, by C−F activation, to give a fluoride-bridged dinuclear titanium complex. It is remarkable that no product resulting from a C−H activation was found in this case. Pentafluoropyridine reacts with **1** to give a similar perfluorinated product.

A fluoride-bridged dinuclear titanium complex is formed in the reaction with 2,4,6-trifluoro-1,3,5-triazine by C−F activation (Scheme 14).

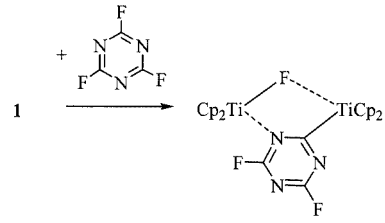

Scheme 14

The reaction of complex **3** with pentafluoropyridine or cyanuric fluoride forms, after C−F activation, mononuclear fluorotitanium(IV) complexes as intermediates, as proved by ^1H and ^{19}F NMR measurements, which go on to react with an excess of the substrates to give the difluoride [$Cp^*_2TiF_2$] (Scheme 15).

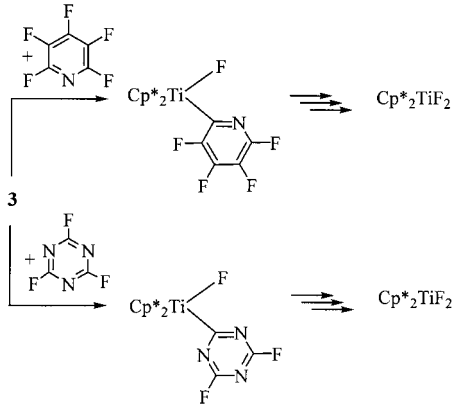

Scheme 15

The corresponding zirconocene complexes **2b** and **6** behave completely differently in such reactions.[48] Tetrafluoropyridine reacts with **2b** or **6** by C−H activation to give 4-substituted pyridyl complexes that contain alkylidene groups with agostic interactions to the metal center (Scheme 16).

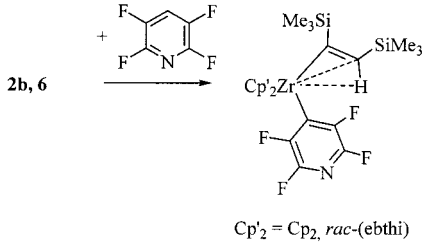

Cp'$_2$ = Cp$_2$, *rac*-(ebthi)

Scheme 16

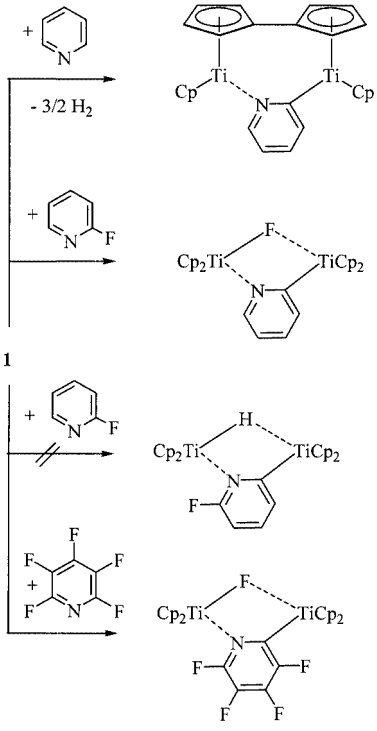

Scheme 13

 © 2004 Wiley-VCH Verlag GmbH & Co. KGaA, Weinheim

This result is opposite to the above-mentioned titanium case in which C−F activation was preferred over C−H activation and the 2-position reacted. The reason for this could be a bimolecular reaction with precoordination of the N-atom of the pyridine and an attack of a second zirconocene in the 4-position. Such a coordination of the pyridine is impossible for complex **1**.

Mach and coworkers have recently described some reactions of substituted zirconocene complexes of bis(trimethylsilyl)acetylene with terminal acetylenes and lithium acetylides.[49] For example, complex **4** reacts with $HC{\equiv}CSiMe_3$ to give the agostic alkenyl-alkynyl complex $[Cp^*_2Zr\{\eta^3\text{-}[C(SiMe_3){=}CHSiMe_3]\}(\eta^1\text{-}C{\equiv}CSiMe_3)]$, as described before for the permethyltitanocene complex **3**. The corresponding complex $[(\eta^5\text{-}C_5HMe_4)_2Zr(\eta^2\text{-}Me_3SiC_2SiMe_3)]$ yielded the diamagnetic zirconate complex $Li[\{(\eta^5\text{-}C_5HMe_4)_2Zr\}\{\eta^1\text{-}(C{\equiv}CSiMe_3)\}\{\eta^2\text{-}(Me_3SiC{\equiv}CSiMe_3)\}]$ with $LiC{\equiv}CSiMe_3$ (Scheme 17).

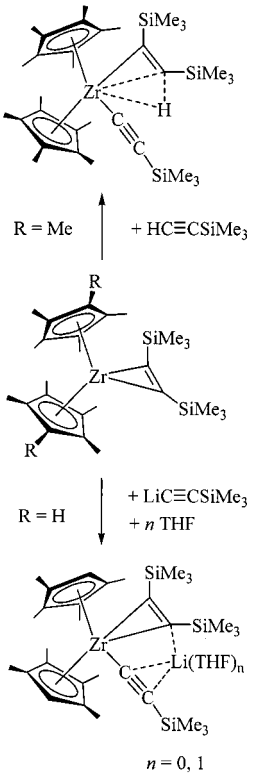

Scheme 17

New Reactions with Lewis Acids

One of the most remarkable discoveries during the past few decades was that the activity of metallocene-based Ziegler−Natta polymerization catalysts is based on cationic $[Cp'_2MR]^+$ complexes containing a metal atom in the +4 oxidation state. Such cationic moieties can easily be prepared by interaction of metallocene complexes $[Cp'_2MX_2]$ (Cp′ = substituted or unsubstituted η^5-cyclopentadienyl, X = Me, CH_2Ph, H etc.) with strong Lewis acids (LA) such as $B(C_6F_5)_3$, Ph_3C^+ etc. After abstraction of X, the metallocenium ion-pair complexes with noncoordinating anions to give $[Cp'_2MX]^+[(\mu\text{-}X)\text{-}LA]^-$ complexes.

As well as the above-mentioned $[Cp'_2MX_2]$ complexes, the titana- and zirconacyclopropenes **1**−**6** also possess two M−C σ-bonds and their reactions with Lewis acids such as $B(C_6F_5)_3$, Al*i*Bu$_3$, and HAl*i*Bu$_2$ have been investigated in detail. The reaction of alkynyl- and alkenylmetallocene complexes with organoaluminum or -boron compounds has been intensively investigated by Erker[50] and Binger;[51] it leads to dimetallic systems of the type $[Cp_2M^1](\mu\text{-}\eta^1{:}\eta^2\text{-}RCCR)(\mu\text{-}X)[M^2R^2_2]$ (M^1 = Zr, Hf, X = Cl, H, M^2 = Al, Ga; M^1 = Ti, X = H, M^2 = B) containing a planar-tetracoordinate carbon atom bridging between a group-4 transition metal and a main group element.

The reactions of the alkynyltitanocene and -zirconocene complexes **1**, **2b**, and **6** with Al*i*Bu$_3$ lead to similar heterodimetallic complexes, along with formation of isobutene and HAl*i*Bu$_2$.[52] These complexes are better prepared, however, by the direct reaction of the alkyne complexes with HAl*i*Bu$_2$ (Scheme 18).

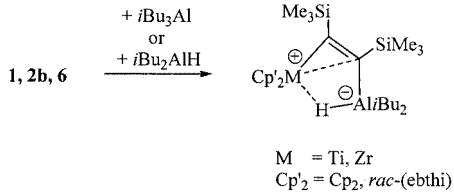

Scheme 18

The X-ray crystal structure analyses of the complexes show planar, bicyclic, five-membered-ring systems containing the metal atom, the hydridic hydrogen, Al, C_β, and C_α. Some of these complexes are very active catalysts for the ring-opening polymerization of ε-caprolactone.[52]

Interestingly, the reaction of **4** with HAl*i*Bu$_2$ gave no such complexes. Instead, an electrophilic substitution of a hydrogen atom from one of the methyl groups of the Cp* ring by the HAl*i*Bu$_2$ moiety occurred.[53] No hydrogen or alkyne were liberated, and a product with an agostic σ-alkenyl group at the zirconium center and a μ-H atom between Al and Zr was isolated (Scheme 19).

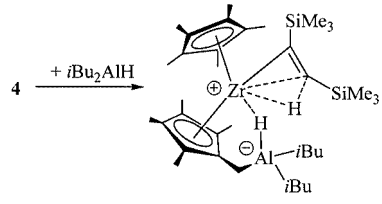

Scheme 19

In the reaction of **1** with $B(C_6F_5)_3$ in toluene at room temperature the titanium(III) complex of $[TiCp\{\eta^5\text{-}C_5H_4B(C_6F_5)_3\}]$, a novel type of zwitterionic complex containing the $B(C_6F_5)_3$ group in the Cp ligand and no σ-bonded organic substituents at the titanium atom, was

 © 2004 Wiley-VCH Verlag GmbH & Co. KGaA, Weinheim

formed. Hydrogen, alkyne, and 1,2-bis(trimethylsilyl)ethane are liberated by the electrophilic substitution of a hydrogen atom of one of the η^5-C_5H_5 rings by a $B(C_6F_5)_3$ group (Scheme 20).[54,55]

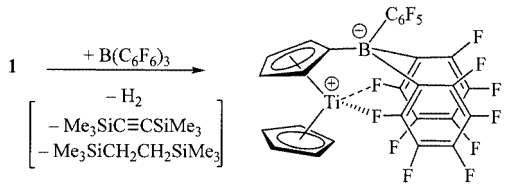

Scheme 20

The reaction of $[Cp_2Ti(PhC_2SiMe_3)]$ with $B(C_6F_5)_3$ under the same conditions gives an identical product, but with a strongly diminished rate of reaction. The complex $[Cp_2Ti(PhC_2Ph)]$ does not react with $B(C_6F_5)_3$ at all under the same conditions, not even after one month. Thus, the replacement of the Me_3Si groups of the acetylene ligand by Ph substituents sharply decreases the reactivity of the corresponding acetylene complexes $[Cp_2Ti(R^1C_2R^2)]$ toward $B(C_6F_5)_3$.[56]

An attempt to electrophilically mercuriate the Cp rings in **1** by reaction with $Hg(OCOCF_3)_2$ was undertaken to obtain the complex $[TiCp(OCOCF_3)\{\eta^5$-$C_5H_4Hg(OCOCF_3)\}]$. It appeared, however, that the process proceeds in another way, and $[Cp_2Ti(OCOCF_3)_2]$ was isolated after the liberation of metallic mercury and alkyne (Scheme 21).[57]

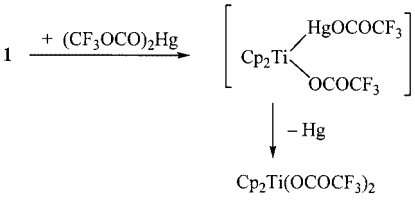

Scheme 21

The reaction of $[(\eta^5$-$iPrC_5H_4)_2Ti(\eta^2$-$Me_3SiC_2SiMe_3)]$ with $B(C_6F_5)_3$ in toluene at room temperature also produces the zwitterionic titanium(III) complex $[Ti(\eta^5$-$iPrC_5H_4)\{\eta^5$-1,3-$iPrC_5H_3B(C_6F_5)_3\}]$ in which the 3-H atom of one of the C_5 rings has been substituted by a $B(C_6F_5)_3$ group (Scheme 22).[56] This complex is analogous in its structure to the titanium(III) zwitterion $[TiCp\{\eta^5$-$C_5H_4B(C_6F_5)_3\}]$ formed from the reaction of $B(C_6F_5)_3$ with **1** (Scheme 20). In this reaction, 1,2-bis(trimethylsilyl)ethene was also detected in addition to the silylated alkyne and 1,2-bis(trimethylsilyl)ethane. A characteristic feature of both zwitterionic complexes is the presence of coordinative bonds between the *ortho*-fluorine atoms of two C_6F_5 substituents and the positively charged titanium center.

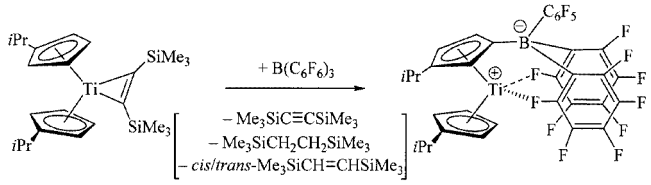

Scheme 22

An electrophilic substitution of a hydrogen atom of one of the methyl groups of the Cp* ring by a $B(C_6F_5)_3$ moiety was also found in the reaction of $B(C_6F_5)_3$ with $[Cp^*_2Ti(\eta^2$-$PhC_2SiMe_3)]$ — the zwitterionic Ti^{III} complex $[TiCp^*\{\eta^5$-$C_5Me_4CH_2B(C_6F_5)_3\}]$ was isolated (Scheme 23).[58]

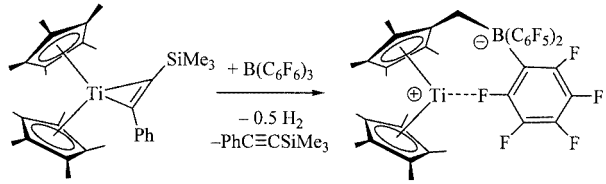

Scheme 23

The oxidation of $[TiCp\{\eta^5$-$C_5H_4B(C_6F_5)_3\}]$ and $[Ti(\eta^5$-$iPrC_5H_4)\{\eta^5$-1,3-$iPrC_5H_3B(C_6F_5)_3\}]$ by atmospheric oxygen affords the isostructural zwitterionic titanoxanes $[Cp\{\eta^5$-$C_5H_4B(C_6F_5)_3\}Ti]_2(\mu$-O) and $[(\eta^5$-$iPrC_5H_4)\{\eta^5$-1,3-$iPrC_5H_3B(C_6F_5)_3\}Ti]_2(\mu$-O), respectively, which contain two zwitterionic units in the molecule (Scheme 24).[56] In each of these units only one *ortho*-fluorine atom of a $B(C_6F_5)_3$ group is involved in coordination to the titanium atom.

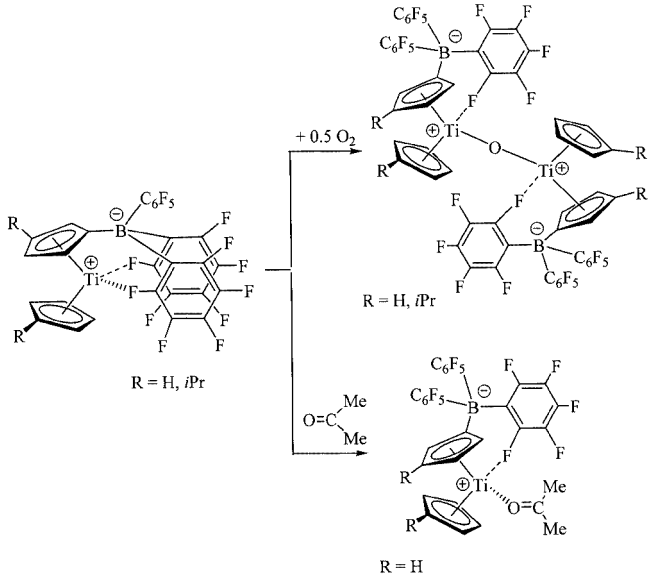

Scheme 24

 © 2004 Wiley-VCH Verlag GmbH & Co. KGaA, Weinheim

These complexes are active catalysts for the cationic ring-opening polymerization of ε-caprolactone, THF, and propylene oxide, whereas γ-butyrolactone and 1-methyl-2-pyrrolidone are not polymerized under the same conditions.[59]

[TiCp{η^5-$C_5H_4B(C_6F_5)_3$}] also reacts readily with acetone to give the zwitterionic adduct [(Me_2CO)TiCp{η^5-$C_5H_4B(C_6F_5)_3$}], where the acetone is bonded to the Ti^{III} center through the oxygen atom and only one *ortho*-fluorine atom of the $B(C_6F_5)_3$ group is coordinated to the metal (Scheme 24).[56]

The monohalide complexes [TiXCp{η^5-$C_5H_4B(C_6F_5)_3$}] (X = Cl, Br) are produced by the reaction of [TiCp{η^5-$C_5H_4B(C_6F_5)_3$}] with alkyl halides (Scheme 25). A characteristic feature of the resulting complex is the coordination between one *ortho*-fluorine atom of one C_6F_5 group and the titanium center. As found for the zwitterionic titanoxanes, the chloride complex catalyses the cationic ring-opening polymerization of THF.[60,61]

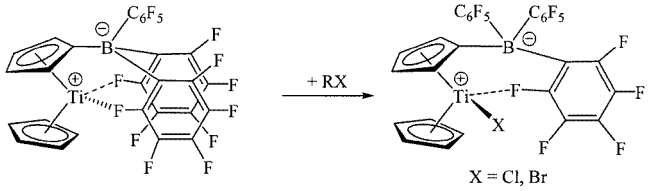

Scheme 25

The reactions of the corresponding zirconium complexes with $B(C_6F_5)_3$ differ from the reaction mode presented above. No hydrogen or alkyne are liberated in the reaction of [$Cp^*_2Zr(\eta^2$-$RC_2SiMe_3)$] (R = Ph, Me_3Si) with $B(C_6F_5)_3$ and the zwitterionic Zr^{IV} derivative [ZrCp*{η^5-$C_5Me_4CH_2B(C_6F_5)_3$}{C(R)=CH($SiMe_3$)}], which contains a σ-alkenyl group at the zirconium center, is produced (Scheme 26).[58]

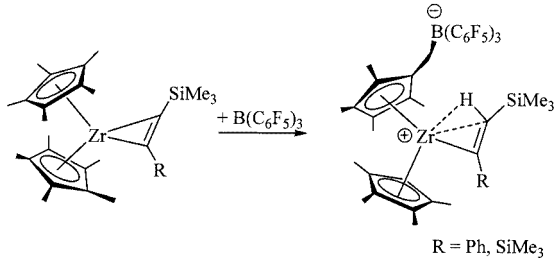

Scheme 26

The reactions of the *rac*-ebthi complexes **5** and **6** with $B(C_6F_5)_3$ also proceed totally differently for Ti and Zr.[62] For **6** an electrophilic substitution of one H atom of the Cp ring in the 3-position occurs to give a zwitterionic alkenyl complex without liberation of hydrogen or alkyne (Scheme 27).

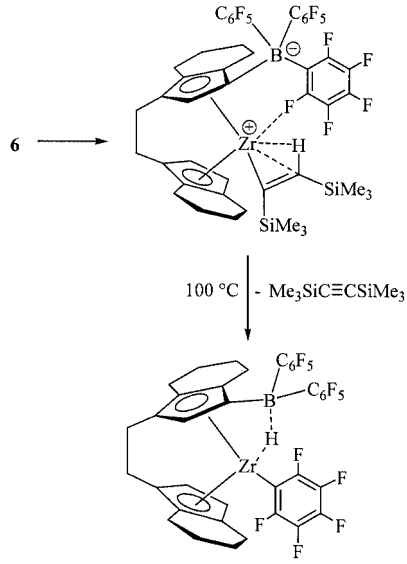

Scheme 27

When this complex is heated to 100 °C in solution the alkyne is eliminated and one B−C bond is cleaved, with a subsequent transfer of one C_6F_5 group from boron to zirconium, to give a complex with one μ-H atom between B and Zr (Scheme 27).

Both complexes are important for the understanding of deactivation processes in the polymerization of olefins and demonstrate the importance of the proper addition sequence when adding reagents in order to achieve catalytic activity. If **6** is first treated with ethene, the zirconacyclopentane formed is subsequently activated by $B(C_6F_5)_3$ to give a catalyst that is active for the polymerization of ethylene. However, if the borane is added to **6** first, neither the obtained complex nor the thermolysis product (Scheme 27) react with ethylene. Interestingly, the analogous complexes [ZrCp*{η^5-$C_5Me_4CH_2B(C_6F_5)_3$}{C(R)=CH($SiMe_3$)}] (R = Ph, $SiMe_3$; Scheme 26) are active in ethylene polymerization, presumably because they have no C−F interactions due to steric reasons.

In the reaction of **5** with $B(C_6F_5)_3$ neither an electrophilic substitution of an H atom nor an elimination of the alkyne was observed. Instead, after substitution of one of the $SiMe_3$ groups in the coordinated bis(trimethylsilyl)acetylene by $B(C_6F_5)_3$, the first zwitterionic titanium(III) η^2-(trimethylsilyl)alkynylboranate complex *rac*-[{(ebthi)Ti}$^+$-{[η^2-$Me_3SiC_2B(C_6F_5)_3$]}−] was obtained (Scheme 28).

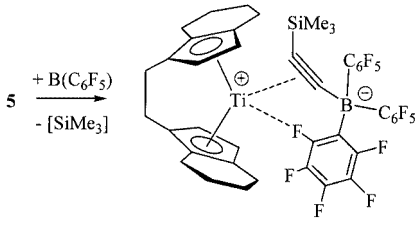

Scheme 28

 © 2004 Wiley-VCH Verlag GmbH & Co. KGaA, Weinheim

In this complex the $[Me_3SiC_2B(C_6F_5)_3]^-$ ligand is unsymmetrically and weakly bonded to the Ti center by its C≡C bond as well as by one of the *ortho*-F atoms of the $B(C_6F_5)_3$ group. Complexes of alkynylboranates have not been isolated or characterized before, although they have frequently been postulated as reactive intermediates, for example in the $B(C_6F_5)_3$-catalyzed C−C coupling of alkynyl groups by bis(alkynyl)zirconocene(IV) complexes[63] and in the reaction of alkynylstannanes with boranes.[64]

Reaction of **5** with the Brönsted acid $B(C_6F_5)_3{\cdot}H_2O$ gives a mixture of the blue complexes [*rac*-(ebthi)Ti]$^+$-$[HOB(C_6F_5)_3]^-$ and [*rac*-(ebthi)Ti]$^+[HB(C_6F_5)_3]^-$ (Scheme 29).[65]

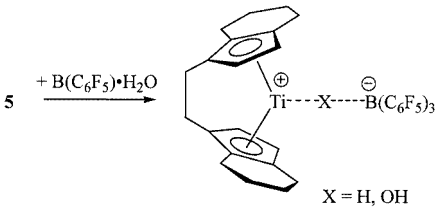

Scheme 29

These complexes form a series of compounds of the type [*rac*-(ebthi)Ti]$^+[XB(C_6F_5)_3]^-$ with X = $Me_3SiC{\equiv}C$, OH, and H.

Conclusion

The reactions presented here show once again that the metallocene bis(trimethylsilyl)acetylene complexes $[Cp_2M(L)(\eta^2\text{-}Me_3SiC_2SiMe_3)]$ [M = Ti, without L (**1**); M = Zr, L = THF (**2a**); M = Zr, L = pyridine (**2b**)], the pentamethylcyclopentadienyl complexes $[Cp^*_2M(\eta^2\text{-}Me_3SiC_2SiMe_3)]$ [M = Ti (**3**), Zr (**4**)], and the complexes *rac*-[(ebthi)M(η^2-$Me_3SiC_2SiMe_3$)] [ebthi = ethylenebis(tetrahydroindenyl); M = Ti (**5**), Zr (**6**)] offer a number of compelling advantages over other, widely used metallocene reagents as they are readily prepared directly from the dichlorides $[Cp'_2MCl_2]$, are stable at room temperature for a long time under argon atmosphere, and allow a control over the stoichiometry of reactions at elevated temperatures. The side-products of the reactions — bis(trimethylsilyl)acetylene, THF, and pyridine — are soluble and volatile and thus easy to remove. These complexes allow reactions in a broad variety of solvents, in particular nonpolar solvents such as pentane.

Acknowledgments

This work was supported by the Deutsche Forschungsgemeinschaft (SPP 1118, Project No. Ro 1269/6), the Fonds der Chemischen Industrie, the Land Mecklenburg-Vorpommern, and the Russian Foundation for Basic Research (Project No. 02-03-32589). Funding and facilities provided by the Leibniz-Institut für Organische Katalyse an der Universität Rostock are gratefully acknowledged. The work reported in this contribution would not have been possible without the excellent efforts by various former Ph.D. students and scientists and a lot of other colleagues whose names appear in the list of references, as well as our technical staff, in particular Petra Bartels and Regina Jesse. We thank Dr. Barbara Heller and Professor Rüdiger Beckhaus for many useful suggestions and discussions.

[1] E. Negishi, T. Takahashi, *Aldrichim. Acta* **1985**, *18*, 31−47.
[2] E. Negishi, *Acc. Chem. Res.* **1987**, *20*, 65−72.
[3] S. L. Buchwald, R. B. Nielsen, *Chem. Rev.* **1988**, *88*, 1047−1058.
[4] E. Negishi, T. Takahashi, *Synthesis* **1988**, 1−19.
[5] S. L. Buchwald, R. A. Fisher, *Chem. Scr.* **1989**, *29*, 417−421.
[6] E. Negishi, *Chem. Scr.* **1989**, *29*, 457−568.
[7] G. Erker, *Angew. Chem.* **1989**, *101*, 411−450; *Angew. Chem. Int. Ed. Engl.* **1989**, *28*, 397−406.
[8] E. Negishi, T. Takahashi, *Acc. Chem. Res.* **1994**, *27*, 124−130.
[9] S. L. Buchwald, R. D. Broene, *Science* **1993**, 1696−1701.
[10] E. Negishi, T. Takahashi, *Bull. Chem. Soc. Jpn.* **1998**, *71*, 755−769.
[11] R. Beckhaus, *Nachr. Chem. Tech. Lab.* **1998**, *46*, 611−623.
[12] E. Negishi, J.-L. Montchamp, in *Metallocenes, Synthesis, Reactivity, Applications* (Eds.: A. Togni, R. L. Halterman), Wiley-VCH, Weinheim, **1998**, vol. 1, chapter 5, p. 241−319.
[13] R. Beckhaus, in *Metallocenes, Synthesis, Reactivity, Applications* (Eds. A. Togni, R. L. Halterman), Wiley-VCH, Weinheim, **1998**, vol. 1, chapter 4, p. 153−239.
[14] E. Negishi, S. Huo, in *Titanium and Zirconium in Organic Synthesis* (Ed.: I. Marek), Wiley-VCH, Weinheim, **2002**, chapter 1, p. 1−49.
[15] T. Takahashi, Y. Li, in *Titanium and Zirconium in Organic Synthesis* (Ed.: I. Marek), Wiley-VCH, Weinheim, **2002**, chapter 2, p. 50−85.
[16] A. Ohff, S. Pulst, C. Lefeber, N. Peulecke, P. Arndt, V. V. Burlakov, U. Rosenthal, *Synlett* **1996**, 111−118.
[17] U. Rosenthal, P.-M. Pellny, F. G. Kirchbauer, V. V. Burlakov, *Acc. Chem. Res.* **2000**, *33*, 119−129.
[18] U. Rosenthal, V. V. Burlakov, in *Titanium and Zirconium in Organic Synthesis* (Ed.: I. Marek), Wiley-VCH, Weinheim, **2002**, chapter 10, p. 355−390.
[19] U. Rosenthal, V. V. Burlakov, P. Arndt, W. Baumann, A. Spannenberg, *Organometallics* **2003**, *22*, 884−900.
[20] U. Rosenthal, P. Arndt, W. Baumann, V. V. Burlakov, A. Spannenberg, *J. Organomet. Chem.* **2003**, *670*, 84−96.
[21] U. Rosenthal, *Angew. Chem.* **2003**, *115*, 1838−1842; *Angew. Chem. Int. Ed.* **2003**, *42*, 1794−1798.
[22] A. Spannenberg, P. Arndt, W. Baumann, U. Rosenthal, *J. Organomet. Chem.* **2003**, *683*, 261−266.
[23] U. Rosenthal, *Angew. Chem.* **2004**, *116*, 3972−3977; *Angew. Chem. Int. Ed.* **2004**, *43*, 3882−3887.
[24] U. Rosenthal, V. V. Burlakov, P. Arndt, W. Baumann, A. Spannenberg, *Organometallics*, submitted.
[25] U. Rosenthal, in *Acetylene Chemistry II. Chemistry, Biology, and Material Science* (Eds.: F. Diederich, P. J. Stang, R. R. Tykwinski), Wiley-VCH, Weinheim, **2003**, chapter 4, p. 139−171.
[26] M. Horacek, V. Kupfer, U. Thewalt, P. Stepnicka, M. Polasek, K. Mach, *Organometallics* **1999**, *18*, 3572−3578.
[27] L. Lukesova, M. Horacek, P. Stepnicka, K. Feifarova, R. Gyepes, I. Cisarova, J. Kubista, K. Mach, *J. Organomet. Chem.* **2002**, *663*, 134−144.
[28] H. Sun, V. V. Burlakov, A. Spannenberg, W. Baumann, P. Arndt, U. Rosenthal, *Organometallics* **2001**, *20*, 5472−5477.
[29] D. Thomas, W. Baumann, A. Spannenberg, R. Kempe, U. Rosenthal, *Organometallics.* **1998**, *17*, 2096−2102.
[30] H. Sun, V. V. Burlakov, A. Spannenberg, W. Baumann, P. Arndt, U. Rosenthal, *Organometallics.* **2002**, *21*, 3360−3366.
[31] V. V. Burlakov, P. Arndt, W. Baumann, A. Spannenberg, U. Rosenthal, P. Parameswaran, E. D. Jemmis, *Chem. Commun.* **2004**, 2074−2075.

 © 2004 Wiley-VCH Verlag GmbH & Co. KGaA, Weinheim

[32] N. Suzuki, M. Nishiura, Y. Wakatsuki, *Science* **2002**, *295*, 660−663.
[33] N. Suzuki, N. Ahihara, H. Takahara, T. Watanabe, M. Iwasaki, M. Saburi, D. Hashizume, T. Chihara, *J. Am. Chem. Soc.* **2004**, *126*, 60−61.
[34] E. D. Jemmis, A. K. Phukan, U. Rosenthal, *J. Organomet. Chem.* **2001**, *635*, 204−211.
[35] K. C. Lam, Z. Lin, *Organometallics* **2003**, *22*, 3466−3470.
[36] E. D. Jemmis, A. K. Phukan, H. Jiao, U. Rosenthal, *Organometallics* **2003**, *22*, 4958−4965.
[37] A. Spannenberg, P. Arndt, W. Baumann, V. V. Burlakov, U. Rosenthal, S. Becke, T. Weiß, *Organometallics* **2004**, *23*, 3819−3825.
[38] J. R. Nitschke, S. Zürcher, T. D. Tilley, *J. Am. Chem. Soc.* **2000**, *122*, 10345−10352.
[39] J. R. Nitschke, T. D. Tilley, *Angew. Chem.* **2001**, *113*, 2200−2203; *Angew. Chem. Int. Ed.* **2001**, *40*, 2142−2145.
[40] L. L. Schafer, J. R. Nitschke, S. S. H. Mao, F.-Q. Liu, G. Harder, M. Haufe, T. D. Tilley, *Chem. Eur. J.* **2002**, *8*, 74−83.
[41] J. R. Nitschke, T. D. Tilley, *J. Am. Chem. Soc.* **2001**, *123*, 10183−10190, and references cited therein.
[42] A. Tillack, I. G. Castro, C. G. Hartung, M. Beller, *Angew. Chem.* **2002**, *114*, 2646−2648, *Angew. Chem. Int. Ed.* **2002**, *41*, 2541−2543.
[43] A. Tillack, H. Jiao, I. G. Castro, C. G. Hartung, M. Beller, *Chem. Eur. J.* **2004**, *10*, 2409−2420.
[44] I. G. Castro, A. Tillack, C. G. Hartung, M. Beller, *Tetrahedron Lett.* **2003**, *44*, 3217−3221.
[45] Y. Shi, C. Hall, J. T. Ciszewski, C. Cao, A. L. Odom, *Chem. Commun.* **2003**, 586−587.
[46] S. Kraft, R. Beckhaus, D. Haase, W. Saak, *Angew. Chem.* **2004**, *116*, 1609−1614, *Angew. Chem. Int. Ed.* **2004**, *43*, 1583−1587.
[47] I. M. Piglosiewicz, S. Kraft, R. Beckhaus, D. Haase, W. Saak, *Eur. J. Inorg. Chem.*, in press.
[48] U. Jäger-Fiedler, P. Arndt, W. Baumann, V. V. Burlakov, A. Spannenberg, U. Rosenthal, *7th North-German Colloquium of PhD Students of Inorganic Institutes*, Hamburg, September 29−30, **2004**, abstract 4.1.
[49] M. Horacek, P. Stepnicka, J. Kubista, R. Gyepes, K. Mach, *Organometallics* **2004**, *23*, 3388−3397.
[50] D. Röttger, G. Erker, *Angew. Chem.* **1997**, *109*, 840−856; *Angew. Chem. Int. Ed. Engl.* **1997**, *36*, 812−827.
[51] P. Binger, F. Sandmeyer, K. Krüger, *Organometallics* **1995**, *14*, 2969−2976.
[52] P. Arndt, A. Spannenberg, W. Baumann, S. Becke, U. Rosenthal, *Eur. J. Inorg. Chem.* **2001**, 2885−2890.
[53] V. V. Burlakov, P. Arndt, A. Spannenberg, W. Baumann, U. Rosenthal, *14th International Symposium on Homogeneous Catalysis*, München, Germany, July 5−9, **2004**, book of abstracts, p. 298.
[54] V. V. Burlakov, S. I. Troyanov, A. V. Letov, E. I. Mysov, G. G. Furin, V. B. Shur, *Izv. Akad. Nauk. Ser. Khim.* **1999**, 1022−1023; *Russ. Chem. Bull.* **1999**, *48*, 1012−1013; *Chem. Abstr.* **1999**, *131*, 257665.
[55] V. V. Burlakov, S. I. Troyanov, A. V. Letov, G. G. Furin, U. Rosenthal, V. B. Shur, *J. Organomet. Chem.* **2000**, *598*, 243−247.
[56] V. V. Burlakov, P. Arndt, W. Baumann, A. Spannenberg, U. Rosenthal, A. V. Letov, K. A. Lyssenko, A. A. Korlyukov, L. I. Strunkina, M. Kh. Minacheva, V. B. Shur, *Organometallics* **2001**, *20*, 4072−4079.
[57] L. I. Strunkina, M. Kh. Minacheva, K. A. Lyssenko, Z. S. Klemenkova, A. Yu. Volkonsky, P. V. Petrovskii, V. V. Burlakov, V. B. Shur, *Izv. Akad. Nauk. Ser. Khim.* **2003**, 1299−1301; *Russ. Chem. Bull.* **2003**, *52*, 1372−1375; *Chem. Abstr.* **2004**, *140*, 303788.
[58] V. V. Burlakov, P.-M. Pellny, P. Arndt, W. Baumann, A. Spannenberg, V. B. Shur, U. Rosenthal, *Chem. Commun.* **2000**, 241−242.
[59] V. V. Burlakov, A. V. Letov, P. Arndt, W. Baumann, A. Spannenberg, Ch. Fischer, L. I. Strunkina, M. Kh. Minachova, Ya. S. Vygodskii, U. Rosenthal, V. B. Shur, *J. Mol. Catal.* **2003**, *200*, 63−67.
[60] L. I. Strunkina, M. Kh. Minacheva, K. A. Lyssenko, O. I. Chaustova, V. V. Burlakov, U. Rosenthal, V. B. Shur, *Izv. Akad. Nauk. Ser. Khim.* **2003**, 737−738; *Russ. Chem. Bull.* **2003**, *52*, 773−774; *Chem. Abstr.* **2004**, *140*, 217747.
[61] L. I. Strunkina, M. Kh. Minachova, K. A. Lisenko, P. V. Petrovskii, V. V. Burlakov, U. Rosenthal, V. B. Shur, *International Conference dedicated to the 50th Anniversary of A. N. Nesmeyanov Institute of Organoelement Compounds (INEOS)*, Russian Academy of Sciences, Moscow, Russia, Modern Trends in Organoelement and Polymer Chemistry, May 30−June 4, **2004**, book of abstracts, p. 69.
[62] P. Arndt, W. Baumann, A. Spannenberg, U. Rosenthal, V. V. Burlakov, V. B. Shur, *Angew. Chem.* **2003**, *115*, 1455−1458; *Angew. Chem. Int. Ed.* **2003**, *42*, 1414−1418.
[63] G. Erker, S. Venne-Dunker, G. Kehr, N. Kleigrewe, R. Fröhlich, C. Mück-Lichtenfeld, S. Grimme, *Organometallics* **2004**, *23*, 4391−4395, and references cited therein.
[64] B. Wrackmeyer, G. Kehr, S. Willbold, S. Ali, *J. Organomet. Chem.* **2002**, *646*, 125−133.
[65] A. Spannenberg, V. V. Burlakov, P. Arndt, W. Baumann, V. B. Shur, U. Rosenthal, *Z. Kristallogr.* **2002**, *217*, 546−548.

Received September 10, 2004

 © 2004 Wiley-VCH Verlag GmbH & Co. KGaA, Weinheim

Vinylic Deprotonation in the Coordination Sphere of Platinum(II): Regioselective Formation of Alkenyl Complexes

Giuseppe Lorusso,[a] Giovanni Boccaletti,[a] Nicola G. Di Masi,[a] Francesco P. Fanizzi,[b,c] Luciana Maresca,*[a] and Giovanni Natile[a]

Keywords: Platinum / Alkenes / Brönsted acidity / Deprotonation reaction / (*E*)/(*Z*) isomerization

Reaction of [PtCl(η^2-CH_2=CHAr)(tmeda)](ClO_4) (**1**) [Ar = C_6H_5 (**1a**), 4-$CH_3OC_6H_4$ (**1b**), 3-$NO_2C_6H_4$ (**1c**); tmeda = *N*,*N*,*N*′,*N*′-tetramethylethylenediamine) with triethylamine, or even with inorganic carbonate, leads to the abstraction of a vinylic proton and formation of the (alkenyl)platinum species [PtCl{(*E*)-CH=CHAr}(tmeda)] (**2**) in high yield. The initially formed (*E*) isomer, in solution of chlorinated solvents, partly isomerizes into the (*Z*) form [equilibrium ratio (*E*)/(*Z*) ≈ 4:1]; the isomerization reaction is rather slow and is catalyzed by visible light. The nature of the phenyl substituent (electron donor OMe or electron-withdrawing NO_2 group) does not appear to affect the rate of deprotonation. The nature and stereochemistry of the formed (alkenyl)platinum species has been elucidated through 1D and 2D ^1H and ^{13}C NMR spectroscopy.

(© Wiley-VCH Verlag GmbH & Co. KGaA, 69451 Weinheim, Germany, 2004)

Introduction

In a recent paper we described the allylic deprotonation of the alkene in cationic [PtCl(η^2-alkene)(tmeda)]$^+$ complexes (tmeda = *N*,*N*,*N*′,*N*′-tetramethylethylenediamine). The reaction requires the use of a noncoordinating base (NEt_3) and, under suitable conditions, it can lead to the removal of two allylic protons and formation of a dimeric species with an η^1,η^3-allyl bridging ligand.[1] We have extended the investigation to styrene analogues of the previous compounds, [PtCl(η^2-styrene)(tmeda)](ClO_4), for which only vinylic protons can be removed. The Brönsted acidity of vinylic protons has already been reported for styrenes coordinated to a metal center and in a cationic substrate.[2−6] There is, however, only one report concerning platinum complexes, which involves dicationic species that are known to be rather reactive towards deprotonation.[7]

Results and Discussion

[PtCl(η^2-CH_2=CHPh)(tmeda)](ClO_4) (**1a**) is readily deprotonated by a base in chlorinated solvents. The reaction is fast and quantitative in the presence of a moderate excess of triethylamine (3 h, 25 °C, **1a**/NEt_3 = 1:2.5), but slower in the presence of anhydrous sodium carbonate in heterogeneous conditions (ca. 80% yield at 25 °C after 3 d). Moreover, it is completely regioselective and leads to the exclusive formation of the (*E*) isomer [PtCl{(*E*)-CH=CHPh}(tmeda)] [(*E*)-**2a**] (Scheme 1).

The stereochemistry of **2a** was unequivocally determined on the basis of NMR spectroscopic data. The signals of the vinylic protons appear at δ = 6.46 and 7.31 ppm with $^3J_{H,H}$ = 16.3 Hz which is typical for protons that are mutually *trans* with respect to a carbon−carbon double bond.[8] ^{13}C and $^1H/^{13}C$ INVERSE HETCOR spectra set the signals of the vinylic carbon atoms at δ = 121.3 and 135.8 ppm with $J_{Pt,C}$ = 1009 Hz for the former and < 60 Hz for the latter (Figure 1 and Table 1). The more shielded and strongly Pt-coupled carbon atom is the one directly bound to the metal center. It is worth noting that this carbon atom carries the less shielded proton (δ = 7.31 ppm).

Complex (*E*)-**2a** in chloroform solution partially isomerizes to the (*Z*) form. The transformation is photocatalyzed since at ambient temperature (ca. 25 °C) the equilibrium is attained in the dark after ca. 100 d and if the sample is exposed to visible light after ca. 35 h. At equilibrium the (*E*)/(*Z*) ratio is ca. 4:1. In the (*Z*) isomer the two vinylic protons have $^3J_{H,H}$ = 10.7 Hz consistent with their mutual *cis* position.[9] All other proton resonances change slightly on going from the (*E*) to the (*Z*) form, with the only exception being the phenyl *ortho*-proton signals which are shifted by more than 1 ppm at lower field [δ = 7.27 and 8.50 ppm for the (*E*) and (*Z*) isomer, respectively]. In the (*Z*) isomer the phenyl ring is *cis* to the platinum atom with respect to

[a] Dipartimento Farmaco-Chimico, Università di Bari,
Via E. Orabona 4, 70125 Bari, Italia
Fax: (internat.) + 39-0805442230
E-mail: maresca@farmchim.uniba.it
[b] Dipartimento di Scienze e Tecnologie Biologiche ed Ambientali, Università di Lecce,
Via Monteroni, 73100 Lecce, Italia
[c] Consortium C.A.R.S.O., Cancer Research Center,
70010 Valenzano-Bari, Italia

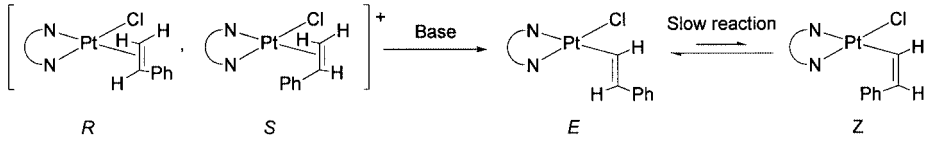

Scheme 1. Deprotonation and isomerization reactions

the olefin double bond, the *ortho* protons are close to and deshielded by the metal center.[10]

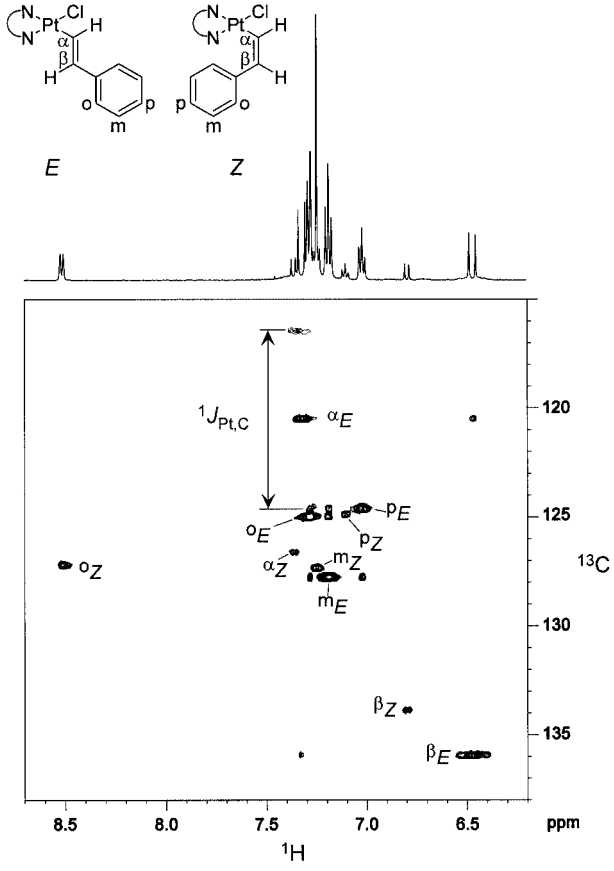

Figure 1. Aromatic portion of the $^1H/^{13}C$ HETCOR spectrum (500 MHz, $CDCl_3$, 25 °C) for an equilibrated solution of (*E*)- and (*Z*)-**2a**; some two-bond carbon-to-hydrogen correlation peaks are also visible

An interesting aspect of the present reaction is its complete stereoselectivity leading to the exclusive formation of the (*E*) isomer. The (*E*) isomer is also thermodynamically preferred because of smaller intramolecular steric interactions. However, the kinetic preference for the (*E*) isomer is greater than the thermodynamic preference for the same isomer, therefore, starting from the pure (*E*) isomer (kinetically determined composition), a significant amount of the (*Z*) form (ca. 20%) is also found at equilibrium.

The behavior of [PtCl(η^2-4-MeO-styrene)(tmeda)](ClO_4) (**1b**) in which the phenyl ring carries an electron-donor substituent, and that of [PtCl(η^2-3-NO_2-styrene)(tmeda)](ClO_4) (**1c**) carrying an electron-withdrawing substituent, is practically the same as that of **1a**. Therefore, the presence of substituents of different types on the styrene phenyl ring does not appear to significantly affect the rate of deprotonation.

Treatment of the alkenyl complexes with mineral acids ($HClO_4$, 0.02 M in water) reverses the reaction, reforming the parent η^2-alkene complexes.

In a thorough work by Gladysz on C−H bond activation of coordinated olefins in cationic complexes of rhenium(II) promoted by K(*t*BuO), the attention was focused on the two different deprotonation pathways involving either allylic or vinylic protons.[3d] It was shown that both types of deprotonation can take place depending upon the experimental conditions. Vinylic deprotonation was preferred in THF or DMSO, while allylic deprotonation was preferred in *t*BuOH. A greater thermodynamic stability of the alkenyl species (sp^2 carbon atom bound to the metal atom), as compared to the η^1-allyl complex (sp^3 carbon atom bound to the metal atom), was given as a rationale for the observed preference in THF and DMSO. On the contrary, the formation of large hydrogen-bonded aggregates of solvent molecules, around the tBuO$^-$ anion, was proposed to be responsible for the enhanced selectivity for less hindered allylic protons in *tert*-butyl alcohol. The relevance of steric

Table 1. ^1H NMR spectroscopic data (300 MHz, $CDCl_3$, 25 °C) for [PtCl(η^1-$C_\alpha H{=}C_\beta HAr$)(tmeda)] complexes **2**; coupling constants in Hz are reported in parentheses ($^3J_{H,H}$), brackets [$J_{Pt,H}$] and braces {$J_{Pt,C}$}; *ortho*, *meta*, and *para* protons of the aryl substituents are indicated by *o*, *m* and *p*, respectively

	Pt−$C_\alpha H_\alpha{=}C_\beta H_\beta$−Ar				Ar			tmeda	
Compound	H_α	H_β	C_α	C_β	*o*	*m*	*p*	CH_2	NCH_3
(*E*)-**2a**	7.31 (16.3) [48]	6.46 (16.3) [50]	121.3 {1009}	135.8 {< 60}	7.27	7.18	7.01	2.62, 2.83	2.77, 2.91
(*Z*)-**2a**	7.35 (10.7)	6.79 (10.7)	126.8	134	8.50	7.24	7.10	2.60, 2.71	2.82, 2.97
(*E*)-**2b**	7.06 (16.2) [46]	6.38 (16.2) [50]	117.6 {1009}	134.0 {79}	7.18	6.74	3.74 (OCH_3)	2.60, 2.81	2.76, 2.90
(*Z*)-**2b**	7.14 (10.7)	6.71 (10.7)	122.5	133.0	8.43	6.80	3.78 (OCH_3)	2.60, 2.68	2.81, 2.95
(*E*)-**2c**	7.61 (16.4) [48]	6.57 (16.4) [53]	125.9	134.2	7.53, 8.11	7.31	7.84	2.65, 2.85	2.79, 2.94

 © 2004 Wiley-VCH Verlag GmbH & Co. KGaA, Weinheim

factors was also supported by the observation that vinylic deprotonation in *t*BuOH increased as the number of substituents on the allylic carbon increased.

In our investigations (ref.[1] and present work), we always use a very bulky base (NEt_3) since the use of less bulky nucleophiles such as OH^-, OMe^- or even $NHEt_2$ leads to stable addition products {[PtCl{η^1-$CH_2CHR(X)$}(tmeda)]; R = H, alkyl or aryl; X = OH, OMe or $NHEt_2$} which have no tendency, whatsoever, to lose HX and form allyl- or alkenylplatinum species.[11] Also triethylamine can add to the coordinated olefin, leading to the formation of an alkylplatinum derivative, but only in the case of unsubstituted ethylene.[11] Having used a bulky base it is obvious that, in the presence of allylic protons (more exposed to the solvent than vinylic protons), these are preferentially removed leading to formation of allylplatinum species. Only in the absence of allylic protons (such as in the case of styrene), will vinylic deprotonation take place. Moreover, it is very likely that both allylic and vinylic deprotonations take place through a direct attack of the base (NEt_3) on the leaving proton. The understanding of the reaction on the basis of a simple Brönsted acid-base model is also supported by the observation that mineral acids can protonate the alkenyl species leading back to the π-olefin complex.

The kinetic preference for the (*E*) isomer is also worthy of further discussion. The alkene complex [PtCl(η^2-CH_2=CHAr)(tmeda)]$^+$ is present in solution in two enantiomeric forms having opposite configurations at the =CHAr stereocenter (Scheme 1). The proton abstraction by an achiral base (such as NEt_3) will occur at a similar rate for the two enantiomers and the (*E*) or (*Z*) configuration of the formed alkenyl complex will depend exclusively upon the *trans* or *cis* position of the abstracted proton with respect to the Ar substituent. The kinetic preference for the (*E*) isomer indicates that the proton is removed exclusively in the position *trans* to Ar, which is more exposed to the solvent and more susceptible to undergo attack by a bulky nucleophile. In this context it could be worth mentioning that acidity data for the free styrene indicate that the most acidic protons are not those on the unsubstituted atom, but on the carbon atom bearing the phenyl substituent.[13,14]

The formation of an alkenyl complex by deprotonation of a coordinated alkene is unprecedented in platinum chemistry except for a recent report on dicationic platinum species of formula [Pt(PNP)(alkene)]$^{2+}$ [PNP = 2,6-bis(diphenylphosphanylmethyl)pyridine]. In methanol the styrene derivative exhibited a spontaneous deprotonation leading to formation of the alkenyl complex [Pt(PNP)(HC=CHPh)]$^+$ which precipitated from solution.[7] The authors did not specifically discuss the (*E*) or (*Z*) configuration of the obtained alkenyl complex; however, their NMR spectroscopic data are in full agreement with those found in our case for the (*E*) isomer. Moreover, since the (*E*) isomer is usually preferred, also on a thermodynamic basis, it is not clear if the obtained isomer was also the one preferred on a kinetic basis. Our alkene complexes, being monocationic, have a smaller propensity to undergo deprotonation than the dicationic complex mentioned above and require the use of a base. Moreover, in the case of the dicationic alkene complex, the formed alkenyl species, being insoluble in methanol, precipitated from the solution and this could have favored its formation.

Conclusion

This study, besides providing a quick and clean route to the synthesis of (*E*)-alkenyl complexes, has also given valuable information on the possible reaction mechanism. Abstraction of the proton *trans* to the phenyl substituent leads to the exclusive formation of the (*E*) isomer. The (*E*) isomer is also thermodynamically favored but not to the extent of precluding the formation of a small amount of (*Z*) isomer (ca. 20%) at equilibrium. The equilibration reaction is rather slow (at room temperature in the dark it requires some weeks) and can be accelerated by visible light. There appears to be a direct correlation between overall charge of the complexes and deprotonation propensity of the coordinated alkene.

Experimental Section

General Methods: The reagents and solvents employed are commercially available and were used as received without further purification. The complex [PtCl(η^2-propene)(tmeda)](ClO_4) was prepared as already reported.[11] All complexes described in this work gave satisfactory elemental analysis. ^1H and ^{13}C NMR spectra were recorded with DRX500 Avance and DPX300 Avance Bruker instruments equipped with probes for inverse detection and with *z* gradient for gradient-accelerated spectroscopy. ^1H and ^{13}C NMR spectra were referenced to TMS; the residual proton signal of the solvent was used as internal standard. Standard Bruker automation programs and pulse sequences were used for $^1H/^{13}C$ inversely detected gradient-sensitivity enhanced heterocorrelated 2D NMR for normal coupling (INVIEAGSSI). ^1H 2D NOESY experiments were performed at room temperature by collecting a 512 × 1024 matrix with 64 scans per t_1, and a mixing time of 1200 ms. Each block of data was preceded by eight dummy scans. The data were processed in the phase-sensitive mode.

Preparation of Alkene Complexes: [PtCl(η^2-CH_2=CHC_6H_4X)(tmeda)](ClO_4) [X = H, (**1a**), 4-OCH_3 (**1b**), 3-NO_2 (**1c**)]. Complexes **1a**−**c** were prepared by propene exchange in the cationic complex [PtCl(η^2-propene)(tmeda)](ClO_4).[11] In a typical experiment [PtCl(η^2-propene)(tmeda)](ClO_4) (250 mg, 0.51 mmol) was suspended in 4 mL of dichloromethane and treated with a 10-fold excess of the incoming olefin (**a** = styrene, **b** = 4-MeO-styrene, **c** = 3-NO_2-styrene). After 24 h of stirring at room temperature, the solid was recovered on a sintered glass filter, washed with diethyl ether and dried. The yield was always above 90%.

Preparation of Alkenyl Complexes: [PtCl(η^1-CH=CHC_6H_4X)(tmeda)] {X = H [(*E*)-**2a**], 4-OCH_3 [(*E*)-**2b**], 3-NO_2 [(*E*)-**2c**]}, by deprotonation with NEt_3. In a typical experiment the styrene complex **1** (0.4 mmol) was suspended in dichloromethane (8 mL) and triethylamine was added whilst stirring at room temperature (2.5-fold the stoichiometric amount). The mixture was left stirring for several hours, while dissolution of the solid was observed. The resulting solution was concentrated under vacuum; the viscous resi-

 © 2004 Wiley-VCH Verlag GmbH & Co. KGaA, Weinheim

due was triturated with diethyl ether and dried. The obtained solid was then washed with water (to remove the alkylammonium salt) and dried again under vacuum leaving a pale yellow compound which was identified as the alkenyl complex **2**. The isolated yield, based on platinum, was ca. 85% for (*E*)-**2a** and (*E*)-**2b** and ca. 50% for (*E*)-**2c**, which required purification of the crude reaction product (Sefadex; eluent chloroform/acetone, 98:2, v/v). All manipulations were carried out by shielding the reaction vessel from light. The alkenyl complexes (*E*)-**2** were also prepared by deprotonation of the corresponding alkene complexes with Na_2CO_3. In a typical experiment **1** (0.25 mmol) was suspended in chloroform (5−6 mL), where it is sparingly soluble, treated with powdered Na_2CO_3 (0.50 mmol), and the mixture stirred for 70 h at 25 °C. After filtration, the mother liquor was concentrated under vacuum and the viscous residue was triturated with diethyl ether and dried. The obtained solid was the alkenyl species **2**, the yield (always based on platinum) was 80% for (*E*)-**2a** and 85% for (*E*)-**2b**.

The Reverse Reaction: The alkenyl species (*E*)-**2** (0.10 mmol) was treated with an aqueous solution (6 mL) containing $HClO_4$ (0.02 M). After 48 h of stirring, the solid was recovered by filtration of the mother liquor, washed with very small amounts of cold water, and dried in a dessicator. It always corresponded to the parent π-alkene complex.

(*E*)/(*Z*) Isomerization of the Alkenyl Ligand: NMR tubes containing $CDCl_3$ solutions (0.7 mL of a 6 mM solution) of the (*E*)-alkenyl species, were exposed to a neon lamp (75 W) and the ^1H NMR spectrum scanned every 4−6 h. The intensity ratio of two well-separated signals, one belonging to the (*E*) and the other to the (*Z*) isomer [the high-field vinylic signal of the (*E*) isomer and the *ortho*-phenyl signals of the (*Z*) form], was plotted against time. A constant ratio was reached at about 35 h for all compounds.

Acknowledgments

We thank the University of Bari, and the Italian Ministero dell'Istruzione, Università e Ricerca (MIUR) (Cofin. 2003 no. 2003039774-005) for financial support.

[1] [1a] G. Bandoli, A. Dolmella, F. P. Fanizzi, N. G. Di Masi, L. Maresca, G. Natile, *Organometallics* **2001**, *20*, 805−807. [1b] G. Bandoli, A. Dolmella, F. P. Fanizzi, N. G. Di Masi, L. Maresca, G. Natile, *Organometallics* **2002**, *21*, 4595.

[2] [2a] W. P. Giering, S. Raghu, M. Rosenblum, A. Cutler, D. Ehntholt, R. W. Fish, *J. Am. Chem. Soc.* **1972**, *94*, 8251. [2b] A. Cutler, D. Ehntholt, P. Lennon, K. Nicholas, D. F. Marten, M. Madhavarao, S. Raghu, A. Rosan, M. Rosenblum, *J. Am. Chem. Soc.* **1975**, *97*, 3149. [2c] A. Cutler, D. Ehntholt, W. P. Giering, P. Lennon, S. Raghu, A. Rosan, M. Rosenblum, J. Tancrede, D. Wells, *J. Am. Chem. Soc.* **1976**, *98*, 3495. [2d] P. Lennon, M. Rosenblum, *J. Am. Chem. Soc.* **1983**, *105*, 1233.

[3] [3a] G. S. Bodner, K. Emerson, R. D. Larsen, J. A. Gladysz, *Organometallics* **1989**, *8*, 2399. [3b] T. S. Peng, J. A. Gladysz, *Organometallics* **1990**, *9*, 2884. [3c] J. J. Kowalczyk, A. M. Arif, J. A. Gladysz, *Chem. Ber.* **1991**, *124*, 729. [3d] T. S. Peng, J. A. Gladysz, *Organometallics* **1995**, *14*, 898.

[4] L. Giannini, G. Guillemot, E. Solari, C. Floriani, N. Re, A. Chiesi-Villa, C. Rizzoli, *J. Am. Chem. Soc.* **1999**, *121*, 2797.

[5] [5a] S. A. Benyunes, M. Green, M. McPartlin, C. B. M. Nation, *J. Chem. Soc., Chem. Commun.* **1989**, 1887. [5b] S. A. Benyunes, R. J. Deeth, A. Fries, M. Green, M. McPartlin, C. B. M. Nation, *J. Chem. Soc., Dalton Trans.* **1992**, 3453.

[6] A. M. Gull, P. E. Fanwick, C. P. Kubiak, *Organometallics* **1993**, *12*, 2121.

[7] C. Hahn, P. Morvillo, E. Herdtweck, A. Vitagliano, *Organometallics* **2002**, *21*, 1807.

[8] The coupling constants with the ^{195}Pt nucleus are $J_{Pt,H}$ = 50 and 48 Hz for the more and the less shielded proton, respectively.

[9] In the (*Z*) isomer the vinyl hydrogen signals appear at δ = 6.79 and 7.35 ppm, and the vinyl carbon signals at δ = 126.8 and 134.0 ppm; also in this case the more shielded carbon atom is bound to the less shielded proton.

[10] Large downfield shifts are typical for signals of protons at a pseudoaxial position above the platinum center in a square-planar complex: A. Albinati, P. J. Pregosin, F. Wombacher, *Inorg. Chem.* **1990**, *29*, 1812; Y. Liu, C. Pacifico, G. Natile, E. Sletten, *Angew. Chem. Int. Ed.* **2001**, *40*, 1226. It has been proposed that a C−H bond, close to the apical position of the Pt atom, may undergo 3-center-4-electron interaction with a filled orbital of the Pt atom. This interaction, unlike the 3-center-2-electron agostic interactions, would cause a downfield shift in the ^1H NMR spectrum: W. Yao, O. Eisenstein, R. H. Crabtree, *Inorg. Chim. Acta* **1997**, *254*, 105; L. Bremmer, J. M. Charnock, P. L. Goggin, R. J. Goodfellow, A. G. Orpen. T. F. Koetzle, *J. Chem. Soc., Dalton Trans.* **1991**, 1789.

[11] F. P. Fanizzi, L. Maresca, G. Natile, C. Pacifico, *Gazz. Chim. Ital.* **1994**, *124*, 184.

[12] L. Maresca, G. Natile, *Comments Inorg. Chem.* **1994**, *16*, 95.

[13] [13a] When the vinylic C−H bond is closely parallel to the π electrons of the benzene ring, it is activated by σ−π* orbital interaction; similarly, the vinyl anion, generated by proton abstraction, is stabilized by delocalization to the phenyl ring. [13b] H. Mori, T. Matsuo, Y. Yoshioka, S. Katsumura, *Tetrahedron Lett.* **2001**, *42*, 3093.

[14] M. Meot-Ner, S. A. Kafafi, *J. Am. Chem. Soc.* **1988**, *110*, 6297.

Received June 14, 2004

 © 2004 Wiley-VCH Verlag GmbH & Co. KGaA, Weinheim

$(AgI)_2Te_6$ and $(AgI)_2Se_6$: New Composite Materials with Cyclic Te_6 and Se_6 Molecules Stabilized in the "Solid Solvent" AgI

Hans-J. Deiseroth,*[a] Michael Wagener,[a] and Elmar Neumann[a]

Dedicated to Prof. Dr. H. Oppermann on the occasion of his 70th birthday

Keywords: Composite materials / Cyclic hexaselenium / Cyclic hexatellurium / Solid solvent silver iodide / Selenium / Tellurium

The new deeply colored solids $(AgI)_2Te_6$ and $(AgI)_2Se_6$ are obtained under hydrothermal conditions in hydroiodic acid. They contain molecules of cyclic hexatellurium and hexaselenium (Te_6, Se_6, respectively, both chair conformations) stabilized in a matrix of AgI. Whereas Se_6 molecules are well known as isolated species in rhombohedral selenium, Te_6 molecules are not known to exist in any modification of that element. They can be stabilized only in an appropriate "solid solvent" like AgI. To date, the new compound $(AgI)_2Te_6$ is the second example only of a composite material containing cyclic Te_6 molecules [the first example is $Re_6Te_{10}Cl_6(Te_6)$].

(© Wiley-VCH Verlag GmbH & Co. KGaA, 69451 Weinheim, Germany, 2004)

Introduction

The stabilization of unusual molecules of group 15 and 16 elements in composite materials based on a matrix of solid CuI has been generally known for about 30 years.[1] In particular, those molecules that do not exist as free molecules in one of the known element modifications of the respective group 15 or 16 element have attracted great attention in the past (for example see ref.[2]). Among others, the scientific interest in the field of those materials is focused on the chemical bonding nature in "nonexistent" molecules of, for example, phosphorus[3] as potential candidates for a suitable stabilizing matrix. The possibility of isolating the molecules from the solid composite by either dissolving the CuI matrix in a suitable liquid or vice versa is another area of interest.[4] The only known example in which AgI serves as a "solid solvent" instead of CuI is AgITe[5] with a Te_∞ screw.

In the course of a sequence of hydrothermal syntheses under strongly acidic conditions (concentrated hydroiodic acid) aiming to form new argyrodites (argyrodite: Ag_8GeS_6) with improved silver ionic conduction by systematic substitution of S with Se/Te and/or halides,[6] we repeatedly obtained deeply colored by-products of initially unknown chemical character. Analytical scanning electron microscopy, in combination with X-ray investigations, revealed the unexpected formation of the two new compounds $(AgI)_2Te_6$ (= $AgITe_3$) and $(AgI)_2Se_6$ (= $AgISe_3$) with cyclic Te_6 and Se_6 molecules (chair conformation) that are embedded in a matrix of AgI. Although we have not been able to produce the title compounds without any contaminants, we decided to publish our preliminary results. The reason for this is that it was explicitly stated in ref.[7] that $(AgI)_2Ch_6$ (Ch: Se, Te) should not exist. Furthermore, to the best of our knowledge, $(AgI)_2Te_6$ is only the second literature example of cyclic Te_6, which, in contrast to Se_6, is *not* known to exist in one of the elemental modifications of tellurium.

Results and Discussion

Both title compounds crystallize isotypically to $CuBrSe_3$[8] but *not* to $CuISe_3$,[9] although the latter was claimed to be more likely in a former paper.[10] The difference between $CuBrSe_3$ and $CuISe_3$ is related to the stacking and coordination of the cyclic Se_6 molecules only, but not to the molecular structure of Se_6.

To date, $(AgI)_2Te_6$ and $(AgI)_2Se_6$ can only be obtained as components of hydrothermal reaction products containing at least two phases. Because of the characteristic color and morphology of the crystalline samples, it is possible to separate them mechanically under the light microscope. Typically single crystals of the tellurium compound show a significantly better quality for structure determinations than those of the selenium compound. The latter crystals are unfortunately characterized by extended intergrowth. On the other hand, an excellent X-ray powder diagram can only be obtained for the selenium compound (Figure 1). It is for

[a] Anorganische Chemie, Universität Siegen,
57068 Siegen, Germany
Fax: (internat.) + 49-271-7402555
E-mail: deiseroth@chemie.uni-siegen.de

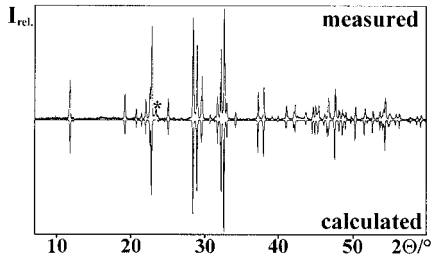

Figure 1. X-ray powder diagram for $(AgI)_2Se_6$ (Cu-$K_{\alpha 1}$, Siemens D5000) relative to a calculated pattern based on single crystal data (*: α-Se)

this reason that we restrict the subsequent structure discussion involving structural details of $(AgI)_2Se_6$ (e.g. bond lengths) to reasonably rounded values. Table 1 contains a summary of all relevant X-ray data for $(AgI)_2Te_6$ and $(AgI)_2Se_6$, whereas in Table 2 and 3 the atomic coordinates and relevant interatomic distances are given.

The structure projection of $(AgI)_2Te_6$ (Figure 2), which is representative for $(AgI)_2Se_6$ also, clearly shows the composite character of this material with respect to the Te_6/Se_6 units embedded in a matrix of AgI. The silver and iodine atoms form zigzag chains along [001] that are separated by Te_6 units. In addition to the two iodine atoms, each silver atom is coordinated by two tellurium/selenium atoms from different Te_6/Se_6 units that are stacked along [010], such that each Ag has a total coordination number of four. Only four of the six Te/Se atoms of each Te_6/Se_6 unit coordinate

Table 2. Atomic coordinates, Wyckoff notations and equivalent isotropic displacement parameters U_{eq} /10^4 pm^2 for $AgISe_3$ and $AgITe_3$ (second line); U_{eq} is defined as one third of the trace of the orthogonalized U_{ij} *tensor, s.o.f. = 1*

Atom	Wyckoff	*x*	*y*	*z*	U_{eq}
Ag	4*g*	0.75	0.75015(5)	0.25	0.0420(5)
		0.75	0.7057(3)	0.25	0.0333(2)
Se1	4*h*	0.5	0.6023(5)	0.2401(2)	0.0291(5)
Te1		0.5	0.6324(2)	0.21725(6)	0.0218(2)
Se2	8*i*	0.61862(8)	0.3710(3)	0.3749(3)	0.0275(4)
Te2		0.62483(2)	0.35589(8)	0.36338(5)	0.0176(2)
I	4*e*	0.66265(8)	1	0	0.0338(4)
		0.67345(3)	1	0	0.0228(2)

Table 3. Selected interatomic distances *d* [pm] for $AgICh_3$

		$AgISe_3$	$AgITe_3$
Ag	Se/Te2 (2 ×)	268.6(2)	279.7(1)
	I (2 ×)	279.9(1)	288.9(1)
Se/Te1	Se/Te2	234.6(2)	272.9(1)
Se/Te2	Se/Te2	238.1(2)	276.0(1)

Table 1. Summary of data collection and refinement details for $AgICh_3$ (Ch = Se, Te)

Name	Silver triseleniumiodide	Silver tritelluriumiodide
Chemical formula	$AgISe_3$	$AgITe_3$
Molecular mass [g·mol^{-1}]	471.65	617.57
Temperature [K]	293(2)	
Wavelength [pm]	Mo-K_α, λ = 71.073	
Crystal system, space group	orthorhombic, *Pmna* (No. 53)	
Cell dimensions [pm]	a = 1493.5(3), b = 458.9(1), c = 825.4(2)	a = 1623.0(3), b = 469.6(1), c = 880.5(2)
Volume [10^6 pm^3]	565.7(2)	671.1(2)
Z, X-ray crystal density [Mg·m^{-3}]	4, 5.538	4, 6.113
Absorption coefficient [mm^{-1}]	28.156	20.248
F(000)	808	1024
Diffractometer	IPDS (Stoe), oriented graphite monochromator	
Scan type	φ	
Crystal size [mm]	0.26 × 0.06 × 0.03	0.31 × 0.01 × 0.01
Measured range (Θ) [°]	2.82−30.52	2.63−30.33
Index ranges	$-21 \le h \le 17$, $-6 \le k \le 6$, $-11 \le l \le 11$	$-23 \le h \le 22$, $-5 \le k \le 6$, $-11 \le l \le 12$
Measured reflections; unique; significant	1991; 748; 442	5406; 1048; 853
$R_{int.}$, R_σ	0.1294, 0.0961	0.0835, 0.0440
Completeness to Θ = 30.33°	82.6%	99.3%
$T_{min.}$, $T_{max.}$	0.1576, 0.8258	0.1576, 0.8258
Structure solution	Direct methods[a]	
Structure refinement	Full-matrix least-squares on F^2[b]	
Data/restraints/parameter	748 / 0 / 27	1048 / 0 / 27
$S(F^2)$	0.901	0.995
Absorption correction	numerical[c]	
R_1, $wR2$ [$1 > 2\sigma(I)$]	0.0518, 0.1437	0.0285, 0.0694
R_1, $wR2$ (all data)	0.0879, 0.1581	0.0388, 0.0726
Extinction coefficient	0.005(2)	0.0005(2)
$\rho_{min.}$, $\rho_{max.}$ [10^{-6}e·pm^{-3}]	−2.0(5), 1.6(5)	−1.8(4), 2.5(4)

[a] G. M. Sheldrick, SHELXS-97, Program for the solution of Crystal Structures, Universität Göttingen, **1997**. [b] G. M. Sheldrick, SHELXL-97, Program for Structure Refinement, Universität Göttingen, Germany, **1997**. [c] STOE & CIE, X-SHAPE 1.06, − Crystal Optimisation for Darmstadt, **1999**.

 © 2004 Wiley-VCH Verlag GmbH & Co. KGaA, Weinheim

directly to a silver atom. This feature is consistent with the corresponding coordination for the cyclic Se_6 units in $(CuBr)_2Se_6$ and $(CuI)_2Se_6$, and indicates a bonding interaction between Ag and Te/Se (see below).

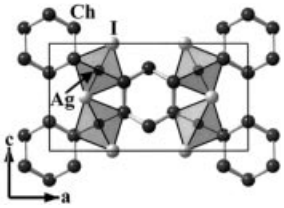

Figure 2. Crystal structure of $(AgI)_2Ch_6$ (Ch: Se, Te) projected along [010]; the coordination of Ag ($2 \times$ Ch, $2 \times$ I) is emphasized by a shaded polyhedral representation; the distance between neighboring Ch_6 molecules along [010] corresponds to the lattice constant *b*

In further compounds with cyclic Se_6 molecules, for example $(PdCl_2)Se_6$ and $Rb_3AsSe_4(Se_6)_2$ (see ref.[11,12] and papers cited therein), *differences* in the coordination of the Se_6 units with respect to the matrix are found relative to the title compounds [e.g. in $(PdCl_2)Se_6$ only *two* of the six Se atoms are coordinated to Pd].

However, in the cluster compound $Re_6Te_{16}Cl_6$ [13] [= $Re_6Te_{10}Cl_6(Te_6)$], the analogous Te_6 molecules are *similar* to those in $(AgI)_2Te_6$ as *four* of the six Te atoms are coordinated directly to surrounding Re_6 clusters. The comparison with $(AgI)_2Te_6/Se_6$ has to be restricted to the cyclic Te_6 molecules only, because $Re_6Te_{16}Cl_6$ is a unique cluster compound with a completely different structural chemistry.

A closer inspection of the bond lengths (Table 3 and Figure 3) shows that the average Te−Te distance for Te_6 in $(AgI)_2Te_6$ ($d_{av(Te-Te)}$ = 273.9 pm) is slightly shorter than for the infinite helices in α-Te[14] (d_{Te-Te} = 283.4 pm) and for Te_6 in $Re_6Te_{10}Cl_6(Te_6)$ (d_{av} = 281 pm). Interestingly, the $d_{av(Se-Se)}$ value of 237 pm for Se_6 in $(AgI)_2Se_6$ is closer to, for example, Se_6 in $(CuBr)_2Se_6$ ($d_{av(Se-Se)}$ = 237 pm), Se_6 in $(PdCl_2)Se_6$ ($d_{av(Se-Se)}$ = 236 pm) and Se_6 in rhombohedral selenium[15] (d_{av} = 235.6 pm]. For a more detailed discussion of the geometry see ref.[6]

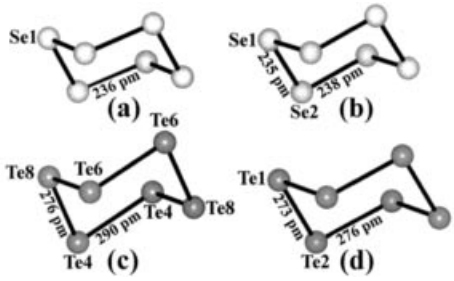

Figure 3. Cyclic Ch_6 molecules (chair conformation) in rhombohedral selenium (a), $(AgI)_2Se_6$ (b), $Re_6Te_{10}Cl_6(Te_6)$ (c), and $(AgI)_2(Te_6)$ (d)

In addition, the bond length d_{Ag-I} = 288 pm in $(AgI)_2Te_6$ [280 pm in $(AgI)_2Se_6$] compares well with d_{Ag-I} = 281.7 pm in β-AgI.[16]

The bond lengths $d_{Ag-Te/Se}$ are somewhat puzzling because the values d_{Ag-Te} = 279.6 pm and d_{Ag-Se} = 269 pm are in the range expected for covalent interactions $d_{Ag-Te/Se}$ (sum of atomic radii for Ag^0 and Te^0/ Se^0: 288/261 pm) in a variety of compounds (for an overview concerning the range of experimental d_{Ag-Te} see ref.[17]). This finding does not seem to be consistent with the conventional formulation $Ag^{1+}I^{1-}(Te_6)^{\pm 0}$ and $Ag^{1+}I^{1-}(Se_6)^{\pm 0}$, and suggests a van der Waals interaction between Ag and Te (Se) rather than a covalent one, and thus emphasizes the special bonding character in composite materials such as the title compounds. A similar ambiguity was found and discussed in the context of those materials that contain copper halides as a stabilizing matrix instead of silver iodide.[2]

Calculations of densities of states, crystal orbital Hamilton populations (COHP) and ELF representations (ELF: electron localization function,[18] Figure 4) based on the TB-LMTO-ASA formalism[6,19] clearly show significant differences between the Te (Se) atoms that are coordinated directly to Ag (Te2, Se2) and those that are not (Te1, Se1). From Figure 4 it is evident that, in contrast to Te1 (Se1), *one lone pair* of each Te2 (Se2) is involved in a bonding interaction with neighboring Ag atoms, resulting in a charge transfer from Te2 (Se2) to Ag. Further, it is interesting to note that the COHP values for the electronic states that are dominated by the cyclic Te_6 (Se_6) indicate that these electronic states are exclusively bonding below the Fermi energy (E_F) with an unusual steep transition to antibonding states immediately above E_F. This finding might be one of the keys to a deeper understanding of why Te_6 is stabilized in appropriate matrices like AgI only and is not known as a free molecule in an elemental Te modification. Raman and IR spectroscopic measurements, together with more detailed calculations of the electronic structure, are currently under progress.

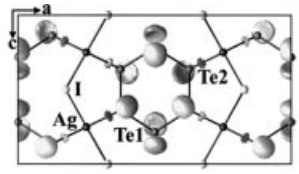

Figure 4. Projection of the crystal structure of $(AgI)_2Te_6$ with a superimposed ELF pattern (0.9-localization domain); the polarizing interaction between Ag^+ and *one* lone pair at each of the four Te2 is indicated by a significant reduction in the effective volume of the interacting lone pair relative to those of the noninteracting lone pairs

Experimental Section

$AgISe_3$ was repeatedly obtained as major component of a hydrothermal reaction product. A stoichiometric mixture of the roughly homogenized elements [silver powder (Degussa), selenium metal grey (Fluka AG- 99.995%, typical weight sum: 0.5 g)] was placed in a quartz tube ($l \approx 8$ cm, $\varnothing = 8$ mm, $V \approx 4$ cm^3), together with about 0.5 mL of concentrated HI (Merck- 57%). Subsequently, the glass tube was sealed and transferred to a steel autoclave (Berghof BAR 845, internal volume: approximately 240 cm^3). The pressure

 © 2004 Wiley-VCH Verlag GmbH & Co. KGaA, Weinheim

balance inside the autoclave was achieved with water as counter pressure medium. The autoclave was then heated up to 220 °C and kept at this temperature for 5 days. Finally, the temperature was lowered at a rate of 2 °C/h down to room temperature. Red transparent hexagonal crystals of $(AgI)_2Se_6$, characterized by strong intergrowth were separated mechanically from the other products under the light microscope. $(AgI)_2Se_6$ is not significantly air sensitive. Crystals of the grey-metallic-black $(AgI)_2Te_6$ were obtained by a similar procedure [tellurium powder (Johnson Matthey GmbH, 99.5%)] with traces of GeO_2 as "mineralizer". The chemical composition of the selected crystals was checked by EDX analyses prior to X-ray structure determination. Further details of the crystal-structure investigation of $(AgI)_2Se_6$ and $(AgI)_2Te_6$ may be obtained from the Fachinformationzentrum Karlsruhe, 76344 Eggenstein-Leopoldshafen (Germany), on quoting the depository number CSD-414116 and -414117.

Acknowledgments

The authors are grateful to the "Deutsche Forschungsgemeinschaft" and the "Fonds der Chemischen Industrie" for their continuous financial support.

[1] A. Rabenau, H. Rau, G. Rosenstein, *Z. Anorg. Allg. Chem.* **1970**, *374*, 43−53.
[2] A. Pfitzner, *Chem. Eur. J.* **2000**, *6*, 1891−1898.
[3] S. Böcker, M. Häser, *Z. Anorg. Allg. Chem.* **1995**, *621*, 258−286.
[4] A. Pfitzner, M. F. Bräu, J. Zweck, G. Brunklaus, H. Eckert, *Angew. Chem.*, in press.
[5] F. Schnieders, P. Boettcher, *Z. Kristallogr.* **1995**, *210*, 323−327.
[6] M. Wagener, Universität Siegen, PhD thesis, in progress.
[7] A. Rabenau, H. Rau, *Inorg. Synth.* **1973**, *14*, 160−173.
[8] H. M. Haendler, P. M. Carkner, *J. Solid State Chem.* **1979**, *29*, 35−39.
[9] W. Milius, A. Rabenau, *Mater. Res. Bull.* **1987**, *22*, 1493−1497.
[10] A. Pfitzner, S. Zimmerer, *Z. Kristallogr.* **1997**, *212*, 203−207.
[11] K. Neininger, H. W. Rotter, G. Thiele, *Z. Anorg. Allg. Chem.* **1996**, *622*, 1814.
[12] M Wachhold, W. S. Sheldrick, *Z. Naturforsch., Teil B* **1997**, *52*, 169.
[13] Y. V. Mironov, M. A. Pell, J.A. Ibers, *Angew. Chem.* **1996**, *108*, 2999.
[14] J. Donohue, *The Structures of the Elements*, J. Wiley & Sons, New York, **1974**, p. 386.
[15] Y. Miyamoto, *J. Appl. Phys., Jpn.* **1980**, *19*, 1813.
[16] R. J. Cava, F. Reidinger, B. J. Wuensch, *Solid State Commun.* **1977**, *24*, 411.
[17] J. Peters, O. Conrad, B. Bremer, B. Krebs, *Z. Anorg. Allg. Chem.* **1996**, *622*, 1823.
[18] M. Kohout, F. R. Wagner, Y. Grin, *Theor. Chem. Acc.* **2002**, *108*, 150.
[19] G. Krier, O. Jepsen, A. Burkhardt, O. K. Andersen, *TB-LMTO-ASA*, version 47, Max Planck Institut fuer Festkörperforschung, Stuttgart, **1997**.

Received June 23, 2004

 © 2004 Wiley-VCH Verlag GmbH & Co. KGaA, Weinheim

Synthesis of (Indenylidene)phosphoranes − A Novel Class of Ligand Precursors for Main-Group and Transition Metal Organometallics[‡]

Konstantin A. Rufanov,*[a] Burkhard Ziemer,[a] Markus Hummert,[b] and Stefan Schutte[b]

Dedicated to Professor Manfred Meisel on the occasion of his 65th birthday

Keywords: Bridging ligands / Constrained geometry catalysts / Cyclopentadienyl ligands / Isoelectronic analogues / Isolobal relationship / Phosphoranes / Phosphorus ylides / Indenyl / Sodium

$IndPPh_2$ (**1**) reacts with RCH_2Br to form the phosphonium salts $[RCH_2P(Ph)_2Ind]^+Br^-$ (**2**: R = Ph; **3**: R = C_6F_5) in high yields. Oxidation of **1** with H_2O_2 in THF proceeds smoothly to give the phosphane oxide $IndP(O)Ph_2$ (**4**). Dehydrobromination of **2** and **3** with NaH in THF yields the corresponding indenylidenephosphoranes $C_9H_6{=}P(Ph)_2CH_2R$ (**5**: R = Ph; **6**: R = C_6F_5). Further deprotonation of **6** with excess NaH results in formation of sodium 1-{[(pentafluorophenyl)methylidene]-diphenylphosphoranyl}indenide (**7**), isolated as a solvate with three THF molecules. A detailed NMR study of new ligand precursors and X-ray structure studies of **5** and **7** have been accomplished. A short F→Na coordination contact in the molecular structure of **7** has been detected.

(© Wiley-VCH Verlag GmbH & Co. KGaA, 69451 Weinheim, Germany, 2004)

Introduction

Linked (cyclopentadienylsilyl)amine systems **A** (Scheme 1) became one of the best established and developed classes of specially designed ligand precursors[1−5] for bridged cyclopentadienyl−amido early transition metal complexes, the so-called "constrained geometry catalysts".[6] Depending on the nature of the ligand framework, these complexes give high molecular weight PE with long-chain branching. Furthermore, because of their more open coordination spheres (relative to *ansa*-metallocenes), they have the pronounced ability to incorporate higher olefins.[7−12] Isoelectronic analogues of systems **A** are the linked cyclopentadienylphosphoranylidene systems (**B**, left). These compounds do exist in the thermodynamically more stable form of the cyclopentadienylidenephosphoranes (**B**, right). Some examples of similar compounds are known from the literature;[13] however, neither a general synthetic route towards these ligand precursors for organometallic chemistry nor their organometallic derivatives have been explored.

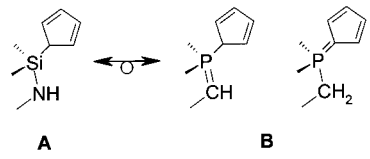

Scheme 1

In this paper we describe a synthetic approach towards and a detailed NMR study of type **B** ligand precursors on the basis of stable Ph_2PInd (**1**), as well as the first alkali metal derivative of one such new ligand, along with their crystal structures.

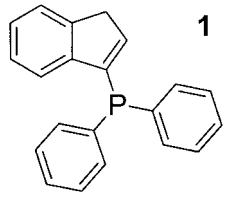

Results and Discussion

As the simple (cyclopentadienyl)phosphanes are eager to dimerise by Diels−Alder reaction, **1** was chosen for our preliminary studies. Of the two isomers of this compound, earlier described by Anderson and co-workers,[14] the thermodynamically most stable is the vinylic isomer. It was synthesised in 89% yield by a slightly modified procedure starting from IndLi and Ph_2PCl in toluene.[15] Quaternisation of **1** with bulky $tBuCH_2Br$ or Me_3SiCH_2Br was un-

[‡] Organophosphorus(V) Ligands for Coordination and Organometallic Chemistry, I

[a] Institut für Chemie, Humboldt-Universität zu Berlin, Brook-Taylor-Strasse 2, 12489 Berlin, Germany
[b] Institut für Chemie, Technische Universität Berlin, Strasse des 17. Juni 135, 10623 Berlin, Germany

successful,[16] we therefore decided to use the more electrophilic $C_6H_5CH_2Br$ and $C_6F_5CH_2Br$. In both cases, using 20% molar excess of benzyl bromides, complete quaternisation was achieved in THF at room temperature after 2 d (Scheme 2). Corresponding phosphonium salts **2** and **3** are only slightly soluble in THF and were isolated as white powders in practically quantitative yields.[17]

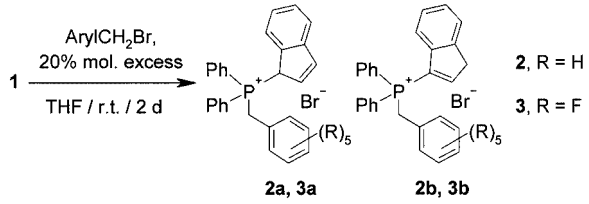

Scheme 2

According to ^{31}P NMR spectroscopic data, **2** and **3** exist as mixtures of allylic (**2a**: δ = 32.8 ppm; **3a**: δ = 15.6 ppm) and vinylic (**2b**: δ = 31 ppm; **3b**: δ = 13 ppm) isomers depending on the position of the double bond in the indenyl ring. The ratio of isomers differs from one sample to another in an irregular way, which precludes accurate assignment of arylic and vinylic signals in ^1H and ^{13}C NMR spectra that have been measured in [D$_6$]DMSO. ^1H NMR benzylic signals are located between δ = 5.0 and 5.5 ppm and ^{13}C signals at δ = 30.0 ppm for **2** and δ = 19.0 ppm for **3**. Allylic signals of isomers **a** are located at $\delta \approx 6.3$ ppm ($^2J_{PH}$ = 21 Hz) and 44 ppm ($^1J_{P,C}$ = 42 Hz), while those of isomers **b** are shifted downfield to δ = 4 ppm and 42 ppm in the ^1H and ^{13}C NMR spectra, respectively.

Interestingly, a similar situation arises when phosphane oxide **4** is synthesised by oxidation of **1** with H_2O_2 in THF (Scheme 3).[18] Compound **4**, obtained quantitatively, exists as a 1:4 isomeric mixture of corresponding allylic and vinylic phosphane oxides **4a** and **4b**, respectively.[19]

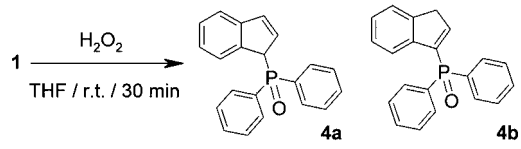

Scheme 3

The reaction of the phosphonium salt **2** with a five-fold molar excess of NaH in THF was rather slow, took 3 d, and resulted in a dark green solution (Scheme 4). Upon concentration of the solution to one quarter of its initial volume, the desired indenylidenephosphorane **5** precipitated at −78 °C after 1 d as a yellow-green, light-sensitive microcrystalline powder.[20] Crystallisation from CH_2Cl_2 gave block crystals. The X-ray structure of **5** was determined and showed nearly ideal tetrahedral coordination of the central phosphorus atom with C−P−C angles between 104° and 116°. The C−P bond lengths are also not very different: 1.828(4) Å for $PhCH_2$−P, 1.797(4) Å for C_{Ph}−P and 1.727(4) Å for C_{Ind}=P.[21,22] The molecular structure of **5** with thermal ellipsoids of 50% probability as well as selected bond lengths and angles are shown in Figure 1.

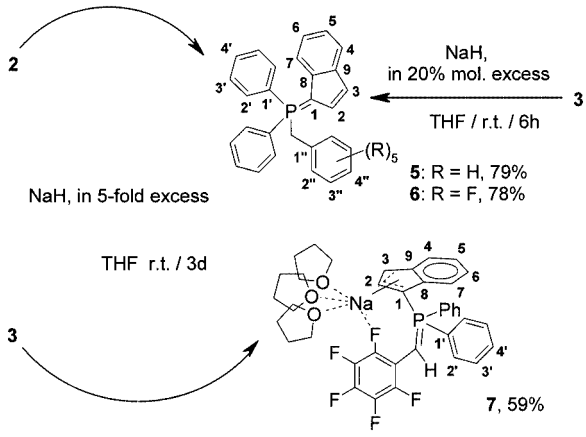

Scheme 4

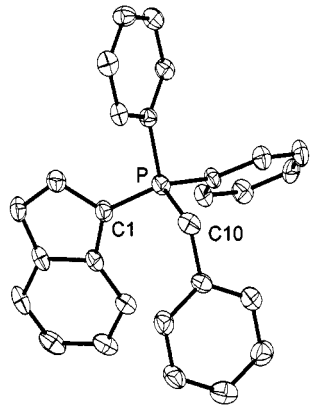

Figure 1. Molecular structure of **5** showing the atom numbering scheme with 50% probability thermal ellipsoids; all hydrogen atoms are omitted for clarity; selected bond lengths [Å] and angles [°]: C(1)−P(1) 1.733(4), C(1)−C(2) 1.420(5), C(10)−P(1) 1.832(4), C(1)−P(1)−C(10) 116.4(2); C(1)−P(1)−C(Ph) 108.9(2), C(Ph)−P(1)−C(Ph′) 108.3(2)

Under the same reaction conditions, phosphonium salt **3** was converted directly into the Na salt **7**. Obviously, CH acidity of the benzylic CH_2 group is much higher in the case of the pentafluorobenzyl derivative, and further deprotonation with NaH (applied in fivefold excess) proceeds quicker and results in the formation of sodium 1-{[(pentafluorophenyl)methylidene]diphenylphosphoranyl}-indenide (**7**).[23] The synthesis of **6** was achieved in another experiment using only 20% molar excess of NaH and a shorter reaction time: after 6 h in THF, it was obtained in 78% yield as a yellow powder.[24] Both indenylidenephosphoranes **5** and **6** are rather stable and can be handled in air without special care for several minutes. They are more soluble in ethereal and aromatic solvents than in aliphatic ones. Gold-yellow Na salt **7** crystallises with three THF molecules (coordinated by sodium) in the asymmetric unit.[25,26] While their O atoms occupy fixed positions

 © 2004 Wiley-VCH Verlag GmbH & Co. KGaA, Weinheim

around the sodium atom, all carbon atoms are disordered. The structure refinement of the latter had to be split on two sides in each case. For this reason only the C atoms of the major components could be refined anisotropically. The ratios between major and minor components vary from 64:36, 66:34 to 83:17, respectively. The sodium atom shows predominantly η^3-coordination with the allylic part of the indenyl fragment, with the shortest distance to the C2 atom (2.67 Å). Similar delocalisation of the carbanionic charge was found by Schmidbaur and co-workers in the crystal structure of the solvent-free potassium salt of dimethylphosphonium bis(benzylide) K[$Me_2P(CHPh)_2$]. The lattice did not contain discrete complex molecules, but was rather a coordination polymer; the metal atoms interacted preferentially with ylidic carbanions and the *ortho* and *para* positions of the benzylide rings.[27] In the molecular structure of **7**, a short F→Na coordination contact was found. The intramolecular distance between the sodium cation and one of the *ortho*-F atoms of the C_6F_5 group is only 2.67 Å, i.e. more than 1 Å shorter than the sum of the van der Waals radii of these elements (3.74 Å).[28] The molecular structure of **7** with thermal ellipsoids of 50% probability as well as selected bond lengths and angles are shown in Figure 2.

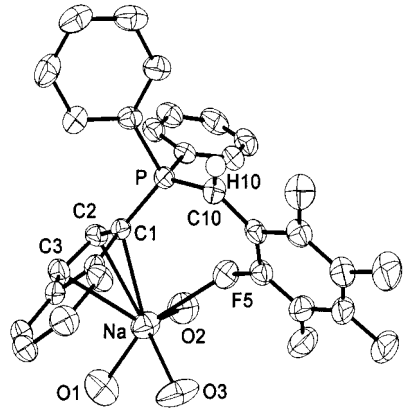

Figure 2. Molecular structure of **7** showing the atom numbering scheme with 50% probability thermal ellipsoids; all hydrogen atoms except for H(10) of the bridging moiety are omitted; only oxygen atoms of coordinated THF molecules are shown for clarity; selected bond lengths [Å] and angles [°]: P−C(10) 1.714(2), P−C(1) 1.747(1), P−C(Ph) 1.827(2), P−C(Ph′) 1.828(2), C(1)−C(2) 1.431(2), C(2)−C(3) 1.383(2), Na−C(1) 2.874(2), Na−C(2) 2.679(2), Na−C(3) 2.741(2), Na−O(1) 2.373(2), Na−O(2) 2.322(2), Na−O(3) 2.271(2), Na−F(5) 2.669(1), F(5)−C(C_6F_5) 1.374(2), F(3)−C(C_6F_5) 1.354(2); C(10)−P−C(1) 118.77(8), C(10)−P−C(Ph) 103.51(8), C(1)−P−C(Ph′) 109.02(8), C(1)−P−C(Ph) 106.37(7), C(Ph)−P−C(Ph′) 103.61(8), P−C(1)−Na 125.21(8), O(3)−Na−O(2) 116.93(6), O(3)−Na−O(1) 87.75(6), O(2)−Na−O(1) 88.00(6), O(3)−Na−F(5) 81.70(5), O(2)−Na−F(5) 78.87(5), O(1)−Na−F(5) 157.07(5), C(C_6F_5)−F(5)−Na 140.0(1)

Because of the importance of **5**, **6** and **7** for further syntheses of organometallic derivatives, a detailed NMR study of these compounds has been performed using $^1H/^{13}C$ COSY, APT and DEPT methods and heteronuclear NMR spectroscopy. The complete set of data obtained is given in Table 1. It is interesting to note that in the ^{13}C NMR spectrum of **7** signals for C1 appear considerably shifted downfield, and the signals for C1′ and P*C*H are shifted upfield, relative to those in the spectrum of **6**. In the ^{19}F NMR spectrum the signals of *ortho*- and *para*-F substituents in **7** also appear at a much lower field than in **6**, while those of *meta*-F substituents are almost unaffected. Also, no difference between the *ortho*-F atoms can be detected, which indicates free rotation of the C_6F_5 substituent of **7** when it is in solution.

Table 1. Assignment of signals in ^1H, ^{13}C, ^{31}P and ^{19}F NMR spectra of **5**, **6** and **7**

	^1H: δ [ppm]			$^{13}C/^{31}P/^{19}F$: δ [ppm]		
	5	**6**	**7**	**5**	**6**	**7**
1	–	–	–	59.9 ($^1J_{P,C}$ = 110 Hz)	62.2 ($^1J_{P,C}$ = 118 Hz)	24.5 ($^1J_{P,C}$ = 135 Hz)
2	6.65, t	6.57, t	6.66, t	126.9 ($^2J_{P,C}$ = 15 Hz)	126.1 ($^2J_{P,C}$ = 16 Hz)	127.4 ($^2J_{P,C}$ = 16 Hz)
3	6.44. t	6.43, t	6.16, t	117.3 ($^3J_{P,C}$ = 13 Hz)	106.9 ($^3J_{P,C}$ = 15 Hz)	101.0 ($^3J_{P,C}$ = 14 Hz)
4, 7	7.57−7.02	7.62−7.39	7.32−7.26	120.1, 117.3	119.6, 117.1	119.6, 119.5
5, 6	6.76−6.57	6.77−6.55	6.57−6.46	117.2, 116.7	116.6, 116.3	115.8, 115.2
8	–	–	–	137.6	137.8	136.7
9	–	–	–	135.1	135.4	135.2
1′	–	–	–	124.6 ($^1J_{P,C}$ = 86 Hz)	123.1 ($^1J_{P,C}$ = 87 Hz)	137.5 ($^1J_{P,C}$ = 88 Hz)
2′	7.57−7.02	7.62−7.39	7.80−7.27	133.3($^2J_{P,C}$ = 10 Hz)	132.6 ($^2J_{P,C}$ = 10 Hz)	133.1 ($^2J_{P,C}$ = 9 Hz)
3′	7.57−7.02	7.62−7.39	7.80−7.27	128.8 ($^3J_{P,C}$ = 12 Hz)	128.5 ($^3J_{P,C}$ = 12 Hz)	128.1 ($^3J_{P,C}$ = 11 Hz)
4′	7.57−7.02	7.62−7.39	7.80−7.27	132.7 ($^4J_{P,C}$ = 3 Hz)	132.8($^4J_{P,C}$ = 3 Hz)	130.2($^4J_{P,C}$ = 2.5 Hz)
1′′	–	–	–	130.2 ($^2J_{P,C}$ = 8 Hz)	–	–
2′′	6.82−6.76	–	–	130.5	–	–
3′′	7.57−7.50	–	–	128.4	–	–
4′′	7.42−7.10	–	–	127.5	–	–
THF	–	–	3.61, 1.76	–	–	68.3, 26.4
P*CH*	4.14 ($^2J_{PH}$ = 14 Hz)	4.16 ($^2J_{PH}$ = 13 Hz)	2.73 ($^2J_{PH}$ = 11Hz)	33.9 ($^1J_{P,C}$ = 53 Hz)	22.0 ($^1J_{P,C}$ = 55 Hz)	81.4 ($^1J_{P,C}$ = 124 Hz)
P	–	–	–	9.7	8.9	4.7
o-F	–	–	–	–	−139	−153
m-F	–	–	–	–	−169	−170
p-F	–	–	–	–	−155	−190

 © 2004 Wiley-VCH Verlag GmbH & Co. KGaA, Weinheim

Conclusion

Series of phosphoranes **B** with different R substituents can be synthesised easily using the developed synthetic scheme or, alternatively, from chlorophosphonium ylides with sterically encumbered {Cp}-type anions. A combination of these two methods allows a wide range of the type **B** ligand precursors to be synthesised (Scheme 5).[29]

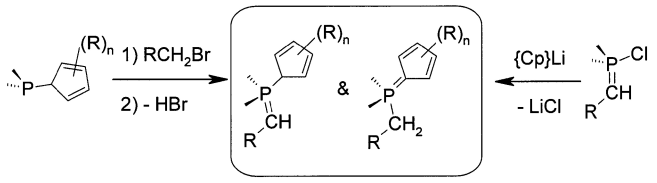

Scheme 5

In this preliminary work we have formed the basis for the further development and revival of organometallic chemistry in the so-called "post-metallocene" epoch. Systematic study of thus developed linked cyclopentadienylphosphoranylidene ligands for the syntheses of alkali, rare-earth and transition metal complexes is the subject of our current efforts.

Acknowledgments

K. R. thanks Dr. Heinz-Jürgen Kroth for multinuclear NMR experiments, Profs. Herbert Schumann (Berlin Technical University) and Igor Fedushkin (Razuvaev-Institute of Chemistry, Nizhnij Novgorod, Russian Federation) for fruitful discussions and the Graduate College Programme 352 of the DFG for a postdoctoral fellowship.

[1] P. J. Shapiro, E. E. Bunel, W. P. Schaefer, J. E. Bercaw, *Organometallics* **1990**, *9*, 867.
[2] J. Okuda, *Chem. Ber.* **1990**, *123*, 1649.
[3] J. Okuda, *Top. Curr. Chem.* **1991**, *160*, 97.
[4] J. C. Stevens, F. J. Timmers, G. W. Rosen, G. W. Knight, S. Y. Lai (Dow Chemical Co.), Eur. Pat. Appl. EP0416815A2, **1991**.
[5] J. A. Canich (Exxon Chemical Co.), Eur. Pat. Appl. EP0420436A1, **1991**.
[6] J. C. Stevens, *Stud. Surface Sci. Cat.* **1994**, *89*, 277.
[7] W. Kaminsky, *J. Chem. Soc., Dalton Trans.* **1998**, 1413.
[8] K. Soga, T. Uozumi, S. Nakamura, T. Toneri, T. Teranishi, T. Sano, T. Arai, *Macromol. Chem. Phys.* **1996**, *197*, 4237.
[9] Y.-X. Chen, C. L. Stern, S. Yang, T. J. Marks, *J. Am. Chem. Soc.* **1996**, *118*, 12451.
[10] L. Jia, X. Yang, C. L. Stern, T. J. Marks, *Organometallics* **1997**, *16*, 842.
[11] A. L McKnight, R. M. Waymouth, *Chem. Rev.* **1998**, *98*, 2587.
[12] G. J. P. Britovsek, V. C. Gibson, D. F. Weiss, *Angew. Chem.* **1999**, *111*, 448.
[13] G. Becker, in *Methoden Org. Chem. (Houben-Weyl)*, Georg Thieme Verlag, Stuttgart, **1985**, Bd. V/2c, p. 494.
[14] K. A. Fallis, G. K. Anderson, N. P. Rath, *Organometallics* **1992**, *11*, 885.
[15] **General Remarks:** All synthetic procedures were performed under purified argon using standard Schlenk techniques. Solvents were distilled from an appropriate drying agent and degassed prior to use. The ^{1}H, ^{13}C, ^{19}F and ^{31}P NMR spectra were obtained with Bruker ARX-200, -300 or -400 spectrometers. Mass spectra were measured with a Varian CH-7a MAT device using electron impact with an excitation energy of 70 eV. Indene, Ph_2PCl, $C_6H_5CH_2Br$, $C_6F_5CH_2Br$, *n*BuLi and NaH were used as supplied (Merck, Aldrich). **Starting Phosphane, Ph_2PInd (1):** Indene (29 g, 250 mmol) was dissolved in pentane (900 mL). While the solution was stirred vigorously and cooled with an ice bath, *n*BuLi (110 mL 2.5 M solution in hexanes, 275 mmol) was added over a period of 2−3 h.. The mixture was stirred overnight. The white precipitate of IndLi was filtered off, washed with pentane (3 × 100 mL) and dried in vacuo for several hours. The thus obtained IndLi (12.2 g, 100 mmol) was suspended in toluene (400 mL), and under continuous stirring a solution of Ph_2PCl (22 g, 100 mmol) in toluene (100 mL) was added over a period of 4−5 h. The reaction mixture was stirred overnight, LiCl was filtered off, toluene was removed in vacuo, the crude product washed with hexane (4 × 50 mL) and dried in vacuo, to afford **1** in 89% yield and 95% purity as a light grey powder. ^{1}H NMR (200 MHz, C_6D_6, 25 °C): δ = 7.52−6.98 (m, 14 H, H_{Aryl}), 6.12 (dd, 1 H, vinylic H), 3.07 (t, 2 H, allylic H) ppm. ^{31}P NMR (200 MHz, C_6D_6, 25 °C): δ = −21 ppm.
[16] No reaction was observed after stirring of **1** with 50% molar excess of RCH_2Br (R = *t*Bu or TMS) at room temperature in THF for 30 h.
[17] **Phosphonium Salts $[C_6H_5CH_2P(Ph)_2Ind]^+Br^-$ (2) and $[C_6F_5CH_2P(Ph)_2Ind]^+Br^-$ (3)**: $C_6H_5CH_2Br$ (8.5 g, 50 mmol) or $C_6F_5CH_2Br$ (13 g, 50 mmol) was added at once to a solution of **1** (12 g, 40 mmol) in THF (300 mL). The reactions were very slow and only after 3 d complete, resulting in a white precipitate of **2** or **3**, which was filtered off, washed with THF and pentane, and dried in vacuo. Yields in both cases > 95%. **2**: M.p. 253−255 °C. EIMS: *m*/*z* (%) = 391.0 (100) $[M]^+$. **3**: M.p. 228−230 °C. EIMS: *m*/*z* (%) = 481.0 (100) $[M]^+$.
[18] **Phosphane Oxide $IndP(O)Ph_2$ (4)**: A 34% aqueous solution of H_2O_2 (2 mL, 20 mmol) was slowly added with a syringe to a stirred solution of **1** (3.0 g, 10 mmol) in THF (50 mL). After 30 min, the solution was quickly dried with Na_2SO_4, and THF was removed in vacuo, yielding an off-white microcrystalline powder of **4**. Yield: 3.15 g (100%). M.p. 137−138 °C. EIMS: *m*/*z* (%) = 316.1 (32) $[M]^+$, 201.0 (100) $[M^+ - Ind]$. $C_{21}H_{17}OP$ (316.34): calcd. C 79.73, H 5.42; found C 80.07, H 5.66.
[19] NMR measured in CD_2Cl_2: ^{1}H: **4a:** δ = 7.8−6.9 (m, aryl, Ph), 6.83, 6.38 (AB system, $^{3}J_{AB}$ = 3 Hz, vinylic protons), 4.72 (d, $^{2}J_{PH}$ = 25 Hz, allylic H); **4b:** δ = 7.8−6.9 (m, aryl, Ph), 6.71 (dt, vinylic H), 3.5 (br. s, 2 allylic H) ppm. ^{31}P: **4a:** δ = 32.3 ppm; **4b:** δ = 23.2 ppm.
[20] **Indenylidenephosphorane $C_9H_6{=}P(Ph)_2CH_2C_6H_5$ (5):** NaH (2.4 g, 100 mmol) was added under argon to a stirred suspension of **2** (9.42 g, 20 mmol) in THF (100 mL). Slowly the solution began to darken. The reaction was complete after 48 h, resulting in a dark green solution and white precipitate, which was filtered off. The filtrate was concentrated to one quarter of its initial volume (ca. 20−25 mL). The desired ylide **5** precipitated from the solution at −78 °C after 1 d as a yellow-green, light-sensitive microcrystalline powder. Yield: 6.16 g (79%). M.p. 224−226 °C. EIMS: *m*/*z* (%) = 390.1 (73) $[M]^+$, 299.0 (18) $[M^+ - C_7H_8]$, 276.1 (22) $[M^+ - Ind]$, 185.1 (100) $[Ph_2P]^+$. $C_{28}H_{23}P$ (390.47): calcd. C 86.13, H 5.94; found C 86.19, H 5.70.
[21] **X-ray Crystallographic Study:** Crystallisation of **5** was achieved from CH_2Cl_2. A suitable light-yellow, nearly colourless crystal with linear dimensions of 0.35 × 0.20 × 0.18 mm was mounted on the end of a glass fibre and investigated with a Siemens SMART CCD at 173(2) K, using graphite-monochromated Mo-K_α radiation (λ = 0.71073 Å). Data were collected with an area detector by use of ω scans. The structure was solved by direct methods and expanded by difference Fourier syntheses using the SHELX-97 software package; the intensities were corrected for Lorentz, polarisation and absorption effects using SADABS ($T_{min.}$ = 0.9601, $T_{max.}$ = 0.9777). G. M. Sheldrick, SADABS, *Programme for absorption correction*, University of Göttingen, **1996**; G. M. Sheldrick, *Programme for the refinement of crystal structures, SHELX-97*, University of Göttingen, **1997**.

 © 2004 Wiley-VCH Verlag GmbH & Co. KGaA, Weinheim

[22] **Crystal Data and Structure Refinements Details:** $C_{28}H_{23}P$, M = 390.43, triclinic, a = 9.5646(3) Å, b = 9.7692(3) Å, c = 11.8500(4) Å, α = 98.242(2)°, β = 94.528(2)°, γ = 109.004(2)°, V = 1026.70(5) Å^3, space group $P1$, Z = 2, μ = 0.145 mm^{-1}, $D_{calcd.}$ = 1.263 g·cm^{-3}, θ range 1.75−26.00°, 6798 reflections measured, 3971 unique (R_{int} = 0.0990) which were used in all calculations. GoF (on F^2) = 0.861. The final residuals R_F and wR_F^2 were 0.0723 [$I > 2\sigma(I)$] and 0.1638 (all). CCDC-233977 contains the supplementary crystallographic data for this paper. These data can be obtained free of charge at www.ccdc.cam.ac.uk/conts/retrieving.html [or from the Cambridge Crystallographic Data Centre, 12 Union Road, Cambridge CB2 1EZ, UK; Fax: (internat.) + 44-1223-336-033; E-mail: deposit@ccdc. cam. ac. uk].

[23] **Sodium 1-{[(Pentafluorphenyl)methylidene]diphenylphosphoranyl}indenide (7):** NaH (0.61 g, 25 mmol) was added under argon to a stirred suspension of **3** (2.72 g, 4.9 mmol) in THF (50 mL). The reaction proceeded exothermally with the evolution of a large amount of gas (H_2). The yellow solution was stirred over a weekend. After concentration of the reaction mixture, it was filtered and an equal amount of pentane was slowly poured onto the solution. Crystallisation began immediately, yielding gold-yellow crystals of Na salt **7** at 0 °C after 1 d. Yield: 1.5 g (59%).

[24] **Indenylidenephosphorane $C_9H_6{=}P(Ph)_2CH_2C_6F_5$ (6)**: Analogous to the preparation of **5** starting from **3** (5.6 g, 10 mmol) and NaH (0.29 g, 12 mmol) but with a shorter reaction time (6 h). Yield: 3.74 g (78%). M.p. 180−182 °C. EIMS: m/z (%) = 480.1 (9) [M^+], 366.1 (18) [M^+ − Ind], 299.0 (10) [M^+ − $C_6F_5CH_3$], 185.1 (50) [Ph_2P^+]. $C_{28}H_{18}F_5P$ (480.42): calcd. C 70.00, H 3.78; found C 68.15, H 4.20.

[25] **X-ray Crystallographic Study**: Crystallisation of **7** was achieved from THF. A suitable gold-yellow specimen with linear dimensions of 0.48 × 0.24 × 0.22 mm was mounted on the end of a glass fibre and investigated with a Siemens SMART CCD at 153(2) K, using graphite-monochromated Mo-K_α radiation (λ = 0.71073 Å). Data were collected with an area detector by use of ω scans. The structure was solved by direct methods and expanded by difference Fourier syntheses using the SHELX-97 software package; the intensities were corrected for Lorentz, polarisation and absorption effects using SADABS ($T_{min.}$ = 0.9324, $T_{max.}$ = 0.9682). G. M. Sheldrick, SADABS, *Programme for absorption correction*, University of Göttingen, **1996**; G. M. Sheldrick, *Programme for the refinement of crystal structures, SHELX-97*, University of Göttingen, **1997**.

[26] **Crystal Data and Structure Refinements Details:** $C_{40}H_{41}F_5NaO_3P$, M = 718.69, monoclinic, a = 12.0079(2) Å, b = 15.8221(2) Å, c = 20.3386(3) Å, $\alpha = \gamma$ = 90°, β = 106.918(1)°, V = 3696.90(9) Å^3, space group $P2_1/c$, Z = 4, μ = 0.148 mm^{-1}, $D_{calcd.}$ = 1.291 g·cm^{-3}, θ range 1.77−25.50°, 22 887 reflections measured, 6866 unique (R_{int} = 0.0993), which were used in all calculations. GoF (on F^2) = 1.012. The final residuals R_F and wR_F^2 were 0.0637 [$I > 2\sigma(I)$] and 0.1488 (all). CCDC-233976 contains the supplementary crystallographic data for this paper. These data can be obtained free of charge at www.ccdc.cam.ac.uk/conts/retrieving.html [or from the Cambridge Crystallographic Data Centre, 12 Union Road, Cambridge CB2 1EZ, UK; Fax: (internat.) + 44-1223-336-033; E-mail: deposit@ccdc.cam.ac.uk].

[27] H. Schmidbaur, U. Deschler, B. Milewski-Mahrla, B. Zimmer-Gasser, *Chem. Ber.* **1981**, *114*, 608.

[28] A. Bondi, *J. Phys. Chem.* **1964**, *68*, 441.

[29] K. Rufanov, *Chem. Eur. J.*, manuscript in preparation.

Received July 29, 2004

 © 2004 Wiley-VCH Verlag GmbH & Co. KGaA, Weinheim

Experimental and Theoretical Studies of Homoleptic Tellurium Cyanides $Te(CN)_x$: Crystal Structure of $Te(CN)_2$

Thomas M. Klapötke,*[a] Burkhard Krumm,[a] Juan Carlos Gálvez-Ruiz,[a][‡] Heinrich Nöth,[a][‡] and Ingo Schwab[a]

Dedicated to Professor H. Schmidbaur on the occasion of his 70th birthday

Keywords: Cyanides / Structure elucidation / Tellurium / Ab initio calculations

The labile tellurium cyanide species $Te(CN)_2$ and $Te(CN)_4$ have been prepared by treatment of tellurium(IV) tetrahalides with cyanide. Both are thermosensitive solids and, in addition, the tetracyanide was found to be pyrophoric. The crystal structure of $Te(CN)_2$ has been determined. The structures of $Te(CN)_2$, $Te(CN)_4$, and $Te(CN)_6$ have been calculated at various levels of theory.

(© Wiley-VCH Verlag GmbH & Co. KGaA, 69451 Weinheim, Germany, 2004)

Introduction

A search for low-valent tellurium pseudohalides leads to few reports on the existence of dicyanotellane, $Te(CN)_2$ (**1**). This almost "forgotten" molecule was first prepared in 1908 by the reaction of $TeBr_4$ with excess AgCN,[1] and since then it has had a scanty publication history.[2−4] Somewhat surprising is the fact that **1** had been investigated by IR spectroscopy,[3] and used for an attempted synthesis only once, respectively.[4] The stable dicyanides of the lighter homologues of **1**, $S(CN)_2$ and $Se(CN)_2$, have been characterized in more detail,[5,6] while the $O(CN)_2$ molecule probably only exists as an intermediate and has been studied by theoretical methods.[7] The Te^{II} dihalides $TeHal_2$ (Hal = Cl, Br, I) are not stable towards disproportionation in the condensed phase,[8] but have been investigated in the gas phase;[9,10] the difluoride TeF_2 does not seem to exist at all. To the best of our knowledge, structurally characterized binary covalent main-group cyanides—apart from HCN, $(CN)_2$, and the halogen derivatives HalCN—are limited to $P(CN)_3$, $As(CN)_3$, $S(CN)_2$, and $Se(CN)_2$, whose reports date back to the 1960s.[11,12] This let us believe that the elucidation of the structural and spectroscopic properties of $Te(CN)_2$ (**1**) might be worthwhile.

Results and Discussion

Similar to the original procedure, $Te(CN)_2$ (**1**) can be obtained in analytically pure form from the reaction of $TeBr_4$ or TeI_4 with excess AgCN by separation of its colorless solutions in Et_2O under meticulously anhydrous conditions [Equation (1)].

$$TeHal_4 + 3\,AgCN \xrightarrow[-\,3\,AgHal]{60\,^\circ C\,/\,C_6H_6} Te(CN)_2\,(\mathbf{1}) + HalCN \qquad (1)$$

Hal = Br, I

After evaporation of the solvents, careful sublimation of the faintly brownish residue in vacuo ($<10^{-4}$ mbar/<80 °C) yielded an almost colorless solid, which is very sensitive towards hydrolysis; above 100 °C slow decomposition to elemental tellurium and cyanogen occurs.

The vibrational spectra (IR/Raman) of solid **1** exhibit the symmetric and antisymmetric C≡N stretching vibrations at 2176/2177 (A_1) and 2168/2170 (B_1), and bands at 410/409 (A_1 Te−C stretch), 398/395 (B_2 Te−C stretch), 296/− (B_1 TeCN deformation), 277/279 (A_2 TeCN deformation), and 147/136 cm^{-1} (A_1 CTeC deformation). The significant differences in frequencies and intensities (see Figure 1) obtained from the calculated values for the gas phase may result from intermolecular interactions in solid **1** (vide infra). Even if appropriate scaling factors for the calculated vibrational frequencies of **1** were available for all methods, this would give only partial improvement of the computed spectra because of a non-linear systematic difference in the Te−C and C≡N stretching vibrations. In the mass spec-

[‡] X-ray structure analysis.
[a] Chair of Inorganic Chemistry, Ludwig-Maximilian University of Munich,
Butenandtstr. 5−13(D), 81377 Munich, Germany
Fax: (internat.) + 49-89-2180-77492
E-mail: tmk@cup.uni-muenchen.de

 © 2004 Wiley-VCH Verlag GmbH & Co. KGaA, Weinheim **DOI: 10.1002/ejic.200400763**

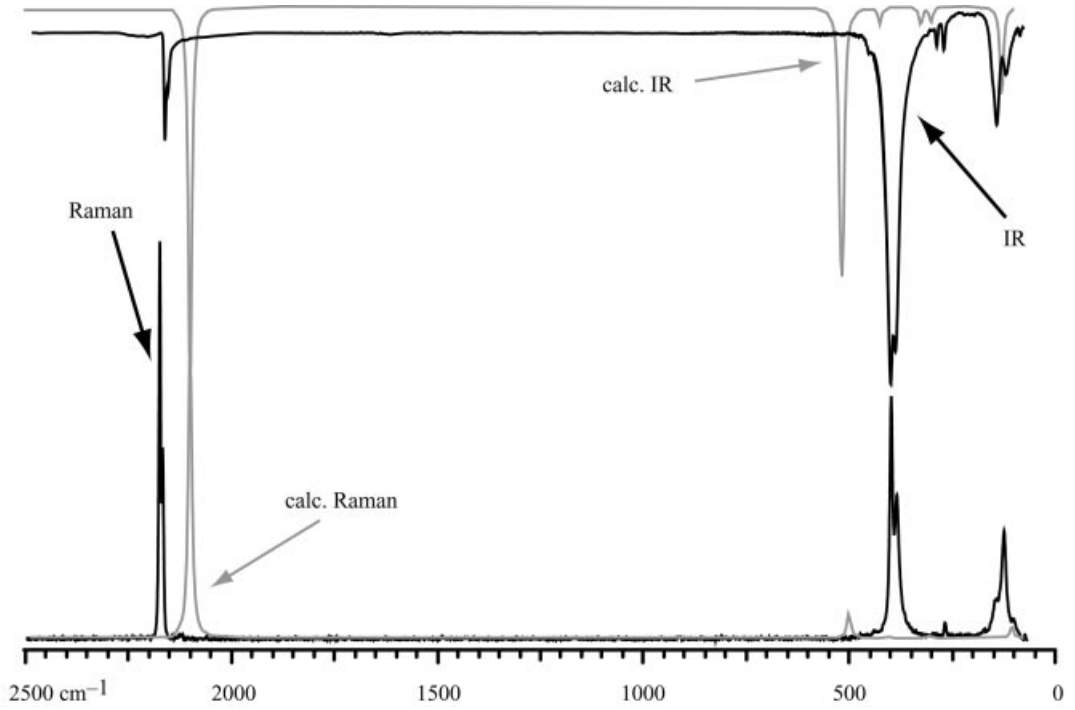

Figure 1. Experimental and calculated vibrational spectra of **1**, unscaled frequencies obtained at the MP2(FC)/MDF28-cc-pVQZ level

trum (EI), the parent ion is detected at m/z = 182, along with the fragments $[TeCN]^+$ at m/z = 156 and Te_2^+ at m/z = 256. The ^{125}Te NMR spectrum shows a single resonance at δ = 567 ppm in [D$_8$]THF (δ = 585 ppm in Et$_2$O). In the ^{13}C NMR spectrum in [D$_8$]THF, a resonance at δ = 86.2 ppm with a coupling $^1J_{C-Te}$ of 330.2 Hz is found. The broad ^{14}N NMR resonance at δ = −70 ppm ($\Delta\nu_{1/2}$ = 1300 Hz) is overlapped by the sharp resonance for dinitrogen at δ = −71.5 ppm. A minor second resonance at δ = −123 ppm ($\Delta\nu_{1/2}$ = 170 Hz) is assigned to cyanogen.

From saturated solutions of **1** in diethyl ether to which small amounts of *n*-heptane were added, off-white needles were formed under strictly anhydrous conditions at −25 °C after an extended period (18 months). In contrast, slow sublimation produced only amorphous solids. A single crystal suitable for X-ray diffraction was obtained only after several attempts because **1** in solution mostly decomposed faster than it crystallized. X-ray diffraction revealed a molecular structure with space group $R\bar{3}c$. Whereas the calculated gas phase structures of **1** at all theoretical levels applied

Table 1. Experimental parameters from X-ray diffraction and calculated parameters of Te(CN)$_2$ (**1**), Te(CN)$_4$ (**2**), and Te(CN)$_6$ in the gas phase at different levels of theory

Molecule	Method	Pseudo-potential	E [a.u.]	zpe [kJ mol^{-1}]	d(Te−C) [Å]	d(C−N) [Å]	<(C−Te−C) [°]	νCN [cm^{-1}][a]
Te(CN)$_2$ (**1**, C_{2v})	exp.	–	–	–	2.090(5)/ 2.091(6)[b]	1.131(7)/ 1.149(7) [b]	85.4(4)	2170/2177[c]
	B3LYP/cc-pVQZ	MDF28	−453.8442	40.57	2.054	1.153	94.46	2266/2274
	MP2(FC)/cc-pVQZ	MDF28	−452.6322	39.05	2.021	1.177	93.19	2100/2101
	CCD/cc-pVQZ	MDF28	−452.6691	–[d]	2.023	1.152	93.57	–[d]
	DHF/(20s18p11d+1s1p1d), cc-pVDZ	all-electron	−6978.4023	–	2.059	1.138	93.75	–
	LL-MP2/(20s18p11d+1s1p1d), cc-pVDZ	all-electron	−6796.9235	–	2.046	1.191	93.60	–
Te(CN)$_4$ (**2**, C_{2v})	B3LYP/cc-pVTZ	MDF28	−639.4585	88.91	2.074/2.227	1.152/1.155	84.35/104.06	2263/2265/ 2295/2300
	MP2(FC)/cc-pVTZ	MDF28	−637.7936	77.00	2.042/2.180	1.176/1.180	83.53/105.60	2053/2057/ 2086/2089
Te(CN)$_6$ (O_h)	B3LYP/cc-pVTZ	MDF28	−825.0674	125.49	2.118	1.153	90	2292−2297
	MP2(FC)/cc-pVTZ	MDF28	−823.0421	118.69	2.078	1.179	90	2062−2070

[a] Vibrational frequencies are unscaled. [b] Two different bond lengths due to lower symmetry of **1** in the crystal. [c] Raman frequencies. [d] Frequency analysis impossible due to exceedingly high memory requirements.

 © 2004 Wiley-VCH Verlag GmbH & Co. KGaA, Weinheim

have the expected C_{2v} symmetry with a C−Te−C angle of about 95° (see Table 1), comparable to $TeCl_2$ in the gas phase with 97.0(6)°,[10] the crystal structure of **1** reveals two almost identical Te−C bond lengths [2.090(5) and 2.091(6) Å], but two slightly different C−N bond lengths [1.131(7) and 1.149(7) Å], with a C−Te−C angle of 85.4(2)° (see Figure 2). The Te−C distance in **1** is in the same range as found for diaryl-substituted tellanes Ar_2Te,[13] but with a more acute C−Te−C angle than the latter. Available structural data for $S(CN)_2$ and $Se(CN)_2$, as far as their poor quality allows conclusions, suggest a different structure in the solid state with C−S and Se−C angles of 96 and 99°, respectively.[5,12] This unusual small angle in **1** is most likely caused by the near square-planar coordination around Te^{II}

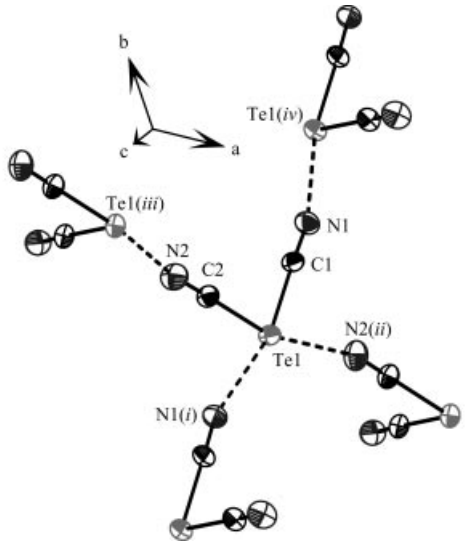

Figure 2. ORTEP plot of the molecular structure of **1** with thermal ellipsoids drawn at 50% probability; selected bond lengths [Å], distances [Å] and angles [°]: Te1−C1 2.090(5), Te1−C2 2.091(6), N1−C1 1.131(7), N2−C2 1.149(7); C1−Te1−C2 85.4(2), N1−C1−Te1 178.3(5), N2−C2−Te1 179.2(5); Te1···N1(*i*) 2.758(5), Te1···N2(*ii*) 2.745(5); C1−Te1···N1(*i*) 163.3(5), C1−Te1···N2(*ii*) 77.8(5), C2−Te1···N1(*i*) 78.0(5), C2−Te1···N2(*ii*) 163.2(5), N1(*i*)···Te1···N2(*ii*) 118.8(1); *i* = −1/3 + *x*, −1/6 + *x* − *y*, −1/6 + *z*; *ii* = 4/3 − *x* + *y*, −1/3 + *y*, −1/6 + *z*; *iii* = 1/3 + *x*, −1/3 + *x* − *y*, 1/6 + *z*; *iv* = 2/3 − *x* + *y*, 1/3 + *y*, −1/6 + *z*

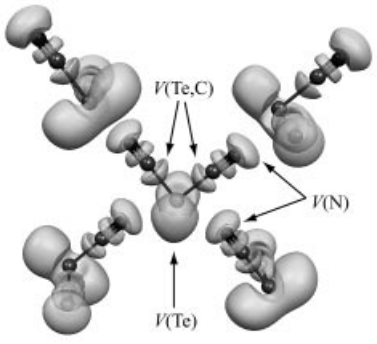

Figure 3. Ball-and-stick model with superimposed ELF isosurface of five $Te(CN)_2$ (**1**) molecules in the arrangement found by X-ray structure analysis (representing the full first coordination sphere for the central molecule, equivalent to Figure 2), single point calculation at the B3LYP/MWB46-VDZ level of theory; η = 0.78, grid increment 0.2 Å

created by the two covalent cyano groups attached to tellurium and two additional strong Te···N secondary interactions [2.745(5) and 2.758(5) Å] with two cyano-N atoms of two neighboring $Te(CN)_2$ molecules (see Figure 2), which are "pushed away" by the two lone pairs of Te^{II}. This can be conveniently visualized by the use of ELF analysis,[14] by using the experimental geometry of a part of the unit cell (see Figure 3). This coordination to adjacent molecules builds up a three-dimensional network, which connects all molecules of **1** contained in the unit cell. Furthermore, this network, when looked upon along the *c* axis, features small tubes of about 8 Å in diameter containing small residual electron densities, which have been assigned to disordered carbon atoms of a solvate, diethyl ether or *n*-heptane that was used during the crystallization process (see Figure 4).

The only report of a reaction of **1** is the attempted reaction with cyanide in MeCN solution, which did not furnish the tricyanotellurate(II) anion, $[Te(CN)_3]^-$.[4] Our experiments to halogenate **1** gave no clear results; reaction with XeF_2 in MeCN or EtCN led to colorless solutions, which were stable at −20°C for several hours. However, at higher temperatures, decomposition/dismutation reactions occurred, and sublimation of the dark residues thereof resulted in the isolation of starting material **1**.

The reaction of TeF_4 with Me_3SiCN, in a manner similar to the synthesis of $Te(N_3)_4$,[15] yields tellurium(IV) cyanide, $Te(CN)_4$ (**2**), one of the elusive neutral main-group tetracyanide species; a highly pyrophoric and thermally unstable solid. Compound **2** is obtained in CH_2Cl_2 or THF suspension at −20 °C [Equation (2)].

$$TeF_4 + 4\ Me_3SiCN \xrightarrow[-\ 4\ Me_3SiF]{-20\ °C\ /\ CH_2Cl_2} Te(CN)_4\ (\mathbf{2}) \qquad (2)$$

Above this temperature, rapid decomposition was observed that yielded a brownish oil, which was shown to contain **1** by ^{125}Te NMR spectroscopy. Reductive decomposition with extrusion of R−R species is also reported for some other R_4Te compounds.[16] After removal of all volatile materials from a suspension of **2** in CH_2Cl_2 at −20 °C, the remaining colorless powder was filled into a small Schlenk tube under argon for further investigations, upon which in two separate attempts a severe explosion destroyed parts of the glassware, presumably owing to thermal decomposition. The characterization of **2** is limited to Raman spectroscopy, since all other methods failed due to the enormous pyrophoric character, thermal sensitivity and insolubility. The fact that four equivalents of Me_3SiCN were consumed strongly suggests full substitution of all four fluorine atoms of TeF_4 to give the tetracyanide **2**. In the experimental Raman spectrum, four different C≡N stretching vibrations were detected, which complies with the basic considerations for two different cyano groups, axial and equatorial. The insolubility in all common solvents prevented crystallization and characterization by NMR spectroscopy.

In order to obtain a derivative of **2**, we probed the possible existence of pentacyanotellurate(IV) $[Te(CN)_5]^-$; re-

 © 2004 Wiley-VCH Verlag GmbH & Co. KGaA, Weinheim

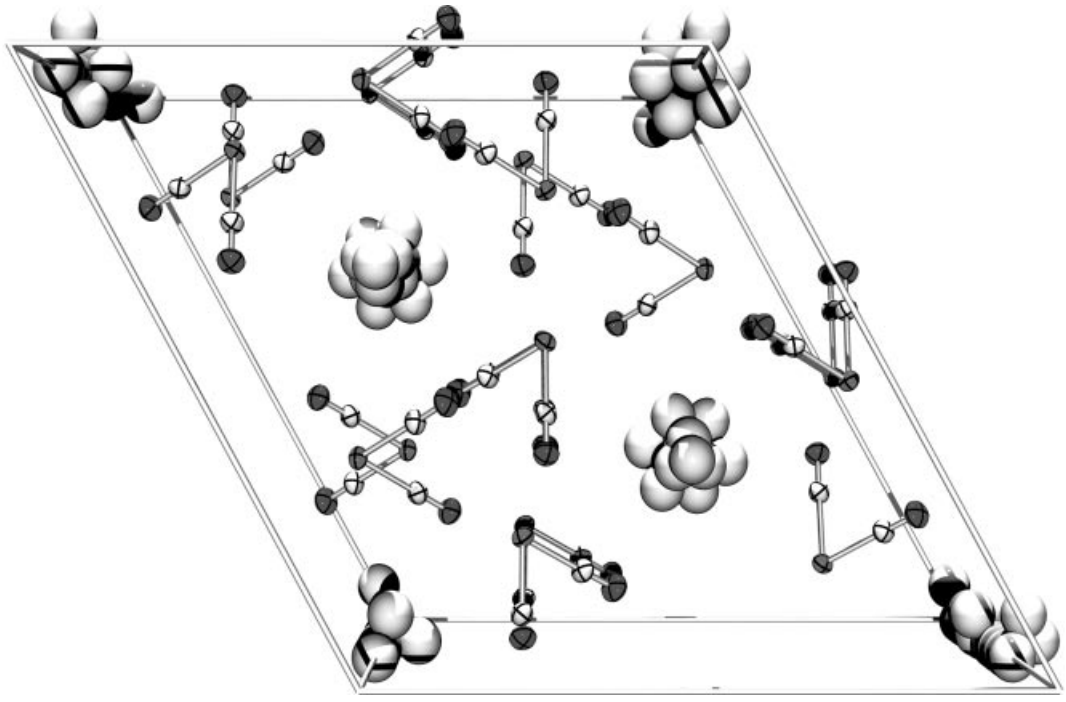

Figure 4. Unit cell of crystalline **1**, atoms within $0.5 \leq z \leq -1$ omitted, view along the *c*-axis (001), the residual electron densities assigned to carbon atoms [C11−C15, site occupation factor (SOF) = 0.207] of disordered solvate molecules are depicted as gray spheres within the free tubular spaces, thereof C11, C12, and C13 on a threefold axis

cently, we were able to characterize the stable azido analogue $[Te(N_3)_5]^-$.[15] Similar anions of the type $[aryl_5Te]^-$ can be trapped and have been proven to exist at low temperatures by ^{125}Te NMR spectroscopy.[17] Unfortunately, the reaction of $[Me_4N][TeF_5]$ with Me_3SiCN causes instantaneous decomposition to elemental tellurium, cyanide ion and cyanogen.

Since $Te(CN)_4$ (**2**) and $Te(N_3)_4$ [15,18] both seem to be highly sensitive compounds, and as examined for the hypothetical hexaazide,[18,19] we also investigated the possible existence of $Te(CN)_6$ with theoretical methods. The electronic structures of the $Te(CN)_2$ (**1**, C_{2v}), $Te(CN)_4$ (**2**, C_{2v}, see Figure 5), and $Te(CN)_6$ (O_h) molecules were calculated by using different ab initio and density functional methods (Table 1). All geometries have been fully optimized within C_1-symmetry and then recalculated in the obtained higher symmetry [**1** and **2**: C_{2v}; $Te(CN)_6$: O_h] at the level chosen, which led to minimum structures without imaginary frequencies. In addition, geometry optimization at the relativistic Dirac−Hartree−Fock level was performed for **1**, by using an energy-minimized relativistic Gaussian basis set for tellurium with either 4-component Dirac−Coulomb or Levy−Leblond Hamiltonians. The reductive decomposition of the $Te(CN)_x$ molecules yields energetic differences for the products $Te(CN)_{x-2}$ and one molecule of cyanogen of 75.78 kJ mol^{-1} ($x = 2$), −357.81 kJ mol^{-1} ($x = 4$), and −343.32 kJ mol^{-1} ($x = 6$) at the MP2(FC)/MDF28-cc-pVDZ level, respectively (corrected for the atomization energy of tellurium: 196.7 kJ mol^{-1}), thereby adding strong evidence for the instability of **2** and, even more for the hypothetical $Te(CN)_6$, relative to **1**.

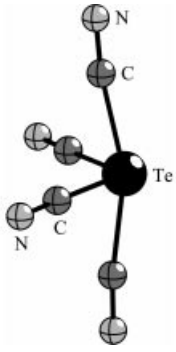

Figure 5. Calculated molecular structure of **2** (C_{2v}) at the MP2(FC)/MDF28-cc-pVTZ level of theory; selected bond lengths [Å] and angles [°]: Te−C_{eq} 2.042, C_{eq}−N_{eq} 1.177, Te−C_{ax} 2.180, C_{ax}−N_{ax} 1.179; C_{eq}−Te−C_{eq} 105.60, C_{ax}−Te−C_{ax} 158.50, Te−C_{eq}−N_{eq} 177.73, Te−C_{ax}−N_{ax} 172.21

Our present study involved the preparation and characterization of homoleptic tellurium cyanide species $Te(CN)_2$ (**1**) and $Te(CN)_4$ (**2**), as well as the calculation of their structures and that of hypothetical $Te(CN)_6$. A first comprehensive investigation of a chalcogen cyanide $Te(CN)_2$ (**1**), including an exact determination of its crystal structure is now at hand.

 © 2004 Wiley-VCH Verlag GmbH & Co. KGaA, Weinheim

Experimental Section

General: All manipulations of air- and moisture-sensitive materials were performed under purified argon using flame-dried glass vessels and Schlenk techniques. Tellurium dioxide, silver cyanide and trimethylsilyl cyanide (Aldrich) were dried or distilled prior to use. Tellurium(IV) tetrahalides were prepared according to the literature.[8c,15] Ethers and hydrocarbons were dried with sodium/benzophenone and freshly distilled, CH_2Cl_2 was dried with CaH_2 and stored over molecular sieves (4 Å). Infrared spectra were recorded with a Bruker IFS 66/vS (as KBr and PE pellets), Raman spectra with a Perkin−Elmer 2000 NIR FT spectrometer fitted with an Nd-YAG laser (1064 nm). NMR spectra were recorded with a JEOL Eclipse 400 instrument, and chemical shifts are reported with respect to Me_4Si (^{13}C), $MeNO_2$ (^{14}N) and Me_2Te (^{125}Te). Mass spectra were recorded with a JEOL MStation JMS 700 spectrometer, tellurium-containing fragments refer to ^{130}Te. Elemental analysis: Analytical service (LMU).

$Te(CN)_2$ (1): In a flame-dried Schlenk tube connected with a D3 glass frit, $TeBr_4$ (3.5 mmol, 1.5 g), AgCN (37.3 mmol, 5.0 g) and benzene (10 mL) were stirred at 60 °C for 3 d. After the supernatant solution was decanted, the remaining residue was extracted with boiling diethyl ether (3 × 15 mL), and the ethereal extracts were filtered through the glass frit. Evaporation of all volatile material at 10^{-3} mbar and ambient temperature left a colorless solid, which was carefully sublimed at $<10^{-4}$ mbar and <80 °C; **1** has an off-white color (yield 68 %). M.p. 80−82 °C. IR: $\tilde{\nu}$ = 2176 (vs, νCN), 2168 (s, νCN), 462 (sh), 410 (vs, νTeC), 398 (vs, νTeC), 296 (w, δTeCN), 277 (w, δTeCN), 147 (m, δCTeC) cm^{-1}. Raman (200 mW, 25 °C): $\tilde{\nu}$ = 2177 (100, νCN), 2170 (50, νCN), 409 (69, νTeC), 395 (40, νTeC), 279 (5, δTeCN), 136 (30, δCTeC) cm^{-1}. ^{13}C NMR (100.6 MHz, [D$_8$]THF, 25 °C): δ = 86.2 ($^1J_{C-Te}$ = 330.2 Hz) ppm. ^{14}N NMR (28.9 MHz, [D$_8$]THF, 25 °C): δ ($\Delta\nu_{1/2}$) = −70 (1300 Hz) ppm. ^{125}Te NMR (126.1 MHz, [D$_8$]THF, 25 °C): δ = 567 ppm. EI MS m/z (%) = 256 (20) [Te_2^+], 182 (90) [M^+], 156 (68) [$TeCN^+$], 130 (100) [Te^+]. C_2N_2Te (179.63): C 13.4, N 15.6; found C 13.6, N 15.4.

$Te(CN)_4$ (2): In a flame-dried Schlenk tube, TeF_4 (1.0 mmol, 0.20 g) was suspended in dry CH_2Cl_2 (5 mL) at −20 °C. After addition of Me_3SiCN (4.4 mmol, 0.44 g) in one portion, the mixture was stirred at −20 °C for 7 h, then all volatile materials were evaporated in vacuo at this temperature. ***CAUTION:*** The remaining colorless powder tends to suddenly decompose when either exposed to temperatures above −20 °C or upon contact with air. Raman (200 mW, −20 °C): $\tilde{\nu}$ = 2204 (25, νCN), 2191 (45, νCN), 2149 (40, νCN), 2129 (15, νCN), 640 (65), 474 (35), 426 (br, 55), 381 (br, 55), 220 (75), 155 (50) cm^{-1}.

Crystal Data for 1: C_2N_2Te (179.63), colorless needle, 0.08 × 0.1 × 0.6 mm, hexagonal, space group $R\bar{3}c$, a = 16.288(1), b = 16.288(1), c = 21.267(1) Å, α = 90°, β = 90°, γ = 120°, V = 4886.3(4) Å^3, Z = 36, $\rho_{calcd.}$ = 2.198 g cm^{-3}, μ = 5.321 mm^{-1}, $F(000)$ = 2808, Siemens P4 diffractometer with CCD Area Detector, Mo-K_α, λ = 0.71073 Å, T = 193 K, 2θ range = 4.80−58.32°, $-10 \le h \le 19$, $-21 \le k \le 13$, $-28 \le l \le 28$, reflections collected: 7815, independent reflections: 1478 (R_{int} = 0.0414), observed reflections: 943 [$I > 4\sigma(I)$], SADABS absorption correction, structure solution: SHELXS-97, heavy-atom method, data/parameters ratio: 24.6:1 [16.8:1 for $I > 4\sigma(I)$], final R indices [$I > 4\sigma(I)$]: $R1$ = 0.0370, $wR2$ = 0.1079, $R1$ = 0.0511, $wR2$ = 0.1159 (all data), GOF on F^2 = 1.084, largest difference peak/hole: 1.319/−1.841 e Å^{-3}. Residual peaks (five with 1.15−2.4 e Å^{-3}) were considered to be carbon atoms (disordered diethyl ether or *n*-heptane) and refined isotropically (U_{eq} = 0.15) with the same SOF (0.207) for all atoms. CCDC-244701 (**1**) contains the supplementary crystallographic data for this paper. These data can be obtained free of charge at www.ccdc.cam.ac.uk/conts/retrieving.html [or from the Cambridge Crystallographic Data Centre, 12 Union Road, Cambridge CB2 1EZ, UK; Fax: (internat.) + 44-1223-336-033; E-mail: deposit@ccdc.cam.ac.uk].

Computational Details: Gaussian03 program package on Itanium2 (64 bit),[20] DFT and MP2(FC) methods, employing the MWB46 large-core and the MDF28 small-core pseudopotentials with the corresponding cc-pVnZ-PP basis sets for tellurium,[21] and the cc-pVnZ basis sets for carbon and nitrogen atoms;[22] (very) tight geometry optimizations for **1** and **2**, and $Te(CN)_6$ until max. force = 2/15 × 10^{-6} a.u., root-mean-square force = 1/10 × 10^{-6} a.u., max. displacement = 6/60 × 10^{-6} a.u., root-mean-square displacement = 4/40 × 10^{-6} a.u. Fully relativistic direct 4-component Dirac−Hartree−Fock and MP2 calculations have been performed with the DIRAC program package[23] on Pentium4 by using the Dirac−Coulomb-Hamiltonian, a relativistic dual family basis set for tellurium (20s18p11d+1s1p1d) applying strict kinetic balance,[24] and cc-pVDZ basis sets for carbon and nitrogen atoms. ELF values have been calculated with the ToPMoD package and visualized with Molekel 4.2.[25]

Acknowledgments

Financial support by the University of Munich and the Fonds der Chemischen Industrie is gratefully acknowledged.

[1] H. E. Cocksedge, *J. Chem. Soc.* **1908**, *93*, 2175−2177.
[2] [2a] F. Challenger, A. T. Peters, J. Halévy, *J. Chem. Soc.* **1926**, 1648−1655. [2b] L. Birckenbach, K. Huttner, *Z. Anorg. Allg. Chem.* **1930**, *190*, 1−26. [2c] H. Rheinboldt, in *Houben-Weyl: Methoden der Organischen Chemie* (Ed.: E. Müller), Thieme, Stuttgart, **1952**, pp. 1075−1086. [2d]E. Montignie, *Z. Anorg. Allg. Chem.* **1962**, *315*, 102−103. [2e] K. J. Irgolic, in *Methoden der Organischen Chemie* (Ed.: D. Klamann), Thieme, Stuttgart, **1990**, pp. 676−706.
[3] H. P. Fritz, H. Keller, *Chem. Ber.* **1961**, *94*, 1524−1533.
[4] T. Austad, S. Esperas, *Acta Chem. Scand., Ser. A* **1974**, *28*, 892−896.
[5] L. Pierce, R. Nelson, C. Thomas, *J. Chem. Phys.* **1965**, *43*, 3423−3431.
[6] F. Cataldo, *Polyhedron* **2000**, *19*, 681−688.
[7] [7a] E. Mayer, *Monatsh. Chem.* **1970**, *101*, 846−849. [7b] T. Nguyen Minh, P. Ruelle, T. K. Ha, *Theochem* **1983**, *13*, 353−364. [7c] H. Rosenberg, J. F. Olsen, J. M. Howell, *J. Mol. Struct.* **1978**, *48*, 249−258.
[8] [8a] A. Damiens, *Compt. Rend.* **1920**, *171*, 1140−1143. [8b] A. Damiens, *Compt. Rend.* **1921**, *173*, 300−303. [8c] L. Gmelin, J. Meyer, E. H. E. Pietsch, A. Kotowski, M. Becke-Goehring, *Gmelin Handbuch der Anorganischen Chemie*, 8th ed., Springer-Verlag, Berlin, **1978**.
[9] H. Oppermann, G. Stoever, E. Wolf, *Z. Anorg. Allg. Chem.* **1976**, *419*, 200−212.
[10] L. Fernholt, A. Haaland, H. V. Volden, R. Kniep, *J. Mol. Struct.* **1985**, *128*, 29−31.
[11] [11a] A. C. Hazell, *Acta Crystallogr.* **1963**, *16*, 843−844. [11b] K. Emerson, D. Britton, *Acta Crystallogr.* **1963**, *16*, 113−118. [11c] K. Emerson, D. Britton, *Acta Crystallogr.* **1964**, *17*, 1134−1139. [11d] K. Emerson, *Acta Crystallogr.* **1966**, *21*, 970−974. [11e] K. H. Linke, F. Lemmer, *Z. Anorg. Allg. Chem.* **1966**, *345*, 203−210.
[12] [12a] K. H. Linke, F. Lemmer, *Z. Anorg. Allg. Chem.* **1966**, *345*, 211−216. [12b] K. H. Linke, F. Lemmer, *Z. Naturforsch., Teil B* **1966**, *21*, 192.

 © 2004 Wiley-VCH Verlag GmbH & Co. KGaA, Weinheim

[13] T. M. Klapötke, B. Krumm, P. Mayer, K. Polborn, O. P. Ruscitti, *Inorg. Chem.* **2001**, *40*, 5169−5176.
[14] [14a] A. Savin, A. D. Becke, J. Flad, R. Nesper, H. Preuss, H. G. von Schnering, *Angew. Chem.* **1991**, *103*, 421−424; *Angew. Chem. Int. Ed. Engl.* **1991**, *30*, 409−412. [14b] B. Silvi, A. Savin, *Nature* **1994**, *371*, 683−686.
[15] T. M. Klapötke, B. Krumm, P. Mayer, I. Schwab, *Angew. Chem.* **2003**, *115*, 6024−6026; *Angew. Chem. Int. Ed.* **2003**, *42*, 5843−5846.
[16] R. W. Gedridge, Jr., K. T. Higa, R. A. Nissan, *Organometallics* **1991**, *10*, 286−291.
[17] [17a] H. J. Reich, D. P. Green, N. H. Phillips, J. P. Borst, I. L. Reich, *Phosphorus Sulfur Silicon Relat. Elem.* **1992**, *67*, 83−97. [17b] M. Minoura, T. Sagami, K.-y. Akiba, *Organometallics* **2001**, *20*, 2437−2439.
[18] R. Haiges, J. A. Boatz, M. Gerken, S. Schneider, T. Schroer, K. O. Christe, *Angew. Chem.* **2003**, *115*, 6027−6031; *Angew. Chem. Int. Ed.* **2003**, *42*, 5847−5851.
[19] T. M. Klapötke, B. Krumm, K. Polborn, I. Schwab, *J. Am. Chem. Soc.* **2004**, *126*, 14166−14175.
[20] M. J. Frisch, G. W. Trucks, H. B. Schlegel, G. E. Scuseria, M. A. Robb, J. R. Cheeseman, J. A. Montgomery, Jr., T. Vreven, K. N. Kudin, J. C. Burant, J. M. Millam, S. S. Iyengar, J. Tomasi, V. Barone, B. Mennucci, M. Cossi, G. Scalmani, N. Rega, G. A. Petersson, H. Nakatsuji, M. Hada, M. Ehara, K. Toyota, R. Fukuda, J. Hasegawa, M. Ishida, T. Nakajima, Y. Honda, O. Kitao, H. Nakai, M. Klene, X. Li, J. E. Knox, H. P. Hratchian, J. B. Cross, C. Adamo, J. Jaramillo, R. Gomperts, R. E. Stratmann, O. Yazyev, A. J. Austin, R. Cammi, C. Pomelli, J. W. Ochterski, P. Y. Ayala, K. Morokuma, G. A. Voth, P. Salvador, J. J. Dannenberg, V. G. Zakrzewski, S. Dapprich, A. D. Daniels, M. C. Strain, O. Farkas, D. K. Malick, A. D. Rabuck, K. Raghavachari, J. B. Foresman, J. V. Ortiz, Q. Cui, A. G. Baboul, S. Clifford, J. Cioslowski, B. B. Stefanov, G. Liu, A. Liashenko, P. Piskorz, I. Komaromi, R. L. Martin, D. J. Fox, T. Keith, M. A. Al-Laham, C. Y. Peng, A. Nanayakkara, M. Challacombe, P. M. W. Gill, B. Johnson, W. Chen, M. W. Wong, C. Gonzalez, J. A. Pople, *Gaussian03*, Revision B01, Gaussian Inc., Pittsburgh PA, **2003**.
[21] [21a] A. Bergner, M. Dolg, W. Küchle, H. Stoll, H. Preuss, *Mol. Phys.* **1993**, *80*, 1431−1441. [21b] J. M. L. Martin, A. Sundermann, *J. Chem. Phys.* **2001**, *114*, 3408−3420. [21c] K. A. Peterson, D. Figgen, E. Goll, H. Stoll, M. Dolg, *J. Chem. Phys.* **2003**, *119*, 11113−11123.
[22] [22a] T. H. J. Dunning, P. J. Hay, in *Modern Theoretical Chemistry*, vol. 3 (Ed.: H. F. Schaefer, III), Plenum, New York, **1976**, pp. 1−28. [22b] T. H. Dunning, Jr., *J. Chem. Phys.* **1989**, *90*, 1007−1023.
[23] T. Saue, V. Bakken, T. Enevoldsen, T. Helgaker, H. J. A. Jensen, J. K. Lærdahl, K. Ruud, J. Thyssen, L. Visscher, Release 3.2 ed., http://dirac.chem.sdu.dk, **2000**.
[24] [24a] K. Fægri, Jr., *Theor. Chem. Acc.* **2001**, *105*, 252−258. [24b] K. Fægri, Jr., personal communication.
[25] [25a] S. Noury, X. Krokidis, F. Fuster, B. Silvi, Université Pierre et Marie Curie (Paris), **1997**. [25b] S. Portmann, H. P. Lüthi, *Chimia* **2000**, 766−770.

Received September 14, 2004

 © 2004 Wiley-VCH Verlag GmbH & Co. KGaA, Weinheim

A Novel Dinuclear Fe^{II} Spin-Crossover Complex Based on a 2,2-Bipyrimidine Bridge Ligand: $[Fe(CH_3bipy)(NCS)_2]_2bpym$

Ana B. Gaspar,[a] Vadim Ksenofontov,[a] Víctor Martinez,[c] M. Carmen Muñoz,[b] José A. Real,*[c] and Philipp Gütlich*[a]

Keywords: Spin crossover / Iron(II) bpym-bridged dinuclear compounds / Pressure-induced spin transition / Mössbauer spectroscopy

The dinuclear iron(II) complex $\{[Fe(CH_3bipy)(NCS)_2]_2bpym\}$ has been synthesised and its crystal structure determined at 293 K. The magnetic properties display intramolecular antiferromagnetic coupling at 1 bar ($J = -4.2$ cm^{-1}), and the onset of a pressure-induced spin conversion is observed at 11 kbar. Magnetic field Mössbauer measurements have been carried out at 4.2 K, and indicate that the HS species correspond to [HS-HS] pairs.
(© Wiley-VCH Verlag GmbH & Co. KGaA, 69451 Weinheim, Germany, 2004)

Introduction

Spin crossover (SCO) materials present magnetic and optical bistability due to a high-spin (HS) to low-spin (LS) cooperative spin transition driven by an external perturbation such as a change in temperature and/or pressure or irradiation with light.[1] Many publications stress the potential for applications of such compounds in information storage, as sensors, or as molecular switches.[2] The characteristics of this class of bistable compounds, for example, transition temperatures, hysteresis, thermochromism, photochromism as well as thermodynamic and kinetic properties, depend on the interplay between the ligand-field strength at the transition-metal ion and the interactions between the metal complex, the counterions, and solvate molecules as governed by crystal packing. In comparison with monomers, a little is known on cooperativity in small clusters or extended coordination polymers of Fe^{II}. Understanding the cooperativity between clusters and the synergy, if any, between intracluster magnetic exchange coupling and the SCO phenomenon has been the subject of investigation,[3] and continues to present other fundamental challenges.

Dinuclear iron(II) complexes of the type $\{[Fe(L)(NCX)_2]_2bpym\}$ (L: 2,2′-bipyrimidine, 2,2′-bithiazoline, 2,2′-dipyridylamine, X: S, Se) and $\{[Fe(phdia)(NCS)_2]_2(phdia)\}$ (phdia: 4,7-phenanthroline-5,6-diamine) provide a first step in the research line aimed at combining magnetic exchange and SCO phenomena in a molecule or polymeric network.[4] Extensive research has led to the conclusion that the plateau of the spin-transition curve, a special feature of this class of compounds, is constituted mainly of [HS−LS] pairs. This result confirmed that the spin conversion in these dinuclear entities proceeds through [HS-HS] ⇄ [HS−LS] ⇄ [LS−LS] pairs. The appearance of [HS−LS] species should be interpreted in terms of a synergy between intramolecular and intermolecular cooperative interactions (short- and long range) that energetically stabilises the mixed pairs, gives rise to the plateau region of a two-step transition curve and determines its width. Further, a form of synergy between spin-crossover and magnetic-coupling phenomena has been observed under the application of hydrostatic pressure or by light irradiation. Presently, the question is posed as to whether all dinuclear compounds will exhibit this two-step behaviour and/or synergy between electronic properties. In this respect, a very gradual SCO behaviour without a plateau has been observed in the $\{[Fe(dpa)(NCS)_2]_2bpym\}$ derivative,[5] the lack of such a plateau being ascribed to interdimer interactions. Murray[6] and Kaizaki[7] and their groups have reported new dinuclear iron(II) SCO systems based on pyrazolate bridges in which the conversion takes place through [HS−HS] ⇄ [LS−LS] pairs.

Here we report on the synthesis and characterisation by means of X-ray, magnetic and Mössbauer spectroscopic studies of a novel dinuclear SCO system $\{[Fe(CH_3bipy)(NCS)_2]_2bpym\}$ (**1**), where CH_3bipy = 6-methyl-2,2′-bipyridine.

The crystal structure determination on **1** was performed at 293 K. The structure of **1** consists of centrosymmetric

[a] Institut für Anorganische und Analystiche Chemie, Johannes Gutenberg Universität,
Staudinger Weg 9, 55099 Mainz, Germany
[b] Departament de Física Aplicada, Universitat Politécnica de València,
Camí de Vera s/n, 46071 València, Spain
[c] Institut de Ciéncia Molecular, Universitat de València,
Doctor Moliner 50, 46100 Burjassot, València, Spain

 © 2004 Wiley-VCH Verlag GmbH & Co. KGaA, Weinheim **DOI: 10.1002/ejic.200400586**

discrete dinuclear molecules, in which two iron(II) ions are bridged by a bpym ligand in a bis-bidentate fashion. A perspective view of the molecule with the labeling of the atoms is shown in Figure 1. The Fe···Fe intramolecular distance is 6.052(5) Å. Each iron atom is bound to six nitrogen atoms that belong to two NCS^- groups in a *cis*-position, one CH_3bipy ligand, which occupies the terminal positions in the iron surrounding, and one bridging bpym ligand. The Fe−N bond lengths involving NCS^- [2.060(16) and 2.148(10) Å] are much shorter than those involving the CH_3bipy and bpym ligands [from 2.144(8) to 2.222(9) Å,] (Table 1). The [FeN_6] chromophore is rather distorted with Fe−N bond lengths characteristic for an iron(II) ion in the HS state. Whereas the N−C−S groups are quasi-linear, the Fe−*N*−C(S) linkages are significantly bent [Fe−N3−C5 = 156.3(11)° and Fe−N4−C6 = 159.2(11)°]. There is no π−π stacking between dimers. The shortest intermolecular Fe···Fe separation is 8.250(4) Å ($i = x, 1 - y, z$).

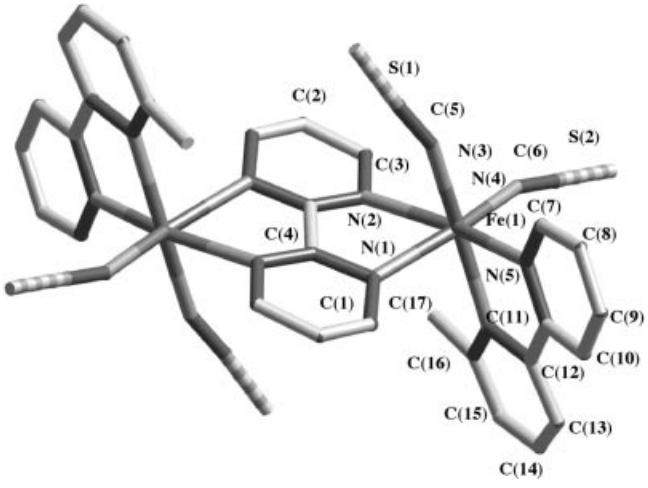

Figure 1. Molecular structure of {[Fe(CH_3bipy)$(NCS)_2]_2$bpym} (**1**) solved at 293 K with the corresponding atom numbering scheme; thermal ellipsoids are shown at 40% probability levels

Table 1. Selected bond lengths [Å] and angles [°] for **1**

Fe−N(1)	2.292(13)	N(1)−Fe−N(2)	69.6(4)
Fe−N(2)	2.272(9)	N(1)−Fe−N(3)	85.2(5)
Fe−N(3)	2.148(10)	N(3)−Fe−N(6)	164.9(4)
Fe−N(4)	2.060(16)	N(6)−Fe−N(5)	75.6(4)
Fe−N(5)	2.144(8)	N(5)−Fe−N(4)	105.3(5)
Fe−N(6)	2.222(9)	N(4)−Fe−N(2)	93.8(5)

The $\chi_M T$ vs. T curve for **1** at ambient pressure shows that the iron(II) centres of the dinuclear entities are antiferromagnetically coupled with a typical value for the magnetic coupling constant[3,4] $J = -4.2$ cm^{-1} and $g = 2.21$ [$\hat{H} = -J\hat{S}_a\hat{S}_b + g\beta(\hat{S}_a + \hat{S}_b)H$ (Figure 2)]. The maximum of the χ_M vs. T curve is centred at $T_c = 15$ K. Up to applied pressures of about 7 kbar, the magnetic properties of **1** remain practically unaltered. Further increase in the pressure up to 11 kbar induces a very incomplete spin transition around 100 K that involves 10% of the metal ions, the rest are antiferromagnetically coupled. Zero-field Mössbauer measurements of compound **1** have been carried out at 4.2 K (see a in Figure 3). At this temperature, the spectra consist of one doublet corresponding to the $S = 2$ high-spin state characterised by a quadrupole splitting of ΔE_Q(HS) = 2.91(3) mm s^{-1} and an isomer shift of δ(HS) = 0.87(1) mm s^{-1} (relative to α-Fe). The application of an external magnetic field of 50 kOe at 4.2 K causes only a broadening of the paramagnetic doublet lines of the HS species, which indicates that the HS species of **1** correspond to the [HS−HS] pairs[4] (see b in Figure 3). The effective magnetic field at the iron nuclei may be estimated by using the expression $H_{eff} \approx H_{ext} - [220 - 600(g - 2)] <S>$ (1). The effective field felt by the iron nuclei, H_{eff}, estimated from the spectrum was 14 kOe. To explain this value, one must consider the electronic levels of a dinuclear unit in the presence of antiferromagnetic coupling.[3−4] Admixture of upper levels of higher multiplicity with $S \geq 1$ to the singlet ground state $S = 0$ of the antiferromagnetically coupled pair caused by temperature and magnetic field splitting leads to a non-zero expectation value of $<S>$.

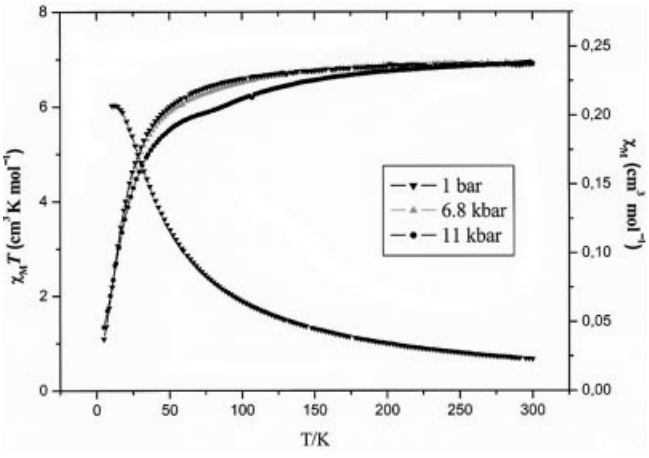

Figure 2. $\chi_M T$ and χ_M vs. T curves for {[Fe(CH_3bipy)$(NCS)_2]_2$-bpym} (**1**) at different pressures, 1 bar, 6.8 kbar, 11 kbar

The significantly higher pressures required to trigger the spin transition in **1** than the analogous dinuclear system {[Fe(bpym)$(NCS)_2]_2$bpym}[3,4] is not surprising despite the fact that the molecular structures of both compounds are similar. At ambient pressure, the complex {[Fe(bpym)-$(NCS)_2]_2$bpym} is paramagnetic in the temperature region 4−300 K and shows the intramolecular antiferromagnetic interaction. At $p = 9$ kbar, {[Fe(bpym)$(NCS)_2]_2$bpym} undergoes spin transition at $T_{1/2} \approx 150$ K involving 50% of iron atoms and ultimately causing the disappearance of antiferromagnetic coupling. The average Fe−N bond lengths are 2.188 Å and 2.180 Å for **1** and {[Fe(bpym)$(NCS)_2]_2$bpym}, respectively. Hence, the strength of the ligand field is expected to be weaker for **1** than for {[Fe(bpym)$(NCS)_2]_2$bpym}, which should be the

 © 2004 Wiley-VCH Verlag GmbH & Co. KGaA, Weinheim

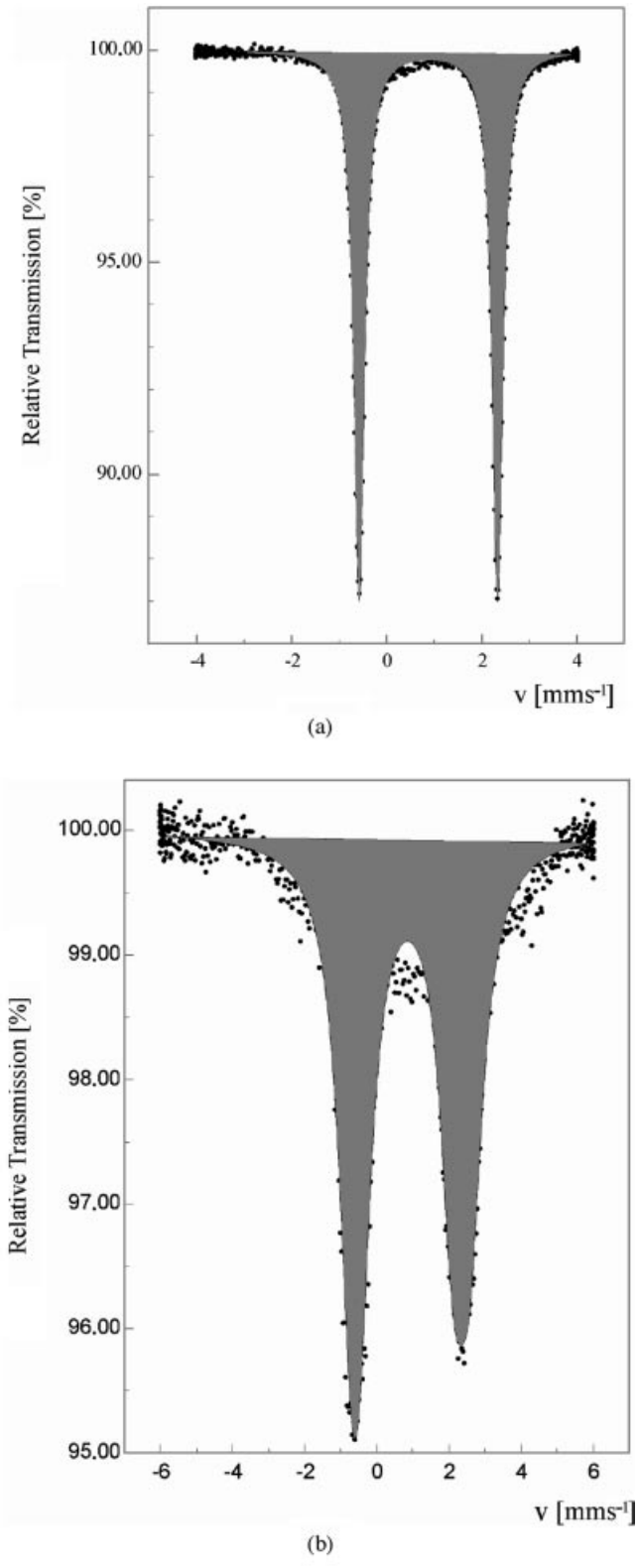

Figure 3. (a) Mössbauer spectra of {[Fe(CH_3bipy)($NCS)_2$]$_2$bpym} (**1**) at 4.2 K; (b) at 4.2 K and $H = 50$ kOe

reason for the difference in sensitivity to pressure-induced spin conversion.

Further dinuclear iron(II) examples of the present and related types are being sought.

Experimental Section

General Remarks: All reactions were carried out under Ar using standard Schlenk techniques. The ligand 6-methyl-2,2′-bipyridine (CH_3bipy) was synthesised according to a procedure described previously.[1] 2,2′-Bipyrimidine (Lancaster), $FeSO_4 \cdot 7H_2O$ (Panreac), and KNCS (Aldrich) were used as received.

{[Fe(CH_3bipy)($NCS)_2$]$_2$bpym} (1): To a solution of $FeSO_4 \cdot 7H_2O$ (0.25 mmol) in methanol (15 mL) was added a methanol solution (15 mL) of KNCS (0.5 mmol). The solution was stirred for 15 min, and the resulting precipitate (K_2SO_4) was filtered. The colourless solution containing Fe/NCS^- (1:2) was mixed with a solution of CH_3bipy (0.5 mmol) in methanol (25 mL), and the colour of the solution changed to orange. To this solution was added dropwise bpym (0.25 mmol) dissolved in methanol (15 mL). The final dark red solution was filtered and allowed to evaporate for a week, giving cubic black crystals of {[Fe(CH_3bipy)($NCS)_2$]$_2$bpym} (**1**) suitable for X-ray studies. Yield: 70%. $C_{34}H_{26}Fe_2N_{12}S_4$ (842.6): calcd. C 48.47, H 3.11, N 19.95; found C 48.16, H 3.15, N 19.18.

X-ray Crystallographic Study: Diffraction data for {[Fe(CH_3bipy)($NCS)_2$]$_2$bpym} was collected at room temperature with an Enraf−Nonius CAD-4 diffractometer by using graphite-monochromated Mo-K_α radiation with the ω-2θ scan method. The unit cell parameters were determined from least-squares refinement on the setting angles from 25 centered reflections in the range $12° < \theta < 20°$. No significant fluctuations were observed in the intensities of three standard reflections monitored periodically throughout data collections. The structure of {[Fe(CH_3bipy)($NCS)_2$]$_2$bpym} was solved by standard Patterson methods and refined by the full-matrix least-squares method on F^2. The computations were performed using SHELXS-86 and SHELXL-93.[8] All non-hydrogen atoms were refined anisotropically. Details are listed in Table 2. CCDC-239827 contains the supplementary crystallographic data for this paper. These data can be obtained free of charge at www.ccdc.cam.ac.uk/conts/retrieving.html [or from the Cambridge Crystallographic Data Centre, 12 Union Road, Cambridge CB2 1EZ, UK; Fax: (internat.) + 44-1223-336-033; E-mail: deposit@ccdc.cam.ac.uk].

Table 2. Crystal data of compound **1**

Empirical formula	$C_{34}H_{26}Fe_2N_{12}S_4$
M	842.61
Crystal system	monoclinic
Space group	$P2_1/c$
a [Å]	14.048(8)
b [Å]	18.250(3)
c [Å]	17.357(7)
β [°]	113.78(3)
V [Å^{3}9	1840.9(14)
Z	2
D_c [mg·cm^{-3}]	1.520
F(000)	860
μ (Mo-K_α) [mm^{-1}]	1.059
Crystal size [mm]	0.04 × 0.06 × 0.08
Temperature [K]	293(2)
No. of total reflections	2425
No. of independent reflections	1272
No. of parameters	237
R_1	0.0715
wR_2	0.0950
S	0.922

 © 2004 Wiley-VCH Verlag GmbH & Co. KGaA, Weinheim

Magnetic Susceptibility Measurements under Hydrostatic Pressure: The variable-temperature magnetic susceptibility measurements were performed on small single crystals by using a Quantum Design MPMS2 SQUID susceptometer equipped with a 5.5 T magnet and operating at 1 T and 1.8−375 K, the PAR 151 Foner-type magnetometer, equipped with a cryostat operating in the temperature range 2−300 K. The hydrostatic pressure cell made of hardened beryllium bronze with silicon oil as the pressure-transmitting medium operates in the pressure range 1 bar $< p <$ 13 kbar Cylindrically shaped powder sample holders with dimensions of 1 mm in diameter and 5−7 mm in length were used. The pressure was measured by using the pressure dependence of the superconducting transition temperature a of built-in pressure sensor made of high purity tin.[9] Experimental data were corrected for diamagnetism using Pascal's constants.

Mössbauer Spectroscopy: ^{57}Fe Mössbauer spectra were recorded with a constant-acceleration conventional spectrometer and helium bath cryostat. A superconducting magnet was applied to create a magnetic field directed parallel to the wave vector of the γ-quanta. The sample and the Mössbauer source ^{57}Co/Rh were immersed in liquid helium. About 40 mg of microcrystalline powder were placed in a 16 mm diameter absorber holder made of polished transparent acryl. The Recoil 1.03a Mössbauer Analysis Software was used to fit the experimental spectra.

Acknowledgments

A. B. G. thanks the Alexander von Humboldt Foundation for financial assistance. We also acknowledge the Deutsche Forschungsgemeinschaft (Priority Program SPPU37 "Molecular Magnetism"), the Fonds der Chemischen Industrie and the Materialwissenschaftliches Forschungszentrum der Universität Mainz for financial help. M. C. M. and J. A. R. thank the Ministerio Español de Ciencia y Tecnología (project BQU 2001−2928).

[1] P. Gütlich, A. Hauser, H. Spiering, *Angew. Chem. Int. Ed. Engl.* **1994**, *33*, 2024; P. Gütlich, *Struc. Bonding* **1981**, *44*, 83; P. Gütlich, Y. Garcia, H. A. Goodwin, *Chem. Soc., Rev.* **2000**, *29*, 419; J. A. Real, A. B. Gaspar, V. Niel, M. C. Muñoz, *Coord. Chem. Rev. Ed.* **2003**, *236*, 121.

[2] O. Kahn, C. J. Martinez, *Science* **1998**, *279*, 44; O. Kahn, C. Kröber, *Adv. Mater.* **1992**, *4*, 367; J. A. Real, E. Andrés, M. C. Muñoz, M. Julve, T. Trainer, A. Bousseksou, *Science* **1995**, *268*, 265; G. J. Halder, C. J. Kepert, B. Mourabaki, K. S. Murray, J. D. Cashion, *Science* **2002**, *298*, 1762.

[3] J. A. Real, A. B. Gaspar, M. C. Muñoz, P. Gütlich, V. Ksenofontov, H. Spiering, *Top. Curr. Chem.* **2004**, *233*; S. Brooker, P. G. Plieger, B. Moubaraki, K. Murray, *Angew. Chem. Int. Ed.* **1999**, *38*, 408.

[4] J. A. Real, H. Bolvin, A. Bousseksou, A. Dworkin, O. Kahn, F. Varret, J. Zarembowitch, *J. Am. Chem. Soc.* **1992**, *114*, 4650; V. Ksenofontov, A. B. Gaspar, J. A. Real, P. Gütlich, *J. Chem. Phys. B.* **2001**, *105*, 12266; A. B. Gaspar, V. Ksenofontov, H. Spiering, S. Reiman, J. A. Real, P. Gütlich, *Hyp. Interact.* **2002**, 144/145, 297; V. Ksenofontov, H. Spiering, S. Reiman, Y. Garcia, A. B. Gaspar, N. Moliner, J. A. Real, P. Gütlich, *Chem. Phys. Lett.* **2001**, *348*, 381; V. Ksenofontov, H. Spiering, S. Reiman, Y. Garcia, A. B. Gaspar, N. Moliner, J. A. Real, P. Gütlich, *Hyper. Inter.* **2001**, *141/142*, 47; V. Ksenofontov, A. B. Gaspar, S. Reiman, V. Niel, J. A. Real, P. Gütlich, *Chem. Eur. J.* **2004**, *10*, 1291.

[5] A. B. Gaspar, V. Ksenofontov, J. A. Real, P. Gütlich, *Chem. Phys. Lett.* **2003**, *373*, 385.

[6] B. A. Leita, B. Moubaraki, K. Murray, J. P. Smith, J. D. Cashion, *Chem. Commun.* **2004**, 156.

[7] K. Nakano, N. Suemura, S. Kawata, A. Fuyuhiro, T. Yagi, S. Nasu, S. Morimoto, S. Kaizaki, *Dalton Trans.* **2004**, 982.

[8] G. M. Sheldrick, SHELX97, *Program for Crystal Structure Determination*, University of Göttingen, Germany, **1997**.

[9] M. Baran, G. G. Levchenko, V. P. Dyakonov, G. Shymchak G, *Physica C* **1995**, *241*, 383.

Received July 6, 2004

 © 2004 Wiley-VCH Verlag GmbH & Co. KGaA, Weinheim

Spin Glass Behaviour in a 1D Mixed Molybdenum-Vanadium Heteropolyoxometalate-Bridged Coordination Polymer

Cai-Ming Liu,*[a] Jian-Lin Luo,[b] De-Qing Zhang,*[a] Nan-Lin Wang,[b] Zhao-Jia Chen,[b] and Dao-Ben Zhu*[a]

Keywords: Nickel / Hydrothermal synthesis / Polyoxometalate / Crystal structure / Magnetic properties

A 1D trimetallic coordination polymer containing mixed molybdenum-vanadium heteropolyoxometalate bridges, {[Ni(phen)$_2$(H$_2$O)]$_2$[Ni(phen)$_2$][V$^{IV}_8$Mo$^{VI}_6$Mo$^{V}_2$O$_{40}$(PO$_4$)]}{[Ni(phen)$_2$(H$_2$O)]$_2$[V$^{IV}_8$Mo$^{VI}_6$Mo$^{V}_2$O$_{40}$(PO$_4$)$_2$]}·5H$_2$O·2EtOH (**1**) (phen = 1,10-phenanthroline, EtOH = ethanol), has been synthesised hydrothermally. An X-ray crystallographic study revealed that **1** is composed of 1D zigzag chains of {[Ni(phen)$_2$(H$_2$O)]$_2$[Ni(phen)$_2$][V$^{IV}_8$Mo$^{VI}_6$Mo$^{V}_2$O$_{40}$(PO$_4$)]}$_n^{n+}$ cations, {[Ni(phen)$_2$(H$_2$O)]$_2$ [V$^{IV}_8$Mo$^{VI}_6$Mo$^{V}_2$O$_{40}$(PO$_4$)$_2$]}$^-$ anions and solvent molecules. Both the cation and the anion in **1** are mixed molybdenum-vanadium heteropolyoxometalates with covalently linked nickel complex fragments. Magnetic investigations of **1** indicate spin glass behaviour and several magnetic transitions occur at low temperatures (below 20 K). (© Wiley-VCH Verlag GmbH & Co. KGaA, 69451 Weinheim, Germany, 2004)

Introduction

Heteropolyoxometalates with specific topological structural characteristics have a large range of potential applications in catalysis, nanotechnology, material science, medicine, biochemistry, magnetochemistry and other important areas.[1] One powerful strategy for the preparation of new heteropolyoxometalates with large clusters or high-dimensional extended solid frameworks has involved the hybrid reaction of a metal oxide and a traditional polymolybdate under hydrothermal conditions.[1a,2] On the other hand, use of the bridging capabilities of transitional metal complex fragments has recently been exploited to build more and more high-dimensional organic-inorganic hybrid oxide materials.[3−5] Therefore, connecting heteropolyoxometalate ions with transition metal complex fragments via covalent bonds forming heteropolyoxometalate coordination polymers is considerably appealing.[5] To date, many mixed molybdenum-vanadium polyoxometalate coordination polymers have been reported which include 1D chain-like complexes such as [Ni(en)$_2$]$_2$[Ni(en)$_2$Mo$^{VI}_6$V$^{VI}_{10}$O$_{40}$(V^{IV}O$_4$)]·4H$_2$O,[5f] 2D layer complexes such as [Co(en)$_2$][Co(bpy)$_2$]$_2$[PMo$^{VI}_5$Mo$^{V}_3$V$^{IV}_8$O$_{44}$]·4.5H$_2$O (en = ethylenediamine, bpy = 2,2′-bipyridine),[5a] [en]$_{0.5}$[Cu(en)$_2$]$_2$[Cu(en)$_2$Mo^{VI}Mo$^{V}_2$V$^{VI}_8$O$_{40}$(Mo^{IV}O$_4$)]·0.5H$_2$O[5f] and [Cu(en)$_2$(H$_2$O)]{PMo$^{VI}_8$V$^{IV}_6$O$_{42}$[Cu(en)$_2$][Cu$_{0.5}$(en)]$_3$}·5.5H$_2$O (en = ethylenediamine)[5e] and the 3D framework complex H$_3${V^{V}Mo$^{VI}_8$V$^{IV}_6$O$_{42}$[Cu(en)$_2$]$_4$}[MoO$_4$]$_2$·14H$_2$O (en = ethylenediamine).[5e] However, to the best of our knowledge, no heteropolyoxometalate coordination polymer exhibiting spin glass behaviour has been found although spin glass has become one of fundamental and general forms of magnetism[6] and many crystalline molecular materials have been reported to exhibit this important phenomenon.[7] In this paper, we report the hydrothermal synthesis, crystal structure and magnetic properties of a 1D coordination polymer with mixed molybdenum-vanadium heteropolyoxometalate bridges, namely {[Ni(phen)$_2$(H$_2$O)]$_2$[Ni(phen)$_2$][V$^{IV}_8$Mo$^{VI}_6$Mo$^{V}_2$O$_{40}$(PO$_4$)]}{[Ni(phen)$_2$(H$_2$O)]$_2$[V$^{IV}_8$Mo$^{VI}_6$Mo$^{V}_2$O$_{40}$(PO$_4$)$_2$]}·5H$_2$O·2EtOH (**1**) (phen = 1,10-phenanthroline, EtOH = ethanol). Both the cation and the anion are heteropolyoxometalates with covalently linked transitional metal complex fragments. Interestingly, this complex exhibits spin glass behaviour and several magnetic transitions at low temperature.

Results and Discussion

A single-crystal X-ray structure analysis revealed that complex **1** consists of 1D zigzag cationic {[Ni(phen)$_2$(H$_2$O)]$_2$[Ni(phen)$_2$][V$^{IV}_8$Mo$^{VI}_6$Mo$^{V}_2$O$_{40}$(PO$_4$)]}$_n^{n+}$ chains and {[Ni(phen)$_2$(H$_2$O)]$_2$[V$^{IV}_8$Mo$^{VI}_6$Mo$^{V}_2$O$_{40}$(PO$_4$)$_2$]}$^-$ anions as well as solvent water molecules and solvent ethanol molecules (Figure 1 and 2). There are mixed molybdenum-vanadium polyoxoanion clusters [V$^{IV}_8$Mo$^{VI}_6$Mo$^{V}_2$O$_{40}$(PO$_4$)]$^{5-}$ in both the anion and the cation. This heteropolyanion shows a tetra-capping Keggin structural

[a] Beijing National Laboratory for Molecular Sciences, Institute of Chemistry
Chinese Academy of Sciences,
Beijing 100080, P. R. China
E-mail: cmliu@iccas.ac.cn
[b] Institute of Physics, Chinese Academy of Sciences,
Beijing 100080, P. R. China

 © 2004 Wiley-VCH Verlag GmbH & Co. KGaA, Weinheim **DOI: 10.1002/ejic.200400593**

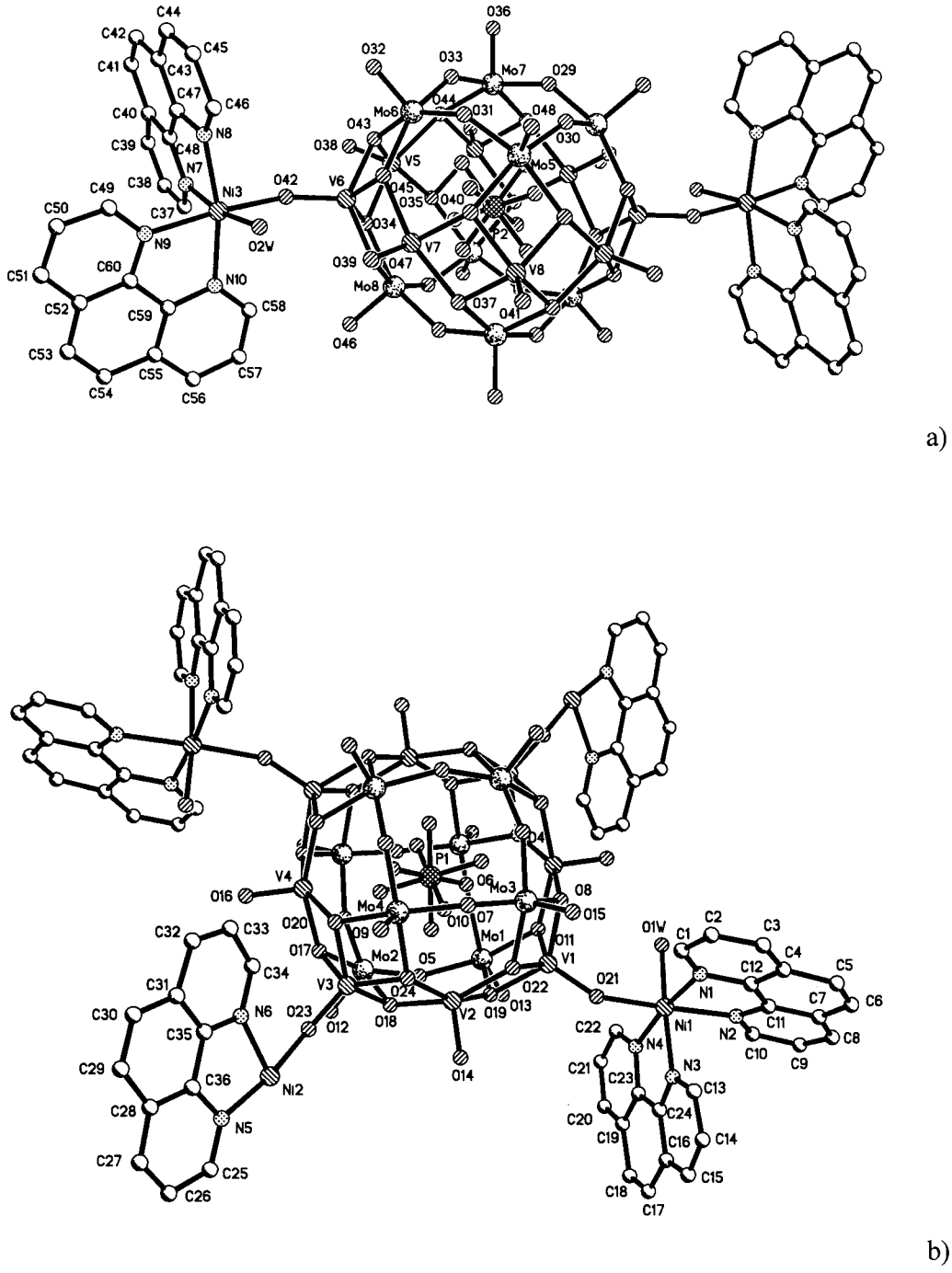

Figure 1. ORTEP view of the anion (a) and a unit of the cation (b) in **1** (50% probability displacement ellipsoids). The H atoms are omitted for clarity

feature and is very similar to that in $[Ni(tea)_2]_3[PMo^{VI}_5Mo^{V}_3V^{IV}_8O_{44}]\cdot tea\cdot H_2O$ (tea = triethylenediamine),[2] $\{Co(tea)_2\}_2Na[PMo^{VI}_6Mo^{V}_2V^{IV}_8O_{44}]\cdot 8H_2O$,[2] $[Co(en)_2][Co(bpy)_2]_2[PMo^{VI}_5Mo^{V}_3V^{IV}_8O_{44}]\cdot 4.5H_2O$,[5a] $\{Mo^{VI}_6Mo^{V}_2V^{IV}_8O_{40}(PO_4)[Co(phen)_2(H_2O)]_2\}\text{-}[Co_2(phen)_2(OH)_2(H_2O)_4]_{1/2}$ [5b] and $\{Mo^{VI}_5Mo^{V}_3V^{IV}_8O_{40}(PO_4)[Co(phen)(en)(H_2O)]_2\}[Co(phen)_3]\cdot 1.5H_2O$ (en = ethylenediamine).[5b] The $[V^{IV}_8Mo^{VI}_6Mo^{V}_2O_{40}(PO_4)]^{5-}$ unit is constructed from eight VO_5 square pyramids by sharing square edges thus forming a central belt and two Mo_4 rings are bonded above and below this V_8 belt. A disordered PO_4^{3-} anion is located in the centre as a guest.

Two terminal nickel(II) complex fragments $[Ni(phen)_2(H_2O)]^{2+}$ link to two terminal V-O groups of the heteropolyoxoanion cluster $[V^{IV}_8Mo^{VI}_6Mo^{V}_2O_{40}(PO_4)]^{5-}$ from the opposite sides to generate the anion $\{[Ni(phen)_2(H_2O)]_2[V^{IV}_8Mo^{VI}_6Mo^{V}_2O_{40}(PO_4)_2]\}^{-}$ which is quite similar to the trimetallic nanocluster anion $\{Mo^{VI}_6Mo^{V}_2V^{IV}_8O_{40}(PO_4)[Co(phen)_2(H_2O)]_2\}^{-}$ in $\{Mo^{VI}_6Mo^{V}_2V^{IV}_8O_{40}(PO_4)[Co(phen)_2(H_2O)]_2\}[Co_2(phen)_2(OH)_2(H_2O)_4]_{1/2}$.[5b]

 © 2004 Wiley-VCH Verlag GmbH & Co. KGaA, Weinheim

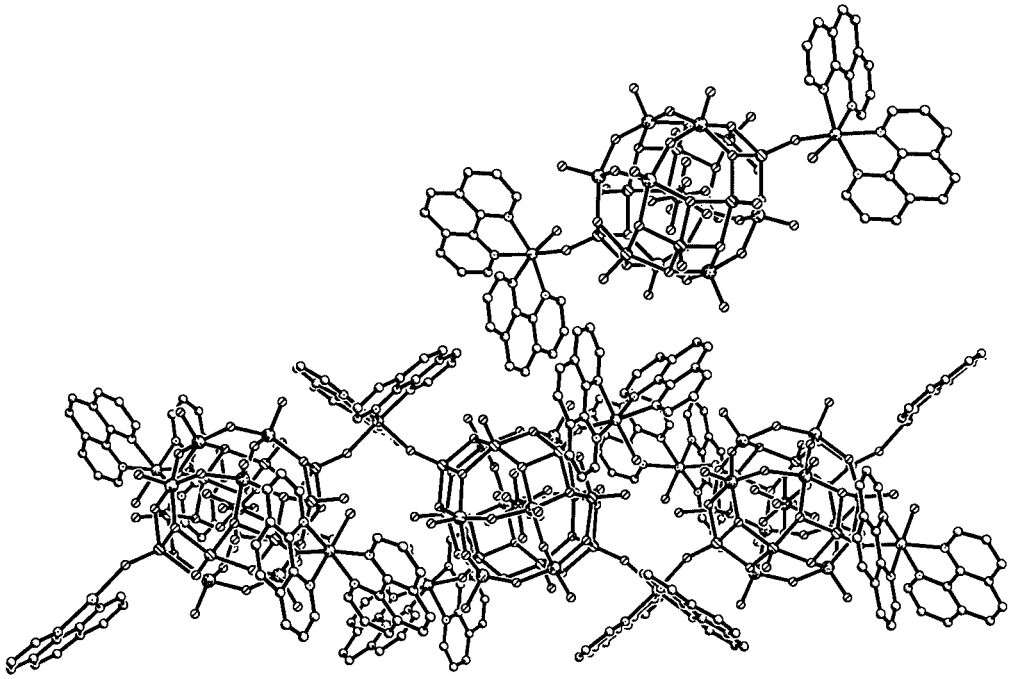

Figure 2. Molecular structure of complex **1** showing the zigzag cation chain (below) and an isolated anion (above); all solvent water molecules and ethanol molecules as well as H atoms are omitted for clarity

The Ni···Ni separation distance of 15.131Å is a little longer than the corresponding Co···Co separation distance of 14.843Å in $\{Mo^{VI}_6Mo^{V}_2V^{IV}_8O_{40}(PO_4)[Co(phen)_2(H_2O)]_2\}$-$[Co_2(phen)_2(OH)_2(H_2O)_4]_{1/2}$.[5b] The cation $\{Ni(phen)_2$-$(H_2O)\}_2[Ni(phen)_2][V^{IV}_8Mo^{VI}_6Mo^{V}_2O_{40}(PO_4)]\}^+$ also contains $\{[Ni(phen)_2(H_2O)]_2[V^{IV}_8Mo^{VI}_6Mo^{V}_2O_{40}(PO_4)_2]\}^-$ components but they are further connected to each other through *cis*-nickel complex fragments, $[Ni(phen)_2]^{2+}$, acting as bridges. Both $[Ni(phen)_2(H_2O)]^{2+}$ and $[Ni(phen)_2]^{2+}$ fragments connect the terminal V−O groups in the cation $\{Ni(phen)_2(H_2O)\}_2[Ni(phen)_2][V^{IV}_8Mo^{VI}_6Mo^{V}_2O_{40}(PO_4)]\}^+$. The Ni···Ni separation distance between two opposite $[Ni(phen)_2(H_2O)]^{2+}$ fragments (15.272 Å) is a little longer than that between two opposite $[Ni(phen)_2]^{2+}$ fragments (15.077 Å). These zigzag cationic chains are arranged parallel to the *c*-axis to form a layer along the *bc* plane with an interchain distance of about 15.7Å, whereas the isolated anions are located between cation layers to form the anion layer. It is noteworthy that although polyoxometalates with covalently linked transitional metal complex fragments have been extensively observed in many organic-inorganic hybrid oxide materials,[1e,3][5b][5c,8] cases of polyoxometalates with covalently linked transitional metal complex fragments acting as both the cations and the anions are quite rare. Complex **1** is the first coordination polymer of this type. The other reported complex with heteropolyoxocations and heteropolyoxoanions coexisting is $[PMo^{VI}_6Mo^{V}_2V^{IV}_8O_{44}$-$\{Co(2,2'\text{-bipy})_2(H_2O)\}_4][PMo^{VI}_4Mo^{V}_4V^{IV}_8O_{44}\{Co(2,2'$-$bipy)_2(H2O)\}_2]\cdot 4H_2O$ (2,2′-bipy = 2,2′-bipyridine, phen = 1,10-phenanthroline)[5d] which is a zero-dimensional polyoxometalate.

As shown in Table 1, the Mo−O and V−O bond lengths are $Mo-O_t$ 1.654(6)−1.676(6)Å, $Mo-O_b$ 1.854(7)−2.004(7) Å, $V-O_t$ 1.600(6)−1.640(6) Å and $V-O_b$ 1.915(6)−2.019(7) Å for the anion $\{[Ni(phen)_2(H_2O)]_2$-$[V^{IV}_8Mo^{VI}_6Mo^{V}_2O_{40}(PO_4)_2]\}^-$ and $Mo-O_t$ 1.658(6)−1.672(6) Å, $Mo-O_b$ 1.859(7)−1.994(6) Å, $V-O_t$ 1.591(6)−1.643(5) Å and $V-O_b$ 1.923(6)−2.007(6) Å for the cation $\{Ni(phen)_2(H_2O)\}_2[Ni(phen)_2][V^{IV}_8Mo^{VI}_6Mo^{V}_2$-$O_{40}(PO_4)]\}^+$. The assignments of the oxidation states for the Mo atoms and the V atoms are consistent with the electric charge and can be confirmed by bond valence sum calculations[9] which give values of 5.840 for Mo1, 5.851 for Mo2, 5.673 for Mo3, 5.815 for Mo4, 4.040 for V1, 3.910 for V2, 4.098 for V3, 3.909 for V4 (the cation part), and 5.871 for Mo5, 5.723 for Mo6, 5.804 for Mo7, 5.780 for Mo8, 3.875 for V5, 4.063 for V6, 3.906 for V7 and 4.065 for V8 (the anion part), respectively. The average values calculated for the oxidation state of V are 3.988 for the cation $\{Ni(phen)_2(H_2O)\}_2[Ni(phen)_2][V^{IV}_8Mo^{VI}_6Mo^{V}_2O_{40}(PO_4)]\}^+$ and 3.977 for the anion $\{[Ni(phen)_2(H_2O)]_2[V^{IV}_8$-$Mo^{VI}_6Mo^{V}_2O_{40}(PO_4)_2]\}^-$ (expected value for V^{IV}_8 is 4.000). Both the average values calculated for the oxidation state of Mo in the cation $\{Ni(phen)_2(H_2O)\}_2[Ni(phen)_2][V^{IV}_8$-$Mo^{VI}_6Mo^{V}_2O_{40}(PO_4)]\}^+$ and in the anion $\{[Ni(phen)_2(H_2O)]_2[V^{IV}_8Mo^{VI}_6Mo^{V}_2O_{40}(PO_4)_2]\}^-$ are 5.795 (expected value for $Mo^{VI}_6Mo^{V}_2$ is 5.750) and the calculated result is in good agreement with the formula of **1**.

The 2−300 K magnetic susceptibility, χ, of a polycrystalline sample of **1** could be fitted to the Curie−Weiss law above 70 K with C = 9.77 $cm^{-3}\cdot mol^{-1}\cdot K$ and θ = −36.49 K, indicating antiferromagnetic interactions of

 © 2004 Wiley-VCH Verlag GmbH & Co. KGaA, Weinheim

Table 1. Selected bond lengths (Å) and angles (°) for **1**

Cation part			
Ni1−N4	2.063(8)	Ni1−N1	2.084(8)
Ni1−N2	2.085(7)	Ni1−N3	2.103(8)
Ni1−O21	2.066(6)	Ni1−O1W	2.094(8)
Ni2−O23	2.068(5)	Ni2−N6	2.073(7)
Ni2−N5	2.088(7)	Mo1−O13	1.658(6)
Mo1−O5	1.874(7)	Mo1−O7	1.880(7)
Mo1−O11	1.975(6)	Mo1−O19	1.981(6)
Mo2−O12	1.667(6)	Mo2−O5	1.859(7)
Mo2−O18	1.989(6)	Mo3−O15	1.672(6)
Mo3−O10	1.864(7)	Mo3−O4	1.868(8)
Mo3−O8	1.964(6)	Mo3−O22	1.970(6)
Mo4−O9	1.668(6)	Mo4−O7	1.862(7)
Mo4−O10	1.871(6)	Mo4−O20	1.980(6)
Mo4−O24	1.982(6)	V1−O21	1.627(6)
V1−O8	1.926(6)	V1−O11	1.935(6)
V1−O22	1.943(6)	V1−O19	1.952(6)
V2−O14	1.591(6)	V2−O24	1.980(6)
V2−O18	1.987(6)	V2−O22	1.991(6)
V3−O23	1.643(5)	V3−O24	1.923(6)
V3−O20	1.932(6)	V3−O18	1.934(6)
V3−O17	1.946(7)	V4−O16	1.602(6)
V4−O20	1.977(6)	V4−O17	1.979(6)
N1−Ni1−N2	79.2(3)	N4−Ni1−N3	80.2(3)
O21−Ni1−N1	93.0(3)	O21−Ni1−N2	171.7(3)
O21−Ni1−N3	93.7(3)	N4−Ni1−O21	89.5(3)
N4−Ni1−O1W	93.4(4)	O21−Ni1−O1W	93.1(3)
O1W−Ni1−N3	170.6(3)	N6−Ni2−N5	79.8(3)
O23−Ni2−N6	94.3(3)	O23−Ni2−N5	172.8(3)
O23−Ni2−O23[a]	90.1(3)		
Anion part			
Ni3−O42	2.045(6)	Ni3−N10	2.084(7)
Ni3−O2W	2.085(7)	Ni3−N7	2.088(8)
Ni3−N9	2.110(7)	Ni3−N8	2.088(8)
Mo5−O48	1.676(6)	Mo5−O30	1.854(7)
Mo5−O31	1.868(7)	Mo5−O40	1.966(6)
Mo6−O32	1.656(7)	Mo6−O33	1.860(7)
Mo6−O31	1.866(6)	Mo6−O45	1.986(6)
Mo6−O43	1.988(5)	Mo7−O36	1.671(6)
Mo7−O29	1.854(7)	Mo7−O33	1.862(7)
Mo7−O44	1.992(6)	Mo8−O46	1.654(6)
Mo8−O39	1.973(6)	Mo8−O34	1.989(7)
V5−O38	1.602(6)	V5−O44	1.993(6)
V5−O43	2.000(6)	V5−O35	2.006(7)
V5−O34	2.019(7)	V6−O42	1.640(6)
V6−O45	1.915(6)	V6−O39	1.918(6)
V6−O34	1.936(6)	V6−O43	1.937(6)
V7−O47	1.600(6)	V7−O40	1.964(6)
V7−O37	1.981(7)	V7−O39	1.993(6)
V7−O45	1.995(7)	V8−O41	1.618(7)
V8−O37	1.935(6)	V8−O40	1.939(6)
O42−Ni3−N10	94.7(3)	O42−Ni3−O2W	89.6(3)
N7−Ni3−N8	79.5(4)	N10−Ni3−N9	79.1(3)
O42−Ni3−N7	85.2(3)	O42−Ni3−N8	95.3(3)
N10−Ni3−O2W	95.9(3)	N10−Ni3−N7	93.0(3)
O2W−Ni3−N7	170.1(3)	O2W−Ni3−N9	93.0(3)
O42−Ni3−N9	173.5(3)	O2W−Ni3−N8	92.6(4)

[a] Symmetry transformations used to generate equivalent atoms: $-x, y, -z + 3/2$.

nearest-neighbour spin units. As shown in Figure 3, χT has a value of 8.90 emu·K·mol^{-1} at room temperature which is smaller than that expected for the total value of 16 uncoupled $S = 1/2$ spins of the V^{4+} atoms, 4 uncoupled $S = 1/2$ spins from the Mo^{5+} atoms and 5 uncoupled $S = 1$ spins from the Ni^{2+} atoms (≈ 13.83 emu·K·mol^{-1} assuming $g = 2.0$ for V^{4+} and Mo^{5+} and $g = 2.25$ for Ni^{2+}). This is due to spin pairing[5,10] which is favoured by electron delocalisation in the cluster $[V^{IV}{}_8Mo^{VI}{}_6Mo^{V}{}_2O_{40}(PO_4)]^{5-}$. The value of χT decreases upon cooling but a sharp increase in $\chi T(T)$ occurs near 50 K and a maximum of 27.02 emu K·mol^{-1} is reached at 16 K. Below 16 K, $\chi T(T)$ decreases abruptly down to 2 K because of saturation effects and/or increasing antiferromagnetic interactions.

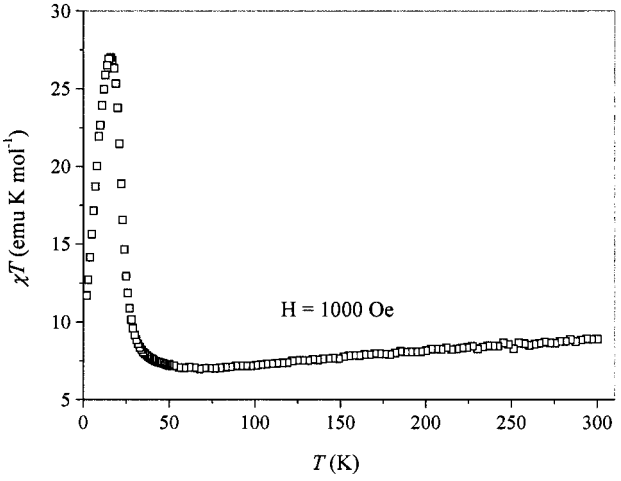

Figure 3. χT vs. T plot of **1** at 1000 Oe

The ac susceptibility measurements indicated that both real χ' and imaginary χ'' components of the susceptibility show rather complicated behaviour (Figure 4). Firstly, there are two peaks in the $\chi'(T)$ and $\chi''(T)$ curves: both the cusped one and the rounded one are frequency dependent while the latter is more sensitive to frequency, suggesting unusual spin glass behaviour. Secondly, below 8 K, $\chi'(T)$ increases gradually, possibly indicating the existence of another phase transition. This peculiar ac susceptibility behaviour may occur for a *ferroglass* system (also called a re-

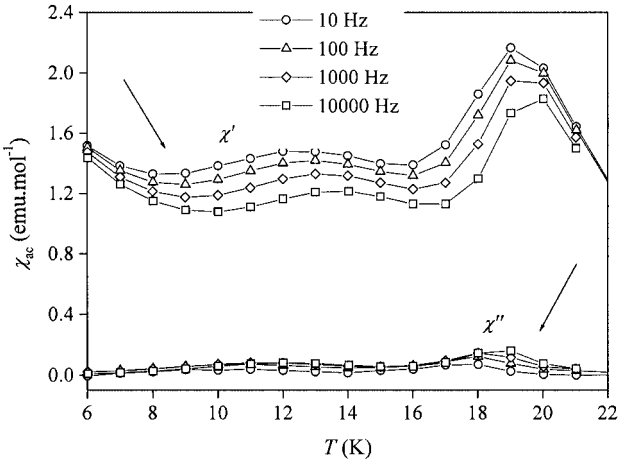

Figure 4. Real(χ') and imaginary(χ'') parts of the *ac* susceptibility at a bias DC field of 10 Oe for **1**

 © 2004 Wiley-VCH Verlag GmbH & Co. KGaA, Weinheim

entrant spin glass system) because it generally undergoes multiple magnetic phase transitions.[11] Therefore, the cusped peak could be assigned to a spin glass transition while the rounded one probably corresponds to a ferroglass transition.[11b] The spin-freezing temperature T_f (= 19 K) may be defined approximately by the sharp cusp in χ' at 10 Hz and the spin-freezing at a lower temperature T_{fg} may be estimated by the rounded peak in χ' at 10 Hz (T_{fg} = 12 K). The spin-glass state was also confirmed by the divergence of the zero-field-cooled (ZFC) and field-cooled (FC) $\chi(T)$ data of **1** below 20 K, indicating the occurrence of irreversibility of magnetisation. Furthermore, hysteresis can be observed with coercive fields (*Hc*) of 191 Oe at 20 K (Figure 5), 386 Oe at 12.5 K and 660 Oe at 5 K, respectively. However, the field dependent magnetisation of **1** measured at 5 K shows that at the highest field measured (50 kOe), a low magnetisation value of 7.4 $N\beta$ is achieved and saturation does not occur, this being consistent with weak ferromagnetism owing to spin glass.

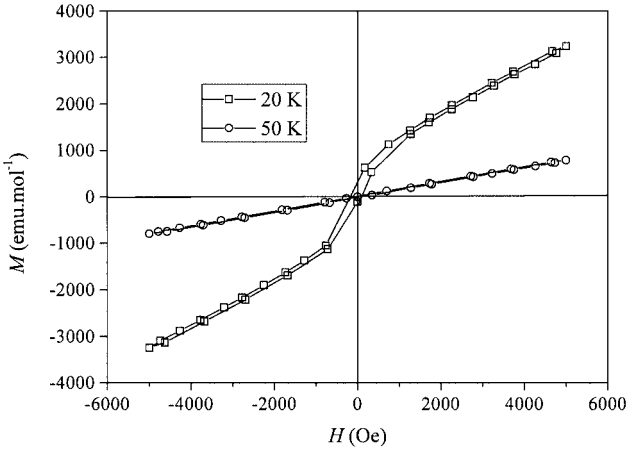

Figure 5. Hysteresis loops at 20 K and 50 K

In summary, the successful synthesis of $Ni_5[V^{IV}{}_8Mo^{VI}{}_6Mo^{V}{}_2O_{40}(PO_4)]_2(phen)_{10}(H_2O)_9(EtOH)_2$ **1** indicates that a new type of organic-inorganic hybrid oxide material in which polyoxometalate clusters act as both the cation and the anion can be prepared hydrothermally. The anion in **1** is a trimetallic nanocluster $\{Mo^{VI}{}_6Mo^{V}{}_2V^{IV}{}_8O_{40}(PO_4)[Ni(phen)_2(H_2O)]_2\}^-$ and the cation $\{Ni(phen)_2(H_2O)\}_2[Ni(phen)_2][V^{IV}{}_8Mo^{VI}{}_6Mo^{V}{}_2O_{40}(PO_4)]\}^+$ also contains trimetallic units $\{Mo^{VI}{}_6Mo^{V}{}_2V^{IV}{}_8O_{40}(PO_4)[Ni(phen)_2(H_2O)]_2\}^-$ which are further connected to each other through *cis*-nickel complex fragments, $Ni(phen)_2{}^{2+}$, to form a zigzag chain. Both the cation and the anion in **1** are high-spin systems which would generate randomness either in the positions of the spins or the signs of the neighbouring couplings in a field and spin glass behaviour is then expected.

Experimental Section

Materials and Methods: All reagents were obtained from commercial sources and used without further purification. The elemental analyses were performed with a Heraeus Chn-Rapid elemental analyser. The inductively coupled plasma (ICP) analysis was conducted with a Perkin−Elmer Optima 3300DV spectrometer. The infrared spectra were recorded with a Pekin-Elmer 2000 spectrophotometer with pressed KBr pellets. X-ray photoelectron spectroscopy data were obtained with an ESCALab220i-XL electron spectrometer from VG Scientific using 300-W Al-K_α radiation. The base pressure was around 3×10^{-9} mbar. The binding energies were referenced to the C 1s line at 284.6 eV from adventitious carbon. The magnetic susceptibility measurements for **1** were carried out on a polycrystalline sample (202.84 mg) using a MagLab System 2000 magnetometer in a field up to 5 T. Diamagnetic corrections were estimated from Pascal's constants.[12]

Synthesis of 1: A mixture of NH_4VO_3 (3 mmol), $H_3[P(Mo_3O_{10})_4]\cdot xH_2O$ (0.5 mmol), $Ni(NO_3)_2$ (1 mmol), 1,10-phenanthroline (1 mmol), *N*,*N*′-diethylethylenediamine (3 mmol), ethanol (0.2 mL) and H_2O (18 mL) was stirred for 20 min and then transferred into a 30 mL Teflon-lined steel autoclave. The mixture was heated at 170 °C for 6 days and black block crystals of **1** were separated from the blue supernatant solution in ca. 40% yield (463 mg) based on V. $C_{124}H_{110}Mo_{16}N_{20}Ni_5O_{99}P_2V_{16}$ (6169.89): calcd. C 24.14, H 4.54, N 1.80, Mo 24.9, Ni 4.8, V 13.2; found C 24.06, H 4.60, N 1.75, Mo 24.8, Ni 4.7, V 13.2. IR (KBr): $\tilde{\nu}$ = 1055(w) [$\nu_{(P-O)}$], 951(vs) [$\nu_{(M=O)}$], 792(s) cm^{-1} [$\nu_{(M-O-M)}$] (M = V or Mo). XPS: calcd. C 1s 284.75, O 1s 530.10, P 2p 132.90, Ni $2p_3$ 855.90, V $2p_3$ 516.10, Mo 3d 231.80 eV.

X-ray Crystal Structure Determination: A black single crystal of **1** with dimensions 0.37 × 0.27 × 0.17 mm was selected and mounted on a Rigaku RAXIS RAPID IP imaging plate system with Mo-K_α radiation (λ = 0.71073Å) at 300(2) K in the range $1.38° < \theta < 27.48°$. An empirical absorption correction from Ψ scans was applied. A total of 28115 reflections were collected ($-64 \le h \le 64$, $-20 \le k \le 20$, $-33 \le l \le 33$) of which 18729 were unique (R_{int} = 0.0441) and 15227 with $I > 2\sigma(I)$. The structure was solved by the Patterson method and refined using full-matrix least-squares techniques based on F^2 using the SHELXL 97 program. All nonhydrogen atoms were refined anisotropically and all hydrogen atoms but those in water molecules were placed as riding atoms.

Crystal Data For 1: $C_{124}H_{110}Mo_{16}N_{20}Ni_5O_{99}P_2V_{16}$, monoclinic, space group *C*l*2c*, *Mr* = 6169.89, *a* = 49.658(10), *b* = 15.675(3), *c* = 25.916(5) Å, β = 115.39(3)°, *V* = 18225(6) Å^3, *Z* = 4, $D_{calcd.}$ = 2.242 g·cm^{-3}, *T* = 293(2) K, μ = 2.457 mm^{-1}, R_1 = 0.0694, wR_2 = 0.1855 for 15227 observed reflections [$I > 2\sigma(I)$], GOF = 1.087.

CCDC-213185 contains the supplementary crystallographic data for this paper. These data can be obtained free of charge at www.ccdc.cam.ac.uk/conts/retrieving.html [or from the Cambridge Crystallographic Data Centre, 12, Union Road, Cambridge CB2 1EZ, UK; Fax: (internat.) +44-1223-336-033; E-mail: deposit@ccdc.cam.ac.uk].

Acknowledgments

This work was supported by the National Natural Science Foundation of China (No. 20201012, 90101025), the Major State Basic Research Development Program of the People's Republic of China (G2000077500 and 2001CB610507) and the Chinese Academy of Sciences. The authors also thank the anonymous reviewers for their excellent suggestions for improving the manuscript.

[1] [1a] C. L. Hill, *Chem. Rev.* **1998**, *98*, 1−390 (Ed.: C. L. Hill; special issue on polyoxometalates). [1b] M. T. Pope, A. Müller, *Angew. Chem. Int. Ed. Engl.* **1991**, *30*, 34−48. [1c] R. C. Howell,

F. G. Perez, S. Jain, W. D. Horrocks, Jr., A. L. Rheingold, L. C. Francesconi, *Angew. Chem. Int. Ed.* **2001**, *40*, 4031−4034. [1d] A. Müller, H. Reuter, S. Dillinger, *Angew. Chem. Int. Ed. Engl.* **1995**, *34*, 2328−2361. [1e] V. Kogan, Z. Aizenshtat, R. Neumann, *Angew. Chem. Int. Ed.* **1999**, *38*, 3331−3334. [1f] K. Wassermann, M. H. Dickman, M. T. Pope, *Angew. Chem. Int. Ed. Engl.* **1997**, *36*, 1445−1448. [1g] R. Ben-Daniel, R. Neumann, *Angew. Chem. Int. Ed.* **2003**, *42*, 92−95. [1h] C.-D. Wu, C.-Z. Lu, H.-H. Zhuang, J.-S. Huang, *J. Am. Chem. Soc.* **2002**, *124*, 3836−3837. [1i] J. T. Rhule, W. A. Neiwert, K. I. Hardcastle, B. T. Do, C. L. Hill, *J. Am. Chem. Soc.* **2001**, *123*, 12101−12102. [1j] J. M. Maestre, X. Lopez, C. Bo, J.-M. Poblet, N. Casañ-Pastor, *J. Am. Chem. Soc.* **2001**, *123*, 3749−3758. [1k] L. Zhang, X. Zhao, J. Xu, T. Wang, *Dalton Trans.* **2002**, 3275−3276.

[2] [2a] Y. Xu, D.-R. Zhu, Z.-J. Guo, Y.-J. Shi, K.-L. Zhang, X.-Z. You, *J. Chem. Soc., Dalton Trans.* **2001**, 772−773. [2b] L. Zhang, X. Zhao, J. Xu, T. Wang, *Dalton Trans.* **2002**, 3275−3276.

[3] [3a] Y. Zhang, J. R. D. DeBord, C. J. O'Connor, R. C. Haushater, A. Clearfield, J. Zubieta, *Angew. Chem. Int. Ed. Engl.* **1996**, *35*, 989−991. [3b] L.-M. Zheng, T. Whitfield, X. Wang, A. Jacobson, *Angew. Chem. Int. Ed.* **2000**, *39*, 4528−4531. [3c] Z. Shi, L.-R. Zhang, G.-L. Zhu, G.-Y. Yang, J. Hua, H. Ding, S.-H. Feng, *Chem. Mater.* **1999**, *11*, 3565−3570. [3d] L.-R. Zhang, Z. Shi, G.-Y. Yang, X.-M. Chen, S.-H. Feng, *J. Chem. Soc., Dalton Trans.* **2000**, 275−278. [3e] R. L. LaDuca, M. Desciak, M. Laskoski, R. S. Rarig, J. Zubieta, *J. Chem. Soc., Dalton Trans.* **2000**, 2255−2258. [3f] P. J. Hagrman, C. Bridges, J. E. Greedan, J. Zubieta, *J. Chem. Soc., Dalton Trans.* **1999**, 2901−2904. [3g] R. C. Finn, E. Burkholder, J. Zubieta, *Chem. Commun.* **2001**, 1852−1853. [3h] E. E. Burkholder, J. Zubieta, *Chem. Commun.* **2001**, 2056−2057. [3i] R. C. Finn, J. Zubieta, *Inorg. Chem.* **2001**, *40*, 2466−2467. [3j] R. C. Finn, E. Burkholder, J. Zubieta, *Inorg. Chem.* **2002**, *41*, 2109−2123. [3k] P. J. Zapf, C. J. Warren, R. C. Haushalter, J. Zubieta, *Chem. Commun.* **1997**, 1543−1544. [3l] E. Burkholder, V. Golub, C. J. O'Conner, J. Zubieta, *Inorg. Chem.* **2003**, *42*, 6729−6740.

[4] [4a] P. J. Hagrman, D. Hagrman, J. Zubieta, *Angew. Chem. Int. Ed.* **1999**, *38*, 2638. [4b] X.-B. Cui, J.-Q. Xu, Y. Li, Y.-H. Sun, G.-Y. Yang, *Eur. J. Inorg. Chem.* **2004**, 1051−1055. [4c] D. Xiao, Y. Xu, Y. Hou, E. Wang, S. Wang, Y. Li, L. Xu, C. Hu, *Eur. J. Inorg. Chem.* **2004**, 1385−1388. [4d] S.-T. Zheng, J. Zhang, G.-Y. Yang, *Eur. J. Inorg. Chem.* **2004**, 2004−2007.

[5] [5a] C.-M. Liu, D.-Q. Zhang, M. Xiong, D.-B. Zhu, *Chem. Commun.* **2002**, 1416−1417. [5b] C.-M. Liu, D.-Q. Zhang, D.-B. Zhu, *Crystal Growth & Des.* **2003**, *3*, 363−368. [5c] C.-L. Pan, J.-Q. Xu, Y. Sun, D.-Q. Chu, L. Ye, Z.-L. Lü, T.-G. Wang, *Inorg. Chem. Commun.* **2003**, *6*, 233−237. [5d] M. Yuan, Y. Li, E. Wang, C. Tian, L. Wang, C. Hu, N. Hu, H. Jia, *Inorg. Chem.* **2003**, *42*, 3670−3676. [5e] L.-M. Duan, C.-L. Pan, J.-Q. Xu, X.-B. Cui, F.-T. Xie, T.-G. Wang, *Eur. J. Inorg. Chem.* **2003**, 2578−2581. [5f] W.-M. Bu, L. Ye, G.-Y. Yang, J.-S. Gao, Y.-G. Fan, M.-C. Shao, J.-Q. Xu, *Inorg. Chem. Commun.* **2001**, *4*, 1−4.

[6] J. A. Mydosh, *Spin glasses: An Experimental Introduction*, Taylor and Francis, London, **1993**.

[7] See for example: [7a] B.-Q. Ma, S. Gao, G. Su, G.-X. Xu, *Angew. Chem. Int. Ed.* **2001**, *40*, 434−436. [7b] T.-F. Liu, D. Fu, S. Gao, Y.-Z. Zhang, H.-L. Sun, G. Su, Y.-J. Liu, *J. Am. Chem. Soc.* **2003**, *125*, 13976−13977. [7c] M. T. Johnson, A. M. Arif, J. S. Miller, *Eur. J. Inorg. Chem.* **2000**, 1781−1787. [7d] M. L. Taliaferro, T. D. Selby, J. S. Miller, *Chem. Mater.* **2003**, *15*, 3602−3606. [7e] H. Miyasaka, R. Clerac, K. Mizushima, K.-I. Sugiura, M. Yamashita, W. Wernsdorfer, C. Coulon, *Inorg. Chem.* **2003**, *42*, 8203−8213. [7f] J. L. Manson, C. R. Kmety, F. Palacio, A. J. Epstein, J. S. Miller, *Chem. Mater.* **2001**, *13*, 1068−1073.

[8] [8a] P. J. Zapf, C. J. Warren, R. C. Haushalter, J. Zubieta, *Chem. Commun.* **1997**, 1543−1544. [8b] C.-M. Liu, S. Gao, H.-M. Hu, Z.-M. Wang, *Chem. Commun.* **2001**, 1636−1637. [8c] Y. Xu, J.-Q. Xu, K.-L. Zhang, Y. Zhang, X.-Z. You, *Chem. Commun.* **2000**, 153−154. [8d] J.-Q. Xu, R.-Z. Wang, G.-Y. Yang, Y.-H. Xing, D.-M. Li, W.-M. Bu, L. Ye, Y.-G. Fan, G.-D. Yang, Y. Xing, Y.-H. Lin, H.-Q. Jia, *Chem. Commun.* **1999**, 983−984.

[9] M. O'Keeffe, A. Navrotsky (Ed.), *Structure and Bonding in Crystals*, Academic Press, New York, **1981**, vol. II, p. 1.

[10] [10a] A.-L. Barra, D. Gatteschi, L. Pardi, A. L. Barra, A. Müller, J. Döring, *J. Am. Chem. Soc.* **1992**, *114*, 8509−8514. [10b] A. Müller, R. Sessoli, E. Krickemeyer, H. Bögge, J. Meyer, D. Gatteschi, L. Pardi, J. Westphal, K. Hovermeier, R. Rohlfing, J. Döring, F. Hellweg, C. Beugholt, M. Schmidtmann, *Inorg. Chem.* **1997**, *36*, 5239−5250.

[11] [11a] T. Wasiutyński, Z. Szeglowski, A. W. Pacyna, M. Balanda, *Physica B* **1998**, *253*, 305−312. [11b] R. B. Goldfarb, K. V. Rao, H. S. Chen, *Solid State Commun.* **1985**, *54*, 799−801.

[12] O. Kahn, *Molecular Magnetism*, VCH Publishers, New York, **1993**.

Received July 9, 2003

 © 2004 Wiley-VCH Verlag GmbH & Co. KGaA, Weinheim

One-Pot Synthesis of Pyridyltellurium Derivatives from a Reaction with Isopropylmagnesium Chloride and X-ray Crystal Structures of Various Pyridyl Ditellurides

Kuldip K. Bhasin,*[a] Veena Arora,[a] Thomas M. Klapötke,[b] and Margaret-Jane Crawford[b]

Dedicated to the memory of Prof. R. C. Paul (1919−2002)

Keywords: Grignard reaction / Pyridyl telluride / Tellurium / Transmetallation

A one-pot synthesis of various symmetrical and unsymmetrical 2-pyridyl-, 2-bromo-5-pyridyl-, and 2,5-dibromo-3-pyridyltellurium compounds has been carried out, at room temperature, by selective single bromine-magnesium exchange of 2-bromo-, 2,5-dibromo- and 2,3,5-tribromopyridine, respectively, with isopropylmagnesium chloride. This exchange reaction gives the corresponding pyridylmagnesium chlorides, which, upon insertion of elemental tellurium (activated), give the pyridyltelluromagnesium chlorides, and, subsequently, the corresponding dipyridyl ditellurides upon aerial oxidation. The pyridyltelluromagnesium chlorides give unsymmetrical pyridyltellurium derivatives in good yield upon treatment with alkyl halides. The X-ray crystal structures of bis(2-pyridyl) ditelluride, bis(2,5-dibromo-6-methyl-3-pyridyl) ditelluride and bis(2,5-dibromo-3-pyridyl) ditelluride are discussed.
(© Wiley-VCH Verlag GmbH & Co. KGaA, 69451 Weinheim, Germany, 2004)

Introduction

Organic synthesis using tellurium-based methodologies has recently become increasingly important.[1,2] Compared to alkyl- and aryltellurium compounds,[3,4] the use of pyridyltellurium derivatives in organic synthesis has been relatively less studied. This may primarily be due to the lack of a convenient and efficient synthesis of these compounds. Most recently developed methods for the syntheses of dipyridyl ditellurides involve either deprotonation of BF_3-complexed pyridine[5] or bromine-lithium exchange[6] of 2-bromopyridine with BuLi at −78 °C followed by tellurium insertion and subsequent aerial oxidation. The low temperature invariably required in these preparations restricts its utility in large-scale preparations (Scheme 1).

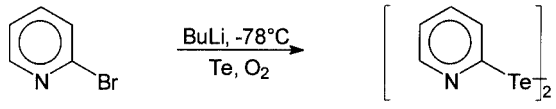

Scheme 1. Preparation of dipyridyl ditellurides at low temperature

[a] Department of Chemistry and Centre of Advanced Studies in Chemistry, Panjab University, Chandigarh-160014, India
[b] Department of Chemistry, University of Munich, Butenandtstrasse 5−13 (D), 81377 Munich, Germany

Owing to the instability of the lithiated pyridine the reaction has to be carried out at low temperature in order to avoid its decomposition. The corresponding pyridylmagnesium halides are comparatively stable even at higher temperatures (>25 °C). However, pyridylmagnesium halides are extremely difficult to generate directly from the corresponding halides and magnesium.[7−10] Meunier et al.[11] have reported a magnesium-halogen exchange reaction that generates pyridylmagnesium halides, although the successful quenching of pyridylmagnesium halides with electrophiles was achieved only recently.[12−14] In continuation of our ongoing project on the chemistry of pyridyltellurium compounds,[15−18] we decided to examine the reactivity of pyridylmagnesium halides for the synthesis of pyridyltellurium derivatives. Colonna et al. have also reported the synthesis of dipyridyl ditelluride in very low yield by employing magnesium-halogen exchange of 2-bromopyridine with ethylmagnesium bromide, although the results were later found to be non-reproducible.[19]

Result and Discussion

We found that elemental tellurium adds smoothly to 2-pyridylmagnesium chloride (**1a**), generated in situ by the bromine-magnesium exchange reaction between 2-bromopyridine and *i*PrMgCl in THF, at room temperature, to afford a species chemically equivalent to 2-pyridyltelluromag-

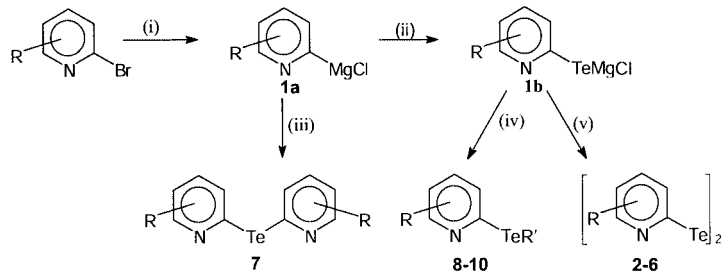

R = H, CH_3 and R' = CH_3, allyl, i-C_3H_7

Scheme 2. Reagents and conditions: (i) *i*PrMgCl (1.2 equiv.), THF, room temp.; (ii) Te, 15 min; (iii) R-Py_2Te_2; (iv) R′X (X = Br, I), (v) H_2O, O_2

nesium chloride (**1b**). Its aerial oxidation gave dipyridyl ditelluride in moderate to excellent yields. Reaction of **1b** with a number of electrophiles gives unsymmetrical 2-alkyltelluropyridines in good yields (Scheme 2).

This protocol was extended to the selective synthesis of various symmetrical 3,3′-dipyridyl and 5,5′-dipyridyl ditellurides. We found that when *i*PrMgCl reacts with 2,5-dibromopyridine, a single bromine-magnesium exchange takes place at C-5 of the pyridine ring, which is attributed to the fact that electrophilic attack at C-5 is more favorable than atC-2. The bromine-magnesium exchange with 2,3,5-tribromopyridine occurs at C-3 due to the *ortho* activating effect of the bromine present at C-2. Further bromine-magnesium exchange was not possible even after the addition of a twofold excess of *i*PrMgCl, as shown in Scheme 3. The present methodology was also successfully extended to a variety of methyl-substituted 2-bromopyridines. The scope and efficiencies are summarized in the Exp. Sect.

As a part of our ongoing study, we also compared the efficiency of the reaction by employing different Grignard reagents, such as ethylmagnesium bromide, *n*-propylmagnesium bromide, isopropylmagnesium chloride and butylmagnesium chloride. The results are given for the formation of bis(2-pyridyl) ditelluride in Table 1. These results show that a more sterically hindered Grignard reagent gives a better yield. This may be attributed to the fact that a more hindered Grignard reagent imparts stability to the pyridylmagnesium halide, thereby increasing the yield.

Table 1. Influence of the different Grignard reagents on the efficiency of the reaction

Grignard reagent	Compound	Solvent	Yield (%)
EtMgBr	Bis(2-pyridyl) ditelluride	THF	5
*i*PrMgCl	Bis(2-pyridyl) ditelluride	THF	80
*n*BuMgCl	Bis(2-pyridyl) ditelluride	THF	70
*n*PrMgBr	Bis(2-pyridyl) ditelluride	THF	27

It is important to note that the use of an equimolar amount of bromopyridine and *i*PrMgCl resulted in a poor yield; however, a slight excess of *i*PrMgCl increased the yield considerably. We must emphasise that the conditions throughout the reaction have to be extremely dry as even traces of moisture can hinder the insertion of tellurium into the species **1a**.

Among the various applications of organotellurium compounds, transmetallation with organolithium or organocuprate reagents[20] is considered to be synthetically important. As a representative example, the transmetallation reaction of isopropyltelluropyridine with *i*PrMgCl was also carried out for C−C bond formation. Subsequent quenching with benzaldehyde in THF at room temperature gave phenyl(2-pyridyl)methanol in 65% yield, indicating a clean tellurium-magnesium exchange as shown in Scheme 4. This exchange is operationally simple and represents a consider-

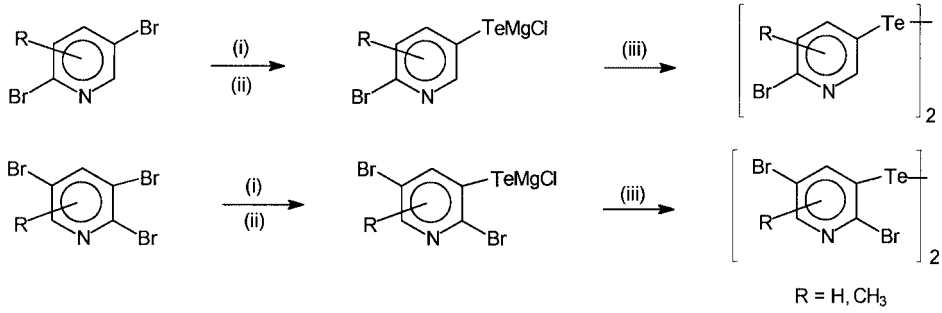

Scheme 3. Reagents and conditions: (i) *i*PrMgCl, THF, room temp., 2 h; (ii) Te, 15 min; (iii) H_2O, O_2

 © 2004 Wiley-VCH Verlag GmbH & Co. KGaA, Weinheim

able improvement over the reported method[21] in terms of the reaction conditions, ease and efficiency of the reaction on a molar scale.

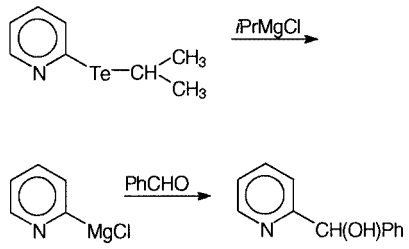

Scheme 4. Transmetalation reaction of isopropyltelluropyridine with *i*PrMgCl

Table 2. Chemical-shift values (δ) of various symmetrical pyridyltellurium derivatives[a]

Compound	^{1}H (CH_3)	^{13}C (CH_3)	^{125}Te
Py_2Te_2	–	–	439
$(3\text{-}CH_3Py)_2Te_2$	2.449	24.679	473
$(4\text{-}CH_3Py)_2Te_2$	2.224	20.741	422
$(5\text{-}CH_3Py)_2Te_2$	2.286	17.807	436
$(3\text{-}CH_3\text{-}5\text{-}Br\text{-}Py)_2Te_2$	2.432	24.484	485
$(5\text{-}Br\text{-}Py)_2Te_2$	–	–	440
$(2,5\text{-}Br_2\text{-}Py)_2Te_2$	–	–	414
$(6\text{-}CH_3\text{-}2,5\text{-}Br_2\text{-}Py)_2Te_2$	2.609	23.881	407

[a] ^{125}Te chemical shift values could not be determined for unsymmetrical pyridyltellurium derivatives due their instability, particularly in solution.

^{125}Te NMR chemical shifts are listed in Table 2 and are found to be sensitive to the nature of the substituents present on the pyridine ring. The chemical shift for $(Br_2PyTe)_2$ is found at the most shielded position (δ = 407 ppm) and that for $(3\text{-}CH_3\text{-}5\text{-}BrPyTe)_2$ is found at the most deshielded position (δ = 485 ppm). For compounds **3** and **4**, in which a methyl group is substituted on the pyridine ring at the *meta* and *para* positions to the tellurium atom, respectively, the observed signals at δ = 422 and 436 ppm, respectively, indicate that the ^{125}Te resonance is influenced by polar effects due to shielding by an electron-donating group[22] i.e. the methyl group. Interestingly, when the methyl group is present *ortho* to tellurium on the ring, deshielding of the ^{125}Te resonance is observed (signals at δ = 473 and 485 ppm for compounds **2** and **7**, respectively). Conformational constraints and through-space interactions between the methyl group and tellurium are suggested as possible reasons for this observation. It is also noted that the ^{125}Te resonances for **8** and **9** are at δ = 407 and 414 ppm, respectively, which is attributed to intramolecular through-space interactions between the bromine and tellurium atoms. These interactions, being intramolecular, are also likely to be found in solution ppm. ^{125}Te NMR spectra of alkylpyridyltellurium compounds could not be recorded, as these compounds are exceedingly unstable in solution.

Solid-State Structures

Molecular Geometry and Crystal Structure of Bis(2-pyridyl) Ditelluride (1)

A single crystal of **1** was obtained by slow evaporation of a solution of **1** in diethyl ether and hexane. The molecular structure of **1** with the atom numbering scheme is given in Figure 1. Selected bond angles and bond lengths are given in Table 3. The molecule crystallizes in the triclinic $P\bar{1}$ space group with unit-cell dimensions a = 6.2870(4) Å, b = 8.4928(7) Å, c = 11.7370(12) Å and α = 109.101°, β = 99.717°, γ = 89.829(6)°. The molecular geometry of the pyridine rings is as expected in terms of bond angles and bond lengths. The two pyridine rings have an average C–C bond length of 1.37 Å and C–C–C bond angle of 119° (slightly distorted). The Te–Te bond length is significantly shorter (2.6759 Å) than the single covalent Te–Te bond length (2.74 Å) on the Pauling scale.[23] The Te(1)–C(1) [2.136(7) Å] and Te(2)–C(6) [2.144(6) Å] distances are also slightly longer than the some of the Pauling single-bond covalent radii for Te–C(sp^2) single bonds (2.11 Å), but are similar to the values found in bis(2-naphthyl) ditelluride[24] [2.135(6), 2.127(5) Å]. The C–E–E–C torsion angles are similar: 87.1° for E = S,[25] 84.3(2)° for E = Se[26] and 86.3(2)° for E = Te.

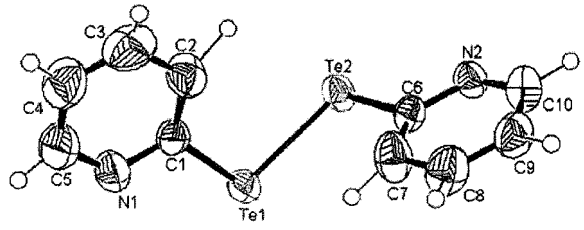

Figure 1. Perspective view of bis(2-pyridyl) ditelluride

Molecular Geometry and Crystal Structure of Bis(2,5-dibromo-3-pyridyl) Ditelluride (8)

Needle-shaped copper-colored crystals of compound **8** were obtained by slow evaporation of a solution in dichloromethane and hexane. The molecular structure of **8** with atom numbering scheme is given in Figure 2 (a). Selected bond angles and bond lengths are given in Table 4. The molecule crystallizes in the monoclinic space group $C2/c$ with cell dimensions a = 12.5073(15) Å, b = 9.4521(11) Å, c = 14.1713(13) Å and α = 90.00°, β = 111.707°, γ = 90.00°. The Te(1)–Te(2) bond length of this ditelluride [2.6830(15) Å] is significantly shorter than the sum of the Pauling single-bond covalent radii but is quite similar to the value found for compound **1**. The Te(1)–C(1) [2.127(13) Å] distance is also quite similar to the single C–Te bond in compound **1**. The Te(1)–N(1) distance (3.421 Å) is much higher than the sum of the covalent radii but is within the van der Waal distance of 3.61 Å[27] and therefore can be

 © 2004 Wiley-VCH Verlag GmbH & Co. KGaA, Weinheim

Table 3. Bond lengths (Å) and angles (°) and torsion angles (°) for bis(2-pyridyl) ditelluride

Te(1)−C(1)	2.14(7)	C(1)−Te(1)−Te(2)	101.2(18)
Te(1)−Te(1)	2.68(6)	C(6)−Te(2)−Te(1)	100.6(17)
Te(2)−C(6)	2.14(6)	C(6)−N(2)−C(10)	116.9(6)
N(1)−C(1)	1.32(9)	N(1)−C(1)−C(2)	123.9(7)
N(1)−C(5)	1.33(11)	N(1)−C(1)−Te(1)	111.5(5)
N(2)−C(6)	1.33(9)	C(2)−C(1)−Te(1)	124.7(5)
N(2)−C(10)	1.37(10)	C(1)−C(2)−C(3)	117.3(8)
C(1)−C(2)	1.37(10)	C(1)−C(2)−H(2)	134.0(5)
C(2)−C(3)	1.40(13)	C(3)−C(2)−H(2)	105.0(5)
C(2)−H(2)	1.20(11)	C(4)−C(3)−C(2)	119.2(9)
C(3)−C(4)	1.34(15)	C(4)−C(3)−H(3)	127.0(5)
C(3)−H(3)	0.82(7)	C(2)−C(3)−H(3)	113.0(5)
C(4)−C(5)	1.38(14)	C(3)−C(4)−C(5)	119.2(9)
C(4)−H(4)	0.62(11)	C(3)−C(4)−H(4)	134.0(10)
C(5)−H(5)	1.06(8)	C(5)−C(4)−H(4)	107.0(10)
C(6)−C(7)	1.32(10)	N(1)−C(5)−C(4)	122.7(9)
C(7)−C(8)	1.37(12)	N(1)−C(5)−H(5)	114.0(5)
C(8)−C(9)	1.36(13)	N(2)−C(6)−C(7)	123.7(7)
C(8)−H(8)	0.97(8)	N(2)−C(6)−Te(2)	113.8(5)
C(9)−C(10)	1.38(12)	C(7)−C(6)−Te(2)	122.4(5)
C(9)−H(9)	0.92(6)	C(6)−C(7)−C(8)	119.0(7)
C(10)−H(10)	0.97(9)	C(6)−C(7)−H(7)	122.0(10)
C(1)−Te(1)−Te(2)−C(6)	86.30(2)	C(5)−N(1)−C(1)−C(2)	−2.0(12)
C(5)−N(1)−C(1)−Te(1)	178.50(8)	Te(2)−Te(1)−C(1)−N(1)	168.4(5)
Te(2)−Te(1)−C(1)−C(2)	−11.00(7)	N(1)−C(1)−C(2)−C(3)	2.0(13)
Te(1)−C(1)−C(2)−C(3)	−178.60(7)	C(1)−C(2)−C(3)−C(4)	−0.3(15)
Te(2)−C(6)−C(7)−C(8)	179.00(7)	C(10)−N(2)−C(6)−C(7)	1.5(11)
C(10)−N(2)−C(6)−Te(2)	178.80(5)	Te(1)−Te(2)−C(6)−N(2)	169.5(4)

Table 4. Bond lengths (Å) and angles (°) and torsion angles (°) for bis(2,5-dibromo-3-pyridyl) ditelluride[a]

Te(1)−C(1)[a]	2.13(13)	C(1)−Te(1)−Te(1)#1	100.1(3)
Te(1)−Te(1)#1	2.68(15)	C(2)−N(1)−C(3)	119.1(10)
Br(1)−C(2)	1.90(12)	C(5)−C(1)−C(2)	117.6(11)
Br(2)−C(4)	1.89(12)	C(5)−C(1)−Te(1)	123.6(8)
N(1)−C(2)	1.31(17)	C(2)−C(1)−Te(1)	118.8(9)
N(1)−C(3)	1.33(18)	N(1)−C(2)−C(1)	124.8(11)
C(1)−C(5)	1.39(16)	N(1)−C(2)−Br(1)	116.7(8)
C(1)−C(2)	1.40(16)	C(1)−C(2)−Br(1)	118.4(9)
C(3)−C(4)	1.39(16)	N(1)−C(3)−C(4)	120.6(11)
C(3)−H(3)	0.93	N(1)−C(3)−H(3)	119.7
C(4)−C(5)	1.42(16)	C(4)−C(3)−H(3)	119.7
C(5)−H(5)	0.93	C(3)−C(4)−Br(2)	119.2(9)
Te(1)#1−Te(1)−C(1)−C(5)	−11.90(9)	Te(1)#1−Te(1)−C(1)−C(2)	169.1(8)
C(3)−N(1)−C(2)−C(1)	0.00(18)	C(3)−N(1)−C(2)−Br(1)	176.9(8)
C(5)−C(1)−C(2)−N(1)	0.80(17)	Te(1)−C(1)−C(2)−N(1)	179.8(9)
Te(1)−C(1)−C(2)−Br(1)	3.00(12)	Te(1)−C(1)−C(5)−C(4)	−179.8(8)

[a] Symmetry transformations used to generate equivalent atoms: #1 $-x + 1, y, -z + 3/2$.

considered as a weak interaction. The Te(1)−Br(1) distance (3.82 Å) is shorter than the sum of the van der Waal radii (4.06 Å). The Br(1)···Br(1) contacts (3.61 Å) are shorter than the Br(1)···Br(2) and Br(2)···Br(2) short contacts (3.948 Å and 3.960 Å, respectively). These observations clearly indicate that the molecules are bridged together by intermolecular secondary interactions. The crystal packing depicting these secondary interactions is shown in Figure 2 (b) and the distances are given in Table 5.

Table 5. Secondary interactions in bis(2,5-dibromo-3-pyridyl) ditelluride

Atoms	Interatomic distances	Symmetry transformations
Te1···Br2	3.821	$x, 1 - y, z - 0.5$
Br1···Br1	3.607	$2x, y, 1.5 - z$
Br1···Br2	3.948	$1.5 - x, 0.5 - y, 2 - z$
Br1···Br2	3.980	$x, 1 - y, z - 0.5$
Br2···Br2	3.960	$1.5 - x, 1.5 - y, 2 - z$

 © 2004 Wiley-VCH Verlag GmbH & Co. KGaA, Weinheim

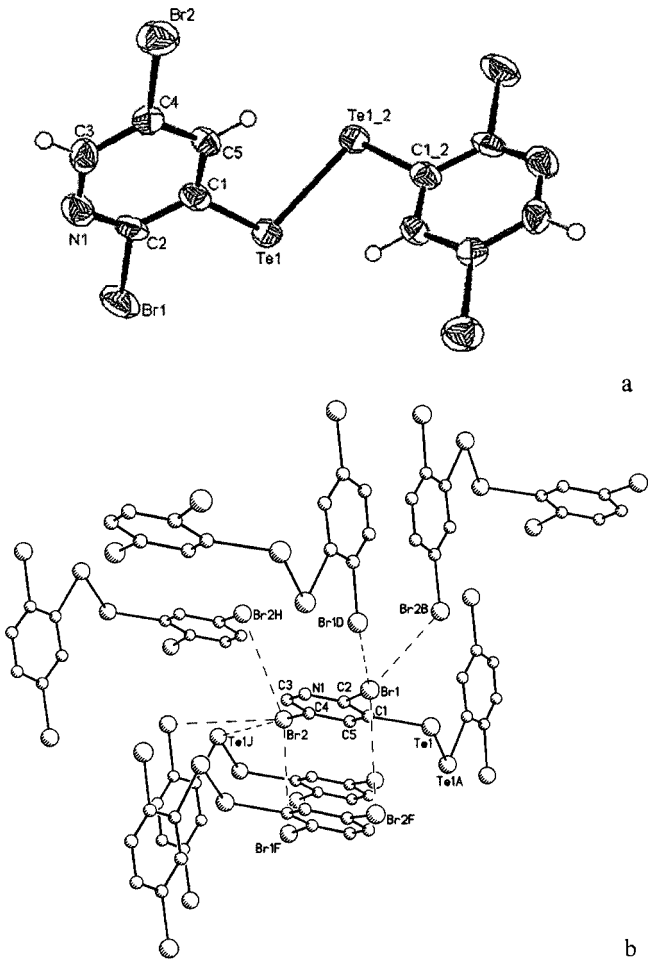

Figure 2. a) Perspective view of bis(2,5-dibromo-3-pyridyl) ditelluride; b) secondary interactions

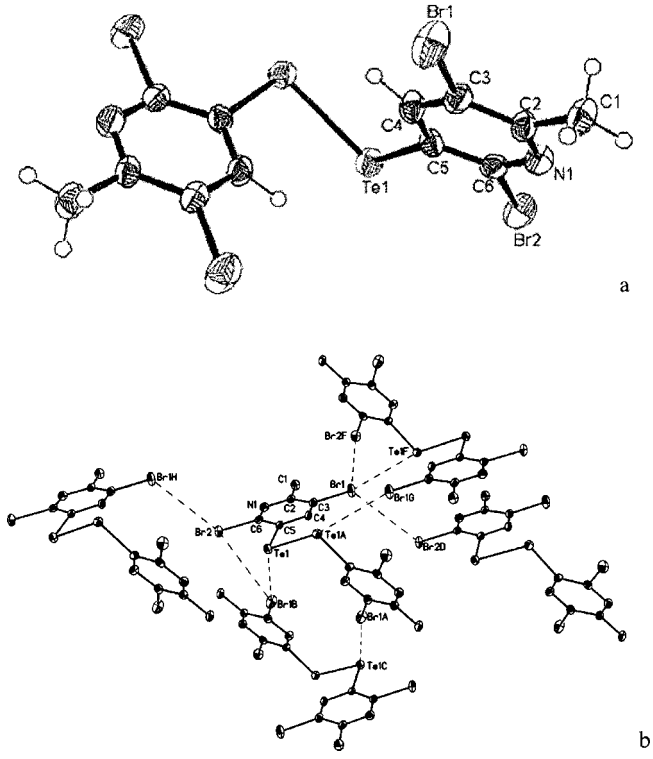

Figure 3. a) Perspective view of bis(2,5-dibromo-6-methyl-3-pyridyl) ditelluride; b) secondary interactions

Molecular Geometry and Crystal Structure of Bis(2,5-dibromo-6-methyl-3-pyridyl) Ditelluride (9)

Deep-red plates of **9** were obtained by slow evaporation of a solution in diethyl ether and hexane. The molecular

Table 6. Bond lengths (Å) and angles (°) and torsion angles (°) for bis(2,5-dibromo-6-methyl-3-pyridyl) ditelluride[a]

Te(1)−C(5)[a]	2.130(8)	C(5)−Te(1)−Te(1)#1	99.5(2)
Te(1)−Te(1)#1	2.69(11)	C(6)−N(1)−C(2)	119.1(7)
Br(1)−C(3)	1.89(9)	C(2)−C(1)−H(1A)	109.5
Br(2)−C(6)	1.91(9)	C(2)−C(1)−H(1B)	109.5
N(1)−C(6)	1.32(12)	H(1A)−C(1)−H(1B)	109.5
N(1)−C(2)	1.34(12)	C(2)−C(1)−H(1C)	109.5
C(1)−C(2)	1.50(12)	H(1A)−C(1)−H(1C)	109.5
C(1)−H(1A)	0.96	H(1B)−C(1)−H(1C)	109.5
C(1)−H(1B)	0.96	N(1)−C(2)−C(3)	119.6(8)
C(1)−H(1C)	0.96	N(1)−C(2)−C(1)	117.4(7)
C(2)−C(3)	1.39(11)	C(3)−C(2)−C(1)	123.0(8)
C(3)−C(4)	1.38(12)	C(4)−C(3)−Br(1)	118.6(6)
C(4)−C(5)	1.39(12)	C(3)−C(4)−H(10)	114.0(6)
C(4)−H(10)	0.98(11)	C(6)−C(5)−C(4)	116.1(8)
C(5)−C(6)	1.38(12)	C(6)−C(5)−Te(1)	121.1(6)
C(6)−N(1)−C(2)−C(3)	−1.10(12)	N(1)−C(2)−C(3)−C(4)	0.1(13)
C(1)−C(2)−C(3)−C(4)	177.50(8)	N(1)−C(2)−C(3)−Br(1)	−179.0(6)
C(3)−C(4)−C(5)−Te(1)	175.40(6)	Te(1)#1−Te(1)−C(5)−C(6)	−163.1(6)
Te(1)#1−Te(1)−C(5)−C(4)	19.60(7)	Te(1)−C(5)−C(6)−N(1)	−176.3(6)
Te(1)−C(5)−C(6)−Br(2)	3.40(9)	C(4)−C(5)−C(6)−Br(2)	−179.1(6)

[a] Symmetry transformations used to generate equivalent atoms: #1 $-x + 1$, y, $-z + 3/2$.

 © 2004 Wiley-VCH Verlag GmbH & Co. KGaA, Weinheim

structure of **9** with atom numbering scheme is given in Figure 3a. Selected bond angles and bond lengths are given in Table 6. The molecule crystallizes in the monoclinic space group *C*2/*c* with cell dimensions a = 13.7342(15) Å, b = 12.1460(6) Å, c = 11.8950(10) Å and α = 90.00°, β = 116.663(8)°, γ = 90.66(8)°. The Te(1)−Te(2) bond length of this ditelluride [2.6847(11) Å] is only slightly longer than in molecule **8**, and the C(1)−Te(1) distance [2.130(8) Å] is also slightly longer than in **8**. The Te(1)−Br(1) distance [3.868 Å] is shorter than the sum of the van der Waal radii (4.06 Å) and therefore can be considered as a weak interaction. The various secondary interactions observed in the molecule are shown in Figure 3b and listed in Table 7.

Table 7. Secondary interactions in bis(2,5-dibromo-6-methyl-3-pyridyl) ditelluride

Atoms	Interatomic distances	Symmetry transformations
Te1···Br1	3.868	$x, -y, 0.5 + z$
Br1···Br2	3.937	$0.5 + x, 0.5 + y, z$
Br1···Br2	4.039	$x, -y, z - 0.5$

Conclusion

We have presented a mild and efficient protocol for hitherto difficult to synthesize pyridyltellurium compounds in moderate to excellent yields using readily available reagents, at room temperature, and studied their application in transmetallation reactions.

Experimental Section

All experiments were carried out under a dry, oxygen-free nitrogen atmosphere. All the reagents and solvents were purified and dried by standard techniques and deoxygenated by bubbling oxygen-free dry nitrogen gas through them prior to use. Infrared spectra were recorded between KBr pellets on a Perkin-Elmer Model 1430 ratio recording spectrometer. ^{1}H and ^{13}C NMR spectra were recorded in $CDCl_3$ using TMS as an internal standard — ^{125}Te NMR spectra are referenced to dimethyl telluride — on a Jeol 300 MHz spectrometer. The mass spectra were obtained on a VG 705 11 250J Mass spectrometer. Carbon, hydrogen and nitrogen were estimated microanalytically on a Perkin- Elmer 2400 CHN elemental analyzer. Bromopyridines were prepared from the corresponding 2-aminopyridines by literature methods.[28,29]

General Method for the Preparation of Symmetrical Dipyridyl Ditellurides: Bromopyridine (20 mmol) was added dropwise to a vigorously stirred mixture of isopropylmagnesium chloride (22 mmol) in THF. After stirring for 2 h at room temperature the mixture was cooled in an ice bath and elemental tellurium (20 mmol) was added. After all the tellurium had dissolved, the stirring was stopped and the reaction was diluted with acidified water. The mixture was then extracted with diethyl ether (4 × 100 mL) and the organic layer was dried over anhydrous sodium sulfate. The solvent was removed on a rotary evaporator and the residue was purified by silica gel column chromatography with hexane/ethyl acetate (5:1) as eluent.

Bis(2-pyridyl) Ditelluride{[(C_5H_4N)Te]$_2$} (1): Yield: 2.8 g (70%). M.p. 48−50 °C. ^{1}H NMR (300 MHz, $CDCl_3$, 25 °C): δ = 6.98 (dt, $^4J_{H,H}$ = 2.0, $^3J_{H,H}$ = 8.0 Hz, 2 H, *m* to N), 7.35 (dt, $^4J_{H,H}$ = 2.0, $^3J_{H,H}$ = 8.0 Hz, 2 H, *p* to N), 7.94 (d, $^3J_{H,H}$ = 8.0 Hz, 2 H, *o* to Te), 8.42 (d, $^3J_{H,H}$ = 8.0 Hz, 2 H, *o* to N) ppm. ^{13}C NMR: δ = 121.57, 131.15, 135.3, 137.0, 149.9 ppm. ^{125}Te NMR: δ = 439 ppm. IR (KBr): $\tilde{\nu}$ = 3060, 2960, 2920, 1565, 1552, 1444, 1105, 1076, 1031, 983, 748, 660, 543, 458 cm^{-1}. $C_{10}H_8N_2Te_2$: calcd. C 29.26, H 1.95, N 6.82; found C 29.16, H 1.91, N 6.85.

Bis(3-methyl-2-pyridyl) Ditelluride {[(3-MeC_5H_3N)Te]$_2$} (2): Yield: 3.5 g (70%). M.p. 120−125 °C. ^{1}H NMR (300 MHz, $CDCl_3$, 25 °C): δ = 2.4 (s, 6 H, CH_3), 7.05 (t, $^3J_{H,H}$ = 8.0 Hz, *m* to N), 7.47 (dd, $^4J_{H,H}$ = 2.3, $^4J_{H,H}$ = 8.0 Hz, 2 H, *p* to N), 8.24 (dd, $^4J_{H,H}$ = 2.3, $^4J_{H,H}$ = 8.0 Hz, 2 H, *o* to N) ppm. ^{13}C NMR: δ = 24.6, 122.46, 135.29, 138.33, 140.6, 148.3 ppm. ^{125}Te NMR: δ = 473 ppm. IR (KBr): $\tilde{\nu}$ = 3060, 2960, 1580, 1540, 1430, 1120, 1090, 1020, 1090, 1020, 840, 780, 660, 540 cm^{-1}. EI-MS: *m*/*z* (%) = 444 (7.33) [M]$^+$, 314 (14.51) [M − Te]$^+$, 183 (76.62) [M − Te_2H]$^+$, 92 (100) [M − CH_3PyTe_2]$^+$. $C_{12}H_{12}N_2Te_2$: calcd. C 32.43, H 2.70, N 6.30; found C 32.60, H 2.42, N 6.18.

Bis(4-methyl-2-pyridyl) Ditelluride {[(4-MeC_5H_3N)Te]$_2$} (3): Yield: 3.2 g (68%). M.p. 92−92 °C. ^{1}H NMR (300 MHz, $CDCl_3$, 25 °C): δ = 2.24 (s, 6 H, CH_3), 6.81 (d, $^3J_{H,H}$ = 4.8 Hz, 2 H, *m* to N), 7.82 (s, 2 H, *o* to Te), 8.25 (d, $^3J_{H,H}$ = 4.8 Hz, 2 H, *o* to N) ppm. ^{13}C NMR: δ = 20.7, 122.86, 131.68, 135.0, 148.27, 149.39 ppm. ^{125}Te NMR: δ = 422 ppm. IR (KBr): $\tilde{\nu}$ = 3025, 2963, 2908, 1573, 1546, 1261, 1097, 1020, 865, 685, 473 cm^{-1}. EI-MS: *m*/*z* (%) = 444 (1.8) [M]$^+$, 314 (41.15) [M − Te]$^+$, 183 (37.5) [M − Te_2]$^+$, 92 (100) [CH_3Py]$^+$. $C_{12}H_{12}N_2Te_2$: calcd. C 32.43, H 2.70, N 6.30; found C 32.74, H 2.13, N 6.92.

Bis(5-methyl-2-pyridyl) Ditelluride {[(5-MeC_5H_3N)Te]$_2$} (4): Yield: 3.5 g (70%). M.p. 110−112 °C. ^{1}H NMR (300 MHz, $CDCl_3$, 25 °C): δ = 2.28 (s, 6 H, CH_3), 7.18 (d, $^3J_{H,H}$ = 4.8 Hz, 2 H, *o* to Te), 7.91 (d, $^3J_{H,H}$ = 4.8 Hz, 2 H, *p* to N), 8.27 (s, 2 H, *o* to N) ppm. ^{13}C NMR: δ = 17.8, 131.0, 131.4, 134.9, 137.8, 150.2 ppm. ^{125}Te NMR: δ = 436 ppm. IR (KBr): $\tilde{\nu}$ = 3033, 2969, 2917, 1582, 1544, 1526, 1368, 1272, 1073, 983, 835, 694, 520 cm^{-1}. EI-MS: *m*/*z* (%) = 444 (8.2) [M]$^+$, 314 (12.1) [M − Te]$^+$, 183 (67.3) [M − Te_2H]$^+$, 92 (100) [M − CH_3PyTe_2]$^+$. $C_{12}H_{12}N_2Te_2$: calcd. C 32.43, H 2.70, N 6.30; found C 32.83, H 2.12, N 6.19.

Bis(6-methyl-2-pyridyl) Ditelluride {[(6-MeC_5H_3N)Te]$_2$} (5): Yield: 3.2 g (68%). M.p. 55−56 °C. ^{1}H NMR (300 MHz, $CDCl_3$, 25 °C): δ = 2.48 (s, 6 H, CH_3), 6.63 (d, $^3J_{H,H}$ = 7.6 Hz, 2 H, *m* to N), 7.19 (t, $^3J_{H,H}$ = 7.6 Hz, 2 H, *p* to N), 7.63 (d, $^3J_{H,H}$ = 7.6 Hz, 2 H, *o* to Te) ppm. ^{13}C NMR: δ = 24.1, 121.1, 127.9, 134.6, 156.6, 156.6 ppm. IR (KBr): $\tilde{\nu}$ = 3033, 2969, 2917, 1582, 1544, 1526, 1368, 1272, 1073, 983, 835, 694, 520 cm^{-1}. EI-MS: *m*/*z* (%) = 444 (5.5) [M]$^+$, 314 (5.5) [M − Te]$^+$, 183 (30.9) [M − Te_2H]$^+$, 92 (100) [M − CH_3PyTe_2]$^+$. $C_{12}H_{12}N_2Te_2$: calcd. C 32.43, H 2.70, N 6.30; found C 32.21, H 2.52, N 6.18.

Bis(2-bromo-5-pyridyl) Ditelluride {[(2-Br-5-C_5H_3N)Te]$_2$} (6): Yield: 3.53 g (62%). M.p. 180 °C (dec.). ^{1}H NMR (300 MHz, $CDCl_3$, 25 °C): δ = 8.63 (d, $^4J_{H,H}$ = 2.0 Hz, 2 H, *m* to N), 7.86 (dd, $^4J_{H,H}$ = 2.0, $^3J_{H,H}$ = 8.0 Hz, 2 H, *p* to N), 7.34 (d, $^4J_{H,H}$ = 8.0 Hz, 2 H, *o* to N) ppm. ^{13}C NMR: δ = 103.6, 129.2, 143.0, 148.0, 157.7 ppm. ^{125}Te NMR: δ = 440 ppm. EI-MS: *m*/*z* (%) = 574 (40.4) [M(^{130}Te)]$^+$, 442 (12.8) [($BrPy)_2$Te]$^+$, 286 (61.7) [BrPyTeH]$^+$, 78 (100) [PyH]$^+$. $C_{10}H_6Br_2N_2Te_2$: calcd. C 21.12, H 1.05, N 4.92; found C 21.20, H 1.00, N 4.85.

Bis(2-bromo-3-methyl-5-pyridyl) Ditelluride {[(2-Br-3-Me-5-C_5H_2N)Te]$_2$} (7): Yield: 3.0 g (60%). M.p. 110−112 °C. ^{1}H NMR

 © 2004 Wiley-VCH Verlag GmbH & Co. KGaA, Weinheim

(300 MHz, $CDCl_3$, 25 °C): δ = 2.43 (s, 2 H, CH_3), 7.46 (d, $^4J_{H,H}$ = 2.0 Hz, 2 H, *p* to N), 8.31 (d, $^4J_{H,H}$ = 2.0 Hz, 2 H, *o* to N) ppm. ^{13}C NMR: δ = 24.4, 120.5, 137.6, 137.9, 139.6, 149.1 ppm. ^{125}Te NMR: δ = 485 ppm. EI-MS: *m*/*z* (%) = 602 (43.8) [M (^{130}Te)]$^+$, 570 (5.1) [(BrPyTe)$_2$]$^+$, 457 (15.2) [(CH_3BrPy)$_2$Te]$^+$, 444 (4.8) [CH_3PyTe]$_2^+$, 299 (20.5) [CH_3BrPyTeH]$^+$, 78 (100) [PyH]$^+$. $C_{12}H_{10}Br_2N_2Te_2$: calcd. C 24.08, H 2.00, N 4.68; found C 24.21, H 1.94, N 4.63.

Bis(2,5-dibromo-3-pyridyl) Ditelluride{[(2,5-Br$_2$-3-C$_5$H$_2$N)Te]$_2$} (8): Yield: 4.32 g (60%). M.p. 185 °C. ^1H NMR (300 MHz, $CDCl_3$, 25 °C): δ = 8.05 (d, $J_{H,H}$ = 2.0 Hz, 2 H, p to N), 8.21 (d, $J_{H,H}$ = 2.0 Hz, 2 H, o to N) ppm. ^{13}C NMR: δ = 113.0, 122.3, 143.6, 148.2, 150.3 ppm. ^{125}Te NMR: δ = 414 ppm. EI-MS: *m*/*z* (%) = 600 (27.5) [(Br$_2$Py)$_2$Te]$^+$, 520 (3.1) [BrPyTeBr$_2$PyH]$^+$, 440 (21.6) [(BrPy)$_2$TeH]$^+$, 366 (100) [Br$_2$PyTeH]$^+$. $C_{10}H_4Br_4N_2Te_2$: calcd. C 16.52, H 0.55, N 3.85; found C 16.38, H 0.51, N 3.79.

Bis(2,5-dibromo-6-methyl-3-pyridyl) Ditelluride {[(2,5-Br$_2$-6-Me-3-C$_5$HN)Te]$_2$} (9): Yield: 3.6 g (55%). M.p. 85−88 °C. ^1H NMR (300 MHz, $CDCl_3$, 25 °C): δ = 2.58 (s, 6 H, CH_3), 7.48 (s, 2 H, p to N) ppm. ^{13}C NMR: δ = 22.7, 120.1, 136.3, 138.8, 142.3, 150.3 ppm. ^{125}Te NMR: δ = 407 ppm. EI-MS: *m*/*z* (%) = 630 (12.2) [(CH_3Br_2Py)$_2$TeH]$^+$, 600 (1.0) [Br$_2$PyTe]$^+$, 444 (3.8) [CH_3PyTe]$_2^+$, 380 (41.9) [CH_3Br_2PyTeH]$^+$, 207 (26.0) [PyTeH$^+$], 78 (100) [PyH]$^+$. $C_{12}H_8Br_4N_2Te_2$: calcd. C 19.09, H 1.06, N 3.71; found C 18.95, H 1.09, N 3.78.

General Method for the Preparation of Unsymmetrical Pyridyl Tellurides and Dipyridyl Monotellurides: A solution of bromopyridine (20 mmol) in THF (20 mL) was treated with *i*PrMgCl (22 mmol) at room temperature. After two hours of stirring elemental tellurium (20 mmol) was added in parts. When all the tellurium had dissolved, the mixture was cooled in an ice bath and an equivalent amount of alkyl halide/bromopyridine was added. The reaction was monitored by TLC. When the spot corresponding to ditelluride had disappeared, the reaction mixture was washed with distilled water and extracted with dichloromethane. The product was purified by column chromatography using 1% ethyl acetate in hexane as eluent.

Bis(4-methyl-2-pyridyl) Telluride [(4-MeC$_5$H$_3$N)$_2$Te] (10): Viscous liquid. Yield: 40%. ^1H NMR (300 MHz, $CDCl_3$, 25 °C): δ = 2.27 (s, 6 H, CH_3), 6.92 (d, $^3J_{H,H}$ = 4.8 Hz, 2 H, *m* to N), 7.56 (s, 2 H, *o* to Te), 8.35 (d, $^3J_{H,H}$ = 4.8 Hz, 2 H, *o* to N) ppm. ^{13}C NMR: δ = 20.85, 124.05, 132.06, 135.70, 148.17, 150.23 ppm. ^{125}Te NMR: δ = 378 ppm. EI-MS: *m*/*z* (%) = 314 (51.1) [M − Te]$^+$, 183 (43.5) [M − Te$_2$]$^+$, 92 (100) [CH_3Py]$^+$. IR (KBr): $\tilde{\nu}$ = 3023, 2969, 2917, 1654, 1582, 1544, 1451, 1261, 1368, 694, 520, 473 cm^{-1}. $C_{12}H_{12}N_2Te$: calcd. C 46.21, H 3.85, N 8.98; found C 46.13, H 3.71, N 8.7.

(3-Methyl-2-telluropryridyl)methane [(3-MeC$_5$H$_3$N)TeCH$_3$] (11): Viscous liquid. Yield: 1.39 g (60%). ^1H NMR (300 MHz, $CDCl_3$, 25 °C): δ = 2.31 (s, 3 H, py CH_3), 2.15 (s, 3 H,CH_3), 6.93 (dd, $J_{H,H}$ = 4.6 Hz, 7.2 Hz, 1 H, *m* to N), 7.10 (d, $J_{H,H}$ = 7.2 Hz, 1 H, *p* to N), 8.31 (d, $J_{H,H}$ = 4.6 Hz, 1 H, *o* to N) ppm. ^{13}C NMR: δ = 153.08, 133.48, 121.72, 136.65, 147.69, 20.53, 10.52 ppm. EI-MS: *m*/*z* (%) = 237 (2.3) [CH_3PyTeCH$_3$]$^+$, 222 (4.8) [CH_3PyTeH]$^+$, 145 (21.3) [CH_3TeH]$^+$, 107 (53.7) [CH_3PyCH_2]$^+$, 92 [(100.0) CH_3Py]$^+$, 78 (71.0) [PyH]$^+$. C_7H_9NTe: calcd. C 36.20, H 3.87, N 6.03; found C 35.88, H 3.45, N 5.93.

2-(3-Methyl-2-telluropyridyl)-2-methylethane [(3-MeC$_5$H$_3$N)-TeCH(CH$_3$)$_2$] (12): Viscous liquid. Yield: 1.56 g (60%). ^1H NMR

Table 8. Crystal and structure refinement data for **1**, **8** and **9**

	1	**8**	**9**
Empirical formula	$C_{10}H_8N_2Te_2$	$C_{10}H_4Br_4N_2Te_2$	$C_6H_4Br_2NTe$
Molecular mass	411.38	726.99	377.52
Crystal system, space group	triclinic, P$\bar{1}$	monoclinic, *C*2/*c*	monoclinic, *C*2/*c*
a (Å)	6.2870(4)	12.5073(15)	13.7340(15)
b (Å)	8.4920(7)	9.4521(11)	12.1460(6)
c (Å)	11.7370(12)	14.1713(15)	11.8950(10)
α (°)	109.101(8)	90.000	90.000(6)
β (°)	99.717(7)	111.707(10)	116.663(8)
γ (°)	89.829(6)	90.000	90.000(6)
V (A^3)	582.71(9)	1556.5(3)	1773.2(3)
Z, $D_{calcd.}$ (Mg/m^3)	2, 2.345	4, 3.102	8, 2.828
Absorption coefficient (mm^{-1})	4.970	14.000	12.294
F(000)	372	1288	1352
Crystal size (mm)	0.35 × 0.30 × 0.25	0.40 × 0.25 × 0.25	0.25 × 0.25 × 0.225
θ range for data collection (°)	1.86 to 24.93	2.78 to 24.97	2.35 to 24.92
Index ranges	$0 \le h \le 7$ $-9 \le k \le 10$ $-13 \le l \le 13$	$-14 \le h \le 0$ $-11 \le k \le 0$ $-15 \le l \le 16$	$0 \le h \le 16$ $0 \le k \le 14$ $-14 \le l \le 12$
Reflections collected/unique	1980/1980 [*R*(int.) = 0.0000]	1431/1365 [*R*(int.) = 0.1066]	1471/1471 [*R*(int.) = 0.0000]
Completeness to 2θ (%)	96.7	46.8	44.8
Absorption correction	Psi-scan	Psi-scan	Psi-scan
Max./min. transmission	1.000/0.907	1.000/0.863	1.000/0.895
Refinement method	Full-matrix least-squares on F^2		
Data/restraints/parameters	1980/0/159	1365/0/83	1471/0/96
Goodness-of-fit on F^2	1.192	1.084	1.097
Final *R* indices [$I > 2\sigma(I)$]	*R*1 = 0.0353, ωR2 = 0.1015	*R*1 = 0.0567, ωR2 = 0.1617	*R*1 = 0.0551, ωR2 = 0.1409
R indices (all data)	*R*1 = 0.0361, ωR2 = 0.1021	*R*1 = 0.0670, ωR2 = 0.1692	*R*1 = 0.0586, ωR2 = 0.1453
Largest diff. peak and hole (e·Å^{-3})	1.213 and −1.403	1.664 and −2.908	2.904 and −1.276

 © 2004 Wiley-VCH Verlag GmbH & Co. KGaA, Weinheim

(300 MHz, $CDCl_3$, 25 °C): δ = 1.58 (d, $J_{H,H}$ = 15.5 Hz, 6 H, $2CH_3$), 2.15 (s, 3 H, $pyCH_3$), 3.70 (m, $J_{H,H}$ = 15.5 Hz, 1 H, CH), 6.93 (dd, $J_{H,H}$ = 4.6 Hz, 7.2 Hz, 1 H, *m* to N), 7.10 (d, $J_{H,H}$ = 7.2 Hz, 1 H, *p* to N), 8.31 (d, $J_{H,H}$ = 4.6 Hz, 1 H, *o* to N) ppm. ^{13}C NMR: δ = 17.58, 26.63, 20.53, 153.08, 133.48, 121.72, 136.65, 147.69 ppm. EI-MS: *m/z* (%) = 265 (18.7) $[CH_3PyTeC_3H_7]^+$, 222 (55.3) $[CH_3PyTeH]^+$, 174 (11.5) $[C_3H_7TeH]^+$, 92 (100.0) $[CH_3Py]^+$, 78 (48.8) $[PyH]^+$. $C_9H_{13}NTe$: calcd. C 41.53, H 5.00, N 5.38; found C 41.05, H 4.89, N 5.04.

2-(3-Methyl-2-telluropyridyl)-1-propene [(3-MeC_5H_3N)Te(CH_2-CH=CH_2)] (13): Viscous liquid. Yield: 1.47 g (57%). ^1H NMR (300 MHz, $CDCl_3$, 25 °C): δ = 2.19 (s, 3 H, CH_3), 3.94 (d, $J_{H,H}$ = 7.8 Hz, 2 H, $TeCH_2$), 4.29 (d, $J_{H,H}$ = 9.9 Hz, 1 H, $=CH_2$), 5.07 (d, $J_{H,H}$ = 9.9 Hz, 1 H, $=CH_2$), 6.07(m, $J_{H,H}$ = 8.0, 1.7, 7.6 Hz, 1 H, CH), 6.93 (dd, $J_{H,H}$ = 4.6 Hz, 7.2 Hz, 1 H, *m* to N), 7.10 (d, $J_{H,H}$ = 7.2 Hz, 1 H, *p* to N), 8.31 (d, $J_{H,H}$ = 4.6 Hz, 1 H, *o* to N) ppm. ^{13}C NMR: δ = 12.28, 21.44, 136.71, 114.66, 120.30, 134.96, 137.01, 147.48, 148.13 ppm. EI-MS: *m/z* (%) = 263 (1.8) $[(CH_3PyTeC_3H_5]^+$, 237 (4.7) $[(CH_3PyTeCH_3]^+$, 222 (15.2) $[CH_3PyTeH]^+$, 171 (14.2) $[C_3H_5TeH]^+$, 92 (100.0) $[CH_3Py]^+$, 78 (53.0) $[PyH]^+$. IR (KBr): $\tilde{\nu}$ = 3067, 3043, 2977, 2929, 1662, 1571, 1451, 1346, 1277, 1148, 698, 539, 467 cm^{-1}. $C_9H_{11}NTe$: calcd. C 41.22, H 4.20, N 5.34; found C 40.17, H 4.16, N 5.39.

Crystal Structure Determination and Refinement: A crystal of **1**, **8** or **9** were mounted on an Enraf−Nonius CAD-4 diffractometer in Lindeman glass capillaries at 293(2) K. Final cell dimensions and reflection intensities were measured with graphite-monochromated Mo-K_α radiation in the ω-2θ scan mode. Anisotropic thermal parameters were used for heavier atoms Te and Br only. Carbon atoms were refined isotropically and hydrogen atoms were placed in calculated positions riding their respective bonded atoms. All other relevant information about the data collection and the refinement id presented in Table 8. The crystal structure was solved by direct methods and refined on F^2 using SHELX-97.[30]
CCDC-225524 (for **1**), -229371 (for **8**) and -220146 (for **9**) contain the supplementary crystallographic data for this paper. These data can be obtained free of charge at www.ccdc.cam.ac.uk/conts/retrieving.html [or from the Cambridge Crystallographic Data Centre, 12 Union Road, Cambridge CB2 1EZ, UK; Fax: (internat.) + 44-1223-336-033; E-mail: deposit@ccdc.cam.ac.uk].

Acknowledgments

K. K. B. would like to thank the Department of Science and Technology, New Delhi, for financial assistance (grant no. DST SR/ SI/ IC-02/2003). We are also indebted to Prof. P. Mathur, Head of the X-ray Diffraction facility, IIT Mumbai for X-ray diffraction studies of the crystals and Prof. Ray Butcher (Harvard University, USA) for valuable discussions on secondary interactions and Dr. B. Krumm (LMU, Germany) for ^{125}Te NMR. K. K. B. is also thankful to the German Academic Exchange Service (DAAD) for a study and research visit to the Federal Republic of Germany.

[1] N. Petragnani, *Tellurium in Organic Synthesis*; Academic Press, New York, **1994**.
[2] J. V. Comasseto, R. E Barrientos-Astigarraga, *Aldrichimica Acta* **2000**, *66*, 33.
[3] H. Miyazoe, S. Yamago, J. Yoshida, *Angew. Chem. Int. Ed.* **2000**, *39*, 3669−71.
[4] T. Hiiro, N. Kambe, A. Ogawa, N. Miyoshi, S. Murai, N. Sonada, *Angew. Chem. Int. Ed. Engl.* **1987**, *26*, 1187−82.
[5] K. K. Bhasin, B. S. Bhandal, J. Singh, N. Singh, K. N. Singh, P. Singh, *Synth. Commun.* **2002**, *9*, 1319−25.
[6] L. Engman, M. P. Cava, *Organometallics.* **1982**, *1*, 470−75.
[7] J. Overhoff, W. Proost, *Recl. Trav. Chim.* **1938**, *57*, 179−84.
[8] W. Proost, J. P. Wilbaut, *Recl. Trav. Chim.* **1940**, *59*, 971−75.
[9] Y.-H. Lai, *Synthesis* **1981**, 585.
[10] M. Nakane, C. R. Hutchinson, *J. Org. Chem.* **1978**, *43*, 3922.
[11] G. J. Martin, B. Mechin, Y. Leroux, C. L. Paulmier, J. C. Meunier, *J. Organomet. Chem.* **1974**, *67*, 327−339.
[12] F. Trecourt, G. Breton, V. Bonnet, F. Mongin, F. Marsais, G. Queguiner, *Tetrahedron Lett.* **1999**, *40*, 4339−4343.
[13] M. Abarbri, J. Thibonnet, L. Berillon, F. Dehmel, M. Rottlander, P. Knochel, *J. Org. Chem.* **2000**, *65*, 4618−4634.
[14] A. Lepretre, A. Turck, N. Ple, P. Knochel, G. Queguiner, *Tetrahedron* **2000**, *56,* 265−271.
[15] S. Dey, V. K. Jain, J. Singh, V. Trehan, K. K. Bhasin, B. Varghese, *Eur. J. Inorg. Chem.* **2003,** 744−750.
[16] K. K. Bhasin, V. K. Jain, H. Kumar, S. Sharma, S. K. Mehta, J. Singh, *Synth. Commun.* **2003**, *33*, 977.
[17] K. K. Bhasin, P. Venugopalan, J. Singh, *Phosphorous Sulfur Silicon* **2002**, *177*, 2579.
[18] K. K. Bhasin, J. Singh, K. N. Singh, *Phosphorous Sulfur Silicon* **2002**, *177*, 597.
[19] F. P. Colonna, G. Distefano, V. Galasso, K. Irgolic, G. C. Pappalarado, L. Pope, *J. Chem. Soc., Perkin Trans. 2* **1981**, 281−285.
[20] T. Hiiro, Y. Morita, T. Inoue, N. Kambe, A. Ogawa, I. Ryu, N. Sonoda, *J. Am. Chem. Soc.* **1990**, *112*, 455−457.
[21] Y. Kondo, M. Shilai, M. Uchiyama, T. Sakamoto, *J. Chem. Soc., Perkin Trans. 1* **1996**, 1781−1782.
[22] N. P. Luthra, A. M. Boccanfuso, R. B. Dunlap, J. D. Odom, *J. Organomet. Chem.* **1988**, *354*, 51−62.
[23] L. Pauling, *The Nature of the Chemical Bond*, 3rd edition, Cornell University Press, Ithaca, NY, **1960**.
[24] S. C. Menon, H. B. Singh, J. M. Jasinki, J. P. Jasinki, R. J. Butcher, *Organometallics* **1996**, *15*, 707−1712.
[25] N. V. Raghvan, K. Seff, *Acta Crystallogr., Sect. B* **1977**, *33*, 386−388.
[26] C. O. Kienitz, C. Thone, P. G. Jones, *Inorg. Chem.* **1996**, *35*, 3990−3997.
[27] A. Bondi, *J. Phys. Chem.* **1964**, *68*, 441.
[28] V. Canibeno, J. F. Rodriguez, M. Santos, M. A. S. Tejedor, M. C. Carreno, C. Gonzalez, J. L. G. Ruano, *Synthesis* **2001**, *10*, 2175−2178.
[29] L. C. Craig, *J. Am. Chem. Soc.* **1934**, *56*, 231−233.
[30] G. M. Sheldrick, *SHELX-97, Program for the solution and refinement of crystal structures*, University of Göttingen, Göttingen, Germany.

Received April 13, 2004
Early View Article
Published Online November 10, 2004

 © 2004 Wiley-VCH Verlag GmbH & Co. KGaA, Weinheim

Manganese(II) Complexes Coordinated by a New Derivative of Bipyridine: 9′-[4,5-Bis(methylthio)-1,3-dithiol-2-ylidene]-4′,5′-diazafluorene

Qin-Yu Zhu ,[a] Jie Dai,*[a−c] Ding-Xian Jia,[a] Li-Hui Cao,[a] and Hai-Hong Lin[a]

Keywords: Diazafluorene / Manganese(II) complex / Crystal structure / Catalysis

Manganese(II) complexes with the ligand 9′-[4,5-bis(methylthio)-1,3-dithiol-2-ylidene]-4′,5′-diazafluorene (L) have been synthesized, and the single-crystal structures of complexes $[Mn(L)_2(H_2O)_2](ClO_4)_2·(L)_2·2C_2H_5OH·2CH_3CN$ (**1**), $[Mn(L)_2Cl_2]·1.5CH_2Cl_2$ (**2**) and $[Mn(L)_2(NO_3)_2]$ (**3**) have been characterized. Complex **1** is *trans*-coordinated with N···H–O and S···S contacts, while the other two complexes are *cis*-coordinated with short π···π stacking. Solvent-free powder samples were also obtained and these complexes showed catalytic activity in the decomposition of H_2O_2 in the presence of added imidazole; the perchlorate compound was the most effective.
(© Wiley-VCH Verlag GmbH & Co. KGaA, 69451 Weinheim, Germany, 2004)

Introduction

Recent decades have seen considerable interest in the design and synthesis of manganese complexes because of their potential use as magnetic materials[1] and catalysts, such as for the disproportionation of hydrogen peroxide.[2] The role of manganese ions in biological systems has been increasingly recognized,[3] e.g. in manganese superoxide dismutase (MnSOD).[4] 1,10-Phenanthroline, bipyridine and their derivatives are well-known excellent N ligands used in manganese model compounds for biological simulations.[5] Consequently, we became interested in ligands of 9′-(4,5-disubstituted-1,3-dithiol-2-ylidene)-4′,5′-diazafluorenes (L),[6] which include a bipyridine moiety and have a similar structure to 1,10-phenanthroline. These ligands also have a conjugated dithiole moiety that influences the relative energy levels of orbitals compared with those of 1,10-phenanthroline and bipyridine. In this paper, we present the synthesis, crystal structures and catalytic properties of a series of Mn^{II} complexes with this type of ligands, $[Mn(L)_2(H_2O)_2](ClO_4)_2$, $[Mn(L)_2Cl_2]$ and $[Mn(L)_2(NO_3)_2]$. Manganese complexes with such ligands are expected to be a new molecular system.

[a] Department of Chemistry, Suzhou University,
Suzhou 215006, P. R. China
P. O. Box 174, 1 Shizi Street, Suzhou 215006, P. R. China
E-mail: daijie@suda.edu.cn
[b] State Key Laboratory of Coordination Chemistry, Nanjing University,
Nanjing 210093, P. R. China
[c] Laboratory of Organic Solids, Center for Molecular Sciences, Institute of Chemistry, Chinese Academy of Sciences,
Beijing 100080, P. R.China

Results and Discussion

Structural Descriptions

$[Mn(L)_2(H_2O)_2](ClO_4)_2·2L·2C_2H_5OH·2CH_3CN$ (1)

In the crystal structure of compound **1** (see a in Figure 1) the manganese atom is symmetrically chelated by four nitrogen atoms from two ligands L, forming a quasi-planar structure that includes the manganese(II) ion with a mean deviation of 0.1119 Å. Perpendicular to the plane are two coordinated water molecules at *trans*-axial positions. Mn(1)−N(1) and Mn(1)−N(2) distances are 2.321 and 2.283 Å, respectively, and in the perpendicular position the Mn(1)−O(1) distance is 2.171 Å, forming an axial-pressed octahedral geometry. Table 1 lists selected bond lengths, angles and interaction distances for **1**−**3** (shorter than the sum of van der Waals radii).

Compound **1** crystallizes in the triclinic space group with co-crystallized free ligand and solvents. Complex molecules form one layer and two free ligands form another layer (see b in Figure 1). These parallel layers are alternately arranged and are linked with N···H−O hydrogen bonds (2.700 Å) and an S···S contact (3.526 Å). These blocks are further linked to a 1D column structure along the *a* axis by hydrogen bonds between coordinated water molecules and the solvent molecules. There are also short S···S interactions (3.311 Å) between the columns.

$[Mn(L^1)_2Cl_2]·1.5CH_2Cl_2$ (2)

Figure 2 (a) shows the X-ray crystal structure of the compound **2**. The complex crystallizes in a monoclinic system with eight complex molecules and 12 dichloromethane molecules in a unit cell. In the crystal structure of **2**, the Mn

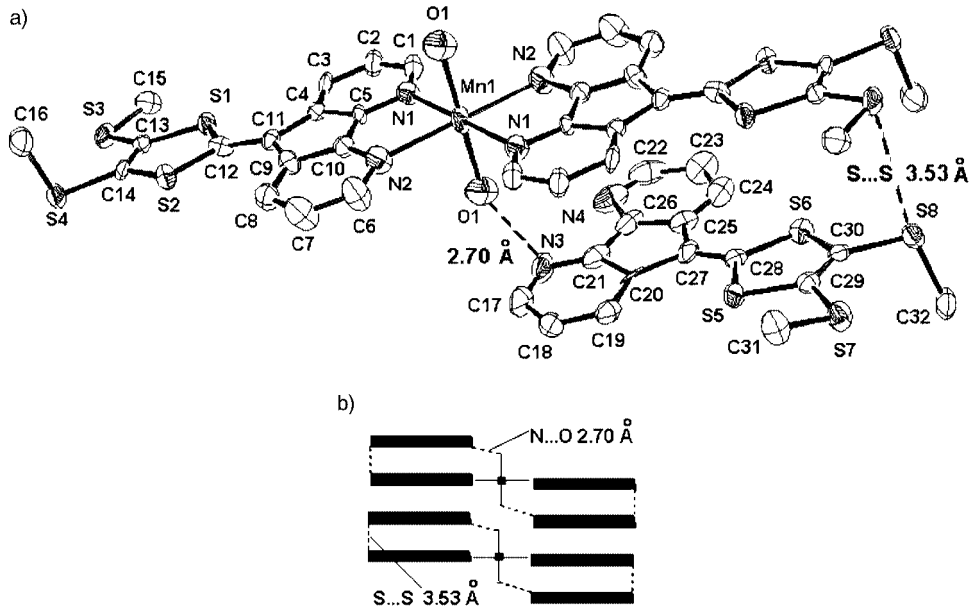

Figure 1. (a) ORTEP view of **1** showing the atom labels; solvents omitted for clarity; (b) schematic view of the layered arrangement of the complex and the co-crystallized free ligand; broken lines show intermolecular interactions

Table 1. Selected bond lengths [Å], angles [°] and interaction distances for **1** − **3**; i: 1 − *x*, −*y*, 1 − *z*; ii: 1 − *x*, −*y*, −*z*; iii: 1/2 − *x*, 1/2 + *y*, 1/2 − *z*; iv: 1/2 + *x*, −*y*, *z*; v: −*x*, 1 − *y*, *z*

1		**2**		**3**	
Mn(1)−O(1)	2.171(9)	Mn(1)−Cl(1)	2.458(2)	Mn(1)−O(1)	2.113(5)
Mn(1)−N(1)	2.32(1)	Mn(1)−Cl(2)	2.425(2)	Mn(1)−O(4)	2.118(3)
Mn(1)−N(2)	2.282(9)	Mn(1)−N(1)	2.304(5)	Mn(1)−N(1)	2.333(3)
O(1)−Mn(1)−N(1)	93.23	Mn(1)−N(2)	2.422(6)	Mn(1)−N(2)	2.322(3)
O(1)−Mn(1)−N(1′)	86.77	Mn(1)−N(3)	2.431(6)	Mn(1)−N(3)	2.310(4)
O(1)−Mn(1)−N(2)	90.36	Mn(1)−N(4)	2.299(6)	Mn(1)−N(4)	2.340(3)
O(1)−Mn(1)−N(2′)	89.64	Cl(1)−Mn(1)−Cl(2)	99.34(8)	O(1)−Mn(1)−O(4)	84.2(2)
N(1)−Mn(1)−N(2)	78.93	N(1)−Mn(1)−N(2)	75.98	N(1)−Mn(1)−N(2)	78.01
		N(3)−Mn(1)−N(4)	76.50	N(3)−Mn(1)−N(4)	77.69
S(3)···S(8)^{i}	3.526(5)	C(17)···C(7)^{iii}	3.37(1)	C(27)···C(23)^{iv}	3.390(5)
S(7)···S(7)^{ii}	3.311(5)	C(18)···C(6)^{iii}	3.28(1)	C(2)···C(11)^{v}	3.371(7)
O(1)···N(3)	2.70(1)	C(20)···C(8)^{iii}	3.38(1)		
		C(21)···C(8)^{iii}	3.354(9)		

atom also exhibits a six-coordinate environment that consists of the four nitrogen atoms from the two ligands and two *cis* chloride ions, but the geometry is distorted far from formal octahedral. The mean deviation from the plane of the two ligands is 0.0720 and 0.1478 Å, respectively. The dihedral angle between the least-squares planes of the two ligands is 92.671°.

Mn(1)−Cl(1), 2.458 Å, and Mn(1)−Cl(2), 2.425 Å, bond lengths are similar to those of $[Mn(phen)_2Cl_2]$,[5c] a (dichloro)Mn^{II} complex showing a coordination environment resembling that of **2**. The bonds of Mn(1)−N(3) (2.431 Å) and Mn(1)−N(2) (2.420 Å) *trans* to Cl(1) and Cl(2), are longer than those of Mn(1)−N(1) (2.304 Å) and Mn(1)−N(4) (2.298 Å). This suggests that the axes Cl(1)−Mn(1)−N(3) and Cl(2)−Mn(1)−N(2) are elongated and the octahedral geometry is distorted. There is short π···π stacking between the conjugated ligands (in the range of about 3.3−3.5 Å, Table 1). These interactions and the coordination bonds result in 1D zigzag chains along the *b* axis (Figure 2, b).

$[Mn(L^1)_2(NO_3)_2]$ (3)

Figure 3 (a) shows the X-ray crystal structure of **3**. The complex crystallizes as a monoclinic system with two complex molecules in a unit cell. In the crystal structure of **3**, the coordination environment around the manganese(II) center is a distorted octahedral coordination geometry, like that of **2**. The Mn^{II} ion is coordinated by four nitrogen atoms from two chelating ligands and the two *cis*-oxygen atoms from two nitrate anions. The mean deviation from the plane of the two ligands is 0.0563 and 0.0590 Å, respec-

 © 2004 Wiley-VCH Verlag GmbH & Co. KGaA, Weinheim

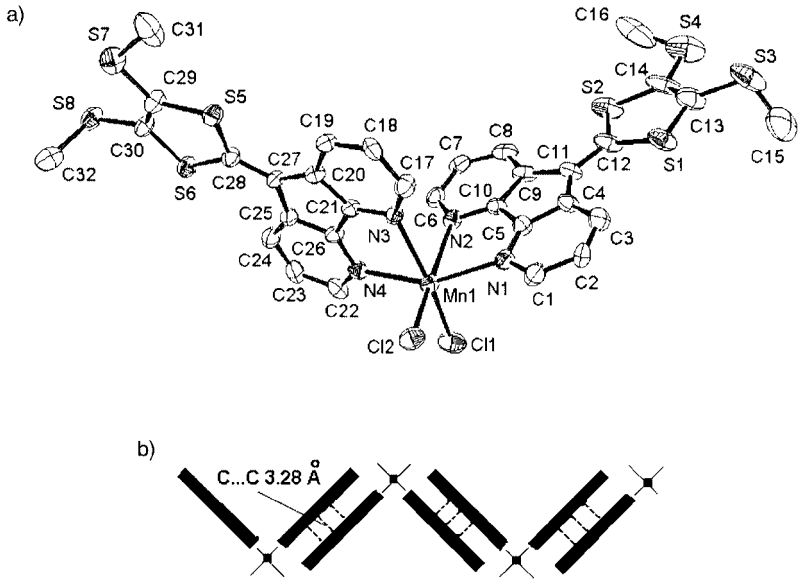

Figure 2. (a) ORTEP view of **2** showing the atom labels; solvents omitted for clarity; (b) schematic view of the 1D arrangement and intermolecular π···π stacking

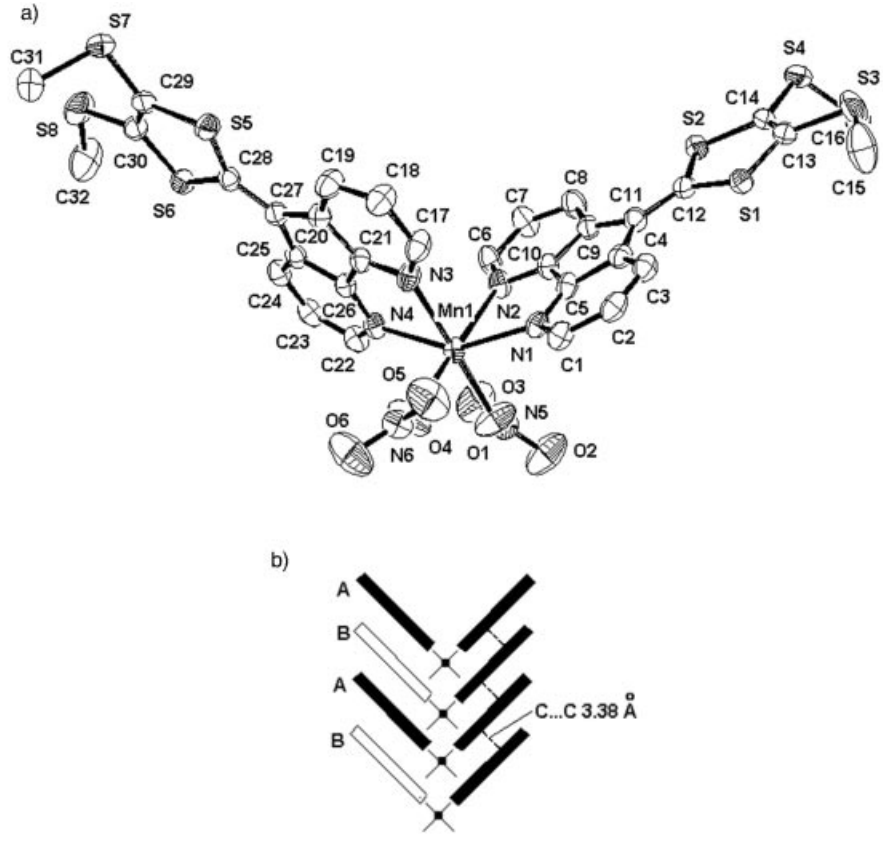

Figure 3. (a) ORTEP view of **3** showing the atom labels; (b) schematic view of molecular packing and π···π stacking; A and B represent ligands orientated in different directions

tively, which are better than those of **2**. The dihedral angle between least-squares planes of the two ligands is 95.09°. The crystal is also stabilized by interligand π···π stacking, but the crystal packing is quite different from that of **2**. Ligand planes from two different symmetrical molecules are arranged alternately with C···C distances of 3.37 or 3.38 Å, forming 1D ligand columns along the *a* axis (Figure 3, b). In Figure 3 (b), A and B represent ligands orientated in

 © 2004 Wiley-VCH Verlag GmbH & Co. KGaA, Weinheim

different directions and those molecules interact further with others in the same manner as described above (1D ligand columns). By the metal coordination linkage these π···π-assembled ligand columns form a 2D structure parallel with the (001) plane.

Synthesis and Properties

Table 2 gives selected IR vibration bands of the powder samples and their assignments. The shift of the ν(C=N) band is not very notable for the coordination of Mn^{II}, whereas the ν(C=C) band at 1488 cm^{-1} for the free ligand L is clearly shifted to lower energy for complexes, due to the metal coordination. In contrast to the C=C bands, the S−C−S vibrations at about 857 cm^{-1} are enhanced. The ClO_4^- and NO_3^- vibrations of the complexes **1′** and **3** at around 1130 and 1442 cm^{-1} confirm the presence of these counterions.

Table 2. Characteristic IR bands of the ligand and its complexes [cm^{-1}]; **1′** and **2′** are solvent-free compounds corresponding to **1** and **2**

Compound	ν(C=N)	ν(C=C)	ν(S−C−S)	Anion
L	1540 vs	1488 vs	857 m	
1′	1538 vs	1478 vs	868 m	1130 vs
2′	1536 vs	1473 vs	867 m	
3	1539 vs	1479 s	868 m	1442 s

Although single crystals suitable for X-ray diffraction were obtained and the structures of **1**−**3** have been successfully determined, the composition of the powder samples of **1′** and **2′** differ from those of the crystals. Crystals of **1** and **2** contain solvent molecules that are easily lost from the powder samples in vacuo. Interestingly, free ligand is not contained in **1′**, unlike crystals of **1**. Both the results of elemental analysis and IR measurement suggest this conclusion. IR spectra of the three powder complexes are essentially the same, except for the band of the anions and no peak splits (for free L) were found for **1′**. Unlike the synthesis of powder **1′**, **1** was obtained by adding some ethanol solvent to the reaction filtrate, which decreased the solubility of the ligand and therefore free L co-crystallized with the molecules of complex and solvents. Owing to the space filling of those free L molecules, **1** has a different structure (C_i) to those of **2** and **3** (C_2) (see Figure 1−3).

To further understand the structure of **1′**, ESR spectra of **1′** and **3** were recorded (Figure 4). A *trans* structure would show an axial field character in the ESR spectra with *g* values of 2 and 6 for monomeric Mn^{II} complexes,[7] but the ESR patterns of **1′** and **3** do not satisfy an axially symmetric electron environment. A higher rhombic distortion from octahedral geometry can be deduced for the complexes owing to the *cis* instead of *trans* structure. Examples of Mn^{II} complexes have been discussed in detail.[8] The results are in accord with the structure determination of **3**. Since the signal characters of **1′** and **3** are similar, the most promising structure of **1′** is a *cis*-coordination geometry, as in the crystal structures of **2** and **3**.

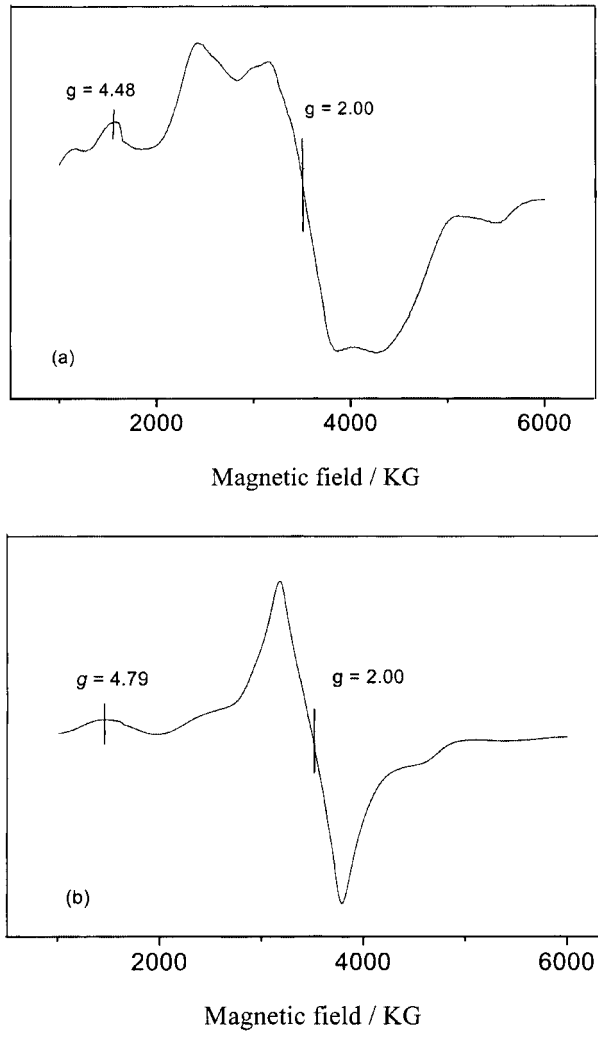

Figure 4. ESR spectra of **1′** (a) and **3** (b) powder samples measured at room temperature

Several manganese(II) complexes have been studied for catalytic activity in decomposing H_2O_2. Since our new ligands are derivatives of bipy and phen (ligands that are widely used in such catalytic systems), it seemed worthwhile to study the catalytic activity of the new Mn^{II} compounds. Unfortunately, unlike Mn^{II} complexes of bipy and phen, compounds **1**−**3** are all insoluble in water; therefore, it is impossible to discuss the influences of the conjugated electron-donor moiety of dithiole on activity by direct comparison with those of bipy or phen complexes. However, catalytic activities of **1**−**3** were determined in a heterogeneous reaction system (Figure 5). All the complexes showed activity for the catalytic decomposition of H_2O_2 in the presence of added imidazole. Among them $[Mn(L)_2(H_2O)_2](ClO_4)_2$ (**1′**) is the most effective. Experiments were repeated several times to ensure consistency of the results. The higher

 © 2004 Wiley-VCH Verlag GmbH & Co. KGaA, Weinheim

activity of **1′** is attributed to the coordinated water molecules, which are exchangeable in the catalytic system.

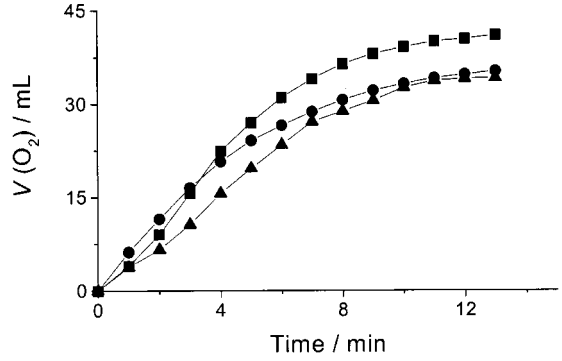

Figure 5. Activity in the catalytic decomposition of H_2O_2 in the presence of imidazole: **1′** (squares), **2′** (triangles) and **3** (circles)

Experimental Section

General Remarks: The ligand L, 9′-[4,5-bis(methylthio)-1,3-dithiol-2-ylidene]-4′,5′-diazafluorene, was prepared according to ref.[9] Acetonitrile was dried and distilled by a standard method before use. Elemental analyses of C, H and N were performed using an EA1110 elemental analyzer. IR spectra were recorded as KBr discs with a Nicolet Magma 550 FT-IR spectrometer. ESR spectra were recorded with a Jeol-FE1XG spectrometer at room temperature.

Synthesis of Complexes

$[Mn(L)_2(H_2O)_2](ClO_4)_2$ (1′): A dichloromethane solution (20 mL) of the ligand L (0.1 mmol, 36 mg) was slowly added dropwise to an acetonitrile solution (4 mL) of $Mn(ClO_4)_2{\cdot}6H_2O$ (0.05 mmol, 18.1 mg). The resultant orange precipitate, formed after the mixture was stirred at room temperature for 30 min, filtered off, washed with acetonitrile and dichloromethane and, finally, dried in vacuo over silica gel (yield: 48 mg, 65%). $C_{32}H_{28}Cl_2MnN_4O_{10}S_8$ (1010.9): calcd. C 38.02, H 2.79, N 5.54; found C 37.96, H 2.87 N 5.69.

$[Mn(L)_2Cl_2]$ (2′): To an ethanol solution (10 mL) of $MnCl_2{\cdot}4H_2O$ (0.05 mmol, 10.0 mg) was slowly added dropwise a dichloromethane solution (20 mL) of the ligand L (0.1 mmol, 36 mg). Then, all the procedures were similar to that of **1** (yield: 49 mg, 67%). $C_{32}H_{24}Cl_2MnN_4S_8$ (846.9): calcd. C 45.39, H 2.84, N 6.62; found C 45.27, H 2.78, N 6.56.

$[Mn(L)_2(NO_3)_2]$ (3): A dichloromethane solution (20 mL) of the ligand L (0.1 mmol, 36 mg) was slowly added dropwise to an ethanol solution (5 mL) of $Mn(NO_3)_2$ ca. 0.1 mmol, 20 μL, 50% w/w aqueous solution). Subsequent procedures were similar to that of **1** (yield: 45 mg, 65%). $C_{32}H_{24}MnN_6O_6S_8$ (900.0): calcd. C 42.71, H 2.67, N 9.34; found C 37.12, H 2.38, N 5.49.

$[Mn(L)_2(H_2O)_2](ClO_4)_2{\cdot}(L)_2{\cdot}2C_2H_5OH{\cdot}2CH_3CN$ (1): Crystals of complex **1** was prepared by slowly adding dropwise a dichloromethane solution (10 mL) of the ligand L (0.02 mmol, 7.2 mg) to an acetonitrile solution (3 mL) of $Mn(ClO_4)_2{\cdot}6H_2O$ (0.01 mmol, 3.62 mg). The resultant mixture was stirred at room temperature for 30 min and then filtered. Ethanol was then gently layered on the filtrate, which was sealed in bottles and left undisturbed at room temperature for several days. The so-obtained orange, single crystals were suitable for X-ray diffraction.

$[Mn(L)_2Cl_2]{\cdot}1.5CH_2Cl_2$ (2) or $Mn(L)_2(NO_3)_2]$ (3): Crystals of **2** or **3** were prepared in dilute solutions by similar procedures to that above. Filtrates were sealed in bottles and left undisturbed at room temperature for several days to afford orange single crystals suitable for X-ray diffraction.

Hydrogen Peroxide Disproportionation Studies: Aqueous H_2O_2 (2 wt.%, 5 mL) was added to a solid mixture consisting of the complex (2.3×10^{-3} mmol) and imidazole (5 mg). This combination was

Table 3. Crystallographic data for complexes **1**−**3**

	1	**2**	**3**
Empirical formula	$C_{72}H_{68}Cl_2MnN_{10}O_{12}S_{16}$	$C_{33.50}H_{27}Cl_5MnN_4S_8$	$C_{32}H_{24}MnN_6O_6S_8$
Formula mass	1904.19	974.29	900.00
Crystal size [mm]	0.22 × 0.42 × 0.05	0.10 × 0.40 × 0.20	0.70 × 0.15 × 0.30
Crystal system	triclinic	monoclinic	monoclinic
Space group	$P\bar{1}$ (no. 2)	$C2/c$ (no. 15)	Pa (no. 7)
a [Å]	7.564(2)	25.044(3)	9.113(1)
b [Å]	11.980(4)	16.0260(13)	14.019(2)
c [Å]	24.331(7)	22.654(3)	14.955(2)
α [°]	102.461(13)	90	90
β [°]	92.462(9)	115.720(4)	107.621(7)
γ [°]	100.986(13)	90	90
V [Å^3]	2105.4(11)	8191.8(15)	1820.8(4)
Z	1	8	2
$D_{calcd.}$ [mg·m^{-3}]	1.502	1.580	1.641
$F(000)$	981.00	3952.00	918.00
$2\theta_{max.}$ [°]	55.0	55.0	55.0
No. of reflections measured	14203	83234	24388
No. of unique reflections	8877	9650	7747
No. of reflections [$I > 3.0\sigma(I)$]	3654	4630	6456
Goodness-of-fit (S)	1.014	1.001	1.011
R_1	0.090	0.063	0.037
wR_2	0.179	0.178	0.104

$R_1 = \Sigma||F_o| - |F_c||/\Sigma|F_o$ and $wR_2 = [\Sigma w(F_o^2 - F_c^2)^2]/\Sigma w(F_o^2)^2]^{1/2}$

 © 2004 Wiley-VCH Verlag GmbH & Co. KGaA, Weinheim

then stirred and thermostatted at 25 °C. Evolved O_2 was measured volumetrically.

X-ray Crystallographic Study: X-ray crystallographic data for complexes **1**−**3** were obtained using a Rigaku Mercury CCD area detector with graphite-monochromated Mo-K_α (λ = 0.71070 Å) radiation, at 193 K. Table 3 lists selected crystallographic data for three complexes and details of data collection. An empirical absorption correction was applied and data were corrected for Lorentz and polarization effects. All structures were solved by direct methods[10] and expanded using Fourier techniques.[11] Non-hydrogen atoms were refined anisotropically. Hydrogen atoms were refined using the riding model. The final cycle of full-matrix least-squares refinement on F^2 was based on observed reflections and variable parameters and converged to unweighted and weighted agreement factors. Calculations were performed using the CrystalStructure software package. CCDC-236214 to -236216 contain the supplementary crystallographic data for this paper. These data can be obtained free of charge at www.ccdc.cam.ac.uk/conts/retrieving.html [or from the Cambridge Crystallographic Data Centre, 12 Union Road, Cambridge CB2 1EZ, UK; Fax: + 44-1223-336-033; E-mail: deposit@ccdc.cam.ac.uk].

Acknowledgments

This work was supported by the National Natural Science Foundation (20071024, 20371033), P. R. China. The authors are also grateful to the Key Laboratory of Organic Synthesis of Jiangsu Province, Suzhou University for financial support.

[1] [1a] A. J. Amoroso, J. C. Jeffery, P. L. Jones, J. A. McCleverty, P. Thornton, M. D. Ward, *Angew. Chem. Int. Ed. Engl.* **1995**, *34*, 1443−1446. [1b] A. Caneschi, F. Ferraro, D. Gatteschi, M. C. Melandri, P. Rey, R. Sessoli, *Angew. Chem. Int. Ed. Engl.* **1989**, *28*, 1365−1367. [1c] W. Lin, M. E. Chapman, Z. Wang, G. T. Yee, *Inorg. Chem.* **2000**, *3*, 4169−4173. [1d] E-Q. Gao, S-Q. Bai, Y-F. Yue, Z-M. Wang, C-H. Yan, *Inorg. Chem.* **2003**, *42*, 3642−3649. [1e] D. J. Price, S. R. Batten, B. Moubaraki, K. S. Murray, *Chem. Commun.* **2002**, 762−763.

[2] [2a] C. Palopoli, B. Chansou, J-P. Tuchagues, S. Signorella, *Inorg. Chem.* **2000**, *39*, 1458−1462. [2b] L. Dubois, R. Caspar, L. Jacquamet, P.-E. Petit, M.-F. Charlot, C. Baffert, M-N. Collomb, A. Deronzier, J-M. Latour, *Inorg. Chem.* **2003**, *42*, 4817−4827. [2c] J. Brinksma, R. Hage, J. Kerschner, B. L. Feringa, *Chem. Commun.* **2000**, 537−538. [2d] M. Maneiro, M. R. Bermejo, M. I. Fernandez, E. Gomez-Forneas, A. M. Gonzalez-Noya, A. M. Tyryshkin, *New J. Chem.* **2003**, 727−733. [2e] C. E. Dubé, D. W. Wright, W. H. Armstrong, *Angew. Chem. Int. Ed.* **2000**, *39*, 2169−2172.

[3] [3a] C. Baffert, M-N. Collomb, A. Deronzier, S. Kjaergaard-Knudsen, J-M. Latour, K. H. Lund, C. J. McKenzie, M. Mortensen, L. P. Nielsen, N. Thorup, *J. Chem. Soc., Dalton Trans.* **2003**, 1765−1772. [3b] R. J. Debus, K. A. Campbell, D. P. Pham, A-M. A. Hays, R. D. Britt, *Biochemistry* **2000**, *39*, 6275−6287. [3c] R. J. Debus, K. A. Campbell, J. M. Peloquin, D. P. Pham, R. D. Britt, *Biochemistry* **2000**, *39*, 470−478. [3d] K. Wieghardt, *Angew. Chem. Int. Ed. Engl.* **1989**, *28*, 1153−1172.

[4] [4a] M. W. Epperly, V. E. Kagan, C. A. Sikora, J. E. Gretton, S. J. Defilippi, D. Bar-Sagi, J. S. Greenberger, *Int. J. Cancer* **2001**, *96*, 221−231. [4b] F. Semrau, R-J. Kühl, S. Ritter, K. Ritter, *J. Med. Virol.* **1998**, *55*, 161−167.

[5] [5a] M. J. Knapp, D. N. Hendrickson, V. A. Grillo, J. C. Bollinger, G. Christou, *Angew. Chem. Int. Ed. Engl.* **1996**, *35*, 1818−1820. [5b] G. G. D. Munno, M. Julve, G. Viau, F. Lloret, J. Faus, D. Viterbo, *Angew. Chem. Int. Ed. Engl.* **1996**, *35*, 1807−1810. [5c] S. McCann, M. McCann, R. M. T. Casey, M. Jackman, M. Devereux, V. Mckee, *Inorg. Chim. Acta* **1998**, *279*, 24−29. [5d] M. McCann, M. T. Casey, M. Devereux, M. Curran, G. Ferguson, *Polyhedron* **1997**, *16*, 2547−2552. [5e] X. S. Tan, D. F. Xiang, W. X. Tang, J. Sun, *Polyhedron* **1997**, *16*, 689−694.

[6] [6a] Q. Y. Zhu, G. Q. Bian, J. Dai, D. X. Jia, J. S. Zhang, L. Guo, *Inorg. Chim. Acta* **2003**, *351*, 177−182. [6b] Q. Y. Zhu, J. Dai, G. Q. Bian, X. Wang, W. Yang, Z. M. Yan, *Synth. React. Inorg. Met.-Org. Chem.* **2002**, *32*, 1001−1012. [6c] Q. Y. Zhu, Y. Zhang, J. Dai, G. Q. Bian, D. X. Jia, J. S. Zhang, L. Guo, *Chem. Lett.* **2003**, *32*, 762−763.

[7] R. D. Dowsing, J. F. Gibson, *J. Chem. Phys.* **1969**, *50*, 294.

[8] [8a] L. Yang, S. Yan, D. Liao, Z. Jiang, G. Wang, P. Shen, *Polyhedron* **1995**, *14*, 1565−1570. [8b] E. Garribba, G. Micera, M. Zema, *Inorg. Chim. Acta* **2004**, *357*, 2038−2048.

[9] [9a] L. J. Henderson, J. Frank, R. Fronczek, R. William, *J. Am. Chem. Soc.* **1984**, *106*, 5876−5879. [9b] N. Svenstrup, K. M. Rasmussen, T. K. Hansen, J. Becher, *Synthesis* **1994**, 809. [9c] N. Svenstrup, J. Becher, *Synthesis* **1995**, 215−235. [9d] K. Sako, M. Kusakabe, H. Tatemitsu, *Mol. Cryst. Liq. Cryst.* **1996**, *285*, 101−106.

[10] SHELX97: G.M. Sheldrick, University of Göttingen, **1997**.

[11] DIRDIF99: P. T. Beurskens, G. Admiraal, G. Beurskens, W. P. Bosman, R. de Gelder, R. Israel, J. M. M. Smits, *Technical Report of the Crystallography Laboratory*, University of Nijmegen, The Netherlands, **1999**.

Received April 26, 2004
Early View Article
Published Online November 15, 2004

 © 2004 Wiley-VCH Verlag GmbH & Co. KGaA, Weinheim

Synthesis and Characterization of Lithium Complexes of 2-(Diphenylphosphanylamino)pyridine and *N*,2-Bis(diphenylphosphanyl)benzeneamine

Kochappilly O. Xavier,[a] Elena Smolensky,[a] Moshe Kapon,[a] Stephen M. Aucott,[b] J. Derek Woollins,[b] and Moris S. Eisen*[a]

Keywords: Lithium complexes / (Diphenylphosphanylamino)pyridine / *N*,2-Bis(diphenylphosphanyl)benzeneamine / Hard-soft interactions / *N*,*N*-chelation / *N*,*P*-chelation / X-ray diffraction

Lithium complexes of 2-(diphenylphosphinoamino)pyridine and *N*,2-bis(diphenylphosphanyl)benzeneamine have been synthesized from the corresponding neutral compounds. In the former complex, the metal ion is coordinated to both nitrogen atoms, forming a constrained four-membered ring, whereas the latter complex forms a five-membered ring as the metal ion coordinates preferentially to the phosphorus atom. Coordination of the metal ion in both complexes is dictated primarily by soft–hard interactions and, subsequently, by the constrained geometry of the ring formed. Both lithium complexes and the corresponding neutral compounds have been characterized by single-crystal X-ray diffraction.
(© Wiley-VCH Verlag GmbH & Co. KGaA, 69451 Weinheim, Germany, 2004)

Introduction

Alkali metal salts play an important role in advanced organic and organometallic transformations.[1] The most extensively used salts contain lithium because this metal cation has the highest charge density of all alkali-metal cations, and inorganic and organic lithium compounds are reasonably soluble in organic solvents.[2] Over 95% of natural products syntheses employ at least one lithium-containing species.[3] *N*-Lithiated species, a very important family in organic chemistry, are the favorite bases in forming ketone enolates,[4] generating low steady-state concentrations of some relatively unstable carbanions,[5] and in preparing heterocyclic thiazenes that incorporate an RC(=N−)N< moiety using lithium amidinates.[6] They are also the main synthons used to introduce an amido group to either early or late transition metal complexes.[7] Since the bonding in these lithium complexes is ionic, the solid-state structures are highly dependent on the steric and electronic properties of the substituents at the anionic center. In addition, the presence of coordinative solvents reduces the high tendency of organolithium compounds to self-assemble into higher aggregates.[3,8]

In the last decade lithium complexes containing *N*,*N*- and *P*,*N*-ligations have attracted much attention. Representative examples of these ligations (Scheme 1) are amidinate,[9] β-diketiminate,[10] pyridylamine,[11] diaminobenzene,[12] phosphanamide,[13] phosphane *Janus Head*,[14] phospha-amidinate,[15] and amidophosphane.[16]

Recently, we have shown that lithium benzamidinates can form dimeric and trimeric species, depending on the solvent,[17] and that the coordination of TMEDA (tetramethylethylenediamine) to lithium benzamidinates guarantees the formation of mononuclear species.[18] These lithium complexes are useful reagents for the bidentate chelation of main group, early- and late-transition metal centers that produce, in some cases, homogeneous complexes as catalysts for the stereoregular polymerization of α-olefins.[18,19]

In the lithium benzamidinate/TMEDA complex the metal ion is coordinated symmetrically by both nitrogen atoms of the benzamidinate moiety, forming an η^2-ligation and, with the two nitrogen atoms of TMEDA, a tetrahedral environment (Figure 1).

With pyridylamine and amidophosphane ligations η^2-coordination to the metal ion is normally observed since both heteroatoms (P or N) are located *ortho* to the lithiated position of the aromatic ring (aminobenzene or pyridine), forming a "single side arm coordination". In such coordination there is still space for donor solvent coordination and, commonly, the dimer four-membered ring is the favorite aggregation state.[20]

A basic conceptual question regards the coordination of the alkali metal ion in non-symmetrical systems where, as well as a hard atom (N), the competitive chelation of additional soft and/or hard atoms is also possible. Two systems were selected for this study. The first asymmetric ligation contains the N−C−N−P backbone in which the cen-

[a] Department of Chemistry and Institute of Catalysis Science and Technology, Technion − Israel Institute of Technology, Haifa 32000, Israel
E-mail: chmoris@tx.technion.ac.il
[b] School of Chemistry, University of St. Andrews, Fife, KY16 9ST, U.K.

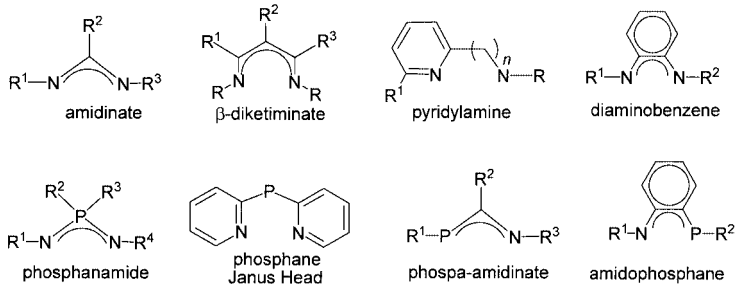

Scheme 1. Representative *P,N*- and *N,N*-ancillary ligations in lithium complexes

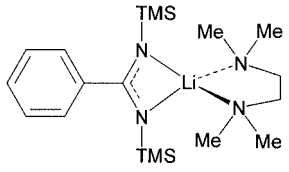

Figure 1. Lithium benzamidinate complex with TMEDA ligation

tral nitrogen atom belongs to a pyridine ring, whereas the second asymmetric system includes a P−C−C−N−P backbone in which the C−C moiety is part of an aromatic ring.

Regarding the former system, only one known structure contains an N−C−N−P moiety in which the nitrogen atoms are attached to a lithium ion and the phosphorus atom is part of a P−N−P−N cyclobutane moiety.[21] Interestingly, 13 structures are known in which an *ortho*-amidopyridinium moiety is anchored to a lithium center, although without the presence of soft (phosphane) atoms.[22,11] Regarding the latter system, structures of late transition metal complexes anchoring the ligand to the metal ion by one or two phosphane P atoms are known but no crystal structure has been reported for alkali or early transition metals of this unsymmetrical ligation.[23] We present here the solid-state characterization of lithium complexes for both N−C−N−P and P−C−C−N−P backbones. To compare the effect of the alkali center, crystallographic parameters of the neutral systems are also described.

Results and Discussion

2-(Diphenylphosphanylamino)pyridine (**1**) was prepared according to a published procedure[23b] and recrystallized before use [Equation (1)]. X-ray diffraction (Figure 2, Table 1) shows that **1** is a dimeric polymorph that crystallizes in a different space group to the structure known in the literature[23b] although with almost identical bond lengths and angles.

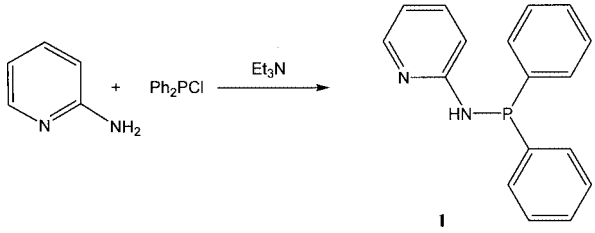

(1)

Lithium complex **2** was prepared quantitatively from the reaction of the neutral compound **1** with butyllithium (1:1)

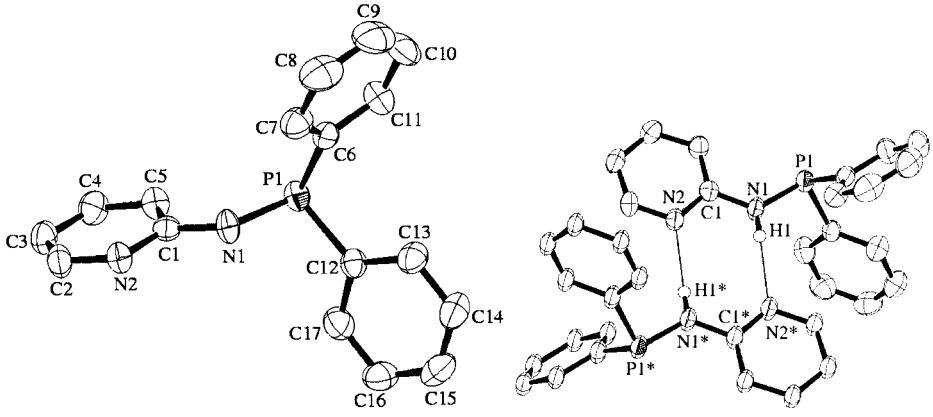

Figure 2. Crystal structure of complex **1** and its dimer in the crystal structure (N1−N2* = 3.050 Å and H1−N2* = 2.18 Å); thermal ellipsoids given at 50% probability

 © 2004 Wiley-VCH Verlag GmbH & Co. KGaA, Weinheim

Table 1. Comparison of bond lengths [Å] and angles [°] for complexes **1**−**4**

Compound **1**		Complex **2**		Compound **3**		Complex **4**	
P(1)−N(1)	1.695(3)	P(1)−N(2)	1.676(3)	P(2)−N(1)	1.699(2)	P(2)−N(1)	1.681(2)
N(1)−C(1)	1.391(4)	N(2)−C(25)	1.355(4)	N(1)−C(18)	1.402(3)	N(1)−C(18)	1.386(3)
N(1)−H(1)	0.8700			P(1)−C(13)	1.830(2)	P(1)−C(13)	1.817(3)
N(2)−C(1)	1.341(4)	N(1)−C(25)	1.364(4)	C(13)−C(18)	1.411(3)	C(13)−C(18)	1.421(4)
C(1)−C(5)	1.384(5)	C(25)−C(24)	1.419(4)			N(1)−Li	1.985(5)
		N(1)−Li(1)	2.043(6)			P(1)−Li	2.618(3)
		N(2)−Li(1)	2.012(7)			O(1)−Li	1.963(4)
		O(1)−Li(1)	1.949(6)			O(2)−Li	1.901(4)
		O(2)−Li(1)	1.939(6)				
				C(7)−P(1)−C(1)	102.63(12)	C(7)−P(1)−C(1)	104.02(14)
N(1)−P(1)−C(6)	104.09(16)	N(2)−P(1)−C(1)	104.24(14)	C(7)−P(1)−C(13)	102.18(11)	C(7)−P(1)−C(13)	103.90(13)
N(1)−P(1)−C(12)	100.01(14)	N(2)−P(1)−C(7)	100.29(15)	C(1)−P(1)−C(13)	100.07(11)	C(1)−P(1)−C(13)	101.84(12)
C(6)−P(1)−C(12)	101.76(15)	C(1)−P(1)−C(7)	97.10(13)	N(1)−P(2)−C(19)	100.65(11)	N(1)−P(2)−C(19)	106.86(12)
C(1)−N(1)−P(1)	124.7(2)	C(25)−N(2)−P(1)	118.9(2)	N(1)−P(2)−C(25)	102.92(10)	N(1)−P(2)−C(25)	100.36(12)
P(1)−N(1)−H(1)	117.6 (3)			C(19)−P(2)−C(25)	100.92(12)	C(19)−P(2)−C(25)	100.40(12)
C(1)−N(2)−C(2)	117.1(3)	C(25)−N(1)−C(21)	118.5(3)	C(18)−N(1)−P(2)	125.88(17)	C(18)−N(1)−P(2)	116.45(18)
N(2)−C(1)−N(1)	115.1(3)	N(1)−C(25)−N(2)	113.3(3)	P(1)−C(13)−C(18)	117.83(18)	P(1)−C(13)−C(18)	115.30(18)
		C(21)−N(1)−Li(1)	152.7(3)	N(1)−C(18)−C(13)	120.0(2)	N(1)−C(18)−C(13)	118.4(2)
		C(25)−N(1)−Li(1)	88.4(3)			C(13)−P(1)−Li	88.99(12)
		C(25)−N(2)−Li(1)	89.9(3)			C(7)−P(1)−Li	110.91(12)
		P(1)−N(2)−Li(1)	148.7(2)			C(1)−P(1)−Li	139.66(14)
						C(18)−N(1)−Li	114.99(19)
						P(2)−N(1)−Li	126.34(14)
						N(1)−Li−P(1)	76.31(11)
		N(1)−Li(1)−N(2)	68.1(2)			N(1)−Li−O(2)	129.3(2)
		N(2)−Li(1)−O(1)	118.0(3)			N(1)−Li−O(1)	120.2(2)
		N(2)−Li(1)−O(2)	117.5(3)			O(1)−Li−O(2)	100.31(18)
		O(1)−Li(1)−O(2)	111.0(3)			P(1)−Li−O(1)	102.93(15)
		O(2)−Li(1)−N(1)	113.2(3)			P(1)−Li−O(2)	125.4(2)
		O(1)−Li(1)−N(1)	123.3(3)				

in a tetrahydrofuran solution [Equation (2)]. Complex **2** is bright yellow and is highly soluble in organic solutions. By cooling to −78 °C a crystallized product was obtained and subsequently characterized by low-temperature X-ray diffraction (Figure 3, Table 1) and spectroscopic methods.

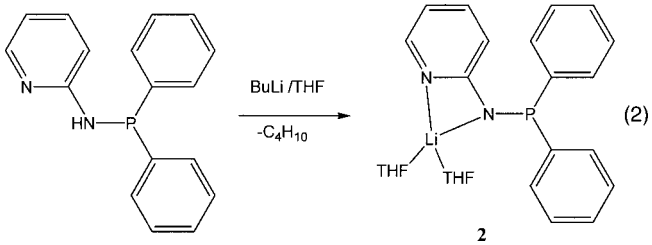

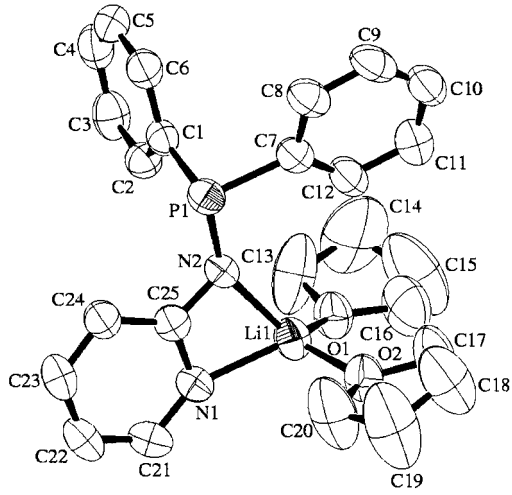

Figure 3. Molecular structure of complex **2**; thermal ellipsoids given at 50% probability

X-ray analysis shows that the complex has a structure containing one symmetrical diazaallyl moiety as the core unit [Li(1)−N(1)−C(25)−N(2)] bonded in addition to two equidistant molecules of tetrahydrofuran, forming a tetracoordinated lithium atom.

Comparison of the neutral and the lithiated complex indicates the electronic effects introduced by the lithium atom. In the neutral compound the aromatic carbon atom exhibits a shorter distance to the pyridine nitrogen atom [N(2)−C(1) = 1.341(4) Å] than to the aminophosphane nitrogen atom [N(1)−C(1) = 1.391(4) Å]. In the lithiated complex the distances become almost equivalent [N(1)−C(25) = 1.364(4) Å and N(2)−C(25) = 1.355(4) Å] and are very close to the geometrical average in the neutral compound. The N(1)−C(25) and C(25)−C(24) bonds [1.418(4) Å] are longer than those in the neutral compound, for which N(2)−C(1) and C(1)−C(5) = 1.384(5) Å, respec-

 © 2004 Wiley-VCH Verlag GmbH & Co. KGaA, Weinheim

tively. The charge has little effect on the N−P bond length as N(2)−P(1) = 1.676(3) Å and N(1)−P(1) = 1.695(3) Å for **2** and **1**, respectively.

The Li−N(Py) bond length in complex **2** [2.043(6) Å] lies in the middle of the range (1.96−2.19 Å) indicated by other well-defined lithium complexes bearing a pyridine ring (Table 2).

Table 2. Li−N(Py) bond lengths in representative complexes

Complex	Li−N(Py) [Å]	Ref.
$[(THF)_2Li(2\text{-}Py)_2CH]$	1.966(4), 1.973(4)	[24]
$[\{(2\text{-}Py)NP(\mu\text{-}N\textit{t}Bu\}Li_2\cdot\{Li(\textit{t}BuN)_2P\}]$	2.002(6)	[11d]
$[Li_8(C_5H_3NMeNH)_6(O)(OEt_2)_2]$	2.01(1), 2.01(1)	[11a]
$[Li(Py)_2(PNSiMe_3)]_2$	2.028(3), 2.038(3)	[25]
$\{[Li(A\text{-}PySiMe_3)](THF)\}_2$[a]	2.042(7)	[11b]
$[Li(PyNPPh_2)_2(THF)_2]$ (**2**)	2.043(6)	this paper
$[MeSi(2\text{-}Py)_3LiX]$ (X = $Br_{0.2}Cl_{0.8}$)	2.051(5), 2.081(4)	[26]
$[\{\textit{t}BuNP(\mu\text{-}N\textit{t}Bu)_2PN(2\text{-}Py)\}Li_2]$	2.093(3)	[11b]
$[Li(bpg)(H_2O)]\cdot H_2O$[b]	2.152(3), 2.187(3)	[27]

[a] A-PySiMe$_3$ = 6-methyl-2-(trimethylsilylamino)pyridine. [b] bpg = *N*,*N*-bis(2-pyridylmethyl)glycine.

The organic compound *N*,2-bis(diphenylphosphanyl)benzenamine (**3**) was prepared from deprotonated 2-(diphenylphosphanyl)benzeneamine with butyllithium and concomitant addition of chlorodiphenylphosphane [Equation (3)].[14] Pale yellow single crystals of **3** suitable for X-ray diffraction (Figure 4, Table 1) were obtained by recrystallization from toluene at −40 °C.

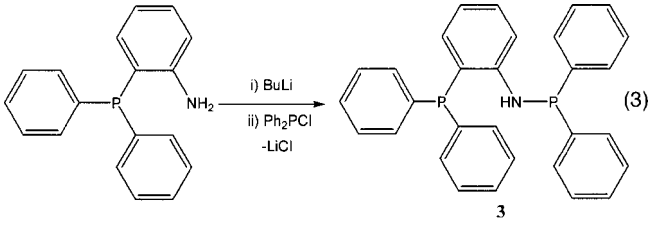

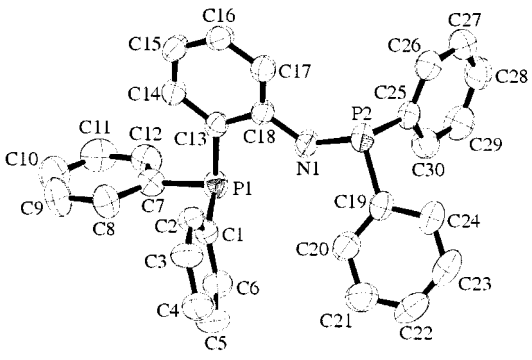

Figure 4. Molecular structure of compound **3**; thermal ellipsoids given at 50% probability

The corresponding lithium *N*,2-bis(diphenylphosphanyl)-benzenamine (**4**) was prepared by deprotonation of *N*,2-bis(diphenylphosphanyl)benzenamine (**3**) with butyllithium [Equation (4)]. The reaction proceeds in THF in good yield (85%), producing a yellow product that can be easily recrystallized from THF at −20 °C.

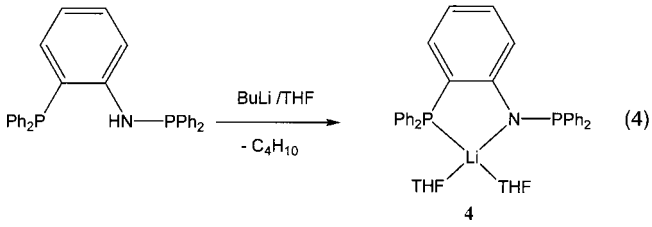

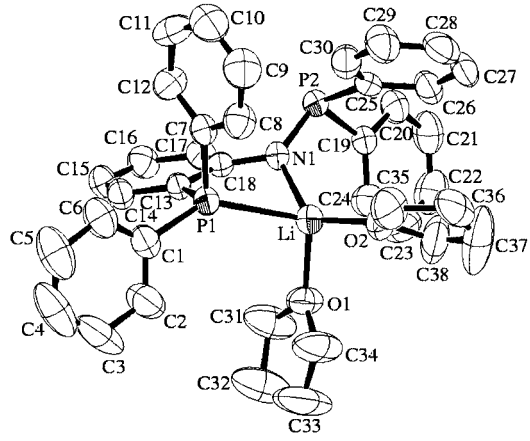

Figure 5. Molecular structure of complex **4**; thermal ellipsoids given at 50% probability

The X-ray structure of complex **4** (Figure 5, Table 1) shows a core unit of a five-membered ring, P(1)−C(13)−C(18)−N(1)−Li, with the lithium atom tilted down from the plane formed by the four additional atoms. The lithium atom is coordinated by the nitrogen atom and *ortho*-phosphorus atom in addition to two molecules of THF, forming a highly distorted tetrahedron. Whereas the average Li−O bond length in lithiated complexes is normally around 1.92−1.94 Å, in complex **4** one bond is rather short and the second is rather long [O(2)−Li = 1.901(4) Å and O(1)−Li = 1.963(4) Å]. This increase is a result of the rejection of the lone pair of electrons of one oxygen atom and one of the phosphorus atoms [O(1)−P(1) = 3.61 Å]. Interestingly, no interaction is exhibited between the lithium atom and the phosphorus atom attached to the nitrogen atom. Seemingly, this interaction induces a higher energy and is observed only when no other donating atoms are present in sterically less demanding positions.[28] Comparison of the neutral and lithiated complexes shows that the increase in charge at the nitrogen atom causes almost no change in aromatic C−C bond lengths, although the bonds connecting the substituents to the aromatic ring do lengthen, i.e. C(13)−C(18) = 1.421(4) Å, N(1)−C(18) =

 © 2004 Wiley-VCH Verlag GmbH & Co. KGaA, Weinheim

Table 3. Comparison of bond angles and lengths in four- and five-membered ring *N*,*N*- and *N*,*P*-ligated lithium complexes

	Complex	Bond angles [°] Bond lengths [Å]	Ref.
Four-membered ring complexes:			
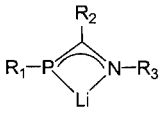	$[Li\{P(Ph)C(Ph)NSiMe_2tBu\}(THF)]_2$	N–Li–P = 68.0(3) Li–N = 1.991(10) Li–P = 2.641(9)	[15]
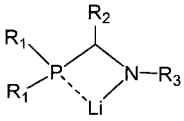	$[Ph_2PC\{NiPr\}_2Li(TMEDA)]$	N–Li–P = 66.54(16) Li–N = 1.927(5) Li–P = 2.625(5)	[29]
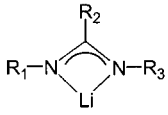	[Li(FIso)(THF)$_2$][a]	N(1)–Li–N(2) = 68.2(1) Li–N(1) = 2.036(4) Li–N(2) = 2.041(4)	[9a]
	$[PhC(NSiMe_3)_2Li(TMEDA)]$	N(1)–Li–N(2) = 69.19(19) Li–N(1) = 2.019(6) Li–N(2) = 2.033(6)	[19]
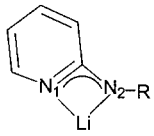	$\{[Li(A\text{-}PySiMe_3)](thf)\}_2$[b]	N(1)–Li–N(2) = 67.4(2) Li–N(1) = 2.042(7) Li–N(2) = 2.097(7)	[11b]
	$[Li(PyNPPh_2)_2(thf)_2]$ (**2**)	N(1)–Li–N(2) = 68.1(2) Li–N(1) = 2.043(6) Li–N(2) = 2.012(7)	this work
Five-membered ring coplexes:			
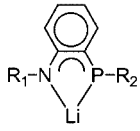	$[Ph_2PC_6H_4\{2\text{-}N(2,6\text{-}Me_2Ph)\}Li(thf)_2]$	N–Li–P = 76.63(17) Li–N = 1.990(5) Li–P = 2.620(5)	[16a]
	$[Ph_2PC_6H_4\{2\text{-}N(C_6H_4PPh_2)\}Li(thf)_2]$	N–Li–P = 73.09(15), 73.35(15) Li–N = 2.039(5) Li–P = 2.779(5), 2.824(5)	[16b]
	$[PPh_2PC_6H_4(2\text{-}NPPh_2)Li(thf)_2]$ (**4**)	N–Li–P = 76.31(11) Li–N = 1.985(5) Li–P = 2.618(3)	this work

[a] Fiso = *N*,*N*-bis(2,6-diisopropylphenyl)formamidine. [b] A-PySiMe$_3$ = 6-methyl-2-(trimethylsilylamino)pyridine.

1.386(3) Å, P(1)−C(13) = 1.817(3) Å, and C(14)−C(19) = 1.411(3) Å, N(1)−C(18) = 1.402(3) Å, P(1)−C(13) = 1.830(3) Å, for **4** and **3**, respectively. Notably, the distance between the *ortho* substituents decreases only slightly upon the attachment of the lithium atom: N(1)−P(1) = 2.99 and 2.80 Å in **3** and **4**, respectively.

Comparison of the Li−N bond lengths in complexes **2** and **4** is of interest. In complex **2** the average bond length of 2.02 Å is a result of resonance among the aminopyridine ring whereas in complex **4** a shorter bond length [1.985(6) Å] is observed. This difference in bonding also occurs in other lithium benzamidinate complexes.[9]

The rings formed by the metal atom and the *N*,*P*- and *N*,*N*-ancillary ligations are also of interest. When four-membered rings are formed, the N−Li−P or N−Li−N bond angle is within 66.5−69.2°, while for five-membered rings this angle is between 73.0 and 76.6° (Table 3). The N−Li−N angle in the four-membered ring in complex **2** is similar to that found in benzamidinate complexes, whereas the N−Li−P angle in the five-membered ring in complex **4** exhibits an angle close to the highest observed value (76.31°).

Conclusions

Two lithium complexes and their corresponding parent neutral ligands have been characterized by single-crystal X-ray diffraction. In the phosphanylpyridine complex **2** the metal ion is coordinated to the hard nitrogen ligands, forming a constrained four-membered metallacycle, regardless of possible coordination with the soft phosphorus atom to form a less constrained five-membered ring. In the diphosphane complex **4** the metal ion forms a five-membered ring that connects soft and hard moieties. Coordination to the second phosphorus moiety is sterically hindered.

Experimental Section

General Remarks: All manipulations of air-sensitive materials were carried out with the vigorous exclusion of oxygen and moisture in

 © 2004 Wiley-VCH Verlag GmbH & Co. KGaA, Weinheim

flame dried Schlenk-type glassware connected to a dual-manifold Schlenk line, or interfaced to a high-vacuum (10^{-6} Torr) line, or in a nitrogen-filled Vacuum Atmospheres glove box with a medium-capacity recirculator (1−2 ppm O_2). Argon and nitrogen were purified by passage through an MnO oxygen-removal column and a Davison molecular sieves (4-Å) column. THF and [D_8]THF solvents were distilled under argon from sodium/benzophenone. Hydrocarbon solvents (C_6D_6, toluene) were distilled under nitrogen from Na/K alloy. All solvents for vacuum-line manipulations were stored in vacuo over Na/K alloy in resealable bulbs. The neutral ligands Ph_2PNPy (**1**) (Py = pyridine) and *ortho*-$Ph_2PNHC_6H_4PPh_2$ (**3**) were prepared according to literature methods.[23] NMR spectra were recorded with Bruker Avance 300 and 500 spectrometers. Chemical shifts for ^1H and ^{13}C NMR are referenced to internal solvent resonance and are reported relative to tetramethylsilane. Experiments were conducted in Schlenk vessel sealed tubes (J. Young stopcock) after vacuum transfer of the solvent in a high-vacuum line.

Synthesis of Li(Ph_2PNPy)$(THF)_2$ (2): *n*BuLi (0.24 g, 3.78 mmol as a 1.6 M solution in hexane) was added dropwise at −78 °C under nitrogen to a stirred solution of the ligand Ph_2PNHPy (1.05 g, 3.78 mmol) in THF (20 mL). After stirring at −78 °C for 30 min, the resultant solution was allowed to warm to room temperature and stirred for a further 12 h. After the resulting solution was concentrated to 3 mL and cooled slowly to −78 °C, yellow crystals precipitated; 1.45 g (95%). $C_{25}H_{30}LiN_2O_2P$ (428.4 g): calcd. C 70.09, H 7.06, N 6.54; found C 69.69, H 7.40, N 6.27. ^1H NMR (C_4D_8O, 300 MHz): δ = 1.73 (m, 4 H, CH_2CH$_2$O), 3.57 (m, 4 H, CH$_2$O), 6.05 (dd, ^3J = 5.1 Hz; ^3J = 6.3 Hz, 1 H, NCHC*H*CHCHC), 6.56 (d, ^3J = 8.1 Hz, 1 H, NCHCHCHC*H*C), 7.12 (dd, ^3J = 6.3, ^3J = 8.1 Hz, 1 H, NCHCHC*H*CHC), 7.15 (m, 6 H, 2 × C_6H_5 *m*- and *p*-H), 7.32 (m, 4 H, 2 × C_6H_5 *o*-H), 7.63 (d, ^3J = 5.1 Hz, 1 H, NC*H*CHCHCHC) ppm. ^{13}C NMR (C_4D_8O, 150 MHz): δ = 22.5, 64.1, 105.3, 107.2 (d, $^1J_{c\text{-}p}$ = 30.0 Hz), 124.5, 124.9, 125.0, 128.5, 128.7, 133.9 (d, $^3J_{c\text{-}p}$ = 7.5 Hz), 144.4 ppm. ^{31}P NMR (C_6D_6): δ = 32.14 ppm.

Synthesis of $Ph_2PNHC_6H_4PPh_2$ (3): $Ph_2PNHC_6H_4PPh_2$ was synthesized according to a reported method.[12] This procedure involves the deprotonation of 2-(diphenylphosphanyl)benzeneamine with BuLi, followed by reaction with PPh_2Cl to obtain the product.[12] Single crystals for X-ray diffraction were obtained by recrystallization from toluene at −40 °C. ^1H NMR (C_6D_6, 300 MHz): δ = 5.88 (m, 1 H, C_6H_4 3-H), 6.68 (m, 1 H, C_6H_4 5-H), 6.96 (m, 1 H, C_6H_4 6-H), 7.03−7.19 (m, 14 H, C_6H_5 2′-,6′′-H and non-marked rings), 7.30−7.41 (m, 6 H, C_6H_5 3′-,5′-H), 7.72 (m, 1 H, C_6H_4 4-H) ppm. ^{13}C NMR (C_6D_6, 150 MHz): δ = 115.5, 116.0, 120.4, 127.8, 128.3, 128.8, 129.0, 129.1, 129.29, 129.35, 131.5, 131.9, 134.3, 134.6, 135.1, 135.2, 150.5 ppm. ^{31}P NMR (C_6D_6): δ = 21.01 (P_A), 28.01 (P_X) ppm.

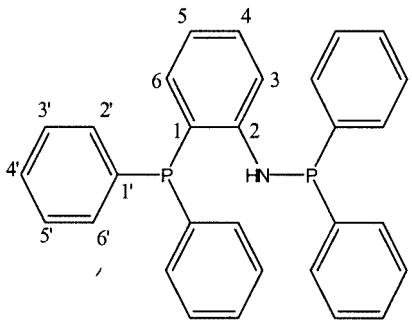

Synthesis of Li($Ph_2PNC_6H_4PPh_2$)$(THF)_2$ (4): *n*BuLi (0.347 g, 5.42 mmol, 1.6 M solution in hexane) was added dropwise at −78 °C under nitrogen to a stirred solution of the ligand $Ph_2PNHC_6H_4PPh_2$ (2.50 g, 5.42 mmol) in THF (50 mL). After stirring at −78 °C for 30 min, the obtained solution was allowed to warm to room temperature and stirred for a further 12 h. The resulting solution was then concentrated to dryness to obtain 2.15 g (85%) of yellow product. Single crystals for X-ray diffraction were obtained by recrystallization of the solid from THF at −20 °C. $C_{38}H_{40}LiNP_2O_2$ (611.2 g): calcd. C 74.61, H 6.60, N 2.29; found C 72.71, H 6.61, N 2.59. ^1H NMR (C_4D_8O, 300 MHz): δ = 1.76 (m, 4 H, CH_2CH_2O), 3.62 (m, 4 H, CH_2O), 6.09 (m, 1 H, C_6H_4 3-H), 6.37 (m, 1 H, C_6H_4 5-H), 6.78 (m, 1 H, C_6H_4 6-H), 6.91−7.02 (m, 6 H, C_6H_5 1′-,3′-,5′-H), 7.18−7.22 (m, 6 H, C_6H_5 1′′-,3′′-,5′′-H), 7.23−7.28 (m, 8 H, C_6H_4 2′-,2′′-,4′-,4′′-H), 7.34 (m, 1 H, C_6H_4 4-H) ppm. ^{13}C NMR (C_4D_8O, 150 MHz): δ = 26.5, 68.6, 114.5 (d, $^1J_{c\text{-}p}$ = 30.0 Hz), 119.6, 120.2, 120.3, 128.1, 129.1, 129.2, 130.0, 130.08, 130.16, 131.9, 131.9, 133.2, 133.6, 134.8, 134.8, 135.7, 136.0, 140.1, 149.6 (d, $^2J_{c\text{-}p}$ = 20.0 Hz) ppm. ^{31}P NMR: (C_6D_6): δ = 12.99 (P_A), 42.46 (P_X) ppm.

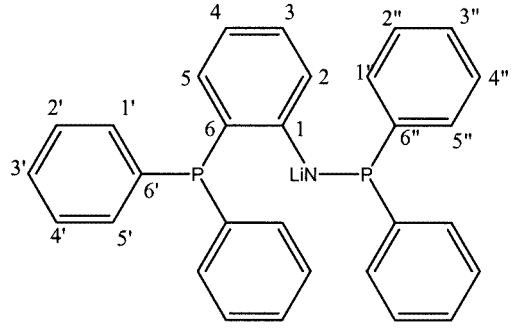

X-ray Crystallographic Study: X-ray crystallographic experiments were carried out with a Nonius Kappa CCD diffractometer with graphite-monochromatized Mo-K_α radiation (λ = 0.71073 Å). Crystals were placed in a Parothone N oil in a glove box. Single crystals were mounted on the diffractometer under a stream of cold N_2 at 230 K. Data were collected using ω and φ scans to cover the Ewald sphere. Accurate cell parameters were obtained with refined collections of intensities and were corrected in the usual way. Structures were solved by direct methods and completed using successive Fourier difference maps. Refinements were performed anisotropically with respect to the non-hydrogen atoms. Hydrogen atoms were placed at calculated positions and refined using the riding model until convergence was reached. Data collection and reduction, cell refinements were carried out with the Nonius software package.[30] Structure solution and refinement were carried out by the SHELXS-97[31] and SHELXL-97[32] software packages, respectively. The ORTEP program incorporated in the TEXRAY Structure Analysis Package was used for molecular graphics.[33] Details are listed in Table 4. CCDC-250098 to -250101 contain the supplementary crystallographic data for this paper. These data can be obtained free of charge at www.ccdc.cam.ac.uk/conts/retrieving.html [or from the Cambridge Crystallographic Data Centre, 12 Union Road, Cambridge CB2 1EZ, UK; Fax: + 44-1223-336-033; E-mail: deposit@ccdc.cam.ac.uk].

Acknowledgments

This research was supported by the German−Israel Foundation under contract I-621-27.5/1999 and by the Fund for the Promotion of Research at Technion.

Table 4. Crystal data collection for complexes **1**−**4**

	1	**2**	**3**	**4**
Empirical formula	$C_{17}H_{15}N_2P$	$C_{25}H_{30}OLiN_2O_2P$	$C_{30}H_{25}NP_2$	$C_{38}H_{40}LiNO_2P_2$
Formula mass	278.28	428.42	461.45	611.59
Temperature [K]	230.0(1)	230.0(2)	230.0(1)	230.0(2)
Wavelength [Å]	0.71070	0.71070	0.71070	0.71070
Crystal system, space group	monoclinic, *C*2/*c*	monoclinic, *P*21/*n*	triclinic, $P\bar{1}$	monoclinic, *P*21/*n*
Unit cell dimensions:				
a [Å]	27.0230(15)	10.1860(3)	10.4130(8)	11.2180(3)
b [Å]	8.2640(6)	14.4800(5)	10.5580(11)	17.0050(6)
c [Å]	14.2330(11)	16.2270(7)	12.1650(11)	18.7330(6)
α [°]	90	90	77.967(6)	90
β [°]	114.444(3)	95.5900(16)	75.626(6)	106.1630(19)
γ [°]	90	90	75.058(4)	90
V [Å^3]	2893.6(3)	2381.99(15)	1236.8(2)	3432.30(19)
Z	8	4	2	4
$D_{calcd.}$ [g/cm^3]	1.278	1.195	1.239	1.184
μ [mm^{-1}]	0.181	0.138	0.194	0.160
F(000)	1168	912	484	1296
Crystal size [mm]	0.15 × 0.10 × 0.10	0.30 × 0.18 × 0.09	0.25 × 0.33 × 0.42	0.30 × 0.21 × 0.15
θ range for data collection [°]	2.60−25.05	2.27−25.04	1.75−25.05	1.65−25.02
Limiting indices:				
h	$0 \le h \le 32$	$-12 \le h \le 12$	$0 \le h \le 12$	$0 \le h \le 13$
k	$0 \le k \le 9$	$17 \le k \le 16$	$-11 \le k \le 12$	$0 \le k \le 20$
l	$-16 \le l \le 15$	$9 \le l \le 19$	$-13 \le l \le 14$	$-22 \le l \le 21$
Reflections collected/unique	2561/2561 [*R*(int) = 0.0000]	7201/4159 [*R*(int) = 0.0461]	4381/4381 [*R*(int) = 0.0000]	6043/6043 [*R*(int) = 0.0000]
Completeness to θ = 25.05°	99.7%	98.8%	99.8%	99.7%
Max./min. transmission	0.9821/0.9734	0.9877/0.9597	0.9857/0.9689	0.9765/0.9537
Refinement method	full-matrix least squares on F^2	full-matrix least squares on F^2	full-matrix least squares on F^2	full-matrix least squares on F^2
Data/restraints/parameters	2561/0/196	4159/0/302	4381/0/323	6043/0/506
Goodness-of-fit on F^2	1.065	0.916	1.027	1.046
Final *R* indices [$I > 2\sigma(I)$]	*R*1 = 0.0676, *wR*2 = 0.1450	*R*1 = 0.0594, *wR*2 = 0.1583	*R*1 = 0.0486, *wR*2 = 0.1133	*R*1 = 0.0547, *wR*2 = 0.1257
R indices (all data)	*R*1 = 0.1159, *wR*2 = 0.1650	*R*1 = 0.1242, *wR*2 = 0.1728	*R*1 = 0.0934, *wR*2 = 0.1240	*R*1 = 0.1022, *wR*2 = 0.1405
Largest difference peak/hole [e·A^{-3}]	0.295/−0.331	0.460/−0.412	0.176/−0.234	0.312/−0.246

[1] [1a] W. N. Setzer, P.v. R. Schleyer, *Adv. Organomet. Chem.* **1985**, *24*, 353−451. [1b] C. Schade, P. v. R. Schleyer, *Adv. Organomet. Chem.* **1987**, *27*, 169−278. [1c] K. Gregory, P. v. R. Schleyer, R. Snaith, *Adv. Inorg. Chem.* **1991**, *37*, 47−142. [1d] R. E. Mulvey, *Chem. Soc. Rev.* **1991**, *20*, 167−209. [1e] J. D. Smith, *Adv. Organomet. Chem.* **1998**, *43*, 267−348. [1f] R. Kempe, *Angew. Chem. Int. Ed.* **2000**, *39*, 468−493.

[2] A. Streitwieser, S. M. Bacharach, A. Dorigo, P. v. R. Schleyer, *Lithium Chemistry: A Theoretical and Experimental Overview* (Eds.: A. M. Sapse, P. v. R. Schleyer), John Wiley, New York, **1995**, chapter 1.

[3] [3a] D. B. Collum, J. S. DePue, *J. Am. Chem. Soc.* **1988**, *110*, 5518−5524. [3b] D. B. Collum, *Acc. Chem. Res.* **1993**, *5*, 227−234 and references cited therein. [3c] D. Seebach, *Angew. Chem. Int. Ed. Engl.* **1988**, *27*, 1624−1654.

[4] [4a] G. L. J. v. Vliet, H. Luitjes, M. Schakel, G. W. Klumpp, *Angew. Chem. Int. Ed.* **2000**, *39*, 1643−1645 and references cited therein. [4b] C. H. Heatcock, *Comprehensive Carbanion Chemistry* (Eds.: E. Buncel, T. Durst); Elsevier, New York, **1980**, vol. B, chapter 4.

[5] V. Snieckus, *Chem. Rev.* **1990**, *90*, 879−933 and references cited therein.

[6] R. T. Boeré, R. T. Oakley, R. W. Reed, *J. Organomet. Chem.* **1987**, *331*, 161−167.

[7] [7a] J. Barker, M. Kilner, *Coord. Chem. Rev.* **1994**, *133*, 219−300. [7b] F. T. Edelmann, *Coord. Chem. Rev.* **1994**, *137*, 403−481.

[8] [8a] D. B. Collum, J. S. DePue, *J. Am. Chem. Soc.* **1988**, *110*, 5524−5533. [8b] A.-M. Sapse, D. C. Jain, K. Raghavachari, *Lithium Chemistry: A Theoretical and Experimental Overview* (Eds.: A. M. Sapse, P. v. R. Schleyer), John Wiley, New York, **1995**, chapter 2. [8c] R. Snaith, D. S. Wright, *Lithium Chemistry: A Theoretical and Experimental Overview* (Eds.: A. M. Sapse, P. v. R. Schleyer), John Wiley, New York, **1995**, chapter 8.

[9] [9a] M. L. Cole, A. J. Davies, C. Jones, P. C. Junk, *J. Organomet. Chem.* **2004**, *689*, 3093−3107. [9b] C. L. Boyd, B. R. Tyrrell, P. Mountford, *Acta Crystallogr., Sect. B* **2002**, *58*, m597−m598. [9c] J. A. R. Schmidt, J. Arnold, *J. Chem. Soc., Dalton Trans.* **2002**, 2890−2899.

[10] [10a] P. B. Hitchcock, M. F. Lappert, D. S. Liu, *J. Chem. Soc., Chem. Commun.* **1994**, 1699−1670. [10b] L. Bourget−merle, M. F. Lappert, J. R. Servern, *Chem. Rev.* **2002**, *102*, 3031−3066. [10c] X. Chen, D. Chenxia, G. Jianping, W. Xuehong, L. Dian-Sheng, *J. Organomet. Chem.* **2002**, *655*, 89−95. [10d] M.-S. Zhou, S.-P. Huang, L.-H. Weng, W.-H. Sun, L. Dian−Sheng, *J. Organomet. Chem.* **2003**, *665*, 237−245. [10e] N. Takeda, H. Hamaki, N. Tokitoh, *Chem. Lett.* **2004**, *33*, 134−135.

[11] [11a] C. Jones, P. C. Junk, S. G. Leary, N. A. Smithies, *J. Chem. Soc., Dalton Trans.* **2000**, 3186−3190. [11b] J. Baldamus, M. L. Cole, U. Helmstedt, E.-M. Hey-Hawkins, C. Jones, P. C. Junk, F. Lange, N. A. Smithies, *J. Organomet. Chem.* **2003**, *665*,

 © 2004 Wiley-VCH Verlag GmbH & Co. KGaA, Weinheim

33−42. [11c] R. J. Bowen, M. A. Fernandes, M. Layh, *J. Organomet. Chem.* **2004**, *689*, 1230−1237. [11d] A. D. Bond, E. L. Doyle, S. J. Kidd, A. D. Woods, D. S. Wright, *Chem. Commun.* **2001**, 777−778.

[12] S. Daniéle, C. Drost, B. Gehehus, S. M. Hawkins, P. B. Hitchcock, M. F. Lappert, P. G. Merle, S. G. Bott, *J. Chem. Soc., Dalton Trans.* **2001**, 3179−3188.

[13] [13a] E. Muller, J. Muller, H.-G. Schmidt, M. Noltemeyer, F. T. Edelmann, *Phosphorus, Sulfur Silicon Relat. Elem.* **1996**, *119*, 121−126. [13b] A. Steiner, D. Stalke, *J. Chem. Soc., Chem. Commun.* **1994**, 2607−2608. [13c] M. Schultz, B. F. Straub, P. Hofmann, *Acta Crystallogr., Sect. B* **2002**, *58*, m256−m257. [13d] N. Poetschke, M. Nieger, M. A. Khan, E. Niecke, M. T. Ashby, *Inorg. Chem.* **1997**, *36*, 4087−4093. [13e] G. Trinquier, M. T. Ashby, *Inorg. Chem.* **1994**, *33*, 1306−1313.

[14] [14a] F. Baier, Z. Fei, H. Gornitzka, A. Murso, S. Neufeld, M. Pfeiffer, I. Rüdenauer, A. Steiner, T. Stey, D. Stalke, *J. Organomet. Chem.* **2002**, *661*, 111−127. [14b] A. Steiner, D. Stalke, *Organometallics* **1995**, *14*, 2422−2429. [14c] T. L. Schull, S. L. Brandow, W. J. Dressick, *Tetrahedron Lett.* **2001**, *42*, 5373−5376.

[15] W. Zhong-Xia, W. Da-Qi, D. Jian-Min, *J. Organomet. Chem.* **2003**, *665*, 205−213.

[16] [16a] M.-H. Huang, L.-C. Liang, *Organometallics* **2004**, *23*, 2813−2816. [16b] L.-C. Liang, J.-M. Lin, C.-H. Hung, *Organometallics* **2004**, *22*, 3007−3009.

[17] A. Lisovskii, M. Botoshansky, M. S. Eisen, *J. Chem. Soc., Dalton Trans.* **2001**, 1692−1698.

[18] [18a] V. Volkis, E. Nelkenbaum, A. Lisovskii, G. Hasson, R. Semiat, M. Kapon, M. Botoshansky, Y. Eishen, M. S. Eisen, *J. Am. Chem. Soc.* **2003**, *125*, 2179−2194. [18b] M. S. Eisen, M. Kapon, *J. Chem. Soc., Dalton Trans.* **1994**, 3507−3510.

[19] [19a] D. Herscovics-Korine, M. S. Eisen, *J. Organomet. Chem.* **1995**, *503*, 307−314. [19b] R. Gomez, R. Duchateau, A. N. Chernega, A. Meetsma, F. T. Edelmann, J. H. Teuben, M. L. H. Green, *J. Chem. Soc., Dalton Trans.* **1995**, 217−225. [19c] R. Gomez, M. L. H. Green, J. L. Haggitt, *J. Chem. Soc., Chem. Commun.* **1994**, 2607−2608. [19d] V. Volkis, M. Shmulinson, C. Averbuj, A. Lisovskii, F. T. Edelmann, M. S. Eisen, *Organometallics* **1998**, *17*, 3155−3157. [19e] C. Averbuj, E. Tish, M. S. Eisen, *J. Am. Chem. Soc.* **1998**, *120*, 8640−8648.

[20] T. Stey, D. Stalke, *Organolithium Compounds* (Eds.: Z. Rappoport, I. Marek), John Wiley, New York, **2004**, chapter 2.

[21] A. D. Bond, E. L. Doyle, S. J. Kidd, A. D. Woods, D. S. Wright, *Chem. Commun.* **2001**, 777−778.

[22] [22a] D. Barr, W. Clegg, R. E. Mulvey, R. Snaith, *Chem. Commun.* **1984**, 469−470. [22b] D. Barr, W. Clegg, R. E. Mulvey, R. Snaith, *J. Chem. Soc., Chem. Commun.* **1984**, 700−701. [22c] L. M. Engelhardt, G. E. Jacobsen, P. C. Junk, C. L. Raston, B. W. Skelton, A. H. White, *J. Chem. Soc., Dalton Trans.* **1988**, 1011−1020. [22d] M. Tayebani, S. Gambarotta, G. Yap, *Organometallics* **1998**, *17*, 3639−3641. [22e] M. S. Hill, P. B. Hitchcock, *Angew. Chem. Int. Ed.* **2001**, *40*, 4089−4092. [22f] S. R. Boss, R. Haigh, D. J. Linton, A. E. H. Wheatly, *J. Chem. Soc., Dalton Trans.* **2002**, 3129−3134. [22g] N. Feeder, R. Snaith, A. E. H. Wheatly, *Eur. J. Inorg. Chem.* **1998**, 879−883. [22h] S. T. Liddle, W. Clegg, *J. Chem. Soc., Dalton Trans.* **2001**, 402−408. [22i] M. Polamo, M. Leskelä, *J. Chem. Soc., Dalton Trans.* **1996**, 4345−4349. [22j] R. Kempe, A. Spannenberg, S. Brenner, *Z. Krystallogr.* **1996**, *211*, 569−570.

[23] [23a] S. M. Aucott, A. M. Z. Slawin, J. D. Woollins, *J. Organomet. Chem.* **1999**, *582*, 83−89. [23b] S. M. Aucott, A. M. Z. Slawin, D. Woollins, *J. Chem. Soc., Dalton Trans.* **2000**, 2559−2576.

[24] H. Gornitzka, D. Stalke, *Organometallics* **1994**, *13*, 4398−4405.

[25] S. Wingerter, M. Pfeiffer, A. Murso, C. Lustig, T. Stey, V. Chandrasekhar, D. Stalke, *J. Am. Chem. Soc.* **2001**, *123*, 1381−1388.

[26] F. Garc, A. D. Hopkins, S. M. Humphrey, M. McPartlin, M. C. Rogers, D. S. Wright, *Dalton Trans.* **2004**, 361−362.

[27] K. W. So, C.-T. Yang, J. J. Vittal, J. D. Ranford, *Inorg. Chim. Acta* **2003**, *349*, 135−141.

[28] O. Kühl, T. Koch, F. B. Somoza, Jr., P. C. Junk, E. Hey-Hawkins, D. Plat, M. S. Eisen, *J. Organomet. Chem.* **2000**, *604*, 116−125.

[29] M. P. Coles, P. B. Hitchcock, *Chem. Commun.* **2002**, 2794−2795.

[30] *Nonius*, Kappa CCD Collect Program for data collection and HKL, Schalepack and Denzo (Otwinowski & Minor, **1997**), software package for data reduction and cell refinement.

[31] G. M. Sheldrick, *Acta Crystallogr., Sect. A* **1990**, *46*, 467−473.

[32] G. M. Sheldrick, *SHELXL-97, Program for the refinement of crystal structures*, University of Göttingen, Germany, **1997**.

[33] Molecular Structure Corporation, *ORTEP*, TEXRAY Structure Analysis Package, MSC, 3200, Research Forest Drive, The Woodlands, TX 77381, USA, **1999**.

Received April 29, 2004
Early View Article
Published Online November 4, 2004

 © 2004 Wiley-VCH Verlag GmbH & Co. KGaA, Weinheim

Thallium−Arene Contacts in a Rare Yttrium Tris(pyrazolyl)hydroborate "ate" Complex

Fábio A. Kunrath,[a] Osvaldo L. Casagrande Jr.,*[b] Loic Toupet,[c] and Jean-François Carpentier*[d]

Keywords: Arene ligands / N ligands / Noncovalent interactions / Thallium / Yttrium

A salt elimination reaction between $[YCl_3(THF)_{3.5}]$ and 1 or 2 equiv. of $Tl(Tp^{Ms*})$ [Tp^{Ms*} = HB(3-mesitylpyrazolyl)$_2$(5-mesitylpyrazolyl)$^-$] leads in both cases to single metathesis, giving a mixture of the mono-Tp^{Ms*} complex $[YCl_3(Tp^{Ms*})Tl]$ (**1**) and another complex, $[YCl_2(Tp^{Ms**})]$ (**2**) [Tp^{Ms**} = HB(3-mesitylpyrazolyl)(5-mesitylpyrazolyl)$_2^-$], that results from the transfer of a second mesityl group to the 5-position of the pyrazolyl ring. The solid-state structure of **1** shows a unique "ate" dimeric structure with the Tl^+ cations coordinated by two μ^2- and two μ^3-bridging Cl atoms as well as two η^3-mesityl ligands.

(© Wiley-VCH Verlag GmbH & Co. KGaA, 69451 Weinheim, Germany, 2004)

Introduction

Tris(pyrazolyl)hydroborate (Tp) ligands, first introduced by Trofimenko,[1] are an attractive class of sterically demanding ancillaries for a wide variety of ionic metal centers.[2] Of particular interest is the case of group 3 metals,[3] due to their predominant ionic character. Indeed, one of the most attractive features of the Tp ligands is their steric tunability. This is a crucial advantage in lanthanide chemistry, which is recognized to be largely affected by steric factors.[4] Half-sandwich trivalent lanthanide Tp halide complexes are commonly prepared by salt metathesis (elimination) routes from the corresponding $LnX_3(L)_n$ (L = donor solvent) and $M(Tp^R)$ salts, leading to the desired neutral $[Ln(Tp^R)X_2]$ or $[Ln(Tp^R)_2X]$ complexes.[3] This procedure is sometimes plagued by the formation of ionic "ate" complexes, a feature very often observed in lanthanide chemistry with alkali metal salts.[4] A few examples of such lanthanide Tp "ate" complexes have indeed been reported, for example $[Na(THF)_3][YbCl_3(Tp^{Me2})]$ and $[H_2pz^{Me2}][YbCl_3(Tp^{Me2})]$.[5] The use of thallium salts has so far been considered to prevent this undesired formation, as TlCl usually precipitates irreversibly from solution. In this contribution, we report the first example of a lanthanide "ate" complex containing a thallium atom, which shows unusual thallium−arene contacts with the aromatic rings of a Tp ligand bearing mesityl substituents in the solid state. Migration of a mesityl group during coordination of the Tp^{Ms*} ligand to the yttrium atom is also described.

[a] Instituto de Química de Araraquara, UNESP,
C. P. 355, Araraquara, SP 14800-900, Brazil
[b] Laboratório de Catálise Molecular, Instituto de Quimica-Universidade Federal do Rio Grande do Sul,
Av. Bento Goncalves, 9500 Porto Alegre, RS 90501-970, Brazil
[c] Groupe Matière Condensée et Matériaux, Cristallochimie, UMR 6626 CNRS-Université de Rennes 1,
35042 Rennes Cedex, France
[d] Laboratoire Organométalliques et Catalyse, UMR 6509 CNRS-Université de Rennes 1,
35042 Rennes Cedex, France
Fax: + 33-2-23236939
E-mail: jean-francois.carpentier@univ-rennes1.fr

Results and Discussion

We are interested in the coordination of the Tp^{Ms*} ligand [Tp^{Ms*} = HB(3-mesitylpyrazolyl)$_2$(5-mesitylpyrazolyl)$^-$] to group 3 metal centers because of its particular steric properties that confer very high polymerization activity towards ethylene to some related catalyst species.[6] Salt-elimination reactions of $[YCl_3(THF)_{3.5}]$ with 1 or 2 equiv. of $Tl(Tp^{Ms*})$ in THF under different conditions (20−60 °C, 1−7 d) led only to mono-Tp complexes. This observation likely reflects the high steric hindrance of the Tp^{Ms*} ligand to the small yttrium atom. These reactions are, however, not as selective as with the ubiquitous Tp^{Me2} ligand. In fact, besides significant amounts of free 3-mesitylpyrazole (Hpz^{Ms}; ca. 10−20% based on initial Tp^{Ms*}) arising from the decomposition of the Tp^{Ms*} ligand,[5] mixtures of two Tp complexes were invariably produced [Equation (1)]. The most abundant complex formed (NMR yield in the range 20−50% based on Y, depending on the reaction conditions) is the mono-Tp^{Ms*} complex $[YCl_3(Tp^{Ms*})Tl]$ (**1**), which is readily separated from the mixtures by recrystallization due to its poor solubility in toluene, consistent with its ionic "ate"

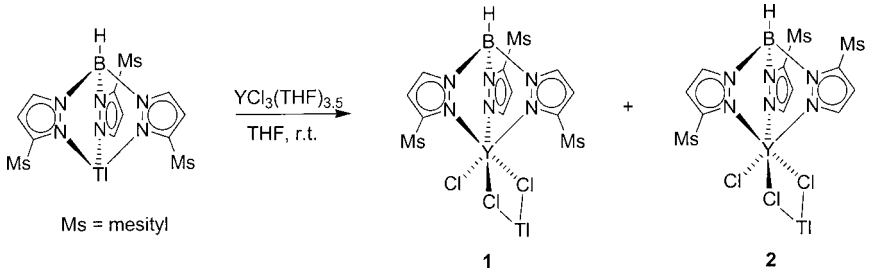

(1)

nature. Complex **1** is, to the best of our knowledge, the first structurally characterized example of a group 3 metal complex incorporating a thallium cation, irrespective of the nature of the other ancillary ligands. The identity of **1** was unambiguously established by a single-crystal X-ray diffraction study, elemental analysis, and NMR spectroscopy. Key ^{1}H NMR resonances for **1** in [D$_8$]THF include a set for one 5-mesitylpyrazolyl ring and a set for the two 3-mesitylpyrazolyl rings. The 3-H signal of the 5-mesitylpyrazolyl ring appears at lower field (δ = 8.08 ppm) than the 5-H signals of the 3-mesitylpyrazolyl rings (δ = 7.65 ppm), as observed previously in [Tp^{Ms*}ZrCl$_3$].[6c] The second complex present in the mixture (**2**; ca. 15−30% based on Y) shows an inversion (2:1 vs. 1:2 in **1**) of the relative intensities of the 5-mesityl- and 3-mesitylpyrazolyl sets. This pattern is consistent with the formation "[YCl$_2$(Tp^{Ms**})]" (**2**) [Tp^{Ms**} = HB(3-mesitylpyrazolyl)(5-mesitylpyrazolyl)$_2^-$].[7−9] This Tp^{Ms*}/Tp^{Ms**} rearrangement indicates that the B−N bonds in these yttrium systems are labile, as also observed recently in the preparation of [NiCl(Tp^{Ms**})][6f] and the hydrolysis product [{(Tp^{Ms**})ZrCl$_2$}$_2$(μ-O)].[6c] Crystal data and refinement details for **1** are summarized in the Exp. Sect., and selected bond lengths and angles are listed in Table 1. Two independent molecules were found in the asymmetric unit of **1**, but both are quite similar, so that only the distances and the angles for one of them are listed in Table 1. As depicted in Figure 1, complex **1** is dimeric in the solid state with a structure that can be described as two pseudo-octahedral [Y(Tp^{Ms*})Cl$_3$]$^-$ anions that are bound to two Tl$^+$ cations by three bridging Cl atoms. The Cl(1) and Cl(3) atoms are doubly bridging between Y(1) and Tl(2)/Tl(2)* and the Cl(2) atom is triply bridging between Tl(2), Tl(2)* and Y(1). The Tl···Tl separation of 4.870 Å is non-bonding considering the sum of the van der Waals

Table 1. Selected bond lengths [Å] and angles [°] for [(Tp^{Ms*})YCl$_3$]-Tl·2THF (**1**)

Y(1)−Cl(1)	2.5750(15)	Tl(2)−Cl(2)	3.1155(13)
Y(1)−Cl(2)	2.5955(15)	Tl(2)−Cl(3)	3.1240(15)
Y(1)−Cl(3)	2.5667(14)	Tl(2)−Cl(2)*	3.1320(15)
Y(1)−N(2)	2.460(4)	Tl(2)−Cl(1)*	3.1420(15)
Y(1)−N(4)	2.457(4)	Ct(01)−Tl(2)*	3.224
Y(1)−N(6)	2.401(5)	Ct(02)−Tl(2)*	3.312
Cl(1)−Y(1)−Cl(2)	94.62(5)	Cl(3)−Y(1)−N(4)	91.31(12)
Cl(1)−Y(1)−Cl(3)	95.29(5)	Cl(3)−Y(1)−N(6)	90.55(12)
Cl(2)−Y(1)−Cl(3)	95.20(5)	N(2)−Y(1)−N(4)	78.91(15)
Cl(1)−Y(1)−N(2)	92.83(1)	N(2)−Y(1)−N(6)	78.82(15)
Cl(1)−Y(1)−N(4)	167.70(11)	N(4)−Y(1)−N(6)	78.31(15)
Cl(1)−Y(1)−N(6)	91.23(11)	Cl(2)−Tl(2)−Cl(3)	75.32(4)
Cl(2)−Y(1)−N(2)	94.54(11)	Y(1)−Cl(2)−Tl(2)	94.47(4)
Cl(2)−Y(1)−N(4)	95.11(11)	Y(1)−Cl(3)−Tl(2)	94.85(5)
Cl(2)−Y(1)−N(6)	171.38(12)		
Cl(3)−Y(1)−N(2)	166.77(11)		

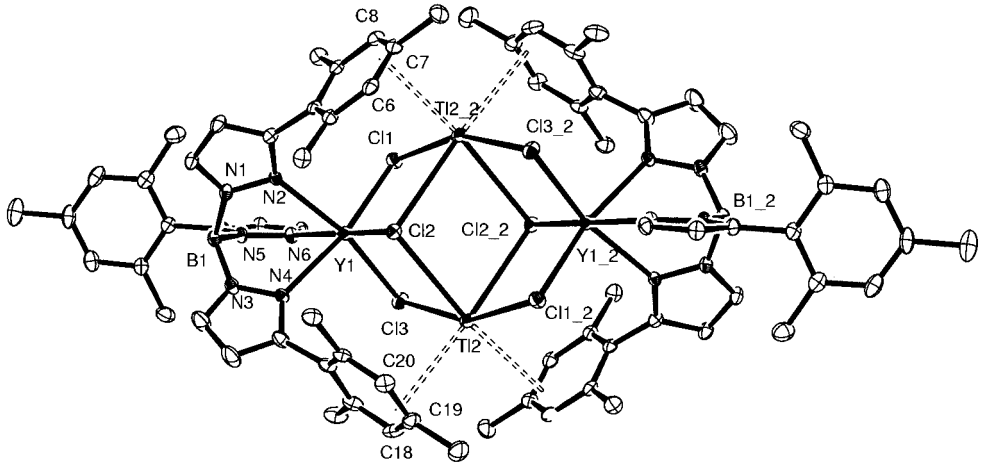

Figure 1. Molecular structure of compound **1** (ellipsoids at 30% probability level; hydrogen atoms omitted for clarity)

 © 2004 Wiley-VCH Verlag GmbH & Co. KGaA, Weinheim

radii (4.00 Å).[10] Each thallium cation is coordinated to four Cl atoms with similar distances [average Tl−Cl = 3.1283(15) Å]. Interestingly, in addition to the chloro ligands, there are six Tl···C contacts from two mesityl groups at less than 3.60 Å [C(6)*−C(8)*: 3.280−3.542 Å; C(18)−C(20): 3.374−3.565 Å]; this value is slightly lower than the sum of the van der Waals radii of Tl[10] and an aromatic ring (3.73 Å).[11] These contacts are in the upper limit of the range (3.10−3.50 Å) for Tl−C bonds in complexes with discrete arenes η^6-bonded to Tl^+.[12] Although others have considered 3.74 Å as an upper bonding limit,[13] the remaining six Tl···C(mesityl) contacts in **1** (3.635−3.859 Å and 3.696−3.850 Å for the two rings) are significantly longer and we prefer to view them as essentially non-interacting. Overall, the geometry around the thallium atoms can thus be described as distorted octahedral by considering the centroid of the η^3-mesityl ligands as a monodentate ligand [Cl(2)−Tl(2)−Ct(01)* = 157.14°; Cl(2)*−Tl(2)−Ct(02)* = 159.27°; Cl(3)−Tl(2)−Ct(01)* = 160.33°]. The average thallium−centroid distance is 3.268 Å.

The yttrium center features a distorted octahedral geometry as evidenced by the *cis*-L−Y−L angles [78.31(15)−95.29(5)°]. As expected, the N−Y−N angles involving the pyrazolyl-ring donor atoms are all smaller than 90°, allowing the face formed by three chloride ligands to open considerably. The average Y−N and Y−Cl distances of 2.439(4) and 2.579(15) Å, respectively, are comparable to those found in other yttrium−Tp^{Me2} complexes, such as [$Y(Tp^{Me2})Cl_2$(phen)][14] [2.448(6) and 2.600(2) Å, respectively]. The modest torsion-angle values in **1** [B(1)−N(1)−N(2)−Y(1) = −3.0(6)°; B(1)−N(3)−N(4)−Y(1) = 0.3(7)°; B(1)−N(5)−N(6)−Y(1) = −5.7(6)°] are diagnostic of relatively low steric congestion around the yttrium center due to the coordination of just one Tp^{Ms*} ligand to the metal center.

Conclusion

In conclusion, we have described an unusual dimeric "ate" species that features Tl^+ cations coordinated by μ^2,μ^3-bridging Cl atoms as well as two η^3-mesityl ligands. The present Tl···C contacts can be viewed as supramolecular interactions which fill the large gap in the Tl coordination sphere,[15] but they may also be the origin of the formation of this unique Y−Tl "ate" complex. Decomposition and isomerization processes, generating a free pyrazole group and an isomerized Tp^{Ms**} ligand coordinated to a lanthanide metal center, have also been seen. These new elements further show the complexity of lanthanide−Tp chemistry when using salt-elimination routes.

Experimental Section

Salt Elimination Reaction between Tl(Tp^{Ms*}) and [$YCl_3(THF)_{3.5}$]. Synthesis of [$YCl_3(Tp^{Ms*})Tl$] (1) and "[$Y(Tp^{Ms**})Cl_2$]" (2): All manipulations were performed under purified argon using standard high-vacuum Schlenk techniques or in a glovebox. Solvents were distilled from Na/benzophenone (THF) and Na/K alloy (toluene) under argon and degassed thoroughly prior to use. In a typical procedure, [$YCl_3(THF)_{3.5}$] (0.380 g, 0.85 mmol) and THF (40 mL) were introduced into a Schlenk flask and the suspension was stirred at 70 °C for 3 h. The clear solution was cooled slowly to room temperature and a solution of Tl(Tp^{Ms*})[17] (0.650 g, 0.85 mmol) in THF (30 mL) was added dropwise with a cannula over 15 min. A grayish solid precipitated immediately. The mixture was stirred for 2 h, and then it was filtered and volatiles were removed from the filtrate under vacuum. The ^{1}H NMR spectrum ([D_8]THF, 300 MHz, 20 °C) of the residue showed the absence of initial reagents and the presence of free 3-mesitylpyrazole [δ = 7.57 (s, 1 H, 5-H pz), 6.85 (s, 2 H, *m*-C_6H_2 Ms), 6.06 (s, 1 H, 4-H pz), 2.32 (s, 3 H, 4-Me Ms), 2.01 (s, 6 H, 2-,6-Me Ms) ppm], [$YCl_3(Tp^{Ms*})Tl$] (**1**) [δ = 8.08 (s, 1 H, 3-H pz), 7.69 (s, 2 H, 5-H pz), 6.97 (s, 2 H, C_6H_2 Ms), 6.82 (s, 4 H, C_6H_2 Ms), 6.10 (s, 1 H, 4-H pz), 6.00 (s, 2 H, 4-H pz), 2.36 (s, 3 H, Me Ms), 2.26 (s, 6 H, 2 Me Ms), 2.05 (s, 9 H, 3 Me Ms), 1.87 (s, 6 H, 2 Me Ms), 1.72 (s, 6 H, 2 Me Ms) ppm] and another species assigned to "[$YCl_2(Tp^{Ms**})$]" (**2**) [key resonances: δ = 8.17 (d, $J_{H,H}$ = 2.0 Hz, 2 H, 3-H pz), 7.42 (d, $J_{H,H}$ = 2.1 Hz, 1 H, 5-H pz), 6.81 (s, 2 H, C_6H_2 Ms), 6.71 (s, 4 H, C_6H_2 Ms), 5.96 (d, $J_{H,H}$ = 2.1 Hz, 2 H, 4-H pz), 5.90 (d, $J_{H,H}$ = 2.1 Hz, 1 H, 4-H pz) ppm] in a ratio of 5:2:1. The residue was extracted with toluene (2 × 40 mL) and filtered. The clear solution was left at room temperature for 48 h, during which time a colorless crystalline material precipitated. This was filtered off, washed with toluene (2 × 15 mL) and dried under vacuum to afford **1** as a white crystalline solid (0.310 g, 33%), from which X-ray quality crystals were collected. $C_{36}H_{40}BCl_3N_6TlY$ (967.22): calcd. C 44.71, H 4.17, N 8.69; found C 44.26, H 4.35, N 9.12.

Crystallographic Data for 1·2THF: $C_{88}H_{112}B_2Cl_6N_{12}O_4Tl_2Y_2$, M = 2222.78, triclinic, T = 120 K, space group $P\bar{1}$, a = 14.8421(2), b = 17.1968(3), c = 19.1037(3) Å, α = 83.200(1), β = 78.279(1), γ = 78.986(1)°, V = 4670.3(1) Å^3, Z = 2, D_c = 1.581 g·cm^{-3}, μ(Mo-K_α) = 4.896 mm^{-1}; 21392 reflections collected, 15501 unique, full-matrix least squares on F^2 refinement, R_1 = 0.0486 [$I > 2\sigma(I)$], wR_2 = 0.1060 [$I > 2\sigma(I)$] (0.1224 for all data). An orange crystal of dimensions 0.45 × 0.38 × 0.30 mm was coated with oil, mounted on a fiber and X-ray diffraction data were collected using a Nonius KappaCCD diffractometer with graphite-monochromated Mo-K_α radiation (λ = 0.71073 Å) employing CCD scans to cover the reciprocal space up to 27.50° with 99.7% completeness. Integration of raw data yielded a total of 60449 reflections, merged into 15501 unique reflections with R_{int} = 0.0823 after applying Lorentz, polarization and absorption correction. The structure was solved by Patterson methods using SHELXS-97.[16] Atomic positions and displacement parameters, at the anisotropic level for all non-hydrogen atoms, were refined using full-matrix least-squares procedures based on F^2 using SHELXL-97.[16] Refinement of 1016 parameters using all reflections converged at R_1 = 0.0486, wR_2 = 0.1060. The locations of the largest peaks in the final difference Fourier map calculation as well as the magnitude of the residual electron densities (highest residual electron density peak of 1.2 Å^3) were of no chemical significance. The cell of **1** was found to contain four molecules of crystallization (THF). CCDC-237703 contains the supplementary crystallographic data for this paper. These data can be obtained free of charge at www.ccdc.cam.ac.uk/conts/retrieving.html [or from the Cambridge Crystallographic Data Centre, 12 Union Road, Cambridge, CB2 1EZ, UK; Fax: + 44-1223-336-033; E-mail: deposit@ccdc.cam.ac.uk].

 © 2004 Wiley-VCH Verlag GmbH & Co. KGaA, Weinheim

Acknowledgments

This work was financially supported by the Brazilian-French Capes-Cofecub (Grant 382/02) and the Centre National de la Recherche Scientifique (CNRS).

[1] [1a] S. Trofimenko, *J. Am. Chem. Soc.* **1967**, *89*, 3170−3177. [1b] S. Trofimenko, *J. Am. Chem. Soc.* **1967**, *89*, 6288−6294.

[2] [2a] S. Trofimenko, *Chem. Rev.* **1993**, *93*, 943−980. [2b] N. Kitajima, W. B. Tolman, *Prog. Inorg. Chem.* **1995**, *43*, 419−531. [2c] G. Parkin, *Adv. Inorg. Chem.* **1995**, *42*, 291−393. [2d] D. L. Reger, *Coord. Chem. Rev.* **1996**, *147*, 571−595. [2e] S. Trofimenko, *Scorpionate: The Coordination Chemistry of Polypyrazolylborate Ligands*, Imperial College Press, London, **1998**.

[3] N. Marques, A. Sella, J. Takats, *Chem. Rev.* **2002**, *102*, 2137−2160.

[4] Recent organolanthanide reviews: [4a] H. Schumann, J. A. Meese-Marktscheffel, L. Esser, *Chem. Rev.* **1995**, *95*, 865−986. [4b] R. Anwander, W. A. Herrmann, *Top. Curr. Chem.* **1996**, *179*, 1−32. [4c] F. T. Edelmann, *Top. Curr. Chem.* **1996**, *179*, 247−276. [4d] R. Anwander, in *Applied Homogeneous Catalysis with Organometallic Compounds* (Eds.: B. Cornils, W. A. Herrmann), Wiley, Weinheim, **1996**, vol. 2, p. 866−892. [4e] R. Anwander, *Top. Organomet. Chem.* **1999**, *2*, 1−61. [4f] G. A. Molander, E. C. Dowdy, *Top. Organomet. Chem.* **1999**, *2*, 119−154. [4g] S. Arndt, J. Okuda, *Chem. Rev.* **2002**, *102*, 1953−1976.

[5] C. Apostolidis, A. Carvalho, A. Domingos, B. Kanellakopoulos, R. Maier, N. Marques, A. Pires de Matos, J. Rebizant, *Polyhedron* **1999**, *18*, 263−272.

[6] [6a] S. Murtuza, O. L. Casagrande Jr., R. F. Jordan, *Organometallics* **2002**, *21*, 1882−1890. [6b] K. Michiue, R. F. Jordan, *Macromolecules* **2003**, *36*, 9707−9709. [6c] K. Michiue, R. F. Jordan, *Organometallics* **2004**, *23*, 460−470. [6d] L. G. Furlan, M. P. Gil, O. L. Casagrande Jr., *Macromol. Rapid Commun.* **2000**, *21*, 1054−1057. [6e] M. P. Gil, J. H. Z. dos Santos, O. L. Casagrande Jr., *Macromol. Chem. Phys.* **2001**, *202*, 319−324. [6f] F. A. Kunrath, O. L. Casagrande Jr., R. F. De Souza, N. Brooks, V. Young Jr., *Organometallics* **2003**, *22*, 4739−4743. [6g] M. P. Gil, O. L. Casagrande Jr., *J. Organomet. Chem.* **2004**, *689*, 286−292.

[7] Complex **2** could not be isolated in pure form (samples were still contaminated by **1**) and no elemental analysis could be run to establish if it is a neutral or an "ate" complex.

[8] Similar salt-elimination reactions using 2 equiv. of the symmetrically bonded Tl(Tp^{Ms}) [instead of Tl(Tp^{Ms*})] in THF under different conditions led systematically to mixtures of products, of which the NMR spectra in [D_8]THF indicated the presence of the isomerization complexes **1** (> 30%) and **2** (> 10%) and other unidentified products. Attempts to isolate products from these mixtures were unsuccessful.

[9] Tp^{Ms} and Tp^{Ms*} complexes of Yb^{II} have been prepared, and isomerization of Tp^{Ms} to Tp^{Ms*} has been observed to take place during the salt-metathesis process: I. Lopes, R. Dias, A. Domingos, N. Marques, *J. Alloys Compd.* **2002**, *344*, 60−64.

[10] A. Bondi, *J. Phys. Chem.* **1964**, *68*, 441−451.

[11] L. C. Pauling, *The Nature of the Chemical Bond*, Cornell University Press, Ithaca, NY, **1960**.

[12] [12a] M. D. Noirot, O. P. Anderson, S. H. Straus, *Inorg. Chem.* **1987**, *26*, 2216−2223. [12b] H. Schmidbaur, W. Bublak, B. Huber, J. Hofmann, G. Müller, *Chem. Ber.* **1989**, *122*, 265−270. [12c] W. Frank, G. Korrell, G. J. Reiss, *Z. Anorg. Allg. Chem.* **1995**, *621*, 765−770. [12d] W. Frank, G. Korrell, G. J. Reiss, *J. Organomet. Chem.* **1996**, *506*, 293−300.

[13] [13a] F. Wiesbrock, H. Schmidbaur, *J. Am. Chem. Soc.* **2003**, *125*, 3622−3630. [13b] C. H. Galka, L. H. Gade, *Inorg. Chem.* **1999**, *38*, 1038−1039.

[14] D. Roitershtein, A. Domingos, L. C. J. Pereira, J. R. Ascenso, N. Marques, *Inorg. Chem.* **2003**, *42*, 7666−7673.

[15] G. B. Deacon, E. E. Delbridge, C. M. Forsyth, B. W. Skelton, A. H. White, *J. Chem. Soc., Dalton Trans.* **2000**, 745−751.

[16] [16a] G. M. Sheldrick, *SHELXS-97, Program for the Determination of Crystal Structures*, University of Göttingen, Germany, **1997**. [16b] G. M. Sheldrick, *SHELXL-97, Program for the Refinement of Crystal Structures*, University of Göttingen, Germany, **1997**.

[17] A. L. Rheingold, C. B. White, S. Trofimenko, *Inorg. Chem.* **1993**, *32*, 3471−3477.

Received May 4, 2004
Early View Article
Published Online October 26, 2004

 © 2004 Wiley-VCH Verlag GmbH & Co. KGaA, Weinheim

Synthesis and Structural Characterization of Three-Coordinate Mn^{II}, Fe^{II}, and Zn^{II} Complexes Containing a Bulky Diamide Ligand $[DippN(CH_2)_3NDipp]^{2-}$ (Dipp = 2,6-*i*$Pr_2C_6H_3$)

Jianfang Chai,[a] Hongping Zhu,[a] Qingjun Ma,[a] Herbert W. Roesky,*[a] Hans-Georg Schmidt,[a] and Mathias Noltemeyer[a]

Keywords: Iron / Manganese / N ligands / Zinc

The reaction of $DippNH(CH_2)_3NHDipp$ (**1**) (Dipp = 2,6-*i*$Pr_2C_6H_3$) with 2 equiv. of MeLi in diethyl ether resulted in the formation of the monomeric dilithium salt $[(Dipp)N(CH_2)_3N(Dipp)][Li(OEt_2)]_2$ (**2**) in high yield. Further reactions of **2** with $MnCl_2$, $FeCl_2$, and $ZnCl_2$, respectively, afforded the complexes $[M_2\{N(Dipp)(CH_2)_3N(Dipp)\}_2]$ [M = Mn (**3**), Fe (**4**), Zn (**5**)] with three-coordinate metal centers. Complexes **2**–**5** were characterized by X-ray structural analysis. The complexes contain a nonplanar MNMN central core. The diamide ligand in complexes **3**–**5** displays a boat conformation and is both chelating and bridging, so that one of the nitrogen atoms is three-coordinate and the other four-coordinate. Complexes **3**–**5** are the first examples with diamide ligands in such a bonding mode. The magnetic investigations of compounds **3** and **4** reveal an antiferromagnetic exchange between the metal atoms.
(© Wiley-VCH Verlag GmbH & Co. KGaA, 69451 Weinheim, Germany, 2004)

Introduction

Transition metal complexes with three-coordinate metal centers are rare, since it is difficult to reach the preferred stable configurations with 16 or 18 valence electrons around the metal center using only three donor ligands.[1] Metal amide complexes are of wide interest as they show a broad range of structures and reaction types.[2] Transition metal amides, for instance, are the first examples with unusually low coordinate metal centers due to the strong M−N bonds and flexible steric properties of the amine ligands.[2b] In addition, transition metal amides are a useful hydrocarbon-soluble source of M^{n+} cations and have proved to be good starting materials to prepare other species.[3] However, reports of saturated hydrocarbon-bridged bidentate diamide ligands are rare.[2b] Considering the recent success in the synthesis of complexes of main-group elements, transition metals and lanthanides of unusual properties with the Dippnacnac ligand $[HC(CMeNDipp)_2]^-$ (Dipp = 2,6-*i*$Pr_2C_6H_3$),[4] we were interested in investigating the behavior of the bulky chelating diamide ligand $[DippN(CH_2)_3NDipp]^{2-}$, which has similar steric properties to Dippnacnac and is expected to result in interesting new organometallic chemistry.

The bulky chelating diamide ligand $[DippN(CH_2)_3NDipp]^{2-}$ was previously used by McConville and co-workers as a non-cyclopentadienyl ligand to prepare group 4 complexes that can catalyze olefin polymerization under "living" conditions.[5] Cloke and Roesky et al. have reported lanthanide complexes bearing this ligand.[6] Recently, we obtained the aluminum hydride $[DippN(CH_2)_3NDipp]AlH(NMe_3)$ and its derivatives $\{[DippNH(CH_2)_3NDipp]Al\}_2(\mu\text{-}E)_2$ (E = S, Se and Te) by hydrogen transfer from chalcogen to nitrogen.[7] Herein we describe the synthesis and structural analysis of the dilithium salt $[N(Dipp)(CH_2)_3N(Dipp)][Li(OEt_2)]_2$ (**2**) and the resulting complexes with three-coordinate Mn^{II}, Fe^{II}, and Zn^{II} of composition $[M_2\{N(Dipp)(CH_2)_3N(Dipp)\}_2]$ [M = Mn (**3**), Fe (**4**), Zn (**5**)].

Results and Discussion

Synthesis of Compounds 2−5

The lithiation of $DippNH(CH_2)_3NHDipp$ (**1**) with 2 equiv. of MeLi in diethyl ether proceeds smoothly to afford $[(Dipp)N(CH_2)_3N(Dipp)][Li(OEt_2)]_2$ (**2**) as colorless crystals in high yield (Scheme 1). The existence of the coordi-

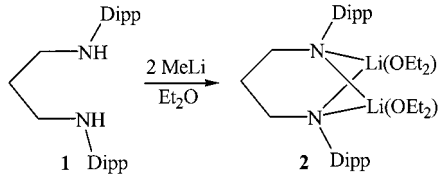

Scheme 1

[a] Institut für Anorganische Chemie, Universität Göttingen, Tammannstrasse 4, 37077 Göttingen, Germany
Fax: + 49-551-393-373
E-mail: hroesky@gwdg.de

nated diethyl ether molecules was confirmed by ^{1}H NMR spectroscopy, elemental analysis, and an X-ray solid-state structural analysis. The dilithium salt **2** is soluble in diethyl ether and stable under an inert gas and is a useful reagent for metathesis reactions with metal halides.

The reaction of **2** with 1 equiv. of anhydrous $MnCl_2$, $FeCl_2$, or $ZnCl_2$, respectively, in diethyl ether at low temperature smoothly provided the corresponding dimeric compounds $[M_2\{N(Dipp)(CH_2)_3N(Dipp)\}_2]$ [M = Mn (**3**), Fe (**4**), Zn (**5**)] in good yield (Scheme 2). The same products were obtained even when 2 equiv. of MCl_2 were employed. Complexes **3**−**5** are soluble in CH_2Cl_2 and THF and have a moderate solubility in diethyl ether and toluene.

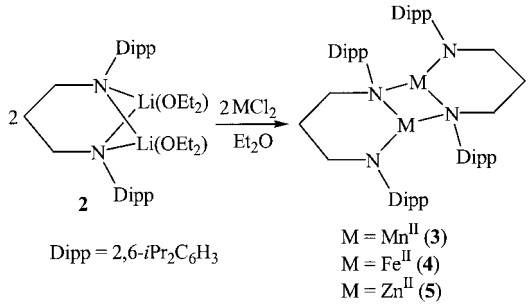

Scheme 2

Complexes **2**−**5** were characterized by EI-MS, ^{1}H NMR and IR spectroscopy and X-ray solid-state structural analysis. The molecular ion peaks of **3**−**5** in the EI mass spectra were all observed. However, the most intense peaks of these complexes show different fragments: **3**: *m*/*z* = 705 [M − CH_2NDipp]$^+$; **4**: *m*/*z* = 504 [M − N(Dipp)$(CH_2)_3$N-(Dipp)]$^+$; **5**: *m*/*z* = 456 [1/2 M]$^+$. In the the monomeric compounds {such as [N(Dipp)$(CH_2)_3$N(Dipp)]AlX·NMe_3 (X = H, F)}[7] the four isopropyl methine groups (C*H*Me_2) are not equivalent and give two resonances in the ^{1}H NMR spectra, whereas compound **5** gives four isopropyl methine resonances, which is consistent with restricted rotation about the N−C_{ipso} bond. The doublets in the range of δ = 0.16−1.36 ppm correspond to the protons of methyl groups (CH*Me*$_2$).

X-ray Solid-State Structural Analyses

The X-ray solid-state structural analyses for complexes **2**−**5** were undertaken. Crystallographic data for these complexes are given in the Exp. Sect. and selected bond lengths and angles in Tables 1 and 2.

Table 1. Selected bond lengths [Å] and bond angles [°] for **2**

Li(1)−O(1)	1.894(11)	O(1)−Li(1)−N(2)	118.3(5)
Li(1)−N(1)	1.999(10)	N(1)−Li(1)−N(2)	96.8(5)
Li(1)−N(2)	1.971(10)	O(1)−Li(1)−Li(2)	163.6(6)
Li(1)−Li(2)	2.514(13)	N(1)−Li(1)−Li(2)	51.9(3)
Li(2)−N(1)	2.028(10)	N(2)−Li(1)−Li(2)	52.4(3)
Li(2)−N(2)	2.039(10)	O(2)−Li(2)−N(1)	144.0(5)
Li(2)−O(2)	1.949(10)	O(2)−Li(2)−N(2)	114.2(5)
O(1)−Li(1)−N(1)	142.8(6)	N(1)−Li(2)−N(2)	93.7(4)

Table 2. Selected bond lengths [Å] and bond angles [°] for **3**−**5**

Compound **3**			
Mn(1)−N(1)	1.932(2)	N(1)−Mn(1)−N(2)	106.79(10)
Mn(1)−N(2)	2.126(3)	N(1)−Mn(1)−N(3)	146.55(9)
Mn(1)−N(3)	2.078(3)	N(2)−Mn(1)−N(3)	96.72(10)
Mn(1)−Mn(2)	2.690(2)	N(1)−Mn(1)−Mn(2)	133.93(8)
Mn(2)−N(2)	2.093(3)	N(2)−Mn(1)−Mn(2)	49.86(8)
Mn(2)−N(3)	2.128(3)	N(3)−Mn(1)−Mn(2)	51.07(8)
Mn(2)−N(4)	1.935(2)	Mn(1)−N(2)−Mn(2)	79.20(9)
Compound **4**			
Fe(1)−N(1)	1.878(3)	N(1)−Fe(1)−N(2A)	146.98(12)
Fe(1)−N(2)	2.085(3)	N(2)−Fe(1)−N(2A)	97.94(12)
Fe(1)−N(2A)	2.022(3)	N(1)−Fe(1)−Fe(1A)	137.06(9)
Fe(1)−Fe(1A)	2.557(2)	N(2)−Fe(1)−Fe(1A)	50.39(9)
Fe(1A)−N(2)	2.022(3)	N(2A)−Fe(1)−Fe(1A)	52.61(9)
N(1)−Fe(1)−N(2)	108.89(12)	Fe(1)−N(2)−Fe(1A)	77.00(11)
Compound **5**			
Zn(1)−N(1)	1.8537(16)	N(1)−Zn(1)−N(2A)	111.45(6)
Zn(1)−N(2)	1.9969(16)	N(2)−Zn(1)−N(2A)	92.92(6)
Zn(1)−N(2A)	2.0798(15)	N(1)−Zn(1)−Zn(1A)	136.14(5)
Zn(1)−Zn(1A)	2.6505(5)	N(2)−Zn(1)−Zn(1A)	50.82(4)
Zn(1A)−N(2)	2.0798(15)	N(2A)−Zn (1)−Zn(1A)	48.10(5)
N(1)−Zn(1)−N(2)	148.69(6)	Zn(1)−N(2)−Zn(1A)	81.08(5)

The X-ray structural analysis of **2** (Figure 1) reveals a monomer with two three-coordinate lithium atoms. Each of the lithium atoms is bonded to two nitrogen atoms of the chelating ligand and one oxygen atom of the coordinated ether ligand. It is better to describe the coordination sphere of the Li atoms as trigonal-planar rather than trigonal-pyramidal. Two C_3N_2Li six-membered rings are formed, one of which displays a boat conformation while the other is in a chair conformation. The interplanar angle between the two central LiN_2 planes is 43.8°. The Li−N distances are in the normal range (1.94−2.15 Å).[2b] In addition, there are some very close contacts between Li(1), Li(2) and various carbon and hydrogen atoms from the chelating ligand [Li(1)−H(26a): 2.29(4) Å; Li(2)−C(2): 2.36(2) Å; Li(2)−H(2a): 2.02(4) Å]. Similar contacts have been observed in [Li(Dipp)NCH_2CH_2N(Dipp)Li]$_2$.[2b]

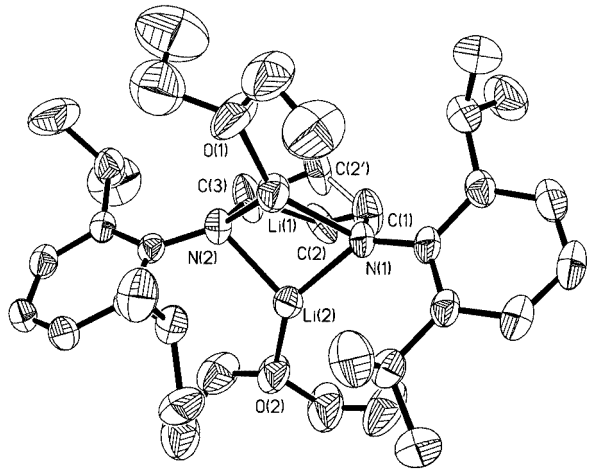

Figure 1. ORTEP drawing for **2** (50% probability ellipsoids)

 © 2004 Wiley-VCH Verlag GmbH & Co. KGaA, Weinheim

The X-ray solid-state structural analysis reveals that complexes **3**−**5** are isostructural and dimeric. The dimers are formed through two bridging nitrogen atoms. Compound $[Mn_2\{N(Dipp)(CH_2)_3N(Dipp)\}_2]$ (**3**; Figure 2) crystallizes in the triclinic space group $P\bar{1}$, while compounds $[Fe_2\{N(Dipp)(CH_2)_3N(Dipp)\}_2]$ (**4**; Figure 3) and $[Zn_2\{N(Dipp)(CH_2)_3N(Dipp)\}_2]$ (**5**; Figure 4) crystallize in the monoclinic space group *C*2/*c*. The central core of these compounds contains a nonplanar MNMN four-membered ring, which is in a butterfly configuration, with dihedral angles of 28.6° in **3**, 30.9° in **4**, and 35.0° in **5**. This arrangement is caused by the strain of the bulky aryl groups. Each metal atom is surrounded by three nitrogen atoms and always lies out of the plane formed by these nitrogen atoms (0.33 Å in **3**, 0.26 Å in **4**, and 0.26 Å in **5**), so that all the metal atoms are in a trigonal-pyramidal geometry. The two ligands chelate two metal atoms to fuse two six-membered MN_2C_3 rings, which display a boat conformation with the two metal atoms at the stern and the corresponding opposite carbon atoms at the bow. The metal atoms are about 0.20 Å (av. 0.17 Å in **3**, 0.22 Å in **4**, and 0.18 Å in **5**) out of the plane formed by the two carbon and two nitrogen atoms. The opposite carbon atoms are about 0.70 Å (av. 0.72 Å in **3**, 0.71 Å in **4**, and 0.73 Å in **5**) out of the plane.

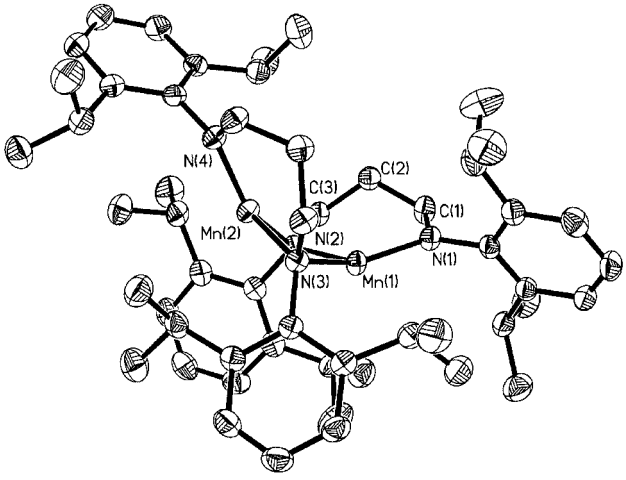

Figure 2. ORTEP drawing for **3** (50% probability ellipsoids)

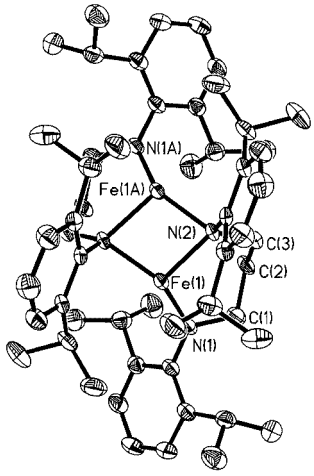

Figure 3. ORTEP drawing for **4** (50% probability ellipsoids)

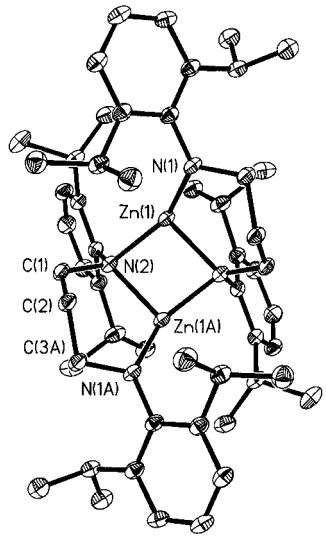

Figure 4. ORTEP drawing for **5** (50% probability ellipsoids)

The ligand in complexes **3**−**5** is both chelating and bridging, so that one of the nitrogen atoms is three-coordinate and the other four-coordinate. To the best of our knowledge, complexes **3**−**5** are the first examples with the diamide ligands in such a bonding mode. The terminal M−N distances in these complexes (Mn−N: 1.93 Å; Fe−N: 1.88 Å; Zn−N: 1.85 Å) are significantly shorter than those of the corresponding bridging ones (Mn−N: 2.10 Å; Fe−N: 2.05 Å; Zn−N: 2.04 Å). The M−N distances decrease in the order Mn−N > Fe−N > Zn−N, while the N−M−N angles increase in the order N−Mn−N < N−Fe−N < N−Zn−N, which is consistent with the relative sizes of the cations: $Mn^{2+} > Fe^{2+} > Zn^{2+}$.[8] The terminal and bridging M−N distances in **3** and **4** are about 0.06 Å shorter than the corresponding distances in the dimeric silylamides $Mn_2[N(SiMe_3)_2]_4$ [9] and $Fe_2[N(SiMe_3)_2]_4$.[10] The terminal M−N bond lengths in complexes **3** and **4** are even shorter than those found in amides with two coordinate metal centers $[Mn\{N(SiMePh_2)_2\}_2]$ (Mn−N 1.99 Å) and $[Fe\{N(SiMe_2Ph)_2\}_2]$ (Fe−N 1.92 Å).[11] This possibly results from the strong N→Si interaction in the silylamide.[10]

The M−M distances and the M−N−M angles in complexes **3** and **4** are 2.69 Å and 79.2°, and 2.56 Å and 77.0°, respectively, which indicates that there is some contact between the metal centers. The M−M distances are significantly shorter than those in the commonly planar MNMN four-membered rings.[9,10]

Magnetic Susceptibility Measurements

The temperature dependence of the molar magnetic susceptibility, χ_m and $\chi_m T$, for compounds **3** and **4** are displayed in Figures 5 and 6, respectively. The plots of $\chi_m T(T) - T$ for the two compounds indicate a magnetic behavior with an antiferromagnetic exchange interaction between the nearest neighboring spins. The value of $\chi_m T$ at 300 K is estimated to 6.82 emu·K·mol^{-1} for **3** and 5.16 emu·K·mol^{-1} for **4**. These values are lower than those of

 © 2004 Wiley-VCH Verlag GmbH & Co. KGaA, Weinheim

the spin-only value ($S = 5/2$ for Mn^{II} dimer and $S = 2$ for Fe^{II} dimer). This reveals that there is an antiferromagnetic exchange interaction between the two metal atoms in both compounds.

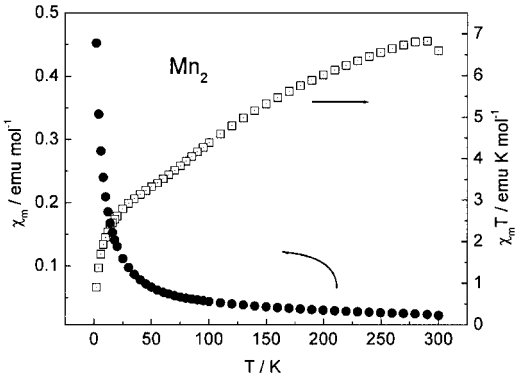

Figure 5. Plots of $\chi_m(T) - T$ and $\chi_m T(T) - T$ for compound **3**

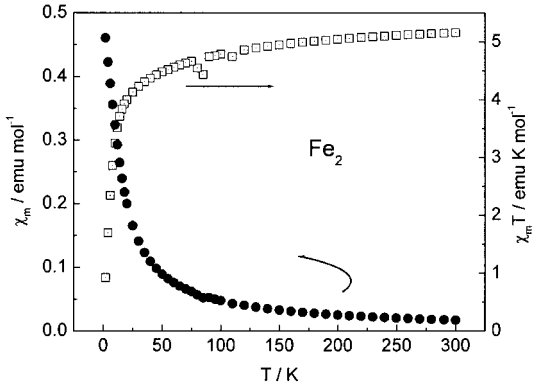

Figure 6. Plots of $\chi_m(T) - T$ and $\chi_m T(T) - T$ for compound **4**

In summary, we have successfully synthesized and characterized novel dimeric Mn^{II}, Fe^{II}, and Zn^{II} complexes, which contain three-coordinate metal centers by using the bulky diamide ligand $DippNH(CH_2)_3NHDipp$. In complexes **3**−**5** the ligand is both chelating and bridging, so that one of the nitrogen atoms is three-coordinate and the other four-coordinate. Complexes **3**−**5** are the first examples with diamide ligands in such a bonding mode.

Experimental Section

General: All reactions were performed using standard Schlenk and dry-box techniques. Solvents were appropriately dried and distilled under dinitrogen prior to use. ^1H and ^7Li NMR spectra were recorded with Bruker AM-250, AM-300 and AM-500 instruments. The chemical shifts are reported in ppm with reference to external standards: $SiMe_4$ for ^1H and $LiCl/D_2O$ for ^7Li. The magnetic susceptibility measurements were carried out with a Quantum-Design-MPMS-5S SQUID magnetometer in the range from 300 K to 2 K. The powdered samples were placed in a gel bucket and fixed in a nonmagnetic sample holder. Elemental analyses were performed by the Analytisches Labor des Instituts für Anorganische Chemie der Universität Göttingen. Mass spectra were recorded with a Finnigan Mat 8230. IR spectra were measured with a Bio-Rad Digilab FTS-7 spectrometer as Nujol mulls between KBr plates. [DippNH$(CH_2)_3$NH(Dipp)] (**1**) was prepared according to a literature method.[5c]

[N(Dipp)$(CH_2)_3$N(Dipp)][Li(OEt_2)]$_2$ (2): MeLi (5.5 mL, 1.6 M in diethyl ether, 8.8 mmol) was added at −78 °C to a diethyl ether (35 mL) solution of **1** (1.58 g, 4 mmol). The mixture was warmed to room temperature and stirred for an additional 14 h. The precipitate was removed by filtration. The filtrate was concentrated to about 10 mL and kept at −26 °C for 24 h to give colorless crystals. The crystals were collected by filtration and the mother liquor was concentrated to about 4 mL and kept at −26 °C for 24 h to give colorless crystals. Total yield: 2.04 g (92%). M.p. 110 °C (dec). ^1H NMR (250 MHz, C_6D_6): $\delta = 0.95$ (t, 12 H, $J = 7.1$ Hz, MeCH$_2$O), 1.23 (d, 12 H, $J = 6.8$ Hz, Me_2CH), 1.34 (d, 12 H, Me_2CH), 1.79 (br., 2 H, NCH$_2CH_2$), 3.00−3.25 (m, 4 H, $J = 7.2$ Hz, NCH_2CH$_2$), 3.12 (t, 8 H, $J = 7.0$ Hz, MeCH$_2$O), 3.38 (sept, 4 H, $J = 6.9$ Hz, CHMe$_2$), 6.91−7.22 (m, C_6H_3, 6 H) ppm. ^7Li NMR (300 MHz, C_6D_6): $\delta = 1.90$ ppm. $C_{35}H_{60}Li_2N_2O_2$ (554.75): calcd. C 75.78, H 10.90, N 5.05; found C 75.92, H 11.02, N 4.85.

[Mn$_2${N(Dipp)$(CH_2)_3$N(Dipp)}$_2$] (3): A solution of **2** (1.1 g, 2 mmol) in diethyl ether (10 mL) was added to a suspension of $MnCl_2$ (0.25 g, 2 mmol) in diethyl ether (30 mL) at −78 °C. The mixture was warmed to room temperature and stirred for additional 14 h. The precipitate was removed by filtration and extracted with dichloromethane (10 mL). A yellow-green solid was obtained by removing the solvent in vacuo. The mother liquor was concentrated to about 10 mL and yellow-green crystals were obtained at room temperature after 5 d. Total yield: 0.64 g (72%). M.p. 220 °C (dec). EI-MS: *m/z* (%) = 894 (49) $[M]^+$, 705 (100) $[M - CH_2NDipp]^+$, 447 (68) $[1/2\ M]^+$. $C_{54}H_{80}Mn_2N_4$ (895.10): calcd. C 72.39, H 8.94, N 6.26; found C 72.15, H 8.94, N 6.17. IR (KBr, nujol mull): $\tilde{\nu}$ = 1426 (w), 1308 (w), 1260 (w), 1243 (w), 1169 (w), 1092 (w), 1073 (w), 1041(w), 1019 (w), 857 (w), 800 (w), 786 (w), 722 (w) cm^{-1}.

[Fe$_2${N(Dipp)$(CH_2)_3$N(Dipp)}$_2$] (4): A solution of **2** (1.1 g, 2 mmol) in diethyl ether (10 mL) was added to a suspension of $FeCl_2$ (0.25 g, 2 mmol) in diethyl ether (30 mL) at −78 °C. The mixture was warmed to room temperature and stirred for additional 14 h. The precipitate was removed by filtration. The dark-blue filtrate was concentrated to about 10 mL and crystals of **4** were obtained at room temperature after 5 d. Yield: 0.67 g (75%). M.p. 228 °C (dec). EI-MS: *m/z* (%) = 896 (68) $[M]^+$, 504 (100) $[M - N(Dipp)(CH_2)_3N(Dipp)]^+$, 448 (13) $[1/2\ M]^+$. $C_{54}H_{80}Fe_2N_4$ (896.92): calcd. C 72.25, H 8.92, N 6.24; found C 72.08, H 8.63, N 6.13. IR (KBr, nujol mull): $\tilde{\nu}$ = 1403 (w), 1308 (w), 1262 (w), 1201 (w), 1155 (w), 1094 (m), 1030 (m), 973 (w), 933 (w), 918 (w), 890 (w), 801 (m), 750 (w), 722 (m), 658 (w), 597 (w), 564 (w), 540 (w), 465 (w) cm^{-1}.

[Zn$_2${N(Dipp)$(CH_2)_3$N(Dipp)}$_2$] (5): The procedure is the same like that described for **3**. Yield: 0.72 g (79%). M.p. 223 °C (dec). EI-MS: *m/z* (%) = 916 (7) $[M]^+$, 456 (100) $[1/2\ M]^+$. ^1H NMR (500 MHz, $CDCl_3$): $\delta = 0.16$ (d, 6 H, $J = 6.8$ Hz, Me_2CH), 0.43 (d, 6 H, Me_2CH), 0.99 (d, 6 H, Me_2CH), 1.21−1.28 (m, 24 H, Me_2CH), 1.36 (d, 6 H, Me_2CH), 2.20−2.34 (m, 4 H, $J = 9.7$ Hz, NCH$_2CH_2$), 2.71(t, 2 H, $J = 7.1$ Hz, NCH_2CH$_2$), 2.81 (m, 2 H, $J = 6.9$ Hz, CHMe$_2$), 3.02 (t, 2 H, NCH_2CH$_2$), 3.12 (m, 4 H, NCH_2CH$_2$), 3.27 (m, 2 H, CHMe$_2$), 3.72 (m, 2 H, NCH_2CH$_2$), 3.97 (t, 2 H, NCH_2CH$_2$), 4.04 (m, 2 H, CHMe$_2$), 3.72 (m, 2 H, CHMe$_2$), 6.78−7.45 (m, 12 H, C_6H_3) ppm. $C_{54}H_{80}N_4Zn_2$ (915.96): calcd. C 70.75, H 8.73, N 6.11; found C 70.34, H 8.68, N 5.85. IR

 © 2004 Wiley-VCH Verlag GmbH & Co. KGaA, Weinheim

Table 3. Crystallographic data for compounds **2**−**5**

	2	**3**	**4**	1/2 **5**
Empirical formula	$C_{35}H_{60}Li_2N_2O_2$	$C_{54}H_{80}Mn_2N_4$	$C_{54}H_{80}Fe_2N_4$	$C_{27}H_{40}N_2Zn$
Formula mass	554.73	895.10	896.92	457.98
Temperature [K]	200(2)	203(2)	203(2)	133(2)
Wavelength [Å]	0.71073	0.71073	0.71073	1.54178
Crystal system	monoclinic	triclinic	monoclinic	monoclinic
Space group	$P2_1/n$	$P\bar{1}$	$C2/c$	$C2/c$
Unit cell dimensions [Å]	a = 11.224(2)	a = 11.545(9)	a = 25.14(2)	a = 25.057(2)
	b = 9.6466(19)	b = 13.642(10)	b = 11.472(12)	b = 11.447(2)
	c = 32.070(6)	c = 18.014(15)	c = 18.121(9)	c = 17.881(2)
	α = 90°	α = 105.26(8)°	α = 90°	α = 90°
	β = 92.19(3)°	β = 94.01(3)°	β = 108.12(6)°	β = 108.00(2)°
	γ = 90°	γ = 111.954(18)°	γ = 90°	γ = 90°
Volume [Å^3]	3469.7(12)	2490(1)	4970(1)	4877.7(11)
Crystal size [mm]	1.00 × 0.70 × 0.60	1.00 × 0.50 × 0.30	1.30 × 0.40 × 0.40	0.10 × 0.10 × 0.10
Z	4	2	4	8
Absorption coefficient [mm^{-1}]	0.063	0.545	0.623	1.491
θ range for data collection	3.60 to 22.53°	3.54 to 25.04°	3.55 to 22.51°	3.71 to 60.69°
F(000)	1224	964	1936	1968
Reflections collected	7629	11007	3256	11348
Independent reflections	4515 (R_{int} = 0.0710)	8774 (R_{int} = 0.0616)	3219 (R_{int} = 0.0799)	3661 (R_{int} = 0.0383)
Data/restraints/parameters	4515/0/393	8774/0/557	3219/0/279	3661/0/279
Goodness-of-fit on F^2	1.115	1.023	1.044	1.032
Final R indices [$I > 2\sigma(I)$]	0.0979, 0.2922	0.0461, 0.1150	0.0591, 0.1561	0.0295, 0.0736
R (all data)	0.1357, 0.3219	0.0601, 0.1258	0.0661, 0.1665	0.0328, 0.0754
Largest difference peak/hole [e·Å^{-3}]	0.527/−0.427	0.533/−0.638	0.491/−1.112	0.032/−0.460

(KBr, nujol mull): $\tilde{\nu}$ = 1587 (w), 1320 (w), 1309 (m), 1273 (w), 1262 (w), 1245 (w), 1167 (m), 1100 (m), 1073 (w), 1043 (w), 967 (w), 931 (w), 888 (w), 861 (w), 801 (w), 788 (m), 759 (w), 746 (w), 722 (m), 610 (w), 556 (w), 479 (w) cm^{-1}.

X-ray Crystallography: Crystallographic data for **2**−**4** (Table 3) were collected with a Stoe−Siemens−Huber four-circle diffractometer coupled to a Siemens CCD area-detector with graphite-monochromated Mo-K_α radiation (λ = 0.71073 Å) and for **5** with a Bruker three-circle diffractometer equipped with a SMART 6000 CCD area-detector using Cu-K_α radiation (λ = 1.54178 Å). All structures were solved by direct methods (SHELXS-97)[12] and refined against F^2 using SHELXL-97.[13] All non-hydrogen atoms were refined anisotropically. The central carbon atom C(2) in **2** is disordered over two positions C(2) and C(2′), which were isotropically refined with site-occupation factors of 0.34 and 0.66, respectively. CCDC-233452 (**2**), -233453 (**3**), -233454 (**4**), and -233455 (**5**) contain the supplementary crystallographic data for this paper. These data can be obtained free of charge at www.ccdc.cam.ac.uk/conts/retrieving.html or from the Cambridge Crystallographic Data Centre, 12 Union Road, Cambridge CB2 1EZ, UK [Fax: + 44-1223-336-033; E-mail: deposit@ccdc.cam.ac.uk].

Acknowledgments

The work was supported by the Deutsche Forschungsgemeinschaft, the Göttinger Akademie der Wissenshaften and Ciba company. We are thankful to Dr. Xiaoming Ren and Mr. Björn Sass for performing the magnetic measurements.

[1] P. L. Holland, T. R. Cundari, L. L. Perez, N. A. Eckert, R. J. Lachicotte, *J. Am. Chem. Soc.* **2002**, *124*, 14416−14424.
[2] [2a] M. F. Lappert, P. P. Power, A. R. Sanger, R. C. Srivastava, *Metal and Metalloid Amides*, Ellis Horwood, Chichester, England, **1980**. [2b]H. Chen, R. A. Bartlett, H. V. R. Dias, M. M. Olmstead, P. P. Power, *Inorg. Chem.* **1991**, *30*, 2487−2494.
[3] A. Panda, M. Stender, R. J. Wright, M. M. Olmstead, P. Klavins, P. P. Power, *Inorg. Chem.* **2002**, *41*, 3909−3916.
[4] L. Bourget-Merle, M. F. Lappert, J. R. Severn, *Chem. Rev.* **2002**, *102*, 3031−3066.
[5] [5a] J. D. Scollard, D. H. McConville, N. C. Payne, J. J. Vittal, *Macromolecules* **1996**, *29*, 5241−5243. [5b] J. D. Scollard, D. H. McConville, *J. Am. Chem. Soc.* **1996**, *118*, 10008−10009. [5c] J. D. Scollard, D. H. McConville, J. J. Vittal, *Organometallics* **1997**, *16*, 4415−4420.
[6] [6a] F. G. N. Cloke, B. R. Elvidge, P. B. Hitchcock, V. M. E. Lamarche, *J. Chem. Soc., Dalton Trans.* **2002**, 2413−2414. [6b] P. W. Roesky, *Organometallics* **2002**, *21*, 4756−4761.
[7] H. Zhu, J. Chai, H. W. Roesky, M. Noltemeyer, H.-G. Schmidt, D. Vidovic, J. Magull, *Eur. J. Inorg. Chem.* **2003**, 3113−3119.
[8] R. D. Shannon, *Acta Crystallogr., Sect. A* **1976**, *32*, 751−767.
[9] [9a] D. C. Bradley, M. B. Hursthouse, K. M. A. Malik, R. Möseler, *Transition Met. Chem.* **1978**, *3*, 253−254. [9b] B. D. Murray, P. P. Power, *Inorg. Chem.* **1984**, *23*, 4584−4588.
[10] M. M. Olmstead, P. P. Power, S. C. Shoner, *Inorg. Chem.* **1991**, *30*, 2547−2551.
[11] H. Chen, R. A. Bartlett, H. V. R. Dias, M. M. Olmstead, P. P. Power, *J. Am. Chem. Soc.* **1989**, *111*, 4338−4345.
[12] G. M. Sheldrick, *Acta Crystallogr., Sect. A* **1990**, *46*, 467−473.
[13] G. M. Sheldrick, *SHELXL-97, Program for Crystal Structure Refinement*, Universität Göttingen, **1997**.

Received May 12, 2004
Early View Article
Published Online November 10, 2004

 © 2004 Wiley-VCH Verlag GmbH & Co. KGaA, Weinheim

Mono- and Dinuclear Rhenium Polyhydride Complexes Bearing the Chelating Ligand 1,2-Bis(dicyclohexylphosphanyloxy)ethane

Sandra Bolaño,[a] Jorge Bravo,*[a] and Soledad García-Fontán*[a]

Dedicated to the memory of Dr. Juan Carlos del Amo[‡]

Keywords: Rhenium / Hydrido ligands / P ligands / Fluxionality

Variable-temperature NMR spectroscopic studies of new rhenium polyhydride compounds of the type $[ReH_7(dcype)]$ (**1**), $[Re_2H_8(dcype)_2]$ (**3**) and $[ReH_5(dcype)L]$ (**5a–f**) [dcype = $Cy_2PO(CH_2)_2OPCy_2$; L = $PPh_n(OR)_{3-n}$, n = 0–2, R = Me, Et] show them to be highly fluxional classical hydride complexes. In the case of the ethoxy compounds **5b**, **5d** and **5f**, three hydride interchange processes were observed in the temperature range 283–173 K and their activation parameters were determined by NMR line-shape analysis. A mechanism is proposed for each. Protonation of **1** and **5** with $HBF_4{\cdot}OMe_2$ gave the nonclassical hydrides $[ReH_8(dcype)]BF_4$ (**2**) and $[ReH_6(dcype)L]BF_4$ (**6**) which are relatively stable. Compound **2** decomposes at 273 K in solution releasing H_2,whereas compound **6** can be stored at room temperature for more than 24 h without decomposition. Protonation of **3** with $HBF_4{\cdot}OMe_2$ gave the classical dinuclear hydride $[Re_2H_9(dcype)_2]BF_4$.

(© Wiley-VCH Verlag GmbH & Co. KGaA, 69451 Weinheim, Germany, 2004)

Introduction

Transition metal polyhydride complexes are notable for exhibiting H−H distances that range from 1.6 Å or more in the case of "classical" hydrides to 0.8−1.0 Å in "nonclassical" hydrides,[1] with intermediate distances having been observed in "elongated dihydrogen" or "stretched dihydride" complexes[2] such as $[ReH_7\{P(p\text{-tolyl})_3\}_2]$, in which there is an H−H distance of 1.35 Å.[3] The exact length of the H−H bond in such elongated η^2-H_2 ligands appears to depend heavily on the nature of the non-hydrogen ligand {e.g. the phosphane ligand in the $[ReH_7\{P(C_6H_4\text{-}p\text{-}X)_3\}_2]$ family to which the above compound belongs and in other $[ReH_7(PR_3)_2]$ compounds[4]} which can also have a marked influence on the stability of the complex[5] and on properties such as the susceptibility to protonation of the hydride ion in $[ReH_2(CO)(NO)(PR_3)_2]$.[6] Structures with elongated dihydrogen have been regarded as the result of a process of oxidative addition of dihydrogen that has been arrested at an intermediate stage but theoretical calculations have suggested, alternatively, that two of their hydrogen atoms move freely in a large region of the coordination sphere of the metal atom.[7]

Transition metal polyhydrides are also notable for their fluxionality. Because of their intermediate electronegativity, the nondirectionality of the 1s orbital and the absence of steric hindrance, the hydrogen ligands readily switch positions. The nature of these exchange processes and their thermodynamics can be explored by means of variable-temperature NMR spectroscopy.

Complexes of rhenium polyhydrides have proved useful in organometallic chemistry for the activation of C−H bonds by various routes.[8] They can also undergo a variety of thermal, photochemical or oxidative substitution reactions in which H_2 is replaced by a two-electron donor.[9] Although many rhenium polyhydride complexes of phosphanes are known, less attention has been given to complexes of phosphites $[P(OR)_3]$, phosphonites $[PR_1(OR)_2]$ and phosphinites $[PR_2(OR)_1]$. These ligands are all weaker σ-donors and stronger π-acceptors than phosphanes[10] and can therefore be expected to have different influences on the above-mentioned ligand-sensitive properties of the complex. Further control over these properties might come from the use of chelating ligands which afford two or more conformers, if it can be proved possible to favour one or another of these different forms.[11]

In previous work we synthesised, characterised and investigated the protonation of rhenium polyhydride complexes of the chelating ligand 1,2-bis(diphenylphosphanyloxy)-

[a] Departamento de Química Inorgánica, Facultade de Química, Universidade de Vigo,
36310 Vigo, Spain
Fax: (internat.) + 34-986-813798
E-mail: jbravo@uvigo.es
sgarcia@uvigo.es

[‡] Member of the RSEQ, killed in Madrid on March 11, 2004

Supporting information for this article is available on the WWW under http://www.eurjic.org or from the author.

 © 2004 Wiley-VCH Verlag GmbH & Co. KGaA, Weinheim **DOI: 10.1002/ejic.200400405**

ethane.[12] Here we describe the ligand dependence of the properties of an analogous series in which the ligand is 1,2-bis(dicyclohexylphosphanyloxy)ethane (dcype), with or without a monodentate phosphorus ligand (a methyl or ethyl phosphite, phosphonite or phosphinite).

Results and Discussion

Synthesis and Properties of $[ReH_7(dcype)]$ (1) and $[ReH_8(dcype)]BF_4$ (2)

Treatment of the complex $[ReOCl_2(OMe)(dcype)]$ (prepared as previously reported[13]) with a 30-fold excess of $NaBH_4$ in absolute ethanol produced the violet complex **1** which is stable in air at room temperature in both the solid state and solution. Its IR spectrum shows two medium bands at 1933 and 1956 cm^{-1} which are attributable to ν(Re−H) vibrations.[14]

$[ReH_7\{Cy_2PO(CH_2)_2OPCy_2\}]$ **1** $[ReH_8\{Cy_2PO(CH_2)_2OPCy_2\}](BF_4)$ **2**

$[Re_2H_8\{Cy_2PO(CH_2)_2OPCy_2\}_2]$ **3** $[Re_2H_9\{Cy_2PO(CH_2)_2OPCy_2\}_2](BF_4)$ **4**

$[ReH_5\{Cy_2PO(CH_2)_2OPCy_2\}\{PPh_n(OR)_{3-n}\}]$ **5**

R = Me		R = Et	
$n = 0$	**5a**	$n = 0$	**5b**
$n = 1$	**5c**	$n = 1$	**5d**
$n = 2$	**5e**	$n = 2$	**5f**

$[ReH_6\{Cy_2PO(CH_2)_2OPCy_2\}\{PPh_n(OR)_{3-n}\}](BF_4)$ **6**

R = Me		R = Et	
$n = 0$	**6a**	$n = 0$	**6b**
$n = 1$	**6c**	$n = 1$	**6d**
$n = 2$	**6e**	$n = 2$	**6f**

At room temperature, the ^1H NMR spectrum of **1** in C_6D_6 shows the hydride resonance as a seven-proton triplet at $\delta = -6.55$ ppm ($J_{PH} = 17$ Hz), while the $^{31}P\{^1H\}$ NMR spectrum displays a singlet at $\delta = 157.0$ ppm which becomes an octuplet when an off-resonance experiment is performed [$J_{PH(residual)} = 15$ Hz]. These results confirm the number of hydride ions coordinated to the rhenium atom and show the magnetic equivalence of the two phosphorus atoms in the bidentate ligand. When the NMR experiments were performed at 183 K in CD_2Cl_2, both the ^1H and the ^{31}P signals broadened slightly which can be seen as reflecting a step towards resolution of a very fast fluxional process which renders the hydrido ligands equivalent. The value of T_1(min) at 400 MHz as measured by the standard inversion-recovery method is 88 ms at 217 K, confirming the classical nature of this complex.[1c]

Treatment of a solution of compound **1** in CD_2Cl_2 with 2 equiv. of $HBF_4{\cdot}OMe_2$ in an NMR tube at 183 K yielded the nonclassical polyhydride complex $[ReH_8(dcype)]BF_4$ (**2**).[15] At that temperature its $^{31}P\{^1H\}$ NMR spectrum shows a single very broad signal at $\delta = 144.7$ ppm, while a broad signal at $\delta = -5.38$ ppm in its ^1H NMR spectrum corresponds to the hydrido ligands. This cationic complex is therefore, like compound **1**, stereochemically nonrigid on the NMR time scale. The value of T_1(min) of this signal at 400 MHz is 13 ms at 226 K (Figure 1), denoting the presence of at least one dihydrogen ligand.

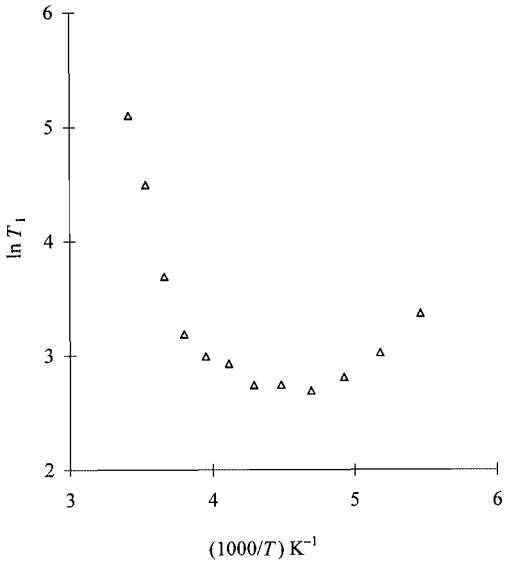

Figure 1. Plot of ln T_1 (CD_2Cl_2, 400 MHz) versus 1000/T for **2**

Between 183 and 273 K, the ^1H NMR spectrum of **2** shows just a slight sharpening of its signals, but between 273 and 293 K the hydride signal becomes a broad quintuplet integrating to nine protons ($J_{PH} = 8$ Hz) and a new singlet appears at $\delta = 4.6$ ppm which is attributable to H_2 (Figure 2).

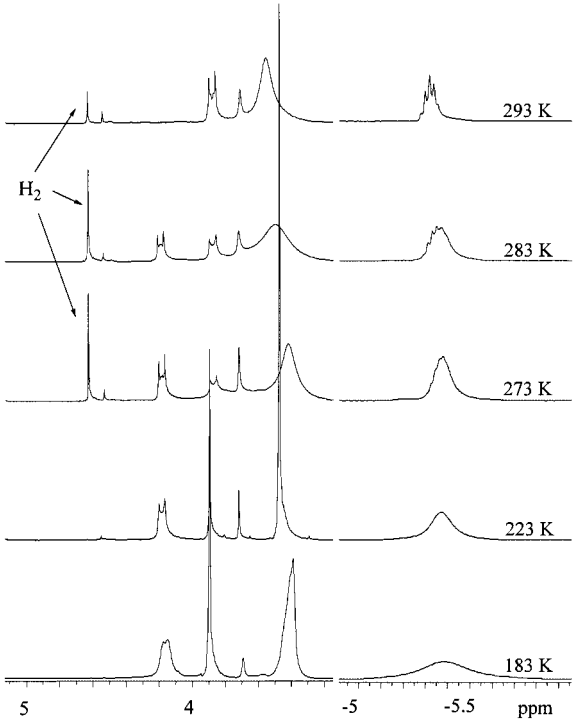

Figure 2. Selected regions of the ^1H NMR spectra obtained at various temperatures following protonation of $[ReH_7(dcype)]$ **(1)** with $HBF_4{\cdot}OMe_2$ in CD_2Cl_2

 © 2004 Wiley-VCH Verlag GmbH & Co. KGaA, Weinheim

In the $^{31}P\{^1H\}$ NMR spectrum, the broad signal at δ = 144.7 ppm sharpens when the temperature is raised and between 273 and 293 K is progressively replaced by a new singlet at δ = 151.3 ppm (Figure 3). This signal remains unaltered when the sample is maintained at 293 K for 24 h.

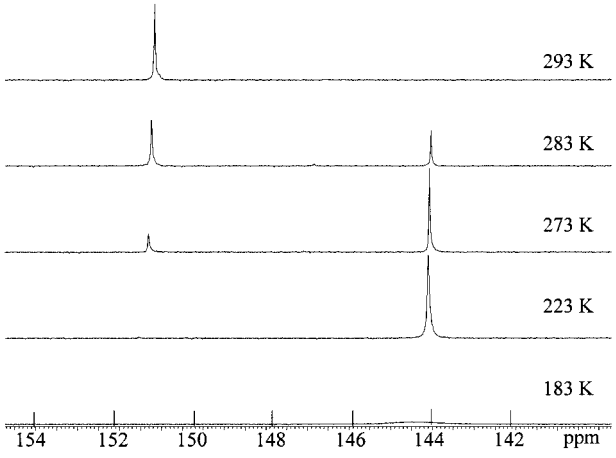

Figure 3. $^{31}P\{^1H\}$ NMR spectra obtained at various temperatures following protonation of [ReH_7(dcype)] **(1)** with an excess of $HBF_4{\cdot}OMe_2$ in CD_2Cl_2

The spectroscopic features observed at room temperature coincide with those of [Re_2H_9(dcype)$_2$]BF_4 (**4**) (see next subsection). It seems likely that at temperatures above 273 K the dinuclear compound [Re_2H_8(dcype)$_2$] (**3**) is formed from the nonclassical compound **2** with release of H_2 and immediately reacts with the excess $HBF_4{\cdot}OMe_2$ which is present in solution, thus yielding compound **4**.

Synthesis and Properties of [Re_2H_8(dcype)$_2$] (3) and [Re_2H_9(dcype)$_2$]BF_4 (4)

Heating of a solution of the heptahydride **1** to reflux in toluene for 24 h[14] resulted in the precipitation of a yellow solid with analytical and spectroscopic data in accordance with the formulation [Re_2H_8(dcype)$_2$] (**3**). The $^{31}P\{^1H\}$ NMR spectrum of a solution of **3** in CD_2Cl_2 exhibits a single singlet at δ = 162.4 ppm showing the magnetic equivalence of the four P nuclei, while the ^1H NMR spectrum shows an eight-proton quintuplet at δ = −7.37 ppm ($^2J_{PH}$ = 9 Hz). The postulated structure of this compound (Scheme 1) has four bridging and four terminal H atoms as has been described for similar systems.[10a,16]

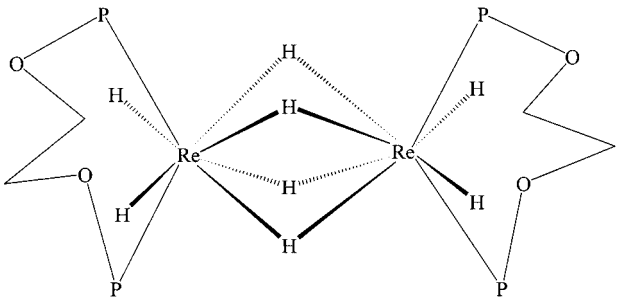

Scheme 1

Unfortunately, the poor solubility of compound **3** in dichloromethane prevented variable-temperature (VT) NMR spectroscopy. However, treatment of a suspension of **3** in CD_2Cl_2 in an NMR tube at 174 K with an excess of $HBF_4{\cdot}OMe_2$ resulted in the disappearance of the precipitate and the appearance of new NMR signals [$^{31}P\{^1H\}$ NMR: δ = 151.9 ppm (s); ^1H NMR: δ = −5.61 ppm (br. s)] corresponding to a protonated compound, **4**, which was amenable to a VT NMR study. Raising of the temperature from 174 to 293 K converted the broad singlet in the hydride region into a quintuplet (J_{PH} = 8 Hz) which remained unaltered for several days. There was no evidence of evolution of H_2 gas. The T_1(min) value for the hydride signal at 400 MHz was 94 ms at 239 K showing the classical nature of this compound. These findings suggest the formulation (μ-H_3) [Re_2H_9(dcype)$_2$]BF_4 indicating protonation of a hydride bridge as proposed for a similar system.[10a]

Syntheses and Properties of [ReH_5(dcype)L] (5a−f) and [ReH_6(dcype)L]BF_4 (6a−f) (L = $PPh_n(OR)_{3-n}$, n = 0−2, R = Me, Et)

Treatment of compound **1** with the monodentate ligands L = $PPh_n(OR)_{3-n}$ (n = 0−2, R = Me, Et) yielded the pentahydrides [ReH_5(dcype)L] as solids which are stable in air. Their IR spectra exhibit 3−4 bands between 1895 and 2000 cm^{-1} which correspond to Re−H stretching vibrations. Room-temperature ^1H NMR spectra of CD_2Cl_2 solutions of these compounds display, at high field (δ = −7 to −8 ppm), a double triplet which integrates to five protons. $^{31}P\{^1H\}$ NMR spectra show a doublet and a triplet in a 2:1 intensity ratio which are attributable to the dcype and L ligands, respectively, and form an AX_2 system. These spectroscopic features reflect fluxional processes which make the hydride nuclei equivalent. When the ^1H NMR spectra were recorded with decoupling of the ^{31}P nuclei, the hydride signals became singlets, showing the absence of coupling among the hydrido ligands. As the number of OR groups in the monodentate ligand L increased, the hydride signal shifted upfield in response to the increased electron-withdrawing character of L.

As representative examples of the VT NMR spectra of compounds **5**, Figures 4 and 5 (a) show the $^{31}P\{^1H\}$ spectrum and the hydride region of the $^1H\{^{31}P\}$ spectrum of [ReH_5(dcype){$P(OEt)_3$}] (**5b**). As was mentioned above, at 298 K this compound like other transition metal polyhydrides[17] shows marked fluxionality. As the temperature is lowered from 298 K to 198 K, the triplet observed at δ = 145 ppm in the $^{31}P\{^1H\}$ NMR spectrum becomes a double doublet in which the outer peaks are less intense than the inner ones, indicating that the coupling constants between the P nucleus of the monodentate ligand and the two dcype P nuclei have different signs.[18] At the same time, the doublet at δ = 157.5 ppm first becomes a single broad hump (at 228 K) and then a broad singlet and a broad doublet which narrows progressively, showing the transition from an AX_2 to an AMX system. Lowering of the temperature below 198 K broadens all these signals which probably reflects the initial stages of the freezing of the interconversion equilib-

 © 2004 Wiley-VCH Verlag GmbH & Co. KGaA, Weinheim

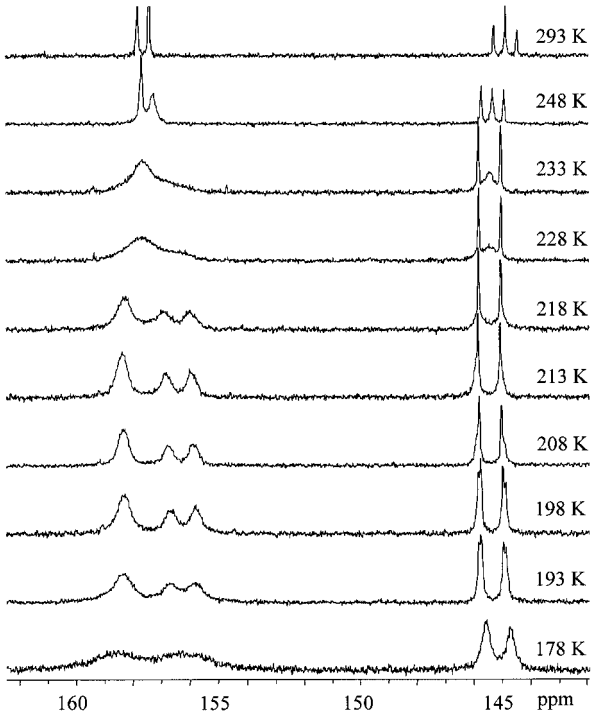

Figure 4. $^{31}P\{^{1}H\}$ NMR spectra of compound **5b** at various temperatures

rium between the conformers of the chelate ring of the bidentate ligand.

Their VT $^{1}H\{^{31}P\}$ NMR spectra [Figure 5, a) shows that of **5b**] show compounds **5** to be more rigid than the analogous complexes of 1,2-bis(diphenylphosphanyloxy)-ethane,[12] since in most cases there is a separate signal for each hydrido ligand at the lowest temperature attainable. This afforded an opportunity to investigate the interchange processes in which the hydrido ligands are involved. From 198 to 173 K the five signals become slightly broader (for example, the signal of **5b** at $\delta = -8.40$ ppm broadens from $W_{1/2} = 16$ Hz to $W_{1/2} = 38$ Hz) which is in keeping with the behaviour of the ^{31}P NMR signals and is likewise attributable to the initial stages of the freezing of the chelate ring conformer interconversion. As the temperature is progressively increased above 198 K, three signals ($\delta = -6.50$, -8.09 and -10.19 ppm in the spectrum of **5b**) coalesce to form a signal so broad that at 218 K it disappears into the baseline. Meanwhile, at 213 K the two remaining signals (located at $\delta = -8.40$ and -6.80 ppm in the case of **5b**) also begin to coalesce, suggesting the existence of a second interchange process involving the other two hydrido ligands. Finally, a third process which makes all five protons equivalent, appears at 233 K and results in the room-temperature spectrum showing a single signal which for **5b** is located at $\delta = -8.00$ ppm.

Plausible mechanisms for the above processes are indicated in Scheme 2. Cyclic interchange of three hydride ions defining one of the triangular faces of a distorted dodecahedral coordination polyhedron, as proposed by Crabtree et al.[19] for $[ReH_5(PPh_3)_2(py)]$, may account for the lowest-temperature process. The second process, which was not observed in the case of Crabtree's complex, may be the interchange of the other two protons. Finally, the equivalence of all five protons at high temperature may be due to the pseudorotation illustrated in Scheme 2 (b).

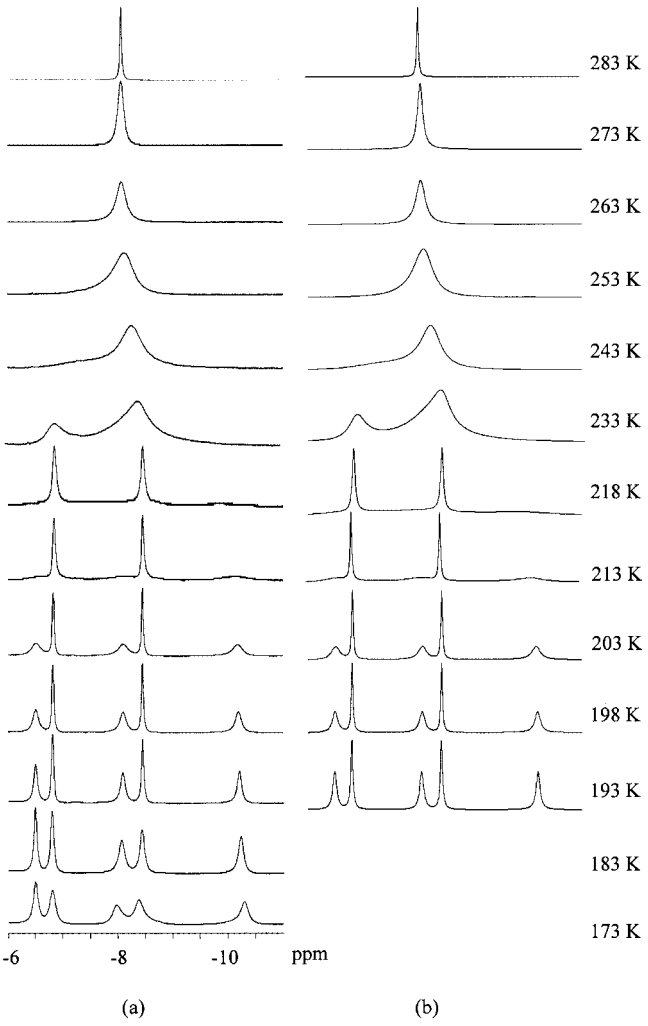

Figure 5. The observed (a) and simulated (b) hydride region of the $^{1}H\{^{31}P\}$ NMR spectra of compound **5b** at various temperatures

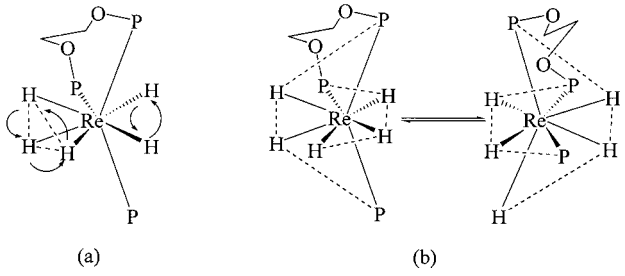

Scheme 2

Line-shape analysis performed using g NMR software[20] [Figure 5, b) shows the hydride region of the simulated VT ^{1}H NMR spectrum of **5b**] allowed us to calculate the thermodynamic parameters of the above interchange processes from the Eyring plots shown in Figure 6. Table 1 lists the results for the series of ethoxy compounds **5b**, **5d** and

 © 2004 Wiley-VCH Verlag GmbH & Co. KGaA, Weinheim

Table 1. Activation parameters obtained by Eyring analysis for **5b**, **5d** and **5f**

Compound	Activation parameters[a] Low-temperature process	Medium-temperature process	High-temperature process
$[ReH_5(dcype)\{P(OEt)_3\}]$ (**5b**)	$\Delta H^{\ddagger}$ = 11.4±0.2 $\Delta S^{\ddagger}$ = 8.9±0.1	$\Delta H^{\ddagger}$ = 13.6±0.4 $\Delta S^{\ddagger}$ = 12.0±0.4	$\Delta H^{\ddagger}$ = 14.1±0.8 $\Delta S^{\ddagger}$ = 12.5±0.7
$[ReH_5(dcype)\{PPh(OEt)_2\}]$ (**5d**)	$\Delta H^{\ddagger}$ = 10.6±0.6 $\Delta S^{\ddagger}$ = 5.7±0.3	$\Delta H^{\ddagger}$ = 12.5±0.3 $\Delta S^{\ddagger}$ = 8.9±0.2	$\Delta H^{\ddagger}$ = 13.1±0.5 $\Delta S^{\ddagger}$ = 8.9±0.3
$[ReH_5(dcype)\{PPh_2(OEt)\}]$ (**5f**)	$\Delta H^{\ddagger}$ = 10.3±0.5 $\Delta S^{\ddagger}$ = 4.9±0.2	$\Delta H^{\ddagger}$ = 12.2±1.6 $\Delta S^{\ddagger}$ = 9.6±1.3	$\Delta H^{\ddagger}$ = 12.3±1.2 $\Delta S^{\ddagger}$ = 9.3±0.9

[a] $\Delta H^{\ddagger}$ [kcal/mol], $\Delta S^{\ddagger}$ [cal/mol].

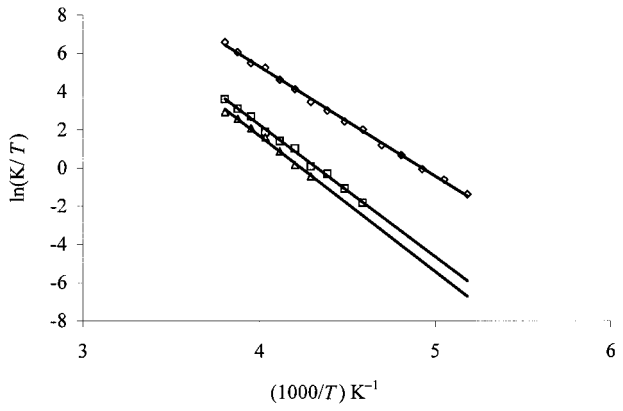

Figure 6. Eyring plots for the low- (open diamonds), medium- (open squares) and high-temperature (open triangles) interchange processes

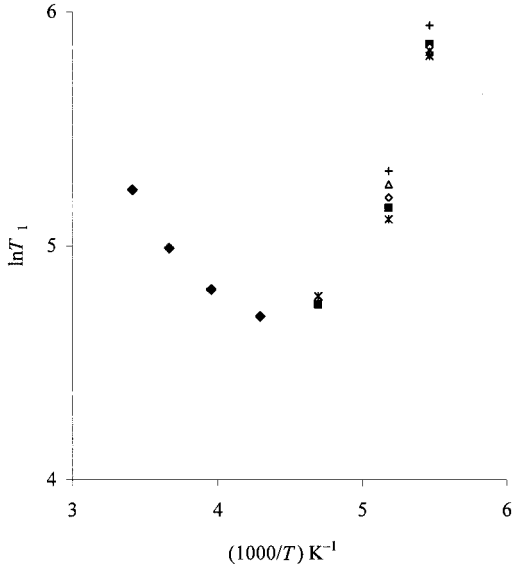

Figure 7. Plots of $\ln T_1$ values vs. temperature for the hydride signals of compound **5b** in CD_2Cl_2, at 400 MHz; solid diamonds indicate the signal at $\delta = -8.15$ ppm (fast-exchange motion), solid squares the signal at $\delta = -6.82$ ppm; * the signal at $\delta = -8.45$ ppm, triangles the signal at $\delta = -6.51$ ppm, open diamonds the signal at $\delta = -8.09$ ppm; + the signal at $\delta = -10.19$ ppm

5f. The activation energy of each process shows a clear trend, falling as the donor capacity of L increases.

Figure 7 shows plots of $\ln T_1$ against the temperature for the hydride signals of **5b** in CD_2Cl_2 at 400 MHz. At about the lowest coalescence temperature, all five signals have similar T_1 values of about 110 ms, values which increase as the temperature is lowered further. Similar behaviour is exhibited by the rest of compounds **5**, with the minimum T_1 values listed in Table 2. These compounds can, accordingly, all be regarded as classical in nature.

Table 2. T_1(min.) data at 400 MHz for compounds **5a**−**f** and **6a**−**f**

Compound	T [K]	T_1 [ms]
$[ReH_5(dcype)\{P(OMe)_3\}]$ (**5a**)	227	114
$[ReH_5(dcype)\{P(OEt)_3\}]$ (**5b**)	215	116
$[ReH_5(dcype)\{PPh(OMe)_2\}]$ (**5c**)	229	115
$[ReH_5(dcype)\{PPh(OEt)_2\}]$ (**5d**)	226	113
$[ReH_5(dcype)\{PPh_2(OMe)\}]$ (**5e**)	212	103
$[ReH_5(dcype)\{PPh_2(OEt)\}]$ (**5f**)	230	108
$[ReH_4(\eta^2\text{-}H_2)(dcype)\{P(OMe)_3\}]^+$ (**6a**)	226	25
$[ReH_4(\eta^2\text{-}H_2)(dcype)\{P(OEt)_3\}]^+$ (**6b**)	225	24
$[ReH_4(\eta^2\text{-}H_2)(dcype)\{PPh(OMe)_2\}]^+$ (**6c**)	226	26
$[ReH_4(\eta^2\text{-}H_2)(dcype)\{PPh(OEt)_2\}]^+$ (**6d**)	226	21
$[ReH_4(\eta^2\text{-}H_2)(dcype)\{PPh_2(OMe)\}]^+$ (**6e**)	225	42
$[ReH_4(\eta^2\text{-}H_2)(dcype)\{PPh_2(OEt)\}]^+$ (**6f**)	226	32

Protonation of compounds **5a**−**f** with $HBF_4{\cdot}O_2Me$ at 183 K in CD_2Cl_2 yielded the cationic complexes $[ReH_6(dcype)L]^+$ (**6a**−**f**) which in view of their T_1(min.) values (24−42 ms at 400 MHz) (Table 2) must each contain at least one dihydrogen ligand.[21] As a result of their marked fluxionality, their ^1H NMR spectra show single broad hydride resonances between $\delta = -5$ ppm and −6 ppm (Table 3) at 183 K. As the temperature is raised to 293 K, these signals become broad quadruplets (**6a**−**d**) or double triplets (**6e**,**f**). These compounds are fairly stable, showing the first sign of decomposition [loss of H_2(g)] only when kept at room temperature for more than 24 h. As reported for the related compound $[ReH_6\{Ph_2PO(CH_2)_2OPPh_2\}]BF_4$,[12] their thermal stability increases with the electron-withdrawing character of the monodentate phosphorus ligand L. When they were treated with Et_3N, the starting pentahydrides **5a**−**f** were obtained. At 183 K the $^{31}P\{^1H\}$ NMR spectra of the compounds show two broad signals which resolve into a typical AX_2 system when the temperature is raised (see Table 3).

Conclusions

The new rhenium polyhydride compounds $[ReH_7(dcype)]$ (**1**), $[Re_2H_8(dcype)_2]$ (**3**) and $[ReH_5(dcype)L]$ (**5a**−**f**) [dcype =

 © 2004 Wiley-VCH Verlag GmbH & Co. KGaA, Weinheim

Table 3. Selected VT NMR spectroscopic data for the cationic complexes **6a−f**

Compound[a]	^{1}H NMR[b] T = 183 K δ [ppm]; J [Hz]	T = 293 K δ [ppm]; J [Hz]	Assignment	^{31}P{^{1}H} NMR T = 183 K δ [ppm]; J [Hz]	T = 293 K δ [ppm]; J [Hz]
6a	−5.98 (br)[c]	−5.71 (q); $J_{P,H}$ = 14	H/η^2-H$_2$	126.48 (t)[c]	145.54 (d)
		3.62 (d); $J_{P,H}$ = 12	CH_3 (L)	142.66 (br)	123.69 (t)
		4.09 (m)	−$(CH_2)_2$− (dcype)	150.22 (br)	J = 36
				J = 39	
6b	−5.87 (br)	−5.66 (q); $J_{P,H}$ = 14	H/η^2-H$_2$	117.59 (t)	145.84 (d)
		1.34 (t); $J_{H,H}$ = 7	CH_3 (L)	146.4 (br)	115.20 (t)
		3.97 (quin); $J_{P,H}$ = 7	CH_2 (L)	J = 38	J = 34
		4.09 (m)	−$(CH_2)_2$− (dcype)		
6c	−5.58 (br)	−5.31 (q); $J_{P,H}$ = 15	H/η^2-H$_2$	141.88 (s)	145.20 (d)
		3.56 (d); $J_{P,H}$ = 13	CH_3 (L)	144.12 (br)	139.73 (t)
		4.06 (m)	−$(CH_2)_2$− (dcype)		J = 23
6d	−5.55 (br)[c]	−5.30 (q); $J_{P,H}$ = 15	H/η^2-H$_2$	133.54 (vbr)[c]	145.40 (d)
		1.36 (t); $J_{P,H}$ = 7	CH_3 (L)	151.13 (vbr)	131.39 (t)
		3.80 (m)	CH_2 (L)		J = 23
		4.00 (m); 4.07 (m)	−$(CH_2)_2$− (dcype)		
6e	−5.19 (br)	−4.89 (dt); $J_{PB,H}$ = 19;		111.07 (s)	144.91 (d)
		$J_{PA,H}$ = 17	H/η^2-H$_2$	145.79 (br)	144.91 (d)
		3.44 (d); $J_{P,H}$ = 14	CH_3 (L)	113.70 (t)	113.70 (t)
		4.12 (m)	−$(CH_2)_2$− (dcype)		J = 9
6f	−5.30 (br)	−4.89 (dt); $J_{PB,H}$ = 19;		106.09 (t)[d]	
		$J_{PA,H}$ = 17	H/η^2-H$_2$	146.31 (d)	
		1.33 (t); $J_{H,H}$ = 7	CH_3 (L)	J = 13	
		3.67 (quin); $J_{P,H}$ = 7	CH_2 (L)		
		4.11 (m)	−$(CH_2)_2$− (dcype)		

[a] In CD_2Cl_2 at 400 MHz. [b] Cyclohexyl and phenyl proton resonances are omitted. [c] Temperature 174 K. [d] Temperature 233 K.

$Cy_2PO(CH_2)_2OPCy_2$; L = $PPh_n(OR)_{3-n}$, n = 0−2, R = Me, Et] are all highly fluxional classical hydride complexes but the combination of both the chelating ligand dcype and the monodentate ligand L in compounds **5** results in pentahydrides that are rigid enough to allow investigation of the various hydride interchange processes and calculation of the corresponding energy barriers. In contrast to other rhenium pentahydride systems, for which two interchange processes have been proposed (cyclic permutation of three hydride ions and a pseudorotation),[19] compounds **5** show signs of three processes, the third being the interchange of two hydride ions. Protonation of pentahydrides **5** with $HBF_4{\cdot}OMe_2$ provided the relatively stable dihydrogen complexes $[ReH_6(dcype)L]BF_4$ (**6**) which can be stored at room temperature for more than 24 h without decomposition.

Experimental Section

General Methods: All operations were carried out under argon using standard Schlenk techniques. Solvents were purified by distillation from the appropriate drying agents and degassed before use.[22] All other reagents and chemicals were reagent grade and, unless otherwise stated, were used as received from commercial suppliers. The ligand $Cy_2PO(CH_2)_2OPCy_2$ (dcype) and the complex $[ReOCl_2(OMe)(dcype)]$ were prepared as described in the literature.[13] Deuterated solvents for NMR measurements (Merck and Aldrich) were dried with molecular sieves (4 Å). Combustion C,H analyses were performed with a Fisons EA-1108 apparatus. NMR spectra were recorded with a Bruker AMX 400 spectrometer. Chemical shifts are reported in ppm relative to tetramethylsilane and were calibrated against the residual solvent resonance for ^{1}H. Peak positions in ^{31}P{^{1}H} spectra were measured relative to external H_3PO_4 (85%) with downfield shifts considered positive. Variable-temperature spin-lattice relaxation times T_1 were determined in deuterated dichloromethane by the inversion-recovery method using a standard 180°−τ−90° pulse sequence and 16 different values of τ at each temperature. Infrared spectra (IR) of samples in KBr pellets were recorded with a Bruker Vector IFS28 FT spectrometer.

$[ReH_7(dcype)]$ (1): An excess of $NaBH_4$ (0.30 g, 7.91 mmol) in ethanol (20 mL) was added to a suspension of $[ReOCl_2(OMe)(dcype)]$ (0.20 g, 0.26 mmol) in ethanol (10 mL). After 6 h of vigorous stirring, the solvent was removed under vacuum and the product was extracted with benzene (30 mL). This solution was concentrated in vacuo and the oil obtained was treated with ethanol (5 mL) giving a tan solid which was filtered, washed with ethanol and dried under vacuum (0.127 g, 75% yield). $C_{26}H_{55}O_2P_2Re$ (648.32): calcd. C 48.12, H 8.5; found C 47.70, H 8.6. IR (KBr pellets): $\tilde{\nu}_{(Re-H)}$ = 1933 (m), 1956 (m) cm^{-1}. ^{1}H NMR (C_6D_6, 400 MHz): δ = −6.55 (t, $J_{P,H}$ = 17 Hz, 7 H, Re*H*), 1.10−2.20 (m, 44 H, Cy), 3.8 [m, 4 H, −$(CH_2)_2$−] ppm. ^{31}P{^{1}H} NMR (C_6D_6, 161 MHz): δ = 157.0 (s) ppm.

$[Re_2H_8(dcype)_2]$ (3): When compound **1** (0.10 g, 0.10 mmol) was dissolved in toluene (10 mL) and heated to reflux for 24 h, a yellow solid was obtained. This solid was filtered and dried under vacuum (0.08 g, 80% yield). $C_{52}H_{104}O_4P_4Re_2$ (1289.70): calcd. C 48.43, H 8.13; found C 48.01, H 7.98. IR (KBr pellets): $\tilde{\nu}_{(Re-H)}$ = 2012 (w), 2028 (w) cm^{-1}. ^{1}H NMR (CD_2Cl_2, 400 MHz): δ = −7.37 (quint, $J_{P,H}$ = 9 Hz, 8 H, Re*H*), 0.70−1.94 (m, 88 H, Cy), 3.77 [m, 8 H, −$(CH_2)_2$−] ppm. ^{31}P{^{1}H} NMR (CD_2Cl_2, 161 MHz): δ = 162.4 (s) ppm.

 © 2004 Wiley-VCH Verlag GmbH & Co. KGaA, Weinheim

[ReH_5(dcype)L] (5) [L = $P(OMe)_3$ (5a), $P(OEt)_3$ (5b), $PPh(OMe)_2$ (5c), $PPh(OEt)_2$ (5d), $PPh_2(OMe)$ (5e), $PPh_2(OEt)$ (5f)]: The appropriate phosphinite, phosphonite or phosphite (L) was added in a 1:3 mol ratio to a solution of **1** (0.10 g, 0.15 mmol) in benzene (20 mL). The mixture was heated to reflux for 7 h. The solution obtained was vacuum concentrated and the resultant oil was treated with ethanol or methanol, as required, affording a solid which was filtered, washed with the same alcohol as had been used for its precipitation and dried under vacuum.

5a: 0.081 g, 68% yield. $C_{29}H_{62}O_5P_3Re$ (770.34): calcd. C 45.18, H 8.11; found C 45.40, H 8.42. IR (KBr pellets): $\tilde{\nu}_{(Re-H)}$ = 1901 (vw), 1928 (w), 1943 (w), 1987 (vw) cm^{-1}. ^1H NMR (CD_2Cl_2, 400 MHz): $\delta = -8.05$ (dt, $J_{P(A),H} = 16$, $J_{P(B),H} = 20$ Hz, 5 H, Re*H*), 1.25−2.02 (m, 44 H, Cy), 3.45 (d, $J_{H,P} = 12$ Hz, 9 H, $-CH_3$), 3.87 [m, 4 H, $-(CH_2)_2-$] ppm. $^{31}P\{^1H\}$ NMR (CD_2Cl_2, 161 MHz): δ = 152.9 (t, P_B), 157.5 (d, P_A) ppm; $J_{P,P} = 51$ Hz.

5b: 0.093 g, 75% yield. $C_{32}H_{68}O_5P_3Re$ (812.38): calcd. C 47.27, H 8.44; found C 46.95, H 8.73. IR (KBr pellets): $\tilde{\nu}_{(Re-H)}$ = 1923 (w), 1943 (w), 1963 (vw) cm^{-1}. ^1H NMR (CD_2Cl_2, 400 MHz): $\delta = -8.01$ (dt, $J_{P(A),H} = 16$, $J_{P(B),H} = 19$ Hz, 5 H, Re*H*), 1.22 (t, $J_{H,H} = 7$ Hz, 9 H, $-CH_3$), 1.25−2.11 (m, 44 H, Cy), 3.89 (quint, $J_{H,H} = J_{H,P} = 7$ Hz, 6 H, $-O-CH_2-CH_3$), 3.86 [m, 4 H, $-(CH_2)_2-$] ppm. $^{31}P\{^1H\}$ NMR (CD_2Cl_2, 161 MHz): δ = 144.8 (t, P_B), 157.7 (d, P_A) ppm; $J_{P,P} = 49$ Hz.

5c: 0.075 g, 60% yield. $C_{34}H_{64}O_4P_3Re$ (816.01): calcd. C 50.05, H 7.91; found C 49.60, H 7.71. IR (KBr pellets): $\tilde{\nu}_{(Re-H)}$ = 1896 (w), 1943 (vw), 1968 (vw), 1990 (vw), cm^{-1}. ^1H NMR (CD_2Cl_2, 400 MHz): $\delta = -7.63$ (dt, $J_{P(A),H} = 15$, $J_{P(B),H} = 20$ Hz, 5 H, Re*H*], 1.21−1.88 (m, 44 H, Cy), 3.43 (d, $J_{P,H} = 12$ Hz, 9 H, $-CH_3$), 3.88 [m, 4 H, $-(CH_2)_2-$], 7.30−7.66 (m, 5 H, Ph) ppm. $^{31}P\{^1H\}$ NMR (CD_2Cl_2, 161 MHz): δ = 157.4 (d, P_A), 160.8 (t, P_B) ppm; $J_{P,P}$ = 40 Hz.

5d: 0.075 g, 58% yield. $C_{36}H_{68}O_4P_3Re$ (844.06): calcd. C 51.23, H 8.12; found C 50.81, H 8.33. IR (KBr pellets): $\tilde{\nu}_{(Re-H)}$ = 1920 (w), 1943 (w), 1962 (vw), cm^{-1}. ^1H NMR (CD_2Cl_2, 400 MHz): $\delta = -7.63$ (dt, $J_{P(A),H} = 16$, $J_{P(B),H} = 20$ Hz, 5 H, Re*H*), 1.24 (t, $J_{H,H} = 7$ Hz, 6 H, $-CH_3$), 1.28−2.05 (m, 44 H, Cy), 3.67 (m, 2 H, $O-CH_2-CH_3$), 3.86 [m, 4 H, $-(CH_2)_2-$], 3.99 (m, 2 H, $O-CH_2-CH_3$), 7.26−7.69 (m, 5 H, Ph) ppm. $^{31}P\{^1H\}$ NMR (CD_2Cl_2, 161 MHz): δ = 152.6 (t, P_B), 157.8 (d, P_A) ppm; $J_{P,P}$ = 37 Hz.

5e: 0.087 g, 65% yield. $C_{39}H_{66}O_3P_3Re$ (862.08): calcd. C 54.34, H 7.72; found C 53.90, H 8.04. IR (KBr pellets): $\tilde{\nu}_{(Re-H)}$ = 1910 (w), 1945 (w), 1964 (vw), cm^{-1}. ^1H NMR (CD_2Cl_2, 400 MHz): $\delta = -7.33$ (dt, $J_{P(A),H} = 16$, $J_{P(B),H} = 21$ Hz, 5 H, Re*H*), 1.18−2.07 (m, 44 H, Cy), 3.36 (d, $J_{P,H} = 13$ Hz, 3 H, $-CH_3$), 3.91 [m, 4 H, $-(CH_2)_2-$], 7.23−7.76 (m, 10 H, Ph) ppm. $^{31}P\{^1H\}$ NMR (CD_2Cl_2, 161 MHz): δ = 133.2 (t, P_B), 156.9 (d, P_A) ppm; $J_{P,P}$ = 34 Hz.

5f: 0.054 g, 40.% yield. $C_{40}H_{68}O_3P_3Re$ (876.11): calcd. C 54.84, H 7.82; found C 54.75, H 7.92. IR (KBr pellets): $\tilde{\nu}_{(Re-H)}$ = 1903 (w), 1943 (w), 1983 (vw), cm^{-1}. ^1H NMR (CD_2Cl_2, 400 MHz): $\delta = -7.31$ (dt, $J_{P(A),H} = 16$, $J_{P(B),H} = 21$ Hz, 5 H, Re*H*), 1.28 (t, $J_{H,H} = 7$ Hz, 3 H, $-CH_3$), 1.34−1.80 (m, 44 H, Cy), 3.71 (quint, $J_{H,H} = J_{H,P} = 7$ Hz, 2 H, $O-CH_2-CH_3$), 3.91 [m, 4 H, $-(CH_2)_2-$], 7.22−7.80 (m, 10 H, Ph) ppm. $^{31}P\{^1H\}$ NMR (CD_2Cl_2, 161 MHz): δ = 126.6 (t, P_B), 157.1 (d, P_A) ppm; $J_{P,P}$ = 32 Hz.

Protonation Reactions Polyhydrides **1**, **3** and **5a**−**f** were protonated according to a procedure reported in the literature for similar compounds.[10a]

Supporting Information: Plot of $\ln T_1$ vs. temperature for compounds **5a**−**f** and **6a**−**f** in $[D_2]CH_2Cl_2$ at 400 MHz (see also footnote on the first page of this article).

Acknowledgments

Financial support from the Xunta de Galicia (Projects PGIDT-PX130102PR and PGIDT03-PXIB30101PR) is gratefully acknowledged. We thank the University of Vigo CACTI NMR service for recording the NMR spectra and Dr. Luis Muñoz for helpful discussions on dynamic NMR spectroscopy.

[1] [1a] Z. Lin, M. B. Hall, *Coord. Chem. Rev.* **1994**, *135/136*, 845−879. [1b] R. H. Crabtree, *Angew. Chem. Int. Ed. Engl.* **1993**, *32*, 789−805. [1c] D. M. Heinekey, W. J. Oldham Jr., *Chem. Rev.* **1993**, *93*, 913−926. [1d] P. J. Jessop, R. H. Morris, *Coord. Chem. Rev.* **1992**, *121*, 155−284. [1e] R. H. Crabtree, *Acc. Chem. Res.* **1990**, *23*, 95−101. [1f] G. J. Kubas, *Acc. Chem. Res.* **1988**, *21*, 120−128. [1g] R. H. Crabtree, D. G. Hamilton, *Adv. Organomet. Chem.* **1988**, *28*, 299−338.

[2] [2a] *Recent Advances in Hydride Chemistry* (Eds.: M. Peruzzini, R. Poli), Elsevier, Amsterdam, NL, **2001**. [2b] *MetalDihydrogen and σ-Bond Complexes; Structure, Theory, and Reactivity* (Ed.: G. J. Kubas), Kluwer Academic/Plenum Publishers, New York, **2001**.

[3] L. Brammer, J. A. K. Howard, O. Johnson, T. F. Koetzle, J. L. Spencer, A. M. Stringer, *J. Chem. Soc., Chem. Commun.* **1991**, 241−243.

[4] [4a] D. Michos, X.-L. Luo, J. A. K. Howard, R. H. Crabtree, *Inorg. Chem.* **1992**, *31*, 3914−3916. [4b] G. R. Haynes, R. L. Martin, P. J. Hay, *J. Am. Chem. Soc.* **1992**, *114*, 28−36. [4c] X.-L. Luo, D. Baudry, P. Boydell, P. Charpin, M. Nierlich, M. Ephritikhine, R. H. Crabtree, *Inorg. Chem.* **1990**, *29*, 1511−1517. [4d] X.-L. Luo, R. H. Crabtree, *J. Am. Chem. Soc.* **1990**, *112*, 4813−4821. [4e] X.-L. Luo, R. H. Crabtree, *Inorg. Chem.* **1989**, *28*, 3775−3777. [4f] J. A. K. Howard, S. A. Mason, O. Johnson, I. C. Diamond, S. Crennell, P. A. Keller, J. L. Spencer, *J. Chem. Soc., Chem. Commun.* **1988**, 1502−1503. [4g] M. T. Costello, R. A. Walton, *Inorg. Chem.* **1988**, *27*, 2563−2564. [4h] D. G. Hamilton, R. H. Crabtree, *J. Am. Chem. Soc.* **1988**, *110*, 4126−4133.

[5] N. Mathew, B. R. Jagirdar, R. S. Gopalan, G. U. Kulkarni, *Organometallics* **2000**, *19*, 4506.

[6] L. M. Epstein, N. V. Belkova, E. S. Shubina, in *Recent Advances in Hydride Chemistry* (Eds.: M. Peruzzini, R. Poli), Elsevier, Amsterdam, **2001**, chapter 14.

[7] F. Maseras, A. Lledós, E. Clot, O. Eisenstein, *Chem. Rev.* **2000**, *100*, 601−636.

[8] J. M. O'Connor, in *Comprehensive Organometallic Chemistry II* (Ed.: C. P. Casey), Elsevier Science, Oxford, **1995**, vol. 6, p. 180−186.

[9] C. C. Romao, in *Encyclopedia of Inorganic Chemistry* (Ed.: R. B. King), John Wiley & Sons, New York, **1994**, vol. 6, p. 3443−3444.

[10] [10a] S. García-Fontán, A. Marchi, L. Marvelli, R. Rossi, S. Antoniutti, G. Albertin, *J. Chem. Soc., Dalton Trans.* **1996**, 2779−2785. [10b] L. F. Rhodes, K. J. Caulton, W. K. Rybak, J. J. Ziolkowski, *Polyhedron* **1986**, *5*, 1891−1893. [10c] M. Freni, P. Romiti, *Inorg. Nucl. Chem. Lett.* **1970**, *6*, 167−170.

[11] J. M. Harrowfield, S. B. Wild, in *Comprehensive Coordination Chemistry* (Eds.: S. G. Wilkinson, R. D. Gillard, J. A. McCleverty), Pergamon Press, Oxford, **1987**, vol. 1, chapter 5.

[12] [12a] S. Bolaño, J. Bravo, S. García-Fontán, J. Castro, *J. Organomet. Chem.* **2003**, *667*, 103−111. [12b] S. Bolaño, J. Bravo, S. García-Fontán, *Inorg. Chim. Acta* **2001**, *315*, 81−87.

[13] S. Bolaño, J. Bravo, R. Carballo, E. Freijanes, S. García-Fontán, P. Rodríguez-Seoane, *Polyhedron* **2003**, *22*, 1711−1717.

 © 2004 Wiley-VCH Verlag GmbH & Co. KGaA, Weinheim

[14] J. Chatt, R. S. Coffey, *J. Chem. Soc. A* **1969**, 1963−1972.
[15] When this reaction is carried out with only 1 equiv. of acid, the protonation is not complete, some acid coexisting with compounds **1** and **3**.
[16] [16a] R. Bau, W. E. Carroll, R. G. Teller, T. F. Koetzle, *J. Am. Chem. Soc.* **1977**, *99*, 3872−3874. [16b] F. A. Cotton, R. L. Luck, *Inorg. Chem.* **1989**, *28*, 4522−4527.
[17] D. G. Gusev, H. Berke, *Chem. Ber.* **1996**, *129*, 1143−1155 and references cited therein.
[18] This conclusion was reached by simulating the signal using the gNMR software package.[20]
[19] [19a] R. H. Crabtree, J. C. Lee Jr., W. Yao, H. Rüegger, *Inorg. Chem.* **1996**, *35*, 695−699. [19b] R. Bosque, F. Maseras, O. Eisenstein, B. P. Patel, W. Yao, R. H. Crabtree, *Inorg. Chem.* **1997**, *36*, 5505−5511.
[20] P. H. M. Budzelaar, *gNMR* version 4.1, Cherwell Scientific Limited, Oxford, **1999**.
[21] The structure of a tridentate phosphane analogue $[ReH_4(\eta^2\text{-}H_2)\{PPh[CH_2CH_2CH_2P(C_6H_{11})_2]_2\}]^+$ has been determined by X-ray crystallography: Y. Kim, H. Deng, D. Meek, W. Devon, A. Wojcicki, *J. Am. Chem. Soc.* **1990**, *112*, 2798−2800.
[22] D. D. Perrin, W. L. F. Armarego, *Purification of Laboratory Chemicals*, 3rd ed., Butterworth and Heinemann, Oxford, **1988**.

Received May 14, 2004
Early View Article
Published Online October 21, 2004

 © 2004 Wiley-VCH Verlag GmbH & Co. KGaA, Weinheim

The Role of Secondary Interactions in Group 11 Metal Complexes Containing the Ferrocene Ligand $FcCH_2NHpyMe$ in Supramolecular Structures

Eva M. Barranco,[a] Olga Crespo,[a] M. Concepción Gimeno,*[a] Peter G. Jones,[b] and Antonio Laguna[a]

Keywords: Ferrocenyl derivatives / Group 11 compounds / Supramolecular chemistry / Aurophilic attractions / N ligands

The ferrocene ligand 6-[(ferrocenylmethyl)amino]-2-picoline, $FcCH_2NHpyMe$ [Fc = $(\eta^5\text{-}C_5H_5)Fe(\eta^5\text{-}C_5H_4)$], has been prepared by treatment of $FcCH_2NMe_2$ with 6-amino-2-picoline, NH_2pyMe. The coordination chemistry with group 11 metals has been studied and several complexes with coordination of the metal atom to the pyridine nitrogen atom, such as $[M(PPh_3)(FcCH_2NHpyMe)]OTf$, $[Au(C_6F_5)(FcCH_2NHpyMe)]$ and $[AuR_3(FcCH_2NHpyMe)]$ (M = Au, Ag; R_3 = $(C_6F_5)_3$, $(C_6F_5)_2Cl$; OTf = trifluoromethanesulfonate), have been obtained. The complex $[Cu(FcCH_2NHpyMe)_2]PF_6$ has also been synthesised with a probable coordination of the copper centre to the pyridine and amine nitrogen atoms. Deprotonation of the NH group allows the synthesis of dinuclear complexes of the type $[M_2(PPh_3)_2(FcCH_2NpyMe)]X$ or $[Au_2(C_6F_5)(PPh_3)(FcCH_2NpyMe)]$ with a mixed pyridine–amide ligand. Some of the complexes have been characterised by X-ray diffraction and show the presence of intramolecular aurophilic interactions in the dinuclear complex and intermolecular interactions leading to chains in the mononuclear complex. Other types of secondary bonds are present in these structures, such as hydrogen bonding and weak η^2 interactions between the gold centre and the cyclopentadienyl ring.

(© Wiley-VCH Verlag GmbH & Co. KGaA, 69451 Weinheim, Germany, 2004)

Introduction

Gold complexes with nitrogen ligands, especially with amine ligands, have not been extensively studied until recently perhaps because of their limited stability.[1] This can be rationalised in terms of incompatibility between the soft metal centre and the hard nitrogen donor. Additional stabilisation of these compounds may be provided by aurophilic interactions or by formation of N−H···X hydrogen bonds. In this manner, several complexes of stoichiometry [AuClL] have been recently reported.[2] Stabilisation of these complexes with a phosphane ligand is also possible and several examples of the type $[AuL(PR_3)]^+$ are known.[3] However, complexes in which there are more than one type of nitrogen donor atoms in the same ligand are not frequent. As far as we are aware there is only one gold(I) derivative, namely $[(AuPPh_3)_4NQuin]BF_4$ (NQuin = 8-quinolinaminato),[4] with a pyridine−imido ligand as well as some gold(III) compounds with amine−amide ligands.[5] Here we report the synthesis of several gold, silver and copper complexes containing the ligand $FcCH_2NHpyMe$ which has two types of nitrogen donor atoms belonging to the amine and the pyridine groups. In our work with ferrocene derivatives[6] we have observed that the ferrocenyl group confers a great deal of stability on these types of ligands. Consequently, in this case, it is possible to coordinate the pyridine nitrogen atom to the metal fragments and also to substitute the proton in the NH group with the isolobal fragments $AgPPh_3^+$ or $AuPPh_3^+$, leading to the formation of the mixed gold or silver complexes with the pyridine−amide ligands. The crystal structure determinations provide experimental evidence for the importance of secondary bonds in the molecular architectures. Here, aurophilic interactions and hydrogen bonding are present in some of the complexes as illustrated by X-ray diffraction.

[a] Departamento de Química Inorgánica, Instituto de Ciencia de Materiales de Aragón, Universidad de Zaragoza-C.S.I.C., 50009 Zaragoza, Spain
[b] Institut für Anorganische und Analytische Chemie der Technischen Universität Braunschweig, Postfach 3329, 38023 Braunschweig, Germany

Results and Discussion

Synthesis of the Complexes

The reaction of $FcCH_2NMe_2$ with 6-amino-2-picoline (NH_2pyMe) in acetic acid gives the ferrocene ligand $FcCH_2NHpyMe$ (**1**) [Equation (1)]. A closely related ferrocene derivative, FcCONHpyMe, has previously been reported and the effect of protonation on the spectroscopic and redox properties was studied.[7] Compound **1** has been characterised by NMR spectroscopy and its ^1H NMR spectrum shows the three resonances for the three types of pyridine protons as two doublets and a doublet of doublets

 © 2004 Wiley-VCH Verlag GmbH & Co. KGaA, Weinheim DOI: 10.1002/ejic.200400479

with the NH signal at $\delta = 4.73$ ppm, the signal of the methylene protons at $\delta = 4.12$ ppm and the cyclopentadienyl proton signals at $\delta = 4.10$, 4.19 and 4.22 ppm in a ratio of 2:5:2, respectively. The positive liquid secondary-ion mass spectrum (LSIMS) exhibits the molecular peak at m/z = 306 as the most intense.

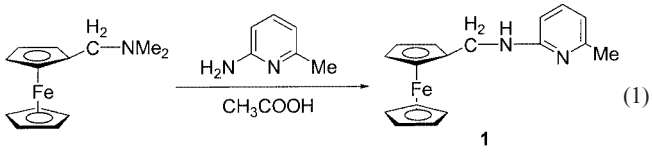

(1)

1

The reactivity of ligand **1** towards several gold, silver and copper compounds has been studied. Thus, treatment of **1** with [M(OTf)PPh_3] in a 1:1 molar ratio affords complexes of stoichiometry [M(PPh_3)($FcCH_2NHpyMe$)]OTf [M = Au (**2**), Ag (**3**)] (see Scheme 1).

Complexes **2**−**3** are air- and moisture-stable yellow solids. Their IR spectra show bands for the trifluoromethanesulfonate group at $\tilde{\nu} \approx 1265$ [vs, br., $\nu_{as}(SO_3)$], 1223 [s, $\nu_s(CF_3)$], 1150 [s, $\nu_{as}(CF_3)$] and 1023 [s, $\nu_s(SO_3)$] cm^{-1}. The ^1H NMR spectra for both complexes show broad signals at $\delta \approx 4.3$ ppm where the resonances for the ferrocenyl, methylene and NH protons are overlapping. The signals of only two of the pyridine protons can be observed because that of the other is also overlapping with those of the phenyl protons. In the $^{31}P(^1H)$ NMR spectra one sharp (in **2**) or broad (in **3**) resonance appears. At −55 °C the broad singlet from **3** splits into two doublets because of the coupling with the $^{109,107}Ag$ nuclei. The positive liquid secondary-ion mass spectra (LSIMS+) exhibit the molecular peaks at m/z (%) = 917 (5) [**2**] or 825 (12) [**3**] or the cationic peaks [M − OTf] at m/z (%) = 765 (95) [**2**] or 676 (30) [**3**].

The reaction of ligand **1** with the oxonium compound $[O(AuPPh_3)_3]ClO_4$ proceeds with the deprotonation of the NH group and coordination of two $AuPPh_3^+$ fragments to the amine nitrogen atom and to the pyridine group, giving the complex $[Au_2(PPh_3)_2(FcCH_2NpyMe)]ClO_4$ (**4**). This derivative, with triflate as counter anion, is also accessible by treatment of complex **2** with [Au(acac)(PPh_3)]. The analogous silver derivative $[Ag_2(PPh_3)_2(FcCH_2NpyMe)]OTf$ (**5**) can be obtained by treatment of **3** with [Ag(OTf)(PPh_3)] in the presence of triethylamine. The IR spectra show absorptions from the perchlorate anion at $\tilde{\nu} = 1096$ (vs, br.) and 623 (m) cm^{-1} for **4** and for **5** the typical absorptions for the trifluoromethanesulfonate anion can be observed. In the ^1H NMR spectra the resonances for the ferrocenyl protons appear as two singlets for the methyl and unsubstituted Cp groups, three multiplets for the α and β protons of the substituted Cp group and for the methylene protons. The resonance of the NH group disappears. For the pyridine protons, only two resonances can be observed because the third overlaps with the signals from the phenyl protons. The $^{31}P(^1H)$ NMR spectrum of complex **4** shows two resonances for the two inequivalent phosphorus atoms. For compound **5** the spectrum at room temperature consists of two

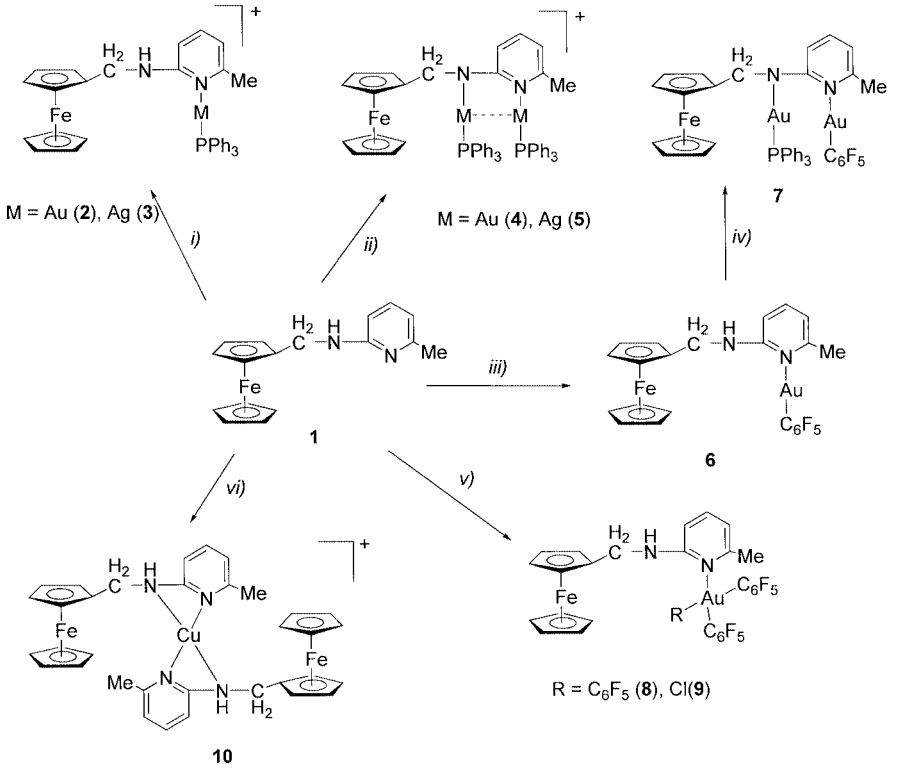

Scheme 1. i) [M(OTf)(PPh_3)], ii) $[O(AuPPh_3)_3]ClO_4$ or 2 [Ag(OTf)(PPh_3)] + NEt_3, iii) [Au(C_6F_5)(tht)], iv) [Au(acac)(PPh_3)], v) [Au(C_6F_5)$_3$(OEt_2)] or 1/2 $[Au(C_6F_5)_2Cl]_2$, vi) 1/2 $[Cu(NCMe)_4]PF_6$

 © 2004 Wiley-VCH Verlag GmbH & Co. KGaA, Weinheim

broad signals that split at −55 °C into four doublets as a consequence of the coupling of two inequivalent phosphorus atoms with the two silver nuclei. In the LSIMS+ mass spectra the cationic molecular peaks appear at *m/z* (%) = 1223 (20) [**4**] and 1044 (40) [**5**].

Treatment of **1** with an equimolar amount of $[Au(C_6F_5)(tht)]$ (tht = tetrahydrothiophene) affords the compound $[Au(C_6F_5)(FcCH_2NHpyMe)]$ (**6**). Complex **6** is an air- and moisture-stable yellow solid which is a nonconductor in acetone solution. The IR spectrum shows bands arising from the pentafluorophenyl group at $\tilde{\nu}$ = 1500 (vs), 954 (s) and 793 (m) cm^{-1}. In the ^1H NMR spectrum of **6** the typical resonances for the ferrocenyl, methyl and methylene (as a doublet) protons are apparent. The three pyridine protons appear as two doublets and a doublet of doublets and the resonance for the NH proton has shifted downfield to δ = 6.73 ppm. The ^{19}F NMR spectrum shows the three resonances for a pentafluorophenyl group as two multiplets for the *ortho*- and *meta*-fluorine atoms and a triplet for the *para*-fluorine atom. The LSIMS+ mass spectrum shows the molecular peak at *m/z* (%) = 670 (85) and a peak arising from loss of the pentafluorophenyl group at *m/z* (%) = 503 (7) can also be observed. The reaction of complex **6** with 1 equiv. of $[Au(acac)(PPh_3)]$ leads to deprotonation of the amine group and coordination of the nitrogen atom to the $AuPPh_3^+$ fragment. The compound $[Au_2(C_6F_5)(PPh_3)(FcCH_2NpyMe)]$ (**7**) is an air- and moisture-stable yellow solid which is a nonconductor in acetone solution. The ^1H NMR spectrum shows the resonances for the ferrocenyl unit, a singlet for the unsubstituted cyclopentadienyl Cp ligand and a broad multiplet for the substituted cyclopentadienyl Cp unit. The methylene and the methyl protons appear as a multiplet and a singlet, respectively, and the resonances for the phenyl and pyridine groups are overlapping. The signal for the NH proton disappears. The ^{31}P NMR spectrum shows one singlet for the phosphorus atom and the ^{19}F NMR spectrum has a typical pattern for the pentafluorophenyl group. In the LSIMS+ spectrum the molecular peak at *m/z* (%) = 1128 (5) and the $[M + AuPPh_3]^+$ fragment at *m/z* (%) = 1587 (10) may be observed.

Ligand **1** also reacts with gold(III) complexes of the type $[Au(C_6F_5)_3(OEt_2)]$ or $[Au(C_6F_5)_2Cl]_2$ to afford the compounds $[Au(C_6F_5)_3(FcCH_2NHpyMe)]$ (**8**) or $[Au(C_6F_5)_2Cl(FcCH_2NHpyMe)]$ (**9**), respectively. Complexes **8** and **9** are air- and moisture-stable yellow solids which are nonconductors in acetone solution. Their IR spectra show typical bands for the pentafluorophenyl fragments bonded to gold(III) at $\tilde{\nu} \approx$ 1507 (s), 972 (s), 800 (s) and 795 (m) cm^{-1}. The ^{19}F NMR spectrum of **8** shows the typical pattern of an $Au(C_6F_5)_3$ group in which the *trans*-pentafluorophenyl groups are equivalent. Six resonances in a 2:1 ratio are observed corresponding to the *ortho*-, *meta*- and *para*-fluorines of the inequivalent C_6F_5 moieties. For compound **9**, two inequivalent pentafluorophenyl units may be observed corresponding to a *cis* configuration. The ^1H NMR spectrum is in agreement with the formula. In the LSIMS+ spectra the molecular peaks appear at *m/z* (%) = 1004 (5) and 872 (100), respectively.

A copper derivative $[Cu\{(FcCH_2NHpyMe)\}_2]PF_6$ (**10**) has been obtained by treatment of **1** with $[Cu(NCMe)_4]PF_6$ in a molar ratio of 2:1. Because of the tendency of Cu^I to adopt higher coordination numbers than gold, we propose a tetrahedral derivative with the copper atom bonded to both pyridine and amine nitrogen atoms. In the ^1H NMR spectrum both ferrocene units are equivalent and the protons appear as a broad resonance. A singlet for the methyl protons and a multiplet for the methylene protons also appear. The pyridine units show two multiplets for the two different types of protons.

Crystal Structure Determinations

The crystal structure of the cyclohexane solvate of $[Au_2(PPh_3)_2(FcCH_2NpyMe)]ClO_4$ (**4**) has been determined by a single-crystal X-ray diffraction study (Figure 1). A selection of bond lengths and angles are shown in Table 1. The gold atoms have a distorted linear geometry with angles N(1)−Au(1)−P(1) of 172.8(2)° and N(2)−Au(2)−P(2) of 170.26(14)°. This distortion may be a consequence of a short intramolecular gold(I)−gold(I) interaction of 2.9732(5) Å. The Au−N distances are 2.091(5) Å to the pyridine nitrogen atom and 2.052(5) Å to the amine nitrogen atom which are among the longest found in

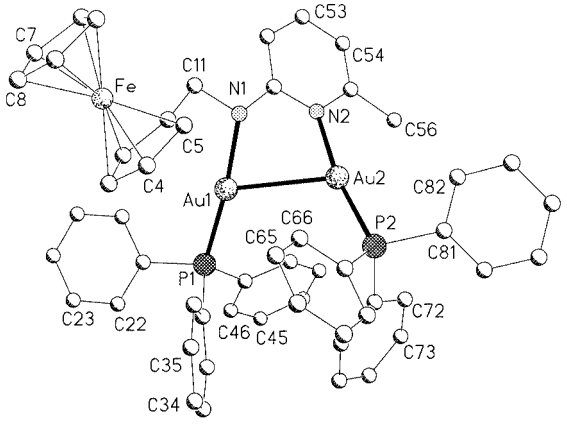

Figure 1. Structure of the cation of complex **4** showing the atom labelling scheme; radii are arbitrary, H atoms are omitted for clarity

Table 1. Selected bond lengths [Å] and angles [°] for **4**

Au(1)−N(1)	2.054(5)	Au(2)−P(2)	2.2341(18)
Au(1)−P(1)	2.2412(16)	C(11)−N(1)	1.469(8)
Au(1)−Au(2)	2.9733(5)	N(1)−C(51)	1.352(8)
Au(2)−N(2)	2.093(5)		
N(1)−Au(1)−P(1)	172.85(16)	C(61)−P(2)−Au(2)	116.3(2)
N(1)−Au(1)−Au(2)	71.67(15)	C(71)−P(2)−Au(2)	111.9(2)
P(1)−Au(1)−Au(2)	114.49(5)	C(81)−P(2)−Au(2)	110.1(2)
N(2)−Au(2)−P(2)	170.25(14)	N(1)−C(11)−C(1)	109.6(5)
N(2)−Au(2)−Au(1)	75.80(13)	C(51)−N(1)−Au(1)	119.0(4)
P(2)−Au(2)−Au(1)	113.94(5)	C(11)−N(1)−Au(1)	115.9(4)
C(31)−P(1)−Au(1)	112.6(2)	C(51)−N(2)−Au(2)	117.1(4)
C(41)−P(1)−Au(1)	112.2(2)	C(55)−N(2)−Au(2)	119.8(4)
C(21)−P(1)−Au(1)	110.9(2)		

 © 2004 Wiley-VCH Verlag GmbH & Co. KGaA, Weinheim

complexes with the unit $N_{pyridinic}-Au-PPh_3$. The latter generally range from 1.986(3)[8] to 2.108[9] Å. The longer Au−P bond in **4** is opposite to the shorter Au−N bond. The values are similar to those observed in other complexes with the N−Au−P unit.[8,9] The two P−Au−N units are skewed with respect to each other as shown by the torsion angle P(1)−Au(1)−Au(2)−P(2) of −45.8(1)°. The cyclopentadienyl rings display an essentially eclipsed geometry [torsion angle C(1)−Cp−Cp−C(6) 0.3°]. The gold atom Au(1) is located close to and with short contacts to the C(1)−C(2) bond of the cyclopentadienyl group [distances to C(1) and C(2): 3.150 and 3.357 Å] indicating a weak η^2 interaction with the Cp ring in a similar manner as has already been observed in other gold and silver complexes with ferrocene derivatives.[10,11] In the lattice there are several O···H interactions involving the oxygen atoms of the perchlorate anion and the protons of the phenyl and cyclopentadienyl moieties. These contacts are around 2.6 Å and are mostly of such a linearity as to be considered hydrogen bonds.

The structure of complex **6** has been confirmed by X-ray diffraction and is shown in Figure 2. Selected bond lengths and angles are shown in Table 2. The gold centre has a linear geometry with an angle C−Au−N of 177.65(13)°. The Au−N distance is 2.073(4) Å. Few examples of compounds with the $N_{pyridinic}-Au-C_6F_5$ moiety have been characterised by X-ray analysis and this value is shorter than the Au−N bond length of 2.124(15) Å in [Au(C_6F_5)(3-Fcpy)] (3-Fcpy = 3-ferrocenylpyridine).[12] It is similar, however, to that in [Au(C_6F_5)(3-Mepy)] (2.066 Å)[2a] or the Au−N(sp^2) value of 2.069(5) Å found in [Au(C_6F_5)($N_2C_2Ph_4$)].[13] The Au−C distance is 1.988(5) Å and resembles the values found in the complexes cited above. The cyclopentadienyl ring deviates slightly from an eclipsed geometry [torsion angle C(31)−Cp−Cp−C(41) 7.7°]. The NH group does not participate in hydrogen bonding but has a short intramolecular contact of 2.55 Å to the gold atom (N−H···Au 117°). The molecules are associated through intermolecular aurophilic interactions of 3.429 Å giving a chain of gold atoms parallel to the short axis (Figure 3). The chain structure is reinforced by offset ring stacking, with a perpendicular distance of ca. 3.33 Å and a centroid−plane distance of 3.48 Å. The molecules are further linked to form a 3D structure through C−H···F hydrogen bonds.

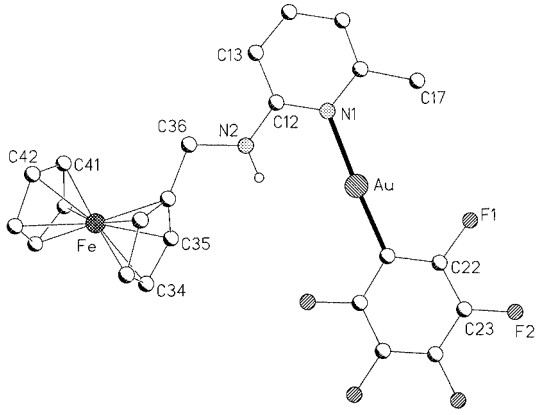

Figure 2. Molecular structure of complex **6** with the atom labelling scheme; H atoms (expect NH) are omitted for clarity

Table 2. Selected bond lengths [Å] and angles [°] for **6**

Au−C(21)	1.988(4)	C(21)−C(22)	1.382(6)
Au−N(1)	2.073(4)	C(21)−C(26)	1.397(6)
N(1)−C(12)	1.345(5)	C(22)−F(1)	1.362(5)
N(1)−C(16)	1.370(5)	C(22)−C(23)	1.365(6)
C(12)−N(2)	1.358(5)	C(23)−F(2)	1.343(5)
C(12)−C(13)	1.392(6)	C(23)−C(24)	1.378(7)
C(13)−C(14)	1.375(6)	C(24)−F(3)	1.338(6)
C(14)−C(15)	1.395(7)	C(24)−C(25)	1.368(7)
C(15)−C(16)	1.355(7)	C(25)−F(4)	1.345(5)
C(16)−C(17)	1.507(6)	C(25)−C(26)	1.375(7)
N(2)−C(36)	1.460(5)	C(26)−F(5)	1.352(5)
C(21)−Au−N(1)	177.65(13)	C(16)−C(15)−C(14)	119.0(4)
C(12)−N(1)−C(16)	119.1(4)	C(15)−C(16)−N(1)	121.7(4)
C(12)−N(1)−Au	120.6(3)	C(15)−C(16)−C(17)	121.7(4)
C(16)−N(1)−Au	120.3(3)	N(1)−C(16)−C(17)	116.6(4)
N(1)−C(12)−N(2)	116.5(4)	C(12)−N(2)−C(36)	124.2(4)
N(1)−C(12)−C(13)	121.9(4)	C(22)−C(21)−C(26)	113.2(4)
N(2)−C(12)−C(13)	121.6(4)	C(22)−C(21)−Au	121.3(3)
C(14)−C(13)−C(12)	118.0(4)	C(26)−C(21)−Au	125.5(3)
C(13)−C(14)−C(15)	120.4(4)		

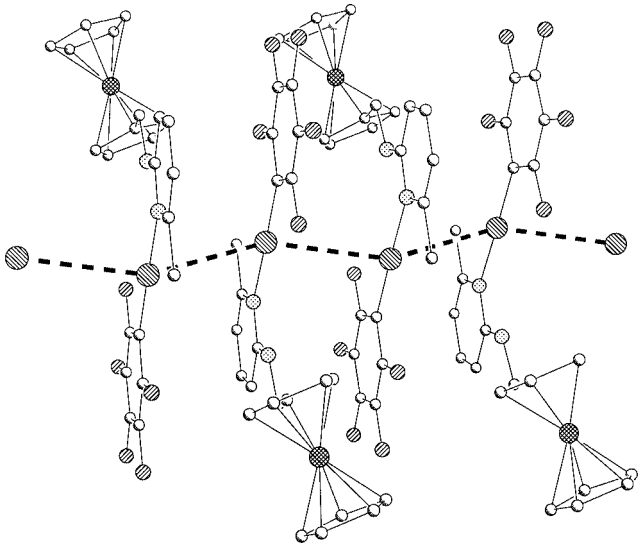

Figure 3. Association of molecules in complex **6** through aurophilic interactions; H atoms (expect NH) are omitted for clarity

The structures of complexes **8** and **9** have also been established by X-ray diffraction studies and the molecules are shown in Figures 4 and 5, respectively. Selected bond lengths and angles are collected in Tables 3 and 4. In both complexes the gold(III) centres are in a square-planar geometry with the mean deviations from the ideal angles being 3.6° (**8**) and 3.8° (**9**). In **8** the Au−C bond lengths are 2.026(6), 2.064(5) and 2.071(5) Å, the shortest is to the pentafluorophenyl group *trans* to the pyridine ligand. In **9** the distances are 2.012(2) and 2.028(3) Å which are similar to the shortest distance in compound **8**. This shows the higher *trans* influence of the pentafluorophenyl group compared with amine or chloro ligands. The Au−N distances are 2.104(4) and 2.101(2) Å and are very similar because

 © 2004 Wiley-VCH Verlag GmbH & Co. KGaA, Weinheim

both have a pentafluorophenyl group *trans* to them. Few examples with the units N−Au(C_6F_5)$_3$ or N−Au−*trans*-(C_6F_5)$_2$Cl have been structurally characterised but the values are similar to those reported, as for example in [{Au(C_6F_5)$_3$}$_2${Fc(Spy)$_2$}].[6f] The cyclopentadienyl rings in these complexes are eclipsed with torsion angles C(1)−Cp−Cp−C(6) of 0.9° in **8** and 8.8° in **9**. Both complexes show intramolecular N−H···Au hydrogen contacts of 2.62(8) and 2.67(9) Å, respectively, but these are better considered as the weaker parts of three-centred interactions involving F5 or Cl, respectively, as the main hydrogen bond acceptor. Additional C−H···F (and C−H···Cl for **9**) hydrogen bonds between various molecules create a 3D extended structure in **8** or the disposition of the molecules into planes in **9** (Figure 6). Table 5 lists the hydrogen bonds found in these complexes.

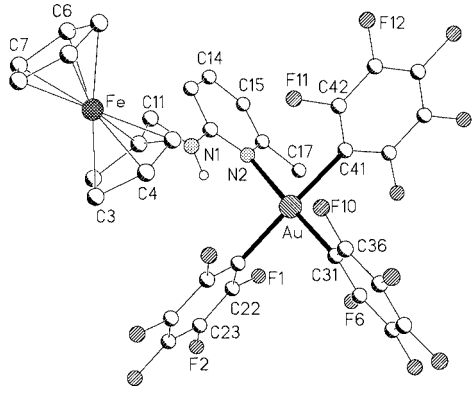

Figure 4. Perspective view of complex **8** with the atom labelling scheme; H atoms (except NH) are omitted for clarity

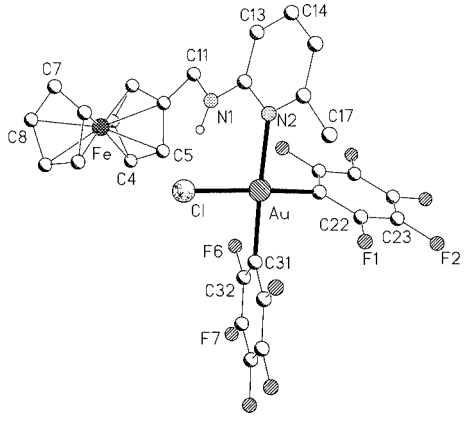

Figure 5. Molecular structure of complex **9** with the atom labelling scheme; H atoms (except NH) are omitted for clarity

Table 3. Selected bond lengths [Å] and angles [°] for **8**

Au−C(31)	2.026(6)	N(1)−C(12)	1.340(6)
Au−C(21)	2.064(5)	N(1)−C(11)	1.455(6)
Au−C(41)	2.071(5)	N(2)−C(12)	1.352(6)
Au−N(2)	2.104(4)	N(2)−C(16)	1.379(7)
C(31)−Au−C(21)	88.9(2)	C(16)−N(2)−Au	119.8(4)
C(31)−Au−C(41)	89.1(2)	C(22)−C(21)−Au	124.7(4)
C(21)−Au−C(41)	177.9(2)	C(26)−C(21)−Au	120.4(4)
C(31)−Au−N(2)	176.60(19)	C(32)−C(31)−Au	122.5(4)
C(21)−Au−N(2)	93.64(18)	C(36)−C(31)−Au	120.1(4)
C(41)−Au−N(2)	88.38(18)	C(42)−C(41)−Au	122.4(4)
C(12)−N(2)−Au	119.4(4)	C(46)−C(41)−Au	122.1(4)

Table 4. Selected bond lengths [Å] and angles [°] for **9**

Au−C(31)	2.012(2)	Au−N(2)	2.101(2)
Au−C(21)	2.028(3)	Au−Cl	2.3303(7)
C(31)−Au−C(21)	86.25(10)	N(2)−Au−Cl	91.03(6)
C(31)−Au−N(2)	177.22(9)	C(12)−N(2)−Au	120.96(17)
C(21)−Au−N(2)	91.52(9)	C(16)−N(2)−Au	118.51(17)
C(31)−Au−Cl	91.28(7)	C(22)−C(21)−Au	122.8(2)
C(21)−Au−Cl	176.22(7)	C(36)−C(31)−Au	122.39(19)

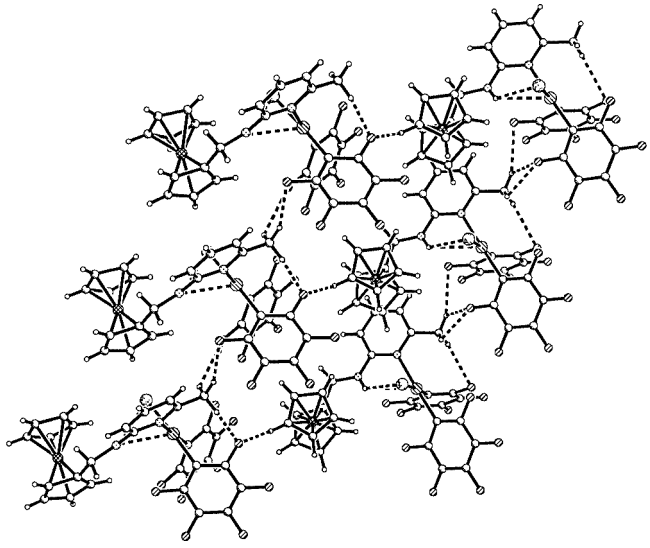

Figure 6. Supramolecular structure through hydrogen bonding in complex **9**

Conclusions

The ligand $FcCH_2NHpyMe$ can form several complexes with copper, silver or gold with different geometries and coordination modes. Coordination through the pyridine nitrogen atom is ususally preferred by the three metals but bonding to the amine nitrogen atom can be achieved using deprotonating agents causing substitution of the proton for the isolobal $AgPPh_3^+$ or $AuPPh_3^+$ fragments. In the structures of these derivatives it is worth mentioning the presence of intra- and intermolecular gold−gold interactions. In some cases the aurophilic interactions provide a supramolecular chain-like structure. The presence of other secondary interactions is also noteworthy, for example the weak η^2 interaction between the gold centre and the cyclopendienyl ring and the intra- and intermolecular hydrogen bonds.

 © 2004 Wiley-VCH Verlag GmbH & Co. KGaA, Weinheim

Table 5. Hydrogen bonds for compounds **4**, **6**, **8** and **9**

Compound **4** D−H···A	*d*(D−H)	*d*(H···A)	*d*(D···A)	∠(DHA)
C(32)−H(32)···O(1)	0.95	2.53	3.256(8)	133.5
C(83)−H(83)···O(2)#1	0.95	2.57	3.500(9)	165.1
C(53)−H(53)···O(3)#2	0.95	2.57	3.465(11)	158.2
C(73)−H(73)···O(3)#3	0.95	2.58	3.258(9)	128.6
C(23)−H(23)···O(4)	0.95	2.55	3.232(10)	128.6
C(64)−H(64)···O(4)#4	0.95	2.47	3.376(9)	160.4
C(10)−H(10)···N(1)#5	0.95	2.64	3.492(8)	149.6
Symmetry transformations used to generate equivalent atoms: #1: $x + 1, -y + 3/2, z - 1/2$; #2: $-x + 1, y - 1/2, -z + 1/2$; #3: $x + 1, y, z$; #4: $x, -y + 3/2, z - 1/2$; #5: $-x + 1, -y + 1, -z$.				
Compound **6** D−H···A	*d*(D−H)	*d*(H···A)	*d*(D···A)	∠(DHA)
C(32)−H(32)···F(1)#1	0.95	2.49	3.130(6)	125.0
C(35)−H(35)···F(1)#2	0.95	2.55	3.316(6)	137.7
C(42)−H(42)···F(2)#3	0.95	2.43	3.335(7)	159.9
C(34)−H(34)···F(3)#4	0.95	2.60	3.520(6)	164.3
C(17)−H(17C)···F(4)#5	0.98	2.52	3.299(6)	136.2
Symmetry transformations used to generate equivalent atoms: #1: $-x + 1, -y + 1, -z + 1$; #2: $-x, -y + 1, -z + 1$; #3: $x + 1, y, z - 1$; #4: $-x, -y + 2, -z + 1$; #5: $x, y - 1, z$.				
Compound **8** D−H···A	*d*(D−H)	*d*(H···A)	*d*(D···A)	∠(DHA)
C(11)−H(11B)···F(3)#1	0.99	2.35	3.328(7)	169.4
C(10)−H(10)···F(4)#1	0.95	2.57	3.459(8)	155.6
N(1)−H(1)···F(5)	0.88	2.26	3.105(6)	161.8
C(13)−H(13)···F(9)#2	0.95	2.47	3.404(7)	169.5
C(14)−H(14)···F(5)#2	0.95	2.38	3.112(7)	134.0
C(9)−H(9)···F(15)#3	0.95	2.59	3.435(8)	147.7
N(1)−H(1)···Au	0.88	2.62	3.128(5)	117.6
C(4)−H(4)···F(14)#3	0.95	2.59	3.435(8)	147.7
Symmetry transformations used to generate equivalent atoms: #1: $x - 1, y, z$; #2: $x - 1/2, -y + 1/2, z - 1/2$; #3: $-x + 3/2, y - 1/2, -z + 1/2$.				
Compound **9** D−H···A	*d*(D−H)	*d*(H···A)	*d*(D···A)	∠(DHA)
N(1)−H(01)···Au	0.88	2.67	3.143(2)	115.2
N(1)−H(01)···Cl	0.88	2.93	3.580(2)	132.1
C(8)−H(8)···F(1)#1[a]	0.95	2.60	3.298(4)	130.8
C(17)−H(17A)···F(6)#2	0.98	2.51	2.967(3)	108.3
C(17)−H(17B)···F(6)#2	0.98	2.56	2.967(3)	108.3
C(4)−H(4)···Cl#3	0.95	2.86	3.759(3)	157.4
C(11)−H(11A)···Cl#4	0.99	2.91	3.882(3)	167.9
Symmetry transformations used to generate equivalent atoms: #1: $x + 1/2, -y + 1/2, z - 1/2$, #2: $x - 1, y, z$; #3: $x + 1, y, z$; #4: $0.5 + x, 0.5 + y, 0.5 - z$.				

Experimental Section

Instrumentation: Infrared spectra were recorded in the range 4000−200 cm^{-1} with a Perkin−Elmer 883 spectrometer using Nujol mulls between polyethylene sheets. Conductivities were measured in ca. 5×10^{-4} mol·dm^{-3} solutions with a Philips 9509 conductimeter. C, H, N and S analyses were carried out with a Perkin−Elmer 2400 microanalyser. Mass spectra were recorded with a VG Autospec instrument with the liquid secondary-ion mass spectroscopy (LSIMS) technique using nitrobenzyl alcohol as a matrix. NMR spectra were recorded with a Varian Unity 300 spectrometer or a Bruker ARX 300 spectrometer in $CDCl_3$. Chemical shifts are given relative to $SiMe_4$ (^1H, external), $CFCl_3$ (^{19}F, external) or 85% H_3PO_4 (^{31}P, external).

Starting Materials: The starting materials [Au(acac)(PPh_3)],[14] [$O(AuPPh_3)_3$]ClO_4,[15] [Au(C_6F_5)(tht)],[16] [Au(C_6F_5)$_3$(OEt_2)],[17] [Au(C_6F_5)$_2$Cl]$_2$ [18] and [Ag(OTf)(PPh_3)][19] were prepared according to published procedures. All other reagents were commercially available.

Synthesis of $FcCH_2NHpyMe$ (1): To a solution of 6-amino-2-picoline (0.756 g, 7 mmol) in acetic acid (30 mL) was added $FcCH_2NMe_2$ (1.7 g, 14 mmol) and the mixture was heated at 80 °C for 3 h. The solution was then cooled and an aqueous solution of $NaHCO_3$ was added in order to raise the pH to 7. The organic phase was extracted with CH_2Cl_2 (3 × 1 mL) and dried with $MgSO_4$. The solution was then concentrated to ca. 2 mL and chromatographed on alumina with diethyl ether/hexane (4:1) as eluent. Evaporation of the solvent to ca. 5 mL and addition of hexane gave the ligand **1** as an orange solid. Yield 40%, 856.9 mg. Λ_M = 0.4 Ω^{-1}·cm^2·mol^{-1}. $C_{17}H_{18}FeN_2$ (306.2): calcd. C 66.69, H 5.92, N 9.15; found C 66.57, H 5.90, N 9.10. ^1H NMR: δ = 2.39 (s, 3 H, Me), 4.10 (m, 2 H, C_5H_4), 4.12 (m, 2 H, CH_2), 4.19 (s, 5 H, C_5H_5), 4.22 (m, 2 H, C_5H_4), 4.73 (br. m, 1 H, NH), 6.23 [d, *J*(H,H) = 8.3 Hz, 1 H, py], 6.46 [d, *J*(H,H) = 7.7 Hz, 1 H, py], 7.35 [dd, *J*(H,H) = 8.3, 7.7 Hz, 1 H, py] ppm.

Synthesis of [M(PPh_3)($FcCH_2NHpyMe$)]OTf, M = Au (2), Ag (3): To a solution of **1** (0.031 g, 0.1 mmol) in dichloromethane (20 mL) was added [Au(OTf)(PPh_3)] (0.061 g, 0.1 mmol) or [Ag(OTf)(PPh_3)] (0.052 g, 0.1 mmol) and the mixture was stirred for 30 min. Evaporation of the solvent to ca. 5 mL and addition of hexane (10 mL) gave complexes **2** or **3** as orange solids.

Complex 2: Yield 72%, 65.8 mg. Λ_M = 120 Ω^{-1}·cm^2·mol^{-1}. $C_{36}H_{33}AuF_3FeN_2O_3PS$ (914.27): calcd. C 47.30, H 3.63, N 3.06, S 3.50; found C 46.86, H 3.29, N 2.90, S 3.64. ^1H NMR: δ = 2.58 (s, 3 H, Me), 4.3 (br. m, 10 H, C_5H_4, C_5H_5, NH, CH_2), 6.46 [d, *J*(H,H) = 6.6 Hz, 1 H, py], 6.63 [d, py, *J*(H,H) = 7.4, 1 H], 7.2−7.8 (m, 16 H, Ph, py) ppm. $^{31}P(^1H)$ NMR: δ = 30.6 (s, 1 P, PPh_3) ppm.

Complex 3: Yield 85%, 70.31 mg. Λ_M = 110 Ω^{-1}·cm^2·mol^{-1}. $C_{36}H_{33}AgF_3FeN_2O_3PS$ (827.171): calcd. C 52.38, H 4.03, N 3.41, S 3.88; found C 52.24, H 4.22, N 3.33, S 3.87. ^1H NMR: δ = 2.44 (s, 3 H, Me), 4−5 (br. m, 10 H, C_5H_4, C_5H_5, CH_2), 6.47 (m, 1 H, py), 6.52 (m, 1 H, py), 6.76 (s, 1 H, NH), 7.2−7.8 (m, 16 H, py, Ph) ppm. $^{31}P(^1H)$ NMR (−55 °C): δ = 11.3 [2 d, *J*(^{107}AgP) = 475.1, *J*(^{109}AgP) = 547.4 Hz, 1 P, PPh_3] ppm.

Synthesis of [M_2(PPh_3)$_2$($FcCH_2NpyMe$)]X, M = Au, X = ClO_4 (4), M = Ag, X = OTf (5)

Complex 4: To a solution of **1** (0.031 g, 0.1 mmol) in dichloromethane (20 mL) was added [$O(AuPPh_3)_3$]ClO_4 (0.149 g, 0.1 mmol) and the mixture was stirred for 2 h. Evaporation of the solvent to ca. 5 mL and addition of diethyl ether (10 mL) gave complex **4** as a yellow solid. Yield 95%, 124.33 mg. Λ_M = 110 Ω^{-1}·cm^2·mol^{-1}. $C_{52}H_{45}Au_2ClFeN_2O_4P_2$ (1308.806): calcd. C 48.11, H 3.58, N 2.12; found C 47.98, H 3.39, N 1.99. ^1H NMR: δ = 2.56 (s, 3 H, Me), 4.04 (m, 2 H, C_5H_4), 4.16 (s, 5 H, C_5H_5), 4.18 (m, 2 H, CH_2), 4.23 (m, 2 H, C_5H_4), 6.44 [d, *J*(H,H) = 7.0 Hz, 2 H, py], 6.68 [d, *J*(H,H) = 8.4 Hz, 2 H, py], 7.1−7.8 (m, 31 H, py, Ph) ppm. $^{31}P(^1H)$ NMR: δ = 30.5 (s, 1 P, PPh_3), 24.3 (s, 1 P, PPh_3) ppm.

 © 2004 Wiley-VCH Verlag GmbH & Co. KGaA, Weinheim

The triflate salt $[Au_2(PPh_3)_2(FcCH_2NpyMe)]OTf$ is also accessible by treatment of complex **2**, $[Au(PPh_3)(FcCH_2NHpyMe)]OTf$, with $[Au(acac)(PPh_3)]$ in dichloromethane. Yield, 89%.

Complex 5: To a solution of **1** (0.031 g, 0.1 mmol) in dichloromethane (20 mL) was added $[Ag(OTf)(PPh_3)]$ (0.104 g, 0.2 mmol) and NEt_3 (0.021 mL, 0.15 mmol) and the mixture was stirred for 1 h. Evaporation of the solvent to ca. 5 mL and addition of hexane (10 mL) gave complex **5** as a red solid. Yield 70%, 82.61 mg. Λ_M = 100 $\Omega^{-1}\cdot cm^2\cdot mol^{-1}$. $C_{53}H_{45}Ag_2F_3FeN_2O_3P_2S$ (1180.226): calcd. C 54.30, H 3.96, N 1.17, S 2.68; found C 54.13, H 4.05, N 1.31, S 2.34. ^1H NMR: δ = 2.50 (s, 3 H, Me), 4.04 (m, 2 H, C_5H_4), 4.10 (m, 2 H, CH_2), 4.14 (s, 5 H, C_5H_5), 4.23 (m, 2 H, C_5H_4), 6.49 (m, 1 H, py), 6.56 (m, 1 H, py), 7.1−7.8 (m, 31 H, py, Ph) ppm. $^{31}P(^1H)$ NMR (−55 °C): δ = 10.4 [2 d, $J(^{107}AgP)$ = 402.9, $J(^{109}AgP)$ = 465.9 Hz, 1 P, PPh_3], 11.2 [2 d, $J(^{107}AgP)$ = 430.1, $J(^{109}AgP)$ = 492.5 Hz, 1 P, PPh_3] ppm.

Synthesis of $[Au(C_6F_5)(FcCH_2NHpyMe)]$ (6): To a solution of **1** (0.031 g, 0.1 mmol) in dichloromethane (20 mL) was added $[Au(C_6F_5)(tht)]$ (0.045 g, 0.1 mmol) and the mixture was stirred for 30 min. Evaporation of the solvent to ca. 5 mL and addition of hexane (10 mL) gave complex **6** as a yellow solid. Yield 76%, 49.86 mg. Λ_M = 4 $\Omega^{-1}\cdot cm^2\cdot mol^{-1}$. $C_{22}H_{16}AuF_5FeN_2$ (656.056): calcd. C 41.22, H 2.71, N 4.18; found C 41.09, H 2.50, N 3.99. ^1H NMR: δ = 2.80 (s, 3 H, Me), 4.07 [d, J(H,H) = 5.1 Hz, 2 H, CH_2], 4.20 (s, 5 H, C_5H_5), 4.20 (m, 2 H, C_5H_4), 4.27 (m, 2 H, C_5H_4), 6.55 [d, J(H,H) = 7.2 Hz, 1 H, py], 6.64 [d, J(H,H) = 8.7 Hz, 1 H, py], 6.73 (m, 1 H, NH), 7.58 [dd, J(H,H) = 8.7, 7.2 Hz, 1 H, py] ppm. ^{19}F NMR: δ = −117.3 (m, 2 F, *m*-F), 160.5 [t, J(F,F) = 20.6 Hz, 1 F, *p*-F], −164.1 (m, 2 F, *o*-F) ppm.

Synthesis of $[Au_2(C_6F_5)(PPh_3)(FcCH_2NpyMe)]$ (7): To a solution of complex **6** (0.067 g, 0.1 mmol) in dichloromethane (20 mL) was added $[Au(acac)(PPh_3)]$ (0.056 g, 0.1 mmol) and the mixture was stirred for 2 h. Evaporation of the solvent to ca. 5 mL and addition of diethyl ether (10 mL) gave complex **7** as a yellow solid. Yield 66%, 72.74 mg. Λ_M = 8 $\Omega^{-1}\cdot cm^2\cdot mol^{-1}$. $C_{39}H_{30}Au_2F_5FeN_2P$ (1102.21): calcd. C 43.64, H 2.86, N 2.48; found C 43.42, H 2.80, N 2.33. ^1H NMR: δ = 2.67 (s, 3 H, Me), 3.80 (m, 2 H, CH_2), 4.12 (s, 5 H, C_5H_5), 4.31 (m, 4 H, C_5H_4), 6.26 [d, J(H,H) = 6.0 Hz, 1 H, py], 6.53 [d, J(H,H) = 8.7 Hz, 1 H, py], 7.1−7.8 (m, py, Ph) ppm. ^{19}F NMR: δ = −116.0 (m, 2 F, *m*-F), 163.3 [t, 1 F, *p*-F, J(F,F) = 20.6 Hz], −164.5 (m, 2 F, *o*-F) ppm. $^{31}P(^1H)$ NMR: δ = 30.7 (s, 1 P, PPh_3) ppm.

Synthesis of $[Au(C_6F_5)_2X(FcCH_2NHpyMe)]$, X = C_6F_5 (8), Cl (9): To a solution of **1** (0.031 g, 0.1 mmol) in dichloromethane (20 mL) was added $[Au(C_6F_5)_3(OEt_2)]$ (0.077 g, 0.1 mmol) or $[Au(C_6F_5)_2Cl]_2$ (0.056 g, 0.05 mmol) and the mixture was stirred for 1 h. Evaporation of the solvent to ca. 5 mL and addition of hexane (10 mL) gave complexes **8** or **9** as yellow solids.

Complex 8: Yield 75%, 75.25 mg, Λ_M = 4 $\Omega^{-1}\cdot cm^2\cdot mol^{-1}$. $C_{35}H_{18}AuF_{15}FeN_2$ (1004.35): calcd. C 41.86, H 1.81, N 2.79; found C 41.79, H 1.56, N 2.34. ^1H NMR: δ = 2.71 (s, 3 H, Me), 4.11 (m, 2 H, CH_2), 4.20 (m, 9 H, C_5H_5, C_5H_4, NH), 5.89 (m, 1 H, py), 6.57 (m, 2 H, py), 7.53 (m, 1 H, py) ppm. ^{19}F NMR: δ = −121.6

Table 6. X-ray data for complexes **4**, **6**, **8** and **9**

Compound	**4**·C_6H_{12}	**6**	**8**·C_5H_{12}	**9**
Formula	$C_{59}H_{59}Au_2ClFeN_2O_4P_2$	$C_{23}H_{18}AuF_5FeN_2$	$C_{40}H_{30}AuF_{15}FeN_2$	$C_{29}H_{18}AuClF_{10}FeN_2$
M_r	1407.26	670.21	1076.48	872.72
Habit	orange tablet	orange prism	orange pyramid	orange tablet
Crystal size [mm]	0.45 × 0.25 × 0.15	0.55 × 0.45 × 0.3	0.50 × 0.45 × 0.25	0.18 × 0.15 × 0.09
Crystal system	monoclinic	triclinic	monoclinic	monoclinic
Space group	$P2_1/c$	$P(-1)$	$P2_1/n$	$P2_1/n$
Cell constants:				
a [Å]	10.879(2)	6.641(3)	10.3534(16)	8.1587(8)
b [Å]	21.245(3)	11.151(4)	22.911(3)	14.5039(14)
c [Å]	23.773(3)	14.737(5)	16.993(2)	23.688(2)
α [°]	90	84.66(2)	90	90
β [°]	97.687(10)	77.56(2)	100.170(12)	94.312(3)
γ [°]	90	85.54(2)	90	90
V [Å^3]	5445.3	1059.2	3967.6	2795.1
Z	4	2	4	4
D_x [Mg·m^{-3}]	1.717	2.101	1.802	2.074
μ [mm^{-1}]	5.8	7.7	4.2	5.9
F(000)	2760	640	2096	1672
T [°C]	−100	−130	−100	−130
$2\theta_{max.}$ [°]	50	50	50	60
No. of reflections				
Measured	10394	4425	7479	59912
Independent	9552	3723	6936	8194
Transmissions	0.45−0.96	0.46−0.81	0.50−0.99	0.69−0.86
R_{int}	0.036	0.024	0.025	0.059
Parameters	641	295	498	398
Restraints	632	274	149	138
$wR(F^2$, all refl.)	0.073	0.062	0.069	0.052
R [F, > 4σ(F)]	0.034	0.024	0.033	0.023
S	0.88	1.07	0.89	0.99
max. $\Delta\rho$ [e·Å^{-3}]	1.9	1.7	0.8	1.8

 © 2004 Wiley-VCH Verlag GmbH & Co. KGaA, Weinheim

(m, 4 F, *m*-F), −123.0 (m, 2 F, *m*-F), −156.2 [t, *J*(F F) = 19.5 Hz, 2 F, *p*-F], −156.7 (t, *J*(F,F) = 19.6 Hz, 1 F, *p*-F], −160.8 (m, 4 F, *o*-F), −161.4 (m, 2 F, *o*-F) ppm.

Complex 9: Yield 74%, 64.39 mg, Λ_M = 18 $\Omega^{-1}\cdot cm^2\cdot mol^{-1}$. $C_{29}H_{18}AuClF_{10}FeN_2$ (872.61): calcd. C 39.91, H 2.08, N 3.22; found C 39.89, H 1.65, N 2.93. ^{1}H NMR: δ = 2.85 (s, 3 H, Me), 4.12 (m, 2 H, CH_2), 4.20 (m, 9 H, C_5H_5, C_5H_4), 4.41 (m, 1 H, NH), 6.04 (m, 1 H, py), 6.60 [2 d, *J*(H,H) = 7.3, 8.5 Hz, 2 H, py], 7.58 [dd, *J*(H,H) = 7.3, 8.5 Hz, 1 H, py] ppm. ^{19}F NMR: δ = −122.0 (m, 2 F, *m*-F), −123.0 (m, 2 F, *m*-F), −154.7 [t, *J*(F,F) = 19.6 Hz, 1 F, *p*-F], −156.0 [t, *J*(F,F) = 19.6 Hz, 1 F, *p*-F], −160.0 (m, 2 F, *o*-F), −161.2 (m, 2 F, *o*-F) ppm.

Synthesis of $[Cu(FcCH_2NHpyMe)_2]PF_6$ (10): To a solution of **1** (0.031 g, 0.1 mmol) in dichloromethane (20 mL) was added $[Cu(NCMe)_4]PF_6$ (0.037 g, 0.1 mmol) and the mixture was stirred for 2 h. Evaporation of the solvent to ca. 5 mL and addition of hexane (10 mL) gave complex **10** as a yellow solid. Yield 72%, 54.83 mg. Λ_M = 134 $\Omega^{-1}\cdot cm^2\cdot mol^{-1}$. $C_{32}H_{32}CuF_6Fe_2N_4$ (761.592): calcd. C 49.75, H 4.42, N 6.82; found C 49.55, H 4.40, N 6.83. ^{1}H NMR: δ = 2.53 (s, 6 H, Me), 4.0 (m, 4 H, CH_2), 4.35 (m, 18 H, C_5H_5, C_5H_4), 5.60 (m, 2 H, NH), 6.58 (m, 3 H, py), 7.57 (m, 1 H) ppm.

X-ray Crystallography: Data were recorded with a Stoe-STADI-4 (**6**), Siemens P4 (**4**, **8**) or Bruker SMART 1000 CCD (**9**) diffractometer. Data collection type: ω/θ-scans (**6**), ω-scans (**4**, **8**) or ω- and φ-scans (**9**). The structures were refined on F^2 using the program SHELXL-97.[20] All non-hydrogen atoms were refined anisotropically. Aminic hydrogen atoms were identified from difference syntheses but were refined freely only for **6**. Other hydrogen atoms were included either as rigid methyl groups (not well resolved for **4** and **8**) or using a riding model. Refinement special details: The structure of **4** contains one well-resolved cyclohexane solvate molecule. Additionally, two peaks of ca. 2 e/Å^3 near the cyclohexane may represent an alternative disordered solvent site. The structure of **8** contains one poorly resolved pentane solvate molecule which was refined isotropically. The molecular weights and related parameters correspond to the idealised compositions including solvent. Further crystallographic data are collected in Table 6. CCDC-229959 to -229962 contain the supplementary crystallographic data for this paper. These data can be obtained free of charge at www.ccdc.cam.ac.uk/conts/retrieving.html [or from the Cambridge Crystallographic Data Centre, 12 Union Road, Cambridge CB2 1EZ; Fax: (internat.) + 44-1223-336-033; E-mail: deposit@ccdc.cam.ac.uk].

Acknowledgments

We thank the Dirección General de Investigación Científica y Técnica (No. BQU2001-2409-C02-C01) and the Fonds der Chemischen Industrie for financial support.

[1] M. C. Gimeno, A. Laguna, *Comprehensive Coordination Chemistry II* (Eds.: J. A. McCleverty, T. J. Meyer), Elsevier, New York **2003**, vol. 5, p. 911.
[2] See for example: [2a] N. H. Adams, W. Hiller, J. Strähle, *Z. Anorg. Allg. Chem.* **1982**, *485*, 81. [2b] W. Conzelmann, W. Hiller, J. Strähle, *Z. Anorg. Allg. Chem.* **1984**, *512*, 169. [2c] P. G. Jones, B. Ahrens, *New. J. Chem.* **1998**, 1041. [2d] P. G. Jones, B. Ahrens, A. Fischer, *Eur. J. Inorg. Chem.* **1999**, 1103.
[3] See for example: [3a] R. Usón, A. Laguna, A. Navarro, R. V. Parish, L. S. Moore, *Inorg. Chim. Acta* **1986**, *112*, 205. [3b] J. Vicente, M. T. Chicote, R. Guerrero, P. G. Jones, *J. Chem. Soc., Dalton Trans.* **1995**, 1251. [3c] M. Munakata, S. G. Yam, M. Maekawa, M. Akiyama, S. Kitagawa, *J. Chem. Soc., Dalton Trans.* **1997**, 4257. [3d] A. Grohmann, J. Riede, H. Schmidbaur, *Z. Naturforsch., Teil B* **1992**, *47*, 1255. [3e] U. M. Tripathi, G. L. Wegner, A. Schier, A. Jockisch, H. Schmidbaur, *Z. Naturforsch., Teil B* **1998**, *53*, 939. [3f] J. Zou, P. Taylor, J. Dornan, S. P. Robinson, M. D. Walkinshaw, P. J. Sadler, *Angew. Chem. Int. Ed.* **2000**, *39*, 2931. [3g] J. F. Vollano, D. H. Picker, J. A. Statler, *Inorg. Chim. Acta* **1989**, *155*, 31.
[4] H. Schmidbaur, A. Kolb, P. Bissinger, *Inorg. Chem.* **1992**, *31*, 4370.
[5] [5a] L. Messori, F. Abbate, P. Orioli, C. Tempi, G. Marcon, *Chem. Commun.* **2002**, 612. [5b] G. Nardin, L. Randaccio, G. Annibale, G. Natile, B. Pitteri, *J. Chem. Soc., Dalton Trans.* **1980**, 220. [5c] T. K. Best, T. K. Chattopadhyay, M. I. Djuran, R. A. Palmer, P. G. Sadler, I. Sovago, K. Varnagy, *J. Chem. Soc., Dalton Trans.* **1997**, 2587. [5d] U. Abram, K. Ortner, R. Gust, K. Sommer, *J. Chem. Soc., Dalton Trans.* **2000**, 735.
[6] [6a] M. C. Gimeno, A. Laguna, *Gold Bull.* **1999**, *32*, 90. [6b] E. M. Barranco, M. C. Gimeno, A. Laguna, M. D. Villacampa, P. G. Jones, *Inorg. Chem.* **1999**, *38*, 702. [6c] E. M. Barranco, O. Crespo, M. C. Gimeno, A. Laguna, P. G. Jones, B. Ahrens, *Inorg. Chem.* **2000**, *39*, 680. [6d] M. C. Gimeno, P. G. Jones, A. Laguna, C. Sarroca, *J. Organomet. Chem.* **2000**, *596*, 10. [6e] S. Canales, O. Crespo, M. C. Gimeno, P. G. Jones, A. Laguna, *J. Organomet. Chem.* **2000**, *613*, 50. [6f] E. M. Barranco, O. Crespo, M. C. Gimeno, P. G. Jones, A. Laguna, C. Sarroca, *J. Chem. Soc., Dalton Trans.* **2001**, 2523. [6g] S. Canales, O. Crespo, A. Fortea, M. C. Gimeno, P. G. Jones, A. Laguna, *Dalton Trans.* **2002**, 2250.
[7] J. D. Carr, S. J. Coles, W. W. Hassan, M. B. Hursthouse, K. M. A. Malik, J. H. R. Tucker, *J. Chem. Soc., Dalton Trans.* **1999**, 57.
[8] R. Usón, L. A. Oro, J. Gimeno, M. A. Ciriano, J. A. Cabeza, A. Tiripicchio, M. Tiripicchio Camellini, *J. Chem. Soc., Dalton Trans.* **1983**, 323.
[9] D. Li, Z. Y. Qi, Q. Peng, R. Z. Li, X. L. Peng, J. M. Cai, *Acta Chim. Sin.* **2002**, *60*, 1637.
[10] O. Crespo, M. C. Gimeno, P. G. Jones, A. Laguna, C. Sarroca, *Chem. Commun.* **1998**, 1481.
[11] M. C. Gimeno, P. G. Jones, A. Laguna, C. Sarroca, M. J. Calhorda, L. F. Veiros, *Chem. Eur. J.* **1998**, *4*, 2308.
[12] E. M. Barranco, O. Crespo, M. C. Gimeno, P. G. Jones, A. Laguna, M. D. Villacampa, *J. Organomet. Chem.* **1999**, *592*, 258.
[13] S. Bordón, L. Busetto, M. C. Cassani, V. G. Albano, P. Sabatino, *Inorg. Chim. Acta* **1994**, *222*, 267.
[14] [14a] D. Gibson, B. J. G. Johnson, J. Lewis, *J. Chem. Soc., A* **1970**, 367. [14b] J. Vicente, M. T. Chicote, *Inorg. Synth.* **1998**, *32*, 172.
[15] [15a] A. N. Nesmeyanov, E. G. Perevalova, Yu T. Struchkov, M. Yu Antipin, K. I. Grandberg, V. P. Dyadchenko, *J. Organomet. Chem.* **1980**, *201*, 343. [15b] M. I. Bruce, B. K. Nicholson, O. B. Shawkataly, *Inorg. Synth.* **1989**, *26*, 324.
[16] R. Usón, A. Laguna, M. Laguna, *Inorg. Synth.* **1989**, *26*, 85.
[17] R. Usón, A. Laguna, M. Laguna, J. Jiménez, E. Durana, *Inorg. Chim. Acta* **1990**, *168*, 89.
[18] R. Usón, A. Laguna, M. Laguna, M. Abad, *J. Organomet. Chem.* **1983**, *249*, 437.
[19] M. Bardají, O. Crespo, A. Laguna, A. Fisher, *Inorg. Chim. Acta* **2000**, *304*, 7.
[20] G. M. Sheldrick, SHELXL-97, *A Program for Crystal Structure Refinement*, University of Göttingen, **1997**.

Received June 7, 2004
Early View Article
Published Online November 5, 2004

 © 2004 Wiley-VCH Verlag GmbH & Co. KGaA, Weinheim

A Kinetic Study on the Reactions of Azolato-Bridged Dinuclear Platinum(II) Complexes with Guanosine 5′-Monophosphate

Seiji Komeda,[a,b] Hirotoshi Yamane,[b] Masahiko Chikuma,[b] and Jan Reedijk*[a]

Keywords: Azoles / Platinum complexes / Cisplatin / Antitumor agents

By using ^{1}H NMR spectroscopy the reactions of [{*cis*-Pt(NH_3)$_2$}$_2$(μ-OH)(μ-pz)](NO_3)$_2$ (**1**), [{*cis*-Pt(NH_3)$_2$}$_2$(μ-OH)(μ-1,2,3-ta-*N1,N2*)](NO_3)$_2$ (**2**) and [{*cis*-Pt(*R,R*-dach)}$_2$(μ-OH)(μ-pz)](NO_3)$_2$ (**3**) with guanosine 5′-monophosphate (GMP) were monitored spectroscopically in 0.1 M phosphate D_2O solutions at three different pD values (5.4, 6.9, 8.4). From the investigations some kinetic information was obtained. The reaction rate for all these complexes become higher when the pD decreases. In addition, for the reactions performed in unbuffered solutions (pD 8.2), the reactivity of all the complexes for GMP was found to increase dramatically. The 1:2 reaction products were characterized by ^{1}H, ^{195}Pt, and ^{31}P NMR spectroscopy. Reactions of **2** with GMP include an unusual ligand-binding isomerization, resulting from the Pt atom migration along the 1,2,3-triazolato ring.

(© Wiley-VCH Verlag GmbH & Co. KGaA, 69451 Weinheim, Germany, 2004)

Introduction

The antitumor activity of the square-planar platinum(II) complex, *cis*-diamminedichloroplatinum(II) (cisplatin), was discovered by Rosenberg[1,2] in the mid 1960's. Cisplatin was subsequently approved for clinical use in 1979 and is now one of the most well-established and most sold successful antitumor drugs. Not exceptionally for an antitumor drug, its chemotherapy involves some serious side effects[3−6] and it also may result in acquired drug resistance.[7,8] It has been generally accepted that the local DNA kink resulting from the formation of the 1,2-intrastrand crosslink at d(GpG) site is connected with cisplatin's antitumor activity.[9,10] Therefore, a successful approach to circumvent the cross-resistance is likely to be the design of a Pt^{II} complex which would react with DNA in a different way from that of cisplatin.[11,12]

Earlier reports by some of us have shown that the azolato-bridged dinuclear platinum(II) complexes, [{*cis*-Pt(NH_3)$_2$}$_2$(μ-OH)(μ-pz)](NO_3)$_2$ (pz = pyrazolate) (**1**) and [{*cis*-Pt(NH_3)$_2$}$_2$(μ-OH)(μ-1,2,3-ta-*N1,N2*)](NO_3)$_2$ (1,2,3-ta = 1,2,3-triazolate) (**2**), exhibit remarkably high in vitro cytotoxicity on several human tumor cell lines[13] and largely circumvent the cross-resistance to cisplatin.[14,15] These complexes were aimed to provide a 1,2-intrastrand GG crosslink with a minimal kink of DNA. This type of DNA adducts would sufficiently induce the desired cytotoxic effect[16] and may expect a different biological consequence compared to cisplatin (Figure 1).

On the other hand, replacing the terminal ammine ligands with primary and secondary amines, such as ethylenediamine, diaminocyclohexane, and isopropylamines, this series of azolato-bridged dinuclear Pt^{II} complexes exhibits a decrease in cytotoxicity.[13,17] This tendency agrees with the general structure-activity relationship in mononuclear cisplatin derivatives. Full interpretation of this relationship requires a proper way to investigate their DNA binding (coordination) rate, and to compare them with the reported cytotoxic profiles.[13] In this paper we report a kinetic study on the reactions of these three azolato-bridged dinuclear Pt^{II} complexes with guanosine 5′-monophosphate (GMP), the most simple DNA fragment, in solution at different pH.

Results and Discussion

Reactions of compounds **1**, **2**, and [{*cis*-Pt(*R,R*-dach)}$_2$(μ-OH)(μ-pz)](NO_3)$_2$ (**3**) with GMP (stoichiometric (2 equiv.) or excess (4 equiv.) per Pt complex) were monitored by ^{1}H NMR in D_2O solution with/without 0.1 M phosphate buffer. These azolato-bridged dinuclear platinum(II) complexes react with 2 equiv. of GMP to yield the final products, **I**-(GMP)$_2$, **II**-(GMP)$_2$, and **III**-(GMP)$_2$ (see Schemes 1 and 2). Upon incubating these compounds with GMP, the ^{1}H NMR signals corresponding to azolates of **1**−**3** and an H8 signal of the free GMP decreases in intensity with time (see Figures 2−4). The supposed intermediates could hardly be traced for all the reactions, not even in

[a] Leiden Institute of Chemistry, Gorlaeus Laboratories, Leiden University,
PO Box 9502, 2300 RA Leiden, The Netherlands
Fax: (internat.) + 31-715274671
E-mail: reedijk@chem.leidenuniv.nl
[b] Osaka University of Pharmaceutical Sciences,
4-20-1 Nasahara, Takatsuki, 569-1094, Japan

 © 2004 Wiley-VCH Verlag GmbH & Co. KGaA, Weinheim **DOI: 10.1002/ejic.200400492**

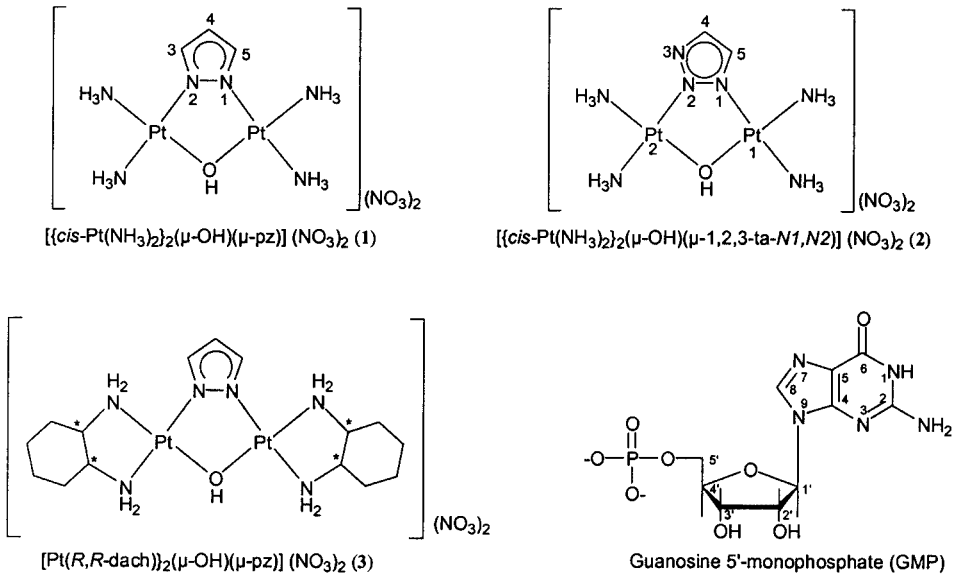

Figure 1. Schematic representation of [{*cis*-Pt(NH_3)$_2$}$_2$(μ-OH)(μ-pz)](NO_3)$_2$ (**1**), [{*cis*-Pt(NH_3)$_2$}$_2$(μ-OH)(μ-1,2,3-ta-*N1*,*N2*)](NO_3)$_2$ (**2**), [Pt(*R*,*R*-dach)}$_2$(μ-OH)(μ-pz)] (NO_3)$_2$ (**3**), and guanosine 5′-monophosphate (GMP)

the reactions with stoichiometric (2 equiv.) GMP at 310 K. Therefore, the rate-determining step is obviously the reaction in which an N7 of the first GMP displaces the leaving hydroxo groups. Hence, the first substitution reaction of these complexes with GMP appears to proceed by an associative process which is followed by the second substitution reaction, in which the hydroxyl or water ligand undergoes relatively rapid substitution by the second nucleotide.

Characterization of the Reaction Products

The ^{1}H, ^{31}P, and ^{195}Pt NMR spectroscopic data for the reaction products, [{*cis*-Pt(NH_3)$_2$(GMP-*N7*)}$_2$(μ-pz)]$^-$(**I**-(GMP)$_2$], [{*cis*-Pt(NH_3)$_2$(GMP-*N7*)}$_2$(μ-1,2,3-ta-*N1*,*N3*)]$^-$ [**II**-(GMP)$_2$], and [{*cis*-Pt(*R*,*R*-dach)(GMP-*N7*)}$_2$(μ-pz)]$^-$ [**III**-(GMP)$_2$] measured in 0.1 M phosphate D_2O (pD 7.0) solution at 298 K are summarized in Table 1.

^{1}H NMR

As mentioned above, **1** reacts with GMP in a bifunctional way to provide **I**-(GMP)$_2$ (Scheme 1). The signal of the H8 proton appears at slightly lower field as a completely broadened signal at 310 K, indicating a hindered rotation about the Pt−N7 bonds.[14,15] The signal becomes sharper to some extent upon increase of the temperature.[14] Referred to the H8 signal of free GMP, cisplatin-platinated GMP shows a 0.44 ppm downfield shift[18] owing to the inductive effect by platinum coordination (Figure 2). On the other hand, the H8 of **I**-(GMP)$_2$ appears at only 0.09 ppm lower field (323 K), indicating a ring-currency effect caused by well-stacked intramolecular guanine bases and by close proximity to the pyrazolate ring, which will compensate for the inductive effect.[14,15] The smaller $J_{1'-2'}$ (3.873 Hz) indicates the increase in N-type population of the sugar puckering.[19,20] Significant upfield shifts are observed for the H1′, H4′, and H5′ protons, but no significant changes are seen for H2′ and H3′. This phenomenon could have the same origin as for the H8 proton, but no proof is available as yet.

The reaction of GMP with **2** (Scheme 2), results in a sharp peak assigned to the H8 of the platinated GMP (observed at $\delta = 0.46$ ppm lower field than that of a free GMP, Figure 3), which is comparable to that of cisplatin-platinated GMP. This implies less stacked guanine ligands and allowance of a relatively free rotation about the Pt−N7

Table 1. The ^{1}H, ^{31}P, and ^{195}Pt NMR spectroscopic data of 1:2 complexes, **I**-(GMP)$_2$, **II**-(GMP)$_2$, and **III**-(GMP)$_2$ measured in 0.1 M phosphate D_2O (pD 7) solution at 298 K

Compound	δ(^{1}H), ppm H8	H1′ ($J_{1'-2'}$, Hz)	azolates	δ(^{31}P), ppm	δ(^{195}Pt), ppm
GMP	8.18	5.92 (6.036)	−	3.95	−
I-(GMP)$_2$	8.27[a]	5.73 (3.873)	6.34 [pz(4)], 7.60 [pz(3,5)]	4.07	−2393
II-(GMP)$_2$	8.64	5.89 (5.637)	7.51 (ta 4,5)	4.04	−2480
III-(GMP)$_2$	7.86	5.74 (4.959)	6.54 [pz(4)], 7.92 [pz(3,5)]	3.86	−2579

[a] Broad peaks that sharpen upon increase of temperature (323 K).

 © 2004 Wiley-VCH Verlag GmbH & Co. KGaA, Weinheim

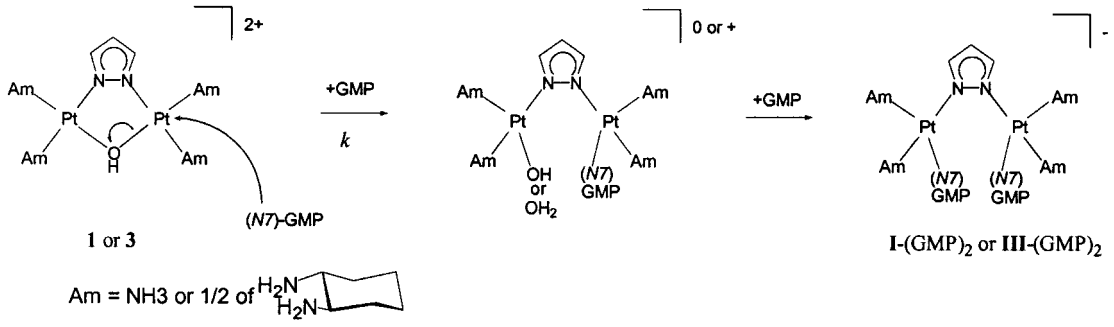

Scheme 1. Two-step reaction of compound **1** (and **3**) with 5′GMP

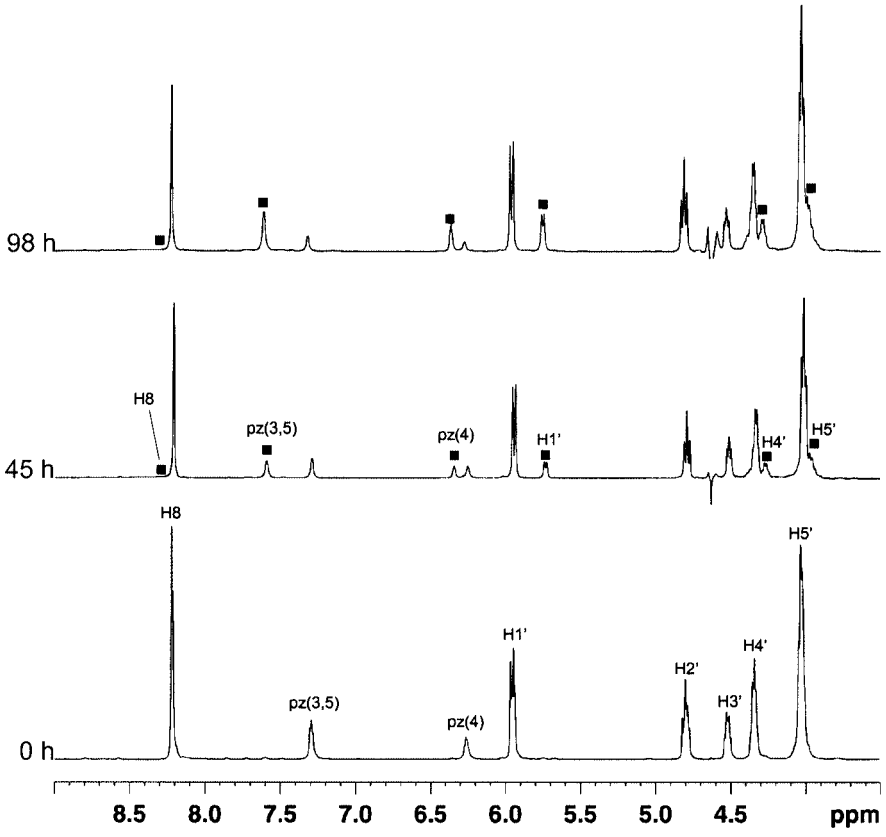

Figure 2. ^{1}H NMR spectra on the reaction of **1** with excess (4 equiv.) of GMP in unbuffered D_2O solution (pD 8.2) measured at 310 K as a function of time. The symbol (filled black squares) shows the newly appeared H8 and sugar ring proton signals (H1′, H4′ and H5′) of GMP ligands, and pz protons in a 1:2 complex, $[\{cis\text{-}Pt(NH_3)_2(GMP\text{-}N7)\}_2(\mu\text{-}pz)]^-$ (**I**-$(GMP)_2$]

bonds.[14] An interesting aspect that should be emphasized, is that the signals of ta(4) and (5) in the bridging 1,2,3-triazolate have shifted to higher field and now appear as a single peak (i.e. a highly symmetric species must be present). This phenomenon clearly indicates that the present reaction includes the same isomerization as we reported earlier for the reaction of **2** with 9EtG.[14] Thus, after the first substitution by N7 of GMP, the Pt atom initially coordinating to N2 of the 1,2,3-triazolate ring migrates from N2 to N3, to provide the symmetric 1:2 complex, **II**-$(GMP)_2$. This migration of the platinum(II) is to be seen as a novel isomerization reaction, since substitution reactions of square-planar metal complexes usually proceed via penta-coordination transition states. It seems obvious that N3 is not able to coordinate at the axial Pt position as long as N2 is coordinating to Pt2. Unlike the products of the pyrazolato-bridged complexes, no significant upfield shifts on the sugar ring proton signals are observed. The $J_{1'\text{-}2'}$ is found to be 5.637 Hz, indicating a sugar puckering with a similar N/S population as that of free GMP.[19,20]

 © 2004 Wiley-VCH Verlag GmbH & Co. KGaA, Weinheim

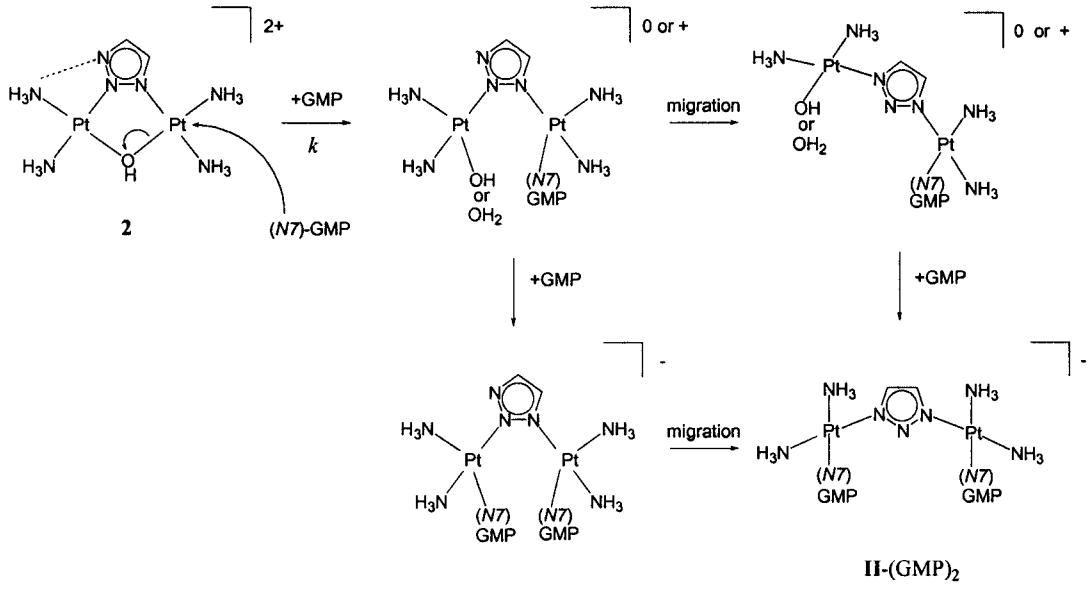

Scheme 2. Reaction steps of compound **2** with 5′GMP

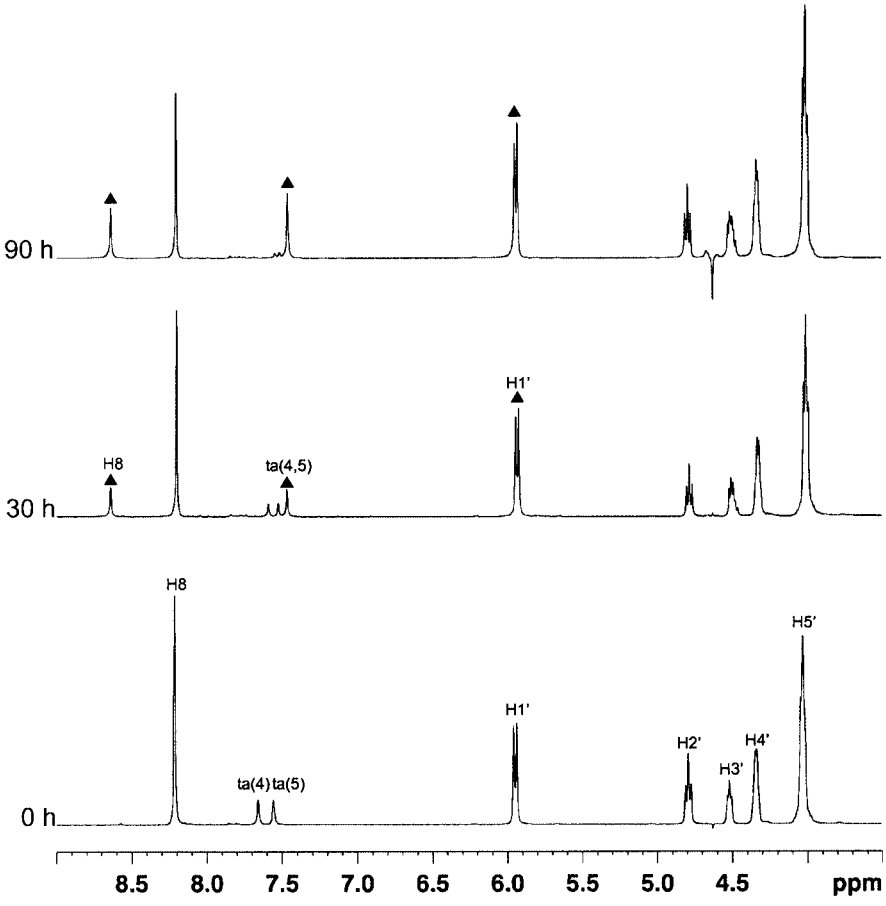

Figure 3. ^1H NMR spectra on the reaction of **2** with excess (4 equiv.) of GMP in unbuffered D_2O solution (pD 8.2) measured at 310 K as a function of time. The symbol (filled black triangles) shows the newly appeared H8 and sugar ring proton signals (H1′) of GMP ligands, and azolate protons in a 1:2 complex, $[\{cis\text{-}Pt(NH_3)_2(GMP\text{-}N7)\}_2(\mu\text{-}1,2,3\text{-}ta\text{-}N1,N3)]^-$ [**II**-$(GMP)_2$]

 © 2004 Wiley-VCH Verlag GmbH & Co. KGaA, Weinheim

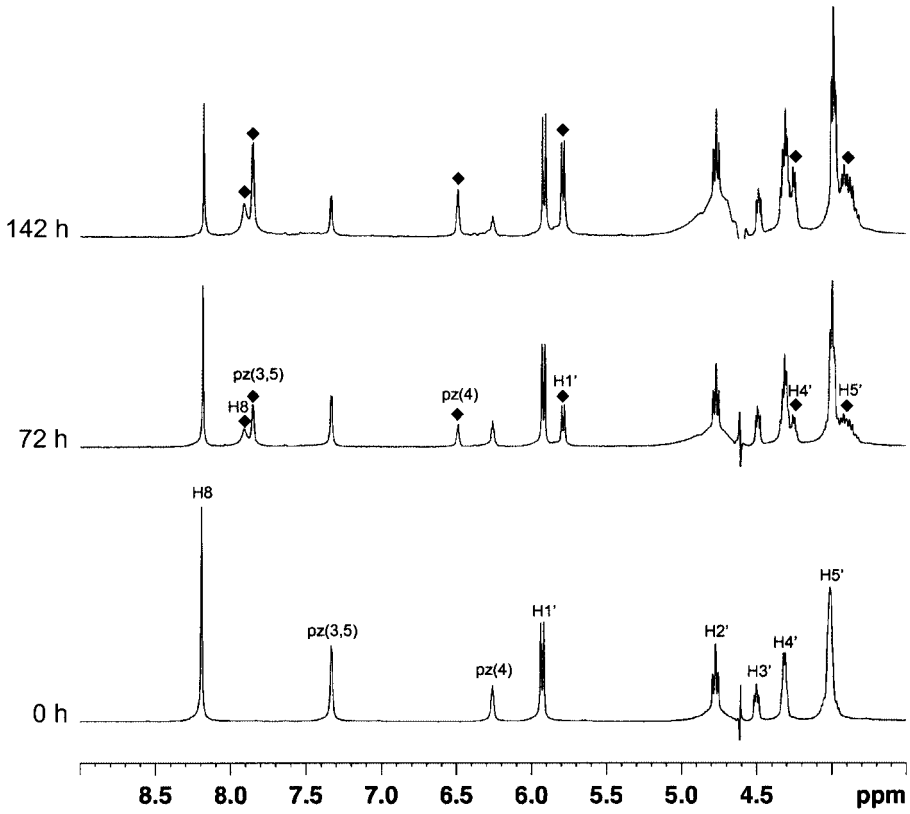

Figure 4. ^{1}H NMR spectra on the reaction of **3** with excess (4 equiv.) of GMP in unbuffered D_2O solution (pD 8.2) measured at 310 K as a function of time. The symbol (filled black diamonds) shows the newly appeared H8 and sugar ring proton signals (H1′, H4′ and H5′) of GMP ligands, and azolate protons in a 1:2 complex, [{Pt(*R*,*R*-dach)$_2$(GMP-*N7*)}$_2$(μ-pz)]$^-$ (**III**-(GMP)$_2$]

The ^{1}H NMR profiles of **III**-(GMP)$_2$ are similar to those of **I**-(GMP)$_2$ (Figure 4). A broad H8 signal is observed at higher field compared to free GMP. This upfield shift also agrees with well-stacked guanine ligands. The H1′ ($J_{1'-2'}$ = 4.959 Hz), H4′ and H5′ protons show significant upfield shifts, just as found for **I**-(GMP)$_2$.

^{195}Pt NMR

The ^{195}Pt NMR chemical shifts for the **I**-(GMP)$_2$, **II**-(GMP)$_2$, and **III**-(GMP)$_2$ are all found in the region expected for a [PtN$_4$] coordination sphere, further confirming the platinum coordination to N7 of GMP. The spectrum found for compound **2** is split into two signals,[13] owing to the two slightly different [PtN$_3$O] environments. On the other hand, the single peak observed for **II**-(GMP)$_2$, is supportive for the isomerization reaction, just as expected from the ^{1}H NMR study.

^{31}P NMR

Given that the 1:2 complexes have strong intramolecular hydrogen bonding between the ammine ligands and phosphate group, higher field shifts of their ^{31}P NMR signals, compared to free GMP (pD = 7.0), could be expected. The signals of the phosphate groups for **I**-(GMP)$_2$ and **II**-(GMP)$_2$ are observed at δ = 0.09−0.12 ppm lower field, and that for **III**-(GMP)$_2$ appeared at only 0.09 ppm higher field. These deviations from free GMP are not considered to be significant.

pH-Titration Experiments

The pH titration curves for GMP, **II**-(GMP)$_2$ and **III**-(GMP)$_2$ are depicted in Figure 5. As is clear from the plots, the N7 (*de*)protonation effects of the GMP ligands of **II**-(GMP)$_2$ and **III**-(GMP)$_2$ are absent, confirming the plati-

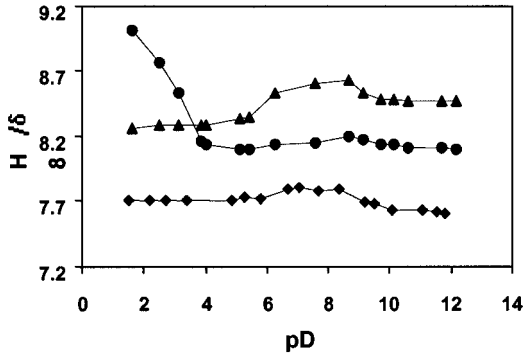

Figure 5. Plots of chemical shift (δ) of H8 resonance vs. pD for free GMP (filled black circles), **II**-(GMP)$_2$ (filled black triangles) and **III**-(GMP)$_2$ (filled black diamonds). pH titrations were performed in unbuffered D_2O solution at 298 K with adjusting pD with 0.1 M DNO_3 and 0.1 M NaOD

 © 2004 Wiley-VCH Verlag GmbH & Co. KGaA, Weinheim

num coordination at the N7 site for these complexes. A pH-titration graph of H8 of **I**-$(GMP)_2$ is uninformative, due to the complete broadening at room temp. as stated above.

Kinetic Aspects

The reactions of **1**−**3** with GMP were monitored by ^1H NMR spectroscopy at 310 K. The reactions with stoichiometric quantities (2 equiv.) of GMP do fit to second-order plots (Figure 6). The reaction rates as determined for the reaction of the complexes are presented in Table 2.

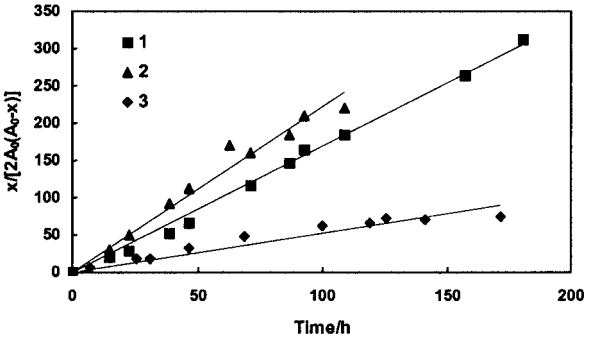

Figure 6. Second-order plots of the reactions of **1** (filled black squares), **2** (filled black triangles) and **3** (filled black diamonds) with 2 equiv. of GMP in unbuffered D_2O solution (pD 8.2) at 310 K. Values for k were calculated from the slope of the lines, as given in Equation (1)

Table 2. Obtained second-order rate constants (k in $M^{-1}s^{-1}$) of the platinum complexes for the reactions of **1**−**3** with 2 equiv. of GMP at 310 K in D_2O with or without 0.1 M phosphate

	Reaction rates k [$M^{-1}s^{-1}$]		
pD/compound	**1**	**2**	**3**
5.4[a] (2 equiv.)	$2.36\cdot10^{-4}$	$3.34\cdot10^{-4}$	$1.53\cdot10^{-4}$
6.9[a] (2 equiv.)	$1.39\cdot10^{-4}$	$2.64\cdot10^{-4}$	$1.11\cdot10^{-4}$
8.4[a] (2 equiv.)	$1.25\cdot10^{-4}$	$2.36\cdot10^{-4}$	$6.94\cdot10^{-5}$
8.2[b] (2 equiv.)	$4.67\cdot10^{-4}$	$6.15\cdot10^{-4}$	$1.46\cdot10^{-4}$

[a] Reactions were performed in 0.1 M phosphate D_2O solution. [b] Reactions were performed in unbuffered D_2O solution.

Compound **2** is found to react faster with GMP than **1**. Even though the amino groups in dach ligands of **3** should have similar *trans* effects on the leaving OH group as the ammine ligands,[21] the dach-containing complex reacts with GMP at a significantly slower rate compared to **1**. The kinetic rate of ligand-exchange reactions with associative mechanism are known to be negatively influenced by steric hindrance of the substrates, and more than those with dissociative reactions. Therefore, the observed kinetic difference could be ascribed to the steric effects of the bulky cyclohexane rings. Another contribution might be the reduced potential of dach to form hydrogen bonds compared to ammonia, since the first contact of these cationic azolato-bridged compounds is supposed to be non-covalent interactions, such as ionic and hydrogen bonds. Comparison of all the kinetic data shows that the reaction rates for all the complexes are faster when the pD decreases (see Figure 7). The pK_b value for the bridging OH group of this series of azolato-bridged dinuclear Pt complexes is very low [e.g. pK_b = 0.4 for complex **1** (unpublished observations)], and no direct contribution to the kinetics can be expected within the pD range applied for this study. However, an increase in H^+ concentration could catalytically act on the hydroxo bridge to promote the first substitution reaction.

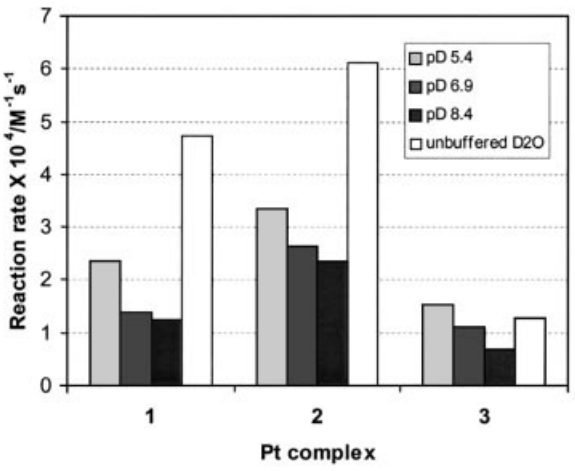

Figure 7. Column graph showing the second-order rate constants for the reaction of **1**−**3** with 2 equiv. of GMP in 0.1 M phosphate D_2O solutions with different pD (5.4, 6.9, and 8.4) and unbuffered D_2O solution (pD 8.2)

Interestingly, in unbuffered D_2O solutions, the reactivity of all complexes for GMP dramatically increases. This may be indicative for the affinity of the OH bridge and/or amine ligands of the platinum complexes for phosphate, i.e. the phosphate in the buffer competitively binds to the platinum complexes electrostatically and competes with the phosphate groups of GMP. This tendency is more pronounced in the reactions of **1** and **2**, thereby clearly demonstrating the importance of the non-covalent (dipolar) interaction with the phosphate group of the GMP as an initial step of the reaction. For confirmation, we undertook a similar kinetic study in other salts, or buffer solutions, such as MES buffer, using HPLC (data not shown). No such a large decrease in the kinetic rate compared to an unbuffered solution was found, and therefore, a high non-covalent (dipolar) affinity of these complexes can be expected also for the phosphate backbone of DNA. This interaction might be important for the processes, such as major-groove or minor-groove binding. Cisplatin, as a neutral molecule, is known to be activated and positively charged by hydrolysis (a first-order reaction with $t_{1/2}$ = 2 h[23]), and the activated species appears to coordinate to nucleic acids, promptly. Therefore, for these azolato-bridged dinuclear platinum(II) non-covalent accumulation on DNA must be more probable.

 © 2004 Wiley-VCH Verlag GmbH & Co. KGaA, Weinheim

Conclusion

Interactions between transition-metal complexes and DNA have been investigated, since DNA has been believed and accepted to be one of the critical targets of cisplatin. The azolato-bridged dinuclear Pt^{II} complexes react with GMP at a relatively slow rate, and show a clear tendency to faster reactions with GMP, when the solution pH decreases. This series of Pt^{II} complexes was aimed to generate a 1,2-intrastrand crosslinks with a minimum kink of DNA. According to our recent report using the hairpin-stabilized double-stranded DNA, d(TATGGCATT$_4$ATGCCATA),[16] **1** indeed yields only the 1,2-intrastrand GG crosslink on a hairpin-stabilized double-stranded DNA, while **2** serves not only as the intrastrand crosslinker, but also generates interstrand GC crosslinks as a minor product. This behaviour appears to, depend on the different configuration about the triazolate ring, such as *N1*,*N2*- and *N1*,*N3*-coordination of the two Pt^{II} atoms. It is as yet too early to conclude that only such coordination interactions would trigger the cytotoxic effects. Accordingly, also ionic (non-coordination) interactions with DNA should also be taken into consideration[24] for the following reasons:

i) The reactions with small DNA fragments proceed at much slower rate compared with cisplatin.

ii) The complexes possess a 2+ charge.

iii) The complexes appear to have a significant affinity with the phosphate group.

Therefore, dipolar or ionic interactions, in addition to coordination, may indeed have a significant influence on the cytotoxicity of such compounds.

Experimental Section

Materials: Guanosine 5′-monophosphate (GMP) was obtained from Sigma. The azolato-bridged dinuclear platinum complexes, [*cis*-{Pt(NH$_3$)$_2$}$_2$(μ-OH)(μ-pz)](NO$_3$)$_2$ (**1**), [*cis*-{Pt(NH$_3$)$_2$}$_2$(μ-OH)(μ-1,2,3-ta-*N1*,*N2*)](NO$_3$)$_2$ (**2**) were prepared as reported before.[12,13]

Preparation of [{Pt(*R*,*R*-dach)}$_2$(μ-OH)(μ-pz)](NO$_3$)$_2$ (3): 50 mL of a water solution containing 0.224 g of Hpz (3.24 mmol) and 0.62 g of [{Pt(*R*,*R*-dach)}(μ-OH)]$_2$(NO$_3$)$_2$ (0.81 mmol) was stirred and heated at 60 °C in the dark. After 3 h incubation, the solution was filtered and the solvents evaporated to dryness, and the resulting white material was washed with 200 mL of ice-cold EtOH and diethyl ether. Recrystallization was carried out from water. Yield: 0.39 g (57%). $C_{15}H_{32}N_8O_7Pt_2{\cdot}H_2O$: calcd. C 21.33, H 4.06, N 13.27; found C 21.44, H 3.86, N 13.23%. ^{1}H NMR (D$_2$O, ppm): δ = (pz resonance) 7.39 (2 H, d), 6.30 (1 H, t), (cyclohexane resonance) 2.40 (4 H, b), 2.07 (4 H, b), 1.59 (4 H, b), 1.32 (4 H, b), 1.17 (4 H, b). ^{195}Pt NMR (D$_2$O, ppm): δ = −2272 (reference: Na$_2$PtCl$_6$).

NMR Measurements: All the NMR spectra were recorded on a Bruker DPX300 spectrometer at 300 MHz. For the monitoring of the GMP reactions, kinetic samples were measured at 310 K. Regarding the characterization for the resulting products, ^{1}H, ^{31}P, and ^{195}Pt NMR spectra were measured at 298 K in a 50 mM phosphate buffer solution (pD = 7.0) and referred to TSP and Na$_2$PtCl$_6$, and H$_3$PO$_4$ (85% in D$_2$O), respectively. For a pH titration study, the pD was adjusted with 0.1 and 1 M solutions of NaOD and DNO$_3$, and the ^{1}H NMR spectra were measured at 298 K.

Reactions in the NMR Tube: The reactions of complexes **1**−**3** with GMP were performed in the NMR tube at 310 K and followed by ^{1}H NMR spectroscopy as a function of time. The reactions of the platinum complexes (4 mM) with stoichiometric (2 equiv., 8 mM) and excess amount (4 equiv., 16 mM) of GMP were carried out in unbuffered D$_2$O solutions (pD of the reaction solution at $T = 0$ is 8.2) and 0.1 M phosphate buffered D$_2$O solutions (pD 5.4, 6.9, and 8.4). The reactions performed in pD 5.4 solutions increased the pD value by approximately 0.2 units after 1 week, and the pD values did not change for those performed in unbuffered D$_2$O solutions during the reaction.

Kinetic Analysis: To determine the time-dependent concentration of the reactants (**1**−**3**) and final product (**I**-(GMP)$_2$, **II**-(GMP)$_2$, and **III**-(GMP)$_2$], the relative integration values for the azolate protons [pz(3,5), ta(4,5), and pz(4) for **1**, **2**, and **3**, respectively) were applied. The kinetic data obtained from the stoichiometric reactions fit to the second-order kinetics [Equation (1); correlation coefficients are 0.963−0.998], Therefore, for the determination of the second-order rate constants (k), the following equation was applied:

$$x/[2A_0(A_0 - x)] = kt \quad (1)$$

where A_0 is the initial concentration of the reactant (**1**−**3**) and x is the concentration of the final product (1:2 complex) at time t. The k values obtained correspond to the first steps of the series of the reactions.

pH Titration Experiments: After each reaction of **2** and **3** with 2 equiv. of GMP in unbuffered D$_2$O solution was completed, the pD of the samples was adjusted by 0.1 M DNO$_3$ and NaOD and measured at 298 K using a PHM 80 pH meter (Radiometer) before and after each ^{1}H NMR measurement.

Acknowledgments

The author is indebted to The Kidani Memorial Trust for a fellowship. Also travel support and sponsorship by COST Action D20/0001/00 (biocoordination chemistry) is kindly acknowledged. The authors are grateful to Johnson & Matthey (Reading, UK) for their generous loan of K$_2$PtCl$_4$.

[1] B. Rosenberg, L. Van Camp, T. Krigas, *Nature* **1965**, *205*, 698−699.
[2] B. Rosenberg, L. Van Camp, J. E. Trosko, V. H. Mansour, *Nature* **1969**, *222*, 385−386.
[3] E. Cvitkovic, J. Spaulding, V. Bethune, J. Martin, W. F. Whitmore, *Cancer* **1977**, *39*, 1357−1361.
[4] D. M. Hayes, E. Cvitkovic, R. B. Golbey, E. Scheimer, L. Helson, I. H. Krakoff, *Cancer* **1977**, *39*, 1372−1381.
[5] D. D. Von Hoff, R. Schilsky, C. M. Reichert, *Cancer Treat. Rep.* **1979**, *63*, 1527−1531.
[6] R. S. Goldstein, B. Noordewier, J. T. Bond, J. B. Hook, G. H. Mayor, *Toxicol. Appl. Pharmacol.* **1981**, *60*, 163−175.
[7] J. H. Burchenal, K. Kalaher, K. Dew, L. Lokys, G. Gale, *Biochimie.* **1978**, *60*, 961.
[8] A. Eastman, E. Bresnick, *Biochem. Pharmacol.* **1981**, *30*, 2721−2723.
[9] [9a] J. Reedijk, *Chem. Commun.* **1996**, 801−806. [9b] J. Reedijk, *Proc. Natl. Acad. Sci. (USA)* **2003**, *100*, 3611−3616.

 © 2004 Wiley-VCH Verlag GmbH & Co. KGaA, Weinheim

[10] E. R. Jamieson, S. J. Lippard, *Chem. Rev.* **1999**, *99*, 2467−2498.
[11] N. Farrell, *Cancer Invest.* **1993**, *11*, 578−589.
[12] S. Komeda, G. V. Kalayda, M. Lutz, A. L. Spek, Y. Yamanaka, T. Sato, M. Chikuma, J. Reedijk, *J. Med. Chem.* **2003**, *46*, 1210−1219.
[13] S. Komeda, M. Lutz, A. L. Spek, M. Chikuma, J. Reedijk, *Inorg. Chem.* **2000**, *39*, 4230−4236.
[14] S. Komeda, M. Lutz, A. L. Spek, Y. Yamanaka, T. Sato, M. Chikuma, J. Reedijk, *J. Am. Chem. Soc.* **2002**, *124* 4738−4746.
[15] S. Komeda, H. Ohishi, H. Yamane, M. Harikawa, K. Sakaguchi, M. Chikuma, *J. Chem. Soc., Dalton Trans.* **1999**, 2959−2962.
[16] J. Kozelka, G. Segal, C. Bois, *J. Inorg. Biochem.* **1992**, *47*, 67−80.
[17] M. Harikawa, Master Dissertation, Osaka Univ. Pharmaceut. Sci., **1995**.
[18] A. T. M. Marcelis, C. G. van Kralingen, J. Reedijk, *J. Inorg. Biochem.* **1980**, *13*, 213−222.
[19] C. Altona, M. Sundaralingam, *J. Am. Chem. Soc.* **1973**, *95*, 2333−2344.
[20] J. H. J. den Hartog, C. Altona, J.-C. Chottard, J.-P. Girault, J. Y. Lallemand, F. A. A. M. de Leeuw, A. T. M. Marcelis, J. Reedijk, *Nucleic Acids Res.* **1982**, *10*, 4715−4730.
[21] A. von Zelewsky, *Stereochemistry of Coordination Compounds*, Wiley, Chichester, **1996**, p. 203.
[22] S. Komeda, S. Bombard, S. Perrier, J. Reedijk, J. Kozelka, *J. Inorg. Biochem.* **2003**, *96*, 357−366.
[23] D. P. Bancroft, C. A. Lepre, S. J. Lippard, *J. Am. Chem. Soc.* **1990**, *112*, 6860−6871.
[24] N. J. Wheate, J. G. Collins, *J. Inorg. Biochem.* **2003**, *96*, 313−320.

Received June 9, 2004
Early View Article
Published Online October 18, 2004

 © 2004 Wiley-VCH Verlag GmbH & Co. KGaA, Weinheim

Synthesis, X-ray Crystal Structure and Magnetic Properties of Oxalato-Bridged Copper(II) Complexes with 2,3-Bis(2-pyridyl)pyrazine, 2,3-Bis(2-pyridyl)quinoxaline and 2,2′-Bipyrazine as Peripheral Ligands

José Carranza,[a,b] Hilde Grove,[c] Jorunn Sletten,*[c] Francesc Lloret,[a] Miguel Julve,*[a] Paul E. Kruger,[d] Chad Eller,[e] and D. Paul Rillema[e]

Keywords: Copper / Magnetic properties / N ligands / Oxalate

Five oxalate-containing copper(II) complexes of formula $[Cu(dpq)(H_2O)(ox)]\cdot 5H_2O$ (**1**), $[Cu(dpp)(H_2O)(ox)]\cdot H_2O$ (**2**), $[Cu(bpz)(ox)]_n$ (**3**), $[Cu_2(dpp)_2(H_2O)_2(NO_3)_2(ox)]\cdot 4H_2O$ (**4**) and $[Cu_2Cl_2(bpz)_2(H_2O)_2(ox)][Cu(bpz)(H_2O)_2(ox)]\cdot 2H_2O$ (**5**) [dpq = 2,3-bis(2-pyridyl)quinoxaline; dpp = 2,3-bis(2-pyridyl)-pyrazine; bpz = 2,2′-bipyrazine; ox = oxalate] were prepared and their structures were determined by X-ray diffraction on single crystals. Complexes **1** and **2** are discrete mononuclear complexes with oxalate and dpq (**1**)/dpp (**2**) acting as bidentate ligands. Complex **3** is a neutral oxalato-bridged (2,2′-bipyrazine)copper(II) chain where the oxalate adopts a bidentate/monodentate coordination mode, whereas **4** is an oxalato-bridged copper(II) dinuclear complex with ox and dpp acting as bis-bidentate and bidentate ligands, respectively. The structure of **5** contains neutral $[Cu(bpz)(H_2O)_2(ox)]$ (mononuclear) and $[Cu_2(bpz)_2(H_2O)_2Cl_2(ox)]$ (dinuclear) units where the bpz acts as a bidentate ligand and the oxalate group adopts the bidentate (mononuclear) and bis-bidentate (dinuclear) coordination modes. The copper atoms have distorted square pyramidal (**1** and **2**) and elongated octahedral (**3**–**5**) geometries: two nitrogen atoms from heterocyclic N-donors and two oxalate-oxygen atoms occupy the equatorial positions (**1**–**5**) and a water molecule (**1** and **2**), two oxalate-oxygen atoms (**3**), a water molecule and a nitrate-oxygen (**4**), and either two water molecules (**5**), mononuclear) or a chlorine atom and a water molecule (**5**, dinuclear) fill the axial ones. Magnetic susceptibility measurements for **3**–**5** in the temperature range 1.9–290 K reveal the occurrence of weak (J = –1.4 cm^{-1}, **3**) and strong (–312 and –345 cm^{-1} for **4** and **5**, respectively; $\hat{H} = -J\cdot\hat{S}_A\cdot\hat{S}_B$) antiferromagnetic interactions between the copper(II) atoms in agreement with the out-of-plane (**3**) and in-plane (**4** and **5**) exchange pathways involved.

(© Wiley-VCH Verlag GmbH & Co. KGaA, 69451 Weinheim, Germany, 2004)

Introduction

An impressive amount of work has been devoted to magneto-structural studies of oxalato-bridged copper(II) complexes.[1−5] The four main reasons accounting for this continuous interest are: (i) the remarkable efficiency of the oxalate ligand (the dianion of oxalic acid H_2ox) to mediate strong magnetic interactions between copper(II) ions when adopting the bis-bidentate bridging mode (singlet-triplet energy gap up to -386 cm^{-1} between a pair of copper(II) ions separated by more then 5.4 Å);[1,5] (ii) the copper(II) ion is the simplest case of magnetic exchange given that it corresponds to a doublet spin state without orbital contribution; (iii) the great plasticity of the coordination sphere of the copper(II) ion (four-, five- and six-coordinate geometries are commonly observed), which allows variations of the orientation and symmetry of the molecular orbital describing its unpaired electron (magnetic orbital) simply by changing the nature of the blocking N-donor ligand used;[1a,1c,1e] (iv) X-ray quality crystals which are commonly air- and moisture-stable can be obtained from aqueous solutions containing oxalate, copper(II) and organic ligands by slow evaporation of the solvent at room temperature.

The major synthetic problem chemists had to overcome when investigating the formation of discrete oxalate-containing copper(II) complexes is the formation of the insoluble, oxalato-bridged copper(II) chain $Cu(C_2O_4)\cdot$

[a] Departament de Química Inorgánica, Facultat de Química de la Universitat de Valencia,
Avda. Dr. Moliner 50, 46100 Burjassot (València), Spain
E-mail: miguel.julve@uv.es
[b] Facultad de Ciencias Químicas, Universidad de Zacatecas,
Jardín Juárez s/n, 98000 Zacatecas, Mexico
[c] Department of Chemistry, University of Bergen,
Allégaten 41, 5007 Bergen, Norway
E-mail: jorunn.sletten@kj.uib.no
[d] Department of Chemistry, Trinity College,
Dublin 2, Ireland
[e] Department of Chemistry, Wichita State University,
Wichita, KS 67260-0051, USA
Supporting information for this article is available on the WWW under http://www.eurjic.org or from the author.

 © 2004 Wiley-VCH Verlag GmbH & Co. KGaA, Weinheim **DOI: 10.1002/ejic.200400500**

$1/3H_2O$.[3b,6] The formation of this chain is precluded in the presence of polydentate nitrogen-donor ligands (L) allowing the formation of mixed-ligand species [CuL(ox)], which, in turn, can be used as ligands in designing higher nuclearity species. Two representative examples of this versatility are $[Cu(tmen)(ox)\cdot 4H_2O]$ and $[Cu(terpy)(H_2O)(ox)]\cdot 4H_2O$ (tmen = *N*,*N*,*N*′,*N*′-tetramethylethylenediamine; terpy = 2,2′:6′,2′′-terpyridine).[1c,1e,7] The reaction of the former neutral mononuclear complex with the preformed species $[Cu(tmen)]^{2+}$ and $[Cu(dien)]^{2+}$ (dien = diethylenetriamine) in aqueous solution provides a direct route towards the centrosymmetric and asymmetric oxalato-bridged copper(II) complexes of formula $[Cu_2(tmen)_2(H_2O)_2(ox)](ClO_4)_2\cdot 1.25H_2O$ and $[Cu(dien)(ox)Cu(H_2O)_2(tmen)](ClO_4)_2$.[1c,1e] As for the terpy-containing precursor, its reaction with the partially blocked species $[Cu(terpy)]^{2+}$ and $[VO(ox)]\cdot 4H_2O$[8] affords the oxalato-bridged homo- and heterometallic compounds $[Cu_2(terpy)_2(H_2O)_2(ox)][Cu_2(terpy)_2(ox)](ClO_4)_4\cdot 2H_2O$ and $[Cu(terpy)(ox)VO(ox)(H_2O)]\cdot H_2O$.[7,9]

Following our previous magneto-structural works where the nitrogen heterocycles 2,2′-bipyridine (bipy),[1d,1i,1m,3g,10] 1,10-phenanthroline (phen),[1f,11] 2,2′-dipyridylamine (dpa)[1p] and 2,2′-bipyrimidine (bpym)[4a] were used as blocking ligands in the copper(II)-oxalate system, we tried to extend these studies to less-common nitrogen donors such as 2,3-bis(2-pyridyl)quinoxaline (dpq), 2,3-bis(2-pyridyl)pyrazine (dpp) and 2,2′-bipyrazine (bpz; Scheme 1). Our first attempts afforded the copper(II) complexes of formula $[Cu(dpq)(H_2O)(ox)]\cdot 5H_2O$ (**1**), $[Cu(dpp)(H_2O)(ox)]\cdot H_2O$ (**2**), $[Cu(bpz)(ox)]_n$ (**3**), $[Cu_2(dpp)_2(H_2O)_2((NO_3)_2(ox)]\cdot 4H_2O$ (**4**) and $[Cu_2(bpz)_2(H_2O)_2Cl_2(ox)][Cu(bpz)(H_2O)_2(ox)]\cdot 2H_2O$ (**5**). Their preparation, structural characterization and magnetic investigation are presented here.

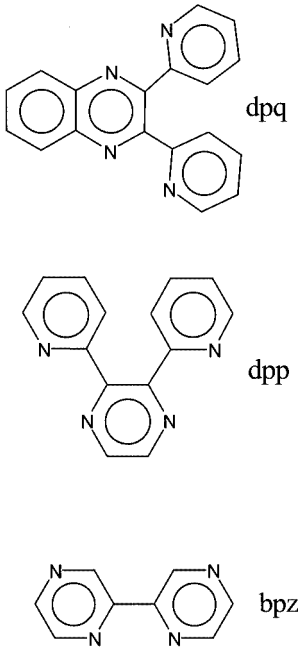

Scheme 1

Results and Discussion

Short Description of the Synthesis

Compound **2** was synthesized by treating a suspension of copper(II) oxalate (insoluble) and the N-donor ligand (dpp). Preparations of complexes **1**, **3**, **4** and **5** were in each case accomplished by treating a common, soluble copper(II) salt with the chosen N-donor ligand, and subsequently adding a solution containing oxalate. The reaction medium was H_2O/EtOH in the cases of **1**, **2** and **4**, H_2O in the case of **3** and **5**. For **1**, **2** and **4** the stoichiometric amounts of reactants used are reflected in the stoichiometry of the products; for **3** and **5** (L = bpz) deficiency and excess, respectively, of oxalate are present in the reaction mixture as compared to the products formed, the Cu^{II}/bpz/ox reactants ratios being 2:2:1 and 1.5:1.5:1, respectively.

Description of the Structures

$[Cu(dpq)(H_2O)(ox)]\cdot 5H_2O$ (1)

The structure of compound **1** is composed of discrete, neutral $[Cu(ox)(H_2O)(dpq)]$ molecules (Figure 1) and water of hydration. The copper atom has a distorted square-pyramidal environment (tetragonality parameter $\tau = 0.17$),[12] binding equatorially to two oxalate oxygen atoms [1.9344(15) and 1.9677(14) Å for Cu−O] and two dpq nitrogen atoms [1.9718(17) and 2.1244(16) Å for Cu−N(pyridyl) and Cu−N(pyrazine), respectively]; a water molecule coordinates in the apical position [2.1867(15) Å for $Cu-O_w$]. The equatorial plane of copper is tetrahedrally distorted (maximum atomic deviation 0.092 Å), with the metal atom displaced by 0.234 Å from the best mean plane toward the apical ligand. The dihedral angle between the equatorial plane and the best plane through the oxalate group is 7.6°. The quinoxaline group makes dihedral angles of 12.9 and 58.2° with the coordinated and uncoordinated pyridyl rings, respectively.

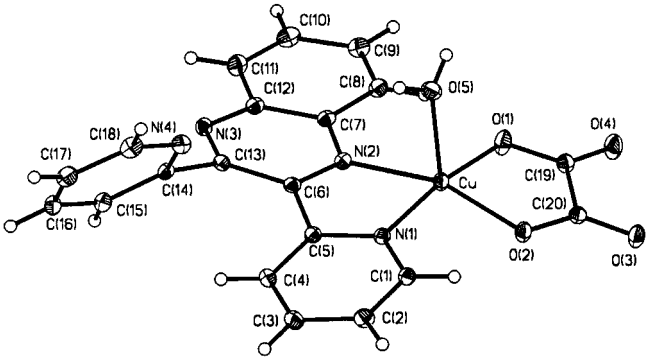

Figure 1. The complex unit $[Cu(dpq)(H_2O)(ox)]\cdot 5H_2O$ in compound **1**, showing the atomic numbering scheme; thermal ellipsoids are plotted at the 30% probability level

Centrosymmetrically related molecules are arranged in the crystals so as to give some overlap between the copper-

 © 2004 Wiley-VCH Verlag GmbH & Co. KGaA, Weinheim

Table 1. Selected bond lengths (Å) and angles (°) for $[Cu(dpq)(H_2O)(ox)]\cdot 5H_2O$ (**1**)[a]

Cu−O(1)	1.9344(15)	Cu−N(2)	2.1244(16)
Cu−O(2)	1.9677(14)	Cu−O(5)	2.1867(15)
Cu−N(1)	1.9718(17)		
O(1)−Cu−O(2)	84.00(6)	N(1)−Cu−N(2)	80.76(7)
O(1)−Cu−N(1)	170.59(7)	O(1)−Cu−O(5)	97.35(7)
O(2)−Cu−N(1)	90.88(6)	O(2)−Cu−O(5)	107.21(6)
O(1)−Cu−N(2)	101.63(6)	N(1)−Cu−O(5)	91.69(6)
O(2)−Cu−N(2)	160.52(6)	N(2)−Cu−O(5)	90.70(6)
O(1)−C(19)	1.289(2)	O(4)−C(19)	1.225(2)
O(2)−C(20)	1.281(2)	C(19)−C(20)	1.558(3)
O(3)−C(20)	1.238(2)		
C(19)−O(1)−Cu	114.31(13)	O(1)−C(19)−C(20)	113.90(17)
C(20)−O(2)−Cu	113.20(13)	O(3)−C(20)−O(2)	126.06(19)
O(4)−C(19)−O(1)	126.1(2)	O(3)−C(20)−C(19)	119.53(18)
O(4)−C(19)−C(20)	120.03(18)	O(2)−C(20)−C(19)	114.41(17)
N(1)−C(1)	1.343(3)	C(6)−C(13)	1.443(3)
N(1)−C(5)	1.360(3)	C(7)−C(8)	1.417(3)
N(2)−C(6)	1.337(3)	C(7)−C(12)	1.430(3)
N(2)−C(7)	1.381(2)	C(8)−C(9)	1.380(3)
N(3)−C(13)	1.327(3)	C(9)−C(10)	1.416(3)
N(3)−C(12)	1.365(3)	C(10)−C(11)	1.369(3)
N(4)−C(18)	1.346(3)	C(11)−C(12)	1.423(3)
N(4)−C(14)	1.354(3)	C(13)−C(14)	1.496(3)
C(1)−C(2)	1.389(3)	C(14)−C(15)	1.392(3)
C(2)−C(3)	1.388(39	C(15)−C(16)	1.387(3)
C(3)−C(4)	1.396(3)	C(16)−C(17)	1.390(3)
C(4)−C(5)	1.391(3)	C(17)−C(18)	1.388(3)
C(5)−C(6)	1.497(3)		
C(1)−N(1)−C(5)	119.54(17)	N(2)−C(7)−C(12)	119.19(18)
C(1)−N(1)−Cu	123.66(14)	C(8)−C(7)−C(12)	119.22(18)
C(5)−N(1)−Cu	116.70(13)	C(9)−C(8)−C(7)	119.5(2)
C(6)−N(2)−C(7)	118.86(179	C(8)−C(9)−C(10)	121.2(2)
C(6)−N(2)−Cu	110.51(13)	C(11)−C(10)−C(9)	120.58(19)
C(7)−N(2)−Cu	129.53(13)	C(10)−C(11)−C(12)	119.8(2)
C(13)−N(3)−C(12)	118.55(17)	N(3)−C(12)−C(11)	119.25(18)
C(18)−N(4)−C(14)	117.04(18)	N(3)−C(12)−C(7)	120.92(18)
N(1)−C81)−C82)	122.04(19)	C(11)−C(12)−C(7)	119.64(19)
C(3)−C(2)−C(1)	118.87(19)	N(3)−C(13)−C(6)	120.99(18)
C(2)−C(3)−C(4)	119.2(29	N(3)−C(13)−C(14)	115.57(17)
C(5)−C(4)−C(3)	119.14(19)	C(6)−C(13)−C(14)	123.14(18)
N(1)−C(5)−C(4)	121.00(18)	N(4)−C(14)−C(15)	123.45(19)
N(1)−C(5)−C(6)	113.71(17)	N(4)−C(14)−C(13)	114.41(17)
C(4)−C(5)−C(6)	125.26(18)	C(15)−C(14)−C(13)	122.08(19)
N(2)−C(6)−C(13)	120.45(18)	C(16)−C(15)−C(14)	118.5(2)
N(2)−C(6)−C(5)	116.39(17)	C(15)−C(16)−C(17)	118.8(2)
C(13)−C(6)−C(5)	123.15(17)	C(18)−C(17)−C(16)	119.2(2)
N(2)−C(7)−C(8)	121.59(18)	N(4)−C(18)−C(17)	123.1(2)

D−H···A	D···A (Å)	H···A (Å)	D−H···A (°)
O(5)−H(51)···O(9)	2.707(2)	1.92	174
O(5)−H(52)···O(10b)	2.843(2)	2.11	174
O(6)−H(61)···O(7c)	2.922(3)	2.06	171
O(6)−H(62)···O(8d)	2.732(2)	1.93	174
O(7)−H(71)···O(6e)	2.753(2)	2.01	164
O(7)−H(72)···N(3)	3.029(2)	2.31	171
O(8)−H(81)···O(3f)	2.886(2)	2.17	162
O(8)−H(82)···O(4)	2.840(2)	2.06	170
O(9)−H(91)···O(10g)	2.834(2)	2.09	179
O(9)−H(92)···O(7h)	2.765(2)	2.03	168
O(10)−H(101)···N(4b)	2.866(2)	2.10	172
O(10)−H(102)···O(3)	2.781(2)	1.99	172

[a] Symmetry transformations used to generate equivalent atoms: (b) $1-x, 1-y, -z$; (c) $1+x, y, z$; (d) $1+x, y, z-1$; (e) $1-x, -y, -1-z$; (f) $-x, 1-y, 1-z$; (g) $x, y-1, z$; (h) $-x, -y, -z$.

oxalate region of one molecule and the pyrazine ring of the other, the distances from individual pyrazine atoms to the oxalate plane ranging from 3.22 to 3.50 Å. This arrangement gives rise to the shortest metal···metal distance in the crystal [4.4193(5) Å for Cu···Cu(1a); (a) = $-x, 1-y, -z$], and also effectively screens the sixth coordination position of the copper atom, the Cu···N(2a) distance being 3.58 Å. There is additionally a slight π-π overlap between the benzo parts of the quinoxaline ligands of centrosymmetrically related molecules, the distances from the quinoxaline plane to three overlapping atoms ranging from 3.43 to 3.48 Å. The molecules are laced together through an extensive network of hydrogen bonds where oxalate, uncoordinated nitrogen and all water molecules are involved (see Table 1). The supramolecular arrangement features parallel sheets of molecules (Figure S1 in the Supporting Information).

The oxalate and dpq groups both coordinate in a monobidentate fashion, and thus have sites available for further metal binding. The bond lengths in the oxalate group are as typically found for this ligand in the didentate coordination mode, the C−O bonds of the coordinated oxygens [1.289(2) and 1.281(2) Å] being significantly longer than those of the uncoordinated ones [1.238(2) and 1.225(2) Å]. dpq is known to act as a chelate ligand either by forming a five-membered ring involving one pyridyl and one pyrazine nitrogen, or by forming a seven-membered ring involving the two pyridyl nitrogen atoms.[13,14] To the best of our knowledge, only two copper(II) complexes with unsubstituted dpq have been structurally characterized previously.[14] In one of these a seven-membered chelate ring was found[14a] and in the second ($[CuBr(dpq)]HSO_4\cdot$dpq) both chelate modes are present.[14b] In addition, the structures of two copper(II) complexes with methyl- or methoxy-substituted dpq (substitution at benzo carbon atoms) have been reported, and in both cases seven-membered chelate rings occur.[13h,15] Compound **1** is therefore the second example of a dpq-containing copper(II) complex with a five-membered chelate ring. It is noteworthy that the Cu−N(2)(pyrazine) bond length of 2.1244(16) Å is rather long for a copper−nitrogen bond in the equatorial plane of a square pyramid, and it is much longer than the Cu−N(1)(pyridyl) bond [1.9718(17) Å]. A similar feature was observed in $[CuBr(dpq)]HSO_4\cdot$dpq [2.101(8) vs. 2.016(8) Å].[14b] A certain difference in pyrazine and pyridyl Cu−N bond lengths is to be expected due to the weaker σ-donor strength of the pyrazine group.[13e] However, it is likely that steric effects also play a role in lengthening the Cu−N(pyrazine) bond in cases where the quinoxaline moiety is close to coplanar with the equatorial plane. In compound **1** this is indicated by the fact that the O(1)−Cu−N(2) angle of 101.63(6)° is much wider than the O(2)−Cu−N(1) angle of 90.88(6)°, possibly to make more room for the benzo part of the dpq ligand. A further indication of the steric effect is found when making a comparison with related dpp-containing copper(II) complexes where no benzo group is present. Studies of these compounds have shown that, although weak, axial bonds are often formed to the pyrazine nitrogen, presumably due to the weaker σ-donor strength mentioned above; the Cu−N(pyrazine) bond is comparable to, or only slightly longer than, the Cu−N(pyridyl) bond in cases where dpp chelates in two equatorial positions to a copper atom with square planar or square pyramidal geometry.[16] Analogous features have also been observed in

 © 2004 Wiley-VCH Verlag GmbH & Co. KGaA, Weinheim

the copper(II) complexes of the more rigid pap ligand (pap = pyrazino[2,3-*f*][4,7]phenanthroline).[16b,17]

[Cu(dpp)(H_2O)(ox)]·H_2O (2)

The structure of compound **2** consists of neutral, mononuclear [Cu(dpp)(H_2O)(ox)] units (Figure 2) and water of hydration. The copper coordination sphere is square pyramidal with bidentate oxalate and dpp binding in the equatorial plane [1.941(2) and 1.953(2) Å for Cu−O and 1.988(2) and 1.989(2) Å for Cu−N] and a water molecule in the apical position [2.250(2) Å for Cu−O_w]. The mean equatorial plane of copper has a very slight tetrahedral distortion (maximum deviation 0.024 Å), and copper is displaced by 0.169 Å from this plane in the direction toward the apical oxygen atom. The oxalate group is essentially coplanar with the equatorial plane (dihedral angle 0.9°). The pyrazine ring makes a dihedral angle of 12.2° with the coordinated pyridyl ring, and a dihedral angle of 66.6° with the free pyridyl ring.

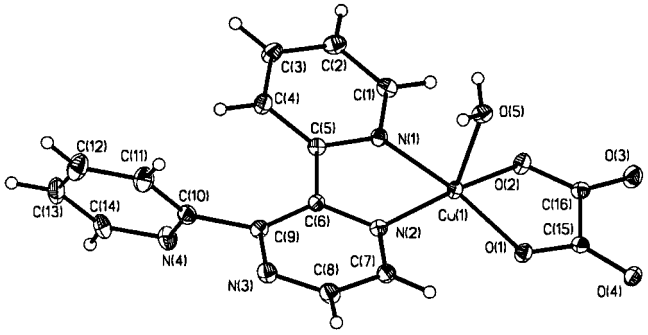

Figure 2. The complex unit [Cu(dpp)(H_2O)(ox)] in compound **2** showing the atomic numbering scheme; thermal ellipsoids are plotted at the 30% probability level

In the crystal there is a slight π-π overlap between the oxalate group of the reference molecule and the coordinated pyridyl ring of a molecule displaced by the unit-cell translation along the *a* axis, with distances from the oxalate plane to the overlapping atoms being 3.30−3.42 Å. This arrangement also screens the sixth coordinating position of copper. There is also a slight π-π overlap between the uncoordinated and coordinated pyrazine of two molecules related by a screw-axis translation (3.46−3.62 Å). The complex molecules are connected by hydrogen bonds into a three-dimensional network: the coordinated water links neighbouring molecules to oxalate groups through hydrogen bonds, and the crystal water connects to pyridyl nitrogen atoms through hydrogen bonds (see Table 2 and Figure S2). The shortest intermolecular metal···metal distance is 5.911(1) Å [Cu(1)···Cu(1a); (a) = $-x$, $y - 0.5$, $2 - z$] and occurs between molecules connected by a hydrogen bond between coordinated water and oxalate oxygen.

The oxalate shows the typical features of bidentate bonding, with two long [1.281(4), 1.297(3) Å] and two short [1.218(3), 1.235(3) Å] C−O bonds. dpp bond lengths and angles compare well with previous findings.[16] The rotation of the uncoordinated pyridyl ring is also of a similar magnitude to that observed in other complexes with bidentate dpp.[16b,16e] In compound **2** the bonds from pyrazine and pyridyl nitrogen atoms to copper are comparable in length [1.982(2) and 1.988(2) Å, respectively], as has been observed earlier for equatorially coordinated, bidentate dpp,[16] but in contrast to the observation in **1** where the pyrazine ring is part of the quinoxaline moiety.

Table 2. Selected bond lengths (Å) and angles (°) for [Cu(dpp)(H_2O)(ox)]·H_2O (**2**)[a]

Cu−O(2)	1.941(2)	Cu−N(2)	1.989(2)
Cu−O(1)	1.953(2)	Cu−O(5)	2.250(2)
Cu−N(1)	1.988(2)		
O(2)−Cu(1)−O(1)	85.40(8)	N(1)−Cu(1)−N(2)	81.02(9)
O(1)−Cu(1)−N(1)	95.85(9)	O(2)−Cu(1)−O(5)	97.88(8)
O(1)−Cu(1)−N(1)	171.32(9)	O(1)−Cu(1)−O(5)	91.85(8)
O(2)−Cu(1)−N(2)	168.53(9)	N(1)−Cu(1)−O(5)	96.48(8)
O(1)−Cu(1)−N(2)	96.08(9)	N(2)−Cu(1)−O(5)	93.44(9)
O(1)−C(15)	1.281(4)	O(4)−C(15)	1.235(3)
O(2)−C(16)	1.297(3)	C(15)−C(16)	1.565(4)
O(3)−C(16)	1.218(3)		
C(15)−O(1)−Cu(1)	112.1(2)	O(1)−C(15)−C(16)	115.3(2)
C(16)−O(2)−Cu(1)	112.4(2)	O(3)−C(16)−O(2)	125.6(3)
O(4)−C(15)−O(1)	126.4(4)	O(3)−C(16)−C(15)	120.4(2)
O(4)−C(15)−C(16)	118.2(3)	O(2)−C(16)−C(15)	114.0(2)
N(1)−C(1)	1.345(4)	C(3)−C(4)	1.385(4)
N(1)−C(5)	1.365(4)	C(4)−C(5)	1.389(3)
N(2)−C(7)	1.338(4)	C(5)−C(6)	1.497(4)
N(2)−C(6)	1.348(3)	C(6)−C(9)	1.407(4)
N(3)−C(8)	1.334(4)	C(7)−C(8)	1.390(4)
N(3)−C(9)	1.352(4)	C(9)−C(10)	1.500(4)
N(4)−C(10)	1.341(4)	C(10)−C(11)	1.390(4)
N(4)−C(14)	1.354(4)	C(11)−C(12)	1.390(5)
C(1)−C(2)	1.386(4)	C(12)−C(13)	1.384(6)
C(2)−C(3)	1.390(4)	C(13)−C(14)	1.381(5)
C(1)−N(1)−C(5)	119.5(2)	N(2)−C(6)−C(9)	119.4(2)
C(1)−N(1)−Cu(1)	124.2(2)	N(2)−C(6)−C(5)	114.0(2)
C(5)−N(1)−Cu(1)	115.7(2)	C(9)−C(6)−C(5)	126.6(2)
C(7)−N(2)−C(6)	119.8(2)	N(2)−C(7)−C(8)	119.7(3)
C(7)−N(2)−Cu(1)	124.3(2)	N(3)−C(8)−C(7)	121.9(3)
C(6)−N(2)−Cu(1)	115.8(2)	N(3)−C(9)−C(6)	120.6(2)
C(8)−N(3)−C(9)	118.1(2)	N(3)−C(9)−C(10)	115.2(2)
C(10)−N(4)−C(14)	117.2(3)	C(6)−C(9)−C(10)	124.1(2)
N(1)−C(1)−C(2)	122.7(3)	N(4)−C(10)−C(11)	123.0(3)
C(1)−C(2)−C(3)	117.7(3)	N(4)−C(10)−C(9)	115.9(3)
C(4)−C(3)−C(2)	120.3(3)	C(11)−C(10)−C(9)	121.1(3)
C(3)−C(4)−C(5)	119.3(3)	C(10)−C(11)−C(12)	118.5(3)
N(1)−C(5)−C(4)	120.5(3)	C(13)−C(12)−C(11)	119.5(3)
N(1)−C(5)−C(6)	112.9(2)	C(14)−C(13)−C(12)	118.0(3)
C(4)−C(5)−C(6)	126.5(3)	N(4)−C(14)−C(13)	123.7(3)

D−H···A	D···A (Å)	H···A (Å)	D−H···A (°)
O(5)−H(51)···O(4b)	2.689(2)	1.93	173
O(5)−H(52)···O(2a)	2.841(3)	2.10	175
O(6)−H(61)···N(4)	2.899(4)	1.94	162
O(6)−H(62)···N(3c)	2.969(4)	2.03	166

[a] Symmetry transformations used to generate equivalent atoms: (a) $-x$, $y - 0.5$, $2 - z$; (b) $x - 1$, y, z; (c) $-x$, $0.5 + y$, $1 - z$.

[Cu(bpz)(ox)]$_n$ (3)

The structural building blocks in **3** are the neutral [Cu(bpz)(ox)] units. Both ox and bpz are bidentate ligands and they surround the copper atom in a close to square-planar geometry [1.9252(14) and 1.9258(15) Å for Cu−O and 1.9837(17) and 1.9869(16) Å for Cu−N]. Copper also has, however, two weak axial connections to semicoordinated oxalate oxygen atoms of centrosymmetrically related mol-

 © 2004 Wiley-VCH Verlag GmbH & Co. KGaA, Weinheim

ecules [2.6170(18) and 2.7518(17) Å for Cu(1)−O(3a) and Cu(1)−O(1b); (a) = $-x$, $-y$, $-z$ and (b) = $1-x$, $-y$, $-z$] resulting in a 4+2 coordination sphere for copper, and formation of a chain with double out-of-plane oxalato bridges (Figure 3). The equatorial plane of copper has a moderate tetrahedral distortion (maximum atomic deviation 0.101 Å), the copper atom being displaced by only 0.004 Å from this plane toward O(3b). The dihedral angles between the equatorial plane and the oxalate and bpz planes are 12.8° and 5.3°, respectively.

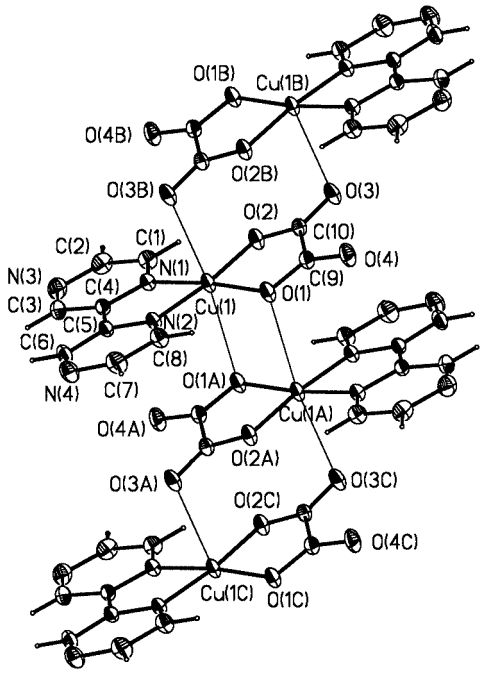

Figure 3. Section of the chain in $[Cu(bpz)(ox)]_n$ (**3**) showing the atomic numbering scheme; thermal ellipsoids are plotted at the 30% probability level; symmetry operations: (a) $1-x$, $-y$, $-z$; (b) $-x$, $-y$, $-z$; (c) $1+x$, y, z

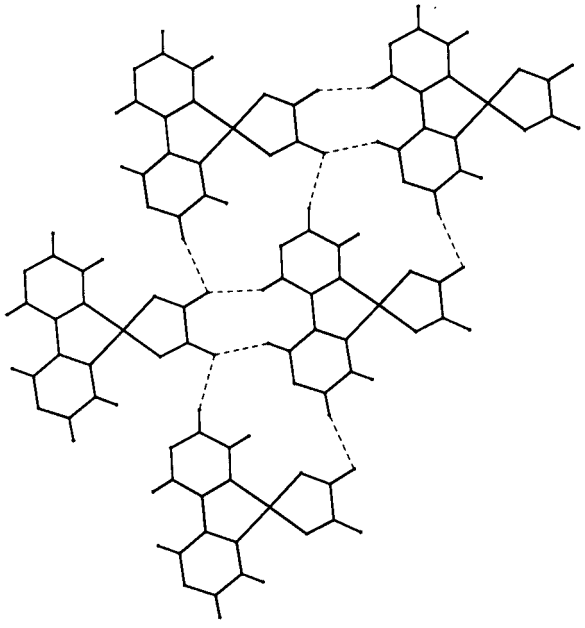

Figure 4. Complex units [Cu(bpz)(ox)] in **3** connected into layers through C−H···O contacts

Table 3. Selected bond lengths (Å) and angles (°) for $[Cu(bpz)(ox)]_n$ (**3**)[a]

Cu(1)−O(2)	1.9252(14)	Cu(1)−N(2)	1.9869(16)
Cu(1)−O(1)	1.9258(15)	Cu(1)−O(3b)	2.6170(18)
Cu(1)−N(1)	1.9837(17)	Cu(1)−O(1a)	2.7518(17)
O(2)−Cu(1)−O(1)	85.76(6)	N(1)−Cu(1)−O(3b)	87.50(6)
O(2)−Cu(1)−N(1)	96.37(6)	N(2)−Cu(1)−O(3b)	85.73(6)
O(1)−Cu(1)−N(1)	173.60(7)	O(2)−Cu(1)−O(1a)	99.73(6)
O(2)−Cu(1)−N(2)	173.99(7)	O(1)−Cu(1)−O(1a)	83.69(6)
O(1)−Cu(1)−N(2)	96.52(6)	N(1)−Cu(1)−O(1a)	90.00(6)
N(1)−Cu(1)−N(2)	81.96(7)	N(2)−Cu(1)−O(1a)	86.07(6)
O(2)−Cu(1)−O(3b)	88.43(6)	O(3b)−Cu(1)−O(1a)	171.69(4)
O(1)−Cu(1)−O(3b)	98.61(6)		
O(1)−C(9)	1.291(2)	O(4)−C(9)	1.215(2)
O(2)−C(10)	1.280(2)	C(9)−C(10)	1.556(3)
O(3)−C(10)	1.224(2)		
C(9)−O(1)−Cu(1)	111.67(13)	O(4)−C(9)−C(10)	120.10(19)
C(9)−O(1)−Cu(1a)	106.77(13)	O(1)−C(9)−C(10)	114.49(17)
Cu(1)−O(1)−Cu(1a)	96.31(6)	O(3)−C(10)−O(2)	125.57(19)
C(10)−O(2)−Cu(1)	111.88(12)	O(3)−C(10)−C(9)	120.05(18)
C(10)−O(3)−Cu(1b)	102.29(13)	O(2)−C(10)−C(9)	114.38(17)
O(4)−C(9)−O(1)	125.36(19)		
N(1)−C(1)	1.336(3)	N(4)−C(6)	1.339(3)
N(1)−C(4)	1.341(3)	C(1)−C(2)	1.338(3)
N(2)−C(8)	1.338(3)	C(3)−C(4)	1.387(3)
N(2)−C(5)	1.342(2)	C(4)−C(5)	1.479(3)
N(3)−C(2)	1.333(3)	C(5)−C(6)	1.386(3)
N(3)−C(3)	1.339(3)	C(7)−C(8)	1.385(3)
N(4)−C(7)	1.333(3)		
C(1)−N(1)−C(4)	118.78(18)	N(3)−C(3)−C(4)	122.3(2)
C(1)−N(1)−Cu(1)	127.01(15)	N(1)−C(4)−C(3)	120.01(19)
C(4)−N(1)−Cu(1)	114.20(13)	N(1)−C(4)−C(5)	114.92(17)
C(8)−N(2)−C(5)	118.25(17)	C(3)−C(4)−C(5)	125.06(18)
C(8)−N(2)−C(1)	127.49(14)	N(2)−C(5)−C(6)	120.31(19)
C(5)−N(2)−Cu(1)	114.24(13)	N(2)−C(5)−C(4)	114.64(17)
C(2)−N(3)−C(3)	116.4(2)	C(6)−C(5)−C(4)	125.05(18)
C(7)−N(4)−C(6)	116.5(2)	N(4)−C(6)−C(5)	122.1(2)
N(1)−C(1)−C(2)	119.8(2)	N(4)−C(7)−C(8)	122.5(2)
N(3)−C(2)−C(1)	122.7(2)	N(2)−C(8)−C(7)	120.3(2)

D−H···A	D···A (Å)	H···A (Å)	D−H···A (°)
C(3)−H(3)···O(3c)	3.192(3)	2.39	144
C(7)−H(7)···O(3d)	3.370(3)	2.48	160
C(6)−H(6)···O(4c)	3.077(3)	2.25	148
C(62)−H(2)···O(4e)	3.247(3)	2.35	162

[a] Symmetry operations used to generate equivalent atoms: (a) $1-x$, $-y$, $-z$; (b) $-x$, $-y$, $-z$; (c) $1+x$, $1+y$, $1+z$; (d) $1+x$, $1+y$, z; (e) x, y, $1+z$.

The overlap between parallel oxalate groups across the Cu(1)···O(3b)/Cu(1b)···O(3) bridge is associated with π-π stacking, with an interplanar spacing of 2.88 Å. The other pair of axial bonds [Cu(1)···O(1a)/Cu(1a)···O(1)] leads to overlap between oxalate and bpz groups, the distance from the oxalate plane to the overlapping bpz atoms ranging from 2.90 to 3.37 Å. The shortest intermetallic distance in the crystal, 3.5279(6) Å, is found between copper atoms linked by the latter type of oxalate bridge [Cu(1)···Cu(1a)]. The intermetallic distance across the Cu(1)−O(3b)/Cu(1b)−O(3) bridge is 4.8952(9) Å. The chains in the crystal are linked through C−H···O interactions, forming parallel layers (Figure 4, Figure S3 and Table 3).

To the best of our knowledge the only copper(II) bpz complex previously characterized by X-ray crystallography is $[Cu(bpz)(H_2O)(C_5O_5)]$ (C_5O_5 is the dianion of croconic acid).[18] In this compound an axially bound water molecule precludes a chain formation analogous to that found in **3**;

 © 2004 Wiley-VCH Verlag GmbH & Co. KGaA, Weinheim

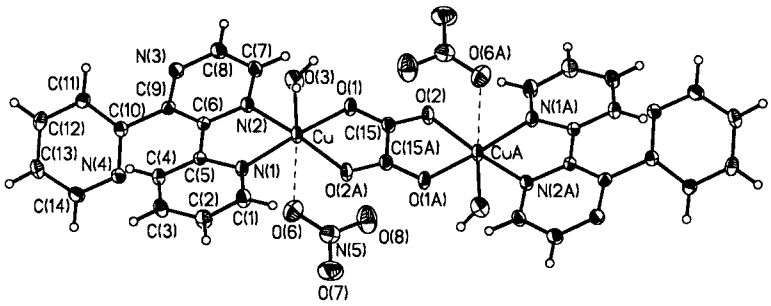

Figure 5. The complex unit $[Cu_2(dpp)_2(H_2O)_2((NO_3)_2(ox)]\cdot 4H_2O$ (**4**), showing the atomic numbering scheme; thermal ellipsoids are plotted at the 30% probability level; symmetry operations: (a) $1 - x$, $1 - y$, $1 - z$

instead the complex units are connected pairwise through weak Cu···O(croconate) interactions. The two pyrazine rings in **3** are practically coplanar (dihedral angle 3.3°), as was the case in the croconato compound. The bond lengths and angles involving bpz are similar in the two bpz-containing copper(II) compounds. Structures of a number of bpz complexes with Ag^{I},[19] Fe^{II},[20] Co^{II},[21] Ru^{II} and Ru^{I},[22] Pd^{II} and Pt^{II} [23] have been reported. In several of these polynuclear complexes the simultaneous occurrence of the chelating and monodentate binding modes for this ligand[19,23] imposes a twist between the two pyrazine ligands.

$[Cu_2(dpp)_2(H_2O)_2(NO_3)_2(ox)]\cdot 4H_2O$ (4)

The structure of **4** is built of centrosymmetric oxalato-bridged dinuclear $[Cu_2(dpp)_2(H_2O)_2(NO_3)_2(ox)]$ units (Figure 5) and water of hydration. The copper coordination may be described as elongated octahedral of the 4+1+1′ type, where two oxalate oxygen atoms and two dpp nitrogen atoms occupy the equatorial positions [1.982(2) and 1.990(2) Å for Cu−O and 1.960(2) and 1.981(2) Å for Cu−N]; a water molecule coordinates in one axial position [2.238(2) Å for $Cu-O_w$] and a semicoordinated nitrate oxygen atom completes the coordination sphere [2.750(3) Å for Cu−O]. The equatorial plane of copper is essentially planar [maximum atomic deviation 0.013 Å] and the copper atom is displaced by 0.160 Å toward the axial water molecule. The bis-bidentate bridging oxalate group is planar and makes a dihedral angle of 7.3° with the mean copper equatorial plane. The dihedral angles between the pyrazine ring and the coordinated and uncoordinated pyridyl rings are 13.0° and 39.4°, respectively. The plane of the nitrate makes dihedral angles of 15.3° and 19.4° with the oxalate group and the equatorial plane, respectively, the average distances between the individual nitrate atoms and the oxalate and equatorial planes being 3.01 and 2.96 Å, respectively. The intramolecular copper···copper distance across the oxalate bridge is 5.171(1) Å.

The packing of the dinuclear units in the crystal results in partial π-π overlap between the pyrazine ring and pyridyl rings of two neighbouring molecules, the distances from the pyrazine plane to the overlapping pyridyl atoms being in the range 3.29−3.63 Å (Figure S4). The molecules are connected by hydrogen bonds involving water, oxalate and nitrate (Table 4 and Figure S4). The shortest intermolecular metal···metal distance occurs between atoms displaced by a unit translation along the *b*-axis (7.2598 Å). The corresponding molecules are connected by hydrogen bonds between coordinated water and nitrate.

The oxalate shows the typical features of bis-bidentate bonding, with the four Cu−O bonds being of the same length [1.254(3)/1.248(3) Å], intermediate between the bond lengths found in bidentate oxalate. The dpp bond lengths and angles compare well with those of compound **2** and with previous findings.[16] The Cu−N(pyrazine) bond [1.981(2) Å] is slightly longer than the Cu−N(pyridyl) bond [1.960(2) Å], but they are still similar, in contrast to the observation in **1** where the pyrazine ring is part of the quinoxaline moiety and steric effects probably tend to lengthen the bond to pyrazine.

$[Cu_2(bpz)_2(H_2O)_2Cl_2(ox)][Cu(bpz)(H_2O)_2(ox)]\cdot 2H_2O$ (5)

Two types of neutral complex units have cocrystallized in this compound: dinuclear $[Cu_2(bpz)_2(H_2O)_2Cl_2(ox)]$ and mononuclear $[Cu(bpz)(H_2O)_2(ox)]$ (Figure 6). The oxalate bridges the metal atoms in the bis-bidentate mode in the dinuclear unit whereas it acts as a bidentate ligand in the mononuclear one. A corresponding situation with coexistence of two analogous complex units in the same crystal was observed by some of us several years ago in copper(II) complexes of formula $[Cu_2(bipy)_2(H_2O)_2(ox)]X_n\cdot[Cu(bipy)(ox)]$ [X = NO_3^-, BF_4^-, ClO_4^- (n = 2) and SO_4^{2-} (n = 1)] where the bidentate bipy ligand was used instead of bpz.[1d,1i,10b] Each copper atom in the dinuclear unit of **5** has an elongated octahedral coordination sphere (4+1+1′ coordination) with two oxalate oxygen atoms [1.956(6) to 1.987(6) Å for Cu−O] and two bpz nitrogen atoms [1.988(7) to 2.009(7) Å for Cu−N] in the equatorial plane and a water molecule [2.509(7) and 2.514(7) Å for $Cu-O_w$] and a chlorine atom [2.629(3) and 2.649(3) Å for Cu−Cl] in the axial positions. The equatorial plane of each copper atom has a small tetrahedral distortion (maximum atomic deviations from the mean plane of 0.053 and 0.047 Å, respectively), and the copper atoms are displaced by 0.103 and 0.089 Å from this plane toward the axial chlorine atom. The dihedral angle between the bridging oxalate and either of the equatorial planes is 4.9°. The copper···copper distance across the bridging oxalate in the dinuclear unit is 5.1345(16) Å. The copper coordination geometry in the

 © 2004 Wiley-VCH Verlag GmbH & Co. KGaA, Weinheim

Table 4. Selected bond lengths (Å) and angles (°) for $[Cu_2(dpp)_2(H_2O)_2((NO_3)_2(ox)]\cdot 4H_2O$ (**4**)[a]

Cu−N(1)	1.960 (2)	Cu−O(2a)	1.990(16)
Cu−N(2)	1.981(2)	Cu−O(3)	2.238(2)
Cu−O(1)	1.982(2)	Cu−O(6)	2.750(3)
N(1)−Cu−N(2)	85.76(6)	O(1)−Cu−O(3)	96.24(8)
N(1)−Cu−O(1)	169.51(8)	O(2a)−Cu−O(3)	93.87(8)
N(2)−Cu−O(1)	95.02(7)	N(1)−Cu−O(6)	77.92(8)
N(1)−Cu−O(2a)	97.85(7)	N(2)−Cu−O(6)	88.80(7)
N(2)−Cu−O(2a)	171.53(8)	O(1)−Cu−O(6)	92.26(8)
O(1)−Cu−O(2a)	84.39(6)	O(2a)−Cu−O(6)	82.78(7)
N(1)−Cu−O(3)	93.84(8)	O(3)−Cu−O(6)	170.53(7)
N(2)−Cu−O(3)	94.60(8)		
O(1)−C(15)	1.254(3)	C(15)−C(15a)	1.532(5)
O(2)−C(15)	1.248(3)		
C(15)−O(1)−Cu	110.93(14)	O(2)−C(15)−C(15a)	117.2(3)
C(15)−O(2)−Cu(a)	110.65(14)	O(1)−C(15)−C(15a)	116.8(3)
O(2)−C(15)−O(1)	126.0(2)		
N(1)−C(1)	1.331(3)	C(3)−C(4)	1.387(3)
N(1)−C(5)	1.356(3)	C(4)−C(5)	1.381(3)
N(2)−C(7)	1.328(3)	C(5)−C(6)	1.494(3)
N(2)−C(6)	1.358(39	C(6)−C(9)	1.405(3)
N(3)−C(8)	1.326(3)	C(7)−C(8)	1.374(3)
N(3)−C(9)	1.348(3)	C(9)−C(10)	1.496(3)
N(4)−C(10)	1.340(3)	C(10)−C(11)	1.386(3)
N(4)−C(14)	1.341(3)	C(11)−C(12)	1.385(3)
C(1)−C(2)	1.375(4)	C(12)−C(13)	1.375(4)
C(2)−C(3)	1.373(3)	C(13)−C(14)	1.374(4)
N(5)−O(6)−Cu	109.7(2)	N(2)−C(6)−C(9)	118.2(2)
C(1)−N(1)−C(5)	119.8(2)	N(2)−C(6)−C(5)	112.7(2)
C(1)−N(1)−Cu	124.0(2)	C(9)−C(6)−C(5)	129.0(2)
C(5)−N(1)−Cu	116.13(15)	N(2)−C(7)−C(8)	120.2(2)
C(7)−N(2)−C(6)	120.2(2)	N(3)−C(8)−C(7)	121.4(2)
C(7)−N(2)−Cu	124.2(2)	N(3)−C(9)−C(6)	120.4(2)
C(6)−N(2)−Cu	115.56(14)	N(3)−C(9)−C(10)	112.3(2)
C(8)−N(3)−C(9)	118.9(2)	C(6)−C(9)−C(10)	127.2(2)
C(10)−N(4)−C(14)	116.5(2)	N(4)−C(10)−C(11)	123.2(2)
N(1)−C(1)−C(2)	122.6(2)	N(4)−C(10)−C(9)	117.0(2)
C(3)−C(2)−C(1)	118.3(2)	C(11)−C(10)−C(9)	119.6(2)
C(2)−C(3)−C(4)	119.7(2)	C(12)−C(11)−C(10)	118.8(2)
C(5)−C(4)−C(3)	119.4(2)	C(13)−C(12)−C(11)	118.7(2)
N(1)−C(5)−C(4)	120.1(2)	C(14)−C(13)−C(12)	118.7(2)
N(1)−C(5)−C(6)	113.6(2)	N(4)−C(14)−C(13)	124.1(2)
C(4)−C(5)−C(6)	126.2(2)		
O(6)−N(5)	1.238(3)	O(8)−N(5)	1.247(3)
O(7)−N(5)	1.224(3)		
O(7)−N(5)−O(6)	121.0(3)	O(6)−N(5)−O(8)	119.4(3)
O7)−N(5)−O(8)	119.6(3)	Cu−O(6)−N(5)	109.67(18)

D−H···A[b]	D···A (Å)	H···A (Å)	D−H···A (°)
O(3)−H(31)···O(5a)	2.830(3)	2.10	156
O(3)−H(32)···O(8b)	2.819(3)	2.07	169
O(4)−H(41)···O(1)	3.032(3)	2.35	163
O(4)−H(42)···O(5c)	2.798(4)	1.94	145
O(5)−H(51)···O(7)*	2.981(4)	2.08	167
O(5)−H(51)···O(8)*	2.967(4)	2.26	134
O(5)−H(52)···O(4d)	2.813(4)	1.94	144

[a] Symmetry transformations used to generate equivalent atoms: (a) $1-x, 1-y, 1-z$; (b) $x, y-1, z$; (c) $1-x, 2-y, 1-z$; (d) $1+x, y, z$. [b] Bifurcated hydrogen bond.

mononuclear unit is also elongated octahedral. The equatorial bonds between copper and oxalate oxygen atoms are somewhat shorter [1.928(6) and 1.937(6) Å] than those found in the dinuclear compound, while the Cu−N bonds are of similar lengths [1.992(7) and 2.013(7) Å]. Both of the axial ligands are water molecules [2.506(7) and 2.541(7) Å for $Cu-O_w$]. The copper equatorial plane is close to planar (maximum atomic deviation 0.015 Å). It is essentially coplanar with oxalate (dihedral angle 1.4°) and makes an angle of 8.7° with the bpz best plane.

The standard deviations in the bond lengths and angles of compound **5** are somewhat higher than in **1**−**4**, but the typical feature of two long C−O oxalate bonds (for oxygen coordinated to copper) and two shorter bonds involving non-coordinated oxygen is clearly seen in the mononuclear unit, while in the dinuclear unit all the C−O bonds are equal within the limits of errors. In the dinuclear unit the two pyrazine rings within each bpz moiety are practically coplanar (dihedral angles 2.8 and 3.1°), as was found in **3** and the $[Cu(bpz)(H_2O)(C_5O_5)]$ complexes.[18] In the mononuclear unit of **5** the bpz ligand is slightly more twisted, the dihedral angle between the two pyrazine rings being 12.1°.

In the crystal the molecules are linked through hydrogen bonds (see Table 5) and partial π-π overlap, resulting in an arrangement of wave-type layers (Figure S5). The most pronounced π-π interaction appears to be between the bpz and oxalate groups of neighbouring mononuclear units, the average distance from oxalate atoms to bpz plane being 3.22 Å.

IR Spectroscopy

The IR spectra of **1**−**5** have in common the occurrence of a strong and broad absorption centred at about 3420 cm^{-1} which is due to the OH stretching of both coordinated and crystallization water molecules participating in hydrogen bonds.[24] The C−H stretching vibrations of dpp in **2** and **4** (triplet between 3200 and 3060 cm^{-1}) and bpz in **3** and **5** (quadruplet between 3100 and 2925 cm^{-1}) are also observed in the high-frequency region. In the case of complex **1**, the C−H stretching vibrations of dpq are obscured by the strong and broad OH absorption of the water molecules. The characteristic bands of bidentate (**1**, **2** and **5**) and bridging (**3**−**5**) oxalate are also observed in the IR spectra of this series:[1i,1o,1p,18,25,26] ν_{as}(CO) vibration at 1708, 1650 and 1680 cm^{-1} (**1**), 1705, 1685 and 1660 cm^{-1} (**2**), 1712, 1680 and 1650 cm^{-1} (**3**), 1640 cm^{-1} (**4**) and 1710 sh, 1665 and 1640 cm^{-1} (**5**); ν_s(CO) stretching at 1411, 1357 and 1268 cm^{-1} (**1**), 1395, 1295 and 1255 cm^{-1} (**2**), 1406 and 1245 cm^{-1} (**3**), 1360 and 1310 cm^{-1} (**4**) and 1410, 1345, 1310 and 1275 cm^{-1} (**5**); δ(OCO) vibration at 790 (**1**), 792 (**2**), 789 (**3**), 790 (**4**) and 794 cm^{-1} (**5**). Finally, the bands observed at 1380, 1320 and 1080 cm^{-1} in the IR spectrum of **4** suggest the occurrence of monodentate coordination of the nitrate ion.[27]

Magnetic Properties

Compounds **3**−**5** were magnetically characterised by following the thermal variation of the magnetic susceptibility (χ_M). The magnetic properties of compounds **1** and **2** were not investigated because they are mononuclear.

The temperature dependence of the $\chi_M T$ product for **3** is shown in Figure 7. At room temperature, $\chi_M T$ is equal to 0.41 $cm^3\cdot mol^{-1}\cdot K$, a value which is as expected for a magnetically isolated spin doublet. Upon cooling, $\chi_M T$ smoothly decreases to reach a value of about 0.26 $cm^3\cdot mol^{-1}\cdot K$ at 1.9 K. The shape of this plot is indicative of a weak antiferromagnetic interaction. In agreement with

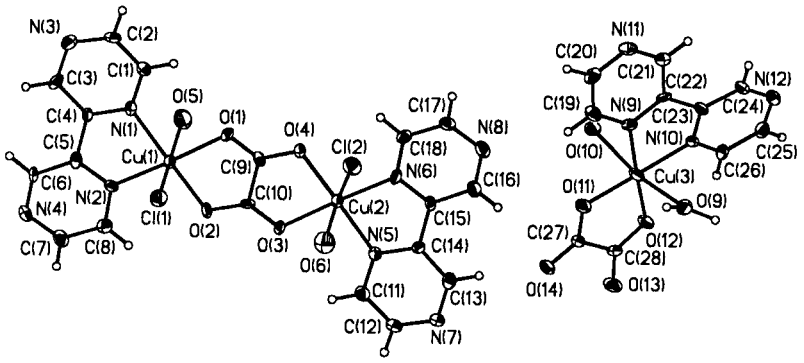

Figure 6. The dinuclear and mononuclear building blocks in $[Cu_2(bpz)_2(H_2O)_2Cl_2(ox)][Cu(bpz)(H_2O)_2(ox)]\cdot 2H_2O$ (**5**) showing the atom numbering scheme; thermal ellipsoids are plotted at the 30% probability level

the alternating chain structure of **3**, we analysed its magnetic data by the alternating-chain spin-exchange model through the Hamiltonian $\hat{H} = -J\Sigma(\hat{S}_{2i} \cdot \hat{S}_{2i-1} + \alpha\hat{S}_{2i} \cdot \hat{S}_{2i+1})$ where J and αJ are the alternating exchange-coupling parameters. The best-fit parameters are: $J = -1.44$ cm^{-1}, $\alpha J = -0.69$ cm^{-1}, $g = 2.10$ and $R = 1.4 \times 10^{-6}$; R is the agreement factor defined as $\Sigma_i[(\chi_M T)_{obs}(i) - (\chi_M T)_{calc}(i)]^2/\Sigma_i[(\chi_M T)_{obs}(i)]^2$. The calculated curve reproduces the experimental data very well. The weak intrachain magnetic interactions in **3** are as expected taking into account the out-of-plane exchange coupling involved. In fact, the unpaired electron on each copper(II) ion in this compound is defined by a $d_{x^2-y^2}$-type magnetic orbital (the x and y axes corresponding roughly to the copper−nitrogen bonds) that is mainly centred on the metal atom. The interchain exchange pathway involves axially coordinated oxalate oxygen atoms [2.75 and 2.62 Å for Cu(1)−O(1a) and Cu(1)−O(3b), respectively] whose spin density must be very weak. Consequently, simple symmetry considerations show that the overlap between the planar magnetic orbitals through the out-of-plane exchange pathway has to be very small and a weak magnetic interaction (either antiferro- or ferromagnetic depending on structural parameters such as the angle at the atom of the bridge and value of the axial bond) is expected,[29] as observed. Looking at the different intrachain out-of-plane exchange pathways occurring in **3**, [Cu(1)O(1)O(1a)Cu(1a) and Cu(1)O(2)-C(10)O(3)O(3b)C(10b)O(2b)Cu(1b)], most likely the strongest antiferromagnetic interaction ($J = -1.44$ cm^{-1}) corresponds to the shorter pathway (double oxalate−oxygen bridge) whereas the weakest one ($\alpha J = -0.69$ cm^{-1}) is ascribed to the longer pathway. Concerning the significance of these coupling values, it should be noted that: (i) weak antiferromagnetic interactions between copper(II) ions through double oxalate−oxygen bridge were observed in the complexes $H_2Im[Cu(ox)_2]$ (Him = imidazole, $J = -1.09$ cm^{-1})[2e] and $Na_2[Cu(ox)_2]\cdot 2H_2O$ ($J = -1.2$ cm^{-1}),[2b] and (ii) either weak antiferro- or ferromagnetic interactions were reported for the copper(II) complexes $M_2[Cu(ox)_2]\cdot 2H_2O$ [M = K$^+$ ($J = -0.7$ cm^{-1}) and NH_4^+ ($J = -0.6$ cm^{-1})],[2a] $[Cu(pyim)(H_2O)(ox)]\cdot 2H_2O$ [pyim = 2-(2-pyridyl)imidazole, $J = +0.04$ cm^{-1}][18] and $[Cu(H_2bim)(H_2O)(ox)]\cdot H_2O$ [H_2bim = 2,2′-biimidazole, $J = -0.08$][18] where the longer out-of-plane exchange pathway occurs.

The temperature dependence of χ_M for **4** [χ_M is the magnetic susceptibility per two copper(II) ions] is shown in Figure 8. The thermal dependence of the $\chi_M T$ product is shown in the inset of this figure. At room temperature, $\chi_M T$ is equal to 0.45 cm^3·mol^{-1}·K, a value which is well below that expected for two magnetically isolated spin doublets [0.75 cm^3·mol^{-1}·K for $g = 2.0$]. This value strongly decreases when cooling and it vanishes at low temperatures. The susceptibility plot exhibits a maximum at 260 K. These features are characteristic of a strong antiferromagnetic interaction between the two copper(II) ions in **4**. The experimental data closely follow Equation (1)

$$\chi_M = (2N\beta^2g^2/kT)[3 + \exp(-J/kT)]^{-1} + \text{tip} \quad (1)$$

which is the Bleaney−Bowers expression for a coupled dinuclear copper(II) complex, the Hamiltonian being $\hat{H} = -J\hat{S}_A \cdot \hat{S}_B$. N, g and β have their usual meanings and the tip is the temperature-independent paramagnetism for two copper(II) ions (120 cm^3·mol^{-1}). The best-fit parameters are: $J = -312$ cm^{-1}, $g = 2.09$ and $R = 1.9 \times 10^{-5}$ (R is the agreement factor defined as $\Sigma_i[(\chi_M)_{obs}(i) - (\chi_M)_{calc}(i)]^2/\Sigma_i[(\chi_M)_{obs}(i)]^2$). The strong intramolecular antiferromagnetic interaction in **4** is as expected keeping in mind the effective σ in-plane overlap between the two $d_{x^2-y^2}$ magnetic orbitals on each copper(II) ion [the x and y axes being roughly defined by the Cu(1)−N(1) and Cu(1)−N(2) bonds].[1c,1i,1e,5] This remarkable efficiency of the oxalato bridge to mediate strong antiferromagnetic interactions in dinuclear copper(II) complexes through the σ in-plane exchange pathway is well-known and it is illustrated by the magneto-structural data listed in Table 6. The small structural distortions in this series account for the differences observed in the magnetic coupling values.

The thermal dependence of the $\chi_M T$ product [per two copper(II) ions] for **5** is shown in Figure 9. $\chi_M T$ decreases upon cooling, tends to a quasi plateau at temperatures below 80 K and further decreases at very low temperatures. Keeping in mind that the structure of compound **5** contains both an oxalato-bridged copper(II) dinuclear unit and a

 © 2004 Wiley-VCH Verlag GmbH & Co. KGaA, Weinheim

Table 5. Selected bond lengths (Å) and angles (°) for $[Cu_2(bpz)_2(H_2O)_2Cl_2(ox)][Cu(bpz)(H_2O)_2(ox)]\cdot 2H_2O$ (**5**)[a]

Cu(1)−O(2)	1.956(6)	Cu(2)−N(6)	1.998(8)
Cu(1)−O(1)	1.980(6)	Cu(2)−O(6)	2.509(7)
Cu(1)−N(2)	1.994(7)	Cu(2)−Cl(2)	2.649(3)
Cu(1)−N(1)	2.009(7)	Cu(3)−O(11)	1.928(6)
Cu(1)−O(5)	2.514(7)	Cu(3)−O(12)	1.937(6)
Cu(1)−Cl(1)	2.629(3)	Cu(3)−N(10)	1.992(7)
Cu(2)−O(3)	1.984(6)	Cu(3)−N(9)	2.013(7)
Cu(2)−O(4)	1.987(6)	Cu(3)−O(9)	2.506(7)
Cu(2)−N(5)	1.988(7)	Cu(3)−O(10)	2.541(7)
O(2)−Cu(1)−O(1)	85.2(2)	N(5)−Cu(2)−O(6)	82.5(3)
O(2)−Cu(1)−N(2)	96.1(3)	N(6)−Cu(2)−O(6)	92.1(3)
O(1)−Cu(1)−N(2)	176.6(3)	O(3)−Cu(2)−Cl(2)	92.2(2)
O(2)−Cu(1)−N(1)	170.7(3)	O(4)−Cu(2)−Cl(2)	96.4(2)
O(1)−Cu(1)−N(1)	97.0(3)	N(5)−Cu(2)−Cl(2)	91.3(2)
N(2)−Cu(1)−N(1)	81.2(3)	N(6)−Cu(2)−Cl(2)	90.2(2)
O(2)−Cu(1)−O(5)	89.5(3)	O(6)−Cu(2)−Cl(2)	173.1(2)
O(1)−Cu(1)−O(5)	84.2(3)	O(11)−Cu(3)−O(12)	86.5(2)
N(2)−Cu(1)−O(5)	92.7(3)	O(11)−Cu(3)−N(10)	176.9(3)
N(1)−Cu(1)−O(5)	81.8(3)	O(12)−Cu(3)−N(10)	95.8(3)
O(2)−Cu(1)−Cl(1)	94.4(2)	O(11)−Cu(3)−N(9)	95.6(3)
O(1)−Cu(1)−Cl(1)	91.5(2)	O(12)−Cu(3)−N(9)	177.9(3)
N(2)−Cu(1)−Cl(1)	91.5(2)	N(10)−Cu(3)−N(9)	82.1(3)
N(1)−Cu(1)−Cl(1)	94.5(2)	O(11)−Cu(3)−O(9)	95.6(3)
O(5)−Cu(1)−Cl(1)	173.96(19)	O(12)−Cu(3)−O(9)	96.6(3)
O(3)−Cu(2)−O(4)	85.4(2)	N(10)−Cu(3)−O(9)	82.2(3)
O(3)−Cu(2)−N(5)	96.0(3)	N(9)−Cu(3)−O(9)	83.0(3)
O(4)−Cu(2)−N(5)	172.1(3)	O(11)−Cu(3)−O(10)	90.1(3)
O(3)−Cu(2)−N(6)	176.9(3)	O(12)−Cu(3)−O(10)	91.7(3)
O(4)−Cu(2)−N(6)	96.3(3)	N(10)−Cu(3)−O(10)	91.8(3)
N(5)−Cu(2)−N(6)	81.9(3)	N(9)−Cu(3)−O(10)	170.2(2)
O(4)−Cu(2)−O(6)	89.8(3)		
O(1)−C(9)	1.239(10)	O(12)−C(28)	1.280(10)
O(2)−C(10)	1.262(10)	O(13)−C(28)	1.241(10)
O(3)−C(10)	1.239(10)	O(14)−C(27)	1.225(10)
O(4)−C(9)	1.253(10)	C(9)−C(10)	1.551(10)
O(11)−C(27)	1.293(11)	C(27)−C(28)	1.522(12)
C(9)−O(1)−Cu(1)	110.6(6)	O(3)−C(10)−O(2)	126.8(8)
C(10)−O(2)−Cu(1)	111.4(5)	O(3)−C(10)−C(9)	117.4(7)
C(10)−O(3)−Cu(2)	110.2(6)	O(2)−C(10)−C(9)	115.6(6)
C(9)−O(4)−Cu(2)	109.8(6)	O(14)−C(27)−O(11)	121.5(8)
C(27)−O(11)−Cu(3)	110.3(5)	O(14)−C(27)−C(28)	121.8(8)
C(28)−O(12)−Cu(3)	111.3(6)	O(11)−C(27)−C(28)	116.5(8)
O(1)−C(9)−O(4)	125.7(8)	O(13)−C(28)−O(12)	125.0(9)
O(1)−C(9)−C(10)	117.2(7)	O(13)−C(28)−C(27)	119.7(8)
O(4)−C(9)−C(10)	117.1(7)	O(12)−C(28)−C(27)	115.3(8)
N(1)−C(4)	1.325(11)	N(11)−C(21)	1.311(11)
N(1)−C(1)	1.349(11)	N(11)−C(20)	1.348(13)
N(2)−C(5)	1.325(11)	N(12)−C(24)	1.330(12)
N(2)−C(8)	1.337(11)	N(12)−C(25)	1.348(12)
N(3)−C(2)	1.323(12)	C(1)−C(2)	1.344(12)
N(3)−C(3)	1.348(12)	C(3)−C(4)	1.394(12)
N(4)−C(6)	1.313(12)	C(4)−C(5)	1.516(13)
N(4)−C(7)	1.324(13)	C(5)−C(6)	1.377(12)
N(5)−C(14)	1.337(10)	C(7)−C(8)	1.392(13)
N(5)−C(11)	1.344(11)	C(11)−C(12)	1.386(13)
N(6)−C(15)	1.325(11)	C(13)−C(14)	1.384(12)
N(6)−C(18)	1.342(11)	C(14)−C(15)	1.487(12)
N(7)−C(12)	1.316(12)	C(15)−C(16)	1.393(12)
N(7)−C(13)	1.340(11)	C(17)−C(18)	1.383(13)
N(8)−C(16)	1.333(12)	C(19)−C(20)	1.375(13)
N(8)−C(17)	1.336(12)	C(21)−C(22)	1.394(12)
N(9)−C(22)	1.324(11)	C(22)−C(23)	1.481(12)
N(9)−C(19)	1.336(12)	C(23)−C(24)	1.385(12)
N(10)−C(26)	1.285(10)	C(25)−C(26)	1.374(12)
N(10)−C(23)	1.365(11)		
C(4)−N(1)−C(1)	118.2(8)	N(2)−C(5)−C(6)	121.1(9)
C(4)−N(1)−Cu(1)	114.5(6)	N(2)−C(5)−C(4)	113.9(7)
C(1)−N(1)−Cu(1)	127.2(6)	C(6)−C(5)−C(4)	124.9(8)
C(5)−N(2)−C(8)	118.2(8)	N(4)−C(6)−C(5)	122.9(8)
C(5)−N(2)−Cu(1)	115.3(6)	N(4)−C(7)−C(8)	124.4(10)
C(8)−N(2)−C(1)	126.3(6)	N(2)−C(8)−C(7)	118.3(9)
C(2)−N(3)−C(3)	116.3(8)	N(5)−C(11)−C(12)	120.8(8)
C(6)−N(4)−C(7)	115.2(8)	N(7)−C(12)−C(11)	122.6(9)
C(14)−N(5)−C(11)	117.5(7)	N(7)−C(13)−C(14)	123.0(9)
C(14)−N(5)−C(2)	113.7(6)	N(5)−C(14)−C(13)	120.0(8)
C(11)−N(5)−Cu(2)	128.7(6)	N(5)−C(14)−C(15)	115.2(7)
C(15)−N(6)−C(18)	117.9(8)	C(13)−C(14)−C(15)	124.8(8)
C(15)−N(6)−Cu(2)	114.0(6)	N(6)−C(15)−C(16)	120.9(8)
C(18)−N(6)−Cu(2)	128.0(6)	N(6)−C(15)−C(14)	114.8(7)
C(12)−N(7)−C(13)	116.0(8)	C(16)−C(15)−C(14)	124.2(8)
C(16)−N(8)−C(17)	117.2(8)	N(8)−C(16)−C(15)	121.4(9)
C(22)−N(9)−C(19)	117.7(7)	N(8)−C(17)−C(18)	121.6(8)
C(22)−N(9)−Cu(3)	113.7(6)	N(6)−C(18)−C(17)	120.8(8)
C(19)−N(9)−Cu(3)	128.2(6)	N(9)−C(19)−C(20)	120.5(9)
C(26)−N(10)−C(23)	119.3(8)	N(11)−C(20)−C(19)	122.5(9)
C(26)−N(10)−Cu(3)	127.3(6)	N(11)−C(21)−C(22)	122.6(9)
C(23)−N(10)−Cu(3)	112.5(5)	N(9)−C(22)−C(21)	120.7(8)
C(21)−N(11)−C(20)	115.9(8)	N(9)−C(22)−C(23)	115.4(8)
C(24)−N(12)−C(25)	115.7(8)	C(21)−C(22)−C(23)	123.8(9)
C(2)−C(1)−N(1)	119.2(8)	N(10)−C(23)−C(24)	118.5(8)
N(3)−C(2)−C(1)	124.9(9)	N(10)−C(23)−C(22)	114.8(7)
N(3)−C(3)−C(4)	120.0(9)	C(24)−C(23)−C(22)	126.6(9)
N(1)−C(4)−C(3)	121.4(8)	N(12)−C(24)−C(23)	123.0(9)
N(1)−C(4)−C(5)	114.6(7)	N(12)−C(25)−C(26)	122.2(9)
C(3)−C(4)−C(5)	124.0(8)	N(10)−C(26)−C(25)	121.3(9)

D[b]	A	D···A (Å)
O(5)	Cl(1a)	3.323(8)
O(6)	Cl(2b)	3.379(8)
O(7)	Cl(1d)	3.263(9)
O(8)	Cl(2)	3.292(10)
O(5)	O(8)	2.868(11)
O(6)	O(7c)	2.828(12)
O(7)	O(4)	3.032(10)
O(8)	O(2d)	3.108(11)
O(9)	O(10b)	2.783(9)
O(10)	O(14d)	2.696(9)
O(9)	N(3e)	2.924(10)
O(10)	N(7d)	2.923(10)

[a] Symmetry transformations used to generate equivalent atoms: (a) $1 + x, y, z$; (b) $-1 + x, y, z$; (c) $x, y, 1 + z$; (d) $x, y, -1 + z$; (e) $-1 + x, 0.5 + y, -z$. [b] Possible hydrogen bonds. D = donor; A = acceptor.

mononuclear one, this plot is interpreted as follows: the strong decrease of $\chi_M T$ in the high temperature range is due to a strong antiferromagnetic interaction within the dinuclear entity whereas the quasi plateau corresponds to the Curie law behaviour expected for the mononuclear copper(II) unit; the decrease of $\chi_M T$ in the very low temperature range is attributed to intermolecular magnetic interactions between the mononuclear copper(II) entities. Consequently, the magnetic data of **5** were analysed with Equation (2)

$$\chi_M = (2N\beta^2 g_d^2/kT)[3 + \exp(-J/kT)]^{-1} + [N\beta^2 g_m^2/k(T - \theta)] + \text{tip} \quad (2)$$

which is the sum of the Bleaney−Bowers equations for a coupled dinuclear copper(II) species, the Curie law for a mononuclear copper(II) unit (with a θ term accounting for the magnetic interaction between the mononuclear entities) and the temperature-independent paramagnetism [180 $cm^3 \cdot mol^{-1}$ for three copper(II) ions]. J is the magnetic coupling through the oxalate bridge in the dinuclear complex, and g_d and g_m are the mean g factors for the di- and mononuclear complexes, respectively. A least-squares fit of the experimental data of **5** with Equation (2) leads to the following set of parameters:

 © 2004 Wiley-VCH Verlag GmbH & Co. KGaA, Weinheim

Table 6. Selected magneto-structural data for oxalato-bridged copper(II) complexes of the type $[(AA)Cu(\mu\text{-ox})Cu(AA)]X_n$ exhibiting the σ in-plane exchange pathway

AA[a]	X	Donor set	Dihedral angle[b]	h_{Cu}[c]	$d_{Cu\cdots Cu}$[d]	J[e]	Ref.
phen	NO_3	O_2N_2/O	16.9	0.27	5.158(1)	−330	[1f]
bipy	NO_3	O_2N_2/O	3.2	0.16	5.154(1)	−386	[1d,1i]
bipy	ClO_4	O_2N_2/O	12.0	0.18	5.150(1)	−376	[1i]
bipy	BF4	O_2N_2/O	10.4	0.16	5.144(1)	−378	[1i]
dpa	NO_3	O_2N_2/O_2	7.2	0.08	5.22	−305	[1p]
tmen	ClO_4	O_2N_2/O	8.4	0.18	5.147/5.167	−385.4	[1c,1e]
deen	ClO_4	O_2N_2/O_2	3.9	[f]	[f]	−300	[4d]
mpz	PF_6	O_2N_2/O	13.9	0.24	[f]	−402	[1g]
mpz	NO_3	$O_2N_2O_2$	2.1	0.06	[f]	−312	[1g]
mpz	NO_3	O_2N_2/O_2	[f]	0.12	5.217	−284	[1h]
dpp (**4**)	NO_3	O_2N_2/O_2	7.3	0.16	5.171(1)	−312	this work
bpz (**5**)	Cl	O_2N_2/OCl	4.9	0.10/0.09	5.1345(16)	−345	this work

[a] Abbreviations: phen = 1,10-phenantholine; bipy = 2,2′-bipyridine; dpa = 2,2′-dipyridylamine; tmen = *N*,*N*,*N*′,*N*′-tetramethylethylenediamine; deen = *N*,*N*-diethylethane-1,2-diamine; mpz = mepirizole; dpp = 2,3-bis(2-pyridyl)pyrazine; bpz = 2,2′-bipyrazine. [b] Dihedral angle (°) between the mean oxalate and equatorial planes. [c] Out-of-plane displacement of the copper atom (Å). [d] Metal-metal separation across the oxalate bridge (Å). [e] Magnetic coupling in cm^{-1}. [f] Not reported.

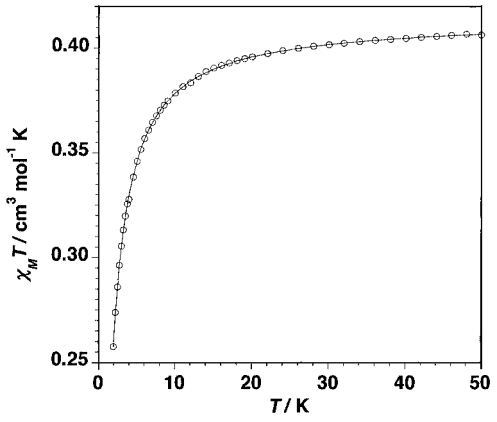

Figure 7. Thermal dependence of the $\chi_M T$ product for **3**: (o) experimental data; (−) best-fit curve (see text)

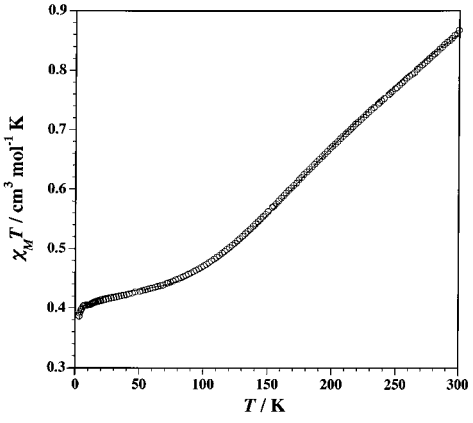

Figure 9. Thermal dependence of the $\chi_M T$ product for **5**: (o) experimental data; (−) best-fit curve from Equation (2) (see text)

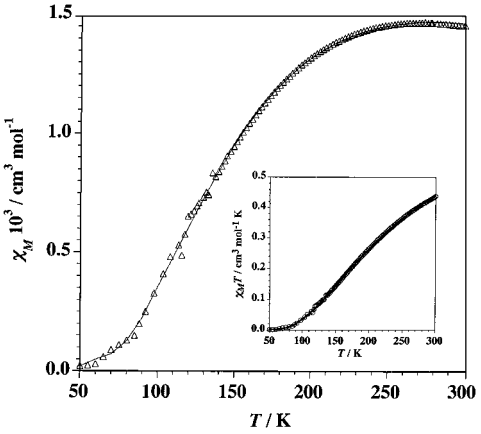

Figure 8. Thermal dependence of χ_M (Δ) and $\chi_M T$ (o) for **4**; the solid line is the best-fit curve through Equation (1) (see text)

$J = -345\ cm^{-1}$, $g_d = 2.05$, $g_m = 2.10$, $\theta = -0.3$ K and $R = 4.8 \times 10^{-5}$ (R is the agreement factor defined as $\Sigma_i[(\chi_M T)_{obs}(i) - (\chi_M T)_{calc}(i)]^2/\Sigma_i[(\chi_M T)_{obs}(i)]^2$). The calculated curve reproduces very well the experimental data in the whole temperature range. The magnetic coupling in **5** compares well with that in complex **4** in agreement with the same σ in-plane exchange pathway that is involved in them. The slightly longer copper···copper separation across the bridging oxalate in **4** versus **5**, together with the somewhat larger dihedral angle between the oxalate and the mean equatorial plane in **4**, weaken somewhat the antiferromagnetic coupling in **4** as compared to that of **5** (see end of Table 6). The intermolecular interactions between the mononuclear units in the crystal of **5** (Figure S5 and Table 5) provide the exchange pathway for the weak antiferromagnetic coupling ($\theta = -0.3$ K) observed in the very low temperature range.

Finally, complex **5** provides an additional example of coexistence in the same crystal of the magnetic orbital [represented by the mononuclear copper(II) unit] and its combination through the oxalato bridge (dinuclear unit). Four examples of oxalate-containing copper(II) complexes with this special feature have previously been described, the blocking ligand being the parent bipy molecule.[1d,1i,10b]

 © 2004 Wiley-VCH Verlag GmbH & Co. KGaA, Weinheim

Conclusions

The use of oxalate with the blocking ligands dpq, dpp and bpz has led to the preparation of five new copper(II) complexes with terminal (**1**, **2** and **5**) and bridging (**3**−**5**) oxalate. Strong (**4** and **5**) and weak (**3**) antiferromagnetic interactions between the copper(II) ions across bridging oxalato are observed, in agreement with the σ in-plane (**4** and **5**) and out-of-plane (**3**) exchange pathways involved. This study illustrates once more the importance of a detailed structural knowledge when interpreting magnetic properties.

Experimental Section

Materials: Copper(II) nitrate trihydrate, copper(II) chloride dihydrate, copper(II) triflate and potassium oxalate monohydrate were purchased from commercial sources and used as received. Cu(ox)·1/3H_2O and the ligands dpp, dpq and bpz were prepared as reported in the literature.[6,30−32] Elemental analyses (C,H,N) were carried out by the Microanalytical Service of the Universidad Autónoma de Madrid.

Compound 1: dpq (0.106 g, 0.5 mmol) was added to 100 mL of an H_2O/EtOH (80:20, v/v) mixture containing $Cu(NO_3)_2·3H_2O$ (0.17 g, 0.5 mmol) and the resulting brown solution was gently refluxed for fifteen minutes. Then, $K_2ox·H_2O$ (0.092 g, 0.5 mmol) was added whilst stirring and the solution turned olive green in a few minutes. Dark green parallelepipeds of **1** suitable for X-ray diffraction were obtained by slow evaporation of the solvent at room temperature. Yield 75%. $C_{20}H_{24}CuN_4O_{10}$ (543.97): calcd. C 44.18, H 4.41, N 10.30; found C 43.96, H 4.35, N 10.21.

Compound 2: Cu(ox)·1/3H_2O (g, 0.5 mmol) and dpp (g, 0.5 mmol) were suspended in 50 mL of an H_2O/EtOH (50:50 v/v) mixture and refluxed during half an hour under continuous stirring. The resulting blue solution was filtered and allowed to evaporate at room temperature. Single crystals of **2** were obtained as deep-blue parallelepipeds after a few days. Yield 85%. $C_{16}H_{14}CuN_4O_6$ (421.85): calcd. C 45.57, H 3.32, N 13.28; found C 45.36, H 3.25, N 13.19.

Compound 3: Solid bpz (0.030 g, 0.20 mmol) was added with stirring to an aqueous solution (20 mL) containing $Cu(CF_3SO_3)_2$ (0.072 g, 0.20 mmol). Then, $K_2ox·H_2O$ (0.018 g, 0.10 mmol) dissolved in a minimum amount of water (5 mL) was slowly added. X-ray quality crystals of **3** were grown as blue polyhedra from the resulting solution on standing at room temperature. Yield 70% (on the basis of oxalate). $C_{10}H_6CuN_4O_4$ (309.73): calcd. C 38.79, H 1.94, N 18.09; found C 38.50, H 1.88, N 17.96.

Compound 4: $Cu(NO_3)_2·3H_2O$ (0.032 g, 0.26 mmol) was dissolved in 5 mL of EtOH/H_2O (1:1 mixture) and added to a solution of dpp (0.060 g, 0.26 mmol) in 15 mL of EtOH/H_2O. $K_2ox·H_2O$ (0.023 g, 0.13 mmol) (3:4 mixture) was then added to the resulting solution whilst stirring. After evaporation of the solvents at room temperature, green prisms of **4** suitable for X-ray diffraction appeared. Yield 70%. $C_{30}H_{32}Cu_2N_{10}O_{16}$ (915.74): calcd. C 39.35, H 3.52, N 15.30; found C 39.21, H 3.37, N 15.20.

Compound 5: Solid bpz (0.030 g, 0.20 mmol) was added with stirring to an aqueous solution (20 mL) containing $CuCl_2·2H_2O$ (0.034 g, 0.20 mmol). Then, $K_2ox·H_2O$ (0.018 g,0.10 mmol) dissolved in a minimum amount of water (5 mL) was slowly added with continuous stirring. X-ray quality crystals of **5** were grown as green polyhedra from the resulting solution on standing at room temperature. Yield 60% (on the basis of oxalate). $C_{28}H_{30}Cl_2Cu_3N_{12}O_{14}$ (1020.2): calcd. C 32.98, H 2.94, N 16.47; found C 32.79, H 2.83, N 16.38.

Physical Measurements: IR spectra of **1**−**5** (4000−400 cm^{-1}) were recorded on a Bruker IF S55 spectrophotometer with samples prepared as KBr pellets. Variable-temperature (2−290 K) magnetic susceptibility measurements on polycrystalline samples of **3**−**5** were carried out with a Quantum Design SQUID susceptometer using an applied magnetic field of 1000 G over the whole temperature range. The complex $(NH_4)_2Mn(SO_4)_2·6H_2O$ was used as a susceptibility standard. Diamagnetic corrections for the constituent atoms were estimated from Pascal's constants[33] as -132×10^{-6} (**3**), -433×10^{-6} (**4**) and -604×10^{-6} $cm^3·mol^{-1}$ (**5**). Corrections for the sample holder were also applied.

Crystal Structure Determination: Diffraction data for **1**, **2**, **3** and **5** were collected with a Bruker-AXS SMART 2 K CCD area detector diffractometer at 173 K (**1**, **2**) and 293 K (**3**, **5**). In the case of **4**, data were collected at 293 K with an Enraf-Nonius CAD-4 diffractometer. Crystal parameters and refinement results are listed in Table 7. Empirical absorption corrections were carried out using SADABS for compounds **1**, **2**, **3** and **5**,[34a] while a semiempirical correction based on psi-scans of six reflections was used for **4**.[34b] The structures were solved by direct methods and refined by full-matrix least-squares based on F^2, including all reflections. All non-hydrogen atoms were refined anisotropically. Hydrogen atoms bound to carbon were included at idealized positions, whereas those of water molecules were located in Fourier difference maps (the hydrogen atoms of only one of the water molecules were detectable in the difference map of compound **5**). All hydrogen atoms included in the structure factor calculation were refined according to the riding model. The two triclinic compounds (**1** and **3**) were both found to belong to the centrosymmetric space group. In the case of compound **3**, the structure was initially solved in the non-centrosymmetric space group $P1$, but conversion to $P\bar{1}$ was later done, as solution and refinement showed this to be the correct choice. For the two monoclinic compounds where the space groups were not determined uniquely by the systematic absences (**2** and **5**), the structure solutions and refinements confirmed the non-centrosymmetric choice ($P2_1$). Refinement of racemic twinning was performed for compound **5** yielding 0.38:0.62 as the fractional contributions of the twin components.

Data collection and data reduction for **1**, **2**, **3** and **5** were done with the SMART and SAINT programs,[35a,35b] whereas for **4** the CAD-Express and XCAD programs[35c,34b] were used. All other calculations were performed with SHELXS-86, SHELXL-93, SHELXS-97, SHELXL/PC and XP.[36]

CCDC-240026 to -240030 for **1**−**5**, respectively, contain the supplementary crystallographic data for this paper. These data can be obtained free of charge at www.ccdc.cam.ac.uk/conts/retrieving.html [or from the Cambridge Crystallographic Data Centre, 12 Union Road, Cambridge CB2 1EZ, UK; Fax: + 44-1223-336-033; E-mail: deposit@ccdc.cam.ac.uk].

Supporting Information (see also footnote on the first page of this article): Figures of the crystal packing (Figures S1−S5) for complexes **1**−**5**.

Acknowledgments

The work described here was supported by the Spanish Ministry of Science and Technology (Project BQU2001-2928). Thanks are due to the University of Bergen and the NFR (Research Council of Norway) for grants allowing the purchase of X-ray equipment. One of us (J. C.) acknowledges the Mexican Government for a predoctoral fellowship through the PROMEP Program.

 © 2004 Wiley-VCH Verlag GmbH & Co. KGaA, Weinheim

Table 7. Crystal data and structure refinement for complexes **1**−**5**

	1	**2**	**3**	**4**	**5**
Empirical formula	$C_{20}H_{24}CuN_4O_{10}$	$C_{16}H_{14}CuN_4O_6$	$C_{10}H_6CuN_4O_4$	$C_{30}H_{32}Cu_2N_{10}O_8$	$C_{28}H_{30}Cl_2Cu_3N_{12}O_{14}$
Molecular mass	543.97	421.85	309.73	915.74	1020.16
Temperature (K)	173	173	293	293	293
λ (Å)	0.71073	0.71073	0.71073	0.71073	0.71073
Crystal system	triclinic	monoclinic	triclinic	monoclinic	monoclinic
Space group	$P\bar{1}$	$P2_1$	$P\bar{1}$	$P2_1/c$	$P2_1$
a (Å)	9.2591(3)	6.4964(2)	7.1385(11)	9.704(29	6.7920(14)
b (Å)	10.3134(4)	11.0218(39	8.9032(13)	7.2598(6)	40.908(8)
c (Å)	12.6911(4)	11.8647(3)	9.4900(14)	25.865(3)	6.9587(14)
α (°)	86.187(1)		108.092(3)		
β (°)	74.485(19	102.5180(10)	97.066(3)	97.395(9)	105.980(5)
γ (°)	83.804(1)		108.374(3)		
V (Å^3)	1160.03(7)	829.34(4)	527.53(14)	1807.0(4)	1858.7(6)
Z	2	2	2	2	2
ρ (Mg·m^{-3})	1.557	1.689	1.950	1.683	1.823
μ (mm^{-1})	1.005	1.362	2.088	1.266	1.929
Max. 2θ (°)	56.0	56.5	64.1	49.9	50.1
Refl. collected	16730	6362	4945	3593	11317
Independent refl.	5602 [R(int) = 0.0436]	3724 [R(int) = 0.0301]	3304 [R(int) = 0.0198]	3171 [R(int) = 0.0163]	6112 [R(int) = 0.0636]
Refl. with $I > 2\sigma(I)$	4424	3585	2638	2677	4307
Data/restraints/param.	5602/0/316	3724/1/244	3304/0/172	3171/0/262	6112/1/533
Goodness-of-fit on F^2	1.041	1.035	1.029	1.051	0.977
R [$I > 2\sigma(I)$]	0.0365	0.0325	0.0331	0.0296	0.0571
R_w [$I > 2\sigma(I)$]	0.0764	0.0860	0.0777	0.0672	0.1226
Flack parameter		0.011(12)			
Twin comp. contributions					0.38(2)/0.62(2)

[1] [1a] T. R. Felthouse, E. J. Laskowski, D. N. Hendrickson, *Inorg. Chem.* **1977**, *16*, 1077. [1b] J. Sletten, *Acta Chem. Scand., Ser. A* **1983**, *37*, 569. [1c] M. Julve, M. Verdaguer, O. Kahn, A. Gleizes, M. Philoche-Levisalles, *Inorg. Chem.* **1983**, *22*, 368. [1d] M. Julve, J. Faus, M. Verdaguer, A. Gleizes, *J. Am. Chem. Soc.* **1984**, *106*, 8306. [1e] M. Julve, M. Verdaguer, A. Gleizes, M. Philoche-Levisalles, O. Kahn, *Inorg. Chem.* **1984**, *23*, 3808. [1f] A. Bencini, A. C. Fabretti, C. Zanchini, P. Zanini, *Inorg. Chem.* **1987**, *26*, 1445. [1g] L. Soto, J. Garcia, E. Escrivá, J. P. Legros, J. P. Tuchagues, F. Dahan, A. Fuertes, *Inorg. Chem.* **1989**, *28*, 3378. [1h] L. S. Tuero, J. García-Lozano, E. E. Moltó, M. B. Borja, F. Dahan, J. P. Tuchagues, J. P. Legros, *J. Chem. Soc., Dalton Trans.* **1991**, 2619. [1i] A. Gleizes, M. Julve, M. Verdaguer, J. A. Real, J. Faus, X. Solans, *J. Chem. Soc., Dalton Trans.* **1992**, 3209. [1j] J. Glerup, P. A. Goodson, D. J. Hodgson, K. Michelsen, *Inorg. Chem.* **1995**, *34*, 6255. [1k] Y. Akhriff, J. Server-Carrión, J. García-Lozano, E. Escrivá, J. V. Folgado, L. Soto, *Inorg. Chem.* **1999**, *38*, 1174. [1l] Z. Smékal, Z. Trávnicek, F. Lloret, J. Marek, *Polyhedron* **1999**, *18*, 2787. [1m] O. Castillo, I. Muga, A. Luque, J. M. Gutiérrez-Zorrilla, J. Sertucha, P. Vitoria, P. Román, *Polyhedron* **1999**, *18*, 1235. [1n] L. Zhang, W. M. Yan, Z. H. Jiang, D. Z. Liao, G. L. Wang, *Polyhedron* **2000**, *19*, 1105. [1o] M. L. Calatayud, I. Castro, J. Sletten, F. Lloret, M. Julve, *Inorg. Chim. Acta* **2000**, *300*−*302*, 846. [1p] S. Youngme, G. A. van Albada, N. Chaichit, P. Gunnasoot, P. Kongsaeree, I. Mutikainen, O. Roubeau, J. Reedijk, U. Turpeinen, *Inorg. Chim. Acta* **2003**, *353*, 119. [1q] F. Tuna, G. I. Pascu, J. P. Sutter, M. Andruh, S. Golhen, J. Guillevic, H. Pritzkow, *Inorg. Chim. Acta* **2003**, *342*, 131. [1r] S. P. Foxon, O. Walter, R. Koch, H. Rupp, P. Müller, S. Schindler, *Eur. J. Inorg. Chem.* **2004**, *2*, 344.

[2] [2a] D. Y. Jeter, W. E. Hatfield, *Inorg. Chim. Acta* **1972**, *6*, 523. [2b] A. Gleizes, F. Maury, J. Galy, *Inorg. Chem.* **1980**, *19*, 2074. [2c] D. R. Bloomquist, J. J. Hansen, C. P. Landee, R. D. Willett, R. Buder, *Inorg. Chem.* **1981**, *20*, 3308. [2d] U. Geiser, B. L. Ramakrishna, R. D. Willettt, F. B. Hulsbergen, J. Reedijk, *Inorg. Chem.* **1987**, *26*, 3750. [2e] S. K. Chattopadhyay, T. C. W. Mak, B. S. Luo, L. K. Thompson, A. Rana, S. Ghosh, *Polyhedron* **1995**, *14*, 3661. [2f] J. Carranza, C. Brennan, J. Sletten, B. Vangdal, P. Rillema, F. Lloret, M. Julve, *New J. Chem.* **2003**, *27*, 1775.

[3] [3a] L. Cavalca, A. C. Villa, A. G. Manfredotti, A. Mangia, *J. Chem. Soc., Dalton Trans.* **1972**, 391. [3b] A. Michalowicz, J. J. Girerd, J. J. Goulon, *Inorg. Chem.* **1979**, *18*, 3004. [3c] J. J. Girerd, O. Kahn, M. Verdaguer, *Inorg. Chem.* **1980**, *40*, 5526. [3d] M. Verdaguer, M. Julve, A. Michalowicz, O. Kahn, *Inorg. Chem.* **1983**, *22*, 2624. [3e] H. Oshio, *Chem. Lett.* **1991**, 227. [3f] M. R. Sundberg, R. Kivekäs, J. K. Koskimies, *J. Chem. Soc., Chem. Commun.* **1991**, 526. [3g] H. Oshio, U. Nagashima, *Inorg. Chem.* **1992**, *31*, 3295. [3h] J. Suárez-Varela, J. M. Domínguez-Vera, E. Colacio, J. C. Avila-Rosón, M. A. Hidalgo, D. Martín-Ramos, *J. Chem. Soc., Dalton Trans.* **1995**, 2143. [3i] O. Castillo, A. Luque, J. Sertucha, P. Román, F. Lloret, *Inorg. Chem.* **2000**, *39*, 6142. [3j] O. Castillo, A. Luque, M. Julve, F. Lloret, P. Román, *Inorg. Chim. Acta* **2001**, *315*, 9. [3k] O. Castillo, A. Luque, P. Román, F. Lloret, M. Julve, *Inorg. Chem.* **2001**, *40*, 5526.

[4] [4a] G. De Munno, M. Julve, F. Nicolò, F. Lloret, J. Faus, R. Ruiz, E. Sinn, *Angew. Chem. Int. Ed. Engl.* **1993**, *32*, 613. [4b] S. Kitagawa, T. Okubo, S. Kawata, M. Kondo, M. Katada, H. Kobayashi, *Inorg. Chem.* **1995**, *34*, 4790. [4c] R. Vicente, A. Escuer, X. Solans, M. Font-Bardía, *J. Chem. Soc., Dalton Trans.* **1996**, 1835. [4d] R. Vicente, A. Escuer, J. Ferretjans, H. Stoeckli-Evans, X. Solans, M. Font-Bardía, *J. Chem. Soc., Dalton Trans.* **1997**, 167. [4e] P. S. Mukherjee, T. K. Magi, G. Mostafa, W. Hibbs, N. R. Chaudhuri, *New J. Chem.* **2001**, *25*, 760. [4f] M. Hernández-Molina, P. A. Lorenzo-Luis, C. Ruiz-Pérez, *Cryst. Eng. Commun.* **2001**, *16*, 1. [4g] T. D. Keene, H. R. Ogilvie, M. B. Hursthouse, D. J. Price, *Eur. J. Inorg. Chem.* **2004**, 1007.

[5] [5a] M. F. Charlot, M. Verdaguer, Y. Journaux, P. de Loth, J. P. Daudey, *Inorg. Chem.* **1984**, *23*, 3802. [5b] S. Alvarez, M. Julve, M. Verdaguer, *Inorg. Chem.* **1990**, *29*, 4500. [5c] J. Cano, P. Alemany, S. Alvarez, M. Verdaguer, E. Ruiz, *Chem. Eur. J.* **1998**, *4*, 476. [5d] J. Cano, E. Ruiz, P. Alemany, F. Lloret, S. Alvarez, *Inorg. Chem.* **1999**, 1669. [5e] J. Cabrero, N. Ben Amor, C. de Graaf, F. Illas, R. Caballol, *J. Phys. Chem. A* **2000**, *104*, 9983.

 © 2004 Wiley-VCH Verlag GmbH & Co. KGaA, Weinheim

[6] L. Dubicki, C. M. Harris, E. Kokot, R. L. Martin, *Inorg. Chem.* **1966**, *5*, 93.
[7] I. Castro, J. Faus, M. Julve, A. Gleizes, *J. Chem. Soc., Dalton Trans.* **1991**, 1937.
[8] O. N. Sathyanarayana, C. C. Patel, *J. Inorg. Nucl. Chem.* **1965**, *27*, 297.
[9] R. Cortés, M. K. Urtiaga, L. Lezama, M. I. Arriortua, T. Rojo, *Inorg. Chem.* **1994**, *33*, 829.
[10] [10a] W. Fitzgerald, J. Foley, D. McSweeney, N. Ray, D. Sheahan, S. Tyagi, B. Hathaway, P. O'Brien, *J. Chem. Soc., Dalton Trans.* **1982**, 1117. [10b] I. Castro, J. Faus, M. Julve, M. C. Muñoz, W. Díaz, X. Solans, *Inorg. Chim. Acta* **1991**, *179*, 59.
[11] [11a] A. C. Fabretti, G. Franchini, P. Zanini, *Inorg. Chim. Acta* **1985**, *105*, 187. [11b] O. Castillo, A. Luque, P. Román, *J. Mol. Struct.* **2001**, *570*, 181.
[12] A. W. Addison, T. N. Rao, J. Reedijk, J. Van Rijn, G. C. Verschoor, *J. Chem. Soc., Dalton Trans.* **1984**, 1349.
[13] [13a] S. C. Rasmussen, M. M. Richter, E. Yi, H. Place, K. J. Brewer, *Inorg. Chem.* **1990**, *29*, 3926. [13b] S. M. Scott, K. C. Gordon, A. K. Burell, *J. Chem. Soc., Dalton Trans.* **1999**, 2669. [13c] N. Moliner, M. C. Muñoz, P. J. Kroningsbruggen, J. A. Real, *Inorg. Chim. Acta* **1998**, *274*, 1. [13d] M. R. Waterland, T. J. Simpson, K. C. Gordon, A. K. Burell, *J. Chem. Soc., Dalton Trans.* **1998**, 185. [13e] D. P. Rillema, D. G. Taghdiri, D. S. Jones, C. D. Keller, L. A. Worl, T. J. Meyer, H. A. Levy, *Inorg. Chem.* **1987**, *26*, 578. [13f] K. C. Gordon, A. H. R. Al-Obaidi, P. M. Jayaweera, J. McGarvey, J. F. Malone, S. E. J. Bell, *J. Chem. Soc., Dalton Trans.* **1996**, 1591. [13g] J. Granifo, M. E. Vargas, M. T. Garland, R. Baggio, *Inorg. Chim. Acta* **2000**, *305*, 143. [13h] O. S. Jung, S. H. Park, Y. J. Kim, Y. A. Lee, H. G. Jang, U. Lee, *Inorg. Chim. Acta* **2001**, *312*, 93. [13i] X. H. Bu, H. Liu, M. Du, K. M. C. Wong, V. W. W. Yam, M. Shionoya, *Inorg. Chem.* **2001**, *40*, 4143. [13j] X. H. Bu, H. Liu, M. Du, K. M. C. Wong, V. W. W. Yam, *Inorg. Chim. Acta* **2002**, *333*, 32.
[14] [14a] A. Escuer, S. B. Kumar, M. Font-Bardía, X. Solans, R. Vicente, *Inorg. Chim. Acta* **1999**, *286*, 62. [14b] K. V. Goodwin, W. T. Pennington, J. D. Petersen, *Acta Crystallogr., Sect. C* **1990**, *46*, 898.
[15] A. Escuer, T. Comas, J. Ribas, R. Vicente, X. Solans, C. Zanchini, D. Gatteschi, *Inorg. Chim. Acta* **1989**, *162*, 97.
[16] [16a] J. Sletten, O. Bjørsvik, *Acta Chem. Scand.* **1998**, *52*, 770. [16b] H. Grove, PhD Thesis, University of Bergen, **2002**. [16c]H. Grove, J. Sletten, M. Julve, F. Lloret, L. Lezama, *Inorg. Chim. Acta* **2000**, *310*, 217. [16d] H. Grove, J. Sletten, M. Julve, F. Lloret, *J. Chem. Soc., Dalton Trans.* **2001**, 2487. [16e] H. Grove, M. Julve, F. Lloret, P. E. Kruger, K. W. Törnroos, J. Sletten, *Inorg. Chim. Acta* **2001**, *325*, 115.
[17] [17a] H. Grove, J. Sletten, M. Julve, F. Lloret, *J. Chem. Soc., Dalton Trans.* **2000**, 515. [17b] H. Grove, J. Sletten, M. Julve, F. Lloret, J. Cano, *J. Chem. Soc., Dalton Trans.* **2001**, 259.
[18] J. Carranza, C. Brenan, J. Sletten, B. Vangdal, P. D. Rillema, F. Lloret, M. Julve, *New J. Chem.* **2003**, *27*, 1775.
[19] [19a] A. J. Blake, N. R. Champness, P. A. Cooke, J. E. B. Nicolson, *Chem. Commun.* **2000**, 665. [19b] A. J. Blake, N. R. Champness, P. A. Cooke, J. E. B. Nicolson, C. Wilson, *J. Chem. Soc., Dalton Trans.* **2000**, 3811.
[20] L. M. Toma, C. Ellis, P. D. Rillema, C. Ruiz-Pérez, M. Julve, *Inorg. Chim. Acta*, in press.
[21] [21a] D. M. Adams, A. Dei, A. L. Reinhold, D. N. Hendrickson, *Angew. Chem. Int. Ed. Engl.* **1993**, *32*, 880. [21b] D. M. Adams, A. Dei, A. L. Reinhold, D. N. Hendrickson, *J. Am. Chem. Soc.* **1993**, *115*, 8221.
[22] [22a] H. Lai, D. S. Jones, D. C. Schwind, P. D. Rillema, *J. Crystallogr. Spectr. Res.* **1990**, *20*, 321. [22b] A. Gerli, J. Reedijk, M. T. Lakin, A. L. Spek, *Inorg. Chem.* **1995**, *34*, 1836. [22c] P. A. Anderson, R. F. Anderson, M. Furue, P. C. Funk, F. R. Keene, B. T. Patterson, B. D. Yeomans, *Inorg. Chem.* **2000**, *39*, 2721.
[23] [23a] R. D. Schnebeck, L. Randaccio, E. Sangrado, B. Lippert, *Angew. Chem. Int. Ed.* **1998**, *37*, 119. [23b] R. D. Schnebeck, E. Freisinger, B. Lippert, *Angew. Chem. Int. Ed.* **1999**, *38*, 168. [23c] R. D. Schnebeck, E. Freisinger, B. Lippert, *Chem. Commun.* **1999**, 675. [23d] R. D. Schnebeck, E. Freisenger, F. Glahé, B. Lippert, *J. Am. Chem. Soc.* **2000**, *122*, 1381. [23e] R. D. Schnebeck, E. Freisinger, B. Lippert, *Eur. J. Inorg. Chem.* **2000**, 1193.
[24] K. Nakamoto, *Infrared and Raman Spectra of Inorganic and Coordination Compounds*, 4th edition, Wiley, New York, **1986**, p. 228.
[25] J. Fujita, A. E. Martell, K. Nakamoto, *J. Chem. Phys.* **1962**, *36*, 324.
[26] [26a] N. F. Curtis, *J. Chem. Soc., A* **1968**, 1584. [26b] K. Nonoyama, H. Ojima, K. Ohki, M. Nonoyama, *Inorg. Chim. Acta* **1980**, *41*, 155.
[27] J. Tang, E. Gao, W. Bu, D. Liao, S. Yan, Z. Jiang, G. Wang, *J. Mol. Struct.* **2000**, *525*, 271.
[28] W.E. Hatfield, W. E. Estes, W. E. Marsh, M. W. Pickens, L. W. Ter van Haar, R. R. Weller, in *Extended Linear Chain Compounds* (Ed.: J. S. Miller), Plenum, New York, **1983**, vol 3, p. 43.
[29] O. Kahn, *Molecular Magnetism*, VCH Verlagsgesellschaft, Weinheim, Germany, **1993**.
[30] [30a] B. N. Figgis, D. J. Martin, *Inorg. Chem.* **1966**, *5*, 100. [30b] K. T. Mc Gregor, Z. G: Soos, *Inorg. Chem.* **1976**, *15*, 2159.
[31] H. A. Goodwin, F. Lions, *J. Am. Chem. Soc.* **1959**, *81*, 6415.
[32] R. J. Crutchley, A. B. P. Lever, *Inorg. Chem.* **1982**, *21*, 2276.
[33] A. Earnshaw, *Introduction to Magnetochemistry*, Academic Press, London, **1968**.
[34] [34a] Bruker 2000, *SADABS*, Versión 2.03, Bruker AXS Inc., Madison, Wisconsin, USA. [34b] K. Harms, *XCAD*, Philipps University of Marburg, Germany, **1996**.
[35] [35a] Bruker **1999**, *SMART*, Version 5.054, Data Collection Software, Bruker AXS Inc., Madison, Wisconsin, USA. [35b] Bruker **2001**, *SAINT*, Version 6.02a, Data Integration Software, Bruker AXS Inc., Madison, Wisconsin, USA. [35c] *CAD-4-Express*, Delft X-ray Diffraction Instruments, Delft, The Netherlands, **1992**.
[36] [36a] G. M. Sheldrick, *Acta Crystallogr., Sect. A* **1990**, *46*, 467. [36b] G. M. Sheldrick, *SHELXL-93*, University of Göttingen, Göttingen, Germany, **1993**. [36c] G. M. Sheldrick, *SHELXTL/PC*, Version 6.12, Bruker AXS Inc., Madison, Wisconsin, USA, **1998**. [36d] G. M. Sheldrick, *XP*, Version 5.1, Bruker AXS Inc., Madison, Wisconsin, USA, **1998**.

Received June 10, 2004
Early View Article
Published Online October 21, 2004

 © 2004 Wiley-VCH Verlag GmbH & Co. KGaA, Weinheim

The Anderson-Type Anion $(TeMo_6O_{24})^{6-}$ – A Multidentate Ligand for Trivalent Rare Earth Cations

Daniel Drewes,[a] Eva Melanie Limanski,[a] and Bernt Krebs*[a]

Dedicated to Professor Philipp Gütlich on the occasion of his 70th birthday

Keywords: Polyoxometalates / Molybdenum / Lanthanides / Tellurium / Self-assembly

The syntheses and structural characterizations of four novel lanthanide polyoxomolybdates containing the Anderson-type anion $(TeMo_6O_{24})^{6-}$ are presented. Depending on the size of the trivalent rare earth cations, in the solid-state structures of $\{[La(H_2O)_6]_2(TeMo_6O_{24})\}_n \cdot 6nH_2O$ (**1**), $\{[Ce(H_2O)_7]_2(TeMo_6O_{24})\}_n \cdot 7nH_2O$ (**2**), $\{[Pr(H_2O)_7]_2(TeMo_6O_{24})\}_n \cdot 8nH_2O$ (**3**) and $\{[Nd(H_2O)_7]_2(TeMo_6O_{24})\}_n \cdot 8nH_2O$ (**4**) two different arrangements of the building unit are present. The $(TeMo_6O_{24})^{6-}$ anion acts as a hexadentate ligand for La^{III} and as a tetradentate ligand for Ce^{III}, Pr^{III} and Nd^{III}, leading to two different infinite one-dimensional chains. The crystal structures of the new compounds are compared with known lanthanide polyoxomolybdates containing the $(TeMo_6O_{24})^{6-}$ anion and the influence of the Ln^{III} ionic radii is discussed.
(© Wiley-VCH Verlag GmbH & Co. KGaA, 69451 Weinheim, Germany, 2004)

Introduction

Polyoxotungstates and -molybdates[1,2] have been investigated extensively over the last years. Owing to their unusual properties such as high charges and ionic masses etc., they attract current attention in view of their potential in medicine, material science, and catalysis.[3–6] The fascination of polyoxometalate chemistry arises from the remarkable size and challenging geometry of several mixed-valence nanostructured polyoxomolybdates synthesized by the group of A. Müller.[7–10] However, complex and largely unknown self-assembly reaction mechanisms are responsible for the formation of polyoxometalates and make it difficult to develop a straightforward reaction route for their syntheses.

Lanthanide containing polyoxoanions differ fundamentally from transition metal substituted anions and exhibit unique structures because of the lanthanides' preferred coordination numbers eight and nine. In order to establish a consistent picture of lanthanide containing polyoxomolybdates, we started synthesizing and characterizing novel exponents in this class of compounds. In 2004, we were able to report the crystal structures of $[(CH_3)_4N]_x(NH_4)_{14-x}[Ln_4(MoO_4)(H_2O)_{16}(Mo_7O_{24})_4] \cdot nH_2O$ (Ln = La^{III}, Ce^{III}, Pr^{III}, Sm^{III}, Gd^{III}).[11] We affirmed that the well-known $[Eu_4(MoO_4)(H_2O)_{16}(Mo_7O_{24})_4]^{14-}$ anion reported by Yamase et al.[12] can be formed by a wide range of lanthanides.

In the case of the $(LnW_{10}O_{36})^{9-}$ anions (Ln = Pr^{III}, Nd^{III}, Sm^{III}, Gd^{III}, Tb^{III}, Dy^{III}), the effect of lanthanide contraction on these anions was discussed by Ozeki and Yamase.[13] Sécheresse et al. showed that the linkage of the monovacant lacunary $(SiW_{11}O_{39})^{8-}$ anions by lanthanide cations is dependent on the nature of the rare earth cation.[14] This example shows the necessity to investigate the dependency of the arrangement of different polyoxo building units on the size of the Ln^{III} atoms.

Recently, we have reported the syntheses and crystal structures of six novel lanthanide polyoxomolybdates containing the Anderson-type anion $(TeMo_6O_{24})^{6-}$. The polyoxometalates $K_{6n}(TeMo_6O_{24})_n\{[Ln(H_2O)_7]_2(TeMo_6O_{24})\}_n \cdot 16nH_2O$ (Ln = Eu^{III}, Gd^{III}) and $K_{3n}\{Ln(H_2O)_5(TeMo_6O_{24})\}_n \cdot 6nH_2O$ (Ln = Tb^{III}, Dy^{III}, Ho^{III}, Er^{III}) exhibit lanthanide cations and $(TeMo_6O_{24})^{6-}$ anions at a ratio of 1:1. Depending on the size of the rare earth cations, two different arrangements of the building units could be found.[15] This paper describes the syntheses and structures of four novel lanthanide polyoxomolybdates with a $(TeMo_6O_{24})^{6-}$:Ln^{III} ratio of 1:2 (Ln = La, Ce, Pr, Nd). While the cerium, praseodymium and neodymium compound show a linkage of the $(TeMo_6O_{24})^{6-}$ building units which can also be found in the europium and gadolinium compounds mentioned above, the lanthanum compound shows a novel type of combination.

Results and Discussion

The four novel compounds $\{[La(H_2O)_6]_2(TeMo_6O_{24})\}_n \cdot 6nH_2O$ (**1**), $\{[Ce(H_2O)_7]_2(TeMo_6O_{24})\}_n \cdot 7nH_2O$ (**2**),

[a] Institut für Anorganische und Analytische Chemie, Westfälische Wilhelms-Universität,
Corrensstraße 30, 48149 Münster, Germany
Fax: (internat.) + 49-(0)251-83-38-366
E-mail: krebs@uni-muenster.de

$\{[Pr(H_2O)_7]_2(TeMo_6O_{24})\}_n \cdot 8nH_2O$ (**3**) and $\{[Nd(H_2O)_7]_2(TeMo_6O_{24})\}_n \cdot 8nH_2O$ (**4**) were synthesized in a two-step reaction. At first, the $(TeMo_6O_{24})^{6-}$ anion was formed by potassium molybdate and telluric acid at pH 5.5. Afterwards, the trivalent rare earth cations were added as chloride or nitrate. Single crystals of **1**−**4** formed after a few days.

All compounds crystallize in the triclinic crystal system, space group $P\bar{1}$. The asymmetric unit contains half a formula unit. The tellurium atom Te(1) is situated at an inversion center in all cases. It is located at the center of a nearly regular hexagon which is formed by the six molybdenum atoms of the $(TeMo_6O_{24})^{6-}$ anion. Consequently, all Te···Mo distances are almost identical in **1**−**4**. The molybdenum and tellurium atoms are nearly planar since the Te(1) atom is situated at a distance of less than 0.06 Å from the [Mo(1), Mo(2), Mo(3)] plane in all compounds. The Te^{VI} atom is surrounded octahedrally by six oxygen atoms. The Te−O bond lengths and O−Te−O bond angles summarized in Table 1 show only little distortion of the TeO_6 octahedra. The corresponding bond lengths and angles differ only slightly in all four compounds.

The corresponding molybdenum−oxygen bond lengths of the $(TeMo_6O_{24})^{6-}$ anions show great similarities in **1**−**4**. The Mo−O distances can be divided into three groups: terminal oxygen atoms, molybdenum-bridging oxygen atoms with middle oxygen−molybdenum bond lengths and oxygen atoms bound to one tellurium and two molybdenum atoms with long oxygen−molybdenum bond lengths. As expected, the terminal oxygen atoms show the shortest molybdenum−oxygen bond lengths [between 1.69(1) and 1.73(1) Å]. The long Mo−O bond lengths are located *trans* to the short Mo−O bonds and show M−O distances between 2.22(1) Å and 2.32(1) Å. The intermediate Mo−O bonds show Mo-O distances between 1.89(1) Å and 1.96(1) Å. As usual for polyoxomolybdates, the O−Mo−O bond angles differ significantly from the ideal 90° and 180° bond angles and confirm the distortion of the MoO_6 octahedra. The Mo−O bond lengths and O−Mo−O bond angles are summarized in Table 1.

In the lanthanum compound **1**, the $(TeMo_6O_{24})^{6-}$ anion acts as a hexadentate ligand for the lanthanum atoms and is bound to four La^{III} atoms. Each La atom achieves ninefold coordination by six water molecules and three terminal oxygen atoms of two $(TeMo_6O_{24})^{6-}$ anions. These nine oxygen atoms build up a tricapped-trigonal prism. Figure 1 shows a detail of the resulting infinite one-dimensional $\{[La(H_2O)_6]_2(TeMo_6O_{24})\}_n$ chain. The one-dimensional chains are linked by an extensive hydrogen bond network.

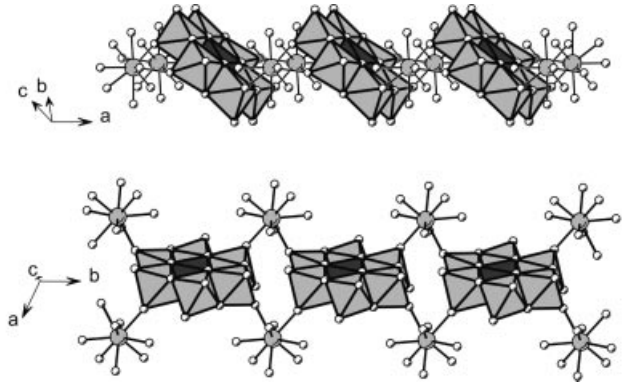

Figure 1. Details of the infinite one-dimensional chains of $\{[La(H_2O)_6]_2(TeMo_6O_{24})\}_n$ in **1** (top) and of $\{[Ln(H_2O)_7]_2(TeMo_6O_{24})\}_n$ (Ln = Ce, Pr, Nd; bottom) in **2**−**4**

In the cerium, praseodymium and neodymium containing compounds **2**−**4**, the Anderson anion acts as a tetradentate ligand coordinating four Ce^{III}, Pr^{III} or Nd^{III} atoms by terminal oxygen atoms. The lanthanide atoms are coordinated by two terminal oxygen atoms of two $(TeMo_6O_{24})^{6-}$ anions and seven water molecules, forming a tricapped-trigonal prism. Figure 1 shows the infinite one-dimensional $\{[Ln(H_2O)_7]_2(TeMo_6O_{24})\}_n$ chain (Ln = Ce, Pr, Nd) in detail. As in **1**, the chains are connected via a hydrogen bond network. This type of chain can also be found in $K_{6n}(TeMo_6O_{24})_n\{[Eu(H_2O)_7]_2(TeMo_6O_{24})\}_n \cdot 16nH_2O$ (**5**) and $K_{6n}(TeMo_6O_{24})_n\{[Gd(H_2O)_7]_2(TeMo_6O_{24})\}_n \cdot 16nH_2O$ (**6**).[15] In contrast to **2**−**4**, the com-

Table 1. Bond lengths (Å) and angles (°) with standard deviations in parentheses of the polyoxometalates **1**−**4**

	1 (Ln = La)	**2** (Ln = Ce)	**3** (Ln = Pr)	**4** (Ln = Nd)
Te−O	1.903(3)−1.942(3)	1.926(4)−1.945(5)	1.921(3)−1.934(3)	1.922(3)−1.935(3)
$Mo-O_t$ [a]	1.686(3)−1.734(3)	1.696(5)−1.733(5)	1.689(3)−1.730(3)	1.691(3)−1.732(3)
$Mo-O_{Mo2}$ [b]	1.914(3)−1.948(3)	1.900(5)−1.962(4)	1.889(3)−1.953(3)	1.891(3)−1.960(3)
$Mo-O_{TeMo2}$ [b]	2.223(3)−2.315(3)	2.257(5)−2.310(5)	2.253(3)−2.313(3)	2.243(3)−2.312(3)
$Ln-O_{Mo}$ [b]	2.512(3)−2.535(3)	2.517(5)−2.548(5)	2.488(3)−2.526(3)	2.479(3)−2.512(3)
$Ln-OH_2$	2.511(3)−2.631(3)	2.506(5)−2.569(6)	2.471(3)−2.553(3)	2.465(3)−2.538(3)
Mo···Te	3.238(1)−3.278(1)	3.273(1)−3.290(2)	3.265(2)−3.282(2)	3.267(1)−3.279(2)
$O-Te-O_{cis}$	84.8(2)−95.2(2)	85.2(2)−94.8(2)	85.1(2)−94.9(2)	85.0(2)−95.0(2)
$O-Te-O_{trans}$	180.0	180.0	180.0	180.0
$O-Mo-O_{cis}$	70.2(1)−107.5(2)	70.2(2)−106.7(3)	70.1(1)−106.8(2)	70.1(1)−106.8(2)
$O-Mo-O_{trans}$	151.6(2)−164.3(2)	151.4(2)−161.3(2)	151.8(3)−161.7(2)	152.2(2)−161.8(2)
O−Ln−O	65.2(1)−141.6(1)	64.2(2)−143.4(2)	63.9(2)−142.6(2)	64.2(2)−142.7(2)

[a] Terminal. [b] The subscripts indicate the atoms bound to the oxygen atom.

 © 2004 Wiley-VCH Verlag GmbH & Co. KGaA, Weinheim

pounds **5** and **6** contain two crystallographically independent $(TeMo_6O_{24})^{6-}$ anions. One of these ions acts as a tetradentate ligand for the lanthanide ions, the second one is surrounded by potassium ions and crystal water and has no bonding to the lanthanide cations.

The crystal structures of **1**−**4** differ not only in the coordination sphere of the lanthanide atoms. Figure 2 and 3 show the different arrangements of the one-dimensional chains for **1** on the one hand and **2**−**4** on the other. In **1**, the $\{[La(H_2O)_6]_2(TeMo_6O_{24})\}_n$ chains run along [100], while the $\{[Ln(H_2O)_7]_2(TeMo_6O_{24})\}_n$ chains in **2**−**4** run along [010]. While the lattice parameters in **2**−**4** are very similar, they differ clearly from those found for **1**. The differences in the crystal structures can also be fixed on the Ln···Ln distances. Within the $\{[Ln(H_2O)_x]_2(TeMo_6O_{24})\}_n$ chains (x = 6, 7), the shortest La···La distance [7.82(1) Å] in **1** differs clearly from the shortest Ln···Ln distances in **2**−**4** [8.70(1) Å for **2**, 8.65(1) Å for **3**, 8.62(1) Å for **4**, respectively]. In contrast to that, the shortest Ln···Ln distances between two different chains are shorter in **2**−**4** [6.25(1) Å for **2**, 6.18(1) Å for **3**, 6.16(1) Å for **4**, respectively] than in **1** [6.77(1) Å].

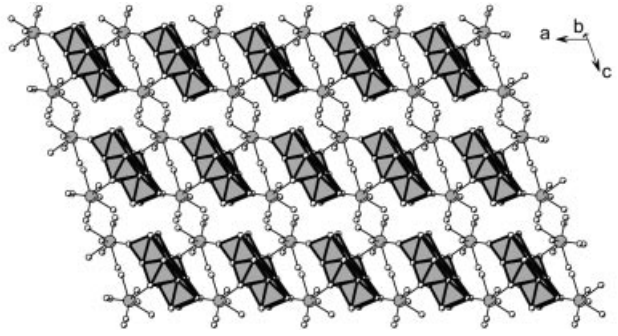

Figure 2. View of the crystal structure of $\{[La(H_2O)_6]_2(TeMo_6O_{24})\}_n \cdot 6nH_2O$ (**1**). The $\{[La(H_2O)_6]_2(TeMo_6O_{24})\}_n$ chains run along [100]. The hydrate water molecules are omitted partially for clarity

We have reported recently that for terbium(III), dysprosium(III), holmium(III) and erbium(III) a further linkage

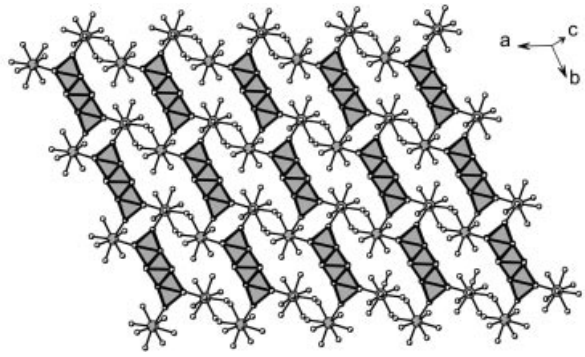

Figure 3. View of the crystal structure of $\{[Pr(H_2O)_7]_2(TeMo_6O_{24})\}_n \cdot 8nH_2O$ (**3**). The $\{[Pr(H_2O)_7]_2(TeMo_6O_{24})\}_n$ chains run along [010]. The hydrate water molecules are omitted partially for clarity

of the Anderson-type anions can be found.[15] In $K_{3n}\{Tb(H_2O)_5(TeMo_6O_{24})\}_n \cdot 6nH_2O$ (**7**), $K_{3n}\{Dy(H_2O)_5(TeMo_6O_{24})\}_n \cdot 6nH_2O$ (**8**), $K_{3n}\{Ho(H_2O)_5(TeMo_6O_{24})\}_n \cdot 6nH_2O$ (**9**) and $K_{3n}\{Er(H_2O)_5(TeMo_6O_{24})\}_n \cdot 6nH_2O$ (**10**), the $(TeMo_6O_{24})^{6-}$ anion acts as a tridentate ligand for the lanthanide atoms. As a result of the lanthanide contraction, the coordination number of these smaller rare earth cations is only eight. Within the $\{Ln(H_2O)_5(TeMo_6O_{24})\}_n^{3n-}$ chains, the Ln^{III} atoms are coordinated by five water molecules, two terminal oxygen atoms of two Anderson anions and one molybdenum-bridging oxygen atom. These eight oxygen atoms form a square-antiprismatic prism.

The oxidation states of the lanthanide cations were checked by the bond valence method.[16] New bond-valence parameters for Ln−O bonds have been reported recently.[17] Table 2 summarizes the calculated bond valences for the lanthanide atoms of the new compounds **1**−**4** and the compounds **5**−**10** reported previously. The calculated valences vary only slightly and affirm that the lanthanide atoms are trivalent in all compounds, although the yellow color of the cerium containing compound **2** could lead to the assumption that Ce^{III} was oxidized to Ce^{IV}. The average Ln−O bond lengths show not only the influence of the lanthanide contraction but also point to the additional decrease of the

Table 2. Comparison of Ln−O bond lengths and calculated bond valences of **1**−**10**

	Ln atom	Coordination number	Range of Ln−O bond lengths	Average Ln−O bond length	Bond-valence (calcd.)
1	La(1)	9	2.511(3)−2.631(3)	2.545	3.01
2	Ce(1)	9	2.506(5)−2.569(6)	2.533	2.87
3	Pr(1)	9	2.471(3)−2.553(3)	2.511	2.95
4	Nd(1)	9	2.465(3)−2.538(3)	2.496	2.97
5	Eu(1)	9	2.398(3)−2.489(3)	2.448	2.99
6[a]	Gd(1)	9	2.393(4)−2.498(4)	2.444	2.95
	Gd(2)	9	2.391(4)−2.497(4)	2.442	2.96
7	Tb(1)	8	2.347(3)−2.422(3)	2.379	2.98
8	Dy(1)	8	2.339(5)−2.401(6)	2.367	2.97
9	Ho(1)	8	2.324(5)−2.394(5)	2.360	2.95
10	Er(1)	8	2.319(6)−2.388(6)	2.350	2.93

[a] The gadolinium compound contains two crystallographically independent Gd^{III} atoms.

 © 2004 Wiley-VCH Verlag GmbH & Co. KGaA, Weinheim

Ln−O bond lengths which is caused by the change of the coordination number from 9 to 8.

Conclusions

The decrease of radii of the trivalent rare earth cations leads to three different one-dimensional chains in **1**, **2**−**6** and **7**−**10**. As a result, the solid-state structures show varieties which are not only limited to slight changes of Ln−O bond lengths, but also cause diverse coordination spheres, lattice parameters and distances between the one-dimensional chains. The influence of the size of the Ln^{III} atoms can be watched closely in the $(TeMo_6O_{24})^{6-}/Ln^{III}$ system because the $(TeMo_6O_{24})^{6-}$ anions exhibit numerous potential bonding partners for the lanthanide cations and therefore enable different arrangements of the building units with different coordination spheres of the lanthanide atoms. In the crystal structures reported, the $(TeMo_6O_{24})^{6-}$ anion can act as a tridentate, tetradentate and hexadentate ligand, respectively. Linking these discrete entities to build up solid-state materials is of great interest beyond the structural point of view, but also for possible applications in different fields of chemistry. It still remains a challenge to investigate the dependency of the crystal structures on the lanthanide radii to establish a consistent picture of lanthanide containing polyoxomolybdates.

Experimental Section

Instrumentation and Analytical Procedures: IR spectra were measured with a Perkin−Elmer 683 spectrometer as KBr pellets. The atomic ratios of the heavy elements were determined by energy dispersive X-ray fluorescence analysis (EDX). Diffraction experiments were performed with a STOE IPDS imaging plate system (for **2**) and a BRUKER SMART APEX diffractometer with CCD detector (for **1**, **3** and **4**), both using graphite-monochromated Mo-K_α radiation (λ = 0.71073 Å). Structures were solved by Patterson Synthesis with the SHELXS-97[18] and refined with the SHELXL-97 program.[19] No hydrogen atoms were included during the refinement. All atoms were refined anisotropically by full-matrix least-squares calculations based on F^2. The programs SADABS[20] (for **1**, **3** and **4**) and DECAY[21] (for **2**) were applied for the absorption correction. As usual for polyoxometalates, the crystal structures of **2**−**4** show disorder in the crystal water part of the structure.

Table 3. Crystallographic data for $\{[La(H_2O)_6]_2(TeMo_6O_{24})\}_n \cdot 6nH_2O$ (**1**), $\{[Ce(H_2O)_7]_2(TeMo_6O_{24})\}_n \cdot 7nH_2O$ (**2**), $\{[Pr(H_2O)_7]_2(TeMo_6O_{24})\}_n \cdot 8nH_2O$ (**3**) and $\{[Nd(H_2O)_7]_2(TeMo_6O_{24})\}_n \cdot 8nH_2O$ (**4**)

	1	**2**	**3**	**4**
Formula	$La_2TeMo_6O_{42}H_{36}$	$Ce_2TeMo_6O_{45}H_{42}$	$Pr_2TeMo_6O_{46}H_{44}$	$Nd_2TeMo_6O_{46}H_{44}$
M (g·mol^{-1})	1689.34	1745.81	1765.41	1772.07
Crystal size (mm^3)	0.10 × 0.06 × 0.02	0.14 × 0.12 × 0.07	0.23 × 0.14 × 0.05	0.18 × 0.16 × 0.09
Crystal color	colorless	yellow	light green	purple
Crystal system	triclinic	triclinic	triclinic	triclinic
Space group	$P\bar{1}$ (No. 2)	$P\bar{1}$ (No. 2)	$P\bar{1}$ (No. 2)	$P\bar{1}$ (No. 2)
a (Å)	9.396(2)	9.626(2)	9.569(2)	9.569(2)
b (Å)	10.188(2)	10.285(2)	10.230(2)	10.236(2)
c (Å)	10.694(2)	11.632(2)	11.572(2)	11.563(2)
α (°)	101.64(3)	97.72(3)	98.01(3)	98.30(3)
β (°)	108.09(3)	101.27(3)	101.29(3)	101.21(3)
γ (°)	106.50(3)	114.33(3)	114.13(3)	114.17(3)
V (Å^3)	884.6(3)	998.9(3)	982.9(3)	981.3(3)
Z	1	1	1	1
$\rho_{calcd.}$ (g·cm^{-3})	3.171	2.902	2.983	2.999
μ (mm^{-1})	5.350	4.888	5.133	5.305
T (K)	173(2)	213(2)	173(2)	173(2)
2θ Range	$4.22 \le 2\theta \le 62.68$	$8.84 \le 2\theta \le 52.30$	$3.70 \le 2\theta \le 63.08$	$3.70 \le 2\theta \le 62.98$
Index range	$-13 \le h \le 13$	$-11 \le h \le 11$	$-13 \le h \le 13$	$-13 \le h \le 13$
	$-14 \le k \le 14$	$-12 \le k \le 12$	$-14 \le k \le 14$	$-14 \le k \le 14$
	$-15 \le l \le 15$	$-14 \le l \le 14$	$-16 \le l \le 16$	$-16 \le l \le 16$
Reflections collected	10455	7260	11723	11718
Independent reflections	5309 [R(int) = 0.0321]	3640 [R(int) = 0.0818]	5917 [R(int) = 0.0342]	5882 [R(int) = 0.0291]
Parameters	232	260	268	268
R_1[a] [$I > 2\sigma(I)$]	0.0313	0.0387	0.0328	0.0307
wR_2[b] [$I > 2\sigma(I)$]	0.0827	0.1079	0.0827	0.0746
R_1[a] (all data)	0.0334	0.0430	0.0373	0.0354
wR_2[b] (all data)	0.0839	0.1111	0.0846	0.0763
GooF[c] on F_0^2	1.131	1.068	1.042	1.045
Weighting scheme[b]	a = 0.0393; b = 0.3916	a = 0.0523; b = 4.6743	a = 0.0362; b = 1.0403	a = 0.0300; b = 1.9405
$(\Delta/\rho)_{max.}$ (e$^-$/Å^3)	1.440	1.745	1.660	1.242
$(\Delta/\rho)_{min.}$ (e$^-$/Å^3)	−2.592	−2.190	−2.255	−1.358

[a] $R_1 = \Sigma \, | \, |F_{obsd.}| - |F_{calcd.}| \, | / \Sigma \, |F_{obsd.}|$. [b] $wR_2 = \{\Sigma \, [w(F_{obsd.}^2 - F_{calcd.}^2)^2] / \Sigma \, [w(F_{obsd.}^2)^2]\}^{1/2}$. $w = 1/[\sigma^2(F_{obsd.}^2) + (aP)^2 + bP]$; with $P = [\max.(F_{obsd.}^2, 0) + 2F_{calcd.}^2]/3$. [c] goof = $[\Sigma w(F_{obsd.}^2 - F_{calcd.}^2)^2/(n - p)]^{1/2}$, n = number of reflections, p = parameters used.

 © 2004 Wiley-VCH Verlag GmbH & Co. KGaA, Weinheim

Syntheses of Heteropolymolybdates: All starting materials and chemicals were used without further purification.

Preparation of $\{[La(H_2O)_6]_2(TeMo_6O_{24})\}_n \cdot 6nH_2O$ (1): K_2MoO_4 (1 g, 4.2 mmol) was dissolved in 30 mL of water, to which telluric acid (0.160 g, 0.7 mmol), dissolved in 10 mL of water, was added. The pH was adjusted to 5.5 by adding 4 M hydrochloric acid. The colorless solution was heated to 80 °C and stirred for 30 min. $La(NO_3)_3 \cdot 6H_2O$ (0.303 g, 0.7 mmol) was dissolved in 4 mL of water and added slowly to the hot solution while stirring. After 15 minutes, the solution was filtered. Colorless single crystals suitable for X-ray diffraction were obtained from the solution after two days. $La_2TeMo_6O_{42}H_{36}$ (1689.34). Yield: 340 mg (57%, based on La). IR (KBr disc, cm^{-1}): $\tilde{\nu}$ = 3434 vs (br), 3245 s (br), 1638 s, 1454 w, 1385 w, 1120 w, 941 s, 914 s, 893 s, 869 m, 679 s, 614 s, 446 s. EDX: found (calcd.) for $La_2TeMo_6O_{42}H_{36}$: La:Te:Mo = 1.95:0.97:6.00 (2.00:1.00:6.00).

Preparation of $\{[Ce(H_2O)_7]_2(TeMo_6O_{24})\}_n \cdot 7nH_2O$ (2): This compound was prepared similarly to **1**, with $CeCl_3 \cdot 7H_2O$ (0.261 g, 0.7 mmol) instead of $La(NO_3)_3 \cdot 6H_2O$. Yellow single crystals were obtained from the solution after two days. $Ce_2TeMo_6O_{45}H_{42}$ (1745.81). Yield: 349 mg (57%, based on Ce). IR (KBr disc, cm^{-1}): $\tilde{\nu}$ = 3444 vs (br), 3164 s, 1636 s, 1384 w, 942 s, 918 s, 890 s, 665 s, 614 m, 494 s, 449 s. EDX: found (calcd.) for $Ce_2TeMo_6O_{45}H_{42}$: Ce:Te:Mo = 1.88:0.93:6.00 (2.00:1.00:6.00).

Preparation of $\{[Pr(H_2O)_7]_2(TeMo_6O_{24})\}_n \cdot 8nH_2O$ (3): This compound was prepared similarly to **1**, with $Pr(NO_3)_3 \cdot 6H_2O$ (0.305 g, 0.7 mmol) instead of $La(NO_3)_3 \cdot 6H_2O$. Green single crystals suitable for X-ray diffraction were obtained from the solution after two days. $Pr_2TeMo_6O_{46}H_{44}$ (1765.41). Yield: 362 mg (58%, based on Pr). IR (KBr disc, cm^{-1}): $\tilde{\nu}$ = 3437 vs (br), 3167 s, 1634 s, 1385 s, 940 s, 914 s, 872 s, 668 s, 614 s, 492 m, 449 m. EDX: found (calcd.) for $Pr_2TeMo_6O_{46}H_{44}$: Pr:Te:Mo = 2.10:0.93:6.00 (2.00:1.00:6.00).

Preparation of $\{[Nd(H_2O)_7]_2(TeMo_6O_{24})\}_n \cdot 8nH_2O$ (4): This compound was prepared similarly to **1**, with $NdCl_3 \cdot 6H_2O$ (0.251 g, 0.7 mmol) instead of $La(NO_3)_3 \cdot 6H_2O$. After one day light pink single crystals suitable for X-ray diffraction were obtained from the solution. $Nd_2TeMo_6O_{46}H_{44}$ (1772.02). Yield: 297 mg (48%, based on Nd). IR (KBr disc, cm^{-1}): $\tilde{\nu}$ = 3386 vs (br), 1634 s, 1384 w, 942 s, 914 s, 870 m, 673 s, 614 s, 490 m, 448 s. EDX: found (calcd.) for $Nd_2TeMo_6O_{46}H_{44}$: Nd:Te:Mo = 1.88:1.03:6.00 (2.00:1.00:6.00).

Further details on the crystal structure investigations may be obtained from the Fachinformationzentrum Karlsruhe, 76344 Eggenstein-Leopoldhafen, Germany [Fax: (internat.) +49-7247-808666; E-mail: crysdata@fiz-karlsruhe.de], on quoting the depository number CSD-414132 (for **1**), -414133 (for **2**), -414134 (for **3**) and -414135 (for **4**).

Acknowledgments

Support by the Deutsche Forschungsgemeinschaft, the Fonds der Chemischen Industrie, and the Bundesministerium für Bildung und Forschung is gratefully acknowledged.

[1] M. T. Pope, *Heteropoly and Isopoly Oxometalates*, Springer, Berlin, **1983**.
[2] *Polyoxometalate Chemistry: From Topology via Self-Assembly to Applications* (Eds.: M. T. Pope, A. Müller), Kluwer, Dordrecht, The Netherlands, **2001**.
[3] *Polyoxometalates: from Platonic Solids to Anti-Retroviral Activity* (Eds.: M. T. Pope, A. Müller), Kluwer, Dordrecht, The Netherlands, **1994**.
[4] M. T. Pope, A. Müller, *Angew. Chem.* **1991**, *103*, 56−70; *Angew. Chem. Int. Ed. Engl.* **1991**, *30*, 34−48.
[5] C. L. Hill, X. Zhang, *Nature* **1995**, *373*, 324−326.
[6] Y. Inouye, Y. Tokutake, T. Yoshida, A. Yamamoto, T. Yamase, S. Nakamura, *Chem. Pharm. Bull.* **1991**, *39*, 1638−1640.
[7] A. Müller, P. Kögerler, C. Kuhlmann, *Chem. Commun.* **1999**, 1347−1358.
[8] A. Müller, S. Q. N. Shah, H. Bögge, M. Schmidtmann, *Nature* **1999**, *397*, 48−50.
[9] A. Müller, E. Krickemeyer, H. Bögge, M. Schmidtmann, F. Peters, *Angew. Chem.* **1998**, *110*, 3567−3571; *Angew. Chem. Int. Ed.* **1998**, *37*, 3360−3363.
[10] A. Müller, S. Polarz, S. K. Das, E. Krickemeyer, H. Bögge, M. Schmidtmann, B. Hauptfleisch, *Angew. Chem.* **1999**, *111*, 3439−3443; *Angew. Chem. Int. Ed.* **1999**, *38*, 3241−3245.
[11] K. Burgemeister, D. Drewes, E. M. Limanski, I. Küper, B. Krebs, *Eur. J. Inorg. Chem.* **2004**, 2690−2694.
[12] H. Naruke, T. Ozeki, T. Yamase, *Acta Crystallogr., Sect. B* **1991**, *47*, 489−492.
[13] T. Ozeki, T. Yamase, *Acta Crystallogr., Sect. B* **1994**, *50*, 128−134.
[14] P. Mialane, L. Lisnard, A. Mallard, J. Marrot, E. Antic-Fidancev, P. Aschehoug, D. Vivien, F. Sécheresse, *Inorg. Chem.* **2003**, *42*, 2102−2108.
[15] D. Drewes, E. M. Limanski, B. Krebs, *Dalton Trans.* **2004**, 2087−2091.
[16] I. D. Brown, D. Altermatt, *Acta Crystallogr., Sect. B* **1985**, *41*, 244−247.
[17] A. Trzesowska, R. Kruszynski, T. J. Bartczak, *Acta Crystallogr., Sect. B* **2004**, *60*, 174−178.
[18] G. M. Sheldrick, *SHELXS-97*, University Göttingen **1997**.
[19] G. M. Sheldrick, *SHELXL-97*, University Göttingen **1997**.
[20] SADABS: Area-Detector Absorption Correction, Siemens Industrial Automation, Inc., Madison, WI, **1996**.
[21] Stoe IPDS Software, Version 2.75, Stoe & Cie GmbH, **1996**.

Received June 16, 2004
Early View Article
Published Online November 10, 2004

 © 2004 Wiley-VCH Verlag GmbH & Co. KGaA, Weinheim

Mechanistic Investigation of the Oxidation of Glyoxylic and Pyruvic Acids by Tris(biguanide)manganese(IV) in Weakly Acidic Aqueous Media

Basab Bijayi Dhar,[a] Ritam Mukherjee,[a] Subrata Mukhopadhyay,*[a] and Rupendranath Banerjee*[a]

Keywords: Kinetics / Mechanism / Redox reaction / Manganese(IV) / Glyoxylic acid / Pyruvic acid

In this study the kinetics of two electron transactions between the reducing substrates glyoxylic and pyruvic acids and the oxidising complex cation, tris(biguanide)manganese(IV) in aqueous acidic media have been examined. Under the experimental conditions (pH = 1.50–3.78) only the fully protonated form of the oxidant reacts with the anions of the substrates whereas the parent acids, viz. glyoxylic and pyruvic acids, were found to be unreactive. The second-order rate constants for the oxidations of glyoxylate and pyruvate by the title Mn^{IV} species are $(2.24 \pm 0.10) \times 10^{-1}$ and $(5.40 \pm 0.30) \times 10^{-2}$ $M^{-1}s^{-1}$, respectively, at 25.0 °C and at I = 1.0 M ($NaNO_3$ or $NaClO_4$). A rate-liming one-electron change between the redox partners seems justified.

(© Wiley-VCH Verlag GmbH & Co. KGaA, 69451 Weinheim, Germany, 2004)

Introduction

Tris(biguanide)manganese(IV) {Figure 1; $[Mn(LH_2)_3]^{4+}$ (LH_2 = biguanide, $C_2N_5H_7$)} is a rare example of a water-soluble mononuclear Mn^{IV} complex stable over a wide range of acidity levels (10^{-6} to 2 M).[1] In aqueous solutions the title Mn^{IV} complex behaves as a mild dibasic acid (pK_{a1} = 5.30 ± 0.20, pK_{a2} = 7.60 ± 0.30) and the deprotonations are believed to originate from the protons bound to the ligand sp^2 nitrogen atoms.[2] Though quite a few di-, tri- and tetranuclear Mn^{IV} complexes can be stabilised in aqueous solution[3] and have interesting solution chemistry,[4] the aqueous solution chemistry of mononuclear Mn^{IV} remained unexplored until recently when we reported[2] the oxidation of Fe^{2+} by Mn^{IV}. Parallel to our report, Gould et al.[5] observed that the oxidation of Fe^{2+} by this Mn^{IV} species is noticeably accelerated by chloride ions in what the authors viewed as the accelerating effect of the polarisable anion on the redox reaction between two positively charged metal centres.

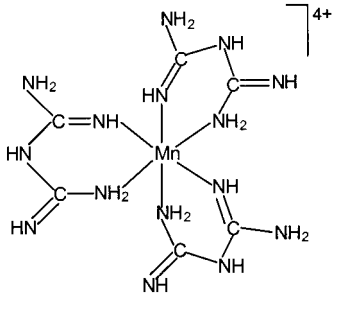

Figure 1. Structure of $[Mn(LH_2)_3]^{4+}$ drawn on the basis of its crystal structure

The present investigation deals with the kinetic and mechanistic aspects of the oxidation of two small carboxylic acids of biological relevance, viz. glyoxylic and pyruvic acid. Detailed kinetic studies of their oxidations are of importance because Mn^{III} species are involved in metabolic processes such as glycine catabolism[6a] and plant physiology,[6b] whereas the reducing substrate pyruvic acid is involved in a major metabolic sequence (TCA cycle) in living systems.[6c] Complete oxidation of these carboxylic acids with α-carbonyl groups ultimately leads to CO_2 with generation of energy in the metabolic processes. We also note that examples of oxidations of these substrates by higher valent oxidising species are only scarce in the literature.[7]

Results and Discussion

Equilibrium Studies and Preliminary Observations

Using a Metrohm 736 GP Titrino auto-titrator yielded pK_a values for glyoxylic and pyruvic acid from the pH-titration curves of 3.20 ± 0.10 and 2.50 ± 0.10, respectively, at 25.0 °C and at I = 1.0 M ($NaNO_3$ or $NaClO_4$). These values are in agreement with those previously reported.[7h,7i] Most of the kinetic runs were performed at 433 nm, i.e. the observed visible absorption maximum of the Mn^{IV} complex. At this wavelength, all other reaction components ex-

[a] Department of Chemistry, Jadavpur University, Calcutta 700032, India
E-mail: subrataju@vsnl.net

 © 2004 Wiley-VCH Verlag GmbH & Co. KGaA, Weinheim DOI: 10.1002/ejic.200400547

cept Mn^{IV} are transparent. No additional buffer was used in the kinetic experiments since the pH drift was well within 0.05 units during the reaction. We observed no Mn^{2+} catalysis (studied up to 0.10 M) in the title reaction.

Stoichiometry and Reaction Products

Results of the stoichiometry experiments yielded $\Delta[Mn^{IV}]/\Delta[\text{Reductant}] = 0.98 \pm 0.10$ for glyoxylic oxidation and 1.07 ± 0.05 for pyruvic acid oxidation. The presence of the oxidation product formic acid in the oxidation of glyoxylic acid was tested for by the addition of chromotropic acid which gave a violet colour.[8] Acetic acid was detected in the pyruvate oxidation by the addition of lanthanum nitrate and iodine which produced a deep blue precipitate.[8] We verified that the reaction products, Mn^{2+} or the released biguanide did not interfere with these qualitative experiments. The generation of gaseous CO_2 in both the reactions was confirmed by GC analysis as described earlier.[9] The overall redox processes for glyoxylic acid and pyruvic acid are thus described by Equation (1) and (2), respectively.

$$Mn^{IV} + CHOCOOH + H_2O \rightarrow Mn^{2+} + HCO_2H + CO_2 + 2\,H^+ \quad (1)$$

$$Mn^{IV} + CH_3COCOOH + H_2O \rightarrow Mn^{2+} + CH_3CO_2H + CO_2 + 2\,H^+ \quad (2)$$

The small amounts of evolved gas in these reactions did not interfere with the kinetic measurements. Iodometric determination of copper in the cupric biguanide which precipitated[10] from the solution indicated release of more than 90% biguanide.

Kinetics

No immediate spectroscopic change was observed on mixing either glyoxylic or pyruvic acid with the Mn^{IV} complex over the entire range of experimental pH values examined (1.50−3.78). The whole reaction course follows first-order kinetics and the $\log(A_t - A_\infty)$ versus time plots were found to be linear to more than three half-lives. In all the kinetic runs, A_∞ values were less than 0.01. The first-order rate constants, k_o, as described by Equation (3), were obtained from least-squares slopes of these plots and are presented in Table 1. Moreover, a tenfold variation in the initial $[Mn^{IV}]$ value (0.02−0.20 mM) resulted in no change in the k_o values within experimental uncertainty (± 5%).

$$-d[Mn^{IV}]/dt = k_o[Mn^{IV}] \quad (3)$$

Table 1. Some representative first-order rate constants for oxidation of glyoxylic and pyruvic acid by $[Mn(LH_2)_3]^{4+}$ at $T = 25.0$ °C, $I = 1.0$ M ($NaNO_3$), $\lambda = 433$ nm [concentration of complex used 0.10 mM; the k_o values calculated using Equation (7a) are given in parentheses]

pH	RCOCOOH [M]	$10^4 k_o$ (R = H) [s^{-1}]	$10^4 k_o$ (R = CH_3) [s^{-1}]
1.46	0.02	0.8 (0.79)	0.8 (0.79)
1.70		1.4 (1.37)	1.4 (1.30)
1.96		2.4 (2.43)	2.2 (2.16)
2.20		4.1 (4.06)	3.3 (3.28)
2.37		5.8 (5.76)[a]	4.3 (4.23)[b]
2.80		13 (12.7)[c]	6.8 (6.85)[c]
3.03		18 (18.1)	8.0 (8.06)
3.02		18 (18.1)[d]	8.2 (8.05)[d]
3.25		23 (23.7)[e]	8.9 (8.96)[e]
3.50		30 (30.3)	9.6 (9.66)
3.78		35 (35.4)	10 (10.2)
2.37	0.01	2.8 (2.88)	2.1 (2.11)
	0.03	8.7 (8.64)	6.3 (6.34)
	0.05	15 (14.4)	11 (10.6)

[a] $10^4\,k_o$ (R = H) [s^{-1}] values are 8.3 and 11 at $I = 0.5$ and 0.2 M ($NaNO_3$), respectively. [b] $10^4\,k_o$ (R = CH_3) [s^{-1}] values are 6.5 and 8.2 at $I = 0.5$ and 0.2 M ($NaNO_3$), respectively. [c] $10^4\,k_o$ [s^{-1}] values are 16 and 8.8 for glyoxylic and pyruvic acid, respectively, at $I = 1.0$ M ($LiClO_4$). [d] Reactions carried out in the presence of externally added 1.00 m M biguanide. [e] $10^4\,k_o$ [s^{-1}] values are 23 and 9.0 for glyoxylic and pyruvic acid, respectively, at $I = 1.0$ M (NaCl).

For both the reducing agents, the k_o values were found to increase significantly with the pH of the reaction medium (Table 1). The title Mn^{IV} complex is a weak acid ($pK_{a1} = 5.30$) and thus its deprotonation may be disregarded, whereas the concentration of both the neutral and anionic forms of the reducing agents are substantial under the pH interval studied (1.46−3.78).

The observed rate constants depend remarkably on the ionic strength of the reaction medium maintained by $NaNO_3$ or $NaClO_4$ (Table 1). A considerable increase in the reaction rate over the entire pH range for both the reductants with a decrease in ionic strength indicates a reaction between oppositely charged ions. The rate constants were also found to increase substantially when $LiClO_4$ was used instead of Na^+ salts for maintaining the ionic strength of the reaction mixture. As the redox partners of the title reactions are oppositely charged, conventional metal ion catalysis can be ruled out.[11] We also verified that the reactions are not accelerated by addition of chloride. A possible reason for the rate enhancement in the presence of Li^+ may be explained by the very high approximate hydration number of Li^+ (25.3), as estimated by transference data,[12] compared with that of Na^+ (16.6). This results in a major lowering of the effective concentration of solvent water which in turn increases the activity of the redox partners.[7h]

Reactions studied in the presence of 6% (v/v) acrylonitrile showed slow polymerisation after consumption of ca. 40−50% of the initial Mn^{IV} amount. The $\log(A_t - A_\infty)$ versus time plots under these conditions showed a definite up-

 © 2004 Wiley-VCH Verlag GmbH & Co. KGaA, Weinheim

ward curvature after ca. 50% completion of the reaction, probably due to heterogeneity in the reaction media. Polymerisation of acrylonitrile is more prominent in the case of glyoxylic acid than in that of pyruvic acid.

Scheme 1 provides a reasonable explanation for the kinetic observations considering the acid dissociation constants of the complex in aqueous solution (K_{a1} and K_{a2} are 5.01×10^{-6} and 2.50×10^{-8} M, respectively) and K_a values (i.e. the measured acid dissociation constants of glyoxylic and pyruvic acid under experimental condition, 6.31×10^{-4} M for glyoxylic and 3.16×10^{-3} M for pyruvic acid).

$$RCOCOOH \overset{K_a}{\rightleftharpoons} RCOCOO^- + H^+ \quad (4)$$

$$[Mn(LH_2)_3]^{4+} + RCOCOOH \xrightarrow{k_1} Products \quad (5)$$

$$[Mn(LH_2)_3]^{4+} + RCOCOO^- \xrightarrow{k_2} Products \quad (6)$$

(R = H for glyoxylic and CH_3 for pyruvic acid)

Scheme 1

Scheme 1 leads to the rate law of Equation (7), where $T_R = [RCOCOOH] + [RCOCOO^-]$.

$$k_o(K_a + [H^+])/T_R = k_1[H^+] + k_2K_a \quad (7)$$

The left-hand-side values of Equation (7) were found to be nearly a constant within allowable uncertainty in the entire pH range studied, both for glyoxylic [$(1.40 \pm 0.02) \times 10^{-4}$ s^{-1}] and pyruvic acid [$(1.60 \pm 0.06) \times 10^{-4}$ s^{-1}]. We thus found no contribution from k_1 for both the reducing agents to the overall rates. Equation (7) can thus be simplified to Equation (8).

$$T_R/k_o = 1/k_2 + [H^+]/(k_2K_a) \quad (8)$$

Plots of T_R/k_o versus $[H^+]$ yielded straight lines (Figure 2) with intercepts yielding k_2 values of $(2.24 \pm 0.10) \times 10^{-1}$ and $(5.40 \pm 0.30) \times 10^{-2}$ M^{-1}s^{-1} for glyoxylic and pyruvic acid, respectively. From the slopes, using such k_2 values, K_a values could be determined. These kinetically evaluated K_a values agree well (within 10%) with the literature values supporting the proposed reaction scheme.

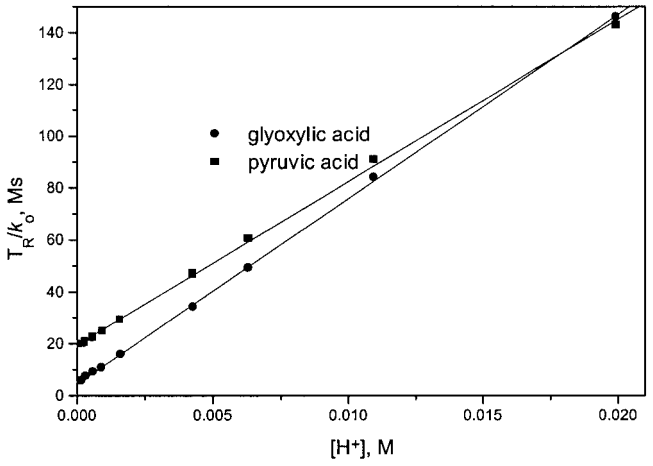

Figure 2. Plot of T_R/k_o versus $[H^+]$; [complex] = 0.10 mM, T_R = 0.02 M, I = 1.0 M ($NaNO_3$), T = 25.0 °C

Mechanism

The reducing anions glyoxylate and pyruvate have been found to be the only reactive species and this result supports the well-accepted concept that deprotonated reductants are more effective than their conjugate acids in reducing higher valent metal centres.[2,7h,9,13] However, we were astonished at the extent of this behaviour since we recently observed that both glyoxylic and pyruvic acids are reactive in reducing ethylenebis(biguanide)silver(III).[7h,7j] (One of the referees of this article commented that these reducing agents have inherent equilibria between the gem-diol and carbonyl forms in aqueous solution. Literature reports also support this.[7c] The reactivity of glyoxylate and pyruvate anions as found in this investigation is thus the combined reactivities of their gem-diol and carbonyl forms.)

The reduction of Mn^{IV} to Mn^{II} and the oxidation of the reductants chosen in this study are both net two-electron transactions. Nevertheless, it is extremely unlikely that the Mn^{IV} reduction proceeds in a single step. Moreover, polymerisation experiments also lend support to single-electron steps which generate polymerisation initiating radicals. Generation of these substrate radicals by one-electron oxidation has been well established by EPR spectroscopy.[14]

Pyruvate oxidation by the Mn^{IV} complex was found to be slower than glyoxylate oxidation. The increase in reaction rate may originate from the weaker C−C bond energy in glyoxylic acid compared with that in pyruvic acid due to the presence of an electron-donating methyl group in pyruvic acid which increases the electron density at the carbonyl carbon atom. The weakening of the C−C bond in glyoxylic acid may be a driving force for a faster initial electron transfer leading to a quicker overall oxidation of glyoxylic acid.[7g] A similar explanation was also offered for the oxidation of these reducing agents by Cr^{VI} [7g] and ethylenebis(biguanide)silver(III).[7h,7j] Moreover, the presence of a strongly reducing aldehyde function in glyoxylic acid may also be another explanation, at least in part, for obtaining a higher rate.

The Mn^{IV} centre in the title complex is coordinatively saturated and thus replacement of the strong field chelating biguanide ligand by the substrate anions seems to be unlikely. The estimated maximum value for the pre-equilibrium formation of a 1:1 adduct between Mn^{IV} and $RCOCOO^-$ (R = H for glyoxylate and CH_3 for pyruvate) lies between 1 and 10 and this does not confirm a strong inner-sphere attachment. However, we note that among the three s^2 metal-ion centres studied for the reduction of Mn^{IV}, only the reaction of In^I with $[Mn(LH_2)_3]^{4+}$ is subject to kinetic saturation for which an association constant of 6×10^3 M^{-1} for the formation of this adduct (believed to be due to strong hydrogen bonding) was estimated by Gould et al.[5] The estimated low value for the formation of adducts in the present study may be due to electrostriction[15] or a

 © 2004 Wiley-VCH Verlag GmbH & Co. KGaA, Weinheim

process aided by hydrogen bonding[16] involving the reductants and the NH or NH_2 fragments of the ligand biguanide moiety of the title complex. The presence of a strong chelating ligand can be expected to stabilise Mn^{IV} to a great extent and render the complex a mild oxidant. Cyclic voltammetric studies of an aqueous solution (deoxygenated by purging with nitrogen) of the Mn^{IV} complex (0.10 mM) in the presence of 0.1 M Et_4NClO_4 as a supporting electrolyte revealed a single irreversible wave corresponding to Mn^{IV}/Mn^{III} reduction at ca. 0.4 V versus Ag/AgCl (ΔE_p = 400 ± 50 mV depending on scan rate, 50−300 mV s^{-1}). A direct outer-sphere oxidation by this weakly oxidising Mn^{IV} may thus be eliminated. We observed that more than 90% of the biguanide ligand is released at the end of the reaction (tested using an ammoniacal $CuSO_4$ solution)[10] and the high protonation constants of biguanide[17] encourages the overall reactions to completion.

Experimental Section

Materials: The complex salt $[Mn(C_2N_5H_7)_3]_2SO_4(NO_3)_6{\cdot}3H_2O$ was prepared by a known procedure. The crystals obtained were sufficiently pure as indicated by satisfactory C, H, N analyses: $C_{12}H_{48}Mn_2N_{36}O_{25}S$ (1238): calcd. C 11.63, H 3.88, N 40.71; found C 11.3, H 3.9, N 39.9. Biguanide sulfate $[C_2N_5H_7{\cdot}H_2SO_4]$ was prepared by a known method reported previously.[10b] An aqueous solution of glyoxylic acid was prepared by dissolving solid glyoxylic acid monohydrate (98%, Lancaster) in water and this was standardised either with standard alkali using Weslow's indicator or by spectrophotometry[18] at 520 nm (ε = 17990 $M^{-1}cm^{-1}$ as estimated by us, in agreement with the literature value of 17870 $M^{-1}cm^{-1}$)[18] after converting glyoxylic acid to 1,5-diphenylformazancarboxylic acid. Both results agree well with each other (within 4%). We found that an aqueous solution of ca. 0.5 M glyoxylic acid is stable for at least one weak when kept at low temperature (ca. 5−10 °C) and in the dark. Pyruvic acid (98%, Sigma) was used and standardised using spectrophotometry[19] at 515 nm (ε = 1400 $M^{-1}{\cdot}cm^{-1}$). An aqueous solution of $NaNO_3$ or $NaClO_4$ (G. R., E. Merck) was standardised by passing through a Dowex 50 W X-8 strong cation exchange resin in the H^+ from and titrating the liberated acid with standard NaOH to a phenolphthalein end point. All other chemicals were of reagent grade. Most of the kinetic measurements were carried out at I = 1.0 M ($NaNO_3$ or $NaClO_4$ resulted in almost the same k_o values). All solutions were prepared in water which had been deionised and doubly distilled.

Equilibrium Measurements: The acid dissociation constants, K_a, of both the glyoxylic[7h] and pyruvic acids were determined by titrating several aliquots of different strengths with carbonate-free deoxygenated NaOH solution at 1.0 M $NaNO_3$ using a Titrino Autotitrator (Metrohm, 736 GP) at (25.0 ± 0.1) °C.

Physical Measurements and Kinetics: All absorbance versus time data were recorded with a Shimadzu (1601 PC) spectrophotometer using 1.00-cm quartz cells. The kinetics were monitored in situ in the "kinetic mode" of the instrument at 433 nm which is one of the absorption peaks of the Mn^{IV} complex. An electrically controlled thermostat (25 ± 0.1) °C cell housing (CPS-240) was employed. For faster reactions, the reductant solution (adjusted to the desired pH) was injected directly into the spectrophotometer cell containing other components of the reaction mixture kept at the same pH. The desired concentrations of the complex and the reducing agent were achieved after mixing. The solution pH values were adjusted with HNO_3 or NaOH. Solution pH values ranged from 1.52 to 3.78 and were measured with an Ag/AgCl combined glass electrode attached to a Metrohm 736 GP Titrino autotitrator. The electrode calibration was carried out as reported previously.[20] Production of CO_2 as the gaseous reaction product was qualitatively confirmed by GC analysis. The gaseous product formed during the reaction was analysed by gas chromatography using a Chemito (India) GCHT 8610 instrument equipped with TCD (a Porapak Q and molecular sieves 13X column). A splitless mode of injection of 500 μL of the sample was used. The oven, injector, and detector temperatures were kept at 50, 100 and 150 °C, respectively. The carrier hydrogen gas flow was adjusted to 30 mL·min^{-1}. Cyclic voltammetric studies were performed with an Electrochemical Analyser (Model 600A, CH Instruments, USA) using a three-component electrode system consisting of Pt wire working and auxiliary electrodes and an Ag/AgCl reference electrode.

Stoichiometry and Reaction Products: The stoichiometries were evaluated by estimating unchanged glyoxylic or pyruvic acid spectrophotometrically. Reaction mixtures containing an excess of 4−6 equiv. of glyoxylic or pyruvic acid relative to the title complex were allowed to react under nitrogen until the solutions turned colourless. To estimate the unspent glyoxylic acid[18] freshly prepared phenylhydrazine hydrochloride (1%) solution was added (3.0 mL) into the reaction mixture. The resultant solution was incubated at ca. 110 °C for 10 min and then cooled to room temperature (ca. 25 °C) followed by successive addition of 2.5-mL aliquots of concentrated HCl and 1% $K_3Fe(CN)_6$. The reaction mixtures were allowed to stand for ca. 5 min for the quantitative formation of a pink formazan derivative of glyoxylic acid which was analysed at 520 nm (ε = 17990 $M^{-1}cm^{-1}$).[18] To estimate unchanged pyruvic acid[19] freshly prepared 2,4-dinitrophenylhydrazine solution in MeOH (1 mL, 1%) and 0.1 M HCl (1 mL) were added to the reaction mixture along with K-phosphate (K_2HPO_4) buffer (0.1 M) of pH = 7.5. The resultant solution was incubated at ca. 80 °C for 10 min and then cooled in an ice box for 10 min. A 50% KOH solution (5 mL) was then added to the solution which was again incubated at room temperature for 10 min. The red colour of the 2,4-dinitrophenylhydrazone pyruvate derivative was then analysed at 515 nm (1400 $M^{-1}{\cdot}cm^{-1}$).[19] The biguanide ligand in the product solution was isolated as $[Cu(LH_2)_2]SO_4$ by the addition of Cu^{II} sulfate. The amount of Cu^{II} thus consumed was determined iodometrically after decomposing the copper complex.[10]

Acknowledgments

The award of a junior research fellowship to B. B. D. by the University Grants Commission, New Delhi is gratefully acknowledged. S. M. acknowledges the Council of Scientific and Industrial Research, New Delhi, for funding.

[1] [1a] G. Das, P. K. Bharadwaj, D. Ghosh, B. Chaudhuri, R. Banerjee, *Chem. Commun.* **2001**, 323−324; see also the Addendum, *Chem. Commun.* **2002**, 2278. [1b] L.-P. Lu, M.-L. Zhu, P. Yang, *Acta Crystallogr., Sect. B* **2004**, *60*, m18−m20.
[2] B. B. Dhar, R. Mukherjee, S. Mukhopadhyay, R. Banerjee, *Eur. J. Inorg. Chem.* **2004**, 2950−2955.
[3] [3a] K. R. Reddy, M. V. Rajasekharan, S. Padhye, F. Dahan, J. P. Tuchagues, *Inorg. Chem.* **1994**, *33*, 428−433. [3b] K. R. Reddy, M. V. Rajasekharan, N. Arulsamy, D. J. Hodgson, *Inorg. Chem.* **1996**, *35*, 2283−2286. [3c] K. Wieghardt, *Angew. Chem. Int. Ed. Engl.* **1994**, *33*, 725−728. [3d] H. J. Mok, J. A. Davis, S. Pal, S. K. Mandal, W. H. Armstrong, *Inorg. Chim.*

 © 2004 Wiley-VCH Verlag GmbH & Co. KGaA, Weinheim

Acta **1997**, *263*, 385−394. [3e] C. E. Dube, D. W. Wright, S. Pal, P. J. Bonitatebus, Jr., W. H. Armstrong, *J. Am. Chem. Soc.* **1998**, *120*, 3704−3716. [3f] S. Mukhopadhyay, R. J. Staples, W. H. Armstrong, *Chem. Commun.* **2002**, 864−865.

[4] [4a] A. K. Bhattyacharya, A. B. Mondal, R. Banerjee, *J. Chem. Soc., Dalton Trans.* **1997**, 2351−2355. [4b] B. Mondal, S. Kundu, R. Banerjee, *J. Chem. Soc., Dalton Trans.* **1997**, 4341−4344. [4c] S. Banerjee, U. Roy Choudhury, R. Banerjee, S. Mukhopadhyay, *Dalton Trans.* **2002**, 2047−2052. [4d] B. Mondal, A. K. Bhattyacharya, R. Banerjee, *Polyhedron* **2000**, *19*, 1213−1218. [4e] D. Maji, P. K. Das, R. Banerjee, *Transition Met. Chem.* **2002**, *27*, 80−84. [4f] U. R. Choudhury, S. Banerjee, R. Banerjee, *Transition Met. Chem.* **2002**, *27*, 42−46. [4g] D. Maji, R. Banerjee, *Transition Met. Chem.* **2001**, *26*, 544−550. [4h] U. R. Choudhury, S. Banerjee, R. Banerjee, *J. Chem. Soc., Dalton Trans.* **2000**, 589−592.

[5] O. A. Babich, E. S. Gould, *Inorg. Chem.* **2004**, *43*, 1779−1783.

[6] [6a] A. White, *Principles of Biochemistry*, 2nd ed., McGraw-Hill, New York, **1954**, p. 548. [6b] E. H. Rodd, *Chemistry of Carbon Compounds*, Elsevier, Amsterdam, **1952**, part B, vol. 1, p. 850. [6c] E. S. G. Barron, *Trends in physiology and Biochemistry*, Academic Press, New York, **1952**, p. 471.

[7] [7a] W. J. Albery, R. P. Bell, A. L. Powel, *Trans. Farad. Soc.* **1965**, *61*, 1194. [7b] P. Manikyamba, *React. Kinet. Catal. Lett.* **2003**, *78*, 169−173. [7c] L. Maros, I. Molnar-Perl, L. Kover, *J. Chem. Soc., Perkin Trans. 2.* **1976**, 1337−1342. [7d] K. K. Sengupta, *J. Indian Chem. Soc.* **1964**, *41*, 423. [7e] R. Banerjee, R. Das, A. K. Chakraborty, *J. Chem. Soc., Dalton Trans.* **1990**, 3277−3281. [7f] K. K. Sengupta, H. R. Chatterjee, *Inorg. Chem.* **1978**, *17*, 2429−2431. [7g] K. K. Sengupta, T. Sarkar, *Tetrahedron* **1975**, *31*, 123−127. [7h] A. Das, S. Mukhopadhyay, *Polyhedron* **2004**, *23*, 895−901. [7i] A. E. Martel, R. Smith, *Critical Stability Constants*, Plenum Press, New York, **1977**, vol. 3, p. 66. [7j] A. Das, S. Mukhopadhyay, *Transition Met. Chem.*, in press.

[8] F. Feigl, *Spot Tests in Organic Analysis*, 5th ed., Elsevier, London, **1956**, p. 331, 332.

[9] P. Bandopadhyay, B. B. Dhar, J. Bhattacharyya, S. Mukhopadhyay, *Eur. J. Inorg. Chem.* **2003**, 4308−4312.

[10] [10a] B. Rathke, *Ber. Dtsch. Chem. Ges.* **1879**, *12*, 774. [10b] P. Ray, *Chem. Rev.* **1961**, *61*, 314−359. [10c] R. Banerjee, K. Das, A. Das, S. Dasgupta, *Inorg. Chem.* **1989**, *28*, 585−588.

[11] M. Gupta, S. K. Saha, P. Banerjee, *J. Chem. Soc., Perkin Trans. 2.* **1988**, 1781−1785.

[12] F. A. Cotton, G. Wilkinson, C. A. Murillo, M. Bochmann, *Advanced Inorganic Chemistry*, 6th ed., Wiley, New York, **1999**, chapter 3, p. 102.

[13] P. Bandopadhyay, S. Mukhopadhyay, *Polyhedron* **2002**, *21*, 1893−1898.

[14] B. Neumann, O. Steinbock, S. C. Muller, N. S. Dalal, *J. Phys. Chem.* **1996**, *100*, 12342−12348.

[15] [15a] M. G. Evans, G. H. Nancollas, *Trans. Farad. Soc.* **1953**, *49*, 363−366. [15b] C. Postmus, E. L. King, *J. Phys. Chem.* **1955**, *59*, 1208−1211. [15c] F. Basolo, R. G. Pearson, *Mechanisms of Inorganic Reactions*, 2nd ed., Wiley, New York, **1967**, p. 34. [15d] M. Grant, R. B. Jordan, *Inorg. Chem.* **1981**, *20*, 55−59.

[16] [16a] C. D. Hubbard, A. Gerhard, R. van Eldik, *J. Chem. Soc., Dalton Trans.* **2001**, 1069−1073. [16b] M. C. Ghosh, J. W. Reed, R. N. Bose, E. S. Gould, *Inorg. Chem.* **1994**, *33*, 73−78.

[17] L. Fabbrizzi, M. Micheloni, P. Paoletti, G. Schwarzenbach, *J. Am. Chem. Soc.* **1977**, *99*, 5574−5579.

[18] D. N. Kramer, N. Klein, R. A. Baselice, *Anal. Chem.* **1959**, *30*, 250−252.

[19] S. Takenaka, S. Murakami, R. Shinke, K. Aoki, *Arch. Microbiol.* **1998**, *170*, 132−137.

[20] S. Banerjee, U. R. Choudhury, B. C. Ray, R. Banerjee, S. Mukhopadhyay, *Anal. Lett.* **2001**, *34*, 2797−2815.

Received June 22, 2004
Early View Article
Published Online October 21, 2004

 © 2004 Wiley-VCH Verlag GmbH & Co. KGaA, Weinheim

Diastereomeric Halfsandwich Rhenium Complexes Containing Hemilabile Phosphane Ligands[‡]

Stefan Dilsky[a] and Wolfdieter A. Schenk*[a]

Dedicated to Professor Johann Weis on the occasion of his 60th birthday

Keywords: Rhenium / Chiral complexes / Chiral P ligands / Hemilabile P ligands / Sandwich complexes

The syntheses and some typical reactions of diastereomeric rhenium complexes $[CpRe(NO)(CO)\{P(Ph)(R)(R')\}]BF_4$ (R = Me, Ph; R′ = 2-C_6H_4OMe, $CH_2C_4H_3S$, $CH_2C_4H_7O$) (**3a**–**e**) are described. Reduction of the carbonyl ligand with $NaBH_4$ in THF gave the corresponding methyl complexes $[CpRe(NO)\{P(Ph)(R)(R')\}(CH_3)]$ (**4a**–**e**). Acid treatment of the methyl complexes leads to liberation of methane and coordination of the additional donor site of the potentially bidentate phosphane ligand. Of the chelate complexes **5a**–**e**, those with R′ = 2-C_6H_4OMe (**5a**, **d**) decomposed in solution at room temperature. In donor solvents, the chelate ring opens giving the stable solvated complexes $[CpRe(NO)\{P(Ph)(R)(R')\}](solvent)]BF_4$ (solvent = CH_3CN, THF) (**6b**–**e**, **7d**). The new compounds are thus suitable starting materials for the syntheses of diastereomeric rhenium complexes $[CpRe(NO)\{P(Ph)(R)(R')\}(L)]BF_4$.
(© Wiley-VCH Verlag GmbH & Co. KGaA, 69451 Weinheim, Germany, 2004)

Introduction

Since the first successful enantiomer separation of the pseudotetrahedral *at-metal* chiral complex $[CpMn(CO)(NO)(PPh_3)]PF_6$ by Brunner,[1] a large variety of different *at-metal* chiral, kinetically stable or labile complexes has been synthesised. Some of them have been of synthetic interest, e.g. (R_{Fe})-$[CpFe(CO)(PPh_3)\{C(O)Me\}]$ which has been used, inter alia, in the total synthesis of Captopril.[2,3] Other complexes of this type were investigated as potential catalysts[2] and the chiral Lewis acidic rhenium complex $[CpRe(NO)(PPh_3)]^+$ has been studied in great detail by Gladysz et al.[4,5] We have recently extended this work to thiolate and thioaldehyde complexes of $[CpRe(NO)(PPh_3)]^+$ and its congeners $[CpRe(NO)\{P(OPh)_3\}]^+$ and $[CpRe(NO)\{P(iPr)_3\}]^+$.[6–9] By introducing a second stereogenic centre at the phosphane ligand, higher selectivities in reactions at coordinated ligands might be achieved. Moreover, by introducing a second donor atom into the phosphane, a hemilabile[10,11] ligand can be created which should serve to stabilise reactive intermediates.

Results

Phosphane Synthesis

The hemilabile ligands which are central to this study are shown in Scheme 1.

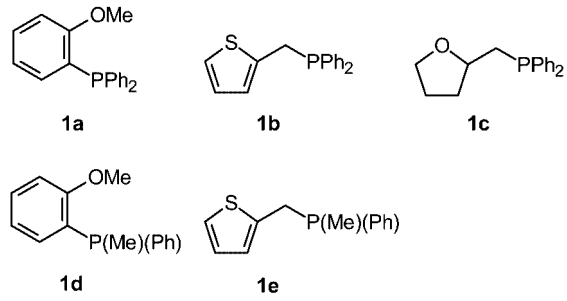

Scheme 1

The prototypic **1a** is commercially available, whereas **1b** was obtained by a slight modification of a known[12] synthesis as follows. Cleavage of PPh_3 with lithium in THF and alkylation of the resultant lithium diphenylphosphide with 2-(chloromethyl)thiophene gave **1b** in 87% yield. *C*-chiral racemic **1c** has been obtained previously via a similar approach.[13] Cleavage of bis(2-anisyl)phenylphosphane with sodium in liquid ammonia followed by alkylation with methyl iodide gave the *P*-chiral racemic ether phosphane ligand **1d**[14] in 63% yield. Deprotonation of methylphenylphosphane with butyllithium in THF followed by alky-

[‡] Enantioselective Organic Syntheses with Chiral Transition Metal Complexes, 13. For part 12 see: G. Bringmann, A. Wuzik, J. Kümmel, W. A. Schenk, *Organometallics* **2001**, *20*, 1692–1694.

[a] Institut für Anorganische Chemie der Universität Würzburg, Am Hubland, 97074 Würzburg, Germany
Fax: (internat.) + 49-931-8884605
E-mail: wolfdieter.schenk@mail.uni-wuerzburg.de

lation with 2-(chloromethyl)thiophene gave *P*-chiral **1e** (73%).

The phosphanes **1a**, **1b** and **1d** are colourless solids which are readily soluble in most organic solvents. They can be recrystallised from alcohols or saturated hydrocarbons and may be handled in air for short periods of time. Compound **1c** had been reported as a waxy solid, whereas the phosphane **1e** is a colourless, air-sensitive oil with an unpleasant odour. The ^{31}P NMR signals are shifted to high field as the number of alkyl substituents increases. The methylene group of **1e** can be observed as an ABX system with $^{2}J_{H,H} = 14.4$ Hz and $^{2}J_{P,H} = 3.6$ Hz.

Crystal and Molecular Structure of 1b·BH_3

Compound **1b** was converted into its borane adduct by treatment with BH_3·SMe_2 in THF. Recrystallisation from ethanol/hexane gave crystals suitable for a single-crystal X-ray structure determination (Figure 1).

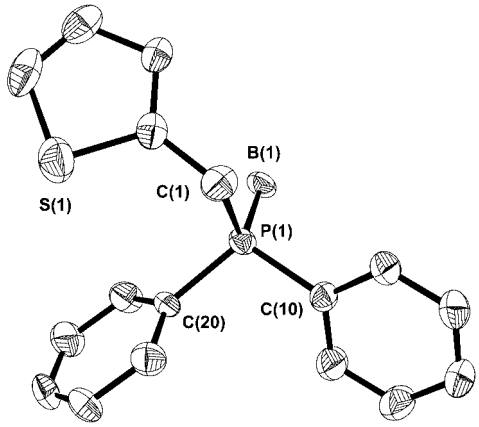

Figure 1. Molecular structure of $PPh_2(CH_2C_4H_3S)$·BH_3 (**1b**·BH_3), hydrogen atoms omitted for clarity. Space group $Pna2_1$; selected distances [pm] and angles (°) (standard deviations in parentheses): P(1)−B(1) 190.4(4), P(1)−C(1) 182.9(3), P(1)−C(10) 181.2(3), P(1)−C(20) 180.6(3); C(1)−P(1)−B(1) 111.98(19), C(10)−P(1)−B(1) 110.52(17), C(20)−P(1)−B(1) 117.02(17), C(1)−P(1)−C(10) 105.82(16), C(1)−P(1)−C(20) 104.13(17), C(10)−P(1)−C(20) 106.58(15)

As expected, the BH_3 group is bound to phosphorus rather than to the sulfur atom of the thiophene moiety. The P−B and P−C bond lengths are in agreement with those of similar borane adducts.[15,16] The angles at the tetrahedral phosphorus atom are slightly distorted reflecting the low electronegativity of the BH_3 substituent.

Carbonyl Complexes

The chiral racemic rhenium complex $[CpRe(CO)(NO)(NCCH_3)]BF_4$ (**2**) was the common starting material for the following syntheses and is readily accessible from $[Re_2(CO)_{10}]$ in three steps.[4] The acetonitrile ligand is known to be easily replaceable by phosphanes[7,17,18] and this methodology was also successful with the phosphanes **1a**−**e** [Equation (1)].

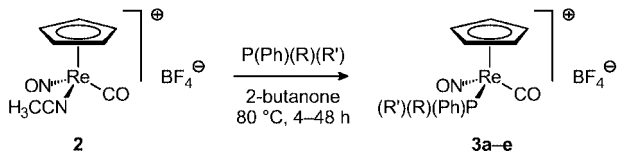

(1)

R \ R'	2-C_6H_4OMe	$CH_2C_4H_3S$	$CH_2C_4H_7O$
Ph	**3a** (85%)	**3b** (83%)	**3c** (95%)
Me	**3d** (62%)	**3e** (76%)	

Compounds **3d** and **3e** were obtained as 1:1 mixtures of diastereoisomers, i.e. Re−P bond formation proceeds without diastereoselectivity. All new complexes $[CpRe(CO)(NO)(PR_3)]BF_4$ (**3a**−**e**) are yellow to yellow-brown air-stable solids (e.g. **3d** melts in air without decomposition). While **3c** is soluble in THF, **3b** and **3d** are insoluble in THF and **3e** is insoluble even in acetone. Due to the stereogenic metal centre, the PCH_2-protons in **3b** can be observed as an ABX system with $^{2}J_{H,H} = 15$ Hz and $^{2}J_{P,H} = 10$ Hz. Diastereomeric **3e** exhibits two such sets of signals. The ^{31}P NMR signals are shifted 25 to 30 ppm downfield compared with the free ligand. The CO and NO stretching frequencies appear in the ranges expected for cationic complexes of this kind.

Crystal and Molecular Structures of 3a, 3b and 3d−AlF_4

Three of the new complexes were investigated by X-ray diffraction. Figure 2−4 show views of the cations.

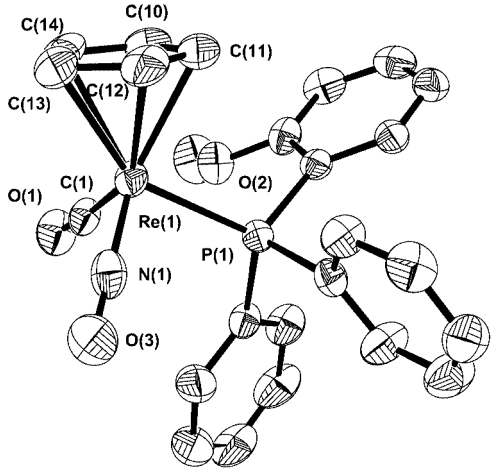

Figure 2. Structure of the cation of $[CpRe(CO)(NO)\{PPh_2(2\text{-}C_6H_4OMe)\}]BF_4$ (**3a**), hydrogen atoms omitted for clarity. Space group $P2_1/c$; selected distances [pm] and angles (°) (standard deviations in parentheses): Re(1)−C(10) 228.2(7), Re(1)−C(11) 229.7(6), Re(1)−C(12) 231.8(6), Re(1)−C(13) 229.9(6), Re(1)−C(14) 229.9(7), Re(1)−C(1) 191.6(6), Re(1)−N(1) 180.1(6), Re(1)−P(1) 239.26(14); Re(1)−C(1)−O(1) 175.1(6), Re(1)−N(1)−O(3) 178.8(5), N(1)−Re(1)−C(1) 97.2(3), P(1)−Re(1)−N(1) 91.37(17), P(1)−Re(1)−C(1) 88.32(18)

Due to the similar sizes of the CO and NO ligands these two groups are usually disordered.[19] Since the extent of this disorder is variable, the apparent Re−C and Re−N bond lengths can vary from their normal values as in **3a** to

 © 2004 Wiley-VCH Verlag GmbH & Co. KGaA, Weinheim

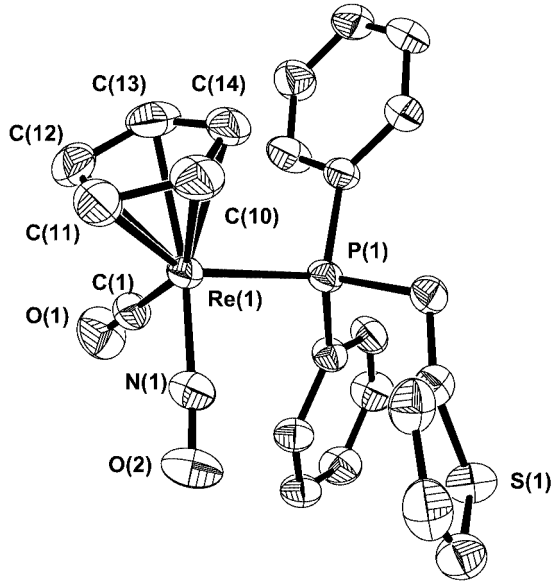

Figure 3. Structure of the cation of [CpRe(CO)(NO){PPh_2-($CH_2C_4H_3S$)}]BF_4 (**3b**), hydrogen atoms omitted for clarity. Space group $P\bar{1}$; selected distances [pm] and angles (°) (standard deviations in parentheses): Re(1)−C(10) 231.4(5), Re(1)−C(11) 227.8(6), Re(1)−C(12) 227.1(6), Re(1)−C(13) 228.1(6), Re(1)−C(14) 231.5(5), Re(1)−C(1) 188.4(5), Re(1)−N(1) 182.6(4), Re(1)−P(1) 239.05(12); Re(1)−C(1)−O(1) 179.7(5), Re(1)−N(1)−O(2) 175.7(4), N(1)−Re(1)−C(1) 92.4(2), P(1)−Re(1)−N(1) 95.56(14), P(1)−Re(1)−C(1) 89.70(16)

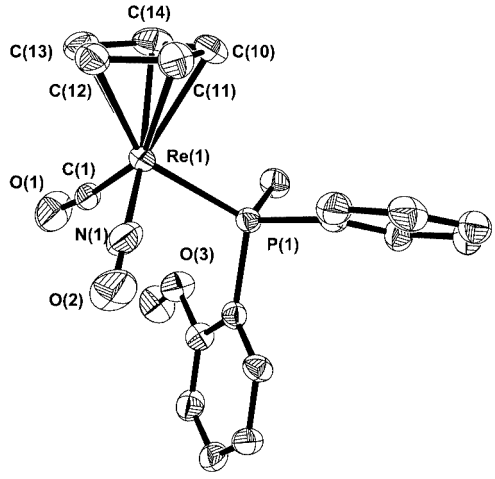

Figure 4. Structure of the cation of [CpRe(CO)(NO){P(Ph)(Me)(2-C_6H_4OMe)}]AlF_4 (**3d-AlF$_4$**), hydrogen atoms omitted for clarity. Space group $P2_1/n$; selected distances [pm] and angles (°) (standard deviations in parentheses): Re(1)−C(10) 231.7(7), Re(1)−C(11) 229.3(7), Re(1)−C(12) 227.7(7), Re(1)−C(13) 229.4(7), Re(1)−C(14) 227.5(7), Re(1)−C(1) 186.2(6), Re(1)−N(1) 183.3(7), Re(1)−P(1) 239.65(17); Re(1)−C(1)−O(1) 173.1(7), Re(1)−N(1)−O(2)−176.3(8), N(1)−Re(1)−C(1) 95.8(3), P(1)−Re(1)−N(1) 89.6(2), P(1)−Re(1)−C(1) 91.1(2)

almost equal values as in **3d**. The topological similarity of the CO and NO ligands also thwarted any attempts to separate the diastereoisomers of **3c**−**e** by crystallisation. Moreover, the disorder makes it impossible to determine the relative configuration of the cation of **3d**−**AlF$_4$**.

Neither the NO ligands are bent nor are the cyclopentadienyl ligands slipped in any of the three structures. The rhenium atoms are octahedrally surrounded with the cyclopentadienyl ligand serving as a six-electron donor. In **3a** and **3d**−**AlF$_4$**, the N(1)−Re(1)−C(1) angles are significantly larger [97.2(3)° and 95.8(3)°, respectively] than in **3b** [92.4(2)°]. As the structure of the prototypic $[CpRe(CO)(NO)(PPh_3)]^+$ reveals the same widened N(1)−Re(1)−C(1) angle [95.5(5)°],[20] we have to conclude that the angle in **3b** is abnormally small. This is surprising since the phosphorus ligands of this study all have similar steric and electronic properties.

The surprising appearance of AlF_4^- as a counterion in the structure of **3d**−**AlF$_4$** was traced back to an impurity in the $[NO]BF_4$ which was used in the synthesis of [CpRe-(CO)(NO)($NCCH_3$)]BF_4 (**2**).

Methyl Complexes

The hydride reduction of a Re−CO group has already been described by Gladysz,[4,17] Casey,[21] Graham[22] and our group.[7] The new methyl complexes **4a**−**e** were obtained in the same way in good yields as orange or orange-red solids [Equation (2)].

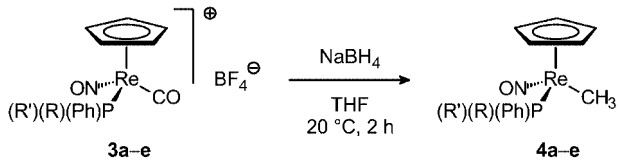

(2)

R \ R'	2-C_6H_4OMe	$CH_2C_4H_3S$	$CH_2C_4H_7O$
Ph	**4a** (87%)	**4b** (75%)	**4c** (82%)
Me	**4d** (82%)	**4e** (81%)	

Complexes **4a**−**e** are readily soluble in common organic solvents except aliphatic hydrocarbons. This again makes a separation of the diastereomeric complexes **4c**−**e** difficult. Nevertheless, a diastereomeric excess of 35% was achieved during the workup of **4e**. This helped in the assignment of the spectroscopic data of the two diastereoisomers. Characteristic spectroscopic features for all methyl complexes are the low frequency of the NO stretching vibration and the high-field shift of the Re−CH_3 resonance in ^{13}C NMR spectroscopy. Furthermore, the phosphorus resonances are shifted downfield compared with those of the cationic starting materials.

Crystal and Molecular Structure of 4d

Crystals of the *unlike* isomer (R_{Re},S_P/S_{Re},R_P)-**4d** suitable for X-ray diffraction were grown at −30 °C by layering a toluene solution of the diastereomeric mixture with petroleum ether. A comparison of this structure with those of similar alkyl complexes (e.g. [CpRe(NO){P(*i*Pr)$_3$}(CH_3)][7]

 © 2004 Wiley-VCH Verlag GmbH & Co. KGaA, Weinheim

and [CpRe(NO)(PPh_3)(CH_2Ph)][23]) did not reveal any significant differences (Figure 5).

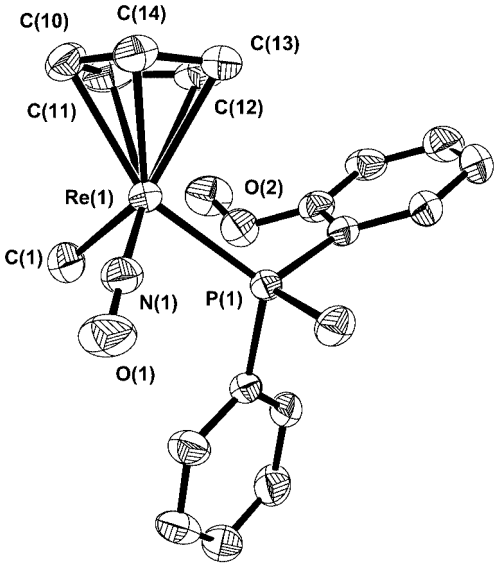

Figure 5. Molecular structure of (R_{Re},S_P/S_{Re},R_P) [CpRe(NO){P(Ph)(Me)(2-C_6H_4OMe)}(CH_3)] (**4d**), hydrogen atoms omitted for clarity. Space group *P*1; selected distances [pm] and angles (°) (standard deviations in parentheses): Re(1)−C(10) 228.4(4), Re(1)−C(11) 234.0(4), Re(1)−C(12) 233.6(4), Re(1)−C(13) 225.7(4), Re(1)−C(14) 222.8(4), Re(1)−C(1) 214.1(4), Re(1)−N(1) 175.6(3), Re(1)−P(1) 234.30(9); Re(1)−N(1)−O(1) 177.9(3), N(1)−Re(1)−C(1) 95.55(18), P(1)−Re(1)−N(1) 88.89(11), P(1)−Re(1)−C(1) 90.24(12)

The P(1)−Re(1) bond in **4d** is 3 pm shorter than in [CpRe(NO){P(*i*Pr)$_3$}(CH_3)] and even 2 pm shorter than in [CpRe(NO)(PPh_3)(CH_2Ph)], reflecting the smaller size of the phosphane ligand. Moreover, the C(1)−Re(1) distance is remarkably shorter [214.1(4) pm] than in [CpRe(NO){P(*i*Pr)$_3$}(CH_3)] [218.2(5)].[7] The cyclopentadienyl ligand is slightly slipped such that the two carbon atoms which are approximately *trans* to the strongly π-accepting NO ligand have moved about 8 pm away from the rhenium atom. As in [CpRe(NO){P(*i*Pr)$_3$}(CH_3)] and [CpRe(NO)(PPh_3)(CH_2Ph)], the N(1)−Re(1)−C(1) angle is widened [95.55(18)°], although the NO and CH_3 ligands are the smallest substituents.

Chelate Ring Closure

It is known that methylrhenium complexes liberate methane when treated with acids.[5,24,25] In the absence of donors, the solvent dichloromethane stabilises the resultant 16 valence electron complex. The CH_2Cl_2 complex thus obtained served as a starting material for a variety of compounds,[5] although it tends to undergo side reactions[6,26] and to decompose above −20 °C.[24,26] The phosphane ligands in this study offer donor functionalities (e.g. oxygen or sulfur), which should serve to stabilise the complex by intramolecular coordination. When the methyl complexes were treated with HBF_4 in dichloromethane, three complexes with chelate structures could be isolated, namely **5b**, **5c** and **5e** [Equation (3)].

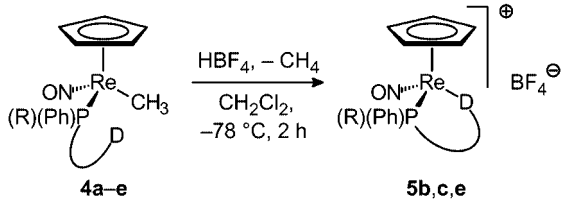

(3)

R \ D	2-C_6H_4OMe	$CH_2C_4H_3S$	$CH_2C_4H_7O$
Ph	dec	**5b** (86%)	**5c** (99%)
Me	dec	**5e** (91%)	

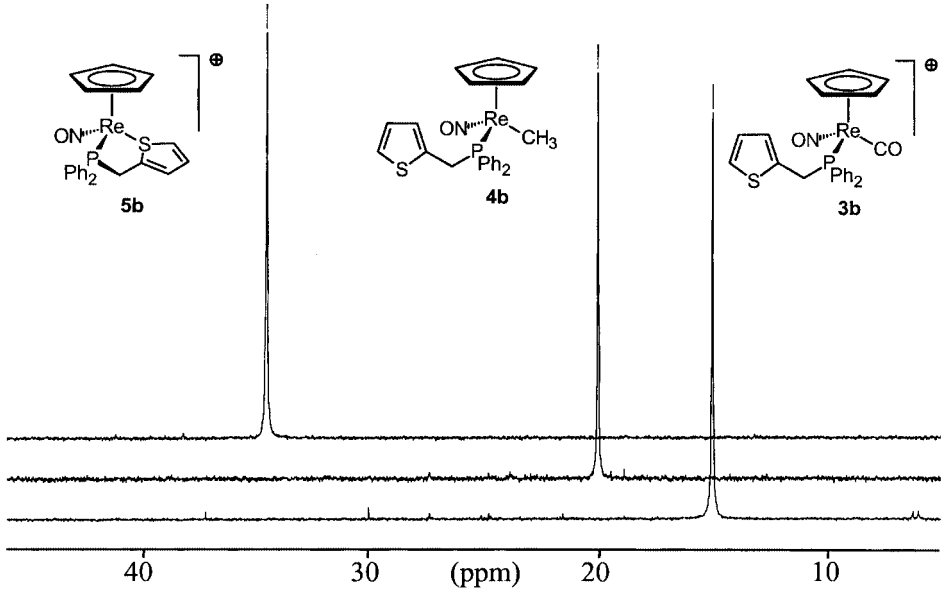

Figure 6. ^{31}P NMR spectra of the complexes [CpRe(NO){PPh_2($CH_2C_4H_3S$)}(X)]Y; X = CO, Y = BF_4 **3b**, X = CH_3, Y = −**4b**, X = −, Y = BF_4 **5b**

 © 2004 Wiley-VCH Verlag GmbH & Co. KGaA, Weinheim

Attempts to obtain ring-closed products from the anisyl-substituted phosphane complexes **4a** and **4d** were only partially successful (see below). Two different samples of **4e** with 0 and 34% *de*, respectively, were employed in this reaction in order to gain some insight into the stereochemistry of the demethylation step. In both cases the *de* was retained in the product **5e**.

Although no crystals suitable for X-ray diffraction could be grown, the ring closure can be unambiguously inferred from ^{31}P NMR spectroscopic data. It is known that in chelate complexes the phosphorus chemical shift depends on the ring size. For five-membered rings, an additional 20−30 ppm downfield shift is typical.[27,28] The ^{31}P NMR spectra of **5b**, **5c** and **5e** exhibit this feature, an example is shown in Figure 6. The NO stretching frequency was found in the typical range for cationic ether[29] or thioether[6,30,31] complexes of the general formula $[CpRe(NO)(PR_3)(L)]^+$. All other spectroscopic data are also in agreement with a cationic structure.

The reaction of **4d** with HBF_4 was investigated by low-temperature NMR spectroscopy. The phosphorus spectrum at −50 °C shows, aside from the expected downfield signals of two diastereomeric ring-closed complexes, a second pair of signals belonging to a cationic, ring-opened complex. Raising the temperature to 20 °C led to a decrease of the downfield signals and an increase of the upfield signals. Continued measurements at 20 °C revealed a slow decrease of both signal sets and, after 24 h, none of the signals could be observed any more. This can be interpreted in terms of a low stability of the ring-closed complex. At temperatures around −30 °C, there seems to be an equilibrium between ring-closed and ring-opened species, were the dichloromethane solvent acts as a ligand. The dichloromethane complex slowly decomposes at temperatures above −20 °C and is removed from the equilibrium which eventually leads to complete decomposition (Scheme 2). Nevertheless, this process is slowed down by the hemilabile ligand, compared with the rapid decomposition of $[CpRe(NO)(PPh_3)(ClCH_2Cl)]BF_4$.[24]

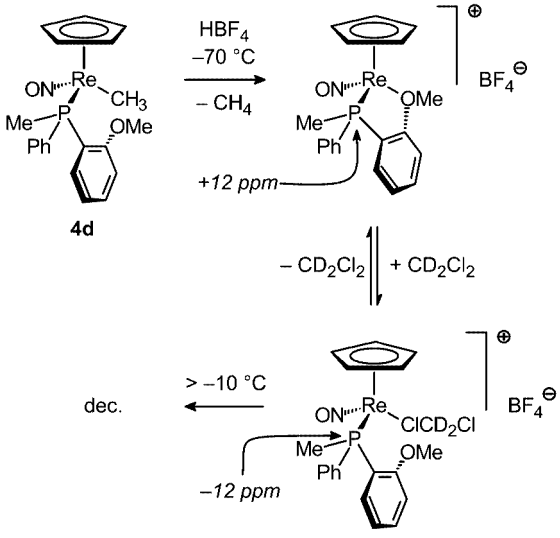

Scheme 2

Stabilitiy of the Ring-Closed Complexes and Preparation of Solvated Complexes

In the acid-promoted ring closure reactions of **5c** and **5e**, no diastereoselectivity was observed thus so far ruling out the possibility of a kinetic diastereoisomeric enrichment. If the diastereomeric complexes differ in energy, a thermodynamic enrichment might be possible. To check this, complexes **5b**, **5c** and **5e** were dissolved in polar solvents (e.g. THF, acetone or acetonitrile at 20 °C or reflux) and the mixtures analysed by ^{31}P NMR spectroscopy. While the acetone solutions did not show any enrichment or decomposition even after being heated to reflux for 24 h, a small diastereomeric enrichment was observed for **5e** in THF. Due to the different solubility of the diastereomers, only a suspension of **5e** in THF could be obtained with one diastereomer preferentially dissolved. The extraction of **5e** with THF led to a *de* of 60%, allowing the assignment of the spectroscopic data to the respective isomers. Upon dissolving the complexes in acetonitrile, new upfield signals in the ^{31}P NMR spectra appeared immediately. After 4 h, only the upfield signals remained. NMR and IR spectroscopic analyses suggested a ring-opening with the acetonitrile occupying the vacated coordination site as shown for **6b**, **6c** and **6e** [Equation (4)].

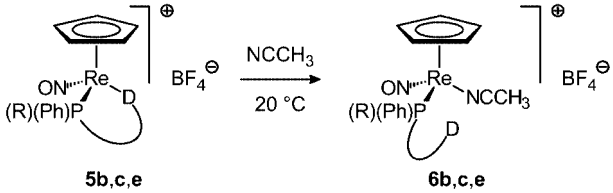

(4)

R \ D	$CH_2C_4H_3S$	$CH_2C_4H_7O$
Ph	**6b** (90%)	**6c** (82%)
Me	**6e** (93%)	

Crystal and Molecular Structure of 6e

The compositions of the acetonitrile complexes were corroborated by X-ray crystallography. Suitable crystals of the *unlike* diastereomer (R_{Re},S_P/S_{Re},R_P)-$[CpRe(NO)\{P(Ph)(Me)(CH_2C_4H_3S)\}(NCCH_3)]BF_4$ (**6e**) were obtained at 20 °C by layering a THF solution of the diastereomeric mixture with hexane. Figure 7 shows a view of the cation.

 © 2004 Wiley-VCH Verlag GmbH & Co. KGaA, Weinheim

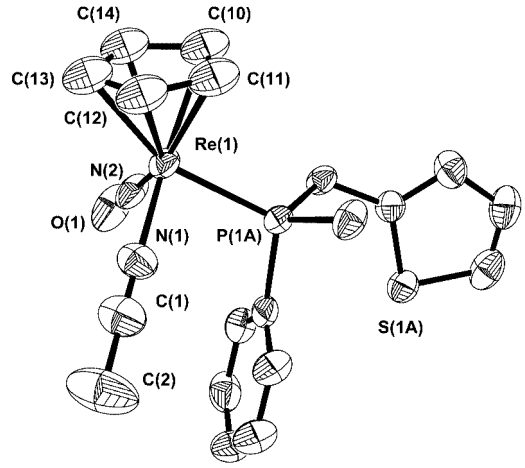

Figure 7. Structure of the cation of (R_{Re},S_P/S_{Re},R_P)-[CpRe(NO){P(Ph)(Me)($CH_2C_4H_3S$)}($NCCH_3$)]BF_4 (**6e**), hydrogen atoms omitted for clarity. Space group $P2_1/c$; selected distances [pm] and angles (°) (standard deviations in parentheses): Re(1)−C(10) 222.3(8), Re(1)−C(11) 228.3(8), Re(1)−C(12) 231.9(8), Re(1)−C(13) 226.9(7), Re(1)−C(14) 221.6(8), Re(1)−N(1) 205.5(6), Re(1)−N(2) 176.0(6), Re(1)−P(1A) 236.3(2); Re(1)−N(2)−O(1) 178.9(5), Re(1)−N(1)−C(1) 176.9(6), N(1)−C(1)−C(2) 178.6(8), N(1)−Re(1)−N(2) 96.9(2), P(1A)−Re(1)−N(1) 85.03(17), P(1A)−Re(1)−N(2) 92.86(18)

The cyclopentadienyl moiety is again slightly slipped such that the two carbon atoms *trans* to the NO ligand have moved away from the rhenium atom. The nitrosyl and nitrile ligands are perfectly linear and the N(1)−Re(1)−N(2) angle is in the typical range. This is somewhat in contrast to the structure of (S_{Re},S_C)-[CpRe(NO)(PPh_3){NCCH-(Ph)CH_2CH_3}]PF_6 where a significantly bent nitrile ligand and a widened N(1)−Re(1)−N(2) angle were observed.[32]

The refinement of the structure of **6e** indicated some disorder which revealed the presence, in the crystal, of ca. 10% of the *like* isomer. This is related to the predominating *unlike* isomer through a reflection of the phosphane ligand at a mirror plane which bisects the N(1)−Re(1)−N(2) angle and passes through the centre of the cyclopentadienyl ring, the rhenium atom and two carbon atoms of the thiophene ring (Figure 8).

Treatment of the methyl complex **4d** with HBF_4 either in a mixture of dichloromethane and acetonitrile or in pure THF gave the cationic solvated complexes **6d** and **7d** without any decomposition. Complex **7d** could be isolated with a *de* of 30% [Equation (5)].

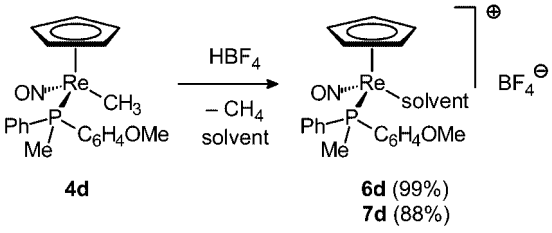

(5)

solvent = CH_3CN (**6d**), THF (**7d**)

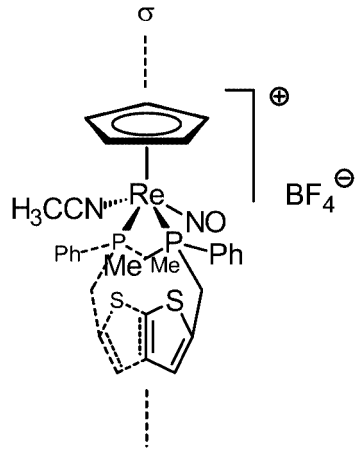

Figure 8. Disorder in the structure of *unlike*-**6e**; the phosphane ligand is reflected along an imaginary mirror plane which contains the Cp centre, the rhenium atom and two carbon atoms of the thiophene moiety giving rise to the *like* diastereoisomer

Crystal and Molecular Structure of 7d

The structure of the *like* isomer of the THF complex **7d** was determined by X-ray diffraction. Figure 9 shows the cation.

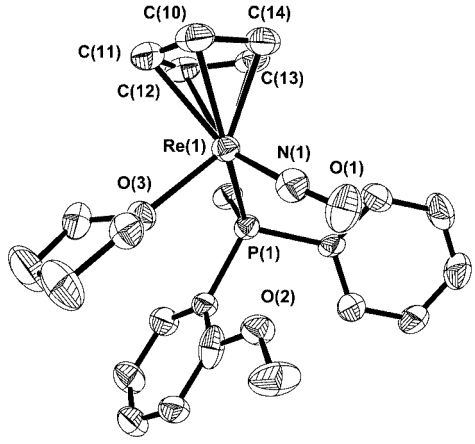

Figure 9. Structure of the cation of (S_{Re},S_P/R_{Re},R_P)-[CpRe(NO){P(Ph)(Me)(2-C_6H_4OMe)}(THF)]BF_4 (**7d**), hydrogen atoms omitted for clarity. Space group $P2_1/c$; selected distances [pm] and angles (°) (standard deviations in parentheses): Re(1)−C(10) 228.9(8), Re(1)−C(11) 235.0(8), Re(1)−C(12) 230.6(8), Re(1)−C(13) 220.8(7), Re(1)−C(14) 217.7(8), Re(1)−N(1) 174.9(7), Re(1)−O(3) 214.6(5), Re(1)−P(1) 238.64(18); Re(1)−N(1)−O(1) 176.0(7), N(1)−Re(1)−O(3) 96.9(3), P(1)−Re(1)−N(1) 90.8(2), P(1)−Re(1)−O(3) 87.60(14)

As for the methyl complex **4d** and the acetonitrile complex **6e** the cyclopentadienyl ligand is slipped, the difference between the longest and the shortest Re−C distances being 17 pm. Once again, the angle between the smallest ligands THF and NO is widened [96.9(3)°]. Since this widening has been observed for all N−Re−X angles in all structures discussed herein, the origin of this distortion must be electronic in nature.

 © 2004 Wiley-VCH Verlag GmbH & Co. KGaA, Weinheim

All acetonitrile complexes were isolated in high yields as yellow or brown solids. Except for [CpRe(NO){P(Ph)(Me)($CH_2C_4H_7O$)}($NCCH_3$)]BF_4 (**6c**), the compounds are stable in acetone and even in dichloromethane solution, whereas **6c** decomposes rapidly in both solvents.

The formation of the THF complex **7d** deserves some comment. It implies that the superior donor ability of THF compared with the aryl methoxy group overrides the entropy effect of the five-membered chelate ring.

Discussion

It was the goal of this work to prepare diastereomeric rhenium complexes which contain stereogenic centres both at the metal and the phosphane ligand. Furthermore, the phosphanes bear a donor function (e.g. oxygen or sulfur) to allow intramolecular stabilisation of reactive intermediates. Five such hemilabile phosphanes were investigated. Adapting published methods, the phosphanes could be coordinated successfully to the rhenium complexes.

The phosphanes **1a** and **1d** which contain an *ortho*-anisyl group as a potential donor did not give stable chelate complexes. Although low temperature NMR experiments revealed that at −50 °C the intramolecularly stabilised complex [CpRe(NO){P(Ph)(Me)(2-C_6H_4OMe)}]BF_4 (**5d**) is formed, the ring opens at temperatures above −30 °C giving rise to another cationic complex, probably the dichloromethane adduct which itself decomposes at temperatures above −10 °C. The oxygen of the anisyl group is even less efficient as a donor than THF. On the other hand, ring closure was observed with the phosphanes **1b**, **1c** and **1e**. In these cases, neither THF nor acetone are strong enough donors to break the Re−O or Re−S bonds, while acetonitrile opens the rings irreversibly. As yet, no complete separation of the diastereoisomers could be achieved either during the formation of the ring-closed complexes or by fractional crystallisation (except for **4e**, **5e** and **7d**). On the other hand, once a sample enriched in one diastereomer is employed, then the degree of enrichment is carried over to the next step. This is in line with earlier observations that substitution reactions at half-sandwich complexes of rhenium proceed with retention of configuration.[33,34]

Conclusions

Diastereomeric rhenium complexes containing a stereogenic metal centre and a chiral phosphane ligand are readily accessible. Furthermore, if the phosphanes contain a second donor atom, e.g. oxygen or sulfur, chelate ring closure can occur. The stability of the chelate ring can be tuned by an appropriate choice of donor function. Further modifications of the system are necessary to give access to diastereomerically pure complexes.

Experimental Section

All experiments were carried out in Schlenk tubes under nitrogen using suitably purified solvents. IR: Bruker IFS 25. ^{1}H NMR: Bruker AMX 400, Jeol JNM-LA 300, δ values relative to TMS. ^{13}C NMR: Bruker AMX 400, Jeol JNM-LA 300, δ values relative to TMS, assignments were routinely checked by DEPT procedures. In some cases the ^{13}C NMR signals of quaternary carbon atoms were too weak to be detected. The ^{1}H and ^{13}C NMR signals of the phenyl groups attached to phosphorus are very similar for all compounds and have therefore been omitted from the lists of spectroscopic data. ^{31}P NMR: Bruker AMX 400, Jeol JNM-LA 300, δ values relative to 85% H_3PO_4. Elemental analyses: Analytical Laboratory of the Institut für Anorganische Chemie. BF_4^- salts occasionally give low carbon values due to trace formation of fluorocarbon compounds which escape detection. GC-MS: Fisons Instruments Trio-1000. The following starting materials were obtained as described in the literature: 2-(chloromethyl)thiophene,[35] $PPh_2(CH_2C_4H_7O)$ (**1c**),[13] $PPh(2\text{-}C_6H_4OMe)_2$,[36] PPh(Me)(H)[37] and [CpRe(CO)(NO)($NCCH_3$)]BF_4 (**2**).[4] All other reagents were used as purchased.

$PPh_2(CH_2C_4H_3S)$ (1b): This compound has been obtained previously via Li reduction of Ph_2PCl.[12] However, no yields or physical data were given. We found the following synthesis to be more convenient. A solution of $LiPPh_2$, prepared from PPh_3 (8.00 g, 30.5 mmol) and excess lithium in THF (50 mL), was treated with NH_4Cl (1.45 g, 27.1 mmol) to quench LiPh. Freshly distilled 2-(chloromethyl)thiophene (5.00 g, 37.7 mmol) was added dropwise to the red solution at 20 °C. After stirring for 1 h at 20 °C, water (15 mL) was added. The organic layer was separated, the aqueous phase extracted four times with diethyl ether (50 mL) and the combined organic phases dried with $MgSO_4$. The solvent was removed under vacuum and the colourless residue purified by recrystallisation from methanol or by column chromatography over silica (20 cm, petroleum ether/diethyl ether, 1:2). Yield 7.50 g (87%), white solid, m.p. 50 °C. ^{1}H NMR (400 MHz, $CDCl_3$, 20 °C): δ = 3.53 (s, br, 2 H, PCH_2), 6.60 (m, 1 H, thiophene *H*), 6.74 (m, 1 H, thiophene *H*), 6.96 (m, 1 H, thiophene *H*) ppm. ^{13}C NMR (100 MHz, $CDCl_3$, 20 °C): δ = 30.0 (d, $^1J_{P,C}$ = 15 Hz, P*C*H_2), 123.7 (d, $^4J_{P,C}$ = 3 Hz, thiophene *C*H), 125.7 (d, $^3J_{P,C}$ = 7 Hz, thiophene *C*H), 126.8 (d, $^4J_{P,C}$ = 1 Hz, thiophene *C*H), 139.8 (d, $^2J_{P,C}$ = 11 Hz, PCH_2*C*) ppm. ^{31}P NMR (162 MHz, $CDCl_3$, 20 °C): δ = −10.7 (s) ppm. $C_{17}H_{15}PS$ (282.35): calcd. C 72.32, H 5.35, S 11.36; found C 72.10, H 5.54, S 10.87.

P(Me)(Ph)(2-C_6H_4OMe) (1d): The preparation of **1d** starting from $PPh(2\text{-}C_6H_4OMe)_2$ was briefly mentioned in the literature, but no details were given.[14] To a solution of sodium (4.00 g, 174 mmol) in liquid ammonia (400 mL) was added $PPh(2\text{-}C_6H_4OMe)_2$ (28.0 g, 86.9 mmol) and the mixture kept at −78 °C for 6 h. NH_4Cl (4.50 g, 84.1 mmol) was then added followed by the dropwise addition of MeI (6.00 mL, 13.7 g, 96.5 mmol). The ammonia was evaporated overnight, the remaining pasty solid was washed twice with water (50 mL) and distilled (kugelrohr, oven temperature 180 °C). The colourless distillate solidified upon cooling to 20 °C. Yield 12.5 g (63%) (ref.[14] 56%), white solid, m.p. 46 °C (ref.[38] 46−47 °C). The NMR spectroscopic data were consistent with those given in ref.[38].

P(Ph)(Me)($CH_2C_4H_3S$) (1e): P(Ph)(Me)(H) (2.52 g, 20.3 mmol) was dissolved in THF (10 mL) and deprotonated with BuLi (8.5 mL 2.5 M, 21.3 mmol) at −78 °C. The orange solution thus obtained was slowly added to a cooled (−78 °C) solution of freshly distilled 2-(chloromethyl)thiophene (2.69 g, 20.3 mmol) in THF (10 mL). The mixture was warmed to 20 °C overnight, water (3 mL) was added, the organic layer was separated and the aqueous layer extracted three times with diethyl ether (20 mL). The combined extracts were dried with $MgSO_4$, the solvent removed and the residue distilled under vacuum. Yield 3.26 g (73%), colourless

 © 2004 Wiley-VCH Verlag GmbH & Co. KGaA, Weinheim

oil, b.p. 100−113 °C/0.1 mbar. ^{1}H NMR (400 MHz, C_6D_6, 20 °C): δ = 1.03 (d, $^2J_{P,H}$ = 4.1 Hz, 3 H, PCH_3), 2.88, 3.00 (ABX system, $^2J_{H,H}$ = 14.4, $^2J_{P,H}$ = 3.6 Hz, 2 H, PCH_2), 6.51 (m, 1 H, thiophene *H*), 6.65 (m, 1 H, thiophene *H*), 6.73 (m, 1 H, thiophene *H*) ppm. ^{13}C NMR (100 MHz, C_6D_6, 20 °C): δ = 10.7 (d, $^1J_{P,C}$ = 17 Hz, P*C*H$_3$), 32.3 (d, $^1J_{P,C}$ = 17 Hz, P*C*H$_2$), 123.5 (d, $^4J_{P,C}$ = 3 Hz, thiophene *C*H), 125.4 (d, $^3J_{P,C}$ = 6 Hz, thiophene *C*H), 126.9 (d, $^4J_{P,C}$ = 1 Hz, thiophene *C*H), 140.2 (d, $^2J_{P,C}$ = 6 Hz, PCH$_2$*C*). ^{31}P NMR (162 MHz, C_6D_6, 20 °C): δ = −29.9 (s) ppm. MS: *m*/*z* (%) = 222 (1) [^{34}S-M$^+$], 221 (3) [M + H]$^+$, 220 (25) [M$^+$], 219 (11) [M − H]$^+$, 97 (100) [$CH_2C_4H_3S^+$]. $C_{12}H_{13}PS$ (220.27).

[CpRe(CO)(NO)(PPh$_2$(2-C$_6$H$_4$OMe))]BF$_4$ (3a): A solution of acetonitrile complex **2** (500 mg, 1.14 mmol) and phosphane **1a** (500 mg, 1.71 mmol) in 2-butanone (10 mL) was heated to reflux for 48 h. Acetone (10 mL) was added, the mixture filtered through silica gel and the silica layer washed twice with acetone (10 mL). The combined filtrate was evaporated to dryness and the residue recrystallised from acetone/diethyl ether. Yield 665 mg (85%), yellow-brown crystalline solid, m.p. 199 °C (dec.). ^{1}H NMR (400 MHz, CD_2Cl_2, 20 °C): δ = 3.74 (s, 3 H, OCH_3), 5.79 (s, 5 H, C_5H_5) ppm. ^{13}C NMR (100 MHz, CD_2Cl_2, 20 °C): δ = 56.1 (s, O*C*H$_3$), 94.7 (s, *C*$_5$H$_5$), 194.9 (d, $^2J_{P,C}$ = 10 Hz, *C*O) ppm. ^{31}P NMR (162 MHz, CD_2Cl_2, 20 °C): δ = 0.9 (s) ppm. IR (CH_2Cl_2): $\tilde{\nu}$ = 2029 (CO), 1763 (NO) cm^{-1}. $C_{25}H_{22}BF_4NO_3PRe$ (688.44): calcd. C 43.62, H 3.22, N 2.03; found C 44.03, H 3.48, N 2.00.

[CpRe(CO)(NO){PPh$_2$(CH$_2$C$_4$H$_3$S)}]BF$_4$ (3b): A solution of acetonitrile complex **2** (615 mg, 1.41 mmol) and phosphane **1b** (500 mg, 1.77 mmol) in 2-butanone (15 mL) was heated to reflux for 48 h. Acetone (10 mL) was added, the mixture filtered through silica gel and the silica layer washed twice with acetone (8 mL). The combined filtrate was evaporated to dryness and the residue recrystallised twice from dichloromethane/diethyl ether and finally washed with petroleum ether. Yield 840 mg (83%), yellow crystalline solid, m.p. 106 °C (dec.). ^{1}H NMR (400 MHz, CD_2Cl_2, 20 °C): δ = 4.41, 4.51 (ABX system, $^2J_{H,H}$ = 15.0 Hz, $^2J_{P,H}$ = 10.4 Hz, 2 H, PCH_2), 5.74 (s, 5 H, C_5H_5), 6.64 (m, 1 H, thiophene *H*), 6.87 (m, 1 H, thiophene *H*), 7.17 (m, 1 H, thiophene *H*) ppm. ^{13}C NMR (100 MHz, CD_2Cl_2, 20 °C): δ = 35.1 (d, $^1J_{P,C}$ = 35 Hz, P*C*H$_2$), 94.4 (s, *C*$_5$H$_5$), 126.9 (d, $^4J_{P,C}$ = 4 Hz, thiophene *C*H), 127.7 (d, $^4J_{P,C}$ = 3 Hz, thiophene *C*H), 129.7 (d, $^3J_{P,C}$ = 7 Hz, thiophene *C*H), 132.5 (d, $^2J_{P,C}$ = 6 Hz, PCH$_2$*C*), 194.7 (d, $^2J_{P,C}$ = 9 Hz, *C*O) ppm. ^{31}P NMR (162 MHz, CD_2Cl_2, 20 °C): δ = 14.6 (s) ppm. IR (CH_2Cl_2): $\tilde{\nu}$ = 2016 (CO), 1767 (NO) cm^{-1}. $C_{23}H_{20}BF_4NO_2PReS\cdot(C_2H_5)_2O$ (715.53): calcd. C 41.97, H 3.52, N 1.96, S 4.48; found C 41.47, H 3.30, N 1.96, S 4.57.

[CpRe(CO)(NO){PPh$_2$(CH$_2$C$_4$H$_7$O)}]BF$_4$ (3c): A solution of acetonitrile complex **2** (1.00 g, 2.29 mmol) and phosphane **1c** (0.88 g, 3.26 mmol) in 2-butanone (20 mL) was heated to reflux for 48 h. Acetone (20 mL) was added, the mixture filtered through silica gel and the silica layer washed twice with acetone (10 mL). The combined filtrate was evaporated to dryness and the residue washed with diethyl ether. Yield 1.45 g (95%), yellow crystalline solid, m.p. 156 °C (dec.). Both diastereomers: ^{1}H NMR (400 MHz, CD_2Cl_2, 20 °C): δ = 1.60−2.11 (m, 8 H, CH_2CH_2), 2.92−3.19 (m, 4 H, PCH_2), 3.53−3.85 (m, 6 H, CH_2OCH), 5.77 (d, $^3J_{P,H}$ = 0.4 Hz, 5 H, C_5H_5), 5.78 (d, $^3J_{P,H}$ = 0.4 Hz, 5 H, C_5H_5) ppm. ^{13}C NMR (100 MHz, CD_2Cl_2, 20 °C): δ = 25.1 (s, *C*H$_2$), 25.2 (s, *C*H$_2$), 33.5 (d, $^3J_{P,C}$ = 12 Hz, *C*H$_2$), 33.6 (d, $^3J_{P,C}$ = 12 Hz, *C*H$_2$), 37.9 (d, $^1J_{P,C}$ = 37 Hz, P*C*H$_2$), 38.3 (d, $^1J_{P,C}$ = 37 Hz, P*C*H$_2$), 68.3 (s, O*C*H$_2$), 68.4 (s, O*C*H$_2$), 74.2 (d, $^2J_{P,C}$ = 3 Hz, O*C*H), 74.5 (d, $^2J_{P,C}$ = 3 Hz, O*C*H), 94.3 (s, *C*$_5$H$_5$), 195.4 (d, $^2J_{P,C}$ = 8 Hz, *C*O), 195.5 (d, $^2J_{P,C}$ = 8 Hz, *C*O) ppm. ^{31}P NMR (162 MHz, CD_2Cl_2, 20 °C): δ = 2.6 (s) ppm. IR (CH_2Cl_2): $\tilde{\nu}$ = 2019 (CO), 1763 (NO) cm^{-1}. $C_{23}H_{24}BF_4NO_3PRe$ (666.43): calcd. C 41.45, H 3.63, N 2.10; found C 41.34, H 3.88, N 1.90.

[CpRe(CO)(NO){P(Ph)(Me)(2-C$_6$H$_4$OMe)}]BF$_4$ (3d): A solution of acetonitrile complex **2** (1.00 g, 2.29 mmol) and phosphane **1d** (1.00 g, 4.34 mmol) in 2-butanone (20 mL) was heated to reflux for 30 h. Acetone (20 mL) was added, the mixture filtered through silica gel and the silica layer washed twice with acetone (10 mL). The solvent was removed under vacuum and the oily residue dissolved in THF (10 mL). Upon stirring, a yellow solid separated which was collected by filtration and washed repeatedly with THF until the washings remained almost colourless. Yield 0.88 g (62%), bright yellow crystalline solid, m.p. 134 °C. Both diastereomers: ^{1}H NMR (400 MHz, CD_2Cl_2, 20 °C): δ = 2.46 (d, $^2J_{P,H}$ = 10.4 Hz, 3 H, PCH_3), 2.52 (d, $^2J_{P,H}$ = 10.4 Hz, 3 H, PCH_3), 3.73 (s, 3 H, OCH_3), 3.79 (s, 3 H, OCH_3), 5.82 (s, 10 H, C_5H_5) ppm. ^{13}C NMR (100 MHz, CD_2Cl_2, 20 °C): δ = 20.3 (d, $^1J_{P,C}$ = 42 Hz, P*C*H$_3$), 20.4 (d, $^1J_{P,C}$ = 42 Hz, P*C*H$_3$), 56.0 (s, O*C*H$_3$), 56.2 (s, O*C*H$_3$), 94.2 (s, *C*$_5$H$_5$), 94.2 (s, *C*$_5$H$_5$), 195.2 (d, $^2J_{P,C}$ = 9 Hz, *C*O), 195.8 (d, $^2J_{P,C}$ = 9 Hz, *C*O) ppm. ^{31}P NMR (162 MHz, CD_2Cl_2, 20 °C): δ = −15.0 (s), −13.0 (s) ppm. IR (CH_2Cl_2): $\tilde{\nu}$ = 2021 (CO), 1763 (NO) cm^{-1}. $C_{20}H_{20}BF_4NO_3PRe$ (626.37): calcd. C 38.35, H 3.22, N 2.24; found C 38.60, H 3.35, N 2.22.

[CpRe(CO)(NO){P(Ph)(Me)(CH$_2$C$_4$H$_3$S)}]BF$_4$ (3e): A solution of acetonitrile complex **2** (600 mg, 1.37 mmol) and phosphane **1e** (400 mg, 1.82 mmol) in 2-butanone (15 mL) was heated to reflux for 4 h. Upon cooling, a yellow precipitate formed. Diethyl ether (15 mL) was added and the solid was collected by filtration and washed with THF. Yield 640 mg (76%), yellow crystalline solid, m.p. 233 °C. Both diastereomers: ^{1}H NMR (400 MHz, CD_3CN, 20 °C): δ = 2.19 (d, $^2J_{P,H}$ = 10.4 Hz, 3 H, PCH_3), 2.19 (d, $^2J_{P,H}$ = 10.4 Hz, 3 H, PCH_3), 4.04, 4.13 (ABX system, $^2J_{H,H}$ = 15.7, $^2J_{P,H}$ = 9.3 Hz, 2 H, PCH_2), 4.07, 4.11 (ABX system, $^2J_{H,H}$ = 15.4, $^2J_{P,H}$ = 10.0 Hz, 2 H, PCH_2), 5.88 (d, $^3J_{P,H}$ = 0.6 Hz, 5 H, C_5H_5), 5.90 (d, $^3J_{P,H}$ = 0.6 Hz, 5 H, C_5H_5), 6.80 (m, 2 H, thiophene *H*), 6.93 (m, 2 H, thiophene *H*), 7.27 (m, 2 H, thiophene *H*) ppm. ^{13}C NMR (100 MHz, CD_3CN, 20 °C): δ = 16.1 (d, $^1J_{P,C}$ = 40 Hz, P*C*H$_3$), 16.2 (d, $^1J_{P,C}$ = 40 Hz, P*C*H$_3$), 35.2 (d, $^1J_{P,C}$ = 34 Hz, P*C*H$_2$), 35.4 (d, $^1J_{P,C}$ = 34 Hz, P*C*H$_2$), 94.7 (d, $^2J_{P,C}$ = 1 Hz. *C*$_5$H$_5$), 94.8 (d, $^2J_{P,C}$ = 1 Hz. *C*$_5$H$_5$), 127.1 (d, 4$J_{P,C}$ = 4 Hz, thiophene *C*H), 127.1 (d, 4$J_{P,C}$ = 4 Hz, thiophene *C*H), 128.3 (d, 4$J_{P,C}$ = 4 Hz, thiophene *C*H), 128.3 (d, 4$J_{P,C}$ = 4 Hz, thiophene *C*H), 129.7 (d, 3$J_{P,C}$ = 7 Hz, thiophene *C*H), 129.8 (d, 3$J_{P,C}$ = 7 Hz, thiophene *C*H), 134.1 (d, $^2J_{P,C}$ = 10 Hz, PCH$_2$*C*), 134.2 (d, $^2J_{P,C}$ = 10 Hz, PCH$_2$*C*), 195.9 (d, $^2J_{P,C}$ = 7 Hz, *C*O), 195.9 (d, $^2J_{P,C}$ = 7 Hz, *C*O) ppm. ^{31}P NMR (162 MHz, CD_3CN, 20 °C): δ = −6.4 (s), −5.5 (s) ppm. IR (Nujol): $\tilde{\nu}$ = 2016 (CO), 1763 (NO) cm^{-1}. $C_{18}H_{18}BF_4NO_2PReS$ (616.40): calcd. C 35.07, H 2.94, N 2.27, S 5.20; found C 34.83, H 2.92, N 2.30, S 5.09.

[CpRe(NO){PPh$_2$(2-C$_6$H$_4$OMe)}(CH$_3$)] (4a): To a suspension of carbonyl complex **3a** (300 mg, 0.44 mmol) in THF (15 mL) was added $NaBH_4$ (50 mg, 1.32 mmol). The colour of the mixture changed from brown to red and a gas was evolved. After 2 h, the solution was evaporated to dryness, the residue dissolved in benzene (15 mL), filtered through silica gel and the silica washed with benzene. The clear, orange filtrate was evaporated to 1 mL and the product precipitated upon addition of petroleum ether and storing overnight at −30 °C. Yield 220 mg (87%), orange crystalline solid, m.p. 55 °C (dec.). ^{1}H NMR (400 MHz, C_6D_6, 20 °C): δ = 1.45 (d, $^3J_{P,H}$ = 6.4 Hz, 3 H, ReCH_3), 3.05 (s, 3 H, OCH_3), 4.61 (s, 5 H, C_5H_5) ppm. ^{13}C NMR (100 MHz, C_6D_6, 20 °C): δ = −35.7 (d, $^2J_{P,C}$ = 7 Hz, Re*C*H$_3$), 55.0 (s, O*C*H$_3$), 89.6 (d, $^2J_{P,C}$ = 2 Hz, *C*$_5$H$_5$)

 © 2004 Wiley-VCH Verlag GmbH & Co. KGaA, Weinheim

ppm. ^{31}P NMR (162 MHz, C_6D_6, 20 °C): δ = 21.4 (s) ppm. IR (THF): $\tilde{\nu}$ = 1637 (NO) cm^{-1}. $C_{25}H_{25}NO_2PRe$ (588.66): calcd. C 51.01, H 4.28, N 2.38; found C 50.86, H 4.37, N 2.27.

[CpRe(NO){PPh$_2$(CH$_2$C$_4$H$_3$S)}(CH$_3$)] (4b): To a suspension of carbonyl complex **3b** (270 mg, 0.40 mmol) in THF (15 mL) was added $NaBH_4$ (50 mg, 1.32 mmol). The colour of the mixture changed from brown to red and a gas was evolved. After 2 h, the solution was evaporated to dryness, the residue dissolved in benzene (20 mL), filtered through silica gel and celite and the filter aid washed with benzene. The solvent was removed under vacuum and the residue dissolved in boiling hexane (40 mL). The solution was filtered hot over celite and the solvents evaporated to 10 mL. The initial crystallisation was completed by storing the mixture overnight at −30 °C. Yield 174 mg (76%), orange crystalline solid, m.p. 86 °C (dec.). ^{1}H NMR (400 MHz, C_6D_6, 20 °C): δ = 1.42 (d, $^3J_{P,H}$ = 5.8 Hz, 3 H, ReCH_3] 3.95, 4.01 (ABX system, $^2J_{H,H}$ = 15.0, $^2J_{P,H}$ = 9.0 Hz, 2 H, PCH_2), 4.50 (s, 5 H, C_5H_5), 6.46 (m, 1 H, thiophene *H*), 6.54 (m, 1 H, thiophene *H*), 6.64 (m, 1 H, thiophene *H*) ppm. ^{13}C NMR (100 MHz, C_6D_6, 20 °C): δ = −38.7 (d, $^2J_{P,C}$ = 8 Hz, ReCH$_3$), 32.9 (d, $^1J_{P,C}$ = 29 Hz, PCH$_2$), 89.0 (d, $^2J_{P,C}$ = 2 Hz. C_5H_5), 124.4 (d, $^4J_{P,C}$ = 3 Hz, thiophene *C*H), 126.8 (d, $^4J_{P,C}$ = 2 Hz, thiophene *C*H), 136.7 (d, $^2J_{P,C}$ = 6 Hz, PCH$_2$*C*) ppm. ^{31}P NMR (162 MHz, C_6D_6, 20 °C): δ = 19.7 (s) ppm. IR (THF): $\tilde{\nu}$ = 1634 (NO) cm^{-1}. $C_{23}H_{23}NOPReS$ (578.69): calcd. C 47.74, H 4.01, N 2.42, S 5.54; found C 48.17, H 4.18, N 2.32, S 5.60.

[CpRe(NO){PPh$_2$(CH$_2$C$_4$H$_7$O)}(CH$_3$)] (4c): To a solution of carbonyl complex **3c** (390 mg, 0.59 mmol) in THF (20 mL) was added $NaBH_4$ (70 mg, 1.85 mmol) at −78 °C. After 30 min at that temperature, the mixture was allowed to warm to 20 °C which was accompanied by gas evolution. The mixture was filtered through silica gel and the silica washed with THF. After evaporation of the solvent, the residue was dissolved in benzene (20 mL), the solution filtered through celite and the solvents evaporated again. The residue was finally recrystallised at −78 °C from toluene (2 mL) and hexane (10 mL). Yield 265 mg (80%), orange powder, m.p. 40 °C. Both diastereomers: ^{1}H NMR (400 MHz, C_6D_6, 20 °C): δ = 0.66−0.97 (m, 2 H, CH_2), 1.03−1.44 (m, 4 H, CH_2), 1.49 (d, $^3J_{P,H}$ = 5.5 Hz, 3 H, ReCH_3), 1.52 (d, $^3J_{P,H}$ = 5.6 Hz, 3 H, ReCH_3), 2.53−2.88 (m, 2 H, CH_2), 3.22−3.64 (m, 4 H, CH_2), 4.13−4.41 (m, 2 H, C*H*), 4.49 (s, 5 H, C_5H_5), 4.61 (s, 5 H, C_5H_5) ppm. ^{13}C NMR (100 MHz, C_6D_6, 20 °C): δ = −39.8 (d, $^2J_{P,C}$ = 7 Hz, Re*C*H$_3$), −38.6 (d, $^2J_{P,C}$ = 7 Hz, Re*C*H$_3$), 25.9 (s, *C*H$_2$), 26.2 (s, *C*H$_2$), 32.7 (d, $^3J_{P,C}$ = 3 Hz, *C*H$_2$), 32.9 (d, $^3J_{P,C}$ = 8 Hz, *C*H$_2$), 37.5 (d, $^1J_{P,C}$ = 31 Hz, P*C*H$_2$), 39.2 (d, $^1J_{P,C}$ = 35 Hz, P*C*H$_2$), 67.0 (s, O*C*H$_2$), 67.4 (s, O*C*H$_2$), 76.3 (d, $^2J_{P,C}$ = 7 Hz, O*C*H), 77.0 (d, $^2J_{P,C}$ = 2 Hz, O*C*H), 89.2 (d, $^2J_{P,C}$ = 2 Hz. C_5H_5), 89.3 (d, $^2J_{P,C}$ = 2 Hz. C_5H_5) ppm. ^{31}P NMR (162 MHz, C_6D_6, 20 °C): δ = 8.1 (s), 11.1 (s) ppm. IR (THF): $\tilde{\nu}$ = 1632 (NO) cm^{-1}. $C_{23}H_{27}NO_2PRe$ (588.65): calcd. C 48.75, H 4.80, N 2.47; found C 48.56, H 4.70, N 2.36.

[CpRe(NO){P(Ph)(Me)(2-C$_6$H$_4$OMe}](CH$_3$)] (4d): To a suspension of carbonyl complex **3d** (500 mg, 0.80 mmol) in THF (15 mL) was added $NaBH_4$ (95 mg, 2.50 mmol). The colour of the mixture changed from brown to red and a gas was evolved. After 2 h, the reaction was worked up as described for **4b**. Yield 344 mg (82%), orange-red crystalline powder, m.p. 206 °C (dec.). Both diastereomers: ^{1}H NMR (400 MHz, C_6D_6, 20 °C): δ = 1.25 (d, $^3J_{P,H}$ = 6.2 Hz, 3 H, ReCH_3), 1.26 (d, $^3J_{P,H}$ = 6.4 Hz, 3 H, ReCH_3), 1.97 (d, $^2J_{P,H}$ = 8.8 Hz, 3 H, PCH_3), 1.99 (d, $^2J_{P,H}$ = 9.1 Hz, 3 H, PCH_3), 2.89 (s, 3 H, OCH_3), 3.02 (s, 3 H, OCH_3), 4.65 (s, 5 H, C_5H_5), 4.71 (s, 5 H, C_5H_5) ppm. ^{13}C NMR (100 MHz, C_6D_6, 20 °C): δ = −38.7 (d, $^2J_{P,C}$ = 6 Hz, Re*C*H$_3$), −38.7 (d, $^2J_{P,C}$ = 6 Hz, Re*C*H$_3$), 15.9 (d, $^1J_{P,C}$ = 35 Hz, P*C*H$_3$), 16.5 (d, $^1J_{P,C}$ = 35 Hz, P*C*H$_3$), 54.7 (s, O*C*H$_3$), 55.0 (s, O*C*H$_3$), 88.5 (d, $^2J_{P,C}$ = 2 Hz, C_5H_5), 88.7 (d, $^2J_{P,C}$ = 2 Hz, C_5H_5]) ppm. ^{31}P NMR (162 MHz, C_6D_6, 20 °C): δ = −1.2 (s), 0.5 (s) ppm. IR (THF): $\tilde{\nu}$ = 1636 (NO) cm^{-1}. $C_{20}H_{23}NO_2PRe$ (526.59): calcd. C 45.62, H 4.40, N 2.66; found C 45.95, H 4.50, N 2.62.

[CpRe(NO){P(Ph)(Me)(CH$_2$C$_4$H$_3$S)}(CH$_3$)] (4e): To a suspension of carbonyl complex **3e** (350 mg, 0.57 mmol) in THF (15 mL) was added $NaBH_4$ (65 mg, 1.72 mmol). The mixture turned red and a gas was evolved. After 2 h, the reaction was worked up as described for **4a**. Yield 237 mg (81%), orange crystalline powder, m.p. 67 °C. Recrystallisation from hot petroleum ether gave a sample enriched in one diastereomer. Major (68%) diastereomer: ^{1}H NMR (400 MHz, C_6D_6, 20 °C): δ = 1.12 (d, $^3J_{P,H}$ = 6.2 Hz, 3 H, ReCH_3), 1.44 (d, $^2J_{P,H}$ = 8.6 Hz, 3 H, PCH_3), 3.47, 3.61 (ABX system, $^2J_{H,H}$ = 15.0, $^2J_{P,H}$ = 8.6 Hz, 2 H, PCH_2), 4.52 (s, 5 H, C_5H_5), 6.40 (m, 1 H, thiophene *H*), 6.57 (m, 1 H, thiophene *H*), 6.64 (m, 1 H, thiophene *H*) ppm. ^{13}C NMR (100 MHz, C_6D_6, 20 °C): δ = −39.3 (d, $^2J_{P,C}$ = 7 Hz, Re*C*H$_3$), 15.1 (d, $^1J_{P,C}$ = 36 Hz, P*C*H$_3$), 33.7 (d, $^1J_{P,C}$ = 30 Hz, P*C*H$_2$), 87.9 (d, $^2J_{P,C}$ = 2 Hz. C_5H_5), 124.2 (d, $^4J_{P,C}$ = 3 Hz, thiophene *C*H), 126.8 (d, $^4J_{P,C}$ = 2 Hz, thiophene *C*H), 127.5 (d, $^3J_{P,C}$ = 5 Hz, thiophene *C*H), 137.2 (d, $^2J_{P,C}$ = 8 Hz, PCH$_2$*C*) ppm. ^{31}P NMR (162 MHz, C_6D_6, 20 °C): δ = −0.9 (s) ppm. Minor (32%) diastereomer: ^{1}H NMR (400 MHz, C_6D_6, 20 °C): δ = 1.22 (d, $^3J_{P,H}$ = 6.1 Hz, 3 H, ReCH_3), 1.40 (d, $^2J_{P,H}$ = 8.6 Hz, 3 H, PCH_3), 3.67, 3.69 (ABX system, $^2J_{H,H}$ = 15.7, $^2J_{P,H}$ = 7.5 Hz, 2 H, PCH_2), 4.54 (s, 5 H, C_5H_5), 6.23 (m, 1 H, thiophene *H*), 6.53 (m, 1 H, thiophene *H*), 6.62 (m, 1 H, thiophene *H*) ppm. ^{13}C NMR (100 MHz, C_6D_6, 20 °C): δ = −40.2 (d, $^2J_{P,C}$ = 7 Hz, Re*C*H$_3$), 11.2 (d, $^1J_{P,C}$ = 32 Hz, P*C*H$_3$), 33.2 (d, $^1J_{P,C}$ = 30 Hz, P*C*H$_2$), 88.0 (d, $^2J_{P,C}$ = 2 Hz. C_5H_5), 124.3 (d, $^4J_{P,C}$ = 3 Hz, thiophene *C*H), 126.7 (d, $^4J_{P,C}$ = 3 Hz, thiophene *C*H), 127.3 (d, $^3J_{P,C}$ = 5 Hz, thiophene *C*H), 136.9 (d, $^2J_{P,C}$ = 10 Hz, PCH$_2$*C*) ppm. ^{31}P NMR (162 MHz, C_6D_6, 20 °C): δ = −4.0 (s) ppm. Both diastereomers: IR (THF): $\tilde{\nu}$ = 1631 (NO) cm^{-1}. $C_{18}H_{21}NOPReS$ (516.62): calcd. C 41.85, H 4.10, N 2.71, S 6.21; found C 42.00, H 4.09, N 2.67, S 5.84.

Chelate Complexes 5b−e: At −78 °C, HBF_4 in diethyl ether (150 µL, ca. 1.50 mmol) was added to a solution of the respective methyl complex (0.38 mmol) in dichloromethane (10 mL). Gas evolution and a change of colour from red to brown was observed. After 1 h, the temperature was raised to 20 °C and the solvents were evaporated to 2 mL. The product, which was precipitated by addition of diethyl ether, was filtered off and washed with diethyl ether and petroleum ether.

[CpRe(NO)(κPPh$_2$(CH$_2$C$_4$H$_3$κS))]BF$_4$ (5b): Yield 212 mg (86%), yellow crystalline solid, m.p. 218 °C (dec.). ^{1}H NMR (400 MHz, CD_2Cl_2, 20 °C): δ = 3.64, 4.01 (ABMX system, $^2J_{H,H}$ = 16.2, $^2J_{P,H}$ = 11.2, $^4J_{H,H}$ = 1.2 Hz, 2 H, PCH_2), 5.49 (s, 5 H, C_5H_5) ppm. ^{13}C NMR (100 MHz, CD_2Cl_2, 20 °C): δ = 27.7 (d, $^1J_{P,C}$ = 32 Hz, P*C*H$_2$), 91.8 (d, $^2J_{P,C}$ = 1 Hz, C_5H_5), 132.0 (d, $^4J_{P,C}$ = 3 Hz, thiophene *C*H), 133.2 (d, $^4J_{P,C}$ = 3 Hz, thiophene *C*H), 134.9 (d, $^3J_{P,C}$ = 3 Hz, thiophene *C*H), 161.4 (d, $^2J_{P,C}$ = 3 Hz, PCH$_2$*C*) ppm. ^{31}P NMR (162 MHz, CD_2Cl_2, 20 °C): δ = 34.5 (s) ppm. IR (CH_2Cl_2): $\tilde{\nu}$ = 1722 (NO) cm^{-1}. $C_{22}H_{20}BF_4NOPReS$ (650.46): calcd. C 40.62, H 3.10, N 2.15, S 4.93; found C 39.67, H 3.27, N 2.02, S 4.68.

[CpRe(NO){κPPh$_2$(CH$_2$C$_4$H$_7$κO)}]BF$_4$ (5c): Yield 243 mg (99%), brownish solid, m.p. 182 °C (dec.). Both diastereomers: ^{1}H NMR (400 MHz, CD_2Cl_2, 20 °C): δ = 1.90−2.04 (m, 1 H, CH_2), 2.05−2.49 (m, 9 H, CH_2), 2.73−2.89 (m, 2 H, CH_2), 4.06−4.18

 © 2004 Wiley-VCH Verlag GmbH & Co. KGaA, Weinheim

(m, 1 H, C*H*), 4.27−4.33 (m, 1 H, C*H*), 4.35−4.54 (m, 4 H, PCH_2), 5.49 (s, 5 H, C_5H_5), 5.52 (s, 5 H, C_5H_5) ppm. ^{13}C NMR (100 MHz, CD_2Cl_2, 20 °C): δ = 28.2 (s, *C*H_2), 28.5 (s, *C*H_2), 29.7 (d, $^3J_{P,C}$ = 11 Hz, *C*H_2), 31.6 (d, $^3J_{P,C}$ = 10 Hz, *C*H_2), 31.8 (d, $^1J_{P,C}$ = 28 Hz, P*C*H_2), 35.8 (d, $^1J_{P,C}$ = 27 Hz, P*C*H_2), 88.7 (s, O*C*H_2), 89.7 (s, O*C*H_2), 90.8 (d, $^2J_{P,C}$ = 2 Hz, C_5H_5), 91.1 (d, $^2J_{P,C}$ = 2 Hz, C_5H_5), 95.8 (s, O*C*H), 97.9 (s, O*C*H) ppm. ^{31}P NMR (162 MHz, CD_2Cl_2, 20 °C): δ = 35.3 (s), 37.5 (s) ppm. IR (CH_2Cl_2): $\tilde{\nu}$ = 1690 (NO) cm^{-1}. $C_{22}H_{24}BF_4NO_2PRe$ (638.42): calcd. C 41.39, H 3.79, N 2.19; found C 41.09, H 3.93, N 1.97.

[CpRe(NO){κP(Ph)(Me)(CH$_2$C$_4$H$_3$κS)}]BF$_4$ (5e): Yield 204 mg (91%), yellow crystalline powder, m.p. 69 °C (dec.). Careful extraction with THF gave a sample enriched in one diastereomer. Major diastereomer: ^{1}H NMR (400 MHz, CD_2Cl_2, 20 °C): δ = 2.19 (d, $^2J_{P,H}$ = 10.2 Hz, 3 H, PCH_3), 3.06−3.63 (m, 2 H, PCH_2), 5.45 (d, $^3J_{P,H}$ = 0.3 Hz, 5 H, C_5H_5). ^{13}C NMR (100 MHz, CD_2Cl_2, 20 °C): δ = 14.7 (d, $^1J_{P,C}$ = 39 Hz, P*C*H$_3$), 26.3 (d, $^1J_{P,C}$ = 32 Hz, P*C*H$_2$), 91.6 (s, C_5H_5), 161.5 (d, $^2J_{P,C}$ = 2 Hz, PCH$_2$*C*). ^{31}P NMR (162 MHz, CD_2Cl_2, 20 °C): δ = 11.3 (s) ppm. Minor diastereomer: ^{1}H NMR (400 MHz, CD_2Cl_2, 20 °C): δ = 2.21 (d, $^2J_{P,H}$ = 10.0 Hz, 3 H, PCH_3), 3.06−3.63 (m, 2 H, PCH_2), 5.83 (d, $^3J_{P,H}$ = 0.2 Hz, 5 H, C_5H_5) ppm. ^{13}C NMR (100 MHz, CD_2Cl_2, 20 °C): δ = 18.1 (d, $^1J_{P,C}$ = 36 Hz, P*C*H$_3$), 26.5 (d, $^1J_{P,C}$ = 33 Hz, P*C*H$_2$), 90.7 (s, C_5H_5), 163.0 (s, PCH$_2$*C*) ppm. ^{31}P NMR (162 MHz, CD_2Cl_2, 20 °C): δ = 15.6 (s) ppm. Both diastereomers: IR (CH_2Cl_2): $\tilde{\nu}$ = 1718 (NO) cm^{-1}. $C_{17}H_{18}BF_4NOPReS$ (588.39): calcd. C 34.70, H 3.08, N 2.38, S 5.45; found C 34.62, H 3.36, N 2.28, S 5.19.

Acetonitrile Complexes 6b−e: A solution of the respective chelate complex (0.20 mmol) in acetonitrile (5 mL) was kept for 24 h at 20 °C. The solvents were evaporated to dryness and the product recrystallised from dichloromethane/diethyl ether.

[CpRe(NO){PPh$_2$(CH$_2$C$_4$H$_3$S)}(NCCH$_3$)]BF$_4$ (6b): Yield 125 mg 90%), yellow crystalline solid, m.p. 232 °C (dec.). ^{1}H NMR (400 MHz, CD_2Cl_2, 20 °C): δ = 2.63 (d, $^5J_{P,H}$ = 1.2 Hz, 3 H, NCCH_3), 4.31, 4.46 (ABX system, $^2J_{H,H}$ = 15.1, $^2J_{P,H}$ = 10.1 Hz, 2 H, PCH_2), 5.40 (s, 5 H, C_5H_5), 6.72 (m, 1 H, thiophene *H*), 6.87 (m, 1 H, thiophene *H*), 7.13 (m, 1 H, thiophene *H*) ppm. ^{13}C NMR (100 MHz, CD_2Cl_2, 20 °C): δ = 4.9 (s, NC*C*H$_3$), 33.0 (d, $^1J_{P,C}$ = 33 Hz, P*C*H$_2$), 91.9 (s, C_5H_5), 126.0 (d, $^4J_{P,C}$ = 4 Hz, thiophene *C*H), 127.4 (d, $^4J_{P,C}$ = 3 Hz, thiophene *C*H), 129.4 (d, $^3J_{P,C}$ = 7 Hz, thiophene *C*H), 134.5 (d, $^2J_{P,C}$ = 4 Hz, PCH$_2$*C*), 141.3 (s, N*C*CH$_3$) ppm. ^{31}P NMR (162 MHz, CD_2Cl_2, 20 °C): δ = 9.2 (s) ppm. IR (CH_2Cl_2): $\tilde{\nu}$ = 1705 (NO) cm^{-1}. $C_{24}H_{23}BF_4N_2OPReS$ (691.51): calcd. C 41.69, H 3.35, N 4.05, S 4.64; found C 40.65, H 3.54, N 3.67, S 4.48.

[CpRe(NO){PPh$_2$(CH$_2$C$_4$H$_7$O)}(NCCH$_3$)]BF$_4$ (6c): Yield 112 mg (82%), yellow-brown solid, m.p. 139 °C (dec.). Both diastereomers: ^{1}H NMR (400 MHz, [D$_6$]acetone, 20 °C): δ = 1.66−2.17 (m, 6 H, CH_2), 2.89 (d, $^5J_{P,H}$ = 1.2 Hz, 3 H, NCCH_3), 2.95 (d, $^5J_{P,H}$ = 1.2 Hz, 3 H, NCCH_3), 2.86−3.10 (m, 4 H, PCH_2), 3.14−3.29 (m, 2 H, CH_2), 3.50−3.58 (m, 2 H, CH_2), 3.65−3.75 (m, 2 H, CH_2), 3.95−4.05 (m, 2 H, C*H*), 5.70 (s, 5 H, C_5H_5), 5.75 (s, 5 H, C_5H_5) ppm. ^{13}C NMR (100 MHz, [D$_6$]acetone, 20 °C): δ = 4.5 (s, NC*C*H$_3$), 4.5 (s, NC*C*H$_3$), 25.9 (s, *C*H$_2$), 25.9 (s, *C*H$_2$), 33.6 (d, $^3J_{P,C}$ = 10 Hz, *C*H$_2$), 33.7 (d, $^3J_{P,C}$ = 10 Hz, *C*H$_2$), 37.0 (d, $^1J_{P,C}$ = 34 Hz, P*C*H$_2$), 37.4 (d, $^1J_{P,C}$ = 35 Hz, P*C*H$_2$), 68.1 (s, O*C*H$_2$), 68.2 (s, O*C*H$_2$), 75.9 (s, O*C*H), 76.4 (s, O*C*H), 92.7 (d, $^2J_{P,C}$ = 1 Hz, C_5H_5), 92.8 (d, $^2J_{P,C}$ = 1 Hz, C_5H_5) ppm, N*C*CH$_3$ not observed. ^{31}P NMR (162 MHz, [D$_6$]acetone, 20 °C): δ = 1.9 (s), 2.7 (s) ppm. IR (CH_3CN): $\tilde{\nu}$ = 1702 (NO) cm^{-1}. $C_{24}H_{27}BF_4N_2O_2PRe$ (679.48): calcd. C 42.42, H 4.01, N 4.12; found. C 41.96, H 4.03, N 3.97.

[CpRe(NO){P(Ph)(Me)(CH$_2$C$_4$H$_3$S)}(NCCH$_3$)]BF$_4$ (6e): Yield 117 mg (93%), dark yellow crystalline solid, m.p. 114 °C. Both diastereomers: ^{1}H NMR (400 MHz, CD_2Cl_2, 20 °C): δ = 2.04 (d, $^2J_{P,H}$ = 9.5 Hz, 3 H, PCH_3), 2.04 (d, $^2J_{P,H}$ = 9.6 Hz, 3 H, PCH_3), 2.42 (d, $^5J_{P,H}$ = 1.3 Hz, 3 H, NCCH_3), 2.80 (d, $^5J_{P,H}$ = 1.3 Hz, 3 H, NCCH_3), 3.95 (m, 4 H, PCH_2), 5.44 (s, 5 H, C_5H_5), 5.53 (s, 5 H, C_5H_5), 6.74 (m, 1 H, thiophene *H*), 6.82 (m, 1 H, thiophene *H*), 6.90 (m, 1 H, thiophene *H*), 6.96 (m, 1 H, thiophene *H*), 7.15 (m, 1 H, thiophene *H*), 7.23 (m, 1 H, thiophene *H*) ppm. ^{13}C NMR (100 MHz, CD_2Cl_2, 20 °C): δ = 4.3 (s, NC*C*H$_3$), 5.1 (s, NC*C*H$_3$), 13.3 (d, $^1J_{P,C}$ = 37 Hz, P*C*H$_3$), 13.5 (d, $^1J_{P,C}$ = 37 Hz, P*C*H$_3$), 33.2 (d, $^1J_{P,C}$ = 31 Hz, P*C*H$_2$), 33.8 (d, $^1J_{P,C}$ = 35 Hz, P*C*H$_2$), 91.1 (d, $^2J_{P,C}$ = 1 Hz, C_5H_5), 91.4 (d, $^2J_{P,C}$ = 1 Hz, C_5H_5), 125.7 (d, $4J_{P,C}$ = 4 Hz, thiophene *C*H), 125.9 (d, $4J_{P,C}$ = 4 Hz, thiophene *C*H), 127.5 (d, $^4J_{P,C}$ = 3 Hz, thiophene *C*H), 127.7 (d, $^4J_{P,C}$ = 3 Hz, thiophene *C*H), 128.7 (d, $^3J_{P,C}$ = 7 Hz, thiophene *C*H), 128.7 (d, $^3J_{P,C}$ = 7 Hz, thiophene *C*H), 134.2 (d, $^2J_{P,C}$ = 10 Hz, PCH$_2$*C*), 134.5 (d, $^2J_{P,C}$ = 8 Hz, PCH$_2$*C*), 139.7 (s, N*C*CH$_3$), 140.8 (s, N*C*CH$_3$) ppm. ^{31}P NMR (162 MHz, CD_2Cl_2, 20 °C): δ = −11.8 (s), −6.9 (s) ppm. IR (CH_2Cl_2): $\tilde{\nu}$ = 1699 (NO) cm^{-1}. $C_{19}H_{21}BF_4N_2OPReS$ (629.44): calcd. C 36.26, H 3.36, N 4.45, S 5.09; found. C 36.16, H 3.50, N 4.29, S 4.93.

[CpRe(NO){P(Ph)(Me)(2-C$_6$H$_4$OMe)}(NCCH$_3$)]BF$_4$ (6d): To a cold (−78 °C) solution of methyl complex **4d** (65 mg, 0.12 mmol) in dichloromethane (3 mL) and acetonitrile (1 mL) was added ethereal HBF_4 (25 μL, ca. 0.25 mmol). The mixture was kept cold for 1 h and was then allowed to warm to room temperature. The solvent was removed under vacuum, the residue dissolved in dichloromethane (1 mL) and the product precipitated by the addition of diethyl ether. Yield 78 mg (99%), yellow crystalline solid, m.p. 183 °C (dec.). Both diastereomers: ^{1}H NMR (400 MHz, CD_2Cl_2, 20 °C): δ = 2.24 (d, $^2J_{P,H}$ = 9.5 Hz, 3 H, PCH_3), 2.36 (d, $^2J_{P,H}$ = 9.8 Hz, 3 H, PCH_3), 2.42 (d, $^5J_{P,H}$ = 1.5 Hz, 3 H, NCCH_3), 2.63 (d, $^5J_{P,H}$ = 1.4 Hz, 3 H, NCCH_3), 3.59 (s, 3 H, OCH_3), 3.67 (s, 3 H, OCH_3), 5.57 (s, 5 H, C_5H_5), 5.60 (s, 5 H, C_5H_5) ppm. ^{13}C NMR (100 MHz, CD_2Cl_2, 20 °C): δ = 4.0 (s, NC*C*H$_3$), 4.5 (s, NC*C*H$_3$), 16.8 (d, $^1J_{P,C}$ = 38 Hz, P*C*H$_3$), 18.9 (d, $^1J_{P,C}$ = 39 Hz, P*C*H$_3$), 56.0 (s, O*C*H$_3$), 56.0 (s, O*C*H$_3$), 91.3 (d, $^2J_{P,C}$ = 1 Hz, C_5H_5), 91.7 (d, $^2J_{P,C}$ = 1 Hz, C_5H_5), 139.5 (s, N*C*CH$_3$), 140.2 (s, N*C*CH$_3$) ppm. ^{31}P NMR (162 MHz, CD_2Cl_2, 20 °C): δ = −12.1 (s), −11.2 (s) ppm. IR (CH_2Cl_2): $\tilde{\nu}$ = 1705 (NO) cm^{-1}. $C_{21}H_{23}BF_4N_2O_2PRe$ (639.41): calcd. C 39.45, H 3.63, N 4.38; found C 38.26, H 3.95, N 4.06.

[CpRe(NO){P(Ph)(Me)(2-C$_6$H$_4$OMe)}(THF)]BF$_4$ (7d): To a cold (−78 °C) solution of methyl complex **4d** (210 mg, 0.40 mmol) in THF (20 mL) was added ethereal HBF_4 (100 μL, ca. 1.0 mmol). The mixture was kept cold for 1 h and was then warmed to room temperature. The solvents were evaporated to 10 mL and the product precipitated upon the addition of diethyl ether. Yield 235 mg (88%) pink powder, m.p. 88 °C (dec.). Major diastereomer: ^{1}H NMR (400 MHz, [D$_6$]acetone, 20 °C): δ = 1.72−1.82 (m, 4 H, CH_2), 2.41 (d, $^2J_{P,H}$ = 9.4 Hz, 3 H, PCH_3), 3.56−3.65 (m, 4 H, OCH_2), 3.63 (s, 3 H, OCH_3), 5.97 (s, 5 H, C_5H_5) ppm. ^{13}C NMR (100 MHz, [D$_6$]acetone, 20 °C): δ = 18.4 (d, $^1J_{P,C}$ = 39 Hz, P*C*H$_3$), 26.1 (s, *C*H$_2$), 56.0 (s, O*C*H$_3$), 68.0 (s, O*C*H$_2$), 92.5 (d, $^2J_{P,C}$ = 1 Hz, C_5H_5) ppm. ^{31}P NMR (162 MHz, [D$_6$]acetone, 20 °C): δ = −6.2 (s) ppm. Minor diastereomer: ^{1}H NMR (400 MHz, [D$_6$]acetone, 20 °C): δ = 1.55−1.62 (m, 4 H, CH_2), 2.47 (d, $^2J_{P,H}$ = 10.1 Hz, 3 H, PCH_3), 3.35−3.42 (m, 4 H, OCH_2), 3.72 (s, 3 H, OCH_3), 5.90 (s 5 H, C_5H_5) ppm. ^{13}C NMR (100 MHz, [D$_6$]acetone, 20 °C): δ = 16.3 (d, $^1J_{P,C}$ = 38 Hz, P*C*H$_3$), 27.4 (s, *C*H$_2$), 56.1 (s, O*C*H$_3$), 71.1 (s, O*C*H$_2$), 93.2 (d, $^2J_{P,C}$ = 1 Hz, C_5H_5) ppm. ^{31}P NMR (162 MHz,

 © 2004 Wiley-VCH Verlag GmbH & Co. KGaA, Weinheim

Table 1. Details of the structure determinations of compounds **1b**·BH_3, **3a**, **3b**, **3d**−**AlF_4**, **4d**, **6e** and **7d**·CH_2Cl_2

	1b·BH_3	**3a**	**3b**	**3d**−**AlF_4**	**4d**	**6e**	**7d**·CH_2Cl_2
Empirical formula	$C_{14}H_{18}BOP$	$C_{25}H_{22}BF_4NO_3Pre$	$C_{23}H_{20}BF_4NO_2PReS$	$C_{20}H_{20}AlF_4NO_3PRe$	$C_{20}H_{23}NO_2PRe$	$C_{19}H_{21}BF_4N_2OPReS$	$C_{24}H_{30}BClF_4NO_3PRe$
Formula mass	244.06	688.42	678.44	642.52	526.56	629.42	755.40
Crystal colour/habit	colourless plate	yellow block	yellow block	yellow block	red block	yellow plate	red prism
Crystal system	orthorhombic	monoclinic	triclinic	monoclinic	triclinic	monoclinic	monoclinic
Space group	$Pna2_1$	$P2_1/c$	$P\bar{1}$	$P2_1/n$	$P\bar{1}$	$P2_1/c$	$P2_1/c$
a (Å)	10.5951(8)	16.1437(13)	9.954(2)	11.1876(7)	9.0940(8)	11.1343(10)	9.920(3)
b (Å)	9.6350(8)	8.9379(7)	10.401(2)	13.8896(9)	10.2778(9)	9.7129(9)	18.071(5)
c (Å)	15.7090(12)	19.4659(16)	12.264(3)	14.3243(9)	12.2877(10)	20.4158(19)	16.858(5)
α (°)	90	90	79.742(3)	90	66.838(1)	90	90
β (°)	90	114.265(1)	75.758(3)	107.106(1)	83.946(1)	90.767(2)	106.823(4)
γ (°)	90	90	77.036(3)	90	64.057(1)	90	90
V (Å^3)	1603.6(2)	2560.6(4)	1189.1(5)	2127.4(2)	946.42(14)	2207.7(4)	2892.8(15)
Θ (°)	2.48−28.27	2.30−26.44	2.45−28.24	2.04−28.23	1.81−28.25	2.32−28.27	1.69−28.11
h	−13 to 13	−20 to 18	−13 to 12	−14 to 14	−12 to 12	−14 to 14	−13 to 13
k	−12 to 12	−11 to 11	−13 to 13	−17 to 18	−13 to 13	−12 to 12	−23 to 23
l	−19 to 20	−23 to 24	−16 to 16	−18 to 18	−16 to 16	−26 to 26	−22 to 22
Z	4	4	2	4	2	4	4
μ(Mo-K_α) (mm^{-1})	0.288	4.865	5.318	5.886	6.517	5.718	4.493
Crystal size (mm)	0.20 × 0.10 × 0.05	0.25 × 0.20 × 0.15	0.20 × 0.20 × 0.15	0.20 × 0.20 × 0.15	0.15 × 0.15 × 0.10	0.15 × 0.10 × 0.05	0.15 × 0.15 × 0.10
$D_{calcd.}$ (g·cm^{-3})	1.227	1.786	1.895	2.006	1.848	1.894	1.734
T (K)	173(2)	173(2)	173(2)	173(2)	173(2)	173(2)	173(2)
Reflections collected	15200	20004	26949	35350	21707	48267	60709
Independent reflections	3600	5212	5489	5991	4397	5262	6827
Parameter	183	308	289	282	229	299	346
R_1 [$I > 2\sigma(I)$]	0.0617	0.0394	0.0352	0.0474	0.0244	0.0418	0.0492
R_1 (overall)	0.0646	0.0482	0.0357	0.0490	0.0260	0.0538	0.0542
wR_2 [$I > 2\sigma(I)$]	0.1449	0.1037	0.0898	0.1022	0.0581	0.0968	0.1164
wR_2 (overall)	0.1496	0.1084	0.0900	0.1037	0.0585	0.1010	0.1180
Diff. peak/hole (e·Å^{-3})	0.482/−0.342	1.994/−1.678	1.564/−1.850	2.163/−1.798	3.488/−1.133	1.781/−1.276	2.097/−3.014
CCDC	242558	242219	242220	242221	242222	242223	242224

[D_6]acetone, 20 °C): δ = −5.8 (s) ppm. Both diastereomers: IR (CH_2Cl_2): $\tilde{\nu}$ = 1701 (NO) cm^{-1}. $C_{23}H_{28}BF_4NO_3PRe$ (670.47): calcd. C 41.20, H 4.21, N 2.09; found C 40.49, H 4.18, N 2.00.

X-ray Structure Determinations: Single crystals of **1b**·BH_3, **3a**, **3b**, **3d**−**AlF_4**, **4d**, **6e** and **7d**·CH_2Cl_2 were bonded to a glass fibre with frozen hydrocarbon oil in each case. A Bruker Smart Apex CCD instrument was used for data collection (graphite monochromator, Mo-K_α radiation, λ = 0.71073 Å). The structures were solved using Patterson methods and refined with full-matrix least-squares against F^2 (SHELXS-97).[39] Hydrogen atoms were included in their calculated positions and refined using a riding model. The details of the measurements are summarised in Table 1. Further data may be obtained from the Cambridge Crystallographic Data Centre. CCDC-242558 (for **1b**·BH_3), -242219 (for **3a**), -242220 (for **3b**), -242221 (for **3d**−**AlF_4**), -242222 (for **4d**), -242223 (for **6e**) and -242224 (for **7d**·CH_2Cl_2) contain the supplementary crystallographic data for this paper. These data can be obtained free of charge at www.ccdc.cam.ac.uk/conts/retrieving.html [or from the Cambridge Crystallographic Data Centre, 12 Union Road, Cambridge CB2 1EZ, UK; Fax: (internat.) +44-1223-336-033; E-mail: deposit@ccdc.cam.ac.uk].

[1] H. Brunner, *Angew. Chem.* **1969**, *81*, 395−396; *Angew. Chem. Int. Ed. Engl.* **1969**, *8*, 382.
[2] H. Brunner, *Angew. Chem.* **1999**, *111*, 1248−1263; *Angew. Chem. Int. Ed.* **1999**, *38*, 1194−1208.
[3] S. G. Davies, *Aldrichimica Acta* **1990**, *23*, 31−37.
[4] F. Agbossou, E. J. O'Connor, C. M. Garner, N. Q. Méndez, J. M. Fernández, A. T. Patton, J. A. Ramsden, J. A. Gladysz, *Inorg. Synth.* **1992**, *29*, 211−225.
[5] J. A. Gladysz, B. J. Boone, *Angew. Chem.* **1997**, *109*, 566−602; *Angew. Chem. Int. Ed. Engl.* **1997**, *36*, 551−583.
[6] W. A. Schenk, N. Burzlaff, H. Burzlaff, *Z. Naturforsch., Teil B* **1994**, *49*, 1633−1639.
[7] N. Burzlaff, M. Hagel, W. A. Schenk, *Z. Naturforsch., Teil B* **1998**, *53*, 893−899.
[8] N. Burzlaff, W. A. Schenk, *Eur. J. Inorg. Chem.* **1998**, 2055−2061.
[9] N. Burzlaff, W. A. Schenk, *Eur. J. Inorg. Chem.* **1999**, 1435−1443.
[10] A. Bader, E. Lindner, *Coord. Chem. Rev.* **1991**, *108*, 27−110.
[11] C. S. Slone, D. A. Weinberger, C. A. Mirkin, *Progr. Inorg. Chem.* **1999**, *48*, 233−350.
[12] D. W. Allen, S. J. Grayson, I. Harness, B. G. Hutley, I. W. Mowat, *J. Chem. Soc., Perkin Trans. 2* **1973**, 1912−1915.
[13] E. Lindner, H. Rauleder, C. Scheytt, H. A. Mayer, W. Hiller, R. Fawzi, P. Wenger, *Z. Naturforsch., Teil B* **1984**, *39*, 632−642.
[14] K. Burgess, M. J. Ohlmeyer, K. H. Whitmire, *Organometallics* **1992**, *11*, 3588−3600.
[15] S. Jugé, M. Stephan, R. Merdès, J. P. Genet, S. Halut-Desportes, *J. Chem. Soc., Chem. Commun.* **1993**, 531−533.
[16] A. J. Rippert, A. Linden, H.-J. Hansen, *Helv. Chim. Acta* **2000**, *83*, 311−321.
[17] W. Tam, G.-Y. Lin, W.-K. Wong, W. A. Kiel, V. K. Wong, J. A. Gladysz, *J. Am. Chem. Soc.* **1982**, *104*, 141−152.
[18] W. Mohr, G. A. Stark, H. Jiao, J. A. Gladysz, *Eur. J. Inorg. Chem.* **2001**, 925−933.
[19] G. W. Stowell, R. R. Whittle, C. M. Whaley, D. P. White, *Organometallics* **2001**, *20*, 1050−1052.

 © 2004 Wiley-VCH Verlag GmbH & Co. KGaA, Weinheim

[20] A. J. Amoroso, A. M. Arif, J. A. Gladysz, *Bull. Soc. Chim. Fr.* **1997**, *134*, 793−799.
[21] C. P. Casey, M. A. Andrews, D. R. McAlister, J. E. Rinz, *J. Am. Chem. Soc.* **1980**, *102*, 1927−1933.
[22] J. R. Sweet, W. A. G. Graham, *J. Am. Chem. Soc.* **1982**, *104*, 2811−2815.
[23] J. H. Merrifield, C. E. Strouse, J. A. Gladysz, *Organometallics* **1982**, *1*, 1204−1211.
[24] J. M. Fernández, J. A. Gladysz, *Organometallics* **1989**, *8*, 207−219.
[25] M. A. Dewey, Y. Zhou, Y. Liu, J. A. Gladysz, *Organometallics* **1993**, *12*, 3924−3932.
[26] J. J. Kowalczyk, S. K. Agbossou, J. A. Gladysz, *J. Organomet. Chem.* **1990**, *397*, 333−346.
[27] P. E. Garrou, *Chem. Rev.* **1981**, *81*, 229−266.
[28] B. de Klerk-Engels, J. H. Groen, K. Vrieze, A. Möckel, E. Lindner, K. Goubitz, *Inorg. Chim. Acta* **1992**, *195*, 237−243.
[29] S. K. Agbossou, J. M. Fernández, J. A. Gladysz, *Inorg. Chem.* **1990**, *29*, 476−480.
[30] N. Q. Méndez, A. M. Arif, J. A. Gladysz, *Organometallics* **1991**, *10*, 2199−2209.
[31] M. Otto, B. J. Boone, A. M. Arif, J. A. Gladysz, *J. Chem. Soc., Dalton Trans.* **2001**, 1218−1229.
[32] J. H. Merrifield, G.-Y. Lin, W. A. Kiel, J. A. Gladysz, *J. Am. Chem. Soc.* **1983**, *105*, 5811−5819.
[33] J. H. Merrifield, J. H. Fernández, W. E. Buhro, J. A. Gladysz, *Inorg. Chem.* **1984**, *23*, 4022−4029.
[34] J. H. Fernández, J. A. Gladysz, *Inorg. Chem.* **1986**, *25*, 2672−2674.
[35] W. A. Archer, R. Cook, R. Taylor, *J. Chem. Soc., Perkin Trans. 2* **1983**, 813−819.
[36] W. E. McEwen, W.-I. Shiau, Y.-I. Yeh, D. N. Schulz, R. U. Pagilagan, J. B. Levy, C. Symmes Jr., G. O. Nelson, I. Granoth, *J. Am. Chem. Soc.* **1975**, *97*, 1787−1794.
[37] W. Wolfsberger, *Chemiker-Zeitung* **1988**, *112*, 379−381.
[38] D. Magiera, J. Omelanczuk, K. Dziuba, K. M. Pietrusiewicz, H. Duddeck, *Organometallics* **2003**, *22*, 2426−2471.
[39] G. M. Sheldrick, *SHELX-97, Programs for Crystal Structure Analysis*, University of Göttingen, Göttingen, Germany, **1997**.

Received June 23, 2004
Early View Article
Published Online October 26, 2004

 © 2004 Wiley-VCH Verlag GmbH & Co. KGaA, Weinheim

Hydrogen-Bonded Network and Layered Supramolecular Structures Assembled from ClO_4^- Counterions with Unprecedented Monomeric $[AgL_2]^+$ and Chain Polymeric $[AgL_2]_n^{n+}$ Complex Cations (L = Thioamide or Thiourea-Like Ligands)

Joan Sola,*[a] Alexandre López,[a] Robert A. Coxall,[b] and William Clegg*[b]

Dedicated to Professor Heribert Barrera on the occasion of his 87th birthday

Keywords: X-ray diffraction / Silver / Supramolecular chemistry / S ligands / Bridging ligands

The complexes $[Ag(etu)_2]ClO_4$ (**1**) and $[\{Ag(py2tH)_2\}(ClO_4)(H_2O)_{0.5}]_n$ (**2**) have been obtained from the reactions of $AgClO_4$ with the corresponding thioamide ligands (etu = imidazolidine-2-thione; py2tH = pyridine-2-thione). Complex **1**, consisting of centrosymmetric monomeric $[Ag(etu)_2]^+$ cations and ClO_4^- counterions, constitutes the first bis[thio(mono- or di)amide] complex (M = Cu, Ag) known thus far to possess a linear MS_2 mononuclear core. Component ions behave in the crystal structure as complementary partners, with all four N–H groups of each $[Ag(etu)_2]^+$ cation and all four oxygen atoms of each ClO_4^- anion involved in N–H···O–Cl hydrogen bonding associations. This leads to the assembly of a three-dimensional supramolecular network. Complex **2**, whose previously reported structure has been redetermined with higher precision, contains *catena*-$[Ag(py2tH)_2]_n^{n+}$ polymeric cations consisting of linear chains of linked $Ag_2(\mu\text{-}S)_2$ rings, with distorted tetrahedral AgS_4 centres. Supramolecular association through N–H···O–Cl, N–H···O(water) and Cl–O···H–O–H···O–Cl hydrogen bonding, where all N–H groups and H_2O molecules and only one or two oxygen atoms of each ClO_4^- anion are involved, leads to the formation of a two-dimensional layered supramolecular structure. A correlation of some stereochemical parameters and a simple qualitative sulfur-bridge bonding model has been developed for **2** and other related thioamide complexes containing $M_2(\mu\text{-}S)_2$ rings or M–S–M′ single bridges. For these structural units, suitable ranges of tilt and twist dihedral angles have been estimated and assigned to different bonding types.

(© Wiley-VCH Verlag GmbH & Co. KGaA, 69451 Weinheim, Germany, 2004)

Introduction

Considerable attention is currently directed to the study of metal−thioamide coordination chemistry with both heterocyclic and thiourea-like ligands. This interest is mainly encouraged by the flexible coordination capability of the thioamide group which, as a neutral ligand, may be involved, as shown in Scheme 1, in equilibrium with its imino−thiol and amino−thione tautomers. The latter form, with sulfur as donor atom, is dominant for metal coordination, while a "zwitterionic" immonium−thiolate resonance form contributes to the delocalisation of the π-electron density and to some electron enrichment at the thione sulfur atom, which may be seen as formally close to a thiolate sulfur atom. On the other hand, thioamide ligands are easily deprotonated to give their thionate anionic form. In this case, and because of the accumulation of the actual anionic

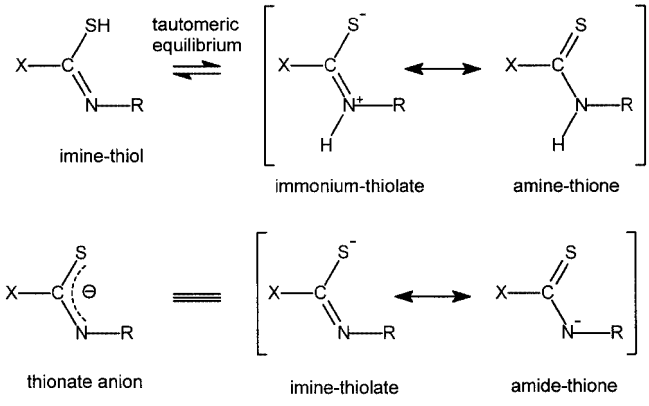

Scheme 1. The equilibrium and structure of the thioamide group in neutral and basic solutions; likely resonance forms contributing to the electronic structure are indicated

[a] Departament de Química, Universitat Autònoma de Barcelona, 08193 Bellaterra, Barcelona, Catalonia, Spain
Fax: (internat.) + 34-93-581-3101
E-mail: joan.sola@uab.es
[b] School of Natural Sciences (Chemistry), University of Newcastle,
Newcastle upon Tyne NE1 7RU, United Kingdom
Fax: (internat.) + 44-191-222-6929
E-mail: w.clegg@ncl.ac.uk

charge mainly at the sulfur atom, its coordination potential is not only closer to that of a thiolate group, but also further enhanced by the donor capacity of the nitrogen atom via the S-to-N backbone.

Extensive reviews and publications, mainly from Raper, focus on the study of the donor behaviour of heterocyclic thioamides and related ligands towards transition and non-transition metal ions,[1−5] silver being the least referenced within the Group 11 metals. One of the points of interest arises from the Cu^{II}-thione redox chemistry as a way of modelling the electronic and structural properties of Cu−cysteine environments in "blue" copper proteins.[2] Additional attention is directed to the employment of thioamide ligands, with the aim of reducing the toxicity associated with coinage metal thiolate complexes and their heteroleptic phosphane derivatives (M^{I} = Au, Ag), which are used as both effective antiarthritic and antitumour (Au),[6] and potential antimicrobial (Ag)[7] drugs. Current research on inorganic-organic hybrid materials containing S,N-donor ligands has led to the characterization of silver thioamide coordination polymers,[8−10] which show interesting infinite chain (1D), layered (2D), and network (3D) structures containing these ligands in a variety of coordination modes.

A bibliographic and database search covering homoleptic complexes of neutral thioamide ligands with monovalent Group 11 metals of known structure, with general formula $[M_x(L)_y]^{x+}$, has revealed an extensive and varied family of compounds, which possess many different stoichiometries ranging from M/L = 1:1 to 1:4 ratios. Although we restrict our attention here to homoleptic complexes, unexpected variations are found when comparing observed structures, and this even occurs, in some cases, for compounds of almost the same chemical formula. No 1:1 cationic complex has so far been crystallographically characterised.[11]

The adamantane-like tetrahedral cage $M_4(\mu\text{-}S)_6$, which is the most frequently encountered structural unit in polynuclear thiolates,[12,13] is also present in cationic thioamide complexes. This tetrahedral cage is known to exist, with no terminal ligands and thus with trigonal coordination of all four metal atoms, in $[Cu_4L_6]^{4+}$ species [L = tu (thiourea),[14,15] thpym2tH$_2$ (tetrahydropyrimidine-2-thione),[16] and with the accommodation of some terminal ligands and both tetrahedral and trigonal metal sites in complexes $[Cu_4(tu)_7](SO_4)_2$,[17] $[Cu_4(tu)_9](NO_3)_4$,[18] and $[\{Cu_4(tu)_6(tu)_{3/2}\}(SO_4)_2]_n$.[19] To the best of our knowledge, none of the reported $[Cu_4L_{10}]^{4+}$ complexes of thioamide ligands contains such a tetrahedral cage with all four metal centres tetrahedrally coordinated.

An alternative structure to the tetrahedral $M_4(\mu\text{-}S)_6$ cage has been found in the complex $[Cu_4(mpym2tH)_6](BF_4)_4$ (mpym2tH = 1-methylpyrimidine-2-thione).[20] It consists of an $M_4(\mu\text{-}S)_4$ eight-membered ring with a rhomboidal planar array of metal atoms. In this case, two S-terminal, two μ_2-S bridging and two μ_3-S,N bridging ligands give rise to CuS_3 and CuS_2N trigonal-planar environments. A silver complex of the same stoichiometry, $[\{Ag_4(py2tH)_6\}(NO_3)_4]_n$ (py2tH = pyridine-2-thione), shows a third structural pattern consisting of a double chain polymeric framework, where silver atoms are linked in a tetrahedral fashion by two μ_2-S and two remarkable μ_4-S bridging ligands.[21]

The structural diversity already noted for some $[M_4L_6]^{4+}$ cations also extends to $[M_4L_9]^{4+}$ species. As cited above, a *tetrahedro*-$[M_4(\mu\text{-}SR)_6]$ cage is present in $[Cu_4(tu)_9]^{4+}$,[18] whereas a *quadro*-$[M_4(\mu\text{-}SR)_4]$ ring containing a planar M_4 arrangement has been established in the complex $[Cu_4(etu)_9](NO_3)_4\cdot 6H_2O$ [etu = imidazolidine-2-thione (ethylenethiourea)],[1,22] where four μ_2-S bridging, four S-terminal and one central μ_4-S bridging ligand account for the tetrahedral geometry of each metal atom. A third structure for this stoichiometry has been encountered in the infinite polymer $[\{Cu_4(tu)_9\}(NO_3)_4]_n$,[23] consisting of chains of linked *quadro*-$[M_4(\mu\text{-}SR)_6(SR)_2(SR)_{2/2}]$ rings, with a planar arrangement of the four metal atoms and tetrahedral MS_4 environments.

The reported structures of the cationic complexes with the general formula $[ML_2]_n^{n+}$ include monomeric (the only cationic thioamide complexes known for Au^{I}) and cyclic tetrameric discrete species, and infinite chain polymers (we return later to some details of these structures).

Two discrete and two polymeric structures have been described for cationic thioamide complexes of stoichiometry M/L = 2:5, none of which contains a *tetrahedro*-$[M_4(\mu\text{-}SR)_6]$ cage. Two trigonal-planar CuS_3 units share a unique μ_2-S bridging ligand in the dinuclear complex $[Cu_2(mimtH_2)_5]SO_4$ (mimtH$_2$ = 1-methylimidazoline-2-thione).[24] A planar core of four tetrahedrally coordinated metal atoms, which is encompassed by four S-terminal and six μ_2-S bridging ligands, *quadro*-$[(MSR)_4(\mu\text{-}SR)_6]$, constitutes the structural unit adopted by the discrete tetranuclear compound $[Cu_4(bzimtH_2)_{10}](ClO_4)_4$ (bzimtH$_2$ = benzimidazoline-2-thione).[25] Making allowances for the different thioamide ligands and counter-anions present in this complex and in the previously cited $[\{Cu_4(tu)_9\}(NO_3)_4]_n$,[23] detachment of one of the terminal ligands from the discrete structure gives rise to the repeat unit *quadro*-$[M_4(\mu\text{-}SR)_6(SR)_3]$ that generates the polymeric framework of the latter.

While the structure of the infinite polymer $[\{Cu_2(tu)_5\}SO_4]_n$ is formed by cationic chains of alternating trigonal-planar MS_3 and tetrahedral MS_4 sites,[26] that of the polymeric compound $[\{Cu_4(tu)_{10}\}(SiF_6)_2]_n$[27] is somewhat more complicated. It consists of infinite chains of alternating $[(MSR)_3(\mu\text{-}SR)_3]$ six-membered rings and μ_2-S bridging ligands, which are in turn cross-linked via $[\{M(SR)_2\}_2(\mu\text{-}SR)_2]$ four-membered rings to give a three-dimensional polymer with all the metals in tetrahedral MS_4 sites.

Cationic thioamide complexes of stoichiometry corresponding to the general formula $[ML_3]_n^{n+}$ are the most numerous for Cu and Ag, with crystallographically demonstrated nuclearities *n* of 1, 2, and (in only one case) 4. While monomers, as in $[Ag(mimtH_2)_3](NO_3)$, show a trigonal planar MS_3 coordination,[28−31] dimeric cations, as in $[Ag_2(dmtu)_6](ClO_4)_2$ (dmtu = *N*,*N*′-dimethylthiourea), contain $[\{M(SR)_2\}_2(\mu\text{-}SR)_2]$ four-membered rings with tetrahedral MS_4 sites.[32−36] These latter sites are also present in

 © 2004 Wiley-VCH Verlag GmbH & Co. KGaA, Weinheim

the complex $[Cu_4(tu)_{12}](SO_4)_2$,[37] which contains a *quadro*-$[\{Cu(SR)_2\}_4(\mu\text{-}SR)_4]$ cationic eight-membered ring. Finally, the structural pattern richest in thioamide ligands possesses a stoichiometry M/L = 1:4 and corresponds, as in $[Ag(mpy2tH)_4]BF_4$ (mpy2tH = 1-methylpyridine-2-thione), to monomeric complexes with an MS_4 (M = Cu, Ag) tetrahedral coordination environment.[38−40]

As evidenced by the stoichiometry-structure relationships outlined above, an extensive range of stereochemical arrangements is available for $[M_xL_n]^{x+}$ thioamide complexes. These, however, are significantly less explored for silver than for the other two coinage metals.

With the aim of obtaining further structural data, particularly for cationic thio(mono- or di)amide complexes, as well as examining their relationship to previous structures, we have carried out the synthesis and crystal structure determination of the compounds $[Ag(etu)_2]ClO_4$ (**1**) and $[\{Ag(py2tH)_2\}(ClO_4)(H_2O)_{0.5}]_n$ (**2**). Complex **1**, containing mononuclear $[M(thioamide)_2]^+$ cations with a linear MS_2 coordination, represents the first reported Ag complex displaying this structural pattern. Although not yet encountered for Cu, this pattern corresponds to the only structural type established thus far for related Au complexes. The structure of complex **2** was previously reported with a misprinted space group and only a brief discussion;[21] the redetermination reported here, from low-temperature data, is of considerably greater precision (standard uncertainties reduced by a factor of 3 or more) and permits more detailed analysis.

Results and Discussion

Spectroscopic Properties

In agreement with the increasing participation of the immonium-thiolate resonance form (Scheme 1) to the electronic structure of a thioamide complex on S-coordination, the IR bands possessing significant contribution from ν(CS) or ν_{as}(N−C−N) vibrations (at 510, 1500 cm^{-1} in etu as free ligand) shift to lower[41] and higher[42] frequencies (495, 1522 cm^{-1}), respectively, in the spectrum of complex **1**; ν(SH), which appears as a weak band near 2500 cm^{-1} in free py2tH, is absent in the IR spectrum of complex **2**. This fact, together with the positive shift of the ring breathing mode[43] of py2tH itself (984 cm^{-1}) to 995 cm^{-1} in the same complex, is also in accordance with S-coordination. As expected from the role of the perchlorate as counter-anion, no significant splitting of its IR-active bands, associated with $\nu(T_2)$ (centred at 1090 cm^{-1}) and $\delta(T_2)$ (626 cm^{-1}) vibrational modes, is observed in the spectra of the two complexes.

S-coordination causes small downfield shifts relative to the free ligand in the ^1H NMR spectra, the largest [$\Delta\delta$ = 1.0 (**1**), 0.7 (**2**) ppm] occurring for the N−H protons.[44] The chemical shifts of these [8.90 (**1**), 14.10 (**2**) ppm], as well as their positive coordination shifts, reflect, as in the IR spectra, the relevant contribution of the immonium-thiolate resonance form in both complexes. ^{13}C NMR spectra are more sensitive to S-donation, the carbon atom of the thione group being the most affected, with high-field coordination shifts[45,46] of δ = −5.2 and −10.2 ppm, respectively, for complexes **1** and **2**.

Structures of the Complexes

Homoleptic complexes of general formula $[ML_2]X$, where M = Cu^I or Ag^I, X^- is an uncoordinated anion, and L is a neutral thio(mono- or di)amide ligand, are not very numerous. To the best of our knowledge, seven complexes have so far been crystallographically characterised. Six of them are $[M(dmtu)_2]X$ (M = Cu, X = NO_3^-;[47] M = Ag, X = ClO_4^- [36]), $[Cu(quinoline\text{-}2\text{-}thione)_2]X$ (X = ClO_4^-, $PO_2F_2^-$),[48] and $[Ag(py2tH)_2]X$ (X = BF_4^-, ClO_4^-),[21] all consisting of linear-chain $[M(\mu\text{-}S)_2]_\infty$ polymeric cations formed by distorted MS_4 tetrahedra, which are linked by sharing opposite edges. The structures of the last two compounds have appeared recently, ostensibly as anhydrous and isomorphous in space group *P*1, though the corresponding entries (with refcodes MOGNAF and MOGNEB) in the Cambridge Structural Database (CSD, version 5.24, November 2002)[49] actually show them to be hydrates and in space group $P\bar{1}$. As only a brief description of the cationic chains was given by the previous authors, with no information on other aspects of the structures, and as our results for the perchlorate are more precise, from low-temperature data, further details of the crystal structure will be given here for complex **2**. The remaining previously reported compound of M/L = 1:2 stoichiometry, $[Ag(1\text{-}azacycloheptane\text{-}2\text{-}thionato)_2]_4(NO_3)_4$, has a totally different structure consisting of discrete $[(AgSR)_4(\mu\text{-}SR)_4]$ cationic rings with trigonal AgS_3 sites.[50]

By contrast, corresponding complexes with Au^I are more numerous and all of those known have mononuclear structures with strictly or essentially linear AuS_2 coordination. Reported $[AuL_2]X$ complexes include those with L = etu, X = $[AuI_2]^-$ [51] or Cl^-;[52] L = tu, X = Br^- [53] or ClO_4^-;[54] L = py2tH, X = ClO_4^-;[55] L = dmtu or detu, X = ClO_4^-.[56] The $[Au(etu)_2]^+$ cation in $[Au(etu)_2]Cl\cdot H_2O$ is somewhat more distorted, with an S−Au−S angle of 167.1°, owing to the *cis* configuration of the heterocyclic rings of the two ligands. This is favoured by the formation of hydrogen bonds that involve the O atom of water and two N−H groups belonging to different ligands.[52]

Despite the fact that $Ag(tu)_2Cl$ is not genuinely homoleptic, its polymeric structure may be referred to here for comparison.[57] It contains both nearly trigonal-planar AgS_3 and flattened tetrahedral $AgS_3\cdots Cl$ environments. The corresponding complex $Cu(tu)_2Cl$[58] adopts a similar structure.

Complex 1

This consists of ClO_4^- anions and mononuclear $[Ag(etu)_2]^+$ cations. The cation (Figure 1) lies on a crystallographic inversion centre, and thus the coordination of Ag is strictly linear (Table 1). The anion lies on a two-fold rotation axis and is disordered over two orientations. Interac-

 © 2004 Wiley-VCH Verlag GmbH & Co. KGaA, Weinheim

tions among the ions appear to be of normal electrostatic and van der Waals character, together with hydrogen bonding as described below, with no significant influence on metal coordination. This is supported by the fact that the shortest Ag···Ag separation, 3.513 Å, is more than twice the van der Waals radius (3.44 Å), and the closest inter-cation Ag···S contact, 3.275 Å, is markedly greater than the sum of the corresponding covalent radii (2.55 Å) and only slightly less than the sum of the van der Waals radii (3.50 Å).[59] This is the first homoleptic silver complex of thio-(mono- or di)amide ligands with a silver/sulfur stoichiometry of 1:2 for which a monomeric cation has been crystallographically established. The closest previous approach to this is in the structure of [Ag(*N*-(diethylaminothiocarbonyl)benzamidine-*S*)$_2$]NO_3, where a secondary Ag···S interaction between two adjacent molecules (3.034 Å) induces a significant bending at the primary S−Ag−S centre (159.4°).[60]

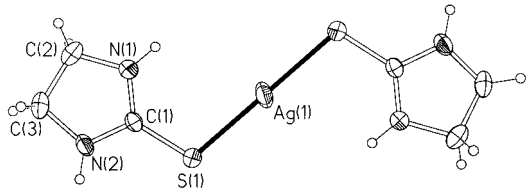

Figure 1. The structure of the cation in complex **1**, with 50% probability displacement ellipsoids and the labelling of the crystallographically independent atoms

Table 1. Selected bond lengths [Å] and angles [°] for **1**

Ag(1)−S(1)	2.4058(8)	Ag(1)−S(1A)	2.4058(8)
S(1)−Ag(1)−S(1A)[a]	180	Ag(1)−S(1)−C(1)	105.80(10)

[a] Symmetry operation for equivalent atoms: A: 1 − *x*, 1 − *y*, 1 − *z* (inversion centre).

The etu ligand is approximately planar and forms a twist dihedral angle (see later for a definition and discussion of twist and tilt dihedral angles with respect to the coordination of bridging ligands) of 11.4° with the central C−S−Ag−S−C segment, so that the whole cation does not deviate greatly from planarity. This near-planarity, together with the 105.8° bond angle at S(1), suggests that coordination of the ligand to Ag^I is essentially through a sulfur lone pair in an in-plane sp^2 hybrid orbital. The cations are arranged in planes corresponding to the (202) lattice planes of the crystal structure, as shown in Figure 2, with the anions lying between these planes. The main deviation of the ligand from planarity is a small distortion towards an envelope conformation, with C(3) as the flap; this can also be seen in Figure 2.

A three-dimensional framework of N−H···O−Cl hydrogen bonding, involving both the amine N−H groups of each ligand and all four perchlorate oxygen atoms, reinforces the ionic interactions and gives rise to a supramolecular assembly of complex cations and ClO_4^- anions, shown in Figure 3 (where only one disorder component of each anion is included). Despite the two-fold disorder of

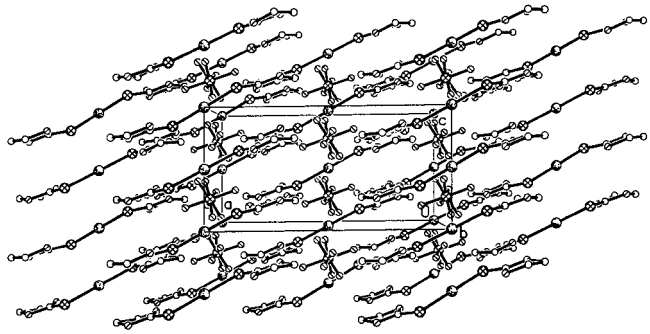

Figure 2. The crystal structure of complex **1**, viewed along the *b* axis, showing the parallel stacking of cation sheets with anions between them; H atoms are omitted

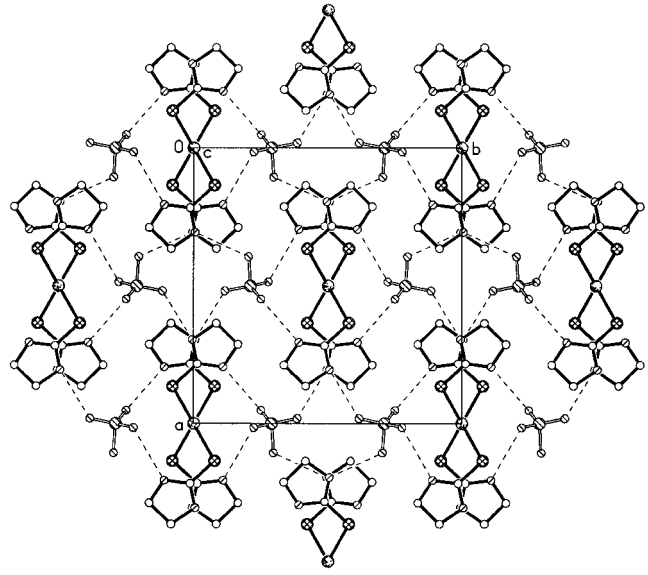

Figure 3. The crystal structure of complex **1**, viewed along the *c* axis, showing NH···O hydrogen bonding interactions; only one disorder component is included for each anion; H atoms are omitted for clarity

the anions, the hydrogen bonding interactions appear to be significant; details of their geometry are given in Table 2. Comparable N···O distances are found in similar Ag^I com-

Table 2. Geometry of hydrogen bonds [Å, °] in the structures of **1** and **2** (symmetry operation for equivalent atoms: B: 1 − *x*, *y*, 1/2 − *z*; C: 1/2 + *x*, 1/2 + *y*, *z*; D: 3/2 − *x*, 1/2 + *y*, 1/2 − *z*; E: 1 − *x*, 1 − *y*, 1 − *z*; F: *x*, 1 + *y*, *z*; G 1 + *x*, *y*, *z*)

D−H...A	D−H	H···A	D···A	D−H···A
Compound **1**				
N(1)−H(1)...O(1)	0.88	2.16	2.950(11)	149
N(1)−H(1)...O(3B)	0.88	2.29	3.109(10)	154
N(2)−H(2)...O(2C)	0.88	2.26	2.998(6)	141
N(2)−H(2)...O(4D)	0.88	2.38	2.904(7)	118
Compound **2**				
N(1)−H(1)...O(22)	0.88	2.03	2.893(4)	165
N(2)−H(2)...O(31E)	0.88	2.01	2.867(3)	165
N(3)−H(3)...O(31)	0.88	2.09	2.946(4)	165
N(4)−H(4)...O(14)	0.88	2.02	2.895(5)	170
O(31)−H(31a)...O(13F)	0.82(3)	2.00(3)	2.805(4)	164(4)
O(31)−H(31b)...O(22G)	0.82(3)	2.30(3)	3.036(4)	149(4)

 © 2004 Wiley-VCH Verlag GmbH & Co. KGaA, Weinheim

plexes of thiourea and thioamide ligands recorded in the CSD.

Complex 2

The complex $[\{Ag(py2tH)_2\}(ClO_4)\cdot 0.5(H_2O)]_n$ contains polymeric $[Ag(py2tH)_2]_n^{n+}$ cations, discrete ClO_4^- anions, and uncoordinated water molecules. All three chemically distinct components are linked together by a network of hydrogen bonds, in addition to the ionic interactions involving the polymeric cations and the anions.

All the py2tH ligands employ only sulfur atoms for coordination to Ag^I, each ligand bridging a pair of metal atoms in distorted AgS_4 tetrahedral environments, to give linear polymeric chains of linked $Ag_2(\mu\text{-}S)_2$ rings, which run parallel to the crystallographic *b* axis. Figure 4 shows the three crystallographically independent Ag_2S_2 rings, and Figure 5 the resultant chain polymer. The two outer rings in Figure 4 are crystallographically centrosymmetric, and hence are strictly planar, with the ligands in *anti* configurations. The central ring, by contrast, is not planar but folded, with its ligands in the *syn-exo* configuration; the two AgS_2 planes define a dihedral (hinge) angle of 152° about the S···S diagonal. Planar *anti* and folded *syn* Ag_2S_2 rings thus alternate along the chain. Ag−S bond lengths span the range

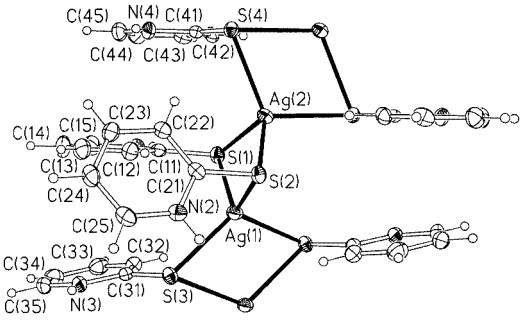

Figure 4. The asymmetric unit of the polymeric cation chain of complex **2**, together with additional Ag^I ions and ligands to complete the bonding environment of this unit; the crystallographically independent atoms are labelled, and displacement ellipsoids are drawn at the 50% probability level

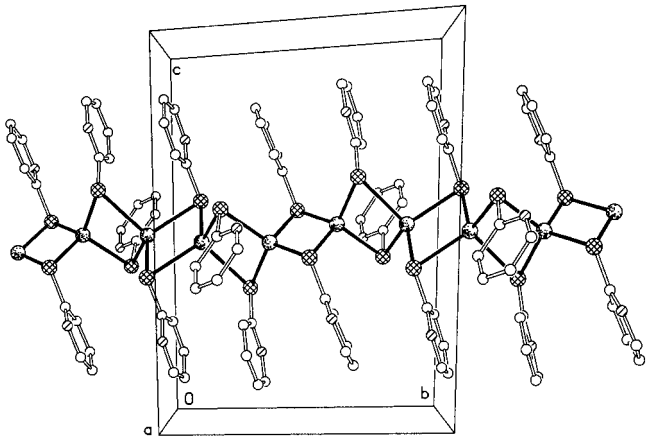

Figure 5. A section of the polymeric cation chain of complex **2**; H atoms are omitted

Table 3. Selected bond lengths [Å] and angles [°] for **2** (symmetry operations for equivalent atoms: H: $-x$, $1-y$, $1-z$; I: $-x$, $-y$, $1-z$)

Ag(1)−S(1)	2.5491(7)	Ag(1)−S(2)	2.6122(7)
Ag(1)−S(3)	2.5724(7)	Ag(1)−S(3H)	2.6900(7)
Ag(2)−S(1)	2.7770(7)	Ag(2)−S(2)	2.5901(7)
Ag(2)−S(4)	2.5873(7)	Ag(2)−S(4I)	2.6322(7)
S(1)−Ag(1)−S(2)	115.40(2)	S(1)−Ag(1)−S(3)	120.29(2)
S(1)−Ag(1)−S(3H)	89.62(2)	S(2)−Ag(1)−S(3)	100.80(2)
S(2)−Ag(1)−S(3H)	115.20(2)	S(3)−Ag(1)−S(3H)	116.542(17)
S(1)−Ag(2)−S(2)	108.71(2)	S(1)−Ag(2)−S(4)	103.94(2)
S(1)−Ag(2)−S(4I)	104.60(2)	S(2)−Ag(2)−S(4)	119.39(2)
S(2)−Ag(2)−S(4I)	108.48(2)	S(4)−Ag(2)−S(4I)	110.658(18)
Ag(1)−S(1)−Ag(2)	64.735(17)	Ag(1)−S(2)−Ag(2)	66.641(16)
Ag(1)−S(3)−Ag(1H)	63.458(17)	Ag(2)−S(4)−Ag(2I)	69.342(18)

2.5491(7)−2.7770(7) Å (Table 3), the sum of the corresponding covalent radii being about 2.55 Å.[59] The nonplanar ring contains the least and the most symmetrical bridges, with the difference in Ag−S bond lengths being approximately 0.23 Å for S(1) and only 0.02 Å for S(2), while it is 0.12 Å for S(3) and 0.04 Å for S(4). Other structural parameters characteristic of these Ag_2S_2 rings are the Ag···Ag distances ranging from 2.769 to 2.969 Å (less than twice the covalent radius, 3.06 Å[59]) and the markedly acute Ag−S−Ag angles, between 63.5 and 69.3°.

Distortion of the two crystallographically independent AgS_4 centres from a regular tetrahedron is clearly reflected in the S−Ag−S angles [Table 2; a range of 30.7° for Ag(1) and 15.5° for Ag(2)], and in the dihedral angles formed by the two AgS_2 half-ring planes at each Ag atom [74.5° for Ag(1) and 86.9° for Ag(2); these would be 90° for a regular tetrahedron]. These figures show that the tetrahedral coordination is substantially less regular for Ag(1). The surrounding sheaths of pyridine rings prevent secondary covalent interactions between Ag and S atoms of different chains. However, the N−H amine groups of these rings, together with the ClO_4^- anions and the uncoordinated water molecules, provide a hydrogen-bonding pathway linking neighbouring cationic chains, causing these to assemble into a two-dimensional sheet supramolecular structure, as shown in Figure 6, where parts of two chains are included, together with the anions and water molecules lying between them. Contacts between hydrogen-bonded sheets involve only ligand C−H groups and perchlorate oxygen atoms, which do not take part in the interactions within the sheets.

Details of the hydrogen bonds are given in Table 2. Each water molecule (there is one for every two Ag^I centres and two anions) acts as a donor in two hydrogen bonds to perchlorate oxygen atoms, and as an acceptor of two hydrogen bonds from amine groups. Thus, two of the four crystallographically independent amine groups form hydrogen bonds to water molecules, while the other two form hydrogen bonds to perchlorate anions. There are two crystallographically distinct anions; for one of them, two oxygen atoms act as hydrogen-bond acceptors (O13 from water, O14 from amine), while the other has just one oxygen atom (O22) accepting two hydrogen bonds, one from water and

 © 2004 Wiley-VCH Verlag GmbH & Co. KGaA, Weinheim

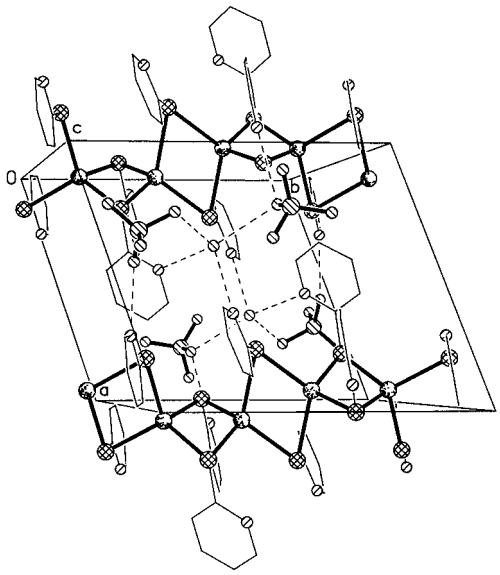

Figure 6. The crystal structure of complex **2**, showing hydrogen bonding interactions as dashed lines; H atoms are omitted for clarity

the other from an amine group. There is no disorder in the structure, and the hydrogen bonds are somewhat stronger (shorter and more linear) than those in the structure of complex **1** discussed above.

Stereochemistry and Sulfur-Bridge Bonding

The bonding of the ligands to Ag^I in the polymeric complex **2** is clearly not as simple as the single lone-pair donation from the sulfur sp^2 orbital to the metal atom for the terminal ligands in **1**. Examination of some details of the varied orientation of the bridging ligands may be informative in order to rationalise the stereochemistry and metal−ligand bonding for the Ag_2S_2 rings of the polymeric cation in **2**, in terms of electron donation by a combination of suitable molecular orbitals of the ligands. These include one or both of the two non-bonding sulfur sp^2 in-plane hybrid orbitals and the thioamide pπ-molecular orbital of the heterocycle; this orbital is perpendicular to the others and is concentrated in the C−S portion of the ligand molecule, with a major contribution of the sulfur atom.[61] These bridging ligand molecular orbitals (HOMOs), each accommodating one electron pair, are able to interact with two

Table 4. Some angular parameters and proposed sulfur-bridge bonding for **2** and other related thioamide complexes containing $M_2(\mu_2\text{-}S)_2$ rings or M−S−M′ single bridges

Bridging sulfur atom	Tilt angle[a]	Twist angles[b]	Δ_{tw}[c]	M–S–M' bond angle	M–S–M bonding mode[d]	Ref.
[{Ag(py2tH)$_2$}(ClO$_4$)(H$_2$O)$_{0.5}$]$_n$ (**2**)						
S(1) (ring 1)	79.2	(−31.1, 36.1)	67.2	64.7	sp^2 (C)	this work
S(2) (ring 1)	84.6	(21.5, 88.8)	67.3	66.6	sp^2 + C=S pπ (B)	
S(3) (ring 2)	82.4	(−32.1, 34.0)	66.1	63.5	sp^2 (C)	
S(4) (ring 3)	85.5	(−1.7, 70.0)	71.7	69.3	sp^2 + C=S pπ (B)	
[{Ag(*N*,*N*'-dimethylthiourea)$_2$}(ClO$_4$)]$_n$						
S(1) (ring1)	83.0	(18.5, 94.5)	76.0	74.9	sp^2 + C=S pπ (B)	[36]
S(2) (ring 2)	73.7	(18.0, 98.0)	80.0	76.6	sp^2 + C=S pπ (B)	
(μ_4-S) in [{Ag$_4$(py2tH)$_6$}(NO$_3$)$_4$]$_n$						
S(2)[e]	88.6	(−36.9, 41.9)	78.8	72.3	sp^2 (C)	[21]
Cu$_2$(μ_2-S)$_2$ rings in [Cu$_2$(py2tH)$_6$]X$_2$ (X = Cl; X = Cl, Br; X = *p*-MeC$_6$H$_4$SO$_3$)						
(X = Cl) S	80.6	(6.5, 84.5)	78.0	74.3	sp^2 + C=S pπ (B)	[33]
(X = Cl) S	79.9	(7.0, 85.0)	78.0	74.6	sp^2 + C=S pπ (B)	[62]
(X = Br) S	82.0	(6.5, 83.5)	77.0	73.8	sp^2 + C=S pπ (B)	[62]
(X = *p*-MeC$_6$H$_4$SO$_3$) S	86.1	(−37.0, 38.0)	75.0	69.6	sp^2 (C)	[35]
[{Cu(quinoline-2-thione)$_2$}(PO$_2$F$_2$)]$_n$						
S(1) (chain 1)	90[f]	(−45.0, 45.0)	90.0	84.0	sp^2 + C=S pπ (B)	[48]
S(2) (chain 2)	90[f]	(−44.0, 44.0)	88.0	84.0	sp^2 + C=S pπ (B)	
Cu$_2$(μ_2-S)$_2$ rings in [*cyclo*-{(μ_2-L)$_6$(CuL)$_4$}](ClO$_4$)$_4$·14 H$_2$O [L = benzimidazoline-2-thione]						
S(3)	88.3	(−28.5, 44.5)	73.0	69.1	sp^2 (C)	[25]
S(4)	86.0	(−17.5, 54.5)	72.0	66.8	sp^2 + C=S pπ (B)	
M–S–M' bridges in [MCl(tu)$_2$]$_n$ (M = Ag, Cu)						
(M = Ag) S(2)	76.2	(−42.1, 58.8)	79.1	77.3	C=S pπ (D)	[57]
(M = Ag) S(3)	26	(7.5, 167.0)	159.5[g]	133.5	sp^2 + sp^2 (A)	
(M = Cu) S(2)	69.8	(−39.3, 54.6)	86.1	82.5	C=S pπ (D)	[58]
(M = Cu) S(3)	14.8	(0.6, 169.6)	169.0[g]	138.1	sp^2 + sp^2 (A)	
Cu–S–Cu bridge in [Cu$_2$Cl$_2$(etu)$_3$(μ-etu)]						
S(2)	12.6	(−4.8, 167.0)	171.8[g]	137.3	sp^2 + sp^2 (A)	[63]

[a] Dihedral angle of each independent planar thioamide ligand with respect to its M_2S_2 planar lozenge or its M−S−M′ unit. [b] Pair of dihedral angles of each independent ligand about its respective M−S−C and M′−S−C planes, (α_1, α_2), where $\alpha_2 > \alpha_1$. [c] For bonding modes A, B and C, $\Delta_{tw} = \alpha_2 - \alpha_1$; for mode D, $\Delta_{tw} = 180 - (\alpha_2 + |\alpha_1|)$. [d] Sulfur-localised molecular orbitals, each with one electron pair, mainly contributing to the bridge bonding. [e] S2 lies on a mirror plane, so that the two Ag−S2−Ag′ and Ag−S2−Ag′ equivalent moieties constituting the quadruple bridge correspond to a pair of bonding systems of type C. [f] Crystallographically imposed value. [g] For this bonding mode A, there is no relationship between Δ_{tw} and the M−S−M′ bond angle.

 © 2004 Wiley-VCH Verlag GmbH & Co. KGaA, Weinheim

vacant tetrahedral sp^3 or other hybrid orbitals, one for each silver atom of the Ag−S−Ag bridge. Considerations of this kind, aimed at proposing an M−S bonding model from an analysis of the stereochemistry, have previously been performed for dinuclear[1,32] and some polymeric[22,23,27,55,56] sulfur-bridged complexes of thioamide or thiourea ligands. All these earlier examples, however, contain both bridging and terminal ligands, which is not the case here.

Two structural parameters may be used to describe the orientation of each of the four independent planar bridging ligands in the complex cation of **2**. These are: (a) the "tilt" angle of each ligand S−C bond with respect to its Ag−S−Ag′ planar unit, and (b) the pair of "twist" dihedral angles of each ligand plane relative to its respective Ag−S−C and Ag′−S−C planes (Figure 7). Values of these parameters have been calculated for **2** and for related complexes (in this case from the corresponding crystallographic data in the CSD), and they are listed in Table 4.

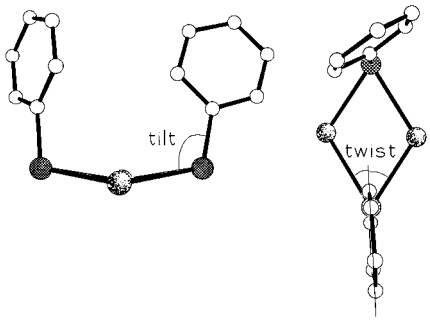

Figure 7. Two views of an M_2S_2 ring with bridging ligands, illustrating the tilt and twist angles characterising the stereochemistry of the ligand arrangement

As defined above, a "tilt" angle close to 0° would imply that the ligand plane and the Ag_2S moiety tend to be coplanar, so that the two S−Ag bonds are formed primarily from the two sulfur sp^2 orbitals with their two electron pairs. This corresponds to an Ag−S−Ag three-centre, four-electron bonding system (type **A**), with ideal "twist" angles of 0° and 180° and an Ag−S−Ag bond angle of 120°; here the line defined by the two N atoms (in thiourea ligands) or its corresponding N···C vector (in thiomonoamides) would be essentially parallel to the Ag···Ag line. Some examples of this arrangement[57,58,63] are included in Table 4, which also shows that all four ligands in complex **2** have tilt angles between 79 and 85° and pairs of "twist" angles markedly different from 0 or 180°. Thus, each of these ligands is almost normal to the Ag_2S unit to which it is attached, making the simultaneous involvement of both sulfur sp^2 orbitals and electron pairs in the formation of Ag−S−Ag bridges unlikely.

On the other hand, a "twist" angle close to 0° would indicate that one of the two silver atoms of a given Ag−S−Ag′ bridge lies nearly in the ligand plane, allowing conventional electron donation from one sulfur sp^2 orbital to an orbital of the Ag atom. In order to complete the bonding scheme for the Ag−S−Ag′ bridge, taking into account that the planar bridging ligands are approximately normal to the Ag−S−Ag′ fragment (Table 4), optimal overlap of an orbital on the Ag′ atom would be obtained by using the thioamide (C=S) pπ-MO, which is perpendicular to the sp^2 orbital. In this case, the Ag−S−Ag′ three-centre, four-electron bridge bonding system (type **B**) would be related to a pair of ideal "twist" angles of 0° and 90° for the atoms Ag and Ag′, respectively (difference, $\Delta_{tw} = 90°$), provided the corresponding "tilt" angle is close to 90°. While this optimal bonding model presumes an ideal value of about 90° for the Ag−S−Ag′ bond angle, this is actually significantly lower in most M_2S_2 rings formed with thioamide ligands (in the range 67−80°, with a few reaching 90°; below 70° in our case).[1,64]

The results in Table 4 show that, for complex **2**, only ligands 2 and 4 [i.e. those containing S(2) and S(4)] approach the above ideal conditions, as can be seen by comparison of Figures 4 and 7. Whereas one of the two twist angles of these ligands closely matches the value of 90° [S(2)] or 0° [S(4)], the second twist in each of the two pairs departs by about 20° from the ideal value. However, the differences between the two twist angles within the pairs, $\Delta_{tw} = 67.3°$ [S(2)] and 71.7° [S(4)], are very close to the respective values of the Ag−S−Ag′ bond angles (66.6, 69.3°), both being far from 90° in contrast to the bonding model initially assumed. These features suggest that maximal overlap of either one sulfur sp^2 or (C=S) pπ-MO orbital on the bridging thioamide ligand is not accomplished in the Ag(1)−S(2)−Ag(2) unit nor in the ring containing ligand 4, so that the proposed bonding mode needs some modification to allow for the actual value of Δ_{tw}. This parameter corresponds, in fact, to the dihedral angle defined by the Ag−S−C and Ag′−S−C planes about the common S−C line, and is always slightly larger than the corresponding Ag−S−Ag′ in-plane angle. Exact coincidence of these two angles would only be attained if the S−C internuclear vector were normal to the Ag−S−Ag′ plane, the difference between the two values increasing as the inclination of the S−C vector decreases.

In order to identify a better correlation of a given pair of twist angles (α_1, α_2 with $\alpha_2 > \alpha_1$ and $\Delta_{tw} = \alpha_2 - \alpha_1$) with the bonding mode **B**, we consider angles within the limits $-45 \le \alpha_1 \le 45$ and $45 \le \alpha_2 \le 135°$. These, with associated tilt angles close to 90°, would correspond to the full set of possible orientations of the bridging thioamide ligands, given by (α_1, $\alpha_1 + \Delta_{tw}$), to which both sulfur sp^2 and (C=S) pπ-MO orbitals would contribute. Among all these geometries, optimal overlap with one of the two Ag orbitals would be achieved through the sp^2 orbital in the (0, Δ_{tw}) ideal case ($\alpha_1 = 0$), but through the (C=S) pπ orbital for the (90 − Δ_{tw}, 90) ideal pair ($\alpha_2 = 90°$). Conversely, poor overlap would be expected for orientations close to those defined by the extreme values of the given ranges, (−45, 45) and (45, 135). A combination of the steric requirements of the bridging ligands, hydrogen-bonding effects and crystal packing requirements affects to some extent the ideal geometry based on electronic factors alone, and gives rise to the large variations observed in the structural parameters α_i and Δ_{tw} (see Table 4). This bonding model **B**, which allows

 © 2004 Wiley-VCH Verlag GmbH & Co. KGaA, Weinheim

us to rationalise the stereochemistry of the ligands 2 and 4 in complex **2**, has been proposed to be involved in most of the $M_2(\mu\text{-}S)_2$ (M = Ag, Cu) rings in reported thio(mono- or di)amide complexes.[1,57]

Although all four ligands in complex **2** show tilt angles close to 90°, ligands 1 and 3 behave differently from the case of ligands 2 and 4 considered above, in that their respective twist angles have opposite signs and very close absolute values (Table 4). As can be seen in Figures 4 and 7, this means that the planes corresponding to ligands 1 and 3 are not only almost normal to their respective Ag−S−Ag′ units, but virtual bisectors of these. With this geometry, the only orbital that a thioamide ligand can contribute to bridge bonding is one sulfur non-bonding sp^2 orbital with its electron pair. In either of these ligands, this orbital with two orbitals of a pair of Ag atoms would lead to delocalised three-centre, two-electron, electron-deficient bonding systems (type **C**) at the S(1) and S(3) bridges, as was previously proposed for the Cu_2S_2 rings present in the $[Cu_4(tu)_9]_n(NO_3)_{4n}$ polymer.[23] This assessment is supported by the short metal−metal distances and accompanying sharp bridge angles [Ag(1)···Ag(1A) 2.769 Å, Ag(1)−S(3)−Ag(1A) 63.46°; and Ag(1)···Ag(2) 2.858 Å, Ag(1)−S(1)−Ag(2) 64.74°], while corresponding values for bridges at S(2) and S(4), assumed to be three-centre, four-electron conventional bonding systems, are larger [Ag(1)···Ag(2) 2.858 Å, Ag(1)−S(2)−Ag(2) 66.64°; and Ag(2)···Ag(2B) 2.969 Å, Ag(2)−S(4)−Ag(2B) 69.34°]. Therefore, a pair of twist angles (−α, α), where $\Delta_{tw} = 2\alpha$, would correspond to the above ideal orientation in which a thioamide plane is exactly bisecting the M−S−M′ angle, the bridge bonding being probably related to an electron-deficient system to which sulfur supplies only two electrons from one of its two sp^2 orbitals. However, other geometry-determining factors such as crystal packing, hydrogen bonding or steric demands of the ligands, can cause the thioamide plane to deviate somewhat from the bisector of the M−S−M′ plane while preserving the close perpendicularity between these planes. This results in general orientations for this bonding mode, which are more accurately denoted by pairs of different twist angles ($-\alpha_1$, α_2), with suitable α_i values in the approximate range $25° < |\alpha_i| < 45°$ and where $\Delta_{tw} = \alpha_2 + |\alpha_1| < 80°$. This latter condition ensures a relatively sharp bridge angle and concomitant short metal−metal distance, both characteristic features of this bonding mode **C**.

Although not present in complex **2**, it is worth mentioning here another ideal orientation in which a thioamide plane, also tending to be orthogonal to its M−S−M′ unit, would not lie in the bisector plane of the latter but perpendicular to it. Here, the N···N line (in thiourea ligands) or its corresponding N···C vector (in thiomonoamides) would be parallel to the M···M′ line. In this geometry, the (C=S) pπ-MO orbital, with the sulfur atom as the major contributor, would extend nearly along the bisector of the M−S−M′ angle, thus allowing the interaction of this ligand-based orbital, accommodating one electron pair, with two empty orbitals of the metal atoms. This would also give rise to a delocalised three-centre, two-electron, electron-deficient bridge bonding system (type **D**). Whereas (−α, α) is a general notation for twist angles that would hold for the two ideal orientations attributable to electron-deficient bridge bonding, the relation $\Delta_{tw} = 180 - 2\alpha$ applies only to the present situation. As reported for $M(tu)_2Cl$ (M = Cu, Ag),[55,56] to the best of our knowledge the only known complexes for which sulfur-bridge bonding has been explained according to model **D**, the overall effect of both stereochemical constraints and electronic factors leads to a deviation of the thiourea plane, and thus of the N···N line, by about 8° from the direction of the M···M′ line, the tilt angle being reasonably close to 90°. For electron-deficient sulfur-bridged bonding with only two electrons supplied by the thioamide (C=S) pπ-MO (type **D**), probable general orientations would be given, though on the basis of only those two complexes, by pairs of twist angles ($-\alpha_1$, α_2), with $\Delta_{tw} = 180 - (\alpha_2 + |\alpha_1|)$ and suitable α_i values both falling within the approximate range $40 \leq |\alpha_i| < 65°$. This should result in a relatively short metal−metal distance.

Assignment of one of the four sulfur-bridge bonding modes here described for thioamide complexes can, therefore, be made quite confidently from the observed stereochemistry, provided the values corresponding to the defined tilt and twist angles lie in the ranges given above. According to these criteria, some selected complexes containing M−S−M′ angular bridges have been included in Table 4, with an indication of the bonding mode thereby deduced. Thus, the four crystallographically independent Ag−S−Ag′ bridges in complex **2**, all with a tilt angle in the range 79.2−85.5° and with different pairs of twist angles for S(2) and S(4) versus S(1) and S(3), are associated with four-electron sp^2 + C=S (mode **B**) and two-electron sp^2 electron-deficient (mode **C**) sulfur-bridging bonding modes, respectively. Although some correlation might be expected between the sulfur-bridge bonding mode (as evidenced by the tilt and twist angles) and Ag−S distances, no simple pattern is found in complex **2**. In particular, mode **C** does not give more symmetrical Ag−S−Ag′ bridges than mode **B**, despite the approximately equal contributions of S orbitals to the two corresponding Ag−S bonds. Clearly, the situation is more complex, with Ag−S distances also depending on the coordination geometry at the soft Ag centre, which is somewhat distorted tetrahedral for Ag(2) and highly distorted for Ag(1), with one S−Ag−S angle as small as 89.62(2)°.

Conclusion

Two silver cationic complexes with perchlorate as the counterion and neutral thio(mono- or di)amide ligands have been prepared and structurally characterised. The centrosymmetric monomeric $[Ag(etu)_2]^+$ complex species in **1** contains a linear MS_2 mononuclear core, unprecedented for bis(thioamide) complexes (M = Cu, Ag). These cations and ClO_4^- counterions assemble as complementary partners involving all available hydrogen bond donor (4 N−H of each

 © 2004 Wiley-VCH Verlag GmbH & Co. KGaA, Weinheim

cation) and acceptor (4 O of each ClO_4^-) sites in a three-dimensional supramolecular network. Despite having the same stoichiometry, a sulfur-bridged polymeric cation with tetrahedral AgS_4 centres is obtained instead in **2**. There are in this case fewer available hydrogen bond donor (4 N−H + 2 water O−H) than potential acceptor [8 O (ClO_4^-) + 2 O (H_2O)] sites, and so the two crystallographically distinct ClO_4^- counterions act as two connectors (through one or two oxygen atoms, respectively). A two-dimensional layered supramolecular structure assembled through N−H···O−Cl, N−H···O(water) and Cl−O···H−O−H···O−Cl hydrogen bonding results, with no significant connections of this type between sheets. Stereochemical parameters (tilt and twist dihedral angles) for **2** indicate two different sulfur-bridge bonding modes, one conventional four-electron and the other electron-deficient two-electron.

Experimental Section

General Remarks: Reagent-grade solvents were used with no further purification. Ethylenethiourea (Fluka) and pyridine-2-thione (Aldrich) were used as received, while silver(I) perchlorate (Alfa) was recrystallized from acetonitrile. Microanalyses (C, N, H, S) were performed with a Carlo-Erba CHN EA-1108 analyser at the Servei d'Anàlisi Química de la UAB. Infrared spectra (4000−400 cm^{-1}) were recorded from KBr pellets with Perkin-Elmer FT-1710 and FT-2000 spectrometers, and ^1H and ^{13}C NMR spectra from [D_6]DMSO solutions with a Bruker AC-250 spectrometer operating at 250 MHz for ^1H NMR nuclei.

[Ag(etu)$_2$](ClO$_4$) (1): A solution of $AgClO_4$ (0.409 g, 4.0 mmol) in 60 mL of a mixture of methanol/water (2:1, v/v) was added dropwise with stirring to a methanol solution (10 mL) of the ligand (0.414 g, 2.0 mmol). After stirring for 2 h, the volume of the solution was reduced to about 30 mL by passing a slow stream of N_2 through it, and then cooled to 0°C. A precipitate separated, which was filtered, washed with 5 mL of cold ethanol and then with 10 mL of diethyl ether, and dried in vacuo. Colourless crystals of the product, suitable for X-ray diffraction, were isolated by slow concentration of an acetonitrile solution of the complex at room temperature. Total yield 60%. This compound is soluble in methanol, acetonitrile, acetone and DMSO. $C_6H_{12}AgN_4S_2{\cdot}ClO_4$ (438.7): calcd. C 11.64, H 1.95, N 9.05, S 10.36; found C 11.68, H 2.15, N 8.78, S 10.27. IR (KBr): $\tilde{\nu}$ = 3350−3270, 2890, 1522, 1355, 1319, 1280, 1200, 1087, 990, 920, 670, 626, 560, 495 cm^{-1}. ^1H NMR ([D_6]DMSO): δ = 8.90, 3.67 ppm. ^{13}C NMR ([D_6]DMSO): δ = 178.4, 44.9 ppm.

[{Ag(py2tH)$_2$}(ClO$_4$)(H$_2$O)$_{0.5}$]$_n$ (2): A solution of 0.311 g (1.5 mmol) of $AgClO_4$ in 10 mL of ethanol was added dropwise with stirring to an ethanol solution (15 mL) of the ligand (0.334 g, 3.0 mmol). A yellow precipitate formed immediately. After stirring for 1 h, the resulting mixture was kept in an ice bath for 15 min, and then filtered. The yellow solid was washed with 15 mL of diethyl ether and dried in vacuo. Yield 80%. Light yellow crystals of the product were isolated by slow vapour diffusion of diethyl ether into a concentrated acetonitrile solution of the complex at room temperature. This compound is soluble in acetonitrile, acetone and DMSO. $C_{10}H_{10}AgN_2S_2{\cdot}ClO_4{\cdot}0.5H_2O$ (411.6): calcd. C 27.38, H 2.52, N 6.38, S 14.62; found C 27.54, H 2.69, N 6.40, S 14.36. IR (KBr): $\tilde{\nu}$ = 3160, 3100, 3075, 3020, 2908, 1605, 1570, 1500, 1440, 1366, 1257, 1132, 1090, 995, 747, 726, 627, 484, 444 cm^{-1}. ^1H NMR ([D_6]DMSO): δ = 14.10, 8.10, 7.69, 7.19 ppm. ^{13}C NMR ([D_6]DMSO): δ = 167.6, 141.1, 141.0, 131.9, 118.4 ppm.

X-ray Crystallographic Study: Crystals of both complexes were examined with a Bruker AXS SMART CCD diffractometer with graphite-monochromated Mo-K_α radiation (λ = 0.71073 Å), at 173 or 160 K. Almost a whole sphere of data was collected in each case,

Table 5. Crystal data

	1	**2**
Empirical formula	$C_6H_{12}AgN_4S_2^+{\cdot}ClO_4^-$	$C_{10}H_{10}AgN_2S_2^+{\cdot}ClO_4^-{\cdot}0.5H_2O$
Formula mass	411.6	438.7
Crystal system	monoclinic	triclinic
Space group	*C*2/*c*	$P\bar{1}$
a [Å]	13.964(3)	9.8871(5)
b [Å]	13.564(3)	10.9878(6)
c [Å]	7.0256(15)	14.8197(8)
α [°]	90	82.816(2)
β [°]	90.642(6)	73.570(2)
γ [°]	90	72.209(2)
V [Å^3]	1330.6(5)	1469.07(14)
Z	4	4
d [g cm^{-3}]	2.055	1.983
μ [mm^{-1}]	2.04	1.85
T [K]	173	160
Crystal size [mm]	0.30 × 0.11 × 0.11	0.60 × 0.21 × 0.16
θ range [°]	2.1−28.6	2.0−28.7
Reflections measured	3972	11929
Unique data, R_{int}	1567, 0.027	6660, 0.024
Transmission factors	0.58−0.81	0.40−0.76
Refined parameters	103	376
R (F; $F^2 > 2\sigma$)	0.032 (1315 data)	0.030 (6023 data)
R_w (F^2; all data)	0.088	0.082
Max./min. electron density [e Å^{-3}]	+0.92/−0.69	+1.10/−1.25

 © 2004 Wiley-VCH Verlag GmbH & Co. KGaA, Weinheim

using narrow-slice ω scans;[65] semi-empirical absorption corrections were based on repeated and symmetry-equivalent data.[66] The structures were solved by heavy-atom or automatic direct methods, and refined by full-matrix least-squares methods on all unique F^2 values, with anisotropic displacement parameters for all non-H atoms. H atoms bonded to C and N were placed in idealised positions and constrained with a riding model; those of the water molecule in **2** were found in difference maps and were freely refined, with the O−H bond lengths restrained to be similar. Largest features in final difference maps were close to heavy atoms and disordered groups. Details are given in Table 5. CCDC-220964 and -220965 contain the supplementary crystallographic data for this paper. These data can be obtained free of charge at www.ccdc.cam.ac.uk/conts/retrieving.html [or from the Cambridge Crystallographic Data Centre, 12 Union Road, Cambridge CB2 1EZ, UK; Fax: (internat.) + 44-1223-336-033; E-mail: deposit@ccdc. cam. ac. uk].

Acknowledgments

Financial support from the Ministerio de Ciencia y Tecnología of Spain (DGICYT: BQU2001-1976) and from EPSRC (U. K.) is gratefully acknowledged.

[1] E. S. Raper, *Coord. Chem. Rev.* **1994**, *129*, 91−156.
[2] E. S. Raper, *Coord. Chem. Rev.* **1996**, *153*, 199−255.
[3] E. S. Raper, *Coord. Chem. Rev.* **1997**, *165*, 475−567.
[4] J. A. García-Vázquez, J. Romero, A. Sousa, *Coord. Chem. Rev.* **1999**, *193−195*, 691−745.
[5] P. D. Akrivos, *Coord. Chem. Rev.* **2001**, *213*, 181−210.
[6] P. D. Cookson, E. R. T. Tiekink, *J. Chem. Soc., Dalton Trans.* **1993**, 259−263.
[7] K. Nomiya, R. Noguchi, T. Shigeta, Y. Kondoh, K. Tsuda, K. Ohsawa, N. Chikaraishi-Kasuga, M. Oda, *Bull. Chem. Soc. Jpn.* **2000**, *73*, 1143−1152.
[8] M. Hong, W. Su, R. Cao, W. Zhang, J. Lu, *Inorg. Chem.* **1999**, *30*, 600−602.
[9] W. Su, R. Cao, M. Hong, W. Wong, J. Lu, *Inorg. Chem. Commun.* **1999**, *2*, 241−243.
[10] W. Su, M. Hong, J. Weng, R. Cao, S. Lu, *Angew. Chem. Int. Ed.* **2000**, *39*, 2911−2914.
[11] A. A. Isab, *Transition. Met. Chem.* **1992**, *17*, 374−376.
[12] I. G. Dance, *Polyhedron* **1986**, *5*, 1037−1104.
[13] J. J. Vittal, *Polyhedron* **1996**, *15*, 1585−1642.
[14] E. H. Griffith, G. W. Hunt, E. L. Amma, *Chem. Commun.* **1976**, 432−433.
[15] M. Van Meerssche, R. Kamara, G. Germain, J. P. Declercq, *Bull. Soc. Chim. Belg.* **1982**, *91*, 553−564.
[16] S. Kitagawa, Y. Nozaka, M. Munakata, S. Kawata, *Inorg. Chim. Acta* **1992**, *197*, 169−175.
[17] R. C. Bott, G. A. Bowmaker, C. A. Davis, G. A. Hope, B. E. Jones, *Inorg. Chem.* **1998**, *37*, 651−657.
[18] E. H. Griffith, G. W. Hunt, E. L. Amma, *Chem. Commun.* **1976**, 432−433.
[19] J. P. Declercq, R. Kamara, C. Moreaux, J. M. Dereppe, G. Germain, M. Van Meerssche, *Acta Crystallogr., Sect. B* **1978**, *34*, 1036−1037.
[20] D. M. L. Goodgame, G. A. Leach, A. C. Skapski, K. A. Woode, *Inorg. Chim. Acta* **1978**, *31*, L375−L376.
[21] W. Su, M. Hong, J. Weng, Y. Liang, Y. Zhao, R. Cao, Z. Zhou, A. S. C. Chan, *Inorg. Chim. Acta* **2002**, *331*, 8−15.
[22] A. L. Crumbliss, L. J. Gestaut, R. C. Rockard, A. T. McPhail, *Chem. Commun.* **1974**, 545−546.
[23] R. G. Vranka, E. L. Amma, *J. Am. Chem. Soc.* **1966**, *88*, 4270−4271.
[24] E. R. Atkinson, E. S. Raper, D. J. Gardiner, H. M. Dawes, N. P. C. Walker, A. R. W. Jackson, *Inorg. Chim. Acta* **1985**, *100*, 285−291.
[25] E. S. Raper, J. R. Creighton, J. D. Wilson, W. Clegg, A. Milne, *Inorg. Chim. Acta* **1988**, *149*, 265−271.
[26] M. B. Ferrari, G. F. Gasparri, *Cryst. Struct. Commun.* **1976**, *5*, 935−940.
[27] A. G. Gash, E. H. Griffith, W. A. Spoffford III, E. L. Amma, *Chem. Commun.* **1973**, 256−257.
[28] J. S. Casas, E. G. Martínez, A. Sánchez, A. S. González, J. Sordo, U. Casellato, R. Graziani, *Inorg. Chim. Acta* **1996**, *241*, 117−123.
[29] R. Kamara, J. P. Declercq, G. Germain, M. Van Meerssche, *Bull. Soc. Chim. Belg.* **1982**, *91*, 339−340.
[30] M. S. Weininger, G. W. Hunt, E. L. Amma, *Chem. Commun.* **1972**, 1140−1141.
[31] Y. Okaya, C. Knobler, *Acta Crystallogr.* **1964**, *17*, 928−930.
[32] I. F. Taylor Jr., M. S. Weininger, E. L. Amma, *Inorg. Chem.* **1974**, *13*, 2835−2842.
[33] E. C. Constable, P. R. Raithby, *J. Chem. Soc., Dalton Trans.* **1987**, 2281−2283.
[34] E. S. Raper, J. R. Creighton, D. Robson, J. D. Wilson, W. Clegg, A. Milne, *Inorg. Chim. Acta* **1988**, *143*, 95−100.
[35] S. C. Davies, M. C. Durrant, D. L. Hugues, K. Leidenberger, C. Stapper, R. L. Richards, *J. Chem. Soc., Dalton Trans.* **1997**, 2409−2418.
[36] C. Pakawatchai, K. Sivakumar, H. K. Fun, *Acta Crystallogr., Sect. C* **1996**, *52*, 1954−1957.
[37] O. E. Piro, R. C. V. Piatti, A. E. Bolzan, R. C. Salvarezza, A. J. Arvia, *Acta Crystallogr., Sect. B* **2000**, *56*, 993−997.
[38] G. Giusti, G. Geier, A. Currao, R. Nesper, *Acta Crystallogr., Sect. C* **1996**, *52*, 1914−1917.
[39] S. C. Kokkou, V. Schramm, P. Karagiannidis, *Acta Crystallogr., Sect. C* **1985**, *41*, 1040−1043.
[40] G. W. Hunt, N. W. Terry III, E. L. Amma, *Acta Crystallogr., Sect. B* **1979**, *35*, 1235−1236.
[41] K. Jensen, P. H. Nielsen, *Acta Chem. Scand.* **1966**, *20*, 597−620.
[42] K. Dwarakanath, D. N. Sathyanarayana, *Bull. Chem. Soc. Japan* **1979**, *52*, 2699−2704.
[43] C. N. R. Rao, P. Vankataraghavan, *Spectrochim. Acta* **1962**, *18*, 541−547.
[44] S. C. Davies, M. C. Durrant, D. L. Hugues, K. Leidenberger, C. Stapper, R. L. Richards, *J. Chem. Soc., Dalton Trans.* **1997**, 2409−2418.
[45] P. M. Henrichs, J. J. H. Ackerman, G. E. Maciel, *J. Am. Chem. Soc.* **1977**, *99*, 2544−2548.
[46] A. A. Isab, *Polyhedron* **1989**, *8*, 2823−2827.
[47] E. Dubler, W. Bensch, *Inorg. Chim. Acta* **1986**, *125*, 37−42.
[48] S. Kitagawa, S. Kawata, Y. Nozaka, M. Munakata, *J. Chem. Soc., Dalton Trans.* **1993**, 1399−1404.
[49] F. H. Allen, *Acta Crystallogr., Sect. B* **2002**, *58*, 380−388.
[50] S. Bernès, J. C. Aguilar, E. Rodríguez de San Miguel Guerrero, M. E. Núñez Gaytán, J. De Gyves, *Acta Crystallogr., Sect. C* **1999**, *55*, 1627−1631.
[51] S. Friedrichs, P. G. Jones, *Acta Crystallogr., Sect. C* **1999**, *55*, 1625−1627.
[52] P. G. Jones, J. J. Guy, G. M. Sheldrick, *Acta Crystallogr., Sect. B* **1976**, *32*, 3321−3322.
[53] L. C. Porter, J. P. Fackler Jr, J. Costamagna, R. Schmidt, *Acta Crystallogr., Sect. C* **1992**, *48*, 1751−1754.
[54] L. Chi-Chang, L. Shi-Xiong, Y. Rong-Sheng, *Chin. J. Struct. Chem.* **1990**, *9*, 42−45.
[55] R. Usón, A. Laguna, M. Laguna, J. Jiménez, M. P. Gómez, A. Sainz, P. G. Jones, *J. Chem. Soc., Dalton Trans.* **1990**, 3457−3463.
[56] R. J. Staples, J. P. Fackler Jr., J. Costamagna, *Acta Crystallogr., Sect. C* **1997**, *53*, 1555−1558.
[57] E. A. Vizzini, I. F. Taylor, E. L. Amma, *Inorg. Chem.* **1968**, *7*, 1351−1357.

 © 2004 Wiley-VCH Verlag GmbH & Co. KGaA, Weinheim

[58] W. A. Spofford III, E. L. Amma, *Acta Crystallogr., Sect. B* **1970**, *26*, 1474−1477.
[59] W. W. Porterfield, *Inorganic Chemistry: A Unified Approach*, 2nd ed., Academic Press, New York, **1993**.
[60] U. Braun, J. Sieler, R. Richter, B. Hettich, A. Simon, *Z. Anorg. Allg. Chem.* **1988**, *557*, 134−142.
[61] P. Aslanidis, P. Karagiannidis, P. D. Akrivos, B. Krebs, M. Läge, *Inorg. Chim. Acta* **1997**, *254*, 277−284.
[62] G. A. Stergioudis, S. C. Kokkou, P. J. Rentzeperis, P. Karagiannidis, *Acta Crystallogr., Sect. C* **1987**, *43*, 1685−1688.
[63] L. P. Battaglia, A. Bonamartini Corradi, M. Nardelli, M. E. V. Tani, *J. Chem. Soc., Dalton Trans.* **1976**, 143−146.
[64] E. S. Raper, J. D. Wilson, W. Clegg, *Inorg. Chim. Acta* **1992**, *194*, 51−55.
[65] *SMART* (diffractometer control) and *SAINT* (data integration) software, Bruker AXS Inc., Madison, Wisconsin, USA, **2001**.
[66] G. M. Sheldrick, *SHELXTL*, version 6.1, Bruker AXS Inc., Madison, Wisconsin, USA, **2001**.

Received October 16, 2003
Early View Article
Published Online October 21, 2004

 © 2004 Wiley-VCH Verlag GmbH & Co. KGaA, Weinheim

Construction of Nano-Channels Based on Zinc(II) Pyrazine-2-carboxylate Complexes

Tetsuya Sunahara,[a] Satoru Onaka,*[a] Mitsuhiro Ito,[a] Hiroyuki Imai,[b] Katsuya Inoue,[b] and Tomoji Ozeki[c]

Keywords: Carboxylato ligands / Nanostructures / Self-assembly / Zinc

The reaction of pyrazine-2-carboxylate (pca) and bis(pyridine) derivatives, such as 4,4′-bipyridine (bipy), 1,2-bis(4-pyridyl)ethylene (bpen), 1,2-bis(4-pyridyl)ethane (bpea), 1,3-bis(4-pyridyl)propane (bpp), and 4,4′-azopyridine (azp), with zinc perchlorate gives supramolecules with grid and/or channel structures. The new complexes reported here are *trans*-[Zn(bipy)(pca)(H_2O)]ClO_4·$(EtOH)_{0.5}$·$(H_2O)_{0.5}$ (**1**), [Zn(μ-bpen)(bpen)(pca)(H_2O)]·ClO_4·$2H_2O$ (**2**), [Zn(bpea)(pca)]-ClO_4·$(EtOH)_{0.5}$ (**3**), and [Zn(bpp)(pca)(MeOH)]ClO_4 (**4**). Their structures have been established by single-crystal X-ray diffraction. Some of these complexes contain voids with nanometer dimensions. Small molecules such as H_2O, MeOH, and EtOH contained in these voids can be removed without destruction of the parental suprastructure.
(© Wiley-VCH Verlag GmbH & Co. KGaA, 69451 Weinheim, Germany, 2004)

Introduction

The basic concepts for constructing supramolecules by self-assembly techniques have been well developed over the past two decades, especially by Lehn's group.[1−4] The entries to this new field are classified from the structural viewpoint into sphere-like molecules, infinite one-dimensional molecules (molecular wires), multi-dimensional molecules, including interwoven coordination polymers and grid and/or channel-like molecules, and dendrimers; we have used the term "molecular dot" for globular molecules.[5] There has been a plethora of reports on grids and/or channel-like networks composed from metal−ligand components, especially with Mn, Co, Ni, Cu, and Zn as metal ions and 4,4′-bipy, aromatic carboxylates, pyrazine, and pyridylporphyrins as organic linkers.[1−4,6−15] These molecules can also be divided into the following categories with regards to their possible applications to nanotechnologies: chemical sensors, microreactors, molecular devices, optoelectronic devices, drug-delivery systems, thin-film technologies, etc.[16−21] One of our current interests in supramolecules has been directed to the trapping of small environmental gaseous molecules such as CO_2, NO_2, and SO_2 into channel-like structures and their possible conversion into more useful chemicals. Since there have been several reports of the trapping of CO_2 by mononuclear Zn complexes and its subsequent reduction into organic species,[22,23] the design of a microreactor prepared from Zn^{II} supramolecules is especially intriguing for the activation of CO_2 molecules and their conversion into organic derivatives, a process that is the key step in C_1 chemistry. As the first step to achieve this goal, we decided to construct new channel-like and/or cage-like nanostructures containing Zn^{II} and a pyrazine-2-carboxylate linker. The reason for the choice of the pyrazine-2-carboxylate (pca) ligand is its potential multidentate coordination ability, depicted in Scheme 1, where several possible new bridging modes are shown. Such multidentate ex-

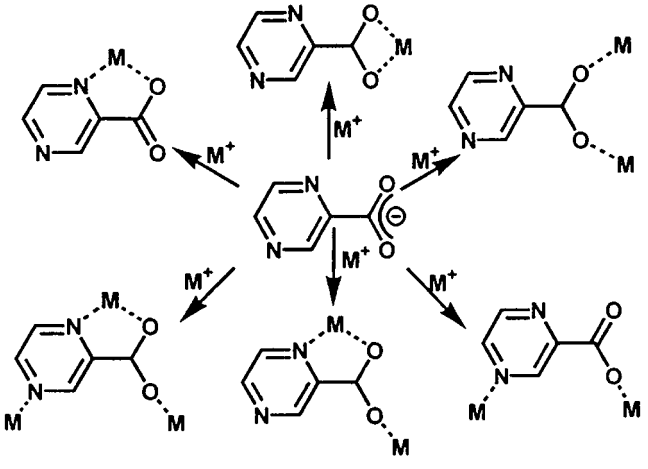

Scheme 1

[a] Department of Environmental Technology, Graduate School of Engineering, Nagoya Institute of Technology,
Gokiso-cho, Showa-ku, Nagoya 466-8555, Japan
Fax: + 81-52-735-5160
E-mail:onaka.satoru@nitech.ac.jp
[b] Institute for Molecular Science,
Myodaiji, Okazaki 444-8585, Japan
[c] Department of Chemistry and Materials Science, Tokyo Institute of Technology,
O-okayama, Meguro-ku, Tokyo 152-8551, Japan

 © 2004 Wiley-VCH Verlag GmbH & Co. KGaA, Weinheim **DOI: 10.1002/ejic.200400438**

amples of pca have not been reported to the best of our knowledge. Here we report on the synthesis of new zinc(II) pyrazine-2-carboxylate complexes with various bis(pyridine) ligands and a structural study of their interlaced supramolecular structures by single-crystal X-ray diffraction.

Results and Discussion

Synthetic Reactions

As described in the Exp. Sect., simply mixing the three components [pcn, the bis(pyridine) ligand, and zinc(II) perchlorate] in EtOH/H_2O at room temperature yielded new cage-type supramolecules. It seems worthy to mention why pcn is employed to build such supramolecules in most reactions instead of simply using pyrazine-2-carboxylic acid (Hpca). At first Hpca was indeed used for such attempts, because several recent reports have shown the versatile nature of pyridine-2-carboxylates and pca was expected to exhibit a similar behavior.[24] However, only limited results were obtained, as described below. Lin et al. have demonstrated that 4-cyanopyridine is susceptible to hydrolysis under hydro(solvo)thermal conditions to yield isonicotinic acid.[24b] With this in mind, zinc perchlorate, 2-cyanopyrazine, and bipy were mixed in EtOH/H_2O in a 1:1:1 molar ratio. After standing at room temperature for several days, pale-yellow crystals of [Zn(pca)(bipy)(H_2O)]ClO_4 (**1**) were obtained. An X-ray diffraction study revealed a grid-like structure in the solid state. A more detailed discussion of this nano-grid can be found below. Thus, we have verified that pcn undergoes hydrolysis under ambient conditions to give pca.

Similar reactions were attempted for various combinations of other ligands; these results are also described below for **2**−**4**. The crux of our synthesis is that the CN group of pcn is oxidized to CO_2^- during the reaction and/or upon exposure to air for several days, thus creating a potentially multidentate linker ligand. The essential contribution of the CO_2^- group in the pca ligand becomes clear when the cage structure of **1** is compared with a similar cage architecture with pyrazine as bridging ligand reported previously by Bourne's group.[25] Their network structures are significantly different from ours: the carboxylate group in pca induces a more sophisticated multidimensional structure which is dependent on the coexistence of bridging ligands, as described in the crystal structure section below. The most common function of pca in **1**−**4** is as a chelating bridging ligand, as depicted in the bottom center of Scheme 1. However, the bridging mode of the O atom of pca in **2** is highly unusual, as described in the following section. Another interesting finding from the present synthesis merits a comment; pcn and/or pca are not incorporated into the final products when pyrazine, 4,4′-bipyridine *N*,*N*′-dioxide (bpyO), and/or azp are used as co-ligands. It is possible that the pcn ligand, which is initially coordinated to the Zn ion by an N atom of the pyrazine skeleton, is affected by the steric and/or electronic influence of the co-ligand and is expelled from the coordination sphere during the hydrolysis of the CN group; the hydrolysis mechanism of the CN group is still unclear. These results strongly suggest that the combination of pca with other potentially bidentate ligands and suitable hydrolysis conditions should allow the synthesis of more sophisticated channel-like structures with multifunctional binding modes of pca different from those in Scheme 1. The next challenge should be to realize other coordination modes such as those of the left and right at the bottom of Scheme 1, where pca functions as a longer grid than those of **1**−**4**.

Molecular and Cage Structures

The minimum units needed to delineate the molecular structure of each product are shown below. Complexes **1**, **4**, and **5** exhibit distorted octahedral skeletons around the Zn ions, whereas **2** has a distorted edge-shared dinuclear octahedral skeleton and **3** exhibits a distorted five-coordinate square-pyramidal one. In **1** (Figure 1a), pca functions as a tridentate bridging ligand as shown in Scheme 1. The sixth coordination site is occupied by the O atom (O1) of a water molecule.

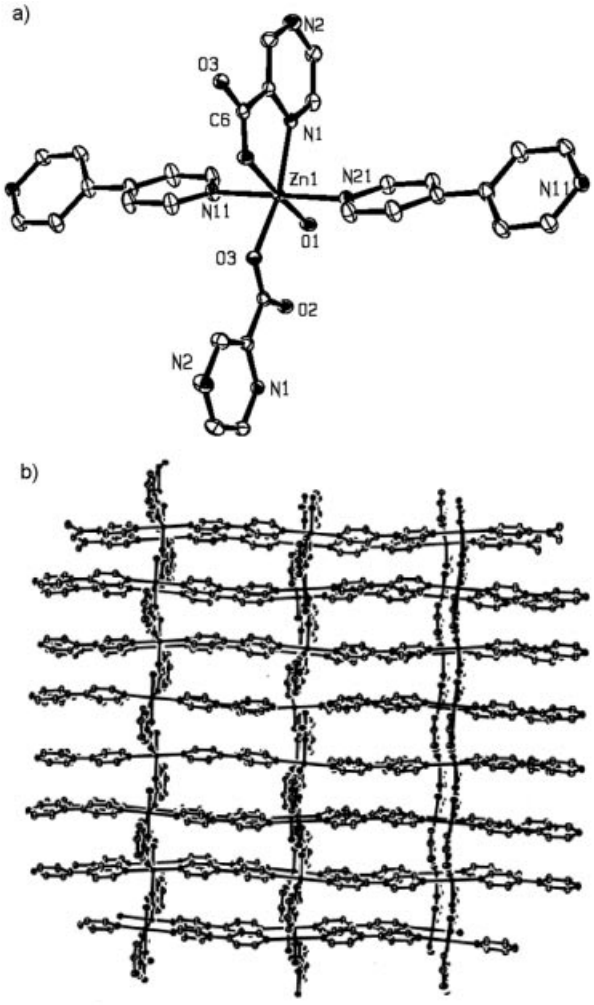

Figure 1. (a) ORTEP drawing of *trans*-[Zn(bipy)(pca)(H_2O)]ClO_4 (**1**); (b) view of the crystal structure of **1** along the *a* axis

 © 2004 Wiley-VCH Verlag GmbH & Co. KGaA, Weinheim

The coordination mode of pca in **2** is rather complicated. It binds as a chelating ligand to a single Zn ion through N and O atoms, and the same O atom also bridges two Zn ions, as shown in Figure 2a. This type of coordination mode was not expected and is not shown in Scheme 1. The O atom (O3) from a water molecule occupies the sixth coordination site.

The coordination mode of pca in **3** is the same as in **1**, although the fundamental structure of the Zn ion is square-pyramidal (Figure 3a). The function of pca in **4** (Figure 4a) is also the same as in **1**, with a molecule of methanol loosely bound in the sixth coordination site. Although the bridging O atom appears to be free in Figures 1a, 3a, and 4a, which show only the independent part of each molecule, it actually straddles the neighboring Zn ions, thereby forming a multidimensional array by linking the Zn ions.

The two pyrazine rings in **5** (Figure 5a) connect two Zn sites; four water molecules occupy the equatorial *trans* positions, and thus form *trans*-linear infinite chains. The mononuclear Zn complex **6** does not merit special comments.

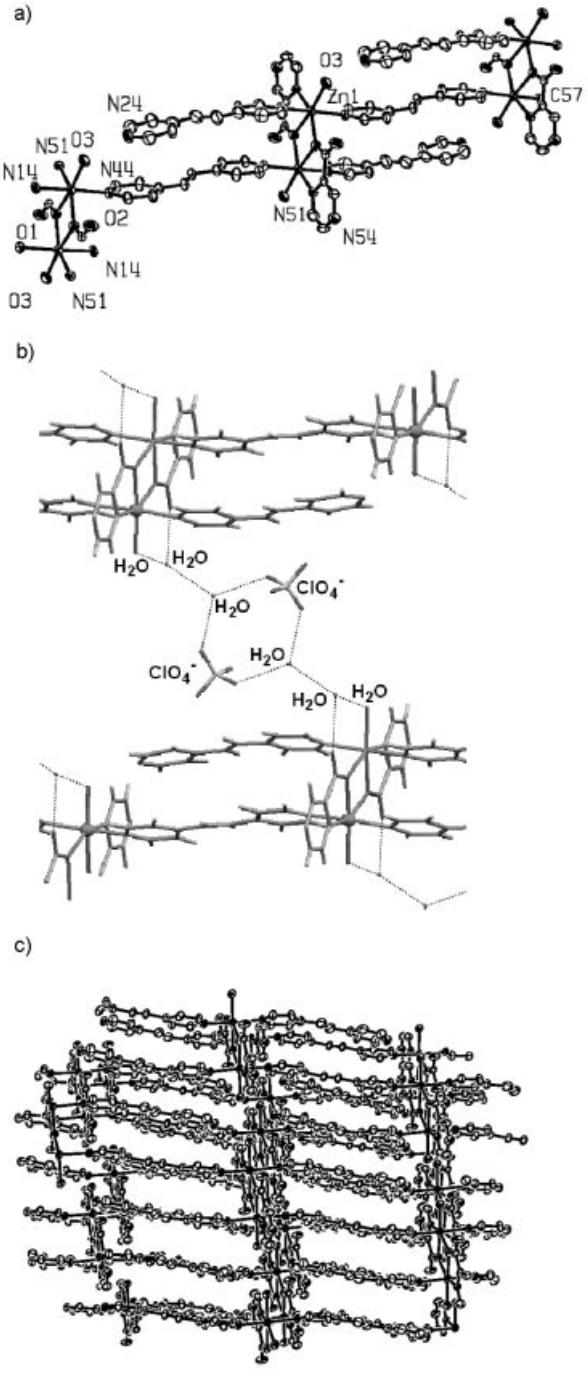

Figure 2. (a) ORTEP drawing of [Zn(μ-bpen)(bpen)(pca)(H_2O)] (**2**); (b) close-up of hydrogen bonds between H_2O, ClO_4^-, and H_2O coordinated to Zn^{II}; (c) side view of the 2D layers of **2** along the *b* axis

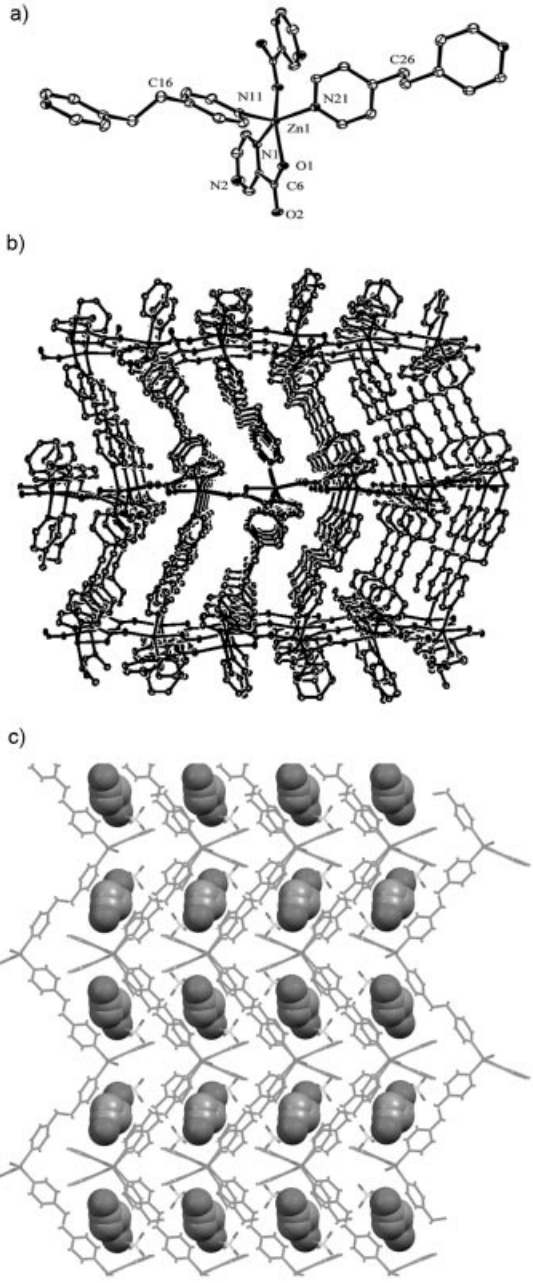

Figure 3. (a) ORTEP drawing of *trans*-[Zn(bpea)($pca)_2$] (**3**); (b) two-dimensional sheet of **3** along the *a* axis; (c) guest ethanol molecules in the channels

 © 2004 Wiley-VCH Verlag GmbH & Co. KGaA, Weinheim

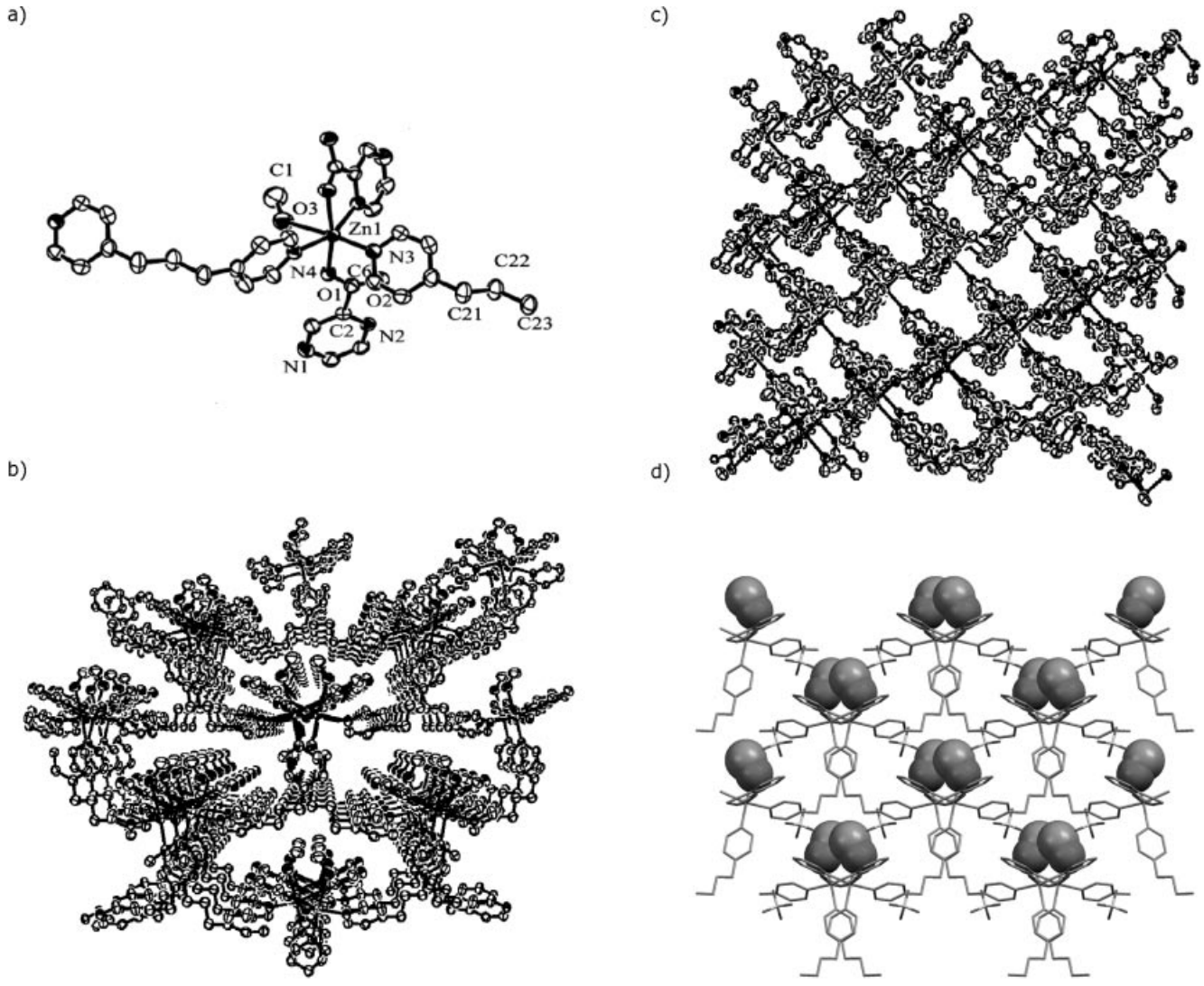

Figure 4. (a) ORTEP drawing of [Zn(bpp)(pca)(MeOH)] (**4**); (b) top view of the multidimensional structure of **4** along the *c* axis; (c) side view of the 3D layers of **4** along the *a* axis; (d) view of the weakly bound methanol molecules in the channels

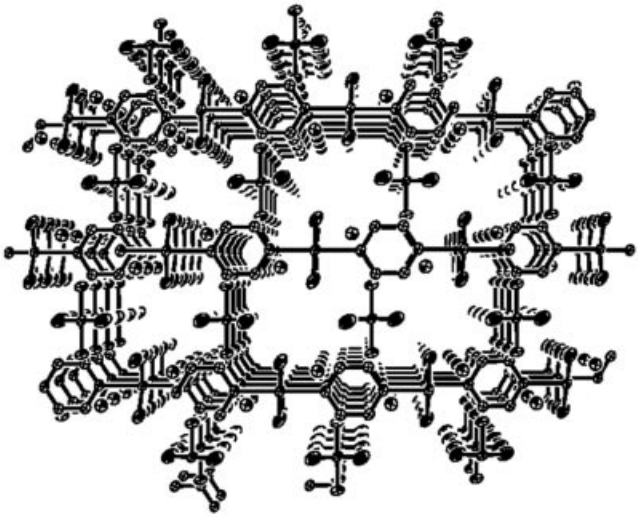

Figure 5. 2D grids built up by hydrogen-bonded networks between 1D chains of **5** and SiF_6^{2-}

The Zn−N and Zn−O bond lengths of pca are 2.082−2.190 and 2.028−2.166 Å, respectively, which are in the normal range for these compounds.[12,13,15,25] One methanol molecule is loosely coordinated to Zn [Zn−O = 2.431(4) Å] in **4**. The Zn−OH_2 distances in **2** and **5** are normal.

The grid architecture of **1** is shown in Figure 1b. It is constructed by pca and bipy linkers with Zn^{II} corners. The approximate size of the cages is 5.9 Å × 11.4 Å; hereafter, the size of the cage is defined by the N·· N distances unless stated otherwise. One H_2O molecule, one EtOH molecule, and a ClO_4 anion are contained in each channel and the ClO_4^- anion tethers solvate molecules through hydrogen bonds.

The function of bpen in **2** is twofold: one bpen ligand connects the neighboring Zn ions directly through two N atoms (two strong interactions) to form a quasi one-dimensional chain, while, at first glance, the other bpen acts as a monodentate ligand through one N atom. However, a

 © 2004 Wiley-VCH Verlag GmbH & Co. KGaA, Weinheim

closer inspection of the packing diagram reveals that the remaining N atom is connected to the O atom in H_2O, which is coordinated to another Zn ion by a hydrogen bond (weak interactions; Figure 2b). Thus, the fundamental unit of the grid is composed from the dimer $[Zn(bpen)(pca)(H_2O)]_2$. In addition, layers composed from these dimers are connected by other hydrogen bonds among O atoms in ClO_4^- and coordinated H_2O and free H_2O, and thus three-dimensional cages are formed by hydrogen bonds (Figures 2b and c). The ClO_4^- anion is essential for the formation of these three-dimensional architectures. The approximate size of the cages is 3.4 Å × 13.6 Å.

Substituting the $-CH_2-CH_2-$ unit (bpea) in **3** for the $-CH=CH-$ unit (bpen) in **2** causes significant changes in the crystal structure. First, the six-coordination around the Zn ion in **2** is reduced to five in **3**. The basic skeleton around the Zn ion is regarded as a square pyramid. The basal square is constructed from N, O (chelating pca), O (bridging pca), and N (bpea) atoms, and the apex is occupied by the N atom from another bpea ligand (Figure 3a). Next, the main motif (the longer grid) of the supramolecule of **3** contains polymeric, pleated (Z-shaped) chains around the corner zinc ions, which are then interlaced by pca by coordination of O atoms to Zn ions (the shorter grids) yielding a two-dimensional sheet (Figure 3b). The size of the grids is approximately 13.3 Å × 5.7 Å, and the distance between the sheets is 8.96 Å. The ClO_4^- anion and EtOH molecule are situated between the sheets and are not connected to the cages by hydrogen bonds. The incorporated EtOH molecules are depicted in Figure 3c. The cage structure is maintained after the loss of EtOH upon heating, as described below and thus **3′**, which is complex **3** without EtOH, exhibits quite similar lattice constants and the same space group. This phenomenon is important for the construction of a microreactor from these coordination polymers. The thermal behavior is described below.

The polymeric structure of **4** is topologically more complicated (Figure 4b, projected almost along the *c* axis). The skeletal motif looks like an atoll. The other crystal-packing diagram has been shown to emphasize how the organic scaffolds are used to bridge the Zn ions and/or how the motif of the atoll is built up (Figure 4c, projected almost along the *a* axis); the minimum numbers of atoms are employed in this diagram to represent the organic linkers. The side view (Figure 4c) demonstrates clearly that the horizontal layer (which is the vertical column in Figure 4b) is composed of bridging pca ligands thus giving rise to a shorter period. The perpendicular grids in Figure 4b are then constructed by tethering the horizontal layers to different Zn ions by another bpp linker (Figure 4b) and thus these two-dimensional grids are built up to form the three-dimensional framework. One methanol molecule coordinates loosely to each zinc ion to complete the six-coordination (Figure 4d). The whole architecture is best described as an oblate honeycomb; one ClO_4^- anion per Zn ion is positioned in each lacuna. The methanol ligand is easily removed upon heating. The approximate size of the cages is 12.4 Å × 5.3 Å when the methanol is neglected.

Figure 5 shows the almost square grids of **5**, the main component of which is an infinite one-dimensional chain of (pyrazine)Zn units. The chains are "glued" to each other by hydrogen bonds between the F atoms in SiF_6^{2-} and the aromatic protons. Two-dimensional sheets are thus formed in the solid state. The approximate size of the cages is 9.9 Å × 9.3 Å.

We suggested in our previous paper that the length of the linker determines the type and the structure of the polymer formed, and that the dimensionality of the polymer is reduced from two to one if a longer linker is used; these complexes were Mn derivatives containing pyridin-2-ylmethanol and another bridging bis(pyridine) ligand.[26] However, the present exploration suggests that the grid structure becomes highly undulated with the elongation of the distance between two pyridine rings used in this study. For **1**−**4**, pca is an indispensable lattice constituent, although the lattice length made by pca is rather short. An appropriate combination of short and long lattice constituents [pca and bis(pyridine) ligand], together with the multiple coordination modes of pca, will be required to form sophisticated structures containing nano-channels, especially the three-dimensional channels of **4**.

Thermogravimetric Measurements

Our stated aim is the construction of cage-like cavities and/or grid structures which contain enough lacuna to accommodate small gaseous molecules. As was described above, the supramolecules **2**, **3**, and **4** are good candidates for this purpose because their caged structures are maintained after the removal of the solvent molecules. In this section, the process of the loss of H_2O, EtOH, and/or MeOH is explored by the use of thermogravimetric analysis. The samples were exposed to air for 1 h before analyzing them. The results of the thermogravimetric measurements are shown in Figures 6a and b for **2** and **4**, respectively. The TG-DTA plot for **2** (Figure 6a) exhibits two steps of H_2O loss. The first step is assigned to the loss of included H_2O and the latter step to loss of coordinated H_2O. The residual cage is stable up to 280 °C. The TG-DTA plot for **3** (not shown), however, exhibits only a small step corresponding to the loss of ethanol. This indicates that the weakly trapped ethanol molecules are easily lost upon exposure to air during the pre-treatment of the sample; the cage structure is stable up to 300 °C. The TG-DTA plot for **4** (Figure 6b) indicates that the weakly coordinated methanol is easily lost upon heating in the range from 60 to 110 °C. The remaining cage is stable up to 270 °C. These thermogravimetric analyses strongly suggest that the nano-channels in **2**−**4** after the loss of ethanol and/or methanol are good candidates for porous materials to trap small molecules. Therefore, gas-absorption measurements were performed for the residual porous-channel-containing supramolecules **2′**−**4′** {**2′** = $[Zn(\mu\text{-bpen})(bpen)(pca)]ClO_4$; **4′** = $[Zn(pca)(bpp)]ClO_4$} with N_2. However, our preliminary gas-absorption measurements are not indicative of a decent absorption ability, especially at low N_2 pressure. Therefore,

 © 2004 Wiley-VCH Verlag GmbH & Co. KGaA, Weinheim

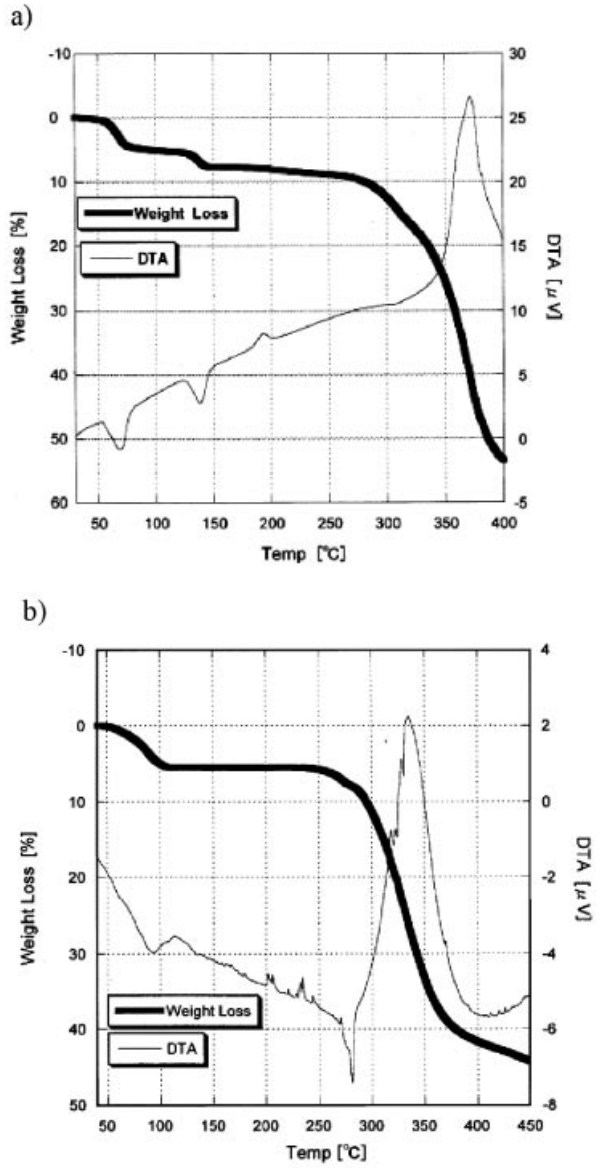

Figure 6. TG-DTA plots for **2** (a) and **4** (b) vs. temperature

our efforts to determine the ability of these porous molecules for this purpose are continuing with other gases.

Conclusion

New caged and/or porous supramolecules have been synthesized from pyrazine-2-carbonitrile, bis(pyridine) ligands, and zinc perchlorate. Hydrolysis of the CN group to CO_2^- during the crystallization process is essential for the success of the synthesis. The channel architectures of the complexes survive after removal of solvent molecules for the three supramolecules chosen as new examples of coordination polymers.

Experimental Section

Materials and General Procedures: Syntheses and manipulations were generally performed in the open air unless otherwise described. Pyrazine-2-carboxylic acid, pyrazine-2-carbonitrile, and pyrazine were purchased from Tokyo Kasei Kogyo Co., Ltd. 4,4′-Bipyridine (bipy) and the other pyridines NC_5H_4-R-C_5NH_4 (R = CH=CH, CH_2-CH_2, $CH_2-CH_2-CH_2$) were purchased from Wako Pure Chemical Ind., Ltd. or Aldrich. The following abbreviations are used for pyrazine derivatives and bis(pyridine) ligands: pcn (pyrazine-2-carbonitrile), Hpca (pyrazine-2-carboxylic acid), bpen [1,2-bis(4-pyridyl)ethylene], bpea [1,2-bis(4-pyridyl)ethane], bpp [1,3-bis(4-pyridyl)propane]. 4,4′-Azopyridine (azp) was synthesized according to a literature method.[27] $Zn(ClO_4)_2·6H_2O$, other ligands, and solvents were also purchased from Wako Pure Chemical Ind., Ltd. or Aldrich. Thermogravimetric measurements were carried out with a Rigaku TAS-300 and TG8101D thermoflex. Gas-absorption measurements were performed with a Yuasa-ionics Autosorb1. ***Caution:*** *Organic perchlorate salts are potentially explosive; all perchlorates salts should be handled with care!*

Synthesis of *trans*-[Zn(bipy)(pca)(H_2O)]ClO_4·$(EtOH)_{0.5}(H_2O)_{0.5}$ (1): A 1:1 mixture of pyrazine-2-carbonitrile (pcn; 105 mg, 1 mmol) and bipyridine (bipy; 155 mg, 1 mmol) was dissolved in 15 mL of EtOH/H_2O (2:1) and the mixture was stirred at room temperature for 2 h. An aqueous solution (5 mL) of $Zn(ClO_4)_2·6H_2O$ (380 mg, 1 mmol) was then added and the mixture stirred for 7 h. The mixture was left standing at room temperature for several days to yield a pale-yellow precipitate. Yield: 240 mg (46%). $C_{17}H_{19}ClN_4O_9Zn$ (524.2): calcd. C 38.89, H 3.47, N 11.34; found C 38.23, H 3.47, N 11.14.

Synthesis of [Zn(μ-bpen)(bpen)(pca)(H_2O)]$ClO_4·2H_2O$ (2): pcn (105 mg, 1 mmol) and bpen (182 mg, 1 mmol) were dissolved in 10 mL of EtOH/H_2O (3:2) and the mixture was stirred at room temperature for 1 h. An aqueous solution (5 mL) of $Zn(ClO_4)_2·6H_2O$ (380 mg, 1 mmol) was then added. The resulting yellow solution immediately became a white suspension upon stirring. After 2 h of stirring, the precipitates were removed by filtration. The filtrate was then left standing at room temperature for several days to yield pale-yellow, plate-like single crystals. X-ray quality single crystals were grown from MeOH/H_2O. Yield: 210 mg (33%). $C_{23}H_{22}ClN_5O_9Zn·2H_2O$ (613.3):calcd. C 44.90, H 3.93, N 11.38; found C 44.70, H 3.90, N 11.35. Upon heating, three H_2O (one coordinated and two free) molecules were lost. Judging from the color and the appearance of the thermally treated compound, the structure of the compound seems unchanged after loss of H_2O, as described in the thermogravimetric section.

Synthesis of [Zn(bpea)(pca)]$ClO_4·(EtOH)_{0.5}$ (3): pcn (105 mg, 1 mmol) and bpea (185 mg, 1 mmol) were dissolved in 15 mL of EtOH/H_2O (2:3) and the mixture was stirred at room temperature for 1 h. An aqueous solution (5 mL) of $Zn(ClO_4)_2·6H_2O$ (380 mg, 1 mmol) was then added. The solution became a white suspension and the mixture was stirred for 10 h. The colorless precipitates were removed by filtration and the filtrate was left standing at room temperature for several days to yield colorless, needle-shaped crystals. The cycle of precipitation and filtration was repeated several times and finally pale-yellow block single crystals were obtained. The yield of combined colorless crystals of **3** was 240 mg (46%) after recrystallization from MeOH/H_2O. $C_{19}H_{21}ClN_4O_7Zn$ (519.6): calcd. C 43.66, H 3.66, N 11.31; found C 43.41, H 3.63, N 11.28. The yellow crystals were determined to be $[Zn(bpea)_2(H_2O)_2](ClO_4)_2(H_2O)_2$ by single-crystal X-ray diffraction.[28] [Zn(bpea)(pca-

 © 2004 Wiley-VCH Verlag GmbH & Co. KGaA, Weinheim

)](ClO4) (**3′**) was obtained upon heating **3**, as demonstrated by a single-crystal X-ray diffraction study. The structural details of **3** and **3′** are described in the text.

Synthesis of [Zn(bpp)(pca)(MeOH)]ClO_4 (4): pcn (60 mg, 0.5 mmol) and bpp (100 mg, 0.5 mmol) were dissolved in 15 mL of EtOH/H_2O (1:2). After stirring of the solution for 1 h, an aqueous solution (5 mL) of $Zn(ClO_4)_2{\cdot}6H_2O$ (190 mg, 0.5 mmol) was added to this mixture with stirring. After stirring at room temperature for 10 h, the solution was left standing at room temperature for several days to give a white, flocculent precipitate. The product was collected on a frit and was recrystallized from MeOH/H_2O to give pale-yellow, pillar-like single crystals of **4**. Yield 190 mg (75%). $C_{19}H_{21}ClN_4O_7Zn$ (518.2): calcd. C 44.03, H 4.08, N 10.81; found C 43.84, H 4.02, N 10.78. Compound **4** was also obtained from the reaction of pca, bpp, and $Zn(ClO_4)_2{\cdot}6H_2O$ in a similar yield.

[Zn(pyz)$(H_2O)_4$]$(SiF_6)(H_2O)$ (5): pcn (210 mg, 2 mmol) and pyrazine (pyz; 170 mg, 2 mmol) were dissolved in 4 mL of EtOH/H_2O (3:1). An EtOH/H_2O (1:1) solution (4 mL) of $Zn(SiF_6){\cdot}xH_2O$ (420 mg, 2 mmol) was then added with stirring. The mixture was left standing at room temperature for several days to give colorless crystals of **5**, whose structure was confirmed by a single-crystal X-ray diffraction study. Yield 270 mg (36%).

[Zn(pca)$_2$$(H_2O)_2$] (6): pca (130 mg, 1 mmol) was dissolved in 10 mL of EtOH/H_2O (1:1) and then 1 mmol of pyrazine (85 mg) was added. An aqueous solution (5 mL) of $Zn(ClO_4)_2{\cdot}6H_2O$ (380 mg, 1 mmol) was added with stirring. After 10 h of stirring, the reaction mixture was left standing at room temperature for several days to yield colorless cubic crystals of **6**, whose structure was confirmed by a single-crystal X-ray diffraction study.[29]

[Zn(bpy-O)$(H_2O)_4$](ClO_4)·(bpy-O)$_2$(7): An ethanol solution (5 mL) of pcn (110 mg, 1 mmol) was mixed with an aqueous solution (10 mL) of bpy-O (185 mg, 1 mmol) with stirring. After 1 h, an EtOH/H_2O solution (2:5; 7 mL) of $Zn(ClO_4)_2{\cdot}6H_2O$ (380 mg, 1 mmol) was added and the mixture stirred for 19 h. The solution was left standing at room temperature to afford colorless plates. A single-crystal X-ray diffraction study showed that the product is [Zn(bpy-O)$(H_2O)_4$](ClO_4)·(bpy-O)$_2$ (**7**).[27] When pca was employed instead of pcn, **6** was isolated. Yield 190 mg (59%).

[Zn(azp)$_2$$(H_2O)_2$]$(ClO_4)$(MeOH) (8), [Zn(azp)$_2$$(H_2O)_4$]$(ClO_4)_2$·(azp)$_{2.5}$ (9) and [Zn$_2$(μ-azp)$_2$(azp)$_4$$(H_2O)_6$]$(ClO_4)_2$ (10): azp (190 mg, 1 mmol) and pcn (110 mg, 1 mmol) were mixed in 6 mL of EtOH/H_2O (1:1) with stirring. An aqueous solution (6 mL) of $Zn(ClO_4)_2{\cdot}6H_2O$ (380 mg, 1 mmol) was then added. After 4 h of stirring, the resulting orange-red precipitate was collected on a frit and recrystallized from MeOH to give red rectangular crystals of **8**; a single-crystal X-ray diffraction study supported the identification.[30] Two kinds of red single crystals (**9** and **10**) were also isolated from the original filtrate. Identification of these crystals was performed by a single-crystal X-ray diffraction study.[30] When pca was employed instead of pcn, **5** was obtained.

X-ray Crystallography: Selected crystals of compounds **1**−**10** were attached on a nylon loop for low-temperature measurements. A Bruker SMART-APEX CCD diffractometer with graphite-monochromated Mo-K_a radiation (λ = 0.71073Å) was used for data collection on these crystals at 100 K. The structures were solved by direct methods using Sir-97 in a WinGx program package and refined with anisotropic thermal parameters by full-matrix least-squares techniques with SHELXS-97 in a WinGx program package.[31] The refinements were made on F^2 data; the final R and wR_2 values are given in Table 1 for **1**−**5**. Crystal data for **6**−**10** are not cited because these are known compounds. Selected bond lengths and angles are given in Table 2. The molecular structures of these compounds are given in the text. CCDC-232435 for (**1**), -232436 (**2**), -232437 (**3**), -232438 (**3′**), -232439 (**4**) and -232440 (**5**) contain the supplementary crystallographic data for this paper. These data can be obtained free of charge at www.ccdc.cam.ac.uk/conts/retrieving.html [or from the Cambridge Crystallographic Data Centre, 12 Union Road, Cambridge CB2 1EZ, UK; Fax: (internat.) + 44-1223-336-033; E-mail: deposit@ccdc.cam.ac.uk].

Table 1. Crystal data

	1	**2**	**3**	**3′**	**4**	**5**
Empirical formula	$C_{17}H_{19}ClN_4O_9Zn$	$C_{23}H_{26}ClN_5O_{11}Zn$	$C_{19}H_{21}ClN_40_7Zn$	$C_{18}H_{18}ClN_40_{6.5}Zn$	$C_{19}H_{21}ClN_40_7Zn$	$C_4H_{14}N_2O_6F_6SiZn$
Formula mass	524.2	613.3	519.6	438.1	518.2	393.6
Crystal system	monoclinic	triclinic	monoclinic	monoclinic	monoclinic	monoclinic
Space group	$P2_1/c$	$P\bar{1}$	$P2_1/n$	$P2_1/n$	Cc	$P2/m$
Temperature [K]	100	293	100	293	100	293
a [Å]	10.492(6)	10.401(1)	10.1459(6)	10.282(4)	14.786(1)	7.0204(8)
b [Å]	9.410(5)	10.905(1)	20.402(1)	20.760(8)	16.528(1)	6.9920(8)
c [Å]	22.685(1)	13.543(2)	11.1216(6)	11.214(4)	10.2302(8)	7.1791(8)
α [°]	90	94.060(3)	90	90	90	90
β [°]	100.12(9)	106.279(3)	114.78(1)	115.25(7)	119.104(1)	104.324(2)
γ [°]	90	114.713(3)	90	90	90	90
V [Å^3]	2204.6(4)	1308.34(3)	2090.2(1)	2164.9(8)	2184.4(1)	341.44(2)
Z	4	2	4	4	4	4
$D_{calcd.}$ [g/cm^3]	1.58	1.56	1.72	1.45	1.58	1.90
μ [mm^{-1}]	1.291	1.101	1.362	1.296	1.296	1.982
θ range [°]	1.8−28.4	1.6−28.4	2.0−28.4	2.0−28.5	2.0−28.4	2.9−28.1
Reflections collected	12648	7903	11955	13038	6503	2097
Unique reflections	4984	5634	4754	5004	4472	834
No. of parameters	349	417	349	299	370	68
R_1	0.044	0.077	0.070	0.061	0.052	0.040
wR_2	0.116	0.151	0.189	0.186	0.145	0.111

 © 2004 Wiley-VCH Verlag GmbH & Co. KGaA, Weinheim

Table 2. Selected bond lengths [Å] and angles [°] (bis-py = bipy, bpen, bpea, and bpp)

	1	2	3	3′	4	5
Zn−N(pca)	2.183(2)	2.189(5)	2.094(3)	2.041(4)	2.189(4)	
Zn−N(pyz)						2.199(3)
Zn−N(bis-py)	2.151(3)	2.137(5)	2.043(3)	2.024(4)	2.093(4)	
	2.139(3)	2.160(5)	2.046(3)	2.104(4)	2.116(4)	
Zn−O(pca)	2.107(2)	2.156(4)	2.124(3)	2.035(3)	2.048(3)	
	2.102(2)	2.203(5)	2.026(2)	2.131(3)	2.111(3)	
Zn−O(ROH)	2.111(2)	2.123(5)			2.431(5)	2.077(2)
N(pca)−Zn−N(bis-py)	91.40(8)	94.3(2)	109.1(1)	102.6(2)	101.2(2)	
	88.85(8)	95.5(2)	148.1(1)	148.1(2)	158.4(2)	
N(pyz)−Zn−N(pyz)						180.0
N(bis-py)−Zn−N(bis-py)	179.58(9)	169.1(2)	101.7(1)	108.2(2)	94.6(2)	
O(pca)−Zn−O(pca)	83.75(7)	75.7(2)	154.8(1)	155.1(2)	165.9(2)	
O(pca)−Zn−N(pca)	76.91(8)	149.5(2)	78.5(1)	91.3(1)	100.2(2)	
	160.63(8)	73.8(2)	85.7(1)	92.9(2)	75.8(1)	
O(pca)−Zn−N(bis-py)	90.86(8)	88.3(2)	94.8(1)	77.8(1)	97.2(2)	
	89.87(8)	94.7(2)	91.1(1)	96.2(2)	92.3(2)	
	89.52(8)	92.7(2)	108.9(1)	106.8(2)	96.9(2)	
	90.01(8)	85.7(2)	92.3(1)	85.9(1)	87.8(1)	
N(pca)−Zn−O(ROH)	97.06(9)	96.2(2)			83.0(2)	
N(bis-py)−Zn−O(ROH)	87.15(8)	87.6(2)			175.2(2)	91.70(8)
	92.48(8)	86.6(2)			82.0(2)	88.30(8)
O(pca)−Zn−O(ROH)	102.19(8)	114.3(2)			79.6(2)	
	173.19(7)				86.5(2)	
O(ROH)−Zn−O(ROH)						180.00(9)
						90.2(1)
						89.9(1)

Acknowledgments

This research was funded by Grants-in-Aid for scientific research in Priority Area (no. 12023221 "Metal-Assembled Complexes") and by Grants-in-Aid for scientific research [nos. 14540514 (S. O.) and 15550047 (T. O.)] from the Ministry of Education, Science, Sports and Culture, Japan. Thanks are also due to CREST, JST (T. O.).

[1] J.-M. Lehn, *Supramolecular Chemistry*, VCH, New York, **1995**, and references cited therein.
[2] *Transition Metals in Supramolecular Chemistry* (Eds.: L. Fabbrizzi and A. Poggi), NATO ASI Series, Kluwer Academic Publishers, Dordrecht**, 1994**, p. 448.
[3] *Supramolecular Materials and Technologies − Perspectives in Supramolecular Chemistry* (Ed.: D. N. Reinhoudt), John Wiley & Sons Ltd., Chichester, **1999**, vol. 4, and references cited therein.
[4] *Supramolecular Organometallic Chemistry* (Eds.: I. Haiduc, F. T. Edelmann), John Wiley & Sons Ltd., Weinheim, **1999**, and references cited therein.
[5] S. Onaka, Y. kasukawa, M. Shiotsuka, *J. Organomet. Chem.* **1998**, *570*, 113−119.
[6] S. Noro, R. Kitaura, M. Kondo, S. Kitagawa, T. Ishii, H. Matsuzaka, M. Yamashita, *J. Am. Chem. Soc.* **2002**, *124*, 2568−2583, and references cited therein.
[7] M. J. Zaworotko, *Chem. Commun.* **2001**, 1−9, and references cited therein.
[8] M. E. Braun, C. D. Steffek, J. Kim, P. G. Rasmussen, O. M. Yaghi, *Chem. Commun.* **2001**, 2532−2533.
[9] L. Carlucci, G. Ciani, D. M. Proserpio, S. Rizzato, *Chem. Commun.* **2001**, 1198−1199.
[10] B.-Q. Ma, H.-l. Sun, S. Gao, G.-X. Xu, *Inorg. Chem.* **2001**, *40*, 6247−6253.
[11] S. Subramanian, M. J. Zaworotko, *Angew. Chem. Int. Ed. Engl.* **1995**, *34*, 2127−2129.
[12] [12a] R.-G. Xiong, X. Xue, H. Zhao, X.-Z. You, B. F. Abrahams, Z. Xue, *Angew. Chem. Int. Ed.* **2002**, *41*, 3800−3803. [12b] R.-G. Xiong, X.-Z. You, B. F. Abrahams, C.-M. Che, *Angew. Chem. Int. Ed.* **2001**, *40*, 4422−4425.
[13] M. Kondo, T. Yoshitomi, K. Seki, H. Matuzaka, S. Kitagawa, *Angew. Chem. Int. Ed. Engl.* **1997**, *36*, 1725−1727.
[14] M.-L. Tong, B.-H. Ye, J.-W. Cai, X.-M. Chen, S. W. Ng, *Inorg. Chem.* **1998**, *37*, 2645−2650.
[15] L. Carlucci, G. Ciani, D. M. Prosperio, A. Sironi, *J. Chem. Soc., Dalton Trans.* **1997**, 1801−1803.
[16] *Mesomolecules − from Molecules to Materials* (Eds.: G. D. Mendenhall, A. Greenberg, J. F. Liebman), Search Series, vol. 1, Chapman & Hall, New York, **1995**, and references cited therein.
[17] *Atomic and Molecular Wires* (Ed.: C. Joachim, S. Roth), NATO ASI Series, vol. 341, Kluwer Academic Publishers, Dordrecht, **1997**, and references cited therein.
[18] *Supramolecular Engineering of Synthetic Metallic Materials-Conductors and Magnets* (Eds.: J. Veciana, C. Rovira, D. B. Amabilino), NATO ASI Series, vol. 518, Kluwer Academic Publishers, Dordrecht, **1999**, and references cited therein.
[19] *Nanoscale Materials in Chemistry* (Ed.: K. Klabunde), John Wiley & Sons Ltd., New York, **2001**, and references cited therein.
[20] S. Martín, M. G. Barandika, L. Lezama, J. L. Pizarro, Z. E. Serna, J. I. R. de Larramendi, M. I. Arriortua, T. Rojo, R. Cortés, *Inorg. Chem.* **2001**, *40*, 4109−4115.
[21] W. W. Ellis, M. Schmitz, A. A. Arif, P. J. Stang, *Inorg. Chem.* **2001**, *39*, 2547−2557.
[22] N. Kitajima, S. Hikichi, M. Tanaka, Y. Moro-oka, *J. Am. Chem. Soc.* **1993**, *115*, 5496−5508.

 © 2004 Wiley-VCH Verlag GmbH & Co. KGaA, Weinheim

[23] X. Yin, J. R. Moss, *Coord. Chem. Rev.* **1999**, *181*, 27−59 and references cited therein.
[24] [24a] S. Noro, S. Kitagawa, M. Yamashita, T. Wada, *Chem. Commun.* **2002**, 222−223. [24b] O. R. Evans, R.-G. Xiong, Z. Wang, G. K. Wong, W. Lin, *Angew. Chem. Int. Ed.* **1999**, *38*, 536−538.
[25] S. A. Bourne, M. Killenny, L. R. Nassimbeni, *J. Chem. Soc., Dalton Trans.* **2001**, 1176−1179.
[26] M. Ito, S. Onaka, *Inorg. Chim. Acta* **2004**, *357*, 1039−1046.
[27] E. B. Brown, R. Granneman, *J. Am. Chem. Soc.* **1975**, *97*, 621−627.
[28] M. L. Hernández, M. K. Urtiaga, G. Barandika, R. Cortes, L. Lezama, N. de la Pinta, M. I. Arriortua, T. Rojo, *J. Chem. Soc., Dalton Trans.* **2001**, 3010−3014.
[29] A. Takenaka, *Nihon Kagakuzasshi* **1970**, *91*, 921−927; *Chem. Abstr.* **1971**, *74*, 7526n.
[30] B. Li, H. Liu, Y. Xu, J. Chen, H. Wang, Z. Xu, *J. Mol. Struct.* **2001**, *597*, 21−30; C. He, B.-G. Zhang, C.-Y. Duan, J.-H. Li, Q.-J. Meng, *Eur. J. Inorg. Chem.* **2000**, 2549−3554.
[31] G. M. Sheldrick, *SHELX-97, Program for Analysis of Crystal Structures*, University of Göttingen, Germany, **1997**.

Received May 26, 2004
Early View Article
Published Online November 4, 2004

 © 2004 Wiley-VCH Verlag GmbH & Co. KGaA, Weinheim

Syntheses, Structures, and Luminescent Properties of [Bis(iminoalkyl)pyridine]cadmium(II) Complexes

Rui-Qing Fan,[a] Dong-Sheng Zhu,[a] Ying Mu,*[a] Guang-Hua Li,[b] Yu-Lin Yang,[b] Qing Su,[a] and Shou-Hua Feng[b]

Keywords: Cadmium / Luminescence / N ligands / X-ray diffraction

Four new Cd^{II} complexes of 2,6-bis[1-(phenylimino)ethyl]-pyridine ($\mathbf{L^1}$), 2,6-bis[1-(2,6-diisopropylphenylimino)ethyl]-pyridine ($\mathbf{L^2}$), 2,6-bis[1-(2,6-dimethylphenylimino)ethyl]-pyridine ($\mathbf{L^3}$), 2,6-bis[1-(2-methylphenylimino)ethyl]pyridine ($\mathbf{L^4}$) have been synthesized. These complexes have the formulas $[Cd(\mathbf{L^1})Cl_2]\cdot 1.5CH_3CN$ (**1**), $[Cd(\mathbf{L^2})Cl_2]$ (**2**), $[Cd(\mathbf{L^3})Cl_2]\cdot CH_3CN$ (**3**), and $[Cd(\mathbf{L^4})Cl_2]\cdot CH_3CN$ (**4**). The molecular structures of complexes **1**–**4** were determined by single-crystal X-ray diffraction. Crystallographic studies of **1**–**4** reveal all four complexes to be five-coordinate with geometries that can be best described as distorted trigonal-bipyramidal. All eight compounds ($\mathbf{L^1}$–$\mathbf{L^4}$ and **1**–**4**) are luminescent at room temperature in solution and the solid state. At 298 K in dichloromethane solution, all compounds have fluorescent emissions at about 368–409 nm. The fluorescent emission of these compounds originates from ligand-centered π^*–π transitions. The Cd^{II} centers play a key role in enhancing the fluorescent emission of the ligands.
(© Wiley-VCH Verlag GmbH & Co. KGaA, 69451 Weinheim, Germany, 2004)

Introduction

Luminescent coordination compounds with pyridine-type ligands have attracted much attention recently due to their good performance in sensor technologies and electroluminescent devices.[1−7] Several d^{10} metal complexes with pyridine-type ligands have been synthesized and their luminescence behavior studied.[1−3] Among these, luminescent cadmium complexes have been widely investigated as potential luminescent materials.[1b,1d,2a,2b,2d] [Bis(iminoalkyl)pyridine]metal complexes have also been the subject of intense research due to their interesting coordination chemistry and applications in catalysis.[8−17] Many complexes containing one or two bis(iminoalkyl)pyridine ligands with small aryl substituents have been synthesized and characterized.[8−9] Recently, iron and cobalt complexes with bulky aryl-substituted bis(iminoalkyl)pyridine ligands were reported by Brookhart and Gibson et al.[10−12] These complexes exhibit high activity for olefin polymerization. Brookhart et al. have also reported [bis(iminoalkyl)pyridine]ruthenium complexes that can catalyze the epoxidation of olefins.[17] To the best of our knowledge, no investigation has been carried out on the luminescent properties of [bis(iminoalkyl)-pyridine]metal complexes. We explored this possibility and selected four [bis(iminoalkyl)pyridine]cadmium complexes for the present study. Herein we report the syntheses, crystal structures, and luminescent properties of a series of Cd^{II} complexes of ligands $\mathbf{L^1}$−$\mathbf{L^4}$.

Results and Discussion

Synthesis and Characterization

2,6-Bis[1-(phenylimino)ethyl]pyridine ($\mathbf{L^1}$), 2,6-bis[1-(2,6-diisopropylphenylimino)ethyl]pyridine ($\mathbf{L^2}$), 2,6-bis[1-(2,6-dimethylphenylmino)ethyl]pyridine ($\mathbf{L^3}$), and 2,6-bis[1-(2-methylphenylimino)ethyl]pyridine ($\mathbf{L^4}$) were synthesized according to modified published procedures in good yield by condensation of 2,6-diacetylpyridine with the corresponding aniline in refluxing absolute methanol in the presence of a catalytic amount of formic acid (Scheme 1).[8a,10] Cadmium complexes of these ligands were prepared by reaction of $CdCl_2\cdot 2.5H_2O$ with a stoichiometric amount of the corresponding 2,6-bis(iminoalkyl)pyridine ligand in acetonitrile (complexes **1** and **3**) or in dichloromethane (complexes **2** and **4**) at room temperature (Scheme 1). Complexes **1**−**4** were obtained as yellowish crystals in good yield.

[a] Key Laboratory for Supramolecular Structure and Materials of Ministry of Education, School of Chemistry, Jilin University, Changchun 130012, People's Republic of China
[b] State Key Laboratory of Inorganic Synthesis and Preparative Chemistry, Jilin University, Changchun 130012, People's Republic of China
Fax: + 86-431-519-3421
E-mail: ymu@mail.jlu.edu.cn
Supporting information for this article is available on the WWW under http://www.eurjic.org or from the author.

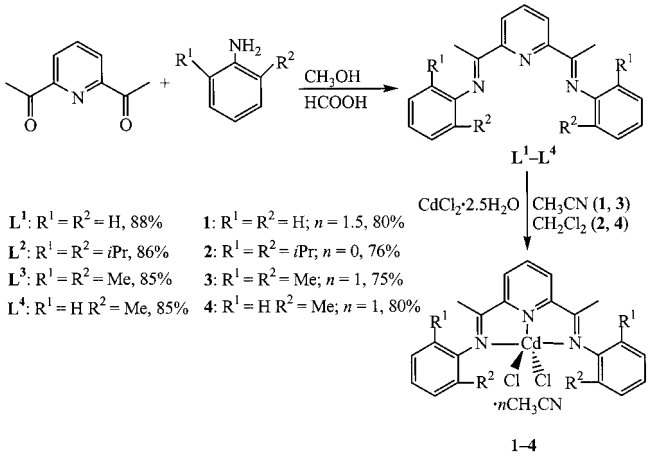

Scheme 1

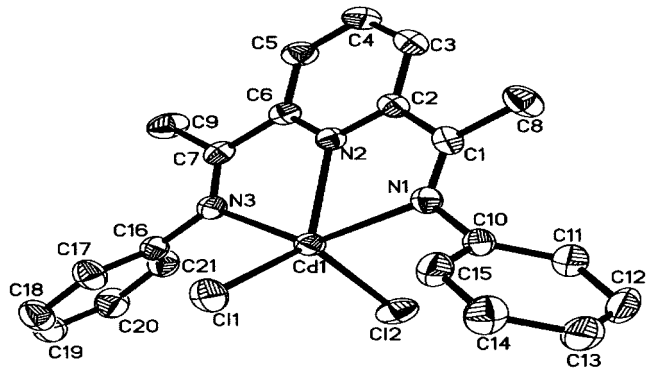

Figure 1. Molecular structure of complex **1** (the other molecule and CH_3CN molecules have been omitted for clarity)

All compounds were characterized by ^1H NMR, UV/Vis, and IR spectroscopy, and elemental analysis. Complexes **1**−**4** were also studied by single-crystal X-ray diffraction.

Structures

Crystals of **1**−**4** suitable for X-ray structural determination were grown from acetonitrile/dichloromethane (2:1) solution (**1**, **3,** and **4**), or from a concentrated dichloromethane solution (**2**). The molecular structures of complexes **1**−**4** are shown below, and selected bond lengths and angles are presented in Table 1.

There are two independent complex molecules and three acetonitrile molecules in the asymmetric unit in the cadmium complex **1** (Figure 1); the two molecules show an approximate C_s symmetry about a plane containing the cadmium atom, two chlorine atoms, and the pyridine nitrogen atom. The dihedral angles between the phenyl rings and the plane formed by three coordinated nitrogen atoms are 75.23(17)° and 82.09(20)° in one of these molecules; these values are larger than those in the other molecule [62.86(17)° and 67.23(14)°, respectively]. The dihedral angles between the two phenyl rings are 83.98(18)° and 74.49(15)°, respectively, in the two molecules. The cadmium atom deviates by 0.077 Å from the coordination plane in one molecule, while in the other the metal atom is displaced by 0.084 Å. For both molecules the central cadmium atom is coordinated to five atoms and the geometry about the cadmium atom is distorted trigonal-bipyramidal, with the equatorial plane defined by the N(2)(pyridine), Cl(1)and Cl(2) atoms and the N(1) and N(3)(imino) atoms in the axial positions. The mean deviation of the cadmium atom from the equatorial plane in one molecule is only 0.019 Å, while in the other the metal atom is displaced by 0.009 Å. In the two molecules, the angles in the equatorial plane range between 113.36(8)° and 128.50(8)°, and the axial Cd−N(imino) bonds subtend an angle of 137.99(11)° [in the other this angle is 137.92(11)°]. The Cd−N(imino) bonds [2.407(3) and 2.419(3) Å] are longer than the Cd−N(pyridine) bonds [2.310(3) Å], as is the case in the other molecule. The imino C=N bonds in **1** have a distinc-

Table 1. Selected bond lengths [Å] and angles [°] for complexes **1**−**4**

	1		**2**	**3**	**4**	
	Molecule 1	Molecule 2			Molecule 1	Molecule 2
Cd−N(2)	2.310(3)	2.313(3)	2.331(5)	2.300(6)	2.316(12)	2.330(11)
Cd−N(1)	2.407(3)	2.378(3)	2.480(5)	2.426(6)	2.359(12)	2.420(10)
Cd−Cl(1)	2.417 (1)	2.411(1)	2.411(2)	2.420(2)	2.450(4)	2.436(5)
Cd−N(3)	2.419(3)	2.390(3)	2.467(5)	2.431(5)	2.438(10)	2.420(11)
Cd−Cl(2)	2.434(1)	2.436 (1)	2.451(2)	2.434(2)	2.422(5)	2.458(4)
N(1)−C(1)	1.271(5)	1.278(5)	1.307(8)	1.282(8)	1.270(20)	1.262(16)
N(3)−C(7)	1.279(5)	1.271(5)	1.299(8)	1.275(8)	1.289(17)	1.263(18)
N(2)−Cd−N(1)	69.25(11)	68.79(11)	68.14(16)	69.50(20)	71.00(40)	68.50(40)
N(2)−Cd−Cl(1)	128.50(8)	126.81(9)	139.19(14)	118.52(15)	116.60(30)	125.70(30)
N(1)−Cd−Cl(1)	101.16(8)	103.49(9)	100.81(13)	99.62(16)	98.10(30)	102.90(30)
N(2)−Cd−N(3)	68.82(11)	69.20(11)	68.29(17)	69.00(20)	68.30(40)	68.80(40)
N(1)−Cd−N(3)	137.99(11)	137.92(11)	131.99(16)	138.40(20)	139.20(40)	137.30(40)
Cl(1)−Cd−N(3)	102.57(8)	103.24(9)	99.01(14)	102.15(14)	101.00(30)	102.50(30)
N(2)−Cd−Cl(2)	113.43(8)	113.36(8)	98.71(14)	124.25(15)	121.30(30)	117.60(30)
N(1)−Cd−Cl(2)	99.25(9)	95.79(9)	103.80(13)	102.69(16)	99.90(40)	98.70(30)
Cl(1)−Cd−Cl(2)	118.07(5)	119.81(5)	122.05(9)	117.22(8)	122.12(17)	116.72(16)
N(3)−Cd−Cl(2)	99.44(8)	98.38(10)	101.71(13)	98.16(14)	99.90(30)	99.80(30)

 © 2004 Wiley-VCH Verlag GmbH & Co. KGaA, Weinheim

tive double-bond character, with C=N distances in the range 1.271(5)−1.279(5) Å.

Complexes **2** (Figure 2) and **3** (Figure 3) possess structures with approximate C_s symmetry about a plane bisecting the central pyridine ring and containing the cadmium atom and two chlorine atoms, while complex **4** (Figure 4) adopts C_2 symmetry. The central cadmium atom in **2**−**4** is coordinated to five groups and the geometry about

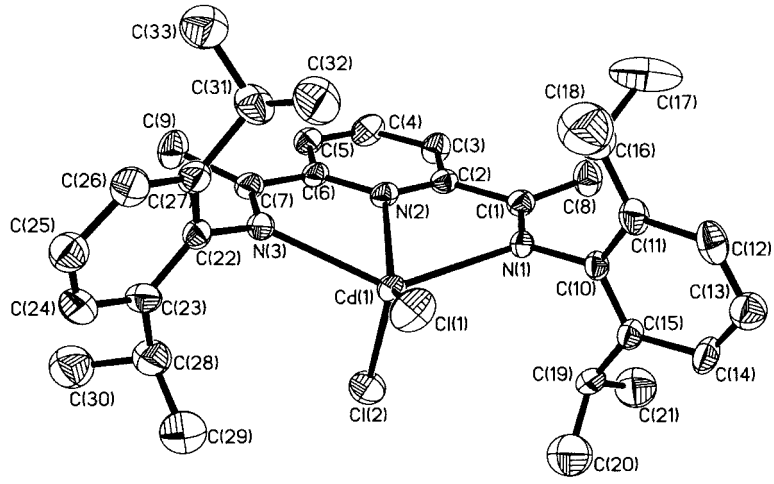

Figure 2. Molecular structure of complex **2**

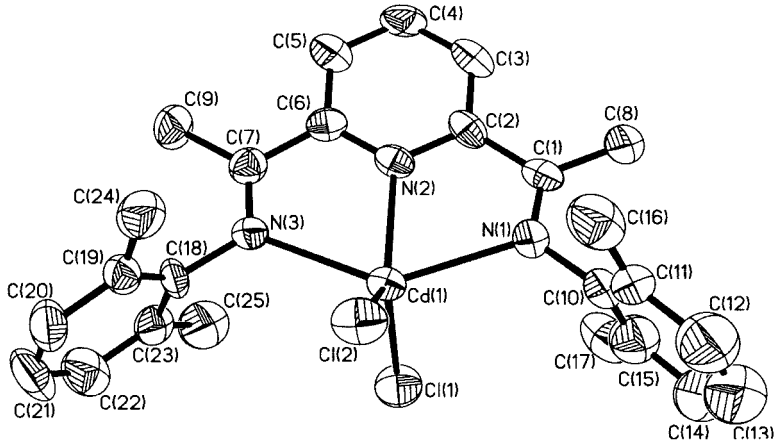

Figure 3. Molecular structure of complex **3** (the CH_3CN molecule has been omitted for clarity)

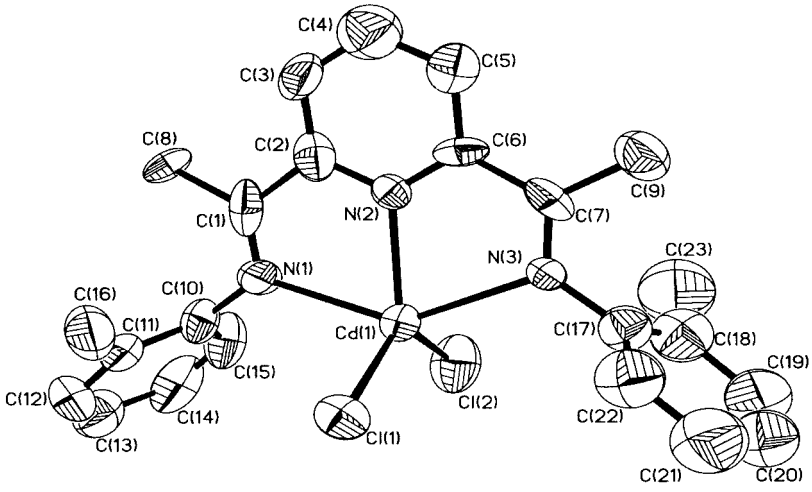

Figure 4. Molecular structure of complex **4** (the other molecule and CH_3CN molecules have been omitted for clarity)

 © 2004 Wiley-VCH Verlag GmbH & Co. KGaA, Weinheim

the cadmium atom is a distorted trigonal bipyramid, with the equatorial plane defined by the N(2)(pyridine), Cl(1) and Cl(2) atoms and the N(1) and N(3)(imino) atoms in the axial positions. Complex **3** contains one independent molecule and one acetonitrile molecule, where as there are two independent molecules and two acetonitrile molecules in the asymmetric unit in the cadmium complex **4**. The mean deviation of the cadmium atoms in **2**−**4** from the equatorial planes is 0.027, 0.020 and 0.002 Å (0.007 Å for the other molecule in **4**), respectively, and the axial Cd−N(imino) bonds subtend angles of 131.99(16)°, 138.40(20)° and 139.20(40)° [137.30(40)° for the other molecule in **4**], respectively. The cadmium atoms in **2**−**4** deviate by 0.652, 0.087 and 0.040 Å (0.037 Å for the other molecule in **4**), respectively, from the coordination plane. The Cd−N(pyridine) bonds in **2**−**4** range from 2.300(6)−2.331(5) Å, while the distances between the cadmium atom and the imino nitrogen atoms in the three complexes are almost the same [2.467(5) and 2.480(5) Å] in **2**, [2.426(6) and 2.431(5) Å] in **3** and [2.359(12) and 2.438(10) Å] in **4** [2.420(10) and 2.420(11) Å for the other molecule in **4**]. The planes of the phenyl rings in **2**−**4** are oriented essentially orthogonal to the coordination plane [ranging between 75.62(46)° and 89.59(52)°]. In each complex the Cd−N(pyridine) bond is significantly shorter than the Cd−N(imino) bonds, with the formal double-bond character of the imino linkages N(1)−C(1) and N(3)−C(7) being retained [C=N distances in range 1.262(16)−1.307(8) Å]. There are no intermolecular packing features of interest in any of the four complexes.

Luminescence Properties

Table 2 presents the absorption and emission data for the new complexes **1**−**4** in dichloromethane solution and in the solid state at room temperature, together with those for ligands $\mathbf{L^1}$−$\mathbf{L^4}$. The four complexes show two main absorption bands, which are similar to ligands $\mathbf{L^1}$−$\mathbf{L^4}$ in the UV region, as shown in Figure 5. The electronic absorption spectra of the complexes show low-energy absorption bands at about 339−350 nm (329−340 nm for ligands $\mathbf{L^1}$−$\mathbf{L^4}$), and higher energy absorption bands at about 301−313 nm (281−291 nm for ligands $\mathbf{L^1}$−$\mathbf{L^4}$), attributed to ligand-centered π−π* transitions. The electronic absorption spectra of the complexes are red-shifted relative to the ligands due to perturbation of the intraligand π−π* transition of the bis(iminoalkyl)pyridine unit by the metal atom. The energy trends of this band for the series **1**−**4** and $\mathbf{L^1}$−$\mathbf{L^4}$ are found to follow the order **3** < **4** < **2** < **1** and $\mathbf{L^3} < \mathbf{L^4} < \mathbf{L^2} < \mathbf{L^1}$, which is in line with the electron-donating ability of the alkyl group (2,6-dimethylphenyl > 2-methylphenyl > 2,6-diisopropylphenyl > phenyl).

Table 2. Photoluminescent data for ligands $\mathbf{L^1}$−$\mathbf{L^4}$ and complexes **1**−**4**[a]

	Absorption [nm] (ε [$dm^3\ mol^{-1}\ cm^{-1}$])	Emission λ_{max} [nm]	Conditions
$\mathbf{L^1}$	281 (16025), 329 (7485)	368	CH_2Cl_2, 298K
		471	solid, 298K
$\mathbf{L^2}$	284 (16180), 334 (7640)	375	CH_2Cl_2, 298K
		475	solid, 298K
$\mathbf{L^3}$	291 (16528), 340 (7998)	381	CH_2Cl_2, 298K
		480	solid, 298K
$\mathbf{L^4}$	287 (16335), 337 (7843)	378	CH_2Cl_2, 298K
		476	solid, 298K
1	301 (16944), 339 (7950)	397	CH_2Cl_2, 298K
		482	solid, 298K
2	305 (17195), 343 (8153)	399	CH_2Cl_2, 298K
		485	solid, 298K
3	313 (17456), 350 (8511)	409	CH_2Cl_2, 298K
		488	solid, 298K
4	309 (17253), 347 (8259)	402	CH_2Cl_2, 298K
		486	solid, 298K

[a] Concentration ca. 10^{-5} M.

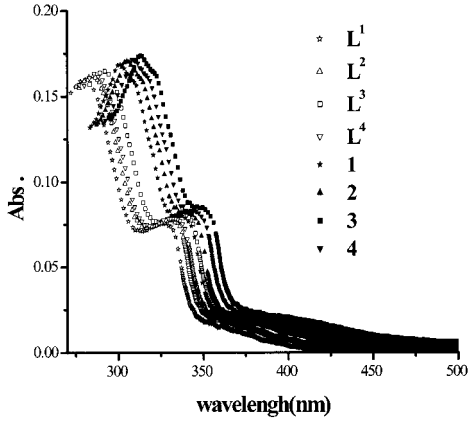

Figure 5. UV/Vis absorption spectra of ligands $\mathbf{L^1}$−$\mathbf{L^4}$ and complexes **1**−**4**

Complexes **1**−**4** have broad fluorescent emission bands in degassed CH_2Cl_2 solution at room temperature, with maxima at 397, 399, 409, and 402 nm for **1**−**4**, respectively (λ_{max} = 368, 375, 381, and 378 nm for $\mathbf{L^1}$−$\mathbf{L^4}$; Figure 6). Similar to the electronic absorption data, the emission energies are found to depend on the bis(iminoalkyl)pyridine ligand. For complexes **1**−**4** and ligands $\mathbf{L^1}$−$\mathbf{L^4}$, emission-energy trends in the order **3** < **4** < **2** < **1** and $\mathbf{L^3} < \mathbf{L^4} < \mathbf{L^2}$

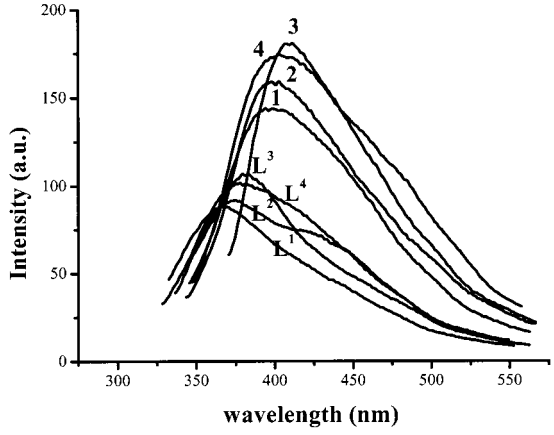

Figure 6. Emission spectra of ligands $\mathbf{L^1}$−$\mathbf{L^4}$ and complexes **1**−**4** in solution at room temperature

 © 2004 Wiley-VCH Verlag GmbH & Co. KGaA, Weinheim

< $\mathbf{L^1}$ are observed, again in line with the electron-donating ability of the alkyl group. The Cd^{II} centers in complexes **1**−**4** play a key role in enhancing the fluorescent emission of the ligands. The chelation of the ligands to the metal center also contributes to the enhancement of the fluorescent emission by increasing the rigidity of the ligands, thus reducing the loss of energy by thermal vibrational decay. However, in the solid state at room temperature complexes **1**−**4** exhibit a bright, greenish-blue emission band with maxima at 482, 485, 488, and 486 nm, respectively (λ_{max} = 471, 475, 480, and 476 nm for $\mathbf{L^1}$−$\mathbf{L^4}$); these values are red-shifted by about 80 nm (100 nm for $\mathbf{L^1}$−$\mathbf{L^4}$) from the emission in solution. This dramatic red-shift of the emission energy for complexes **1**−**4** and ligands $\mathbf{L^1}$−$\mathbf{L^4}$ from solution to the solid state is probably caused by intermolecular interactions in the solid state that effectively decrease the energy gap.

Conclusion

A series of [bis(iminoalkyl)pyridine]cadmium(II) complexes have been synthesized and characterized. Complexes **1**−**4** and ligands $\mathbf{L^1}$−$\mathbf{L^4}$ have fluorescent emission at 368−409 nm in dichloromethane solution at room temperature. Complexes **1**−**4** and ligand $\mathbf{L^1}$−$\mathbf{L^4}$ have broad fluorescent emission bands in the solid state at room temperature, with λ_{max} = 482, 485, 488, 486 nm for **1**−**4,** and 471, 475, 480, 476 nm for $\mathbf{L^1}$−$\mathbf{L^4}$, respectively. Their luminescent properties show that they are a new class of luminescent metal compounds with potential applications in optoelectronic devices.

Experimental Section

General: All manipulations were carried out under nitrogen using standard Schlenk and cannula techniques or in a conventional nitrogen-filled glove box. Elemental analyses were performed with a Perkin−Elmer 240c elemental analyzer. IR spectra were obtained with a Nicolet Impact 410 FTIR spectrometer using KBr pellets. NMR spectra were recorded with a Varian Mercury 300 MHz spectrometer. UV/Vis spectra were obtained with a Perkin−Elmer Lambda 20 spectrometer. Luminescence spectra were measured with a Perkin−Elmer LS55 Luminescence spectrometer at room temperature. Aniline, 2,6-diisopropylaniline, 2,6-dimethylaniline, and 2-methylaniline were purchased from Aldrich Chemical Co. and used as received. Solvents were refluxed in the presence of an appropriate drying agent, and distilled and degassed prior to use. For methanol, Mg ribbon was used as drying agent, whereas acetonitrile and dichloromethane were dried with calcium hydride. 2,6-Diacetylpyridine was prepared according to a published procedure.[18]

Preparation of 2,6-Bis[1-(phenylimino)ethyl]pyridine ($\mathbf{L^1}$): Aniline (2.8 mL, 31.0 mmol) was added to a solution of 2,6-diacetylpyridine (1.70 g, 10.4 mmol) in absolute methanol (30 mL). After the addition of several drops of formic acid, the reaction mixture was refluxed for 8 h and then allowed to cool down to room temperature. The crude product precipitated as a yellow powder. Pure $\mathbf{L^1}$ was obtained in 88% yield (2.87 g) upon recrystallization from methanol. ^{1}H NMR (300 MHz, $CDCl_3$): δ = 8.36 (d, J = 7.8 Hz, 2 H, Py-H_m), 7.89 (t, J = 7.8 Hz, 1 H, Py-H_p), 7.42−6.85 (m, 10 H, Ar-*H*), 2.42 (s, 6 H, N=C*Me*) ppm. IR (KBr): $\tilde{\nu}$ = 3059 (w), 2919 (w), 2860 (w), 1638 (vs), 1594 (m), 1574 (m), 1482 (s), 1445 (m), 1417 (w), 1361 (s), 1319 (m), 1294 (w), 1255 (w), 1220 (s), 1173 (m), 1150 (w), 1118 (m), 1091 (m), 1076 (m), 1027 (m), 992 (w), 969 (w), 912 (w), 874 (w), 823 (s), 808 (m), 774 (s), 762 (m), 743 (m), 707 (s), 697 (m), 658 (w), 645 (w), 551 (w), 520 (m), 468 (w), 443 (w) cm^{-1}. $C_{21}H_{19}N_3$ (313.4): calcd. C 80.48, H 6.11, N 13.41; found C 80.28, H 6.00, N 13.32.

Preparation of 2,6-Bis[1-(2,6-diisopropylphenylimino)ethyl]pyridine ($\mathbf{L^2}$): 2,6-Diisopropylaniline (8.7 mL, 46.1 mmol) was added to a solution of 2,6-diacetylpyridine (2.5 g, 15.3 mmol) in absolute methanol (50 mL). After the addition of several drops of formic acid, the reaction mixture was refluxed for 24 h and then allowed to cool down to room temperature. The crude product precipitated as yellow powder. Pure $\mathbf{L^2}$ was obtained in 86% yield (6.35 g) upon recrystallization from methanol. ^{1}H NMR (300 MHz, $CDCl_3$): δ = 8.60 (d, J = 7.8 Hz, 2 H, Py-H_m), 7.98 (t, J = 7.8 Hz, 1 H, Py-H_p), 7.21−7.13 (m, 6 H, Ar-*H*), 2.78 (sept, J = 6.8 Hz, 4 H, C*H*Me$_2$), 2.30 (s, 6 H, N=C*Me*), 1.19 (dd, J = 6.8 Hz, 24 H, CH*Me*$_2$) ppm. IR (KBr): $\tilde{\nu}$ = 3068 (w), 2960 (s), 2925 (w), 2870 (w), 1646 (vs), 1588 (w), 1571 (w), 1455 (m), 1438 (m), 1406 (w), 1383 (w), 1368 (s), 1321 (w), 1301 (w), 1255 (w), 1240 (m), 1195 (m), 1121 (m), 1103 (w), 1079 (w), 1059 (w), 1041 (w), 994 (w), 961 (w), 936 (w), 886 (w), 829 (m), 801 (w), 770 (s), 758 (w), 744 (w), 691 (w), 634 (w), 533 (w), 443 (w) cm^{-1}. $C_{33}H_{43}N_3$ (481.7): calcd. C 82.28, H 9.00, N 8.72; found C 82.50, H 8.91, N 8.65.

Preparation of 2,6-Bis[1-(2,6-dimethylphenylimino)ethyl]pyridine ($\mathbf{L^3}$): 2,6-Dimethylaniline (6.4 mL, 51.7 mmol) was added to a solution of 2,6-diacetylpyridine (2.81 g, 17.2 mmol) in absolute methanol (50 mL). After the addition of several drops of formic acid, the reaction mixture was refluxed for 24 h and then allowed to cool down to room temperature. The crude product precipitated as a yellow powder. Pure $\mathbf{L^3}$ was obtained in 85% yield (5.4 g) upon recrystallization from methanol. ^{1}H NMR (300 MHz, $CDCl_3$): δ = 8.56 (d, J = 7.8 Hz, 2 H, Py-H_m), 7.95 (t, J = 7.8 Hz, 1 H, Py-H_p), 7.11−6.95 (m, 6 H, Ar-*H*), 2.27 (s, 6 H, N=C*Me*), 2.07 (s, 12 H, C*Me*) ppm. IR (KBr): $\tilde{\nu}$ = 3068 (w), 3019 (w), 2970 (w), 2944 (w), 2915 (w), 2851 (w), 2727 (w), 1646 (vs), 1594 (m), 1567 (m), 1468 (s), 1437 (m), 1366 (s), 1324 (w), 1297 (m), 1247 (m), 1203 (s), 1160 (w), 1148 (w), 1126 (s), 1093 (s), 1071 (w), 1029 (w), 991 (w), 972 (w), 920 (w), 886 (w), 875 (w), 826 (s), 817 (s), 804 (w), 777 (s), 762 (vs), 744 (w), 692 (m), 623 (m), 576 (w), 541 (w), 530 (w), 493 (w), 422 (w) cm^{-1}. $C_{25}H_{27}N_3$ (369.5): calcd. C 81.26, H 7.37, N 11.37; found C 80.98, H 7.40, N 11.56.

Preparation of 2,6-Bis[1-(2-methylphenylimino)ethyl]pyridine ($\mathbf{L^4}$): 2-Methylaniline (2.2 mL, 20.5 mmol) was added to a solution of 2,6-diacetylpyridine (1.1 g, 6.7 mmol) in absolute methanol (25 mL). After the addition of several drops of formic acid, the reaction mixture was refluxed for 24 h and then allowed to cool down to room temperature. The crude product precipitated as a yellow powder. Pure $\mathbf{L^4}$ was obtained in 85% yield (1.96 g) upon recrystallization from methanol. ^{1}H NMR (300 MHz, $CDCl_3$): δ = 8.42 (d, J = 7.6 Hz, 2 H, Py-H_m), 7.92 (t, J = 7.6 Hz, 1 H, Py-H_p), 7.23−6.69 (m, 8 H, Ar-*H*), 2.34 (s, 6 H, N=C*Me*), 2.14 (s, 6 H, C*Me*) ppm. IR (KBr): $\tilde{\nu}$ = 3068 (w), 3019 (w), 2920 (w), 2856 (w), 1648 (vs), 1601 (m), 1569 (m), 1480(s), 1450 (m), 1363 (s), 1321 (m), 1294 (w), 1255 (w), 1220 (s), 1187 (w), 1155 (w), 1118 (s), 1095 (w), 1073 (m), 1041(m), 964 (w), 933 (w), 880 (w), 851 (w), 817 (s), 780 (s), 740 (s), 727 (s), 651 (w), 642 (w), 567 (w), 533 (w), 446 (m), 405 (w) cm^{-1}. $C_{23}H_{23}N_3$ (341.5): calcd. C 80.90, H 6.79, N 12.31; found C 80.89, H 6.82, N 12.27.

 © 2004 Wiley-VCH Verlag GmbH & Co. KGaA, Weinheim

Preparation of {2,6-Bis[1-(phenylimino)ethyl]pyridine}dichlorocadmium(II)·1.5CH$_3$CN (1): A mixture of **L^1** (124 mg, 0.39 mmol) and $CdCl_2·2.5H_2O$ (90 mg, 0.39 mmol) in acetonitrile (30 mL) was stirred under nitrogen at room temperature for 12 h. Evaporation of the solvent gave the crude product as a yellowish powder. Pure **1** was obtained in 80% yield (174 mg) upon recrystallization from acetonitrile/dichloromethane (2:1). ^{1}H NMR (300 MHz, CD_3CN): δ = 8.50 (quint, J = 7.2 Hz, 3 H, Py-*H*), 7.52−7.17 (m, 10 H, Ar-*H*), 2.52 (s, 6 H, N=C*Me*) ppm. ^{13}C NMR (CD_3CN, ^{1}H gated decoupled): δ = 166.30 (N=*C*), 148.41 (Py-C_o), 147.39 (Ar-C_i), 143.44 (Ar-C_o), 129.27 (Ar-C_p), 128.09 (Py-C_p), 126.37 (Py-C_m), 121.66 (Ar-C_m), 17.46 (N=C*Me*) ppm. IR (KBr): $\tilde{\nu}$ = 3089 (w), 3029 (w), 2960 (w), 2915 (w), 2247 (w), 1631 (s), 1591 (s), 1487 (s), br 1450 (m), 1371 (s), 1309 (w), 1284 (w), 1252 (s), 1227 (s), 1185 (w), 1148 (w), 1103 (w), 1071 (w), 1019 (m), 981 (w), 909 (w), 859 (w), 820 (s), 777 (s), 758 (m), 743 (m), 725 (m) 697 (s), 674 (w), 654 (w), 576 (w), 552 (w), 533 (m), 468 (w), 407 (w) cm^{-1}. $C_{21}H_{19}CdCl_2N_3·1.5CH_3CN$ (558.1): calcd. C 51.63, H 4.24, N 11.29; found C 51.60, H 4.31, N 11.25.

Preparation of {2,6-Bis[1-(2,6-diisopropylphenylimino)ethyl]pyridine}dichlorocadmium(II) (2): A mixture of **L^2** (169 mg, 0.35 mmol) and $CdCl_2·2.5H_2O$ (80 mg, 0.35 mmol) in dichloromethane (40 mL) was stirred under nitrogen at room temperature for 12 h. The volume of the reaction mixture was reduced to about 10 mL and the mixture left to stand at 0 °C for several days. Yellowish crystals of **2** formed and were separated from the solution. Yield: 177 mg (76%). ^{1}H NMR (300 MHz, CD_3CN): δ = 8.51 (quint, J = 6.9 Hz, 3 H, Py-*H*), 7.27−7.18 (m, 6 H, Ar-*H*), 2.89 (sept, J = 6.6 Hz, 4 H, C*H*Me$_2$), 2.40 (s, 6 H, N=C*Me*), 1.22 (dd, J = 6.6 Hz, 24 H, CH*Me*$_2$) ppm. IR (KBr): $\tilde{\nu}$ = 3084 (w), 3063 (w), 2965(s), 2925 (m), 2870 (w), 1636 (s), 1584 (s), br 1457 (m), 1371 (s), 1329 (w), 1306 (w), 1249 (s), 1203 (m), 1106 (m), 1054 (w), 1039 (w), 1017 (w), 979 (w), 937 (w), 819 (m), 796 (m), 775 (m), 758 (w), 744 (w), 716 (w), 697 (w), 637 (w), 529 (w), 468 (w), 445 (w), 432 (w) cm^{-1}. $C_{33}H_{43}CdCl_2N_3$ (664.7): calcd. C 59.60, H 6.52, N 6.32; found C 59.99, H 6.85, N 6.68.

Preparation of {2,6-Bis[1-(2,6-dimethylphenylimino)ethyl]pyridine}dichlorocadmium(II)·CH$_3$CN (3): A mixture of **L^3** (137 mg, 0.37 mmol) and $CdCl_2·2.5H_2O$ (85 mg, 0.37 mmol) in acetonitrile (30 mL) was stirred under nitrogen at room temperature for 12 h. Evaporation of the solvent gave the crude product as a yellowish powder. Pure product **3** was obtained in 75% yield (165 mg) upon recrystallization from acetonitrile/dichloromethane (2:1). ^{1}H NMR (300 MHz, CD_3CN): δ = 8.53 (quint, J = 6.3 Hz, 3 H, Py-*H*), 7.25−7.08 (m, 6 H, Ar-*H*), 2.41 (s, 6 H, N=C*Me*), 2.20 (s, 12 H, C*Me*) ppm. IR (KBr): $\tilde{\nu}$ = 3084 (w), 3024 (w), 2969 (w), 2920 (w), 2742 (w), 2247 (w), 1928 (w), 1854 (w), 1633 (s), 1584 (s), 1470 (s), 1443 (s), 1371(s), 1304 (m), 1255 (s), 1215 (s), 1163 (w), 1105 (m), 1093 (m), 1036 (m), 1022 (s), 980 (m), 966 (w), 917 (m), 902 (w), 823 (s), 814 (s), 782 (s), 768 (s), 740 (m), 695 (m), 633 (m), 582 (m), 554 (m), 530 (w), 516 (w), 495 (w), 419 (w) cm^{-1}. $C_{25}H_{27}CdCl_2N_3·CH_3CN$ (593.6): calcd. C 54.61, H 5.09, N 9.43; found C 54.83, H 5.21, N 9.03.

Preparation of {2,6-Bis[1-(2-methylphenylimino)ethyl]pyridine}dichlorocadmium(II)·CH$_3$CN (4): A mixture of **L^4** (131 mg, 0.38 mmol) and $CdCl_2·2.5H_2O$ (86 mg, 0.38 mmol) in dichloromethane (30 mL) was stirred under nitrogen at room temperature

Table 3. Crystallographic data and structure refinement for complexes **1**−**4**

	1	**2**	**3**	**4**
Empirical formula	$C_{24}H_{23.5}CdCl_2N_{4.5}$	$C_{33}H_{43}CdCl_2N_3$	$C_{27}H_{30}CdCl_2N_4$	$C_{25}H_{26}CdCl_2N_4$
Formula mass	558.08	664.67	593.61	565.59
Crystal system	triclinic	triclinic	monoclinic	triclinic
Space group	$P\bar{1}$	$P\bar{1}$	$P2_1/n$	$P\bar{1}$
a [Å]	9.048 (2)	8.884 (2)	13.418(4)	9.455(9)
b [Å]	12.686(3)	9.967(2)	14.941(4)	13.035(8)
c [Å]	22.661(5)	21.213(4)	14.547(4)	21.739(16)
α [°]	91.95(3)	81.02(3)	90	93.71(7)
β [°]	97.52(3)	88.52(3)	108.36(1)	90.31(7)
γ [°]	93.68(3)	66.52(3)	90	98.09(8)
Volume [Å^3]	2571.0(9)	1700.3(6)	2768.2(13)	2647.0(40)
Z	4[a]	2	4	4[a]
D_{calcd} [g m^{-3}]	1.432	1.969	3.042	1.379
μ [mm^{-1}]	1.075	2.805	6.170	1.044
F(000)	1108	960	2291	1080
θ range for data collection [°]	0.91−27.46	2.26−27.48	1.80−24.96	2.36−25.11
Limiting indices	$-11 \le h \le 11$	$-11 \le h \le 11$	$-15 \le h \le 15$	$-5 \le h \le 10$
	$-16 \le k \le 16$	$-12 \le k \le 12$	$-17 \le k \le 17$	$-15 \le k \le 12$
	$-29 \le l \le 29$	$-27 \le l \le 27$	$-17 \le l \le 8$	$-25 \le l \le 16$
Absorption correction	semi-empirical	semi-empirical	empirical	empirical
Data/restraints/parameters	11565/9/668	7213/78/352	4826/24/307	6225/106/577
Goodness-of-fit on F^2	1.053	1.019	0.949	1.047
Final R indices [$I > 2\sigma(I)$]				
R_1[b]	0.0429	0.0736	0.0502	0.0756
wR_2[c]	0.1251	0.1603	0.0982	0.1791
R indices (all data)				
R_1[b]	0.0525	0.1131	0.1209	0.1490
wR_2[c]	0.1368	0.1813	0.1104	0.2159
Largest difference peak/hole [e·Å^{-3}]	0.649/−1.231	1.160/−0.877	0.741/−0.376	1.296/−0.609

[a] There are two crystallographically independent molecules in the asymmetric unit. [b] $R_1 = ||F_o| - |F_c||/|F_o|$. [c] $wR_2 = \{[w(F_o^2 - F_c^2)^2]/[w(F_o^2)^2]\}^{1/2}$.

 © 2004 Wiley-VCH Verlag GmbH & Co. KGaA, Weinheim

for 12 h. Evaporation of the solvent gave the crude product as yellowish powder. Pure product **4** was obtained in 80% yield (172 mg) upon recrystallization from acetonitrile/dichloromethane (2:1). ^{1}H NMR (300 MHz, CD_3CN): δ = 8.49 (quint, J = 6.6 Hz, 3 H, Py-*H*), 7.33−6.97 (m, 8 H, Ar-*H*), 2.38 (s, 6 H, N=C*Me*). 2.18 (s, 6 H, C*Me*) ppm. IR (KBr): $\tilde{\nu}$ = 3079 (w), 3029 (w), 2975 (w), 2920 (w), 2947 (w), 1638 (s), 1599 (m), 1584 (s), 1487 (s), br 1463 (m), 1368 (s), 1311 (w), 1255 (s), 1230 (s), 1200 (s), 1148 (w), 1113 (m), 1041 (m), 1019 (s), 982 (w), 941 (w), 863 (m), 817 (s), 795 (s), 786 (s), 755 (s), 731 (m), 716 (m), 704 (w), 667 (w), 652 (w), 594 (w), 568 (w), 547 (w), 527 (w), 446 (m), 413 (w) cm^{-1}. $C_{23}H_{23}CdCl_2N_3{\cdot}CH_3CN$ (565.6): calcd. C 53.07, H 4.63, N 9.90; found C 53.43, H 4.91, N 9.65.

X-ray Crystallography of 1−4: The data were collected with a Rigaku R-AXIS RAPID IP or a Siemens SMART 1000 CCD diffractometer equipped with graphite-monochromated Mo-K_α radiation (λ = 0.71073 Å) at 293 ± 2 K. The structure was solved by direct methods and refined by full-matrix least squares based on F^2 using the SHELXTL 5.1 software package.[19] The cadmium and chlorine atoms were located first, and the carbon and nitrogen atoms were found in difference Fourier maps. The hydrogen atoms residing on the carbon atoms were located geometrically. All non-hydrogen atoms were refined anisotropically. Crystallographic data are given in Table 3. CCDC-232412 (**1**), -232417 (**2**), -232418 (**3**) and -232413 (**4**) contain the supplementary crystallographic data for this paper. These data can be obtained free of charge at www.ccdc.cam.ac.uk/conts/retrieving.html [or from the Cambridge Crystallographic Data Centre, 12 Union Road, Cambridge CB2 1EZ, UK; Fax: + 44-1223-336-033; E-mail: deposit@ccdc.cam.ac.uk].

Acknowledgments

This work was supported by the National Natural Science Foundation of China (grant no. 20374023) and by the Ministry of Science and Technology of China (grant no. 2002CB6134003).

[1] [1a] Q. Wu, J. A. Lavigne, Y. Tao, M. D'Iorio, S. Wang, *Inorg. Chem.* **2000**, *39*, 5248−5254. [1b] V. W. W. Yam, Y. L. Pui, K. M. C. Wong, K. K. Cheung, *Chem. Commun.* **2000**, 1751−1752. [1c] W. Yang, H. Schmider, Q. Wu, Y. S. Zhang, S. Wang, *Inorg. Chem.* **2000**, *39*, 2397−2404. [1d] W. Y. Wong, K. Y. Tsang, K. H. Tam, G. L. Lu, C. Sun, *J. Organomet. Chem.* **2000**, *601*, 237−245.

[2] [2a] K. S. Anjali, Y. L. Pui, V. W. W. Yam, J. J. Vittal, *Inorg. Chim. Acta* **2001**, *319*, 57−62. [2b] H. Zhu, M. Ströbele, Z. Yu, Z. Wang, H. J. Meyer, X. You, *Inorg. Chem. Commun.* **2001**, *4*, 577−581. [2c] Y. Kang, C. Seward, D. Song, S. Wang, *Inorg. Chem.* **2003**, *42*, 2789−2797. [2d] V. W. W. Yam, Y. L. Pui, K. K. Cheung, *New J. Chem.* **1999**, *23*, 1163−1169.

[3] [3a] V. W. W. Yam, Y. L. Pui, K. K. Cheung, *J. Chem. Soc., Dalton Trans.* **2000**, 3658−3662. [3b] H. Kunkely, A. Vogler, *J. Photochem. Photobiol. A* **2001**, *144*, 69−72.

[4] V. Balzani, A. Juris, M. Venturi, S. Campagna, S. Serroni, *Chem. Rev.* **1996**, *96*, 759−833.

[5] [5a] A. Adachi, R. C. Kwong, P. Djurovich, V. Adamovich, M. A. Baldo, M. E. Thompson, S. R. Forrest, *Appl. Phys. Lett.* **2001**, *79*, 2082−2084. [5b] M. A. Baldo, S. Lamansky, P. E. Burrows, M. E. Thompson, S. R. Forrest, *Appl. Phys. Lett.* **1999**, *75*, 4−6.

[6] [6a] S. Sprouse, K. A. King, P. J. Spellane, R. J. Watts, *J. Am. Chem. Soc.* **1984**, *106*, 6647−6653. [6b] S. Lamansky, P. Djurovich, D. Murphy, F. Abdel-Razzag, H. E. Lee, C. Aadachi, P. E. Burrows, S. R. Forrest, M. E. Thompson, *J. Am. Chem. Soc.* **2001**, *123*, 4304−4312.

[7] W. L. Jia, Q. D. Liu, R. Wang, S. Wang, *Organometallics* **2003**, *22*, 4070−4078.

[8] [8a] E. C. Alyea, P. H. Merrell, *Synth. React. Inorg. Met.-Org. Chem.* **1974**, *4*, 535−544. [8b] R. J. Restivo, G. Ferguson, *J. Chem. Soc., Dalton Trans.* **1976**, 518−521. [8c] E. C. Alyea, P. H. Merrell, *Inorg. Chim. Acta* **1978**, *28*, 91−97.

[9] [9a] E. C. Alyea, *Inorg. Chim. Acta* **1983**, *76*, L239−L240. [9b] D. A. Edwards, M. F. Mahon, W. R. Martin, K. C. Molloy, P. E. Fanwick, R. A. Walton, *J. Chem. Soc., Dalton Trans.* **1990**, 3161−3168. [9c] H. E. Toma, T. E. Chavez-Gil, *Inorg. Chim. Acta* **1997**, *257*, 197−202 and references cited therein.

[10] [10a] B. L. Small, M. Brookhart, A. M. A. Bennett, *J. Am. Chem. Soc.* **1998**, *120*, 4049−4050. [10b] G. J. P. Britovsek, V. C. Gibson, B. S. Kimberley, P. J. Maddox, S. J. McTavish, G. A. Solan, A. J. P. White, D. J. Williams, *Chem. Commun.* **1998**, 849−850.

[11] [11a] A. M. A. Bennett, *CHEMTECH* **1999**, *29*, 24−28. [11b] S. D. Lttel, L. K. Johnson, *Chem. Rev.* **2000**, *100*, 1169−1203. [11c] B. L. Small, A. J. Marcucci, *Organometallics* **2001**, *20*, 5738−5744.

[12] [12a] A. S. Abu-Surrah, K. Lappalainen, U. Piirone, P. Lehmus, T. Repo, M. Leskelä, *J. Organomet. Chem.* **2002**, *648*, 55−61. [12b] V. C. Gibson, S. K. Spitzmesser, *Chem. Rev.* **2003**, *103*, 283−315.

[13] B. Göbelt, K. Matyjaszewski, *Macromol. Chem. Phys.* **2000**, *201*, 1619−1624.

[14] M. A. Esteruelas, A. M. López, L. Méndez, M. Oliván, E. Oñate, *Organometallics* **2003**, *22*, 395−406.

[15] [15a] D. Reardon, G. Aharonian, S. Gambarotta, G. P. A. Yap, *Organometallics* **2002**, *21*, 786−788. [15b] V. C. Gibson, S. McTavish, C. Redshaw, G. A. Solan, A. J. P. White, D. J. Williams, *Dalton Trans.* **2003**, 221−226.

[16] D. Reardon, F. Conan, S. Gambarotta, G. Yap, Q. Wang, *J. Am. Chem. Soc.* **1999**, *121*, 9318−9325.

[17] B. Cetinkaya, E. Cetinkaya, M. Brookhart, P. S. White, *J. Mol. Catal. A* **1999**, *142*, 101−112.

[18] J. Z. Zhong, F. Wang, *Acta Acad. Med. Jiangxi* **1999**, *39*, 93−94.

[19] *SHELXTL NT Crystal Structure Analysis Package*, version 5.10, Bruker AXS, Analytical X-ray System, Madison, WI, **1999**.

Received May 27, 2004
Early View Article
Published Online October 21, 2004

 © 2004 Wiley-VCH Verlag GmbH & Co. KGaA, Weinheim

Hydroalumination of Carbon Dioxide, Carbon Disulfide, and Phenyl Isocyanate with an Aluminum Ketiminate Compound

Pei-Cheng Kuo,[a] I-Chun Chen,[a] Jr-Chiuan Chang,[a] Ming-Tsung Lee,[a] Chin-Han Hu,[a] Chen-Hsiung Hung,[a] Hon Man Lee,[a] and Jui-Hsien Huang*[a]

Keywords: Aluminum / Carbon dioxide / Hydrides / Hydroalumination / Insertion / N ligands

The reaction of MeC(O)C(H)=C(Me)NHAr (Ar = 2,6-diisopropylphenyl) (**1**) with excess $LiAlH_4$ in diethyl ether at –78 °C generates [AlH(OCMeCHCMeNAr)$_2$] (**2**) in 76% yield. The aluminum formate compound [Al(OCMeCHCMeNAr)$_2$(OCOH)] (**3**) can be isolated from the reaction of **2** with CO_2 in 93% yield. Compound **3** is thermally stable and remains unchanged when heated under vacuum at 100 °C for 24 h. Similarly, a solution of **2** in dichloromethane reacts with carbon disulfide or phenyl isocyanate at room temperature to yield the insertion products [Al(OCMeCHCMeNAr)$_2$(SCHS)] (**4**) and [Al(OCMeCHCMeNAr)$_2$(OCH=NPh)] (**5**), respectively, in 80% and 92% yield. Reaction of **2** with 1 equiv. of urethane in toluene at refluxing temperature for 1 h yields the aluminum isocyanate compound [Al(OCMeCHCMeNAr)$_2$(NCO)] (**6**). The molecular structures of compounds **2**–**6** have been determined by X-ray crystallography. Density functional calculations show that the isomer of compound **2** with an N–N *trans* arrangement is 3.1 kcal·mol^{-1} lower in energy than the O–O *trans* isomer. Inserting CO_2 into the Al–H bond of compound **2** results in the formation of the formate compound **3**; this reaction is predicted to be exothermic by 29.8 kcal·mol^{-1}.
(© Wiley-VCH Verlag GmbH & Co. KGaA, 69451 Weinheim, Germany, 2004)

Introduction

Metal−hydride bonds are important in organometallic chemistry because a wide variety of unsaturated small organic molecules can insert into them to yield stable species or intermediates. Among these reactions, the insertion of CO_2 into metal−hydride bonds is particularly interesting. The use of carbon dioxide as a C_1 source is a current research area which is important not only for reducing the dependence on fossil-fuel consumption but also the reduction of greenhouse gases.[1,2] Various methods have been developed for CO_2 activation, and the use of transition-metal compounds as catalysts is common.[3−5] One way to convert CO_2 into functionalized organic molecules is by inserting CO_2 into a transition metal−hydride bond (Scheme 1). Reactions between CO_2 and transition metal hydrides have been reported for many metals, with the main focus on late transition metals.[6−13] The insertion of CO_2 into an aluminum hydride bond has not been reported so far.

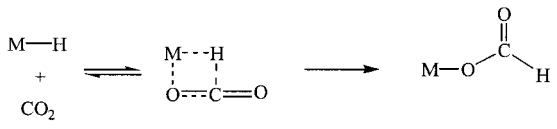

Scheme 1

Highly reactive metal−hydrogen bonds also play an important role in catalytic reactions.[14−18] Among these, aluminum hydrides are well known and widely used due to their high reactivity and low cost.[19−27] In this paper we present the synthesis and characterization of aluminum hydride compounds containing substituted ketiminate ligands and their reactions with carbon dioxide, carbon disulfide, and phenyl isocyanate. A related reaction of the aluminum hydride compound with urethane to yield a novel aluminum isocyanate compound is also presented.

Results and Discussion

Reactivity Studies of Ketiminatoaluminum Hydride Compounds

Ketimine **1** [MeC(O)C(H)=C(Me)NHAr; Ar = 2,6-diisopropylphenyl] can be easily synthesized in high yield by an imine condensation reaction between 2,4-pentanedione and 2,6-diisopropylaniline in a 1:1 ratio in methanol.[28] The reaction of compound **1** with an excess of $LiAlH_4$ in diethyl ether at −78 °C, followed by stirring at −10 °C for 2 h, generates [AlH(OCMeCHCMeNAr)$_2$] (**2**) in 76% yield after recrystallization of the crude solids from diethyl ether at −20 °C (Scheme 2). The ^{1}H NMR spectrum of compound **2** in C_6D_6 indicates C_2 symmetry of the molecule, with the two methyl resonances of the ligand backbone appearing at

[a] Department of Chemistry, National Changhua University of Education,
50058 Changhua, Taiwan
Supporting information for this article is available on the WWW under http://www.eurjic.org or from the author.

 © 2004 Wiley-VCH Verlag GmbH & Co. KGaA, Weinheim DOI: 10.1002/ejic.200400567

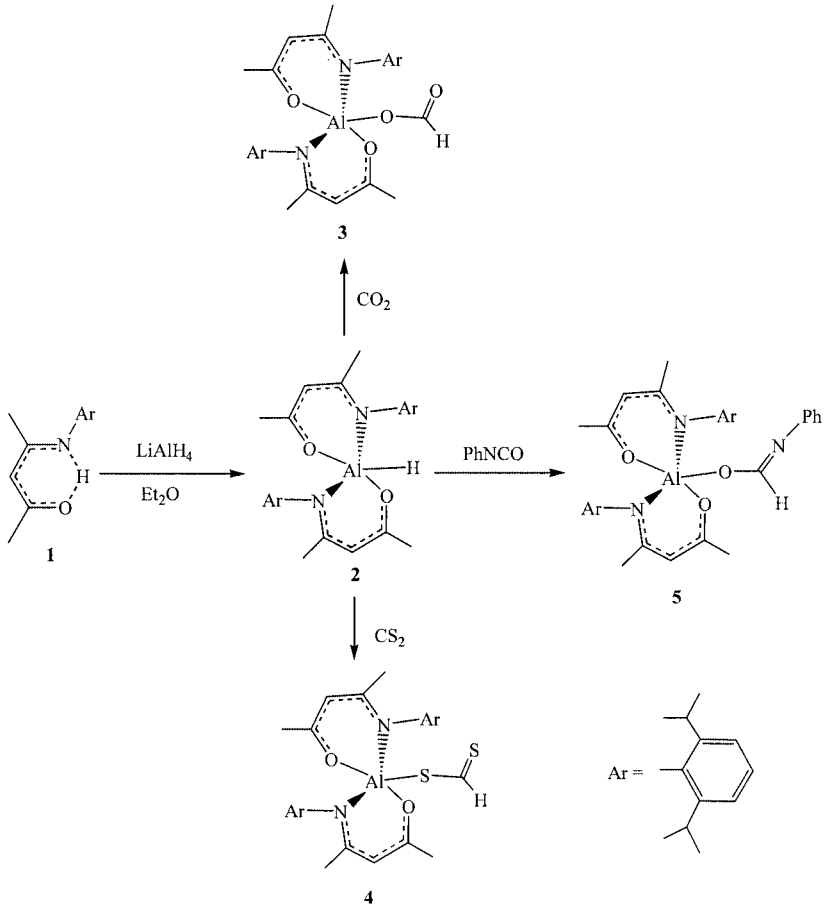

Scheme 2

δ = 1.50 and 1.32 ppm. The N−Ar rotation of compound **2** in solution at ambient temperature is slow due to the high steric hindrance between the isopropyl group and the methyl groups of the ligand backbone. The ^{1}H and ^{13}C NMR spectra of compound **2** confirm this (two sets of isopropyl resonances). The hydride resonance was not observed, presumably due to the interaction of the hydrogen atom with ^{27}Al (I = 5/2).[29] The solid-state IR spectrum shows a ν_{Al-H} band at 1788 cm^{-1}. Moreover, the deuterated compound [AlD(OCMeCHCMeNAr)$_2$] (**2D**), synthesized by treating compound **1** with $LiAlD_4$, exhibits exactly the same ^{1}H NMR spectrum as compound **2**. The ν_{Al-D} band of this compound appears at 1297 cm^{-1} (calculated value 1287 cm^{-1} from the isotope shift). Compound **2** is thermally unstable and decomposes in C_6D_6 at 80 °C, forming unidentified compounds.

The aluminum hydride compound **2** is reactive toward the C=O, C=S, and C=N functional groups in carbon dioxide, carbon disulfide, and phenyl isocyanate, respectively. The reactions are summarized in Scheme 2. Reaction of compounds **2** or **2D** with CO_2 in dichloromethane solution were completed within minutes after admitting CO_2 gas into the solution. The reactions are exothermic. The aluminum formate compounds [Al(OCMeCHCMeNAr)$_2$(OCOH)] (**3**) and [Al(OCMeCHCMeNAr)$_2$(OCOD)] (**3D**) were isolated in 93% yield from diethyl ether solutions at −20 °C. Compound **3** is thermally stable and remains unchanged even when heated under vacuum at 100 °C for 24 h. The ketiminate backbone of **3** exhibits the same pattern of ^{1}H and ^{13}C NMR resonances as **2**. However, the ^{1}H NMR spectrum of **3** exhibits a singlet at δ = 8.0 ppm for the formate proton, which was not observed for compound **3D**. The ^{13}C{^{1}H} NMR spectrum of compound **3** shows a singlet at δ = 163.8 ppm for the formate carbon atom; this signal is a triplet for compound **3D** with a $^1J_{C,D}$ coupling constant of 31 Hz.

Similarly, reactions of **2** with carbon disulfide and phenyl isocyanate in dichloromethane at room temperature yielded the insertion products [Al(OCMeCHCMeNAr)$_2$(SCHS)] (**4**) and [Al(OCMeCHCMeNAr)$_2$(OCH=NPh)] (**5**) in 80% and 92% yield, respectively. The ^{1}H NMR spectrum of **4** exhibits a downfield singlet at δ = 11.66 ppm for the dithioformate proton, comparable to the values of other metal dithioformate compounds.[30,31] The dithioformate proton resonance was not observed for the corresponding deuterated compound **4D**. In the ^{13}C{^{1}H} NMR spectrum, the carbon resonance of C=S for **4** appears at δ = 240.5 ppm, which is downfield relative to that of the C=O resonance of **3**, but similar to the values of reported metal dithioformate compounds.[30,31] Again, the ^{13}C{^{1}H} NMR spectrum shows that the carbon resonance of C=S for compound **4D** also appears as a triplet at δ = 240.5 ppm with a $^1J_{C,D}$

 © 2004 Wiley-VCH Verlag GmbH & Co. KGaA, Weinheim

coupling constant of 28 Hz. The ^{1}H NMR spectrum of **5** displays a singlet at δ = 7.74 ppm for the formimidato proton, which was not observed in **5D**. Similarly, the carbon resonance of the C=N fragment appears at δ = 157.8 ppm as a singlet for compound **5**. However, even with very high concentrations of **5D**, no signal was observed for the carbon resonance of the C=N fragment.

An intriguing reaction of **2** occurs with urethane, $H_2NCOOEt$. Reaction of **2** with 1 equiv. of urethane in refluxing toluene for 1 h yielded the aluminum isocyanate compound [Al(OCMeCHCMeNAr)$_2$(NCO)] (**6**) as white crystals in 57% yield (Scheme 3). The ^{1}H and ^{13}C{^{1}H} NMR spectra of **6** show similar patterns for the ketiminate fragments as those of **3** and **4**. The isocyanate functional group exhibits two strong infrared absorptions at 2267 and 2206 cm^{-1}, which are similar to those of other M−NCO compounds in the literature.[32−34] The reaction was also monitored by ^{1}H NMR spectroscopy in a C_6D_6 solution. A possible mechanistic pathway for the formation of **6** is shown in Scheme 3. The first step involves hydrogen elimination to form the aluminum carbamidate intermediate **7**, followed by successive loss of ethanol to form the final aluminum isocyanate compound **6**. Precise control of the reaction time and recrystallization procedure are necessary to avoid further reaction of the by-product, ethanol, with the aluminum ketiminate compounds, which regenerates the ketimine ligands. A related reaction converting an NCO fragment to urethane was reported by Knoth[35] et al. in 1967. A boron compound containing B−NCO, derived from the reaction of B−CO with azide, was converted into B−NHCO$_2$C$_2$H$_5$ in the reactions of 1,12-$B_{12}H_{10}(NCO)_2^{2-}$ and 1,10-$B_{10}Cl_8(NCO)_2^{2-}$ with ethanol/hydrogen chloride, resulting in the formation of the urethanes 1,12-$B_{12}H_{10}(NHCO_2C_2H_5)_2^{2-}$ and 1,10-$B_{10}Cl_8(NHCO_2C_2H_5)_2^{2-}$, respectively.

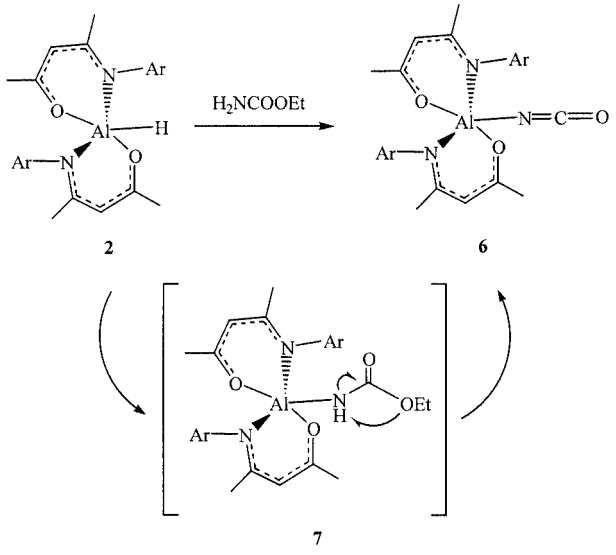

Scheme 3

Molecular Structures of Ketiminatoaluminum Compounds 2−6

The molecular structures of compounds **2**−**6** are shown in Figures 1−5, and selected bond lengths and angles are listed in Table 1. Compounds **2**−**6** are all five-coordinate trigonal-bipyramidal structures. The two nitrogen atoms of the ketiminate backbone for compound **2** occupy the axial positions while the two oxygen atoms and the hydrido ligand form the equatorial plane. However, the most distinct structural difference between **3**−**6** and **2** is that the two oxygen atoms of the two ketiminate backbones in **3**−**6** occupy the axial positions. A schematic description of the molecular structures of **2**−**6** is shown in Scheme 4. The molecular structures of a series of ketiminatoaluminum halide and alkyl compounds reported in the literature are all shown with an O−O *trans* geometry.[36] A theoretical calculation of the geometry of **2** was therefore performed (vide infra).

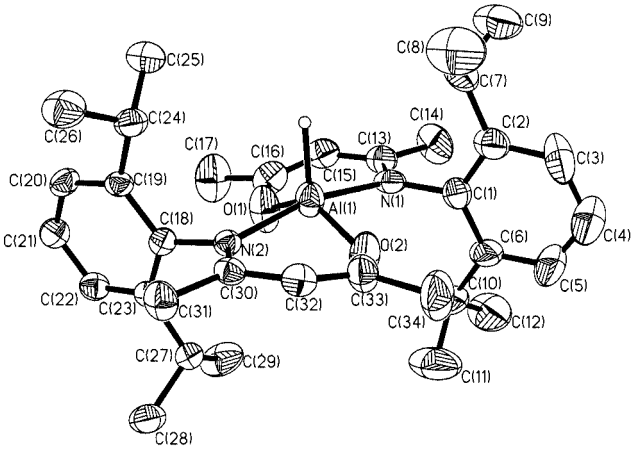

Figure 1. The molecular structure of compound **2**, with ellipsoids drawn at the 50% probability level; all hydrogen atoms except the aluminum hydride have been omitted for clarity

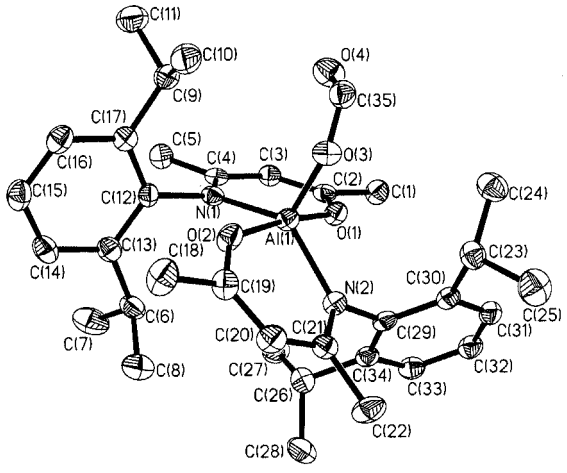

Figure 2. The molecular structure of compound **3**, with ellipsoids drawn at the 50% probability level; all hydrogen atoms have been omitted for clarity

 © 2004 Wiley-VCH Verlag GmbH & Co. KGaA, Weinheim

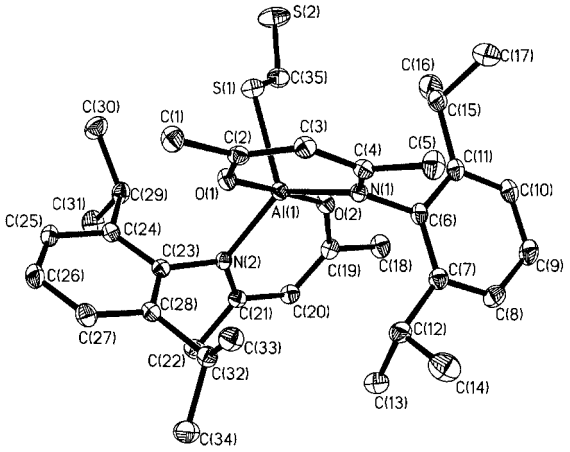

Figure 3. The molecular structure of compound **4**, with ellipsoids drawn at the 50% probability level; toluene and all hydrogen atoms have been omitted for clarity

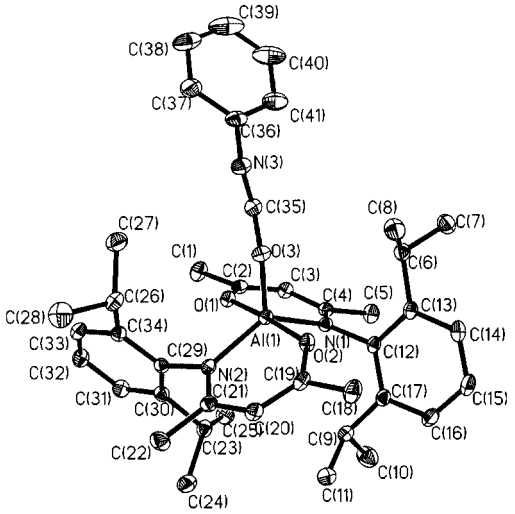

Figure 4. The molecular structure of compound **5**, with ellipsoids drawn at the 50% probability level; all hydrogen atoms have been omitted for clarity

Table 1. Selected bond lengths [Å] and angles [°] for compounds **2**–**6**

2					
Al(1)–O(1)	1.763(3)	Al(1)–O(2)	1.757(3)	Al(1)–N(1)	2.079(3)
Al(1)–N(2)	2.064(3)	Al(1)–H(1)	1.61(3)		
O(1)–Al(1)–O(2)	133.6(2)	O(1)–Al(1)–N(1)	88.3(1)	O(1)–Al(1)–N(2)	86.96(13)
O(1)–Al(1)–H(1)	111.8(11)	O(2)–Al(1)–N(1)	85.31(14)	O(2)–Al(1)–N(2)	88.21(13)
O(2)–Al(1)–H(1)	114.5(11)	N(1)–Al(1)–H(1)	95.3(11)	N(1)–Al(1)–N(2)	165.69(13)
N(2)–Al(1)–H(1)	99.0(1)				
3					
Al(1)–O(1)	1.807(2)	Al(1)–O(2)	1.813(2)	Al(1)–O(3)	1.798(2)
Al(1)–N(1)	1.976(2)	Al(1)–N(2)	1.997(2)	O(4)–C(35)	1.213(3)
O(3)–C(35)	1.296(3)				
O(1)–Al(1)–O(2)	171.20(8)	O(1)–Al(1)–O(3)	96.95(8)	O(1)–Al(1)–N(1)	90.45(7)
O(1)–Al(1)–N(2)	87.00(7)	O(2)–Al(1)–O(3)	91.77(8)	O(2)–Al(1)–N(1)	86.73(7)
O(2)–Al(1)–N(2)	89.17(8)	O(3)–Al(1)–N(1)	116.10(8)	O(3)–Al(1)–N(2)	108.30(8)
N(1)–Al(1)–N(2)	135.50(8)	O(3)–C(35)–O(4)	127.6(3)		
4					
Al(1)–O(1)	1.8093(16)	Al(1)–O(2)	1.8018(16)	Al(1)–N(1)	1.9685(18)
Al(1)–N(2)	1.9864(17)	Al(1)–S(1)	2.3342(8)	S(2)–C(35)	1.642(2)
S(1)–C(35)	1.689(2)				
O(1)–Al(1)–O(2)	177.84(7)	O(1)–Al(1)–N(1)	91.24(7)	O(1)–Al(1)–N(2)	87.48(7)
O(1)–Al(1)–S(1)	85.58(5)	O(2)–Al(1)–N(1)	90.39(7)	O(2)–Al(1)–N(2)	90.39(7)
O(2)–Al(1)–S(1)	95.16(6)	N(1)–Al(1)–N(2)	129.30(7)	N(1)–Al(1)–S(1)	110.70(5)
N(2)–Al(1)–S(1)	119.69(6)	S(1)–C(35)–S(2)	126.35(15)		
5					
Al(1)–O(1)	1.8263(12)	Al(1)–O(2)	1.8054(12)	Al(1)–O(3)	1.7852(13)
Al(1)–N(1)	2.0019(14)	Al(1)–N(2)	1.9799(14)	O(3)–C(35)	1.305(2)
N(3)–C(35)	1.267(2)	N(3)–C(36)	1.418(2)		
O(1)–Al(1)–O(2)	174.26(6)	O(1)–Al(1)–N(1)	89.24(5)	O(1)–Al(1)–N(2)	88.31(6)
O(1)–Al(1)–O(3)	94.25(6)	O(2)–Al(1)–O(3)	91.41(6)	O(2)–Al(1)–N(1)	87.65(5)
O(2)–Al(1)–N(2)	90.18(6)	O(3)–Al(1)–N(1)	113.40(6)	O(3)–Al(1)–N(2)	114.59(6)
O(3)–C(35)–N(3)	122.95(17)	N(1)–Al(1)–N(2)	131.99(6)		
6					
Al(1)–O(1)	1.7875(15)	Al(1)–O(2)	1.7946 (15)	Al(1)–N(1)	1.9991(17)
Al(1)–N(2)	1.9961(18)	Al(1)–N(3)	1.837(2)	N(3)–C(35)	1.147(3)
O(3)–C(35)	1.189(3)				
O(1)–Al(1)–O(2)	168.17(9)	O(1)–Al(1)–N(1)	89.44(7)	O(1)–Al(1)–N(2)	86.73(7)
O(1)–Al(1)–N(3)	96.02(9)	O(2)–Al(1)–N(1)	86.22(7)	O(2)–Al(1)–N(2)	89.33(7)
O(2)–Al(1)–N(3)	95.81(8)	N(1)–Al(1)–N(2)	138.95(8)	N(1)–Al(1)–N(3)	111.70(9)
N(2)–Al(1)–N(3)	109.34(8)	N(3)–C(35)–O(3)	179.5(4)		

 © 2004 Wiley-VCH Verlag GmbH & Co. KGaA, Weinheim

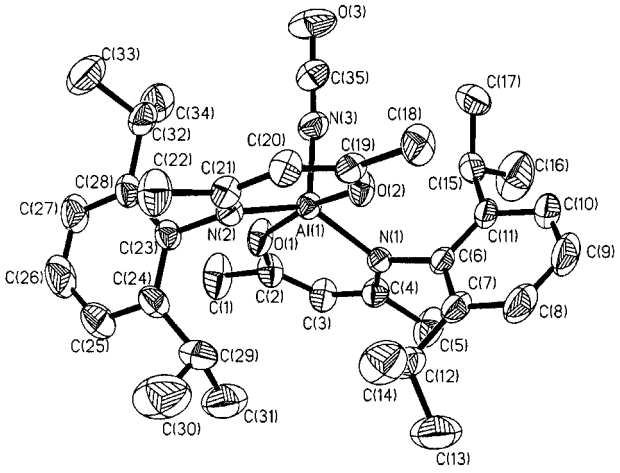

Figure 5. The molecular structure of compound **6**, with ellipsoids drawn at the 50% probability level; all hydrogen atoms have been omitted for clarity

As described above, the molecular structure of **2** is trigonal-bipyramidal with two Al−N(axial) bond lengths of 2.079(3) and 2.064(3) Å. For comparison, the Al−N(equatorial) bonds in compounds **3**−**6**, which range from 1.976(2) to 2.002(1) Å, are generally shorter than the Al−N(axial) bonds. Similarly, the Al−O(equatorial) bonds in compound **2** [1.763(3) and 1.757(3) Å] are shorter than the Al−O(axial) bonds for compounds **3**−**6** [ranging from 1.795(1) to 1.826(1) Å]. A better hybridization of the trigonal-planar sp^2 orbitals of aluminum with the equatorial oxygen or nitrogen atoms forming σ-bonds may be the reason for these shorter distances.

Molecular Structures of Group 13 Metal−NCO Compounds

Compounds containing NCO ligands are very common for late transition metals. However, only a few group 13 metal NCO compounds have been structurally characterized. When searching the Cambridge Crystallographic Database, there are only three M(NCO) (M = group 13) compounds, two B−NCO compounds and one In−NCO compound.[37−39] A comparison of the bond angles and bond lengths of these M(NCO) (M = group 13) compounds is given in Table 2. The NCO angles for all the compounds listed in the table are almost linear [177.8(4)° to 179.5(4)°]. However, the M−NCO angles vary depending on the metals. The In−N−C angle of 147.1(8)° is much smaller than those of compound **6** and the B−N−C compounds; this is probably due to crystal packing effects.[37] The C−N and C−O bond lengths are very similar in all the compounds listed in Table 2 and can be viewed as C≡N triple bonds (normally at 1.16 Å) and C=O double bonds (normally at 1.22 Å), respectively.

Density Functional Theory (DFT) Calculations on the Reaction between CO_2 and 2

The intriguing reactivity of compound **2** toward CO_2 has been carefully calculated. Four structures were considered:

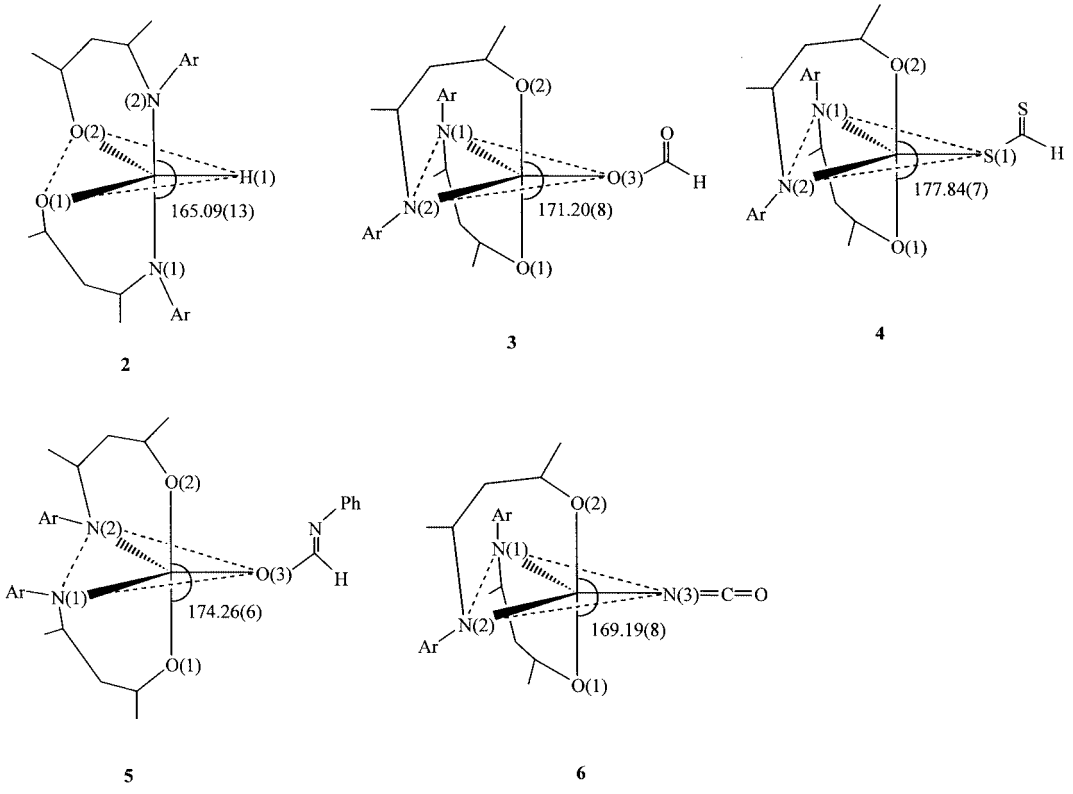

Scheme 4

 © 2004 Wiley-VCH Verlag GmbH & Co. KGaA, Weinheim

Table 2. Comparisons of bond lengths and angles for M(NCO) (M = group 13) compounds

Compound	Bond angles [°]		Bond lengths [Å]			Ref.
	∠ A	∠ B	a	b	c	
[*closo*-2-$B_{10}H_9NCO]^{2-}$	172.3(3)	177.8(4)	1.498(7)	1.128(7)	1.187(7)	[37]
6	172.4(2)	179.5(4)	1.836(2)	1.151(3)	1.188(3)	this work
$[(Pc)_2In(NCO)_2][PNP]$	147.1(8)	178 (1)	2.155(9)	1.15(1)	1.17(2)	[39]
	164.4(9)	179(1)	2.165(9)	1.17(2)	1.23(2)	[39]

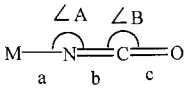

the N−N *trans* and O−O *trans* forms of compound **2**, and the N−N *trans* and O−O *trans* forms of compound **3**, as shown in Scheme 5.

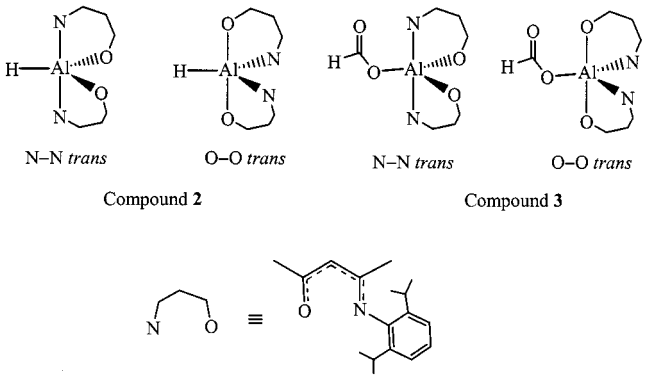

Scheme 5

Density functional theory, which includes Becke's three-parameter nonlocal exchange potential and the nonlocal correlation functional of Lee, Yang, and Parr, was used, along with the 6-31G* basis sets.[40,41] For compound **2**, the isomer with the N−N *trans* arrangement is found to be 3.1 kcal·mol^{-1} lower in energy than the O−O *trans* isomer. This observation is consistent with the solid-state structure of compound **2**, in which the two nitrogen atoms of the ketiminate ligands are found in the axial positions. Inserting CO_2 into the Al−H bond of compound **2** results in the formation of the formate compound **3** in a reaction which was predicted to be exothermic by 29.8 kcal·mol^{-1}. For compound **3**, the N−N *trans* and O−O *trans* isomers are very close in energy, with the former being 0.05 kcal·mol^{-1} more stable. The predicted geometrical parameters at the B3LYP/6-31G* level[42] agree reasonably well with those obtained by X-ray crystallography.

In conclusion, we have synthesized aluminum hydride compounds containing ketiminate ligands. These aluminum hydride compounds show novel reactivity toward CO_2, CS_2, and phenyl isocyanate insertion, which has not been seen before in main-group chemistry. A first example of an aluminum NCO compound, $[Al(OCMeCHCMeNAr)_2(NCO)]$ (**6**), has also been structurally characterized from the reaction of aluminum hydride with urethane. A theoretical calculation proved that the CO_2 insertion product has a lower energy than that of the corresponding aluminum hydride compounds.

Experimental Section

General Procedures: All reactions were performed under dry nitrogen using standard Schlenk techniques or in a glove box. Toluene and diethyl ether were dried by refluxing in the presence of sodium benzophenone ketyl. CH_2Cl_2 was dried with P_2O_5. All solvents were distilled and stored in solvent reservoirs which contained molecular sieves (4 Å) and were purged with nitrogen. ^1H and ^{13}C NMR spectra were recorded with a Bruker AC200 or an Avance 300 M Hz spectrometer. Chemical shifts for ^1H and ^{13}C spectra were recorded in ppm relative to the internal deuterated solvent ($CDCl_3$: ^1H: δ = 7.24 ppm; ^{13}C: δ = 77.0 ppm). Elemental analyses were performed with a Heraeus CHN-OS Rapid Elemental Analyzer at the Instrument Center, NCHU. Ketimine **1** [MeC(O)C(H)=C(Me)NHAr; Ar = 2,6-diisopropylphenyl] was prepared according to a previously reported procedure.[36] $AlCl_3$ (Strem), MeLi, and EtLi (Aldrich) were used as received.

$[AlH(OCMeCHCMeNAr)_2]$ (2): A diethyl ether solution (30 mL) of **1** (10.0 g, 38.6 mmol) was added dropwise whilst stirring at −78 °C to a 100-mL Schlenk flask containing a suspension of $LiAlH_4$ (0.73 g, 19.2 mmol) in diethyl ether (20 mL). The mixture was allowed to warm to −10 °C and then stirred for 2 h. The resulting suspension was filtered through Celite. The filtrate was dried under vacuum to remove volatiles, and the resulting solid was recrystallized from diethyl ether to give 8.0 g of **2** (76% yield). ^1H NMR (C_6D_6): δ = 1.08 (d, 6 H, CHMe_2), 1.12 (d, 6 H, CHMe_2), 1.32 (s, 6 H, C*Me*), 1.34 (d, 6 H, CHMe_2), 1.38 (d, 6 H, CHMe_2), 1.50 (s, 6 H, C*Me*), 3.13 (m, 2 H, C*H*Me_2), 3.40 (m, 2 H, C*H*Me_2), 5.06 (s, 2 H, CMeC*H*CMe), 7.15 (m, 6 H, *Ph*) ppm. ^{13}C NMR (C_6D_6): δ = 23.4 (q, $J_{C,H}$ = 128 Hz, CHMe_2), 24.0 (q, $J_{C,H}$ = 126 Hz, CHMe_2), 24.3 (q, $J_{C,H}$ = 126 Hz, CHMe_2), 24.5 (q, $J_{C,H}$ = 128 Hz, CHMe_2), 24.6 (q, $J_{C,H}$ = 125 Hz,), 25.9 (q, $J_{C,H}$ = 125 Hz,), 28.2 (q, $J_{C,H}$ = 133 Hz,), 28.5 (q, $J_{C,H}$ = 130 Hz,), 100.1 (d, $J_{C,H}$ = 160 Hz,), 123.5 (d, $J_{C,H}$ = 152 Hz,), 123.9 (d, $J_{C,H}$ = 153 Hz,), 125.6 (d, $J_{C,H}$ = 158 Hz,), 129.4 (s), 142.0 (s, Ph C_{ipso}), 145.2 (s, Ph C_{ipso}), 173.0 (s, *C*N), 177.2 (s, *C*O) ppm. IR (KBr): ν_{Al-H} = 1788 cm^{-1}. $C_{34}H_{49}AlN_2O_2$ (544.75): calcd. C 74.96, H 9.07, N 5.14; found C 74.14, H 8.92, N 6.20. **2D** was synthesized following the same procedure except that $LiAlD_4$ was used. The ^1H and ^{13}C

 © 2004 Wiley-VCH Verlag GmbH & Co. KGaA, Weinheim

NMR spectra of **2D** and **2** are identical. IR (KBr): ν_{Al-D} = 1297 cm^{-1}.

[Al(OCMeCHCMeNAr)$_2$(OCOH)] (3): Carbon dioxide was bubbled through a 30-mL Schlenk flask charged with 15 mL of dichloromethane and **2** (1.0 g, 1.8 mmol) at room temperature for 1 min. The solution was then stirred for 3 min and the volatiles were removed under vacuum to yield a pure white solid (1.0 g) of **3** in 92.6% yield. ^{1}H NMR ($CDCl_3$): δ = 1.05 (d, 6 H, CHMe_2), 1.08 (d, 6 H, CHMe_2), 1.10 (d, 6 H, CHMe_2), 1.16 (d, 6 H, CHMe_2), 1.18 (s, 6 H, C*Me*), 1.65 (s, 6 H, C*Me*), 2.85 (m, 2 H, C*H*Me$_2$), 3.05 (m, 2 H, C*H*Me$_2$), 5.21 (s, 2 H, CMeC*H*CMe), 7.03−7.23 (m, 6 H, *Ph*), 8.23 (s, CO*H*) ppm. ^{13}C NMR ($CDCl_3$): δ = 23.7 (q, $J_{C,H}$ = 127 Hz, C*Me*), 23.9 (q, CHMe_2), 24.3 (q, CHMe_2), 24.8 (br. q, two overlapping peaks, CHMe_2), 25.3 (q, $J_{C,H}$ = 128 Hz, *C*Me), 27.3 (d, $J_{C,H}$ = 126 Hz, *C*HMe$_2$), 28.2 (d, $J_{C,H}$ = 127 Hz, *C*HMe$_2$), 100.1 (d, $J_{C,H}$ = 159 Hz, CMe*C*HCMe), 123.1(d, $J_{C,H}$ = 158 Hz, Ph *C*H), 123.9 (d, $J_{C,H}$ = 158 Hz, Ph *C*H), 125.6 (d, $J_{C,H}$ = 159 Hz, Ph *C*H), 140.6 (s, Ph C_{ipso}), 143.0 (s, Ph C_{ipso}), 145.1 (s, Ph C_{ipso}), 163.8 (d, $J_{C,H}$ = 204 Hz, *C*HO), 177.8 (s, *C*N), 180.6 (s, *C*O) ppm. $C_{35}H_{49}AlN_2O_4$ (588.756): calcd. C 71.40, H 8.39, N 4.76; found C 71.83, H 8.90, N 5.05. The ^{1}H and ^{13}C NMR spectra of **3D** are similar to those of **3** except that the formate proton of **3** (δ = 8.01 ppm) is not present in **3D** and the formate carbon atom (δ = 163.8 ppm) for **3D** appears as a triplet ($^1J_{C,D}$ = 31 Hz).

[Al(OCMeCHCMeNAr)$_2$(SCSH)] (4): An excess of carbon disulfide was added at room temperature to a 30-mL Schlenk flask containing 15 mL of dichloromethane and **2** (1.0 g, 1.8 mmol). The solution was stirred for 1 h and the volatiles were removed under vacuum to yield **4** (0.91 g) as a yellow solid in 80% yield. ^{1}H NMR ($CDCl_3$): δ = 1.03 (d, 6 H, CHMe_2), 1.10 (two overlapping doublets, 12 H, CHMe_2), 1.18 (d, 6 H, CHMe_2), 1.24 (s, 6 H, C*Me*), 1.71 (s, 6 H, C*Me*), 2.89 (m, 2 H, C*H*Me$_2$), 3.07 (m, 2 H, C*H*Me$_2$), 5.20 (s, 2 H, CMeC*H*CMe), 7.06−7.24 (m, 6 H, *Ph*), 11.66 (s, CS*H*) ppm. ^{13}C NMR ($CDCl_3$): δ = 23.6 (q, $J_{C,H}$ = 128 Hz, C*Me*), 23.9 (q, CHMe_2), 24.7 (q, CHMe_2), 25.0 (q, CHMe_2), 25.1 (q, CHMe_2), 25.3 (q, $J_{C,H}$ = 129 Hz, *C*Me), 28.1 (d, *C*HMe$_2$), 28.4 (d, *C*HMe$_2$), 100.4 (d, $J_{C,H}$ = 162 Hz, CMe*C*HCMe), 123.1 (d, $J_{C,H}$ = 159 Hz, Ph *C*H), 124.3 (d, $J_{C,H}$ = 156 Hz, Ph *C*H), 126.1 (d, $J_{C,H}$ = 160 Hz, Ph *C*H), 140.8 (s, Ph C_{ipso}), 143.6 (s, Ph C_{ipso}), 143.7 (s, Ph C_{ipso}), 178.9 (s, *C*N), 180.9 (s, *C*O), 240.5 (d, $J_{C,H}$ = 178 Hz, S*C*SH) ppm. $C_{35}H_{49}AlN_2O_2S_2$ (620.89): calcd. C 67.71, H 7.95, N 4.51; found C 67.36, H 9.05, N 4.49. The ^{1}H and ^{13}C NMR spectra of **4D** are similar to those of **4** except that the resonance of the dithioformate proton of **4** at δ = 11.66 ppm is not observed in **4D** and the resonance of the dithioformate carbon atom (δ = 240.5 ppm) of **4D** appears as a triplet ($^1J_{C,D}$ = 28 Hz).

[Al(OCMeCHCMeNAr)$_2$(OCHNPh)] (5): Phenyl isocyanate (0.40 mL, 3.69 mmol) was added with a syringe at room temperature to a 30-mL Schlenk flask containing 15 mL of dichloromethane and **2** (2.0 g, 3.67 mmol). The solution was stirred for 1 h and volatiles were removed under vacuum to yield a yellow solid. The solid was washed with heptane in several portions to remove unreacted phenyl isocyanate, and was then dried under vacuum to give 2.25 g of **5** (92% yield). ^{1}H NMR ($CDCl_3$): δ = 1.06 (d, 6 H, CHMe_2), 1.10 (d, 6 H, CHMe_2), 1.11 (d, 6 H, CHMe_2), 1.20 (s, 6 H, C*Me*), 1.22 (d, 6 H, CHMe_2), 1.65 (s, 6 H, C*Me*), 2.82 (m, 2 H, C*H*Me$_2$), 3.17 (m, 2 H, C*H*Me$_2$), 5.18 (s, 2 H, CMeC*H*CMe), 6.81−7.25 (m, 6 H, *Ph*), 7.74 (s, CNPh*H*) ppm. ^{13}C NMR ($CDCl_3$): δ = 23.6 (q, $J_{C,H}$ = 127 Hz, C*Me*), 23.8 (q, CHMe_2), 24.3 (q,

Table 3. Summary of crystallographic data for compounds **2**−**6**

	2	**3**	**4**	**5**	**6**
Empirical formula	$C_{34}H_{49}AlN_2O_2$	$C_{35}H_{49}AlN_2O_4$	$C_{42}H_{57}AlN_2O_2S_2$	$C_{41}H_{54}AlN_3O_3$	$C_{35}H_{48}AlN_3O_3$
Formula mass	544.73	588.74	713.00	663.85	585.74
Crystal system	rhombohedral	triclinic	triclinic	monoclinic	triclinic
Space group	$R\bar{3}$	$P\bar{1}$	$P\bar{1}$	$P2_1/n$	$P\bar{1}$
a [Å]	35.358(3)	10.4508(13)	12.433(1)	11.2660(7)	11.0971(9)
b [Å]	36.358(3)	12.1431(14)	12.494(1)	11.6265(8)	13.2319(10)
c [Å]	13.0454(14)	14.4459(17)	15.031(1)	29.8774(19)	13.8907(11)
α [°]	90	69.713(2)	101.124(2)	90	71.086(2)
β [°]	90	84.803(2)	111.020(2)	99.793(1)	88.583(2)
γ [°]	120	71.539(2)	102.898(2)	90	66.344(2)
Volume [Å^3]/*Z*	14935(2)/18	1630.7(3)/2	2026.7(3)/2	3856.4(4)/4	1754.3(2)/2
D_{calcd} [Mg/m^3]	1.090	1.199	1.168	1.143	1.109
μ [mm^{-1}]	0.091	0.102	0.189	0.092	0.093
F(000)	5328	636	768	1432	632
Crystal size [mm]	0.47 × 0.30 × 0.22	0.28 × 0.24 × 0.20	0.35 × 0.30 × 0.25	0.35 × 0.28 × 0.22	0.47 × 0.43 × 0.34
θ(min)−θ(max) [°]	1.12−27.52	1.50−27.57	1.52−27.55	1.38−27.52	2.07−27.51
Reflections collected	31448	10381	13027	23811	11319
Independent reflections	7566 (R_{int} = 0.1037)	7215 (R_{int} = 0.0401)	9009 (R_{int} = 0.0506)	8794 (R_{int} = 0.0395)	7807 (R_{int} = 0.0696)
Max./min. transmission	0.9486/0.7467	0.9486/0.5879	0.9486/0.7267	0.9486/0.5620	
Data/restraints/parameters	7566/0/368	7215/ 0 /391	9009/ 0 /455	8794/ 0 /445	7807/0 /379
Goodness-of-fit on F^2	0.996	0.809	0.611	0.816	0.706
R [$I > 2\sigma(I)$]	$R1$ = 0.0586 $wR2$ = 0.1180	$R1$ = 0.0510 $wR2$ = 0.1111	$R1$ = 0.0497 $wR2$ = 0.1441	$R1$ = 0.0420 $wR2$ = 0.0948	$R1$ = 0.0470 $wR2$ = 0.1084
R (all data)	$R1$ = 0.1998 $wR2$ = 0.1729	$R1$ = 0.0991 $wR2$ = 0.1244	$R1$ = 0.0809 $wR2$ = 0.1702	$R1$ = 0.0798 $wR2$ = 0.1140	$R1$ = 0.1193 $wR2$ = 0.1219
Largest difference peak/hole [eÅ^3]	0.423/−0.302	0.320/−0.429	0.579/−0.361	0.224/−0.325	0.198/−0.171

 © 2004 Wiley-VCH Verlag GmbH & Co. KGaA, Weinheim

CH*Me*$_2$), 24.6 (q, CH*Me*$_2$), 25.0 (q, CH*Me*$_2$), 25.1 (q, $J_{C,H}$ = 127 Hz, C*Me*), 27.3 (d, $J_{C,H}$ = 129 Hz, *C*HMe$_2$), 28.1 (d, $J_{C,H}$ = 127 Hz, *C*HMe$_2$), 100.0 (d, $J_{C,H}$ = 162 Hz, CMe*C*HCMe), 121.5 (d, $J_{C,H}$ = 161 Hz, Ph *C*H), 122.2 (d, $J_{C,H}$ = 161 Hz, Ph *C*H), 122.9 (d, $J_{C,H}$ = 155 Hz, Ph *C*H), 123.8 (d, $J_{C,H}$ = 154 Hz, Ph *C*H), 125.4 (d, $J_{C,H}$ = 159 Hz, Ph *C*H), 128.6 (d, $J_{C,H}$ = 160 Hz, Ph *C*H), 140.6 (s, Ph C_{ipso}), 142.9 (s, Ph C_{ipso}), 145.3 (s, Ph C_{ipso}), 151.2 (s, Ph C_{ipso}), 157.8 (d, $J_{C,H}$ = 180 Hz, *C*NPhH), 177.3 (s, *C*N), 180.2(s, *C*O) ppm. A small amount of phenyl isocyanate was present in the product which resulted in inaccuracy of the elemental analysis. The ^{1}H and ^{13}C NMR spectra of **5D** are similar to those of **5** except that the resonance of the *N*-phenyl formimidato proton of **5** at δ = 7.74 ppm was not observed for **5D**.

[Al(OCMeCHCMeNAr)$_2$(NCO)] (6): A toluene (10 mL) solution of $H_2NCOOEt$ (0.32 g, 3.67 mmol) was added dropwise at room temperature to a 50-mL Schlenk flask containing 20 mL of toluene and **2** (2.0 g, 3.67 mmol). The solution was refluxed for 1 h and the volatiles were removed under vacuum to yield an off-white solid. The solid was washed with a small amount of heptane in several portions to remove free ketiminate ligand. The resulting solid was recrystallized from a toluene solution at −20 °C to yield colorless crystals of **6** (1.23 g) in 57% yield. ^{1}H NMR ($CDCl_3$): δ = 1.05 (2 d, overlapping, 12 H, CH*Me*$_2$), 1.17 (d, 6 H, CH*Me*$_2$), 1.19 (s, 6 H, C*Me*), 1.28 (d, 6 H, CH*Me*$_2$), 1.65 (s, 6 H, C*Me*), 2.75 (m, 2 H, C*H*Me$_2$), 3.14 (m, 2 H, C*H*Me$_2$), 5.17 (s, 2 H, CMe*CH*CMe), 7.03−7.17 (m, 6 H, *Ph*) ppm. ^{13}C NMR ($CDCl_3$): δ = 23.6 (q, $J_{C,H}$ = 127 Hz, C*Me*), 23.7 (q, $J_{C,H}$ = 128 Hz, CH*Me*$_2$), 24.3 (q, $J_{C,H}$ = 127 Hz, CH*Me*$_2$), 24.7 (q, $J_{C,H}$ = 127 Hz, CH*Me*$_2$), 24.8 (q, $J_{C,H}$ = 127 Hz, CH*Me*$_2$), 24.9 (q, $J_{C,H}$ = 128 Hz, C*Me*), 27.9 (d, $J_{C,H}$ = 130 Hz, *C*HMe$_2$), 28.3 (d, $J_{C,H}$ = 130 Hz, *C*HMe$_2$), 100.0 (d, JC,H = Hz, CMe*C*HCMe), 123.0, 123.8, 125.4, 140.0, 142.5, 145.3, 176.7 (s, *C*N), 178.9 (s, *C*O) ppm. $C_{35}H_{48}AlN_3O_3$ (585.35): calcd. C 71.75, H 8.26, N 7.18; found C 71.24, H 7.72, N 7.05.

X-ray Structure Determination of Compounds 2−6: Crystals of compound **2** were obtained from a concentrated diethyl ether solution at −20 °C. Crystals of **4** and **6** were obtained from saturated toluene solutions at −20 °C. Crystals of **3** and **5** were obtained from saturated dichloromethane/diethyl ether solutions at −20 °C. The crystals were sealed in glass capillaries and mounted on a goniostat. All data sets were collected at 150(2) K, except for **6**, which was measured at 298(2) K. Data were collected with a Bruker SMART CCD diffractometer with graphite-monochromated Mo-K_α radiation. Structural determinations were performed using the SHELXTL package of programs. All refinements were carried out by full-matrix least squares using anisotropic displacement parameters for all non-hydrogen atoms. All the hydrogen atoms were placed geometrically and included through the use of a riding model. The crystal data are summarized in Table 3. CCDC-234262 (**2**), -234264 (**3**), -234265 (**4**), -234263 (**5**) and -234261 (**6**) contain the crystallohgraphic data for this paper. These data can be obtained free of charge at www.ccdc.cam.ac.uk/conts/retrieving.html [or from the Cambridge Crystallographic Data Centre, 12 Union Road, Cambridge CB2 1EZ, UK; Fax: + 44-1223-336-033; E-mail: deposit@ccdc.cam.ac.uk].

Acknowledgments

We thank the National Science Council of Taiwan for financial support and the National Changhua University of Education for supporting the CCD X-ray facility. We would also like to thank Dr. Darin Tiedtke for helpful discussion.

[1] A. Behr, *Catalysis in C1 Chemistry* (Ed.: W. Keim), Reidel, Dordrecht, **1983**.
[2] B. P. Sullivan, K. Krist, H. E. Guard, *Electrochemical and Electrocatalytic Reactions of Carbon Dioxide*, Elsevier, Amsterdam, **1993**.
[3] W. Leitner, *Coord. Chem. Rev.* **1996**, *153*, 257−284.
[4] P. G. Jessop, Y. Hsiao, T. Ikariya, R. Noyori, *J. Am. Chem. Soc.* **1996**, *118*, 344−355.
[5] R. Fornika, H. Görls, B. Seemann, W. Leitner, *J. Chem. Soc., Chem. Commun.* **1995**, 1479−1481.
[6] D. Walther, *Coord. Chem. Rev.* **1987**, *79*, 135−174.
[7] P. Braunstein, D. Matt, D. Nobel, *Chem. Rev.* **1988**, *88*, 747−764.
[8] X. Yin, J. R. Moss, *Coord. Chem. Rev.* **1999**, *181*, 27−59.
[9] J.-C. Tsai, K. M. Nicholas, *J. Am. Chem. Soc.* **1992**, *114*, 5117−5124.
[10] M. A. McLouglin, N. L. Keder, W. T. A. Harrison, R. J. Flesher, H. A. Mayer, W. C. Kaska, *Inorg. Chem.* **1999**, *38*, 3223−3227.
[11] C. Bianchini, C. A. Ghilardi, A. Meli, S. Midollini, A. Orlandini, *Inorg. Chem.* **1985**, *24*, 924−931.
[12] M. G. Bradley, D. A. Roberts, G. L. Geoffroy, *J. Am. Chem. Soc.* **1981**, *103*, 379−384.
[13] M. K. Whittlesey, R. W. Perutz, M. H. Moore, *Organometallics* **1996**, *15*, 5166−5169.
[14] M. Booij, J. Blenkers, J. C. M. Sinnema, A. Meetsma, F. van Bolhuis, J. H. Teuben, *Organometallics* **1988**, *7*, 1029−1032.
[15] N. Etkin, A. J. Hoskin, D. W. Stephan, *J. Am. Chem. Soc.* **1997**, *119*, 11420−11424.
[16] K. Khan, C. L. Raston, *Organometallics* **1997**, *16*, 3252−3254.
[17] S.-I. Murahashi, H. Takaya, *Acc. Chem. Res.* **2000**, *33*, 225−233.
[18] T. D. Tilley, *Acc. Chem. Res.* **1993**, *26*, 22−29.
[19] M. G. Gardiner, C. L. Raston, *Coord. Chem. Rev.* **1997**, *166*, 1−34.
[20] S. Cucinella, A. Mazzei, W. Marconi, *Inorg. Chim. Acta* **1970**, *4*, 51−71.
[21] C. Jones, G. A. Koutsantonis, C. L. Raston, *Polyhedron* **1993**, *12*, 1829−1848.
[22] A. J. Downs, C. R. Pulham, *Chem. Soc. Rev.* **1994**, *23*, 175−184.
[23] A. J. Downs, C. R. Pulham, *Adv. Inorg. Chem.* **1994**, *41*, 171−232.
[24] A. H. Cowley, F. P. Gabbaï, H. S. Isom, A. Decken, *J. Organomet. Chem.* **1995**, *500*, 81−88.
[25] A. J. Downs, *Coord. Chem. Rev.* **1999**, *189*, 59−100.
[26] R. J. Wehmschulte, P. P. Power, *Polyhedron* **2000**, *19*, 1649−1661.
[27] C. L. Raston, *J. Organomet. Chem.* **1994**, *475*, 15−24.
[28] J. E. Parks, R. H. Holm, *Inorg. Chem.* **1968**, *7*, 1408−1416.
[29] Similar phenomena have been seen, for example: M. P. Coles, D. C. Swenson, R. F. Jordan, *Organometallics* **1997**, *16*, 5183−5194.
[30] D. J. Darensbourg, A. Rokicki, *Organometallics* **1982**, *1*, 1685−1693.
[31] L. D. Field, E. T. Lawrenz, W. J. Shaw, P. Turner, *Inorg. Chem.* **2000**, *39*, 5632−5638.
[32] A. W. Kaplan, J. L. Polse, G. E. Ball, R. A. Anderson, R. G. Bergman, *J. Am. Chem. Soc.* **1998**, *120*, 11649−11662.
[33] R. E. Blake, D. M. Antonelli, L. M. Henling, W. P. Schaefer, K. I. Hardcastle, J. E. Bercaw, *Organometallics* **1998**, *17*, 718−725.
[34] P. Jeske, G. Haselhorst, T. Weyhermüller, K. Wieghardt, B. Nuber, *Inorg. Chem.* **1994**, *33*, 2462−2471.
[35] W. H. Knoth, J. C. Sauer, J. H. Balthis, H. C. Miller, E. L. Muetterties, *J. Am. Chem. Soc.* **1967**, *89*, 4842−4850.
[36] R.-C. Yu, J.-C. Chang, C.-H. Hung, J.-H. Huang, H.-I. Lee, J.-T. Chen, *Inorg. Chem.* **2002**, *41*, 6450−6455.
[37] S. J. Andrews, A. J. Welch, *Inorg. Chim. Acta* **1984**, *88*, 153−160.

 © 2004 Wiley-VCH Verlag GmbH & Co. KGaA, Weinheim

[38] K. Shelly, C. B. Knobler, M. F. Hawthorne, *Inorg. Chem.* **1992**, *31*, 2889−2892.
[39] B. Assmann, A. Franken, H. Homborg, *Z. Naturforsch., Teil B* **1996**, *51*, 325−332.
[40] A. D. Becke, *J. Chem. Phys.* **1993**, *98*, 5648−5652.
[41] C. Lee, W. Yang, R. G. Parr, *Phys. Rev. B* **1988**, *37*, 785−789.
[42] A comparison of bond lengths and angles between the calculated structures and the crystal structures can be found in the Supporting Information.

Received June 29, 2004
Early View Article
Published Online October 21, 2004

 © 2004 Wiley-VCH Verlag GmbH & Co. KGaA, Weinheim

Syntheses, Structures and Magnetic Properties of Novel Oxamido-Bridged Tetranuclear Complexes [Cu_3M] (M = Cu, Mn)

Shi-bin Wang,[a,b] Guang-ming Yang,*[a] Rong-fang Li,[a] Yuan-fang Wang,[a] and Dai-zheng Liao[a]

Keywords: Oxamido bridge / Tetranuclear / Macrocyclic complex / Magnetic property

Three oxamido-bridged tetranuclear complexes with the formulae [(LCu)Cu(LCuSCN)$_2$]·H_2O (**1**), [(LCu)Mn(LCuSCN)$_2$]·1.38CH_3OH (**2**) and {(LCu)Mn[LCuN(CN)$_2$]$_2$}·0.75DMF·0.25H_2O (**3**) (where H_2L = 2,3-dioxo-5,6:15,16-dibenzo-1,4,8,13-tetraazacylotetradeca-7,13-diene) have been prepared and characterised. Their structures were deduced using X-ray crystallography. All three complexes crystallise in the triclinic system, space group $P\bar{1}$. The three copper ions of the complex ligands and the central metal ions (Cu, Mn) remain in the plane and form a scalene triangle. Three copper ions occupy the vertexes and the M(Cu, Mn) ions are located at the centre. Magnetic susceptibility measurements in the 5–300 K temperature range have been carried out for this series of complexes. The experimental data have been fitted according to the Heisenberg Hamiltonian and led to J values equal to –61.80 cm^{-1}, –14.54 cm^{-1} and –12.10 cm^{-1} for complex **1**, **2** and **3**, respectively. Their interaction parameters have been compared with each other. The deviation of the copper ions from the oxamide-bridge plane results in the J value of complex **1** being different from those of other oxamide-bridged copper complexes.

(© Wiley-VCH Verlag GmbH & Co. KGaA, 69451 Weinheim, Germany, 2004)

Introduction

A lot of work has been devoted to the study of the exchange interactions in polynuclear systems. One of the challenges in this field is the design of complexes with predictable magnetic properties. To achieve this goal, one of the best strategies for designing and synthesising complexes is the complex-as-ligand approach, i.e. using mononuclear complexes which contain potential donor groups towards another metal ion.[1−5] The attractive feature of this is that the second metal ion will usually be in a different coordination environment from the first, potentially allowing the facile synthesis of homonuclear complexes in which the metals have different geometries and/or oxidation states,[6−11] or heteronuclear complexes.[12−14] At the same time, it was also discovered that the oxamido group is an efficient bridging mediator of magnetic exchange between neighbouring metal ions[15] because (i) the lower electronegativity of nitrogen with respect to oxygen leads to the gap between the oxamide-bridge molecular orbitals and the d metal orbitals being smaller; (ii) the metal-nitrogen and metal-oxygen distances are very close and contribute to maintaining a good overlap between the bridge and the d-metal orbitals.[16] Many complexes including this bridge have been synthesised and their magnetic properties characterised.[17−21] Antiferromagnetic interactions have been observed in these complexes, the magnitudes of which basically depend upon two factors: one is the nature and magnitude of the overlap between the metal d orbitals containing the unpaired electrons and the bridging ligand orbitals. The other is the energy difference between the two magnetic orbitals.

Polymetallic complexes of macrocyclic ligands have been of great interest to supramolecular and coordination chemists because of their special structures. The macrocyclic oxamido, in which an *exo-cis* conformation of the oxygen donors is enforced, allows us to design heterometallic systems and model magnetic systems in a more controlled fashion via the stepwise complication of the macrocyclic *exo* donors.

With these considerations in mind and continuing our work on polynuclear macrocyclic complexes,[19−25] we designed and synthesised a macrocyclic complex ligand LCu (where H_2L = 2,3-dioxo-5,6:15,16-dibenzo-1,4,8,13-tetraazacylotetradeca-7,13-diene) with oxamido bridging. Based on this complex ligand, we described the syntheses, crystal structures and the magnetic properties of three tetranuclear complexes, namely [(LCu)Cu(LCuSCN)$_2$]·H_2O (**1**), [(LCu)Mn(LCuSCN)$_2$]·1.38CH_3OH (**2**) and [(LCu)Mn[LCuN(CN)$_2$]$_2$]·0.75DMF·0.25H_2O (**3**). Although there have been a few papers concerning tetranu-

[a] Department of Chemistry, Nankai University, Tianjin 300071, People's Republic of China
Fax: (internat.) + 86-22-23502458
E-mail: yanggm@nankai.edu.cn
[b] Department of Materials and Chemical Engineering, Guilin Institute of Technology, Guilin, People's Republic of China
E-mail: sbinwang@hotmail.com

clear complexes in recent years,[26−32] the structures of the three complexes that we are reporting in this paper are different because the structures of those complexes are square or cubic and little work has been devoted to triangular frameworks in a plane.

Results and Discussion

Description of the Structures

The structure of **1** is shown in Figure 1. It consists of a neutral tetranuclear unit and a large number of disordered waters.

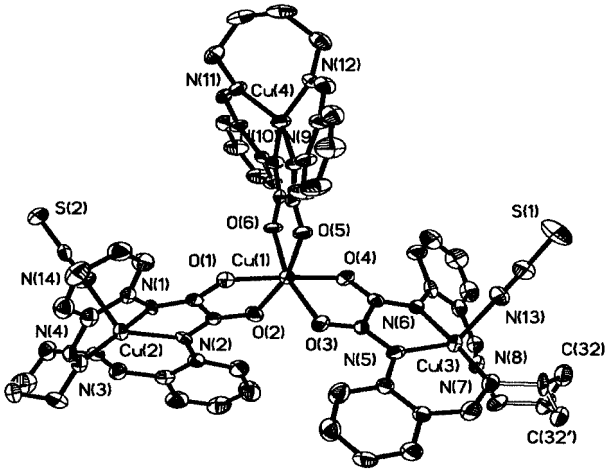

Figure 1. ORTEP plot of **1**; thermal ellipsoids are shown at the 30% probability level

The four copper ions remain in a plane and form a scalene triangle. Cu2, Cu3 and Cu4 occupy the vertexes. Cu1 almost stands on the epicenter since its distances to Cu2, Cu3 and Cu4 are 5.21(2) Å, 5.25 (1) Å and 5.23(2) Å, respectively. The Cu ions deviate from the mean triangular plane by 0.0114(3) Å (Cu1), −0.0040(2) Å (Cu2), −0.0042(2) Å (Cu3) and −0.0032 (1) Å (Cu4). In this molecule, there are three coordination frameworks to every four copper ions. The Cu1 ion is connected to other copper ions via the *exo-cis* oxygen atoms of the oxamido macrocyclic ligands and its coordination polyhedron can be considered as a distorted octahedron. The basal plane of the octahedron consists of O1, O2, O4 and O5 and the apical positions are occupied by O3 and O6. The value that Cu1 deviates from the plane is 0.0463 Å. Cu2 and Cu3 show a (4+1) coordination environment, the four nitrogen atoms of the macrocyclic ligand are situated in the basal position and the coordination is completed by the nitrogen of the SCN^-. The four nitrogen atoms of the macrocyclic ligand deviate significantly from the basal plane [for Cu2, the values are −0.41(2) Å (N1), 0.41 (3) Å (N2), −0.36 (2) Å (N3) and 0.37 (1) Å (N4)]. The coordination environment of Cu2 can be considered as a square pyramid. The Cu−N bond lengths in the plane range from 1.912(1) Å to 1.973 (3) Å for Cu2 and from 1.891(1) Å to 1.995 (3) Å for Cu3. The axial Cu−N bond length is 2.107(1) Å for Cu2 and 2.081 (3) Å for Cu3. These are elongated due to the Jahn−Teller effect of the d^9 electronic configuration. For Cu4, the four-coordinate structure of the complex ligand is maintained. Cu2, Cu3 and Cu4 deviate from the plane of the oxamido bridge ($C_2O_2N_2$) by −0.274(4) Å, 0.166 (1) Å and 0.0457 (1) Å, respectively. Figure 1 indicates that C32 is disordered over two sides.

Complexes **2** and **3** are similar in structure and both consist of a neutral tetranuclear Cu_3Mn unit. Figures 2 and 3 show the common metal part of **2** and **3** with atomic labelling schemes. Within each tetranuclear fragment the Cu1 and Cu2 centres of **2** and the Cu2 and Cu3 centres of **3** are in a (4+1) coordination environment and show square pyramidal structures. The four nitrogen atoms of the macrocyclic ligand form their basal planes and the axial positions are occupied, respectively, by the nitrogen atom from thiocyanate ion for complex **2** and one of the nitrogen atoms of the dicyanamide ion for complex **3**. The Cu3 centre of complex **2** and Cu1 in complex **3** both maintain the four-coordinate structure of the macrocyclic complex ligand. The four copper ions which have pentahedral configurations in these two complexes are displaced from the least-squares basal plane towards the apical ligand by 0.36 (1) Å (Cu1) and 0.47(3) Å (Cu2) for complex **2** and by −0.31(2) Å (Cu2) and 0.39(1) Å (Cu3) for complex **3**. The metal atoms Cu1, Cu2, Cu3 and Mn1 of the two complexes are almost in a plane and form a triangle. The Mn(II) ions in the two complexes are both coordinated to the six oxygen atoms of the oxamido bridges of the three complex ligands. The Mn(II) ions have octahedral geometries and the Mn−O bond lengths range from 2.152(1) Å to 2.179(1) Å for complex **2** and from 2.094 (2) Å to 2.187 (3) Å for complex **3**. The distances from Mn to Cu are 5.514(2) Å (Cu1), 5.547(2) Å (Cu2) and 5.461(2) Å (Cu3) for complex **2** and 5.433 (1) Å (Cu1), 5.441(1) Å (Cu2) and 5.485 (1) Å (Cu3) for complex **3**, respectively. There are many free solvent molecules in both crystal structures. On average, there are 1.38 methanol molecules in the crystalline lattice of complex **2**. However, 0.75 DMF molecules and 0.25 water molecules are distributed in the crystalline lattice of complex **3**.

Selected bond lengths and angles are listed in Tables 1, 2 and 3.

Spectroscopic Characterisation

The $\nu_{(C=O)}$ bands of the oxamido group of the tetranuclear complexes can be observed around 1640cm^{-1} which is lower relative to that of mononuclear CuL (1670cm^{-1}). The IR bands around 1570cm^{-1} can be assigned to the $\nu_{(C=N)}$ mode of the macrocycle. A strong band at ca. 2100cm^{-1} is characteristic of a C−N bond.

The electronic absorption spectra of the three tetranuclear complexes in DMF below 420 nm are dominated by intense bands due to intraligand and charge-transfer transitions in the Cu(II) chromophore. Bands at 670 nm can be attributed to the spin allowed d-d transitions of Cu(II). The coordination environments of manganese in 2 and 3 are distorted octahedral. Thus, according to ligand field theory

 © 2004 Wiley-VCH Verlag GmbH & Co. KGaA, Weinheim

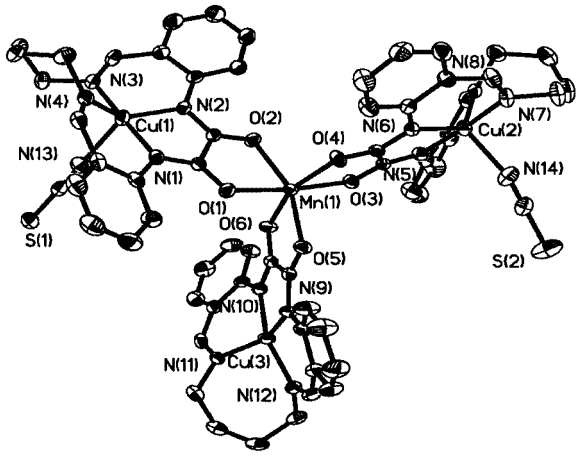

Figure 2. ORTEP plot of **2**; thermal ellipsoids are shown at the 30% probability level

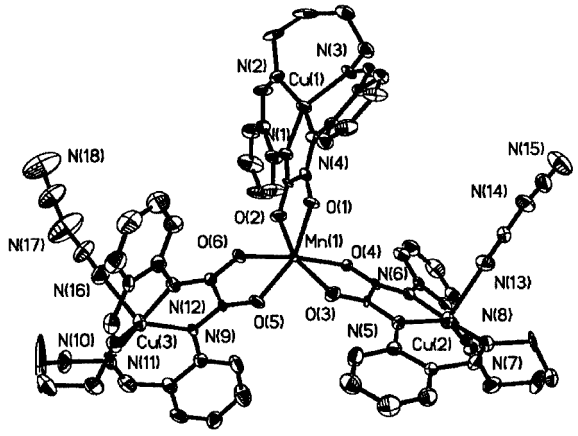

Figure 3. ORTEP plot of **3**; thermal ellipsoids are shown at the 30% probability level

and assuming O_h symmetry, the ground state of manganese is $^6A_{1g}$. Because d-d transitions of manganese [$^6A_{1g} \rightarrow {}^4T_{1g}(G)$. $^4T_{2g}(G)$, $^4A_{1g}$ ···] are spin forbidden, no characteristic bands of manganese were found in the spectra of the complexes.

Magnetic Properties

Variable temperature (5−300 K) magnetic susceptibility data were collected for microcrystalline samples of complexes **1**−**3** in a magnetic field of 10000 G. The χ_M and $\chi_M T$ versus T plot for complex **1** is shown in Figure 4. At 300 K $\chi_M T$ is equal to 1.35cm^{3}mol^{-1}K which is lower than that expected for the four isolated copper ions ($\chi_M T$ = 1.50 cm^{3}mol^{-1}K). This decreases smoothly upon cooling and reaches a minimum at about 70 K with $\chi_M T$ = 1.05cm^{3}mol^{-1}K and increases upon cooling further. At 5 K, $\chi_M T$ is equal to 1.30 cm^{3}mol^{-1}K. The experimental data were fitted using the theoretical expression of the magnetic susceptibility [Equation (1)] which was deduced from the spin Hamiltonian:

Table 1. Selected bond lengths (Å) and angles (°) in **1**

Cu(1)−O(4)	1.883(6)	Cu(2)−N(14)	2.107(9)
Cu(1)−O(1)	1.900(6)	Cu(3)−N(7)	1.995(7)
Cu(1)−O(5)	2.030(6)	Cu(3)−N(13)	2.081(9)
Cu(1)−O(2)	2.064(6)	Cu(3)−N(8)	1.891(8)
Cu(1)−O(6)	2.061(6)	Cu(3)−N(6)	1.903(7)
Cu(1)−O(3)	2.117(7)	Cu(4)−N(12)	1.896(7)
Cu(2)−N(1)	1.924(7)	Cu(4)−N(9)	1.898(8)
Cu(2)−N(2)	1.959(7)	Cu(4)−N(10)	1.901(7)
Cu(2)−N(4)	1.973(8)	Cu(4)−N(11)	1.911(8)
O(4)−Cu(1)−O(1)	176.8(2)	N(3)−Cu(2)−N(4)	93.9(3)
O(4)−Cu(1)−O(5)	95.3(3)	N(1)−Cu(2)−N(4)	89.9(3)
O(1)−Cu(1)−O(5)	86.9(2)	N(2)−Cu(2)−N(4)	133.1(3)
O(4)−Cu(1)−O(2)	98.2(2)	N(3)−Cu(2)−N(14)	91.0(3)
O(1)−Cu(1)−O(2)	79.9(2)	N(1)−Cu(2)−N(14)	89.7(3)
O(5)−Cu(1)−O(2)	164.7(2)	N(2)−Cu(2)−N(14)	120.9(3)
O(4)−Cu(1)−O(6)	87.6(3)	N(4)−Cu(2)−N(14)	105.5(3)
O(1)−Cu(1)−O(6)	95.1(2)	N(8)−Cu(3)−N(7)	92.1(3)
O(5)−Cu(1)−O(6)	79.2(2)	N(6)−Cu(3)−N(7)	89.0(3)
O(2)−Cu(1)−O(6)	94.1(2)	N(5)−Cu(3)−N(7)	131.2(3)
O(4)−Cu(1)−O(3)	79.1(3)	N(8)−Cu(3)−N(13)	93.4(3)
O(6)−Cu(1)−O(3)	164.4(2)	N(6)−Cu(3)−N(13)	90.0(3)
O(1)−Cu(1)−O(3)	98.4(3)	N(5)−Cu(3)−N(13)	118.4(3)
O(5)−Cu(1)−O(3)	93.7(3)	N(7)−Cu(3)−N(13)	109.7(3)
O(2)−Cu(1)−O(3)	95.8(3)	N(9)−Cu(4)−N(10)	85.5(3)
N(3)−Cu(2)−N(1)	175.8(3)	N(12)−Cu(4)−N(11)	98.9(3)
N(3)−Cu(2)−N(2)	92.2(3)	N(9)−Cu(4)−N(11)	150.9(3)
N(1)−Cu(2)−N(2)	83.9(3)	N(10)−Cu(4)−N(11)	92.5(3)

Table 2. Selected bond lengths (Å) and angles (°) in **2**

Cu(1)−N(3)	1.949(5)	Cu(2)−N(6)	2.030(4)
Cu(1)−N(1)	1.961(4)	Cu(2)−N(8)	2.058(4)
Cu(1)−N(2)	2.011(4)	Cu(2)−N(14)	2.111(6)
Cu(1)−N(4)	2.024(4)	Cu(3)−N(10)	1.945(4)
Cu(1)−N(13)	2.196(5)	Cu(3)−N(12)	1.962(4)
Cu(2)−N(5)	1.954(4)	Cu(3)−N(11)	1.966(4)
Cu(2)−N(7)	1.967(4)	Cu(3)−N(9)	1.972(4)
Mn(1)−O(3)	2.151(3)	Mn(1)−O(1)	2.171(3)
Mn(1)−O(5)	2.151(3)	Mn(1)−O(2)	2.178(3)
Mn(1)−O(6)	2.160(3)	Mn(1)−O(4)	2.195(3)
N(1)−Cu(1)−N(2)	83.94(16)	N(5)−Cu(2)−N(14)	91.09(19)
N(3)−Cu(1)−N(4)	93.38(19)	N(7)−Cu(2)−N(14)	93.4(2)
N(1)−Cu(1)−N(4)	91.25(18)	N(6)−Cu(2)−N(14)	117.96(18)
N(2)−Cu(1)−N(4)	135.77(16)	N(8)−Cu(2)−N(14)	112.15(18)
N(3)−Cu(1)−N(13)	91.02(18)	N(10)−Cu(3)−N(12)	161.14(16)
N(1)−Cu(1)−N(13)	88.12(17)	N(10)−Cu(3)−N(11)	92.69(17)
N(2)−Cu(1)−N(13)	120.03(16)	N(12)−Cu(3)−N(11)	97.94(17)
N(4)−Cu(1)−N(13)	103.64(17)	N(10)−Cu(3)−N(9)	85.36(17)
N(5)−Cu(2)−N(7)	175.09(18)	N(12)−Cu(3)−N(9)	93.35(17)
N(5)−Cu(2)−N(6)	83.16(16)	N(11)−Cu(3)−N(9)	148.77(16)
N(7)−Cu(2)−N(6)	92.99(17)	O(6)−Mn(1)−O(2)	96.06(13)
N(5)−Cu(2)−N(8)	88.04(17)	O(3)−Mn(1)−O(5)	99.72(13)
O(5)−Mn(1)−O(6)	75.77(12)	O(3)−Mn(1)−O(6)	89.18(13)
O(3)−Mn(1)−O(1)	173.21(12)	O(3)−Mn(1)−O(4)	74.12(12)
O(5)−Mn(1)−O(1)	85.81(13)	O(5)−Mn(1)−O(4)	95.63(13)
O(6)−Mn(1)−O(1)	96.04(13)	O(6)−Mn(1)−O(4)	159.84(13)
O(3)−Mn(1)−O(2)	100.59(13)	O(1)−Mn(1)−O(4)	101.55(13)
O(5)−Mn(1)−O(2)	157.97(12)	O(2)−Mn(1)−O(4)	98.05(14)
O(1)−Mn(1)−O(2)	74.59(13)		

 © 2004 Wiley-VCH Verlag GmbH & Co. KGaA, Weinheim

Table 3. Selected bond lengths (Å) and angles (°) in **3**

Mn(1)−O(4)	2.092(7)	Cu(2)−N(13)	2.318(12)
Mn(1)−O(6)	2.098(7)	Cu(2)−N(8)	1.956(10)
Mn(1)−O(1)	2.148(7)	Cu(2)−N(6)	1.966(9)
Mn(1)−O(2)	2.146(7)	Cu(2)−N(5)	2.009(8)
Mn(1)−O(3)	2.159(7)	Cu(2)−N(7)	2.025(10)
Mn(1)−O(5)	2.187(7)	Cu(3)−N(9)	2.023(8)
Cu(1)−N(2)	1.952(9)	Cu(3)−N(12)	1.947(9)
Cu(1)−N(4)	1.961(9)	Cu(3)−N(10)	1.975(9)
Cu(1)−N(3)	1.969(9)	Cu(3)−N(11)	2.035(10)
Cu(1)−N(1)	1.972(9)	Cu(3)−N(16)	2.195(12)
O(6)−Mn(1)−O(1)	88.4(3)	N(2)−Cu(1)−N(3)	99.6(4)
O(4)−Mn(1)−O(2)	86.8(3)	N(4)−Cu(1)−N(3)	91.4(4)
O(6)−Mn(1)−O(2)	98.0(3)	N(2)−Cu(1)−N(1)	93.3(4)
O(1)−Mn(1)−O(2)	76.5(3)	N(4)−Cu(1)−N(1)	85.2(4)
O(4)−Mn(1)−O(3)	76.0(3)	N(3)−Cu(1)−N(1)	148.5(4)
O(6)−Mn(1)−O(3)	99.9(3)	N(8)−Cu(2)−N(6)	174.0(4)
O(1)−Mn(1)−O(3)	95.6(3)	N(8)−Cu(2)−N(5)	92.3(4)
O(2)−Mn(1)−O(3)	160.1(3)	N(6)−Cu(2)−N(5)	84.3(4)
O(4)−Mn(1)−O(5)	99.7(3)	N(8)−Cu(2)−N(7)	95.0(4)
O(6)−Mn(1)−O(5)	75.5(3)	N(6)−Cu(2)−N(7)	90.7(4)
O(1)−Mn(1)−O(5)	160.1(3)	N(5)−Cu(2)−N(7)	140.1(4)
O(2)−Mn(1)−O(5)	94.1(3)	N(8)−Cu(2)−N(13)	89.3(4)
N(6)−Cu(2)−N(13)	87.8(4)	N(10)−Cu(3)−N(11)	94.1(4)
N(5)−Cu(2)−N(13)	115.7(4)	N(9)−Cu(3)−N(11)	135.1(4)
N(7)−Cu(2)−N(13)	103.6(4)	N(12)−Cu(3)−N(16)	89.4(4)
N(12)−Cu(3)−N(10)	176.6(4)	N(10)−Cu(3)−N(16)	92.3(4)
N(12)−Cu(3)−N(9)	83.6(4)	N(9)−Cu(3)−N(16)	115.5(4)
N(10)−Cu(3)−N(9)	93.0(4)	N(11)−Cu(3)−N(16)	108.4(4)
N(12)−Cu(3)−N(11)	88.2(4)		

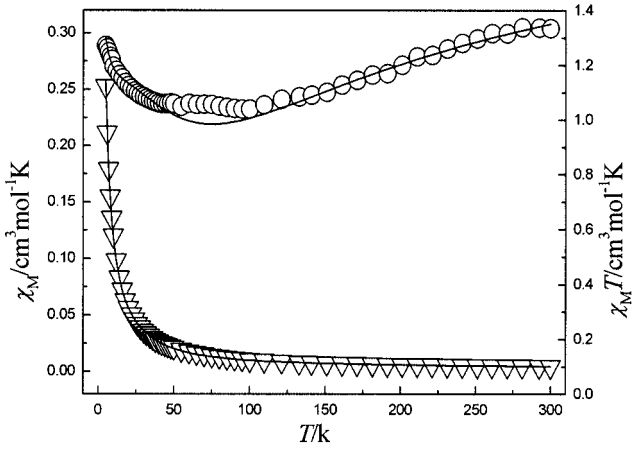

Figure 4. Experimental and calculated variations of the product χ_M and $\chi_M T$ versus T for **1**

$$\chi_M = \frac{2Ng^2\beta^2}{k(T-\theta)}\left[\frac{A}{B}\right] + N\alpha$$

$$A = 5\times\exp(2J/kT) + \exp(-2J/kT) + 2$$
$$B = 5\times\exp(2J/kT) + 3\times\exp(-2J/kT) + 2\times\exp(-2J/kT) + 6 \quad (1)$$

where J is the exchange integral between the Cu(II) ions. (Because Cu2, Cu3 and Cu3 all link to Cu1 through the oxamido bridge and the distances between them are almost similar, we assumed the interaction between them is equal.) $N\alpha$ is the temperature-independent paramagnetic (240×10^{-6} cm^3mol^{-1}) and the other symbols have their usual meanings. The best fitting of the experimental data leads to $J = -61.80 cm^{-1}$, $g = 2.09$, $\theta = 0.8$ and $R = 2.23 \times 10^{-4}$ (R is the agreement factor defined as $\Sigma(\chi_{obs.} - \chi_{calcd.})^2/\Sigma\chi^2_{obs.}$). The results indicate that there is an antiferromagnetic interaction between the copper(II) ions within complex **1**.

According to the Kahn model[33] for the copper complexes, the magnetic exchange pathway is dominated by the interaction between the metal $x^2 - y^2$ orbitals and the oxamido σ orbitals and the antiferromagnetic interaction between the copper(II) ions arises from the nonzero overlap between the magnetic orbitals. The magnitude of the antiferromagnetic interaction is related to the square of the overlap between the magnetic orbitals central to each copper. The antiferromagnetic interaction between the copper(II) ions within complex **1** is weaker than that within other oxamido bridge copper complexes reported previously ($J = 210-80.9$ cm^{-1}).[34−36] This may be attributed to the difference in the ligand environments of the copper ions because the former has less co-planarity between the coordination environments of copper(II) and that of the adjacent copper(II) ions than the latter, resulting in a decrease in overlap between the two magnetic orbitals within the present complex.[37]

Plots of χ_M and $\chi_M T$ versus temperature for complexes **2** and **3** are shown in Figures 5 and 6, respectively. At room temperature, $\chi_M T$ is equal to 5.04 $cm^3mol^{-1}K$ for complex **2** and 5.19 $cm^3mol^{-1}K$ for complex **3**, both of which are lower than 5.50 $cm^3mol^{-1}K$ which would be expected for noninteracting ions [three coppers(II) ions and one manganese(II) ion]. The $\chi_M T$ value decreases steadily upon cool-

$$\chi_M = \frac{N\beta^2}{kT}\left[\frac{A}{B}\right] + N\alpha$$

$$A = 60\times g^2_{4,3/2}\times\exp(18J/kT) + 28\times g^2_{3,3/2}\times\exp(4J/kT) + 10\times g^2_{2,3/2}\times\exp(4J/kT) + 2\times g^2_{1,3/2} + 56\times g^2_{3,1/2}\times\exp(13J/kT) + 20\times g^2_{2,1/2}\times\exp(7J/kT)$$

$$B = 9\times\exp(18J/kT) + 7\times\exp(10J/kT) + \exp(4J/kT) + 3 + 14\times\exp(13J/kT) + 10\times\exp(7J/kT) \quad (2)$$

$$g_{4,3/2} = \frac{3}{8}\times g_{Cu} + \frac{5}{8}\times g_{Mn} \qquad g_{3,3/2} = \frac{7}{24}\times g_{Cu} + \frac{17}{24}\times g_{Mn}$$
$$g_{2,3/2} = \frac{1}{12}\times g_{Cu} + \frac{13}{12}\times g_{Mn} \qquad g_{1,3/2} = \frac{-3}{4}\times g_{Cu} + \frac{7}{4}\times g_{Mn}$$
$$g_{3,1/2} = \frac{1}{6}\times g_{Cu} + \frac{5}{6}\times g_{Mn} \qquad g_{2,1/2} = \frac{-1}{6}\times g_{Cu} + \frac{7}{6}\times g_{Mn}$$

 © 2004 Wiley-VCH Verlag GmbH & Co. KGaA, Weinheim

ing, showing that an antiferromagnetic interaction between the copper and manganese ions occurs. In the 5−15 K temperature range the $\chi_M T$ plot exhibits a plateau at 1.03 $cm^3mol^{-1}K$ for complex **2** and at 0.96 $cm^3mol^{-1}K$ for complex **3**. The experimental data were fitted using the theoretical expression of the magnetic susceptibility [Equation (2)] which was deduced from spin the Hamiltonian: In Equation (2), the value of $N\alpha$ is 180×10^{-6}.

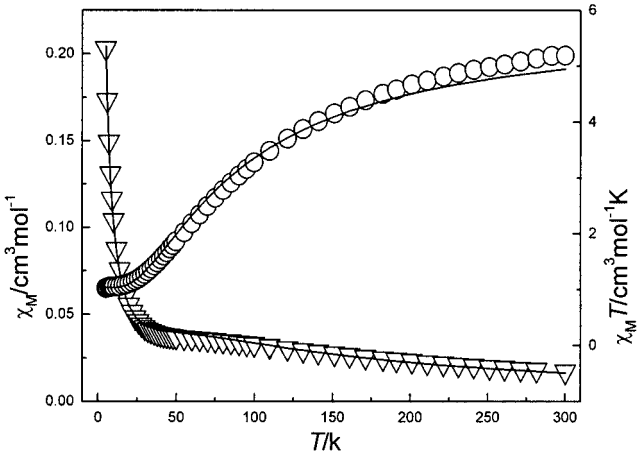

Figure 5. Experimental and calculated variations of the product χ_M and $\chi_M T$ versus T for **2**

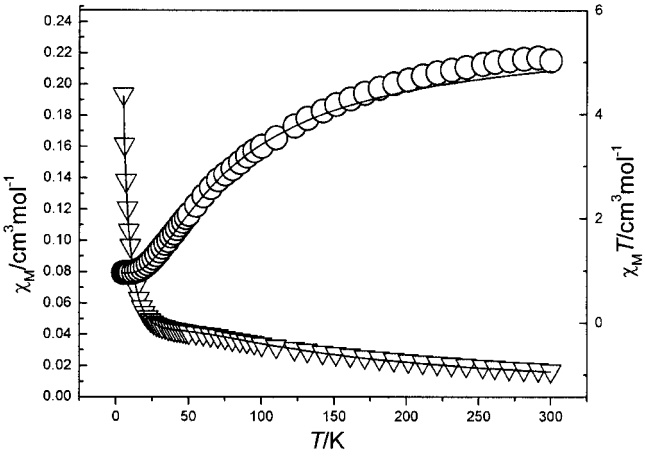

Figure 6. Experimental and calculated variations of the product χ_M and $\chi_M T$ versus T for **3**

The best fit of the data was obtained with the following parameters $J = -14.63\ cm^{-1}$, $g_{Cu} = 2.06$, $g_{Mn} = 1.99$ and $R = 1.05\times10^{-3}$ for complex **2** and $J = -12.22 cm^{-1}$, $g_{Cu} = 2.06$, $g_{Mn} = 1.98$ and $R = 1.20\times10^{-4}$ for complex **3**. The J values of 2 and 3 are in the range of other reported complexes[16,24] with similar structures.

If we compare the J value of complex **1** with those of complexes **2** and **3**, we see that the latter values are lower than the former. The difference may be attributed to the following reasons: (i) the M−O distance is larger for Mn (2.17 Å) than for Cu (2.01Å) or (ii) the energies of the 3d orbitals of Mn(II) are higher than the corresponding ones in Cu(II). The two factors lead to less delocalisation of the d electron towards the oxamido bridge in **2** and **3** than in complex 1, therefore decreasing the antiferromagnetic interaction in **2** and **3**.[38]

Conclusion

By using the macrocyclic oxamido-copper complex as a complex ligand and SCN^{-1} or $N(CN)^{-1}$ as auxiliary ligands, three novel oxamide-bridge tetranuclear complexes have been obtained. In all complexes, the Cu atoms lie at the apexes of a triangle with the M atom located in the plane and at the centre of this triangle. All attempts to crystallise these types of complexes without smaller ions such as SCN^{-1} and $N(CN)^{-1}$ have previously been unsuccessful. It has been confirmed that the smaller ions can make the crystals grow easily in the present systems. Furthermore, we analysed the variable temperature magnetic susceptibilities of the three complexes. The results indicate that there are antiferromagnetic interactions between metal ions in the complexes. We are attempting to replace the metal ion in the centre of the triangle with a diamagnetic ion in order to research further the spin frustration.

Experimental Section

Physical Measurements: Elemental analyses (C, H, N) were performed on a Perkin−Elmer 240 analyser. IR spectra were recorded on a Shimadzu IR spectrometer as KBr pellets. Variable-temperature magnetic susceptibilities from 5−300 K were measured on a Quantum Design MPMS-7 SQUID magnetometer. Diamagnetic corrections were made with Pascal's constants for all the constituent atoms. The electronic absorption spectra were recorded on a JASCO V-5700 spectrometer.

Caution! Perchlorate salts are potentially explosive and should only be handled in small quantities only.

All starting materials were obtained from commercial suppliers and were of AR grade and were used without further purification. The mononuclear precursors were synthesised using the methods reported previously.[12,38]

Preparation of the Complexes: All complexes were prepared using the same method which is described in detail here using $[(LCu)Cu(LCuSCN)_2]\cdot H_2O$ (**1**) as an example. Copper perchlorate (0.2 mmol, 0.0730 g) dissolved in methanol (5 mL) was added to a DMF solution (25 mL) of LCu (0.7 mmol, 0.2860 g). An aqueous solution (5 mL) of KSCN (0.3 mmol, 0.030 g) was then added dropwise to this mixture. After heating to reflux for 2 hours, the resultant green solution was cooled and filtered and the filtrate was allowed to stand for one month until deep green crystals suitable for X-ray analysis separated out. Yield 40%. $C_{62}H_{59}Cu_4N_{14}O_7S_2$ (1430.51): calcd. C 52.12, H 3.92, N 13.73; found C 52.08, H 4.10, N 13.85. IR (KBr): $\tilde{\nu}$ = 2065 (C−N), 1675 (C=O), 1599 (C=O), 1557 cm^{-1}.

$[(LCu)Mn(LCuSCN)_2]\cdot 1.38CH_3OH$ (2): This complex was obtained following the procedure described above for $[Cu_4]$ except that Cu perchlorate was substituted with Mn perchlorate. The solution was left undisturbed and well-formed grey crystals were obtained after about a month. The yield was ca. 54%.

 © 2004 Wiley-VCH Verlag GmbH & Co. KGaA, Weinheim

Table 4. Crystallographic data for complexes **1**, **2** and **3**

	1	**2**	**3**
Empirical formula	$C_{62}H_{59}Cu_4N_{14}O_7S_2$	$C_{63.38}H_{59.50}Cu_3MnN_{14}O_{7.38}S_2$	$C_{66.25}H_{59.75}Cu_3MnN_{18.75}O_7$
Molecular mass	1430.51	1444.93	1476.14
Temperature	293(2) K	293(2) K	293(2) K
Wavelength	0.71073 Å	0.71073 Å	0.71073 Å
Crystal system, space group	triclinic, $P\bar{1}$	triclinic, $P\bar{1}$	triclinic, $P\bar{1}$
Unit cell dimensions			
a (Å)	13.960(11)	13.976(4)	14.349(8)
b (Å)	16.051(13)	16.458(5)	16.395(9)
c (Å)	16.773(12)	17.743(6)	17.402(10)
α (°)	103.024(15)	104.775(6)	102.323(10)
β (°)	107.071(15)	106.467(6)	106.740(10)
γ (°)	108.467(14)	107.267(6)	108.975(10)
Volume (Å^3)	3191(4)	3471.6(19)	3488(3)
Z	2	2	2
Density (mg·m^{-3})	1.489	1.382	1.406
Absorption coeff. (mm^{-1})	1.444	1.204	1.144
F(000)	1466	1482	1513
Crystal size (mm)	0.30 × 0.20 ×0.10	0.30 × 0.24 × 0.20	0.35 × 0.30 × 0.30
θ range for data collection	1.67 to 25.03°	1.66 to 26.44°	1.63 to 25.03°
Data/restraints/parameters	10522/0/811	13938/22/841	11901/38/892
Goodness-of-fit on F^2	0.951	0.988	1.021
Final *R* indices	$R1 = 0.0750$	$R1 = 0.0596$	$R1 = 0.1017$
$[I > 2\sigma(I)]$	$wR2 = 0.1612$	$wR2 = 0.1155$	$wR2 = 0.2061$
R indices (all data)[a]	$R1 = 0.1797$	$R1 = 0.1456$	$R1 = 0.2386$
	$wR2 = 0.2062$	$wR2 = 0.1484$	$wR2 = 0.2780$
Largest diff. peak and hole e·Å^{-3}	1.084 and −0.540	0.612 and −0.421	1.198 and −0.642

[a] $R = \Sigma||F_o| - |F_c||/\Sigma|F_o|$ $wR = [\Sigma w(F_o^2 - F_c^2)^2/\Sigma w(F_o^2)^2]^{1/2}$

$C_{63.38}H_{59.50}Cu_3MnN_{14}O_{7.38}S_2$ (1444.93): C 52.60, H 4.11, N 13.57; found C 53.64, H 4.17, N 13.69. IR (KBr): $\tilde{\nu}$ = 2066 (C−N), 1636 (C=O), 1601 (C=N), 1576 cm^{-1}.

[(LCu)Mn[LCuN(CN)$_2$]$_2$]·0.75DMF·0.25H$_2$O (3): This compound was obtained by using the method used to synthesise complex **2** except that KSCN was substituted with $NaN(CN)_2$. The crystals were also grey. Yield 47%. $C_{66}H_{60.50}N_{18.50}O_{7.50}Cu_3Mn$ (1476.14) : calcd. C 53.86, H 4.04, N 17.79; found C 53.02, H 4.21, N 17.45. IR (KBr): $\tilde{\nu}$ = 2148 (C−N), 1636 (C=O), 1600 (C=N), 1558 cm^{-1}.

X-ray Data Collections and Structure Determinations

Complex 1: A dark green crystal (0.30 × 0.20 × 0.10 mm) was selected and coated with epoxy resin and mounted on a glass fibre for X-ray data collection. Intensity data were colleted on a BRUKER SMART 1000 diffractometer, using Mo-K_α (λ = 0.71073 Å) radiation. The unit cell constants were determined from a least-squares fit of the setting angles for 25 reflections ($1.67° < \theta < 25.03°$). A total of 10522 unique reflections were observed with $I > 2\sigma(I)$ and were used in the calculations.

The structure was solved by direct methods by using SHELXS-97[39] and refined by least-squares procedures. The hydrogen atoms of the water molecules were not added and the other hydrogen atoms were located geometrically and refined isotropically. The final refinement included 811 variable parameters and converged to $R = 0.0750$, $R_w = 0.1612$.

Complexes 2 and 3: The structure determinations of complexes **2** and **3** were similar to that of complex **1**. The grey prism-like crystals of the two complexes, respectively, were used for X-ray data collection. The unit constants were determined from 25 reflections [$1.66° < \theta < 26.44°$ (**2**), $1.63° < \theta < 25.03°$ (**3**)].

A total of 13938 (**2**) and 11901 (**3**) unique reflections were observed with $I > 2\sigma(I)$ and were used in the calculations. The final refinement included 809 variable parameters for complex **2** and 886 for complex **3** and converged to $R = 0.0596$, $R_w = 0.1155$ (**2**) and $R = 0.1017$, $R_w = 0.2061$ (**3**).

The crystallographic data for **1**, **2** and **3** are listed in Table 4.

CCDC-217659 to -217661 contain the supplementary crystallographic data for this paper. These data can be obtained free of charge at www.ccdc.cam.ac.uk/conts/retrieving.html [or from the Cambridge Crystallographic Data Centre, 12 Union Road, Cambridge CB2 1EZ, UK; Fax: (internat.) +44-1223-336-033; E-mail: deposit@ccdc.cam.ac.uk].

Acknowledgments

This work was supported by the National Science Foundation of China (Grant No.59973008 and 20071019) and the Natural Science Foundation of Tianjin (Grant No. No.013603711).

[1] O. Kahn, *Adv. Inorg. Chem.* **1996**, 179.
[2] N. B. O'Bryan, T. O. Marier, I. C. Paul, R. S. Drago, *J. Am. Chem. Soc.* **1973**, *95*, 6640−6645.
[3] J. P. Costes, J. P. Laurent, J. M. M. Sanchez, J. S. Varela, M. Ahlgren, M. Sundberg, *Inorg. Chem.* **1997**, *36*, 4641−4646.
[4] O. Kahn, Y. Pei, M. Verdaguer, J. P. Renard, J. Sletten, *J. Am. Chem. Soc.* **1988**, *110*, 782−789.
[5] H. Okawa, Y. Kawahara, M. Mikuriya, S. Kida, *Bull. Chem. Soc., Jpn.* **1980**, *53*, 549−550.
[6] J. Ribas, C. Diaz, R. Costa, Y. Journaux, C. Mathoniere, O. Kahn, A. Gleizes, *Inorg. Chem.* **1990**, *29*, 2042−2047.
[7] J. C. Livermore, R. D. Willett, R. M. Gaura, C. P. Landee, *Inorg. Chem.* **1982**, *21*, 1403−1405.
[8] M. F. Charlot, S. Jeannin, Y. Jeannin, O. Kahn, J. Lucrèce-Abaul, J. Martin Frere, *Inorg. Chem.* **1979**, *18*, 1675−1681.
[9] M. A. S. Goher, F. A. Mautner, *J. Chem. Soc., Dalton Trans.* **1999**, 1923−1924.

 © 2004 Wiley-VCH Verlag GmbH & Co. KGaA, Weinheim

[10] E. Q. Gao, Q. H. Zhao, J. K. Tang, D. Z. Liao, Z. H. Jiang, S. P. Yan, *J. Chem. Soc., Dalton Trans.* **2001**, 1537−1540.
[11] T. S. Billson, J. D. Crane, O. D. Fox, S. L. Heath, *Inorg. Chem. Commun.* **2000**, *3*, 718−720.
[12] L. Zhang, S. B. Wang, G. M. Yang, J. K. Tang, D. Z. Liao, Z. H. Jiang, S. P. Yan, P. Chen, *Inorg. Chem.* **2003**, *42*, 1462−1466.
[13] C. Diaz, J. Ribas, R. Costa, J. Tercero, M. S. E. Fallah, X. Solans, M. Font-Boadía, *Eur. J. Inorg. Chem.* **2000**, *4*, 675−681.
[14] Y. Pei, Y. Joumaux, O. Kahn, *Inorg. Chem.* **1989**, *28*, 100−103.
[15] L. Soto, J. Garcia, E. Escriva, J.-P. Legros, J.-P. Tuchagues, F. Dahan, A. Fuertes, *Inorg. Chem.* **1989**, *28*, 3378−3386.
[16] F. Loret, Y. Journaux, M. Julve, *Inorg. Chem.* **1990**, *29*, 3967−3972.
[17] J. Larionova, S. A. Chavan, J. V. Yakhmi, A. G. Froystein, J. Sletten, C. Sourisseau, O. Kahn, *Inorg. Chem.* **1997**, *36*, 6374−6381.
[18] G. Brewer, C. T. Brewer, P. Kamaras, S. Prytkov, M. Y. Shang, W. R. Scheidt, *Inorg. Chim. Acta* **2001**, *321*, 175−180.
[19] E. Q. Gao, J. K. Tang, S. P. Yan, D. Z. Liao, Z. H. Jiang, *Trans. Met. Chem.* **2001**, *26*, 473−476.
[20] E. Q. Gao, D. Z. Liao, Z. H. Jiang, S. P. Yan, *Polyhedron* **2001**, *20*, 923−927.
[21] E. Q. Gao, J. K. Tang, D. Z. Liao, Z. H. Jiang, S. P. Yan, G. L. Wang, *Helv. Chim. Acta* **2001**, *84*, 908−917.
[22] E. Q. Gao, G.-M. Yang, J. K. Tang, D. Z. Liao, Z. H. Jiang, S. P. Yan, *Polyhedron* **1999**, *18*, 3643−3646.
[23] J. K. Tang, L.-Y. Wang, L. Zhang, E.-Q. Gao, D. Z. Liao, Z. H. Jiang, S. P. Yan, P. Cheng, *Dalton Trans.* **2002**, 1607−1612.
[24] J. K. Tang, Q. L. Wang, E. Q. Gao, J. J. Chen, D. Z. Liao, Z. H. Jiang, S. P. Yan, P. Cheng, *Helv. Chim. Acta* **2002**, *85*, 175−182.
[25] E. Q. Gao, W. M. Bu, G. M. Yang, D. Z. Liao, Z. H. Jiang, S. P. Yan, G. L. Wang, *J. Chem. Soc., Dalton Trans.* **2000**, 1431−1436.
[26] E. A. Vinogradova, O. Y. Vassilyeva, V. N. Kokozay, B.W. Skelton, J. K. Bjernemosee, P. R. Raithby, *Dalton Trans.* **2002**, 4248−4252.
[27] M. Murugesu, R. Clerac, B. Pilawa, A. Mandel, C. E. Anson, A. K. Powell, *Inorg. Chim. Acta* **2002**, *337*, 328−336.
[28] L. H. Yin, W. H. Gu, P. Cheng, L. Z. Zhang, Z. Liao, J. Li, X. L. Yang, X. Q. Fu, S. P. Yan, *Eur. J. Inorg. Chem.* **2002**, *8*, 1937−1940.
[29] E. Colacio, C. Lopez-Magana, V. McKee, A. Romerosa, *J. Chem. Soc., Dalton Trans.* **1999**, 2923−2926.
[30] D. J. Brauer, G. Hessler, P. C. Knuppel, O. Stelzer, *Inorg. Chem.* **1990**, *29*, 2370−2375.
[31] D. Coucouvanis, S. Kanodia, D. Swenson, S.-J. Chen, T. Stüdemann, N. C. Baeziger, R. Pedelty, M. Chu, *J. Am. Chem. Soc.* **1993**, *115*, 11271−11278.
[32] J. Dai, M. Munakata, Y. Ohno, G.-Q. Bian, Y. Suenaga, *Inorg. Chim. Acta* **1999**, *285*, 332−335.
[33] [33a] M. Julve, M. Verdaguer, O. Kahn, A. Gleizes, M. Philochelevisalles, *Inorg. Chem.* **1983**, *22*, 368−370. [33b] O. Kahn, *Molecular Magnetism,* VCH, New York, **1993**.
[34] E. Q. Gao, H. Y. Sun, D. Z. Liao, Z.H. Jiang, S. P. Yan, *Polyhedron* **2002**, *21*, 359−364.
[35] M. M. Miao, D. Z. Liao, Z. H. Jiang, S. P. Yan, G. L. Wang, *Polyhedron* **1995**, *14*, 1577−1580.
[36] S.W. Bi, C. B. Liu, H. Q. Hu, *J. Phys. Chem. B* **2002**, *106*, 10786−10792.
[37] D. Z. Liao, Q. H. Zhao, Z. Y. Zhang, G. L. Wang, *Trans. Met. Chem.* **1991**, *16*, 209−211.
[38] O. Kahn, *Angew. Chem. Int. Ed. Engl.* **1985**, 24, 834−850.
[39] L. I. Smith, J. W. Opie, *Organic Syntheses*; Wiley: New York, **1995**: Collect. Vol. 3. P. 56.
[40] G. M.Sheldrick, *SHELXS*-97 and *SHELXL*-97, *Software for Crystal Structure Analysis*, Siemens Analytical X-ray Instruments Inc., Madison, WI, USA, **1997**.

Received March 29, 2004
Early View Article
Published Online November 4, 2004

 © 2004 Wiley-VCH Verlag GmbH & Co. KGaA, Weinheim

Incorporation of a (Cyclopentadienyl)molybdenum Oxo Complex in MCM-41 and Its Use as a Catalyst for Olefin Epoxidation

Marta Abrantes,[a] Sandra Gago,[b] Anabela A. Valente,[b] Martyn Pillinger,[b] Isabel S. Gonçalves,*[b] Teresa M. Santos,[b] João Rocha,[b] and Carlos C. Romão*[a]

Keywords: Molybdenum / Sandwich complexes / Mesoporous materials / Supported catalysts / Epoxidation

The tricarbonyl complex [(η^5-C_5H_4-COOMe)$Mo(CO)_3Cl$]-was prepared from the reaction of sodium (methoxycarbonyl)-cyclopentadienide, (C_5H_4-CO_2Me)Na, with (Bu_4N)[Mo-$(CO)_5I$]. Heating the ester with 3-(triethoxysilyl)propylamine gave the amide derivative {[η^5-C_5H_4-CONH-$C_3H_6Si(OEt)_3$]-$Mo(CO)_3Cl$}. The functionalised tricarbonyl complex was immobilised in the ordered mesoporous silica MCM-41 with a loading of 13 wt.-% Mo (1.4 mmol·g^{-1}) by carrying out a grafting reaction in dichloromethane. Powder X-ray diffraction and nitrogen adsorption–desorption analysis indicated that the structural integrity of the support was preserved during the grafting and that the channels remained accessible, despite significant reductions in surface area, pore volume and pore size. The success of the coupling reaction was confirmed by ^{29}Si and ^{13}C (CP) MAS NMR spectroscopy. A supported dioxo complex of the type [(η^5-C_5H_4R)MoO_2Cl] was subsequently prepared by oxidative decarbonylation of the tethered tricarbonyl complex using *tert*-butyl hydroperoxide (TBHP). The oxidised material is an active catalyst for the liquid phase epoxidation of cyclooctene with TBHP as the oxygen source. Similar catalytic results were obtained using the tethered tricarbonyl complex directly as a pre-catalyst since fast oxidative decarbonylation occurs under the reaction conditions used. For both systems, the desired epoxide was the only product and the initial activities were about 13 mol·mol^{-1}_{Mo}·h^{-1}. The solid catalysts were recycled several times. Some activity was lost between the first and second runs but thereafter tended to stabilise.
(© Wiley-VCH Verlag GmbH & Co. KGaA, 69451 Weinheim, Germany, 2004)

Introduction

Molybdenum(VI) complexes are versatile catalysts for the oxidation of organic compounds.[1] The most significant reaction in industry is the epoxidation of propylene to propylene oxide by alkyl hydroperoxides, catalysed with high activity and selectivity by soluble Mo^{VI} compounds.[2] In recent years, complexes of the type [$MoO(O_2)_2(L_1)(L_2)$] and [$MoO_2X_2(L_1)(L_2)$] (X = Cl, Br, CH_3) with different combinations of base ligands L_1 and L_2 have been extensively investigated as catalysts for epoxidation reactions, usually employing *tert*-butyl hydroperoxide (TBHP) as the monooxygen source.[3,4] In contrast, cyclopentadienyl oxo complexes of the type [(η^5-C_5R_5)MoO_2Cl], which are isoelectronic with the [$MoO_2X_2(L_1)(L_2)$] complexes, have been less well studied, even though it was reported in 1991 that the pentamethylcyclopentadienyl complex [Cp*MoO_2Cl] is able to catalyse the olefin epoxidation reaction with TBHP.[5] The lack of a convenient synthesis of [(η^5-C_5R_5)MoO_2X] complexes is one reason why their catalytic potential has not been studied in more detail. However, some of us recently reported a simple entry to (η^5-C_5R_5)chlorodioxomolybdenum(VI) complexes (R = H, CH_3, CH_2Ph) based on the oxidative decarbonylation of the readily available [(η^5-C_5R_5)$Mo(CO)_3Cl$] precursors with TBHP.[6] It was found that the dioxomolybdenum(VI) complexes catalyse the epoxidation of cyclooctene, styrene and 1-octene with TBHP as the oxidising agent. Turnover frequencies (TOF) of up to 21000 mol·mol^{-1}_{Mo}·h^{-1} were found and these even surpass that of the well-known CH_3ReO_3/H_2O_2 system. Preliminary results also indicated that the parent tricarbonyl complexes can be applied directly as catalyst precursors in the olefin epoxidation, without isolation of the dioxo complexes prior to use.

Despite the good results obtained for oxomolybdenum(VI) complexes in homogeneous catalysis, increasing attention is being focussed on studying and developing heterogeneous catalysts since these can be easily separated from a reaction mixture and recycled and this is of significant industrial interest.[7] One approach is to link metal complexes to inorganic oxides by way of Lewis base ligands functionalised with alkylalkoxysilanes. For example, Thiel and co-workers prepared covalently anchored complexes of the type [$MoO(O_2)_2$(L−L)] using the mesoporous silica

[a] Instituto de Tecnologia Química e Biológica da Universidade Nova de Lisboa,
Quinta do Marquês, EAN, Apt. 127, 2781-901 Oeiras, Portugal
Fax: (internat.) + 351-21-4411277,
E-mail: ccr@itqb.unl.pt
[b] Department of Chemistry, CICECO, University of Aveiro, 3810−193 Aveiro, Portugal
Fax: (internat.) + 351-234-370084,
E-mail: igoncalves@dq.ua.pt

 © 2004 Wiley-VCH Verlag GmbH & Co. KGaA, Weinheim **DOI: 10.1002/ejic.200400386**

MCM-41 derivatised with a bidentate pyrazolylpyridine ligand.[8] The hybrid system was highly active and truly heterogeneous for the liquid-phase epoxidation of cyclooctene with TBHP as the oxygen source. Molybdenum(VI) complexes of the type $[MoO_2Cl_2(L_1)(L_2)]$ have also been immobilised in MCM-41 derivatised with monodentate nitrile and bidentate bipyridyl ligands.[9] Unfortunately, these catalysts proved to be unstable towards molybdenum leaching which accounted for nearly complete loss of activity in a second reaction cycle. Better results were obtained using 1,4-diazabutadiene ligands covalently linked to the support, although significant catalytic activity was still lost between the first and second runs.[10] In order to obtain more stable catalysts, it would be preferable if the oxomolybdenum fragment was covalently linked to the support, rather than relying on an interaction between the metal centre and a Lewis base ligand. In the present work we set out to prepare an immobilised $[(\eta^5\text{-}C_5R_5)MoO_2Cl]$ complex by oxidative decarbonylation of a monosubstituted $[(\eta^5\text{-}C_5H_4R)Mo(CO)_3Cl]$ precursor covalently anchored to MCM-41. The resultant material has been examined as a catalyst for the epoxidation of olefins using TBHP.

Results and Discussion

Synthesis and Characterisation

The tricarbonyl complex $[(\eta^5\text{-}C_5H_4\text{-}COOMe)Mo(CO)_3Cl]$ (**2**) was prepared from the reaction of sodium (methoxycarbonyl)cylopentadienide, $(C_5H_4\text{-}COOMe)Na$, with $(Bu_4N)[Mo(CO)_5I]$ in THF at reflux. Compound **2** is air sensitive and very insoluble in noncoordinating solvents. As expected, the IR spectrum (KBr) of **2** showed three strong terminal carbonyl absorptions (at 2056, 1990 and 1973 cm^{-1}) and a strong organic carbonyl absorption at 1725 cm^{-1}. For comparison, $[CpMo(CO)_3Cl]$ (**1**) in CCl_4 exhibits three ν_{CO} bands at 2056, 1986 and 1962 cm^{-1}.[11] The ^1H NMR spectrum of **2** contains a pair of pseudo triplets (A_2B_2 pattern) at $\delta = 5.72$ and 6.03 ppm for the cyclopentadienyl protons $H^{3,4}$ and $H^{2,5}$, respectively. A singlet was also observed at $\delta = 3.83$ ppm for the methoxycarbonyl protons ($-OCH_3$). Heating the ester **2** with 3-(triethoxysilyl)propylamine at 120 °C for 3 hours gave the amide derivative $\{[\eta^5\text{-}C_5H_4\text{-}CONH\text{-}C_3H_6Si(OEt)_3]Mo(CO)_3Cl\}$ (**3**) as an oil which was dried under vacuum and used without further purification. A similar method was used by Jia et al. to functionalise a pyrazolylpyridine ligand with (triethoxysilyl)propyl groups.[8] The presence of the amide functional group in **3** was indicated by the IR spectrum which showed the absence of the peak at 1725 cm^{-1} from the starting material and new bands at 3298 (ν_{NH}), 1617 and 1577 cm^{-1} (NHCO). The last two frequencies are similar to those reported for $[(\eta^5\text{-}C_5H_4\text{-}CONH\text{-}R)W(CO)_3CH_3]$ (1641 and 1554 cm^{-1}) and $[(\eta^5\text{-}C_5H_4\text{-}CONH\text{-}R)W(CO)_3I]$ (1642 and 1556 cm^{-1}).[12] Further evidence for the success of the reaction was provided by the ^{13}C spectrum of **3** which contained a weak resonance at $\delta = 163.2$ ppm which was assigned to the carbon atoms of the CONH groups.

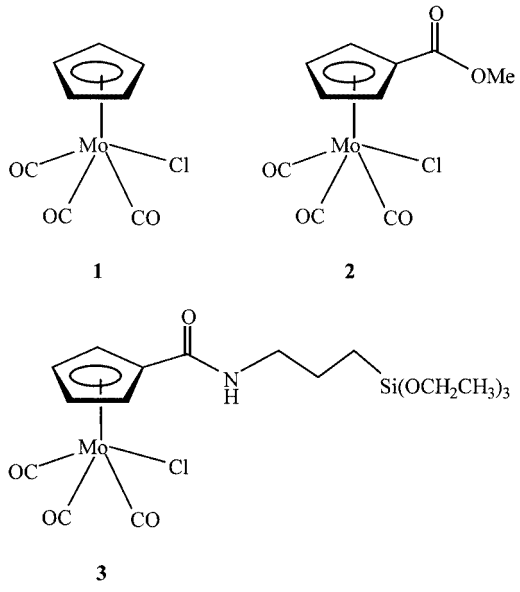

Treatment of calcined and dehydrated MCM-41 (MCM-41-1) with a solution of the triethoxysilane compound **3** in dichloromethane at reflux gave the modified material MCM-41-2 containing 13 wt.-% Mo ($1.4\ mmol \cdot g^{-1}$) (Scheme 1). If the surface area is taken as $500\ m^2 \cdot g^{-1}$ (see below), the metal content corresponds to a surface coverage

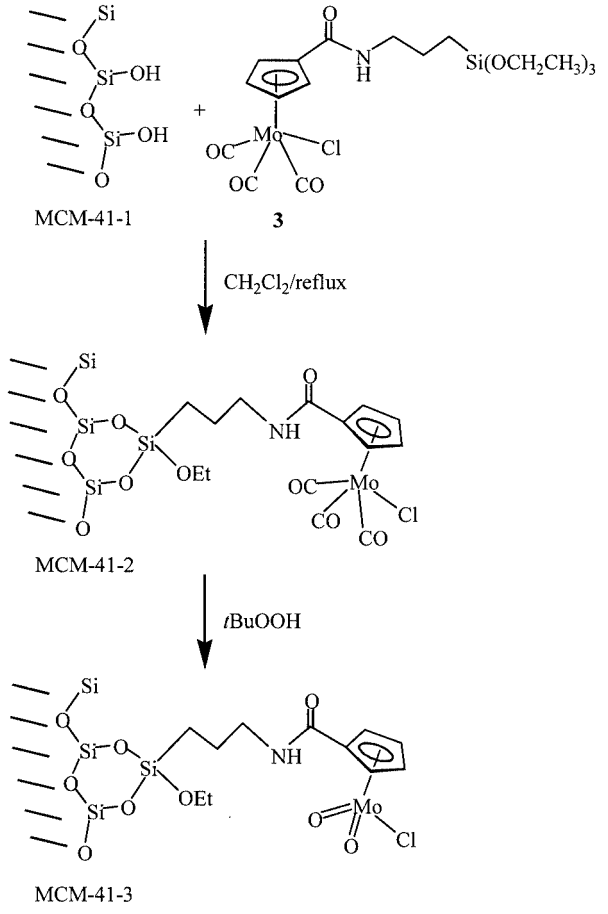

Scheme 1

 © 2004 Wiley-VCH Verlag GmbH & Co. KGaA, Weinheim

of about 1.7 Mo atom per nm^2. This value is similar to experimentally determined values for the concentration of free silanol groups on the surface of pristine MCM-41.[13] Direct evidence for the incorporation of the covalently linked organic system in MCM-41-2 was obtained by recording ^{29}Si MAS NMR spectra (Figure 1). The ^{29}Si MAS NMR spectrum of the parent support MCM-41-1 exhibits two broad resonances at $\delta = -109.9$ and -102.4 ppm, assigned to the species Q^4 and Q^3 of the silica framework, respectively, [$Q^n = Si(OSi)_n(OH)_{4-n}$]. The ^{29}Si CP MAS NMR spectrum shows a marked increase in the relative intensity of the Q^3 peak, confirming that these silicon centres are attached to hydroxy groups. A weak resonance is also present at about -91 ppm corresponding to the Q^2 species. For the grafted material MCM-41-2, both the ^{29}Si MAS and CP MAS NMR spectra clearly show the diminished relative intensity of the Q^2 and Q^3 peaks, indicating the esterification of the isolated silanol groups (single and geminal) by nucleophilic substitution at the silicon atom in the organic ligand. Three additional signals can be observed in the CP MAS spectrum at $\delta = -46.7$, -53.1 and -60.3 ppm, and can be assigned to the T^1, T^2 and T^3 organosilica species, respectively, [$T^m = RSi(OSi)_m(OEt)_{3-m}$]. The presence of residual OEt groups in MCM-41-2 was confirmed by the ^{13}C CP MAS NMR spectrum which contains peaks at $\delta = 23.0$ and 17.6 ppm. Additional peaks were readily assigned to the carbon atoms of the propyl, cyclopentadienyl and CO groups (see Exp. Sect.).

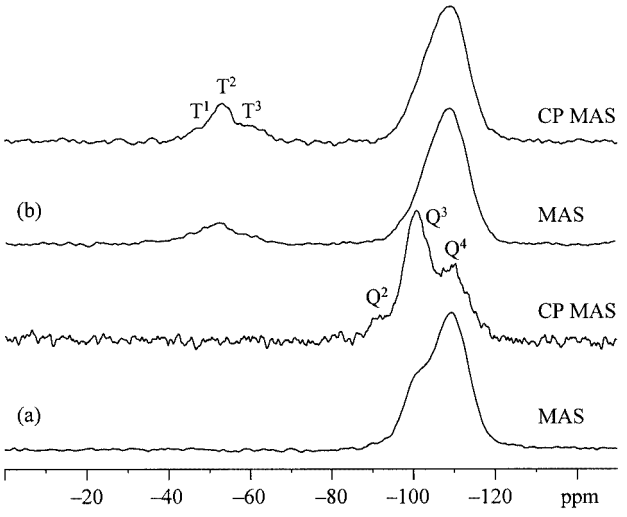

Figure 1. ^{29}Si MAS and CP MAS NMR spectra of (a) MCM-41-1 and (b) MCM-41-Si(OEt)$_n$C$_3$H$_6$NHCOCpMo(CO)$_3$Cl (MCM-41-2)

The powder X-ray diffraction (XRD) pattern of the unmodified MCM-41 sample (MCM-41-1) is typical of a well-ordered mesoporous phase (Figure 2). Several distinct Bragg peaks are present in the range $2\theta = 2-8°$ which can be indexed to different *hkl* reflections for a hexagonal unit cell (using the strongest reflection, d_{100}, $a = 2d_{100}/\sqrt{3} = 41.0$ Å). Upon grafting with **3**, several peaks were still observed indicating retention of the long-range hexagonal symmetry. The significant attenuation of the XRD peak intensities was not interpreted as a loss of crystallinity. Instead, it is likely that there is a reduction in the X-ray scattering contrast between the silica framework and the metal-organic moieties which are located inside the channels of the host.[8b,9b,10a,14] Figure 3 shows the N_2 isotherms of the MCM materials. Unmodified MCM-41 exhibits a reversible type IV adsorption–desorption isotherm, characteristic of a mesoporous solid (pore width between 2 and 50 nm, according to the IUPAC).[15] The values of S_{BET} and V_p are listed in Table 1. A sharp step in the capillary condensation in the primary mesopores can be observed at a relative

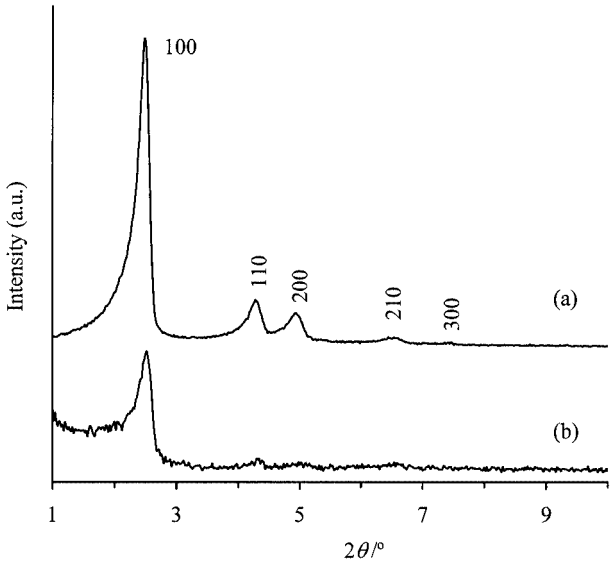

Figure 2. Powder XRD patterns of (a) MCM-41-1 and (b) MCM-41-Si(OEt)$_n$C$_3$H$_6$NHCOCpMo(CO)$_3$Cl (MCM-41-2). The relative intensities for MCM-41-2 have been multiplied by five with respect to those for MCM-41-1

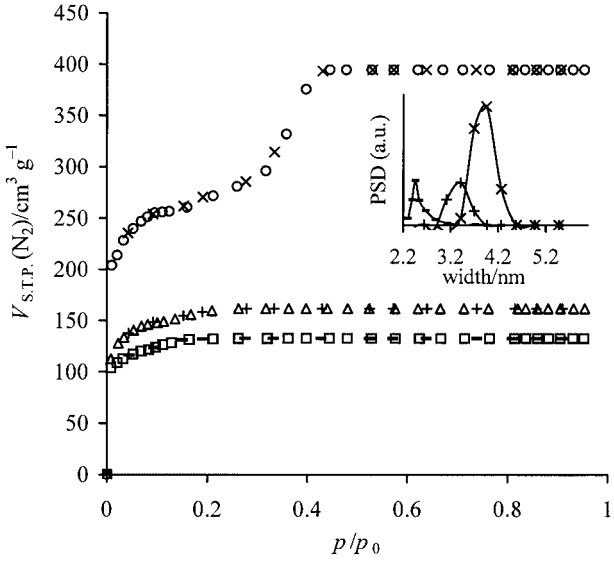

Figure 3. N_2 adsorption (circles: MCM-41-1; squares: MCM-41-2; triangles: MCM-41-3) and desorption (×: MCM-41-1; –: MCM-41-2; +: MCM-41-3) isotherms at 77 K and pore size distribution profiles (inset) of MCM-41-1 (×), MCM-41-2 (–) and MCM-41-3 (+)

 © 2004 Wiley-VCH Verlag GmbH & Co. KGaA, Weinheim

pressure of ca. 0.3, indicating a narrow pore size distribution. The adsorption isotherm is flat in the high-pressure region ($p/p_0 > 0.6$) which shows that the material has a low external surface area and insignificant secondary mesoporosity. After modification in the preparation of MCM-41-2, S_{BET} and V_p decreased significantly, suggesting that grafting of the bulky complex on the internal silica surface was accomplished (Figure 3, Table 1). This conclusion is also supported by the decrease in the p/p_0 coordinates of the inflection points of the isotherms upon the post-synthesis treatment.[16] The capillary condensation step becomes less pronounced, suggesting that the pore size distribution of the MCM-41 support was partly affected by the modification. The maximum of the PSD curve for MCM-41 determined by the BJH method, d_{BJH}, decreased by 36% after the tethering procedure.

Table 1. Texture parameters of MCM-41 samples from N_2 isotherms at 77 K

Sample	S_{BET} [$m^2 \cdot g^{-1}$]	ΔS_{BET}[a] (%)	V_P [$cm^3 \cdot g^{-1}$]	ΔV_P[b] (%)	d_{BJH} [nm]
MCM-41-1	1010	–	0.61	–	3.9
MCM-41-2	493	−51	0.21	−66	2.5
MCM-41-3	581	−42	0.25	−59	3.4

[a] Variation of surface area in relation to parent MCM-41-1. [b] Variation of total pore volume in relation to parent MCM-41-1.

Oxidative decarbonylation of the supported metal complex in MCM-41-2 was carried out by treatment of the material with an excess of TBHP (Scheme 1). During the reaction, the material changed colour from brown to pale yellowish-brown. The product, designated as MCM-41-3, was isolated by filtration and the excess TBHP removed by washing with dichloromethane. The presence of an MoO_2 unit in MCM-41-3 was indicated by the IR spectrum which showed two bands for the symmetric (943 cm^{-1}) and asymmetric (911 cm^{-1}) Mo=O stretching vibrations. For comparison, the corresponding stretching frequencies for the complexes (η^5-C_5R_5)chlorodioxomolybdenum(VI) (R = H, CH_3, CH_2Ph) are located at ca. 920/890 cm^{-1} (ν_{sym}/ν_{asym}).[6] In the Raman spectrum of MCM-41-3, bands were observed at 358 and 266 cm^{-1} which can be attributed to symmetric Mo−Cp stretching and MoO_2 wagging modes, respectively (cf. 328 and 261 cm^{-1} for [$CpMoO_2Cl$][6]). The reaction of MCM-41-2 with TBHP was accompanied by some metal leaching, as evidenced by a decrease in the molybdenum content from 13 to 9 wt.-% and a slight increase in the values of S_{BET} and V_p (Figure 3, Table 1).

Catalytic Olefin Epoxidation

The modified materials MCM-41-2 and MCM-41-3 were tested as catalysts or catalyst precursors for the liquid phase epoxidation of cyclooctene with TBHP at 55 °C (Figure 4, Table 2). For comparison, the tricarbonyl complexes **1**−**3** were also tested as homogeneous pre-catalysts for the same reaction. Cyclooctene conversion in the absence of a catalyst or in the presence of the parent MCM-41 sample was negligible after 6 h and the catalytic activity exhibited by the modified mesoporous materials and the tricarbonyl complexes can therefore be attributed to active species containing molybdenum. For all systems, cyclooctene oxide was the only observed reaction product. The kinetic profiles for MCM-41-2 and MCM-41-3 were quite similar (Figure 4). Initially, the reaction is fast but it then slows down somewhat and conversion after 24 hours is far from quantitative (< 63%). Similar kinetic profiles have been reported for complexes belonging to the [$MoO_2X_2(L_1)(L_2)$] family, in which case an auto retardation effect can be observed due to the formation of *tert*-butyl alcohol, a competitive inhibitor for the attack of TBHP at the molybdenum centre.[4e] The initial activity of epoxidation using MCM-41-2, expressed as initial rate per unit weight of solid, is higher than that for MCM-41-3 (Table 2, values in brackets). However, when the initial activities are expressed as initial rate per mol of MCM-41-supported Mo species, the values are practically the same for both samples since MCM-41-2 (13 wt.-% Mo) possesses a higher Mo loading than MCM-41-3 (9 wt.-% Mo). This suggests that the in-situ oxidative decarbonylation of MCM-41-2 by TBHP is fast and probably gives rise to the same type of active metal species present in MCM-41-3 under the catalytic conditions.

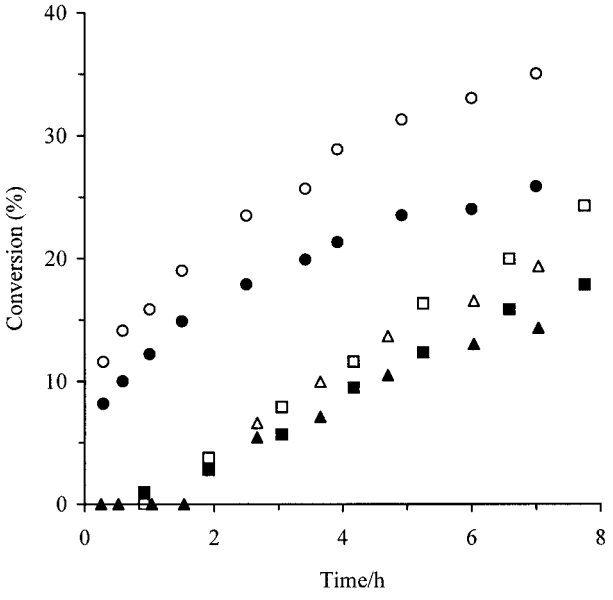

Figure 4. Conversion profiles for the epoxidation of cyclooctene with TBHP at 55 °C using MCM-41-2 (open symbols) or MCM-41-3 (solid symbols): run 1 (circles); run 2 (squares); run 3 (triangles)

The kinetic profile for the homogeneous reaction using the pre-catalyst **3** was similar to that observed using the modified MCM materials (Figure 5). In fact, the initial activities are almost identical (12−13 $mol \cdot mol_{Mo}^{-1} \cdot h^{-1}$). Considerably higher activities were obtained using the tricarbonyl complexes **1** and **2** as precatalysts, particularly in the

 © 2004 Wiley-VCH Verlag GmbH & Co. KGaA, Weinheim

Table 2. Catalytic epoxidation of cyclooctene with TBHP at 55 °C using homogeneous (**1**−**3**) and heterogenised (MCM-41-2, MCM-41-3) molybdenum catalysts

Catalyst	Initial activity [mol·mol$_{Mo}^{-1}$·h^{-1}][a]	Conversion[b] (%)
1	140	100
2	40	100
3	13	82
MCM-41-2 (run, 1)	12 (17)[c]	63
MCM-41-2 (run, 2)	−[d]	57
MCM-41-2 (run, 3)	−[d]	51
MCM-41-3 (run, 1)	13 (12)[c]	52
MCM-41-3 (run, 2)	−[d]	46
MCM-41-3 (run, 3)	−[d]	39

[a] Turnover frequency calculated at ca. 18 min. [b] Cyclooctene conversion after 24 h. [c] The values in parentheses are the initial activities expressed per unit weight of catalyst (mmol g_{cat}^{-1}·h^{-1}). [d] An induction period was observed.

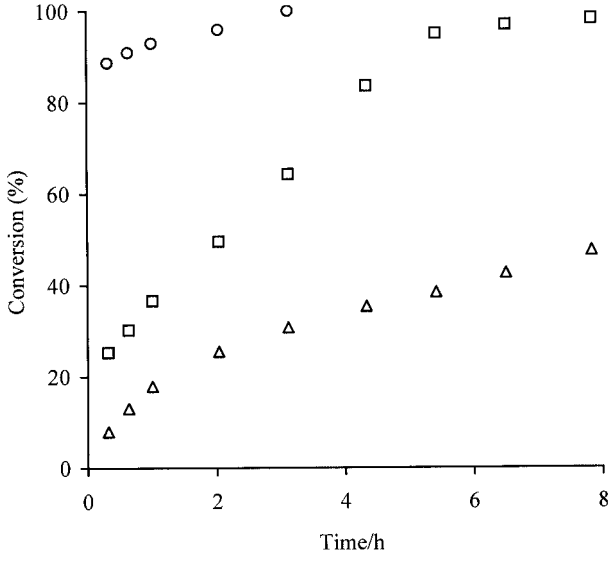

Figure 5. Conversion profiles for the epoxidation of cyclooctene with TBHP at 55 °C using complexes **1** (circles), **2** (squares) and **3** (triangles)

case of the unsubstituted cyclopentadienyl complex (turnover frequency = 140 mol·mol$_{Mo}^{-1}$·h^{-1}). No induction periods were observed using the tricarbonyl complexes **1**−**3** directly, suggesting that the conversion into the corresponding dioxo complexes is quite fast under the applied reaction conditions. Previous studies have shown that the epoxidation of cyclooctene in a homogeneous phase proceeds at practically the same rate in the presence of $CpMo(CO)_3Cl$ or the corresponding $CpMoO_2Cl$ complex and that catalyst/cyclooctene molar ratios as small as 1:10000 give turnover frequencies as high as 21000 mol·mol$_{Mo}^{-1}$·h^{-1} {for [(η^5-C_5Bz_5)MoO_2Cl]}.[6] In the presence of complex **3**, the epoxidation reaction is much slower probably due to the pendant triethoxysilyl groups which may lead to the formation of less reactive dimers/oligomers.

The stabilities of the modified materials MCM-41-2 and MCM-41-3 were studied by recycling the recovered solids twice. Before each reuse, the solid was separated from the reaction solution, thoroughly washed with dichloromethane and dried at room temperature. Some loss of catalytic activity was observed for both samples from the first to the second run but afterwards the activity tended to remain constant (Table 2, Figure 4). After the first run the catalytic results obtained with the two materials were quite similar, suggesting that the materials become much alike after the first run. As mentioned above, the synthesis of MCM-41-3 by treatment of MCM-41-2 with excess TBHP was accompanied by some metal leaching. Hence, one would expect the same to occur when using MCM-41-2 directly under the oxidising catalytic conditions. Indeed, the molybdenum loading after the first run was ca. 83% of the original value which may partly explain the observed catalyst deactivation. In the case of MCM-41-3, no measurable metal leaching occurred during the first run but a significant decrease in activity was nevertheless observed. Both catalyst systems exhibit induction periods of nearly 90 min for the second and third runs, leading to TOFs (calculated for ca. 2.5 h of the third reaction cycle) of 2.5 and 2.0 mol·mol$_{Mo}^{-1}$·h^{-1} for MCM-41-2 and MCM-41-3, respectively. According to studies by Trost and Bergman,[5] the (pentamethyl)cyclopentadienyl analogue [Cp*MoO_2Cl] can react with TBHP to give the peroxo complex [Cp*$MoO(O_2)Cl$] which is inactive as a catalyst for olefin epoxidation.[5] We suspect, therefore, that another reason for the loss of activity between the first and second runs for the systems initially containing MCM-41-2 and MCM-41-3 is because of the formation of supported peroxo complexes. Leaching tests were performed for MCM-41-3 by removing the catalyst from the reaction mixture by hot filtration after 20 minutes. The filtrate was then allowed to react for a further 340 minutes. The conversion of cyclooctene increased by 7%, whereas with the catalyst it increased by 21%. These results suggest that epoxidation in the presence of MCM-41-3 (for the first run) is, to a certain extent, homogeneously catalysed by leached molybdenum species. However, since a sintered glass filter was used it is possible that small catalyst particles were not completely separated by this porous media and that MCM-41-3 is a truly heterogeneous catalyst.[17]

The modified materials MCM-41-2 and MCM-41-3 were tested for the epoxidation of other olefins, namely cyclododecene, *trans*-2-octene and 1-octene. Olefin conversion after 24 hours decreases in the following order for both materials: cyclooctene > cyclododecene > *trans*-2-octene > 1-octene (Figure 6). In the case of *trans*-2-octene the corresponding epoxide is the only product at less than 10% conversion. When the substrate is 1-octene, an unsubstituted and much less reactive olefin, conversion is negligible (< 1%). In the case of cyclododecene, a more bulky substrate, the reaction proceeds to 34−38% conversion after 24 h and the epoxide is the main product, while the corresponding diol is a secondary reaction product obtained in less than 5% yield.

 © 2004 Wiley-VCH Verlag GmbH & Co. KGaA, Weinheim

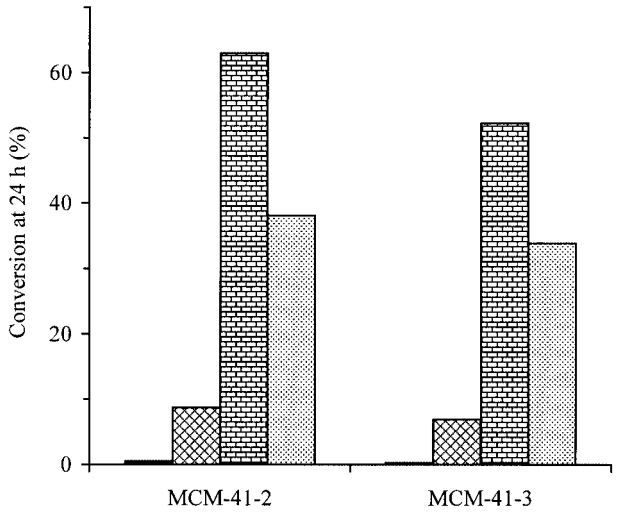

Figure 6. Olefin conversion after 24 h with TBHP at 55 °C using MCM-41-2 or MCM-41-3: 1-octene (solid); *trans*-2-octene (diamonds); cyclooctene (bricks); cyclododecene (dots)

Conclusions

A method has been presented for the immobilisation of a monosubstituted cyclopentadienyltricarbonylchloro molybdenum complex in mesoporous silica. The material can be used as a pre-catalyst for the reaction of *tert*-butyl hydroperoxide and cyclooctene to yield the corresponding epoxide. Upon recycling, some activity is lost between the first and second runs but thereafter it tends to remain constant. According to the leaching test carried out for MCM-41-3, it is possible that epoxidation (in the first run) also occurs in a homogeneous phase. Although the selectivity to the epoxide is very high, the activities are moderate paralleling that observed for the precursor complex (containing the triethoxysilyl group) in a homogeneous phase. We have also noted in this work that the methoxycarbonyl-substituted complex [(η^5-C_5H_4-COOMe)$Mo(CO)_3Cl$] can be used as a pre-catalyst for the olefin epoxidation reaction but the observed activity is much lower than that obtained when the unsubstituted [$CpMo(CO)_3Cl$] is used. These results indicate that a more effectively supported catalyst might be possible by preparing a precursor complex of the type [(η^5-C_5R_5)$Mo(CO)_3X$] where the ligand X terminates in a trialkoxylsilyl group.

Experimental Section

Materials and Methods: All preparations and manipulations were performed using standard Schlenk techniques under oxygen-free and water-free nitrogen. Solvents were dried by standard procedures (THF, *n*-hexane and Et_2O over Na/benzophenone ketyl; CH_2Cl_2 and NCMe over CaH_2), distilled under nitrogen and used immediately (THF) or kept over 4-Å molecular sieves (3-Å for NCMe). Microanalyses for C, H, N were performed at the ITQB (C. Almeida) and Mo was determined by ICP-AES at the Central Laboratory for Analysis, University of Aveiro (E. Soares). Room-temperature powder XRD data were collected with a Philips X'pert diffractometer with a curved graphite monochromator (Cu-K_α radiation) in a Bragg−Brentano para-focusing optics configuration. Samples were step-scanned in 0.02 °2θ steps with a counting time of 2 s per step. The values of the BET specific surface area (S_{BET}, determined in the p/p_0 range 0.03−0.13) and specific total pore volume, V_p, were estimated from N_2 adsorption isotherms measured at 77 K, as described previously.[18] The pore size distributions (PSD) were calculated by the BJH method using the modified Kelvin equation with a correction for the statistical film thickness on the pore walls.[19] The statistical film thickness was calculated using the Harkins-Jura equation in the p/p_0 range 0.1−0.95. IR spectra were measured with a Mattson 7000 FT-IR spectrometer using KBr pellets. Raman spectra were recorded with a Bruker RFS100/S FT instrument (Nd:YAG laser, 1064 nm excitation, InGaAs detector). NMR spectra in solution were recorded with Bruker CXP-300 (^1H) and Bruker AMX-300 (^{13}C) spectrometers. Room temperature ^{29}Si and ^{13}C solid state NMR spectra were recorded at 79.49 and 100.62 MHz, respectively, with a Bruker Avance 400P spectrometer. ^{29}Si MAS NMR spectra were recorded with 40° pulses, spinning rates of 5.0−5.5 kHz and 60 s recycle delays. ^{29}Si CP MAS NMR spectra were recorded with 5.5 μs ^1H 90° pulses, 8 ms contact time, a spinning rate of 5 kHz and 4 s recycle delays. ^{13}C CP MAS NMR spectra were acquired with a 3.5 μs 90° proton pulse and 2 ms contact time with spinning rates of 7−8.5 kHz and 4 s recycle delays. ^{13}C spectra were also recorded in the solid state at 125.76 MHz with a Bruker Avance 500 spectrometer. Chemical shifts are quoted in ppm relative to TMS.

The liquid-phase oxidation of a variety of olefins was carried out at 55 °C under air (atmospheric pressure) in a micro reaction vessel equipped with a magnetic stirrer which was loaded with complex (0.036 mmol) or MCM-catalyst (43.8 mg), olefin (1.8 mmol) and TBHP (2.8 mmol, 5.5 M in decane). Samples were withdrawn periodically and analysed using a gas chromatograph (Varian 3800) equipped with a capillary column (SPB-5, 20 m × 0.25 mm × 0.25 μm) and a flame ionization detector. Undecane was used as an internal standard added after the reaction.

Published procedures were used to prepare the compounds (C_5H_4-COOMe)Na,[20] (Bu_4N)[$Mo(CO)_5I$][21] and [$CpMo(CO)_3Cl$] (**1**).[6] Pure siliceous MCM-41 (MCM-41-1) was synthesised hydrothermally at 100 °C under basic conditions using [($C_{14}H_{29}$)NMe_3]Br as the templating agent and sodium silicate solution as the silica source.[9b] The calcined product (540 °C/6 h) was dehydrated prior to use by heating at 180 °C for 2 h under vacuum.

[(η^5-C_5H_4-COOMe)$Mo(CO)_3Cl$] (2): A solution of (Bu_4N)[$Mo(CO)_5I$] (0.96 g, 1.60 mmol) in THF (20 mL) was mixed with a solution of (C_5H_4-COOMe)Na (0.28 g, 1.9 mmol) in THF (20 mL) and heated to reflux overnight (18 h). The THF was removed from the resultant yellow-brown solution affording an oily residue. Diethyl ether (20 mL), distilled water (20 mL) and acetic acid (0.1 mL) were then added and, after stirring for 20 min, CCl_4 (5 mL) was added and the colour of the emulsion turned red. The mixture was stirred for a further 20 min. The ether phase was then separated and the remaining aqueous phase extracted five times with 20 mL aliquots of diethyl ether. After evaporation of the solvent from the combined ether extracts a red residue was obtained. This was redissolved in acetone (20 mL) and activated charcoal and anhydrous Na_2SO_4 were added. After stirring for 30 min the mixture was filtered. Evaporation of the red filtrate gave an orange solid which was thoroughly washed with water and cold hexane. Yield: 0.22 g, 41%. Selected IR (KBr): $\tilde{\nu}$ = 3114 (m), 2958 (m), 2056 (vs, ν_{CO}), 1990 (vs, ν_{CO}), 1973 (vs, ν_{CO}), 1725 (s, ν_{CO}), 1476 (m), 1434 (m), 1372 (m), 1283 (s), 1194 (m), 1144 (s), 961 (m), 772 (m), 557 (m), 525 (m), 469 (m) cm^{-1}. ^1H NMR (300 MHz, $CDCl_3$, 25 °C, TMS):

 © 2004 Wiley-VCH Verlag GmbH & Co. KGaA, Weinheim

δ = 3.83 (s, 3 H, $-OCH_3$), 5.72 (t, 2 H, $H^{3,4}$), 6.03 (t, 2 H, $H^{2,5}$) ppm. $C_{10}H_7ClMoO_5$ (338.56): calcd. C 35.48, H 2.08; found C 35.53, H 2.22.

{[η^5-C_5H_4-CONH-$C_3H_6Si(OEt)_3$]Mo(CO)$_3$Cl} (3): One equivalent of 3-triethoxysilylpropylamine was added to [(η^5-C_5H_4-COOMe)-Mo(CO)$_3$Cl] (**2**) (2.27 g, 6.7 mmol) and the mixture stirred at 120 °C for 3 h. After this, low boiling volatiles were removed in vacuo at 50 °C. The resultant brown oil was used without further purification. Selected IR (neat): $\tilde{\nu}$ = 3298 (sh, ν_{NH}), 3108 (w), 2975 (m), 2928 (m), 2886 (m), 2044 (vs, ν_{CO}), 1965 (vs, ν_{CO}), 1926 (vs), 1617 (m, CONH), 1577 (m, CONH), 1470 (m), 1443 (m), 1390 (m), 1280 (m), 1237 (w), 1102 (s), 1077 (s), 958 (s), 786 (vs), 596 (m), 540 (m) cm^{-1}. ^{13}C NMR (75.5 MHz, $CDCl_3$, 25 °C, TMS): δ = 13.8 (C^9), 18.4 (C^{11}), 24.3 (C^8), 46.6 (C^7), 59.4 (C^{10}), 94.9 (C^{1-5}), 95.1, 97.3, 163.2 (C^6), 218 (CO) ppm.

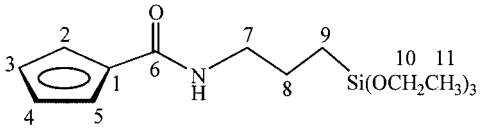

MCM-41-2: A solution of {[η^5-C_5H_4-CONH-$C_3H_6Si(OEt)_3$]Mo-(CO)$_3$Cl} (**3**) (5.0 mmol) in CH_2Cl_2 (10 mL) was added to a suspension of MCM-41-1 (2 g) in toluene (15 mL) and the mixture stirred under reflux for 44 h. The suspension was filtered and the brown powder washed several times with CH_2Cl_2, before drying under vacuum at 40 °C. Selected IR (KBr): $\tilde{\nu}$ = 3419 (br), 3246 (sh, ν_{NH}), 2982 (m), 2939 (sh), 1979 (w, ν_{CO}), 1624 (m, CONH), 1484 (m), 1444 (m), 1393 (m), 1237 (s), 1082 (vs), 954 (br), 797 (s), 564 (br), 454 (vs) cm^{-1}. ^{13}C CP MAS NMR: δ = 8.4 (C^9), 17.6 (C^{11}), 23.0 (C^8), 42.6 (C^7), 58.3 (C^{10}), 86.3 (br., C^{1-5}), 166.7 (C^6) ppm. Elemental analysis found C 16.63, H 3.23, N 1.97, Mo 13.0.

MCM-41-3: MCM-41-2 (0.3 g) was suspended in CH_2Cl_2 (10 mL). Under continuous magnetic stirring, *tert*-butyl hydroperoxide solution (4.1 mmol, 5.0−6.0 M in *n*-decane, 10 equiv.) was added dropwise and the mixture stirred at room temperature for 4 h. The resultant light brown powder was filtered, washed several times with CH_2Cl_2 and dried under vacuum at room temperature. Selected IR (KBr): $\tilde{\nu}$ = 3431 (br), 3262 (sh, ν_{NH}), 2982 (w), 2938 (sh), 1629 (m, CONH), 1508 (w), 1469 (w), 1445 (w), 1384 (w), 1364 (w), 1237 (vs), 1080 (vs), 943 (m, ν_{sym} Mo=O), 911 (m, ν_{asym} Mo=O), 799 (m), 739 (sh), 568 (w), 454 (vs) cm^{-1}. Selected Raman: 2962, 2932, 2895, 1590, 1455, 1321, 1045, 967, 942, 915, 358, 266 cm^{-1}. Elemental analysis found C 11.9, H 2.80, N 1.96, Mo 9.0.

Acknowledgments

The authors are grateful to FCT, POCTI and FEDER for financial support (including Project POCTI//QUI/37990/2001 and a Ph.D. grant to M. A.). S. G. thanks the University of Aveiro for a research grant. Paula Esculcas is acknowledged for assistance with the NMR experiments.

[1] [1a] K. A. Jörgensen, *Chem. Rev.* **1989**, *89*, 431−458. [1b] M. H. Dickman, M. T. Pope, *Chem. Rev.* **1994**, *94*, 569−584.
[2] [2a] J.-M. Brégeault, *Dalton Trans.* **2003**, 3289−3302. [2b] G. W. Parshall, S. D. Ittel, *Homogeneous Catalysis: The Applications and Chemistry of Catalysis by Soluble Transition Metal Complexes*, Wiley, New York, **1992**.
[3] [3a] W. R. Thiel, M. Angstl, T. Priermeier, *Chem. Ber.* **1994**, *127*, 2373−2379. [3b] W. R. Thiel, M. Angstl, N. Hansen, *J. Mol. Catal. A: Chem.* **1995**, *103*, 5−10. [3c] W. R. Thiel, T. Priermeier, *Angew. Chem. Int. Ed. Engl.* **1995**, *34*, 1737−1738. [3d] W. R. Thiel, J. Eppinger, *Chem. Eur. J.* **1997**, *3*, 696−705.
[4] [4a] F. E. Kühn, E. Herdtweck, J. J. Haider, W. A. Herrmann, I. S. Gonçalves, A. D. Lopes, C. C. Romão, *J. Organomet. Chem.* **1999**, *583*, 3−10. [4b] F. E. Kühn, A. D. Lopes, A. M. Santos, E. Herdtweck, J. J. Haider, C. C. Romão, A. G. Santos, *J. Mol. Catal. A: Chem.* **2000**, *151*, 147−160. [4c] F. E. Kühn, A. M. Santos, A. D. Lopes, I. S. Gonçalves, E. Herdtweck, C. C. Romão, *J. Mol. Catal. A: Chem.* **2000**, *164*, 25−38. [4d] F. E. Kühn, A. M. Santos, I. S. Gonçalves, C. C. Romão, A. D. Lopes, *Appl. Organomet. Chem.* **2001**, *15*, 43−50. [4e] F. E. Kühn, M. Groarke, É. Bencze, E. Herdtweck, A. Prazeres, A. M. Santos, M. J. Calhorda, C. C. Romão, I. S. Gonçalves, A. D. Lopes, M. Pillinger, *Chem. Eur. J.* **2002**, *8*, 2370−2383. [4f] R. Clarke, D. J. Cole-Hamilton, *J. Chem. Soc., Dalton Trans.* **1993**, 1913−1914. [4g] M. Miggins, U. K. Kakarla, D. A. Knight, J. C. Fettinger, *An. Quim. Int. Ed.* **1996**, *92*, 59−61. [4h] F. J. Arnaiz, R. Aguado, J. M. M. Ilarduya, *Polyhedron* **1994**, *13*, 3257−3259.
[5] M. K. Trost, R. G. Bergman, *Organometallics* **1991**, *10*, 1172−1178.
[6] M. Abrantes, A. M. Santos, J. Mink, F. E. Kühn, C. C. Romão, *Organometallics* **2003**, *22*, 2112−2118.
[7] [7a] R. A. Sheldon, I. W. C. E. Arends, H. E. B. Lempers, *Catal. Today* **1998**, *41*, 387−407. [7b] R. A. Sheldon, M. Wallau, I. W. C. E. Arends, U. Schuchardt, *Acc. Chem. Res.* **1998**, *31*, 485−493. [7c] D. C. Sherrington, *Catal. Today* **2000**, *57*, 87−104.
[8] [8a] M. Jia, W. R. Thiel, *Chem. Commun.* **2002**, 2392−2393. [8b] M. Jia, A. Seifert, W. R. Thiel, *Chem. Mater.* **2003**, *15*, 2174−2180.
[9] [9a] P. Ferreira, I. S. Gonçalves, F. E. Kühn, A. D. Lopes, M. A. Martins, M. Pillinger, A. Pina, J. Rocha, C. C. Romão, A. M. Santos, T. M. Santos, A. A. Valente, *Eur. J. Inorg. Chem.* **2000**, 2263−2270. [9b] C. D. Nunes, A. A. Valente, M. Pillinger, A. C. Fernandes, C. C. Romão, J. Rocha, I. S. Gonçalves, *J. Mater. Chem.* **2002**, *12*, 1735−1742.
[10] [10a] C. D. Nunes, M. Pillinger, A. A. Valente, J. Rocha, A. D. Lopes, I. S. Gonçalves, *Eur. J. Inorg. Chem.* **2003**, 3870−3877. [10b] C. D. Nunes, M. Pillinger, A. A. Valente, A. D. Lopes, I. S. Gonçalves, *Inorg. Chem. Commun.* **2003**, *6*, 1228−1233.
[11] A. S. Goldman, D. R. Tyler, *Organometallics* **1984**, *3*, 449−456.
[12] A. Gorfti, M. Salmain, G. Jaouen, M. J. McGlinchey, A. Bennouna, A. Mousser, *Organometallics* **1996**, *15*, 142−151.
[13] X. S. Zhao, G. Q. Lu, A. K. Whittaker, G. J. Miller, H. Y. Zhu, *J. Phys. Chem. B* **1997**, *101*, 6525−6531.
[14] [14a] B. Marler, U. Oberhagemann, S. Vortmann, H. Gies, *Microporous Mater.* **1996**, *6*, 375−383. [14b] W. Hammond, E. Prouzet, S. D. Mahanti, T. J. Pinnavaia, *Micropor. Mesopor. Mater.* **1999**, *27*, 19−25.
[15] S. J. Gregg, K. S. W. Sing, *Adsorption, Surface Area and Porosity*, 2nd edn., Academic Press, London, **1982**.
[16] D. Brunel, A. Cauvel, F. Fajula, F. DiRenzo, *Zeolites: A Refined Tool for Designing Catalytic Sites* (Eds.: L. Bonneviot et al.), Elsevier Science B. V., **1995**, p. 173.
[17] Y. Deng, C. Lettmann, W. F. Maier, *Appl. Catal. A: Gen.* **2001**, *214*, 31−45.
[18] C. D. Nunes, M. Pillinger, A. A. Valente, I. S. Gonçalves, J. Rocha, P. Ferreira, F. E. Kühn, *Eur. J. Inorg. Chem.* **2002**, 1100−1107.
[19] [19a] M. Kruk, M. Jaroniec, A. Sayari, *Langmuir* **1997**, *13*, 6267−6273. [19b] M. Kruk, V. Antochshuk, M. Jaroniec, *J. Phys. Chem. B* **1999**, *103*, 10670−10678.
[20] W. P. Hart, D. Shihua, M. D. Rausch, *J. Organomet. Chem.* **1985**, *282*, 111−121.
[21] S. J. N. Burgmayer, J. L. Templeton, *Inorg. Chem.* **1985**, *24*, 2224−2230.

Received May 11, 2005
Early View Article
Published Online October 21, 2004

 © 2004 Wiley-VCH Verlag GmbH & Co. KGaA, Weinheim

Publicationdates for issues of 2004

Issue	Pagination	Print	Online*
1	1−192	January 5	December 18
2	193−430	January 22	January 14
3	431−660	February 4	January 26
4	661−914	February 20	February 16
5	915−1130	March 5	Feburary 24
6	1131−1352	March 19	March9
7	1353−1570	April 2	March 22
8	1571−1770	April 19	April 6
9	1771−1970	May 4	April 20
10	1971−2188	May 17	May 4
11	2189−2392	June 8	May 25
12	2393−2594	June 21	June 8
13	2595−2796	July 5	June 22
14	2797−2990	July 19	July 6
15	2991−3186	August 6	July 27
16	3187−3378	August 23	August 10
17	3379−3570	September 6	August 23
18	3571−3764	September 20	September 7
19	3765−3958	October 4	September 21
20	3959−4146	October 18	October 6
21	4147−4338	November 5	October 25
22	4339−4532	November 19	November 8
23	4533−4724	December 3	November 23
24	4725−4920	December 17	December 7

*The complete issue was published online on the given date.
Selected articles were previously available in EarlyView.

 © 2004 Wiley-VCH Verlag GmbH & Co. KGaA, Weinheim

Author Index

Afzaal, M., 171
Akine, S., 3779
Akkerman, O. S., 154
Al-Mandhary, M. R. A., 329
Alberdi, G., 2937
Alberto, R., 2013
Albrecht, M., 1175
Albrecht-Gary, A.-M., 51
Alcock, N. W., 3981
Alemany, P., 143
Alexiou, M., 3822
Almeida Paz, F. A., 2759
Almeida, M., 1318
Álvarez, E., 707
Alvarez, R., 2937
Alvarez, S., 143
Alves, H., 1318
Amberger, H.-D., 98
Amorós, P., 1799, 1804
Anda, C., 857
Anderson, C. J., 3310
Anderson, T. M., 3462
Andruh, M., 2914
Anson, C. E., 2933
Antiñolo, A., 260, 1299, 3353
Antipin, M. Y., 629
Antonaroli, S., 732
Antoniotti, P., 1125
Antoniutti, S., 1922
Anxolabéhère-Mallart, E., 1225
Aragoni, M. C., 2008, 2363, 3099
Arca, M., 2008, 2363, 3099, 4660
Arezzini, B., 646
Arii, H., 4140
Arion, V., 1530
Arliguie, T., 4502
Arndt, P., 4739
Arnold, D. P., 510, 518, 1262
Arnold, P. L., 3724
Arora, V., 4781
Arrais, A., 1505
Artaud, I., 1545
Aucott, S. M., 3798, 4795
Aullón, G., 4430
Auner, N., 1253
Avarvari, N., 2646, 3409
Axenov, K. V., 695, 4702
Bacchi, A., 1922, 1985
Baceiredo, A., 3533
Bačkovský, J., 1402, 3605
Bacsa, J., 368
Bader, C., 4115
Badraoui, B., 3828
Baerends, E. J., 1675
Baisch, U., 1219
Bakardjiev, M., 3601, 3605
Baldeau, S. M., 783, 879
Balland, V., 301, 1225
Balula, M. S., 619
Balzarini, J., 1420
Banci, L., 1583
Bandoli, G., 1092
Banerjee, R., 2950, 4854
Banerjee, S., 2533
Banse, F., 301, 1225
Baradello, L., 3358
Baran, E. J., 322
Baratta, W., 524
Barba, V., 118
Barbier, J.-P., 1285
Barkigia, K. M., 1545
Barloy, L., 3987
Barral, M. C., 4491
Barranco, E. M., 4820
Bartholomä, M., 4177
Bartoli, J.-F., 301
Bartolomé, C., 2326
Baruah, B., 1873
Battioni, P., 301, 3127
Bauer-Siebenlist, B., 2413
Baumann, W., 4739
Baumgartner, J., 3254
Baux, C., 2173
Baxter, P. N. W., 2379
Beck, J., 2019
Beck, W., 1330
Begnouf-de-Vains, J.-B., 2514
Béguin, C., 1552
Beitia, J. I., 1886
Belai, N., 276, 4132
Belaj, F., 4510
Beley, M., 3984
Belkova, N. V., 3453
Belle, C., 4036
Bellemin-Laponnaz, S., 3436
Beller, M., 1330
Belletti, D., 3564
Belli Dell'Amico, D., 1219, 3938
Beloso, I., 635
Beltrán, A., 1799, 1804
Beltrán, D., 1799, 1804
Ben Salah, M., 2272
Bencini, A., 4061
Benelli, C., 500
Beneš, L., 570, 2493
Benet-Buchholz, J., 1601
Benetollo, F., 1714
Benetsky, E. B., 629
Benkič, P., 1827
Bensch, W., 2553
Bera, J. K., 368
Bergamini, P., 1277
Berke, H., 3544
Bermejo, M. R., 2769, 3696
Berndt, A., 3063
Berni, E., 4061
Berssen, E., 2301
Bertagnolli, M., 2784
Berthet, J.-C., 1996
Berthet, P., 3462
Bertini, I., 1583
Bertolasi, V., 1277
Bertotti, M., 1879
Bertrand, G., 381, 3533
Bhasin, K. K., 4781
Bi, W., 2144, 2228, 2747
Bian, N., 4072
Bianchi, A., 4061
Biaso, F., 1552
Bick, T., 689
Bickelhaupt, F., 154, 1175, 2045
Biesemans, M., 445, 2908
Bigoli, F., 960
Bildstein, B., 1740, 2827
Bill, E., 301, 984, 4209
Billard, I., 1190
Binnemans, K., 3538
Biricik, N., 4232
Blagodatskikh, I. V., 1253
Blais, J.-C., 973
Blasius, R., 3971
Blazina, D., 4381
Bley-Escrich, J., 492
Blockhuys, F., 3798
Blok, A. N. J., 2385
Blunck, T., 4046
Boccaletti, G., 4751
Bochkorev, M. N., 4396
Böck, B., 3612
Böhn, K., 4242
Bolaño, S., 4812
Bolzati, C., 1902
Bondarev, O. G., 629
Bonetti, M., 810
Borak, B., 1411
Borbone, F., 2467
Borocci, S., 1125
Borrás, J., 635
Borrmann, T., 2452
Børsting, P., 376
Boschi, A., 1902
Bosetti, E., 1985
Bothe, E., 984
Botteman, F., 463
Böttger, U. A., 3852
Boubekeur, L., 2013
Bouhmaida, N., 3172
Bourcier, S., 1225
Bourissou, D., 1939
Bousseksou, A., 3017, 4353
Bouwman, E., 1963, 4572
Brandt, C. D., 469
Brasey, T., 964
Bratsos, I., 3118
Braun, U., 3612, 3629
Braun, W., 2235
Bravo, J., 4812
Brečević, L., 4579
Brechin, E., 2219
Bregadze, V. I., 3453
Brellochs, B., 3605
Brenčič, J. V., 1611
Bressan, M., 810
Brito, J. A., 4278
Bronisz, R., 3688
Brooker, S., 2570
Brown, D., 3269
Bruneau, C., 418
Brunetta, A., 1030
Brusko, V. V., 423
Bu, X.-H., 1701, 3228
Budzelaar, P. H. M., 1204, 2385
Budzisz, E., 4412
Bueno Toro, J. D., 3498
Bulach, V., 453
Bünzli, J.-C. G., 51, 1190, 2173, 2348
Burg, A., 3675
Burgemeister, K., 2690
Burlakov, V. V., 4739
Burrows, A. D., 4686
Buryak, A., 964
Burzlaff, N., 2151
Busetto, L., 1494
Butcher, R. J., 1014, 1107
Butler, I. S., 4324
Cabras, M. C., 960
Cabrera, M. M. M., 3508
Cabrera, S., 1799
Cagnolini, A., 1902
Cai, C.-X., 1039
Calabrò, G., 1447
Calderazzo, F., 1219, 3938
Calhorda, M. J., 3038
Calmuschi, B., 2235
Cameron, T. S., 3865
Caminade, A.-M., 2459
Caminiti, R., 2739
Campion, M., 1817
Campo, J. A., 3089
Camus, J.-M., 1081
Canadell, E., 3409
Caneschi, A., 3887
Cangiotti, M., 2853
Cano, J., 335, 3074
Cano, M., 3089
Canovese, L., 732
Cao, L.-H., 4789
Cao, R., 37, 2144, 21228, 2747, 3353
Capes, L., 3017
Capó, M., 3405
Capozzi, M. A. M., 3445
Carapuça, H. M., 619
Carbó, M., 2338
Carcelli, M., 1985
Cardellicchio, C., 3445
Cardon, T. B., 1073
Carlos, L. D., 3913
Carmago, A. J., 1879
Carmalt, C. J., 4286, 4470
Carmona, D., 4586
Carpentier, J.-F., 943, 3247, 4803
Carranza, J., 4836
Carrea, M. B., 4660
Carriedo, G. A., 3668
Caruso, F., 3484
Caruso, U., 2467
Casagrande Jr., O. L., 4803
Casella, L., 2203
Casellato, U., 3887
Castellano, E. E., 322
Castro, J., 635
Cauzzi, D., 1063
Cavaleiro, A. M. V., 619
Centore, R., 2467
Cerasino, L., 3445
Cerecetto, H., 322
César, V., 3436
Çetinkaya, B., 418
Çetinkaya, E., 418
Chai, J., 2673, 4046, 4807
Chakrabarti, S., 3846
Chakravarty, A. R., 1440
Chakravorty, A., 178, 1873
Champness, N. R., 2008
Chan, A. S. C., 37, 1595, 3751
Chan, H.-S., 286
Chan, T. C., 1788
Chandra, M., 3555
Chang, H., 1753
Chang, J.-C., 4898
Chang, J.-Y., 1753
Chaniotakis, N., 2283
Charbonnière, L., 2348
Charlot, M.-F., 301
Chastanet, G., 3017
Chaudhuri, P., 984, 4209
Chaudhuri, S., 3110
Chauvin, A.-S., 2173
Che, C.-M., 956., 1341
Cheah, K.-W., 829, 837
Chen, C., 1454, 3316, 3522
Chen, F., 1454, 3316
Chen, H.-L., 2180
Chen, H.-Y., 4072, 4653
Chen, I.-C., 4898
Chen, J., 2167
Chen, J.-D., 1488, 4696
Chen, J.-L., 3837
Chen, J.-T., 2533
Chen, J.-X., 4247
Chen, Q., 1165, 1474, 1478

 © 2004 Wiley-VCH Verlag GmbH & Co. KGaA, Weinheim

INDEX

Chen, X., 3147
Chen, X.-M., 1024
Chen, X.-Y., 562, 2369
Chen, Z.-J., 4774
Chen, Z.-N., 4247
Chen, Z.-X., 1813
Cheng, D. Y. Y., 3806
Cheng, H.-W., 3147
Cheng, P., 562, 1514, 2130, 2369
Cheng, Y.-T., 2180
Chérioux, F., 2405
Cherkasov, V. K., 388
Chernikov, A. V., 2008
Chikuma, M., 4828
Chinnakali, K., 872
Choi, C.-F., 3806
Choukroun, R., 317, 2861
Chubarova, E. V., 63
Chudakova, V. A., 388
Chung, Y. K., 1522
Churakov, A. V., 771, 2123
Ciccarella, G., 1234
Çiçek, M., 418
Cinellu, M. A., 4484
Cingolani, A., 3484
Ciofi-Baffoni, S., 1583
Ciunik, Z., 1411
Claramunt, R. M., 549
Claver, C., 4193
Clegg, W., 3223, 4871
Clerac, R., 2933
Clinet, J.-C., 4278
Cohen, H., 3675
Cohen, S., 207
Cokoja, M., 4161
Coles, M. P., 2662
Collin, J.-P., 575
Collomb, M.-N. 3880
Comba, P., 4640
Consiglio, G., 2701, 4561
Contant, R., 276, 4132
Cordeiro Santos, I., 1318
Corma, A., 1143
Cornago, P., 549
Cortés-Llamas, S., 3743
Costa, P. J., 3038
Costas, M., 857
Costes, J.-P., 1530, 1808
Coxall, R. A., 4871
Crane, J. D., 4237
Crawford, M.-J., 4781
Crawforth, C. M., 2706
Crespo, O., 423, 3038, 4820
Crestini, C., 4477
Crochet, P., 3668
Crociani, B., 732
Crouch, D., 171
Císařová, I., 1402, 3605
Cucos, A., 2914
Cuenca, T., 3154
Cuffe, L. P., 4525
Cui, A.-L., 4608
Cui, H., 4681
Cui, X.-B., 1051, 1566
Cui, Y., 3662, 4317, 4669
Cusumano, M., 4710
d'Alessandro, N., 810
Dahan, F., 1530
Dahlén, A., 3020, 3393
Dahlenburg, L., 888
Dai, J., 4789
Dai, J.-C., 2096
Dai, L., 237
Dalal, N. S., 3792
Dan, M., 1733
Dang, D.-B., 160
Danovich, D., 207
Daran, J.-C., 4108
Darbost, U., 4371
Darensbourg, M. Y., 231
Dashjav, E., 1183
Davankov, V. A., 629
Debaerdemaeker, T., 3057
Debay, A., 3017
Debbabi, M., 3828
de Castro, B., 2027
de Cian, A., 2107
De Clercq, E., 1420
de Gelder, R., 1675
de Jesús, E., 3287
de Kanter, F. J. J., 2045
de la Mata, F. J., 3287
de los Rios, I., 293
De Maria, A., 2467
de Pater, B. C., 1675
de Visser, S. P., 207
de Vos, W. M., 2847
Dechert, S., 2421, 4681
Decken, A., 3865, 4420
Deeken, S., 2301
Deglmann, P., 349
Deiseroth, H. J., 4755
Del Zotto, A., 524
Della Pergola, R., 3901
Delgado, F. S., 3873
Demartin, F., 2363, 3099, 4660
Demeshko, S., 2413
Dendrinou-Samara, C., 3822
Deplano, P., 960
Derakhshan, S., 1183
Devillanova, F. A., 2008, 2363, 3099, 4660
Dey, B. K., 4115
Dey, S., 4510
Díaz, A., 3353
Díez, J., 2078
Dhar, B. B., 2950, 4854
Diana, E., 1505
Dias, S., 685
Di Bella, S., 2701, 4561
Di Deo, M., 810
Di Marco, V., 2524
Di Masi, N. G., 4751
Di Pietro, M. L., 4710
Di Vaira, M., 293
Dick, A. K. J., 1992
Dietrich-Bucheker, C. O., 575
Dikarev, E. V., 4006
Dilsky, S., 4859
Dimitrov, A., 3842
Ding, B., 562
Ding, J., 4028
Dixneuf, P. H., 418
Djukic, J.-P., 2107
Dobrzyńska, D., 110
Dolbecq, A., 33
Dolmella, A., 1092, 1902
Dombi, G., 2524
Domingos, A., 243
Dong, W., 1514
Dong, Z.-C., 538
Donnadieu, B., 1808, 2459, 2861
Donovan, A. S., 4686
Doppiu, A., 2244
Dorado, I., 1299
Dorogov, K. Y., 771
Dötz, K. H., 2107
Dou, J., 3806
Drabent, K., 110
Draper, P., 322
Dreos, R., 4266
Drew, M. G. B., 3110, 4633
Drewes, D., 2690, 4849
Driessen, W. L., 1963
Drommi, D., 1447
Dronskowski, R., 2313, 2989
Du, M., 3228
Du, W.-X., 2096
Duan, L.-M., 4375
Duatti, A., 1902
Duboc, C., 3880
Duckett, S. B., 4381
Duczmal, M., 110
Duddeck, H., 2160
Dumartin, G., 2908
Duñach, E., 4278
Dunbar, K. R., 368, 3783
Dybal, J., 570, 2493
Dybtsev, D. N., 63
Dyson, P. J., 530, 4232, 4381
Eckenrath, H. J., 1396
Eckert, M., 1330
Eichhöfer, A., 93, 349, 1100
Eisen, M. S., 4795
El Haskouri, J., 1799, 1804
El-Hamdan, A., 969
Elangovan, S. P., 4547
Elgin, J. D., 3345
Elguero, J., 549
Elhabiri, M., 51
Elim, H. I., 86
Eller, C., 4836
Englert, U., 1234, 3938, 4011
Enoki, T., 933
Enzmann, A., 1330
Ephritikhine, M., 1996, 4502, 4624
Epstein, L. M., 3453
Erker, G., 1175, 2260, 4586
Escuer, A., 309, 2885
Espinet, P., 2326
Espino, G., 2542
Esteruelas, M. A., 2477
Fabrizi de Biani, F., 3901
Failla, S., 2701
Fairlamb, I. J. S., 2706
Fajardo, M., 1299
Falini, G., 4579
Falk, K., 335
Falvello, L. R., 2338
Fan, J., 1465
Fan, R.-Q., 4891
Fan, W., 4547
Fan, Y., 3946
Fang, G.-S., 1341
Fang, Q., 185
Fanizzi, F. P., 1234, 1705, 4751
Faraone, F., 1447
Farfán, N., 118
Fátima, M., 1411
Fedin, V. P., 63
Fedorova, E. A., 4396
Fedushkin, I. L., 388, 2421
Fei, Z., 530, 4232
Feige, C., 2053
Félix, V., 3038
Felluga, A., 653
Fenet, B., 3172
Feng, M.-L., 3712
Feng, S.-H., 4891
Feng, Y., 2923
Fenske, D., 63, 93, 1100, 2933
Ferbinteanu, M., 1963
Feringa, B. L., 846
Fermani, S., 4579
Fernandes, J. A., 3913
Fernández, A., 2937
Fernández, M. I., 2769, 3696
Fernández-Baeza, J., 260, 3353
Ferrali, M., 646
Ferrari, E., 646
Feth, M. P., 2784
Figueiredo, J. L., 2027
Fild, M., 749
Filin, A. M., 3453
Filippov, O. A., 3453
Finocchiaro, P., 2701
Fischer, A., 4011
Fischer, B., 4124
Fischer, R., 1243, 2001
Fischer, R. A., 4161
Flamigni, L., 2557
Flores, J. C., 3287
Flores-Parra, A., 601
Flörke, U., 984
Fontanella, C., 2739
Fontecave, M., 3163
Forgó, P., 2524
Formica, M., 2853
Fort, A., 2467
Fort, Y., 3984
Fourmigué, M., 2646, 3409, 4502
Fox, T., 3544
Foxon, S. P., 335, 344
Fragalà, I., 2701, 4561
Fragalà, I. L., 500
Franco, D. W., 1879
Frantz, S., 2902
Fregolent, B., 1922
Freire, C., 2027
Freitas, M. M. A., 2027
Frenking, G., 4388
Freund, C., 1939
Friedrich, A., 4300
Fröhlich, R., 394, 1175, 2260, 2683
Frühauf, H.-W., 1675
Fu, Z.-Y., 2096
Fujimura, Y., 1621
Fukin, G. K., 388, 4396
Fukuda, T., 1621
Fumagalli, A., 3901
Fun, H. K., 872
Fusco, M., 2467
Fusi, V., 2853
Gade, L. H., 2716, 3424, 3436
Gago, S., 1389, 4914
Gaillard, C., 1190
Gais, H.-J., 629
Gal, A. W., 1675
Galán-Mascarós, J.-R., 3783
Galindo, A., 707
Galka, C. H., 3424
Gallego, M. L., 3089
Gálvez-Ruiz, J. C., 4764
Gama, V., 1318
Gamasa, M. P., 2078
Gambino, D., 322
Gamelas, J. A., 619
Gamez, P., 591, 3025, 4036, 4566
Gangopadhyay, J., 2533
Ganin, A. Yu., 3233
Ganzaroli, E., 3127
Gao, S., 557, 956, 1169, 1311, 2968, 3262, 3681
Gao, Y.-C., 866
Garau, A., 2363, 4660
Garcés, A., 1299
Garcia, H., 1143
García, L., 2706
García Alonso, F. J., 3668
García-España, E., 4061
García-Fontán, S., 4812
García-Granda, S., 2078
García-Montalvo, V., 3743
García-Vázquez, J. A., 635
Gardiner, M. G., 1992
Garlaschelli, L., 3901
Garoufis, A., 1427, 3326
Gaspar, A. B., 4770
Gáti, T., 2160
Gávalez-Ruiz, J. C., 601

Gavrilenko, V. V., 3453
Gavrilov, K. N., 629
Gayoso, E., 2937
Ge, N., 2819
Gedanken, A., 1859
Geiseler, G., 3063
Gemel, C., 4161
Gerasko, O. A., 63
Gervasio, G., 1505
Geyer, R. G., 2434
Ghermani, N., 3172
Ghosh, A., 2442, 2533, 3110, 4555
Ghosh, B. K., 250
Ghoshal, D., 4675
Ghule, A., 1753
Ghule, K., 1753
Gielen, M., 445
Giester, G., 4412
Gil, A. Mendoza, L., 4061
Gili, P., 3873
Gimenco, M. C., 3038
Gimeno, J., 2078, 3668
Gimeno, M. C., 423, 4820
Giorgi, L., 2853
Giorgi, M., 1817, 4371
Girerd, J.-J., 301, 1225
Gisselbrecht, J.-P., 492
Glaser, T., 394, 2356, 2683
Gleiter, R., 2585, 4021
Glukhov, I. V., 1379
Gobetto, R., 1505
Goh, L. Y., 2504
Goldberg, I., 1724
Golden, M. L., 231
Golen, J. A., 3310
Golubinskaya, L. M., 3453
Gómez, M., 4278
Gómez, R., 3287
Gómez-García, C. J., 1799
Gómez-Sal, P., 3287, 3814
Gonçalves, I. S., 1389, 3913, 4914
Gong, Y., 3751
Gonzalez, J., 3405
González, M., 322
González-Arellano, C., 1955
González-Duarte, P., 3223, 3585, 4146
González-Noya, A. M., 2769, 3696
González-Prieto, R., 4491
Görls, H., 1243, 2001
Gornitzka, H., 2289, 2823
Gorol, M., 2678
Goswami, A., 2635, 4223
Götz, R., 888
Gould, I. R., 1865
Graff, R., 3987
Graiff, C., 1063, 1447, 3564
Grandi, R., 646
Grandinetti, F., 1125
Grandjean, F., 3345
Green, M. A., 3846
Gribkov, D. V., 4091
Griffe, L., 2459
Griffith, D., 3003
Grimaldi, P., 2363
Grirrane, A., 707
Grisaru, H., 1859
Gromada, J., 3247
Gros, P., 3984
Gross, M., 492
Gross, Z., 1724
Grosshans, P., 453
Grove, H., 4836
Gruber, N., 1285
Grüner, B., 1402
Gu, W., 2130
Guadarrama-Pérez, C., 601
Guedes da Silva, C., 1411
Guerrero, A., 549
Guillem, C., 1799, 1804
Guo, H., 2819
Guo, J., 267, 829, 837
Guo, Q.-L., 1311
Guo, Y.-M., 3228
Guo, Z., 4028
Gutiérrez-Puebla, E., 1955
Gutiérrez-Zorrilla, J. M., 1886
Gütlich, P., 4770
Guyon, F., 2646
Haase, W., 335
Haberland, J., 2235, 3629
Hadjikakou, S. K., 1420, 4324
Hadjiliadis, N., 1420, 1427, 3326, 4324
Hage, R., 846
Hamacek, J., 51
Hampel, F., 4091
Hamza, M. S. A., 653
Han, L., 2695, 3751, 4457
Han, W., 2130
Hanack, M., 2877
Hannon, M. J., 3981
Hanssen, R. W. J. M., 675
Hao, N., 4102
Harms, K., 2123, 2498
Harrington, R. W., 4686
Harrowfield, J. M., 227
Hartl, F., 1675
Hartnell, R. D., 1262
Hartwich, I., 3842
Harvey, P. D., 4420
Hashimoto, M., 2632
Hassler, K., 4259
Hausmann, J., 4402
Hayashi, K., 4646
Hazari, S. K. S., 4115
He, H., 837
He, M., 237
Hector, A. L., 4470
Heeg, M. J., 2652
Hegetschweiler, K., 4177
Hein, K., 3136
Heinemann, F. W., 581, 1847, 3136, 4291, 4591
Heinz, U., 4177
Heinze, K., 2053, 2974, 3498
Heirtzler, F., 685
Heiser, D., 2107
Helliwell, M., 2219
Henry, W., 2001
Henzan, N., 743
Heras, J. V., 3089
Herber, R. H., 3476
Herberich, G. E., 1396, 4011
Herbst-Irmer, R., 3508
Herdtweck, E., 3074, 3154, 3305
Hernández-Molina, M., 3873
Hérold, A., 1661
Hérold, C., 1661
Hervé, M., 973
Hesemann, P., 1190
Hetterscheid, D., 1204
Hey-Hawkins, E., 3277
Hilbert, T., 2019
Hill, A. F., 818
Hill, C. L., 3462
Hilmersson, G., 3020, 3393
Hilpert, K., 1212
Hiratani, K., 4216
Hitchcock, P. B., 2662
Hnatejko, Z., 2379
Hnyk, D., 3605
Ho, K. P., 1056
Hoffmann, R.-D., 2356
Hofmann, M., 3063, 3605
Hogenbirk, M., 1175, 2045
Holman, K. T., 1014
Holub, J., 3601, 3605
Hong, J.-M., 4072
Hong, M., 37, 1595, 2144, 2695, 3751
Hong, M.-C., 4457
Hor, T. S. A., 69, 2504
Hosseini, M. W., 453
Hou, B., 1165
Hou, H., 3946
Hou, Y., 1169, 1385
Houjou, H., 4216
Howard, J. A. K., 771
Hsu, S.-C., 459
Hsu, Y.-F., 1488
Hu, C., 1385
Hu, C.-H., 4898
Hu, C.-W, 4102
Hu, H., 1785
Hu, H.-L., 4696
Hu, Q.-M., 866, 3147
Hu, S.-M., 2096
Hu, X.-X., 1566, 4375
Huang, D., 1454
Huang, J., 1894
Huang, J.-H., 4898
Huang, J.-S., 1341
Huang, K., 2956
Huang, R.-B., 125
Huang, S.-L., 459
Huang, X.-C., 1024
Huang, Z., 2923
Huber, M., 1963
Hüber, M., 335
Hübner, E., 2151
Huisman, M., 591, 4036
Huitrón-Rattinger, E., 3743
Hultzsch, K. C., 4091
Hummel, W., 2235
Hummeltenberg, R., 4259
Hummert, M., 4759
Hung, C.-H., 4898
Hung, W. Y., 2837
Hursthouse, M. B., 1007
Hussain, F., 2733
Hyuga, R., 4140
Ienco, A., 707
Iglesias, M., 1955
Iida, M., 3920
Ikeue, T., 798
Ilg, K., 469
Ilyin, E. G., 3865
Imai, H., 4882
Inohara, T., 322
Inoue, K., 4882
Inoue, M., 3920
Isaia, F., 2008, 2363, 3099, 4660
Isobe, K., 356
Ito, M., 4882
Ito, T., 3084
Itoh, K., 3651
Jabbour, D., 2036
Jabin, I., 4371
Jacob, V., 2053
Jäger, M., 2001
Jagirdar, B. R., 3048
Jain, V. K., 4510
Jakusch, T., 2524
Jalón, F. A., 549, 2542
Jameson, G. B., 2570
Janas, Z., 1639
Jancik, V., 3508, 4056
Jank, S., 98
Jaouen, G., 2013
Jasimuddin, S., 250
Jayaswal, M. N., 2646
Jeffery, J. C., 2570
Jeffery, S. P., 231
Jelínek, T., 3605
Jenkins, H. D. B., 3273
Jerzykiewicz, L. B., 110, 1639
Jeß, I., 2868
Jeunesse, C., 4602
Ji, M., 409
Ji, W., 86
Jia, D.-X., 4789
Jia, G., 2837
Jiang, C., 3662, 4521, 4669
Jiang, C.-W., 2277
Jiang, F., 2695, 3370
Jiang, J., 510, 518, 3806
Jiang, Y.-B., 4608
Jiang, Z.-H., 562, 1514, 2130, 2266, 2369
Jiao, C., 3662, 4669
Jiménez-Aparicio, R., 4491
Jiménez-Tenorio, M., 17
Jin, L., 3262
Jin, L.-P., 2968
Jin, X., 78, 3370
Jitsukawa, K., 4140
Jones, C., 3277
Jones, P. G., 3038, 4820
Jouaiti, A., 453
Journaux, Y., 2914
Jubert, C., 1285
Julve, M., 335, 3873, 4081, 4836
Jung, S., 469, 3415
Jupa, M., 1835
Jurkschat, K., 2283
Kaburagi, Y., 134
Kahlal, S., 1063
Kaifer, E., 1646
Kaim, W., 2902, 4510
Kaizaki, S., 4463
Kaizer, J., 2253
Kajiwara, T., 3084
Kalck, P., 791
Kandasamy, K., 1014
Kandaswamy, M., 872
Kanesato, M., 4216
Kang, Y., 3415
Kapon, M., 4795
Karlov, S. S., 2123, 2498
Karmazin-Brelot, L., 3907
Käss, S., 4402
Katsaros, N., 3118
Katsoulis, D., 1253
Kawabata, K., 2137
Keene, T. D., 1007
Kehr, G., 1175, 4586
Kehr, S. G., 2260
Keita, B., 276, 2036, 3462, 4132
Kellogg, R. M., 846
Kempe, R., 3297
Kempter, A., 4161
Keppler, B. K., 4412
Kerscher, M., 4640
Kersting, B., 4402
Kessissoglou, D. P., 3822
Kheradmandan, S., 3544
Khoo, S. B., 69
Kickelbick, G., 1835
Kiebach, R., 2553
Kienle, L., 3233
Kilyen, M., 2524
Kim, H.-S., 3415
Kim, J.-J., 3415
Kim, T. H., 1522
Kim, Y.-S., 3415
Kimpe, K., 3538
Kimura, K., 356
Kinoshita, I., 356

 © 2004 Wiley-VCH Verlag GmbH & Co. KGaA, Weinheim

INDEX

Kirchner, K., 2609
Kirillov, E., 943
Kirin, V., 1045
Kirsch-De Mesmaeker, A., 3971
Kiss, T., 2524
Kitakoga, Y., 4646
Kivekäs, R., 1402
Klapötke, T. M., 4764, 4781
Klein, A., 2784, 4510
Kleinke, H., 1183
Kleinpeter, E., 4402
Klinga, M., 695, 4702
Klinowski, J., 2759, 3031
Klod, S., 4402
Klopstra, M., 846
Kloskowski, M., 879
Knapp, C., 2446
Knijnenburg, Q., 1204
Knorr, M., 2646
Kobayashi, N., 906, 1621, 3806
Koch, R., 344, 2301
Koh, L. L., 1056
Kölle, P., 2313, 2989
Koller, J., 1611
Komeda, S., 4828
Konar, S., 4202
Konarev, D. V., 1794
Kondoh, H., 1169
Kong, L.-Y., 1465
Kontrec, J., 4579
Kontturi, M., 2627
Kooijman, H., 1175, 2045
Kooistra, T. M., 1204
Kopacka, H., 1740, 2827
Korlyukov, A. A., 1253
Kortz, U., 2036, 2733, 3792
Korybut-Daszkiewicz, B., 3335
Kosaka, Y., 134
Koszinowski, K., 44
Kotov, V. V., 695, 4702
Kou, H.-Z., 401, 4608
Koval, I. A., 591, 4036, 4566
Kozuch, S., 207
Krajete, A., 1740, 2827
Kralj, D., 4579
Kravtsov, V., 2914
Krebs, B., 783, 2690, 4036, 4849
Kreisel, G., 2001
Krinninger, C., 2488
Kristen, M. O., 1740
Krüger, P., 481
Kruger, P. E., 4836
Krumm, B., 4764
Ksenofontov, V., 4770
Kubicki, M. M., 1299, 2379, 4324
Kudinov, A. R., 3476
Kufelnicki, A., 4412
Kuge, K., 134
Kuhn, P., 4602
Kumar, D., 207
Kumar, S., 1014
Kumar, S. S., 4056
Kumar P., R., 1107
Kumbhare, L. B., 4510
Kunkely, H., 4242
Kunrath, F. A., 4803
Küper, I., 2690
Kuo, P.-C., 4898
Kuo, T.-S., 2180
Kurmoo, M., 2272
Kuzmina, L. G., 771
Kwon, S.-K., 3415
Kyritsakas, N., 453, 3987
Kyritsakas-Gruber, N., 2107
Kyritsis, P., 2885
Labat, G., 3907
Labella, L., 1219, 3938
Labet, A., 1190
Lacaze-Dufaure, C., 791
Laforgia, M., 3445
Lagrange, P., 1661
Laguna, A., 423, 3038, 4820
Lahoz, F. J., 2477, 4586
Lai, Y.-H., 2086
Lanfranchi, M., 1705
Lanfredi, A. M. M., 3025
Lang, J.-P., 86, 4247
Lange, K. C. H., 4681
Lanza, S., 3358
Lappert, M. F., 2754
Lara-Sánchez, A., 260
Laschi, F., 3901
Latorre, J., 1799, 1804
Lau, C. P., 1788
Laurent, S., 463, 3538
Lavalette, A., 3981
Lavallo, V., 2289
Lavanant, H., 973
Lawrance, G. A., 3981
Laye, R. H., 2811
Laz, M. M., 3873
Le Floch, P., 3017
Le Hénanf, M., 1687
Le Mest, Y., 1817
Le Roux, C., 2823
Le Roy, C., 1687
Lebrun, C., 3163
Lee, B. Y., 1522
Lee, C.-H., 286
Lee, C.-L., 3415
Lee, G.-H., 4616
Lee, H. M., 4898
Lee, M.-T., 4898
Lee, S.-K., 3415
Lehmann, C. W., 943
Lehmus, P., 3201
Lehn, J.-M., 2379
Lehtonen, A., 3201
Leibeling, G., 2413
Leino, R., 3201
Leising, F., 3247
Lelj, F., 2363, 3099
Lennartz, C., 4242
Lenoble, G., 791
Leonardi, N., 2701, 4561
Leong, W. K., 2504
LeRoy, S., 1545
Leskelä, M., 695, 4702
Leszczynski, J., 1212
Létard, J.-F., 3017
Lezama, L., 1886
Li, C., 1785
Li, C.-H., 2369
Li, D.-F., 1894
Li, F., 2775
Li, G., 1478
Li, G.-H., 4891
Li, J., 3662, 4669
Li, J.-R., 1701
Li, K.-F., 829, 837
Li, L., 1454, 3316, 3522
Li, L.-C., 2266
Li, Q., 1234, 1785, 2819
Li, Q.-X., 4447
Li, R., 3806, 4907
Li, S.-A., 1894
Li, S.-D., 2232
Li, X., 1595, 2144, 2228, 2747
Li, Y., 946, 1051, 1385, 1478, 1595, 2754, 2956, 3718
Li, Y.-G., 4102
Li, Y.-Z., 1039, 4447
Liang, H., 829
Liang, M., 1514
Liao, D., 1454, 3316, 3522, 4907
Liao, D.-Z., 562, 1514, 2130, 2266, 2369
Liao, F., 3262
Liao, F.-H., 2968
Liao, F.-L., 2180
Liebman, J. F., 1349, 3273
Liese, A., 2235
Limanski, E. M., 2690, 4849
Limberg, C., 3644
Lin, H.-H., 4789
Lin, J.-L., 2223
Lin, L., 4028
Lin, Y.-C., 459, 4616
Lin, Z., 2066
Lin, Z.-E., 953
Lin, Z.-Z., 4457
Ling, Y. C., 1753
Lipkowski, J., 1530, 2914
Lippolis, V., 2008, 2363, 3099, 4660
Liptau, P., 4586
Liratzis, I., 2683
Liu, C.-M., 4774
Liu, C.-P., 4457
Liu, H., 459
Liu, L., 2066
Liu, Q., 1454, 3316, 3522
Liu, W., 286
Liu, X.-W., 2369
Liu, Y.-B., 4375
Liu, Y.-H., 459, 4253
Liu, Z., 4521
Liu, Z.-Q., 2130
Lledós, A., 3223, 3585, 4146
Llobet, A., 612, 857, 1601
Lloret, F., 335, 4081, 4836
Llusar, R., 63
Lo, M. F., 2837
Lo, W.-K., 829, 837
Lo, Y.-H., 4616
Lo Nigro, R., 500
Lo Schiavo, S., 3358
Lobana, T. S., 356
Loginov, D. A., 3476
Long, G. J., 3345, 4572
Longato, B., 1092
opatin, M. A., 388
Lopes, M. I., 98
López, A., 4871
López, G., 2706
López-Honorato, E., 3743
López-Mardomingo, C., 1299
López-Solera, I., 1299
Lorber, C., 317, 2861
Lorberth, J., 2123, 2498
Lorenz, I.-P., 2488
Lorenzo-Luis, P., 3873
Lorigan, G. A., 1073
Lork, E., 2446, 2452
Lorusso, G., 4751
Lozinsky, E., 3675
Lu, C.-Z., 2533
Lu, F., 510, 3806
Lu, G.-L., 2066
Lu, K.-L. 4253
Lu, S., 3262
Lu, T.-H., 250
Lu, X. L., 2504
Lu, Y. W., 276, 3462, 4132
Lügger, T., 394. 2356, 2683
Lüken, M., 4036
Lukoyanov, A. N., 2421
Luo, J., 37
Luo, J.-L., 4774
Luo, L., 837
Luo, Q.-H., 4447
Luo, T.-T., 4253
Luobeznova, I., 1724
Lutz, M., 154, 591, 1675, 4036
Lutz, P., 4602
Lützen, A., 2301
Lyssenko, K. A., 1253, 1379
Lyubimov, S. E., 629
Lyubovskaya, R. N., 1794
Ma, C., 518, 2775, 3316, 3522, 3806
Ma, J. S., 1474, 1478
Ma, Q., 4807
Ma, S.-L., 1311
Maestro, M., 2542
Maestro, M. A., 4278
Magiera, D., 2160
Magull, J., 4046, 4056
Mahon, M. F., 4686
Maier, C.-J., 2635
Maimon, E., 4002
Majoral, J.-P., 2459
Mak, T. C. W., 286
Makal, A., 3335
Malaisé, G., 3987
Malandrino, G., 500
Malandrinos, G., 3326
Malatesta, M. C., 3901
Maldotti, A., 3127
Malget, J. M., 818
Malik, M. A., 171
Mallah, T., 2219, 4202, 4675
Manassero, M., 3901, 4484
Mancini, A., 3099
Maneiro, M., 2769, 3696
Manfredi, C., 2739
Mani, F., 293
Manna, S. C., 4202
Manning, T. D., 4470
Manotti Lanfredi, A. M., 4566
Mansuy, D., 301, 3127
Mantel, C. 3880
Manzano, B. R., 549, 2542
Mao, J.-G., 538, 1270, 3706, 3712
Mao, L., 2923
Marabello, D., 1505
Marcelis, A. T. M., 2847
Marchetti, F., 1219, 1494, 3484, 3938
Marchió, L., 960
Marconi, G., 2557
Marcos, M. D., 1799
Maresca, L., 4751
Margiotta, N., 1705, 3445
Mariet, C., 1190
Marinescu, G., 2914
Mariño, M., 2937
Marmion, C. J., 3003
Marotta, E., 1902
Marques, N., 98
Marrot, J., 33
Marschner, C., 3254
Marsden, C. J., 1939
Marsura, A., 3172
Martín, A., 1914
Martin, D., 3533
Martín-Álvarez, J. M., 2326
Martin-Vaca, B., 1939
Martineau, D., 3984
Martinez, V., 4770
Martínez-Agudo, J. M., 3783
Martins, J. C., 2908
Martins, M., 2027
Mas-Ballesté, R., 3223, 3585, 4146
Maschmeyer, T., 978
Masi, S., 2013
Masllorens, E., 1601
Massa, W., 3063
Massera, C., 3025, 4566
Mastrorilli, P., 1234
Masuda, H., 4140

Mathieu, D., 3127
Mathieu, J., 3172
Mathivet, T., 3247
Matouzenko, G., 4353
Matsubayashi, G., 2137
Matt, D., 4602
Mattioli, T. A., 301
Mautner, F. A., 309
May, A. M., 2160
Mayer, C. R., 973
Mayer, P., 2488
Mazej, Z., 1827
Maziéres, S., 2823
Mazzeo, M., 1292
Mbokalle, I.-M., 4132
Mbomekalle, I.-M., 276, 2036, 3462
McCormack, D., 1675
McInnes, E. J. L., 2811
Mealli, C., 707
Mechtler, C., 3254
Meder, M. B., 2716, 3424
Mehdoui, T., 1996
Mehring, M., 3240
Meier, U. W., 3057
Meisel, M., 3842
Mekki, S., 1190
Mekmouche, Y., 3163
Melánová, K., 570, 2493
Mena, M., 1914
Ménage, S., 3163
Mendoza, A., 4061
Mendoza, O., 4525
Mercier, F. A. G., 2908
Mercuri, M. L., 960
Merigo, A., 1219
Merkel, M., 783
Messina, M. A., 4710
Mews, R., 2446, 2452
Meyer, F., 1646, 2413
Meyer, S., 2001
Meyerstein, D., 3675, 4002
Mhiri, T., 2272
Miah, H. A., 4115
Mialane, P., 33
Miao, C.-Q., 2232
Michaelides, A., 1420
Michalik, M., 1538
Micheloni, M., 2853
Michels, M., 492
Michon, C., 2107
Mickoleit, M., 1538
Mijoule, C., 791
Milani, F., 1277
Milata, V., 549
Milios, C. J., 2885
Milius, W., 3601
Miller, M., 1212
Miller, M. L., 231
Mills, A. M., 1963, 4193, 4572
Milton, H. L., 3798
Minghetti, G., 4484
Miqueu, K., 381, 2289
Mirosavljevic, K., 3930, 4579
Mitewa, M., 2173
Miyabe, Y., 3651
Mo, M., 1785
Mochida, K., 2961
Modec, B., 1611
Moeller, S., 2160
Mohamadou, A., 1285, 3733
Mok, K. F., 2086
Molinari, A., 3127
Molnár, G., 4353
Mondal, A., 4633
Monfort, M., 250
Muñoz-Hernández, M.-Á., 3743
Montefusco, P., 1292
Monti, S., 646
Montiel-Palma, V., 3743
Montilla, F., 707
Monzani, E., 2203
Moragues-Cánovas, M., 2219
Morales-Varela, M. C., 949, 1914
Moreton, D. J., 4237
Mori, V., 1879
Mortreux, A., 3247
Morvillo, A., 810
Mösch-Zanetti, N. C., 2678
Mostafa, G., 250
Motevalli, M., 171
Moucheron, C., 3971
Moutiers, G., 1190
Mu, Y., 4891
Muga, I., 1886
Mügge, C., 3852
Muir, K. W., 1687
Mukherjee, P. S., 4675
Mukherjee, R., 2950, 4854
Mukherjee, S., 4209
Mukhopadhyay, S., 2950, 4854
Müller, D., 2283
Muller, G., 2348, 4278
Müller, P., 344
Müller, R., 2151
Muller, R. N., 463, 3538
Müller-Buschbaum, K., 4330
Münchow, V., 718
Mundwiler, S., 2013
Muñoz, M. C., 4770
Murso, A., 4272
Mutikainen, I., 3733
Myari, A., 1427
Nabeshima, T., 3779
Nadjo, L., 276, 2036, 3462, 4132
Nagawa, Y., 4216
Nahum, V., 4124
Nair, B. U., 1840
Nakai, K., 1621
Nakamura, M., 798
Nakano, M., 2137
Nanishankar, H. V., 3048
Nanjo, E., 2961
Nanjo, M., 2961
Narayanan, V., 872
Nardin, G., 4266
Naso, F., 3445
Nassimbeni, L. R., 2943
Natarajan, S., 762, 3846
Näther, C., 2553, 2868
Natile, G., 1705, 3445, 4751
Natrajan, L. S., 3724
Navarro, R., 2338
Nawrot, B., 4412
Neculai, A. M., 3508
Neculai, D., 3508
Nellutla, S., 3792
Nelson, J., 2570
Neretin, I. S., 1794
Nethaji, M., 1440, 3048
Neubauer, P., 3842
Neuburger, M., 685
Neumann, E., 4755
Newport, A., 4286
Neya, S., 1621
Ng, D. K. P., 286, 3806
Ng, S. M., 1788
Nick, H., 4177
Nickel, T., 2235
Nicolis, S., 2203
Nicoló, F., 3358, 4710
Nie, Y., 1630, 2425
Nierlich, M., 1225
Nikiforov, G. B., 3865
Nikolova, D., 2321
Nikonov, G. I., 771
Nishida, D., 3779
Nishioka, T., 356
Nitta, M., 743
Niu, J.-Y., 160
Niu, W., 3310
Nobile, C. F., 1234
Noblía, P., 322
Noethig-Laslo, V., 3930, 4579
Nolan, K. B., 3003
Noltemeyer, M., 2673, 2678, 3508, 4046, 4052, 4056, 4807
Nomiya, K., 4646
Nomoto, T., 154
Nöth, H., 601, 1115, 3612, 3629, 4764
Novais, H., 1318
Novaković, S. B., 2215
Novitchi, G., 1530, 1808
Nowik, I., 1859, 3476
Nowogrocki, G., 3247
O'Brien, P., 171
O'Neill, S. A., 4286
O'Sullivan, B., 3852
Obejero, P., 3089
Oehme, H., 1538
Ogata, H., 906, 1621
Ogilvie, H. R., 1007
Ogita, M., 4463
Ogliaro, F., 207
Ogura, M., 4547
Ohgo, Y., 798
Ohta, K., 3920
Ohta, T., 1169
Okamura, T., 1465
Okeya, S., 2632
Okubo, T., 4547
Okuda, J., 3724
Olabe, J. A., 2902
Olenev, A. V., 4006
Oleneva, O. S., 4006
Olkowska-Oetzel, J., 1100
Onaka, S., 4882
Ongania, K.-H., 1740, 2827
Oro, L. A., 2477, 4586
Ortigueira, J. M., 2937
Ortiz, M., 3353
Osborn, J. A., 3987
Otero, A., 260, 1299, 3353
Otero, L., 322
Otsuka, A., 1794
Ottaviani, M. F., 2853
Ouahab, L., 933
Oxtoby, N. S., 2008
Özdemir, I., 418
Ozeki, T., 4882
Pacchioni, G., 1705
Padma Malar, E. J., 2723
Pal, S., 4718
Pala, J. S., 3783
Pala, L., 3099
Palladino, G., 2739
Pan, C.-L., 1566
Pan, N., 510, 518
Pan, Z.-Q., 4447
Panda, B. K., 178
Pandey, D. S., 3555
Pandey, K. K., 4388
Pantenburg, I., 689
Panunzi, B., 2467
Pap, J., 2253
Papakyriakou, A., 3118
Pappalardo, D., 1292
Parac-Vogt, T. N., 3538
Parella, T., 612, 857
Park, J.-H., 171
Párkányi, L., 2253
Parkin, I. P., 4286, 4470
Pasán, J., 4081
Passarelli, V., 1714, 4439
Passmore, J., 3865
Pastor, A., 707
Pastorini, A., 4477
Pati, S. K., 3846
Patroniak, V., 2379
Pattacini, R., 1063, 3564
Patton, J. T., 3370
Paulo, A., 243
Paulusse, J. M. J., 4193
Pawlowski, V., 4242
Paz, F. A. A., 3031
Peacock, E. J., 1992
Pécaut, J., 3163
Pedersen, J. Z., 335
Pedrido, R., 2769, 3696
Peindy, H. N., 2646
Pelagatti, P., 1985
Pelizzi, G., 1922
Pellecchia, C., 1292
Peng, Y., 2673, 3310
Peng, Z., 1165
Perdikaki, K., 2283
Pereira, M. T., 2937
Pérez, J., 2706
Pérez-Lourido, P., 635
Pérez-Manrique, M., 2542
Perlepes, S. P., 2885
Peräniemi, S., 2627
Peruzzini, M., 293
Pescarmona, P. P., 978
Peters, E. S., 4470
Peters, K. P., 581
Pétillon, F. Y., 1687
Pettinari, C., 3484
Pettinari, R., 3484
Peyronneau, M., 2823
Pfeffer, M., 2107
Pfister-Guillouzo, G., 381, 2289
Phillips, C., 3484
Philouze, C. 3880
Piérart, C., 3538
Pierre, J.-L., 4036
Pietrusiewicz, K. M., 2160
Pillinger, M., 1389, 3913, 4914
Pinilla, E., 857, 3089
Piotrowski, H., 2488
Piro, O. E., 322
Planeix, J.-M., 453
Poater, A., 612
Pol, V. G., 1859
Polborn, K., 1330
Poli, R., 726, 1081, 4108
Pombeiro, A. J. L., 1411
Ponikvar, M., 1349, 3273
Ponikwar, W., 1330
Pope, M. T., 276, 4132
Potvin, P. G., 1763
Pozdniakova, Y. A., 1253
Prakash, R., 1847, 4291
Pramanik, K., 4633
Präsang, C., 3063
Prashar, S., 1299
Predieri, G., 1063, 3564
Preishuber-Pflügl, P., 1740, 2827
Presa-Soto, A., 3668
Prestwich, T. G., 4381
Price, D. J., 1007
Priego, J. L., 4491
Pritzkow, H., 1630, 1646, 2413, 2425, 2635, 3644, 4223
Prosvirin, A. V., 3706
Protasiewicz, J. D., 998
Pruvost, S., 1661
Przybylak, K., 1639
Psychogios, N., 2514
Puerta, M. C., 17

 © 2004 Wiley-VCH Verlag GmbH & Co. KGaA, Weinheim

INDEX

Pursche, D., 879
Qian, X., 557
Qian, Y., 1785, 4521
Qiu, S., 185
Quesada, M., 4566
Quitmann, C. C., 4330
Radius, U., 4300
Rager, M.-N., 4371
Rais, D., 1865
Rajak, K. K., 4633
Ramdeehul, S., 3987
Ramirez, A. P., 2434
Ramírez, F. de M., 2348
Ramírez de Arellano, C., 3814
Randaccio, L., 653, 4266
Rao, C. N. R., 1733
Raptopoulou, C. P., 2885, 3822
Rath, S. P., 1873
Rau, S., 2001
Raubenheimer, H. G., 2943
Rausch, B. J., 2585
Ray, M. S., 3110
Ray, U., 250
Ray Chaudhuri, N., 4202, 4675
Razavi, A., 943
Real, J. A., 4770
Rebbouh, L., 3345
Rebière, B., 726
Reddig, N., 879
Reddmann, H., 98
Reddy, P. A. N., 1440
Reedijk, J., 591, 1963, 3025, 3733, 4036, 4566, 4572, 4828
Reeske, G., 2283
Refosco, F., 1902
Reger, D. L., 3345
Regnouf-de-Vains, J.-B., 2514
Rehder, D., 4115
Rehmann, F.-J. K., 4525
Reibenspies, J. H., 231
Reicke, M., 2733
Reilly, L., 3163
Reinaud, O., 1817, 4371
Ren, G.-M., 2232
Repo, T., 695, 4702
Rheingold, A. L., 3310, 3370
Ribas, J., 250, 3110, 3228, 4202, 4633
Ribeiro-Claro, P. J. A., 3913
Ricard, L., 2219
Richard, P., 1081
Richmond, W. R., 227
Rieger, B., 3057
Rigo, P., 524
Rillema, D. P., 4836
Rivarola, E., 3484
Rivière, E., 33, 1225, 2219
Robé, E., 4108
Rocha, J., 1389, 2759, 3031, 4914
Röder, J. C., 1646
Rodríguez, A., 549
Rodríguez, A. M., 260
Rodríguez, M., 612, 1601
Rodríguez, M. J., 2769
Rodríguez, Y., 2078
Rodríguez-Fortea, A., 143
Roelfes, G., 846
Roesky, H. W., 2673, 2678, 3508, 4046, 4052, 4056, 4807
Roesky, P. W., 1045
Rogerson, E., 4237
Roglans, A., 1601
Rogolino, D., 1985
Román, P., 1886
Romanenko, V., 381
Romanenko, V. D., 2289
Romão, C. C., 3305, 4914
Romero, I., 612
Romero, J., 635
Rominger, F., 2585, 4021, 4223
Rompel, A., 879
Roncaroli, F., 2902
Roncone, R., 2203
Ronig, B., 689
Ronson, T. K., 2570
Roodt, A., 4640
Roques, N., 2823
Rosa, P., 707, 3017
Rosenthal, E. C. E., 4681
Rosenthal, U., 4739
Ross, S., 984
Rossi, M., 3484
Roszak, S., 1212
Roth, R. S., 2434
Rothenberger, A., 2933
Rotondo, A., 4710
Rotondo, E., 4710
Rotthaus, O., 1545
Roubeau, O., 4036
Roviello, A., 2467
Roy, T. G., 4115
Royo, B., 3305
Royo, P., 3074, 3814
Rudolf, M., 2001
Rudzevich, V., 381
Rudzevich, V. L., 2289
Rufanov, K. A., 4759
Ruiz, E., 143
Ruiz-Hitzky, E., 949
Ruiz-Pérez, C., 3873, 4081
Ruiz-Ramírez, L., 4061
Rupp, H., 344
Ruppert, R., 4216
Ryeng, H., 4555
Sá Ferreira, R. A., 3913
Saak, W., 2301
Sabolovic, J., 3930
Sadun, C., 2739
Sahin, Y., 3063
Saiki, T., 3779
Saillard, J.-Y., 1063
Saint-Aman, E., 4036
Saito, G., 1794
Saito, M., 743
Sakai, Y., 4646
Sakellariou, E. G., 575
Sakurai, H., 322
Sala, X., 612
Saladini, M., 646
Saloni, J., 1212
Salzer, A., 2235, 2244
Sampaolesi, S., 2853
Sánchez, F., 1955
Sánchez, G., 2706
Sánchez-Barba, L., 260
Sánchez-Méndez, A., 3287
Sanchiz, J., 4081
Sandri, M., 524
Sansoni, M., 3901
Santamaría, C., 1914
Santillan, R., 118
Santos, I., 243
Santos, T. M., 612, 1389, 4914
Sanz, N., 309
Saravanakumar, D., 872
Sarkar, B., 2902
Sarkar, S., 4633
Sauvage, J.-P., 575
Scagliola, S., 4266
Scarpellini, M., 1879
Schäfer, B., 2001
Schareina, T., 3297
Schat, G., 1175, 2045
Scheer, M., 2062
Scheer, P., 93
Schenk, W. A., 4859
Schindler, S., 335, 344
Schisler, A., 3277
Schlenker, M., 2974
Schlindwein, W., 619
Schlünken, C., 2477
Schmalle, H. W., 3544
Schmid, R., 2609
Schmidt, H.-G., 2673, 2678, 3508, 4046, 4052, 4807
Schmohl, K., 1538
Schneider, N., 4216
Schneiderbauer, S., 1330
Schnieders, D., 783
Schollhammer, P., 1687
Schottek, J., 1175
Schröder, D., 44
Schubert, U., 776, 1835, 2658
Schuenemann, V., 3163
Schulte, J. H., 2585
Schumann, H., 2421, 3852
Schurr, T., 4510
Schutte, S., 4759
Schwab, I., 3612, 4764
Schwan, K.-C., 2062
Schwartz, M., 3612
Schwarz, H., 44
Schwiegk, S., 1630
Scopelliti, R., 530, 964, 1630, 2173, 4232
Scott, N. M., 3297
Sebastián, A., 3814
Sebastián, R.-M., 2459
Sécheresse, F., 33, 973
Sedej, B., 1349
Seebacher, J., 409
Sellmann, D., 581, 1847, 3136, 4291, 4591
Sémeril, D., 418, 4602
Sénèque, O., 1817
Sengottuvelan, N., 872
Sengupta, S., 178
Senthilkumar, G., 872
Serpe, A., 960
Serrano, J. L., 2706
Serratrice, G., 1552
Severin, K., 964
Sevillano, P., 1100
Shaban, S. Y., 4591
Shahin, A. M., 4572
Shaik, S., 207
Shakirov, M. M., 2452
Shamir, D., 4002
Shan, X., 1474
Shan, Y., 237
Shapiro, P. J., 3370
Sharma, P., 1107
Sharma, P. K., 207
Sharma, S., 3555
Shaw, J. L., 1073
Shchegolikhina, O. I., 1253
Shen, E., 4102
Shen, M.-C., 4447
Shen, Q., 2167
Sheng, E., 2923
Sheng, T., 1198
Shevelkov, A. V., 4006
Shi, F.-N., 2759, 3031
Shi, J.-X., 2066
Shi, Q., 1595, 2747
Shi, X., 185
Shieh, D.-L., 2223
Shin, D. M., 1522
Shiomi, D., 356
Shiryaev, A. A., 629
Shiu, K.-B., 2223
Shmyrova, Y. V., 3453
Shova, S., 1530
Shubina, E. S., 3453
Shur, V. B., 4739
Shutov, P. L., 2123, 2498
Si, S.-F., 401
Siebert, W., 1630, 2425, 2635, 4223
Siega, P., 4266
Sieger, M., 2902
Siegrist, T., 2434
Sierka, M., 2933
Sierra, J. C., 2260
Siggelkow, B., 3424
Sillanpää, R., 1402
Silva, A. R., 2027
Silva, A. S., 1879
Silverstru, C., 3743
Silvestri, G. F., 3287
Simão, D., 1318
Simkhovich, L., 1724
Simon, A., 2160
Simonov, Y. A., 2914
Singh, A. K., 1107
Singh, H. B., 1014
Singh, S., 2673, 4052
Sinha, C., 250
Skatova, A. A., 388
Skelton, B. W., 227, 1992
Skoulika, S., 1420
Sletten, J., 4836
Slinn, C., 879
Slovokhotov, Y. L., 1794
Smith, M. D., 3345
Smith, R. C., 998
Smolensky, E., 4795
Smucker, B. W., 368
Sobota, P., 1639
Sokolov, M. N., 63
Sola, J., 4871
Solans, X., 612
Soler, T., 2338
Solladié, N., 2557
Song, J.-F., 4375
Song, J.-L., 538, 3706
Song, L.-C., 866, 3147
Song, Y., 2754, 3025, 3681, 3718
Song, Y. F., 4566
Song, Y.-L., 866, 3147
Sooambar, C., 2557
Sorace, L., 3887
Soriano, C., 4061
Sortino, S., 4561
Sotiropoulos, J.-M., 381, 2289
Sousa, A., 635
Spannenberg, A., 4739
Specos, M., 3938
Speier, G., 2253
Spek, A. L., 154, 591, 1175, 1675, 1963, 2045, 4036, 4193, 4572
Spingler, B., 2013
Sreerama, S. G., 4718
Stalke., D., 4272
Stamatatos, T. C., 2885
Stanghellini, P. L., 1505
Starikova, Z. A., 3476
Stasch, A., 4046, 4052, 4056
Stassen, A. F., 591, 4036
Steel, P. J., 329, 376
Steiner, G., 1740, 2827
Steinhauser, S., 4177
Steinke, T., 4161
Stelzer, O., 2235
Steudel, R., 718, 3513
Steudel, Y., 3513
Štíbr, B., 1402, 3601, 3605
Stoccoro, S., 4484
Stoeckli Evans, H., 857, 2514
Stoffelbach, F., 726
Stoppioni, P., 293
Stowe, A. C., 3792
Strasdeit, H., 2301

 © 2004 Wiley-VCH Verlag GmbH & Co. KGaA, Weinheim

Strukul, G., 1030
Studt, F., 2553
Sturmayr, D., 776, 2658
Stuzhin, P. A., 1621, 2877
Su, C.-C., 2180,42 53
Su, F.-H., 866
Su, Q., 4891
Suardíaz, R., 3353
Sudhölter, E. J. R., 2847
Sudupe, M., 3074
Sugibayashi, M., 3920
Sugimoto, H., 4550
Sun, C., 3262
Sun, D., 2144, 2228, 2747
Sun, L., 1454, 3316
Sun, R.-Q., 2096
Sun, W.-Y., 1465, 1894
Sun, X., 518, 3806
Sun, Y., 37
Sun, Y.-H., 1051
Sun, Y.-Q., 1514, 3837
Sunada, Y., 134
Sunahara, T., 4882
Sundermeyer, J., 2498
Suranna, G. P., 1234
Süss-Fink, G., 2405, 3907
Suzuki, H., 2632
Suzuki, T., 4463
Szczegot, K., 1639
Szmigielska, A., 2160
Tabernero, V., 3154
Tacke, M., 4525
Tagliatesta, P., 4477
Takahashi, H., 4140
Takahashi, M., 798
Takeda, M., 798
Takeuchi, T., 3920
Talarico, A. M., 2557
Talarmin, J., 1687
Tamura, H., 2137
Tanaka, K., 4550
Tanase, S., 1963, 4572
Tanase, T., 3920
Tang, K., 78
Tang, W.-X., 1894
Tangen, E., 2442, 2442
Tangoulis, V., 3822
Tanski, J., 3484
Tao, J., 125
Taraszewska, J., 3335
Tatsumi, K., 86, 134
Tauzher, G., 653, 4266
Taylor, P. R., 4555
Taylor, R. J. K., 2706
Tedesco, C., 1292
Teives Henriques, R., 1318
Teixidor, F., 1402
Tejeda, J., 260
Tekautz, G., 4259
Teplitskaya, L. N., 3453
Tersago, K., 3798
Teruel, H., 4278
Terzis, A., 2885, 3822
Therrien, B., 2405
Thétiot, F., 3783
Thewalt, U., 3057
Thirumurugan, A., 762
Thomas, F., 1552
Thöne, C., 749
Thouvenot, R., 3828
Thuéry, P., 1996, 4502, 4624
Thummel, R. P., 3269
Tian, G., 185
Tian, Y.-Q., 1039, 1813
Tiekink, E. R. T., 445
Tijmensen, J. A., 4193
Tiripicchio, A., 1063, 1447, 1705, 3564
Tisato, F., 1902
Toftlund, H., 335
Tok, O., 3297
Toledo, J. C., 1879
Tomas, A., 1545
Tomasin, P., 3887
Tomić, Z. D., 2215
Tong, Q.-X., 1948
Tonucci, L., 810
Top, S., 2013
Tornil, M. L., 423
Torres, G. R., 335, 3089, 4491
Toscano, R. A., 1107
Tóth, G., 2160
Tötös, S., 749
Toupet, L., 4803
Trautwein, A., 3163
Trchová, M., 570, 2493
Tresoldi, G., 3358
Tressaud, A., 1827
Trifonov, A. T., 4396
Triki, S., 3783
Trindade, T., 2759, 3031
Trogu, E. F., 960
Truflandier, L., 1939
Trzeciak, A. M., 1411
Tsai, H.-L., 4253
Tsai, S.-Y., 2180
Tsai, Y. C., 2180
Tsang, H.-S., 2180
Tsarev, V. N., 629
Tschan, M. J.-L., 2405
Tsukube, H., 4550
Tsukuda, T., 4463
Tsutsumi, Y., 134
Tu, C., 4028
Tubaro, M., 1902
Tung, C.-H., 1948
Turpeinen, U., 3733
Turrin, C.-O., 2459
Tuzi, A., 2467
Twamley, B., 3370
Tyurin, D. A., 2498
Tzing, S.-H., 1753
Uccelli, L., 1902
Udayakumar, D., 1733
Ueng, C.-H., 4253
Ueyama, N., 1465
Uguagliati, P., 732
Uhl, W., 969
Urbanos, F. A., 4491
Urriolabeitia, E. P., 2338
Urrutigoïty, M., 791
Vaduvescu, S., 1763
Vagin, S., 2877
Vahrenkamp, H., 409, 1198
Vaidyanathan, V. G., 1840
Vajenine, G. V., 3233
Valente, A. A., 4914
Valerga, P., 17
van Albada, G. A., 3733
Van Alsenoy, C., 3798
van der Vlugt, J. I., 4193
van der Waal, J. C., 978
Van Droogenbroeck, J., 3798
van Eldik, R., 653
van Klink, G. P. M., 154
van Oort, B., 2442
Van Poeck, M., 2908
van Santen, R. A., 675
Vanderah, T. A., 2434
Vander Elst, L., 463, 3538
Varbanov, S., 2173
Vasca, E., 2739
Vatsadze, S. Z., 2008
Vázquez, M., 2769, 3696
Vendier, L., 317
Venkatesan, K., 3544
Ventura, B., 2557
Vepsäläinen, J. J., 2627
Verani, G., 2008, 2363, 3099, 4660
Verardo, G., 524
Vermonden, T., 2847
Vetrichelvan, M., 2086
Vicent, C., 63
Vicente, R., 309, 2885
Videva, V., 2173
Vidovic, D., 4046
Vieille-Petit, L., 3907
Vigato, P. A., 3887
Vila, J. M., 2937
Vilar, R., 1865
Villafañe, F., 2326
Villanueva, A., 949
Villiers, C., 4624
Vilminot, S., 2272
Viñas, C., 1402
Vincendeau, S., 4108
Virovets, A. V., 63
Visentin, F., 732
Visinescu, D., 2914
Vitali, I., 3127
Vitoria, P., 1886
Vittal, J. J., 1056
Vives, J., 2706
Vogel, E., 492
Vogel, U., 2062
Vogler, A., 4242
Vogt, D., 4193
von Hänisch, C., 2321
Vos, J. G., 2001
Vrieze, K., 1675
Vujovic, D., 2943
Wachter, J., 1367
Wagener, M., 4755
Wagner, T., 1396
Walter, O., 335, 344
Walther, D., 1243
Wang, D., 3806, 4521
Wang, E., 1385
Wang, E.-B., 4102
Wang, G., 2956
Wang, G.-L., 2369
Wang, H., 4653
Wang, H.-T., 866
Wang, J., 1165, 1992
Wang, J.-P., 160
Wang, L.-Y., 2266
Wang, N.-L., 4774
Wang, P., 2819
Wang, R., 37, 185, 1396, 1595, 2695, 3751
Wang, R.-J., 401, 4608
Wang, S., 1385, 2923, 3662, 3681, 4669, 4907
Wang, S.-L., 2180
Wang, T.-C., 1668
Wang, T.-F., 1668
Wang, T.-G., 1566
Wang, W., 1454, 3522
Wang, X., 946, 4028
Wang, Y., 459, 2144, 2819, 4616, 4907
Wang, Z., 1474, 3662, 4669
Wang, Z.-M., 2968
Wang, Z. Y., 4317
Warchhold, M., 1115
Warchulska, J., 110
Weber, S., 3612
Wei, J.-C., 1039
Wei, M.-L., 160
Wei, Y., 2819, 3946
Wei, Z.-B., 125
Weißhoff, H., 3852
Weisman, G. R., 3310
Welter, R., 4602
Wen, T. B., 2837
Wen, Y.-S., 1668
Weng, L.-H., 1813
Werner, H., 469, 481, 2477
Wernsdorfer, W., 2219
Werz, D. B., 2585, 4021
Wesemann, L., 689
Weyhermüller, T., 984, 4177, 4209
White, A. H., 227, 1992
White, A. J. P., 818, 1865
Wiebelhaus, D., 4011
Wieber, S., 2933
Wieghardt, K., 984
Wietelmann, U., 3612
Wilberger, R., 2488
Wilhelm, M., 2301
Willem, R., 445, 2908
Williams, D. J., 818, 1865
Williams, I. D., 2837
Wilson, C., 2008, 3724
Winter, C. H., 2652
Wippert Rodrigues, C., 3644
Wolf, J., 469
Wolf, R., 3277
Wolff, F., 2861
Won, Y. C., 1522
Wong, E. H., 3310
Wong, K.-Y., 1056
Wong, W.-K., 267, 829, 837
Wong, W.-T., 829
Wong, W.-Y., 267, 829, 837, 2066
Woollins, J. D., 171, 3798, 4795
Woźniak, K., 3335
Wozniczka, M., 4412
Wrackmeyer, B., 3601, 3605
Wu, B., 2695
Wu, G., 185
Wu, J., 1056
Wu, L.-Z., 1948
Wu, P., 2819
Wu, X.-T., 2096
Wu, Y., 2923
Wu, Z.-X., 1948
Wurst, K., 1740, 2827
Xavier, C., 243
Xavier, K. O., 4795
Xiao, D., 1385
Xie, C.-Z., 2369
Xie, F.-T., 4375
Xie, X., 78
Xie, Y., 557
Xin, X., 2754
Xin, X.-Q., 4653
Xiong, S., 1478
Xochipa, R., 118
Xu, H.-J., 1813
Xu, J.-Q., 1051, 1566, 4375
Xu, L., 37, 1039, 1385, 1595, 3751, 4102
Xu, M.-Q., 1311
Xu, Q.-F., 86, 4247
Xu, R., 2956, 3718
Xu, S., 4653
Xu, X., 69
Xu, Y., 1385, 4247, 4457, 4547
Xue, M., 185, 2167
Yamamoto, Y., 134, 3651
Yamane, H., 4828
Yan, C.-H., 2968
Yan, S.-P., 562, 1514, 2130, 2266, 2369
Yang, B., 1785
Yang, D.-X., 1894
Yang, G., 2923, 4907
Yang, G.-D., 1566
Yang, G.-J., 1051
Yang, G.-M., 1514
Yang, G.-Y., 953, 2004, 3837

 © 2004 Wiley-VCH Verlag GmbH & Co. KGaA, Weinheim

INDEX

Yang, L., 1474, 1478
Yang, Q.-Z., 1948
Yang, X., 1785
Yang, Y.-L., 4891
Yang, Z., 4028
Yao, Y., 2167
Yates, B. F., 1992
Ye, L., 4375
Yeh, C.-W., 4696
Yeung, C. H., 1788
Yi, L., 2130
Yin, C., 1788
Yin, X., 125
Ying, S.-M., 1270
Yip, J. H. K., 1056
Yong, G.-P., 4317
Yoshioka, M., 743
You, X.-Z., 1039, 1813, 3681
Yoza, K., 4646
Yu, G.-A., 866
Yu, J., 2956, 3718
Yu, S., 237
Yu, Z., 3662, 4669
Yuan, D., 37, 2228, 3695
Yuan, D.-Q., 4457
Zabirov, N. G., 423
Zacchini, S., 1494
Zachariadis, P. C., 1420
Zaitseva, G. S., 2123, 2498
Zakherov, L. N., 3310
Zàliš, S., 2784, 2902
Zander, L., 492
Zanella, P., 1714, 3901, 4439
Zangrando, E., 4202, 4675
Zanotti, V., 1494
Žarić, S. D., 2215
Žemva, B., 1827
Zeng, H.-Y., 538
Zeng, X., 4371
Zhang, D., 185
Zhang, D.-Q., 4774
Zhang, H.-H., 2096
Zhang, J., 953, 956, 2004, 2775, 3837, 4028
Zhang, J.-J., 2096
Zhang, J.-P., 1024, 1948
Zhang, M., 3718
Zhang, R., 2775
Zhang, R.-H., 1701
Zhang, S., 510, 4028
Zhang, X., 1454, 3522
Zhang, X.-M., 544
Zhang, Y., 78, 2167, 4247
Zhao, B., 562, 2369
Zhao, D.-Y., 1813
Zhao, F., 69
Zhao, H.-H., 3706
Zhao, L., 78
Zhao, Y., 4072
Zhao, Z., 837
Zheng, H., 2754
Zheng, L.-S., 125
Zheng, S.-L., 1024
Zheng, S.-T., 953, 2004
Zheng, W., 2652
Zheng, X., 3262
Zheng, X.-J., 2968
Zhou, B. C., 401
Zhou, H.-C., 3681
Zhou, J., 2754
Zhou, L., 2167
Zhou, S., 2923
Zhou, Y., 2695, 3751
Zhou, Y.-F., 4457
Zhou, Z. Y., 2837
Zhou, Z., 829, 1595
Zhu, D.-B., 4774
Zhu, D.-S., 4891
Zhu, G., 185
Zhu, H., 2673, 3522, 4046, 4807
Zhu, H.-F., 1465
Zhu, J.-J., 4072, 4653
Zhu, L., 557
Zhu, N., 1341
Zhu, P., 510, 518, 3806
Zhu, Q.-Y., 4789
Zhu, W.-X., 1311
Zhu, Y., 3946
Zhuang, J., 946
Zibarev, A. V., 2446, 2452
Zięba, K., 3335
Ziegler, C. J., 1073
Ziemer, B., 3852, 4759
Ziener, U., 2877
Zijp, E. J., 4193
Zilbermann, I., 4002
Zima, V., 570, 2493
Ziółkowski, J. J., 1411
Zirngast, M., 3254
Zong, R., 3269
Zou, G., 4521
Zucca, A., 4484
Zuo, J.-L., 3681

 © 2004 Wiley-VCH Verlag GmbH & Co. KGaA, Weinheim

1. General Information

The *European Journal of Inorganic Chemistry* (*EurJIC*) is published twice monthly.

Manuscripts should be submitted online using our online submission service at http://webeos.wiley-vch.de/osm/jsp/osm.jsp. You should prepare a **single file containing all tables, graphics, supporting information (where appropriate) etc.** Acceptable file formats are **Microsoft Word, Rich Text Format, Postscript and PDF**. Avoid the use of page breaks even between the title page and the introduction, and try to fit as many graphics as possible onto a single page if they are not inserted into the correct position in the text. The file should have margins of 2 cm and be 1.5-line spaced.

Authors can follow the progress of their manuscript on their **personal homepage**, which is created automatically upon initial registration. This homepage is the same for the family of Wiley-VCH European journals and can be used to **store all versions of a submitted paper** and to **upload the revised manuscript after acceptance**. Your referee reports for the family of Wiley-VCH European journals are also archived here.

No paper copies of the manuscript are required when using this system.

- The author must inform the editor of all manuscripts submitted, soon to be submitted, or in press at other journals that have a bearing on the manuscript being submitted.
- The correspondence author of a Microreview will receive a complimentary copy of the journal along with a PDF file of his/her paper restricted to 50 printouts; the correspondence author of other articles will receive a PDF file restricted to 25 printouts. Colour figures can be reproduced. Unless essential for the understanding of a paper, authors will be requested to make a contribution towards the costs of colour reproduction. Details will be provided after acceptance of the manuscript.
- We encourage authors to submit pictures for the cover page.

IMPORTANT: Any manuscript already available on personal/group web pages will be considered by the editors as already published and will not be accepted.

2. Types of Contributions

EurJIC publishes articles on synthetic organic chemistry, bioorganic chemistry and physical organic chemistry. All contributions undergo peer review. An author may appeal against the decision on his/her manuscript, in writing. Three types of contributions are accepted for publication:

- **Full Papers** are articles with an Experimental Section that describe a significant contribution to the development of an area of research of importance. There are no restrictions placed on the length of a Full Paper.
- **Short Communications** are brief reports on results of high significance and urgency. Generally, they are no longer than 12−16 double-spaced pages or 3−4 typeset pages. An Experimental Section (as a separate paragraph or as part of the references) is desirable; if it is not included in the paper, the experimental data should be submitted as Supplementary Material for refereeing purposes, and marked as such.
- **A Microreview** introduces the reader to a particular area of an author's research through a concise overview of a selected topic. As a rule, Microreviews are written on invitation, although unsolicited articles are also welcome. It is recommended, however, to contact the editor before submitting an unsolicited Microreview. The content should balance scope with depth; it should be a focused review of 25−30 double-spaced pages or 6−8 typeset pages. Reference to important work from others that is significant to the topic should be included. Microreviews will be refereed but will have no Experimental Section.

A modular version of these Guidelines is available as separate PDF files on the internet at http://www.eurjic.org.

3. Document Templates

Document template files have been created to assist authors in preparing manuscripts for the *European Journal of Inorganic Chemistry*. Use of this easy-to-follow tool facilitates manuscript preparation, reduces revision and shortens publication times.

The files **eurjournw97.dot** for PC, **eurjourn.dot** for Mac (Mac Word 6) or **eurjournoffice2001mac.dot** (Mac Word 2001) can be downloaded from our Guidelines on the World Wide Web (http://www.eurjic.org), where more information on their use may be found.

4. Manuscript Preparation

4.1 General

The whole of the manuscript should be 1.5-line spaced and in a large script (Times New Roman, 12 pt). We recommend that you prepare your text with **Microsoft Word (PC or Macintosh versions)** (see Section 4.2). Use the automatic pagination function incorporated in your word processor to number the pages; do not insert page numbers by hand. Leave a 2-cm margin around the perimeter of each page. **The figures, schemes and graphical abstract in the accepted version should be camera-ready**. Consult a current issue of the journal for an overview of the format. A manuscript should comprise: □ Title Page □ Keywords □ Main Text □ Experimental Section □ Acknowledgments (optional) □ Captions □ Tables □ References □ Schemes and Figures □ Graphical Abstract (without text). □ For Microreviews only: Biographical sketch and a portrait-quality photograph.

4.2 Text

The text should be typed with carriage returns (hard returns) only at the end of a paragraph, title, heading, and similar features. Avoid end-of-line word divisions.

 © 2004 Wiley-VCH Verlag GmbH & Co. KGaA, Weinheim

Use character formatting for italic and bold characters. Avoid any *special style sheets* to format these features. Write *capital letters* using the keyboard (shift + letter key), **not** the format "Capital letter" in Word.

Use only characters from the Symbol and Normal Text character sets, especially when inserting Greek letters and characters with umlauts, accents, tildes, etc.: α, Å, ã, ä, à.

There are three types of hyphens: normal dashes (-), N-dashes (–), and M-dashes (—) on your keyboard. Use these as illustrated — spacing is important too — in the following examples:

well-known reaction	C–H bond
six-membered ring	Tables 2–4
3-position of the ring	carbon–oxygen bond
signal-to-noise ratio	C–N stretch
Mo-K_α	Diels–Alder reaction
1,2-dicyanobutane	structure–activity relationship
p-tert-butylphenol	
(–)-tartaric acid	
$[M^+ - CH_3]$	carried out at −10°C
80–100 mg	cm^{-1}

Use the symbol × where appropriate, rather than the letter x:
... washed with water (2 × 150 mL) ...
Use the double quotation marks "..." rather than „...“, "..." or «...»

Graphics (including structural formulas, schemes, figures, equations, small graphical items that appear in captions, and tables containing graphical items) must be submitted camera-ready on separate sheets after acceptance of the manuscript (see Section 4.5).

The Field, Object, or Formula-Editor commands on the Insert menu should be avoided, consult the table below to create the depicted graphical symbols.

Instead of these graphical symbols	$P\bar{1}$	L_2^{2+}	$\tilde{\nu}$	$[\alpha]_D^{20}$
please use these text alternatives	*P*1bar	$L_2{}^{2+}$	nu(tilde)	$[\alpha]_D{}^{20}$

Lines or **arcs**, for example to indicate ring compounds, cannot be used within the text. Another method for indicating such compounds must be devised. Please contact the Editorial Office if any help is needed.

4.3 Tables

Use the Insert Table command from the Table menu or use the Insert Table button on the Standard toolbar for creating tables. Exception: Tables *containing* embedded graphical items are treated as graphics and will be scanned. Please do not use hard returns or tabs within the cells of a table; instead use a *soft return* (shift + return).

4.4 References

We strongly recommend the use of the Endnotes feature of Word. If you prefer not to use this function, references should be indicated by numbers in square brackets as superscripts and, if applicable, after punctuation (example: text.[1]). Use the Format Font menu. In the case of Endnotes the square brackets are not needed.

The Author is responsible for correct citations. The *European Journal of Inorganic Chemistry* is a member of Cross Ref. (http://www.crossref.org), a service which links reference citations to the online content that those references cite. This can only function if the citations are accurate. Please ensure that only one reference is cited under each reference number. For example:

[1] A. Einstein, A. N. Other, *Eur. J. Inorg. Chem.* **2003**, 1–15.
[2] P. Pat, A. Pandy, *Chem. Eur. J.* **2003**, *7*, 222–229.

rather than:

[1] A. Einstein, A. N. Other, *Eur. J. Inorg. Chem.* **2003**, 1–15; P. Pat, A. Pandy, *Chem. Eur. J.* **2001**, *7*, 222–229.

References subdivided into parts a, b, etc. are, however, acceptable. For example:

[1] [1a] A. Einstein, A. N. Other, *Eur. J. Inorg. Chem.* **2003**, 1–15.
[1b] P. Pat, A. Pandy, *Chem. Eur. J.* **2001**, *7*, 222–229.

4.5 Graphics

Graphics are schemes, figures, equations, small graphical items that appear in captions, and tables containing graphical items. Graphics differ fundamentally from the text portion of your manuscript in that they must be scanned or electronically processed and will appear in the journal exactly as they are submitted. In the revised version please submit **each graphic in its own file** within a graphic folder. The following formats are preferred: *.chm, *.cdr, *.cdx, *.doc, *.wmf (windows metafile), *.pdf, *.pct, *.tif, *.eps. For good reproduction the resolution should be a minimum of 300 dpi. If you wish to embed graphics in Winword, please send us two files only, one containing the text and one containing all graphics.

Consult the following table for the appropriate size of lettering. Lettering smaller than 3.0 mm will reproduce poorly. Use only one size of lettering per graphic, and please use a font like Times (or Times New Roman) which distinguishes between l (small L) as in HCl (hydrochloric acid) and I (capital i) as in HCI (iodocarbene).

Table 1. Guide for preparing graphics

Letter Size	Font	Maximum Graphic Width[a] 1-Column Format	2-Column Format
	Times New Roman		
3.0 mm	12	13 cm	26 cm
3.5 mm	**14**	**15 cm**[b]	–
4.0 mm	**16**	**17 cm**[b]	–
4.5 mm	18	19 cm	–

[a] Most graphics are in 1-column format. [b] We prefer lettering of 3.5 or 4.0 mm with maximum graphic widths of 15 or 17 cm, respectively.

Note that the graphical abstract must be in one-column format. Typically, one-column graphics constructed with ChemDraw should have the following settings: Print Setup: Orientation Portrait. Caption and Label Settings: Font Times New Roman, Font Style Standard, Size 12. **It is not possible to use colour in the Table of Contents**.

These settings help ensure the correct letter-size-to-graphic-width ratio for best reproduction.
Use abbreviations such as R^1, R^2 (not R_2), R′, R″, Ph, Me, Et, *i*Pr, *t*Bu, Ph, Bzl (benzyl), Bz (benzoyl), Hal, L, M (metal, not Me), X (heteroatom).

Attention **Macintosh** users: Please note that we cannot handle Mac-formatted Zip media.

Please note these details regarding the graphics files:
If the formula schemes of your manuscript are prepared with ChemDraw, please **save them as separate files when you come to submit your revised version**. They can then be collected in a single zip file for upload on your personal homepage.

All other graphics (formulae, schemes and figures not prepared with ChemDraw) should be saved separately as a *.doc file (Word) or in a Word-compatible graphics format [e.g., bitmap (*.bmp), windows metafile (*.wmf), pict (*.pct)].

 © 2004 Wiley-VCH Verlag GmbH & Co. KGaA, Weinheim

6. Crystallographic Data

Authors must deposit the data of X-ray structure analyses in a crystallographic database before submitting their manuscript, so that referees can access the information electronically. The two databases, the Cambridge Crystallographic Data Centre (CCDC) and the Fachinformationszentrum Karlsruhe (FIZ) have the same procedure for the deposition of data and both will be pleased to provide help. In general, you will receive a depository number from the database two working days after electronic deposition. Send your data to the appropriate address below and quote the standard text, including the depository number, in your manuscript.

- **For all compounds without C-H bonds:**

Fachinformationszentrum Karlsruhe (FIZ)
76344 Eggenstein-Leopoldshafen, Germany
Phone: +49-(0)7247/808-205
Fax: +49-(0)7247/808-666;
E-mail: crysdata@fiz-karlsruhe.de
FTP: ftp.fiz-karlsruhe.de (under path /pub/csd)
WWW: http://www.fiz-karlsruhe.de (under "Products and Services ")

Further details of the crystal-structure investigation(s) may be obtained from the Fachinformationszentrum Karlsruhe, 76344 Eggenstein-Leopoldshafen, Germany, on quoting the depository number(s) CSD-....

- **For all compounds with at least one C-H bond:**

Cambridge Crystallographic Data Centre (CCDC)
12 Union Road, Cambridge CB2 1EZ, UK
Phone: +44-(0)1223/336-408
Fax: +44-(0)1223/336-033
E-mail: deposit@ccdc.cam.ac.uk
WWW: http://www.ccdc.cam.ac.uk

CCDC-****** contains the supplementary crystallographic data for this paper. These data can be obtained free of charge at www.ccdc.cam.ac.uk/conts/retrieving.html [or from the Cambridge Crystallographic Data Center, 12 Union Road, Cambridge CB2 1EZ, UK; fax: (internat.) +44-1223/336-033; E-mail: deposit@ccdc.cam.ac.uk].

NOTE: The International Union of Crystallography has set up a free service to check CIF files. This is based on a rich set of experience with such data: "Checkcif" thoroughly examines crystallographic data in the CIF format for completeness and consistency, and performs geometry and symmetry checks to detect possible errors of analysis, such as high residual electron densities. Authors who submit manuscripts with structural analyses (to be deposited with either FIZ or CCDC) are kindly asked to supply the report generated by the checkcif service.

Finally, before you return your revised manuscript, please update your database entry if necessary.

7. Electronic Supporting Information

A manuscript may include Electronic Supporting Information which will be accessible only on the WWW. Authors must keep a copy to make available to readers who do not have access to the internet. As this material [text, tables, schemes, figures **but not crystallographic (CIF) data** which must be submitted to either the FIZ or the CCDC] undergoes the peer review process, it must be included, clearly marked as "Supporting Information to be published electronically", when the paper is submitted. The following file formats are accepted: MS Winword or ASCII (*.doc, *.txt), MS Excel (*.xls), Encapsulated Postscript (*.eps), Portable Document Format (*.pdf), graphics embedded in MS Winword; if you wish to submit other formats, please consult the Editorial Office. When preparing such material, authors should keep in mind that — once accepted — it will be made available as provided by the author and not edited. Material accepted for electronic publication will be available mostly as PDF files (Adobe Acrobat Reader required) by following the Table of Contents link of EurJIC's WWW home page. A standard text will be added on the first page of the article in the printed version:

- Supporting information for this article is available on the WWW under http://www.eurjoc.org or from the author.

The supporting information file must start with the title of the paper, the authors, and the CASSI abbreviation of the journal to which it was submitted (e.g. *Eur. J. Inorg. Chem.*).

8. Basic Keyword List

An interjournal browsing facility has been developed for the readers of the WILEY-VCH journals *Advanced Synthesis and Catalysis, Angewandte Chemie International Edition, Chemistry − A European Journal, European Journal of Inorganic Chemistry, European Journal of Organic Chemistry, Zeitschrift für Anorganische und Allgemeine Chemie*, and the precursor journals *Chemische Berichte, Liebigs Annalen*, and *Journal für Praktische Chemie*. On the Internet you will be able to jump between thematically related contributions by mouse click.
To be able to offer this option on the WWW we have compiled a common keyword catalogue that is printed here and is also available online (http://www.eurjic.org).

To assist you in finding keywords they are listed according to categories. You may choose keywords from any category. As with all such records, a few guidelines facilitate the catalogue's use, and these are briefly explained below:
1. As many as possible, but at least two, of the maximum of five keywords assigned to an article must come from this list.
2. Named reactions will be incorporated only in exceptional cases. Generally the reaction type is selected instead. For example, Diels-Alder reactions will be found under "Cycloadditions" and Claisen rearrangements under "Rearrangements".
3. Heteroanalogues of compounds are mainly classified under the C variants, for example, (hetero)cumulenes, (hetero)dienes. A few aza and phospha derivatives are exceptions.
4. Compounds with inorganic components that are central to the article are listed under the element, for instance, iron complexes under "Iron". Some group names like "Alkali metals" exist alongside the names of important members of the group like "Lithium". In such cases the group name is used for these members only when comparative studies are described. The members not appearing separately are also categorised under the group name.
5. A keyword in the form "N ligand" is only chosen if a considerable portion of the paper deals with the coordination of any ligand ligating through the atom concerned.
6. Spectroscopic methods are assigned as keywords only if the article is about the method itself, or if the spectroscopic technique has made an important contribution to the problem under investigation.
7. "Structure elucidation" is intended only if the crux of the paper is a structural elucidation or if a combination of several spectroscopic techniques were needed for conclusive solution of the structure.
8. An attempt has been made to avoid synonyms and to select more general concepts rather than specialized terms. Thus the term "Double-decker complexes" is excluded in favour of "Sandwich complexes".

This list will be a "living" catalogue to be flexible enough to absorb the new developments in chemistry. We therefore welcome all suggestions from our authors that might improve its user-friendliness.

 © 2004 Wiley-VCH Verlag GmbH & Co. KGaA, Weinheim

Guidelines for Authors

Analytical Chemistry and Spectroscopic Methods

Analytical methods
Circular dichroism
Cyclic voltammetry
Electron diffraction
Electron microscopy
Electrophoresis
ENDOR spectroscopy
EPR spectroscopy
EXAFS spectroscopy
Fluorescence spectroscopy
Gas chromatography
High-throughput screening
Ion chromatography
Ion exchange
IR spectroscopy
Isotopic labeling
Laser spectroscopy
Liquid chromatography
Luminescence
Mass spectrometry
Moessbauer spectroscopy
Neutron diffraction
NMR spectroscopy
Photoelectron spectroscopy
Plasma chemistry
Raman spectroscopy
Rotational spectroscopy
Scanning probe microscopy
Sensors
Surface analysis
Trace analysis
Surface plasmon resonance
UV/Vis spectroscopy
Vibrational spectroscopy
Water chemistry
X-ray absorption spectroscopy
X-ray diffraction
ZEKE spectroscopy

Biological Chemistry and Chemical Biology (including Biochemistry, Bioinorganic Chemistry, Bioorganic Chemistry, Medicinal Chemistry, and Molecular and Cell Biology

Allosterism
Amino acids
Angiogenesis
Antibiotics
Antibodies
Antifungal agents
Antigens
Antisense agents
Antitumor agents
Antiviral agents
Azapeptides
Azasugars
Bioinformatics
Bioinorganic chemistry
Biological activity
Biomimetic synthesis
Bioorganic chemistry
Biophysics
Biosensors
Biosynthesis
Biotransformations
C-Glycosides
Carbohydrates
Carbon dioxide fixation
Carotenoids
Cell adhesion
Cell recognition
Cerebrosides
Chaperone proteins
Cobalamines
Cofactors
Combinatorial chemistry
Cyclitols
Cyclodextrins
Cytokines
DNA
DNA cleavage
DNA damage
DNA methylation
DNA recognition
DNA replication
DNA structures
Dopamines
Drug delivery
Drug design
Electron transport
Enzyme models
Enzymes
Fibrous proteins
Fluorescent probes
Gene expression
Gene sequencing
Gene technology
Genomics
Glycoconjugates
Glyolipids
Glycopeptides
Glycoproteins
Glycosides
Glycosylation
Growth factors
Helical structures
Heme proteins
Hormones
Hydrolases
Immobilization
Immunoassays
Immunochemistry
Immunology
Inhibitors
Ion channels
Ionophores
Isomerases
Ligases
Lipids
Lipophilicity
Lipoproteins
Liposomes
Lyases
Medicinal chemistry
Membrane proteins
Membranes
Metabolism
Metalloenzymes
Metalloproteins
Micelles
Molecular evolution
mRNA
Mutagenesis
Natural products
Neurochemistry
Neurotransmitters
Nitrogen fixation
Nitrogenases
Nucleic acids
Nucleobases
Nucleosides
Nucleotides
Oligonucleotides
Oligosaccharides
Oligoreductases
Peptide nucleic acids
Peptides
Peptidomimetics
Pheromones
Phospholipids
Photoaffinity labeling
Photosynthesis
Phytochemistry
Polyketides
Polymerase chain reaction
Prodrugs
Prostaglandins
Protein design
Protein engineering
Protein folding
Protein models
Protein modifications
Protein structures
Proteins
Proteomics
Proton transport
Radiopharmaceuticals
Receptors
Redox chemistry
Ribonucleosides
Ribozymes
RNA
RNA recognition
RNA structures
Sensitizers
Sequence determination
Sialic acids
Siderophores
Signal transduction
Sphingolipids
Steroids
Structure-activity relationships
Terpenoids
Toxicology
Transferases
tRNA
Vesicles
Vitamins

Catalysis

Asymmetric catalysis
Autocatalysis
Biphasic catalysis
Catalytic antibodies
Enzyme catalysis
Heterogeneous catalysis
Homogeneous catalysis
Phase-transfer catalysis
Supported catalysts

 © 2004 Wiley-VCH Verlag GmbH & Co. KGaA, Weinheim

Coordination Chemistry: Compound Classes

Cage compounds
Chelates
Clathrates
Cluster compounds
Cuprates
Dendrimers
Heterometallic complexes
Metallacycles
Metallocenes
Nitrogen oxides
Polyoxometalates
Sandwich complexes
Ylides

Coordination Chemistry: Ligand Classes

Alkene ligands
Alkyne ligands
Allyl ligands
Arene ligands
As ligands
Bridging ligands
Carbene ligands
Carbonyl ligands
Carboxylate ligands
Carbyne ligands
Cyclopentadienyl ligands
Diene ligands
Dioxygen ligands
Hydride ligands
Isocyanide ligands
Macrocyclic ligands
N ligands
N,O ligands
N,P ligands
O ligands
Oxo ligands
P ligands
Peroxo ligands
Phosphane ligands
P ligands
S ligands
Si ligands
Tridentate ligands
Tripodal ligands
Vinylidene ligands

Coordination Chemistry: Methodology and Reactions

Carbon dioxide fixation
Chemical vapor deposition
Chiral resolution
Crystal engineering
Ligand design
Matrix isolation
Metathesis
Neighboring-group effects
Nitrogen fixation
O-O activation
Oxidation
Radical reactions
Reduction
Ring-opening polymerization
Solvent effects
Solvolysis
Substituent effects
Template synthesis

Coordination Chemistry: Structure

Agostic interactions
Aurophilicity
Charge transfer
Cooperative effects
Coordination modes
Donor-acceptor systems
Electron deficient compounds
Electronic structure
Electrostatic interactions
Fluxionality
Helical structures
Host-guest systems
Hydrogen bonds
Inclusion compounds
Isolobal relationship
Jahn-Teller distortion
Ligand effects
Metal-metal interactions
Multiple bonds
Noncovalent interactions
Pi interactions
Stacking interactions
Structure elucidation
Through-bond interactions
Through-space interactions

Elements and Element Groups

Actinides
Alkali metals
Alkaline earth metals
Aluminum
Antimony
Argon
Arsenic
Barium
Beryllium
Bismuth
Boron
Bromine
Cadmium
Calcium
Carbon
Cerium
Cesium
Chalcogens
Chlorine
Chromium
Cobalt
Copper
Deuterium
Fluorine
Gallium
Germanium
Gold
Group 13 elements
Group 14 elements
Hafnium
Halogens
Helium
Hydrogen
Indium
Iodine
Iridium
Iron
Krypton
Lanthanides
Lanthanum
Lead
Lithium
Magnesium
Manganese
Mercury
Molybdenum
Neon
Nickel
Niobium
Nitrogen
Noble gases
Osmium
Oxygen
Palladium
Phosphorus
Platinum
Pnicogens
Potassium
Rare earths
Rhenium
Rhodium
Rubidium
Ruthenium
Samarium

 © 2004 Wiley-VCH Verlag GmbH & Co. KGaA, Weinheim

Scandium
Selenium
Silicon
Silver
Sodium
Strontium
Sulfur
Tantalum
Technetium
Tellurium
Thallium
Tin
Titanium
Tungsten
Uranium
Vanadium
Xenon
Ytterbium
Yttrium
Zinc
Zirconium

Environmental and Atmospheric Chemistry

Anions
Atmospheric chemistry
Cations
Chlorine
Computer chemistry
Crop protection agents
Cycloaddition
Denitrification
Desulfurization
Environmental chemistry
Fluorine
Gas-phase reactions
Green chemistry
Halogenation
Kinetics
Molecular dynamics
Molecular modeling
Nitrogen oxides
Oxidation
Ozone
Peroxides
Photochemistry
Photolysis
Photooxidation
Radical ions
Radical reactions
Radicals
Reaction mechanisms
Reaction intermediates
Sensors
Toxicology
Trace analysis
Waste prevention
Water chemistry

Inorganic Chemistry

Alanes
Allotropy
Alloys
Aluminosilicates
Amalgams
Amorphous materials
Anions
Automerization
Autoxidation
Azides
Bond theory
Boranes
Borates
Carbene homologues
Carbides
Carboranes
Cations
Chain structures
Chromates
Clathrates
Cluster compounds
Cyanides
Electron-deficient compounds
Fluorides
Halides
High-pressure chemistry
Host-guest systems
Hydrates
Hydrides
Hypervalent compounds
Inclusion compounds
Intercalations
Intermetallic phases
Isoelectronic analogues
Isomers
Layered compounds
Lewis acids
Lewis bases
Main group elements
Metal-metal interactions
Mixed-valent compounds
Nitrides
Nonstoichiometric compounds
Organic-inorganic hybrid composites
Perovskite phases
Peroxides
Phosphaalkenes
Phosphaalkynes
Phosphanes
Phosphazenes
Platinates
Pnictides
Polyanions
Polycations
Polychalcogenides
Polyhalides
Polymorphism
Polyoxometalates
Radical ions
Radicals
Silanes
Silicates
Sol-gel processes
Solid-phase synthesis
Solid-state reactions
Solid-state structures
Solvothermal synthesis
Spinel phases
Stannanes
Subvalent compounds
Synthesis design
Titanates
Topochemistry
Transition metals
Transuranium elements
Valence isomerization
Vanadates
Zeolite analogues
Zeolites
Zincates
Zintl anions
Zintl phases

Materials Science: General

Alloys
Amorphous materials
Automerization
Block copolymers
Ceramics
Charge-carrier injection
Chemical vapor deposition
Chemical vapor transport
Clays
Cluster compounds
Colloids
Conducting materials
Copolymerization
Crystal engineering
Crystal growth
Cyclooligomerization
Cyclotrimerization
Dendrimers
Doping
Energy conversion
Fullerenes
Gels
Glasses
Holography
Imprinting
Intercalations
Interfaces
Intermetallic phases
Ladder polymers
Layered compounds
Liquid crystals
Materials science
Membranes
Mesophases
Mesoporous materials
Metal-metal interactions

 © 2004 Wiley-VCH Verlag GmbH & Co. KGaA, Weinheim

Metallomesogens
Micelles
Microporous materials
Monolayers
Nanostructures
Nanotechnology
Nanotubes
Nonlinear optics
Polymerization
Polymers
Ring-opening polymerization
Scanning probe microscopy
Semiconductors
Sensitizers
Sensors
Superconductors
Surface chemistry
Thin films
Vesicles
Zeolite analogues
Zeolites

Organic Chemistry: Compound Classes

Alcohols
Aldehydes
Alkaloids
Alkanes
Alkenes
Alkynes
Allenes
Allylic compounds
Amides
Amines
Amino acids
Amino alcohols
Amino aldehydes
Amphiphiles
Anhydrides
Anions
Annulenes
Arenes
Arynes
Azides
Azo compounds
Azomethine ylides
Betaines
Biaryls
Calixarenes
Carbanions
Carbenes
Carbenoids
Carbocations
Carbocycles
Carbohydrates
Carboxylic acids
Carotenoids
Catenanes
Cations
Cavitands
Crown compounds
Cryptands
Cumulenes
Cyanides
Cyanines
Cyclodextrins
Cyclophanes
Dendrimers
Diazo compounds
Dyes/Pigments
Enols
Enones
Enynes
Fatty acids
Fragrances
Fullerenes
Fused-ring systems
Heterocycles
Hydrazones
Hydrides
Hydrocarbons
Ketones
Lactams
Lactones
Ladder polymers
Macrocycles
Mannich bases
Medium-ring compounds
Metallacycles
Natural products
Nitrogen heterocycles
Oxygen heterocycles
Peroxides
Pheromones
Phosphorus heterocycles
Phthalocyanines
Polycycles
Polymethines
Porphyrinoids
Quinodimethanes
Quinones
Radical ions
Radicals
Rotaxanes
Schiff bases
Small ring systems
Spiro compounds
Steroids
Sulfonamides
Sulfur heterocycles
Surfactants
Terpenoids
Ylides
Zwitterions

Organic Chemistry: Methodology and Reactions

Acylation
Aldol reactions
Alkylation
Allylation
Amination
Annulation
Aromatic substitution
Aromaticity
Asymmetric amplification
Asymmetric catalysis
Asymmetric synthesis
Automerization
Autoxidation
Biomimetic synthesis
C-C activation
C-C coupling
C-H activation
C1 building blocks
Carbonylation
Chiral auxiliaries
Chiral pool
Cleavage reactions
Combinatorial chemistry
Cracking
Cross-coupling
Cyclization
Cycloaddition
Cyclotrimerization
Dehydrogenation
Dihydroxylation
Dimerization
Domino reactions
Electrocyclic reactions
Electrophilic addition
Electrophilic substitution
Elimination
Ene reaction
Epoxidation
Flash pyrolysis
Glycosylation
Grignard reaction
Halogenation
Heck reaction
High-pressure chemistry
Hydroamination
Hydroboration
Hydroformylation
Hydrogen transfer
Hydrogenation
Hydrolysis
Hydrosilylation
Hydrostannation
Hydroxylation
Immobilization
Insertion
Ionic liquids
Isomerization
Lithiation
Metalation
Michael addition
Molecular diversity
Multicomponent reactions
Nucleophilic addition
Nucleophilic substitution
Olefination
Oligomerization
Oxidation
Oxygenation
Ozonolysis
Perfluorinated ligands
Pericyclic reaction
Phosphorylation
Photooxidation
Polymerization
Protecting groups
Protonation
Radical reactions
Rearrangement
Reduction
Retro reactions
Ring contraction
Ring expansion
Sigmatropic rearrangement
Solid-phase synthesis
Solvent effects
Solvolysis
Steric hindrance
Substituent effects
Synthesis design
Synthetic methods
Template synthesis
Topochemistry
Total synthesis
Transesterification
Umpolung
Wittig reactions

 © 2004 Wiley-VCH Verlag GmbH & Co. KGaA, Weinheim

Guidelines for Authors

Organic Chemistry: Stereochemistry and Structures

Atropisomerism
Chemoselectivity
Chiral resolution
Chirality
Configuration
determination
Conformation analysis
Conjugation
Enantioselectivity
Hyperconjugation
Kinetic resolution
Regioselectivity
Strained molecules
Structure elucidation
Tautomerism
Valence isomerization

Physical Chemistry (including Electrochemistry, Kinetics, Photochemistry, Radiochemistry, Thermodynamics and Theoretical Chemistry)

Ab initio calculations
Absorption
Acidity
Adsorption
Basicity
Biophysics
Bond energy
Bond theory
Calorimetry
CARS (Coherent Anti-Stokes Raman Scattering)
Charge carrier injection
Charge transfer
Chemisorption
Chromophores
Colloids
Computer chemistry
Conducting materials
Conical intersections
Crystal engineering
Crystal growth
Cyclic voltammetry
Density functional calculations
Donor-acceptor systems
Doping
Electrochemistry
Electron microscopy
Electron transfer
ELF (Electron Localization Function)
Energy conversion
Exchange interactions
Femtochemistry
Fluorescence
Fluorescent probes
Fractals
FRET (Fluorescence Resonant Energy Transfer)
Gas-phase reactions
Gels
Glasses
Group theory
Heats of formation
High-pressure chemistry
High-temperature chemistry
Hot-atom chemistry
Hydrophobic effect
Imaging agents
Intermediates
Ion pairs
Ion-molecule reactions
Ionization potentials
Isotope effects
Isotopes
Kinetics
Langmuir-Blodgett films
Laser chemistry
Lewis acids
Lewis bases
Linear free energy relationships
Liquid crystals
Liquids
Low-temperature chemistry
Magnetic properties (including magnetochemistry)
Matrix isolation
Mesophases
Metallomesogens
Metastable compounds
Microreactors
Molecular dynamics
Molecular electronics
Molecular modeling
Monolayers
Nanotechnology
Neighboring-group effects
Nonequilibrium processes
Phase diagrams
Phase transitions
Photochemistry
Photochromism
Photolysis
Physisorption
Plasma chemistry
Polarized spectroscopy
Quantum chemistry
Radiochemistry
Radiopharmaceuticals
Reaction mechanisms
Reactive intermediates
Redox chemistry
Salt effect
Semiempirical calculations
Single-molecule studies
Singlet oxygen
Sol-gel processes
Solvatochromism
Spin crossover
Statistical mechanics
Statistical thermodynamics
Structure-activity relationships
Superacidic systems
Supercritical fluids
Thermochemistry
Thermodynamics
Time-resolved spectroscopy
Transition states
Viruses
Voltammetry

Supramolecular Chemistry

Aggregation
Host-guest systems
Molecular devices
Molecular evolution
Molecular recognition
Nanostructures
Pi interactions
Receptors
Self-assembly
Supramolecular chemistry

 © 2004 Wiley-VCH Verlag GmbH & Co. KGaA, Weinheim